The Chemistry of the Actinide and Transactinide Elements

Third Edition

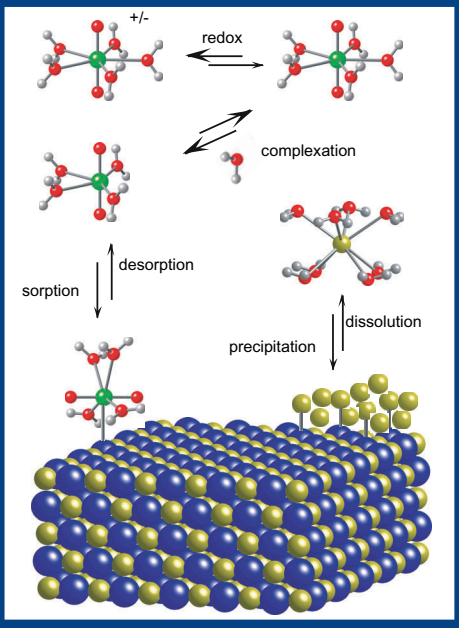

Edited by
Lester R. Morss,
Norman M. Edelstein &
Jean Fuger

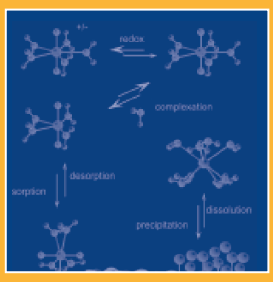

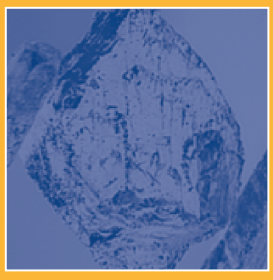

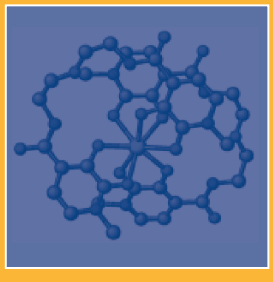

THE CHEMISTRY OF THE ACTINIDE AND TRANSACTINIDE ELEMENTS

Joseph J. Katz

Glenn T. Seaborg

This work is dedicated to
Joseph J. Katz and Glenn T. Seaborg,
authors of the first and second editions of
The Chemistry of the Actinide Elements
and leaders in the field of actinide chemistry.

THE CHEMISTRY OF THE ACTINIDE AND TRANSACTINIDE ELEMENTS

THIRD EDITION

Volume 1

EDITED BY

Lester R. Morss
Argonne National Laboratory,
Argonne, Illinois, USA

Norman M. Edelstein
Lawrence Berkeley National Laboratory,
Berkeley, California, USA

Jean Fuger
University of Liège,
Liège, Belgium

Honorary Editor
Joseph J. Katz
Argonne National Laboratory

Springer

Library of Congress Control Number: 2008922620

ISBN-10 1-4020-3555-1 (HB)
ISBN-10 1-4020-3598-5 (e-book)
ISBN-13 978-1-4020-3555-5 (HB)
ISBN-13 978-1-4020-3598-2 (e-book)

Published by Springer,
P.O. Box 17, 3300 AA Dordrecht, The Netherlands.

www.springer.com

Printed on acid-free paper

First published in 2006
Reprinted 2006
Reprinted with corrections in 2008

CONTENTS

Volume 1

Volume 2

Volume 3

Volume 4

Volume 5

CONTRIBUTORS

Irshad Ahmad
Argonne National Laboratory, USA

Thomas E. Albrecht-Schmitt
Auburn University, Alabama, USA

Mark R. Antonio
Argonne National Laboratory, USA

A. J. Arko
Los Alamos National Laboratory, USA (retired)

James V. Beitz
Argonne National Laboratory, USA (retired)

Jean Blaise
Laboratoire Aimé Cotton, Orsay, France

Jean-Philippe Blaudeau
High Performance Technologies, Inc., Wright-Patterson Air Force Base, Ohio, USA

Nicholas J. Bridges
The University of Alabama, USA

Edgar C. Buck
Pacific Northwest National Laboratory, Richland, Washington, USA

Carol J. Burns
Los Alamos National Laboratory, USA

Bruce E. Bursten
The University of Tennessee, USA

Gregory R. Choppin
Florida State University, USA

David L. Clark
Los Alamos National Laboratory, USA

Claude Degueldre
Paul Scherrer Institute, Switzerland

Peter K. Dorhout
Colorado State University, USA

Janusz Drożdżyński
University of Wroclaw, Poland

Patricia W. Durbin
Lawrence Berkeley National Laboratory, USA

Norman M. Edelstein
Lawrence Berkeley National Laboratory, USA

Moris S. Eisen
Technion -Israel Institute of Technology, Israel

P. Gary Eller
Los Alamos National Laboratory, USA (retired)

Mark Fred
Argonne National Laboratory, USA (deceased)

Blandine Fourest
Institut de Physique Nucléaire, Orsay, France

Jean Fuger
University of Liège, Belgium

Takeo Fujino
Tohoku University, Japan (retired)

Ingmar Grenthe
Royal Institute of Technology, Stockholm, Sweden

Keith E. Gutowski
The University of Alabama, USA

Richard G. Haire
Oak Ridge National Laboratory, USA

John M. Haschke
Actinide Science Consulting, Harwood, TX, USA

Ladia Havela
Charles University, Czech Republic

P. Jeffrey Hay
Los Alamos National Laboratory, USA

Siegfried S. Hecker
Los Alamos National Laboratory, USA

David E. Hobart
Los Alamos National Laboratory, USA

Darleane C. Hoffman
Lawrence Berkeley National Laboratory, USA

Gordon D. Jarvinen
Los Alamos National Laboratory, USA

Mark P. Jensen
Argonne National Laboratory, USA

Stephen G. Johnson
Idaho National Laboratory, USA

John J. Joyce
Los Alamos National Laboratory, USA

Nikolas Kaltsoyannis
University College London, UK

Joseph J. Katz
Argonne National Laboratory, USA (retired)

Takaumi Kimura
Japan Atomic Energy Agency, Japan

Harold W. Kirby *(deceased)*
Mound Laboratory, Miamisburg, Ohio, USA

Rudy J. M. Konings
European Commission, Joint Research Centre
Institute for Transuranium Elements, Karlsruhe, Germany

John R. Krsul
Argonne National Laboratory, USA (retired)

Jérôme Lacquement
CEA-Valrho, Marcoule, France

Gerard H. Lander
European Commission, Joint Research Centre
Institute for Transuranium Elements, Karlsruhe, Germany

Diana M. Lee
Lawrence Berkeley National Laboratory, USA

Jun Li
Pacific Northwest National Laboratory, Richland, Washington, USA

Guokui Liu
Argonne National Laboratory, USA

Gregg J. Lumetta
Pacific Northwest National Laboratory, Richland, Washington, USA

Charles Madic
CEA-Saclay, Gif-sur-Yvette, France

Jagdish N. Mathur
Bhabha Atomic Research Centre, Mumbai, India

Lester R. Morss
Argonne National Laboratory (retired) and
U.S. Department of Energy, Washington DC, USA

Boris F. Myasoedov
Russian Academy of Sciences, Moscow, Russia

Kenneth L. Nash
Washington State University, USA

Mary P. Neu
Los Alamos National Laboratory, USA

Robert A. Penneman
Los Alamos National Laboratory, USA (retired)

Valeria Pershina
Gesellschaft für Schwerionenforschung, Darmstadt, Germany

Joseph R. Peterson
The University of Tennessee, USA and
Oak Ridge National Laboratory, USA (retired)

Robin D. Rogers
The University of Alabama, USA

Wolfgang Runde
Los Alamos National Laboratory, USA

Wallace W. Schulz
Albuquerque, New Mexico, USA

Robert J. Silva
Lawrence Livermore National Laboratory, USA (retired)

Lynda Soderholm
Argonne National Laboratory, USA

Jerry L. Stakebake
Boulder, Colorado, USA

Ivan G. Tananaev
Russian Academy of Sciences, Moscow, Russia

Major C. Thompson
Savannah River National Laboratory, USA (retired)

Norbert Trautmann
Universität Mainz, Germany

Mathias S. Wickleder
Carl von Ossietzky Universität, Oldenburg, Germany

Stephen F. Wolf
Indiana State University, Terre Haute, Indiana, USA

Earl F. Worden, Jr.
Lawrence Livermore National Laboratory, USA (retired)

Jean-François Wyart
Laboratoire Aimé Cotton, Orsay, France

Zenko Yoshida
Japan Atomic Energy Agency, Japan

PREFACE

The first edition of this work (*The Chemistry of the Actinide Elements* by J. J. Katz and G. T. Seaborg) was published in 1957, nearly a half century ago. Although the chemical properties of thorium and uranium had been studied for over a century, and those of actinium and protactinium for over fifty years, all of the chemical properties of neptunium and heavier elements as well as a great deal of uranium chemistry had been discovered since 1940. In fact, the concept that these elements were members of an "actinide" series was first enunciated in 1944. In this book of 500 pages the chemical properties of the first transuranium elements (neptunium, plutonium, and americium) were described in great detail but the last two actinide elements (nobelium and lawrencium) remained to be discovered. It is not an exaggeration to say that *The Chemistry of the Actinide Elements* expounded a relatively new branch of chemistry.

The second edition was published in 1986, by which time all of the actinide elements had been synthesized and chemically characterized, at least to some extent. At this time the chemistry of the actinide elements had reached maturity. The second edition filled two volumes, with a chapter for each of the elements (the elements beyond einsteinium were combined in one chapter) and systematic treatment of various aspects of the chemical and electronic properties of the actinide elements, ions, and compounds due to the filling of the 5f subshell. Six transactinide elements had been synthesized by 1986 but their experimentally determined chemical properties occupied only 1.5 pages of text in the second edition.

This edition was initiated by the editors of the second edition (J. J. Katz, G. T. Seaborg, and L. R. Morss) in 1997. They realized that the study of the chemical properties of the actinide elements had advanced to produce distinct subdisciplines of actinide chemistry, for example actinide coordination chemistry, actinide X-ray absorption spectroscopy, itinerancy in actinide intermetallics, organoactinide chemistry, and actinide environmental chemistry. These fields had sufficiently matured so that scientists could make more substantial contributions to predicting and controlling the fate of actinides in the laboratory, in technology, and in the environment. We now understand and are able to predict with some degree of confidence the chemical bonding and reactivity of actinides in actinide materials, in actual environmental matrices and in proposed nuclear waste repositories. Most of the unique properties of the actinides are caused by their accessible and partly filled 5f orbitals. In addition to advances with the actinides, there have been research groups at nuclear research centers in several countries that have dedicated themselves to carry out significant and systematic experimental studies on the transactinide elements for several decades. For these reasons the editors initiated the writing of a third edition, with the

enlarged title *The Chemistry of the Actinide and Transactinide Elements* that is both broader and deeper than the second edition.

The third edition follows the plan enunciated by the authors of the first edition: "This book is intended to provide a comprehensive and uniform treatment of the chemistry of the actinide [and transactinide] elements for both the nuclear technologist and the inorganic and physical chemist." To fulfill this plan consistent with the maturity of the field, the third edition is organized in three parts.

The first group of chapters follows the format of the first and second editions by beginning with chapters on individual elements or groups of elements that describe and interpret their chemical properties. A chapter on the chemical properties of the transactinide elements is included.

The second group, chapters 15-26, summarizes and correlates physical and chemical properties that are in general unique to the actinide elements, because most of these elements contain partially-filled shells of 5f electrons whether present as isolated atoms or ions, as metals, as compounds, or as ions in solution.

The third group of chapters (chapters 27-31) focuses on specialized topics that encompass contemporary fields related to actinide species in the environment, in the human body, and in storage or wastes. There are also two appendices that tabulate important nuclear properties of all actinide and transactinide isotopes.

Each chapter has been written to provide sufficient background for the substantial parts of the readership that are not specialists in actinide science, nuclear-science-related areas (nuclear physics, health physics, nuclear engineering), spectroscopy, or solid-state science (metallurgy, solid state physics). The editors hope that this work educates and informs those readers who are scientists and engineers that are unfamiliar with the field and wish to learn how to deal with actinides in their research or technology.

The editors are deeply indebted to the contributors of each chapter, all of whom agreed enthusiastically to write their chapters and all of whom did so as a labor of love as well as a long-term professional responsibility. We take special pleasure in thanking Dr. Emma Roberts, Senior Publishing Editor of Springer, who provided the resources to turn more than thirty manuscripts into this attractive and useful professional series of volumes. We also thank Roger Wayman and Aaliya Jetha of Springer and all the other professional staff at Springer and SPI Publisher Services who brought this work to completion.

The editors dedicate this work to Joseph J. Katz and Glenn T. Seaborg, the first authors of the first edition and second editions of *The Chemistry of the Actinide Elements.* They provided inspiration for the generations of scientists who followed them and they set high standards in their research. Dr. Katz guided and motivated the editors and authors of the third edition to produce a work that followed the model of the first and second editions and provided leadership as this edition was unfolding. Because of his insights and leadership as an inorganic, physical, and actinide chemist, we have asked Dr. Katz to be

listed on the title page as honorary editor, and he has agreed to accept this role. The editors also dedicate this work to the memory of Professor Seaborg, the co-discover of plutonium and many other actinide and transactinide elements, and pioneer in actinide chemistry. We note with sadness that he participated in planning this edition but passed away before any of the chapters had been written. We believe that he would have been pleased to see how productive has been the research of the authors and many other actinide and transactinide scientists who follow his leadership.

All of us who have participated in the writing, editing, and publishing *The Chemistry of the Actinide and Transactinide Elements* express our hope that this new edition will make a substantive contribution to research in actinide and transactinide science, and that it will be an appropriate source of factual information on these elements for teachers, researchers, and students and for those who have the responsibility for utilizing the actinide elements to serve humankind and to control and mitigate their environmental hazards.

Lester R. Morss
Norman M. Edelstein
Jean Fuger

CHAPTER ONE

INTRODUCTION

Joseph J. Katz, Lester R. Morss,
Norman M. Edelstein, and Jean Fuger

The actinide elements are the 15 chemical elements with atomic numbers 89 through 103, the first member of which is actinium and the last member is lawrencium (Fig. 1.1). The transactinide elements (those beyond the actinides) are the heaviest known chemical elements. Both the actinide and the transactinide elements have chemical properties that are governed by their outermost electronic subshells. Each of these groups of elements is a unique transition series (a group of elements in which d or f electronic subshells are being filled).

The actinides are the transition elements that fill the 5f subshell. The actinide series is unique in several respects:

- Most of the elements (those heavier than uranium) were first discovered by synthetic methods: bombardment of heavy atoms with neutrons in nuclear reactors, bombardment with other particles in accelerators, or as the result of nuclear detonations.
- All actinide isotopes are radioactive, with a wide range of nuclear properties, especially that of spontaneous and induced nuclear fission.
- They are all metals with very large radii, and exist in chemical compounds and in solution as cations with very large ionic radii.
- The metals exhibit an unusual range of physical properties. Plutonium, with six allotropes, is the most unusual of all metals.
- Many of the actinide elements have a large number of oxidation states. In this respect plutonium is unique, being able to exist in aqueous solution simultaneously in four oxidation states.
- In metallic materials and in some other compounds with elements lighter than plutonium, the 5f orbitals are sufficiently diffuse that the electrons in these orbitals are "itinerant" (delocalized, chemically bonding, often with unique magnetic moments and electrical conductivity). In metallic materials and in most compounds with elements heavier than plutonium the 5f electrons are "localized" (not contributing significantly to electrical conductivity or to chemical bonds). Materials with plutonium and adjacent

elements can exhibit both itinerant and localized behavior, depending on conditions such as temperature and applied pressure.

- Actinium (which has no 5f electrons in the metal, free atom, or in any of its ions) and the elements americium through lawrencium are similar in many respects to the lanthanide elements (the elements that fill the 4f electron subshell). The elements thorium through neptunium have some properties similar to those of the d transition elements.
- Relativistic contributions to electronic properties and spin–orbit effects are important in the chemical properties of actinides.

The transactinide elements are at the frontier of both the periodic table (Fig. 1.1) and the chart of the nuclides. Transactinide chemistry has been in existence since 1970. Although these elements have unique properties, they are very difficult to study because their synthesis and identification require unique nuclear reactions and rapid separations. The heaviest transactinide element for which chemical properties have been identified (at the time of writing of this work) is hassium (atomic number 108). Experimental evidence and theoretical studies to date indicate that the elements through 112 are part of a 6d transition series of elements.

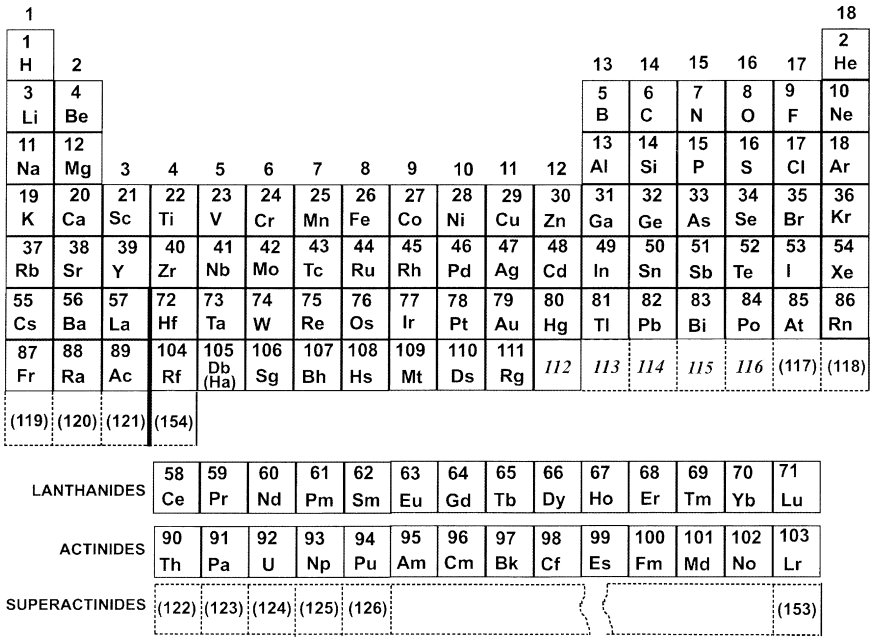

Fig. 1.1 *The periodic table of the elements, showing placement of transactinides and superactinides through element* 154 (*see Chapter* 14). (*Italics indicate elements reported but not yet confirmed as of* 2005. *Undiscovered elements are shown in parentheses.*)

The transactinides are also unique in several respects:

- One-atom-at-a-time chemistry is required to compensate for low nuclear yields and short isotopic half-lives. Ingenious techniques have been developed to study their chemical properties in both gas phase and solution.
- Relativistic effects cause substantial contraction of the 7s (occupied), 7p (empty), and 6d (partially filled) orbitals. (Many electronic configurations have been calculated; see Chapter 14.) The contraction of the 7s orbitals stabilizes the $7s^2$ electron pair. The contraction of the 7p orbitals makes 7p terms accessible, e.g., the first excited multiplet of rutherfordium (element 104) outside the [Xe $5f^{14}$] core is calculated to be $6d7s^27p$.
- The first part of the transactinides constitutes a 6d transition series, with the calculated ionic radii intermediate between those of the 5d ions and actinide ions of the same charge. Relativistic effects decrease the polarizability of transactinide ions.
- Fundamental properties – electronic configurations, ionization energies of atoms and ions, oxidation–reduction potentials in solution – remain to be calculated theoretically and measured experimentally.

In the six decades that have elapsed since the "actinide concept" was enunciated by G. T. Seaborg, great advances have taken place in actinide and transactinide chemistry. As in many other important areas of science, new information and new concepts have accumulated to an extraordinary extent. This, in itself, would be ample justification for a comprehensive examination of the scientific aspects of the actinide elements. Of equal, or perhaps even greater, importance in the preparation of this third edition are the contributions that its many authors have made to provide the foundations for the solution of some of the most urgent technological and environmental problems that face humanity worldwide. We refer, of course, to the problems created by nuclear reactors used for electricity production; nuclear weapons production and dismantlement; the treatment and storage of nuclear wastes; and the cleanup of Cold War nuclear material sites. These are sources of acute global concern, in all of which the actinide elements are intimately involved.

In 1957, when the first edition of this work was published, the chemistry of the actinide elements was remarkably well developed, considering that the actinide concept itself had first been publicly described in 1945. (See Chapter 15, section 1.2, of this book) The elements thorium and uranium had already been studied by chemists for more than 100 years. Uranium enjoyed some small distinction as the heaviest element in nature, and as the terminus of the classical periodic table. In 1895 Becquerel had discovered that uranium undergoes radioactive decay, a discovery that permanently divested uranium of its obscurity, and that inaugurated the era of the Curies, Rutherford, Soddy, Hahn and Meitner, Fajans, and others who mapped the very complex radioactive transformations of the naturally occurring elements. The crucial importance of uranium, however, became fully apparent only after Fermi and his colleagues irradiated many of the

elements, including uranium, with neutrons in the 1930s. They produced new radioactive species with chemical properties that were not identical with any of the known heavy elements. The Fermi group believed that they had created new elements heavier than uranium. In 1938 Hahn, Meitner, and Strassmann conducted definitive chemical experiments showing that the radioactive species produced by neutron irradiation of uranium were in fact fission fragments resulting from the cleavage of the uranium nucleus into smaller nuclei. Their experiments constituted the discovery of nuclear fission. The earlier formation of transuranium elements had been disproved, but the way to their synthesis was now open.

The first transuranium element, neptunium, was nevertheless the by-product of an investigation by McMillan and Abelson into the details of the fission process. While fission fragments recoil with enormous energy from a uranium nucleus undergoing fission, a radioactive species with a half-life of 2.3 days was observed to be formed with insufficient energy to escape from a thin film of irradiated uranium. Chemical investigation confirmed that a new element, neptunium, unknown in nature, with atomic number 93 and mass number 239, had been formed by neutron capture in ^{238}U.

$$^{238}_{92}\mathrm{U} + ^{1}_{0}\mathrm{n} \rightarrow ^{239}_{92}\mathrm{U} \xrightarrow[23.5\,\mathrm{min}]{\beta^-} ^{239}_{93}\mathrm{Np} \quad (t_{1/2} = 2.36 \text{ days}) \tag{1.1}$$

The new prospects opened up by the discovery of the first transuranium element were rapidly explored, and soon the trickle became a flood. Table 1.1 lists the transuranium elements, the discoverers and the date of discovery, and the date of first isolation in weighable amount. The first of the transuranium elements to be synthesized on purpose, so to speak, was element 94 as the isotope of mass number 238. In 1940, Seaborg, McMillan, Kennedy, and Wahl at the University of California in Berkeley bombarded uranium oxide with 16 MeV deuterons produced in the 60 in. cyclotron and succeeded in isolating a long-lived alpha-particle emitter, chemically separable from both uranium and neptunium, which was identified as an isotope of element 94 and later given the name plutonium:

$$^{238}_{92}\mathrm{U} + ^{2}_{1}\mathrm{H} \rightarrow ^{238}_{93}\mathrm{Np} + 2^{1}_{0}\mathrm{n} \tag{1.2}$$

$$^{238}_{93}\mathrm{Np} \xrightarrow[2.1\mathrm{d}]{\beta^-} ^{238}_{94}\mathrm{Pu} \quad (t_{1/2} = 87.7 \text{ years}) \tag{1.3}$$

Twenty isotopes of plutonium are now known. The plutonium isotope of major importance has always been the isotope of mass number 239. Research with ^{239}Pu has been strongly motivated by the fact that it was shown to be fissile by slow neutrons in the same way as ^{235}U, and would thus be able to sustain a neutron chain reaction. The isotope ^{239}Pu can thus be used for both military and nuclear energy purposes. To separate ^{235}U from ^{238}U requires an isotope separation of

Table 1.1 *The transuranium elements.*

Atomic number	*Element*	*Symbol*	*Discoverers and date of discovery*	*First isolation in weighable amount*
93	Neptunium	Np	E. M. McMillan and P. H. Abelson, 1940	L. B. Magnusson and T. J. LaChapelle, 1944
94	Plutonium	Pu	G. T. Seaborg, E. M. McMillan, J. W. Kennedy, and A. C. Wahl, 1940–41	
	Plutonium-239		J. W. Kennedy, G. T. Seaborg, E. Segrè, and A. C. Wahl, 1941	B. B. Cunningham and L. B. Werner, 1942
95	Americium	Am	G. T. Seaborg, R. A. James, L. O. Morgan, and A. Ghiorso, 1944–45	B. B. Cunningham, 1945
96	Curium	Cm	G. T. Seaborg, R. A. James, and A. Ghiorso, 1944	L. B. Werner and I. Perlman, 1947
97	Berkelium	Bk	S. G. Thompson, A. Ghiorso, and G. T. Seaborg, 1949	S. G. Thompson and B. B. Cunningham, 1958
98	Californium	Cf	S. G. Thompson, K. Street, Jr, A. Ghiorso, and G. T. Seaborg, 1950	B. B. Cunningham and S. G. Thompson, 1958
99	Einsteinium	Es	A. Ghiorso, S. G. Thompson, G. H. Higgins, G. T. Seaborg, M. H. Studier, P. R. Fields, S. M. Fried, H. Diamond, J. F. Mech, G. L. Pyle, J. R. Huizenga, A. Hirsch, W. M. Manning, C. I. Browne, H. L. Smith, and R. W. Spence, 1952	B. B. Cunningham, J. C. Wallmann, L. Phillips, and R. C. Gatti, 1961
100	Fermium	Fm	A. Ghiorso, S. G. Thompson, G. H. Higgins, G. T. Seaborg, M. H. Studier, P. R. Fields, S. M. Fried, H. Diamond, J. F. Mech, G. L. Pyle, J. R. Huizenga, A. Hirsch, W. M. Manning, C. I. Browne, H. L. Smith, and R. W. Spence, 1953	
101	Mendelevium	Md	A. Ghiorso, B. G. Harvey, G. R. Choppin, S. G. Thompson, and G. T. Seaborg, 1955	
102	Nobelium	No	A. Ghiorso, T. Sikkeland, J. R. Walton, and G. T. Seaborg, 1958	

Table 1.1 (*Contd.*)

Atomic number	*Element*	*Symbol*	*Discoverers and date of discovery*	*First isolation in weighable amount*
103	Lawrencium	Lr	A. Ghiorso, T. Sikkeland, A. E. Larsh, and R. M. Latimer, 1961	
104	Rutherfordium	Rf	A. Ghiorso, M. Nurmia, J. Harris, K. Eskola, and P. Eskola, 1969; Y. T. Oganessian, Y. V. Lobanov, S. P. Tretyakova, Y. A. Lasarev, I. V. Kolesov, K.A. Gavrilov, V. M. Plotko, and Y. V. Poluboyarinov, 1974	
105	Dubnium	Db	A. Ghiorso, M. Nurmia, K. Eskola, J. Harris, and P. Eskola, 1970; G. N. Flerov, Y.T. Oganessian, Y.V. Lobanov, Y. A. Lasarev, and S. P. Tretyakova, 1970	
106	Seaborgium	Sg	A. Ghiorso, J. M. Nitschke, J. R. Alonso, C. T. Alonso, M. Nurmia, G. T. Seaborg, E. K. Hulet, and R. W. Lougheed, 1974	
107	Bohrium	Bh	G. Münzenberg, S. Hofmann, F. P. Hessberger, W. Reisdorf, K. H. Schmidt, J. H. R. Schneider, P. Armbruster, C. C. Sahm, and B. Thuma, 1981	
108	Hassium	Hs	G. Münzenberg, P. Armbruster, H. Folger, F. P. Hessberger, S. Hofmann, J. Keller, K. Poppensieker, W. Reisdorf, K. H. Schmidt, H. J. Schott, M. E. Leino, and R. Hingmann, 1984	
109	Meitnerium	Mt	G. Münzenberg, P. Armbruster, F. P. Hessberger, S. Hofmann, K. Poppensieker, W. Reisdorf, J. R. H. Schneider, W. F. W. Schneider, K. H. Schmidt, C. C. Sahm, and D. Vermeulen, 1982	
110	Darmstadtium	Ds	S. Hofmann, V. Ninov, F. P. Hessberger, P. Armbruster, H. Folger, G. Münzenberg, H. J. Schött, A. G. Popeko, A. V. Yeremin, A. N. Andreyev, S. Saro, R. Janik, and M. Leino, 1995	

111	Roentgenium	Rg	S. Hofmann, V. Ninov, F. P. Hessberger, P. Armbruster, H. Folger, G. Münzenberg, H. J. Schött, A. G. Popeko, A. V. Yeremin, A. N. Andreyev, S. Saro, R. Janik, and M. Leino, 1995
112			S. Hofmann, F. P. Hessberger, D. Ackermann, G. Münzenberg, S. Antalic, P. Cagarda, B. Kindler, J. Kojouharova, M. Leino, B. Lonnel, R. Mann, A. G. Popeko, S. Reshitko, S. Saro, J. Uusitalo, and V. Yeremin, 2002[a]
113			Same as element 115[a]
114			Yu. Ts. Oganessian, V. K. Utyonkov, Yu. V. Lobanov, F. Sh. Abdullin, A. N. Polyakov, I. V. Shirokovsky, Yu. Ts. Tsyganov, G. G. Gulbekian, S. L. Bogomolov, B. N. Gikal, A. N. Metsentsev, S. Iliev, V. G. Subbotin, A. M. Sukhov, O. V. Ivanov, G. V. Buklanov, K. Subotic, M. G. Itkis, K. J. Moody, J. F. Wild, N. J. Stoyer, M. A. Stoyer, and R. W. Lougheed, 2000[a]
115			Yu. Ts. Oganessian, V. K. Utyonkov, Yu. V. Lobanov, F. Sh. Abdullin, A. N. Polyakov, I. V. Shirokovsky, Yu. Ts. Tsyganov, G. G. Gulbekian, S. L. Bogomolov, A. N. Metsentsev, S. Iliev, V. G. Subbotin, A. M. Sukhov, A. A. Voinov, G. V. Buklanov, K. Subotic, V. I. Zagrebaev, M. G. Itkis, J. J. Patin, K. J. Moody, J. F. Wild, M. A. Stoyer, N. J. Stoyer, D. A. Shaughnessy, J. M. Kenneally, and R. W. Lougheed, 2004[a]
116			Yu. Ts. Oganessian, V. K. Utyonkov, Yu. V. Lobanov, F. Sh. Abdullin, A. N. Polyakov, I. V. Shirokovsky, Yu. Ts. Tsyganov, G. G. Gulbekian, S. L. Bogomolov, B. N. Gikal, A. N. Metsentsev, S. Iliev, V. G. Subbotin, A. M. Sukhov, O. V. Ivanov, G. V. Buklanov, K. Subotic, M. G. Itkis, K. J. Moody, J. F. Wild, N. J. Stoyer, M. A. Stoyer, R. W. Lougheed, C. A. Laue, Ye. A. Karelin, and A. N. Tatarinov, 2000[a]

[a] Discovery claimed and published but not confirmed by IUPAC/IUPAP.

formidable proportions, but separating ^{239}Pu in pure form requires only a chemical separation from other elements, likewise an intimidating problem, but one that is in principle a considerably simpler undertaking.

In 1941, Kennedy, Seaborg, Segré, and Wahl successfully obtained ^{239}Pu by radioactive decay from ^{239}Np, which was first produced by irradiating natural ^{238}U with cyclotron-generated neutrons:

$$^{238}_{92}\mathrm{U} + {}^{1}_{0}\mathrm{n} \rightarrow {}^{239}_{92}\mathrm{U} + \gamma \tag{1.4}$$

$$^{239}_{92}\mathrm{U} \xrightarrow[23.5\ \mathrm{min}]{\beta^-} {}^{239}_{93}\mathrm{Np} \xrightarrow[2.36\ \mathrm{days}]{\beta^-} {}^{239}_{94}\mathrm{Pu} \quad (t_{1/2} = 24\,110\ \mathrm{years}) \tag{1.5}$$

The isotope plutonium-239 indeed turned out to be fissionable, with a slow neutron cross section 1.7 times that of uranium-235. Later work at the wartime Los Alamos Laboratory established conclusively that sufficient neutrons were emitted in the act of fission to sustain a nuclear chain reaction. The exigencies of World War II soon made available the massive resources necessary to convert the scientific possibilities of the transuranium elements into actuality, and the nuclear age was truly upon us. Seaborg (1982, 1992) has given a vivid eyewitness account of the discovery and early experiments with plutonium. This chronicle describes in unusual detail the problems that confronted the investigators in this strange and intimidating new field of research, and how they were solved.

Twelve transplutonium elements were added to the periodic table in the 30 years between 1944 and 1974. The syntheses of the elements with atomic number 95 through 106 required the development of new and ingenious experimental techniques as well as new conceptual frameworks, and these were elaborated with remarkable speed. Elements 95 and 96, named americium and curium, respectively, were first prepared in 1944 by bombardment of ^{239}Pu; curium was synthesized by irradiation of plutonium with helium ions (alpha particles), and soon thereafter americium was synthesized by multiple neutron capture in plutonium in a nuclear reactor. As was the case for neptunium and plutonium, chemical identification was essential; it was not until these elements were predicted to be part of an actinide (5f) transition series with +3 oxidation states that they were isolated and identified. By 1946 the chemical properties of americium and curium were already well defined, and by 1949 sufficient amounts of americium-241 and curium-242 had been accumulated to make it possible to undertake a search for the next members of the actinide series. Bombardment of elements 95 and 96 by helium ions accelerated in the 60 in. Berkeley cyclotron produced alpha-particle-emitting species that could be identified as isotopes of elements 97 and 98. These in turn were named berkelium and californium after their place of discovery. Again, prediction of their behavior as +3 ions in aqueous solution was essential. During this same period of time, magnetic and spectroscopic evidence confirmed that the transuranium elements were indeed members of a 5f series of elements; see the review by Gruen (1992).

The detonation of a thermonuclear device is capable of producing enormously high fluxes of neutrons. The first test thermonuclear explosion was set off at Eniwetok Atoll by the United States at the end of 1952. The huge numbers of neutrons produced by the explosion resulted in multineutron captures in the uranium-238 that was a part of the device. The capture of no fewer than 15 neutrons by a ^{238}U nucleus yielded an isotope of element 98:

$$^{238}_{92}U + 15\,^{1}_{0}n \rightarrow {}^{253}_{92}U \xrightarrow{\text{multiple } \beta^- \text{ decays}} {}^{253}_{98}Cf \tag{1.6}$$

Capture of the 15 neutrons must have been accomplished in a fraction of a microsecond, and the subsequent radioactive decay of uranium-253 via a series of beta-particle emissions to form californium-253 must have been completed in a short time. Californium-253 then undergoes decay by beta-particle emission (with a half-life of 17.8 days) to form einsteinium-253. Close examination of the debris from the nuclear explosion revealed another alpha-particle-emitting radioactive species that was identified as an isotope of element 100 with the mass number 255. The new elements were named einsteinium and fermium in honor of two of the most important progenitors of the nuclear age. The unexpected consequences of the vast numbers of neutrons released by the nuclear chain reaction thus led to the synthesis of two new elements and revealed the potential utility of high-flux nuclear reactors in the production of transplutonium elements. Following the earlier use of other reactors in the 1950s, the High-Flux Isotope Reactor (HFIR) and the transuranium processing facility, currently named Radiochemical Engineering Development Center (REDC) were built at Oak Ridge National Laboratory in the 1960s for the production of transcurium elements. The HFIR starting material is highly irradiated plutonium-239 already containing substantial amounts of heavier isotopes of plutonium. Prolonged exposure to the intense neutron flux of HFIR produces considerable amounts of plutonium-242, americium-243, and curium-244, which have been isolated and refabricated into new targets for irradiation in the HFIR. Work-up of these targets, a task of no mean proportions because of the intense radioactivity from fission products and the newly formed transcurium elements, yields heavy isotopes of curium, berkelium, and californium plus smaller quantities of einsteinium and fermium.

The discovery of elements 99 and 100 in a sense was a watershed in the search for elements of ever higher atomic number. The experimental methods developed to isolate and identify neptunium and plutonium, refined and elaborated, were adequate for the task of isolation and characterization of the transplutonium elements up to element 100. With the transfermium elements, matters became much more difficult. Among the isotopes of the elements uranium, neptunium, plutonium, and curium, there is at least one that has a half-life of 10^6 years or more. For americium and berkelium, the longest-lived isotopes, produced by neutron irradiation, have half-lives of the order of 10^4 years and 1 year, respectively. The most stable californium isotope has a half-life less than

1000 years, einsteinium a half-life less than a year, and fermium a half-life of about 3 months. The elements of atomic number greater than 100 have isotopes with lifetimes measured in days, hours, minutes, seconds, and fractions of a second. The short half-lives severely limit the amount of a heavier isotope that can be made. Whereas the elements up to atomic number 100 could be characterized with amazingly small amounts of material, these, nevertheless, still contained large numbers of atoms. All of the actinides with atomic numbers up to 99 have been studied with weighable amounts (Table 1.1) but there is no prospect for producing weighable amounts of heavier elements. The elements of higher atomic number had to be identified with as little as one atom of a new element. That this feat was achievable was a result of the rapid developments in nuclear systematics, which made it possible to predict the nuclear properties of new isotopes; the actinide concept, which predicted the chemical properties of transuranium elements; and the development of new experimental techniques, which made it possible to isolate a single atom of a new isotope almost simultaneously with its formation in a nuclear reaction, and to measure half-lives in the millisecond range.

On the complex subject of nuclear systematics, it will be sufficient here to mention that the great progress made in the theoretical understanding of the behavior of atomic nuclei allowed predictions about lifetimes and the nature of radioactive emissions and their energetics to be made with considerable confidence, and this played a major role in the search for new elements. The actinide concept similarly played a crucial part. When the first transuranium elements were studied in the laboratory, it soon became apparent that the new members of the periodic table did not have the chemical properties that might be expected of them if they were placed in traditional sequence after uranium. Neptunium did not behave like rhenium, and in no way did plutonium resemble osmium, which would have been positioned directly above plutonium had the first two transuranium elements merely been inserted in the next vacant positions in the periodic table directly after uranium. Because similarities in chemical behavior arise in the periodic table from similarities in electronic configuration of the ions of homologous elements, simple insertion of the transuranium elements into the periodic table would have precluded its use as a reliable guide to the chemistry of the new elements.

The actinide hypothesis advanced by Seaborg systematized the chemistry of the transuranium elements, and thus greatly facilitated the search for new elements. From the vantage point of the actinide concept, the transuranium elements are considered to constitute a second inner transition series of elements similar to the rare-earth elements. In the rare-earth series, successive electrons are added to the inner 4f shell beginning with cerium and ending with lutetium. In the actinide series, fourteen 5f electrons are added beginning, formally, with thorium (atomic number 90) and ending with lawrencium (atomic number 103). Although the regularities are not as pronounced in the actinide as in the lanthanide series, the concept of the actinide elements as members of a 5f

transition series is now accepted and has served as a unifying principle in the evolution of the chemistry of the actinide elements. A more detailed discussion of the actinide hypothesis can be found in Chapter 15.

The first chemical studies on neptunium and plutonium were made using classical radiochemical techniques in the 1940s. Amounts far too small to be weighed were studied by tracer methods, where solutions are handled in ordinary-sized laboratory vessels. Concentrations of the order of 10^{-12} mol L^{-1} or less are not unusual in tracer work, and valuable information could be acquired on solutions containing only a few million atoms. The radioactive element is detected by its radioactivity, and the chemistry is inferred from its behavior relative to that of an element of known chemistry present in macro amounts. When weighable amounts were available, ultramicrochemical methods were used. These manipulations were and still are carried out with microgram or even lesser amounts of material in volumes of solution too small to be seen by the naked eye at concentrations normally encountered in the laboratory. Ultramicro methods make possible the isolation of small samples of pure chemical compounds, which can then be identified by X-ray crystallography or electron diffraction in a transmission electron microscope. All of the actinide elements are radioactive, and, except for thorium and uranium, special containment and shielded facilities are mandatory for safe handling of these substances. Gloved boxes are required (Fig. 1.2)

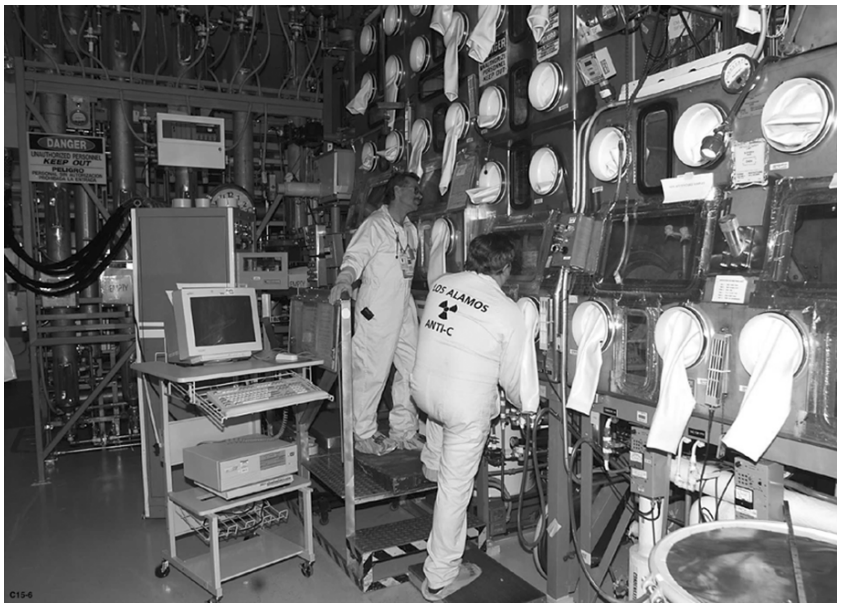

Fig. 1.2 *A modern laboratory with a bank of gloved boxes for carrying out experimental chemistry of transuranium elements.* (*Reproduced by permission of Los Alamos National Laboratory*.)

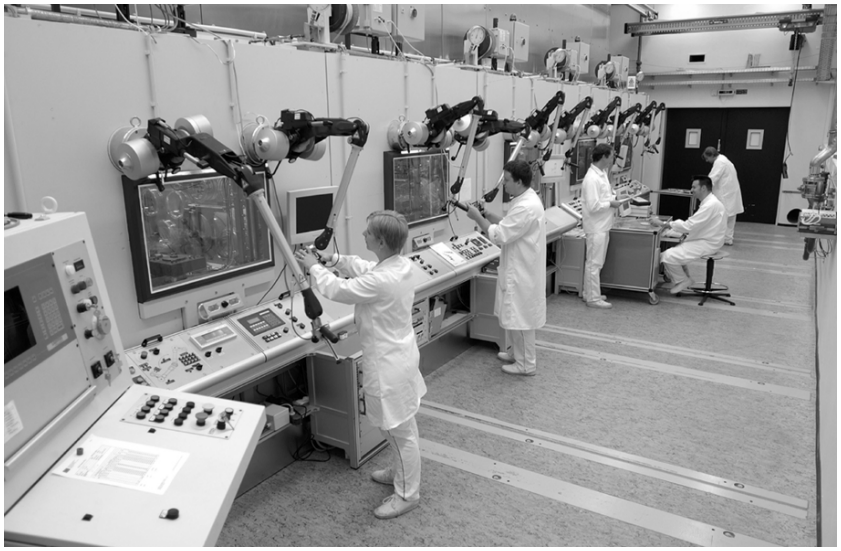

Fig. 1.3 *A hot-cell facility for remote synthesis and characterization of gram-scale transuranium materials.* (*Reproduced by permission of Institute for Transuranium Elements, Karlsruhe, part of the Joint Research Centre, European Commission.*)

and, where high levels of penetrating radiation (gamma rays or neutrons) are encountered, which is not infrequent, all manipulations may need to be performed by remote control (Figs. 1.3 and 1.4). Even when radiation can easily be shielded, as is the case with alpha-particle emitters, containment to prevent inhalation is still essential because of the toxicity of the transuranium elements. Inhaled transuranium isotopes may be deposited in the lungs and ingested isotopes may be translocated to the bone, where the intense alpha radioactivity over a period of time can give rise to neoplasms. The shorter the half-life, i.e., the higher the specific activity of the radioactive isotope, the more serious are the difficulties of experiments with macro amounts of material. Consequently, every effort has been made to produce long-lived isotopes. There are available isotopes of neptunium, plutonium, and curium with half-lives longer than 10^5 years, and isotopes of americium and californium that have half-lives of the order of 1000 years can be used in chemical studies. These long-lived isotopes greatly reduce the extent of radiolysis of water or other solvents for experiments in the liquid phase, they minimize radiation damage in the solid phase, and they also considerably reduce the health hazards in the experiment. Even with the longest-lived isotopes, most laboratory research with transuranium elements is carried out on the milligram or smaller scale.

The syntheses of the transfermium elements presented an even more challenging set of problems. Because of the short lifetimes of these isotopes, production by successive neutron capture in a high-flux reactor was not possible. Methods

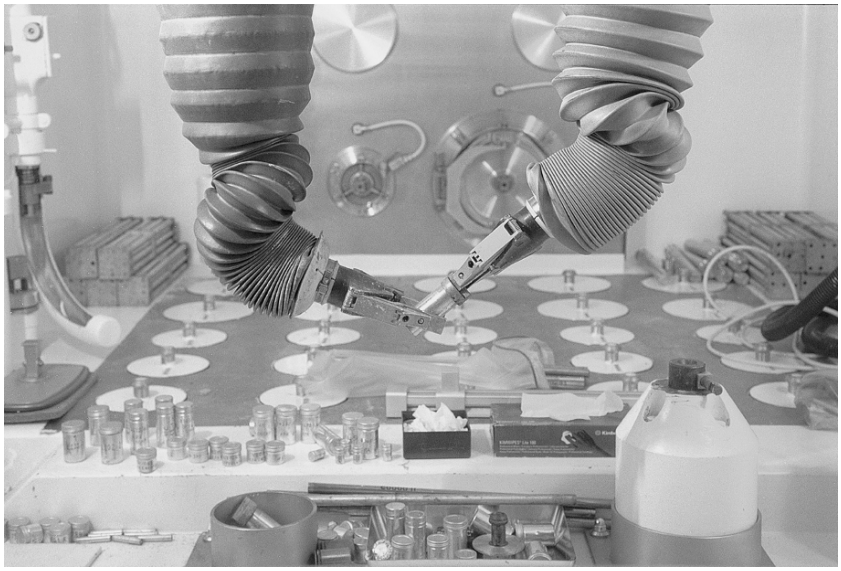

Fig. 1.4 *Example of an experimental setup within a hot-cell facility.* (*Reproduced by permission of Institute for Transuranium Elements, Karlsruhe, part of the Joint Research Centre, European Commission.*)

for the rapid collection of the newly formed isotopes had to be developed and very rapid separation procedures were required to isolate a pure product for identification. Ghiorso (1982) described in fascinating detail how these problems were surmounted. A newly formed nucleus contains sufficient energy to eject it from a target undergoing bombardment; the atom that recoils can be caught on a clean foil placed in close proximity to the target. The catcher foil can then be dissolved and the solution examined. For identification, ion-exchange chromatography proved to be ideal. Elution from an ion-exchange column can be carried out very rapidly. The order of elution is very specific and provides an unmistakable fingerprint for identification. In this way, it was possible to synthesize and identify element 101, subsequently named mendelevium, in experiments in which it was made one atom at a time. Even more highly refined collection procedures were evolved to complete the actinide series of elements by the discovery of nobelium (atomic number 102) and lawrencium (atomic number 103).

The transactinide elements 104 through 112 have been discovered at Berkeley and Darmstadt (see Table 1.1). Scientists at the Dubna Laboratory in Russia also made claims for the discovery of a number of these elements, but their evidence did not meet the accepted criteria for the discovery of new elements (Wilkinson *et al.*, 1991, 1993). No names have been suggested for elements

heavier than 111, in conformity with the IUPAC rules for the naming of new elements (Koppenol, 2002). A surprising amount of information has accumulated about the oxidation states of the transfermium and transactinide ions in solution even though only a few atoms of any of these were available at any one time. Evidence for isotopes of elements heavier than 112 has been published by a consortium of scientists from Dubna and Livermore (Table 1.1). The chemistry of transactinide elements, and predicted chemical properties of these elements, is presented in Chapter 14.

One frontier is the synthesis of longer-lived isotopes and determination of chemical properties of additional transactinide elements (Chapter 14 of this work; Schädel, 2003). Numerous theoretical calculations have been made that indicate that there may be more than one "island" of relatively stable nuclei near the presently defined limits of the periodic table. In addition to the island of spherical stability originally predicted to be around atomic number $Z = 114$ and neutron number $N = 184$, other islands of spherical nuclei have been predicted at $Z = 120$ or 126 and $N = 184$ and at $Z = 120$ and $N = 172$. A predicted island of deformed nuclei at $Z = 108$ and $N = 162$ has already been confirmed experimentally. Because of the relatively long half-lives of isotopes conferred by closed nuclear shells, the goal of carrying out chemical studies with the elements at or near these islands is considered to be attainable by some scientists. The new techniques and theoretical understanding required to attain this goal will undoubtedly have profound consequences for nuclear and inorganic chemistry.

There are outstanding questions in actinide chemistry. One is the understanding of the bonding and electronic structure of the 5f electrons in condensed phases containing plutonium and adjacent elements. Another is the bonding and chemical behavior of actinides that may be released into the environment. To advance both of these frontiers, heavy-element chemists utilize modern instrumental techniques – X-ray absorption spectroscopy, laser fluorescence spectroscopy, electron microscopy, mass spectroscopy, neutron scattering, to name only a few – that make it possible to study the elements described in the subsequent chapters as pure materials, at extremely low concentrations, and under many unique conditions. Theoretical actinide and transactinide chemistry is advancing rapidly. Relativistic contributions to electronic properties that incorporate spin–orbit interactions are being calculated for bulk actinide solids, actinide metal surfaces, actinide complexes in solution, and transactinide atoms. Relativistic electronic structure theory utilizes time-dependent density functional theory and relativistic effective core potentials.

The actinide and transactinide elements in the last 65 years have played an important role in inorganic chemistry, in nuclear chemistry and physics, and in many other branches of science and technology. The actinide elements are also of crucial importance in energy resource development and, regrettably, in warfare. These elements are destined to continue to occupy the attention of scientists, engineers, environmentalists, and statesmen. We hope that these

volumes will help provide the factual basis so necessary for the important research breakthroughs and technical decisions that will have to be made in future years.

REFERENCES

Ghiorso, A. (1982) *Actinides in Perspective* (ed. N. M. Edelstein), Pergamon Press, Oxford, pp. 23–56.

Gruen, D. M. (1992) *Transuranium Elements – A Half Century* (eds. L. R. Morss and J. Fuger), American Chemical Society, Washington, DC, pp. 63–77.

Koppenol, W. H. (2002) *Pure Appl. Chem.,* **74**, 787–791.

Schädel, M. (2003) *Chemistry of Superheavy Elements,* Kluwer Academic Publishers, Dordrecht.

Seaborg, G. T. (1982) *Actinides in Perspective* (ed. N. M. Edelstein), Pergamon Press, Oxford, pp. 1–22.

Seaborg, G. T. (1992) *Transuranium Elements – A Half Century* (eds. L. R. Morss and J. Fuger), American Chemical Society, Washington, DC, pp. 10–49.

Wilkinson, D. H., Wapstra, A. H., Uhelea, I., Barber, R. C., Greenwood, N. N., Hrynkiewicz, A., Jeannin, Y. P., Lefort, M., and Sakai, M. (1991) *Pure Appl. Chem.,* **63**, 879–886.

Wilkinson, D. H., Wapstra, A. H., Uhelea, I., Barber, R. C., Greenwood, N. N., Hrynkiewicz, A., Jeannin, Y. P., Lefort, M., and Sakai, M. (1993) *Pure Appl. Chem.,* **65**, 1764–1814.

ADDITIONAL SUGGESTED READINGS

Bagnall, K. W. (1972) *The Actinide Elements,* Elsevier, Amsterdam.

Bagnall, K. W. (ed.) (1972, 1975) *Lanthanides and Actinides* (MTP International Review of Science, Inorganic Chemistry, series 1, vol. 7, set. 2, vol. 7), Butterworths, London.

Blank, H. and Lindner, R. (eds.) (1976) *Plutonium 1975 and Other Actinides,* North Holland, Amsterdam.

Brown, D. (1968) *Halides of the Lanthanides and Actinides,* Wiley-Interscience, London.

Burney, G. A. and Harbour, R. M. (1974) *Radiochemistry of Neptunium*, Report NAS-NS 3060.

Carnall, W. T. and Choppin, G. R. (eds.) (1983) *Plutonium Chemistry* (ACS Symp. Ser. 216), American Chemical Society, Washington, DC.

Cleveland, J. M. (1979) *The Chemistry of Plutonium,* 2nd edn, American Nuclear Society, La Grange Park, IL.

Cordfunke, E. H. P. (1969) *The Chemistry of Uranium,* Elsevier, Amsterdam.

Edelstein, N. M. (ed.) (1980) *Lanthanide and Actinide Chemistry and Spectroscopy* (ACS Symp. Ser. 131), American Chemical Society, Washington, DC.

Edelstein, N. M. (ed.) (1982) *Actinides in Perspective,* Pergamon Press, Oxford and New York.

Edelstein, N. M., Navratil, J. D., and Schulz, W. W. (eds.) (1985) *Americium and Curium Chemistry and Technology,* Reidel, Dordrecht.

Erdös, P. and Robinson, J. M. (1983) *The Physics of Actinide Compounds,* Plenum, New York.

Fields, P. R. and Moeller, T. (eds.) (1967) *Lanthanide/Actinide Chemistry* (ACS Adv. Ser. 71), American Chemical Society, Washington, DC.

Freeman, A. J. and Darby, J. B. (eds.) (1974) *The Actinides: Electronic Structure and Related Properties,* Academic Press, New York.

Handbook on the Physics and Chemistry of Rare Earths, North-Holland, Amsterdam, New York; Elsevier Science, New York, NY, vols 17–19, 1993–1994.

Handbook on the Physics and Chemistry of the Actinides, North-Holland, Amsterdam, New York; Elsevier Science, New York, NY, 1984–1991, 6 volumes.

Hoffman, Darleane C. (2002) *Advances in Plutonium Chemistry, 1967–2000*, American Nuclear Society, La Grange Park, IL.

Kaltsoyannis, N. and Scott, P. (1999) *The f Elements,* Oxford University Press, Oxford.

Katz, J. J. and Rabinowitch, E. (1951) *The Chemistry of Uranium,* McGraw-Hill, New York. (Reprinted 1961 by Dover Publications, New York.)

Katz, J. J. and Rabinowitch, E. (eds.) (1958) *Chemistry of Uranium, 2 vols.* U.S. Atomic Energy Commission, Technical Information Service, Oak Ridge, TN, TID-5290.

Keller, C. (1971) *The Chemistry of the Transuranium Elements,* Verlag Chemie, Weinheim.

Los Alamos National Laboratory (2000) *Challenges in plutonium science*, *Los Alamos Science No. 26*, 2 vols, Los Alamos National Laboratory, Los Alamos, NM. http://www.fas.org/sgp/othergov/doe/lanl/pubs/number26.htm

Milyukova, M. S., Gusev, N. L., Sentyurin, I. G., and Sklyarenko, I. S. (1967) *Analytical Chemistry of Plutonium,* Israel Program for Scientific Translations, Jerusalem.

Myasoedov, B. F., Guseva, L. I., Lebedev, I. A., Milyukova, M. S., and Chmutova, M. S. (1974) *Analytical Chemistry of the Transplutonium Elements* (Engl. transl.), Wiley, New York.

Meyer, G. and Morss, L. R. (eds.) (1991) *Synthesis of Lanthanide and Actinide Compounds,* Kluwer Academic Publishers, Dordrecht.

Morss, L. R. and Fuger, J. (eds.) (1992) *Transuranium Elements – A Half Century,* American Chemical Society, Washington, DC.

Müller, W. and Blank, H. (eds.) (1976) *Heavy Element Properties,* North-Holland, Amsterdam.

Müller, W. and Lindner, R. (eds.) (1976) *Transplutonium 1975*, North-Holland, Amsterdam.

National Academy of Sciences (1959–86) *Series on Radiochemistry:* Stevenson, P. C. and Nervik, W. E. (1961) *Actinium,* NAS-NS-3020; Hyde, E. (1960) *Thorium,* NAS-NS-3004; Kirby, H. W. (1959) *Protactinium,* NAS-NS-3016; Gindler, J. (1961) *Uranium,* NAS-NS-3050; Burney, G. A. and Harbour, R. M. (1974) *Neptunium,* NAS-NS-3060; Coleman, G. H. and Hoff, R. W. (1965) *Plutonium,* NAS-NS-3058; Penneman, R. A. and Keenan, R. K. (1960) *Americium and Curium,* NAS-NS-3006; Higgins, G. H. (1960) *The Transcurium Elements,* NAS-NS-3031; Roberts, R. A., Choppin, G. R., and Wild, J. F. (1986). *Uranium, Neptunium and Plutonium, An Update,* NA-NS-3063. Volumes of this series can be found at http://lib-lanl.gov/radiochemistry/elements.htm.

Navratil, J. D. and Schulz, W. W. (eds.) (1980) *Actinide Separations* (ACS Symp. Ser. 117), American Chemical Society, Washington, DC.

Navratil, J. D. and Schulz, W. W. (eds.) (1981) *Transplutonium Elements – Production and Recovery* (ACS Symp. Ser. 161), American Chemical Society, Washington, DC.

Schädel, M. (2003) *Chemistry of Superheavy Elements,* Kluwer Academic Publishers, Dordrecht.

Schädel, M. (2006) *Angew. Chem. Int. Ed.*, **45**, 368–401.

Seaborg, G. T. (1958) *The Transuranium Elements,* Yale University Press, New Haven.

Seaborg, G. T. (1963) *Man-Made Transuranium Elements,* Prentice-Hall, Englewood Cliffs, NJ.

Seaborg, G. T. (1978) *Transuranium Elements, Products of Modern Alchemy,* Dowden, Hutchison and Ross, Stroudsburg, PA.

Seaborg, G. T. and Katz, J. J. (eds.) (1954) *The Actinide Elements* (Natl Nucl. Eng. Ser., Div. IV, 14A), McGraw-Hill, New York.

Seaborg, G. T., Katz, J. J., and Manning, W. M. (eds.) (1949) *The Transuranium Elements* (Natl Nucl. Eng. Ser., Div. IV, 14B), McGraw-Hill, New York.

Seaborg, G. T. and Loveland, W. D. (1990) *The Elements Beyond Uranium,* Wiley-Interscience, New York.

Schulz, W. W. (1976) *The Chemistry of Americium,* Report TID-26971, US Dept of Energy, Technical Information Center, Oak Ridge, TN.

Sterne, P. A., Gonis, A., and Borovoi, A. A. (1998) *Actinides and the Environment,* Kluwer Academic Publishers, Dordrecht.

Taube, M. (1974) *Plutonium – A General Survey,* Verlag Chemie, Weinheim.

Trotman-Dickenson, A. F. (exec. ed.) (1973) *Comprehensive Inorganic Chemistry,* vol. 5, The Actinides, Pergamon, Oxford.

Wick, O. J. (ed.) (1967) *Plutonium Handbook,* Gordon and Breach, New York, 2 vols.

CHAPTER TWO

ACTINIUM

H. W. Kirby and L. R. Morss

2.1 INTRODUCTION

The actinide series of elements encompasses all the 15 chemical elements that have properties attributable to the presence of low-lying 7p, 6d, and 5f orbitals such that their tripositive ions have electronic configurations $7p^0 6d^0 5f^n$, where $n = 0,1,2,\ldots,14$. According to this definition, actinium, element 89, is the first member of the actinide series of elements, although it has no 5f electrons in its metallic, gaseous, or ionic forms. As such, its position in group 3 (in current IUPAC terminology) or group 3B (commonly used in some American textbooks) of the periodic table is analogous to that of its homolog, lanthanum, in the lanthanide series. This definition, which includes actinium as the first of the actinides (Seaborg, 1994), parallels the accepted inclusion of lanthanum as the first member of the lanthanide series (Moeller, 1963).

The chemistry of actinium closely follows that of lanthanum. There are no qualitative differences between them; the only quantitative differences are those attributable to the difference in their ionic radii (1.12 Å for Ac^{3+} and 1.032 Å for La^{3+} in six-fold coordination) (Shannon, 1976 and Chapter 15, section 7.5, of this book). Because of this similarity, lanthanum is a nearly ideal surrogate for actinium in the development of preparative or analytical procedures. As a carrier for trace amounts of actinium, lanthanum suffers from only one disadvantage: Once mixed, the two elements behave like any pair of adjacent rare earths and can be separated only by ion-exchange chromatography, solvent extraction, or fractional crystallization.

The most important isotope of actinium is ^{227}Ac, a member of the naturally occurring uranium–actinium $(4n + 3)$ family of radioelements. Its applications

are derived from its unique radioactive properties. Although ^{227}Ac itself is essentially ($\geq$98%) a weak β^- emitter, with a moderately long half-life (21.773 years), its decay chain includes five short-lived α emitters. The net effect is one of high specific power and long service life, a combination that makes ^{227}Ac suitable as a heat source in thermoelectric generators on space missions to the outer planets and beyond. Recently ^{225}Ac and ^{228}Ac have found applications (see Section 2.9).

The early actinium literature (up to January 1940) was comprehensively reviewed by the staff of the Gmelin Institute, and an English translation is available (Gmelin, 1942). Later reviews and bibliographies have appeared with the waxing and waning of interest in possible applications of actinium (Clarke, 1954, 1958; Hagemann, 1954; Bagnall, 1957; Katz and Seaborg, 1957; Bouissières, 1960; Stevenson and Nervik, 1961; Salutsky, 1962; Sedlet, 1964; Kirby, 1967; Keller, 1977). The most recent monograph on actinium chemistry is the *Gmelin Handbook* supplement (Gmelin, 1981).

2.1.1 Historical

In 1899, André Debierne, in the laboratory of Pierre and Marie Curie, reported that he had found a new radioactive substance, whose chemistry closely followed that of titanium (Debierne, 1899). Six months later, he said that the titanium fraction was no longer very active, but that the radioactive material he was now recovering exhibited the same chemical behavior as thorium (Debierne, 1900). Debierne claimed the right of discovery and named the new substance actinium (*aktis*, ray). His claim was accepted uncritically at the time, but, in the light of what we now know of the chemical and nuclear properties of actinium, it is clear that his 1899 preparation contained no actinium at all and that his 1900 preparation was a mixture of several radioelements, possibly including actinium as a minor constituent (Kirby, 1971; Adloff, 2000).

In 1902, Friedrich Giesel reported a new 'emanation-producing' substance among the impurities he had separated with radium from pitchblende residues (Giesel, 1902). He correctly established many of its chemical properties, including the important fact that it followed the chemistry of the cerium group of rare earths. By 1903, he had concentrated and purified it to a point where lanthanum was the chief impurity and thorium was spectroscopically undetectable (Giesel, 1903). A year later, he proposed the name, emanium, for what was clearly a new radioelement (Giesel, 1904a).

Giesel's claim was vigorously attacked by Debierne (1904), who now had an emanation-producing substance of his own, which, he insisted, was the same as the substance he had originally named actinium, although the 1900 preparation had titanium- or thorium-like properties (Adloff, 2000). Debierne's claim prevailed, and has been propagated by historians (Ihde, 1964; Partington, 1964; Weeks and Leicester, 1968), largely because of the prestige of the Curies and the support of Rutherford (1904). The latter based his conclusion solely on

the similarity in the decay characteristics of the "emanations" (i.e. ^{219}Rn) and the "active deposits" (^{211}Pb) given off by the samples supplied to him by the two claimants. Although some historical studies (Weeks and Leicester, 1968; Adloff, 2000) give both Debierne and Giesel credit for the discovery, Kirby (1971), Keller (1977), and the second author of this chapter believe that it is more appropriate to give credit for discovery of actinium to Giesel.

The actinium decay chain was sorted out rather quickly. In 1905, Godlewski (1904–5, 1905) and Giesel (1904b, 1905) independently reported the existence of actinium X (also referred to as "emanium X"), now known as ^{223}Ra, and showed it to be the direct source of the actinium emanation and its active deposit. The following year, Hahn (1906a,b) discovered radioactinium (^{227}Th), the immediate descendant of actinium and the parent of actinium X. ^{231}Pa, the parent of actinium, was discovered independently in 1918 by Soddy and Cranston (1918a,b) and by Hahn and Meitner (1918). The primordial origin of the actinium series ($4n + 3$ or uranium–actinium series, Fig. 2.1) was not finally resolved until 1935, when Dempster (1935) detected the uranium isotope of atomic weight 235 by mass spectroscopy.

2.2 NUCLEAR PROPERTIES

Of the 29 known isotopes of actinium (Table 2.1) only three are of particular significance to chemists. Two of these isotopes are the naturally occurring isotopes, ^{227}Ac (Fig. 2.1, $4n + 3$ or uranium–actinium series) and ^{228}Ac (mesothorium II, Fig. 2.2, $4n$ or thorium series). The third is ^{225}Ac, a descendant of reactor-produced ^{233}U (Fig. 2.3, $4n + 1$ or neptunium series).

2.2.1 Actinium–227

The isotope ^{227}Ac, a β^- emitter, is a member of the naturally occurring ^{235}U (AcU) decay series (Fig. 2.1). It is the daughter of ^{231}Pa and the parent of ^{227}Th (RdAc). It is also the parent, by a 1.38% α branch (Kirby, 1970; Monsecour *et al.*, 1974), of ^{223}Fr, which was discovered in 1939 by Perey (1939a,b). The half-life of ^{227}Ac is (21.772 ± 0.003) years (Jordan and Blanke, 1967; Browne, 2001), as determined by calorimetric measurements made over a period of 14 years. The thermal-neutron-capture cross section σ_t and the resonance integral are (762 ± 29) barn and (1017 ± 103) barn, respectively (1 barn = 10^{-28} m^2) (Monsecour and De Regge, 1975).

The β^- radiation of ^{227}Ac is so weak (0.045 MeV maximum) (Beckmann, 1955; Novikova *et al.*, 1960) that the nuclide was once thought to be 'rayless' (Marckwald, 1909; Rutherford, 1911). Even with modern nuclear spectrometers, neither the β^- nor the γ radiation is useful for analytical purposes because of interference from the rapidly growing decay products. On the other hand, ^{227}Ac is readily identified, even in the presence of its decay products,

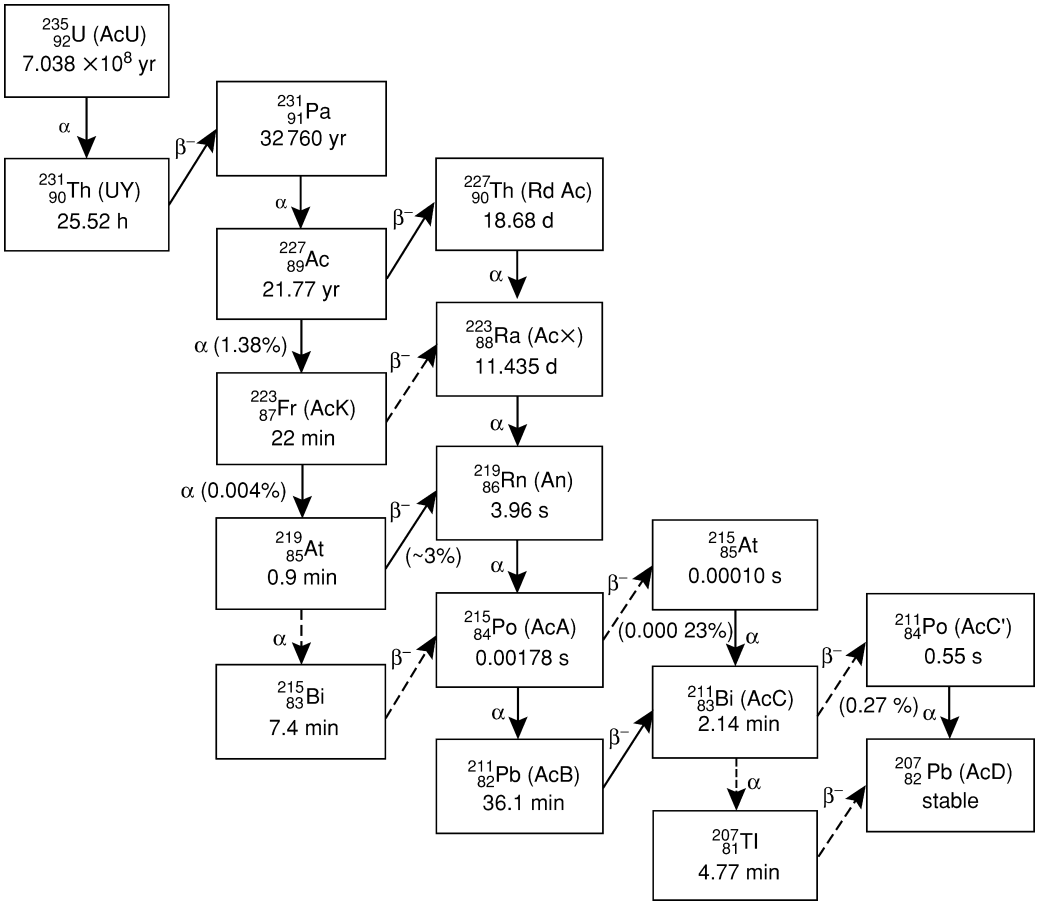

Fig. 2.1 *Uranium–actinium series* $(4n + 3)$.

Table 2.1 *Nuclear properties of actinium isotopes.*[a]

Mass number	*Half-life*	*Mode of decay*	*Main radiations* (MeV)	*Method of production*
206	33 ms	α	α 7.750	^{175}Lu(^{40}Ar,9n)
	22 ms	α	α 7.790	
207	22 ms	α	α 7.712	^{175}Lu(^{40}Ar,8n)
208	95 ms	α	α 7.572	^{175}Lu(^{40}Ar,7n)
	25 ms	α	α 7.758	
209	0.10 s	α	α 7.59	^{197}Au(^{20}Ne,8n)
210	0.35 s	α	α 7.46	^{197}Au(^{20}Ne,7n)
				^{203}Tl(^{16}O,9n)
211	0.25 s	α	α 7.48	^{197}Au(^{20}Ne,6n)
				^{203}Tl(^{16}O,8n)
212	0.93 s	α	α 7.38	^{203}Tl(^{16}O,7n)
				^{197}Au(^{20}Ne,5n)
213	0.80 s	α	α 7.36	^{197}Au(^{20}Ne,4n)
				^{203}Tl(^{16}O,6n)
214	8.2 s	α ≥ 86%	α 7.214 (52%)	^{203}Tl(^{16}O,5n)
		EC ≤ 14%	7.082 (44%)	^{197}Au(^{20}Ne,3n)
215	0.17 s	α 99.91%	α 7.604	^{203}Tl(^{16}O,4n)
		EC 0.09%		^{209}Bi(^{12}C,6n)
216	~0.33 ms	α	α 9.072	^{209}Bi(^{12}C,5n)
216 m	0.33 ms	α	α 9.108 (46%)	
			9.030 (50%)	
217	69 ns	α	α 9.650	^{208}Pb(^{14}N,5n)
218	1.08 μs	α	α 9.20	^{222}Pa daughter
219	11.8 μs	α	α 8.66	^{223}Pa daughter
220	26.4 ms	α	α 7.85 (24%)	^{208}Pb(^{15}N,3n)
			7.68 (21%)	^{224}Pa daughter
			7.61 (23%)	
221	52 ms	α	α 7.65 (70%)	^{205}Tl(^{22}Ne,α2n)
			7.44 (20%)	^{208}Pb(^{18}O,p4n)
222	5.0 s	α	α 7.00	^{226}Ra(p,5n)
				^{208}Pb(^{18}O,p3n)
222 m	63 s	α > 90%	α 7.00 (15%)	^{208}Pb(^{18}O,p3n)
		EC ~ 1%	6.81 (27%)	^{209}Bi(^{18}O,αn)
		IT < 10%		
223	2.10 min	α 99%	α 6.662 (32%)	^{227}Pa daughter
		EC 1%	6.647 (45%)	
224	2.78 h	EC ~ 90%	α 6.211 (20%)	^{228}Pa daughter
		α ~ 10%	6.139 (26%)	
225	10.0 d	α	α 5.830 (51%)	^{225}Ra daughter
			5.794 (24%)	
			γ 0.100 (1.7%)	
226	29.37 h	β^- 83%	α 5.399	^{226}Ra(d,2n)
		EC 17%	β^- 1.10	
		α 6×10^{-3}%	γ 0.230 (27%)	
227	21.772 yr	β^- 98.62%	α 4.950 (47%)	Nature
		α 1.38%	4.938 (40%)	
			β^- 0.045	
			γ 0.086	

Table 2.1 (*Contd.*)

Mass number	*Half-life*	*Mode of decay*	*Main radiations* (MeV)	*Method of production*
228	6.15 h	β^-	β^- 2.18 γ 0.991	Nature
229	62.7 min	β^-	β^- 1.09 γ 0.165	^{229}Ra daughter ^{232}Th(γ,p2n)
230	122 s	β^-	β^- 1.4 γ 0.455	^{232}Th(γ,pn)
231	7.5 min	β^-	β^- 2.1 γ 0.282	^{232}Th(γ,p) ^{232}Th(n,pn)
232	119 s	β^-		^{238}U + Ta
233	145 s	β^-		^{238}U + Ta
234	44 s	β^-		^{238}U + Ta

[a] Appendix II.

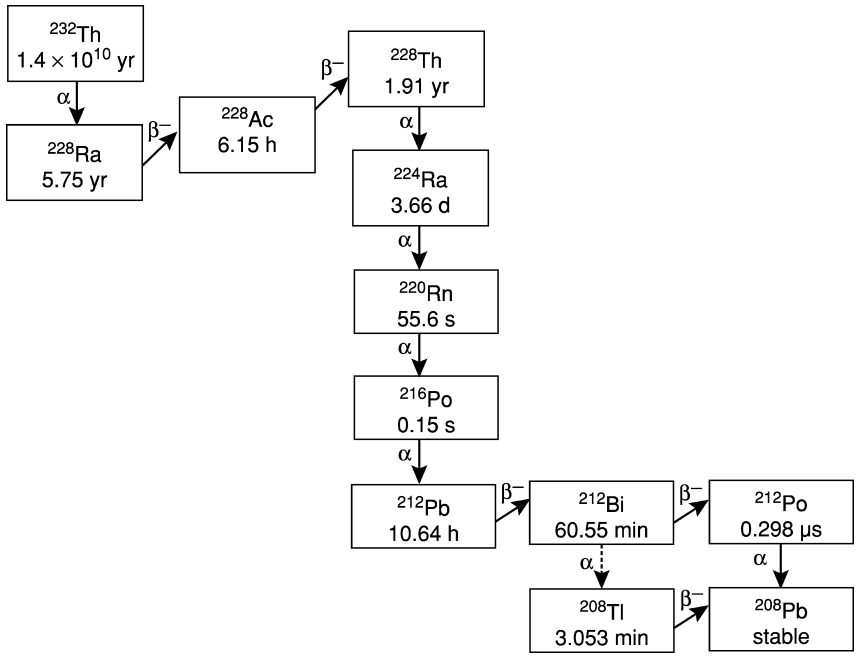

Fig. 2.2 *Thorium series* (4*n*).

by α spectrometry (Fig. 2.4), and a computational technique has been described for its quantitative determination by this method (Kirby, 1970).

The γ spectrum of ^{227}Ac in equilibrium with its decay products is shown in Fig. 2.5. The 235.9-keV γ-ray, which has an intensity of (12.3 $\pm$ 1.3)% of ^{227}Th

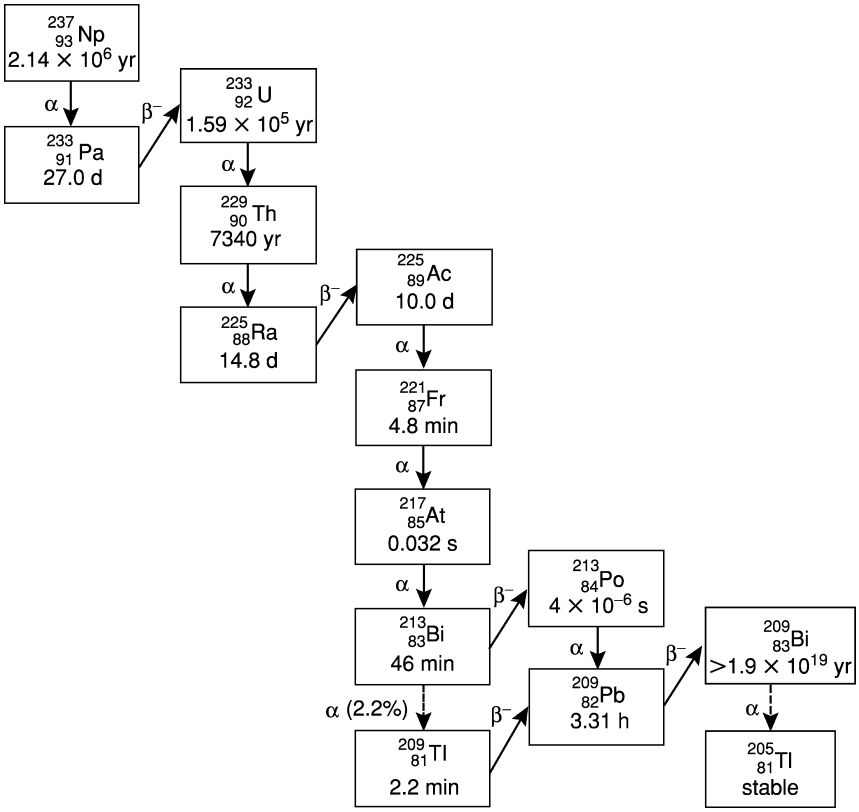

Fig. 2.3 *Neptunium series* $(4n + 1)$.

α decay, can be used for quantitative analysis of ^{227}Ac. For a detailed level scheme, see the most recent critical compilation (Firestone and Shirley, 1996).

2.2.2 Actinium–228 (MsTh II or $MsTh_2$)

The isotope ^{228}Ac (mesothorium II or $MsTh_2$) is a member of the naturally occurring ^{232}Th decay chain. It is the daughter of 5.77-year ^{228}Ra (mesothorium I or $MsTh_1$) and the parent of 1.9116-year ^{228}Th (radiothorium).

All three nuclides were discovered by Otto Hahn (1905, 1907, 1908). The long-accepted half-life of ^{228}Ac (6.13 ± 0.03) h, reported in 1926 (Hahn and Erbacher, 1926), was redetermined to be (6.15 ± 0.02) h in 1985 (Skarnemark and Skalberg, 1985).

^{228}Ac has a complex β^- spectrum (Bjornholm *et al.*, 1957; Arnoux and Giaon, 1969; Dalmasso *et al.*, 1974), but, unlike ^{227}Ac, more than 99% of the β^- particles have maximum energies greater than 0.5 MeV so that its γ-ray spectrum (Novikova *et al.*, 1960) is a useful analytical tool. By contrast, the

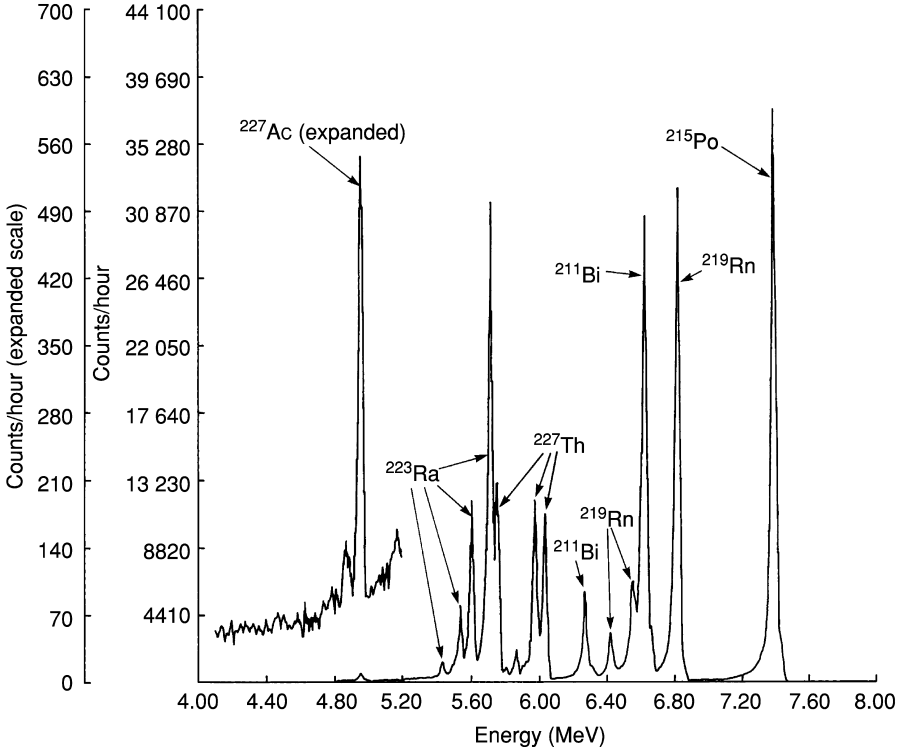

Fig. 2.4 *Alpha spectrum of* ^{227}*Ac in equilibrium with its decay products* (*Kirby,* 1970).

β^- and γ radiations from ^{228}Ra are too weak for routine detection; consequently, nearly all methods for the determination of ^{228}Ra are based on the isolation and counting of ^{228}Ac (Hahn and Erbacher, 1926). ^{228}Ac is frequently used as a tracer for other actinium isotopes (Bhatki and Adloff, 1964; Chayawattanangkur *et al.*, 1973).

A level scheme and a critical compilation of γ-ray energies for ^{228}Ac have been published (Horen, 1973).

2.2.3 Actinium-225

The isotope ^{225}Ac is an α emitter. It is a member of the $4n + 1$ decay series, of which ^{237}Np is the longest-lived member and progenitor (Fig. 2.3). In practice, however, ^{225}Ac is most easily obtained by milking a sample of ^{229}Th that was previously separated from aged ^{233}U (Valli, 1964). The latter isotope is itself produced by neutron bombardment of natural thorium (St. John and Toops, 1958; Hyde *et al.*, 1964):

$$^{232}\mathrm{Th}(\mathrm{n},\gamma)^{233}\mathrm{Th} \xrightarrow[22.3\ \mathrm{min}]{\beta^-} {}^{233}\mathrm{Pa} \xrightarrow[26.967\ \mathrm{d}]{\beta^-} {}^{233}\mathrm{U} \qquad (2.1)$$

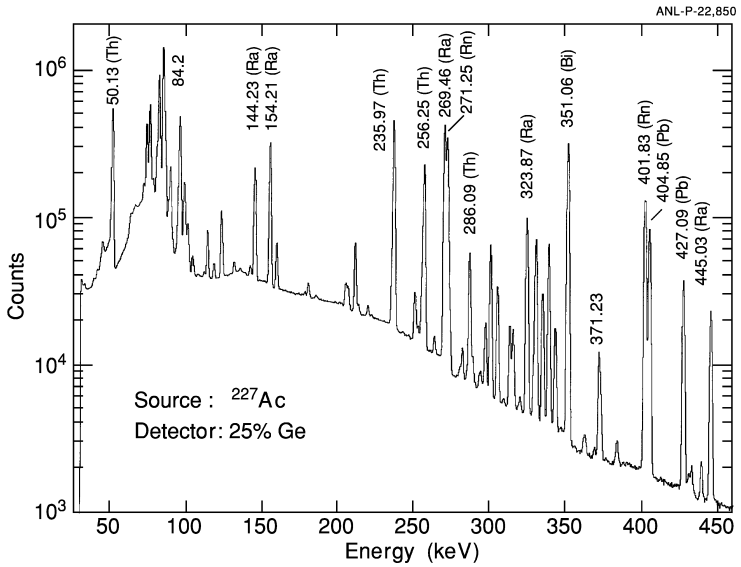

Fig. 2.5 *Gamma spectrum of ^{227}Ac in equilibrium with its decay products* (*I. Ahmad,* 2002).

Unfortunately, ^{229}Th is always more or less contaminated with ^{228}Th because of side reactions during the production of ^{233}U:

$$^{232}\mathrm{Th}(\mathrm{n},2\mathrm{n})^{231}\mathrm{Th} \xrightarrow[25.52\ \mathrm{h}]{\beta^-} {}^{231}\mathrm{Pa} \tag{2.2}$$

$$^{231}\mathrm{Pa}(\mathrm{n},\gamma)^{232}\mathrm{Pa} \xrightarrow[1.31\ \mathrm{d}]{\beta^-} {}^{232}\mathrm{U} \xrightarrow[68.9\,\mathrm{y}]{\alpha} {}^{228}\mathrm{Th} \tag{2.3}$$

To obtain pure samples of ^{225}Ac, the presence of ^{228}Th in ^{229}Th is not a serious problem, because the ^{224}Ra daughter of ^{228}Th can be chemically separated from he ^{225}Ac, together with ^{225}Ra, after its milking from thorium. The ^{224}Ra must be removed to ensure the absence of its progeny ^{208}Tl, which emits a 2.6-MeV γ-ray.

The complex fine structure of the ^{225}Ac α spectrum was thoroughly investigated by Dzhelepov *et al*. (1967) and by Bastin-Scoffier (1967). A level scheme is given in a critical compilation (Maples, 1973).

2.3 OCCURRENCE IN NATURE

The natural occurrence of ^{227}Ac is proportional to that of its primordial ancestor, ^{235}U, which is widely distributed in the Earth's crust (Kirby, 1974). The average crustal abundance of uranium is 2.7 ppm (Taylor, 1964), of which

0.720 mass% is ^{235}U (Holden, 1977). Therefore, the natural abundance of ^{227}Ac (calculated from its half-life and that of ^{235}U) is 5.7×10^{-10} ppm. Based upon a crustal mass of 2.5×10^{25} g (to a depth of 36 km) (Heydemann, 1969), the global inventory of ^{227}Ac is estimated to be 1.4×10^{4} metric tons.

Although the $4n + 1$ family is not ordinarily considered to be 'naturally occurring' because its primordial ancestor has become extinct, both ^{237}Np and ^{225}Ac have been detected in uranium refinery wastes and ^{225}Ac has been found in ^{232}Th isolated from Brazilian monazite (Peppard *et al.*, 1952). These nuclides are believed to be formed continually in nature by the bombardment of natural thorium and uranium with neutrons arising from spontaneous fission of ^{238}U and from neutrons produced by (α,n) reactions on light elements:

$$^{238}\mathrm{U}(\mathrm{n}, 2\mathrm{n})\ ^{237}\mathrm{U} \xrightarrow[6.75\mathrm{d}]{\beta^-}\ ^{237}\mathrm{Np} \tag{2.4}$$

$$^{232}\mathrm{Th}(\mathrm{n}, \gamma)\ ^{233}\mathrm{Th} \xrightarrow[22.3\,\mathrm{min}]{\beta^-}\ ^{233}\mathrm{U} \tag{2.5}$$

2.4 PREPARATION AND PURIFICATION

Uranium ores always contain large amounts of rare earths, and were thus generally unsatisfactory as sources of actinium before modern methods of rare earth separations were developed. The most concentrated actinium sample ever prepared from a natural raw material consisted of 0.5 mCi ($\sim$7 μg) of ^{227}Ac in less than 0.1 mg of La_2O_3 (Lecoin *et al.*, 1950).

In 1949, Peterson reported that ^{227}Ac could be synthesized by irradiating ^{226}Ra with thermal neutrons (Peterson, 1949):

$$^{226}\mathrm{Ra}(\mathrm{n}, \gamma)\ ^{227}\mathrm{Ra} \xrightarrow[42.2\,\mathrm{min}]{\beta^-}\ ^{227}\mathrm{Ac} \quad (\sigma_\mathrm{t} \cong 20 \text{ barn}) \tag{2.6}$$

This reaction greatly simplified the chemical separations required to prepare macroscopic amounts of pure ^{227}Ac and, in 1950, Hagemann reported the isolation of 1.27 mg of ^{227}Ac from 1 g of neutron-irradiated ^{226}Ra (Hagemann, 1950).

Later work (Kirby *et al.*, 1956; Cabell, 1959; Monsecour and De Regge, 1975) showed that the neutron-capture cross section of ^{227}Ac is many times greater than that of ^{226}Ra (Fig. 2.6). A new problem is introduced, namely that of separating ^{227}Ac from the large amounts of 1.9-year ^{228}Th produced by the second-order reactions:

$$^{227}\mathrm{Ac}(\mathrm{n}, \gamma)\ ^{228}\mathrm{Ac} \xrightarrow[6.15\ \mathrm{h}]{\beta^-}\ ^{228}\mathrm{Th} \quad (\sigma_\mathrm{t} = 762 \text{ barn}) \tag{2.7}$$

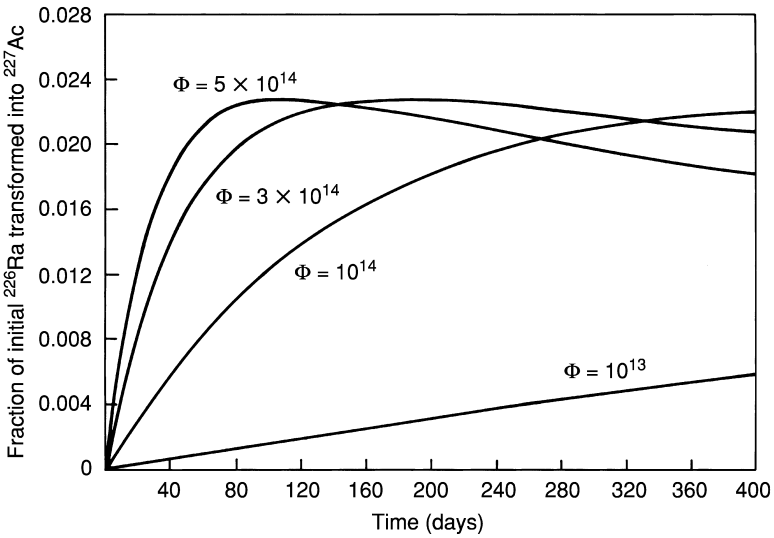

Fig. 2.6 *Growth of ^{227}Ac in neutron-irradiated ^{226}Ra at various thermal-neutron fluxes* Φ (*in* $cm^{-2}\ s^{-1}$). *The calculations assume* $\sigma_t(^{226}Ra) = 20$ *barn and* $\sigma_t(^{227}Ac) = 795$ *barn* (*Gomm and Eakins,* 1968).

Nevertheless, neutron irradiation of ^{226}Ra remains the method of choice for the preparation of ^{227}Ac at either the tracer or the macroscopic level.

The isotope ^{225}Ac is best generated by separating it from the generator ^{229}Th (Geerlings *et al.*,1993; Tsoupko-Sitnikov *et al.*, 1996; Khalkin *et al.*, 1997). The ^{229}Th generator must be separated from ^{233}U. The isotope ^{233}U is synthesized by neutron irradiation of ^{232}Th, which contaminates the ^{229}Th with some ^{228}Th and its daughters.

The isotope ^{228}Ac can be generated by separating it from the generator ^{228}Ra, which can be isolated from natural ^{232}Th (Gmelin, 1981). Detailed procedures were given by Sekine *et al.* (1967). Sani (1970) and Mikheev *et al.* (1995) removed ^{228}Ra from aged ^{232}Th by cocrystallization with $Ba(NO_3)_2$. The ^{228}Ac that grew into ^{228}Ra was removed by extraction or by adding $GdCl_3$ to an aqueous solution of the ^{228}Ra in $Ba(NO_3)_2$ and coprecipitating Ac^{3+} with $Gd(OH)_3$ using NH_3(g).

2.4.1 Purification by liquid–liquid extraction

Hagemann (1950, 1954) isolated the first milligram of ^{227}Ac from neutron-irradiated ^{226}Ra by liquid–liquid extraction with 2-thenoyltrifluoroacetone (TTA). Experience has shown (Engle, 1950; Stevenson and Nervik, 1961; Kirby, 1967), however, that TTA is not a suitable reagent for quantitative extraction of actinium because a relatively high pH ($\geq$5.5, Fig. 2.7) is required

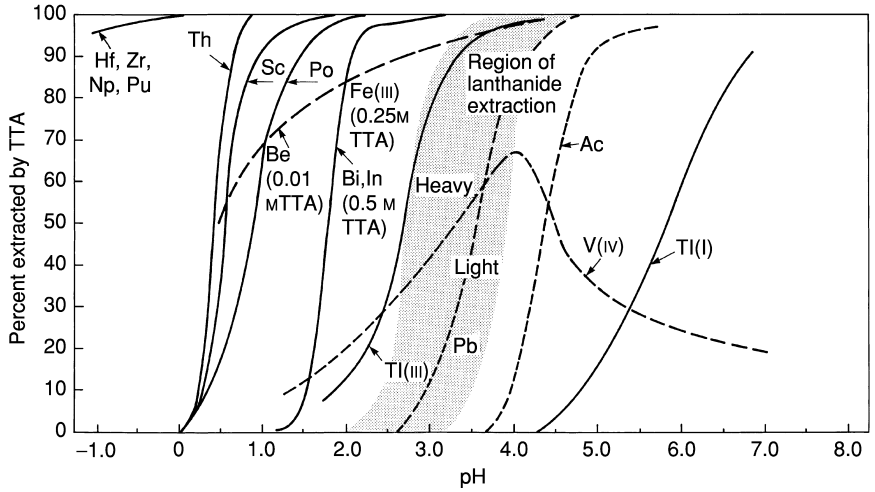

Fig. 2.7 *Extraction of various elements with thenoyltrifluoroacetone (TTA). (After Stevenson and Nervik,* 1961).

for efficient chelation but Ac^{3+} hydrolyzes above pH 7 and forms inextractable polymeric species when the pH is in the 'desirable' range, 6–7. The recovery of actinium requires tight pH control and speed of operation for satisfactory yields (Allison *et al.*, 1954; Tousset, 1961) that are usually not quantitative. The most effective application of TTA in the purification of ^{227}Ac is to remove ^{227}Th, which can be selectively and quantitatively extracted from moderately acid solutions. For this extraction, the pH_{50} (the pH at which 50% of the Th^{4+} is extracted or partitioned equally between the phases, i.e. $D = 1$) is 0.48 (Poskanzer and Foreman, 1961).

On the other hand, Sekine *et al.* (1967) found that, while the extraction of ^{228}Ac with TTA alone was not quantitative, a mixture of 0.1 M TTA and 0.1 M tri(*n*-butyl)phosphate (TBP) in CCl_4 gave reproducible distribution ratios and quantitative extraction of Ac^{3+} at pH $\geq$ 4.

Solvent extraction systems that have been applied to other actinide and lanthanide separations have also been applied to actinium separations from thorium and radium. Thus, Karalova *et al.* (1977a) studied the extraction of Ac(III) in aqueous nitrate solution by trioctylphosphine oxide dissolved in cyclohexane, *o*-xylene, carbon tetrachloride, octyl alcohol, or chloroform. Optimum extraction conditions were: $[NaNO_3] \geq 2$ M, pH 2, and cyclohexane as the partition solvent. Making the aqueous phase 8 M in lithium chloride appears to facilitate extraction with 0.1 M trioctylphosphine oxide (Karalova *et al.*, 1977b).

Trialkylphosphine oxide in aliphatic hydrocarbon solvents was used by Xu *et al.* (1983) for the solvent extraction separation of Ac(III) from La(III) in nitric acid solution. Amines and quaternary ammonium bases have also been used in

solvent extraction systems for the separation of Ac(III) from rare earths and Am(III). Karalova *et al.* (1979a) examined the separation of Ac(III) from Eu(III) by extraction from aqueous solutions containing lithium nitrate at pH 2.5–3 with tri-*n*-octylamine in cyclohexane, and concluded that this partition system shows promise for the separation of Ac(III) from rare earths. A 0.5 M solution of the quaternary ammonium base Aliquat 336 (methyltrioctylammonium chloride) in xylene extracts Ac, Am, and Eu efficiently from aqueous alkaline (pH $>$ 11) solutions containing ethylenediaminetetraacetic acid (EDTA) or 2-hydroxydiaminopropanetetraacetic acid; separation factors for Ac(III)/Am(III) and Ac(III)/Eu(III) greater than 100 were attained (Karalova *et al.*, 1978a, 1979b). A mixture of trialkylmethylammonium nitrate and TBP was reported by Mikhailichenko *et al.* (1982) to exert a weak synergistic effect on La(III) extraction and an antagonistic effect on Ac(III) extraction. Bis(2-ethylhexyl) phosphoric acid (HDEHP) has been successfully employed in the solvent extraction separation of ^{227}Ac(III), ^{227}Th(IV), ^{223}Ra(II), and ^{223}Fr(I) (Mitsugashira *et al.*, 1977). Karalova *et al.* (1978b) established that the actinium species extracted from 1 M perchloric acid is $AcX_3 \cdot 2HX$, and at higher perchloric acid concentrations is $HAc(C1O_4)_4 \cdot 2HX$.

The use of bis(2-ethylhexyl)phosphoric acid (HDEHP) as an extractant for Ac^{3+} has been little explored. Two studies have explored the fundamental mechanism of this extractant with Ac^{3+} (Szeglowski and Kubica, 1991) and the influence of colloidal rare earth particles on this extraction (Szeglowski and Kubica, 1990).

An unusual purification procedure is one in which actinium must be removed from rare earths on a commercial scale to minimize the level of radioactive contamination of the rare earth products (Kosynkin *et al.*, 1995). Uranium–rare earth phosphorites [fibrous apatites, generic formula $Ca_5(PO_4)_3(OH,F,Cl)$] have been processed commercially to remove both uranium and rare earths. After uranium was extracted from the dissolved phosphorite, cerium was removed by oxidation and precipitation from dilute acid. The trivalent rare earths and actinium remained in the aqueous phase and the actinium was removed from the rare earth fraction using mixer-settlers with mixtures of TBP and trialkyl amine (TAA) extractants in kerosene. Decontamination from a level of $\sim 10^{-8}$ Ci/(g rare earth oxides) to a level of $\sim 2 \times 10^{-11}$ Ci/(g rare earth oxides) has been achieved on an industrial scale.

2.4.2 Purification by ion-exchange chromatography

Cation-exchange chromatography is the simplest and most consistently effective method of separating sub-milligram amounts of ^{227}Ac from its principal decay products, 18.68-day ^{227}Th and 11.43-day ^{223}Ra (Gmelin, 1981). The resin most commonly employed is a strong cation-exchange resin such as Dowex 50 (Andrews and Hagemann, 1948; Cabell, 1959; Farr *et al.*, 1961; Eichelberger *et al.*, 1964; Nelson, 1964; De Troyer and Dejonghe, 1966; Baetslé *et al.*, 1967;

Baetslé and Droissart, 1973; Kraus, 1979; Boll *et al.*, 2005), but inorganic ion exchangers have also been used successfully (Huys and Baetslé, 1967; Monsecour and De Regge, 1975). The method is applicable to milking of ^{228}Ac tracer from its parent, 5.76 year ^{228}Ra (Bjornholm *et al.*, 1956, 1957; Duyckaerts and Lejeune, 1960; Bryukher, 1963; Bhatki and Adloff, 1964; Gomm and Eakins, 1966; Arnoux and Giaon, 1969; Monsecour *et al.*, 1973). A typical separation is illustrated in Fig. 2.8.

Anion-exchange chromatography is now used for bulk separation of ^{225}Ac and ^{223}Ra from ^{229}Th. The ^{225}Ac and ^{223}Ra are eluted in 2–4 bed volumes of 8 M HNO_3 and then ^{229}Th is stripped from the resin in 0.1 M HNO_3, after which the ^{229}Th can be recycled (Boll *et al.*, 2004).

Partition chromatography by reverse-phase and ion-exchange chromatography has been explored (Sinitsyna *et al.*, 1977, 1979). The radioisotopes of actinium were separated from other elements using trioctylamine, bis(2-ethylhexyl)phosphoric acid, and TBP as stationary phases on Teflon. Chromatography on a Teflon support was also investigated by Korotkin (1981). He used a mixture of TTA and TBP impregnated in Teflon to sorb the metal ions. Elution

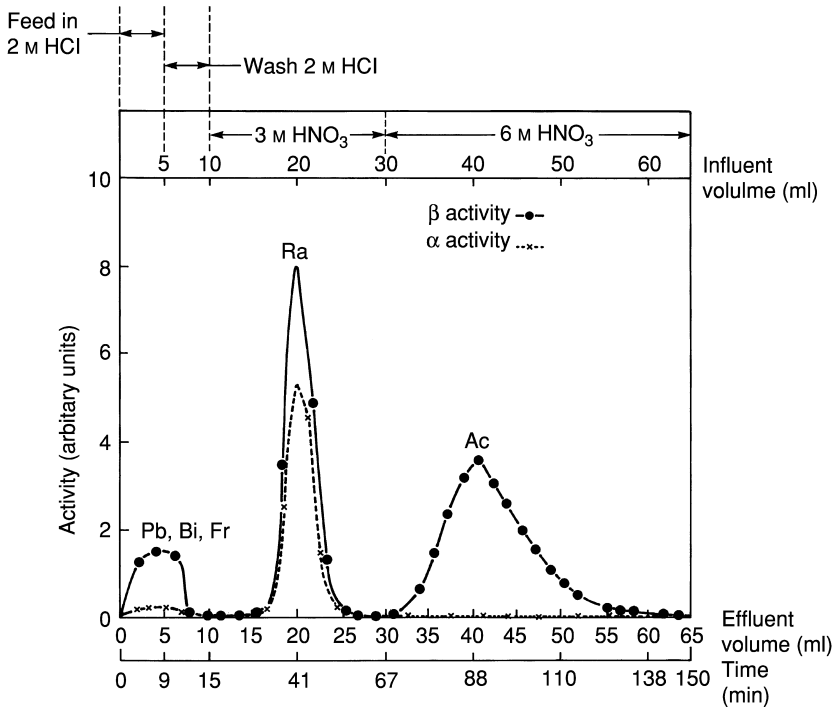

Fig. 2.8 *Separation of* ^{227}Ac *from its decay products by cation-exchange chromatography on Dowex* 50, *hydrogen form,* 200–400 *mesh,* 60°C (*Cabell,* 1959).

was by oxalate in a phthalate buffer. The procedure appears to have general utility for the rapid separation of actinides, lanthanides, and other metal ions. ^{227}Ac was separated from irradiated radium samples containing Pb, Tl, Bi, Po, and Th, and ^{225}Ac was separated from ^{233}U containing the same elements.

The inorganic cation exchanger, cryptomelane MnO_2 [a sorbent for large cations related to the mineral cryptomelane, $K(Mn^{4+},Mn^{2+})_8O_{16}$] is highly radiation-resistant and has distribution ratios (K_d values) for trivalent lanthanides and actinides that are orders of magnitude smaller than for Ra^{2+}. This ion exchanger has been used to separate $^{225}Ac^{3+}$ or $^{228}Ac^{3+}$ from $^{225}Ra^{2+}$ or $^{228}Ra^{2+}$ in radioisotope generators (Włodzimirska *et al.*, 2003).

2.4.3 Isolation of gram quantities of actinium

The history of large-scale actinium production is littered with the mutilated corpses of carefully designed processes, developed at the laboratory scale, which failed utterly, or required innumerable *ad hoc* modifications, when they were applied to the recovery of multi-Curie amounts of ^{227}Ac and ^{228}Th from multigram quantities of neutron-irradiated ^{226}Ra (Andrews and Hagemann, 1948; Engle, 1950; Kirby, 1951, 1952; Eichelberger *et al.*, 1964, 1965; De Troyer and Dejonghe, 1966; Foster, 1966; Baetslé *et al.*, 1967; Huys and Baetslé, 1967; Baetslé and Droissart, 1973).

Not the least of the problems is that posed by 3.824-day ^{222}Rn, a noble gas, which is evolved copiously and continuously by the decay of ^{226}Ra. The radioactive gaseous exhaust from the facility must be trapped and immobilized for several weeks while it decays to levels at which it can safely be released to the environment. (The maximum permissible concentration [inhalation derived air concentration (DAC)] of ^{222}Rn and its progeny in air in the workplace is very low, 3×10^{-8} μCi mL^{-1}) (U.S. Nuclear Regulatory Commission, 2005) Until now, this low level has been achieved by adsorbing the radon on activated charcoal at −75 to −180°C (Baetslé *et al.*, 1972), or by replacing the air at a sufficiently high rate, but chemical methods for removing radon and its daughters from the air by reaction with powerful fluorination reagents were also shown to bear promise for the removal of radon from air (Stein and Hohorst, 1982).

At the Belgian Nuclear Research Center (SCK-CEN, Mol), the irradiated $RaCO_3$ was dissolved in dilute nitric acid, and then precipitated as $Ra(NO_3)_2$ from 80% HNO_3, leaving nearly all the ^{227}Ac and ^{228}Th in solution. This step made the ^{226}Ra immediately available for recycling to the reactor; it also eliminated many of the severe radiolytic problems that develop when organic solvents or ion-exchange resins are in contact with large amounts of ^{226}Ra for extended periods of time.

The solution was then filtered, adjusted to 5 M HNO_3, and passed through a column of Dowex AG 1 × 8, an anion-exchange resin. ^{228}Th was quantitatively

adsorbed (Danon, 1956, 1958), while the non-complexing cations (Fe, Ni, Cr) passed through the column unimpeded. ^{227}Ac, which appeared to be adsorbed to a slight extent by the resin, followed after a brief delay. The actinium was finally purified by oxalate precipitation (Salutsky and Kirby, 1956) and ignited to Ac_2O_3 at 700°C. The process gave excellent Ac/Th separations (<0.01% ^{228}Th) and 'reasonable' Ac purifications (Baetslé *et al.*, 1972; Baetslé, 1973).

The production capacity at Mol was about 20 g ^{227}Ac and 4 g ^{228}Th per year. As of the end of 1972, 2 g of Ac_2O_3 had been encapsulated as a prototype 30 W heat source and about 700 mg had been purified for the preparation of Ac–Be neutron sources. The ^{227}Ac production and separation facility at Mol was dismantled a few years later (Deworm *et al.*, 1979).

2.5 ATOMIC PROPERTIES

Meggers, Fred, and Tomkins (Meggers *et al.*, 1951, 1957; Meggers, 1957; Sugar, 1984) examined the emission spectra of actinium excited in a hollow cathode and in arcs and sparks between copper or silver electrodes. They reported some 500 lines characteristic of actinium in the spectral range 2062.00–7886.82 Å. Of these about 140 lines were assigned to the neutral atom, Ac I, more than 300 to singly ionized actinium, Ac II, and eight to doubly ionized actinium, Ac III. The lowest energy levels for identified configurations are given in Chapter 16 of this work (Table 16.1). The electron configuration of the Ac I (neutral Ac) ground state was found to be [Rn](6d7s^2) $^2D_{3/2}$; that of Ac II (Ac^+), (7s^2) $^1S_0$; and that of Ac III (Ac^{2+}), (7s) $^2S_{1/2}$. The first two ionization potentials were estimated to be 5.17 and 11.87 eV (Sugar, 1973, 1984). Similar values were calculated by Eliav *et al.* (1998), who also calculated the third ionization potential to be 17.518 or 17.512 eV by relativistic coupled-cluster methods. The first ionization potential was recently measured to be 5.3807(3) eV by resonant excitation of ^{227}Ac by laser spectroscopy in an external electric field (Backe *et al.*, 2002).

Analysis of interference spectrograms of the ^{227}Ac nucleus yielded the nuclear spin $I = 3/2$ (Tomkins *et al.*, 1951), and values of $\mu = (1.1 \pm 0.1)$ nuclear magnetons and $Q = +1.7$ barns for the magnetic and electric quadrupole moments, respectively (Fred *et al.*, 1955).

The foregoing comprises essentially all the experimentally determined data presently available on the properties of isolated actinium atoms and ions in the gas phase (see also Chapters 16 and 19). Theoretical calculations on such properties as energy levels (Brewer, 1971a,b; Nugent and Vander Sluis, 1971; Vander Sluis and Nugent, 1972, 1974; Nugent *et al.*, 1973b), ionization potentials (Carlson *et al.*, 1970; Sugar, 1973; Eliav *et al.*, 1998), and electron affinities (Eliav *et al.*, 1998) of actinium atoms and its free ions have also been made. There remain some discrepancies among some of these calculations or estimates

that will only be resolved by better theoretical treatments and experimental measurements.

Consistent with the difference between the ionic radii of La^{3+} and Ac^{3+} (0.088 Å = 8.8 pm) (Shannon, 1976 and Section 15.7.5, Chapter 15), *ab initio* nonrelativistic and quasi-relativistic calculations of the bond lengths in monohydrides, monoxides, and monofluorides of all the lanthanide and actinide elements indicated a difference between La–X and Ac–X bond lengths of 10 pm (Küchle *et al.*, 1997). Another set of fully relativistic *ab initio* calculations of the bond lengths in monofluorides, monohydrides, and trihydrides revealed similar La–X and Ac–X bond-length differences; for LaH_3 and AcH_3 the bond-length difference calculated was also 10 pm (Laerdahl *et al.*, 1998).

2.6 THE METALLIC STATE

In 1953, Farr *et al.* (1953, 1961) prepared 10 μg of ^{227}Ac metal in an X-ray capillary by reduction of $AcCl_3$ with potassium vapor at 350°C. The diffraction pattern yielded two face-centered cubic (fcc) structures, which were attributed (by analogy to a parallel experiment with lanthanum) to actinium metal ($a_0 = 5.311 \pm 0.010$ Å) and actinium hydride ($a_0 = 5.670 \pm 0.006$ Å). The calculated densities were 10.07 and 8.35 g cm^{-1}, respectively. (The hydrogen in the 'actinium hydride' was of unknown origin.)

Milligram amounts of actinium metal were prepared by reduction of AcF_3 with lithium vapor in a molybdenum crucible (Stites *et al.*, 1955). The temperature range, 1100–1275°C, was critical for the reduction of AcF_3; at lower temperatures reduction was incomplete because the product metal did not melt, whereas at higher temperatures the yield was low because some of the AcF_3 was lost by volatilization.

The metal was reported to be silvery white in color, sometimes with a golden cast. It oxidizes rapidly in moist air to form a white coating of Ac_2O_3, which is somewhat effective in preventing further oxidation. Stites *et al.* (1955) estimated the melting point to be (1050 ± 50)°C. This melting point has been criticized as 'unreasonably low' (Matthias *et al.*, 1967) but is accepted in this work. A melting point of 1227°C has been estimated more recently (Arblaster, 1995). Based upon bonding contributions to the cohesive energy by 7s, 7p, and 6d electrons, Fournier (1976) estimated the melting point to be 1430°C and the enthalpy of sublimation ($\Delta_f H°$, Ac, g, 298 K) to be 396 kJ mol^{-1}. Other estimates of the enthalpy of sublimation are 406 kJ mol^{-1} (Wagman *et al.*, 1982) and 418 kJ mol^{-1} (David *et al.*, 1978; Ward *et al.*, 1986). The boiling point, estimated by extrapolation from vapor pressure measurements, is (3200 ± 300)°C (Foster and Fauble, 1960).

Subsequently, two metal preparations were made by the reduction of Ac_2O_3 with metallic thorium in high vacuum at 1750°C (Baybarz *et al.*, 1976), subliming the metal onto a tantalum condenser, and resubliming the metal to further

purify it. X-ray data on these preparations of Ac metal suggest an fcc lattice with a_0 parameter of (5.317 ± 0.009) and (5.314 ± 0.001) Å in the two preparations (Baybarz *et al.*, 1976). Arblaster (1995) predicted that actinium metal should parallel metallic lanthanum and americium, with a double close-packed hexagonal allotrope at lower temperature and a body-centered cubic (bcc) allotrope at higher temperature.

Farr *et al.* (1953, 1961) reported that the metallic radius of actinium is 1.88 Å, but Zachariasen (1961, 1973) regarded this value as unreasonably similar to that of lanthanum (1.87 Å), because, in all isostructural compounds, the bond distances for actinium compounds are approximately 0.1 Å greater than those for the corresponding lanthanum compounds. By interpolation between the metallic radii of Ra and Th (2.293 and 1.798 Å, respectively), he predicted a value of 1.977 Å for Ac. On the other hand, Hill (1972) suggested that the lack of an appreciable increase in the metallic radius is a manifestation of a pronounced relativistic shrinkage in the 7s orbital of the neutral Ac atom, relative to such an effect on the 6s orbital of lanthanum. The fcc Ac prepared by Baybarz *et al.* (1976) corresponded to a metallic radius of 1.878 Å, supporting Hill's argument.

2.7 COMPOUNDS

With the sole exception of the questionable hydride mentioned in Section 2.6, almost all the compounds of actinium that have been positively identified by X-ray diffraction analysis are the result of a single study by Fried, Hagemann, and Zachariasen (Fried *et al.*, 1950). Each of the compounds was prepared from 10 μg of actinium or less, which was purified by TTA extraction (Hagemann, 1950) immediately before the start of the preparation. The small sample size was chosen to minimize the radiation health hazard and to reduce the fogging of the X-ray film by γ radiation from the rapidly growing actinium decay products. Even, so, it was necessary to prepare and photograph the compound within 24 h after purification. After purification of actinium from neutron-irradiated ^{226}Ra (Baetslé and Droissart, 1973) by ion exchange, Weigel and Hauske (1977) precipitated actinium oxalate on the 10 μg scale and identified it as the decahydrate from its X-ray powder pattern. It is isomorphous with similar compounds of the rare earths, plutonium, and americium.

Table 2.2 summarizes the preparative work and some of the properties of the ten known compounds of actinium. In addition, compounds thought to be the iodide, hydroxide, oxalate, oxyiodide, phosphate, and double salt with potassium sulfate were prepared but could not be identified (Fried *et al.*, 1950). Other unidentified compounds, suggested by chemical or thermogravimetric evidence, include the basic carbonate (Butterfield and Woollatt, 1968), the 8-hydroxyquinolate (Mosdzelewski, 1966; Keller and Mosdzelewski, 1967), and a double salt with ammonium nitrate (Kirby, 1969).

Table 2.2 *Preparation and properties of actinium compounds* (*Fried* et al., 1950; *Weigel and Hauske*, 1977; *Gmelin*, 1981).

	Preparation		*Crystal structure data*					
					Lattice parameters			
Compound	*Reaction*	*Temp.* (°C)	*Symmetry*	*Structure type*	a_0 (Å)	b_0 (Å)	c_0 (Å)	β (deg)
AcF_3	$Ac(OH_3)_3 + 3HF \rightarrow AcF_3 + 3H_2O$	700	trigonal	LaF_3	7.41 ± 0.01		7.53 ± 0.02	
	$Ac^{3+} + 3F^- \rightarrow AcF_3$	25						
$AcCl_3$	$2Ac(OH)_3 + 3CCl_4 \rightarrow 2AcC1_3 + 3CO_2 + 6HCl$	subl 960	hexagonal	UCl_3	7.62 ± 0.02		4.55 ± 0.02	
$AcBr_3$	$Ac_2O_3 + 2AlBr_3 \rightarrow 2AcBr_3 + A1_2O_3$	800	hexagonal	UCl_3	8.06 ± 0.04		4.68 ± 0.02	
AcOF	$AcF_3 + 2NH_3 + H_2O \rightarrow AcOF + 2NH_4F$	900–1000	cubic	CaF_2	5.931 ± 0.002			
AcOCl	$AcCl_3 + H_2O \rightarrow AcOCl + 2HCl$	1000	tetragonal	PbClF	4.24 + 0.02		7.07 ± 0.03	
AcOBr	$AcBr_3 + 2NH_3 + H_2O \rightarrow AcOBr + 2NH_4Br$	500	tetragonal	PbClF	4.27 ± 0.02		7.40 ± 0.03	
Ac_2O_3	$Ac_2(C_2O_4)_3 \rightarrow Ac_2O_3 + 3CO_2 + 3CO$	1100	hexagonal	La_2O_3	4.07 ± 0.01		6.29 ± 0.02	
Ac_2S_3	$Ac_2O_3 + 3H_2S \rightarrow Ac_2S_3 + 3H_2O$	1400	cubic	Ce_2S_3	8.97 ± 0.01			
$AcPO_4 \cdot 1/2H_2O$	$Ac^{3+} + PO_4^{3-} \rightarrow AcPO_4$	25	hexagonal	$LaPO_4 \cdot 1/2H_2O$	7.21 ± 0.02		6.64 ± 0.03	
$Ac_2(C_2O_4)_3 \cdot 10H_2O$[a]	$2Ac^{3+} + 3C_2O_4^{2-} \rightarrow Ac_2(C_2O_4)_3 \cdot 10H_2O$	25	monoclinic	$La_2(C_2O_4)_3 \cdot 10H_2O$	11.26	9.97	10.65	111.3

[a] From Weigel and Hauske (1977).

2.8 SOLUTION AND ANALYTICAL CHEMISTRY

All available evidence supports the conclusion (Moeller and Kremers, 1945), derived primarily from tracer and coprecipitation studies, that actinium is a homolog of lanthanum, fitting into the 7th period in the periodic table. The Ac^{3+}(aq) ion is more basic (less subject to hydrolysis) than the La^{3+}(aq) ion. As such, Ac^{3+} is the most basic tripositive ion known.

Aqueous solutions of actinium are colorless. In the only reported spectrophotometric study (Hagemann, 1954), no absorption was observed over the range 400–1000 nm. There was a slight amount of absorption between 300 and 400 nm, and a pronounced absorption maximum at 250 nm.

There has been limited work on the fundamental properties of Ac^{3+}(aq). Abramov *et al*. (1998) calculated the hydration Gibbs energy of Ac^{3+} to be -3034.7 kJ mol^{-1}.

2.8.1 Redox behavior

The only stable oxidation state of actinium in aqueous solution is 3+. A transitory Ac(II) ion has been postulated by Bouissières, David, and coworkers (Bouissières *et al*., 1961; Bouissières and Legoux, 1965; David and Bouissières, 1965, 1968; David, 1970a) to account for the amalgamation behavior of actinium, which resembled that of Eu(II) and Sm(II) more than that of La(III). This hypothesis was reinforced by polarographic evidence: David (1970b,c) reported two waves in the polarogram of ^{228}Ac in $HClO_4$ at pH 1.9–3.1. He attributed the first wave to the reversible reaction:

$$Ac^{2+} + 2e^- + Hg \leftrightarrows Ac(Hg) \tag{2.8}$$

and the second to the irreversible reaction:

$$Ac^{3+} + 3e^- + Hg \rightarrow Ac(Hg) \tag{2.9}$$

From the half-wave potentials, he estimated the formal potential of the Ac(III)/Ac(II) couple to be -1.6 V and that of the Ac(III)/Ac(0) couple to be -2.62 V. A later estimate was $E^\circ(Ac^{3+}/Ac) = -2.13$ V (David *et al*., 1978). However, Maly (1969) performed extractions of actinium and other elements from sodium amalgam in sodium acetate solutions as a function of pH and found that actinium extraction behavior was similar to that of the elements thorium to berkelium, i.e. that actinium reduction did not show evidence of the Ac(II) ion.

Yamana *et al.* (1983) attempted to increase the stability of Ac^{2+}(aq) by complexing it with 18-crown-6. They noted a shift of the half-wave potential of about 0.15 V due to a complex, which they attributed to formation of an Ac^{2+}–crown complex and an Ac^{2+}(aq) ion with electronic configuration [Rn]6d^1 and ionic radius 1.25 Å. The [Rn]6d^1 configuration lies only 801 cm^{-1} above the [Rn]7s state in the free ion, so that the change of configuration is plausible.

However, Mikheev *et al.* (1995) noted that Nugent *et al.* (1973a) and Bratsch and Lagowski (1986) had calculated $E^\circ(Ac^{3+}/Ac^{2+})$ to be -4.9 and -3.3 V, respectively; the value $E^\circ(Ac^{3+}/Ac^{2+}) = -4.9$ V is adopted in Chapter 19 of this work. Either of these much more negative E° values would preclude the observation of $Ac^{2+}(aq)$. Mikheev *et al.* (1994) found no evidence for Ac^{2+} in co-crystallization experiments with Gd_2Cl_3 clusters or with Sm^{2+} in aqueous ethanol solution, a medium that should enhance the stability of Ac^{2+}. They recommended that the polarographic reduction of $Ac^{3+}(aq)$ (David, 1970b,c) was actually reduction of water but they recommended further research on the Ac^{3+}/Ac^{2+} couple.

The electrolysis of actinium at a mercury cathode has been used to separate tracer amounts of ^{228}Ac and 1.24 μg of ^{227}Ac from 3.10 mg of ^{231}Pa and an equilibrium amount of ^{227}Th. After 50 min of electrolysis in 0.17 M lithium citrate solution at a current density of 15 mA cm^{-2} the actinium was recovered by washing the amalgam with 0.1 M HCl. The overall yield was 85% and the decontamination factor was greater than 10^8 with respect to protactinium and thorium (David and Bouissières, 1966; Monsecour *et al.*, 1973).

2.8.2 Solubility

At the tracer level, actinium is carried quantitatively by any quantitative lanthanum precipitate, as well as by a wide variety of isomorphous and non-isomorphous carriers. The coprecipitation behavior of actinium was summarized in a useful table by Kahn (1951) and was exhaustively discussed in reviews (Bouissières, 1960; Sedlet, 1964; Kirby, 1967; Gmelin, 1981).

The relative amounts of actinium in partial precipitations of actinium tracer with lanthanum or other carriers are consistent with the relative solubilities of the compounds precipitated, where these are known or predictable. Unfortunately, however, with only two exceptions, quantitative solubility information is generally unavailable, because the dissolutions and precipitations that have been reported were usually incidental to some other objective, e.g. the preparation of compounds for crystallographic analysis (Table 2.2) (Weigel and Hauske, 1977).

Salutsky and Kirby (1956) precipitated tens of milligrams of ^{227}Ac from homogeneous solution with dimethyl oxalate and estimated the solubility of $Ac_2(C_2O_4)_3$ in 0.25 M $H_2C_2O_4$ (pH 1.2) to be 24 mg L^{-1}. That result is consistent with a more detailed study by Ziv and Shestakova (1965a), which shows, as expected, that the solubility of $Ac_2(C_2O_4)_3$ varies with both the acidity and the oxalate concentration (Table 2.3). In a parallel study, the authors found that the solubility of $La_2(C_2O_4)_3$ in 0.01 M HNO_3 (pH 2.2) was 4.28×10^{-5} M, about half that of $Ac_2(C_2O_4)_3$ under the same conditions. This unusual solubility of $Ac_2(C_2O_4)_3$ may be due to radiolysis.

Ziv and Shestakova (1965b) also studied the solubility of $Ac(OH)_3$ in NH_4NO_3 solutions ($\mu = 0.001$ M). They observed a pronounced aging effect

Table 2.3 *Solubility of actinium oxalate in aqueous media at* 25°C (*Ziv and Shestakova,* 1965a).

Solvent	*pH*	*Solubility*		*Activity product*
		Ac^{3+} (mg L^{-1})	$Ac_2(C_2O_4)_3$ (M)	
0.01 M HNO_3	1.85	41.0	9.0×10^{-5}	7.5×10^{-27}
0.01 M HNO_3	2.00	40.0	8.8×10^{-5}	6.7×10^{-27}
0.01 M HNO_3	2.00	34.0	7.5×10^{-5}	2.1×10^{-27}
0.01 M HNO_3	2.00	30.0	6.5×10^{-5}	1.5×10^{-27}
H_2O	–	0.86	1.9×10^{-6}	2.7×10^{-27}
H_2O	–	1.5	3.3×10^{-6}	4.2×10^{-26}
H_2O	–	1.7	3.7×10^{-6}	8.0×10^{-26}
5×10^{-5} M $H_2C_2O_4$	3.4	2.5	5.5×10^{-6}	–
5×10^{-4} M $H_2C_2O_4$	3.0	1.2	2.6×10^{-6}	–
5×10^{-3} M $H_2C_2O_4$	2.3	0.96	2.1×10^{-6}	–
5×10^{-1} M $H_2C_2O_4$	0.9	7.85	1.73×10^{-5}	–

on both its solubility and the pH of its saturated solutions. For example, 1 h after precipitation the solubility was 3.6×10^{-8} g L^{-1} (1.59×10^{-8} M) and the pH was 10.4; 15 h later, the solubility had increased to 1.73×10^{-4} g L^{-1} and the pH had decreased to 9.1. After 27 days, the pH was 4.2. The authors attributed this decrease in pH to radiolysis of the solution by adsorbed ^{227}Th. Gamma radiation of aerated water also causes the pH to decrease: radiolysis by γ-rays produces nitric acid from dissolved O_2 and N_2 (Barkatt *et al.*, 1982). Another reason for the decrease of pH is that radiolysis of air by α particles at an air–water interface (Burns *et al.*, 1982) oxidizes nitrogen to acidic nitrogen oxides, which slowly acidifies the adjacent aqueous solution.

When ^{227}Ac was radiochemically purified before precipitation, the pH declined from 10.4 to only 8.3 in 166 days. From the activity product in various concentrations of NH_4NO_3, the solubility of aged $Ac(OH)_3$ was calculated to be 0.74 mg L^{-1}, which is higher than that for $La(OH)_3$. The corresponding equilibrium constants

$$M(OH)_3(s) + 3H^+(aq) \rightarrow M^{3+}(aq) + 3H_2O \; {}^*K_{s,0} \qquad (2.10)$$

(see Chapter 19, section 9, this book, for further discussion of $^*K_{s,0}$) at ionic strength 0.1 are $(1.26 \pm 0.04) \times 10^{24}$ for $Ac(OH)_3$ and 2.0×10^{20} for $La(OH)_3$. The higher solubility of $Ac(OH)_3$ can be attributed to the more basic character of the large Ac^{3+} ion, radiation damage of the crystallites, and/or to the tendency of radiolysis to produce more acidic conditions (Barkatt *et al.*, 1982; Burns *et al.*, 1982). A comparison of some solubility products for rare earth and actinide hydroxides is given in Chapter 19. The above evidence that $Ac(OH)_3$ is the most soluble of all f-element trihydroxides is consistent with Ac^{3+} being the most basic tripositive cation.

More recently, Kulikov *et al.* (1992) used electromigration to determine that ^{225}Ac is unhydrolyzed in aqueous solution of ionic strength 0.1 at 298 K until pH > 10. They determined the $^{*}K_{s,0}$

$$Ac(OH)_3(s) + 3H^+(aq) \rightarrow Ac^{3+}(aq) + 3H_2O \; ^{*}K_{s,0} \qquad (2.11)$$

to be 7.9×10^{31}. This value is much higher than that derived by Ziv and Shestakova or that expected by extrapolating from trivalent rare earths and actinide hydroxides.

2.8.3 Complexation

As in all its reactions, actinium closely resembles lanthanum in its behavior toward complexing agents. To the extent that they have been determined experimentally, the stability constants of actinium complexes (a selection is given in Table 2.4) are the same as, or slightly smaller than, those of the corresponding lanthanum complexes (Rao *et al.*, 1968, 1970; Shahani *et al.*, 1968; Sekine *et al.*, 1969; Sekine and Sakairi, 1969; Gmelin, 1981), in agreement with prediction from the similarity in their electronic configurations and their ionic radii (Kirby, 1967; Section 15.7.5). There is a linear dependence of log (formation constant) upon ionic radius, with Ac^{3+} always having the extreme position of largest ionic radius (Gmelin, 1981 and Section 15.7.5).

The hydrolysis of $Ac^{3+}(aq)$ is the smallest of all 3+ ions. Moutte and Guillaumont (1969) determined the equilibrium constant for the reaction

$$AcOH^{2+}(aq) + H_2O \rightarrow Ac(OH)_2^+(aq) + H^+(aq) \qquad (2.12)$$

to be 3.5×10^{-9} mol L^{-1}. Using the isotope ^{228}Ac, they determined that, at pH 8, 74% of the actinium in solution exists as $Ac(OH)^{2+}$ and 26% exists as $Ac(OH)_2^+$.

The Ac^{3+}–citrate complexes are sufficiently strong that citrate complexes almost all Ac^{3+} in 0.001 M citrate even at pH 8.1 (Moutte and Guillaumont, 1969). In addition to the complexes listed in Table 2.4, Ac^{3+} complexes have been studied with *trans*-1,2-diaminocyclohexanetetraacetic acid (DCTA), TTA and other diketones, arsenazo III, and other organic ligands (Gmelin, 1981).

Fukusawa *et al.* (1982) determined stability constants for chloro and bromo complexes of Ac(III), among many others, by a solvent extraction procedure. A much larger contribution from inner-sphere complex formation was observed in chloro than in bromo complexes for tripositive actinide ions. An empirical approach for predicting the stability of metal-ion complexes has been applied to actinium (Kumok, 1978).

On the basis of known and estimated ionic radii, Abramov *et al.* (1998) calculated the extraction constant K_{ex} of Ac^{3+} with bis(2-ethylhexyl)phosphoric acid (HDEHP) into toluene. The calculated K_{ex} value for Ac^{3+} is nearly an order of magnitude smaller than that for La^{3+}.

Table 2.4 *Cumulative stability constants of selected actinium complexes.*

Ligand	*Ionic strength* (μ)	[H^+] (M)	*Stability constant*[a]	*Reference*
F^-	0.5	0.00025	$\beta_1 = 529 \pm 8$ $\beta_2 = (1.67 \pm 0.09) \times 10^5$ $\beta_3 = 8 \times 10^7$	Aziz and Lyle (1970)
F^-	0.1	0.016	$\beta_1 = 885$	Makarova *et al.* (1973)
Cl^-	1.0	1.0	$\beta_1 = 0.80 \pm 0.09$ $\beta_2 = 0.24 \pm 0.08$	Shahani *et al.* (1968)
Cl^-	4.0	0.01	$\beta_1 = 0.9$ $\beta_2 = 0.09$ $\beta_3 = 0.05$	Sekine and Sakairi (1969)
Br^-	1.0	1.0	$\beta_1 = 0.56 \pm 0.07$ $\beta_2 = 0.30 \pm 0.06$	Shahani *et al.* (1968)
NO_3^-	1.0	1.0	$\beta_1 = 1.31 \pm 0.12$ $\beta_2 = 1.02 \pm 0.12$	Shahani *et al.* (1968)
SO_4^{2-}	1.0–1.16	1.0	$\beta_1 = 15.9 \pm 1.3$ $\beta_2 = 71.4 \pm 7.3$	Shahani *et al.* (1968)
SO_4^2	1.0	pH 3–3.5	$\beta_1 = 22.9$ $\beta_2 = 479$	Sekine and Sakairi (1969)
SCN^-	1.0	pH 2	$\beta_1 = 1.11 \pm 0.07$ $\beta_2 = 0.82 \pm 0.08$	Rao *et al.* (1968)
SCN^-	5.0	pH 3–3.5	$\beta_1 = 0.18$ $\beta_2 = 0.35$	Sekine and Sakairi (1969)
$C_2O_4^{2-}$	1.0	pH 3–3.5	$\beta_1 = 3.63 \times 10^3$ $\beta_2 = 1.45 \times 10^6$	Sekine and Sakairi (1969)
$H_2PO_4^-$	0.5	pH 2–3	$\beta_1 = 38.8 \pm 5$	Rao *et al.* (1970)
Citrate	0.1	pH 2–3	$\beta_1 = 9.55 \times 10^6$	Makarova *et al.* (1974)
NTA^{-}[b]	0.1	pH $\approx$ 5	$\beta_3 = 4.3 \times 10^{14}$	Keller and Schreck (1969)
EDTA[c]	0.1	pH 2.8	$\beta_1 = 1.66 \times 10^{14}$	Makarova *et al.* (1972)

[a] $\beta_n = [ML_n]/[M][L]^n$.

[b] HNTA, 2-naphthoyltrifluoroacetone.

[c] EDTA, ethylenediaminetetraacetic acid.

2.8.4 Radiocolloid formation

Kirby (1969) noted that when acidic aqueous solutions containing tracer amounts of Ac^{3+} and its progeny $^{227}Th^{4+}$ and $^{223}Ra^{2+}$ are dried on platinum disks, the actinium can be separated by redissolution in dilute NH_4NO_3(aq) and the radium by redissolution in dilute HF(aq), leaving the thorium on the disk. He described this separation as an application of 'residue adsorption'; it may represent radiocolloid formation and selective redissolution at the metal surface.

Rao and Gupta (1961) studied the adsorption of ^{228}Ra and ^{228}Ac onto sintered glass and paper, and found that the adsorption of ^{228}Ac onto the glass increased with pH and time of aging. They studied the phenomenon by

centrifugation; the ^{228}Ac fraction could be centrifuged at pH $\geq$ 5. Paper chromatography showed that the ^{228}Ac was immobile at a pH of 3 and higher, whereas Ba remained in solution. They concluded that the ^{228}Ac formed radiocolloids at pH $\geq$ 5.

2.8.5 Analytical chemistry of actinium

Sedlet (1964) published a complete set of procedures for analytical chemistry of actinium, primarily radiochemical procedures for ^{227}Ac. Kirby (1967) published a review that selected published and unpublished procedures that "will be of most value to the modern analytical chemist." Kirby also wrote the section on analytical chemistry in Gmelin (1981). Karalova (1979) reviewed the analytical chemistry of actinium. The analytical procedures that they described were based upon separation of actinium from other radioelements and then determination by measurement of the α, β, or γ radioactivity of a sample that has reached secular equilibrium with its daughters. The techniques suitable for tracer-level determination of ^{227}Ac are neutron activation analysis, by which ^{227}Ac can be determined at the level of 10^{-17} g, and total α, β, and γ radioactivity of a sample that has reached secular equilibrium with its daughters, by which ^{227}Ac can be determined at the level of 10^{-20} g. Recently a procedure for determination of ^{227}Ac in environmental samples by coprecipitation with lead sulfate, ion exchange, and α spectrometry after allowing the daughter isotopes ^{227}Th and ^{223}Ra to reach secular equilibrium (2–3 months) has been published (Martin *et al.*, 1995). The method requires the use of a short-lived actinium yield tracer, ^{225}Ac or ^{228}Ac. The lower limit of detection is $\sim$0.2 mBq per sample (7.5×10^{-16} g) at 95% confidence level.

The isotope ^{225}Ac, which is useful for tumor radiotherapy (see below), can be determined by α-spectrometric measurement of its α-emitting progeny ^{217}At (Martin *et al.*, 1995) or by γ spectrometry of the progeny ^{221}Fr and ^{213}Bi (McDevitt *et al.*, 2001).

2.9 APPLICATIONS OF ACTINIUM

2.9.1 Heat sources for radioisotope thermoelectric generators

The first practical use of actinium was to produce multi-Curie amounts of ^{227}Ac in order to take advantage of the energy released from the five α particles that are generated during its decay (Fig. 2.1) to produce electrical power for spacecraft and other devices that must operate for long periods of time in remote locations. An ambitious radioisotope thermoelectric generator (RTG) program was undertaken in Belgium to produce a 250 W_{th} thermoelectric generator fueled with 18 g of ^{227}Ac (Baetslé and Droissart, 1973). A prototype heat source that contained 2 g of ^{227}Ac was prepared but was not put into use (Baetslé and

Droissart, 1973). Kirby (Gmelin, 1981) listed the radioisotopes that can be used as thermoelectric heat sources. Of these, ^{238}Pu has been the most suitable; it has been used in almost all U.S. spacecrafts that utilized RTGs, beginning with 2.7-W SNAP–3B (Space Nuclear Auxiliary Power) generators for Transit 4A and 4B satellites in 1961 (Lange and Mastal, 1994; U.S. Department of Energy, 1987) and continuing to the three 276-W general purpose heat source (GPHS) RTGs in the Cassini probe, which was launched in 1997 and reached Saturn in 2004. (See also relevant sections in Chapter 7 and Chapter 15, section 11.2, this book.)

2.9.2 Neutron sources

Isotopes of elements with $Z \leq 20$ emit neutrons when they are bombarded by $\sim$5 MeV α particles. Kirby (Gmelin, 1981) listed the properties of important (α,n) generators. The advantages of ^{227}Ac as a heat source are also those that make it attractive as an (α,n) generator. A few ^{227}Ac (α,n) generators have been constructed and used (Gmelin, 1981).

2.9.3 Alpha-particle generators for tumor radiotherapy

The 10-day α emitter ^{225}Ac has desirable properties for destroying rapidly growing cancer cells. After decay of ^{225}Ac to ^{221}Fr, four additional high-energy α decays and two β^- decays occur rapidly (Fig. 2.3), delivering $\sim$40 MeV of high linear-energy-transfer radiation over a range of less than 100 μm. None of the decay events emits hard γ-rays, so that ^{225}Ac can deliver large doses to a tumor cell and negligible doses to surrounding healthy tissue (Tsoupko-Sitnikov *et al.*, 1996; Khalkin *et al.*, 1997; Boll *et al.*, 2005). To utilize this isotope for therapy, the principal challenges are to generate the isotope free of other radioisotopes, to deliver it to the cancer cell for a long enough period of time, to bind it firmly to the target call, and to retain the daughter radioisotopes (especially the $^{221}Fr^+$ ion) at the target site. The *in vivo* stability of several macrocyclic complexes of ^{225}Ac have been evaluated. Deal *et al.* (1999) found the most promising complex to be that with 1,4,7,10,13,16-hexaazacyclohexadecane-*N*,*N*′,*N*″,*N*‴,*N*⁗-hexa-acetic acid (HEHA); Ouadi *et al.* (2000) bifunctionalized an isothiocyanate derivative of HEHA for good covalent bonding to biomolecules. A procedure for delivering ^{225}Ac to tumors via bifunctional chelators related to the ligand 1,4,7,10-tetraazacyclododecane-1,4,7,10-tetraacetic acid (DOTA) has been described (McDevitt *et al.*, 2001). Kennel *et al.* (2000, 2002) evaluated radio-immunotherapy of mice with lung and other tumors using ^{225}Ac–HEHA conjugates with monoclonal antibodies; their studies concluded that the radio-toxicity of ^{225}Ac can only be controlled if conjugates that bind strongly with the daughters as well as with Ac^+ can be discovered.

As described in the earlier paragraph and in Section 2.2.3, ^{229}Th (α, $t_{1/2}$=7340 years) is an appropriate generator from which ^{225}Ac can be removed periodically. At the time of writing, Oak Ridge National Laboratory is producing

50–60 mCi of ^{225}Ac from ^{229}Th every 8 weeks. Additional shipments of 5–20 mCi of ^{225}Ac are produced by ORNL every 2 weeks from the decay of the ^{225}Ra parent. The ^{225}Ac is shipped to hospitals and other research facilities (Boll *et al*., 2005).

The isotope ^{225}Ac can also serve as a ^{213}Bi generator, which decays with a 45.6-min half-life (97.8% β, 2.2% α). The decay is accompanied by a 440-keV γ-ray, so that ^{213}Bi can be delivered to tumors with a bifunctional chelating agent for radioimmunotherapy as well as for imaging (Pippin *et al*., 1995; Nikula *et al*., 1999). Generators have been delivered to hospitals, where radioisotopically pure, chemically active ^{213}Bi can be eluted for radiotherapy, with minimum shielding every 5–6 h for at least 10 days. At the time of writing, the Institute for Transuranium Elements (Joint Research Centre of the European Commission, located at Karlsruhe, Germany) is producing and distributing ^{225}Ac/^{213}Bi generators.

2.9.4 Actinium-227 as a geochemical tracer

Nozaki (1984) demonstrated that the concentration of ^{227}Ac is higher than that of its progenitor ^{231}Pa in deep seawater; he proposed the use of natural ^{227}Ac as a tracer for circulation and mixing of seawater in deep ocean basins. Geibert *et al*. (2002) confirmed this phenomenon in several other oceanic locations and proposed that ^{227}Ac be used as a tracer for deep seawater circulation (diapycnal mixing, i.e. mixing across lines of equal density).

REFERENCES

Abramov, A. A., Eliseeva, O. V., and Iofa, B. Z. (1998) *Radiochemistry,* **40**, 302–5; *Radiokhimiya*, **40**, 292–5.

Adloff, J. P. (2000) *Radiochim. Acta,* **88**, 123–7.

Ahmad, I. (2002) Unpublished; personal communication to L. Morss.

Allison, M., Moore, R. W., Richardson, A. E., Peterson, D. T., and Voight, A. F. (1954) *Nucleonics,* **12**(5), 32–4.

Andrews, H. C. and Hagemann, F. (1948) in *Summary Report for April, May, and June 1948. Chemistry Division, Section C-I, ANL–4176* (eds. W. M. Manning and D. W. Osborne), pp. 13–6.

Arblaster, J. W. (1995) *Calphad,* **19**, 373.

Arnoux, M. and Giaon, A. (1969) *C. R. Acad. Sci. Paris,* **269B**, 317–20.

Aziz, A. and Lyle, S. J. (1970) *J. Inorg. Nucl. Chem.,* **32**, 1925–32.

Backe, H., Dretzke, A., Eberhardt, K., Fritsche, S., Grüning, C., Gwinner, G., Haire, R. G., Huber, G., Kratz, J. V., Kube, G., Kunz, P., Lassen, J., Lauth, W., Passler, G., Repnow, R., Schwalm, D., Schwamb, P., Sewtz, M., Thörle, P., Trautmann, N., and Waldek, A. (2002) *J. Nucl. Sci. Technol.*, (Suppl. 3), 86–9.

Baetslé, L. H., Dejonghe, P., Demildt, A. C., De Troyer, A., Droissart, A., and Dumont, G. (1967) *Ind. Chim. Belge,* **32** (2), 56–60.

Baetslé, L. H., Brabers, M. J., Dejonghe, P., Demildt, A. C., De Troyer, A., Droissart, A., and Poskin, M. (1972) *Proc. 4th UN Int. Conf. on Peaceful Uses of Atomic Energy*. A/CONF.49/P/287, United Nations, New York, pp. 191–203.

Baetslé, L. H. (1973) in *CEN-SCK Annual Scientific Report, 1972, Belgian Report BLG–481* (eds. R. Billiau, K. Bobin, W. Drent, and L. Hespeels), ch. 6.

Baetslé, L. H. and Droissart, A. (1973) Production and Applications of ^{227}Ac. Belgian Report BLG 483.

Bagnall, K. W. (1957) in *Chemistry of the Rare Radioelements: Polonium–Actinium,* Butterworths, London, pp. 15–45.

Barkatt, A., Barkatt, A., and Sousanpour, W. (1982) *Nucl. Technol.,* **60**, 218–27.

Bastin-Scoffier, G. (1967) *C. R. Acad. Sci. Paris,* **265B**, 863–5.

Baybarz, R. D., Bohet, J., Buijs, K., Colson, L., Müller, W., Reul, J., Spirlet, J. C., and Toussaint, J. C. (1976) *Transplutonium Elements. Proc. 4th Int. Transplutonium Elements Symp., 1975* (eds. W. Müller and R. Lindner), North Holland, Amsterdam, pp. 61–8.

Beckmann, W. (1955) *Z. Phys.,* **142**, 585–601.

Bhatki, K. S. and Adloff, J. P. (1964) *Radiochim. Acta,* **3**, 123–6.

Bjornholm, S., Nielsen, B., and Sheline, R. K. (1956) *Nature,* **178**, 1110–1.

Bjornholm, S., Nathan, O., Nielsen, O. B., and Sheline, R. K. (1957) *Nucl. Phys.,* **4**, 313–24.

Boll, R. A., Malkemus, D., and Mirzadeh, S. (2004) *Appl. Radiat. Isot.*, **62**, 667–9.

Bouissières, G. (1960) in *Nouveau Traité de Chimie Minérale* (ed. P. Pascal), Masson, Paris 7, pp. 1413–46.

Bouissières, G., Haïssinsky, M., and Legoux, Y. (1961) *Bull. Soc. Chim. Fr.*, 1028–30.

Bouissières, G. and Legoux, Y. (1965) *Bull. Soc. Chim. Fr.*, 386–8.

Bratsch, S. G. and Lagowski, J. J. (1986) *J. Phys. Chem.,* **90**, 307–12.

Brewer, L. (1971a) *J. Opt. Soc. Am.,* **61**, 1101–11.

Brewer, L. (1971b) *J. Opt. Soc. Am.,* **61**, 1666–82.

Browne, E. (2001) *Nucl. Data Sheets,* **93**, 763.

Bryukher, E. (1963) *Sov. Radiochem.,* **5**, 123–5; *Radiokhimiya*, **5**, 142–3.

Burns, W. G., Hughes, A. E., Marples, J. A. C., Nelson, R. S., and Stoneham, A. M. (1982) *J. Nucl. Mater.,* **107**, 245–70.

Butterfield, D. and Woollatt, R. (1968) *J. Inorg. Nucl. Chem.,* **30**, 801–5.

Cabell, M. J. (1959) *Can. J. Chem.,* **37**, 1094–1103.

Carlson, T. A., Nestor, C. W. J., Wasserman, N., and McDowell, J. F. (1970) Comprehensive Calculation of Ionization Potentials and Binding Energies for Multiply-Charged Ions, US Report ORNL-4562.

Chayawattanangkur, K., Herrmann, G., and Trautmann, N. (1973) *J. Inorg. Nucl. Chem.,* **35**, 3061–73.

Clarke, R. W. (1954) Actinium. A Bibliography of Unclassified and Declassified Atomic Energy Project Reports and References to the Published Literature (1906–1953), UK Report AERE Inf/Bib 95.

Clarke, R. W. (1958) Abstracts of Atomic Energy Project Unclassified Reports and Published Literature on the Actinide Elements (Papers dated 1957 noted up to February, 1958), Part I. Actinium, Protactinium, Neptunium, UK Report AERE C/R 2472.

Dalmasso, J., Herment, M., and Ythier, C. (1974) *C. R. Acad. Sci. Paris,* **278B**, 97–100.

Danon, J. (1956) *J. Am. Chem. Soc.,* **78**, 5953–4.

Danon, J. (1958) *J. Inorg. Nucl. Chem.,* **5**, 237–9.
David, F. (1970a) *Rev. Chim. Minér.,* **7**, 1–11.
David, F. (1970b) *C. R. Acad. Sci. Paris,* **271**, 440–2.
David, F. (1970c) *Radiochem. Radioanal. Lett.,* **5**, 279–85.
David, F. and Bouissières, G. (1965) *Bull. Soc. Chim. Fr.*, 1001–7.
David, F. and Bouissières, G. (1966) in *Physico-Chimie du Protactinium*, Colloques internationaux du CNRS, Paris, No. 154, pp. 301–6.
David, F. and Bouissières, G. (1968) *Inorg. Nucl. Chem. Lett.,* **4**, 153–9.
David, F., Samhoun, K., Guillaumont, R., and Edelstein, N. (1978) *J. Inorg. Nucl. Chem.,* **40**, 69–74.
Deal, K. A., Davis, I. A., Mirzadeh, S., Kennel, S. J., and Brechbiel, M. W. (1999) *J. Med. Chem.,* **42**, 2988–92.
Debierne, A. (1899) *C. R. Acad. Sci. Paris,* **129**, 593–5.
Debierne, A. (1900) *C. R. Acad. Sci. Paris,* **130**, 906–8.
Debierne, A. (1904) *C. R. Acad. Sci. Paris,* **139**, 538–40.
Dempster, A. J. (1935) *Nature,* **136**, 180.
De Troyer, A. and Dejonghe, P. (1966) in *Large Scale Production and Applications of Radioisotopes,* US Report DP–1066, edn 1, session III, pp. 63–9.
Deworm, J. P., Fieuw, G., and Marlein, J. (1979) *Ann. Belg. Ver. Stralingsbescherming,* **4**, 107–28; *Chem. Abstr.*, 93, 83093b.
Duyckaerts, G. and Lejeune, R. (1960) *J. Chromatogr.,* **3**, 58–62.
Dzhelepov, B. S., Ivanov, R. B., Mikhailova, M. A., Moskvin, L. N., Nazarenko, O. M., and Rodionov, V. F. (1967) *Bull. Acad. Sci. USSR, Phys. Ser.,* **31**, 563–74; *Dokl. Akad. Nauk USSR, Fiz. Ser.*, **31**, 568–80.
Eichelberger, J. F., Grove, G. R., and Jones, L. V. (1964) Mound Laboratory Progress Report for April, 1964. US Report MLM-1196, pp. 9–11.
Eichelberger, J. F., Grove, G. R., and Jones, L. V. (1965) Mound Laboratory Progress Report for November, 1964. US Report MLM-1227.
Eliav, E., Shmulyian, S., and Kaldor, U. (1998) *J. Chem. Phys.,* **109**, 3954–8.
Engle, P. M. (1950) Preliminary Report on the Actinium Separation Project. US Report MLM-454.
Farr, J. D., Giorgi, A. L., Money, R. K., and Bowman, M. G. (1953) The Crystal Structure of Actinium Metal and Actinium Hydride. US Report LA-1545, Los Alamos National Laboratory.
Farr, J. D., Giorgi, A. L., Bowman, M. G., and Money, R. K. (1961) *J. Inorg. Nucl. Chem.,* **18**, 42–7.
Firestone, R. B. and Shirley, V. S. (eds.) (1996) *Table of Isotopes,* Wiley, New York.
Foster, K. W. (1966) Radioisotopes for Heat Sources. II. Calculations for preparation of Ac-227 by Neutron Irradiation of Ra-226. US Report MLM-1297.
Foster, K. W. and Fauble, L. G. (1960) *J. Phys. Chem.,* **64**, 958–9.
Fournier, J. M. (1976) *J. Phys. Chem. Solids,* **37**, 235–44.
Fred, M., Tomkins, F. S., and Meggers, W. F. (1955) *Phys. Rev.,* **98**, 1514.
Fried, S., Hagemann, F., and Zachariasen, W. H. (1950) *J. Am. Chem. Soc.,* **72**, 771–5.
Fukusawa, T., Kawasuji, I., Mitsugashira, T., Sato, A., and Suzuki, S. (1982) *Bull. Chem. Soc. Jpn.,* **55**, 726–9.
Geerlings, M. W., Kaspersen, F. M., Apostolidis, C., and Van Der Hout, R. (1993) *Nucl. Med. Commun.,* **14**, 121–5.

Geibert, W., Rutgers van der Loeff, M. M., Hanfland, C., and Dauelsberg, H.-J. (2002) *Earth Planet. Sci. Lett.,* **198**, 147–65.
Giesel, F. (1902) *Ber. Dtsch. Chem. Ges.,* **35**, 3608–11.
Giesel, F. (1903) *Ber. Dtsch. Chem. Ges.,* **36**, 342–7.
Giesel, F. (1904a) *Ber. Dtsch. Chem. Ges.,* **37**, 1696–9.
Giesel, F. (1904b) *Ber. Dtsch. Chem. Ges.,* **37**, 3963–6.
Giesel, F. (1905) *Ber. Dtsch. Chem. Ges.,* **38**, 775–8.
Gmelin (1942) *Handbuch der Anorganischen Chemie, 8. Auflage, System-Nummer 40, Actinium und Isotope (MsTh2),* Verlag Chemie, Berlin, (English translation by G. A. Young (1954)). U.S. Report AEC-tr-l734.
Gmelin (1981) *Handbook of Inorganic Chemistry, Actinium*, 8th edn, System Number 40 Suppl. vol. 1, Springer-Verlag, Berlin.
Godlewski, T. (1904–5) *Nature,* **71**, 294–5.
Godlewski, T. (1905) *Phil. Mag.,* **10**, 35–45.
Gomm, P. J. and Eakins, I. D. (1966) The Determination of Actinium-227 in Urine. UK Report AERE-R 4972.
Gomm, P. J. and Eakins, J. D. (1968) *Analyst,* **93**, 228–34.
Hagemann, F. (1950) *J. Am. Chem. Soc.,* **72**, 768–71.
Hagemann, F. T. (1954) The Chemistry of Actinium, in *The Actinide Elements, Nat. Nucl. En. Ser. Div. IV, 14A* (eds. G. T. Seaborg and J. J. Katz), McGraw-Hill, New York, pp. 14–44.
Hahn, O. (1905) *Jahrb. Radioaktivitat Elektronik,* **2**, 233–66.
Hahn, O. (1906a) *Ber. Dtsch. Chem. Ges.,* **39**, 1605–7.
Hahn, O. (1906b) *Phys. Z.,* **7**, 855–64.
Hahn, O. (1907) *Ber. Dtsch. Chem. Ges.,* **40**, 1462–9.
Hahn, O. (1908) *Phys. Z.,* **9**, 146–8.
Hahn, O. and Meitner, L. (1918) *Phys. Z.,* **19**, 208–18.
Hahn, O. and Erbacher, O. (1926) *Phys. Z.,* **27**, 531–3.
Heath, R. L. (1974) Gamma-ray Spectrum Catalogue. Ge(Li) and Si(Li) Spectrometry. US Report ANCR-1000-2, 3rd edn, vol. 2.
Heydemann, A. (1969) in *Handbook of Geochemistry* (ed. K. H. Wedepohl), Springer-Verlag, New York, vol. 1, pp. 276–412.
Hill, H. H. (1972) *Chem. Phys. Lett.,* **16**, 114–8.
Holden, N. E. (1977) *Isotopic Composition of the Elements and Their Variation in Nature – A Preliminary Report, BNL-NCS–50605*; (1979) *Pure Appl. Chem.,* **52**, 2371.
Horen, D. J. (1973) *Nucl. Data Sheets,* **10**, 387–90.
Huys, D. and Baetslé, L. H. (1967) Separation of ^{226}Ra, ^{227}Ac and ^{228}Th by Ion Exchange. Belgian Report BLG 422.
Hyde, E. K., Perlman, I., and Seaborg, G. T. (1964) *The Nuclear Properties of the Heavy Elements*, vol. 2, Prentice-Hall, Englewood Cliffs, NJ, pp. 584–6.
Ihde, A. J. (1964) *The Development of Modern Chemistry,* Harper & Row, New York, p. 492.
Jordan, K. C. and Blanke, B. C. (1967) in *Standardization of Radionuclides, IAEA Proc. Series STI/PUB/139*. IAEA, Vienna, pp. 567–78.
Kahn, M. (1951) in *Radioactivity Applied to Chemistry* (eds. A. C. Wahl and N. A. Bonner) Wiley, New York, pp. 403–33.

Karalova, Z. K., Rodionova, L. M., Pyzhova, Z. I., and Myasoedov, B. F. (1977a) *Soviet Radiochem.,* **19**, 31–3; *Radiokhimiya*, **19**, 38–41.
Karalova, Z. K., Rodionova, L. M., Pyzhova, Z. I., and Myasoedov, B. F. (1977b) *Sov. Radiochem.,* **19**, 34–7; *Radiokhimiya,* **19**, 42–5.
Karalova, Z. K., Nekrasova, V. V., Pyzhova, Z. I., Rodionova, L. M., and Myasoedov, B. F. (1978a) *Radiokhimiya,* **20**, 845–50.
Karalova, Z. K., Rodionova, L. M., Pyzhova, Z. I., and Myasoedov, B. F. (1978b) *Sov. Radiochem.,* **20**, 30–3; *Radiokhimiya,* **20**, 42–6.
Karalova, Z. K. (1979) *Sov. Radiochem.,* **20**, 712–20; *Radiokhimiya,* **20**, 834–44.
Karalova, Z. K., Rodionova, L. M., Pyzhova, Z. I., and Myasoedov, B. F. (1979a) *Sov. Radiochem.,* **21**, 7–10; *Radiokhimiya*, **21**, 11–4.
Karalova, Z. K., Rodionova, L. M., Pyzhova, Z. I., and Myasoedov, B. F. (1979b) *Sov. Radiochem.,* **21**, 335–9; *Radiokhimiya*, **21**, 394–9.
Katz, J. J. and Seaborg, G. T. (1957) in *The Chemistry of the Actinide Elements*, Methuen, London, pp. 5–15.
Keller, C. and Mosdzelewski, K. (1967) *Radiochim. Acta,* **7**, 185–8.
Keller, C. and Schreck, H. (1969) *J. Inorg. Nucl. Chem.,* **31**, 1121–32.
Keller, C. (1977) *Chem.-Z.,* **101**, 500–7.
Kennel, S. J., Chappell, L. L., Dadachova, K., Brechbiel, M. W., Lankford, T. K., Davis, I. A., Stabin, M., and Mirzadeh, S. (2000) *Cancer Biotherapy Radiopharm.,* **15**, 235–44.
Kennel, S. J., Brechbiel, M. W., Milenic, D. E., Schlom, J., and Mirzadeh, S. (2002) *Cancer Biotherapy Radiopharm.,* **17**, 219–31.
Khalkin, V. A., Tsupko- Sitnikov, V. V., and Zaitseva, N. G. (1997) *Radiochemistry,* **39**, 481–90; *Radiokhimiya,* **39**, 483–92.
Kirby, H. W. (1951) Mound Laboratory Report for General Research. December 11, 1950 to April 2, 1951 (Actinium volume). US Report MLM-558, pp. 13–4.
Kirby, H. W. (1952) Tentative Procedure for the Analysis of Mixtures Containing Radium-226, Actinium-227 and Thorium-228. US Report MLM-773.
Kirby, H. W., Grove, G. R., and Timma, D. L. (1956) *Phys. Rev.,* **102**, 1140–1.
Kirby, H. W. (1967) *Prog. Nucl. Energy, Ser. IX,* **8(1)**, 89–139.
Kirby, H. W. (1969) *J. Inorg. Nucl. Chem.,* **31**, 3375–85.
Kirby, H. W. (1970) *J. Inorg. Nucl. Chem.,* **32**, 2823–37.
Kirby, H. W. (1971) *Isis,* **62**, 290–308.
Kirby, H. W. (1974) Geochemistry of the Naturally Occurring Radioactive Series. US Report MLM-2111.
Korotkin, Y. S. (1981) *Sov. Radiochem.,* **23**, 145–9; *Radiokhimiya,* **23**, 181–5.
Kosynkin, V. D., Moiseev, S. D., and Vdovichev, V. S. (1995) *J. Alloys Compds.,* **225**, 320–3.
Kraus, K. A. (1979) *J. Chromatogr.,* **178**, 163–8.
Küchle, W., Dolg, M., and Stoll, H. (1997) *J. Phys. Chem. A,* **101**, 7128–33.
Kulikov, E. V., Novgorodov, A. F., and Schumann, D. (1992) *J. Radioanal. Nucl. Chem., Lett.,* **164**, 103–8.
Kumok, V. N. (1978) *Sov. Radiochem.,* **20**, 590–4; *Radiokhimiya*, **20**, 691–4.
Laerdahl, J. K., Faegri, J., Visscher, L., and Saue, T. (1998) *J. Chem. Phys.,* **109**, 10806–17.

Lange, R. G. and Mastal, E. F. (1994) A tutorial review of radioisotope power systems in *A Critical Review of Space Nuclear Power and Propulsion, 1984–1993* (ed. M. S. El-Genk), American Institute of Physics, New York, pp. 1–20.
Lecoin, M., Perey, M., Riou, M., and Teillac, J. (1950) *J. Phys. Radium.,* **11**, 227–34.
Maly, J. (1969) *J. Inorg. Nucl. Chem.,* **31**, 1007–17.
Makarova, T. P., Sinitsyna, G. S., Stepanov, A. V., Shestakova, I. A., and Shestakov, B. I. (1972) *Sov. Radiochem.,* **14**, 555–8; *Radiokhimiya*, **14**, 538–41.
Makarova, T. P., Stepanov, A. V., and Shestakov, B. I. (1973) *Russ. J. Inorg. Chem.,* **18**, 783–785; *Zh. Neorg. Khim.,* **18**, 1845–9.
Makarova, T. P., Sinitsyna, G. S., Stepanov, A. V., Gritschenko, I. A., Shestakova, I. A., and Shestakov, B. I. (1974) *Chem. Abs.,* **82**, 176644.
Maples, C. (1973) *Nucl. Data Sheets,* **10**, 643–71.
Marckwald, W. (1909) *Am. Chem. J.,* **41**, 515–57.
Martin, P., Hancock, G. J., Paulka, S., and Akber, R. A. (1995) *Appl. Radiat. Isot.,* **46**, 1065–70.
Matthias, B. T., Zachariasen, W. H., Webb, G. W., and Engelhardt, J. J. (1967) *Phys. Rev. Lett.,* **18**, 781–4.
McDevitt, M. R., Ma, D., Lai, L. T., Simon, J., Borchardt, P., Frank, R. K., Wu, K., Pellegrini, V., Curcio, M. J., Miederer, M., Bander, N. H., and Scheinberg, D. A. (2001) *Science,* **294**, 1537–40.
Meggers, W. F., Fred, M., and Tomkins, F. S. (1951) *J. Opt. Soc. Am.,* **41**, 867–8.
Meggers, W. F. (1957) *Spectrochim. Acta,* **10**, 195–200.
Meggers, W. F., Fred, M., and Tomkins, F. S. (1957) *J. Res. NBS,* **58**, 297–315.
Mikhailichenko, A. I., Goryacheva, E. G., Aksenova, N. M., and Denisov, A. F. (1982) *Sov. Radiochem.,* **24**, 173–5; *Radiokhimiya,* **24**, 207–9.
Mikheev, N. B., Kamenskaya, A. N., Rumer, I. A., Kulyukhin, S. A., and Novichenko, V. L. (1994) *Radiokhimiya,* **36**, 160–2; *Radiochemistry,* **36**, 173–5.
Mikheev, N. B., Veleshko, I. E., Kamenskaya, A. N., and Rumer, I. A. (1995) *Radiokhimiya,* **37**, 322–5; *Radiochemistry,* **37**, 297–9.
Mitsugashira, T., Yamana, H., and Suzuki, S. (1977) *Bull. Chem. Soc. Jpn,* **50**, 2913–6.
Moeller, T. and Kremers, H. E. (1945) *Chem. Rev.,* **37**, 97–159.
Moeller, T. (1963) *The Chemistry of the Lanthanides*, Reinhold, New York.
Monsecour, M., De Regge, P., and Demildt, A. (1973) *Radiochem. Radioanal. Lett.,* **14**, 365–71.
Monsecour, M., De Regge, P., Demildt, A., and Baetslé, L. H. (1974) *J. Inorg. Nucl. Chem.,* **36**, 719–23.
Monsecour, M. and De Regge, P. (1975) *J. Inorg. Nucl. Chem.,* **37**, 1841–3.
Mosdzelewski, K. (1966) Die Extraktion der Elemente Radium, Actinium, Protactinium, Americium, und Curium mit 8-Hydroxychinolin, Thesis. German Report KFK–432.
Moutte, A. and Guillaumont, R. (1969) *Rev. Chim. Minér.,* **6**, 603–10.
Nelson, F. (1964) *J. Chromatogr.,* **16**, 538–40.
Nikula, T. K., McDevitt, M. R., Finn, R. D., Wu, C., Kozak, R. W., Garmestani, K., Brechbiel, M. W., Curcio, M. J., Pippin, C. G., Tiffany-Jones, L., Geerlings, M. W., Sr., Apostolidis, C., Molinet, R., Geerlings, M. W. Jr., Gansow, O. A., and Scheinberg, D. A. (1999) *J. Nucl. Med.,* **40**, 166–76.
Novikova, G. I., Volkova, E. A., Gol'din, L. L., Ziv, D. M., and Tret'yakov, E. F. (1960) *Sov. Phys. JETP,* **37**, 663–9; *Zh. Eks. Teor. Fiz.,* **37**, 928–37.

Nozaki, Y. (1984) *Nature,* **310**, 486–8.
Nugent, L. J., Baybarz, R. D., Burnett, J. L., and Ryan, J. L. (1973a) *J. Phys. Chem.,* **77**, 1528–39.
Nugent, L. J., Burnett, J. L., and Morss, L. R. (1973b) *J. Chem. Thermodyn.,* **5**, 665–78.
Nugent, L. J., and Vander Sluis, K. L. (1971) *J. Opt. Soc. Am.,* **61**, 1112–5.
Ouadi, A., Loussouarn, A., Remaud, P., Morandeau, L., Apostolidis, C., Musikas, C., Fauve-Chauvet, A., and Gestin, J.-F. (2000) *Tetrahedron Lett.,* **41**, 7207–9.
Partington, J. R. (1964) *A History of Chemistry*, Macmillan, London, vol. 4, p. 938.
Peppard, D. F., Mason, G. W., Gray, P. R., and Mech, J. F. (1952) *J. Am. Chem. Soc.,* **74**, 6081–4.
Perey, M. (1939a) *C. R. Acad. Sci. Paris,* **208**, 97–9.
Perey, M. (1939b) *J. Phys. Radium,* **10**, 435–8.
Peterson, S. (1949) *Natl. Nucl. En. Ser., Div. IV*, in *The Transuranium Elements* (eds. G. Seaborg, J. J. Katz, and W. M. Manning), McGraw-Hill, New York, vol. 14B, pp. 1393–4.
Pippin, C. G., Gansow, O. A., Brechbiel, M. W., Koch, L., Molinet, R., van Geel, J., Apostolidis, C., Geerlings, M. W., and Scheinberg, D. A. (1995) in *Chemist's Views of Imaging Centers* (ed. A. M. Emran), Plenum Press, New York, pp. 315–25.
Poskanzer, A. M. and Foreman, B. M. J. (1961) *J. Inorg. Nucl. Chem.,* **16**, 323–36.
Rao, C. L. and Gupta, A. R. (1961) *J. Chromatogr.,* **5**, 147–52.
Rao, C. L., Shahani, C. I., and Mathew, K. A. (1968) *Inorg. Nucl. Chem. Lett.,* **4**, 655–9.
Rao, V. K., Shahani, C. J., and Rao, C. L. (1970) *Radiochim. Acta,* **14**, 31–4.
Rutherford, E. (1904) *Phil. Trans. R. Soc. Lond.,* **204A**, 169–219.
Rutherford, E. (1911) in *Encyclopaedia Britannica*, 11th edn, vol. 22, pp. 795–802.
Salutsky, M. L. (1962) in *Comprehensive Analytical Chemistry* (eds. C. L. Wilson and D. W. Wilson), Elsevier, Amsterdam, 1C, pp. 492–6.
Salutsky, M. L. and Kirby, H. W. (1956) *Anal. Chem.,* **28**, 1780–2.
Sani, A. R. (1970) *J. Radioanal. Chem.,* **4**, 127–9.
Seaborg, G. T. (1994) Origin of the Actinide Concept, in *Handbook on the Chemistry and Physics of the Rare Earths* (eds. K. A. Gschneidner, L. Eyring, G. R. Choppin, and G. Lander), North-Holland, Amsterdam, 18, 1–27.
Sedlet, J. (1964) Actinium, Astatine, Francium, Polonium, and Protactinium, in *Treatise on Analytical Chemistry*, Part II, vol. 6 (eds. I. M. Kolthoff, P. J. Elving, and E. B. Sandell), Wiley, New York, pp. 435–610.
Sekine, T., Koike, Y., and Sakairi, M. (1967) *J. Nucl. Sci. Technol.,* **4**, 308–11.
Sekine, T., Koike, Y., and Hasegawa, Y. (1969) *Bull. Chem. Soc. Japan,* **42**, 432–6.
Sekine, T. and Sakairi, M. (1969) *Bull. Chem. Soc. Jpn.,* **42**, 2712–3.
Shahani, C. J., Mathew, K. A., Rao, C. L., and Ramaniah, M. V. (1968) *Radiochim. Acta,* **10**, 165–7.
Shannon, R. D. (1976) *Acta Crystallogr.,* **A32**, 751–67.
Sinitsyna, G. S., Shestakova, I. A., Shestakov, B. I., Plyushcheva, N. A., and Malyshev, N. A., Belyatskii, A. F. (1977) *Tezisy Dokl.-Konf. Anal. Khim. Radioakt*., Nauka, Moscow.
Sinitsyna, G. S., Shestakova, I. A., Shestakov, B. I., Plyushcheva, N. A., Malyshev, N. A., Belyatskii, A. F., and Tsirlin, V. A. (1979) *Sov. Radiochem.,* **21**, 146–51; *Radiokhimiya,* **21**, 172–7.
Skarnemark, G. and Skalberg, M. (1985) *Int. J. Appl. Radiat. Isot.,* **36**, 439–41.

Soddy, F. and Cranston, J. A. (1918a) *Nature,* **100**, 498–9.
Soddy, F. and Cranston, J. A. (1918b) *Proc. R. Soc. Lond.,* **94A**, 384–404.
Stein, L. and Hohorst, F. A. (1982) *Envir. Sci. Technol.,* **16**, 419–22.
Stevenson, P. C. and Nervik, W. E. (1961) The Radiochemistry of the Rare Earths, Scandium, Yttrium and Actinium. US Report NAS-NS 3020. All the volumes of the series "The Radiochemistry of..." can be found on the site http://lib-www.lanl.gov/radiochemistry/elements.htm
Stites, J. G. Jr., Salutsky, M. L., and Stone, B. D. (1955) *J. Am. Chem. Soc.,* **77**, 237–40.
St. John, D. S. and Toops, E. C. (1958) Formation of U-232 During the Irradiation of Thorium. US Report DP-279.
Sugar, J. (1973) *J. Chem. Phys.,* **59**, 788–91.
Sugar, J. (1984) Personal communication to L. R. Morss.
Szeglowski, Z. and Kubica, B. (1990) *J. Radioanal. Nucl. Chem.,* **143**, 389–95.
Szeglowski, Z. and Kubica, B. (1991) *J. Radioanal. Nucl. Chem. Lett.,* **153**, 67–74.
Taylor, S. R. (1964) *Geochim. Cosmochim. Acta,* **28**, 1273–85.
Tomkins, F. S., Fred, M., and Meggers, W. F. (1951) *Phys. Rev.,* **84**, 168.
Tousset, J. (1961) Les Spectres Béta de Faible Energie de Que1ques Eléments Lourds, Thesis, Univ. Lyon (F.) French Report NP-13367.
Tsoupko-Sitnikov, V., Norseev, Y., and Khalkin, C. (1996) *J. Radioanal. Nucl. Chem.,* **205**, 75–83.
U.S. Department of Energy (1987) Atomic Power in Space: a History (excerpted in *Nuclear News*, May 2003, pp. 37–44).
U.S. Nuclear Regulatory Commission (2005) U.S. Code of Federal Regulations, 10 CFR 20.
Valli, K. (1964) *Ann. Acad. Sci. Fenn., Ser. A*, VI, no. 165.
Vander Sluis, K. L. and Nugent, L. J. (1972) *Phys. Rev. A,* **6**, 86–94.
Vander Sluis, K. L. and Nugent, L. J. (1974) *J. Opt. Soc. Am.,* **64**, 687–95.
Wagman, D. D., Evans, W. E., Parker, V. B., Schumm, R. H., Halow, I., Bailey, S. M., Churney, K. L., and Nuttall, R. L. (1982) *J. Phys. Chem. Ref. Data*, **11**, Suppl. No. 2.
Ward, J. W., Kleinschmidt, P. D., and Peterson, D. E. (1986) in *Handbook on the Physics and Chemistry of the Actinides*, vol. 4 (eds. A. J. Freeman and C. Keller), ch. 7.
Weeks, M. E. and Leicester, H. M. (1968) *Discovery of the Elements*, Journal of Chemical Education, Easton, PA, p. 794.
Weigel, F. and Hauske, H. (1977) *J. Less-Common Met.,* **55**, 243–7.
Włodzimirska, B., Bartoś, B., and Bilewicz, A. (2003) *Radiochim. Acta,* **91**, 553–6.
Xu, J., He, P., and Zhu, Y. (1983) *He Huaxue Yu Fangshe Huaxue,* **5**, 202–10; *Chem. Abstr.*, **99**, 192397.
Yamana, H., Mitsugashira, T., and Shiokawa, Y. (1983) *J. Radioanal. Nucl. Chem.,* **76**, 19–26.
Zachariasen, W. H. (1961) in *The Metal Plutonium* (eds. W. N. Miner and A. S. Coffinberry), University of Chicago Press, Chicago, pp. 99–107.
Zachariasen, W. H. (1973) *J. Inorg. Nucl. Chem.,* **35**, 3487–97.
Ziv, D. M. and Shestakova, I. A. (1965a) *Sov. Radiochem.,* **7**, 168–75; *Radiokhimiya,* **7**, 166–75.
Ziv, D. M. and Shestakova, I. A. (1965b) *Sov. Radiochem.,* **7**, 176–86; *Radiokhimiya,* **7**, 175–87.

CHAPTER THREE

THORIUM

Mathias S. Wickleder, Blandine Fourest, and Peter K. Dorhout

3.1 HISTORICAL

In 1815 Berzelius analyzed a rare mineral from the Falun district. He assumed that the mineral contained a new element, which he named thorium after the ancient Scandinavian god of thunder and weather, Thor (Weeks and Leicester, 1968).

Unfortunately, 10 years later the mineral turned out to be simply xenotime, e.g. yttrium phosphate. However, in 1828, Berzelius was given a mineral by the Reverend Hans Morten Thrane Esmark. In that mineral Berzelius really discovered a new element and gave it the same name (Berzelius, 1829; Gmelin, 1955, 1986a; Weeks and Leicester, 1968). Consequently, he called the mineral from which he isolated the new element thorite. It is a silicate that contains significant amounts of uranium and should therefore be written as $(Th,U)SiO_4$. Although thorium was discovered in 1828, it virtually had no application until the invention of the incandescent gas mantle in 1885 by C. Auer von Welsbach. Thereafter the application of thorium developed into a wide array of products and processes (Gmelin, 1988b). Besides the above-mentioned incandescent gas mantles, the production of ceramics, carbon arc lamps, and strong alloys may serve as examples. To be mentioned is also its use as coating for tungsten welding rods, because it provides a hotter arc. Furthermore, when added to refractive glass, it allows for smaller and more accurate camera lenses. As minor important applications, the use of ThO_2 in producing more heat-resistant laboratory crucibles and its occasional use as a catalyst for the oxidation of ammonia to nitric acid and other industrial chemical reactions can be

mentioned. Nevertheless, during the last decade the demand for thorium in non-nuclear applications has sharply decreased due to environmental concerns related to its radioactivity. The radioactivity of thorium is helpful for the dating of very old materials, e.g. seabeds or mountain ranges. Maybe the largest potential for thorium is its usage in nuclear energy. This is because ^{232}Th can be converted by thermal (slow) neutrons to the fissionable uranium isotope ^{233}U via the following reaction sequence:

$$^{232}\mathrm{Th}(\mathrm{n},\gamma) \rightarrow {}^{233}\mathrm{Th} \xrightarrow{\beta^-} {}^{233}\mathrm{Pa} \xrightarrow{\beta^-} {}^{233}\mathrm{U}$$

Fission of the ^{233}U can provide neutrons to start the cycle again. This cycle of reactions is known as the thorium cycle (Seaborg *et al*., 1947; Katzin, 1952).

Conversion of ^{232}Th into ^{233}U provides the possibility to gain large amounts of slow-neutron-fissile material, several times the amount of uranium naturally present on Earth, and several hundred times the amount of the naturally occurring fissile uranium isotope ^{235}U (Seaborg and Katzin, 1951).

A number of advantages of thorium-based nuclear fuels exist in comparison with the presently utilized uranium–plutonium fuels (Rand *et al*., 1975; Trauger, 1978). These include the inherent detectability of ^{233}U, its higher neutron yield, the fact that ^{233}U, unlike ^{239}Pu, can be mixed with ^{238}U so that it cannot directly be used in weapons manufacture, and the superior physical properties of thorium-based fuels that enhance reactor core safety and performance. The disadvantage of the use of thorium-based fuels is that thorium must be irradiated and reprocessed before the advantages of ^{232}Th can be realized. This reprocessing step, requiring more advanced technology than that needed for uranium fuels, and other factors have projected greater costs for thorium fuels. The nuclear technology has nevertheless matured with the development of high-temperature gas-cooled reactors.

3.2 NUCLEAR PROPERTIES

Thorium refined from ores free of uranium would be almost monoisotopic ^{232}Th, with less than one part in 10^{10} of ^{228}Th (radiothorium) produced by its own radioactivity decay chain ($4n$ family). If the ore contains uranium, as is usually the case, practically undetectable concentrations of ^{231}Th (uranium Y) and ^{227}Th (radioactinium) are present, products of the $(4n + 3)$ decay chain that starts with ^{235}U. Also present are greater quantities of ^{230}Th (ionium), as well as lesser amounts of ^{234}Th (uranium X_1), which originate from the $(4n + 2)$ decay chain whose progenitor is ^{238}U. ^{229}Th is the first product in the $(4n + 1)$ decay series (English *et al*., 1947; Hagemann *et al*., 1947, 1950) derived from man-made ^{233}U formed as indicated in Section 3.1. The remaining thorium isotopes listed in Table 3.1 (see also Appendix II) are also synthetic, being formed directly by bombardment of lead or bismuth targets with energetic

Table 3.1 *Nuclear properties of thorium isotopes.*[a]

Mass number	*Half-life*	*Mode of decay*	*Main radiations* (MeV)	*Method of production*
209	3.8 ms	α	α 8.080	$^{32}S + ^{182}W$
210	9 ms	α	α 7.899	$^{35}Cl + ^{181}Ta$
211	37 ms	α	α 7.792	$^{35}Cl + ^{181}Ta$
212	30 ms	α	α 7.82	$^{176}Hf(^{40}Ar,4n)$
213	140 ms	α	α 7.691	$^{206}Pb(^{16}O,9n)$
214	100 ms	α	α 7.686	$^{206}Pb(^{16}O,8n)$
215	1.2 s	α	α 7.52 (40%) 7.39 (52%)	$^{206}Pb(^{16}O,7n)$
216	28 ms	α	α 7.92	$^{206}Pb(^{16}O,6n)$
217	0.237 ms	α	α 9.261	$^{206}Pb(^{16}O,5n)$
218	0.109 μs	α	α 9.665	$^{206}Pb(^{16}O,4n)$ $^{209}Bi(^{14}N,5n)$
219	1.05 μs	α	α 9.34	$^{206}Pb(^{16}O,3n)$
220	9.7 μs	α	α 8.79	$^{208}Pb(^{16}O,4n)$
221	1.68 ms	α	α 8.472 (32%) 8.146 (62%)	$^{208}Pb(^{16}O,3n)$
222	2.8 ms	α	α 7.98	$^{208}Pb(^{16}O,2n)$
223	0.60 s	α	α 7.32 (40%) 7.29 (60%)	$^{208}Pb(^{18}O,3n)$
224	1.05 s	α	α 7.17 (81%) 7.00 (19%) γ 0.177	^{228}U daughter $^{208}Pb(^{22}Ne,\alpha 2n)$
225	8.0 min	α ≈ 90% EC ≈ 10%	α 6.478 (43%) 6.441 (15%) γ 0.321	^{229}U daughter $^{231}Pa(p,\alpha 3n)$
226	30.57 min	α	α 6.335 (79%) 6.225 (19%) γ 0.1113	^{230}U daughter
227	18.68 d	α	α 6.038 (25%) 5.978 (23%) γ 0.236	nature
228	1.9116 yr	α	α 5.423 (72.7%) 5.341 (26.7%) γ 0.084	nature
229	7.340×10^3 yr	α	α 4.901 (11%) 4.845 (56%) γ 0.194	^{233}U daughter
230	7.538×10^4 yr	α	α 4.687 (76.3%) 4.621 (23.4%) γ 0.068	nature
231	25.52 h	β^-	β^- 0.302 γ 0.084	nature $^{230}Th(n,\gamma)$
232	1.405×10^{10} yr $> 1 \times 10^{21}$ yr	α SF	α 4.016 (77%) 3.957 (23%)	nature

Table 3.1 (*Contd.*)

Mass number	*Half-life*	*Mode of decay*	*Main radiations* (MeV)	*Method of production*
233	22.3 min	β^-	β^- 1.23 γ 0.086	^{232}Th(n,γ)
234	24.10 d	β^-	β^- 0.198 γ 0.093	nature
235	7.1 min	β^-		^{238}U(n,α)
236	37.5 min	β^-	γ 0.111	^{238}U(γ,2p) ^{238}U(p,3p)
237	5.0 min	β^-		^{18}O + ^{238}U
238	9.4 min	β^-		^{18}O + ^{238}U

[a] Appendix II.

multi-nucleon projectiles, by decay of lightweight uranium isotopes, which are themselves synthetic and formed by nuclear bombardment, or by other miscellaneous nuclear reactions. Uranium ores that are relatively thorium-free can be processed to prepare multigram amounts of material with significant proportions of ionium, ^{230}Th. From one unselected ore residue, after removal of uranium, thorium was obtained (Hyde, 1952, 1960) that was 26.4% ionium and 73.6% ^{232}Th (Roll and Dempster, 1952).

3.3 OCCURRENCE OF THORIUM

Two volumes of the *Gmelin Handbook of Inorganic Chemistry* deal with the natural occurrence of thorium and give a comprehensive review of known thorium minerals (Gmelin, 1990a, 1991a). So only the most important features will be emphasized here. Thorium has a much wider distribution than is generally thought. In the Earth's crust it is three times as abundant as Sn, twice as abundant as As, and nearly as abundant as Pb and Mo. It occurs in the tetravalent state in nature and is frequently associated with U(IV), Zr(IV), Hf(IV), and Ce(IV) but also with the trivalent rare earth elements that are relatively close in ionic radii (Cuthbert, 1958; Frondel, 1958; Shannon, 1976).

Due to the isotypism of ThO_2 and UO_2 solid state solutions can be formed and depending on the uranium content the mixtures are named thorianite (75–100 mol% ThO_2), uranothorianite (25–75 mol% ThO_2), thorian uraninite (15–25 mol% ThO_2) and uraninite (0–15 mol% ThO_2). A second mineral with a high thorium content is thorite, $ThSiO_4$, from which the element has originally been discovered. Thorite has the tetragonal zircon-type of structure but also a monoclinic variant of $ThSiO_4$ is known, which is called huttonite (Taylor and

Table 3.2 *Thorium content of various minerals.*

Accessory mineral	*Th* (ppm)
monazite	25000 to 2×10^5
allanite	1000 to 20000
zircon	50 to 4000
titanite	100 to 600
epidote	50 to 500
apatite	20 to 150
magnetite	0.3 to 20
xenotime	Low

Ewing, 1978). In both modifications of $ThSiO_4$, substitution of PO_4^{3-} for SiO_4^{4-} is frequently observed with additional replacement of Th^{4+} by trivalent rare earth ions for charge compensation. SiO_4^{4-} ions may be also replaced by OH^- groups according to $Th(SiO_4)_{1-x}(OH)_{4x}$ leading to a new mineral, thorogummite.

However, in all the minerals given in Table 3.2, Th occurs as the minor constituent. From these minerals, monazite is of significant commercial interest because it is distributed throughout the world, and some of the deposits are very large. Monazite is a phosphate of high specific gravity that is found in the form of yellow to brown sand in nature (monazite sand). The chemical inertness of monazite makes it hard to process.

3.4 THORIUM ORE PROCESSING AND SEPARATION

Monazite can be only attacked by strong acid, which essentially transforms the phosphate ion to $H_2PO_4^-$ and H_3PO_4 and leaves the metal ions as water-soluble salts, or by strong alkali, which transforms the insoluble phosphates to insoluble metal hydroxides that can easily be dissolved in acid after removal from the supernatant solution of alkali phosphates.

Thorium in monazite follows the rare earths in either the acid or the alkali processes. Thorium can be separated from the rare earths in strong sulfuric acid solution (Fig. 3.1) by partial dilution and reduction of acidity (by ammonia addition) to about pH 1.0, at which point hydrated thorium phosphates, containing only small amounts of entrained rare earths, precipitate (Fig. 3.2). The acidity must be reduced to about pH 2.3 to ensure precipitation of the bulk of the rare earths. (Any uranium present in the process solution is separated from the rare earths at this step.) The crude precipitate of thorium phosphate is then treated with alkali to remove undesired sulfate and phosphate anions, and the thorium hydroxide residue may then be dissolved in nitric acid for subsequent

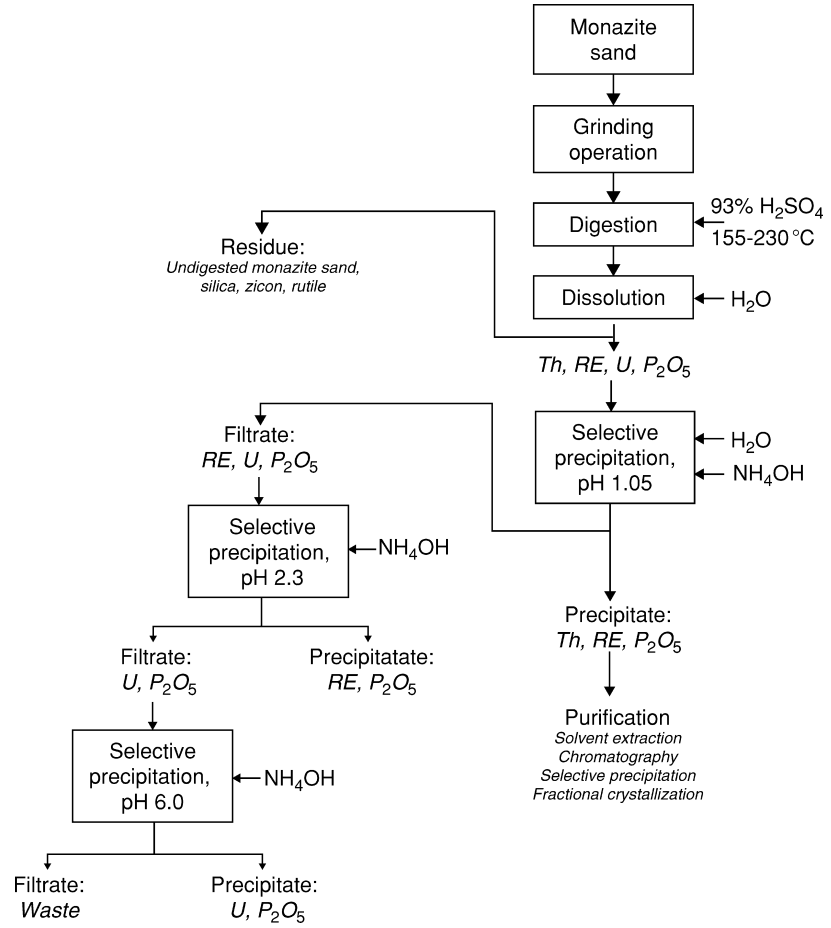

Fig. 3.1 *Simplified schematic diagram of sulfuric acid digestion of monazite sand and recovery of thorium, uranium, and the rare earths.*

purification. Purification is achieved efficiently by solvent extraction of the thorium with tri(*n*-butyl)phosphate (TBP) dissolved in kerosene, a procedure that separates thorium nitrate from rare earths and other non-extractable species. Numerous further extractants have been employed as pointed out in the *Gmelin Handbook* (Gmelin, 1985a).

The solid reaction product of the alkaline digestion of monazite (Fig. 3.3) may be dissolved in acid after separation from the supernatant solution. The solubility of the thorium-containing fraction, however, is a function of the conditions under which the alkaline digestion is performed. Too prolonged

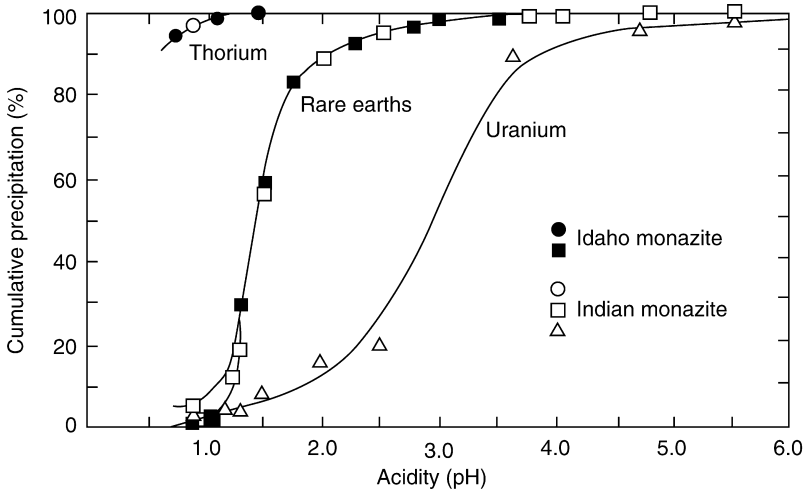

Fig. 3.2 *Effect of acidity on precipitation of thorium, rare earths, and uranium from a monazite–sulfuric acid solution of Idaho and Indian monazite sands: agitation time* 5 min; *dilution ratio,* 45 *to* 50 *parts water per one part monazite sand; digestion ratio of* 93% *sulfuric acid to digestion sands,* 1.77*; neutralizing agent,* 3.1% *ammonium hydroxide* (*Cuthbert,* 1958).

digestion at too high temperature may produce a product in which a large fraction of the thorium will not react readily with the acid used to dissolve the hydroxide cake. Presumably this is a consequence of the formation of ThO_2. Depending on whether hydrochloric, nitric, or sulfuric acid is used to dissolve the hydroxide cake, different procedures may be used in subsequent purification. Assuming the use of hydrochloric acid, which involves the fewest complications, a solution of thorium and rare earth chlorides is obtained. Differential precipitation of thorium from this solution again offers several choices: hydroxide (preferred), peroxide, or phosphate may be used to precipitate the thorium, or precipitation by carbonate may be used to separate the rare earths from thorium (and uranium), which form soluble anionic complexes. Final purification of thorium, again, is preferably made by solvent extraction (Marcus and Kertes, 1969; Gmelin, 1985a), but also chromatographic methods are applied (Kiriyama and Kuroda, 1978; Mayankutty *et al.*, 1982; Gmelin, 1990c, 1991b).

Thorium may also be recovered as a by-product from the treatment of uraninite or uranothorianite to obtain uranium. The thorium remaining in the solution of sulfuric acid after removal of the uranium is extracted into kerosene with the aid of long-chain amines. The thorium is part of a complex sulfate anion, which accompanies the protonated cationic amine into the organic phase. Neutralization of the quaternary ammonium cation precipitates the thorium from the organic phase or allows it to be back-extracted into an aqueous phase.

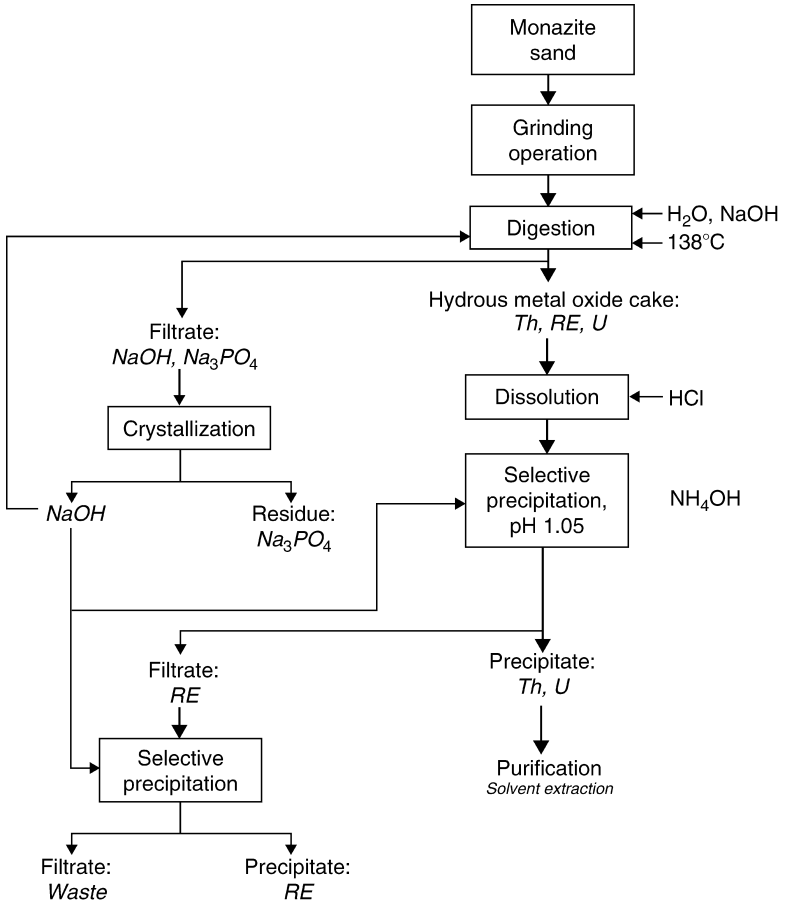

Fig. 3.3 *Simplified schematic diagram of caustic soda digestion of monazite sand and recovery of thorium, uranium, and the rare earths.*

3.5 ATOMIC SPECTROSCOPY OF THORIUM

The atomic spectroscopy of thorium provides not only information about the electronic states of thorium but also clues to the properties expected for elements of higher atomic number. The electronic structure of thorium and the related spectra will be discussed in more detail in Chapter 16 and are only summarized briefly here. Further details are also given in a volume of *Gmelin's Handbook* (Gmelin, 1989).

The four valence electrons of the neutral atom have available to them, in principle, the 5f, 6d, 7s, and 7p orbitals. The stable ground state configuration of the neutral thorium atom turns out to be $6d^27s^2$ ($^3F_2$) (Giacchetti *et al.*, 1974).

The $6d^37s$ ($^5F_1$) level is at higher energy by 5563.143 cm^{-1} and it is only at 7795.270 cm^{-1} that one encounters $5f6d7s^2$ ($^3H_4$). Still higher lie $6d7s^27p$ (10783.153 cm^{-1}), $6d^27s7p$ (14465.220 cm^{-1}), and $5f6d^27s$ (15618.98 cm^{-1}) (Zalubas, 1968).

The ionization potential of neutral Th was recently measured by resonance ionization mass spectrometry (RIMS) (Köhler *et al.*, 1997) as 6.3067(2) eV. The value obtained earlier (Sugar, 1974; Ackermann and Rauh, 1972) by extrapolation of spectroscopic data was 6.08 eV. The ground level of singly ionized Th is d^2s, followed by ds^2 (1859. 938 cm^{-1}), fs^2 (4490.256 cm^{-1}), fds (6168.351 cm^{-1}), d^3 (7001.425 cm^{-1}), and fd^2 (12485.688 cm^{-1}) (Zalubas and Corliss, 1974). It is a major step up in energy to configurations with either p contribution or to configurations that contain paired f-electrons: dsp is at 23372.582 cm^{-1}, followed by f^2s (24381.802 cm^{-1}), fsp (26488.644 cm^{-1}), d^2p (28243.812 cm^{-1}), fdp (30452.723 cm^{-1}), s^2p (31625.680 cm^{-1}), and f^2d (32620.859 cm^{-1}).

The ground state of doubly ionized thorium is 5f6d but the $6d^2$ configuration is only 63.267 cm^{-1} and the 5f7s is 2527.095 cm^{-1} higher (Racah, 1950). These are followed by 6d7s (5523.881 cm^{-1}), $7s^2$ (11961.133 cm^{-1}), $5f^2$ (15148.519 cm^{-1}), 5f7p (33562. 349 cm^{-1}), 6d7p (37280.229 cm^{-1}), and 7s7p (42259.714 cm^{-1}). These trends are continued in the triply ionized form (Klinkenberg and Lang, 1949), in which the ground level is 5f, and 6d is at 9193.245 cm^{-1}, 7s at 23130.75 cm^{-1}, and 7p at 60239.10 cm^{-1}.

Thus, with increasing ionic charge, configurations that include 5f electrons are stabilized with respect to others and the configurations containing 7p electrons become grossly destabilized. Effects in 7s and 6d systems are less but are still significant. The stabilization of the 5f electron in the triply charged ion is not sufficient however to make triply charged thorium a stable chemical species. The stable form is tetrapositive Th^{4+}, in which only the radon core of electrons is present.

Solid metallic thorium with the ground state configuration d^2s^2 has the 5f electrons in a reasonably broad energy band (Koelling and Freeman, 1971), about 5 eV above the Fermi level of 7.5–8.0 eV. This presumably is because the fds^2 level lies so low and interacts with the d^2s^2 level. Electron-binding energies for the various core levels of the atom have been determined (Nordling and Hagström, 1964), and the X-ray transitions have been determined with precision (Bearden, 1967; Bearden and Burr, 1967; Murthy and Redhead, 1974).

3.6 THORIUM METAL

A comprehensive treatment of the physical and chemical properties of thorium metal is given in the *Gmelin Handbook* (Gmelin, 1989, 1997). A brief summary on the most important properties shall be given here.

The preparation of thorium has been done by reducing halides or double halides by sodium, potassium, or calcium (Berzelius, 1829; Chydenius, 1863;

Nilson, 1876; Chauvenet, 1911). Furthermore, $ThCl_4$ can be reduced by sodium or electrolysis can be applied to a melt of thorium chloride or fluoride in sodium chloride or potassium chloride (Matignon and Delepine, 1901; Moissan and Hönigschmid, 1906; von Bolton, 1908; von Wartenberg, 1909; Chauvenet, 1911; Kaplan, 1956). Also, ThO_2 can be used as starting material and various reductants may be used (Ruff and Brintzinger, 1923; Marden and Rentschler, 1927). Care has to be taken when carbon or silicon is used because the formation of carbides and silicides may occur (Berzelius, 1829; Moissan and Étard, 1896, 1897; Hönigschmid, 1906a,b). In the so-called 'Sylvania process' calcium is used as the reducing agent (Dean, 1957; Smith *et al.*, 1975). Other reduction processes involve ThO_2 and aluminum or magnesium (Winkler, 1891; Leber, 1927). Both reactions are preferably carried out in the presence of zinc, making the reduction process thermodynamically favorable due to the formation of the intermetallic compound Th_2Zn_{17} (Spedding *et al.*, 1952). Zinc can easily be removed by vacuum distillation and leaves the metal mainly as a powder (Meyerson, 1956; Fuhrman *et al.*, 1957). Zinc is usually introduced as chloride or fluoride in the process (Briggs and Cavendish, 1971), but attempts have been made to use a zinc–magnesium alloy as reductant (Capocchi, 1971).

Unusual reductions include, for example, the reaction of $ThCl_4$ with $DyCl_2$ (Mikheev *et al.*, 1993). A method leading to high-purity thorium is the thermal decomposition of ThI_4 on a hot tungsten filament, known as the van Arkel–de Boer process (van Arkel and de Boer, 1925). This reaction is also used for the purification of thorium because the iodine formed in the reaction can be used to transport the crude metal from the low-temperature source to the hot wire. Another method to gain very pure thorium is the electrotransport that refines the high-grade thorium from the van Arkel–de Boer process further to a material containing less than 50 ppm impurities in total (Peterson and Schmidt, 1971).

Thorium appears as a bright silvery metal that has the highest melting point among the actinide elements while its density is the lowest one in the series except for Ac. Under ambient conditions, Th adopts the face-centered cubic (fcc) structure of copper that transforms to the body-centered cubic (bcc) structure of tungsten above 1360°C. Under high pressure, a third modification with a body-centered tetragonal lattice has been observed (Bridgman, 1935; Vohra, 1991, 1993; Vohra and Akella, 1991, 1992). Note that the transition conditions between the modifications depend remarkably on the amount of impurities in the metal (Smith *et al.*, 1975; Oetting *et al.*, 1976). The same is true for the properties like melting point, density (James and Straumanis, 1956), resistance, and others shown in Table 3.3, which summarizes selected properties of thorium as reported in two monographs (Smith *et al.*, 1975; Oetting *et al.*, 1976), and in the *Gmelin Handbook* (Gmelin, 1997).

Thorium metal is paramagnetic (ground state $6d^27s^2$) and shows a specific magnetic susceptibility of $0.412 \times 4\pi \times 10^{-9}$ m^3 kg^{-1} at room temperature (Greiner and Smith, 1971). The magnetic susceptibility is nearly

Table 3.3 *Some physical properties of thorium metal.*

melting point	2023 K
crystal structure	
face-centered cubic up to 1633 K	$a = 5.0842$ Å (298 K)
body-centered cubic from 1633–2023 K	$a = 4.11$ Å (1723 K)
body-centered tetragonal at high pressure	$a = 2.282$ Å, c = 4.411 Å (102 GPa)
atomic radius (from fcc structure)	1.798 Å
density	
from X-ray lattice parameters	11.724 g cm^{-3}
bomb reduced, as-cast	11.5–11.6 g cm^{-3}
arc melted, van Arkel metal	11.66 g cm^{-3}
enthalpy of sublimation (298 K)[a]	602 ± 6 kJ mol^{-1}
vapor pressure of the solid (1757–1956 K)	$\log p(\text{atm}) = -28780\ (\text{T/K})^{-1} + 5.991$
vapor pressure of the liquid (2020–2500 K)	$\log p(\text{atm}) = -(29770 \pm 218)\ (\text{T/K})^{-1} - (6.024 \pm 0.098)$
enthalpy of fusion	14 kJ mol^{-1}
elastic constants	
Young's modulus	7.2×10^7 kPa
shear modulus	2.8×10^7 kPa
Poisson's ratio	0.265
compressibility	17.3×10^{-8} cm^2 N^{-1}
coefficient of thermal expansion (298–1273 K)	12.5×10^{-6} K^{-1}
electric resistivity	
electrorefined metal (298 K)	15.7×10^{-6} Ω cm
temperature coefficient of resistance	3.6×10^{-3} K^{-1}
thermal conductivity (298 K)	0.6 W cm^{-1} K^{-1}
work function	3.49 eV
Hall coefficient (297 K)	-11.2×10^{-5} cm^3 C^{-1}
emissivity (solid, 1600 K)	0.31

[a] Cox *et al.* (1989).

temperature-independent but it depends on the amount of impurities or dopants, respectively (Sereni *et al.*, 1987). Thorium is superconducting at low temperature (Meissner, 1929; de Haas and van Alphen, 1931). The transition temperature T_c is between 1.35 and 1.40 K, the critical magnetic field H_c has been found to be (159.22 ± 0.10) G for a high-purity sample (Decker and Finnemore, 1968). Thorium is an excellent example of a weakly coupled type-I superconductor that exhibits a complete Meissner effect and whose critical field curve $H_c(T)$ has a parabolic temperature dependence and is in good agreement with the predictions of the theory of Bardeen, Cooper, and Schrieffer (Bardeen *et al.*, 1957). The pressure dependence of H_c has been determined (Fertig *et al.*, 1972)

and the specific heat discontinuity at T_c has been reported by several authors to be around 8.4 mJ mol^{-1} K^{-1} (Gordon *et al.*, 1966; Satoh and Kumagai, 1971, 1973; Luengo *et al.*, 1972a,b). Calculations on electron–phonon coupling have been also reported (Winter, 1978; Skriver and Mertig, 1985; Allen, 1987; Skriver *et al.*, 1988). The pressure dependence of the critical temperature has been followed up to 20 GPa (Palmy *et al.*, 1971; Rothwarf and Dubeck, 1973). Below 2.5 GPa T_c decreases linearly with pressure. The decrease flattens to a minimum around 7.4 GPa, increases slightly up to 10 GPa, before it smoothly decreases again. The pressure dependence of T_c has also been recently examined theoretically (Rosengren *et al.*, 1975; Mahalingham *et al.*, 1993). Furthermore, the dependence of T_c on impurities has been investigated (Guertin *et al.*, 1980).

The chemical reactivity of thorium is high. It is easily attacked by oxygen, hydrogen (Winkler, 1891; Matignon and Delepine, 1901; Sieverts and Roell, 1926; Nottorf *et al.*, 1952), nitrogen (Matignon, 1900; Kohlschütter, 1901; Matignon and Delepine, 1901), the halogens (Nilson, 1876; Moissan and Étard, 1896, 1897; von Wartenberg, 1909), and sulfur (Berzelius, 1829; Nilson, 1876; von Wartenberg, 1909) at elevated temperatures. Also carbon and phosphorus are known to form binary compounds with thorium (Strotzer *et al.*, 1938; Meisel, 1939; Wilhelm and Chiotti, 1950). Finely divided thorium is even pyrophoric (Raub and Engles, 1947). The reaction of bulky thorium with air under ambient conditions is low, but nevertheless corrosion is observed according to the investigations of several authors. Thorium reacts vigorously with hydrochloric acid. The reaction with hydrochloric acid always leaves a certain amount of a black residue (12 to 15%) behind, which was first thought to be ThO_2 that was originally present in the metal (Matignon and Delepine, 1901; Meyer, 1908; von Wartenberg, 1909). As discussed in Section 3.7.3, other studies have suggested that a lower-valent thorium oxide hydrate, $ThO{\cdot}H_2O$, is formed but it is much more likely that this compound is in fact an oxide hydride containing hydroxide and chloride ions according to ThO(X)H (X = combination of OH^- and Cl^-) (von Bolton, 1908; Karstens, 1909, Katzin, 1944, 1958; Karabash, 1958; Katzin *et al.*, 1962). This assumption is also supported by mass spectroscopic investigations that show Cl^- to be present in the residue (Ackermann and Rauh, 1973a). The reaction of thorium with other acids occurs slowly, with nitric acid even passivation is observed (Smithells, 1922; Schuler *et al.*, 1952). The latter can be overcome by adding small amounts of fluoride or fluorosilicate ions.

A great number of thorium alloys are known, including those with iron, cobalt, nickel, copper, gold, silver, platinum, molybdenum, tungsten, tantalum, zinc, bismuth, lead, mercury, sodium, beryllium, magnesium, and aluminum. Other systems, like Th/Cr and Th/U, are simply eutectics, and complete miscibility is found in the liquid and solid states with cerium. An overview of thorium alloys with main group metals can be found in the *Gmelin Handbook* (Gmelin, 1992a, 1997).

3.7 IMPORTANT COMPOUNDS

As Chapter 19 is devoted to the thermodynamic properties of the actinides and their compounds, data such as enthalpies of formation or entropies will not be given here, except when needed for the clarity of the discussion.

3.7.1 Hydrides

Reaction of thorium with hydrogen, and formation of two hydrides, ThH_2 and Th_4H_{15}, has been known for more than a century (Winkler, 1891). A substoichiometric dihydride with the fluorite-type of structure was observed by X-ray diffraction (XRD) along with the tetragonal ThH_{2-x} in a preparation of overall composition $ThH_{1.73}$ (Korst, 1962) as well as in dihydrides containing some ThO_2 (Peterson *et al.*, 1959). The well-known dihydride, which can be significantly substoichiometric, has a tetragonal structure (Nottorf *et al.*, 1952; Rundle *et al.*, 1952; Flotow and Osborne, 1978). The compound contains two metal atoms in the unit cell and is isotypic with ZrH_2 (Rundle *et al.*, 1948a; Nottorf *et al.*, 1952). The higher hydride (Matignon and Delepine, 1901; Sieverts and Roell, 1926; Rundle *et al.*, 1948a, 1952; Nottorf *et al.*, 1952; Zachariasen, 1953; Mueller *et al.*, 1977), Th_4H_{15} (= $ThH_{3.75}$), has a unique cubic structure, with the Th atom in 12-fold coordination of hydrogen atoms. The hydrogen atoms are coordinated by three and four thorium atoms as may be expressed by the formula $ThH_{9/3}H_{3/4}$ according to Niggli's formalism. The structure has also been determined for the deuterated analog Th_4D_{15} (Mueller *et al.*, 1977). Th_4H_{15} was the first metal hydride to be found to show superconductivity (Satterthwaite and Toepke, 1970; Satterthwaite and Peterson, 1972; Dietrich *et al.*, 1974). The transition temperature for superconductivity is 7.5–8 K, which is narrow, but not isothermal. Metallic conduction is exhibited at room temperature. Both the hydride and the deuteride are superconducting, with no apparent isotope effect. The existence of another crystalline form, with a 1% tetragonal distortion, that is non-superconducting has been suggested (Caton and Satterthwaite, 1977). The transition temperature is reversibly pressure-sensitive, with a slope of about 42 mK $kbar^{-1}$, up to a pressure of about 28 kbar. The heat capacities of ThH_2 and Th_4H_{15} have been measured from 5 to 350 K (Schmidt and Wolf, 1975; Miller *et al.*, 1976; Flotow and Osborne, 1978). As pointed out in more detail in Chapter 19, experimental values have been extrapolated to 800 K by Flotow *et al.* (1984).

The electronic structure of these binary thorium hydrides has been investigated by photoelectron spectroscopy (Weaver *et al.*, 1977) and nuclear magnetic resonance (NMR) spectroscopy (Schreiber, 1974; Lau *et al.*, 1977; Peretz *et al.*, 1978; Maxim *et al.*, 1979).

Powdered or sintered thorium metal reacts immediately and exothermically with hydrogen at room temperature, whereas massive metal may require heating to 300–400°C before reaction takes place. For the reaction with massive

metal, an induction period that is a function of the impurity content of the metal was found (Nottorf *et al.*, 1952). In general, it is taken for granted that a consequence of the reaction of hydrogen on massive metal is a crumbling and powdering of the mass. However, it has been found (Satterwaithe and Peterson, 1972) that, at temperatures around 850°C, massive metal yields massive ThH_2, and then massive Th_4H_{15}, whereas even at 500°C the reaction fractures and cracks the massive metal. It is assumed that at high temperature, there is a sufficiently close match between the crystal structures of the metal and the hydride formed at that temperature that the incorporation of hydrogen can proceed without causing disruption of the solid.

At 900°C, in high vacuum, thorium hydride is completely decomposed to its elements. The decomposition product is grey to black, powdered, or in the form of an easily disintegrated mass. When it is desired to prepare thorium metal for some subsequent reaction, formation and decomposition of the hydride is generally used to accomplish this goal. The dissociation pressures of the two hydrides have been reported as (Nottorf *et al.*, 1952):

$$\log p(\text{mmHg}) = -7700\ (T/K)^{-1} + 9.54 \quad (\text{Th}/\text{ThH}_2\ \text{system})$$

$$\log p(\text{mmHg}) = -4220\ (T/K)^{-1} + 9.50 \quad (\text{ThH}_2/\text{Th}_4\text{H}_{15}\ \text{system})$$

Flotow *et al.* (1984) discuss in greater detail the hydrogen pressures associated with the Th–H_2 system as a function of the hydrogen composition of the solid phases and the temperatures.

Thorium hydride reacts readily with oxygen to form ThO_2. Many hydride preparations are in fact pyrophoric. ThO_2 can also be formed smoothly by reaction of thorium hydride with steam at 100°C. The reactions with oxygen and with steam are typical for the procedures commonly used for the synthesis of binary compounds of thorium. Pure thorium is necessary to prepare thorium hydride that is free of oxygen or moisture. Subsequent manipulation in the absence of air or moisture then assures the formation of pure binary compounds. Thus, in the range of 250–350°C, the hydride reacts smoothly with halogens as well as with hydrogen compounds of the halogens, sulfur, phosphorus, or nitrogen to give the corresponding binary compounds of thorium (Foster, 1945, 1950; Lipkind and Newton, 1952). Methane or carbon dioxide does not react with thorium hydride.

A number of ternary hydrides and deuterides has been reported (Table 3.4). The iron compounds $Th_2Fe_{17}D_x$ are structurally related to the respective alloy Th_2Fe_{17} and show interesting magnetic properties (Isnard *et al.*, 1993). The deuterides $ThZr_2D_x$ can be described as stuffed variant of the cubic Laves phases as it has been shown by neutron diffraction (van Houten and Bartram, 1971; Bartscher *et al.*, 1986). $ThZr_2H_{7+x}$ (and also the hexagonal $ThTi_2H_{6+x}$) combine an extremely large amount of hydrogen per unit volume with relatively low equilibrium vapor pressures of hydrogen at elevated temperatures. Both of

Table 3.4 *Crystallographic data of thorium hydrides and deuterides.*

		Lattice parameters			
Compound	*Space group*	*a* (Å)	*b* (Å)	*c* (Å)	*References*
ThH_2	I4/mmm	4.055		4.965	Flotow and Osborne, 1978[a]
Th_4H_{15}	I$\bar{4}$3d	9.11			Mueller *et al.* (1977)
Th_4D_{15}	I$\bar{4}$3d	9.11			Mueller *et al.* (1977)
$Th_2Fe_{17}D_{4.956}$	R$\bar{3}$m	8.7116		12.624	Isnard *et al.* (1993)
$Th_2Fe_{17}D_{4.668}$	R$\bar{3}$m	8.682		12.56	Isnard *et al.* (1993)
$Th_6Mn_{23}D_{16.2}$	Fm$\bar{3}$m	12.922			Hardman *et al.* (1980)
$Th_6Mn_{23}D_{16}$	Fm$\bar{3}$m	12.921			Hardman *et al.* (1980)
$Th_6Mn_{23}D_{16}$	P4/mmm	9.076		12.961	Hardman-Rhyne *et al.* (1984)
$Th_6Mn_{23}D_{28.5}$	Fm$\bar{3}$m	13.203			Hardman-Rhyne *et al.* (1984)
$ThZr_2D_6$	Fd$\bar{3}$m	9.151			Bartscher *et al.* (1986)
$ThZr_2D_{3.6}$	Fd$\bar{3}$m	9.042			Bartscher *et al.* (1986)
$ThZr_2D_{4.8}$	Fd$\bar{3}$m	9.112			Bartscher *et al.* (1986)
$ThZr_2D_{6.3}$	Fd$\bar{3}$m	9.154			Bartscher *et al.* (1986)
$ThNi_2D_2$	P6/mmm	3.87		3.951	Andresen *et al.* (1984)
$ThNi_2D_{2.6}$	P6/mmm	4.405		4.360	Andresen *et al.* (1984)
Th_2AlD_2	I4/mcm	7.702		6.23	Bergsma *et al.* (1961)
Th_2AlD_3	I4/mcm	7.676		6.383	Bergsma *et al.* (1961)
Th_2AlD_4	I4/mcm	7.629		6.517	Bergsma *et al.* (1961)
$Th_2AlD_{3.71}$	I4/mcm	7.6260		6.5150	Sorby *et al.* (2000)
$Th_2AlD_{2.75}$	P$\bar{4}$2m	7.6796		19.073	Sorby *et al.* (2000)
$Th_2AlD_{2.29}$	I4/mcm	7.7014		6.2816	Sorby *et al.* (2000)

[a] These authors use the F4/mmm setting with a = 5.734 Å. The F-centered cell has the diagonal of the ab-plane as axis, i.e. square root of twice the a axis of the I-centered cell.

these ternary hydrides are apparently stable in air. Unlike thorium hydride itself, the Th–Zr hydride is not superconducting (Satterthwaite and Peterson, 1972). Also the nickel phases $ThNi_2D_x$ are derived from the alloy $ThNi_2$ and show the deuterium atom in tetrahdral interstices of the metal atom network (Andresen *et al.*, 1984). The thorium manganese compounds $Th_6Mn_{23}D_x$ have been investigated frequently with respect to the D atom distribution in the lattice (Hardman *et al.*, 1980, 1982; Jacob, 1981; Carter, 1982; Hardman-Rhyne *et al.*, 1984). Furthermore, the ternary aluminum hydrides Th_2AlD_x have been reported in great detail (Bergsma *et al.*, 1961; Sorby *et al.*, 2000). Other hydrides, for example with cobalt and palladium are known, however not very well characterized in the most cases (Buschow *et al.*, 1975; Oesterreicher *et al.*, 1976).

3.7.2 Borides, carbides, and silicides

Three binary thorium borides are well characterized (du Jassonneix, 1905; Allard, 1932; Stackelberg and Neumann, 1932; Lafferty, 1951; Post *et al.*, 1956; Konrad *et al.*, 1996). ThB_6 contains a network of linked $[B_6]$ octahedra;

in ThB_4, [B_2] dumbbells accompany the octahedra (Brewer *et al.*, 1951; Zalkin and Templeton, 1951; Blum and Bertaut, 1954). Investigations of the thorium–boron system at low boron concentrations showed that non-stoichiometric varieties of ThB_4 can be prepared (Rand *et al.*, 1975; Chiotti *et al.*, 1981). On the other hand, certain impurities (for example ThO_2) have been suggested to be accountable for the non-stoichiometry (Brewer *et al.*, 1951). The third boride, ThB_{12}, is isotypic with UB_{12} (Cannon and Hall, 1977; Cannon and Farnsworth, 1983). Furthermore, the borides ThB_{66} and ThB_{76} have been reported (Naslain *et al.*, 1971; Schwetz *et al.*, 1972), but it was not clear whether they are truly thorium–boron phases or if they are a metal-stabilized form of a boron allotrope.

Various ternary thorium borides have been prepared, especially those containing transition metals. The orthorhombic borides Th_2MB_{10} were obtained from the elements by arc melting and show a structure that is closely related to that of ThB_6 (Konrad and Jeitschko, 1995). Borides of the composition $ThMB_4$ have been recognized for M = V, Mo, W, Re, Cr, and Mo (Pitman and Das, 1960; Rogl and Nowotny, 1974; Konrad *et al.*, 1996). The crystal structures have been determined for M = Cr and Mo, in which the boron atoms form infinite layers with the metal atoms in between similar to MgB_2. The chromium compound $ThCr_2B_6$ is isotypic with $CeCr_2B_6$ and shows metallic conduction and Pauli paramagnetism (Konrad and Jeitschko, 1995). The hexagonal borides $ThIr_3B_2$ and $ThRu_3B_2$ have been characterized magnetically and structurally. They contain discrete boride ions in prismatic coordination of the platin metal atoms (Hiebl *et al.*, 1980; Ku *et al.*, 1980). The magnetic properties have also been also determined for the rather complicated borides $R_{2-x}Th_xFe_{14}B$ (R = Y, Dy, Er) (Pedziwiatr *et al.*, 1986).

Further boron-containing thorium compounds are the borohydrides $Th(BH_4)_4$, $LiTh(BH_4)_5$, and $Li_2Th(BH_4)_6$ (Ehemann and Nöth, 1971). They contain the tetrahedral BH_4^- ion.

Carbides of thorium have been discussed in great detail in the *Gmelin Handbook* (Gmelin, 1992b). Thus only the most important items shall be given here briefly. Binary thorium carbides were obtained by the reaction of ThO_2 with carbon or the direct fusion of the elements (Troost, 1883; Moissan and Étard, 1896, 1897; Wilhelm and Chiotti, 1949, 1950). Three compositions, ThC_2, Th_2C_3, and ThC, are known (Fig. 3.4). ThC_2 occurs in three different modifications. At room temperature, a monoclinic unit cell is found (Jones *et al.*, 1987). Between 1430 and 1480°C, a rotation of the C_2 dumbbells starts, leading to a tetragonal structure that changes to cubic above 1480°C with complete rotational disorder of the C_2 units (Hunt and Rundle, 1951; Gantzel and Baldwin, 1964; Hill and Cavin, 1964; Langer *et al.*, 1964; Bowman *et al.*, 1968). The monocarbide, ThC, has the cubic NaCl structure. Both ThC_2 and ThC are refractory solids with high melting points (2655 ± 25 and 2625 ± 25, respectively). For ThC, the specific heat has been measured from 1.5 to 300 K (Danan, 1975). The third binary thorium carbide, Th_2C_3, has been observed at pressures

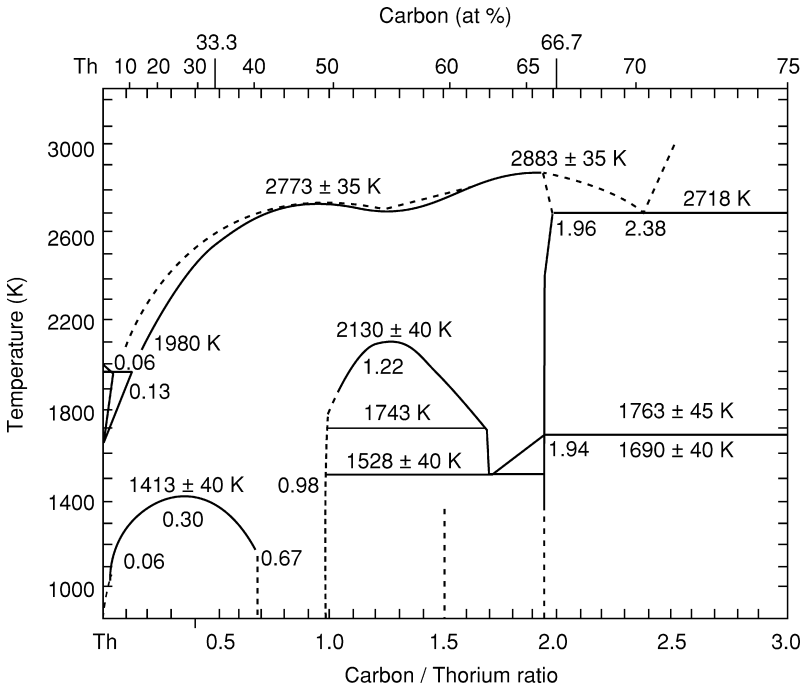

Fig. 3.4 *Phase diagram of the thorium–carbon system* (*Chiotti* et al., 1981).

above 33 kbar in the region of 1200°C (Krupka, 1970). It has the cubic structure of Pu_2C_3 and is a superconductor with T_c decreasing with increasing pressure (Giorgi *et al.*, 1976). Besides these three carbides, several non-stoichiometric phases have been found that can be seen as solid state solutions between α-Th and γ-ThC_2 (Chiotti *et al.*, 1967; Storms, 1967) that have cubic symmetry.

Upon heating ThC_2 to high temperature on a graphite filament, ThC_4^+ ions were observed (Asano *et al.*, 1974). ThC_2 burns in the air to form ThO_2 and reacts with sulfur or selenium vapor (Moissan and Étard, 1896, 1897). Halogens react with the carbide to give anhydrous halides. According to an early study (Lebeau and Damiens, 1913) the hydrolysis of the carbide produces a mixture of almost 60% hydrogen, 3.16% methane, 10.7% ethane, ~15% acetylene, ~3% ethylene, ~8% propylene and propane, and higher products. Other studies on the hydrolysis of ThC and ThC_2 report the formation of methane in the ThC case and the formation of ethane and hydrogen in the ThC_2 case (Kemper and Krikorian, 1962). It seems evident that not only the composition and purity of the carbide but also the actual hydrolysis conditions may be important factors.

A number of ternary carbides have been reported (Table 3.5). The boride carbides have the compositions ThBC, $Th_3B_2C_3$, and ThB_2C (Rogl, 1978, 1979;

Rogl and Fischer, 1989). ThBC and $Th_3B_2C_3$ contain CBBC units; in $Th_3B_2C_3$ additional C atoms are found (Fig. 3.5). For ThB_2C extended layers of connected B and C atoms are found with the thorium atoms located between the layers. In the nitride carbide ThCN (Benz, 1969; Benz and Troxel, 1971), dumbbell-shaped C_2 units and nitride ions are present (Benz *et al.*, 1972).

Several ternary carbide systems have been investigated, Th–M–C, with M being a transition metal element or a lanthanide, and a huge number of compounds are believed to exist (Gmelin, 1992b). However, only a few of them are structurally characterized. Specifically, for ruthenium and nickel, several structure determinations have been performed. In the former case, the compounds $Th_{11}Ru_{12}C_{18}$, $Th_2Ru_6C_5$, and $ThRu_3C$ were investigated (Aksel'rud *et al.*, 1990a,b; Wachtmann *et al.*, 1995). The carbon-rich species contain both C_2 units and single C atoms while $ThRu_3C$ can be regarded as a cubic closest packing of metal atoms with the carbon atoms in octahedral interstices. Two series of thorium iron carbides have been structutrally and magnetically investigated recently. They have the composition $ThFe_{11}C_{1+x}$ ($0 < x < 1$) and $Th_2Fe_{17}C_x$ ($0 < x < 1$), respectively (Isnard *et al.*, 1992a,b; Singh Mudher *et al.*, 1995). In the nickel system, three compounds were found: Th_2NiC_2, $Th_3Ni_5C_5$, and $Th_4Ni_3C_6$. According to the structure determination the latter two should be more correctly described as $Th_3Ni_{4.96}C_{4.79}$ and $Th_4Ni_{2.88}C_6$, respectively (Moss and Jeitschko, 1991a,b). Two carbides have been prepared in the system Th–Al–C, namely $Th_2Al_2C_3$ and $ThAl_4C_4$ (Gesing and Jeitschko, 1996). They are both methanides in the sense that they contain isolated carbon atoms. One lanthanide compound that has been structurally characterized is $CeThC_2$ (Stecher *et al.*, 1964).

According to the phase diagram Th–Si (Fig. 3.6) four binary thorium silicides exist (Stecher *et al.*, 1963; Chiotti *et al.*, 1981; Gmelin, 1993b): Th_3Si_5, Th_3Si_2, ThSi, and $ThSi_2$. The latter three are structurally known (Brauer and Mitius, 1942; Jacobson *et al.*, 1956; Brown, 1961). $ThSi_2$ is dimorphic and both the hexagonal (AlB_2 type) and the tetragonal modifications show the thorium atoms in 12-fold coordination of silicon atoms. In ThSi the silicon atoms are linked to zigzag chains (Si—Si distance: 2.49 Å) while Si_2 dumbbells (2.33 Å) are found in Th_3Si_2. Further silicides have been reported, for example Th_6Si_{11} (Brown and Norreys, 1961), but have not be confirmed up to now.

Various ternary silicides of thorium are known (Table 3.5). The largest group among them contains compounds of the composition ThM_2Si_2 with M being a transition metal element. For M = Cr, Mn, Fe, Co, Ni, Cu, and Tc, structure determinations have been performed (Ban and Sikirica, 1965; Leciejewicz *et al.*, 1988; Wastin *et al.*, 1993) and for part of the silicides, magnetic properties are known (Omejec and Ban, 1971; Ban *et al.*, 1975). The compounds are isotypic with each other and have tetragonal symmetry. The stucture consists of layers of edge connected [$ThSi_8$] cubes that are separated by the transition metal atoms. Other silicides have the composition Th_2MSi_3 (M = M, Fe, Co, Ni, Cu, Ru, Rh, Pd, Os, Ir, Pt, Au) and are derived from the two modifications of $ThSi_2$ by

substitution of transition metal atoms for silicon atoms (Ban *et al.*, 1975; Wang *et al.*, 1985; Albering *et al.*, 1994). In the same way, the silicides ThMSi (M = Au, Pd, Ni) are derived from the hexagonal form of $ThSi_2$ (Ban *et al.*, 1975; Wang *et al.*, 1985). Two new silicides of thorium have been reported recently with $ThCo_9Si_2$ and $ThRe_4Si_2$ (Albering and Jeitschko, 1995; Moze *et al.*, 1996).

In a few cases, quaternary compounds have also been investigated. For example the silicide–carbides $Th_2Re_{2.086}Si_xC$ ($x = 1.914$ and 1.904), $ThOs_{2.04}Si_{0.96}C$, and $ThOs_{2.284}Si_{0.716}C$ have been reported (Hüfken *et al.*, 1998, 1999), and the two lanthanide nitride carbides CeThNC and DyThNC are known (Ettmayer *et al.*, 1980).

3.7.3 Oxides, hydroxides, and peroxides

Thorium oxides have received considerable attention in the recent decades. They have been reviewed in the *Gmelin Handbook* (Gmelin, 1976, 1978), but the diverse chemistry of the simple binary oxide of thorium has yielded 435 patents since these days, out of which 53 are related to the catalytic behavior of ThO_2. An recent search of the Chemical Abstract Services database revealed over 540 journal articles and some 50 reports on catalysis. While ThO_2 has been studied as a complement to CeO_2 and HfO_2 in its chemistry, ThO has been postulated as a defect form of the fluorite or a ZnS structure (Katzin, 1958; Ackermann and Rauh, 1973b). Table 3.6 lists the binary oxides and the other chalcogenides (cf. Section 3.7.5) with their lattice constants. Thorium monoxide has been reported to form on the surface of thorium metal exposed to air (Rundle *et al.*, 1948b) but its preparation and isolation as a bulk black suspension was first reported in 1958 by Katzin as a result of the action of 2 to 12 N HCl solutions on thorium metal. The black powder reported appeared later to be a form of low-valent thorium oxide stabilized by HCl and H_2O. XRD studies revealed a cubic phase with a lattice constant of 5.302 Å and a pattern indicative of an fcc lattice – either a defect fluorite or ZnS-type (Ackermann and Rauh, 1973b). However, the 'monoxide' solid state compound appears to be a Th(IV) phase with the formula Th(H)(O)X, where X is a combination of OH^- and Cl^- (Katzin *et al.*, 1962). This seemed to explain the reaction of the black solid upon heating to yield HCl, H_2, H_2O, and ThO_2 under various conditions (Ackermann and Rauh, 1973b). This phase was also reported to be unstable to disproportionation under dynamic vacuum. Until now, however, there is no report on bulk-phase ThO available that is without question. On the other hand, ThO was reported in the vapor phase above a mixture of Th and ThO_2 at high temperatures (Darnell and McCollum, 1961; Ackermann and Rauh, 1973b; Hildenbrand and Murad, 1974a,b; Neubert and Zmbov, 1974).

Thorium dioxide (thoria) is somewhat hygroscopic. Reaction with nitric or hydrochloric acids followed by evaporation yields hydrates that have in the past been thought to resemble the so-called 'metaoxides' of tin and zirconium. The material may be dispersed as a positively charged colloid following evaporation

Table 3.5 *Crystallographic data of thorium borides, carbides, and silicides.*

Compound	*Space group*	*Lattice parameters*				*References*
		a (Å)	*b* (Å)	*c* (Å)	*Angles* (°)	
ThB_4	P4/mbm	7.256		4.113		Zalkin and Templeton (1950, 1953); Konrad *et al.* (1996)
ThB_6	Pm$\bar{3}$m	4.113				Konrad *et al.* (1996), Blum and Bertaut (1954)
ThBC	P$4_1$22	3.762		25.246		Rogl (1978)
ThB_2C	R$\bar{3}$m	6.676		11.376		Rogl and Fischer (1989)
$Th_3B_2C_3$	P2/m	3.703	3.773	9.146	$\beta = 100.06$	Rogl (1979)
$ThB_{66.8}O_{0.36}$	Fm$\bar{3}$c	23.53				Naslain *et al.* (1971)
$Na_{0.77}Th_{0.23}B_6$	Pm$\bar{3}$m	4.151				Blum and Bertaut (1954)
Th_2FeB_{10}	Pbam	5.627		4.183		Konrad and Jeitschko (1995)
Th_2CoB_{10}	Pbam	5.624		4.185		Konrad and Jeitschko (1995)
Th_2NiB_{10}	Pbam	5.646	11.204	4.173		Konrad and Jeitschko (1995)
$ThCrB_4$	Pbam	6.057	11.712	3.640		Konrad *et al.* (1996)
$ThCr_2B_6$	Immm	3.158	6.591	8.364		Konrad *et al.* (1996)
$ThMoB_4$	Cmmm	7.481	9.658	3.771		Rogl and Nowotny (1974)
$ThIr_3B_2$	P6/mmm	5.449		3.230		Ku *et al.* (1980)
$ThRu_3B_2$	P6/mmm	5.528		3.070		Hiebl *et al.* (1980)
ThC	Fm$\bar{3}$m	5.346				Kemper and Krikorian (1962)
ThC_2	C2/c	6.53	4.24	6.56	β =104.0	Hunt and Rundle (1951)
ThC_2	C2/c	6.684	4.220	6.735	$\beta = 103.91$	Jones *et al.* (1987)
$ThC_{1.97}$	C2/c	6.692	4.223	6.744	$\beta = 103.1$	Bowman *et al.* (1968)
$ThC_{1.97}$	I4/mmm	4.221		5.394		Bowman *et al.* (1968)
$ThC_{1.97}$	Fm$\bar{3}$m	5.806				Bowman *et al.* (1968)
ThCN	C2/m	7.0249	3.9461	7.2763	$\beta = 95.67$	Benz *et al.* (1972)
$Th_2Al_2C_3$	Pnnm	5.406	11.556	3.5201		Gesing and Jeitschko (1996)
$ThAl_4C_4$	I4/m	8.231		3.3273		Gesing and Jeitschko (1996)
$ThFe_{11}C_{1+x}$	$I4_1$/amd	~10.20		~6.61		Isnard *et al.* (1992a)

Table 3.5 (*Contd.*)

Compound	*Space group*	*Lattice parameters*				*References*
		a (Å)	*b* (Å)	*c* (Å)	*Angles* (°)	
$Th_2Fe_{17}C_x$	$R\bar{3}m$	~8.6		~12.5		Isnard *et al*. (1992b)
Th_2NiC_2	I4/mmm	3.758		12.356		Moss and Jeitschko (1991b, 1989b)
$Th_3Ni_{4.96}C_{4.79}$	Cmca	13.961	7.174	7.07		Moss and Jeitschko (1991b, 1989b)
$Th_4Ni_{2.88}C_6$	C2/m	15.369	3.751	7.628	$\beta = 113.29$	Moss and Jeitschko (1991a, 1989a)
$ThRu_3C$	$Pm\bar{3}m$	4.227				Wachtmann *et al.* (1995)
$Th_2Ru_6C_5$	P4/mbm	9.113		4.186		Aksel'rud *et al*. (1990a)
$Th_{11}Ru_{12}C_{18}$	$I4\bar{3}m$	10.764				Aksel'rud *et al*. (1990b)
$Th_2Ru_6C_5$	P4/mbm	9.096		4.177		Wachtmann *et al.* (1995)
$Th_{11}Ru_{12}C_{18}$	$I4\bar{3}m$	10.754				Wachtmann *et al.* (1995)
$ThCeC_2$	$Fm\bar{3}m$	5.280				Stecher *et al*. (1964)
ThSi	Pbnm	5.89	7.88	4.15		Jacobson *et al*. (1956)
$ThSi_2$	P6/mmm	4.136		4.126		Brown (1961)
$ThSi_2$	$I4_1/amd$	4.126		14.346		Brauer and Mitius (1942)
$ThSi_2$	P6/mmm	3.985		4.220		Jacobson *et al*. (1956)
Th_3Si_2	P4/mbm	7.835		4.154		Jacobson *et al*. (1956)

$ThCr_2Si_2$	I4/mmm	4.043		10.577	Ban and Sikirica (1965)
$ThCr_2Si_2$	I4/mmm	4.0414		10.588	Leciejewicz *et al*. (1988)
$ThMn_2Si_2$	I4/mmm	4.021		10.493	Ban and Sikirica (1965)
$ThMn_2Si_2$	I4/mmm	4.0225		10.475	Leciejewicz *et al*. (1988)
$ThMn_2Si_2$	I4/mmm	4.019		10.483	Ban *et al*. (1975)
$ThFe_2Si_2$	I4/mmm	4.038		9.820	Ban and Sikirica (1965)
$ThFe_2Si_2$	I4/mmm	4.038		9.812	Leciejewicz *et al*. (1988)
$Th(Co_{0.5}Si_{1.5})$	P6/mmm	4.043		4.189	Wang *et al*. (1985)
$ThCo_9Si_2$	$I4_1$/amd	9.7914		6.3138	Moze *et al*. (1996)
$ThCo_2Si_2$	I4/mmm	4.015		9.760	Ban and Sikirica (1965)
$ThCo_2Si_2$	I4/mmm	4.0128		9.754	Leciejewicz *et al*. (1988)
$ThNi_2Si_2$	I4/mmm	4.076		9.551	Ban and Sikirica (1965)
$ThNi_2Si_2$	I4/mmm	4.0789		9.555	Leciejewicz *et al*. (1988)
$ThCu_2Si_2$	I4/mmm	4.104		9.864	Ban and Sikirica (1965)
$ThCu_2Si_2$	I4/mmm	4.1031		9.866	Leciejewicz *et al*. (1988)
$ThTc_2Si_2$	I4/mmm	4.184		10.063	Wastin *et al*. (1993)
$ThRe_4Si_2$	$Pn\bar{n}m$	7.294	15.500	4.124	Albering and Jeitschko (1995)
ThAuSi	$P\bar{6}m2$	4.260		4.164	Albering *et al*. (1994)

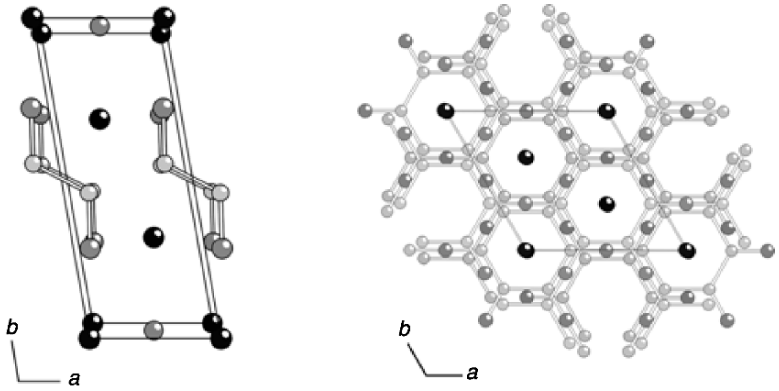

Fig. 3.5 *Crystal structures of* $Th_3B_2C_3$ (*left*) *and* ThB_2C (*right*).

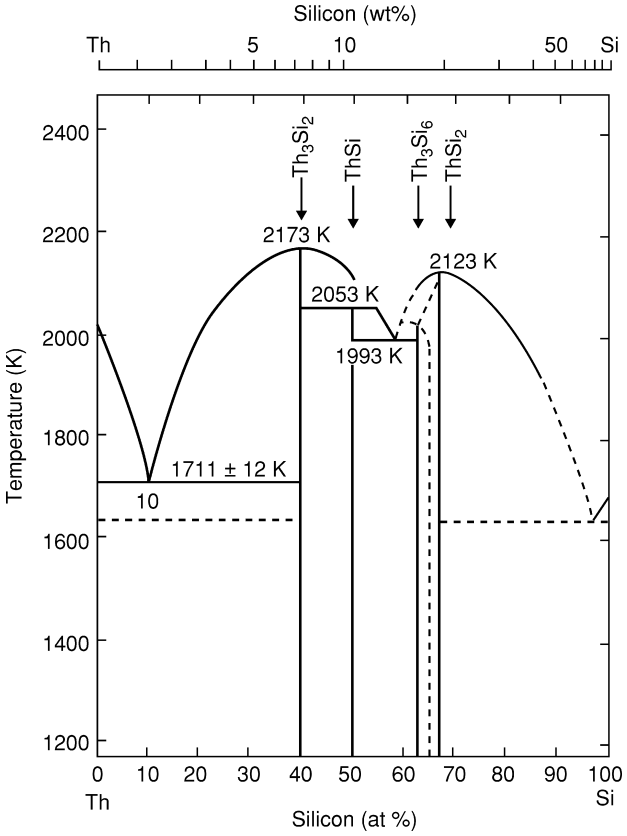

Fig. 3.6 *Phase diagram of the thorium–silicon system* (*Chiotti* et al., 1981).

Table 3.6 *Crystallographic data of thorium chalcogenides.*

		Lattice parameters				
Compound	*Space group*	*a* (Å)	*b* (Å)	*c* (Å)	*Angles* (°)	*References*
ThO	cubic	5.302				Katzin (1958); Ackermann and Rauh (1973b)
ThO_2	$Fm\bar{3}m$	5.592				Gmelin (1976, 1978)
ThOS	P4/nmm	3.963		6.747		Zachariasen (1949c)
ThS	$Fm\bar{3}m$	5.682				Zachariasen (1949c)
Th_2S_3	Pbnm	10.990	10.850	3.960		Zachariasen (1949c)
Th_7S_{12}	$P6_3/m$	11.063		3.991		Zachariasen (1949d)
ThS_2	Pmnb	4.267	7.264	8.617		Zachariasen (1949c)
Th_2S_5	Pcnb	7.623	7.677	10.141		Nöel and Potel (1982)
ThOSe	P4/nmm	4.038		7.019		D'Eye *et al.* (1952)
ThSe	$Fm\bar{3}m$	5.875				D'Eye *et al.* (1952)
Th_2Se_3	Pbnm	11.36	11.59	4.28		D'Eye *et al.* (1952)
Th_7Se_{12}	$P6_3/m$	11.570		4.230		D'Eye (1953)
$ThSe_2$	Pmnb	4.420	7.611	9.065		D'Eye (1953)
Th_2Se_5	Pcnb	7.922	7.937	10.715		Kohlmann and Beck (1999)
$ThSe_3$	$P2_1/m$	5.72	4.21	9.64	$\beta = 97.05$	Nöel (1980)
ThOTe	P4/nmm	4.120		9.563		D'Eye and Sellman (1954)
ThTe	$Pm\bar{3}m$	3.827				D'Eye and Sellman (1954)
Th_2Te_3	hexagonal	12.49		4.35		Graham and McTaggart (1960)
Th_7Te_{12}	$P\bar{6}$	12.300		4.566		Tougait *et al.* (1998)
$ThTe_2$	hexag. (?)	8.49		9.01		Graham and McTaggart (1960)
$ThTe_3$	monoclinic	6.14	10.44	4.31	$\beta = 98.4$	Graham and McTaggart (1960)

and the colloid can be 'salted out' by addition of electrolytes. The ignited oxide or the oxide sintered into larger particles is one of the most refractory substances known, showing limited reactivity with hot sulfuric acid or fusion with potassium hydrogen sulfate. Aqueous nitric acid with a few percentage of HF or sodium fluorosilicate provides a reasonable solution of the oxide (Smithells, 1922). Hot aqueous HF or gaseous HF at 250–750°C converts thoria to ThF_4 (Newton *et al.*, 1952b).

Amorphous thoria is said to crystallize from a suitable flux, for example sodium carbonate, potassium orthophosphate, or borax (Nordenskjöld and Chydenius, 1860; Nordenskjöld, 1861; Chydenius, 1863; Rammelsberg, 1873; Troost and Ouvrard, 1889; Duboin, 1909a,b). However, the use of borax as a

flux is questionable, because ThO_2 is known to form ThB_2O_5 in the reaction with B_2O_3 (Baskin *et al.*, 1961).

Thorium dioxide has been studied as an active catalyst because of its reactivity with many gases, in addition to water. Dehydration of alcohols (Frampton, 1979; Siddham and Narayanan, 1979), dehydrogenation of alcohols (Thomke, 1977), and the hydration (Frampton, 1979) and hydrogenation of alkenes (Tanaka *et al.*, 1978) have been demonstrated. Other examples include copper–thorium oxide catalysts studied for the selective hydrogenation of isoprene (Bechara *et al.*, 1990a,b), decomposition of isopropanol (Aboukais *et al.*, 1993), and the oxidative coupling of methane (Zhang *et al.*, 2001). Indeed, the development of mixed-metal rare earth/thorium/copper oxides based on a perovskite parent structure have been shown to decompose NO_x (Gao and Au, 2000), to catalyze the reduction of NO by CO (Wu *et al.*, 2000), and to dehydroxylate phenol (Liu *et al.*, 1997). Lastly, thorium oxide, when heated, produces an intense blue light and mixed with ceria at 1%, produces a more intense white light. It is this property that was the basis for the thoriated gas mantle industry (Mason, 1964; Manske, 1965).

Thorium hydroxide is formed as a gelatinous precipitate when alkali or ammonium hydroxide is added to a solution of a thorium salt. This precipitate dissolves in dilute acids and, when fresh, in ammonium oxalate, alkali carbonates, sodium citrate, or sodium potassium tartrate solutions (Chydenius, 1863; Glaser, 1897; Jannasch and Schilling, 1905; Sollman and Brown, 1907). The hydroxide is also precipitated by the action of sodium nitrate (Baskerville, 1901) or potassium azide (Dennis and Kortright, 1894; Glaser, 1897; Wyrouboff and Verneuil, 1898a). Electrolysis of thorium nitrates is also said to yield a precipitate of hydroxide at the anode (Angelucci, 1907). Material dried at 100°C has been reported to correspond closely in composition to $Th(OH)_4$ (Clève, 1874), but other reports claim to find higher hydrates even at higher temperatures (Wyrouboff and Verneuil, 1905). Two forms of $ThO_2{\cdot}2H_2O$ (=$Th(OH)_4$), from precipitation in basic aqueous solution, have been distinguished, one of which is amorphous (Guymont, 1977). Further studies indicate that $Th(OH)_4$ is stable in the temperature range 260–450°C and is converted to the oxide at temperatures of 470°C and higher (Dupuis and Duval, 1949). Thermal analysis has shown that the decomposition of the hydroxide is a continuous process (Tiwari and Sinha, 1980). Thorium hydroxide absorbs atmospheric carbon dioxide very readily (Chydenius, 1863; Dennis and Kortright, 1894; Chauvenet, 1911). When boiled with thorium nitrate, $Th(OH)_4$ forms a positively charged colloid (Müller, 1906). The colloid formation is also observed if thorium hydroxide is treated with hydrous aluminum chloride, ferric chloride, uranyl nitrate, or hydrochloric acid (Szilard, 1907). The solubility product of $Th(OH)_4$ is discussed in Section 3.8.5.

Thorium peroxide had been reportedly known since 1885 as the product of the reaction between hydrogen peroxide and salts of thorium in solution

(de Boisbaudran, 1885). The precipitate that forms can be a dense solid or a gelatinous paste. The solid has initially been described in the literature as hydrated thorium peroxide, 'Th_2O_7' (de Boisbaudran, 1885; Pissarsjewski, 1900; Schwarz and Giese, 1928). The existence of peroxide species was confirmed but it was pointed out that the respective anions of the initial thorium salt are part of the solid (Clève, 1885; Wyrouboff and Verneuil, 1898a; Hamaker and Koch, 1952a,b; Johnson *et al.*, 1965; Hasty and Boggs, 1971; Raman and Jere, 1973a,b; Jere and Santhamma, 1977). XRD studies revealed two phases if the precipitation occurs from thorium sulfate solution: $Th(OO)SO_4{\cdot}3H_2O$ precipitated from solutions of high H_2SO_4 concentration and a second phase is obtained from more weakly acidic solutions with a variable sulfate content and 3.0–3.8 peroxide oxygen atoms per thorium atom (Hamaker and Koch, 1952a). A Raman analysis of $Th(OO)SO_4{\cdot}3H_2O$ has been performed (Raman and Jere, 1973a,b) and suggests a formulation of the compound as 'tetraaquo-μ-peroxy-disulfatodithorium(IV)', with two bridging sulfato groups. Raman investigations have been also carried out for the peroxide obtained from a nitrate solution (Raman and Jere, 1973b). According to these measurements thorium peroxide nitrate showed a 'free' (D_{3h}) nitrate anion along with a bridging peroxide molecule between thorium atoms. However, also a nitrate-free peroxide has been obtained from the reaction of a refluxing aqueous solution of $Th(NO_3)_4{\cdot}4H_2O$, urea, and 30% hydrogen peroxide (Gantz and Lambert, 1957). The precipitate, described as a granular light blue-green powder, decomposes at 120°C to yield ThO_2 and water. Chemical analysis revealed a formula of $Th(OH)_3OOH$, equivalent to tin and zirconium analogs. The dried peroxide is insoluble in neutral solutions (aqueous) but is soluble in concentrated mineral acids. Thorium peroxide has also been reported by the action of hydrogen peroxide or sodium hypochlorite on thorium hydroxide, or by anodic oxidation of an alkaline thorium hydroxide suspension containing sodium chloride (Pissarsjewsky, 1902).

Like the double salts of the halides, thorium dioxide will form a similar 'double salt' of oxide with BaO and alkali metal oxides (K_2O, for example) in phases such as $BaThO_3$ and K_2ThO_3 (Brunn and Hoppe, 1977); however, neither the Sr form nor the Li form of these structures have been reported (Hoffmann, 1935; Naray-Szabo, 1951; Scholder *et al.*, 1968; Fava *et al.*, 1971; Nakamura, 1974). No reaction was seen with BeO (Ohta and Sata, 1974) and, although there is solid solution formation with the rare earth oxides, no reaction to form the 'double salt' phase Ln_2ThO_5 has been observed (Diness and Roy, 1969; Sibieude, 1970). Because of the reactivity of ThO_2–CuO mixtures, reactions that have included other transition metal oxides have yielded a number of unique phases including tetragonal perovskite phases such as $La_{1-x}Th_xCoO_3$ (Tabata and Kido, 1987), $La_{1-1.333x}Th_xNiO_3$ (Yu *et al.*, 1992), $Na_{.6667}Th_{.3333}TiO_3$ (Zhu and Hor, 1995), and the Ruddlesden–Popper manganites $Ca_{3-x}Th_xMn_2O_7$ (Lobanov *et al.*, 2003).

3.7.4 Halides

(a) Binary halides

The halides of thorium had been treated comprehensively in 1968 by Brown (1968), and the fluorides in particular have been reviewed by Penneman *et al.* (1973) and Taylor (1976). In addition, a later volume of the *Gmelin Handbook* has discussed thorium halides (Gmelin, 1993a).

The tetrahalides of thorium are known for the whole halogen series (Table 3.7). Thorium fluoride, ThF_4, can be obtained by various procedures (Moissan and Martinsen, 1905; Duboin, 1908a; Chauvenet, 1911; Lipkind and Newton, 1952). Precipitation from aqueous Th^{4+}-containing solutions leads to hydrates of ThF_4 that are, however, not easily dehydrated due to the formation of hydroxide or oxide fluorides (Briggs and Cavendish, 1971). Under careful conditions, for example under streaming HF or F_2 gas, dehydration to pure ThF_4 is possible (Pastor and Arita, 1974). Alternative routes avoiding aqueous media are the reaction of thorium metal or thorium carbide with fluorine (Moissan and Étard, 1896, 1897), or the action of hydrogen fluoride on other thorium halides, thorium oxide or hydroxide, and thorium oxalate or oxide carbonate (Newton *et al.*, 1952a). As mentioned in the Section 3.7.1, the reaction of thorium hydrides with fluorine provides a route to ThF_4 (Lipkind and Newton, 1952). An elegant way to obtain pure ThF_4 is the reaction of ThO_2

Table 3.7 *Crystallographic data of binary thorium halides.*

		Lattice parameters				
Compound	*Space group*	*a* (Å)	*b* (Å)	*c* (Å)	*Angles* (°)	*References*
ThF_4	C2/c	13.049	11.120	8.538	$\beta = 126.31$	Benner and Müller (1990)
β-$ThCl_4$	$I4_1/amd$	8.491		7.483		Brown *et al.* (1973)
α-$ThCl_4$	$I4_1/a$	6.408		12.924		Mason *et al.* (1974a)
β-$ThBr_4$	$I4_1/amd$	8.971		7.912		Madariaga *et al.* (1993)
α-$ThBr_4$	$I4_1/a$	6.737		13.601		Mason *et al.* (1974b)
ThI_4	$P2_1/n$	13.216	8.068	7.766	$\beta = 98.68$	Zalkin *et al.* (1964)
β-ThI_3	Cccm	8.735	20.297	14.661		Beck and Strobel (1982)
β-ThI_2	$P6_3/mmc$	3.97		31.75		Guggenberger and Jacobson (1968)

with NH_4HF_2. Ammonium hydrogen fluoride serves as the fluorinating agent and is much easier to handle than hydrogen fluoride itself. The reaction yields the ternary fluoride NH_4ThF_5 that decomposes above 300°C to the tetrafluoride (Asprey and Haire, 1973). The disadvantage of the method compared to the direct hydrofluorination is that an eight-fold excess of NH_4HF_2 is needed.

The monoclinic crystal structure of ThF_4 is isotypic with those of zirconium and hafnium fluoride and contains Th^{4+} ions in slightly distorted square antiprismatic coordination of fluoride ions (Zachariasen, 1949a; Asprey and Haire, 1973; Benner and Müller, 1990). Each of the fluorine atoms is attached to another thorium ion, leading to a three-dimensional structure according to $^3_\infty[ThF_{8/4}]$. Surprisingly, the thorium fluoride hydrate that can be precipitated from aqueous solution (Berzelius, 1829; Chydenius, 1863) has not been structurally characterized up to now. It is believed to be an octahydrate, which decomposes to a tetrahydrate on further drying and then finally to a dihydrate on heating (Chauvenet, 1911). The only hydrate of ThF_4 that is structurally known is $Th_6F_{24}{\cdot}H_2O$ ($=ThF_4{\cdot}1/6H_2O$) (Cousson *et al.*, 1978). Similarly to the anhydrous fluoride it consists of three-dimensionally connected square antiprisms [ThF_8]. Six of these aniprisms are arranged in a way that empty voids are formed in which the water molecule resides having contact to two of the six Th^{4+} ions (Fig. 3.7). It is assumed that this compound can be obtained by

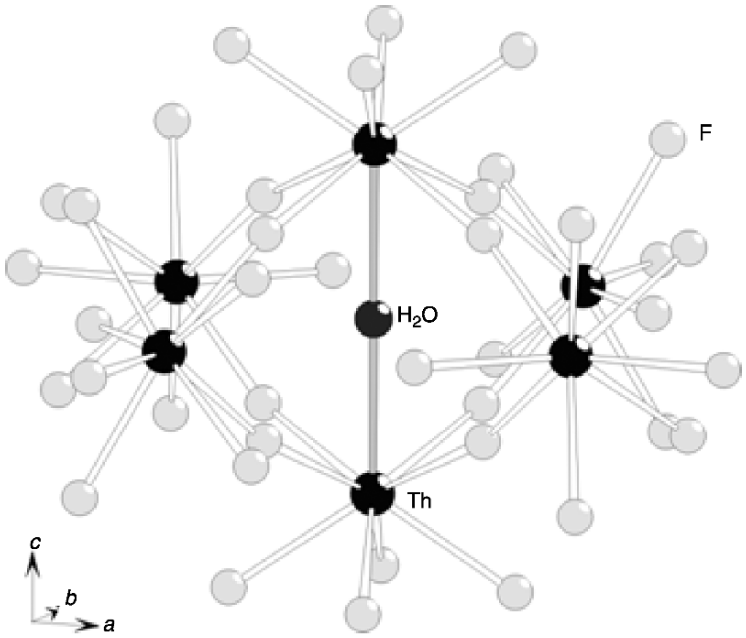

Fig. 3.7 *Detail of the crystal structure of $Th_6F_{24}{\cdot}H_2O$; the H_2O molecule resides in a void formed by six square antiprismatic [ThF_8] polyhedra.*

careful dehydration of higher hydrates but usually hydrolysis is observed yielding $Th(OH)F_3 \cdot H_2O$ and then finally $ThOF_2$ (Marden and Rentschler, 1927; Zachariasen, 1949a; D'Eye, 1958). The structure of neither of the latter two compounds is known without some question. For $ThOF_2$, however, an orthorhombic unit cell has been determined, which has a close relationship to the hexagonal one of LaF_3. Probably the structure can be seen as an ordering variant of the LaF_3-type of structure. The treatment of $ThOF_2$ with steam at 900°C will yield thoria (Chydenius, 1863; Cline *et al.*, 1944).

Thorium tetrachloride, $ThCl_4$, can be crystallized from aqueous solution as an octahydrate, which is easily transformed to basic chlorides upon heating above 100°C (Chauvenet, 1911; Dergunov and Bergman, 1948; Knacke *et al.*, 1972a,b). Dehydration has also been done by refluxing the hydrates with thionyl chloride but the product was hard to get free of $SOCl_2$. Other routes have been employed to produce pure $ThCl_4$ (Chydenius, 1863) including the reaction of ThH_4 with HCl and the action of chlorine on thorium metal (Krüss and Nilson, 1887a; Lipkind and Newton, 1952), ThH_4, or thorium carbide (Nilson, 1876, 1882a,b, 1883; Moissan and Étard, 1896, 1897; von Wartenberg, 1909). Furthermore mixtures of chlorine and carbon or S_2Cl_2 were used for the chlorination of ThO_2 (Matignon and Bourion, 1904; Meyer and Gumperz, 1905; Bourion, 1909; von Wartenberg, 1909; Yen *et al.*, 1963), and also carbon tetrachloride (Matignon and Delepine, 1901; von Bolton, 1908; Knacke *et al.*, 1972a), phosgene (Baskerville, 1901; Karabasch, 1958), and phosphorus pentachloride (Smith and Harris, 1895; Matignon, 1908) were applied as chlorinating agents and mixtures of chlorine and CO or CO_2 for the chlorination of thorium oxalate and nitrate, respectively (Dean and Chandler, 1957). A facile synthesis of $ThCl_4$ is provided in the reaction of thorium metal with NH_4Cl in sealed tubes (Schleid *et al.*, 1987). Purification of $ThCl_4$ can be achieved by sublimation. $ThCl_4$ melts at 770°C (Moissan and Martinsen, 1905; Fischer *et al.*, 1939) and boils at 921°C. The results of vapor pressure measurements as a function of the temperature have been compiled (Fuger *et al.*, 1983).

$ThCl_4$ is dimorphic and exhibits a phase transition at 405°C (Mooney, 1949; Mucker *et al.*, 1969; Mason *et al.*, 1974a). The phase transition can only be observed under special conditions and in very pure samples. Usually the high-temperature phase β-$ThCl_4$ remains even at temperatures below 405°C as a metastable compound. Both the low-temperature phase α-$ThCl_4$ and the high-temperature phase β-$ThCl_4$ are tetragonal and show eight-fold coordinated Th^{4+} ions. The coordination polyhedra are slightly distorted dodecahedra that are connected via four edges to a three-dimensional structure. Thus, each of the chloride ligands are connected to two Th^{4+} ions. The difference in the two polymorphs results from small differences in the orientation of the $[ThCl_8]$ polyhedra with respect to each other (Fig. 3.8). The symmetry decreases from $I4_1/amd$ for β-$ThCl_4$ to $I4_1/a$ for α-$ThCl_4$. The two modifications of $ThCl_4$ are related in much the same way as are zicon ($ZrSiO_4$) and scheelite ($CaWO_4$).

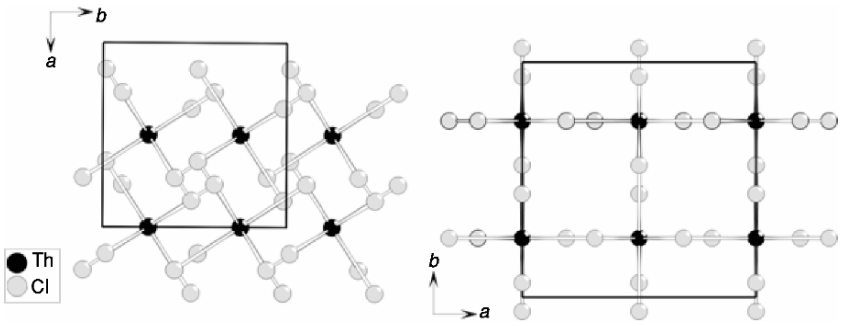

Fig. 3.8 *Projections of the crystal structures of* α*-$ThCl_4$ (right) and* β*-$ThCl_4$ (left) onto* (001).

In fact the structures of $ThCl_4$ result if the atoms in the tetrahedral centers (Si and W, respectively) are removed in the oxo-compounds. More recent investigations gave some evidence that there is a third modification of $ThCl_4$ below 70 K that has a complicated incommensurate structure related to that of α-$ThCl_4$ (Khan Malek *et al.*, 1982; Bernard *et al.*, 1983; Krupa *et al.*, 1987).

Structural data of $ThCl_4$ hydrates are not known up to now but the enthalpies of formation of the di-, tetra-, hepta- and octahydrates have been evaluated (Fuger *et al.*, 1983) from enthalpy of solution measurements (Chauvenet, 1911). Also the basic chlorides that are frequently observed as the products of the thermal treatment of the hydrates are poorly investigated (Bagnall *et al.*, 1968). It is only for the oxychloride $ThOCl_2$ that lattice parameters have been calculated from powder diffraction data based on the data given for $PaOCl_2$ (Bagnall *et al.*, 1968). The heat of formation of $ThOCl_2$ has been reported several times (Yen *et al.*, 1963; Korshunov and Drobot, 1971; Knacke *et al.*, 1972b; Fuger *et al.*, 1983) and will be discussed in proper context in Chapter 19. Chlorides of lower-valent thorium have been reported to form by electrochemical reduction of a $ThCl_4$/KCl melt (Chiotti and Dock, 1975) but these observations are still in need of confirmation.

Analogous to the tetrachloride, $ThBr_4$ can be obtained from aqueous solution, for example, by adding $Th(OH)_4$ to aqueous HBr. Depending on the drying conditions various hydrates may form. The main disadvantage of the wet route for preparing $ThBr_4$ is the contamination of the product with hydrolysis products like $ThOBr_2$. Dry routes to $ThBr_4$ include the action of bromine on thorium metal, ThH_4, ThC, or on mixtures of ThO_2 and C (Nilson, 1876; Troost and Ouvrard, 1889; Moissan and Étard, 1896, 1897; Matthews, 1898; Moissan and Martinsen, 1905; Fischer *et al.*, 1939; Young and Fletcher, 1939; Lipkind and Newton, 1952). Moreover, the reaction of gaseous HBr with ThH_4 (Lipkind and Newton, 1952) and of a mixture of S_2Cl_2 and gaseous HBr with ThO_2 have been employed (Bourion, 1907). Sublimation above 600°C in

vacuum should be applied for purification. The temperature dependence of the vapor pressure has been investigated (Fischer *et al.*, 1939) and melting (679°C) and boiling (857°C) points have been reported (Fischer *et al.*, 1939; Mason *et al.*, 1974b).

As found for the tetrachloride, $ThBr_4$ is also dimorphic (D'Eye, 1950; Brown *et al.*, 1973; Fuger and Brown, 1973; Mason *et al.*, 1974b; Guillaumont, 1983). Both modifications, β-$ThBr_4$ and α-$ThBr_4$, are isotypic to the respective chlorides. The transition temperature is slightly higher compared to $ThCl_4$ and is determined to be 426°C. Again, the β-phase is found to remain metastable even below 426°C. The phase transition has been investigated in detail by means of nuclear quadrupolar resonance (NQR) on the ^{79}Br isotope (Kravchenko *et al.*, 1975). According to these experiments, the time to achieve complete conversion is strongly dependent on the previous treatment of the sample and is reduced after one conversion cycle has passed. Analogous to $ThCl_4$ another phase transition is found at lower temperature. According to NQR and electron paramagnetic resonance (EPR) measurements as well as neutron and X-ray diffractions, the transition is second order and occurs at 92 K (Kravchenko *et al.*, 1975). It is only observed in β-$ThBr_4$ and can be described as a continuous modulation of the bromide ions along the *c*-axis, leading to a complicated incommensurate structure (Madariaga *et al.*, 1993). The incommensurate low-temperature modifications of $ThBr_4$ and $ThCl_4$ have also been investigated spectroscopically on U^{4+}-doped samples (Krupa *et al.*, 1995).

There are two reports on the low-valent thorium bromides, $ThBr_3$ and $ThBr_2$ (Hayek and Rehner, 1949; Shchukarev *et al.*, 1956). They have been prepared from the elements in the desired molar ratio or, in the case of $ThBr_3$, by reduction of $ThBr_4$ with hydrogen. These bromides are highly reactive and show disproportionation at higher temperatures. Unfortunately no structural data are known. More recently the molecular species, $ThBr_3$, $ThBr_2$ and ThBr, have been identified by mass spectrometry in the bromination of thorium between 1500 and 2000 K (Hildenbrand and Lau, 1990).

None of the various hydrates of $ThBr_4$ that have been reported to contain 12, 10, 8, and 7 molecules of water, respectively (Lesinsky and Gundlich, 1897; Rosenheim and Schilling, 1900; Rosenheim *et al.*, 1903; Moissan and Martinsen, 1905; Chauvenet, 1911), are well characterized to date. The heat of solution has been determined in some cases and the thermal decomposition of the hydrates is known to lead to $Th(OH)Br_3$ and finally to $ThOBr_2$ (Chauvenet, 1911). The powder diffraction pattern of the oxybromide shows that this compound is not isotypic with $ThOCl_2$ but seems to have a lower symmetry (Bagnall *et al.*, 1968). $ThBr_4$ is also known to form solvates with amines (Rosenheim and Schilling, 1900; Rosenheim *et al.*, 1903), acetonitrile (Young, 1935), and trimethylphosphine (Al-Kazzaz and Louis, 1978).

Thorium tetraiodide (ThI_4) is most conveniently prepared by the reaction of the elements in sealed silica ampoules (Nilson, 1876; Moissan and Étard, 1896, 1897; Zalkin *et al.*, 1964). It is very important to exclude any traces of water or

oxygen during the reaction to avoid contamination of the product with $ThOI_2$ or even ThO_2. Alternative procedures involve the reactions between ThH_4 and HI, and between thorium metal and a H_2/I_2 mixture (Lipkind and Newton, 1952). If only small amounts of ThI_4 are needed, the action of AlI_3 on ThO_2 might also be appropriate (Chaigneau, 1957). In the temperature range from 500 to 550°C, ThI_4 can be sublimed for purification under dynamic vacuum yielding yellow crystals. Knudsen cell effusion studies of ThI_4 have suggested dissociation through ThI_3, ThI_2, and ThI to thorium metal (Knacke *et al.*, 1978). On heating, ThI_4 reacts with ThO_2 to form the basic iodide $ThOI_2$ (Scaife *et al.*, 1965; Corbett *et al.*, 1969).

ThI_4 is not isotypic with the other tetrahalides. It has monoclinic symmetry and contains eight-fold coordinated Th^{4+} ions (Zalkin *et al.*, 1964). The coordination polyhedron can be seen as a distorted square antiprism. The polyhedra are linked in chains via two triangular faces leading to Th–Th distances of 4.48 Å. The chains are further connected via the two remaining iodine ligands into layers. The connectivity may be formulated as $^{2}_{\infty}[ThI^{f}_{6/2}I^{e}_{2/2}]$ (f = face; e = edge). These layers are held together only by van der Waals interactions (Fig. 3.9).

Two lower-valent thorium iodides, ThI_3 and ThI_2, are known. Both can be obtained by reduction reactions of ThI_4 with appropriate amounts of thorium metal in sealed tantalum tubes (Anderson and D'Eye, 1949; Hayek and Rehner, 1949; Hayek *et al.*, 1951; Clark and Corbett, 1963; Scaife and Wylie, 1964; Guggenberger and Jacobson, 1968). If hydrogen is used as the reducing reagent, the formation of iodide hydrides is observed (Struss and Corbett, 1978).

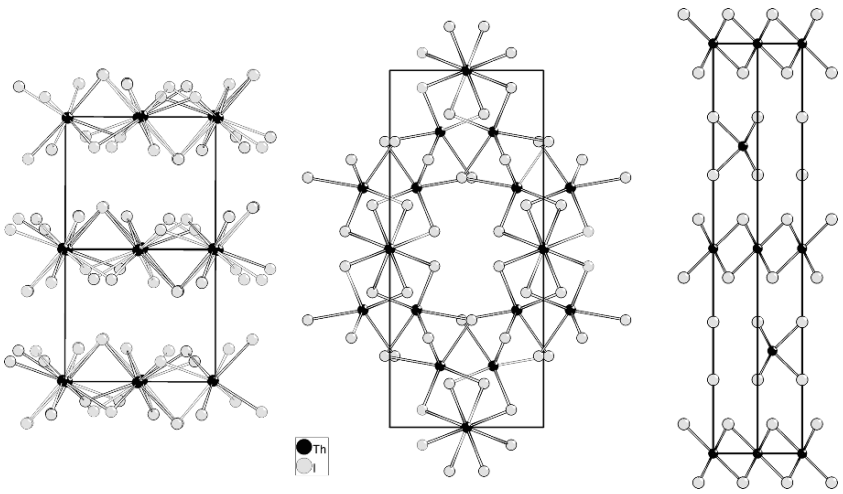

Fig. 3.9 *Crystal structures of the thorium iodides* ThI_4 (*left, as a projection onto the* (101) *plane*), β-ThI_3 (*middle, as a projection onto the* (001) *plane*), *and* β-ThI_2 (*right, as a projection onto the* (110) *plane*).

For the preparation of ThI_2, another route has been developed. The electrolysis of thorium metal in a solution of iodine and tetraethyl ammonium perchlorate in acetonitrile affords $ThI_2 \cdot 2CH_3CN$ that can be decomposed into ThI_2 *in vacuuo* (Kumar and Tuck, 1983).

Depending on the time, the reaction of ThI_4 and Th leads to two modifications of ThI_3 (Beck and Strobel, 1982). After a short period of 2–3 days, thin shiny rods of α-ThI_3 were obtained while long heating times led to compact crystals of β-ThI_3 that show a slight green to brass-colored luster. For α-ThI_3 only the lattice constants are known while a complete structure determination has been performed for β-ThI_3 (Beck and Strobel, 1982). It shows three crystallographically different thorium atoms in the unit cell, each of them in an eightfold coordination of iodide ions. Two of the $[ThI_8]$ polyhedra are square antiprismatic, the third one is a slightly elongated cube. The $[ThI_8]$ cubes are connected via four rectangular faces to $[ThI_8]$ square antiprisms (Fig. 3.9). One half of the square antiprisms is further connected to other cubes and, the second half to other square antiprisms, leading to a three-dimensional network. The Th–I bond distances suggest that thorium is in the tetravalent state in ThI_3 and has to be formulated according to $Th^{4+}(I^-)_3(e^-)$ with the electrons delocalized or involved in metal–metal bonds. The latter assumption is supported by the relatively short Th–Th distances of 3.46 to 3.80 Å.

ThI_2 is also found to adopt two different crystal structures (Clark and Corbett, 1963; Scaife and Wylie, 1964). Lustrous gold crystals of β-ThI_2 are obtained at 700 to 850°C while α-ThI_2 forms at 600°C. Both compounds are hexagonal but a structure determination has been performed only for β-ThI_2 (Guggenberger and Jacobson, 1968). The structure can be seen as a stacking variant of the CdI_2 structure (Fig. 3.9). It has a remarkable long *c*-axis (31 Å) and the stacking sequence of the iodide ions is …ABCCBA… with the thorium atoms in octahedral and trigonal prismatic sites (Fig. 3.9). Judging from the Th–I bond distances, Th^{4+} is present in the structure and the free electrons, according to $Th^{4+}(I^-)_2(e^-)_2$, should be responsible for the electrical conductivity of the compound. The metal–metal distances, however, are remarkably longer than those found in ThI_3. Both subiodides, ThI_3 and ThI_2, exhibit peritectic decomposition above 850°C caused by disproportionations to ThI_4 and ThI_2 or ThI_4 and Th, respectively (Scaife and Wylie, 1964).

The formation of pseudo-halides of thorium (such as thiocyanate or selenocyanate) in organic solvents has been reported, but up to now, no binary compound is known (Golub and Kalibabchuk, 1967; Laubscher and Fouché, 1971; Golub *et al.*, 1974).

(b) Polynary halides

The systems AF/ThF_4, where A is an alkali or another monovalent metal ion, have been widely investigated (Brunton *et al.*, 1965). Phase diagrams of the

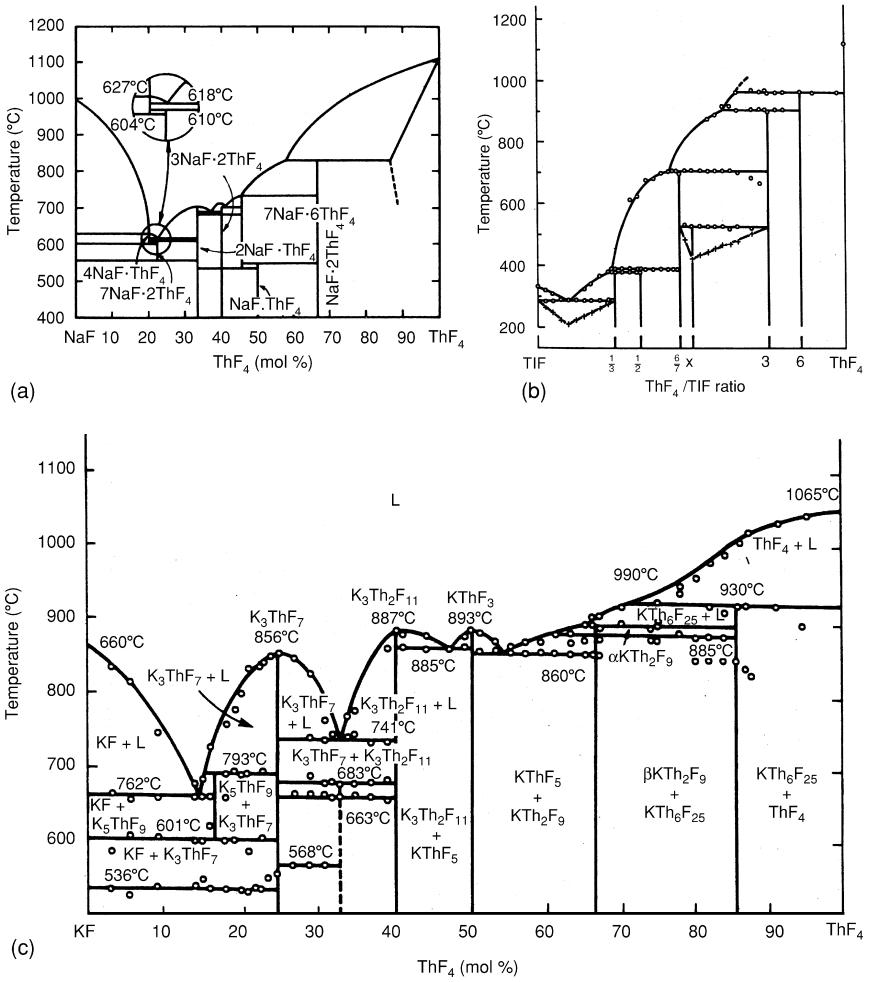

Fig. 3.10 *Phase diagrams of three AF/ThF*$_4$ *systems.* (*a*) *NaF/ThF*$_4$ (*Thoma,* 1972). (*b*) *TlF/ThF*$_4$ (*Avignant and Cousseins,* 1970). (*c*) *KF/ThF*$_4$ (*Kaplan,* 1956).

systems NaF/ThF_4 (Thoma, 1972), KF/ThF_4 (Kaplan, 1956), and TIF/ThF_4 (Avignant and Cousseins, 1970) are given as examples in Fig. 3.10. Furthermore, the binary and also some ternary phase diagrams of ThF_4 with several other fluorides were determined. Table 3.8 surveys the phases that are reported to exist along with those found in the other halide systems. Unfortunately, only very few of these phases have been carefully characterized. In some cases lattice parameters of the compounds were determined by powder diffraction; moreover,

Table 3.8 *Detected phases in the systems with ThX_4 ($X = F, Cl, Br$).*

System	*Compounds*	*References*
$LiF–ThF_4$	Li_3ThF_7, $LiThF_5$, $LiTh_2F_9$, $LiTh_4F_{17}$	Thoma and Carlton (1961)
$NaF–ThF_4$	Na_4ThF_8, Na_3ThF_7, Na_2ThF_6, $Na_3Th_2F_{11}$, $Na_7Th_6F_{31}$, $NaThF_5$, $NaTh_2F_9$	Thoma and Carlton (1961); Thoma (1972); Brunton *et al.* (1965)
$KF–ThF_4$	K_5ThF_9, K_2ThF_6, $K_7Th_6F_{31}$, $KThF_5$, KTh_2F_9, KTh_6F_{25}	Thoma and Carlton (1961); Dergunov and Bergman (1948); Harris (1960)
$RbF–ThF_4$	Rb_3ThF_7, Rb_2ThF_6, $Rb_7Th_6F_{31}$ $RbTh_3F_{13}$, $RbTh_6F_{25}$	Thoma and Carlton (1961); Dergunov and Bergman (1948)
$CsF–ThF_4$	Cs_3ThF_7, Cs_2ThF_6, $CsThF_5$, $Cs_2Th_3F_{14}$, $CsTh_2F_9$, $CsTh_3F_{13}$, $CsTh_6F_{25}$	Thoma and Carlton (1961); Brunton *et al.* (1965)
$NH_4F–ThF_4$	$(NH_4)_4ThF_8$, $(NH_4)_3ThF_7$, $(NH_4)_2ThF_6$	Ryan *et al.* (1969); Penneman *et al.* (1971, 1976, 1968)
$N_2H_5F–ThF_4$	$(N_2H_5)_3ThF_7$, $(N_2H_5)ThF_5$	Glavic *et al.* (1973); Sahoo and Patnaik (1961)
$NH_3OH–ThF_4$	$(NH_3OH)ThF_4$	Satpathy and Sahoo (1968); Rai and Sahoo (1974)
$TlF–ThF_4$	Tl_3ThF_7, Tl_2ThF_6, $Tl_7Th_6F_{31}$, $TlThF_5$, $TlTh_3F_{13}$, $TlTh_6F_{25}$	Avignant and Cousseins (1970); Keller and Salzer (1967)
$LiCl–ThCl_4$	Li_4ThCl_8	Vdovenko *et al.* (1974)
$NaCl–ThCl_4$	$NaThCl_5$	Vdovenko *et al.* (1974)
$KCl–ThCl_4$	K_3ThCl_7, K_2ThCl_6, $KThCl_5$	Gershanovich and Suglobova (1980)
$RbCl–ThCl_4$	Rb_3ThCl_7, Rb_2ThCl_6, $RbThCl_5$, $RbTh_{1.6}Cl_{5.6}$	Gershanovich and Suglobova (1980)
$CsCl–ThCl_4$	Cs_3ThCl_7, Cs_2ThCl_6, $CsThCl_5$, $CsTh_3Cl_{13}$	Gershanovich and Suglobova (1980)
$BaCl_2–ThCl_4$	Ba_3ThCl_{10}, $Ba_3Th_2Cl_{14}$	Gorbunov *et al.* (1974)
$NaBr–ThBr_4$	$NaThBr_5$	Gershanovich and Suglobova (1981)
$KBr–ThBr_4$	K_2ThBr_6	Gershanovich and Suglobova (1981)
$RbBr–ThBr_4$	Rb_2ThBr_6	Gershanovich and Suglobova (1981)
$CsBr–ThBr_4$	Cs_2ThBr_6	Gershanovich and Suglobova (1981)

careful structure determinations remain scarce. Known crystallographic data are summarized in Table 3.9.

In the system LiF/ThF_4 four compounds are known to exist (Brown, 1968; Cousson *et al.*, 1977; Penneman *et al.*, 1973; Taylor, 1976), namely Li_3ThF_7, $LiThF_5$, $LiTh_2F_9$, and $LiTh_4F_{17}$. A complete structure analysis has been done for only one of these phases, namely Li_3ThF_7 (Cousson *et al.*, 1978;

Table 3.9 *Crystallographic data of polynary thorium halides (in italics: powder data).*

Compound	*Space group*	*Lattice parameters*				*References*
		a (Å)	*b* (Å)	*c* (Å)	*Angles* (°)	
Li_3ThF_7	Ccca	8.788	8.768	12.958		Laligant *et al.* (1989)
Li_3ThF_7	P4/ncc	6.206		12.940		Cousson *et al.* (1978); Laligant *et al.* (1992)
$LiThF_5$	*$I4_1/a$*	*15.10*		*6.60*		Keenan (1966)
$LiTh_2F_9$	*tetragonal*	*11.307*		*6.399*		Harris *et al.* (1959)
α-$(Na_2ThF_6)_{1.333}$	$Fm\bar{3}m$	5.687				Zachariasen (1949a)
β_2-Na_2ThF_6	P321	5.989		3.835		Zachariasen (1948a)
δ-*Na_2ThF_6*	*hexagonal*	*6.14*		*7.36*		Zachariasen (1948b)
$NaTh_2F_9$	$I4\bar{3}m$	8.722				Zachariasen (1948a, 1949b)
Na_4ThF_8	*cubic*	*12.706*				Zachariasen (1948b)
$Na_7Th_6F_{31}$	*$R\bar{3}$*	*14.96*		*9.912*		Keenan (1966)
$Na_3Li_4Th_6F_{31}$	P3c1	9.906		13.282		Brunton and Sears (1969)
$Na_3BeTh_{10}F_{45}$	$P4_2/ncm$	11.803		23.420		Brunton (1973)
$Na_3ZnTh_6F_{29}$	P321	10.166		13.255		Cousson *et al.* (1979b)
Li_2CaThF_8	$I\bar{4}m2$	5.109		11.013		Vedrine *et al.* (1973)
$KNaThF_6$	$P\bar{3}$	6.307		7.891		Brunton (1970)
α-$(K_2ThF_6)_{1.333}$	$Fm\bar{3}m$	5.994				Zachariasen (1948b, 1949a)
β-K_2ThF_6	$P\bar{6}2m$	6.578		3.822		Zachariasen (1948a)
K_5ThF_9	$Cmc2_1$	7.848	10.840	12.785		Ryan and Penneman (1971)
$K_7Th_6F_{31}$	$R\bar{3}$	15.293		10.449		Brunton (1971a)
KTh_6F_{25}	$R\bar{3}m$	8.313		25.262		Brunton (1972)
$RbTh_3F_{13}$	$P2_1ma$	8.649	8.176	7.445		Brunton (1971b)
Rb_3ThF_7	*$Fm\bar{3}m$*	*9.62*				Dergunov and Bergman (1948)
Rb_2ThF_6	*$P\bar{6}2m$*	*6.85*		*3.83*		Harris (1960)
$Rb_7Th_6F_{31}$	*$R\bar{3}$*	*9.58*			$\alpha = 106.9^a$	Brunton *et al.* (1965)
$RbTh_6F_{25}$	*$R\bar{3}m$*	*8.330*		*25.40*		Brunton *et al.* (1965)
Cs_3ThF_7	*$Fm\bar{3}m$*	*10.04*				Brunton *et al.* (1965)
$CsTh_6F_{25}$	*$P6_3/mmc$*	*8.31*		*16.91*		Brunton *et al.* (1965)

Table 3.9 (*Contd.*)

Compound	*Space group*	*Lattice parameters*				*References*
		a (Å)	*b* (Å)	*c* (Å)	*Angles* (°)	
$(NH_4)_4ThF_8$	$P\bar{1}$	8.477	8.364	7.308	$\alpha = 88.38$ $\beta = 96.08$ $\gamma = 106.33$	Ryan *et al.* (1969)
$(NH_4)_3ThF_7$	Pnma	13.944	7.928	7.041		Penneman *et al.* (1971)
$(NH_4)_7Th_2F_{15}\cdot H_2O$	$P2_13$	12.573				Penneman *et al.* (1968)
Tl_3ThF_7	$P2_1/m$	9.793	8.464	10.712	$\beta = 117.20$	Gaumet *et al.* (1995)
$Tl_7Th_6F_{31}$	*$R\bar{3}$*	*15.60*		*10.84*		Avignant and Cousseins (1970)
$TlTh_6F_{25}$	*$P6_3/mmc$*	*8.31*		16.86		Avignant and Cousseins (1970)
$(SmTh_2F_{11})_{1.333}$	Pnma	8.610	4.137	7.225		Abaouz *et al.* (1997)
Zr_2ThF_{12}	I2/m	9.895	10.488	7.856		Taoudi *et al.* (1996)
$CaThF_6$		*6.994*		*7.171*		Keller and Salzer (1967); Salzer (1966)
$SrThF_6$		*7.150*		*7.313*		Keller and Salzer (1967); Salzer (1966)
$BaThF_6$		*7.419*		*7.516*		Keller and Salzer (1967); Salzer (1966)
$CdThF_6$		*6.963*		*7.109*		Keller and Salzer (1967); Salzer (1966)
$PbThF_6$		*7.245*		*7.355*		Keller and Salzer (1967); Salzer (1966)
$EuThF_6$		*7.124*		*7.360*		Keller and Salzer (1967); Salzer (1966)
Cs_2ThCl_6	$P\bar{3}m1$	7.614		6.038		Siegel (1956)
K_2ThCl_6	*Orthorh.*	*8.16*	*14.13*	*8.62*		Gershanovich and Suglobova (1981)
Rb_2ThCl_6	*Orthorh.*	*8.31*	*14.39*	*8.74*		Gershanovich and Suglobova (1981)
In_2ThBr_6	C2/c	8.791	14.670	9.046	$\beta = 91.15$	Dronskowski (1995)
K_2ThBr_6	*trigonal*	*7.52*		*11.80*		Siegel (1956); Gershanovich *et al.* (1981);
	tetragonal	*11.478*		*7.94*		Brunton *et al.* (1965)
Rb_2ThBr_6	trigonal	*7.58*		*12.24*		Gershanovich and Suglobova (1981)

Cs_2ThBr_6	*tetragonal*	*11.37*		*10.69*	Siegel (1956); Gershanovich and Suglobava (1981)
	trigonal	*9.537*		*8.10*	Brunton *et al.* (1965)
$CaThBr_6$	Pmma	9.764	4.109	12.104	Beck and Kühn (1995)
$SrThBr_6$	Pmma	9.878	4.286	12.255	Beck and Kühn (1995)
$BaThBr_6$	Pmma	9.992	4.490	12.526	Beck and Kühn (1995)
$SnThBr_6$	*Pmma*	*9.143*	*4.209*	*12.716*	Beck *et al.* (1993)
$PbThBr_6$	*Pmma*	*9.191*	*4.228*	*12.68*	Beck *et al.* (1993)
$FeTh_6Br_{15}$	Im$\bar{3}$m	11.488			Böttcher *et al.* (1991a)
$CoTh_6Br_{15}$	Im$\bar{3}$m	11.507			Böttcher *et al.* (1991a)
$NaFeTh_6Br_{15}$	Im$\bar{3}$m	11.605			Böttcher *et al.* (1991a)
$Th_6Br_{15}H_7$	Im$\bar{3}$m	11.390			Böttcher *et al.* (1991a)
$Th_6Br_{15}D_7$	Im$\bar{3}$m	11.376			Böttcher *et al.* (1991a)
$Th_6H_7Br_{15}$	Im$\bar{3}$m	11.470			Böttcher *et al.* (1991b)
$Th_6D_7Br_{15}$	Im$\bar{3}$m	11.376			Böttcher *et al.* (1991b)
$Th_6Br_{14}C$	Cmca	15.764	14.160	13.123	Böttcher *et al.* (1991)
$K(Th_{12}N_6Br_{29})$	Pnnm	17.524	11.943	14.031	Braun *et al.* (1995)
ThNI	P4/nmm	4.107		9.242	Juza and Sievers (1968)
β-$PbThI_6$	P$\bar{3}$1c	7.748		13.789	Beck *et al.* (1993)
γ-$PbThI_6$	Cmcm	4.387	13.956	10.005	Beck *et al.* (1993)
β-$SnThI_6$	P$\bar{3}$1c	7.748		13.789	Beck *et al.* (1993)
β-$PbGeI_6$	*P$\bar{3}$1c*	*7.526*		*13.783*	Beck *et al.* (1993)
β-$CaThI_6$	*P$\bar{3}$1c*	*7.697*		*13.959*	Beck *et al.* (1993)
γ-$GeThI_6$	*Cmcm*	*4.248*	*13.92*	*9.991*	Beck *et al.* (1993)
γ-$SnThI_6$	*Cmcm*	*4.376*	*13.937*	*9.995*	Beck *et al.* (1993)
γ-$CaThI_6$	*Cmcm*	*4.278*	*14.02*	*10.10*	Beck *et al.* (1993)
γ-$SrThI_6$	*Cmcm*	*4.455*	*13.991*	*10.052*	Beck *et al.* (1993)
γ-$BaThI_6$	*Cmcm*	*4.685*	*13.76*	*10.015*	Beck *et al.* (1993)
γ-$EuThI_6$	*Cmcm*	*4.420*	*13.964*	*10.038*	Beck *et al.* (1993)

[a] rhombohedral setting.

Laligant *et al.*, 1989; Pulcinelli and de Almeida Santos, 1989). It is dimorphic but the linkage of the monocapped square antiprisms [ThF_9] is the same in the two modifications. They are connected via two common edges to layers according to the formulation $^{2}_{\infty}[ThF^{e}_{4/2}F^{t}_{5/1}]$ (e = edge, t = terminal). The layers are stacked along the *c*-axis. The different symmetry of the two modifications arises from the different positions of the Li^+ ions in the interlayer spacings, and their positions are temperature-dependent, making the compound a good ionic conductor (Laligant *et al.*, 1992). According to powder diffraction measurements, $LiThF_5$ is isotypic with $LiUF_5$ and contains a three-dimensional network of vertex-connected monocapped square antiprisms [ThF_9] that incorporate the Li^+ in a six-fold coordination (Keenan, 1966). The lattice parameter of the other two fluorides have been obtained by powder XRD (Harris *et al.*, 1959; Cousson *et al.*, 1978).

The system NaF/ThF_4 shows the formation of seven compounds (Table 3.8) (Rosenheim *et al.*, 1903; Dergunov and Bergman, 1948; Brunton *et al.*, 1965; Kaplan, 1956; Ryan and Penneman, 1971; Thoma, 1972). Na_2ThF_6 may either be cubic (α-Na_2ThF_6) or trigonal (β_2-Na_2ThF_6) (Table 3.9). The cubic modification is a variant of the CaF_2-type of structure with Na^+ and Th^{4+} occupying Ca^{2+} sites in a disordered fashion (Zachariasen, 1949b). The trigonal structure of Na_2ThF_6 is very similar to the structure of LaF_3 and contains both the Na^+ and the Th^{4+} ions in tricapped trigonal prismatic coordination of fluoride anions (Zachariasen, 1948b). The polyhedra are connected via triangular faces in the [001] direction and via common edges in the (001) plane. A third modification, δ-Na_2ThF_6, has been reported to be also trigonal but has not been proved yet (Zachariasen, 1948c; Penneman *et al.*, 1973). In $NaTh_2F_9$ the Th^{4+} are nine-fold coordinated by F^- ions. The polyhedra are connected via vertices according to $^{3}_{\infty}[ThF_{9/2}]^{-0.5}$ to a three-dimensional network with the Na^+ ions incorporated for charge compensation (Zachariasen, 1948b, 1949a). In the complex structure of $Na_7Th_6F_{31}$ nine- and ten-fold coordinated Th^{4+} ions are present (Keenan, 1966; Penneman *et al.*, 1973).

An X-ray structure analysis is available for all of the six compounds that exist in the KF/ThF_4 system (Kaplan, 1956), except for $KThF_5$ (Table 3.9). α_1-K_2ThF_6 is isotypic with the respective sodium compound, while a slight difference is found between β_1-K_2ThF_6 and β_1-Na_2ThF_6 (Zachariasen, 1948c; Ryan and Penneman, 1971). The Th/F sublattice is the same in the two compounds, however, in the former the K^+ ions are located in tricapped trigonal prismatic voids, in the latter, Na^+ occupies octahedral sites. The complex fluoride $K_7Th_6F_{31}$ (Zachariasen, 1948c; Brunton, 1971a) shows isotypism to the sodium compound. K_5ThF_9, which has also been prepared from aqueous media (Wells and Willis, 1901), consists of monomeric distorted square antiprismatic $[ThF_8]^{4-}$ anions that are connected via K^+ ions (Ryan and Penneman, 1971). Furthermore there are isolated F^- ions in the structure that are not bonded to Th^{4+}. The structure of KTh_6F_{25} is a polymorph of the CsU_6F_{25}-type with the Th^{4+} ions in nine-fold coordination by fluoride ions (Brunton, 1972).

The tricapped trigonal prismatic polyhedra are linked via shared edges and vertices. The resulting three-dimensional network incorporates the K^+ ions in voids. Finally, a mixed sodium potassium fluoride is known: $NaKThF_6$ (Brunton, 1970).

Among the compounds found in the RbF/ThF_4 system (Dergunov and Bergman, 1948; Thoma and Carlton, 1961), Rb_2ThF_6, $Rb_7Th_6F_{31}$ and $RbTh_6F_{25}$ are isotypic to their respective potassium fluorides (Harris, 1960; Penneman *et al.*, 1973). Rb_3ThF_7 has the same cubic structure as K_3UF_7 and shows a highly disordered fluoride sublattice (Dergunov and Bergman, 1948).

The same is true for Cs_3ThF_7, which is one of the seven phases that are known to exist in the CsF/ThF_4 system (Thoma and Carlton, 1961; Penneman *et al.*, 1973). Unfortunately, lattice parameters are only available for one additional compound, $CsTh_6F_{25}$. It is isotypic to CsU_6F_{25} and can be seen as a polymorph of the KTh_6F_{25}-type wherein the Th^{4+} ions are in nine-fold and the Cs^+ ions in 12-fold coordination by fluoride ions (Brunton, 1971b; Penneman *et al.*, 1973).

Although the size of the ammonium ion is comparable to the radii of K^+ and Rb^+, the NH_4F/ThF_4 system contains only a few phases, namely $(NH_4)_2ThF_6$, $(NH_4)_3ThF_7$, and $(NH_4)_4ThF_8$ (Ryan *et al.*, 1969; Penneman *et al.*, 1971). The latter two have been structurally characterized. $(NH_4)_3ThF_7$ is not isotypic with the respective potassium or cesium compounds but crystallizes with orthorhombic symmetry (Penneman *et al.*, 1971). It contains chains of edge-sharing $[ThF_9]$ polyhedra with the formulation ${}^1_\infty[ThF_{4/2}F_{5/1}]$ that are separated by the NH_4^+ ions. Similar chains are found in the unique crystal structure of $(NH_4)_4ThF_8$. This latter compound contains, however, an additional fluoride ion that is not coordinated to any Th^{4+} so that it should be formulated as $(NH_4)_4[ThF_7]F$ (Ryan *et al.*, 1969).

As far as structural data are known, the compounds found in the TlF/ThF_4 system show a close relationship to the respective fluorides of the larger alkali metal ions (Avignant and Cousseins, 1970). Slight deviations may be observed as can be seen from the structure of Tl_3ThF_7 and are usually attributed to the stereochemical activity of the lone electron pair on Tl^+ (Gaumet *et al.*, 1995).

Several other systems with ThF_4 have been investigated with unusual components like N_2H_5F or even NH_3OH (Table 3.8) (Sahoo and Patnaik, 1961; Satpathy and Sahoo, 1968; Glavic *et al.*, 1973; Rai and Sahoo, 1974). Single crystal structures are not known in these cases. In addition, compounds with higher valent ions have been investigated. With divalent cations, a number of compounds are known that have essentially the LaF_3 structure type, wherein the La^{3+} positions are filled by Th^{4+} and the divalent cation, respectively (Zachariasen, 1949a; Keller and Salzer, 1967; Brunton, 1973). Anion-rich fluorides can be obtained when a small amount of Th^{4+} is doped in the CaF_2 lattice and complicated phases with severe disorder in the cation and anion lattice are described for lanthanide-containing compounds like $SmTh_2F_{11}$ (Abaouz *et al.*, 1997). Finally, the zirconium thorium fluoride $ThZr_2F_{12}$ is completely ordered and contains layers of vertex-shared $[ZrF_8]$ polyhedra that alternate with layers of Th^{4+} ions in nine-fold coordination by F^- ions (Taoudi *et al.*, 1996).

A few hydrates of ternary thorium fluorides are known. Probably the most remarkable hydrate has the composition $(NH_4)_7Th_2F_{15} \cdot H_2O$ (Penneman *et al.*, 1968, 1976) and contains the dimeric anion $[Th_2F_{15}(H_2O)]^{7-}$ in which the Th^{4+} ions are linked via three fluoride ions. Furthermore the lanthanide-containing phases $LaTh_4F_{19} \cdot H_2O$ and $ThEr_2F_{10} \cdot H_2O$ have been reported in which the lanthanide and the Th^{4+} ions occupy the same sites (Guery *et al.*, 1994; Le Berre *et al.*, 2000). Finally, the fluoride hydroxide $Li_3Th_5F_{22}OH$ should be mentioned, which incorporates the Li^+ ions in a three-dimensional network of $[ThF_9]$ and $[ThF_8OH]$ polyhedra (Cousson *et al.*, 1979a).

Polynary thorium fluorides with more than one additional cation have been rarely characterized (Table 3.9). Structural data are available for $Na_3Li_4Th_6F_{31}$ (Brunton and Sears, 1969), $KNaThF_6$ (Brunton, 1970), Li_2CaThF_8 (Vedrine *et al.*, 1973), $Na_3BeTh_{10}F_{45}$ (Brunton, 1973), and $Na_3ZnTh_6F_{29}$ (Cousson *et al.*, 1979b). $Na_3Li_4Th_6F_{31}$ has the same structure as $Na_7Th_6F_{31}$, with some of the Na^+ ions being substituted by Li^+. Similarly, the structure of $KNaThF_6$ is closely related to the structure of the potassium-only compound. Li_2CaThF_8 adopts the structure of $CaWO_4$, even if the symmetry is slightly different. The Li^+ ions occupy the tetrahedral positions of the tungsten atoms, while both Ca^{2+} and Th^{4+} are found on the calcium sites of $CaWO_4$. $Na_3BeTh_{10}F_{45}$ and $Na_3ZnTh_6F_{29}$ (Fig. 3.11) have crystal structures wherein the Th^{4+} ions are found mainly in an eight-fold coordination of fluoride ions (Brunton, 1973). The thorium polyhedra are linked in complicated three-dimensional networks

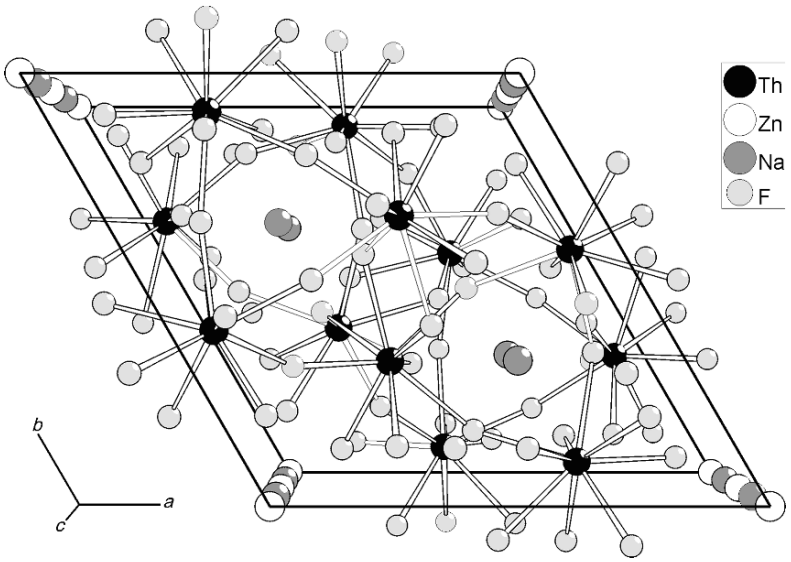

Fig. 3.11 *Crystal structure of the polynary $Na_3ZnTh_6F_{29}$.*

that incorporate the Na^+, Be^{2+}, and Zn^{2+} ions, respectively. The coordination number of the sodium ions range from six to eight. Be^{2+} is tetrahedrally coordinated, and Zn^{2+} is in the center of an octahedron.

Mixed chloride–fluorides, namely $LiThClF_4$, $CsTh_2ClF_8$, $SrThCl_2F_4$, and $BaThCl_2F_8$, have been reported but these compounds are in need of further characterization (Gudaitis *et al.*, 1972; Desyatnik *et al.*, 1974a,b).

Compared to the respective fluorides the number of well-characterized polynary thorium chlorides, bromides, or iodides is quite limited. According to phase diagram investigations containing $ThCl_4$, the compounds included in Table 3.8 are known to exist (Vdovenko *et al.*, 1974; Gershanovich and Suglobova, 1980). However, additional chlorides, which were not found in their respective phase diagrams, have been prepared by several authors (Rosenheim and Schilling, 1900; Rosenheim *et al.*, 1903; Chauvenet, 1911; Siegel, 1956; Ferraro, 1957; Adams *et al.*, 1963; Brown, 1966; Vokhmyakov *et al.*, 1973; Gorbunov *et al.*, 1974; Desyatnik and Emel'yanov, 1975). Unfortunately, the structure of only a few chlorides is known, all of them being exclusively hexachlorothorates containing the octahedral $[ThCl_6]^{2-}$ anion. Alkaline metal ions, Tl^+ and Cu^+, as well as divalent ions, for example Ba^{2+} or Pb^{2+}, may serve as counter-ions (Binnewies and Schäfer, 1973, 1974; Gorbunov *et al.*, 1974; Westland and Tarafder, 1983). Furthermore, alkyl ammonium ions can be used to crystallize the hexachlorothorate (Brown, 1966; Woodward and Ware, 1968). Occasionally, complex $[ThCl_5]^-$ and $[ThCl_7]^{3-}$ ions have been mentioned in the literature (Oyamada and Yoshida, 1975; Yoshida *et al.*, 1978). The enthalpies of formation of several thorium–alkali metal ternary chlorides have been reported. Experimental data on these chlorides, together with those on other actinide ternary halides are assembled and briefly discussed in Chapter 19.

Chloro compounds of thorium in which one or more chloride ions in $ThCl_4$ are replaced by other ligands have been prepared. These ligands can be trimethysilylamide, benzaldehyde, and methylsalicylate, for example (Bradley *et al.*, 1974).

The phase diagrams of $ThBr_4$ and the alkali metal bromides NaBr–CsBr show one compound to exist in each case (Ribas Bernat and Ramos Alonso, 1976; Ribas Bernat *et al.*, 1977; Gershanovich and Suglobova, 1981). For sodium, $NaThBr_5$ melts incongruently, and for the remaining alkali metals, the bromides A_2ThBr_6 (A = K – Cs) melt congruently. The structure of the equivalent sodium compound is not known, but for the compounds with heavier alkali metals, the lattice parameters have been derived from powder diffraction data. Although the data are not in entire agreement, it seems very likely that these compounds are (nearly) isotypic with the respective iodides and thus contain the octahedral $[ThBr_6]^{2-}$ anion. The same anion also occurs in the family of bromides, $AThBr_6$, with A being a divalent cation (cf. Table 3.9) (Beck and Kühn, 1995). An interesting exception is the unique crystal structure of In_2ThBr_6. It contains square antiprismatic $[ThBr_8]$ polyhedra that are linked in

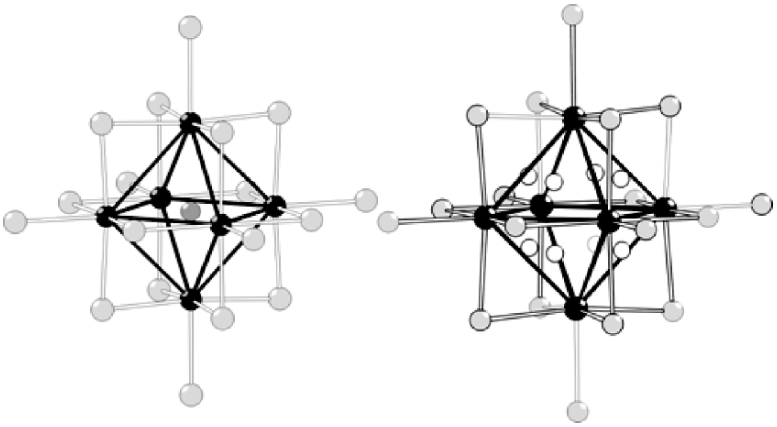

Fig. 3.12 *Octahedral* [Th_6] *cluster in the crystal structures of* $Th_6Br_{15}Co$ *and* $Th_6Br_{14}H_7$, *respectively. The cobalt atom as well as the hydrogen atoms are stabilizing the cluster, which are surrounded by* 18 Br^- ions. *The hydrogen position are only occupied to* 7/8.

chains along [001] according to the formula $^1_\infty[ThBrF_{4/2}Br_{4/1}]$ via shared edges. The chains are held together by nine-fold coordinated In^+ ions (Dronskowski, 1995).

A series of reduced thorium bromides containing octahedral [Th_6] clusters has been described recently. They have been prepared from $ThBr_4$ and thorium metal in the presence of either hydrogen, carbon, or a transition metal, leading to the compounds: MTh_6Br_{15} (M = Mn, Fe, Co, Ni), $Th_6Br_{14}C$, and $Th_6Br_{15}H_7$ (Böttcher *et al.*, 1991a,b). The transition metal and the carbon atom act as a stabilizing interstitial atom within the octahedron whereas the hydrogen atoms are located above the triangular faces of the empty octahedra. In each case, the [Th_6] core is surrounded by 12 Br^- ions that are bridging the edges of the octahedron, and six additional anions attached to the vertices. The linkage of the $[(Th_6Br_{12})Br_6]$ units is different in $Th_6Br_{14}C$ compared to the metal-centered cubic phases, causing the slightly higher Th/Br ratio (Fig. 3.12). Another unique cluster compound is $KTh_{12}N_6Br_{29}$. It shows a core of six [NTh_4] tetrahedra that are connected by sharing edges (Fig. 3.13) (Braun *et al.*, 1995).

Ternary iodides containing the octahedral $[ThI_6]^{2-}$ anion have been prepared with a number of different counter-cations, for example alkali metal ions, tetraalkyl ammonium ions, or $[As(C_6H_5)_4]^+$ (Bagnall *et al.*, 1965; Brown *et al.*, 1970a, 1976; Brendel *et al.*, 1985). The ThI_4/AI_2 systems with A being Ca, Sr, Sn, or Pb, have been investigated and for selected examples crystal structures have even been determined (Beck *et al.*, 1993). Ternary iodides have also been synthesized by the fusion of the binary iodides at elevated temperature with other divalent cations (Beck *et al.*, 1993). Finally, the mercury iodides $Hg_2ThI_8 \cdot 12H_2O$ and $Hg_5ThI_{14} \cdot 18H_2O$ have been reported (Duboin, 1909a).

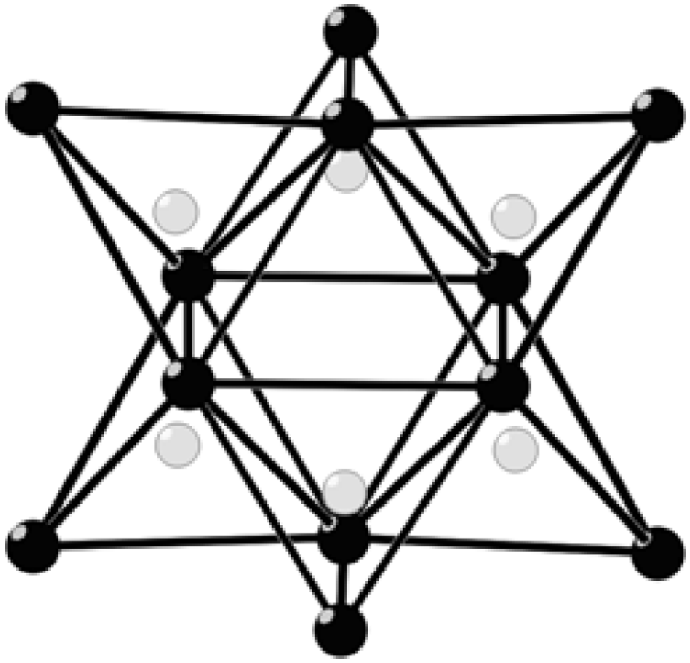

Fig. 3.13 $[Th_{12}N_6]$ *core in the crystal structure of* $KTh_{12}N_6Br_{29}$. The unit consists of six linked $[NTh_4]$ *tetrahedra. It might also be seen as an* $[Th_6]$ *octahedron whith four of the six triangular faces capped by an additional thorium atom.*

3.7.5 Chalcogenides

The heavier analogs of oxides, the chalcogenides S, Se, and Te, all form compounds with thorium (Table 3.6). While some are based on simple crystal structures such as fluorite or NaCl, the richness of the electronic structures of sulfur, selenium, and tellurium lend themselves to forming more complex structures than the oxides. Binary thorium sulfur compounds can be prepared by the action of H_2S on the metal (Berzelius, 1829; Nilson, 1876; Moissan and Étard, 1896, 1897), the metal halide (Krüss and Volck, 1894; Duboin, 1908b), the metal hydride (Eastman *et al*., 1950; Lipkind and Newton, 1952), or on thoria itself in the presence of carbon (Eastman *et al*., 1950). Sulfur will react at elevated temperatures with the metal or thorium carbide and CS_2 with thoria will also form the binary sulfides. There are six generally recognized structurally characterized sulfides (including ThOS, which is not isostructural with ThS_2 or ThO_2) listed in Table 3.6 (Shalek, 1963). The sulfide with the lowest sulfur content (Khan and Peterson, 1976), ThS, stands out against ThO as not being like ZnS but rather forming the NaCl structure type (Zachariasen, 1949c). However, as mentioned earlier, the characterization of ThO remains a puzzle. ThS is metallic in appearance with a density of 9.56 g cm^{-3}. The compound

sinters above 1950°C with no appreciable vapor pressure above its melting point (2200°C). The compound can be machined or polished and becomes superconducting near 0.5 K (Moodenbaugh *et al.*, 1978). The disulfide of thorium, ThS_2, is a purple-brown solid with the $PbCl_2$ structure and a density of 7.36 g cm^{-3}. It is reported to melt at 1905°C with considerable decomposition starting at 1500°C (Eastman *et al.*, 1950, 1951). Heating the disulfide in vacuum will yield a black phase, Th_7S_{12}, which melts around 1770°C (Zachariasen, 1949d; Eastman *et al.*, 1950, 1951). This compound has been mislabeled as Th_4S_7. The sesquisulfide is a brown-metallic phase, isotypic with stibnite, Sb_2S_3 (Zachariasen, 1949c). This phase also melts with no appreciable vapor pressure at high temperatures (2000°C), making it a useful high-temperature crucible material. An orange-brown material has been prepared via a lower-temperature reaction (400°C) between thorium metal and sulfur or between the hydride and excess H_2S. A 'polysulfide' phase was first identified as Th_3S_7 (Strotzer and Zumbusch, 1941) and later found (Graham and McTaggart, 1960) to evolve sulfur around 150°C to yield Th_2S_5, of tetragonal structure, although more recent studies found that it is correctly reported in the orthorhombic cell (Noël and Potel, 1982). ThOS, a yellow phase prepared from the action of thoria and CS_2 or thoria and sulfur (Krüss, 1894; Heindl and Loriers, 1974), forms in the PbFCl structure type, analogous with the rare earth series of compounds (Zachariasen, 1949c). ThOS hydrolyzes in acid solutions as do all the other binary sulfides of thorium (Dubrovskaya, 1971).

Selenium and tellurium form a series of compounds with thorium that are homologs of the sulfides. These compounds, listed in Table 3.6, are ThOSe, ThSe, Th_7Se_{12}, Th_2Se_3, $ThSe_2$, Th_2Se_5, and $ThSe_3$ (D'Eye *et al.*, 1952; D'Eye, 1953; Graham and McTaggart, 1960; Noël, 1980; Kohlmann and Beck, 1999). These phases have all been obtained by the reaction of selenium on thorium metal (D'Eye *et al.*, 1952) on the carbide, the halide, or the silicide of thorium (Moissan and Martinsen, 1905). Thorium selenides have also been produced by the reaction of hydrogen selenide gas on thorium bromide (Moissan and Martinsen, 1905). It has been reported that ThSe becomes superconducting at 1.6 K (Moodenbaugh, 1978), in contrast to earlier observations (Bucher and Staundenmann, 1968). A selenium analog to the polysulfide phase may be Th_7Se_{12} (D'Eye, 1953) or Th_2Se_5 (Graham and McTaggart, 1960). Another reported polyselenide is $ThSe_3$ (Noël and Potel, 1982), which is isotypic with USe_3 (Ben Salem *et al.*, 1984). Finally, the reaction of selenium with thoria yields ThOSe (D'Eye, 1953).

The tellurides of thorium exist in phases of similar stoichiometry but with slightly differing structures from those of the sulfides or selenides. For example, ThTe is found in the CsCl structure rather than the NaCl-type (D'Eye and Sellman, 1954). Several conflicting reports exist about the identity of a higher telluride, Th_3Te_8, although it has been confirmed to be $ThTe_3$, in a structure type analogous to the low-dimensional $ZrSe_3$-type (Graham and McTaggart, 1960). This same report also suggests that $ThTe_2$ is hexagonal rather than

orthorhombic as in the $PbCl_2$-type found for $ThSe_2$. Recently, the missing link in the series, Th_7Te_{12}, was prepared and characterized as isostructural with the selenide (Tougait *et al.*, 1998). An early report on 'Th_3Te' has not been confirmed up to now and seems to be not very reliable (Montignie, 1947).

During the past decade, a series of interesting ternary and quaternary thorium chalcogenide phases have been prepared (Cody and Ibers, 1996; Wu *et al.*, 1997; Tougait *et al.*, 1998; Narducci and Ibers, 1998a,b, 2000; Choi *et al.*, 1998; Briggs-Piccoli *et al.*, 2000, 2001, 2002; Hess *et al.*, 2001). The series of layered tellurides and selenides of thorium, ATh_2Te_6, are based on the sesquiselenide or telluride structure type that has been, in effect, pried apart, reduced, and intercalated by an alkali metal (Cody and Ibers, 1996; Wu *et al.*, 1997; Tougait *et al.*, 1998). The review by Narducci and Ibers describes these reactions in detail (1998a). Indeed, a series of related transition metal compounds such as $KCuThSe_3$, $CuTh_2Te_6$, and $SrTh_2Se_5$ have been prepared from the action of tellurium or selenium, or their alkali metal salts, on thorium metal (Narducci and Ibers, 1998a, 2000).

Attempts were also made to prepare chalcophosphate analogs of the thorium phosphates discussed in Section 3.7.7e. The unique chemistry of thiophosphates and selenophosphates provided a rich set of compounds from homoleptic clusters of $[Th_2(PS_4)_6]^{10-}$ (Briggs-Piccoli *et al.*, 2002) to complex three-dimensional phases with a unique $(P_2Se_9)^{6-}$ anion building block in $Cs_4Th_4P_4Se_{26}$ (Briggs-Piccoli *et al.*, 2001).

3.7.6 Pnictides

The nitride of thorium, Th_3N_4, can be prepared by a variety of methods (Gmelin, 1987). One is the strong heating of the metal in the presence of N_2. At the turn of the last century, there was significant debate about the composition and color (chestnut, citron yellow, maroon, and black) of the thorium nitride that could be obtained by heating the metal in presence of N_2 (Matignon and Delepine, 1907; Düsing and Hüniger, 1931). The debate lingered into the 1960s and the variations in color have been attributed to vacancies in nitrogen and oxygen impurities. Indeed, the tan-colored Th_2N_3 is actually Th_2N_2O (Aronson and Auskern, 1966; Benz and Zachariasen, 1966). The golden yellow ThN (Chiotti, 1952; Olson and Mulford, 1965) may likely be seen as a thin layer on the surface of Th_3N_4 as it is the thermally stable product of all decomposition reactions of the other thorium nitrides (Aronson and Auskern, 1966). ThN displays metallic character when prepared as a thin film (Gouder *et al.*, 2002). The ThN phase is isotypic with all other actinide mononitrides and has the NaCl fcc structure (Auskern and Aronson, 1967; Benz *et al.*, 1967). ThN is a superconductor at low temperatures with an inverse dependence of pressure on the critical temperature (Dietrich, 1974).

The synthesis of the binary nitrides listed in Table 3.10 can be achieved most easily by the action of ammonia or nitrogen on heated thorium hydride

Table 3.10 *Crystallographic data of thorium pnictides.*

Compound	*Lattice symmetry*	*Lattice parameters*				*References*
		a (Å)	*b* (Å)	*c* (Å)	*Angles* (°)	
ThN	cubic	5.180				Evans and Raynor (1959)
Th_3N_4	rhombohedral	3.87		27.38		Bowman and Arnold (1971)
Th_2N_3	rhombohedral	3.883		6.187		Zachariasen (1949a)
ThP	cubic	5.840				Gingerich and Wilson (1965)
Th_3P_4	cubic	8.600				Meisel (1939); Zumbusch (1941)
Th_2P_{11}	monoclinic	17.384	10.104	19.193	$\beta = 117.62$	von Schnering *et al.* (1980)
ThP_7	orthorhombic	10.218	10.401	5.671		von Schnering and Vu (1986)
ThAs	cubic	5.978				Ferro (1955)
Th_3As_4	cubic	8.843				Ferro (1955)
$ThAs_2$	tetragonal	4.086		8.575		Ferro (1955); Pearson (1985)
ThSb	cubic	6.318				Ferro (1956)
Th_3Sb_4	cubic	9.371				Ferro (1956)
$ThSb_2$	tetragonal	4.352		9.172		Ferro (1956)
$ThBi_2$	tetragonal	4.492		9.298		Pearson (1985)

(Katzin, 1983). Metal powder heated in nitrogen will yield the nitrides; in the presence of ammonia, a hydride intermediate can be formed (Juza and Gerke, 1968). These hydrogen-containing species might be nitride-imides, nitride-amides, or pure amides of thorium, as investigations of the system Th–N–H have shown. Thoria treated with carbon and heated in a nitrogen atmosphere will also yield nitrides where a finely divided metal powder can be seen as an intermediate.

The reaction of binary nitrides with thorium halides leads to the halide nitrides ThNX (X = F, Cl, Br, I). They have been shown to adopt the BiOCl-type of structure (Juza and Sievers, 1968; Blunck and Juza, 1974). Complex metal nitrides such as Th_2NOP can be prepared by heating binary nitrides with thoria and thorium phosphides (Benz and Zachariasen, 1969; Barker and Alexander, 1974). Heating the nitrides in oxygen generally yields thoria as the product and the nitrides are moisture-sensitive. Several complex mixtures of double salts have been prepared recently, namely $Ca_xTh_{3-x}N_{4-2x}O_{2x}$, $Sr_xTh_{3-x}N_{4-2x}O_{2x}$, and $Sr_xTh_{1-x}N_xO_{1-x}$ (Brese and DiSalvo, 1995a). Ternary nitrides are the lithium compound Li_2ThN_2 (Palisaar and Juza, 1971) as well as the very unique nitride perovskite phase, $TaThN_3$ (Brese and DiSalvo, 1995b).

This latter cubic perovskite was prepared by the action of Ta_3N_5 and Th_3N_4 at 1400°C as well as by the reaction of $Ta_2Th_2O_9$ and Ca_3N_2 at 1500°C.

The heavier pnictide analogs all form similar binary phases to the nitride that have been characterized by single crystal XRD analysis except for ThBi that is conspicuously absent (Ferro, 1957). Analogously to ThN, ThP, ThAs, and ThSb adopt the fcc NaCl structure (Ferro, 1955, 1956; Gingerich and Wilson, 1965; Javorsky and Benz, 1967; Baskin, 1969). The same structure has been reported for all of the actinide and lanthanide mononitrides and pnictides, respectively. Interestingly, the lattice constant has been shown to decrease when going from Th to U, then to increase through Cm, and finally to decrease again (Lam *et al.*, 1974; Damien and de Novion, 1981) (Fig. 3.14).

Adachi and Imoto reported that the cubic ThP could be made as ThP_{1-x} where x varied from 0 to 0.6. This behavior dramatically affected the hardness of the phase as well as its conductivity (Adachi and Imoto, 1968). Indeed, at 1200°C, the phase ranges from $ThP_{0.4}$ to $ThP_{0.6}$. The non-stoichiometric phases show a weak paramagnetism and the room temperature resistivity of the metallic ThP decreased with an increasing P/Th ratio for the ThP_{1-x} phases. ThP forms a solid solution with UP and displays an antiferromagnetic phase transition at 23 K with up to 40% ThP (Adachi *et al.*, 1973). ThP undergoes a

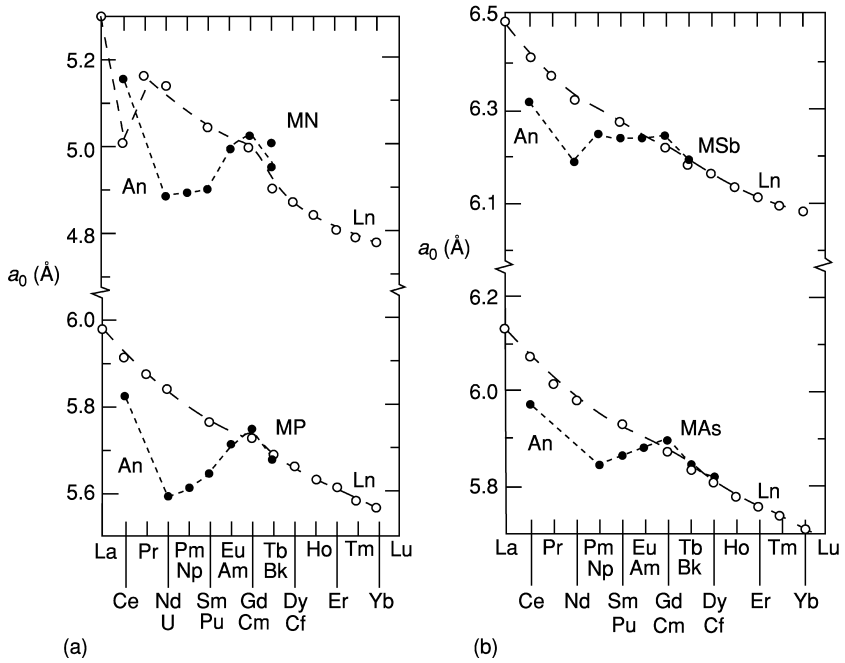

Fig. 3.14 *Lattice constants of actinide and lanthanide monopnicnitides: mononitrides and monophosphides* (*a*)*; monoantimonides and monoarsenides* (*b*) (*Damien and de Novion*, 1981).

structural phase transition from the NaCl-type to the CsCl-type at 30 GPa (Staun Olsen *et al.*, 1988). The reaction between Th and Th_3P_4 at 1100°C will yield ThP (Gingerich and Wilson, 1965; Gingerich and Aronson, 1966; Javorsky and Benz, 1967). Th_3P_4 can be made by the direct combination of the elements (Gingerich and Wilson, 1965; Price and Warren, 1965), by heating $ThCl_4$ with phosphorus vapors (Moissan and Martinsen, 1905), and by the reaction of the hydride with phosphine gas (Lipkind and Newton, 1952). This phase of phosphide is a dark gray material, unlike the black ThP, and is unreactive in water. It releases phosphine upon action by acids and can be ignited to thorium phosphate by heating in air (Strotzer *et al.*, 1938; Meisel, 1939). Th_3P_4 is an n-type semiconductor with a band gap of 0.4 eV (Henkie *et al.*, 1976; Suzuki *et al.*, 1982). A very unique, phosphorus-rich Zintl phase was prepared by the action of phosphorus on thorium metal at 1040°C, yielding Th_2P_{11} (von Schnering *et al.*, 1980). This phase comprises chains of phosphorus atoms linked into two-dimensional nets comprising open and closed P_6 rings. This black, semiconducting phase (band gap of 0.3 eV) decomposes to Th_3P_4 upon heating to 1040°C in vacuum. Other complex ternary phosphides are known including $Th_5Fe_{19}P_{12}$, $ThFe_4P_2$, and $Th_2Mn_{12}P_7$ (Albering and Jeitschko, 1992; Jeitschko *et al.*, 1993). Finally, a dense, magnetoresistive skutterudite phase can be prepared from the elements to yield $ThFe_4P_{12}$ (Dordevic *et al.*, 1999).

In the thorium–arsenic system, ThAs and Th_3As_4 are black-gray compounds that are isomorphous with the associated phosphides and nitrides (Benz, 1968). Th_3As_4 is an n-type semiconductor with a band gap of 0.43 eV (Ferro, 1955; Warren and Price, 1964; Henkie and Markowski, 1978). In contrast to the Th–P system, a diarsenide, $ThAs_2$, is formed, which displays two modifications: a low-temperature phase (α), with the PbCl structure and a high-temperature phase (β) with the Fe_2As structure (Ferro, 1955; Hulliger, 1966). More complex mixtures of ThAs and ThS or ThSe have yielded compounds such as ThAsSe that display unique anomalous Kondo-like behavior (Henkie and Wawryk, 2002). Thorium antimony compounds form in the same structures as the arsenides, with ThSb, Th_3Sb_4, and $ThSb_2$ (Ferro, 1956; Hulliger, 1966, Chiotti *et al.*, 1981). Like the arsenide, ThSb undergoes a high-pressure phase transition from NaCl to the CsCl-type (Palanivel *et al.*, 1995). Kondo-like resistivity behavior was observed for solid solutions of USb and ThSb. The dilution of USb by ThSb lead to large modifications of the electrical transport properties, reflecting the change from antiferromagnetism to ferromagnetism with a concomitant decrease of the ordered magnetic moment per U atom (Frick *et al.*, 1982). In the thorium–bismuth system, three binary compounds with familiar structures are found: ThBi, $ThBi_2$, and Th_3Bi_4 (Ferro, 1957; Dahlke *et al.*, 1969). ThBi was reported as part of an alloy structure although a single crystal structure has not been determined (Borzone *et al.*, 1982). Another phase with the Mn_5Si_3-type was observed as well but was not confirmed by elemental analysis (Borzone *et al.*, 1982). Bismuth can be distilled from ThBi, yielding the thorium-rich Th_5Bi_3 hexagonal structure. During the U.S. breeder reactor

program of the mid–1950s, breeder-blanket liquid Bi with a slurry of $ThBi_2$ suspended in the liquid bismuth showed promise but there was significant difficulty in suspending the inhomogeneous particles of $ThBi_2$ (Bryner and Brodsky, 1959).

3.7.7 Complex anions

Thorium compounds with complex anions play an important role in various fields, for example in separation techniques (cf. Section 3.4) and nuclear waste disposal, to name only two of them. Thus, this chemistry has been widely investigated, although often not in very detail, what is especially true with respect to structural characterizations. In the following the most important and more recent findings are summarized. For each complex anion an extra subdivision has been created and reliable crystallograhic data are presented in Table 3.11.

(a) Perchlorates

Thorium perchlorate is highly soluble in water and crystallizes, generally from acidic solution, in the form of the tetrahydrate $Th(ClO_4)_4{\cdot}4H_2O$ (Murthy and Patel, 1965). The structure of the tetrahydrate is not known, but the compound has been shown to decompose at 280°C to form $ThO(ClO_4)_2$ that finally forms ThO_2 at 335°C (Murthy and Patel, 1965). The oxide–perchlorate apparently will dissolve in water, and from XRD this is interpreted to be due to the formation of a tetrameric species (Bacon and Brown, 1969). An elegant (but somewhat dangerous) route to prepare anhydrous $Th(ClO_4)_4$ is the reaction of $ThCl_4$ with Cl_2O_6 (Koulkès-Pujo *et al.*, 1982). From X-ray powder diffraction, an orthorhombic lattice has been deduced with the space group probably being $P2_12_12$ (Ramamurthy and Patel, 1963). Due to the weak coordination tendency of the ClO_4^- ion, $Th(ClO_4)_4$ is frequently used to prepare coordination compounds of thorium in which the perchlorate anion in not included in the coordination sphere (Gmelin, 1985b, 1993a).

(b) Sulfates (VI, IV)

A detailed discussion of the older literature on thorium sulfates has been given by Mellor (1941). Thorium sulfates can be prepared by the reaction of various thorium salts, for example thorium nitrate, with concentrated sulfuric acid. Upon crystallization from aqueous solution, different hydrates can be obtained. At lower temperatures (0–45°C), $Th(SO_4)_2{\cdot}9H_2O$ has the lowest solubility (Clève, 1874; Roozeboom, 1890; Dawson and Williams, 1899). Nevertheless, the octahydrate is usually obtained even under these conditions (Clève, 1874; Krüss and Nilson, 1887b; Roozeboom, 1890; Koppel and Holtkamp, 1910). Furthermore, a hexahydrate has been mentioned and at higher temperature,

Table 3.11 *Crystallographic data of thorium compounds with oxo anions.*

Compound	*Space group*	*Lattice parameters*				*References*
		a (Å)	*b* (Å)	*c* (Å)	*Angles* (°)	
$Th(SO_4)_2{\cdot}8H_2O$	$P2_1/n$	8.51	11.86	13.46	$\beta = 92.65$	Habash and Smith (1983)
$Th(OH)_2SO_4$	Pnma	11.733	6.040	7.059		Lundgren (1950)
$K_4Th(SO_4)_4{\cdot}2H_2O$	$C\bar{1}$	10.096	16.75	9.762	$\alpha = 95.15$ $\beta = 95.22$ $\gamma = 91.00$	Arutyunyan *et al.* (1963)
$Na_2Th(SO_4)_3{\cdot}6H_2O$	$P2_1/c$	5.567	16.81	15.76	$\beta = 91.925$	Habash and Smith (1990)
$Cs_2Th(SO_4)_3{\cdot}2H_2O$	$P2_1/c$	6.415	15.95	13.078	$\beta = 90.88$	Habash and Smith (1992)
$Th(NO_3)_4{\cdot}5H_2O$	Fdd2	11.191	22.89	10.579		Taylor *et al.* (1966)
$Th(NO_3)_4{\cdot}4H_2O$	$P2_1/n$	7.438	17.530	9.183	$\beta = 99.72$	Charpin *et al.* (1987)
$ThOH(NO_3)_3{\cdot}4H_2O$	$P2_1/c$	6.772	11.693	13.769	$\beta = 102.63$	Johansson (1968a)
$(NH_4)_2Th(NO_3)_6$	$P2_1/n$	8.321	6.890	13.097	$\beta = 91.55$	Spirlet *et al.* (1992)
$MgTh(NO_3)_6{\cdot}8H_2O$	$P2_1/c$	9.080	8.750	13.610	$\beta = 97.03$	Scavnicar and Prodic (1965)
$(C(NH_2)_3)_6Th(CO_3)_5{\cdot}4H_2O$	B11b	16.15	16.70	13.23	$\gamma = 108.42$	Voliotis and Rimsky (1988)
$Na_6Th(CO_3)_5(H_2O)_{12}$	$P\bar{1}$	9.60	9.92	13.64	$\alpha = 90.47$ $\beta = 104.38$ $\gamma = 95.52$	Voliotis and Rimsky (1975)
$(C(NH_2)_3)_5(Th(CO_3)_3F_3)$	$P2_12_12_1$	9.53	29.79	9.11		Voliotis (1979)
$Na_6BaTh(CO_3)_6(H_2O)_6$	$R\bar{3}$	14.175		8.605		Yamnova *et al.* (1990)
$Th(P_2O_7)$	$Pa\bar{3}$	8.721				Burdese and Borlera (1963)
$KTh_2(PO_4)_3$	C2/c	17.57	6.863	8.138	$\beta = 101.77$	Matkovic *et al.* (1968)
$NaTh_2(PO_4)_3$	C2/c	17.37	6.81	8.13	$\beta = 101.13$	Matkovic *et al.* (1970)
$Pb_{0.5}Th_2(PO_4)_3$	C2/c	17.459	6.8451	8.1438	$\beta = 101.25$	El-Yacoubi *et al.* (1997)
$CuTh_2(PO_4)_3$	C2/c	22.029	6.7430	7.0191	$\beta = 108.58$	Louer *et al.* (1995)
$Na_2Th(PO_4)_2$	C2/c	7.01	21.50	9.12	$\beta = 111.02$	Galesic *et al.* (1984)

$KTh(P_3O_{10})$	$P2_12_12_1$	8.234	10.187	10.015		Ruzic Toros *et al.* (1974)
$Na_6(Th(PO_4)(P_2O_7))_2$	$P\bar{1}$	8.734	8.931	6.468	$\alpha = 93.33$ $\beta = 108.29$ $\gamma = 110.10$	Kojic-Prodic *et al.* (1982)
$Na_2Th(PO_4)_2$	$P2_1/c$	7.055	21.66	9.095	$\beta = 111.56$	Galesic *et al.* (1984)
$Th_4(PO_4)_4(P_2O_7)$	Pcam	12.865	10.437	7.0676		Bénard *et al.* (1996)
$KTh_2(VO_4)_3$	C2/c	18.564	7.157	8.077	$\beta = 101.05$	Quarton and Kahn (1979)
ThV_2O_7	Pnnm	7.216	6.964	22.80		Quarton *et al.* (1970)
$Pb_{0.5}Th_{0.5}(VO_4)$	$I4_1/a$	5.175		11.943		Andreetti *et al.* (1984)
$Pb_{0.5}Th_{0.5}(VO_4)$	$I4_1/amd$	7.428		6.590		Andreetti *et al.* (1984)
$Pb_{0.5}Th_{0.5}(VO_4)$	$P2_1/n$	7.046	7.3089	6.8066		Andreetti *et al.* (1984)
$Th(VO_3)_2O$	$Pn2_1a$	7.201	22.771	6.945		Launay *et al.* (1992)
$Th(MoO_4)_2$-I	Pbca	10.318	9.737	14.475		Cremers *et al.* (1983)
$Th(MoO_4)_2$-II	$P\bar{3}$	17.593		6.238		Larson *et al.* (1989)
$K_2Th(MoO_4)_3$	C2/c	17.649	12.143	5.3688	$\beta = 105.76$	Huyghe *et al.* (1991a)
$K_4Th(MoO_4)_4$	$I4_1/a$	11.586		13.069		Huyghe *et al.* (1991b)
$K_8Th(MoO_4)_6$	$P\bar{1}$	10.255	10.260	14.466	$\alpha = 75.87$ $\beta = 96.81$ $\gamma = 118.43$	Huyghe *et al.* (1993)
$Cu_2Th_4(MoO_4)_9$	$I4\bar{3}d$	14.477				Launay *et al.* (1998)
$CdTh(MoO_4)_3$	$P6_3/m$	9.803		6.350		Launay and Rimsky (1980)
$Th(OH)_2CrO_4 \cdot H_2O$	$P2_1/m$	7.67	6.11	6.94	$\beta = 113.91$	Lundgren and Sillen (1949)
$ThSiO_4$	$I4_1/amd$	7.133		6.319		Taylor and Ewing (1978)
$ThSiO_4$	$P2_1/n$	6.784	6.974	6.500	$\beta = 104.92$	Taylor and Ewing (1978)
$Ca_2ThSi_8O_{20}$	I422	7.483		14.893		Szymanski *et al.* (1982)
$Na_{12}Th_3(Si_8O_{19})_4 \cdot 18H_2O$	$R\bar{3}c$	29.124		17.260		Li *et al.* (2000)

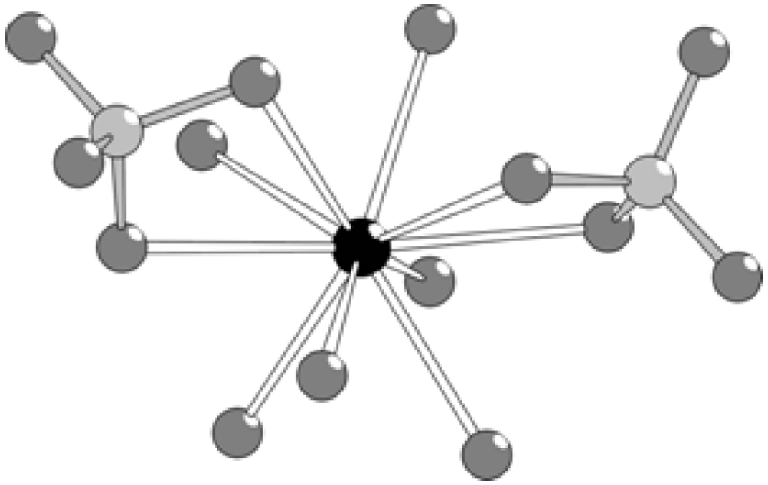

Fig. 3.15 *The* $[Th(SO_4)_2(H_2O)_6]$ *molecule in the crystal structure of* $Th(SO_4)_2{\cdot}8H_2O$.

a tetrahydrate is said to form (Roozeboom, 1890; Dawson and Williams, 1899; Wirth, 1912). A dihydrate was observed as an intermediate of the dehydration of higher hydrates (Rollefson, 1947) and $Th(SO_4)_2{\cdot}8H_2O$ has been structurally characterized (Fig. 3.15). It shows the Th^{4+} ions in a ten-fold coordination by oxygen atoms, which belong to six water molecules and two chelating sulfate ions. The coordination polyhedron is a distorted bicapped squared antiprism. The crystal structure is completed by two crystal water molecules (Habash and Smith, 1983).

The formation of basic thorium sulfates has also been frequently observed but these compounds are not well characterized (Krüss and Nilson, 1887b; Wyrouboff and Verneuil, 1898b, 1899; Meyer and Gumperz, 1905). $ThOSO_4$ has been reported to form upon dehydration of $ThOSO_4{\cdot}3H_2O$ but none of these compounds has been further investigated (Wyrouboff, 1901; Wöhler *et al*., 1908; Hauser and Wirth, 1908; Barre, 1910, 1911; Halla, 1912). The structure is known only for $Th(OH)_2SO_4$, which has been thought to be $ThOSO_4{\cdot}H_2O$ (Lundgren, 1950). The thorium ions are connected as dimers by two OH^- ions. The coordination sphere of Th^{4+} is completed by four monodentate sulfate groups and the dimeric $[Th_2(OH)_2(SO_4)_8]$ units are linked into a three-dimensional network.

Various polynary sulfates containing alkali metals are thought to exist (Colani, 1909; Barre, 1912). The phase diagram of $Na_2SO_4/Th(SO_4)_2$ has been determined recently wherein the compound $Na_{12}Th(SO_4)_8$ is found (Fedorov and Fedorov, 2001). Solid state reactions of ThO_2 with $KHSO_4$, $K_2S_2O_8$, and $K_2S_2O_7$ afforded $K_4Th(SO_4)_4$ (Keskar *et al*., 2000). Also the reactions of ThO_2 with $(NH_4)_2SO_4$, and mixtures of $(NH_4)_2SO_4$ with NH_4NO_3 or NH_4HF, have

been studied (Singh Mudher *et al.*, 1995). Furthermore, the rubidium compound, $Rb_2Th(SO_4)_3$, has been synthesized. Despite these investigations no structural data of the anhydrous species have been reported until now. A little more information is available for the hydrated polynary sulfates (Cleve, 1874; Manuelli and Gasparinetti, 1902; Rosenheim *et al.*, 1903; Barre, 1910, 1911). According to very old data, they may contain alkali and thorium metal ions in a ratio of 1:1, 2:1, 3:1, and 4:1, but newer investigations determined the compositions as $A_2Th(SO_4)_3{\cdot}xH_2O$ and $A_4Th(SO_4)_4{\cdot}xH_2O$ (A = Na–Cs, NH_4) (Gmelin, 1986b), where the water content x varies from 2 to 6. Additionally, $M_6Th(SO_4)_5{\cdot}3H_2O$ (M = Cs, NH_4) and $(NH_4)_8Th(SO_4)_6{\cdot}2H_2O$ are known (Gmelin, 1986b). For several compounds, infrared spectroscopy (IR) data are available (Evstaf'eva *et al.*, 1966) and structure determinations have been done for $Na_2Th(SO_4)_3{\cdot}6H_2O$ (Habash and Smith, 1990), $Cs_2Th(SO_4)_3{\cdot}2H_2O$ (Habash and Smith, 1992), and $K_4Th(SO_4)_4{\cdot}2H_2O$ (Arutyunyan *et al.*, 1963). The sodium compound exhibits chains of $^{1}_{\infty}[Th(H_2O)_{3/1}(SO_4)_{6/2}]$ running along [100] in which the Th^{4+} ions are surrounded by six monodentate SO_4^{2-} ions and three H_2O molecules to form a tricapped trigonal prism. The chains are linked by the Na^+ ions and three non-coordinating water molecules are found in the unit cell. In $Cs_2Th(SO_4)_3{\cdot}2H_2O$ the $[Th(H_2O)_2(SO_4)_5]$ polyhedra are linked to layers according to $^{2}_{\infty}[Th(H_2O)_2(SO_4)_{4/2}(SO_4)_{1/1}]$ that are connected by the Cs^+ ions. For the Th^{4+} ions a coordination number of nine arises due to the chelating nature of two of the SO_4^{2-} groups. In $K_4Th(SO_4)_4{\cdot}2H_2O$ zigzag chains are found with the formula $^{1}_{\infty}[Th(H_2O)_{2/1}(SO_4)_{4/2}(SO_4)_{2/1}]$. One of the SO_4^{2-} ions acts as chelating ligand leading to a coordination number of 9 for Th^{4+}.

Thorium sulfates containing other counter-cations besides alkali metals are rarely described. They include the manganese compound $MnTh(SO_4)_3{\cdot}7H_2O$ that was obtained from an aqueous solution of the binary sulfates at 30°C, the tin compound, $Sn_2Th(SO_4)_4{\cdot}2H_2O$ (Weinland and Kühl, 1907), and the poorly characterized thallium sulfates (Fernandes, 1925). Finally, the organic guanidinium ion has been used for the precipitation of thorium sulfato complexes (Molodkin *et al.*, 1964).

With $Th(SO_3F)_4$, one fluorosulfate of thorium has been synthesized by the reaction of HSO_3F with thorium acetate. According to IR measurements the anions act as bidentate ligands. The thermal decomposition of the compound yields SO_2F_2 and $Th(SO_4)_2$ (Paul *et al.*, 1981).

Thorium sulfate (IV), $Th(SO_3)_2{\cdot}xH_2O$, is said to form as a white precipitate when SO_2 is passed through a solution containing Th^{4+} ions or when an alkali metal sulfite is added (Clève, 1874; Chavastelon, 1900; Baskerville, 1901; Grossmann, 1905). Based on differential thermal analysis (DTA) investigations, the water content x is believed to be four (Golovnya *et al.*, 1967a,b). Hydrolysis of the thorium sulfites or their thermal decomposition leads to basic compounds with different compositions (Golovnya *et al.*, 1964, 1967a). Furthermore, various ternary sulfites containing alkali metal ions or the ammonium ion have been mentioned, but a more precise characterization is needed for these compounds

(Chavastelon, 1900; Golovnya *et al.*, 1967b,c). A number of organic solvates of thorium sulfites are reported, but again, further characterization is still needed (Golovnya *et al.*, 1967b).

(c) Nitrates

Nitrates of thorium may be prepared by dissolving $Th(OH)_4$ in nitric acid. Depending on the concentration of the acid, three different hydrates form upon evaporation. If the acid concentration is in the range between 1 and 54%, a pentahydrate crystallizes while a tetrahydrate is obtained at concentrations up to 75% (Ferraro *et al.*, 1954). Both hydrates have molecular structures. The tetrahydrate contains $[Th(NO_3)_4(H_2O)_4]$ molecules with all of the nitrate groups being attached in a chelating manner to the Th^{4+} ions, leading to a coordination number of 12 (Charpin *et al.*, 1987). In the non-centrosymmetric pentahydrate, $Th(NO_3)_4 \cdot 5H_2O$, there are also four chelating nitrate groups around Th^{4+} but only three additional H_2O molecules, yielding a coordination number of 11. The remaining water molecules are held via hydrogen bonds in the structure so that the compound has to be formulated according to $[Th(NO_3)_4(H_2O)_3] \cdot 2H_2O$ (Ueki *et al.*, 1966). The structure of the pentahydrate has also been determined by neutron diffraction so that exact hydrogen positions are known (Taylor *et al.*, 1966). Furthermore, thermodynamic data have been provided for the pentahydrate (Ferraro *et al.*, 1956; Cheda *et al.*, 1976; Morss and McCue, 1976).

From nearly neutral solutions, a hexahydrate was said to crystallize (Fuhse, 1897; Misciatelli, 1930a,b). Unfortunately it has not been structurally characterized and due to the well-known tendency of Th^{4+} compounds to hydrolyze, it might be possible that the hexahydrate is in fact a basic species. With $ThOH(NO_3)_3 \cdot 4H_2O$, another basic nitrate is known (Johansson, 1968a,b). As seen in Fig. 3.16, it contains the dimers $[Th_2(OH)_2(NO_3)_6(H_2O)_6]$, with the Th^{4+} ions in an 11-fold coordination by three H_2O molecules, two hydroxide ions, and three chelating nitrate groups. The dimers are arranged in the lattice with additional crystal water molecules. The thermal decomposition of thorium nitrate hydrates leads to ThO_2. According to DTA and thermogravimetry (TG) measurements, various intermediates can be observed (Tiwari and Sinha, 1980). Acidic thorium nitrates have been reported, for example $H_2Th(NO_3)_6 \cdot 3H_2O$, but unfortunately they have not been characterized (Moseley *et al.*, 1971). Also $Th(NO_3)_4 \cdot 2N_2O_5$, which is said to form in highly concentrated HNO_3, has not been investigated further (Kolb, 1913; Misciatelli, 1930a,b; Ferraro *et al.*, 1954, 1955).

Thorium nitrate is well soluble in water and various oxygen-containing organic solvents such as alcohols, ketones, ethers, and esters (Imre, 1927; Misciatelli, 1929; Templeton and Hall, 1947; Rothschild *et al.*, 1948; Yaffe, 1949; Bock and Bock, 1950). The solid solvate $Th(NO_3)_4 \cdot 3H_2O \cdot 3C_2H_5OCH_2CH_2OC_2H_5$ has been crystallized from a solution of thorium

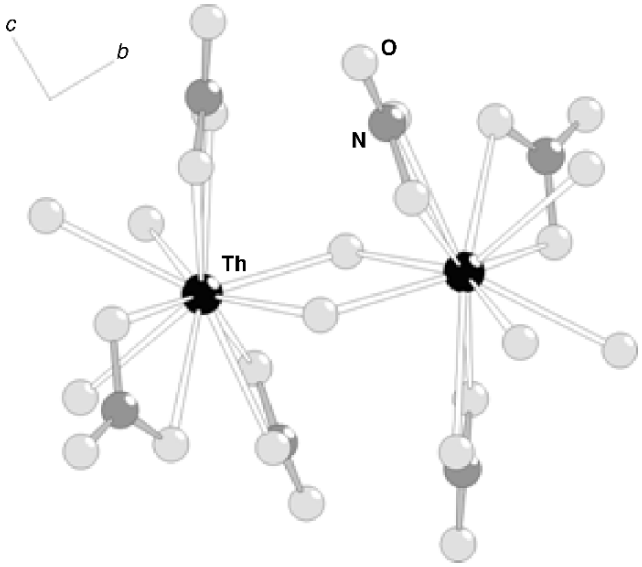

Fig. 3.16 *The dimeric unit* $[Th_2(OH)_2(NO_3)_6(H_2O)_6]$ *in the crystal structure of* $ThOH(NO_3)_3{\cdot}4H_2O$.

nitrate in the diethylether of ethyleneglycol (Katzin, 1948), and compounds with a variety of nitrogen bases in place of water are known (Kolb *et al*., 1908; Kolb, 1913). It is possible to extract thorium nitrate from aqueous solution with an immiscible organic solvent if the aqueous phase is extremely concentrated, or if it contains high concentrations of ammonium nitrate (Templeton and Hall, 1947; Rothschild *et al*., 1948; Hyde and Wolf, 1952; Newton *et al*., 1952b). Since the rare earth metal ions do not extract well under the same conditions, being almost totally restricted to the aqueous phase, the procedure finds application in the preparation of pure thorium salts from ores containing rare earth elements.

A particularly useful liquid extractant is tri(*n*-butyl)phosphate (TBP) (Warf, 1949; Anderson, 1950), as well as other phosphate esters (Peppard, 1966, 1971; Shoun and McDowell, 1980). These compounds differ from ordinary nucleophilic solvents in that they interact specifically with the metal ion through the oxygen atom of the phosphoryl group to form a very strong solvation bond. In the case of thorium nitrate, this results in the formation of very stable complexes in the organic phase, with two and three molecules of phosphate per molecule of thorium nitrate (Katzin *et al*., 1956). The TBP adduct is stable even against considerable dilution with 'inert' fluids such as benzene, CCl_4, or aliphatic hydrocarbons, which are themselves not solvents for thorium nitrate (Anderson, 1950; Katzin *et al*., 1956). The coordination interaction of Th^{4+} in aqueous solution with phosphate esters is the basis of an important commercial

process for the extraction and purification of thorium. Normally, addition of ammonia to the aqueous phase causes the formation of hydroxo complexes that reduce the efficiency of the thorium nitrate extraction. If this is coupled with addition of a neutral salting agent such as lithium nitrate, it is found that extraction is enhanced by formation of a hydroxynitrate of thorium. The polymeric complex has been formulated as $[Th_4(OH)_{10}(NO_3)_6(TBP)_4]$, thus contains one tri(*n*-butyl)phosphate molecule per thorium atom in contrast to the monomeric unhydrolyzed thorium nitrate complex (Klyuchnikov *et al.*, 1972). Thorium nitrate forms 1:1 or 1:2 complexes with crown ethers, depending on the size of the crown (Zhou *et al.*, 1981; Rozen *et al.*, 1982; Wang *et al.*, 1982). These can also be used as extractants (Wang *et al.*, 1983).

Organic donor molecules such as butylamine, dimethylamine, aromatic amine *N*-oxides, and others have been frequently used to prepare complexes with thorium nitrate (Rickard and Woolard, 1978). A compound with trimethylphosphine oxide, $Th(NO_3)_4 \cdot 3/8(Me_3PO)$, has been crystallographically characterized (Alcock *et al.*, 1978). It contains $[Th(NO_3)_3(Me_3PO)]^+$ cations and $[Th(NO_3)_6]^{2-}$ anions, a structural feature that is frequently displayed by transition metal–halide complexes (Katzin, 1966).

A number of ternary thorium nitrates with mono or divalent counter-cations are known (Jacoby, 1901; Meyer and Jacoby, 1901; Sachs, 1901). Those of the type $A_2Th(NO_3)_6$ contains the complex anion $[Th(NO_3)_6]^{2-}$ that shows the Th^{4+} ion in 12-fold coordination by oxygen atoms (Spirlet *et al.*, 1992). The latter contains six chelating nitrate groups, as it was shown from the structure determination of the ammonium compound. The same complex anion is found in the nitrates $BTh(NO_3)_6 \cdot 8H_2O$ with B = Mg, Mn, Co, Ni, Zn (Geipel, 1992). In this case, the counter-ions are octahedral $[B(H_2O)_6]^{2+}$ complexes according to the formulation $[B(H_2O)_6][Th(NO_3)_6] \cdot 2H_2O$ (Scavnicar and Prodic, 1965). Another series of ternary nitrates with monovalent cations includes members of the composition $ATh(NO_3)_5 \cdot xH_2O$, with A = NH_4, Na, K. They have not been fully characterized, so the amount of crystal water is not known (Meyer and Jacoby, 1901; Molodkin *et al.*, 1971; Volkov *et al.*, 1974). Furthermore, the nitrates $K_3Th(NO_3)_7$ and $K_3H_3Th(NO_3)_{10} \cdot 4H_2O$ have been reported, but again structural data are not known (Meyer and Jacoby, 1901; Molodkin *et al.*, 1971).

(d) Carbonates

Thorium hydroxide absorbs CO_2 readily (Berzelius, 1829; Chydenius, 1863; Clève, 1885; Chauvenet, 1911), where the end product is the hydrated $ThOCO_3$, and finally $Th(CO_3)_2 \cdot 0.5H_2O$ under high CO_2 pressures. The composition of this latter product has also been given as $Th(OH)_2CO_3 \cdot 2H_2O$ (Kharitonov *et al.*, 1969). Hydrates of the oxycarbonate are also produced by the action of sodium or ammonium carbonate on a solution of a thorium salt. The carbonate is somewhat soluble in excess alkali carbonate solution (Clève, 1885) because of the formation of complexes strong enough to prevent

precipitation of thorium by ammonia, fluoride, or phosphate. Sodium hydroxide, however, will bring about precipitation (Sollman and Brown, 1907). The nature of the carbonato complexes (Dervin and Faucherre, 1973a,b; Shetty *et al.*, 1976) will be discussed in more detail in Section 3.8. Crystallization of these complexes is possible using various counter-cations, and compounds with Na^+, K^+, Tl^+, NH_4+, $(HGua)^+$ (guanidinium), Ca^{2+}, Ba^{2+}, and $[Co(NH_3)_6]^{3+}$ have been reported (Clève, 1874; Rosenheim *et al.*, 1903; Canneri, 1925; Rosenheim and Kelmy, 1932; Chernyaev *et al.*, 1958; Kharitonov *et al.*, 1969; Ueno and Hoshi, 1970; Dervin and Faucherre, 1973b; Dervin *et al.*, 1973; Voliotis and Rimsky, 1975, 1988). All of the salts are hydrated and the sodium compound, $Na_6Th(CO_3)_5 \cdot xH_2O$, has been reported to occur with a considerable range of hydration. In the crystal structures of $Na_6Th(CO_3)_5 \cdot 12H_2O$ and $[C(NH_2)_3]_6Th(CO_3)_5 \cdot 4H_2O$, the Th^{4+} ions are in ten-fold coordination by oxygen atoms (Voliotis *et al.*, 1977). In the mineral tuliokite, $Na_6BaTh(CO_3)_6 \cdot 6H_2O$, six chelating carbonate groups are attached to the Th^{4+} ion leading to a $[ThO_{12}]$ icosahedron (Yamnova *et al.*, 1990). Carbonates containing additional anions have been reported, for example $Na_5Th(CO_3)_4OH \cdot 9H_2O$, $Na_4Th(CO_3)_4 \cdot 7H_2O$, $(HGua)_4Th(CO_3)_4 \cdot 6H_2O$, $(HGua)_2Th(CO_3)_3 \cdot 5H_2O$, $K_3Th(CO_3)_3(OH) \cdot 5H_2O$, $(NH_4)_2Th(CO_3)_3 \cdot 6H_2O$, $Na_2Th(CO_3)_2(OH)_2 \cdot 10H_2O$, $K_2Th(CO_3)_2(OH)_2 \cdot 10H_2O$, and the fluoride carbonate $(HGua)_5Th(CO_3)_3F_3$ (Voliotis, 1979).

(e) Phosphates

Phosphates of thorium have been investigated for many years (Troost and Ouvrard, 1885; Johnson, 1889; Kauffmann, 1899; Hecht, 1928; King, 1945; Dupuis and Duval, 1949; Burdese and Borlera, 1963; Hubin, 1971; Laud, 1971). More recent studies were carried out in relation with the potential of phosphate matrices to be used as radioactive waste storage material, due to their resistance to radiation effects and their low solubilities (Baglan *et al.*, 1994; Merigou *et al.*, 1995; Genet *et al.*, 1996; Dacheux *et al.*, 1998; Volkov, 1999; Brandel *et al.*, 2001a,b). The system ThO_2/P_2O_5 has been studied in the 1960s and the phosphates $Th_3(PO_4)_4$, $(ThO_3)(PO_4)_2$, $(ThO)_2P_2O_7$, ThP_2O_7, and $ThO_2 \cdot 0.8P_2O_5$ have been reported. Recent investigations, however, show that $ThO_2 \cdot 0.8P_2O_5$ and the orthophosphate, $Th_3(PO_4)_4$, do not exist (Bénard *et al.*, 1996; Brandel *et al.*, 1998). Instead, the phosphate–diphosphate $Th_4(PO_4)_4P_2O_7$ has been obtained under similar conditions. Subsequently it has been shown that the compound can be synthesized applying dry or wet preparative routes and even single crystals have been grown. Besides ThP_2O_7 (Burdese and Borlera, 1963), the orthophosphate–disphosphate is the only structurally known binary thorium phosphate to date, although various other species, for example $ThOH(PO_4)$ and $Th_2(PO_4)_2HPO_4 \cdot H_2O$, have been reported (d'Ans and Dawihl, 1929; Merkusheva, 1967; Molodkin *et al.*, 1968a; Brandel *et al.*, 2001a,b). In the crystal structure of the orthophosphate–diphosphate

(Bénard *et al*., 1996), Th^{4+} is surrounded by four monodentate and one chelating PO_4^{3-} groups and one diphosphate ion. The latter suffers from a positional disorder. In ThP_2O_7, the Th^{4+} ions are octahedrally surrounded by six monodentate $P_2O_7^{4-}$ ions and the polyhedra are linked in a three-dimensional cubic network. The compound is thought to exhibit a second modification that has unfortunately not been structurally characterized.

Several ternary thorium phosphates are known, especially those with additional monovalent cations like alkali metals, silver, copper, and thallium (Wallroth, 1883; Palmer, 1895; Haber, 1897; Schmid and Mooney, 1964; Matkovic and Sljukic, 1965; Matkovic *et al*., 1966, 1968, 1970; Molodkin *et al*., 1970; Topic *et al*., 1970; Popovic, 1971; Laügt, 1973; Ruzic Toros *et al*., 1974; Kojic-Prodic *et al*., 1982; Galesic *et al*., 1984; Arsalane and Ziyad, 1996). Phosphates with the composition $MTh_2(PO_4)_3$ (M = Na, K) show ferroelectric properties and are thus of special interest. In the crystal structure, the Th^{4+} ions are nine-fold coordinated by oxygen atoms that belong to seven PO_4^{3-} ions. Two of the latter are chelating ligands. The linkage of the polyhedra leads to parallel layers (100) that are further linked into a three-dimensional network in [100] direction. The Na^+ or K^+ ions in $MTh_2(PO_4)_3$ can be replaced by Pb^{2+} ions, leading to the composition $Pb_{0.5}Th_2(PO_4)_3$ without structural changes (El-Yacoubi *et al*., 1997). The structure of $CuTh_2(PO_4)_3$ is very similar, although the coordination number of Th^{4+} is lowered to eight. Another characteristic feature of the structure is the linear two-fold coordination of the Cu^+ ions (Louer *et al*., 1995).

(f) Vanadates

The vanadates of thorium have been investigated to a much lesser extent than the respective phosphates. They seem to parallel the structural chemistry of the phosphates (Le Flem and Hagenmuller, 1964; Le Flem *et al*., 1965; Quarton *et al*., 1970; Baran *et al*., 1974; Elfakir *et al*., 1987), but high-quality structure determinations are rare. For example, such determinations have been performed for $MTh_2(VO_4)_3$ (M = K, Rb) and 'ThV_2O_7' (Quarton and Kahn, 1979; Elfakir *et al*., 1987, 1989; Nabar and Mangaonkar, 1991; Launay *et al*., 1992; Pai *et al*., 2002). The latter compound is not a divanadate but a mixed *ortho*-vanadate–*catena*-vanadate with the formula $Th(VO_4)(VO_3)$ (Fig. 3.17). Other structurally characterized vanadates include $BaMTh(VO_4)_3$ (M = La, Pr) that adopt the monazite structure type (Nabar and Mhatre, 2001) and the silver compound, $AgTh_2(VO_4)_3$, in the zircon-type (Elfakir *et al*., 1990). Monazite-, scheelite-, and zircon-type structures have also been frequently observed for other ternary or quaternary thorium *ortho*-vanadates, namely $Pb_{0.5}Th_{0.5}(VO_4)$ (Botto and Baran, 1981; Andreetti *et al*., 1984; Calestani and Andreetti, 1984), $MLaTh(VO_4)_3$ (M = Sr, Pb) (Nabar and Mhatre, 1982), and $CdMTh(VO_4)_3$ (M = La, Yb) (Nabar *et al*., 1981). Furthermore, a hydrogenvanadate, $Th(HVO_4)_2{\cdot}5H_2O$, is said to precipitate, when VO_4^{3-} is added to solution of a thorium salt (Clève, 1874; Volck, 1894; Neish, 1904).

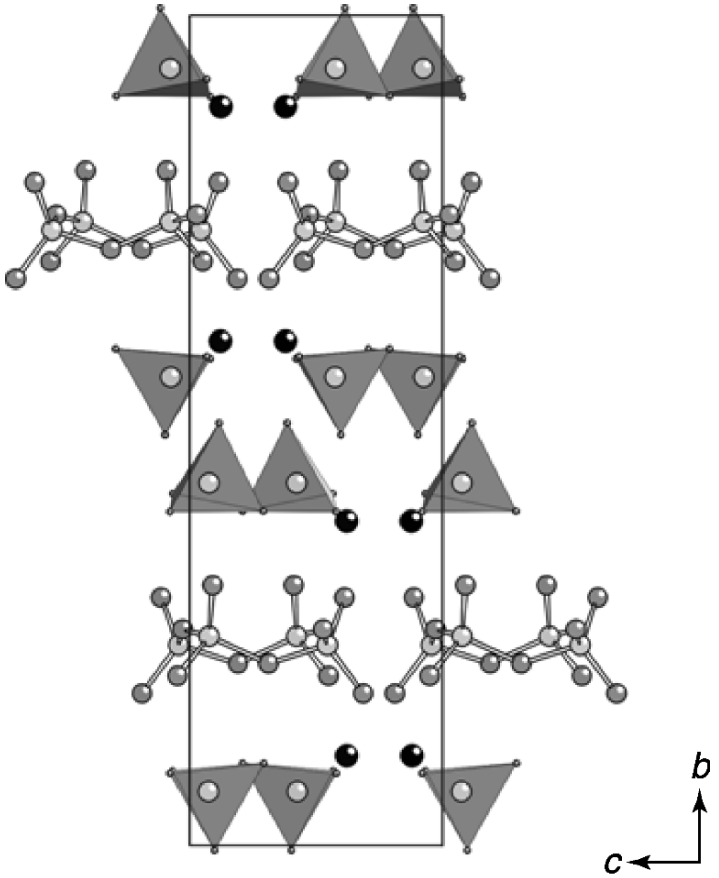

Fig. 3.17 *Crystal structure of* $Th(VO_4)(VO_3)$ (*or* ThV_2O_7). *The structure contains isolated* ortho-*vanadate ions* (*drawn as tetrahedra*) *and* catena-*vanadate strands*.

(g) Molybdates

One compound, $Th(MoO_4)_2$, is found in the system ThO_2/MoO_3 (Zambonini, 1923; Thoret *et al*., 1970; Pagès and Freundlich, 1971; Thoret, 1971, 1974). It can be obtained by fusion of the binary oxides or as a hydrate by adding ammonium or alkali metal molybdate to Th^{4+} solutions (Metzger and Zons, 1912; Banks and Diehl, 1947; Trunov and Kovba, 1963; Trunov *et al*., 1966; Thoret *et al*., 1968). $Th(MoO_4)_2$ is dimorphic. The orthorhombic low-temperature form shows the Th^{4+} ion in an eight-fold coordination by eight monodentate MoO_4^{2-} groups (Thoret *et al*., 1970; Thoret, 1974). The molybdate tetrahedra are coordinated to four Th^{4+} ions, leading to a three-dimensional

network. In the high-temperature trigonal modification, one set of thorium ions are coordinated by six oxygen atoms while the other set has tricapped trigonal-prismatic coordination polyhedra (Cremers *et al.*, 1983; Larson *et al.*, 1989).

With alkali metal molybdates, M_2MoO_4, $Th(MoO_4)_2$ forms a great variety of compounds (Barbieri, 1913; Thoret, 1971, 1974; Bushuev and Trunov, 1974). The compositions $M_2Th_4(MoO_4)_9$, $M_2Th_2(MoO_4)_5$, $M_2Th(MoO_4)_3$, $M_4Th(MoO_4)_4$, $M_6Th(MoO_4)_5$, and $M_8Th(MoO_4)_6$ have been reported, but only very few of them are properly characterized. In $K_2Th(MoO_4)_3$ the Th^{4+} ions are coordinated by eight oxygen atoms that belong to one chelating and six monodentate MoO_4^{2-} ions (Huyghe *et al.*, 1991a). The $[Th(MoO_4)_7]$ polyhedra are linked to chains along [001] that are held together by K^+ ions. $K_4Th(MoO_4)_4$ consists of a three-dimensional network with the formula $^3_\infty[Th(MoO_4)_{8/2}]$, where the potassium ions are found in holes in the structure (Huyghe *et al.*, 1991b). All of the MoO_4^{2-} groups are monodentate, leading to a coordination number of eight for Th^{4+}. The potassium-rich molybdate $K_8Th(MoO_4)_6$ contains isolated $[Th(MoO_4)_6]^{8-}$ ions in which Th^{4+} attains a coordination number of eight due to the chelating nature of two of the six molybdate groups (Huyghe *et al.*, 1993). The cadmium compound $CdTh(MoO_4)_3$ shows the Th^{4+} ions in tricapped trigonal-prismatic coordination of nine monodentate MoO_4^{2-} groups (Launay and Rimsky, 1980). The prisms are connected to columns along the *c*-axis that are stacked in a hexagonal fashion. In this way channels are formed in which the Cd^{2+} ions reside in an octahedral coordination. $Cu_2Th_4(MoO_4)_9$ has a complicated three-dimensional structure with nine-fold coordinated thorium ions (Launay *et al.*, 1998).

(h) Chromates

Upon addition of dichromate to a solution containing Th^{4+}, the thorium chromate $Th(CrO_4)_2{\cdot}3H_2O$ precipitates at room temperature (Palmer, 1895; Haber, 1897; Britton, 1923). At higher temperatures, a monohydrate precipitates (Palmer, 1895). Both hydrates have been investigated by optical microscopy and seem to be hexagonal or rhombic (Vasilega *et al.*, 1980). According to thermal investigations $Th(CrO_4)_2{\cdot}3H_2O$ dehydrates by a three-step mechanism (Vasilega *et al.*, 1980). Above 280°C, the anhydrous chromate is obtained that remains stable up to 620°C where it decomposes to ThO_2 and Cr_2O_3. Under acidic conditions, for example in concentrated chromic acid, $Th(CrO_4)_2{\cdot}CrO_3{\cdot}3H_2O$ is found as the equilibrium solid in the system $ThO_2/CrO_3/H_2O$ (Palmer, 1895; Britton, 1923). None of these compounds is structurally characterized, but the basic chromate, $Th(OH)_2CrO_4{\cdot}H_2O$ (Palmer, 1895; Britton, 1923), has been investigated by means of XRD (Lundgren and Sillen, 1949). Its crystal structure contains zigzag-chains of hydroxo-bridged Th^{4+} ions along [010]. Further linkage of the thorium ions is achieved through bonding to CrO_4^{2-} ions.

(i) Miscellaneous oxometallates

A limited number of thorium compounds with oxo-anions other than those discussed above have been mentioned in the literature. The arsenates of thorium are obviously related to the phosphates (Le Flem, 1967; Hubin, 1971; Chernorukov *et al.*, 1974a,b), while the tungstates resemble the molybdates (de Maayer *et al.*, 1972; Thoret, 1974). Thorium *ortho*-germanate, $ThGeO_4$, has been shown to be dimorphic (Bertaut and Durif, 1954; Perezy Jorba *et al.*, 1961; Harris and Finch, 1972) and adopts either the zircon or the scheelite structure type (Ennaciri *et al.*, 1986). This compound has been used as a host lattice for trivalent lanthanides (Gutowska *et al.*, 1981). Besides the most important silicate minerals thorite, huttonite, and thorogummite already mentioned in Section 3.3, a number of complex silicate minerals is known, which are, however, often not characterized completely. Structural data are, for example, available for ekanite, $Ca_2ThSi_8O_{20}$ (Szymanski *et al.*, 1982), and $Ca_6Th_4(SiO_4)_6O_2$, which has the apatite type of structure (Engel, 1978). Furthermore the structure of the mineral thornasite, $Na_{12}Th_3(Si_8O_{19})_4{\cdot}18H_2O$, has been reported recently (Li *et al.*, 2000). One borate, $Th(B_2O_5)$, has been structurally investigated. It contains $B_2O_5^{4-}$ ions and eight-fold coordinated Th^{4+} ions (Baskin *et al.*, 1961; Cousson and Gasperin, 1991).

Additional thorium compounds with transition metal oxo-anions such as the perrhenates should be mentioned. $Th(ReO_4)_4 \cdot 4H_2O$ was obtained from $Th(OH)_4$ and $HReO_4$ (Silvestre *et al.*, 1971; Zaitseva *et al.*, 1984). Its structure is not known but is has been shown to dehydrate in four steps yielding $Th(ReO_4)_4$, which finally decomposes to $Th_2O(ReO_4)_6$ (Zaitseva *et al.*, 1984). $Th(ReO_4)_4$ forms ternary compounds with alkali perrhenates and mixed anionic species with WO_4^{2-} and MoO_4^{2-} (Silvestre, 1978).

Other oxo-metallates reported are the titanate $ThTi_2O_6$ (brannerite structure) (Perezy Jorba *et al.*, 1961; Radzewitz, 1966; Ruh and Wadsley, 1966; Loye *et al.*, 1968; Kahn-Harari, 1971; Zunic *et al.*, 1984; Mitchell and Chakhmouradian, 1999), the niobate $ThNb_4O_{12}$ (Keller, 1965; Trunov and Kovba, 1966; Alario-Franco *et al.*, 1982), and the tantalates $ThTa_2O_7$, $Th_2Ta_2O_9$ (Keller, 1965; Schmidt and Gruehn, 1989, 1990), $Th_2Ta_6O_{19}$ (Busch *et al.*, 1996), and $Th_4Ta_{18}O_{53}$ (Busch and Gruehn, 1996) have been reported. Structurally, however, they are preferably described as double oxides rather than oxo-metallates. Values for the enthalpies of formation of thorite, huttonite (Mazeina *et al.*, 2005) and thorium brannerite (Helean *et al.*, 2003) are given in Chapter 19.

(j) Carboxylates and related organic salts

Carboxylate complexes of thorium have been frequently investigated with respect to the role they may play in solvent extraction processes. Carboxylates and related salts have also been employed in gravimetric analyses for thorium, either by direct weighing if the compound is stoichiometric, or after ignition to thorium dioxide. Thus, there are a large number of papers describing these

compounds. Most of them have been mentioned in the *Gmelin Handbook* (Gmelin, 1988a), so only selected examples will be presented here.

The most investigated groups among the carboxylates are formates and acetates. Formates and formato complexes can be obtained by the reaction of formic acid with $ThCl_4$ or other salts of Th^{4+}. In acid solution, $Th(OOCH)_4$, is formed, which has been shown to be polymorphic (Mentzen, 1969, 1971a,b; Greis *et al.*, 1977) and may contain different amounts of crystal water (Claudel and Mentzen, 1966; Thakur *et al.*, 1980). If the pH of the solution increases above 6, basic formates start to form. They may have different compositions like $ThOH(OOCH)_3$, $Th(OH)_2(OOCH)_2$, and $Th(OH)_3(OOCH)$ (Gmelin, 1988a) but they have not been structurally characterized. Various metal ions have been used to crystallize formato complexes, such as $MTh(OOCH)_5$ (M = K, Rb, Cs, NH_4) and $MTh(OOCH)_6$ (M = Sr, Ba). All these complexes have been characterized by thermal analysis and vibrational spectroscopy (Molodkin *et al.*, 1968b; Gmelin, 1988a).

The structural knowlegde of thorium acetates and acetato complexes is also quite limited, although quite a number of compounds have been described. The tetraacetate, $Th(CH_3COO)_4$, is said to be isotypic with the respective uranium acetate (Eliseev *et al.*, 1967; Bressat *et al.*, 1968; Gmelin, 1988a), and similar to the formates, various hydrates and basic salts are known. Derivatives of acetic acid such as CF_3COOH, CCl_3COOH, $CHCl_2COOH$, $CH_2ClCOOH$, $C_6H_5CH_2COOH$, $C_6H_5CH(OH)COOH$, naphtyl acetic acid, and others, have been used to prepare the respective salts (Katzin and Gulyas, 1960; Gmelin, 1988a). Even bromo- and iodoacetates are known. Among the chloroacetates, one compound has been investigated crystallographically. It has the composition $[Th_6(CHCl_2\ COO)_{12}(OH)_{12}(H_2O)_2]$ and shows an octahedral $[Th_6]$ core surrounded by the ligands.

With increasing complexity of the carboxylic acids, less is known structurally about their thorium compounds. The compounds prepared include glycolates, propionates, butyrates, and their derivatives. Furthermore, compounds with unsaturated mono carboxylic acids have been reported, for example crotonates and cinnamates.

The largest group of thorium salts of dicarboxylic acids are the oxalates and oxalato complexes, for which some crystallographic data are available (Gmelin, 1988a). More complex dicarboxylic acids have been employed, and even the thorium salts of long-chain acids like sebacic acid, $HOOC(CH_2)_8COOH$, are known. The latter has been used, along with *m*-nitrobenzoic acid (Neish, 1904), picrolonic acid (Hecht and Ehrmann, 1935; Dupuis and Duval, 1949), or 'ferron' (7-iodo-8-hydroxyquinoline-5-sulfonic acid), for analytical purposes (Dupuis and Duval, 1949).

3.7.8 Coordination compounds

Coordination compounds of thorium are of special interest because the knowledge of their behavior and their properties is fundamental for the understanding

of separation processes (for example, the thorium extraction [THOREX] process that involves tri(*n*-butyl)phosphate complexes) (Peppard and Mason, 1963), see Chapter 24, the development of decontamination methods, and the treatment of radioactive waste. Thus, the number of compounds reported in literature is very large. The *Gmelin Handbook* provides a comprehensive overview of the compounds investigated until 1983 (literature closing date) (Gmelin, 1985b). A more recent review (Agarwal *et al.*, 2000) covers thorium compounds with neutral oxygen donor ligands. These ligands can be divided with respect to the atom to which the oxygen donor is bonded: ligands containing a C–O group may, for example, be alcohols, phenols, ketones, esters, ethers, formamide, acetamide, those containing a N–O group are typically pyridine and quinoline *N*-oxides or even nitrosyl chloride and P=O, As=O, and S=O groups are known for the respective phosphine, arsine, and sulfoxides. The group of neutral oxygen donor ligands is probably the most investigated, but also a great number of complexes with neutral nitrogen donor ligands are known (Vigato *et al.*, 1977). Besides NH_3 (Matthews, 1898; von Bolton, 1908; Clark, 1924), the ligands are higher amines, hydrazine and its derivatives, and pyridine and its derivatives (Matthews, 1898;Adi and Murty, 1978; Al-Daher and Bagnall, 1984). Coordination compounds with charged ligands besides the above-mentioned carboxylates have been also frequently investigated. Among these ligands are the diketonates and related ligands, tropolone and its derivatives, and a great number of Schiff base ligands (Biradar and Kulkarni, 1972).

One of the most important thorium coordination compounds is thorium tetrakis(acetylacetonate), $Th(acac)_4$, which can be sublimed at temperatures below its melting point of 171°C (Urbain, 1896). This is also true for most of the substituted acetylacetonates, for example the trifluoromethylacetylacetonate, whose structure has been determined and that shows the thorium atoms in square antiprismatic coordination of oxygen atoms (Wessels *et al.*, 1972). These compounds are generally efficiently extracted into water-immiscible solvents, a property that has been used, for example, with thenoyltrifluoroacetone, to measure complexation of thorium with various anions (Calvin, 1944; Day and Stoughton, 1950). Another ligand that has been studied in more detail is 8-hydroxyquinoline ('oxine') and its derivatives (Frazer and Rimmer, 1968; Abraham and Corsini, 1970; Corsini and Abraham, 1970; Singer *et al.*, 1970; White and Ohnesorge, 1970). Also heteroleptic species involving oxine and another ligand, for example dimethylsulfoxide, are known (Singer *et al.*, 1970; Andruchow and Karraker, 1973). As a thorium complex with eight-fold thorium coordination with sulfur atoms, thorium(IV) tetrakis(*N*,*N*-diethyldithiocarbamate) should be mentioned (Brown *et al.*, 1970b). A path to related compounds is through intermediates such as $Th(NEt_2)_4$ (Bradley and Gitlitz, 1969; Watt and Gadd, 1973), which, when treated with CXY (X,Y = O, S, Se etc.), gives carbamates, thiocarbamates, mixed compounds like $Th[OSCN(CH_3)_2]_4$, and even $Th(Se_2CNEt_2)_4$ (Bagnall and Yanir, 1974). It is very surprising that despite the large number of complexes that have been prepared, the number of structure determinations is very limited.

3.7.9 Organothorium compounds

As Chapters 25 and 26 are devoted to the synthesis, the characterization and the properties of the organoactinide compounds, only selected examples shall be mentioned briefly here.

Thorocene, $Th(COT)_2$ (COT = cyclo-octatetraene), has been prepared by treating $ThCl_4$ in tetrahydrofuran (THF) with $K_2(COT)$ at dry-ice temperature (Streitwieser and Yoshida, 1969). The yellow crystals of $Th(COT)_2$ sublime at 0.01 mmHg pressure and 160°C. Thorocene, isomorphous with $U(COT)_2$ (uranocene) (Avdeef *et al.*, 1972), is unstable in air, decomposes in water, and undergoes thermal decomposition without melting above 190°C. Gas-phase photoelectron spectra have been used to elucidate the bonding in thoracene (Fragala *et al.*, 1976; Clark and Green, 1977). This compound has also been prepared by treating ThF_4 with Mg(COT) (Starks *et al.*, 1974). In addition, a number of half-sandwich Th(IV) complexes with COT have been reported (LeVanda *et al.*, 1980; Zalkin *et al.*, 1980).

Numerous complexes with the cyclopentadienyl (Cp^-) anion have been reported. $Th(Cp)_4$ was first prepared by the reaction of $ThCl_4$ with KCp (Fischer and Treiber, 1962). This compound sublimes between 250 and 290°C at 10^{-3} to 10^{-4} mmHg. Tris(cyclopentadienyl) halides and alkoxides of thorium have been synthesized (Ter Haar and Dubeck, 1964; Marks *et al.*, 1976), and, in general, these air-sensitive compounds sublime below 200°C and 10^{-3} to 10^{-4} mmHg pressure. Related tris(indenyl)thorium halides and alkoxides have been prepared (Laubereau *et al.*, 1971; Goffart *et al.*, 1975, 1977). The only bis (cyclopentadienyl)thorium dihalide reported is $ThI_2(Cp)_2$, prepared from ThI_4 and $Mg(Cp)_2$ (Reid and Wailes, 1966), whereas it is believed that the chloride analog would be unstable, similar to the uranium compound (Ernst *et al.*, 1979). In contrast, the permethylated Cp derivative $C_5(CH_3)_5^-$ (=Cp*) has been used to prepare stable dichlorides, $(Cp^*)_2ThCl_2$ (Manriquez *et al.*, 1978; Blake *et al.*, 1998). The CpTh trihalides have been described to exist as adducts with ethers, $CpThX_3 \cdot 2L$ (L = tetrahydrofurane or 1/2 dimethoxyethane [DME]) (Bagnall *et al.*, 1978). Analogous indenyl (Goffart *et al.*, 1980) and Cp* compounds have also been reported (Mintz *et al.*, 1982).

Tetrabenzylthorium, $Th(CH_2C_6H_5)_4$, is the best-characterized thorium homoalkyl compound reported to date (Köhler *et al.*, 1974). The light-yellow, air-sensitive, crystalline compound decomposes slowly at room temperature. A second tetrahydrocarbyl thorium complex has been reported, $Th(CH_3)_4(dmpe)_2$ (dmpe = bis(dimethylphosphino)ethane), prepared by the reaction of $ThCl_4(dmpe)_2$ with CH_3Li (Edwards *et al.*, 1981). It is stable up to –20°C in the absence of air and moisture. These two thorium phosphine complexes, along with $Th(OC_6H_5)_4(dmpe)_2$ and $Th(CH_2C_6H_5)_4(dmpe)_2$, were the first isolated and characterized species of their kind (Edwards *et al.*, 1984). Tetraallylthorium, $Th(C_3H_5)_4$, has been reported and decomposes slowly above 0°C (Wilke *et al.*, 1966).

The reaction of the Cp– (Marks and Wachter, 1976), indenyl– (Goffart *et al.*, 1977), and Cp*–thorium chlorides (Fagan *et al.*, 1981; Fendrick, 1984) with alkylating or arylating reagents has yielded the corresponding π-ligand thorium hydrocarbyls. In a thermodynamic study on the series $(Cp^*)_2ThR_2$, it was observed that the bond disruption enthalpies of the thorium–ligand σ-bonds were about 250–335 kJ mol^{-1}, significantly greater than similar transition metal bond enthalpies (Bruno *et al.*, 1983).

More recent investigations on organothorium chemistry were intended to introduce new ligands in that field and to synthesize low-valent thorium compounds. For example, the bicyclic pentalene dianion $C_8H_6^{2-}$ has been used to prepare a new type of thorium sandwich complex. The crystal structure, as well as the photoelectron spectra, of $[Th\{C_6H_4(Si^iPr_3\text{–}1,5)_2\}_2]$ was reported (Cloke and Hitchcock, 1997; Cloke *et al.*, 1999). Another very interesting ligand, the dicarbollide anion $C_2B_9H_{11}^{2-}$, should be mentioned: it is found in the complexes $[Li(THF)_4]_2[Th(\eta^5\text{-}C_2B_9H_{11})_2X_2]$ (X = Cl, Br, I) (Rabinovich *et al.*, 1997).

The number of potentially low-valent organothorium complexes is still very limited. Two forms of $Th(C_5H_5)_3$ have been reported. Purple $Th(C_5H_5)_3$ was prepared by sodium naphtalide reduction of $Th(C_5H_5)_3Cl$ in THF. The latter was removed under vacuum (Kanellakopulos *et al.*, 1974). According to X-ray powder diffraction measurements, the compound is isotypic with the analogs of heavier 5f elements and has an effective magnetic moment of $0.331\mu_B$. The green form of $Th(C_5H_5)_3$ was formed via photolysis of $Th(C_5H_5)_3[(CH(CH_3)_2]$ in benzene solution and has a magnetic moment of $0.404\mu_B$ (Kalina *et al.*, 1977). A recent example is $[Th\{COT(TBS)_2\}_2][K(DME)_2]$ – with $COT(TBS)_2$ = $\eta\text{-}C_8H_6(t\text{BuMe}_2\text{Si})_2\text{–}1,4$ – that has been prepared by the reaction of a suspension of $[Th\{COT(TBS)_2\}_2]$ in DME with elemental potassium (Parry *et al.*, 1999). Furthermore, the first organometallic compounds of divalent thorium have been reported recently. They contain the complex Et_8-calix[4]tetrapyrrole ligand and are potentially divalent synthons (Korobkov *et al.*, 2003).

3.8 SOLUTION CHEMISTRY

3.8.1 Redox properties

Thorium is known to have only one stable oxidation state in aqueous solution, the tetravalent state, $Th^{4+}(aq)$ (Gmelin, 1988c).

Th(III) has been recently claimed by Klapötke and Schulz (1997) to be formed by reaction of $ThCl_4$ with HN_3 in slightly acidic solution and to be stable for at least 1 h. Reportedly, the reaction involved:

$$Th^{4+} + HN_3 \rightarrow Th^{3+} + 1.5N_2 + H^+$$

Yet, the reaction has been shown to be thermodynamically impossible by Ionova *et al.* (1998). First, the stabilization of d-electrons by the crystal field effect is not

sufficient to assign, as suggested by Bratsch and Lagowski (1986), a value of –3.0 V to the redox potential of the couple M^{4+}/M^{3+}. Besides, a value between –3.35 and –3.82 V, in the same range as the previously published one, –3.7 V (Nugent *et al.*, 1973), is much more probable. Secondly, the reducing ability of HN_3 has been overestimated and the authors concluded that the spectra published by Klapötke and Schulz (1997), as a proof of the existence of Th^{3+}(aq) (broad absorption signal centered around 460 nm and intense peaks at 392, 190 and below 185 nm), correspond, in fact, to azido–chloro complexes of Th(IV).

3.8.2 Structure of the aqueous Th^{4+} ion

The LIII-edge extended X-ray fine structure (EXAFS) experiments on 0.03–0.05 M Th(IV) in 1.5 M $HClO_4$ solutions have clearly defined the structure of the Th(IV) aqua ion (Moll *et al.*, 1999). A least-squares refinement of the data leads to a Th–O distance of (2.45 ± 0.01) Å and a coordination number of (10.8 ± 0.5) which is larger than the older values estimated by Johansson *et al.* (1991) from low-angle X-ray scattering (LAXS) results (8.0 ± 0.5 water molecules at 2.485 Å) or by Fratiello *et al.* (1970) from ^1H NMR data at low temperatures and higher concentrations (nine water molecules in the first hydration sphere).

The results of Moll *et al.* are consistent with the structural parameters obtained in the same study for U^{4+}(aq) (CN = 10 ± 1; R = 2.42 ± 0.01 Å) and previously by Allen *et al.* (1997) for Np^{4+}(aq) (CN = 11.2 ± 0.4; R = 2.40 ± 0.01 Å). A correlation between the hydration number (higher than 6) of highly charged metal ions and the bond distance shows also that a M–O distance of 2.45 Å is in favor of a hydration number closer to 10 (Sandström *et al.*, 2001). More precise systematics and correlation between the space around the cation and its charge have been proposed by David and Vokhmin (2003). They give consistent coordination numbers of Th^{4+}, U^{4+}, Np^{4+}, and Pu^{4+}: 11.0, 10.65, 10.2, and 10.0, respectively. The same authors have evaluated the corresponding ionic radii, 1.178 Å for Th^{4+}, and a size of the coordinated water molecule of 1.335 Å, by assuming a pure electrostatic bond. It would result in a larger cation–oxygen distance of 2.51 Å. The observed difference with experimental data (0.06 Å) has been interpreted by a covalent effect and the effective charge of the Th^{4+} aquo ion has been evaluated to be 3.82 (David and Vokhmin, 2003). Finally, the same authors have determined the number of water molecules in a second hydration sphere as 13.4.

3.8.3 Thermodynamics of the Th^{4+}(aq) ion

The data on the standard enthalpy of formation, entropy, and corresponding Gibbs energy, adopted in this review and shown in Table 3.12, are those given in the compilation of Martinot and Fuger (1985), except for a small difference in the standard Gibbs energy of formation, due to the use of a more recent value for the entropy of Th(cr) (see Chapter 19).

Table 3.12 *Main thermodynamic properties of the thorium aqueous ion at* 25°C (*see text for references*).

$E°(Th^{4+}/Th)$	$\Delta_f H°$(kJ mol^{-1})	$\Delta_f G°$(kJ mol^{-1})	$S°$ (J K^{-1} mol^{-1})
–(1.828 ± 0.015) V/NHE	–(769.0 ± 2.5)	–(705.5 ± 5.6)	–(422.6 ± 16.7)

Thermodynamic models have been proposed recently by David and Vokhmin (2001) to evaluate the Gibbs hydration energy and the entropy of the aquo ions. Corresponding values are $\Delta_{hyd}G°(Th^{4+}) = -6100$ kJ mol^{-1} and $S°(Th^{4+},aq) = -438$ J mol^{-1} K^{-1} (David and Vokhmin, 2003). The entropy value is consistent with the experimental value, –(422.6 ± 16.7) J K^{-1} mol^{-1} (Martinot and Fuger, 1985).

The standard state partial molar heat capacities and volumes of Th^{4+}(aq) have been recently determined from 10 to 55°C under conditions minimizing complications due to hydrolysis and ion-pairing equilibria or ion–ligand complexation (measurements on aqueous solutions containing $Th(ClO_4)_4$ in dilute $HClO_4$ (Hovey, 1997)). The values obtained at 25°C, $C_p°(Th^{4+},aq) = -(224 \pm 3)$ J K^{-1}mol^{-1} and $V°(Th^{4+},aq) = -(60.6 \pm 0.5)$ cm^3 mol^{-1}, appear as more negative than those of any monoatomic aqueous ion. These results are also quite different from the previous estimations: $C_p°(Th^{4+},aq) = -(1 \pm 11)$ J K^{-1} mol^{-1} (Morss and McCue, 1976) recalculated as –(60 ± 11) J K^{-1} mol^{-1} using a newer $C_p°(NO_3^-,aq)$ value, –72 J K^{-1} mol^{-1} (Hovey, 1997) and $V°(Th^{4+},aq) =$ –53.5 and –54.6 cm^3 mol^{-1} from the values given in the International Critical Tables (1928) for the standard state partial molar volumes of $ThCl_4$(aq) and $Th(NO_3)_4$(aq), respectively.

3.8.4 Hydrolysis behavior

Being the largest actinide tetravalent ion, Th^{4+}(aq) is also the least hydrolyzable of them (Onosov, 1971). Because of its size, it is less hydrolyzable than many other multi-charged ions such as iron(III); tetravalent thorium may therefore be studied over a larger range of concentrations, at pH values up to 4. However, its tendency to undergo polynucleation reactions and colloid formation, as well as the low solubility of its hydroxide or hydrous oxide, limit the possibilities of investigation. For these reasons, the oxide/hydroxide solubility products and hydrolysis constants published in the literature show great discrepancies.

Very recently, Neck and Kim (2001) have proposed a critical review and a comprehensive set of thermodynamic constants at zero ionic strength and 25°C. In the first part of their work, they compared the frequently accepted constants of Baes *et al.* (1965), Baes and Mesmer (1976), Brown *et al.* (1983), Grenthe and Lagerman (1991), and Ekberg and Albisson (2000). All these data, which are

reported in Table 3.13, are based on potentiometric titrations at 15, 25, or 35°C with relatively low thorium concentrations (2×10^{-4} to 10^{-5} M).

Ekberg and Albinsson have performed, in addition, solvent extraction experiments with a total concentration of Th(IV) in the range 10^{-5} to 10^{-7} M. It should be outlined that, under the conditions usually applied in potentiometric and solvent extraction studies ($[Th]_{tot} = 2 \times 10^{-4}$ to 2×10^{-2} M; pH = 2.5–4; Kraus and Holmberg, 1954; Hietanen and Sillen, 1964; Baes *et al.*, 1965; Nakashima and Zimmer, 1984), polynuclear species are of major importance and laser-induced breakdown detection (LIBD) has shown that a considerable amount of colloids were present at $\log[H^+] \leq -(1.90 \pm 0.02)$ for $\log[Th]_{tot} = -(2.04 \pm 0.02)$ and at $\log [H^+] \leq -(2.40 \pm 0.03)$ for $\log[Th]_{tot} = -(4.05 \pm 0.02)$ (Bundschuh *et al.*, 2000). We can also cite the work of Moulin *et al.* (2001) who recently applied electrospray ionization–mass spectrometry to determine the hydrolysis of Th(IV) in dilute solution, but the equilibrium constants so-determined $\log K^\circ_{11} = -(2.0 \pm 0.2)$, $\log K^\circ_{12} = -(4.5 \pm 0.5)$, and $\log K^\circ_{13} = -(7.5 \pm 1.0)$ are so large, compared to those obtained from the above-cited well-established methods, that it is difficult to consider them as reliable.

As we can see from Table 3.13, the first mononuclear hydrolysis constants found by Brown *et al.* (1983) and Ekberg and Albinsson (2000) are about one order of magnitude higher than the constants derived by Baes and Mesmer (1976) and Grenthe and Lagerman (1991). Moreover, the hydrolysis constants reported for $Th(OH)_2^{2+}$, $Th(OH)_3^+$, and $Th(OH)_4(aq)$ differ between authors by several orders of magnitude. In order to select the best available data, Neck and Kim (2000) estimated the 'unknown' formation constants of $Th(OH)_n^{(4-n)+}$ by two methods.The first one, method A, is based on the empirical intercorrelation between hydrolysis constants of actinide ions at different oxidation states. The second method, B, developed by the authors consists of applying a semiempirical approach, in which the decrease of the stepwise complexation constants for a given metal–ligand system is related to the increasing electrostatic repulsion between the ligands. From their results collected in Table 3.13, Neck and Kim concluded that the higher $\log \beta^\circ_{11}$ values, in the range 11.7–11.9, and the lower $\log \beta^\circ_{13}$ and $\log \beta^\circ_{14}$ values (Ekberg and Albinsson, 2000) should be preferred. Consequently, their selected values are $\log \beta^\circ_{1n} = (11.8 \pm 0.2)$, (22.0 ± 0.6), (31.0 ± 1.0), and (39.0 ± 0.5) for $n = 1$, 2, 3, and 4, respectively (Neck and Kim, 2000). These data have been used to plot the speciation diagrams given in Fig. 3.18.

Following a similar approach, Moriyama *et al.* (1999) analyzed the mononuclear hydrolysis constants of actinide ions by using a simple hard sphere model. Systematic trends were thus obtained, from which the values given in Table 3.13 have been deduced ($\log \beta^\circ_{1n} = 12.56$, 23.84, 32.76, and 40.40 for $n = 1$, 2, 3, and 4, respectively). These values are intermediate between the two series calculated by Neck and Kim (2000) and are in rather good agreement with the averages of literature data ($\log \beta^\circ_{1n} = 11.27$, 22.43, 33.41, and 40.94 for $n = 1$, 2, 3, and 4, respectively) given by Moriyama *et al.* (1999).

Table 3.13 *Experimental and estimated hydrolysis constants proposed for Th(IV) at 25°C and defined as follows ([i] and γ_i denoting the concentration and the activity coefficient of the species i):*

$$K_{1-n} = [Th(OH)_n^{(4-n)+}][H^+]^n/[Th^{4+}]$$

$$\beta^\circ_{1-n} = [Th(OH)_n^{(4-n)+}](\gamma_{Th(OH)n})/[Th^{4+}](\gamma_{Th})[OH^-]^n(\gamma_{OH})^n$$

The values at I = 0 (log β°_{1n}) have been calculated by Neck and Kim (2001) *by applying the specific interaction theory (SIT) following the NEA Thermochemical Data Base project* (*Grenthe* et al., 1992).

References	*Method*	*Medium*	log β^o_{1-1} (*log* K_{1-1})	log β^o_{1-2} (*log* K_{1-2})	log β^o_{1-3} (*log* K_{1-3})	log β^o_{1-4} (*log* K_{1-4})
Hietanen and Sillen (1964)	potentiometry and coulometry	3 M NaCl	(–2.65/ <–2.33)			
Baes *et al.* (1965); Baes and Mesmer (1976)	potentiometry	1 M $NaClO_4$	11.0 ± 0.2 (–4.12 ± 0.03)[a]	22.2 ± 0.2 (–7.81 ± 0.03)[a]	<30.3[b]	40.1 ± 0.3[b]
Brown *et al.* (1983)	potentiometry	0.1 M KNO_3	11.7 ± 0.1 (–2.98 ± 0.07)			
Nakashima and Zimmer (1984)	solvent extraction	0.5 M KNO_3	11.8 ± 0.2 (–3.28)			
Bruno *et al.* (1987)	potentiometry	3 M $NaClO_4$	(–4.13 ± 0.06)			(–15.07 ± 0.2)
Moon (1989)	ThO_2 solubility	0.1 M $NaClO_4$	12.42 ± 0.02[c]	22.46 ± 0.15[c]	34.36 ± 0.07[c]	42.58 ± 0.08[c]
	$Th(OH)_4$ solubility	0.5 M $NaClO_4$	12.58 ± 0.02[c]	22.35 ± 0.15[c]	34.42 ± 0.07[c]	42.76 ± 0.08[c]
Grenthe and Lagerman (1991)	potentiometry	3 M $NaClO_4$	10.9 ± 0.3 (–4.35 ± 0.09)		32.7 ± 0.4 (–12.3 ± 0.2)	42.4 ± 0.4 (–16.65 ± 0.04)
Ekberg and Albinsson (2000)	potentiometry and solvent extraction	1 M $NaClO_4$	11.9 ± 0.2 (–3.3 ± 0.1)	21.4 ± 0.2 (–8.6 ± 0.1)	30.6[d] (–13.8)[d]	39.0 ± 0.5 (–19.4 ± 0.5)
Moriyama *et al.* (1999)	hard sphere model		12.56	23.84	32.76	40.40
Neck and Kim (2001)	estimation A		13.4	26.5	36.7	43.9
	estimation B		11.9	22.9	31.4	37.0
	selection		11.8 ± 0.2	22.0 ± 0.6	31.0 ± 1.0	38.5 ± 1.0

[a] Values based on the data of Kraus and Holmberg (1954).
[b] Values based on the data of Nabivanets and Kudritskaya (1964).
[c] Not extrapolated to zero ionic strength.
[d] Interpolated values (15–35°C).

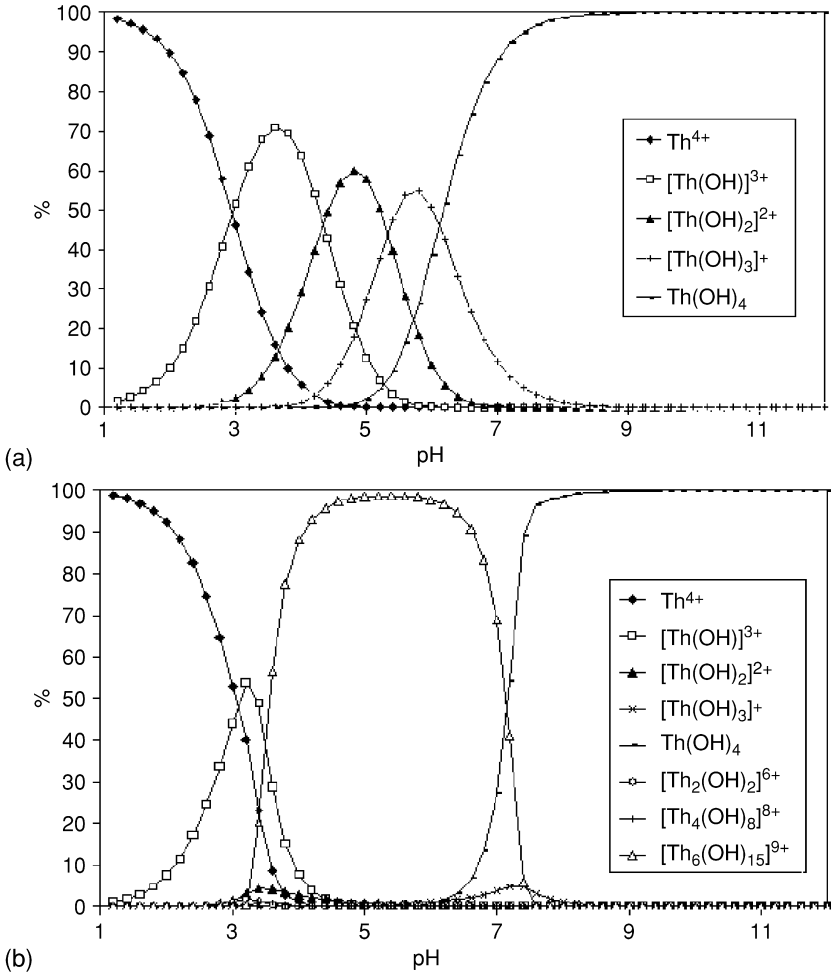

Fig. 3.18 *Thorium speciation diagrams in non-complexing aqueous solution* (*calculated for* 0.1 M *NaCl by using the hydrolysis constants given in Tables* 3.13 *and* 3.14 (*Neck and Kim,* 2001*; Ekberg and Albinsson,* 2000) *and the PHREEQUE program, version* 2.2). (*a*) *Species distribution for low concentrations of Th*(IV) (= 10^{-8}M *in the present case*). (*b*) *Species distribution for* $[Th]_{tot}$ = 0.1 M, *considering the possible formation of only three polynuclear species:* $Th_2(OH)_2^{6+}$, $Th_4(OH)_8^{8+}$, *and* $Th_6(OH)_{15}^{9+}$.

3.8.5 Solubility

(a) In non-complexing media

In perchlorate media, an average hydroxyl number, n (OH^- groups bound per thorium), of about 2.5 can be reached without delayed precipitation. All hydrolyzed solutions contain polymeric species and the weight-average degree of

polymerization increases with the degree of hydrolysis (Danesi *et al.*, 1968; Hietanen and Sillen, 1964). The presence of the $Th_2(OH)_2^{6+}$ polymer is well recognized in most of the studies (Hietanen and Sillen, 1964; Baes *et al.*, 1965; Milic, 1971, 1981; Milic and Suranji, 1982; Moon, 1989), but other polymers such as $Th_2(OH)_3^{5+}$ (Milic, 1981, Moon, 1989), $Th_2(OH)_4^{5+}$ (Moon, 1989), $Th_4(OH)_8^{8+}$ (Baes *et al.*, 1965; Ekberg and Albinsson, 2000), $Th_4(OH)_{12}^{4+}$ (Brown *et al.*, 1983), $Th_5(OH)_{12}^{8+}$ (Lefèbvre, 1957), $Th_6(OH)_{14}^{10+}$ (Milic, 1981), $Th_6(OH)_{15}^{9+}$ (Baes *et al.*, 1965; Brown *et al.*, 1983; Ekberg and Albinsson, 2000) have been found as well. The corresponding conditional constants collected in Table 3.14 show a rather reasonable agreement between the different studies for the species commonly detected. The experimental conditions, especially the total thorium concentration involved in the measurements, may explain why different sets of polynuclear species are discussed in the different studies (some species can have a too low concentration to be detected and/or can precipitate). However, it is interesting to note that $Th_6(OH)_{15}^{9+}$ is the only polynuclear species expected to predominate in the simple Th(IV)/H_2O system, when the total Th(IV) concentration exceeds $\sim 10^{-3}$ M (and up to at least 1 M) and for a pH range centered around 4.5–5 (see Fig. 3.18(b)).

The structure of highly hydrolyzed thorium salt solutions has been studied by electronic microscopy (Dobry *et al.*, 1953; Dzimitrowickz *et al.*, 1985) and light or X-ray scattering techniques (Dobry *et al.*, 1953; Hentz and Johnson, 1966; Magini *et al.*, 1976). The details of this structure are dependent on sample history. At room temperature, the hydrolysis complexes contain a small number of Th(IV) atoms probably situated at the corners of slightly distorted face-sharing tetrahedral. At higher temperatures, small crystallites (~40 Å) are formed, which have the ThO_2 structure. These crystallites tend to join to other crystallites, in random orientation, to form particles of up to 170 Å in diameter (Magini *et al.*, 1976). Finally, the small fragments of fluorite can be connected (e.g. cross-linking by oxide bridges) in a random manner into larger, porous agglomerates irregular in shape and size up to 800–15000 Å (Dzimitrowickz *et al.*, 1985). In dilute colloidal solutions ($[Th]_{tot} < 10^{-2}$ mol L^{-1}), filamentous particles with a statistic average length of 700 Å are observed; they are wound into compact balls in more concentrated solutions (Dobry *et al.*, 1953).

The solubility products reported for the thorium oxide and hydroxide species show considerable discrepancies (Table 3.15). The reasons can be found in: (1) the characteristics of the solid phase (degree of crystallization, morphology, etc.), which depend on the history of its preparation (hydrolysis reaction, pretreatment, aging); (2) the composition of the solution (pH range, ionic strength); (3) the method of evaluating the total concentration of thorium in solution (cutting size for the phase separation); (4) the generally too simplified chemical model used to derive the solubility product; and (5) the set of hydrolysis constants used in the data treatment.

Concerning the first point, it is important to distinguish between the amorphous fresh hydroxide precipitate, just washed prior to experiments,

Table 3.14 *Conditional hydrolysis constants proposed for the polynuclear species of Th(IV) and defined as follows ([i] denoting the concentration of the species i):*

$$K_{x-y} = [Th_x(OH)_y^{(4x-y)+}]\,[H^+]^y/[Th^{4+}]^x.$$

Medium (reference)	$-logK_{2-2}$	$-logK_{2-3}$	$-logK_{2-4}$	$-logK_{4-8}$	$-logK_{4-12}$	$-logK_{6-14}$	$-logK_{6-15}$
3 M $NaClO_4$ (Hietanen and Sillen, 1964)	4.70 ± 0.05	8.83 ± 0.21				36.53 ± 0.19	40.37 ± 0.23
1 M $NaClO_4$ (Baes *et al.*, 1965)	4.61 ± 0.02			19.01 ± 0.02			36.76 ± 0.02
3 M $NaClO_4$ (Brown *et al.*, 1983)					30.55 ± 0.03		34.4 ± 0.03
3 M $NaClO_4$ (Bruno *et al.*, 1987)	4.74 ± 0.04			19.15 ± 0.04		33.83 ± 0.03	
0.5 M $NaClO_4$	−2.05 ± 0.04	9.79 ± 0.11	−3.07 ± 0.04				
0.1 M $NaClO_4$ (Moon, 1989)	5.89 ± 0.10						
3 M $NaClO_4$ (Grenthe and Lagerman, 1991)	5.10 ± 0.17	7.87 ± 0.05		19.6 ± 0.2	34.86 ± 0.05	33.67 ± 0.05	
1 M $NaClO_4$ (Ekberg and Albinsson, 2000)				19.1[a]			39.5[a]

[a] Values used, after correction for the ionic strength, in the PHREEQUE program in order to calculate the speciation curves plotted in Fig. 3.18.

Table 3.15 *Conditional solubility product, K_{sp}, and estimated value at infinite dilution, K°_{sp}, proposed for Th oxide and hydroxide species at* 17–25°C *and defined as follows* ([*i*] *and* γ_i *denoting the concentration and the activity coefficient of the species i*):

$$K_{sp} = [Th^{4+}][OH^{-}]^4$$

$$K^{\circ}_{sp} = K_{sp}(\gamma_{Th})(\gamma_{OH})^4 (for\, Th(OH)_4, am)$$

$$K^{\circ}_{sp} = K_{sp}(\gamma_{Th})(\gamma_{OH})^4 (a_w)^{(x=2)} (for\, ThO_2.xH_2O, s).$$

References	*Solid*	*Solution*	*$log[Th]_{tot}$ at $pH > 5$*	K_{sp}	K°_{sp}
Nabivanets and Kudritskaya (1964)	Th(IV) hydroxide or hydrous oxide	0.1 M $NaClO_4$ (17°C)	−6.3	−44.7	−46.8
Ryan and Rai (1987)	$ThO_2.\cdot xH_2O$(am) (hydrous oxide)	0.1 M $NaClO_4$	−8.8 ± 0.2	−45.2	−45.5
Felmy *et al.* (1991)		0.6 M NaCl and KCl (room temp.)	−8.5 ± 0.6		−47.3[b]
Moon (1989)	$Th(OH)_4$(am)	0.5 M $NaClO_4$ (18°C)	−8.2 ± 0.3	−50.52 ± 0.08 −43.5[a]	−46.6 −52.9
	ThO_2(cr) (700°C)	0.1 M $NaClO_4$(25°C)	−8.2 ± 0.3	−50.76 ± 0.08	−53.6[b]
Östhols *et al.* (1994)	microcrystalline $ThO_2{\cdot}2.5H_2O$	0.5 M $NaClO_4$ (25°C)		−45.1	−48.7 −48.2[b]
Bundschuh *et al.* (2000)	colloidal ThO_2(cr)	0.5 M NaCl (25°C)		−49.54 ± 0.22	−52.8 ± 0.3
Neck and Kim (2001)	$Th(OH)_4$(am)		−8.5 ± 0.6		−47.0 ± 0.8
	ThO_2(cr)		−8.5 ± 0.6		−53.5 ± 0.7

[a] Value calculated by Neck and Kim (2001) with the use of an other set of hydrolysis constants.
[b] Values calculated by Neck and Kim (2001) by applying the specific interaction theory (SIT) following the NEA Thermochemical Data Base project (Grenthe *et al.*, 1992).

the hydrous oxide or microcrystalline $ThO_2 \cdot nH_2O$ showing very broad X-ray powder diffraction peaks, and the well-crystallized thorine, obtained after appropriate heating steps. The four other points have to be taken into account to select and interpret the various solubility curves published in the literature. This task has been recently accomplished by Neck and Kim (2001). First, they analyzed the solubility data obtained for amorphous Th(IV) precipitates (not treated at higher temperature but only washed with water) at $I \leq 1$ M by using a chemical model that includes all mononuclear species $Th(OH)_n^{(4-n)+}$ up to $n = 4$ and two polynuclear species, $Th_4(OH)_{12}^{4+}$ and $Th_6(OH)_{15}^{9+}$. For this purpose, they chose the hydrolysis constants, $\log K_{4-12}$ and $\log K_{6-15}$, given in Table 3.14 and derived by Brown *et al.* (1983) from potentiometric titrations at pH = 3–4, in combination with their selected data for the mononuclear hydrolysis species (see Table 3.13).

By monitoring the initial colloid generation (with size of 16–23 nm) as a function of pH and Th(IV) concentration with the use of LIBD, Bundschuh *et al.* (2000) determined a value of $\log K_{sp}^{\circ}$ equal to $-(52.8 \pm 0.3)$ (also calculated with the specific interaction theory (SIT) coefficients of Nuclear Energy Agency Thermochemical Database Project [NEA-TDB] data), which corresponds both to the solubility products of crystalline ThO_2 (values of Moon (1989) revisited by Neck and Kim (2001) [see Table 3.15]) and to the value calculated from thermochemical data for ThO_2, $\log K_{sp}^{\circ} = -(54.2 \pm 1.3)$ (Rai *et al.*, 1987). The difference is ascribed to a particle size effect and it is concluded that the colloids formed in the coulometric pH titration experiments consist of crystalline thorium dioxide. This conclusion is also supported by the work of Dzimitrowickz *et al.* (1985).

Moreover, it is evident from Fig. 3.19 that the degree of crystallization of ThO_2 influences its solubility behavior essentially in acidic media. At pH < 2.5, the experimental solubility curve of ThO_2(cr) seems to indicate an equilibrium between the solid phase and Th^{4+}(aq) (slope of -4 for the microcrystalline precipitates only). However, such an equilibrium has never been observed when the dissolution process is studied from under-saturation (Hubert *et al.*, 2001; Neck, 2002). With increasing pH, the solubility data deviate more and more from the expected curve. The hydrolysis of the Th^{4+} ions leads to increased Th(IV) concentrations, which are not in equilibrium with ThO_2(cr), but with an amorphous surface layer of $Th(OH)_4$ covering the crystalline solid, as judiciously explained by Neck and Kim (2001). In fact, kinetic effects play an important role in the overall process, as outlined by Hubert *et al.* (2001).

(b) In complexing media

The precipitation of thorium by various inorganic and organic ligands and the characterization of the resulting solids were treated at some length in Section 3.7.7. Therefore the discussion here will be limited to the role of the carbonate

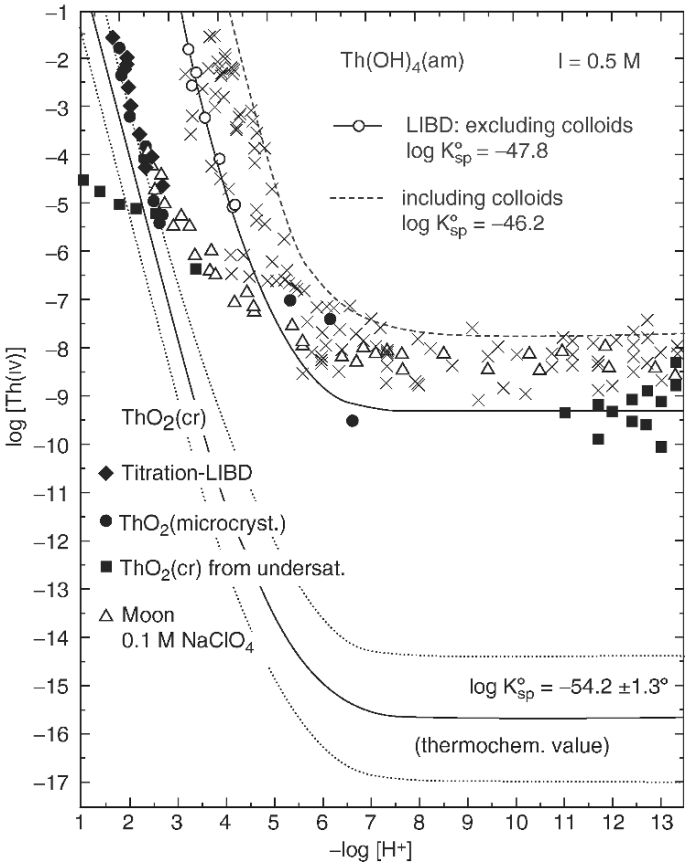

Fig. 3.19 *Experimental and calculated solubility of $ThO_2(cr)$ in comparison with that of Th(IV) hydroxide or hydrous oxide at $I = 0.5$ M and 25°C (Neck,* 2002). *The experimental data for $ThO_2(cr)$ are those determined by Neck* (2002) *by titration–LIBD and from under- and oversaturation (filled symbols) and by Moon* (1989) *in* 0.1 M *$NaClO_4$ at* 18°C (*open triangles*). *The solubility data for amorphous precipitates (crosses) are taken from Moon* (1989), *Felmy et al.* (1997), *Östholsetal.* (1994), *Rai et al.* (1997), *Neck and Kim* (2000), *all data being at $I = 0.5$–0.6 M and* 18–25°C. *The curves calculated for the two kinds of solids and for $I = 0.5$ M are based on the hydrolysis constants selected by Neck and Kim* (2001) *and on the solubility products $\log K^{\circ}_{sp}(ThO_2, cr) = -(54.2 \pm 1.3)$ (Rai et al.,* 1987) *and $\log K^{\circ}_{sp}(Th(OH)_4, am) = -(47.0 \pm 0.8)$ (Neck and Kim,* 2001).

and the phosphate ions on the solubility of thorium and, consequently, on its behavior in natural waters.

The presence of carbonates in solution greatly increases the solubility of thorium dioxide. An increase by one order of magnitude of the carbonate

concentration (in the range 0.1–2.0 M Na_2CO_3) leads to an increase by about five orders of magnitude of the solubility of hydrous ThO_2(am) (Rai *et al.*, 1995). Moreover, for a fixed carbonate concentration [1 M Na_2CO_3 (Rai *et al.*, 1995) or $pCO_2 = 0.1$ atm (Östhols *et al.*, 1994)], a large pH dependency is observed. The fitting of their solubility data has lead Östhols *et al.* (1994) to propose the following equilibrium constants:

$$ThO_2 + H^+ + H_2O + CO_3^{2-} \leftrightarrow Th(OH)_3CO_3^-;\ \log K_{131} = 6.11 \pm 0.19, \log K^\circ_{131} = 6.78 \pm 0.30$$

$$ThO_2 + 4H^+ + 5CO_3^{2-} \leftrightarrow Th(CO_3)_5^{6-};\ \log K_{105} = 42.12 \pm 0.32, \log K^\circ_{105} = 39.64 \pm 0.40$$

that were calculated by using the hydrolysis constants determined in 3 M $NaClO_4$ by Grenthe and Lagerman (1991) and were corrected to 0.5 M $NaClO_4$ (Grenthe *et al.*, 1992) .

The ion interaction model of Pitzer has been developed, extending to high concentration, and applied satisfactorily by Felmy *et al.* (1997) to describe, on the basis of the above equilibria, the solubility data obtained by both Rai *et al.* (1995) and Östhols *et al.* (1994) in the aqueous Na^+–HCO_3^- – CO_3^{2-}–OH^-–ClO_4^- –H_2O system. They have estimated $\log K^\circ_{105}$ to be 37.6 and log K°_{131} to be 6.78; these values are identical or close to those previously determined by Östhols *et al.* (1994). However, a considerable uncertainty in the determination of the value for $\log K^\circ_{105}$, due to the introduction of large mixing terms with the bulk anionic species, has been outlined by the authors.

The effect of phosphate on the solubility of microcrystalline ThO_2 has been observed to be very limited (Östhols, 1995). The only data for which there is a significant deviation from the solubility of ThO_2(am) as predicted in the absence of phosphates, are those obtained in 0.1 M phosphate solutions in the pH range 10.5–13. Here, a small increase in solubility has been found. However, an analysis of the solid phase has shown a small but significant phosphate content. This suggests the formation of a sparingly soluble thorium phosphate in the experiments, meaning that there will eventually be a decrease of the thorium solubility in the presence of excess amounts of phosphate.

It has been concluded from other solubility measurements (Fourest *et al.*, 1999) carried out on a synthesized thorium phosphate–diphosphate, $Th_4(PO_4)_4P_2O_7$ (incorrectly named 'Th orthophosphate' in a previous study (Baglan *et al.*, 1994)) that the total concentration of Th(IV) in solution ($-3 < \log [Th] < -7$ for $0 < pH < 5$) is mainly controlled by the precipitation of two compounds: $Th(HPO_4)_2$ in acidic media ($pH < 4.5$) and $Th(OH)_4$ in basic and near-neutral media. However, more recently, Thomas *et al.* (2000) and Brandel *et al.* (2001b) have characterized by electron probe microanalysis (EPMA), XRD, IR, TGA, and DTA, the crystallized phase formed during the dissolution of $Th_4(PO_4)_4P_2O_7$, when the saturation of the leachate is reached. They have shown that the thorium concentration in phosphate-containing solutions is controlled by the precipitation of the thorium phosphate–hydrogenphosphate hydrate, $Th_2(PO_4)_2(HPO_4) \cdot H_2O$, which has a very low solubility product: $\log K^\circ_{sp} = -(66.6 \pm 1.2)$ (Thomas *et al.*, 2001).

3.8.6 Complexation

(a) Inorganic ligands

To our knowledge, the formation of Th(IV) complexes with most of the common inorganic ligands, such as F^-, Cl^-, SO_4^{2-}, andNO_3^{2-}, has not been re-investigated recently (Hogfeld, 1982). The stability constants of the corresponding equilibria, collected in Table 3.16, are those previously reported by Langmuir and Herman (1980) in their review paper. From these values, it can be concluded that weak 1:1 complexes are formed with chloride and nitrate anions and that higher order complexes, even if they have been pointed out in the literature (Langmuir and Herman, 1980; Fuger *et al*., 1992), are unimportant. Colin-Blumenfeld (1987) has thus shown, through thermodynamic calculations, that $Th(NO_3)_2^{2}+$ can only exist in acidic solutions (pH < 3.2) containing high concentrations of nitrates (>0.1 M). Similarly, $Th(Cl)_2^{2+}$ is expected to be found only at pH < 4 and for $[Cl^-]_{tot} > 0.5$ M (Colin-Blumenfeld, 1987).

On the contrary, strong complexes of Th(IV) are formed with F^- and SO_4^{2-} and particularly with carbonate and phosphate ligands which are known to appreciably affect the speciation of Th(IV) in natural waters. A very strong complexation of Th(IV) by the HPO_4^{2-} species is indicated by the stability constants published by Moskvin *et al*. (1967) (see Table 3.16). These data are found in many databases used for geochemical modeling, but they were derived from solubility of an ill-defined solid thorium phosphate in acidic phosphate media (hydrogen concentration of 0.35 M). They cannot explain the ThO_2 solubility results obtained by Östhols (1995). Moreover, extraction experiments by acetylacetone in the two-phase system 1 M $Na(H)ClO_4$/toluene carried out by Engkvist and Albinsson (1994) at pH 8 and 9 (HPO_4^{2-} being thus the dominant species) give cumulative stability constants of Th^{4+}/HPO_4^{2-} much lower than the values published earlier; these new β values suffer, however, from large uncertainties.

The stability constants known for $Th^{4+}/H_2PO_4^-$ and Th^{4+}/H_3PO_4, and reported in Table 3.16, are those collected by Langmuir and Herman (1980). They have not been checked by subsequent studies, but their role is of minimal importance in the speciation of thorium in neutral and basic media. No data have been published on the complexation of Th^{4+} by the PO_4^{3-} ions, except the following equilibrium proposed by Östhols (1995):

$$Th^{4+} + 4H_2O + PO_4^{3-} \leftrightarrow Th(OH)_4PO_4^{3-} + 4H^+ \quad \log K = -(14.90 \pm 0.36)(0.35\ \text{M})$$

Finally, mention can be made of the study of Fourest *et al*. (1994). The solubility curves obtained by equilibrating solid thorium phosphate-diphosphate and highly concentrated phosphate solutions have led to the determination of $ThO(HPO_4)_3(H_2PO_4)^{5-}$ and $ThO(HPO_4)_3(H_2PO_4)_2^{6-}$ as the presumed complex forms of Th(IV) at pH 6–7 and for $0.3 < [PO_4]_{tot} < 0.8$ and $0.8 < [PO_4]_{tot} < 1.5$ M, respectively.

Table 3.16 *Cumulative formation constants of the Th(IV) complexes formed with the main inorganic ligands at* 25°C.

Complex	*log* β_{1xn}	*I* (M)	*References*
ThF^{3+}	8.03	0	Langmuir and Herman (1980)
ThF_2^{2+}	14.25	0	Langmuir and Herman (1980)
ThF_3^{+}	18.93	0	Langmuir and Herman (1980)
ThF_4	22.31	0	Langmuir and Herman (1980)
$ThCl^{3+}$	1.09	0	Langmuir and Herman (1980)
$ThCl_2^{2+}$	0.80	0	Langmuir and Herman (1980)
$ThCl_3^{+}$	1.65	0	Langmuir and Herman (1980)
$ThCl_4$	1.26	0	Langmuir and Herman (1980)
$ThSO_4^{2+}$	5.45	0	Langmuir and Herman (1980)
$Th(SO_4)_2$	9.73	0	Langmuir and Herman (1980)
$Th(SO_4)_3^{2-}$	10.50	0	Langmuir and Herman (1980)
$Th(SO_4)^{4-}$	8.48	0	Langmuir and Herman (1980)
$ThNO_3^{3+}$	0.94	0	Langmuir and Herman (1980)
$Th(NO_3)_2^{2+}$	1.97	0	Langmuir and Herman (1980)
$Th(OH)_4PO_4^{3-}$	-14.9 ± 0.36	0.35	Östhols (1995)
$Th(HPO_4)^{2+}$	10.8	0.35	Langmuir and Herman (1980)
	(8.7 – 9.7)	1	Engkvist and Albinsson (1994)
$Th(HPO_4)_2$	22.8	0.35	Langmuir and Herman (1980)
	(15 – 17.3)	1	Engkvist and Albinsson (1994)
$Th(HPO_4)_3^{2-}$	31.3	0.35	Langmuir and Herman (1980)
	(21–23)	1	Engkvist and Albinsson (1994)
$ThH_2PO_4^{3+}$	4.52	0	Langmuir and Herman (1980)
$Th(H_2PO_4)_2^{2+}$	8.88	0	Langmuir and Herman (1980)
$ThH_3PO_4^{4+}$	1.9	2	Langmuir and Herman (1980)
$Th(OH)_3CO_3^{-}$	41.5	0	Östhols *et al.* (1994)
$Th(CO_3)_5^{6-}$	21.6[a]	0.05	Joao *et al.* (1995)
	32.3	0	Östhols *et al.* (1994)
	27.1[b]	0	Felmy *et al.* (1997)

[a] Recalculated by Östhols *et al.* (1994) (see text) to be 33.2 in 1 M carbonate media.
[b] Derived by using the K_{sp}° value of Ryan and Rai (1987) given in Table 3.15.

Despite the studies mentioned above, the thermodynamic database for tetravalent actinides remains rather poor for the complexation with inorganic anions, such as carbonate, phosphate, sulfate, fluoride, and chloride, which are dominant in natural aquatic systems. Consequently, a new semiempirical approach (based on an energy term describing the interligand electrostatic repulsion) has been developed by Neck and Kim (2000) with a first application for the mononuclear complexes with a high number of carbonate ligands. For such a ligand, this model predicts a slight decrease from $\log\beta_4^{\circ}$ to $\log\beta_5^{\circ}$ and a strong decrease from $\log\beta_5^{\circ}$ to $\log\beta_6^{\circ}$. Hence the pentacarbonate complex is expected to be the limiting Th(IV)–carbonate complex at high carbonate concentration. Moreover, the existence of $Th(CO_3)_5^{6-}$ has been confirmed by several experiments using various methods: cryoscopy, conductometry, and ionic

exchange (Dervin and Faucherre, 1973a), solvent extraction followed by neutron activation (Joao *et al.*, 1987, 1995), solubility of amorphous or microcrystalline ThO_2 (Rai *et al.*, 1995; Felmy *et al.*, 1997; Östhols *et al.*, 1994) and X-ray absorption (Felmy *et al.*, 1997). The pentacarbonate complex structure is also well established in solid phase investigations (Voliotis and Rimsky, 1975). The stability constant values published in the frame of these works for the corresponding reaction:

$$Th^{4+} + 5CO_3^{2-} \leftrightarrow Th(CO_3)_5^{6-}$$

are collected in Table 3.16. The value obtained by Joao *et al.* (1987) recalculated by taking into account the complex really formed between Th(IV) and ethylenediaminetetraacetic acid (EDTA) at high pH (Th(OH)Y and not ThY) (Östhols *et al.*, 1994) is in general agreement with the value estimated by these authors. The estimation of Faucherre and Dervin (1962) from measurements of freezing point depressions is open to criticism, because only the dominant reaction is postulated and Th(IV) hydrolysis is neglected in the data treatment. The remaining values (Östhols *et al.*, 1994; Rai *et al.*, 1995; Felmy *et al.*, 1997) depend on the hydrolysis constants applied for their evaluation.

X-ray absorption spectroscopy (XAS) data (Felmy *et al.*, 1997) have clearly shown a change in speciation at low bicarbonate concentrations (0.01 M solution), but the total thorium concentration was too low to allow a definitive identification of the species. Solubility data of amorphous or microcrystalline ThO_2 have been most satisfactorily explained by the introduction of a mixed $Th(OH)_3CO_3$ (Östhols *et al.*, 1994; Felmy *et al.*, 1997) with $\log K^{\circ}_{131} = 41.5$ (see Table 3.16).

(b) Organic ligands

The organic species, such as oxalate ($C_2O_4^{2-}$), citrate ($C_6H_5O_7^{3-}$), and EDTA ($C_{10}H_{12}O_8N_2^{4-}$), form strong complexes with thorium and 'organic' complexation can predominate in natural waters over 'inorganic' by orders of magnitude, even when the concentrations of organic ligands are low as compared with inorganic ones (Langmuir and Herman, 1980).

The interaction of Th(IV) with citrate has been investigated both by potentiometry in 0.1 M chloride solution (Raymond *et al.*, 1987) and solvent extraction (thenoyltrifluoro-acetone [TTA] or dibenzoylmethane [DBM] in toluene) in perchlorate (0.1–14 M $NaClO_4$; pH: 1.8–4.0) and chloride (0.1–5.0 M NaCl; pH: 3) solutions (Choppin *et al.*, 1996). The former study covers a wider pH range (pH: 1–6) and a larger set of stability constants has been derived from the results than in the latter one. However, attention should be paid to the choice of hydrolysis constants used to fit the results. Moreover, the contribution of mixed hydroxy species, not yet identified, can be expected to be more important in basic media. Nevertheless, a relatively good agreement is observed for the two $Th(Cit)^+$ formation constants (see Table 3.17).

Table 3.17 *Cumulative formation constants of the Th(IV) complexes with some organic ligands at* 25°C.

Complex	$\log \beta^{o}_{1n}$	*References*
$Th(Cit)^{+}$	16.17	Nebel and Urban (1966)
	14.13	Raymond *et al.* (1987)
	13.7 ± 0.1	Choppin *et al.* (1996)
$Th(Cit)_2^{2-}$	24.94	Nebel and Urban (1966)
	24.29	Raymond *et al.* (1987)
$ThH(Cit)_2^{-}$	16.6 ± 0.1	Choppin *et al.* (1996)
$ThH_2(Cit)_2$	31.9 ± 0.1	Choppin *et al.* (1996)
$Th(Cit)_2(OH)_2^{4-}$	14.67	Raymond *et al.* (1987)
$Th(Cit)_3^{5-}$	28.0	Raymond *et al.* (1987)
$ThH(Cit)_3^{4-}$	33.31	Raymond *et al.* (1987)
$ThC_2O_4^{2+}$	10.6	Moskvin and Essen (1967)
	9.30	Langmuir and Herman (1980)
	9.8	Erten *et al.* (1994)
$Th(C_2O_4)_2$	20.2	Moskvin and Essen (1967)
	18.54	Langmuir and Herman (1980)
	17.5	Erten *et al.* (1994)
$Th(C_2O_4)_3^{2-}$	26.4	Moskvin and Essen (1967)
	25.73	Langmuir and Herman (1980)
$Th(C_2O_4)_4^{4-}$	29.6	Moskvin and Essen (1967)
$Th(HC_2O_4)^{3+}$	11.0	Erten *et al.* (1994)
$Th(HC_2O_4)_2^{2+}$	18.13	Erten *et al.* (1994)
ThEDTA	25.30	Langmuir and Herman (1980)
$ThHEDTA^{+}$	17.02	Langmuir and Herman (1980)

The Th(IV)/oxalate constants determined by using solvent extraction techniques (TTA and bis(2-ethylhexyl)phosphoric acid [HDEHP] in toluene; pH: 1.3–4.0; $I = 1$, 3, 5, 7, and 9 M) (Erten *et al.*, 1994) appear somewhat different from the values previously obtained from solubility measurements, but the approach of Moskvin and Essen (1967) has already been subjected to some criticism in the case of the phosphate ligands (Östhols, 1995).

Other anions of organic acids, such as formate, acetate, chloroacetate, tartrate, malate, salicylate, sulfosalicylate, and so on, form complexes with Th(IV). They are too numerous to be listed in Table 3.16, but the corresponding stability constants can be found in various compilations: Sillen and Martell (1964, 1971), Perrin (1982), or the most recent database issued by the National Institute of Standards and Technology (NIST, 2002).

Humic and fulvic acids have been identified as efficient complexing agents for ions such as Th^{4+}. Their influence on thorium mobilization in natural waters have been discussed in several publications (Choppin and Allard, 1985; Cacheris and Choppin, 1987; Miekeley and Küchler, 1987). The Th(IV)–humate complex has been recently analyzed by X-ray photoelectron spectroscopy (XPS)

(Schild and Marquardt, 2000). The XPS study corroborates EXAFS results (Denecke *et al.*, 1999) according to which Th(IV) is predominantly bound to carboxylic groups of humic acids.

3.8.7 Analytical chemistry

As Chapter 30 is devoted to trace analysis of actinides in geological, environmental, and biological matrices, only summarized considerations will be given here, centered on the determination of thorium in natural waters. Extensive information on the techniques used in analytical chemistry of thorium, including the 'classical' gravimetric, titrimetric, and photometric methods, is also given in the *Gmelin Handbook* (1990b).

Because of its low solubility and its ability to be sorbed as hydroxo complexes, the concentration of thorium in natural waters is, in general, below 0.1 μg L^{-1} and its quantitative determination is difficult. The most important analytical methods for the determination of Th(IV) in the range of low concentrations have been compiled and discussed by Hill and Lieser (1992). In most cases, a preconcentration step – coprecipitation, solvent extraction, and/or ion exchange separation – is performed prior to the measurement.

Inductively coupled plasma mass spectrometry (ICP-MS) is the most sensitive method with usual limits of detection around 0.01 μg kg^{-1} (Gray, 1985) and a reported limit value as low as 0.2 ng kg^{-1} (Chiappini *et al.*, 1996), but this method needs costly pieces of equipment. Two other methods exhibit low detection limits (0.1 μg kg^{-1}) and are well suited for routine analysis (Hill and Lieser, 1992):

- Spectrophotometry, with the procedure described by Keil (1981) coupling preliminary extraction and Th(IV) complexation with arsenazo;
- Voltammetry, with the procedure reported by Wang and Zadeii (1986) using a chelating reagent (with a concentration to be optimized).

However, in practical applications, drawbacks are encountered with both methods due to the presence of uranium and aluminium, respectively. To avoid these drawbacks, a selective preconcentration of Th(IV) is thus necessary (Hill and Lieser, 1992).

Gamma- and alpha-spectrometries, with sensitivity around 1 μg kg^{-1} (Singh *et al.*, 1979; Kovalchuk *et al.*, 1982; Jiang and Kuroda, 1987), are essentially used for isotopic determinations. However, these standard radiochemical techniques require preconcentration and long counting times. ^{228}Th can be determined from two successive gamma-measurements of the ^{224}Ra daughters, but a delay of 20 days is necessary to obtain reliable results for ^{228}Th (Surbeck, 1995). The chemical separation techniques for the classical alpha-spectrometry have been reviewed by De Regge and Boden (1984). These techniques often need optimization because around 50% of the initial activity can be lost at the chemical separation stage (Vera Tomé *et al.*, 1994). Liquid scintillation

spectrometers, which allow discrimination between alpha and beta decays, and are commercially available, offer, in combination with selective extractive scintillators, a more advantageous solution to the problem of the isotopic determination of ^{232}Th, ^{230}Th, and ^{228}Th, in spite of a low-energy resolution compared to alpha-spectrometry (Dacheux and Aupiais, 1997). With the PERALS (name registered to Ordela, Inc.) system, a limit of detection as low as 0.2 μg kg^{-1} can be reached for ^{232}Th [value obtained for 250 mL and 3 days of counting (Dacheux and Aupiais, 1997)]. Moreover, PERALS spectrometry can be associated to six short liquid–liquid extraction steps to isolate Th from other actinides (U, Pu, Am, and Cm) prior to its detection at very low levels (the use of spikes during the chemical procedure is necessary for complex matrices).

REFERENCES

Abaouz, A., Taoudi, A., and Laval, J. P. (1997) *J. Solid State Chem.*, **130**, 277–83.

Aboukais, A., Bechara, R., Aissi, C. F., Bonnelle, J. P., Ouqour, A., Loukah, M., Coudurier, G., and Vedrine, J. C. (1993) *J. Chem. Soc., Faraday Trans.*, **89**, 2545–9.

Abraham, J. and Corsini, A. (1970) *Anal. Chem.*, **42**, 1528–31.

Ackermann, R. J. and Rauh, E. G. (1972) *J. Chem. Thermodyn.*, **4**, 521–32.

Ackermann, R. J. and Rauh, E. G. (1973a) *High Temp. Sci.*, **5**, 463–73.

Ackermann, R. J. and Rauh, E. G. (1973b) *J. Inorg. Nucl. Chem.*, **35**, 3787–94.

Adachi, H. and Imoto, S. (1968) *Technol. Rep. Osaka Univ.*, **18**, 377.

Adachi, H., Imoto, S., and Kuki, T. (1973) *Phys. Lett. A*, **44**, 491–2.

Adams, D. M., Chatt, J., Davidson, J. M., and Gerratt, J. (1963) *J. Chem. Soc.*, 2189–94.

Adi, M. B. and Murty, A. S. R. (1978) *Curr. Sci.*, **47**, 539–41.

Agarwal, R. K., Agarwal, H., and Arora, K. (2000) *Rev. Inorg. Chem.*, **20**, 1–61.

Aksel'rud, L. G., Bodak, O. I., Aslan, A. N., Marusin, E. P., and Mazus, M. D. (1990a) *Kristallografiya*, **35**, 199–201; (1990a) *Sov. Phys., Crystallogr.*, **35**, 120–1.

Aksel'rud, L. G., Bodak, O. I., Marusin, E. P., and Aslan, A. M. (1990b) *Kristallografiya*, **35**, 487–90.

Alario-Franco, M. A., Grey, I. E., Joubert, J. C., Vincent, H., and Labeau, M. (1982) *Acta Crystallogr.*, **A38**, 177–86.

Albering, J. H. and Jeitschko, W. (1992) *Z. Naturforsch.*, **47b**, 1521–5.

Albering, J. H. and Jeitschko, W. (1995) *Z. Kristallogr.*, **210**, 686.

Albering, J. H., Poettgen, R., Jeitschko, W., Hoffmann, R.-D., Chevalier, B., and Etourneau, J. (1994) *J. Alloys*, **206**, 133–9.

Alcock, N. W., Esperas, S., Bagnall, K. W., and Wang, H.-Y. (1978) *J. Chem. Soc. Dalton Trans.* 638–46.

Al-Daher, A. G. M. and Bagnall, K. W. (1984) *J. Less Common Metals*, **97**, 343–8.

Al-Kazzaz, Z. M. S. and Louis, R. A. (1978) *Z. Anorg. Allg. Chem.*, **440**, 286–8.

Allard, G. (1932) *Bull. Soc. Chim.*, **51**, 1213–5.

Allen, P. B. (1987) *Phys. Rev.*, **B36**, 2920–3.

Allen, P. G., Bucher, J. J., Shuh, D. K., Edelstein, N. M., and Reich, T. (1997) *Inorg. Chem.*, **36**, 4676–83.

Anderson, J. S. and D'Eye, R. W. M. (1949) *J. Chem. Soc.*, (Suppl. Issue 2), S244–8.

Anderson, M. R. (1950) USAEC Document ISC-116.
Andreetti, G. D., Calestani, G., and Montenero, A. (1984) *Z. Kristallogr.*, **168**, 41–51.
Andresen, A. F., Fjellvag, H., and Maeland, A. J. (1984) *J. Less Common Metals*, **103**, 27–31.
Andruchow, W. J. and Karraker, D. G. (1973) *Inorg. Chem.*, **12**, 2194–6.
Angelucci, O. (1907) *Atti Acad. Nazl. Lincei*, **16**, 196–8.
Aronson, S. and Auskern, A. B. (1966) *J. Phys. Chem.*, **70**, 3937–41.
Arsalane, S. and Ziyad, M. (1996) *Mater. Res. Bull.*, **31**, 156–71.
Arutyunyan, E. G., Porai-Koshits, M. A., and Molodkin, A. K. (1963) *Zh. Strukt. Khim.*, **4**, 276–7.
Asano, M., Kubo, K., and Sasaki, N. (1974) *Kyoto Daigaku Genshii Enerugi Kenkyosho Iho*, **46**, 33.
Asprey, L. B. and Haire, R. G. (1973) *Inorg. Nucl. Chem. Lett.*, **9**, 1121–8.
Auskern, A. B. and Aronson, S. (1967) *J. Phys. Chem. Solids*, **28**, 1069–71.
Avdeef, A., Raymond, K. N., Hodgson, K. O., and Zalkin, A. (1972) *Inorg. Chem.*, **11**, 1083–8.
Avignant, D. and Cousseins, J. C. (1970) *C. R. Acad. Sci. Paris C*, **271**, 1446–8.
Bacon, W. E. and Brown, G. H. (1969) *J. Phys. Chem.*, **73**, 4163–6.
Baes, C. F. Jr, Meyer, N. J., and Roberts, C. E. (1965) *Inorg. Chem.*, **4**, 518–27.
Baes, C. F. and Mesmer, R. E. (1976) *The Hydrolysis of Cations*, Reprint edn, Krieger Publishing company, Malabar, FL, Copyright 1976 by John Wiley, p. 158.
Baglan, N., Fourest, B., Guillaumont, R., Blain, G., Le Du, J. F., and Genet, M. (1994) *New J. Chem.*, **18**, 809–16.
Bagnall, K. W., Brown, D., Jones, P. J., and du Preez, J. G. H. (1965) *J. Chem. Soc.*, 350–3.
Bagnall, K. W., Brown, D., and Easey, J. F. (1968) *J. Chem. Soc. A*, 288–91.
Bagnall, K. W. and Yanir, E. (1974) *J. Inorg. Nucl. Chem.*, **36**, 777–9.
Bagnall, K. W., Behesti, A., and Heatley, F. (1978) *J. Less Common Metals*, **61**, 63–9.
Ban, Z. and Sikirica, M. (1965) *Acta Crystallogr.*, **18**, 594–9.
Ban, Z., Omejec, L., Szytula, A., and Tomkowicz, Z. (1975) *Physica Status Solidi A*, **27**, 333–8.
Banks, C. V. and Diehl, H. (1947) *Anal. Chem.*, **19**, 222–4.
Baran, E. J., Gentil, L. A., Pedregosa, J. C., and Aymonino, P. J. (1974) *Z. Anorg. Allg. Chem.*, **410**, 301–12.
Barbieri, G. A. (1913) *Atti Acad. Nazl. Lincei*, **22**, 781–6.
Bardeen, J., Cooper, L. N., and Schrieffer, J. R. (1957) *Phys. Rev.*, **108**, 1175–204.
Barker, M. G. and Alexander, I. C. (1974) *J. Chem. Soc., Dalton Trans.*, 2166–70.
Barre, M. (1910) *C. R. Acad. Sci. Paris*, **150**, 1599–602.
Barre, M. (1911) *Ann. Chim. Phys.*, **8** (24), 145–256.
Barre, M. (1912) *Bull. Soc. Chim.*, **11**, 646–8.
Bartscher, W., Rebizant, J., Boeuf, A., Caciuffo, R., Rustichelli, F., Fournier, J. M., and Kuhs, W. F. (1986) *J. Less Common Metals*, **121**, 455–6.
Baskerville, C. (1901) *J. Am. Chem. Soc.*, **23**, 761–4.
Baskin, Y., Harada, Y., and Handwerk, J. H. (1961) *J. Am. Ceram. Soc.*, **44**, 456–9.
Baskin, Y. (1969) *J. Am. Ceram. Soc.*, **52**, 54–5.
Bearden, J. A. (1967) *Rev. Mod. Phys.*, **39**, 78–124.
Bearden, J. A. and Burr, A. F. (1967) *Rev. Mod. Phys.*, **39**, 125–42.

Bechara, R., D'Huysser, A., Aissi, C. F., Guelton, M., Bonnelle, J. P., and Abou-Kais, A. (1990a) *Chem. Mater.*, **2**, 522–6.
Bechara, R., Wrobel, G., Aissi, C. F., Guelton, M., Bonnelle, J. P., and Abou-Kais, A. (1990b) *Chem. Mater.*, **2**, 518–22.
Beck, H. P. and Strobel, C. (1982) *Angew. Chem.*, **94**, 558–9.
Beck, H. P., Thiel, W., and Schuster, M. (1993) *Z. Anorg. Allg. Chem.*, **619**, 221–7.
Beck, H. P. and Kühn, F. (1995) *Z. Anorg. Allg. Chem.*, **621**, 1649–54.
Ben Salem, A., Meerschaut, A., and Rouxel, J. (1984) *C. R. Acad. Sci. Paris*, **299**, 617–9.
Bénard, P., Brandel, V., Dacheux, N., Jaulmes, S., Launay, S., Lindecker, C., Genet, M., Louer, D., and Quarton, M. (1996) *Chem. Mater.*, **8**, 181–8.
Benner, G. and Müller, B. G. (1990) *Z. Anorg. Allg. Chem.*, **588**, 33–42.
Benz, R. and Zachariasen, W. H. (1966) *Acta Crystallogr.*, **21**, 838–40.
Benz, R., Hoffmann, C. G., and Rupert, G. N. (1967) *J. Am. Chem. Soc.*, **89**, 191–7.
Benz, R. (1968) *J. Nucl. Mater.*, **25**, 233–5.
Benz, R. (1969) *J. Nucl. Mater.*, **31**, 93–8.
Benz, R. and Zachariasen, W. H. (1969) *Acta Crystallogr. B*, **25**, 294–6.
Benz, R. and Troxel, J. E. (1971) *High Temp. Sci.*, **3**, 422–32.
Benz, R., Arnold, G. P., and Zachariasen, W. H. (1972) *Acta Crystallogr. B*, **28**, 1724–7.
Bergsma, J., Goedkoop, J. A., and van Vucht, J. H. N. (1961) *Acta Crystallogr.*, **14**, 223–8.
Bernard, L., Currat, R., Delamoye, P., Zeyen, C. M. E., and Hubert, S. (1983) *J. Phys. Chem.*, **16**, 433–56.
Bertaut, F. and Durif, A. (1954) *C. R. Acad. Sci. Paris*, **238**, 2173–5.
Berzelius, J. J. (1829) *K. Sven. Vetenskapsakad. Handl.*, **9**, 1–30; (1829) *Pogg. Ann.*, **16**, 385–415.
Binnewies, M. and Schäfer, H. (1973) *Z. Anorg. Allg. Chem.*, **395**, 77–81; (1974) *Z. Anorg. Allg. Chem.*, **407**, 327–44.
Binnewies, M. and Schäfer, H. (1974) *Z. Anorg. Allg. Chem.*, **410**, 149–55.
Biradar, N. S. and Kulkarni, V. H. (1972) *Z. Anorg. Allg. Chem.*, **387**, 275–9.
Blake, P. C., Edelman, M. A., Hitchcock, P. B., Hu, J., Lappert, M. F., Tian, S., Müller, G., Atwood, J. L., and Zhang, H. (1998) *J. Organomet. Chem.*, **551** (1–2), 261–70.
Blum, P. and Bertaut, F. (1954) *Acta Crystallogr.*, **7**, 81–6.
Blunck, H. and Juza, R. (1974) *Z. Anorg. Allg. Chem.*, **410**, 9–10.
Bock, R. and Bock, E. (1950) *Z. Anorg. Chem.*, **263**, 146–8.
Borzone, G., Borsese, A., and Ferro, R. (1982) *J. Less Common Metals*, **84**, 165–72.
Böttcher, F., Simon, A., Kremer, R. K., Buchkremer-Hermanns, H., and Cockcroft, J. K. (1991a) *Z. Anorg. Allg. Chem.*, **598**, 25–44.
Böttcher, F., Simon, A., Kremer, R. K., Buchkremer-Hermanns, H., and Cockcroft, J. K. (1991b) *Angew. Chem.*, **103**, 79–80.
Botto, I. L. and Baran, E. J. (1981) *Acta Sud. Am. Quim.*, **1**, 143–50.
Bourion, F. (1907) *C. R. Acad. Sci. Paris*, **145**, 243–6.
Bourion, F. (1909) *C. R. Acad. Sci. Paris* **148**, 170–1; (1910).
Bowman, A. L., Krikorian, N. H., Arnold, G. P., Wallace, T. C., and Nereson, N. G. (1968) *Acta Crystallogr. B*, **24**, 1121–3.
Bowman, A. L. and Arnold, G. P. (1971) *Acta Crystallogr. B*, **27**, 243–4.
Bradley, D. C. and Gitlitz, M. H. (1969) *J. Chem. Soc. A*, 980–4.

Bradley, D. G., Ghotra, J. S., and Hart, F. A. (1974) *Inorg. Nucl. Chem. Lett.*, **10**, 209–11.
Brandel, V., Dacheux, N., Pichot, E., and Genet, M. (1998) *Chem. Mater.*, **10**, 345–50.
Brandel, V., Dacheux, N., and Genet, M. (2001a) *Radiochemistry* **43**, 16–21. (Moscow, Russian Federation) (Translation of Radiokhimiya)
Brandel, V., Dacheux, N., Genet, M., and Podor, R. (2001b) *J. Solid State Chem.*, **159**, 139–48.
Bratsch, S. G. and Lagowski, J. J. (1986) *J. Phys.Chem.*, **90**, 307–12.
Brauer, G. and Mitius, A. (1942) *Z. Anorg. Allg. Chem.*, **249**, 325–39.
Braun, T. P., Simon, A., Böttcher, F., and Ueno, F. (1995) *Angew. Chem.*, **107**, 647–8.
Brendel, W., Samartzis, T., Brendel, C., and Krebs, B. (1985) *Thermochim. Acta*, **83**, 167–72.
Brese, N. E. and Di Salvo, F. J. (1995a) *J. Solid State Chem.*, **120**, 372–5.
Brese, N. E. and Di Salvo, F. J. (1995b) *J. Solid State Chem.*, **120**, 378–80.
Bressat, R., Claudel, B., Giorgio, G., and Mentzen, B. (1968) *J. Chim. Phys.*, **65**, 1615–7.
Brewer, L., Sawyer, D. L., Templeton, D. H., and Dauben, C. H. (1951) *J. Am. Ceram. Soc.*, **34**, 173–9.
Bridgman, P. W. (1935) *Phys. Rev.*, **48**, 825–47.
Briggs, G. G. and Cavendish, J. H. (1971) AEC Report NLCO-1080.
Briggs-Piccoli, P. M., Abney, K. D., Schoonover, J. R., and Dorhout, P. K. (2000) *Inorg. Chem.*, **39**, 2970–6.
Briggs-Piccoli, P. M., Abney, K. D., Schoonover, J. R., and Dorhout, P. K. (2001) *Inorg. Chem.*, **40**, 4871–5.
Briggs-Piccoli, P. M., Abney, K. D., and Dorhout, P. K. (2002) *J. Nucl. Sci. Tech.*, **3**, 611–5.
Britton, H. T. S. (1923) *J. Chem. Soc.*, 1429–35.
Brown, A. (1961) *Acta Crystallogr.*, **14**, 860–5.
Brown, A. and Norreys, J. J. (1961) *J. Inst. Methods*, **89**, 238–40.
Brown, D. (1966) *J. Chem. Soc.*, 766–9.
Brown, D. (1968) *Halides of the Lanthanides and Actinides,* John Wiley, London.
Brown, D., Fowles, G. W. A., and Walton, R. A. (1970a) *Inorg. Synth.*, **12**, 225–32.
Brown, D., Holah, D. G., and Rickard, C. E. F. (1970b) *J. Chem. Soc. A*, 423–5.
Brown, D., Hall, T. L., and Moseley, P. T. (1973) *J. Chem. Soc., Dalton Trans.*, 686–91.
Brown, D., Lidster, P., Whittaker, B., and Edelstein, N. (1976) *Inorg. Chem.*, **15**, 511–4.
Brown, P. L., Ellis, J., and Sylva, R. N. (1983) *J. Chem. Soc., Dalton Trans.*, 31–4.
Brunn, H. and Hoppe, R. (1977) *Z. Anorg. Allg. Chem.*, **430**, 144–54.
Bruno, J. W., Marks, T. J., and Morss, L. R. (1983) *J. Am. Chem. Soc.*, **105**, 6824–32.
Bruno, J., Casas, I., Lagerman, B., and Munoz, M. (1987) in *Scientific Basis for Nuclear Waste Management X (Pittsburg, PA)* (eds. J. K. Bates and W. B. Seefelt), *M R S Symposium Proceedings* ANL-IL (USA): pp. 153–60.
Brunton, G. D., Insley, H., McVay, T. N., and Thoma, R. E. (1965) ORNL-3761.
Brunton, G. and Sears, D. R. (1969) *Acta Crystallogr. B*, **25**, 2519–27.
Brunton, G. (1970) *Acta Crystallogr. B*, **26**, 1185–7.
Brunton, G. (1971a) *Acta Crystallogr. B*, **27**, 2290–2.
Brunton, G. (1971b) *Acta Crystallogr. B*, **27**, 1823–6.
Brunton, G. (1972) *Acta Crystallogr. B*, **28**, 144–7.
Brunton, G. (1973) *Acta Crystallogr. B*, **29**, 2976–8.

Bryner, J. S. and Brodsky, M. B. (1959) *Proc. Second UN Int. Conf. on the Peaceful Uses of Atomic. Energy*, 2nd, Geneva, 1958, **7**, 207–15.
Bucher, E. and Staundenmann, J. L., private communication cited by Hulliger, F. (1968) *Struct. Bonding*, **4**, 83–229.
Bundschuh, T., Knopp, R., Kim, J. I., and Fanghänel, Th (2000) *Radiochim. Acta*, **88**, 625–9.
Burdese, A. and Borlera, M. L. (1963) *Ann. Chim.*, **53**, 344–55.
Busch, J. and Gruehn, R. (1996) *Z. Anorg. Allg.*, **622**, 640–8.
Busch, J., Hofmann, R., and Gruehn, R. (1996) *Z. Anorg. Allg.*, **622**, 67–75.
Buschow, K. H. J., Van Mal, H. H., and Miedema, A. R. (1975) *J. Less Common Metals*, **42**, 163–78.
Bushuev, N. N. and Trunov, V. K. (1974) *Dokl. Akad. Nauk SSSR*, **217**, 827–9; *Dokl. Chem.*, **217**, 533–5.
Cacheris, W. P. and Choppin, G. R. (1987) *Radiochim. Acta*, **42**, 185–90.
Calestani, G. and Andreetti, G. D. (1984) *Z. Kristallogr.*, **168**, 41–51.
Calvin, M. (1944) Report CN-2486.
Canneri, G. (1925) *Gazz. Chim. Ital.*, **55**, 39–44.
Cannon, J. F. and Hall, H. T. (1977) in *The Rare Earths in Modern Science and Technology* (eds. G. J. McCarthy and J. J. Rhyne), Plenum, New York, pp. 219–24.
Cannon, J. F. and Farnsworth, P. B. (1983) *J. Less Common Metals*, **92**, 359–68.
Capocchi, J. D. T. (1971) *Met. Ass. Brasil Metais.*, **27**, 881–90.
Carter, F. L. (1982) *Rare Earth Mod. Sci. Technol*, **3**, 479–80.
Caton, R. and Satterthwaite, C. B. (1977) *J. Less Common Metals*, **52**, 307–21.
Chaigneau, M. (1957) *Bull. Soc. Chim. Fr.*, 886–8.
Charpin, P., Chevrier, G., Lance, M., Nierlich, M., and Vigner, D. (1987) *Acta Crystallogr. C*, **43**, 1239–41.
Chauvenet, E. (1911) *Ann. Chim. Phys.*, **8** (23), 425–90.
Chavastelon, R. (1900) *C. R. Acad. Sci. Paris*, **130**, 781–2.
Cheda, J. A. R., Westrum, E. F. Jr, and Morss, L. R. (1976) *J. Chem. Thermodyn.*, **8**, 25–9.
Chernorukov, N. G., Moskvichev, E. P., and Zhuk, M. I. (1974a) *Kristallographiya*, **19**, 1084–5.
Chernorukov, N. G., Sibrina, G. F., and Moskvichev, E. P. (1974b) *Radiokhimiya*, **16**, 412–3.
Chernyaev, I. I., Golovina, V. A., and Molodkin, A. K. (1958) *Proc. Second UN Int. Conf. on the Peaceful Uses of Atomic Energy*, **28**, 203–9.
Chiappini, R., Taillade, J. M., and Brébion, S. (1996) *J. Anal. At. Spectrom.*, **11**, 497–503.
Chiotti, P. (1952) *J. Am.Ceram. Soc.*, **35**, 123–30.
Chiotti, P., Korbitz, F. W., and Dooley, G. J. (1967) *J. Nucl. Mater.*, **23**, 55–67.
Chiotti, P. and Dock, C. H. (1975) *J. Less Common Metals*, **41**, 225–39.
Chiotti, P., Akhachinskij, V. V., Ansara, I., and Rand, M. H. (1981) in *The Chemical Thermodynamics of Actinide Elements and Compounds,* part 5, *The Actinide Binary Alloys* (eds. F. L. Oetting, V. A. Medvedev, M. H. Rand, and E. F. Westrum Jr), STI/PUB/424/5, IAEA, Vienna.
Choi, K.-S., Patschke, R., Billinge, S. J. L., Waner, M. J., Dantus, M., and Kanatzidis, M. G. (1998) *J. Am. Chem. Soc.*, **120**, 10706.

Choppin, G. R. and Allard, B. I. (1985) in *Handbook on the Physics and Chemistry of Actinides,* vol. 3, ch. 11 (eds. A. J. Freeman and C. Keller), Elsevier, Amsterdam, 407–29.
Choppin, G. R., Erten, H. N., and Xia, Y.-X. (1996) *Radiochim. Acta*, **74**, 123–7.
Chydenius, J. J. (1863) *Pogg. Ann.*, **119**, 43.
Clark, G. L. (1924) *Am. J. Sci.*, **7**, 1–23.
Clark, R. J. and Corbett, J. D. (1963) *Inorg. Chem.*, **2**, 460–3.
Clark, J. P. and Green, J. C. (1977) *J. Chem. Soc., Dalton Trans.*, 505–8.
Claudel, B. and Mentzen, B. (1966) *Bull. Soc. Chim. France*, 1547–52.
Clève, P. T. (1874) *Bull. Soc. Chim. Paris*, **21**, 115–23.
Clève, P. T. (1885) *Bull. Soc. Chim. Paris*, **43**, 53–8.
Cline, D., Tevebaugh, R., and Warf, J. (1944) Report CC-1981.
Cloke, F. G. N. and Hitchcock, P. B. (1997) *J. Am. Chem. Soc.*, **119**, 7899–900.
Cloke, F. G. N., Grenn, J. C., and Jardine, C. N. (1999) *Organometalics*, **18**, 1080–6.
Cody, J. A. and Ibers, J. A. (1996) *Inorg. Chem.*, **35**, 3836.
Colani, A. (1909) *C. R. Acad. Sci. Paris*, **149**, 207–10.
Colin-Blumenfeld, M. (1987) Thesis, University of Nancy I (France), 182–4.
Corbett, J. D., Guidotti, R. A., and Adolphson, D. G. (1969) *Inorg. Chem.*, **8**, 163–5.
Corsini, A. and Abraham, J. (1970) *Talanta*, **17**, 439–42.
Cousson, A., Pagès, M., Cousseins, J. C., and Vedrine, A. (1977) *J. Cryst. Growth*, **40**, 157–60.
Cousson, A., Pagès, M., and Chevalier, R. (1978) *Acta Crystallogr. B*, **34**, 1776–8.
Cousson, A., Pagès, M., and Chevalier, R. (1979a) *Acta Crystallogr. B*, **35**, 1564–6.
Cousson, A., Tabuteau, A., Pagès, M., and Gasperin, M. (1979b) *Acta Crystallogr. B*, **35**, 2674–6.
Cousson, A. and Gasperin, M. (1991) *Acta Crystallogr. C*, **47**, 10–2.
Cox, J. D., Wagman, D. D., and Medvedev, V. A. (1989) *CODATA Key Values for Thermodynamics,* Hemisphere Publishers, New York.
Cremers, T. L., Eller, P. G., and Penneman, R. A. (1983) *Acta Crystallogr. C*, **39**, 1165–7.
Cuthbert, F. L. (1958) *Thorium Production Technology,* Addison-Wesley, Reading, MA.
d'Ans, J. and Dawihl, W. (1929) *Z. Anorg. Allg. Chem.*, **178**, 252–6.
Dacheux, N. and Aupiais, J. (1997) *Anal. Chem.*, **69**, 2275–82.
Dacheux, N., Podor, R., Chassigneux, B., Brandel, V., and Genet, M. (1998) *J. Alloys Compds*, **271–273**, 236–9.
Dahlke, O., Gans, W., Knacke, O., and Müller, F. (1969) *Z. Metallk.*, **60**, 465–8.
Damien, D. and de Novion, C. H. (1981) *J. Nucl. Mater.*, **100**, 167–77.
Danan, J. (1975) *J. Nucl. Mater.*, **57**, 280–2.
Danesi, P. R., Magini, M., Margherita, S., and D'Alessandro, G. (1968) *Energy. Nucl.*, **15**, 333–9.
Darnell, A. J. and McCollum, W. A. (1961) USAEC Report NAA-SR-6498.
Dawson, H. M. and Williams, P. (1899) *Proc. Chem. Soc.*, **15**, 210–1.
David, F. and Vokhmin, V. (2001) *J. Phys. Chem.*, **105**, 9704–9.
David, F. and Vokhmin, V. (2003) *New J. Chem.*, **27**, 1627–32.
Day, R. A. Jr and Stoughton, R. W. (1950) *J. Am. Chem. Soc.*, **72**, 5662–6.
de Boisbaudran, L. (1885) *C. R. Acad. Sci. Paris*, **100**, 605–7.
de Haas, W. J. and van Alphen, P. V. (1931) *Proc. Acad. Sci. Amsterdam*, **34**, 70–4.

de Maayer, P., de Bruyne, R., and Brabers, M. J. (1972) *J. Am. Ceram. Soc.*, **55**, 113.
de Regge, P. and Boden, R. (1984) *Nucl. Instrum. Methods Phys. Res.*, **223**, 181–7.
Dean, O. C. (1957) *Adv. Nucl. Eng., Proc. Second Nucl. Eng. Sci. Conf.*, **1**, 66–73. Philadelphia.
Dean, O. C. and Chandler, J. M. (1957) *Nucl. Sci. Eng.*, **2**, 57–72.
Decker, W. R. and Finnemore, D. K. (1968) *Phys. Rev.*, **172**, 430–6.
Denecke, M. A., Bublitz, D., Kim, J. I., Moll, H., and Farkes, I. (1999) *J. Synchrotron Radiat.*, **6**, 394–6.
Dennis, L. M. and Kortright, F. L. (1894) *Am. Chem. J.*, **16**, 79–83.
Dergunov, E. P. and Bergman, A. G. (1948) *Dokl. Akad. Nauk SSSR*, **60**, 391–4.
Dervin, J. and Faucherre, J. (1973a) *Bull. Soc. Chim. Fr.*, 2926–9.
Dervin, J. and Faucherre, J. (1973b) *Bull. Soc. Chim. Fr.*, 2929–33.
Dervin, J., Faucherre, J., Herpin, P., and Voliotis, S. (1973) *Bull. Soc. Chim. Fr.*, 2634–7.
Desyatnik, V. N., Kurbatov, N. N., Raspopin, S. P., and Trifonov, I. I. (1974a) *Zh. Fiz. Khim.*, **48**, 237; *Russ. J. Phys. Chem.,* **48**, 145.
Desyatnik, V. N., Raspopin, S. P., and Trifonov, I. I. (1974b) *Zh. Neorg. Khim.*, **19**, 842–3; *Russ. J. Inorg. Chem.,* **19**, 459–60.
Desyatnik, V. N. and Emel'yanov, N. M. (1975) *Zh. Prikl. Khim.*, **48**, 1382–4.
D'Eye, R. W. M. (1950) *J. Chem. Soc.*, 2764–6.
D'Eye, R. W. M., Sellman, P. G., and Murray, J. R. (1952) *J. Chem. Soc.*, 255–62.
D'Eye, R. W. M. (1953) *J. Chem. Soc.*, 1670–2.
D'Eye, R. W. M. and Sellman, P. G. (1954) *J. Chem. Soc.*, 3760–6.
D'Eye, R. W. M. (1958) *J. Chem. Soc.*, 196–9.
Dietrich, M. (1974) Report KFK-2098.
Dietrich, M., Gey, W., Rietschel, A., and Satterthwaite, C. B. (1974) *Solid State Commun.*, **15**, 941–3.
Diness, A. M. and Roy, R. (1969) *J. Mater. Sci.*, **4**, 613–24.
Dobry, A., Guinand, S., and Mathieu-Sicaud, A. (1953) *J. Chim. Phys. et Phys. Chim. Biol.*, **50**, 501–11.
Dordevic, S. V., Dilley, N. R., Bauer, E. D., Basov, D. N., Maple, M. B., and Degiorgi, L. (1999) *Phys. Rev. B: Conden. Matter Mater. Phys.*, **60**, 11321.
Dronskowski, R. (1995) *Inorg. Chem.*, **34**, 4991–5.
du Jassonneix, B. (1905) *C. R. Acad. Sci. Paris*, **141**, 191–3; (1906) *Bull. Soc. Chim.*, **3** (35), 278–80.
Duboin, A. (1908a) *C. R. Acad. Sci. Paris*, **146**, 489–91.
Duboin, A. (1908b) *C. R. Acad. Sci. Paris*, **146**, 815–7.
Duboin, A. (1909a) *Ann. Chim. Phys.*, **8** (16), 256–88.
Duboin, A. (1909b) *Ann. Chim. Phys.*, **8** (17), 354–64.
Dubrovskaya, G. N. (1971) *Zh. Neorg. Khim.*, **16**, 12–5; *Russ. J. Inorg. Chem.*, **16**, 6–8.
Dupuis, T. and Duval, C. (1949) *C. R. Acad. Sci. Paris*, **228**, 401–2.
Düsing, W. and Hüniger, M. (1931) *Techn. Wiss. Abhandl. Osram-Konzern*, **2**, 357–65.
Dzimitrowickz, D. J., Wiseman, P. J., and Cherns, D. (1985) *J. Colloid Interface Sci.*, **103**(1), 170–7.
Eastman, E. D., Brewer, L., Bromley, L. A., Gilles, P. W., and Lofgren, N. L. (1950) *J. Am Chem. Soc.*, **72**, 4019–23.
Eastman, E. D., Brewer, L., Bromley, L. A., Gilles, P. W., and Lofgren, N. L. (1951) *J. Am. Ceram. Soc.*, **34**, 128–34.

Edwards, P. G., Andersen, R. A., and Zalkin, A. (1981) *J. Am. Chem. Soc.*, **103**, 7792–4.
Edwards, P. G., Andersen, R. A., and Zalkin, A. (1984) *Organometallics*, **3**, 293–8.
Ehemann, M. and Nöth, H. (1971) *Z. Anorg. Allg. Chem.*, **386**, 87–101.
Ekberg, C. and Albinsson, Y. (2000) *J. Solution Chem.*, **29**(1), 63–86.
Elfakir, A., Mahe, P., and Quarton, M. (1987) *Z. Kristallogr.*, **181**, 235–9.
Elfakir, A., Souron, J. P., and Quarton, M. (1989) *Powder Diffraction*, **4**, 165–7.
Elfakir, A., Souron, J. P., and Quarton, M. (1990) *Powder Diffraction*, **5**, 219–20.
Eliseev, A. A., Molodkin, A. K., and Ivanova, O. M. (1967) *Russ. J. Inorg. Chem.*, **12**, 1507–8.
El-Yacoubi, A., Brochu, R., Serghini, A., Louer, M., Alami Talbi, M., and Louer, D. (1997) *Powder Diffraction*, **12**, 76–80.
Engel, G. (1978) *Mater. Res. Bull.*, **13**, 43–8.
Engkvist, I. and Albinsson, Y. (1994) *Radiochim. Acta*, **58/59**, 139–42.
English, A. C., Cranshaw, T. E., Demers, P., Harvey, J. A., Hincks, E. P., Jelly, J. V., and May, A. N. (1947) *Phys. Rev.*, **72**, 253–4.
Ennaciri, A., Kahn, A., and Michel, D. (1986) *J. Less Common Metals.*, **124**, 105–9.
Ernst, R. D., Kennelly, W. J., Day, V. W., and Marks, T. J. (1979) *J. Am. Chem. Soc.*, **101**, 2656–64.
Erten, H. N., Mohammed, A. K., and Choppin, G. R. (1994) *Radiochim. Acta*, **66/67**, 123–8.
Ettmayer, P., Waldhart, J., Vendl, A., and Banik, G. (1980) *Monatsh. Chem.*, **111**, 1185–8.
Evans, D. S. and Raynor, G. V. (1959) *J. Nucl. Mater.*, **1**, 281–8.
Evstaf'eva, O. N., Molodkin, A. K., Dvoryantseva, G. G., Ivanova, O. M., and Struchkova, M. I. (1966) *Russ. J. Inorg. Chem.*, **11**, 697–702.
Fagan, P. J., Manriquez, J. M., Maatta, E. A., Seyam, A. M., and Marks, T. J. (1981) *J. Am. Chem. Soc.*, **103**, 6650–7.
Faucherre, J. and Dervin, J. (1962) *C. R. Acad. Sci.*, **255**, 2264–6.
Fava, J., Le Flem, G., Devalette, M., Rabardel, L., Coutures, J.-P., Foëx, M., and Hagenmuller, P. (1971) *Rev. Int. Hautes Temp. Refract.*, **8**, 305–10.
Fedorov, P. I. and Fedorov, P. P. (2001) *Zh. Neorg. Khim.*, **46**, 1571–2; *Russ. J. Inorg. Chem.*, **46**, 1422–4.
Felmy, A. R., Rai, D., and Mason, M. J. (1991) *Radiochim. Acta*, **55**, 177–85.
Felmy, A. R., Rai, D., Sterner, S. M., Mason, M. J., Hess, N. J., and Conradson, S. D. (1997) *J. Solution. Chem.*, **26**, 233–48.
Fendrick, C. M., Mintz, E. A., Schertz, L. D., Marks, T. J., and Day, V. W. (1984) *Organometallics*, **3**, 819–21.
Fernandes, L. (1925) *Gazz. Chim. Ital.*, **55**, 3–6.
Ferraro, J. R., Katzin, L. I., and Gibson, G. (1954) *J. Am. Chem. Soc.*, **76**, 909–11.
Ferraro, J. R., Katzin, L. I., and Gibson, G. (1955) *J. Am. Chem. Soc.*, **77**, 327–9.
Ferraro, J. R., Katzin, L. I., and Gibson, G. (1956) *J. Inorg. Nucl. Chem.*, **2**, 118–24.
Ferraro, J. R. (1957) *J. Inorg. Nucl. Chem.*, **4**, 283–6.
Ferro, R. (1955) *Acta Crystallogr.*, **8**, 360
Ferro, R. (1956) *Acta Crystallogr.*, **9**, 817–8.
Ferro, R. (1957) *Acta Crystallogr.*, **10**, 476–7.
Fertig, W. A., Moodenbaugh, A. R., and Maple, M. B. (1972) *Phys. Lett.*, **38A**, 517–8.
Fischer, E. O. and Treiber, A. (1962) *Z. Naturforsch. B*, **17**, 276–7.

Fischer, W., Gewehr, R., and Wingchen, H. (1939) *Z. Anorg. Allg. Chem.*, **242**, 161–92.
Flotow, H. E. and Osborne, D. W. (1978) *J. Chem. Thermodyn.*, **10**, 537–51.
Flotow, H. E., Haschke, F. M., Yamauchi, S. (1984) in *The Chemical Thermodynamics of Actinide Elements and Compounds* (eds. V. A. Medredev, M. H. Raud, E. F. Westrum Jr., part 9, The Actinide Hydrides), STI/PuB/424/9, IAEA, Vienna.
Foster, L. S. (1945) Report CT-3370.
Foster, L. S. (1950) Report AECD-2942.
Fourest, B., Baglan, N., Guillaumont, R., Blain, G., and Legoux, Y. (1994) *J. Alloys Compds*, **213/214**, 219–25.
Fourest, B., Lagarde, G., Perrone, J., Brandel, V., Dacheux, N., and Genet, M. (1999) *New J. Chem.*, **23**, 645–9.
Fragala, I., Condorelli, G., Zanella, P., and Tondello, E. (1976) *J. Organomet. Chem.*, **122**, 357–63.
Frampton, O. D. (1979) *Res. Discl.*, **183**, 364.
Fratiello, A., Lee, R. E., and Schuster, R. E. (1970) *Inorg. Chem.*, **9**, 391–2.
Frazer, M. J. and Rimmer, B. (1968) *J. Chem. Soc. A*, 2273–5.
Frick, B., Schoenes, J., Vogt, O., and Allen, J. W. (1982) *Solid State Commun.*, **42**, 331.
Frondel, C. (1958) *Systematic Mineralogy of Uranium and Thorium*, Geological Survey Bulletin no. 1064, U.S. Govt.
Fuger, J. and Brown, D. (1973) *J. Chem. Soc., Dalton Trans.*, 428–34.
Fuger, J., Parker, V. B., Hubbard, W. N., and Oetting, F. L. (1983) in *The Chemical Thermodynamics of Actinide Elements and Compounds,* part 8, *The Actinide Halides* (eds. F. L. Oetting, V. A. Medvedev, M. H. Rand, and E. F. Westrum Jr), STI/PUB/424/8, IAEA, Vienna.
Fuger, J., Khodakovsky, I. L., Sergeyeva, E. I., Medvedev, V. A., and Navratil, J. D. (1992) in *The Chemical Thermodynamics of Actinide Elements and Compounds,* part 12, *The Actinide Aqueous Inorganic Complexes* (eds. F. L. Oetting, V. A. Medvedev, M. H. Rand, and E. F. Westrum Jr), STI/PUB/424/12, IAEA, Vienna.
Fuhrman, N., Holden, R. B., and Whitman, C. I. (1957) USAEC Report SCNC-185.
Fuhse, O. (1897) *Z. Angew. Chem.*, **10**, 115–6.
Galesic, N., Matkovic, B., Topic, M., Coffou, E., and Sljukic, M. (1984) *Croat. Chem. Acta*, **57**, 597–608.
Gantz, D. E. and Lambert, J. L. (1957) *J. Phys. Chem.*, **61**, 112–4.
Gantzel, P. K. and Baldwin, N. L. (1964) *Acta Crystallogr.*, **17**, 772–3.
Gao, L. Z. and Au, C. T. (2000) *Catalysis Lett.*, **65**, 91–8.
Gaumet, V., El-Ghozzi, M., and Avignant, D. (1995) *Eur. J. Solid State Inorg. Chem.*, **32**, 893–905.
Geipel, G. (1992) *Z. Kristallogr.*, **35**, 608–28.
Genet, M., Brandel, V., Dacheux, N., and Lindecker, C. (1996) in *PCT Int. Appl.* (Centre National De La Recherche Scientifique, Fr.). WO 9630300, 35 pp.
Gershanovich, A. Y. and Suglobova, I. G. (1980) *Sov. Radiochem.*, **22**, 201–5.
Gershanovich, A. Y. and Suglobova, I. G. (1981) *Sov. Radiochem.*, **23**, 170–3.
Gesing, T. M. and Jeitschko, W. (1996) *J. Alloys Compds*, **240**, 9–15.
Giacchetti, A., Blaise, J., Corliss, C. H., and Zalubas, R. (1974) *J. Res. NBS*, **78A**, 247–81.
Gingerich, K. A. and Wilson, D. W. (1965) *Inorg. Chem.*, **4**, 987–93.
Gingerich, K. A. and Aronson, S. (1966) *J. Phys. Chem.*, **70**, 2517–23.

Giorgi, A. L., Hill, H. H., Szklarz, E. G., and White, R. W. (1976) Report LA-UR-76-1535.
Glaser, C. (1897) *Chem. News*, **75**, 145–7, 157–8.
Glavic, P., Slivnik, J., and Bole, A. (1973) *J. Inorg. Nucl. Chem.*, **35**, 427–32.
Gmelin Handbook of Inorganic Chemistry, 8th edn, Thorium, System No. 44, Springer Verlag, Berlin.
(1955) Main volume (reprint 1978).
(1976) vol. C2, Ternary and Polynary Oxides.
(1978) vol. C1, Compounds with Noble Gases, Hydrogen, Oxygen.
(1985a) vol. C2, Solvent Extraction.
(1985b) vol. E, Coordination Compounds.
(1986a) vol. A2, History, Isotopes, Recovery.
(1986b) vol. C5, Compounds with S, Se, Te, B.
(1987) vol. C3, Compounds with Nitrogen.
(1988a) vol. C7, Compounds with Carbon: Carbonates, Thiocyanates, Alkoxides, Carboxylates.
(1988b) vol. A3, Technology, Uses, Irradiated Fuel, Reprocessing.
(1988c) vol. D1, Properties of Ions in Solutions.
(1989) vol. A4, General Properties. Spectra. Recoil Reactions.
(1990a) vol. A1a, Natural Occurrence. Minerals(Excluding Silicates).
(1990b) vol. C5, Analysis, Biological Behavior.
(1990c) vol. D3, Ion Exchange.
(1991a) vol. A1b, Minerals (Silicates). Deposits.Mineral Index.
(1991b) vol. D4, Chromatography. Chemistry in Nonaqueous Solutions.
(1992a) vol. B2, Alloys with Metals of Group I to IV.
(1992b) vol. C6, Carbides.
(1993a) vol. C4, Compounds with F, Cl, Br, I.
(1993b) vol. C8, Compopunds with Si, P, As,Sb, Bi, and Ge.
(1997) vol. B1, Thorium Metal.
Goffart, J., Fuger, J., Gilbert, B., Hocks, L., and Duyckaerts, G. (1975) *Inorg. Nucl. Chem. Lett.*, **11**, 569–83.
Goffart, J., Gilbert, B., and Duyckaerts, G. (1977) *Inorg. Nucl. Chem. Lett.*, **13**, 189–96.
Goffart, J., Piret-Meunier, J., and Duyckaerts, G. (1980) *Inorg. Nucl. Chem. Lett.*, **16**, 233–4.
Golovnya, V. A., Molodkin, A. K., and Tverdokhlebov, V. N. (1964) *Zh. Neorg. Khim.*, **9**, 2032–34; *Russ. J. Inorg. Chem.*, **9**, 1097–8.
Golovnya, V. A., Molodkin, A. K., and Tverdokhlebov, V. N. (1967a) *Zh. Neorg. Khim.*, **12**, 2377–87; *Russ. J. Inorg. Chem.*, **12**, 1254–9.
Golovnya, V. A., Molodkin, A. K., and Tverdokhlebov, V. N. (1967b) *Zh. Neorg. Khim.*, **12**, 2729–39; *Russ. J. Inorg. Chem.*, **12**, 1439–44.
Golovnya, V. A., Molodkin, A. K., and Tverdokhlebov, V. N. (1967c) *Zh. Neorg. Khim.*, **12**, 2075–85; *Russ. J. Inorg. Chem.*, **12**, 1092–8.
Golub, A. M. and Kalibabchuk, V. A. (1967) *Zh. Neorg. Khim.*, **12**, 2370–6; *Russ. J. Inorg. Chem.*, **12**, 1249–53.
Golub, A. M., Dabeka, R. V., and Koval, V. T. (1974) *Komplexobrazovanie Ekstr. Aktinoidov Lantanoidov*, 97–101.

Gorbunov, L. V., Desyatnik, V. N., Raspopin, S. P., and Trifonov, I. I. (1974) *Zh. Neorg. Khim.*, **19**, 3093–5; *Russ. J. Inorg. Chem.*, **19**, 1692–3.
Gordon, J. E., Montgomery, H., Noer, R. J., Pickett, G. R., and Tobóu, R. (1966) *Phys. Rev.*, **152**, 432–7.
Gouder, T., Havela, L., Black, L., Wastin, F., Rebizant, J., Boulet, P., Bouexiere, D., Heathman, S., and Idiri, M. (2002) *J. Alloys Compds*, **336**, 73–6.
Graham, J. and McTaggart, F. K. (1960) *Aust. J. Chem.*, **13**, 67–73.
Gray, A. L. (1985) *Spectrochim. Acta*, **40B**, 1525–37.
Greiner, J. D. and Smith, J. F. (1971) *Phys. Rev. B.*, **4**, 3275–7.
Greis, O., Bohres, E. W., and Schwochau, K. (1977) *Z. Anorg. Allg. Chem.*, **433**, 111–8.
Grenthe, I. and Lagerman, B. (1991) *Acta Chem. Scand.*, **45**, 231–8.
Grenthe, I., Fuger, J., Konings, R. J. M., Lemire, R. J., Muller, A. B., Nguyen-Trung, C., and Wanner, H. (1992) OECD, NEA-TDB: Chemical Thermodynamics, vol. 1, *The Chemical Thermodynamics of Uranium,* Elsevier, North-Holland, Amsterdam, pp. 683–98.
Grossmann, H. (1905) *Z. Anorg. Chem.*, **44**, 229–36.
Gudaitis, M. N., Desyatnik, V. N., Raspopin, S. P., and Trifonov, I. I. (1972) *Zh. Neorg. Khim.*, **17**, 2841–2; *Russ. J. Inorg. Chem.*, **17**, 1489.
Guertin, R. P., Bulman, J. B., Huber, J. G., and Parks, R. D. (1980) *Physica B/C*, **102**, 151–4.
Guery, J., Gao, Y., Guery, C., and Jacoboni, C. (1994) *Eur. J. Solid State Inorg. Chem.*, **31**, 187–96.
Guggenberger, L. J. and Jacobson, R. A. (1968) *Inorg. Chem.*, **7**, 2257–60.
Guillaumont, R. (1983) *Radiochim. Acta*, **32**, 129–37.
Gutowska, M., Wanklyn, B. M., and Porcher, P. (1981) *Physica B*, **111**, 257.
Guymont, M. (1977) *C. R. Acad. Sci. Paris C*, **285**, 345–8.
Habash, J. and Smith, A. J. (1983) *Acta Crystallogr. C*, **39**, 413–5.
Habash, J. and Smith, A. J. (1990) *Acta Crystallogr. C*, **46**, 957–60.
Habash, J. and Smith, A. J. (1992) *J. Crystallogr. Spectr. Res.*, **22**, 21–4.
Haber, L. (1897) *Monatsh. Chem.*, **18**, 687–99.
Hagemann, F., Katzin, L. I., Studier, M. H., Ghiorso, A., and Seaborg, G. T. (1947) *Phys. Rev.*, **72**, 252.
Hagemann, F., Katzin, L. I., Studier, M. H., Seaborg, G. T., and Ghiorso, A. (1950) *Phys. Rev.*, **79**, 435–43.
Halla, F. (1912) *Z. Anorg. Chem.*, **79**, 260–2.
Hamaker, J. W. and Koch, C. W. (1952a) in Katzin (1952), paper 7.2, p. 318.
Hamaker, J. W. and Koch, C. W. (1952b) in Katzin (1952), paper 7.3, p. 339.
Hardman, K., Rhyne, J. J., Smith, K., and Wallace, W. E. (1980) *J. Less Common Metals*, **74**, 97–102.
Hardman, K., Rhyne, J. J., Prince, E., Smith, H. K., Malik, S. K., and Wallace, W. E. (1982) *Rare Earth Mod. Sci. Technol.*, **3**, 477–8.
Hardman-Rhyne, K., Smith, H. K., and Wallace, W. E. (1984) *J. Less Common Metals*, **96**, 201–11.
Harris, L. A., White, G. D., and Thoma, R. E. (1959) *J. Phys. Chem.*, **63**, 1974–5.
Harris, L. A. (1960) *Acta Crystallogr.*, **13**, 502.
Harris, L. A. and Finch, C. B. (1972) *Am. Mineral.*, **57**, 1894–8.
Hasty, R. A. and Boggs, J. E. (1971) *J. Inorg. Nucl. Chem.*, **33**, 874–6.

Hauser, O. and Wirth, F. (1908) *Z. Anorg. Chem.*, **60**, 242–6.
Hayek, E. and Rehner, T. (1949) *Experientia*, **5**, 114.
Hayek, E., Rehner, T., and Frank, A. (1951) *Monatsh. Chem.*, **82**, 575–87.
Hecht, F. (1928) *Z. Anal. Chem.*, **75**, 28–39.
Hecht, F. and Ehrmann, W. (1935) *Z. Anal. Chem.*, **100**, 87–98.
Heindl, F. and Loriers, J. (1974) *Bull. Soc. Chim. Fr.*, 377–8.
Helean, K. B., Navrotsky A., Lumpkin, G. R., Colella, M., Lian, J., Ewing, R. C., Ebbinghaus B., and Catalano, J. G. (2003) *J. Nucl. Mater.*, **320**, 231–44.
Henkie, Z., Markowski, P. J., and Zdanowicz, E. (1976) *Proc. Second Int. Conf. on Electronic Structure of Actinides,* Wroclaw (Poland), pp. 425–9.
Henkie, Z. and Markowski, P. J. (1978) *J. Phys. Chem. Solids*, **39**, 39–43.
Henkie, Z. and Wawryk, R. (2002) *Solid State Commun.*, **122**, 1–6.
Hentz, F. C. and Johnson, J. S. (1966) *Inorg. Chem.*, **5**, 1337–44.
Hess, R. F., Abney, K. D., Burris, J. L., Hochheimer, H. D., and Dorhout, P. K. (2001) *Inorg. Chem.*, **40**, 2851–9.
Hiebl, K., Rogl, P., Uhl, E., and Sienko, R. J. (1980) *Inorg. Chem.*, **19**, 3316–20.
Hietanen, S. and Sillen, L. G. (1964) *Acta Chem. Scand.*, **18**, 1018–9.
Hildenbrand, D. L. and Murad, E. (1974a) *J. Chem. Phys.*, **61**, 5466–7.
Hildenbrand, D. L. and Murad, E. (1974b) *J. Chem. Phys.*, **61**, 1232–7.
Hildenbrand, D. L. and Lau, K. H. (1990) *J. Chem. Phys.*, **93**, 5983–9.
Hill, N. A. and Cavin, O. B. (1964) *J. Am. Ceram. Soc.*, **47**, 360–1.
Hill, R. and Lieser, K. H. (1992) *Fresenius J. Anal. Chem.*, **342**, 337–40.
Hoffmann, A. (1935) *Z. Phys. Chem. B*, **28**, 65–77.
Hogfeldt, E. (1982) *Stability Constants of Metal-ion Complexes.* part A, *Inorganic Ligands, IUPAC Chemical Data Series*, no. 21, Pergamon Press, Oxford, p. 122.
Hönigschmid, O. (1906a) *Monatsh. Chem.*, **27**, 205–12.
Hönigschmid, O. (1906b) *C. R. Acad. Sci. Paris*, **142**, 157–9.
Hovey, J. K. (1997) *J. Phys. Chem.*, **101**, 4321–34.
Hubert, S., Barthelet, K., Fourest, B., Lagarde, G., Dacheux, N., and Baglan, N. (2001) *J. Nucl. Mater.*, **297**, 206–13.
Hubin, R. (1971) *Spectrochim. Acta*, **27A**, 311–9.
Hüfken, T., Witte, A. M., and Jeitschko, W. (1998) *J. Alloys Compds*, **266**, 158–63.
Hüfken, T., Witte, A. M., and Jeitschko, W. (1999) *J. Solid State Chem.*, **142**, 279–87.
Hulliger, F. (1966) *Nature*, **209**, 499–500; (1968) *J. Less Common Metals*, **16**, 113–7.
Hunt, E. B. and Rundle, R. E. (1951) *J. Am. Chem. Soc.*, **73**, 4777–81.
Huyghe, M., Lee, M.-R., Quarton, M., and Robert, F. (1991a) *Acta Crystallogr.*, **C47**, 244–6.
Huyghe, M., Lee, M.-R., Quarton, M., and Robert, F. (1991b) *Acta Crystallogr.*, **C47**, 1797–9.
Huyghe, M., Lee, M.-R., Jaulmes, S., and Quarton, M. (1993) *Acta Crystallogr.*, **C49**, 950–4.
Hyde, E. K. (1952) in Katzin (1952), paper 9.7, p. 554.
Hyde, E. K. and Wolf, M. J. (1952) in Katzin (1952), paper 3.12, p. 197.
Hyde, E. K. (1960) *The Radiochemistry of Thorium,* NAS-NS–3004, National Research Council, Springfield, VA.
Imre, L. (1927) *Z. Anorg. Allg. Chem.*, **164**, 214–8; **166**, 1–15.
International Critical Tables (1928) vol. 3, McGraw-Hill, New York, pp. 51–95.

Ionova, G., Madic, C., and Guillaumont, R. (1998) *Polyhedron*, **17**, 1991–5.
Isnard, O., Soubeyroux, J. L., Fruchart, D., Jacobs, T. H., and Buschow, K. H. J. (1992a) *J. Phys.: Conden. Matter*, **4**, 6367–74.
Isnard, O., Soubeyroux, J. L., Fruchart, D., Jacobs, T. H., and Buschow, K. H. J. (1992b) *J. Alloys Compds*, **186**, 135–45.
Isnard, O., Miraglia, S., Soubeyroux, J. L., Fruchart, D., Deportes, J., and Buschow, K. H. J. (1993) *J. Phys.: Cond. Matter*, **5**, 5481–90.
Jacob, I. (1981) *Solid State Commun.*, **40**, 1015.
Jacobson, E. L., Freeman, R. D., Tharp, A. G., and Searcy, A. W. (1956) *J. Am. Chem. Soc.*, **78**, 4850–2.
Jacoby, R. (1901) *Die Doppelnitrate des vierwertigen Ceriums und des Thoriums, Berlin,* as cited in Mellor, J. W. (1941) *A Comprehensive Treatise on Inorganic and Theoretical Chemistry*, vol. VII, Longmans, Green & Co., London, p. 251.
James, W. J. and Straumanis, M. E. (1956) *Acta Crystallogr.*, **9**, 376–9.
Jannasch, P. and Schilling, J. (1905) *J. Prakt. Chem.* **72**, 26–34.
Javorsky, C. A. and Benz, R. (1967) *J. Nucl. Mater.*, **23**, 192–8.
Jeitschko, W., Pollmeier, P. G., and Meisen, U. (1993) *J. Alloys Compds*, **196**, 105–9.
Jere, G. V. and Santhamma, M. T. (1977) *J. Less Common Metals*, **55**, 281–4.
Jiang, F. S. and Kuroda, P. K. (1987) *Radiochim. Acta*, **42**, 23–28.
Joao, A., Bigot, S., and Fromage, F. (1987) *Bull. Soc. Chim.*, **1**, 42–4.
Joao, A., Burrows, H. D., Zikovsky, L., and Lipponen, M. (1995) *Radiochim. Acta*, **68**, 177–83.
Johansson, G. (1968a) *Acta Chem. Scand.*, **22**, 389–98.
Johansson, G. (1968b) *Acta Chem. Scand.*, **22**, 399–409.
Johansson, G., Magini, M., and Ohtaki, H. (1991) *J. Solution Chem.*, **20**(8), 775–92.
Johnson, G. L., Kelly, M. I., and Cuneo, D. R. (1965) *J. Inorg. Nucl. Chem.*, **27**, 1787–91.
Johnson, K. R. (1889) *Berl. Dtsch. Chem. Ges.*, **22**, 976–80.
Jones, D. W., McColm, I. J., Steadman, R., and Yerkess, J. (1987) *J. Solid State Chem.*, **68**, 219–26.
Juza, R. and Gerke, H. (1968) *Z. Anorg. Allg. Chem.*, **363**, 245–57.
Juza, R. and Sievers, R. (1968) *Z. Anorg. Allg. Chem.*, **363**, 258–72.
Kahn-Harari, A. (1971) *Rev. Int. Hautes Temp. Refract.*, **8**, 71–84.
Kalina, D. G., Marks, T. J., and Wachter, W. A. (1977) *J. Am. Chem. Soc.*, **99**, 3877–9.
Kanellakopulos, B., Dornberger, E., and Baumgärtner, F. (1974) *Inorg. Nucl. Chem. Lett.*, **10**, 155–60.
Kaplan, G. E. (1956) *Proc. Int. Conf. on the Peaceful Uses of Atomic Energy*, Geneva, 1955, vol. 8, pp. 184–7.
Karabasch, A. G. (1958) *Zh. Neorg. Khim.*, **3**, 986–95.
Karstens, H. (1909) *Z. Elektrochem.*, **15**, 33–4.
Katz, J. J. and Seaborg, G. T. (1957) *The Chemistry of the Actinide Elements,* Methuen, London, 58.
Katzin, L. I. (1944) Memorandum to G. T. Seaborg on October 14.
Katzin, L. I. (1948) Report AECD-2213.
Katzin, L. I. (1952) *Production and Separation of U^{233}: Collected Papers*, Natl. Nucl. En. Ser., Div. IV, 17B, Report TID–5223, USAEC, Oak Ridge, Tenn.
Katzin, L. I., Ferraro, J. R., Wendlandt, W. W., and McBeth, R. L. (1956) *J. Am. Chem. Soc.*, **78**, 5139–44.

Katzin, L. I. (1958) *J. Am. Chem. Soc.*, **30**, 5908–10.
Katzin, L. I. and Gulyas, E. (1960) *J. Phys. Chem.*, **64**, 1347–50.
Katzin, L. I., Kaplan, L., and Seitz, T. (1962) *Inorg. Chem.*, **1**, 963–4.
Katzin, L. I. (1966) in *Transition Metal Chemistry, A Series of Advances,* vol. 3 (ed. R. L. Carlin), Marcel Dekker, New York, pp. 56–88.
Katzin, L. I. (1983) *Kirk-Othmer Encyclopoedia of Chemical Technology,* 3rd edn, **22**, 989–1002.
Kauffmann, O. (1899) PhD Thesis, University of Rostok, Germany.
Keenan, T. K. (1966) *Inorg. Nucl. Chem. Lett.*, **2**, 153–6; 211–4.
Keil, R. (1981) *Fresenius Z. Anal. Chem.*, **305**, 374–8.
Keller, C. (1965) *J. Inorg. Nucl. Chem.*, **27**, 1233–46.
Keller, C. and Salzer, M. (1967) *J. Inorg. Nucl. Chem.*, **29**, 2925–34.
Kemper, C. P. and Krikorian, N. H. (1962) *J. Less Common Metals*, **4**, 244–51.
Keskar, M., Kasar, U. M., and Singh Mudher, K. D. (2000) *J. Nucl. Mater.*, **282**, 146–51.
Khan Malek, C., Péneau, A., and Guibé, L. (1982) *J. Mol. Struct.*, **83**, 201–12.
Khan, A. S. and Peterson, D. T. (1976) *J. Less Common Metals*, **50**, 103–6.
Kharitonov, Yu. Ya., Molodkin, A. K., and Balakaeva, T. A. (1969) *Zh. Neorg. Khim.*, **14**, 2761–7; *Russ. J. Inorg.Chem.*, **14**, 1453–6.
King, E. L. (1945) Ph.D. Thesis, University of California.
Kiriyama, T. and Kuroda, R. (1978) *Anal. Chim. Acta*, **101**, 207–10.
Klapötke, T. M. and Schulz, A. (1997) *Polyhedron*, **16**(6), 989–91.
Klinkenberg, P. F. A. and Lang, R. J. (1949) *Physica*, **15**, 774–88.
Klyuchnikov, V. M., Zaitsev, L. M., and Apraksin, I. A. (1972) *Zh. Neorg. Khim.*, **17**, 2269–73.
Knacke, O., Müller, F., and van Rensen, E. (1972a) *Phys. Chem.*, **80**, 82–90.
Knacke, O., Müller, F., and van Rensen, E. (1972b) *Z. Phys. Chem.*, **80**, 91–100.
Knacke, O., Münstermann, E., and Probst, H. (1978) *Ber. Bunsen Ges.*, **82**, 154–9.
Koelling, D. D. and Freeman, A. J. (1971) *Solid State Commun.*, **9**, 1369–72.
Köhler, E., Brüser, W., and Thiele, K.-H. (1974) *J. Organomet. Chem.*, **76**, 235–40.
Köhler, S., Deißenberger, R., Eberhardt, K., Erdmann, N., Herrmann, G., Huber, G., Kratz, J. V., Nunnemann, M., Passler, G., Rao, P. M., Riegel, J., Trautmann, N., and Wendt, K (1997) *Spectrochim. Acta B*, **52**, 717–26.
Kohlmann, H. and Beck, H. P. (1999) *Z. Kristallogr.*, **214**, 341–5.
Kohlschütter, V. (1901) *Liebig's Ann.*, **317**, 158–89.
Kojic-Prodic, B., Slukic, M., and Ruzic Toros, Z. (1982) *Acta Crystallogr.*, **B38**, 67–71.
Kolb, A., Melzer, G., Merckle, A., and Teufel, C. (1908) *Z. Anorg. Chem.*, **60**, 123–33.
Kolb, A. (1913) *Z. Anorg. Chem.*, **83**, 143–8.
Konrad, T. and Jeitschko, W. (1995) *Z. Naturforsch.*, **50b**, 1195–9.
Konrad, T., Jeitschko, W., Danebrock, M. E., and Evers, C. B. H. (1996) *J. Alloys Compds*, **234**, 56–61.
Koppel, I. and Holtkamp, H. (1910) *Z. Anorg. Chem.*, **67**, 266–92.
Korobkov, I., Gambarotta, S., and Yap, G. P. A. (2003) *Angew. Chem.*, **115**, 838–42.
Korshunov, B. G. and Drobot, D. V. (1971) *Zh. Neorg. Khim.*, **16**, 556–7.
Korst, W. L. (1962) *Acta Crystallogr.*, **15**, 287–8.
Koulkès-Pujo, A. M., Martin-Rovet, D., Folcher, G., Plissionier, M., and Pascal, J. L. (1982) *Nouv. J. Chim.*, **6**, 571–2.
Kovalchuk, E. L., Smolnikov, A. A., and Temmoev, A. H. (1982) *Phys. Appl.*, **8**, 297–303.

Kraus, K. A. and Holmberg, R. W. (1954) *J. Phys. Chem.*, **58**, 325–30.
Kravchenko, E. A., Ivanova, O. M., and Ilin, E. G. (1975) *Zh. Neorg. Khim.*, **20**, 2556–7.
Krupa, J. C., Khan Malek, C., Delamoye, P., Moine, B., and Pedrini, C. (1987) *Phys. Status Solidi B*, **140**, 289–300.
Krupa, J. C., Delamoye, P., and Milicic-Tang, A. (1995) *Zh. Prikl. Spek.*, **62**, 167–78.
Krupka, M. C. (1970) *J. Less Common Metals*, **20**, 135–40.
Krüss, G. and Volck, C. (1894) *Z. Anorg. Chem.*, **5**, 75–9.
Krüss, G. and Nilson, L. F. (1887a) *Z. Phys. Chem.*, **1**, 301–6.
Krüss, G. and Nilson, L. F. (1887b) *Ber. Dtsch. Chem. Ges.*, **20**, 1665–76.
Krüss, G. (1894) *Z. Anorg. Chem.*, **6**, 49–56.
Ku, H. C., Meisner, G. P., Acker, F., and Johnston, D. C. (1980) *Solid State Commun.*, **35**, 91–6.
Kumar, N. and Tuck, D. G. (1983) *Inorg. Chem.*, **22**, 1951–2.
Lafferty, J. M. (1951) *J. Appl. Phys.*, **22**, 299–309.
Laligant, Y., Le Bail, A., Avignant, D., Cousseins, J. C., and Ferey, G. (1989) *J. Solid State Chem.*, **80**, 206–12.
Laligant, Y., Ferey, G., El Ghozzi, M., and Avignant, D. (1992) *Eur. J. Solid State Inorg. Chem.*, **29**, 497–504.
Lam, D. J., Darby, J. B. Jr, and Nevitt, M. V. (1974) in *The Actinides: Electronic Structure and Related Properties,* ch. 4 (eds. A. J. Freeman and J. B. Darby), Academic Press, New York.
Langer, S., Baldwin, N., Gantzel, P., Kester, F., and Hancock, C. (1964) in *Nuclear Metallurgy,* vol. 10 (eds. J. T. Waber, P. Chiotti, and W. N. Miner), Edward Bros., Ann Arbor, p. 359.
Langmuir, D. and Herman, J. S. (1980) *Geochim. Cosmochim. Acta*, **44**, 1753–66.
Larson, E. M., Eller, P. G., Cremers, T. L., Penneman, R. A., and Herrick, C. C. (1989) *Acta Crystallogr.*, **C45**, 1669–72.
Lau, K. F., Vaughan, R. W., and Satterthwaite, C. B. (1977) *Phys. Rev. B*, **15**, 2449–57.
Laubereau, P. G., Ganguly, J., Burns, J. H., Benjamin, B. M., Atwood, J. L., and Selbin, J. (1971) *Inorg. Chem.*, **10**, 2274–80.
Laubscher, A. E. and Fouché, K. F. (1971) *J. Inorg. Nucl. Chem.*, **33**, 3521–35.
Laud, K. R. (1971) *J. Am. Ceram. Soc.*, **54**, 296–8.
Laügt (1973) *J. Appl. Crystallogr.*, **6**, 299–301.
Launay, S. and Rimsky, A. (1980) *Acta Crystallogr.*, **B36**, 910–2.
Launay, S., Mahe, P., Quarton, M., and Robert, F., J. (1992) *J. Solid State Chem.*, **97**, 305–13.
Launay, S., Jaulmes, S., Lucas, F., and Quarton, M. (1998) *J. Solid State Chem.*, **136**, 199–205.
Le Berre, F., Boucher, E., Allain, M., and Courbion, G. (2000) *J. Mater. Chem.*, **10**, 2578–86.
Le Flem, G. (1967) Thése de Doctorat, Bordeaux.
Lebeau, P. and Damiens, A. (1913) *C. R. Acad. Sci. Paris*, **156**, 1987–9.
Leber, A. (1927) *Z. Anorg. Allg. Chem.*, **166**, 16–26.
Leciejewicz, J., Siek, S., and Szytula, A. (1988) *J. Less Common Metals*, **144**, 9–13.
Lefèbvre, J. (1957) *Bull. Soc. Chim.*, **14**, 227–33.
Le Flem, G. and Hagenmuller, P. (1964) *Rev. Hautes Temp. Refract.*, **1**, 149–52.

Le Flem, G., Hardy, A., and Hagenmuller, P. (1965) *C. R. Acad. Sci. Paris C*, **260**, 1663–5.
Lesinsky, J. and Gundlich, C. (1897) *Z. Anorg. Chem.*, **15**, 81–3.
Le Vanda, C., Solar, J. R., and Streitwieser, A. Jr (1980) *J. Am. Chem. Soc.*, **102**, 2128–9.
Lipkind, H. and Newton, A. S. (1952) in Katzin (1952), paper 7.8, p. 398.
Li, Y.-P., Krivovichev, S. V., and Burns, P. C. (2000) *Am. Miner.*, **85** 1521–5.
Liu, C., Zhao, Z., Yang, X., Ye, X., and Wu, Y. (1997) *Sci. China, Ser. A: Math., Phys., Astron.*, **40**, 1210.
Lobanov, M. V., Li, S., and Greenblatt, M. (2003) *Chem. Mater.*, **15**, 1302–8.
Louer, M., Brochu, R., Louer, D., Arsalane, S., and Ziyad, M. (1995) *Acta Crystallogr.*, **B51**, 908–13.
Loye, O., Laurelle, P., and Harari, A. (1968) *C. R. Acad. Sci. Paris C*, **266**, 454–6.
Luengo, C. A., Cotiguola, J. M., Sereni, J. G., Sweedler, A. R., and Maple, M. B. (1972a) *Proc. 13th Int. Conf. Low Temp. Phys.,* Boulder, Colorado, 585–9.
Luengo, C. A., Cotiguola, J. M., Sereni, J. G., Sweedler, A. R., Maple, M. B., and Huber, J. G. (1972b) *Solid State Commun.*, **10**, 459–63.
Lundgren, G. (1950) *Ark. Kem.*, **2**, 535–49.
Lundgren, G. and Sillen, L. G. (1949) *Naturwiss.*, **36**, 345–6.
Madariaga, G., Perez-Mato, J. M., and Aramburu, I. (1993) *Acta Crystallogr.*, **B49**, 244–54.
Magini, M., Cabrini, A., Scibona, G., Johansson, G., and Sandström, M. (1976) *Acta Chem. Scand. A*, **30**, 437–47.
Mahalingham, A., Kalpana, G., Kansalaya, B., Palanivel, B., and Rajagopalan, M. (1993) *Phys. Status Solidi B*, **178**, 185–97.
Manriquez, J. M., Fagan, P. J., and Marks, T. J. (1978) *J. Am. Chem. Soc.*, **100**, 3939–41.
Manske, W. J. (1965) *Luminescent Gas Mantles and Their Mountings*, Minnesota Mining and Manufacturing Company, 32 pp.
Manuelli, C. and Gasparinetti, B. (1902) *Gazz. Chim. Ital.*, **32**, 523–31.
Marcus, Y. and Kertes, A. S. (1969) *Ion Exchange and Solvent Extraction of Metal Complexes,* Wiley-Interscience, London.
Marden, J. W. and Rentschler, H. C. (1927) *Ind. Eng. Chem.*, **19**, 97–103.
Marks, T. J. and Wacher, W. A. (1976) *J. Am. Chem. Soc.*, **98**, 703–10.
Marks, T. J., Seyam, A. M., and Wachter, W. A. (1976) *Inorg. Synth.*, **16**, 147–51.
Mason, D. M. (1964) Technical Report – Institute of Gas Technology (Chicago), No. 9, 19 pp.
Mason, J. T., Jha, M. C., and Chiotti, P. (1974a) *J. Less Common Metals*, **34**, 143–51.
Mason, J. T., Jha, M. C., Bailey, D. M., and Chiotti, P. (1974b) *J. Less Common Metals*, **35**, 331–8.
Martinot, L. and Fuger, J. (1985) in *Standard Potentials in Aqueous Solution* (eds. A. J. Bard, R. Parsons, and J. Jordan), IUPAC, Marcel Dekker, New York, ch. 21, p. 640.
Matignon, C. (1900) *C. R. Acad. Sci. Paris*, **131**, 837–9.
Matignon, C. and Delepine, M. (1901) *C. R. Acad. Sci. Paris.*, **132**, 36–8.
Matignon, C. A. and Bourion, R. (1904) *C. R. Acad. Sci. Paris*, **138**, 631–3.
Matignon, C. and Delepine, M. (1907) *Ann. chim. phys.*, **10**, 130–44.
Matignon, C. A. (1908) *C. R. Acad. Sci. Paris*, **147**, 1292–3.
Matkovic, B. and Sljukic, M. (1965) *Croat. Chem. Acta*, **37**, 115–6.

Matkovic, B., Sljukic, M., and Prodic, B. (1966) *Croat. Chem. Acta*, **38**, 69–70.
Matkovic, B., Prodic, B., and Sljukic, M. (1968) *Bull. Soc. Chim. Fr.*, 1777–9.
Matkovic, B., Kojic-Prodic, B., Sljukic, M., Topic, M., Willett, R. D., and Pullen, F. (1970) *Inorg. Chim. Acta*, **4**, 571–6.
Matthews, J. M. (1898) *J. Am. Chem. Soc.*, **20**, 815–39; 839–43.
Maxim, P., Müller, R., and Schnabel, B. (1979) *Physica*, **24**, 53–6.
Mayankutty, P. C., Jangida, B. L., and Sundaresan, M. (1982) *Separat. Sci. Technol.*, **17**, 1327–37.
Mazeina, L., Ushakov, S. V., Navrotsky, A., and Boatner, L. A. (2005) *Geochim. Cosmochim. Acta* **69**, 4675–783.
Meisel, K. (1939) *Z. Anorg. Allg. Chem.*, **240**, 300–2.
Meissner, W. (1929) *Naturwissenschaften*, **17**, 390–1; (1930) *Z. Phys.*, **61**, 191–8.
Mellor, J. W. (1941) *A Comprehensive Treatise on Inorganic and Theoretical Chemistry,* vol. VII, Longmans, Green & Co., London, p. 241.
Mentzen, B. F. (1969) *Rev. Chim. Miner.*, **6**, 713–25.
Mentzen, B. F. (1971a) *J. Solid State Chem.*, **3**, 12–9.
Mentzen, B. F. (1971b) *J. Solid State Chem.*, **3**, 20–5.
Merigou, C., Le Du, J. F., Genet, M., Ouillon, N., and Chopin, T. (1995) *New J. Chem.*, **19**, 1037–45.
Merkusheva, S. A., Skorik, N. A., Kumok, V. N., and Serebrennikov, V. V. (1967) *Radiokhimiya*, **9**, 723–5; *Sov. Radiochem.*, **9**, 683–5.
Metzger, F. J. and Zons, F. W. (1912) *Ind. Eng. Chem.*, **4**, 493–5.
Meyer, R. J. and Jacoby, R. (1901) *Z. Anorg Chem.*, **27**, 359–89.
Meyer, R. J. and Gumperz, A. (1905) *Berl. Dtsch. Chem. Ges.*, **38**, 817–25.
Meyer, R. J. (1908) *Z. Elektrochem.*, **14**, 809–10; (1909) *Z. Elektrochem.*, **15**, 105–6.
Meyerson, G. A. (1956) *Proc. Int. Conf. on the Peaceful Uses of Atomic Energy*, Geneva, 1955, vol. 8, pp. 188–93.
Miekeley, N. and Küchler (1987) *Inorg. Chim. Acta*, **140**, 315–9.
Mikheev, N. B., Kulyhukin, S. A., and Kamenskaya, A. N. (1993) *Radiokhimiya*, **35**, 1; *Sov. Radiochem.*, **35**, 249.
Milic, N. A. (1971) *Acta Chem. Scand.*, **25**, 2487–98.
Milic, N. B. (1981) *J. Chem. Soc. Dalton*, 1445–9.
Milic, N. A. and Suranji, T. M. (1982) *Can. J. Chem.*, **60**, 1298–303.
Miller, J. F., Caton, R. H., and Satterthwaite, C. B. (1976) *Phys. Rev. B*, **14**, 2795–800.
Mintz, E. A., Moloy, K. G., Marks, T. J., and Day, V. W. (1982) *J. Am Chem. Soc.*, **104**, 4692–5.
Misciatelli, P. (1929) *Phil. Mag.*, **7**, 670–4.
Misciatelli, P. (1930a) *Gazz. Chim. Ital.*, **60**, 833–8.
Misciatelli, P. (1930b) *Gazz. Chim. Ital.*, **60**, 882–5.
Mitchell, R. H. and Chakhmouradian, A. R. (1999) *Phys. Chem. Miner.*, **26**, 396–405.
Moissan, H. and Étard, A. (1896) *C. R. Acad. Sci. Paris*, **122**, 573
Moissan, H. and Étard, A. (1897) *Ann. Chim. Phys.*, **7** (12), 427–32.
Moissan, H. and Martinsen, M. (1905) *C. R. Acad. Sci. Paris*, **140**, 1510–5.
Moissan, H. and Hönigschmid, O. (1906) *Ann. Chim. Phys.*, **8** (8), 182–92.
Moll, H., Denecke, M. A., Jalilehvand, F., Sandström, M., and Grenthe, I. (1999) *Inorg. Chem.*, **38**, 1795–9.

Molodkin, A. K., Skotnikova, E. G., and Arutyunyan, E. (1964) *Zh. Neorg. Khim.*, **9**, 2705–9; *Russ. J. Inorg. Chem.*, **9**, 1458–61.
Molodkin, A. K., Petrov, K. I., Balakayeba, T. A., and Kuchumova, A. N. (1968a) *Zh. Neorg. Khim.*, **13**, 3209–15; *Russ. J. Inorg. Chem.*, **13**, 1654–7.
Molodkin, A. K., Ivanova, O. M., Kozina, L. E., and Petrov, K. I. (1968b) *Russ. J. Inorg. Chem.*, **13**, 694–9.
Molodkin, A. K., Balakayeva, T. A., and Kuchumova, A. N. (1970) *Zh. Neorg. Khim.*, **15**, 1152–3; *Russ. J. Inorg. Chem.*, **15**, 589–90.
Molodkin, A. K., Belyakova, Z. V., and Ivanova, O. M. (1971) *Zh. Neorg. Khim.*, **16**, 1582–9; *Russ. J. Inorg. Chem.*, **16**, 835–9.
Montignie, E. (1947) *Bull. Soc. Chim. Fr.*, 748–9.
Moodenbaugh, A. R., Johnston, D. C., Viswanathan, R., Shelton, R. N., Delong, L. E., and Fertig, W. A. (1978) *J. Low Temp. Phys.*, **33**, 175–203.
Moon, H. C. (1989) *Bull. Korean Chem. Soc.*, **10**(3), 270–2.
Mooney, R. C. L. (1949) *Acta Crystallogr.*, **2**, 189–91.
Morss, L. R. and McCue, M. C. (1976) *J. Chem. Eng. Data*, **21**, 337–41.
Moriyama, H., Kitamura, A., Fujiwara, K., and Yamana, H. (1999) *Radiochim. Acta*, **87**, 97–104.
Morss, L. R. and McCue, M. C. (1976) *J. Chem. Eng. Data*, **21**, 337–41.
Moseley, P. T., Sanderson, S. W., and Wheeler, V. J. (1971) *J. Inorg. Nucl. Chem.*, **33**, 3975–6.
Moss, M. A. and Jeitschko, W. (1989a) *Z. Kristallogr.*, **186**, 204–5.
Moss, M. A. and Jeitschko, W. (1989b) *Z. Kristallogr.*, **186**, 204.
Moss, M. A. and Jeitschko, W. (1991a) *Z. Anorg. Allg. Chem.*, **603**, 57–67.
Moss, M. A. and Jeitschko, W. (1991b) *Z. Metallkunde*, **82**, 669–74.
Moskvin, A. I. and Essen, L. N. (1967) *Russ. J. Inorg. Chem.*, **12**, 359–62.
Moskvin, A. I., Essen, L. N., and Bukhtiyarova, T. N. (1967) *Russ. J. Inorg. Chem.*, **12**, 1794–5.
Moulin, C., Amekraz, B., Hubert, S., and Moulin, V. (2001) *Anal. Chim. Acta*, **441**, 269–79.
Moze, O., Brueck, E., de Boer, F. R., and Buschow, K. H. J. (1996) *J. Magn. Magn. Mater.*, **152**, 341–4.
Mucker, K., Smith, G. S., Johnson, Q., and Elson, R. E. (1969) *Acta Crystallogr. B*, **25**, 2362–5.
Mueller, M. H., Beyerlein, R. A., Jorgensen, J. D., Brun, T. O., Satterthwaite, C. B., and Caton, R. (1977) *J. Appl. Crystallogr.*, **10**, 79–83.
Müller, A. (1906) *Berl. Dtsch. Chem. Ges.*, **39**, 2857–9; (1908) *Z. Anorg. Chem.*, **57**, 311–22.
Murthy, M. S. and Redhead, P. A. (1974) *J. Vac. Sci. Technol.*, **11**, 837–42.
Murthy, P. R. and Patel, C. C. (1965) *Indian Chem.*, **3**, 134–5.
Nabar, M. A., Mhatre, B. G., and Vasaikar, A. P. (1981) *J. Appl. Crystallogr.*, **14**, 469–70.
Nabar, M. A. and Mhatre, B. G. (1982) *J. Solid State Chem.*, **45**, 135–9.
Nabar, M. A. and Mangaonkar, S. S. (1991) *Eur. J. Solid State Inorg. Chem.*, **28**, 549–52.
Nabar, M. A. and Mhatre, B. G. (2001) *J. Alloys Compds*, **323–4**, 83–5.
Nabivanets, B. I. and Kudritskaya, L. N. (1964) *Ukr. Khim. Zh.*, **30**, 891–5.

Nakamura, T. (1974) *Chem. Lett.*, 429–34.
Nakashima, T. and Zimmer, E. (1984) *Radiochim. Acta*, **37**, 165–7.
Naray-Szabo, L. (1951) in *Crystal Structures,* vol. 1 (ed. R. W. Wyckoff), Interscience Publishers, New York, no. 1, 30.
Narducci, A. A. and Ibers, J. A. (1998a) *Chem. Mater.*, **10**, 2811–23.
Narducci, A. A. and Ibers, J. A. (1998b) *Inorg. Chem.*, **37**, 3798–801.
Narducci, A. A. and Ibers, J. A. (2000) *Inorg. Chem.*, **39**, 688–91.
Naslain, R., Etourneau, J., and Kasper, J. S. (1971) *J. Solid State Chem.*, **3**, 101–11.
Nebel, D. and Urban, G. (1966) *Z. Phys. Chem. (Leipzig)*, **233**, 73–84.
Neck, V. and Kim, J. I. (2000) *Radiochim. Acta*, **88**, 815–22.
Neck, V. and Kim, J. I. (2001) *Radiochim. Acta*, **89**, 1–16.
Neck, V (2002) *ANDRA project: Solution Chemistry of Actinides and Radium; Lot 2: Cement water Environment, 3rd Annual and Final Report to Phase 3* "*Experimental Programme*", FZK-INE 002/02 Report.
Neck, V., Müller, R., Bouby, M., Altmaier, M., Rothe, J., Denecke, M. A., and Kim, J. I. (2002) *Radiochim. Acta*, **90**, 485–94.
Neish, A. C. (1904) *J. Am. Chem. Soc.*, **26**, 780–3.
Neubert, A. and Zmbov, K. F. (1974) *High Temp. Sci.*, **6**, 303–8.
Newton, A. S., Lipkind, H., Keller, W. H., and Iliff, J. E. (1952a) in Katzin (1952), paper 8.3, p. 419.
Newton, A. S., Johnson, O., Tucker, W., Fisher, R. W., and Lipkind, H. (1952b) in Katzin (1952), paper 8.6, p. 462.
Nilson, L. F. (1876) *Berl. Dtsch. Chem. Ges.*, **9**, 1142.
Nilson, L. F. (1882a) *Berl. Dtsch. Chem. Ges.*, **15**, 2537.
Nilson, L. F. (1882b) *C. R. Acad. Sci. Paris*, **95**, 727.
Nilson, L. F. (1883) *Berl. Dtsch. Chem. Ges.*, **16**, 153.
NIST (2002) NIST Critically Selected Stability Constants of Metal Complexes:version 7.0.NIST Standard Reference Database 46, National Institute of Standards and Technology, Gaithersburg, MD.
Noël, H. (1980) *J. Inorg. Nucl. Chem.*, **42**, 1715–7.
Noël, H. and Potel, M. (1982) *Acta Crystallogr. B*, **38**, 2444–5.
Nordenskjöld, A. E. and Chydenius, J. J. (1860) *Pogg. Ann.*, **110**, 642.
Nordenskjöld, A. E. (1861) *Pogg. Ann.*, **114**, 612.
Nordling, C. and Hagström, S. (1964) *Z. Phys.*, **178**, 418–32.
Nottorf, R. W., Wilson, A. S., Rundle, R. E., Newton, A. S., and Powell, J. E. (1952) in Katzin (1952), paper 7.6, p. 350.
Nugent, L. J., Baybarz, R. D., Burnett, J. L., and Ryan, J. L. (1973) *J. Phys. Chem.*, **77**, 1528–39.
Oesterreicher, H., Clinton, J., and Bittner, H. (1976) *J. Solid State Chem.*, **16**, 209–10.
Oetting, F. L., Rand, M. H., and Ackermann, R. J. (1976) in *The Chemical Thermodynamics of Actinide Elements and Compounds*, part 1, *The Actinide Elements* (eds. F. L. Oetting, V. A. Medvedev, M. H. Rand, and E. F. Westrum Jr), STI/PUB/424/1, IAEA, Vienna.
Östhols, E., Bruno, J., and Grenthe, I. (1994) *Geochim. Cosmochim. Acta*, **58**, 613–23.
Östhols, E. (1995) *Radiochim. Acta*, **68**, 185–90.
Ohta, T. and Sata, T. (1974) *Yogyo Kyoka Shi*, **82**, 387–401.
Olson., W. M. and Mulford, R. N. R. (1965) *J. Phys. Chem.*, **69**, 1223–6.

Omejec, L. and Ban, Z. (1971) *Z. Anorg Allg. Chem.*, **380**, 111–7.
Onosov, V. N. (1971) *Tr. Ural. Politekh. Inst.*, **193**, 21–7.
Oyamada, R. and Yoshida, S. (1975) *J. Phys. Soc. Japan*, **38**, 1786.
Pagès, M. and Freundlich, W. (1971) *C. R. Acad. Sci. Paris C*, **272**, 1861–2.
Pai, M. R., Wani, B. N., and Gupta, N. M. (2002) *J. Mater. Sci. Lett.*, **21**, 1187–90.
Palanivel, B., Kalpana, G., and Rajagopalan, M. (1995) *Mater. Res. Soc. Symp. Proc.*, **364**, 1095.
Palisaar, A.-P. and Juza, R. (1971) *Z. Anorg. Allg. Chem.*, **384**, 1–11.
Palmer, C. (1895) *Am. Chem. J.*, **17**, 374–9.
Palmy, C., Flach, R., and De Trey, P. (1971) *Physica*, **55**, 663–8.
Parry, J. S., Cloke, F. G. N., Coles, S. J., and Hursthouse, M. B. (1999) *J. Am. Chem. Soc.*, **121**, 6867–71.
Pastor, R. C. and Arita, K. (1974) *Mater. Res. Bull.*, **9**, 579–83.
Paul, R. C., Singh, S., and Verma, R. D. (1981) *J. Indian Chem. Soc.*, **58**, 24–5.
Pearson, W. B. (1985) *Z. Kristallogr.*, **171**, 23–39.
Pedziwiatr, A. T., Wallace, W. E., and Burzo, E. (1986) *J. Magn. Magn. Mater.*, **61**, 177–82.
Penneman, R. A., Ryan, R. R., and Rosenzweig, A. (1968) *J. Chem. Soc. Chem. Commun.*, 990–1.
Penneman, R. A., Ryan, R. R., and Kressin, I. K. (1971) *Acta Crystallogr. B*, **27**, 2279–83.
Penneman, R. A., Ryan, R. R., and Rosenzweig, A. (1973) *Struct. Bonding*, **13**, 1–52.
Penneman, R. A., Ryan, R. R., and Larson, A. C. (1976) *Proc. Moscow Symp. on Chem. Transuranium Elements, 1972,* Pergamon Press, Oxford, , pp. 265–9.
Peppard, D. F. and Mason, G. W. (1963) *Nucl. Sci. Eng.*, **16**, 382–8.
Peppard, D. F. (1966) *Adv. Inorg. Chem. Radiochem.*, **9**, 1–80.
Peppard, D. F. (1971) *Annu. Rev. Nucl. Sci.*, **21**, 365–96.
Peretz, M., Zamir, D., and Hadari, Z. (1978) *Phys. Rev. B*, **18**, 2059–65.
Perezy Jorba, M., Mondange, H., and Collongues, R. (1961) *Bull. Soc. Chim. Fr.*, 79–81.
Perrin, D. D. (1982) *Stability Constants of Metal-ion Complexes, Part B-Organic Ligands,* IUPAC Chemical Data Series, n°21, Pergamon Press, Oxford.
Peterson, D. T. and Schmidt, F. A. (1971) *J. Less Common Metals*, **24**, 223–8.
Peterson, D. T., Westlake, D. G., and Rexer, J. (1959) *J. Am. Chem. Soc.*, **81**, 4443–5.
Pissarsjewski, L. (1900) *J. Russ. Phys.-Chem. Ges.*, **32**, 609–27.
Pissarsjewsky, L. (1902) *Z. Anorg. Chem.*, **31**, 359–67.
Pitman, D. T. and Das, D. K. (1960) *J. Electrochem. Soc.*, **107**, 763–6.
Popovic, S. (1971) *J. Appl. Cryst.*, **4**, 240–1.
Post, B., Moskowitz, D., and Glaser, F. S. (1956) *J. Am. Chem. Soc.*, **78**, 1800–2.
Price, C. E. and Warren, I. H. (1965) *J. Electrochem. Soc.*, **112**, 510–3.
Pulcinelli, S. H. and de Almeida Santos, R. H. (1989) *J. Fluorine Chem.*, **42**, 41–50.
Quarton, M., Rimsky, H., and Freundlich, W. (1970) *C. R. Acad. Sci. Paris C*, **271**, 1439–41.
Quarton, M. and Kahn, A. (1979) *Acta Crystallogr.*, **C35**, 2529–32.
Rabinovich, D., Chamberlin, R. M., Scott, B. L., Nielsen, J. B., and Abney, K. D. (1997) *Inorg. Chem.*, **36**, 4216–7.
Racah, G. (1950) *Physica*, **16**, 651–66.
Radzewitz, H. (1966) Report KFK-433.

Rai, H. C. and Sahoo, B. (1974) *Indian J. Chem.*, **12**, 1302–3.
Rai, D., Swanson, J. L., and Ryan, J. L. (1987) *Radiochim. Acta*, **42**, 35–41.
Rai, D., Felmy, A. R., Moore, D. A., and Mason, M. J. (1995) *Mater. Res. Soc. Symp. Proc.*, **353**, 1143–50.
Rai, D., Felmy, A. R., Sterner, S. M., Moore, D. A., Mason, M. J. M., and Novak, C. F. (1997) *Radiochim. Acta*, **79**, 239–47.
Ramamurthy, P. and Patel, C. C. (1963) *J. Inorg. Nucl. Chem.*, **25**, 310–2.
Raman, V. and Jere, G. V. (1973a) *Indian J. Chem.*, **11**, 1318–9.
Raman, V. and Jere, G. V. (1973b) *Indian J. Chem.*, **11**, 31–4.
Rammelsberg, C. (1873) *Pogg. Ann.*, **150**, 198.
Rand, M. H., von Goldbeck, O., Ferro, R., Girgis, K., and Dragoo, A. L. (1975) in *Thorium: Physico-Chemical Properties of its Compounds and Alloys* (ed. O. Kubaschewski), IAEA, Vienna.
Raub, E. and Engles, M. (1947) *Metallforsch.*, **2**, 115–9.
Raymond, D. P., Duffield, J. R., and Williams, D. R. (1987) *Inorg. Chim. Acta.*, **140**, 309–13.
Reid, A. F. and Wailes, P. C. (1966) *Inorg. Chem.*, **5**, 1213–6.
Ribas Bernat, J. G. and Ramos Alonso, V. (1976) *Ion (Madrid)*, **36**, 11–3.
Ribas Bernat, J. G., Ramos Alonso, V., and Balcazar Pinal, J. L. (1977) *Ann. Quim.*, **73**, 1425–7.
Rickard, C. E. F. and Woolard, D. C. (1978) *Inorg. Nucl. Chem. Lett.*, **14**, 207–10.
Rogl, P. and Nowotny, H. (1974) *Monatsh. Chem.*, **105**, 1082–98.
Rogl, P. (1978) *J. Nucl. Mater.*, **73**, 198–203.
Rogl, P. (1979) *J. Nucl. Mater.*, **79**, 154–8.
Rogl, P. and Fischer, P. (1989) *J. Solid State Chem.*, **78**, 294–300.
Roll, W. and Dempster, A. J. (1952) in Katzin (1952), paper 9.22, p. 639.
Rollefson, G. K. (1947) unpublished work cited in Report CB-3717.
Roozeboom, H. W. B. (1890) *Z. Phys. Chem.*, **5**, 198–216.
Rosengren, A., Ebbsjö, I., and Johansson, B. (1975) *Phys. Rev. B*, **12**, 1337–42.
Rosenheim, A. and Schilling, J. (1900) *Berl. Dtsch. Chem. Ges.*, **33**, 977–80.
Rosenheim, A., Samter, V., and Davidsohn, J. (1903) *Z. Anorg. Chem.*, **35**, 424–53.
Rosenheim, A. and Kelmy, M. (1932) *Z. Anorg. Allg. Chem.*, **206**, 31–43.
Rothschild, B. F., Templeton, C. C., and Hall, N. F. (1948) *J. Phys. Col. Chem.*, **52**, 1006–20.
Rothwarf, F. and Dubeck, L. W. (1973) *Solid State Commun.*, **13**, 1645–9.
Rozen, A. M., Nikolotova, Z. A., Kartasheva, N. A., Luk'yanenko, N. G., and Bogatskii, A. V. (1982) *Dokl. Akad. Nauk SSSR*, **263**, 1165–9.
Ruff, O. and Brintzinger, H. (1923) *Z. Anorg. Allg. Chem.*, **129**, 267–75.
Ruh, R. and Wadsley, A. D. (1966) *Acta Crystallogr.*, **21**, 974–8.
Rundle, R. E., Wilson, A. S., Nottorf, R., and Rauchle, R. F. (1948a) Report AECD-2120.
Rundle, R. E., Baenziger, N. C., Wilson, A., McDonald, R. A., Chiotti, P., and Rundle, R. E. (1948b) *Acta Crystallogr.*, **1**, 180–7.unpublished data cited in
Rundle, R. E., Schull, C. G., and Wollan, E. O. (1952) *Acta Crystallogr.*, **5**, 22–6.
Ruzic Toros, Z., Kojic-Prodic, B., Liminga, R., and Popovic, S. (1974) *Inorg. Chim. Acta*, **8**, 273–8.

Ryan, R. R., Penneman, R. A., and Rosenzweig, A. (1969) *Acta Crystallogr. B*, **25**, 1958–62.
Ryan, R. R. and Penneman, R. A. (1971) *Acta Crystallogr. B*, **27**, 829–33.
Ryan, J. L. and Rai, D. (1987) *Inorg. Chem.*, **26**, 4140–2.
Sachs, A. (1901) *Z. Kristallogr.*, **34**, 162–70.
Sahoo, B. and Patnaik, D. (1961) *Curr. Sci.*, **30**, 293–4.
Salzer, M. (1966) Report KFK-385.
Sandström, M., Persson, I., Jalilehvand, F., Lindquist- Reis, P., Spangberg, D., and Hermansson, K. (2001) *J. Synchrotron Radiat.*, **8**, 657–9.
Satoh, T. and Kumagai, K. (1971) *Proc. 12th Int. Conf. Low Temp. Phys.*, Tokyo, 347–9.
Satoh, T. and Kumagai, K. (1973) *J. Phys. Soc. Jpn.*, **34**, 391–5.
Satpathy, K. C. and Sahoo, B. (1968) *Curr. Sci.*, **37**, 435–6.
Satterthwaite, C. B. and Toepke, I. L. (1970) *Phys. Rev. Lett.*, **25**, 741–3.
Satterthwaite, C. B. and Peterson, D. T. (1972) *J. Less Common Metals*, **26**, 361–8.
Scaife, D. E. and Wylie, A. W. (1964) *J. Chem. Soc.*, 5450–8.
Scaife, D. E., Turnbull, A. G., and Wylie, A. W. (1965) *J. Chem. Soc.*, 1432–7.
Scavnicar, S. and Prodic, B. (1965) *Acta Crystallogr.*, **18**, 698–702.
Schleid, ThMeyer, and G., Morss, R. L. (1987) *J. Less Common Metals*, **132**, 69–77.
Schmid, W. F. and Mooney, R. W. (1964) *J. Electrochem. Soc.*, **111**, 668–73.
Schmidt, H. G. and Wolf, G. (1975) *Solid State Commun.*, **16**, 1085–7.
Schmidt, H. G. and Gruehn, R. (1989) *J. Less Common Metals*, **156**, 75–86.
Schmidt, H.G. and Gruehn, R. (1990) *J. Less Common Metals*, **158**, 275–85.
Scholder, R., Räde, D., and Schwarz, H. (1968) *Z. Anorg. Allg. Chem.*, **362**, 149–68.
Schild, D. and Marquardt, C. M. (2000) *Radiochim. Acta*, **88**, 587–91.
Schreiber, D. S. (1974) *Solid State Commun.*, **14**, 177–9.
Schuler, F. W., Steahly, F. L., and Stoughton, R. W. (1952) in Katzin (1952), paper 7.1, p. 307.
Schwarz, R. and Giese, H. (1928) *Z. Anorg. Allg. Chem.*, **176**, 209–32.
Schwetz, K., Ettmayer, P., Kieffer, R., and Lipp, A. (1972) *J. Less Common Metals*, **26**, 99–104.
Seaborg, G. T., Gofman, J. W., and Stoughton, R. W. (1947) *Phys. Rev.*, **71**, 378.
Seaborg, G. T. and Katzin, L. I. (1951) *Production and Separation of U^{233}: Survey*, Natl. Nucl. En. Ser., Div. IV, 17A, Report TID–5222, USAEC, Oak Ridge, Tenn.
Sereni, J. G., Nieva, G., Huber, J. G., Braun, E., Oster, F., Brück, E., Roden, B., and Wohlleben, D. (1987) *J. Magn. Magn. Mater.*, **63/64**, 597–9.
Shalek, P. D. (1963) *J. Am. Ceram. Soc.*, **46**, 155–61.
Shannon, R. D. (1976) *Acta Crystallogr. A,* **32**, 751–67.
Shchukarev, S. A., Novikov, G. I., and Suvorov, A. V. (1956) *Russ. J. Inorg. Chem.*, **9**, 13–8.
Shetty, S. Y., Sathe, R. M., and Shanker Das, M. (1976) *Indian J. Chem.*, **14A**, 719–20.
Shoun, R. R. and McDowell, W. J. (1980) in Actinide Separations (ACS Symp. Ser. no. 117), American Chemical Society, Washington, DC, pp. 71–87.
Sibieude, F. (1970) *C. R. Acad. Sci. Paris C*, **271**, 130–3.
Siddham, S. and Narayanan, K. (1979) *J. Catal.*, **59**, 405–22; Karuppannasamy, S., Narayanan, K., and Pilai, C. N. (1980) *J. Catal.*, **63**, 433–7.

Siegel, S. (1956) *Acta Crystallogr.*, **9**, 827.
Sieverts, A. and Roell, E. (1926) *Z. Anorg. Allg. Chem.*, **153**, 289–308.
Sillen, L. G. and Martell, A. (1964) *Stability Constants of Metal-ion Complexes*, Special Publication n°17, The Chemical Society, Burlington House, London, p. 534.
Sillen, L. G. and Martell, A. (1971) Stability Constants of Metal-ion Complexes, Supplement n°1, Special Publication n°25, The Chemical Society, Burlington House, London, p. 203.
Silvestre, J. P. (1978) *Rev. Chim. Miner.*, **15**, 412–22.
Silvestre, J. P., Pagès, M., and Freundlich, W. (1971) *C. R. Acad. Sci. Paris C*, **272**, 1808–10.
Singer, N., Studd, B. F., and Swallow, A. G. (1970) *J. Chem. Soc. Chem. Commun.*, 342–8.
Singh, N. P., Ibrahim, S. A., Cohen, N., and Wrenn, M. E. (1979) *Anal. Chem.*, **51**, 207–10; 1978–81.
Singh Mudher, K. D., Keskar, M., and Venugopal, V. (1995) *Proceedings of Nuclear and Radiochemistry Symposium* (eds. S. G. Kulkarni, S. B. Manohar, D. D. Sood), Kalpakkam, India, pp. 234–5.
Skriver, H. L. and Mertig, I. (1985) *Phys. Rev.*, **B32**, 4431–41.
Skriver, H. L., Eriksson, O., Mertig, I., and Mrosan, E. (1988) *Phys. Rev.*, **B37**, 1706–10.
Smith, E. F. and Harris, H. B. (1895) *J. Am. Chem. Soc.*, **17**, 654–6.
Smith, J. F., Carlson, O. N., Peterson, D. T., and Scott, T. E. (1975) *Thorium: Preparation and Properties,* Iowa State University Press, Ames, Iowa.
Smithells, C. J. (1922) *J. Chem. Soc.*, 2236–8.
Sollman, T. and Brown, E. D. (1907) *Am. J. Physiol.*, **18**, 426–56.
Sorby, M. H., Fjellvag, H., Hauback, B. C., Maeland, A. J., and Yartys, V. A. (2000) *J. Alloys Compds*, **309**, 154–64.
Spedding, F. H., Wilhelm, H. A., Keller, W. H., Iliff, J. E., and Neher, C. (1952) in Katzin (1952), paper 8.4, p. 428.
Spirlet, M. R., Rebizant, J., Apostolidis, C., Kanellakopoulos, B., and Dornberger, E. (1992) *Acta Crystallogr.*, **C48**, 1161–4.
Stackelberg, M. V. and Neumann, F. (1932) *Z. Phys. Chem. B*, **19**, 314–20.
Starks, D. V., Parsons, T. C., Streitwieser, A. Jr, and Edelstein, N. (1974) *Inorg. Chem.*, **13**, 1307–8.
Staun Olsen, J., Gerward, L., Benedict, U., Luo, H., and Vogt, O. (1988) Report KU-HCOE-FL-R-88-8(Fys. Lab., Univ. Copenhagen, Copenhagen, Den.) 15 pp.; (1989) *J. Appl.Crystallogr.*, 22, 61–3.
Stecher, P., Benesovsky, F., and Nowotny, H. (1963) *Monatsh. Chem.*, **94**, 549–64.
Stecher, P., Neckel, A., Benesovsky, F., and Nowotny, H. (1964) *Planseeber. Pulvermetall.*, **12**, 181–95.
Storms, E. K. (1967) *Refractory Carbides,* Academic Press, New York and London, p. 160.
Streitwieser, A. Jr and Yoshida, N. (1969) *J. Am. Chem. Soc.*, **91**, 7528.
Strotzer, E. F., Biltz, W., and Meisel, K. (1938) *Z. Anorg. Allg. Chem.*, **238**, 69–80.
Strotzer, E. F. and Zumbusch, M. (1941) *Z. Anorg. Allg. Chem.*, **247**, 415–28.
Struss, A. W. and Corbett, J. D. (1978) *Inorg. Chem.*, **17**, 965–9.
Sugar, J. (1974) *J. Chem. Phys.*, **60**, 4103.
Surbeck, H. (1995) *Sci. Total Environ.*, **173–174**, 91–9.

Suzuki, T., Takagi, S., Niitsuma, N., Takegahara, K., Kasuya, T., Yanase, A., Sakakibara, T., Date, M., Markowski, P. J., and Henkie, Z. (1982) *High Field Magnetism, Proc. Int. Symp.*, pp. 183–7.
Szilard, B. (1907) *J. Chem. Phys.*, **5**, 488–94.
Szymanski, J. T., Owens, D. R., Roberts, A. C., Ansell, H. G., and Chao, G. Y. (1982) *Can. Mineral.*, **20**, 65–75.
Tabata, K. and Kido, H. (1987) *Phys. Status Solidi A*, **99**, K121.
Tanaka, Y., Hattori, H., and Tanabe, K. (1978) *Bull. Chem. Soc. Jpn*, **51**, 3641–2; Tanaka, K. and Okuhara, T. (1980) *J. Catal.*, **65**, 1–8.
Taoudi, A., Mikou, A., and Laval, J. P. (1996) *Eur. J. Solid State Inorg. Chem.*, **33**, 1051–62.
Taylor, J. C., Mueller, M. H., and Hitterman, R. L. (1966) *Acta Crystallogr.*, **20**, 842–51.
Taylor, J. C. (1976) *Coord. Chem. Rev.*, **20**, 197–273.
Taylor, M. and Ewing, R. C. (1978) *Acta Crystallogr.*, **B34**, 1074–5.
Templeton, C. C. and Hall, N. F. (1947) *J. Phys. Coll. Chem.*, **51**, 1441–9.
Ter Haar, G. L. and Dubeck, M. (1964) *Inorg. Chem.*, **3**, 1648–50.
Thakur, L., Thakur, A. K., and Ahmad, M. F. (1980) *Indian J. Chem.*, **A19**, 792–5.
Thoma, R. E. and Carlton, T. S. (1961) *J. Inorg. Nucl. Chem.*, **17**, 88–97.
Thoma, R. E. (1972) *J. Inorg. Nucl. Chem.*, **34**, 2747–60.
Thomas, A. C., Dacheux, N., Le Coustumer, P., Brandel, V., and Genet, M. (2000) *J.Nucl. Mater.*, **281**, 91–105.
Thomas, A. C., Dacheux, N., Le Coustumer, P., Brandel, V., and Genet, M. (2001) *J.Nucl. Mater.*, **295**, 249–64.
Thomke, K. (1977) *Z. Phys. Chem.*, **107**, 99–108.
Thoret, J., Rimsky, A., and Freundlich, W. (1968) *C. R. Acad. Sci. Paris C*, **267**, 1682–4.
Thoret, J., Rimsky, A., and Freundlich, W. (1970) *C. R. Acad. Sci. Paris C*, **270**, 2045–7.
Thoret, J. (1971) *C. R. Acad. Sci. Paris C*, **273**, 1431–4.
Thoret, J. (1974) *Rev. Chim. Minér.*, **11**, 237–61.
Tiwari, R. N. and Sinha, D. N. (1980) *Indian Chem. J.*, **14**, 25–8.
Topic, M., Prodic, B., and Popovic, S. (1970) *Czech J. Phys.*, **20**, 1003–6.
Tougait, O., Potel, M., and Noël, H. (1998) *Inorg. Chem.*, **37**, 5088–91.
Trauger, D. B. (1978) *Ann. Nucl. Energy*, **5**, 375–403.
Troost, L. (1883) *C. R. Acad. Sci. Paris*, **116**, 1229
Troost, L. and Ouvrard, L. (1885) *C. R. Acad. Sci. Paris*, **101**, 210–2; (1886) *C. R. Acad. Sci. Paris*, **102**, 1422–7; (1887) *C. R. Acad. Sci. Paris*, **105**, 30–4.
Troost, L. and Ouvrard, L. (1889) *Ann. Chim. Phys.*, **6** (17), 227–45.
Trunov, V. K. and Kovba, L. M. (1963) *Vestn. Mosk. Univer., Ser. II, Khim.*, **18**, 60–3.
Trunov, V. K. and Kovba, L. M. (1966) *Zh. Strukt. Khim.*, **7**, 896–7.
Trunov, V. K., Efremova, A., and Kovba, L. M. (1966) *Radiokhimiya*, **8**, 717–18; *Sov. Radiochem.*, **8**, 658–9.
Ueki, T., Zalkin, A., and Templeton, D. H. (1966) *Acta Crystallogr.*, **20** 836–41.
Ueno, K. and Hoshi, M. (1970) *J. Inorg. Nucl. Chem.*, **32**, 3817–22.
Urbain, G. (1896) *Bull. Soc. Chim.*, **3** (15), 347–9.
van Arkel, A. E. and de Boer, J. H. (1925) *Z. Anorg. Allg. Chem.*, **148**, 345–50.
Van Houten, R. and Bartram, S. (1971) *Metall. Trans.*, **2**, 527–30.
Vasilega, N. D., Tishchenko, A. F., Lugovskaya, E. S., Badaev, Yu. V., and Pavlikov, V. N. (1980) *Dopov. Akad. Nauk Ukr. RSR*, **B11**, 34–8.

Vdovenko, V. M., Gershanovich, A. Y., and Suglobova, I. G. (1974) *Sov. Radiochem.*, **16**, 863–5.
Vedrine, A., Barackic, L., and Cousseins, J. C. (1973) *Mater. Res. Bull.*, **8**, 581–8.
Vera Tomé, F., Jurado Vargas, M., and Martin Sanchez, A. (1994) *Appl. Radiat. Isot.*, **45**, 449–52.
Vigato, P. A., Casellato, U., and Vidali, M. (1977) *Gazz. Chim. Ital.*, **107**, 61–6.
Vohra, Y. K. (1991) *Scr. Met. Mater.*, **25**, 2787–9.
Vohra, Y. K. and Akella, J. (1991) *Phys. Rev. Lett.*, **67**, 3563–6.
Vohra, Y. K. and Akella, J. (1992) *High Pressure Res.*, **10**, 681–5.
Vohra, Y. K. (1993) *Physica B*, **190**, 1–4.
Vokhmyakov, A. N., Desyatnik, V. N., and Kurbatov, N. N. (1973) *At. Energy (USSR)*, **35**, 424.
Volck, C. (1894) *Z. Anorg. Chem.*, **6**, 161–7.
Voliotis, S. and Rimsky, A. (1975) *Acta Crystallogr.*, **B31**, 2615–20.
Voliotis, S. (1979) *Acta Crystallogr. B*, **35**, 2899–904.
Voliotis, S., and Rimsky, A. (1988) *Acta Crystallogr.*, **B44**, 77–88.
Volkov, Yu. F., Kapshukov, I. I., and Vasil'ev, V. Ya. (1974) *1st Vses. Konf. Khim. Urana*, p. 26.
Volkov, Yu. F. (1999) *Radiochemistry (Moscow) (Translation of Radiokhimiya)*, **41**, 168–74.
Voliotis, S., Fromage, F., Faucherre, J., and Dervin, J. (1977) *Rev. Chim. Minér.*, **14**, 441–6.
von Bolton, W. (1908) *Z. Elektrochem.*, **14**, 768–70.
von Schnering, H. G., Wittmann, M., and Nesper, R. (1980) *J. Less Common Metals*, **76**, 213–26.
von Schnering, H. G. and Vu, D. (1986) *J. Less Common Metals*, **116**, 259–70.
von Wartenberg, H. (1909) *Z. Elektrochem.*, **15**, 866–72.
Wachtmann, K. H., Moss, M. A., Hoffmann, R.-D., and Jeitschko, W. J. (1995) *J.Alloys Compds*, **219**, 279–84.
Wallroth, K. A. (1883) *Bull. Soc. Chim.*, **2** (39), 316–22.
Wang, W., Chen, B., Wang, A., Yu, M., and Liu, X. (1982) *He Huaxue Yu Fangshe Huaxue*, **4**, 139–46.
Wang, W., Chen, B., Jin, Z., and Wang, A. (1983) *J. Radioanal. Chem.*, **76**, 49–62.
Wang, X. Z., Ng, W. L., Chevalier, B., Etourneau, J., and Hagenmuller, P. (1985) *Mater. Res. Bull.*, **20**, 1229–38.
Wang, J. and Zadeii, J. M. (1986) *Anal. Chim. Acta*, **188**, 187–94.
Warf, J. C. (1949) *J. Am. Chem. Soc.*, **71**, 3257–8.
Warren, I. H. and Price, C. E. (1964) *Adv. Energy Conversion*, **4**, 169.
Wastin, F., Rebizant, J., Spirlet, J. C., Sari, C., Walker, C. T., and Fuger, J. (1993) *J.Alloys Compds*, **196**, 87–92.
Watt, G. W. and Gadd, K. F. (1973) *Inorg. Nucl. Chem. Lett.*, **9**, 203–5.
Weaver, J. H., Knapp, J. A., Eastman, D. E., Peterson, D. T., and Satterthwaite, C. B. (1977) *Phys. Rev. Lett.*, **39**, 639–42.
Weeks, M. E. and Leicester, H. M. (1968) *Discovery of the Elements*, 7th edn, Easton, PA.
Weinland, R. F. and Kühl, H. (1907) *Z. Anorg. Chem.*, **54**, 244–52.
Wells, H. L. and Willis, J. M. (1901) *Am. J. Sci.*, **12**, 191–2.

Wessels, G. F. S., Leipoldt, J. G., and Bok, L. D. C. (1972) *Z. Anorg. Allg. Chem.*, **393**, 284–94.
Westland, A. D. and Tarafder, M. T. H. (1983) *Can. J. Chem.*, **61**, 1573–7.
White, G. M. and Ohnesorge, W. E. (1970) *Anal. Chem.*, **42**, 504–8.
Wilhelm, H. A. and Chiotti, P. (1949) Report AECD-2718.
Wilhelm, H. A. and Chiotti, P. (1950) *Trans. Am. Soc. Met.*, **42**, 1295–310.
Wilke, G., Bogdanivic, B., Hardt, P., Heimbach, P., Keim, W., Kröner, M., Oberkirch, W., Tanaka, K., Steinrücke, E., Walter, D., and Zimmermann, H. (1966) *Angew. Chem.* (*Int. Edn. Engl.*), **5**, 151–64.
Winkler, C. (1891) *Berl. Dtsch. Chem. Ges.*, **24**, 873–99.
Winter, H. (1978) *Conf. Ser. Inst. Phys.*, **39**, 713–5.
Wirth, F. (1912) *Z. Anorg. Chem.*, **76**, 174–200.
Wöhler, L., Plüddemann, W., and Wöhler, P. (1908) *Ber. Dtsch. Chem. Ges.*, **41**, 703–17.
Woodward, L. A. and Ware, M. J. (1968) *Spectrochim. Acta*, **24A**, 921–5.
Wu, E. J., Pell, M. A., and Ibers, J. A. (1997) *J. Alloys Compds.*, **255**, 106
Wu, Y., Zhao, Z., Liu, Y., and Yang, X. (2000) *J. Mol. Catal. A. Chem.*, **155**, 89–100.
Wyrouboff, G. and Verneuil, A. (1898a) *Bull. Soc. Chim.*, **3** (19), 219–27.
Wyrouboff, G. and Verneuil, A. (1898b) *C. R. Acad. Sci. Paris*, **128**, 1573–5.
Wyrouboff, G. and Verneuil, A. (1899) *Bull. Soc. Chim.*, **3** (21), 118–43.
Wyrouboff, G. (1901) *Bull. Soc. Miner.*, **24**, 105–16.
Wyrouboff, G. and Verneuil, A. (1905) *Ann. Chim. Phys.*, **6**, 441–507.
Yaffe, L. (1949) *Can. J. Res. B*, **27**, 638–45.
Yamnova, N. A., Pushcharovskii, D. Y., and Voloshin, A. V. (1990) *Dokl. Akad. Nauk SSSR*, **310**, 99–102.
Yen, K.-F., Li, S.-C., and Novikov, G. I. (1963) *Zh. Neorg. Khim.*, **8**, 89–93; *Russ. J. Inorg. Chem.*, **8**, 44–7.
Yoshida, S., Oyamada, R., and Kawamura, K. (1978) *Bull. Chem. Soc. Japan*, **51**, 25–7.
Young, R. C. (1935) *J. Am. Chem. Soc.*, **57**, 997–9.
Young, R. C. and Fletcher, H. G. (1939) in *Inorganic Synthesis,* vol. I (ed. H. S. Booth), McGraw-Hill, New York, pp. 51–4.
Yu, Z., Gao, L., Yuan, S., and Wu, Y. (1992) *J. Chem. Soc., Faraday Trans.*, **88**, 3245–9.
Zachariasen, W. H. (1948a) Report AECD-2163.
Zachariasen, W. H. (1948b) *Acta Crystallogr.*, **1**, 265–8.
Zachariasen, W. H. (1948c) *J. Am. Chem. Soc.*, **70**, 2147–51.
Zachariasen, W. H. (1949a) *Acta Crystallogr.*, **2**, 388–90.
Zachariasen, W. H. (1949b) *Acta Crystallogr.*, **2**, 390–3.
Zachariasen, W. H. (1949c) *Acta Crystallogr.*, **2**, 291–6.
Zachariasen, W. H.(1949d) *Acta Crystallogr.*, **2**, 288–91.
Zachariasen, W. H. (1953) *Acta Crystallogr.*, **6**, 393–5.
Zaitseva, L. L. Vakhrushin, YuA., and Shepel'kov, S. V. (1984) *Zh. Neorg. Khim.*, **29**, 768–72; *Russ. J. Inorg. Chem.*, **29**, 443–5.
Zalkin, A. and Templeton, D. H. (1950) *J. Chem. Phys.*, **18**, 391.
Zalkin, A. and Templeton, D. H. (1953) *Acta Crystallogr.*, **6**, 269–72.
Zalkin, A., Forrester, J. D., and Templeton, D. H. (1964) *Inorg. Chem.*, **3**, 639–44.
Zalkin, A., Templeton, D. H., Le Vanda, C., and Streitwieser, A. Jr (1980) *Inorg. Chem.*, **19**, 2560–3.

Zalubas, R. (1968) *J. Opt. Soc. Am.*, **58**, 1195–9.
Zalubas, and R. Corliss, C. H.(1974) *J. Res. NBS*, **78A**, 163–246.
Zambonini, F. (1923) *C. R. Acad. Sci. Paris*, **176**, 1473–5.
Zhang, H. B., Lin, G. D., Wan, H. L., Liu, Y. D., Weng, W. Z., Cai, J. X., Shen, Y. F., and Tsai, K. R. (2001) *Catal. Lett.*, **73**, 141–7.
Zhou, M. L., Jin, J. N., Xu, S. C., Liu, M. Z., Xu, D. Q., Peng, Q. X., Qi, and Sh., J. (1981) *Huaxue Yu Fangshe Huaxue*, **3**, 136–40.
Zhu, W. J. and Hor, P. H. (1995) *J. Solid State Chem.*, **120**, 208–9.
Zumbusch, M. (1941) *Z. Anorg. Allg. Chem.*, **245**, 402–8.
Zunic, T. B., Scavnicar, S., and Grobenski, Z. (1984) *Croat. Chem. Acta*, **57**, 645–51.

CHAPTER FOUR

PROTACTINIUM

Boris F. Myasoedov, H. W. Kirby, and Ivan G. Tananaev

4.1 INTRODUCTION

Protactinium, element 91, is one of the most rare of the naturally occurring elements and may well be the most difficult of all to extract from natural sources. Protactinium is, formally, the third element of the actinide series and the first having a 5f electron. The superconducting properties of protactinium metal provide clear evidence that Pa is a true actinide element (Smith *et al.*, 1979). Its chemical behavior in aqueous solution, however, would seem to place it in group VB of the Mendeleev's table, below Ta and Nb.

The predominant oxidation state is 5+. Pa(v) forms no simple cations in aqueous solution and, like Ta, it exhibits an extraordinarily high tendency to undergo hydrolysis, to form polymers, and to be adsorbed on almost any available surface. These tendencies undoubtedly account for the many reports of erratic and irreproducible behavior of protactinium as well as for its frustrating habit of disappearing in the hands of inexperienced or unwary investigators. A useful review of the chemical properties of Pa important in an analytical context has been made by Pal'shin *et al.* (1970) and Myasoedov *et al.* (1978).

The most important natural isotope is ^{231}Pa, but the industrial importance of Pa stems chiefly from the role of its artificial isotope, ^{233}Pa, as an intermediate in the production of fissile ^{233}U in thorium breeder reactors. It was, in fact, the need for a relatively stable isotope that could be used for macroscopic chemical studies, which was responsible for the revival of interest in the recovery of ^{231}Pa from natural sources (Katzin, 1952). The result has been a rapid growth in our

understanding of Pa chemistry, as summarized in numerous critical review articles (Gmelin, 1942, 1977; Elson, 1954; Katz and Seaborg, 1957; Haïssinsky and Bouissières, 1958; Kirby, 1959; Salutsky, 1962; Brown and Maddock, 1963; Sedlet, 1964; Guillaumont and deMiranda, 1966; Keller, 1966a; Brown and Maddock, 1967; Guillaumont *et al*., 1968; Brown, 1969; Muxart *et al*., 1969; Muxart and Guillaumont, 1974; Morgan and Beetham, 1990), books (Cotton *et al*., 1999) and presentations (Weigel 1978; Jung *et al*., 1993; Greenwood and Earnshaw 1997; Sime, 1997).

4.1.1 Discovery of protactinium

During the preparation of the periodic table Mendeleev (1872) placed in the vacant space in group V between Th(IV) and U(VI) an unknown hypothetical element No. 91 named 'eka-tantalum' with atomic mass of about 235, and chemical properties similar to Nb and Ta. Forty years later, Russell (1913), Fajans (1913a,b), and Soddy (1913a,b) independently proposed the radioactive displacement principles, i.e. two simple rules for reconciling the chemical and radioactive properties of the 33 radioelements known at that time: (1) if a radioelement emits an α particle, its position in the Mendeleev's table is shifted two places to the left, or (2) if it emits a β^--particle, its position is shifted one place to the right. When the rules were applied systematically, there was one obvious discrepancy: the only known link between ^{238}U and ^{234}U, both in group VI, was element UX, a β^--emitter whose chemistry was identical with that of thorium, in group IV. It was necessary to postulate the existence of an unknown β^--emitter, in the space in the periodic table reserved by Mendeleev (1872).

Before the end of 1913, Fajans and his student, Göhring, had shown that element UX was actually a mixture of two distinct radioelements: UX_1 (^{234}Th) and UX_2 (^{234m}Pa), which gave off hard β^--rays, had a half-life of 1.15 min, and was chemically similar to Ta (Göhring, 1914a,b). They named the new element, '*brevium*' (Bv) (*brĕvis* (Latin): short, brief), because of its short half-life (Göhring, 1914b).

An analogous problem existed with respect to the origin of actinium (Göhring, 1914a). It was clear that Ac could not be a 'primary' radioelement, because its half-life was only about 30 years (Curie, 1911). On the other hand, although there was a constant ratio of Ac to U in nature (Boltwood, 1906, 1908), Ac could not be part of the main U–Ra series, because the ratio was far too low. According to the displacement laws, Ac, in group III, could only be the product either of a β^--emitter in group II or of an α-emitter in group V. The first possibility was eliminated when Soddy (1913b) proved that Ra, the only group II element in the U–Ra series, was not the parent of Ac. The only remaining alternative was an α-emitting isotope of UX_2.

In 1913, Soddy had reported the growth of Ac in two lots of UX, separated from 50 kg of uranium 4 years earlier (Soddy, 1913a). This suggested that Ac was being produced from UX 'through an intermediate substance'. Five years

later Soddy and Cranston (1918) [see also Sackett (1960)] had confirmed the growth beyond doubt and had separated the parent of Ac by sublimation from pitchblende in a current of air containing CCl_4 at incipient red heat. This method was later applied by Malm and Fried (1950, 1959) to the separation of ^{233}Pa from neutron-irradiated ^{232}Th.

Almost simultaneously, Hahn and Meitner (1918) reported their independent discovery of the parent of Ac in the siliceous residue resulting from the treatment of pulverized pitchblende with hot concentrated HNO_3. They proposed the name, *protactinium*. Preliminary estimates indicated that the half-life of the new isotope was between 1200 and 180 000 years. Since the name, *brevium*, was obviously inappropriate for such a long-lived radioelement, Fajans and Morris (1913) proposed that the name of element-91 be changed to *protactinium* (linguistic purists at first insisted on calling it *protoactinium*, because '*proto* is better Greek' (Grosse, 1975), but the name *protactinium* (Pa) was restored officially in 1949 (Anonymous, 1949)).

There was still no direct evidence as to the origin of protactinium. In 1911, Antonoff (1911) had separated uranium Y – UY (^{231}Th) from a purified U solution. UY was chemically similar to Th and Antonoff (1913) suggested that this might be the point at which the Ac series branched off from the U series. In 1917, Piccard (1917) suggested that, in addition to the two known isotopes of uranium, uranium I and II (UI and UII), there might also exist a third long-lived isotope, actinouranium (AcU). AcU would decay by α-emission to yield UY, which, in turn, would decay by β^--emission to give an isotope of *brevium*. Piccard's hypothesis was confirmed experimentally in 1935, when Dempster (1935) discovered AcU (^{235}U) by mass spectrography.

4.1.2 Isolation of protactinium

The new element was isolated for the first time in 1927, when Grosse (1927, 1928) reported that he had prepared about 2 mg of essentially pure Pa_2O_5. By the end of 1934, Grosse with Agruss had developed a process for the large-scale recovery and purification of Pa (Grosse, 1934a; Grosse and Agruss, 1934, 1935a). They had isolated more than 0.15 g of Pa_2O_5, reduced it to the metal, and determined its atomic weight to be 230.6 ± 0.5 (Grosse, 1934b). In the same year, Graue and Kading (1934a,b) recovered 0.5 g of pure Pa (as K_2PaF_7) from 5.5 tons of pitchblende residues, an achievement that would not be equaled, let alone surpassed, for the next quarter of a century.

The development of atomic energy led to the processing of most of the world's known reserves of high-grade uranium ores and to the accumulation of vast stockpiles of process wastes. Among these, at the Springfields refinery of the United Kingdom Atomic Energy Authority (UKAEA) was the '*ethereal sludge*', a siliceous precipitate that had separated during the ether extraction of U from dilute HNO_3 solution. This material, amounting to some 60 tons, contained about 4 ppm of Pa, or more than ten times its equilibrium concentration in

unprocessed pitchblende. Since the sludge also contained about 12 tons of U, it was economically attractive to recover both elements, with most of the development and production cost being borne by the U recovery. The process that was finally adopted yielded 127 g of 99.9% pure ^{231}Pa (Goble *et al.*, 1958; Nairn *et al.*, 1958; Jackson *et al.*, 1960a,b; Collins *et al.*, 1962; Hillary and Morgan, 1964) at a cost of about US$500 000 (CRC Handbook, 1997).

The UKAEA has generously made its stockpile of Pa available to the rest of the world at nominal cost, thereby touching off intensive investigation of Pa chemistry at many laboratories. Thanks to this concentrated effort, the new era in Pa research that started in the mid-1950s has now reached maturity. Three international conferences were convened, devoted entirely to the chemical, physical, and nuclear properties of Pa (Oak Ridge National Laboratory, 1964; Bouissières and Muxart, 1966; Born, 1971).

4.2 NUCLEAR PROPERTIES

At present, there are 29 known isotopes of Pa (Table 4.1), but only three are of particular significance to chemists. They are the naturally occurring isotopes, ^{231}Pa and ^{234}Pa, and reactor-produced ^{233}Pa. The characteristics of α-decay of Pa isotopes with mass numbers (A) till 224 were presented by Andreev *et al.* (1996b). Hyde (1961, undated) and Hyde *et al.* (1964) had exhaustively reviewed the nuclear properties of all the isotopes with A ranging from 225 to 237.

A new nuclide ^{239}Pa produced recently by multi-nucleon transfer reactions ^{238}U(p,2n)^{239}Pa (Yuan *et al.*, 1996). Protactinium was chemically separated from the uranium target and other produced elements. From the ^{239}Pa β^--decay a half-life of (106 ± 30) min was observed.

For details concerning the more recently discovered isotopes, the reader should consult the original references (Meitner *et al.*, 1938; Ghiorso *et al.*, 1948; Gofman and Seaborg, 1949; Hyde *et al.*, 1949; Meinke *et al.*, 1949, 1951, 1952, 1956; Harvey and Parsons, 1950; Barendregt and Tom, 1951; Keys, 1951; Browne *et al.*, 1954; Crane and Iddings, 1954; Zijp *et al.*, 1954; Wright *et al.*, 1957; Hill, 1958; Arbman *et al.*, 1960; Takahashi and Morinaga, 1960; Albridge *et al.*, 1961; Baranov *et al.*, 1962; Bjørnholm and Nielsen, 1962, 1963; Subrahmanyam, 1963; Wolzak and Morinaga, 1963; McCoy, 1964; Bastin *et al.*, 1966; Bjørnholm *et al.*, 1968; Hahn *et al.*, 1968; Trautmann *et al.*, 1968; Briand *et al.*, 1969; Borggreen *et al.*, 1970; dePinke *et al.*, 1970; Laurens *et al.*, 1970; Varnell, 1970; Holden and Walker, 1972; Sung-Ching-Yang *et al.*, 1972; Lederer and Shirley, 1978; Folger *et al.*, 1995; Yuan *et al.*, 1995, 1996; Andreev *et al.*, 1996a; Nishinaka *et al.*, 1997).

4.2.1 Protactinium-231

^{231}Pa, an α-emitter with fixed atomic weight 231.03588 ± 0.0002 (Delaeter and Heumann, 1991), is a member of the naturally occurring ^{235}U decay ($4n + 3$) chain. It is the daughter of ^{231}Th and the parent of ^{227}Ac, from which it derives

Table 4.1 *Nuclear properties of protactinium isotopes.*

Mass number	*Half-life*	*Mode of decay*	*Main radiations* (MeV)	*Method of production*
212	5.1 ms	α	α 8.270	^{182}W(^{35}Cl,5n)
213	5.3 ms	α	α 8.236	^{170}Er(^{51}V,8n)
214	17 ms	α	α 8.116	^{170}Er(^{51}V,7n)
215	14 ms	α	α 8.170	^{181}Ta(^{40}Ar,6n)
216	0.2 s	α	α 7.865	^{197}Au(^{24}Mg,5n)
217	4.9 ms	α	α 8.340	^{181}Ta(^{40}Ar,4n)
	1.6 ms	α	α 10.160	
218	0.12 ms	α	α 9.614 (65%)	^{206}Pb(^{16}O,4n)
219	53 ns	α	α 9.900	^{204}Pb(^{19}F,4n)
220	0.78 μs	α	α 9.15	^{204}Pb(^{19}F,3n)
221	5.9 μs	α	α 9.080	^{209}Bi(^{16}O,4n)
222	5.7 ms	α	α 8.54 (∼30%)	^{209}Bi(^{16}O,3n)
			∼8.18 (50%)	^{206}Pb(^{19}F,3n)
223	6 ms	α	α 8.20 (45%)	^{208}Pb(^{19}F,4n)
			8.01 (55%)	^{205}Tl(^{22}Ne,4n)
224	0.9 s	α	α 7.49	^{208}Pb(^{19}F,3n)
225	1.8 s	α	α 7.25 (70%)	^{232}Th(p,8n)
			7.20 (30%)	^{209}Bi(^{22}Ne,α2n)
226	1.8 min	α 74%	α 6.86 (52%)	^{232}Th(p,7n)
		EC 26%	6.82 (46%)	
227	38.3 min	α ∼85%	α 6.466 (51%)	^{232}Th(p,6n)
		EC ∼15%	6.416 (15%)	
			γ 0.065	
228	22 h	EC ∼98%	α 6.105 (12%)	^{232}Th(p,5n)
		α ∼2%	6.078 (21%)	^{230}Th(p,3n)
			γ 0.410	
229	1.5 d	EC 99.5%	α 5.669 (19%)	^{230}Th(d,3n)
		α 0.48%	5.579 (37%)	^{229}Th(d,2n)
230	17.7 d	EC 90%	α 5.345	^{230}Th(d,2n)
		β^- 10%	β^- 0.51	^{232}Th(p,3n)
		α 3.2×10^{-3}%	γ 0.952	
231	3.28×10^4 yr	α	α 5.012 (25%)	nature
			4.951 (23%)	
			γ 0.300	
232	1.31 d	β^-	β^- 1.29	^{231}Pa(n,γ)
			γ 0.969	^{232}Th(d,2n)
233	27.0 d	β^-	β^- 0.568	^{233}Th daughter
			γ 0.312	^{237}Np daughter
234	6.75 h	β^-	β^- 1.2	nature
			γ 0.570	
234 m	1.175 min	β^- 99.87%	β^- 2.29	nature
		IT 0.13%	γ 1.001	
235	24.2 min	β^-	β^- 1.41	^{235}Th daughter
				^{235}U(n,p)
236	9.1 min	β^-	β^- 3.1	^{236}U(n,p)
			γ 0.642	^{238}U(d,α)
237	8.7 min	β^-	β^- 2.3	^{238}U(γ,p)
			γ 0.854	^{238}U(n,pn)
238	2.3 min	β^-	β^- 2.9	^{238}U(n,p)
			γ 1.014	
239	106 min	β^-		^{18}O + ^{238}U

its name (Fig. 4.1). Reported half-lives have ranged from 32 000 years ± 10% (Grosse, 1932) to (34 300 ± 300) years (Van Winkle *et al.*, 1949); three recent determinations (Kirby, 1961; Brown *et al.*, 1968a; Robert *et al.*, 1969) yield a weighted average of (32 530 ± 250) years (at the 95% confidence level). Therefore ^{231}Pa is the only isotope easy to access in multi-gram quantities. The thermal-neutron cross section is (211 ± 2) barn (Simpson *et al.*, 1962; Gryntakis and Kim, 1974). The spontaneous fission half-life is 1.1×10^{16} years (Segrè, 1952), which gives the correlation of 0.3 of a fission per 1 g Pa per min.

The complex fine structure of the ^{231}Pa alpha-spectrum can be resolved with a passivated implanted planar silicon detector (Fig. 4.2). Baranov *et al.* (1962, 1968), using a double-focusing magnetic spectrometer, found at least 19 α-groups with energies ranging from 4.51 to 5.06 MeV and additional low-abundance groups have been detected by α–γ coincidence measurements (Lange and Hagee, 1968). Predictably, the γ-ray spectrum, as recorded with a high-resolution Ge detector, is even more complex (Fig. 4.3): 92 γ-rays have been reported, with energies up to 609 keV (dePinke *et al.*, 1970; Leang, 1970). A detailed level scheme is given in the critical compilation by Artna-Cohen (1971). The prominent γ photopeak at 27.35 keV is easily detectable even with a NaI(Tl) crystal; it uniquely identifies ^{231}Pa in the presence of other naturally occurring γ-emitters (Fig. 4.4).

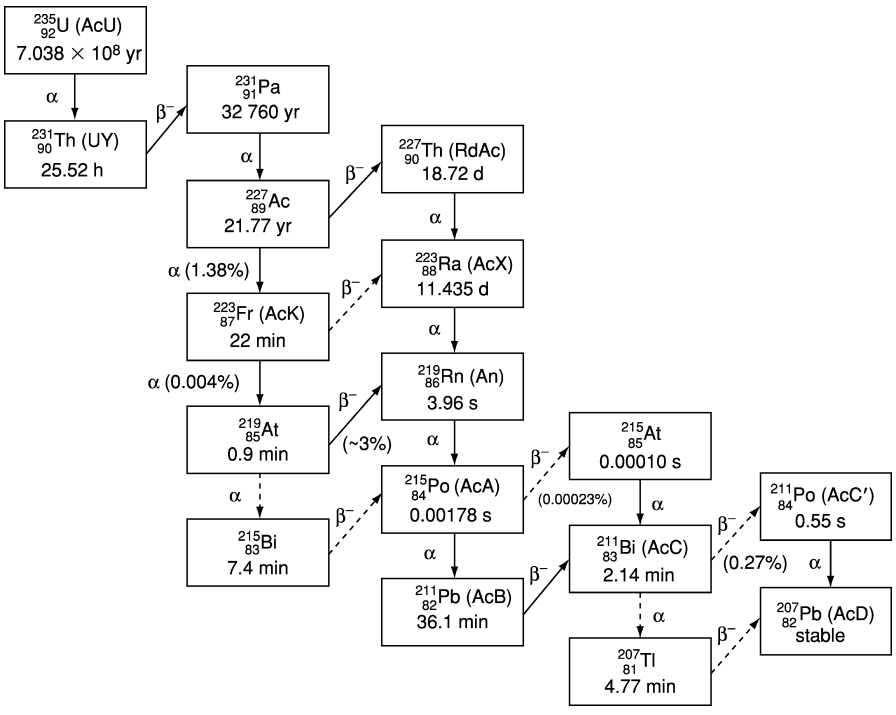

Fig. 4.1 *Uranium–actinium series* (4*n* + 3).

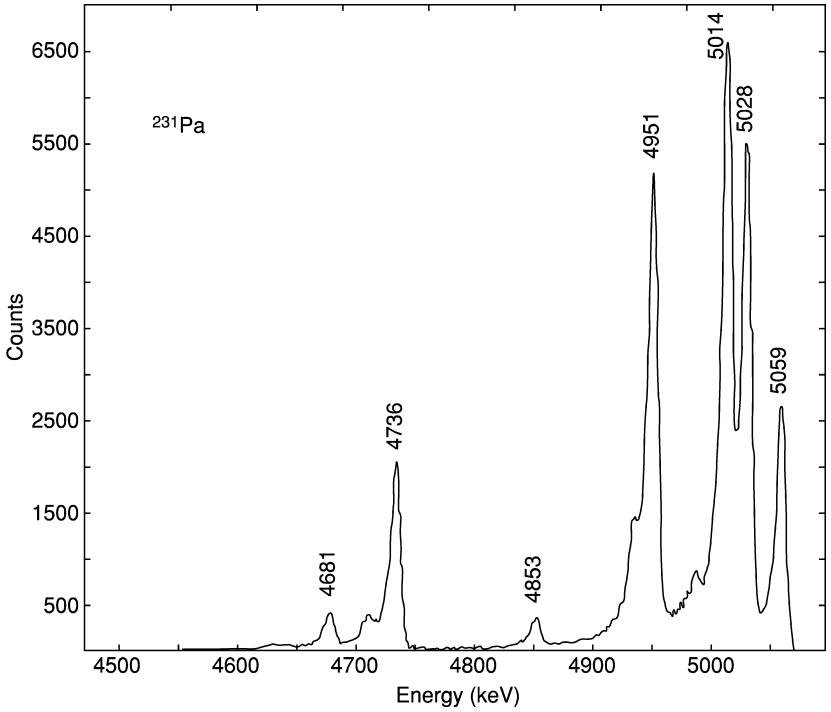

Fig. 4.2 *Alpha-spectrum of* ^{231}*Pa measured with a passivated implanted planar silicon detector* (*Ahmad,* 2004).

^{231}Pa can be separated from reprocessed U ores, or alternatively, produced by either of the two nuclear reactions: ^{232}Th(n,2n)^{231}Th (Nishina *et al*., 1938) or ^{230}Th(n,γ)^{231}Th (Hyde, 1948). In principle, this would eliminate many of the problems attendant on the isolation of ^{231}Pa. However, neutron irradiation of ^{232}Th yields large amounts of ^{233}Pa and other undesirable contaminants, but relatively little ^{231}Pa (Table 4.2) (Schuman and Tromp, 1959; Codding *et al*., 1964). The ^{230}Th route is only superficially more attractive, since the richest sources of ^{330}Th found thus far in U refinery waste streams and residues have always been associated with at least eight times as much ^{232}Th (Figgins and Kirby, 1966). Protactinium was not formed in the amalgam and could be also separated from thorium (David and Bouissières, 1966).

4.2.2 Protactinium-233

^{233}Pa is the only artificial isotope of Pa thus far produced in weighable amounts; the first gram was isolated in 1964 by a group at the National Reactor Testing Station in Idaho (Codding *et al*., 1964). ^{233}Pa derives its importance from the

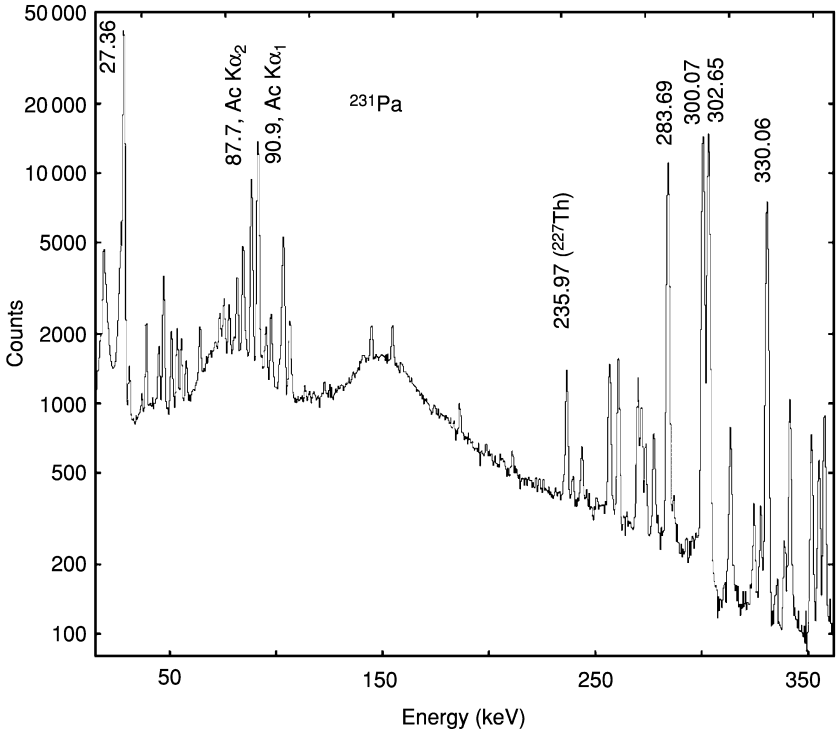

Fig. 4.3 *γ-Ray spectrum of* ^{231}*Pa measured with a* 25% *efficiency germanium detector* (*Ahmad*, 2004).

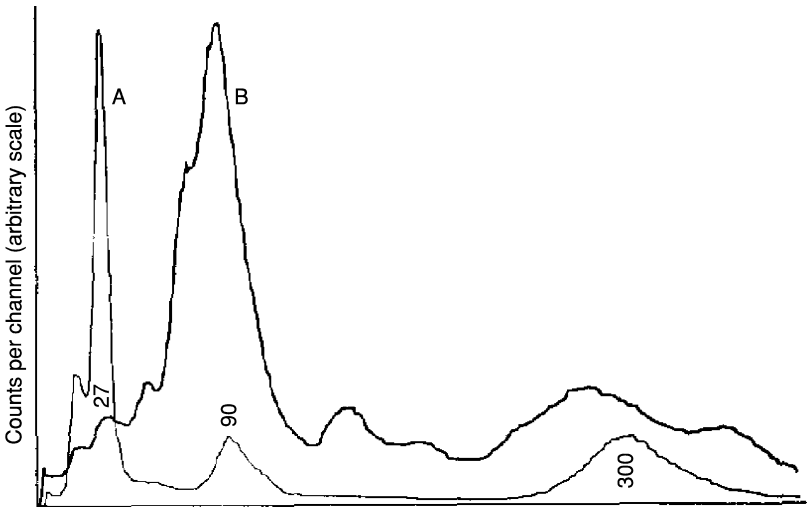

Fig. 4.4 *γ-Ray spectrum of* ^{231}*Pa observed with a NaI(Tl) crystal: curve A, freshly purified* ^{231}*Pa; curve B, raw material* (∼0.3 *ppm* ^{231}*Pa*).

Table 4.2 *Calculated composition of* 100 g *of* ^{232}*Th after thermal-neutron irradiation* (*Codding* et al., 1964) (*thermal flux* $= 5 \times 10^{14}$ n cm^{-2}s^{-1}*; resonance flux* = (*thermal flux*)/12*; nvt* $= 1.2 \times 10^{21}$ n cm^{-2}).

Nuclide	*Amount*
^{231}Pa	98.6 g
^{232}Th	~1 mg
^{233}Pa	950 mg
^{233}U	320 mg
^{235}U	65 mg
^{235}U	5 mg
fission products	60 mg

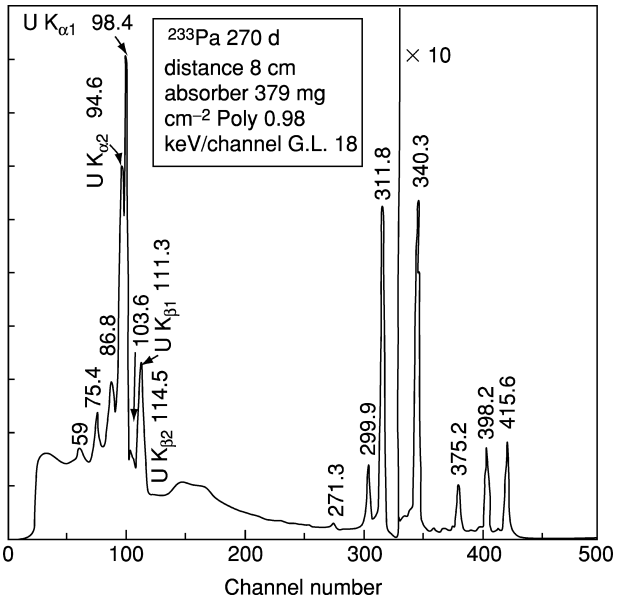

Fig. 4.5 *γ-Ray spectrum of* ^{233}*Pa observed with a Ge*(*Li*) *detector. Reproduced from Crouthamel* et al. (1970) *with permission from Pergamon Press.*

fact that it is an intermediate in the production of fissile ^{233}U. The reaction, discovered in 1938 by Meitner *et al.* (1938) (Sime, 1997) is:

$$^{232}\mathrm{Th}\,(\mathrm{n},\gamma)\,^{233}\mathrm{Th}\,(\beta^{-};22\ \mathrm{min}) \rightarrow {}^{233}\mathrm{Pa}(\beta^{-};\,27\,\mathrm{days}) \rightarrow {}^{233}\mathrm{U}$$

^{233}Pa has largely replaced ^{234}Pa as a tracer because of its favorable half-life (26.95 ± 0.06) days (Wright *et al.*, 1957), its relative ease of preparation (cf. Table 4.2), and its readily detectable gamma spectrum (Fig. 4.5). Using this isotope a large volume of important data on protactinium chemistry had been provided.

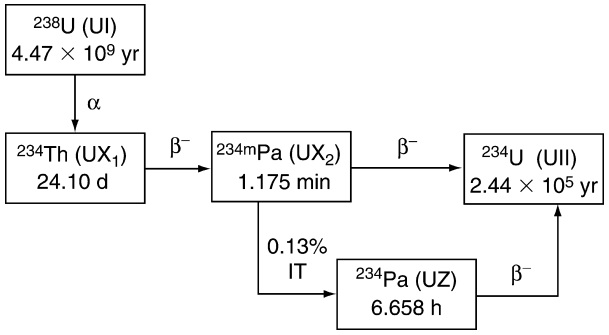

Fig. 4.6 *Genetic relationships of the UX_1–UX_2–UZ complex.*

4.2.3 Protactinium-234

The nuclide ^{234}Pa occurs naturally in two isomeric forms: ^{234m}Pa, discovered by Fajans and Göhring (1913a,b), and ^{234}Pa, discovered afterward by Hahn (1921). Their genetic relationships are indicated in Fig. 4.6. Both are β^--emitters, decaying to ^{234}U, but ^{234m}Pa is metastable and, in 0.13% of its disintegrations, it decays to its ground state by isomeric transition, yielding ^{234}Pa (Bjørnholm and Nielsen, 1963). The extraordinarily complex decay scheme of ^{234}Pa (Ellis, 1970; Ardisson and Ardisson, 1975) is difficult to study, because the intense sources needed for high-resolution spectrometry are not readily available. However, 0.8 Ci of ^{234}Th was extracted from several tons of ^{238}U, making possible the definitive study by Bjørnholm *et al.* (1967, 1968). The gamma-spectrum of ^{234}Pa (in equilibrium with ^{238}U and ^{234}Th) is shown in Fig. 4.7 (Crouthamel *et al.*, 1970).

4.3 OCCURRENCE IN NATURE

Since the half-life of ^{231}Pa is short in geological terms, its natural occurrence is closely tied to that of ^{235}U, its primordial ancestor. Uranium isotopes are widely distributed in the Earth's crust (Kirby, 1974). The average crustal abundance of U is 2.7 ppm (Taylor, 1964), of which 0.711 wt% is ^{235}U (Grundy and Hamer, 1961); therefore, the natural abundance of ^{231}Pa (calculated from its half-life and that of ^{235}U) is 0.87×10^{-6} ppm – only slightly less than that of ^{226}Ra. Assuming that the crustal mass (to a depth of 36 km) is 2.5×10^{25} g (Heydemann, 1969), the global inventory of ^{231}Pa is 2.2×10^7 metric tons.

The pronounced hydrolytic tendency of Pa is the basis of a method for dating marine sediments less than 10^6 years old (Sackett, 1960; Roshalt *et al.*, 1961, 1962; Sakanoue *et al.*, 1967; Thomson and Walton, 1971, 1972; Kirby, 1974). In an undisturbed geological formation, thematic Pa:U $= 3.2 \times 10^{-7}$, but this ratio

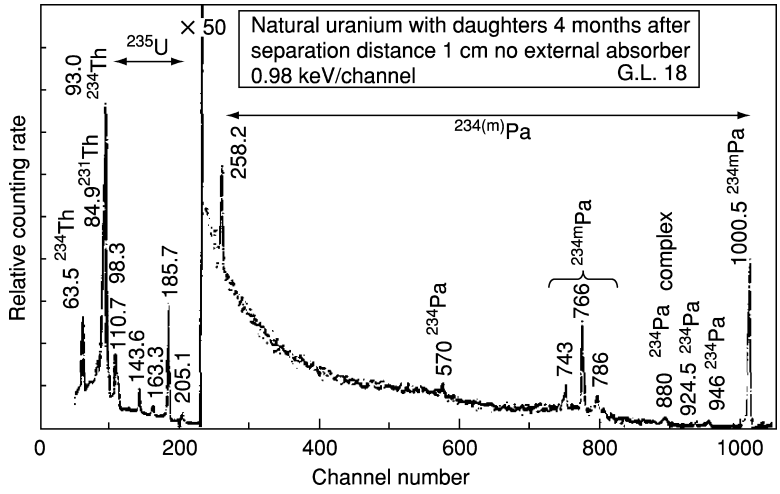

Fig. 4.7 *γ-Ray spectrum of UX_1–UX_2–UZ in equilibrium with ^{238}U. Reproduced from Crouthamel* et al. (1970) *with permission from Pergamon Press.*

is altered when the deposit is leached with groundwater and the U is carried to sea. At the pH of seawater, both Pa and Th hydrolyze and deposit together on the ocean floor, leaving the U in solution as UO_2^{2+}. Because ^{231}Pa and ^{230}Th decay moved at different rates, their ratio at various depths can be used to determine the rate of sedimentation.

$^{231}Pa/^{235}U$ ages were also determined for 17 carnotites from two areas in Israel (Kaufman *et al.*, 1995). For the determination of ^{231}Pa in solids, a new method, more than ten times more precise than those determined by decay counting, based on thermal ionization mass spectroscopy (TIMS) of protactinium in carbonates was created. Carbonates between 10 and 250 000 years old can now be dated with this ^{231}Pa method. Barbados corals that have identical ^{231}Pa and ^{230}Th ages indicate that the timing of sea level change over parts of the last glacial cycle is consistent with the predictions of the Astronomical Theory (Edwards *et al.*, 1997).

^{233}Pa has not itself been detected in nature, but traces of both ^{237}Np, its parent, and ^{225}Ac, its descendant, have been identified in a U refinery waste stream (Peppard *et al.*, 1952). It may, therefore, be inferred that ^{233}Pa is being continually formed in nature by the reaction:

$$^{238}\mathrm{U}\,(\mathrm{n},2\mathrm{n})\,^{237}\mathrm{U}\,(\beta^-;\,6.75\,\mathrm{days}) \rightarrow {}^{237}\mathrm{Np}\,(\alpha;\,2.14\times10^{6}\,\mathrm{years}) \rightarrow {}^{233}\mathrm{Pa}.$$

The natural neutron output in pitchblende is about 0.05 $ng^{-1}\,s^{-1}$, attributable about equally to spontaneous fission of ^{238}U and (α,n) reactions of light elements (McKay, 1971).

4.4 PREPARATION AND PURIFICATION

No large-scale separation of ^{231}Pa has ever been made from virgin ores because the element has little commercial value. Weighable amounts of Pa have always been obtained from U refinery residues. Indeed, the economic realities are such that it is rarely possible even to optimize the segregation of Pa in a single waste stream or residue. More typically, the Pa is fractionated at every stage in the beneficiation and extraction of U from its ores.

Before the development of atomic energy, pitchblende ores were processed primarily for their Ra content. The pulverized ore, after being roasted with Na_2CO_3, was leached with aqueous solutions of H_2SO_4 or HNO_3 (or both) and the acid-insoluble material was digested with NaOH or Na_2CO_3 solutions. The residue was then leached with hydrochloric acid to recover the Ra (Curie, 1913). The final residue retained a greater or lesser fraction of the original Pa according to the relative proportions of the acids used in the digestion; a higher H_2SO_4 concentration and higher total acidity favored the dissolution of Pa (Reymond, 1931). This *Rückrückstände,* or 'residue of residues', was the raw material used by Hahn and Meitner (1918) for their discovery of ^{231}Pa, by Grosse (1927, 1928) in the isolation of the first milligram amounts, and by Graue and Kading (1934a) in the recovery of 0.5 g of the element. The analysis of one such residue is given in Table 4.3.

During and after World War II, an ether extraction process was used for the purification of U. The acid solution resulting from the ore digestion was treated with Na_2CO_3 to precipitate some of the less basic metals, while leaving the U in solution as a carbonate complex. Katzin *et al.* (1950) found that the carbonate precipitate contained 0.30–0.35 ppm of Pa and subsequent processing of this material yielded about 25 mg of pure Pa (Kraus and Van Winkle, 1952; Larson *et al.*, 1952; Thompson *et al.*, 1952). When the process was modified to eliminate the carbonate precipitation, the Pa passed through the ether extraction step into the aqueous raffinate, from which Elson *et al.* (1951) recovered 35 mg of pure material.

A later modification produced a precipitate in the aqueous waste stream, which, according to Salutsky *et al.* (1956), carried down nearly all the Pa. This material was periodically filtered off and eventually yielded a total of about 2 g of Pa (Kirby, 1959; Hertz *et al.*, 1974; Figgins *et al.*, 1975).

The aqueous raffinate from the ether extraction was treated with lime and the filtered precipitate was stored for future recovery of U and other commercially valuable metals. The accumulated material was later treated by a process of which the relevant steps were: digestion with sulfuric acid, followed by extraction with bis(2-ethylhexyl)phosphoric acid (HDEHP), and finally back-extraction with sodium carbonate solution. The waste solutions and residues were discharged to a tailings pond, where, for all practical purposes, much of the Pa and ^{230}Th were irretrievably lost. In 1972, the process was modified by

Table 4.3 *Analyses of some* ^{231}*Pa raw materials.*

Riickriickstände (*Grosse and Agruss*, 1935*a*)		*Ethereal sludge* (*Nairn* et al., 1958)		*Cotter concentrate* (*Ishida*, 1975)	
Constituent	*Amount* (%)	*Constituent*	*Amount* (%)	*Constituent*	*Amount* (%)
SiO_2	60	U	28.3	U_3O_8	13.8
Fe_2O_3	22	Fe	7.7	Fe	~30
PbO	8	Si	6.4	Si	~4
Al_2O_3	5	Ba	~3	Na	~60
MnO	1	Zr	2.7	Mo	$\leq$2
CaO	0.6	Mo	2.7	V	$\leq$1
MgO	0.5	F^-	1.8	Al	$\geq$0.3
Ti	0.3	NH_4^+	1.7	Th	0.15
Zr	0.1	Ca	1.5	Ti	0.1
HF and others	–	V	0.9	Ca	0.07
Graphite	0.1	Ti	0.44	Cu	0.05
Pa_2O_5	3×10^{-3}	Pb	0.4	Zr	0.04
		Al	0.27	Mg	0.04
		P	0.15	Ni	0.03
		Sr	0.09	Mn	0.01
		Nb, Ta	<0.1	Cr	0.01
		Mg, Ni, Cr, Co, Mn, & Sn	<0.01	B	0.002
				Be	7×10^{-4}
		Pa	$3.7 \times I0^{-4}$	Pa	4×10^{-5}

adding enough sodium hydroxide to the Na_2CO_3 strip solution to cause total precipitation of the U, thus minimizing any further loss of Pa and ^{230}Th (Haubach, 1967; Figgins and Hertz, 1972a,b, 1973). The filtered precipitate ('*Cotter concentrate*') consists of some 2000 tons (dry weight) of mixed oxides and carbonates (Table 4.3) and contains an estimated 30 tons of U_3O_8, 14 kg of ^{230}Th, and 75 g of Pa. This material has been processed at Mound Laboratory.

At the Windscale refinery of the UKAEA, after removal of a sulfate precipitate containing the Ra, the solution was buffered to pH ~2 and the U was precipitated by the addition of hydrogen peroxide. The peroxide precipitate carried down more than 80% of the Pa and, when it was redissolved in nitric acid, the low acidity encouraged the formation of a siliceous Pa-containing sludge, which deposited on the walls of the ether extraction plant and its ancillary vessels. This '*ethereal sludge*' was collected and drummed, pending future recovery of U. It proved to be the richest source of Pa ever found, ultimately yielding 127 g of the pure element (Goble *et al.*, 1958; Nairn *et al.*, 1958; Jackson *et al.*, 1960a; Collins *et al.*, 1962). The gross chemical composition of '*ethereal sludge*' is shown in Table 4.3.

4.4.1 Industrial-scale enrichment of siliceous residues

At ultra-micro concentrations with respect to other metals ions, Pa scarcely exhibits a chemistry of its own. Consequently, the procedure adopted to recover Pa from 'natural' sources is usually dictated less by the chemistry of Pa than by the gross chemical and physical characteristics of the source and, sometimes, by the sheer quantity of material to be processed.

The problems are magnified by the extreme complexity and variability of the sources from which ^{231}Pa is obtained, but one problem common to nearly all natural sources has been the ubiquitous presence of silica, and nearly all authors have resorted, at one stage or another, to alkaline fusion or digestion for its removal. Grosse (1934a) and Grosse and Agruss (1934, 1935a) recovered more than 100 g of pure Pa_2O_5 from 1.2 tons of *Rückrückstände,* a material composed largely of SiO_2 and Fe_2O_3 (Table 4.3). The principal steps in the enrichment process were: (1) leaching with hydrochloric acid to eliminate Fe and the more basic oxides; (2) fusing the residue with NaOH and leaching the cooled melt with water to remove soluble silicates and Pb; (3) dissolving the residue in hydrochloric acid and heating to coagulate the remaining SiO_2; (4) washing the precipitate with 20% NaOH solution and dissolving the residue in hydrochloric acid; (5) precipitating Zr (and Pa) by the addition of phosphoric acid; and (6) fusing the ZrP_2O_7 with KOH to eliminate PO_4^{3-} and the last of the SiO_2. The plant product contained more than 85% of the original Pa in a concentration of 1:5000 – an enrichment factor of about 600. Graue and Kading (1934a,b) recovered 700 mg of Pa from 5.5 tons of *Rückrückstände* by essentially the same process, except that the raw material was first fused with NaOH and then leached with hydrochloric acid. The large quantity of SiO_2 that remained in the residue was eliminated by fuming with hydrofluoric acid.

4.4.2 Enrichment of carbonate precipitates

Pa in trace amounts may fractionate unpredictably during dissolution or precipitation of a multi-component mixture. To inhibit such fractionation, many authors have introduced carriers such as Ta (Hahn and Meitner, 1918), Zr (Graue and Kading, 1934a; Grosse and Agruss, 1935a), or Ti (Zavizziano, 1935; Emmanuel-Zavizziano, 1936; Kirby, 1959), which carry Pa quantitatively when they are precipitated as phosphates or hydrated oxides.

Larson *et al.* (1952) leached a carbonate precipitate with nitric acid and digested the resultant SiO_2 gel with 10% NaOH solution to which La carrier was added to minimize losses of Pa in the alkaline solution. However, Thompson and co-workers (1952), by first digesting the carbonates with 40% NaOH, were able to remove enough SiO_2 to prevent gel formation when the metathesized residue was dissolved in 1 M HNO_3. There was no loss of Pa to the alkaline solution, probably because the residue already contained appreciable amounts of both Zr and Ti. The Pa was concentrated from the 1 M HNO_3

solution by adsorption on a MnO_2 precipitate formed *in situ* (Grosse and Agruss, 1935b; Katzin and Stoughton, 1956). Two additional cycles of MnO_2 precipitation and redissolution in HNO_3 were followed by a hydrolytic precipitation of Ti and Zr from 5 M HNO_3. The precipitate that carried down the Pa was taken up in hydrofluoric acid and evaporated to dryness in the presence of perchloric acid to eliminate SiO_2, giving a 1000-fold enrichment of the Pa with a 65% yield.

Carrying by MnO_2 is a key step in the recovery of Pa from *Cotter concentrate* (Hertz *et al.*, 1974). The solids are digested in HNO_3 solution and filtered to yield a solution that is 2–3 M in HNO_3. Essentially all the U and ^{230}Th and 50–85% of the Pa are dissolved; the undissolved residue is reserved for further digestion. The U is extracted with di-*S*-butylphenyl phosphonate (DSBPP) and the Pa and ^{230}Th are quantitatively extracted with tri-*n*-octylphosphine oxide (TOPO). ^{230}Th is stripped from the TOPO with 0.3 M H_2SO_4 and the Pa with 0.5 M $H_2C_2O_4$. Addition of potassium permanganate to the oxalic acid solution yields a precipitate of 5 g of MnO_2 containing 1–6 mg of Pa, for an enrichment factor of 500–2500.

4.4.3 Enrichment of aqueous raffinates

After the sodium carbonate precipitation step was omitted from the Mallinckrodt process, the aqueous raffinate from the diethyl ether extraction of U contained about 0.2 mg L^{-1} of Pa and 1–10 g L^{-1} for other elements (chiefly Ca, Fe, and rare earths). Elson *et al.* (1951) extracted this weakly acid solution of nitrates with 5% of its volume of tri(*n*-butyl)phosphate (TBP) and stripped the TBP with one-fourth of its volume of 0.5 M HF solution. Rare earths and Th isotopes precipitated, but the Pa remained in solution. Al^{3+} was added to complex the F^- and the solution was contacted with di-isopropylcarbinol (DIPC), which extracted 70–90% of the Pa. Back-extraction into 10% H_2O_2 gave another 20-fold volume reduction and yielded a product that contained about 4% Pa by weight, with Ca and U as the principal impurities. The overall yield was only 5–35%, however, primarily because of the poor extractability of Pa into TBP at low acidity. Peppard *et al.* (1957) later found that Pa is efficiently extracted by TBP from 5 M HCl.

In a Russian process (Shevchenko *et al.*, 1958b), the U ore is digested with nitric acid and extracted as slurry with a 10% solution of TBP in kerosene. About 75–85% of the ^{230}Th and 50–55% of the Pa pass into solution, but neither is appreciably extracted by the TBP. After phase separation and filtration, the aqueous solution is made 2 M in HNO_3 and contacted with a 15% solution of mixed mono- and di-isoamylphosphoric acids (DIAPA) in isoamylacetate. A single-stage extraction with an organic:aqueous volume ratio of 1:20 recovers 75–85% of the ^{230}Th and 82–89% of the Pa. After back-extraction with saturated aqueous $(NH_4)_2CO_3$, Fe and other heavy metals are precipitated as sulfides and the carbonate is decomposed by heating and acidification.

The ^{230}Th and Pa are precipitated with NH_4OH and calcined to yield a concentrate containing up to 1% ^{230}Th and about 0.01% Pa in a matrix of U, P, Ti, Zr, Sc, and other impurities. The Pa is separated from ^{230}Th and Sc by fluoride precipitation, which leaves Pa in the solution, from which it is coprecipitated with Zr as a phosphate in the presence of H_2O_2. The Pa:Zr ratio in the concentrate is usually 1:400 or higher.

The adsorption behavior of protactinium on zirconium phosphate cation exchanger from ammonium chloride, hydrochloric acid, and hydrochloric acid–alcohol media has been investigated (Souka *et al*., 1975c). The distribution coefficients in solvent mixtures of hydrochloric acid and various alcohols depend on both alcohol content and acid concentration. Similar investigations have been carried out for nitric acid systems (Souka *et al*., 1976a). Sorption of protactinium on silica gel has also attracted attention. Adsorption of ^{233}Pa on silica gel has been investigated as a possible procedure for obtaining isotopically pure uranium-233 (Chang and Ting, 1975a). Protactinium-233 sorption from oxalic acid system has been studied; a 1:1 complex of Pa and oxalate is formed in these systems and the observed adsorption is well correlated to the concentration of the oxalate complexes (Bykhovskii *et al*., 1977). Hydrophobic silica gel has been prepared by silylation; uptake of protactinium from mixtures of hydrochloric acid and lower aliphatic alcohols increases with increasing molecular weight of the aliphatic alcohol (Caletka and Spěváčkova, 1975).

4.4.4 Enrichment of ethereal sludge

Aqueous hydrofluoric acid is the most consistently effective solvent for Pa(V), with which it forms strong anionic complexes (Guillaumont and deMiranda, 1966; Guillaumont *et al*., 1968). It has the added advantage of dissolving the oxides of most of the elements with which Pa is normally associated in nature (Si, Fe, Ta, Zr, Ti, etc.). If Al^{3+} is added to such a solution in sufficient quantity to mask all the F^-, a precipitate forms, which carries the Pa quantitatively.

In an enrichment method reported by Goble *et al.* (1958), ethereal sludge was leached with 0.5 M HNO_3, which dissolved about 90% of the U. The residue, which retained more than 95% of the Pa, was leached with 0.5 M HF and Al sheets were suspended in the solution. After 5 days or more, the Pa separated quantitatively as a black deposit on the aluminum, from which it was loosened by treatment with 0.2 M NaOH. The precipitate was washed with dilute NaOH solution and dissolved in 8 M HCl, from which it was extracted with di-isobutylketone (DIBK). The DIBK was stripped with 8 M HCl containing a little HF. Addition of $AlCl_3$ permitted a second cycle of DIBK extraction and stripping. The crude HCl–HF product from 100 kg of sludge was 200 mg of Pa (77% yield) in 0.5 L of solution containing about 10 g of solids.

Unfortunately, this ingenious and inexpensive process failed when attempts were made to apply it on a tonnage scale, apparently because fluorides (from CaF_2 slag) had been dispersed throughout the sludge during a re-drumming

operation. This resulted in unacceptable losses of Pa during the initial leaching with dilute HNO_3 solution. Furthermore, the deposition of Pa on Al plates proved too slow and cumbersome for operation on a tonnage scale.

The process that was finally adopted is outlined in Fig. 4.8 (Nairn *et al.*, 1958; Collins *et al.*, 1962). The U and Pa were dissolved by leaching the sludge with a mixture of HNO_3 and HF. After extraction of the U with TBP, Al^{3+} as chloride was added to the raffinate. A precipitate is formed, which carried down 80–95% of the Pa, with an enrichment factor of approximately 10. The precipitate was

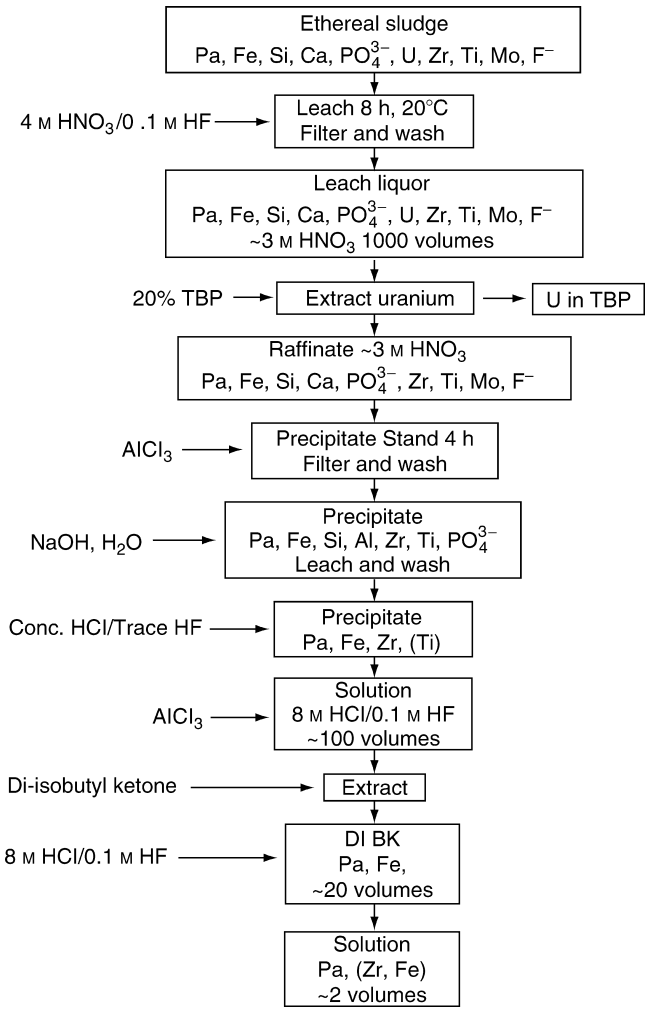

Fig. 4.8 *Recovery of protactinium and uranium from ethereal sludge* (*Nairn* et al., 1958).

digested with 10–35% NaOH to remove Si, Al, and, especially, PO_4^{3-}. The residue was dissolved in 8 M HCl and 0.1 M HF and aluminum chloride was added in a molar ratio of Al:F > 5. The solution was extracted with DIBK and stripped with 8 M HCl and 0.1 M HF. A second cycle of DIBK extraction and stripping yielded 52.4 L of an aqueous solution containing 126.75 g of Pa, 3.25 g of Zr, and 1.42 g of Fe (it was later learned that the product also contained 0.1–4% Nb) (Walter, 1963; Brown *et al.*, 1966a; Jenkins *et al.*, 1975).

Salutsky *et al.* (1956) recovered 0.5 mg of Pa from 5 kg of a material similar to ethereal sludge but only one-tenth as rich. The principal features of the method were: (1) dissolution in 1 M HCl, (2) saturation of the solution with sodium chloride, and (3) boiling to coagulate a small precipitate (chiefly Ca and Si), which quantitatively carried down the Pa. The precipitate was digested with NaOH solution to solubilize silicates and the residue was dissolved in 9 M HCl; this became the feed solution for purification of the Pa by anion exchange. However, attempts to apply this simple process to other batches of the same material failed because of the inhomogeneity of the raw material. Batchwise development and processing ultimately recovered approximately 2 g of Pa from 20 tons of residue, but only after substantial modification of the process, including (Kirby, 1959): addition of Ti as a carrier; dissolution of HCl-insoluble residues in sulfuric acid; extraction with isopropyl ether to reduce the Fe concentration to manageable proportions; and concentration of the Pa by several cycles of extraction into di-isobutylcarbinol (DIBC) and stripping with H_2O_2.

4.4.5 Purification of macroscopic amounts of ^{231}Pa

Preliminary enrichment processes such as those described above afford a high degree of decontamination from Si, Fe, U, Th, Ti, and most bivalent and trivalent elements, including the ^{231}Pa decay products (Fig. 4.1). However, Zr, Ta, and Nb are usually enriched along with the Pa and most recent work has been directed primarily at the separation of those elements, of which Nb is the most troublesome.

Methods reported for the purification of Pa after its enrichment from natural sources are so numerous that only a selected few can be mentioned here. For details of other methods, readers should consult the following reviews (Gmelin, 1942, 1977; Haïssinsky and Bouissières, 1958; Brown and Maddock, 1963, 1967; Pal'shin *et al.*, 1970) and the original publications cited therein.

(a) Precipitation and crystallization

The addition of KF to a solution of Pa(v) in hydrofluoric acid quantitatively precipitates K_2PaF_7 and separates Pa from Zr, Nb, Ti, and Ta (Grosse, 1928; Graue and Kading, 1934b; Bouissières and Haïssinsky, 1951; Cunningham, 1966).

On the other hand, during the fractional crystallization of the double ammonium fluorides, Pa crystallizes before Zr, but after Ti and Ta (Bachelet and Bouissières, 1947). Haïssinsky (Haïssinsky and Bouissières, 1951; Bouissières and Haïssinsky, 1951) separated Pa from Ta, Zr, and Ti by reducing Pa(V) to Pa(IV) with Zn amalgam in 2 M HF. The PaF_4 precipitate was redissolved in aqueous HF or H_2SO_4 in the presence of H_2O_2 or a current of air, which reoxidized the Pa.

Precipitation by H_2O_2 has been widely used to separate Pa from Nb, Ta, and Ti (Grosse, 1930; Bachelet and Bouissières, 1944, 1947; Goble *et al.*, 1958). Walter (1963) decontaminated 500 mg of Pa of about 4% Nb by adding H_2O_2 to a 40% H_2SO_4 solution of the Pa and neutralizing with ammonium hydroxide. Pal'shin *et al.* (1968a) mixed 4.1 mg of Pa with 8 mg each of Nb, Ta, and Zr in 0.25–0.5 M $H_2C_2O_4$, then precipitated the Pa by adding H_2O_2 (to 7.5%) and HCl (to 1.2 M). The precipitate, which formed during an 8–12 h period at room temperature, contained less than 1% total impurities.

The hydrolytic behavior of Pa was used by Kirby (1966) and by Kirby and Figgins (1966) to separate it from up to 13 times as much Nb. When hydrochloric acid was added to a 1 M $H_2C_2O_4$ solution containing equal amounts of the two elements, the precipitate, which developed on heating, contained 94.4% of the Pa and 2.0% of the Nb. Final purification was achieved by dissolution of the precipitate in 7 m H_2SO_4 and evaporation to fumes of SO_3, yielding Pa crystals of undetermined composition, in which the Nb content was reduced from 0.3 to 0.05% in a single stage. According to Brown and Jones (1964) and Bagnall *et al.* (1965), Pa crystallizes quantitatively as $H_3PaO(SO_4)_3$ when Pa_2O_5 is dissolved in a mixture of HF and H_2SO_4 and the solution is evaporated until all F^- has been eliminated. Two recrystallizations of a 10 g batch of Pa reduced the Nb contamination from 4 to 0.18%.

Myasoedov *et al.* (1968c) reported that Pa is quantitatively precipitated by phenylarsonic acid (PAA) from 1 to 7 N HCl, HNO_3, or H_2SO_4. In the absence of $H_2C_2O_4$, Sn(IV), Zr, Nb, Ta, and Ti are also precipitated; however, Pa is separated from Nb and Zr (but not from Ta) when PAA is added to a 2.5 M H_2SO_4 solution containing 0.1 M $H_2C_2O_4$. Both trace and major amounts of Pa have been separated from Nb, Zr, and Fe by this method.

Protactinium was isolated from liquid radioactive waste by sodium silicate, potassium silicate, and an alumina sol mixed in ratios by volume of 1:0.1 to 1. As an example, 0.94 mL of water glass containing 200 g L^{-1} of sodium silicate, and 100 mL of liquid waste containing 20 ppm of uranium was stirred, then 0.94 mL of the same water glass was added and stirred into the mixture along with 1.88 mL of an alumina sol for 10 min. Negatively charged silica particles and positively charged alumina particles absorb U and β^--decay nuclides (Pa) (Mitsubishi, 1995).

The protactinium distribution in a fluoride melt in the presence of solid oxide phases has been calculated (Alekseev *et al.*, 1988, 1989).

(b) Ion exchange

Numerous studies have demonstrated that Pa(v) at trace levels can be separated from the usual contaminants by sorption on anion-exchange resins from hydrochloric acid solutions (Kraus and Moore, 1950, 1951, 1955; Kahn and Hawkinson, 1956; Kraus *et al.*, 1956; Maddock and Pugh, 1956; Hill, 1958; Bunney *et al.*, 1959; Lebedev *et al.*, 1961; D'yachkova *et al.*, 1962; El-Dessouky, 1966; Hicks *et al.*, 1978; Kluge and Lieser, 1980; Alhassanieh *et al.*, 1999; Raje *et al.*, 2001). Typically, the feed solution is 9–10 M HCl, from which Pa(v) is strongly sorbed in anion-exchange resins such as Dowex-1, along with Fe(III), Ta(v), Nb(v), Zr(IV), U(IV), and U(VI); Th(IV) is only weakly sorbed and appears in the feed effluent. The eluent is a mixture of HCl and HF acids, the concentration of each depending upon the separation required. For example, Zr and Pa are both eluted with 9 M HCl and 0.004 M HF, but Zr may be eluted with 6–7 M HCl, without significant desorption of Pa (Fig. 4.9).

However, attempts to apply this procedure to the purification of weighable amounts of Pa have usually been unsatisfactory, primarily because of the low capacity of the resin (5–50 μg of Pa per gram of resin) and the strong tendency of Pa to hydrolyze in HCl solutions in the absence of complexing anions (Nairn *et al.*, 1958; Kirby, 1959; Collins *et al.*, 1962). Nevertheless, several authors (Jackson *et al.*, 1960a; Stein, 1966; Suzuki and Inoue, 1966) have reported the successful purification of gram quantities of Pa by anion-exchange procedures in which a stable feed solution was prepared by first dissolving the Pa in 9 M HCl

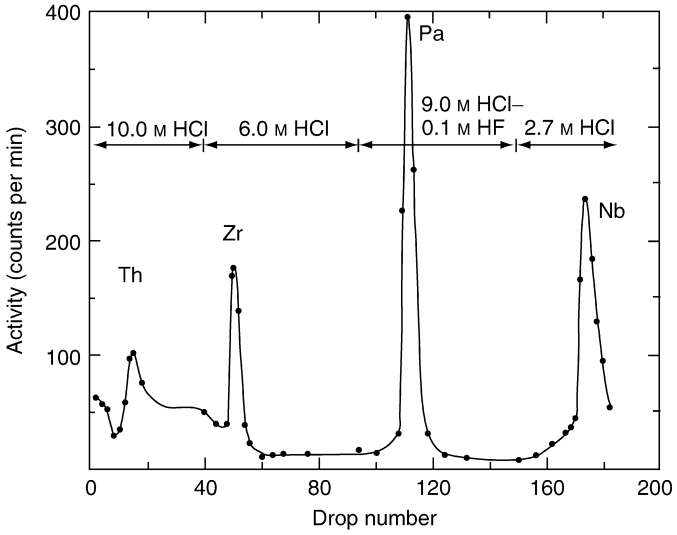

Fig. 4.9 *Separation of Th, Zr, Pa, and Nb on Dowex-1 anion-exchange column* (*Hill*, 1958).

containing some HF and then eliminating the F^- by complexing it with Al^{3+} or by evaporation. Sorption properties of Zr, HF, Nb, Ta, and Pa at trace levels towards a macroporous anion exchanger in HF and HCl media were investigated with two ion-exchange methods: static and dynamic. Variations of the distribution coefficients as a function of HCl and HF concentration in the range 0.02–0.8 M for both acids were presented in the form of contour plots and some of the most promising separation possibilities were pointed out (Trubert *et al*., 1998).

Keller (1963) found that Pa(V), Nb(V), and Ta(V) are all strongly sorbed by an anion exchanger (Dowex-1) from pure hydrofluoric acid solution. However, an increase in $[H^+]$ suppresses the dissociation of HF and sharply reduces the distribution coefficient (K_d) of Pa. Chetham-Strode and Keller (1966) observed that, in >10 M HF, the K_d of Pa was more than an order of magnitude lower than that of Nb and they applied these observations to the separation of Nb and various alkali- and alkaline-earth metal ions from 1 g of Pa_2O_5. The impure Pa was loaded on Dowex-1-Ax10 in 2.5 M HF and eluted with 17 M HF; the product was contaminated only by ^{227}Th, a decay product of ^{231}Pa. Jenkins *et al.* (1975) have reported the purification of approximately 35 g of Pa by this method, with high decontamination factors for Si, Mg, Fe, Al, Cu, and Nb.

The separation of Zr, Ha, Nb, Ta, and Pa was performed on a macroporous anion-exchange resin BIO-RAD AG MP1® in HF media (Monroy-Guzman *et al*., 1996) and a mixture of 0.01–4.0 M NH_4SCN and 0.05–3.0 M HF media to determine its analytical potential for the quantitative separation of these elements. It was found that the SCN^- concentration in mixtures NH_4SCN–HF had a strong influence on the adsorption of these ions. The K_d of these elements could be explained in terms of the formation of species: $[MF_x]^{(n-x)-}$, $[M(SCN)_y]^{(n-y)-}$, or $[MOF_x]^{(n-x-y)-}$ and $[MO(SCN)_y]^{(n-(2+y)-}$, and mixed fluorothiocyanates of the type $[M(F)_x(SCN)_y]^{(n-x-y)-}$ anionic complexes (Monroy-Guzman *et al*., 1997).

El-Sweify *et al*. (1985) calculated the distribution of Pa, other actinides, and fission products between the chelating ion exchanger Chelex–100 and certain carboxylic acid solutions.

(c) Solvent extraction and extraction chromatography

Pal'shin *et al.* (1970) have exhaustively reviewed the analytical applications of solvent extraction and Guillaumont and deMiranda (1971) have reviewed the published data as they relate to the ionic species of Pa and the mechanism of its extraction. At tracer levels ($<10^{-4}$ M), Pa(V) is efficiently extracted from aqueous solutions by a wide variety of organic solvents (Hyde and Wolf, 1952; Elson, 1954; Sedlet, 1964); however, only a few have been found useful at macroscopic levels. Dimethyl sulfoxide (DMSO) and the related compounds, diphenyl sulfoxide, and dibenzyl sulfoxide, have received some scrutiny, but it is not clear whether these complexing agents have particular utility for protactinium

separation (Reddy and Reddy, 1977; Reddy *et al.*, 1977; Chakravortty and Mohanly, 1979; Chakravortty *et al.*, 1986). As with ion exchange, the chief problems encountered in scaling up tracer-level procedures have been the low capacities of most solvents and the hydrolysis of Pa(v) in the aqueous phase, leading to the formation of 'inextractable polymers'. The most successful extractions of Pa at concentrations up to about 10 g L^{-1} have been with certain ketones, such as di-isopropylketone (DIPK) and DIBK (Goble and Maddock, 1958; Brown *et al.*, 1966a; Myasoedov *et al.*, 1966b) and long-chain alcohols, notably DIBC (Moore, 1955; Kirby, 1959; Brown and Jones, 1964; Scherff and Hermann, 1964; Brown *et al.*, 1966a; Sotobayashi *et al.*, 1977; Pathak *et al.*, 1999a,b).

DIBK was used in some studies for isolation of protactinium from raw materials (Katzin *et al.*, 1950; Katzin, 1952; Kraus and VanWinkle, 1952; Larson *et al.*, 1952; Thompson *et al.*, 1952) and from neutron-irradiated thorium (Meinke, 1946; Hyde and Wolf, 1952; Hill, 1958; Van Winkle and Kraus, 1959; Hyde *et al.*, 1951). Brown *et al.* (1966a) dealt with the problem of hydrolysis by precipitating Pa(v) from aqueous acid solutions with NH_4OH, redissolving the hydrated oxide in either 9 M H_2SO_4 and 0.5 M HF or 9 M HCI and 0.5 M HF, and then complexing the F^- with H_3BO_3. The use of sulfuric acid systems is preferred because of the greater stability of the Pa(v) complexes in that medium. In HCl and HF solutions, hydrolysis proceeds rapidly after the F^- is masked by reaction with $A1^{3+}$ or BO_3^{3-}. After adjustment of the aqueous phase to 4.5 M H_2SO_4 and 6 M HCl, the Pa(v) is extracted with DIBK, stripped with 9 M H_2SO_4 containing some H_2O_2, and re-extracted with DIBC (Fig. 4.10).

The method is said to give good decontamination from nearly all the usual impurities, including Si, Al, Fe, Nb, Zr, Ta, and ^{231}Pa decay products.

DIBC was also used for extraction studies of Pa, Nb, and element 105 – dubnium (Db) from aqueous HBr and HCl. It was shown that the extraction behavior of Db is closer to that of Nb than to Pa. The decreasing extractability from HBr (Pa > Nb > Db) is likely to be due to an increasing tendency of these elements to form a non-extractable polynegative complex species in concentrated HBr in the sequence Pa < Nb < Db (Gober *et al.*, 1992).

Milligram amounts of Pa(v) were extracted from H_2SO_4, HCl or HNO_3 acid solutions by isoamyl alcohol containing 1% PAA or 4% benzeneseleninic acid; good separation from many impurities was reported (Myasoedov *et al.*, 1966a, 1968a). Tetraphenylarsonium chloride has also been studied as a possible extractant for protactinium from hydrochloric or oxalic acid solutions (Abdel Gawad *et al.*, 1976; Souka *et al.*, 1976b). Other extraction agents have also been explored. Thus, l-phenyl-2-methyl-3-hydroxy-4-pyridone dissolved in chloroform (Tamhina *et al.*, 1976, 1978; Herak *et al.*, 1979) quantitatively extracted Pa from hydrochloric acid solution, and Pa can be separated from uranium and/or thorium by appropriate adjustment of the acidity. The antibiotic, tetracycline, was used in radiochemical analytical separations of protactinium from other actinide elements (Saiki *et al.*, 1981) and 5,7-dichloro-8-hydroxyquinoline

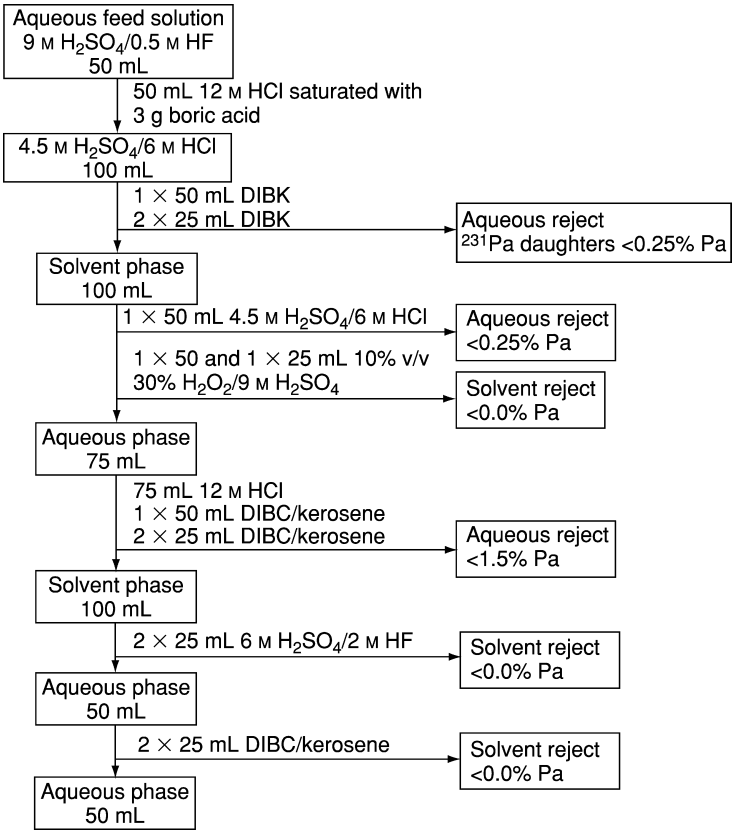

Fig. 4.10 *Purification scheme for* 555 mg *of Pa.* (*According to Brown* et al., 1966*a*.) *Reproduced with permission from Pergamon Press.*

was investigated for the separation of protactinium from niobium, tantalum, and zirconium by solvent extraction (Vaezi-Nasr *et al*., 1979).

Myasoedov and Pal'shin (1963) and Davidov *et al*. (1966c) proposed an effective method for isolation of Pa from uranium ores and products of their reprocessing by liquid–liquid extraction with the chelating complexing reagent 3,6-bis-[(2-arsenophenyl)azo]-4,5-dihydroxy-2,7-naphthalene disulfo acid (Arsenazo-III) in isoamyl alcohol. It was shown that an effective extraction of Pa from strong acid media, even in the presence of a great amount of Al, Fe(III), Mn(II), rare earth metals, and other elements, took place. The growth of U, Zr, Th, and particularly Nb concentrations in the solutions led to a diminution of Pa isolation. This method was used for analytical control of the separation of gram amounts of Pa(V) under plant conditions.

Thenoyltrifluoroacetone (TTA) had been used for separation and purification of Pa from several elements (Meinke and Seaborg, 1950; Meinke, 1952; Bouissières *et al.*, 1953; Moore, 1955, 1956; Brown *et al.*, 1959; Moore *et al.*, 1959; Poskanzer and Foreman, 1961a,b; Myasoedov and Muxart, 1962a). TTA extraction has been applied to the extraction of Pa from 10 M HCI in which $PaOCl_6^{3-}$ appears to be a principal species (Duplessis and Guillaumont, 1979). Triphenylphosphine oxide (TPPO), triphenylarsine oxide (Maghrawy *et al.*, 1989), and mixtures of TTA and either TBP, TOPO, or TPPO have been investigated (Kandil *et al.*, 1980); a combination of TTA and TOPO has found use in the separation of protactinium and thorium by solvent extraction (Kandil and Ramadan, 1978). TBP (Peppard *et al.*, 1957; Souka *et al.*, 1975b; Svantesson *et al.*, 1979), HDEHP (Shevchenko *et al.*, 1958a; Brown and Maddock, 1963; Myasoedov and Molochnikova, 1968; Myasoedov *et al.*, 1968b; Maghrawy *et al.*, 1988), and di-2-ethyl-hexyl isobutylamide (D2EHIBA) (Pathak *et al.*, 1999a,b) have high capacities for Pa(V), but are relatively unselective.

The extraction by *N*-benzoylphenylhydroxylamine (BPHA) from HCl, and H_2SO_4 solutions was used for the separation of Pa(V) from other elements by Pal'shin *et al.* (1963) and Myasoedov *et al.* (1964). It was found that protactinium complexes with BPHA were extracted by benzene or other solvents from aqueous solutions with a wide range of acid concentrations. D'yachkova and Spitsyn (1964) studied the protactinium, zirconium, and niobium behavior by extraction with BPHA from sulfuric acid solutions. The isolation of the above elements was carried out with 0.2–0.5% solution BPHA in chloroform. The largest difference in extraction ability for these elements was observed with H_2SO_4 concentrations in the aqueous phase greater than 7 N. Rudenko *et al.* (1965) and Lapitskii *et al.* (1966) carried out the separation of protactinium from uranium and thorium by extraction with 0.1 M BPHA solution in chloroform from 4 M HCl.

The Pa(V) extraction by cupferron (CP) had been studied by Maddock and Miles (1949). It was found that Pa was easily extracted by CP in both oxygen-containing and inert solvents from inorganic acid media. Spitsyn and Golutvina (1960) used the extraction with CP for the separation of ^{233}Pa from large amounts of manganese. Rudenko *et al.* (1965) and Lapitskii *et al.* (1965) reported that the neocupferron (NCP), an analog of CP, can be also used for the separation of protactinium from uranium, thorium, and other elements. Uranium and thorium are not extracted by NCP from 2 M HCl solutions, whereas protactinium isolation by a 0.01 M solution of this reagent in chloroform is about 90%. These authors used NCP for isolation of ^{233}Pa from irradiated thorium.

The extraction of Pa by 1-phenyl-3-methyl-4-benzoylpyrazolone (PMBP) in benzene solution from H_2SO_4 media effectively isolated this element from large amounts of Fe(III), La, Nb(V), Th(IV), and U(VI) (Pal'shin *et al.*, 1970). Hence, Pa extraction and isolation by 0.1 M solution of PMBP in benzene from 5 N H_2SO_4 is greater than 98%. For the complete separation of Pa from Zr by this method, a 12% solution of H_2O_2 had been used.

The quantitative extraction of protactinium salicylate with acetone at pH 4 from saturated calcium chloride solutions was reported by Nikolaev *et al.* (1959). Under these conditions zirconium, thorium, uranium, and plutonium are extracted with protactinium. The extraction with salicylate can be used for the separation of protactinium from rare earth and other di- and tervalent elements. The quantitative extraction of protactinium oxychinolate with chloroform from solutions with pH 3–9 was described (Keller, 1966a).

Extraction by tertiary amines in early work was explored only at levels of 10^{-4} M or less, but this procedure shows promise because it permits the extraction of Pa(V) from HF-containing solutions (Moore, 1960; Muxart and Arapaki-Strapelias, 1963; Guillot, 1966; Muxart *et al.*, 1966b; Pal'shin *et al.*, 1971; Moore and Thern, 1974).

The extraction behavior of protactinium in mixtures of uranium, thorium, and neptunium with trilaurylamine from sulfonic acid solutions (Souka *et al.*, 1975c) indicates low distribution coefficients at high acid concentrations; the addition of hydrochloric acid appreciably enhances extraction. The extraction of protactinium (V) with trioctylamine (TOA) dissolved in xylene from thiocyanate solutions containing uranium and thorium have been successfully accomplished (Nekrasova *et al.*, 1975a); tracer amounts of Pa can exist in monomeric form in thiocyanate media for several months, but at Pa(V) concentrations greater than 10^{-6} M, polymers form and the efficacy of TOA as an extractant is seriously impaired (Nekrasova *et al.*, 1975b). Columns impregnated with TOA in a liquid chromatographic system were also used for the separation of ^{262,263}Db in HCl–HF media from Pa and Nb. The data obtained confirm the non-tantalum-like behavior of dubnium in 0.5 M HCl and 0.01 M HF media, and corroborate previously suggested structural differences between the halide complexes of dubnium, niobium, and protactinium, on the one hand, and those of tantalum on the other hand (Zimmerman *et al.*, 1993). Dubnium was shown to be adsorbed on the column from 12 M HCl and 0.02 M HF solutions together with its lighter homologs Nb, Ta, and the pseudohomolog Pa. In elutions with 10 M HCl and 0.025 M HF, 4 M HCl and 0.02 M HF, and 0.5 M HCl and 0.01 M HF, the extraction sequence Ta > Nb > Db > Pa was observed (Paulus *et al.*, 1998, 1999).

The formation of polymers of Pa(V) in the extractions by quaternary ammonium base Aliquat 336 from strongly alkaline solutions can be minimized by the addition of a hydroxycarboxylic acid or aminopolycarboxylic acid (Myasoedov *et al.*, 1980). While the extractability of Pa(V) can be enhanced, the separations are poor. For the systematic study of halide complexation of the group V elements, new batch extraction experiments for Nb, Ta, and Pa were performed with the Aliquat 336 in pure HF, HCl, and HBr solutions. Based on these results, new chromatographic column separations were designed to study separately the fluoride and chloride complexation of Db with Automated Rapid Chemistry Apparatus II (ARCA II). In the system Aliquat 336-HF, after feeding the activity onto the column in 0.5 M HF, dubnium did not elute in 4 M HF (Pa fraction) but showed a higher distribution coefficient close to that of

Nb (and Ta). In the system Aliquat 336-HCl, after feeding onto the column in 10 M HCl, dubnium showed a distribution coefficient in 6 M HCl close to that of Nb establishing an extraction sequence Pa > Nb greater than or equal to Db > Ta, which was theoretically predicted by considering the competition between hydrolysis and complex formation (Paulus *et al.*, 1998, 1999). Separation of ^{231}Pa from U and other impurities has been provided by an extraction-chromatographic method using quaternary ammonium-Kel-F materials (Zhang Xianlu *et al.*, 1993).

Extraction of protactinium(V) chloro complexes by tricaprylamine and its separation from Th(IV), U(VI), and rare earths has been described (El-Yamani and Shabana, 1985).

(d) Large-scale recovery of protactinium-231

Brown and Whittaker (1978) have described a new, 'relatively simple' method for the recovery and purification of protactinium-231. It has been applied with signal success to the recovery of Pa from various residues containing 1.73 g of protactinium in a state of high chemical and radiochemical purity. Efficient separation of ^{231}Pa was readily effected by dissolving the ^{231}Pa-containing residues in 5 M hydrofluoric acid. Excess ammonia is added to precipitate the hydrous oxides, which after several washes with water are redissolved in 2 M nitric acid. This precipitate is considerably enriched in ^{231}Pa. Washing the precipitated hydrous oxides with 0.5–4.0 M HNO_3 and/or 0.5 M HNO_3 and 0.3 M H_2O_2, in which protactinium(V) hydrous oxide, is essentially insoluble, removes much of the impurities carried in the initial hydrous oxide precipitation. Repetition of this cycle twice more yields Pa_2O_5 of high purity. The final traces of silicon are then removed by dissolving the hydrous oxides in 20 M HF and evaporating the solution to dryness. Recovery yields range from 92 to 96% from initial samples containing 30–75 wt% ^{231}Pa. The purity of the product is generally greater than 99%; it is also radiochemically pure.

4.4.6 Preparation of pure ^{234}Pa and ^{234m}Pa

Because of its short half-life, 1.17 min ^{234m}Pa is frequently used for classroom demonstrations of radioactive decay and growth (Booth, 1951; Carsell and Lawrence, 1959; Overman and Clark, 1960). Pure ^{234m}Pa (and its ground-state isomer, 6.7 h ^{234}Pa) can be coprecipitated directly from a 6 M HCl solution of $(NH_4)_2U_2O_7$ with BPHA (Cristallini and Flegenheimer, 1963). The procedure is rapid and gives a high degree of decontamination from both U and Th.

However, most authors prefer to make a preliminary separation of 24.1 day ^{234}Th, from which the ^{234m}Pa (and ^{234}Pa) can be repeatedly 'milked'. The classical procedure of Crookes (1900) is still one of the most widely used for this purpose (Harvey and Parsons, 1950; Barendregt and Tom, 1951;

Bouissières *et al.*, 1953; Forrest *et al.*, 1960; Bjørnholm and Nielsen, 1963): 10–200 g of $UO_2(NO_3)_2 \cdot 6H_2O$ are dissolved in diethyl ether. The aqueous phase formed by the water of crystallization retains the ^{234}Th and some U. Repeated extraction with fresh ether removes the remaining U. Alternatively, the ^{234}Th is purified and concentrated by coprecipitation with $Fe(OH)_3$ in the presence of $(NH_4)_2CO_3$ (Hahn, 1921; Harvey and Parsons, 1950), by cation exchange from HCl solution (Zijp *et al.*, 1954; Suner *et al.*, 1974), by anion exchange from HNO_3 solution (Bunney *et al.*, 1959), or by extraction with tertiary amines (Moore and Thern, 1974; Carswell and Lawrence, 1959).

Once the ^{234}Th has been purified, the ^{234m}Pa and ^{234}Pa quickly regain equilibrium and can be isolated by any of the methods described above for the purification of ^{231}Pa, except, of course, carrier-free precipitation. Solvent extraction is the most suitable, because of its speed and selectivity, at tracer levels, Pa(V) is rapidly and quantitatively separated from Th(IV) by extraction from 6 M HCl solution with any number of organic solvents, notably DIPK, DIBK, DIPC, and DIBC (Moore, 1955; Myasoedov *et al.*, 1966a). The ^{234}Th remains in the aqueous phase. To prepare ^{234m}Pa free of ^{234}Pa, the first two or three organic extracts are discarded and, after 10–15 min, the re-grown ^{234m}Pa is extracted with fresh solvent (Bjørnholm and Nielson, 1963).

Fajans and Göhring (1913b) first separated *brevium* by selective adsorption on lead plates and by coprecipitation with Ta_2O_5. The addition of ^{232}Th keeps the mixture of ^{234}Th and ^{234m}Pa more quantitatively in solution (Guy and Russell, 1923; Jacobi, 1945). Hahn (1921) coprecipitated the mixture of ^{234}Th and ^{234m}Pa with LaF_3, leaving ^{234}Pa in the filtrate. Zijp *et al.* (1954) concentrated ^{234}Pa by MnO_2 precipitations (Maddock and Miles, 1949), alternating with extraction by TTA (Meinke, 1952).

Bjørnholm *et al.* (1967) milked 0.5–1 mCi of ^{234}Pa from 0.8 mCi of ^{234}Th by extraction into hexone (methyl isobutyl ketone, MIK) from 6 M HC1 solution. It is noteworthy, however, that many of the same problems were encountered in the initial concentration of ^{234}Th from 2 tons of U metal as in scaling up laboratory procedures for the concentration of macroscopic amounts of ^{231}Pa from natural sources.

4.4.7 Preparation of pure ^{233}Pa

Irradiation of 1 g ^{232}Th (as metal, oxide, chloride, nitrate, or basic carbonate) for 1 day in a thermal-neutron flux of 2×10^{14} n cm^{-2} s^{-1} will produce approximately 5 Ci of ^{233}Pa (Schuman and Tromp, 1959). Detailed procedures for the isolation of ^{233}Pa from Th targets are given in several review articles (Hyde and Wolf, 1952; Hyde, 1954, 1956; Haïssinsky and Bouissières, 1958; Kirby, 1959; Pal'shin *et al.*, 1970). In general, the target is dissolved in concentrated HCl or HNO_3 (usually containing 0.01–0.1 M HF as a catalyst) and the ^{233}Pa is separated from Th and other impurities by one, or a combination, of the

anion-exchange and solvent extraction methods described above. Alternatively, 3 g of Th metal irradiated in a reactor with an irradiation time of 1 day in a thermal flux of 3×10^{13} n cm^{-2} s^{-1} are dissolved in nitric acid. The ^{233}Pa is adsorbed on an anion-exchange column, eluted, then is extracted by TOPO (Kuppers and Erdtmann, 1992).

A preliminary concentration by coprecipitation (Katzin and Stoughton, 1956; Fudge and Woodhead, 1957; Katzin, 1958) is often used, and was, in fact, the method adopted by Codding *et al.* (1964) to isolate 1 gram of ^{233}Pa after solvent extraction with MIK or DIPK gave unaccountably poor yields. Leaching the MnO_2 with a mixture of HNO_3 and H_2O_2 removed the Mn without loss of ^{233}Pa, which was subsequently dissolved in 6 M H_2SO_4 and re-precipitated with HNO_3. On the other hand, Schulz (1972) reported good extraction of ^{233}Pa by DIBC from 7.4 M HNO_3 solutions containing 1.4 M Th $(NO_3)_4$ and 480 Ci L^{-1} of ^{233}Pa. Macroscopic amounts of ^{233}Pa have also been recovered from HNO_3 solutions of irradiated ThO_2 by adsorption on powdered unfired Vycor glass and silica gel (Moore and Rainey, 1964; Goode and Moore, 1967); at tracer levels, ^{233}Pa has been separated from Th targets by adsorption on silica gel (Davydov *et al.*, 1965; Spitsyn *et al.*, 1969; Chang *et al.*, 1974; Chang and Ting, 1975b), on quartz sand (Sakanoue and Abe, 1967), and on activated charcoal saturated with PAA (Pal'shin *et al.*, 1966). Separations with cation and chelating resins (Kurodo and Ishida, 1965; Myasoedov *et al.*, 1969), by paper chromatography and paper electrophoresis (Vernois, 1958, 1959; Myasoedov *et al.*, 1969), and by reversed-phase partition chromatography (Fidelis *et al.*, 1963) have also been reported.

4.4.8 Toxic properties

^{231}Pa is dangerous to organisms, similar to other α-emitters with comparatively short half-lives. Once in organisms it accumulates in kidneys and bones. The maximum amount of protactinium considered not harmful after absorption by an organism is 0.03 μCi. It corresponds to 0.5 μg ^{231}Pa. Protactinium-231, contained in the air as an aerosol, is 2.5×10^8-fold more toxic than hydrocyanic acid at the same concentrations (Bagnall, 1966a). Therefore all operations with weighable amounts of ^{231}Pa are carried out in special isolated boxes.

4.4.9 Applications of protactinium

Pa was used for the preparation of a scintillator for detecting X-rays, comprising complex oxides of Gd, Pa, Cs, rare earth metals and other elements. This scintillator, which can significantly increase relative light emission outputs without increasing background, is used in for detecting X-rays, particularly in an X-ray computed tomography apparatus (Hitachi Metals, 1999). The coating

material for a color cathode ray tube with bright green fluorescence was created by doping wih Pa (Toshiba, 1995).

Mixed oxides of Nb, Mg, Ga and Mn, doped with 0.005–0.52% Pa_2O_5, were used as high temperature dielectrics (up to 1300°C) for ceramic capacitors (Fujikawa *et al.*, 1996).

One of the important applications of Pa can be in the determination of ancient subjects using a $^{231}Pa/^{235}U$ dating method. This method was used for the dating of one of the Qafzeh human skulls, Qafzen 6, excavated in 1934 by Neuville and Stekelis and conserved at the Institut de Paléontologie Humaine in Paris, by non-destructive gamma-ray spectroscopy. A long-term measurement resulted in an age of (94 ± 10) Ka and confirmed the great antiquity of the Proto-Cro-Magnons of the Near East, contributing to the establishment of modern man's chronology (Yokoyama *et al.*, 1997). The Neanderthal hominid Tabun C1, found in Israel by Garod and Bate, was attributed to either layer B or C of their stratigraphic sequence. Gamma-ray spectroscopy of the $^{231}Pa/^{235}U$ ratios of two bones from this skeleton was used to determine their age. Calculations gave the age of the Tabun C1 mandible as 345 Ka. This suggests that Neanderthals did not necessarily coexist with the earliest modern humans in the region. The early age determined for the Tabun skeleton would suggest that Neanderthals survived as late in the Levant as they did in Europe (Schwarcz *et al.*, 1998). Uranium-series dating of bones and teeth from the Chinese Paleolithic sites has also been used (Chen and Yuan, 1988).

As a result of the development of the nuclear industry (e.g. nuclear power engineering and nuclear powered fleets), a considerable amount of radioactive wastes and spent nuclear fuel is accumulating in the world. Geological disposal of solid and solidified nuclear waste is considered as being economical, technically and ecologically the most feasible approach to completion of the nuclear fuel cycle. Thus determination of chemical behavior of actinides elements, Pa included, is an important problem of environmental science.

The sorption behavior of Pa, which is a decay product of uranium, was studied on the principal rock types from the potential areas selected for construction of a repository. The sorption distribution coefficients (K_d) of Pa were determined under ambient conditions in oxic and anoxic (N_2) atmospheres using natural fresh and brackish groundwater; and the values obtained were 0.07–2.3 and 1.7–12 $m^3\ kg^{-1}$, respectively (Kulmala *et al.*, 1998). Pickett and Murrell (1997) presented the first survey of $^{231}Pa/^{235}U$ ratios in volcanic rocks; such measurements were made possible by new mass spectrometric techniques. It was shown that the high $^{231}Pa/^{235}U$ ratios in basalts reflect a large degree of discrimination between two incompatible elements, posing challenges for modeling of melt generation and migration. Fundamental differences in $^{231}Pa/^{235}U$ ratios among different basaltic environment are likely related to differences in melting zone conditions (e.g. melting rate). Strong disequilibria in continental basalts demonstrate that Pa–U fractionation is possible in both garnet and spinel mantle stability fields.

4.5 ATOMIC PROPERTIES

Experimental measurements (Marrus *et al.*, 1961; Giaechetti, 1966; Richards *et al.*, 1968) and theoretical calculations (Judd, 1962; Wilson, 1967, 1968) agree that the ground state configuration of the neutral Pa atom is almost certainly [Rn] $5f^2 6d^1 7s^2$. However, some unpublished calculations by Maly (cited by Cauchois (1971)) indicated that the total relativistic energy of that structure was 0.9 eV higher than that of a $5f^1 6d^2 7s^2$ configuration, implying that the latter may be the more stable of the two. Giaechetti (1967) found that the ground state configuration of the first ion of Pa (Pa^{1+}) was $5f^2 7s^2$ and this was confirmed by theoretical calculations, which also yielded $5f^2 6d^1$, $5f^2$ and $5f^1$ as the ground state configurations of Pa^{2+}, Pa^{3+} and Pa^{4+}, respectively. Crystal structure stabilities and the electronic structure of Pa have been discussed by Wills and Ericsson (1992).

The emission spectrum of Pa was first recorded by Schüler and Gollnow (1934), who reported a large number of lines in the visible region, many of which showed hyperfine splitting patterns, indicating a nuclear spin of 3/2 for ^{231}Pa. Tomkins and Fred (1949) listed 263 lines in the ultraviolet region sensitive to copper spark excitation. The emission spectrum excited by a microwave discharge tube was measured by Richards and co-workers (1963, 1968), who recorded some 14 000 lines between 3 μm and 400 nm, about half of which were fitted into a level scheme of about 200 even and 300 odd levels.

Table 4.4 lists recommended X-ray atomic energy levels, based on the X-ray wavelengths re-evaluated by Bearden (1967) and by Bearden and Burr (1967).

The Mössbauer effect has been studied by Croft *et al.* (1968) with the 84.2 keV γ-ray of ^{231}Pa, following β^--decay of ^{231}Th; resonance absorption was detected

Table 4.4 *Recommended values of the atomic energy levels* (eV) *of Pa* (*measured values of the X-ray absorption energies are shown in parentheses*) (*Bearden and Burr*, 1967).

Level	*Energy* (eV)	*Level*	*Energy* (eV)
K	1 12 601.4 ± 2.4	N_I	1387.1 ± 1.9
L_I	21 104.6 ± 1.8 (21 128)	N_{II}	1224.3 ± 1.6
L_{II}	20 313.7 ± 1.5 (20 319)	N_{III}	1006.7 ± 1.7
L_{III}	16 733.1 ± 1.4 (16 733)	N_{IV}	743.4 ± 2.1
M_I	5366.9 ± 1.6	N_V	708.2 ± 1.8
M_{II}	5000.9 ± 2.3	N_{VI}	371.2 ± 1.6
M_{III}	4173.8 ± 1.8	N_{VII}	359.5 ± 1.6
M_{IV}	3611.2 ± 1.4 (3608)	O_I O_{II}	309.6 ± 4.3
M_V	3441.8 ± 1.4 (3436)	O_{III}	222.9 ± 3.9
		O_{IV}	94.1 ± 2.8
		O_V	

with absorbers of both Pa_2O_5 and PaO_2. No isomer shift between the valence states was observed.

4.6 THE METALLIC STATE

Grosse (1934a) prepared metallic Pa by two methods: (1) Pa_2O_5 was bombarded for several hours with 35 kV electrons at a current strength of 5–10 mA and (2) the pentahalide (Cl, Br, I) was heated on a tungsten filament at a pressure of 10^{-6} to 10^{-5} torr. Later authors have prepared the metal by reduction of PaF_4 with the vapors of Ba (Sellers *et al.*, 1954; Bansal, 1966; Cunningham, 1966, 1971; Dod, 1972), Li (Fowler *et al.*, 1965; Cunningham, 1971), or Ca (Marples, 1966). A Zn–Mg reductant is said to yield an impure Pa product (Lee and Marples, 1973).

In the method used by Cunningham and his co-workers at Berkeley (Cunningham, 1971; Dod, 1972), PaF_4 is mixed with barium in a crucible fabricated from a single crystal of BaF_2 (or LiF) and supported in a tantalum foil cylinder. The assembly is evacuated to below 10^{-6} torr and heated inductively to 1250–1275°C for 4–5 min. The BaF_2 crucible is then melted by raising the temperature to 1600°C for 1.5 min and then molten Pa metal agglomerates as a small sphere at the bottom of the Ta support ring. Individual preparations are limited to about 15 mg.

Subsequently, individual preparations of Pa metal of up to 0.5 g have been successfully executed by a modified Van Arkel technique (Baybarz *et al.*, 1976; Brown *et al.*, 1977; Bohet and Muller, 1978; Brown, 1982; Spirlet, 1982). The starting material is protactinium carbide obtained by reduction of Pa_2O_5 with carbon. Heating the protactinium carbide with I_2 generates volatile PaI_5, which is then decomposed on a heated tungsten filament or, better, a sphere (Spirlet, 1979) using induction heating. Protactinium can be precipitated from diluted HF, H_2SO_4 solutions as a fine film on several metal plates (Zn, Al, Mn, and other) (Camarcat *et al.*, 1949; Haïssinsky and Bouissières, 1958; Stronski and Zelinski, 1964). The electrolytic reduction of Pa from NH_4F solutions in the presence of triethylamine at pH 5.8 and 10–20 mA cm^{-2} also has been realized (Emmanuel-Zavizziano and Haïssinsky, 1938). Preparation of a protactinium measurement source by the electroplating method also has been reported by Li Zongwei *et al.* (1998).

The availability of pure, single-crystal Pa metal has made possible the measurement of important physical parameters that cast light on the electronic structure of Pa and for the calculation of its optical properties (Gasche *et al.*, 1996). A theoretical calculation by Soderling and Eriksson (1997) predicted that protactinium metal will undergo a phase transition to the α-U orthorhombic structure below 1 Mbar (1 Mbar ~100 GPa) pressure. At higher pressures, the β-phase re-enters into the phase diagram and at the highest pressures an ideal *hcp* structure becomes stable. Hence, Soderling and Eriksson expect Pa to

undergo a sequence of transitions, with the first transition taking place at 0.25 Mbar and the subsequent ones above 1 Mbar. The β→α-U transition is triggered by the pressure-induced promotion of the spd-valence electrons to 5f states. In this regard Pa approaches uranium, which at ambient conditions has one more 5f electron than Pa at similar conditions. At higher compression of Pa, the 5f band broadens and electrostatic interactions in combination with Born–Mayer repulsion become increasingly important and drive Pa gradually to more close-packed structures. At ultra-high pressures, the balance between electrostatic energy, Born–Mayer repulsion, and one-electron band energy stabilizes the *hcp* (ideal packing) structure.

Recent experimental results (Haire *et al.*, 2003) confirm that the stable room temperature and pressure phase of Pa metal is the body-centered tetragonal (*bct*) phase. Under high pressure this phase is stable until 77(5) GPa (77 GPa ~0.77 Mbar) where it is converted to orthorhombic, the α-uranium phase, with a small (0.8%) volume collapse. The relative volume of the *bct* phase decreased smoothly from 1 atm down to a volume ratio of ~0.7 before the high-pressure phase transformation. Experiments continued to a pressure of 130 GPa with no further phase change but with a smooth decrease in the volume of the orthorhombic phase of ~0.62. Haire *et al.* (2003) attribute the structural phase change to an increase in 5f bonding at the higher pressures.

The superconducting properties of Pa metal have been described by Smith *et al.* (1979), who determined the superconducting transition temperature and upper critical magnetic field. Since the superconducting properties of Pa are markedly affected by its 5f electronic structure, it is now evident that Pa is a true actinide element. The heat capacity of a single Pa crystal in the temperature range 4.9–18 K has been reported (Stewart *et al.*, 1980). The unit cell volume of Pa metal first decreases and then increases on cooling from 300 to 50 K (Benedict *et al.*, 1979). The importance of the expansion coefficient in the explanation of specific-heat parameters has been discussed by Mortimer (1979). A Mössbauer resonance of ^{231}Pa at 84.2 keV in Pa metal has been reported; the electric field gradient in Pa metal is $|eq_Z| = (2.05 \pm 0.15) \times 10^{18}$ V cm^{-2} (Friedt *et al.*, 1978; Rebizant *et al.*, 1979). The vapor pressure of liquid Pa metal in the temperature range 2500–2900 K has been measured by a combination of mass spectrometry and Knudsen effusion techniques; the vapor pressure (in Pascals) is given (Bradbury, 1981) by:

$$\log[P(\text{Pa(liq)})] = -[(31\,328 \pm 375)/T] + (10.83 \pm 0.13).$$

Pa metal is malleable and ductile (Zachariasen, 1952; Sellers *et al.*, 1954). Other physical properties are summarized in Table 4.5. The enthalpy of sublimation of Pa(s) at 298 K has been calculated to be 660 (Bradbury, 1981) or 570 kJ mol^{-1} (Kleinschmidt *et al.*, 1983).

Metallic Pa is attacked by 8 M HCl, 12 M HF, or 2.5 M H_2SO_4, but the initial reaction ceases quickly, possibly because of the accumulation of a protective layer resulting from the hydrolysis of Pa(V) or Pa(IV) at the metal surface.

Table 4.5 *Some physical properties of protactinium metal.*

Property	*Observed or calculated value(s)*	*References*
crystal structure	body-centered tetragonal (14/*mmm*) high temp. form is fcc or bcc	Zachariasen (1952); Asprey *et al.* (1971)
lattice parameters (Å)	$a = 3.925 \pm 0.005$, $c = 3.238 \pm 0.007$ (RT)	Zachariasen (1952); Sellers *et al.* (1954)
	$a = 3.924 \pm 0.001$, $c = 3.239 \pm 0.0005$ (18°C) (*a/c* approaches 1 with increased temperature)	Marples (1966)
	$a = 3.929 \pm 0.001$, $c = 3.241 \pm 0.002$ (RT)	Cunningham (1966)
	$a = 3.921 \pm 0.001$, $c = 3.235 \pm 0.001$ (RT)	Bohet (1977)
	$a = 5.02$ (high temperature form fcc)	Asprey *et al.* (1971)
	$a = 5.018$ (high temperature form fcc)	Bohet (1977)
	$a = 3.81$ (high temperature form bcc)	Marples (1965)
X-ray density (g cm^{-3})	15.37 ± 0.08	Zachariasen (1952)
metallic radius (Å)	1.63 for coordination number 12	Zachariasen (1952)
melting point (°C)	1575 ± 20	Marples (1966)
	1560 ± 20	Cunningham (1966)
	1565 ± 20	Cunningham (1971)
	1562 ± 15	Dod (1972)
vapor pressure (atm)	1×10^{-8} at ~2400 K	Cunningham (1971)
	5.1×10^{-5} at 2200 K	Murbach (1957)
magnetic susceptibility (emu mol^{-1}; 20–298 K)	$(250 \pm 50) \times 10^{-6}$ (temperature-independent)	Cunningham (1966)
	$(268 \pm 14) \times 10^{-6}$ (temperature-independent)	Bansal (1966)
	$(189 \pm 6.5) \times 10^{-6}$ (temperature-independent)	Dod (1972)
superconducting transition temperature (K)	1.4	Fowler *et al.* (1965, 1974)
	?	Smith *et al.* (1979)
	2	Francis and Theng-Da Tchang (1935)
	2	Launay and Dolechek (1947)

Table 4.6 *Preparation and structure of protactinium–noble-metal alloy phases* (*Erdmann*, 1971; *Erdmann and Keller*, 1971, 1973).

Compound	*Reduction temperature* (°C)	*Structure type*	*Lattice parameters* (Å)	
			a	*c*
Pt_3Pa	1250 ± 50	Cd_3Mg (hex)	5.704	4.957
Pt_5Pa	1200 ± 50	Ni_5U	7.413	
Ir_3Pa	1550 ± 50	Cu_3Au	4.047	
Rh_3Pa	1550 ± 50	Cu_3Au	4.037	
$Be_{13}Pa$	1300 ± 50	$NaZn_{13}$	10.26	

The metal does not react with 8 M HNO_3 even in the presence of 0.01 M HF. The most effective solvent found thus far is a mixture of 8 M HCl and 1 M HF (Cunningham, 1971).

According to Dod (1972), metal samples exposed to air at room temperature show little or no tarnishing over a period of several months. A slight loss of metallic luster was observed when a sample of Pa metal was heated in air for 1 h at 100°C. Heating for 1 h at 300°C caused the sample to turn grayish white and begin to disintegrate. Pa metal exposed to O_2, H_2O, or CO_2 at 300 and 500°C yielded Pa_2O_5; reaction with NH_3 and H_2 produced PaN_2 and PaH_3, respectively. The metal reacts quantitatively with excess I_2 above 400°C to yield a sublimate of crystalline, black PaI_5 (Sellers *et al.*, 1954; Brown *et al.*, 1967b).

4.6.1 Alloys

Erdmann and Keller (Erdmann, 1971; Erdmann and Keller, 1971, 1973) have prepared Pa–noble-metal alloy phases by reduction of Pa_2O_5 with highly purified H_2 in the presence of Pt, Ir, and Rh. Preparation conditions and some properties of these intermetallic compounds are listed in Table 4.6. Reaction of Pa_2O_5 with beryllium metal has been reported by Benedict *et al.* (1975) to form $Be_{13}Pa$.

4.7 SIMPLE AND COMPLEX COMPOUNDS

4.7.1 Protactinium hydride

Perlman and Weisman (1951) and Sellers *et al.* (1954) reacted H_2 with Pa metal at about 250°C and a pressure of about 600 torr, and obtained a black flaky substance, isostructural with β-UH_3. The compound was cubic, with a unit cell constant $a = (6.648 \pm 0.005)$ Å. However, Dod (1972) reported the formation at 100, 200, and 300°C of a gray, powdered substance that is isostructural with α-UH_3. The unit cell constant of α-PaH_3 is (4.150 ± 0.002) Å for the product obtained at 100 and 200°C and (4.154 ± 0.002) Å at 300°C. Subsequently, Brown (1982) prepared α- and β-PaH_3 at 250 and 400°C, respectively.

4.7.2 Protactinium carbides

Lorenz *et al.* (1969) prepared PaC by reduction of Pa_2O_5 with graphite at reduced pressure and temperatures above 1200°C. The product obtained at 1950°C was face-centered cubic (*fcc*) (NaCl type) with $a = (5.0608 \pm 0.0002)$ Å. At 2200°C, some additional weak lines, attributable to PaC_2, were observed; this structure was body-centered tetragonal with $a = (3.61 \pm 0.01)$ Å and $c = (6.11 \pm 0.01)$ Å. According to Sellers *et al.* (1954), PaC was 'probably' prepared by the reduction of PaF_4 with Ba in a carbon crucible. The magnetic susceptibility of PaC between 4 K and room temperature was measured by Hery *et al.* (1977). The magnetic susceptibility of PaC is weak (about -50×10^6 (emu cg)·mol^{-1}) and essentially independent of temperature, which may be taken to indicate the absence of 5f electrons and the presence of Pa(v) in the compound. Theoretical calculations by Maillet (1982) suggest that in ThC 5f electron participation in the bonding is minimal, but that in PaC the 5f electron bonding contribution is important.

4.7.3 Protactinium oxides

The known binary oxides of Pa are listed in Table 4.7. White Pa_2O_5 is obtained when the hydrated oxide, $Pa_2O_5 \cdot nH_2O$, and a wide variety of protactinium compounds as well are heated in oxygen or air above 500°C (Kirby, 1961) or 650°C (Sellers *et al.*, 1954; Keller, 1977). Thermochemical studies (Kleinschmidt and Ward, 1986) and differential thermal analysis shows three endothermic peaks, with maxima at 80, 390, and 630°C, and an exothermic peak, whose maximum occurs at 610°C (Stchouzkoy *et al.*, 1968). Several crystal modifications can be prepared, depending on the temperature to which the Pa_2O_5 is heated (Stchouzkoy *et al.*, 1964, 1966b; Roberts and Walter, 1966).

Black PaO_2 is prepared by the reduction of Pa_2O_5 with H_2 at 1550°C (Sellers *et al.*, 1954). Pa dioxide did not dissolve in H_2SO_4, HNO_3, or HCl solutions but reacted with HF because of the Pa(IV) oxidation to the pentavalent state by O_2 (Pal'shin *et al.*, 1970). Four intermediate phases have been identified by reduction of the pentoxide and oxidation of the dioxide (Roberts and Walter, 1966). A monoxide has been claimed to exist as a coating on metal preparations (Sellers *et al.*, 1954).

The heat of formation of Pa_2O_5 is about 106 kJ mol^{-1} as calculated by Augoustinik (1947). Pa_2O_5 did not dissolve in concentrated HNO_3 (Jones, 1966), but dissolved in HF and in a HF + H_2SO_4 mixture (Codding *et al.*, 1964) and reacted at high temperatures with solid oxides of metals of groups I and II of the periodic table (Pal'shin *et al.*, 1970).

Ternary oxides and oxide phases of different compositions and structures have been prepared by reaction of PaO_2 and Pa_2O_5 with the oxides of other elements (Table 4.8) (Keller, 1964a,b, 1965a–c, 1966a,b, 1971; Keller and Walter, 1965; Keller *et al.*, 1965; Iyer and Smith, 1966).

Table 4.7 *Binary oxides of protactinium.*

Composition	*Symmetry*	*Lattice constants*				*Temp, range of existence* (°C)	*References*
		a (Å)	*b* (Å)	*c* (Å)	α (deg.)		
PaO	cubic (NaCl)	4.961					Sellers *et al.* (1954)
PaO_2	fcc (CaF_2)	5.509					Roberts and Walter (1966)
PaO_2	fcc	5.505					Sellers *et al.* (1954)
$PaO_{2.18}$–$PaO_{2.21}$	fcc	5.473					Roberts and Walter (1966)
$PaO_{2.33}$	tetragonal	5.425		5.568			Roberts and Walter (1966)
$PaO_{2.40}$–$PaO_{2.42}$	tetragonal	5.480		5.416			Roberts and Walter (1966)
$PaO_{2.42}$–$PaO_{2.44}$	rhombohedral	5.449			89.65		Roberts and Walter (1966)
Pa_2O_5	fcc	5.446				650–700	Sellers *et al.* (1954)
Pa_2O_5	tetragonal	5.429		5.503		700–1000	Roberts and Walter (1966)
Pa_2O_5	tetragonal	10.891		10.992		700–1050	Stchouzkoy *et al.* (1968)
Pa_2O_5	hexagonal	3.820		13.225		1050–1500	Stchouzkoy *et al.* (1968)
Pa_2O_5	hexagonal	3.817		13.220		1000–1500	Roberts and Walter (1966)
Pa_2O_5	orthorhombic	6.92	4.02	4.18		?	Sellers *et al.* (1954)
Pa_2O_5	rhombohedral	5.424			89.76	1240–1400	Roberts and Walter (1966)

Table 4.8 *Polynary oxides of protactinium* (*Keller*, 1966*a*, 1971; *Palshin* et al., 1970).

		Lattice constants			
Compound	*Structure type*	*a* (Å)	*b* (Å)	*c* (Å)	*β* (deg.)
$LiPaO_3$	unknown				
Li_3PaO_4	tetragonal (Li_3UO_4)	4.52		8.48	
Li_7PaO_6	hexagonal (Li_7BiO_6)	5.55		15.84	
$(2–4)Li_2O \cdot Pa_2O_5$	cubic (fluorite phase)				
$(2–4)Na_2O \cdot Pa_2O_5$					
$NaPaO_3$	orthorhombic ($GdFeO_3$)	5.82	5.97	8.36	
Na_3PaO_4	tetragonal (Li_3SbO_4)	6.68			
$KPaO_3$	cubic ($CaTiO_3$)	4.341			
$RbPaO_3$	cubic ($CaTiO_3$)	4.368			
$CsPaO_3$	unknown				
$BaPaO_3$[a]	cubic ($CaTiO_3$)	4.45			
$SrPaO_3$[a]	unknown				
$Ba(Ba_{0.5}Pa_{0.5})O_{2.75}$	cubic (Ba_3WO_6)	8.932			
$GaPaO_4$	unknown				
$(La_{0.5}Pa_{0.5})O_2$	cubic (CaF_2)	5.525			
$Ba(LaO_{0.5}Pa_{0.5})O_3$	cubic (Ba_3WO_6)	8.885			
α-$PaGeO_4$	tetragonal ($CaWO_4$)	5.106		11.38	
β-$PaGeO_4$[a]	tetragonal ($ZrSiO_4$)	7.157		6.509	
α-$PaSiO_4$[a]	tetragonal ($ZrSiO_4$)	7.068		6.288	
β-$PaSiO_4$[a]	monoclinic ($CePO_4$)	6.76	6.92	6.54	104.83
Pa_2O_5/ThO_2	cubic (fluorite phase)				
$PaO_2 \cdot 2Nb_2O_5$[a]	tetragonal ($Th_{0.25}NbO_3$)	7.76		7.81	
$PaO_2 \cdot 2Ta_2O_5$[a]	tetragonal ($Th_{0.25}NbO_3$)	7.77		7.79	
$Pa_2O_5 \cdot 3Nb_2O_5$	hexagonal ($UTa_3O_{0.67}$)	7.48		15.81	
$Pa_2O_5 \cdot 3Ta_2O_5$	hexagonal ($UTa_3O_{10.67}$)	7.425		15.76	

[a] Could not be prepared in the pure state; always contained varying amounts of Pa(v).

The pale yellow product, which precipitates upon addition of H_2O_2 to a solution of Pa(v) in 0.25 M H_2SO_4, has been assigned the formula $Pa_2O_9 \cdot 3H_2O$ (Stchouzkoy *et al.*, 1966b). It is considered to be an unstable peroxide with a composition that varies with time over the range $Pa_2O_x \cdot 3H_2O$ with $5 < x < 9$.

4.7.4 Protactinium halides

Methods for preparing all the binary halides and many of the oxyhalides of Pa(IV) and Pa(V) are summarized schematically in Figs. 4.11, 4.12, and 4.13; those compounds which have been fully characterized are listed in Table 4.9. The preparative methods shown in Figs. 4.11 and 4.12 use an aqueous acid solution of Pa(V) as the starting material for the synthesis of binary protactinium halides. PaF_5 can be prepared by fluorination of PaC at 570 K or $PaCl_5$ at 295 K. The reaction products are isostructural with β-UF_5 (Brown *et al.*, 1982a). $PaF_5 \cdot 2H_2O$ is prepared by the evaporation of Pa solution in 30% HF

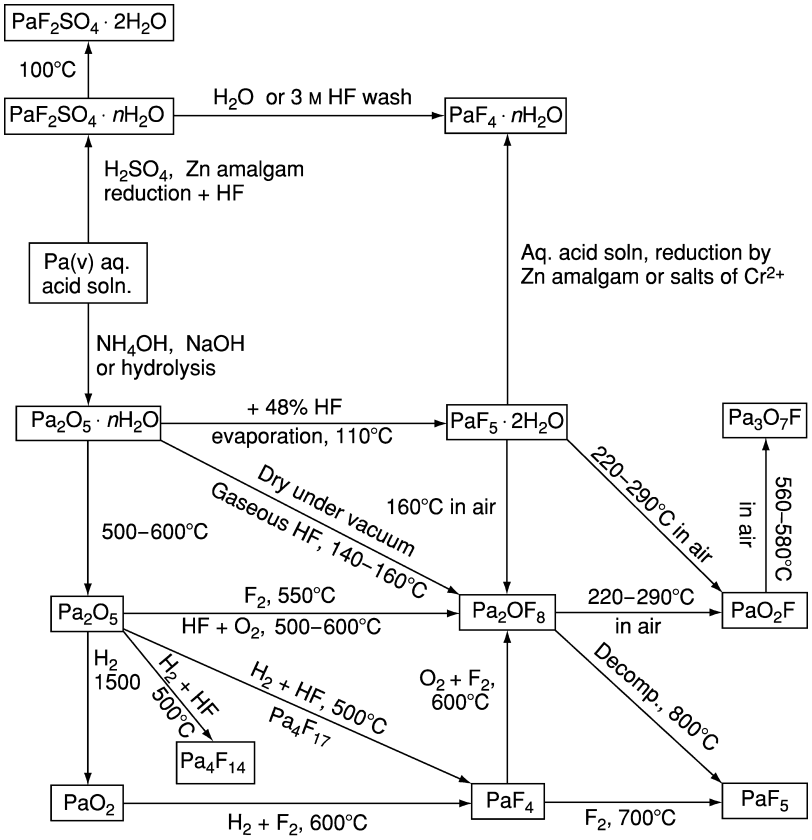

Fig. 4.11 *Preparation of some fluoride derivatives of Pa(IV) and Pa(V)* (*Muxart and Guillaumont*, 1974; *Pal'shin* et al., 1968a).

(Grosse, 1934c). Protactinium carbide is also useful in the preparation of other binary penta- and tetrahalides. Brown *et al.* (1976a) treated PaC with I_2 at 400°C, Br_2 at 350°C, and $SOCl_2$ at 200°C to obtain PaI_5, $PaBr_5$, and $PaCl_5$, respectively. PaI_4 was obtained by reaction of PaC with PaI_5 at 600°C or by the treatment with HgI_2 at 500°C. These compounds were also prepared by reactions of Pa_2O_5 with $Cl_2 + CCl_4$ at 300°C ($\rightarrow PaCl_5$) (Pissot *et al.*, 1966); CCl_4 at 400°C ($\rightarrow PaCl_4$) (Sellers *et al.*, 1954); $AlBr_3$ at 317°C ($\rightarrow PaBr_5$); and AlI_3 at $\leq$300°C ($\rightarrow PaI_5$) (D'Ege *et al.*, 1963) and so on.

Protactinium pentafluoride is reduced to PaF_4 by PF_3 but no reaction occurs with AsF_3. $PaCl_5$ and $PaCl_4$ are formed from PaF_5 and PaF_4 by reaction with PCl_3 and $SiCl_4$, respectively. PaF_5 reacts with CCl_4 to give $PaCl_xF_{5-x}$ (x probably 1), but no reaction is observed with PaF_4 (O'Donnell *et al.*, 1977). Whereas UF_5 is very soluble in acetonitrile, PaF_5 forms a sparingly soluble complex. An adduct $PaF_5 \cdot 2Ph_3PO$ forms on addition of TPPO to PaF_5 in acetonitrile

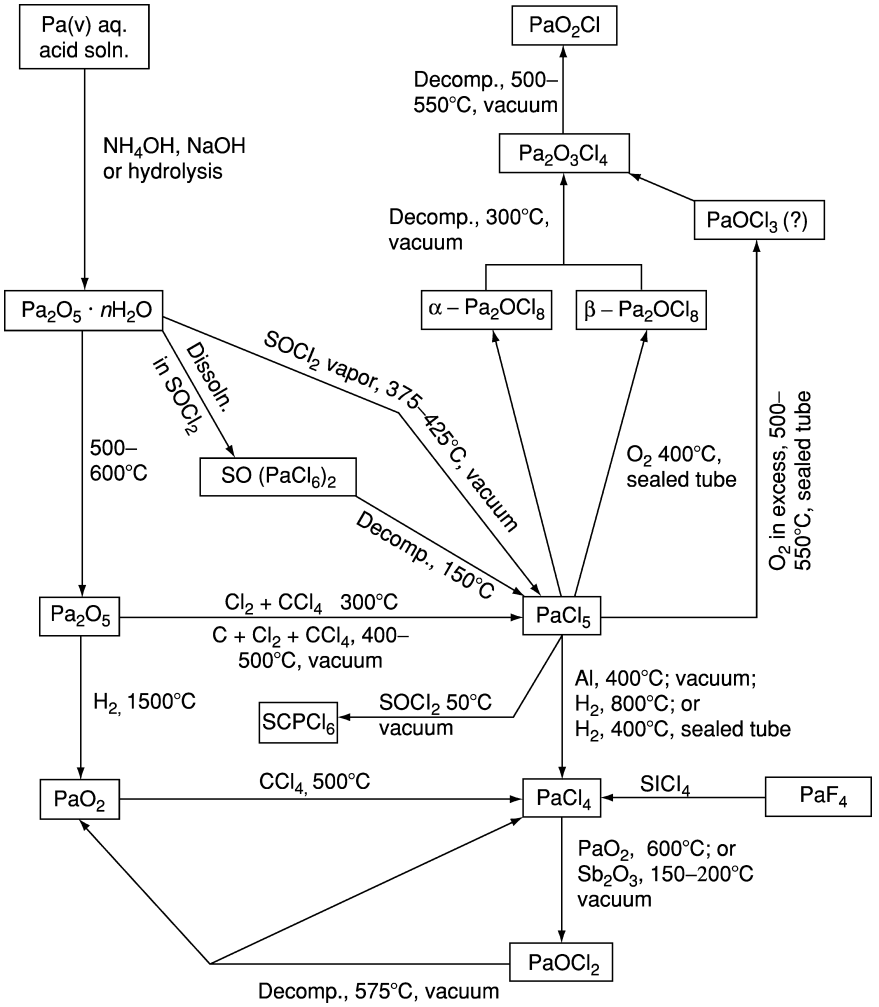

Fig. 4.12 *Preparation of some chlorides and oxychlorides of Pa(IV) and Pa(V)* (*Muxart and Guillaumont*, 1974; *Pal'shin* et al., 1968*a*).

(Brown *et al.*, 1982b). Brown (1979) found still another $PaBr_5$ crystal structure, designated γ, isostructural with β-UCl_5.

Of the possible halides of Pa(III), only PaI_3 has been reported so far (Scherer *et al.*, 1967). It is a dark brown compound (not black as originally reported) (Wilson, 1967), prepared by heating PaI_5, for several days at 10^{-6} torr and 360–380°C. Its tentative identification is based primarily on the similarity of its X-ray powder pattern to that of CeI_3.

All the binary halides are volatile at moderate temperatures, a property that has been used for the separation of ^{233}Pa from irradiated ThO_2 as well as for the

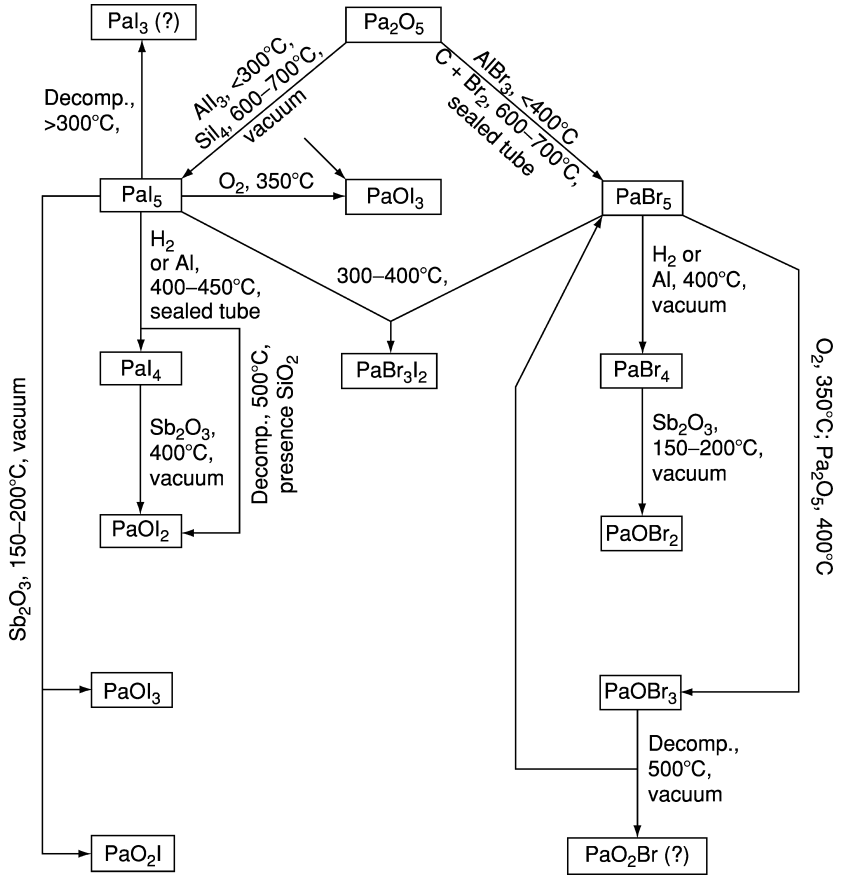

Fig. 4.13 *Preparation of some bromide and iodide derivatives of Pa(IV) and Pa(V)* (*Muxart and Guillaumont*, 1974; *Pal'shin* et al., 1968*a*).

preparation of radiochemically pure ^{231}Pa and ^{234}Pa (Malm and Fried, 1950; Merinis *et al.*, 1966; Brown, 1971). The vapor pressures of $PaCl_5$ and $PaBr_5$ have been measured by Weigel *et al.* (1969, 1974) in the temperature range 490–635 K; the boiling points, extrapolated to 760 torr, were 420 and 428°C, respectively. The thermal stability studies of Brown and co-workers (1976b) show that PaI_4 is stable up to a temperature of 330°C, and that PaI_5 is stable to 200–300°C.

Numerous alkali fluoro complexes of Pa(v) have been identified (Table 4.10) . The first, K_2PaF_7, was prepared by Grosse (1934a) for use in determining the atomic weight of ^{231}Pa. Complexes of the form $MPaF_6$ (M = Li, Na, K, Rb, Cs, Ag, NH_4) can be prepared by crystallization from aqueous HF solutions containing equimolar amounts of Pa(v) and the alkali fluorides, but $LiPaF_6$ and $NaPaF_6$ are best prepared by evaporating the equimolar mixture to dryness and

Table 4.9 *Halides and oxyhalides of protactinium.*

Compound	*Symmetry*	*Structure type or space group*	*Lattice constants*				*References*
			a (Å)	*b* (Å)	*c* (Å)	*Angle* (deg.)	
PaF_4	monoclinic	UF_4	12.86	10.88	8.54	$\beta = 126.34$	Soddy and Cranston (1918); Sellers *et al.* (1954); Asprey *et al.* (1967)
Pa_2F_9 (or Pa_4F_{17})	bcc cubic	U_2F_9	8.507				Brown (1966); Stein (1966)
PaF_5	tetragonal	β-UF_5	11.525		5.218		Brown (1971)
			11.53		5.19		Stein (1964)
Pa_2OF_8	bcc	U_2F_9	8.406				Stein (1964)
							Brown and Easey (1970)
PaO_2F	orthorhombic	–	6.894	12.043	4.143		Brown and Easey (1970)
Pa_3O_7F	orthorhombic	$Cmm2(C_{20}^{11})$	6.947	12.030	4.203		Brown and Easey (1970)
$PaCl_4$	tetragonal	UCl_4	8.377		7.479		Brown and Jones (1967c)
					7.482		Sellers *et al.* (1954)
$PaCl_5$	monoclinic	C2/*c*	10.35	12.31	8.82	$\beta = 111.8$	Brown and Maddock (1963)
$PaOCI_2$	orthorhombic	*Pbam*	15.332	17.903	4.012		Dodge *et al.* (1968); Bagnall *et al.* (1968a)
$PaBr_4$	tetragonal	UCl_4	8.824		7.957		Brown and Jones (1967c)
α-$PaBr_5$	monoclinic	$P2_1/c$	12.69	12.82	9.92	$\beta = 108$	Brown and Petcher (1969)
β-$PaBr_5$	monoclinic	$P2_1/n$	8.385	11.205	8.950	$\beta = 91.1$	Brown *et al.* (1968b); Brown and Petcher (1969)
γ-$PaBr_5$	triclinic	P1	7.52(1)	10.21(1)	6.74(1)	$\alpha = 89.27(5)$; $\beta = 117.55(6)$; $\gamma = 109.01(5)$	Merinis *et al.* (1966)
			9.25	12.12	9.13		D'Ege *et al.* (1963)
$PaOBr_3$	monoclinic	C2	16.911	3.871	9.334	$\beta = 113.67$	Brown *et al.* (1968b)
PaI_3(?)	orthorhombic	CeI_3	4.33	14.00	10.02		Scherer *et al.* (1967)
PaI_4							Brown *et al.* (1976b)
PaI_5	orthorhombic	–	7.22	21.20	6.85		Maddock (1960)
PaO_2I	hexagonal	–	12.64		4.07		Brown *et al.* (1967b)

Table 4.10 *Some fluoro complexes of Pa(IV) and Pa(V).*

Compound	*Symmetry*	*Structure type or space group*	*Lattice constant*				*References*
			a (Å)	*b* (Å)	*c* (Å)	*Angle* (deg.)	
$LiPaF_5$	tetragonal	$LiUF_5$	14.96		6.58		Asprey *et al.* (1967)
$Na_7Pa_6F_{31}$	rhombohedral	$Na_7Zr_6F_3$,	9.16			$\alpha = 107.09$	Asprey *et al.* (1967)
$K_7Pa_6F_{31}$	rhombohedral	$Na_7Zr_6F_3$,	9.44			$\alpha = 107.15$	Asprey *et al.* (1967)
$Rb_7Pa_6F_{31}$	rhombohedral	$Na_7Zr_6F_{31}$	9.64			$\alpha = 107.00$	Asprey *et al.* (1967)
$(NH_4)_4PaF_8$	monoclinic	–	13.18	6.71	13.22	$\beta = 17.17$	Asprey *et al.* (1967)
$NaPaF_6$	tetragonal	–	5.35		3.98		Asprey *et al.* (1966)
NH_4PaF_6	orthorhombic	$RbPaF_6$	5.84	11.90	8.03		Asprey *et al.* (1966); Brown (1973)
$KPaF_6$	orthorhombic	$RbPaF_6$	5.64	11.54	7.98		Asprey *et al.* (1966); Brown (1973)
$RbPaF_6$	orthorhombic	*Cmca*	5.86	11.97	8.04		Asprey *et al.* (1966); Brown (1973)
$CsPaF_6$	orthorhombic	$RbPaF_6$	6.14	12.56	8.06		Asprey *et al.* (1966); Brown (1973)
K_2PaF_7	monoclinic	*C2/c*	13.760	6.742	8.145	$\beta = 125.17$	Brown and Easey (1966)
Cs_2PaF_7	monoclinic	K_2PaF_7	14.937	7.270	8.266	$\beta = 125.32$	Brown *et al.* (1967a)
Li_3PaF_8	tetragonal	$P4_22_12(D^6)$	10.386		10.89		Brown and Easey (1965, 1966)
Na_3PaF_8	tetragonal	14 *mmm*	5.487		10.89		Brown and Easey (1965, 1966)
K_3PaF_8	fcc	F*m3m*	9.235				Brown and Easey (1966)
Cs_3PaF_8	fcc	F*m3m*	9.937				Brown and Easey (1966)
Rb_3PaF_8	fcc	F*m3m*	9.6				Asprey *et al.* (1966); Brown (1973)

fluorinating the dried residue (Asprey *et al.*, 1966). The heptafluoroprotactinates, M_2PaF_7 (M = K, NH_4, Rb, Cs), are precipitated by the addition of acetone to a 17 M HF solution containing Pa(V) and an excess of the appropriate alkali fluoride. NaF in a 3:1 molar ratio to Pa(V) yields Na_3PaF_8, but the other octafluoroprotactinates (V) are most easily prepared by the reaction:

$$M_2PaF_7 + MF \rightarrow M_3PaF_8$$

at 450°C in an atmosphere of dry argon or by fluorination of the product obtained by evaporation of an HF solution containing 3:1 MF and Pa(V) (Brown and Easey, 1966).

The fluoro complexes of Pa(IV) are prepared either by H_2 reduction of a Pa(V) complex at 450°C or by heating stoichiometric amounts of the alkali fluoride with PaF_4 in a dry argon atmosphere (Asprey *et al.*, 1967).

$Pa_2O_5 \cdot nH_2O$ reacts vigorously with $SOCl_2$ at room temperature to yield stable solutions containing up to 0.5 M Pa(V). The product is probably $SO(PaCl_6)_2$ which decomposes at 150°C under vacuum. Hexa- and octachloroprotactinates (V) are precipitated when CS_2 is added to $SOCl_2$ solutions containing equal amounts of $PaCl_5$ and MCl (M = $N(CH_3)_4$, $N(C_2H_5)_4$, $NH_2(CH_3)_2$, and $(C_6H_5)_4As$). Hexachloro complexes with Cs^+ and NH_4^+ precipitate when the component halides are reacted in $SOCl_2$/ICl mixtures (Bagnall and Brown, 1964). Hexabromoprotactinate (V) complexes, $MPaBr_6$ (M = $N(CH_3)_4$, $N(C_2H_5)_4$), have been prepared by vacuum evaporation of stoichiometric quantities of $PaBr_5$ and the tetraalkylammonium bromide dissolved in anhydrous CH_3CN (Brown and Jones, 1967b).

Axe and co-workers (Axe, 1960, Axe *et al.*, 1960, Axe *et al.*, 1961) observed the paramagnetic resonance spectrum of Pa^{4+} in single crystal of Cs_2ZrCl_6, crystallized from a melt containing approximately 500 μg of $^{231}PaCl_4$. The $5f^1$ structure was confirmed, as was the nuclear spin of 3/2. The resonance spectrum was found to be isotropic, with a spectroscopic splitting factor $g = -1.14$. Hendricks *et al.* (1971) measured the magnetic susceptibility of $PaCl_4$ from 3.2 to 296 K and found a ferromagnetic transition at about 182 K.

$PaCl_4$ is virtually insoluble in $SOCl_2$, but hexachloro- and hexabromoprotactinates (IV), M_2PaX_6 (X = Cl, Br; M = $N(CH_3)_4$ and $N(C_2H_5)_4$), have been prepared by reaction of PaX_4 with the tetraalkylammonium halide in CH_3CN. Cs_2PaCl_6 is precipitated on the addition of CsCl to a solution of $PaCl_4$ in concentrated HCl. The hexaiodo complex, $[(C_6H_5)_3CH_3As]_2PaI_6$, was also prepared from the component iodides dissolved in CH_3CN (Brown and Jones, 1967a). The electronic structures and optical transition energies of PaX_6^{2-} (X = F, Cl, Br, I) were calculated by quasi-relativistic density functional methods (Kaltsoyannis and Bursten 1995; Kaltsoyannis 1998). Analysis of the $5f^1 \rightarrow 6d^1$ transitions in PaX_6^{2-} (X = Cl, Br) and $ThBr_4$:Pa^{4+} was reported by Edelstein *et al.* (1988), and the EPR spectra of $ThBr_4$:Pa^{4+} in the incommensurate phase was detected (Zwanenburg *et al.*, 1988). The fluorescence and absorption spectra between the ground $5f^1$ and the excited $6d^1$ configurations of

Pa^{4+} diluted into a single crystal of Cs_2ZrCl_6 were analyzed (Piehler *et al.*, 1991; Edelstein *et al.*, 1992).

Numerous halide complexes of Pa(IV) and Pa(V) are formed with oxygen donor ligands, such as substituted phosphine oxides (Brown *et al.*, 1966b, 1970a,b), hexamethylphosphoramide (Brown and Jones, 1966a), DMSO (Bagnall *et al.*, 1968b), tropolone (Brown and Rickard, 1970), *N*,*N*-dimethylacetamide (Bagnall *et al.*, 1969), acetylacetone (Brown and Rickard, 1971b), and *N*,*N*-diethyldithiocarbamate (Heckley *et al.*, 1971). In addition, complexes with sulfur and selenium donors have been reported (Brown *et al.*, 1971).

The ground state electronic structures of PaX_6^{2-} (X = F, Cl, Br, I), UX_6^- (X = F, Cl, Br), and NpF_6 have been calculated using both non-relativistic and relativistic implementations of the discrete-variational X alpha (DV-X alpha) method. A significant amount of metal–ligand covalent bonding is found, involving both 6d and 5f metal orbitals. The 5f contribution to the bonding levels increases significantly from PaX_6^{2-} to UX_6^- to NpX_6 but remains approximately constant as the halogen is altered in PaX_6^{2-} and UX_6^-. In contrast, the 6d atomic orbital character of the halogen-based levels increases from UF_6^- to UBr_6^- and a similar, though less marked, trend is observed in PaX_6^{2-}. The electronic transition energies have been calculated using the transition-state method. The relativistic calculations are far superior to the non-relativistic ones in both qualitatively and quantitatively describing the electronic spectra. The stabilization of the metal 5f atomic orbitals with respect to the halogen *n*p levels from Pa to Np results in the more energetic f→f transitions in NpF_6 being masked by the onset of a ligand-to-metal charge transfer band. In the remaining molecules, the f→f transitions occur well removed from charge transfer bands (Kaltsoyannis, 1998).

Several chloro complexes and one bromo complex for which crystallographic data are available are listed in Table 4.11.

4.7.5 Protactinium pnictides

Protactinium pnictide compounds have been prepared and constitute a new category of Pa compounds that have several features of more than usual interest. The protactinium phosphide, PaP_2, was prepared by reaction of elemental phosphorus with protactinium hydride; thermal dissociation of PaP_2 forms Pa_3P_4 (Table 4.12) (Wojakowski *et al.*, 1982). The diarsenide, $PaAs_2$, can be obtained by heating together PaH_3 and elemental arsenic at 400°C; heating $PaAs_2$ to 840°C results in decomposition of $PaAs_2$ to form Pa_3As_4 (Hery *et al.*, 1978). $PaAs_2$ has a tetragonal structure of the anti-Fe_2As type, and Pa_3As_4 crystallizes in a body-centered structure of the Th_3P_4-type (Table 4.12). Single crystals of $PaAs_2$, Pa_3As_4, PaAs, and Pa_3Sb_4 were prepared from the elements by a Van Arkel procedure using vapor transport; iodine was the transporting agent and deposition occurred on an induction-heated tungsten support (Calestani *et al.*, 1979a,b). Hery and co-workers (1979) have obtained Pa_3Sb_4 and $PaSb_2$ by heating PaH_3 with antimony.

Table 4.11 *Some chloro and bromo complexes of Pa(IV) and Pa(V).*

Compound	*Symmetry*	*Lattice constants*				*References*
		a (Å)	*b* (Å)	*c* (Å)	*Angle* (deg.)	
Cs_2PaCl_6	trigonal	7.546		6.056		Brown and Jones (1967a)
$(NMe_4)_2PaCl_6$	fcc	13.08				Brown and Jones (1967a)
$(NEt_4)_2PaCl_6$	orthorhombic	14.22	14.75	13.35		Brown and Jones (1966a,b)
$(NMe_4)_2PaBr_6$	fcc	13.40				Brown and Jones (1967a,b)
$Pa(Trop)_4Cl$,DMSO	triclinic	9.87	12.60	15.96	$\alpha = 119.8$; $\beta = 103.6$; $\gamma = 103.0$	Brown and Rickard (1970)
$(NEt_4)_2PaOCl_5$	monoclinic	14.131	14.218	13.235	$\beta = 91.04$	Brown and Rickard (1971a); Brown *et al.* (1972)
$Pa(Acac)_2Cl_3$	monoclinic	8.01	23.42	18.63	$\beta = 98.9$	Bagnall *et al.* (1969)

Me, methyl; Et, ethyl; Trop, tropolonate; DMSO, dimethyl sulfoxide; Acac, acetylacetonate.

Table 4.12 *Crystallographic data for some miscellaneous compounds of protactinium.*

Compound	*Symmetry*	*Lattice parameters*				*References*
		a (Å)	*b* (Å)	*c* (Å)	γ (deg.)	
$H_3PaO(SO_4)_3$	hexagonal	9.439		5.506		Bagnall *et al.* (1965)
$H_3PaO(SeO_4)_3$	hexagonal	9.743		5.679		Bagnall *et al.* (1965)
PaOS	tetragonal	3.832		6.704		Sellers *et al.* (1954)
$[N(C_2H_5)_4]_4Pa(NCS)_8$	tetragonal	11.65		23.05		Al-Kazzaz *et al.* (1972)
$[N(C_2H_5)_4]_4Pa(NCSe)_8$	tetragonal	11.82		23.49		Al-Kazzaz *et al.* (1972)
$Pa(HCOO)_4$	tetragonal	7.915		6.517		Bohres (1974); Greis *et al.* (1977)
$HPaOP_2O_7$	fcc	5.92				LeCloarec (1974)
$(PaO)_4(P_2O_7)_3$	monoclinic	12.23	13.44	8.96	113.88	LeCloarec (1974); Lux *et al.* (1980)
$Pa_2O_5{\cdot}Pa_2O_5$	orthorhombic	5.683	12.06	14.34		LeCloarec (1974); Lux *et al.* (1980)
PaP_2	tetragonal	3.898		7.845		Bhandari and Kulkarni (1979)
[a]$Pa(Trop)_5$	tetragonal	9.759		9.46		Bhandari and Kulkarni (1979)

[a] Trop, tropolone.

The magnetic susceptibility of $PaAs_2$ and $PaSb_2$ has been measured from 4 K to room temperature. PaAs, $PaAs_2$, and $PaSb_2$ exhibit temperature-independent paramagnetism (Hery *et al.*, 1978). Self-consistent band structure calculations show that PaN and PaAs have about one f-electron, and hence they are expected to be paramagnetic; these results have been confirmed by experiment (Hery, 1979; Brooks *et al.*, 1980).

4.7.6 Miscellaneous compounds

Pa_2O_5 is insoluble in nitric acid but the freshly prepared hydroxide, the pentachloride, the pentabromide, and the complex $SO(PaCl_6)_2$ all dissolve in fuming HNO_3 to form stable solutions of at least 0.5 M Pa(V). Vacuum evaporation of such solutions yields $PaO(NO_3)_3 \cdot xH_2O$ ($1 < x < 4$). The reaction of Pa(V) halides with N_2O_5 in anhydrous CH_3CN yields $Pa_2O(NO_3)_4 \cdot 2CH_3CN$. Complexes of the type $MPa(NO_3)_6$ (M = Cs, $N(CH_3)_4$, $N(C_2H_5)_4$) have been prepared by reaction of the hexachloroprotactinates (V) with liquid N_2O_5 at room temperature (Brown and Jones, 1966b; Jones, 1966).

When a solution of Pa(V) in a mixture of HF and H_2SO_4 is evaporated until all F^- ion has been eliminated, $H_3PaO(SO_4)_3$ crystallizes almost quantitatively. The analogous selenato complex, more stable in acid (6 M HCl) or basic (NH_4OH) media, is obtained from HF/H_2SeO_4 mixtures. The sulfato-complex decomposes to $HPaO(SO_4)$ at 375°C (Bagnall *et al.*, 1965; Bagnall, 1966b) and to Pa_2O_5 at 750°C (Pal'shin *et al.*, 1968b). The binary chalcogenides, β-PaS_2 and γ-$PaSe_2$, have been prepared by Hery (1979). PaOS was obtained by the reaction of $PaCl_5$ with a mixture of H_2S and CS_2 at 900°C (Sellers *et al.*, 1954). $PaF_2SO_4 \cdot 2H_2O$ is precipitated when a solution of Pa(IV) in 4.5 M H_2SO_4 is added to 3 M HF (Stein, 1966). Crystallographic data for some S and Se compounds are given in Table 4.12.

The addition of hydrochloric acid to a solution of Pa(V) oxalate causes the precipitation of $PaO(C_2O_4)(OH) \cdot xH_2O$ ($x \sim 2$) (Muxart *et al.*, 1966a). On the other hand, the addition of acetone instead of acid yields $Pa(OH)(C_2O_4)_2 \cdot 6H_2O$ (Davydov and Pal'shin, 1967).

Phenylarsonic acid forms a white flocculent precipitate with Pa(V) in neutral or acid solutions. The compound is believed to have the composition $H_3PaO_2(C_6H_6AsO_3)_2$ (Myasoedov *et al.*, 1968c).

Complexes of the type $[N(C_2H_5)_4]_4PaR_8$ (R = NCS or NCSe) have been prepared by reaction of $PaCl_4$ with stoichiometric amounts of KCNS or KCNSe in anhydrous CH_3CN (Table 4.12) (AI-Kazzaz *et al.*, 1972). The bis(phthalocyaninato)complexes of Pa(IV), $(C_{32}H_{16}N_8)_2Pa$, have been prepared by neutron irradiation of the corresponding thorium $^{233}ThPc_2$ complex by the reactions (Lux *et al.*, 1970, 1971):

$$^{232}ThPc_2(n,\gamma)\,^{233}ThPc_2 \rightarrow {}^{233}PaPc_2 + \beta^-$$

Spectroscopically pure bis(phthalocyaninato)protactinium(IV) ($PaPc_2$) was prepared by reaction between $PaI_4 \cdot 4CH_3CN$ and *o*-phthalic dinitrile in

1-chloronaphthalene followed by purification by sublimation. $PaPc_2$ is isostructural with $ThPc_2$ and UPc_2 (Lux *et al.*, 1980). Tetrakis(cyclopentadienyl)Pa(IV), $(C_5H_5)_4Pa$, was prepared by treating Pa_2O_5 with a mixture of $Cl_2 + CCl_4$ in an argon stream at 600°C, then fusing the reaction product with $Be(C_2H_5)_2$ at 65°C (Keller, 1964b; Baumgartner *et al.*, 1969). Protactinium(IV) tropolone, $Pa(Trop)_4$, has been prepared by reaction of $PaCl_4$ or $PaBr_4$ with lithium tropolonate, Li(Trop) in methylene chloride; in the presence of excess Li (Trop) in dimethyl formamide, $LiPa(Trop)_5$ is formed (Brown and Richard, 1970). However, when protactinium pentethoxide, which is obtained by reaction of $PaCl_5$ with sodium ethoxide in anhydrous alcohol (Maddock and Pires deMatos, 1972; Bagnall *et al.*, 1975), is treated with tropolone, the complex Pa $(Trop)_5$ is obtained. $Pa(Trop)_5$ has been crystallized and its crystal structure parameters are determined (Table 4.12) (Bhandari and Kulkarni, 1979). Complexes of the actinide elements with cyclooctatetrene have been obtained by reaction of an actinide halide with cyclooctatetrene anion. The bis(η^8-tetramethylcyclooctatetradiene) complex of Pa has been prepared by reaction of Pa borohydride, $Pa(BH_4)_4$, with tetramethylcyclooctatetrene dianion (Solar *et al.*, 1980). The preparation of the anhydrous tetraformate, $Pa(HCOO)_4$, has been reported by the reaction of $PaCl_4$ with O_2-free HCOOH at 60°C in an argon atmosphere for 4 h (Table 4.12) (Bohres, 1974; Bohres *et al.*, 1974).

Freshly precipitated Pa(V) hydroxide or peroxide dissolves readily in 14 M H_3PO_4. However, upon aging, the hydrated orthophosphate, $PaO(H_2PO_4)_3 \cdot 2H_2O$, crystallizes out. Calcination of this product yields, successively: the anhydrous orthophosphate, $PaO(H_2PO_4)_3$ between room temperature and 300°C; the trimetaphosphate, $PaO(PO_3)_3$, stable to 900°C; the pyrophosphate, $(PaO)_4(P_2O_7)_3$, at 1000°C; and an unidentified phase with the gross composition $Pa_2O_5 \cdot P_2O_5$ at 1200°C (LeCloarec *et al.*, 1970, 1976; LeCloarec and Muxart, 1971; LeCloarec, 1974). Crystallographic data for several phosphates are given in Table 4.12. Protactinium(V) perrhenate, $PaO(ReO_4)_3 \cdot xH_2O$, has been prepared by reaction of Pa_2O_5 and Re_2O_7 (Silvestre *et al.*, 1977).

Protactinium(IV) borohydride, $Pa(BH_4)_4$, has been prepared by treating PaF_4 with aluminum borohydride, $Al(BH_4)_3$. It is a relatively unstable solid at 20°C, but exhibits high volatility as do other actinide borohydrides. $Pa(BH_4)_4$ is isostructural with $U(BH_4)_4$ (Banks *et al.*, 1978; Banks, 1979; Banks and Edelstein, 1980). The molecular compound, $Pa(BH_3CH_3)_4$, has been synthesized from the reaction of $PaCl_5$ or $PaCl_4$ with $Li(BH_3CH_3)$. Its optical and NMR spectra have been obtained. Because of the T_d symmetry at the Pa^{4+} site, the dipolar shift is zero and the temperature-dependent proton and ^{11}B shifts are attributed to spin delocalization mechanisms. The ^1H NMR peaks of both the bridging and terminal protons shift to lower field as the temperature is decreased. These observations are inconsistent with a spin-polarization mechanism, which assumes that the temperature-dependent shifts are proportional to the average value of the electron spin in the 5f orbitals. In addition, new synthetic routes to $Pa(BH_4)_4$ and $Pa(MeCp)_4$ (MeCp = methylcyclopentadienyl) are described. They are simpler and more convenient than the earlier

published methods and take advantage of the unexpected solubility of $PaCl_5$ in aromatic hydrocarbons (Kot and Edelstein, 1995). The 5f–6d absorption spectrum of $Pa^{4+}/CsZrCl_6$ (Edelstein *et al.*, 1992) and magnetic data of tetravalent protactinium(IV) (Edelstein and Kot, 1993) also were reported.

4.8 SOLUTION CHEMISTRY

Two oxidation states, Pa(IV) and Pa(V), have been definitely established in aqueous solution (Haïssinsky and Bouissières, 1948, 1951; Bouissières and Haïssinsky, 1949), but all attempts to demonstrate the existence of Pa(III) in solution have led to negative or inconclusive results (Elson, 1954; deMiranda and Maddock, 1962; Musikas, 1966). Both Pa(IV) and Pa(V) show strong tendencies to hydrolyze in the absence of complexing agents and most studies of the ionic species of Pa in aqueous solution have therefore been carried out at the tracer level. Furthermore, the instability of Pa(IV) toward reoxidation has made it difficult to obtain reproducible data on this oxidation state, so that, until quite recently, little quantitative information has been available about the aqueous chemistry of Pa(IV).

The behavior of protactinium in aqueous solution has been very thoroughly reviewed by Guillaumont, Bouissières, and Muxart (Guillaumont *et al.*, 1968; Bouissières, 1971; Muxart and Guillaumont, 1974) and by Pal'shin *et al.* (1970); those reviews should be consulted for more detail than can be given here. For a general discussion of the techniques used in the determination of stability constants, see Rossotti and Rossotti (1961), Fronaeus (1963), or Ahrland *et al.* (1973).

4.8.1 Hydrolysis of Pa (V) in non-complexing media

The hydrolytic behavior of Pa(V) has been studied by a large number of investigators (Jakovac and Lederer, 1959; Guillaumont, 1966a, 1971; Liljenzin and Rydberg, 1966; Scherff and Hermann, 1966; Suzuki and Inoue, 1966, 1969; Kolarich *et al.*, 1967; Mitsuji and Suzuki, 1967; D'yachkova *et al.*, 1968a; Mitsuji, 1968; Liljenzin, 1970; Cazaussus *et al.*, 1971) whose conclusions are summarized schematically in Figs. 4.14 and 4.15 (Bouissières, 1971).

The hydrolysis of Pa(V) is usually studied in perchloric acid solutions, because ClO_4^- is considered to be a non-complexing anion. However, the presence of small amounts of weakly complexing anions does not affect the results. Thus, <0.5 M HNO_3, <1 M HCl, <0.01 M H_2SO_4, or <0.01 M $H_2C_2O_4$, are all equivalent to $HClO_4$ of the same acidity.

In solutions of constant ionic strength ($\mu = 3$; 10^{-5} M$< [H^+] < 3$ M), the least hydrolyzed cation is $PaOOH^{2+}$. At $[H^+] < 1$ M, $PaO(OH)_2^+$ begins to form and becomes predominant at pH $\sim$3. At higher pH values, the neutral species, $Pa(OH)_5$, is formed. At tracer levels these species are in equilibrium (Fig. 4.14), but, at concentrations of Pa(V) close to saturation, polymers are

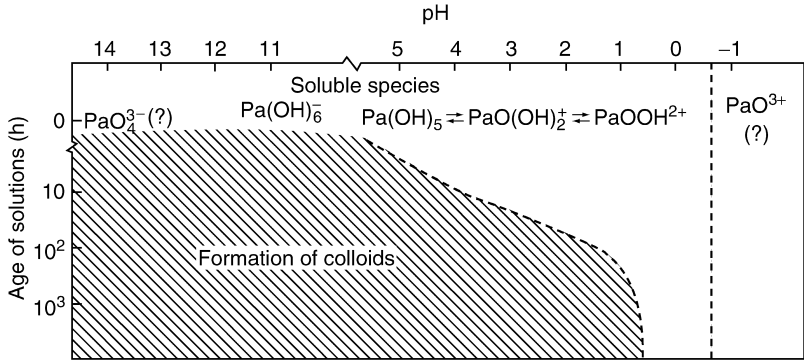

Fig. 4.14 *Hydrolysis of tracer-level Pa(v) in $HClO_4$ solution* (*Bouissières*, 1971).

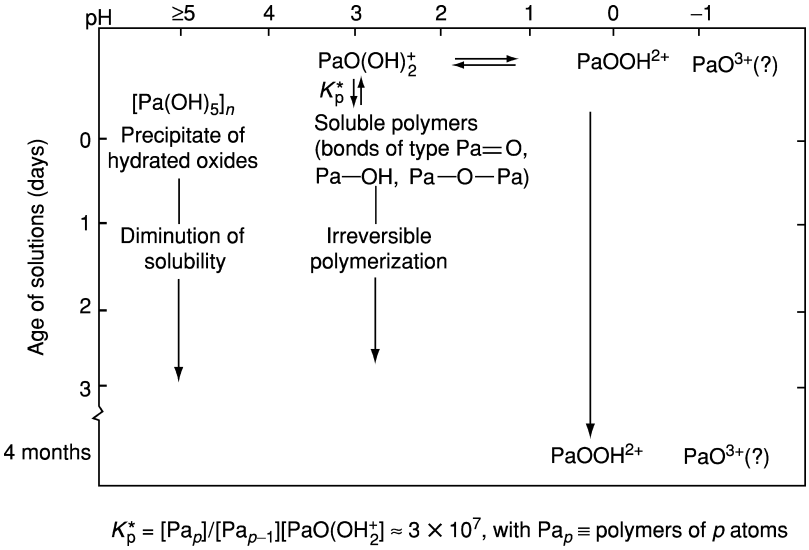

Fig. 4.15 *Hydrolysis of Pa(v) in $HClO_4$ solution at $[Pa(v)] = 10^{-5}$* M (*Bouissières*, 1971).

formed, a process that rapidly becomes irreversible (Fig. 4.15). At pH 5–6, the hydrated oxide is precipitated. In alkaline solution ($\mu = 0.1$) minute concentrations of $Pa(OH)_6^-$ are formed, and at $[H^+] \geq 3$ M the existence of PaO^{3+} has been suggested.

The hydrolysis reactions of Pa(v) may be written as:

$$PaO^{3+} + H_2O \leftrightarrow PaO(OH)^{2+} + H^+ \qquad (4.1)$$

$$PaO(OH)^{2+} + H_2O \leftrightarrow PaO(OH)_2^+ + H^+ \quad (4.2)$$

$$PaO(OH)_2^+ + 2H_2O \leftrightarrow Pa(OH)_5 + H^+ \quad (4.3)$$

with the corresponding equilibrium reaction constants K_1, K_2, and K_3. Since the species PaO^{3+} has only been suggested but never proven, only the latter two hydrolysis reactions and corresponding hydrolysis constants can be measured. Early studies on Pa(v) hydrolysis were reported by Guillaumont (1966a) and Bouissières (1971).

Recently Trubert *et al.* (Le Naour *et al.*, 2003; Trubert *et al.*, 1998, 2002, 2003) have obtained the hydrolysis constants for Pa(v) at the tracer level ($\sim 10^{-12}$ M using ^{233}Pa) from the variations of the partition coefficient of Pa(v) in the system: TTA/toluene/Pa(v)/H_2O/H^+/Na^+/ClO_4^- . These experiments were performed as a function of the concentrations of TTA and H^+ at ionic strengths of $0.1 \leq \mu \leq 3$ M and temperatures of $10°C \leq T \leq 60°C$. From the hydrolysis constants obtained under these conditions extrapolations to zero ionic strength were performed using the specific ion interaction theory (SIT) (Grenthe and Puigdomenech, 1997). The equilibrium constants obtained are given in Table 4.13. Thermodynamic data related to the hydrolysis equilibria were derived from the temperature dependence of the hydrolysis constants at infinite dilution and are given in Table 4.14.

Table 4.13 *Equilibrium constants for the hydrolysis of Pa(v) at zero ionic strength (from Trubert* et al., 2003).

T (°C)	$\log K_2^0$ $PaO(OH)^{2+} + H_2O \leftrightarrow PaO(OH)_2^+ + H^+$	$\log K_3^0$ $PaO(OH)_2^+ + 2H_2O \leftrightarrow Pa(OH)_5 + H^+$
10	–1.32 ± 0.15	–6.7 ± 0.4
25	–1.24 ± 0.02	–7.03 ± 0.15
40	–1.22 ± 0.1	–5.3 ± 1.0
60	–1.19 ± 0.12	–5.4 ± 0.9

Table 4.14 *Standard thermodynamic data at* 25°C *derived from the experimental hydrolysis equilibria of Pa(v). The thermodynamic values for the hydrolysis reaction forming $Pa(OH)_5$ are considered to be estimates (from Trubert* et al., 2003).

$PaO(OH)^{2+} + H_2O \leftrightarrow PaO(OH)_2^+ + H^+$	$PaO(OH)_2^+ + 2H_2O \leftrightarrow Pa(OH)_5 + H^+$
$\Delta_r H^\circ = (5.7 \pm 1.3)$ kJ mol^{-1}	$\Delta_r H^\circ = (61 \pm 31)$ kJ·mol^{-1}
$\Delta_r C_p^\circ = (-200 \pm 89)$ J K^{-1} mol^{-1}	
$\Delta_r G^\circ = (7.1 \pm 0.1)$ kJ mol^{-1}	$\Delta_r G^\circ = (36.3 \pm 4)$ kJ mol^{-1}
$\Delta_r S^\circ = (-4.5 \pm 4.7)$ J K^{-1} mol^{-1}	$\Delta_r S^\circ = (81 \pm 118)$ J K^{-1} mol^{-1}

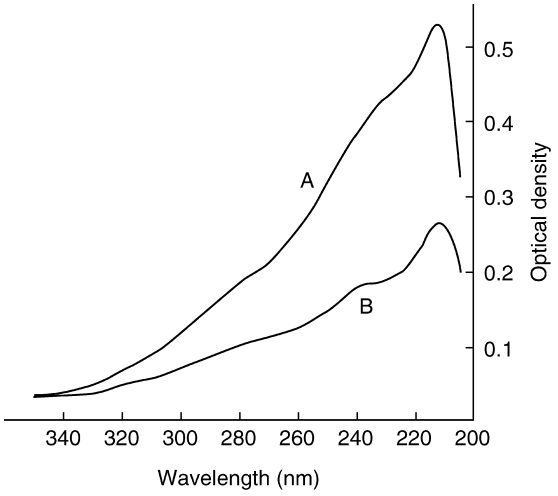

Fig. 4.16 *Absorption spectra of Pa(v) in* 11.5 M $HClO_4$. *The solution was prepared by dissolution of the hydroxide. Curve A, fresh solution; curve B, solution aged for* 1 *day or longer.* $[Pa(v)] \sim 10^{-5}$ M (*Guillaumont*, 1966*c*).

The absorption spectrum of Pa(v) in 11.5 M $HClO_4$ is shown in Fig. 4.16 (Guillaumont, 1966c); similar spectra are obtained at lower acidities. The absorption maximum at about 200–210 nm is attributed to the Pa=O bond in $PaO(OH)_2^+$ and $PaOOH^{2+}$; this bond persists even in sulfuric acid media up to 4 M concentration.

4.8.2 Complexes of Pa(v) in mineral acid solutions

In the absence of strong complexing agents, such as F^- and certain organic reagents, the aqueous complexes of Pa(v) are all oxo- or hydroxo complexes. Consequently, Pa(v) in aqueous solution is rarely present as a single species but rather exists as a mixture of several complexes or hydrolyzed species. These may be characterized by solvent extraction or ion-exchange methods, which, because of differences in the experimental conditions, such as ionic strength, acidity, concentration of the ligand, age of the solution, etc., may yield ambiguous or mutually contradicting interpretations.

The relative complexing tendencies of inorganic anions with respect to Pa(v) are:

$$F^- > OH^- > SO_4^{2-} > Cl^- > Br^- > I^- > NO_3^- \geq ClO_4^-$$

(a) Ionic species of Pa(v) in nitric acid solution

In general, NO_3^- is a poor complexing anion for Pa(v) but freshly prepared solutions, in which $[Pa(v)] \leq 10^{-5}$ M and $[HNO_3] \geq 1$ M, are fairly stable. Such

systems contain monomeric nitratohydroxo complexes of the form $[Pa(OH)_n(NO_3)_m]^{5-n-m}$, where $n \geq 2$ and $m \leq 4$ (Hardy *et al.*, 1958). The transition from cationic to anionic forms occurs at $[HNO_3] \approx 4$–5 M. Stability constants for several suggested species in this medium are listed in Table 4.15.

(b) Ionic species of Pa(V) in hydrochloric acid solution

Solutions of Pa(V) in hydrochloric acid are generally unstable with respect to hydrolytic condensation when $[Pa] \geq 10^{-3}$ M, although complete precipitation may take as long as several weeks (Kirby, 1966). If the freshly precipitated hydroxide is dissolved in 12 M HCl and then diluted to $[Pa] \leq 10^{-4}$ M and 1 M $<$ $[HCl] < 3$ M, the solution is reasonably stable and will then contain a mixture of monomeric chloro complexes in thermodynamic equilibrium. It is generally agreed that, for $[HCl] < 1$ M and $[Pa] < 10^{-5}$ M, the species present are the same as those described above for perchloric acid media, while, for $[HCl] \approx 3$ M, the predominant species is $PaOOHCl^+$. The complexes that have been proposed to explain the solvent extraction and ion-exchange behavior of Pa(V) at higher acidities are summarized in Table 4.16. The study of complex formation of Pa in aqueous HCl solutions of medium and high concentrations and the electronic structures of anionic complexes of $[PaCl_6]^-$, $[PaOCl_4]^-$, $[Pa(OH)_2Cl_4]^-$, and $[PaOCl_5]^{2-}$ have been calculated using the relativistic Dirac–Slater discrete-variational method. The charge density distribution analysis has shown that protactinium has a slight preference for the $[PaOCl_5]^{2-}$ form or for the pure halide complexes with coordination number higher than six under these conditions. On the other hand, Ta occupies a specific position in the group and has the highest tendency to form the pure halide complex $[TaCl_6]^-$; niobium has equal tendencies to form the $NbCl_6$ and $[NbOCl_5]^{2-}$ species (Pershina *et al.*, 1994).

There are no data on the species of protactinium in HBr and HI solutions. Goble and co-workers (1956, 1958) suggested on the basis of ^{231}Pa extraction from HBr and HI aqueous solutions that bromide and iodide complexes of protactinium are less stable than the chloride complexes.

(c) Fluoro complexes of Pa(V)

The solubility of Pa(V) is relatively high at all concentrations of hydrofluoric acid; thus, 0.05 M HF dissolves 3.9 g L^{-1} of ^{231}Pa and 20 M HF dissolves at least 200 g L^{-1} of the pentoxide (Bagnall *et al.*, 1965). The solubility of Pa(V) is estimated to be 11.2 g L^{-1} in 8 M HCl and 0.6 M HF and at least 125 g L^{-1} in 8 M HCl and 5 M HF (Chilton, 1964). Solutions of Pa(V) in aqueous HF are very stable with respect to hydrolysis and are probably the only systems that contain no polymeric species.

A great many complexes have been proposed to explain the behavior of Pa(V) in aqueous HF (deMiranda and Muxart, 1965; Bukhsh *et al.*, 1966a,b;

Table 4.15 *Stability constants for some suggested nitrate complexes of Pa(V).*

μ	$[H^+]$ (M)	$[NO_3^-]$ (M)	*Suggested species*	*Stability constants*	*References*
1	1	≤ 1	$[PaO_x(OH)_{4-2x}NO_3]^\circ$	$K_1 = 0.68$	Nowikow and Pfrepper (1963)[a]
			$[PaO_x(OH)_{4-2x}(NO_3)_2]^-$	$K_2 = 3.0$	
			$[PaO_x(OH)_{2-2x}(NO_3)_3]^-$	$K_4 = 11.93$	
2	2	≤ 1		$K_1 = 0.79$	
				$K_2 = 0.74$	
4	4	≤ 1		$K_1 = 0.63$	
				$K_2 = 0.21$	
1	1	≤ 1	$(PaNO_3)^{4+}$	$K_1 = 1.43$	Kolarich *et al.* (1967)
			$[Pa(NO_3)_2]^{3+}$	$K_2 = 0.07$	
6	6	1–3	$[Pa(NO_3)_5]^0$		Stanik and Ilmenkova (1963)
6	6	3–6	$[Pa(NO_3)_6]^-$	$K_6 = 0.141$	
			$[Pa(NO_3)_7]^{2-}$	$K_7 = 1.09$	
5–6	5	0.4–5	$[Pa(OH)_2(NO_3)]^{2+}$	$K_1 = 17$	Spitsyn *et al.* (1964); Khlebnikov *et al.* (1966)
			$[Pa(OH)_2(NO_3)_2]^+$	$K_2 = 127$	
			$[Pa(OH)_2(NO_3)_3]^0$	$K_3 = 540$	
			$[Pa(OH)_2(NO_3)_4]^-$	$K_4 = 1380$	

[a] Only the ratio $[Pa]:[NO_3^-]$ was determined.

Table 4.16 *Suggested chloro complexes of Pa(v) as a function of HCl concentration (after Guillaumont* et al., 1968).

$[HCl]$ (M)	$Pa(OH)_nCl_m^{5-n-m}$			
1	$PaOOH^{2+}$	$PaOOH^{2+}$		
2	$PaOOHCl^{+}$	$PaOOHCl^{+}$		$Pa(OH)Cl_3^{+}$
3	$PaO_2Cl_2^{-}$	$PaOOHCl_2$	$Pa(OH)Cl_3^{+}$	$Pa(OH)_3Cl^{+}$
		$PaOCl_3$	$Pa(OH)_2Cl_3$	$Pa(OH)_2Cl_2^{+}$
4	PaO_3^{+}	$POOHCl_3^{-}$	$Pa(OH)Cl_4$	$Pa(OH)_2Cl_3$
				$Pa(OH)Cl_4$
5	$PaOCl_4^{-}$	$PaOCl_4^{-}$	$Pa(OH)_2Cl_4^{-}$	$Pa(OH)_2Cl_4^{-}$
6	$PaOHCl_6^{2-}$	$PaOCl_5^{2-}$	$Pa(OH)Cl_5^{-}$	$Pa(OH)Cl_5^{-}$
7	$PaCl_6^{-}$		$PaCl_6^{-}$	$PaCl_6^{-}$
8	$PaCl_7^{2-}$		$PaCl_7^{2-}$	
>8	$PaCl_8^{3-}$ or $POHCl_7^{3-}$	$PaOCl_6^{3-}$		
References	Scherff and Herrman (1966)	Guillaumont (1966c); Muxart *et al.* (1966a,b)	Casey and Maddock (1959a,b)	Shankar *et al.* (1963)

deMiranda, 1966; Guillaumont, 1966a,c; Guillaumont and deMiranda, 1966; Guillot, 1966; Kolarich *et al.*, 1967; Bonnet and Guillaumont, 1969; Plaisance and Guillaumont, 1969); their regions of existence are summarized in Fig. 4.17. Those for which stability constants have been determined are listed in Table 4.17. Only two species exist in a pure state: PaF_7^{2-}, which is present over the range 10^{-3} M < [HF] < 4–8 M, and PaF_8^{3-}, which can exist only when $[F^-] > 0.5$ M and 10^{-7} M < $[H^+]$< 10^{-2} M. In more acid media, 1 M < $[H^+]$ < 3 M and $[F^-] \approx 10^{-4}$ M, the dominant heptafluoro complex is $HPaF_7^-$; this species would also exist in 10–12 M HF, because the $[F^-]$ is limited to about 10^{-2} M by the equilibrium constants: $K_1 = ([HF]/([H^+] \cdot [F^-])) = 935$ M^{-1} and $K_2 = ([HF_2]/([HF] \cdot [F^-])) = 3.12$ M^{-1} (Plaisance and Guillaumont, 1969). At [HF] < 10^{-3} M, PaF_7^{2-} is replaced by complexes of successively lower F:Pa ratios, then by oxo and hydroxyfluoro complexes and, finally, by uncomplexed species.

(d) Behavior of Pa(v) in sulfuric acid solution

Freshly precipitated Pa(v) hydroxide is readily soluble in moderately concentrated H_2SO_4 and permanently stable solutions, containing up to 90 g L^{-1} of ^{231}Pa in approximately 2.5 M H_2SO_4, have been reported (Thompson, 1952; Kirby, 1959, 1966; Brown *et al.*, 1961; Campbell, 1964; Bagnall *et al.*, 1965; Takagi and Shimojima, 1965; Kirby and Figgins, 1966). The solubility falls off sharply at both ends of the acid concentration range, yielding amorphous hydrated oxides or colloids in <1 M H_2SO_4 and crystalline $H_3PaO(SO_4)_3$ in

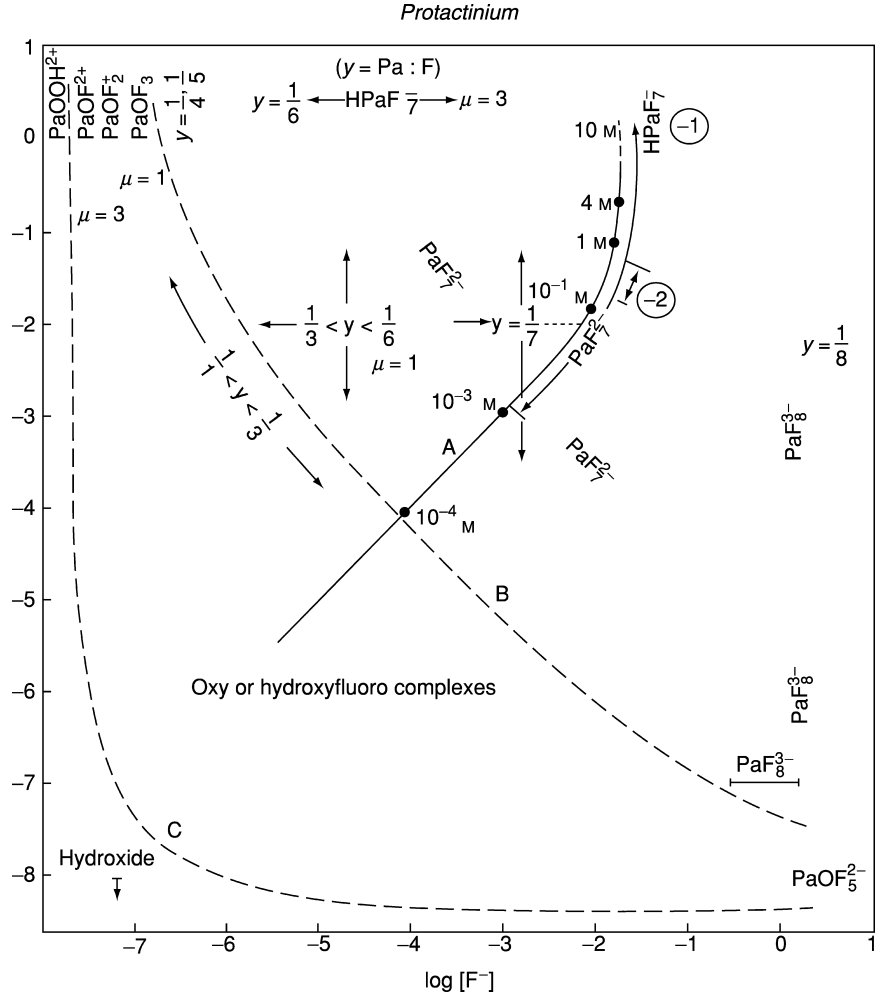

Fig. 4.17 *Fluoro complexes of Pa(v) as a function of* [*HF*], [H^+], *and* [F^-] (*Guillaumont* et al., 1968).

concentrated H_2SO_4 (Bagnall *et al.*, 1965; Takagi and Shimojima, 1965; Stchouzkoy *et al.*, 1966b, 1968).

The sulfate complexes of Pa(v) that have been deduced from tracer-level studies ([Pa] $\leq 10^{-4}$ M) are listed in Table 4.18. The absorption spectra of Pa(v) in H_2SO_4 are shown in Fig. 4.18 (Guillaumont *et al.*, 1960; Guillaumont, 1966c).

Table 4.17 *Stability constants for some suggested fluoride complexes of Pa(v).*

μ	$[H^+]$ (M)	$[F^-]$ (M)	*Suggested species*	*Stability constants*	*References*
1	≤0.1	≤0.1	PaF_3^{2+}	$\log K_3 = 4.9$	Bukhsh *et al.* (1966a)
			PaF_4^+	$\log K_4 = 4.8$	
			PaF_5	$\log K_5 = 4.5$	
			PaF_6^-	$\log K_6 = 4.4$	
			PaF_7^{2-}	$\log K_7 = 3.7$	
			PaF_8^{3-}	$\log K_8 = 1.7$	
3	1–3	$\leq 10^{-6}$	$Pa(OH)_2F^{2+}$	$K_1 = 3.6 \times 10^3$	Guillaumont (1966a,c)
			$Pa(OH)_2F_2^+$	$K_2 = 4.45 \times 10^7$	
			$Pa(OH)_2F_3$	$K_3 = 8.2 \times 10^{10}$	
1	1	$\leq 10^{-6}$	PaF^{4+}	$K_1 = 9 \times 10^3$	Kolarich *et al.* (1967)
			PaF_2^{3+}	$K_2 = 3 \times 10^3$	
			PaF_3^{2+}	$K_3 = 1.1 \times 10^3$	

Table 4.18 *Stability constants for some suggested sulfate complexes of Pa(v).*

μ	$[H^+]$ (M)	$[SO_4^{2-}]$ (M)	*Suggested species*	*Stability constants*	*References*
1	1	≤1	$[PaO_x(OH)_{4-2x}SO_4]^-$	$K_1 = 0.94$	Nowikow and
				$K_2 = 7.39$	Pfrepper (1963)[a]
2	2	≤1	$[PaO_x(OH)_{2-2x}(SO_4)_2]^-$	$K_1 = 1.14$	
				$K_2 = 14.70$	
3	1–3	≤3	$PaOSO_4^+$	$K_1 = 19.3$	Guillaumont (1966c)
			$PaO(SO_4)_2^-$	$K_2 = 320$	
1	1	≤1	$PaSO_4^{3+}$	$K_1 = 120$	Kolarich *et al.* (1967)[a]
			$Pa(SO_4)_2^+$	$K_2 = 1.7$	
1.38	0.3	≤0.4	$Pa(OH)_2SO_4^+$	$K_1 = 6.4$	Mitsuji and Suzuki (1967c)
1	0.1–1	≤0.2	$PaOOH(HSO_4)^+$	$K_1 = 31$	LeCloarec *et al.* (1973)
		≤0.2	$PaO(HSO_4)_2^+$	$K_2 = 250$	

[a] Only the ratio [Pa]:$[SO_4^{2-}]$ was determined.

(e) Miscellaneous complexes of Pa(v) with inorganic ligands

The absorption spectra and the formation constants of complexes formed by tracer-level Pa(v) in phosphoric acid solution have been reported by LeCloarec and Muxart (1973), LeCloarec *et al.* (1973), and LeCloarec (1974). The species identified were $PaO(OH)^-(H_2PO_4)^+$, $HPaO(H_2PO_4)_2^{2+}$, $PaO(H_2PO_4)_2^+$, and $PaO(H_2PO_4)_3$.

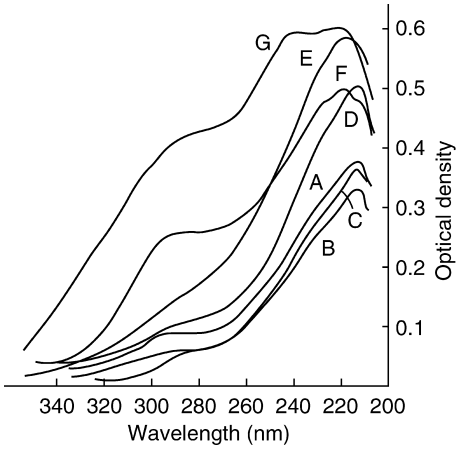

Curve	$[H_2SO_4]$ (M)	$[Pa(v)]$ (M)
A	0.7	0.35×10^{-4}
B	1.32	0.40×10^{-4}
C	2.2	0.45×10^{-4}
D	4.1	0.42×10^{-4}
E	6.5	0.49×10^{-4}
F	9	0.18×10^{-4}
G	18	0.19×10^{-4}

Fig. 4.18 *Absorption spectra of Pa(v) in H_2SO_4 solution* (*Guillaumont*, 1966*c*).

The addition of $\leq$1 M H_2O_2 to a solution of ^{233}Pa in aqueous $HClO_4$ (1 M $\leq [H^+] \leq$3 M) leads to the formation of the following peroxy complexes: $PaO(OH)(HO_2)^+$, $PaO(OH)(HO_2)_2$, $PaO(HO_2)^{2+}$, and $PaO(HO_2)_2^+$, according to Stchouzkoy *et al.* (1969). Association constants for the 1:1 and 1:2 complexes of Pa(v) with IO_3^- have been reported by Kolarich *et al.* (1967).

Pa(v) forms mixed complexes in solutions containing more than one type of ligand. For example, a species identified as $PaO(H_2PO_4)_3(HSO_4)^-$ is found in a mixture of 0.35 M H_3PO_4 and 0.22 M H_2SO_4 (LeCloarec *et al.*, 1973). Mixed complexes are also formed in hydrochloric or nitric acid solutions containing $\leq 10^{-2}$ M HF (Hardy *et al.*, 1958; Casey and Maddock, 1959b; Shankar *et al.*, 1963; Plaisance and Guillaumont, 1969). Formation constants have been determined for the unidentified mixed complexes formed by Pa(v) in 3–6 M HNO_3 to which HCl, $(NH_4)_2SO_4$, $(NH_4)_2HPO_4$, or H_3AsO_4 was added (Davydov *et al.*, 1966b).

Finally, the existence of a perprotactinate ion with a charge of 3– is suggested by the fact that Pa(v) ($\sim 3 \times 10^{-4}$ M) is soluble in alkaline media in the presence of H_2O_2 (Stchouzkoy *et al.*, 1966a).

4.8.3 Organic complexes of Pa(v) in aqueous solution

Only a few systematic studies have been done of the aqueous complexes of Pa(v) with organic reagents. Galateanu and co-workers (1962a,b, 1966), Moskvin *et al.* (1963) used the ion-exchange method to determine the stability constants of the complexes formed with a number of organic acids (Table 4.19). Stability constants have also been reported for complexation by acetylacetone (Liljenzin and Rydberg, 1966; D'yachkova *et al.*, 1968b; Liljenzin, 1970),

Table 4.19 *Stability constants of complexes formed by Pa(v) with various organic acids* ($\mu = 0.25$) (*Galateanu and Lapitskii,* 1962*a,b*; *Moskvin* et al., 1963; *Galateanu*, 1966; *Lapitskii and Galateanu*, 1963).

		Stability constant for Pa:ligand ratio		
Acid	*pH*	1:1	1:2	1:3
lactic (≤0.1 M)	1.5–2.7	1.75×10^2		
α-hydroxyisobutyric (≤0.5 M)	0.98–1.2		3.0×10^3	1.0×10^7
mandelic (≤0.5 M)	1.0–1.1	9.1×10^2		
malic (≤0.65 M)	0.8–0.87	8.3×10^2	6.3×10^4	
tartaric (≤0.65 M)	0.75–0.8	1.7×10^2	2.1×10^4	
trihydroxyglutaric (≤0.7 M)	0.95–1.2	9.1×10^2	7.7×10^7	
oxalic (≤0.7 M)[a]	0.7–0.8	3.6×10^2	8.0×10^5	1.1×10^6
citric (≤0.7 M)[b]	0.7–0.95	4.5×10^3	2.3×10^5	6.3×10^8
aconitic (≤0.7 M)	0.75–0.8	1.5×10^2		
ethylenediaminetetraacetic acid (≤0.02 M)[c]	2.4–2.7	1.5×10^8	9.1×10^{11}	
amygdalic (≤0.5 M)	1.1	8.5×10^2		

[a] cf. Carrere (undated); Davydov *et al.* (1966a,b); Guillaumont (1966a,c).
[b] cf. Guillaumont (1968).
[c] cf. Shiokawa *et al.* (1969).

DIAPA (Mikhailov, 1960), and TTA (Guillaumont, 1965a; D'yachkova *et al.*, 1968a).

Oxalic acid has been singled out for special attention because of its importance in the analytical and process chemistry of ^{231}Pa. Davydov and Pal'shin (1967) found that the solubility of Pa(v) at 25°C remained low in <0.05 M $H_2C_2O_4$, but increased sharply from 0.33 to 4 g L^{-1} or more between 0.05 and 0.5 M $H_2C_2O_4$. The low solubility was attributed to the formation of hydroxy complexes with a Pa:C_2O_4 ratio of 1:1, while the higher solubility was explained by the formation of complexes with a 1:2 ratio. Casey and Maddock (1959b) suggested the existence of complexes of the form $Pa(C_2O_4)_3^-$, and $Pa(C_2O_4)_4^{3-}$, but Guillaumont (1966a,c) suggested that these were preceded by the formation of $PaOC_2O_4^+$ and $PaO(C_2O_4)_2^+$.

It was shown that protactinium(v) forms a colored compound with Arsenazo-III in highly acidic solutions with a 1:1 ratio (Pal'shin *et al.*, 1962). Complex compounds formed with a large number of other organic reagents, such as 8-oxyquinoline (Maddock and Miles, 1949; Vernois *et al.*, 1963), BPHA (Cristallini and Flegenheimer, 1963; D'yachkova and Spitsyn, 1964), tannin (Elson *et al.*, 1951; Casey and Maddock, 1959a), 1-phenyl-3-methyl-4-benzoyl-pyrazolone-5 (Myasoedov and Molochnikova, 1968), pyrogallol, catechol, and gallic acid (Casey and Maddock, 1959a), and are used in the analytical chemistry of protactinium. However, literature data on the composition and stability of these compounds are absent.

4.8.4 Redox behavior in aqueous solution

The standard electrode potential of the Pa(V)/Pa(IV) couple has been estimated to be –0.1 V (vs. normal hydrogen electrode [NHE]) by Fried and Hindman (1954) and –0.25 V by Haïssinsky and Pluchet (1962), the latter value being based on a measured electrochemical potential of -0.29 ± 0.03 V in 6 M HCl.

Pa(IV) was prepared by Haïssinsky (Haïssinsky and Bouissières, 1948, 1951; Bouissières and Haïssinsky, 1949), who reduced 0.1–2 mg of ^{231}Pa(V) with solid Zn amalgam or $CrCl_2$ in 1–3 N HCl or H_2SO_4. Brown *et al.* (1959) found that Zn amalgam gave complete reduction in 5–6 h only if the initial solution was $\geq$6 M in HCl; lower acidities led to the formation of colloidal Pa(V), which was difficult to reduce. Mitsuji (1967a,b) used liquid Zn amalgam to obtain complete reduction in a few minutes of 4×10^{-4} M ^{231}Pa(V) in 1–11 M HCl or 0.05–9 M H_2SO_4. Tracer-level Pa(V) could not be completely reduced unless Cr(III) was added to the system. ^{233}Pa(IV) has also been obtained by dissolution of neutron-irradiated ^{232}Th metal in 1 M HCl by Manier and co-workers (1969, 1970) or of neutron-irradiated $^{232}ThX_4$ (X = Cl, Br, I) in 0.02 M $ThCl_4$ (Carlier, 1971; Carlier and Genet, 1972a,b). In the first case, the yield of Pa(IV) was about 20%; in the second, it varied with the nature of the irradiated halogen and the pH of dissolution, ranging from less than 20% at pH $\leq$ 3 to approximately 80% for $ThCl_4$ at pH 5.5.

Musikas (1966) has described the electrolytic reduction of 10^{-3} M ^{231}Pa(V) in 8 M HCl, 0.5 M H_2SO_4, and 5 M NH_4F (pH 7.2). Electrolysis at 50 mA for 5 h completely reduced Pa(V) in 8 M HCl to Pa(IV). The reduction of 10^{-13} M Pa(V) on a Pt–H_2 electrode in aqueous solutions of acetylacetone at pH > 7 has also been reported (Liljenzin and Rydberg, 1966).

The polarography of Pa has been studied in various aqueous media (Elson, 1954; deMiranda and Maddock, 1962; Musikas, 1966; Schwochau and Astheimer, 1970; Astheimer and Schwochau, 1973). All solutions gave at least one wave, corresponding to the one-electron change, Pa(V)→Pa(IV), and in some cases a second wave, which might represent either the reduction, Pa(IV)→Pa(III), or, more probably, the catalytic reduction of H^+. For example, with $[NH_4F] =$ 3.84 M, pH 7.2, $[^{231}Pa(V)] = (2.3–9.5) \times 10^{-4}$ M, the wave height at $E_{1/2} = -1.29$ V (vs. standard calomel electrode [SCE]) was proportional to [Pa], but that of the second wave ($E_{1/2} = -1.57$ V) was not (deMiranda and Maddock, 1962). In DMSO, the reduction of $PaCl_4$ led directly to Pa(0) in a single step ($E_{1/2} =$ –1.49 V), with the 3+ oxidation state omitted (Astheimer and Schwochau, 1973).

The behavior of protactinium in the TmI_2–TmI_3–THF system (THF, tetrahydrofuran) was studied by the cocrystallization method. In the presence of Tm^{2+}, microamounts of Pa cocrystallize with the solid phase of TmI_3 solvate, the cocrystallization coefficient (K_c) being nearly 1. A similar K_c for this system was obtained with Ce. Thus, in THF in the presence of Tm^{2+}, protactinium is probably reduced to the oxidation state 3+ (Kulyukhin *et al.*, 1996, 1997). Attempts to reduce Pa(V) to the trivalent state by Sm(II) or Tm(II) in chloride

melts at high temperatures were reported by Mikheev *et al.* (1992). Using a cocrystallization method of Pa with the Sm(II) and Tm(II) system, the authors proposed that under these conditions the stabilization of the Pa(III) species was obtained. In the system with PrOCl, the Pa(III) reduction to Pa(II) has been detected. The standard redox potential of Pa(III)/Pa(II) couple has been calculated as –2.59 ± 0.1 V (vs. NHE) (Mikheev *et al.*, 1993a,b). Pa(II) also was produced by interaction of ^{233}Pa(V) with the cluster PrI_2 (Kazakevich *et al.*, 1993). It was shown that An = Pa, U, Np, Pu with the electronic configuration ($5f^{n-1}6d$) in the divalent state, were stabilized in clusters of the type $(Pr,An)I_2$ in the LiI–PrI_2–PrI_3 system (Kulyukhin and Mikheev, 1998). The influence of the electronic configurations of Pa^{2+} (f^3 and f^2d) and Pa^{3+} (f^2 and fd) upon the stability of divalent and trivalent protactinium and their redox potentials was examined by Guillaumont *et al.* (1996). An analysis of the stabilization of the configuration $5f^26d$ (Pa^{2+}) led to predictions of the relative scale for the $E^{\circ}_{Pa(III)/Pa(II)}$ potentials which depend on the medium and on ligands. For this purpose the relation between the energy ($f^3 \rightarrow f^2d$) for Pa(II) in water (Pa^{2+}·aq) and in solid (Pa^{2+}:CaF_2) was established. The values of the redox potentials were discussed on the basis of the 6d electron stabilization of Pa^{2+} and destabilization of Pa^{3+} ions. The standard redox potential $E^{\circ}_{Pa(III)/Pa(II)}$ was estimated to be around −4.0 V, and for the couple Pa(IV)/Pa(III) about –2.1 V (vs. NHE). This result was confirmed by a measurement of E_{fd} in Pa^{4+}(aq) and by correlation of E_{fd} for Pa^{2+}(aq), Pa^{3+}(aq), and Pa^{4+}(aq) with the corresponding redox potentials (Guillaumont *et al.* 1996). Standard reduction potentials are given in Chapter 19, Fig. 19.9.

Pa(IV) in aqueous solution is rapidly oxidized by air, but the rate of oxidation is decreased by the exclusion of O_2 and by the presence of complexing anions (Brown *et al.*, 1959; Brown and Wilkins, 1961; Guillaumont, 1966b; Bagnall and Brown, 1967; Mitsuji, 1967a). Guillaumont *et al.* (1960) found that the stability of ^{231}Pa(IV) increased with increase in [H_2SO_4] or [HCl], but Myasoedov *et al.* (1966b) reported the opposite effect. The oxidation rate was increased by ultraviolet light or heat. In the absence of air, Pa(IV) in a neutral solution of 2.2 M $N(CH_3)_4F$ was oxidized at the rate of about 1% per day (deMiranda and Muxart, 1964). Mitsuji (1967a) has proposed the reaction:

$$2Pa^{4+} + 2H^{+} \leftrightarrow 2Pa^{5+} + H_2$$

The half-life for the oxidation of ^{233}Pa(IV) in the absence of redox buffers decreases exponentially with increase in [H^+], but the formation of complexes tends to stabilize the 4+ oxidation state. The stability of Pa(IV) is greatly enhanced by a decrease in the dielectric constant; thus, in 0.6 M $HClO_4$ (10% H_2O/90% C_2H_5OH), the half-life for oxidation was 40 h, as compared with $\tau_{1/2} \sim 1$ h in a pure aqueous solution (Manier *et al.*, 1969; Manier, 1970; Manier and Genet, 1970). The oxidation of Pa(IV) by molecular halogens is first-order with respect to both [^{233}Pa(IV)] and [Cl_2, or Br_2, or I_2] (Carlier, 1971; Carlier and Genet, 1972a).

4.8.5 Aqueous chemistry of Pa(IV)

The most characteristic property of Pa(IV) in aqueous solution is that, unlike Pa(V), it is precipitated by hydrofluoric acid (Haïssinsky and Bouissières, 1948; Bouissières and Haïssinsky, 1949). It is also precipitated by IO_3^-, PO_4^{3-}, $P_2O_6^{4-}$, phenylarsonate, and saturated K_2SO_4, but forms soluble carbonate, citrate, and tartrate complexes (Haïssinsky and Bouissières, 1951). PaF_4 is soluble in 15 M NH_4F (Haïssinsky *et al.*, 1961).

The spectrophotometry of Pa(IV) has been investigated in perchloric (Brown and Wilkins, 1961), hydrochloric (Fried and Hindman, 1954; Brown *et al.*, 1959; Guillaumont *et al.*, 1960; Brown and Wilkins, 1961; Bagnall and Brown, 1967; Mitsuji, 1967a), hydrobromic (Brown and Wilkins, 1961), and sulfuric (Guillaumont *et al.*, 1960; Brown and Wilkins, 1961; Myasoedov *et al.*, 1966b; Mitsuji, 1967a) acid solutions and in neutral fluoride media (Haïssinsky *et al.*, 1961; deMiranda and Muxart, 1964; Asprey *et al.*, 1967). The reduction of Pa(V) in acid solutions is accompanied by the disappearance of the prominent absorption band at 210–215 nm (Figs. 4.16 and 4.18) and the appearance of bands at 225–230, 255–265, and 275–290 nm. Beer's law is not followed in hydrochloric acid solutions, but, for $(0.65–1.5) \times 10^{-4}$ M Pa(IV) in 0.5–6 M H_2SO_4, the molar extinction coefficient (ε) is about 1500 L M^{-1} cm^{-1} at 290 nm (Myasoedov *et al.*, 1966b). In neutral fluoride media, the spectrum is different according to the nature of the medium: in NH_4F, bands are observed at 355 and 250 nm (Haïssinsky *et al.*, 1961); but in $N(CH_3)_4F$, the absorption maxima are at 344 and 323 nm, with $\varepsilon = 0.08$ and 0.037 M^{-1} cm^{-1}, respectively (deMiranda and Muxart, 1964).

Pa(IV) hydrolyzes less readily than Pa(V). In 3 M $HClO_4$, the dominant species are Pa^{4+} and $PaOOH^{2+}$ (cf. Fig. 4.14). As the acidity is decreased at constant ionic strength ($\mu = 3$), $Pa(OH)^{3+}$, PaO^{2+} or $Pa(OH)_2^{2+}$, and $PaO(OH)^+$ or $Pa(OH)_3^-$ appear successively; their hydrolysis constants, as determined by Guillaumont (1965b, 1966b), are 0.725, 0.302, and 0.017, respectively. Estimates of the relative amounts of these species as a function of $[H^+]$ are indicated in Fig. 4.19.

Mitsuji (1968), however, finds that $Pa(OH)_2^{2+}$ is the most probable ionic species at pH 0.4–1.1 ($\mu = 0.5$). Lundqvist (1974c,d, 1975) believes that PaO^{2+} is more probable, because of the high stability of that ion toward both ethylenediaminetetraacetic acid (EDTA) and acetylacetone. He finds no evidence for species either more or less hydrolyzed than $Pa(OH)_2^{2+}$ at pH 0–10.

There is, as yet, little information about the complexes formed by Pa(IV). Guillaumont (1966a,c) has calculated the formation constants of the following complexes at $\mu = 3$, $[H^+] = 3$ M, and $[Cr^{2+}] = 10^{-2}$ M: $PaCl^{3+}$ ($K_1 < 1$). $PaCl_2^{2+}$ ($K_2 = 1$), $PaSO_4^{2+}$ ($K_1 = 42$), $Pa(SO_4)_2$ ($K_2 = 153$), PaF^{3+} ($K_1 = 5.34 \times 10^4$), and PaF_2^{2+} ($K_2 = 1.8 \times 10^3$). Muxart *et al.* (1966b) found no anionic chloro complexes except at high acidity, e.g. $PaCl_6^{2-}$ in ~8 M HCl. Mitsuji (1968) finds that $Pa(SO_4)(OH)^+$ ($K = 320$) is the most probable ionic species formed by HSO_4^- at

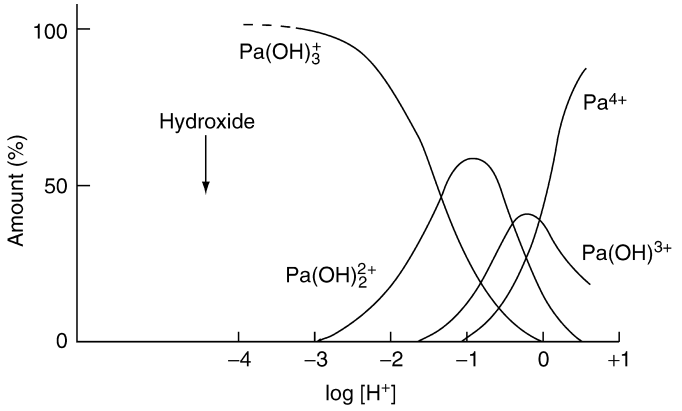

Fig. 4.19 *Distribution of the ionic species of* ^{233}*Pa*(IV) *as a function of* $[H^+]$ *in non-complexing media of ionic strength* $\mu = 3$ (*Guillaumont*, 1966*a*).

pH 0.4–1.1, $\mu = 0.5$, 10°C. A comparable value is reported by Lundqvist (1974c), who has also determined stability constants for the complexes formed by ^{233}Pa(IV) with acetylacetone (Lundqvist, 1974a; Lundqvist and Rydberg, 1974), TOPO (Lundqvist, 1974b), EDTA (Lundqvist and Andersson, 1974), and benzoylacetone (Lundqvist, 1975).

Recently, the $6d^1 \rightarrow 5f^1$emission spectrum of Pa^{4+} in aqueous acidic solution was reported. The peak maximum was at 460 nm with a half-width of (61.6 ± 1.4) nm and a lifetime of (16 ± 2) ns (Marquardt *et al.*, 2004).

4.9 ANALYTICAL CHEMISTRY

Protactinium determination in natural materials is very complicated because of the extremely small content of Pa in the samples, as well as its tendency to hydrolyze. The presence of other elements, with chemical properties similar to protactinium, highly influences the behavior of protactinium in solutions.

Spectral, spectrophotometric, gravimetric, and other methods are used for the determination of macroquantities of protactinium. However, they are often invalid for the analysis of natural objects that contain very small amounts of protactinium. In these cases radiometric methods are preferable but they need careful purification of protactinium from macroelements and other radioactive materials.

4.9.1 Radiometric methods

The basis of the simplest methods for the determination of the long-lived protactinium isotope, ^{231}Pa, in natural objects (the ores, rocks, waste products), various solutions, and other samples is the measurements of α-activity and

γ-rays. The determination of the artificial protactinium isotope, ^{233}Pa, also is usually carried out by measurements of its γ-rays or β-particles.

(a) The determination of ^{231}Pa by α-counting

The large specific activity of ^{231}Pa isotope, equal to 10^6 alpha decays min^{-1} mg^{-1} of element (Bagnall, 1966a) allows the use of this method for the determination of submicrogram amounts of protactinium after its isolation in the radiochemically pure state.

α-Counters, such as ionization chambers, scintillation or proportional counters, are utilized for the measurements of α-activity of protactinium samples. Absolute quantities of protactinium are determined by comparison of the α-activity of the protactinium sample without other α-emitting isotopes with the activity of standard samples of ^{231}Pa, ^{239}Pu, RaD (^{210}Pb) + RaE (^{210}Bi) + RaF (^{210}Po), ^{210}Po, measured under the same conditions.

Usually protactinium samples for α-counting are prepared by evaporation of a known aliquot of the solution under investigation, after placing it on a platinum, stainless steel, or glass plate.

Thin layers are formed by placing the organic phase directly on a plate for counting, for instance, after extraction of protactinium with DIBK (Scherff and Hermann, 1964; Rona *et al.*, 1966).

Multichannel alpha-spectrometers are used for control of radiochemical purity of isolated samples (Salutsky *et al.*, 1957; Spitsyn and D'yachkova, 1960; Myasoedov and Pal'shin, 1963; Suzuki and Inoue, 1966). ^{231}Pa also can be characterized with enough reliability by its γ-rays spectrum (Salutsky *et al.*, 1956, 1957; Barnett, 1957; Suzuki and Inoue, 1966). Samples for alpha-spectrometers can be prepared by the electrolytic technique (Ko, 1956, 1957; Shimojima and Takagi, 1964; Smith and Barnett, 1965).

The application of alpha-spectrometers with high resolution (~0.5%) in some cases allows the determination of protactinium without separation from other α-emitters (Glover *et al.*, 1959; Jackson *et al.*, 1960b; Brown and Maddock, 1967). The alpha-spectrum of ^{231}Pa has the following main groups of α-particles: 5.046 (10%), 5.017 (23%), 5.001(24%), 4.938 (22%), and 4.722–4.666 MeV (13%) (Hyde, 1961). So 79% of ^{231}Pa α-particles emitted have energies within the interval 4.85–5.15 MeV. Measurements in this energy range with the alpha-spectrometer, previously calibrated with a pure ^{231}Pa sample, allow the determination of protactinium in the presence of other radioactive elements. Only ^{227}Ac (α-particles energy is 4.947 MeV) slightly influences measurements in this case. The effect of ^{227}Ac may be excluded completely if the protactinium α-particle energies in the interval 5.001–5.041 MeV are measured with a spectrometer that has a silicon detector with resolution of about 0.1%. The alpha-spectrometric method, developed by Glover *et al.* (1959), allows the determination of up to 10^{-4}% of protactinium in various natural objects with a relative precision of ±5%.

(b) The determination of ^{231}Pa by the γ-rays

The measurement of ^{231}Pa γ-rays is widely used for the quick determination of the protactinium concentration in the absence of other radioactive admixtures in solutions, in salts, and compounds of protactinium after their dissolution, and also for control of the protactinium behavior during its separation from waste solutions and solid residue (Barnett, 1957, 1958; Guillaumont *et al.*, 1960; Haïssinsky *et al.*, 1961; Stchouzkoy and Muxart, 1962; Miranda and Muxart, 1964a,b; Guillaumont, 1966a,c; Pissot *et al.*, 1966; Stchouzkoy *et al.*, 1966a,b).

In the γ-ray spectrum of ^{231}Pa there are three maxima, corresponding to the energies of γ-rays 27, 95, and 300 keV. The quantitative determination of protactinium is carried out with γ-spectrometers by comparison of γ-ray intensities from the sample under investigation in the region 300 keV with the intensity of the standard, containing a known amount of radiochemically pure protactinium. The sensitivity of this method is approximately 1×10^{-6} g Pa. So, for instance, it can determine 1.4×10^{-6} g Pa in a 5 g sample. The precision of this method is ±5% (Salutsky *et al.*, 1957). ^{227}Ac (0.095 and 280 keV) and ^{226}Ra (0.080 and 320 keV) prevent the determination.

(c) The determination of ^{234}Pa

The immediate short-lived daughters of U-238 are Th-234 and Pa-234. These nuclides are β^--emitters having energy bands that overlap the uranium bands in a liquid scintillation spectrum. ^{234}Pa is a high-energy β^--emitter that can be further identified and quantified from its Cerenkov radiation. Energy spectra were collected on the Packard 2500AB liquid scintillator analyzer for uranium solutions in diisopropylnaphthalene and pseudocumene-based scintillator cocktails. Calibration curves were prepared for nitric, hydrochloric, and sulfuric acid media (Huntley *et al.*, 1986; Grudpan *et al.*, 1990; Bower *et al.*, 1994).

(d) The determination of ^{233}Pa

Quantitative determination of ^{233}Pa is carried out by β^--particles (Fudge and Woodhead, 1956; McIsaak and Freinling, 1956; McCormac *et al.*, 1960; Sakanoue *et al.*, 1964) as well as γ-rays (Fudge and Woodhead, 1956; Moore and Reynolds, 1957; Arden *et al.*, 1962; Stricos, 1966) by comparison of the intensity of the sample under investigation with the intensity of a standard containing a known amount of ^{233}Pa.

The absolute amount of ^{233}Pa in a standard is determined by the β^--activity measurement on 4π-counters (Fudge and Woodhead, 1956; McCormac *et al.*, 1960).

A method, developed for the determination of absolute amounts ^{233}Pa in irradiated metallic thorium, consists of the measurement of ^{233}Pa β-particles

after its chemical separation (McCormac *et al.*, 1960). This method is quick and simple and provides 70–80% protactinium yield and high degree of purification of protactinium from fission elements (10^6 times). For the separation of ^{233}Pa in a radiochemically pure state for its determination in neutron-irradiated thorium, Moore and Reynolds (1957) used the extraction with DIBC from 6 M HCl in the presence of oxalic acid, with almost all admixtures remaining in aqueous phase.

Fudge and Woodhead (1956) carried out the radiochemical purification of protactinium by ^{233}Pa precipitation with niobium tannate in the presence of EDTA. The separation of niobium and protactinium was carried out by paper chromatography or by protactinium precipitation with barium fluorozirconate.

4.9.2 Radioactivation methods

A quite large value of the thermal-neutron cross-section (^{231}Pa, 211 barns) (Smith *et al.*, 1956; Holtzman, 1962) allows the use of the nuclear reaction ^{231}Pa(n,γ)^{232}Pa for protactinium determination. In some cases it is better to measure ^{232}U, the daughter of the ^{232}Pa decay product, after the separation of uranium in a radiochemically pure state. This method allows the determination of 10^{-8} to 10^{-10} g of ^{231}Pa (Sakanoue *et al.*, 1965).

4.9.3 Spectral and X-ray methods

Spectral methods are not practical for the direct determination of protactinium in natural samples and other materials because of the low sensitivity and experimental complications. Usually emission spectral analysis is applied only for the detection of admixtures (Nb, Fe, Mg, Al, Sn, Cu, Si, and others) in pure samples of protactinium (Sackett, 1960; Spitsyn and D'yachkova, 1960; Walter, 1963; Birks *et al.*, 1965; Cunningham, 1966; Kirby and Figgins, 1966; Roberts and Walter, 1966).

The emission spectrum of protactinium has been investigated (Schüller and Gollnow, 1934; Thompson, 1951; Richards and Atherton, 1961, 1963; Richards *et al.*, 1961; Giaechetti, 1966). There are a few thousand lines in the range 2650–25 000 Å, and many of them have hyperfine structure. Tomkins and Fred (1949) observed 263 lines in the range 2640.3–4371.4 Å; the most sensitive and definite lines are at 3957.8, 3054.6, and 3053 Å. The sensitivity of protactinium determination is 0.2 μg Pa by use of these lines with the copper spark method. According to the data of Spitsyn and D'yachkova (1960), lines at 2732.2, 2743.9, and 2755.9 Å are also characteristic for protactinium. The X-ray spectrum of Pa_2O_5 has been investigated by Russell (1913) and Grosse and co-workers (Beuthe and Grosse, 1930; Pierce and Grosse, 1935; Grosse, 1939). Twenty-one lines of the L-series were found in the range 1088.5×10^{-11} to 586.6×10^{-11} cm and 14 lines of M-series in the range 518.2×10^{-11} to 252.2×10^{-11} cm. The information about other lines in these series has been reported in the literature (Dolejsek and

Kunzl, 1936; Cauchois and Hulubel, 1947; Cauchois and Bonnelle, 1966). A more recent compilation is given in Browne *et al.* (1954).

A comparative study of the photoacoustic spectra of lanthanide and actinide oxides (protactinium included) has been given by Heinrich *et al.* (1986).

4.9.4 Electrochemical methods

(a) Polarographic

The application of the polarographic method for the determination of protactinium is limited by the irreversibility of the Pa reduction process on the mercury drop electrode in many media.

(b) Potentiometric and amperometric

An oxidimetric method for Pa(IV) determination in chloride and sulfate solutions by titration with 6.7×10^{-2} M $FeCl_3$ solution was described by Musikas (1966). The final point was determined by a potentiometric method at a given current of 5 μA and an amperometric method at a given potential of 0.2 V. The platinum electrode was used as the indicator electrode, and a saturated calomel electrode was used as reference electrode. The titration was carried out in a special cell with a magnetic stirrer under nitrogen atmosphere.

The relative error for 3.65×10^{-2} to 4.08×10^{-2} M Pa in 6–8 N HCl or 1.0–1.8 N H_2SO_4 was nearly ±3%. The method is used for determination of the extent of Pa(V) reduction by an electrolytic method with the application of an amalgamated silver electrode.

4.9.5 Spectrophotometric methods

(a) Methods based on the Pa light absorption in mineral acids solutions

The absorption spectra of penta- and tetravalent protactinium in aqueous solutions of hydrochloric acid (Fried and Hindman, 1954; Nairn *et al.*, 1958; Brown *et al.*, 1959; Casey and Maddock, 1959a; Guillaumont *et al.*, 1959, 1960; Guillaumont, 1966c), sulfuric (Guillaumont *et al.*, 1960; Brown *et al.*, 1961; Brown and Wilkins, 1961; Guillaumont, 1966c; Myasoedov *et al.*, 1966b), perchloric (Guillaumont *et al.*, 1960; Brown and Wilkins, 1961; Guillaumont, 1966a,c) acids, and in neutral fluoride solutions (Miranda and Muxart, 1964a,b) have been studied rather completely. Protactinium complexes with inorganic ligands highly absorb in the ultraviolet part of spectrum at wavelength <250 nm. Protactinium determination by light absorption in solutions of inorganic acids is used very rarely because of the low sensitivity and selectivity of these methods, and also because of complications connected with work in ultraviolet part of the spectrum. Nevertheless the existence of characteristic

bands in the absorption spectra of protactinium allow their use for the determination of protactinium concentration and for identification of protactinium valence state in some cases.

(b) Methods based on reactions with organic reagents

Effective spectrophotometric methods for the determination of microgram amounts of protactinium with application of organic reagents have been described. The advantage of such methods is their high sensitivity and the possibility of protactinium determination without previous separation from other radioactive elements that usually prevent radiometric determination of protactinium. Spectrophotometric methods for the determination in very acidic solutions are especially worthwhile. In this case complications connected with the hydrolysis of protactinium ions are excluded, and the selectivity of determination, reproducibility, and reliability of the methods increase considerably.

Pentavalent protactinium forms a stable complex with Arsenazo-III, hence this reaction is accompanied by the change of the red color of the reagent to green after mixing. The formation of the colored compound takes place in a wide interval of acidity: from slightly acidic media to 10 N H_2SO_4 or HCl and even in more concentrated solutions. Absorbance of the solution of protactinium complex compound reaches a maximum immediately after the reagent addition and does not change for at least 24 h. The reaction of Pa with the reagent is rather sensitive; the molar extinction coefficient at 660 nm is equal to 2.2×10^4 L· M^{-1} cm^{-1}. The error of the protactinium determination at the concentration 0.3–3.1 mg L^{-1} in the absence of interfering elements is $\pm 3.5\%$ (Pal'shin *et al.*, 1962).

According to the data of Pal'shin *et al.* (1962) the complex compound of protactinium with Arsenazo-III is quantitatively extracted by an equal volume of isoamyl alcohol from solutions with sulfuric acid concentration >2 M. The extraction of the protactinium compound from very acidic solutions of sulfuric acid gave high selectivity. In addition there is no necessity for the previous separation of contaminants. The error of the protactinium determination at a concentration 3 mg L^{-1} is less than 3% in the presence of a 10^4-fold amounts of Fe(III), Al, Ni; 10^3-fold amounts of Cr(III), La, Mn(II); 200-fold amounts of Bi(III), Sn(IV), Zr, Nb, Mo(VI), U(VI); and 100-fold amounts of Th and Ti(IV).

Pa(V) forms with TTA a colored complex compound, slightly soluble in aqueous solutions, but very soluble in many organic solvents (Myasoedov and Muxart, 1962a,b; Pal'shin and Myasoedov, 1963). The extraction-photometric method of protactinium determination with TTA is rather sensitive ($\sim$1 mg L^{-1} Pa) and highly selective. The molar extinction coefficient of protactinium complex with TTA is equal to 1.4×10^4 and 0.9×10^4 L· M^{-1} cm^{-1} at 430 and 440 nm, respectively. Beer's law is followed for concentrations of Pa in the solution over the range from 1.3 to 8.7 mg L^{-1}.

4.9.6 Gravimetric methods

Gravimetric methods of protactinium determination are used relatively rarely because of their low sensitivity. Nowadays this method is applied mainly for the determination of milligram amounts of Pa in solutions and in compounds. Protactinium is isolated from solutions in the form of insoluble compounds with inorganic or organic reagents. The choice of reagent for precipitation depends on the presence of other elements in solution.

The weighing of Pa_2O_5 is the final operation in most gravimetric determinations of protactinium after its precipitation in the form of hydroxide, peroxide, iodate, phenylarsonate, cupferronate, and following calcinations at 600–1000°C under air for 1–2 h. Pa_2O_5 is suitable and stable weight form for the determination, but it has a large conversion coefficient to protactinium, equal to 0.852. This limits the application of the determination to relatively large amounts of protactinium. The use of phenylarsonate of protactinium is more preferable as the weight form (Myasoedov *et al.*, 1968a). In this case the conversion coefficient is equal to 0.346. The calcinations of the protactinium compounds usually are carried out in platinum crucibles in order to regenerate the element. Concentrated HF or a mixture of HF + H_2SO_4 is used for dissolution of Pa_2O_5.

(a) Protactinium hydroxide

For weight determination protactinium hydroxide is obtained usually by precipitation of protactinium ions from solutions of mineral acids or their mixtures with ammonium hydroxide. The composition of the formed precipitate depends on precipitation conditions and can be represented as $Pa_2O_5 \cdot xH_2O$. Under precipitation by NaOH or KOH solutions it is necessary to wash thoroughly the precipitate to remove the adsorbed alkali metal ions. The precipitation of protactinium hydroxide is often used for analysis of some protactinium compounds (Grosse, 1934c; Sellers *et al.*, 1954; Bagnall and Brown, 1964; Bagnall *et al.*, 1965; Bukhsh *et al.*, 1966a,b; Stchouzkoy *et al.*, 1966a; Davydov and Pal'shin, 1967).

(b) Protactinium phenylarsonate

Phenylarsonic acid precipitates Pa(V) practically quantitatively from neutral solutions and from solutions of HCl, HNO_3, H_2SO_4, and $HClO_4$ at acids concentration <5 N. The precipitate composition, dried at 120–180°C, corresponds to the formula $H_3PaO_2(C_6H_5AsO_3)_2$. The precipitate is stable and is not changed in weight during heating for few hours at the above-mentioned temperature. As described above, protactinium phenylarsonate can be used for gravimetric determination. This compound may also be converted to Pa_2O_5 by calcination at 1000°C.

The precipitation of protactinium as phenylarsonate from acid solutions can be carried out in the presence of Ni, Co, Cr, La, Fe(III), Mn, Cu, Ti, Th, U, and other elements. Zr, Nb, Ta, fluoro-, and phosphate ions prevent the determination (Myasoedov *et al.*, 1968a).

(c) Protactinium peroxide

Hydrogen peroxide precipitates protactinium from solutions of mineral acids (HNO_3, HCl, H_2SO_4, and $HClO_4$) in the form of amorphous white protactinium peroxide, $Pa_2O_5 \cdot 3H_2O$ (Stchouzkoy and Muxart, 1962; Marples, 1965; Stchouzkoy *et al.*, 1966b). This compound is not stable in air, therefore, the protactinium determination is performed with the calcination of the precipitate to Pa_2O_5. The precipitation of protactinium peroxide from acid solutions can be carried out in the presence of Ni, Co, Cr, Mg, Mn, and other elements, and small quantities of iron. La, Th, U, Zr, and F^- ions prevent the determination. Stchouzkoy and Muxart (1962) recommend carrying out the $Pa_2O_5 \cdot 3H_2O$ precipitation from 0.25 M H_2SO_4 solution, obtained by dissolution of freshly precipitated protactinium hydroxide in sulfuric acid or by some other method.

Pal'shin *et al.* (1968a) applied oxalic acid to increase the selectivity of precipitation with hydrogen peroxide. It was shown that the extent of precipitation of protactinium peroxide from oxalic acid solutions increases with increasing HCl concentration. When the molar relation $H_2C_2O_4$:HCl is equal to 1:5 the extent of precipitation reaches a steady value, and at sufficient excess of hydrogen peroxide the precipitation is quantitative. The method allows determining protactinium in complex solutions and also in the presence of large amounts of zirconium, niobium, and tantalum.

(d) Protactinium iodate

Iodic acid and its salts precipitate Pa(V) from acid solutions in the form of a white volumetric precipitate. Upon standing, especially after heating on a water bath, the precipitate is compressed and is transformed into crystalline form. The composition of protactinium iodate precipitate is not established. According to the data of Kirby (1959) the quantitative precipitation of protactinium (~99.5%) occurs from previously heated solution of protactinium in 0.7 M H_2SO_4 under the addition of a drop at a time of excess 15% HNO_3. The weight determination is performed by calcination of the precipitate to Pa_2O_5 at 800°C (Codding *et al.*, 1964; 1966).

(e) Protactinium cupferronate

There is an indication that CP quantitatively precipitates protactinium from tartaric acid solutions (SalesGrande, 1950) and from solutions of mineral acids (Maddock and Miles, 1949). However, conditions of protactinium precipitation

and composition of the formed precipitate have not been investigated in detail. The calcination of protactinium cupferronate at 1000°C leads to the formation of Pa_2O_5 that can be used for weight determination of protactinium.

4.9.7 Determination of protactinium in the environment

High-sensitivity mass spectrometric measurements of the naturally occurring radionuclides ^{231}Pa and ^{230}Th in the deep Canada Basin and on the adjacent shelf indicate high particle fluxes and scavenging rates in this region. The data obtained suggest that offshore advection of particulate material from the shelves contributes to scavenging of reactive materials in areas of permanent ice cover (Edmonds *et al.*, 1998). The scavenging of ^{231}Pa and ^{230}Th was investigated also in the Atlantic Sector of the Pacific Ocean (Yang *et al.*, 1986), and Southern Ocean by combining results from sediment trap and *in situ* filtration studies (Walter *et al.*, 2001). The U–Th–Pa model was realized for environment samples aging (Cheng *et al.*, 1998).

A new technique for the determination of ^{231}Pa in silicate rocks by isotope dilution mass spectroscopy was described (Bourdon *et al.*, 1999). This technique permits the determination down to a 100 fg of ^{231}Pa with a 1–2% uncertainty at the 2 sigma level. The first high-precision ^{231}Pa measurements in a manganese crust applying TIMS using the double filament techniques were described (Pickett *et al.*, 1994). The detection limit using TIMS is at least one order of magnitude lower, and the statistical uncertainty – six to eight times better than for alpha-spectroscopy. Thus, the older section of manganese crust from the Northern Equatorial Pacific could be measured precisely for their Pa-231 activity. The data described by Fietzky *et al.* (1999) reveal significant variations in ^{231}Pa activity for the last 150 ka, which corroborate existing alpha-spectroscopy results. If the growth rate was constant between 0 and 450 ka, the protactinium flux from the water column into manganese encrustations must have been variable. Thus, ^{231}Pa is not suitable for dating marine Mn/Fe deposits.

The determination of ^{231}Pa in environmental and soil materials (Harbottle and Evans, 1997) and in uranium ore samples is provided by gamma-ray spectrometer with high-purity germanium (Zhang Qingwen *et al.*, 1991).

LIST OF ABBREVIATIONS

Arsenazo-III	3,6-bis-[(2-arsonophenyl)azo]-4,5-dihydroxy-2,7-naphthalene disulfo acid
BPHA	*N*-benzoylphenylhydroxylamine
CP	Cupferron
HDEHP	bis(2-ethylhexyl)phosphoric acid
DIAPA	di-isoamylphosphoric acids
DIBC	di-isobutylcarbinol

DIBK	di-isobutylketone
DIPC	di-isopropylcarbinol
DIPK	di-isopropylketone
DMSO	dimethyl sulfoxide
DSBPP	di-*S*-butylphenyl phosphonate
EDTA	ethylenediaminetetraacetic acid
fg	femtogram
Hexone (or MIK)	methyl isobutyl ketone
Ka	thousand years ago
ng	nanogram
NCP	neocupferron
NHE	normal hydrogen electrode
PAA	phenylarsonic acid
Pc	phthalocyaninato
PMBP	1-phenyl-3-methyl-4-benzoylpyrazolone
SCE	standard calomel electrode
TBP	tri(*n*-butyl)phosphate
THF	tetrahydrofuran
TIMS	thermal ionization mass spectroscopy
TOA	trioctylamine
TOPO	tri-*n*-octylphosphine oxide
TPPO	triphenylphosphine oxide
TTA	thenoyltrifluoroacetone
UKAEA	United Kingdom Atomic Energy Authority

REFERENCES

Abdel Gawad, A. S., Souka, N., and Girgis, C. (1976) *J. Radioanal.*, **31**, 377–82.

Ahmad, I. (2004) Argonne National Laboratory, unpublished work.

Ahrland, S., Liljenzin, J. O., and Rydberg, J. (1973) in Comprehensive Inorganic Chemistry, vol. 5 (eds. J. C. Bailor, Jr., H. J. Emeleus, R. Nyholm, and A. F. Trotman-Dickenson), Pergamon, Oxford, pp. 465–635.

Albridge, R. G., Hollander, J. M., Gallagher, C. J., and Hamilton, J. H. (1961) *Nucl. Phys.*, **27**, 529–53.

Alekseev, V. A., Morozova, Z. E., and Ziv, V. S. (1988) *Radiokhimiya*, **29**, 344–9.

Alekseev, V. A., Morozova, Z. E., and Ziv, V. S. (1989) *Radiokhimiya*, **30**, 322–6.

Alhassanieh, O., Abdul-Hadi, A., Ghafar, M., and Aba, A. (1999) *Appl. Rad. Isotopes*, **51**, 493–8.

Al-Kazzaz, A. M. S., Bagnall, K. W., Brown, D., and Whittaker, B. (1972) *J. Chem. Soc. Dalton Trans.*, 2273–7.

Andreev, A. M., Bogranov, D. D., Yeremin, A. V., Kabachenko, A. P., Malyshev, O. N., Ter Akopian, T. A., and Chepigin, V. I. (1996a) *Izvestiya Akademii Nauk. Ser. Fiz.*, **60**, 186–8.

Andreev, A. M., Popeko, A. G., Yeremin, A. V., Hofman, S., Hessberger, F. P., Folder, H., Ninov, V., and Saro, S. (1996b) *Izvestiya Akademii Nauk. Ser. Fiz.*, **60**, 148–53.

Anonymous (1949) *Chem. Eng. News*, **27**, 2996–9.
Antonoff, G. N. (1911) *Phil. Mag.*, **22**, 419–32.
Antonoff, G. N. (1913) *Phil. Mag.*, **26**, 1058.
Arbman, E., Bjornholm, S., and Nielsen, O. B. (1960) *Nucl. Phys.*, **21**, 406–37.
Arden, I. W., Booth, E., and Perkins, M. (1962) U.K. Atomic Energy Authority Research Group. Report No AERE-AM90.
Ardisson, G. and Ardisson, C. (1975) *Radiochem. Radioanal. Lett.*, **21**, 357–64.
Artna-Cohen, A. (1971) *Nucl. Data B*, **6**, 225–55.
Asprey, L. B., Kruse, F. H., Rosenzweig, A., and Penneman, R. A. (1966) *Inorg. Chem.*, **6**, 659–61.
Asprey, L. B., Kruse, F. H., and Penneman, R. A. (1967) *Inorg. Chem.*, **6**, 544–8.
Asprey, L. B., Fowler, R. D., Lindsay, J. D., White, R. W., and Cunningham, B. B. (1971) *Inorg. Nucl. Chem. Lett.*, **7**, 977–80.
Astheimer, L. and Schwochau, K. (1973) *J. Inorg. Nucl. Chem.*, **35**, 223–30.
Augoustinik, A. I. (1947) *Zh. Prikl. Khim.*, **20**, 327.
Axe, J. D. (1960) U.S. Report UCRL-9293.
Axe, J. D., Kyi, R.-T., and Stapleton, H. J. (1960) *J. Chem. Phys.*, **32**, 1261.
Axe, J. D., Stapleton, H. J., and Jeffries, C. D. (1961) *Phys. Rev.*, **121**, 1630–7.
Bachelet, M. and Bouissières, G. (1944) *Bull. Soc. Chim.*, **11**, 169–71.
Bachelet, M. and Bouissières, G. (1947) *Bull. Soc. Chim.*, **14**, 281–3.
Bagnall, K. W. and Brown, D. (1964) *J. Chem. Soc.*, 3021–5.
Bagnall, K. W., Brown, D., and Jones, P. J. (1965) *J. Chem. Soc.*, 176–81.
Bagnall, K. W. (1966a) *Radiochim. Acta*, **5**, 1.
Bagnall, K. W. (1966b) in *Physico-Chimie du Protactinium* (eds. G. Bouissières and R. Muxart), Centre National de la Recherche Scientifique, Orsay, Paris, pp. 88–92.
Bagnall, K. W. and Brown, D. (1967) *J. Chem. Soc. A*, 275–8.
Bagnall, K. W., Brown, D., and Easey, J. F. (1968a) *J. Chem. Soc. A*, 288–91.
Bagnall, K. W., Brown, D., Holah, D. H., and Lux, F. (1968b) *J. Chem. Soc. A*, 465–70.
Bagnall, K. W., Brown, D., Lux, F., and Wirth, G. (1969) *Z. Naturforsch.*, **B24**, 214–21.
Bagnall, K. W. (1972) *The Actinide Elements,* Elsevier, Amsterdam.
Bagnall, K. W., Bhandari, A. M., Brown, D., Lidster, P. E., and Whittaker, B. (1975) *J. Chem. Soc. Dalton Trans.*, 1249–52.
Banks, R. H., Edelstein, N. M., Rietz, R. R., Templelon, D. H., and Zalkin, A. (1978) *J. Am. Chem. Soc.*, **100**, 1857–8.
Banks, R. H. (1979) Lawrence Berkeley Laboratory Report LBL-10292.
Banks, R. H. and Edelstein, N. M. (1980) *Am. Chem. Soc. Symp. Ser.*, **131**, 331–48.
Bansal, B. M. (1966) U.S. Report UCRL-16787.
Baranov, A. A., Kulakov, V. M., Samilov, P. S., Zelenkov, A. G., Rodinov Yu, F., and Pirozhkov, S. V. (1962) *Sov. Phys. JETP*, **14**, 1052–9.
Baranov, A. A., Kulakov, V. M., and Shatinskii, V. M. (1968) *Sov. J. Nucl. Phys.*, **7**, 442–5.
Barendregt, F. and Tom, S. (1951) *Physica*, **17**, 817–20.
Barnett, M. K. (1957) *J. Inorg. Nucl. Chem.*, **4**, 358.
Barnett, M. K. (1958) *Khimiya & Khim. Tekhnologiya*, **3**, 150.
Bastin, G., Leang, C. F., and Walen, R. J. (1966) *Compt. Rend. Acad. Sci. Paris B*, **262**, 89–92.

Baumgartner, F., Fischer, E. O., Kanellakopulos, B., and Laubeneau, P. (1969) *Angew. Chem.*, **8**, 202.
Baybarz, R. D., Bohet, J., Buijs, K., Colson, L., Muller, W., Reul, J., and Spirlet, J. C. (1976) in *Proc. 4th Int. Transptutonium Element Symp*., Baden, pp. 61–8.
Bearden, J. A. (1967) *Rev. Mod. Phys.*, **39**, 78–124.
Bearden, J. A. and Burr, A. F. (1967) *Rev. Mod. Phys.*, **39**, 125–42.
Benedict, V., Buijs, K., Dufour, C., and Toussaint, J. C. (1975) *J. Less Common Metals*, **42**, 345–54.
Benedict, U., Dufour, C., and Mayne, K. (1979) *J. Phys. Colloq.*, **4**, 103–5.
Beuthe, H. and Grosse, A. (1930) *A. Phys. Z*, **61**, 170.
Bhandari, A. M. and Kulkarni, D. K. (1979) *Curr. Sci.*, **48**, 577–8.
Birks, F. T., Tomas, A. M., and Milner, G. W. C. (1965) UK Atomic Energy Authority Research Group. Report NAER-E-R-4615, p. 17.
Bjørnholm, S. and Nielsen, O. B. (1962) *Nucl. Phys.*, **30**, 488–512.
Bjørnholm, S. and Nielsen, O. B. (1963) *Nucl. Phys.*, **42**, 642–59.
Bjørnholm, S., Westgaard, L., Mason, T., and Nielsen, H. S. (1967) *Radiochim. Acta*, **8**, 204–6.
Bjørnholm, S., Borggreen, J., Davies, D., Hansen, N. J. S., Pedersen, J., and Nielsen, H. S. (1968) *Nucl. Phys. A*, **118**, 261–301.
Bohet, J. (1977) *Comm. Eur. Communities (Rep.) EUR 5882.*
Bohet, J. and Muller, W. (1978) *J. Less Common Metals*, **57**, 185–9.
Bohres, E. W. (1974) German Report JUL-1080-NC.
Bohres, E. W., Hauck, J., Schenk, H. J., and Schwochau, K. (1974) in *Proc. 16th Int. Conf. Coord. Chem.*, **2**, 166.
Boltwood, B. B. (1906) *Am. J. Sci.*, **22**, 537–8.
Boltwood, B. B. (1908) *Am. J. Sci.*, **25**, 269–98.
Bonnet, M. and Guillaumont, R. (1969) *Radiochim. Acta*, **12**, 98–107.
Booth, A. H. (1951) *J. Chem. Educ.*, **28**, 144–5.
Borggreen, J., Valli, K., and Hyde, E. K. (1970) *Phys. Rev. C*, **2**, 1841–62.
Born, H.-J. (ed.) (1971) *Tagungsber. 3 Int. Pa-Konf.*, Schloss-Elmau. 15–18 April 1969, German Report BMBW-FBK 71–17.
Bouissières, G. and Haïssinsky, M. (1949) *J. Chem. Soc. Suppl.*, **2**, 256–8.
Bouissières, G. and Haïssinsky, M. (1951) *Bull. Soc. Chem.*, **18**, 557–60.
Bouissières, G., Marty, N., and Teillac, J. (1953) *Compt. Rend. Acad. Sci. Paris*, 324–6.
Bouissières, G. and Muxart, R. (eds) (1966) *Physico-Chimie du Protactinium*, Centre National de la Recherche Scientifique, Orsay, Paris , 2–8 July 1965.
Bouissières, G. (1971) in *Tagungsber. 3 Int. Pa-Konf.* (ed. H.-J. Born), Schloss-Elmau, 15–18 April 1969, German Report BMBW-FBK 71–17, Paper No. 26.
Bourdon, B., Joron, J. L., and Allegre, C. J. (1999) *Chem. Geol.*, **157**, 147–51.
Bower, K., Angel, A., Gibson, R., Robinson, T., Knobeloch, D., and Smith, B. (1994) *J. Radioanal. Nucl. Chem. Articles*, **181**, 97–107.
Bradbury, M. H. (1981) *J. Less Common Metals*, **78**, 207–18.
Briand, J.-P., Chevallier, P., Borg, J., and Teillas, J. (1969) *Compt. Rend. Acad. Sci. Paris B*, **269**, 582–5.
Brooks, M. S. S., Calestani, G. J., Spirlet, C., Rebizant, J., Mueller, W., Fournier, J. M., and Blaise, A. (1980) *Physica B&C*, **102**, 84–7.
Brown, D., Smith, A. J., and Wilkins, R. G. (1959) *J. Chem. Soc*., 1463–6.

Brown, D. and Wilkins, R. G. (1961) *J. Chem. Soc*., 3804–7.
Brown, D., Sato, T., Smith, A. J., and Wilkins, R. G. (1961) *J. Inorg. Nucl. Chem.*, **23**, 91–101.
Brown, D. and Maddock, A. G. (1963) *Quart. Rev.*, **17**, 289–341.
Brown, D. and Jones, P. J. (1964) *J. Inorg. Nucl. Chem.*, **26**, 2296–7.
Brown, D. and Easey, J. F. (1965) *Nature*, **205**, 589.
Brown, D. (1966) in *Physico-Chimie du Protactinium* (eds. G. Bouissières and R. Muxart), Centre National de la Recherche Scientifique, Orsay, Paris, 2–8 July 1965, pp. 147–53.
Brown, D. and Easey, J. F. (1966) *J. Chem. Soc. A*, 254–8.
Brown, D. and Jones, P. J. (1966a) *Chem. Commun*., 280.
Brown, D. and Jones, P. J. (1966b) *J. Chem. Soc. A*, 733–7.
Brown, D. and Jones, P. J. (1966c) *J. Chem. Soc. A*, 874–8.
Brown, D., Dixon, S. N., and Jones, P. J. (1966a) *J. Inorg. Nucl. Chem.*, **28**, 2529–33.
Brown, D., Easey, J. F., and DuPreez, J. G. H. (1966b) *J. Chem. Soc. A*, 258–61.
Brown, D. and Jones, P. J. (1967a) *J. Chem. Soc. A*, 243–7.
Brown, D. and Jones, P. J. (1967b) *J. Chem. Soc. A*, 247–51.
Brown, D. and Jones, P. J. (1967c) *J. Chem. Soc. A*, 719–23.
Brown, D. and Maddock, A. G. (1967) in *Prog. Nucl. Energy Ser*., IX, pp. 3–47.
Brown, D., Easey, J. F., and Holah, D. G. (1967a) *J. Chem. Soc. A*, 1979–80.
Brown, D., Easey, J. F., and Jones, P. J. (1967b) *J. Chem. Soc. A*, 1698–702.
Brown, D., Kettle, S. F. A., and Smith, A. J. (1967c) *J. Chem. Soc. A*, 1429–34.
Brown, D., Dixon, S. N., Glover, K. M., and Rogers, F. J. G. (1968a) *J. Inorg. Nucl. Chem.*, **30**, 19–22.
Brown, D., Petcher, T. J., and Smith, A. J. (1968b) *Nature*, **271**, 737–8.
Brown, D. (1969) *Adv. Inorg. Chem. Radiochem.*, **12**, 1–51.
Brown, D. and Petcher, T. J. (1969) *Acta Crystallogr. B*, **25**, 178–82.
Brown, D. and Easey, J. F. (1970) *J. Chem. Soc. A*, 3378–81.
Brown, D. and Rickard, C. E. F. (1970) *J. Chem. Soc. A*, 3373–7.
Brown, D., Hill, J., and Rickard, C. E. F. (1970a) *J. Chem. Soc. A*, 476–80.
Brown, D., Hill, J., and Rickard, C. E. F. (1970b) *J. Chem. Soc. A*, 497–501.
Brown, D. (1971) in *Tagungsber. 3 Int. Pa-Konf*. (ed. H.-J. Born), Schloss-Elmau, 15–18 April 1969, German Report BMBW-FBK 71-17, Paper No. 32.
Brown, D. and Rickard, C. E. F. (1971a) *J. Chem. Soc. A*, 81–7.
Brown, D. and Rickard, C. E. F. (1971b) in *Tagungsber. 3 Int. Pa-Konf*. (ed. H.-J. Born), Schloss-Elmau, 15–18 April 1969, German Report BMBW-FBK 71-17, Paper No. 21.
Brown, D., Hill, J., and Rickard, C. E. F. (1971) in *Tagungsber. 3 Int. Pa-Konf*. (ed. H.-J. Born), Schloss-Elmau, 15–18 April 1969, German Report BMBW-FBK 71-17, Paper No. 22.
Brown, D., Reynolds, C. T., and Mosely, P. T. (1972) *J. Chem. Soc. Dalton Trans*., 857–9.
Brown, D. (1973) in *Comprehensive Inorganic Chemistry*, vol. 5 (eds. J. C. Bailar, Jr, H. J., Emeleus, R. Nyholm, and A. F. Trotman-Dickenson), Pergamon, Oxford, pp. 151–217.
Brown, D., De Paoli, G., and Whittaker, B. (1976a) *J. Chem. Soc. Dalton Trans*., 1336–8.
Brown, D., Whittaker, B., and Di Paoli, G. (1976b) UK Report, Atomic Energy Research Establishment AERE-R8367.

Brown, D., Tso, T. C., and Whittaker, B. (1977) *J. Chem. Soc. Dalton Trans.*, 2291–6.
Brown, D. and Whittaker, B. (1978) *J. Less Common Metals*, **61**, 161–70.
Brown, D. (1979) *Inorg. Nucl. Chem. Lett.*, **15**, 219–23.
Brown, D. (1982) in *Actinides in Perspective* (ed. N. Edelstein), Pergamon Press, Oxford, pp. 343–59.
Brown, D., Barry, J. A., and Holloway, J. H. (1982a) UK Report, Atomic Energy Research Eslablishment, AERE-R10415.
Brown, D., Whittaker, B., Benny, J. A., and Holloway, J. H. (1982b) *J. Less Common Metals*, **86**, 75–84.
Browne, C. I., Hoffman, D. C., Smith, H. L., Bunker, M. E., Mize, J. P., Stanner, J. W., Moore, R. L., and Bologna, J. P. (1954) *Phys. Rev.*, **95**, 827.
Bukhsh, M. N., Flegenheimer, J., Hall, F. M., Maddock, A. G., and deMiranda, C. F. (1966a) *J. Inorg. Nucl. Chem.*, **28**, 421–31.
Bukhsh, M. N., Flegenheimer, J., Hall, F. M., Maddock, A. G., and deMiranda, C. F. (1966b) in *Physico-Chimie du Protactinium* (eds. G. Bouissières and R. Muxart), Centre National de la Recherche Scientifique, Orsay, Paris, pp. 195–207.
Bunney, L. R., Ballou, N. E., Pascual, J., and Foti, S. (1959) *Anal. Chem.*, **31**, 324–6.
Bykhovskii, D. N., Kuzmina, M. A., and Lazkhina, G. S. (1977) *Radiokhimiya*, **19**, 178–84.
Calestani, G., Spirlet, J. C., and Mueller, W. (1979a) *J. Phys. Colloq.*, **4**, 106–7.
Calestani, G., Spirlet, J. C., Rebizant, J., and Mueller, W. (1979b) *J. Less Common Metals*, **68**, 207–12.
Caletka, R. and Spěváčkova, V. (1975) *Radiochem. Radioanal. Lett.*, **23**, 37–42.
Camarcat, M., Bouissières, G., and Haïssinsky, M. (1949) *J. Chem. Phys.*, **46**, 153.
Campbell, D. O. (1964) in *Proc. Protactinium Chem. Symp.,* 25–26 April 1963, U.S. Report TID-7675, Gatlinburg, Tennessee, pp. 87–103.
Carlier, R. (1971) French Report FRNC-TH-91.
Carlier, R. and Genet, M. (1972a) *Radiochem. Radioanal. Lett.*, **10**, 91–7.
Carlier, R. and Genet, M. (1972b) *Radiochim. Acta*, **18**, 11–16.
Carrere, J. P. (undated) unpublished results cited by Muxart and Guillaumont (1974) in *Complements au Noueveau Traite de Chimie Minerale* (eds. A. Pacault and G. Pannetier), Masson, Paris, p. 2.
Carsell, O. J. and Lawrence, J. J. (1959) *J. Chem. Educ.*, **36**, 499–501.
Carswell, D. J. and Lawrence, J. J. (1959) *J. Inorg. Nucl. Chem.*, **11**, 69–74.
Casey, A. T. and Maddock, A. G. (1959a) *J. Inorg. Nucl. Chem.*, **10**, 58.
Casey, A. T. and Maddock, A. G. (1959b) *J. Inorg. Nucl. Chem.*, **10**, 289–305.
Cauchois, Y. and Hulubel, H. (1947) Constantes selectionees Longueurs D'onde des Emmissions X et des Discont. D'Adsorption X. Hermann, Paris.
Cauchois, Y. and Bonnelle, C. (1966) in *Physico-Chimie du Protactinium* (eds. G. Bouissières and R. Muxart), Centre National de la Recherche Scientifique, Orsay, Paris, 2–8 July 1965, p. 21.
Cauchois, Y. (1971) in *Tagungsher. Int. Pa-Konf.* (ed. H.-J. Born), Schloss-Elmau, 15–18 April 1969, German Report BMBW-FBK 71–17.
Cazaussus, A., Arapaki-Strapelius, H., and Muxart, R. (1971) *Radiochem. Radioanal. Lett.*, **6**, 297–306.
Chakravortty, V. and Mohanly, S. R. (1979) *Radiochem. Radioanal. Lett.*, **41**, 275–8.
Chakravortty, V., Mohanly, S. R., and Dash, K. C. (1986) *Radiochim. Acta*, **40**, 89–94.

Chang, H.-P., Ho, C.-K., Ting, G., and Wu, S.-C. (1974) *Nucl. Sci. J.*, **11**, 73–81.
Chang, H.-P. and Ting, G. (1975a) *Ho Tzu K'oHsueh.*, **12**, 119–32.
Chang, H.-P. and Ting, G. (1975b) Taiwan Report INER-64-D–0167.
Chen, T. and Yuan, S. (1988) *Archaeometry*, **30**, 59–76.
Cheng, H., Edwards, R. L., Murrell, M. T., and Benjamin, T. M. (1998) *Geochimica et Cosmochimica Acta*, **62**, 3437–52.
Chetham-Strode, A., Jr. and Keller, O. L., Jr. (1966) in *Physico-Chimie du Protactinium* (eds. G. Bouissières and R. Muxart), Centre National de la Recherche Scientifique, Orsay, Paris, 2–8 July 1965, pp. 189–93.
Chilton, J. M. (1964) in *Proc. Protactinium Chem. Symp*., 25–26 April 1963, U.S. Report TID-7675, Gatlinburg, Tennessee, pp. 157–9.
Codding, J. W., Berreth, J. R., Schuman, R. P., Burgus, W. H., and Deal, R. A. (1964) U.S. Report IDO-17007.
Codding, J. W., Berreth, J. R., Schuman, R. P., Burgus, W. H., Deal, R. A., and Simpson, F. B. (1966) in *Physico-Chimie du Protactinium* (eds. G. Bouissières and R. Muxart), Centre National de la Recherche Scientifique, Orsay, Paris, 2–8 July 1965, p. 325.
Collins, D. A., Hillary, J. J., Nairn, J. S., and Phillips, G. M. (1962) *J. Inorg. Nucl. Chem.*, **24**, 441–59.
Cotton, F. A., Wilkinson, G., Murillo, C. A., and Bochmann, M. (1999) in *Advanced Inorganic Chemistry*, 6th edition. John Wiley & Sons. Inc. Technical and Medical Division 605 Third Avenue; NY 10158–0012 ISBN 0-471-19957-5; Chapter 20 The Actinide Elements, P. 1130.
Crane, W. W. T. and Iddings, G. M. (1954) *Phys. Rev.*, **95**, 1702–3.
CRC Handbook of Chemistry and Physics and the American Chemical Society, Last Updated 12/19/1997, CST Information Service Team.
Cristallini, O. and Flegenheimer, J. (1963) *Radiochim. Acta*, **1**, 157–61.
Croft, W. L., Stone, J. A., and Pillinger, W. L. (1968) *J. Inorg. Nucl. Chem.*, **30**, 3203–8.
Crookes, W. (1900) *Proc. R. Soc.*, **66**, 409–22.
Crouthamel, C. E., Adams, F., and Dams, R. (1970) *Applied Gamma-Ray Spectrometrv,* Pergamon, Oxford.
Cunningham, B. B. (1966) in *Physico-Chimie du Protactinium* (eds. G. Bouissières and R. Muxart), Centre National de la Recherche Scientifique, Orsay, Paris, 2–8 July 1965, pp. 45–8.
Cunningham, B. B. (1971) in *Tagungsber. 3 Int. Pa-Konf*. (ed. H.-J. Born), Schloss-Elmau, 15–18 April 1969, German Report BMBW-FB-K, Paper No. 14.
Curie, P. (1911) *Le Radium*, **8**, 353–4.
Curie, M. (1913) *Ann. Chim. Phys.*, **30**, 125–6.
David, F. and Bouissières, G. (1966) in *Physico-Chimie du Protactinium* (eds. G. Bouissières and R. Muxart), Centre National de la Recherche Scientifique, Orsay, Paris, 2–8 July 1965, p. 301.
Davydov, A. V., Myasoedov, B. F., Novikov, Yu. P., Palei, P. N., and Pal'shin, E. S. (1965) *Nucl. Sci. Abst.*, **20**, 27–62.
Davydov, A. V., Marov, I. N., and Palei, P. N. (1966a) *Sov. J. Inorg. Chem.*, **11**, 1316.
Davydov, A. V., Marov, I. N., and Palei, P. N. (1966b) in *Physico-Chimie du Protactinium* (eds. G. Bouissières and R. Muxart), Centre National de la Recherche Scientifique, Orsay, Paris, 2–8 July 1965, pp. 181–8.

Davydov, A. V., Myasoedov, B. F., Novikov, Yu. P., Palei, P. N., and Pal'shin, E. S. (1966c) *Tr. Kom. Anal. Khim. Akad. Nauk SSSR*, **15**, 64–79.
Davydov, A. V. and Pal'shin, E. S. (1967) *Atomnaya Energiya*, **32**, 487–90.
D' Ege, R., Maddock, A. G., and Toms, D. I (1963). Unpublished observations cited by Brown.
Delaeter, J. R. and Heumann, K. G. (1991) *J. Phys. Chem. Refer. Data*, **20**, 1313–35.
deMiranda, C. F. and Maddock, A. G. (1962) *J. Inorg. Nucl. Chem.*, **24**, 1623–33.
deMiranda, C. F. and Muxart, R. (1964) *Bull. Soc. Chim. Fr.*, 2174–6.
deMiranda, C. F. and Muxart, R. (1965) *Bull. Soc. Chim. Fr.*, 387–9.
deMiranda, C. F. (1966) in *Physico-Chimie du Protactinium* (eds. G. Bouissières and R. Muxart), Centre National de la Recherche Scientifique, Orsay, Paris, 2–8 July 1965, pp. 127–34.
Dempster, A. J. (1935) *Nature*, **136**, 180.
dePinke, A. G., deSilviera, E. F., and Costa, N. L. (1970) *Phys. Rev. C*, **2**, 572–86.
Dod, R. L. (1972) U.S. Report LBL-659.
Dodge, R. P., Smith, G. S., Johnson, Q., and Elson, R. E. (1968) *Acta Crystallogr. B*, **24**, 304–12.
Dolejsek, V. and Kunzl, V. (1936) *Nature*, **138**, 590.
Duplessis, J. and Guillaumont, R. (1979) *Radiochem. Radioanal. Lett.*, **37**, 159–63.
D'yachkova, R. A., Spitsyn, V. I., and Nazarov, P. P. (1962) *Radiokhimiya*, **4**, 77–81.
D'yachkova, R. A. and Spitsyn, V. I. (1964) *Radiokhimiya*, **6**, 102.
D'yachkova, R. A., Khlebnikov, V. P., and Spitsyn, V. I. (1968a) *Sov. J. Inorg Chem.*, **13**, 439–42.
D'yachkova, R. A., Khlebnikov, V.P., and Spitsyn, V. I. (1968b) *Radiokhimiya*, **10**, 17–21.
Edelstein, N. M., Brown, D., Whittaker, B., Rajnak, K., Naik, R. C., and Krupa, J. C. (1988) *Inorg. Chem.*, **27**, 3186–9.
Edelstein, N. M., Krupa, J. C., and Kot, W. K. (1992) *J. Chem. Phys.*, **96**, 1–4.
Edelstein, N. M. and Kot, W. K. (1993) *J. Alloys & Comp.*, **193**, 82–7.
Edmonds, H. N., Moren, S. B., Hoff, J. A., Smith, J. N., and Edwards, R. L. (1998) *Science*, **280**, 405–7.
Edwards, R. L., Cheng, H., Murrell, M. T., and Goldstein, S. J. (1997) *Science*, **276**, 782–6.
El- Dessouky, M. M. (1966) *Microchim. Acta*, **2**, 461–6.
Ellis, Y. A. (1970) *Nucl. Data B*, **4**, 581–621.
Elson, R. E., Mason, G. W., Peppard, D. F., Sellers, P. O., and Studier, M. H. (1951) *J. Am. Chem. Soc.*, **73**, 4974–5.
Elson, R. E. (1954) *The Actinide Elements* (eds. G. T. Seaborg and J. J. Katz), McGraw-Hill, New York, pp. 103–29.
El-Sweify, F. H., Aly, H. F., Abdel-Rahman, A., and Shabana, R. (1985) *Radiochim. Acta*, **38**, 211–4.
El-Yamani, I. S. and Shabana, E. I. (1985) *J. Radioanal. Nucl. Chem. Lett.*, **88**, 209–16.
Emmanuel-Zavizziano, H. and Mme (1936) *Compt. Rend. Acad. Sci. Paris*, **202**, 1052–4.
Emmanuel-Zavizziano, H. and Haïssinsky, M. (1938) *Compt. Rend. Acad. Sci. Paris*, **206**, 1102.
Erdmann, B. (1971) German Report KFK-1444.
Erdmann, B. and Keller, C. (1971) *Inorg. Nucl. Chem. Lett.*, **7**, 675–83.

Erdmann, B. and Keller, C. (1973) *J. Solid State Chem.*, **7**, 40–8.
Fajans, K. (1913a) *Phys. Z*, **14**, 131–6.
Fajans, K. (1913b) *Phys. Z*, **14**, 136–42.
Fajans, K. and Göhring, O. (1913a) *Naturwissenschaften*, **I**, 339.
Fajans, K. and Göhring, O. (1913b) *Phys. Z*, **14**, 877–84.
Fajans, K. and Morris, D. F. C. (1913) *Nature*, **244**, 137–8.
Fidelis, J., Gwozdz, R., and Siekierski, S. (1963) *Nukleonika*, **8**, 224–7.
Fietzke, J., Bollhofer, A., Frank, N., and Mangini, A. (1999) *Nuclear Instr. Meth. Phys. Res. Sec. B*, **149**, 353–60.
Figgins, P. E. and Kirby, H. W. (1966) U.S. Report MLM-1349.
Figgins, P. E. and Hertz, M. R. (1972a) U.S. Report MLM-1903, pp. 6–17.
Figgins, P. E. and Hertz, M. R. (1972b) U.S. Report MLM-1955, pp. 7–13.
Figgins, P. E. and Hertz, M. R. (1973) U.S. Report MLM-2013, pp. 48–55.
Figgins, P. E., Hertz, M. R., and Stringham, W. S. (1975) U.S. Report MLM-2198, pp. 33–8.
Folger, H., Hartmann, W., Hessberger, F. P., Hoffman, S., Klemm, J., Munzenberg, G., Nilov, V., Thalheimer, W., and Armbruster, P. (1995) *Nucl. Instrum. Meth. Phys. Res. A*, **362**, 64–9.
Forrest, J. H., Lyle, S. J., Martin, G. R., and Maulden, J. J. (1960) *J. Inorg. Nucl. Chem.*, **15**, 210–4.
Fowler, R. D., Matthias, B. T., Asprey, L. B., Hill, H. H., Lindsay, J. D. G., Olsen, C. E., and White, R. W. (1965) *Phys. Rev. Lett.*, **15**, 860–7.
Fowler, R. D., Asprey, L. B., Lindsayand, J. D. G., and White, R. W. (1974) in *Low-Temperature Physics, LT13*, vol. 3 (ed. K. D. Timmerhaus), Plenum, New York, pp. 377–81.
Francis, M. and Theng-Da Tchang. (1935) *Phil. Mag.*, **20**, 626.
Fried, S. and Hindman, J. C. (1954) *J. Am. Chem. Soc.*, **76**, 4863–4.
Friedt, J. M., Kalvius, G. M., Poinsot, R., Rebizant, J., and Spirlet, J. C. (1978) *Phys. Lett. A*, **69**, 225–7.
Fronaeus, S. (1963) *Technique of Inorganic Chemistry*, vol. 1 (eds. H. B. Jonassen and A. Weissberger), Interscience, New York, pp. 1–36.
Fudge, A. J. and Woodhead, J. L. (1956) *Analyst*, **81**, 417.
Fudge, A. J. and Woodhead, J. L. (1957) *Chem. Ind.*, **17**, 1122.
Fujikawa, N., Fujioka, Y., Ojima, H., Osawa, S., and Yamakuchi, Y. (1996) Japan Patent 08151260-A, U.S. Patent 5650367-A, C04B-035/46, H01B-003/12.
Galateanu, I. and Lapitskii, A. V. (1962a) *Dokl. Akad. Nauk. SSSR (Angl. Transl.)*, **147**, 983–7.
Galateanu, I. and Lapitskii, A. V. (1962b) *Radiokhimiya*, **4**, 371–5.
Galateanu, I. (1966) *Can. J. Chem.*, **44**, 647–55.
Gasche, T., Johansson, B., and Brooks, M. S. (1996) *Phys. Rev. B. (Cond. Matt.)*, **54**, 2446–52.
Ghiorso, A., Meinke, W. W., and Seaborg, G. T. (1948) *Phys. Rev.*, **74**, 695–6.
Giaechetti, A. (1966) *J. Opt. Soc. Am.*, **56**, 653–7.
Giaechetti, A. (1967) *J. Opt. Soc. Am.*, **57**, 728–33.
Glover, K. M., Golden, A. J., Maddock, A. G., and Toms, D. J. (1959) Atomic Energy Research Establ. (GB), Report AERE-R-2971.

Gmelin (1942) *Gmelin Handbuch der Anorganischen Chemie – Protactinium und Isotope. System-Nummer 51 Verlag Chemie (1942) Verlag Chemie*. Springer Verlag, Berlin.

Gmelin (1977) *Gmelin Handbuch der Anorganischen Chemie – Protactinium und Isotope. System-Nummer 51Verlag Chemie (1977). Weinheim: Suppl.*, Vols. 1 and 2, Springer-Verlag, Berlin.

Gober, M. K., Kratz, J. V., Zimmermann, H. P., Schädel, M., Bruchle, W., Schimpf, E., Gregorich, K., Turler, E. A., Hannink, N. J., Czerwinski, K. R., Kadkhodayan, B., Lee, D. M., Nurmia, M. J., Hoffman, D. C., Gaggeler, H., Jost, D., Kovacs, J., Cherer, U. W., and Weber, A. (1992) *Radiochim. Acta*, **57**, 77–84.

Goble, A. G., Golden, J., and Maddock, A. G. (1956) *Can. J. Chem.*, **34**, 284.

Goble, A. G. and Maddock, A. G. (1958) *J. Inorg. Nucl. Chem.*, **7**, 94.

Goble, A. G., Golden, J., Maddock, A. G., and Toms, D. J. (1958) in *Prog. Nuct. Energy Ser. III*, 2: pp. 86–98.

Gofman, J. W. and Seaborg, G. T. (1949) *The Transuranium Elements. Div. IV, Natl. Nucl. En. Ser., 14B* (eds. G. T. Seaborg, J. J. Katz, and W. M. Manning), McGraw-Hill, New York, pp. 1427–30.

Göhring, O. (1914a) *Phys. Z*, **15**, 642–5.

Göhring, O. (1914b) Dissertation, p. 21. T. H., Karlsruhe.

Goode, J. H. and Moore, J. G. (1967) U.S. Report ORNL-3950.

Graue, G. and Kading, H. (1934a) *Naturwissenschaften*, **22**, 386–8.

Graue, G. and Kading, H. (1934b) *Angew. Chem.*, **47**, 650–3.

Greenwood, N. N. and Earnshaw, A. (1997) in *Chemistry of the Elements*, 2nd edn, Elsevier, Butterworth-Hainman, London, UK, Chapters 30–31.

Greis, O., Bohres, E. W., and Schwochau, K. (1977) *Z. Anorg. Allg. Chem.*, **433**, 111–8.

Grenthe, I. and Puigdomenech, I. (eds) (1997) *Modeling in Aquatic Chemistry*, OECD/NEA, Paris.

Grosse, A. V. (1927) *Naturwissenschaften*, **15**, 766–7.

Grosse, A. V. (1928) *Ber. Dtsch. Chem. Ges.*, **61B**, 233–45.

Grosse, A. V. (1930) *J. Am. Chem. Soc.*, **52**, 1742–7.

Grosse, A. V. (1932) *Naturwissenschaften*, **20**, 505.

Grosse, A. V. (1934a) *J. Am. Chem. Soc.*, **56**, 2200–1.

Grosse, A. V. (1934b) *J. Am. Chem. Soc.*, **56**, 2501.

Grosse, A. V. (1934c) *Science*, **80**, 512.

Grosse, A. V. and Agruss, M. S. (1934) *J. Am. Chem. Soc.*, **56**, 2200.

Grosse, A. V. and Agruss, M. S. (1935a) *Ind. Eng. Chem.*, **27**, 422–6.

Grosse, A. V. and Agruss, M. S. (1935b) *J. Am. Chem. Soc.*, **57**, 438–9.

Grosse, A. V. (1939) *Phys. Rev.*, **55**, 584.

A. V. Grosse, (1975) Personal communication.

Grudpan, K., Punyodom, W., and Singjanusong, P. (1990) in *Nuclear Science and Techn. Conf.,* 23–25 April 1990, Bangkok, Thailand.

Grundy, B. R. and Hamer, A. N. (1961) *J. Inorg. Nucl. Chem.*, **23**, 148–50.

Gryntakis, E. M. and Kim, J. I. (1974) *J. Inorg. Nucl. Chem.*, **36**, 1447–52.

Guillaumont, R., Muxart, R., Bouissières, G., and Haïssinsky, M. (1959) *Compt. Rend. Acad. Sci. Paris*, **248**, 3298.

Guillaumont, R., Muxart, R., Bouissières, G., and Haïssinsky, M. (1960) *J. Chim. Phys.*, **57**, 1019–28.

Guillaumont, R. (1965a) *Bull. Soc. Chim. Fr*., 135–9.
Guillaumont, R. (1965b) *Compt. Rend. Acad. Sci. Paris*, **260**, 1416–8.
Guillaumont, R. (1966a) *Rev. Chim. Miner.*, **3**, 339–73.
Guillaumont, R. (1966b) in *Physico-Chimie du Protactinium* (eds. G. Bouissières and R. Muxart), Centre National de la Recherche Scientifique, Orsay, Paris, 2–8 July 1965, pp. 165–79.
Guillaumont, R. (1966c) Theses. La faculte des sciences de l'universite de Paris.
Guillaumont, R. and deMiranda, C. F. (1966) *Rev. Chim. Miner.*, **3**, 861–72.
Guillaumont, R. (1968) *Bull. Soc. Chim. Fr.*, 1956–61.
Guillaumont, R., Bouissières, G., and Muxart, R. (1968) *Actinides Rev.*, **1**, 135–63.
Guillaumont, R. (1971) in *Tagungsber. 3 Int. Pa-Konf.* (ed. H.-J. Bom). Schloss-Elmau, 15–18 April 1969, German Report BMBW-FBK 71–17, Paper No. 31.
Guillaumont, R. and deMiranda, C. F. (1971) *Solvent Extr. Rev.*, **1**, 105–49.
Guillaumont, R., Ionova, G. V., Krupa, J. C., and David, F. (1996) *Radiochim. Acta*, **75**, 97–103.
Guillot, P. (1966) in *Physico-Chimie du Protactinium* (eds. G. Bouissières and R. Muxart), Centre National de la Recherche Scientifique, Orsay, Paris, 2–8 July 1965, pp. 239–48.
Guy, W. G. and Russell, A. S. (1923) *J. Chem. Soc.*, **123**, 2618–31.
Hahn, O. and Meitner, L. (1918) *Phys. Z*, **19**, 208–18.
Hahn, O. (1921) *Ber. Dtsch Chem. Ges. B*, **54**, 1131–42.
Hahn, R. L., Roche, M. F., and Toth, K. S. (1968) *Nucl. Phys. A*, **113**, 206–14.
Haire, R. G., Heathman, S., Idiri, M., Le Bihan, T., Lindbaum, A., and Rebizant, J. (2003) *Phys. Rev. B*, **67**, 134101-1-10.
Haïssinsky, M. and Bouissières, G. (1948) *Compt. Rend. Acad. Sci. Paris*, **226**, 573–94.
Haïssinsky, M. and Bouissières, G. (1951) *Bull. Soc. Chim.*, 146–8.
Haïssinsky, M. and Bouissières, G. (1958) *Noweau Traits de Chimie Minérale* (ed. P. Pascal), Masson, Paris, pp. 617–80.
Haïssinsky, M., Muxart, R., and Arapaki, H. (1961) *Bull. Soc. Chim. Fr.*, 2248.
Haïssinsky, M. and Pluchet, E. (1962) *J. Chim. Phys*., 608–10.
Harbottle, G. and Evans, C. V. (1997) *Radioact. Radiochem.*, **8**, 38–46.
Hardy, C. J., Scargill, D., and Fletcher, J. M. (1958) *J. Inorg. Nucl. Chem.*, **7**, 257–75.
Harvey, B. G. and Parsons, B. I. (1950) *Phys. Rev.*, **80**, 1098–9.
Haubach, W. J. (1967) Unpublished memorandum, 15 August.
Heckley, P. R., Holah, D. G., and Brown, D. (1971) *Can. J. Chem.*, **49**, 1151–60.
Heinrich, G., Ache, H. J., and Guesten, H. (1986) *Appl. Spectrosc.*, **40**, 363–8.
Hendricks, M. E., Jones, E. R. Jr, Stone, J. A., and Karraker, D. G. (1971) *J. Chem. Phys.*, **55**, 2993–7.
Herak, M. J., Prpic, I., and Tamhina, B. (1979) in *CIM Spec. Vol., Proc. Int. Solvent Extr. Conf.* 1977, pp. 462–6.
Hertz, M. R., Figgins, P. E., and Watrous, R. M. (1974) U.S. Report MLM–2168, pp. 31–5.
Hery, Y., Wojakowski, A., Baidron, M., and De Novion, C. H. (1977) in *Proc. 2nd Int. Conf. Electron. Structure Actinides, Zakl. Norimienia Ossolinskich, Wydawn. Polish Akad. Nauk*, Wroclaw, Poland, pp. 343–7.
Hery, Y., Damien, D., Haessler, M., and De Novion, E. H. (1978) *Radiochem. Radioanal. Lett.*, **32**, 283–92.

Hery, Y. (1979) Report CEA-R-4971.
Hery, Y., Damien, D., and Charvillat, J. P. (1979) *Radiochem. Radioanal. Lett.*, **37**, 17–26.
Heydemann, A. (1969) *Handbook of Geochemistry*, vol. 1 (ed. K. H. Wedepohl), Springer-Verlag, New York, pp. 376–412.
Hicks, H. G., Stevenson, P. C., and Schweiger, J. S. (1978) *J. Chromatogr*, 527–33.
Hill, M. W. (1958) U.S. Report UCRL-8423.
Hillary, J. J. and Morgan, A. R. (1964) *Ind. Chemist*, **40**, 131–6.
Hitachi Metals Ltd (1999) Japan Patent JP11166177-A, C09K–011/00.
Holden, N. E. and Walker, F. W. (1972) *Chart of the Nuclides,* 11th edn, General Electric Co., Schenectady, New York.
Holtzman, R. B. (1962) Atomic Energy Commission, Report ANL-6474. p. 42.
Huntley, D. J., Calvert, S. E., Thomson, J., and Nissen, M. K. (1986) *Can. J. Earth Sci.*, **23**, 959–66.
Hyde, E. K. (1948) U.S. Report ANL-4183.
Hyde, E. K., Studier, M. H., Hopkins, H. H. Jr, and Ghiorso, A. (1949) *The Transuranium Elements, Div. IV. 14B* (eds. G. T. Seaborg, J. J. Katz, and W. M. Manning), Natl. Nucl. Energy Ser., McGraw-Hill, New York, pp. 1439–41.
Hyde, E. K., Katzin, L. I., and Wolf, M. J. (1951) U.S. Patent 2978294.
Hyde, E. K. and Wolf, M. J. (1952) U.S. Report T1D-5223 (ed. L. I. Katzin), pp. 197–222.
Hyde, E. K. (1954) *The Actinide Elements, Div. IV, 14A* (eds. G. T. Seaborg and J. J. Katz), Natl. Nucl. Energy Ser., McGraw-Hill, New York, pp. 542–95.
Hyde, E. K. (1956) in *Proc. Int. Conf. on Peaceful Uses of Atomic Energy,* vol. 7, 8–20 August 1955 (Geneva). United Nations, New York, pp. 281–303.
Hyde, E. K. (1961) U.S. Report UCRL-9458.
Hyde, E. K., Perlman, J., and Seaborg, G. T. (1964) *The Nuclear Properties of the Heavy Elements,* vol. 2. Prentice-Hall, Englewood Cliffs, New York.
Hyde, E. K. (undated) U.S. Report UCRL-10612.
Ishida, Y. E. (1975) Unpublished results.
Iyer, P. N. and Smith, A. J. (1966) in *Physico-Chimie du Protactinium* (eds. G. Bouissières and R. Muxart), Centre National de la Recherche Scientifique, Orsay, Paris, 2–8 July 1965, pp. 81–5.
Jackson, N., Rogers, F. J. G., and Short, J. F. (1960a) UK Report AERE-R 3311.
Jackson, N., Rogers, F. J. G., and Short, J. F. (1960b) UK Report AERE-R 3377.
Jacobi, E. (1945) *Helv. Chim. Acta*, **28**, 757–8.
Jakovac, Z. and Lederer, M. (1959) *J. Chromatogr.,* **2**, 411–7.
Jenkins, I. L., Scargell, D., and Wain, A. G. (1975) *J. Inorg. Nucl. Chem.*, **37**, 257–9.
Jones, P. J. (1966) in *Physico-Chimie du Protactinium* (eds. G. Bouissières and R. Muxart), Centre National de la Recherch Scientifique, Orsay, Paris, 2–8 July 1965, pp. 93–8.
Judd, B. R. (1962) *Phys. Rev.*, **125**, 613–25.
Jung, B., Seaborg, G. T., and Edelstein, N. M. (1993) in *205th American Chemical Society National Meeting*, 28 March–2 April, 1993, Denver, CO.
Kahn, S. and Hawkinson, D. E. (1956) *J. Inorg. Nucl. Chem.*, **3**, 155–6.
Kaltsoyannis, N. and Bursten, B. E. (1995) *Inorg. Chem.*, **34**, 2735–44.
Kaltsoyannis, N. (1998) *J. Alloys Comp.*, **271–273**, 859–62.

Kandil, A. T. and Ramadan, A. (1978) *Radiochim. Acta*, **25**, 107–9.
Kandil, A. T., Abdel Gawad, A. S., and Ramadan, A. (1980) *Radiochim. Acta*, **27**, 39–42.
Katz, J. J. and Seaborg, G. T. (1957) *The Chemistry of the Actinide Elements*, Methuen, London, pp. 67–93.
Katzin, L. I., Van Winkle, Q., and Sedlet, J. (1950) *J. Am. Chem. Soc.*, **72**, 4815–7.
Katzin, L. I. (ed.) (1952) *Production and Separation of* ^{233}U, U.S. Report TID-5223.
Katzin, L. I. and Stoughton, R. W. (1956) *J. Inorg. Nucl. Chem.*, **3**, 229–32.
Katzin, L. I. (1958) USA Patent 2847273, August 12, 1958. *Cit Nucl. Sci. Abstr. 13*. 1007, 1959.
Kaufman, A., Ku, T. L., and Luo, S. D. (1995) *Chem. Geol.*, **120**, 175–81.
Kazakevich, M. Z., Mikheev, N. B., Kulyukhin, S.A., and Rumer, I.A. (1993) *Radiokhimiya*, **5**, 28–30.
Keller, C. (1963) *Radiochim. Acta*, **1**, 147–56.
Keller, C. (1964a) *J. Inorg. Nucl. Chem.*, **26**, 2069–74.
Keller, C. (1964b) German Report KFK 225.
Keller, C. (1965a) *J. Inorg. Nucl. Chem.*, **27**, 321–7.
Keller, C. (1965b) *J. Inorg. Nucl. Chem.*, **27**, 797–800.
Keller, C. (1965c) *J. Inorg. Nucl. Chem.*, **27**, 1233–46.
Keller, C. and Walter, K. H. (1965) *J. Inorg. Nucl. Chem.*, **27**, 1253–60.
Keller, C., Koch, L., and Walter, K. H. (1965) *J. Inorg. Nucl. Chem.,* **27**, 1225–32.
Keller, C. (1966a) *Angew. Chem.*, **5**, 23–35.
Keller, C. (1966b) in *Physico-Chimie du Protactinium* (eds. G. Bouissières and R. Muxart), Centre National de la Recherche Scientifique, Orsay, Paris, 2–8 July 1965, pp. 71–9.
Keller, C. (1971) in *Tagungsber 3 Int. Pa-Konf*. (ed. H.-J. Born). Schloss-Elmau, 15–18 April 1969, German Report BMBW-FBK 71–17, Paper No. 8.
Keller, C. (1977) in *Gmelin Handbuch der Anorganischen Chemie – Protactinium, Suppl.,* vol. 2, Springer-Berlag, Berlin, pp. 6–34.
Keys, J. D. (1951) Thesis. McGill University.
Khiebnikov, V. P., D'yachkova, R. A., and Spitsyn, V. I. (1966) *Radiokhimiya*, **8**, 119–24.
Kirby, H. W. (1959) *The Radiochemistry of Protactinium*, U.S. Report NAS-NS-3016, p. 440.
Kirby, H. W. (1961) *J. Inorg. Nucl. Chem.*, **18**, 8–12.
Kirby, H. W. (1966) *Physico-Chimie du Protactinium* (eds. G. Bouissières and R. Muxart), Centre National de la Recherche Scientifique, Orsay, Paris, 2–8 July 1965, pp. 283–91.
Kirby, H. W. and Figgins, P. E. (1966) in *Physico-Chimie du Protactinium* (eds. G. Bouissières and R. Muxart), Centre National de la Recherche Scientifique, Orsay, Paris, 2–8 July 1965, pp. 275–81.
Kirby, H. W. (1974) U.S. Report MLM-2111.
Kleinschmidt, P. D., Ward, J. W., and Haire, R. G. (1983) in *Proc. Symp. High Temp. Materials Chem. II* (eds. D. Cubiciotti and Z. A. Munir), Electrochemical Society, Pennington, NJ, pp. 23–31.
Kleinschmidt, P. D. and Ward, J. W. (1986) *J. Less Common Metals*, **121**, 121.
Kluge, E. and Lieser, K. H. (1980) *Radiochim. Acta*, **27**, 161–70.
Ko, R. (1956) *Nucleonics*, **14**, 74.
Ko, R. (1957) *Nucleonics*, **15**, 72.

Kolarich, R. T., Ryan, V. A., and Schuman, R. P. (1967) *J. Inorg. Nucl. Chem.*, **29**, 783–97.
Kot, W. K. and Edelstein, N. M. (1995) *New J. Chem.*, **19**, 641–54.
Kraus, K. A. and Moore, G. E. (1950) *J. Am. Chem. Soc.*, **72**, 4293–4.
Kraus, K. A. and Moore, G. E. (1951) *J. Am. Chem. Soc.*, **73**, 2900–2.
Kraus, K. A. and Van Winkle, Q. (1952) U.S. Report TID-5223, pp. 259–71.
Kraus, K. A. and Moore, G. E. (1955) *J. Am. Chem. Soc.*, **77**, 1383.
Kraus, K. A., Moore, G. E., and Nelson, F. (1956) *J. Am. Chem. Soc.*, **78**, 2692–5.
Kulmala, S., Hakanen, M., and Lindgerg, A. (1998) *Radiokhimiya*, **40**, 519–21.
Kulyukhin, S. A., Kamenskaya, A. N., Mikheev, N. B., and Rumer, I. A. (1996) in *Fourth Conf.: Nucl. & Radiochem. C-P21*, 8–13 September, St. Malo, France.
Kulyukhin, S. A., Kamenskaya, A. N., Mikheev, N. B., Rumer, I. A., Novichenko, V. L., and Kazakevich, M. Z. (1997) *Radiokhimiya*, **39**, 501–3.
Kulyukhin, S. A. and Mikheev, N. B. (1998) *Radiokhimiya*, **40**, 296–8.
Kuppers, G. and Erdtmann, G. L. (1992) *J. Radioanal. Nucl. Chem. Articles*, **160**, 425–34.
Kurodo, R. and Ishida, V. (1965) *J. Chromatogr.*, **18**, 438–40.
Lange, R. C. and Hagee, G. R. (1968) *Nucl. Phys. A*, **124**, 412–28.
Lapitskii, A. V. and Galateanu, I. (1963) *Radiokhimiya*, **5**, 298–302.
Lapitskii, A. V., Rudenko, N. P., and Saed A. Gavad (1965) *Radiokhimiya*, **7**, 139.
Lapitskii, A. V., Rudenko, N. P., and Saed, A. Gavad (1966) in *Physico-Chimie du Protactinium* (eds. G. Bouissières and R. Muxart), Centre National de la Recherche Scientifique, Orsay, Paris, 2–8 July 1965, p. 249.
Larson, R. G., Katzin, L. I., and Hausman, E. (1952) U.S. Report TID-5223, pp. 272–5.
Launay, J. and Dolechek, R.L. (1947) *Phys. Rev.*, **72**, 141.
Laurens, W., Ten Brink, B. O., and Wapstra, A. H. (1970) *Nucl. Phys. A*, **152**, 463–80.
Leang, C. F. (1970) *J. Phys.*, **31**, 269–76.
Lebedev, I. A., Pirozhkov, S. V., Semochkin, V. M., and Yakovlev, G. N. (1961) *Radiokhimiya*, **3**, 258–60.
Le Cloarec, M.-F., Kovacevic, S., and Muxart, R. (1970) *Rev. Chim. Miner.*, **7**, 735–45.
Le Cloarec, M.-F. and Muxart, R. (1971) in *Tagungsber. 3 Int. Pa-Konf.* (ed. H.-J. Born), Schloss-Elmau, German Report BMBW-FBK 71–17, 15–18 April 1969, Paper No. 11.
Le Cloarec, M. F. and Muxart, R. (1973) *Radiochim. Acta*, **20**, 7–10.
Le Cloarec, M. F., Guillaumont, R., deMiranda, C. F., and Franck, J. C. (1973) *Radiochim. Acta*, **20**, 1–6.
Le Cloarec, M.-F. (1974) Thesis, University of Paris.
Le Cloarec, M.-F., Dartyge, J. M., Kovacevic, S., and Muxart, R. (1976) *J. Inorg. Nucl. Chem.*, **38**, 737–9.
Lederer, C. M. and Shirley, V. S. (eds) (1978) *Table of Isotopes*, 7th edn, Wiley, New York.
Lee, J. A. and Marples, J. A. C. (1973) in *Comprehensive Inorganic Chemistry*, vol. 5 (eds. J. C. Bailar Jr, H. J. Emeleus, R. Nyholm, and A. F. Trotman-Dickenson), Pergamon, Oxford, pp. 5–73.
Le Naour, C., Trubert, D., and Jaussaud, C. (2003) *J. Solution Chem.*, **32**, 489–504.
Liljenzin, J. O. and Rydberg, J. (1966) in *Physico-Chimie du Protactinium* (eds. G. Bouissières and R. Muxart). Centre National de la Recherche Scientifique. Orsay, Paris, 2–8 July 1965, pp. 255–72.
Liljenzin, J. O. (1970) *Acta Chem. Scand.*, **24**, 1655–61.

Li, Z., Pan, Q., Guo, J., Yuan, S., Fang, K., and Yang, W. (1998) *Nucl. Technol.*, **21**, 7–10.
Lorenz, R., Scherff, H. L., and Toussaint, N. (1969) *J. Inorg. Nucl. Chem.*, **31**, 2381–90.
Lundqvist, R. (1974a) *Acta Chem. Scand. A*, **28**, 243–7.
Lundqvist, R. (1974b) *Acta Chem. Scand. A*, **28**, 358–61.
Lundqvist, R. (1974c) in *Int. Solvent Extr. Conf.*, Lyon, 8–14 September, Paper No. 143.
Lundqvist, R. (1974d) Thesis. Chalmers University of Technology and University of Gothenburg, Sweden.
Lundqvist, R. and Andersson, J. E. (1974) *Acta Chem. Scand. A*, **28**, 700–2.
Lundqvist, R. and Rydberg, J. (1974) *Acta Chem. Scand. A*, **28**, 399–406.
Lundqvist, R. (1975) *Acta Chem. Scand. A*, **29**, 231–5.
Lux, F., Ammentorp-Schmidt, F., Dempf, D., Graw, D., and Hagenberg, W. (1970) *Radiochim. Acta*, **14**, 57–61.
Lux, F., Brown, D., Dempf, D., Fischer, R. D., and Hagenberg, W. (1971) in *Tagungsber. 3 Int. Pa-Konf.* (ed. H.-J. Born), Schloss-Elmau, 15–18 April 1969, German Report BMBW-FBK 71–17, Paper No. 23.
Lux, F., Beck, O. F., Kraus, H., Brown, D., and Tso, C. (1980) *Z. Naturforsch. B. Anorg. Chem. Org. Chem. B*, **35**, 564–7.
Maddock, A. G. and Miles, G. L. (1949) *J. Chem. Soc. Suppl.*, **2**, 253–6.
Maddock, A. G. and Pugh, W. (1956) *J. Inorg. Nucl. Chem.*, **2**, 114–17.
Maddock, A. G. (1960) Unpublished observations cited by Brown (1969).
Maddock, A. G. and Pires de Matos, A. (1972) *Radiochim. Acta*, **18**, 71–4.
Maghrawy, H. B., Marie, S. A., and Ayoub, E. J. (1988) *J. Radioanal. Nucl. Chem. Lett.*, **121**, 429–40.
Maghrawy, H. B., Aly, H. F., and El-Reefy, S. A. (1989) *Radiochim. Acta*, **46**, 127–30.
Maillet, C. P. (1982) *J. Phys. Chem. C*, **15**, 6371–8.
Malm, J. G. and Fried, S. (1950) U.S. Report ANL-4490, pp. 53–5.
Malm, J. G. and Fried, S. (1959) U.S. Patent 2 893 825.
Manier, M., Carlier, R., and Genet, M. (1969) *Radiochem. Radioanal. Lett.*, **2**, 133–8.
Manier, M. (1970) French Report NP-18348.
Manier, M. and Genet, M. (1970) *Rev. Chim. Miner.*, **7**, 1087–100.
Marples, J. A. C. (1965) *Acta Crystallogr.*, **18**, 815.
Marples, J. A. C. (1966) in *Physico-Chimie du Protactinium* (eds. G. Bouissières and R. Muxart), Centre National de la Recherche Scientifique, Orsay, Paris, 2–8 July 1965, pp. 39–43.
Marquardt, C. M., Panak, P. J., Apostolidis, C., Morgenstern, A., Walther, C., Klenze, R., and Fanghänel, Th. (2004) *Radiochim. Acta*, **92**, 445–447.
Marrus, R., Nierenberg, W. A., and Winocur, J. (1961) *Nucl. Phys.*, **23**, 90–106.
McCormac, J. J., Cripps, F. H., and Wiblin, W. A. (1960) *Anal. Chim. Acta*, **22**, 408.
McCoy, J. D. (1964) *Soc. Sci. Fenn. Commentat. Phys. Math.*, **30**, 1–37.
McIsaac, L. D. and Freinling, E. C. (1956) *Nucleonics*, **14**, 10–65.
McKay, H. A. C. (1971) *Principles of Radiochemistry*, CRC Press, Cleveland, Ohio, p. 232.
Meinke, W. W. (1946) U.S. Report AECD-2738.
Meinke, W. W., Ghiorso, A., and Seaborg, G. T. (1949) *Phys. Rev.*, **75**, 314–5.
Meinke, W. W. and Seaborg, G. T. (1950) *Phys. Rev.*, **78**, 475.
Meinke, W. W., Ghiorso, A., and Seaborg, G. T. (1951) *Phys. Rev.*, **81**, 782–98.

Meinke, W. W. (1952) *J. Chem. Phys.*, **20**, 754.
Meinke, W. W., Ghiorso, A., and Seaborg, G. T. (1952) *Phys. Rev.*, **85**, 429–31.
Meinke, W. W., Wick, G. C., and Seaborg, G. T. (1956) *J. Inorg. Nucl. Chem.*, **3**, 69–92.
Meitner, L., Strassmann, F., and Hahn, O. (1938) *Z. Phys.*, **109**, 538–52.
Mendeleev, D. I. (1872) *Ann. Chem. Pharm. Suppl.*, **8**, 133–229.
Merinis, J., Legoux, Y., and Bouissières, G. (1966) in *Physico-Chimie du Protactinium* (eds. G. Bouissières and R. Muxart), Centre National de la Recherche Scientifique, Orsay, Paris, 2–8 July 1965, pp. 307–14.
Mikhailov, V. A. (1960) *Radiokhimiya*, **1**, 188–94.
Mikheev, N. B., Kulyukhin, S. A., and Konovalova, N. A. (1992) *Radiokhimiya*, **3**, 23–6.
Mikheev, N. B., Kamenskaya, A. N., Kulyukhin, S. A., and Rumer, I. A. (1993a) *Mendeleev Comm.*, 198.
Mikheev, N. B., Kamenskaya, A. N., Rumer, I. A., Kulyukhin, S. A., and Auerman, L. N. (1993b) *Radiokhimiya*, **5**, 24–6.
Miranda, C. F. and Muxart, R. (1964a) *Bull. Soc. Chim. France*, 387.
Miranda, C. F. and Muxart, R. (1964b) *Bull. Soc. Chim. France*, 2174.
Mitsubishi Materials, Corporation (1995) Japan Patent. B01J-020/10, G21F-009/10.
Mitsuji, T. (1967a) *Bull. Chem. Soc. Japan*, **40**, 2091–5.
Mitsuji, T. (1967b) *Bull. Chem. Soc. Japan*, **40**, 2822–5.
Mitsuji, T. and Suzuki, S. (1967) *Bull. Chem. Soc. Japan*, **40**, 821–6.
Mitsuji, T. (1968) *Bull. Chem. Soc. Japan*, **41**, 115–19.
Monroy-Guzman, F., Constantinescu, O., Hussonnois, M., Kim, J. B., Brillard, L., and Trubert, D. (1996) *J. Radioanal. Nucl. Chem. Lett.*, **208**, 461–6.
Monroy-Guzman, F., Trubert, D., Brillard, L., Hussonnois, M., and Le Naour, C. (1997) *Quimica Anal.*, **16**, 43–7.
Moore, F. L. (1955) *Anal. Chem.*, **27**, 70–2.
Moore, F. L. (1956) *Anal. Chem.*, **28**, 997.
Moore, F. L. and Reynolds, S. A. (1957) *Anal. Chem.*, **29**, 1596.
Moore, F. L., Fairman, W. D., Ganchoff, J. G., and Surac, J. G. (1959) *Anal. Chem.*, **31**, 1148.
Moore, F. S. (1960) U.S. Report NAS-NS 3101.
Moore, J. G. and Rainey, R. H. (1964) in *Proc. Protactinium Chem. Symp.*, Gatlinburg, Tenn., 25–26 April 1963, U.S. Report TID-7675, pp. 16–34.
Moore, F. L. and Thern, G. G. (1974) *Radiochem. Radioanal. Lett.*, **19**, 117–25.
Morgan, J. and Beetham, C. (1990) Report No.: NSS/R-220, ANS-2358-R4.
Mortimer, M. J. (1979) *J. Phys. Colloq.*, **4**, 124–9.
Moskvin, A. I., Galateanu, I., and Lapitskii, A. V. (1963) *Dokl. Akad. Nauk. SSSR*, **149**, 264–6.
Murbach, E. W. (1957) U.S. Report NAA-SR-1988.
Musikas, C. (1966) French Report CEA-R-3023.
Muxart, R. and Arapaki-Strapelias, H. (1963) *Bull. Soc. Chim.*, 888–91.
Muxart, R., Guillaumont, R., and Vernois, J. (1966a) *Compt. Rend. Acad. Sci. Paris C*, **262**, 888–9.
Muxart, R., Guillaumont, R., and Arapaki-Strapelias, H. (1966b) *Physico-Chimie du Protactinium* (eds. G. Bouissières and R. Muxart), Centre National de la Recherche Scientifique, Orsay, Paris, 2–8 July 1965, pp. 225–38.

Muxart, R., Guillaumont, R., and Bouissières, G. (1969) *Actinides Rev.*, **1**, 223–74.
Muxart, R. and Guillaumont, R. (1974) *Complements au Noueveau Traite de Chimie Minerale* (eds. A. Pacault and G. Pannetier), Masson, Paris, p. 2.
Myasoedov, B. F. and Muxart, R. (1962a) *J. Anal. Chem. (USSR)*, **17**, 340–2.
Myasoedov, B. F. and Muxart, R. (1962b) *Bull. Soc. Chim. France*, 237–9.
Myasoedov, B. F. and Pal'shin, E. S. (1963) *Zhurn. Anal. Khim.*, **18**, 596–602.
Myasoedov, B. F., Pal'shin, E. S., and Paley, P. N. (1964) *Zhurn. Anal. Khim.*, **19**, 105–10.
Myasoedov, B. F., Pal'shin, E. S., and Molochnikova, N. P. (1966a) *Zhurn. Anal. Khim.*, **21**, 599–606.
Myasoedov, B. F., deMiranda, C. F., and Muxart, R. (1966b) *Zhurn. Anal. Khim.*, **21**, 946–50.
Myasoedov, B. F. and Molochnikova, N. P. (1968) *Zhurn. Anal. Khim.*, **23**, 681.
Myasoedov, B. F., Pal'shin, E. S., and Molochnikova, N. P. (1968a) *Zhurn. Anal. Khim.*, **23**, 66–71.
Myasoedov, B. F., Pal'shin, E. S., and Molochnikova, N. P. (1968b) *Zhurn. Anal. Khim.*, **23**, 786–7.
Myasoedov, B. F., Pal'shin, E. S., and Molochnikova, N. P. (1968c) *Zhurn. Anal. Khim.*, **23**, 1312–17.
Myasoedov, B. F., Eliseeva, O. P., and Sawwin, S. B. (1969) *J. Radioanal. Chem.,* **2**, 369–76.
Myasoedov, B. F., Davydov, A. V., and Nekrasova, V. V. (1978) *Radiokhimiya*, **6**, 851–8.
Myasoedov, B. F., Karalova, Z. K., Nekrasova, V. V., and Rodionova, I. M. (1980) *J. Inorg. Nucl. Chem.*, **42**, 1495–9.
Nairn, J. S., Collins, D. A., McKay, H. A. C., and Maddock, A. G. (1958) in *Proc. 2nd UN Int. Conf. on Peaceful Uses of Atomic Energy*, 1–13 September 1958, Geneva, vol. 17, pp. 216–35.
Nekrasova, V. V., Pal'shin, E. S., and Myasoedov, B. F. (1975a) *Zh. Anal. Khim.*, **30**, 1122–6.
Nekrasova, V. V., Pal'shin, E. S., and Myasoedov, B. F. (1975b) *Zh. Anal. Khim.*, **30**, 2267–9.
Nikolaev, A. V., Kurnakova, A. G., and Rumyantseva, Z. G. (1959) *Zhurn. Neorg. Khim.*, **4**, 1682.
Nishina, Y., Yasaki, T., Kimura, K., and Ikawa, M. (1938) *Nature*, **142**, 874.
Nishinaka, I., Nagame, Y., Tsukada, K., Ikezoe, H., Sueki, K., Nakahara, H., Tanikawa, M., and Ohtsuki, T. (1997) *Phys. Rev. C*, **56**, 891–9.
Nowikow, J. and Pfrepper, G. (1963) *Z. Naturforsch. B*, **18**, 993–1001.
Oak Ridge National Laboratory (1964) in *Proc. Protactinium. Chem. Symp.*, Gatlinburg, Tenn., 25–26 April 1963. U.S. Report T1D 7675.
O'Donnell, T. A., Waugh, A. B., and Randall, C. H. (1977) *J. Inorg. Nucl. Chem.*, **39**, 1597–600.
Overman, R. T. and Clark, H. M. (1960) *Radioisotope Techniques*, McGraw-Hill, New York, pp. 326–9.
Pal'shin, E. S., Myasoedov, B. F., and Palei, P.N. (1962) *Zhurn. Anal. Khim.*, **17**, 471.
Pal'shin, E. S. and Myasoedov, B. F. (1963) *Zhurn. Anal. Khim.*, **18**, 750
Pal'shin, E. S., Myasoedov, B. F., and Novikov, Yu. P. (1963) *Zhurn. Anal. Chim.*, **18**, 657.

Pal'shin, E. S., Myasoedov, B. F., and Novikov, Yu. P. (1966) *Zhurn. Anal. Khim.*, **21**, 851–6.
Pal'shin, E. S., Myasoedov, B. F., and Ivanova, L. A. (1968a) *Zhurn. Anal. Khim.*, **23**, 758–61.
Pal'shin, E. S., Myasoedov, B. F., and Davydov, A. V. (1968b) *Analytical Chemistry of Protactinium* (ed. A. P. Vinogradov), Nauka, Moscow, pp. 16–19 (in Russian).
Pal'shin, E. S., Myasoedov, B. F., and Davydov, A. V. (1970) *Analytical Chemistry of Protactinium*, Ann Arbor-Humphrey, Ann Arbor.
Pal'shin, E. S., Davydov, A. V., Palei, P. N., and Ivanova, L. A. (1971) in *Tagungsher. 3 Int. Pa-Konf.* (ed. H.-J. Born), Schloss-Elmau, 15–18 April 1969, German Report BMBW-FBK 71–17.
Pathak, P. N., Manchnda, V. K., Ruikar, P. B., and Veeraraghavan, R. (1999a) *Radiochim. Acta*, **86**, 129–34.
Pathak, P. N., Manchnda, V. K., Purushotham, D. S. C., Rama Rao, G. A., Manohar, S. B., and Reddy, A. V. R. (1999b) in *Conference: NUCAR 99: Nuclear and Radiochemistry Symposium*, Mumbai, India.
Paulus, W., Kratz, J. V., Strub, E., Zauner, S., Bruchle, W., Pershina, V., Schädel, M., Schausten, B., Adams, J. L., Gregorich, K. E., Hoffman, D. C., Lane, M. R., Laue, C., Lee, D. M., McGrath, C. A., Shaughnessy, D. K., Strellis, D.A., and Sylwester, E. R. (1998) *J. Alloys Comp.*, **271**, 292–5.
Paulus, W., Kratz, J. V., Strub, E., Zauner, S., Bruchle, W., Pershina, V., Schädel, M., Schausten, B., Adams, J. L., Gregorich, K. E., Hoffman, D. C., Lane, M. R., Laue, C., Lee, D. M., McGrath, C. A., Shaughnessy, D. K., Strellis, D. A., and Sylwester, E. R. (1999) *Radiochim. Acta*, **84**, 69–77.
Peppard, D. F., Mason, G. W., Grayand, P. R., and Mech, J. F. (1952) *J. Am. Chem. Soc.*, **74**, 6081–4.
Peppard, D. F., Mason, G. W., and Gergel, M. V. (1957) *J. Inorg. Nucl. Chem.*, **3**, 370–8.
Perlman, M. N. and Weisman, S. J. (1951) USA Patent 2558377, June 26, 1951.
Pershina, V., Fricke, B., Kratz, J. V., and Ionova, G. V. (1994) *Radiochim. Acta*, **64**, 37–48.
Piccard, A. (1917) *Arch. Sci. Phys. Naturelles*, **44**, 161–4.
Pickett, D. A., Williams, R. W., and Murrell, M. T. (1994) *Anal. Chem.*, **66**, 1044–9.
Pickett, D. A. and Murrell, M. T. (1997) *Earth Planet. Sci. Lett.*, **148**, 259–71.
Piehler, D., Kot, W. K., and Edelstein, N. (1991) *J. Chem. Phys.*, **94**, 942–8.
Pierce, W. E. and Grosse, A. (1935) *Phys. Rev.*, **47**, 532.
Pissot, A. M., Muxart, R., and Miranda, C. F. (1966) *Bull. Soc. Chim. France*, 1757.
Plaisance, M. L. and Guillaumont, R. (1969) *Radiochim. Acta*, **12**, 32–7.
Poskanzer, A. M. and Foreman, B. M. (1961a) *Atomnaya Tekhnika za Rubezhom*, **8**, 33.
Poskanzer, A. M. and Foreman, B. M. (1961b) *J. Inorg. Nucl. Chem.*, **16**, 323.
Rajaram, M. and Scott, C. E. (2000) U.S. Patent C03C-013/04. 2000-6136736-A.
Raje, N., Swain, K. K., Kumar, S. R., Parthasarathy, R., and Mathur, P. K. (2001) *J. Radioanal. Nucl. Chem. Lett.*, **247**, 115–20.
Rebizant, J., Spirlet, J. C., Friedt, J. M., Poinsot, R., and Kalvius, G. M. (1979) *J. Phys. Colloq.*, **4**, 133.
Reddy, A. S. and Reddy, S. K. (1977) *Sep. Sci.*, **12**, 661–4.
Reddy, A. S., Ramakrishna, V. V., and Patel, S. K. (1977) *Radiochem. Radioanal. Lett.*, **28**, 445–52.

Reymond, F. (1931) *J. Chim. Phys.*, **28**, 409–10.
Richards, E. W. T. and Atherton, N. J. (1961) Atomic Energy Research Establishment (Great Britain). Report AERE-R-3851.
Richards, E. W. T., Ridgeliy, A., Atherton, N. J., and Wise, H. S. (1961) *Nature*, **192**, 4444.
Richards, E. W. T. and Atherton, N. J. (1963) *Spectrochim. Acta*, **19**, 971–87.
Richards, E. W. T., Stephen, J., and Wise, H. S. (1968) *Spectrochim. Acta B*, **23**, 635–42.
Robert, J., deMiranda, C. F., and Muxart, R. (1969) *Radiochim. Acta*, **11**, 104–7.
Roberts, L. E. J. and Walter, A. J. (1966) in *Physico-Chimie du Protactinium* (eds. G. Bouissières and R. Muxart), Centre National de la Recherche Scientifique, Orsay, Paris, 2–8 July 1965, pp. 51–9.
Rona, E., Muse, L., and Brandau, B. L. (1966) in *Physico-Chimie du Protactinium* (eds. G. Bouissières and R. Muxart), Centre National de la Recherche Scientifique, Orsay, Paris, 2–8 July 1965, p. 333.
Roshalt, J. N., Emiliani, C., Geise, J., Koczy, F. F., and Wangersky, P. J. (1961) *J. Geol.*, **69**, 162–85.
Roshalt, J. N., Emiliani, C., Geiss, J., Koczy, F. F., and Wangersky, P. J. (1962) *J. Geophys. Res.*, **67**, 2907–11.
Rossotti, F. J. C. and Rossotti, H. (1961) *The Determination of Stability Constants and Other Equilibrium Constants in Solution*, McGraw-Hill, New York.
Rudenko, N. P., Saed A. Gavad, and Lapitskii, A. V. (1965) *Radiokhimiya*, **7**, 32.
Russell, A. S. (1913) *Chem. News*, **107**, 49–52.
Sackett, W. M. (1960) *Science*, **132**, 1761–2.
Saiki, M., Nestasi, M. J. C., and Lima, F. W. (1981) *J. Radioanal. Chem.*, **64**, 83–116.
Sakanoue, M., Oosawa, M., Sakai, T., and Ishida, K. J. (1964) *J. At. Energy Soc. Japan*, **6**, 503.
Sakanoue, M., Takagi, E., Abe, M., and Oosawa, M. (1965) *J. At. Energy Soc. Japan*, **7**, 404.
Sakanoue, M. and Abe, M. (1967) *Radioisotopes*, **16**, 645–51.
Sakanoue, M., Konishi, K., and Komura, K. (1967) Paper SM–87/28, in *Symp. on Radioactive Dating and Methods of Low-Level Counting. Monaco*, 2–10 March 1967, IAEA Report STI/PUB/152, Vienna.
Sales Grande, M. R. (1950) *Rev. Quim. Appl.*, **1**, 184.
Salutsky, M. L., Shaver, K., Elmlinger, A., and Curtis, M. L. (1956) *J. Inorg. Nucl. Chem.*, **3**, 995–8.
Salutsky, M. L., Curtis, M. L., Shaver, K., Elmlinger, A., and Miller, R. A. (1957) *Anal. Chem.*, **29**, 373.
Salutsky, M. L. (1962) *Comprehensive Analytical Chemistry* (eds. C. L. Wilson and D. W. Wilson), EIsevier, Amsterdam, pp. 570–80.
Scherer, V., Weigel, F., and Van Ghemen, M. (1967) *Inorg. Nucl. Chem. Lett.*, **3**, 589–95.
Scherff, H.-L. and Hermann, G. (1964) *Radiochim. Acta*, **2**, 141–6.
Scherff, H.-L. and Hermann, G. (1966) *Radiochim. Acta*, **6**, 53–61.
Schüler, H. and Gollnow, H. (1934) *Naturwissenschaften*, **22**, 511.
Schulz, W. W. (1972) U.S. Report ARH-2420.
Schuman, R. P. and Tromp, R. L. (1959) U.S. Report IDO-16571.
Schwarcz, H. P., Simpson, J. J., and Stringer, C. B. (1998) *J. Human Evol.*, **35**, 635–45.
Schwochau, V. and Astheimer, L. (1970) *J. Inorg. Nucl. Chem.*, **32**, 119–26.

Sedlet, J. (1964) *Treatise on Analytical Chemistry*, part II, vol. 6 (eds. I. M. Kolthof, T. P. J. Elving, and E. B. Sandell), Wiley, New York, pp. 435–610.
Seelmann-Eggebert, M., Keller, C., and Zundel, G. (1961) Kernforschungszentrum Karlsruhe, Report KFK-41.
Segrè, E. (1952) *Phys. Rev.*, **86**, 21–8.
Sellers, P. A., Fried, S., Elson, R. F., and Zachariasen, W. H. (1954) *J. Am. Chem. Soc.*, **76**, 5935–8.
Shankar, J., Venkateswarlu, K. S., and Gopinathan, C. (1963) *J. Inorg. Nucl. Chem.*, **25**, 57–66.
Shevchenko, V. B., Mikhailov, V. A., and Zavalsky, Yu. P. (1958a) *Sov. J. Inorg. Chem.*, **3**, 1955.
Shevchenko, V. B., Zolotulcha, S. I., Kascheyev, N. F., Tsaryov, S. A., Mikhailov, V. A., and Toropchenova, G. A. (1958b) in *Proc. 2nd UN Int. Conf. on Peaceful Uses of Atomic Energy*, vol. 4, 1–13 September 1958, Geneva, pp. 40–3.
Shimojima, H. and Takagi, J. (1964) *J. Inorg. Nucl. Chem.*, **26**, 253.
Shiokawa, T., Kikuchi, M., and Omori, T. (1969) *Inorg. Nucl. Chem. Lett.*, **5**, 105–9.
Silvestre, J. P., Le Cloarec, M.-F., and Cazaussus, A. (1977) *Radiochem. Radioanal. Lett.*, **31**, 367–71.
Sime, R. L. (1997) Abstracts of Papers of the American Chemical Society **213**, 15.
Simpson, F. B., Burgus, W. H., Evans, J. E., and Kirby, H. W. (1962) *Nucl. Sci. Eng.*, **12**, 243–9.
Smith, G. and Barnett, G. A. (1965) *J. Inorg. Nucl. Chem.*, **27**, 975.
Smith, J. L., Spirlet, J. C., and Mueller, W. (1979) *Science*, **151**, 188–90.
Smith, R. R., Alloy, H. P., Lewis, R. H., and Does, A. V. (1956) *Phys. Rev.*, **101**, 1053.
Soddy, F. (1913a) *Chem. News*, **107**, 97–9.
Soddy, F. (1913b) *Nature*, **91**, 634–5.
Soddy, F. and Cranston, J. A. (1918) *Proc. R. Soc. A*, **94**, 384–404.
Soderling, P. and Eriksson, O. (1997) *Phys. Rev. B*, **56**, 10719–21.
Solar, J. P., Burghard, H. P. G., Banks, R. H., Streitwieser, A., and Brown, D. (1980) *Inorg. Chem.*, **19**, 2186–8.
Sotobayashi, T., Suzuki, T., and Kudo, H. (1977) *J. Radioanal. Chem.*, **36**, 145–52.
Souka, N., Shabana, R., and Hafey, F. (1975a) *Radiochim, Acta*, **22**, 45–8.
Souka, N., Shabana, R., and Hafey, F. (1975b) *J. Radioanal. Chem.*, **27**, 401–10.
Souka, N., Abdel- Gawad, A. S., Shabana, R., and Farah, K. (1975c) *Radiochim, Acta*, **22**, 180–2.
Souka, N., Shabana, R., and Farah, K. (1976a) *J. Radioanal. Chem.*, **33**, 215–22.
Souka, N., Shabana, R., and Girgis, C. (1976b) *Isotopenpraxis*, **12**, 164–6.
Spirlet, J. C. (1979) *J. Phys. Colloq.*, **40**, 87–94.
Spirlet, J. C. (1982) *Actinides in Perspective* (ed. N. Edelstein), Pergamon Press, Oxford, pp. 361–80.
Spitsyn, V. I. and D'yachkova, R. A. (1960) *Dokl. Akad. Nauk. SSSR*, **134**, 1111.
Spitsyn, V. I. and Golutvina, M. M. (1960) *Atomnaya Energiya*, **8**, 117.
Spitsyn, V. I., D'yachkova, R. A., and Khlebnikov, V. P. (1964) *Dokl. Akad. Nauk. SSSR*, **157**, 677–80.
Spitsyn, V. I., D'yachkova, R. A., and Kamenskaya, A. N. (1969) *Dokl. Akad. Nauk. SSSR*, **184**, 35–7.
Stanik, I. E. and Il'menkova, L. I. (1963) *Radiokhimiya*, **5**, 209–15.

Stchouzkoy, T. and Muxart, R. (1962) *Bull. Soc. Chim. France*, 2176.
Stchouzkoy, T., Pezeral, H., Bouissières, G., and Muxart, R. (1964) *Compt. Rend. Acad. Sci. Paris*, **259**, 3016–18.
Stchouzkoy, T., Muxart, R., and Bouissières, G. (1966a) *Compt. Rend. Acad. Sci. Paris C*, **262**, 1845–7.
Stchouzkoy, T., Pezerat, H., and Muxart, R. (1966b) in *Physico-Chimie du Protactinium* (eds. G. Bouissières and R. Muxart), Centre National de la Recherche Scientifique, Orsay, Paris, 2–8 July 1965, pp. 61–77.
Stchouzkoy, T., Muxart, R., Pezerat, H., and Dhers, J. (1968) *Rev. Chim. Miner.*, **5**, 1085–101.
Stchouzkoy, T., Muxart, R., and Guillaumont, R. (1969) *Rev. Chim. Miner.*, **6**, 411–25.
Stein, L. (1964) *Inorg. Chem.*, **3**, 995–8.
Stein, L. (1966) in *Physico-Chimie du Protactinium* (eds. G. Bouissières and R. Muxart), Centre National de la Recherche Scienlifique, Orsay, Paris, 2–8 July 1965, pp. 101–6.
Stewart, G. R., Smith, J. L., Spirlet, J. C., and Mueller, W. (1980) in *Superconductivity in d- and f-band Metals (Proc. Conf.) 1979* (eds. H. Subl and M. B. Maple), Academic Press, New York, pp. 65–70.
Stricos, D. P. (1966) Kholes At. Power Lab. KAPL-M-6554. Contract W-31–109-eng. 52.
Stronski, I. and Zelinski, A. (1964) *Nucleonica*, **9**, 801.
Subrahmanyam, V. B. (1963) U.S. Report UCRL-11082.
Suner, A., La Gamma de Bastioni, A. M., and Botbol, J. (1974) in Preparasion de Microcuries de ^{234}Th, Argentine Report CNEA 380.
Sung-Ching-Yang, G. Y., Druin, V. A., and Trofimov, A. S. (1972) *Sov. J. Nucl Phys.*, **14**, 725–6.
Suzuki, S. and Inoue, Y. (1966) *Bull. Chem. Soc. Japan*, **39**, 1705–15.
Suzuki, S. and Inoue, Y. (1969) *Bull. Chem. Soc. Japan*, **42**, 1916–21.
Svantesson, J., Hagstrom, I., Persson, G., and Liljenzin, G. (1979) *J. Inorg. Nucl. Chem.*, **41**, 383–9.
Takagi, J. and Shimojima, H. (1965) *J. Inorg. Nucl. Chem.*, **27**, 405–9.
Takahashi, K. and Morinaga, H. (1960) *Nucl. Phys.*, **15**, 664–77.
Tamhina, B., Gojnierac, A., and Herak, M. J. (1976) *Microchim. Acta*, **2**, 569–78.
Tamhina, B., Gojnierac, A., and Herak, M. J. (1978) *J. Inorg. Nucl. Chem.*, **40**, 335–8.
Taylor, S. R. (1964) *Geochim. Cosmochim. Acta*, **28**, 1273–85.
Thompson, R. C. (1951) U.S. Atomic Energy Commission, Report TID-5222.
Thompson, R. C. (1952) *Production and Separation of'U*^{233} (ed. L. I. Katzin), U.S. Report T1D-5223, pp. 291–5.
Thompson, R. C., Van Winkle, Q., and Malm, J. G. (1952) U.S. Report TID-5223, pp. 276–86.
Thomson, J. and Walton A. (1971–72) *Proc. R. Soc. Edinburgh (B)*, **72/73**, 167–82.
Tomkins, F. S. and Fred, M. (1949) *J. Opt. Soc. Am.*, **39**, 357–63.
Toshiba Denshi Eng KK (1995) Japan Patent 07188653-A; C09K-011/56; C09K-011/84.
Trautmann, N., Denig, R., Kaffnell, N., and Herrmann, G. (1968) *Z. Naturforsch. A*, **23**, 2127–30.
Trubert, D., Guzman, F. M., Le Nauor, C., Brillard, L., Hussonnois, M., and Constantinescu, O. (1998) *Analytica Chim. Acta*, **374**, 149–58.
Trubert, D., Le Naour, C., and Jaussaud, C. (2002) *J. Solution Chem.*, **31**, 261–9.

Trubert, D., Le Naour, C., Jaussaud, C., and Mrad, O. (2003) *J. Solution Chem.*, **32**, 505–17.
Vaezi- Nasr, F., Duplessis, J., and Guillaumont, R. (1979) *Radiochem. Radioanal. Lett.*, **37**, 153–7.
Van Winkle, Q., Larson, R. G., and Katzin, L. I. (1949) *Am. Chem. Soc.*, **7**, 2585–96.
Van Winkle, Q. and Kraus, K. A. (1959) U.S. Patent 2910345.
Varnell, L. (1970) *Nucl. Phys. A*, **144**, 429–40.
Vernois, J. (1958) *J. Chromatogr.*, **1**, 52–61.
Vernois, J. (1959) *J. Chromatogr.*, **2**, 155–61.
Vernois, J., Conte, P., and Muxart, R. (1963) *Bull. Soc. Chim. France*, 403.
Walter, A. J. (1963) *J. Inorg. Nucl. Chem.*, **25**, 1301.
Walter, H. J., Geigert, W., van der Loeff, M. M. R., Fischer, G., and Bathmann, U. (2001) *Deep-Sea Res. Part I*, **48**, 471–93.
Weigel, F., Hoffman, G., and Ter Meer, N. (1969) *Radiochim. Acta*, **11**, 210–14.
Weigel, F., Hoffman, G., Wishnevsky, V., and Brown, D. (1974) *J. Chem. Soc. Dalton Trans.*, 1473–6.
Weigel, F. (1978) in *Handbuch der Präparativen Anorganischen Chemie, Aktiniden*, vol. 2 (ed. G. Brauer), Ferdinand Enke, Stuttgart, pp. 1117–322.
Wills, J. M. and Ericsson, O. (1992) *Phys. Rev. B. (Cond. Mat.)*, **45**, 13879–90.
Wilson, M. (1967) *J. Opt. Soc. Am.*, **57**, 429–30.
Wilson, M. (1968) *J. Opt. Soc. Am.*, **58**, 855–6.
Wojakowski, A., Damien, D., and Hery, Y. (1982) *J. Less Comm. Metals*, **83**, 169–74.
Wolzak, G. and Morinaga, H. (1963) *Radiochim. Acta*, **1**, 225–6.
Wright, H. W., Wyatt, E. I., Reynolds, S. A., Lyon, W. S., and Handley, T. H. (1957) *Nucl. Sci. Eng.*, **2**, 427–30.
Yang, H. S., Masuda, A., Sokai, H., and Nozaki, Y. (1986) *Geocimica Cosmochim. Acta*, **50**, 81–9.
Yokoyama, Y., Falgueres, C., and deLumley, M. A. (1997) *Compt. Rend. Acad. Sci. Paris. Séries II. Fasc. Sciences de la terre et des planètes*, **324**, 773–9.
Yuan, S., Yang, W., Mou, W., Zhang, X., Li, Z., Yu, X., Gu, J., Guo, Y., Gan, Z., Liu, H., and Guo, J. (1995) *Zeit. für Phys. A*, **352**, 235–6.
Yuan, S., Yang, W., Mou, W., Zhang, X., and Li, Z. (1996) *Chinese Physics Lett.*, **13**, 896–98.
Zachariasen, W. H. (1952) *Acta Crystallog.*, **5**, 19–21.
Zavizziano, H. (1935) *Compt. Rend. Acad. Sci. Paris*, **200**, 1843–5.
Zhang Qingwen, Tan Fuwen, Lin Chao, and Chen Yingqiang (1991) *Uranium Geology. China*, **7**, 251–3.
Zhang Xianlu, Xia Kailan, and Liu Husheng (1993) *Uranium Mining Metallurgy*, **12**, 189–93.
Zijp, W. L., Tom, S., and Sizoo, G. J. (1954) *Physica*, **20**, 727–35.
Zimmerman, H. P., Gober, M. K., Kratz, J. V., Schädel, M., Bruchle, W., Schimpf, E., Gregorich, K. E., Turler, A., Czerwinski, K. R., Hannink, N. J., Kadkhodan, B. D. M., Lee Nurmia, M. J., Hoffman, D. C., Gaggeler, H., Jost, D., Kovacs, J., Scherer, U. W., and Weber, A. (1993) *Radiochim. Acta*, **60**, 11–6.
Zwanenburg, G. J., Krupa, C., de Boer, E., and Keijzers, C. P. (1988) *J. Molec. Struct.*, **173**, 397–404.

CHAPTER FIVE

URANIUM*

Ingmar Grenthe, Janusz Drożdżyński, Takeo Fujino, Edgar C. Buck, Thomas E. Albrecht-Schmitt, and Stephen F. Wolf

5.1 HISTORICAL

Uranium compounds have been used as colorants since Roman times (Caley, 1948). Uranium was discovered as a chemical element in a pitchblende specimen by Martin Heinrich Klaproth, who published the results of his work in 1789. Pitchblende is an *impure* uranium oxide, consisting partly of the most reduced oxide uraninite (UO_2) and partly of U_3O_8. Earlier mineralogists had considered this mineral to be a complex oxide of iron and tungsten or of iron and zinc, but Klaproth showed by dissolving it partially in strong acid that the solutions yielded precipitates that were different from those of known elements. Therefore he concluded that it contained a new element (Mellor, 1932); he named it after the planet Uranus, which had been discovered in 1781 by William Herschel, who named it after the ancient Greek deity of the Heavens.

* Part of this chapter is based on Chapter 5 in the previous edition authored by the late Fritz Weigel.

The name 'Uranus' was first proposed by Johann Elert Bode in conformity with the other planetary names from classical mythology, but this name for the planet did not come into common use until 1850. However, uranium was accepted as the name for the chemical element.

The pure oxide UO_2 isolated by Klaproth by reduction was believed to be the elemental form until 1841, when Eugène-Melchior Péligot (1841a,b) showed that Klaproth's 'partially metallic' substance was in reality the oxide UO_2. Péligot (1841b, 1842, 1844) succeeded in preparing metallic uranium by reducing the tetrachloride with potassium. Péligot may thus properly be considered the founder of modern uranium chemistry; he was the first to use the word 'uranyl' to designate the yellow salts of uranium.

In the elaboration of the periodic table, Mendeleev assigned in 1872 an atomic weight of 240 and a highest valence of six to uranium, rather than the value of 120 that was then commonly used based on the assumption that uranium was trivalent. Mendeleev's reason was that he could not place an element with atomic weight 120 in group III of the periodic table; thus he conferred upon uranium the distinction of having the highest atomic weight in the periodic table. An atomic weight of nearly 240 was firmly established by Zimmerman (1882) by determining the mass ratios of several oxides and sodium uranyl acetate. The valence and atomic weight were confirmed by determination of the vapor density of UCl_4 and later of UF_6 and the atomic number 92 was established (Hahn, 1925) from nuclear decay systematics.

The principal use of uranium during the first century after its discovery (and for the previous two millenia) was as a colorant for ceramics and glasses. The obscurity surrounding the element was permanently dissipated by the discovery of Henri Becquerel (1896) that uranium emits penetrating rays. In connection with investigations of the fluorescence and phosphorescence of uranium salts that had been undertaken by generations of Becquerels (Zhang and Pitzer, 1999), H. Becquerel placed photographic plates that were covered with black paper near any salt or other material containing uranium. Whether the material was phosphorescent or not, he found that the emulsion was blackened by emanations that passed through the paper. He compared this phenomenon to that of X-rays, which had been announced only a few weeks earlier by Roentgen. Later Becquerel showed that the penetrating rays could discharge an electroscope. Shortly thereafter, Marie Curie developed quantitative techniques for measuring the radioactivity of uranium. She and others also found thorium to be radioactive and discovered by chemical separations that there were other elements present at trace levels in the uranium ore. Working with her husband Pierre, she discovered and named polonium and radium and described this property of these heavy elements as 'radioactivity'.

Because the Curies recognized that ores of uranium and thorium are much more radioactive than purified compounds of these elements, they and other radiochemists (e.g. Rutherford, Fajans, and Soddy) separated other radioelements and identified their chemical and nuclear transformations. The

luminescent and medical properties of radium created a market for uranium ores and the processed radium that far exceeded the use of uranium as a colorant for glasses.

By 1911, the atomic weight of uranium had been refined to 238.5 (Gmelin, vol. A2, 1980a). The natural isotope ^{235}U was discovered in 1935 by mass spectrometry. The artificial isotope ^{239}U, which is the precursor of ^{239}Np and ^{239}Pu, was postulated and identified by Hahn and coworkers (Hahn *et al*., 1937; Meitner *et al*., 1937) as a 23 min half-life intermediate to transuranium elements that were not identified until the famous studies of Seaborg and coworkers 3 years later.

Despite these important discoveries, the crucial importance of uranium was not established until Hahn and Strassman (1939) discovered nuclear fission in late 1938. Since then, the chemistry, materials science, and nuclear properties of uranium have occupied a central position in the field of nuclear energy. Most schemes so far proposed for the release of nuclear energy involve the naturally occurring fissionable ^{235}U, fertile ^{238}U, or the artificial fissionable ^{233}U in one way or another, so that the chemistry and technology of uranium have become of great scientific and technical importance. For these reasons many reviews dealing with uranium chemistry, technology, and metallurgy have been published. The main volume on uranium of the *Gmelin Handbook of Inorganic Chemistry* (Gmelin, 1936) and a chapter by Mellor (1932) are the earliest comprehensive reviews of uranium chemistry prior to the discovery of fission. The Manhattan Project work was summarized in a number of volumes of the National Nuclear Energy Series (Katz and Rabinowitch, 1951, 1958; Seaborg and Katzin, 1951; Vance and Warner, 1951; Katzin, 1952; Warner, 1953; Wilkinson, 1962). These volumes deal with the chemistry of uranium and its compounds, ^{233}U, metallurgy, and technology of uranium, respectively. The most recent monograph on the chemistry of uranium is that by Cordfunke (1969). The most comprehensive treatment of all phases of uranium chemistry is the multi-volume uranium supplement to the *Gmelin Handbook of Inorganic Chemistry* (1975–1996).

5.2 NUCLEAR PROPERTIES

Uranium, as it occurs in nature, consists of a mixture of the three isotopes ^{238}U, ^{235}U, and ^{234}U. The relative abundances of ^{238}U, ^{235}U, and ^{234}U have been measured by various investigators, and 'best values' for the ^{238}U, ^{235}U, and ^{234}U relative abundances have been chosen through a review of the literature by Holden (1977). We have accepted these values and they are listed in Table 5.1. One has to keep in mind, however, that the isotopic ratio of the uranium isotopes in nature may vary as much as 0.1%. By utilizing mass spectrometric and nuclear disintegration data, the (chemical) atomic weight of natural uranium is calculated to be (238.0289 ± 0.0001). The isotope ^{238}U is the parent of the

Table 5.1 *Natural abundance of the uranium isotopes* (*Holden*, 1977).

Abundance (*at%*)		
Mass number	*Range*	*'Best' value*
234	0.0059–0.0050	0.005 ± 0.001
235	0.7202–0.7198	0.720 ± 0.001
238	99.2752–99.2739	99.275 ± 0.002

natural $4n + 2$ radioactive series, and the isotope ^{235}U is the parent of the natural $4n + 3$ radioactive series. ^{234}U arises from ^{238}U by radioactive decay and these two isotopes are thus linked to each other, but ^{235}U appears to be of independent origin.

The isotope ^{235}U, which exists in nature to the extent of 0.72%, and was identified by Dempster (1935) using mass spectrometry. This isotope is of special importance since it undergoes fission with slow neutrons.

Complete fission of ^{235}U gives rise to an energy equivalent of about 2×10^7 kWh kg^{-1} (corresponding to about 200 MeV per fission). Advantage can be taken of the fissionability of ^{235}U not only to generate large amounts of power but also to synthesize other important actinide elements. Uranium with its natural isotopic composition can be used in nuclear reactors to generate neutrons. The chain reaction is sustained by the excess neutrons produced by the fission of ^{235}U, while neutrons in excess of those required to propagate the chain reaction can be captured by the other natural isotope to produce plutonium:

$$^{235}U + n \rightarrow \text{fission products} + \text{energy} + 2.5\,\text{neutrons}$$

$$^{238}U + n \rightarrow {}^{239}U$$

$$^{239}U \xrightarrow{\beta^-} {}^{239}Np \xrightarrow{\beta^-} {}^{239}Pu$$

The abundant isotope ^{238}U can in this way be converted to plutonium-239, which, like ^{235}U, is also fissionable with slow neutrons.

A large number of synthetic isotopes of uranium have been prepared. The isotope ^{233}U, which was discovered by Seaborg, Gofman, and Stoughton (Katzin, 1952, paper 1.1), is particularly noteworthy, because it also undergoes fission with slow neutrons. Separation of this isotope from neutron-irradiated ^{232}Th is discussed (Thorex Process) in Chapter 24. Some of the other synthetic isotopes have particular utility as tracers for uranium. This is the case for beta-emitting ^{237}U and alpha-emitting ^{232}U, both of which have found extensive use in chemical and physical studies. The isotope ^{232}U is formed by alpha bombardment on ^{232}Th, or in the decay of the short-lived ^{232}Pa, which in turn may be obtained by neutron irradiation of ^{231}Pa. Procedures for the isolation of ^{232}U from this source have been described (Leuze *et al.*, 1962, 1963; Chilton, 1963).

The naturally occurring ^{234}U appears also in the α decay of ^{238}Pu (87.7 years). Separation of this ^{234}U from its parent furnishes a simple way to obtain isotopically pure ^{234}U (Figgins and Bernardinelli, 1966).

The various isotopes of uranium are listed in Table 5.2.

5.3 OCCURRENCE IN NATURE

The most important oxidation states of uranium in natural environments are 4+ and 6+. Compounds containing tetravalent uranium are insoluble in mildly acidic to alkaline conditions, whereas, those containing the linear uranyl moiety $(O{=}U{=}O)^{2+}$ are highly soluble and mobile. In solution, UO_2^{2+} forms soluble complexes with carbonate, oxalate, and hydroxide; UO_2^{2+} is also highly susceptible to adsorption either by organic matter, Fe oxyhydroxides, or by precipitation with various anions, such as hydroxide, silicate, vanadate, arsenate, and phosphate. In groundwater systems U(VI) is reduced to U(IV) if an effective reductant is present, such as H_2S. Other reducing agents may be fossil plants, methane, and transported humic material. Uranium minerals display an extraordinary wide structural and chemical variability, resulting from the different chemical conditions under which U minerals are formed.

Elucidation of the mechanisms of uranium sorption by mineral surfaces, refinements of complex U-mineral structures, and chemical bonding are needed to improve current models from uranium cycling in the aquo- and geospheres in order to describe the behavior of uranium in the environment. In past years, uranium mineralogy was more concerned with the economic quality of U-deposits; however, today we are equally concerned with the hazard presented by former uranium mines and nuclear waste sites to the local environment and population. This has placed greater emphasis on understanding the role of uranium sorption and for developing accurate thermodynamic and kinetic models for uranium attenuation. There are $\sim$200 minerals that contain uranium as an essential component (Burns, 1999a; Finch and Murakami, 1999). Of these, the U(VI) minerals constitute the largest portion. Burns and coworkers have developed a novel approach for describing and classifying the uranyl phases, based on polymerization of coordination polyhedra of higher bond valence, which permits easy visualization of these extremely complex structures (Burns *et al.*, 1996; Burns, 1999a). Mineral descriptions are divided according to the major anionic component and structural similarities. In Table 5.3 a list of uranium minerals with the current information on composition, space group, and lattice parameters has been provided. Hill (1999) provided a similar list of uranium minerals and related synthetic phases; recent studies have identified new phases and errors in the previous entries.

Improved understanding of uranium mineralogy gives insight into the evolution of uranium deposits, possible mechanisms for uranium and radionuclide retardation following the weathering of nuclear waste materials, and the fate of

Table 5.2 *Nuclear properties of uranium isotopes.*[a]

Mass number	*Half-life*	*Mode of decay*	*Main radiations* (MeV)	*Method of production*
217	16 ms	α	α 8.005	^{182}W(^{46}Ar,5n)
218	1.5 ms	α	α 8.625	^{197}Au(^{27}Al,6n)
219	42 μs	α	α 8.680	^{197}Au(^{27}Al,x)
222	1.0 μs	α	α 9.500	W(^{40}Ar,xn)
223	18 μs	α	α 8.780	^{208}Pb(^{20}Ne,5n)
224	0.9 ms	α	α 8.470	^{208}Pb(^{20}Ne,4n)
225	59 ms	α	α 7.879	^{208}Pb(^{22}Ne,5n)
226	0.35 s	α	α 7.430	^{232}Th(α,10n)
227	1.1 min	α	α 6.87	^{232}Th(α,9n) ^{208}Pb(^{22}Ne,3n)
228	9.1 min	α ≥ 95% EC ≤ 5%	α 6.68 (70%) 6.60 (29%) γ 0.152	^{232}Th(α,8n)
229	58 min	EC ∼ 80% α ∼ 20%	α 6.360 (64%) 6.332 (20%) γ 0.123	^{230}Th(^{3}He,4n) ^{232}Th(α,7n)
230	20.8 d	α	α 5.888 (67.5%) 5.818 (31.9%) γ 0.072	^{230}Pa daughter ^{231}Pa(d,3n)
231	4.2 d	EC > 99% α 5.5×10^{-3}%	α 5.46 γ 0.084	^{230}Th(α,3n) ^{231}Pa(d,2n)
232	68.9 yr ≈ 8×10^{13} yr	α SF	α 5.320 (68.6%) 5.264 (31.2%) γ 0.058	^{232}Th(α,4n)
233	1.592×10^{5} yr 1.2×10^{17} yr	α SF	α 4.824 (82.7%) 4.783 (14.9%) γ 0.097	^{233}Pa daughter
234	2.455×10^{5} yr 2×10^{16} yr	α SF	α 4.777 (72%) 4.723 (28%)	nature
235	7.038×10^{8} yr 3.5×10^{17} yr	α SF	α 4.397 (57%) 4.367 (18%) γ 0.186	nature
235 m	25 min	IT		^{239}Pu daughter
236	2.3415×10^{7} yr 2.43×10^{16} yr	α SF	α 4.494 (74%) 4.445 (26%)	^{235}U(n,γ)
237	6.75 d	β$^-$	β$^-$ 0.519 γ 0.60	^{236}U(n,γ) ^{241}Pu daughter
238	4.468×10^{9} yr 8.30×10^{15} yr	α SF	α 4.196(77%) 4.149 (23%)	nature
239	23.45 min	β$^-$	β$^-$ 1.29 γ 0.075	^{238}U(n,γ)
240	14.1 h	β$^-$	β$^-$ 0.36 γ 0.044	^{244}Pu daughter
242	16.8 min	β$^-$	β$^-$ 1.2 γ 0.068	^{244}Pu(n,2pn)

[a] Appendix II.

Table 5.3 *List of natural minerals with uranium as an essential component.*

Mineral	*Formula*	*Space group*	*a* (Å)	*b* (Å)	*c* (Å)	*Angle* (°)	*References*
uranium oxide	UO_2	*Fm*3*m*	5.4682				Roberts *et al.* (1990)
natural uraninite	$[U^{4+}_{1-x-y-z-u}U^{6+}_{x}(Th^{4+})_{u}REE^{3+}_{y}M^{z+}_{z}]O_{2+x-(0.5y)-z}$	*Fm*3*m*	5.470–5.443				Janeczek and Ewing (1992)
uranyl oxide hydrates							
dehydrated schoepite	$(UO_2)_4O(OH)_6 \cdot H_2O$		6.86	4.26	10.20		Finch *et al.* (1998)
ianthinite	$[U^{4+}_2(UO_2)_4O_6(OH)_4(H_2O)_4](H_2O)_5$	$P2_1cn$	7.178	11.473	30.39		Burns *et al.* (1997a)
meta-schoepite	$(UO_2)_4O(OH)_6 \cdot 5H_2O$	*Pbcn*	14.6861	13.9799	16.7063		Weller *et al.* (2000)
schoepite	$[(UO_2)_8O_2(OH)_{12}](H_2O)_{12}$	$P2_1ca$	14.337	16.813	14.731		Finch *et al.* (1996a)
wyartite	$Ca[U^{5+}(UO_2)_2(CO_3)O_4(OH)](H_2O)_7$	$P2_12_12_1$	11.2706	7.1055	20.807		Burns and Finch (1999)
peroxides							
meta-studtite	$(UO_2)O_2(H_2O)_2$		6.50	8.78	4.21		Deliens and Piret (1983a)
studtite	$[(UO_2)(O_2)(H_2O)_2](H_2O)_2$	C2/c	14.068	6.721	8.428	$\beta = 123.356$	Burns and Hughes (2003)
metal uranyl oxyhydroxides							
agrinierite	$K_2(Ca_{0.65}Sr_{0.35})[(UO_2)_3O_3(OH)_2]_2 \cdot 5H_2O$	*F*2*mm*	14.094	14.127	24.106		Cahill and Burns (2000)
bauranoite	$BaU_2O_7 \cdot 4.5H_2O$	No unit cell data					Rogova *et al.* (1973)
becquerelite	$Ca[(UO_2)_3O_2(OH)_3]_2(H_2O)_8$	$Pn2_1a$	13.8378	12.3781	14.9238		Burns and Li (2002)
billietite	$Ba[(UO_2)_3O_2(OH)_3]_2(H_2O)_4$	$Pbn2_1$	12.0720	30.167	7.1455		Pagoaga *et al.* (1987)
compreignacite	$K_2[(UO_2)_3O_2(OH)_3]_2(H_2O)_7$	*Pmmn*	14.8591	7.1747	12.1871		Burns (1998c)
protasite	$Ba[(UO_2)_3O_3(OH)_2](H_2O)_3$	*Pn*	12.2949	7.2206	6.9558	$\beta = 90.401$	Pagoaga *et al.* (1987)
rameauite	$K_2CaU_6O_{20} \cdot 9H_2O$	*C*2/*c*	13.97	14.26	14.22	$\beta = 121.02$	Gaines *et al.* (1997)
uranosphaerite	$Bi(UO_2)O_2OH$	$P2_1/n$	7.559	7.811	7.693	$\beta = 92.88$	Hughes *et al.* (2003)
vandenbrandeite	$(UO_2)Cu(OH)_4$	$P\bar{1}$	7.855	5.449	6.089	$\alpha = 91.44$ $\beta = 101.90$ $\gamma = 89.2$	Rosenzweig and Ryan (1977)

Table 5.3 (*Contd.*)

Mineral	*Formula*	*Space group*	*a* (Å)	*b* (Å)	*c* (Å)	*Angle* (°)	*References*
Pb–uranyl oxyhydroxides							
calciouranoite	$(Ca,Ba,Pb)U_2O_7 \cdot 5H_2O$	No data					
clarkeite	$(NaCa_{0.5}Pb_{0.5})[(UO_2)O(OH)](H_2O)_{0-1}$	*R*-3*m*	3.954		17.73		Finch and Ewing (1997)
curite	$Pb_{3+x}(H_2O)_2[((UO_2)_4O_{4+x}(OH)_{3-x}]_2$	*Pnam*	12.551 (12.53–12.58)	13.003 (13.01–13.03)	8.390 (8.39–8.40)		Taylor *et al.* (1981)
fourmarierite	$Pb_{1-x}[(UO_2)_4O_{3-2x}(OH)_{4+2x}](H_2O)_4$	*Bb*2$_1$*m*	13.986 (14.00–14.03)	16.400 (16.40–16.48)	14.293 (14.32–14.38)		Piret (1985)
masuyite	$Pb[(UO_2)_3O_3(OH)_2](H_2O)_3$	*Pn*	12.241	7.008	6.983	$\beta = 90.40$	Burns and Hanchar (1999)
meta-calciouranoite	$(Ca,Ba,Pb,K,Na)O \cdot UO_3 \cdot 5H_2O$	No data					
meta-vandendriesscheite	$PbU_7O_{22} \cdot nH_2O \quad n < 12$	*Pmma*	14.07	41.31	43.33		Roberts *et al.* (1990)
richetite	$M_xPb_{8.57}[(UO_2)_{18}(OH)_{12}]_2(H_2O)_{41}$	*P*1	20.9391	12.1000	16.3450	$\alpha = 103.87$ $\beta = 115.37$ $\gamma = 90.27$	Burns (1998b)
sayite	$Pb_2[(UO_2)_5O_6(OH)_2](H_2O)_4$	*P*2$_1$/*c*	10.704	6.960	14.533	$\beta = 116.81$	Piret *et al.* (1983)
spriggite	$Pb_3[(UO_2)_6O_8(OH)_2](H_2O)_3$	*C*2/*c*	28.355	11.990	13.998	$\beta = 104.248$	Brugger *et al.* (2004)
vandendriesscheite	$Pb_{1.57}[(UO_2)_{10}O_6(OH)_{11}](H_2O)_{11}$	*Pbca*	14.1165	41.478	14.5347		Burns (1997)
wölsendorfite	$Pb_{6.2}Ba_{0.4}[(UO_2)_{14}O_{19}(OH)_4](H_2O)_{12}$	*Cmcm*	14.131	13.885	55.969		Burns (1999b)
uranyl silicates							
haiweeite group (*U:Si = 1:3*)							
coutinhoite	$Th_xBa_{(1-2x)}(H_2O)_y(UO_2)_2Si_5O_{13} \cdot H_2O$ With $0 \leq x \leq 0.5$ and $0 \leq y \leq (2+x)$	*Cmmb*	14.1676	14.1935	35.754		Atencio *et al.* (2004)
haiweeite	$Ca[(UO_2)_2Si_5O_{12}(OH)_2](H_2O)_3$	*Cmcm*	7.125	17.937	18.342		Burns (2001b)
weeksite	$K_{1.26}Ba_{0.25}Ca_{0.12}[(UO_2)_2(Si_5O_{13})]H_2O$	*Cmmb*	14.209	14.248	35.869		Jackson and Burns (2001)

uranophane group (*U:Si = 1:1*)							
boltwoodite	$K_{0.56}Na_{0.42}[(UO_2)(SiO_3OH)](H_2O)_{1.5}$	$P2_1/m$	7.0772	7.0597	6.6479	$\beta = 104.982$	Burns (1998d)
cuprosklodowskite	$Cu(UO_2)_2(SiO_3OH)_2 \cdot 6H_2O$	$P\bar{1}$	7.052	9.267	6.655	$\alpha = 109.23$ $\beta = 89.84$ $\gamma = 110.01$	Rosenzweig and Ryan (1975)
kasolite	$Pb[(UO_2)(SiO_4)](H_2O)$	$P2_1/c$	6.704	6.932	13.252	$\beta = 104.22$	Ryan and Rosenzweig (1977)
oursinite	$(Co_{0.86}Mg_{0.10}Ni_{0.04}) \cdot O_2 \cdot UO_2 \cdot 2SiO_2 \cdot 6H_2O$	*Aba*2 *or Abam*	12.74	17.55	7.050		Deliens and Piret (1983b)
sklodowskite	$Mg(H_3O)_2[(UO_2)(SiO_4)]_2 \cdot 4H_2O$	*C2/m*	17.382	7.047	6.610	$\beta = 105.9$	Ryan and Rosenzweig (1977)
sodium boltwoodite	$(Na,K)(H_3O)[(UO_2)(SiO_4)] \cdot H_2O$	$P2_12_12_1$	27.2	7.02	6.65		Stohl and Smith (1981)
swamboite	$(UO_2)_{0.33}[(UO_2)(SiO_4)]_2 \cdot 6H_2O$	$P2_1/a$	17.64	21.00	20.12	$\gamma = 103.4$	Deliens and Piret (1981)
α-uranophane	$Ca(UO_2)_2(SiO_3OH)_2(H_2O)_5$	$P2_1$	15.909	7.002	6.665	$\beta = 97.27$	Ginderow (1988)
β-uranophane	$Ca(UO_2)_2(SiO_3OH)_2(H_2O)_5$	$P2_1/a$	13.966	15.443	6.632	$\gamma = 91.38$	Viswanathan and Harnett (1986)
other U silicates							
arapovite	$U(Ca,Na)_2(K_{1-x}\square_x)(Si_8O_{20})$, $x \sim 0.5$	*P4/mcc*	7.5505		14.7104		Uvarova *et al.* (2004)
ciprianiite	$Ca_4[(Th,U)(REE)]Al_2(Si_4B_4O_{22})(OH, F)_2]$	*P2/a*	19.032	4.746	10.248	$\gamma = 110.97$	della Ventura *et al.* (2002)
lepersonnite-Gd	$CaO(Gd,Dy)_2O_3 \cdot 24UO_3 \cdot 8CO_2 \cdot 4SiO_2 \cdot 60H_2O$	*Pnnm or Pnn*2	16.23	38.74	11.73		Deliens and Piret (1982)
soddyite	$(UO_2)_2[SiO_4](H_2O)_2$	*Fddd*	8.334	11.212	18.688		Demartin *et al.* (1992)
uranosilite	$(Mg,Ca)_4(UO_2)_4(Si_2O_5)_{5.5}(OH)_5 \cdot 13H_2O$	*Pmmb or Pmcb*	11.60	14.68	12.83		Walenta (1983)
orthosilicates							
coffinite	$U(SiO_4)_{1-x}(OH)_{4x}$	$I4_1/amd$	6.979		6.252		Fuchs and Gebert (1958)
uranyl carbonates							
albrechtschraufite	$Ca_4Mg(UO_2)_2(CO_3)_6F_2 \cdot 17H_2O$	$P\bar{1}$	13.562	13.406	11.636	$\alpha = 115.72$ $\beta = 107.66$ $\gamma = 92.86$	Mereiter (1984)

Table 5.3 (*Contd.*)

Mineral	*Formula*	*Space group*	*a* (Å)	*b* (Å)	*c* (Å)	*Angle* (°)	*References*
andersonite	$Na_2Ca[(UO_2)(CO_3)_3](H_2O)_5$	*R*-3*m*	17.904		23.753		Mereiter (1986)
astrocyanite-Ce	$Cu_2(Ce,Nd,La)_2UO_2(CO_3)_5(OH)_2 \cdot 1.5H_2O$	*P6/mmm*	14.96		26.86		Deliens and Piret (1990b)
bayleyite	$Mg_2[(UO_2)(CO_3)_3](H_2O)_{18}$	$P2_1/a$	26.560	15.256	6.505	$\gamma = 92.90$	Mayer and Mereiter (1986)
bijvoetite-Y	$[M_8^{3+}(H_2O)_{25}(UO_2)_6O_8(OH)_8(CO_3)_{16}](H_2O)_{14}$	$B12_11$	21.234	12.958	44.911	$\beta = 90.00$	Li et *al.* (2000)
blatonite	$UO_2CO_3 \cdot H_2O$		15.79		23.93		Vochten and Deliens (1998)
čejkaite	$Na_4(UO_2)(CO_3)_3$	*P*1 *or* $P\bar{1}$	9.291	9.292	12.895	$\alpha = 90.73$ $\beta = 90.82$ $\gamma = 120$	Ondruš *et al.* (2003)
fontanite	$Ca[(UO_2)_3(CO_3)_2O_2](H_2O)_6$	$P2_1/n$	6.968	17.276	15.377	$\beta = 90.064$	Hughes and Burns (2003)
grimselite	$K_3Na[(UO_2)(CO_3)_3](H_2O)$	*P*-62*c*	9.302		8.260		Li and Burns (2001b)
joliotite	$UO_2CO_3 \cdot nH_2O \quad n = 1.5–2.0$	*P*222	8.16	10.35	6.32		Walenta (1976)
kamotoite-Y	$Y_2O_4(UO_2)_4(CO_3)_3 \cdot 14H_2O$	$P2_1/a$	21.22	12.93	12.39	$\gamma = 115.3$	Gaines *et al.* (1997)
liebigite	$Ca_2UO_2(CO_3)_3 \cdot 11H_2O$	*Bba*2	16.699	17.557	13.697		Mereiter (1982a)
mckelveyite-Y	$Ba_3Na(Ca,U)Y(CO_3)_6 \cdot 3H_2O$	$P\bar{1}$	9.142	9.141	7	$\alpha = 102.51$ $\beta = 115.67$ $\gamma = 59.99$	Roberts *et al.* (1990)
meta-zellerite	$CaUO_2(CO_3)_2 \cdot 3H_2O$	*Pbnm*	9.718	18.226	4.965		Roberts *et al.* (1990)
oswaldpeetersite	$(UO_2)_2CO_3(OH)_2 \cdot 4H_2O$	$P2_1/c$	4.1425	14.098	18.374	$\beta = 103.62$	Vochten *et al.* (2001)
rabbittite	$Ca_3Mg_3(UO_2)_2(CO_3)_6(OH)_4 \cdot 18H_2O$		32.6	23.8	9.45	$\beta = 90$	Gaines *et al.* (1997)
roubaultite	$Cu_2[(UO_2)_3(CO_3)_2O_2(OH)_2](H_2O)_4$	$P\bar{1}$	7.767	6.924	7.850	$\alpha = 92.16$ $\beta = 90.89$ $\gamma = 93.48$	Ginderow and Cesbron (1985)
rutherfordine	UO_2CO_3	*Pmmn*	4.845	9.205	4.296		Finch *et al.* (1999b)
schröckingerite	(*listed under uranyl sulfates*)						
shabaite-Nd	$Ca(Nd,Sm,Y)_2UO_2(CO_3)_4(OH)_2 \cdot 6H_2O$	*P*2, *Pm*, *or* $P2_1/m$	9.208	32.09	8.335	$\beta = 90.3$	Deliens and Piret (1990a)
sharpite	$Ca(UO_2)_6(CO_3)_5(OH)_4 \cdot 6H_2O$		21.99	15.63	4.48		Gaines *et al.* (1997)
swartzite	$CaMgUO_2(CO_3)_3 \cdot 12H_2O$	$P2_1/m$	11.080	14.634	6.439	$\beta = 99.43$	Mereiter (1986)

urancalcarite	$Ca(UO_2)_3CO_3(OH)_6 \cdot 3H_2O$	*Pmcm* or $P2_1cn$	15.42	6.97	16.08		Deliens and Piret (1984a)
voglite	$Ca_2CuUO_2(CO_3)_4 \cdot 6H_2O$	$P2_1$	25.97	24.5	10.7	$\beta = 104$	Gaines *et al.* (1997)
widenmannite	$Pb_2UO_2(CO_3)_3$		8.99	9.36	4.95		Walenta (1976)
zellerite	$Ca(UO_2)(CO_3)_2(H_2O)_5$	*Pbnm*	11.22	19.25	4.93		Roberts *et al.* (1990)
znucalite	$CaZn_{11}(UO_2)(CO_3)_3(OH)_{20}(H_2O)_4$	$P\bar{1}$	12.692	25.096	11.85	$\alpha = 89.08$ $\beta = 91.79$ $\gamma = 90.37$	Ondruš *et al.* (1990)
uranyl phosphates							
althupite	$ThAl(UO_2)[(UO_2)_3(PO_4)_2O(OH)]_2(OH)_3(H_2O)_{15}$	$P\bar{1}$	10.953	18.567	13.504	$\alpha = 72.64$ $\beta = 68.20$ $\gamma = 84.21$	Piret and Deliens (1987)
ankoleite	$K_2(UO_2)_2(PO_4)_2 \cdot 6H_2O$	*P4/nmm*	6.993		8.891		Gaines *et al.* (1997)
asselbornite	$(Pb,Ba)(UO_2)_6(BiO)_4[(As,P)O_4]_2(OH)_{12} \cdot 3H_2O$	*Im3m*	15.66				Gaines *et al.* (1997)
autunite	$Ca[(UO_2)(PO_4)]_2 \cdot 11H_2O$	14*/mmm*	7.00		20.67		Locock and Burns (2003a)
bassetite	$Fe^{2+}(UO_2)_2(PO_4)_2 \cdot 8H_2O$	$P2_1/m$	6.98	17.07	7.01	$\beta = 90.32$	Roberts *et al.* (1990)
bergenite	$Ca_2Ba_4[(UO_2)_3O_2(PO_4)_2]_3(H_2O)_{16}$	$P2_1/c$	10.092	17.245	17.355	$\beta = 113.678$	Locock and Burns (2003c)
chernikovite	$(H_3O)_2(UO_2)(PO_4)_2 \cdot 6H_2O$	*P4/nmm*	7.02		9.043		Gaines *et al.* (1997)
coconinoite	$Fe_2Al_2(UO_2)_2(PO_4)_4SO_4(OH)_2 \cdot 20H_2O$	*C2/c*	12.5	12.97	23	$\beta = 106.6$	Young *et al.* (1966)
dewindtite	$Pb(UO_2)_3(PO_4)_2(OH)_2 \cdot 3H_2O$	*Bmmb*	16.031	17.264	13.605		Piret *et al.* (1990)
dumontite	$Pb_2[(UO_2)_3(PO_4)_2(OH)_4](H_2O)_5$	$P2_1/m$	8.118	16.819	6.983	$\beta = 109.03$	Locock and Burns (2003b)
françoisite-Nd	$Nd[(UO_2)_3(PO_4)_2O(OH)](H_2O)_6$	$P2_1/c$	9.298	15.605	13.668	$\beta = 112.77$	Piret *et al.* (1988)
furongite	$Al_2UO_2(PO_4)_2 \cdot 8H_2O$	$P\bar{1}$	17.87	14.18	12.18	$\alpha = 67.8$ $\beta = 77.5$ $\gamma = 79.9$	Shen and Peny (1981)
kamitugaite	$PbAl(UO_2)_5[(P,As)O_4]2(OH)_9 \cdot 5H_2O$	$P\bar{1}$	10.98	15.96	9.068	$\alpha = 95.1$ $\beta = 96.1$ $\gamma = 80$	Deliens and Piret (1984b)
lehnerite	$Mn(UO_2)_2(PO_4)_2 \cdot 8H_2O$	$P2_1/n$					Gaines *et al.* (1997)
lermontovite	$U^{4+}PO_4 \cdot OH \cdot H_2O$		9.74	19	10.01		Gaines *et al.* (1997)
meta-autunite	$Ca[(UO_2)(PO_4)]_2 \cdot 6H_2O$	*P4/nmm*	6.96		8.40		Gaines *et al.* (1997)

Table 5.3 (*Contd.*)

Mineral	*Formula*	*Space group*	*a* (Å)	*b* (Å)	*c* (Å)	*Angle* (°)	*References*
meta-torbenite	$Cu[(UO_2)(PO_4)]_2(H_2O)_8$	*P4/n*	6.9756		17.349		Locock and Burns (2003d)
meta-uranocircite-I	$Ba[(UO_2)(PO_4)]_2(H_2O)_7$	$P2_1$	6.943	17.634	6.952	$\beta = 89.95$	Locock *et al.* (2005b)
meta-vanmeersscheite	$U(UO_2)_3(PO_4)_2(OH)_6 \cdot 2H_2O$		34.18	33.88	14.07		Piret and Deliens (1982)
mundite	$Al(UO_2)_3(PO_4)_2(OH)_3 \cdot 5.5H_2O$		17.08	30.98	13.76		Gaines *et al.* (1997)
ningyoite	$(U^{4+},Ca,Ce)_2[PO_4]_2 \cdot 1–2H_2O$		6.8040	12.0117	6.3504		Gaines *et al.* (1997)
parsonsite	$Pb_2[(UO_2)(PO_4)_2](H_2O)n$, where $0 \leq n \leq 0.5$	$P\bar{1}$	6.842	10.383	6.670	$\alpha = 101.5$ $\beta = 110.84$ $\gamma = 88.09$	Sejkora *et al.* (2002)
phosphatian walpurgite	$(UO_2)Bi_4O_4[(As,P)O_4]_2 \cdot 2H_2O$	$P\bar{1}$	7.124	10.392	5.492	$\alpha = 101.22$ $\beta = 109.93$ $\gamma = 87.93$	Sejkora *et al.* (2004)
phosphuranylite	$KCa(H_3O)_3(UO_2)[(UO_2)_3(PO_4)_2O_2]_2(H_2O)_8$	*Cmcm*	15.899	13.740	17.300		Demartin *et al.* (1991)
phuralumite	$Al_2(UO_2)_3(PO_4)_3(OH)_2 \cdot 13H_2O$	$P2_1/a$	13.836	20.918	9.428		Piret *et al.* (1979)
phurcalite	$Ca_2(UO_2)_3O_2(PO_4)_2 \cdot 7H_2O$	*Pbca*	17.415	16.035	13.598		Atencio *et al.* (1991)
przhevalskite	$Pb_2(UO_2)_3(PO_4)_2(OH)_4 \cdot 3H_2O$	*Cmmm*	8.57	11.01	6.93		Gmelin (1981d)
ranunculite	$HAlUO_2PO_4(OH)_3 \cdot 4H_2O$		11.1	17.7	18.0	$\beta = 90$	Gaines *et al.* (1997)
renardite	(not a mineral species possible mixture of dewindtite and phosphuranylite (Čejka, 1999)						
sabugalite	$HAl(UO_2)_4(PO_4)_4 \cdot 16H_2O$		6.96		19.3		Frondel (1951a)
saléeite	$Mg[(UO_2)(PO_4)]_2 \cdot 10H_2O$	$P2_1/c$	6.951	19.947	9.896	$\beta = 135.17$	Miller and Taylor (1986)
threadgoldite	$Al(UO_2)_2(PO_4)_2OH \cdot 8H_2O$	*C2/c*	20.168	9.847	19.719		Khosrawan-Sazedj (1982b)
torbernite	$Cu[(UO_2)(PO_4)]_2(H_2O)_{12}$	*P4/nnc*	7.0267		20.807		Locock and Burns (2003d)
triangulite	$Al_3(UO_2)_4(PO_4)_4(OH)_5 \cdot 5H_2O$		10.39	10.56	10.6	$\alpha = 116.4$ $\beta = 107.8$ $\gamma = 113.4$	Gaines *et al.* (1997)

tristramite	*listed under uranyl sulfates*						
ulrichite	$Cu[Ca(H_2O)_2(UO_2)(PO_4)_2](H_2O)_2$	$P2_1/c$	12.84	6.996	13.007	$\beta = 91.92$	Kolitsch and Giester (2001)
upalite	$Al(UO_2)_3(PO_4)_2O(OH) \cdot 7H_2O$	$P2_1/a$	13.704	16.82	9.332	$\gamma = 111.5$	Piret and Declercq (1983)
uramphite	$NH_4UO_2PO_4 \cdot 3H_2O$		7.01		9.05		Gmelin (1981d)
uranocircite	$Ba[(UO_2)(PO_4)]_2(H_2O)_{10}$	$P2/c$	7.01	6.99	21.2	$\beta = 103.7$	Locock *et al.* (2005b)
uranospathite	$Al_{1-x}\square_x[(UO_2)(PO_4)]_2(H_2O)_{20+3x}F_{1-3x}$, $0 < x < 0.33$	$Pmn2$	30.020	7.0084	7.0492		Locock *et al.* (2005c)
vochtenite	$(Fe,Mg)Fe[(UO_2)(PO_4)]_2 \cdot 8H_2O$		12.606	19.99	9.99	$\beta = 102.52$	Gaines *et al.* (1997)
vanmeersscheite	$U(OH)_4[(UO_2)_3(PO_4)_2(OH)_2](H_2O)_4$	$P2_1mn$	17.06	16.76	7.023		Piret and Deliens (1982)
vyacheslavite	$UPO_4(OH) \cdot nH_2O$		6.96	9.1	12.38		Gaines *et al.* (1997)
xiangjiangite	$(Fe,Al)(UO_2)_4(PO_4)_2(SO_4)_2OH \cdot 22H_2O$	$C2/c$	12.54	12.98	23.8	$\beta = 108.6$	Zhang *et al.* (1992)
yingjiangite	$(K_{1-x}Ca_x)(UO_2)_3(PO_4)_2(OH)_{1+x} \cdot 4H_2O \quad x = 0.35$	$Bmmb$	15.707	17.424	13.692		Zhangru *et al.* (1986)
uranyl arsenates							
arsenuranospathite	$HAl(UO_2)_4(AsO_4)_4 \cdot 40H_2O$	$P4_2/n$	7.16		30.37		Gaines *et al.* (1997)
arsenuranylite	$Ca(UO_2)_4(AsO_4)_2(OH)_4 \cdot 6H_2O$		15.4	17.4	13.77		Gaines *et al.* (19970
asselbornite	$(Pb,Ba)(UO_2)_6(BiO)_4(AsO_4)_2(OH)_{12} \cdot 3(H_2O)$	$Im3m$	15.66				Sarp *et al.* (1983)
abernathyite	$K[(UO_2)(AsO_4)]_2(H_2O)_3$	$P4/ncc$	7.176		18.126		Ross and Evans (1964)
chadwickite	$(UO_2)H(AsO_3)$		11		15.96		Walenta (1998)
hallimondite	$Pb_2[(UO_2)(AsO_4)_2](H_2O)_n$, where $0 \leq n \leq 0.5$	$P\bar{1}$	7.123	10.469	6.844	$\alpha = 100.57$ $\beta = 94.80$ $\gamma = 91.27$	Walenta (1965)
heinrichite	$Ba[(UO_2)_2(AsO_4)]_2(H_2O)_{10}$	$P2/c$	7.1548	7.1340	21.290	$\beta = 104.171$	Locock *et al.* (2005b)
hügelite	$Pb_2[(UO_2)_3O_2(AsO_4)_2](H_2O)_5$	$P2_1/m$	31.066	17.303	7.043	$\beta = 96.492$	Locock and Burns (2003b)
kahlerite	$Fe(UO_2)_2(AsO_4)_2 \cdot 12H_2O$	$P4_2/n$	14.3		21.97		Gaines *et al.* (1997)
meta-heinrichite	$Ba[(UO_2)(AsO_4)]_2(H_2O)_7$	$P2_1$	7.08	17.7	7.09	$\beta = 90.02$	Locock *et al.* (2005b)
meta-kahlerite	$Fe(UO_2)_2(AsO_4)_2 \cdot 8H_2O$	$P4/mmm$	7.16		8.62		Gaines *et al.* (1997)
meta-kirchheimerite	$Co(UO_2)_2(AsO_4)_2 \cdot 8H_2O$	$P4/mmm$	7.16		8.60		Gaines *et al.* (1997)
meta-lodevite	$Zn(UO_2)_2(AsO_4)_2 \cdot 10H_2O$	$P4_2/m$	7.16		17.20		
meta-novácekite	$Mg(UO_2)_2(AsO_4)_2 \cdot 4–8H_2O$	$P4/n$	7.16		8.58		Roberts *et al.* (1990)

Table 5.3 (*Contd.*)

Mineral	*Formula*	*Space group*	*a* (Å)	*b* (Å)	*c* (Å)	*Angle* (°)	*References*
meta-zeunerite	$Cu[(UO_2)(AsO_4)]_2(H_2O)_8$	*P4/n*	7.1094		17.416		Locock and Burns (2003d)
novacekite	$Mg(UO_2)_2(AsO_4)_2 \cdot 12H_2O$	$P4_1/n$	7.16		20.19		Frondel (1951b)
orthowalpurgite	$(UO_2)Bi_4O_4(AsO_4)_2 \cdot 2H_2O$	*Pbcm*	5.492	13.324	20.685		Krause *et al.* (1995)
séelite	$Mg(UO_2)(AsO_3)_{0.7}(AsO_4)_{0.3} \cdot 7\beta\beta H_2O$	*C2/m*	18.207	7.062	6.661	$\beta = 99.65$	Frondel (1951b)
trögerite	$(UO_2)_3(AsO_4)_2 \cdot 12H_2O$	*P4/mmm*	7.16		8.8		Gaines *et al.* (1997)
uranospinite	$Ca[(UO_2)(AsO_4)]_2(H_2O)_{11}$	*Pnma*	14.35	20.66	7.17		Lockock *et al.* (2005b)
walpurgite	$(UO_2)Bi_4O_4(AsO_4)_2 \cdot 2H_2O$	$P\bar{1}$	7.135	10.426	5.494	$\alpha = 101.47$ $\beta = 110.82$ $\gamma = 88.20$	Mereiter (1982b)
zeunerite	$Cu[(UO_2)(AsO_4)]_2(H_2O)_{12}$	*P4/nnc*	7.1797		20.857		Locock and Burns (2003d)
uranyl molybdates							
calcurmolite	$Ca(UO_2)_3(MoO_4)_3(OH)_2(H_2O)_{11}$						Gaines *et al.* (1997)
deloryite	$Cu_4(UO_2)(MoO_4)_2(OH)_6$	*C2/m*	19.94	6.116	5.52	$\beta = 104.2$	Pushcharovsky *et al.* (1996)
iriginite	$[(UO_2)Mo_2O_7(H_2O)_2](H_2O)$	*Pbcm*	6.705	12.731	11.524		Krivovichev and Burns (2000)
moluranite	$U^{4+}(UO_2)_2Mo_5O_{19} \cdot 12H_2O$	*amorphous*					Roberts *et al.* (1990)
mourite	$U^{4+}Mo_5O_{12}(OH)_{10}$	*P2/c*	24.443	7.182	9.901	$\beta = 102.22$	Gaines *et al.* (1997)
tengchongite	$CaO_6UO_3 \cdot 2MoO_3 \cdot 12H_2O$		15.616	13.043	17.716		Chen *et al.* (1986)
sedovite	$U(MoO_4)_2$		3.36	11.08	6.42		Roberts *et al.* (1990)
umohoite	$[(UO_2)MoO_4(H_2O)](H_2O)$	$P2_1/c$	6.3748	7.5287	14.628	$\alpha = 82.64$ $\beta = 85.95$ $\gamma = 89.91$	Krivovichev and Burns (2000b)
uranyl vanadates							
carnotite	$[K_2(UO_2)_2(VO_4)_2 \cdot 1\text{–}3H_2O]$	*P21/a*	10.51	8.45	7.32	$\gamma = 106.08$	Appleman and Evans (1965)
curienite	$Pb[(UO_2)_2(V_2O_8)](H_2O)_5$	*Pcan*	10.40	8.45	16.34		Borène and Cesbron (1971)

francevillite	$Ba_{0.96}Pb_{0.04}[(UO_2)_2(V_2O_8)](H_2O)_5$	*Pcan*	10.419	8.510	16.763		Mereiter (1986)
fritzscheite	$Mn(UO_2)_2(PO_4,VO_4)_2 \cdot 10H_2O$	*Pnam*	10.59	8.25	15.54		Roberts *et al.* (1990)
margaritasite	$(Cs,K,H_3O)_2(UO_2)_2(VO_4)_2 \cdot H_2O$	$P2_1/a$	10.514	8.425	7.25	$\gamma = 106.01$	Roberts *et al.* (1990)
meta-tyuyamunite	$Ca(UO_2)_2(VO_4)_2 \cdot 3–5H_2O$	*Pnam*	10.54	8.49	17.34		Roberts *et al.* (1990)
meta-vanuralite	$Al(UO_2)_2(VO_4)_2OH \cdot 8H_2O$	*P*1	10.46	8.44	10.43	$\alpha = 75.88$ $\beta = 102.83$ $\gamma = 90$	Roberts *et al.* (1990)
rauvite	$Ca(UO_2)_2V_{10}O_{28} \cdot 16H_2O$	(*no unit cell data*)					
sengierite	$Cu_2[(UO_2)_2(V_2O_8)](OH)_2(H_2O)_6$	$P2_1/a$	10.599	8.093	10.085	$\gamma = 103.42$	Piret *et al.* (1980)
strelkinite	$NaUO_2VO_4 \cdot 3H_2O$	*Pnmm*	10.64	8.36	32.72		Gaines *et al.* (1997)
tyuyamunite	$Ca(UO_2)_2(VO_4)_2 \cdot 5–8H_2O$	*Pnan*	10.36	8.36	20.4		Roberts *et al.* (1990)
uvanite	$U_2V_6O_{21} \cdot 15H_2O$	(*no unit cell data*)					
vanuralite	$Al(UO_2)_2(V^{5+}O_4)_2(OH) \cdot 11H_2O$		10.55	8.44	24.52	$\beta = 103$	Roberts *et al.* (1990)
vanuranylite	$(H_3O,Ba,Ca,K)_{1.6}(UO_2)_2(VO_4)_2 \cdot 4H_2O$	*C*2/*c*	10.49	8.37	20.2	$\beta = 90$	Roberts *et al.* (1990)
uranyl tungstates							
uranotungstite	$(Fe^{2+},Ba,Pb)(UO_2)_2WO_4(OH)_4(H_2O)_{12}$		9.22	13.81	7.17		Walenta (1985)
uranyl sulfates							
deliensite	$Fe(UO_2)_2(SO_4)_2(OH)_2 \cdot 3H_2O$	*Pnnm or Pnn*2	15.908	16.274	6.903		Vochten *et al.* (1997)
Co-zippeite	$Co(H_2O)_{3.5}[(UO_2)_2(SO_4)O_2]$	*C*2/*m*	8.650	14.252	17.742	$\beta = 104.092$	Burns *et al.* (2003)
coconinoite	$Fe_2Al_2(UO_2)_2(PO_4)_4SO_4(OH)_2 \cdot 20H_2O$		12.5	12.97	23	$\beta = 106.6$	Young *et al.* (1966)
jáchymovite	$(UO_2)_8(SO_4)(OH)_{14} \cdot 13H_2O$	(*no unit cell data*)					Brugger *et al.* (2003)
johannite	$Cu(UO_2)_2(SO_4)_2(OH)_2 \cdot 8H_2O$	$P\bar{1}$	8.903	9.499	6.812	$\alpha = 109.87$ $\beta = 112.01$ $\gamma = 100.40$	Mereiter (1982c)
marecottite	$Mg_3(H_2O)_{18}[(UO_2)_4O_3(OH)(SO_4)_2]_2(H_2O)_{10}$	$P\bar{1}$	10.815	11.249	13.851	$\alpha = 66.224$ $\beta = 72.412$ $\gamma = 69.95$	Brugger *et al.* (2003)
Mg-zippeite	$Mg_2(H_2O)_{11}[(UO_2)_2(SO_4)O_2]_2$	$P2_1/c$	8.6457	17.2004	18.4642	$\beta = 102.119$	Burns *et al.* (2003)
meta-uranopilite	$(UO_2)_6SO_4(OH)_{10} \cdot 5H_2O$	no unit cell data					Roberts *et al.* (1990)
Ni-zippeite	$Ni_2(UO_2)_6(SO_4)_3(OH)_{10} \cdot 16H_2O$	no unit cell data					Roberts *et al.* (1990)

Table 5.3 (*Contd.*)

Mineral	*Formula*	*Space group*	*a* (Å)	*b* (Å)	*c* (Å)	*Angle* (°)	*References*
rabejacite	$Ca(UO_2)_4(SO_5)_2(OH)_6 \cdot 6H_2O$		8.73	17.09	15.72		Deliens and Piret (1993)
schröckingerite	$NaCa_3(UO_2)(CO_3)_3(SO_4)F \cdot 10H_2O$		9.341		12.824		Li *et al.* (2001a)
Na-zippeite	$Na_5(H_2O)_{12}[(UO_2)_8(SO_4)_4O]_5(OH)_3$	$P2_1/n$	17.6425	14.6272	17.6922	$\beta = 104.461$	Burns *et al.* (2003)
tristramite	$(Ca,U^{4+},Fe^{3+})(PO_4,SO_4) \cdot 2H_2O$	$P6_222$	6.919		6.422		Gaines *et al.* (1997)
uranopilite	$(UO_2)_6[(SO_4)O_2(OH)_6(H_2O)]_6(H_2O)_8$	$P\bar{1}$	8.896	14.029	14.33	$\alpha = 96.610$ $\beta = 98.472$ $\gamma = 99.802$	Burns (2001a)
Zn-zippeite	$Zn(H_2O)_{3.5}[(UO_2)_2(SO_4)O_2]$	$C2/m$	8.6437	14.1664	17.701	$\beta = 104.041$	Burns *et al.* (2003)
zippeite	$K_3(H_2O)_3[(UO_2)_4(SO_4)_2O_3(OH)]$	$C2$	8.7524	13.9197	17.6972	$\beta = 104.178$	Burns *et al.* (2003)
uranyl selenites and tellurites							
cliffordite	$UO_2(Te_3O_7)$	$Pa\bar{3}$	11.335				Branstätter (1981)
derriksite	$Cu_4[(UO_2)(SeO_3)_2](OH)_6$	$Pn2_1m$	5.570	19.088	5.965		Ginderow and Cesbron (1983a)
demesmaekerite	$Cu_5Pb_2(UO_2)_2(SeO_3)_6(OH)_6(H_2O)_2$	$P\bar{1}$	11.955	10.039	5.639	$\alpha = 89.78$ $\beta = 100.36$ $\gamma = 91.34$	Ginderow and Cesbron (1983b)
guilleminite	$Ba[UO_2)_3(SeO_3)_2O_2](H_2O)_3$	$P2_1nm$	7.084	7.293	16.881		Cooper and Hawthorne (1995)
haynesite	$(UO_2)_3(OH)_2(SeO_3)_2 \cdot 5H_2O$	$Pncm$	8.025	17.43	6.953		Gaines *et al.* (1997)
larisaite	$Na(H_3O)(UO_2)_3(SeO_3)_2O_2 \cdot 4H_2O$	$P11m$	6.9806	7.646	17.249	$\beta = 90.039$	Chukanov *et al.* (2004)
marthozite	$Cu^{2+}[(UO_2)_3(SeO_3)_2O_2](H_2O)_8$	$Pbn2_1$	6.9879	16.4537	17.2229		Cooper and Hawthorne (2001)
moctezumite	$PbUO_2(TeO_3)_2$	$P2_1/c$	7.813	7.061	13.775	$\beta = 93.71$	Swihart *et al.* (1993)
piretite	$Ca(UO_2)_3(SeO_3)_2(OH)_4 \cdot 4(H_2O)$	$Pmnm$	7.01	17.135	17.606		Vochten *et al.* (1996)
schmitterite	UO_2TeO_3	$Pca2_1$	10.161	5.363	7.862		Meunier and Galy (1973)

euxenite–pyrochlore (mineral structures obtained by heating)							
betafite	$(Ca,Na,U)_2(Ti,Nb,Ta)_2O_6(OH)$	*Fd*$\bar{3}$*m*	10.31				Gaines *et al.* (1997)
calciobetafite	$(Ca,RE,Th,U)_2(Nb,Ta,Ti)_2O_7$	*Fd*$\bar{3}$*m*	10.2978				Mazzi and Munno (1983)
calciosamarskite	$(Ca,Fe^{3+},U,Y)NbO_4$	Metamict					Hanson *et al.* (1999)
euxenite-y	$(Y,Ca,Ce,U,Th)(Nb,Ta,Ti)_2O_6$	*Pcan*	5.52	14.57	5.166		Gaines *et al.* (1997)
ishikawaite	$(U,Fe,Y,Ce)(Nb,Ta)O_4$	Metamict					Hanson *et al.* (1999)
kobeite-y	$(Y,U)(Ti,Nb)_2(O,OH)_6$		5.021				Gaines *et al.* (1997)
liandratite	$U^{6+}(Nb,Ta)_2O_8$	*P*$\bar{3}$1*m*	6.36		4.01		Mucke and Strunz (1978)
petscheckite	$U^{4+}Fe^{2+}(Nb,Ta)_2O_8$	*P*$\bar{3}$1*m*	6.42		4.02		Mucke and Strunz (1978)
samarskite	$(Fe,Y,Ce,U)(Nb,Ta,Ti)O_4$	*Pbcn*	5.498	14.34	5.12		Warner and Ewing (1993)
uranopyrochlore	$(U,Ca,Ce)_2(Nb,Ta)_2O_6(OH,F)$	*Fd*$\bar{3}$*m*	10.44				Gaines *et al.* (1997)
uranmicrolite	$(U,Ca,Ce)_2(Ta,Nb)_2O_6(OH,F)$	*Fd*$\bar{3}$*m*	10.4				Gaines *et al.* (1997)
uranopolycrase	$(U,Y)(Ti,Nb)_2O_6$	*Pbcn*	14.51	5.558	5.173		Gaines *et al.* (1997)
brannerites							
brannerite	$(U,Ca,Y,Ce)(Ti,Fe)_2O_6$	*C*2/*m*	9.79	3.72	6.87	$\beta = 118.25$	Pabst (1954)
thorutite	$(Th,U,Ca)Ti_2(O,OH)_6$	*C*2/*m*	9.822	3.824	7.036	$\beta = 118.83$	Roberts *et al.* (1990)
Fe–Ti oxides							
davidite-la	$(La,Ce)(Y,U,Fe)(Ti,Fe)_{20}(O,OH)_{38}$	*R*$\bar{3}$	10.375		20.909		Gatehouse *et al.* (1979)
dessauite	$(Sr,Pb)(Y,U)(Ti,Fe^{3+})_{20}O_{38}$	*R*$\bar{3}$	9.197			$\alpha = 68.75$	Orlandi *et al.* (1997)

other anthropogenic sources of uranium of environmental concern. The long-term behavior of nuclear waste materials such as high-level waste (HLW) glass, spent UO_2 nuclear fuel (SNF), and U-bearing waste forms, can be predicted, in part, by understanding the geochemical behavior of uranium. Other forms of uranium contamination of immediate concern are located at uranium production facilities, mines, and, more recently, battlefields where depleted uranium weapons have been used. Concerns about the fate of uranium in the environment have been addressed by employing several micro-analytical techniques to identify and characterize the nature of the contaminants (Bertsch *et al.*, 1994; Buck *et al.*, 1996; Morris *et al.*, 1996; Duff *et al.*, 1997, 2002).

Burns *et al.* (1997a) have theorized that many of the alteration phases that form during waste form corrosion may be capable of incorporating key radionuclides, including Np, Tc, and Pu. The potential for uranium secondary phases to incorporate radionuclides and thus curtail their migration is of significant scientific interest (Buck *et al.*, 1997; Chen *et al.*, 1999, 2000; Li and Burns, 2001a; Burns *et al.*, 2004a). A key to predicting the thermodynamic properties of these complex U(VI) minerals is to understand the nature of the connectivity between uranium polyhedra. Finch and Murakami (1999) have reported measured and estimated thermodynamic data for 14 uranyl silicate and carbonate minerals. Additional data is published elsewhere on uranium phases (Grenthe *et al.*, 1995), studtite (Hughes-Kubatko *et al.*, 2003), and new experimental thermodynamic measurements have now been obtained from the uranyl carbonates, uranophane, and uranyl phosphates (Hughes-Kubatko *et al.*, 2005). In addition to the natural U-minerals, a wealth of complex synthetic U(VI) phases have now been explored as potential, mesoporous materials, catalysts, and waste forms.

5.3.1 Mineralogy and classification of uranium deposits

Extensive reviews of uranium mineralogy and the origin of uranium deposits have been made by Finch and Murakami (1999) and Plant *et al.* (1999), respectively. Uranium deposits can be classified into 14 groups. These are: unconformity related, sandstone, quartz–pebble conglomerate, veins, breccia complex, intrusive, phosphorite, collapse breccia, volcanic, surficial, metasomatite, metamorphic, lignite, and black shale. Uranium is precipitated in reducing environments, sandstones rich in organic matter or iron sulfides, phosphate-rich sediments, shales where uranium is concentrated in organic matter, and lignite and coals. Enrichment of uranium in lignite or coal can create environmental problems when these sources are burned. Uranium undergoes a series of complex fractionation events, resulting in highly variable levels in different rock types. Owing to its relatively large size (the ionic radius of U^{4+} is 0.940 Å) in eight-fold coordination with oxygen (Farges *et al.*, 1992), tetravalent uranium is incompatible in silicate melts, depending on alkali content and the presence of nonbonding oxygens. Uranium is preferentially partitioned into small volume,

low-temperature melts, and becomes progressively more concentrated, so that certain types of highly evolved granite, rhyolite,[1] and alkaline complexes contain significant quantities of uranium (Plant *et al.*, 1999). Uranium is usually present in accessory minerals such as zircon ($ZrSiO_4$), monazite {(Ce, La, Nd, Th)PO_4}, and pyrochlore (general formula AB_2O_7), many of which are also observed in synthetic ceramic HLW forms (Ewing, 1999). Although the levels of Th and U in terrestrial igneous rocks are variable, the Th/U ratio is relatively constant at about 3.8 (Taylor and McLennan, 1985). Although the most important uranium oxidation states of environmental and geological significance are considered to be U(IV) and U(VI), there is increasing evidence for the role of U(V) in uranium minerals (Burns and Finch, 1999; Colella *et al.*, 2005).

There are numerous U-deposits worldwide and some of these have been studied in great detail, some owing to their relevance to HLW disposal and the environmental fate of uranium, as well as being sources for unique uranium minerals. Understanding the geochemical behavior of uranium at these sites provides the basis for predictive modeling of uranium in the environment and also helps build confidence in the feasibility of geological waste isolation. Uranium deposits at Oklo, Peña Blanca, Shinkolobwe, and Koongarra will be described briefly below.

(a) Oklo, Gabon (Sandstone deposit)

The geochemical behavior of the natural fission reactors at Oklélobondo and Bangombé (Oklo), located in a Precambrian[2] sedimentary basin in Gabon (Africa) have been discussed by Brookins (1990), Hidaka and Holliger (1998), and Janeczek (1999). The Bamgombé site in the Oklo region is of particular interest as it is located at shallow depths. Furthermore, as full-scale mining was never commenced, the ore deposit has been left almost intact. Electron microprobe analysis (EMPA) of uraninite in contact with U(VI) phases indicates that the alteration resulted in increased concentrations of Si, P, S, Zr, Ce, and Nd. The dissolution of accessory apatite {$Ca_5(PO_4)_3(OH,Cl,F)$}, monazite and sulfides resulted in the retardation of uranium through the formation of secondary minerals, including phosphatian coffinites and iron–uranyl phosphate hydroxide hydrates (i.e. bassetite {$Fe^{2+}(UO_2)_2(PO_4)_2 \cdot 8H_2O$}). Jensen *et al.* (2002) investigated the mineralogy of the uranium deposits at Bamgombé and compared their experimental observations with thermodynamic predictions based on groundwater conditions. The primary U-minerals at Bamgombé are uraninite and minor coffinite [$U(SiO_4)_{4-x}(OH)_{4x}$]. The uranyl minerals include fourmarierite {$Pb_{1-x}[(UO_2)_4O_{3-2x}(OH)_{4+2x}] \cdot 4H_2O$}, bassetite possibly associated with {$U(HPO_4)_2 \cdot 2H_2O$} or chernikovite {$(H_3O)_2[(UO_2)(PO_4)]_2 \cdot 6H_2O$},

[1] Derived from the rapid cooling of a very viscous granitic magma.
[2] Between 2.5 and 1.8 billion years ago.

torbernite $\{Cu[(UO_2)(PO_4)]_2 \cdot 8–12H_2O\}$, Ce-rich françoisite $\{(Nd,Y,Sm,Ce)(UO_2)_3(PO_4)_2O(OH)(H_2O)_6\}$, and uranopilite $\{(UO_2)_6(SO_4)O_2(OH)_6(H_2O)_6 \cdot 8H_2O\}$. Autunite $\{Ca[(UO_2)(PO_4)]_2 \cdot 11H_2O\}$ has also been reported. Eh–pH diagrams predict that coffinite, $U(HPO_4)_2 \cdot H_2O$, and $UOF_2 \cdot H_2O$ are the only stable U(IV) phases and that uranopilite, torbernite, and bassetite will become stable during oxidative alteration.

(b) Peña Blanca, Chichuhua District, Mexico (Breccia Pipe)

The Sierra de Peña Blanca District, Chihuahua, Mexico consists of a gently dipping Tertiary[3] volcanic pile that covers a calcareous basement of Cretaceous age[4] (Cesbron *et al*., 1993; Pearcy *et al*., 1994). Peña Blanca is part of a much more extensive range of volcanic uranium deposits that extend from the McDermitt caldera at the Oregon–Nevada border through the Marysvale district of Utah and Date Creek Basin in Arizona and south into the Peña Blanca (Finch, 1996). In the Nopal I deposit, the ignimbritic tuffs[5] have been hydrothermally altered and U-mineralization is located within a breccia pipe structure at the intersection of several faults. The uraninite deposition under reducing conditions (8 ± 5) Ma ago has precluded the accumulation of significant amounts of lead. Later tectonic forces elevated the deposit above the local water table, exposing it to oxidizing conditions. The site is a convincing geochemical analog of the proposed HLW repository at Yucca Mountain, Nevada. The initial corrosion products from the oxidative dissolution of uraninite are uranyl oxide hydrates, including ianthinite $\{[U_2^{4+}(UO_2)_4O_6(OH)_4(H_2O)_4](H_2O)_5\}$ (Burns *et al*., 1997b), schoepite $\{[(UO_2)_8O_2(OH)_{12}](H_2O)_{12}\}$, and dehydrated schoepite $\{(UO_2)_4O(OH)_6 \cdot H_2O\}$ (Leslie *et al*., 1993). Ianthinite is unusual in that it contains both U^{6+} and U^{4+}. The phase has a narrow stability range and will easily degrade. It will form in oxygen-deficient environments, such as under localized reducing environments at Shinkolobwe (Finch and Ewing, 1992).

Uranyl silicates, uranophane $\{Ca(UO_2)_2(SiO_3OH)_2(H_2O)_5\}$, are the predominant U-phases at Nopal I, comprising more than 95% of all U-bearing minerals. They either replace earlier formed U-phases or form euhedral[6] crystals within open voids and fractures. The uranophanes at Nopal I have been dated at 3.2 Ma, suggesting that alteration of the initial uraninite took millions of years under the oxidizing environment. The paragenesis[7] of U-phases was similar to that observed in laboratory tests by Wronkiewicz *et al*. (1992) on synthetic UO_2 apart from the occurrence of the mixed uranium valence phase,

[3] ~5–45 million years ago.
[4] ~65–130 million years ago.
[5] Deposits of hot incandescently glowing ash (tuff) from volcanic activity.
[6] Well-formed crystal with regular shape.
[7] Refers to the order of mineral formation.

ianthinite that has not been observed in corrosion tests with UO_2 (Wronkiewicz *et al.*, 1996) or SNF (Finch *et al.*, 1999a; Wronkiewicz and Buck, 1999).

(c) Shinkolobwe (Sandstone U-deposit)

Uranium minerals from the 1.8-Ga-old Shinkolobwe deposit, located in the Katanga District of the Democratic Republic of the Congo, have been extensively described and discussed by Finch and Ewing (1992) and in references therein. The deposit has been exposed since Tertiary times and extensive weathering has significantly altered or replaced uraninite. Uranium mineralization occurs along fracture zones where meteoric[8] waters have penetrated. The uranyl silicates, uranophane and cuprosklodowskite $\{Cu(UO_2)_2(SiO_3OH)_2 \cdot 6H_2O\}$, are ubiquitous and replace becquerelite, compreignacite $\{K_2[(UO_2)_3O_2(OH)_3]_2(H_2O)_7\}$, vandendriesscheite $\{Pb_{1.57}[(UO_2)_{10}O_6(OH)_{11}](H_2O)_{11}\}$, fourmarierite, billietite $\{Ba[(UO_2)_3O_2(OH)_3]_2(H_2O)_4\}$ and schoepite by reaction with the silica-rich groundwater. As the groundwater interacts with the host rocks, it becomes increasingly more enriched in silica, resulting in the precipitation of uranophane. Finch *et al.* (1995) argued that the cyclical weather pattern explained the simultaneous occurrence of both becquerelite and uranophane. Becquerelite has been estimated to be 10^5 to 10^6 years old based on the $^{230}Th/^{234}U$ ratios being close to 1.0 in these minerals (Finch *et al.*, 1996b).

(d) Koongarra

Koongarra is located in a tropical monsoon climate with long dry seasons (Edghill, 1991). The host rock is quartz-rich schist[9] and the primary uranium mineral, uraninite, has been subjected to weathering for more than 1 million years. The alteration of chlorite produces Fe^{3+} minerals that become associated with some uranium. In the primary ore deposit uraninite has been altered to curite $\{Pb_3[(UO_2)_8O_8(OH)_6] \cdot 3H_2O\}$, and sklodowskite $\{Mg(H_3O)_2[(UO_2)(SiO_4)]_2 \cdot 4H_2O\}$. However, Murakami *et al.* (1997) have shown that upstream from the deposit, saléeite $\{Mg[(UO_2)(PO_4)]_2 \cdot 10H_2O\}$, has replaced sklodowskite and granular apatite and is the predominant mechanism for fixing uranium. In a transmission electron microscopy (TEM) study by Lumpkin *et al.* (1999) on Koongarra mineral substrates, uranium was observed to preferentially sorb to the iron oxide minerals (goethite, α-FeOOH, and possibly ferrihydrite) rather than the clay minerals.

[8] Groundwater of atmospheric origin (i.e. rain, snow, etc.).
[9] A thinly layered crystalline rock.

5.3.2 Reduced uranium phases

Uraninite is a common accessory mineral in pegmatites and peraluminous granites and is the most important source of dissolved uranium in groundwaters emanating from weathered granite terrains. Uraninite possesses the fluorite structure, nominally UO_{2+x}. U(IV) is coordinated by eight O atoms in a cubic arrangement, and each O atom bonds to four U^{4+} ions. Stoichiometric UO_2 is unknown in nature and is always partially oxidized in addition to containing radiogenic lead and commonly thorium, calcium, and lanthanides. Stoichiometric UO_2 ($a = 5.47$ Å) forms a complete solid solution with ThO_2 ($a = 5.6$ Å) following Végard's Law. Janeczek and Ewing (1992) proposed the formula $\{(U^{4+}_{1-x-y-z}U^{6+}_{x}Ln^{3+}_{y}M^{2+}_{z}\square_{v})O_{2-x-0.5y-z-2v}\}$ (where $\square$ denotes a vacancy).

It is possibly inappropriate to term uraninite (as well as coffinite and brannerite), as a primary uranium mineral as it can precipitate from aqueous solutions under reducing conditions or through microbial processes (e.g. sulfur-reducing bacteria (Spirakis, 1996; Fredrickson *et al*., 2002)). Primary reduced uranium minerals are usually coarse grained and present in granites and pegmatites. They have high Th and consequently larger unit cells. Hydrothermal vein[10] uraninites typically have minor lanthanides, Y, Ca, and Th absent. Low-temperature sedimentary uraninites are devoid of lanthanides and Th, but may contain Ca, Si, and P. Grandstaff (1976) observed a correlation between dissolution rate and the mole fraction of impurity cations (Pb and Th). The decrease was attributed to the buildup of low-solubility impurities in the surface as U was preferentially leached. Similar processes have been observed in corroded SNF (Buck *et al*., 2004).

The most common U-ore is fine grained uraninite, sometimes termed pitchblende, similar to the term used for fine-grained quartz (chalcedony); pitchblende is not a mineral name but a textural term. The name 'pitch' does not come from its black, resinous appearance, and botyroidal habit[11] but from the german word 'pech' meaning bad luck (Piekarski and Morfeld, 1997). Radiogenic lead can reach levels of 15–20 wt.% in ancient uraninites. Janeczek and Ewing (1991) observed lead contents of 14 wt.% in an 1800-Ma-old uraninite specimen from the Eldorado mine in Canada. The presence of lead in uraninite results in auto-oxidation and can lead to high U(VI)/U(IV) ratios in uraninite. Auto-oxidation at the uraninite deposit at Cigar Lake has led to U (VI)/U(IV) ratios from 0.02 to as high as ~0.75 according to X-ray photoelectron spectroscopy (XPS) studies by Sunder *et al*. (1996), despite the highly anoxic conditions prevalent in the deposit. Sunder and coworkers also examined uraninites from Oklo and found a similar range of ratios for uraninites.

[10] A vein formed by the crystallization of minerals from predominantly hot water solutions of igneous origin.
[11] A globular growth of minerals.

Oxidation of uraninite results in a decrease of the unit cell parameter, whereas α-decay damage has the opposite effect through the formation of defects and voids. Uraninites typically experience more than 10 displacements per atom over periods of millions of years; yet, the high rate of self-annealing prevents metamictization[12] of the uraninite. Cationic substitutions (radiogenic Pb, Th, Ca, and Ln) increase the unit cell parameter (Janeczek and Ewing, 1991). The large ionic radius of Pb^{2+} results in a substantial increase in the unit cell with increasing age of the uraninite. The presence of silicium and phosphorus in partly altered uraninite is due most likely due to the precipitation of phosphatian coffinite.

(a) U(IV) phosphates and molybdates

The UO_2–P_2O_5 system includes uranium meta-phosphate $U(PO_3)_4$, uranium diphosphate UP_2O_7, uranium oxide phosphate $(UO)_3(PO_4)_2$, and uranium oxide diphosphate $(UO)_2P_2O_7$. Douglass (1962) first characterized both orthorhombic $U(PO_3)_4$ and its isostructural plutonium analog. Brandel *et al.* (1996) synthesized two additional phosphates, uranium uranyl phosphate $U(UO_2)(PO_4)_2$, that formed in air at 1000–1200°C, which may be the only mixed valence uranium phosphate known, and diuranium oxide phosphate $U_2O(PO_4)_2$ that was formed at 1350°C in an inert atmosphere. Attempts by Brandel *et al.* (1996) to produce uranium orthophosphate, $U_3(PO_4)_4$, were unsuccessful confirming earlier data, indicating that this phase does not exist (Gmelin, 1981d).

A number of hydrous U(IV) phosphates exist in nature and some of these have been observed in secondary alteration phases formed during laboratory corrosion tests on HLW glass (Bates *et al.*, 1992). These phases have been described as brockite- and rhabdophane-related phases and contain U, Th, Ln, and Pu (Buck and Bates, 1999). Ningyoite, $\{(U^{4+},Ca,Ce)_2[PO_4]_2 \cdot 1\text{–}2H_2O\}$, is a member of the rhabdophane group of phosphates (Gaines *et al.*, 1997). Ningyoite is a translucent brown to greenish mineral observed at the Ningyo-Toge mine, Japan. The phase may form a solid solution with U-bearing brockite, $\{Ca_{z-y}(U^{4+}_{1-x}Th^{4+}_{x})_{y/2}(PO_4)_2 \cdot nH_2O\}$; in addition CO_3 and SO_4 may substitute for PO_4.

Lermontovite $\{U^{4+}(PO_4)OH\}$ and vyacheslavite $\{U^{4+}(PO_4)(OH) \cdot 2.5H_2O\}$ form under reduced conditions in hydrothermal deposits associated with sulfides.

(b) Uranium orthosilicate

Coffinite and the thorium orthosilicate, thorite, $(Th,U)SiO_4$, are widespread in igneous and metamorphic rocks and are important ore minerals in some uranium and thorium deposits (Speer, 1982). These silicates are tetragonal and

[12] Process of alteration of crystalline to non-crystalline structure through radioactive decay.

isostructural with zircon (Fuchs and Gebert, 1958). Because they can be primary in origin, they have been used in geochronological studies. Coffinite occurs as a primary uranium ore mineral in unoxidized, uranium–vanadium ores of the Colorado Plateau, USA; however, it is also found in hydrothermal, vein deposits with pitchblende, with variable composition where $(OH)^-$ substitutes for $(SiO_4)^{4-}$. Some studies have suggested that the ubiquitous occurrence of organic matter with secondary coffinite indicates a possible biogenic origin (Spirakis, 1996).

(c) Uranium in silicate melts and glasses

The partitioning of uranium into silicate melts depends on the oxygen fugacity, melt composition, and redox conditions. Under mildly reducing conditions, U(V) is present as an octahedrally coordinated species. Under very reducing conditions, such as that prevailing in silicate magmatic melts, U(IV) is the dominant uranium species. Data obtained by Farges *et al.* (1992) with extended X-ray absorption fine structure analysis (EXAFS) indicated that U(IV) is present in six coordinated sites in silicate glasses with a mean U–O distance of $\approx$ 2.26–2.29 Å. Uranium(IV) is expected to occupy similar sites in the melt. The solubility of uranium in silicate liquids is enhanced by high alkali content and the presence of nonbonding oxygens (NBO)[13] and non-framework oxygens (NFO).[14] There is a strong correlation between uranium solubility and the NBO/T ratio (where T is the number of tetrahedral cations). Up to 18 wt% U(IV) can be dissolved in sodium trisilicate glass; whereas less than 1 wt% of U(IV) will dissolve in a glass with albite (Na alumino-silicate) composition. The formation of bonds between NBO and NFO is favored because these oxygens have lower bond strength. The solubility of actinides in alkali silicate glasses decreases in the order Th > U > Np > Pu owing to decreasing ionic size and increasing actinide–oxygen bond strength. The solubilities of U(V) and U(IV) are also affected by alkali content due to variation in bond strength. Uranium(IV) and U(V) are generally incompatible with magmatic systems and tend to partition strongly into late stage formed minerals, such as zircon, titanite, or apatite. Farges *et al.* (1992) suggest that if melts have a heterogeneous distribution of bonding oxygens (BO) and NBO, uranium will become enriched in the NBO-enriched regions. With increasing magmatic differentiation,[15] the BO content of the melt increases, as a consequence U(IV) will partition to late crystallizing minerals, such as pyrochlore or zircon.

Farges *et al.* (1992) determined the U–O bond lengths in U(VI)-containing silicate glasses as $U–O_{ax} \approx 1.77–1.85$ Å and $U–O_{eq} \approx 2.18–2.25$ Å, characteristic

[13] Oxygen bonded to one Si^{4+} and an indeterminate number of other cations (Ellison *et al.*, 1994).
[14] Oxygen bonded exclusively to cations other than Si^{4+}.
[15] The process of chemical and mechanical evolution of a magma in the course of its crystallization such that different rock types are formed from the same original magma.

of the uranyl species. U(VI) is the dominant oxidation state observed in radioactive borosilicate waste glasses. XPS measurements performed on SON68-type borosilicate waste glass by Ollier *et al.* (2003) revealed two oxidation states in the glass: about 20% U(IV) and 80% U(VI) present in two different environments, uranate- and uranyl-sites, respectively. As a consequence of bond strength considerations, U(VI) also bonds primarily to NBO and NFO in both crystalline and amorphous silicates. U(V) is six-coordinated with a mean U–O bond distance of 2.19–2.24 Å (Farges *et al.*, 1992).

Karabulut *et al.* (2000) have investigated the local structure of uranium in a series of iron phosphate glasses with EXAFS and determined that the all uranium was present as U(IV).

(d) Uranium niobates, tantalates, and titanates

There are a number of complex tantalum, niobium, and titanium oxides that may contain uranium as an essential element. These phases are mainly observed in granitic rocks and granite pegmatites[16] and have been difficult to characterize as they commonly occur in the aperiodic metamict state owing to their age and radionuclide content. A common feature of these minerals is that niobium, tantalum, and titanium atoms occupy octahedral sites, and a structural framework that is formed by octahedral corner or edge sharing (Finch and Murakami, 1999).

The structures of the ixiolite, samarskite, and columbite groups, ideally $A^{3+}B^{5+}O_4$, are all derivatives of the α-PbO_2 structure. Ishikawaite $\{(U^{4+},Fe,Y,Ce)(Nb,Ta)O_4\}$ is the U-rich variety of samarskite and calciosamarskite is the Ca-rich variety. Because these minerals are chemically complex, metamict, and pervasively altered, their crystal chemistry and structure are poorly understood (Hanson *et al.*, 1999). Many of these phases are of interest because of their occurrence in designer crystalline ceramic waste forms for immobilization of actinides (Gieré *et al.*, 1998; Ewing, 1999). In particular, zirconolites, pyrochlores, and brannerites have been proposed for immobilizing transuranics. These phases will be discussed in more detail.

(*i*) *Zirconolite*

Zirconolite is an accessory mineral crystallizing under different geological conditions and in a wide range of generally SiO_2-poor rock types (Gieré *et al.*, 1998). Zirconolite has been found in mesostasis areas of ultrabasic cumulates, in granitic pegmatites, in carbonatites,[17] in nepheline syenites, and in other igneous formations. Zirconolite has been observed commonly in lunar late-stage

[16] Late stage crystallization from an igneous intrusion.
[17] Rock consisting of >50% carbonate minerals.

mesostasis areas of lunar basalts.[18] It is also a common constituent of designer titanate ceramic waste forms (Gieré *et al*., 1998; Ewing, 1999). Natural zirconolite is a reddish-brown mineral with an appearance similar to that of ilmenite; however, the grains are typically anhedral and <0.1 mm in diameter, and easily overlooked.

Zirconolite, $CaZrTi_2O_7$, belongs to a group of anion-deficient superstructures of the fluorite-type, which have been found to be the most versatile phases for the incorporation of HLW elements. Zirconolite is termed the aristotype of the group (i.e. the structurally simplest member of the series). All have the general formula $[A_2B_2X_7]$ (A = Ca, Na, Ln, U, Th, Zr, Ti; B = Ti, Nb, Ta, Al, Fe; X = O, F) (Mazzi and Munno, 1983; Bayliss *et al*., 1989). Zirconolite does not appear to incorporate uranium and lanthanides by isomorphic substitution; rather, distinct phases form depending on the particular elements present in the mineral. Elements may not be distributed uniformly throughout the zirconolite but concentrated in extended defects, which can lead to the formation of zirconolite polytypes (White, 1984). These are constructed by stacking modular units in a variety of orientations with respect to the arrangement of the interlayer cations. Each module consists of two hexagonal tungsten bronze layers and interposed cations. The zirconolite-type phases have been described in the literature as zirconolite, zirkelite, pyrochlore, and polymignyte. The three natural zirconolites are orthorhombic zirconolite, known as zirconolite-3O, trigonal zirconolite, known as as zirconolite-3T, and the more common monoclinic zirconolite called zirconolite-2M. The cubic form is termed zirkelite and for metamict minerals, the name polymignyte is used.

Geochemical studies by Lumpkin and coworkers (Lumpkin *et al*., 1988, 1995; Lumpkin and Ewing, 1995) have shown that zirconolite is highly durable in the presence of hydrothermal fluids and low-temperature groundwaters. Uranium in zirconolite is mobilized only under conditions of high temperature and pressure in hydrothermal fluids. At lower temperatures alteration takes place because previous radiation induced damage; this may result in the release of radiogenic lead. However, uranium remains relatively unaffected by the alteration process.

(*ii*) *Pyrochlore*

Minerals of the pyrochlore group have the general formula $A_{1-2}B_2O_6X_{0-1}$ (Greegor *et al*., 1989). Three subgroups are defined on the basis of the major B-site cations. The B-site is occupied by Ti, Nb, or Ta; however, Al, Fe^{3+}, Zr, Sn, and W may also be possible. Microlite and natural pyrochlore both contain more niobium and tantalum than titanium (see Fig. 5.1a). The H_2O content in

[18] Zirconolite was reported in rocks collected on Apollo 10 (mare basalt) and Apollo 14 (recrystallized breccia) moon missions.

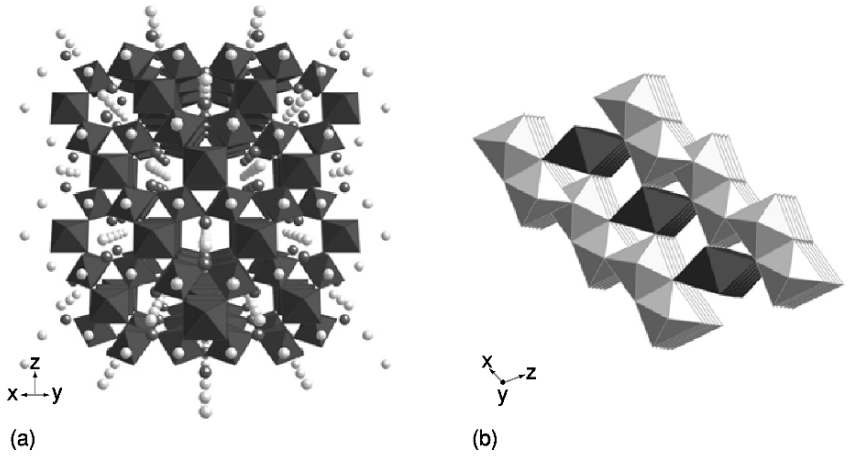

Fig. 5.1 *Structure of* (*a*) *pyrochlore* (*diagram displays grey circles = A site, dark circles = B site, and* TiO_6 *octahedra*) *and* (*b*) *brannerite* (*diagram shows uranium as dark-colored polyhedra and* TiO_6 *octahedra as gray*) (*courtesy of Prof. R. Gieré, University of Freiberg, Germany*).

the natural minerals ranges from 10 to 15 wt%, but will increase if the mineral has undergone alteration. These groups can be further subdivided based on the A-site occupation which can be Na, Ca, Mn, Fe^{2+}, Sr, Sb, Cs, Ba, rare earths, Pb, Bi, Th, and U. Natural pyrochlore minerals occur predominantly in three host rock categories: carbonatites, nepheline syenites, and granitic pegmatites.

(*iii*) *Evidence for U*(*v*) *in pyrochlores and zirconolite*

Fortner *et al.* (2002) used X-ray absorption spectroscopy near-edge structure (XANES) analysis to suggest that U(v) is present in a synthetic pyrochlore ceramic produced under reducing (Ar/H_2) conditions. The authors argue that uranium substitutes for titanium on the B-site in pyrochlore and suggest that this will also occur in natural pyrochlore-type minerals. This result is partially supported by findings by Vance *et al.* (2001) who determined that zirconolite, ($CaU_xZr_{1-x}Ti_2O_7$) oxidized at 1400°C in air, formed U(v) at the expense of U(IV) and that zirconolites with available charge-compensating lanthanides, also resulted in U(IV) to U(v) oxidation, even when sintered in an argon gas environment. The oxidation of U(IV) to U(v) is accompanied by a significant decrease in ionic size, suggesting that uranium is unlikely to enter the calcium site, but rather prefers the zirconium site. Although the presence of significant amounts of U(v) in these titanate phases has not been established by quantitative EMPA data on synthetic (Gieré *et al.*, 2002) and natural zirconolites and pyrochlores (Gieré *et al.*, 1998), the strong observed correlation between Ca and U in natural zirconolites, indicates substitution on the A-site rather than the B-site.

(*iv*) *Brannerite*

After uraninite and coffinite, brannerite is the most important uranium ore mineral. At the large uranium deposit of the El'kon District of the Aldan Shield, Siberia, brannerite is the dominant uranium phase (Miguta, 1997). Ifill *et al.* (1996) report that brannerite at the Elliot lake U-deposit in Canada formed mainly by replacement of uranium in TiO_2-rich relicts of magnetite–ilmenite intergrowths. The uranium was derived from diagenetic dissolution of uraninite. Brannerite, ideally $\{(U,Th)_{1-x}Ti_{2+x}O_6\}$, is a monoclinic accessory phase that is completely metamict (amorphous) as a result of the α-decay damage from the constituents uranium and thorium. As with many of these metamict U-minerals, the structure can be recrystallized on heating. Many cation substitutions have been identified for both uranium (Pb, Ca, Th, Y and Ce) and titanium (Si, Al, Fe) in natural brannerites (Vance *et al.*, 2001) (see Fig. 5.1b).

Brannerite is also formed in the titanate-based nuclear waste-form crystalline ceramics under reducing conditions. Finnie *et al.* (2003) and Colella *et al.* (2005) examined synthetic U(v) phases and natural brannerites with XPS and electron energy-loss spectroscopy. The average valence state in the natural brannerites was close to 5.0.

5.3.3 Uranium(VI) phases

Carbonate dominates the speciation of uranium in alkaline environments, while sulfate complexation is of importance in slightly acidic oxidizing media. The U(VI) phases represent an extremely diverse and complex series of minerals. In this section, the U(VI) minerals will be discussed by first introducing the various uranium mineral structures and then their occurrence on the basis of the major complexing anion, and finally a mention of uranium sorption on soil minerals.

Uranyl oxyhydroxides that form in U-rich aqueous solutions can be represented by the general formula $\{M_n[UO_2)_xO_y(OH)_z](H_2O)_m\}$, where M represents divalent cations, including Ca^{2+}, Pb^{2+}, Ba^{2+}, and Sr^{2+}. However, uranyl oxyhydroxides are only stable in groundwaters devoid of carbonate, sulfate, and/or vanadate ligands.

(a) Bonding in uranyl polyhedra

Burns *et al.* (1996) developed a hierarchical structural classification for U(VI) minerals and other inorganic phases, based on the polymerization of coordination polyhedra. The linear uranyl (Ur) ion is coordinated by four, five, or six anions (ϕ: O^{2-}, OH^-, H_2O), with the oxygen atoms of the uranyl ion forming the apices of square ($Ur\phi_4$), pentagonal ($Ur\phi_5$), and hexagonal ($Ur\phi_6$) bipyramids. The equatorial U–O bond lengths for $Ur\phi_4$, $Ur\phi_5$, and $Ur\phi_6$, are 2.26(8), 2.34(10), and 2.46(12) Å, respectively. The polyhedra possess very asymmetrical charge distributions, $O_{Ur} \sim -1.7$and $U\text{–}O_{eq} \sim -0.5$ as discussed in more detail in

Section 5.8. Uranyl minerals with uranium as the only high-valence cation invariably contain sheets [the exception being studtite (Burns and Hughes, 2003)], as do the naturally occurring uranyl vanadates, uranyl molybdates, and most uranyl sulfates. A majority of the uranyl silicates contain sheets except for soddyite $\{(UO_2)_2[SiO_4](H_2O)_2\}$ and weeksite $\{K_{1.26}Ba_{0.25}Ca_{0.12}[(UO_2)_2(Si_5O_{13})]H_2O\}$ (Jackson and Burns, 2001), which involve frameworks of U(VI) polyhedra. Uranyl carbonates are exceptional because they often contain isolated uranyl tricarbonate clusters, although rutherfordine, UO_2CO_3 (cf. Fig. 5.54), and roubaultite $\{Cu_2(UO_2)_3(CO_3)_2O_2(OH)_2](H_2O)_4\}$, contain uranyl carbonate sheets. The uranyl selenites demesmaekerite $\{Cu_5Pb_2(UO_2)_2(SeO_3)_6(OH)_6(H_2O)_2\}$, and derriksite, $\{Cu_4[(UO_2)(SeO_3)_2](OH)_6]\}$, contain chains of polyhedra, whereas guillemenite, $\{Ba[UO_2)_3(SeO_3)_2O_2](H_2O)_3\}$, and haynesite, $\{(UO_2)_3(OH)_2(SeO_3)_2 \cdot 5H_2O\}$, both contain uranyl selenite sheets. Uranyl arsenates either contain autunite-type sheets or chains, as in the structures of walpurgite, $\{(UO_2)Bi_4O_4(AsO_4)_2 \cdot 2H_2O\}$, and orthowalpurgite, $\{(UO_2)Bi_4O_4(AsO_4)_2 \cdot 2H_2O\}$.[19] Relatively few uranium minerals are based upon chains, although recent structural refinements indicate that these types of U^{6+} minerals are more common that previously thought. Examples include: the only know peroxide mineral, studtite (Burns and Hughes, 2003); the uranyl tellurides, moctezumite $\{PbUO_2(TeO_3)_2\}$, derriksite, and demesmaekerite; the uranyl sulfate uranopilite; the uranyl arsenates, walpurgite, orthowalpurgite, and their phosphate analog, phosphowalpurgite $\{(UO_2)Bi_4O_4(PO_4)_2 \cdot 2H_2O\}$ (Sejkora *et al.* 2004); and parsonsite $\{Pb_2[(UO_2)(PO_4)_2]\}$. Locock *et al.* (2005a) have also shown that the synthetic arsenic-bearing analog of parsonsite, hallimondite $\{Pb_2[(UO_2)(AsO_4)_2]\}$, is also a chain structure.

(b) Geometries of uranyl polyhedra

The crystal chemistry of U(VI) is rich in diversity, yet it is relatively rare for uranyl solids to form frameworks. The distribution of bond strengths within uranyl bipyramidal polyhedra generally permits polymerization only through the equatorial ligands, resulting in chains or sheets. Linkages in the third dimension may be facilitated by additional polyhedra such as silicate, molybdate, vanadate, or phosphate.

The U(VI) minerals that are based on infinite polyhedra sheets with edge- and corner-sharing polyhedra can be better described by the topological arrangement of anions that occur within the sheets (Miller *et al.*, 1996; Burns and Hill, 2000a). Similar to a method described by Aléonard *et al.* (1983) for U_3O_8 structures, the procedure is as follows: Each anion that is not bonded to at least two cations within the sheet, and not an equatorial anion of a bipyramid or

[19] The compositions of orthowalpurgite and walpurgite as written are identical; however, the structures are not (Mereiter, 1982b; Krause *et al.*, 1995).

pyramid within the sheet, is removed from further consideration. Cations are removed along with all cation–anion bonds, leaving an array of unconnected anions. Anions are joined by lines, with only those anions that may be considered as part of the same coordination polyhedra being connected. Anions are removed from further consideration, leaving a series of lines that represent the anion topology. The anion topology does not contain any information about the cation population of the sheet from which the topology was derived (see Fig. 5.2). The P chain is composed of edge-sharing pentagons, the R chain contains rhombs, and the H chain contains edge-sharing hexagons. The arrowhead chains (U and D), which have a directional aspect, contain both pentagons and triangles, arranged such that each triangle shares an edge with a pentagon and the opposite corner with another pentagon in the chain. Generation of anion topologies using chain-stacking sequences is an elegant method for describing the relationships among the complex U(VI) sheet recently found in several minerals. The following describes a number of the possible anion topologies in the U(VI) minerals (see Burns, 1999a for a more complete list).

(*i*) *Protasite* (α-U_3O_8) *anion topology*

The protasite anion topology is the basis of sheets that occur in protasite $\{Ba[(UO_2)_3O_3(OH)_2](H_2O)_3\}$, becquerelite (Burns and Li, 2002), billietite (Pagoaga *et al.*, 1987), richetite $\{M_xPb_{8.57}[(UO_2)_{18}(OH)_{12}]_2(H_2O)_{41}\}$ (Burns, 1998b), compreignacite (Burns, 1998c), agrinierite $\{K_2(Ca_{0.65}Sr_{0.35})[(UO_2)_3O_3(OH)_2]_2 \cdot 5H_2O\}$ (Cahill and Burns, 2000), and masuyite $\{Pb[(UO_2)_3O_3(OH)_2](H_2O)_3\}$ (Burns and Hanchar, 1999), as well as a synthetic cesium uranyl oxide hydrate (Hill and Burns, 1999). As such, it is apparent that sheets based on this topology are compatible with a range of interlayer configurations involving Ba, Ca, Pb, K, and Cs. This simple anion topology contains only triangles and pentagons (see Fig. 5.2a).

Only P and D chains are required to develop the protasite anion topology, with the repeat sequence PDPD... The protasite anion topology does not distinguish between O^{2-} and OH^- anions and the distribution of anions is not identical between different minerals possessing the protasite structure type. Becquerelite, billietite, and compreignacite have identical anion distributions, $[(UO_2)O_3(OH_3)]^-$ but masuyite and protasite do not.

(*ii*) *Fourmarierite anion topology*

Sheets based upon the fourmarierite anion topology (see Fig. 5.2b) occur in fourmarierite (Piret, 1985) and schoepite (Finch *et al.*, 1996a). In schoepite, the sheets are neutral, with H_2O groups being the only constituents of the interlayer. In fourmarierite, the sheets have a different distribution of O and OH^-, resulting in a charged sheet that is balanced by Pb^{2+} in the interlayer. The anion topology

can be obtained with a chain-stacking sequence involving P, D, and U chains, with the sequence PDUPUD.... Li and Burns (2000a) have refined the structures of several fourmarierite specimens from various localities. All the crystals are orthorhombic.

(*iii*) *Vandendriesscheite anion topology*

Vandendriesscheite is the most common Pb-bearing uranyl oxyhydroxide, occurring at numerous weathered uraninite deposits, often in association with schoepite. The anion topology of vandendriesscheite (see Fig. 5.2c) is exceptionally complex, with a primitive repeat of 41.4 Å (Burns, 1997). Only vandendriesscheite contains a sheet based upon this topology, which can be constructed using P, U and D chains in the sequence PDUPUPUPU DPDPDPDUPUPUP.... It contains sections that are identical to the PDPD... (or PUPU...) repeats of the protasite anion topology, with the junction between such sections involving the DU sequence of the fourmarierite anion topology. Thus, the vandendriesscheite anion topology is a structural intermediate between these two simpler anion topologies.

(*iv*) *Sayrite anion topology*

Sayrite $\{Pb_2[(UO_2)_5O_6(OH)_2](H_2O)_4\}$ (Piret *et al.*, 1983), is the only mineral that contains sheets based upon the sayrite anion topology, which involves U, D, P and R chains. The chains are arranged in such a way that each P chain is flanked by two arrowhead chains with the same sense (direction), giving UPU or DPD sequences. These two sequences alternate in the anion topology, and are separated by R chains, giving the sequence RUPURDPDRUPU...

(*v*) *Curite anion topology*

The structure of curite (Taylor *et al.*, 1981; Li and Burns, 2000b) contains sheets based upon the curite anion topology, which cannot be described as a simple chain-stacking sequence using only the U, D, P and R chains. A chain with pentagons, triangles, and squares is required. It has a directional sense owing to the presence of an arrowhead (a pentagon and a triangle sharing an edge), and is designated U_m and D_m, for up and down (modified) pointing chains, respectively. The curite anion topology can be characterized by the chain-stacking sequence U_mDU_mD...

(*vi*) *β-U_3O_8 anion topology*

The β-U_3O_8 sheet anion topology (see Fig. 5.2d) is the basis of the sheets in ianthinite (Burns *et al.*, 1997b), as well as the sheets in β-U_3O_8. This topology can conveniently be described using a chain-stacking sequence involving U, D, and R chains with the repeat sequence DRUDRU...

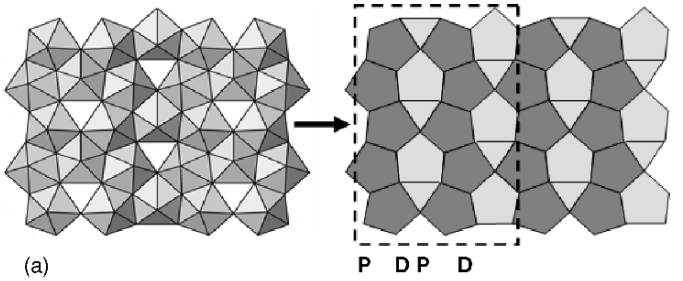

(a)

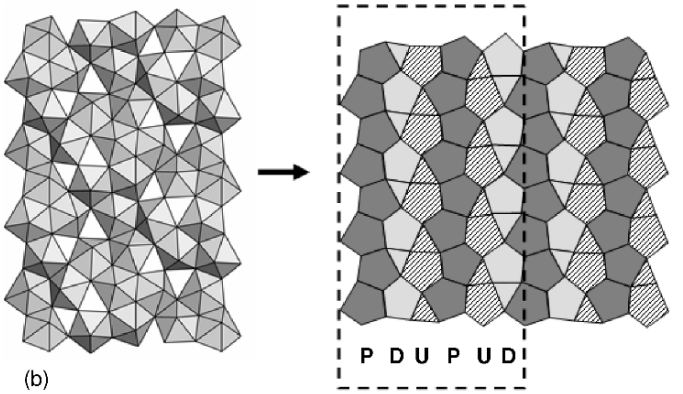

(b)

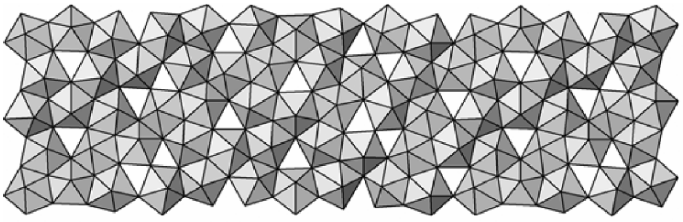

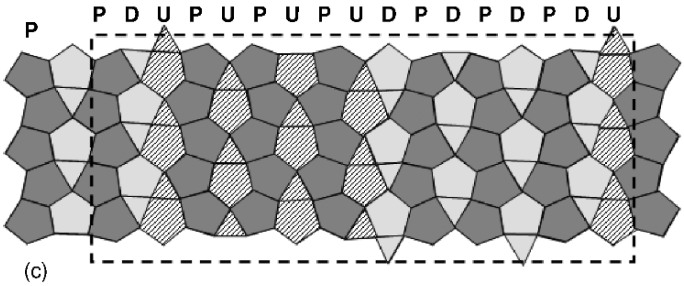

(c)

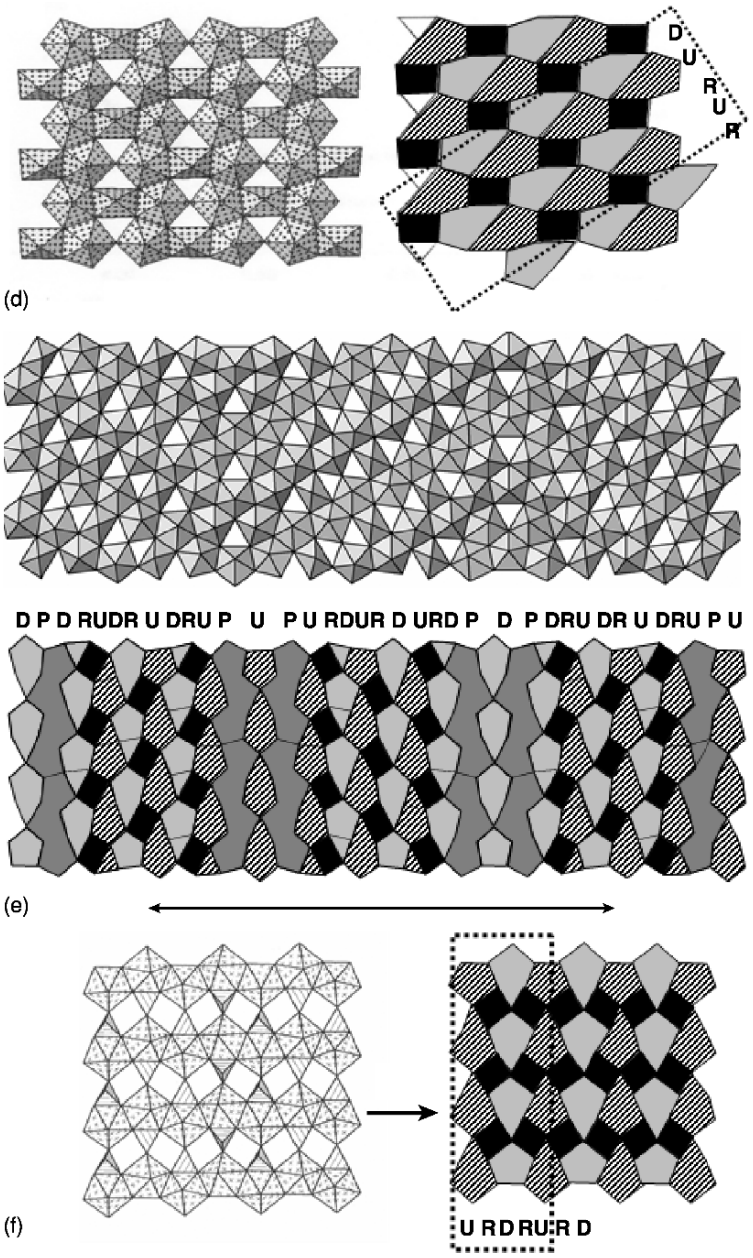

Fig. 5.2 (*a*) *Protasite* (α-U_3O_8) *structure and anion topology with anion repeat* (*adapted from Burns,* 1999). (*b*) *Fourmarierite structure and anion topology, showing the structural repeat.* (*c*) *Vandendriesscheite structure and anion topology.* (*d*) β-U_3O_8 *structure and anion topology* (*adapted from Brugger* et al., 2004). (*e*) *Wölsendorfite anion topology and the complex anion topology.* (*f*) *Uranophane anion topology showing anion repeat* (*adapted from Burns*, 1999).

(*vii*) *Wölsendorfite anion topology*

The versatility of this method for visualizing complex structures is beautifully demonstrated in the description of the structure of wölsendorfite (Burns, 1999b). The structure contains unique $Ur\phi_4$ square bipyramids and six unique $Ur\phi_5$ pentagonal bipyramids that link by sharing equatorial corners and edges to form infinite sheets that are parallel to (100). The interlayer between the uranyl sheets contains Pb^{2+} and Ba^{2+} cations, as well as H_2O groups that are either bonded to the interlayer cations or are held in the structure by H-bonding only. This complex anion topology possesses a primitive repeat of 56 Å (see Fig. 5.2e). It may be constructed using R, D, P, and U chains, with the repeat sequence DRUDRUDRUPDPDRUDRUDRUPDP... The repeat sequence involves the strings DRUDRUDRU and PDP, which are slabs of the β-U_3O_8 and protasite anion topologies, respectively. Thus, the wölsendorfite anion topology is structurally intermediate between the β-U_3O_8 and protasite anion topologies.

(*viii*) *Uranophane anion topology*

All minerals based on the uranophane topology contain pentagons of the anion topology (see Fig. 5.2f).

The uranophane sheet consists of chains of $Ur\phi_5$ bipyramids linked by bridging, isolated SiO_4 tetrahedra, and is common to uranophane, boltwoodite $\{K_{0.56}Na_{0.42}[(UO_2)(SiO_3OH)](H_2O)_{1.5}\}$, cuprosklodowskite, kasolite $\{Pb[(UO_2)(SiO_4)](H_2O)\}$, and sklodowskite. The difference between α-uranophane and β-uranophane depends on the orientation of the silicate tetrahedron. In kasolite, the apical O atoms of the SiO_4 tetrahedra bond to two Pb^{2+} cations in the interlayer (Catalano and Brown, 2004).

(c) Prediction of crystal morphology of U(VI) sheet minerals

The bond valence approach is commonly used to evaluate the analysis of a crystal structure. It provides a means to check bond lengths, the valence state of ions with the structure, as well as providing a method to describe hydrogen bonding (Burns, 1999a). The bond valence approach can be used to identify the valence state of the U cation in well-refined crystal structures. Schindler *et al.* (2004) and Schindler and Hawthorne (2004) have developed a method for predicting the stability of sheet uranyl minerals using the bond-valence deficiency of the sheet edges. Schindler *et al.* (2004) have shown that the surface structure of an edge is characterized by the bond-valence deficiency of anion terminations along chains of polyhedra parallel to the edge, and by the shift and orientation of adjacent layers. The stability of the edges also depends on the arrangement of the interstitial cations between the layers. The edges of the sheet-like uranyl minerals are more reactive than the basal surfaces because the equatorial O-atoms on the edges bond to fewer U^{6+} atoms than oxygen in the sheet, and hence must satisfy their individual bond-valence requirements through a higher degree of protonation (Schindler *et al.*, 2004). The interaction

of the uranyl mineral edge surface with aqueous species controls crystal growth, dissolution, and sorption of other species, including other actinides. These interactions depend on the surface structure of an edge, the pH, and saturation index with respect to the mineral.

(d) Uranyl oxyhydroxides

The uranyl oxyhydrates are not only of importance in the geochemistry of uranium, but they are also one of the primary phases generated during the oxidative dissolution of SNF. Uranyl oxyhydroxides form in U-rich aqueous solutions and develop early during the oxidative dissolution of uraninite ores deposits; hence, they are expected to be the older U(VI) minerals in an oxidized deposit. The complexity of these structures combined with their propensity to dehydrate made their structure characterization difficult; Finch *et al.* (1996a) reported the full structure determination of schoepite and Weller *et al.* (2000) refined the structure of meta-schoepite $\{(UO_2)_4O(OH)_6 \cdot 5H_2O\}$. The uranyl oxyhydroxides are based on electrostatically neutral polyhedral sheets of the form $[(UO_2)_xO_y(OH)_z]$ and no interlayer cations. Water molecules occupy the interlayer sites, linking adjacent sheets through H-bonds. Meta-schoepite possesses one less water molecule than schoepite, leading to 2.8% reduction in the *c*-axis and 0.6 and 0.9% in the *a*- and *b*-directions, respectively. Hughes-Kubatko *et al.* (2005) have shown that meta-schoepite is thermodynamically unstable relative to dehydrated schoepite and have suggested that sodium may be an essential element in natural meta-schoepite. The $U–O_{ax}$ and $U–O_{eq}$ bond lengths in schoepite vary with pH. Allen *et al.* (1996a) determined that $U–O_{ax}$ distances are 1.80, 1.84, and 1.86 Å and $U–O_{eq}$ distances are 2.38, 2.36 and 2.32 Å, at pH 7, 9, and 11, respectively. At pH 11, the uranyl group becomes elongated and the $U–O_{eq}$ bond contracts, such that the structure resembles a clarkeite-like alkali metal uranate. Clarkeite-like sodium uranates have been observed during dissolution of soddyite (Giammar and Hering, 2002) and in the highly caustic environment of the Hanford tank wastes in Washington, USA (Deutsch *et al.*, 2004). Pseudomorphic replacement of pegamatic uraninite by clarkeite $\{(NaCa_{0.5}Pb_{0.5})[(UO_2)O(OH)](H_2O)_{0–1}\}$ may occur during metasomatic alteration by oxidizing hydrothermal fluids (Finch and Ewing, 1997).

The alkali uranyl oxyhydroxides may play an important role in attenuating radionuclides in the environment, including neptunium (Li and Burns, 2001a; Burns *et al.*, 2004a), strontium (Burns and Li, 2002), and cesium (Hoskins and Burns, 2003).

(e) Pb–uranyl oxyhydroxides

As uranium decays to lead, the lead enters cation vacancies in the interlayer, leaving a uranium vacancy in the structural sheet. Although Pb–uranyl oxyhydroxides will form directly from uraninite alteration, many Pb–uranyl minerals are formed though the accumulation of radiogenic lead in nominally Pb-free uranium phases. Accumulation of lead will also destabilize the structure

of some U(VI) minerals. For example, Finch and Ewing (1997) have demonstrated that clarkeite will eventually transform to wölsendorfite or curite. Lead is not incorporated into rutherfordine, soddyite, or uranophane, minerals that may replace early-formed lead uranyl oxyhydroxides. However, several uranyl phosphates and arsenates will incorporate lead. Indeed, Finch and Ewing (1992) suggested that curite, one of the last minerals remaining after complete oxidative dissolution of uraninite, may act as substrate for nucleation of certain phosphates. Burns and Hill (2000b) have synthesized a strontium analog of curite that may be relevant to HLW disposal.

Spriggite, $\{Pb_3[(UO_2)_6O_8(OH)_2](H_2O)_3\}$, has been identified by Brugger *et al.* (2004). The structure is based on $[(UO_2)_6O_8(OH)_2]^{6+}$ sheets of uranyl polyhedra of the β-U_3O_8 anion topology with Pb^{2+} and H_2O in the interlayer. Spriggite has the highest Pb:U ratio (1:2.00) of all known lead uranyl oxide hydrates. Finch and Murakami (1999) have suggested a reaction pathway for increasing alteration of hydrated lead uranyl oxyhydroxides where the molar proportion of PbO can be correlated with the molar proportion of H_2O. With increasing PbO content, charge compensation in the sheet structure results in OH^- substitution for O^{2-}. The U–O_{eq} bonds in the Urϕ_5 pentagonal bipyramids are considerably longer and of lower bond valence than the U^{6+}–O bonds in the Urϕ_4 square bipyramids. The change in uranyl ion coordination from pentagonal to square helps satisfy bond-valence requirements of OH^- in the anion site. Hence, the spriggite adopts Urϕ_4 square bipyramids, whereas the structure of vandendriesscheite (Pb:U = 1:6.36) consists entirely of Urϕ_5 pentagonal bipyramids. Vandendriesscheite, one of the most common Pb-bearing uranyl oxyhydroxides, contains two symmetrically distinct Pb^{2+} cations in the interlayer; both bonded to H_2O groups. The two Pb^{2+} cations (Pb(1) and Pb(2)) are bonded to five and six O_{ur} atoms of adjacent sheets of uranyl polyhedra, respectively. Richetite possesses an extraordinarily complex structure (Burns, 1998b). The phase has been reported at the Shinkolobwe and Jáchymov U-deposits.

(f) Uranyl peroxides

The U-bearing phases, studtite and meta-studtite $\{(UO_2)O_2(H_2O)_2\}$, are the only known peroxide minerals that form during the buildup of α-generated H_2O_2 on the surface of natural uraninite (Walenta, 1974; Deliens and Piret, 1983a; Finch and Ewing, 1992). Burns and Hughes (2003) determined that the structure of studtite is monoclinic, contains one symmetrically distinct U^{6+} cation and four O atoms, two of which occur as H_2O groups. The U^{6+} cation occurs as part of a linear uranyl ion, and each U^{6+} cation is bonded to six additional O atoms, two of which are H_2O groups, and four that are O atoms of the peroxide groups. Unlike all other uranyl oxide hydrate minerals, studtite is not based upon sheet of uranyl polyhedra, but contains polymerized uranyl polyhedra in only one dimension. The occurrence of chains rather sheets in U(VI) minerals is usually due to distortions in the polyhedra, normally the result of lone pairs (e.g. in Se- and Bi-bearing uranium minerals); however, in studtite,

the presence of peroxide at the equatorial positions of the uranyl polyhedra results in distorted hexagonal bipyramids, with the peroxide O–O edge length of 1.46 Å. Typical O–O edge length in uranyl hexagonal bipyramid is 2.4 Å with nitrate or carbonate ligands. This distortion may prevent the formation of two-dimensional layer structures (see Fig. 5.56a).

Radiolysis of water at spent nuclear fuel may create an additional complexity for predicting UO_2 paragenesis in a geological repository (Satonnay *et al*., 2001; Amme, 2002). Studtite and meta-studtite have been identified by McNamara *et al*. (2003) on the surface of corroding commercial spent fuel replacing the meta-schoepite that precipitated earlier. As the H_2O_2 concentration increased with time, studtite and meta-studtite became the dominant alteration phases. H_2O_2 is consumed in the presence of carbonate (Sunder *et al*., 2004), forming peroxo complexes with H_2O_2 and U(VI) (Amme, 2002).

(g) Uranyl carbonates and calcite

Uranyl carbonates tend to form in evaporative environments or under high p_{CO_2} conditions. They are structurally diverse and only relatively few of the uranyl carbonates (rutherfordine (Finch *et al*., 1999b), roubaultite, bijvoetite $\{[M_8^{3+}(H_2O)_{25}(UO_2)_{16}O_8(OH)_8(CO_3)_{16}](H_2O)_{14}\}$, where M is Y or Ln (Li *et al*., 2000), and wyartite (Burns and Finch, 1999) consist of sheets of polyhedra that contain a cation of high valence. Other uranium carbonates contain isolated clusters similar to those observed in solution (Allen *et al*., 1995). The optical signature of the UO_2^{2+} bands in liebigite $\{Ca_2UO_2(CO_3)_3 \cdot 11H_2O\}$, andersonite $\{Na_2Ca[(UO_2)(CO_3)_3](H_2O)_5\}$, and schröckingerite $\{NaCa_3(UO_2)(CO_3)_3(SO_4)F \cdot 10H_2O\}$, that all contain uranyl tricarbonate clusters, are almost identical (Čejka, 1999).

The uranyl monocarbonates (rutherfordine, joliotite $[UO_2CO_3 \cdot nH_2O]$, blatonite $[UO_2CO_3 \cdot H_2O]$, and urancalcarite $\{Ca(UO_2)_3CO_3(OH)_6 \cdot 3H_2O)\}$) are thermodynamically stable, having solubilities comparable to some uranyl oxide hydrates. The uranyl carbonate mineral grimselite, $\{K_3Na[(UO_2)(CO_3)_3](H_2O)\}$ (Li and Burns, 2001b), contains uranyl tricarbonate complexes of composition $[(UO_2)(CO_3)_3]^{4-}$, which occur as an isolated polyhedra in each of the structures, cf. Fig. 5.53. Schröckingerite contains $Na\phi_6$ octahedron, an SO_4 tetrahedron, and three symmetrically distinct $Ca\phi_8$ polyhedra (Hayden and Burns, 2002). The structure contains isolated units of uranyl tricarbonate and sulfate tetrahedra that are coordinated to low-valence cations. Bayleyite, $\{Mg_2[(UO_2)(CO_3)_3](H_2O)_{18}\}$, contains three symmetrically distinct $Mg(H_2O)_6$ octahedra, as well as a $(UO_2)(CO_3)_3$ cluster, and six symmetrically distinct H_2O groups. Swartzite, $\{CaMgUO_2(CO_3)_3 \cdot 12H_2O\}$, contains $Ca\phi_8$ polyhedra and a $Mg(H_2O)_6$ octahedron.

At a partial pressure of $CO_2 > 10^{-2.2}$ atm, rutherfordine becomes the stable uranium phase with respect to dehydrated schoepite; however, the schoepite–rutherfordine equilibrium indicates that p_{CO_2} must be $>10^{-1.9}$ atm before schoepite becomes unstable with respect to rutherfordine. Schoepite is thus expected

to be the U-solubility-controlling phase in waters exposed to atmospheric conditions. Rutherfordine would be expected to replace schoepite in environments where the p_{CO_2} pressure is higher, possibly in a repository environment or in saturated soils. Replacement of schoepite by rutherfordine has been observed at the Shinkolobwe U-deposit (Finch and Ewing, 1992). The structure of rutherfordine was elucidated by Finch *et al.* (1999b) and can be represented by an anion topology that consists of edge-sharing hexagons that share corners, creating pairs of edge-sharing triangles. The rutherfordine sheet is obtained by populating all the hexagons in the anion topology with uranyl ions and one half of the triangles are populated with CO_3 groups. The sheets are held together via van der Waals forces. An identical sheet structure occurs in synthetic $(UO_2)(SeO_3)$.

Burns and Finch (1999) reported the structure of a mixed uranium valence mineral, wyartite that contains U(V) and U(VI). The structure of wyartite contains three symmetrically distinct U positions. The U1 and U2 cations are each strongly bonded to two O atoms with U–O bond lengths of ~1.8 Å, consistent with a linear uranyl ion, whereas the U3 site has seven anions at the corners of a pentagonal bipyramid, with U–O bond lengths of 2.07 and 2.09 Å. A bond valence analysis showed that the U3 site is coordinated by six O atoms and one H_2O group. Two of the O atoms of the bipyramid are shared with a CO_3 group and the sum of bond valences incident at the U3 site is 5.07, in agreement with the assignment of U(V) in this site. Urancalcarite is structurally similar to wyartite and commonly associated with wyartite in nature. Finch and Murakami (1999) suggest that wyartite may oxidize to uranocalcarite. Schindler and coworkers (Schindler and Hawthorne, 2004; Schindler *et al.*, 2004) proposed the formation of the mixed U(V)–U(VI) mineral, wyartite II, on surface of calcite during interaction of acidic and basic uranyl-bearing solutions with calcite.

The structure of fontanite, $\{Ca[(UO_2)_3(CO_3)_2O_2](H_2O)_6$, has been refined by Hughes and Burns (2003) as a monoclinic phase that consists of two symmetrically distinct $Ur\phi_5$ units, one $Ur\phi_6$ unit, and two CO_3 triangles. It is observed in the weathered zone of the Rabejac uranium deposit in Lodève, Hérault, France, where it is associated with billietite and uranophane. Both fontanite and roubaultite possess anion topologies similar to phosphuranylite $\{KCa(H_3O)_3(UO_2)[(UO_2)_3(PO_4)_2O_2]_2(H_2O)_8\}$.

Several uranyl carbonates that contain lanthanides have been described. Bijvoetite is found in association with uraninite, sklodowskite, and uranophane in the oxidized zone at the Shinkolobwe mine (Li *et al.*, 2000). The structure of bijvoetite is extremely complex and contains 16 unique carbonate groups, 39 symmetrically distinct H_2O groups, and 8 unique M^{3+} sites that are occupied by variable amounts of yttrium, dysprosium, and other lanthanides. Astrocyanite $\{Cu_2(Ce,Nd,La)_2UO_2(CO_3)_5(OH)_2 \cdot 1.5H_2O\}$, is another rare earth-bearing uranyl carbonate that is observed as an oxidation product of uraninite. These complex rare earth uranyl carbonates may play an important role in the long-term behavior of released transuranic elements following corrosion of nuclear materials in a geologic repository.

The occurrence of trace amounts of uranyl ions in natural calcite has posed a long-standing problem in crystal chemistry because of speculation that the size and shape of the uranyl ion may preclude its incorporation in a stable lattice position in calcite. The incorporation of uranium in calcite and aragonite provides the basis for U-series age-dating which are commonly adopted for marine and terrestrial carbonates. Uranium is enriched in aragonite relative to calcite owing to the nature of the coordination environment in U-bearing aragonite. Reeder *et al.* (2000) have demonstrated using EXAFS that the dominant aqueous species $UO_2(CO_3)_3^{4-}$ is retained by the uranyl in aragonite, essentially intact. In contrast, a different equatorial coordination occurs in calcite, characterized by fewer nearest oxygens at a closer distance, reflecting that the CO_3 groups are monodentate. The uranyl ion has a more stable and well-defined local environment when co-precipitated with aragonite; however, Reeder *et al.* (2000) argue that as aragonite is metastable with respect to calcite, retention of U(VI) by calcite is likely to be temporary. In contrast, Kelly *et al.* (2003) examined a 13 700-year-old U-rich calcite from a speleothem in northernmost Italy. X-ray absorption spectroscopy data indicated substitution of U(VI) for a Ca^{2+} and two adjacent CO_3^{2-} ions in calcite. This data implied that uranyl has a stable lattice position in natural calcite and suggested that uranium may become incorporated in calcite over long time scales.

Sturchio *et al.* (1998) reported the occurrence of U^{4+} in calcite based on XANES core spectroscopic analysis and concluded that this explained the anomalously high concentrations of uranium observed in calcite in reducing environments. Substitution of Ca^{2+} by Na^{+} was suggested as a possible mechanism to charge balance the structure. The calculated U–O distances reported by Sturchio *et al.* (1998) were (2.21 ± 0.02) Å and (2.78 ± 0.03) Å for U^{4+} in calcite, whereas Reeder *et al.* (2001) estimated $U–O_{eq}$ to be 2.33 Å and $U–O_{ax}$ as 1.80 Å. Interestingly, Sturchio *et al.* (1998) showed a good match of their measured U–O bond lengths with a natural brannerite, where U–O bond lengths were reported as 2.28 and 2.82 Å. However, natural brannerite minerals have recently been shown to be U(V) phases (Finnie *et al.*, 2003; Colella *et al.*, 2005).

(h) Uranyl sulfates

Uranyl sulfates are important in systems where sulfides (e.g. pyrite) are being oxidized. Initial oxidation causes an increase in acidity of the system; however, the acidity may be buffered by the dissolution of carbonate in the surrounding rock, leading to the formation of gypsum. Uranyl sulfates usually occur where uranyl carbonates are absent (and vice versa), owing to the different pH conditions where these minerals will dominate. Uranyl sulfate minerals typically occur as microcrystalline crusts, finely intergrown with other uranyl sulfates and/or monocarbonates. They are common at uranium mines where they form during evaporation of acid sulfate-rich mine drainage waters.

Burns (2001a) and Burns *et al.* (2003) have performed structural refinements on a number of monoclinic zippeite-group U(VI) phases, including zippeite

$\{K_3(H_2O)_3[(UO_2)_4(SO_4)_2O_3(OH)]\}$, sodium-zippeite $\{Na_5(H_2O)_{12}[(UO_2)_8(SO_4)_4O_5(OH)_3]\}$, Mg-zippeite $\{Mg(H_2O)_{3.5}[(UO_2)_2(SO_4)O_2]\}$, Zn-zippeite $\{Zn(H_2O)_{3.5}[(UO_2)_2(SO_4)O_2]\}$, and Co-zippeite $\{Co(H_2O)_{3.5}[(UO_2)_2(SO_4)O_2]$. Each structure contains the zippeite-type layers that consist of chains of edge-sharing $Ur\phi_5$ units that are cross-linked by vertex sharing with sulfate tetrahedra. Marecottite, $\{Mg_3(H_2O)_{18}[(UO_2)_4O_3(OH)(SO_4)_2]_2(H_2O)_{10}\}$, is based on uranyl layers composed of chains of edge-sharing $Ur\phi_5$ biyramids that are linked by vertex-sharing sulfate tetrahedra, identical to zippeite (Brugger *et al.*, 2003). Marecottite and zippeite can co-exist as has been observed in samples from the Jáchymov mine in the Czech Republic. Uranopilite is the only known uranyl sulfate mineral to form chains. The structure consists of clusters of six distinct $Ur\phi_5$ bipyramids that are linked together into a chain by sulfate tetrahedra bonded to two oxygens from each cluster. Adjacent chains are only hydrogen-bonded (Burns, 2001a).

(i) Uranyl silicates

Because of the ubiquity of dissolved silica in most groundwaters, uranyl silicates are the most abundant U(VI) minerals. The uranyl silicates are divided into three groups based on their U:Si ratios (Stohl and Smith, 1981). Accordingly, the structural trends in the uranyl silicates are also dependent on the U:Si ratio (Stohl and Smith, 1981; Finch and Murakami, 1999; Burns, 2001b). In phases with the U:Si ratio of 2:1 and 1:1, no polymerization of the SiO_4 tetrahedra occurs, whereas phases with 1:3 ratios contain chains of vertex-sharing silica tetrahedra. As the U:Si ratio approaches 1:4, the structures contain sheets of SiO_4 tetrahedra. In soddyite, with a ratio of 2:1, each silica tetrahedron shares two of its edges with other uranyl polyhedra, but in structures with the ratio 1:1, only one edge of each silica tetrahedron is shared with a second uranyl polyhedron and each silica tetrahedron is linked to other uranyl polyhedra by vertex sharing.

Uranophane is one of the most common uranyl minerals, and its ubiquity suggests that the uranyl silicates are important phases controlling uranium concentrations in groundwater (Finch and Ewing, 1992). α-Uranophane and β-uranophane have distinctly different crystallographic data and stabilities. Differences in stability were amply illustrated in the study by Cesbron *et al.* (1993) where they failed to synthesize β-uranophane whereas α-uranophane was produced. Both calcium uranyl silicates are common in most oxidized uranium deposits.

The 1:3 silicates (weeksite and haiweeite) are only known from Si-rich environments such as tuffaceous rocks but are commonly observed during the laboratory weathering of borosilicate waste glasses (Ebert *et al.*, 1991; Feng *et al.*, 1994). The structure of weeksite, originally described by Outebridge *et al.* (1960), has been refined by Jackson and Burns (2001). Haiweeite, named for the Haiwee reservoir, California, USA, has been identified at the Nopal I deposit in Peña Blanca, Mexico, where it is associated with uranophane. The structure of weeksite consists of chains of edge-sharing $Ur\phi_5$ pentagonal bipyramids that share edges with SiO_4 tetrahedra. The chains are linked through

disordered SiO_4 tetrahedra to form complex sheets, which in turn form a framework through linkage with SiO_4 tetrahedra (Burns, 1999b).

The only known thorium uranyl silicate mineral, coutinhoite, has been described by Atencio *et al.* (2004) as being isostructural with weeksite. The open channels created by the silicate framework structure are thought to permit the incorporation of Th^{4+}. Oursinite, $\{(Co_{0.86}Mg_{0.10}Ni_{0.04}) \cdot O_2 \cdot UO_2 \cdot 2SiO_2 \cdot 6H_2O\}$, was first reported by Deliens and Piret (1983b) from Shinklolobwe. The phase formed from the oxidation of Co- and Ni-bearing sulfides and demonstrates the ability for U(VI) phases to incorporate a range of elements. Lepersonnite, $\{CaO(Gd,Dy)_2O_3 \cdot 24UO_3 \cdot 8CO_2 \cdot 4SiO_2 \cdot 60H_2O\}$, is a pale yellow uranyl silicate from the Shinkolobwe mine that was first described by Deliens and Piret (1982). The reported compositions of oursinite, lepersonnite, and coutinhoite have immediate implications for radioactive waste disposal for the possible retention of radionuclides, including plutonium, in the environment.

Soddyite is the only known mineral with a U:Si ratio of 2:1; it is also the most common of the uranyl minerals that have structures based on frameworks of polyhedra of higher valence. The structure of soddyite consists of $Ur\phi_5$ units that share equatorial edges to form chains. The chains are cross-linked by sharing edges with SiO_4 tetrahedra in such a way that each tetrahedron shares two of its edges with adjacent chains (Burns, 1999b). Based on observations at the Nopal I site, Pearcy *et al.* (1994) suggested that the precipitation of soddyite may be kinetically more favorable than the formation of other U^{6+} silicates. Soddyite may form from uranophane exposed to dilute metoric waters that are low in carbonate and with a pH below 7. Uranosilite, $\{(Mg,Ca)_4(UO_2)_4(Si_2O_5)_{5.5}(OH)_5 \cdot 13H_2O\}$, has only been reported in nature at a site in Menzenschwand, Germany (Walenta, 1983). Burns *et al.* (2000) reported the occurrence of a new U(VI) silicate from the corrosion of a borosilicate glass with formula $\{KNa_3(UO_2)_2(Si_4O_{10})_2(H_2O)_4\}$, with a U:Si ratio of 1:4. This phase was demonstrated to be structurally distinct from the phase synthesized by Plesko *et al.* (1992). Burns and co-authors suggested that this novel U(VI) silicate may incorporate Np(V).

(j) Uranyl phosphates and arsenates

Uranyl phosphates and arsenates constitute about one-third of the ~200 described uranium minerals (see Table 5.3); yet only a fraction of these have well-defined structures. In groundwaters where $\log\{[PO_4^{3-}]_T/[CO_3^{2-}]_T\} > -3.5$, uranyl phosphate complexes dominate over uranyl carbonate complexes (Sandino and Bruno, 1992). Finch and Ewing (1992) suggested that the occurrence of uranyl phosphates in the most weathered zones of the Koongarra U-deposit indicated that higher oxidation potentials may be necessary for uranyl phosphate precipitation, as uranyl silicates were observed at depth. However, saléeite $(Mg(UO_2)_2(PO_4)_2 \cdot 10H_2O)$ was observed on the surface of apatite where the groundwater was undersaturated with respect to saléeite, indicating that the mineralization occurred by local saturation (Murakami *et al.*, 1997).

Laboratory studies have demonstrated that surface mineralization of saléeite on fluoro-apatite where localized release of Ca and P facilitates autunite formation and U^{6+} uptake (Ohnuki *et al.*, 2004).

Uranyl arsenates are often structurally analogous to the corresponding uranyl phosphates; e.g. the isostructural mineral species abernathyite, $\{K[(UO_2)(AsO_4)](H_2O)_3\}$, and meta-ankoleite, $\{K[(UO_2)(PO_4)](H_2O)_3\}$. Many of the natural uranyl phosphates and arsenates may exhibit complete solid solution formation between end-members. However, in hügelite, $\{Pb_2[(UO_2)_3O_2(AsO_4)_2](H_2O)_5\}$, the presence of arsenic makes the unit cell four times larger than that reported for dumontite, $\{Pb_2[(UO_2)_3(PO_4)_2(OH)_4](H_2O)_5\}$ (Locock and Burns, 2003b). Both structures possess the phospuranylite anion topology. In hügelite, the interlayer contains four symmetrically distinct Pb^{2+} cations. Unlike the lead uranyl oxyhydroxides, hügelite contains only $Ur\phi_5$ and $Ur\phi_6$ polyhedra; yet, it possesses a high U:Pb ratio.

Uranyl arsenates and phosphates may be divided into groups depending on the U:P or U:As ratio. However, a structural classification is more encompassing. The uranium phosphates and arsenates can be separated into four groups: (i) autunite structure; (ii) 3:2 phosphuranylite structure; (iii) uranophane structure; and (iv) chain structures.

(*i*) *Autunite structures*

The most important uranyl phosphates in terms of natural abundance are the autunites and meta-autunite groups. The autunite group of minerals is tetragonal uranyl arsenates and phosphates. The group possesses the general formula $M(UO_2)_2(XO_4)_2 \cdot 8\text{–}12H_2O$ where M may be Ba, Ca, Cu, Fe^{2+}, Mg, Mn^{2+} or $\frac{1}{2}$(HAl) and X is As or P. Takano (1961) obtained unit cell parameters for an autunite specimen from Ningyo Pass, Japan ($a = 6.989$ Å and $c = 20.63$ Å). These were virtually identical to those obtained by Locock and Burns (2003a) on a synthetic autunite. The Pb uranyl oxide hydrate, curite is commonly associated with uranium phosphates such as autunite, torbernite, and parsonsite (Vochten and Deliens, 1980). Finch and Ewing (1992) suggested that the (010) face of curite consists of $\equiv (UO_2) - OH_2^+$ surface species that may provide a reactive pathway for attachment of $(HPO_4)^{2-}$ groups, forming $\equiv (UO_2)$-OPO_3-H_3O^0. This species, once deprotonated, would have the equivalent stoichiometry of chernikovite. Heinrichite $\{Ba[(UO_2)(AsO_4)]_2(H_2O)_{10}\}$ was originally assumed by Gross *et al.* (1958) to be tetragonal, despite the observation of biaxial optical properties. Locock *et al.* (2005b) have refined the structures of several of the barium-bearing phases that possess the autunite sheet structure, including heinrichite and meta-uranocircite $\{Ba[(UO_2)(PO_4)]_2(H_2O)_7\}$ type I and II. There is only the loss of one H_2O group and a slight decrease in the interlayer spacing, from $d_{020} = 8.82$ Å to $d_{020} = 8.43$ Å from going from meat-uranocircite I to II; however, there is a significant re-arrangement in the Ba atomic positions. Table 5.3 lists new refinements from Locock *et al.* (2005b) for these autunite structures; however, because of the difficulties in obtaining

suitable natural specimens, some are based synthetic phases and predictions. These have been listed owing to the apparent inconsistencies in earlier published data. Locock *et al.* (2005c) have published a refinement of uranospathite $\{Al_{1-x}\square_x[(UO_2)(PO_4)]_2(H_2O)_{20+3x}\ F_{1-3x}\}$ with $0 < x < 0.33$ and confirmed the presence of fluorine, the absence of H_3O^+, and a higher Al content in the structure; the empty square in the formula indicates a vacancy. Locock *et al.* (2005c) have described uranospathite as the "Dogwood sandwich" of the autunite group with an interlayer spacing, d_{200} of 15.01Å, possessing 21 H_2O groups per formula unit (*pfu*). The discovery that uranospathite and other aluminum uranyl phosphates possess a number of different hydration states has called into question the traditional division of these minerals into autunite and meta-autunite sub-groups based on the 10-12 H_2O *pfu* and 6-8 H_2O *pfu*, respectively.

(*ii*) *Phosphuranylite structures*

The phosphuranylite group consists of mainly orthorhombic phases with structure sheets of the composition $[(UO_2)_3(O,OH)_2(PO_4)_2]$. Phosphuranylite is remarkable because it contains all three types of Ur polyhedra. The $Ur\phi_5$ and $Ur\phi_6$ occur in the uranyl sheet and the $Ur\phi_4$ occur in the interlayer (Burns, 1999a). It is one of the few minerals with uranium in an interlayer position. Torbernite and meta-torbernite are hydrous copper uranium phosphates, the only difference between the two being the number of water molecules present; the length of the *c*-axis depends on the water content. The structure of monoclinic bergenite, the barium phosphuranylite phase $\{Ca_2Ba_4[(UO_2)_3O_2(PO_4)_2]_3(H_2O)_{16}\}$, has been refined by Locock and Burns (2003c).

(*iii*) *Uranophane structures*

The uranophane structure type occurs in only a few uranium phosphates and arsenates. Ulrichtite, $Cu[Ca(H_2O)_2(UO_2)(PO_4)_2](H_2O)_2$, and the mixed valence arsenite–arsenate uranyl mineral, Séelite, $\{Mg(UO_2)(AsO_3)_{0.7}(AsO_4)_{0.3} \cdot 7H_2O\}$. The name ulrichite was once used as a term for pitchblende; however, the structure of this $Ca–Cu^{2+}$ mineral has now been refined by Kolitsch and Giester (2001).[20] The structure consists of elongated CuO_6 octahedra that are corner linked by two PO_4 octahedra, edge- and corner-sharing $Ur\phi_5$, CaO_8, and PO_4 polyhedra. These form heteropolyhedral sheets parallel to (001) that are linked by the elongated CuO_6 octahedra.

(*iv*) *Chain structures*

Chain structures occur in walpurgite, orthowalpurgite, phosphowalpurgite, hallimondite, and parsonsite. Burns (2000) solved the structure of parsonsite

[20] Problems with the ulrichite structure as described by Birch *et al.* (1988) were recognized by Burns (1999a).

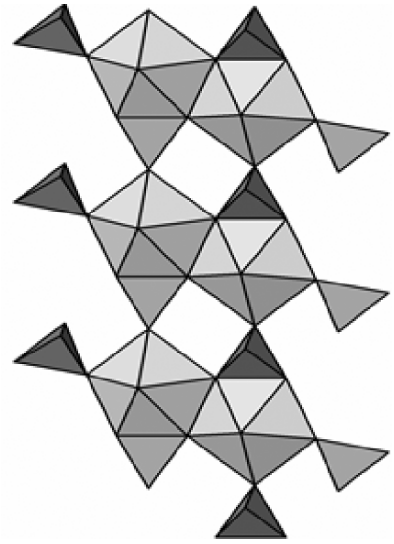

Fig. 5.3 *Parsonsite, the chain uranyl phosphate phase* (*adapted from Locock and Burns*, 2003).

and found that it was composed of uranyl phosphate chains rather than sheets as observed in the autunite and phosphuranylite minerals. The structure consists of $Ur\phi_5$ polyhedra edge-sharing dimers that are cross-linked with two distinct phosphate tetrahedra by edge- and vertex- sharing. Two symmetrically distinct Pb^{2+} cations link the uranyl phosphate chains (see Fig. 5.3).

One of the Pb positions, Pb(1) is coordinated by 9 oxygen atoms, with Pb–O bond lengths ranging from 2.35 to 3.16 Å. Pb(2) is coordinated by 6 oxygens with a distinctly one-sided polyhedral geometry owing to the presence of a lone pair of electrons on the Pb cation. The Pb(2)–O bond lengths range from 2.28 to 3.15 Å. Common to other uranium phases, the lone pair distortion may be responsible for the formation of chains rather than sheets.

Based on structural refinements and infrared spectroscopy, Locock *et al.* (2005a) have shown that parsonsite does not contain any structural water. In most uranyl phosphates and arsenates, water occurs as a hydrate H_2O, either coordinating interlayer cations, or occurring as interstitial H_2O groups. Although Locock *et al.* (2005a) detected water in hallimondite, this was determined not to be critical to structural integrity.

(*v*) *Synthetic uranyl phosphates and arsenates*

Synthetic varieties have also revealed structural differences between phosphate and arsenate uranyl phases that contain the large alkali cations cesium and rubidium. These phosphate and arsenate phases are not isostructural. For

example, cesium uranyl arsenates are not isostructural with cesium uranyl phosphates, but show a homeotypic framework with identical coordination geometries and polyhedral connectivity. The presence of arsenic expands the framework relative to phosphorus and so the cesium uranyl arsenate has a unit-cell volume ~7% greater than the corresponding phosphate.

(*vi*) *Uranium*(*VI*) *phosphates in the environment*

Because of their low solubilities, phosphate and arsenate minerals are of considerable environmental importance for understanding the mobility of uranium in natural systems and they may control the concentration of uranium in many groundwaters. In alkaline environments, dewindite $\{Pb(UO_2)_3(PO_4)_2(OH)_2 \cdot 3H_2O\}$ is stable at low lead concentrations; whereas dumontite is the stable phase in Pb-rich environments. In acid environments, parsonsite is prevalent at high lead levels and przhevalskite $\{Pb_2(UO_2)_3(PO_4)_2(OH)_4 \cdot 3H_2O\}$ occurs under low lead concentrations (Nriagu, 1984). Jerden and Sinha (2003) examined the long-term sequestration of uranium by U(VI) phosphate mineral precipitation at the Coles Hill uranium deposit in Virginia, USA where uranium is released by the oxidation and chemical weathering of an apatite-rich, coffinite–uraninite orebody. Meta-autunite was observed by Buck *et al.* (1996) and Morris *et al.* (1996) in contaminated soils from a former uranium processing plant at Fernald, Ohio, USA.

Significant uraniferous phosphorite deposits occur in Tertiary sediments in Florida, Georgia, and North and South Carolina and in the Hahotoé-Kpogamé U-deposits in Togo, West Africa (Gnandi and Tobschall, 2003). The Florida Phosphorite Uranium Province has yielded large quantities of uranium as a by-product of the production of phosphoric acid fertilizer (Finch, 1996). The discovery that bacteria can reduce U(VI), which appears to precipitate as uraninite, has led to the concept of *in situ* bioremediation of U-contaminated groundwater; however, another possible microbial process for uranium immobilization is the precipitation of U-phosphates. Macaskie *et al.* (2000) have demonstrated that *Citrobacter* sp. will bioprecipitate uranyl phosphate with exocellularly produced phosphatase enzyme. In a similar study by Basnakova *et al.* (1998) a nickel uranyl phosphate was observed in experiments with *Citrobacter* sp.

(k) Uranyl vanadates

Uranyl vanadates comprise some of the most insoluble uranyl minerals, forming whenever dissolved uranium comes in contact with dissolved vanadate anions. The K-bearing uranyl vanadate, carnotite, is possibly the most important source of secondary (U^{6+}) uranium ore minerals, providing ~90% of the uranium production from secondary deposits. It is a lemon-yellow mineral with an earthy luster, a yellow streak, and a specific gravity of about 4. It occurs most commonly in soft, powdery aggregates of finely crystalline material or in thin films or stains on rocks or other minerals. The most noted occurrences of

carnotite are in the Colorado Plateau (Zhao and Ewing, 2000), on the western edge of the Black Hills, South Dakota, USA, and in the Ferghana basin in Kyrgyzstan. It occurs in sandstones in flat-lying, irregular, partially bedded ore bodies. If present in sufficient quantity, carnotite will color the rock bright yellow; but in poorer deposits, particularly below 0.20 percent U_3O_8, it may be difficult to distinguish the uranium mineral from the sandstone itself.

Using solid state reactions, Dion *et al.* (2000) synthesized two new alkali uranyl vanadates, $M_6(UO_2)_5(VO_4)_2O_5$ with M = Na, K, by and determined their structures from single-crystal XRD. Both structures consisted of $[(UO_2)_5(VO_4)_2O_5]^{6-}$ corrugated layers parallel to the (100) plane. The layers contained VO_4 tetrahedra, Urϕ_5 pentagonal bipyramids, and distorted Urϕ_4 octahedra. The Urϕ_5 units were linked by sharing opposite equatorial edges to form zigzag infinite chains parallel to the *c*-axis. These chains were linked together on one side by VO_4 tetrahedra and on other side by Urϕ_4 and Urϕ_5 corner-sharing units.

(l) Uranyl selenites and tellurites

In nature, uranyl selenite minerals form where Se-bearing sulfides are undergoing oxidative dissolution. Selenium occurs as Se(IV), in the selenite anion, SeO_3^{2-}, however, Finch and Murakami (1999) suggested that Se(VI) minerals may be expected under sufficiently oxidizing conditions. Natural uranyl selenites and tellurites include the minerals derriksite, demesmaekerite, guilleminite, larisaite $\{Na(H_3O)(UO_2)_3(SeO_3)_2O_2 \cdot 4H_2O\}$ (Chukanov *et al.*, 2004), and marthozite, $\{Cu[(UO_2)_3(SeO_3)_2O_2](H_2O)_8\}$. The three known uranyl tellurites are cliffordite $\{UO_2(Te_3O_7)\}$, moctezumite $\{PbUO_2(TeO_3)_2\}$, and schmitterite $\{UO_2(TeO_3)\}$. The selenites and tellurites are based upon infinite chains of polymerized polyhedra of higher valence. The chain structures observed with moctezumite and derriksite contains Urϕ_5 and Urϕ_4 bipyramids as well as $Te^{4+}O_3$ and $Se^{4+}O_3$ triangles. They are strongly distorted owing to the presence of a lone pair of electrons on the cation. The crystal structure of marthozite has been refined by Cooper and Hawthorne (2001). There are two unique selenium sites, each occupied by Se^{4+} and coordinated by three O atoms, forming a triangular pyramid with Se at the apex, indicative of the presence of a stereoactive lone pair. The Se–O bond length is ~1.70 Å. The structure possesses one Cu site coordinated by 4 H_2O groups and two O atoms. The structural unit is a sheet of composition $[(UO_2)_3(SeO_3)_2O_2]$, which is topologically identical to the structural unit in guilleminite $\{Ba[(UO_2)_3(SeO_3)_2O_2](H_2O)_3\}$. Adjacent sheets are linked through interstitial Cu^{2+} cations *via* Cu^{2+}-O bonds and *via* H-bonds that involve both (H_2O) groups bonded to Cu^{2+} and interstitial (H_2O) groups.

A number of uranyl selenites containing alkaline metals (Almond *et al.*, 2002), as well as Ag and Pb (Almond and Albrecht-Schmitt, 2002) have been prepared. The structures consist of $[(UO_2)(SeO_3)_2]^{2-}$ sheets constructed from Urϕ_5 units that are linked by SeO_3^{2-} anions, similar to the natural minerals. Synthetic $Sr[(UO_2)_3(SeO_3)_2O_2] \cdot 4H_2O$ prepared in supercritical water was

found to possess the same anion topology as is found in guilleminite and marthozite; however, this phase could not be prepared under ambient or hydrothermal conditions (Almond and Albrecht-Schmitt, 2004).

(m) Uranyl molybdates

Uranyl molybdates are common minerals formed by weathering of uraninite and Mo-bearing minerals (Finch and Murakami, 1999). Umohoite $\{[(UO_2)(MoO_2)](H_2O)_4\}$, is commonly partially replaced by iriginite $\{[(UO_2)(MoO_3OH)_2(H_2O)](H_2O)\}$, which also consists of polyhedra sheets. Iriginite, however, has a distinctive anion-topology arrangement of chains of pentagons and squares that share edges, and zigzag chains of edge sharing squares and triangles (Krivovichev and Burns, 2000a). In the structure of iriginite, each pentagon of the anion topology is populated by an $Ur\phi_5$ polyhedron, two-thirds of the squares are populated with $Mo^{6+}O_6$ octahedra that occur as edge-sharing dimers; the triangles, as well as one-third of the squares, are empty. There have been reports of substantial variability of the *c* dimension of umohoite possibly due to variation of the H_2O content or polytypism that may account for the observed variation in unit-cell parameters (Krivovichev and Burns, 2000b).

The sheets of uranyl and molybdate polyhedra in iriginite and umohoite have features in common. The umohoite to iriginite transformation during alteration of U–Mo deposits, corresponding to a change of the U:Mo ratio from 1:1 to 1:2, involves a change of anion topology to one with a smaller number of edges shared between coordination polyhedra. The uranophane anion-topology is the basis of the umohoite sheet. Construction of the anion topology requires the U and D arrowhead chains as well as the R chain, with the chain-stacking sequence URDRURDR... The iriginite anion-topology contains the same chains as the umohoite (uranophane) anion-topology, but the chain-stacking sequence is DRRRURRRDRRRURRR... The ratio of arrowhead (U and D) chains to R chains in the umohoite and iriginite anion topologies is 1:1 and 1:3, respectively. In the umohoite sheet, all rhombs of the R chains are populated with Mo^{6+} cations, whereas in the iriginite sheet, only two-thirds of the rhombs contain Mo^{6+}, with the remaining third empty. The result is U:Mo ratios of 1:1 and 1:2 in the umohoite and iriginite sheets, respectively. The iriginite anion-topology may be derived from that of umohoite by expansion of the umohoite anion-topology along a vector within the sheet that is perpendicular to the arrowhead chain, together with the insertion of two additional **R** chains between adjacent arrowhead chains. This transformation mechanism requires addition of Mo^{6+} to populate the rhombs of the **R** chains. Another mechanism for obtaining the iriginite anion-topology from that of umohoite is the replacement of every second URD sequence in the umohoite anion-topology with an **R** chain. This mechanism requires the removal of the U^{6+} that populated the **D** and **U** arrowhead chains. Krivovichev and Burns (2000a,b) have suggested that this may appear to be the most likely mechanism of the umohoite-to-iriginite transformation (see Fig. 5.4).

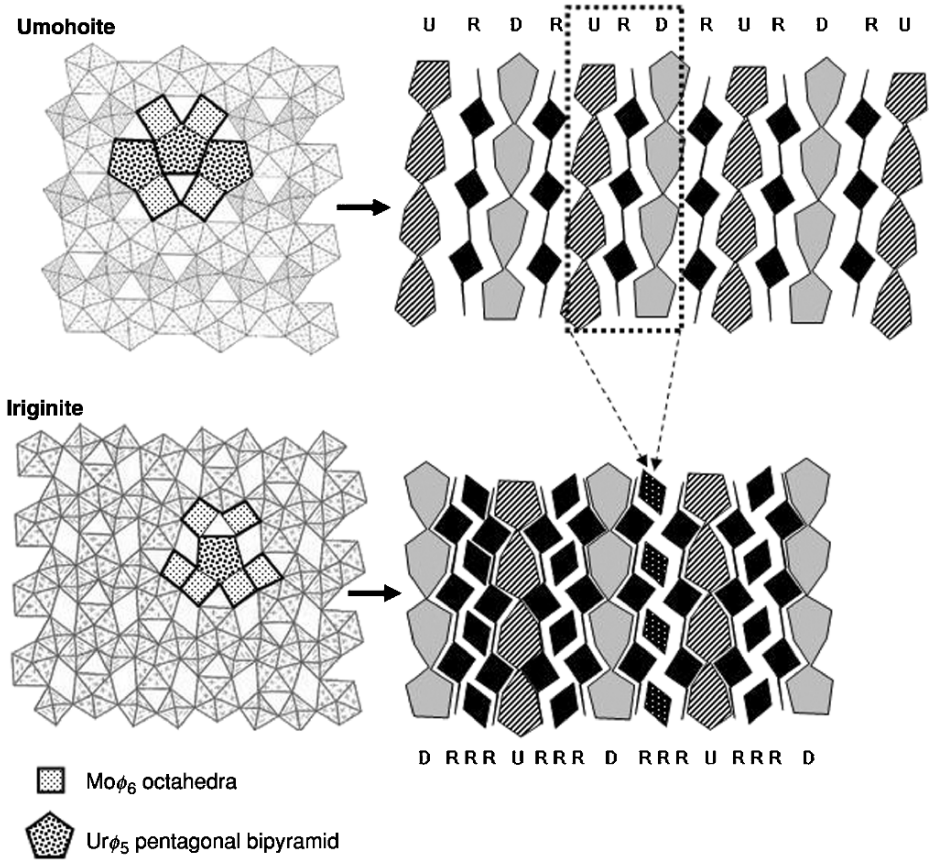

Fig. 5.4 *Diagram showing a possible mechanism for the umohoite to iriginite transformation (adapted from Krivovichev and Burns, 2000a,b). The iriginite structure can be obtained from umohoite through the replacement of every second URD sequence in the unmohoite anion topology with an R chain. This mechanism requires removal of the U^{6+} that occupied the D and U arrowhead chains.*

Mourite $\{U^{4+}Mo^{6+}{}_5O_{12}(OH)_{10}\}$, is a rare U^{4+} mineral containing molybdenum that is observed in oxidized zones in association with umohoite occurring as dark violet crusts and scaly aggregates in the Kyzylsai uranium deposit in Kazakhstan associated with umohoite. Krivovichev and Burns (2002a–c, 2003a) have described several synthetic uranyl molybdates, including Rb, Cs, Ag, and Tl species, respectively.

(n) Uranyl tungstates

Only one natural uranium tungstate is known, uranotungstite $\{(Fe^{2+},Ba,Pb)(UO_2)_2WO_4(OH)_4(H_2O)_{12}\}$; however, there are a wealth of synthetic U(IV) and U(VI) tungstates that have been reported in the literature. The phase UO_2WO_4 is isostructural with UO_2MoO_4, suggesting that the W^{6+} cations are tetrahedrally coordinated by O atoms. Given the structural similarities of Mo(VI) and W(VI), it might be expected that a variety of U(VI)–W(VI) phases should form. The phases $UO_2W_3O_{10}$ and $Na_2UO_2W_2O_8$, has been described but their structures are unknown. U(IV) tungsten bronzes have received considerable attention. The structures consist of ReO_3-type slabs of corner-sharing $W^{6+}O_6$ octahedra. A number of lithium uranyl tungstates ion conductors, such as $Li_2(UO_2)(WO_4)_2$ and $Li_2(UO_2)_4(WO_4)_4O$, have been prepared by high-temperature solid state reactions (Obbade *et al.*, 2004).

(o) Uranium association with clay minerals and zeolites

Chisholm-Brause *et al.* (2001) have identified four distinct uranyl complexes on montmorillonite that co-exist under certain conditions. Inner sphere and exchange-site complexes persist over a range of solution conditions. The uranyl ion sorbs onto montmorillonite at low pH *via* ion exchange, leaving the inner-sphere uranyl aquo-ion structure intact (Dent *et al.*, 1992; Sylwester *et al.*, 2000). At near neutral pH and in the presence of a competing cation, inner-sphere complexation with the surface predominates. Adsorption of the uranyl onto silica and γ-alumina surfaces appears to occur *via* an inner-sphere, bidentate complexation with the surface, with the formation of polynuclear surface complexes occurring at near-neutral pH (Sylwester *et al.*, 2000). Pabalan *et al.* (1993) have performed laboratory tests on the sorptive properties of zeolitic materials for uranium; the sorption is strongly dependent on pH. At near neutral pH U(VI) was strongly sorbed but under conditions where carbonate- and ternary hydroxyl-carbonate-complexes are present the sorption decreased substantially. Della Ventura *et al.* (2002) have discovered a new lanthanide borosilicate minerals of the hellandite group where uranium appears to be incorporated into a borosilicate cage structure. The phase, called ciprianiite $\{Ca_4[(Th,U)(REE)]Al_2(Si_4B_4O_{22})(OH,F)_2]\}$, formed with a syenitic ejectum[21] collected close at

[21] Literally, the violent volcanic explosion of mainly alkali feldspar (syenite) intrusive rock.

Tre Croci within a pyroclastic formation belonging to the Vico volcanic complex (Latium, Italy). Uvarova *et al*. (2004) reported another U^{4+} bearing silicate, arapovite $\{U(Ca,Na)_2(K_{1-x}\square_x)Si_8O_{20}\}$ from the Dara-i-Pioz moraine, Tien-Shan Mountains, Tajikistan.

The thorium and uranium uptake from their aqueous solutions by pristine and NaCl-pretreated zeolite-bearing volcanoclastic rock samples from Metaxades (Thrace, Greece) has been studied using a batch-type method (Misaelides *et al*., 1995). The concentration of the solutions varied between 50 mg L^{-1} and 20 g L^{-1}. The NaCl pretreatment of the materials improved the thorium, but not the uranium, uptake. The absolute thorium uptake by the pretreated material, determined using neutron activation and X-ray fluorescence techniques, reached 12.41 mg g^{-1}, whereas the uranium uptake by the raw material was 8.70 mg g^{-1}. The distribution coefficients (K_d) indicated that the relative thorium and uranium uptake is higher for initial concentrations below 250 mg L^{-1}. The zeolitic materials were very stable despite the initial low pH of the solutions used; however, the pH increased significantly with time due to the simultaneous hydrogen-ion uptake. The thorium and uranium uptake is a complex function of the aqueous chemistry of the elements, the nature of the constituent minerals, and the properties of the zeolitic rock specimens. The various metal species are bound through different sorption processes such as ion-exchange, adsorption, and surface precipitation. Microporous minerals (zeolites, phyllosilicates) are mainly responsible for the large sorption capacity of the rock samples studied.

5.4 ORE PROCESSING AND SEPARATION

Because of the complexity of many uranium ores and the usual low concentrations of uranium present, the economic recovery of uranium often poses a difficult problem for the chemist. Physical concentration methods (flotation, gravitational, electromagnetic, etc.) have met with only limited success for uranium. The chemical methods used for the recovery of uranium from ores thus have to be designed to treat large ore volumes economically. Because of this and because uranium is a very electropositive metal, most direct pyrochemical methods are not applicable and processes usually involve modern aqueous extractive metallurgy. In this section the more important aspects of the extractive metallurgy of uranium will be described with emphasis on the chemical principles involved.

Uranium ores vary in chemical complexity from the relatively simple pitchblendes, which are accompanied by perhaps 10 other minerals, to exceedingly complex and refractory uranium-bearing titanites, niobates, and tantalates containing rare earths and many other metals. Included are uranium minerals accompanied by major admixtures of ill-defined organic compounds. Some pitchblende ores may have as many as 40 elements present from which

uranium must be separated. Many uranium deposits are variable in composition, resulting in an almost daily variation in the composition of the starting materials. Such variations are minimized by stockpiling methods. Nevertheless there have been many *ad hoc* procedures elaborated to meet special chemical situations. Most such highly specialized methods will have little interest for this discussion. The general features common to most procedures will, however, be pertinent. All methods that have been commonly used comprise the following steps: (1) pre-concentration of the ore; (2) a leaching operation to extract the uranium into an aqueous phase – this step frequently being preceded by roasting or calcination to improve the extraction; and (3) recovery of the uranium from the pregnant leach liquors by ion exchange, solvent extraction, or direct precipitation, and in the case of ion-exchange or solvent extraction products by a final precipitation. Special methods may be used for recovery of by-product uranium. The product of these operations is a high-grade concentrate, which is usually further purified at a site other than the uranium mill.

The extractive metallurgy of uranium has been discussed in detail in various books (Vance and Warner, 1951; Clegg and Foley, 1958; Harrington and Ruehle, 1959; Chervet, 1960; Bellamy and Hill, 1963; Gittus, 1963; Galkin and Sudarikov, 1966; Merritt, 1971) and in collections of papers (United Nations, 1955, 1958, 1964; IAEA, 1966, 1970). There is also a bibliography on feed materials (Young, 1955). The most comprehensive collection of data is the multi-volume supplement to the *Gmelin Handbook of Inorganic Chemistry* (Gmelin, 1975–1996), more particularly its volume (A3) on Technology and Uses (Gmelin, 1981a). Many other references can be found in these sources.

5.4.1 Pre-concentration

Most uranium ores contain only small amounts of uranium, and because leaching is a relatively expensive operation, much effort has been expended to reduce the magnitude of the leaching operation by pre-concentration of the ore. Physical concentration methods (gravitational, electrostatic, flotation) and various sorting methods have been either used or proposed for upgrading of uranium ores. Unfortunately such beneficiation methods have not achieved great success, only a few of the uranium ores processed being amenable to physical beneficiation processes. Only in a few cases can appreciable concentration of uranium be achieved without excessive loss to tailings.

Uranium minerals as well as other minerals, with which they are closely associated, are denser than many gangue materials and successful gravity separation methods are sometimes possible. Such gravity separations are complicated by the fact that uranium minerals tend to concentrate in the fines upon crushing or grinding of some ores. This property has been used to some advantage in that a certain degree of mechanical concentration can be achieved by a gentle grinding followed by screening. Electrostatic methods generally give low recoveries or low concentration factors. Magnetic separation methods have

generally been used to remove gangue materials such as magnetite, ilmenite, garnet, etc. Flotation methods have received considerable laboratory attention although they do not appear to have been widely applied. Flotation of undesirable gangue materials such as sulfides has met with some success, but no flotation agents have been developed for uranium minerals that give concentration factors approaching those obtained in the processing of sulfide minerals. Flotation has met with some success in splitting carbonate-containing ores into a carbonate and a non-carbonate fraction so that the former fraction can be leached by the carbonate method and the other with sulfuric acid. Both manual and mechanical sorting methods have been applied to the upgrading of uranium ores. In this procedure individual lumps of ore are sorted either by hand or by mechanical devices usually on the basis of radiation readings for the individual lumps. Merritt (1971) reviewed various mechanical upgrading techniques in some detail.

5.4.2 Roasting or calcination

It is frequently desirable to subject ores to high-temperature calcination prior to leaching. Several functions can be performed by such roasting operations. An oxidizing roast can remove carbonaceous material and put the uranium in soluble form. It can oxidize sulfur compounds to avoid subsequent polythionate and sulfur poisoning of ion-exchange resins. It removes other reductants, which might consume oxidant during the leaching step. Reducing roasts can convert uranium to the reduced state and prevent dissolution of uranium during by-product recovery.

Roasting also improves the characteristics of many ores. Many of them contain clays (particularly of the montmorillonite class), which cause thixotropic slurries and create problems in leaching, settling, and filtering. Dehydration of these clays alters their physical properties and decreases these problems.

Roasting with sodium chloride is commonly used with vanadium-containing ores to convert the vanadium to a soluble form. Sodium vanadate is formed, which is believed to form soluble uranyl vanadates (Merritt, 1971). Salt roasting has also been used to convert silver to silver chloride for easier separation from soluble components.

5.4.3 Leaching or extraction from ores

The object of this procedure is to extract the uranium present in the ore into solution, usually aqueous, from which the recovery and purification of the uranium from accompanying metals can be carried out. The leaching operation is usually the first of the chemical manipulations to which the ore is subjected, and all present chemical processing methods for any type of ore involve digestion of the ore with either acid or alkaline reagents. The acid reagent may be

generated *in situ* by bacterial or high-pressure oxidation of sulfur, sulfides and Fe(II) in the ore to sulfuric acid and ferric [Fe(III)] species. The choice of a reagent for a particular case will be determined primarily by the chemical nature of the uranium compounds present in the ore and the gangue materials that accompany them.

The extraction of uranium from the majority of the ores is generally more complete by acid leaching than with alternative leaching procedures and is therefore used in most mills. While other acids can be used, sulfuric acid is employed because of its lower price, except when hydrochloric acid is available as a by-product of salt roasting. As a general principle only uranium (VI) minerals are readily dissolved in sulfuric acid. For uranium minerals, such as uraninite, pitchblende, and others, containing uranium in lower oxidation states, oxidizing conditions must be provided to ensure complete extraction. Oxidizing conditions are provided by agents such as manganese dioxide, chlorate ion, ferric ion, chlorine, or molecular oxygen. Manganese dioxide and chlorate ion are most commonly used and iron must be present in solution as a catalyst in order for either of them to be effective.

Manganese dioxide to the extent of perhaps 5 kg per ton (but typically about one-half of this in U.S. practice) or up to 1.5 kg $NaClO_3$ per ton of ore are usually adequate for all but the very refractory ores. Free ferric-ion concentrations larger than 0.5 g L^{-1} generally give adequate dissolution rates. Sufficient iron is normally provided by the ores themselves and by the ore-grinding process. Typical dissolution reactions are

$$UO_2 + 2Fe^{3+} \rightarrow UO_2^{2+} + 2Fe^{2+}$$

$$2Fe^{2+} + MnO_2 + 4H^+ \rightarrow 2Fe^{3+} + Mn^{2+} + 2H_2O$$

$$6Fe^{2+} + ClO_3^- + 6H^+ \rightarrow 6Fe^{3+} + Cl^- + 3H_2O$$

To avoid excessive consumption of oxidant this is in general not added to the acidified ore until the reaction with free iron and sulfides is practically complete. Manganese can be recovered at later stages as manganese(II) hydroxide followed by ignition in air at 300°C to the dioxide. When only a small fraction of the uranium is in reduced form, agitation with air is often sufficient to maintain oxidation by ferric ion. Various other oxidants are effective, including chlorine, permanganate, bromine, etc., but cost or difficulty of handling (corrosiveness, etc.), have relegated their use to very special situations. Proper addition of oxidizing agent can be controlled by an empiric potentiometric measurement of the redox potential. If the potential between a platinum and a calomel electrode inserted into the digesting ore mixture is adequately controlled, the iron will be present principally as Fe^{3+} and suitable oxidizing conditions will have been imposed (Woody and George, 1955).

The most common form in which acid leaching is applied is in the form of aqueous leaching with agitation. The sulfuric acid concentration is adjusted so that it close to pH 1.5 at the end of the leaching period; the period of extraction

is generally 4–48 h, in U.S. practice typically 4–24 h. Elevated temperatures and higher acid concentrations increase the rate of extraction but are often uneconomic and result in higher reagent consumption, increased corrosion, and increased dissolution of non-uranium minerals. Counter-current leaching in several stages is sometimes used but is less common than single stage processes. Recycle circuits have also been devised to use the acid leachant more efficiently. A less common procedure is acid pugging, in which a small amount of dry, ground ore is mixed with a more concentrated acid to form a plastic mass, which is allowed to cure and then leached with water. Percolation leaching, in which solution percolates slowly through an ore bed, is well-suited to ores in which the uranium minerals occur as coatings on sand grains, particularly when the ore is of low grade. A variation of percolation leaching that has important application to low-grade ores is heap leaching, in which 5–10 m deep piles of ore of about 100 m length are leached by slow percolation of an acid solution that is collected in the pile drainage. *In situ* leaching is another method that has been applied to certain ore bodies with low permeability of the rock underlying the deposit and adequate porosity of the ore body itself. In this procedure, wells are drilled into the ore body and leachant is pumped into some of these while the enriched solutions are pumped from other wells.

Two acid leaching methods require no reagent addition in some ores containing sulfides or sulfur. These methods are pressure leaching, in which air is the oxidant at elevated temperatures ($\sim$150°C) and pressures, and bacterial leaching, where air is also the oxidant but at temperatures near ambient. In both cases uranium dissolution is brought about by the oxidation of iron and sulfur compounds to Fe^{3+} and sulfuric acid. Typical reactions in pressure leaching are

$$4FeS_2 + 15O_2 + 2H_2O \rightarrow 2Fe_2(SO_4)_3 + 2H_2SO_4$$
$$UO_2 + Fe_2(SO_4)_3 \rightarrow UO_2SO_4 + 2FeSO_4$$
$$4FeSO_4 + 2H_2SO_4 + O_2 \rightarrow 2Fe_2(SO_4)_3 + 2H_2O$$

Similar overall reactions occur in bacterial leaching through the action of bacteria, such as *Thiobacillus ferrooxidans* and others, on ferrous ion, sulfur, and sulfides. Although there are several reported advantages of high-pressure leaching, such as improved extraction and shorter extraction times, particularly with refractory ores, there is also larger corrosion and higher maintenance costs and the method has received little actual use. Bacterial leaching appears to be particularly attractive as a low-cost recovery method for very low-grade ores when used with heap or *in situ* leaching.

While acid leaching is excellent for many ores, and is essential for primary refractory ores such as euxenite, davidite, and brannerite, it is subject to certain limitations. Most uranium minerals are soluble in dilute sulfuric acid with an oxidant present, but many ores contain other minerals such as calcite, dolomite, and magnesite, which consume sufficient amounts of acid to make

acid leaching uneconomic. In such cases, carbonate solutions are used to extract uranium.

Carbonate leaching is usually carried out with sodium carbonate. The utility of carbonate solutions arises from the high stability of the uranyl(VI) tricarbonate ion, $UO_2(CO_3)_3^{4-}$, in aqueous solution at low hydroxide-ion concentration. Uranium(VI) is thus soluble in carbonate solution, unlike the vast majority of other metal ions, which form insoluble carbonates or hydroxides in these solutions. The sodium carbonate leaching is thus inherently more selective than the sulfuric acid procedure. In general, compounds of uranium(VI) are readily soluble in carbonate leach solutions although silicates dissolve, albeit with some difficulty. Minerals containing uranium in its lower oxidation states are insoluble in carbonate solutions, and oxidants are required. Under oxidizing conditions, simple uranium oxides and some other uranium(IV) minerals such as coffinite can be leached, particularly at elevated temperature.

In addition to the advantage of low reagent consumption in carbonate-containing ores, carbonate leaching is relatively (but not completely) specific for uranium and carbonate solutions, which are moderately non-corrosive. Disadvantages include lower uranium extraction than by acid leaching and that the method is not suitable for ores having high gypsum or sulfide content. Important refractory minerals such as euxenite, brannerite, and davidite are not attacked significantly without a prior fusion step. Since few ore components other than uranium minerals are attacked to any appreciable extent by carbonate solutions, any uranium imbedded in gangue will escape leaching. A carbonate leach thus requires sufficiently fine grinding to liberate the uranium. Economics dictate that the reagents must be recovered and recycled in the carbonate leach process.

Oxygen (often under pressure) is the commonly used oxidant in carbonate leaching and the dissolution of simple uranium oxide follows the reactions (Merritt, 1971).

$$2UO_2 + O_2 \rightarrow 2UO_3$$
$$UO_3 + H_2O + 3CO_3^{2-} \rightarrow UO_2(CO_3)_3^{4-} + 2OH^-$$
$$OH^- + HCO_3^- \rightarrow CO_3^{2-} + H_2O$$

As shown in the equations above, bicarbonate is used to prevent increase in the hydroxide concentration, which would result in precipitation of uranates or polyuranates by the reaction

$$2UO_2(CO_3)_3^{4-} + 6OH^- + 2Na^+ \rightarrow Na_2U_2O_7 + 6CO_3^{2-} + 3H_2O$$

The detailed dissolution mechanisms are more complex than represented here and several possible alternatives have been proposed (Clegg and Foley, 1958; Wilkinson, 1962; Merritt, 1971). Although air is the most commonly used oxidant in carbonate leaching, other oxidants have been used. Potassium permanganate was commonly used in the past but was expensive and replaced

by pressurized leaching at 95–120°C in air. This was followed by the use of cupric–ammonia complexes, a catalyst for air oxidation, but current practice is toward simply using air at atmospheric pressure and longer dissolution times at about 75–80°C in Pachuca-type (air-agitated) tanks (Merritt, 1971). Pure oxygen has been used (Woody and George, 1955) in place of air with some advantages. Other oxidants that have been considered are NaOCl, H_2O_2, and $K_2S_2O_8$. Various catalysts such as $MgCl_2$, Ag_2SO_4, $K_3Fe(CN)_6$, copper–cyanide complexes, and copper–, nickel–, and cobalt–ammonia complexes have also been studied.

Although sodium carbonate is the only reagent used commercially in alkaline leaching, ammonium carbonate has been extensively tested in the laboratory and pilot plant (Merritt, 1971). Since the concentrations of sodium carbonate and bicarbonate used are typically 0.5–1.0 M, the recovery of reagents is necessary. The specificity of carbonate leaching for uranium is such that the uranium can usually be recovered from the leach solution by precipitation as sodium polyuranates ('diuranate') with sodium hydroxide. The filtrate is then treated with carbon dioxide to regenerate the desired carbonate/bicarbonate ratio.

While the amounts of carbonate, bicarbonate, and oxygen consumed during leaching are usually very small, side reactions may occur with other constituents of the ores, which consume substantial amounts of carbonate. Particularly important parasitic reactions are due to sulfide minerals and gypsum and, at higher temperatures and pressures, silica and alumina:

$$2FeS_2 + 15/2O_2 + 8CO_3^{2-} + 7H_2O \rightarrow 2Fe(OH)_3 + 4SO_4^{2-} + 8HCO_3^-$$

$$CaSO_4 + CO_3^{2-} \rightarrow CaCO_3 + SO_4^{2-}$$

$$SiO_2 + H_2O + 2CO_3^{2-} \rightarrow SiO_3^{2-} + 2HCO_3^-$$

$$Al_2O_3 \cdot 3H_2O + 2CO_3^{2-} \rightarrow 2AlO_2^- + 2HCO_3^- + 2H_2O$$

Flotation may be used to reduce the initial sulfide content to tolerable limits.

Organic materials in some ores cause difficulties in the carbonate leach process and various schemes for handling this problem are reviewed by Merritt (1971). A simplified flow sheet for carbonate leaching is shown in Fig. 5.5.

Clarification is the separation of ore slimes from the aqueous uranium extract and constitutes the final step in ore extraction of uranium. It is a necessary step except when the resin-in-pulp ion-exchange process is used, in which case only partial clarification is necessary, and when *in situ*, heap, or percolation leaching has been used, since the ore itself acts as an effective filter medium in these leaching techniques and clear solutions are obtained. Solution clarification has in the past been one of the most difficult problems in uranium recovery, but flocculants have been developed (Clegg and Foley, 1958) to improve settling of clays and other slimy ore constituents. These have greatly improved liquid–solid separation technology and most ores can now be handled satisfactorily in liquid–solid separation equipment with the proper choice and use of flocculants.

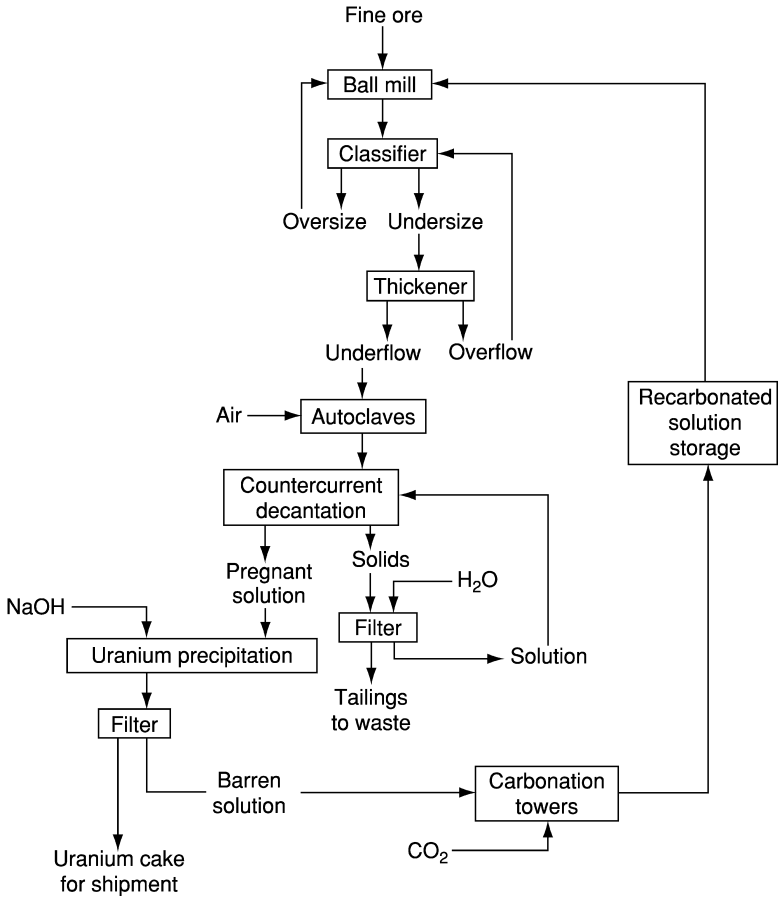

Fig. 5.5 *Flow sheet of raw ore leach for unoxidized or primary uranium of Eldorado Mining and Refining Ltd, Beaverlodge, Saskatchewan* (*Stephens and McDonald*, 1956).

Flocculants used include polyacrylamides, guar gums, and animal glues. For the resin-in-pulp process, only the coarser ore particles (325 mesh) are removed and slime contents of 5% to as high as 20% solids can be handled depending on exact process design. Clegg and Foley (1958) and Merritt (1971) review clarification in detail.

5.4.4 Recovery of uranium from leach solutions

The recovery of uranium from leach solutions can be achieved by a variety of methods including ion exchange, solvent extraction, and chemical precipitation. Each of the various procedures listed above can be applied to acid or alkaline

leach liquors, although in general they will not be equally applicable. Although various precipitation methods were extensively used in the past, they were generally cumbersome and complex if significant uranium purification was to be achieved. Currently operating uranium mills, with the exception of some that employ carbonate leaching, all use ion exchange or solvent extraction, or both, to purify and concentrate the uranium before a final product precipitation. Because of the selectivity of carbonate leaching, precipitation from carbonate leach solutions produces a fairly pure uranium concentrate, but for acid leach solutions, ion exchange or solvent extraction is always employed.

(a) Ion exchange

The recovery of uranium by ion exchange is of great importance. Uranium(VI) is selectively absorbed from both sulfate and carbonate leach solutions as anionic complexes using anion-exchange resins. The loaded resin is rinsed, and the uranium eluted with a sodium chloride or an acid solution. The uranium is then precipitated from the eluate and recovered as a very pure uranium concentrate. This process can be carried out with either stationary columns of ion-exchange resin through which clarified leach liquors are passed; alternatively the resin may be moved through the leach liquor in agitated baskets. This resin-in-pulp process does not require complete clarification of the leach liquor.

The degree of purification of the uranium by these ion-exchange processes is related to the selectivity of the anion-exchange resins for the anionic uranyl sulfate or carbonate complexes relative to that of impurity species. Cationic impurities are not absorbed and many anionic species are absorbed less strongly than are the uranyl complexes and are displaced by them. The impurities can be left in the ion exchangers during uranium elution, but often they are so strongly absorbed as to act as exchanger poisons that require elaborate removal steps.

The uranyl species absorbed by the exchangers from carbonate solution appears to be exclusively the $UO_2(CO_3)_3^{4-}$ complex, but from sulfate solutions more than one species is absorbed (Ryan, 1962). Although it has been reported (OECD-NEA, 1982) that below pH 2 the only uranyl sulfate complex in the resin is $UO_2(SO_4)_3^{4-}$, spectral studies of the resin phase (Ryan, 1962) indicate that, although $UO_2(SO_4)_3^{4-}$ is present over at least the pH range 0.5–4.5, it is not the only uranyl species. The ratio of uranyl species in the resin phase changes with pH but is almost unaffected by change in total aqueous phase sulfate concentration at any given pH. Even if the affinity of anion-exchange resins for complex anions may be very high, high distribution coefficients do not necessarily mean that an appreciable fraction of the uranium is present as anionic species in the aqueous phase. Both weak-base or strong-base resins can be used with the sulfate system, but only the strong-base resins in the basic carbonate solutions. In practice, the resin choice is governed by several factors, including absorption and elution kinetics, resin particle size, the physical and

chemical stability of the resin, the selectivity and ease of removal of resin poisons, hydraulic characteristics, and exchange capacity. Typically, resins of moderately low cross-linking and moderately large particle size are used and several resins have been marketed specifically for uranium processing.

Elution of the uranium from anion-exchange resins in either the sulfate or the carbonate processes is normally made with approximately 1 M sodium or ammonium chloride or nitrate solutions. In the sulfate process the eluent is acidified, and in the carbonate process some carbonate or bicarbonate is added to prevent hydrolysis. Special elution techniques are used for vanadium recovery when it is co-absorbed in the carbonate process (Merritt, 1971).

Although uranyl sulfate and carbonate complexes have a higher affinity for the resin than most impurity ions, they are not extremely strongly sorbed and some impurity ions are more strongly absorbed. In the acid system such ions include pentavalent vanadates, molybdenum sulfate complexes, polythionates, and in South African ores treated for gold recovery, cobalt cyanide complexes and thiocyanate. Vanadates are more strongly absorbed than uranium in the carbonate process except at high pH values. In addition, some other weakly sorbed ions may be present in sufficiently high concentration to compete for resin sites, resulting in decreased uranium loading; some of these may also alter absorption kinetics. Some of the strongly held ions and others such as silicate, titanium, thorium, hafnium, niobium, antimony, and arsenate and phosphate complexes, which polymerize or hydrolyze in the resin phase, are not readily removed during the normal elution process. They gradually build up in the resins where they act as poisons and require special removal procedures (Merritt, 1971).

Merritt (1971) and Clegg and Foley (1958) have reviewed the uranium ion-exchange processes in detail along with the various specialized problems encountered and their treatment. They have discussed specific flow sheets, processing rates, back-cycle methods for reagent conservation, and processing equipment for fixed-bed, moving-bed, basket resin-in-pulp, and continuous resin-in-pulp ion-exchange processes.

(b) Solvent extraction

Solvent extraction has a distinct advantage over ion exchange for uranium purification from leach liquors because of the ease with which it can be operated in a continuous counter-current flow process. It has a disadvantage, however, in the incomplete phase separation, due to emulsion formation, third-phase formation, etc. In addition solvent losses constitute both a monetary loss and a potential pollution problem in the disposal of spent leach liquor. Because solvent losses are related to overall solution volume, solvent extraction usually has an advantage for leach solutions with concentrations above about 1 g U per liter, and ion exchange has an advantage for low-grade solutions with concentrations appreciably less than 1 g U per liter (Merritt, 1971). Solvent extraction

processes are not economically advantageous for carbonate leach solutions. Two types of alkyl phosphoric acids and secondary and tertiary alkylamines, have been used industrially for uranium extraction from sulfate leach liquors. These extraction reagents are normally used as relatively dilute solutions in an inert diluent such as kerosene. Modifiers such as long-chain alcohols and neutral phosphate esters are typically added to prevent third-phase formation to increase amine salt solubility in the diluent, and to improve phase separation.

Amine extraction from sulfate leaching is analogous to anion exchange in that anionic uranyl sulfate complexes are extracted by the alkylammonium cations. The species extracted, at least by tertiary amines, is predominantly the $UO_2(SO_4)_3^{4-}$ complex in the pH range ($1 < pH < 2$) normally used in commercial processing. The concentration of other uranyl species increases with decreasing pH (Ryan, 1962). There is considerable variation in affinity and selectivity for uranium with the structure of the amine. Typical commercially used tertiary amines give extraction coefficients of 100–140, whereas *N*-benzylheptadecylamine gives extraction coefficients as high as 8000 (Merritt, 1971). Such specialized amines, if made available at a reasonable cost, will be capable of recovering uranium from very dilute leach solutions but might require more complex stripping procedures. Amines extract other anions to varying degree and thereby decrease uranium extraction efficiency. Nitrate interference is severe and chloride interference is more severe for secondary than for tertiary amines. These factors are important for the choice of stripping agent and the recycling of solutions. Molybdenum is extracted more strongly than uranium. It builds up as a poison in the amine, finally causing serious problems by precipitating at the organic–aqueous interface, and special molybdenum stripping procedures are used to counteract this problem (Merritt, 1971). Vanadium is also extracted to some extent. Various ions are effective in stripping uranium from the solvent. Nitrate has such high affinity for the amine that it must be removed in the carbonate or hydroxide regeneration step before the next extraction cycle; however this is not necessary in solutions containing chloride, except with secondary amines having high chloride affinity. Another procedure uses ammonium sulfate with pH carefully controlled in the range 4.0–4.3, since poor stripping or poor phase separation occurs outside this range. Direct precipitation of uranium from the organic phase has been proposed (Brown *et al*., 1958).

The alkylphosphoric acid extractants have the advantage over amines of fewer phase separation problems due to suspended solids and of having good extraction efficiency in the presence of dilute nitrate, chloride, and sulfate. On the other hand, they suffer from lower selectivity for uranium since the alkyl phosphates extract cations and many of the impurities including iron in the leach solutions. Special methods for removing or rendering these impurities non-extractable have been devised. Alkylphosphoric acid extraction has been referred to as 'liquid cation exchange'. The dialkyl phosphates appear to be

dimers and four dialkyl phosphates are required to extract one uranyl ion (Baes *et al.*, 1958; Blake *et al.*, 1958). Addition of neutral phosphate esters increases the uranium extraction coefficient of alkylphosphoric acids (synergistic effect). Stripping of bis(2-ethylhexyl)phosphoric acid is normally carried out with carbonate solution, but monodecylphosphoric acid requires 10 M HCl for stripping.

In addition to the solvent extraction procedures discussed above, mixed amine–alkylphosphoric acids have also been used. Other processes include both ion-exchange and solvent-extraction steps as well as special methods for removing and in some cases recovering interfering ions such as molybdenum. Solvent extraction methods have also been studied in cases where the leach solution is not clarified, solvent-in-pulp, but solvent losses are then very high. Merritt (1971) has reviewed the commercial practice in detail and gives many further references.

(c) Chemical precipitation

Before the use of ion-exchange and solvent extraction methods for the removal and purification of uranium from leach liquors, precipitation techniques were used on clarified leach liquors. Much effort was spent during the late 1940s to develop selective precipitation processes; most of these techniques are obsolete and will not be discussed here but they are reviewed by Wilkinson (1962) and by Merritt (1971).

The product from typical acid process anion-exchange or solvent extraction processes is an acid solution of mixed nitrate or chloride and sulfate. The two principal methods of precipitation of uranium from these are neutralization with sodium hydroxide, magnesia, or ammonia, or the precipitation of the peroxide $UO_4 \cdot xH_2O$ in the pH range 2.5–4.0 with hydrogen peroxide. In the neutralization procedure a preliminary pH adjustment to 3.5–4.2 is made to precipitate and remove iron if it exceeds specifications. Phosphate, if present, is also removed in this step as iron phosphate. Uranium precipitation is then accomplished at a pH of 6.5–8.0. Since the cations used (Na^+, M^{2+}, or NH_4^+) contaminate the product by formation of insoluble polyuranates, the choice of precipitant will depend on cost, physical nature of the precipitate formed, product specifications, etc. Most U.S. plants now use ammonia, which can be removed by heating of the product, but there is also some use of magnesia. The peroxide precipitation process is more specific although the cost is somewhat higher, a higher-purity product is obtained. Ferric ions must be removed to a concentration less than 0.5 g L^{-1} in order to prevent catalytic decomposition of hydrogen peroxide in a preliminary precipitation step; alternatively the decomposition is prevented by precipitation from very cold solutions or by complexing the iron. The precipitates ('yellow cake') are dried, and in the case of the ammonia, precipitated material of composition approximately $(NH_4)_2U_2O_7$ (ammonium diuranate) may be heated to form U_3O_8 or UO_3, depending on

temperature. The magnesium and sodium polyuranates are stable to low-temperature calcination.

Precipitation from alkaline solution is carried out with either clarified carbonate leach solution or with alkaline eluting or stripping solutions from ion exchange or solvent extraction. The three methods include addition of strong base, acidification followed by CO_2 removal and neutralization, and reduction to U(IV). The latter method is the only one capable of direct recovery of any vanadium present; the other ones do not result in complete recovery or complete separation. Sodium hydroxide does not completely precipitate uranium from carbonate solution; despite this, the filtrate is recarbonated and recycled. The product consists of sodium polyuranates. Acidification, carbon dioxide removal by boiling, and neutralization (usually with ammonia or magnesia) is preferred for the high-uranium-concentration carbonate strip solutions from solvent extraction since the volume is low and recycling of reagents is not so important. Reduction of uranyl(VI) carbonate solutions results in precipitation of hydrated U(IV) oxide. Reduction methods include hydrogen reduction under pressure in the range 100–200°C with appropriate catalyst, electrolytic reduction, and sodium amalgam reduction. Vanadium is reduced and co-precipitated with uranium. Merritt (1971) has reviewed precipitation conditions, flow sheets, and plant practice in detail.

(d) By-product uranium

In South Africa, uranium is recovered as a by-product of gold recovery by conventional methods after the recovery of gold by cyanide leaching. Uranium has also been recovered as a by-product from crude phosphoric acid by both ion exchange and solvent extraction methods. In anion exchange, U(VI) is absorbed and concentrated by absorption of uranyl phosphate complexes, but resin capacities are uneconomically low. Solvent extraction has normally involved use of alkyl pyrophosphate extraction of U(IV) (Greek *et al.*, 1957), but other schemes utilize extraction of U(VI) and synergistic combinations of phosphates. References to previous work in this field are given in a paper on this subject (Deleon and Lazarević, 1971).

(e) Refining to a high-purity product

The normal product of uranium milling operations, 'yellow cake' or calcined 'yellow cake', is not sufficiently pure to be of nuclear grade and is normally further refined to produce nuclear-grade material (IAEA, 1980). There has been some emphasis on further upgrading in the mill to produce a high-grade product by using multiple stages of solvent extraction and/or ion exchange, special stripping methods, more selective precipitation methods, or combinations of these (see Merritt, 1971 for further detail). The usual refining operation has

normally been carried out either by tri(*n*-butyl)phosphate (TBP) extraction from nitric acid solutions or by distillation of uranium hexafluoride, since this is the feed for isotope enrichment plants.

Solvent extraction and fluoride volatility processes are currently used for uranium refining. A schematic flow diagram of a typical TBP/kerosene extraction process is shown in Fig. 5.6; a fluoride volatility process flow sheet is shown in Fig. 5.7. The TBP extraction from nitric acid solution makes use of the very selective tendency of actinides to form nitrate- or mixed nitrate–solvent complexes, as discussed further in Chapters 23 and 24. This process replaces the earlier and more hazardous diethyl ether extraction from nitrate solution. The extraction reaction is

$$UO_2(NO_3)_x^{2-x} + (2-x)NO_3^- + 2TBP \rightarrow UO_2(NO_3)_2(TBP)_2$$

where $x = 0$–2. Thorium is the only normally encountered impurity element having an appreciable distribution coefficient into a kerosene-TBP phase from nitric acid solution, but its distribution is sufficiently low that it can be transferred to the aqueous phase by high uranium loading of the organic phase.

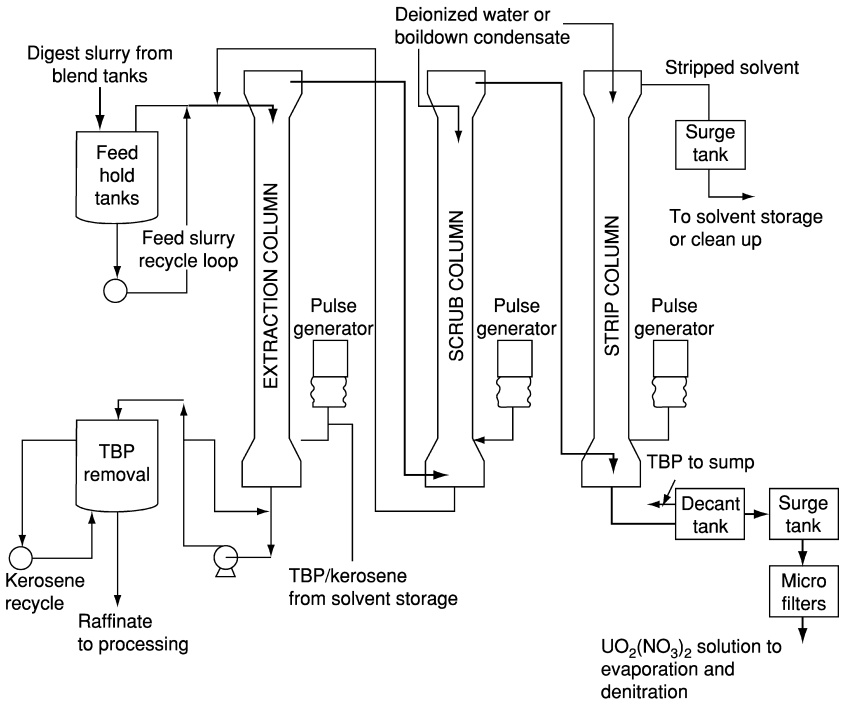

Fig. 5.6 *Schematic flow diagram: TBP/kerosene extraction system at the Fernald refinery* (*Harrington and Ruehle*, 1959).

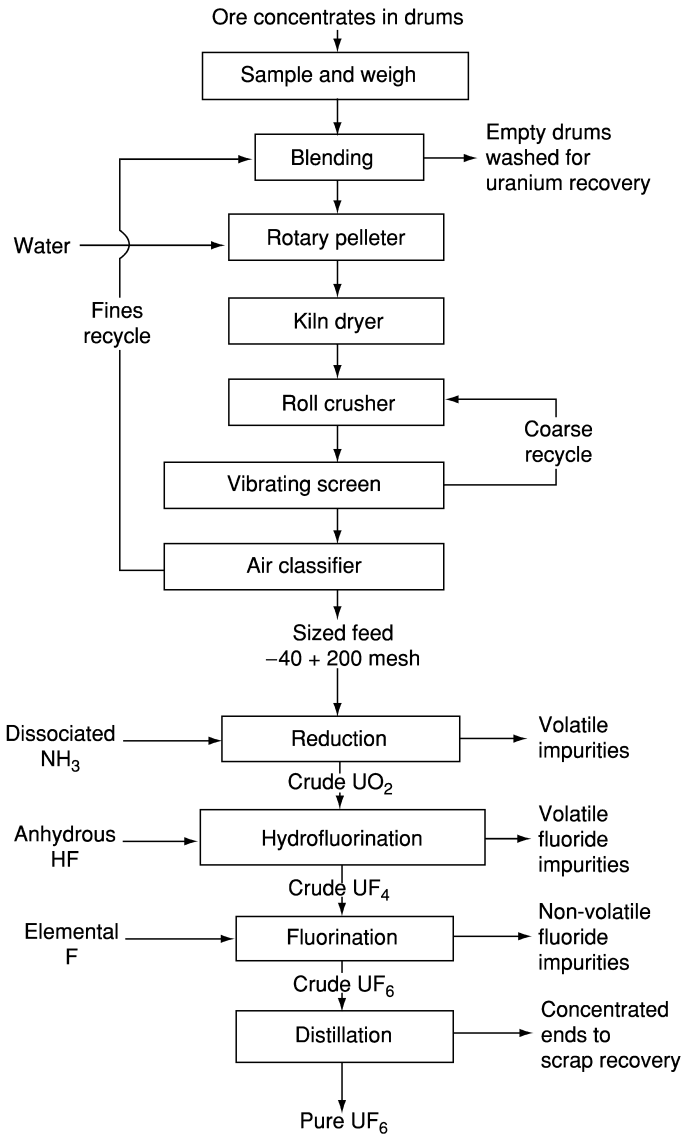

Fig. 5.7 *Overall process flow diagram for fluoride volatility process for the refining of ore concentrates* (*Ruch* et al., 1959).

The purified uranium is stripped from the organic phase with water, converted to UO_3, reduced with hydrogen to UO_2, and converted to UF_4 with hydrogen fluoride at elevated temperatures. The UF_4 can either be reduced to uranium metal for natural uranium reactors or be fluorinated to UF_6 for isotopic

enrichment for production of other types of reactor fuel. The fluoride volatility process makes use of reduction to UO_2 followed by direct fluorination, using the cheaper hydrogen fluoride to make UF_4 followed by F_2 to prepare UF_6. The UF_6 is fractionally distilled to produce a high-purity UF_6 for isotopic enrichment. The chemistry and operating conditions of the TBP refining process, the conversion to UO_3, UO_2, and finally to UF_4 are reviewed in detail in the book edited by Harrington and Ruehle (1959). Ruch *et al.* (1959) have described the refining of ore concentrates by uranium hexafluoride distillation.

Hyman *et al.* (1955) have converted uranium ore concentrates to UF_6 by means of liquid-phase fluorination using bromine trifluoride, BrF_3 (b.p. 126°C). While not applicable to raw ore, the procedure may be readily applied to concentrates. Results of experiments along these lines are summarized in Table 5.4. Since fluorine in the form of BrF_3 is rather expensive, it is worthwhile to introduce as much fluorine as possible via the inexpensive reagent hydrogen fluoride (which cannot, of course, be used to convert lower uranium fluorides to uranium hexafluoride), and then to complete the fluorination process with bromine trifluoride. This reduction of fluorine consumption may be readily accomplished by a preliminary hydrofluorination at 600°C. This treatment fluorinates silica and other gangue materials present in the ore concentrate and converts uranium(IV) to UF_4. Thus, two-thirds of the fluorine in the final UF_6 product is introduced by the relatively inexpensive hydrogen fluoride rather than by bromine trifluoride. Since uranium hexafluoride is used for the isotope separation of uranium, chlorination procedures have not received nearly as extensive investigation, because of the serious corrosion problems created by the use of chlorine at elevated temperatures.

Table 5.4 *Fluorination of various ore concentrates with BrF_3* (*Hyman* et al., 1955).

Ore concentrate			
Source	*U content* (%)	*Uranium retained by residue*[a,b] (%)	*F_2 consumption*[a,c] (cm^3 *F_2(STP) per* g U)
rand concentrate	68.1	0.16, 0.07	383, 419
rand concentrate	68.1	0.73, 0.10[d]	133, 138[d]
intermediate plant concentrate	23.3	1.45, 0.81	805, 767
intermediate plant concentrate	32.6	0.55, 1.00	552, 735

[a] Duplicate runs are given for each sample and treatment.
[b] (Grams U in residue/grams U in initial concentrate) × 100.
[c] To form UF_6 from 1 g U as metal requires 282.5 cm^3 F_2; to form UF_6 from 1 g U as UF_4 requires 94.2 cm^3 F_2.
[d] After hydrofluorination.

5.5 PROPERTIES OF FREE ATOMS AND IONS

Uranium, being one of the elements with the largest atomic number, has a very complex electronic structure. This is manifested in its spectral properties as they appear in the X-ray, UV/visible and fluorescence spectra. Details of the electronic energy levels deduced experimentally and from quantum chemical calculations are discussed in detail in Chapter 16 and in the following sections where the properties of compounds and complexes are described. The focus in Section 5.9 is on the interpretation of solid state spectra using the crystal field model and in Section 5.10 on solution spectra, including fluorescence spectroscopy of uranyl(VI) species.

5.6 URANIUM METAL

Uranium metal was used in earlier reactor systems but is now largely replaced in commercial reactors by ceramic uranium dioxide. Large-scale production of uranium metal requires elevated temperature where the high reactivity of uranium with most common refractory materials and metals makes the selection of reaction vessels a difficult problem. Finely divided uranium reacts even at room temperature with all the components of the atmosphere except the noble gases. However, contrary to the situation with titanium and zirconium, the introduction of small amounts of oxygen or nitrogen does not have an adverse effect on the mechanical properties of the metal. There are three different phases of metallic uranium below the melting point, α-, β-, and γ-uranium, each with its specific structure and physical properties. A detailed discussion of the physical properties is given in Chapter 21 on actinide metals and a short description on uranium metal and alloys in the following section.

5.6.1 Preparation of uranium metal

The element uranium is strongly electropositive, resembling aluminum and magnesium in this respect; consequently uranium metal cannot be prepared by reduction with hydrogen. Uranium metal has been prepared in a number of ways: reduction of uranium oxide with strongly electropositive elements, such as calcium, electro-deposition from molten-salt baths, thermal decomposition, decomposition of uranium halides (van Arkel de Boer 'hot wire' method), and reduction of uranium halides (UCl_3, UCl_4, UF_4) with electropositive metals (Li, Na, Mg, Ca, Ba). Only the last method is of current importance. For details, the reader is referred to two comprehensive surveys (Katz and Rabinowitch, 1951; Warner, 1953) and of older work to a review by Wilkinson (1962) and to the *Gmelin Handbook of Inorganic Chemistry* (1981a).

Both uranium tetrafluoride and tetrachloride are reducible with calcium and magnesium, while uranium dioxide can be reduced with calcium and probably magnesium. Finely divided uranium is pyrophoric and a massive metal product is therefore desired; this can be achieved by ensuring that the entire reaction mixture is fluid for a sufficiently long time for uranium metal to collect; this requires a slag with a moderately low melting point. Calcium oxide and magnesium oxide slags have melting points well above 2500°C, and are therefore less useful than calcium fluoride and magnesium fluoride, with melting points 1423°C and 1261°C, respectively. Uranium tetrachloride is very hygroscopic, and subject to oxidation in air and therefore the much more stable uranium tetrafluoride is preferred. Magnesium is the reagent of choice for reduction, since it is available in large quantities with a high degree of purity and can also be handled in air without special precautions. Details of a process based on these considerations are described by Wilhelm (1956) and in the books by Warner (1953) and by Harrington and Ruehle (1959).

For small-scale production of ^{233}U or ^{235}U in metallic state the batch size is limited by their critical mass of these isotopes and calcium is the preferred reductant. Bertino and Kirchner (1945), have described the special procedures for ^{233}U, and Patton *et al.* (1963) and Baker *et al.* (1946) those for ^{235}U.

Uranium ore concentrates are first purified by solvent extraction with TBP in kerosene as the immiscible solvent in the manner described in Section 5.4.4e. The purified uranyl nitrate is then decomposed thermally to UO_3. The trioxide is reduced with hydrogen to the dioxide, which in turn is converted to uranium tetrafluoride, 'green salt', by high-temperature hydrofluorination. The tetrafluoride is then reduced to metallic uranium with magnesium. A flow sheet of the production of uranium from ore concentrates is given in Fig. 5.8.

The temperature reached during the reduction reaction exceeds 1300°C where magnesium metal has a very high vapor pressure; hence, the reaction must be carried out in a sealed container (bomb). Such bombs are made in various sizes from standard seamless pipes. Their lengths range from 91.4 to 114.3 cm (36 to 45 in.), their diameters up to 33 cm (13 in.).

Uranium prepared by the metallothermic processes described above is of sufficient purity for most purposes. However, it may be further purified by molten-salt electrolysis (Slain, 1950; Noland and Marzano, 1953; Niedrach and Glamm, 1954; Blumenthal and Noland, 1956) using alkali or alkaline-earth chloride as electrolytes. UF_4, UCl_4, or UCl_3 are dissolved in these electrolytes. The material to be purified is used as the anode, molybdenum, or tantalum as the cathode; a diaphragm, usually of a sintered, porous ceramic material, separates the anode and the cathode.

Other methods that have been employed in uranium purification include zone melting (Whitman *et al.*, 1955; Antill, *et al.*, 1961) and hot-wire deposition (Fine *et al.*, 1945; Prescott *et al.*, 1946). Because of the low melting point of uranium, the latter method is only of limited value.

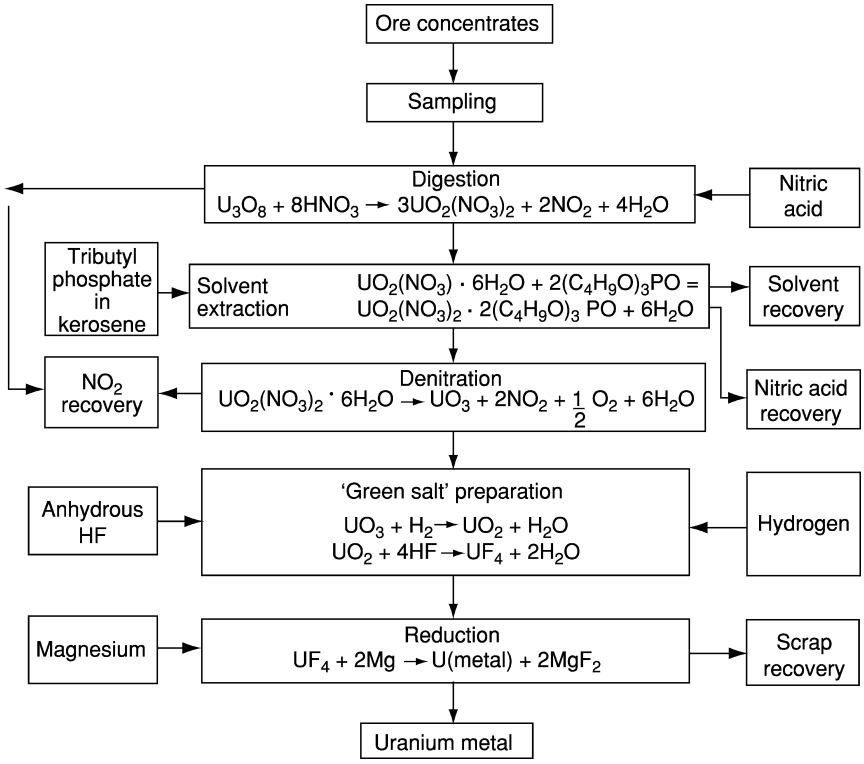

Fig. 5.8 *Flow sheet for the production of uranium metal by reduction of* UF_4 *with magnesium* (*Kelley,* 1955).

(a) Physical properties of uranium metal

(*i*) *Crystal structure*

Uranium metal has three crystalline phases below the melting point at (1134.8 ± 2.0)°C. The α-phase is the room-temperature modification of uranium; it is orthorhombic with space group No. 63, *Cmcm* and unit cell parameters $a = 2.854$ Å, $b = 5.87$ Å, and $c = 4.955$ Å (Barrett *et al.*, 1963; Lander and Müller, 1970) and one uranium at the site 4c in the space group.

The structure consists of corrugated sheets of atoms, parallel to the *ac*-plane and perpendicular to the *b*-axis. Within the sheets the atoms are tightly bonded, whereas the forces between atoms in adjacent sheets are relatively much weaker (Fig. 5.9). This arrangement is highly anisotropic and resembles the layer structures of arsenic, antimony, and bismuth. In the α-uranium structure, the U–U distances in the layer are (2.80 ± 0.05) Å and between adjacent layers

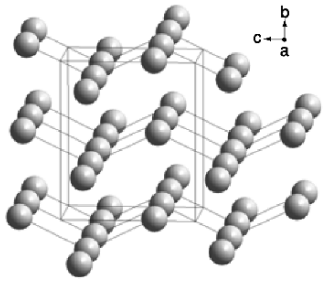

Fig. 5.9 *The structure of α-uranium from Lander and Müller* (1970). *It is a layer structure with puckered ac-layers perpendicular to the b-axis; the uranium–uranium distances in the layer are* (2.80 ± 0.05) Å *and between the layers* 3.26 Å.

3.26 Å. The physical properties of the α-phase are a reflection of its structure, e.g. the strongly anisotropic coefficient of thermal expansion. The average value of the thermal expansion coefficient over the temperature range 25–325°C is 26.5, –2.4, and 23.9 × 10^{-6} $°C^{-1}$, respectively, along *a*, *b*, and *c*. A chemical consequence of the unique orthorhombic structure of α-uranium is that the formation of solid solutions with metals of the common structure types is severely restricted.

The β-phase of uranium exists between 668 and 775°C; it has a complex structure with six crystallographically independent atoms in the tetragonal unit cell (Donohue and Einspahr, 1971). The space group is $P4_2/mnm$, $P4_2nm$, or $P4n2$, with unit cell parameters $a = 5.656$ Å and $b = c = 10.759$ Å. The lattice parameters were determined in an alloy with 1.4% chromium at 720°C, and in uranium powder in the temperature range where the phase is stable. The tetragonal lattice is a stacked layer structure with layers parallel to the *ab* plane of the unit cell at *c*/4, *c*/2, and 3*c*/4. Additional high-precision measurements are required to solve the structure completely (Donohue and Einspahr, 1971).

The γ-phase of uranium is formed at temperatures above 775°C; it has a body-centered cubic (bcc) structure with the cell parameter $a = 3.524$ Å; the phase stabilized at room temperature by the addition of molybdenum that forms an extensive series of solid solutions with γ-uranium.

(b) General properties

Foote (1956), Holden (1958), and Wilkinson and Murphy (1958) have described the physical metallurgy of uranium and Oetting *et al.* (1976) and Rand and Kubaschewski (1963) the thermodynamic properties of uranium metal.

A number of physical and thermal properties of elemental uranium are collected in Table 5.5. Uranium is not a refractory metal like chromium, molybdenum, or tungsten; it is among the densest of all metals, being exceeded in this respect only by some of the platinum metals and by α-Np and α-Pu.

Table 5.5 *Physical and thermal properties of uranium* (*Oetting* et al., 1976).

melting point	(1408 ± 2) K
vapor pressure	
1720–2340 K	$\log p(\text{atm}) = -(26210 \pm 270)\ T^{-1}$
(Pattoret *et al.*, 1964)	$+ (5.920 \pm 0.135)$
1480–2420 K	$\log p(\text{atm}) = -(25230 \pm 370)\ T^{1}$
(Ackerman and Rauh, 1969)	$+ (5.71 \pm 0.17)$
X-ray density (α-uranium)	19.04 g cm^{-3}
(Lander and Müller, 1970)	
enthalpy of sublimation	
$\Delta_f H°$(U, g, 298.15 K)	(533 ± 8) kJ mol^{-1}[a]
enthalpy	
$H°(298.15\ K) - H°(0\ K)$	6364 J mol^{-1}
entropy	
$S°(298.15\ K)$	(50.20 ± 0.20) J K^{-1} mol^{-1}[a]
heat capacity	
$C_p°(298.15\ K)$	(27.669 ± 0.050) J K^{-1} mol^{-1}
transformation points	
α to β	(942 ± 2) K
β to γ	(1049 ± 2) K
enthalpies of transformation	
$\Delta_{trs}H$ (α to β)	2791 J mol^{-1}
$\Delta_{trs}H$ (β to γ)	4757 J mol^{-1}
$\Delta_{fus}H$ (γ to liq)	9142 J mol^{-1}
enthalpy and specific heat functions	
α-uranium (298–942 K)	$H_T - H_{298} = 26.920T - 1.251 \times 10^{-3}T^2 + 8.852 \times 10^{-6}T^3 + 0.7699 \times 10^{5}T^{-1} 8407.828$ (J mol^{-1})
	$C_p = 26.920 - 2.502 \times 10^{-3}T + 26.556 \times 10^{-6}T^2 - 0.7699 \times 10^{5}T^{-2}$ (J K^{-1} mol^{-1})
β-uranium (942–1049 K)	$H_T - H_{298} = 42.920T - 14326.020$ (J mol^{-1})
	$C_p = 42.92$(J K^{-1} mol^{-1})
γ-uranium (1049–1408 K)	$H_T - H_{298} = 38.280T - 4698.690$ (J mol^{-1})
	$C_p = 38.28$ (J K^{-1} mol^{-1})
uranium (liquid)	$H_T - H_{298} = 48.650T - 10137.120$ (J mol^{-1})
	$C_p = 48.65$ (J K^{-1} mol^{-1})
thermal conductivity at 298.15 K (Ho *et al.*, 1972)	27.5 J m^{-1} s^{-1} K^{-1}
electrical resistivity (300 K) (Arajs and Colvin, 1964)	28×10^{-8} Ω m

[a] CODATA key value (Cox *et al.*, 1989).

The electrical resistivity of uranium is about 16 times higher than that of copper, 1.3 times that of lead and approximates that of hafnium (Gale and Totemeier, 2003).

An important mechanical property (Table 5.6) of uranium is its plastic character, allowing easy extrusion. The mechanical properties are very sensitive

Table 5.6 *Average mechanical properties of uranium* (*Grossman and Priceman,* 1954; *Wilkinson and Murphy,* 1958).

modulus of elasticity	1758×10^6 kPa
Poisson ratio at zero stress	0.20
shear modulus	73.1×10^6 kPa
bulk modulus	97.9×10^6 kPa
proportional limit	2.068×10^4 kPa
yield strength	
0.1% offset	1.8617×10^5 kPa
0.2% offset	2.2754×10^5 kPa
compressibility	
β_{100}	$0.758 \pm 7\%$
β_{010}	$0.296 \pm 16\%$
β_{001}	$0.141 \pm 16\%$
β_v	$1.195 \pm 6\%$

to the pre-history of the sample, and are strongly dependent on crystal orientation, fabrication, and heat treatment. Despite its plastic nature, uranium has a definite yield point with a well-defined, but very low, proportional limit. The ultimate tensile strength of uranium varies between 3.44×10^5 and 13.79×10^5 kPa, depending on the cold working and previous thermal history of the sample. Uranium rapidly loses strength at elevated temperatures, the tensile strength falling from 1.862×10^5 kPa at 150°C to 0.827×10^5 kPa at 600°C.

The Brinell hardness of rolled polycrystalline α-uranium varies between 2350 and 2750 MN m^{-2} at 23°C (Samsonov, 1968). The hardness is strongly affected by impurities. Cold working increases the hardness with up to 50%. Above 200°C, the hardness falls off rapidly. γ-Uranium is so soft as to make fabrication difficult, while the β-phase is harder and considerably more brittle than the α-phase.

(c) Magnetic susceptibility and related properties

The solid-state properties of uranium have been the subject of a relatively recent exhaustive review (Lander *et al.*, 1994). Some pertinent physical properties taken from this review are given here. Although many measurements have been performed on uranium metal, the description and full understanding of its properties is still not complete. Uranium metal is weakly paramagnetic and exhibits almost temperature-independent paramagnetism with a room temperature value of 390×10^{-9} emu mol^{-1}. (Fournier and Troć, 1985). α-Uranium exhibits an anomaly at 43 K apparent in the magnetic susceptibility data and in other measurements. This anomaly and further phase transformations observed at 37 and 23 K have been attributed to charge density waves. α-Uranium exhibits a superconducting transition at low temperatures that can be described by the Bardeen–Cooper–Schreiffer (BCS) theory. The maximal T_c value for

Table 5.7 *Components of uranium resistivity tensor at* 273 K.

References	ρ[100] (μΩ cm)	ρ[110] (μΩ cm)	ρ[110] (μΩ cm)
Brodsky *et al.* (1969)	36.1 ± 0.2	20.6 ± 0.2	26.0 ± 0.2
Berlincourt (1959)	39.4	25.5	26.2
Pascal *et al.* (1964)	39.1	23.6	30.2
Raetsky (1967)	34.7	23.6	20.3

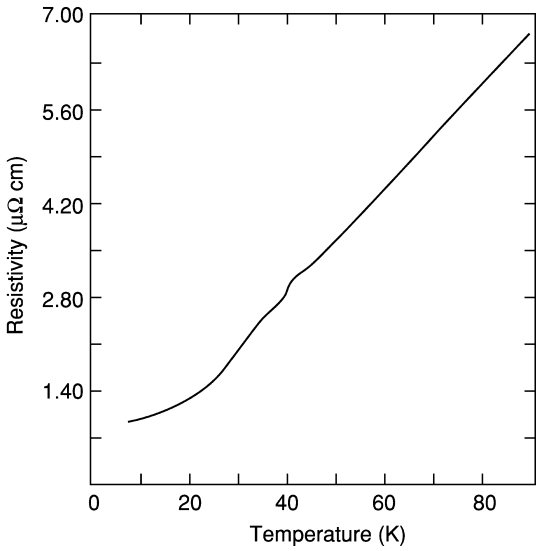

Fig. 5.10 *Resistivity–temperature curve for* α*-uranium along the* [010] *axis* (*Brodsky* et al., 1969).

α-uranium is ∼2–2.3 K at a pressure of ∼1.0–1.1 GPa. The 0.1013 MPa (1 atm) value of T_c is taken as ≤0.1 K.

(d) Electrical and related properties

The temperature dependence of the resistivity of uranium single crystals has been measured by a number of authors and the components of the resistivity tensor are given in Table 5.7. The resistivity–temperature curve for α-uranium along the [010] direction is shown in Fig. 5.10. Many other physical properties of elemental uranium have been determined, such as elastic moduli, heat capacity, de Haas-van Alphen measurements, transport properties and others. The reader is referred to Lander *et al.* (1994) and to Chapter 21 for further discussion.

Table 5.8 *Reactions of uranium with various metals* (*Saller and Rough,* 1955*; Rough and Bauer,* 1958*; Chiotti* et al., 1981). *IS and SS denote intensely studied and slightly studied, respectively*.

Class	*Behavior*		*Metals*
I	form intermetallic compounds	IS	Al, As, Au, B, Be, Bi, Cd, Co, Cu, Fe, Ga, Ge, Hg, Ir, Mn, Ni, Os, Pb, Pd, Pt, Rh, Ru, Sb, Sn
II	form solid solutions but no intermetallic compounds	SS	In, Re, Tc, Tl, Mo, Nb, Pu, Ti, Zr
III	form neither solid solutions nor intermetallic compounds	IS	Ag, Cr, Mg, Ta, Th, V, W
		SS	lanthanides, Li, Na, K, Ca, Sr, Ba

5.6.3 Uranium intermetallic compounds and alloys

The most noticeable features of the behavior of uranium with other metals are the formation of intermetallic compounds with a wide variety of alloying metals and the extensive ranges of solid solutions in α- and β-uranium. Table 5.8 summarizes the alloying behavior with the metallic elements. Saller and Rough (1955), Pfeil (1956), Rough and Bauer (1958), Hansen and Anderko (1958), Elliott (1965), Shunk (1969), and Wilkinson (1962) have given comprehensive and informative descriptions of the general behavior of the alloying elements, including numerous phase diagrams. The thermodynamics of uranium alloy systems was reviewed by Chiotti *et al*. (1981).

A large number of intermetallic compounds have been characterized by X-ray crystallographic methods and by conventional metallographic techniques. The *Gmelin Handbook of Inorganic Chemistry* gives a comprehensive review of the properties of the uranium alloys with alkali metals, alkaline earths, and elements of main groups III and IV (Gmelin, 1989, vol. B2), with transition metals of groups IB to IVB (Gmelin, 1994, vol. B3), and with transition metals of groups VB to VIIB (Gmelin, 1995a, vol. B4), including the effects of irradiation, which are also discussed in the volume on technology and uses of uranium (Gmelin, 1981a, vol. A3).

Among uranium intermetallic phases of interest may be mentioned the transition-metal compounds U_6Mn, U_6Fe, U_6Co, and U_6Ni, which are distinguished by their hard and brittle nature. Uranium forms intermetallic phases with noble metals and the phase diagrams for U–Ru, U–Rh, U–Pd, U–Os, U–Ir, and U–Pt systems have been assessed by Chiotti *et al*. (1981), a compilation that also provides information on a number other intermetallic phases. The compounds of uranium with the light platinum metals, Ru, Rh, and Pd, are of interest in the pyrometallurgical reprocessing of metallic fuels, because the

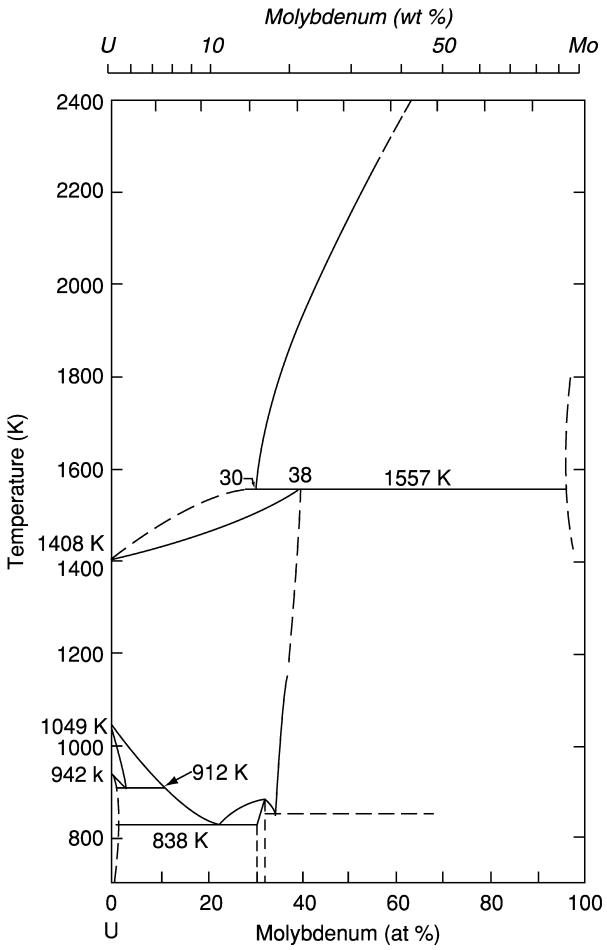

Fig. 5.11 *Phase diagram of the uranium–molybdenum system* (*Chiotti* et al., 1981).

noble metals form alloys that remain with the uranium when the fuel is processed for fission-product removal by oxidative slagging.

Elements of class III in many cases form simple eutectic systems. Molybdenum, titanium, zirconium, niobium, and plutonium form extensive solid solutions with uranium at elevated temperatures. No intermediate phases are detected for the U–Nb system, whereas the U–Mo, U–Pu, U–Ti, and U–Zr systems all show metastable phases. The uranium–molybdenum system is shown in Fig. 5.11 and illustrates the general features of the small but important class of true alloying elements. The uranium alloys have unusual physical properties that are discussed in Chapter 21.

Table 5.9 *Chemical reactions of uranium metal.*

Reactant	*Reaction temperature*[a] (°C)	*Products*
H_2	250	α- and β-UH_3
C	1800–2400	UC; U_2C_3; UC_2
N_2	700	UN, UN_2
P	1000[b]	U_3P_4
O_2	150–350	UO_2, U_3O_8
S	500	US_2
F_2	250	UF_6
Cl_2	500	UCl_4, UCl_5, UCl_6
Br_2	650	UBr_4
I_2	350	UI_3, UI_4
H_2O	100	UO_2
HF(g)	350[b]	UF_4
HCl(g)	300[b]	UCl_3
NH_3	700	$UN_{1.75}$
H_2S	500[b]	US, U_2S_3, US_2
NO	400	U_3O_8
N_2H_4	25	$UO_2(NO_3)_2 \cdot 2NO_2$
CH_4	635–900[b]	UC
CO	750	UO_2 + UC
CO_2	750	UO_2 + UC

[a] Reaction temperature with massive metal.
[b] Reaction temperature with powdered uranium (from decomposition of UH_3).

5.6.4 Chemical properties of uranium and its alloys

Uranium metal is a highly reactive substance that can react with practically all of the elements in the periodic table with the exception of the noble gases. Some of the more important chemical reactions of uranium are listed in Table 5.9.

Wilkinson (1962) has discussed in detail the corrosion of massive uranium by various gaseous agents, such as dry oxygen, dry air, water vapor, carbon monoxide, carbon dioxide, and others, as well as the pyrophoricity of this element. Totemeier (1995) has written a more recent review of the corrosion and pyrophoricity behavior of uranium (and plutonium) with oxygen, water vapor, and aqueous solutions in terms of reaction rates, products, and reaction mechanisms.

From a practical point of view, the reactions of uranium with oxygen, nitrogen, and water are probably the most significant. Uranium metal exposed to oxygen, water, or air undergoes reaction even at room temperature. The kinetics of corrosion of uranium by various reagents such as dry and moist oxygen, dry and moist air, water vapor and hydrogen, and the pyrophoricity of uranium, as well as that of plutonium, are discussed in detail in Chapter 29

devoted to handling, storage, and disposal of these elements and their relevant compounds.

Uranium dissolves very rapidly in aqueous hydrochloric acid. The reaction frequently yields considerable amounts of a black solid, presumably a hydrated uranium oxide but very likely containing some hydrogen. The addition of a small amount of fluorosilicate ion prevents the appearance of the black solid during dissolution in hydrochloric acid. Non-oxidizing acids, such as sulfuric, phosphoric, and hydrofluoric, react only very slowly with uranium, whereas nitric acid dissolves massive uranium at a moderate rate. With finely divided uranium, the dissolution in nitric acid may approach explosive violence. Uranium metal is inert to alkalis. Addition of oxidizing agents such as peroxide to sodium hydroxide solution leads to the dissolution of uranium and to the formation of ill-defined water-soluble peroxyuranates.

5.7 COMPOUNDS OF URANIUM

Ever since the discovery of uranium in 1789, its compounds have been synthesized and studied, so that a wealth of information has accumulated over the years. Much of this information may be found in the books by Katz and Rabinowitch (1951, 1958) and in the various volumes of the Supplement Series of the *Gmelin Handbook of Inorganic Chemistry* (1975–1996), which constitute probably the most comprehensive collection of information on uranium compounds.

For obvious reasons, such as lack of space, it is impossible to give a complete account of every uranium compound known to date. Rather, representative examples will be discussed with emphasis on preparation, structure, and chemical properties; information and discussion of thermodynamic properties of uranium and other actinide compounds are found in Chapter 19. In its compounds, uranium exhibits the oxidation states 3+, 4+, 5+, and 6+, with 4+ and 6+ as the predominant ones. Also, mixed valence and non-stoichiometric compounds are known.

While general features of the structures of uranium compounds, both from coordination and chemical points of view, will be discussed in Section 5.9, structures pertaining to each family of compounds will be described in the following subsections.

5.7.1 The uranium–hydrogen system

The uranium–hydrogen system has been reviewed by Katz and Rabinowitch (1951), Mallett *et al.* (1955), Libowitz (1968), Flotow *et al.* (1984), and Ward (1985). An extensive review has been given in the *Gmelin Handbook* (Gmelin, 1977, vol. C1). The kinetics of the reaction of hydrogen on uranium is discussed

in detail in Chapter 29, describing the handling, storage, and disposition of plutonium and uranium. This topic will therefore not be developed here.

(a) Preparative methods

β-UH_3 forms rapidly as fine black or dark gray powder when uranium turnings or powder, as well as large massive lumps, are heated to 250°C in a vacuum followed by the introduction of H_2 gas into the reaction system (Spedding *et al.*, 1949; Libowitz and Gibb. Jr, 1957). Crystalline β-UH_3 may be prepared as gray, fibrous crystals at 30 atm H_2 and 600–700°C in an autoclave using a uranium nitride crucible as the primary container inside the pressure vessel.

α-UH_3 can only be prepared by slow reaction at temperatures below about −80°C. The α-phase is unstable, and the products are usually a mixture with more than 50% β-UH_3 (Mulford *et al.*, 1954; Abraham and Flotow, 1955). Purer α-UH_3 has been obtained by the diffusion method: Fine reactive uranium metal powder, formed by thermal decomposition of β-UH_3, was kept below −78°C in an Ar (or He) filled cryostat at a pressure of 0.25–0.40 atm, to which H_2 was introduced with an adequately low rate (reaction period: 20 days). More than 80% of the product was α-UH_3 (Wicke and Otto, 1962).

(b) Crystal structures

α-UH_3 is cubic with space group *Pm*3*n*. Two uranium atoms occupy (0,0,0) and (1/2,1/2,1/2), and six hydrogen atoms ±(1/4,0,1/2), ±(1/2,1/4,0), and ±(0,1/2,1/4) positions. The crystallographic data are listed in Table 5.10.

β-UH_3 also has a cubic structure with space group *Pm*3*n*, the same as in α-UH_3, but with different atom positions, $2U_I$ in (0,0,0) and (1/2,1/2,1/2), and

Table 5.10 *Crystallographic data of uranium hydrides.*

Compound	*Symmetry*	*Space group*	*a* (Å)	*z*	*X-ray density* (g cm^{-3})	*References*
α-UH_3	cubic	*Pm*3*n*	4.160(1)	2	11.12	Mulford *et al.* (1954); Wicke and Otto (1962);
			4.153(2)			Caillat *et al.* (1953)
α-UD_3	cubic	*Pm*3*n*	4.150	2	11.34	Wicke and Otto (1962); Grunzweig-Genossar *et al.* (1970);
			4.147(3)		11.36	Johnson *et al.* (1976)
α-UT_3	cubic	*Pm*3*n*	4.142(2)	2	11.55	Johnson *et al.* (1976)
β-UH_3	cubic	*Pm*3*n*	6.6444(8)	8	10.92	Rundle (1947, 1951)
β-UD_3	cubic	*Pm*3*n*	6.633(3)	8	11.11	Rundle (1947, 1951)
β-UT_3	cubic	*Pm*3*n*	6.625(3)	8	11.29	Johnson *et al.* (1976)

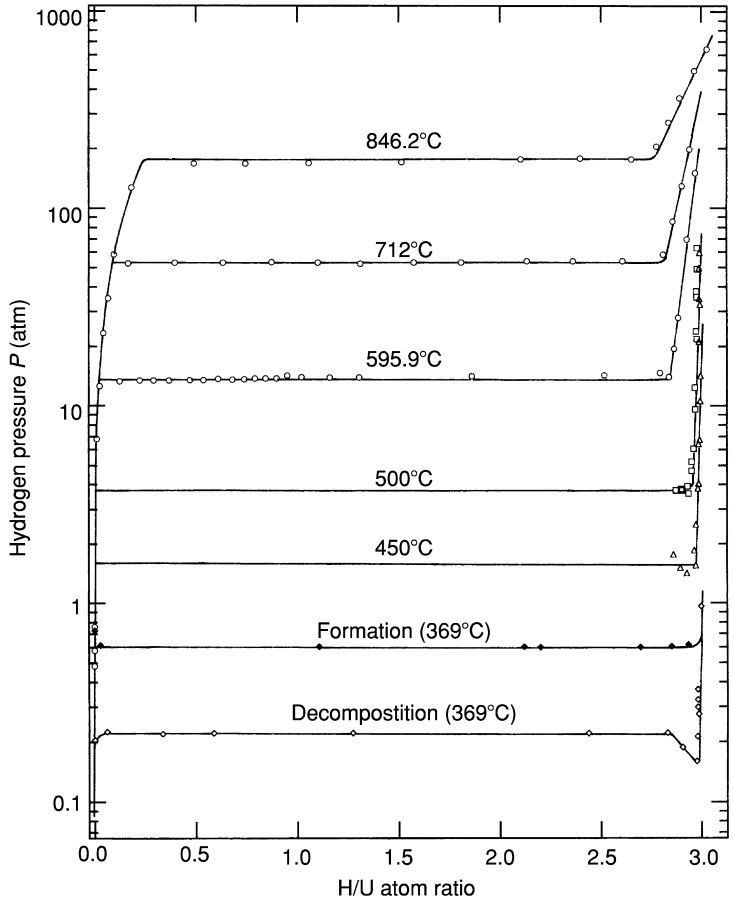

Fig. 5.12 *Hydrogen pressure versus composition isotherms for the system U–UH_3–H_2. Formation and decomposition curves at* 369°C: *Wicke and Otto* (1962); 450 *and* 500°C *curves: Libowitz and Gibb, Jr.* (1957); 595.9, 712, *and* 846.2°C *curves: Northrup, Jr.* (1975).

$6U_{II}$ in $\pm(1/4,0,1/2)$ and their equivalent positions. The hydrogen position was determined by neutron diffraction of β-UD_3 (Rundle, 1951). The hydrogen atoms are located in the 24(*k*) position, where each hydrogen atom is equidistant from four uranium neighbors within the experimental error, i.e., $12H_I$ in $\pm(5/16,0,\pm5/32)$ and $12H_{II}$ in $\pm(11/32,\pm1/2,3/16)$.

(c) Phase relations and dissociation pressures

A pressure–composition (isotherm) diagram of the U–UH_3–H_2 system is shown in Fig. 5.12; the region of the existence of α-hydride phase is not given because this phase is unstable and transforms irreversibly to β-UH_3 at higher

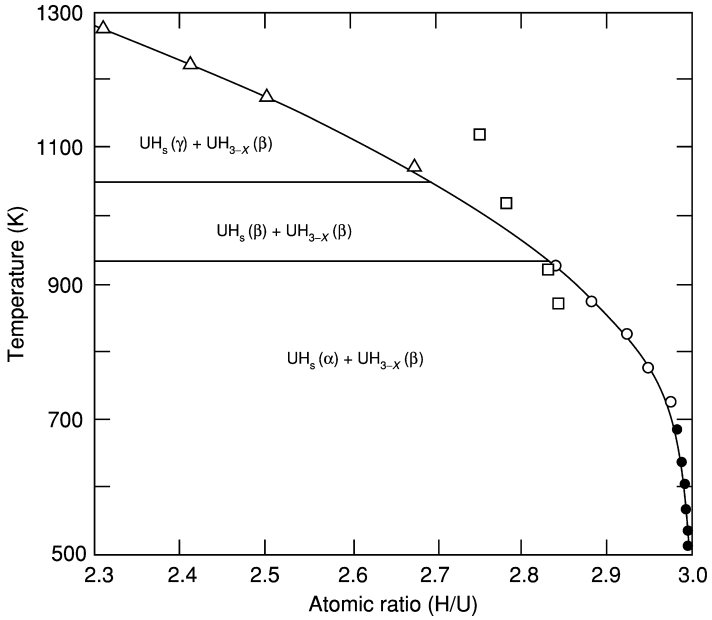

Fig. 5.13 *Phase diagram of the uranium–hydrogen system in the range H/U* = 2.3–3.0 (*from Flotow* et al., 1984). *UH_s (α, β, and γ) represent uranium metal phases (α, β, and γ), respectively, with dissolved hydrogen.* •: *Besson and Chevallier* (1964); ○: *Libowitz and Gibb, Jr.* (1957); □: *Northrup, Jr.* (1975); △: *Lakner* (1978). *Reproduced by the permission of the Atomic Energy Agency, Vienna.*

temperatures. The equilibrium H_2 pressure over α-UH_3 is much higher than that over β-UH_3, but no quantitative data are available. The rate of the α → β transformation is relatively low; α-UH_3 changes to β-UH_3 in a few hours at 250°C (Wicke and Otto, 1962).

The β-hydride phase, β-UH_{3-x}, has a relatively wide range of hydrogen hypostoichiometry at higher temperatures. The slight hyperstoichiometry at 846.2°C shown in Fig. 5.12 is an experimental artefact caused by hydrogen permeation from the sample vessel (Northrup, Jr., 1975).

Fig. 5.13 shows the hypostoichiometric range for uranium trihydride up to 1300 K (Flotow *et al.*, 1984). At 1280 K, the lower limit of the β-hydride phase attains to $UH_{2.3}$.

The solubility of hydrogen in uranium metal increases with increasing temperature (Fig. 5.12). The data determined by Mallett and Trzeciak (1958) obey Sieverts law.

$$\alpha\text{-U: } \log S(\mathrm{H/U}) = 1/2 \log p_{\mathrm{H_2}}(\mathrm{atm}) - 2.874 - 388\, T^{-1} \quad (T < 942\,\mathrm{K}),$$
$$\beta\text{-U: } \log S(\mathrm{H/U}) = 1/2 \log p_{\mathrm{H_2}}(\mathrm{atm}) - 1.778 - 892\, T^{-1} \quad (942 < T < 1049\,\mathrm{K}),$$
$$\gamma\text{-U: } \log S(\mathrm{H/U}) = 1/2 \log p_{\mathrm{H_2}}(\mathrm{atm}) - 2.238 - 227\, T^{-1} \quad (1049 < T < 1408\,\mathrm{K}),$$
$$\text{Liquid U: } \log S(\mathrm{H/U}) = 1/2 \log p_{\mathrm{H_2}}(\mathrm{atm}) - 1.760 - 587\, T^{-1} \quad (T > 1408\,\mathrm{K}),$$

where S is the solubility measured as the atom ratio. It may be noteworthy that finely divided uranium chemisorbs much larger amounts of hydrogen than those given by the previous equations (e.g. about 100 times larger at 295°C and 0.15 mmHg H_2).

Below 400°C the hydrogen pressure for formation of hydrides is not the same as that for the decomposition in the region of two solid phases (plateau region). Spedding *et al.* (1949) reported that the decomposition and formation pressures at 357°C were 0.176 and 0.188 atm, respectively. Wicke and Otto (1962) indicated that this difference is 170% at 369°C as shown in Fig. 5.12. Various explanations of the hysteresis and the dip in the decomposition process have been proposed (Libowitz, 1968; Condon and Larson, 1973); there is a possibility that traces of oxygen play a role. Using very pure uranium samples, no evidence of hysteresis was found and the time to attain equilibrium was quite short (Meusemann and von Erichsen, 1973; Condon, 1980).

The plateau hydrogen pressures are given by the equation

$$\ln p(\text{atm}) = A - BT^{-1}$$

where $A = 14.55$ and $B = 10233$ for UH_3 in the temperature range 298–942 K (Chiotti, 1980). For uranium trideuteride, UD_3, Flotow *et al.* (1984) assessed the measured data by Spedding *et al.* (1949), Wicke and Otto (1962), Destriau and Sériot (1962), and Carlson (1975), and recommended the values $A = 15.046$ and $B = 10362$ (500–800 K), which were obtained by averaging the results of Spedding *et al.* (1949) and Wicke and Otto (1962). The data for uranium tritritide, UT_3, are meager. The recommended A and B values (Flotow *et al.*, 1984) are those obtained by averaging the results of Flotow and Abraham (1951) and of Carlson (1975); they are $A = 14.57$ and $B = 9797$ in the temperature range 600–800 K. The above equilibrium pressures are considerably lower than the pressures derived from calorimetric data for UH_3, UD_3, and UT_3 (Flotow *et al.*, 1984).

(d) Thermodynamic properties

The heat capacity, entropy, and enthalpy of formation of UH_3, UD_3, and UT_3 (β forms) at 298 K are listed in Table 5.11.

Table 5.11 *Heat capacity, entropy, and enthalpy of formation of β-UH_3, β-UD_3, and β-UT_3 at* 298.15 K (*Flotow* et al., 1984).

Compound	C_p°(298.15 K) ($JK^{-1}mol^{-1}$)	S°(298.15 K) ($JK^{-1}mol^{-1}$)	$\Delta_f H^\circ$ (298.15K) ($kJ\ mol^{-1}$)
β-UH_3	49.29 ± 0.08	63.68 ± 0.13	– 126.98 ± 0.13
β-UD_3	64.98 ± 0.08	71.76 ± 0.13	– 129.79 ± 0.13
β-UT_3	74.43 ± 0.75	79.08 ± 0.79	–130.29 ± 0.21

Flotow and Osborne (1967) and Flotow *et al.* (1959) have measured the low-temperature heat capacity of $UH_3(\beta)$ from 1.4 to 23 K and from 5 to 350 K, respectively. Abraham *et al.* (1960) have reported the low-temperature heat capacity of UD_3 from 5 to 350 K and Ward *et al.* (1979) that from 4 to 17 K.

Although no experimental heat capacity data have been published for $UT_3(\beta)$, Flotow *et al.* (1984) obtained the estimated C_p values using semiempirical equations to estimate the optical mode contributions of the hydrogen lattice vibrations. Abraham *et al.* (1960) found that the sum of the lattice heat capacity associated with the acoustic modes, the electronic heat capacity, and the magnetic heat capacity, agreed within 0.08 $JK^{-1}mol^{-1}$ for $UH_3(\beta)$ and $UD_3(\beta)$, which means that this part of heat capacity is virtually the same for UH_3, UD_3, and UT_3. Moreover, they showed that this could be represented by a linear function of temperature. On this basis, Flotow *et al.* (1984) calculated the optical mode contributions of UT_3 by using the Einstein heat capacity function to estimate the heat capacity of UT_3.

The heat capacity of UH_3 and UD_3 up to 800 K was also obtained by this method as shown in Fig. 5.14. The sharp anomaly in the vicinity of 170 K is due to the ferromagnetic–paramagnetic transition of the β-hydride phases.

(e) Electrical resistivity

The electrical resistivity, ρ, of β-hydride increases with increasing temperature as in metals. Ward *et al.* (1979) measured the electrical resistivity of β-UD_3 from 2.4 to 300 K. The ρ vs T curve has an anomaly due to a magnetic transition at 166 K. These resistivities are in good agreement with the unpublished data of Flotow for β-UH_3 communicated to Grunzweig-Genossar *et al.* (1970). The resistivity of β-hydride is about ten times higher than that of uranium metal.

(f) Magnetic properties and the nature of bonding

The history of magnetic studies of uranium hydrides is described in the review of Troć and Suski (1995). In the earlier work, α-UH_3 was considered to be ferromagnetic at low temperatures with T_C the same as, or close to that of β-UH_3. However, the neutron diffraction study on α-UD_3 (Lawson *et al.*, 1991) revealed the α-hydride phase to be non-magnetic at least above 15 K, i.e. the apparent ferromagnetism was due to β-hydride impurities in the α-hydride samples.

β-Hydride is ferromagnetic at low temperatures. The magnetic data for β-UH_3 and β-UD_3 are shown in Table 5.12. At the Curie temperature, the λ-type heat capacity anomaly has also been observed at 170.5 and 167.6 K for β-UH_3 and β-UD_3, respectively (Fig. 5.14). The lower Curie temperature in the deuteride is associated with the somewhat shorter U–U distance, resulting in a change of the exchange integrals for the Weiss field (Ward, 1985). The electrical

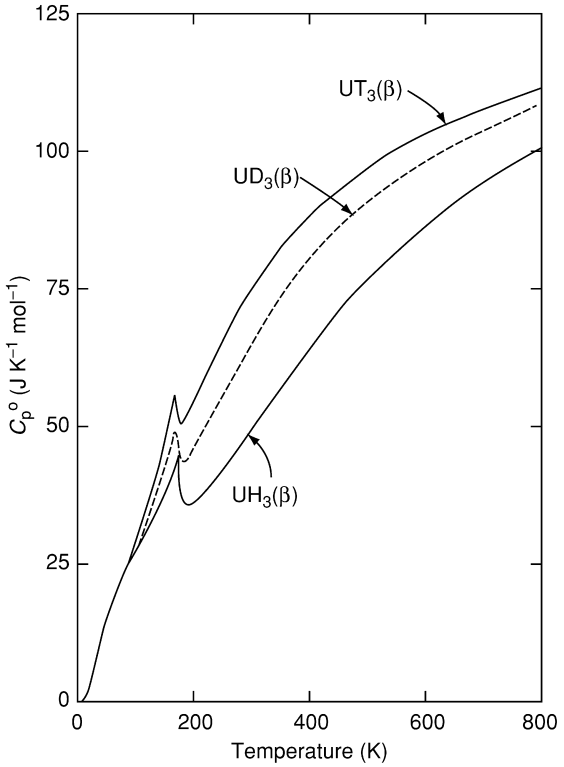

Fig. 5.14 *Heat capacities of $UH_3(\beta)$, $UD_3(\beta)$, and $UT_3(\beta)$* (*Flotow* et al., 1984).

resistivity for β-UD_3 changed at the Curie temperature (166 K) (Ward *et al.*, 1979). Andreev *et al.* (1998) report that the Curie temperature of β-UH_3 decreases with increasing external pressure from 175 K (0 kbar) to 169 K (8 kbar). In Table 5.12, the saturation uranium magnetic moments obtained by neutron diffraction are far larger than those obtained by magnetization measurements, possibly a result of a large magnetic anisotropy in β-UH_3 (Bartscher *et al.*, 1985). The neutron diffraction studies of β-UH_3 carried out at the ferromagnetic temperatures revealed that the two U_I and six U_{II} atoms, which occupy different crystallographic positions in space group *Pm*3*n*, are magnetically equivalent giving the same magnetic moment; no (110) reflection peak was observed in the diffraction patterns (Wilkinson *et al.*, 1955; Bartscher *et al.*, 1985; Lawson *et al.*, 1990). Increased external pressure lowers the saturation magnetic moment of uranium from $1\mu_B$(0 kbar) to $0.985\mu_B$(10 kbar) at 4.2 K (Andreev *et al.*, 1998). The effective uranium moments in Table 5.12 are those obtained from the slope of the Curie–Weiss curves in the paramagnetic range of temperatures.

Table 5.12 *Magnetic data for β-UH_3 and β-UD_3.*

Hydride	*Ferromagnetic Curie temperature* T_C(K)	*Paramagnetic Curie temperature* θ_p(K)	*Saturation uranium moment* $\mu_S(\mu_B)$	*Effective paramagnetic uranium moment* $\mu_{eff}(\mu_B)$	*References*
β-UH_3	174	174	0.65 (80 K)	2.44	Trzebiatowski *et al.* (1954)
	173		0.9 (78 K)	2.79	Gruen (1955)
	181	173	0.9 (2.1 T, 4.2 K)		Lin and Kaufmann (1956)
	168	180	1.18 (6 T, 1.3 K)		Henry (1958)
	181	176	0.7	2.24	Karchevskii and Buryak (1962)
	175		1.0 (40 T, 4.2 K)		Andreev *et al.* (1998)
	175		1.39 (ND)		Shull and Wilkinson (1955)
			1.45 (NMR)		Barash *et al.* (1984)
			1.54 (ND)		Lawson *et al.* (1990)
β-UD_3	172	172		2.44	Trzebiatowski *et al.* (1954)
			0.98 (6 T, 1.3 K)		Henry (1958)
	177.5	175.2		2.24	Karchevskii and Buryak (1962)
		166	0.87 (5.34 T)	2.26	Ward *et al.* (1979)
			1.39 (ND)		Wilkinson *et al.* (1955)
	178		1.45 (ND, 10 K)		Bartscher *et al.* (1985)

ND: neutron diffraction.

Grunzweig-Genossar *et al.* (1970) assume that uranium is composed of uranium ions and protons (deuterons) in a high-density interacting electron gas. The magnetic moments arise from 5f electrons. The uranium ions are magnetically coupled through the polarized conduction electrons by the RKKY interaction, which can explain the ferromagnetic ordering below ~180 K and the large Knight shift obtained by their nuclear magnetic resonance (NMR) measurement, i.e. $K = 0.40\chi_M$, where χ_M is the molar magnetic susceptibility. The second moment and line-shape data suggest that the 5f electrons ($Z \sim 2.5$ conduction electrons per uranium atom) are localized and do not form a band as in metallic uranium.

Cinader *et al.* (1973) measured the NMR spin-lattice relaxation time in the paramagnetic state at 189–700 K. In addition to the time-dependent dipolar interaction through hydrogen diffusion, the relaxation time was dependent on (1) the direct interaction between the conduction electrons and the protons (deuterons) causing Korringa relaxation, and (2) the indirect RKKY (Ruderman-Kittel-Kasuya-Yosida) interaction. The density of states of the s-type conduction electrons at the Fermi level was 1.65 states per eV. A model with a spherical Fermi surface and free electron behavior in the RKKY interaction, results in U^{3+} and H^- as the ionic species.

(g) Chemical properties

Uranium hydride is very reactive and, in most respects its reactions resemble those of the finely divided uranium metal; in fact, reactions that occur at temperatures where the hydrogen decomposition pressures are high may be those of the metal. Uranium hydride ignites spontaneously in air, but gradual oxidation at low oxygen pressures at room temperature results in the formation of a protective film of oxide on the surface of hydride particles, which prevents the hydride from ignition. Adsorption of a variety of electron-pair-donor compounds can reduce the pyrophoric properties.

Uranium hydride is used as a starting material in many reactions, including the preparation of finely divided uranium metal. Hydrogen, deuterium, and tritium may be stored as UH_3, UD_3, and UT_3, respectively. These gases are released when the compounds are heated to the decomposition temperatures. Gram quantities of UH_3 reacts slowly with water, but larger samples react violently and produce high temperatures (Newton *et al.*, 1949). UH_3 reacts slowly with solution of non-oxidizing acids such as HCl and weak acids such as CH_3COOH, but vigorously with HNO_3. UH_3 reacts with H_2SO_4 to form S, SO_2, and H_2S, and with H_3PO_4 to form UPO_4. UH_3 is unstable in strong bases and reduces aqueous solutions of $AgNO_3$ and $HgCl_2$. At elevated temperatures, UH_3 reacts with O_2, hydrogen halides, H_2S, HCN, NH_3, N_2, CO_2, CH_4, and C_2H_2 (acetylene), but not with liquid hydrocarbons and chlorinated solvents, although an explosive reaction occurs with CCl_4. The reactions of UH_3 with most compounds are thermodynamically favored, and many cases where the

Table 5.13 *Reactions of uranium hydride.*

Reagent	*Reaction temperature* (°C)	*Product*
O_2	ignites at room temperature	U_3O_8
H_2O	350	UO_2
H_2S	400–500	US_2
N_2	250	U_2N_3
NH_3	250	U_2N_3
PH_3	400	UP
Cl_2	250	UCl_4
CCl_4	250	UCl_4
	possibility of explosion at 25°C	
HCl	250–300	UCl_3
HF	200–400	UF_4
Br_2	300–350	UBr_4
HBr	300	UBr_3
CO_2	300	UO_2

reactions do not proceed are a result of kinetic inhibition (Haschke, 1991). Typical reactions of uranium hydride are given in Table 5.13.

(h) Other uranium hydride compounds

(*i*) *Uranium*(IV) *borohydride,* $U(BH_4)_4$

The volatile $U(BH_4)_4$ is obtained as dark green crystals by the reaction

$$UF_4 + 2Al(BH_4)_3 \rightarrow U(BH_4)_4 + 2Al(BH_4)F_2.$$

Purification is made by vacuum sublimation (Schlesinger and Brown, 1953).

$U(BH_4)_4$ is tetragonal with space group $P4_32_12$ having four formula units in the unit cell. The lattice parameters are $a = (7.49 \pm 0.01)$ Å and $c = (13.24 \pm 0.01)$ Å. The positions of U, B, and H have been determined by X-ray and neutron diffraction analyses (Bernstein *et al.*, 1972a,b).

In vacuo and in an inert-gas atmosphere, $U(BH_4)_4$ is fairly stable, but it is immediately decomposed by oxygen or moisture. Bernstein and Keiderling (1973) determined the molecular structure from optical and nuclear magnetic resonance spectra.

The vapor pressure of $U(BH_4)_4$ is given by the equation

$$\log p(\text{mmHg}) = 13.354 - 4265T^{-1}.$$

$U(BH_4)_3$ is a red solid, which has been observed as a by-product in the synthesis of $U(BH_4)_4$. Because of its pyrophoric properties, it has not been well characterized (Schlesinger and Brown, 1953).

(*ii*) *$UNiAlH_y$ and related compounds*

The intermetallic compounds UXAl (X = Ni, Co, Mn) absorb hydrogen on heating in the temperature range 20–250°C at high H_2 pressures. The maximum hydrogen content attained at 20°C corresponds to $UNiAlH_{2.74}$ ($p_{H_2} = 55$ atm), $UCoAlH_{1.2}$ (40 atm), and $UMnAlH_{0.15}$ (40 atm) (Drulis *et al.*, 1982). UNiAl absorbs the largest amount of hydrogen in these compounds, though lower maximum hydrogen absorption values have been reported, at room temperature and 70 atm viz. $UNiAlH_{2.5}$ (Jacob *et al.*, 1984), and $UNiAlD_{2.2}$ at 30°C and 50 atm D_2 (Yamamoto *et al.*, 1998). The lower limit of the hydride phase is $y = 0.7$–0.8 (Yamamoto *et al.*, 1994, 1998; Yamanaka *et al.*, 1999). The hydrogen solubility in the UNiAl metal appears to obey Sieverts law in the hydrogen concentration region below 0.02 H per formula unit UNiAl (Yamanaka *et al.*, 1999).

The symmetry and space group of $UNiAlH_y$ are the same as those for UNiAl. The structure consists of alternate planes containing three Al (in 3f) and two Ni (2c) atoms at $z = 0$ and three U (3g) and one Ni (1b) atoms at $z = 1/2$. The hydrogen atoms are located in the center of one of the adjacent U_3Ni tetrahedra, in the bipyramid U_3Al_2, and in the bipyramid Al_3Ni_2 (Kolomiets *et al.*, 2000). The lattice parameter a increases whereas b decreases slightly with increasing value of y (Drulis *et al.*, 1982; Jacob *et al.*, 1984; Yamamoto *et al.*, 1994; Yamanaka *et al.*, 1999; Kolomiets *et al.*, 2000). This variation, expressed in Å, is approximately represented by the equations $a = 6.736 + 0.187y$ and $c = 4.037 - 0.028y$ in the range $0.8 \leq y \leq 2.7$. The hydrogenation of UNiAl is accompanied by a volume change. The quotient $\Delta V/V$ attains a value of 0.124 for both hydride ($y = 2.3$) and deuteride ($y = 2.1$). In addition, the X-ray diffraction peak intensities indicate a positional shift of the U atoms from (0.572, 0, 1/2) in UNiAl to (2/3, 0, 1/2) in $UNiAlH_{2.3}$. These changes are supposed to favor the accommodation of a larger amount of hydrogen (Kolomiets *et al.*, 2000).

The desorption isotherms of $UNiAlH_y$ have two sloping plateaus, which suggests the existence of two hydride phases (Jacob *et al.*, 1984). The partial molar enthalpy and entropy of hydrogen for the non-stoichiometric $UNiAlH_y$ varies with the y value. $\Delta\bar{H}(H_2)$ and $\Delta\bar{S}(H_2)$ were –53 kJ (mol H_2)$^{-1}$ and –88 J K^{-1} (mol H_2)$^{-1}$, respectively, for $UNiAlH_{1.35}$, and –41 kJ (mol H_2)$^{-1}$ and –95 J K^{-1} (mol H_2)$^{-1}$ for $UNiAlH_{2.30}$ (Drulis *et al.*, 1982). The values measured by Jacob *et al.* (1984) are comparable with the above values: $\Delta\bar{H}(H_2)$ and $\Delta\bar{S}(H_2)$ were −64 kJ (mol H_2)$^{-1}$ and –90 J K^{-1} (mol H_2)$^{-1}$, respectively, for $UNiAlH^{1.2}$, and −47 kJ (mol H_2)$^{-1}$ and –94 J K^{-1} (mol H_2)$^{-1}$, respectively, for $UNiAlH_{2.0}$.

The incorporation of hydrogen into UNiAl leads to a large increase in the antiferromagnetic ordering temperature from 19 K to 90–100 K. The transition temperatures for $UNiAlH_{2.3}$ and $UNiAlD_{2.1}$ are 99 and 94 K, respectively (Kolomiets *et al.*, 2000). According to Zogal *et al.* (1984), $UNiAlH_{1.9}$ has

magnetic transitions at 122 and 34 K, where the second transition possibly refers to the hydride at the lower phase limit. The magnetic susceptibility in the paramagnetic region is represented by the modified Curie–Weiss equation. The effective moment, μ_{eff}, the paramagnetic Curie temperature, θ_{p}, and the temperature-independent susceptibility, χ_{o}, are 2.42 μ_{B}/f.u., –42 K and 7×10^{-9} m^3 mol^{-1}, respectively, for $UNiAlH_{2.3}$. The values are 2.43 μ_{B}/f.u., –50 K and 8×10^{-9} m^3 mol^{-1}, respectively, for $UNiAlD_{2.1}$ (Kolomiets *et al.*, 2000).

$U(Fe_{1-x}Ni_x)Al$ with $x \geq 0.7$ absorbs hydrogen forming $U(Fe_{1-x}Ni_x)AlH_y$ hydrides. Raj *et al.* (2000) studied the magnetic properties of $U(Fe_{0.3}Ni_{0.7})AlH_y$, and found that no other hydride phase was formed above or below $y = 0.8$. $U(Fe_{0.3}Ni_{0.7})AlH_y$ is ferromagnetic with $T_{\text{C}} = 15$ K ($y = 0$) and 90 K ($y = 0.8$). Magnetization of $U(Fe_{0.3}Ni_{0.7})Al$ at 5.5 T gave a saturation moment of $\cong 0.3\mu_{\text{B}}$/f.u. The value for the hydride ($y = 0.8$) was much higher, $\cong 0.9\mu_{\text{B}}$/f.u., indicating considerable increase in the ferromagnetic correlations. Other intermetallic hydrides, e.g. $U_5Ni_4PdH_{1.0}$ (Drulis *et al.*, 1982), $UCoH_{2.7}$ (Andreev *et al.*, 1986; Yamamoto *et al.*, 1991), and UTi_2D_y (Yamamoto *et al.*, 1995) have also been studied.

5.7.2 The uranium–oxygen system

(a) Binary uranium oxides

(*i*) *Preparative methods*

Comprehensive information on the preparation of actinide oxides including uranium oxides is given in a monograph by Morss (1991).

UO(*s*)

Although UO gas is one of the main species over U(l)+UO_{2-x} at high temperatures, solid UO ($Fm\bar{3}m$, $a = 4.92$ Å) with NaCl-type structure is very unstable and its formation has not been definitely established. When UO_2 was heated with uranium metal at high temperatures, a fcc phase was produced only in cases of considerable carbon contamination (Rundle *et al.*, 1948). Carbon is thought to promote the reaction. It is possible that UC or UN must be present for the formation of the UO phase (Rundle *et al.*, 1948; Cordfunke, 1969).

UO_2(*s*)

UO_2 is prepared by hydrogen reduction of UO_3 or U_3O_8 between 800 and 1100°C (Katz and Rabinowitch, 1951; Belle, 1961; Wedermeyer, 1984). The H_2 gas used for this purpose should not contain impurity of O_2 in order to avoid oxidation to hyperstoichiometric UO_{2+x}, which occurs on cooling at temperatures below 300°C. The UO_2 pellets for reactor fuel are reduced at much higher temperatures around 1700°C in order to approach the theoretical density. For laboratory use, other reductants such as CO, C, CH_4, and C_2H_5OH may be

used, but they offer no advantages over H_2 (Katz and Rabinowitch, 1951; Wedermeyer, 1984; Roberts and Walter, 1966). NH_3 is not suitable (Belle, 1961). Commercial methods of UO_2 synthesis start from the peroxide $UO_4 \cdot 2H_2O$, ammonium diuranate with the approximate composition $(NH_4)_2U_2O_7$ or ammonium uranyl carbonate $(NH_4)_4UO_2(CO_3)_3$ followed by air calcination at 400–500°C. Subsequent H_2 reduction at 650–800°C yields UO_2 with high surface area. The nuclear fuel pellets are produced by cold pressing of these powders, followed by sintering.

$U_4O_9(s)$

U_4O_9 can be prepared from the stoichiometric amounts of UO_2 and U_3O_8 according to the reaction $5UO_2 + U_3O_8 = 2U_4O_9$. The reactants are ground in an agate mortar and the mixture is sealed in an evacuated quartz ampoule, and then heated at 1000°C for about 2 weeks until the sample is completely homogenized. The sample is slowly cooled to room temperature over a period of 2 weeks (Gotoo and Naito, 1965; Westrum, Jr. *et al.*, 1965). U_4O_9 has three phases: α-U_4O_9 that transforms into β-U_4O_9 on heating to ~350 K, and β-U_4O_9 that transforms into γ-U_4O_9 at ~850 K (Labroche *et al.*, 2003b). These transformations are reversible.

$U_3O_7(s)$

Three polymorphs of α, β, and γ are known for U_3O_7; all of them are tetragonal. α-U_3O_7 with *c/a* ratios 0.986–0.991 is prepared by oxidizing UO_2 at temperatures below 160°C (Hoekstra *et al.*, 1961; Westrum, Jr. and Grønvold, 1962). To prepare a single phase with O/U $\approx$ 2.33, the use of reactive UO_2, which is obtained by low-temperature reduction of UO_3 by H_2, is recommended (Hoekstra *et al.*, 1961). Oxidation of UO_2 in air at 200°C yields β-U_3O_7 with *c/a* ratios between 1.027 and 1.032 (Garrido *et al.*, 2003). The oxidation of standard uranium dioxide ceases at $UO_{2.33}$ at temperatures below 200°C and no formation of U_3O_8 takes place (Hoekstra *et al.*, 1961). Allen and Tyler (1986) report that well-crystallized single-phase β-U_3O_7 was obtained by oxidation at 230°C for 16 h. The γ-U_3O_7 ($U_{16}O_{37}$) phase, which has *c/a* ratios of 1.015–1.017 and smaller O/U ratios of 2.30–2.31 (Hoekstra *et al.*, 1961; Westrum, Jr. and Grønvold, 1962; Hoekstra *et al.*, 1970; Nowicki *et al.*, 2000), is formed when U_4O_9 is oxidized at 160°C (Hoekstra *et al.*, 1961). This compound has also been prepared as a mixture with monoclinic U_8O_{19} on heating a pellet of mixed UO_2 and UO_3 at $\geq$400°C under high pressures (15–60 kbar) (Hoekstra *et al.*, 1970).

$U_2O_5(s)$

High-pressure syntheses by Hoekstra *et al.* (1970) identified three U_2O_5 phases (α-U_2O_5, β-U_2O_5 and γ-U_2O_5). α-U_2O_5 was prepared by heating a mixture of UO_2 and U_3O_8 at 400°C and 30 kbar for 8 h. At 500°C, a pressure of 15 kbar was enough to prepare α-U_2O_5. Hexagonal β-U_2O_5 is formed at 40–50 kbar pressure at temperatures higher than 800°C. Monoclinic γ-U_2O_5 was sometimes

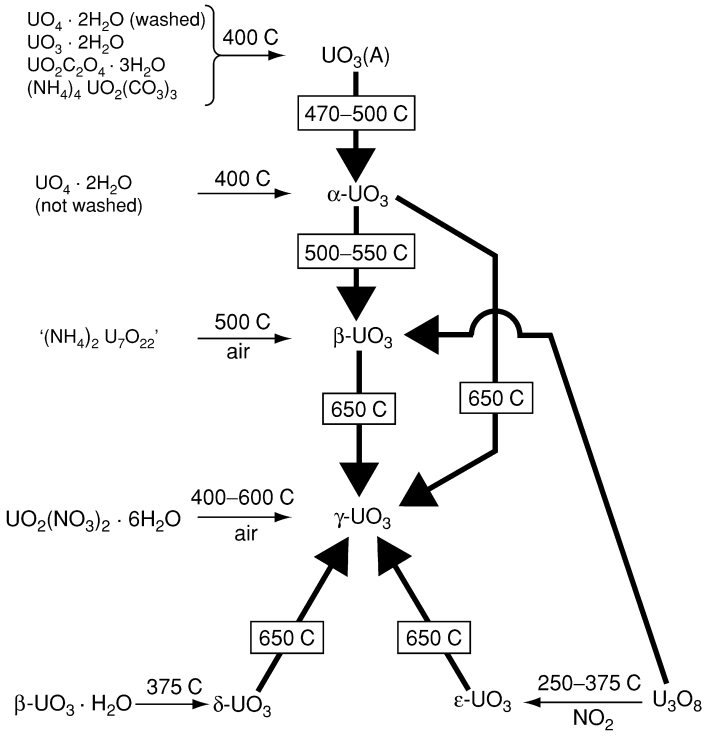

Fig. 5.15 *Flow sheet for the preparation of various UO_3 modifications: Bold lines refer to high O_2 pressure* (*Hoekstra and Siegel,* 1961; *Cordfunke*, 1969).

obtained when the UO_2 and U_3O_8 mixture was heated above 800°C at a pressure of 60 kbar.

$U_3O_8(s)$

α-U_3O_8 is prepared by oxidation of UO_2 in air at 800°C followed by slow cooling (Loopstra, 1970a). β-U_3O_8 is prepared by heating α-U_3O_8 to 1350°C in air or oxygen, followed by slow cooling (cooling rate: 100 K per day) to room temperature (Loopstra, 1970b).

$UO_3(s)$

Seven modifications are known for UO_3: A, α, β, γ, δ, ε, and ζ-UO_3. The methods of their syntheses are outlined in the flow sheet of Fig. 5.15 (Hoekstra and Siegel, 1961; Cordfunke, 1969).

Amorphous UO_3 (A-UO_3) forms when any of the compounds $UO_4 \cdot 2H_2O$ (washed with H_2O), $UO_3 \cdot 2H_2O$, $UO_2C_2O_4 \cdot 3H_2O$ and $(NH_4)_4UO_2(CO_3)_3$ is heated in air at 400°C. Because of the difficulty to remove residual traces of nitrogen and carbon, it is preferable to use either of the first two of the above

compounds (Hoekstra and Siegel, 1961). α-UO_3 is prepared by crystallization of A-UO_3 at 485°C for 4 days. The heating time can be shortened at 500°C but a pressure of 40 atm oxygen is then needed (Hoekstra and Siegel, 1961). β-UO_3 is prepared by heating 'ammonium diuranate' or uranyl nitrate rapidly in air at 450–500°C. The crystallinity of β-UO_3 is improved by keeping the sample at 500°C (not higher) for 4–6 weeks (Debets, 1966). This compound is also obtained by heating at 500–550°C under 30–40 atm O_2. γ-UO_3 is formed slowly at 500–550°C in 6–10 atm O_2. At 650°C and 40 atm O_2, all α, β, δ, and ε-UO_3 compounds convert to the γ-phase. γ-UO_3 can be prepared directly in air by heating uranyl nitrate hexahydrate to 400–600°C (Hoekstra and Siegel, 1958; Engmann and de Wolff, 1963). Stoichiometric δ-UO_3 is obtained by heating β-$UO_2(OH)_2$ (= β-$UO_3 \cdot H_2O$) at 375–400°C for more than 24 h (Hoekstra and Siegel, 1961). At 415°C, the oxygen-deficient δ-phase forms (Wait, 1955). ε-UO_3 is prepared by oxidizing U_3O_8 at 350°C in NO_2(g). The reaction goes to completion in a few seconds (Gruen *et al.*, 1951). At a temperature of 400°C, the reaction rate levels off as the stability limit of ε-UO_3 is approached (Hoekstra and Siegel, 1961). The high-pressure modification ζ-UO_3 forms at 30 kbar and 1100°C (Hoekstra *et al.*, 1970).

UO_3 hydrates

The existence of six compounds, i.e. $UO_3 \cdot 2H_2O$, α-$UO_3 \cdot 0.8H_2O$, α-$UO_2(OH)_2$, β-$UO_2(OH)_2$, γ-$UO_2(OH)_2$, and $U_3O_8(OH)_2$, has been confirmed in the UO_3–water system. $UO_3 \cdot 2H_2O$ is prepared by exposure of anhydrous UO_3 to water at 25–75°C. An alternative method is to add 0.65 g $La(OH)_3$ to 50 mL 0.2 M $UO_2(NO_3)_2$ solution. The hydroxide dissolves slowly, accompanied by an increase in solution pH from 2.2 to 4.0. Digestion of the clear solution at 55°C causes a gradual precipitation of a portion of the uranium as bright yellow crystals of $UO_3 \cdot 2H_2O$ (Hoekstra and Siegel, 1973). Water-deficient α-phase monohydrate, α-$UO_3 \cdot 0.8H_2O$, was prepared by heating $UO_3 \cdot 2H_2O$ in air at 100°C or by heating either $UO_3 \cdot 2H_2O$ or UO_3 in water at 80–200°C (Dell and Wheeler, 1963). Stoichiometric α-$UO_2(OH)_2$ (= α-$UO_3 \cdot H_2O$) was prepared in hydrothermal experiments at temperatures approaching 300°C (Harris and Taylor, 1962; Taylor, 1971).

Stoichiometric β-$UO_2(OH)_2$ (or β-$UO_3 \cdot H_2O$) is prepared by the action of water on $UO_3 \cdot 2H_2O$ or UO_3 at 200–290°C in a sealed reactor (Dawson *et al.*, 1956). It is also formed by the hydrolysis of uranyl salt solutions (cf. γ-$UO_2(OH)_2$). γ-$UO_2(OH)_2$ (or γ-$UO_3 \cdot H_2O$) is obtained when 0.65 g $La(OH)_3$ is added to 50 mL of 0.2 M $UO_2(NO_3)_2$ and subsequent heating of the solution to 80–90°C; digestion of the solution leads to slow precipitation of γ-$UO_2(OH)_2$ (Hoekstra and Siegel, 1973). There may be no region of true thermodynamic stability for the γ-phase. Continued digestion for several weeks eventually gives β-$UO_2(OH)_2$ as the sole product. $U_3O_8(OH)_2$ (= $UO_3 \cdot 1/3H_2O$ or $H_2U_3O_{10}$, i.e. hydrogen triuranate) is prepared by hydrothermal reaction of $UO_3 \cdot 2H_2O$ or UO_3 at temperatures between 300 and 400°C. Although no solid solution range

has been observed for this compound, appreciable variations in water content from 0.33 to 0.50 have been reported (Siegel *et al.*, 1972).

Uranium peroxide tetrahydrate, $UO_4 \cdot 4H_2O$, is obtained when the precipitate, grown from the uranyl nitrate solution of pH = 2 on addition of hydrogen peroxide solution, is dried at room temperature (Silverman and Sallach, 1961); the dihydrate, $UO_4 \cdot 2H_2O$, is prepared by heating $UO_4 \cdot 4H_2O$ at 90°C.

(*ii*) *Preparation of single crystals*

The basic method to prepare single crystals of UO_2 is to melt UO_2 powders. Arc melting (Brit and Anderson, 1962) and solar furnace heating (Sakurai *et al.*, 1968) techniques have been adopted for this purpose. The vapor deposition method has also been used, where an electric current was passed through a hollow cylinder of UO_2. UO_2 sublimed from the hot central part of the inner surface of the cylinder and deposited at the cooler end, forms large hemispherical single crystals of 4–12 mm (van Lierde *et al.*, 1962). Recrystallization also yields single crystals in the central part of UO_2 rod when the current is directly passed through the specimen (Nasu, 1964).

Single crystals of the length 5 cm have been prepared by means of the floating zone technique. In this case, the preheated UO_2 rods were heated by induction eddy-currents (Chapman and Clark, 1965). Robins (1961) obtained single crystals of 3 mm length by electrolysis of uranyl chloride in fused alkali chloride melts.

Formation of single crystals by chemical transport reactions has been studied by a number of researchers. Naito *et al.* (1971) examined the transport of UO_2, U_4O_9, and U_3O_8 from 1000 to 850°C in sealed quartz tubes using the transporting agents HCl, Cl_2, I_2, Br_2, and Br_2+S_2. Although the transport rate was very low in I_2 (0.002 mg h^{-1}), it was high enough in Cl_2 of 4 mmHg pressure (23 mg h^{-1}) and in Br_2+S_2 with partial pressures (2.5 ± 0.2) mmHg (12.5 mg h^{-1}) to obtain single crystals. Single crystals of UO_2 were deposited on UO_2 substrates with (100) and (111) orientations by the chemical transport method using Cl_2 as the transporting agent (Singh and Coble, 1974). At Cl_2 pressures below 10 mmHg and high substrate temperatures (>950°C), good single crystals free from cracking caused by epitaxial growth were obtained.

Faile (1978) reported the formation of large single crystals of UO_2 by the use of $TeCl_4$ as transport agent. UO_2 was transported in a sealed fused quartz tube from the source end at 1050°C over a temperature gradient to the deposition end at 950°C. The maximum weight of the obtained single crystals was 1 g. $TeCl_4$ has also been used successfully for the preparation of single crystals of other actinide dioxides (Spirlet *et al.*, 1979).

(*iii*) *Crystal structures*

The crystal structures of uranium oxides in the composition range $2.00 \leq O/U \leq 2.375$, which includes UO_2 and polymorphs of U_4O_9 and U_3O_7, are closely related to the fluorite structure. On the other hand, the crystal structures of

U_3O_8 and many of the UO_3 polymorphs are based on the layer structures, which are characterized by the existence of UO_2^{2+} uranyl groups arranged normal to the plane of the layers. The lattice parameters of the uranium oxides are shown in Table 5.14.

UO_2, UO_{2+x}

Stoichiometric uranium dioxide crystallizes in a fcc structure (space group $Fm\bar{3}m$), where the uranium atoms occupy the positions 0,0,0; 1/2,1/2,0; 1/2, 0, 1/2 and 0, 1/2, 1/2 and the oxygen atoms occupy the 1/4, 1/4, 1/4 and its equivalent positions. As the temperature is raised, the anisotropic thermal vibration causes the oxygen atoms to move to the $1/4 + \delta$, $1/4 + \delta$, $1/4 + \delta$ positions, where $\delta = (0.016 \pm 0.001)$ at 1000°C (Willis, 1964a).

In the hyperstoichiometric uranium dioxide, UO_{2+x}, the interstitial oxygen atoms occupy two different sites of the UO_2 lattice, which are displaced by about 1 Å along the <110> and <111> directions from the cubic coordinated interstitial position. These oxygen atoms are denoted as O′ and O″, respectively. Together with these interstitial atoms, it was observed that vacancies were formed at the normal oxygen sites, although the uranium sublattice remained undisturbed (Willis, 1964b). Willis (1978) later analyzed the neutron diffraction data for $UO_{2.12}$ at 800°C by taking into account the anharmonic contribution to the Debye–Waller factor. The occupancy numbers of O′ and O″ and the vacant lattice oxygens were calculated to be equal within one standard deviation, indicating that the defect complex has a 2:2:2 configuration of oxygen defects. The two O″ oxygen atoms displace two normal oxygen atoms forming two O′ atoms and two oxygen vacancies.

A model that assumes a chain-like coordination of the 2:2:2 clusters along <110> directions has been proposed (Allen *et al.*, 1982). However, it failed to give a satisfactory agreement between the observed and calculated neutron intensities (Willis, 1987). There may be a similarity between the clusters present in UO_{2+x} and $Fe_{1-x}O$. In the non-stoichiometric $Fe_{1-x}O$, the Roth clusters (Roth, 1960) or Koch–Cohen clusters (Koch and Cohen, 1969) are thought to be statistically distributed. These clusters have different structures but their compositions are close to that of Fe_3O_4 (Anderson, 1970), which is formed as an ordered phase when the concentration of clusters exceeds a certain value. In the case of UO_{2+x}, the possibility of disordered arrangement of cuboctahedral clusters exists, as U_4O_9 might be composed of ordered cuboctahedral clusters.

U_4O_9

The low-temperature phase α-U_4O_9 transforms to β-U_4O_9 at 340–350 K, which is accompanied by an anomaly in the specific heat at 348 K (Westrum, Jr. *et al.*, 1965) or 330 K (Gotoo and Naito, 1965) and of a dilatation at 293–359 K (Grønvold, 1955). The lattice parameter decreases with increasing temperature in this range (Ferguson and Street, 1963), but no anomaly was observed in the

Table 5.14 *Physical properties of the stoichiometric uranium oxides.*

					Lattice parameters					*Density* ($g\ cm^{-3}$)		
Formula	*Color*	*m.p.*(K)	*Space group*	*Symmetry*	*a* (Å)	*b* (Å)	*c* (Å)	*Angle* (deg)	*Z*	*Exp.*	*X-ray or ND*	*References*
UO_2	brown to black	3138	$Fm\bar{3}m$	fcc	5.4704				4	10.95	10.964	IAEA (1965); Winslow (1971)
U_4O_9	black		$I\bar{4}3d$	bcc	5.441 × 4				64		10.299	IAEA (1965); Ishii *et al.* (1970a); Bevan *et al.* (1986)
$U_{16}O_{37}$(*)	black			tetragonal	5.407		5.497				11.366	Hoekstra *et al.* (1970)
U_8O_{19}(*)	black			monoclinic	5.378	5.559	5.378	β = 90.27		11.34	11.402	Hoekstra *et al.* (1968)
α-U_3O_7	black			tetragonal	5.447		5.400			10.62		Hoekstra *et al.* (1961); Westrum, Jr. and Grønvold (1962)
β-U_3O_7	black			tetragonal	5.383		5.547			10.60		Hoekstra *et al.* (1961); Garrido *et al.* (2003)
γ-U_3O_7 ($U_{16}O_{37}$)	black			tetragonal	5.407		5.497					Hoekstra *et al.* (1970)
α-U_2O_5	black			monoclinic	12.40	5.074	5.675	β = 99.2	4	10.5	10.47	Hoekstra *et al.* (1970); Spitsyn *et al.* (1972)
β-U_2O_5	black			hexagonal	3.813		13.18		2	10.76 to 11.38	11.15	Hoekstra *et al.* (1970)
γ-U_2O_5	black			monoclinic	5.410	5.481	5.410	β = 90.49	2	10.36	11.51	Hoekstra *et al.* (1970)
$U_{13}O_{34}$	black		*Cmcm* (or *Cmc* or *Ama*)	orthorhombic	6.740	3.964×13	4.143×2		4		8.40	Spitsyn *et al.* (1972)

U_8O_{21}			*Pmma*	orthorhombic	6.796	3.958×8	4.145×2		4		8.341	Spitsyn *et al.* (1972)
$U_{11}O_{29}$			*Pnma* (or *Pna*$_2$)	orthorhombic	6.765	3.956×11	4.140×2		4		8.40	Spitsyn *et al.* (1972)
α-U_3O_8	green black		*C*2*mm*	orthorhombic	6.716	11.960	4.147		2		8.395	Loopstra (1970b)
β-U_3O_8	green black		*Cmcm*	orthorhombic	7.069	11.445	8.303		4		8.326	Loopstra (1970b)
$U_{12}O_{35}$(*)	olive green			orthorhombic	6.91	3.92	4.16		2	7.72	8.39	Hoekstra *et al.* (1970)
A-UO_3	orange	723(d)		amorphous						6.80		Hoekstra and Siegel (1961)
α-UO_3	beige	723(d)	(*C*222 derived)	orthorhombic	6.84	43.45	4.157		19	7.30	7.44	Siegel and Hoekstra (1971a); Greaves and Fender (1972)
β-UO_3	orange	803(d)	*P*2$_1$	monoclinic	10.34	14.33	3.910	β = 99.03	10	8.25	8.30	Hoekstra and Siegel (1961); Debets (1966)
γ-UO_3	yellow	923(d)	*Fddd*	orthorhombic	9.813	19.93	9.711		32	7.80	8.00	Hoekstra and Siegel (1961); Siegel and Hoekstra (1971b)
δ-UO_3	deep red	673(d)	*Pm*3*m*	cubic	4.16				1	6.69	6.60	Wait (1955); Hoekstra and Siegel (1961)
ε-UO_3	brick red	673(d)		triclinic	4.002	3.841	4.165	α = 98.10 β = 90.20 γ = 120.17	1	8.54	8.67	Hoekstra and Siegel (1961); Kovba *et al.* (1963)
ζ-UO_3	brown		*P*2$_1$2$_1$2$_1$	orthorhombic	7.511	5.466	5.224		4	8.62	8.86	Siegel *et al.* (1966); Hoekstra *et al.* (1970)

(d): decomposes.
(*): Parameters for these phases refer to a pseudo-cell.

magnetic susceptibility (Gotoo and Naito, 1965). The transition was claimed to be due to disordering of oxygen with U^{4+}–U^{5+} rearrangement (Naito *et al.*, 1967; Fournier and Troć, 1985). Belbeoch *et al.* (1967) reported that α-U_4O_9 has a rhombohedral structure, slightly distorted from a cubic structure with the lattice parameters $a = 5.4438n$ (*n*: an integer) and $\alpha = 90.078°$ at 20°C. The transition is possibly of order–disorder type coupled with a small change in crystal structure.

Another transition from β-U_4O_9 to γ-U_4O_9 occurs at higher temperatures around 850 K. An X-ray diffraction analysis showed the transition temperature to be 823–973 K (Blank and Ronchi, 1968), while the heat capacity measurement gave 900–950 K (Grønvold *et al.*, 1970). A transition between 813–893 K was observed for the specimens of $2.228 \leq O/U \leq 2.25$ (Naito *et al.*, 1973) using X-ray diffraction and electrical conductivity measurements. This β/γ transition is assumed to be based on the order–disorder mechanism (Blank and Ronchi, 1968; Naito *et al.*, 1973). According to Seta *et al.* (1982), there was no clear anomaly or variation in the heat capacity curves in the above temperature range. Instead they observed two small peaks for hypostoichiometric U_4O_{9-y} ($UO_{2.22}$ and $UO_{2.235}$) at 1000 and 1100 K.

The crystal structure of α-U_4O_9 has not yet been solved, but it is supposed to be closely related to that of strictly cubic β-U_4O_9, with the space group $I\bar{4}3d$. Electron diffraction measurements on α-U_4O_9 showed that the superlattice reflections all obeyed the special extinction rules for the $\bar{4}$ sites of the space group $I\bar{4}3d$ (Blank and Ronchi, 1968). Bevan *et al.* (1986) suggest that α-U_4O_9 consists of cuboctahedral clusters centered on 12(a) or 12(b) sites similar to the crystal structure of β-U_4O_9, although the anion sublattice may be perturbed.

Bevan *et al.* (1986) collected single-crystal neutron diffraction data for β-U_4O_9 at 230 and 500°C. A partial Patterson synthesis obtained using only the superlattice reflections supported the cuboctahedral cluster model. Fig. 5.16 shows a sketch of the cuboctahedral oxygen cluster formed by 12 anions located at the vertices of a cuboctahedron and with a 13th oxygen atom situated in its center. The cube surrounding the cluster has an edge length close to the lattice parameter of the fcc cell of the uranium sublattice (the individual cations are not shown in the figure). In β-U_4O_9, the discrete U_6O_{37} cuboctahedral clusters are arranged on $\bar{4}$ axes with positions 12(b) of $I\bar{4}3d$.The displacement of oxygen in the cluster gives rise to the O′ interstitial atoms of Willis. The cuboctahedral cluster contains the Willis 2:2:2 clusters as a component. The structure contains twelve U_6O_{37} clusters per unit cell. There are 60 extra anions per unit cell, and the composition is then $U_{256}O_{572}$, i.e. the β-U_4O_9 phase has the composition U_4O_{9-y} with $y = 0.062$.

U_3O_7

The U_3O_7 polymorphs all crystallize in the tetragonal system but none of their space groups have been specified. The axial ratio *c/a* is here an important parameter to classify the different polymorphs. α-U_3O_7, which is prepared by

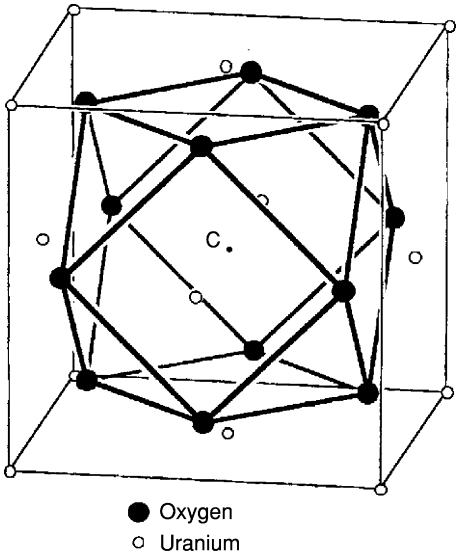

Fig. 5.16 *A schematic diagram of the cuboctahedral cluster. Eight oxygen anions inside the cationic cube are replaced by* 12 *anions located along the* <110> *directions from the center C.* (*from Garrido* et al. (2003), *reproduced by the permission of Elsevier*).

oxidation of UO_2 in air at temperatures of 120–175°C, has *c/a* ratios less than 1 (0.986–0.991) (Pério, 1953b; Westrum, Jr. and Grønvold, 1962). The *c/a* ratios for β-U_3O_7, prepared by oxidizing UO_2 in air at temperatures 160–250°C, are 1.027–1.032 (Hoekstra *et al.*, 1961; Simpson and Wood, 1983; McEachern and Taylor, 1998). In the range of O/U ratios between 2.26 and 2.33, the *c/a* ratio of α-U_3O_7 did not vary in a systematic way between 0.986 and 0.989, while that of β-U_3O_7 seemed to increase very slightly with increasing O/U ratio (Hoekstra *et al.*, 1961). The γ-U_3O_7 ($U_{16}O_{37}$) phase with *c/a* ratios of 1.015–1.016 appears in a range where the O/U ratios are 2.30–2.31 (Westrum, Jr. and Grønvold, 1962; Hoekstra *et al.*, 1970; Tempest *et al.*, 1988), which are significantly smaller than those of α-U_3O_7 and β-U_3O_7.

In the recent studies on β-U_3O_7, it was found that all the uranium atoms and 70% of the oxygen atoms were hardly affected by the oxidation of UO_2 to U_3O_7; however, the remaining 30% of the oxygen atoms changed their location to new sites which are shifted 0.31 Å along $\langle 110 \rangle$ vectors from the holes in the fluorite framework of UO_2. This result, based on a neutron diffraction analysis, is consistent with the assumption that the excess oxygen atoms in β-U_3O_7 are accommodated in the cuboctahedral oxygen clusters (Garrido *et al.*, 2003) as in the case of β-U_4O_9.

According to a theoretical study by Nowicki *et al.* (2000), the crystal structures of U_3O_7 differ from that of UO_2 by the presence of the cuboctahedral

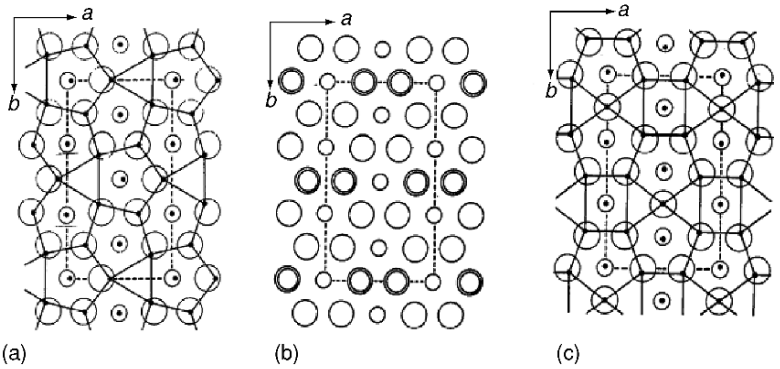

Fig. 5.17 *Atom arrangements on the sections perpendicular to the c-axis* (*Loopstra,* 1970*b*). (*a*) *α-U_3U_8*; (*b*) *hypothetical 'ideal' UO_3*; (*c*) *β-U_3O_8. The dots in the figure represent the actual positions. Isolated dots: uranium atoms; dots connected by full-drawn lines denote oxygen atoms. In* (*a*), *the section is at* $z = 0$, *and in* (*c*), *the origin is shifted b/3 at* $z = 1/4$. *Reproduced by permission of the International Union of Crystallography*.

clusters centered at specified ordered positions, and the arrangement of the clusters can be expressed as a stacking of identical polyatomic modules. A single module contains clusters arranged in a square pattern. The square sides have a length approximately equal to $R_1 = \sqrt{2.5}a_{UO_2} \approx 0.86$ Å. The thickness of the modules is close to $1.5a_{UO_2} \approx 0.82$ Å. The various polytypes found in U_3O_7 can be rationalized with different stacking order of these modules; the small change in the energy of formation of the crystal reflects the interaction between the clusters.

U_3O_8

α-U_3O_8 is orthorhombic (*C*2*mm*; $a = 6.716$ Å, $b = 11.96$ Å, $c = 4.1469$ Å; $z = 2$) (Loopstra, 1962). β-U_3O_8 is also orthorhombic (*Cmcm*; $a = 7.069$ Å, $b = 11.445$ Å, $c = 8.303$ Å; $z = 4$) (Loopstra, 1970b), and the crystal structures of these two modifications are very similar. Fig. 5.17 depicts the relation of α- and β-U_3O_8 with the hypothetical 'ideal' UO_3 structure. The idealized α-U_3O_8 structure (Fig. 5.17a) is derived from a layer of the hypothetical 'ideal' UO_3 (Fig. 5.17b) by removing one oxygen atom from every third row. The idealized β-U_3O_8 structure is obtained by replacing two oxygen atoms by a single one, located halfway between them (Fig. 5.17c). Fig. 5.17a and c show that the actual structures are only slightly distorted from the hypothetical ideal positions, which are represented in Fig. 5.17 by small circles (uranium atoms) and large circles (oxygen atoms). In α-U_3O_8, all uranium atoms are coordinated with oxygen atoms forming pentagonal bipyramids. In β-U_3O_8 the layers are stacked along the *c*-axis so that a set of chains of uranium atoms is formed at $x = 0$, $y = 0$ and $x = 1/2$, $y = 1/2$. The other uranium atoms form chains in the *c* direction, in which the oxygen coordination is alternately pentagonal bipyramidal and distorted octahedral.

α-U_3O_8 shows a λ-type anomaly in the specific heat at 208.5°C (Girdhar and Westrum, Jr., 1968). At this first-order phase transformation temperature, the orthorhombic pseudo-hexagonal α-U_3O_8 changes to a hexagonal structure ($P\bar{6}2m$; $a = 6.812$ Å, $c = 4.142$ Å; $z = 1$) (Loopstra, 1970a). Although the high- and low-temperature phases are closely related, there is an essential difference in the atom arrangement. In the high-temperature phase the uranium atoms occupy a single three-fold position, whereas at room temperature (in the low-temperature phase) they are located at two-fold and four-fold positions making it possible for the uranium atoms to have different localized charges.

Allen and Holmes (1995) pointed out the resemblance in the crystal structures of UO_2 and α-U_3O_8. The UO_2 fluorite structure can be transformed to the layer structure of α-U_3O_8 by displacing the (111) planes in UO_2. A displacement of 2.23 Å along the $\langle 112 \rangle$ direction in the (111) plane brings the outermost uranium layer directly above the second layer of the structure of α-U_3O_8.

UO_3

The crystal structure of α-UO_3 was first reported as trigonal ($P\bar{3}m1$; $a = 3.971$ Å, $c = 4.170$ Å) (Zachariasen, 1948a). However, the later neutron powder diffraction data could not be adequately described in this way. Loopstra and Cordfunke (1966) published a structure assignment using an orthorhombic unit cell ($C2mm$; $a = 3.961$ Å, $b = 6.860$ Å, $c = 4.166$ Å). This structure is close to the former one, since in both cases there are linear chains of O–U–O–U–O with the uranium surrounded by six additional oxygen atoms lying approximately in a plane normal to the chains. The reassignment to the orthorhombic cell reduced the *R*-value from 0.35 to 0.19, but this is still high. Neither of the structures proposed could explain the abnormally low experimental density and the infrared absorption spectrum; the experimental densities were 7.25 g cm^{-3} (Loopstra and Cordfunke, 1966) or 7.30 g cm^{-3} (Siegel and Hoekstra, 1971a), which are much lower than the X-ray density of 8.39 g cm^{-3}. Strong infrared absorption was observed around 930 cm^{-1} (Hoekstra and Siegel, 1961; Carnall *et al.*, 1966). This is typical of the antisymmetric stretching vibration of the linear uranyl group with the U–O bond distance of about 1.7 Å (Jones, 1959), but isolated uranyl groups do not exist in either of the above crystal structures.

A characteristic feature of a large number of solid uranium(VI) oxides is that they contain uranyl groups (UO_2^{2+}) with collinear atom arrangement (O–U–O) (Zachariasen, 1954b). The U–O bond (primary bond) of the uranyl group is a strong covalent bond (cf. Section 5.8.3c), giving short bond distances of 1.7–1.9 Å. The antisymmetric vibration of O_I–U–O_I, where O_I denotes the oxygen atoms in the uranyl group, gives rise to a strong infrared absorption in the frequency range of 600–950 cm^{-1}. The oxygen atoms (O_{II}), bound to uranium in a plane perpendicular to the linear uranyl group, form secondary bonds which are weaker than the U–O_I bonds. The U–O_{II} bond distances are longer, usually between 2.1 and 2.5 Å. The uranyl groups are often seen in the uranium oxides having layer structures. The collinear axis of the uranyl group is along the *c*-axis of such crystals with the four to six U–O_{II} bonds formed in the *a*–*b* plane.

Greaves and Fender (1972) carried out a structure refinement based on the assumption that α-UO_3 is formed by introducing statistically distributed vacancies into the uranium sublattice of α-U_3O_8 so as to re-establish an O/U ratio of three. For each missing uranium atom there were two displaced oxygen atoms in the *z*-direction. Refinement of diffraction data using this model for the α-U_3O_8 structure (space group *C*222) of Andresen (1958) decreased the *R*-value to 0.031 and the theoretical density to 7.44 g cm^{-3}; the U–O distance in the uranyl groups was 1.64 Å. The same refinement based on the *C*2*mm* space group of Loopstra (1962) yielded fairly reasonable values of the uranium occupation number, 0.82, and the U–O distance, 1.58 Å, but the *R*-value (0.13) and the uranium and oxygen temperature factors were somewhat higher. The superlattice reflections observed in both the neutron and electron diffraction patterns could be indexed on an orthorhombic unit cell with dimensions $a = 6.84$ Å, $b = 43.45$ Å, and $c = 4.157$ Å.

The crystal structure of high-pressure phase, ζ-UO_3, is orthorhombic ($P2_12_12_1$; $a = 7.511$ Å, $b = 5.466$ Å, $c = 5.224$ Å) (Siegel *et al.*, 1966). There are no uranium vacancies in this UO_3 modification as shown by the agreement of the measured density (8.62 g cm^{-3}) with the X-ray density (8.85 g cm^{-3}). In this structure each uranium atom is bonded to seven oxygen atoms, leading to shared [UO_7] configurations with bridging oxygen atoms in the plane perpendicular to the UO_2-axis, identified by two short collinear bonds of 1.80 and 1.85 Å. The other five coordinated oxygen atoms form a puckered pentagonal coordination geometry around the uranyl groups.

(*iv*) *Phase relations*

There have been numerous reports on the phase relations and thermodynamic properties of the uranium–oxygen system. Rand *et al.* (1978) made an assessment of thermodynamic data and presented a phase diagram of this system. Recently, Chevalier *et al.* (2002) and Guéneau *et al.* (2002) published critical reviews. In two recent papers Labroche *et al.* (2003a,b) critically assessed the composition range and oxygen potential of uranium oxides in the UO_2–U_3O_8 region taking into account the uncertainties of the published data.

Uranium–uranium dioxide region

Hypostoichiometric UO_{2-x} exists as a single phase or as a mixture with liquid. Since the formation energy of an oxygen vacancy in UO_2 is much higher than that of interstitial oxygen, the lower phase boundary of single phase UO_{2-x} is very close to O/U = 2.0 up to ~1500 K. In the phase diagram of Rand *et al.* (1978), this phase boundary has been obtained up to 2500 K by using the relation $\ln x = (3.877 \pm 0.094) - (13130 \pm 210)T^{-1}$ proposed by Winslow (1973) based on examination of the relevant experimental data. In the recent critical review on the thermodynamic properties in the uranium–oxygen system, Chevalier *et al.* (2002) presented the phase diagram of the U–UO_2 region by careful selection of the experimental data from Blum *et al.* (1963),

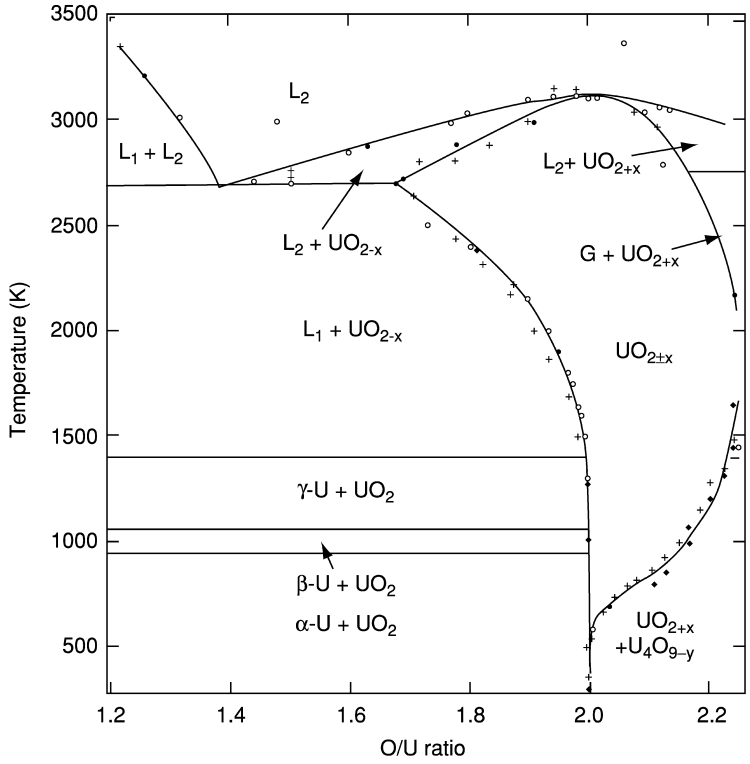

Fig. 5.18 *Partial phase diagram of the U–UO_2 system assembled from values in Rand* et al. (1978), *Chevalier* et al. (2002), *and Guéneau* et al. (2002).

Bates (1964, 1966), Martin and Edwards (1965), Edwards and Martin (1966), Guinet *et al.* (1966), Bannister (1967), Tetenbaum and Hund (1968, 1970), Ackermann *et al.* (1969), Latta and Fryxell (1970), Ackermann and Rauh (1972), Garg and Ackermann (1977, 1980), and Guéneau *et al.* (1998). Guéneau *et al.* (2002) presented the phase diagram of this region using the data from Cleaves *et al.* (1945), Martin and Edwards (1965), Edwards and Martin (1966), Bannister (1967), Hein *et al.* (1968), Ackermann *et al.* (1969), Kjaerheim and Rolstad (1969), Latta and Fryxell (1970), Tachibana *et al.* (1985), and Guéneau *et al.* (1998). Fig. 5.18 shows a phase diagram of the U–UO_2 region ($1.2 \leq O/U \leq 2.0$) and the UO_{2+x} region with $x \leq 0.25$ drawn by using the selected values from Rand *et al.* (1978), Chevalier *et al.* (2002), and Guéneau *et al.* (2002).

The monotectic temperatures for the reaction $L_2 = UO_{2-x} + L_1$ are (2773 ± 30) K (Edwards and Martin, 1966), (2743 ± 30) K (Guinet *et al.*, 1966) and (2693 ± 70) K (Bannister, 1967). The reported compositions of the liquid L_2 phase at the monotectic temperature are $O/U = (1.3 \pm 0.1)$ (Edwards and Martin, 1966), 1.18 (Guinet *et al.*, 1966), (1.53 ± 0.05) (Bannister, 1967) and

1.46 (Latta and Fryxell, 1970). The measured composition of the liquid L_1 phase at this temperature was O/U = 0.05 (Edwards and Martin, 1966; Latta and Fryxell, 1970). The O/U ratios of solid UO_{2-x} are in reasonable agreement: 1.67 (Latta and Fryxell, 1970; Rand *et al.*, 1978), 1.64 (Edwards and Martin, 1966), 1.60 (Guinet *et al.*, 1966), and (1.62 ± 0.06) (Bannister, 1967). The ratio O/U is decreased to ≈1.67 at the lower phase boundary of single phase UO_{2-x} at the monotectic temperature. Above the monotectic temperature the O/U ratio at the lower phase boundary increases to $UO_{2.00}$, until the maximum melting temperature is reached. At the monotectic temperature, three condensed phases, i.e. oxygen-saturated liquid uranium metal L_1 ($UO_{0.05}$), liquid L_2 of a composition $UO_{1.39}$, and solid UO_{2-x} ($UO_{1.67}$) coexist in equilibrium.

$UO_{2.00}$–$UO_{2.25}$ region

Stoichiometric uranium dioxide, UO_2, shows a first-order transition at 30.8 K. This is a magnetic transition, and below that temperature UO_2 is antiferromagnetic, with a structure of type I (Fournier and Troć, 1985), accompanied by an internal distortion in the oxygen sublattice (Faber, Jr. and Lander, 1976). At the transition temperature, a discontinuity in the lattice parameter vs temperature curve (Marples, 1976) and a sharp anomaly in the heat capacity with an entropy increment of 3.6 $J\,K^{-1}\,mol^{-1}$ (Westrum, Jr. and Grønvold, 1962; Huntzicker and Westrum, Jr., 1971) were observed.

Uranium dioxide is stoichiometric at low temperatures, but exhibits a hyperstoichiometric (UO_{2+x}) homogeneity range above 500 K; this range increases with increasing temperature. The upper phase boundary of single phase UO_{2+x} has been extensively studied at temperatures between 500 and 1950 K. The boundary increases with increasing temperature up to (1398 ± 8) K (Blackburn, 1958; Roberts and Walter, 1961; Anthony *et al.*, 1963; Belbeoch *et al.*, 1967; Blank and Ronchi, 1968; van Lierde *et al.*, 1970; Dodé and Touzelin, 1972; MacLeod, 1972; Matsui and Naito, 1975; Labroche *et al.*, 2003b), at which the U_4O_9 phase decomposes to UO_{2+x} and U_3O_{8-z} ($UO_{2.61}$) peritectoidally. The upper phase boundary of UO_{2+x} above that temperature increases only slightly with increasing temperature up to 1950 K.

The phase diagram in the region $2.0 \leq O/U \leq 3.0$ is shown in Fig. 5.19, where the upper phase boundary of UO_{2+x} was obtained by referring to the literature (Blackburn, 1958; Schaner, 1960; Aronson *et al.*, 1961; Roberts and Walter, 1961; Kiukkola, 1962; Markin and Bones, 1962a; Hagemark and Broli, 1966; Kotlar *et al.*, 1967a; Bannister and Buykx, 1974; Saito, 1974; Picard and Gerdanian, 1981; Labroche *et al.*, 2003b). The U_4O_9 phase has a narrow homogeneity range; the reported lower phase boundary is located between the O/U ratios of 2.228 and 2.235 (Blackburn, 1958; Schaner, 1960; Roberts and Walter, 1961; Kotlar *et al.*, 1968; van Lierde *et al.*, 1970; Inaba and Naito, 1973; Picard and Gerdanian, 1981; Labroche *et al.*, 2003b). This boundary is almost unchanged with temperature from room temperature to the peritectic temperature. The reported upper phase boundaries have the O/U values mostly between

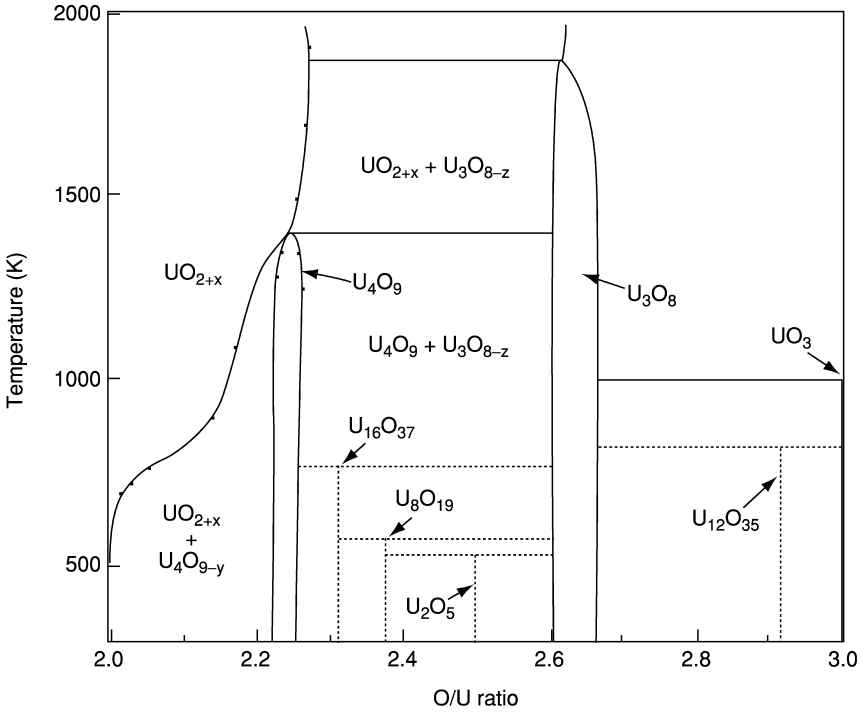

Fig. 5.19 *Phase diagram of the U–O system in the region* $2.0 \leq O/U \leq 3.0$.

2.24 and 2.25 (Blackburn, 1958; Schaner, 1960; Roberts and Walter, 1961; Kotlar *et al.*, 1968; van Lierde *et al.*, 1970; Inaba and Naito, 1973; Picard and Gerdanian, 1981; Labroche *et al.*, 2003b), and many of the papers indicate the uppermost composition to have O/U = 2.242. It is generally assumed that also the upper phase boundary does not change substantially with temperature.

U_4O_9 shows no low-temperature anomaly in the heat capacity due to a magnetic transition observed for UO_2. This is interesting if one considers the close resemblance in the crystal structures between U_4O_9 and UO_2. Instead, the low-temperature modification α-U_4O_9 undergoes a non-magnetic second-order transition to β-U_4O_9 at 340–350 K giving rise to a λ-type specific heat anomaly. The enthalpy and entropy increments of this transition for U_4O_{9-y} with O/U = 2.246–2.254 are 630–710 J mol^{-1} and 1.9–2.2 J K^{-1} mol^{-1}, respectively (Gotoo and Naito, 1965; Westrum, Jr., *et al.*, 1965; Grønvold *et al.*, 1970; Inaba and Naito, 1973). β-U_4O_9 transforms into γ-U_4O_9 at around 850 K. According to Bevan *et al.* (1986), the maximum O/U atom ratio of the β-U_4O_9 phase should be 2.2345 (cf. section on U_4O_9), which supports the hypostoichiometries at the upper phase boundary observed for U_4O_9. The phase transitions α/β and β/γ are reversible, as described in the crystal structure section.

$UO_{2.25}$–$UO_{2.667}$ region

Most compounds in the composition range of $2.25 \leq O/U \leq 2.5$, i.e. α- and β-U_3O_7, γ-U_3O_7 ($U_{16}O_{37}$), U_8O_{19}, and β- and γ-U_2O_5 have fluorite-type structures. α-, β-, and γ-U_3O_7 have been prepared under ambient atmosphere, but U_8O_{19} and α-, β-, and γ-U_2O_5 were formed only at high pressures (15–60 kbar). On this basis, U_8O_{19} and U_2O_5 are regarded as metastable phases, which are thermodynamically unstable at atmospheric pressure (Hoekstra *et al.*, 1970). The phases for which the stability has not been established are indicated in Fig. 5.19 by broken lines. U_3O_7 decomposes at 700°C in air to U_4O_9 and U_3O_8 (Pério, 1953a; Grønvold, 1955). Although β-U_3O_7 shows no low-temperature transitions, α-U_3O_7 exhibits a small λ-type anomaly at 30.5 K with enthalpy and entropy increments of 11 J mol^{-1} and 0.4 J K^{-1} mol^{-1}, respectively. This transition is assumed to be of magnetic origin (Westrum, Jr. and Grønvold, 1962). The other oxides $U_{13}O_{34}$ ($UO_{2.615}$) and $U_{11}O_{29}$ ($UO_{2.636}$) have been described (Kovba *et al.*, 1972; Spitsyn *et al.*, 1972), but no information is given for their stability at low temperatures and pressures.

Two modifications of U_3O_8, i.e. α- and β-U_3O_8, crystallize both in orthorhombic system and their crystal structures are very similar. These compounds are not based on the fluorite structure but are composed of the layer structures related to the hypostoichiometric 'ideal' UO_3 structure (Section 5.7.2a(iii)), which has uranyl bonds perpendicular to the layer planes. The difficulty to rearrange the oxygen atoms in these infinite layer structures is probably the reason for the slow equilibration between U_3O_8 and the gas phase at different temperatures and the oxygen partial pressures. The O/U ratio of the U_3O_8 phase varies with the experimental methods (Gerdanian and Dodé, 1965; Fujino *et al.*, 1981; Srirama Murti *et al.*, 1989). Labroche *et al.* (2003a) suggested that the reason for the scattered data is dissolution of atmospheric nitrogen in the oxides. Although the measured data at the lower phase boundary of U_3O_8 phase are not in good agreement above 1000 K (Labroche *et al.*, 2003b), the ratios O/U are in general between 2.595 and 2.62 (Blackburn, 1958; Hagemark and Broli, 1966; Kotlar *et al.*, 1967b; Ackermann and Chang, 1973; Caneiro and Abriata, 1984). This phase boundary does not change with temperature up to ~1600 K. Above 1000 K, the upper phase boundary was observed to have $O/U = 2.667$ (stoichiometric U_3O_8) up to ~1400 K (Ackermann and Chang, 1973; Caneiro and Abriata, 1984). At an ambient pressure of 0.21 atm O_2, however, the compound becomes hypostoichiometric above 873 K (Cordfunke and Aling, 1965; Rodriguez de Sastre *et al.*, 1967; Ackermann and Chang, 1973). On the other hand, at lower temperatures of 773–873 K, freshly prepared U_3O_8 samples often show hyperstoichiometry with $O/U = 2.670$. Moreover, a hysteresis is seen in the O/U ratio in heating and cooling cycles. Repetition of the heating and cooling cycle results in formation of compounds of lower O/U ratios (Dharwadkar *et al.*, 1975; Fujino *et al.*, 1981). Similar hysteresis phenomena for U_3O_{8-z} have also been observed in oxygen partial pressure vs O/U ratio isotherms (Caneiro and Abriata, 1984) and the electrical conductivity (Ishii *et al.*, 1970b;

Dharwadkar *et al.*, 1978). Slow formation of another phase in α-U_3O_8 may take place at temperatures of 1273–1573 K; according to Hoekstra *et al.* (1955); this is possibly the U_8O_{21} phase with a homogeneity range extending between the compositions $UO_{2.60}$ and $UO_{2.65}$. A slightly different composition range, $UO_{2.617}$–$UO_{2.655}$, has also been reported (Caneiro and Abriata, 1984). It is possible that the proper stoichiometry of β-U_3O_8 is U_8O_{21}, since β-U_3O_8 has been prepared by heating α-U_3O_8 to 1623 K followed by slow cooling to room temperature (Loopstra, 1970b). However in the majority of reports, the phase in this region of compositions is considered to be hypostoichiometric U_3O_8 (i.e. U_3O_{8-z}) (Kotlar *et al.*, 1967a; Ackermann and Chang, 1973; Labroche *et al.*, 2003a,b).

α-U_3O_8 shows a λ-type transition in the heat capacity at 25.3 K with associated enthalpy and entropy increments of 50 J mol^{-1} and 2.3 J K^{-1} mol^{-1}, respectively (Westrum, Jr. and Grønvold, 1959, 1962). This is due to a para-antiferromagnetic transition (Leask *et al.*, 1963). α-U_3O_8 shows three other transitions at higher temperatures: 490, 570, and 850 K. The reported temperature for the 490 K transition varies between 480 and 490 K (Girdhar and Westrum, Jr., 1968; Maglic and Herak, 1970; Inaba *et al.*, 1977; Naito *et al.*, 1982). For the 570 K transition, the reported temperatures are between 562 and 576 K (Inaba *et al.*, 1977; Naito *et al.*, 1982, 1983). The 850 K transition has been observed in one study using adiabatic calorimetry (Inaba *et al.*, 1977). Naito *et al.* (1983) proposed an electronic ordering on uranium atoms with displacement of oxygen atoms as the origin of the above transitions.

$UO_{2.667}$–UO_3 region

Hoekstra and Siegel (1961) regard the $UO_{2.9}$ phase ($U_{12}O_{35}$), which is formed by partial decomposition of amorphous UO_3, as a distinct compound because on heating amorphous UO_3 the O/U ratio remains virtually constant over a 100 K temperature interval from 450 to 550°C. The pycnometric density measured for $UO_{2.9}$ is considerably lower than the theoretical density. This is similar to the case of α-UO_3 assigned to a *C*2*mm* orthorhombic cell with $a = 3.961$ Å, $b = 6.860$ Å, and $c = 4.166$ Å (Loopstra and Cordfunke, 1966). Thus the crystal structure of $UO_{2.9}$ may also have vacant uranium sites as in the α-UO_3 structure.

For UO_3, one amorphous and six crystalline modifications are known. When α-UO_3 is heated in air with a constant heating rate, it decomposes to U_3O_8 passing through a non-stoichiometric range with the O/U ratios between 3.0 and ca. 2.95 (Hoekstra and Siegel, 1961). The δ- and ε-UO_3 compounds convert to U_3O_8 at about 450°C in air with no evidence of a non-stoichiometric oxide range. However, if the heating rate is low, they do not decompose directly, instead re-oxidation of the partially reduced oxides to γ-UO_3 takes place. Also in the γ-UO_3 there is no measurable oxygen non-stoichiometry. The γ-phase is more stable and decomposes to U_3O_8 at higher temperatures of 620–700°C. ζ-UO_3 is formed by heating U_3O_8 at 500°C under high pressures of 15–60 kbar interval produced by a pyrophyllite tetrahedral assembly. This compound is unstable at the ambient pressure (Hoekstra *et al.*, 1970). No magnetic transition has been observed for UO_3 (Jones *et al.*, 1952).

In the uranium trioxide–water system, six compounds have been well established (Dawson *et al.*, 1956; Harris and Taylor, 1962; Debets and Loopstra, 1963; Dell and Wheeler, 1963; Cordfunke and Debets, 1964; Bannister and Taylor, 1970; Taylor, 1971; Siegel *et al.*, 1972; Hoekstra and Siegel, 1973; Vita *et al.*, 1973; Tasker *et al.*, 1988). The physical properties for these compounds are listed in Table 5.15 together with those for uranium peroxide hydrates.

(*v*) *The heat capacity of UO_2*

The low-temperature heat capacity of UO_2 shows a very sharp λ-type anomaly of magnetic origin (Fournier and Troć, 1985) at 30.44 K (Huntzicker and Westrum, Jr., 1971) or 28.7 K (Jones *et al.*, 1952). The entropy increment is 3.6 J K^{-1} mol^{-1} (Westrum, Jr, and Grønvold, 1962). Faber, Jr. and Lander (1976) carried out a neutron diffraction and scattering study on this transition. They showed that the anomaly took place at 30.8 K and that it could be explained as a first-order transition from the low-temperature antiferromagnetic state of type I, associated with an internal distortion of the oxygen sublattice, to the paramagnetic state. The low-temperature (5–346 K) heat capacity data of Huntzicker and Westrum, Jr. (1971) are in good agreement with those of Grønvold *et al.* (1970) (304–1006 K) in the range of overlapping temperatures.

The high-temperature heat capacity of UO_2 has been studied extensively because of the importance of this compound as nuclear fuel; several critical reviews have also been published (Browning, 1981; Browning *et al.*, 1983; Naito, 1989; Ronchi and Hyland, 1994; Fink, 2001; Carbajo *et al.*, 2001). The selected data of heat capacities are shown in Fig. 5.20 together with the correlations calculated by the MATPRO equation (Hagrman, 1995) and by the Fink equations with functional and polynomial forms. In the figure two sets of data of Ronchi *et al.* (1999) are shown for high temperatures, and the data of Huntzicker and Westrum, Jr. (1971) and Grønvold *et al.* (1970) are shown for low and intermediate temperatures. Since the heat capacities of the functional and polynomial equations differ by at most 1%, the latter equation is recommended because of its simplicity (Fink, 2001). This equation, which is based on a combined analysis of the reported data (Moore and Kelley, 1947; Hein and Flagella, 1968; Hein *et al.*, 1968; Ogard and Leary, 1968; Leibowitz *et al.*, 1969; Fredrickson and Chasanov, 1970; Grønvold *et al.*, 1970; Huntzicker and Westrum, Jr., 1971; Ronchi *et al.*, 1999), for $298.15 \leq T \leq 3120$ K is:

$$C_p(T)(\text{J K}^{-1}\,\text{mol}^{-1}) = 52.1743 + 87.951\,\tau - 84.2411\,\tau^2 + 31.542\,\tau^3 - 2.6334\,\tau^4 - 0.71391\,\tau^{-2},$$

where, $\tau = T(\text{K})/1000$. The MATPRO equation (Hagrman, 1995) gives somewhat lower C_p values at higher temperatures.

The λ-type transition found by Bredig (1972) at 2670 K has been confirmed by other researchers (Hutchings *et al.*, 1984; Ralph and Hyland, 1985; Hiernaut *et al.*, 1993). Hiernaut *et al.* (1993) modeled the transition in $UO_{2.00}$ as

Table 5.15 *Physical properties of the uranium trioxide hydrates and of the uranium peroxide hydrates.*

Formula	*Color*	*Space group*	*Symmetry*	*Lattice parameters*				*Z*	*Density* ($g\ cm^{-3}$)		*References*
				a (Å)	*b* (Å)	*c* (Å)	*Angle* (deg)		*Exp.*	*X-ray or ND*	
α-$UO_3 \cdot 0.8H_2O$			orthorhombic	4.27–4.30	10.19–10.24	6.86–6.96		4	6.63		Dawson *et al.* (1956)
α-$UO_2(OH)_2$ (=α-$UO_3 \cdot H_2O$)	greenish yellow	*Cmca*	orthorhombic	4.242	10.302	6.868		4	6.73		Taylor (1971); Hoekstra and Siegel (1973)
β-$UO_2(OH)_2$ (=β-$UO_3 \cdot H_2O$)	yellow-green	*Pbca*	orthorhombic	5.6438	6.2867	9.9372		4	5.73		Bannister and Taylor (1970); Hoekstra and Siegel (1973)
γ-$UO_2(OH)_2$ (=γ-$UO_3 \cdot H_2O$)	gray-chamois	$P2_1/c$	monoclinic	6.419	5.518	5.561	$\beta = 112.77$	2	5.56		Cordfunke and Debets (1964); Hoekstra and Siegel (1973)
$UO_2(OH)_2 \cdot H_2O$ (=$UO_3 \cdot 2H_2O$) (schoepite)	bright yellow	*Pbna*	orthorhombic	13.977	16.696	14.672		32	5.00		Debets and Loopstra (1963); Tasker *et al.* (1988); Hoekstra and Siegel (1973)
$U_3O_8(OH)_2$	violet		triclinic	6.802	7.417	5.556	$\alpha = 108.5$ $\beta = 125.5$ $\gamma = 88.2$	1		6.85	Siegel *et al.* (1972)
$UO_4 \cdot 4H_2O$	pale yellow	*C*2, *Cm* or *C*2/*m*	monoclinic	11.85	6.78	4.245	$\beta = 93.47$	2	5.15		Debets (1966)
$UO_4 \cdot 2H_2O$	pale yellow	*Immm*	orthorhombic	6.502	4.216	8.778		2			Debets (1966)

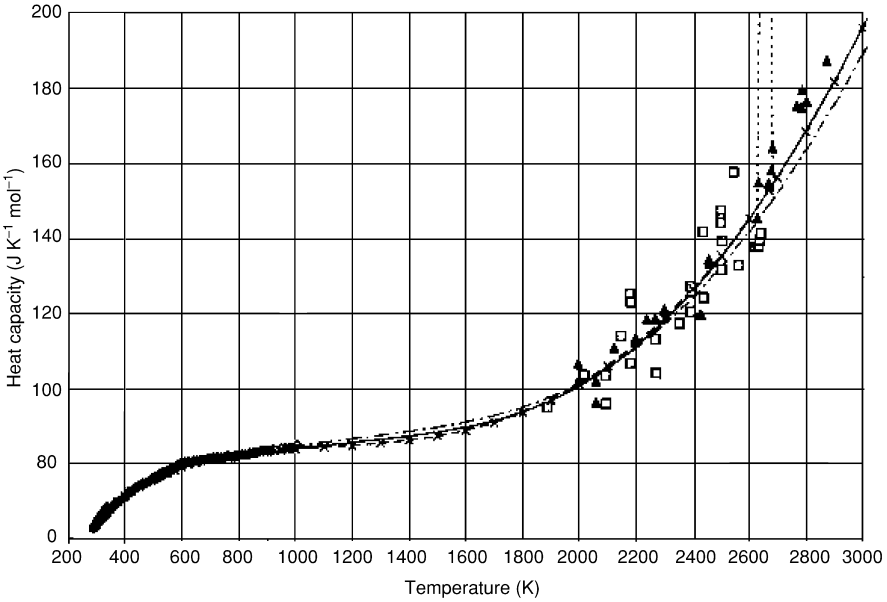

Fig. 5.20 *Recommended equations and data for the heat capacity of UO_2* (*Fink,* 2001). ▲: *Table data of Ronchi* et al. (1999); □: *Graph data of Ronchi* et al. (1999); ◇ *Grønvold* et al. (1970); ○: *Huntzicker and Westrum, Jr.* (1971); ——: *Functional form equation* (*Fink*, 2001); –×–×–: *Polynomial form equation* (*Fink*, 2001); ------: *Phase transition*; —·—·—: *MATPRO equation* (*Hagrman*, 1995).

a second-order transition involving oxygen Frenkel disorder. The transition temperature of hypostoichiometric uranium dioxide (UO_{2-x}) increases with increasing x. Their model explains the shift as due to the change from a λ-transition to a first-order phase transition in UO_{2-x}.

The discussion on the heat capacity of UO_2 can be divided into the following four regions (Ronchi and Hyland, 1994):

(1) *Room temperature – 1000* K *region*. The increase in the heat capacity is caused by the harmonic lattice vibrations with a smaller contribution from thermal excitation of localized electrons of U^{4+} in the crystal field.
(2) *1000–1500* K *region*. The heat capacity increases with increasing anharmonicity of the lattice vibrations as shown by thermal expansion.
(3) *1500–2670* K *region*. The heat capacity increase in this region is mainly ascribed to the formation of lattice and electronic defects. The C_p peak at 2670 K is due to the oxygen Frenkel defects as determined by neutron scattering measurements.
(4) *Region above 2670* K. The peak of the heat capacity drops sharply by rapid saturation of the defects. At temperatures from 2700 K to the melting point, the concentration of Schottky defects increases.

(*vi*) *Oxygen potential and other thermodynamic properties*

A large number of reports have been published on the partial molar thermodynamic quantities $\Delta\bar{G}(O_2)$, $\Delta\bar{H}(O_2)$, and $\Delta\bar{S}(O_2)$ for non-stoichiometric uranium oxides. These studies have been carried out mainly by means of thermogravimetric method (Gerdanian, 1964; Gerdanian and Dodé, 1965; Hagemark and Broli, 1966; Kotlar *et al.*, 1967b; Ugajin, 1983; Matsui and Naito, 1985a) and emf method (Aronson and Belle, 1958; Kiukkola, 1962; Markin and Bones, 1962a,b; Marchidan and Matei, 1972; Saito, 1974; Nakamura and Fujino, 1987); however, tensimetric (Roberts and Walter, 1961), quenching (Anthony *et al.*, 1963), and Knudsen effusion (Blackburn, 1958) techniques have also been used.

In the two-phase regions of solid oxides, the equilibrium oxygen pressure over uranium oxides, p_{O_2}(atm), which is related with the oxygen potential of the oxides $\Delta\bar{G}(O_2)$ by the equation $\Delta\bar{G}(O_2) = RT \ln p_{O_2}$, is a function of only temperature. For the UO_{2+x}–U_4O_{9-y} two-phase region, Saito (1974) showed that $\log p_{O_2}$ is:

$$\log p_{O_2}(\text{atm}) = -105.7 - 5136\, T^{-1} + 33.46 \log T \tag{5.1}$$

The previous equation describes the measured data from the literature (Aronson and Belle, 1958; Blackburn, 1958; Roberts and Walter, 1961; Kiukkola, 1962; Markin and Bones, 1962b; Kotlar *et al.*, 1967b; Marchidan and Matei, 1972; Saito, 1974; Nakamura and Fujino, 1987), although it gives gradually too low values at temperatures above 1323 K (Roberts and Walter, 1961; Nakamura and Fujino, 1987).

For the U_4O_9–U_3O_{8-z} two-phase region, $\log p_{O_2}$ is represented by (Saito, 1974)

$$\log p_{O_2}(\text{atm}) = 7.996 - 16\,330\, T^{-1} \tag{5.2}$$

or (Roberts and Walter, 1961)

$$\log p_{O_2}(\text{atm}) = 8.27 - 16\,760\, T^{-1}. \tag{5.3}$$

The difference in $\log p_{O_2}$ of equations (5.2) and (5.3) is 0.20 at $T = 900$ K, which decreases to 0.033 at $T = 1400$ K.

The oxygen potential of UO_{2+x} in the single-phase region is a function of the composition x and temperature. A number of experimental $\Delta\bar{G}(O_2)$ isotherms plotted against O/U ratio of UO_{2+x} for various temperatures in the range 1173–1773 K have been reported (Aukrust *et al.*, 1962; Markin and Bones, 1962a,b; Hagemark and Broli, 1966; Ugajin, 1983; Matsui and Naito, 1985a). The scatter in the experimental $\Delta\bar{G}(O_2)$ data seems to increase as the O/U ratio decreases in the composition range below 2.01, where $\Delta\bar{G}(O_2)$ rapidly decreases with decreasing O/U ratio.

Fig. 5.21 shows $\Delta\bar{G}(O_2)$ for UO_{2+x} as a function of the O/U ratio expressed by an equation which consists of component equations giving experimental values in polynomial forms (Nakamura and Fujino, 1987) with small modifications for

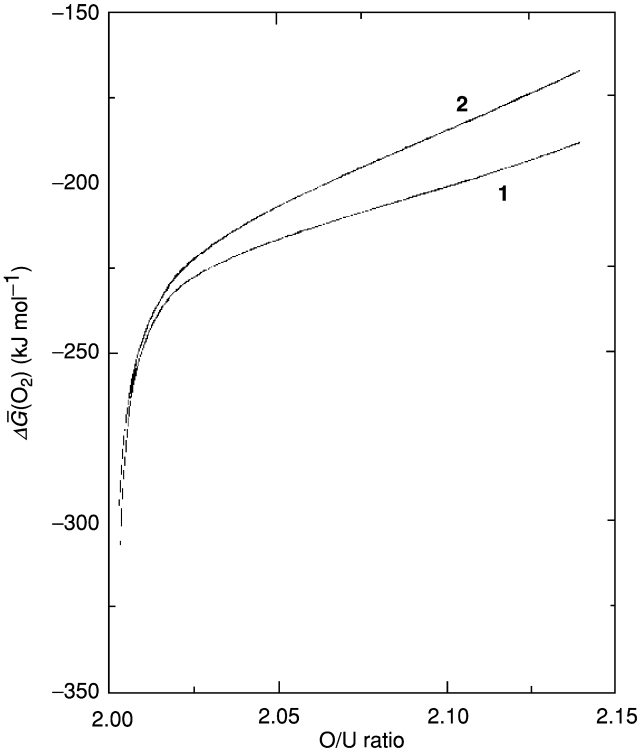

Fig. 5.21 *Oxygen potential as a function of O/U ratio. Curve* 1, 1173 K; *curve* 2, 1373 K.

$\Delta\bar{G}(O_2)$ below O/U = 2.02. The lowest O/U ratio shown in the figure is 2.003, below which the $\Delta\bar{G}(O_2)$ values approach those at $x = 0$, i.e. –633.3 and –588.4 kJ mol^{-1} for 1173 and 1373 K, respectively. These values are obtained from the equation $\Delta\bar{G}(O_2) = -897\,000 + 224.8\,T$ J mol^{-1} at $x = 0$ assessed by Lindemer and Besmann (1985) for temperatures between 873 and 1673 K.

The partial molar entropy of oxygen, $\Delta\bar{S}(O_2) = -d\Delta\bar{G}(O_2)/dT$, was in most papers regarded as temperature independent and on this basis differentiation of $\Delta\bar{G}(O_2)$ was made without specifying temperature. There have been rather wide scattering in the reported values of the partial molar enthalpy of oxygen, $\Delta\bar{H}(O_2)$, and the entropy, $\Delta\bar{S}(O_2)$. This is significantly reduced when $\Delta\bar{S}(O_2)$ is treated as a temperature-dependent quantity: $d\Delta\bar{S}(O_2) = \bar{C}_p(O_2)dT/T$ where $\bar{C}_p(O_2)$ is the partial molar heat capacity of oxygen expressed as a polynomial of $\log x$ (Nakamura and Fujino, 1987). In this case, $\Delta\bar{H}(O_2)$ also becomes temperature-dependent because of the relation $\Delta\bar{H}(O_2) = \Delta\bar{G}(O_2) + T\Delta\bar{S}(O_2)$.

Fig. 5.22a compares the calculated $\Delta\bar{H}(O_2)$ vs x curves obtained by using the above $\bar{C}_p(O_2)$ values with the literature data. Fig. 5.22b compares the $\Delta\bar{S}(O_2)$ vs x curves. The derived $\Delta\bar{H}(O_2)$ curve at 1323 K is in good agreement

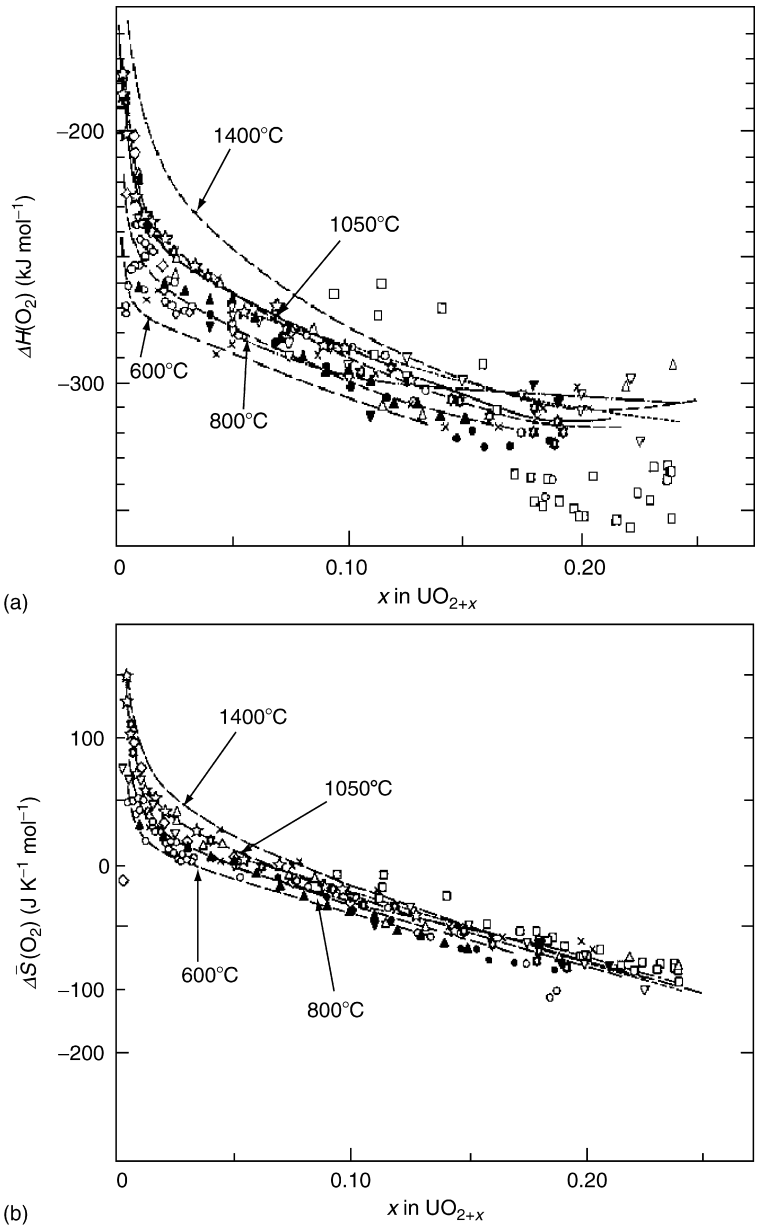

Fig. 5.22 (*a*) and (*b*): *Variation of* $\Delta\bar{H}(O_2)$ *and* $\Delta\bar{S}(O_2)$, *respectively*, *with composition x at* 873, 1073, 1323, *and* 1673 K *in the region* $0 \leq x \leq 0.25$ (*Nakamura and Fujino,* 1987). ★: *sample a* (*Nakamura and Fujino,* 1987); ☆: *sample b* (*Nakamura and Fujino,* 1987); — — —: *least squared* $\Delta\bar{H}(O_2)$ *and* $\Delta\bar{S}(O_2)$ *curves* (*Nakamura and Fujino* 1987); ——: *Picard and Gerdanian* (1981) *at* 1323 K; ○: *Markin and Bones* (1962*a,b*); △: *Kiukkola* (1962); ●: *Saito* (1974); ▲: *Gerdanian and Dodé* (1965); ▽: *Hagemark* et al. (1962, 1966); ▼: *Marchidan and Matei* (*1972*); ×: *Aronson and Belle* (1958); ◇: *Ugajin* (1983); □: *Roberts and Walter* (1961); -----: *Rand and Kubaschewski* (1963) *at* 1273 K; —·—·—: *Rand* et al. (1978). *Reproduced by the permission of Elsevier*.

with the measured curve of Picard and Gerdanian (1981). Most reported values of the temperature-independent $\Delta\bar{H}(O_2)$ and $\Delta\bar{S}(O_2)$ are within the curves derived using temperature-dependent $\Delta\bar{H}(O_2)$ and $\Delta\bar{S}(O_2)$ in the range 1073–1323 K.

Labroche *et al.* (2003a) made a critical assessment of the thermodynamic data for UO_{2+x} taking into account the uncertainties in the measurements. The result showed that $\log p_{O_2}$ could be represented by equations of the form $\log p_{O_2} = A - B\,T^{-1}$ with A and B varying with the O/U ratio in the range 2.01–2.23. On the other hand, this treatment revealed that the x dependence of $\log p_{O_2}$ could not be given with adequate accuracy by the above simple formulas if the temperature range is larger.

Gerdanian and Dodé (1968) determined $\Delta\bar{H}(O_2)$ by measuring the evolved heat when a small amount of oxygen was passed over UO_{2+x} in a Calvet-type microcalorimeter. This technique made it possible to measure $\Delta\bar{H}(O_2)$ close to the stoichiometric composition as shown in Fig. 5.23.

In this figure, $\Delta\bar{H}(O_2)$ increased very sharply with increasing O/U ratio from $<$–800 kJ mol^{-1} at $UO_{2.0003}$, and then attained a maximum of about

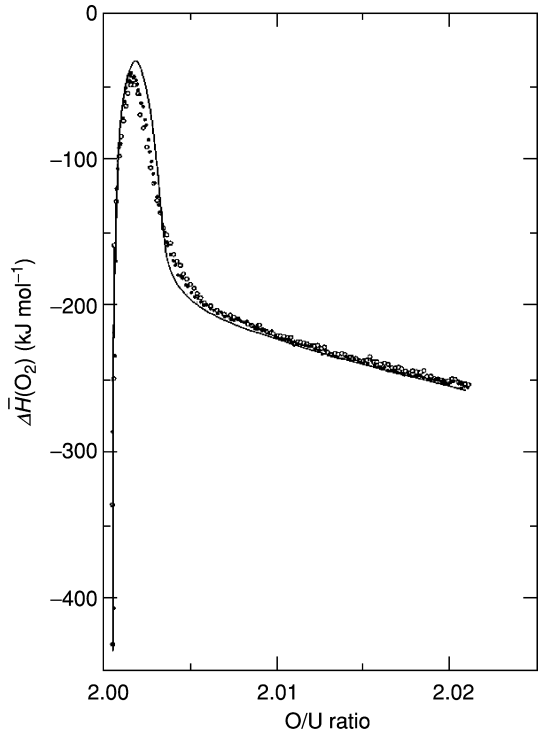

Fig. 5.23 *Change of* $\Delta\bar{H}(O_2)$ *close to stoichiometric* UO_2 (*Gerdanian and Dodé*, 1968). •: run 1; ○: *run* 2;———: $\Delta\bar{H}(O_2)$ *corrected for systematic experimental errors.*

–29 kJ mol^{-1} at $UO_{2.0018}$. The curve afterwards decreased and became progressively linear above O/U = 2.01.

No significant anomaly has been observed for $\Delta\bar{G}(O_2)$ in the above composition range (Markin and Bones, 1962a), though precise determination could not be made at small O/U ratios near stoichiometric UO_2 due to rapid change of $\Delta\bar{G}(O_2)$. When there is no anomaly in $\Delta\bar{G}(O_2)$, $\Delta\bar{S}(O_2)$ should have the sharp peak at the same composition as $\Delta\bar{H}(O_2)$. Gerdanian (1974) showed that the $\Delta\bar{H}(O_2)$ anomaly could be well described by assuming that the formation of the Willis (2:2:2) cluster is the predominant reaction. At the same time he commented that the choice of cluster structures and ionic charges was not crucial and it could be changed if another appropriate and consistent set of $\Delta\bar{H}(O_2)$ and $\Delta\bar{S}(O_2)$ was selected. Actually, the $\Delta\bar{H}(O_2)$ anomaly can also be interpreted by the oxygen Frenkel disorder and Willis (2:1:2) cluster formation reactions coupled with the intrinsic hole–electron formation reaction (Nakamura and Fujino, 1986).

(*vii*) *Vaporization of UO_2*

The vaporization of uranium oxides has been studied mainly on stoichiometric and hypostoichiometric uranium dioxides. The vaporization data concerning U_3O_8 and U_4O_9 phases (Ackermann *et al.*, 1960; Ackermann and Chang, 1973) have attracted only little attention (Naito and Kamegashira, 1976). The vaporization behavior of uranium dioxide may be discussed for the temperature regions below and above the melting point. In the region below the melting point, vaporization has been studied using a variety of techniques such as Knudsen mass effusion, Langmuir surface evaporation, mass spectrometry, and transpiration. The important gaseous species are U(g), UO(g), UO_2(g), UO_3(g), O(g), and O_2(g). The transpiration method can only give total pressures. The partial pressures of each of the uranium-bearing species are measured by means of the Knudsen cell - mass spectrometer technique. In the temperature range 1890–2420 K, the partial pressure of UO_2(g) measured by the latter method (Pattoret *et al.*, 1968) was $\log p_{UO_2}(\text{atm}) = 8.60 - 30850\,T^{-1}$.

In order to obtain the total pressure, it is necessary to measure the pressures of the other gaseous species. However, since the partial pressure p_{UO_2} over uranium dioxide near the stoichiometric composition is (94 ± 3)% of the total pressure at 2150 K (Pattoret *et al.*, 1968; Ackermann *et al.*, 1979), the total pressure is very close to p_{UO_2}. Ackermann *et al.* (1979) compared, at 2150 K, the reported values of the total pressure (10^{-6} atm), the apparent heat of sublimation (kJ mol^{-1}) obtained from a plot of $\log p_{total}$ versus $1/T$, and the apparent entropy of sublimation for UO_2(s) (J K^{-1} mol^{-1}). The values are 1.21, 596.2, and 164 (Ackermann *et al.*, 1956); 1.91, 627.6, and 182 (Ivanov *et al.*, 1962); 0.577, 587.9, and 154 (Voronov *et al.*, 1962); 1.32, 635.1, and 183 (Ohse, 1966); 0.914, 589.5, and 159 (Alexander *et al.*, 1967); 1.97, 617.1, and 178 (Gorban, *et al.*, 1967); 1.81, 590.8, and 165 (Pattoret *et al.*, 1968) and 1.16,

598.7, and 165 (Tetenbaum and Hunt, 1970), respectively. The ΔH_V values spread in a range from 585 to 635 kJ mol^{-1}. The Langmuir method (Voronov *et al.*, 1962) yields low total pressures. The pressure data obtained by the transpiration method (Alexander *et al.*, 1967; Tetenbaum and Hunt, 1970) also tend to be low, which is supposed to be caused by more rapid loss of material giving rise to composition gradient in uranium dioxide during transpiration evaporation. The transpiration total pressures in the form of $\log p_{\text{total}} = A - B\,T^{-1}$, measured at temperatures between 2500 and 2900 K for $UO_{1.88}$(s) (Szwarc and Latta, 1968), were in good agreement with those of Tetenbaum and Hunt (1970) measured over the temperature range 2080–2705 K, but the total pressures for $UO_{1.92}$ (s) and $UO_{1.94}$ (s) were low; approximately two-third to half of the values of Tetenbaum and Hunt (1970).

For hypostoichiometric uranium dioxide, the pressure of UO(g) becomes comparable to p_{UO_2}or, depending on the composition of the solid, higher than p_{UO_2}. Storms (1985) measured p_{UO} as a function of composition between U(l) + UO_{2-x}(s), and $UO_{2.0}$(s) in the temperature range 1667–2175 K using a mass spectrometer equipped with a tungsten Knudsen cell. The gas-phase reaction $2UO_2(g) = UO(g) + U(g)$ was assumed to be in equilibrium in the cell and its equilibrium constant should be independent of the solid composition. Thus, the uranium activity, a_U, and the partial enthalpy of vaporization of U(g), $\Delta\bar{H}_U$, were obtained by adopting the two-phase mixture U(l) + UO_{2-x}(s) as the reference in which a_U was measured to be unity below 2100 K. The partial pressures of U(g), UO(g), and UO_2(g) were expressed as a function of temperature and a_U. From the gas-phase equilibrium $UO_3(g) + UO(g) = 2UO_2(g)$, p_{UO_3} was also given as a (T, a_U) function using the $\Delta_f G^o(UO_3, g)$ data. The pressures p_U and p_{UO_2} were then obtained in terms of temperature, a_U, and $\Delta_f G^o(UO_2, s)$. The partial pressures and the total pressures over various compositions of UO_{2-x}(s) at 2000 K are shown in Fig. 5.24.

The sum of the partial pressures of U(g), UO(g), and UO_2(g) over U(l) + UO_2(s) at 2300 K was in good agreement with that of Ackermann *et al.* (1969), but it was about one-third that of Pattoret *et al.* (1968). The partial pressures of O_2 over U(l) + UO_{2-x} measured recently by Baïchi *et al.* (2002) using the twin-cell method are, for example, $\sim 1 \times 10^{-19}$, $\sim 1 \times 10^{-18}$, and $\sim 1 \times 10^{-17}$ atm for 2000, 2100, and 2200 K, respectively. The above O_2 pressure at 2000 K is in accord with that of Fig. 5.24.

The congruently vaporizing composition (CVC) changes with temperature as reported in the literature (Ackermann *et al.*, 1960, 1969; Pattoret *et al.*, 1968; Edwards *et al.*, 1969). The calculated relation between temperature and the O/U ratio for CVC by Storms (1985) is in reasonable accord with these data: Up to 2100–2200 K, CVC is O/U = 2.00. As the temperature rises above these temperatures, CVC decreases nearly linearly with increasing temperature to O/U = 1.95–1.96 at 2700 K.

The total vapor pressures over uranium dioxide above its melting point measured by the transpiration technique (Reedy and Chasanov, 1972), pulsed

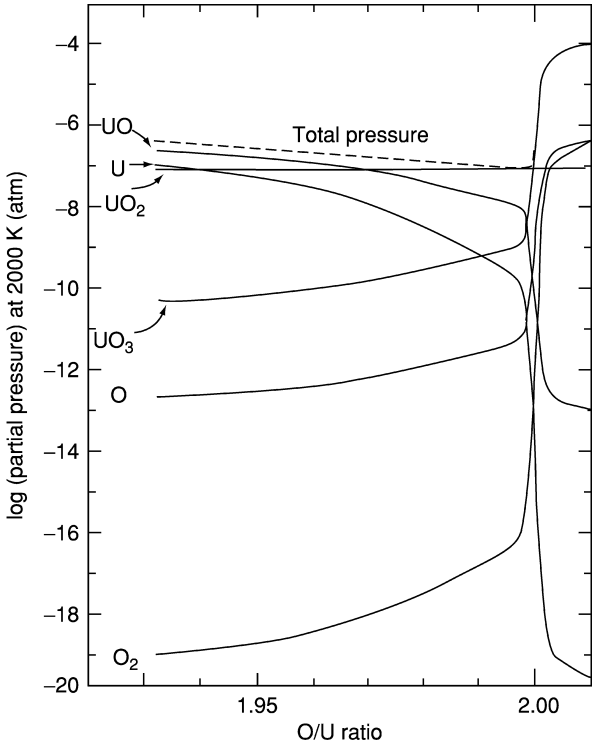

Fig. 5.24 *Partial pressures and total pressure over* UO_{2-x} *of various compositions at* 2000 K (*from Storms*, 1985, *reproduced by the permission of Elsevier*).

laser surface heating (Asami *et al.*, 1975; Bober *et al.*, 1975; Tsai *et al.*, 1975; Babelot *et al.*, 1977), and electron beam heating (Benson, 1977) have been compared by Ohse *et al.* (1979). In the latter monograph, a discussion was made of the methods to measure the equilibrium pressure from the evaporation rate of the gaseous species generated by dynamic, non-equilibrium pulse heating techniques. The upper temperature limit of the transpiration measurements was 3400 K for hypostoichiometric uranium dioxide of O/U = 1.94 (Reedy and Chasanov, 1972). The total pressure data above 4200 K showed a small curvature toward high pressures due to the composition change of liquid uranium dioxide to hypostoichiometry (Babelot *et al.*, 1977). In the case where the correction was made for this deviation by normalizing to O/U = 2.00 in forced congruency evaporation mode, a straight line was obtained in the $\log p_{\text{total}}$ vs. $1/T$ plot. The scattering of the corrected data (Asami *et al.*, 1975; Bober *et al.*, 1975; Tsai *et al.*, 1975; Babelot *et al.*, 1977; Benson, 1977) around the straight line is reasonable in the temperature range 3120–5000 K.

The suggested total pressure up to 5000 K by the IAEA Specialists' Meeting (1978) is

$$\log p_{\text{total}}(\text{MPa}) = 28.65 - 34\,930\,T^{-1} - 5.64 \log T.$$

The data of the equation of state for UO_2 were obtained using the principle of corresponding states (Browning *et al.*, 1978), the method of rectilinear diameters (Partington, 1949; Ohse *et al.*, 1979), and significant structure theory (Vilcu and Misdolea, 1967; Lu *et al.*, 1968). The values of critical temperature, T_c(K), critical pressure, p_c(atm), and critical density, ρ_c(g cm^{-3}) calculated by means of the principle of corresponding states are: 7300, 1915, and 3.16 (Meyer and Wolfe, 1964); 7300, 1900, and 3.16 (Menzies, 1966). The values obtained by the method of rectilinear diameters are 9110, 1230, and 1.59 (Miller, 1965). Gillan (1975) obtained the critical values on the basis of the significant structure theory. The values changed greatly when using the vapor pressures measured over UO_2(s) at lower temperatures from 6960, 1070, and 1.64 (Ohse, 1966) to 9330, 1450, and 1.63 (Tetenbaum and Hunt, 1970), respectively. Fischer *et al.* (1976), obtained the values 7560, 1210, and 1.66 using the experimental data of Ohse (1966).

(*viii*) *Diffusion*

Oxygen self-diffusion in hypostoichiometric uranium dioxide takes place by the vacancy mechanism. The self-diffusion coefficient, D^*, is expressed as

$$D^* \cong D_V^O = A_V \theta_V (1 - \theta_V) \exp(-\Delta H_V^O / RT),$$

where D_V^O, A_V, θ_V and ΔH_V^O are the oxygen self-diffusion coefficient of vacancy, pre-exponential factor, oxygen vacancy concentration (site fraction), and migration enthalpy of vacancy motion, respectively. Most of the observed values for ΔH_V^O are between 48 and 58 kJ mol^{-1} (Matzke, 1981, 1987; Bayovlu and Lorenzelli, 1984). Kim and Olander (1981) report 48.9 kJ mol^{-1}. The theoretically calculated enthalpy is 52 kJ mol^{-1} (Jackson *et al.*, 1986).

For stoichiometric UO_2, the oxygen diffusion mechanism changes with temperature: At low temperatures, thermal oxygen vacancies are the primary species contributing to oxygen mobility, whereas thermal interstitial oxygens predominate at high temperatures. In the range of 800–1800°C, both defects have significant mobility. Calculation suggests $D_i \approx D_V$ at 1400°C (Kim and Olander, 1981). The activation enthalpy of oxygen migration for stoichiometric UO_2, Q, has been determined to be 247 kJ mol^{-1} (Marin and Contamin, 1969), which is related to the enthalpy of oxygen Frenkel defect formation, H_F, by $Q = \Delta H_V^O + H_F/2$. This equation gives $H_F = 396$ kJ mol^{-1} for $\Delta H_V^O = 50$ kJ mol^{-1} (Murch and Catlow, 1987).

For hyperstoichiometric uranium dioxide, UO_{2+x}, the oxygen self-diffusion is considered to occur via the structural interstitial oxygen ions. By plotting D^* against $1/T$, the migration enthalpy of interstitial oxygens, ΔH_i^O, has been measured to be ca. 96 kJ mol^{-1} (Belle, 1969; Contamin *et al.*, 1972; Murch

and Catlow, 1987) or 99.6 kJ mol^{-1} (Breitung, 1978) for x values between 0.01 and 0.1. The calculated ΔH_i^O value is 62 kJ mol^{-1} (Jackson *et al.*, 1986).

The chemical diffusion coefficient of oxygen, $\tilde{D}^O$, describes the movement of oxygen ions under the oxygen concentration gradient of hyperstoichiometric UO_{2+x}; it is expressed as (Lay, 1970; Breitung, 1978):

$$\tilde{D}^O = D^* \frac{(2+x)}{2RT} \frac{d[\Delta\overline{G}(O_2)]}{dx}$$

The $\tilde{D}^O$ values are higher than the oxygen self-diffusion coefficient, D^*, by several orders of magnitude. The $\tilde{D}^O$ values calculated by the above equation are comparable with the experimental values for the x values up to 2.14 (Marin, 1968; Bittel *et al.*, 1969; Carter and Lay, 1970; Lay, 1970).

Uranium self-diffusion in uranium dioxide also depends on oxygen non-stoichiometry. For $x \geq 0$, the uranium vacancies are mainly responsible for uranium diffusion, while in the range of significant hypostoichiometry the interstitial uranium atoms become predominant. The activation enthalpies of uranium migration, Q_U, were measured to be 540 and 250 kJ mol^{-1} for UO_2 and UO_{2+x}, respectively (Matzke, 1987).

The calculated Q_U values are 1200 and 750 kJ mol^{-1} for UO_2 and UO_{2+x}, respectively (Jackson *et al.*, 1986). The uranium self-diffusion coefficient, D_U^*, is smaller than oxygen diffusion coefficient, D^*, by a factor of 10^5 at 1400°C. Another feature is the pronounced dependence of D_U^* on non-stoichiometry. D_U^* increases approximately proportionally with increasing x^2 from UO_2 to $UO_{2.20}$ at 1400–1600°C by about five orders of magnitude (Marin and Contamin, 1969).

(*ix*) *Electrical conductivity*

UO_2, UO_{2+x}

The electrical conductivity of hyperstoichiometric uranium dioxide is caused by positive holes (Tagawa *et al.*, 1975). Although the measured values of mobility of the holes are scattered over a rather wide range, viz. from 0.0015 $cm^2\ V^{-1}\ s^{-1}$ at room temperature (Nagels *et al.*, 1964) to 0.021 $cm^2\ V^{-1}\ s^{-1}$ at 600°C or 0.055 $cm^2\ V^{-1}\ s^{-1}$ at 1100°C (Aronson *et al.*, 1961), these mobilities are much lower than those for usual band-type semiconductors for which the mobility is larger than 1 $cm^2\ V^{-1}\ s^{-1}$ (Tuller, 1981).

To explain the above conduction behavior of uranium dioxide, the small polaron model is used, where the holes are assumed to move in the oxide structure dragging the local distortion of the lattice caused by the electrical interaction. de Coninck and Devreese (1969) measured the electrical conductivity and thermoelectric power of UO_{2+x} having $x = 0.001$ and reported that the small polaron model could be applied with a nearly linear dependence of $\ln(\sigma T^{3/2})$ against $1/T$, where σ is the electrical conductivity. The holes and electrons are localized on individual atoms, giving the species of U^{5+} and U^{3+}, respectively; the electrical conduction occurs as a result of their hopping

in the crystal (Catlow and Pyper, 1979). For wider range of x values of UO_{2+x}, the electrical conductivity follows (Aronson *et al.*, 1961; Winter, 1989)

$$\sigma T = 3.8 \times 10^6 (n+p)(1-n-p)e^{-0.3/kT},$$

where n and p are the electron and hole concentrations, respectively. The activation energy of conduction was measured to be 0.3 eV.

Based on Seebeck data, Winter (1989) claims the same mobility for electrons and holes in UO_{2+x}. The ratio σ_p/σ_n is larger than 1 for $x > 0$, and smaller than 1 for $x < 0$. Since one of the electronic defects always has a concentration higher than that of the ionic defects and the electronic mobilities are much higher, the ionic conductivity is insignificant. The conductivities for nominally stoichiometric UO_2 with $x \sim 10^{-3}$ can be represented by the above equation (Bates *et al.*, 1967; Winter, 1989). At $x = 0$, the intrinsic conductivity by the U^{5+} and U^{3+} charge carriers produced by a disproportionation reaction $2U^{4+} = U^{5+} + U^{3+}$ becomes important. The above reaction parameters were given by a band gap of 2 eV and a vibrational entropy of $2k$ (Winter, 1989).

For UO_{2+x} at 500–1400°C, the electrical conductivities plotted against x decrease nearly linearly with decreasing x below $x = 0.1$ in the direction $\sigma \to 0$. The conductivity changes in the different measurements, but there is a fairly good consistency in the σ values of the samples having larger x values: For $x = 0.1$ at 1000°C, for example, $\sigma \approx 30\ \Omega^{-1}\ cm^{-1}$ (Aronson *et al.*, 1961), which is close to the conductivity obtained by Dudney *et al.* (1981). The other reported values are $\approx 10\ \Omega^{-1}\ cm^{-1}$ (Matsui and Naito, 1985b) and $\approx 1.5\ \Omega^{-1}\ cm^{-1}$ (Ishii *et al.*, 1970c), while the measured values of Lee (1974) are much lower.

U_3O_{8-z}

There are no large differences in the electrical conductivity between U_3O_{8-z} and UO_{2+x}. The conductivities for U_3O_{8-z} are $\sigma \approx 10^{-1}$ and $10^{-3}\ \Omega^{-1}cm^{-1}$ at 730 and 230°C, respectively, when the oxygen partial pressure is 150 mmHg. Contrary to the conduction behavior of UO_{2+x}, however, σ for U_3O_{8-z} increases with decreasing p_{O_2} (in the range 10^2 to 10^{-2} mmHg O_2), suggesting that the main carriers are electrons (George and Karkhanavala, 1963). A change of slope in the $\log\sigma$ vs $1/T$ plots, resulting from a phase transition, was observed at 723 K. The activation energies of conduction were 0.64 and 1.10 eV below and above the transition, respectively. The transition temperature varies with non-stoichiometry from 658 K ($UO_{2.667}$, i.e. stoichiometric U_3O_8) to 923 K ($UO_{2.558}$ to $UO_{2.650}$) (Ishii *et al.*, 1970b). At higher temperatures of 1111–1190 K, another σ anomaly has been measured, presumably due to the formation of U_8O_{21+x} (Dharwadkar *et al.*, 1978).

(*x*) *Chemical properties*

UO_2 is oxidized to U_3O_8 on heating in air at temperatures of 600–1300°C. When UO_3 is heated in air above 600°C, the compound is reduced to U_3O_8. U_3O_8 has been used as a standard material for chemical analysis of uranium oxides

Table 5.16 *Reactions of uranium oxides.*

Reagent	*Temperature* (°C)	*Products of the following oxides*		
		UO_2	*U_3O_8*	*UO_3*
H_2(g)	>750	—	UO_2	UO_2
CO(g)	>750	—	UO_2	UO_2
HF(g)	550	UF_4	$UO_2F_2 + UF_4$	UO_2F_2
F_2(g)	400	UF_6 (>500°C)	UF_6	UF_6
CCl_4(g)	400	UCl_4	$UCl_4 + UCl_5$	$UCl_4 + UCl_5$
$SOCl_2$(g)	450	UCl_4	UCl_4	UCl_4
H_2S(g)	1000	UOS	UOS	UOS
C(s)	1500–1700	UC (UC_2)	UC (UC_2)	UC (UC_2)
C(s) + Cl_2(g)	1000	UCl_4	UCl_4	UCl_4
C(s) + CS_2(g)	1000	US_2	US_2	US_2
C(s) + N_2(g)	1700–1900	UN	UN	UN

because of its high stability in air. However, U_3O_8 is now recognized as a compound that is rather difficult to obtain in strictly stoichiometric composition; the O/U ratio deviates significantly from 8/3 depending on the heating temperature, time, and thermal history.

Stoichiometric UO_2 can be obtained by heating uranium oxides in H_2 or CO gas streams at temperatures 750–1700°C (Table 5.16). However, if the H_2 gas contains an O_2 impurity, the formed UO_2 is oxidized to non-stoichiometric UO_{2+x} during the cooling process at temperatures below 300°C. The reaction of UO_2 with air at room temperature deserves special attention, as the reaction is dependent on particle size and reactivity. Very fine UO_2 powder formed by the hydrogen reduction at lower temperatures below 800°C may be pyrophoric. Even though large particles are usually not pyrophoric, the O/U ratio increases steadily with time of exposure to air. UO_2 can take up appreciable quantities of oxygen for particle diameters of about 0.05–0.08 μm. When the particle size is 0.2–0.3 μm or larger, UO_2 is fairly stable to oxidation (Belle, 1961). UO_2 pellets sintered at around 1700°C are not oxidized for years due to protection by slightly oxidized thin surface films.

Some reactions of uranium oxides with chemical reagents are shown in Table 5.16. For the reaction with C(graphite), the product is UC if the mixing mole ratio of carbon and UO_2 is $C/UO_2 = 3$, and UC_2 if $C/UO_2 = 4$.

An interesting reaction between uranium oxides and liquid N_2O_4 has been observed (Gibson and Katz, 1951). Anhydrous uranium oxides react with liquid N_2O_4 to yield $UO_2(NO_3)_2 \cdot N_2O_4$. A similar reaction with N_2O_5 (Gibson *et al.*, 1960) may be used to prepare anhydrous $UO_2(NO_3)_2$. It was found that the reaction between metal and liquid N_2O_4 also gives $UO_2(NO_3)_2 \cdot N_2O_4$ (Addison and Hodge, 1961).

Uranium oxides dissolve in mineral acids such as HNO_3, $HClO_4$, HCl, and H_2SO_4. In HCl, H_2SO_4, and strong phosphoric acid, the mean valence of

uranium does not change from that in the solid state before dissolution. Sintered UO_2 pellets dissolve in HNO_3 with a slow rate, but the dissolution can be accelerated if a small amount of NH_4F is added, due to the formation of fluoro-complexes of uranium. The addition of a small amount of H_2O_2 to HNO_3 is also effective to enhance the dissolution rate of UO_2 in laboratory experiments; in this way no contamination of the solution takes place.

The mechanism of dissolution of UO_2 in H_2O_2 aqueous solution has been studied by a number of researchers. It is regarded as a second-order reaction with a rate constant 8×10^{-7} m min^{-1} (based on the surface-to-solution volume ratio) (Ekeroth and Jonsson, 2003). The plausible mechanism is a slow electron transfer step producing $UO^{+}_{2(surface)} + OH^{\bullet}$ followed by a rapid reduction of the radical $OH^{\bullet}$ to OH^{-}. The $UO^{+}_{2(surface)}$ ions are oxidized to $UO^{2+}_{2(surface)}$ by $OH^{\bullet}$ or by disproportionation (Shoesmith and Sunder, 1994; Ekeroth and Jonsson, 2003). Carbonate ions increase the solubility of $UO^{2+}_{2(surface)}$ (Grenthe *et al.*, 1984). The above mechanism is consistent with the results by other oxidants, viz. $IrCl_6^{2-}$, MnO_4^{-}, $Fe(EDTA)^{-}$, $CO_3^{\bullet-}$, $HO_2^{\bullet}$, and O_2 (Bard and Parsons, 1985; Wardman, 1989; Huie *et al.*, 1991).

(b) Alkali metal uranates and alkaline-earth metal uranates

In Table 5.17, some physico-chemical properties and crystal structures are shown for ternary alkali metal uranates and alkaline-earth metal uranates.

(*i*) *Uranates*(VI)

The most frequently encountered uranates(VI) are a series of compounds of types $M_2^{+}U_nO_{3n+1}$ (M^{+}: alkali metals) and $M^{2+}U_nO_{3n+1}$ (M^{2+}: alkaline-earth metals), but other compounds such as $M_4^{+}UO_5$, $M_2^{2+}UO_5$, $M_3^{2+}UO_6$, and $M_2^{2+}U_3O_{11}$ are also well known.

Preparation

Carbonates, nitrates, or chlorides of alkali or alkaline-earth elements are mixed with the calculated amounts of U_3O_8 or UO_3. Uranates(VI) are obtained by heating the mixtures in air or oxygen at temperatures 500–1000°C. Because of higher volatility of rubidium and cesium oxides, the uranates of these elements are prepared by heating at lower temperatures of 600–700°C (Hoekstra, 1965). The alkaline-earth oxides are also used as starting materials. Reaction temperatures above 1000°C can be used for the preparation of alkaline-earth uranates on account of very low vapor pressures of alkaline-earth oxides.

A number of stoichiometric sodium uranates (α- and β-Na_2UO_4, $Na_2U_2O_7$, α-Na_4UO_5, etc.) have been prepared following a procedure described by Jayadevan *et al.* (1974) by calcining well-characterized thermally labile double sodium uranium salts such as carbonates, oxalates, and acetates. This technique avoids high-temperature treatment and decreases losses by vaporization. This is

Table 5.17 *Some physico-chemical properties and crystal structures for alkali and alkaline earth metal uranates.*

Formula	*Physico-chemical properties*	*Space group*	*Symmetry*	*Lattice parameters*				*Z*	*Density* ($g\ cm^{-3}$)		*References*
				a (Å)	*b* (Å)	*c* (Å)	*Angle* (deg)		*Exp*	*X-ray or ND*	
U(VI) compounds											
Li_2UO_4	not hygroscopic.	α-phase:	orthorhombic						6.13		Zachariasen (1946); Kovba *et al.*
	α→β transformation	(*Fmmm*)		(6.04	5.11	10.52)					(1958); Efremova *et al.* (1959, 1961c);
	1573 K. excitation	*Pnma*		10.547	6.065	5.134					Neuhaus and Recker (1959); Spitsyn
	and infrared	β-phase:	hexagonal	3.912		16.52					*et al.* (1961a); Bereznikova *et al.*
	spectra										(1961); Prigent and Lucas (1965);
											Hoekstra (1965); Ohwada (1970a);
											Kovba (1971a); O'Hare and Hoekstra
											(1974b); Hauck (1974); Krol (1981);
											Volkovich *et al.* (1998)
Na_2UO_4	yellow.	α-phase:	orthorhombic	9.76	5.73	3.50			5.71		Wisnyi and Pijunowski (1957); Spitsyn
	hygroscopic.	*Cmmm*									*et al.* (1961a,b); Kovba *et al.* (1961a);
	infrared spectra	β-phase:	orthorhombic						5.51		Scholder and Glser (1964); Hoekstra
		(*Fmmm*)		5.98	5.807	11.70					(1965); Ohwada (1970a); Kovba
		Pnma		11.708	5.804	5.970					(1971a); Cordfunke and Loopstra
											(1971); O'Hare and Hoekstra (1973);
											Osborne *et al.* (1974); Gebert *et al.*
											(1978); Volkovich *et al.* (1998)
K_2UO_4	yellow. hygro-	α-phase:	tetragonal	4.344		13.13			4.66		Hoekstra and Siegel (1956); Wisnyi
	scopic. infrared	*I4/mmm*		4.335		13.13					and Pijunowski (1957); Spitsyn *et al.*
	spectra		orthorhombic	7.98	6.91	19.78					(1961a,b); Hoekstra (1965); Ohwada
		β-phase:	pseudo-cubic	4.32							(1970b); Kovba (1971a); O'Hare and
											Hoekstra (1974b); Volkovich *et al.*
											(1998)
Rb_2UO_4	yellow.	*I4/mmm*	tetragonal	4.354		13.86			4.52	6.02	Spitsyn *et al.* (1961a,b); Hoekstra
	hygroscopic.			4.353		13.869					(1965); Ohwada (1970b); Kovba and
	infrared spectra										Trunova (1971); O'Hare and
											Hoekstra (1974b)
Cs_2UO_4	orange. very	*I4/mmm*	tetragonal	4.39		14.82					Spitsyn *et al.* (1961a,b); Hoekstra
	hygroscopic.			4.3917		14.803					(1965); Ohwada (1970b); O'Hare
	infrared spectra										and Hoekstra (1974a); van Egmond
											(1976b)
$MgUO_4$	yellow. not	*Imma*	orthorhombic	6.520	6.595	6.924				7.28	Zachariasen (1954a); Lambertson and
	hygroscopic,										Mueller (1954); Rüdorff and Pfitzer
	infrared spectra										(1954); Klíma *et al.* (1966); Jakeš and
				6.499	6.592	6.921					Schauer (1967); Ohwada (1972); Jakeš
											and Křivý (1974); O'Hare *et al.* (1977)

$CaUO_4$	yellow, not hygroscopic, infrared and far infrared spectra	$R\bar{3}m$	rhombohedral	6.266 6.2683 3.87 3.876		 17.54 17.558	$\alpha = 36.03$ $\alpha = 36.04$	1			Zachariasen (1948b); Wisnyi and Pijunowski (1957); Leonidov (1960); Kovba *et al.* (1961b); Anderson and Barraclough (1963); Carnall *et al.* (1965); Jakeš *et al.* (1966); Loopstra and Rietveld (1969); Voronov *et al.* (1972)
$SrUO_4$	α-phase: orange red. β-phase: yellow, infrared and Raman spectra	α-phase: $R\bar{3}m$ (isostructural with $CaUO_4$)	rhombohedral	6.54 6.551 3.991		 18.361	$\alpha = 35.53$ $\alpha = 34.82°$		7.84		Zachariasen (1948b); Rüdorff and Pfitzer (1954); Ippolitova *et al.* (1959, 1961b); Keller (1962a); Klíma *et al.* (1966); Reshetov and Kovba (1966); Cordfunke and Loopstra (1967); Loopstra and Rietveld (1969); Ohwada (1970a); Brisi (1971); Sawyer (1972); Voronov *et al.* (1972); Fujino *et al.* (1977); Tagawa and Fujino (1977); Tagawa *et al.* (1977)
		β-phase: *Pbcm* (isostructural with $BaUO_4$)	orthorhombic	5.4896	7.9770	8.1297				7.26	
$BaUO_4$	orange yellow. infrared spectra	*Pbcm*	orthorhombic	5.751 5.7553 5.744	8.135 8.1411 8.136	8.236 8.2335 8.237		4			Samson and Sillén (1947); Rüdorff and Pfitzer (1954); Wisnyi and Pijunowski (1957); Ippolitova *et al.* (1961c); Allpress (1964); Klíma *et al.* (1966); Reis, Jr. *et al.* (1976)
$LiU_{0.83}O_3$	α, β, and γ-phases ($Li_2O \cdot 1.60UO_3 = Li_{22}U_{18}O_{65}$)		orthorhombic	20.382	11.511	11.417		2	6.6	6.66	Kovba (1971b); Hauck (1974); Prins and Cordfunke (1983); Griffiths and Volkovich (1999)
$Li_2U_2O_7$	yellow. existence confirmed. electronic and infrared spectra		rhombohedral orthorhombic	 20.4	 11.6	 11.1					Efremova *et al.* (1961c); Kovba *et al.* (1961b); Spitsyn *et al.* (1961c); Hoekstra (1965); Kovba (1971b); Toussaint and Avogadro (1974); Hauck (1974); Prins and Cordfunke (1983); Volkovich *et al.* (1998); Griffiths and Volkovich (1999)
$Na_2U_2O_7$	orange colored. infrared and far-infrared spectra		hexagonal orthorhombic	3.94 3.725	 6.660	17.80 11.88					Sutton (1955); Neuhaus (1958); Kovba *et al.* (1961b); Spitsyn *et al.* (1961c); Hoekstra (1965); Carnall *et al.* (1965, 1966); Kovba (1970, 1972a); Cordfunke and Loopstra (1971); Battles *et al.* (1972); Volkovich *et al.* (1998)
		C2/m	monoclinic	12.796	7.822	6.896	$\beta = 111.42$				
$K_2U_2O_7$	infrared and far-infrared spectra. possibility of two phases	α-phase: $R\bar{3}m$	hexagonal	3.99 3.985 3.998		19.71 19.643 19.77					Kovba *et al.* (1958, 1961b); Ippolitova and Kovba (1961); Spitsyn *et al.* (1961c); Hoekstra (1965); Carnall *et al.* (1965); Allpress *et al.* (1968); Anderson (1969); Kovba (1972a); Volkovich *et al.* (1998)

Table 5.17 (*Contd.*)

Formula	*Physico-chemical properties*	*Space group*	*Symmetry*	*Lattice parameters*				*Z*	*Density* ($g\ cm^{-3}$)		*References*
				a (Å)	*b* (Å)	*c* (Å)	*Angle* (deg)		*Exp*	*X-ray or ND*	
$Rb_2U_2O_7$	decomposes at 1473 K. infrared spectra	$R\bar{3}m$	hexagonal	4.01 4.00 4.004		20.81 20.57 20.83			6.33	6.50	Kovba *et al.* (1961b); Spitsyn *et al.* (1961c); Hoekstra (1965); Allpress *et al.* (1968); Anderson (1969); Kovba and Trunova (1971)
$Cs_2U_2O_7$	orange yellow. infrared spectra	α-phase: $C2/m$ β-phase: $C2/m$ γ-phase: $P6/mmc$	monoclinic monoclinic hexagonal	14.528 14.516 4.106	4.2638 4.3199	7.605 7.46 14.58	$\beta = 112.93$ $\beta = 113.78$		6.62		Hoekstra (1965); Kovba and Trunova (1971); Kovba *et al.* (1974); Cordfunke *et al.* (1975); van Egmond (1976c)
CaU_2O_7	yellow or orange green. infrared spectra	two orthogonal axes with 14.06 and 4.00 Å exist									Hoekstra and Katz (1952); Bereznikova *et al.* (1961); Jakeš *et al.* (1966); Cordfunke and Loopstra (1967); Brochu and Lucas (1967)
SrU_2O_7	magnetic susceptibility. infrared spectra										Hoekstra and Katz (1952); Klíma *et al.* (1966); Cordfunke and Loopstra (1967); Brochu and Lucas (1967)
BaU_2O_7	yellow. infrared spectra	$I4_1/amd$	tetragonal	7.127		11.95					Hoekstra and Katz (1952); Allpress (1964, 1965)
$Li_2U_3O_{10}$	infrared spectra	 α-phase: $P2_1/c$ β-phase: $P2$	tetragonal monoclinic monoclinic	5.63 6.821 6.805	 18.91 19.067	12.28 7.300 7.250	 $\beta = 121.56$ $\beta = 121.12$	2	 6.85	7.62 7.35 7.32	Efremova *et al.* (1961c); Spitsyn *et al.* (1961c); Hoekstra (1965); Kovba (1970, 1972c); Prins and Cordfunke (1983); Volkovich *et al.* (1998)
$K_2U_3O_{10}$	infrared spectra										Prigent and Lucas (1965); Anderson (1969)
$Cs_2U_3O_{10}$	no existence claimed										Efremova *et al.* (1961b); Cordfunke *et al.* (1975)
MgU_3O_{10}	yellow or orange yellow. infrared spectra		hexagonal	3.79 7.57		4.080 16.32					Rüdorff and Pfitzer (1954); Polunina *et al.* (1961); Klíma *et al.* (1966)
$K_2U_4O_{13}$	existence not confirmed	$P6_3$	hexagonal	14.29		14.014			6.7	6.6	Efremova *et al.* (1959); Allpress *et al.* (1968); Anderson (1969); Kovba (1970)
$Rb_2U_4O_{13}$	yellow. decomposes at 1473 K	Pb_3/m (or Pb_3)	hexagonal	14.307		14.298		8	6.85	7.0	Ippolitova *et al.* (1961a); Spitsyn *et al.* (1961c); Kovba and Trunova (1971)
$Cs_2U_4O_{13}$	forms by $Cs_2CO_3 + 4UO_3$ at 873 K	$Cmcm$	orthorhombic	13.494	15.476	39.56			6.8	6.88	Efremova *et al.* (1959); Spitsyn *et al.* (1961c); Cordfunke (1975); Cordfunke *et al.* (1975); van Egmond (1976a)
CaU_4O_{13}	tan colored. decomposes to CaU_2O_7 at 1333 K in air		orthorhombic	6.656	4.161	4.030					Cordfunke and Loopstra (1967)

SrU_4O_{13}	dark purple. decomposes to $Sr_2U_3O_{11}$ at 1403 K		monoclinic (pseudo-orthorhombic)	6.734	4.193	4.065	$\beta = 90.16$				Cordfunke and Loopstra (1967)
$Cs_2U_5O_{16}$	solid solution with $Cs_2U_4O_{13}$		monoclinic	13.465	15.561	15.928	$\beta = 92.78$			6.82	Cordfunke *et al.* (1975); van Egmond (1976a)
$Li_2U_6O_{19}$	decomposes to $Li_2U_{2.7}O_9$ at 1263 K		othorhombic	6.701	4.01	4.148					Kovba (1970); Hauck (1974); Fujino *et al.* (1983)
$K_2U_6O_{19}$	existence doubtful		orthorhombic	6.95	3.90	7.19					Efremova *et al.* (1959); Kovba (1961); Spitsyn *et al.* (1961c); Allpress *et al.* (1968); Anderson (1969)
$K_2U_7O_{22}$	forms by the reaction of K_2CO_3 and $UO_4 \cdot nH_2O$	*Pbam*	orthorhombic	6.945	19.533	7.215		2	7.1	7.11	Kovba (1961, 1970)
$Rb_2U_7O_{22}$	decomposes at 1273 K	*Pbam*	orthorhombic	6.958	19.590	7.279				7.32	Efremova *et al.* (1959); Spitsyn *et al.* (1961c); Kovba and Trunova (1971)
$Cs_2U_7O_{22}$	decomposes at 1273 K	*Pbam*	orthorhombic	6.949	19.711	7.3955				7.485	Efremova *et al.* (1959); Spitsyn *et al.* (1961c); Cordfunke *et al.* (1975); van Egmond (1976b)
Li_4UO_5	gold colored. hygroscopic. excitation and infrared spectra	*I4/m*	tetragonal	6.736 6.720		4.45 4.451			5.28	5.41	Scholder (1958); Efremova *et al.* (1959, 1961c); Kovba (1962); Hoekstra and Siegel (1964); Reshetov and Kovba (1966); Ohwada (1971); Hauck (1974); Krol (1981)
Na_4UO_5	red to salmon pink. very hygroscopic. infrared spectra	*I4/m*	tetragonal	7.576 7.536		4.641 4.630			4.95	5.11	Findley *et al.* (1955); Efremova *et al.* (1959); Kovba (1962); Hoekstra and Siegel (1964); Cordfunke and Loopstra (1971); Ohwada (1971); Battles *et al.* (1972)
K_4UO_5	possibility of no existence remains		othorhombic	3.50	8.58	12.95				4.19	Efremova *et al.* (1959, 1961a); Hoekstra and Siegel (1964)
Rb_4UO_5	preparation $Rb_2CO_3 + UO_3$ at 1273 K		tetragonal	8.18		13.73				6.00	Efremova *et al.* (1959); Ippolitova *et al.* (1961a)
Ca_2UO_5	yellow. infrared spectra	$P2_1/c$	monoclinic	7.9137	5.4409	11.4482	$\beta = 108.803$		5.55	5.67	Bereznikova *et al.* (1961); Sawyer (1963); Jakeš *et al.* (1966); Cordfunke and Loopstra (1967); Loopstra and Rietveld (1969)
Sr_2UO_5	yellow. infrared and Raman spectra	$P2_1/c$	monoclinic	8.1043	5.6614	11.9185	$\beta = 108.985$		6.08	6.34	Sawyer (1963); Keller (1964); Cordfunke and Loopstra (1967); Loopstra and Rietveld (1969); Allen and Griffiths (1977)
Li_6UO_6	yellow. infrared spectra	α-phase:	hexagonal	8.338		7.352					Scholder and Glser (1964); Hauck (1973); Prins and Cordfunke (1983)
Ca_3UO_6	pale yellow. decomposes at 1773 K. infrared spectra	$P2_1$ (cryolite structure)	monoclinic	5.7275	5.9564	8.2982	$\beta = 90.568$		5.1	5.34	Rüdorff and Pfitzer (1954); Ippolitova *et al.* (1959); Bereznikova *et al.* (1961); Jakeš *et al.* (1966); Rietveld (1966); Brisi (1969); Loopstra and Rietveld (1969); Voronov *et al.* (1972); Kemmler-Sack and Seemann (1975)

Table 5.17 (*Contd.*)

Formula	*Physico-chemical properties*	*Space group*	*Symmetry*	*Lattice parameters*				*Z*	*Density* ($g\ cm^{-3}$)		*References*
				a (Å)	*b* (Å)	*c* (Å)	*Angle* (deg)		*Exp*	*X-ray or ND*	
Sr_3UO_6	pale yellow. infrared and Raman spectra	$P2_1$	monoclinic	5.9588	6.1795	8.5535	$\beta = 90.192$	2		6.17	Rüdorff and Pfitzer (1954); Scholder and Brixner (1955); Ippolitova *et al.* (1959); Sleight and Ward (1962); Rietveld (1966); Cordfunke and Loopstra (1967); Loopstra and Rietveld (1969); Kemmler-Sack and Seemann (1975); Allen and Griffiths (1977)
Ba_3UO_6	pale yellow. stable up to high temperatures. infrared and charge transfer spectra	$Fm\bar{3}m$ $(NH_4)_3FeF_6$ type structure	cubic tetragonal orthorhombic	8.922 8.90 6.825 44.63	 44.31	 8.943 8.973			6.75	6.98	Rüdorff and Pfitzer (1954); Scholder and Brixner (1955); Ippolitova *et al.* (1959, 1961c); Rietveld (1966); Kemmler-Sack and Seemann (1975)
$Ca_2U_3O_{11}$	ocher. decomposes to CaU_2O_7 and $CaUO_4$ at 1173 K		triclinic	6.186	6.212	6.186	$\alpha = \gamma = 37.12$ $\beta = 37.56$				Cordfunke and Loopstra (1967)
$Sr_2U_3O_{11}$	cognac colored. stable to 1573 K. infrared and Raman spectra		triclinic	6.484	6.523	6.484	$\alpha = \gamma = 35.44$ $\beta = 36.10$				Cordfunke and Loopstra (1967); Allen and Griffiths (1977)
$Ba_2U_3O_{11}$	orange. stable to 1773 K. infrared spectra										Allpress (1964)
U(v) and U(iv) compounds											
$LiUO_3$	black purple. magnetic properties. electronic spectra	$R3c$ $LiNbO_3$ type	rhombohedral	5.901			$\alpha = 54.60$	1	7.46	7.67	Rüdorff and Leutner (1957); Rüdorff and Menzer (1957); Kovba (1960); Rüdorff *et al.* (1962); Kemmler (1965); Kemmler-Sack *et al.* (1967); Kemmler-Sack (1968b); Keller (1972); Selbin *et al.* (1972a)
$NaUO_3$	red brown. magnetic susceptibility. electronic spectra. no existence of uranyl group	*Pbnm* $GdFeO_3$ type	orthorhombic	5.775 5.776	5.905 5.910	8.25 8.283				7.33	Rüdorff and Leutner (1957); Rüdorff and Menzer (1957); Ippolitova *et al.* (1961d); Rüdorff *et al.* (1962); Prigent and Lucas (1965); Kemmler-Sack *et al.* (1967); Kemmler-Sack and Rüdorff (1967); Kemmler-Sack (1968b); Bartram and Fryxell (1970); Cordfunke and Loopstra (1971); King (1971); Battles *et al.* (1972); Keller (1972); Selbin *et al.* (1972a); Lyon *et al.* (1977)

Na_xUO_3	green. $0 < x \leq 0.14$		orthorhombic ($Na_{0.025}UO_{3-x}$)	6.718	11.90	4.142		8.0	8.29	Greaves *et al.* (1973)
			hexagonal ($Na_{0.10}UO_3$)	3.955		4.163		7.2	7.69	
KUO_3	brown. magnetic susceptibility. electronic spectra	*Pm*3*m* $CaTiO_3$ type	cubic	4.290 4.299				6.85	6.84	Ippolitova *et al.* (1961d); Rüdorff *et al.* (1962); Kemmler-Sack *et al.* (1967); Kemmler-Sack and Rüdorff (1967); Kemmler-Sack (1968b); Selbin *et al.* (1972a)
$RbUO_3$	pale brown. Rb_xUO_3 ($0.8 \leq x \leq 1$). magnetic susceptibility. electronic spectra	*Pm*3*m*	cubic	4.323				7.5	7.63	Ippolitova and Kovba (1961); Rüdorff *et al.* (1962); Kemmler-Sack *et al.* (1967); Kemmler-Sack and Rüdorff (1967); Kemmler-Sack (1968b); Selbin *et al.* (1972a)
$CaUO_3$	black. no existence claimed	*Iam* Mn_2O_3 type	cubic (high pressure form: *fcc*, $a = 5.38$ Å)	10.727						Alberman *et al.* (1951); Young and Schwartz (1963); Brochu and Lucas (1967)
$SrUO_3$	dark brown	(deformed $CaTiO_3$ type)	orthorhombic	6.101 6.03	8.60 6.18	6.17 8.62				Scholder and Brixner (1955); Lang *et al.* (1956); Furman (1957); Brisi (1960); Keller (1964)
$BaUO_3$	brown. magnetic susceptibility	*Pm*3*m* $CaTiO_3$ type	cubic	4.40 4.387 (pseudo-cubic) 4.411				7.98		Rüdorff and Pfitzer (1954); Scholder and Brixner (1955); Lang *et al.* (1956); Furman (1957); Trzebiatowski and Jabloński (1960); Fujino and Naito (1969); Braun *et al.* (1975)
$Ca_{2.5}U_{1.33}O_{5.83}$	electronic spectra	deformed $CaTiO_3$ type	monoclinic	5.767	5.974	8.349	$\beta = 89.8$		6.10	Kemmler-Sack and Seemann (1974)
$Sr_{2.5}U_{1.33}O_{5.83}$	same crystal structure as $Ca_{2.5}U_{1.33}O_{5.83}$.		monoclinic	6.178	6.023	8.629	$\beta = 89.8$	6.33	6.51	Kemmler-Sack and Seemann (1974)
$Ba_{2.67}U_{1.33}O_6$	brown. magnetic susceptibility. electronic spectra		cubic	8.901				7.10	7.34	Kemmler-Sack and Wall (1971)
Ca_2UO_4	forms by the reaction of $CaO+UO_2$ below 2023 K									Alberman *et al.* (1951)
Sr_2UO_4	forms by heating Sr_2UO_5 in H_2.									Scholder and Brixner (1955)
Ba_2UO_4	forms by the same method as Sr_2UO_4. possibility of no existence									Scholder and Brixner (1955); Trzebiatowski and Jabloński (1960)
Ba_3UO_5	no existence reported	α-phase: β-phase: $Fm\bar{3}m$	tetragonal cubic	6.291 8.915		8.982				Trzebiatowski and Jabloński (1960); Keller (1964); Charvillat *et al.* (1970); Braun *et al.* (1975)
Li_3UO_4	ocher colored. magnetic susceptibility. electronic spectra		tetragonal	4.49		8.5				Scholder (1960); Scholder and Glser (1964); Blasse (1964); Kemmler-Sack *et al.* (1967); Kemmler-Sack (1968b)

Table 5.17 (*Contd.*)

Formula	*Physico-chemical properties*	*Space group*	*Symmetry*	*Lattice parameters*				*Z*	*Density* ($g\ cm^{-3}$)		*References*
				a (Å)	*b* (Å)	*c* (Å)	*Angle* (deg)		*Exp*	*X-ray or ND*	
Na_3UO_4	pale brown.	$Fm\bar{3}m$	cubic	4.77					6.5		Scholder (1960); Pepper (1964);
	low temperature C_p.	NaCl type		4.79–4.80							Scholder and Glser (1964); Addison
	high temperature			4.74							(1969); Bartram and Fryxell (1970);
	C_p (298–1200 K).	$P4_232$	cubic	9.543 (to explain superstructure lines)							Marcon (1972); O'Hare *et al.* (1972);
	formula claimed to be $Na_{11}U_5O_{16}$	$Fd3m$	cubic	9.574							Osborne and Flotow (1972); Fredrickson and Chasanov (1972)
Li_7UO_6	pale green. magnetic		rhombohedral	6.61			$\alpha = 53.27$				Scholder and Glser (1964); Keller
	susceptibility.		(hexagonal indexing)	5.52		15.80					*et al.* (1965); Kemmler-Sack *et al.*
	electronic spectra			5.55		15.76					(1967); Kemmler-Sack (1968b); Hauck (1969); Selbin *et al.* (1965)
$Cs_2U_4O_{12}$	$\alpha \rightarrow \beta$ at 898 K, and	α-phase: $R\bar{3}m$	rhombohedral	10.9623			$\alpha = 89.402$				Cordfunke *et al.* (1975); Cordfunke
	$\beta \rightarrow \gamma$ at 968 K. stable	β-phase: $P2_1$	monoclinic	7.886	8.002	10.793	$\beta = 92.62$				(1975); van Egmond (1975); Cordfunke
	in air up to 1523 K	γ-phase: $Fd3m$	cubic	11.2295							and Westrum, Jr. (1979)
MgU_2O_6	black. magnetic	$Fm\bar{3}m$	cubic	5.284							Hoekstra and Katz (1952); Keller
	susceptibility.	CaF_2 type		5.275							(1964); Kemmler-Sack *et al.* (1967);
	electronic spectra.			5.281							Kemmler-Sack and Rüdorff (1967);
	Mg and U atoms statistically distributed.										Kemmler-Sack (1968b); Fujino and Naito (1970); Selbin *et al.* (1972a); Fujino (1972)
CaU_2O_6	black. magnetic susceptibility	$Fm\bar{3}m$ CaF_2 type	cubic	5.379						8.71	Hoekstra and Katz (1952); Hoekstra and Siegel (1956); Brochu and Lucas (1967)
SrU_2O_6	black. magnetic susceptibility	$Fm\bar{3}m$ CaF_2 type	cubic	5.452						9.07	Hoekstra and Katz (1952); Hoekstra and Siegel (1956); Brochu and Lucas (1967); Tagawa *et al.* (1977)
BaU_2O_6	black. magnetic susceptibility (85–300 K)	$Fm\bar{3}m$ CaF_2 type	cubic	5.63							Hoekstra and Katz (1952); Scholder and Brixner (1955); Hoekstra and Siegel (1956); Keller (1964); Brochu and Lucas (1967)
CaU_3O_9	non-stoichiometric region in CaU_3O_{9-x}		cubic	super-structure line							Young and Schwartz (1962, 1963)
$Ba_2U_2O_7$	magnetic susceptibility. electronic spectra		monoclinic (pseudo tetragonal)	11.56	11.31	11.56	$\beta \approx 90$		7.46	7.58	Kemmler-Sack and Rüdorff (1967); Kemmler-Sack (1968a,b)

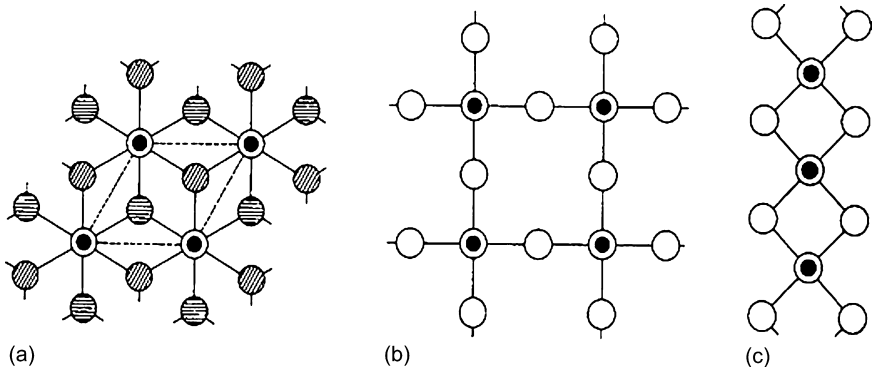

Fig. 5.25 *Schematic atom arrangement around a uranyl group* (*Zachariasen,* 1954*b*); *the notation is as follows:* ◉: *the inner filled circles show U in the plane of the page; the outer empty circles denote* O_I, *one above and the other below the plane of the page*; ○: *denotes* O_{II} *in the plane of the page*; ◍: *denotes* O_{II} *slightly above the plane of the page and* ◍: *denotes* O_{II} *slightly below the plane.* (*a*) *Hexagonal coordination by six* O_{II} *atoms* (β-Li_2UO_4, $CaUO_4$, α-$SrUO_4$). *Each uranium atom is coordinated with six oxygen atoms in an approximately planar arrangement. The axis of the collinear* U_I–U–O_I *group is normal to the plane of the page.* (*b*) *Tetragonal coordination by four* O_{II} *atoms forming an infinite plane* ($BaUO_4$). *Uranium is octahedrally coordinated by four* O_{II} *atoms and two* O_I *atoms. Each octahedron shares four corners with adjacent octahedra forming a layer structure extended in the bc plane. The Ba atoms are located between the layers and link them by electrostatic force.* (*c*) *Tetragonal coordination by four* O_{II} *atoms forming an infinite chain* ($MgUO_4$). *The octahedra share two opposite edges, resulting in formation of chains along the a-axis. Reproduced by the permission of the International Union of Crystallography.*

discussed in Tso *et al.* (1985). Note that the technique is also discussed by Keller (1972) for BaU_2O_7 and $Ba_2U_3O_{11}$.

Crystal structures

An important feature of $M_2^+U_nO_{3n+1}$ and $M^{2+}U_nO_{3n+1}$ type uranates(VI) is their layer structure and the existence of the uranyl groups, UO_2^{2+}, in the crystals.

The structure of monouranates ($n = 1$) is characterized by the layer planes; the oxygen atoms on this plane are coordinated to uranium atoms forming secondary bonds. The primary bonds between the uranium and oxygen atoms of the uranyl group, O_I–U–O_I, are collinear and perpendicular to the layer plane. The atom arrangements around the uranyl groups are schematically drawn in Fig. 5.25 (Zachariasen, 1954b).

For β-Li_2UO_4 (Zachariasen, 1945), $CaUO_4$ and α-$SrUO_4$ (Zachariasen, 1948b), each uranium atom is coordinated to six oxygen atoms (cf. Fig. 5.25a, viewed from the *c*-axis). The axis of the UO_2^{2+} group in the figure is normal to the page, while three of six O_{II} atoms are located about 0.5 Å above and remaining three O_{II} atoms about 0.5 Å below the plane through uranium and perpendicular to the UO_2^{2+} axis. The oxygen atoms coordinated to uranium in

$BaUO_4$ and $MgUO_4$ form a deformed octahedron, where each O_{II} oxygen atom acts as a bridge between two adjacent uranium atoms. In $BaUO_4$ the octahedra share corners (Fig. 5.25b), but in $MgUO_4$ they share edges (Fig. 5.25c). As a consequence, infinite layers are formed in $BaUO_4$ and infinite chains in $MgUO_4$. The alkali or alkaline-earth metals occupy the positions between the layers and bind them together by electrostatic force (Zachariasen, 1954b).

There are no uranyl groups in Li_4UO_5 and Na_4UO_5, and the structure instead contains four orthogonal planar $U–O_I$ bonds (with the distance 1.99 Å in both Li_4UO_5 and Na_4UO_5), yielding UO_4^{2-}; in addition, there are also two collinear $U–O_{II}$ bonds (Li_4UO_5: 2.23 Å; Na_4UO_5: 2.32 Å) (Hoekstra and Siegel, 1964). The octahedra produced in this way are linked to bridges through the diagonally located O_{II} atoms, resulting in formation of a structure containing octahedral chains running along the *c*-axis. $M_3^{2+}UO_6$-type compounds (M = Ca, Sr, Ba) crystallize into distorted perovskite structures ($2[M_{1/4}U_{1/4}][M_{5/4}U_{1/4}]O_3$), where the alkaline-earth atoms and uranium atoms corresponding to $[M_{1/4}U_{1/4}]$ occupy the octahedral sites in an ordered manner (Keller, 1964; Morss, 1982; Williams *et al.*, 1984).

Physicochemical properties

Alkali metal monouranates(VI) are hygroscopic except for Li_2UO_4, and mostly yellow colored; some diuranates are orange or red-orange. The uranates(VI) of the heavy alkali metals are volatile on heating in air. The antisymmetric stretching vibration of UO_2^{2+} in uranates(VI) gives a strong absorption in the IR range of 600–900 cm^{-1}. The frequency changes depending on the bonding strength of the coordinated oxygen atoms. Since the $U–O_I$ bonds of the uranyl group are much stronger, this vibration can be treated approximately as an isolated linear three-atom system of CO_2-type (Jones, 1958). The $U–O_I$ distances calculated from the infrared frequencies using the empirical Badger equation are mostly in good agreement with those obtained by diffraction experiments (Hoekstra and Siegel, 1964; Allpress, 1965; Hoekstra, 1965; Carnall *et al.*, 1966).

A phase transformation coupled with oxygen non-stoichiometry has been observed for $SrUO_4$ and $CdUO_4$ (Tagawa and Fujino, 1978, 1980). α-$SrUO_4$ can be reduced to non-stoichiometric $SrUO_{4-x}$ with the maximum x value of 0.2–0.3. On heating α-$SrUO_4$ at different oxygen partial pressures from 10 to 600 mmHg and heating rates of 1–5 K min^{-1}, the compound is rapidly reduced to $SrUO_{3.8–3.9}$ at about 800°C. The solid is then immediately re-oxidized to stoichiometric composition by absorbing oxygen from the gaseous phase. At the same time, it transforms into β-$SrUO_4$. The atom rearrangement in the phase transformation may be accelerated by the formation of vacancies in the oxygen sublattice of α-$SrUO_4$.

Magnetic susceptibilities have been measured for $MgUO_4$, $SrUO_4$, $BaUO_4$, CaU_2O_7, SrU_2O_7, and BaU_2O_7 (Brochu and Lucas, 1967). In these compounds U(VI) is expected to be diamagnetic, but a weak paramagnetism was observed; this is ascribed to covalency in the uranyl group (Bell, 1969).

(*ii*) *Uranates* (*V*) *and* (*IV*)

Uranates(V) of $M^{+}UO_3$ (M = Li, Na, K, Rb), $M_3^{+}UO_4$ (M = Li, Na), and $M^{2+}U_2O_6$ (M = Mg, Ca, Sr, Ba) types are the most well known, as are the uranates(IV) of $M^{2+}UO_3$ (M = Ca, Sr, Ba) type.

Preparation

To prepare uranates(V), a symproportionation reaction is widely used, where the uranates(IV) and (VI) are first mixed in 1:1 uranium atom ratio, after which the mixture is heated in an evacuated sealed quartz ampoule. An example is the reaction $Li_2UO_4 + UO_2 = 2LiUO_3$, which takes place at 650–750°C. Another method is to reduce uranates(VI) by H_2 at elevated temperatures; the reaction condition should be carefully defined in order to form uranates(V). Since the uranates of alkaline-earth metals are not volatile, the high-temperature reduction method by H_2 can be used to prepare the corresponding uranates(IV).

For some uranates(VI) having high equilibrium oxygen pressures, uranates(V) can be prepared by heating the uranate(VI) in a vacuum at high temperature. The $M^{2+}U_2O_6$ compounds are prepared by the reaction

$$M^{2+}U_2O_7 = M^{2+}U_2O_6 + 1/2O_2$$

at 1100°C (M = Mg, Ca, Sr, Ba). It is, however, rather difficult to obtain stoichiometric uranates(V) by this method.

Crystal structures

Uranates(V) and (IV) do not contain uranyl groups and as a result, their crystal structures are in general not of the layer type and in many cases simpler. The compounds of $M^{+}UO_3$ and $M^{2+}UO_3$, with the exception of $CaUO_3$ (cubic Mn_2O_3-type structure), have perovskite or deformed perovskite-type structures. $LiUO_3$ crystallizes into a rhombohedrally distorted $LiNbO_3$ structure, as a result of the small ionic radius of Li^{+}. $NaUO_3$ has an orthorhombic $GdFeO_3$ structure with small distortions from cubic perovskite structure. KUO_3 and $RbUO_3$ have cubic perovskite structures, and $BaUO_3$ a cubic or pseudo-cubic perovskite structure.

In the uranates(V) of $M_3^{+}UO_4$-type, Li_3UO_4 crystallizes in a tetragonally distorted NaCl-type structure, in which the lithium and uranium atoms are located in the cation sites in an ordered manner with an atom ratio of 3:1. All $M^{2+}U_2O_6$ compounds have cubic fluorite-type structures, where the alkaline-earth metal atoms and uranium atoms are statistically distributed with an atom ratio of 1:2 over the cation sites.

Physico-chemical properties

Most uranates(V) and (IV) are brown to black. An exception is the pale green Li_7UO_6. Uranates(V) and (IV) dissolve in dilute mineral acids. The dissolution rate in HNO_3 is higher than those in HCl and H_2SO_4 (Trzebiatowski and

Jabloński, 1960; Scholder and Gläser, 1964; Brochu and Lucas, 1967). Li_3UO_4 is oxidized to Li_2UO_4 in air even at room temperature. Na_3UO_4 absorbs significant amounts of oxygen, water, and CO_2 at room temperature. On heating the uranates(V) or uranates(IV) in air, they are readily oxidized to uranates(VI).

Electronic spectra have been measured for $LiUO_3$, $NaUO_3$, KUO_3, $RbUO_3$, MgU_2O_6, CdU_2O_6, Li_3UO_4, Li_7UO_6, $Ba_2U_2O_7$, etc. in the range 4000–40000 cm^{-1} (Kemmler-Sack *et al.*, 1967). The crystal field parameters were determined for $LiUO_3$ and Li_3UO_4 from the optical absorption electronic spectra (Lewis *et al.*, 1973; Kanellakopulos *et al.*, 1980; Hinatsu *et al.*, 1992a,b). For KUO_3 and $RbUO_3$, the octahedral crystal field around a U^{5+} atom was consistently calculated with a spin–orbit coupling constant of 1770 cm^{-1} (Kemmler-Sack *et al.*, 1967; Selbin *et al.*, 1972a).

Magnetic susceptibilities have been measured for $LiUO_3$, $NaUO_3$, KUO_3, $RbUO_3$, Li_3UO_4, Li_7UO_6, MgU_2O_6, CdU_2O_6, and $Ba_2U_2O_7$ at temperatures 85–473 K (Rüdorff and Menzer, 1957; Kemmler-Sack, 1968a). In the paramagnetic temperature range, the Curie constant changed with the coordination number. The magnetic susceptibilities for M^+UO_3 (M = Li, Na, K, Rb) were measured in a wider temperature range from 4.2 K to room temperature (Keller, 1972; Miyake *et al.*, 1979, 1982; Kanellakopulos *et al.*, 1980). The electron paramagnetic resonance (EPR) spectra for U^{5+} ions doped in $LiNbO_3$, which has the same crystal structure as $LiUO_3$, gave a signal at $g = 0.727$ (Lewis *et al.*, 1973). The EPR signals were also observed for pure M^+UO_3 but they were very broad (Miyake *et al.*, 1979, 1982). $LiUO_3$ showed a ferromagnetic transition at 16–17 K (Miyake *et al.*, 1979, 1982; Hinatsu *et al.*, 1992b).

Li_3UO_4 has a distorted NaCl-type structure and its magnetic properties have been studied by measuring the EPR spectra and magnetic susceptibility in an extended temperature range down to 4.2 K (Keller, 1972; Lewis *et al.*, 1973; Kanellakopulos *et al.*, 1980; Miyake *et al.*, 1982; Hinatsu *et al.*, 1992a). The experimental magnetic susceptibility can be well described by assuming the $5f^1$ electron of U^{5+} in an octahedral crystal field with a small tetragonal distortion with the crystal field parameters obtained from the electronic spectra (Hinatsu *et al.*, 1992a). $NaUO_3$ gives a magnetic transition at 32 K (Miyake *et al.*, 1977) or 35 K (Keller, 1972), for which a λ-type anomaly has also been observed in the heat capacity (Lyon *et al.*, 1977). The EPR and magnetic susceptibility studies for $M^{2+}U_2O_6$ (M = Mg, Ca, Cd, Sr) have been carried out (Brochu and Lucas, 1967; Miyake *et al.*, 1993; Miyake and Fujino, 1998). The anomalies of magnetic origin have been observed at 4–7 K.

(*iii*) *Non-stoichiometry*

The non-stoichiometry in uranates can be classified into three types. The first type occurs when part of the alkali metal in the uranate is lost as an oxide by vaporization on heating, viz. $Na_{2-2x}U_2O_{7-x}$ is formed from $Na_2U_2O_7$ by the loss of xNa_2O ($0 \leq x \leq 0.07$) (Carnall *et al.*, 1966; Anderson, 1969). The second type

is caused by non-stoichiometric dissolution of alkali metal in a uranium oxide. An example is Na_xUO_3 ($0 \leq x \leq 0.14$) (Greaves *et al.*, 1973). The third type is the most common non-stoichiometry, i.e. the oxygen non-stoichiometry. Examples of such uranates are $Na_2U_2O_{7-x}$ ($0 \leq x \leq 0.5$) (Anderson, 1969), $K_2U_2O_{7-x}$ (Spitsyn *et al.*, 1961b), $Cs_2U_4O_{13-x}$ (Cordfunke *et al.*, 1975), $CaUO_{4-x}$ ($0 \leq x \leq 0.5$) (Anderson and Barraclough, 1963), α-$SrUO_{4-x}$ ($0 \leq x \leq 0.5$) (Tagawa and Fujino, 1977), CaU_2O_{7-x} ($0 \leq x \leq 0.13$) and SrU_2O_{7-x} ($0 \leq x \leq 0.4$) (Hoekstra and Katz, 1952), SrU_4O_{13-x} (Cordfunke and Loopstra, 1967; Tagawa *et al.*, 1977). Rhombohedral $CaUO_4$ and α-$SrUO_4$, which crystallographically are very similar to ionic UO_2, show a wide range of non-stoichiometries, while β-$SrUO_4$ and $BaUO_4$ with increased covalency have virtually no non-stoichiometry. Examples of the third type of non-stoichiometric compounds derived from uranate(v) are MgU_2O_{6+x} ($-0.16 \leq x \leq 0.03$), CaU_2O_{6+x} ($-0.05 \leq x \leq 0.05$), SrU_2O_{6+x} ($-0.05 \leq x \leq 0.4 \sim 0.6$), and BaU_2O_{6+x} ($x \leq 0.86$) (Hoekstra and Katz, 1952).

The non-stoichiometric uranates are produced by heating in reducing atmospheres, but generally the U(VI) state is more stable in ternary uranates than in binary uranium oxides. This trend is more pronounced for the uranates with higher M/U ratios (M = alkali metals or alkaline-earth metals). The experimental fact that alkali and alkaline-earth metal uranates(VI) strictly without U(V) and U(IV) are formed under certain conditions when heated in air was utilized for the determination of oxygen in uranium oxides (Fujino *et al.*, 1978b).

(c) Transition metal uranates

Table 5.18 shows the crystallographic properties of ternary transition metal uranates. In this section the uranates of some non-transition metals such as Sb, Tl, Pb, and Bi are included because of the resemblance of their properties. Here we present an overview of preparation methods and crystal structures. For more detailed information, the reader is referred to the following review articles (Hoekstra and Marshall, 1967; Keller, 1972, 1975).

(*i*) *Preparative methods*

The most general 'dry' method for preparation is to heat thoroughly ground mixtures of transition metal oxides and UO_3 (or U_3O_8) in air. $CrUO_4$, $MnUO_4$, and $CoUO_4$ can be synthesized by heating the mixed oxides for 1 day at 1000–1100°C (Hoekstra and Marshall, 1967). $CuUO_4$ is obtained by heating below 875°C. Triuranates, MU_3O_{10} (M = Mn, Co, Ni, Cu, Zn), are prepared by heating the mixtures of M/U = 1/3 at 875°C. Although Ni, Cu, and Zn triuranates are readily obtained as stoichiometric compounds, Mn and Co triuranates tend to remain oxygen-deficient.

Nitrates, viz. $M(NO_3)_2 + UO_2(NO_3)_2$ (Weigel and Neufeldt, 1961), can also be used as starting materials for preparing MUO_4 (M = Cu, Zn, Cd, Hg),

Table 5.18 *Crystallographic properties of transition metal uranates.*

Formula	*Color*	*Space group*	*Symmetry*	*Lattice parameters*					*Density* ($g\ cm^{-3}$)		*References*
				a (Å)	*b* (Å)	*c* (Å)	*Angle* (deg)	*Z*	*Exp.*	*X-ray or ND*	
$EuUO_3$			orthorhombic	6.020	6.165	8.606					Berndt *et al.* (1976)
$U_{0.25}NbO_3$	brown		tetragonal	7.727		7.792			5.72		Keller (1975)
$U_{0.25}TaO_3$	brown		tetragonal	7.739		7.773			8.23		Keller (1975)
U_xWO_3 (x<0.16–0.2)			cubic	3.78–3.81							Keller (1975)
$CrUO_4$	dark brown	*Pbcn*	orthorhombic	4.871	11.787	5.053			7.72	8.12	Rüdorff *et al.* (1967); Hoekstra and Marshall (1967); Keller (1975)
$MnUO_4$		*Imma*	orthorhombic	6.645	6.983	6.749					Hoekstra and Marshall (1967); Keller (1972)
$FeUO_4$	black	*Pbcn*	orthorhombic	4.888	11.937	5.110					Rüdorff *et al.* (1967); Hoekstra and Marshall (1967); Keller (1972, 1975)
$CoUO_4$	dark brown	*Imma*	orthorhombic	6.497	6.952	6.497				8.17	Hoekstra and Marshall (1967); Keller (1972, 1975)
α-$NiUO_4$		*Pbcn*	orthorhombic	4.820	11.627	5.188					Hoekstra and Marshall (1967); Keller (1972, 1975)
β-$NiUO_4$		*Imma*	orthorhombic	6.472	6.870	6.472					Hoekstra and Marshall (1967); Keller (1972, 1975)
$CuUO_4$	coffee brown	$P2_1/n$	monoclinic	5.475	4.957	6.569	$\beta = 118.87$	2			Hoekstra and Marshall (1967); Siegel and Hoekstra (1968); Keller (1972)
$ZnUO_4$	bright red	*Imma*	orthorhombic	6.492	6.994	6.574					Hoekstra and Marshall (1967); Keller (1972)
α-$CdUO_4$	brownish yellow		orthorhombic	7.01	6.836	3.519					Ippolitova *et al.* (1961e); Keller (1972)

β-$CdUO_4$	brownish yellow	$R\bar{3}m$	rhombohedral	3.587		17.41		2			Ippolitova *et al.* (1961e); Keller (1972)
$HgUO_4$	orange		orthorhombic	11.12	6.87	6.48					Keller (1972)
$PbUO_4$	red	*Pbcm*	orthorhombic	5.528	7.952	8.180					Keller (1972)
$BiUO_4$	gray black	$Fm\bar{3}m$	cubic	5.481				4	10.3	10.31	Rüdorff *et al.* (1967)
α-Ag_2UO_4	deep brown		tetragonal	11.70		5.87			7.57	7.41	Keller (1972)
β-Ag_2UO_4	deep brown		tetragonal	4.66		6.38			6.46	6.20	Keller (1972)
Tl_2UO_4	yellow orange		tetragonal	4.468		13.10					Keller (1972)
Cd_2UO_5	orange yellow	$P2_1/c$	monoclinic	8.074	5.312	11.52	$\beta = 100.52$	4		7.74	Keller (1972)
$UTiO_5$			orthorhombic	6.31	7.35	15.56					Dickens *et al.* (1993)
UVO_5	black	*Pbma*	orthorhombic	12.31	7.19	4.115					Keller (1975)
$UNbO_{5(+x)}$			orthorhombic	6.459	3.785	4.036					Keller (1975)
$UTaO_{5.17}$	dark gray		orthorhombic	6.463	3.780	3.980					Keller (1975)
$UMoO_5$		*Pbcm*	orthorhombic	4.115	12.761	7.338					Keller (1975)
$UTeO_5$		$Pca2_1$	orthorhombic	10.161	5.363	7.862					Meunier and Galy (1973)
CoU_2O_6	dark brown		hexagonal	9.095		4.990			8.55	8.79	Kemmler-Sack and Rüdorff (1967); Keller (1975)
NiU_2O_6	red brown	*P*321	hexagonal	9.015		5.103			8.64	8.75	Kemmler-Sack and Rüdorff (1967); Keller (1975)
CdU_2O_6			cubic	5.357					9.66	9.858	Kemmler-Sack and Rüdorff (1967)
Cr_2UO_6	black	$P\bar{3}1m$	hexagonal	4.988		4.620			7.01	7.31	Keller (1975)
Cd_3UO_6	light orange		monoclinic	8.262	5.733	5.623	$\beta = 89.53$				Keller (1972)
Pb_3UO_6	dark red	*Pnam*	orthorhombic	13.71	12.36	8.21					Keller (1972)
UV_2O_6		$P\bar{3}1m$	hexagonal	4.988		4.768			7.09	7.06	Keller (1975)

Table 5.18 (*Contd.*)

Formula	*Color*	*Space group*	*Symmetry*	*Lattice parameters*				Z	*Density* ($g\ cm^{-3}$)		*References*
				a (Å)	*b* (Å)	*c* (Å)	*Angle* (deg)		*Exp.*	*X-ray or ND*	
CdU_2O_7	yellow										Keller (1972)
$Cd_2U_2O_7$			rhombohedral	10.72			$\alpha = 91.30$				Kemmler-Sack and Rüdorff (1967)
$Tl_2U_2O_7$			orthorhombic	6.902	7.971	19.643					Keller (1972)
$U_{2/3}Nb_2O_7$		*Fd*3	cubic	10.38					5.2	5.4	Keller (1975)
$Co_3U_2O_8$		*Pnnm*	orthorhombic	5.11	10.30	6.15		2			Bacmann (1973); Keller (1975)
UV_2O_8	yellow green	*Pnma*	orthorhombic	5.70	11.78	10.42			4.50	4.45	Keller (1975)
UTa_2O_8	yellow	$P\bar{3}1m$	hexagonal	6.41		3.95			8.3		Keller (1975)
UMo_2O_8		*Pban*	orthorhombic	20.08	7.32	4.11			6.13		Keller (1975)
U_2MoO_8		$P2_12_12$	orthorhombic	6.734	23.24	4.115					Keller (1975)
U_2WO_8		$P2_12_12$	orthorhombic	6.711	23.28	4.091					Keller (1975)
MnU_3O_{10}	light brown		hexagonal	3.80		4.14					Hoekstra and Marshall (1967); Keller (1972)
FeU_3O_{10}			orthorhombic	6.51	7.53	16.14					Keller (1972, 1975)
CoU_3O_{10}	deep brown		hexagonal	3.79		4.08					Hoekstra and Marshall (1967); Keller (1972, 1975)
NiU_3O_{10}	yellow brown		monoclinic	7.525	6.545	16.126	$\beta = 91$				Hoekstra and Marshall (1967); Keller (1972, 1975)
CuU_3O_{10}	deep red		monoclinic	7.575	6.473	16.679	$\beta = 91$				Hoekstra and Marshall (1967); Keller (1972)

ZnU_3O_{10}	red brown		hexagonal	7.56			16.418			Hoekstra and Marshall (1967); Keller (1972)
UV_3O_{10}	black	*Fddd*	orthorhombic	12.00	6.926	16.17				Keller (1975)
$UNb_3O_{10(+x)}$		*Fddd*	orthorhombic	7.38	12.78	15.96		5.95	5.98	Keller (1975)
$UTa_3O_{10(+x)}$			hexagonal	7.416		15.770		8.41		Keller (1975)
$U(WO_4)_2$			orthorhombic	9.545	10.245	14.26				Keller (1975)
$U_2V_2O_{11}$	green	$P2_1/m$	monoclinic	9.29	13.24	7.27	$\beta \approx 100$			Keller (1975)
Y_6UO_{12}	pale yellow-green	$R\bar{3}$	hexagonal	9.934	9.364			5.91	6.00	Aitken *et al.* (1964); Bartram (1966)
La_6UO_{12}	reddish-orange	$R\bar{3}$	hexagonal	10.473		9.984			9.63	Aitken *et al.* (1964); Hinatsu *et al.* (1988)
Pr_6UO_{12}		$R\bar{3}$	hexagonal	10.301		9.800				Aitken *et al.* (1964)
Nd_6UO_{12}		$R\bar{3}$	hexagonal	10.254		9.748				Aitken *et al.* (1964)
Sm_6UO_{12}		$R\bar{3}$	hexagonal	10.148		9.630				Aitken *et al.* (1964)
Gd_6UO_{12}		$R\bar{3}$	hexagonal	10.076		9.529				Aitken *et al.* (1964)
Tb_6UO_{12}		$R\bar{3}$	hexagonal	10.013		9.465				Aitken *et al.* (1964)
Ho_6UO_{12}		$R\bar{3}$	hexagonal	9.935		9.368				Aitken *et al.* (1964)
Tm_6UO_{12}		$R\bar{3}$	hexagonal	9.826		9.248				Aitken *et al.* (1964)
Yb_6UO_{12}		$R\bar{3}$	hexagonal	9.826		9.248				Aitken *et al.* (1964)
Lu_6UO_{12}		$R\bar{3}$	hexagonal	9.797		9.204				Aitken *et al.* (1964); Bartram (1966)
$Y_5U_2O_{12}$		$R\bar{3}$	hexagonal	10.01		9.36		6.88	6.83	Bartram (1966)
$U_2V_6O_{21}$	brown	*Fddd*	orthorhombic	11.995	6.94	16.17				Keller (1975)
$UMo_{10}O_{32}$		*Cccm*	orthorhombic	16.18	14.48	19.18				Keller (1975)
$UMo_{11}O_{35}$			orthorhombic	19.66	14.41	16.11		5.01		Keller (1975)
α-$U_3Mo_{20}O_{64}$		*Cccm*	orthorhombic	8.246	28.76	19.78				Keller (1975)
γ-$U_3Mo_{20}O_{64}$		*Pbmn*	orthorhombic	4.134	14.33	9.873		5.08	5.18	Keller (1975)
$U_5W_{19}O_{67}$		*Pcmm*	orthorhombic	7.814	7.271	38.67				Keller (1975)

because of their high reactivity. In this case, reaction temperatures not higher than 600°C are recommended for M = Cu, Zn, and Cd to avoid the formation of U_3O_8. $HgUO_4$ forms at 400°C. Ag_2UO_4 has been synthesized by heating a mixture of $AgNO_3$ and UO_2 to 500°C and maintaining this temperature for a period of 15 min. Above 500°C, Ag_2UO_4 begins to decompose with precipitation of metallic silver.

For preparing $FeUO_4$ and FeU_3O_{10}, the symproportionation reaction method in a sealed tube gives a good result. $FeUO_4$ is synthesized by heating either a mixture of $FeO + UO_3$ or $2Fe_2O_3 + U_3O_8 + UO_2$ at 1050°C in evacuated sealed quartz tubes. When a mixture of $Fe_2O_3 + U_3O_8 + 3UO_3$ is heated at 880°C, FeU_3O_{10} forms (Hoekstra and Marshall, 1967). $BiUO_4$ is prepared by heating a mixture of $2Bi_2O_3 + U_3O_8 + UO_2$ at 900–1000°C (Rüdorff *et al.*, 1967). The compounds MU_2O_6 (M = Co, Ni, Cd) have been prepared by heating the mixtures of $MUO_4 + UO_2$ at 800°C (Kemmler-Sack and Rüdorff, 1967). Single crystals of CuU_3O_8 and NiU_3O_{10} were grown by the reaction of UO_3 with the molten anhydrous transition metal chlorides in evacuated sealed silica tubes at 600–650°C for several weeks (Hoekstra and Marshall, 1967).

MU_3O_{10} with M = Mn, Co, and Zn were prepared by hydrothermal reactions using a platinum-lined Morey bomb in which the transition metal oxides and γ-UO_3 were heated in 0.06 M H_2SO_4 solution for 5 days at 350°C (Hoekstra and Marshall, 1967).

MUO_4 (M = Ni, Zn, Co, Mn) was successfully synthesized in experiments where a mixture of oxides was heated for 30 min at 1000°C under high pressures of 30–40 kbar using a tetrahedral anvil. However, the triuranates of these transition metals and $FeUO_4$ did not form by this method (Hoekstra and Marshall, 1967).

(*ii*) *Crystal structures*

$MnUO_4$ and $CoUO_4$ have the infinite chains of edge-sharing oxygen octahedra in the direction normal to the *c*-axis, characteristic of the $MgUO_4$ structure; these compounds crystallize in the same space group. The space group of $CrUO_4$, $FeUO_4$, and α-$NiUO_4$ is different from that of the above two compounds, and the lengths of the uranium–oxygen bonds that are expected to belong to uranyl groups are longer (2.05–2.06 Å) than those in $MnUO_4$ and $CoUO_4$. In these three compounds, the distorted UO_6 octahedra form infinite chains along the *c*-axis and less deformed MO_6 (M = Cr, Fe, Ni) octahedra are running parallel in the direction of the *c*-axis. Similar chain structures are also observed in the crystals of $USbO_5$, $UTiO_5$, and $UMoO_5$ (Dickens *et al.*, 1993). These structures are built from parallel layers of edge-sharing UO_m and MO_n polygons, linked together by metal–oxygen–metal chains or pillars running perpendicularly to the layers. In Pb_3UO_6, the infinite chains are formed by sharing the corners of distorted UO_6 octahedra in the direction of the *c*-axis.

The crystal structure of Pb_3UO_6 is wholly different from those of Ca_3UO_6 and Sr_3UO_6 (Sterns, 1967).

In the system PbO–U_2O_5, cubic $Pb_{1.5}U_2O_{6.5}$ ($a = 11.16$ Å) accommodates PbO until the $Pb_{2.5}U_2O_{7.5}$ composition is attained, resulting in a slight distortion to a rhombohedral structure ($a = 11.23$ Å, $\alpha = 90.25°$). This homogeneity range is regarded as derived from pyrochlore-type $Pb_2U_2O_7$ by addition or subtraction of PbO (Kemmler-Sack and Rüdorff, 1966).

$CuUO_4$ comprises a third group of crystal structures among the transition metal monouranates (Siegel and Hoekstra, 1968). The compound is monoclinic with space group $P2_1/n$. The coordination geometry is distorted octahedral with short collinear uranyl bonds, each of length 1.90 Å. The uranyl groups are in the direction nearly normal to a planar and almost square array of secondary uranium–oxygen bonds of lengths 2.15 and 2.24 Å.

Rare-earth oxides form solid solutions with UO_2 in an extended composition range. At the high atom ratio of RE/U = 6 (RE = rare-earth metals), however, the compounds of the composition RE_6UO_{12} crystallize in rhombohedral systems. In RE_6UO_{12} the uranium atom is surrounded by six oxygen atoms that form a distorted octahedron. All the U–O bond distances in the octahedron are 2.34 Å (La_6UO_{12}), and no uranyl groups exist in the crystal (Hinatsu *et al.*, 1988). $Y_5U_2O_{12}$ is produced along with Y_6UO_{12} giving a very similar crystal structure with similar lattice parameters. In $Y_5U_2O_{12}$, half the uranium atoms occupy the Y position (18f) in a disordered manner (Bartram, 1966).

(d) Solid solutions with UO_2

Uranium dioxide forms solid solutions with the oxides of alkaline-earth elements, rare-earth elements, some transition elements (Mn, Zr, Nb, Cd), and actinide elements (Th, Np, Pu, Am, Cm, etc.). The solid solution with PuO_2 (MOX) is important as nuclear fuel. Description on mixed oxide fuel, MOX, is given in Chapter 7.

The solid solutions are prepared by heating intimate mixtures of metal (M) oxides and uranium oxides usually in reducing atmosphere at temperatures between 1000 and 2000°C. The oxide powders are in most cases mechanically mixed, but other techniques such as coprecipitation (Keller *et al.*, 1972; Miyake *et al.*, 1986) and evaporation from aqueous solutions (Markin *et al.*, 1970; Lindemer and Sutton, Jr., 1988) have also been adopted. In the solid solutions, the dissolved foreign metal atoms and host uranium atoms are statistically distributed on the metal sites of the fluorite-type cubic crystals of UO_2 (Rüdorff *et al.*, 1967; Keller *et al.*, 1969; Hutchings *et al.*, 1985; Martin *et al.*, 2003). The solid solution can be written as $M_yU_{1-y}O_{2+x}$, where x is defined (in this section) to take on both positive and negative values. A considerable number of publications on the magnetic properties are available since the magnetic properties of uranium and metals, M, of varying oxidation state can be studied in the same fluorite-type fcc crystal field in these solid solutions; detailed description is given

in Chapter 20. Recent progress on this subject is written in a review (Fujino and Miyake, 1991).

(*i*) *Lattice parameter change with composition*

The lattice parameter of cubic solid solution changes nearly linearly with the increase of y and x in $M_yU_{1-y}O_{2+x}$. The differential coefficient, $\partial a/\partial y$, where a is the lattice parameter in Å, can have both negative and positive values depending on the metal ion M^{n+}. Table 5.19 shows the observed $\partial a/\partial y$ and $\partial a/\partial x$ for various solid solutions (Fujino and Miyake, 1991). The underlined values in the table are those obtained from the lattice parameters of the stoichiometric solid solutions at the upper limit of the y-values, i.e. $M^{3+}_{0.5}U_{0.5}O_{2.00}$ and $M^{2+}_{0.33}U_{0.67}O_{2.00}$.

As seen in the table, the coefficient $\partial a/\partial y$ is large for the metals with large ionic radii, although correction for valence state of the metals is required for a more detailed discussion. Investigations to determine the functional relation between these quantities have been performed (Ohmichi *et al*., 1981; Fujino and Miyake, 1991). The differential coefficient of the oxygen non-stoichiometry, $\partial a/\partial x$, in Table 5.19 have in general the values $-0.3 \leq \partial a/\partial x \leq -0.24$ for $x < 0$ and $-0.13 \leq \partial a/\partial x \leq -0.11$ for $x > 0$ regardless of the M metal.

(*ii*) *The solid solution regions*

$M^{4+}_yU_{1-y}O_{2+x}$

Zr SOLID SOLUTIONS The solubility data on this system are diverse. The Zr solid solution with $y = 0.15$ was obtained by heating at 1500°C (Une and Oguma, 1983a); at 1750°C, solid solutions with y values up to 0.3 were obtained (Aronson and Clayton, 1961). The solid solution with the highest y value, 0.35, has been obtained by heating the mixture of $UO_2(NO_3)_2 \cdot 6H_2O$ and $ZrOCl_2 \cdot 8H_2O$ in H_2 at 1650°C (Hinatsu and Fujino, 1985). The Zr solid solution is regarded as metastable at lower temperatures.

Th SOLID SOLUTIONS Th solid solutions are formed continuously from $y = 0$ to 1 for $x = 0$. However, for $x > 0$, there is an upper limit in the solubility. According to Paul and Keller (1971), the single-phase solid solutions under 1 atm O_2 exist below $y = 0.45$, 0.40, and 0.36 at 1100, 1400, and 1550°C, respectively. The lower limits at $p_{O_2} = 0.2$ atm are $y = 0.383$, 0.359, 0.253, and 0.068 for 700, 1200, 1400, and 1500°C, respectively (Gilpatrick *et al*., 1964), which is in agreement with the value of $y = 0.22$ below 1400°C reported by Anderson *et al*. (1954). The maximum x value is 0.25 at temperatures between 1250 and 1550°C for $y \leq 0.5$. At lower temperatures of 600–1100°C, the upper limit of x decreases to 0.12–0.14 for y values below 0.4 (Cohen and Berman, 1966; Paul and Keller, 1971).

Table 5.19 *Lattice parameter change with composition of solid solutions* $M_yU_{1-y}O_{2+x}$ (*Fujino and Miyake,* 1991).

Element	$\partial a/\partial y$	$\partial a/\partial x$	*References*
Zr	–0.302		Cohen and Schaner (1963);
	–0.301		Hinatsu and Fujino (1985)
Th	0.163 ($y \leq 0.05$)	–0.14 ($x > 0$)	Cohen and Berman (1966)
	0.127		
	($0.1 \leq y \leq 0.5$)		
Np	–0.146		Tabuteau *et al.* (1984)
Pu	–0.0747 ($x = 0$)	–0.345 ($x < 0$)	Schmitz *et al.* (1971);
	–0.0727 ($x < 0$)		
		–0.313 ($x < 0$)	Martin and Shinn (1971);
		–0.274 ($x < 0$)	Mignanelli and Potter (1986)
Sc	–0.438		Hinatsu and Fujino (1986);
	–0.521		Keller *et al.* (1972)
Y	–0.233		Fukushima *et al.* (1981);
	–0.254		Weitzel and Keller (1975);
	–0.266		Ohmichi *et al.* (1981)
La	0.094 ($x > 0$)	–0.131 ($x > 0$)	Hinatsu and Fujino (1987);
	0.06 ($x < 0$)	–0.2 ($x < 0$)	
	0.073 ($x = 0$)		Weitzel and Keller (1975);
		–0.285 ($x < 0$)	Hill *et al.* (1963)
Ce	–0.067		Mignanelli and Potter (1983);
	–0.06		Lorenzelli and Touzelin (1980);
	–0.057 ($x = 0$)		Hinatsu and Fujino (1988a);
		–0.321 ($x < 0$)	Markin *et al.* (1970);
		–0.288	Norris and Kay (1983)
		($y = 0.282$,	
		$-0.015 \leq x < 0$)	
Pr	–0.007	–0.127 ($x > 0$)	Yamashita *et al.* (1985);
		–0.397 ($x < 0$)	
	–0.015		Hinatsu and Fujino (1988c)
Nd	–0.047	–0.112 ($x > 0$)	Hinatsu and Fujino (1988b);
	–0.057		Fukushima *et al.* (1983);
	–0.058		Weitzel and Keller (1975);
	–0.075		Ohmichi *et al.* (1981);
		–0.30 ($x < 0$)	Wadier (1973)
Sm	–0.118		Fukushima *et al.* (1983);
	–0.121		Rüdorff *et al.* (1967)
Eu	–0.138		Fukushima *et al.* (1983);
	–0.144		Ohmichi *et al.* (1981);
	–0.151	–0.30 ($x < 0$)	Fujino *et al.* (1990)
Gd	–0.164		Fukushima *et al.* (1982);
	–0.171		Rüdorff *et al.* (1967);
	–0.173	–0.24 ($x < 0$)	Ohmichi *et al.* (1981)
Ho	–0.267		Weitzel and Keller (1975)
Yb	–0.315		Rüdorff *et al.* (1967)
Lu	–0.356		Weitzel and Keller (1975)
Mg	–0.568	–0.117 ($x > 0$)	Fujino and Naito (1970);
	–0.546		Kemmler-Sack and Rüdorff (1967);
	–0.559		Keller (1964)

Table 5.19 (*Contd.*)

Element	$\partial a/\partial y$	$\partial a/\partial x$	*References*
Ca	–0.310	–0.102 ($x > 0$) –0.190 ($x < 0$)	Yamashita and Fujino (1985);
	–0.213	–0.10 ($x > 0$)	Hinatsu and Fujino (1988d);
	–0.289		Loopstra and Rietveld (1969)
Sr	–0.098	–0.109 ($x > 0$) –0.244 ($x < 0$)	Fujino *et al.* (1988);
	–0.055		Hoekstra and Katz (1952)
Mn	–0.499		Kemmler-Sack and Rüdorff (1967)
Cd	–0.340		Keller (1962b); Kemmler-Sack and Rüdorff (1967)
Bi	0.149		Rüdorff *et al.* (1967)

$M_y^{4+\sim3+}U_{1-y}O_{2+x}$

Ce SOLID SOLUTIONS Ce solid solutions are formed continuously from $y = 0$ to 1 for $x = 0$. For $x < 0$, the region of the single-phase solid solution is restricted to $y \leq 0.35$ (Markin *et al.*, 1970) or $y \leq 0.2$ (Lorenzelli and Touzelin, 1980). Above this value up to $y = 0.7$, the products are two phases $(Ce,U)O_{2.00}$ and $(Ce,U)O_{2-x}$ at room temperature. Further reduction results in formation of single-phase solid solutions. The x values for the single-phase solid solutions are $x < -0.04$, –0.12, –0.19, and –0.24 for $y = 0.1$, 0.3, 0.5, and 0.7, respectively (Lorenzelli and Touzelin, 1980).

In the hyperstoichiometric range of $0 \leq x \leq 0.18$, the solid solutions with $y < 0.5$ are a single phase at room temperature. Air-oxidized hyperstoichiometric solid solutions crystallize in a fluorite-type single phase in the region of high Ce concentrations (Hoch and Furman, 1966). Single-phase regions exist in $y = 0.56$–1.0 (1100°C), 0.43–1.0 (1250 °C), and 0.26–1.0 (1550°C) (Paul, 1970). Single phases with $y = 0.6$–1.0 at 1100°C have also been reported (Tagawa *et al.*, 1981a).

$M_y^{n+}U_{1-y}O_{2+x}$ ($n = 3$ and 2)

SOLID SOLUTIONS IN REDUCING ATMOSPHERE The solid solutions obtained by heating in reducing atmospheres are generally hypostoichiometric. The x values are highly negative when strong reductants such as H_2 or CO are used. The single-phase regions of fcc solid solutions with M metals (M = rare-earth elements, alkaline-earth metals, and Cd) are shown in Table 5.20. In reducing atmosphere, the single-phase solid solution forms essentially in a range starting from $y = 0$. For M^{2+} metals, the maximum y values are around 1/3. If the monoxides of Mg and Ba are heated with UO_2 in a vacuum, the solubility is very low even at high temperatures due to shortage of oxygen (cf. Table 5.20).

Table 5.20 *Single phase regions of fcc solid solutions* $M_yU_{1-y}O_{2+x}$ *with M elements (rare-earth elements, alkaline-earth elements and Cd) prepared in reducing atmospheres. Concentrations of the M elements are shown in* mol%.

	Temperature (°C)					
Element	1100	1250	1400	1550	1700	*References*
Sc	0–1.6	0–1.8	0–2.1	0–2.9 (H_2)		Keller *et al.* (1972)
Y					0–50 (H_2)	Bartram *et al.* (1964);
					0–65 (2000°C, vacuum)	Ferguson and Fogg (1957)
La		0–82				Diehl and Keller (1971);
				0–54 (1750°C, vacuum)		Wilson *et al.* (1961);
				0–75 (1750°C, H_2 or vac.)		Hill *et al.* (1963)
Pr		0–70 (1350°C, vacuum)				Yamashita *et al.* (1985)
Eu		0–42 (Ar)				Berndt *et al.* (1976);
				0–53 (1600°C, vacuum)		Grossman *et al.* (1967);
				0–50∼60 (vacuum)		Fujino *et al.* (1990)
Gd					0–80 (H_2)	Beals and Handwerk (1965)
					0–50 (Ar)	
Mg	0–33 ($MgUO_4$+MgU_3O_{10}+UO_2, 1100–1300°C, He)					Fujino and Naito (1970);
				0–5 (MgO+UO_2, 2350°C, vac.)		Anderson and Johnson (1953)
Ca	0–33 ($CaUO_4$+U_3O_8+UO_2, 1100–1300°C, vacuum)				0–40 (2000°C)	Brisi *et al.* (1972);
						Voronov and Sofronova (1972);
		3–33 (1200–1400°C, He)		0–20(CaO+UO_2, 1650°C, vac.)		Yamashita and Fujino (1985);
						Alberman *et al.* (1951)
Sr	0–30 ($SrUO_4$+U_3O_8+UO_2, 1200–1400°C, ∼1 Pa O_2)					Fujino *et al.* (1988);
	33 (SrU_2O_7, vacuum)					Hoekstra and Siegel (1956);
						Ippolitova *et al.* (1961b);
		0–20 (1300°C)				Brisi *et al.* (1972)
Ba	33 (BaU_2O_7, 1200°C, vacuum)					Hoekstra and Siegel (1956);
	33 (BaU_2O_7, 600°C, NH_3)					Brochu and Lucas (1967);
				0–3 (BaO+UO_2, vac.)		Kleykamp (1985)
Cd	0–33 ($CdUO_4$+UO_2, vacuum sealed tube)					Kemmler-Sack and Rüdorff (1967)

SOLID SOLUTIONS IN OXIDIZING ATMOSPHERE The single-phase regions of fcc solid solutions prepared in oxidizing atmospheres are shown in Table 5.21. UO_2 is oxidized to U_3O_8 when heated in oxidizing atmospheres unless mixed with the M elements. Hence, the lower limit of the fcc single phase is not $y = 0$ but at higher values. The x value changes with y value in a rather simple way for rare-earth solid solutions: For Nd solid solutions heated under $p_{O_2} = 1$ atm at 1100°C for example, the mean uranium valence remains constant (+5) when the y value is in a region between ~0.3 and 0.5, i.e. x changes as $x=1/2-y$. The uranium valence then increases linearly from +5 to +6 when y increases from 0.5 to 0.67, during which $x = 0$. For the solid solutions in a higher y range, 0.67–0.75, the uranium valence is U(VI). Here, the x value decreases linearly from 0 to –0.125 ($x=1-3y/2$) with increasing y value in order to satisfy the charge neutrality condition (Keller and Boroujerdi, 1972).

(*iii*) *Oxygen potentials*

$M_y^{4+}U_{1-y}O_{2+x}$

Zr SOLID SOLUTIONS The oxygen potential of $Zr_yU_{1-y}O_{2+x}$ solid solution is lower than that of UO_{2+x}. At 1250 K, the $\Delta\bar{G}(O_2)$ value for Zr solid solution with $y = 0.3$ is –270 kJ mol^{-1} at $x = 0.05$ (Aronson and Clayton, 1961), while that for UO_{2+x} at $x = 0.05$ is ca. –210 kJ mol^{-1}. The low $\Delta\bar{H}(O_2)$ of $Zr_yU_{1-y}O_{2+x}$ has been suggested to explain the low $\Delta\bar{G}(O_2)$ of this solid solution. The $\Delta\bar{H}(O_2)$ values vary between –480 and –355 kJ mol^{-1} for $Zr_yU_{1-y}O_{2+x}$, which are significantly lower than those between –355 and –270 kJ mol^{-1} for $Th_yU_{1-y}O_{2+x}$ (Aronson and Clayton, 1960, 1961; Une and Oguma, 1983a).

Th SOLID SOLUTIONS Dissolution of Th causes an increase in $\Delta\bar{G}(O_2)$ with increasing value of y. The difference in $\Delta\bar{G}(O_2)$ between Th solid solution and UO_{2+x} is small if the concentration of Th is low (viz., $y = 0.1$). However, at high Th concentration with $y = 0.71$ ($x = 0.05$), $\Delta\bar{G}(O_2)$ of the solid solution at 1250 K is as high as –150 kJ mol^{-1} (Aronson and Clayton, 1960). This value is 60 kJ mol^{-1} higher than $\Delta\bar{G}(O_2)$ of $UO_{2.05}$ at the same temperature. There have been other thermodynamic studies on this solid solution (Tanaka *et al.*, 1972; Ugajin, 1982; Ugajin *et al.*, 1983; Matsui and Naito, 1985a).

$M_y^{4+\sim3+}U_{1-y}O_{2+x}$

Ce SOLID SOLUTIONS Because two oxidation states, Ce^{3+} and Ce^{4+}, are possible for Ce in oxides, the oxygen potential of Ce solid solution changes over a wide range of x-values from negative to positive values, giving rise to a rapid ('vertical') change of $\Delta\bar{G}(O_2)$ at $x = 0$. The shape of the $\Delta\bar{G}(O_2)$ curve is very similar to that of $Pu_yU_{1-y}O_{2+x}$, but the $\Delta\bar{G}(O_2)$ values of $Ce_yU_{1-y}O_{2+x}$ are markedly higher. Namely, $\Delta\bar{G}(O_2)$ for $Ce_{0.25}U_{0.75}O_{1.95}$ is as high as –460 kJ mol^{-1} at 1200°C, compared to the value of –570 kJ mol^{-1} for $Pu_{0.25}U_{0.75}O_{1.95}$.

Table 5.21 *Single-phase regions of fcc solid solutions* $M_yU_{1-y}O_{2+x}$ *with M elements (rare-earth elements and Mg) prepared in oxidizing atmospheres. Atmosphere is* O_2 (1 atm) *unless otherwise described. Concentrations of the M elements are shown in* mol%.

	Temperature (°C)					
Element	1100	1200	1300	1400	1500	*References*
Sc	49.5–63.8	48.5–64.0 (1250°C)		45.5–64.9	42.1–65.5 (1510°C) ~0–65.7 (1550°C)	Keller *et al.* (1972)
Y	33–60 (1000°C, air)	30–65 (air)				Bartram *et al.* (1964); Hund *et al.* (1965)
La	31.5–51.5 68.5 79.5–82 30–45, 70–90 (1000°C, air)	28.5–55 63.5–69.5 79–82	26.5–75 77–82	25–82	24–82 (1550°C) 30–80 (1650°C)	Diehl and Keller (1971); Hill *et al.* (1963); Tagawa *et al.* (1983)
Pr	38.6–71.9	39.9–71.2 30–60 (1250°C)	41.4–70.2 32–71 (1350°C, air)	43.2–69.0	45.3–67.1	de Alleluia *et al.* (1981); Jocher (1978); Yamashita *et al.* (1985)
Nd	35.0–74.5	33–81 (1250°C)		25–81	13–81 (1550°C)	Boroujerdi (1971); Keller and Boroujerdi (1972)
Sm	50–60 (1000°C, air)					Tagawa *et al.* (1981b)
Eu	39–72 38–64 (air)	36–72 (1250°C)		30–72	25–72	Tanamas (1974); Haug and Weigel (1963)
Gd					30–60 (1700°C, air)	Beals and Handwerk (1965)
Dy	48.4–74.9	44.1–72.8 (1250°C)		35.0–72.8	14.2–72.2 (1550°C)	de Alleluia *et al.* (1981)
Ho	47.0–64.0	43.0–64.0 (1250°C)		33.0–64.0	19.0–64.0 (1550°C)	Keller *et al.* (1969)
Er	49.0–62.5	45.0–62.5 (1250°C)		41.0–62.5	21.5–62.5 (1550°C)	Keller *et al.* (1969)
Tm	48.5–64.0	45.0–64.0 (1250°C)		34.0–64.0	15.0–64.0 (1550°C)	Keller *et al.* (1969)
Yb	48.5–64.5	45.0–64.5 (1250°C)		38.5–64.5	16.5–64.5 (1550°C)	Keller *et al.* (1969)
Lu	48.0–65.5	45.0–65.5 (1250°C)		43.0–65.5	41.0–65.5 (1550°C)	Keller *et al.* (1969)
Mg			36–39 (1300°C, air)	12–39 (1500°C, air)	~0–39 (1600°C, air) max. 37 (1600–1700°C, air)	Sugisaki *et al.* (1973); Budnikov *et al.* (1958)

This difference has been attributed to the higher $\Delta\bar{G}(O_2)$ value of CeO_{2-x} (Panlener *et al.*, 1975) compared with that of PuO_{2-x} (Woodley, 1981). The $\Delta\bar{G}(O_2)$ measurements of the Ce solid solutions have been carried out by a number of researchers (Hoch and Furman, 1966; Markin and Crough, 1970; Ducroux and Baptiste, 1981; Norris and Kay, 1983; Nagarajan *et al.*, 1985).

Pr AND Am SOLID SOLUTIONS The Pr solid solutions have lower values of $\Delta\bar{G}(O_2)$ than the solid solutions with solely M^{3+} rare-earth ions, because of the two possible oxidation states, Pr^{3+} and Pr^{4+} (Jocher, 1978; Fujino and Miyake, 1991). The situation is the same for Am solid solutions, although their $\Delta\bar{G}(O_2)$ values are markedly higher than those of Pu and Ce solid solutions (Bartscher and Sari, 1983).

$M_y^{3+}U_{1-y}O_{2+x}$

A large number of oxygen potential measurements for the M^{3+} solid solutions have been carried out. These comprise solid solutions of Y (Aitken and Joseph, 1966; Hagemark and Broli, 1967; Nakajima *et al.*, 2002), La (Hagemark and Broli, 1967; Stadlbauer *et al.*, 1974; Matsui and Naito, 1986), Pr (Jocher, 1978; Fujino and Miyake, 1991), Nd (Wadier, 1973; Une and Oguma, 1983c), Eu (Tanamas, 1974; Lindemer and Brynestad, 1986; Fujino *et al.*, 1990, 1999), and Gd (Une and Oguma, 1982, 1983b; Lindemer and Sutton, Jr. 1988).

$\Delta\bar{G}(O_2)$ for $M_y^{3+}U_{1-y}O_{2+x}$ can be defined from $x = -y/2$ to positive x values; the measured oxygen potential increases with increasing x value, passing through an inflection point at $x = 0$, where $\Delta\bar{G}(O_2)$ increases very rapidly. The dissolution of M^{3+} metals enhances $\Delta\bar{G}(O_2)$ more than do the M^{4+} metals. The $\Delta\bar{G}(O_2)$ value increases with increasing y, but the $\Delta\bar{G}(O_2)$ curve gradually levels off at high M^{3+} concentrations. In a series of rare-earth solid solutions, the La solid solution shows the highest $\Delta\bar{G}(O_2)$ values, which is assumed to be associated with the fact that La^{3+} has the largest ionic radius of these M^{3+} ions. With increasing atomic number of the lanthanides, $\Delta\bar{G}(O_2)$ is lowered, although the $\Delta\bar{G}(O_2)$ difference between the Nd and Gd solid solutions is small. Fig. 5.26 shows the oxygen potential of $Gd_yU_{1-y}O_{2+x}$ as a function of O/(Gd+U) ratio ($=2 + x$).

The Eu solid solutions show a much higher value of $\Delta\bar{G}(O_2)$ than the other M^{3+} solid solutions (Lindemer and Brynestad, 1986). This is possibly due to the coexistence of Eu^{2+} and Eu^{3+} in the solid solutions (Fujino *et al.*, 1990). It is noteworthy that the inflection point of $\Delta\bar{G}(O_2)$ for Eu solid solutions is shifted to a range of $x < 0$ values. This is also observed for $M_y^{2+}U_{1-y}O_{2+x}$, supporting the presence of Eu^{2+} in the Eu solid solutions.

$M_y^{2+}U_{1-y}O_{2+x}$

The oxygen potential of $Mg_yU_{1-y}O_{2+x}$ (Fujino and Naito, 1970; Fujino *et al.*, 1978a; Tateno *et al.*, 1979) is significantly higher than those of $M_y^{3+}U_{1-y}O_{2+x}$. Moreover, the x values at which the 'vertical' change of $\Delta\bar{G}(O_2)$ takes place,

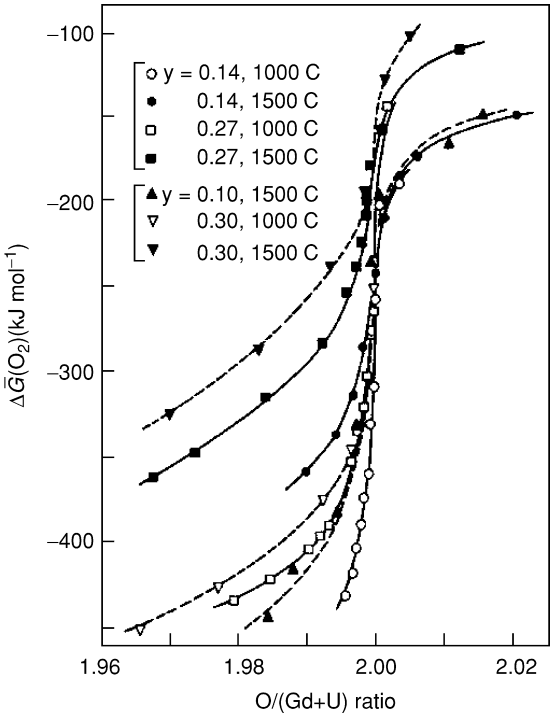

Fig. 5.26 *Oxygen potential of* $Gd_yU_{1-y}O_{2+x}$ *as a function of O/(Gd+U) ratio* (*Fujino and Miyake,* 1991). *Solid lines: Une and Oguma* (1983*b*)*; Broken lines: Lindemer and Sutton, Jr.* (1988). *Reproduced by the permission of Elsevier*.

which are also the inflection points, are negative in contrast to the M^{4+} and M^{3+} solid solutions, where the value of x at the inflection is zero. This negative shift for $Mg_yU_{1-y}O_{2+x}$ becomes more pronounced at higher values of y, viz., $x = -0.07$ at $y = 0.3$ (1200–1500°C) (Sugisaki and Sueyoshi, 1978).

The high $\Delta\bar{G}(O_2)$ values are supposed to be rationalized by a configurational entropy change. Dissolution of M^{2+} metals in UO_2 results in formation of a larger number of U^{5+} ions in the solid solution crystals, which increases the number of ways, W, of arranging the cations on the cation sites. The entropy, $\Delta\bar{S}(O_2)$, described by the relation $\Delta\bar{S}(O_2) = 2R\,\partial \ln W/\partial(xN)$, where N is the Avogadro's number (Aronson and Clayton, 1960; Hagemark and Broli, 1967; Fujino and Miyake, 1991), shows therefore a significant decrease. For the Mg solid solutions Fujino *et al.* (1992, 1995, 1997b) claim that the $\Delta\bar{G}(O_2)$ shift is explained if the charge complexes of the form, ($M^{2+}2U^{5+}$), in which the corresponding cations have their normal sites, are formed together with ($M^{2+}U^{5+}$) complexes. In the oxygen potential curves for $(Mg,Gd,U)O_{2+x}$ (Fujino *et al.*, 2001a) and $(Mg,Ce,U)O_{2+x}$ (Fujino *et al.*, 2001b), the shift to negative x values is even larger than in the Mg solid solution.

When the oxygen partial pressure is very low, high concentrations of Mg cannot dissolve in UO_2. The solubility of Mg is in a range $0.1 < y < 0.15$ for $p_{O_2} = 10^{-15}$–10^{-19} atm at 1200°C (Fujino *et al.*, 1997a).

5.7.3 Uranium borides, carbides, silicides, and related compounds

Non-oxide p-block compounds of uranium represent a large family that share certain similarities with oxides in that non-stoichiometric compounds exist; these are especially well noted for the heavy p-block elements of a semi-metallic nature (e.g. Sb and Te). Oxidation state assignment for uranium in some of these compounds can be very tedious, owing to the presence of homoatomic bonding between main group elements where the E ··· E (E = main group element) contacts between main group elements is intermediate in length between a full single bond and a van der Waals contact. This phenomenon is particularly common in antimonides and tellurides. Full descriptions of all known binaries and especially of ternary and quaternary phases are not possible in the present context. Further historical details can be found in Waber *et al.* (1964), Eding and Carr (1961), Freeman and Darby (1974), and in a series of IAEA bibliographies (Maximov, 1963, 1965, 1967).

(a) Uranium–boron system

The only known binary uranium borides are UB_2, UB_4, and UB_{12}. The crystal structure data for these compounds are given in Table 5.22. The former compounds have been prepared by direct reaction of the elements at high temperatures (Wedekind and Jochem, 1913). Mixtures of UB_{12} and UB_4 have also been deposited by fused-salt electrolysis (Andrieux, 1948; Andrieux and Blum, 1949). It has recently been demonstrated that UB_4 can be prepared by the solid-state metathesis reaction of UCl_4 with MgB_2 at 850°C (Lupinetti *et al.*, 2002).

$$UCl_4 + 2MgB_2 \rightarrow UB_4 + 2MgCl_2$$

A view of the structure of UB_4 is shown in Fig. 5.27.

The phase diagram of the U–B system is shown in Fig. 5.28 (Howlett, 1959, 1960; Elliott, 1965; Chiotti *et al.*, 1981).

In addition, there is mass spectroscopic evidence that supports the existence of UB and UB_2 in the gas phase (Gingerich, 1970). The dissociation energies D_0^o were reported as (318 ± 33) kJ mol^{-1} for UB and (949 ± 42) kJ mol^{-1} for UB_2.

Uranium borides are remarkably inert, and borides have been proposed as a potential form for storing transuranium waste generated from the nuclear fuel cycle (Lupinetti *et al.*, 2002). There are some differences in reactivity of the uranium borides with respect to one another. UB_4 is generally more reactive

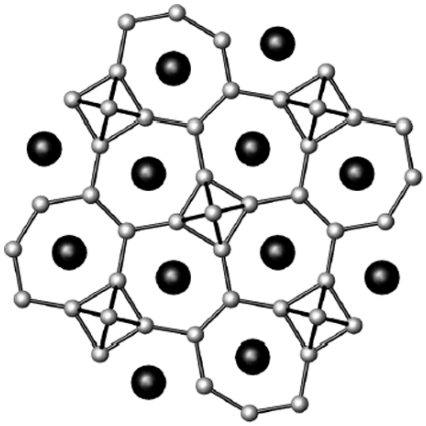

Fig. 5.27 *A view down the c-axis of the structure of UB_4. U–B bonds have been omitted for clarity.*

than UB_{12}. For example, boiling HF, HCl, and H_2SO_4 attack UB_{12} very slowly, but react more rapidly with UB_4, allowing for the separation of the two compounds. Both UB_4 and UB_{12} can be dissolved in HNO_3–H_2O_2 mixtures.

Ternary uranium borides have been extensively investigated for their rich variation in bonding and their complex physical properties. Compounds in this class include $U_5Mo_{10}B_{24}$, which contains three different kinds of B polyanions: two-dimensional puckered sheets formed from six- and eight-membered rings, planar ribbons composed of six-membered B rings, and chains of condensed eight-membered rings (Konrad and Jeitschko, 1996). UNi_4B has been extensively investigated and is a geometrically frustrated antiferromagnetic compound that partially orders below $T_N = 20$ K (Mentink *et al.*, 1998).

(b) Uranium–carbon system

The uranium–carbon system has been studied by a number of teams including Rundle *et al.* (1948), Esch and Schneider (1948), Litz *et al.* (1948), Wilhelm *et al.* (1949), and Mallett *et al.* (1952). The uranium–carbon system bear some similarities with that of uranium with other first-row p-block elements in that in addition to discrete, stoichiometric compounds, there are three known phases, UC, UC_2, and U_2C_3 that can be of variable composition. The complex phase diagram of the uranium–carbon system is shown in Fig. 5.29.

Among other things this diagram demonstrates that UC and UC_2 are completely miscible with one another at elevated temperatures and under these conditions the entire range UC–UC_2 is homogeneous. At lower temperatures, miscibility is much more limited and the exact extent of variability in composition for each of the carbides is still to be determined.

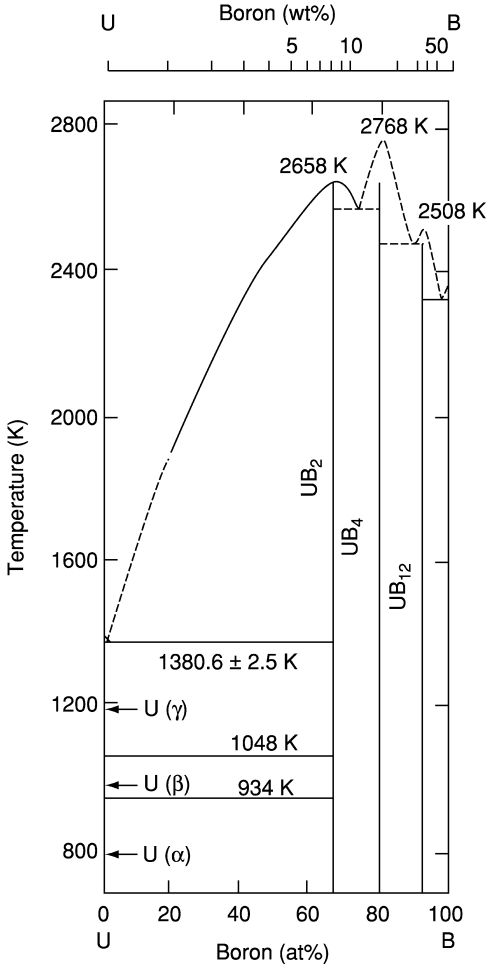

Fig. 5.28 *Phase diagram of the uranium–boron system* (*Chiotti* et al., 1981).

Litz *et al.* (1948) were the first to study the preparation of UC and UC_2. U_2C_3 is an unusual compound in that it has not been prepared by the direct reaction of the elements at high temperatures; this reaction invariably yields UC and UC_2 (Mallet *et al.*, 1952). However, U_2C_3 is obtained when a mixture of UC and UC_2 is heated in the range 1250–1800°C *in vacuo*. It is essential that the fused mixture be given a certain amount of stressing and cold working to initiate the nucleation necessary for the formation of the U_2C_3 phase; once formed it is stable at room temperature. Table 5.22 lists some of the crystallographic data for the uranium carbides. An illustration of the structure of UC_2 is shown in Fig. 5.30.

Table 5.22 *Crystallographic data for the stoichiometric binary uranium compounds with boron and group* IV *elements* (*Chiotti* et al., 1981).[a]

				Lattice parameters				*Density* (g cm^{-3})	
Formula	*Color*	*Space group*	*Symmetry*	*a* (Å)	*b* (Å)	*c* (Å)	*Z*	*Meas.*	*X-ray*
UB_2	metallic	*P*6/*mmm*	hexagonal	3.1293[b]		3.9893[b]	1	12.8	12.82
				3.1314[c]		3.9857[c]			
UB_4	metallic	*P*4/*mbm*	tetragonal	7.075		3.979	4	9.32	9.38
UB_{12}	metallic	*Fm*3*m*	fcc	4.4773			4	5.65	5.825
$UC(\delta_1)$	gray-black	*Fm*3*m*	fcc	4.961			4		13.63
U_2C_3	black	$I\bar{4}3d$	cubic	8.088			8		12.88
$UC_2(\zeta)$	light gray	*I*4/*mmm*	tetragonal	3.5266		6.0023	2		11.68
$UC_2(\delta_2)$	light gray		cubic	5.488			4		
$USi_3(1)$		*Pm*3*m*	cubic	4.060			1		8.15
$USi_{1.88}(\eta)$[d]	silvery	$I4_1/amd$	tetr. bc	3.948		13.67	4	7.27	8.98
				3.930		14.06			
$U_3Si_5(\tau)$[e]	silvery	*P*6/*mmm*	hexagonal	3.843		4.069	1	7.27	9.25
$USi(\zeta)$[f]	black	*Pbnm*	orthorhombic	5.66	7.67	3.91	4	9.30	10.40
$U_3Si_2(\varepsilon)$		*P*4/*mbm*	tetragonal	7.3299		3.9004	2	11.31	12.20
$U_3Si(\delta)$		*I*4/*mcm*	tetr. bc	6.029		9.696	4		15.58
UGe_3	metallic	*Pm*3*m*	cubic	4.2062			1		10.37
UGe_2[g]	metallic	*Cmmm*	orthorhombic	4.036	14.928	4.116	4		10.26
UGe[f]	metallic	*Pbcm*	orthorhombic	9.827	8.932	5.841	12		12.07
U_5Ge_4[k]	metallic	$P6_3/mcm$	hexagonal	8.744		5.863	2		12.67
U_3Ge_3	metallic								
U_5Ge_3[l,m]		$P6_3/mcm$	hexagonal	8.58		5.79	2		12.66
U_7Ge[h,m]									

Table 5.22 (*Contd.*)

Formula	*Color*	*Space group*	*Symmetry*	*Lattice parameters*			*Z*	*Density* (g cm^{-3})	
				a (Å)	*b* (Å)	*c* (Å)		*Meas.*	*X-ray*
USn_3	metallic	*Pm*3*m*	cubic	4.626			1		10.0
U_3Sn_5	metallic								
U_5Sn_4									
UPb_3[g]	metallic	*Fm*3*m*	cubic	4.7915					12.93
UPb[g,i]	metallic		tetr. bc	11.04		10.60			
			tetr. fc	4.579		5.259			13.27

[a] Unless otherwise mentioned, the data are taken from Chiotti *et al.* (1981).
[b] Boron-rich phase.
[c] Boron-poor phase.
[d] $USi_{1.88}$ is also referred to as α-USi_2.
[e] U_3Si_5 is also referred to as β-USi_2.
[f] According to Laugier *et al.* (1971), USi is tetragonal. The orthorhombic structure is due to oxygen.
[g] Boulet *et al.*, (1997a).
[h] Existence of these compounds deduced from vapor pressure data taken by Alcock and Grieveson (1962, 1963).
[i] The different lattice constants are due to different interpretations of powder patterns.
[j] Boulet *et al.* (1997b).
[k] Boulet *et al.* (1997c).
[l] Marakov and Bykov (1959). May be the same phase as U_5Ge_4.
[m] The existence of U_5Ge_3 and U_7Ge has been called into question (Boulet *et al.*, 1997c), and they are likely mixture of U_5Ge_4 and U metal dissolving 3% of germanium.

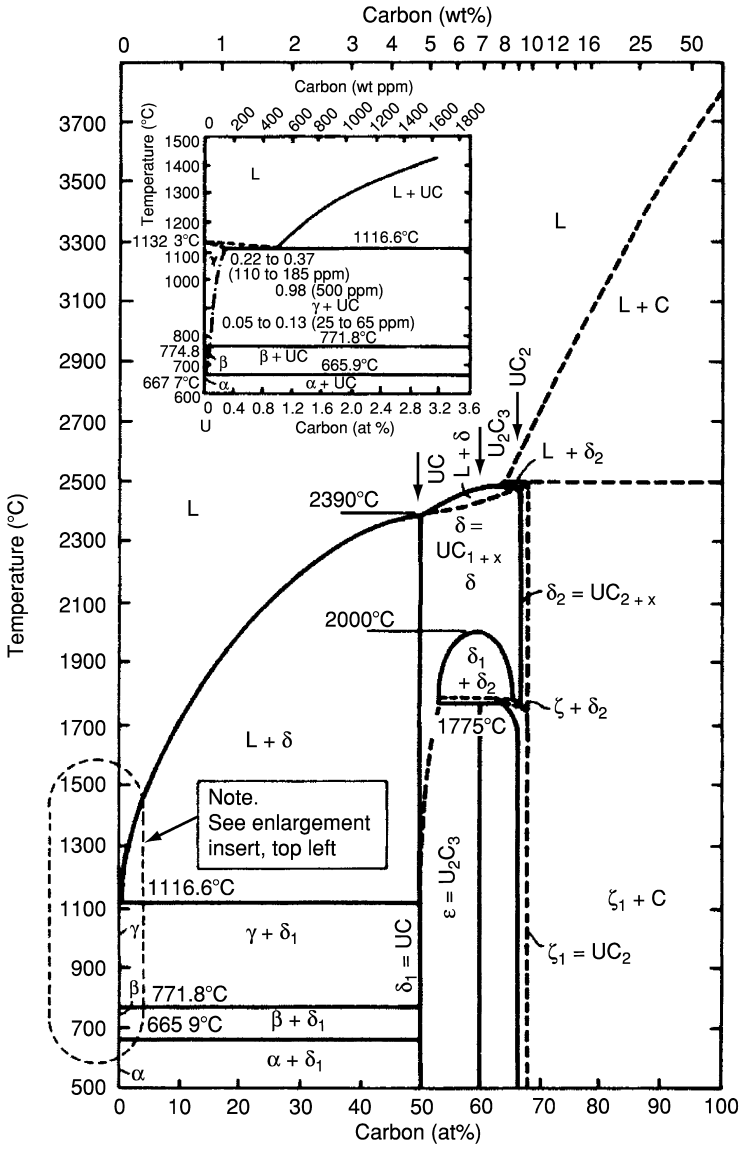

Fig. 5.29 *Phase diagram of the uranium–carbon system* (*Wilkinson,* 1962).

The uranium carbides can undergo a number of hydrolysis reactions; finely divided UC_2 is pyrophoric. The carbides react with water to yield a variety of products. Lebeau and Damien (1913) found that upon hydrolysis of UC_2, in addition to hydrogen, methane, and ethane, significant amounts of liquid and

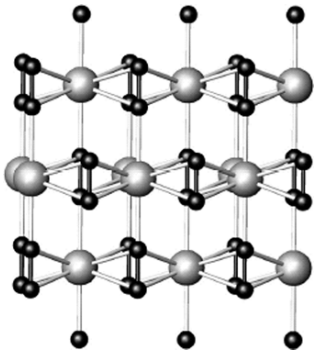

Fig. 5.30 *A view down the a-axis of the structure of UC_2.*

solid hydrocarbons are produced. Litz (1948) made an exhaustive study of the hydrolysis of UC and UC_2, the value of which is limited by the fact that he worked only at temperatures above 83°C and did not measure the quantity of gas evolved or analyze the solid residue for carbon compounds. Bradley and Ferris (1962, 1964) made a very careful study of the hydrolysis of arc-melted UC (1962) and of UC_2, U–UC mixtures, and UC–UC_2 mixtures (1964) at temperatures between 25 and 99°C. In the case of UC, the hydrolysis yielded a gelatinous, hydrous uranium(IV) oxide and a gaseous mixture (93 mL (STP) per gram UC), which consisted of 86 vol% methane, 11 vol% hydrogen, 1.8 vol% ethane, and small quantities of saturated C_3–C_6 hydrocarbons. The gaseous products contained all the carbon originally present in the carbide.

The total amount of carbon originally present in the carbide was also recovered in the hydrocarbon hydrolysis products of UC_2, U–UC, and UC–UC_2 mixtures. In the case of arc-melted $UC_{(1.85 \pm 0.03)}$, 36 different hydrocarbons were identified. The reaction product contained 15 vol% methane, 28 vol% ethane, 7 vol% C_3–C_6 alkanes, 8 vol% alkenes, 0.6 vol% alkynes, 1 vol% unidentified un-saturates, and 40 vol% hydrogen. Approximately 25% of the total carbon was found as a water-insoluble wax. In the hydrolysis of UC–UC_2 mixtures, a linear decrease of the volume percentage of CH_4 and linear increases of the percentages of hydrogen and the C_2–C_8 hydrocarbons were observed as the combined C/U atom ratio increased from 1.0 to 1.85. For UC–UC_2 mixtures, less methane than expected was evolved. This indicates that some polymerization of C units had occurred.

Bunnell *et al.* (1975) studied the hydrolysis of bare and defect-coated UC_2 fuel bead cores by water vapor at $p_{H_2O} = 24$–76 mmHg. They studied the reaction products by optical and scanning electron microscopies, identified hydrogen, methane, and ethane as the major reaction products, and measured the activation energy to be (25.4 ± 2.9) kJ mol^{-1}.

In air, UC_2 decomposes completely in a week, presumably as a result of hydrolysis. According to Mallet *et al.* (1952), U_2C_3 does not react appreciably with water even at 75°C. UC_2 appears to be stable in air at 300°C, but is completely converted to oxide in air within 4 h at 400–500°C. UC_2 reacts at 1100°C with nitrogen to form uranium nitride. Since the reactions of the carbides are greatly affected by the particle size of the solid and the previous thermal history of the sample, no far-reaching conclusions should be drawn regarding the relative reactivity of the uranium carbides.

The uranium carbides have found an important application as nuclear fuels in fast reactors. This type of application and related properties has been discussed in a number of uranium carbide conferences (see Proceedings, 1960a,b, 1961, 1963). One of the problems with reprocessing the spent fuels from these reactors is that oxalic acid is also produced in the dissolution of mixed uranium and plutonium carbides in HNO_3. Complexation of UO_2^{2+} by oxalate can account for the problems of incomplete uranium and plutonium extraction in the PUREX process for fuel reprocessing (Choppin *et al.*, 1983).

Ternary carbides, such as $U_2Al_3C_4$, can be prepared by melting the elements in a carbon crucible in a high-frequency radiofrequency (RF) furnace (Gesing and Jeitschko, 1995). The structure of $U_2Al_3C_4$ is closely related to that of Al_4C_3. Much like binary uranium carbides, $U_2Al_3C_4$ undergoes hydrolysis reactions in dilute HCl resulting in the formation of 74 (wt.)% methane, 8% ethane and ethylene, and 18% saturated and unsaturated higher hydrocarbons.

Laser-ablated U atoms react with CO in a noble gas matrix to form CUO (Li *et al.*, 2002). This molecule exhibits different stretching frequencies in a solid Ar matrix from those in a solid Ne matrix. Further experiments suggest that Ar atoms interact directly with CUO molecules to form an actinide–noble gas compound. The combination of experimental and theoretical methods suggests that multiple Ar atoms interact with a single CUO molecule.

(c) Uranium–silicon system

The uranium–silicon system is remarkably rich and a large number of uranium silicides including U_3Si, U_3Si_2, USi, U_3Si_5, $USi_{1.88}$, and USi_3 have been prepared and crystallographically characterized (Zachariasen, 1949a; Kaufman *et al.*, 1957). The phase diagram, shown in Fig. 5.31, is based on earlier work reported in the compilations by Hansen and Anderko (1958), Elliott (1965), and Shunk (1969), and in the paper by Vaugoyeau *et al.* (1971), which has been assessed and discussed by Chiotti *et al.* (1981).

Further details on the composition ranges of the two phases U_3Si_5 and $USi_{1.88}$ are given by Vaugoyeau *et al.* (1971). U_3Si_5 melts congruently at 2043 K (1770°C) and has a composition range $USi_{1.71}$ to $USi_{1.78}$ (63–64 at % Si) in the temperature range 1000–1300°C. The phase $USi_{1.88}$, in the same temperature range, has a composition span $USi_{1.79}$ to $USi_{1.84}$ (64–64.8 at % Si).

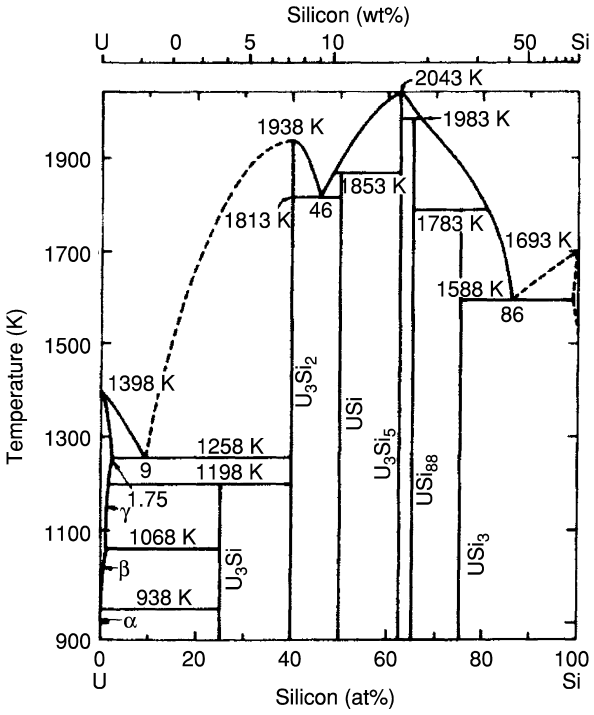

Fig. 5.31 *Phase diagram of the U–Si system* (*Chiotti* et al., 1981).

The two-phase region between the two compounds is very narrow. The compound USi was shown to decompose peritectically at 1580°C and has a narrow homogeneity range. The eutectic between U_3Si_2 and USi occurs at 1540°C and 46 at % Si.

As can be inferred from this information and from the data in Table 5.22, the U–Si phase diagram is very complicated. However, the uranium silicides are of technical importance. For instance, compounds such as $U(Al,Si)_3$ are formed in the layer between the uranium metal and the aluminum can in natural uranium fuel elements (Cunningham and Adams, 1957). Because of the chemical inertness of some of the uranium silicides, these compounds promise more applications. Crystal structures of the U–Si compounds are also summarized in Table 5.22.

Ternary uranium silicides are well established from compounds such as UCu_2Si_2 (Fisk *et al.*, 2003), $U_2Nb_3Si_4$ (Le Bihan *et al.*, 2000), and URu_2Si_2 (Sugiyama and Onuki, 2003). Single crystals of UCu_2Si_2 prepared from a Cu flux undergo a 50 K antiferromagnetic transition below the 100 K ferromagnetic transition (Fisk *et al.*, 2003).

$U_2Nb_3Si_4$ is weakly ferromagnetic below 35 K (Le Bihan *et al.*, 2000). Finally, URu_2Si_2 is one of the most studied heavy fermion materials (Sugiyama and Onuki, 2003).

(d) Uranium–germanium, uranium–tin, and uranium–lead systems

The uranium–germanium system is as complex as that of uranium silicides. U_7Ge (*vide infra*), U_5Ge_3 (*vide infra*), U_5Ge_4, UGe_2, and UGe have all been characterized and subjected to extensive physical property measurements (Onuki *et al*., 1992). The compound originally formulated as U_3Ge_4 has been shown to be a mixture of UGe and U_3Ge_5. Detailed studies including magnetic structure determination via neutron diffraction have been performed on UGe_2, which is an unusual example of a ferromagnetic superconductor (Saxena, 2000; Sheikin *et al*., 2000; Nishioka *et al*., 2002).

This compound was originally reported to crystallize in the $ZrSi_2$ (*Cmcm*) structure type, but in fact crystallizes in the $ZrGa_2$ (*Cmmm*) type (Oikawa *et al*., 1996; Boulet *et al*., 1997a). U_5Ge_3 and U_7Ge both undergo a transition to a superconducting phase below 2 K (Onuki *et al*., 1990). However, the existence of both of these compounds has been called into question (Boulet *et al*., 1997c), and they are likely mixture of U_5Ge_4 and U metal dissolving 3% of germanium.

The uranium–tin phase diagram has been described by Palenzona and Manfrinetti (1995). U_5Sn_4 (Ti_5Ga_4-type), USn (ThIn-type), USn_2 ($ZrGa_2$-type), U_3Sn_7 (Ce_3Sn_7-type), and USn_3 ($AuCu_3$-type) were identified from this work. Dhar *et al*. (1998) have assessed the magnetic properties of these compounds. U_5Sn_4 and USn are ferromagnetically ordered below 62 and 49 K, respectively; USn_2 and U_3Sn_7 attain an antiferromagnetic state near 80 K. Shunk (1969) and Chiotti *et al*. (1981) have reported the phase diagram for the uranium–lead system.

5.7.4 Uranium pnictides

The systems U–N, U–P, U–As, U–Sb, and U–Bi have been studied in great detail. In particular, the monopnictides UN, UP, and UAs have found major interest because of their solid-state properties, which are relatively easy to study because of their cubic (NaCl) structure. Physical and crystallographic data of the pnictides are summarized in Table 5.23.

The thermodynamic properties of uranium and other actinide nitrides are briefly summarized in Chapter 19. Additional information on uranium nitrides and heavier pnictides is available in Gmelin (1981b, vol. C7; 1981d, vol. C14).

(a) Uranium–nitrogen system

Rundle *et al*. (1948) established the existence of the following uranium nitride phases: UN, U_2N_3, and $UN_{1.75}$, while the phase UN_2 could not be confirmed. Berthold *et al*. (1957) and Berthold and Delliehausen (1966) succeeded, however, in preparing a phase $UN_{1.90}$ by reacting uranium hydride with ammonia at

Table 5.23 *Crystallographic data of uranium pnictides* (*Rough and Bauer,* 1958*; Hansen and Anderko,* 1958*; Waber* et al., *1964; Elliot,* 1965*; Shunk,* 1969).[a]

					Lattice parameters			*Density*	
Formula	*Color*	*m.p.* (°C)	*Space group*	*Symmetry*	*a* (Å)	*c* (Å)	Z	*X-ray*	*Exp.*
UN	metallic	2850	$Fm3m$	fcc	4.889		4	14.32	
UN[b]			$R\bar{3}m$	rhombohedral	3.170	8.635	3	16.7	
α-U_2N_3			$Ia3$	cubic	10.678		16	11.24	
β-U_2N_3[c]			$P\bar{3}m1$	hexagonal	3.700	5.825		12.45	
$UN_{1.45}$	black				10.700				
UN_x[d]									
$UN_{1.76}$	black			bcc	10.628				
$UN_{1.90}$	black								
UP	metallic	2610	$Fm3m$	fcc	5.5889		4	10.23	
UP[b]			$R\bar{3}m$	rhombohedral	7.583	9.433	12	11.41	
U_3P_4	metallic		$I\bar{4}3d$	bcc	8.207		4		
UP_2	grey		$P4/nmm$	tetragonal	3.808	7.780	2		
UAs	metallic	2705[e]	$Fm3m$	fcc	5.7788		4	10.77	
U_3As_4	metallic		$I\bar{4}3d$	bcc	8.507		4		

UAs_2	metallic		$P4/nmm$	tetragonal	3.954	8.116	2	9.8	
U_5Sb_4[g]	metallic		$P6_3/mcm$	hexagonal	9.237	6.211	2	12.14	
USb	metallic	1850	$Fm\bar{3}m$	fcc	6.203		4		
U_3Sb_4	metallic	1695[f]	$I\bar{4}3d$	bcc	9.113		4	10.84	10.7
USb_2	metallic	1335[f]	$P4/mmm$	tetragonal	4.272	8.759	2	10.04	10.5
α-UBi(δ_1)	metallic		$Fm\bar{3}m$	cubic	6.364		4	11.52	
β-UBi(δ_2)	metallic	1400–1450[e]	$P4/nmm$	tetr.bc	11.12	10.55	24	13.6	
U_3Bi_4 (ε)	metallic	1150[f]	$I\bar{4}3d$	bcc	9.350		4	12.57	12.8
UBi_2	metallic	1010[f]	$P4/nmm$	tetragonal	4.445	8.908	2	12.38	12.36

[a] Unless otherwise mentioned, the data are taken from Rough and Bauer (1958), Hansen and Anderko (1958), Waber *et al.* (1964), Elliot (1965), Shunk (1969).
[b] High-pressure phase (Olsen *et al.*, 1985, 1988).
[c] Masaki and Tagawa (1975).
[d] Solid solutions ranging from $UN_{1.45}$ through $UN_{1.76}$, lattice constant decreasing from 10.700 to 10.628 Å.
[e] With decomposition.
[f] With peritectic decomposition.
[g] Paixão *et al.* (1994). This phase was originally formulated as U_4Sb_3.

elevated temperatures. Bugl and Bauer (1964) have studied the U–N system in detail.

The nitrides can be prepared by reaction of very pure uranium metal (or uranium hydride prepared from such metal) with nitriding agents. The surface of the uranium metal has to be pickled with nearly concentrated HNO_3, and then washed with organic solvents to remove even traces of oxide and oil films, which might lead to the formation of oxide or carbide contaminants. The nitriding agents also have to be of high purity. Uranium mononitride can be prepared (i) by reaction of uranium metal (or uranium hydride) with nitrogen or ammonia, (ii) by the thermal decomposition of higher nitrides at or above 1300°C, or (iii) by the reduction of higher nitrides with uranium metal. U_2N_3 can be prepared by reacting UC with NH_3 or a N_2/H_2 gas mixture (Nakagawa *et al.*, 1997). The reaction with ammonia is advantageous because NH_3 acts as both a nitriding agent and as a carbon-clearing agent. Fitzmaurice and Parkin (1994) report that various uranium nitrides could be prepared from the self-propagating reaction of UCl_4 with Li_3N.

Mallett and Gerds (1955) made a kinetic study of the reaction of uranium metal with nitrogen in the temperature range 550–900°C and at atmospheric pressure. Surface reaction products were identified by X-ray diffraction methods. At 775–900°C it was found that all three nitride phases were present. The intermediate nitride U_2N_3 is prepared by similar methods or by reduction of $UN_{1.75}$ with hydrogen. Since U_2N_3 loses nitrogen above 700°C *in vacuo*, the preparative procedure must take this into account. The nitride $UN_{1.75}$ cannot be prepared at all by reaction of the metal with nitrogen, unless a high pressure of nitrogen is used. There appears to be a two-phase region between UN and U_2N_3, but the region between U_2N_3 and $UN_{1.75}$ appears to be homogeneous. A tentative phase diagram of the system is shown in Fig. 5.32.

All of the higher uranium nitrides are thermally unstable relative to UN. UN is easily oxidized by air and is decomposed by water vapor; it is not attacked by either hot or cold hydrochloric or sulfuric acids, but is attacked by molten alkali. U_2N_3 can be used for the catalytic cracking of ammonia (Rizzo da Rocha *et al.*, 1995). Schmitz-Dumont *et al.* (1954) described the interesting uranium compound uranyl amide, $UO_2(NH_2)_2$. This compound can be prepared by the reaction of potassium uranyl nitrate, $KUO_2(NO_3)_3$, with potassium amide in liquid ammonia. Uranyl amide is a brown, amorphous substance that is unaffected by dry oxygen at room temperature. Moisture, however, converts the amide to ammonium diuranate. The uranium amido chlorides, UNH_2Cl_2 and $U(NH_2)_2Cl$, can be obtained by reacting UCl_3 with ammonia at 450 to 500°C. Increased heating of these compounds results in their conversion to U(NH)Cl and then $UN_{1.73–1.75}$ (Berthold and Knecht, 1965a).

The reaction of Li_3N with UH_3 at 900°C results in the formation of $LiUN_2$ (Jacobs *et al.*, 2003). The structure is related to the anatase type with the octahedral sites occupied by Li. Ca_3UN_4 can be prepared by reacting Ca $(NH_2)_2$ and UH_3 between 600 and 1000°C (Heckers *et al.*, 2003). X-ray and

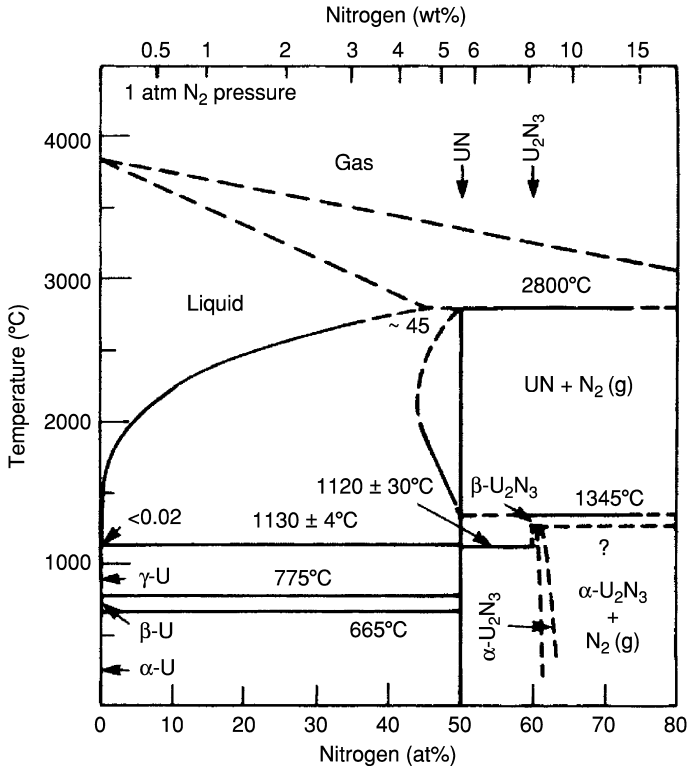

Fig. 5.32 *Phase diagram of the U–N system* (*Shunk*, 1969).

neutron diffraction studies on this phase show that it crystallizes in the NaCl structure type with statistical occupation of the cation site by three Ca atoms and one U atom.

(b) Uranium–phosphorus, uranium–arsenic, and uranium–antimony, and uranium–bismuth systems

In the systems U–P, U–As, U–Sb, and U–Bi, the compounds UX, U_3X_4, and UX_2 (where X = P, As, Sb, or Bi) have been reported. Compounds UX have the cubic NaCl structure for all X, with the exception of β-UBi, which is tetragonal body-centered. U_3X_4 is body-centered cubic and UX_2 tetragonal for all X.

At least four methods have been applied for preparation of the pnictides: direct synthesis from the elements in an autoclave (Albutt *et al.*, 1964) or in a sealed tube, for instance (Iandelli, 1952).

$$2U + P_4 \rightarrow 2UP_2$$

the reaction of uranium hydride with phosphine or arsine, for instance

$$UH_3 + PH_3 \rightarrow UP + 3H_2$$

and finally by circulating gaseous phosphine or arsine over slightly heated hydride (Baskin and Shalek, 1964; Baskin, 1969). For the preparation of the phosphides, a PH_3-loaded stream of argon is passed over the hydride, which is heated at 400–500°C. For the preparation of the arsenides, AsH_3 is reacted with UH_3 at 300°C. The reaction products are annealed at 1200–1400°C. Single crystals of UAs_2 have been grown by reacting uranium metal with a Cs_3As_7 flux (Albrecht-Schmitt *et al.*, 2000). Finally, uranium phosphides, arsenides, and antimonides can be prepared from the reaction of UCl_4 with sodium pnictides (Fitzmaurice and Parkin, 1994).

Buhrer (1969), Spirlet (1979), and Vogt (1982) succeeded in growing single crystals of most uranium pnictides by gas-phase transport, using $TeCl_4$, I_2, and other transporting agents. The crystals grown in this manner allow the determination of physical properties such as magnetic susceptibilities, magnetic phase diagrams (Busch *et al.*, 1979a), or the measurement of the de Haas–van Alphen effect (Henkie *et al.*, 1981); the uranium pnictides are particularly well suited for such measurements. Normally, they should exhibit isotropic behavior because of their structure, but the presence of anisotropy in the cubic crystals suggests the formation of magnetic domains. U_3P_4 and U_3As_4 are both metallic ferromagnets with itinerant 5f electrons (Inada *et al.*, 2001).

The binary compounds of the systems U–Sb and U–Bi may be prepared directly from the elements, or by reacting uranium with alkali metal antimonide and bismuthide fluxes. The binary phase diagram of U–Sb was originally investigated by Beaudry and Daane (1959). Among the binary compounds discovered in this system was a uranium-rich phase (δ) that forms a eutectic with USb at 1770°C. This compound was originally formulated as U_4Sb_3. Magnetic susceptibility measurements on a compound with this nominal composition show ferromagnetic behavior below 86 K (Troć, 1992). However, later microprobe analysis, neutron scattering, and single crystal X-ray diffraction data were utilized to establish that the actual composition of this phase is U_5Sb_4 (Paixão *et al.*, 1994); this compound crystallizes in the Ti_5Ga_4 structure type. Paixão *et al.* (1994) have demonstrated that U_5Sb_4 shows highly anisotropic ferromagnetic behavior below 86 K.

5.7.5 Uranium chalcogenides

The binary, ternary, and quaternary uranium sulfides, selenides, and tellurides have been the subject of intense investigation for more than 160 years. U–Po compounds are currently unknown owing to the high radioactivity and rarity of polonium. A significant number of the chalcogenide phases deduced before 1980 were reinvestigated over the past two decades, primarily by single-crystal X-ray diffraction, as a number of previously known compounds were assigned incorrect space groups, unit cells, and compositions.

(a) Uranium–sulfur system

Uranium sulfide in the form of US_2 was first prepared in the mid-1800s (Péligot, 1842; Herrmann, 1861). This compound was followed by the preparation of US and U_2S_3, which were identified by Alibegoff (1886); these studies pre-date the discovery of X-rays. Systematic X-ray powder diffraction investigations did not take place until 1943 (Strotzer *et al.* 1943), when seven distinct phases were identified from their powder patterns, but these were not indexed. The phase diagram of the uranium–sulfur system is shown in Fig. 5.33.

Based on later systematic studies of the uranium–sulfur system by Eastman *et al.* (1950), Zachariasen (1949b) was able to elucidate the crystal structures of many of the previously synthesized phases. Mills (1974) has compiled thermodynamic data for these phases. Crystal structure data for the uranium chalcogenides and oxychalcogenides are given in Table 5.24.

The uranium sulfides can be prepared by heating uranium or uranium hydride with H_2S, or by heating the elements together in a sealed tube. Lower sulfides may be obtained by thermal decomposition of the higher sulfides *in vacuo* at high temperatures. γ-US_2 can be prepared from what is thought to be a topotactic reaction of U_3S_5 with sulfur (Kohlmann and Beck, 1997).

α-UX_2 compounds (X = S, Se) were previously reported to crystallize in *I*4/*mcm*, but based on single crystal X-ray data they are now known to crystallize in *P*4/*ncc* (Noël and Le Marouille, 1984). U_3S_5 has been the subject of a large number of studies that have concluded that the compound is mixed-valent, containing both U^{3+} and U^{4+}; it can be formulated as $(U^{3+})_2(U^{4+})(S^{2-})_5$ (Noël and Prigent, 1980; Kohlmann and Beck, 2000). A view of the structure of U_3S_5 is shown in Fig. 5.34.

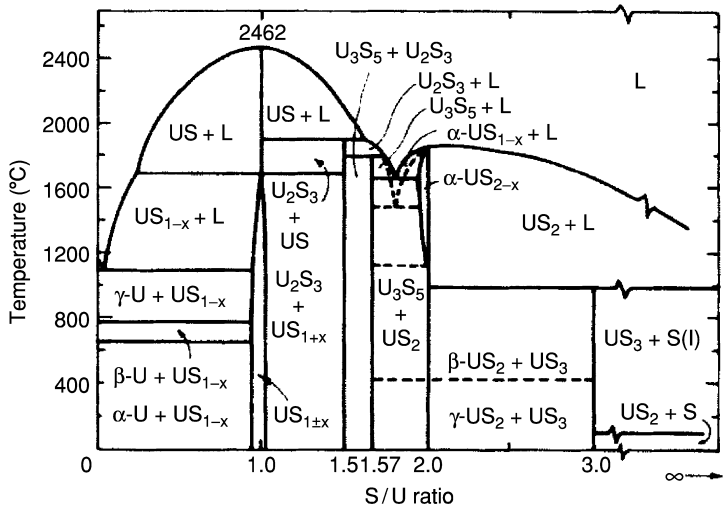

Fig. 5.33 *Tentative phase diagram of the U–S system* (*Cordfunke,* 1969).

Table 5.24 *Crystallographic data for uranium chalcogenides and oxychalcogenides.*[a]

Formula	*Color*	*m.p.* (°C)	*Space group*	*Symmetry*	*Lattice parameters*				*Z*	Density (g/cm^3)		*References*
					a	*b*	*c*	β		*Obs.*	*Calc.*	
UOS	Black		*P4/nmm*	tetrag.	3.483		6.697		2		9.64	Picon and Flahaut (1968)
US	silvery black	2462	*Fm*$\bar{3}$*m*	cubic	5.484				4		10.87	Zachariasen (1949b)
U_2S_3	Blue-black	1850	*Pbnm*	orthor.	10.34	10.58	3.885		4	8.94	8.96	Picon and Flahaut (1968)
U_3S_5	Blue-black			orthor.	7.42	8.11	11.74		4	8.16	8.26	Potol *et al.* (1972)
α-US_2[b]	Steel gray	1850	*P4/ncc*	tetrag.	10.293		6.374		10		8.01	Noël and Le Marouille (1984)
β-US_2	Steel gray		*Pbab*	orthor.	4.4803	7.439	4.1209		4	8.07	8.09	Suski *et al.* (1972)
γ-US_2	Steel gray		*P*$\bar{6}$*2m*	hexag.	7.236		4.062		3	8.12	8.17	Picon and Flahaut (1968); Daoudi *et al.* (1996); Kohlmann and Beck (1997)
US_3	Black, shiny		$P2_1/m$	monoc.	5.40	3.90	18.26	80.5	4	5.9	5.86	Picon and Flahaut (1968); Marcon (1969)
UOSe	black[c]		*P4/nmm*	tetrag.	3.9035		6.9823		2	10.40	10.38	Murasik *et al.* (1968)
USe	Black		*Fm*$\bar{3}$*m*	fcc	5.7399				4		11.13	Kruger and Moser (1967)
U_3Se_4	Black, shiny	1680[d]	*I*$\bar{4}$3*d*	cubic	8.820				4	10.07	9.97	Khodadad (1960); Khodadad (1961); Noël (1985a)

U_2Se_3	Black	1610	*Pnma*	orthor.	10.94	11.33	4.06	4	9.42	9.40	Khodadad (1959, 1961)
U_3Se_5	Black	1560[d]	*Pnma*	orthor.	12.292	8.459	7.799	4	9.04	9.14	Breeze and Brett (1972)
U_7Se_{12}	Black		$P6_3/m$	hexag.	11.385		4.099	1			Breeze and Brett (1972)
α-USe_2[e]	Black	1460	*I4/mcm*	tetrag.	10.765		6.660	10		9.03	Noël and Le Marouille (1984)
β-USe_2	black[f]		*Pnma*	orthor.	7.455	4.2320	8.964	4	9.08	9.3	Breeze and Brett (1972); Noël *et al.* (1996)
γ-USe_2	Black		$P\bar{6}2m$	hexag.	7.6376		4.1924	3	9.07	9.31	Breeze and Brett (1972); Kohlmann and Beck (1997)
USe_3	Black, shiny	1160[d]	$P2_1/m$	monoc.	5.652	4.056	10.469	2	7.25	7.25	Breeze and Brett (1972); Ben Salem *et al.* (1984)
UOTe	Gray-black		*P4/nmm*	tetrag.	4.004		7.491	2	10.55		Klein-Haneveld and Jellinek (1964); Breeze *et al.* (1971)
U_2O_2Te	Gray-black		*I4/m*	tetrag.	3.9640		12.564	2			Breeze *et al.* (1971)
UTe	Gray-black	1740	$Fm\bar{3}m$	fcc	6.150			4	10.37	10.55	Kruger and Moser (1967); Klein-Haneveld and Jellinek (1964)
U_3Te_4	Black	1540[d]	$I\bar{4}3d$	cubic	9.3980			4	9.80	9.81	Matson *et al.* (1963)
α-U_2Te_3	Black, shiny		$I\bar{4}3d$	cubic	9.3960			4	9.02	9.81	Matson *et al.* (1963)

Table 5.24 (*Contd.*)

Formula	*Color*	*m.p.* (°C)	*Space group*	*Symmetry*	*Lattice parameters*				*Z*	Density (g/cm^3)		*References*
					a	*b*	*c*	β		*Obs.*	*Calc.*	
β-U_2Te_3	Black	1500[d]	*Pnma*	orthor.	12.175	4.370	11.828		4		9.06	Suski *et al.* (1976); Tougait *et al.* (1998b)
α-U_3Te_5	Black			hexag.	12.25		4.23					Ellert *et al.* (1975)
β-U_3Te_5	Black	1300[d]		orthor.	7.99	8.73	12.88					Slovyanskikh *et al.* (1977)
γ-U_3Te_5	Black		*Pnma*	orthor.	16.098	4.210	14.060		4		9.42	Tougait *et al.* (1998a)
U_7Te_{12}	Black		$P\bar{6}$	hexag.	12.312		4.260		1		9.49	Breeze *et al.* (1971); Breeze and Brett (1971); Tougait *et al.* (1998c)
$UTe_{1.77}$	Black		*P4/nmm*	tetrag.	4.243		8.946		2		9.8	Klein-Haneveld and Jellinek (1969); Klein-Haneveld and Jellinek (1970)
$UTe_{1.78}$	Black			orthor.	4.162	6.134	13.973		4			Breeze *et al.* (1971)

α-UTe_2	Dark gray	1180[d]	*Immm*	orthor.	4.1619	6.1277	13.961		4	9.20	Klein-Haneveld and Jellinek (1970); Boehme *et al.* (1992)
β-UTe_2	Black		*Pnnn*	orthor.	4.24	6.16	14.52		4	8.68	Ellert *et al.* (1971)
U_3Te_7	Black	950[d]									Montignie (1947)
α-UTe_3	Black	935[d]	$P2_1/m$	monoc.	6.0987	4.2229	10.325	98.2	2	7.83	Breeze *et al.* (1971); Boehme *et al.* (1992); Stoewe (1996a)
β-UTe_3	Black		*Cmcm*	orthor.	4.338	24.743	4.338		4	8.85	Noël and Levet (1989)
U_2Te_5	Black		*C2/m*	monoc.	34.42	4.181	6.074	95.4	4	8.5	Stoewe (1996b); Tougait *et al.* (1997)
$U_{0.9}Te_3$[g]	Black		*Cmcm*	monoc.	4.3537	24.792	4.3541		4	8.4	Stoewe (1997a)
UTe_5		490[d]	*Pnma*	orthor.	17.915	10.407	4.220		4		Slovyanskikh *et al.* (1967); Noël (1985b)

[a] Compiled from Gmelin (1981, vol. C11, 1984, vol. C10) and from original literature.
[b] Old sources listing α-US_2 refer to $US_{1.80}$-$US_{1.93}$. The single crystal structure of α-US_2 is known.
[c] Most of the selenides and tellurides, if prepared in sealed tubes, are obtained as free-running black powders. In some cases, single crystals have been prepared by gas-phase transport.
[d] Peritectic decomposition temperature of the solid-state phase.
[e] α-USe_2 can refer to the phase $USe_{1.88}$ and has variable lattice parameters.
[f] Obtained as black crystals with metallic luster.
[g] This compound has been previously reported in the literature as $UTe_{3.38}$. Powder diffraction data suggests that the uranium content may equal $U_{0.724}Te_3$ (Boehme *et al.*, 1992).

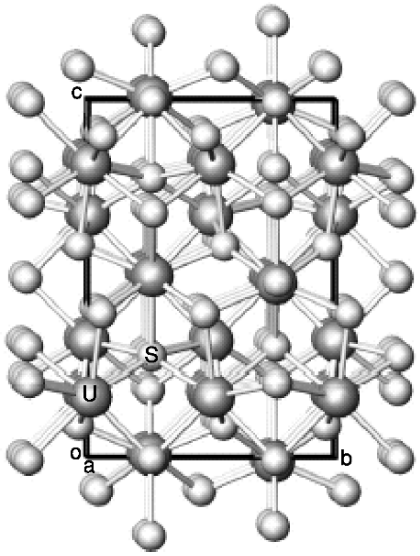

Fig. 5.34 *A view down the a-axis of the structure of* U_3S_5. *This is a mixed valence compound and should be formulated as* $(U^{3+})_2(U^{4+})(S^{2-})_5$.

(b) Uranium–selenium and uranium-tellurium systems

The selenides and tellurides of uranium have also been studied extensively. A large number of individual phases have been identified and characterized by their X-ray patterns. The crystallographic data of the individual phases have also been summarized in Table 5.24. The phase diagrams of the systems U–Se and U–Te are shown in Figs. 5.35 and 5.36, respectively.

The β modification of UTe_3, which was originally thought to adopt the $NdTe_3$ structure type, has been shown to be non-stoichiometric with uranium defects, giving rise to a formulation of $U_{0.9}Te_3$ (Stoewe, 1997a). This compound is identical to the previously known binary uranium telluride, formulated as $UTe_{3.38}$, and shows variable composition with U content ranging from 0.87 to 0.93. X-ray powder diffraction data suggest even a larger defect concentration consistent with a formula of $U_{0.724}Te_3$ (Boehme *et al.*, 1992). Te–Te bonding exists in a number of uranium telluride phases, making oxidation state assignment difficult. For example, one-dimensional tellurium chains exist in UTe_2. Therefore the compound is not $(U^{4+})(Te^{2-})_2$ but rather $(U^{3+})(Te^{2-})(Te^{1-})$ (Stoewe, 1997b). A view of the structure of UTe_2 is shown in Fig. 5.37.

The selenides and tellurides can be prepared by similar methods as the sulfides, i.e. reaction of uranium powder prepared from the hydride with H_2Se or H_2Te, synthesis from the elements at controlled temperatures in sealed tubes, or thermal decomposition of the higher selenides or tellurides. For a more detailed description of the solid-state properties of USe and UTe,

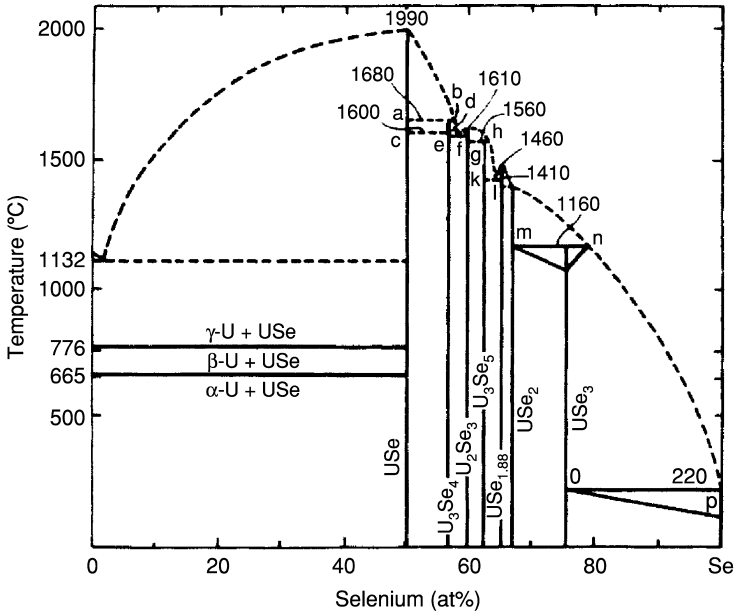

Fig. 5.35 *Phase diagram of the U–Se system* (*Klein-Haneveld and Jellinek*, 1964).

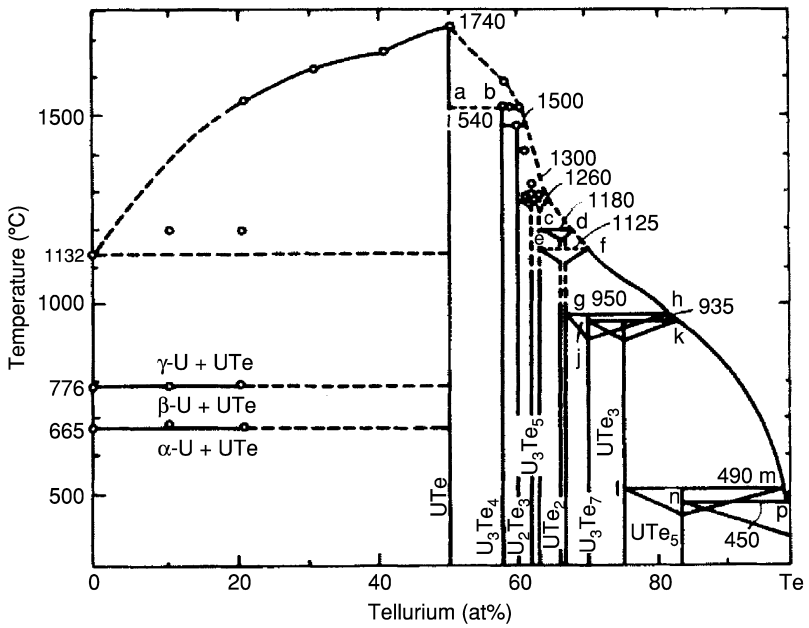

Fig. 5.36 *Phase diagram of the U–Te system* (*Slovyanskikh* et al., 1977).

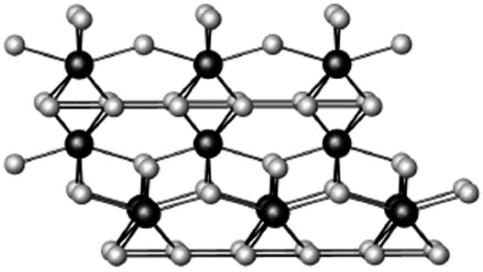

Fig. 5.37 *A view down the a-axis of the structure UTe_2. There are one-dimensional chains formed from Te–Te bonding, leading to the composition $(U^{3+})(Te^{-})(Te^{2-})$.*

see *Gmelin* (1981c, vol. C11) and the Proceedings of the International Conference on the Physics of Actinides and Related 4f Materials (Wachter, 1980). U_2Te_5 has been prepared from the direct reaction of the elements, and single crystals grown by using $TeBr_4$ as a chemical transport reagent (Stoewe, 1996b). Uranium chalcogenides can also be prepared by reacting UCl_4 with Li_2X (X = S, Se, Te) (Fitzmaurice and Parkin, 1994). Narducci and Ibers (1998) have reviewed the ternary and quaternary uranium chalcogenides. These compounds range from simple perovskite-type compounds with ABX_3 (X = S, Se, Te) formula to complex, tellurium-deficient compounds such as one-dimensional $Cs_8Hf_5UTe_{30.6}$ (Cody *et al*., 1995; Cody and Ibers, 1995). The oxidation state of uranium in these compounds is often called into question due to the presence of Te ··· Te contacts on the order of 3 Å, which are considerably shorter than the van der Waals distance (4.10 Å), but longer than a full Te–Te single bond (2.76 Å). This results in a formal oxidation state for the tellurium with a non-integral value; hence, the oxidation state of uranium is ambiguous.

5.7.6 Uranium halides and related compounds

The halides and complex halides are one of the most thoroughly studied classes of uranium compounds. They have found use in many industrial applications, uranium hexafluoride, tetrachloride, and trichloride in large-scale isotope separation of ^{235}U and uranium tetrafluoride as a component of molten-salt reactor fuels as well as for the preparation of uranium metal. The most stable halides are formed with uranium in the 6+ and 4+ oxidation states. Experimental investigations gave evidence for increasing U 5f participation in the chemical bonds in the more covalent compounds. Ionicity is largest for halides with uranium in higher oxidation states and with the more electronegative halogens. An exception to this rule is UF_3, which is reported to be more covalent than UCl_3 (Thibaut *et al*., 1982). Uranium in oxidation states 5+ and 6+ forms linear uranyl groups UO_2^+ and UO_2^{2+}. These possess covalent, substitution inert bonds and act like single species with respect to the halogen atoms. Lau and Hildenbrand (1982, 1984) have presented thermochemical data for gaseous

U–F_n and U–Cl_n species (where $n = 1, 2, 3, 4$, or 5), obtained from mass spectrometric investigations of high-temperature reaction equilibria.

The chemistry of uranium halides has been reviewed in numerous papers and books, e.g. Katz and Sheft (1960), Hodge (1960), Pascal (1962–1970), Bagnall (1967, 1987), Caillat (1961), Chatalet (1967), Brown (1968, 1972, 1973, 1979), Johnson *et al*. (1974), Manes (1985), and Eick (1994). Several reviews were devoted to particular aspects of the halides: the crystallographic data of actinide halides have been reported by Taylor (1976a) and of their binary compounds with non-metallic elements by Benedict (1987); the results of spectroscopic investigations were presented by Carnall (1982), Carnall and Crosswhite (1985), Baer (1984), and Wilmarth and Peterson (1981); the magnetism of actinide compounds by Santini *et al*. (1999); EPR by Kanellakopulos (1983); the thermodynamic data by Kubaschewski and Alcock (1979), Fuger *et al*. (1983), Grenthe *et al*. (1992), and Guillaumont *et al*., (2003); the industrial production of uranium hexafluoride by Hellberg and Schneider (1981), and the properties of uranium in molten salts and metals by Martinot (1984, 1991). A number of review papers have been also devoted to a particular oxidation state or group of uranium halides, e.g. *Structural systematics in actinide fluoride complexes* (Penneman *et al*., 1973), *Verbindungen mit Fluor* (Bacher and Jacob, 1980), *Actinide fluorides* (Freestone and Holloway, 1991), *Uranium hexafluoride. Its chemistry related to its major application* (Bacher and Jacob, 1986), *Compounds of uranium with chlorine, bromine, iodine* (Brown, 1979), *Heptavalent actinides* (Keller, 1985), *Complex compounds of uranium* (Bagnall, 1979), *Comprehensive coordination chemistry II – The Actinides* (Burns *et al*., 2004), *Magnetochemistry of uranium*(v) *complexes and compounds* (Miyake, 1991), *Chemistry of tervalent uranium* (Drożdżyński, 1991). In order to keep the reference number at a reasonable limit these review articles will be frequently cited as the source of chemical and physical properties of the compounds. In each of the following subsections the uranium halides and related compounds are discussed in order of increasing valence state and some of their physical properties summarized in subsequent tables. Although references to original literature data have been kept in these tables, the citation of thermodynamic data have been limited to the most important binary compounds as Chapter 19 of this work is devoted to thermodynamic properties of the actinides.

(a) Tervalent halides and complex halides

The first tervalent uranium compound, UCl_3, was prepared by Péligot (1842), and until the end of the 1960s the binary trihalides have been almost the only ones investigated. The crucial reason was the large sensitivity to oxidation and very poor solubility in aprotic organic solvents of all at that time known uranium(III) compounds. During the last 30 years the development of new experimental methods made it possible to prepare almost 150 uranium(III)

compounds (Drożdżyński, 1991). However, the uranium trihalides and complex halides still remain the only relatively well-investigated group.

The stability of the trihalides decreases with increase in the atomic number of the halide. Apart from UF_3, all the halides are more or less hygroscopic and easily oxidized in air. In aqueous solutions they are rapidly oxidized but in pure, thoroughly deoxygenated solvents the U^{3+} ions are fairly stable. Concentrated hydrochloric acid gives intensely deep-red solutions, characteristic of the $[UCl_n]^{3-n}$ complex anions. With the exception of UF_3, UCl_3 and uranium(III) fluoro complexes, the halides are also readily soluble in some more polar solvents. The compounds exhibit a variety of colors (see Table 5.25). The preparation of somewhat more stable hydrated uranium(III) complexes have also been reported. Since all of them are readily soluble in water they are efflorescent in a humid atmosphere. For binary halides the following anion polyhedra have been identified: five capped trigonal prism (UF_3), tricapped trigonal prism (UCl_3, UBr_3), and bicapped trigonal prism (UI_3).

The synthesis of uranium(III) halides and complex halides requires a rather complex equipment and strictly oxygen-free conditions. At temperatures higher than 600°C the syntheses ought to be carried out in tantalum or molybdenum tubes in order to avoid side reactions with silica; Drożdżyński (1991) has reported a survey of the preparation methods.

Trivalent uranium has a [Rn] $5f^3$ electronic configuration with the $^4I_{9/2}$ ground state. A number of crystal-field analyses of high-resolution low-temperature absorption spectra have been reported for U^{3+}-doped single crystals of $LiYF_4$ (S_4) (Simoni *et al.*, 1995), $LaCl_3$ (C_{3h}) (Crosswhite *et al.*, 1980; Carnall, 1989; Karbowiak *et al.*, 2002a), $LaBr_3$ (C_{3h}) (Sobczyk *et al.*, 2005), RbY_2Cl_7 (C_{2v}) (Karbowiak *et al.*, 1997), K_2UX_5 (C_s) (X = Cl, Br or I) (Karbowiak *et al.* 1998a), Cs_2NaYCl_6 (O_h) and Cs_2LiYCl_6 (O_h) (Karbowiak *et al.*, 1998b), Ba_2YCl_7 (C_1) Karbowiak *et al.*, 2002b, Cs_2NaYBr_6 (Karbowiak *et al.*, 2003a), $CsCdBr_3$ (Karbowiak *et al.*, 2003b), $Cs_3Lu_2Cl_9$(C_{3v}) and $Cs_3Y_2I_9$ (C_{3v}) (Karbowiak *et al.* 2005a). Such analyses have been also performed for polycrystalline samples of UCl_3 and UBr_3 (C_{3h}) (Sobczyk *et al.*, 2003), $UCl_3 \cdot 7H_2O$ (C_i) (Karbowiak *et al.*, 2001), $CsUCl_4 \cdot 3H_2O$ (C_s), $NH_4UCl_4 \cdot 4H_2O$ (C_2) (Karbowiak *et al.*, 2000), and $ZnCl_2$-based glass (Dereń *et al.*, 1998). However, only the U^{3+}-doped single crystals of $LaCl_3$ and $LiYF_4$ exhibit suitable site symmetry for precise energy-level investigations, using selection rules for electric and magnetic dipole transitions. The energy levels of the U^{3+} ion in the different site symmetries were assigned and fitted to a semiempirical Hamiltonian representing the combined atomic and crystal-field interactions. *Ab initio* calculations made it possible to use a simplified parametrization and the determination of the starting values in the angular overlap model in cases where the U^{3+} ion had the lowest site symmetry (Karbowiak *et al.*, 2000). The free ion and crystal-field parameters obtained from an analysis of low-temperature absorption spectra of thin films of UF_3, UCl_3, and UBr_3 are presented in Table 5.25. In addition, an analysis of low-temperature absorption, luminescence, and excitation

Table 5.25 *Properties of selected uranium(III) halides and complex halides.*[a]

Formula	*Selected properties and physical data*[b]	*Lattice symmetry, lattice constants* (Å)*, conformation and density* (g cm^{-3})[c]	*Remarks regarding information available and references*
UF_3	grey to black powder or purplish black crystals. density: 8.9 g cm^{-3}; disproportionates above 1000°C UF_3(cr): $\Delta_f G_m^o = -1432.5$ (4.7)†, $\Delta_f H_m^o = -1501.4$(4.7)†, $S_m^o = 123.4$ (0.4)†; $C_{p,m}^o = 95.1$(0.4)†. UF_3(g): $\Delta_f G_m^o = -1062.9$ (20.2)†, $\Delta_f H_m^o = -1065.0$ (20)†, $S_m^o = 347.5$(10)†; $C_{p,m}^o = 76.2$(5.0)†. $\log p$(mm Hg) = $4187T^{-1} + 3.945$ $\mu_{eff.} = 3.67$ B.M. (125–300 K)[d]; $\theta = -110$ K. $\mu_{eff.} = 3.66$ B.M. (293–723K)[d]; $\theta = -98$ K, Atomic and crystal-field parameters: $E_{avg} = 20\,006$ (30), $F^2 = 38\,068$ (108), $F^4 = 32256$ (177), $F^6 = 16372$ (198), $\zeta_{5f} = 1613$ (11); $\alpha = 26.1$ (6), $\beta = -793$ (40), $\gamma = 2085$ (104); $T^2 = [298.0]$, $T^3 = [48.0]$, $T^4 = [255.0]$, $T^6 = [-285.0]$, $T^7 = [332.0]$, $T^8 = [305.0]$; $M^0 = [0.67]$, $M^2 = [0.37]$, $M^4 = [0.26]$; $P^2 = [1276]$, $P^4 = [608]$, $P^6 = [122]$;$B_0^2 = 216(60)$, $B_2^2 = -319(49)$, $B_0^4 = 1479$ (78), $B_2^4 = 679(62)$, $B_4^4 = 1615(62)$, $B_0^6 = 2373$ (79), $B_2^6 = -2201$ (62), $B_4^6 = -1631(630)$, $B_6^6 = -1106$ (63); $n = 75$; *rms* = 33.6.	hexagonal; C_{6v}^3, $P6_3cm$, No. 185; $Z = 6$; or trigonal: $P\bar{3}c1$, D_{3d}^4, No. 165; Z = 6, CN = 11, $a = 7.173$, $c = 7.341$; d(calc.) = 8.95 to 8.99; d(exp.) = 9.18. LaF_3 structure type; The bond lengths to the corresponding prism atoms in $P\bar{3}cl$ are 3.01 (2×), 2.48 (2×) and 2.63 (2×) and in $P6_3cm$ these are 2.53 (2×), 2.81 (2×), 2.45 and 3.09, respectively. The cap atoms in both structures have fit firmly (bond lengths 2.42–2.48.)	*X-ray single-crystal and neutron diffraction data* (Zalkin *et al.*, 1967; Taylor 1976a; Zachariasen, 1975); *Synthesis* (Runnals, 1953; Warf, 1958; Friedman *et al.*, 1970; Berndt, 1973); *absorption spectra* (Schmieder *et al.*, 1970); *photoelectron spectra* (Thibaut *et al.*, 1982); *crystal-field analysis* (Drożdżyński *et al.*, 2002); *mechanical and thermal properties* (Bacher and Jacobs, 1980); *EPR, NMR and magnetic susceptibility data* (Berger and Sienko, 1967; Dao, Nguyen Nghi *et al.*, 1964; Kanellakopulos, 1983); *fused-salt systems* (Martinot, 1984); *thermodynamic properties* (Brown, 1973, 1979; Grenthe *et al.*, 1992; Guillaumont *et al.*, 2003)

Table 5.25 (*Contd.*)

Formula	*Selected properties and physical data*[b]	*Lattice symmetry, lattice constants* (Å)*, conformation and density* (g cm^{-3})[c]	*Remarks regarding information available and references*
$NaUF_4$	peritectic decomposition point of α-$NaUF_4$: 775°C; α–β transformation temp. 595°C	hexagonal, C_{3h}^1, $P\bar{6}$, No. 174; a = 6.167, c = 3.770; d(calc.) = 5.92; tricapped trigonal prism sharing ends to form chain	*X-ray powder diffraction data; fused salt systems* (Brunton *et al*., 1965; Bacher and Jacob, 1980)
Na_2UF_5		cubic, space centered, Z = 4; a = 7.541(6); d(calc.) = 5.87	*X-ray powder diffraction data; fused salt systems* (D'Eye and Martin, 1957; Bacher and Jacob, 1980)
KUF_4	dark-blue		(Bacher and Jacob, 1980)
K_2UF_5	peritectic point: 848°C	cubic; CaF_2 structure type ; a = 6.62 (1); Z = 1.6; d(calc.) = 3.74	*X-ray powder diffraction data; fused salt systems* (Volkov *et al*., 1979)
K_3UF_6	purple-brown, extremely moisture sensitive	cubic, face centered; a = 9.20	*X-ray powder diffraction data; fused salt systems* (Thoma and Penneman, 1965; Thoma *et al*., 1966)
$K_3U_2F_9$	peritectic point: 750°C	cubic; CaF_2structure type ; a = 6.00 (1); Z = 0.8; d(calc.) = 4.67	*X-ray powder diffraction data; fused salt systems* (Volkov *et al*., 1979)
$RbUF_4$		hexagonal; KYF_4 structure type ; a = 8.54(1), c = 10.72(2); Z = 6, d(calc.) = 5.84	*X-ray powder diffraction data; fused salt systems* (Boraopkova *et al*., 1971)
Rb_3UF_6	purple-brown, extremely moisture sensitive	cubic, face centered; a = 9.5074	*X-ray powder diffraction data; fused salt systems* (Thoma and Penneman, 1965; Thoma *et al*., 1966; Chirkst, 1981)
Cs_3UF_6	purple-brown, extremely moisture sensitive	cubic, face centered; a = 10.6	*X-ray powder diffraction data; fused salt systems* (Thoma and Penneman, 1965; Thoma *et al*., 1966; Chirkst, 1981)

$UZrF_7$	reddish-brown, slowly oxidizes in air at room temperature; $\mu_{eff.} = 3.80$ B.M. (100–300 K)[d]; $\theta = -85$ K	monoclinic, isotypic with $SmZrF_7$, $a = 6.1000(6)$, $b = 5.833(8)$ $c = 8.436(10)$; $\beta = 102.69(7)$; $Z = 2$; $V = 292.81$; d(calc) = 5.25; d(exp.) = 5.40.	*X-ray powder diffraction data; magnetic susceptibility data* (Fonteneau and Lucas, 1974)
UZr_2F_{11}	slowly oxidizes in air at room temperature. $\mu_{eff.} = 3.90$ B.M. (100–300 K)[d]; $\theta = -101$ K	monoclinic; $a = 5.308(6)$, $b = 6.319(8)$, $c = 8.250(8)$, $\beta = 105.41(5)^\circ$, $Z = 2$; $V = 266.81$; d(calc.) = 5.22	*X-ray powder diffraction data; magnetic susceptibility data* (Fonteneau and Lucas, 1974). *general properties* (Bacher and Jacob, 1980)
UCl_3	dark red needles or fine crystalline olive-green powder; hygroscopic; soluble in acetic acid.m.p. = 835°C; b.p. = 1657 °C; density: 5.51 g cm^{-3}; Oxidizes in air at room temperatures; UCl_3(cr): $\Delta_f G^o_m = -796.1$ (2.0)†, $\Delta_f H^o_m = -863.7$ (2.0)†, $S^o_m = 158.1$ (0.5)†; $C^o_{p,m} = 95.10$ (0.5)†. UCl_3(g): $\Delta_f G^o_m = -521.7$ (20.2)†, $\Delta_f H^o_m = -523.0(20)$†, $S^o_m = 380.3$ (10.0)†; $C^o_{p,m} = 82.4$ (5.0)†. $\log p$(mmHg) = $-11149\ T^{-1} + 8.90$ (590–790 K) $\log p$(mmHg) = $-11552 T^{-1} + 8.97$ (>790 K); Atomic and crystal-field parameters: $\mu_{eff.} = 3.76$ B.M. (70–300 K)[d]; $\theta = -75$ K; $T_N = 20$ K; $\mu_{eff.} = 3.03$ B.M. (350–509 K)[d]; $\theta = -29$ K; $E_{avg} = 19331(42)$, $F^2 = 37719(154)$, $F^4 = 30370(202)$, $F^6 = 19477(218)$, $\zeta_{5f} = 1606(13)$; $\alpha = 31(5)$, $\beta = -939(40)$, $\gamma = 2087(115)$; $T^2 = 460(81)$; $T^3 = 59(25)$, $T^4 = 159(39)$, $T^6 = -144(46)$, $T^7 = 356(42)$, $T^8 = [300]$; $M^0 = [0.663]$; $P^2 = 1639(65)$; $B^2_0 = 370(42)$, $B^4_0 = -359(76)$, $B^6_0 = -1704(74)$; $B^6_6 = 935(60)$; $n = 58$; $rms = 35.8$	hexagonal; C^2_{6h}, $P6_3/m$, No. 176; the coordination polyhedron is a symmetrically tricapped trigonal prism arranged in columns in the c-direction; $a = 7.452(6)$, $c = 4.328(4)$; d(U–Cl) = 2.928(3), (6×); d(U–Cl) = 2.934(5), (3×); d(U–Cl) = 4.816(4) (to neighbor chain); d(Cl–Cl) = 3.342(5); d(Cl–Cl) = 3.410(3); (face atom-cape atom); d(calc.) = 5.51	*X-ray single crystal data* (Schleid *et al.*, 1987; Murasik *et al.*, 1985; Taylor and Wilson, 1974f); *synthesis* (Brown, 1968, 1979; Drożdżyński, 1991, 1988a); *thermodynamic properties* (Rand and Kubaschewski, 1963; Brown, 1973, 1979; Grenthe *et al.*, 1992; Guillaumont *et al.*, 2003). *magnetic susceptibility data*, (Handler and Hutchison, 1956; Jones *et al.*, 1974; Dawson, 1951); *NIR, visible and UV low temperature absorption spectra and crystal-field analysis of UCl_3 and U^{3+}:$LaCl_3$*, (Carnall, 1989; Karbowiak *et al.*, 2002; Sobczyk *et al.*, 2003); *photoelectron spectra* (Thibaut *et al.*, 1982)

Table 5.25 (*Contd.*)

Formula	*Selected properties and physical data*[b]	*Lattice symmetry, lattice constants* (Å)*, conformation and density* (g cm^{-3})[c]	*Remarks regarding information available and references*
$UCl_3 \cdot 7H_2O$	grayish-ink-blue needles, readily soluble in numerous organic solvents; relatively resistant to oxidation by air at temperatures lower than 15°C; loses some of its crystallization water at higher temperatures or at high vacuum; may be completely dehydrated at 260°C. $\mu_{eff.} = 2.95$ B.M. (10–300 K)[d]; $\theta = -32.7$ K; Atomic and crystal-field parameters: $E_{avg} = 19827(17)$, $F^2 = 40488(58)$, $F^4 = 32544(81)$, $F^6 = 22866(75)$, $\zeta_{5f} = 1622(10)$; $\alpha = 28(5)$, $\beta = -622(35)$, $\gamma = 1148$; $T^2 = 306$, $T^3 = 42$, $T^4 = 188$, $T^6 = -242$, $T^7 = 447$, $T^8 = 300$; $M^0 = 0.672$, $M^2 = 0.372$, $M^4 = 0.258$; $P^2 = 1216$, $P^4 = 608$, $P^6 = 122$; $B_0^2 = -126(76)$, $B_1^2 = [-109]$, $\mathrm{Im}B_1^2 = -423(47)$, $B_2^2 = -209(53)$, $\mathrm{Im}B_2^2 = -350(55)$, $B_0^4 = 188(106)$, $B_1^4 = [-99]$, $\mathrm{Im}B_1^4[-81]$, $B_2^4 = [-66]$, $\mathrm{Im}B_2^4 = [-238]$, $B_3^4 = [136]$, $\mathrm{Im}B_3^4 = -529(83)$, $B_4^4 = [374]$, $\mathrm{Im}B_4^4 = [-491]$, $B_0^6 = [-130]$, $B_1^6 = 428(90)$, $\mathrm{Im}B_1^6 = [-77]$, $B_2^6 = [171]$, $\mathrm{Im}B_2^6 = 133$ [100], $B_3^6 = [-251]$, $\mathrm{Im}B_3^6 = [-14]$, $B_4^6 = -489(110)$, $\mathrm{Im}B_4^6 = -1832(81)$, $B_5^6 = [160]$, $\mathrm{Im}B_5^6 = 1197(96)$, $B_6^6 = -498(98)$, $\mathrm{Im}B_6^6 = -241(91)$; *rms* = 36; $n = 94$	triclinic; $P\bar{1}$, C_i^1, No.2; $a = 7.902(1)$; $b = 8.210(2)$, $c = 9.188(2)$; $\alpha = 70.53(3)$; $\beta = 73.14(3)$; $\gamma = 81.66(3)$; $V = 537.0(2)$; $Z = 2$; d(calc.) = 2.910. The crystals are built up from separate $[U_2Cl_2(H_2O)_{14}]^{4+}$ units and Cl^- ions. The characteristic features of this structure are dimers, formed by two uranium ions connected through the (Cl1) bridging chlorine atoms. d(U–Cl) = 2.915(1) and 2.894(1); d(U–O) = from 2.515(3) to 2.573(3)	*X-ray single crystal data* (Mech *et al.*, 2005); *magnetic susceptibility data; NIR and visible absorption spectrum, decomposition* (Drożdżyński, 1985); *crystal-field analysis, low temperature absorption spectrum* (Karbowiak *et al.*, 2001)

$UCl_3{\cdot}6H_2O$	purple plates	monoclinic; *P*12/*n*l; $a = 9.732(2)$, $b = 6.593(1)$, $c = 8.066(2)$, $\alpha = 90$, $\beta = 93.56(3)$; $\gamma = 90$; $V = 516.51$; $Z = 2$; d(calc.) = 2.909; The basic units of the crystal structure are Cl^- anions and $[UCl_2(H_2O)_6]^+$ cations. The U as well as O(1), O(2) and O(3) atoms are each eight-coordinated, whereas the Cl(2) and Cl(1) chloride atoms are seven and six coordinated, respectively. The characteristic feature of this structure is the existence of hydrogen bonds, which link the uranium eight–coordinated polyhedra, forming a three–dimensional network	*X-ray single crystal data* (Mech *et al.*, 2005)
$UCl_3{\cdot}CH_3CN{\cdot}5H_2O$	deep-red; soluble in polar organic solvents; IR (cm^{-1}): 2260m, 2270sh (ν_2, symm. C ≡ N stretching); 1367 (ν_3, symm. CH_3 deform.); 926m (ν_4, symm. C–C stretching); 2298 ($\nu_3 + \nu_4$, combination band); 1035 (ν_7, degenerate CH_3 rocking); $\mu_{eff.} = 3.39$ B.M .(65–300 K)[d], $C = 1.430$ emu·K·mol^{-1}, $\theta = -65.7$ K, $T_N = 12$ K	monoclinic; $a = 12.96(2)$, $b = 12.98(3)$, $c = 6.62(1)$; $\beta = 101.7(2)$; $Z = 4$, $V = 1007.2$; d(calc.) = 3.14	*X-ray powder diffraction data; magnetic susceptibility data; IR, NIR and visible absorption spectra; decomposition*, (Zych and Drożdżyński, 1986)
$UCl_3{\cdot}2H_2O{\cdot}2CH_3CN$	deep dark reddish needles	$P\bar{1}$, C_i^1, No.2; $a = 7.153(1)$, $b = 8.639(2)$, $c = 10.541(2)$; $\alpha = 108.85(3)$, $\beta = 105.05(3)$, $\gamma = 93.57(3)$; $V = 587.6(3)$; $Z = 2$; d(calc.) = 2.61; d(U–Cl) = 2.775; d(U–Cl) to the bridging anions = 2.860–2.901; d(U–O) = 2.468–2.485; d(U–U) = 4.605.	*X-ray single crystal data* (Mech *et al.*, 2005)

Table 5.25 (*Contd.*)

Formula	*Selected properties and physical data*[b]	*Lattice symmetry, lattice constants* (Å), *conformation and density* (g cm^{-3})[c]	*Remarks regarding information available and references*
		The U^{3+} ion is eight coordinated by five chloride ions, two water molecules and one methyl cyanide, which are forming a distorted bicapped trigonal prism The characteristic feature of this structure is the link of the uranium atoms through the two common edges of the Cl1 and Cl3 chlorine atoms into an infinitive zigzag chain in the [010] direction	
$CsUCl_4$	deep ink-blue; soluble in polar organic solvents; $\mu_{eff.} = 3.16$ B.M. (60–300 K)[d]; $\theta = -36$ K; $C = 1.2146$ emu·K·mol^{-1}	could not be unambiguously indexed	*X-ray powder diffraction data; magnetic susceptibility data; NIR, Vis, and UV absorption spectra* (Karbowiak and Drożdżyński, 1998a)
K_2UCl_5	purple; soluble in polar organic solvents, m.p. = 608°C – congruently; $\mu_{eff.} = 3.77$ B.M. (130–300 K)[d)]; $\theta = -33.5$ K; $T_N = 13.2$ K; IR(cm^{-1}): ν(U–Cl, stretching) = 140–220	orthorhombic; D_{2h}^{16}, *Pnm*, No. 62; Z = 4; Monocapped trigonal prisms $[UCl_7]$ are connected via two opposite common edges to chains; $a = 12.7224(7)$, $b = 8.8064(6)$, $c = 7.9951(5)$; $V = 1348.8(1)$; d(calc.) = 3.68	*single crystal and X-ray powder diffraction data; IR, NIR, and Vis absorption spectra; magnetic susceptibilities* (Drożdżyński and Miernik, 1978; Krämer *et al*., 1994); *luminescence and low temperature spectra of* U^{3+}*:*K_2LaCl_5 (Andres *et al*., 1996); *magnetic phase transitions* (Keller *et al*., 1995); *crystal-field analysis* (Karbowiak *et al*., 2000); *fused salt systems* (Suglobova and Chirkst, 1981)

Rb_2UCl_5	violet-red; soluble in polar organic solvents; m.p. = 575°C– incongruently; $\mu_{eff.} = 3.44$ B.M. (150–300 K)[d]; $\theta = -32.0$ K; $T_N = 8.6$ K; IR (cm^{-1}): ν(U–Cl, stretching) = 100–260	orthorhombic; D_{2h}^{16}, *Pnma,* No. 62; $Z = 4$; Monocapped trigonal prisms [UCl_7] are connected via two opposite common edges to chains; $a = 13.1175(8)$, $b = 8.9782(6)$, $c = 8.1871(7)$; $V = 1451.19(2)$; d(calc.) = 4.04; d(U–Cl) = 2.774 to 2.846; d(U–U) = 4.651 (interchain); d(U–U) = 7.88 (intrachain)	*X-ray powder diffraction data; IR, NIR and visible absorption spectrum; magnetic susceptibilities* (Drożdżyński and Miernik, (1978); Krämer *et al.*, 1994); *fused salt systems* (Suglobova and Chirkst, 1981)
Cs_2UCl_5	m.p. = 370°C – decomposition in solid state	rhombic; $a = 12.03$, $b = 9.76$, $c = 9.37$; $Z = 4$, d(calc.) = 4.08	*X-ray powder diffraction data; fused salt systems* (Suglobova and Chirkst, 1981)
$(NH_4)_2UCl_5$	violet; $\mu_{eff.} = 3.54$ B.M. (17–220 K)[d]; $\theta = -26.0$ K; $\mu_{eff.} = 3.47$ B.M. (220–300 K)[c]; $\theta = -37.5$ K; $T_N = 7.8$ K; IR(cm^{-1}): ν(U–Cl, stretching) = 140–260		*IR, NIR,and Vis absorption spectra; magnetic susceptibilities* (Drożdżyński and Miernik, 1978)
$SrUCl_5$	deep olive-green; $\mu_{eff.} = 3.65$ B.M. (90–300 K)[d] $C = 1.653$ emu·K·$mole^{-1}$, $\theta = -127$ K	could not be indexed	*X-ray powder diffraction data; magnetic susceptibility data; NIR and Vis absorption spectra*, (Karbowiak and Drożdżyński, 1998b)
$[(CH_3)_3N]_3 \cdot UCl_6$	dark violet-blue; IR (cm^{-1}): 110m [$\delta(UCl_6)$ A_u]; 123m,b [$\delta(UCl_6)$ E_u] 203s [lattice or cation vib.]; 236s [$\nu_s(UCl_6)$ A_u]; 259s [$\nu_{as}(UCl_6)$ E_u]. Raman (cm^{-1}): 79sh [lattice]; 89w [$\delta(UCl_6)$ E_g]; 104w [$\delta(UCl_6)$ B_g]; 131m [lattice or cation vib.]; 226vs [$\nu_{as}(UCl_6)$ A_g]; 237sh [$\nu'(UCl_6)$ A_g]; 268w [$\nu_s(UCl_6)$ B_g]; $\mu_{eff.} = 3.36$ B.M. (200–300K)[d]; $\theta = 17$; $T_N = 4.8$ K; $C = 1.5058$ emu·K·$mole^{-1}$	tetragonal; $a = 13.020$, $c = 7.825$; $Z = 2$; $V = 1326.48$; d(calc.) = 1.68	*X-ray powder diffraction data; IR, Raman, NIR and Vis absorption spectra; magnetic susceptibility data* (Karbowiak *et al.*, 1996a)

Table 5.25 (*Contd.*)

Formula	*Selected properties and physical data*[b]	*Lattice symmetry, lattice constants* (Å), *conformation and density* (g cm^{-3})[c]	*Remarks regarding information available and references*
RbU_2Cl_7	pale-brown; soluble in polar organic solvents; IR (cm^{-1}):281s, 271s, 210s, 202vs, 195sh, 190vs, 181vs, 169vs, 150sh [ν(U–Cl)]; 130m, 125m, 114m, 90m [δ(Cl–U–Cl)]; 83sh, 70m, 55w [T'(Rb/U)]; RS (in cm^{-1}): 262w, 227 s,b, 189s,165s [ν(U–Cl)]; 142m, 120m, 95w [δ(Cl–U–Cl)]; 85m, 62m T'(Rb/U); $\mu_{eff.} = 3.76$ B.M., $C = 1.750$ emu·K·$mole^{-1}$, $\theta = -80$ K	rhombic; $a = 12.86(5)$, $b = 6.89(1)$, $c = 12.55(2)$; $Z = 4$, d(calc) = 4.80(3), $RbDy_2Cl_7$ structure type	*X-ray powder diffraction data* (Suglobova and Chirkst, 1981); Volkov *et al*., 1987); *NIR and Vis low temperature absorption spectrum; magnetic susceptibility data; IR transmission and Raman spectra* (Karbowiak *et al*., 1996b); *luminescence and excitation spectra* (Karbowiak *et al*., 1996d); *low temperature absorption spectrum and crystal-field analysis of* U^{3+}*:*RbY_2Cl_7 (Karbowiak *et al*., 1997)
Ba_2UCl_7	deep black-brown; soluble in polar organic solvents; $\mu_{eff.} = 3.25$ B.M., (105–300 K)[d], $C = 1.310$ emu·K·$mole^{-1}$, $\theta = -95$ K	monoclinic; C_{2h}^5, $P2_1/c$, No. 14; $a = 7.20$, $b = 15.61$, $c = 10.66$; $\beta = 91.1°$, $V = 1197$; d(calc.) = 4.22	*X-ray powder diffraction data* (Volkov *et al*., 1987); Suglobova and Chirkst, 1981); *magnetic susceptibility data; IR, NIR and Vis absorption spectra* (Karbowiak and Drożdżyński, (1998b)
Cs_2LiUCl_6	deep ink-blue; $\mu_{eff.} = 3.56$ B.M. (85–300)[d]; $C = 1.571$ emu·K·$mole^{-1}$, $\theta = -103$ K	regular; O_h^5, $Fm3m$, No. 225; $a = 10.671$; $Z = 4$; $V = 1218.03$; d(calc.) = 3.9444	*X-ray powder diffraction data, NIR, Vis and UV absorption spectra, magnetic susceptibilities* (Karbowiak and Drożdżyński, 1998a); *absorption, vibronic and emission spectra; crystal-field analysis* (Karbowiak *et al*., 1996e; Karbowiak *et al*., 1998b)

K_2NaUCI_6		hexagonal; C_{3v}^1, $P3m1$, No.156; isostructural with α-K_2LiAlF_6; a = 7.28(1), c = 17.79(2); Z = 3; V = 816.53; d(calc.) = 3.35(1)	*X-ray powder diffraction data* (Volkov *et al*., 1987; Aurov *et al*., 1983); *thermodynamic data* (Aurov and Chirkst, 1983)
Rb_2NaUCI_6		trigonal; a = 7.27(2), c = 35.51(10); Z = 6; d(calc.) = 3.93(3), d(exp.) = 3.98(2); Rb_2LiAlF_6 and Cs_2NaCrF_6 structure type	*X-ray powder diffraction data* (Volkov *et al*., 1987; Aurov *et al*., 1983); *thermodynamic data* (Aurov and Chirkst, 1983)
Cs_2NaUCl_6	ink-blue; soluble in polar organic solvents; $\mu_{eff.}$ = 2.49 B.M. (4–20)[d]; θ = 0.53 K. $\mu_{eff.}$ = 2.92 B.M. (25–50)[d]; θ = 9.6 K	cubic; O_h^5, $Fm3m$, No.225; a = 10.937 (1); V = 1308.3(5); Z = 4, d(U–Cl) = 2.723(9), d(U–U) = 7.734; d(calc.) = 3.754	*single crystal data* (Spirlet *et al*., 1988); *magnetic properties* (Hendricks *et al*., 1974); *thermodynamic properties* (Aurov and Chirkst, 1983; Schoebrechts *et al*., 1989); *NIR, Vis and UV low temperature absorption and luminescence spectra; crystal-field analysis* (Karbowiak *et al*., 1998b); *IR spectra* (Mazurak *et al*., 1988).
NaU_2Cl_6 or $(Na^+)(U^{3+})_2(e^-)(Cl^-)_6$		hexagonal; C_{6h}^2, $P6_3/m$., No 176; a = 7.5609(3), c = 4.3143(3); Z = 1; d(U–Cl) = 2.945(6×) and 2.977(3×), d(Na–Cl) = 2.878(6×)].	*single crystal data* (Schleid and Meyer, 1989)
$KUCl_4{\cdot}4H_2O$	violet-red; soluble in polar organic solvents; IR (cm^{-1}): 650, 610 (U–OH_2 rocking); 470s (U–OH_2 wagging); 300w ν(U–OH_2 stretching); 222sh, 214s, 198s ν(U–Cl, stretching); 166s ν(U–Cl–U, stretching or lattice); 130s δ(Cl–U–Cl, stretching or lattice); 107s, 88sh (lattice modes); $\mu_{eff.}$ = 3.72 B.M. (100–300 K)[d]; C = 1.716 emu·K·$mole^{-1}$; θ = −69.3 K	orthorhombic; a = 6.971, b = 6.638, c = 11.317; Z = 2; V = 523.6; d(calc.) = 3.11	*X-ray powder diffraction data; magnetic susceptibility data; IR, NIR and Vis spectra* (Drożdżyński, 1988b)

Table 5.25 (*Contd.*)

Formula	*Selected properties and physical data*[b]	*Lattice symmetry, lattice constants* (Å), *conformation and density* ($g\ cm^{-3}$)[c]	*Remarks regarding information available and references*
$RbUCl_4 \cdot 4H_2O$	violet-red; soluble in polar organic solvents; IR (cm^{-1}): 660 (U–OH_2, rocking); 486s (U–OH_2, wagging); 300sh, 290ms [ν(U–OH_2), stretching]; 228s, 216sh, 197s [ν(U–Cl) stretching]; 165ms [ν(U–Cl–U), stretching or lattice]; 130s [δ(Cl–U–Cl), bending]; 99 ms (lattice modes); $\mu_{eff.} = 3.74$ B.M. (100–300 K)[d]; $C = 1.734$ emu·K·$mole^{-1}$, $\theta = -66.2$ K	orthorhombic; $a = 6.999$, $b = 6.673$, $c = 11.375$; $Z = 2$; $V = 531.3$; d(calc.) = 3.36	*X-ray powder diffraction data; magnetic susceptibility data; IR, NIR and Vis absorption spectra* (Drożdżyński, 1988b)
$NH_4UCl_4 \cdot 4H_2O$	dark red-violet; soluble in polar organic solvents; IR (cm^{-1}): 650, 610 (U–OH_2, rocking); 494s (U–OH_2, wagging); 299ms [ν(U–OH_2) stretching]; 222s, 202s ν(U–Cl, stretching); 175ms [ν(U–Cl–U), stretching or lattice]; 130s [δ(Cl–U–Cl), bending]; 114ms, 84sh (lattice modes); $\mu_{eff.} = 3.53$ B.M. (100–240 K)[d]; $C = 1.560$ emu·K·$mole^{-1}$, $\theta = -72.5$ K. Atomic and crystal-field parameters: $F^2 = 39911(85)$, $F^4 = 33087(149)$, $F^6 = 22048(160)$, $\zeta_{5f} = 1627.3(8.8)$; $\alpha = 33.0(3.7)$, $\beta = -973.1(29.3)$, $\gamma = 1316.9(85.4)$; $T^2 = 306$, $T^3 = 42$, $T^4 = 188$, $T^6 = -242$, $T^7 = 447$, $T^8 = 300$;	orthorhombic; D_2^3, $P2_12_12$, No. 18; $a = 7.002(2)$, $b = 11.354(3)$, $c = 6.603(2)$; $Z = 2$; $V = 524.94(14)$. The U^{3+} cation is coordinated by four Cl^-, ions and four H_2O molecules. The crystal is build up from eight-coordinated U^{3+} polyhedrons, which are connected together by O-H··Cl hydrogen bonds. d(U–Cl) (2×) = 2.845(4); d(U–Cl)) (2×) = 2.847(4); d(U–O) (2×) = 2.510(11); d(U–O) (2×) = 2.568(10); d(calc.) = 2.973, d(exp.) = 2.97	*single crystal diffraction data; magnetic susceptibility data; IR, NIR and Vis low temperature absorption spectra* (Drożdżyński, 1988b); *low temperature absorption spectra and crystal-field analysis* (Karbowiak *et al*., 2000)

	$M^0 = 0.672$, $M^2 = 0.372$, $M^4 = 0.258$; $P^2 = 1216$, $P^4 = 608$, $P^6 = 122$; $B_0^2 =$ 721(47) / [698], $B_2^2 = 428$ (39) / [403], $\mathrm{Im}B_2^2 = -460$ (39) / [–515], $B_0^4 =$ [–814], $B_2^4 =$ [–858], $\mathrm{Im}B_2^4 =$ [118], $B_4^4 =$ [–670], $\mathrm{Im}B_4^4 =$ [–22], $B_0^6 =$ [–403], $B_2^6 =$ [–612], $\mathrm{Im}B_2^6 =$ [838], $B_4^6 =$ [–549], $\mathrm{Im}B_4^6 =$ [–197], $B_6^6 =$ [–1063], $\mathrm{Im}B_6^6 =$ [–96], *rms* = 30, $n = 83$		
$KUCl_4 \cdot 3H_2O$	green; hygroscopic and air sensitive; IR(cm^{-1}): ν(U–OH_2, rocking) = 635s, 575s; ν(U–OH_2, wagging) = 480; *ν*(U–OH), stretching = 425, 280sh; *ν*(U–Cl), stretching = 260s, 238, 202; *ν*(U–Cl–U), stretching or lattice = 169, 125; *δ*(Cl–U–Cl), bending = 144, 125; *ν*(stretching and bending modes of coordinated water) = 1600; (3170, 3215, 3360, 3420); $\mu_{\mathrm{eff.}} = 3.70$ B.M. (150–300 K)[d]; $C =$ 1.7033 emu·K·$mole^{-1}$, $\theta = -80$ K	monoclinic; $a = 6.9373$, $b = 7.2658$, $c = 9.5209$; $\beta = 96.71$; $Z = 2$; $V = 476.62$; *d*(calc.) = 3.30	*X-ray powder diffraction data; IR, NIR and Vis absorption spectra; magnetic susceptibility data* (Karbowiak and Drożdżyński, 1993)
$RbUCl_4 \cdot 3H_2O$	greenish-brown to brown; hygroscopic and air sensitive; IR (cm^{-1}): *ν*(U–OH_2, rocking) = 650, 615, 600; *ν*(U–OH_2, wagging) = 485; *ν*(U–OH), stretching = 380, 285sh; *ν*(U–Cl), stretching = 255s, 220, 190; *ν*(U–Cl–U), stretching or lattice = 151, 157; *δ*(Cl–U–Cl), bending = 132, 127, 121, 118; *ν*(stretching and bending modes of coordinated water) = 1565, 1580, 1605, 3470; (93180, 3210, 3350, 3420, 3470); $\mu_{\mathrm{eff.}} = 3.57$ B.M. (100–300 K)[d], $C =$ 1.5766 emu·K·$mole^{-1}$, $\theta = -64$ K	monoclinic; $a = 8.8986$, $b = 6.9738$; $c = 8{,}0517$; $\beta = 100$; $Z = 2$; $V = 490.75$; *d*(calc.) = 3.51	*X-ray powder diffraction data; IR, NIR and Vis absorption spectra; magnetic susceptibility data* (Karbowiak and Drożdżyński, 1993)

Table 5.25 (*Contd.*)

Formula	*Selected properties and physical data*[b]	*Lattice symmetry, lattice constants* (Å)*, conformation and density* (g cm^{-3})[c]	*Remarks regarding information available and references*
$CsUCl_4 \cdot 3H_2O$	brown-green; soluble in polar organic solvents; $CsUCl_4 \cdot 3H_2O$; $\mu_{eff.} = 3.39$ B.M., $C = 1.430$ emu·K·$mole^{-1}$, $\theta = -67.7$ K. Free ion and crystal-field parameters: $F^2 = 39876(58)$, $F^4 = 33279(77)$, $F^6 = 23598(68)$, $\zeta_{5f} = 1648.3(10.3)$; $\alpha = 26.2(4.3)$, $\beta = -889(38)$, $\gamma = 1131(94)$; $T^2 = 306$, $T^3 = 42$, $T^4 = 188$, $T^6 = -242$, $T^7 = 447$, $T^8 = 300$; $M^0 = 0.672$, $M^2 = 0.372$, $M^4 = 0.258$; $P^2 = 1216$, $P^4 = 608$, $P^6 = 122$; $B_0^2 = -411(46)$ / [–390], $B_2^2 = 614(45)$ / [573], $\mathrm{Im}B_2^2 = 610(46)$ / [614], $B_0^4 =$ [–699], $B_2^4 =$ [–398], $\mathrm{Im}B_2^4 =$ [–525], $B_4^4 =$ [–1039], $\mathrm{Im}B_4^4 =$ [–49], $B_0^6 =$ [–1046], $B_2^6 =$ [–58], $\mathrm{Im}B_2^6 =$ [794], $B_4^6 =$ [–119], $\mathrm{Im}B_4^6 =$ [–173], $B_6^6 =$ [–27], $\mathrm{Im}B_6^6 =$ [–691], *rms* = 34; $n = 77$	monoclinic; C_{2h}^2, $P2_1/m.$, No. 11; $a = 7.116(1)$, $b = 8.672(2)$, $c = 8.071(2)$; $\beta = 99.28(3)$; $Z = 4$; $V = 956.96$; d(U–Cl) = 2.957(3×), d(U–O) = 2.552 (3×) (mean values); tricapped trigonal prism consisting of six Cl and three O atoms (representing the water molecules)	*single crystal diffraction data* (Krämer *et al.*, 1991*)*; *synthesis, magnetic susceptibility data; IR, NIR and Vis low temperature absorption spectra; crystal-field analysis* (Karbowiak *et al.*, 1993, 2000)
$NH_4UCl_4 \cdot 3H_2O$	greenish-brown to brown; hygroscopic and air sensitive; IR (cm^{-1}): ν(U–OH_2, rocking) = 615sh, 590s; ν(U–OH_2, wagging) = 470s; ν(U–OH), stretching = 385, 290sh; ν(U–Cl), stretching = 266s, 232; ν(U–Cl–U), stretching or lattice = 172; δ(Cl–U–Cl), bending = 147, 128; ν(stretching and bending modes	monoclinic; $a = 13.7693$, $b = 8.8990$, $c = 7.8643$; $\beta = 95.65$; $Z = 4$; $V = 956.95$; d(calc.) = 3.12	*X-ray powder diffraction data; IR, NIR and Vis absorption spectra; magnetic susceptibility data* (Karbowiak and Drożdżyński, 1993)

	of coordinated water) = 1585, 1600; $\nu_4(NH_4)$ = 1404 vs; $\nu_2(NH_4)$ = 1670, $\nu_4 + \nu_6(NH_4)$ = 1770, $2\nu_4 - \nu_5(NH_4)$ = 2710, $\nu_1(NH_4)$ = 3040, $\nu_3(NH_4)$ = 3110vs. $\mu_{eff.}$ = 3.71 B.M. (75–300 K)[d]; C = 1.7073 emu·K·mole^{-1}, $\theta = -54$ K		
UOCl	red; UOCl (cr): $\Delta_f G^o_m = -785.7$ (4.9)[†], $\Delta_f H^o_m = -833.9(4.2)^{\dagger}$, S^o_m = 102.5 (8.4)[†]; $C^o_{p,m} = 71.0$ (5.0)[†]. $\mu_{eff.}$ = 3.40 B.M. (240–300 K)[d]; $\theta = -145$ K	tetragonal; D^7_{4h}, $P4/nmm$, No. 129; (PbFCl type of unit cell); a = 4.043, c = 6.882; Z = 2; CN = 9; d(U–Cl) = 2.373(2×), d(U–Cl) = 3.074(1×), d(U–Cl) = 3.150(4×)	*single crystal diffraction data* (Schleid and Meyer; 1988; Brown and Edwards, 1972); *IR and magnetic susceptibility data* (Levet and Noël, 1981); *photo-electron spectra* (Thibaut *et al.*, 1982); *themodynamic data* (Grenthe *et al.*, 1992; Guillaumont *et al.*, 2003)
U(NH)Cl		tetragonal; D^7_{4h}, $P4/nmm$, No.129; a = 3.972(5), b = 3.972(5), c = 6.81 (1); Z = 2; V = 107.44; d(calc.) = 8.91	*crystallographic data* (Berthold, and Knecht, 1966)
$Cs_2U[Cl_9O_3(TaCl)_6]$		trigonal/rhombohedral; D^2_{3d}, $P\bar{3}1c$, No.163; a = 9.1824(5), c = 17.146(2); Z = 2; V = 1252.01; d(calc.) = 5.75	*structural and theoretical studies of bondings in the cluster* (Ogliaro *et al.*, 1998)
UBr_3	reddish-brown; air sensitive; soluble in acetic acid, dimethylacetamid; density: 6.53 g cm^{-3}; m.p. = 835°C, b.p. = 1537°C UBr_3(cr): $\Delta_f G^o_m = -673.2$ (4.2)[†], $\Delta_f H^o_m = -698.7$ (4.2)[†], S^o_m = 192.98 (0.50)[†]; $C^o_{p,m} = 105.83$ (0.50)[†]. UBr_3(g): $\Delta_f G^o_m = -408.1$ (20.5)[†], $\Delta_f H^o_m = -371$ (20)[†], S^o_m = 403.0 (15.0)[†]; $C^o_{p,m} = 85.2$ (5.0)[†]. $\log p(\text{mmHg}) = -16420T^{-1} + 22.95 - 3.02 \log T$ (298–1000 K). $\log p(\text{mmHg}) = -15000T^{-1} + 27.54 - 5.03 \log T$ (1000–1810 K)	hexagonal, (UCl_3 type of structure), C^2_{6h}, $P6_3m$, No.176; a = 7.942(2), c = 4.441(2), (a = 7.9519, c = 4.448; Z = 2, CN = 9; d(calc.) = 6.54; d(U–Br) = 3.145 (3.150) to the three capping Br atoms, d(U–Br) = 3.062(3.069∼) to the six Br atoms at the prism vertices, d(Br–Br) = 3.652(3.663) at the trigonal prism face edge and d(U–U) = 4.441Å (4.448) along the c-direction. The face Br–U–Br angle is 73.21(73.3). Values in parentheses were taken from Krämer and Meyer (1989)	*X-ray single crystal data* (Levy *et al.*, 1975; Krämer and Meyer, 1989); *magnetic susceptibility data*: (Jones *et al.*, 1974); *thermodynamic properties* (Rand and Kubaschewski, 1963; Grenthe *et al.*, 1992; Guillaumont *et al.*, 2003); *NIR, Vis and UV absorption spectra; fused salt systems* (Sobczyk *et al.*, 2003; Karbowiak *et al.*, 2003a; Brown, 1979); *photoelectron spectra* (Thibaut *et al.*, 1982)

Table 5.25 (*Contd.*)

Formula	*Selected properties and physical data*[b]	*Lattice symmetry, lattice constants* (Å)*, conformation and density* ($g\ cm^{-3}$)[c]	*Remarks regarding information available and references*
	$\mu_{eff.} = 3.57$ B.M. (25–76K)[d]; $\theta = -54$ K, $T_N = 15$ K; $\mu_{eff.} = 3.29$ B.M. (350–483K)[d]; $\theta =$ 25K, $T_N = 15$ K; Atomic and crystal-field parameters: $E_{avg} = 19213(74)$, $F^2 = 37796(265)$, $F^4 = 30940(313)$, $F^6 = 20985(315)$, $\zeta_{5f} = 1604(19)$; $\alpha = 27(8)$, $\beta = -823$ (54), $\gamma = 1647(168)$; $T^2 = 374(125)$, $T^3 = 29(34)$, $T^4 = 262(58)$, $T^6 = -258(77)$, $T^7 = 264(60)$, $T^8 = [300]$; $M^0 = [0.6630]$; $P^2 = 1707(89)$; $B_0^2 = 410(50)$, $B_0^4 = -452(86)$, $B_0^6 = -1637$ (77), $B_6^6 = 722(63)$; $n = 47$; *rms* = 36.5		
$UBr_3 \cdot 6H_2O$	red	monoclinic; *P*2/*n*; $a = 10.061$, $b =$ 6.833, $c = 8.288$; $\beta = 92.99$; $V =$ 285.00	*X-ray powder diffraction and thermal decomposition data* (Brown *et al.*, 1968)
K_2UBr_5	dark violet; Polar organic solvents; m.p. = 625°C – congruently; ν(U–Br) stretching vibrations (cm^{-1}): 110m, 124m, and 145s,br	orthorhombic; D_{2h}^{16}, *Pnma,* No. 62; $a = 13.328(1)$, $b = 9.2140(7)$, $c =$ 8.4337(5), $Z = 4$, $V = 1559.5(2)$; CN = 6; *d*(calc.) = 4.53	*X-ray powder diffraction data; magnetic data; NIR, Vis an UV absorption spectra* (Krämer *et al.*, 1993, 1994); *magnetic phase transitions* (Keller *et al.*, 1995); *IR and thermodynamic data* (Suglobova and Chirkst, 1978a; Fuger *et al.*, 1983); melting point diagrams (Vdovenko *et al.*, 1974a)
Rb_2UBr_5	violet; polar organic solvents; m.p. = 600°C – congruently; ν(U–Br) stretching vibrations (cm^{-1}): 111m, 124m, and 144s,br	orthorhombic; D_{2h}^{16}, *Pnma,* No. 62; $a = 13.670(1)$, $b = 9.3900(8)$, $c =$ 8.6046(4); $Z = 4$; $V = 1663.1(2)$. CN = 6	*X-ray powder diffraction data; magnetic data; NIR, Vis an UV absorption spectra* (Krämer *et al.*, 1994); *IR and thermodynamic data*:

			(Suglobova and Chirkst, 1978a; Fuger *et al.*, 1983); melting point diagrams (Vdovenko *et al.*, 1974a)
Cs_2UBr_5	violet; m.p. = 420°C, congruently; ν (U–Br) stretching vibrations(cm^{-1}): 110m, 124m, and 149s,br	rhombic; isostructural with Cs_2DyCl_5; $a = 15.79(4)$, $b = 9.85(5)$, $c = 7.90(1)$; $Z = 4$, CN = 6, d(calc.) = 4.85(4)	*X-ray powder diffraction data* (Volkov *et al.*, (1987); *IR and thermodynamic data* (Suglobova and Chirkst, 1978a,b; Fuger *et al.*, 1983); melting point diagrams (Vdovenko *et al.*, 1974a)
Rb_3UBr_6	dark-violet; m.p. = 695°C, congruently	cubic; face centered; $a = 11.03(2)$, d(calc.) = 4.79	*X-ray powder diffraction data* (Vodovenko *et al.*, 1974a).
Cs_3UBr_6	dark-violet; m.p. = 758°C, congruently;	cubic; face centered; $a = 11.51(2)$; d(calc) = 4.83	*X-ray powder diffraction data; thermodynamic properties* (Aurov and Chirkst, 1983)
K_2NaUBr_6	–	tetragonal; D_{4h}^3, *P4/nbm*, No. 125; $a = 10.81(1)$, $c = 11.30(1)$; $Z = 4$, d(calc.) = 4.09, d(exp.) = 4.04	*X-ray powder diffraction and thermodynamic data* (Aurov *et al.*, 1983); *thermodynamic properties* (Aurov and Chirkst, 1983)
Cs_2NaUBr_6	–	P-cubic; T_h^6, *Pa*3, No. 205; $Z = 4$, $a = 11.439(2)$, d(calc.) = 4.44	*X-ray powder diffraction and thermodynamic data* (Aurov *et al.*, 1983); *thermodynamic properties* (Aurov and Chirkst, 1983)
UOBr	$\mu_{eff.} = 3.67$ B.M. (250–300K)[d]; $\theta = -140$ K	tetragonal; (PbFCl type of unit cell), D_{4h}^7, *P4/nmm*, No.129; $a = 4.063(1)$, $c = 7.447(2)$; CN = 9	*X-ray powder diffraction data; IR and magnetic susceptibility data* (Levet and Noël, 1981; *photoelectron spectra* (Thibaut *et al.*, 1982)
$K_2UBr_5 \cdot 2CH_3CN \cdot 6H_2O$	brown-red		*magnetic susceptibility data; decomposition; IR, NIR and Vis and UV absorption spectra* (Zych and Drożdżyński, 1991)
$Rb_2UBr_5 \cdot CH_3CN \cdot 6H_2O$	blue-violet		*magnetic susceptibility data; decomposition; IR, NIR and Vis absorption spectra* (Zych and Drożdżyński, 1991)

Table 5.25 (*Contd.*)

Formula	*Selected properties and physical data*[b]	*Lattice symmetry, lattice constants* (Å), *conformation and density* ($g\ cm^{-3}$)[c]	*Remarks regarding information available and references*
$(NH_4)[UBr_2 \cdot (CH_3CN)_2 \cdot (H_2O)_5]Br_2$	grayish-green to brown crystalline solid; air sensitive; soluble in organic solvents like methanol, ethanol, formic acid, dimethyl-formamide, tributhylphosphate etc. IR (cm^{-1}): $\nu(H_2O)$ with hydrogen bond character = 3325s,b; (3114s,b; 2952w); $\nu(CH_3)$ = 2921w; (2851w); combination band = 2307w; $\nu_s(C{\equiv}N)$ = 2273w; $\delta(HOH)$ = 1606m; $\delta_{as}(CH_3)$ = 1399s; (1378s); $\delta_s(CH_3)$ = 1189w, 1144w; $\delta(U{-}OH_2)$ = 1078w; $\rho(CH_3)$ = 1044w; $\nu(C{-}C)$ = 971w, 938w, 922w; $\rho(U{-}OH_2)$ = 887w, 770w,721w; $\omega(U{-}OH_2)$ = 663vs,b, 670vs,b, 400–590s,vb; $\nu(U{-}OH_2)$ = 387m, 306m; $\nu(UN_2)$ = 202m; $\nu(UBr_2)$ = 157m,b, 115sh; $\delta(UBr_2)$ = 82w; (62w, 59w,47w, 37w) Raman; $\nu_s(C{\equiv}N)$ = 2280m; $\delta(HOH)$ = 1631m;$\delta_{as}(CH_3)$ = 1415w; (1356m); $\delta_s(CH_3)$ = 1261w, 1186w; $\delta(U{-}OH_2)$ = 1123m; $\rho(CH_3)$ = 1063m; $\nu(C{-}C)$ = 952w, 826w;	orthorhombic; D_{2h}^{16}, *Pnma* No. 62; $a = 8.98(2)$, $b = 9.99(2)$, $c = 20.24(4)$; $Z = 4$; $V = 1816(7)$ Å^3; d(U–Br1) = 3.074(4) (2×), d(U–O1) = 2.538(12) (2×), d(U–O2) = 2.549(14) (2×), d(U–N1) = 2.517(30) (1×), d(U–N2) = 2.688(26) (1×), d(U–O3) = 2.652(20) (1×), d(calc.) = 2.74	*single crystal diffraction data; magnetic susceptibility data; IR, Raman, NIR, Vis and UV spectra; factor group analysis* (Zych *et al.*, 1993; Zych and Drożdżyński, 1990b)

	$\rho(U–OH_2) = 729w$; $\omega(U–OH_2) =$ 651w, 611w, 536w; $\nu(U–OH_2) =$ 536w, 455m,b, 326w; $\nu(UN_2) =$ 282w; $\nu(UBr_2) = 195sh$, 149		
UI_3	black; extremely moisture sensitive, soluble: methanol, ethanol, ethyl acetate, dimethyl-acetamide, acetic acid; m.p. = 766°C; UI_3(cr): $\Delta_f G^o_m = -466.1$ (4.9)†, $\Delta_f H^o_m = -466.9$ (4.2)†, $S^o_m = 221.8$ (8.4)†; $C^o_{p,m} = 112.1$ (6.0)†; UI_3(g): $\Delta_f G^o_m = -198.7$ (25.2)†, $\Delta_f H^o_m = -137$ (25)†, $S^o_m = 431.2$ (10.0)†; $C^o_{p,m} = 86.0$ (5.0)†. $\mu_{eff.} = 3.65$ B.M. (25–200 K)[d]; $\theta = -34$ K, $T_N = 3.4$ K; $\mu_{eff.} = 3.31$ B.M. (350–394 K)[d]; $\theta = 5$ K	orthorhombic; ($TbCl_3$ and $PuBr_3$ structure type); D^{17}_{2h}, *Cmcm*, No. 63; $a = 4.334(6)$, $b = 14.024(18)$, $c = 10.013(13)$; $Z = 4$. The coordination polyhedron is a bicapped trigonal prism the third capping Br^- anion being withdrawn by bonding with another U atom; d(U–I1) = 3.165(12) (2×) and d(U–I2) = 3.244(8) (4×) (to the prism iodine atoms), d(U–I2) (2×) = 3.456(11) (to the cap iodine atoms), d(I2–I2) = 3.679(18) Å and d(U–U) = 4.328(5) Å. d(calc.) = 6.78	*X-ray single crystal and neutron diffraction data* (Zachariasen, 1948a; Levy *et al*., 1975; Murasik *et al*., 1981); *thermodynamic data* (Brown, 1979; Guillaumont *et al*., 2003); *e diffuse reflectance spectra* (Barnard *et al*., 1973); *magnetic data* (Dawson, 1951; Jones *et al*., 1974; Murasik *et al*., 1981; 1985)
$UI_3{\cdot}4CH_3CN$	dark-brown	monoclinic; $a = 9.6168$, $b = 8.7423$, $c = 7.1858$; $\beta = 92.99$; $Z = 2$; $V = 603.31$; d(calc.) = 4.08; d(U–Il) = 3.165(12) (2×) and d(U–I2) (4×) = 3.244(8) (to prism iodines), d(U–I2) (2×) = 3.456(11) (to cap iodine atoms), d(I2–I2) = 3.679(18) and d(U–U) = 4.328(5) Å	*X-ray powder diffraction data; magnetic susceptibility data; IR, NIR, Vis and UV absorption spectra* (Drożdżyński and du Preez, 1994)
$UI_3(THF)_4$	dark-purple	monoclinic; C^5_{2h}, $P2_1/c$; No. 14; $a = 8.750(3)$, $b = 16.706(16)$, $c = 17.697(16)$; $\beta = 93.64(3)$; $Z = 4$; $V = 2582$	*synthesis and reactivity; single crystal X-ray diffraction data; thermal gravimetric analysis; vibrational spectrum;* ^1H *NMR spectrum; electronic absorption spectrum* (Avens *et al*., 1994)

Table 5.25 (*Contd.*)

Formula	*Selected properties and physical data*[b]	*Lattice symmetry, lattice constants* (Å)*, conformation and density* (g cm^{-3})[c]	*Remarks regarding information available and references*
K_2UI_5	deep-blue	orthorhombic; D_{2h}^{16}, *Pnma*, No. 62; monocapped trigonal prisms [UCl_7] are connected via two opposite common edges to chains; CN = 6; $a = 14.293(1)$, $b = 9.8430(5)$, $c = 9.1067(5)$; $Z = 4$; $V = 1929.1(2)$; d(U–I) = 3.182 to 3.275; d(U–U) = 5.143 (interchain); d(U–U) = 7.778 (intrachain)	*X-ray powder diffraction data, magnetic data, NIR, Vis an UV absorption spectra, magnetic phase transitions* (Krämer *et al.*, 1994; Keller *et al.*, 1995); *low temperature absorption spectrum of* U^{3}*:*K_2LaI_5 (Andres *et al.*, 1996); *crystal-field analysis* (Karbowiak *et al.*, 1998a); *IR and thermodynamic data* (Suglobova and Chirkst, 1978)
Rb_2UI_5	blue-violet	orthorhombic; D_{2h}^{16}, *Pnma*, No.62; $a = 14.546(2)$, $b = 9.249(1)$, $c = 10.026(2)$; $Z = 4$; $V = 2031.1(5)$Å, CN = 6	*X-ray powder diffraction data; magnetic data; NIR, Vis and UV absorption spectra* (Krämer *et al.*, 1994); *IR and thermodynamic data* (Suglobova and Chirkst, 1978)
UOI	deep blue; $\mu_{eff.} = 3.56$ B.M. (220–300K)[d]; $\theta = -150$ K	tetragonal; (PbFCl type of unit cell), D_{4h}^{7}, *P4/nmm*; No. = 129; $a = 4.062(1)$, $c = 9.208(2)$; CN = 9	*X-ray powder diffraction data;IR and magnetic susceptibility data* (Levet and Noel, 1981)
$UBrCl_2$	black with a greenish tinge; m.p. = 800°C; $UBrCl_2$(cr): $\Delta_f G_m^o = -760.3(9.8)^{\dagger}$, $\Delta_f H_m^o = -812.1(8.4)^{\dagger}$, $S_m^o = 175.7(16.7)$		*thermodynamic data* (MacWood, 1958; Brown, 1979; Grenthe *et al.*, 1992; Guillaumont *et al.*, 2003)

UBr_2Cl	black with a greenish tinge; m.p. = 775°C; UBr_2Cl(cr) $\Delta_f G^o_m = -714.4$ (9.8)†, $\Delta_f H^o_m = -750.6$ (8.4)†, $S^o_m =$ 192.5 (16.7)†	*thermodynamic data* (MacWood, 1958; Brown,1979; Grenthe *et al.*, 1992; Guillaumont *et al.*, 2003)
other mixed halides: (i) UCl_2I; (ii) $UClI_2$; (iii) UBr_2I; (iv) $UBrI_2$.	extremely moisture sensitive; (i) black, m.p. ~750; (ii) black, m.p. ~725; (iii) black, m.p. ~700; (iv) black, m.p. ~690	

* Estimated values.

† Values recommended by the Nuclear Energy Agency (Guillaumont *et al.*, 2003).

[a] Values have been selected in part from review articles (Brown, 1979; Bacher and Jacob, 1980; Freestone and Holloway, 1991; Grenthe *et al.*,1992; Guillaumont *et al.*, 2003).

[b] m.p. = melting point (°C); b.p.. = boiling point (°C); (cr) = crystalline; (g) = gaseous; thermodynamic values in kJ mol^{-1}, or J K^{-1} mol^{-1} at 298.15 K, unless otherwise mentioned; $\Delta_f G^o_m$, standard molar Gibbs energy of formation; $\Delta_f H^o_m$, standard molar enthalpy of formation; S^o_m, standard molar entropy; $C^o_{p,m}$(J K^{-1} mol^{-1}), standard molar heat capacity; log p (mmHg) = $-AT^{-1} + B - C \log T$: vapor pressure equation for indicated temperature range; IR = infrared active; lat. = lattice vibrations; val. = valence vibrations; def. = deformation vibrations; all values in cm^{-1}; vs: very strong; s: strong; m: medium; ms: medium strong; w: weak; sh: shoulder; b: broad; C, Θ, paramagnetic constants from the Curie Weiss law $C = \chi_M(T-\Theta)$; $\mu_{eff} = 2.84\sqrt{C}$ - effective magnetic moment; T_N, ordering temperature; atomic and crystal-field parameters; F^k and ζ_{5f} = electrostatic and spin–orbit interaction; α, β, γ; = two-body correction terms; $T^i t_i$ (i = 2,3,4,6,7,8) = three-particle configuration interaction; M^j (j = 0, 2 and 4) = spin–spin and spin–other–orbit relativistic corrections; P^k (k = 2, 4 and 6) = electrostatically correlated spin-orbit perturbation; B^k_q, crystal-field parameters; values in brackets indicate parameter errors; parameters in square brackets were kept constant during the final fitting procedure; standard deviation: $rms = \sum \left[(\Delta_i)^2/(n-p)\right]^{1/2}$ [cm^{-1}], where Δ_i is the difference between the observed and calculated energies, n is the number of levels fitted and p is the number of parameters freely varied.

[c] All values are in Å and angles are in degrees; d, density [g cm^{-3}]; CN, coordination number, V = molar volume [cm^3 mol^{-1}].

[d] Temperature range with linear relationship of χ_M^{-1} against T.

spectra of co-doped (U^{4+},U^{3+}):Ba_2YCl_7 single crystals has been also reported (Karbowiak *et al.*, 2003c) Efficient luminescence was observed at 7 K from both the $^4G_{7/2}$ and $^4F_{9/2}$ levels of the U^{3+} ions and from the $^1D_2$ and $^1I_6$ levels of U^{4+}. For the U^{4+}ions a very strong anti-Stokes emission was noticed due to energy transfer processes. Contrary to U^{4+} for which emission was observed even at room temperature the emission of U^{3+} ions is strongly quenched by temperature. Owing to the presence of U^{3+} and U^{4+} ions in the host crystal, an energy transfer between these ions has been proved. Analyses of the nephelauxetic effect and crystal field splittings of the K_2UX_5 (X = Cl, Br or I) series of compounds have also been reported (Karbowiak *et al.*, 1998a).

The absorption spectra of $NH_4UCl_4 \cdot 4H_2O$ and $CsUCl_4 \cdot 3H_2O$ recorded at 298 and 4.2 K, presented in Fig. 5.38 (Karbowiak *et al.*, 2000) are typical for most uranium(III) compounds. In the 4000–15800 cm^{-1} region the spectra consist of relatively intense, sharp, and well-separated absorption lines.

A comparison of the spectra shows significant differences in the visible range connected with the appearance of strong and broad f–d bands, allowed by the Laporte rule. For $CsUCl_4 \cdot 3H_2O$ the first f–d bands are located at about 23000 cm^{-1}, while in $NH_4UCl_4 \cdot 4H_2O$ they are shifted about 5000 cm^{-1} toward the infrared region. For the isostructural series of complex halides of the composition U^{3+}:K_2LaX_5 (X = Cl, Br, I), the substitution of the Cl^- by I^- results in a significantly smaller shift of about 1000 cm^{-1} (Karbowiak *et al.*, 1998a). Drożdżyński (1985, 1991) and Karbowiak *et al.* (1996c) report a close relationship between the increase of covalence/decrease of the uranium–halogenide distances, and the red shift of the first intense f–d bands. The crystal-field symmetry is another factor, which can influence the position of the f–d bands. However, this seems to be a minor factor, since there is no simple dependence of the energy of the first f–d transition on the site symmetry of the U^{3+} ion. For example in K_2UCl_5 (C_s) and Cs_2NaUCl_6 (O_h) (Karbowiak *et al.*, 1998a,b) the first f–d transitions occur at similar energies of 14300 and 15000 cm^{-1}, respectively, while for UCl_3 (D_{3h}) they appear at 23000 cm^{-1} (Karbowiak *et al.*, 2002a). An extensive analysis of the $5f^3 \rightarrow 5f^26d^1$ transitions in low temperature absorption spectra of U^{3+} ions incorporated in various single crystals were reported by Seijo and Barandiran (2001), Karbowiak and Drożdżyński (2004) and Karbowiak (2005a,b). Temperature-induced line broadening and line shift measurements have been chosen as method for the determination of the electron–phonon coupling parameters for U^{3+} doped in K_2LaCl_5 (Ellens *et al.*, 1998), $LaCl_3$ and $LaBr_3$ single crystals (Karbowiak *et al.*, 2003d). The value of the electron–phonon coupling parameter, $\bar{\alpha}$, was found to be considerably lower in $LaCl_3$ than in K_2LaCl_5 but larger than that of Nd^{3+} in $LaCl_3$. The electron–phonon coupling is also stronger for U^{3+} in the tribromide as compared with the trichloride host; this has been attributed to a larger covalency of the first compound.

Intensity calculations of $5f^3 \rightarrow 5f^3$ transitions in tervalent uranium, based on the Judd–Ofelt theory were performed both for solution (Drożdżyński, 1978, 1984) and solid-state spectra (Drożdżyński and Conway, 1972, Karbowiak and

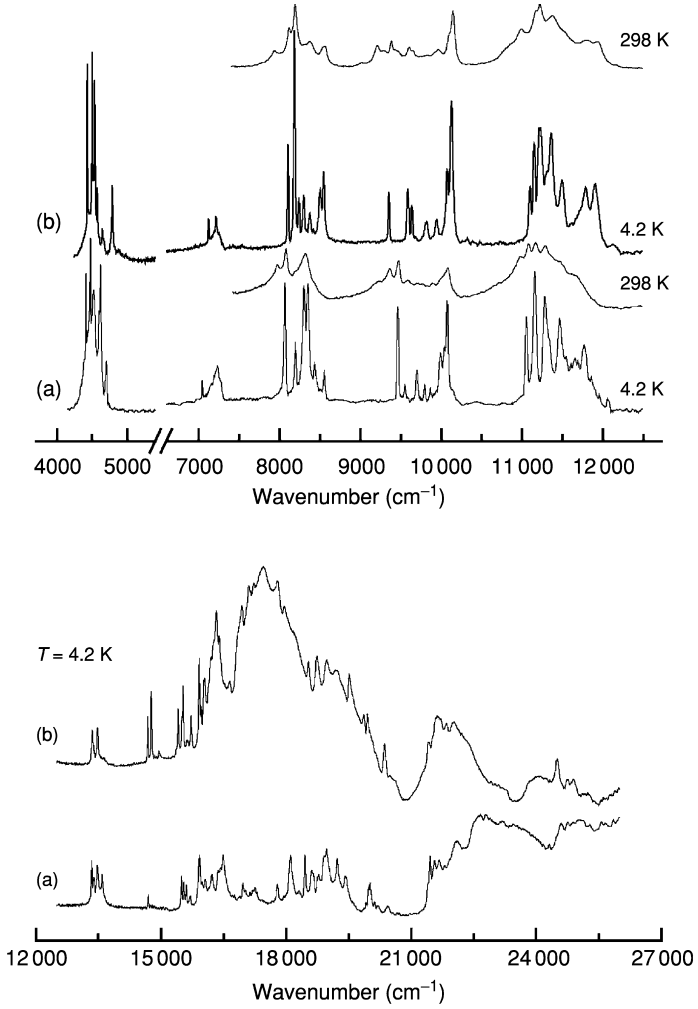

Fig. 5.38 *Absorption spectra of thin films of* $CsUCl_4 \cdot 3H_2O$ (*a*) *and* $NH_4UCl_4 \cdot 4H_2O$ *recorded at* 4.2 *and* 298 K (*from Karbowiak* et al., 2000 *reproduced by the permission of Elsevier*).

Drożdżyński, 2003). The analyses have shown a rather poor agreement between the observed and calculated oscillator strengths. So far, a relatively small r.m.s. deviation, of the order 10^{-6} to 10^{-7}, has been obtained only for the absorption spectra of UCl_3 in hexamethylphosphortriamide (Drożdżyński and Kamenskaya, 1978) and of UCl_3-doped $ZnCl_2$-based glass (Dereń *et al.*, 1998).

For almost all the halides and complex halides, magnetic susceptibility measurements were carried out over wide temperature ranges. The paramagnetic

constants from the Curie–Weiss law $\chi'_{m.} = C/(T - \theta)$ and the effective magnetic moments $\mu_{eff} = 2.84\mu_B$ were determined for a large number of compounds (see Table 5.25). The trihalides show remarkable cooperative effects, which were studied both experimentally (Murasik *et al*., 1980, 1985, 1986) and theoretically (Łyżwa and Erdös, 1987; Plumer and Caillé, 1989). UCl_3 and UBr_3 undergo an unusual magnetic phase transition for actinide compounds. A one-dimensional, short-range magnetic order along the *z*-axis of the hexagonal lattice develops at about 15 K for UBr_3 and 22 K for UCl_3, which results from strong antiferromagnetic interactions between the nearest neighbors. A three-dimensional ordering appears in UBr_3 and UCl_3 when the uranium magnetic moments order to a '0+–' configuration in each plane perpendicular to the *z*-axis at $T_N = 6.5$ and 5.3 K, respectively. At temperatures below $T_t = 2.7$ K for UBr_3 and $T_t = 2.5$ K for UCl_3 the magnetic moments exhibit smaller values and become oriented parallel to the equivalent *x*- or *y*-axis. The observed reorientation of the moments is reported to be rare in the actinide ions due to a usually strong anisotropy, which determines the direction of the moment (Santini *et al*., 1999).

An extensive physical analysis of the magnetic interactions and magnetic ordering phenomena, as well as the crystal-field splitting in the K_2UX_5 (X = Cl, Br or I) series of compounds, were performed on the basis of the Ising model (Keller *et al*., 1995). The application of elastic and inelastic neutron scattering experiments along with specific heat measurements made it possible to obtain a consistent picture of the magnetic phases. An analysis of the IR and Raman spectra of this series of compounds and of RbU_2Cl_7 is also available (Karbowiak *et al*., 1996a; Hanuza *et al*., 1999). Drożdżynski (1991) has summarized paramagnetic resonance measurements for U^{3+} ions substituted in CaF_2, SrF_2, and $LaCl_3$ single crystals. Some physical properties of tervalent uranium halides and related compounds are collected in Table 5.25.

(*i*) *Uranium trifluoride and uranium(III) fluoro complexes*

Uranium trifluoride

Uranium trifluoride is most conveniently prepared by reduction of UF_4 with metallic aluminum or finely powdered uranium. In the former case the reagents are placed in a graphite crucible and heated up to 900°C where the reaction proceeds smoothly and the excess of aluminum and by-products sublime from the reaction zone (Runnals, 1953). In the latter one, stoichiometric quantities of cleaned uranium turnings and UF_4 are placed in a nickel tube and heated to about 250°C in a stream of pure hydrogen (Warf, 1958). The finely divided UH_3 was decomposed at 400°C, after which the tube should be shaken in order to obtain an intimate mixture that was then heated to 700–900°C to give the pure trifluoride (Friedman *et al*., 1970). The reduction with other metals such as Be, Mg, Ti, or Zr, as well as UN or U_2N_3, at 900–950°C has also been found suitable for the synthesis. The use of the nitrates has some technical advantages since they prevent the formation of corrosive by-products. Reduction with Li,

Na, Cs, Mg, Ca, Sr, and Ba yields metallic uranium. The preparation of ultrapure UF_3 by reduction of UF_4 with hydrogen at 1020 to 1050 ($\pm$ 20)°C has been reported by Berndt and Erdman (1973).

Uranium trifluoride is a gray to black solid. Separate crystals show a deep-violet color under the microscope. As compared to other uranium(III) compounds the trifluoride is remarkably stable on air at room temperature. At higher temperatures UF_3 oxidizes and at 900°C it is quantitatively converted into U_3O_8. The compound is thermally unstable even in an inert atmosphere and disproportionates to UF_4 and U at about 1000°C and to a smaller extent (0.1% per hour) also at 800°C. UF_3 is insoluble in water and cold aqueous acids but slowly undergoes oxidation. This proceeds with the formation of uranium(IV) and uranyl compounds at 100°C. UF_3 dissolves rapidly in nitric acid–boric acid mixtures. Chlorine, bromine, and iodine react to give UF_3X (X = Cl, Br or I).

UF_3 has the LaF_3-type structure but the symmetry is reported to be either trigonal (space group $P\bar{3}c1$, D^4_{3d}, No. 185) or hexagonal (space group $P6_3cm$, C^3_{6v}, No. 165). Two coordination numbers 9 and 11 are also taken into consideration (Taylor, 1976a). Both structures may be considered as distorted ideal polyhedra with a bimolecular hexagonal cell (space group $P6_3/mmc$) (Schlyter, 1953). The polyhedra are fully capped trigonal prisms in which fluorine atoms (CN = 11) are located on all corners and outside the two triangular and the three square boundary planes. The main difference between the different structures is a slight displacement of the atoms forming the prism and the atoms outside the triangular surfaces normal to *c*-axis (Taylor, 1976a). Other crystallographic data are listed in Table 5.25.

A good quality absorption spectrum of UF_3 was obtained by means of the teflon disk technique (Schmieder *et al.*, 1970) and in chlorinated naphthalene at 4.2 K (Drożdżyński and Karbowiak, 2005). For the latter data a crystal-field analysis has also been performed. There is a large shift of the L′S′J′ multiplets towards higher wave numbers, as compared with other U^{III} low-temperature spectra. Some absorption spectra were also recorded in fused-salt systems: LiF–Be_2, LiF–BeF_2–ZrF_4, and LiF–NaF–KF (Martinot, 1984).

The magnetic susceptibility of UF_3 has been measured between 2 and 300 K (Berger and Sienko, 1967) and between 293 and 723 K (Nguyen-Nghi *et al.*, 1964). For both temperature ranges a linear relationship of $1/\chi'_M$ vs T was reported. The effective magnetic moment of 3.67 BM is close to the free ion value.

Uranium trifluoride monohydrate and uranium(III) fluoro complexes

$UF_3 \cdot H_2O$ was prepared from an uranium(III) solution in 1 M HCl or in anhydrous methanol by precipitation with ammonium fluoride (Barnard *et al.*, 1973). The green gelatinous precipitate appears in the latter case to be brown after drying due to some U(IV) impurities. The hydrate is reported to be far more reactive than the anhydrous fluoride and is immediately oxidized in air, giving a pale green uranium(IV) substance. The compound was characterized by magnetic susceptibility measurements, but the results may not be reliable.

The formation of a number alkali fluorouranates(III) and complexes of UF_3 with ZrF_4 has been known for a long time (Bacher and Jacob, 1980). KUF_4, K_2UF_5, K_3UF_6, Rb_3UF_6, and Cs_3UF_6 were prepared by heating UF_4 and metallic uranium with the appropriate alkali fluoride at 1000°C (Thoma *et al.*, 1966). $NaUF_4$ and Na_2UF_5 were identified during investigations of the binary fused-salt system $NaF–UF_3$. Some of the complex fluorides were characterized by X-ray powder diffraction (Table 5.25) but more detailed information is still not available.

$UZrF_7$ was prepared by reduction of a mixture of UF_4 and ZrF_4, either with metallic zirconium or with metallic uranium at about 800°C; UZr_2F_{11} was identified in a systematic study of the $UZrF_7–ZrF_4$ binary system (Fonteneau and Lucas, 1974). The fluorides are not stable and slowly oxidize even at room temperature. The compounds were characterized by magnetic susceptibility measurements in the 100–300 K range and by X-ray powder diffraction analyses (Table 5.25).

(*ii*) *Uranium trichloride and uranium(III) complex chlorides*

Uranium trichloride

Uranium trichloride may be prepared by a number of methods (Brown, 1979; Drożdżyński, 1991). One of the most convenient is the action of gaseous hydrogen chloride on uranium hydride. Attractive alternative methods involve the reduction of uranium tetrachloride with zinc, metallic uranium, or uranium hydride.

$$UH_3 + 3HCl \overset{350^\circ C}{\rightarrow} UCl_3 + 3H_2$$

$$3UCl_4 + Al \overset{400^\circ C}{\rightarrow} 3UCl_3 + AlCl_3$$

Small amounts of pure UCl_3 may also be prepared by thermal vacuum decomposition of $NH_4UCl_4 \cdot 4H_2O$ (Drożdżyński, 1988a, 1991). The compound obtained by the latter method is reactive and tractable for synthetic purposes, in contrast to that obtained by reduction with metals.

Uranium trichloride is obtained either in the form of a fine olive-green powder or as dark-red crystals. It is not soluble in anhydrous organic solvents but it dissolves somewhat in glacial acetic acid, showing a characteristic transient red color. UCl_3 dissolves in polar organic solvents, provided the compound or the solvents have absorbed some gaseous hydrogen chloride before. In aqueous solutions it is more or less rapidly oxidized. UCl_3 reacts with chlorine to form a mixture of higher valence chlorides, and with bromine and iodine to yield $UBrCl_3$ and UCl_3I, respectively. The reaction with ammonia, acetonitrile, tetrahydrofuran (THF), and phenazine yields a number of unstable adducts.

UCl_3 is hygroscopic, but in contrast to other uranium halides no absorption of water is reported at p_{H_2O} less than 320 Pa (2.4 mmHg). It is a strong reducing agent both in solution and in solid state. Several metals such as calcium or

lithium reduce UCl_3 to metallic uranium but the reaction has not been widely applied. UCl_3 melts at 837°C and disproportionates to U and UCl_4 at 840°C. A number of fused-salt systems containing UCl_3 have been investigated and the formation of some chloro complexes has also been reported (Bacher and Jacob, 1980).

Uranium trichloride has hexagonal symmetry (Zachariasen, 1948a,c; Murasik *et al.*, 1985; Schleid *et al.*, 1987) with the space group $P6_3/m - C_{6h}^2$. The coordination polyhedron is a symmetric tricapped trigonal prism arranged in columns in the *c*-direction. Each column is surrounded trigonally by three others at 1/2*c* in such a manner that the prism atoms of one chain become the cap atoms of the neighboring one. The packing view of UCl_3 along the [001] direction is shown on Fig. 5.39. The trichlorides Ac–Am and La–Nd have the same type of structure; some of the crystal data are listed in Table 5.25.

High-resolution polarized absorption spectra of $LaCl_3:U^{3+}$ single crystals (Karbowiak *et al.*, 2002) and unpolarized spectra of a polycrystalline UCl_3 sample in chlorinated naphathalene have been recorded at 4.2 K in the 4000–30000 cm^{-1} range (Sobczyk *et al.*, 2003). The experimental energy levels of the U^{3+} ion in the compounds were fitted to a semi-empirical Hamiltonian employing free-ion operators, one-electron crystal-field operators, and two-particle correlation crystal-field (CCF) operators, resulting in the determination of crystal-field parameters and the assignment/reassignment of the recorded $5f^3 \rightarrow 5f^3$ transitions. The effects of selected CCF operators on the splitting of

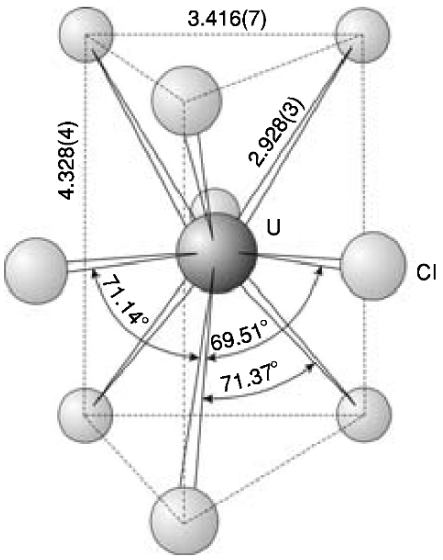

Fig. 5.39 *The tricapped trigonal prism configuration of halogen atoms in UCl_3 and UBr_3 (distances in* Å *are for UCl_3; after Murasik* et al., 1985).

some specific U^{3+} multiplets have also been investigated. The so far most accurate analysis of the band intensity, based on the Judd–Ofelt theory (Karbowiak and Drożdżyński, 2003), has been based on the obtained electronic wave functions and a room temperature absorption spectrum of UCl_3. A good agreement between the observed and calculated oscillator strengths has been obtained by combining the recorded band areas of some multiplets. In order to check the correctness of the calculations, the obtained intensity parameters, Ω_λ, have been used for the determination of transition probabilities and these in turn for the calculations of radiative lifetimes. A good-quality UCl_3 absorption spectrum has been obtained also by means of teflon disk technique (Schmieder *et al.*, 1970).

The magnetic properties of uranium trichloride have been the subject of extensive investigations (Santini *et al.*, 1999; Drożdżyński, 1991). The inverse magnetic susceptibility as a function of the temperature follows the Curie-Weiss law in two different temperature ranges and exhibits an antiferromagnetic transition at 22 K. Neutron diffraction studies revealed the existence of three-dimensional long-range anti-ferromagnetic ordering below the Néel temperature $T_N = 6.5$K (Murasik *et al.*, 1981, 1985).

Uranium trichloride hydrates and hydrated uranium(III) chloro complexes

Two hydrates of UCl_3 are known, the heptahydrate, $UCl_3 \cdot 7H_2O$ and the hexahydrate, $UCl_3 \cdot 6H_2O$. The heptahydrate was obtained by reduction of an UCl_4 solution consisting of acetonitrile, propionic acid, and water (Drożdżyński, 1985) with liquid zinc amalgam in an inert atmosphere whereas the reduction is most conveniently accomplished in an all glass apparatus with provisions for precipitation, filtration, and drying in an inert gas atmosphere (Drożdżyński, 1979). It is interesting to note that a few years earlier Habenschuss and Spedding (1980) predicted the possible formation of this compound on the basis of ionic size considerations. $UCl_3 \cdot 7H_2O$ is a crystalline ink-blue solid, readily soluble in numerous organic solvents. The compound is relatively resistant to oxidation by air at temperatures lower than 15°C. At higher temperatures it loses some of its crystallization water and in high vacuum it may be completely dehydrated at 200°C (Drożdżyński, 1985).

X-ray single crystal analyses of the heptahydrate and of the less hydrated $UCl_3 \cdot 6H_2O$ compound have been reported (Mech *et al.*, 2005) (see Table 5.25). In the heptahydrate the crystals are built from separate $[U_2Cl_2(H_2O)_{14}]^{4+}$ units and Cl^- ions. The characteristic features of this structure are dimers, formed by two uranium ions connected through the (Cl1) bridging chlorine atoms. Whereas the basic units of the crystal structure of $UCl_3 \cdot 6H_2O$ are Cl^- anions and $[UCl_2(H_2O)_6]^+$ cations. The basic units of the crystal structure of $UCl_3 \cdot 6H_2O$ are Cl^- anions and $[UCl_2(H_2O)_6]^+$ cations. The U atom is eight-coordinated through six water molecules and two chlorine atoms. In this structure the characteristic feature is the existence of hydrogen bonds, which link the uranium eight-coordinated polyhedra, forming a three-dimensional network.

The presence of water molecules in the inner coordination sphere was also confirmed by the solid-state absorption spectrum of $UCl_3 \cdot 7H_2O$, which is very similar with that of the U^{3+} aquo ion (Drożdżyński, 1978) and exhibits significant differences in comparison to those of the less hydrated uranium(III) complex chlorides (Zych and Drożdżyński, 1986; Drożdżyński, 1988b). A detailed crystal-field level analysis, based on a very good quality low-temperature spectrum, is also available (Karbowiak *et al.*, 2001). The heptahydrate exhibits Curie–Weiss dependence in the temperature range 10 to 300 K. The derived magnetic moment $\mu_{\text{eff.}} = 2.95$ B.M. is much lower than the 'free ion' value of ca. 3.7 B.M., presumably due to the crystal field of the water molecules.

The synthesis and characterization of a number of hydrated complex chlorides of the formulas $MUCl_4 \cdot 5H_2O$ (Barnard *et al.*, 1972b), $MUCl_4 \cdot 4H_2O$ (M = K, Rb or NH_4) (Drożdżyński, 1988b; Karbowiak and Drożdżyński, 1993), $MUCl_4 \cdot 3H_2O$ (M = Cs, K, Rb, or NH_4) (Karbowiak and Drożdżyński, 1993, 1999), and $UCl_3 \cdot CH_3CN \cdot 5H_2O$ (Zych and Drożdżyński, 1986) have been reported.

The pentahydrates were prepared by shaking a U(III) solution in 11 M HCl with the appropriate halide MCl (M = K, Rb, or NH_4) at 0°C. The U^{III} solution was prepared either by dissolving $U_2(SO_4)_3 \cdot 8H_2O$ or by dissolving a uranium (III) double sulphate in 11 M HCl (Barnard *et al.*, 1972a). The preparation of the tetrahydrates can be achieved using a general route reported by Drożdżyński (1979). In this method the reduction of a solution of UCl_4, methyl cyanide, propionic acid, and water with zinc amalgam in anaerobic conditions generates an immediate precipitation of the tetrachlorouranate(III) tetrahydrate (Drożdżyński, 1988b). The formation of the pentahydrates has not been confirmed by X-ray investigations. Apart from some expected similarities between the compounds of the series, one can also note differences, e.g. that the tetrahydrates are reported to be readily soluble in dry methanol or ethanol, in contrast to the pentahydrates. The tetrahydrates are also much more resistant to oxidation and hydrolysis in dry air and temperatures below 15°C, and can be easily transformed into the anhydrous salts by thermal dehydration at high vacuum. One may note also a red shift of the $5f^3 \rightarrow 5f^3$ transitions and relatively large differences in the plots of the reciprocal susceptibilities as well as in the derived effective magnetic moments.

Structure investigations revealed that $(NH_4)UCl_4 \cdot 4H_2O$ belongs to the orthorhombic system, space group $P2_12_12$. The crystal is built up from separate $[U(H_2O)_4Cl_4]^-$ and NH_4^+ ions. The eight-coordinated U^{3+} polyhedra are connected by O–H $\cdots$ Cl hydrogen bonds forming a three-dimensional network (Karbowiak *et al.*, 1996c). X-ray powder diffraction patterns show that the other members of the series could also be indexed on the basis of the orthorhombic cell (Karbowiak *et al.*, 1996c). $(NH_4)UCl_4 \cdot 4H_2O$ is an excellent starting material for the preparation of numerous other uranium(III) compounds.

The $MUCl_4 \cdot 3H_2O$ series of compounds was also obtained by reduction of appropriate acetonitrile solutions of UCl_4 and MCl (where M = K, Rb, Cs, or NH_4) with liquid zinc amalgam, but using somewhat different conditions than those used to prepare the tetrahydrates (Karbowiak and Drożdżyński, 1993). In contrast to the deep purple-red colors of the penta- and tetrahydrates the latter ones show green to brown colors. In this series the first broad and strong $5f^3 \rightarrow 5f^26d^1$ bands were observed in the absorption spectra at wavenumbers higher than 21000 cm^{-1}.

Single-crystal X-ray analysis is available for $CsUCl_4 \cdot 4H_2O$ (Krämer *et al.*, 1991). The compound crystallizes in the monoclinic system, space group: $P2_1/m$ (Table 5.25). Uranium has a coordination number of nine (tricapped trigonal prism) consisting of six chlorine atoms and three oxygen atoms (representing water) with mean distances of 2.957 and 2.552 Å, respectively. Cesium is surrounded by eight chlorine atoms in the shape of a distorted cube, which is capped by two non-bonded water ligands at a mean distance of 3.602 Å. One can view the structure as a linking of the polyhedra $[U(Cl1)_4(Cl2)_2(H_2O)_3]$ through two common edges of chloride (Cl1) ligands at two triangular faces of the trigonal prism of chloride ions to an infinite zigzag chain in the [010] direction. X-ray powder diffraction analyses show that the remaining three members of the series could be indexed on the basis of the same monoclinic cell, and that they presumably are isostructural.

For the tri- and tetrahydrates the first broad and strong $5f^3 \rightarrow 5f^26d^1$ bands are observed in the absorption spectra at about 21500 and 16000 cm^{-1}, respectively. The red shift of these bands has been attributed to the formation of inner sphere complexes with some of the uranium–ligand bond lengths of a markedly more covalent character than that of the U^{3+} aqua-ion, e.g. in $UCl_3 \cdot 7H_2O$ (Drożdżyński, 1991; Karbowiak *et al.*, 1996c). The magnetic susceptibility constants from the Curie–Weiss law are listed in Table 5.25.

Anhydrous uranium(III) chloro complexes

The largest group of well-characterized uranium(III) compounds is formed by chloro complexes such as $CsUCl_4$ (Karbowiak and Drożdżyński, 1998c), M_2UCl_5 (M = K, Rb, Cs. or NH_4) (Drożdżyński and Miernik, 1978; Meyer *et al.*, 1983), $SrUCl_5$ (Karbowiak and Drożdżyński, 1998b), $[(CH_3)_3N]_3UCl_6$ (Karbowiak *et al.*, 1996a); MU_2Cl_7 (M = K, Rb, Ph_4As or Ph_4P) (Drożdżyński, 1991; Karbowiak *et al.*, 1996b); Ba_2UCl_7 (Karbowiak *et al.* 1998d); M_2NaUCl_6 (M = K, Rb or Cs) (Aurov *et al.*, 1983; Volkov *et al.*, 1987), and Cs_2LiUCl_6 (Karbowiak and Drożdżyński, 1998a).

Most of the complex chlorides can be conveniently prepared by heating stoichiometric amounts of the component halides in graphite-coated quartz tubes. The $(NH_4)_2UCl_5$, $Ph_4AsU_2Cl_7$, and $Ph_4PU_2Cl_7$ compounds were obtained by reduction of appropriate uranium tetrachloride solutions in

acetonitrile with liquid zinc amalgam (Drożdżyński, 1991; Drożdżyński and Miernik, 1978). Also the complexes with the general formulas M_2UCl_5 and MU_2Cl_7 can be prepared in this way (Drożdżyński, 1979). All the syntheses were carried out in an inert atmosphere or high vacuum of ca. 10^{-4} Pa. Spectroscopic studies and crystal-field analysis of U^{3+}:RbY_2Cl_7 and U^{3+}:Li_2NaYCl_6 single crystals were reported by Karbowiak *et al.* (1996b, 1977) and Karbowiak *et al.* (1996e, 1998b), respectively.

The formation of number of uranium(III) chloro complexes has also been observed during investigations of binary and ternary phase systems (Brown, 1979). The complexes display a variety of colors (Table 5.25). All of them are hygroscopic but are somewhat resistant to oxidation in dry air. Unlike UCl_3 the complex chlorides are readily soluble in numerous polar organic solvents.

K_2UCl_5 and Rb_2UCl_5 crystallize in the orthorhombic system and are isotypical with the K_2PrCl_5/Y_2HfS_5 structures, their space group is *Pnma*, $Z = 4$ (Krämer *et al.*, 1994). The coordination polyhedron is a monocapped trigonal prism [UCl_7], connected via two opposite common edges to chains, $[UCl1_{1/1}Cl2_{1/1}Cl3_{1/1}Cl4_{4/2}]^{-2}$, that run in the [010] direction of the unit cell. The relatively short U^{3+}–U^{3+} distance through the common edge, equal to 4.556 Å, is assumed to be responsible for antiferromagnetic transitions at 8.6 to 13.2 K. The temperature dependence of the inverse molar susceptibilities in the 20–300 K range follows the Curie–Weiss law in two temperature ranges, separated by a slight but apparent break at 130, 150, and 220 K, respectively, for K_2UCI_5, Rb_2UCl_5, and $(NH_4)_2UCl_5$. The effective magnetic moments range from 3.47 B.M. for $(NH_4)_2UCl_5$ to 3.99 B.M. for K_2UCI_5 (Drożdżyński and Miernik, 1978). Some other magnetic susceptibility constants determined from the Curie–Weiss law are listed in Table 5.25.

Solid-state electronic spectra of thin mulls of the compounds show all characteristic features of the uranium(III) complex anions with strong $5f^3 \rightarrow 5f^26d^1$ bands starting at ca. 18000 cm^{-1}. The complexes exhibit very similar far-IR spectra with one broad and not well-resolved band in the region 100–240 cm^{-1} assigned to U-Cl stretching modes. An analysis of magnetic phase transitions and crystal-field splittings in the K_2UX_5 (X = Cl, Br, or I) series of complex halides is reported by Keller *et al.*(1995).

Single-crystal X-ray data show that Cs_2NaUCl_6 (Spirlet *et al.*, 1988) crystallizes with the ideal cryolite arrangement. Each of the uranium or sodium ions is octahedrally surrounded by six chloride ions at the distance of 2.723(9) and 2.746(9) Å, respectively. The cesium ions (site symmetry T_d) are surrounded by 12 equidistant chloride ions with d(Cs–Cl) = 3.867(8) Å (for other data see Table 5.25). The enthalpies of formation of the hexachloro complexes are also available (Aurov and Chirkst, 1983; Schoebrechts *et al.*, 1989).

It is interesting to note the preparation of a reduced metallic uranium chloride which has been formulated as NaU_2Cl_6 or $(Na^+)(U^{3+})_2(e^-)(Cl^-)_6$ (Schleid and

Meyer, 1989). The extra electrons provided by the incorporation of the sodium atom are reported to occupy the 6d band of uranium. The compound is isostructural with $NaPr_2Cl_6$ and may be described as a stuffed derivative of UCl_3 (hexagonal symmetry, space group $P6_3/m$). Other available information about the compounds is compiled in Table 5.25.

Complexes of UCl_3 with neutral donor ligands

Ammonia adducts of the composition $UCl_3 \cdot 7NH_3$ and $UBr_3 \cdot 6NH_3$ were obtained by treatment of the halides with gaseous ammonia at room temperature and a pressure of 1013 hPa (Eastman and Fontana, 1958; Berthold and Knecht, 1965b, 1968). Since heating in a stream of nitrogen up to 45°C formed a relatively stable $UCl_3 \cdot 3NH_3$ complex, indicating that the compounds contain some loosely bound ammonia. At higher temperatures this adduct decomposes into $UCl_3 \cdot NH_3$, which is stable up to 300°C.

According to MacCordick and Brun (1970) the heating of UCl_3 with an excess of acetonitrile in sealed tube at 80°C results in the separation of a brown, hygroscopic solid of the formula $UCl_3 \cdot CH_3CN$. However, an attempt to repeat the preparation was unsuccessful (Barnard *et al.*, 1973).

A purple adduct of the composition $UCl_3(THF)_x$ has been prepared by reduction of a UCl_4 solution in THF with stoichiometric amounts of NaH or an excess of Na_2C_2. The obtained purple solution of $UCl_3(THF)_x$ is reported to be a useful starting material for numerous syntheses (Moody and Odom, 1979; Andersen, 1979; Moody *et al.*, 1982).

Hart and Tajik (1983) have reported the preparation of numerous air sensitive uranium(III) complexes with cyclic polyethers and aromatic diamines by reduction with liquid zinc amalgam in acetonitrile or acetonitrile/propionic acid solutions of UCl_4 and the appropriate ligand, e.g. $(UCl_3)_3$(benzo-15-crown-5)$_2 \cdot 1.5CH_3CN$ (yellow-orange), $(UCl_3)_3$(benzo-15-crown-5)$_2$ (deep red), UCl_3 (cyclohexyl-15-crown-5) (red-purple), $(UCl_3)_3$(18-crown-6)$_2$ (red-brown), $(UCl_3)_5$(dibenzo-18-crown-6)$_3$ (deep-red), $(UCl_3)_5$(*cis-syn-cis*-dicyclohexyl-18-crown-6)$_3$ (red), UCl_3(1,10 phenantroline)$_2$ (violet-purple) and UCl_3(2,2′-bipyridile)$_2$. The complexes are insoluble or react with common organic solvents. The preparation of several trivalent uranium complexes with crown ethers, oxygen donor or amine ligands has also been reported by other authors e.g. UCl_3(15-crown-5)(red), UCl_3(18-crown-6), UCl_3(benzo-15-crown-5) (red) by Moody *et al.* (1979, 1982), as well as $(UCl_3)_3$(18-crown-6)$_2$ (red-brown), $(UCl_3)_2$(2,2′-bipyridine)$_3$ (bright-green) and $(UCl_3)_2$(dimethoxyethane)$_3$ (brown) by Rossetto *et al.* (1982). All complexes are hygroscopic and more or less rapidly oxidized by atmospheric air. They exhibit some characteristic features of U(III) absorption spectra with very intense f–d transitions in the visible and/or ultraviolet region. Infrared data are indicative to decide if the coordination takes place through the ligand nitrogen or oxygen atoms. Some of the complexes have also been characterized by magnetic susceptibility measurements at 298 K (Hart and Tajik, 1983).

(*iii*) *Uranium tribromide and uranium(III) bromo complexes*

Uranium tribromide

Uranium tribromide can most conveniently be prepared by the reaction of uranium hydride with gaseous hydrogen bromide at 300°C. The method is also suitable for a large-scale preparation (Brown, 1979). Alternative methods include the reduction of UBr_4 by metallic zinc or finely divided uranium at about 600°C. Since UBr_3 reacts with quartz at that temperature, the reaction ought to be performed in a sealed tantalum or molybdenum vessel. In small quantities it may be readily prepared by thermal vacuum decomposition of $NH_4UBr_4 \cdot 5CH_3CN \cdot 6H_2O$ (Zych and Drożdżynski, 1990a). Other preparation procedures such as a direct combination of the elements or the reaction between uranium oxalate and gaseous hydrogen bromide seem to be less convenient (Brown, 1979).

UBr_3 is a dark-brown substance, much more hygroscopic and sensitive to oxidation in air than UCl_3. Rapid oxidation occurs on dissolution in water and in numerous organic solvents. It gives, however, somewhat more stable solutions in formamide, methyl acetate, dimethylacetamide, and acetic acid. Reactions with chlorine and bromine yield UCl_4 and UBr_4, respectively. UBr_3 is reduced by calcium to metallic uranium at high temperatures.

Uranium tribromide is isostructural with UCl_3. The unit cell data are given in Table 5.25. The interatomic distances of the tricapped trigonal prismatic coordination polyhedron obtained from neutron diffraction studies (Levy *et al.*, 1975) and by Krämer and Meyer (1989) (values in parentheses) are: d(U–Br) = 3.145 Å (3.150 Å) to the three capping Br atoms, d(U–Br) = 3.062 Å (~3.069 Å) to the six Br atoms at the prism vertices, d(Br–Br) = 3.652 Å (3.663 Å) at the trigonal prism face edge and d(U–U) = 4.441 Å (4.448 Å) along the c-direction.

Using low-temperature, high-resolution absorption and fluorescence spectra of UBr_3 doped into single crystals of $LaBr_3$ (Paszek, 1978) and K_2LaBr_5 (Karbowiak *et al.*, 1998a) a complete crystal-field analysis in the 4000–22000 cm^{-1} absorption range has been performed. Magnetic susceptibility measurements in the 4.5–483 K range show an antiferromagnetic transition at $T_N = (15 \pm 0.5)$ K. The effective magnetic moments equal to 3.92 and 3.57 B.M. have been determined from the temperature ranges where a plot of $1/\chi_M$ against T is linear.

Uranium tribromide hexahydrate

Uranium tribromide may be converted to the hexahydrate by controlled exposure to oxygen-free water vapor (Brown *et al.*, 1968). On prolonged pumping the obtained red-colored hexahydrate slowly loses most of the coordinated water until the composition approximates $UBr_3 \cdot H_2O$. Complete dehydration occurs with a slow and gradual increase of temperature to about 100°C. X-ray powder diffraction pattern shows that $UBr_3 \cdot 6H_2O$ is isostructural with the

monoclinic lanthanide trihalide hexahydrates (Table 5.25). Further information is not available.

Uranium(III) bromo complexes

Bromouranates(III) of the composition M_2UBr_5 and M_3UBr_6 (M = K, Rb or Cs) have been identified during investigations of the binary fused-salt systems (Vdovenko *et al.*, 1974a; Volkov *et al.*, 1987). The pentabromouranates(III) may also be prepared by fusion of the appropriate components. Complexes of the M_3UBr_6 type are high-temperature phases and decompose on cooling into the alkali bromide and the corresponding pentabromouranate(III). The melting points and regions of existence of the hexabromouranates(III) increase with an increase in the atomic number of the alkali metal. An opposite tendency is observed in the series of pentabromouranates(III) (Vdovenko *et al.*, 1974a). Suglobova and Chirkst (1978a) have reported the thermodynamic properties of some of the bromo complexes.

X-ray powder diffraction analyses reveal that the hexabromouranates(III) have a face-centered cubic symmetry whereas the pentabromouranates(III) are isostructural with the rhombic Tl_2AlF_6. On this basis, it has been assumed (Suglobova and Chirkst, 1978b) that the structure of the pentabromouranates (III) contains distorted UBr_6 octahedra, which combine into parallel chains through common vertices. Aurov *et al.* (1983) and Aurov and Chirkst (1983) have reported X-ray powder diffraction and thermodynamic data for K_2NaUBr_6 and Cs_2NaUBr_6 by (Table 5.25).

A royal-blue $UBr_3(THF)_4$ adduct has been obtained by a gentle dissolution of uranium metal turnings in THF at a reaction temperature near 0°C (Avens *et al.*, 1994). The compounds $K_2UBr_5 \cdot 2CH_3CN \cdot 6H_2O$, $Rb_2UBr_5 \cdot CH_3CN \cdot 6H_2O$ and $(NH_4)[UBr_2(CH_3CN)_2(H_2O)_5]Br_2$ were obtained from acetonitrile solutions of UBr_4 and the appropriate ammonium or alkali metal bromide, by reduction with liquid zinc amalgam (Zych and Drożdżyński, 1990b, 1991; Zych *et al.*, 1993). All compounds are well characterized by various physical methods (Table 5.25). Single crystal X-ray data are available for $(NH_4)[UBr_2(CH_3CN)_2(H_2O)_5]Br_2$, (Zych *et al.*, 1993).

(*iv*) *Uranium(III) iodide and uranium(III) iodo complexes*

Uranium triiodide

A convenient and widely used method for the preparation of uranium triiodide involves the action of iodine vapors on finely divided uranium metal, either in sealed or flow systems at 570 and 525°C, respectively. Large quantities of high purity UI_3, in the form of black crystals, are collected in the 375–450°C condensing zone of a flow system apparatus first reported by Gregory (1958). Alternative procedures employ the reduction of uranium tetraiodide with zinc metal or finely divided uranium metal, reaction between uranium hydride and

methyl iodide, and vacuum thermal decomposition of UI_4 at 225–235°C (Brown, 1979).

UI_3 is a jet-black, highly hygroscopic crystalline solid, sensitive to oxidation in air. Even at elevated temperatures the triiodide is corrosive and attacks glass, which at 800°C is reduced to silicon. The compound reacts with iodine, methylchloride, and uranium tetrachloride to yield UI_4, UCl_4, and $UClI_3$, respectively. UI_3 dissolves in aqueous solutions, methanol, ethanol, ethyl acetate, dimethylacetamide, and acetic acid forming unstable U(III) solutions. Spontaneous oxidation within 1 min was observed in organic solvents like dioxan, pyridine, acetonitrile, dimethylformamide, or acetone (Barnard *et al.*, 1973).

UI_3 possesses the orthorhombic $PuBr_3$-type structure (Zachariasen, 1948a). The structure (space group *Ccmm* - D_{2h}^{17}) was studied in detail also by neutron diffraction profile analysis (Levy *et al.*, 1975; Murasik *et al.*, 1981). The coordination polyhedron is a distorted bicapped trigonal prism layered in planes perpendicular to the *a*-axis.

Diffuse reflectance spectra have been reported in the 4000–30000 cm^{-1} range at room temperature and 90 K (Barnard *et al.*, 1973). In the series of uranium (III) halides one may observe a pronounced red shift of the first $5f^3 \rightarrow 5f^2 6d^1$ bands from about 23000 cm^{-1} in the spectrum UF_3 to about 13400 cm^{-1} forUI_3.

Magnetic susceptibility measurements have shown an antiferromagnetic transition at $T_N = (3.4 \pm 0.2)$ K as well as a second susceptibility maximum at 1.5 K. UI_3 exhibits a first-order magnetic phase transition. The compound orders antiferromagnetically at $T_N = 2.6$ K, resulting in the appearance of a magnetic sublattice (Parks and Moulton, 1968). Neutron scattering investigations reveal hysteresis of the integretated neutron intensity of the magnetic reflections versus temperature, which confirms that the phase transition is of the first order (Murasik *et al.*, 1986).

Complexes with neutral donor ligands

The reaction of elemental iodine with an excess of oxide-free uranium metal turnings in appropriate coordinating solvents at 0°C yields dark purple $UI_3(THF)_4$, purple $UI_3(dme)_4$, black $UI_3(py)_4$ (Avens *et al.*, 1994), and a dark brown $UI_3(CH_3CN)_4$ (Drożdżyński and du Preez, 1994) (THF, tetrahydrofuran; dme, 1,2-dimethoxyethane; py, pyridine). These organic-solvent soluble Lewis base adducts are reported to be key starting materials for the preparation of variety of inorganic and organometallic uranium complexes. Single-crystal X-ray diffraction data show that $UI_3(THF)_4$ is mononuclear with a pentagonal bipyramidal coordination geometry about the uranium ion. Two iodide atoms, with an average U–I lengths of 3.111(2) Å are axially coordinated. The third iodide atom and the four THF ligands lie in the equatorial plane with the U–I distance of 3.167(2) Å and average U–O distances of 2.52(1) Å (Avens *et al.*, 1994). Other available information is listed in Table 5.25.

(*v*) *Uranium*(III) *oxide halides and mixed halides*

The uranium(III) oxide halides UOCI, UOBr, and UOI were prepared by heating stoichiometric mixtures of UO_2X_2, UO_2, and U or UX_4, U_3O_8 and U (X = Cl, Br or I), for 24 h at 700°C (Levet and Noël, 1981). The chemical properties of UOCI, UOBr, and UOI have not been reported.

The X-ray powder diffraction patterns are consistent with the tetragonal PbFCl-type of structure (*P*4/*nmm*). In a recent investigation, the structure was refined by single-crystal X-ray analysis and the atomic positions were determined (Schleid and Meyer, 1988). A plot of the inverse paramagnetic susceptibility against temperature follows the Curie–Weiss law from about 220 to 300 K with μ_{eff} of 3.40, 3.67, and 3.56 B.M. for UOCl, UOBr, and UOI, respectively. All of the oxide halides are weak ferromagnets with nearly the same transition temperatures ranging from 190 to 183 K. Some IR data are also available (Levet and Noël, 1981).

The preparation of a number of uranium(III) mixed halides with the general formulas UXY_2 and UX_2Y, where X = Cl or Br and Y = Cl or I were reported (Gregory, 1958), but very little information about their properties is available. $UClBr_2$ was obtained by reduction of UCl_3Br with hydrogen at 400°C. The UBr_3 by-product is removed from the substance by treatment with iodine. One of the most convenient methods for the preparation of UCl_2Br is reported to be the fusion of a 2:1 molar ratio of UCl_3 and UBr_3 at 850°C. The solid-state reaction between UCl_3 and UI_3 has been also applied successfully for the preparation of $UClI_2$. The remaining mixed halides, i.e. UCl_2I, UBr_2I, and $UBrI_2$ have usually been obtained by thermal decomposition of UCl_2I_2 and UBr_2I_2 at 400°C, and of $UBrI_3$ at 375°C (see also Table 5.25).

(b) Tetravalent halides and complex halides

Uranium tetrahalides and complex halides have so far been the most extensively investigated group of uranium compounds besides those in the 6+ oxidation state. The tetrahalides are not stable on exposure to air however with some exceptions, e.g. that of UF_4. They are more or less hygroscopic and after a time the compounds get oxidized in air. The large chemical stability of UF_4 is mainly due to its high lattice energy. Apart from the fluorides most of the compounds are readily soluble in polar solvents. Aqueous solutions are slowly oxidized to U(VI) species, but in pure and thoroughly deoxygenated solvents U^{4+} is fairly stable. The typical colors vary from pale olive green to deep bluish-green. In few cases black, brown, and blue colors have also been noticed (Table 5.26). The synthesis of binary uranium(IV) halides usually requires strictly oxygen-free conditions. The coordination polyhedra in the binary tetrahalides are more or less distorted forms of a square antiprism (UF_4), a dodecahedron (UCl_4), or a pentagonal bipyramid (UBr_4). The tetrahalides form stable solid complexes with a large variety of ligands, e.g. of the UX_4L_2-type (X = Cl. Br, or I)

Table 5.26 *Properties of selected uranium(IV) halides and complex halides.*[a]

Formula	*Selected properties and physical constants*[b]	*Lattice symmetry, lattice constants* (Å), *conformation and density* (g cm^{-3})[c]	*Remarks regarding information available and references*
UF_4	emerald green; non-volatile; almost insoluble in water and organic solvents; soluble in oxidizing solutions; m.p. = 1036°C; density: 6.70 g cm^{-3}; $\mu_{eff.} = 3.28$ B.M.; $\theta = -116$ K (77–500 K)[d]; $\mu_{eff.} = 2.83$ B.M.; $\theta = -146$ K (75–295K)[d]; $\mu_{eff.} = 2.79$ B.M; (1–300 K)[d] UF_4(cr): $\Delta_f G^o_m = -1823.5$ (4.2)†, $\Delta_f H^o_m = -1914.2$ (4.2)†, $S^o_m = 151.7$ (0.2)†; $C^o_{p,m} = 116.0$ (0.1)†. UF_4(g): $\Delta_f G^o_m = -1576.9$ (6.7)†, $\Delta_f H^o_m = -1605.2$ (6.5)†, $S^o_m = 360.7$ (5.0)†; $C^o_{p,m} = 95.1$ (3.0)†. log$p$(mmHg) = 22.60–16400T^{-1} – 3.02 log$T$ (298–1309 K). log p(mmHg) = 28.05–15300·T^{-1} –5.03 log$T$ (1309–1755 K); IR (cm^{-1}): 404(s)[ν(U–F)]; 194 (s) [ν(F–U–F), bending]; Energy levels parameters (cm^{-1}): $F^2 = 44\,784$, $F^4 = 43107$, and $F^6 = 25654$; $\zeta_{5f} = 1761.0(3.4)$, $\alpha = 34.74$, $\beta = -767.3$, and $\gamma = 913.9$; $P^2 = 2715$ (94); $B^2_0 = 1183(28)$, $B^2_2 = 29(27)$, $B^4_0 = -2714(99)$, $B^4_2 = 3024(71)$, $B^4_4 = -3791(53)$, $B^6_0 = -1433$ (148),$B^6_2 = 1267(101)$, $B^6_4 = -1391$ (93) and $B^6_6 = 1755(82)$; $rms = 31$; $n = 69$	monoclinic; C^6_{2h}, $C2/2$, No. 15; $a =$ 12.73 [12.7941], $b = 10.753$ [10.7901]; $c = 8.404$ [8.3687 90]; $\beta = 126.33$ [126.25]; [$V = 931.68$]; $Z = 12$; d(calc.) = 6.71], d(exp.) = 6.71; d(U–F) distances: 2.23–2.354. Antiprism linked in 3-dimensions by sharing all corners. Each uranium atom has eight fluorine neighbours arranged in a slightly distorted square antiprism. In square brackets are given the data of Kern *et al*., (1994)	*synthesis* (Halstead *et al*., 1982; Bacher and Jacob, 1980, Freestone and Holloway, 1990); *crystallographic data and temperature variation of structural parameters*, (Larson *et al*., 1964; Keenan and Asprey, 1969; Kern *et al*., 1994); *thermodynamic data* (Grenthe *et al*., 1992; Guillaumont *et al*., 2003); *magnetic data, IR, NIR; Raman spectra; Photo-acoustic spectra, ESCA spectra; redox reactions; applications for nuclear fuel* (Conway, 1959; Bacher and Jacob, 1980; *crystal-field spectra* (Carnall *et al*., 1991); *Vis and UV spectra* (Conway, 1959; Bacher and Jacob, 1980); *photo-electron spectra* (Thibaut *et al*., 1982)

Table 5.26 (*Contd.*)

Formula	*Selected properties and physical constants*[b]	*Lattice symmetry, lattice constants* (Å), *conformation and density* (g cm^{-3})[c]	*Remarks regarding information available and references*
$UF_4 \cdot 4/3H_2O$	grass-green	monoclinic; $d = 5.79$. The water molecules are bonded through O–H–F bridges	*crystallographic data* (Gagarinskii *et al.*, 1965; Khanaev *et al.*, 1967)
$UF_4 \cdot 2H_2O$	IR (cm^{-1}): 2950, 3365, and 3840	cubic; O_h^5, $Fm\bar{3}m$, No.225; a = 5.701(0.012); d(calc.) = 6.32; $Z = 2$; d(U–U) = 2.465, d(F–F) = 2.846	*crystallographic data* (Dawson *et al.*, 1954; Bakakin, 1965), *NMR data* (Gabuda *et al.*, 1969)
$UF_4 \cdot 2.5H_2O$	slightly soluble in water (0.1g L^{-1}), soluble in dimethylammonium acetate; stable up to 100°C; $UF_4 \cdot 2.5H_2O$ (cr): $\Delta_f G_m^o$ = –2440.3 (6.2)†, $\Delta_f H_m^o$ = –2671.5(4.3)†, S_m^o = 263.5(15.0)†; $C_{p,m}^o$ = 263.7 (15.0)†	orthorhombic; D_{2h}^{16}, *Pnam,* No.62; a = 12,75, b = 11.12, c = 7.05; d(calc.) = 4.74; $Z = 8$; d(U1–F) (5×) = 2.29; d(U1–O) (4×) = 2.63–2.84; d(U2—F) (9×) = 2.39	*crystallographic data* (Dawson *et al.*, 1954; Borisov and Zaniedporovski, 1971; Zadneporovskii and Borisov, 1971); *^{1}H-NMR, ^{19}F-NMR, IR data*, *thermodynamic data* (Bacher and Jacob, 1980; Grenthe *et al.*, 1992; Guillaumont *et al.*, 2003).
$UF_4 \cdot 7H_2O$		cubic; O_h^5, $Fm\bar{3}m$, No.225; a = 5.65 (1); V = 180.36; $Z = 2$; d(calc.) = 6.01	*crystallographic data* (Dawson *et al.*, 1954)
$LiUF_5$	dark-green; m.p. 605°C*	tetragonal; C_{4h}^6, $I4_1/a$; No.88; a = 14.8592(96), c = 6.5433(9); $Z = 16$; V = 90.3; d(calc.) = 6.23; the U atom is surrounded by nine F ions in a tricapped trigonal prismatic array. Adjacent prisms share edges and corners to form network	*crystallographic data* (Brunton, 1966; Keenan, 1966; Penneman *et al.*, 1973)

Li_3UF_7		tetragonal; D_{4h}^7, *P*4*nmn*, No.129; $a = 6.132$, $c = 6.391$	*crystallographic data* (Thoma and Penneman, 1965)
Li_4UF_8	m.p. = 496°C (incongr.)	orthorhombic; D_{2h}^{16}, *Pnma*; No.62; $a = 9.960$, $b = 9.883$, $c = 5.986$; $Z = 4$; d(calc.) = 4.71; $V = 589.23$; the coordination polyhedron is a triangular prism with pyramids on two of the prism faces; each U atom has 8 F^- neighbours at 2.29 (0.02) and a ninth at 3.30(0.03); CN. = 8	*crystallographic data; IR spectra* (Barton *et al.*, 1958; Brunton, 1967)
LiU_4F_{17}	yellowish-green or green square prism; 775°C*	$a = 8.990$, $c = 11.387$	*crystallographic data* (Jove and Cousson, 1977; Cousson *et al.*, 1977)
Li_2CaUF_8		tetragonal; D_{2d}^9, $I\bar{4}m2$, No. 119; $a = 5.2290(12)$, $c = 11.0130(18)$; $Z = 2$; $V = 301.12$; d(exp.) = 4.85, d(calc.) = 4.9.	*crystallographic data* (Védrine *et al.*, 1973; 1979)
Li_2CdUF_8		tetragonal; D_{2d}^9, $I\bar{4}$ (or $I\bar{4}m2$), No.119; $a = 5.222(0.002)$, $c = 10.952(0.005)$; $Z = 2$; d(exp.) = 4.85, d(calc.) = 4.86.	*crystallographic data* (Védrine *et al.*, 1973)
α-Na_2UF_6	blue; m.p. = 673°C; IR(cm^{-1}): ν(U–F) = 375(s); ν(F–U–F), bending = 192(s); 258(m), ν(Na–F) = 258(m); other: 146w	cubic; O_h^5, $Fm\bar{3}m$, No 225; $a = 5.565(4)$; $Z = 4$; $V = 172.34$; d(calc.) = 5.11	*crystallographic data* (Zachariasen, 1948d; Mighell and Ondik, 1977)
β_2-Na_2UF_6		trigonal/rhombohedral; D_3^2, *P*321, No 150; $a = 5.95(1)$, $c = 3.7(1)$; $Z = 1$; $V = 114.97$; d(calc.) = 5.75; tricapped trigonal prism sharing ends to form chain	*crystallographic data* (Zachariasen, 1948d)

Table 5.26 (*Contd.*)

Formula	*Selected properties and physical constants*[b]	*Lattice symmetry, lattice constants* (Å), *conformation and density* (g cm^{-3})[c]	*Remarks regarding information available and references*
γ-Na_2UF_6	$\mu_{eff.} = 3.13$ to 3.23 B.M.; $\theta = -84$ to –89 K (14–300 K)[d]	orthorhombic; D_{2h}^{25}, *Immm*, No 71; $a = 5.56$, $b = 4.01$, $c = 11.64$; the coordination geometry in UF_9 chains is a tricapped trigonal prism (structure type of β_1-K_2UF_6)	*crystallographic data* (Zachariasen, 1948d; Mighell and Ondik, 1977); *magnetic data* (Bacher and Jacob, 1980)
δ-Na_2UF_6	m.p. = 648°C	hexagonal; C_3^1, *P*3, No.143; $a = 6.112(2)$, $c = 7.240(2)$; $Z = 2$; $V = 234.23$; d(calc.) = 5.64; in the asymmetric unit cell are two U ions; each has nine nearest F^- ions at the corners of capped trigonal prisms; d(U–F) ranges from 2.23 to 2.42(1)	*crystallographic data* (Brunton *et al.*, 1965; Cousson *et al.*, 1979)
Na_3UF_7	geenish-blue; m.p. = 629°C; $\mu_{eff.} = 3.40$ B.M.; $\theta = 290$ K (74–300 K)[d] or $\mu_{eff.} = 3.30$ B.M.; θ = 81 K $\mu_{eff.} = 3.38$ B.M.; $\theta = 290$ K; (for 195–473 K range). IR (cm^{-1}): ν(U–F) = 380(s); ν(F–U–F), bending = 217(s); ν(Na–F) = 240 (m); other, 146w	tetragonal; D_{4h}^{17}, *I*4/*mmm,* No.139; $a = 5.488$, $c = 10.896$	*crystallographic data* (Zachariasen, 1948a; Mighell and Ondik, 1977); *magnetic data* (Bacher and Jacob, 1980)
NaU_2F_9	yellowish-green; m.p. = 660°C (dec.); IR (cm^{-1}): ν(U–F) = 360(s); ν(F–U–F), bending = 194(s); ν(Na-F) = 260(m); other, 145w		*IR data* (Ohwada *et al.*, 1972)

$Na_7U_2F_{15}$	green	orthorhombic; D_{2h}^{23}, *Fmmm*, No.69; $a = 17{,}7$, $b = 29.8$, $c = 12.7$	*crystallographic data* (Thoma *et al.*, 1963; Mighell and Ondik, 1977)
$Na_5U_3F_{17}$		cubic; $a = 5.589$	*crystallographic data* (Thoma *et al.*, 1963).
$Na_7U_6F_{31}$	green; m.p. = 718°C; IR(cm^{-1}): ν(U–F) = 383(s); ν(F–U–F), bending = 193(s); ν(Na–F) = 241(m)	rhombohedral; C_{3i}^2, $R\bar{3}$, No.148; $a = 14.72$, $c = 9.84$; $Z = 3$; $V =$ 615.5 $Å^3$; CN = 8; isostructural with $Na_7Zr_6F_{31}$ in which the basic coordination geometry about central ion is approx. square antiprismatic, and six antiprisms share corners to form an octahedral cavity which encloses the additional F atom.	*crystallographic data* (Thoma *et al.*, 1963; Mighell and Ondik, 1977)
$NaKUF_6$		hexagonal; C_3^1, *P*3, No.143; $a = 6.24$, $c = 7.80$; $Z = 2$; d(calc.) = 5.23	*crystallographic data* (Brunton *et al.*, 1965)
$NaRbUF_6$	pale green, purple interference	hexagonal; C_3^1, *P*3, No. 143; $a = 6.29$, $c = 8.13$; $Z = 2$; d(calc.) = 5.49	*crystallographic data* (Brunton *et al.*, 1965); *optical data* (Bacher and Jacob, 1980)
α-K_2UF_6	green; $\mu_{eff.} = 3.45$ B.M.; $\theta =$ –108K (74–300 K)[d]; IR(cm^{-1}): ν(U–F)val. = 360s, 292s; ν(F–U–F)def. = 217sv; 161m, ν(F–U–F)def. or ν(K–F)lat. = 147m; ν(K–F)lat. = 84w	cubic with disordered cations; O_h^5, $Fm\bar{3}m$, No 225; $a = 5.946(1)$; $Z = 4$; $V = 210.22$; d(calc.) = 4.53	*crystallographic data* (Zachariasen, 1948d); *magnetic data* (Bacher and Jacob, 1980)
β_1-K_2UF_6	drab olive; m.p. = 755°C[*]; stable between 608 –and 755°C; below 608°C decomposes to K_3UF_7 + $K_7U_6F_{31}$	hexagonal; D_{3h}^3, $P\bar{6}2m$, No.189; $a = 6.5528(2)$, $c = 3.749(1)$; $Z = 1$; $V = 139.41$; d(calc.) = 5.1235; tricapped trigonal prisms share the triangular faces perpendicular to the three fold axis of the ideal polyhedron to form infinite chains	*crystallographic data* (Zachariasen, 1948a; Brunton, 1969a, Penneman *et al.*, 1973; Bacher and Jacob, 1980; *IR spectra* (Soga *et al.*, 1972)

Table 5.26 (*Contd.*)

Formula	*Selected properties and physical constants*[b]	*Lattice symmetry, lattice constants* (Å), *conformation and density* (g cm^{-3})[c]	*Remarks regarding information available and references*
β_2-K_2UF_6	green	hexagonal; D_3^2, *P*321, No.150; a = 6.54(2); c = 4.04; Z = 1; V = 150.02; d(calc.) = 4.76. tricapped trigonal prism sharing ends to form chain	*crystallographic data* (Zachariasen, 1948d); *IR spectra* (Soga *et al.*, 1972)
α-K_3UF_7	deep-green; m.p. = 957°C; IR (cm^{-1}): ν(U–F)val. = 362s; ν(F–U–F)def. = 206s; ν(F–U–F)def. or ν(K–F)lat. = 120m; ν(K–F)lat. = 80w	cubic; O_h^5, $Fm\bar{3}m$, No.225; a = 9.22 (2); Z = 4; V = 783.78, d(calc.) = 4.14; the seven F atoms are statistically distributed over fluorite lattice sites	*crystallographic data, IR spectra* (Zachariasen, 1954c; Burns and Duchamp, 1962; Bacher and Jacob, 1980); *IR spectra* (Soga *et al.*, 1972)
β-K_3UF_7		orthorhombic; D_{2h}^{13}, *Pmmn*, No.59 or $Pmn2_1$, C_{2v}^7, No. 31; a = 6.58, b = 8.31, c = 7.22	*crystallographic data* (Burns and Duchamp, 1962)
$K_7U_6F_{31}$	green; m.p. = 789°C (congr.); IR: ν(U–F)val. = 380s, 319m; 244sh, 200m; ν(F–U–F) def. = 244sh, 200m; ν(F–U–F) def. or ν(K–F) lat. = 153m, 114m; ν(K–F) lat. = 80w	rhombohedral; C_{3i}^2, $R\bar{3}$, No. 148; a = 9.376, α = 107.20; Z = 1; CN = 8; d(calc.) = 5.58; isostructural with $Na_7Zr_6F_{31}$; square antiprisms sharing corners, with one fluorine atom in a cavity	*crystallographic data, IR spectra* (Brunton *et al.*, 1965); *IR spectra* (Soga *et al.*, 1972)
KU_2F_9	green; m.p. = 765°C (incongr.) with formation of UF_6; IR (cm^{-1}): ν(U–F)val. = 360s, 331s, 290sh; ν(F–U–F) def. = 235m, 204m; ν(F–U–F)def. or ν(K–F)lat. = 160m, 148m, 118w; ν(K–F)lat. = 85w	orthorhombic; D_{2h}^{16}, *Pnma,* No 62; a = 8.7021, b = 11.4769, c = 7.0350; Z = 4; V = 702.61; CN = 9; d(calc.) = 6.4851; tricapped trigonal prism, sharing ends and edges; d(U–F) = 2.29–2.39	*X-ray powder diffraction and single crystal data, IR spectra* (Brunton *et al.*, 1965; Brunton, 1969b); *IR spectra* (Soga *et al.*, 1972)

KU_6F_{25}	metastable	hexagonal; D_{6h}^4, $P6_3/mmc$, No.194; $a = 8.18$, $c = 16.42$; d(calc.) = 6.73; $Z = 2$; tricapped trigonal prism, sharing edges and corners to form double rings of six polyhedra each	*crystallographic data* (Burton *et al.*, 1965; Zachariasen, 1948d); *IR spectra* (Soga *et al.*, 1972)
RbU_6F_{25}	deep-green; m.p. = 832°C (incongr. with formation of UF_4)	hexagonal; D_{6h}^4, $P6_3/mmc$, No.194; $a = 8.195$, $c = 16.37$; $Z = 2$; d(calc.) = 6.908; tricapped trigonal prism, sharing edges and corners to form double rings of six polyhedra each	*crystallographic data* (Mighell and Ondik, 1977; Brunton *et al.*, 1965); *IR spectra* (Soga *et al.*, 1973)
Rb_2UF_6	green; m.p. = 818°C (incongr)	orthorhombic; D_{2h}^{17}, *Cmcm*, No.63; $a = 6.958(2)$, $b = 12.042(5)$, $c = 7.605(5)$; $Z = 4$; $V = 637.21$; d(calc.) = 5.45; the structure is of the K_2ZrF_6 type and consists of infinitive chains of UF_8 polyhedra in the form of dodecahedra with triangular faces (ideal symmetry D_{2d})	*X-ray powder and single crystal diffraction data* (Kruse, 1971; Kruse and Asprey, 1962); *IR spectra* (Soga *et al.*, 1973)
Rb_3UF_7	pale green; m.p. = 995°C (congr.)	cubic; O_h^5, $Fm\bar{3}m$, No.225; $a = 9.5667$; the seven F atoms are statistically distributed over fluorite lattice sites	*crystallographic data* (Bacher and Jacob, 1980); *IR spectra* (Soga *et al.*, 1973)
$Rb_7U_6F_{31}$	green; m.p. = 675°C (incongr.)	rhombohedral; C_{3i}^2, $R\bar{3}$, No. 148; $a = 9.595$; $\alpha = 107.67$, $Z = 1$; CN = 8; d(calc.) = 6.02; structure type of $Na_7Zr_6F_{31;}$ square antiprisms sharing corners, with one fluorine atom in a cavity	*crystallographic data* (Burton *et al.*, 1965; Thoma *et al.*, 1958); *IR spectra* (Soga *et al.*, 1973)

Table 5.26 (*Contd.*)

Formula	*Selected properties and physical constants*[b]	*Lattice symmetry, lattice constants* (Å), *conformation and density* (g cm^{-3})[c]	*Remarks regarding information available and references*
other complex fluorides with rubidium: $RbUF_5$ (green blue, m.p. = 735°C; IR(cm^{-1}):ν_{UF} = 370, 330, 302 cm^{-1}, RbU_3F_{13}, $Rb_2U_3F_{14}$ (m.p. = 722°C*)			*general properties* (Bacher and Jacob, 1980)
$CsUF_5$	greenish-blue (or sky blue); m.p. = 735°C.		
CsU_2F_9	deep-green crystals	monoclinic; C_{2h}^6, *C*2/*c*, No.15; *a* = 15.649(3), *b* = 7.087(1), *c* = 8.689 (2); β = 118·11(2); *Z* = 4, *V* = 849.98; CN = 8 1/2 (effective); *d*(exp.) = 6.4; *d*(calc.) = 6.09; tricapped trigonal prism, one prism corner statistically only half-occupied. Contains 8-coordinate U in edge-sharing polyhedra forming U_4F_{16} sheets	*crystallographic data* (Rosenzweig *et al.*, 1973)
CsU_6F_{25}	deep-green; m.p. = 867°C (incongr.) with formation of UF_4	hexagonal; D_{6h}^4, $P6_3/mmc$, No.194; *a* = 8.2424(4), *c* = 16.4120(20); *Z* = 2; *V* = 965.61; *d*(calc.) = 7; tricapped trigonal prism, sharing edges and corners to form double rings of six polyhedra each	*crystallographic data* (Brunton *et al.*, 1965, 1971)

Cs_2UF_6	greenish- blue to light blue; m.p. = 800°C*		*general properties* (Bacher and Jacob, 1980)
$Cs_2U_3F_{14}$	bluish-green; m.p. = 737°C (incongr.) with formation of $Cs_2U_3F_{14}$	monoclinic; C_{2h}^2, $P2_1/m$, No.11 or $P2_1$, C_2^2, No.4; $a = 8.39$, $b = 8.46$, $c = 20.88$; $\beta = 119.89°$	*crystallographic data* (Brunton *et al.*, 1965); *magnetic susceptibilities* (Bacher and Jacob, 1980)
Cs_3UF_7	pale blue; m.p. = 970°C	cubic; O_h^5, $Fm\bar{3}m$, No.225; $a =$ 9.90; CN = 7; structure type of K_3UF_7; d(calc.) = 7.92.	*crystallographic data* (Penneman *et al.*, 1973; Brunton *et al.*, 1965)
α-NH_4UF_5	over 190°C decomposes partly to β-NH_4UF_5	rhombohedral; C_{3i}^2, $R\bar{3}$, No.148; $a = 9.55$; $\alpha = 107.4$	*crystallographic data* (Benz *et al.*, 1963; Penneman *et al.*, 1974); *magnetic susceptibilities* (Bacher and Jacob, 1980)
β-NH_4UF_5	polymeric	monoclinic; C_{2h}^5, $P2_1/c$, No.14; $a =$ 7.799(5), $b = 7.158(5)$, $c = 8.762$ (7); $\beta = 116.45$; $Z = 4$; $V = 437.94$; d(calc.) = 5.32; CN = 9	*crystallographic data* (Penneman and Ryan, 1974) *magnetic susceptibilities* (Bacher and Jacob, 1980)
γ-$(NH_4)_2UF_6$	decomposes under He over 220°C to NH_4F+$(NH_4)_7U_6F_{31}$	orthorhombic; C_{2v}^2, $Pmc2_1$, No.26 or D_{2h}^5, $Pmcm$, No.51; $a = 4.05$, $b = 7.03$, $c = 11.76$; $Z = 2$; d(calc.) = 3.9	*crystallographic data* (Penneman *et al.*, 1964a); *magnetic and optical data* (Bacher and Jacob, 1980)
$(NH_4)_4UF_8$	deep green; over 130°C decomposes in air to NH_4F + $(NH_4)_2UF_6$	monoclinic; C_{2h}^6, $C2/c$, No.15; $a =$ 13.126, $b = 6.692$, $c = 13.717$; $\beta =$ 121.32; $Z = 4$; CN = 8; d(exp.) = 2.96; d(calc.) = 2.982; d(U–F) = 2.25–2.33; discrete distorted tetragonal antiprismatic array	*X-ray powder and single crystal data*; (Rosenzweig and Cromer, 1970); *thermodynamic data, magnetic and optical data* (Bacher and Jacob, 1980)
$NH_4U_3F_{13}$	decomposes in vacuum at 300–400°C to UF_4	orthorhombic; C_{2v}^2, $Pmc2_1$, No. = 26; $a = 8.045(2)$, $b = 8.468(2)$, $c =$ 7.375(2); $V = 502.42$; $Z = 2$; d(calc.) = 6.47	*crystallographic data* (Abazli *et al.*, 1980)

Table 5.26 (*Contd.*)

Formula	*Selected properties and physical constants*[b]	*Lattice symmetry, lattice constants* (Å), *conformation and density* (g cm^{-3})[c]	*Remarks regarding information available and references*
$(NH_4)_7U_6F_{31}$	m.p. > 150°C (dec.); under He gas to UF_4; exists in α, β, γ and δ forms	rhombohedral; C_{3i}^2, $R\bar{3}$, No.148; $a = 9.55$; $\alpha = 107.4$; CN = 8; square antiprisms sharing corners, with one fluorine atom in a cavity; structure type of $Na_7Zr_6F_{31}$.	*crystallographic data* (Benz *et al.*, 1963; Penneman *et al.*, 1964a); *thermodynamic data, magnetic and optical properties* (Bacher and Jacob, 1980)
$(NH_3OH)UF_5$		orthorhombic; D_2^1, $P222$, No.16; C_{2v}^1, $Pmm2$, No.25 or D_{2h}^1, $Pmmm$, No.47; $a = 10.963$, $b = 14.9024$, $c = 10.4391$	*crystallographic data* (Ratho *et al.*, 1969)
$N_2H_5UF_5$		orthorhombic; D_2^1, $P222$, or C_{2v}^1, $Pmm2$; $a = 7.941$, $b = 6.372$, $c = 7.478$; $Z = 4$	*crystallographic data* (Ratho and Patel, 1968); *thermodynamic data; magnetic susceptibilities; IR spectra, decomposition data.* (Bacher and Jacob, 1980)
$[N(C_2H_5)_4]_2UF_6$	white cryst.; air and moisture sensitive; IR (cm^{-1}):ν(U–F) = 405; $F^2 = 49699$, $\varsigma_{5f} = 1970$; $B_0^4 = 10\,067(113)$, $B_0^6 = 22(72)$; *rms* = 67		*general properties* (Ryan *et al.*, 1974); *electronic spectra, crystal-field parameters* (Wagner *et al.*, 1977)
other complex fluorides with hydrazinium: $(N_2H_5)_2UF_6$, $(N_2H_5)_3UF_7$			*general properties* (Bacher and Jacob, 1980)
$UN_{0.95}F_{1.2}$	uranium oxidation number = +4.05	tetragonal; D_{2h}^5, $P4/n$, No.85; $a = 3.951$ $c = 5.724$; $Z = 2$; $V = 89.35$; d(calc.) = 10.19	*crystallographic data* (Jung and Juza, 1973)

$Ca_{0.925}\ U_{0.075}\ F_{2.15}$		cubic; O_h^5; $Fm\bar{3}m$; No.225; a = 5.507(3), $Z = 4$; $V = 167.01$; d(calc.) = 3.81	*neutron diffraction data* (Laval *et al.*, 1987)
$CaUF_6$	green; $\mu_{eff.} = 3.25$ B.M.; $\theta = -101$ (74–300 K)[d]	hexagonal (LaF_3 type); D_{3d}^4, $P\bar{3}c1$, No.165; $a = 6.928$, $c = 7.127$; d(calc.) = 6.59	*crystallographic data* (Keller and Salzer, 1967) *magnetic data* (Bacher and Jacob, 1980)
$SrUF_6$		hexagonal (LaF_3 type); D_{3d}^4, $P\bar{3}c1$, No.165; $a = 7.122$, $c = 7.293$; d(calc.) = 6.83	*crystallographic data* (Keller and Salzer, 1967)
$BaUF_6$		hexagonal (LaF_3 type); D_{3d}^4, $P\bar{3}c1$, No.165; $a = 7.403$, $c = 7.482$; d(calc.) = 6.86	*crystallographic data* (Keller and Salzer, 1967)
$PbUF_6$	green	hexagonal (LaF_3 type); D_{3d}^4, $P\bar{3}c1$, No.165; $a = 7.245$, $c = 7.355$; d(calc.) = 8.33	*crystallographic data* (Keller and Salzer, 1967)
other complex fluorides with lead: $Pb_3U_2F_{14}$, Pb_6UF_{16}.			*general properties* Bacher and Jacob (1980)
$TlUF_5$	m.p. = 640°C	monoclinic; C_{2h}^5, $P2_1/c$; No.14; $a = 8.222(2)$, $b = 13.821(4)$, $c = 8.317(5)$; $\beta = 102.53(3)$; $Z = 8$; $V = 922.6$; d(calc.) = 7.74; tricapped trigonal prismatic at U	*infrared spectra* (Soga *et al.*, 1973); *crystallographic data* (Avignant *et al.*, 1980, 1982)
Tl_2UF_6	m.p. = 598°C (eutec.)	orthorhombic; $a = 4.07$, $b = 6.97$, $c = 11.56$; $Z = 2$; d(calc.) = 7.54	*crystallographic data* (Avignant and Cousseins, 1971)
Tl_3UF_7	m.p. = 542°C (incongr.)	cubic; $a = 9437$; $Z = 2$; $d = 7.92$	*crystallographic data* (Avignant and Cousseins, 1971)
Tl_4UF_8	m.p. = 317°C*		
$Tl_7U_6F_{31}$		hexagonal; $a = 15.39$, $c = 10.80$; $Z = 3$; d(calc.) = 7.74	*crystallographic data* (Avignant and Cousseins, 1977; Avignant *et al.*, 1977)
TlU_3F_{13}	m.p. = 674°C (incongr)	orthorhombic; $a = 8.49$, $b = 8.04$, $c = 7.38$.; Z = 2; d(calc.) = 7.68	*crystallographic data* (Avignant *et al.*, 1977)

Table 5.26 (*Contd.*)

Formula	*Selected properties and physical constants*[b]	*Lattice symmetry, lattice constants* (Å), *conformation and density* (g cm^{-3})[c]	*Remarks regarding information available and references*
TlU_6F_{25}		hexagonal; $a = 8.18$, $c = 16.46$; $d = 7.19$	*crystallographic data* (Avignant *et al.*, 1977)
$TlUO_3F_{11}$		monoclinic; C_s^3, *Cm*, No. 8; $a = 14.051(3)$, $b = 8.106(3)$, $c = 8.389(2)$, $\beta = 90.00(3)$; $Z = 4$; $V = 955.49$; d(calc.) = 7.95	*crystallographic data* (Hsini *et al.*, 1986)
YUF_7		monoclinic; $a = 8.19$, $b = 8.27$, $c = 11.17$; $\beta = 92.66$	*crystallographic data; magnetic properties* (Denes *et al.*, 1973)
$TmUF_7$		monoclinic; $a = 8.19$, $b = 8.27$, $c = 11.19$; $\beta = 92.73$	*crystallographic data; magnetic properties* (Denes *et al.*, 1973)
$YbUF_7$		monoclinic; $a = 8.18$, $b = 8.25$, $c = 11.20$; $\beta = 92.70$; d(calc.) = 6.93	*crystallographic data; magnetic properties* (Denes *et al.*, 1973)
$LuUF_7$		monoclinic; $a = 8.17$, $b = 8.24$, $c = 11.18$; $\beta = 92.48$	*crystallographic data; magnetic properties* (Denes *et al.*, 1973)
$CuU_2F_{10}{\cdot}8H_2O$		orthorhombic; $a = 8.73$, $b = 7.16$, $c = 20.78$, $Z = 4$, d(calc.) = 4.48.	*crystallographic data* (Charpin *et al.*, 1968)
$ZnUF_6{\cdot}5H_2O$		orthorhombic; $a = 14.34$, $b = 15.72$, $c = 8.05$; $Z = 8$; d(calc.) = 3.71	*crystallographic data* (Charpin *et al.*, 1969)
$MnUF_6{\cdot}8H_2O$		monoclinic; $a = 12.37$, $b = 6.98$, $c = 8.06$; $\beta = 93.33$; $Z = 4$; d(calc.) = 4.41	*crystallographic data* (Charpin *et al.*, 1969)
$CoU_2F_{10}{\cdot}5H_2O$		monoclinic; $a = 11.07$, $b = 7.10$, $c = 8.81$; $\beta = 94.17$; $Z = 2$; d(calc.) = 4.16	*crystallographic data* (Charpin *et al.*, 1968)
InU_2F_{11}		monoclinic; $a = 5.430$, $b = 6.407$, c = 8.402, $\beta = 104.62(4)$	*crystallographic data* (Champarnaud-Mesjard and Gaudreau, 1976)

$NiU_2F_{10}{\cdot}8H_2O$		monoclinic; $a = 11.05$, $b = 7.08$, $c = 8.86$; $\beta = 93.33$; $Z = 2$; d(calc.) = 4.17	*crystallographic data* (Charpin *et al.*, 1968)
UOF_2	UOF_2(cr): $\Delta_f G^o_m = -1434.1$ (6.4)†, $\Delta_f H^o_m = -1504.6$ (6.3)†, $S^o_m = 119.2$ (4.2)$^{\dagger.}$		*thermodynamic data* (Grenthe *et al.*, 1992; Guillaumont *et al.*, 2003)
$UO_2F_{0\cdot25}$	dark grey to black; mixed valence compound (U^{IV} and U^{V}); oxidation state 4.25	octahedral; fluorite type of structure; $a = 5.49$; $Z = 4$; d(exp.) = 11.0. One anion per unit cell is occupying inter-net places	(Kemmler-Sack, 1967, 1969)
$UOF_2{\cdot}H_2O$	$UOF_2{\cdot}H_2O$(cr): $\Delta_f G^o_m = -1674.5$ (4.1)†, $\Delta_f H^o_m = -1802.0$(3.3)†, $S^o_m = 161.1$(8.4)†		*IR spectra* (Jacob and Bacher, 1980); *thermodynamic properties*, (Grenthe *et al.*, 1992; Guillaumont *et al.*, 2003)
UCl_4	light green needles or dark-green octahedra; m.p. = 590°C; b.p. = 789°C; density: 4.725 g cm^{-3}; $\mu_{eff.} = 3.29$ B.M.; $\theta = -65$ K (90 – 551 K)[d] hygroscopic; soluble in polar organic solvents; insoluble in ethyl acetate, chloroform and benzene. UCl_4(cr): $\Delta_f G^o_m = -929.6$ (2.5)†, $\Delta_f H^o_m = -1018.8$ (2.5)†, $S^o_m = 197.200$(0.8)†; $C^o_{p,m} = 121.8$ (0.4)†. UCl_4(g): $\Delta_f G^o_m = -789.4$ (4.9)†, $\Delta_f H^o_m = -815.4$ (4.7)†, $S^o_m = 409.3$ (5.0)†; $C^o_{p,m} = 103.5$ (3. 0)† $\log p$ (mmHg) = $-11350T^{-1} + 23.21 - 3.02 \log T$ (298–863 K) $\log p$(mmHg) = $-9950\ T^{-1} + 28.96 - 5.53 \log T$ (863–1062 K); IR and Raman vibrations(cm^{-1}): 311 (R), 270 (R, IR), 240 (R, IR),	tetragonal; D^{19}_{4h}, $I4_1/amd$, No.141; $a = 8.3018(4)$, $c = 7.4813(6)$, $Z = 4$; d(calc.) = 4.87; each uranium atom is bonded to eight chlorine atoms; the coordination polyhedron is a dodecahedron ($\bar{4}2m$); d(U–Cl) = 2.889(1) and 2.644(2) (4 times each); Cl–U–Cl angles: 3.141(8) and 3.540(1). The Cl–Cl approaches are 3.141(8), 3.097(8) and 3.540(1); structure refined data: $a = 8.3018(4)$, $b = 8.3018(4)$, $c = 7.4813(6)$; $V = 515.61$; d(calc.) = 4.89	*crystallograhic data* (Brown, 1979; Taylor and Wilson, 1973a); *structural transitions anticipating melting* (Bros *et al.*, 1987); *structure refinement* (Schleid *et al.*, 1987) *temperature absorption spectra, crystal-field energy level structure* (Malek *et al.*, 1986a,b); Brown, 1979; Hecht and Gruber, 1974; Clifton *et al.*, 1969; McLaughlin, 1962; Żołnierek *et al.*, 1984; *thermodynamic data* (Rand and Kubaschewski, 1963 ; Grenthe *et al.*, 1992; Brown, 1979; Guillaumont *et al.*, 2003); *magnetic properties* (Hendricks *et al.*, 1971; Dawson, 1951; Gamp *et al.*, 1983); *electrical and optical properties* (Brown, 1979); *IR and*

Table 5.26 (*Contd.*)

Formula	*Selected properties and physical constants*[b]	*Lattice symmetry, lattice constants* (Å), *conformation and density* (g cm^{-3})[c]	*Remarks regarding information available and references*
	172 (R), 153 (R, IR), and 102(R, IR); $\mu_{eff.} = 3.29$; $\theta = -62$ K Energy level parameters: $F^2 = 42561(235)$, $F^4 = 39440(634)$, and $F^6 = 24174(185)$; $\zeta_{5f} = 1805$ (8), $\alpha = 30.9(1)$, $\beta = -576(168)$; $B_0^2 = -903(151)$, $B_0^4 = 766(220)$, $B_4^4 = -3091(185)$, $B_0^6 = -1619(482)$ and $B_4^6 = -308(280)$. $F_2 = 172.6$, $F_4 = 38.79$, $F_6 = 2.565$; $M^0 = [0.99]$, $M^2 = [0.55]$ and $M^4 = [0.38]$; $P^2 = P^4 = P^6 = [500]$		*Raman spectra* (Bohres *et al.*, 1974); *photoelectron spectra* (Thibaut *et al.*, 1982)
$UCl_4(CH_3CN)_4$	grey-green cryst; soluble in CH_3CN; loses CH_3CN *in vacuo* >40°C; IR (cm^{-1}): ν(CN) = 2278; $\mu_{eff.} = 2.89$ B.M.; $\theta = -158$ K	monoclinic; C_{2h}^6, *C*2/*c*, No.15; $a = 14.677(4)$; $b = 8.452(2)$; $c = 13.9559(3)$; $\beta = 91.77(2)$; $Z = 4$; d(calc.) = 2.087; d(U–Cl) = 2.624 (2) and 2.614(2); d(U–N) = 2.599 (6) and 2.567(6). The U atom is eight-coordinated with a dodecahedral arrangement. The C atoms occupy the dodecahedral B sites and the N atoms the A site	*crystallographic data* (Cotton *et al.*, 1984; Van den Bossche *et al.*, 1986); *infrared data* (Kumar and Tuck, 1984)
Li_2UCl_6	m.p. = 448.8 °C ; IR (cm^{-1}): ν(U–Cl) = 232w, 258, 287w	hexagonal; D_{6h}^4, $P6_3/mmc$, No. 194; $a = 11.191(5)$, $b = 11.191(5)$, $c = 6.0365(1)$; $Z = 3$; $V = 654.72$; d(calc.) = 3.53	*crystal structure from multiphase powder neutron profile refinement* (Bendall *et al.*, 1983); *magnetic properties* (Trzebiatowski and Mulak, 1970); *thermodynamic data* Vdovenko *et al.*, 1974b; Fuger *et al.*, 1983)

Na_2UCl_6	m.p. = 445.6 °C; IR (cm^{-1}): ν(U–Cl) = 240w, 260, 286w	trigonal/rhombohedral; D^3_{3d}, $P\bar{3}m1$, No.164; a = 11.8062(9), b = 11.8062(9), c = 6.3243(2); Z = 3; V = 763.42; d(calc.) = 3.24	*crystal structure from multiphase powder neutron profile refinement* (Bendall *et al.*, 1983); *magnetic properties* (Trzebiatowski and Mulak, 1970); *thermodynamic data* Vdovenko *et al.*, 1974b; Fuger *et al.*, 1983)
Rb_2UCl_6	IR (cm^{-1}):ν(U–Cl) = 267; 285w	trigonal; D^5_{3d}, $R\bar{3}m$, No.166; a = 7.34, c = 5.89; d(calc.) = 3.68; each U atom is surrounded by six Cl atoms at the vertices of an octahedron	*crystallographic data* (Vdovenko *et al.*, 1972a); *magnetic properties* (Trzebiatowski and Mulak, 1970); *thermodynamic data* (Vdovenko *et al.*, 1974b; Fuger *et al.*, 1983)
α-Cs_2UCl_6	green crystals; m.p. = 670°C; IR and Raman data (cm^{-1}): ν_1 = 307, ν_3 = 262, ν_4 = 115, ν_5 = 125, ν_6 = 88; Energy level parameters (T_d): F_2 = 189.358, F_4 = 33.469, F_6 = 3.927, F^2 = 42605, F^4 = 36447, F^6 = 28909; ς_{5f} = 1800.104; $A^o_4\langle r^4\rangle$ = 901.381 $A^o_6\langle r^6\rangle$ = 85.426; B^4_0 = 7211.0, B^4_4 = (4309) B^6_0 = 1366.8 B^6_4 = (–2554); *rms* = 163; n = 21	trigonal; D^5_{3d}, $R\bar{3}m$, No 166; a = 7.478, c = 6.026; each U atom is surrounded by six Cl atoms at the vertices of an octahedron	*crystallographic data* (Siegel, 1956); *IR and Raman data* (Brown *et al.*, 1975; Brown, 1979); *crystal-field spectra* (Johnston *et al.*, 1966); *magnetic properties* (Trzebiatowski and Mulak, 1970); *thermodynamic data* Vdovenko *et al.*, 1974b; Fuger *et al.*, 1983)
β-Cs_2UCl_6	appears in a polymorphic transition at 510°C; IR and Raman data: ν_1 = 308, ν_2 = 230, ν_3 = 267, ν_4 = 116, ν_5 = 126, ν_6 = 89	trigonal; a = 7.50, c = 12.00; d(calc.) = 4.04; (for a rapidly quenched sample); for the refined structure: trigonal/rhombohedral; D^3_{3d},$P\bar{3}m1$; No.164; a = 7.5037(3), b = 7.5037(3), c = 6.0540(4); Z = 1; V = 295.21; 95.21	*crystallographic data* (Vdovenko *et al.*, 1972b); *structure refinement* (Schleid *et al.*, 1987) *IR and Raman data* (Shamir and Silberstein, 1975; Shamir *et al.*, 1975)
$Cs_2U[O_3Cl_9(Nb\ Cl)_6]$		trigonal/rhombohedral; D^2_{3d}, $P\bar{3}1c$, No.163; a = 9.2080(7), c = 17.0950(30); Z = 2; V = 1255.25; d(calc.) = 4.34	*crystal structure* (Cordier *et al.*, 1997)

Table 5.26 (*Contd.*)

Formula	*Selected properties and physical constants*[b]	*Lattice symmetry, lattice constants* (Å), *conformation and density* (g cm^{-3})[c]	*Remarks regarding information available and references*
$[N(CH_3)_4]_2UCl_6$	green cryst.; soluble in CH_3CN, H_2O; IR and Raman data (cm^{-1}): $\nu_1 = 284$, $\nu_2 = 230$, $\nu_5 = 123$, $\nu_6 = 87$	cubic face centered; $a = 13.06$; d(calc.) = 1.788, d(exp.) = 1.791	*crystallographic data* (Staritzky and Singer, 1952); *IR and Raman data* (Silberstein, 1972; Brown, 1979)
$[N(C_2H_5)_4]_2UCl_6$	green cryst.; soluble in CH_3CN, H_2O; crystals undergo reversible phase change at 94°C; IR and Raman data (cm^{-1}): $\nu_1 = 293$, $\nu_3 = 254$, $\nu_4 = 110$, $\nu_5 = 110$, $\nu_6 = 78$; $F^2 = 43170(2181)$, $\varsigma_{5f} = 1774(35)$; $B_0^4 = 7463(432)$, $B_0^6 = 992(258)$; *rms* = 168	orthorhombic; D_{2h}^{23}, *Fmmm*, No.69; $a = 14.23$, $b = 14.73$, $c = 13.33$; d(calc.) = 1.693	*crystallographic data* (Staritzky and Singer, 1952); *IR and Raman data* (Brown *et al.*, 1975; Brown, 1979); *electronic spectra, crystal-field parameters* (Wagner *et al.*, 1977)
$[P(C_6H_5)_3C_2H_5]_2UCl_6$		triclinic; C_1^1, $P\bar{1}$, No.2; $a = 10.53$ (1), $b = 10.95(1)$, $c = 10.31(1)$; $\alpha = 113.22(5)^o$, $\beta = 105.20(5)$, $\gamma = 80.40(5)$; $Z = 1$; d(calc.) = 1.631, d(exp.) = 1.64; d(U-Cl): = 2.621 (2), 2.627(1) and 2.623(1)	*crystallographic data* (Caira *et al.*, 1978)
$UCl(H_2PO_2)_3(H_2O)_2$		orthorhombic; D_{2h}^{11}, *Pbcm*, No.57; $a = 7.559(2)$, $b = 10.111(2)$, $c = 14.680(2)$; $Z = 4$; $V = 1121.98$, d(calc.) = 2.99	*synthesis, structure, vibrational spectra* (Tanner *et al.*, 1992)
$UCl(PO_4)2H_2O$		tetragonal; C_{4h}^5, *I4/m*, No.87; $a = 14.631(2)$, $b = 14.631(2)$, $c = 6.662$ (1); $Z = 8$; $V = 1426.11$; d(calc.) = 3.77	*crystallographic data* (Benard-Rocherulle *et al.*, 1997)

other uranium(IV) chloro complexes: (i) $KUCl_5$; (ii) $RbUCl_5$; (iii) $CsUCl_5$, (iv) K_2UCl_6; (v) Cs_2UCl_6 (vi) Ag_2UCl_6; (vii) $KNaUCl_6$; (viii) $SrUCl_6$; (ix) $BaUCl_6$; (x) Rb_4UCl_8; (xi) KU_3Cl_{13}; (xii) $KNaUCl_6$; (xiii) CsU_2Cl_9; (xiv) $Cs_3U_2Cl_{11}$	(i) m.p. = 345°C* (ii) m.p. = 360°C* (iii) (iv) IR (cm^{-1}):ν(U–Cl) = 250w, 263, 286w (v) green cryst.; m.p. 670°C (vi) m.p. = 407°C; ΔH^o_{fus} = 35.4 (2.1) (vii) (viii) m.p. = 560°C (ix) m.p. = 382°C* (x) m.p. = 406.3°C (xi) (xii) (xiii)		*thermodynamic and IR data* (Brown, 1979; Suglobova and Chirkst, 1978a, Vdovenko *et al.*, 1974b; Fuger *et al.*, 1983); *magnetic properties* (Brown, 1979)
$UOCl_2$	green; moisture sensitive; insoluble in organic solvents; soluble in H_2O; b.p.>400°C; $UOCl_2$(cr): $\Delta_f G^o_m$ = –998.5 (2.7)†, $\Delta_f H^o_m$ = –1069.3 (2.7)†, S^o_m = 138.32 (0.21)†; $C^o_{p,m}$ = 95.06 (0.42)†; paramagnetic $\mu_{eff.}$ = 3.13 B.M. (above 40 K); exhibits magnetic ordering below 31 K	orthorhombic; D^9_{2h}, *Pbam*, No.55; a = 15.255, b = 17.828, c = 3.992; d(U(1)–O) = 2.20–2.40; d(U(1)–Cl) = 2.66–3.15; d(U(2)–O) = 2.17–2.33; d(U(2)–Cl) = 2.88–3.01; d(U(3)–O) = 2.22–2.35; d(U(3)–Cl) = 2.70–3.51; the arrangement around U(1) is dodecahedral (CN = 8; 3O, 5Cl); that around U(2) is trigonal (CN = 7; 3O, 4Cl) and that around U (3) is approx. dodecahedral-1 (C.N. = 7; 3O, 4Cl)	*crystallographic data, neutron diffraction data* (Bagnall *et al.*, 1968; Taylor and Wilson, 1974a); *infrared spectra* (Bagnall *et al.*, 1968) *thermodynamic data* (Brown, 1979; Grenthe *et al.*, 1992;Guillaumont *et al.*, 2003); *magnetic properties, ir spectra* (Levet.and Noël, 1979); *photoelectron spectra* (Thibaut *et al.*, 1982)
UNCl		tetragonal; D^7_{4h}, *P4/nmm*, No.129; a = 3.979, c = 6.811; Z = 2; V = 107.83; d(calc.) = 8.85; d(exp) = 8.78. The compound is isostructural with PbFCl;	*crystallographic data* (Juza and Sievers, 1965; Juza and Meyer, 1969; Yoshihara *et al.*, 1971)

Table 5.26 (*Contd.*)

Formula	*Selected properties and physical constants*[b]	*Lattice symmetry, lattice constants* (Å), *conformation and density* (g cm^{-3})[c]	*Remarks regarding information available and references*
		d(U–Cl_1) = 3.17 (4×); d(U–N) = 2.30; d(Cl_1–Cl_1) = 3.98; d(Cl_1–Cl_2) = 3.23; d(N–Cl) = 3.29; d(N–N) = 2.81	
$UClF_3$	emerald green cryst.; m.p. = 444°C*; b.p. = 550–650°C (in vacuo subl.) $UClF_3$(cr): $\Delta_f G^o_m$ = –1606 (5.)†, $\Delta_f H^o_m$ = –1690 (5)†, S^o_m = 185.4 (4.2)†; $C^o_{p,m}$ = 120.9 (4.2)†	orthorhombic; *Abam* or C^{17}_{2v}, *Aba*2, No.41; a = 8.673(2), b = 8.69(1), c = 8.663(5); Z = 8; d(calc.) = 6.72	*crystallographic data* (Savage, 1956; Staritzky and Douglass, 1956); *thermodynamic data; fused salt system* (Brown, 1979; Grenthe *et al.*, 1992; Guillaumont *et al.*, 2003)
other chloride fluorides: (i) UCl_2F_2, (ii) UCl_3F.	(i) green; m.p. = 460°C*. UCl_2F_2(cr): $\Delta_f G^o_m$ = –1376(6)†, $\Delta_f H^o_m$ = –1466 (5)†, S^o_m = 174.1 (8.4)†; $C^o_{p,m}$ = 119.7 (4.2)†. (ii) m.p. = 530°C*; UCl_3F(cr): $\Delta_f G^o_m$ = –1147(5)†, $\Delta_f H^o_m$ = –1243 (5)†, S^o_m = 162.8 (4.2)†; $C^o_{p,m}$ = 118.8(4.2)†		*thermodynamic data; fused salt system* (Brown, 1979; Grenthe *et al.*, 1992; Guillaumont *et al.*, 2003)
UBr_4	brown to black-brown cryst; moisture sensitive; soluble in Me_2CO, EtOH; m.p. = 519°C; b.p. = 777°C; sublimes in a Br_2-N_2 stream. $\mu_{eff.}$ = 3.12 B.M; θ = –35 K; (77–569 K)[d] . UBr_4(cr): $\Delta_f G^o_m$ = –767.4 (3.5)†, $\Delta_f H^o_m$ = –802.1 (2.5)†, S^o_m = 238.5 (8.4)†; $C^o_{p,m}$ = 128.0 (4.2)†. UBr_4(g): $\Delta_f G^o_m$ = –634.6 (5.0)†, $\Delta_f H^o_m$ =	monoclinic; C^3_{2h}, *C*2/*m*, No.12; a = 10.92(2), b = 8.69(3), c = 7.05(1); β = 93.9(1); Z = 4; d(calc.) = 5.55, d(exp.) = 5.35. The Br anions form a pentagonal bipyramid around the U atom. The bipyramids are linked into two-dimensional sheets by double bromide bridging of the U cations. d(U–Br) = 2.85(2) to 2.95(2)	*synthesis* (Brauer, 1981) *crystallographic data* (Douglass and Staritzky, 1957; Taylor and Wilson, 1974d,e; Levy *et al.*, 1975; Korba, 1983); *thermodynamic data;* (Grenthe *et al.*, 1992; Guillaumont *et al.*, 2003); *magnetic data* (Dawson, 1951; Hendricks, 1971); *photoelectron spectra* (Thibaut *et al.*, 1982)

	–605.6 (4.7)†, S^o_m = 451.9 (5.0)†; $C^o_{p,m}$ = 106.9 (3.0)†. log*p* (mmHg) = –10800 T^{-1} +23.15–3.02 log*T* (298–792 K) log *p* (mmHg) = –8770 T^{-1} + 27.93 – 5.53 log*T* (792–1050 K); Energy level parameters: F_2 = 191, F_4 = 34, F_6 = 4, ζ_{5f} = 1976, $A(r^4)$ = –490 and $A(r^6)$ = –15 (in cm^{-1}); ν_{U-Br} = 233 cm^{-1} (vapor)	(in the pentagonal ring) and 2.78 (3) and 2.61(4) (to the apical bromides); the axial Br–U–Br angle = 177(1)°	
$[UBr(H_2O)_8]Br_3(H_2O)$		triclinic; C_i^1, $P\bar{1}$, No.2; *a* = 8.234 (4), *b* = 12.781(7), *c* = 7.168(2), α = 97.76(3), β = 98.36(2)° γ = 85.38(4); *Z* = 2; *V* = 738.07; *d*(calc.) = 3.24	*crystallographic data* (Rabinovich *et al*., 1998)
Li_2UBr_6		trigonal/rhombohedral; D^2_{3d}, $P\bar{3}1c$; No = 163; *a* = 6.8896(4), *c* = 12.6465(9); γ = 120; *Z* = 2; *V* = 519.86	*crystallographic data; phase transitions by neutron diffraction* (Maletka *et al*., 1998)
Na_2UBr_6	m.p. = 533°C; ν(U–Br)as. = 164w, 180, 202w	trigonal/rhombohedral; D^3_{3d}, $P\bar{3}m1$; No. = 164; *a* = 12.4368(1), *c* = 6.6653(2); *V* = 892.83; *Z* = 3	*crystallographic data* (Vdovenko *et al*., 1973b; Bogacz *et al*., 1980); *thermodynamic data* (Vdovenko *et al*., 1973a, 1974c; Fuger *et al*., 1983); *Visible and, IR data* (Brown, 1979; Suglobova and Chirkst, 1978)
K_2UBr_6	m.p. = 672°C; ν(U–Br)as. = 185, 208w	trigonal; *a* = 10.94, *c* = 10.67; *d*(calc.) = 4.11, *d*(exp.) = 4.12	*crystallographic data* (Vdovenko *et al*., 1973b); *thermodynamic data* (Vdovenko *et al*., 1973a, 1974c; Fuger *et al*., 1983); *Visible and IR data* (Suglobova and Chirkst, 1978a; Brown, 1979)

Table 5.26 (*Contd.*)

Formula	*Selected properties and physical constants*[b]	*Lattice symmetry, lattice constants* (Å), *conformation and density* (g cm^{-3})[c]	*Remarks regarding information available and references*
Rb_2UBr_6	m.p. = 722°C[*]; ν(U–Br)as. = 192	cubic face centered; O_h^5, $Fm\bar{3}m$, No.225; $a = 10.94$; $V = 1309.34$. The U atoms are surrounded by an octahedral array of Br atoms at distances of 2.74; d(calc.) = 4.48, d(exp.) = 4.048	*crystallographic data* (Vdovenko *et al.*, 1973a; Maletka *et al.*, 1996b); *thermodynamic data* (Vdovenko *et al.*, 1973a, 1974c; Fuger *et al.*, 1983); *visible-near IR data* (Suglobova and Chirkst, 1978a; Brown, 1979)
Cs_2UBr_6	m.p. = 756°C; vibrational modes (cm^{-1}): ν_1(R) = 197, ν_2(R) = (155), ν_3(IR) = 195, ν_4 = (IR) = 84, ν_5(R) = 87, $L = 5$; $F_2 = 84.112$, $F_4 = 35.542$, $F_6 = 3.818$, $\zeta_{5f} = 1792.306$, $B_0^4 = 6593$, $B_0^6 = 1195$	cubic face centered; O_h^5, $Fm\bar{3}m$, No.225; $a = 11.07$; $V = 1356.57$. The U atoms are surrounded by an octahedral array of Br atoms at distances of 2.767; d(Br–Br) = 3.914; d(calc.) = 4.78, d(exp.) = 4.74	*crystallographic data*, (Vdovenko *et al.*, 1973a); *thermodynamic data* (Vdovenko *et al.*, 1973a, 1974c; Fuger *et al.*, 1983); *visible and IR spectral data* (Johnston *et al.*, 1966; Chodos, 1972; Suglobova and Chirkst, 1978a; Brown, 1979); *crystal-field analysis* (Johnston *et al.*, 1966)
UNBr		tetragonal; D_{4h}^7, $P4/nmm$, No.129; $a = 3.944$, $c = 7.950$; $Z = 2$; d(calc.) = 8.913; d(exp.) = 8.64; The compound is isostructural with BiOCl; d(U–Br) = 3.234; d(U–N) = 2.280	*crystallographic data*; (Juza and Meyer, 1969)
$[N(CH_3)_4]_2UBr_6$	vibrational modes (cm^{-1}): ν_3(IR) = 181; ν(U–Br) = 190–195	cubic face centered; O_h^5, $Fm\bar{3}m$, No.225; $a = 13.37$; d(calc.) = 2.405	*crystallographic data* (Brown, 1966)
$[N(C_2H_5)_4]_2UBr_6$	IR (cm^{-1}): ν(U–Br) = 178; energy level parameters: $F_2 = 181.63(12)$ (or $F^2 = 40867$), $\zeta_{5f} = 1756(41)$, $B_0^4 = 6946(609)$, $B_0^6 = 999(252)$; *rms* = 176		*IR and energy level analyses* (Brown, 1966; Wagner *et al.*, 1977)

$[P(C_6H_5)_3C_2H_5]_2UBr_6$		monoclinic; C_{2h}^2, $P2_1/m$, No.11; $a = 10.45(1)$, $b = 13.51(1)$, $c = 15.46(1)$; $\beta = 96.67(5)$; $Z = 2$; d(calc.) = 1.990, d(exp). = 1.96; d(U–Br): = 2.757(2), 2.776 (2) and 2.777(2)	*crystallographic data* (Caira *et al.*, 1978)
$[P(C_6H_5)_4]_2[UBr_6]\cdot 4CH_3CN$	green crystals; extremely sensitive towards oxygen and moisture	monoclinic; C_{2h}^5, $P2_1/c$, No.14; $a = 9.818(3)$, $b = 20.101(4)$, $c = 15.493(3)$, $\beta = 98.79(2)$; $Z = 2$; $V = 3022$; d(calc.) = 1.72; d(U–Br1) = 2.754 (1); d(U–Br2) = 2.778(1); d(U–Br3) or O = 2.768(1); Br(1)–U–Br(2) = 89.2(1); Br(1)–U–Br(3) (or O) = 90.4(1); Br(2)–U–Br(3) (or O) = 89.6(1).	*synthesis and crystallographic data* (Bohrer *et al.*, 1988)
$UBr(PO_2H_2)_3\cdot 2H_2O$		orthorhombic; D_{2h}^{11}, *Pbcm*, No. 57; $a = 7.488(5)$, $b = 10.192(2)$, $c = 15.203(5)$; $Z = 2$; $V = 1160.26$.	*X-ray crystallographic and spectroscopic structural studies* (Tanner *et al.*, 1993)
$UBr(PO_4)(H_2O)_2$		tetragonal; C_{4h}^5, $I4/m$, No.87; $a = 14.7480(7)$, $c = 6.6810(4)$; $V = 1453.14$; $Z = 8$; d(calc.) = 4.1.	*crystallographic data* (Benard-Rocherulle *et al.*, 1997)
$UBrCl_3$	greenish brown; hygroscopic; m.p. = 521°C; b.p. = 784°C; $UBrCl_3$(cr): $\Delta_f G_m^o = -893.5\ (9.2)^\dagger$, $\Delta_f H_m^o = -967.3\ (8.4)^\dagger$, $S_m^o = 213.4\ (12.6)^\dagger$	tetragonal; $a = 8.434$, $c = 7.690$	*thermodynamic data* (MacWood, 1958; Brown, 1979; Grenthe *et al.*, 1992; Guillaumont *et al.*, 2003)
UBr_2Cl_2	dark green; hygroscopic; m.p. = 510°C; b.p. = 1053 °C; UBr_2Cl_2 (cr): $\Delta_f G_m^o = -850.9\ (9.8)^\dagger$, $\Delta_f H_m^o = -907.9\ (8.4)^\dagger$, $S_m^o = 234.3\ (16.7)^\dagger$		*thermodynamic data* (MacWood, 1958; Brown, 1979; Grenthe *et al.*, 1992; Guillaumont *et al.*, 2003)
UBr_3Cl	greenish brown; hygroscopic; m.p. = 502°C; b.p. = 774°C UBr_3Cl(cr): $\Delta_f G_m^o = -807.1\ (9.8)^\dagger$, $\Delta_f H_m^o = -852.3\ (8.4)^\dagger$, $S_m^o = 238.5\ (16.7)^\dagger$		*thermodynamic data* (MacWood, 1958; Brown, 1979; Grenthe *et al.*, 1992; Guillaumont *et al.*, 2003)

Table 5.26 (*Contd.*)

Formula	*Selected properties and physical constants*[b]	*Lattice symmetry, lattice constants* (Å), *conformation and density* (g cm^{-3})[c]	*Remarks regarding information available and references*
$UOBr_2$	greenish yellow: $UOBr_2$(cr): $\Delta_f G^o_m$ = –929.6 (8.4)†, $\Delta_f H^o_m$ = –973.6 (8.4)†, S^o_m = 157.57 (0.29)†; $C^o_{p,m}$ = 98.0 (0.4)†		*thermodynamic data* (Greenberg and Westrum, 1956; Rand and Kubaschewski, 1963; Brown, 1979; Grenthe *et al.*, 1992; Guillaumont *et al.*, 2003); *photoelectron spectra* (Thibaut *et al.*, 1982)
UI_4	black lustrous crystals; moisture sensitive; m.p. = 506°C; density: 5.6 g cm^{-3}; m.p. = 506°C; b.p. = 757°C; $\mu_{eff.}$ = 2.98 B.M; (1–300 K)[d] . UI_4(cr): $\Delta_f G^o_m$ = –512.7 (3.8)†, $\Delta_f H^o_m$ = –518.3 (2.8)†, S^o_m = 263.6 (8.4)†; $C^o_{p,m}$ = 126.4 (4.2)†. UI_4(g): $\Delta_f G^o_m$ = –369.6 (6.2)†, $\Delta_f H^o_m$ = –305.0 (5.7)†, S^o_m = 499.1 (8.0)†; $C^o_{p,m}$ = 108.8 (4.0)†. log p (mmHg) = –12330 T^{-1} + 26.62 – 3.52 log$T$ (298–779 K), log p (mmHg) = –9310 T^{-1} + 28.57 – 5.53 log$T$ (779–1030 K): IR data (cm^{-1}): 178m, 165s, 132,s, 122m, 104vw, 92m, 55m	monoclinic; C^6_{2h}, $C2/c$, No. 15; a = 13.967(6), b = 8.472(4), c = 7.510 (3); β = 90.54(5); Z = 4; V = 888.7; d(calc.) = 5.57. Close-packed hexagonal iodine atoms form zigzag chains of edge-sharing octahedra ($UI_2I_{4/2}$). d(U–I(1) bridging) = 3.08(2) and 3.11(2); d(U-I(2) terminal) = 2.92(2)(2×); d(U—U) = 4.55	*crystallographic and neutron diffraction data* (Levy *et al.*, 1980, Taylor, 1987); *thermodynamic data*; (Fuger and Brown, 1973; Brown, 1979; Guillaumont *et al.*, 2003)
Li_2UI_6		trigonal/rhombohedral; D^2_{3d}, $P\bar{3}1c$, No. = 163; a = 7.3927(8), c = 13.826(2); V = 654.39; Z = 2; d(U–I) = 3.013	*neutron diffraction and electrical conductivity data* (Maletka *et al.*, 1996a)

Na_2UI_6		trigonal/rhombohedral; C_{3i}^2, $R\bar{3}$, No.148; $a = 7.7001(6)$, $c = 20.526$; $Z = 3$; $V = 1053.97$; d(U–I) = 2.992	*crystallographic data* (Maletka *et al*., 1992, 1995)
$EuUI_6$		monoclinic; C_s^4, Cc, No.9; $a = 8.006(4)$, $b = 12.998(5)$, $c = 15.194(5)$; $\beta = 106.2(1)$; $V = 1518.34$; $Z = 4$; d(U–I) = 3.035 to 3.218	*X-ray powder diffraction data* (Beck and Kuehn, 1995)
$BaUI_6$		monoclinic; C_s^4, Cc, No.9; $a = 8.845(5)$, $b = 13.834(7)$, $c = 15.753(8)$; $\beta = 107.5(1)$; $V = 1838.35$; $Z = 4$; d(U–I) = 3.164 to 3.241	*X-ray powder diffraction data* (Beck and Kuehn, 1995)
M_2UI_6 (M = N$(C_2H_5)_4$, N$(C_4H_9)_4$, N$(C_6H_5)(CH_3)_3$, As$(C_6H_5)_4$).	red; extremely moisture sensitive; soluble in anhydrous methyl cyanide and acetone; vibrational mode in (cm^{-1}) UI_6^{2-}: $\nu_1 = 143$ to 156; $\nu_2 = 119$, $\nu_3 = 135$ to 143; $\nu_4 = 60$ to 65, $\nu_5 = 62$ to 66; $\nu_6 = 44$ to 47; energy level parameters for $[N(C_2H_5)_4]_2UI_6$: $F^2 = 38188$ (2422), $\zeta_{5f} = 1724(39)$, $B_0^4 = 6338(676)$, and $B_0^6 = 941$ (289)		*electronic and IR spectra; crystal-field analysis; magnetic susceptibility data* (Wagner *et al*., 1977; Brown, 1979)
UOI_2	rose-brown cryst; decomposes slowly at room temp; hygroscopic; soluble in H_2O; U–O vibrations (cm^{-1}): 520(w), 475(m), 420 (m), 280(w), and 250(sh); paramagnetic; $\mu_{eff.} = 3.34$ B.M	orthorhombic; D_{2h}^9, *Pbam*, No.55; isostructural with $UOCl_2$ ($PaOCl_2$ struct. type); $a = 17.853(5)$, $b = 20.05(2)$, $c = 4.480(5)$	*crystallographic data; magnetic susceptibility data, infrared spectra* (Levet and Noël, 1979)
UNI		tetragonal; D_{4h}^7, *P4/nmm*, No.129; $a = 3.990$, $c = 9.206$; $Z = 2$;	*crystallographic data*; (Juza and Meyer, 1969)

Table 5.26 (*Contd.*)

Formula	*Selected properties and physical constants*[b]	*Lattice symmetry, lattice constants* (Å), *conformation and density* (g cm^{-3})[c]	*Remarks regarding information available and references*
		$V = 146.56$; d(calc.) = 8.58; d(exp) = 8.50; isostructural with BiOCl	
(i) UF_3I; (ii) $UClI_3$; (iii) UCl_2I_2; (iv) UCl_3I; (v) $UBrI_3$; (vi) UBr_2I_2; (vii) UBr_3I; (viii) UCl_2BrI; (ix) $UClBr_2I$.	(i) brownish black; (ii) black, m.p.<500°C; $UClI_3$ (cr): $\Delta_f G^o_m = -615.8\ (11.4)^\dagger$, $\Delta_f H^o_m = -643.8\ (10.0)^\dagger$, $S^o_m = 242\ (18)^\dagger$; (iii) black, m.p.<500°C; UCl_2I_2 (cr): $\Delta_f G^o_m = -723.4\ (11.3)^\dagger$, $\Delta_f H^o_m = -768.8\ (10.0)^\dagger$, $S^o_m = 237\ (18)^\dagger$; (iv) black, m.p.<490°C, UCl_3I(cr): $\Delta_f G^o_m = -829.9\ (8.8)^\dagger$, $\Delta_f H^o_m = -898.3\ (8.4)^\dagger$, $S^o_m = 213.4\ (8.4)^\dagger$; (v) black, m.p.<500°C $UBrI_3$(cr): $\Delta_f H^o_m = -589.6\ (10.0)^\dagger$;		*thermodynamic data*, (MacWood, 1958; Brown, 1979; Grenthe *et al*., 1992; Guillaumont *et al*., 2003)

(vi) dark, brown; m.p.<500°C
UBr_2I_2 (cr): $\Delta_f H_m^o = -660.4$ (10.0)†;
(vii) dark brown, m.p. 478°C,
UBr_3I $\Delta_f H_m^o = -727.6$ (8.4)†,
sublimes without decomposition;
(viii) black, m.p. < 500°C;
(ix) black, m.p. < 500°C.

---

* Peritectic decomposition point.

† Values recommended by the Nuclear Energy Agency (Guillaumont *et al.*, 2003) .

[a] Values have been selected in part from review articles (Brown, 1979, Bacher and Jacob, 1980; Freeman,1991; Grenthe *et al.*,1992; Guillaumont *et al.*, 2003);

[b] m.p. = melting point (°C); b.p(°C). = boiling point; (cr) = crystalline; (g) = gaseous; thermodynamic values in kJ mol^{-1}, or J $K^{-1}mol^{-1}$ at 298.15 K, unless otherwise mentioned; $\Delta_f G_m^o$, standard molar Gibbs energy of formation; $\Delta_f H_m^o$– standard molar enthalpy of formation; S_m^ostandard molar entropy; $C_{p,m}^o$, standard molar heat capacity; log p (mm Hg) $= -AT^{-1} + B - C \log T$: vapour pressure equation for indicated temperature range; IR = infrared active; L = lattice vibrations; val. = valence vibrations; def. = deformation vibrations; all values in cm^{-1}; s:strong; m: medium; w: weak; sh: shoulder; Energy levels parameters: F_k, F^k, ζ_{5f} = electrostatic and spin–orbit interaction parameters; α, β, γ; = two-body correction; M^j ($j = 0$, 2 and 4) = spin-spin and spin-other-orbit relativistic corrections; P^k = the electrostatically correlated spin-orbit perturbation parameters; B_q^k = crystal-field parameters; values in brackets indicate parameter errors; standard deviation: $rms = \sum \left[(\Delta_i)^2/(n-p)\right]^{1/2}$[$cm^{-1}$], where Δ_i is the difference between the observed and calculated energies, n is the number of levels fitted and p is the number of parameters freely varied.

[c] All values are in Å and angles are in degrees; CN, coordination number; d represents density in g cm^{-3}, V = molar volume [cm^3 mol^{-1}].

[d] Temperature range with linear relationship of χ_M^{-1} against T.

with arsine oxides or phosphine oxides (du Preez *et al*., 1977b; du Preez and Zeelie, 1987).

Tetravalent uranium has a [Rn]$5f^2$ electronic configuration. The ground state is nominally $^3H_4$. The earlier studies of absorption spectra of tetravalent halides in the solid state, aqueous solutions, organic solvents, and in doped host crystals have been compiled in a review article by Carnall (1982). Krupa (1987) analyzed the spectroscopic properties of the ions in solids with their characteristic $5f^2 \rightarrow 5f^2$ transitions. In contrast to the uranium(III) spectra, the spin–orbit interactions in different compounds are of the same order of magnitude and the f–d transitions have been observed at higher energies beginning near 40000–45000 cm^{-1}. For a number of halides and complex halides, low-temperature absorption spectra have been recorded and the energy levels of the U^{4+} ion in different site symmetries were assigned and fitted to a semiempirical Hamiltonian representing the combined atomic and crystal-field interactions. An analysis of octahedral UX_6^{2-} spectra for a series of $(NEt_4)_2UX_6$ salts (X = F, Cl, Br or I) was reported by Wagner *et al*. (1977). The authors have noticed that the Slater parameter F^2 diminishes by ~20% for the series and the crystal-field parameters are different from those of the comparable octahedral PaX_6^{2-} and UX_6^{2-} halides. Analyses of the energy-level structure of U^{4+} ion doped in an isomorphic series of tetragonal ($I4_1/amd$) host crystals such as $ThSiO_4$, $ThCl_4$, and $ThBr_4$ (Delamoye *et al*., 1983; Simoni *et al*., 1988; Malek *et al*., 1986a,b; Malek and Krupa, 1994) led to consistent sets of free ion and crystal-field parameters with a least square deviation (r.m.s.) between 36 and 71 cm^{-1}. In these host crystals, U^{4+} experiences a rather weak crystal field, which justifies the same theoretical approach as for the Ln^{3+} ions; this is in contrast to that in higher symmetry sites as found in $U(BD_4)_4/Hf(BD_4)_4$ (site symmetry T_d; Rajnak *et al*., 1998), Cs_2UX_6 (X = Cl or Br) (site symmetry O_h; Johnston *et al*., 1966; Satten *et al*., 1983) or U^{4+}: $CsCdBr_3$ (disturbed O_h site symetry; Karbowiak *et al*., 2005b) where the crystal field splitting is approximately twice as large with the r.m.s. deviation of 100 to 150 cm^{-1}. As a result, mixing of crystal field components of different multiplets in close proximity may occur. In an analysis of the absorption spectrum of Cs_2UBr_6 single crystals, Faucher *et al*. (1996) have shown that the inclusion of configuration interactions with the higher lying $5f^17p^1$ electronic configuration in the fitting procedure may considerably improve the r.m.s. deviation.

An analysis of (U^{4+}, U^{3+}):BaY_2Cl_7 single crystals (Karbowiak *et al*., 2003b) enabled the assignment of 60 observed $5f^2 \rightarrow 5f^2$ transitions from absorption, excitation, and luminescence spectra, which encompasses all but the $^1S_0$ multiplet. A comparison of the scalar crystal field parameters,

$$N_v = \left[\sum_{k,2} (B_2^k)^2 \frac{4\pi}{(2k+1)}\right]^{1/2}$$

(Auzel and Malta, 1983), indicates that the main factor determining the crystal-field strength is not the nature of the ligand but the site symmetry of the central ion; this is in contrast to that for Ln^{3+} and U^{3+} ions. Energy transfer has been demonstrated between uranium ions in the 3+ and 4+ oxidations states. A very strong anti-Stokes emission was observed for the U^{4+} ions.

In all cases in which the uranium ions are occupying sites of inversion symmetry, as in UCl_6^{2-}, the observed band structure consists almost exclusively of vibronic side bands and their progressions could be used to deduce the electronic transitions. The analysis of absorption spectra of UF_4 in a KBr pellet at 4 K as well as of U^{4+}(aq.) at 298 K have been reported by Cohen and Carnall (1960) and Carnall *et al.* (1991). The authors have also compared the crystal-field interactions of UF_4, NpF_4, and PuF_4. The absorption spectrum of thin films of a mixture of UF_4 with chlorinated naphthalene (refraction index 1.635) at 7 K is shown in Fig. 5.40 (Drożdżyński and Karbowiak, 2005) and is typical for most uranium(IV) compounds. In this region the spectra consist of relatively intense and sharp absorption lines. The intra-configurational $5f^3 \rightarrow 5f^3$ transitions result in 91 non-degenerated crystal field levels.

Magnetic susceptibility measurements have been carried out over wide temperature ranges for almost all halides and complex halides. The paramagnetic constants from the Curie–Weiss law $\chi'_m = C/(T - \theta)$ and the effective magnetic moments ($\mu_{eff} = 2.84\sqrt{c}\mu_{B+}$) for some of the compounds are collected in Table 5.26. Hexachloro uranates(IV) show temperature-independent paramagnetism between 4 and 300 K with $\chi_M = 2000 \times 10^{-6}$ emu.

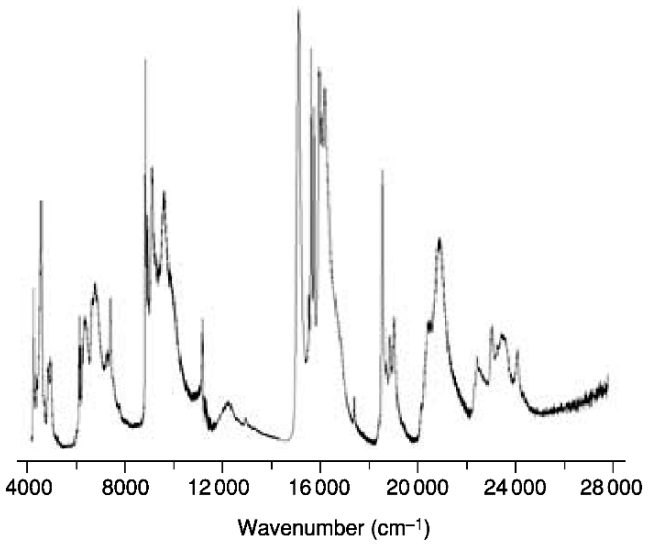

Fig. 5.40 *Absorption spectrum of thin films of a mixture of UF_4 with chlorinated naphthalene at* 7 K (*Drożdżyński and Karbowiak*, 2005).

(*i*) *Uranium tetrafluoride and complex uranium(IV) fluoro compounds*

Uranium tetrafluoride

Uranium tetrafluoride has important industrial applications in the conversion of uranium ore to UF_6 and in the production of UO_2. The former is a key compound in the uranium enrichment process and UO_2 is a nuclear fuel. The usefulness of UF_4 in these two processes depends on its large chemical stability and an almost complete insolubility in aqueous solutions. Fluoride melts containing UF_4 have also proved to be suitable in 'homogeneous reactors'. The preparation of UF_4 has been extensively investigated (Brown, 1968, 1979; Bacher and Jacob, 1980; Freestone and Holloway, 1991). Most of the procedures are based either on precipitation from aqueous solutions or on high-temperature reactions in anhydrous conditions. In the first method, aqueous uranyl solutions are reduced to U(IV) by $SnCl_2$, $Na_2S_2O_4$, $FeSO_4$, CuCl, $CrCl_3$, $TiCl_3$, and SO_2 (combined with Cu^{2+}ions), or electrochemically; after reduction, two hydrates, $UF_4 \cdot 2.5H_2O$ and $UF_4 \cdot nH_2O$, with $0.5 < n < 2$, are obtained by precipitation with F^- (Allen *et al.*, 1950; Anderson *et al.*, 1950; Dawson *et al.*, 1954). The preparation from aqueous solutions based on electrolytic reductions of uranyl solutions has found industrial application in the Excer Process (ion exchange conversion, electrolytic reduction (Higgins and Roberts, 1956; Marinsky, 1956; Bacher and Jacob, 1980).

Since it is difficult to remove water without hydrolytic reactions, UF_4 produced by aqueous processes is not suitable for reduction to metal or for conversion to UF_6. Consequently, it has been customary to prepare UF_4 by high-temperature reactions. One of the most convenient methods to produce UF_4 on a large scale employs heating of UO_2 in an excess of anhydrous HF at 400–600°C.

$$UO_2 + 4HF \overset{550°C}{\rightarrow} UF_4 + 2H_2O$$

This and similar methods result in the formation of a highly reactive form of the dioxide. If the starting material is a non-stoichiometric oxide, it is essential to insert H_2 in order to avoid reactions such as:

$$U_3O_8 + 8HF \rightarrow 2UO_2F_2 + UF_4 + 4H_2O$$

Ruehle (1959) describe the synthesis of UF_4 using a stirred fluidized-bed hydrofluorination reactor. The chemistry of the reaction has been discussed by Dawson *et al*. (1954).

On a large scale the compound may be prepared by thermal decomposition of $UO_4 \cdot 2H_2O$ to UO_3 at 250°C followed by reduction with hydrogen to UO_2 at 600°C and fluorination to UF_4 with NH_4HF_2 at 150°C (Van Impe, 1954). Alternatively, UF_4 may be obtained in a similar route using uranium(IV) acetate or by reaction of UO_2 with SF_4 at 500°C.

Other satisfactory methods involve the direct reduction of UO_3 to UF_4 by ammonia–hydrogen fluoride mixtures at 500–750°C and by NH_4F, NH_4HF_2, or

a mixture of NH_4HF_2 and hydrazine fluoride. Also various freons, in particular, CF_2Cl_2, are useful fluorinating agents for UO_2, UO_3, and $(NH_4)_3U_4O_{16}F_3$ (Evers and Reynolds, 1954; Van Impe, 1954).

Attractive alternatives for the preparation of smaller amounts include the heating of metallic uranium with anhydrous hydrogen fluoride in a sealed tube at 225–250°C and treating UH_3 or uranium with hydrogen fluoride vapours at 250–350°C or with a mixture of $H_2 + HF$ at 250°C (Brown, 1979).

Since UF_6 is the starting material for ^{235}U enrichment, it is also a convenient preparatory material for enriched metallic uranium via uranium tetrafluoride. The preparation of UF_4 from UF_6 may be performed by:

(i) reduction with H_2 in the gaseous phase (Smiley and Brater, 1958, 1960; Bacher and Jacob, 1980)

$$UF_6 + H_2 \overset{630°C}{\rightarrow} UF_4 + 2HF$$

(ii) reduction with chlorinated hydrocarbons C_2HCl_3, C_2Cl_4, and CCl_4 (Bacher and Jacob, 1980, 1986)

$$UF_6 + 2CCl_4 \xrightarrow{200°C,\ p=29\ bar} UF_4 + 2CCl_3F + Cl_2$$

(iii) the reaction with Me_3SiX (Brown *et al.*, 1983)

$$UF_6 + 2Me_3SiX \rightarrow 2Me_3SiF + X_2 + UF_4 (X = Cl \text{ or } Br)$$

On technical scale the reaction (i) may be performed either in a 'hot-wall reactor', by heating the outside wall of the reactor up to 650°C, or in a 'cold-wall reactor' in which the energy is supplied by the reaction

$$F_2 + H_2 \rightarrow 2HF$$

The temperature of the reactor wall is kept between 150 and 200°C. In order to achieve a complete conversion in the reactions (ii) and (iii), a substantial excess of CCl_4 and a molar ratio 1:2 of UF_6 to Me_3SiX is essential (Bacher and Jacob, 1980; Hellberg and Schneider, 1981).

Uranium tetrafluoride is an emerald-green high melting polymeric solid, entirely insoluble in water. However it may be dissolved in the presence of reagents that can form fluoride complexes, such as Fe^{3+}, Al^{3+}, or boric acid, for example. It is a good starting material for the synthesis of UF_6 and production of uranium metal by reduction with calcium or magnesium. The reduction may also be performed with Li, La, or Al whereas Zr, Be, Ti, or hydrogen leads to uranium trifluoride. The compound is stable in air at room temperature, which makes it useful as an intermediate product in the conversion of uranium ore to UF_6. For sublimation *in vacuo*, a stainless steel tube with a molybdenum liner has been used (Dawson *et al.*, 1954). Uranium tetrafluoride reacts with strong oxidizing reagents such as Ce^{4+}, concentrated perchloric acid, nitric acid and, nitric acid–boric acid or sulphuric acid–ammonium persulphate mixtures with the formation of the appropriate uranyl salt solutions.

UF_4 is monoclinic, with the same structures as those of zirconium and hafnium tetrafluorides. The structure at different temperatures has been examined in detail by Kern *et al.* (1994), using neutron diffraction on polycrystalline samples. The unit cell of UF_4 contains 12 formula units with four (U1) and eight (U2) sites having C_2 symmetry. Each uranium atom has eight fluorine neighbors arranged in a slightly distorted square antiprism. A basic repeating unit of five uranium atoms is arranged in a slightly distorted pyramid. Four of them are forming a rhomb-shaped base, and the fifth comprises the apex of the pyramid. For other details see Table 5.26.

The thermodynamic properties of UF_4 have been analyzed in detail by Rand and Kubaschewski (1963), Kubaschewski and Alcock (1979), and Fuger *et al.* (1983). The heat capacity from 1.3 to 20 K has been measured by Burns *et al.* (1960) and between 5 and 300 K by Osborne *et al.* (1955).

Carnall *et al.* (1991) have reported an analysis of the low-temperature crystal-field absorption spectrum of UF_4. The authors found a good agreement between the experimentally observed and calculated band structure using an effective Hamiltonian with orthogonalized free-ion operators. The initial crystal-field parameter values were calculated on the basis of a superposition model for An^{4+} sites with C_2 symmetry. The values obtained are listed in Table 5.26. The parameters have been obtained in a fit of 69 observed crystal-field levels of UF_4; the r.m.s. error is 31 cm^{-1}. The spin–spin and spin–orbit parameters, $M^0 = 0.775$, $M^2 = 0.434$, and $M^4 = 0.294$, were assigned on the basis of *ab initio* calculations and were not varied in the fitting. The electrostatically correlated spin–orbit perturbation parameters P^4 and P^6 were constrained by keeping the ratios P^4/P^2 and P^6/P^2 constant, equal to 0.5 and 0.1, respectively. The magnitude of the total crystal-field strength expressed by the scalar parameter N_v (Auzel and Malta, 1983), is equal to 2700 (assuming the C_{2v} approximation).

Uranium tetrafluoride hydrates

The reaction of U(IV) solutions with 4–20% aqueous fluoride solutions results in the precipitation of $UF_4 \cdot 2.5H_2O$. A number of hydrates with smaller water content, $UF_4 \cdot nH_2O$ (where $0.5 < n < 2$), was obtained by controlled thermal decomposition. $UF_4 \cdot 2.5H_2O$ is the most stable one: in vacuum up to 25°C and in air up to 100°C. The compound may be converted to $UF_4 \cdot 0.5H_2O$ at 100–120°C with the maintenance of its structure. A complete dehydration occurs at 500–550°C in a stream of N_2 or HF. However, it still retains some of the structure of $UF_4 \cdot 2.5H_2O$ and, contrary to UF_4, it may be readily rehydrated to $UF_4 \cdot 2.5H_2O$. All UF_4 hydrates with lower water content may also be gradually converted back to this stable form. The solubility of $UF_4 \cdot 2.5H_2O$ in water is 0.1 $g \cdot L^{-1}$ (Bacher and Jacob, 1980).

$UF_4 \cdot 2.5H_2O$, $UF_4 \cdot 2H_2O$, and $UF_4 \cdot 4/3H_2O$ have orthorhombic *Pnma*, cubic $Fm\bar{3}m$, and a monoclinic structure, respectively, as revealed by X-ray diffraction and NMR data. Crystallographic data are given in Table 5.26.

The three-dimensional network contains channels in which coordinated and free water molecules are located (Zadneporovskii and Borisov, 1971).

Complex uranium(IV) fluorides

Metal fluoride–uranium tetrafluoride fused salt systems have been extensively studied because of their usefulness as fertile fuel materials, coolants, and heat transfer media in the Molten-Salt Reactor Experiment (MSRE), Molten-Salt Breeder Reactor, and the Aircraft Nuclear Propulsion (ANP) projects. Numerous ternary and polynary uranium(IV) fluorides have been characterized by determination of their crystallographic parameters (see Table 5.26) but there are fewer studies of their chemical and thermodynamic properties. The application of the compounds in molten-salt reactor technology has been reviewed in a number of articles (Thoma and Grimes, 1957; Thoma, 1959, 1971, 1972; Grimes and Cuneo, 1960; Rosenthal *et al.*, 1972; Grimes, 1978). Caillat (1961), Brown (1968), Bacher and Jacob (1980), Martinot (1984), Bagnall (1987), Freestone and Holloway (1991) and others have reviewed their general properties. Various complex compounds are listed in Table 5.27 with an indication of their melting behavior when available.

A number of ternary and quaternary fused salt systems such as $LiF–BeF_2–UF_4$ (Thoma, 1959; Jones *et al.*, 1959) and $NaF–BeF_2–UF_4$ (Thoma, 1959) were important for the MSRE and ANP projects. The $MgUF_6$ and $CaUF_6$ fluorides are of importance for the production of uranium by high-temperature reduction of UF_4 with calcium or magnesium. Systems with ammonium or hydrazinium cations have found application in the preparation of high-purity UF_4 by decomposition of the corresponding complex fluorides. A typical phase diagram of some importance for the molten-salt reactor projects is presented in Fig. 5.41.

The general methods for the preparation of the compounds (Bacher and Jacob, 1980; Freestone and Holloway, 1991) include: (i) solid state reaction between the component fluorides in an inert atmosphere; (ii) reactions between UF_4 or UO_2 and the alkali metal fluoride or carbonate in HF or $HF–O_2$ mixtures; (iii) reductions of UF_6 with appropriate alkali metal fluorides; (iv) controlled thermal decomposition of tetravalent uranium fluoro complexes of higher stoichiometry (e.g. $(NH_4)_4U^{IV}F_8$) or the treatment of other fluoro complexes with fluorine, (v) precipitation from aqueous solutions, followed by heating in air, *in vacuo* or fluorine, and (vi) hydrogen reduction of higher valence state fluoro complexes and precipitation from aqueous solutions.

The structures for the majority of the fluoro complexes are well established; typical examples are those with the UF_7^{3-}, UF_8^{4-} anions, but octahedral UF_6^{2-} complexes are also known. The cubic K_3UF_7 structure contains UF_7^{3-} pentagonal bipyramids, while the uranium coordination in Li_4UF_8 is described as a bicapped triangular prism (Brunton, 1967; Freestone and Holloway, 1991). Compounds of the $M^{II}UF_6$ (M^{II} = Ca, Sr, Ba, or Pb) adopt the LaF_3 structure (Keller and Salzer, 1967). U(IV) in $LiUF_5$, KU_2F_9, and $M^IU_3F_{13}$ (M^I = Rb or

Table 5.27 *Melting behavior of uranium(IV) complex fluorides and chlorides.*

System	*Complex fluorides*[a]
$LiF\text{-}UF_4$	LiU_3F_{13}, Li_2UF_6, Li_4UF_8 (P), Li_3UF_7, $LiUF_5$ (P), LiU_4F_{17} (P)
$NaF\text{-}UF_4$	$NaUF_5$, $Na_7U_2F_{15}$, Na_3UF_7 (C), Na_2UF_6 (P), $Na_5U_3F_{17}$ (P), $Na_7U_6F_{31}$ (C), NaU_2F_9 (D)
$KF\text{-}U_4$	KUF_5, K_3UF_7 (C), K_2UF_6 (P), KU_3F_{14}, $K_7U_6F_{31}$ (P), KU_2F_9 (P), KU_6F_{25}
$RbF\text{-}UF_4$	RbU_2F_9, Rb_3UF_7 (C), Rb_2UF_6 (P), $Rb_7U_6F_{31}$ (P), $RbUF_5$ (C), $Rb_2U_3F_{14}$ (P), RbU_3F_{13} (P), RbU_6F_{25} (P)
$CsF\text{-}UF_4$	Cs_3UF_7 (C), Cs_2UF_6 (P), $CsUF_5$ (C), $Cs_2U_3F_{14}$, CsU_2F_9, CsU_6F_{25}
$NH_4F\text{-}UF_4$	$(NH_4)_4UF_8$, $(NH_4)_2UF_6$, $(NH_4)_7U_6F_{31}$, NH_4UF_5, $NH_4U_3F_{13}$
$N_2H_5F\text{-}UF_4$	$(N_2H_5)_3UF_7$, $(N_2H_5)_2UF_6$, $N_2H_5UF_5$
$NH_3OHF\text{-}UF_4$	$(NH_3OH)UF_5$
$LiF\text{-}CaF_2\text{-}UF_4$	Li_2CaUF_8
$LiF\text{-}CdF_2\text{-}UF_4$	Li_2CdUF_8
$MgF_2\text{-}UF_4$	$MgUF_6$
$CaF_2\text{-}UF_4$	$CaUF_6$ (P)
$BaF_2\text{-}UF_4$	$BaUF_6$
$SrF_2\text{-}UF_4$	$SrUF_6$
$TlF\text{-}UF_4$	Tl_4UF_8, Tl_2UF_6, $Tl_7U_6F_{31}$, $TlUF_5$, TlU_3F_{13}, TlU_6F_{25}
$SnF_2\text{-}UF_4$	Sn_2UF_8 (P), $SnUF_6$ (P)
$PbF_2\text{-}UF_4$	$PbUF_6$, Pb_6UF_{16} (C), $Pb_3U_2F_{14}$ (C)
	complex chlorides[a]
$LiCl\text{-}UCl_4$	Li_2UCl_6 (C)
$NaCl\text{-}UCl_4$	Na_2UCl_6 (C)
$KCl\text{-}Ucl_4$	K_2UCl_6 (C), $KUCl_5$ (P), KU_3Cl_{13} (P), K_2UCl_6 (C)
$RbCl\text{-}UCl_4$	Rb_2UCl_6 (C), $Rb_3U_2Cl_{11}$ (P), $RbUCl_5$ (C), RbU_3Cl_{13} (P)
$CsCl\text{-}UCl_4$	Cs_2UCl_6 (C), CsU_2Cl_9 (P), $Cs_3U_2Cl_{11}$ (P), $CsUCl_5$ (P)

[a] C: congruent melting, E: eutectic, P: incongruent melting, D: decomposition.

NH_4) has tricapped trigonal prism coordination geometry. A structure with linear chains of polyhedra with a distorted cubic arrangement has been proposed for $\gamma\text{-}Na_2UF_6$ (Zachariasen, 1948a). Infinite chains are also present in the $\beta_1\text{-}K_2UF_6$ structure, where they are formed by tricapped trigonal prisms that share the triangular faces perpendicular to the three-fold axis of the ideal polyhedron (Zachariasen, 1948a). The structure of Rb_2UF_6 (Kruse, 1971) consists of infinite chains of $[UF_8]$ units with triangular faced dodecahedral geometry (of the K_2ZrF_6-type) whereas in $(NH_4)_2UF_6$ the chains of antiprism are linked by s edges on opposite square faces (Penneman *et al.*, 1974). Compounds of the $M^I_7U_6F_{31}$ type (M^I = Na, K, Rb, or NH_4) are isostructural with $Na_7Zr_6F_{31}$ (Burns *et al.*, 1968) and have a coordination geometry that is approximately square antiprismatic. The six antiprisms share corners to form an octahedral cavity, which encloses one F atom. Additional information on the structures and crystallographic data of uranium(IV) fluoro complexes are given in Table 5.26.

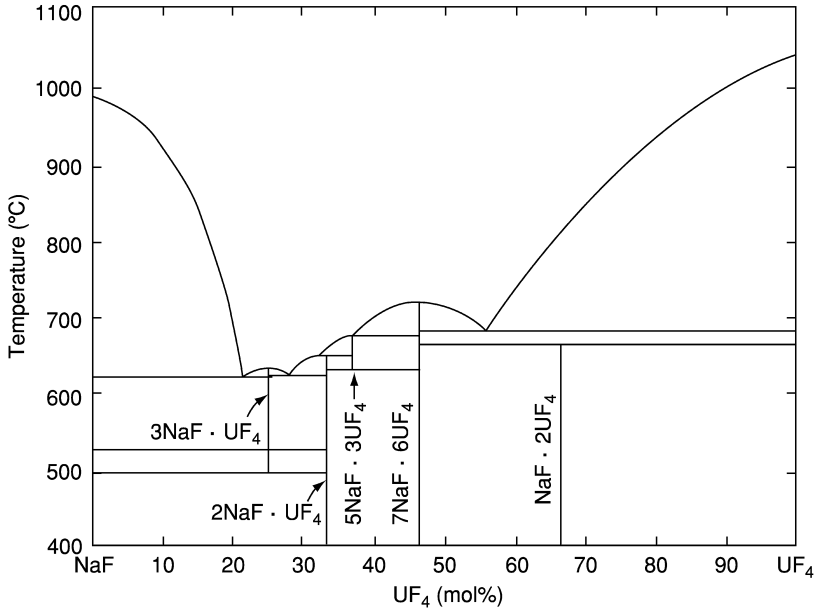

Fig. 5.41 *Phase diagram of the NaF–UF_4 system* (*Thoma,* 1959).

Numerous UF_4 complexes with quaternary ammonium compounds such as amines, pyridine, quinoline, and guanidine have been chemically and structurally characterized (Bacher and Jacob, 1980).

(*ii*) *Uranium*(IV) *oxide fluorides and nitride fluorides*

The melting of stoichiometric amounts of UO_2 and UF_4 yields UOF_2. From aqueous U(IV) solutions, the green hydrates $UOF_2 \cdot 2H_2O$ and $UOF_2 \cdot H_2O$ precipitates. Numerous non-stoichiometric uranium oxide fluorides, rich in oxygen, have been obtained by interactions of UF_4 with uranium oxides in the absence of oxygen at 400–550°C (Bacher and Jacob, 1980). The uranium atoms have an oxidation number that is either 5+, or a mixture of 5+ and 6+. In $UO_2F_{0.25}$, the oxidation number is 4+ and 5+. The compounds are non-volatile or difficult to volatilize; they have structures related to that of uranium oxide. The crystallographic data of $UO_2F_{0.25}$ are given in Table 5.26.

Heating of uranium nitride ($UN_{1.33}$) and uranium tetrafluoride leads to the formation of nitride fluorides of composition between UNF and $UN_{0.98}F_{1.20}$. The formal oxidation number of uranium in these compounds varies between 4 and 4.14. A tetragonal high-temperature and an orthorhombic low-temperature phase have been claimed to exist in this composition range. X-ray investigations of the tetragonal phase revealed a close structural relationship with lanthanum oxide fluoride (Jung and Juza, 1973). The interaction of uranium nitride with an

excess of UF_4 at 950°C leads to UF_3 and with an excess of UN to UNF (Tagawa, 1975).

(*iii*) *Uranium tetrachloride and uranium*(*IV*) *complex chlorides*

Uranium tetrachloride

Uranium tetrachloride is a suitable starting material for the synthesis of a large range of uranium compounds due to its ease of preparation and solubility in numerous polar organic solvents. It has also found application as charge material for calutron ion sources in the electromagnetic separation of uranium isotopes (Akin *et al.*, 1950). Since it has been the subject of an extensive research, numerous methods for the synthesis have been developed (Brown, 1979). Most of them are based on chlorination of uranium oxides with an extensive range of powerful chlorinating agents such as CCl_4, $COCl_2$, $SOCl_2$, S_2Cl_2, Cl_2, $Cl_2C{=}CClCCl_3$ as well as of S_2Cl_2/Cl_2 and Cl_2/He mixtures that can be used both in gaseous and liquid phases. The direct combination of uranium and chlorine leads to a complex mixture of uranium chlorides and does not yield pure UCl_4. This may most conveniently be obtained either by liquid-phase chlorination of UO_3, $UO_4 \cdot 2H_2O$, U_3O_8, UO_2Cl_2 (but not UO_2) with hexachloro propene, $Cl_2C{=}CCl{-}CCl_3$ (Hermann and Suttle, 1957) or by converting UO_2 to the tetrachloride by carbon tetrachloride at 450°C (Brown, 1979):

$$UO_2 + CCl_4 \overset{450^\circ C}{\rightarrow} UCl_4 + CO_2$$

Since the particle size of uranium dioxide is important for the synthesis, a reactive form of UO_2 should be used, formed by decomposition of uranyl oxalate in presence of hydrogen at 300°C. On laboratory scale, the simplest method involves the refluxing of UO_3 with a five-fold excess of hexachloro propene (b.p. 210°C) at atmospheric pressure. Uranium tetrachloride is insoluble in the reaction mixture and precipitates quantitatively as the reaction progresses. Due to extensive hydrolysis, the anhydrous chloride cannot be recovered from aqueous solutions.

In syntheses involving chlorine or the higher uranium oxides, usually small amounts of UCl_5 are formed. This is, however, thermally unstable and loses chlorine by heating in a stream of carbon dioxide or nitrogen. Uranium tetrachloride may be easily purified by sublimation *in vacuo*, or in a stream of a dry inert gas. A recommended route is also vapor-phase transport by the $UCl_4 \cdot AlCl_3$ complex, which proceeds rapidly already at 350°C (Gruen and McBeth, 1968). The chorination of UO_3 using liquid CCl_4 was used on a large scale to obtain UCl_4, which was used as charge material for the calutron ion sources used in the electromagnetic separation of uranium isotopes. Under a pressure of 20 atm, the chlorination yielded UCl_5, which was thermally decomposed to UCl_4 in an inert gas. Details of these processes can be found in Akin *et al.* (1950).

Uranium tetrachloride forms dark-green hygroscopic crystals, which must be handled in a dry atmosphere. At 600°C, in air it converts into U_3O_8. The compound is insoluble in non-polar organic solvents such as chloroform or

carbon tetrachloride but dissolves readily in numerous polar solvents, usually with complex formation, which enables the recovery of the anhydrous compound by evaporation. In water, it undergoes hydrolysis, which is complete at 100°C. The reaction of UCl_4 with hydrogen, zinc, or UN results in the formation of uranium trichloride. Reaction with HBr or HI yields UBr_3 and UI_3, respectively. Reduction to uranium metal takes place when the tetrachloride is heated with Li, Na, K, Mg, Ca, and Al.

Metallic uranium is also obtained by electrolytic reduction of molten UCl_4 or its solutions in fused salts media such as NaCl–KCl. Reduction with magnesium also leads to metallic uranium, whereas insoluble U(III) species are formed on reduction with Zn, Pb, and Bi. Uranium trichloride is formed in a LiCl–KCl melt by reduction with uranium or aluminum. The interaction of UCl_4 with chlorine at 115–125°C yields mixtures of UCl_5 and UCl_6, whereas in fused salt media at 400–700°C it leads to the formation of UCl_6. The reaction with fluorine gas, HBr, or HI converts UCl_4 to UF_6, UBr_4, and mixed chloride iodides, respectively.

Uranium tetrachloride crystallizes in the space group $I4_1/amd$, with tetragonal symmetry; it is isostructural with other actinide tetrachlorides. Each uranium atom is bonded to eight chlorine atoms in a dodecahedral arrangement. The crystallographic data are listed in Table 5.26. High-quality absorption spectra of UCl_4 were obtained (Brown, 1979) both for powdered samples, single crystals, in the vapor phase, and in a nitrogen matrix at 4 K (Clifton *et al.*, 1969). Numerous spectra were also recorded in different non-aqueous solvents. Successful investigations of U^{4+} spectra in the solid state started with a parametric analysis of U^{4+}-doped $ThBr_4$ single crystals by Delamoye *et al.* (1983). On this basis, consistent sets of atomic and crystal field parameters have been obtained also for isomorphic $ThCl_4$:U^{4+} and UCl_4 of D_{2d} symmetry (Malek *et al.*, 1986a,b). The data for UCl_4 are listed in Table 5.26. The parameters have been obtained by fitting 60 observed crystal-field levels of UCl_4 with a r.m.s. error of 60 cm^{-1}. The configuration interaction parameter $\gamma = 1200$, the spin–spin and spin–other orbit parameters, $M^0 = 0.99$, $M^2 = 0.55$ and $M^4 = 0.38$, and the electrostatically correlated spin–orbit perturbation parameters $P^2 = P^4 = P^6 = 500$ (all in cm^{-1}) have been used as constants in the fitting (Malek *et al.*, 1986b). The magnitude of the total crystal-field strength expressed by the scalar parameter (Auzel and Malta, 1983) N_v is equal to 1224.

The magnetic susceptibility of UCl_4 has been measured in wide temperature ranges: 100–350 K, $\mu_{eff} = 3.18$ B.M.; 350–500 K, $\mu_{eff} = 3.18$ B.M., $\theta = -31$ K (Bommer, 1941); 77–500 K, $\mu_{eff} = 3.29$ B.M., $\theta = -62$ K (Dawson, 1951); 77–450–775; 825–1200 K, $\mu_{eff} = 3.33$, 3.50, and 3.60 B.M., respectively (Trzebiatowski and Mulak, 1970). A deviation from the Curie–Weiss law was found at very low temperatures. The best fit between the experimental and the calculated curves was achieved using the values obtained by Hecht and Gruber (1974) with $A_6^4\langle r^6\rangle$ increased to 1561.8 cm^{-1}. The crystal-field parameters deduced by Mulak and Żołnierek (1977) are different from those obtained from spectroscopic data.

It has been shown (Gamp *et al.*, 1983) that the previous susceptibility measurements made on powdered UCl_4 samples are not reproducible because of a re-orientation effect caused by the high anisotropy of the susceptibility of this material. For single crystals, the anisotropic magnetic susceptibility $\chi_{\parallel}$ (along the tetragonal axis), measured between 1.6 and 350 K, is found to be almost temperature-independent and about 30 times smaller than $\chi_{\perp}$ at low temperatures (Gamp *et al.*, 1983). Chlorine-35 nuclear quadrupole resonance has been observed in solid UCl_4 at 77 K and a frequency of (6.24 $\pm$0.03) MHz (Carlson, 1969). Some other physical data are summarized in Table 5.26.

Complex uranium(IV) chlorides

A large number of hexachloro uranium(IV) compounds of the formulas $M^{I}_2UCl_6$ and $M^{II}UCl_6$ have been prepared by reactions in non-aqueous and aqueous media and by solid state reactions of the component halides (where M^{I} = Li, Na, K, Rb, Cs, Ag, $N(CH_3)_4$, $N(C_2H_5)_4$, $As(C_6H_5)_4$, C_5H_5NH, $N(CH_3)_2(C_6H_5CH_2)_2$, $P(C_2H_5)_3H$, $P(C_4H_9)_3H$, $P(C_6H_5)_2H_2$, $P(C_2H_5)_4$ etc. and M^{II} = Be, Ca, Ba, Sr, etc.). The chlorination of a mixture of U_3O_8 and NaCl at high temperatures yields Na_2UCl_6. The formation of numerous complex tetravalent chloro compounds (see Table 5.27) has also been observed during investigations of binary and ternary fused salt systems containing UCl_4.

The results of investigations on phase equilibria, spectroscopic and electrochemical properties of uranium tetrachloride in molten salt systems have been reviewed by Brown (1979) and Martinot (1984). Investigations of Gruen and McBeth (1968, 1969) and Schäfer (1975) and Binnewies and Schäfer (1974) have given evidence for the existence of uranium(IV) vapor phase complexes such as $UCl_4 \cdot AlCl_3$, $TlUCl_5$, $CuUCl_5$, Tl_2UCl_6, TlU_2Cl_9, $BeUCl_8$, In_2UCl_{10}, $ThUCl_8$, and Cu_2UCl_5. In the UCl_4–HCl–H_2O system, five hydrates have been identified among which $UCl_4 \cdot 9H_2O$ and $UCl_4 \cdot 5H_2O$ are stable at 0 and 40°C, respectively (Brown, 1979).

The action of oxygen and nitrogen donor ligands on UCl_4 solutions in non-aqueous solvents results in the formation of stable adducts of different UCl_4 to ligand stoichiometries (Brown, 1979; du Preez and Zeelie, 1989):

- (1:1): methylene bis-diphenylphosphine, ethylene bis-diphenylphosphine, α-α-dimethylmalonamide;
- (1:2): pyridine, triphenylphosphine oxide, 1,2–dimethoxyethane, 1,2-bis-methylthioethane, 1,10-phenanthroline, 1,8-diaminonaphthalene, 1,2-diaminobenzene, dimethyl sulfoxide, di-*tert*-butylsulfoxide;
- (1:2, 1:6): trimethylphosphine oxide;
- (1:2, 1:4): ammonia;
- (1:3): dioxan, tetrahydrofuran, trimethylphosphine, pyrrolidine;
- (1:4): phosphorous oxide trichloride, ROH (R = CH_3, C_2H_5, C_3H_9, i-C_3H_9), ethylenediamine, piperidine, methyl cyanide;
- (1:6): acetamide, hydrazine;

- (1:7, 1:5, 1:3): dimethylsulphoxide;
- (2:3): malonamide, glutaramide, dimethylglutaramide;
- (2:5):dimethylformamide, pyrazine, 1,2-diaminobenzene, pyrazine-2-carboxamide; dimethylacetamide.

In alternative syntheses, the reaction between uranium tetraacetate and acetates of M^I cations (M^I = K, Rb, Cs, NH_4, or $N(CH_3)_4$) in an acetyl chloride–acetic acid mixture has been used. The use of $CsUCl_6$ as a convenient starting material for the preparation of the complexes has also been reported.

The chlorine atoms may by replaced by a variety of anions in metathetic reactions involving uranium tetrachloride in non-aqueous media such as formic acid, acetic acid, sodium diethyldithiocarbamate (Nadtc), tertaethylammonium diethyldiselenocarbamate ($N(C_2H_5)_4$dsc), sodium acetylacetonate (Na-acac), tropolone (Htrop), $LiNR_2$ (R = C_2H_5, C_3H_7, C_6H_5, KC_5H_5), $NaNH_2$ (in NH_3), $NaBH_4$, and many other compounds. Electrochemical oxidation of anodic uranium into acetonitrile solutions of Cl_2 results in the formation of $UCl_4 \cdot 4CH_3CN$ in good yield. The compound may be converted into other UCl_4 adducts, e.g. with dimethylsulfoxide (1:3), 2,2′-bipyridine (1:2), Ph_3PO (1:2) etc. (Kumar and Tuck, 1984).

The chloro complexes are to some extent soluble in organic solvents such as ethanol, methyl cyanide, thionyl chloride, nitromethane, etc. with the exception of the compounds containing alkali metal cations. In aqueous hydrochloric acid solutions, the solubility of the complexes decreases markedly with the increase of the acid concentration. Liquid zinc amalgam reduction of solutions of M_2UCl_6 (where M = NH_4, K, or Rb) with an excess of NH_4Cl, KCl, or RbCl in anhydrous methyl cyanide results in the formation of the trivalent complexes, M_2UCl_5 (Drożdżyński and Miernik, 1978).

The crystallographic data of the hexachloro uranium(IV) compounds are listed in Table 5.26. The compounds with Cs^+, Rb^+, $N(CH_3)_4^+$, $As(C_2H_5)_4^+$, $P(C_6H_5)H^+$, and other cations exhibit a non-magnetic ground state A_1 with no thermal population of the excited states of the ground multiplet $^3H_4$, resulting in a temperature-independent paramagnetism between 4 and 350 K with $\chi_{mole} \cong 2000 \times 10^6$ cm^3 mol^{-1}. The magnetic susceptibility of Rb_2UCl_6 and Cs_2UCl_6 has been measured at higher temperatures and show an approximate Curie–Weiss dependence above 400 K. The magnetic susceptibilities of other chloro compounds (with M = Li, Na, or K) have a somewhat more complex temperature dependence with limited ranges of temperature-independent paramagnetism, e.g. $KUCl_5$ exhibits Curie–Weiss dependence in the 77 to 600 K and 600–1200 K ranges with μ_{eff} = 3.52 and 3.64 B.M., respectively. Solid state reactions of stoichiometric mixtures of Cs_2UCl_6 and Sb_2O_3 at 300°C *in vacuo* yields a dark olive brown uranium(IV) oxochloro compound of the formula Cs_2UOCl_4, for which Watt *et al.* (1974) reported infrared and powder diffraction data.

(*iv*) *Uranium*(IV) *oxychloride and oxochloro complexes*

$UOCl_2$ can be prepared by heating uranium dioxide in an excess of molten uranium tetrachloride followed by vacuum sublimation of the excess of tetrachloride at about 450°C (Brown, 1979), or by the following reaction:

$$3UCl_4 + Sb_2O_3 \rightarrow 3UOCl_2 + 2\,SbCl_3$$

This latter synthesis ought to be carried out *in vacuo* around 400°C where by-products sublimate from the reaction zone (Bagnall *et al*., 1968).

Uranium(IV) oxide dichloride is a green, moisture-sensitive, and thermally unstable solid. It readily dissolves in water and aqueous nitric acid, but is insoluble in organic solvents. At 170°C, CCl_4 may convert the compound to the tetrachloride; anhydrous liquid hydrogen fluoride may convert it to the tetrafluoride.

$UOCl_2$ is isostructural with some $MOCl_2$ oxychlorides (where M = Pa, Th, or Np). The oxychlorides crystallize in the orthorhombic system (see Table 5.26) and the structure contains $U_3O_3Cl_3$ chains running parallel to the *c*-axis that are linked by chlorine bridges. There are three types of polyhedra around the non-equivalent uranium atoms in the chains: around U(1), dodecahedra (CN = 8; from 3O and 5 Cl); around U(2), tricapped trigonal prism (CN = 9; 4O, 5Cl) and around U(3) monocapped trigonal prisms (CN = 7; 3O, 4Cl) (Taylor and Wilson, 1974a); all coordination polyhedra are distorted from the ideal shape. A dark olive-brown to blue-brown oxochloro complex of the formula Cs_2UOCl_4 was prepared by heating together Cs_2UCl_6 with Sb_2O_3 at 300°C *in vacuo* (Watt *et al*., 1974).

(*v*) *Uranium*(IV) *perchlorates*

Uranium(IV) perchlorate, $U(ClO_4)_4$, is unknown, but a few uranium(IV) perchlorato compounds have been isolated. Bagnall *et al*. (1962) and Bagnall and Wakerley (1974) have described the preparation and reactions in non-aqueous media of oxygen donor complexes of the formula $U(ClO_4)_4 \cdot 4L$ (L = octamethyl phosphoramide) and $U(ClO_4)_4 \cdot 4L'$ (L′ = dimethylacetamide, trimethylphosphine oxide, or hexamethylphosphoramide). Interaction of solid $U(HPO_4)_2 \cdot xH_2O$ with 10 M $HClO_4$ results in the formation of hydrated phosphate perchlorates of the formula $U(H_2PO_4)_2(ClO_4)_2 \cdot xH_2O$ ($x = 4$ and 6).

(*vi*) *Uranium tetrabromide and uranium*(IV) *complex bromides*

Uranium tetrabromide

A wide variety of methods for the preparation of uranium tetrabromide have been reported (Brown, 1979); the product may then be purified by sublimation *in vacuo* or in a stream of an inert gas. Since the compound is extremely moisture-sensitive, the carrier gases must be carefully dried. The most convenient and widely used preparation methods involve (i) the conversion of UO_2 or

U_3O_8 to the tetrabromide by heating, with a mixture of carbon, in a stream of bromine at 700–900°C, (ii) reactions between UO_2, UO_3, or $UOBr_3$ with carbon tetrabromide at about 170°C, (iii) reactions between UO_2 and a sulfur–bromine mixture under reflux at about 170°C, and (iv) direct bromination of uranium metal, either in a flow system, for example, a helium–bromine mixture at about 650°C, or in sealed evacuated vessels at 500–700°C.

Uranium tetrabromide is a deep brown, very hygroscopic solid, insoluble in non-polar organic solvents but soluble or reacting with numerous polar solvents. HBr is evolved on dissolution in methanol, ethanol, phenol, acetic acid, aniline, or on exposure to moist air. In non-aqueous solvents, the tetrabromide forms complex compounds with numerous organic ligands such as nitriles, amides, sulfoxides, phosphine oxides, or arsine oxides, e.g. $UBr_4 \cdot 4CH_3CN$, $UBr_4 \cdot 4CH_3CON(CH_3)_2 \cdot CH_3COCH_3$, $UBr_4 \cdot nCH_3CON(CH_3)_2$ ($n = 2.5$ or 5), $UBr_4 \cdot 8CO(NH_2)_2$, $UBr_4 \cdot 6(CH_3)_2SO$, $UBr_4 \cdot 2L$ (L = $(C_6H_5)_3PO$, $[(CH_3)_2N]_3PO$, $(C_2H_5)_3PO$, $(CH_3)_3AsO$, $(C_6H_5)_3AsO$, $(C_2H_5)_3AsO$, $(CH_3)_3AsO$, $UBr_4 \cdot 6(CH_3)_3PO$, $UBr_4 \cdot 6L'$ (L′ = $(CH_3)_3AsO$ and $(C_2H_5)_3AsO$). Reduction with alkali or alkaline earth metals at high temperatures and hydrogen at 450–700°C yields uranium metal and uranium tribromide, respectively. Uranium tetrabromide may be converted to the tetrachloride by chlorine and to UO_2Br_2 by dry oxygen at 150–160°C. The preparation and crystal structure of octaaquabromo uranium(IV) tribromide monohydrate, $[UBr(H_2O)_8]Br_3(H_2O)$ (Table 5.26) have been reported by Rabinovich *et al.* (1998).

Uranium tetrabromide crystallizes in the monoclinic space group *C*2/*m* (see Table 5.26), with pentagonal bipyramid coordination at the uranium atom; the polyhedra are linked into infinite two-dimensional sheets by double bromine bridges between the uranium atoms (Taylor and Wilson, 1974d,e).

Good-quality low-temperature absorption spectra as well as solution, reflectance, and transmission spectra of UBr_4 are available. The energy level parameters obtained from least-squares fitting of the observed and calculated energy levels are listed in Table 5.26. Absorption bands observed in the range 41400–32160 cm^{-1} were assigned to $5f^2 \rightarrow 5f^16d^1$ transitions; a charge transfer band was identified at 30165 cm^{-1}. Magnetic susceptibility measurements reveal a Curie–Weiss behavior in the temperature range 77–569 K, with $\theta = -35$ K and $\mu_{eff} = 3.12$ B.M (Brown, 1979; Dawson, 1951).

Uranium(IV) ternary and polynary bromides and bromo compounds

Cooling curves obtained from melting point diagrams show that only complexes of the M_2UBr_6-type are formed in the UBr_4–MBr system (M = Na, K, Rb, or Cs). They may conveniently be prepared by heating the component bromides in evacuated silica ampoules (Vdovenko *et al.*, 1973a,b). In addition to synthetic methods, phase transitions and crystallographic data for Li_2UBr_6 have been reported (Maletka *et al.*, 1998). Hexabromo compounds containing large organic cations are formed in anhydrous methyl cyanide solutions as a result of reactions at 0°C between UBr_4 and a number of alkylammonium or

phosphonium bromides, e.g. $[N(CH_3)_4]_2UBr_6$, $[N(C_2H_5)_4]_2UBr_6$, (Brown, 1979). Hexabromouranates(IV) may also be prepared by reactions of UBr_4 with aniline, ethylenediamine, and 8-hydroxyquinoline (Sara, 1970).

$UBr_4 \cdot 2CH_3CN$ in good yield is formed by electrochemical oxidation of uranium in CH_3CN/Br_2 solution under an inert atmosphere. Using a two-fold excess of different neutral ligands in a solution of this compound in acetone gives rise to UBr_4 adducts, e.g. $UBr_4 \cdot 2Ph_3O$ and $UBr_4 \cdot 6$dmso (dmso = dimethylsulfoxide) (Kumar and Tuck, 1984). The preparation of UBr_4 adducts has also been reported by du Preez and Zeelie (1989), e.g. $UBr_4 \cdot (tbso)_2$ (tbso = di-*tert*-butyl phosphoxide), $UBr_4(dmso)_2$ (dimethylsulfoxide) and $UBr_4 \cdot 4CH_3CN$. Evaporation of UBr_5 solutions containing 1 or more than 3 mol equivalents of methyl cyanide in dichloromethane yields $UBr_4 \cdot CH_3CN$ and $UBr_4 \cdot 3CH_3CN$, respectively. The synthesis, crystal structure, and IR data of $P(C_6H_5)_4UBr_6$, $P(C_6H_5)_4[UBr_6] \cdot 2CCl_4$, $[P(C_6H_5)_4]_2[UBr_6] \cdot 4CH_3CN$, and $[P(C_6H_5)_4]_2[UO_2\ Br_4] \cdot 2CH_2Cl_2$ were reported by Bohrer *et al.* (1988) (see Table 5.26).

The hexabromo complexes containing large organic cations have green-blue color; they dissolve readily in water, aqueous hydrobromic acid, and a number of polar non-aqueous organic solvents. They may be purified by crystallization, e.g. from methylcyanide or nitromethane. The compounds react with aqueous ammonia and liquid ammonia forming hydrous oxides and the insoluble $[N(C_2H_5)_4]_2UBr_6$ complex, respectively.

Rb_2UBr_6, Cs_2UBr_6, and $[N(CH_3)_4]_2UBr_6$ crystallize with face-centered cubic symmetry. The crystallographic data of these and some other hexabromouranates(IV) are listed in Table 5.26. Spectroscopic and magnetic susceptibility investigations performed for a number of octahedral uranium(IV) chloro- and bromo-complex compounds by Day and Venanzi (1966) show a temperature-independent paramagnetism, which results from interactions between the A_1 ($^3H_4$) ground state and the first excited state T_1 ($^3H_4$). Using the relative field strengths obtained from magnetic data, the authors have obtained the following values of the energy parameters: $\Delta = 1177\ cm^{-1}$ and $\theta = 2096\ cm^{-1}$ [where $\Delta = 8/33\ (B_0^4 + 35/13B_0^6)$ and $\theta = 2/33\ (5B_0^4 - 210/13B_0^6)$; $B_0^4 = 6481.5\ cm^{-1}$, $B_0^6 = 804\ cm^{-1}$]. The observed interactions are in an octahedral field best described by the orbital energy differences $\Delta(a_{2u} \rightarrow t_{2u})$ and $\theta(t_{2u} \rightarrow t_{1u})$.

Spectroscopic investigations reveal a coordination geometry with octahedral geometry both in the solid and in non-aqueous solutions; vibronic side bands are prominent in the spectra of the complexes and permit the assignment of a number of electronic transitions and the determination of the electrostatic, spin–orbit, and crystal-field parameters, e.g. for Cs_2UBr_6: (Johnston *et al.*, 1966) and for $[N(C_2H_5)_4]_2UBr_6$: (Wagner *et al.*, 1977) (see Table 5.26). From the spectral data the following ligand field parameters have been obtained: $\theta = 2378$, $\Delta = 828\ cm^{-1}$, $\zeta_{5f} = 1792\ cm^{-1}$ (or $B_0^4 = 6592.5\ cm^{-1}$, $B_0^6 = 1194.8\ cm^{-1}$) and $\theta = 2336$, $\Delta = 1127\ cm^{-1}$, $\zeta_{5f} = 998.95\ cm^{-1}$ (or $B_0^4 = 6946.5\ cm^{-1}$, $B_0^6 = 998.95\ cm^{-1}$) for Cs_2UBr_6 and $[N(C_2H_5)_4]_2UBr_6$, respectively. As one would

expect the $5f^2 \rightarrow 5f^16d^1$ transitions, recorded for $[N(C_2H_5)_4]_2UBr_6$, lie between those observed for the hexachloro and hexaiodo uranates(IV), i.e. at 27400(sh), 29400, 30400, 31500(sh), 33100, 37000, and 39000 cm^{-1} (Ryan, 1972). Spectral investigations of the compound in non-aqueous solvents reveal hydrogen bonding to primary, secondary, and tertiary alkylammonium ions that partially distorts the octahedral field in the UBr_6^{2-}complex, making the $5f^2 \rightarrow 5f^2$ electronic transitions allowed. The analysis of the visible and near IR spectra demonstrates vibronic frequencies within the ranges: 180–184 cm^{-1} (ν_3), 72–74 cm^{-1} (ν_4), and at 58 cm^{-1} (ν_6).

(*vii*) *Uranium(IV) oxide dibromide and nitride bromides*

Useful preparative methods for $UOBr_2$ (Brown, 1979) involve heating of UO_2 in a stream of CS_2 at 900°C to form $U_3O_2S_4$ followed by bromination at 600°C:

$$U_3O_2S_4 + 6Br_2 \rightarrow 2UOBr_2 + UBr_4 + 2S_2Br_2$$

or by heating of stoichiometric amounts of Sb_2O_3 and UBr_4 at about 150°C *in vacuo* (Bagnall *et al.*, 1968):

$$Sb_2O_3 + 3UBr_4 \rightarrow 3\,UOBr_2 + 2SbBr_3$$

Uranium(IV) oxide dibromide is a non-volatile, pale yellow, air-sensitive solid, readily soluble in water with the formation of a green solution from which a black solid slowly deposits. It decomposes above 600°C *in vacuo* to form UO_2 and UBr_4. The reported thermodynamic data (Greenberg and Westrum, Jr., 1956; Rand and Kubaschewski, 1963; Grenthe *et al.*, 1992; Guillaumont *et al.*, 2003) are listed in Table 5.26.

As in the corresponding chloride systems, the ammonolysis of UBr_4 at elevated temperatures leads to the formation of uranium nitride via amido, imido, and nitride bromides (Burk, 1967; Burk and Naumann, 1969). Since the composition of the decomposition products varies with temperature, the pure phases cannot easily be obtained (Brown, 1959). Juza and Meyer (1966, 1969) have obtained a dark-brown $UN_{1.03}Br_{1.03}$ phase on heating UBr_4-ammoniates at 400°C in gaseous ammonia. The compound can also be prepared by solid-state reactions of UN with UBr_4 at 600–900°C. It is insoluble in water and has the BiOCl-type structure with the space group *P*4/*nmm*. The crystallographic data are listed in Table 5.26.

(*viii*) *Uranium tetraiodide and uranium(IV) complex iodides*

Uranium tetraiodide

The most convenient and widely used method for the preparation of UI_4 involves the direct combination of the elements at about 500°C, either in a gas-flow system or in sealed vessels (see Brown, 1979); it is a black, moisture-sensitive solid. It rapidly decomposes on exposure to air and is also thermally

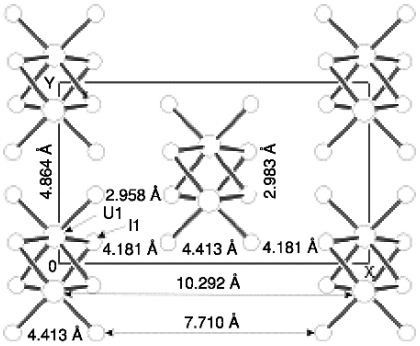

Fig. 5.42 *View along zigzag chains in UI_4 (distances are taken from Levy* et al., 1980).

unstable, liberating iodine with the formation of UI_3. The tetraiodide may also readily be reduced to UI_3 by hydrogen at moderate temperatures. The interaction of UI_4 with chlorine yields UCl_4, and with uranium tetrahalides it forms the mixed halides: UCl_2I_2, $UClI_3$, UBr_2I_2, and $UBrI_3$. Like other uranium halides the tetraiodide also forms complexes with organic ligands, e.g. $UI_4 \cdot 4$dma (dma = dimethylacedamide), $UI_4 \cdot 2$tbso (tbso = di-*tert*-butyl sulfoxide), $UI_4 \cdot 8$dmso (dmso = dimethyl sulfoxide), $UI_4 \cdot 6$dibso (dibso = di-isobutylsulfoxide), $UI_4 \cdot xNH_3$ (x = 4, 5, or 10) and $UI_4 \cdot 8$L (L = ε-caprolactam, α-$UI_4 \cdot tpao_2$, β-$UI_4 \cdot tpao_2$, $UI_4 \cdot tpao_4$, and $UI_4 \cdot tpao_6$ (tpao = triphenylarsine oxide) (Brown, 1979; du Preez and Zeelie, 1987, 1989).

The crystal structure of UI_4 has been solved using X-ray and powder neutron diffractions (Levy *et al.*, 1980; Taylor, 1987). The monoclinic structure (Table 5.26) contains uranium atoms with an approximately octahedral coordination, where the uranium atoms are linked by double iodide bridges, forming zigzag chains (Fig. 5.42). Two terminal iodide ions in the *cis* position are completing the coordination sphere of the uranium atom.

Uranium(IV) iodo complexes

Hexaiodo uranium(IV) compounds of the M_2UI_6-type (where M = $N(C_2H_5)_4$, $N(C_4H_9)_4$, $N(C_6H_5)(CH_3)_3$, and $As(C_6H_5)_4$) have been obtained from reactions of the component halides in anhydrous methyl cyanide followed by crystallization in an ice bath or by vacuum evaporation of the solvent. Alternatively, the treatment of uranium(IV) hexachloro or hexabromo complexes with anhydrous liquid hydrogen iodide may be used (Bagnall *et al.*, 1965; Brown *et al.*, 1976). The hexaiodo uranium(IV) compounds are stable, but extremely moisture-sensitive, red colored solids. Exposure to the atmosphere, addition of dilute aqueous acids, or ammonia results in immediate decomposition. The compounds are soluble in anhydrous methyl cyanide and acetone and liberate iodine on heating above 200°C.

From an analysis of the spectral data for $[N(C_2H_5)_4]_2UI_6$ the following electrostatic, spin–orbit, and crystal-field parameters were obtained (in cm^{-1}): $F^2 = 38188(2422)$, $\zeta_{5f} = 1724(39)$, $B_0^4 = 6338(676)$, and $B_0^6 = 992(252)$ (Wagner *et al.*, 1977). Magnetic susceptibility measurements of $[As(C_6H_5)_4]_2UI_6$ have shown that the compound exhibits a temperature-independent paramagnetism in the 84–300 K range with $\chi_{mole} = 2146(30) \times 10^{-6}$ cm^3 mol^{-1} (Bagnall *et al.*, 1965), analogous to that in the hexachloro and hexabromo uranium(IV) compounds.

(*ix*) *Uranium(IV) oxide di-iodide and nitride iodide*

UOI_2 can be prepared by heating U_3O_8, U, and I_2 at 450°C in a sealed Pyrex tube. The compound is iso-structural with $UOCl_2$ (orthorhombic symmetry in space group *Pbam*, see Table 5.26) and has $\mu_{eff} = 3.34$ B.M, as determined from magnetic susceptibility measurements (Levet and Noël, 1979).

The reaction of uranium tetraiodide with gaseous ammonia at temperatures above ~350°C yields uranium nitride iodide, UNI. It may be also obtained by heating uranium nitride with uranium tetraiodide. The compound has tetragonal symmetry (space group *P4/nmm*) and is iso-structural with the chloride and bromide analogues (see Table 5.26).

(*x*) *Uranium(IV) mixed halides and mixed halogeno compounds*

Phases of the composition of $UClF_3$, UCl_2F_2, and UCl_3F occur in the UCl_4–UF_4 system. All are melting incongruently and are thermally unstable, the order being $UClF_3 > UCl_2F_2 > UCl_3F$. The last compound may be prepared by (i) chlorination of UO_2F_2 in refluxing hexachloropropene, (ii) chlorination of UF_3 with chlorine at 350–380°C and by heating of UF_4 in a CCl_4 vapor at 420°C. UCl_3F, obtained in this way, is somewhat contaminated with unreacted starting materials and by-products (UCl_4 or $UOCl_2$). The X-ray powder data obtained for UCl_3F are listed in Table 5.26. A number of ternary chloride fluorides were identified in the $M^{I}Cl$–UF_4 and $M^{II}Cl_2$–UF_4 phase diagrams (where M^{I} = Li, Na, K, Rb, or Cs and M^{II} = Mg or Ca) (Brown, 1979).

The preparation and thermodynamic data of uranium(IV) mixed halides containing bromine have been reported by MacWood (1958). Solid-state reactions of stoichiometric quantities of UCl_4 and UBr_4 yield $UBrCl_3$ at 750°C and UBr_2Cl_2 and $UBrCl_3$ at 590°C. The former may also be prepared by bromination of UCl_3 at 500°C. Some thermodynamic data of these compounds are listed in Table 5.26.

The following mixed tetravalent halides containing iodide anions: (i) UCl_3I, (ii) UCl_2I_2, (iii) $UClI_3$, (iv) UBr_3I, (v) UBr_2I_2, and (vi) $UBrI_3$ (Brown, 1979) have be obtained in pure form. Satisfactory preparation methods involve: (i) iodination of UCl_3 at 500°C in a atmosphere of iodine, (ii) fusion of equimolar

amounts of UI_4 and UCl_4 in the presence of small amount of iodine, (iii) fusion of UCl_4 and either UI_3 (at 600°C) or UI_4, (iv) iodination of UBr_3 at 500°C, (v) iodination of UBr_2I at 500°C, or fusion of UBr_4 and UI_4 at 520°C followed by sublimation in a stream of iodine, and (vi) fusion of a 1:3 mole ratio of UBr_4 and UI_4, followed by sublimation at a low pressure of iodine. The compounds are dark-brown or black and undergo rapid hydrolysis in a humid atmosphere. Their melting points range from 478 and 490°C for UBr_3I and UCl_3I, respectively, to somewhat less than 500°C for the remaining mixed halides. All compounds readily lose iodine on heating *in vacuo*, except of $UBrI_3$, which can be sublimed without decomposition. A number of thermodynamic data are available for these compounds (see Table 5.26). The stability of the chloride iodides increases with increasing iodide content. A reverse stability trend is reported for the bromide iodides.

The preparation of uranium(IV) mixed halgeno-compounds by fusion methods and mixed halgeno compounds with donor ligand have been also reported, e.g. $M^{I}_2UX_2Y_2$ (where M^{I} = Na, K or Cs, X = Cl, and Y = Br), $K_2UCl_4I_2$, $K_2UBr_4I_2$, $UCl_3I \cdot 8CO(NH_2)_2$, $UI_2Cl_2 \cdot 5DMA$ (DMA = *N*,*N*-dimethylacetamide), and $UClI_3 \cdot 5DMA$ (Gregory, 1958; Brown, 1968).

(*xi*) *Nitrogen-containing uranium halides*

Uranium nitride chlorides, bromides, and iodides

High-temperature ammonolysis of UCl_4, UBr_4, or UI_4 leads to the corresponding uranium nitride chloride, bromide, and iodide. The formation of UNCl and UNBr proceeds via a number of intermediates such as $U(NH_2)Cl_3$, $U(NH)_2Cl_2$, or UNCl. Other routes to UNCl involve high-temperature interaction of UCl_4 and $UN_{1.33}$ as well as solid-state reactions between UCl_4 and aluminium or silicium at about 800°C in a nitrogen atmosphere. Crystallographic data for UNCl (Juza and Sievers, 1965; Juza and Meyer, 1969) are listed in Table 5.26.

A dark brown compound of the formula $UN_{1.03}Br_{1.03}$ was obtained on heating uranium tetrabromide ammoniates in gaseous ammonia for 48–60 h. The compound may also be prepared by heating uranium nitride and the tetrabromide at 600–900°C (Juza and Meyer, 1969). It is insoluble in water but dissolves slowly in 2 M H_2SO_4 with the formation of a green solution. UNBr is converted to uranium nitride in gaseous ammonia at temperatures over 750°C. The compound crystallizes in the BiOCl-type of structure, space group *P4/nmm*, D^7_{4h}, the same as the corresponding UNCl and UNI compounds (see Table 5.26).

The preparation of UNI can be achieved by ammonolysis of uranium tetraiodide at about 350°C or by heating uranium nitride with UI_4. The compound has the BiOCl-type structure and is isostructural with the chloride and bromide analogs (Juza and Meyer, 1969; see Table 5.26).

(c) Pentavalent halides and complex halides

Uranium halides in the pentavalent oxidation state exhibit a tendency to hydrolysis and disproportionation into U(IV) and U(VI) species. However, in the absence of substances that cause hydrolysis, diproportionation does not occur spontaneously (Bacher and Jacob, 1980). Stable solutions of uranium(V) have been obtained, for example, by heating a mixture of UO_3 with thionyl chloride under prolonged refluxing, or by dissolving UF_5 in methyl cyanide, dimethylformamide or Me_2SO as well as of UCl_5 and UBr_5 in some organic solvents (Selbin and Ortego, 1969; Brown, 1979; Halstead *et al.*, 1979). Uranium hexachloride decomposes easily in solvents like carbon tetrachloride, methylene dichloride, or 1,2-dichlorethane and is therefore a suitable starting material for the preparation of uranium(V) compounds on a laboratory scale. The synthesis and properties of various uranium(V) compounds and complexes have been reviewed by Selbin and Ortego (1969). The preparation of UX_6^- (X = F, Cl, Br or I) complexes and the oxohalide complexes $[UOF_5]^{2-}$, $[UOCl_5]^{2-}$, and $[UOBr_5]^{2-}$ has been reported by Ryan (1971). The chemical properties of the compounds, their stability against disproportionation in various non-aqueous halide solutions as well as some aspects of their absorption spectra are also discussed. The halides and complex halides have a variety of colors – from pale blue and red brown to yellow (Table 5.28). The coordination geometry of uranium(V) halides are: octahedral (α-UF_5), pentagonal bipyramidal (β-UF_5), and edge-sharing octahedral (U_2Cl_{10} units).

Uranium(V) has a $[Rn]5f^1$ electronic configuration with the $^4F_{5/2}$ (Γ_7) ground state. A number of spectra in solutions, solids, and gas phase are available (Ryan, 1971; Edelstein *et al.*, 1974; Leung and Poon, 1977; Bacher and Jacob, 1980; Eichberger and Lux, 1980; Carnall and Crosswhite, 1985). The analysis of the spectra has been based on a strong ligand-field model. The site symmetry of the U^{5+} ion is frequently found to be octahedral or distorted octahedral (Carnall and Crosswhite, 1985). The combined ligand field and spin–orbit interaction split the parent ^2F state into the Γ_7, Γ_8, Γ_7', Γ_8', and Γ_6 components. The spectra of U^{5+} in the approximate octahedral sites of the different compounds have very similar f–f band energy and relative intensities, e.g. the spectra of $[N(C_2H_5)_4]_2UOCl_5$ (Selbin *et al.*, 1972a), UCl_5 single crystals (Leung and Poon, 1977), UCl_5 in $SOCl_2$ (Karraker, 1964), and $(UCl_5)_2$ or $UCl_5 \cdot AlCl_3$ in the vapor phase (Gruen and McBeth, 1969). Spectroscopic studies and semi-empirical theoretical calculations of energy levels of UOX_5^{2-} species (X = F, Cl, or Br) in the corresponding tetraethylammonium oxopentahalide complexes reveal that each of the six electronic transitions is shifted to higher energy in the expected order: $Br^- < Cl^- < F^-$. The spin–orbit coupling constants obtained in the best fits also increase in this same order: 1750, 1770, and 1850 cm^{-1}. For a number of uranium(V) halides and complex halides, magnetic susceptibility measurements were carried out over wide temperature ranges. The paramagnetic constants from the Curie–Weiss law $\chi'_M = C/(T-\theta)$ and the effective

Table 5.28 *Properties of selected uranium(v) halides, mixed valence halides and complex halides.*[a]

Formula	*Selected properties and physical constants*[b]	*Lattice symmetry, lattice constants* (Å), *polyhedron type and density* (g cm^{-3})[c]	*Remarks regarding information available and references*
α-UF_5	grayish-white or bluish-white crystals; moisture sensitive; soluble in CH_3CN, C_2H_5CN, DMF and Me_2SO; disproportionate over 150°C to $U_2F_9 + UF_6$; m.p. = 348 (+13, –16)°C in a UF_6 atmosphere of 1.6–4.6 bar; density = 5.81g cm^{-3}; α-UF_5: $\Delta_f G^o_m = -1968.7\ (7.0)^\dagger$, $\Delta_f H^o_m = -2075.3\ (5.9)^\dagger$, $S^o_m = 199.6\ (12.6)^\dagger$, $C^o_{p,m} = 132.2\ (4.2)^\dagger$. UF_5(g): $\Delta_f G^o_m = -1862.1\ (15.3)^\dagger$, $\Delta_f H^o_m = -1913\ (15)^\dagger$, $S^o_m = 386.4\ (10.0)^\dagger$; $C^o_{p,m} = 110.6\ (5.0)$. IR: 580s,br, 398s; $\log p_{solid}(mmHg) = -(8001 \pm 664)/T^{-1} + (13.994 \pm 1.119)\log p_{liquid}(mmHg) = -(5388 \pm 803)\ T^{-1} + (9.819 \pm 1.236)$.Raman (cm^{-1}): 627.5s, 503m, 223m; $\lvert g\rvert = 0.892$;	tetragonal; C^5_{4h}, $I4/m$, No. 87; a = 6.5259(3), c = 4.4717(2), Z = 2; V = 190.44; CN = 6; d(calc.) = 5.81; UF_6 octahedra are bridged by *trans*-fluorides with d(U–F1) = 2.235(1) to give an infinite linear chain parallel to the c-axis. The remaining four F atoms in the octahedron are bound to one U atom with d(U–F2) = 1.995(7)	*crystallographic and neutron powder data; UV, Vis, IR and Raman spectra; heat capacity* (Zachariasen, 1949c; Osborne *et al*., 1955; Burns *et al*., 1960; Paine *et al*., 1976; Eller *et al*., 1979; Howard *et al*., 1982); *thermodynamic data* (Rand and Kubaschewski, 1963; Kubaschewski and Alcock, 1979; Fuger *et al*., 1983; Grenthe *et al*., 1992; Guillaumont *et al*., 2003); *magnetic susceptibility data, chemical properties* (Eller *et al*., 1979; Brown, 1968, 1973); *optical spectra and crystal-field analysis* (Hecht *et al*., 1986b); *photoelectron spectra* (Thibaut *et al*., 1982)
β-UF_5	pale yellow; moisture sensitive; soluble in CH_3CN, C_2H_5CN, DMF and Me_2SO; β-UF_5: $\Delta_f G^o_m = -1970.6(5.6)^\dagger$, $\Delta_f H^o_m = -2083.2\ (4.2)^\dagger$, $S^o_m = 179.5\ (12.6)^\dagger$; $C^o_{p,m} = 132.2\ (12.0)^\dagger$. IR (cm^{-1}): 623s,sh, 567s, 508s, 405s; Raman: 623s, 610s, 280m.	tetragonal; D^{12}_{2d}, $I\bar{4}2d$, No. 122; a = 11.469(5), c = 5.215(2); Z = 8; CN = 7; V = 685.97; d(calc.) = 6.45	*crystallographic and neutron diffraction data, IR and Raman spectra, thermodynamic data, chemical properties* (Brown, 1968; Paine *et al*., 1976; Ryan *et al*., 1976; Bacher and Jacob, 1980; Taylor and Waugh, 1980; Grenthe *et al*., 1992; Guillaumont *et al*.,

	$\mu_{\text{eff.}} = 2.24$ B.M.; $\theta = -75.4$ K (125–420 K)		2003); *magnetic susceptibility data* (Nguyen-Nghi *et al.*, 1964b) *optical spectra and crystal-field analysis* (Hecht *et al.*, 1986b); *solution spectra* (Halstead *et al.*, 1979)
U_2F_9 (mixed valence)	black; uranium oxidation number = +4.5; disproportionates into UF_4 and UF_6; U_2F_9(cr): $\Delta_f G^o_m = -3812$ (17)†, $\Delta_f H^o_m = -4016$ (18)†, $S^o_m = 329$ (20)†; $C^o_{p,m} = 251.0$ (16.7)†	cubic; body centered; T^3_d, $I\bar{4}3m$, No. 217; $a = 8.462(2)$; [$a = 8.4716$: (Howard *et al.* 1982)]; $Z = 4$; $V = 607.99$; CN = 9; d(calc.) = 7.091; the structure consists of a three-dimensionally bridged network composed of tricapped trigonal prismatic UF_9 units; $d(U–F_1) = 2.37(2)$, 2.21(2); $d(U–F_2) = 2.266$ (3); F1–U–F1 = 119.5(1), 71.2(3); F1–U–F2 = 67.0(5), 128.4(9)	*crystallographic and neutron diffraction data; reflectance spectrum* (Zachariasen,1949d; Eller *et al.*, 1979; Laveissière, 1967; Taylor, 1976a,b; Howard *et al.*, 1982); *thermodynamic data* (Bacher and Jacob, 1980; Grenthe *et al.*, 1992; Guillaumont *et al.*, 2003)
U_4F_{17} (mixed valence)	black; uranium oxidation number = +4.25; disproportionates into UF_4 and UF_6; U_4F_{17}(cr) $\Delta_f G^o_m = -7464$ (30)†, $\Delta_f H^o_m = -7850$ (32)†, $S^o_m = 631$ (40)†, $C^o_{p,m} = 485.3$ (33.0)†	monoclinic; deformed UF_4 lattice; C^6_{2h}, $C2/c$, No. 15; $a = 12.09(0.08)$, $b = 10.81(2)$, $c = 8.29(4)$; $\beta = 128.0(8)$; $Z = 12$; CN = 8 (UF_4); d(calc.) = 7.07	*crystallographic data* (Chatelet, 1967); *thermodynamic data* (Bacher and Jacob, 1980; Grenthe *et al.*, 1992; Guillaumont *et al.*, 2003)
$(H_3O)UF_6$	blue-green; above 68(1) °C decomposes to $UF_4 + UO_2F_2$; $(H_3O)UF_6$(cr): $\Delta_f H^o_m = -2641.4$ (3.2)†	cubic; $a = 5.2229(5)$	*X-ray powder diffraction data; VIS, NIR and IR spectra, EPR data* (Masson *et al.*, 1976); *thermodynamic data* (Grenthe *et al.*, 1992; Guillaumont *et al.*, 2003)
Other hydrated fluorides: $HUF_4 \cdot 2.5H_2O$; $HUF_4 \cdot 1.25H_2O$;	blue or light blue		*general properties* (Bacher and Jacob, 1980)

Table 5.28 (*Contd.*)

Formula	*Selected properties and physical constants*[b]	*Lattice symmetry, lattice constants* (Å), *polyhedron type and density* (g cm^{-3})[c]	*Remarks regarding information available and references*
$LiUF_6$	pale blue; EPR: $g_o = -0.768$; $\|\Delta g\| = 0.022$; $\Delta H = 109$ Oe; angle of distortion 0.13°; $\|g\| = 0.768$; $g_\parallel = -0{,}801$, $g\perp = -0.753$; $\varsigma = 1969$; IR and Raman(cm^{-1}): $\nu_1 = 622$, $\nu_2 = 439$, $\nu_3 = 515$, $\nu_4 = 152$, $\nu_5 = 222, 232$, $\nu_6 = 107$[e]	rhombohedral; C_{3i}^2, $R\bar{3}$, No. 148; structure type of $LiSbF_6$; $a = 5.262$, $c = 14.295$	*crystallographic data* (Brown, 1968, 1973; Penneman *et al.*, 1973); *absorption spectra, IR data, ESR data* (Hecht *et al.*, 1986a; Rigny and Plurien, 1967; Allen *et al.*, 1978; Halstead *et al.*, 1979; Bacher and Jacob, 1980)
α-$NaUF_6$	pale blue; air sensitive; EPR: $g_o = -0.745$; angle of distortion 0.65° $g_\parallel = -0.8175$, $g\perp = -0.708$; $\varsigma = 1965$; IR and Raman (cm^{-1}): $\nu_1 = 621$, $\nu_2 = 449$, $\nu_3 = 520$, $\nu_4 = 122$[e], 132[e], $\nu_5 = 206, 209$, $\nu_6 = 72$[e]	rhombohedral; C_{3i}^2, $R\bar{3}$, No.148; structure type of $LiSbF_6$; $a = 5.596$, $c = 15.526$	*crystallographic data* (Brown, 1968, 1973; Penneman *et al.*, 1973); *absorption spectra* (Bacher and Jacob, 1980; Hecht *et al.*, 1986a); *thermodynamic data* (Kudriashov *et al.*, 1978; Fuger *et al.*, 1983); *ESR data* (Rigny and Plurien, 1967; Halstead *et al.*, 1979)
β-$NaUF_6$	pale blue; air sensitive; EPR: $\|g\| = 0.748$; $\|\Delta g\| = 0.107$; $\Delta H = 57$ Oe; angle of distortion = 0.65°	cubic fcc; O_h^5, *Fm*3*m*, No. 225; $NaTaF_6$ structure type; $a = 8.608$	*crystallographic data* (Brown, 1968, 1973; Penneman *et al.*, 1973) *thermodynamic data* (Kudriashov *et al.*, 1978; Fuger *et al.*, 1983); *spectroscopic data* (Moskvin and Zaitseva, 1962)
KUF_6	yellow-green; air sensitive	orthorhombic; D_{2h}^{18}, *Cmca*, No. 64; CN = 6; $RbPaF_6$ structure type; $a = 5.61$, $b = 11.46$, $c = 7.96$; dodecahedron sharing edges to form chains	*crystallographic data* (Brown, 1968, 1973; Penneman *et al.*, 1973); *absorption sp*ectra (Bacher and Jacob, 1980) *thermodynamic data* (Kudriashov *et al.*, 1978; Fuger *et al.*, 1983)
$RbUF_6$	yellow-green;		*crystallographic data* (Penneman *et al.*, 1973 ; Brown, 1968, 1973);

		orthorhombic; D_{2h}^{18}, *Cmca*, No. 64; $RbPaF_6$ structure type; $a = 5.82$, $b = 11.89$, $c = 8.03$	*absorption spectra* (Bacher and Jacob, 1980); *thermodynamic data* (Kudriashov *et al*., 1978; Fuger *et al*., 1983); *crystal-field calculations* (Amberger *et al*., 1983)
$CsUF_6$	pale blue to green blue; (ν(U–F) = 503s; EPR: $\|g\| = 0.709$; $\|g\| = 0.709$; $\|\Delta g\| = 0.210$; angle of distortion = 1.25°; $g_{\|} = -0{,}928$, $g\perp = -0.681$; $\varsigma = 1985\ cm^{-1}$; IR and Raman ($cm^{-1}$): $\nu_1 = 608$, $\nu_2 = 452$, $\nu_3 = 505$, $\nu_4 = 126$–130^e, $\nu_5 = 190, 213$, $\nu_6 = 60^e$	rhombohedral; C_{3i}^2, $R\bar{3}$, No. 148; $KCsF_6$ structure type, $a = 8.04$, $c = 8.39$; dodecahedron sharing edges to form chains	*crystallographic data* (Brown, 1968, 1973; Penneman *et al*., 1973); *absorption spectra, NMR-spectra; IR and Raman spectra* (Bacher and Jacob, 1980, Carnall and Crosswhite, 1985; Hecht *et al*., 1986a; Geichman *et al*., 1962); *magnetic susceptibilities* (Mulak and Żołnierek, 1972); *ESR spectra* (Rigny and Plurien, 1967); *thermodynamic data* (Kudriashov *et al*., 1978; Fuger *et al*., 1983)
NH_4UF_6	yellow-green; $\mu_{eff} = 1.74$ B.M. (93–200 K); $\mu_{eff} = 2.25$ B.M. (200–390 K)[d]	orthorhombic; D_{2h}^{18}, *Cmca*, No.64; $RbPaF_6$ structure type; $a = 5.83$, $b = 11.89$, $c = 8.03$; dodecahedron sharing edges to form chains	*crystallographic data* (Brown, 1968, 1973; Penneman *et al*., 1973; *absorption spectra; magnetic susceptibility* (Nguyen-Nghi *et al*., 1965; Bacher and Jacob, 1980)
$AgUF_6$	decomposes at 230°C to F_2, UF_4 and AgF	tetragonal; $a = 5.42$, $c = 7.95$	*crystallographic data* (Brown, 1968, 1973; Penneman *et al*., 1973)
$TlUF_6$		orthorhombic; D_{2h}^{18}, *Cmca,* No.64; $a = 5.96$, $b = 11.55$, $c = 8.00$.	*crystallographic data* (Charpin, 1965)
$UF_5(SbF_5)_2$		monoclinic; C_{2h}^5, $P2_1/c$, No. = 14; $a = 8.110(4)$, $b = 14.129(6)$, $c = 10.032(6)$; $\beta = 96.97(5)°$; $Z = 4$; $V = 1141.03$; d(calc.) = 4.46	*crystallographic data* (Sawodny *et al*., 1980)

Table 5.28 (*Contd.*)

Formula	*Selected properties and physical constants*[b]	*Lattice symmetry, lattice constants* (Å), *polyhedron type and density* (g cm^{-3})[c]	*Remarks regarding information available and references*
$NOUF_6$	greenish-white; IR (cm^{-1}): ν(U–F) = 2333, 550s, 509sh; Raman: 616, 495, 441, 225, 206; $\|g\| = 0.748$	cubic; T_h^7, *Ia*3, No. 206; a = 10.464; d(exp.) = 4.30(5)	*crystallographic data* (Brown, 1973; Penneman *et al.*, 1973; *chemical reactivity, absorption spectra; IR and Raman spectra* (Geichman *et al.*, 1962; Bacher and Jacob, 1980); *ESR spectra* (Rigny *et al.*, 1971)
$C_{36}H_{30}P_2NUF_6$ bis (triphenylphosphine) iminium hexafluorouranate(V)	exhibits an unusual g-tensor with $\|g_1\| = 0.79$, $\|g_2\| = 0.69$, $\|g_3\| = 0.65$ which is attributed to low site symmetry and/or very small distortions of the UF_6^- octahedron	triclinic; C_i^1, $P\bar{1}$, No. 2; a = 14.553 (9), b = 12.110(7), c = 12.384(8); α = 73.08(4)°, β = 95.40(5)°, γ = 64.64(4)°; Z = 2; d(exp.) = 1.62, d(calc.) = 1.62; the U atom lies in a general position in the cell; d(U–F) = distances range between 2.00(1) and 2.061.	*crystal structure, EPR spectra* (Eastman *et al.*, 1981)
$Co(UF_6)_2{\cdot}4H_2O$		triclinic; a = 11.52, b = 10.11, c = 5.22; α = 91.30°, β = 91.30°, γ = 90.0°; d(exp.) = 4.52	*crystallographic data* (Montoloy and Plurien, 1968)
other hexa- and heptafluoro complexes: (i) K_2UF_7; Rb_2UF_7; (ii) Cs_2UF_7; (iii), (iv) $(NH_4)_2UF_7$; (v) $N_2H_6UF_7$; (vi) $N_2H_6(UF_6)_2$; (vii) NO_2UF_6; (viii) $(NH_3OH)UF_6$; (ix) $As(C_6H_5)_4UF_6$; (x) $Cu(UF_6)_2{\cdot}4H_2O$.			*general properties* (i–iv) Penneman *et al.*, 1964b; (v) Frlec *et al.* (1966), (vi) Frlec and Hyman (1967) (vii) Gleichman *et al.*,1961 (i–x) Bacher and Jacob, 1980

Na_3UF_8	pale blue; $\mu_{eff.} = 2.29$ B.M.	tetragonal; D_{4h}^{17}, *I*4/*mmm*, No.139; Na_3PaF_8 structure type; $a = 5.470$, $c = 10.940$	*crystallographic data* (Brown, 1973; Penneman *et al.*, 1973; Freestone and Holloway, 1991); *magnetic susceptibility, ^{19}F-NMR spectra* (Bacher and Jacob, 1980)
K_3UF_8	pale blue	fcc cubic; O_h^5, $Fm\bar{3}m$, No. 225, $a = 9.20$	*crystallographic data* (Brown, 1973; Penneman *et al.*, 1973; Freestone and Holloway, 1991); *IR spectra* (Bacher and Jacob, 1980)
Rb_3UF_8		fcc cubic; O_h^5, $Fm\bar{3}m$, No. 225, $a = 9.60$	*crystallographic data* (Brown, 1968; Bacher and Jacob, 1980; Freestone and Holloway, 1991); *absorption spectra and spectral data* (Bacher and Jacob, 1980; Penneman *et al.*, 1964b)
Cs_3UF_8		fcc *cubic;* O_h^5, $Fm\bar{3}m$, No.225	*X-ray powder diffraction data, absorption spectra, magnetic susceptibilities* (Bacher and Jacob, 1980)
Ag_3UF_8		cubic; $a = 4.36$; d(exp.) = 6.49	*crystallographic data* (Brown, 1973; Penneman *et al.*, 1973; Freestone and Holloway, 1991); *IR spectra* (Bacher and Jacob, 1980)
Tl_3UF_8		cubic; $a = 4.75$	*crystallographic data* (Bougon and Plurien, 1965; Freestone and Holloway, 1991). (Bacher and Jacob, 1980)

Table 5.28 (*Contd.*)

Formula	*Selected properties and physical constants*[b]	*Lattice symmetry, lattice constants* (Å), *polyhedron type and density* (g cm^{-3})[c]	*Remarks regarding information available and references*
other octafluoro complexes:			
$(NH_4)_3UF_8$.			
$N_2H_6(UF_6)_2$	bluish-green; $\mu_{eff} = 1.61$ B.M. (80–293 K)		*magnetic susceptibility, IR and Raman data* (Frlec *et al*., 1966; Frlec and Hyman, 1967)
$N_2H_6UF_7$	yellow; $\mu_{eff} = 1.66$ B.M. at 273 K (160–280 K); $\theta = 111$ K		*magnetic susceptibility, IR and Raman data* (Frlec *et al*., 1966; Frlec and Hyman, 1967)
$(NH_3OH)UF_6$	blue; $\mu_{eff} = 152$ B.M. at 300 K; (the Curie–Weiss law is not obeyed)		*magnetic susceptibility, IR and Raman data* (Frlec and Hyman, 1967)
$[N(C_2H_5)_4]_2UOF_5$	pink; air sensitive; IR data (cm^{-1}): ν(U–O) = 852, 760 cm^{-1}; $\lvert g \rvert$ = 0.58		*IR data* (Ryan, 1971); *EPR and crystal-field spectra* (Selbin and Sherrill, 1974)
$[N(C_2H_5)_4]_2$ $UOF_5{\cdot}2H_2O$	pink; air sensitive; IR data: ν(U–O) = 872, 780 cm^{-1}		*IR data* (Ryan, 1971)
UO_2F		monoclinic; $a = 8.22$, $b = 6.81$, $c = 32.08$; $\beta = 90.5$	*X-ray powder diffraction, optical and magnetic data* (Kemmler-Sack, 1967, 1969)
$UO_2F_{0.25}$	deep-gray to black	cubic; fluorite type of structure; $a = 5.49$; $Z = 4$; d(calc.) = 11.4; d(exp.) = 11.0	*X-ray powder diffraction, optical and magnetic data* (Kemmler-Sack, 1967, 1969)
(i) $NaSrU_2O_6F$		cubic; O_h^7, $Fd3m$, No. 227;	*crystallographic data* (Kemmler-Sack, 1968c)
(ii) $KSrU_2O_6F$		(i) $a = 11.16$	
(iii) $RbSrU_2O_6F$		(ii) $a = 11.27$	
(iv) $TlSrU_2O_6F$		(iii) $a = 11.34$	
(v) $NaBaU_2O_6F$		(iv) $a = 11.27$	

(vi) $KBaU_2O_6F$ (vii) $RbBaU_2O_6F$ (viii) $TlBaU_2O_6F$ (ix) $KPbU_2O_6F$ (x) $RbPbU_2O_6F$ (xi) $TlPbU_2O_6F$		(v) $a = 11.31$ (vi) $a = 11.39$ (vii) $a = 11.45$ (viii) $a = 11.40$ (ix) $a = 11.33$ (x) $a = 11.36$ (xi) $a = 11.36$	
$UZr_6O_{14}F$		orthorhombic; C_{2v}^9, $Pna2_1$, No.33; $a = 5.328(1)$, $b = 36.64(1)$, $c = 5.065(1)$; $Z = 4$; $V = 988.78$; d(calc.) = 6.91	*crystallographic data* (Papiernik *et al.*, 1980, 1983)
α-UCl_5	red-brown; very moisture sensitive; in water disproportionates to U(IV) and U(VI); soluble in CS_2, CCl_4 and $SOCl_2$. m.p. = dec; density = 3.81 g cm^{-3}. UCl_5(cr): $\Delta_f G_m^o = -930.1$ (3.9)†, $\Delta_f H_m^o = -1039.0$ (3.0)†, $S_m^o = 242.7$ (8.4)†; $C_{p,m}^o = 150.6$ (8.4)†. UCl_5(g): $\Delta_f G_m^o = -849.6$ (15.1)†, $\Delta_f H_m^o = -900$ (15)†, $S_m^o = 438.7$ (10.0)†; $C_{p,m}^o = 123.6$ (5.0)†. log p (mmHg) = $-3307\ T^{-1} + 3.361$ $\mu_{eff.} = 2.00$ B.M, $\theta = -99$ K, (14–300 K); ESR: $\lvert g \rvert = 1.188$; IR (cm^{-1}): 360, 340, 320, 308sh, 263, 227, 177, 169, 150, 127, 116, 102, 64; Raman (cm^{-1}): 367, 324, 130;crystal-field data (cm^{-1}): $B_0^4 = 134.79$ (1125), $B_0^6 = 158.6(745)$, $\varsigma_{5f} = 1559(115)$	monoclinic; C_{2h}^2, $P2_1/n$, No.11; structure based on cubic close packing of Cl atoms in which U atoms occupy one-fifth of the octahedral holes; two such octahedra share one edge forming a U_2Cl_{10} unit; d[U–Cl(1)] = 2.70, d[U–Cl(1')] = 2.67, d[U–Cl(2)] and d[U–Cl(4)] = 2.43, d[U–Cl(3)] and d[U–Cl(5)] = 2.44; $a = 7.99$, $b = 10.69$, $c = 8.48$; $\beta = 91.5$; $Z = 4$; d(calc.) = 3.81	*synthesis:* (Rediess and Sawodny, 1982); *crystallographic data* (Smith *et al.*, 1967; Brown, 1973); *thermodynamic data* (Grenthe *et al.*, 1992; Guillaumont *et al.*, 2003); *electrical properties, optical data and crystal-field analysis* (Leung and Poon, 1977; Brown, 1979; Carnall and Crosswhite, 1985); *photoelectron spectra* (Thibaut *et al.*, 1982); *IR and Raman spectra*; (Brown, 1979); *magnetic properties and electron spin resonance data* (Handler and Hutchison, 1956; Fuji *et al.*, 1979; Miyake, 1991)
β-UCl_5	red-brown	triclinic; C_i^1, $P\bar{1}$, No.2; $a = 7.07$, $b = 9.65$, $c = 6.35$; $\alpha = 89.1$,	*crystallographic data* (Müller and Kolitsch, 1974)

Table 5.28 (*Contd.*)

Formula	*Selected properties and physical constants*[b]	*Lattice symmetry, lattice constants* (Å), *polyhedron type and density* (g cm^{-3})[c]	*Remarks regarding information available and references*
		$\beta = 117.36$, $\gamma = 108.54$; structure based on hexagonal close packing of Cl atoms. In the U_2Cl_{10} units the U–Cl distances of the bridging atoms are 2.70 and those involving the terminal Cl atoms are ranging from 2.43 to 2.45	
$Cl_4UCl_2UCl_4$		triclinic; C_i^1, $P\bar{1}$, No.2; $a = 7.07$, $b = 9.65$, $c = 35.89$; $\alpha = 89.1$, $\beta = 117.36$, $\gamma = 108.54$; $Z = 1$; $V = 360.4$; d(calc.) = 3.83	*crystallographic data* (Müller and Kolitsch, 1974); *spectral data* (Gruen and McBeth, 1969)
$(SCl_3)(UCl_6)$		orthorhombic; D_2^4, $P2_12_12_1$, No. 19; $a = 10.668(10)$, $b = 10.712(4)$, $c = 11.333(6)$; $Z = 4$; $V = 1295.09$; d(calc.) = 3.02	*crystallographic data* (Sawodny *et al*., 1983)
UCl_5 adducts: $UCl_5{\cdot}Cl_2C = CClCOCl$; $UCl_5{\cdot}Ph_3PO$; $UCl_5{\cdot}SOCl_2$; $UCl_5{\cdot}AlCl_3$(g).			*general properties* (Sillén and Martell, 1964; Bagnall *et al*., 1964; Gruen and McBeth, 1969)
$LiUCl_6$	IR data (cm^{-1}): $\nu_1 = 343$; $\nu_2 = 293$; $\nu_5 = 160$		*infrared and Raman data* (Stumpp and Piltz, 1974)
α-$NaUCl_6$	yellow; IR data (cm^{-1}): $\nu_1 = 343$; $\nu_2 = 273$; $\nu_5 = 136$	cubic; O_h^5, $Fm\bar{3}m$, No. 225, $a = 9.86(2)$; $Z = 4$; d(U-Cl) = 4.93; d(calc.) = 3.26	*X-ray powder diffraction data*; *thermodynamic data* (Kudryashov *et al*., 1978; Fuger *et al*., 1983); *infrared and Raman data* (Stumpp and Piltz, 1974)
β-$NaUCl_6$	yellow	trigonal; C_{3i}^2, $R\bar{3}$, No.148; $a = 6.56(1)$, $c = 18.68(3)$; $Z = 3$; d(U-Cl) =	*X-ray powder diffraction data; thermodynamic data* (Kudryashov

		4.90; d(calc.) = 3.37, d(exp.) = 3.15	*et al.*, 1978; Fuger *et al.*, 1983); *infrared and Raman data* (Stumpp and Piltz, 1974)
$KUCl_6$	yellow; IR data (cm^{-1}): $\nu_1 = 343$; $\nu_2 = 286$; $\nu_5 = 141$	orthorhombic; D_{2h}^{18}, *Cmca*, No.64; $a = 6.97(1)$, $b = 14.14(3)$, $c = 9.66(2)$; $Z = 4$; d(U-Cl) = 6.23; d(calc.) = 3.40	*X-ray powder diffraction data; thermodynamic data* (Kudryashov *et al.*, 1978; Fuger *et al.*, 1983); *infrared and Raman data* (Stumpp and Piltz, 1974)
$RbUCl_6$	deep yellow; moisture and oxygen sensitive; m.p. >280 °C;; IR data (cm^{-1}): $\nu_1 = 341$; $\nu_2 = 273$; $\nu_5 = 136$	orthorhombic; D_{2h}^{18}, *Cmca,* No. 64; $a = 6.92(1)$, $b = 14.14(3)$, $c = 9.66(2)$; $Z = 4$; d(U-Cl) = 6.23; d(calc.) = 3.74	*X-ray powder diffraction data*; *thermodynamic data* (Kudryashov *et al.*, 1978; Fuger *et al.*, 1983); *infrared and Raman data* (Stumpp and Piltz, 1974)
$CsUCl_6$	yellow; moisture sensitive; soluble in $SOCl_2$; m.p. = 360°C; μ_{eff} = 1.71 B.M., θ = –161 K, (83–308 K); IR data (cm^{-1}): $\nu_1 = 342$; $\nu_2 = 280$; $\nu_5 = 139$	cubic; O_h^5, $Fm\bar{3}m$, No. 225; a = 10.22(1); $Z = 4$; d(calc.) = 3.61, d(U–Cl) = 5.11	*X-ray powder diffraction data; thermodynamic data* (Kudryashov *et al.*, 1978; Fuger *et al.*, 1983); *infrared and Raman data* (Stumpp and Piltz, 1974)
$TlUCl_6$	orange yellow; IR data (cm^{-1}): $\nu_1 = 348$; $\nu_2 = 283$; $\nu_5 = 147$		*infrared and Raman data* (Stumpp and Piltz, 1974)
$UCl_5 \cdot PCl_5$ (= $[PCl_4]^+[UCl_6^-]$)	orange-red; air sensitive; IR data (cm^{-1}): $\nu_1 = 343$; $\nu_2 = 271$; $\nu_5 = 130$	triclinic; C_i^1, $P\bar{1}$, No.2; a = 7.038(4), b = 7.373(4); c = 13.706(8); α = 89.38(3), β = 88.80(3)°, γ = 105.20(3)°; $Z = 2$; V = 686.09, d(calc.) = 3.02; d(U–Cl) = 2.474(13) to 2.517(14); Cl–U–Cl = 88.6(5) to 92.1(6); the compound is isomorphous with $PCl_5 \cdot NbCl_5$ and $PCl_5 \cdot TaCl_5$, consisting of an assemblage of octahedral $U(1)Cl_6^-$, $U(2)Cl_6^-$ and tetrahedral PCl_4^+ groups. The array of the chlorine atoms are hexagonal	*crystal and molecular structure* (Taylor and Waugh, 1983); *infrared and Raman data* (Stumpp and Piltz, 1974)

Table 5.28 (*Contd.*)

Formula	*Selected properties and physical constants*[b]	*Lattice symmetry, lattice constants* (Å), *polyhedron type and density* (g cm^{-3})[c]	*Remarks regarding information available and references*
		close packed, while the polyhedra are regular within experimental errors	
$[P(C_6H_5)_3CH_2(C_6H_5)]UCl_6$	orange crystals; discolors on exposure to air	monoclinic; C_{2h}^5, $P2_1/c$, No.14; $a = 11.72(1)$, $b = 18.78(1)$, $c = 13.61(1)$; $\beta = 105.71(2)$; $Z = 4$; d(calc.) = 1.851, d(exp.) = 1.85(1). Each uranium atom is surrounded by a slightly distorted octahedron of six crystallographically independent Cl atoms at U–Cl distances ranging from 2.469(7) to 2.513(7)	*crystallographic data* (de Wet *et al.*, 1978)
$[C(N_3)_3]UCl_6$	IR data (cm^{-1}): $\nu_1 = 347$; $\nu_3 = 314$; $\nu_4 = 127$; $\nu_5 = 129$	hexagonal; D_{3d}^1, $P\bar{3}1m$, No.162; $a = 8.19(2)$, $c = 6.43(5)$; d(U–Cl) = 2.56	*crystallographic data; infrared and Raman data* (Kolitsch and Müller, 1974)
$[N(CH_3)_4]UCl_6$	yellow; air sensitive; soluble in $MeNO_2$, MeCN, Me_2CO, Et_2O; $\mu_{eff.} = 1.62$ B.M.; $\theta = -161$K; IR data (cm^{-1}): $\nu_1 = 345$; $\nu_2 = 278$; $\nu_5 = 134$; $\nu_6 = 95$; ν(U–Cl)as = 310		*Infrared and Raman data* (Shamir and Silberstein, 1975, Shamir *et al.*, 1975)
$[N(C_2H_5)_4]UCl_6$	deep yellow cryst.; soluble in $MeNO_2$, MeCN, Me_2CO, Et_2O; IR data (cm^{-1}): $\nu_3 = 310$; $\nu_4 = 122$; ν(U–Cl)as. = 303–310; $\|g\| = 1.12$		*absorption spectra and crystal-field analysis* (Ryan, 1971; Edelstein *et al.*, 1974); *infrared and Raman data* (Ryan, 1971); *ESR data* (Edelstein *et al.*, 1974)

$[N(C_3H_7)_4]UCl_6$	yellow; air sensitive; soluble in $SOCl_2$, $MeNO_2$, MeCN, Me_2CO, Et_2O; IR data (cm^{-1}): $\nu_1 = 340$; $\nu_2 = 278$; $\nu_3 = 310$; $\nu_4 = 121$; $\nu_5 = 129$; $\nu_6 = 91$	*infrared and Raman data* (Shamir and Silberstein, 1975, Shamir *et al*., 1975)
$[As(C_6H_5)_4]UCl_6$	yellow cryst.; soluble in $MeNO_2$, MeCN, Me_2CO, Et_2O; $\mu_{eff.} = 2.14$ B.M.; $\theta = -280$ K; IR data (cm^{-1}): $\nu_1 = 340$; $\nu_2 = 276$; $\nu_3 = 319$; $\nu_4 = 124$; $\nu_5 = 124$	*infrared and Raman data* (Kolitsch and Müller, 1975)
other hexachloro complexes: $AgUCl_6$; $Ba(UCl_6)_2$; $[NH_2(CH_3)_2]UCl_6$; $[N(CH_3)_4]_3UCl_8$;		*general properties* (Brown, 1979)
$[(N(C_2H_5)_4]_2UOCl_5$	blue; assignment of electronic bands in D_4 symmetry: $\Gamma_7 \rightarrow \Gamma_6 = 1555$, $\Gamma_7 \rightarrow \Gamma_7 = 5050$, $\Gamma_7 \rightarrow \Gamma_7 = 6161$, $\Gamma_7 \rightarrow \Gamma_6 = 8584$, $\Gamma_7 \rightarrow \Gamma_7 = 10616$, $\Gamma_7 \rightarrow \Gamma_6 = 16835$; IR data ($cm^{-1}$): ν(U–O) = 913, 813; other observed bands: 296, 253, 197, and 120	*infrared* (Ryan, 1971) *and electronic spectral data* (Selbin *et al*., 1972a)
$UOCl_3$	brown; moisture sensitive, dissolves in alcohols and $MeNO_2$; sl. soluble in acetone and CCl_4; soluble. in water with decomposition; $UOCl_3$(cr): $\Delta_f G^o_m = -1045.6$ (8.3)†, $\Delta_f H^o_m = -1140.0$ (8.0)†, $S^o_m = 170.7$ (8.4)†; $C^o_{p,m} = 117.2$ (4.2)†. IR (cm^{-1}): 450, 615, 750, 845, 965	*synhthesis* (Brauer, 1981); *thermodynamic and infrared data* (Brown, 1979; Grenthe *et al.*, 1992; Guillaumont *et al*., 2003)

Table 5.28 (*Contd.*)

Formula	*Selected properties and physical constants*[b]	*Lattice symmetry, lattice constants* (Å), *polyhedron type and density* (g cm^{-3})[c]	*Remarks regarding information available and references*
UO_2Cl	violet brown or reddish grey; air sensitive; decomposes >600°C and in aqueous media; not soluble in organic solvents; UO_2Cl(cr): $\Delta_f G^o_m = -1095.2\ (8.4)^\dagger$, $\Delta_f H^o_m = -1171.1\ (8.0)^\dagger$, $S^o_m = 112.5\ (8.4)^\dagger$; $C^o_{p,m} = 88\ (5)^\dagger$. $\mu_{eff} = 1.86$ B.M., $\Theta = -95$ K		*thermal and magnetic properties data* (Brown, 1979; Grenthe *et al.*, 1992; Guillaumont *et al.*, 2003); *magnetic properties* (Levet, 1969); *photoelectron spectra* (Thibaut *et al.*, 1982)
$(UO_2)_2Cl_3$ (mixed valence)	black-brown; contains hexa- and pentavalent uranium; hygroscopic, forms $(UO_2)_2Cl_3 \cdot 7H_2O$ on exposure to air; dissolves slowly in H_2O and dilute mineral acids $\Delta_f G^o_m = -2234.8\ (2.9)^\dagger$, $\Delta_f H^o_m = -2404.5\ (1.7)^\dagger$, $S^o_m = 276\ (8)^\dagger$; $C^o_{p,m} = 203.6(5.0)^\dagger$	orthorhombic; $a = 5.833(2)$, $b = 20.978(2)$, $c = 11.9266(5)$; $Z = 8$, d(calc.) = 5.88, d(exp.) = 6.02	*crystallographic data* (Cordfunke *et al.*, 1977); *thermodynamic data* (Cordfunke *et al.*, 1977; Grenthe *et al.*, 1992; Guillaumont *et al.*, 2003)
$U_2O_2Cl_5$	$\Delta_f G^o_m = -2037.3\ (4.9)^\dagger$, $\Delta_f H^o_m = -2197.4\ (4.2)^\dagger$, $S^o_m = 326.3\ (8.4)^\dagger$; $C^o_{p,m} = 219.4(5.0)^\dagger$	orthorhombic; D^{19}_{2h}, *Cmmm*, No.65; $a = 8.431(3)$, $b = 13.663(3)$, $c = 4.106(2)$; $Z = 2$; $V = 472.98$; d(calc.) = 4.81	*crystallographic data* (Levet *et al.*, 1980); *thermodynamic data* (Cordfunke *et al.*, 1983; Grenthe *et al.*, 1992; Guillaumont *et al.*, 2003)
$U_5O_{12}Cl$	$\Delta_f G^o_m = -5518.0\ (12.4)^\dagger$, $\Delta_f H^o_m = -5854.4\ (8.6)^\dagger$, $S^o_m = 465\ (30)^\dagger$	orthorhombic; D^5_{2h}, *Pmma*, No.51; $a = 7.111(9)$, $b = 19.625(12)$, $c = 4.130(2)$; $Z = 2$; $V = 576.36$; d(calc.) = 8.17	*crystallographic data* (Cordfunke *et al.*, 1985); *thermodynamic data* (Cordfunke *et al.*, 1985; Grenthe *et al.*, 1992; Guillaumont *et al.*, 2003)

UBr_5	deep-brown, dec.. UBr_5(cr): $\Delta_f G^o_m$ = –769.3 (9.2)†, $\Delta_f H^o_m$ = –810.4 (8.4)†, S^o_m = 292.9 (12.6)†; $C^o_{p,m}$ = 160.7 (8.0)†. UBr_5(g): $\Delta_f G^o_m$ = –668.2 (15.3)†, $\Delta_f H^o_m$ = –648 (15)†, S^o_m = 498.7 (10.0)†; $C^o_{p,m}$ = 129.0 (5.0) $\mu_{eff.}$ = 1.42 B.M. (χ_g = 1.316×10^{-6} at 291 K), (11–291 K)	triclinic; C_1^1; $P\bar{1}$, No. 2; a = 7.449 (7), b = 10.127(14), c = 6.686(4); α = 89.25(12°), β = 117.56(4)°, γ = 108.87(9)°; Z = 2; V = 417.46; d(calc.) = 5.07; d(U–Br) = 2.81(7) and 2.94(7) for bridging atoms and 2.58(7) to 2.58(7) for terminal atoms	*crystallographic data* (Levy *et al.*, 1978); *magnetic susceptibility data* (Eichberger,, 1979); *photoelectron spectra* (Thibaut *et al.*, 1982); *thermodynamic data* (Grenthe *et al.*, 1992; Guillaumont *et al.*, 2003)
$P(C_6H_5)_4[UBr_6]$	brown crystals; extremely oxygen- and moisture-sensitive; soluble in CH_2Cl_2	monoclinic; C^6_{2h}, $C2/c$, No.15; a = 23.155(4), b = 6,950(3), c = 18.052 (3); β = 96.38(2)°; Z = 4; V = 2887; d(calc.) = 3.07 d(U–Br1 and U–Br2) = 2.669(3); d(U–Br3 or U–O) = 2.654(4); Br–U–Br = 89.9(11) and O–U–O = 88.8(1) or 89.9(1)	*synthesis and crystallographic data* (Bohrer *et al.*, 1988) *absorption spectra; ESR data* (Eichberger and Lux, 1980; Edelstein *et al.*, 1974); *infrared spectra* (Brown, 1979)
$P(C_6H_5)_4[UBr_6]\cdot2CCl_4$	almost black crystals; IR (cm^{-1}): ν(U–Br) = 215	monoclinic; C^5_{2h}, $P2_1/c$; No.14; a = 11.115(3), b = 21.142(5), c = 17.187(5), β = 95.42(3)°; Z = 4; V = 4021; d(calc.) = 2.25; d(U–Br) = 2.603(4) to 2.679(3); d(U–O) = 2.674(4); Br1–U–Br2 = 89.3(1) Br1–U–Br3 (or O) = 89.5(1) Br2–U–Br3 (or O) = 91.1(1)	*synthesis and crystallographic data* (Bohrer *et al.*, 1988)
$MUBr_6$ [M = (i) Na, K, Rb, (ii) Cs, NH_4, (iii) $N(C_2H_5)_4$, $N(C_4H_9)_4$, $As(C_6H_5)_4$,	brown to black; IR data (cm^{-1}) for $N(C_2H_5)_4UBr_6$: ν_3 = 215; ν_4 = 87; ν(lattice) = 62→68; ν_6 (IR and R inactive) = 61; (i) $\|g\|$ = 1.245; (ii) $\|g\|$ = 1.21; (iii) $\|g\|$ = 1.21		*absorption spectra; ESR data* (Eichberger and Lux, 1980; Edelstein *et al.*, 1974); *infrared spectra* (Brown, 1979); *crystal-field analysis for* $[N(C_2H_5)_4]UBr_6$ (Ryan, 1971, Eichberger and Lux, 1980)

Table 5.28 (*Contd.*)

Formula	*Selected properties and physical constants*[b]	*Lattice symmetry, lattice constants* (Å), *polyhedron type and density* (g cm^{-3})[c]	*Remarks regarding information available and references*
M_2UOB_5 (i) M = N $(C_2H_5)_4$ and (ii) As $(C_6H_5)_4$.	IR: 919, 817 (U–O, stetch.), 250, 190 and 80 cm^{-1}; for (i): green solid; $\varsigma_{5f} = 1750\ cm^{-1}$, $\Gamma_6 = 16194$, $\Gamma_7 = 10460$, $\Gamma_6 = 8163$, $\Gamma_7 = 6080$, $\Gamma_7 = 4865$, $\Gamma_7 = 1490$, $\Gamma_7 = 0$; $\|g\| = 1.24$; (ii) green solid		*absorption spectra; ESR data; infrared spec tra* (Selbin and Sherrill, 1974; Brown, 1979)
$[N(C_2H_5)_4]_2UBr_6 \cdot 2.5\ N(C_2H_5)_4Br$	green; IR data (cm^{-1}): ν(M–O) = 919, 817; ν(M–Br) = 190s, 80m.		*infrared data* (Ryan, 1971)
$UOBr_3$	brown; $UOBr_3$ (cr): $\Delta_f G^o_m$ = –901.5 (21.3)†, $\Delta_f H^o_m$ = –954(0)†, S^o_m = 205.0 (12.6)†; $C^o_{p,m}$ = 120.9 (4.2)†	monoclinic; C_2^3, *C*2, No.5; *a* = 16.24, *b* = 3.7, *c* = 9.0; $\beta = 110.5$	*crystallographic data* (Brown, 1973); *thermodynamic data* (Rand and Kubaschewski, 1963; Grenthe *et al*., 1992; Guillaumont *et al*., 2003)
UO_2Br	brown-black; $\mu_{eff} = 1.76$ B.M., $\Theta = -200$ K	orthorhombic; D_{2h}^{17}, *Cmcm*, No. 63; *a* = 4.106(1), *b* = 20.200 (5), *c* = 3.980(1); *d*(calc.) = 6.97. The coordination polyhedron is a pentagonal bipyramid with two Br and three U atoms; *d*(U–Br) = 2.939(3) in the base of the pentagon; *d*(U–O1) = 2.17(1)×2	*crystallographic data* (Levet *et al*., 1977); *magnetic susceptibility data* (Levet, 1969); *thermodynamic data* (Shchukarev *et al*., 1959); *photoelectron spectra* (Thibaut *et al*., 1982)

		and d(U–O'1) = 2.30(3) = 2.30(3) in the base of the pentagon; d(U–O2) = 2.054(1))×2 at the apices; d(Br–Br) = 3.870(6). The angles are: O(2)–U–(O2) = 176.8 (2); O(2)–U–O'(1) = 90.6(4); Br–U–Br = 85.2(2); Br–U–O(1) = 70.7(2)	
$[N(C_2H_5)_4]_2UOBr_5$; $[As(C_6H_5)_4]_2UOBr_5$; $[N(C_2H_5)_4]_2UOBr_5 \cdot 2.5N(C_2H_5)_4Br$	IR vibrations for $UOBr_5^{2-}$ species (cm^{-1}): 919, 817, 250, 190, and 80; ν(U–O, stretch.) = 919, 817		*absorption spectra; crystal-field analysis* (Selbin and Sherrill, 1974); *infrared spectra* (Ryan, 1971)

* Peritectic decomposition point.

† Values recommended by the Nuclear Energy Agency (Grenthe *et al.*, 1992; Guillaumont *et al.*, 2003).

* *R*, *rhombohedral* (*hexagonal parameters given*).

[a] Values have been selected in part from review articles (Brown, 1979; Bacher and Jacob, 1980; Freeman,1991; Grenthe *et al.*, 1992; Guillaumont *et al.*, 2003).

[b] m.p. = melting point (°C); b.p. = boiling point (°C); (cr) = crystalline; (g) = gaseous; thermodynamic values in kJ mol^{-1}, or J K^{-1} mol^{-1} at 298.15 K, unless otherwise mentioned; $\Delta_f G^o_m$ (kJ mol^{-1}), standard molar Gibbs energy of formation; $\Delta_f H^o_m$(kJ mol^{-1}), standard molar enthalpy of formation; S^o_m, standard olar entropy; $C^o_{p,m}$(J K^{-1} mol^{-1}), standard molar heat capacity; log p (mmHg) = $-AT^{-1} + B - C \log T$, vapor pressure equation for indicated temperature range; IR = infrared active; val. = valence vibrations; def. = deformation vibrations; stretch. = stretching; all values in cm^{-1}; s: strong; m: medium; w: weak; sh: shoulder; ς_{5f} = spin-orbit interaction parameter; B^k_2-crystal-field parameters; $\mu_{eff.}$ = effective magnetic moment; B.M. = Bohr magneton.

[c] All values are in Å and angles are in degrees; CN, coordination number; d = density [g cm^{-3}], V = molar volume [cm^3 mol^{-1}].

[d] Temperature range with linear relationship of χ_M^{-1} against T.

[e] Deduced from measurements in excited states spectra.

magnetic moments $\mu_{\text{eff}} = 2.84\sqrt{c}\mu_{\text{B}}$ along with some other physical constants are summarized in Table 5.28.

(*i*) *Uranium pentafluoride and uranium(v) complex fluorides*

Uranium pentafluoride

The pentafluoride exists in two crystalline modifications: a high-temperature α-UF_5 (over 150°C) and a low-temperature β-UF_5 form (below 125°C). The general preparation procedures involve either the oxidation of UF_4 or reduction of UF_6 (Bacher and Jacob, 1980). Halogen fluorides, some noble gas fluorides, and CoF_3, VF_3, and OF_2 may be used as oxidation reagents. The formation of α-UF_5 can be achieved by fluorine oxidation of UF_4 at 150°C, or the conversion of UCl_5 by gaseous HF at 300°C; the low-temperature form may be prepared by the reaction with anhydrous liquid HF (AHF) and UCl_6 or UCl_5. The β-form may be also obtained by reduction of UF_6 by silicium powder, NH_3, or $SOCl_2$. This compound is also formed in AHF in the presence of gold plates, by pyrolysis of NH_4UF_7, photolysis of UF_6 by UV light, and by reaction of $NOUF_6$ in a solution of AHF and BF_3. The reduction of UF_6 to UF_5 has also been achieved in hydrogen bromide and CF_3COOH. Some of the preparation methods are of little practical importance because of small yields, an impure product, or inconvenient starting materials. On laboratory scale the most convenient procedures involve photoreduction of UF_6 in the presence of H_2, CO, or SO_2. The reaction between UF_4 and UF_6 results in the formation of β-UF_5 below 125°C and α-UF_5 at 230–250°C. β-UF_5 is formed also in the following reaction at molar ratios 1.1 to 1 between UF_6 and $(CH_3)_3SiX$ (Brown *et al.*, 1983):

$$UF_6 + (CH_3)_3SiX \rightarrow (CH_3)_3SiF + 1/2X_2 + UF_5 \quad (X = \text{Cl or Br})$$

The pentafluoride is a hygroscopic crystalline solid, which disproportionates even in a humid atmosphere, according to reaction

$$2UF_5 + 3H_2O \rightarrow UF_4 + UO_2F_2 \cdot H_2O + 4HF$$

In aqueous solutions this reaction results in the precipitation of the hydrated tetrafluoride and the formation of a solution of uranyl fluoride. Above 150°C, UF_5 disproportionates slowly to U_2F_9(s) and UF_6(g). The disproportionation reaction can be limited by the presence of UF_6(g); the temperature dependence of the vapor pressure follows the equations (Wolf *et al.*, 1965):

$$\log p_{\text{solid}}(\text{mmHg}) = -8001\, T^{-1} + 13.99$$
$$\log p_{\text{liquid}}(\text{mmHg}) = -5388\, T^{-1} + 9.82$$

UF_5 can be reduced to UF_4 by H_2 or Ni (at 600°C) and by some covalent fluorides such as PF_3, AsF_3, or $AsCl_3$. Halide exchange reactions were observed with BCl_3, $TiCl_4$, and PCl_3, the products being respectively, BF_3, TiF_4, and PF_3, in addition to UF_4 and UCl_6.

Uranium pentafluoride dissolves without hydrolytic decomposition in 48–50% hydrofluoric acid, forming relatively stable blue solutions from which $(H_3O)UF_6 \cdot 1.5H_2O$ crystallizes; by addition of RbF or CsF, the blue MUF_6 salts (M = Rb or Cs) are formed. Uranium pentafluoride dissolves in acetonitrile and reacts with alkali fluorides and sodium ethoxide, NaOEt, to form $M[UF_4]$ and $U_2(OEt)_{10}$, respectively.

The structure of α-UF_5 consists of infinite chains of UF_6 octahedra, bridged by *trans*-fluorides to give a linear chain parallel to the *c*-axis. The remaining four fluorine atoms are single bonded to uranium. The low-temperature β-form is isostructural with PaF_5 and NpF_5 and consists of an eight-coordinate arrangement with a geometry intermediate between dodecahedral and square antiprismatic (Ryan *et al.*, 1976; Eller *et al.*, 1979). The crystal packing of β-UF_5 is shown on Fig. 5.43. Other crystallographic data are listed in Table 5.28.

Theoretical model calculations performed using the vibrational spectrum of monomeric UF_5 molecules isolated in an Ar-matrix indicate a square-pyramidal structure in which the U atoms are located above the equatorial plane formed by the fluorine atoms (Paine *et al.*, 1976).

In non-aqueous solvents such as nitriles, dimethyl sulfoxide, and dimethylformamide, uranium pentafluoride forms stable solutions containing UF_6^- anions and solvated UF_4^+ cations. From these solutions several adducts and complex

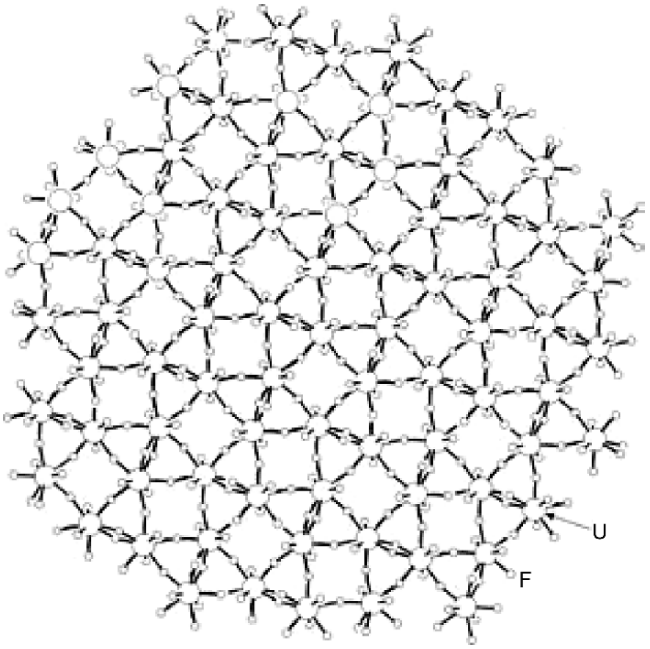

Fig. 5.43 *Crystal packing view of β-UF_5* (*from Ryan* et al., 1976).

fluorides have been isolated, for example, $UF_5 \cdot CH_3CN$, $[UF_4(Me_2SO)_3][UF_6]$, $[UF_4(DMF)_3][UF_6]$, $[(C_6H_5N(CH_3)_3][UF_6]$, $[(C_6H_5)_3PNP(C_6H_5)_3][UF_6]$, Na $[UF_6]$, and K$[UF_6]$ (Berry *et al*., 1977; Halstead *et al*., 1979). The compounds and their solutions have been characterized by electronic, infrared, Raman, and EPR spectra.

Complex uranium(v) fluoro compounds

A number of fluorouranates(v) have been characterized by determination of their crystallographic data and their chemical and thermodynamic properties (see Table 5.28). Additional information in the reviews of Chatalet (1967), Penneman *et al*. (1967), Ryan (1971), Brown (1972), Bacher and Jacob (1980), and Freestone and Holloway (1991). Complex compounds identified in a number of selected fused salt systems are listed in Table 5.29.

The compounds may be prepared by a variety of methods (Bacher and Jacob, 1980; Freestone and Holloway, 1991): (i) solid state reactions between UF_5 and the appropriate alkali fluorides in an inert atmosphere at 300°C constitute a general route to most of the fluoro complexes; (ii) melting of mixtures of hexa- and octafluoro complexes leads to the formation of the heptafluoro complex compounds; (iii) solid state reactions or reduction of UF_6 with NH_3 yield ammonium fluorouranates; (iv) treatment of equimolar mixtures of UF_5 and the appropriate alkali fluoride with anhydrous HF yields the hexafluorouranates(v); (v) oxidation of UF_4–alkli fluoride mixtures with fluorine also leads to the hexafluoruranates; and (vi) $RbUF_6$ may be also obtained by crystallization from solutions of RbF and UF_5 in concentrated HF.

The pentafluoro uranates may disproportionate into U(IV) and U(VI). However, they are relatively stable in the absence of substances that cause hydrolysis. Ohwada (1976) and Soulié (1978) suggest that the U–F bonds in the fluorouranates(v) are partly covalent (68 to 77% as compared to 46.3 and 35%, respectively, in UF_4 and β-K_2UF_5). The bonds in UF_5 are assumed to have

Table 5.29 *Uranium(v) complex fluorides identified in molten salt systems.*

System	*Complex fluorides*
$LiF\text{-}UF_5$	$LiUF_6$
$NaF\text{-}UF_5$	$NaUF_6$, Na_3UF_8
$KF\text{-}UF_5$	KUF_6, K_2UF_7, K_3UF_8
$RbF\text{-}UF_5$	$RbUF_6$, Rb_2UF_7, Rb_3UF_8
$CsF\text{-}UF_5$	$CsUF_6$, Cs_2UF_7, Cs_3UF_8
$NH_4F\text{-}UF_5$	NH_4UF_6, $(NH_4)_2UF_7$, $(NH_4)_3UF_8$
$N_2H_6F_2\text{-}UF_5$	$N_2H_6UF_7$, $N_2H_6(UF_6)_2$
$(NH_3OH)F\text{-}UF_5$	$(NH_3OH)UF_6$

a nearly 100% covalent character. The pentafluoro uranates of the M_2UF_7 type (M = K, Rb, Cs, or NH_4) have the same type of powder patterns ($P2_1/c$, C_{2h}^5, No. 14) as that of K_2NbF_7 where the coordination polyhedon is a monocapped trigonal prism (Brown and Walker, 1966). The analysis of the spectral data for $CsUF_6$ (Carnall and Crosswhite, 1985) made it possible to assign the electronic transitions from the Γ_7 ground state to the excited levels Γ_8, $\Gamma_{7'}$, $\Gamma_{8'}$ and Γ_6 of the $5f^1$ electronic configuration. The spin–orbit coupling parameter ς_{5f} and the B_0^2, B_0^4, and B_0^6 crystal-field parameters determined for the D_{3d} site symmetry are equal to 1910.2(13), 534.2(139), –14866(66) and 3305(78) cm^{-1}, respectively.

Pentavalent oxide fluorides and oxide fluoride complexes

White U_2OF_8 oxide fluoride has been obtained by heating of UF_4 in an intermittent oxygen flow at 850°C (Kirslis *et al.*, 1950; Freestone and Holloway, 1991). The compound disproportionates in vacuo at 300°C to form a mixture of uranyl fluoride and uranium hexa and tetrafluoride. The existence of this compound has not been confirmed by other authors (Ekstrom *et al.*, 1974). A series of uranium oxide fluoride phases, UO_xF_y, containing uranium in the oxidation state 5+ ($UO_{2.33}F_{0.33}$ to $UO_{2.00}F_{1.00}$), a mixture of 5+ and 6+ ($UO_{2.58}F_{0.17}$ to $UO_{2.17}F_{0.83}$) and a mixture of 4+ and 5+ ($UO_{2.00}F_{0.25}$) have been obtained by heating UF_4 with UO_3 or U_3O_8 at 400–500°C *in vacuo* (Kemmler-Sack, 1967, 1969). The possible structures of these phases have been discussed on the basis of X-ray powder, magnetic, and spectral data.

A number of complexes of the $M^IM^{II}U_2O_6F$-type (where M^I = Na, K, Rb, or Tl and M^{II} = Ba, Sr, or Pb) were obtained by heating appropriate mixtures of the component fluorides and oxide fluorides at 500–900°C *in vacuo*, e.g. (i) M^IF with $M^{II}UO_4$, and UO_2; (ii) $M^{II}F_2$ with $M_2{}^IUO_4$, $M^{II}UO_4$, and UO_2, and (iii) M^IUO_2 with $M^{II}O$, UO_3, UO_2, and UF_4 (Kemmler-Sack, 1968a). All complexes have cubic symmetry (Kemmler-Sack, 1968b,c) with similar lattice parameters (Table 5.28). Reflectance spectra of the compound have been analyzed on the basis of the $5f^1$ configuration of the U(v) ion in an octahedral field.

Two additional complex oxide fluoride compounds, $[N(C_2H_5)_4]_2UOF_5$ and $[N(C_2H_5)_4]_2UOF_5 \cdot 2H_2O$, have also been isolated. The hydrated compound is formed by hydrolysis of the corresponding UCl_6 salt in a saturated solution of $[N(C_2H_5)_4]F \cdot nH_2O$ in an ethanol–acetone mixture. The complex is easily dehydrated in vacuum (Ryan, 1971). Both compounds are pink colored and oxygen-sensitive. UOF_5^{2-} solutions may be stabilized by an excess of $[N(C_2H_5)_4]F$. Addition of water results in a rapid disproportionation of UOF_6^{2-} to U^{IV} and U^{VI} species. An analysis of the absorption spectra of $[N(C_2H_5)_4]_2UOF_5$ in solid state and in an acetonitrile solution made it possible to make an assignment of the six electronic transitions based on a D_4 ligand field model (Selbin and Sherrill, 1974).

(*ii*) *Uranium pentachloride and uranium*(*v*) *complex chlorides*

Uranium pentachloride

Uranium pentachloride may be prepared by a number of methods, but only a few of them result in high yields and high purity due to the instability of the compound towards thermal decomposition and disproportionation; these reactions take place below 100°C at pressures between 10^5 Pa (1 atm) and 133×10^{-4} Pa, respectively:

$$UCl_5 \xrightarrow{10^5 Pa} UCl_4 + 1/2Cl_2 \text{ and}$$

$$2UCl_5 \xrightarrow{133 \times 10^{-4} Pa} UCl_4 + UCl_6$$

At normal pressure, the disproportionation is complete in the range 100 to 175°C.

One of the most satisfactory preparative methods is to use liquid phase chlorination of UO_3 or U_3O_8 with carbon tetrachloride at 80–250°C under pressure and UCl_5 as catalyst (Brown, 1979). The most convenient laboratory method involves decomposition of UCl_6 at room temperatures in carbon tetrachloride, methylene dichloride, or 1,2-dichloroethane. Another relatively simple method is the reduction of UO_3 by silicon tetrachloride at 400°C followed by vacuum removal of the excess of reagent from the resulting solution of UCl_5 in $SiCl_4$ (Selbin *et al*., 1968).

Uranium pentachloride is obtained as dark brown crystals, which exist in two crystal modifications. The more often encountered α-UCl_5 is obtained by recrystallization from CCl_4 and the β-UCl_5 is formed by crystallization of UCl_6 from carbon tetrachloride or methylene dichloride (Kolitsch and Müller, 1974). UCl_5 is very hygroscopic and immediately disproportionates into U(IV) and U(VI) in aqueous solutions. It reacts instantly with a number of organic solvents such as alcohols, acetone, dimethyl ether, diethyl ether, ethyl acetate, formamide, or dioxane. In some anhydrous organic solvents such as carbon tetrachloride, carbon disulfide, and thionyl chloride, it forms relatively stable solutions; it is insoluble in benzene, xylene, or isopropyl ether. Impure samples may be recrystallized from carbon tetrachloride and separated from UCl_4 by dissolution and recrystallization from liquid chlorine. Hydrogen reduces UCl_5 to UCl_4 at 250–300°C. Anhydrous gaseous or liquid hydrogen fluoride converts it to UF_5 and fluorine oxidizes it to UF_6. The reactions of UCl_5 with some univalent chlorides yield $N(CH_3)_4UCl_6$, $As(C_6H_5)_4UCl_6$, or $N(CH_3)_2H_2UCl_6$ (Bagnall *et al*., 1964).

The structures of the monoclinic α-UCl_5 (space group $P2_1/n$) and triclinic β-UCl_5 (space group $P\bar{1}$) are based on a cubic or hexagonal close packing of the chlorine atoms. In the first one, the uranium atoms occupy one-fifth of the octahedral holes and two octahedra are forming a dimeric U_2Cl_{10} unit by sharing a common edge. The structure of the β phase contains the same

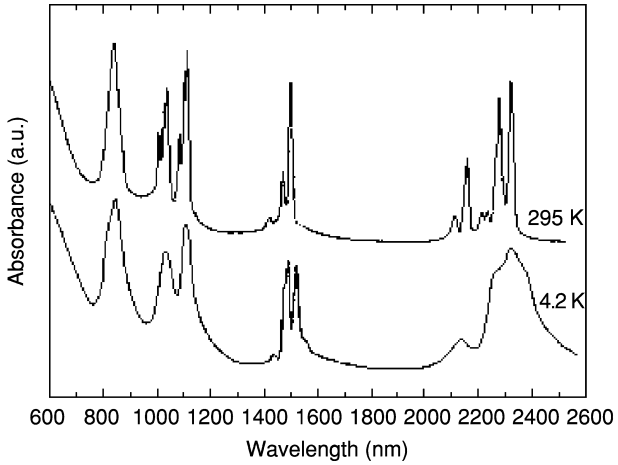

Fig. 5.44 *Absorption spectrum of UCl_5 single crystals at* 4.2 *and* 295 K (*partially adapted from Leung and Poon*, 1977). *Reproduced with the permission of Copyright Clearance on Government of Canada Works.*

U_2Cl_{10} units (Table 5.28). The following ligand-field parameters have been reported from an analysis of the UCl_5 spectrum: $\varsigma_{5f} = 1559(115)$, $B_0^4 = 13479$ (1125) and $B_0^6 = -158.6(745)$ (Leung and Poon, 1977). The electronic absorption spectra of the two UCl_5 crystal modifications (see Fig. 5.44) are identical and similar to those of the hexachlorouranates(v).

The magnetic susceptibility follows the Curie–Weiss law in the 14–300 K temperature range. Different effective magnetic moments were reported: according to Rüdorff and Menzer (1957), they range from 1.05 B.M. at 77 K to 1.42 B.M. at 398 K, while Handler and Hutchison (1956) report $\mu_{eff} = 2.00$ B. M. at 300 K with $\Theta = -99$ K.

Complex uranium(v) chloride compounds

The isolation of numerous pentavalent uranium complexes with ligands containing N, P, As, S, Se, and Te donor atoms has been reported (Selbin and Ortego, 1969; Brown,1972, 1979). Thus, complexes of UCl_5L-type are formed with triphenylphosphine oxide, thionyl chloride, phenazine, 2,2′-bipyridyl, ethylene bis(diphenylphosphine), triphenylphosphine, trioctylphosphine, diarsine, anthrone, benzanthrone, methyleneanthrone, triphenylbismuthine, diphenyldisulphide, Ph_2Se_2, and Ph_2Te_2; those of the $UCl_5{\cdot}2$L-type – with pyrazine, phthalazine, methyl cyanide, pyridine, 1,10-phenanthroline, 2-mercaptopyridine, ethylene bis-salicylaldiamine, 8-hydroxyquinoline, anthrone, benzil, benzanthrone, and triphenylphosphine oxide, while $UCl_5{\cdot}3$L complexes are formed with dioxane and tetramethyl amine.

The preparation of $[N(CH_3)_4]_3UCl_8$ and a number of $MUCl_6$ complexes (where M = $N(CH_3)_4$, $N(CH_3)_2H_2$, $N(C_2H_5)_4$, $N(C_3H_7)_4$, $N(C_3H_9)_4$,

$N(C_4H_9)_4$, $P(C_6H_5)_4$, $As(C_6H_5)_4$, NH_4, K, Rb, etc.) has been achieved by addition of carbon disulfide to thionyl chloride solutions of U(v) using the appropriate MCl compound (Bagnall *et al.*, 1964; Brown, 1979). A convenient alternative method to prepare $MUCl_6$ complexes (where M = $N(C_2H_5)_4$, As $(C_6H_5)_4$, or $N(CH_3)_4$) employs chlorine oxidation in nitromethane solutions (Ryan, 1974). UCl_5tcac (tcac is the acronym for $Cl_2C{=}CClCOCl$) has been reported (Fuji *et al.*, 1979) to be a useful starting material for the preparation of $RbUCl_5$, $(n\text{-}C_3H_7)_4NUCl_5$, and a number of UCl_5 adducts with different donor ligands. Other convenient routes to the U(v) complexes involve the addition of MCl (where M = NH_4, $As(C_6H_5)_4$, or $N(CH_3)_4$) to uranium hexachloride in methylene dichloride (Brown, 1979). The reactions between UO_3, $SOCl_2$, and MCl (M = Na, K, Rb, Cs, NH_4, Ag, Ba, or Tl) in sealed vessels at 180–200°C also lead to uranium(v) hexachloro complexes (Stumpp, 1969); the reaction between UO_3 and PCl_5 results in the formation of $UCl_5 \cdot PCl_5$. The last compound should be formulated as $[PCl_4]^+[UCl_6]^-$ (Brown, 1969). Gruen and McBeth (1969) have reported the formation of a uranium(v) chloro complexes in the vapor phase according to the reaction

$$UCl_4 + \frac{1}{2}Cl_2 + AlCl_3 \rightarrow UCl_5 \cdot AlCl_3$$

The analysis of the high-temperature electronic spectrum indicates that the compound should be formulated as $[AlCl_4]^+[UCl_6]^-$.

The hexachlorouranates(v) are very hygroscopic. On exposure to air they are hydrolyzed with disproportionation to U(IV) and U(VI). With the exception of those containing alkali metal cations, they are soluble in numerous organic solvents such as methyl cyanide, diethyl ether, acetone, nitromethane, or phosphorous oxytrichloride. $CsUCl_6$ is reported to react in inert solvents with oxygen donor ligands forming $UCl_5{\cdot}L$ adducts. Structure data and references to heats of formation determinations of several uranium(v) chloro-complexes are listed in Table 5.28. Spin–orbit and crystal field parameters, $\varsigma_{5f} = (1913)$, B_0^4 = 12209(710), and B_0^6 = –39(776), were determined for $N(C_2H_5)_4UCl_6$ by Edelstein *et al.* (1974). The magnetic susceptibility of $CsUCl_4$, $[(CH_3)_2H_2]$ UCl_6, $[N(CH_3)_4]UCl_6$, and $[As(C_2H_5)_4]UCl_6$ exhibits a Curie–Weiss dependence in two temperture ranges: 140–205 K and 210–310 K. The effective magnetic moments and Weiss constants (in brackets) range between 1.71 (161 K) and 2.14 B.M. (280 K) (Bagnall *et al.*, 1964; Brown, 1979). In the 250–310 K range $[N(CH_3)_4]_3UCl_8$ has a temperature-independent paramagnetism ($\chi_{mole} = 1100 \times 10^{-6}$ cm^3 mol^{-1}).

(*iii*) *Uranium*(*v*) *and mixed valence oxide chlorides*

The most convenient methods for the preparation of $UOCl_3$ involve heating of stoichiometric amounts of (i) UO_3 and $MoCl_5$ at 200–220°C *in vacuo*, (ii) UCl_4 and UO_2Cl_2 at about 370°C, or (iii) UO_2Cl_2 with WCl_5, $ReCl_5$, or $MoOCl_3$ at about 200°C (Brown, 1979). The mechanism of the first reaction is:

$$UO_3 + MoCl_5 \rightarrow UO_2Cl_2 + MoOCl_3$$
$$UO_2Cl_2 + MoOCl_3 \rightarrow UOCl_3 + \uparrow MoO_2Cl_2$$

The brown, moisture-sensitive solid is insoluble in non-polar organic solvents like carbon tetrachloride and benzene, but dissolves without decomposition in anhydrous ethanol. In the latter, it reacts with $C_6H_5N \cdot HCl$ to give $[C_6H_5NH]_2UOCl_5$. In other alcohols, acetone, and water, the compound dissolves with decomposition. Hydrolysis of $UOCl_3$ results in the formation of polymeric –U–O–U–O– chains. The reduction with $MoOCl_3$, $MoCl_5$, or $ReCl_5$ *in vacuo* around 200°C leads to UCl_4.

The preparation of UO_2Cl can be achieved by heating equimolar quantities of UO_2Cl_2 and UO_2 at 590°C *in vacuo* (Levet, 1969) or by reduction of UO_3 with $MoCl_3$ (Eliseev *et al.*, 1972). Uranium(v) dioxide monochloride is a brown-violet, air-sensitive solid. It is insoluble in organic solvents and decomposes to UO_2 and Cl_2 at 600°C in an inert atmosphere. UO_2Cl is reduced to UCl_4 by $MoCl_5$ at about 200°C and to $UOCl_2$ when heated with $MoOCl_3$. It exhibits Curie–Weiss dependence between 86 and 295 K with $\mu_{eff} = 1.86$ B.M. and $\Theta = -95$ K (Levet, 1969).

There is also a mixed valence state oxide chloride, $(UO_2)_2Cl_3$, which may be obtained by thermal decomposition of UO_2Cl_2 in high vacuum at 400–500°C, or by heating UO_2 and $UOCl_2$ in the molar ratio of 1:3 at 500°C; at higher temperature (500–650°C), UO_2Cl is formed. The black-brown solid has orthorhombic symmetry (Table 5.28) and dissolves slowly in water and in dilute mineral acids (Cordfunke *et al.*, 1977, Brown, 1979). On exposure to the atmosphere, the compound converts into the heptahydrate $(UO_2)_2Cl_3 \cdot 7H_2O$.

(*iv*) *Complex uranium*(v) *oxochlorides*

Brown (1979) has described methods for the preparation and characterization of a number of uranium(v) oxochloro-compounds, such as M_2UOCl_5 (where M = $N(C_2H_5)_4$, $N(C_2H_5)_3H$, $As(C_6H_5)_4$, or C_5H_5NH), $[N(C_2H_5)_4]UOCl_5 \cdot L$ (where L = phtalazine or 1,10-phenantroline), $[LH]_2UOCl_5 \cdot L$ (where L = pyridine, quinoline, isoquinoline, α- and β-picoline), and $[C_5H_5NH]_2UOCl_5 \cdot 2.5C_5H_5NHCl$. The complex $[C_5H_5NH]_2UOCl_5$ may be obtained by the addition of pyridine to an ethanolic solution of $UCl_5 \cdot SOCl_2$ saturated with hydrogen chloride; $[N(C_2H_5)_3H]_2UOCl_5$ by photolysis of $UO_2Cl_2 \cdot 2C_5H_5N$ in dry ethanol; and $[N(C_2H_5)_4]_2UOCl_5$ or $[As(C_2H_5)_4]_2UOCl_5$ by controlled hydrolysis in nitromethane of the corresponding hexachloro complexes. They are slightly soluble in nitromethane where they may react with other species to yield different uranium(IV), (V), or (VI) complexes. The oxopentachloro compounds are moisture-sensitive and undergo rapid disproportionation in water-containing solvents with the exception of $[N(C_2H_5)_4]_2UOCl_5$ and $[As(C_2H_5)_4]_2UOCl_5$ that are moderately stable on exposure to air. Reactions

between $[N(C_2H_5)_4]_2UOCl_5$ and nitrogen heterocyclic compounds in nitromethane or nitrobenzene yield complexes of uranyl(VI) or U(IV) (Selbin *et al.*, 1972b, 1973; Brown, 1979).

The electronic absorption spectra of $[UOCl_5]^{2-}$ in solid state and non-aqueous solvents are essentially identical (Ryan, 1971). A good agreement between observed and calculated energy levels of $[N(C_2H_5)_4]_2UOCl_5$ is obtained assuming D_4 symmetry and using the following crystal field parameters: $\tau = 700\ cm^{-1}$ and $\varsigma_{5f} = 1770\ cm^{-1}$, where τ is a parameter which depends on the radial function and ς_{5f} is the spin–orbit coupling parameter (Selbin *et al.*, 1972a).

(*v*) *Uranium pentabromide and uranium(v) complex bromides*

Uranium pentabromide

The most convenient method for the preparation of UBr_5 is bromination of either uranium metal or uranium tetrabromide at 55°C, or at room temperatures in the presence of catalytic amounts of methyl cyanide (Brown, 1979). The compound is a dark brown solid and is extremely sensitive to moisture. It disproportionates rapidly on dissolution in water and in various organic solvents like ethanol, acetone, dioxane, and ethylacetate. In chloroform and bromoform, the rate of disproportionation is much slower. Stable solutions may be obtained on dissolution in anhydrous, oxygen-free methyl cyanide and methylene dichloride. A number of stable $UBr_5{\cdot}L$ complexes with oxygen donors like $L = (C_6H_5)_3PO$ or $[(CH_3)_2N]_3PO$ have been prepared by bromine oxidation of UBr_4 in the presence of the ligand. Interactions with univalent bromides in thionyl bromide result in the formation of hexabromourantes(V), $MUBr_6$. Uranium pentabromide crystallizes with triclinic symmetry, space group $P\bar{1}$ and is isostructural with β-UCl_5 (see Table 5.28).

Ternary and polynary bromides and bromo compounds of uranium(v)

Hexabromouranates(V) of the formula $MUBr_6$ (where M = Na, K, Rb, Cs, NH_4, $N(CH_3)_4$, $N(C_2H_5)_4$, $N(C_4H_9)_4$, $As(C_6H_5)_4$, $P(C_6H_5)_4$, etc.) have been prepared by a variety of methods (Brown, 1979): (i) bromine oxidation of the appropriate tetravalent M_2UBr_6 compounds in non-aqueous solutions, e.g. nitromethane; (ii) halogen exchange reactions between the chloro complexes and an excess of liquid boron tribromide; (iii) reactions between thionyl bromide solutions of pentavalent uranium (prepared by dissolution of UO_3 in the solvent under refluxing) and the appropriate MBr; and (iv) reaction of UBr_6^{2-} and $UO_2Br_4^{2-}$ in nitromethane or methyl cyanide in the presence of anhydrous HBr according to the reaction

$$UBr_6^{2-} + UO_2Br_4^{2-} + 10HBr \rightarrow 2UBr_6^{-} + 2H_3O^{+} + 4HBr_2^{-}$$

The hexabromouranates have a brown-black color and are rapidly decomposed on dissolution in water or in the presence of moisture. $[As(C_6H_5)_4]UBr_6$ and $[N(C_2H_5)_4]UBr_6$ form stable solutions in anhydrous methylene dichloride

and nitromethane. In the last solvent, the presence of bromine is required to avoid reduction to uranium(IV). The complexes with M = $N(CH_3)_4$, $N(C_2H_5)_4$, and $N(C_4H_9)_4$ dissolve also in methylene dibromide and dibromoethane.

Vibronic side-bands dominate in the solid state and solution spectra of the bromo complexes, which indicates an octahedral or close to octahedral stereochemistry. An assignment of the electronic transitions in $[N(C_2H_5)_4]UBr_6$ from the Γ_7 ground level to the Γ_6, Γ_7, and Γ_8 excited levels of the $5f^1$ electronic configuration has been made (Edelstein *et al*., 1974). The spin–orbit coupling parameter ς_{5f} and the B_0^4 and B_0^6 crystal-field parameters determined from the fitting procedure are 1761(31), 10953(350) and –1058(274) cm^{-1}, respectively (Ryan, 1971; Eichberger and Lux, 1980). There are IR vibronic frequencies at 215 (ν_3) and 87 (ν_4) and at 61 cm^{-1} (ν_6); the identification of the infrared (IR) and Raman inactive (ν_6) vibration has been made by Brown *et al*. (1970). The first electron transfer band in a solution of anhydrous nitromethane has been registered at 17400 cm^{-1}, from which a value of 2.22 for the uncorrected optical electronegativity was deduced (Ryan, 1971).

(*vi*) *Uranium*(*V*) *oxide bromides*

Uranium(*V*) *oxide tribromide*

Uranium(V) oxide tribromide, $UOBr_3$, may be conveniently prepared by heating UO_3 in a stream of nitrogen and carbon tetrabromide vapour at 110°C. $UOBr_3$ is a moisture-sensitive and thermally unstable compound, slowly evolving bromine even at room temperatures. It is converted to UO_2Br_2 or UBr_4 by heating in oxygen at 148°C and with CBr_4 at 165°C, respectively. When heated at 200–300°C in a nitrogen atmosphere $UOBr_3$ converts to $UOBr_2$. In water and ethanol, acetone, ethyl acetate, and dioxan, it disproportionates to U(IV) and U(VI) species. The compound is insoluble in non-polar organic solvents like CCl_4 or CS_2.

Uranium(*V*) *dioxide monobromide*

The preparation of UO_2Br can be achieved by thermal decomposition of UO_2Br_2 in a sealed evacuated glass tube (Levet *et al*., 1977) or by heating the latter compound in a nitrogen–bromine mixture around 320°C (Gueguin, 1964). It may also be prepared by heating UO_3 at 250°C in a mixture of H_2 and HBr, or by treating UO_2Cl_2 with HBr (Levet, 1965). UO_2Br is a moisture-sensitive black-brown solid. When heated in an inert atmosphere (400–500°C), it decomposes to UO_2 and Br_2. It reacts with chorine (400°C) and oxygen (300°C) to yield UO_2Cl_2 and UO_3, respectively.

The compound has an orthorhombic symmetry in the space group *Cmcm* (No. 63). The coordination polyhedron is a pentagonal bipyramid with two bromine and three oxygen atoms in the equatorial plane and two oxygen atoms at the apices. The uranium atoms are linked in double chains by the sharing of three coordinated oxygen atoms. The structural arrangement is

similar to those in $PaOBr_3$, U_3O_8 and $PaCl_5$ and the compound is isostructural with PaO_2Br, NbO_2Br, TaO_2Br, NbO_2I and TaO_2I (Levet *et al.*, 1977). Crystallographic data are listed in Table 5.28. Magnetic susceptibility data are reported by Levet (1969) and the effective magnetic moment is 1.76 B.M. with $\Theta = -200$ K.

(*vii*) *Ternary and polynary uranium(v) oxide bromides and oxobromo compounds*

Green oxybromo complexes of the formulas $[As(C_6H_5)_4]_2UOBr_5$, $[N(C_2H_5)_4]_2UOBr_6 \cdot 2.5N(C_2H_5)_4Br$, etc. have been obtained by controlled hydrolysis of hexabromouranates(v) in acetone or acetone–nitromethane mixtures at –75°C (Ryan, 1971; Brown, 1979). The complexes are significantly less stable than their fluoro and chloro analogs. They are moisture-sensitive and rapidly disproportionate in numerous anhydrous solvents, such as nitromethane.

Selbin *et al.* (1972a) and Selbin and Sherrill (1974) have presented an interpretation of the electronic spectra of UBr_6^- and $UOBr_5^{2-}$ and have shown the effect of perturbing the $5f^1$ orbital energy levels successively by a tetragonal distortion of the octahedral field and spin–orbit coupling. Semi-empirical theoretical calculations of energy levels of UBr_6^- and $UOBr_5^{2-}$ have been performed in order to locate and assign all electronic transitions in these $5f^1$ species. The first electron transfer transition was observed at 26700 cm^{-1}. As compared with UBr_6^- species it is shifted by 9300 cm^{-1} to higher frequencies, equivalent to 0.3 eV. This change is reported to result from the pronounced anisotropic nature of the $UOBr_5^{2-}$ complex (Ryan, 1971).

(*viii*) *Intermediate uranium halides*

The reaction of solid UF_4 with gaseous UF_6 results in a gradual formation of intermediate fluorides with a composition between UF_4 and $UF_{4.5}$, depending on the temperature used and the partial pressure of uranium hexafluoride: U_2F_9 (= $UF_{4.5}$), U_4F_{17} (= $UF_{4.25}$), and U_5F_{22} (= $UF_{4.2}$) (Eller *et al.*, 1979; Bacher and Jacob, 1980).

$$3UF_4 + UF_6 \rightleftharpoons 2U_2F_9 \quad (200\,^\circ C)$$

$$7UF_4 + UF_6 \rightleftharpoons 2U_4F_{17} \quad (300\,^\circ C)$$

Agron (1958) has studied the chemical equilibria in these systems; the forward reactions take place at temperatures between 225–300 and 270–350°C, respectively. Agron (1958) has also reported the conditions of formation, equilibrium, dissociation, and the thermodynamics of the disproportionation reactions.

Intermediate uranium fluorides may also be prepared by reduction of UF_6 with HBr by a careful control of the reactant stoichiometry in reactions between

UF_3 and iodine, SiH_4 or PF_3. There are only two oxidation states, U(IV) and U(V), in U_2F_9 as shown by spectroscopic analyses. U_4F_{17} and U_2F_9 are slowly hydrolyzed, in water with the formation of $UF_4 \cdot nH_2O$, UO_2^{2+}, and F^-, and in moist air with the formation of $UO_2F_2 \cdot xHF \cdot yH_2O$. Organic solvents such as C_6H_6, $CHCl_3$, or CCl_4 react with U_2F_9 with reduction to UF_4.

U_4F_{17} has a monoclinic structure that is a distorted version of that of UF_4 (Chatalet, 1967). In U_2F_9 the uranium atoms are nine-coordinated with a tricapped trigonal prismatic arrangement (Zachariasen, 1949d; Taylor, 1976a,b).

Investigation of the UCl_3–UF_4 phase diagram identified mixed valence phases $2UCl_3 \cdot UF_4$ and $UCl_3 \cdot 7UF_4$ that melt incongruently at 625 and 760°C, respectively.

The preparation and characterization of a mixed-valence oxide chloride of the composition $(UO_2)_2Cl_3$ has been reported by Cordfunke *et al*. (1977). The compound is formed by thermal decomposition of anhydrous UO_2Cl_2 at 400–500°C in high vacuum, or by the reaction of UO_2 and UO_2Cl_2 in evacuated quartz tubes at temperatures between 400 and 800°C. On the basis of comparable uranium compounds, such as U_3O_8, the authors have assumed that uranium is present in both oxidation states 6+ and 5+. Structure data of the intermediate halides are given in Table 5.28.

(d) Hexavalent halides and complex halides

Uranium hexahalides and complex halides have been the most extensively investigated uranium compounds due to their commercial applications. The stability of the halides decreases with increasing atomic number of the halide anion, e.g. UCl_6 is much more prone to thermal decomposition than UF_6, and no simple halides are formed with iodine or bromine in this oxidation state. The hexahalides react violently with water at room temperatures to form soluble uranyl halides; they are also readily soluble in polar organic solvents, in many cases with formation of complexes. The uranyl ion (UO_2^{2+}) forms weak complexes with halide ions, with the exception of fluoride cf. Table 5.34, p.349. Hexavalent halides and complex halides are typically yellow and in a few cases colorless (e.g. UF_6) or green (e.g. UCl_6) (see Table 5.30).

Hexavalent uranium has the $[Rn]5f^0$ electronic configuration. The ground state is formally $^1S_0$. There are numerous reports on absorption and fluorescence spectra of hexavalent halides and uranyl halogeno complexes in the solid state, aqueous solutions, and organic solvents that are discussed in a review article by Carnall (1982). The spectra of UO_2^{2+} compounds exhibit a characteristic vibrational fine structure in the visible–ultraviolet region due to coupling with the stretch modes in the linear UO_2 unit. The absorption spectrum of UF_6 displays a similar complex vibronic structure, which is observed to be superimposed on broad and intense charge transfer bands centered near 26670 and 38460 cm^{-1}. An analysis of the spectrum (Lewis *et al*., 1976) has

Table 5.30 *Properties of selected uranium(VI) halides and complex halides.*[a]

Formula	*Selected properties and physical data*[b,c]	*Lattice symmetry, lattice constant* (Å), conformation and density (g cm^{-3})	*Remarks regarding information available and references*
UF_6	colorless; extremely hygroscopic; m.p. = 64.02 (1136 torr); reacts vigorously with water; soluble: liq. Cl_2, Br_2, CCl_4, CH_3Cl; gives dark red fuming solution with nitrobenzene. bond energies (kJ mol^{-1}): average bond: 523.4 first bond: 286; second bond: 422.9. ionization potential: 14.0 eV $\Delta_f H^o_m$(cr) = –2197.7(1.8)[†] $\Delta_f H^o_m$(g) = –2148.6(1.9)[†] S^o_m(g) = 376.3(1.0)[†] $C^o_{p,m}$(cr) = 166.8(0.2)[†] $C^o_{p,m}$(g) = 129.4(0.5[†] sublimation: $\Delta_{sub}H_m$(298.15K) = 49.1(5)[†] fusion: $\Delta_{fus}H_m$ (329.69K) = 18.8 vaporization: $\Delta_{vap}H_f$(337.202K) = 28.8 triple point : 337.20 K at p = 1522 mbar vapor pressure: solid (273.15–337.17K): log p (mmHg)[‡] = 6.38363 + 0.0075377t – [942.76/t+ 183.416)]; liquid (337.17–383.15K):	solid: orthorhombic; D^{16}_{2h}; *Pnma,* No.62; a = 9.900, b = 8.962, c = 5.207; [from neutron diffraction data a = 9.654(3), b = 8.776(4) c = 5.084(3); V = 430.73; d(calc.) = 5.43]; Z = 4; V = 462; d(calc.) = from 4.93 to 5.43, d(exp.) = 4.87; the molecule appears to have an undistorted octahedral structure; distances in the UF_6 octahedron: d(U–F1) = 1.981(4), d(U–F2) = 1.989(4), d(U–F3) (2×) = 1.979 (3), d(U–F4) (2×) = 1.978(3), d(F···F) = from 2.784 to 2.806; F–U–F = 89.78 to 90.20; F2–U–F1 = 179.9°; F4–U–F3 (2×) = 179.6; liquid: octahedral, space group O_h, a = 1.996; gaseous: octahedral, space group O_h, a = 1.996	*X-ray single crystal data* (Hoard and Stroupe, 1959; Levy *et al*., 1976; Rigny, 1965); *neutron diffraction data* (Taylor and Wilson 1975b; Levy *et al*., 1983)*; structure in liquid and gaseous states; NMR, IR, Raman, vis, UV, photoelectron and fluorescence spectra; physical constants* (Stoller and Richards, 1961 Lewis *et al*., 1976; Downs, 1986); *IR and Raman data* (McDowell *et al*., 1974); *mechanical and thermal properties, phase diagram, phase transformation, thermal conductivity, stability, diffusion coefficients, magnetic susceptibility; paramagnetic resonance; sorption on solids, thermal conductivity, dielectric polarization, transport phenomena, electrical properties, chemical properties; handling, reactions with UF_6, industrial applications* (Bacher and Jacob, 1980, 1986)

log p(mmHg)‡ = 6.99646 – [1126.288/(t+ 221.963)];
above 383.15K : log p(mmHg)‡ = 7.69069 – [1683.165/(t + 302.148)]
sublimation point: 56.54°C at 760 mmHg
vapor density(326–405K): may be considered ideal at 298K;
$P(1+1.2328 \times 10^{6}\, T^{-3}\, P)\cdot V = RT$.
critical constants:
temperature: 503.35(20)K
pressure: 45.5(5) atm
density: 1.39 g cm^{-3}
thermal conductivity:
liquid (345.15K):
$k = 16.02\times10^{-4}$ J cm^{-1}s^{-1}K^{-1}
gas‡ $k = (6.104 + 0.002568t)$ $\times10^{-5}$ J cm^{-1} s^{-1} K^{-1}
density (g cm^{-3}):
solid: 5.060 (at 298.15K); 4.87 (at 335.65K);
liquid‡ : $\rho = 3.630–5.805\times10^{-3}$ (t–64.0) –1.36 (t–64.0)^2 (at 333.15 to 436.15K)
viscosity, η (cP):
liquid: 0.731 at 340.35K; 0.663 at 348.15K.
gas‡ : (1.67–0.0044t) $\times10^{-2}$
surface tension, γ (N cm^{-1}):
16.8(3) $\times$ 10^{-5} at 343.15K;
13.1(3) 10^{-5}at 373.15K

Table 5.30 (*Contd.*)

Formula	*Selected properties and physical data*[b,c]	*Lattice symmetry, lattice constant* (Å), conformation and density ($g\ cm^{-3}$)	*Remarks regarding information available and references*
	refractive index: liquid (Na D line): $n_D = 1.3580$ (4) at 343.15K gas (5100 Å): $n-1 = 5.2\times10^{-4}$ pK^{-1} (p in mmHg) fundamental frequencies (IR and Raman, cm^{-1}): ν_1 (R) = 667.1 ; ν_2 (R) = 534.1; ν_3 (IR) = 625.5; ν_4 (IR) = 186.2; ν_5 (R) = 200.3; ν_6 (inact.) = 143 dielectric constants: liquid: $\varepsilon^{-1} = 2.18\cdot10^{-6}$ at 65°C and $p =$ 2745.9 kPa gaseous $\varepsilon^{-1} = 3815.4 \times 10^{-6}$ at 28.2°C $\varepsilon^{-1} = 3221.9 \times 10^{-6}$ at 83.1°C magnetic susceptibility: UF_6 exhibits temperature independent paramagnetism molar susceptibility: $\chi_M = (42.7\pm2.6) \times 10^{-6}\ cm^3 mol^{-1}$ molar polarization: $P_M = 31.453$ (25) $cm^3\ mol^{-1}$ (average value for 326–426 K) dipole moment: $\mu \approx 0$ ($\ll 10^{-18}$ Debye)		

$NaUF_7$	white to pale green; very hygroscopic; decomposes over 20°C to $Na_2UF_8 + UF_6$; Raman (solid): 636, 554, 540, 516, 463, 441, 430, 312, 305sh, 243, 218; (L): 111, 91, 57, 35; $\log p$ (mmHg) = $(11.06 \pm 0.02) - 3.48\times10^3 T^{-1}$ (T in K)	dimorphic; the high-temperature form is cubic, face centered, $a = 8.511$; $Z = 4$. The low-temperature form is monoclinic. The UF_7^- anion is octahedral with predominant covalent character	*crystallographic data* (Bougon *et al.*, 1976a); *IR, Raman, vis and UV spectra; physical constants, thermodynamic data, thermal decomposition; paramagnetic resonance; NMR* (Brown, 1968; Bacher and Jacob, 1980)
Na_2UF_8	yellow; very hygroscopic; decomposes to $UF_6 + NaF$; Raman (cm^{-1}): 607(10), 440(0.2), 410(0.6), 372(0.5), 343(.7) 303 (1.1), 284(1.1), 170(0.7), 141(0.3); $\log p$ (mmHg) = $(9.25 \pm 0.02) - 4.18\times10^3 T^{-1}$	tetragonal; space centered; D_{4h}^{17}; *I4/mmm*, No. 139; $a = 5.27$; $c = 11.20$; each U atom is surrounded by eight equidistant F atoms with d(U–F) = 2.29; d(F–F) = 2.63 and 2.97. Each Na atom is also surrounded by 8 F atoms with d(Na–F) = 2.37 and d(F–F) = 2.63 and 2.97	*crystallographic data* (Malm *et al.*, 1966); *IR, Raman, vis and UV spectra; physical constants, thermodynamic data, thermal decomposition* (Bougon *et al.*, 1976a; Katz, 1964); *magnetic susceptibility; paramagnetic resonance; NMR* (Brown, 1968; Bacher and Jacob, 1980).
KUF_7	extremely hygroscopic; decomposes at 100°C to $K_2UF_8 + UF_6$; IR(cm^{-1}): 626w,580sh, 540,s, 497s, 457w, 438w, 314w, 296sh, 256w, 234s, 202s, 140m, 100(L); Raman (solid): 623, 544, 517, 502, 455, 440, 311, 253, 232, 212, 201, 100L, 31L	dimorphic; the high-temperature form is cubic, $a = 5.22$	*crystallographic data* (Bougon *et al.*, 1976a); *IR and Raman spectra; thermal decomposition* (Brown, 1968; Bacher and Jacob, 1980)
K_2UF_8	extremely hygroscopic; decomposes at 300°C to $UF_6 + F_2 + K_2UF_7 + K_3UF_8$; IR: 598m, 510s,br, 460sh, 390sh, 294vw, 260s, 232s,br	orthorhombic; $a = 6.038$, $b = 12.899$, $c = 8.728$	*crystallographic data* (Bougon *et al.*, 1976a); *IR and Raman spectra; thermal decomposition* (Brown, 1968; Bacher and Jacob, 1980)
K_3UF_9		orthorhombic; $a = 6.974$, $b = 7.534$, $c = 9.768$	*crystallographic data* (Iwasaki *et al.*, 1981)

Table 5.30 (*Contd.*)

Formula	*Selected properties and physical data*[b,c]	*Lattice symmetry, lattice constant* (Å), conformation and density ($g\ cm^{-3}$)	*Remarks regarding information available and references*
$RbUF_7$	extremely hygroscopic: $4RbUF_7 + H_2O \rightarrow Rb_4UO_2F_6 + 3UO_2F_2 + 16HF$; decomposes in vacuum at 210°C to $UF_6 + Cs_2UF_8$; IR(cm^{-1}): 625w, 550, br, 482w, 457m, 442w, 230m, 210m; (L.): 100, 53, 35. at –170°C; Raman: 625(10), 520(0.1), 443 (0,9), 310(0.5), 248(0.5), 215(0.4)	dimorphic; the high temperature form is cubic; $a = 5.385(5)$	*crystallographic data* (Bougon *et al.*, 1976a); *IR and Raman spectra; thermal decomposition* (Brown, 1968; Bacher and Jacob, 1980)
Rb_2UF_8	very hygroscopic; decomposes over 350°C to $UF_6 + F_2 + Rb_2UF_7$ or Rb_3UF_8	orthorhombic; $a = 6.265(16)$, $b = 13.479(37)$, $c = 8.776(21)$	*crystallographic data* (Bougon *et al.*, 1976a); *IR and Raman spectra; thermal decomposition*; (Brown, 1968; Bacher and Jacob, 1980)
Rb_3UF_9		orthorhombic; $a = 8.121$, $b = 7.612$, $c = 9.614$	*crystallographic data* (Iwasaki *et al.*, 1981).
$CsUF_7$	yellow; hygroscopic; decomposes to $Cs_3UF_8 + UF_6$ at 210°C in vacuum; IR(cm^{-1}): 618vw, 605m, 540sh, 507s, 450sh, 200br, 170; Raman: 622, 462sh, 444, 312, 249, 211	the high-temperature form is cubic with $a = 5.517(5)$. At 15(1)°C it transforms to a tetragonal structure with $a = 5.30$ and $c = 5.37$	*crystallographic* data (Bougon *et al.*, 1976a); *IR and Raman spectra; thermal decomposition* (Bacher and Jacob, 1980)
Cs_2UF_8	very hygroscopic; decomposes to $Cs_3UF_8 + UF_6 + F_2$ over 400°C	orthorhombic; $a = 6.480(10)$, $b = 14.036(22)$, $c = 9.272(12)$	*crystallographic data* (Bougon *et al.*, 1976a); *IR and Raman spectra* (Brown, 1968; Bacher and Jacob, 1980)

NH_4UF_7	decomposes at 100–170°C to $UF_5 + NH_4F + HF + N_2$; IR(cm^{-1}): 625(10), 447(1.25), 314(0.55), 250 (0.76), 215(1.74), 195(1.53)	cubic; $a = 5.393(5)$	*crystallographic data* (Bougon *et al.*, 1976a); *IR and Raman spectra; thermal decomposition* (Bacher and Jacob, 1980)
$(NH_4)_2UF_8$	Raman (cm^{-1}): 592(10), 470(0.3), 420(0.3), 321(1.4), 286(1.5), 112 (L), 38(L)	orthorhombic; $a = 6.305(13)$; $b = 13.431(23)$, $c = 9.018(16)$	*crystallographic data* (Bougon *et al.*, 1976a); *IR, Raman spectra* (Bacher and Jacob, 1980).
$N_2H_5UF_7$	yellow		*synthesis* Bacher and Jacob (1980).
$NOUF_7$	hygroscopic; decomposes to $NOF + UF_6$ with reversible formation of $NOUF_7$. IR(cm^{-1}): 624vw, 604m, 540sh, 508s, 450sh, 420vw, 208vw, 188vw, 120(L); Raman (solid): 627, 446sh, 434, 310, 240, 210	cubic (high-temperature form); $a = 5.334(70)$; $Z = 1$; CN = 7; d(exp.) = 4.5. At room temperatures the lattice is composed of NO^+ cations and UF_7^- anions. Below –16°C exists β-$NOUF_7$ of lower symmetry.	*crystallographic data* (Geichman *et al.*, 1963; Bougon *et al.*, 1976a); *NMR, IR and Raman spectra* (Brown, 1968; Bacher and Jacob, 1980)
NO_2UF_7	hygroscopic; decomposes to $NO_2F + UF_6$ with reverse formation of NO_2UF_7	tetragonal; $a = 5.74$, $c = 2$	*crystallographic data* (Geichman *et al.*, 1963); *IR spectra and thermodynamic data* (Brown, 1968; Bacher and Jacob, 1980)
$(NO_2)_2UF_8$	IR (cm^{-1}): 590sh, 534sh, 510s, 498sh, 208w, 160m	orthorhombic; D_{2h}^{15}, *Pbca*, No.61; $a = 8.795(1)$, $b = 13.247(2)$, $c = 11.942(2)$; $Z = 8$; $V = 1391.33$; CN = 8. d(calc.) = 4.3 The lattice is composed of NO^+ cations and UF_8^{2-} anions. The coordination polyhedron around the uranium atom is a slightly distorted cube with an almost O_h symmetry	*crystallographic data* (Bougon *et al.*, 1976b; Seppelt and Hwang, 2000), *NMR, IR and Raman spectra* (Brown, 1968; Bacher and Jacob, 1980)
other fluorouranate (VI): $Na_3U_2F_{15}$, $K_3U_2F_{15}$, Rb_3UF_9, Cs_3UF_9,	$Na_3U_2F_{15}$ and $K_3U_2F_{15}$ are extremely hygroscopic		Bacher and Jacob (1980)

Table 5.30 (*Contd.*)

Formula	*Selected properties and physical data*[b,c]	*Lattice symmetry, lattice constant* (Å), conformation and density (g cm^{-3})	*Remarks regarding information available and references*
$NH_4(UO_2)F(SeO_4) \cdot H_2O$		orthorhombic; D_{2h}^{16}, *Pnma*, No.62; $a = 8.450(4)$, $b = 13.483(5)$, $c = 13.569(5)$; $V = 1545.93$; $Z = 8$; d(calc.) = 4.02	*crystallographic data* (Blatov *et al.*, 1989)
α-UOF_4	orange; hygroscopic; decomposes at 200 to 250°C into $UO_2F_2 + UF_4$; reacts with $H_2O \rightarrow UO_2F_2$. UOF_4(cr): $\Delta_f G_m^o = -1816.3$ (4.3)†, $\Delta_f H_m^o = -1924.6$ (4.0)†, $S_m^o = 195$ (5)†. UOF_4(g): $\Delta_f G_m^o = -1704.814$ (20.142)†, $\Delta_f H_m^o = -1763$ (20)†, $S_m^o = 363.2$ (8.0)†, $C_{p,m}^o = 108.1$ (5.0) IR ($U^{16}OF_4$) (cm^{-1}): ν(U–O, valence, terminal) = 893; ν(U–$F_{trans.}$, terminal) = 667s, ν(U–$F_{cis.}$, valence, terminal) = 558; 478m (L); 375s,br (L); Raman: ν(U–O stretch, terminal) = 890s; ν(U–$F_{trans.}$, stretch, terminal) = 660s, ν(U–$F_{cis.}$, stretch, terminal) = 552m	trigonal/rhombohedral; C_{3v}^5, *R3m*, No.160; $a = 13.095(6)$, $c = 5.658$ (2); $V = 840.24$; $Z = 9$, d(calc.) = 5.87; The idealized coordination sphere of the U atom consists of a pentagonal bipyramid formed by the light atoms; one O and one F atom occupy indistinguishable axial positions with d(U–O) = 1.870(16) and d(U–F1) = 1.884 (17), d(U–F2(a)) = 2.273, d(U–F2 (b)) = 2.270(11), d(U–F3) = 2.050 (5); O–U–F(1) = 179.2, U–F(2)–U = 153.2(7) (received from neutron diffraction analysis)	*crystallographic data* (Paine *et al.*, 1975); *neutron powder diffraction data* (Levy *et al.*, 1977), *electronic, IR and Raman spectra* (Jacob and Polligkeit, 1973; Paine *et al.*, 1975; Bacher and Jacob, 1980). *thermodynamic data* (Grenthe *et al.*, 1992; Guillaumont *et al.*, 2003)
$UOF_4(SbF_5)_2$		monoclinic; C_{2h}^5, $P2_1/c$, No.14; $a = 7.864(16)$, $b = 14.704(8)$, $c = 9.980$ (8); $\beta = 99.8(1)$; $Z = 4$; $V = 1137.17$; d(calc.) = 4.46	*crystallographic data; NMR-investigations* (Bougon, *et al.*, 1979)

$KUOF_5$	hygroscopic	orthorhombic; $a = 8.02(1)$, $b = 11.28(2)$, $c = 5.55(1)$. Each uranium atom is surrounded by eight light atoms forming a dodecahedron. The dodecahedra are linked together by fluorine atoms	*crystallographic data, IR and Raman spectra* (Joubert *et al.*, 1978a)
$RbUOF_5$	hygroscopic	orthorhombic; $a = 8.07(1)$, $b = 11.73(2)$, $c = 5.77(1)$. Each uranium atom is surrounded by eight light atoms forming a dodecahedron. The dodecahedra are linked together by fluorine atoms to form infinite chains	*crystallographic data, IR and Raman spectra* (Joubert *et al.*, 1978a)
$CsUOF_5$		rhombohedral; C_{3i}^2, $R\bar{3}$, No.148; $a = 5.41(1)$; $\alpha = 95.57(8)°$; $V = 155.9$; d(calc.) = 5.13, d(exp.) = 5.1(5). The unit cell is very close to that of $CsUF_6$	*neutron powder diffraction and, NMR data* (Joubert *et al.*, 1978b; Bougon *et al.*, 1978)
NH_4UOF_5	hygroscopic	orthorhombic; $a = 8.08(1)$, $b = 11.59(2)$, $c = 5.77(2)$. Each uranium atom is surrounded by eight light atoms forming a dodecahedron. The dodecahedra are linked together by fluorine atoms to form infinite chains.	*crystallographic data, IR and Raman spectra* (Joubert *et al.*, 1978a)
$AgUOF_5$		tetragonal; $a = 5.370$, $c = 8.043$	*crystallographic data* (Malm, 1980)
UO_2F_2	light yellow-green; decomposes in a He stream at 700–900°C to $UF_6 + U_3O_8 + O_2$; sublimes in the presence of HF over 550°C; may be transported with partial	rhombohedral; D_{3d}^5, $R\bar{3}m$, No = 166; $a = 5.755(1)$; $\alpha = 42{,}72(5)°$; $Z = 1$; CN = 8; d(calc.) = 6.37, d(exp.) = 5.8; d(U–O) = 1.91 (2×); d(U–F) = 2.50 (6×)	*synthesis* (Brauer, 1981); *X-ray and neutron powder diffraction data* (Atoji and McDermott, 1970); Zachariasen, 1948e); Bacher and Jacob, 1980) *IR and*

Table 5.30 (*Contd.*)

Formula	*Selected properties and physical data*[b,c]	*Lattice symmetry, lattice constant* (Å), conformation and density (g cm^{-3})	*Remarks regarding information available and references*
	decomposition in a He stream at 825°C. UO_2F_2(cr): $\Delta_f G_m^o$ = –1557.3 (1.3)†, $\Delta_f H_m^o$ = –1653.5 (1.3)†, S_m^o = 135.56 (0.42)†; $C_{p,m}^o$ = 103.22 (0.42)†. UO_2F_2(g): $\Delta_f G_m^o$ = –1318.1 (10.2)†, $\Delta_f H_m^o$ = –1352.5 (10.1)†, S_m^o = 342.7 (6.0)†; $C_{p,m}^o$ = 86.4 (3.0)†. IR ($U^{16}O_2F_2$)(cm^{-1}): ν_3 ($\nu_{asym.}UO_2$) = 1020vs; ν_4(L.) = inactive; ν_7 (L[$UF_{6/3}$]) = 260; ν_8($\delta_{asym.}UO_2$) = 238s. Raman (cm^{-1}): ν_1 ($\nu_{sym.}UO_2$) = 918vs; ν_2(L) = inactive (?); ν_5(L[$UF_{6/3}$]) = 444vw; ν_6 ($\delta_{sym.}$ UO_2) = 183m; ν_7	neutron powder diffraction data: a = 4.192; $c/3$ = 5.520; d(U–O) = 1.74(0.02) (2×); d(U–F) = 2.429 (0.002) (6×). The structure consists of layers of U atoms, which are 5.22 Å apart from each other. The axes of the UO_2 groups are perpendicular to the there planes. The fluorine atoms are 0.61 Å above and below the uranium planes, and weak O···O and O···F bonds holds the layer together	*Raman spectra, chemical properties, conversion of UO_2F_2 to UF_6.* (Bacher and Jacob, 1980); *photoelectron spectroscopy* (Thibaut *et al.*, 1982) *thermodynamic data* (Grenthe *et al.*, 1992; Guillaumont *et al.*, 2003)
$UO_2F_2{\cdot}nH_2O$ (n = 1,2,3,4) $UO_2FOH{\cdot}H_2O$; $UO_2FOH{\cdot}2H_2O$	monohydrate (yellow solid, soluble in H_2O, $\nu_{U=O}$ = 990 cm^{-1}); dihydrate (yellow solid, soluble in H_2O, $\nu_{U=O}$ = 966 cm^{-1}); formed when anhydrous compound is exposed to moist air. $UO_2F_2{\cdot}3H_2O$ (cr): $\Delta_f G_m^o$ = –2269.7 (6.9)†, $\Delta_f H_m^o$ = –2534.4 (4.4)†, S_m^o = 270 (18)†; $UO_2FOH{\cdot}H_2O$ (cr): $\Delta_f G_m^o$ = –1721.7 (7.5)†, $\Delta_f H_m^o$ = –1894.5 (8.4)†, S_m^o = 178 ($38UO_2F$ $OH{\cdot}2H_2O$ (cr): $\Delta_f G_m^o$ = – 1961.0 (8.4)†, $\Delta_f H_m^o$ = –2190.0 (9.4)†, S_m^o = 223 (38)†		*general properties* (Bacher and Jacob, 1980); *thermodynamic data* (Grenthe *et al.*, 1992; Guillaumont *et al.*, 2003)

$UO_2F_2(SbF_5)_3$		monoclinic; C_{2h}^5, $P2_1/c$, No.14; $a = 11.040(7)$; $b = 12.438(12)$; $c = 12.147(8)$; $\gamma = 111.16(20)$; $Z = 4$; $V = 1555.51$; d(calc.) = 4.09	*crystallographic data and characterization* (Fawcett *et al.*, 1982)
$[UO_2F_2\{CO(NH_2)_2\}_2]_2$		monoclinic; $P2_1/b$; $a = 10.240(1)$, $b = 10.983(1)$, $c = 8.254(1)$; $\beta = 98.65(1)$; $Z = 4$; d(U–F) = 2.23(2)–2.39(2); d(U–O) = 2.36(2) 2× and 1.72(2) 2×	*crystallographic data* (Mikhailov *et al.*, 1976a)
$Rb_2UO_2F_4 \cdot H_2O$		orthorhombic; C_{2h}^{15}, *Pbca*, No. = 61; $a = 8.881(3)$, $b = 14.547(6)$, $c = 11.975(4)$; $Z = 8$; d(calc.) = 4.59; $V = 1547.07$	*crystallographic data* (Brusset *et al.*, 1972)
$Cs_2UO_2F_4 \cdot H_2O$		monoclinic; C_{2h}^5, $P2_1/c$, No.14; $a = 8.06(1)$, $b = 12.18(1)$, $c = 9.29(1)$; $\beta = 109.12(4)$; $Z = 4$; $V = 861.7$, d(calc.) = 4.85	*crystallographic data* (Nguyen Quy Dao, 1972)
$K_3UO_2F_5$	yellow; $\nu_1(UO_2^{2+}) = 803\,cm^{-1}$, $\nu_3(UO_2^{2+}) = 863\,cm^{-1}$	tetragonal; C_{4h}^6, $I4_1/a$, No.88; $a = 9.159(4)$, $c = 18.170(8)$; $Z = 8$; $V = 1524.23$; d(calc.) = 4.2; pentagonal $UO_2F_5^{2-}$ units are held together by potassium ions	*crystallographic data* (Zachariasen, 1954d; Vodovatov *et al.*, 1984; Lychev *et al.*, 1986); *thermodynamic data* (Fuger *et al.*, 1983)
$Cs_3UO_2F_5$	yellow	cubic; T_h^3, $Fm3$, No.202; $a = 9.833(5)$; $Z = 4$; $V = 950.73$; d(calc.) = 5.33	*crystallographic data* (Rebenko *et al.*, 1968; Brusset and Nguyen Quy Dao, 1971); *thermodynamic data* (Fuger *et al.*, 1983).
$(NH_4)_3UO_2F_5$	yellow	monoclinic; C_s^3, Cm, No.8; $a = 29.22$, $b = 9.48$, $c = 13.51$; $\beta = 136.11^o$; $V = 2594.15$; d(calc.) = 3.22. Distorted pentagonal bipyramid	*crystallographic data* (Brusset *et al.*, 1969)

Table 5.30 (*Contd.*)

Formula	*Selected properties and physical data*[b,c]	*Lattice symmetry, lattice constant* (Å), conformation and density (g cm^{-3})	*Remarks regarding information available and references*
$K_2[UO_2F_2(C_2O_4)]$	yellow, stable in air, soluble in water; insoluble in common organic solvents. IR (cm^{-1}): ν_{as}(C=O) = 1650vs,b; ν_s(C–O) + ν(C–C) + δ(O–C=O) = 1355s, 1316s, 1480w, 1455m, 1415w, 1360m, 1315vs.; $\nu_{as}(UO_2)$ = 905. Other bands; 3610s, 3500s, 2920w, 845m, 800vs, 782w, 740w, 490s, 450s	triclinic; C_i^1, $P\bar{1}$, No. 2; $a = 10.981$, $b = 11.038$, $c = 12.629$; $\alpha = 108.00^o$, $\beta = 86.79^o$, $\gamma = 123.99^o$; $Z = 2$; d(calc.) = 1.31, d(exp.) = 1.36	*crystallographic data and IR spectral bands* (Chakravorti *et al.*, 1978)
$K_4[UO_2F_2(C_2O_4)_2]$	yellow, stable in air, soluble in water; insoluble in common organic solvents; ν_{as}(C=O) = 1720vs, 1655vs; ν_s(C–O)+ν(C–C)+δ(O–C=O) = 1410vs, 1295vs; $\nu_{as}(UO_2)$ = 890vs; Other bands: 3500s, 2910w, 830w, 790vs, 485s, 400s, in cm^{-1}	triclinic; C_i^1, $P\bar{1}$, No. 2; $a = 8.768$, $b = 8.777$, $c = 14.857$; $\alpha = 101.58^\circ$, $\beta = 114.27^o$, $\gamma = 85.27$; $Z = 4$; d(calc.) = 4.16, d(exp.) = 4.08	*crystallographic data and IR spectral bands* (Chakravorti *et al.*, 1978)
$K_2[(UO_2)_2F_4(C_2O_4)]$	yellow, stable in air, soluble in water; insoluble in common organic solvents; ν_{as}(C=O) = 1640, 1610vs; ν_s(C–O)+ν(C–C)+δ(O–C=O) = 1365m, 1318vs; $\nu_{as}(UO_2)$ = 920vs; Other bands: 3630s, 3460s, 3220w, 2920w, 855s, 795vs, in cm^{-1}	monoclinic; $a = 10.792$, $b = 12.028$, $c = 10.615$; $\beta = 136.88$; $Z = 2$; d(calc.) = 2.92, d(exp.) = 2.83	*crystallographic data and IR spectral bands* (Chakravorti *et al.*, 1978)

$Na_2(UO_2)_2\ (SiO_4)F_2$	The compound is structurally related to soddyite, and is formed during uranyl silicate synthesis in teflon-lined bombs	tetragonal; D_{4h}^{19}, $I4_1/amd$, No.141; $a = 6.975(8)$, $c = 18.31(2)$; $Z = 4$; $V = 890.79$	*crystallographic data* (Blaton *et al*., 1999)
$Cs_2[(UO_2)_2F_6(H_2O)_2]$		monoclinic; C_{2h}^5, $P2_1/c$, No.14; $a = 6.027(2)$, $b = 11.505(2)$, $c = 9.389(2)$; $\beta = 95.72(2)^\circ$; $Z = 2$; $V = 647.8$; d(calc.) = 4.9	*crystallographic data* (Mikhailov *et al*., 1979)
$[Na_3(UO_2)_2F_7](H_2O)_6$	yellow, transparent crystals: dehydration of the compound gives: $[Na_3(UO_2)_2F_7](H_2O)_2$ at 25–91°C : $[Na_3(UO_2)_2F_7]$ at 150–200°C; at higher temperatures (235–300°C) it decomposes to a mixture of $Na_3UO_2F_5$, UO_2F_2, $NaUO_2F_3$, and $Na(UO_2)_2F_5$	triclinic; C_i^1, $P\bar{1}$, No.2; $a = 6.997(1)$, $b = 7.176(1)$, $c = 8.630(1)$; $\alpha = 77.84(1)^o$, $\beta = 113.30(1)^o$, $\gamma = 104.95(1)^o$; $Z = 1$; $V = 381.62$; d(calc.) = 3.7; d(U–U)single bridge = 4.632(1) and 4.003(1) double bridge; d(U–O1) = 1.79(1), d(U–O2) = 1.77(1); d(U–F) = from 2.21 to 2.39; the structure consists of $[(UO_2)_2F_6{\cdot}F_{2/2}]^{3-}$ chains of complex ions formed by double and single F bridges alternatively	*crystallographic, thermogravimetric and IR data* (Nguyen Quy Dao *et al*., 1981)
$[K_3(UO_2)_2F_7](H_2O)_2$		triclinic; C_i^1, $P\bar{1}$, No.2; the structure consists of $(UO_2)_2F_7^{3-}$ chains of complex ions formed by double and single F bridges alternatively	*crystallographic data and physicochemical properties* (Mikhailov *et al.*, 1972a; Nguyen Quy Dao and Chourou, 1974)
$K_5(UO_2)_2F_9$		monoclinic; C_{2h}^6, $C2/c$, No. = 15; $a = 19.860(1)$, $b = 6.110(1)$, $c = 11.706(4)$; $\beta = 102.58(4)^\circ$; $V = 1386.36$; $Z = 4$; d(calc.) = 4.34	*crystallographic data* (Brusset *et al*., 1974; *Nguyen Quy Dao and Chourou,S.(1972)* Mikhailov *et al*., 1972b); *thermodynamic data* (Fuger *et al*., 1983)
$Cs_2(NH_4)[(UO_2)_2F_7]$		orthorhombic; D_{2h}^{25}, *Immm*, No.71; $a = 6.526(2)$, $b = 8.553(3)$, $c = 12.434(2)$; $Z = 2$; $V = 694.03$; d(calc.) = 4.58	*crystallographic data* (Ivanov *et al*., 1980)

Table 5.30 (*Contd.*)

Formula	*Selected properties and physical data*[b,c]	*Lattice symmetry, lattice constant* (Å), conformation and density (g cm^{-3})	*Remarks regarding information available and references*
$Rb_2[(UO_2)_3F_8(H_2O)]\cdot 3H_2O$		orthorhombic; C_{2v}^{16}, *Ama*2, No. = 40; $a = 8.4624(8)$, $b = 14.343(1)$, $c = 13.916(1)$; $V = 1689.07$; $Z = 4$; d(calc.) = 4.74	*crystallographic data* (Mikhailov *et al.*, 1976b)
$K_2[(UO_2)_3F_8(H_2O)]\cdot 3H_2O$		orthorhombic; C_{2v}^{16}, *Ama*2, No.40; $a = 8.39(5)$, $b = 14.12(8)$, $c = 13.66(8)$; $V = 1618.26$; $Z = 4$; d(calc.) = 4.56	*crystallographic data* (Nguyen Quy Dao., 1979)
$K_2(UO_2F_2)(SO_4)\cdot H_2O$		monoclinic; C_{2h}^5, $P2_1/c$, No. = 14; $a = 9.2634(18)$, $b = 8.6722(18)$, $c = 11.0195(15)$; $\beta = 101.60(1)^\circ$; d(calc.) = 3.83; $V = 867.16$; $Z = 4$	*crystallographic data* (Alcock *et al.*, 1980)
$Ni_2[(UO_2)F_4]_2\cdot 14H_2O$		monoclinic; C_{2h}^5, $P2_1/c$, No.14; $a = 10.141(1)$, $b = 11.901(1)$, $c = 9.510(1)$; $\beta = 96.80(1)$; $V = 1139.67$; $Z = 4$; d(calc.) = 3.09	*crystallographic data* (Ivanov *et al.*, 1982)
$Ni_3[(UO_2)_2F_7]_2\cdot 18H_2O$		monoclinic; C_{2h}^2, $P2_1/m$, No.11; $a = 9.132$, $b = 16.925$, $c = 12.500$; $\gamma = 114.62^o$	*crystallographic data* (Ivanov *et al.*, 1981)
$Cs_3UO_3F_5$		cubic; $a = 9.869$	*crystallographic data* (Rebenko *et al.*, 1968)
$U(OTeF_5)_6$		monoclinic; C_{2h}^3, $C/2m$, No. 12; d(calc) = 3.56; $a = 10.30(1)$, $b = 16.61(2)$, $c = 9.98(1)$; $\beta = 114.14(6)^\circ$; $Z = 2$; $V = 1558.09$; d(calc.) = 3.56	*crystallographic data* (Templeton *et al.*, 1976)

UCl_6	black to dark green crystalline material; extremely moisture sensitive; slightly soluble in some organic solvents: CCl_4, $CHCl_3$; hydrolyzes in moist air; reacts vigorously with water to form UCl_2O_2, m.p. = 177.5°C. UCl_6(cr): $\Delta_f G^o_m = -937.1$ (3.0)†, $\Delta_f H^o_m = -1066.5$ (3.0)†, $S^o_m = 285.5$ (1.7)†; $C^o_{p,m} = 175.7$ (4.2)†. UCl_6(g): $\Delta_f G^o_m = -901.6$ (5.2)†, $\Delta_f H^o_m = -985.5$ (5.0)†, $S^o_m = 438.0$ (5.0)†; $C^o_{p,m} = 147.2$ (3.0)†. vapour pressure: log p (mmHg) = $-4000T^{-1} + 10.20$ (298–450 K). IR and Raman (cm^{-1}): ν_1 (R) = 367, ν_2 (R) = 321, ν_3 (IR) = 343, ν_4 (IR) = 101, and ν_5 (R) = 133	hexagonal; D^3_{3d}, $P\bar{3}m1$, No. 164; $a = 10.95$, $c = 6.016(6)$; $Z = 3$; d(calc.) = 3.594, d(exp.) = 3.17–3.36. Chlorine atoms form an almost regular octahedron around U(1) with d(U–Cl) = 2.47 and Cl–U–Cl angles of 86.6 and 93.4°; the array around U(2) is slightly distorted; d(U–Cl) lie between 2.41(4) and 2.51(4); the Cl–U–Cl angles are of 79.7, 98.0 and 90.4	*synthesis* (Rediess and Sawodny, 1982), *crystallographic and neutron diffraction data* (Zachariasen, 1948c, Taylor and Wilson, 1974b); *thermodynamic data* (Brown, 1973, 1979; Grenthe *et al*., 1992; Guillaumont *et al*., 2003), *UV, vis, infrared and Raman spectra; magnetic susceptibility data* (Brown, 1979 and references therein)
$[P(C_6H_5)_4]UOCl_5$	deep orange-red moisture sensitive crystals. IR (cm^{-1}): ν(U–O) = 834, δ(U–O) = 231; Raman: ν(U–O) = 836, δ(U–O) = 229; . ν(U–Cl) = 345, 341(sh), 302, 298, 291 (IR); and 347, 341, 293 (R)	tetragonal; C^3_{4h}, *P4/n*, No. 85; $a = 13.264(5)$; $c = 7.621(5)$; $Z = 2$; d(calc.) = 1.924, d(exp.) = 1.916; d(U–O) = 1.76(1). The structure is composed of octahedral anions and cations with the $\bar{4}$ (S_4) symmetry. Both ions are forming linear stacks parallel to *c*. d(U–Cl) = 2.636(2) in the equatorial plane and 2.433(4) in the axial bond	*crystallographic data* (de Wet and du Preez, 1978); *infrared data* (Bagnall *et al*., 1975)
UO_2Cl_2	golden-yellow; very hygroscopic; m.p. = 570–578°C very volatile >775°C; soluble H_2O, acetone, alcohol, and common polar organic	orthorhombic; D^{16}_{2h}, *Pnma*, No. 62; $a = 5.725$, $b = 8.409$, $c = 8.720$; $Z = 4$; d(calc.) = 5.349; d(exp.) = 5.28; The U coordination polyhedron is a pentagonal	*crystallographic data* (Debets, 1968; Taylor and Wilson, 1973b); *thermodynamic data* (Cordfunke *et al*., 1976; Grenthe *et al*., 1992; Guillaumont *et al*., 2003)

Table 5.30 (*Contd.*)

Formula	*Selected properties and physical data*[b,c]	*Lattice symmetry, lattice constant* (Å), conformation and density (g cm^{-3})	*Remarks regarding information available and references*
	solvents. UO_2Cl_2 (cr): $\Delta_f G_m^o$ = –1145.9 (1.3)†, $\Delta_f H_m^o$ = –1243.6 (1.3)†, S_m^o = 150.54 (0.21)†; $C_{p,m}^o$ = 107.86 (0.17)†. UO_2Cl_2 (g): $\Delta_f G_m^o$ = –939.0 (15.1)†, $\Delta_f H_m^o$ = –970.3 (15.0)†, S_m^o = 373.4 (6.0)†; $C_{p,m}^o$ = 92.6 (3.0)†. IR (cm^{-1}): ($\nu_{as}(B_{1u}+B_{3u})$ = 958vs, 946vs; $\nu_s(B_{1u})$ = 832s; $\nu_s(B_{3u})$ = 781s; ν(U···O) = 320w; δ(O–U–O)(B_{1u}, B_{2u}, B_{3u}) = 727w, 258m, 200s; ν(U–Cl) = 97s, 80.5s; Raman: $\nu_{as}(A_g)$ = 940m; $\nu_s(B_{2g})$ = 848m; $\nu_s(A_g)$ = 767vs; ν(overtone or combination) = 750w; ν(U···O) = 340w; δ(O–U–O)(B_{1g}, B_{2g}, B_{3g}) = 270w; 255vw, 240w; δ(O–U–O) (A_g) = 197m; ν(U–Cl) = 178s, 105s	bipyramid with uranyl oxygen atoms at the apices: d(U–O, uranyl) = 1.78(2) and 1.73(1). Three Cl and one O atoms form the equatorial pentagon: d(U–Cl) = 2.73 and 2.75; d(U–O, pentagon) = 2.52(2); pentagonal angles in ring: ≈72; uranyl angle O–U–O = 178.8(8); angles in the bipyramid: ≈90°	*electronic absorption, luminescence and fluorescence spectra* (Brown, 1979); *IR and Raman data* (Bullock, 1969; Perrin and Caillet, 1976); *photoelectron spectroscopy* (Thibaut *et al.*, 1982)
$UO_2Cl_2 \cdot H_2O$	yellow powder; hygroscopic; soluble in H_2O, EtOH, Me_2CO; dec. > 300°C. $UO_2Cl_2 \cdot H_2O$(cr): $\Delta_f G_m^o$ = –1405.0 (3.3)†, $\Delta_f H_m^o$ = –1559.8 (2.1)†, S_m^o = 192.5 (8.4)†. IR (cm^{-1}): 150w, 182m, 208m, 240mw, 280m, 962vs, br, 1602vs, 3450ms. Raman: 52mw (sharp), 58w (sharp), 136w, 176m, 203m, br, 245ms, 869vs (sharp)	monoclinic system; C_{2h}^2, $P2_1/m$, No.11; a = 5.847(9), b = 8.596 (13), c = 5.543(9); β = 97.51(8); CN = 7; d(calc.) = 4.34; d(U–Cl) = 2.75(1) and 2.80(1); d(U–O) = 1.70 and 1.74(3); d(U–O)(water) = 2.46	*crystallographic and neutron diffraction data* (Taylor and Wilson, 1974c); *infrared and Raman data* (Gerding *et al.*, 1975); *thermodynamic data* (Grenthe *et al.*, 1992; Guillaumont *et al.*, 2003)

$UO_2Cl_2{\cdot}3H_2O$	yellow-green, fluorescent; deliquescent in air; extremely soluble in water, alcohol and ether $UO_2Cl_2{\cdot}3H_2O$(cr): $\Delta_f G_m^o$ = –1894.6 (3.0)†, $\Delta_f H_m^o$ = –2164.8 (1.7)†, S_m^o = 272.0 (8.4)†. IR (cm^{-1}): (B_{1u}, B_{2u}, B_{3u}): 93w,150m, 220sh, $\nu_2(UO_2^{2+})$ = 255s, ν(free H_2O) = 435br, 590br, $\nu_1(UO_2^{2+})$ = 879 (sharp), $\nu_3(UO_2^{2+})$ = 950s, 955s, $\nu_2(H_2O)$ = 1570sh, 1595m, 1610sh, $(\nu_1+\nu_3)(UO_2^{2+})$ = 1830w, 1835sh, ν(combination) = 2230w, $\nu_1+\nu_3(H_2O)$ = 3250vs,br	orthorhombic; C_{2v}^9, $Pn2_1a$, No.11; a = 12.738(5), b = 10.495(5), c = 5·47(2)	*crystallographic data* (Debets, 1968; Caville and Poulet, 1974; Brown, 1979); *infrared and Raman data* (Caville and Poulet, 1974); *thermodynamic data* (Brown, 1979; Grenthe *et al*., 1992; Guillaumont *et al*., 2003)
$[(UO_2)_4Cl_2O_2(OH)_2(H_2O)_6]\cdot(H_2O)_4$		monoclinic; C_{2h}^5, $P2_1/c$; No.14; a = 11.645(1), b = 10.101(1), c = 10.206(1); β = 105.77(1), Z = 2; V = 1155.31	*crystal structure* (Aberg, 1971, 1976)
$Li_2UO_2Cl_4$		monoclinic; C_{2h}^3, $C2/m$, No.12; a = 11.63, b = 7.56, c = 5.58; β = 95.7°	*crystallographic data* (Vorobei *et al*., 1971); *infrared and thermodynamic data* (Brown, 1979)
$Na_2UO_2Cl_4$		monoclinic; C_{2h}^3, $C2/m$, No.12; a = 11.53, b = 7.56, c = 5.60; β = 94.41	*crystallographic data* (Vorobei *et al*., 1971); *infrared and thermodynamic data* (Brown, 1979)
$Rb_2UO_2Cl_4$		monoclinic; C_{2h}^3, $C2/m$, No.12; a = 11.65, b = 7.42, c = 5.58; β = 98.6	*crystallographic data* (Vorobei *et al*., 1971); *infrared and thermodynamic data* (Brown, 1979)
$Rb_2UO_2Cl_4{\cdot}2H_2O$		triclinic; C_i^1, $P\bar{1}$, No.2; a = 6.795 (5); b = 6.929(5), c = 7.457(4),	*crystallographic data* (Anson *et al*., 1996)

Table 5.30 (*Contd.*)

Formula	*Selected properties and physical data*[b,c]	*Lattice symmetry, lattice constant* (Å), conformation and density (g cm^{-3})	*Remarks regarding information available and references*
		$\alpha = 91.96(5)$, $\beta = 102.13(5)$, $\gamma = 118.82(6)$; $Z = 1$; $V = 296.95$; d(calc.) = 3.46	
$Cs_2UO_2Cl_4$	IR and Raman (symmetry in D_{4h}) (cm^{-1}): A_{1g}(R) ν(O–U–O) sym. str. = 831; A_{2u}(IR) ν(O–U–O) asym. str. = 916; E_u(IR) ν(O–U–O) bend. = 252; A_{1g}(R) ν(U–Cl) sym.str. = 264; B_{2g}(R) ν(U–Cl) str. = 230; E_u(IR) ν(O–Cl) = 238; B_{1g}(R) ν(U–Cl) in plane bend. = 131; E_u(IR) ν(U–Cl) in plane bend. = 112; A_{2u}(IR) ν(U–Cl) out of plane bend. = 112; B_{1u} ν(U–Cl) out of plane bend. = 91****; E_g(R) ν(O–U–O) rock = 205–200; Lattice modes: 93(R), 73(R), 69(R), 56 (IR), 53(R), 48(R)	monoclinic; C_{2h}^3, *C2/m*, No.12; a = 11.92(2), b = 7.71(2), c = 5.83(1); $\beta = 99.66(3)$; d(calc.) = 4.26; d(U–O) = 1.81; d(U–Cl) = 2.62; O–U–O = 180; data from the neutron refinement: monoclinic; C_s^3, *Cm*, No.8; a = 12.005(8), b = 7.697(3), c = 5.850(3); $\beta = 100.00$ (4); $Z = 2$; $V = 532.34$; d(calc.) = 4.23	*crystallographic data* (Hall 1966; Vorobei *et al.*, 1971); *infrared and Raman data* (Denning *et al.*, 1976; Brown, 1979); *neutron diffraction refinement* (Tutov *et al.*, 1991) *thermodynamic data* (Brown, 1979; Fuger *et al.*, 1983)
$Cs(UO_2)_2Cl_5$		orthorhombic; a = 11.17(5), b = 12.80(5), c = 838(5); d(calc.) = 4.715	*crystallographic data* (Bevz *et al.*, 1970)
$[N(CH_3)_4]_2UO_2Cl_4$		tetragonal; D_{4h}^{14}, *P4$_2$/mmm*, No. 136; a = 9.175(5), c = 11.745(6); d(U–O) = 1.724(7); d(U–Cl) = 2.646(4) and 2.660(3); O–U–O = 180°	*crystallographic data* (Di Sipio *et al.*, 1974a); *infrared and Raman data*, *thermodynamic data* (Brown, 1979)

$[N(C_2H_5)_4]_2UO_2Cl_4$	triclinic; C_i^1, $P\bar{1}$, No. 2; $a = 9.997$ (5), $b = 10.064(5)$, $c = 12.914(5)$; $\alpha = 90.00(5)$, $\beta = 90.69(5)$, $\gamma = 90.00(5)$; d(U–O) = 1.76(2) and 1.77(3); d(U–Cl) = 2.65(1), 2.67(1) and 2.68(1)(2×); O–U–O = 180.0(1)	*crystallographic data* (Bois *et al.*, 1976a); *infrared and Raman data*, *thermodynamic data* (Brown, 1979)
$[N(C_2H_5)_3H]_2UO_2Cl_4$	tetragonal; C_{4h}^6, $I4_1/a$, No. 88; $a = 13.465(5)$, $c = 24.18(1)$; d(calc.) = 1.84; d(U–O) = 1.75(1); d(U–Cl) = 2.663(5) and 2.672(5); O–U–O = 179(1)	*crystallographic data* (Bois *et al.*, 1976b); *infrared and Raman, thermodynamic data* (Brown, 1979)
$[N(C_3H_7)_4N]_2UO_2Cl_4$	triclinic; C_i^1, $P\bar{1}$, No.2; $a = 10.890$ (5), $b = 17.257(7)$, $c = 11.076(5)$; $\alpha = 95.4(1)$, $\beta = 106.1(1)$, $\gamma = 114.9(13)$; $Z = 4$. The structure consists of tetrahedral $[CH_3CH_2CH_2]^+$ cations and bipyramidal $[UO_2Cl_4]^{2-}$ anions held together by Van der Waals forces. The U–O(2) bond distances [1.58(2)] are significantly shorter than the usual distances reported for uranyl U–O bonds (1.68–1.77) in hexacoordinated U (VI) compounds	*crystallographic data* (Di Sipio *et al.*, 1974b)
$[N(C_4H_9)_4]_2UO_2Cl_4$	monoclinic; C_{2h}^5, $P2_1/c$, No. 14; $a = 15.533(6)$, $b = 15.466(6)$, $c = 20.438(8)$; $\beta = 118.2(2)$; d(U–O) = 1.68(1) and 1.69(1); d(U–Cl) = 2.646(6), 2.648(5), 2.656(6) and 2.671(5); O–U–O = 178.1(5)°. The structure is built up of flattened $[UO_2Cl_4]^{2-}$ bipyramids and tetrahedral $[Bu_4N]^+$ ions held together by Van der Waals forces	*crystallographic data* (Di Sipio *et al.*, 1974c); *Infrared and Raman, thermodynamic data* (Brown, 1979)

Table 5.30 (*Contd.*)

Formula	*Selected properties and physical data*[b,c]	*Lattice symmetry, lattice constant* (Å), conformation and density ($g\ cm^{-3}$)	*Remarks regarding information available and references*
$[LH]_2UO_2Cl_4$[f]		monoclinic; C_{2h}^3, *C2/m*, No.12; ($P2_1/n$; No.14; non standard setting of P_21/c); $a = 11.199$, $b = 6.968$, $c = 23.675$; $\beta = 97.50$; d(U–O) = 1.78(1); d(U–Cl) = 2.66 (1) and 2.69(1); O–U–O = 180.0.	*crystallographic data* (Marzotto *et al.*, 1973; Clemente *et al.*, 1974)
$[L'H]_2UO_2Cl_4$ CH_3CN[g]		triclinic; C_i^1, $P\bar{1}$, No. 2; $a = 12.77$ (1), $b = 23.12(2)$, $c = 8.11(1)$; $\alpha = 94.33(3)$, $\beta = 89.43(3)$, $\gamma = 98.22$ (3); d(exp.) = 1.60; d(U–O) = 1.784(2) and 1.789(12); d(U–Cl) = 2.705(6), 2.706(4), 2.697(6) and 2.699(6); O–U–O = 179(1)	*crystallographic data* (Graziani *et al.*, 1975)
$UO_2(ClO_4)_2$	forms complexes with various donors ligands, e.g. DMSO and urea; soluble in H_2O; IR (cm^{-1}) (C_s): $\nu_8 = 1270$, 1234, $\nu_6 = 1116$, 1114; $\nu_1 = 1048$, $\nu_2 = 974$, $\nu_7 = 640$, $\nu_9 = 627$, $\nu_3 = 600$, $\nu_5 = 481$, $\nu_4 = 455$, $\nu_3(UO_{2(as)}^{2+}) = 996$, $\nu_3(UO_{2(sym)}^{2+}) = 900$		*infrared data* (Vdovenko *et al.*, 1964)
(i) $UO_2(ClO_4)_2{\cdot}H_2O$ (ii) $UO_2(ClO_4)_2{\cdot}3H_2O$ (iii) $UO_2(ClO_4)_2{\cdot}5H_2O$	(i) IR (cm^{-1})(C_s): $\nu_8 = 1250$, 1231, $\nu_6 = 1136$, 1114; $\nu_1 = 1075$, $\nu_2 = 996$, $\nu_7 = 646$, $\nu_9 = 633$, $\nu_3 = 613$, $\nu_5 = 470$, $\nu_4 = 450$, $\nu_3(UO_{2(as)}^{2+}) = 974$, $\nu_3(UO_{2(sym)}^{2+}) = 896$		*infrared data* (Vdovenko *et al.*, 1964)

	(ii) IR (cm^{-1}) (C_{3v}): $\nu_4 = 1192$, 1162, $\nu_1 = 1035$, 1017; $\nu_2 = 874$, $\nu_5 = 645$, $\nu_3 = 619$, $\nu_6 = 460$, $\nu_3(UO^{2+}_{2(as)}) = 967$, $\nu_3(UO^{2+}_{2(sym)}) = 892$. (iii) IR ($cm^{-1}$) ($T_d$): $\nu_3 = 1030$ to 1160, $\nu_1 = 930$; $\nu_4 = 624$, $\nu_3(UO^{2+}_{2(as)}) = 958$, $\nu_3(UO^{2+}_{2(sym)}) = 898$		
$UO_2(ClO_4)_2{\cdot}7H_2O$	soluble in: H_2O, EtOH, CH_3Cl, pyridine, DMSO etc.: loses H_2O at 270°C, dec. at 375°C; IR (cm^{-1}) (T_d): $\nu_3 = 1110$, $\nu_1 = 932$; $\nu_4 = 624$, $\nu_3(UO^{2+}_{2(as)}) = 958$, $\nu_3(UO^{2+}_{2(sym)}) = 888$	orthorhombic; C^5_{2v}, $Pca2_1$, No. 29; $a = 9.302(4)$, $b = 14.692(6)$, $c = 10.842(5)$; $Z = 4$; $d_{cal.} = 2.75$. The structure contains $[UO_2(OH_2)_5]^{2+}$ and ClO^-_4 ions and two H_2O molecules per U atom. The coordination polyhedron is a distorted bipyramid with d(U–O) = 1.62(7) and 1.80(3) in the uranyl group and 2.35 to 2.55 for the coordinated water molecules.	*crystallographic data* (Alcock and Esperäs, 1977); *Infrared data* (Vdovenko *et al.*, 1964); *absorption ,fluorescence and luminescence spectra* (Carnall, 1982)
$UO_2(HMPTA)_4(ClO_4)_2$; HMPTA = hexamethyl-phosphor-triamide = $[(CH_3)_2N]_3PO$.	$\nu_3(ClO^-_4) = 1095$, $\nu_4(ClO^-_4) = 624$, $\nu_{as}(UO^{2+}_2) = 917$	orthorhombic; D^{15}_{2h}, $Pbca$, No. 61; $a = 45,818(5)$, $b = 14.273(5)$, $c = 15.381(5)$; $V = 10056$	*crystallographic data* (Nassimbeni and Rodgers, 1976); *infrared spectra* (Gusev *et al.*, 1985)
(i) $K_xUO_3Cl_x$($x \approx 0.8$). (ii) $Rb_xUO_3Cl_x$ ($x \approx 0.8$). (iii) $Cs_xUO_3Cl_x$ ($x \approx 0.9$).		monoclinic; C^2_{2h}, $P2_1/m$, No.11. (i) $a = 8.55$, $b = 4.10$, $c = 7.00$; $\beta = 104.22$. (ii) $a = 8.734(2)$, $b = 4.118(2)$, $c = 7.718(2)$; $\beta = 105.34$. (iii) $a = 8.56$, $b = 4.11$, $c = 7.35$; $\beta = 104.56$; d(exp.) = 5.43. d(U–O) = 1.82(6); 1,85(9); 2.30(7); 2.17(7); d(U–Cl) = 2.98(2); O–U–O = 180.	*crystallographic data* (Allpress *et al.*, 1968)

Table 5.30 (*Contd.*)

Formula	*Selected properties and physical data*[b,c]	*Lattice symmetry, lattice constant* (Å), conformation and density (g cm^{-3})	*Remarks regarding information available and references*
(i) $Rb_2U_2O_5Cl_4{\cdot}2H_2O$[d] (ii) $Cs_2U_2O_5Cl_4{\cdot}2H_2O$		monoclinic; C_{2h}^5, $P2_1/c$, No. 14; (i) $a = 8.540(11)$, $b = 8.096(8)$, $c = 21.735(32)$; $\beta = 111.74(11)^\circ$; d(U–O) = 1.78(2×), 2.203*, 2.268*, 2.289* and 2.509; d(U–Cl) = 2.743, 2.781, 2.800*, 2.804*, 2.825*, and 2.845*, O–U–O = 180.0 (ii) $a = 8.82(2)$, $b = 8.27(1)$, $c = 22.17(4)$; $\beta = 112.03(10)$; d(calc.) = 4.30	*crystallographic data* (Perrin, 1977a)
(i) $K_4U_5O_{16}Cl_2$ (ii) $Rb_4U_5O_{16}Cl_2$		monoclinic; C_{2h}^5, $P2_1/c$, No. 14; (i) $a = 9.96$, $b = 6.99$, $c = 19.60$; $\beta = 134.97^\circ$ (ii) $a = 10.21$, $b = 7.01$, $c = 19.64$; $\beta = 134.22$; d(calc.) = 6.13	*crystallographic data* (Allpress *et al*., 1968)
(i) $La_3(UO_6Cl_3)$ (ii) $Pr_3(UO_6Cl_3$ (iii) $Nd_3(UO_6Cl_3)$		hexagonal; C_{6h}^2, $P6_3/m$, No.176; (i) $a = 9.5155(16)$, $c = 5.6132(16)$; $Z = 2$; $V = 440.15$ (ii) $a = 9.3957(6)$, $c = 5.5470(5)$; $Z = 2$; $V = 424.08$ (iii) $a = 9.3668(5)$, $c = 5.5300(7)$; $Z = 2$; $V = 420.18$	*crystallographic data* (Henche *et al*., 1993)
$(NH_4)_2[(UO_2)_4O_2(OH)_2Cl_4(H_2O)_4]{\cdot}2H_2O$		triclinic; $a = 12.12(1)$, $b = 12.31(1)$, $c = 7.99(1)$; $\alpha = 111.2(1)$, $\beta = 95.1(1)$, $\gamma = 138.1(1)$	*crystallographic data* (Perrin, 1977b)

$K_2[(UO_2)_4O_2(OH)_2Cl_4(H_2O)_4] \cdot 2H_2O$[e]		triclinic; $a = 12.15(2)$, $b = 12.33(1)$, $c = 8.026(9)$; $\alpha = 110.5(1)$, $\beta = 96.3(1)$, $\gamma = 138.7(1)$; d[U(1)–O] = 1.767(6), 1.774(7), 2.205(2)*, 2.39(2)*, and 2.45(2)**; d[U(2)–O] = 1.795(6), 1.786(6), 2.246(19)*, 2.256(14)*, 2.39(2)*, and 2.41(1)**; d(U-Cl) = 2.873(9)*; O–U–O = 175.6(7)	*crystallographic data* (Perrin, 1977b; Perrin and Le Marouille, 1977)
$Rb_2[(UO_2)_4O_2(OH)_2Cl_4(H_2O)_4] \cdot 2H_2O$		triclinic; $a = 12.25(2)$, $b = 12.32(2)$, $c = 7.95(1)$; $\alpha = 110.4(1)$, $\beta = 95.6(1)$, $\gamma = 138.4(1)$	*crystallographic data* (Perrin, 1977b)
$Rb_4[(UO_2)_4O_2Cl_8(H_2O)_2] \cdot 2H_2O$		monoclinic; C_{2h}^5, $P2_1/c$, No.14; $a = 8.540(11)$, $b = 8.096(8)$, $c = 21.735(32)$; $\beta = 111.74(11)$; $Z = 2$; $V = 1395.87$; d(calc.) = 4.3	*crystallographic data* (Perrin, 1977a)
$Cs_3[(UO_2)_3O_2(OH)_3]_2Cl \cdot (H_2O)_3$		monoclinic; C_2^3, $C2$, No.5; $a = 19.6150(50)$, $b = 7.239(2)$, $c = 12.064(3)$; $\beta = 127.929(4)$; $Z = 2$; $V = 1351.17$; d(calc.) = 5.59	*synthesis and structural characterization* (Li *et al*., 2001)
$[N(C_6H_5CH_2)(CH_3)_3]_4 \cdot [UO_2Cl_3O]_2$[h]		monoclinic; C_{2h}^5, $P2_1/c$, No. 14; $a = 8.869(5)$, $b = 11.013(5)$, $c = 25.60(1)$; $\beta = 103.66(10)$; $Z = 4$; d(calc.) = 1.89; mean d(U–O, peroxy) = 2.30; the mean d(U–O, uranyl) = 1.78; mean d(U–Cl, uranyl) = 2.71; 1. O–U–O = 179.3 (1.0)	*crystallographyic data* (Boeyens and Haegele, 1976; Haegele and Boeyens, 1977)
UO_2Br_2	bright red; hygroscopic, thermally unstable; soluble in Me_2CO, Et_2O, EtOH, MeCN, H_2O; slowly loses Br_2 at room temp. UO_2Br_2 (cr): $\Delta_f G_m^o = -1066.4\ (1.8)^\dagger$, $\Delta_f H_m^o = -1137.4\ (1.3)^\dagger$, $S_m^o = 169.5\ (4.2)^\dagger$; $C_{p,m}^o = 116\ (8)^\dagger$. IR ($cm^{-1}$): 905s (stretching), 945, 930, and 825		*thermodynamic data* (Prins *et al*., 1978; Grenthe *et al*., 1992; Guillaumont *et al*., 2003); *IR spectra* (Prigent, 1958); *photoelectron spectroscopy* (Thibaut *et al*., 1982)

Table 5.30 (*Contd.*)

Formula	*Selected properties and physical data*[b,c]	*Lattice symmetry, lattice constant* (Å), conformation and density (g cm^{-3})	*Remarks regarding information available and references*
$UO_2Br_2{\cdot}H_2O$; $UO_2Br_2{\cdot}3H_2O$.	$UO_2Br_2{\cdot}H_2O$(cr): $\Delta_f G^o_m = -1328.6$ (2.5)†, $\Delta_f H^o_m = -1455.9$ (1.4)†, $S^o_m = 214$ (7)†. $UO_2Br_2{\cdot}3H_2O$(cr): $\Delta_f G^o_m = -1818.5$ (5.6)†, $\Delta_f H^o_m = -2058.0$ (1.5)†, $S^o_m = 304$ (18)†.		*thermodynamic data* (Grenthe *et al*., 1992; Guillaumont *et al*., 2003)
$(UO_2)_2(OH)_2Br_2(H_2O)_4]$	$UO_2OHBr(H_2O)_2$(cr): $\Delta_f G^o_m = -1744.2$ (4.4)†, $\Delta_f H^o_m = -1958.2$ (1.3)†, $S^o_m = 248$ (14)†	isostructural with the chloride analogue (monoclinic; C^5_{2h}, $P2_1/c$, No.14)	*X-ray powder diffraction data* (Peterson, 1961); *IR spectra* (Perrin, 1970); *thermodynamic data* (Prins *et al*., 1978; Grenthe *et al*., 1992; Guillaumont *et al*., 2003)
$[UO_2Br_2]{\cdot}3C_4H_8O$	light brown cryst.; soluble in THF	monoclinic; C^5_{2h}, $P2_1/c$, No.14; $a = 6.931(3)$, $b = 17.032(4)$, $c = 16.257(4)$; $\beta = 94.25(5)$; $V = 1914$ (2); $Z = 4$; d(calc.) = 2.242; the coordination polyhedron is a bipyramid with a non-planar pentagonal base made up of two Br^- anions three O atoms from the THF molecules. The two uranyl O atoms are in the apical positions; d(U–O) = 1.75(1), 1.77(1), 2.45(2), 2.47(1), 2.46(2); d(U–Br) = 2.845 (3), 2.856(3)	*crystallographic data* (Rebizant *et al*., 1987)
$Cs_2UO_2Br_4$	yellow; IR (cm^{-1}): ν(U–O, asym. stretch.) = 895–934; ν(O–U–O deformation) = 243–263; ν(U–Br	monoclinic; C^5_{2h}, $P2_1/a$, No.14; $a = 9.959(3)$, $b = 9.806(5)$, $c = 6.415$ (5); $\beta = 104.8(2)$; d(calc.) = 4.51;	*crystallographic data* (Mikhailov and Kuznetzov, 1971); *infrared and Raman data* (Brown, 1979);

	stretch.) = 160–180; Raman: ν(U–O sym. stretch.) = 826–835, ν(U–O–Br bend.) = 190–198, ν(U–Br stretch.) = 167–172, 81–83 ν(U–Br bending mode) = 81–83	d(U–O) = 1,70(5); d(U–Br) = 2.83 (1)(2×) and 2.80(1)(2×)	*thermodynamic data* (Fuger *et al.* (1983)
$(NH_4)_2UO_2Br_4(H_2O)_2$		triclinic; C_i^1, $P\bar{1}$, No.2; a = 6.8850 (9), b = 6.887(1), c = 7.7370(7); α = 94.44(1)°, β = 98.78(1), γ = 116.79(1); d(U-O) = 1.766(6); d(U–Br) = 2.813 (average); Z = 1; V = 319.17; d(calc.) = 3.44. The structure consists of $[UO_2Br_4]^{2-}$ and $[NH_4]^+$ ions. The U ions are octahedrally coordinated and the symmetry of $[UO_2Br_4]^{2-}$ is approx. D_{4h}	*crystallographic data* (Van den Bossche *et al.*, 1987)
$[N(CH_3)_4]_2UO_2Br_4$	yellow; IR (cm^{-1}): ν(U–O, asym. stretch.) = 895–934; ν(O–U–O, deformation) = 243–263; ν(U–Br, stetch.) = 160–180; Raman: ν(U–O, sym. stretch.) = 826–835, ν(U–O–Br, bend.) = 190–198, ν(U–Br, stretch.) = 167–172, 81–83; ν(U–Br, bending mode) = 81–83	tetragonal; D_{4h}^{14}, $P4_2/mmm$, No. 136; a = 9.350(5), c = 11.695(6); d(calc.) = 2.40; d(U–O) = 1,76(2); d(U–Br) = 2.783(6)(2×) and 2.828 (4) 2×	*crystallographic data* (Di Sipio *et al*. 1974a); *infrared and Raman data* (Brown, 1979)
$[N(C_3H_7)_4]_2UO_2Br_4$	yellow; IR (cm^{-1}): ν(U–O, asym. stretch.) = 895–934; ν(O–U–O, deformation) = 243–263; ν(U–Br, stetch.) = 160–180; Raman: ν(U–O, sym. stretch.) = 826–835, ν(U–O–Br, bend.) = 190–198, ν(U–Br, stretch.) = 167–172, 81–83 cm^{-1} ν(U–Br, bending mode) = 81–83.	monoclinic; $P2_1/n$; a = 13.706(6), b = 12.270(6), c = 10.758(5); β = 89.9(2); d(U–O) = 1,698(7); d(U–Br) = 2.837(2)(2×) and 2.829(6) 2×	*crystallographic data* (Di Sipio *et al*., 1974d); *Infrared and Raman data* (Brown, 1979)

Table 5.30 (*Contd.*)

Formula	*Selected properties and physical data*[b,c]	*Lattice symmetry, lattice constant* (Å), conformation and density ($g\ cm^{-3}$)	*Remarks regarding information available and references*
$[N(C_4H_9)_4]_2UO_2Br_4$		triclinic; C_i^1, $P\bar{1}$, No.2; $a = 18.62$ (2), $b = 11.52(1)$, $c = 11.50(1)$; $\alpha = 100.75(8)$, $\beta = 93.70(8)$, $\gamma = 115.96$ (8); $Z = 2$. The structure is built up of $[Bu_4N]^+$ and $[UO_2Br_4]^{2-}$ ions. The four Br anions are arranged around the linear UO_2 group to form a distorted to square bipyramidal octahedral coordination polyhedron. The U–Br moiety is strictly planar. The cations are tetrahedral. Alternating layers of anions and cations are linked by Van der Waals forces	*crystallographic data* (Di Sipio *et al.*, 1977)
$[P(C_6H_5)_4]_2$ $[UO_2\ Br_4]$ $\cdot 2CH_2Cl_2$	yellow	monoclinic; C_{2h}^6, $C2/c$, No.15; $a = 20.063(8)$, $b = 13.206(4)$, $c = 20.425(9)$; $\beta = 98.78(4)$; $V = 5348$; $Z = 4$; d(calc.) = 3.07 d(U–Br1) = 2.83.6(3); d(U–Br2) = 2.814(3); d(U–Br3 or U–O) = 1.72(2); Br–U–Br and O–U–O = 92.4(1) and 88.3(5)	*synthesis and crystallographic data* (Bohrer *et al.*, 1988)
$[C_7H_{16}NO_2]_2$ UO_2Br_4[i]	yellow; IR (cm^{-1}): ν(U–O, asym. stretch.) = 895–934; ν(O–U–O deformation) = 243–263; ν(U–Br	orthorhombic; D_{2h}^{16}, *Pnma*, No. 62; $a = 13.60(2)$, $b = 20.943)$, $c = 9.22$ (2); d(calc.) = 2.23; d(U–O) = 1,80	*crystallographic data* (Marzotto *et al.*, 1974); *Infrared and Raman data* (Brown, 1979)

	stetch.) = 160–180; Raman: ν(U–O sym. stretch.) = 826–835, ν(U–O–Br bend.) = 190–198, ν(U–Br stretch.) = 167–172 cm^{-1}, 81–83, ν(U–Br bending mode) = 81–83 cm^{-1}	(3); d(U–Br) = 2.804(4), 2.792 (4) and 2.859(2) 2×	
(i) $K_2[(UO_2)_4 O_2(OH)_2 Br_4(H_2O)_4] \cdot 2H_2O$ (ii) $Rb_2[(UO_2)_4O_2 (OH)_2Br_4(H_2O)_4] \cdot 2H_2O$		triclinic; C_i^1, $P\bar{1}$, No. 2. (i) $a = 12.42(2)$, $b = 12.46(1)$, $c = 8.08(1)$; $\alpha = 109.4(1)^o$, $\beta = 97.2(1)$, $\gamma = 139.0(1)$. (ii) $a = 12.47(2)$, $b = 12.34(2)$, $c = 8.07(3)$; $\alpha = 109.0(1)$, $\beta = 97.2(1)$, $\gamma = 138.6(1)$	*crystallographic data* (Perrin, 1977b)
$K_xUO_3Br_x$ ($x = 0.9$)		monoclinic; C_{2h}^2, $P2_1/m$, No.11; $a = 9.57$, $b = 4.14$, $c = 6.89$; $\beta = 11.77$	*crystallographic data* (Allpress *et al*., 1968)
$UO_2(HMPTA)_4 (BrO_4)_2$ HMPTA = hexamethyl-phosphor-triamide = $[(CH_3)_2N]_3PO$.	IR (cm^{-1}):$\nu_3(BrO_4^-)$ = 871, $\nu_{as}UO_{2(as)}^{2+}$ = 917	orthorhombic; D_{2h}^{15}, *Pbca*, No. 61; $a = 46.18(10)$, $b = 14.40(4)$, $c = 15.56(4)$; $V = 10347$	*crystallographic data and infrared spectra* (Gusev *et al*., 1985)
$K_2[(UO_2)_3 (IO_3)_4 O_2)]$		triclinic; C_i^1, $P\bar{1}$, No.2; $a = 7.0372(5)$, $b = 7.7727(5)$, $c = 8.9851(6)$; $\alpha = 93.386(1)$, $\beta = 105.668(1)$, $\gamma = 91.339(1)$; $Z = 1$; $V = 471.98$	*crystallographic data* (Bean *et al*., 2001b)
$Ba[(UO_2)_2(IO_3)_2 O_2)] H_2O$		monoclinic; C_{2h}^5, $P2_1/c$, No. 14; $a = 8.062(4)$, $b = 6.940(3)$,$c = 21.665(10)$; $\beta = 98.049(10)$; $Z = 4$; $V = 1200.22$	*crystallographic data* (Bean *et al*., 2001b)
$Ag_4(UO_2)_4 (IO_3)_2 (IO_4)_2 O_2$		monoclinic; C_{2h}^5, $P2_1/c$, No.14; $a = 15.040(7)$, $b = 8.051(4)$, $c = 18.3320(80)$; $\beta = 100.738(7)$; $V = 2180.9$; $Z = 4$	*crystallographic data* (Bean *et al*., 2001a)

Table 5.30 (*Contd.*)

Formula	*Selected properties and physical data*[b,c]	*Lattice symmetry, lattice constant* (Å), conformation and density (g cm^{-3})	*Remarks regarding information available and references*
(i) $UO_2(IO_3)_2$;. (ii)$UO_2(HMPTA)_4(IO_4)_2$ HMPTA = hexamethyl-phosphortriamide = $[(CH_3)_2N]_3PO$	(i) $UO_2(IO_3)_2$(cr): $\Delta_f G^o_m = -1250.2$ (2.4)†, $\Delta_f H^o_m = -1461.3$ (3.6)†, $S^o_m = 279$ (9)† (ii) IR (cm^{-1}):$\nu_3(IO_4^-) = 843$, $\nu_{as}(UO_2^{2+}) = 917$	orthorhombic; D^{15}_{2h}; *Pbca*, No. 61; $a = 46.52(10)$, $b = 14.50(4)$, $c = 15.66(4)$; $V = 10563$	*crystallographic data and infrared spectra* (Gusev *et al.*, 1985)

* Bridging oxygen or chlorine distances.
** U–O distances to the water molecule.
*** Estimated values.
**** Value obtained from a force constant calculation (IR inactive).
† Values recommended by the Nuclear Energy Agency (Grenthe *et al.*,1992; Guillaumont *et al.*, 2003).
‡ equation expressed in°C.
[a] Values have been selected in part from review articles (Brown, 1979; Bacher and Jacob 1980; Freeman,1991; Grenthe *et al.*, 1992; Guillaumont *et al.*, 2003.).
[b] m.p. = melting point; b.p(°C). = boiling point; (cr) = crystalline; (g) = gaseous; thermodynamic values in kJ mol^{-1}, or J K^{-1} mol^{-1} at 298.15 K, unless otherwise mentioned; $\Delta_f G^o_m$, - standard molar Gibbs energy of formation; $\Delta_f H^o_m$, standard molar enthalpy of formation; S^o_m (J K^{-1} mol^{-1}), standard molar entropy; $C^o_{p,m}$, standard molar heat capacity; log p (mmHg) = $-AT^{-1} + B - C \log T$: vapor pressure equation for indicated temperature range; R = Raman active; IR = infrared active; vs: very strong; s: strong; m: medium; ms: medium strong; w: weak; sh: shoulder; b: broad; L: lattice; all values are in cm^{-1}.
[c] All values are in Å and angles are in degrees; CN, coordination number; d, density [g cm^{-3}], V = molar volume [cm^3 mol^{-1}].
[d] The anion is $[(UO_2)_4O_2Cl_8(H_2O)_2]^4$.
[e] The anion is $[(UO_2)_4O_2(OH)_2Cl_4(H_2O)_4]^{2-}$.
[f] L = thiamine ($C_{12}H_{16}ClN_4OS$).
[g] L′ = 2,6-diacetylpyridine-bisphenyl hydrazone.
[h] The anion is $[(UO_2)_2Cl_6(\mu\text{-}O_2)]^{4-}$.
[i] Acetylcholine cation.

shown the existence of several progressions in the symmetric stretching frequency (ν_1) coupled with other modes. Two non-phonon transitions, originating at 24564 and 25265 cm^{-1}, are associated with the first band and four other with origins at 30331, 31032 (observed directly), 32120, and 32821 cm^{-1} with the second one; they could be located in the low-temperature spectra of the compound. The observed fine structure has been explained in terms of electric–dipole forbidden transitions from the t_{1u} ($\pi+\sigma$) orbitals of the fluorine atoms to the empty 5f orbitals of the uranium atoms. A strong absorption band without vibronic structure, observed at about 46730 cm^{-1}, has been assigned as a charge transfer transition.

Since the ground state of UO_2^{2+} does not contain unpaired electrons the uranyl compounds are either diamagnetic or weakly paramagnetic. The octahedral hexahalides exhibit a weak, almost temperature-independent, paramagnetism.

(*i*) *Uranium hexafluoride and uranium*(*VI*) *complex fluorides*

Uranium hexafluoride

Uranium hexafluoride is the only uranium compound that is readily volatilized and is therefore used for uranium isotope separation by gas diffusion, gas centrifugation, liquid thermal diffusion, or in mixtures with a light auxiliary gas like H_2 or He (separation nozzle). The uranium enrichment technologies have been surveyed by Becker (1979) and Ehrfeld and Ehrfeld (1980), for example. Due to the importance of UF_6, the physical and chemical properties of UF_6, including commercial syntheses, have been extensively studied. The literature is covered in a number of reviews (Caillat, 1961; Brown, 1968; Bacher and Jacob, 1980, 1982, 1986; Hellberg and Schneider, 1981; Freestone and Holloway, 1991). A scheme of reactions leading to UF_6 is shown in Fig. 5.45.

Some important preparative procedures are based on the following reagents (Bacher and Jacob, 1980; Freestone and Holloway, 1991):

(1) reaction of elemental fluorine with U, UF_4 (at 340°C), U_4F_{17}, U_2F_9 (at 300°C), UF_5 (at 270°C), $NaUF_5$ (at 340°C), UO_2 (at 500°C), UO_3 (at 400°C), U_3O_8 (at 360°C), UO_2F_2 (at 340°C), $Na_2U_2O_7$, CaU_2O_7, UCl_5 (at –20 to 30°C), UO_2HPO_4 (at 370°C), UC_2 (at 350°C); e.g.

$$U_3O_8 + 17F_2 \overset{360°C}{\rightarrow} 3UF_6 + 8F_2O$$

$$CaU_2O_7 + 7F_2 \rightarrow 2UF_6 + CaF_2 + 7/2O_2$$

(2) reaction of bromine trifluoride with U (at 50–125°C), U_2F_9 (at 170°C, leading to UF_4), UO_2, UO_3, U_3O_8, UO_2F_2; e.g.

$$U_3O_8 + 6BrF_3 \rightarrow 3UF_6 + 3Br_2 + 4O_2$$

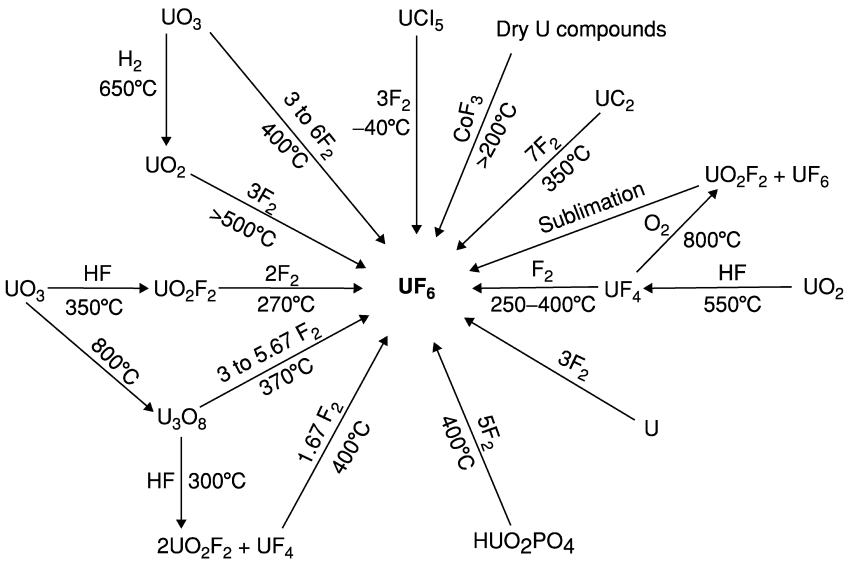

Fig. 5.45 *Reactions leading to UF_6 (adapted from Katz and Rabinowitch, 1951).*

(3) reaction of hydrogen fluoride with UO_2 (at 550°C), $Na_2U_2O_7$, UCl_5; e.g.

$$UCl_5 + 5HF \rightarrow UF_5 + 5HCl$$

followed by reactions (6b) and (6c) below;

(4) reaction with low temperature fluorinating agents: O_2F_2 with U_3O_8; KrF_2 with UF_4, and UO_2 and U_3O_8 in the gaseous phase or at room temperatures in HF solutions;

(5) reaction with other reagents:

(a) $O_2 + 2UF_4$ (at 660–800°C) $\rightarrow UF_6 + UO_2F_2$
(b) $3BrF_5 + U$ (at 50–125°C) $\rightarrow UF_6 + 3BrF_3$
(c) $3ClF_3 + U$ (at 25–75°C) $\rightarrow UF_6 + 3ClF$
(d) $2CoF_3 + UF_4$ (at 250°C) $\rightarrow UF_6 + 2CoF_2$

(6) decomposition reactions with disproportionation:

(a) $2U_4F_{17}$ (at 270–350°C) $\rightarrow 7UF_4 + UF_6$
(b) $3UF_5$ (at 170°C) $\rightarrow U_2F_9 + UF_6$
(c) $2U_2F_9$ (at >500°C) $\rightarrow 3UF_4 + UF_6$
(d) $9UO_2F_2$ (at >700°C) $\rightarrow 3UF_6 + 2U_3O_8 + O_2$.

As indicated above, the fluoride obtained by means of the reaction given in (3) can be converted to UF_6, using double decomposition with subsequent

disproportionation (reactions 6b and 6c). The separation from UF_4 and an excess of HF can be achieved by heating, followed by fractional distillation. The method based on reaction (5a) is also a convenient route, not involving the use of gaseous fluorine; UO_2F_2 is formed as a by-product, but can be converted to UF_4 by reduction and to UF_6 by hydrofluorination. An attractive method on laboratory scale uses reactions (5d) (Weigel, 1958). The by-product CoF_2 can easily be separated from UF_6 and regenerated with fluorine. The general route for purification of UF_6 employs trap-to-trap distillation followed by condensing the hexafluoride at about –80°C.

The production of UF_6 on an industrial scale is achieved mainly by oxidative fluorination of uranium oxides or lower fluorides by fluorine at elevated temperatures. A uranium ore concentrate is first purified by solvent extraction or by ion exchange methods. From this concentrate, $(NH_4)_2U_2O_7$ (ammonium diuranate, ADU, yellow cake) or $UO_2(NO_3)_2 \cdot 6H_2O$ (UNH) is then precipitated. ADU is converted to UO_2 by calcination in the presence of H_2 whereas UNH is first pyrolyzed to UO_3 and then reduced by H_2 to UO_2.

A detailed description of the commonly applied direct fluorination technology of UF_4

$$UF_4(s) + F_2(g) \rightarrow UF_6(g)$$

has been published by Smiley and Brater (1956) and Brater and Smiley (1958). In the conversion flow sheet shown in Fig. 5.46, the fluorination reactor used is either a flame reactor or a fluidized-bed reactor (Harrington and Ruehle, 1959). In the first one UF_4 is fed to the top of the reactor having a length of 3.60 m, diameter of 20 cm, and a capacity of 380 kg per hour. The highly exothermic fluorination reaction takes place over a length of ~1 m at the top of the reactor where a flame with temperatures up to 1100°C is formed. In order to suppress corrosion, the temperature of the reactor walls is maintained below 540°C. For a maximum yield of UF_6 a temperature limit of 450°C, which eliminates the formation of intermediate fluorides, is required. The off-gases contain ~75% UF_6 and have their outlet at the lower part of the reactor. All unreacted solids are collected, powdered, mixed with fresh UF_4 and transmitted again to the feed.

In the second method, UF_4 is fluorinated with F_2 at 500°C in a Monel fluidized-bed reactor with an annual production capacity of 4400 to 7400 tons of UF_6. The UF_4 feed material and fluorine gas are mixed continuously by means of a conveyor screw and a gas distributor (6–20 $cm^3\ s^{-1}$), respectively. For stabilization of the fluidized bed CaF_2 is added to the feed. It serves also to prevent sintering of UF_4 and as a heat transfer material. The product obtained in both types of reactors is passed through Monel filters in order to remove UF_4 dust and is then condensed, first at +4 to –15°C and finally at –40°C. The condensers are then heated to 80°C and UF_6, which liquefies at that temperature under its own pressure, is drained into transport cylinders, which have a volume of up to about 4 m^3, weigh around 2.36 tons, and have a capacity

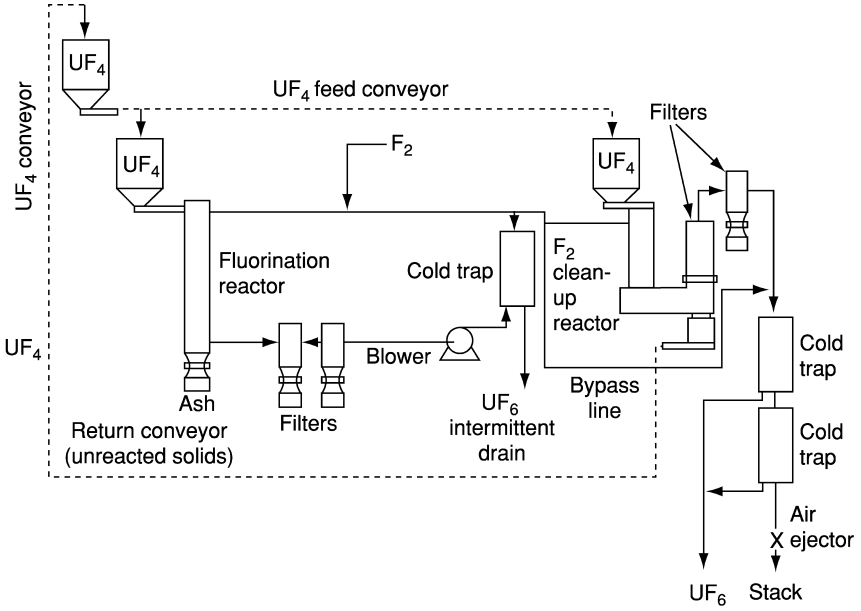

Fig. 5.46. *Schematic flow diagram for uranium hexafluoride production* (*Harrington and Ruehle*, 1959).

of 12.5–14 tons (Keller, 1956). The crude product usually contains numerous volatile impurities such as SiF_6, CF_4, SF_4, MoF_6, CrO_2F_2, or VF_5 as well as some less volatile compounds like MoF_4, VOF_3, and other transition metal fluorides. Since stringent purity specifications are required of commercial UF_6 for isotope separations, the impurities are removed by fractionation at temperatures and pressures above the triple point and by absorption–desorption techniques. At room temperature, UF_6 has a pressure of ca. 120 mmHg; it is thus possible to handle it as a gas in the separation of ^{235}U from natural uranium. For large-scale applications, solid UF_6 is delivered to isotope separation plants in containers, which are then placed into a steam-heated autoclave in which UF_6 builds up a high enough pressure to flow as a gas into the attached diffusion cascade for the separation process (Arendt *et al.*, 1957).

Uranium hexafluoride forms low-melting orthorhombic (space group *Pnma*) colorless crystals which sublime at 56.5°C at atmospheric pressure. The compound has a triple point at 64.02°C and a pressure of 1137 mmHg (Hoard and Stroupe, 1959; Rigny, 1965, 1966; Levy *et al.*, 1976). The structure of solid UF_6 was first determined by Hoard and Stroupe (1959) and later in a number of X-ray and neutron diffraction studies (Levy *et al.*, 1976; Jacob and Bacher, 1980). It consists of hexagonal close-packed fluorine ions with uranium atoms in octahedral holes. The crystallographic data of UF_6 are listed in Table 5.30 together with selected physical data.

The structure of UF_6 in the liquid and gaseous states is perfectly octahedral (point group O_h) with U–F bond lengths in solid UF_6 equal to 1.996 Å. The compound has a temperature-independent paramagnetism with a molar susceptibility of $\chi_{mole} = 43 \times 10^{-6}$ cm^3 mol^{-1}, after correction for a diamagnetic contribution of $\chi_{mole} = 106 \times 10^{-6}$ cm^3 mol^{-1}. Carnall (1982) has published extensive analyses of the absorption and fluorescence spectra of UF_6. The absorption spectrum of UF_6 in visible to the near-UV range is similar to that of the UO_2^{2+} ion; in the range 200–420 nm there is only one broad band at 375 nm.

The compound is highly reactive and extremely moisture-sensitive. It reacts with most elements but is relatively stable towards oxygen, chlorine, bromine, carbon dioxide, and noble gases even at elevated temperatures. UF_6 has a significant solubility in liquid chlorine and bromine. Thermodynamic calculations have shown that UF_6 is thermally stable below 1000 K; dissociation starts between 1100 and 1450 K. Since UF_6 is rapidly hydrolyzed by water with the formation of HF it is recommended to store the compound in teflon, Kel-F, nickel, or Monel containers.

$$UF_6 + 2\,H_2O \rightarrow UO_2F_2 + 4HF$$

It can be also stored in quartz or Pyrex tubes by using NaF and KF as HF 'getters'.

Uranium hexafluoride is a powerful fluorinating agent with a vapor pressure of 115 mm at 25°C. Bacher and Jacob (1982) have classified, as discussed below, a number of reactions of UF_6.

Oxidative fluorination results in a simultaneous formation of lower uranium fluorides. UF_6 oxidizes elements or their fluorides in low oxidation states to yields fluorides in higher oxidation state, e.g. with alkali, alkaline earth metals, B, Al, Ga, In, C, Si, Ge, Sn, Pb, As, Sb, S, Se, and Te binary fluorides are formed; lower fluorides such as PF_3, SF_4, MoF_5, or WF_4 are oxidized to higher fluorides:

$$nUF_6 + M(s) \rightarrow nUF_5(s) + MF_n$$

Lower oxides are converted to oxyfluorides whereas chlorides and bromides yield fluorides in presence of an excess of UF_6 with formation of Cl_2 and Br_2, respectively:

$$nUF_6 + 2MX_n \rightarrow nUF_4 + 2MF_n + nX_2 \quad (X = Cl \text{ or } Br)$$

The high fluorination efficiency of UF_6 is also demonstrated by interactions with SO_3 that leads to the formation of the peroxide $S_2O_6F_2$ (Wilson *et al.*, 1977; Masson *et al.*, 1978). The effective first bond dissociation energy of UF_6, according to the the reaction scheme

$$UF_6 \rightarrow (UF_5)_{solid} + F$$

is equal to (134.0 ± 29.3) kJ mol^{-1}, and is of the same order of magnitude as the bond energy of elemental F_2 (153.2 kJ mol^{-1}, Jacob and Bacher, 1986).

Reaction of UF_6 with other highly electronegative groups may lead to a total or partial substitution of the fluorine atoms with retained oxidation state of uranium as in the vapor phase hydrolysis:

$$UF_6 + 3H_2O \rightarrow UO_2F_2 \cdot H_2O + 4HF$$

and the hydrolysis in liquid HF:

$$UF_6 + nH_2O \rightarrow UO_nF_{(6-2n)} + 2nHF \quad (\text{where } n = 1 \text{ or } 2)$$

or in exchange reactions where fluorine is replaced by groups such as Cl, OCH_3, and $OTeF_5$:

$UF_6 + 6BCl_3 \rightarrow UCl_6 + 6BCl_2F$ (with excess of BCl_3) (O'Donnell *et al.*, 1966)
$UF_6 + 6Si(OCH_3)_4 \rightarrow U(OCH_3)_6 + 6SiF(OCH_3)_3$ (with excess of $Si(OCH_3)_4$) (Jacob, 1982).

UF_6 is a strong Lewis acid that can bind fluoride from Lewis bases such as MF (where M = Na, K, Cs, Rb, NH_4, N_2H_5, NO, and NO_2) under the formation of the corresponding heptafluorouranates(VI), MUF_7 and octafluorouranates(VI), M_2UF_8. UF_6 can oxidize various metals, as well as NO, NO_2, and I_2 in other less common reactions. These reactions are due to the high electron affinity of UF_6 (5.2 eV) and to a favorable lattice energy when fluorouranates(V) are formed, e.g.:

$$NO \rightarrow NO^+ + e \quad + 9.2 \text{ eV}$$

$$UF_6 + e \rightarrow UF_6^- \quad - 5.2 \text{ eV}$$

$$NO^+ + UF_6^- \rightarrow NOUF_6 \quad - \text{lattice energy}$$

The hexafluoride is reduced to the tetravalent state by a number of reagents, e.g. HCl (250°C), PF_3, HBr (80°C), CCl_4, CS_2, H_2S, amorphous carbon as well as $SiCl_4$, $AsCl_3$, $SbCl_3$, PBr_5, and BBr_3, with the formation of the appropriate free halogen. Reduction with H_2 is slow and may be carried out at 650°C, or in pressurized systems at 300°C. Exposure of UF_6 to UV light or photocatalytic reduction with HBr, SO_2, or CO yield β-UF_5:

$$2UF_6 \xrightarrow{h\nu} (UF_5)_{\text{solid}} + 1/2F_2$$

$$2UF_6 + X \xrightarrow{h\nu} 2\beta\text{-}(UF_5)_{\text{solid}} + XF_2 \quad (X = H_2, CO, \text{or } SO_2).$$

Alpha radiation from hexafluoride enriched with ^{235}U or ^{234}U results in significant reduction to lower fluorides.

A number of binary phase diagrams of uranium hexafluoride with fluorine and elements of the 7th main group have been reported (Bacher and Jacob, 1980). Simple eutectic types were observed in the UF_6–BrF_3, UF_6–BrF_5, and UF_6–BrF_2 systems. Some deviation from ideality was found for the UF_6–BrF_3, UF_6–BrF_5, UF_6–ClF_3, and UF_6–BrF_3 systems. In all of these systems, the solid

phases are pure stoichiometric compounds. The UF_6–HF phase diagram investigated by Rutledge *et al.* (1953) has practical importance due to the common presence of HF in UF_6. In the phase diagram shown in Fig. 5.47 there is a complete miscibility above 100°C and above a pressure of 10 atm.

The system possesses an eutectic point at –85°C with less than 0.5 mol% of UF_6. The separation of HF from UF_6–HF solutions by distillation is limited due to the appearance of azeotropes.

Complex uranium(VI) fluorides

Bacher and Jacob (1980) and Freestone and Holloway (1991) have compiled data on the synthesis and characterisation of numerous fluorouranate(VI) compounds listed below in Table 5.31; some of their physical data are presented in Table 5.30.

NaF has found practical application in nuclear processing. It absorbs UF_6 quickly and has the largest absorption capacity of all alkali metal fluorides. The sodium fluorouranates(VI) formed in the process can easily be thermally dissociated to UF_6 (Bacher and Jacob, 1986).

Several methods have been applied for the preparation of the fluoro complexes (Bacher and Jacob, 1980; Freestone and Holloway, 1991), e.g.: (i) most of

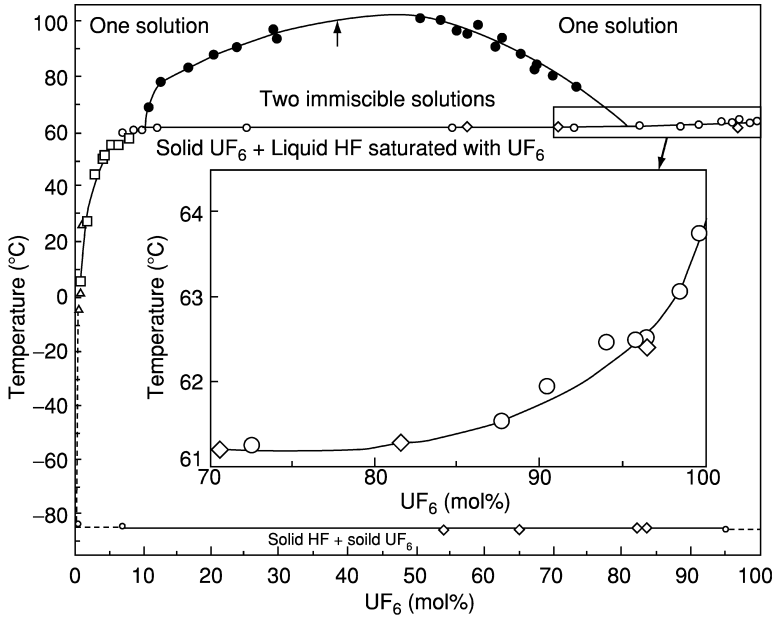

Fig. 5.47 *Phase diagram of the binary system UF_6-HF* (*Rutledge* et al., 1953). •, *Visual observation of disappearance of two liquid layers;* □, *visual observation of precipitation of solid UF_6;* Δ, *filter cell;* ○, *freezing point cell–K2 potentiometer;* ◇, *freezing point cell–white potentiometer. The thin arrow indicates rupture of polyethylene tube.*

Table 5.31 *Identified uranium(VI) complex fluorides.*

System	*Complex fluorides*
$NaF–UF_6$	$NaUF_7$, Na_2UF_8, Na_3UF_9, $Na_3U_2F_{15}$
$KF–UF_6$	KUF_7, K_2UF_8, K_3UF_9, $K_3U_2F_{15}$
$RbF–UF_6$	$RbUF_7$, Rb_2UF_8, Rb_3UF_9
$CsF–UF_6$	$CsUF_7$, Cs_2UF_8, Cs_3UF_9
$NH_4F–UF_6$	NH_4UF_7, $(NH_4)_2UF_8$
$N_2H_5F–UF_6$	$N_2H_5UF_7$, $N_2H_6(UF_6)_2$
$NO_xF–UF_6$	$NOUF_7$, NO_2UF_7, $(NO)_2UF_8$

the compounds can be obtained by the reaction of gaseous UF_6 with solid MF (where M = Na, K, Rb, Cs, or NH_4). In some cases, the reactions are carried out at higher temperatures and pressures. The products may be however contaminated by unreacted solid fluorides; (ii) the interaction of a large excess of liquid UF_6 with solid MF yields MUF_7 (M = K, Rb, or Cs); (iii) complex fluorides of the formula MUF_7 or M_2UF_8 are formed by interaction of UF_6 with NaF, KF, RbF, CsF, AgF, or TlF_3 by using appropriate solutions or suspensions in perfluoroheptane, C_7F_{16}, C_8F_{16}, ClF_3, or anhydrous HF; (iv) fluorination of a M_2UF_6 (M = Rb or Cs) or a $NaF–UF_4$ mixture with F_2 results in the formation of M_2UF_8 and $NaUF_7$, respectively; (v) the M_2UF_8 octafluoro uranate(VI) may also be prepared by thermal decomposition of the corresponding sodium (at 60–145°C), potassium (at 130°C), rubidium (at 150°C), and cesium (180–200°C) heptafluoro uranates; (vi) the reaction between UF_6 and liquid or gaseous ammonia yields NH_4UF_5 and NH_4UF_6, respectively. In the latter case also, a mixture of NH_4UF_5 and UF_5 may be obtained; (vii) the condensing of UF_6 in a suspension of NH_4F in tetrachloroethane yields NH_4UF_7; (viii) the corresponding hydrazinium $N_2H_5UF_7$, nitrosonium $NOUF_7$, and nitronium NO_2UF_7 salts are prepared by direct reaction of the component fluorides, the former in anhydrous hydrofluoric acid.

The fluoro uranates(VI) are extremely moisture-sensitive solids, very susceptible to hydrolysis. With some exception (e.g. NH_4UF_7, which decomposes to UF_5 or UF_4, depending of the applied temperature) they decompose to UF_6 when heated. The UF_6–bromine fluorides and the UF_6–HF systems (HF removal) have also found application in the fluorination reactions in nuclear reprocessing.

(*ii*) *Uranium(VI) oxide fluorides and complex oxide fluorides*

Uranium(VI) oxide tetrafluoride, UOF_4

UOF_4 can most conveniently be prepared either by the interaction of an excess of UF_6 with quartz wool in liquid HF

$$3UF_6 + SiO_2 \overset{\text{HF (liquid)}}{\rightarrow} 3UOF_4 + SiF_4$$

or by reaction with an excess of B_2O_3

$$3UF_6 + B_2O_3 \rightarrow 3UOF_4 + 2BF_3$$

Uranium oxide tetrafluoride is an orange solid with a shade of red. It is non-volatile and decomposes at 200–250°C without melting. At 250°C in vacuum UOF_4 decomposes spontaneously in an exothermic reaction to UF_6 and UO_2F_2. The reaction proceeds quantitatively and may be used for purity checking. UOF_4-hydrate is formed after some time in moist air, but liquid water results in a rapid hydrolysis. UOF_4 reacts with KF and NH_4F in liquid HF to form $MUOF_5$ type of salts. Fluorination of UOF_4 by ClF_5, ClF_3, or $ClOF_3$ at room temperature yields UF_6:

$$ClF_5 + 2UOF_4 \rightarrow ClO_2F + 2UF_6$$

UOF_4(cr) has trigonal symmetry in the space group $R3m$ and a pentagonal bipyramidal coordination geometry formed by the O and F atoms. Some physical data are given in Table 5.30.

Uranium(*VI*) *oxide difluoride* (*uranyl fluoride*), UO_2F_2

One of the simplest methods to prepare UO_2F_2 is by heating of UO_3 in gaseous HF at 300–500°C. Other satisfactory routes employ fluorination of uranium oxides at 350°C and oxidation of UF_4 with O_2 at 600–800°C. The compound is a pale yellow solid with a green hue, slightly soluble in water, methanol, and ethanol. Recrystallization from water results in the formation of $UO_2F_2 \cdot 2H_2O$. Controlled action of H_2O in a closed vessel yields hydrates $UO_2F_2 \cdot nH_2O$ ($n = 1$ to 4). The reaction of an excess of UF_6 with water vapour at 60°C leads to the formation of $UO_2F_2 \cdot 1.53H_2O$. Adducts of the $UO_2F_2 \cdot L(H_2O)$ and $UO_2F_2 \cdot nL$ ($n = 1$ to 4) type are formed by interactions with oxygen or nitrogen donor ligands (L) such as NH_3, pyridine (py), tributylphosphine oxide (tbpo), dimethylsulfoxide (dmso), antipyrine (antypy), 2,2′-dipyridyl (dipy), dimethylformamide (dmf), acetamide (aa), dimethylacetamide (dma), urea (ur), dimethylurea (dmur), and tetramethylurea (tmur) (Shchelokov *et al.*, 1977; Bagnall, 1979, 1987; Mass, 1979). IR and Raman data are available for most of the compounds. The nature of the uranium–oxygen bonds in UO_2^{2+} depends on the electron donor properties of the ligands, which result in variations of the UO_2^{2+} ν_1 and ν_2 frequencies that provide valuable structural information. The k_{UO} force constants, determined from both of these frequencies, decrease in the series (Shchelokov *et al.*, 1977) $H_2O >$ aa $>$ dma $>$ dmur $>$ dmso $>$ dmf $>$ tmur$\sim$antipy $>$ ur.

The total energy, molar entropy, heat capacity, and vibration frequencies of the compound in the gas phase have been calculated by *ab initio* methods to obtain thermodynamic data for reactions. They agree well with experimental values and previous results (Privalov *et al.*, 2002).

UOF_2 is converted to UF_6 by gaseous fluorides such as XeF_6 (25°C), BrF_3 (25°C), ClF_3 (50–160°C), ClF (64–150°C), ClO_2F (100–150°C), ClF_5 (>120°C)

F_2 (>300°C), BrF_5 (250°C), SF_4 (>300°C), and VF_5 (100°C). The reactions proceed with much greater difficulty than oxidative fluorination of UF_4 or UF_5 (Bacher and Jacob, 1980). The compound crystallizes with a rhombohedric structure in the space group $R\bar{3}m$. Selected crystallographic data are given in Table 5.30. Besides, Otey and LeDoux (1967) have identified an oxide fluoride of the composition $U_3O_5F_8$ and suggested the existence of an intermediate, $U_2O_3F_6$ compound.

Hexavalent oxide fluoride complexes

There is a large variability in the stoichiometry of the very large number of reported hexavalent oxide fluorides: M^IUOF_5, $M^I(UO_2)_2F_5$, $M^IUO_2F_3$, $M^I_2UO_2F_4$, $M^I_3UO_2F_5$, $M^I_3(UO_2)F_3$, $M^I_3(UO_2)_2F_7$, $M^I_4(UO_2)_2F_8$, $M^I_5(UO_2)F_9$ (where M^I is usually an alkali metal ion), $M^{II}(UO_2)F_4$ (where M^{II} = Ca, Pb, Cu, Zn, or Cd) and $M^{II}(UO_2)_2F_6$ (where M^{II} = Sr, Ba, or Mg) (Freestone and Holloway, 1991). Many of the compounds were identified from phase diagram investigations. The complexes of the M^IUOF_5-type (M = K, Rb, Cs, NH_4) have been prepared by interaction of UOF_4 with the appropriate MF fluoride in liquid sulfur dioxide or anhydrous HF (Joubert and Bougon, 1975; Joubert *et al.*, 1978a,b). Hydrated complexes of the $M^{II}(UO_2)F_4 \cdot 4H_2O$ (M^{II} = Zn, Cd, Cu, Mn, Co, or Ni) were obtained by crystallization from aqueous solutions. A number of fluoro-oxalato compounds of the $[UO_2F(C_2O_4)_2(H_2O)]^{3-}$ and $[UO_2F_3(C_2O_4)(H_2O)]^{3-}$ types with alkali metals, ammonium, and guanidinium have been reported by Chernyayev (1966) and Shchelokov and Belomestnykh (1968a,b). Fluoro-oxalato compounds of the types $M_2[UO_2F_2(C_2O_4)]$, $M_4[UO_2F_2(C_2O_4)_2]$, and $M_2[(UO_2)_2F_4(C_2O_4)]$ (where M = Rb or K) are obtained by mixing of saturated solutions of $H[UO_2F_3] \cdot H_2O$ with alkali metal oxalates in different mole ratios (Chakravorti *et al.*, 1978). Some crystallographic data and IR spectral bands are collected in Table 5.30.

Numerous hydrated and anhydrous uranyl fluoro compounds have been obtained from aqueous solutions by varying the preparation conditions with a given alkali metal or organic base cation (Brown, 1968; Bacher and Jacob, 1980), e.g. $CsUO_2F_3$, $CsUO_2F_3 \cdot H_2O$, $NaUO_2F_3 \cdot xH_2O$ (x = 2 and 4), $CsUO_2F_4 \cdot H_2O$, $M_3UO_2F_5$ (M = Na, K, Rb, Cs, NH_4), $M_4(UO)_2F_5 \cdot 2H_2O$ (M = K, R, Cs), $M^I(UO_2)_2F_5 \cdot xH_2O$, $M^IUO_2F_3 \cdot xH_2O$ and $M^I(UO_2)_3F_7 \cdot xH_2O$ (where M^I is an organic base and x varies from 0 to 6). The MF/UO_2F_2 ratio in aqueous solutions has a significant influence on the stoichiometry of the complexes obtained. With a large excess of MF one usually obtains the $M_3UO_2F_5$ type of complexes. When the ratio is less than 3 one obtains di- or polynuclear complexes. The compounds obtained using the preparative methods described above can be rationalized from information on the equilibrium constants of the complexes present (cf. Section 5.9).

In $CsUOF_5$, the fluorine and oxygen atoms form a pseudo-octahedral surrounding of the uranium atom. In the other $MUOF_5$ (M = NH_4, K or Rb) oxide fluorides, uranium is eight coordinated with dodecahedral coordination geometry. The structure consists of chains formed by surface sharing of individual

dodecahedra through bridging fluoride ligands. (Joubert *et al.*, 1978a,b). Some structural details are also available for other hexavalent oxide fluoride complexes (see Table 5.30).

(*iii*) *Uranium hexachloride*

Uranium hexachloride may be obtained by thermal decomposition of UCl_5 at 120–150°C *in vacuo*. The green UCl_6 crystals are collected on a cold finger and purified from contaminating UCl_5 by sublimation in vacuum at 75–100°C or distillation in a stream of an inert gas at a low pressure. On laboratory scale it is best prepared by condensing an excess of BCl_3 onto UF_6 at –196°C and allowing the vessel with the compounds to warm up slowly. It is not necessary to purify the product by sublimation since the by-products are volatile at room temperatures (Brown, 1979).

UCl_6 is an extremely moisture-sensitive, black to dark green crystalline solid. The compound is reported to melt at (177.5 ± 2.5)°C, but it readily liberates chlorine at temperatures higher than ≈120°C. It reacts violently with water to form uranyl(VI) solutions. Hydrogen reduces UCl_6 to UCl_4 at 250°C. Reaction of UCl_6 with anhydrous liquid hydrogen fluoride or UF_6 converts it to UF_4 and UF_5, respectively. The hexachloride is slightly soluble in carbon tetrachloride, liquid chlorine, methyl chloride, isobutyl bromide, and thionyl chloride. On prolonged storage in carbon tetrachloride, it decomposes forming crystalline red-brown, volatile U_2Cl_{10}. The decomposition reaction proceeds much faster in 1,2-dichloroethane and methylene dichloride. The reduction in the last solvent appears to be photochemically mediated. Interaction with chlorides such as NH_4Cl, $(C_6H_5)_4AsCl$, and $(CH_3)_4NCl$ yields the appropriate $MUCl_6$ hexachloorouranate(v) compounds.

UCl_6 has hexagonal symmetry, space group D_{3d}^3; $P\bar{3}m1$ (Zachariasen, 1948f). The structure has been refined with neutron and X-ray powder diffraction data by Taylor and Wilson (1974b) and can be described as a hexagonal close packing of chlorine atoms with uranium atoms in one-sixth of the octahedral holes. The chlorine atoms form an almost regular octahedron around the U(1) located at 0,0,0 while the geometry around U(2) at 1/3, 2/3, 0.518 is slightly distorted (Fig. 5.48).

The absorption spectra for UCl_6 in the solid state, vapor phase, and solutions in perfluoroheptane in the UV–Vis range have been reported and analyzed (Brown, 1979). Charge transfer bands were observed at 17000 and 20800 cm^{-1} for solid UCl_6 and at 21000 and 20800 cm^{-1} in the vapor phase. Some X-ray and physical data of the compound are summarized in Table 5.30.

(*iv*) *Uranium(VI) dioxide dichloride, UO_2Cl_2, and related compounds*

Uranium(VI) dioxide dichloride (*uranyl chloride*)

Since the literature on uranium(VI) dioxide dichloride is very extensive (Brown, 1979), the results of investigations presented in this section must necessarily be incomplete. The most attractive methods for the preparation of UO_2Cl_2 involve

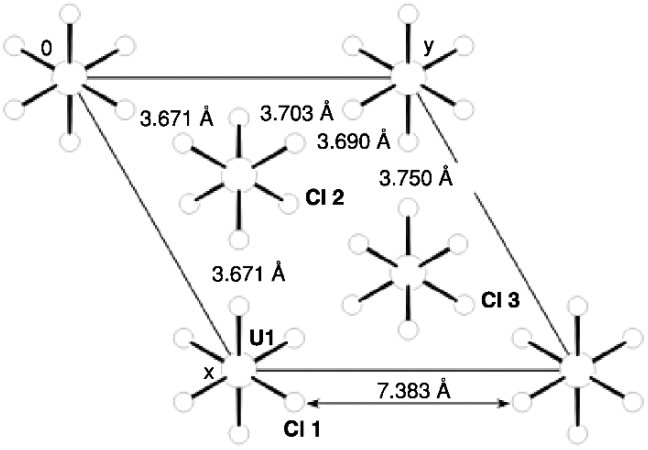

Fig. 5.48 *View of the crystal packing of* UCl_6 (*distances are taken from Taylor and Wilson*, 1974*b*).

the oxidation of UCl_4 at temperatures between 300 to about 350°C or the dehydration of $UO_2Cl_2 \cdot H_2O$. The last method may readily be performed by heating in a stream of gaseous HCl or HCl + Cl_2 mixtures at 400–450°C. UO_2Cl_2 may be also obtained by electrochemical oxidation of uranium in an acetonitrile solution of Cl_2 in the presence of oxygen. This solution of UO_2Cl_2 may be used for the preparation of numerous adducts, e.g. $(Et_4N)_2UO_2Cl_4$ (Kumar and Tuck, 1984).

The anhydrous compound is a yellow, hygroscopic solid, readily soluble in a number of organic solvents, in many cases with complex formation. It is not soluble in non-polar organic solvents. Thermal decomposition in air leads to formation of a mixture of α-UO_3 and $UO_{2.9}$ at 460°C and to U_3O_8 at higher temperature. The compound decomposes to UO_2 and Cl_2 on heating in a nitrogen atmosphere. Vacuum thermal decomposition results first in the formation of an intermediate state $(UO_2)_2Cl_3$ and next, at 450°C, of a mixture of UO_3 and U_3O_8. UO_2Cl_2 may be converted to $UOCl_3$ by reaction with UCl_4 *in vacuo* at 370°C.

The reaction of UO_2Cl_2 solutions with a variety of ligands in both aqueous and non-aqueous media results in the formation of a large number of stable compounds of different UO_2Cl_2:ligand stoichiometry, e.g.:

- (1:1): with methyl cyanide, methylmalonamide, benzophenone; acetyl chloride, 1,10-phenantroline and *N*,*N*,*N*′,*N*′- teramethyl-α,α-dimethylmalonamide;
- (1:1,5): with *N*,*N*,*N*′,*N*′-tetramethylmalonamide, *N*,*N*,*N*′,*N*′-tetramethylglutaramide;
- (1:2): aniline, pyridine, ethanol, acetic anhydride, diethyl ether, acet-*p*-phenetidine, 1,10-phenantroline, dimethylurea, tetramethylurea,

trialkyl-phosphine, triaryl-phosphine, 2,2′-bipyridine, and 4-methoxoy-pyridine-*N*-oxide;
- (1:3): with 4-methylpyridine-*N*-oxide, *N*,*N*-dimethylformamide, ethylurea, diethylurea;
- (1:4): hydrazine, urea, 1,3-dimethylurea and 4-chloropyridine-*N*-oxide etc.

A number of uranyl chloro-complexes have been identified during investigations of the $MCl–UO_2Cl_2$, $CuCl_2–UO_2Cl_2$, and $NaCl–KCl–UO_2Cl_2$ phase diagrams (where M = Li, Na, K, Rb, or Cs) (Brown, 1979).

UO_2Cl_2 has orthorhombic symmetry, space group *Pnma* (see Table 5.30). Uranium has pentagonal bipyramidal coordination geometry with two uranyl oxygen atoms at the apices; there are four chlorine atoms and one oxygen atom in the equatorial plane, the latter an "yl" oxygen atom from neighbouring uranium. The pentagons form chains parallel to the *b* axis by sharing Cl–Cl edges (Taylor and Wilson, 1973b). Electronic absorption spectra in the solid state and solutions in non-aqueous media and luminescence spectra have been discussed in numerous papers (Brown, 1979; Wells, 1990). Some physical data are listed in Table 5.30.

Uranyl(VI) chloride hydrates and hydroxide chlorides

The following compounds have been identified $UO_2Cl_2 \cdot 3H_2O$, $UO_2Cl_2 \cdot H_2O$, $[(UO_2)_2(OH)_2Cl_2(H_2O)_4]$, $[(UO_2)_4O_2(OH)_2Cl_2(H_2O)_6]$, and $4UO_3 \cdot HCl \cdot 8H_2O$ (Brown, 1979). The tri- and monohydrate are most conveniently prepared by slow evaporation from concentrated uranyl(VI) hydrochloric acid solutions over KOH and P_2O_5, or from an aqueous solution in dry air at room temperature; they form yellow hygroscopic powders. The hydrates are readily soluble in water and in various organic solvents such as ether, acetone, ethyl acetate, and a number of alcohols. The trihydrate may be dehydrated to $UO_2Cl_2 \cdot H_2O$ and then readily converted to the anhydrous salt by heating in a stream of dry hydrogen chloride or a $HCl + Cl_2$ mixture. When heated in an inert atmosphere, it is converted at about 220°C to impure UO_2Cl_2 and at temperatures above 400°C to U_3O_8 (Brown, 1979). $UO_2Cl_2 \cdot H_2O$ reacts with $P(C_6H_5)_4Cl$ by refluxing in a thionyl chloride solution to give $[P(C_6H_5)_4]UOCl_5$ on cooling. With smaller cations reductive chlorination to hexachlorouranates(V) occurs.

$UO_2Cl_2 \cdot H_2O$ and $UO_2Cl_2 \cdot 3H_2O$ have monoclinic ($P2_1/m$) and orthorhombic ($Pn2_1a$) symmetry, respectively. Neutron diffraction studies of $UO_2Cl_2 \cdot H_2O$ (Taylor and Wilson, 1974c) show that uranium has the common pentagonal bipyramidal coordination geometry with four chlorine and one water oxygen atoms in the equatorial plane. Infinite chains similar to those in UO_2Cl_2 are formed by sharing two Cl–Cl edges (Table 5.30).

Three basic hydroxide chlorides are observed in the $UO_3–HCl–H_2O$ phase diagram at 25°C, but only one, $[(UO_2)_2(OH)_2Cl_2(H_2O)_4]$, is reported to be congruently soluble (Prins and Cordfunke, 1975). The compound may be easily obtained as hydrolysis product of a UO_2Cl_2 solution prepared by dissolution of

UO_3 in concentrated HCl (Åberg, 1969). Thermal decomposition of the compound in air leads first to the hemi-hydrate $UO_2(OH)Cl \cdot 0.5H_2O$ at 80–120°C, from which the nearly anhydrous salt, $UO_2(OH)Cl$ is formed at about 250°C. The compound crystallizes with monoclinic symmetry (see Table 5.30) and has a structure in which two linear uranyl units are linked through a double OH bridge, the remaining coordination sites are occupied by one Cl atom and four O atoms from two H_2O molecules, resulting in an irregular planar pentagon (Åberg, 1969).

(*v*) *Uranium*(VI) *oxochloro complexes*

The typical representatives of this group have the composition: $M^{I}UOCl_5$ (e.g. M = $P(C_6H_5)_4$, $M^{I}_2UO_2Cl_4$ (e.g. M = Li, Na, K, Rb Cs, NH_4, $P(C_6H_5)_4$, $N(C_2H_5)_4$, and others), $M^{I}_2UO_2Cl_4 \cdot 2H_2O$ (M = Li, Na, K, Rb, or NH_4), $M^{II}UO_2Cl_4 \cdot 2H_2O$ (M = Mg, Ca, Sr, Ba, Zn, Zn, Cd, and others), $M^{I}UO_2Cl_3$ (e.g. M = $P(C_6H_5)_4$, $N(C_{10}H_{21})_4$, and others), $M^{I}(UO_2)_2Cl_5$ (e.g. M = Na, K, Rb, Cs, or NH_4), $M^{I}_2U_2O_5Cl_4$ (M = Na, K, Rb, or Cs), $M^{I}_2U_2O_5Cl_4 \cdot xH_2O$ (M = Na, K, Rb or Cs), $KNa_2(UO_2)_2Cl_7$, KUO_3Cl, $K_2U_3O_8Cl_4$, and $K_2(UO_2)_xCl_{2x+2}$ ($x = 2$, 3, or 4). The compounds have been prepared by variety of methods (Brown, 1979), most commonly by crystallization from organic solvents (methyl cyanide or ethanol solutions) or aqueous hydrochloric acid solutions of the corresponding chlorides, as well as by solid-state reactions. Some of them are air-sensitive (e.g. $[P(C_6H_5)_4]UOCl_6$) or are hydrated on exposure to moist air ($M^{I}_2UO_2Cl_4$ where M = Li to Rb and NH_4); they are soluble in some organic solvents.

Structure data (Brown, 1979) are available for a number of the compounds (see Table 5.30). In $M^{I}_2UO_2Cl_4$ there are discrete $UO_2Cl_4^{2-}$ units with linear O–U–O groups. The structure of $M_2U_2O_5Cl_4 \cdot 2H_2O$ (M = Rb or Cs) consists of discrete planar tetranuclear anions, $[(UO_2)_4O_2Cl_8(H_2O)_2]^{4-}$, in which the uranyl groups in the equatorial plane are linked by oxygen and chloride bridges. In the structure of $[N(C_6H_5CH_2)(CH_3)_3]_4[UO_2Cl_3O]_2$ there are puckered sheets of binuclear $[Cl_3O_2U\text{-}(\mu\text{-}O_2)\text{-}UO_2Cl_3]^{4-}$ anions parallel to (001), which are interleaved by the cations. The anion is built of two identical, distorted pentagonal bipyramides sharing the peroxo-group as a common edge. Oxochlorouranates of the formula $Ln_3UO_6Cl_3$ (Ln = La, Pr, or Nd) were prepared by heating stoichiometric amounts of $LnOCl/Ln_2O_3/U_3O_8$ (Ln = La or Nd) or $PrOCl/Pr_6O_{11}/U_3O_8$ in silica ampoules at 800–1000°C in an excess of chlorine (Henche *et al*., 1993). The crystals were investigated by X-ray diffraction methods (see Table 5.30) and high-resolution electron microscopy.

(*vi*) *Uranium*(VI) *perchlorates and related compounds*

The synthesis and characterization of uranyl(VI) perchlorate, $UO_2(ClO_4)_2$ and its hydrates $UO_2(ClO_4)_2 \cdot xH_2O$ ($x = 0$, 1, 3, 5, or 7) have been investigated by a number of authors (Brown, 1979). The heptahydrate has been obtained by

crystallization from aqueous solution at room temperatures. Vacuum drying of the compound at that temperature leads to the pentahydrate, and vacuum dehydration over sulfuric acid to the trihydrate. Further vacuum drying converts the latter to the monohydrate; in the temperature range 100–140°C anhydrous perchlorate $UO_2(ClO_4)_2$ is formed (Vdovenko *et al.*, 1963). All of the compounds are readily soluble in water and polar organic solvents, in many cases with the formation of stable uranyl(VI) perchlorate complexes. The interaction with oxygen and nitrogen donor ligands leads to the formation of the following types of complexes:

$UO_2(ClO_4)_2$5L: where L = pyridine, pyridine-*N*-oxide, antipyrene, dimethylsulfoxide, dimethylselenoxide, dimethylformamide, diphenylsulfoxide, thioxane oxide, urea, 1,3-dimethylurea, 1,3-diethylurea, hexamethylphosphoramide.

$UO_2(ClO_4)_2$4L: where L = trimethylphosphine oxide, triphenylphosphine oxide, tripropylphosphine oxide.

$UO_2(ClO_4)_2$3L: where L = octamethylphosphoramide, camphor, methyl cyanide, nonamethylimido-diphosphoramide.

$UO_2(ClO_4)_2$2L: where L = tributylphosphate, tributylphosphine oxide, nitromethane, dibutyl ether.

$UO_2(ClO_4)_4 \cdot 7H_2O$ crystallizes in the orthorhombic space group $Pca2_1$ The structure consists of $[UO_2(OH_2)_5]^{2+}$ and ClO_4^- ions, with two additional water of solvation. The crystal structure is held together by an extensive network of hydrogen bonds.The coordination polyhedron is a distorted pentagonal bipyramid (Alcock and Esperas, 1977). Some crystallographic and infrared data are are listed in Table 5.30.

(*vii*) *Uranium*(VI) *oxide bromides and complex oxobromo compounds*

Uranyl(VI) *bromide and related complexes*

One of the most convenient methods for the preparation of UO_2Br_2 is the reaction of anhydrous UBr_4 with oxygen at a carefully controlled temperature in the range 150–160°C; at higher temperature, U_3O_8 is formed (Brown, 1979). An alternative method involves the electrochemical anodic oxidation of uranium in CH_3CN/Br_2 solution in the presence of dry oxygen. The resulting solution of UO_2Br_2 may also be used for the preparation of adducts by adding a two-fold excess of the appropriate ligand (Kumar and Tuck, 1984).

The compound is a bright red, hygroscopic solid which turns yellow on exposure to moisture. It is thermally unstable and appears to lose bromine slowly even at room temperature. The decomposition is complete within 48 h in an inert atmosphere at 350°C. UO_2Br_2 is extremely soluble in water and polar organic solvents. Numerous complex compounds have been prepared by reactions with a variety of ligands in anhydrous solvents, for example, of the following types: UO_2Br_2L (L = methyl cyanide), $UO_2Br_2$2L (L = acetic anhydride, ether, *N*,*N*–dimethylacetamide, antipyrine, *N*-methylacetanilide,

$(CH_3)_3PO$, $(C_2H_5)_3PO$, $(C_6H_5)_3PO$, etc), $UO_2Br_2 3L$ (L = dimethylformamide), $UO_2Br_2 4L$ (L = dimethylsulfoxide) $UO_2Br_2 \cdot xNH_3$ (x = 2, 3, and 4), $UO_2Br_4 \cdot (LH)_2$ (L = 2,2′-dipyridine,1,10-phenanthroline) and $(Et_4N)_2UO_2Br_4$. In addition, a number of oxo-tetrabromo complexes of the $M_2UO_2Br_4$ (M = Cs, $P(C_6H_5)_3CH_3$, $P(C_6H_5)_3H$, $P(CH_3)_3H$, $P(C_6H_5)_3C_6H_5CH_2$, etc.) and $M_2UO_2Br_4 \cdot 2H_2O$ (M = NH_4, K, or Rb) types have been obtained by reaction of UO_2Br_2 with the appropriate ligands in HBr or in anhydrous organic solvents (Brown, 1979, Kumar and Tuck, 1984).

Uranyl(VI) hydroxide bromide and bromide hydrates

A stable hydrate of the formula $UO_2Br_2 \cdot 3H_2O$ is obtained in the form of dark yellow needles by crystallization from an aqueous solution of HBr and UO_2Br_2, followed by vacuum drying (Peterson, 1961). The dehydration of the trihydrate over phosphoric acid leads to the formation of the monohydrate $UO_2Br_2 \cdot H_2O$. The hydrates may be also obtained by other methods (Brown, 1979). Crystallization of UO_2Br_2 from acid-deficient solutions leads to the formation of $UO_2(OH)Br \cdot 2H_2O$ (alternative formulations are: $[U_2O_5(H_2O)]Br_2 \cdot 4H_2O$ or $[UO_2(OH)_2UO_2]Br_2 \cdot 4H_2O$). The compound is isostructural with its chloride analog $[UO_2(OH)_2UO_2]Cl_2 \cdot 4H_2O$; it is converted to $UO_2(OH)Br$ when heated at 200°C.

The hydrates are readily soluble in water and numerous organic solvents like ethanol, ether, amyl alcohol, etc. $M_2UO_3Br_2$ (M = NH_3 or K) is formed by reacting the monohydrate with ammonia gas or a stiochiometric quantity of KOH (Brown, 1979). According to Peterson (1961) the trihydrate is stable in dry air and may lose one molecule of water at 60°C without decomposition.

Uranium(VI) oxobromo complexes

The synthesis and characterization of a large number of complex oxobromo compounds containing uranium(VI) have been summarized by Brown (1979). Oxo-tetrabromo complexes of the $M_2UO_2Br_4 \cdot 2H_2O$ type (M = NH_4, Na, K, or Rb) were prepared from aqueous or alcoholic HBr solutions of uranyl bromide by precipitation with appropriate MBr. The anhydrous analogs were obtained by heating at 120°C in an inert atmosphere. With large cations, for example Cs^+ or pyridinium, only anhydrous complexes of the $M_2UO_2Br_4$-type are formed.

Other anhydrous complexes of this type were prepared by reactions of uranyl bromide solutions in ethanol or methyl cyanide with various phosphonium bromides (e.g. $P(C_6H_5)_3C_4H_9Br$, $P(C_6H_5)_3HBr$, $P(C_6H_5)_3C_6H_5CH_2)Br$, $P(C_2H_5)_3HBr$, and $P(C_3H_7)_3HBr$) as well as with $N(C_2H_5)_4Br$ (in ethanol), $N(CH_3)_4Br$ (in a C_2H_5OH–HBr mixture), choline bromide, $(C_5H_{14}NO)Br$ (in methanol), and acetylcholine bromide, $(C_7H_{16}NO_2)Br$ (in methanol). The reaction of UO_2Br_2 with tetradecylammonium bromide in anhydrous benzene results in the formation of a viscous liquid of the $[N(C_{10}H_{21})_4]UO_2Br_3$. In the presence of traces of water in benzene compound converts into the oxo-tetrabromo complex.

The oxobromo complexes are yellow and readily soluble in aqueous solutions; those with organic cations also in anhydrous solvents such as acetone, benzene, methyl cyanide, and nitromethane. Structure investigations reveal a distorted octahedral geometry in complexes with M = Cs, $N(CH_3)_4$, $N(C_3H_7)_4$, and $C_7H_{16}NO_2$, where the U–O and U–Br bond distances range from 1.70 to 1.90 and 2.78 to 2.86 Å, respectively. For structural data, see Table 5.30. Extensive information on the infrared and Raman spectra is also available (Brown, 1979). On the basis of these data the observed frequencies for various oxotetrabromo complexes can be assigned as follows:

IR (cm^{-1}): ν(U–O, asym. stretch.) = 895–934; ν(O–U–O deformation) = 243–263; ν(U–Br stetch.) = 160–180; Raman (cm^{-1}): ν(U–O sym. stretch.) = 826–835, ν(U–O–Br bend.) = 190–198, ν(U–Br stretch.) = 167–172 ν(U–Br bending mode) = 81–83. The fluorescence spectrum of $Cs_2UO_2Br_4$ measured at 14.3 K reveals the existence of two sites of different symmetry, which has been supported by the observed differences in the fluorescence relaxation time. The solution spectra of $[N(C_{10}H_{21})_4]UO_2Br_3$ and $[N(C_{10}H_{21})_4]UO_2Br_4$ in anhydrous benzene have absorption bands at 508, 491, 483, 447, and 431 nm and at 497, 480, 464, and 449 nm, respectively. For $[P(C_6H_5)_3H]_2 \cdot UO_2Br_3$ in methyl cyanide solution these bands appear at 19800, 20080, 20790, 21550, 20220, and 22880 cm^{-1}. As one should expect, the absorption bands of the solid state reflectance spectra of $[C_5H_{14}NO]_2UO_2Br_4$ and $[C_7H_{16}NO_2]UO_2Br_4$ are somewhat shifted towards longer wavelengths as compared to their chloro analogs.

The reactions of uranyl bromide with various metal bromides in aqueous HBr lead to the formation of the following hydrated bromo compounds:

$MUO_2Br_4 \cdot xH_2O$ (M = Sr, $x = 3$; M = Zn, Mg, $x = 4$; M = Ca, $x = 8$);
$MUO_2Br_5 \cdot xH_2O$ (M = La, $x = 3$; M = Y, $x = 5$);
$MUO_2Br_6 \cdot 4H_2O$ (M = Ce or Th);
$MU_3O_8Br_5 \cdot xH_2O$ (M = Co, $x = 12$; M = Sc, $x = 8$), and
$Be_2UO_2Br_6 \cdot 8H_2O$, $Mn_3UO_2Br_8 \cdot 11H_2O$, and $HgU_3O_8Br_4 \cdot 4H_2O$

The complexes may be dehydrated in an oxygen atmosphere at about 200°C. $LaUO_2Br_5$, YUO_2Br_5, and $CeUO_2Br_5$ are converted to $LaUO_2(O_2)Br$, $YUO_2(O_2)Br$, and $LaUO_2(O_2)Br$, respectively, at 290–305°C. Decomposition at high temperature results in the formation of appropriate uranates, $CaUO_4$, Mn_3UO_6, $Co_2U_6O_{21}$, and HgU_3O_{10}, etc. The heating of $K_2UO_2Br_4$ at 250°C and $(NH_4)_2K_2UO_2Br_4$ at 250–350°C in an oxygen atmosphere results in the formation of $K_2UO_3Br_2$ and $(NH_4)_2UO_3Br_2$, respectively. $K_2UO_3Br_2$ may be also prepared by interaction of uranyl bromide monohydrate with KOH, or by heating K_2UO_4 with gaseous hydrogen bromide, whereas $(NH_4)_2UO_3Br_2$ is obtained by action of gaseous NH_3 on $UO_2Br_2 \cdot H_2O$. Compounds of the composition $K_2U_2O_6Br_2$ and $K_2U_3O_9Br_2$ have been prepared by heating K_2UO_4 or $K_2U_3O_{10}$ with gaseous HBr, respectively. A phase of the composition $K_xUO_3Br_x$ ($x = 0.9$) is obtained when UO_3 and KBr are heated

at 300–550°C *in vacuo*. The compound is isostructural with $K_xUO_3Cl_x$ (see Table 5.30).

The interaction of $M_2UO_2Br_4 \cdot 2H_2O$ (M = K or Rb) with $UO_2(OH)_2$ results in the formation of compounds containing the tetranuclear unit $M_2[(UO_2)_4O_2(OH)_2Br_4(H_2O)_4] \cdot 2H_2O$. The complexes lose four H_2O molecules in an inert atmosphere at 60°C and form $M_2U_4O_{11}Br_4$ at ≈200°C. The compounds are triclinic ($P\bar{1}$) and isostructural with the chloro analogs (see Table 5.30).

(*viii*) *Uranium*(VI) *compounds with iodine*

$UI_4 \cdot 4$dmf is obtained by electrochemical oxidation of uranium anodes in *N*,*N*-dimethylformamide (dmf) (Kumar and Tuck, 1984). The preparation of an extremely unstable UO_2I_2 has been reported in a number of papers (Brown, 1979; du Preez and Zeelie, 1989). The compound has not been obtained in a pure form but relatively stable compounds, such as $UO_2I_2 \cdot 4$dmf (yellow, m.p. = 156°C; dmf = dimethylformamide), $UO_2I_2 \cdot 2$tppo (orange red, m.p. = 268°C; tppo = triphenylphosphine oxide), $UO_2I_2 \cdot 2$tmu (orange, tmu = *N*,*N*,*N*′,*N*′-tetramethylurea), $UO_2I_2 \cdot 5CO(NH_2)_2 \cdot H_2O$ (orange-red), $UO_2I_2 \cdot 2$hmpa (orange, hmpa = hexamethylphosphoric triamide), $UO_2I_2 \cdot xNH_3$ ($x = 2$ or 3), $UO_2I_2 \cdot 2$tbso (yellow-green, tbso = di-*tert*-butyl sulfoxide), $UO_2I_2 \cdot 2$dmeu (dmeu = *N*,*N*′-dimethylethylene urea), $(PPh_4)_2UO_2I_4$ (black), $UO_2I_2 \cdot 2Et_2O$ (decomposes at room temperature by evolving iodine), may be separated from solutions in water and various organic solvents (for example, ether, methanol, ethanol, amyl alcohol, methyl acetate, ethyl acetate, pyridine) (Brown, 1989; du Preez and Zeelie, 1989). A red uranyl(VI) iodo compound, $[P(C_6H_5)_3C_4H_9]_2UO_2I_4$, has been obtained by interaction of uranyl(VI) iodide with phosphonium iodide in a methyl cyanide solution (Day and Venanzi, 1966).

The addition of soluble iodides to uranyl nitrate solutions at room temperatures results in the formation of the uranyl(VI) iodide dihydrate, $UO_2(IO_3)_2 \cdot 2H_2O$. The compound is converted to α-$UO_2(IO_3)_2 \cdot H_2O$ when UO_2NO_3 and iodic acid are mixed in boiling nitric acid. β-$UO_2(IO_3)_2 \cdot H_2O$ is formed by recrystallization from water in the absence of acid. The compound $(UO_2)_2I_2O_9$ has been obtained by addition of potassium periodate to a cold solution of $UO_2(NO)_2$. The preparation of a number of uranium(VI) iodato and periodato complexes has also been reported: $KUO_2(IO_3)_3 \cdot 3H_2O$, $(KIO_4)_2(UO_2)_2O_2 \cdot 5H_2O$, $[Co(NH_3)_6][(UO_2)_2(IO_3)_7] \cdot 10H_2O$, $K_2I_2O_5(UO_2)_2$, $H(UO_2)_2IO_6 \cdot 8H_2O$, $NaH_2UO_2IO_6 \cdot 7H_2O$, $Ba(H_2UO_2IO_6)_2 \cdot xH_2O$ (Brown, 1979).

(*ix*) *Mixed halogeno-complexes*

Mixed uranyl(VI) halogeno-compounds $M^I_2UO_2Cl_2Br_2$ (M^I = NH_4, Na, K, or Cs), $Cs_2UO_2X_3Y$ (X and Y = Cl or Br), $[N(C_{10}H_{21})_4]_2[UO_2X_3I]$ (where X = Cl or Br), and $[P(C_6H_5)_3C_4H_9]_2[UO_2Cl_2Br_2]$, $[P(C_6H_5)_3C_4H_9]_2[UO_2Br_2I_2]$ have

been obtained by interaction of uranyl halides with appropriate univalent bromides or iodides in aqueous HBr solutions, or in anhydrous organic solvents such as benzene and methyl cyanide. Alternative routes to these and similar mixed halogeno complexes have been also reported (Brown, 1968, 1979). $Cs_2UO_2BrCl_3$ and $Cs_2UO_2Br_3Cl$ (Ellert *et al*., 1965) have been obtained by varying the HBr concentration in the interaction between CsBr and $UO_2Cl_2 \cdot H_2O$ The preparation of the dihydrate $K_2UO_2Br_2Cl_2 \cdot 2H_2O$ has been achieved by crystallization from 20% HCl containing KBr and UO_2Cl. Dehydration of the compound in an inert atmosphere at 110°C leads to $K_2UO_2Br_2Cl_2$ (Lucas, 1964). Dihydrates of the composition $M_2UO_2Br_{4-x}Cl_x$ (M = NH_4 or Rb; x = 1, 2, or 3) have also been isolated (Kharitonov *et al*., 1967).

Complexes containing alkali metal cations are soluble in water and aqueous acetic acid solution; those containing phosphonium or tetralkylammonium cations are soluble in numerous non-aqueous solvents like methyl cyanide, benzene, and ethanol. In water, hydrolysis takes place. Dehydration of the compound in an inert atmosphere at ≈110°C leads to the anhydrous complexes (Lucas, 1964).

X-ray powder diffraction data are available for $Cs_2UO_2Cl_2Br_2$, $Cs_2UO_2BrCl_3$, $Cs_2UO_2Br_3Cl$ (Ellert *et al*., 1965), $K_2UO_2Cl_2Br_2$, $K_2UO_2Br_2Cl_2 \cdot 2H_2O$, and $K_2U_2O_5Cl_2Br_2$ (Lucas, 1964). The ν(U–O) asymmetric stretching vibrations occur at 905–910 cm^{-1} for $M_2UO_2Br_{4-x}Cl_x \cdot 2H_2O$ (M = NH_4, K or Rb) and at 907–922 cm^{-1} for various anhydrous complexes. In the IR spectrum of $[P(C_6H_5)_4]UOBr_4Cl$, they appear at 838 cm^{-1}.

The metal–halogen stretching frequencies have been reported for: $[P(C_6H_5)_3C_4H_9]_2UO_2Br_2Cl_2$, ν(U–Cl) = 260 cm^{-1}; $[N(C_{10}H_{21})_4]_2UO_2BrCl_3$, ν(U–Cl) = 255 cm^{-1}, ν(U–Br) = 165 cm^{-1}; $[N(C_{10}H_{21})_4]_2UO_2Cl_3I$, ν(U–Cl) = 236 cm^{-1}, and ν(U–I) = 135 cm^{-1}, with the uranyl deformation mode at 261 cm^{-1} (Brown, 1979). The first high-intensity bands in the visible spectra of $[N(C_{10}H_{21})_4]_2UO_2Cl_3I$, and $[N(C_{10}H_{21})_4]_2UO_2BrCl_2I$ in benzene solutions, were recorded at about 20000 cm^{-1} (Vdovenko *et al*., 1969).

5.8 CHEMICAL BONDING IN URANIUM COMPOUNDS

5.8.1 U(III) and U(IV) compounds

In general, the discussion of chemical bonding in U(III) and U(IV) compounds is related to metal–organic complexes as discussed in Chapters 25 and 26. A recent review of the organometallic chemistry of lanthanides and actinides has been given by Hyeon *et al*. (2005). An early example is given in a study by Bursten and Strittmatter (1987) that discussed the bonding in $[Cp_3UCO]$ and $[Cp_3UCO]^+$, where Cp is cyclopentadiene, η^5-C_5H_5. They suggested an extensive U(III) 5f–CO π-back-bonding, an effect that decreases significantly on oxidation to U(IV). The coordination of dinitrogen in $[\{U(NN'_3)\}_2(\mu_2{-}\eta^2{:}\eta^2{-}N_2)]$, where NN'_3 is $N(CH_2CH_2NSiBu^tMe_2)_3$, was studied by Roussel and Scott (1998). The end-on

coordination is consistent with U → N back-bonding, but the authors suggest that the effect is minor. The role of the 5f orbitals in back-bonding has also been studied by comparison with the bonding in lanthanide compounds in oxidation states 3+ and 4+. A typical example is given in a study by Berthet *et al.* (2002) of the selective complexation of U(III) over Ce(III) and Nd(III) in 2,2′:6,2″-terpyridine complexes. This ligand forms much stronger complexes with uranium than cerium in solution. The authors probed the possible reasons behind this by determination of the X-ray crystal structure of the complexes $[MI_2(terpy)_2]I$, M = Ce, Nd, $[CeI_2(terpy)_2(H_2O)]I$, and $[UI_2(terpy)_2(pyridine)]I$. They suggest that the shortening of the average M–N distance by 0.05 Å in the uranium complex as compared to that of cerium might be a result of a stronger π back-bonding interaction between uranium and the terpyridyl ligand. The evidence for back-bonding is indirect and more direct information is necessary to draw definite conclusions, e.g. Di Bella *et al.* (1996) point out, based on electronic structure calculations and photoelectron spectroscopic data, that the bonding in isoleptic 4f and 5f M(III) bis-(cyclopentadienyl) is very similar. Experimental data and quantum chemical calculations on different model systems indicate 5f orbital participation in chemical bonding, but the extent of this and its chemical effects are far from clear. A detailed discussion of the quantum chemistry of uranium and other actinides is given in Chapter 17.

Roos and Gagliardi have used quantum chemical methods to explore the stability and possible existence of compounds with U–U bonds, similar to those found for some d-transition elements, e.g. Cr, Mo, W, Tc and Re. They predicted stable diatomic U_2 with a quintuple U–U bond and a bond distance of 2.43 Å (Gagliardi and Roos, 2005a). Gagliardi *et al.*, (2005) found that also U_2^{2+} is a stable ion with several low-lying electronic states, all with U–U bond distances around 2.30 Å.

Compounds containing U–U bonds have been identified by matrix isolation techniques; H_2U–UH_2 by Souter *et al.* (1997) and O-U–U-O by Gorokhov *et al.* (1974). In their most recent paper Gagliardi and Roos (2005b) have studied the stability and chemical bonding in U_2Cl_6, $U_2Cl_6^{2-}$, $U_2(OCHO)_4$, $U_2(OCHO)_6^{2-}$, and $U_2(OCHO)_4Cl_2^{2-}$. It seems unlikely that compounds where the formal oxidation state of uranium is +2 can be prepared, but those with the oxidation state of +3 seem more probable. $U_2Cl_6^{2-}$, has a similar structure and bonding as $Re_2Cl_6^{2-}$, with the eclipsed conformation as the most stable one. The weakest bond is found in $U_2(OCHO)_4Cl_2^{2-}$, where the U–U distance is 2.80 Å.

5.8.2 UF_5 and UF_6 compounds

The bonding in these compounds has been discussed by Rosén and Fricke (1979), Wadt and Hay, (1979), and Onoe *et al.* (1993, 1997); these compounds can presumably be used as models for the bonding also in other uranium(V) and uranium(VI) halides. The authors point out that there is extensive involvement of 5f, 6p, and 6d orbitals in the U–F bonds, the orbital population in the 7s and 7p orbitals is smaller, and relativistic effects are of great importance for the

chemical bonding. The participation of the 5f orbitals in the bonding explains the fluxional geometry of UF_5 between C_{4v} and D_{3h} (Onoe *et al.*, 1997).

5.8.3 Uranyl(V) and uranyl(VI) compounds

The linear "yl"-ions in aqueous systems are unique for the actinide elements; in other "yl"-ions, such as VO_2^+, MoO_2^{2+}, and WO_2^{2+}, the oxygen atoms are mutually *cis*, thereby maximizing $(p_\pi) \rightarrow M(d_\pi)$ bonding. A linear MO_2^{2+} group is known in compounds of technetium, rhenium, ruthenium, and osmium, but the corresponding aqua-ions are unknown (a recent discussion of the electronic structure of these *trans*-dioxometal complexes is found in Hummel *et al.*, 2006). The short U(VI)–O_{yl} bond distance, approximately 1.75 Å, indicates a strong multiple uranium–oxygen bonding, one of σ and two of π character. The uranium–"yl" distance in UO_2^+ is somewhat longer due to the smaller effective charge of uranium (Vallet *et al.*, 2004a). The orbitals involved in the uranium–"yl"-oxygen bonds have been extensively discussed (see Denning, 1992; Kaltsyoannis, 2000; Matsika *et al.*, 2001 for a review); the MO diagram in Fig. 5.49 illustrates the bonding.

The bonding molecular orbitals are $\sigma_g^2\ \sigma_u^2\ \pi_g^4\ \pi_g^4$ with 5fδ and 5fφ as the lowest unoccupied orbitals. The bonding orbitals have mainly O 2p character and the uranyl(VI) ion can therefore be described as $O^{2-}{\equiv}U^{6+}{\equiv}O^{2-}$.

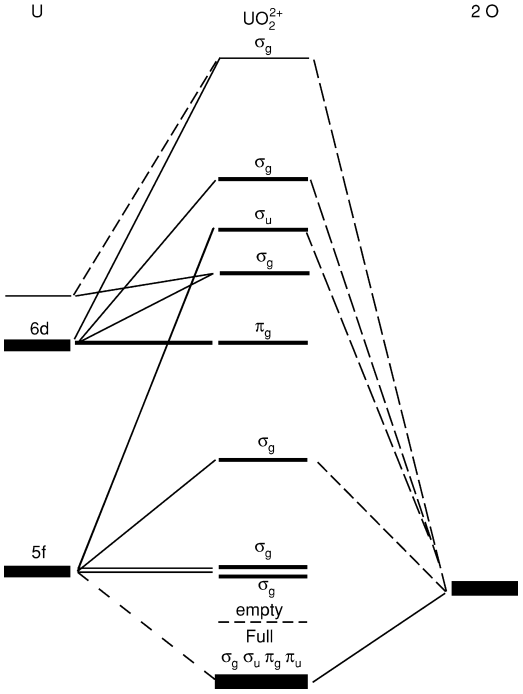

Fig. 5.49 *Schematic molecular orbital diagram for the uranyl(VI) ion.*

The nonbonding and antibonding orbitals have 5f and 6d character. The ordering of the bonding orbitals and the HOMO in UO_2^{2+} is not straightforward (de Jong *et al.*, 1999); Denning (1992) and later Kaltsyoannis (2000) suggested the order $\pi_g < \pi_u < \sigma_g << \sigma_u$, where σ_u is the highest occupied orbital. The significant energy gap between the σ_g and σ_u orbitals is traced to the filled–filled interactions between the semi-core 6p orbitals and the σ_u valence level, the 'pushing from below' mechanism. Triatomic UN_2 and UON^+ are isoelectronic with UO_2^{2+} and Pyykkö *et al.* (1994) suggested that these and other triatomic groups could have a significant stability. This was confirmed in experimental studies by Brown and Denning (1996) who prepared a number of stable compounds containing the linear –N≡U=N– and O=U=N– groups and discussed their chemical bonding. Kaltsyoannis (2000) made a more detailed study using density functional methods and concluded that the U–N bond is significantly more covalent than the U–O bond in UON^+ and UO_2^{2+} and that the uranium f-orbitals play a more important role than the d-orbitals in the metal to ligand bonding. He also pointed out that the U–N bond in iminato complexes is best described as a triple bond.

The previous correlation diagram can also be used to describe the bonding in UO_2^+, where the single 5f electron is located in one of the nonbonding 5fδ or 5fφ orbitals.

Tatsumi and Hoffmann (1980) and Wadt (1981) have discussed the electronic reasons for the change from the linear geometry in UO_2^{2+} to the *cis*-geometry in MoO_2^{2+}. Dyall (1999) and Straka *et al.* (2001) have discussed the bonding in actinyl ions and showed that the 5f character in the M–O bond increases steadily through the actinide series, while the 6d population remains nearly constant. The nonlinear O–M–O bonds are a result of an increased 6d population. As a result of the strong covalent $U–O_{yl}$ bonding, the formal charge of uranium is much lower than +6, +2.43 for $UO_2(H_2O)_5^{2+}$ in gas phase (Vallet *et al.*, 2004a); the charge of the 'yl' oxygen atoms is –0.43. Because of their negative charge, the 'yl' oxygen atoms in UO_2^{2+} and UO_2^+ are Lewis bases, resulting in the formation of 'cation–cation' complexes of type O=U=O- - - M (Section 5.10.2f). The negative charge on the 'yl'-oxygen atoms varies with the nature of the ligands in the equatorial plane and by proper ligand choice, the Lewis basicity of the 'yl'-oxygen atoms can be significantly increased, resulting in coordination of strong Lewis acids such as $B(C_6F_5)_3$ (Sarsfield and Helliwell, 2003). The charges on U and oxygen in $UO_2(H_2O)_5^+$ are 2.19 and –0.66, respectively (Vallet *et al.*, 2004a), making the uranyl(v) oxygen atoms even stronger Lewis bases than in uranyl(vi). A more detailed discussion of the electronic structure and energy levels of the other oxidation states of uranium is given in Chapter 16. The slight variations in the effective charge of uranium in different compounds result in small differences in the $U–O_{yl}$ bond distance and the effect is also noticeable as small changes in the vibrational stretch frequencies of the UO_2 group in infrared and Raman spectra. In the same way the 'yl'-stretch frequency is lower in UO_2^+ than in UO_2^{2+}, indicating a weaker bond in the former ion.

5.9 STRUCTURE AND COORDINATION CHEMISTRY OF URANIUM COMPLEXES IN SOLUTION AND THE SOLID STATE

The structure of complexes in solution is characterized by their coordination geometry, coordination number, and bond distances. The coordination geometry in solid-state structures is also influenced by additional factors, such as the efficiency of packing, the charge distribution in the structure, and the formation of hydrogen bond networks. The solid-state structures are often good models for bond distances and coordination geometry in solution. The structure in solution refers to discrete ions and molecules, more or less solvated, depending on the nature of the solvent and the charge of the complex. In some cases solid-state structures may contain discrete ions and molecules, but in general, the solid is better regarded as a 'polymer'. For example, UO_2CO_3(s) is a layer structure that does not contain isolated UO_2CO_3 units (see Fig. 5.54), while $Na_4UO_2(CO_3)_3$(s) contains discrete complexes of $UO_2(CO_3)_3^{4-}$ (Fig. 5.53).

The three-dimensional structures can be described using polyhedra and nets, and for simple structures, using packing of spheres (Chapters 3 and 4 in Wells, 1990). Polynuclear complexes are more common in the solid state than in solution, presumably as a result of the stronger electrostatic interactions in the solid phase. The water solvent with its high dielectric constant and strong hydrogen bond donor/acceptor properties reduces the stability of polynuclear complexes, except those involving hydroxide and oxide donors. Polynuclear fluoride complexes are very common in the solid state (Allen *et al.*, 2000), but are not formed in significant amounts in aqueous solution. This is presumably a result of the strong hydrogen bond acceptor properties of fluoride that makes hydrogen bonding to the water more favored than fluoride bridge formation between uranium atoms.

The stoichiometry, coordination number, and the number of available donor atoms per uranium atom indicate whether a certain compound contains isolated complexes, or if chains, layer structures, or three-dimensional networks are formed. Networks are common in oxide, uranate, phosphate, arsenate, and silicate compounds where they are a result of the sharing of oxygen donor atoms between two or more metal ions. These compounds are sparingly soluble and have a variable stoichiometry, (*cf.* Section 5.7.2).

The structure principles are demonstrated in the structure models of uranium compounds in oxidation states 3+, 4+, and 6+ described in the following sections. The largest number of structures are found for uranium(VI) compounds, many of which can be prepared from aqueous solution. In these compounds, the linear UO_2 unit is inert and the additional ligands in the coordination sphere are located in, or close to the plane through uranium and perpendicular to the UO_2 axis; the number of coordinated ligands in the plane varies between four and six; in solution, these ligands are labile, i.e. they can rapidly exchange with free ligand or in ligand substitution reactions as discussed in Section 5.10.3.

5.9.1 Uranyl(VI) compounds

The coordination chemistry of U(VI) differs from that of the d-transition and main-group elements. The common coordination geometry in UO_2^{2+} complexes with small ligands is a pentagonal bipyramid, with all labile ligands in the plane perpendicular to the linear UO_2 unit. Other coordination geometries are possible; a number of oxides and uranates have distorted octahedral or pentagonal bipyramidal structure, (Section 5.7.2.2, Fig. 5.25). Isolated ions of $UO_2(OH)_4^{2-}$ are found in the compound $[Co(NH_3)_6]_2[UO_2(OH)_4]_3 \cdot xH_2O$, the X-ray structure of which was determined by Clark *et al.* (1999) (Fig. 5.50), $UO_2(OH)_4^{2-}$ has a square bipyramidal geometry also in solution (Clark *et al.*, 1999; Wahlgren *et al.*, 1999; Moll *et al.*, 2000a); this geometry may also occur in complexes where there is a strong steric interference between coordinated organic ligands. The tetra-hydroxide complex has also been studied using quantum chemical methods (Schreckenbach *et al.*, 1998; Wahlgren *et al.*, 1999; Vallet *et al.*, 2001).

The structure of $K_2UO_2(SO_4)_2 \cdot 2H_2O$ is an example of pentagonal bipyramidal coordination consisting of uranium(VI) bipyramids linked in three dimensions by bridging sulfate groups (Niinistö *et al.*, 1979). Each sulfate acts as a bridge between two uranium atoms, leaving two non-coordinated sulfate oxygen atoms. The remaining coordination site on uranium is occupied by one of the two water molecules (Fig. 5.51).

A different structure (Burns and Hayden, 2002) still with pentagonal bipyramidal coordination is found in $Na_{10}[UO_2(SO_4)_4](SO_4)_2 \cdot 3H_2O$, shown in Fig. 5.52. This structure contains discrete complexes where the five-coordination in the equatorial plane is achieved by one chelating and three monodentate sulfate ions.

A hexagonal bipyramidal geometry with six ligands in the equatorial plane is in general obtained with ligands that can form chelates that have a small distance between their donor atoms. Examples are nitrates, $M[UO_2(NO_3)_3]$, where $M = NH_4$, K, Rb, Cs, and Tl (Zalkin *et al.*, 1989), carbonates such as $K_4UO_2(CO_3)_3$ (Anderson *et al.*, 1980), and acetates (Navaza *et al.*, 1991); these

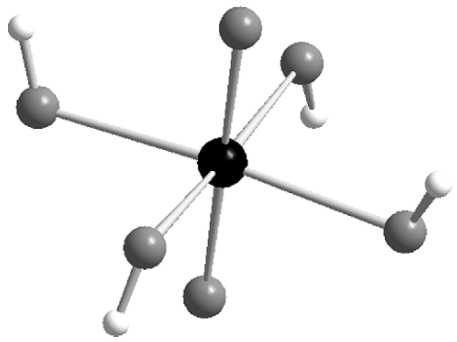

Fig. 5.50 *The structure of* $UO_2(OH)_4^{2-}$ (*from Clark* et al., 1999).

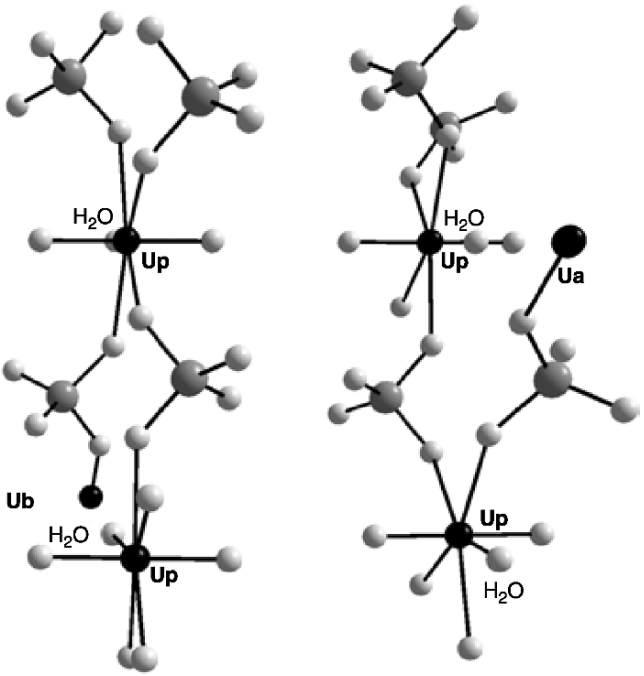

Fig. 5.51 *Coordination geometry and the three-dimensional linking in* $K_2UO_2(SO_4)_2 \cdot 2H_2O$ (*from Niinistö* et al., 1979). *The uranium atoms denoted* U_p *are located in the same plane and those denoted* U_a *and* U_b *in planes above and below this. The potassium atoms and one of the water molecules* (*not shown in the figure*) *provide additional links between the coordination polyhedra through coordination to the back end of the sulfate ions and through hydrogen bonding.*

compounds contain nine oxygen donors per uranium and from the geometry of the ligand, it is obvious that at most two per ligand can be coordinated to the same uranium atom. The donor atoms form hexagonal bipyramidal coordination together with the 'yl'-oxygen atoms. This results in structures that are composed of discrete complexes (Fig. 5.53). However, it is also feasible to have isomers; isolated pentagonal bipyramidal geometry is obtained if one of the ligands is coordinated through a single oxygen atom as in $UO_2(\text{oxalate})_3^{4-}$, discussed by Vallet *et al*. (2003). The only way to distinguish between these alternatives is through a structure determination or by using quantum chemical methods.

In UO_2CO_3(s), there are three oxygen donors per uranium and therefore the structure cannot contain isolated complexes; it turns out to be a layer structure where each oxygen donor is shared between two adjacent uranium atoms giving rise to hexagonal bipyramidal coordination (Fig. 5.54). This coordination geometry is very similar to that in the tris-carbonato complex (Fig. 5.53), but the three-dimensional structure of the latter is very different.

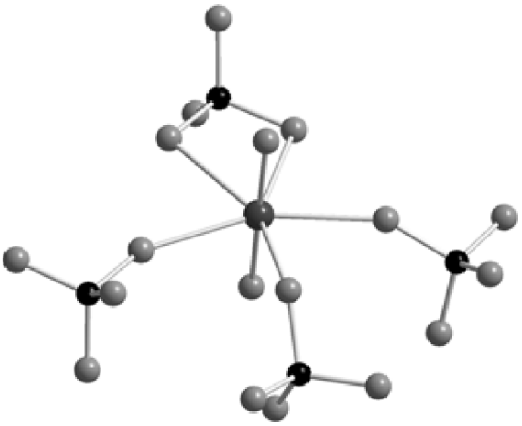

Fig. 5.52 *The coordination geometry of the* $UO_2(SO_4)_4^{6-}$ *ion in* $Na_{10}[UO_2(SO_4)_4](SO_4)_2 \cdot 3H_2O$ (*Burns and Hayden,* 2002). *One sulfate ion forms a chelate while the other three sulfate ions are monodentate.*

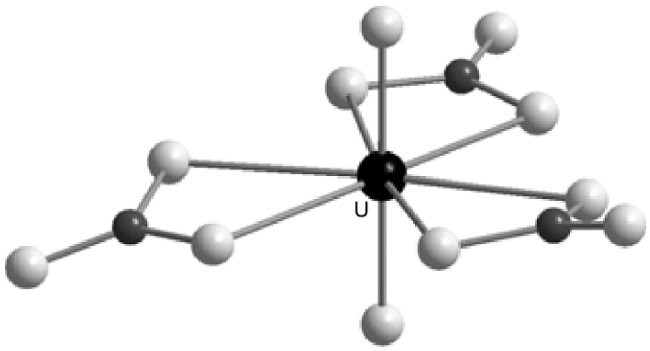

Fig. 5.53 *The coordination geometry, a hexagonal bipyramid, in* $K_4UO_2(CO_3)_3$ (*from the X-ray structure of Anderson* et al., 1980). *The ion* $[UO_2(CO_3)_3]^{4-}$ *occurs as discrete units in the structure; these units are linked through coordination to the counter ion* K^+.

Rare examples of six-coordination are also known in compounds containing organic ligands, e.g. $[UO_2(OTf)_2(bipy)_2]$ and $[UO_2(phen)_3][OTf]_2$, where bpy and phen denote bipyridine and phenantroline, respectively, and OTf^- the weakly coordinating triflate ion. Berthet *et al.* (2003) have determined the structure (Fig. 5.55) of these compounds, where the six nitrogen donors in the ligands are separated into two parallel and staggered equilateral triangles, (N2, N4, N6) and (N1, N3, N5) with the UO_2-axis perpendicular to the triangles. The uranium atom is equidistant, about 0.6 Å from these planes. The distortion is a result of geometric constraints in the chelating ligands.

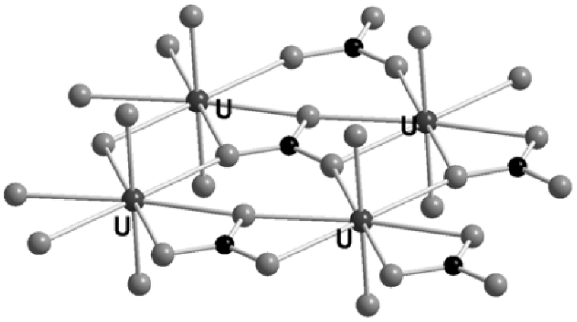

Fig. 5.54 *Part of the layer structure in $UO_2CO_3(s)$ showing the hexagonal bipyramidal coordination geometry of U(VI). By sharing each of the carbonate oxygens between two adjacent uranium atoms, six coordination in the plane perpendicular to the linear UO_2^{2+} ion is achieved. The structure is based on the X-ray study of Christ* et al. (1955).

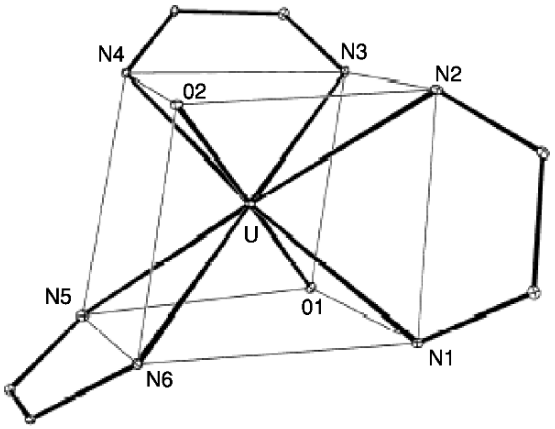

Fig. 5.55 *The coordination geometry for the six-coordinated U(VI) in $[UO_2(OTf)_2(bipy)_2]$ and $[UO_2(phen)_3][OTf]_2$; bpy denotes bipyridine, phen denotes phenantroline, and OTf the weakly coordinating triflate ion* (*from Berthet* et al., 2003, *reproduced by the permission of Royal Society of Chemistry*).

Uranium(VI) forms a number of peroxide complexes both in solution and in the solid state where the peroxide ligand is bonded 'side-on' to uranium as shown in Fig. 5.56a and b. The first one is the very rare mineral studtite, $UO_2(O_2)(H_2O)_2$ (Burns *et al.*, 2003); this compound has also been identified as a corrosion product on $UO_2(s)$ formed as a result of α-radiolysis (Sattonnay *et al.*, 2001); the second one is the structure of $Na_4[UO_2(O_3)_2](H_2O)_9$ from Alcock (1968). A number of other peroxide compounds and complexes in solution have been prepared by adding hydrogen peroxide to uranyl(VI) solutions; the sulfate and malonate systems were studied by Gurevich *et al.* (1971a,b);

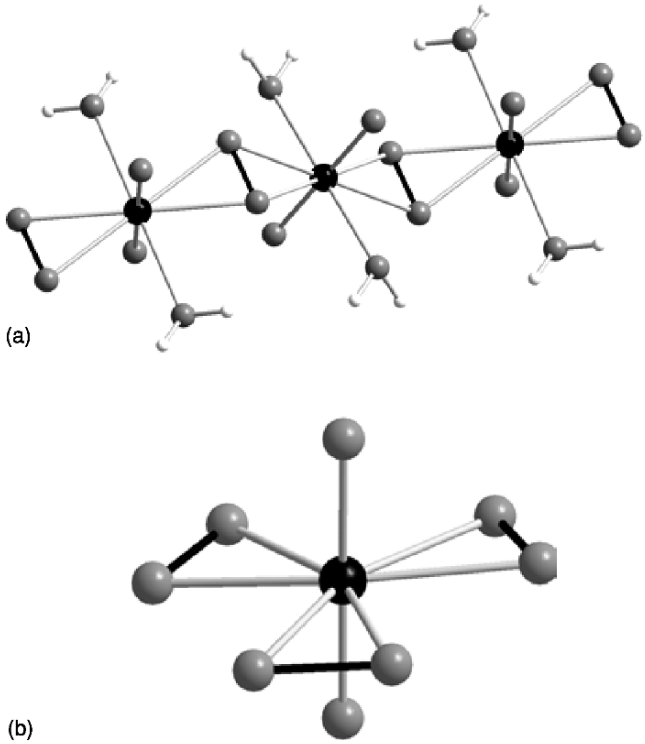

Fig. 5.56 (*a*) *The structure of studtite* (*from Burns* et al., 2003). *The peroxide group* (*black bond*) *is bridging two uranyl*(VI) *ions and forms a hexagonal bipyramidal coordination geometry around uranium together with two coordinated water molecules.* (*b*) *The structure of* $Na_4[UO_2(O_2)_3](H_2O)_9$ (*from Alcock,* 1968). *The structure contains discrete complexes with hexagonal bipyramidal coordination geometry*.

the oxalate system by Moskvin (1968); the uranyl(VI)-monoperoxo species was characterized by Djogic and Branica (1992). Self-assembled uranyl peroxide nanosphere clusters of 24, 28, and 32 polyhedra (some containing neptunyl) that crystallize from alkaline solution have been characterized (Burns *et al*., 2005).

5.9.2 Uranium(III) compounds

The structures of U(III) complexes are expected to be very similar to those of the other trivalent actinides; the coordination chemistry of which has been extensively studied as they are chemically more stable than the corresponding U(III) compounds. A point of interest is if there are differences in bonding between trivalent lanthanides and their actinide homologs. A comparison of equilibrium constants indicates that the actinide complexes are somewhat more stable, but the difference is not large. In the same way there are no large differences in bond distances and coordination geometry; the differences that

do exist may be due to the larger ionic radius of the actinide homologs as compared to the corresponding lanthanides. Uranium(III) compounds are characterized by high coordination numbers, eight and nine coordination are predominating as in the corresponding lanthanide(III) compounds. There are no structure determinations of uranium(III) complexes of simple inorganic ligands in solution, but it is reasonable to assume that their coordination geometry is similar to those of the trivalent lanthanides and transuranium elements (Allen *et al*., 2000). Examples of solid uranium(III) compounds are given by Chernyayev (1966) and Mehdoui *et al*. (2004), the latter also provides comparisons between U(III) and lanthanide(III) compounds.

Fig. 5.57 shows the structure of $K_3U(SO_4)_3 \cdot 3H_2O$ from Barnard *et al*. (1972a); it contains nine-coordinated U(III) through two chelating and two mono-dentate sulfate ions and three coordinated water molecules that form a strongly distorted trigonal prism around uranium.

5.9.3 Uranium(IV) compounds

Uranium(IV) forms both normal and basic salts with most inorganic ligands. The formation of basic salts is the result of the strong hydrolysis of U(IV) and these compounds contain coordinated hydroxide and/or oxide in addition to donor atoms from the other ligand. The relatively large ionic radius, 0.93 Å (eight coordination), and the high charge of U^{4+} results in high and often variable coordination numbers in different compounds, eight, nine and ten are

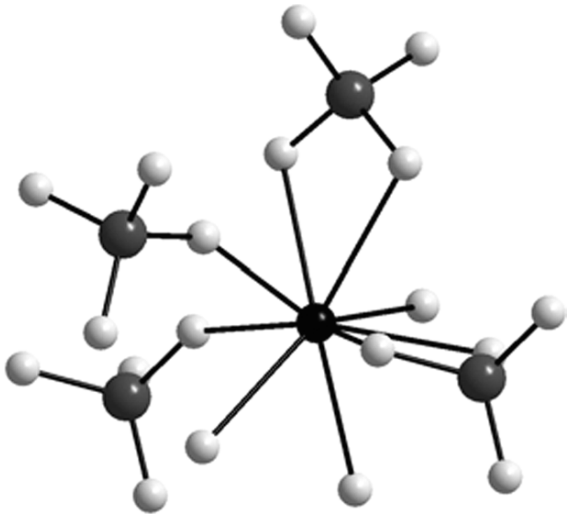

Fig. 5.57 *The coordination geometry of U(III) in* $K_3U(SO_4)_3 \cdot 3H_2O$ (*Barnard* et al., 1972*a*)*; uranium is nine-coordinated through two chelating and two monodentate sulfate ligands and three coordinated water molecules. The coordination polyhedron is strongly distorted from all the ideal geometries.*

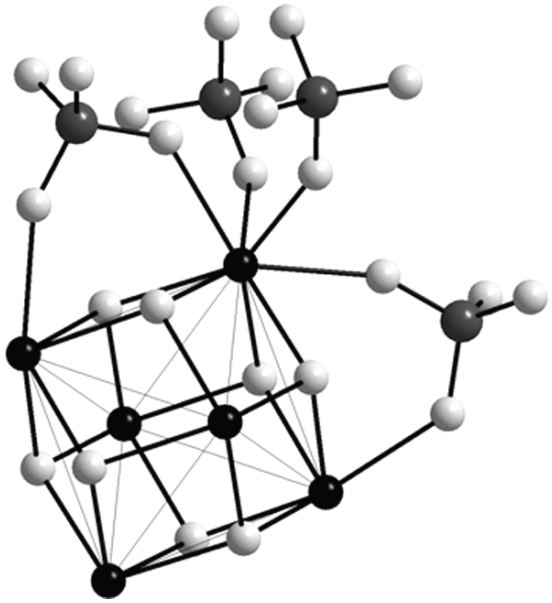

Fig. 5.58 *Structure of* $U_6(SO_4)_6O_4(OH)_4(s)$. *The characteristic structure element is an octahedron of six uranium*(IV) *ions* (*black*) *shown in the lower part of the figure. The oxide and hydroxide ions* (*light gray*) *are placed outside the eight triangular faces of this octahedron. The sulfate ions* (*sulfur is dark gray*) *are coordinated outside the octahedron and act as bridges between the U*(IV) *ions within the octahedron and between adjacent octahedra* (*not shown in the figure*). *Uranium*(IV) *is eight-coordinated in this compound. The structure is based on the X-ray study of Lundgren* (1952).

the most common ones. Uranium(IV) is in this respect similar to the elements in the lanthanide group, notably Ce(IV). Two examples of the coordination geometry of uranium(IV) in solid compounds are given in Figs. 5.58 and 5.59.

Fig. 5.59, based on an X-ray study of Fuchs and Gebert (1958), shows the structure of the mineral coffinite, $USiO_4$. A coordination number of eight can only be achieved by sharing all oxygen atoms in the silicate between two U(IV) atoms. The coordination geometry is best described as a triangular dodecahedron (Kepert, 1982, p. 153), the two 'arms' of which are indicated by the black full drawn lines.

The coordination number of the U(IV) and Th(IV) aqua ions in solution has been discussed based on data from Large-Angle X-ray Scattering (LAXS) and Extended X-ray Absorption Fine structure Spectroscopy (EXAFS). These methods provide accurate bond distances, while the determination of the coordination number is more uncertain, (9 ± 1). The high coordination number is retained in UF^{3+}(aq), as indicated by EXAFS data (Moll *et al.*, 1999); these data demonstrate a pronounced difference in bond distance between coordinated fluoride and water; the U–F distance is 2.15 Å and the U–H_2O distance 2.45 Å. The large variability of the coordination geometry in complexes of tetravalent actinides is demonstrated also by the structure of

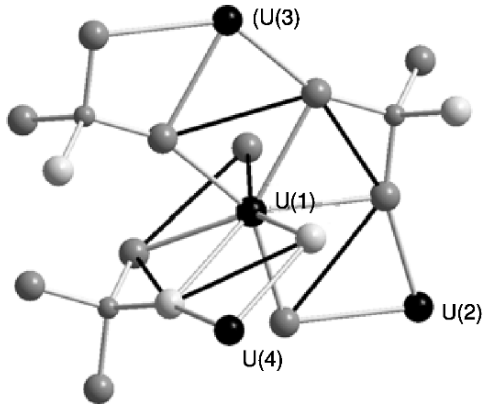

Fig. 5.59 *The structure of $USiO_4$ from Fuchs and Gebert* (1958). *The silicate group forms both a chelate and acts as a bridge between adjacent uranium atoms U*(2–4). *The chelate bonding is shown in the figure; the two remaining oxygen atoms in the silicate group are coordinated to adjacent uranium*(IV) *atoms not shown in the figure. The black full-drawn lines connect the atoms in the 'arms' of the dodecahedral coordination polyhedron. Each arm is approximately planar and the two planes are perpendicular.*

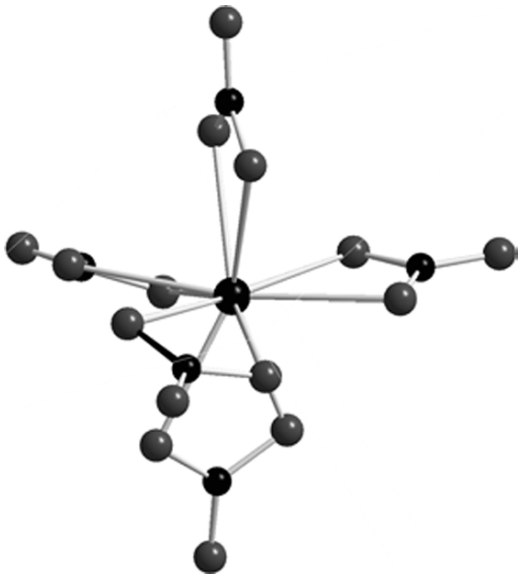

Fig. 5.60 *The structure of $Th(CO_3)_5^{6-}$ and the isostructural $U(CO_3)_5^{6-}$ from Voliotis and Rimsky* (1975).

$Na_6[Th(CO_3)_5] \cdot 12H_2O$ from Voliotis and Rimsky (1975), shown in Fig. 5.60; the corresponding uranium compound is isostructural. The carbonate ligands are arranged in an approximately trigonal bipyramidal arrangement around the central actinide ion; this geometry is very different from the common ones for ten-coordination, as discussed by Kepert (1982, p. 188). We may describe each carbonate ligand with one 'effective' charge because of its small ligand bite, resulting in a trigonal bipyramidal charge distribution in a geometry that minimizes the electrostatic repulsion between the ligands.

Another example of the variable coordination geometry is given by the structure of tetra(glycolato)uranium(IV) dihydrate, $[U(HOCH_2COO)_4] \cdot 2H_2O$ where uranium is ten-coordinated as indicated by Fig. 5.61, based on the structure data of Alcock *et al*. (1980). A recent example of the variable coordination geometry of U(IV) is the structure of the azide complex $U(N_3)_7^{3-}$, with an approximately pentagonal bipyramidal coordination geometry (Crawford *et al*., 2005). The azide ion is linear, but the angle U–N–N–N is highly variable (from 120° to 180°).

5.9.4 Uranyl(v) compounds

There are few experimental data on the structure and bonding of uranyl(v) complexes, the only example is the structure of the uranyl(v) triscarbonate complex studied in solution using EXAFS (Docrat *et al*., 1999). The complex has

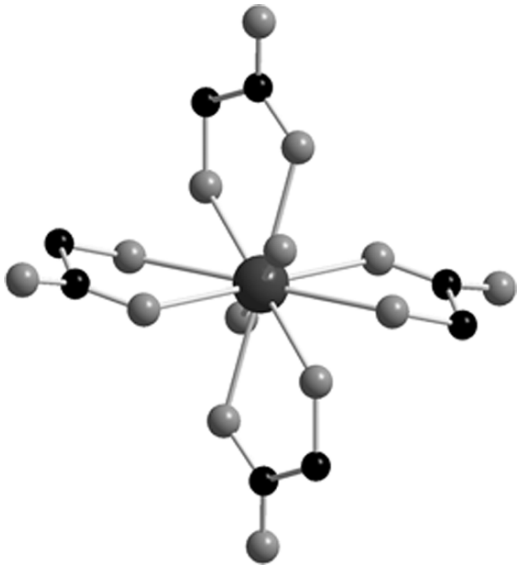

Fig. 5.61 *The coordination geometry in tetra(glycolato)uranium(IV) dihydrate from Alcock* et al. (1980). *The structure contains discrete ten-coordinated complexes* $[U(HOCH_2COO)_4(OH_2)_2]$ *with zero charge.*

hexagonal bipyramidal geometry similar to that of the uranyl(VI) triscarbonate complex, *cf*. Fig. 5.53. The corresponding information on neptunyl(V) complexes should provide good models also for the corresponding U(V) species. The geometry of the uranyl(V) and -(VI) carbonate complexes are supported by quantum chemical calculations by Gagliardi *et al*. (2001). The predominant coordination geometry is presumably a pentagonal or hexagonal bipyramid, with the labile ligands in the plane perpendicular to the linear UO_2 unit. The lower charge of the central atom results in the formation of weaker complexes and somewhat longer U–L distances than for the corresponding U(VI) complexes.

5.9.5 Uranium compounds of organic ligands

There is an abundance of organic ligands that form solid uranium complexes and we will restrict the examples to simple carboxylates, α-hydroxy and amino carboxylates.

The same structural principles as observed with the inorganic ligands are found also among the organic ones; the main difference between the two groups is that the geometry of the organic ligands puts additional constraints on the availability of the various donor atoms for bonding to uranium. In addition, the larger versatility of many organic ligands also opens up the possibility to form structural and bonding isomers.

Stoichiometric information on the constitution of complexes in solution can be obtained by an array of experimental methods (Rossotti and Rossotti, 1961), but this rarely gives information on structure and bonding. As is the case of inorganic ligands, the important methods to obtain structural information from solution are LAXS or EXAFS methods. However, both of them provide only limited structural information in the form of radial distribution functions, i.e. the distance from the central uranium atom to the atoms in the first and second coordination spheres and the number of such distances. In the case of LAXS one can also obtain information on the distances between the coordinated donor atoms. Allen *et al*. (1996b) give examples of the use of EXAFS for the deduction of structure models of uranyl(VI) tartrate, citrate, and malate complexes. Jiang *et al*. (2002) have investigated the structure and bonding of uranyl(VI) imino- and oxy-diacetate compounds and identified different modes of coordination of the ligands, an example that the stoichiometry of a complex does not provide sufficient information to identify the mode of coordination. In order to obtain more precise structure data it is often necessary to obtain additional structural information, such as provided by NMR spectroscopy (Szabó *et al*., 1997, 2000; Moll *et al*., 2000a,b) or by quantum chemical methods (Schreckenbach *et al*., 1998; Tsushima *et al*., 2001; Vallet *et al*., 2001, 2004b; Yang *et al*., 2003). The uranyl(VI) oxalate system provides a good example of different modes of bonding of the oxalate ligand in solid compounds and the structure of $UO_2(\text{oxalate})_3^{4-}$ complex in solution (Vallet *et al*., 2003). The ground state structure predicted by the quantum chemical methods is the one that is found experimentally (Fig. 5.62a–c).

The stoichiometry and the value of the stability constants of the complexes given in Tables 5.33–5.37 give some indications of the mode of bonding of the ligands, in particular whether a certain ligand forms a chelate or not. A comparison between acetate and glycolate is instructive: acetate can only coordinate through the carboxylate group, either using one oxygen donor or both. In the latter case a four-membered chelate ring is formed. Glycolate can bind in the same way if only the carboxylate group is involved and one then expects a stability constant of the same magnitude for both ligands. However, glycolate can also form a chelate by using one donor atom from each of the carboxylate and the α-OH groups, in which case a five-membered chelate ring is formed. Chelate formation results in a large increase in the stability constant, *cf.* the $\log\beta_n$ values for the acetate and glycolate complexes of U(IV) in Table 5.36. The stability constants, with the exception of $\log\beta_1$, are slightly larger for the U(VI) acetate than those for the glycolate complexes, which strongly indicates the same mode of bonding of acetate and glycolate in the U(VI) complexes (Beck and Nagypál, 1990; Grenthe *et al.*, 1997). The stepwise equilibrium constants for the formation of $UO_2(ox)$ ($\log\beta_1 = 5.99$), $UO_2(ox)_2^{2-}$ ($\log K_2 = 4.65$ for the reaction $UO_2(ox) + ox^{2-} \rightleftharpoons UO_2(ox)_2^{2-}$) are large compared to the value for the formation of $UO_2(ox)_3^{4-}$ ($\log K_3 = 0.36$ for the reaction $UO_2(ox)_2^{2-} + ox^{2-} \rightleftharpoons UO_2(ox)_3^{4-}$), indicating that the third oxalate does not form a chelate. This assumption has been verified both by experimental EXAFS data from solution and by quantum chemical calculations (Vallet *et al.*, 2003) as shown in Fig. 5.62a–c. These data also illustrate the possible occurrence of isomers.

5.10 URANIUM CHEMISTRY IN SOLUTION

5.10.1 The uranium aqua ions

The most stable oxidation state of uranium in aqueous solution is 6+, with the linear uranyl(VI) ion, UO_2^{2+}, as the stable entity. The only known uranium ion in the 5+ oxidation state in aqueous solution is the linear dioxouranium(V) ion, UO_2^+. Aqueous solutions containing U^{4+} are stable in the absence of oxidation agents like dissolved oxygen. Aqueous solutions containing U^{3+} are rapidly oxidized under evolution of hydrogen. The relative stability of the various oxidation states is strongly depending on the pH of the solution and on the presence of complexing ligands as indicated in Fig. 5.63. The rate of the redox transformations between the different oxidation states of uranium is rapid when there is no change in chemical composition between the oxidized and reduced forms, otherwise it is very slow. This means that the reactions $UO_2^{2+} + e^- \rightleftharpoons UO_2^+$ and $U^{4+} + e^- \rightleftharpoons U^{3+}$ are fast, while $UO_2^{2+} + 4H^+ + 2e^- \rightleftharpoons U^{4+} + 2H_2O$ is slow.

The kinetics of the redox transformations in aqueous actinide systems has been described in a report by Newton (1975) (Section 5.10.3i). The structures and chemical properties of actinide aqua ions are discussed and compared in

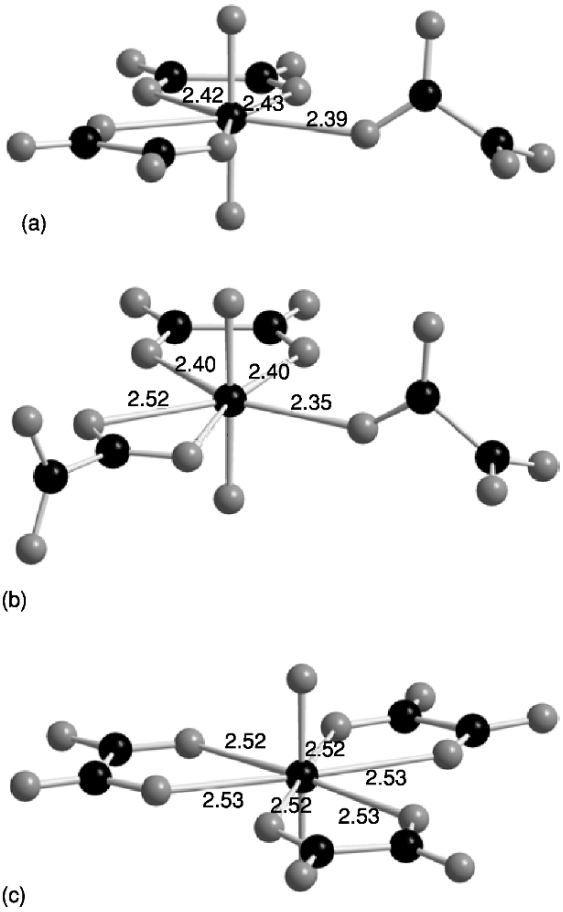

Fig. 5.62 (*a–c*) *Perspective views of three* $[UO_2(oxalate)_3]^{4-}$ *isomers, where* (*a*) *is the most stable one from Vallet* et al. (2003). *By using quantum chemical methods one can estimate the relative stability of the different isomers. The uranium atom and the carbon atoms are black and the oxygen atoms gray; distances are in ångströms. The bond distances for the ground state isomer a obtained from quantum chemical calculations agree with those obtained from EXAFS data in solution within* 0.03 Å. *The same mode of bonding has also been found in solid-state structures, but here there are no discrete complexes as the oxalate ligands act as bridges between adjacent uranium atoms.*

Chapter 23, section 2; a comparison of the complex formation properties of actinides is given in Chapter 23, sections 3–8. The kinetics of actinide reactions are compared and discussed in Chapter 23, sections 10 and 11.

Aqueous solutions of UO_2^+ are prone to disproportionation and the range of stability of U(v) is therefore small, a fact that makes it difficult to study its solution chemistry.

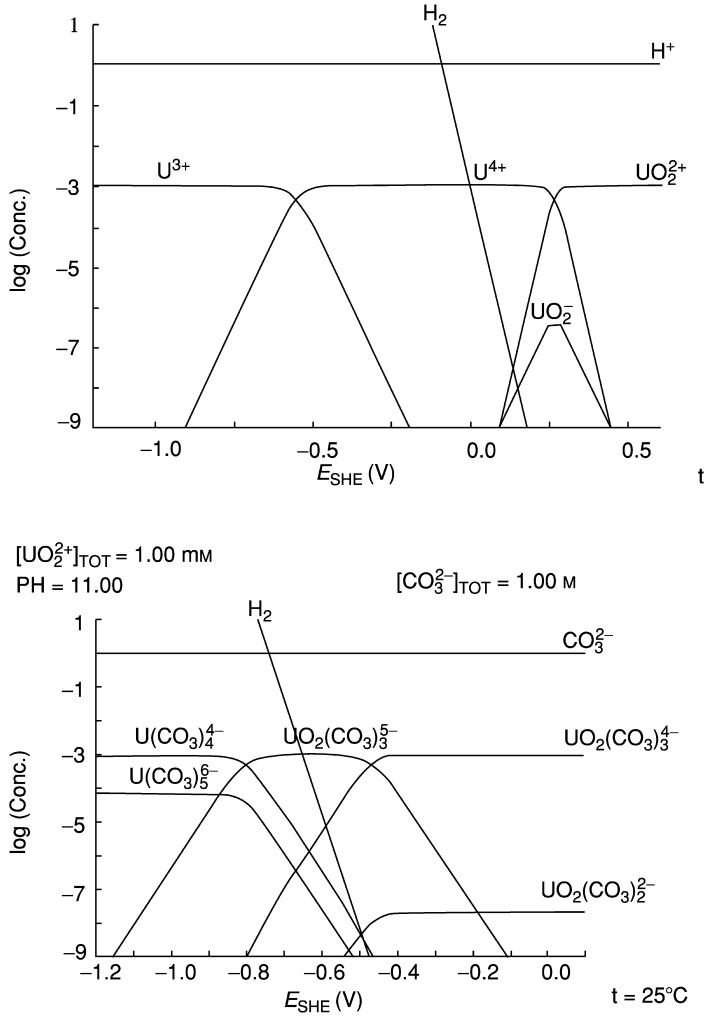

Fig. 5.63 *Logarithmic diagrams showing the distribution of* U^{3+}, U^{4+}, UO_2^+ *and* UO_2^{2+} *as a function of the redox potential in* 1 M *perchloric acid* (*the first diagram*), *and in* 1 M Na_2CO_3 (*the second diagram*). *U*(*V*) *is predominant between* –0.7 *and* –0.4 V *in the second diagram.*

The oxygen atoms in UO_2^{2+} and UO_2^+ are kinetically inert and their rate of exchange with oxygen from water is slow, with a half-life of approximately 5×10^4 h in 1 M perchloric acid for the former (Gordon and Taube, 1961a), but much faster for the latter as indicated by the fact that UO_2^+ catalyzes the oxygen exchange between UO_2^{2+} and water (Gordon and Taube, 1961b).

However no exchange rate has been determined for UO_2^+ alone. The rate of exchange of the 'yl' oxygen atoms with the water solvent is strongly catalyzed by light in the near UV/visible region and varies with the chemical composition of the complexes present in solution as discussed in Section 5.10.3, where also some spectroscopic characteristics of the various species are described.

Solutions of U^{3+}, U^{4+}, and UO_2^{2+} can be used to prepare complexes in solution and various solid compounds using standard techniques. A treatise by Chernyayev (1966) gives an excellent account of the compounds prepared from aqueous media.

(a) Tripositive uranium, U^{3+}

Aqueous solutions of U^{3+} can be prepared by dissolving uranium trichloride in water. Alternatively, solutions of U(IV) or U(VI) can be reduced by electrolysis at a mercury cathode (Barnard *et al.*, 1967, 1972b; Weigel, 1958). The course of the reduction can conveniently be observed by the colour of the solutions in *incandescent* light: Solutions of U(VI) are yellow, while those of U(IV) and U(III) are green and wine red, respectively. These colors cannot be observed in fluorescent light. There are only few studies of the chemical properties of U^{3+} and its complexes in solution (Section 5.8.6); however the properties can often be estimated from those of the trivalent lanthanides. The standard redox potential of the U^{4+}/U^{3+} redox couple and the Gibbs energy and enthalpy of formation, entropy and heat capacity of U^{3+}(aq) have been reviewed by Grenthe *et al.* (1992) and Guillaumont *et al.* (2003). These data are reported in Table 5.32.

There is no structural information available on the U^{3+}(aq) ion, however the structure of Pu^{3+}(aq) has been determined (Matonic *et al.*, 2001) by a single-crystal X-ray diffraction study of $[Pu(H_2O)_9][CF_3SO_3]_3$. In addition, the structures of trivalent lanthanides and Am(III) and Cm(III) have been determined in solution using EXAFS (Allen *et al.*, 2000). The solid Pu(III) compound contains discrete nine-coordinated complexes that are very similar to those found among the trivalent lanthanides, in the same way the bond distances and coordination number determined from the EXAFS data are close to those in lanthanide(III) and actinide(III) complexes, indicating an aqua-ion of the composition $U(H_2O)_9^{3+}$ for trivalent uranium.

(b) Tetrapositive uranium, U^{4+}

U(IV) in the form of U^{4+}(aq) is a very strong acid and accordingly hydrolyzed except in solutions with a hydrogen ion concentration larger than 0.5 M. The hydrolysis will be discussed in Section 5.10.2b. Uranium(IV) species can be prepared by electrolysis of corresponding uranium(VI) solutions at low pH using a two-compartment cell and a mercury cathode, U(III) is formed simultaneously, but is rapidly oxidized by blowing air through the cathode

Table 5.32 *The redox potentials, Gibbs energy and enthalpy of formation, molar entropy, and heat capacity for the different uranium aqua ions under standard state conditions* (298.15 K, 0.1 MPa) *in pure water solvent at zero ionic strength* (*Grenthe* et al., 1992; *Guillaumont* et al., 2003).

Species and redox reaction	E° (V)	$\Delta_f G^\circ_m$ (kJ mol^{-1})	$\Delta_f H^\circ_m$(kJ mol^{-1})	S°_m (J K^{-1} mol^{-1})	$C^\circ_{p,m}$ (J K^{-1} mol^{-1})
$U^{3+}(aq)$		–(476.5 ± 1.8)	–(489.1 ± 3.7)	–(188 ± 14)	–(150 ± 50)
$U^{4+} + e^- \rightleftharpoons U^{3+}$	–(0.553 ± 0.004)				
$U^{4+}(aq)$		–(529.9 ± 1.8)	–(591.2 ± 3.3)	–(417 ± 13)	–(220 ± 50)
$UO_2^+(aq)$		–(961.0 ± 1.8)	–(1025.1 ± 3.0)	–(25 ± 8)	–
$UO_2^{2+} + e^- \rightleftharpoons UO_2^+$	(0.0878 ± 0.0013)				
$UO_2^{2+}(aq)$		–(952.6 ± 1.7)	–(1019.0 ± 1.5)	–(98.2 ± 3.0)	(42.4 ± 3.0)
$UO_2^{2+} + 4H^+ + 2e^- \rightleftharpoons U^{4+} + 2H_2O$	(0.2673 ± 0.0012)				

compartment. Acid solutions of U(IV) are only slowly oxidized by oxygen but the situation is very different in the presence of strong complexing agents where the oxidation is very rapid and great experimental care has to be taken in order to keep the 4+ oxidation state. Uranium(IV) in acid solution can also be obtained by reduction of U(VI) with hydrogen using platinum black as a catalyst. The coordination number of the $U^{4+}(aq)$ in solution has been studied by LAXS (Johansson, 1992) and by EXAFS (Moll *et al.*, 1999); the U–O distance is (2.42 ± 0.01) Å and the coordination number (9 ± 1). The coordination number is not well defined and the energy difference between isomers with different geometries is probably small (Kepert, 1982), an assumption supported by quantum chemical data on $Th^{4+}(aq)$ by Yang *et al.* (2001, 2003). The rate constant for the exchange between coordinated and bulk water has been determined using ^{17}O NMR spectroscopy as discussed in section 5.10.3 (b). Experimental data for the redox potential and other thermodynamic quantities for $U^{4+}(aq)$ have been reviewed (Grenthe *et al.*, 1992; Guillaumont *et al.*, 2003) and selected values are given in Table 5.32.

(c) Dioxouranium(v), UO_2^+

The 5+ oxidation state of uranium has a very narrow range of existence in aqueous solution, (Fig. 5.63). Millimolar solutions of UO_2^+ can be prepared by reduction of UO_2^{2+} with zinc amalgam or hydrogen, or by dissolving UCl_5 in water. A more convenient method is to irradiate a 0.5 M 2-propanol–0.2 M $LiClO_4$ solution of uranium(VI) at a pH between 1.7 and 2.7, with UV radiation from a Hg lamp (Howes *et al.*, 1988). The uranium(V) solution formed is not thermodynamically stable, but the rate of oxidation is so slow that there is little decomposition during 1 h.

There is no experimental information on the structure of $UO_2^+(aq)$ and the number of coordinated water molecules. However, as judged by the chemical similarity between U(V) and Np(V) complexes, it is reasonable to assume that they also have a similar coordination geometry, as exemplified by the coordination geometry of different Np(V) carbonate complexes in solution is given by Clark *et al.* (1996); these structures are also very similar to those of the corresponding U(VI) system (Docrat *et al.*, 1999; Gagliardi *et al.*, 2001). Vallet *et al.* (2004a) have used quantum chemical models to predict that the most probable constitution of $UO_2^+(aq)$ is $UO_2(H_2O)_5^+$, with pentagonal bipyramidal geometry. The thermodynamics of $UO_2^+(aq)$ has been reviewed (Grenthe *et al.*, 1992; Guillaumont *et al.*, 2003) and the redox potential for the reaction: $UO_2^{2+}(aq) + e^- \rightleftharpoons UO_2^+(aq)$, and other thermodynamic data for $UO_2^+(aq)$ from these reviews are given in Table 5.32. U(V) is an intermediate in the photochemical reduction of uranium(VI) (Heidt and Moon, 1953).

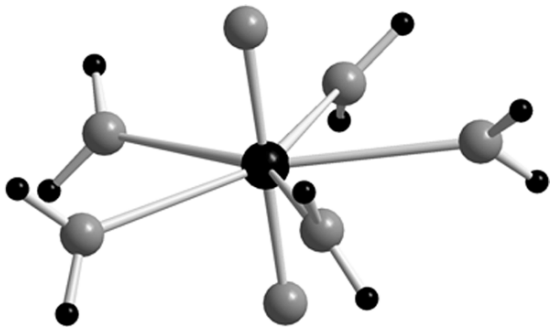

Fig. 5.64 *The coordination geometry of* $UO_2(H_2O)_5^{2+}$ *and* $UO_2(H_2O)_5^{+}$*, deduced from quantum chemical calculations using a solvent model as discussed by Vallet* et al. (2001, 2004). *Only the bond distances differ between the two structures; the U–O water distances are* 2.47 Å *in the uranyl(*VI*) aqua ion and* 2.63 Å *in the corresponding uranyl(*V*) species. The* $U–O_{yl}$ *distance is* 0.1 Å *longer in the uranyl(*V*) compound than in the corresponding uranyl (*VI*) compound.*

(d) Dioxouranium(VI), UO_2^{2+}

The 6+ state is the most stable of the oxidation states of uranium and has accordingly been extensively studied. A large number of different compounds have been prepared from aqueous solution both by simple crystallization, by using hydrothermal techniques and other methods; numerous examples are given in other parts of this chapter. Under certain circumstances, the oxo ligands can undergo ligand exchange, scrambling, and substitution reactions; the ligand exchange reactions are in general slow but are strongly photo-catalyzed and these reactions are discussed in Section 5.10.3. The structure of the aqua ion $UO_2(H_2O)_5^{2+}$ in solution has been determined using LAXS (Åberg *et al.*, 1983) and EXAFS techniques (Wahlgren *et al.*, 1999; Sémon *et al.*, 2001; Neuefeind *et al.*, 2004b); more detailed studies have been made using quantum chemical methods (Spencer *et al.*, 1999; Wahlgren *et al.*, 1999; Hay *et al.*, 2000; Vallet *et al.*, 2001). Guilbaud and Wipff (1993), Hagberg *et al.* (2005) have determined the structure by using molecular dynamics simulations, a method that also gives some information on the structure of the second hydration sphere. The structure of the aqua ion is shown in Fig. 5.64. The redox potentials for reactions involving $UO_2^{2+}(aq)$, and the standard Gibbs energy and enthalpy of formation, the molar entropy, and heat capacity of $UO_2^{2+}(aq)$ from the reviews by Grenthe *et al.* (1992) and Guillaumont *et al.* (2003) are given in Table 5.32. The rate of exchange between coordinated water and the pure water solvent has been studied using ^{17}O NMR (Farkas *et al.*, 2000a), and these data are discussed in section 5.10.3(b).

5.10.2 Aqueous uranium complexes

Uranium is a very strong Lewis acid and a hard electron acceptor in all its different oxidation states. This means that the donor–acceptor interactions follow the sequences:

$$F^- \gg Cl^- > Br^- \approx I^-; O \gg S > Se; N \gg P \approx As$$

where the donors are either simple ions like fluoride, or part of a larger ion/molecule like carbonate. These sequences are expected if the donor–acceptor interactions are dominated by electrostatic forces. There is extensive information in the literature on the chemical thermodynamics of uranium complexes. Most of these data are compiled in *Stability Constants, Special Publications* No. 6 (Bjerrum *et al*., 1957), No. 7 (Bjerrum *et al*., 1958), No. 17 (Sillén and Martell, 1964), No. 25 (Sillén and Martell, 1971), and in the International Union of Physical and Applied Chemistry (IUPAC) Chemical Data Series, *Stability Constants of Metal-Ion Complexes, Part A* (Högfeldt, 1982) and *Part B* (Perrin, 1979). There are several critical evaluations of the compiled data; the series *Critical Stability Constants*, Vols 1–6, by Martell and Smith, is now available in a computer database that also includes the necessary software, *NIST Standard Reference Database* 46 (NIST, 2004). Grenthe *et al*. (1992) and Guillaumont *et al*. (2003) have given a more detailed critical evaluation of thermodynamic data for uranium, including a discussion of many of the experimental investigations on which the selected data are based.

The high Lewis acidity results in extensive hydrolysis of uranium that decreases in the order U(IV) > U(VI) >> U(III) > U(V). Another effect of the high Lewis acidity is that coordinated uranium exerts a very strong inductive effect on coordinated ligands, e.g. the dissociation constant of the proton in the α-hydroxy group of coordinated α-hydroxy carboxylic acids can increase by more than 13 orders of magnitude (Szabó and Grenthe, 2000) on coordination to uranium(VI); a similar effect is also found in some Th(IV) complexes (Toraishi *et al*., 2002) and therefore most likely also in U(IV) complexes:

$$HOCH_2COO^- \rightleftharpoons {}^-OCH_2COO^- + H^+; pK \approx 17$$
$$UO_2(HOCH_2COO^-) \rightleftharpoons UO_2({}^-OCH_2COO^-) + H^+; pK = 3.6.$$

A similar example is found in the structure of the complex $[UO_2L(MeO)(MeOH)]_2$ where L is a thiosemicarbazone (Santos and Abram, 2004); this complex contains one coordinated (MeOH) and one deprotonated (MeO^-) methanol ligand. The 'inductive effect' is an electron redistribution in the coordinated ligand; if this is an organic species it will result in a changed ligand reactivity, a fact that has been used in preparative chemistry (van Axeel Castelli *et al*., 2000).

(a) Uranium(III) and uranyl(V) complexes

Uranium(III) is a very strong reducing agent that is oxidized by water, hence no stable complexes can be maintained in aqueous solution. However, the chemical properties of uranium(III) are expected to be very similar to those of trivalent lanthanides, actinium(III) and the transuranium elements in oxidation state 3+. Guidance on the magnitude of equilibrium constants for U(III) species can therefore be obtained from databases for lanthanide(III) and actinide(III) elements: examples are given in Tables 5.34 and 5.36. The differences in chemical properties between U(III) and other An(III) ions and the corresponding Ln(III) species can be exploited by proper choice of ligand. This is a useful strategy for the design of An(III)/Ln(III) separation processes (Karmazin *et al.*, 2002). The narrow range of existence of uranium(V) in aqueous solution results in very little quantitative information on equilibrium constants. In view of the large chemical similarity between actinides in the same oxidation state, one may use the equilibrium constants for Np(V) complexes as estimates for the corresponding U(V) complexes (Chapter 6, section 9).

(b) Hydrolysis of uranium

A summary of the stoichiometry and equilibrium constants of the various hydroxide complexes are given in Table 5.33: they refer to reactions of the type

$$pM + qH_2O \rightleftharpoons M_p(OH)_q + qH^+$$

where all charges except for H^+ have been omitted for simplicity, and where M denotes, UO_2^{2+} UO_2^+, U^{4+}, or U^{3+}; the equilibrium constants are taken from Grenthe *et al.* (1992), Guillaumont *et al.* (2003) and Baes and Mesmer (1976).

In most of the experimental determinations of hydrolytic equilibria it is not possible to decide if the species formed contain coordinated hydroxide and/or oxide; the reason being that $2OH^- \equiv O^{2-}$ in experiments where the equilibrium constants and the stoichiometry are deduced from measurements of the free hydrogen ion concentration; this is an example of the so-called 'proton ambiguity' (Rossotti and Rossotti, 1961). The following example illustrates the point:

$$3UO_2^{2+} + 5H_2O \rightleftharpoons (UO_2)_3(OH)_5^+ + 5H^+$$
$$3UO_2^{2+} + 5H_2O \rightleftharpoons (UO_2)_3(O)(OH)_3^+ + 5H^+ + H_2O$$

Both reactions result in the formation of five H^+ and can therefore not be distinguished. As the activity of water is a constant, the stability constant is the same for both stoichiometric formulations. This tri-nuclear complex was originally formulated as $(UO_2)_3(OH)_5^+$, but when structural data became available the actual composition turned out to be $(UO_2)_3(O)(OH)_3^+$, with the structure given in Fig. 5.65 (Åberg, 1978).

Table 5.33 *Stoichiometry and stability constants for the hydrolysis complexes of uranium. The stability constants refer to zero ionic strength and a temperature of* 25°C*; data from Grenthe* et al. (1992), *Guillaumont* et al. (2003), *and Baes and Mesmer* (1976).

Uranium(VI) Chemical reaction	$log^*\beta_{p,q}$	*Uranium(IV) Chemical reaction*	$log^*\beta_{p,q}$
$UO_2^{2+} + H_2O \rightleftharpoons UO_2OH^+ + H^+$	–5.25	$U^{4+} + H_2O \rightleftharpoons UOH^{3+} + H^+$	–0.54
$UO_2^{2+} + 2H_2O \rightleftharpoons UO_2(OH)_2(aq) + 2H^+$	–12.15	$U^{4+} + 2H_2O \rightleftharpoons U(OH)_2^{2+} + 2H^+$	–2.6[a]
$UO_2^{2+} + 3H_2O \rightleftharpoons UO_2(OH)_3^- + 3H^+$	–20.25	$U^{4+}3H_2O \rightleftharpoons U(OH)_3^+ + 3H^+$	–5.8[a]
$UO_2^{2+} + 4H_2O \rightleftharpoons UO2(OH)_4^{2-} + 4H^+$	–32.40	$U^{4+} + 4H_2O \rightleftharpoons U(OH)_4(aq) + 4H^+$	–10.3[a]
$2UO_2^{2+} + H_2O \rightleftharpoons (UO_2)_2OH^{3+} + H^+$	–2.7	$6U^{4+} + 15H_2O \rightleftharpoons U_6(OH)_{15}^9 + 15H^+$	–16.9
$2UO_2^{2+} + 2H_2O \rightleftharpoons (UO_2)_2(OH)^{2+} + 2H^+$	–5.62	Uranium(v): Estimates from Np(v) data	
$3UO_2^{2+} + 5H_2O \rightleftharpoons (UO_2)_3(OH)_5^+ + 5H^+$	–15.55	$UO_2^+ + H_2O \rightleftharpoons UO_2OH(aq) + H^+$	≈–11.3
$3UO_2^{2+} + 7H_2O \rightleftharpoons (UO_2)_3(OH)_7^+ + 7H^+$	–32.7	$UO_2^+ + 2H_2O \rightleftharpoons UO_2(OH)_2^- + 2H^+$	≈–23.6
$4UO_2^{2+} + 7H_2O \rightleftharpoons (UO_2)_4(OH)_7^+ + 7H$	–21.9	Uranium(III): Estimates from Cm(III) data	
		$U^{3+} + H_2O \rightleftharpoons UOH^{2+}$	–7.6
		$U^{3+} + 2H_2O \rightleftharpoons U(OH)_2^{2+}$	–15.7

[a] Estimates from Baes and Mesmer (1976).

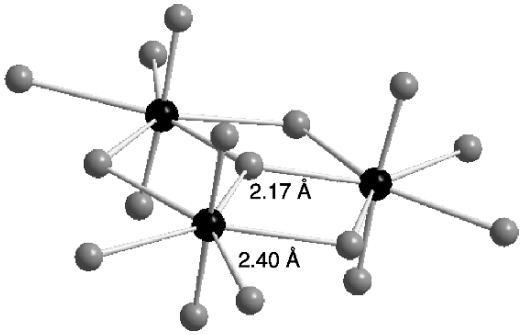

Fig. 5.65 *The structure of* $(UO_2)_3(O)(OH)_3^+$ (*from Åberg,* 1978). *The bond distance between uranium and the bridging oxide and hydroxide groups are* 2.17 Å *and* 2.40 Å, *respectively.*

Except at very low total concentrations of uranium, the polynuclear hydroxide complexes are predominant for all oxidation states, with the possible exception of U(v). There are no experimental data for U(iii), but its behavior can be estimated from the chemically analogous Cm(iii) ion, for which precise data are available.

The coordination chemistry of $U(OH)_4(aq)$ and $UF_4(aq)$ (Section 5.10.2c) deserves a comment. Because of the strong inductive effect of uranium on the dissociation of H^+ from coordinated water one would have expected the formation of anionic hydroxide complexes according to

$$U(OH)_4(H_2O)_n \rightleftharpoons U(OH)_5(H_2O)_{n-1}^- + H^+$$

if water is present in the first coordination sphere. However, there is no experimental indication of the formation of negatively charged hydroxide complexes even in 1 M hydroxide solutions. A coordination number of four is unlikely in view of the large ionic radius of U^{4+}. A possible resolution of this dilemma might be that the complex formulated as $U(OH)_4(aq)$ is a polymer, e.g. a tetramer $U_4(OH)_{16}$ with one of the A_4X_{16}-type structures (Wells, 1990, p. 201), where the coordination number of A, in this case uranium(iv), is six. Hydroxide and fluoride ions have similar size and often replace one another in solid-state structures. One might therefore expect that their coordination geometry is similar also in aqueous solution. However, $UF_4(aq)$ is not the limiting stoichiometry in aqueous solution where two negatively charged fluoride complexes UF_5^- and UF_6^{2-} have been identified (Table 5.34). This indicates a coordination number of at least six in the U(iv)–fluoride system, the same as the coordination number for $U(OH)_4(aq)$ if this has an $U_4(OH)_{16}$ structure. Polynuclear complexes, e.g. $U_4F_{16}(aq)$ do not form because of the poor bridging ability of fluoride in aqueous solution.

Table 5.34 *Stoichiometry and stability constants of uranium complexes of some common inorganic ligands at zero ionic strength and a temperature of* 25°C. *Data from Grenthe* et al. (1992) *and Guillaumont* et al. (2003). *The stability constants for U(III) have been estimated from the corresponding constants for Cm(III). Charges of the complexes have been deleted, to simplify notations.*

	$log\,\beta_n$			
Chemical reaction	$M \equiv UO_2^{2+}$	$M \equiv UO_2^{+}$	$M \equiv U^{4+}$	$M \equiv U^{3+}$
$M + F^- \rightleftharpoons MF$	5.1		9.3	~3.4
$M + 2F^- \rightleftharpoons MF_2$	8.6		16.2	
$M + 3F^- \rightleftharpoons MF_3$	10.9		21.6	
$M + 4F^- \rightleftharpoons MF_4$	11.7		25.6	
$M + 5F^- \rightleftharpoons MF_5$	11.5		27.0	
$M + 6F^- \rightleftharpoons MF_6$	–		29.1	
$M + Cl^- \rightleftharpoons MCl$	0.17		1.7	~0.24
$M + 2Cl^- \rightleftharpoons MCl_2$	–1.1			~–0.74
$M + NO_3^- \rightleftharpoons MNO_3$	0.3		1.5	
$M + SO_4^{2-} \rightleftharpoons MSO_4$	3.15		6.6	~3.3
$M + 2SO_4^{2-} \rightleftharpoons M(SO_4)_2$	4.14		10.5	~3.7
$M + PO_4^{3-} \rightleftharpoons MPO_4$	13.2			
$M + HPO_4^{2-} \rightleftharpoons MHPO_4$	7.2			
$M + H_2PO_4^- \rightleftharpoons MH_2PO_4$	1.12			
$M + CO_3^{2-} \rightleftharpoons MCO_3$	9.68			
$M + 2CO_3^{2-} \rightleftharpoons M(CO_3)_2$	16.9			
$M + 3CO_3^{2-} \rightleftharpoons M(CO_3)_3$	21.6	12.7		
$M + 4CO_3^{2-} \rightleftharpoons M(CO_3)_4$			35.1	
$M + 5CO_3^{2-} \rightleftharpoons M(CO_3)_5^{6-}$			34.0	

(c) Complexes between uranium and other inorganic ligands

Uranium(IV) and uranium(VI) form very strong fluoride complexes, while those formed with Cl^-, Br^-, and I^- are weak. There are no experimental data for halide complexes of U(V) and U(III); however, data from the chemically analogous Np(V) and Cm(III) indicate that they are all weak, the strongest being the fluoride complexes. The strength of complexes containing ligands with oxygen donors, such as sulfate, sulfite, phosphate, carbonate, silicate, and nitrate increases strongly with the charge and base strength of the ligand. However, complexes of the strongest bases such as $HSiO_4^{3-}$ and SiO_4^{4-} are difficult to study in aqueous solution because of competition from OH^- (and the formation of sparingly soluble hydrous oxides) at the high pH where these ions are present in significant amounts.

Strong complexes are also formed between UO_2^{2+} and the peroxide ion and the mode of coordination of the ligand is known from solid state structures (Fig. 5.56a and b). Examples of uranyl(VI) peroxide complex formation in solution have been given by Djogic and Branica (1992), Gurevich *et al.* (1971a,b), and

Moskvin (1968). However, most of the stability constants are uncertain (Sillén and Martell, 1971; NIST, 2004).

Ternary complexes of the type MA_qH_r may be formed when the ligand is the anion of a polyprotic acid.

The stoichiometry and equilibrium constants of uranium complexes of inorganic ligands are given in Table 5.34 where the data are taken from Grenthe *et al.* (1992) and Guillaumont *et al.* (2003). The structure of the complexes may be inferred from the known coordination geometry of the central uranium atom and from the structure of the ligand. However, quantitative information requires other methods, either X-ray or neutron diffraction data from solid compounds containing the ligands, or from EXAFS spectroscopy of solutions. It is interesting to note that the tetrahedral sulfate (Moll *et al.*, 2000b) and phosphate ions (Dusausoy *et al.*, 1996) rarely form chelates in solid compounds. In most cases the ligands are bonded either through a single oxygen donor, or act as a bridge between different uranium atoms (Figs. 5.51, 5.52, 5.57, and 5.58). In solution, however, EXAFS data indicate that the sulfate ion forms a bidentate chelate in $UO_2(SO_4)_2^{2-}$ and in ternary hydroxide–sulfate complexes (Moll *et al.*, 2000b) but not in UO_2SO_4(aq) (Neuefeind *et al.*, 2004a). On the other hand, carbonate invariably forms complexes where the ligand is chelate-bonded to uranium via two oxygen atoms (Fig. 5.66).

The data in Table 5.34 provide the experimental basis for describing uranium as a strong Lewis acid, or as a hard acceptor. Uranium also forms complexes of moderate stability with inorganic nitrogen donors like azide, N_3^-, and thiocyanate, SCN^- (Table 5.35). Uranium does not form ammine complexes in aqueous solution; ammines are strong bases and under the conditions where complexes might form the pH is so high that the stronger uranium hydroxide complexes predominate. However, N-donor complexes are found in organic ligands of various types, some examples are given in Table 5.36.

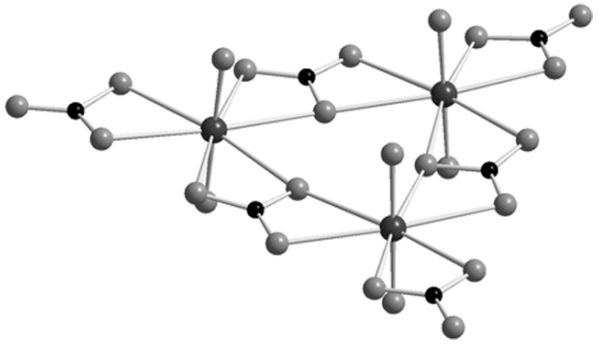

Fig. 5.66 *The structure of* $(UO_2)_3(CO_3)_6^{6-}$ *from Allen* et al. (1995). *Three terminal carbonate ligands form bidentate chelates and the remaining three act as bridges between the uranium atoms. The structure is closely related to that of* $UO_2(CO_3)_3^{4-}$ *containing three bidentate carbonate ligands.*

Table 5.35 *Equilibrium constants for uranium azide and thiocyanate complexes at zero ionic strength and a temperature of* 25°C. *Data from Grenthe* et al. (1992) *and Guillaumont* et al. (2003).

Chemical reaction	$log\,\beta_n$ $U(VI)$	*Chemical reaction*	$log\,\beta_n$ $M^{n+} \equiv U^{4+}$	$log\,\beta_n$ $M^{n+} \equiv UO_2^{2+}$
$UO_2^{2+} + N_3^- \rightleftharpoons UO_2N_3^+$	2.58	$M^{n+} + SCN^- \rightleftharpoons MSCN^{(n-1)+}$	1.4	2.97
$UO_2^{2+} + 2N_3^- \rightleftharpoons UO_2(N_3)_2$	4.3	$M^{n+} + 2SCN^- \rightleftharpoons M(SCN)_2^{(n-2)+}$	1.2	4.3
$UO_2^{2+} + 3N_3^- \rightleftharpoons UO_2(N_3)_3^-$	5.7	$M^{n+} + 3SCN^- \rightleftharpoons M(SCN)_3^{(n-3)+}$	2.1	–
$UO_2^{2+} + 4N_3^- \rightleftharpoons UO_2(N_3)_4^{2-}$	4.9			

(d) Complexes between uranium and some important organic ligands

Two groups of ligands will be discussed, those containing carboxylate functional groups alone and those containing in addition one or more hydroxy or amino/imino groups; the first group is exemplified by acetate and oxalate, and the second by glycolate, glycine, iminodiacetate, and ethylenediaminetetraacetate ($EDTA^{4-}$). The stoichiometry and stability constants for the corresponding UO_2^{2+} and U^{4+} complexes are listed in Table 5.36. There is no experimental information available for U(III) and the equilibrium constants have been estimated from corresponding data for trivalent lanthanides and other trivalent actinides. The first chemical issue to be discussed is the mode of bonding of the ligand; the stoichiometry and the magnitude of the stability constants provide some insight, but more precise information requires direct structure information, either from X-ray or neutron diffraction, EXAFS spectroscopy, or from quantum chemistry. The relative magnitude of the stepwise stability constants often gives indication of changes in the mode of bonding of the ligand and structural changes of the complexes. An example is the stepwise stability constants of oxalate complexes of U(VI) (Table 5.36). It is also tempting to relate the very small equilibrium constant for the reaction $U(CO_3)_4^{4-} + CO_3^{2-} \rightleftharpoons U(CO_3)_5^{6-}$ (Table 5.34) to a structural rearrangement from a trigonal bipyramid arrangement of the carbonate ligands in $U(CO_3)_5^{6-}$ with CN = 10, (Fig. 5.60), to a tetrahedral arrangement with CN = 8 in $U(CO_3)_4^{4-}$ (the carbonate ligand is modelled with a single point change). The small stability constant for $UO_2(Hgly)^{2+}$, where Hgly is the "zwitter-ion" form of glycine, $^+H_3NCH_2COO^-$ indicates that the ligand is bonded only at the carboxylate end.

The equilibrium constants for the glycine complexes also deserve a comment. The predominant form of glycine at pH < 8 is the zwitter-ion; this means that one has to take the possible formation of complex with the formally uncharged zwitter-ion into account, which has not always been done in the

Table 5.36 *Stability constants for complexes between U(VI), U(IV), and U(III), and some organic ligands; acetate (ac^-); glycolate/α-hydroxyactate (α-ac^-), oxalate (ox^{2-}), glycinate ($glyc^-$), iminodiacetate ($IMDA^{2-}$), ethylenediamine-tetraacetate ($EDTA^{4-}$). The equilibrium constants are taken from Smith and Martell* (1989). *For some of the reactions, we have tabulated the equilibrium constant for the corresponding Th(IV) and Ce(III) complexes that should be good models for U(IV) and U(III).*

Chemical reaction	$\log \beta_n$ $U(VI)$	*Chemical reaction*	$\log \beta_n$ $M^{n+} \equiv U^{4+}$	$\log \beta_n$ $M^{n+} \equiv U^{3+}$
$UO_2^{2+} + ac^- \rightleftharpoons UO_2(ac)^+$	2.44	$M^{n+} + ac^- \rightleftharpoons M(ac)^{n-1}$	3.9	1.9
$UO_2^{2+} + 2ac^- \rightleftharpoons UO_2(ac)_{22}$	4.42	$M^{n+} + 2ac^- \rightleftharpoons M(ac)_2^{n-2}$	6.9	3.1
$UO_2^{2+} + 3ac^- \rightleftharpoons UO_2(ac)_3^-$	6.43	$M^{n+} + 3ac^- \rightleftharpoons M(ac)_3^{n-3}$	9.0	3.7
$UO_2^{2+} + \alpha{-}ac^- \rightleftharpoons UO_2(\alpha{-}ac)^+$	2.72	$M^{n+} + 4ac^- \rightleftharpoons M(ac)_4^{n-4}$	10.3	
$UO_2^{2+} + 2\alpha{-}ac^- \rightleftharpoons UO_2(\alpha{-}ac)_2$	4.45	$M^{n+} + 5ac^- \rightleftharpoons M(ac)_5^{n-5}$	11.0	
$UO_2^{2+} + 3\alpha{-}ac^- \rightleftharpoons UO_2(\alpha{-}ac)_3^-$	5.70	$M^{n+} + \alpha - ac^- \rightleftharpoons M(\alpha - ac)^{n-1}$	4.4	2.7
$UO_2^{2+} + ox^{2-} \rightleftharpoons UO_2(ox)$	5.99	$M^{n+} + 2\alpha - ac^- \rightleftharpoons M(\alpha - ac)_2^{n-2}$	8.3	4.5
$UO_2^{2+} + 2ox^{2-} \rightleftharpoons UO_2(ox)_2^{2-}$	10.64	$M^{n+} + 3\alpha - ac^- \rightleftharpoons M(\alpha - ac)_3^{n-3}$	11.8	5.3
$UO_2^{2+} + 3ox^{2-} \rightleftharpoons UO_2(ox)_3^{4-}$	11.0	$M^{n+} + ox^{2-} \rightleftharpoons M(ox)^{n-2}$	8.8	4.9
$UO_2^{2+} + Hgly \rightleftharpoons UO_2(Hgly)^{2+}$	1.16	$M^{n+} + 2ox^{2-} \rightleftharpoons M(ox)_2^{n-4}$	16.8	8.3
$UO_2^{2+} + 2gly^- \rightleftharpoons UO_2(gly)_2^a$	13.0			
$UO_2^{2+} + IMDA^{2-} \rightleftharpoons UO_2(IMDA)$	8.75	$M^{n+} + 3ox^{2-} \rightleftharpoons M(ox)_3^{n-6}$	22.8	10.2
$UO_2^{2+} + HIMDA^- \rightleftharpoons UO_2(HIMDA)$	2.41	$M^{n+} + 4ox^{2-} \rightleftharpoons M(ox)^{n-8}$	27.2	11.7
$UO_2^{2+} + HEDTA^{3-} \rightleftharpoons UO_2(HEDTA)^-$	6.35	$M^{n+} + IMDA^{2-} \rightleftharpoons M(IMDA)^{n-2}$	9.7	6.2
		$M^{n+} + EDTA^{4-} \rightleftharpoons M(EDTA)^{n-4}$	25.7	15.9

[a] From Szabó and Grenthe (2000).

published studies. The corresponding complexes with gly^- are strong as indicated by $\log k = 13.0$ for the reaction $UO_2^{2+} + 2gly^- \rightleftharpoons UO_2(gly)_2(aq)$ (Szabó and Grenthe, 2000). Aliphatic nitrogen donors are strong bases and the competition between H^+ prevents coordination to uranium unless the pH is above 6. The interpretation of experimental results is then complicated by the possible formation of binary and ternary complexes containing hydroxide. Sessler *et al.* (2001) have reviewed complex formation between uranium and macrocyclic ligands; these complexes together with organometallic complexes of uranium are discussed in Chapter 25.

(e) Ternary uranium complexes

Most experimental studies of uranium complexes in aqueous solution have been made in two-component systems (metal ion and ligand). Accordingly, most of the published equilibrium constant data refer to binary M_pL_q complexes. However, in experimental studies performed in water one must also take the possibility of the formation of ternary $M_pL_q(OH)_r$ complexes into account. When the ligand is a polyprotic acid also species of the type $M_pL_qH_r$ may form (the phosphate complexes in Table 5.34). The 'proton ambiguity' referred to in the case of hydroxide complexes, cf. $(UO_2)_3(OH)_5^+$ vs. $(UO_2)_3(O)(OH)_3^+$), is also found in other cases, notably for polyprotic ligands. An example is the UO_2^{2+}–glycolate system where there is a large difference in the dissociation constants of the carboxylate and α-hydroxy group. When studying the complex formation with this ligand using potentiometric methods, it is not possible to distinguish between the following two reactions:

$$UO_2^{2+}(aq) + HOCH_2COO^- \rightleftharpoons UO_2(OCH_2COO) + H^+$$

and

$$UO_2^{2+}(aq) + HOCH_2COO^- + H_2O \rightleftharpoons UO_2(HOCH_2COO)(OH) + H^+$$

To decide on the stoichiometry of the complex formed, it is necessary to use other methods, e.g. NMR spectroscopy as discussed by Szabó *et al.* (2000) and Toraishi *et al.* (2003).

It is possible to use coordination chemical data to decide on the conditions where ternary complexes containing different ligands (except OH^- and protonated ligands) may form; Beck and Nagypál (1990) and Grenthe *et al.* (1997) have discussed this issue and point out that the strength of a ternary complex MA_qB_r depends strongly on the strength of the binary complexes MA_q and MB_r and the steric constraints imposed by metal ion and ligands. Hence, ternary complexes are not common even in multicomponent systems; most of them contain fluoride or hydroxide, both strong donors that do not impose large steric constraints on the second ligand. Table 5.37 gives examples of some ternary uranium(VI) complexes. Note that the presence of the strongly binding oxalate and carbonate ligands has only a moderate influence on the strength of

Table 5.37 *Stoichiometry and stepwise equilibrium constants for reactions of the type* $UO_2AF_r + F^- \rightleftharpoons UO_2AF_{r+1}$. *Charges have been omitted for simplicity. The data are from Aas* et al. (1998) *and refer to a* 1 M $NaClO_4$ *ionic medium at* 25°C. *For comparison* $\log K_q$ *for the stepwise formation of the binary complexes* $UO_2F_q^{2-q}$ *are* 4.54, 3.44, *and* 2.43, *respectively*.

	log K		
A	$UO_2A + F^- \rightleftharpoons UO_2AF$	$UO_2AF + F^- \rightleftharpoons UO_2AF_2$	$UO_2AF_2 + F^- \rightleftharpoons UO_2AF_3$
Oxalate	3.93	2.55	1.72
Carbonate	4.08	2.30	1.91

bonding of fluoride as compared to that in the binary fluoride system. Ternary uranium(IV) complexes containing hydroxide/oxide ligands are abundant both in solid state structures and in solution. An example of the latter is U(EDTA)$(OH)^-$, where the equilibrium constant for the reaction U(EDTA)(aq)+ $H_2O \rightleftharpoons$ U(EDTA)$(OH)^- + H^+$ is equal to $\log^* K = -9.3$ (Smith and Martell, 1989), indicating a very large decrease in the acid strength of coordinated water from that in U^{4+}(aq), where $\log^* K$ is equal to –0.54 (see Table 5.33).

(f) Complex formation between UO_2^+ and other cations

The lower effective nuclear charge on uranium (V) as compared to uranium(VI) in uranyl ions results in a correspondingly larger negative charge of the 'yl' oxygen atoms (Vallet *et al.* (2004a). Electrostatic interactions between the 'yl' oxygen in MO_2^+ and the high positive effective charge of M(VI) in MO_2^{2+} is probably the reason for the formation of weak cation–cation complexes between the two. Newton and Baker (1965) were first to identify these species for UO_2^+ and UO_2^{2+} and Sullivan *et al.* (1961) for NpO_2^+ and UO_2^{2+}; Frolov and Rykov (1979) have reviewed the field.

5.10.3 Reaction mechanisms of ligand substitution reactions

The analysis of the rate and mechanism of chemical reactions requires information on the experimental rate equation and the thermodynamics of the reaction studied; in addition the structure and coordination geometry of reactants, intermediates, and products provide important clues on the microscopic details of the reaction. The rate equation describes how the rate of reaction depends on the concentration of different chemical species in the reacting system, some of them may appear as reactants/products in the total (stoichiometric) reaction, but this is not always the case. The rate equation may be simple or complex depending on the mechanism; details on the analysis of rate equations are given in standard texts on chemical kinetics, e.g. Katakis and Gordon (1987), Wilkins (1991) and Espenson (1995). 'Mechanism' is defined as the sequence of

elementary reactions that transform the reactant(s) to product(s); these different steps can rarely be studied in isolation, but have to be inferred from the experimental rate equation and the activation parameters $\Delta H^{\neq}$, $\Delta S^{\neq}$, and $\Delta V^{\neq}$ of the reaction. The rate equation rarely provides a unique mechanistic model for a certain reaction: one reason is that it contains only stoichiometric information on the rate determining step and the fast equilibria preceding this, but no information on the fast reactions following the rate-determining step. The mechanism deduced from the rate equation is usually referred to as the *stoichiometric mechanism* of the reaction; the *intimate mechanism* describes the molecular details of a certain reaction, e.g. the timing of bond breaking and bond formation.

The information on rates and mechanisms of ligand substitution reactions in uranium complexes is limited and in general only includes information on rate equations, while the mechanistic discussions are much more speculative. Most experimental data refer to uranyl(VI) complexes where three reviews provide some details. Lincoln (1979) and Tomiyasu and Fukutomi (1982) have reviewed reactions that mostly take place in non-aqueous solvents, while Nash and Sullivan (1998) have reviewed the kinetics and mechanism of actinide redox and complexation reactions in aqueous solution. Vallet *et al.* (2004b) have discussed the combination of experimental and quantum chemical methods for the elucidation of the intimate mechanism of solvent exchange and ligand substitution in uranyl(VI) complexes.

Substitution reactions of simple unidentate ligands in uranium complexes are in general very fast and require special experimental methods (stopped-flow, temperature jump and other relaxation methods; NMR spectroscopy). Only the uranyl(VI) fluoride system has been studied in detail (Szabó *et al.*, 1996).

Most of the experimental studies of ligand substitution have been made using multidentate ligands. These reactions involve several elementary reactions, chelate ring opening/ring closure, and ligand dissociation/association steps. In addition, the ligands are often protolytes and the rate equation therefore depends on the hydrogen ion concentration. All these factors result in complicated rate equations from which it is difficult to deduce the reaction mechanism. The activation parameters, $\Delta H^{\neq}$, $\Delta S^{\neq}$, and $\Delta V^{\neq}$ (of which only the first two are known for reactions involving uranium) provide additional mechanistic information that in some cases can be corroborated by quantum chemical methods as will be described later. The ligand substitution reactions with multidentate ligands are conveniently followed using conventional stopped-flow spectrophotometric methods. Experiments of this type start from a system that is not in equilibrium and its evolution is then followed until equilibrium has been attained. In many cases the reaction has to be followed by using a color indicator and this introduces additional complications when deducing the reaction mechanism (Friese *et al.*, 2001).

A more direct method to obtain mechanistic information on ligand exchange reactions is to use NMR equilibrium dynamics with ^{1}H, ^{13}C, ^{17}O, and ^{19}F as the NMR-active nuclei. The use of ^{17}O-enriched UO_2^{2+} and ternary complexes

containing fluoride have been particularly useful as the high sensitivity and wide chemical shift scales of these nuclei makes it possible to study a very large range of exchange rates. A typical example is the exchange reaction

$$UO_2(H_2O)_5^{2+} + H_2O^* \rightleftharpoons UO_2(H_2O^*)_5^{2+} + H_2O$$

that was studied using proton-NMR in mixed water–acetone media by Ikeda *et al*. (1979a) and Bardin *et al*. (1998) and by ^{17}O-NMR in water by Farkas *et al*. (2000a). An analogous example is the exchange between dimethyl sulfoxide (DMSO) and $UO_2(DMSO)_5^{2+}$ in DMSO solvent that was studied by Ikeda *et al*. (1979b). It should be noted that the NMR methods give information on all reactions that contribute to the dynamics at the reaction center. Hence one can use one NMR-active ligand as a probe to provide information on the dynamics of other ligands that are not easily studied using NMR, an example is the use of ^{19}F-NMR to estimate of the rate of water exchange in $UO_2(oxalate)F(H_2O)_2^-$ and $UO_2(oxalate)F_2(H_2O)^{2-}$ (Szabó *et al*., 1997).

The range of rates that can be studied using NMR depends on the magnitude of the chemical shift between the NMR-active nuclei located in different exchanging sites, the larger the chemical shift the faster processes can be studied. The NMR method can be used in different ways: (a) as an analytical tool where the concentration is measured as a function of time. This method can only be used if the rate of exchange is slow in comparison with the time for measurement; (b) using magnetization transfer, which is a method appropriate for reactions with half-lives of a few seconds; (c) by measurement of the line-broadening which is the method for study of the fastest reactions. The NMR-active nuclei may be located in different chemical surroundings in the same complex allowing studies of intramolecular exchange, or located in different species, e.g. a complex and free ligand, making studies of intermolecular exchange possible. In order to provide accurate data the different sites must have similar concentrations.

It is often difficult, or impossible to use the NMR method to study the rate and mechanism of the formation of the first complex in systems where strong complexes are formed (Szabó *et al*., 1996) because the free ligand concentration is here very small. In these cases stopped-flow technique is a useful alternative; on the other hand, NMR spectroscopy is superior when studying the rate and mechanism of limiting complexes (Ikeda *et al*., 1984; Szabó *et al*., 1997). A summary of experimental kinetic data is given in Tables 5.38 and 5.39, and a general discussion of the mechanistic conclusions in the following section.

(a) Reaction mechanisms

The Eigen–Wilkins mechanism describes the stoichiometric mechanism for many ligand substitution reactions; it includes the following two steps where N denotes the coordination number:

$$[(H_2O)_N M]^{n+} + [(H_2O)L^-] \rightleftharpoons [(H_2O)_N M \ldots L]^{(n-1)} + H_2O \quad (1)$$

$$[(H_2O)_N M \ldots L]^{(n-1)+} \rightarrow [M(H_2O)_{N-1}L]^{(n-1)+} + H_2O \quad (2)$$

Table 5.38 *Rate constants at* 25°C *and activation enthalpies for water exchange in* $U^{3+}(aq)$, $U^{4+}(aq)$, *and* UO_2^{2+} (aq). *The rate constant for* U(III) *has been estimated from data on the trivalent lanthanides* (*Helm and Merbach,* 1999). *There is no experimental information on ligand exchange mechanisms in any actinide*(*V*) *species.*

Exchange reaction	k_{ex} (s^{-1})	*Activation enthalpy*, ($\Delta H^{\neq}$) (kJ mol^{-1})	*Activation entropy*, ($\Delta S^{\neq}$) (J K^{-1} mol^{-1})	*References*
$U(H_2O)_9^{3+} + H_2O^* \rightleftharpoons U(H_2O^*)_9^{3+} + H_2O$	$\approx 10^8$	–	–	Helm and Merbach (1999)
$U(H_2O)_9^{4+} + H_2O^* \rightleftharpoons U(H_2O^*)_9^{4+} + H_2O$	5.4×10^6	34	–16	Farkas *et al.* (2000b)
$UO_2(H_2O)_5^{2+} + H_2O^* \rightleftharpoons UO_2(H_2O^*)_5^{2+} + H_2O$; in water at 25°C	1.3×10^6	26	–40	Farkas *et al.* (2000a)
in water–acetone 1/4.38 at –70°C and at 25°C	3.6×10^2 9×10^5	42	12	Ikeda *et al.* (1979a)
In water–acetone 1/1.86 at –70°C and at 25°C	8×10^2 4.6×10^5	32	–30	Bardin *et al.* (1998)

Reaction (1) describes the formation of an outer-sphere ion pair; this is a fast diffusion controlled equilibrium reaction with equilibrium constants K_{os}. The second reaction is rate-determining with the rate constant k_2 (unit s^{-1}); it involves the substitution of water in the first coordination sphere of the metal ion with a ligand from the second coordination sphere. This situation may arise when L is a unidentate ligand, but also for polydentate ligands, when the rate of chelate ring-closure is fast. The rate equation deduced from the two elementary reactions is often approximated by the expression

$$\frac{-\mathrm{d}[M(H_2O)]}{\mathrm{d}t} = \frac{k_2 K_{os}[M(H_2O)][L]}{1 + K_{os}[L]} \cong k_2 K_{os}[M(H_2O)][L]$$

K_{os} is usually estimated using the Fuoss equation (Fuoss, 1958).

For reactions where the experimental rate equation has the form

$$\frac{-\mathrm{d}[M(H_2O)]}{\mathrm{d}t} = k_{obs}[M(H_2O)][L]$$

we have $k_{obs} = k_2 K_{os}$. The analysis of experimental rate data using the Eigen–Wilkins mechanism is described by Katakis and Gordon (1987) and Wilkins (1991). The intimate mechanism of the water–ligand exchange can be associative, A, dissociative, D, or of interchange type, I. The assignment is based on the identification of intermediates (A and D); if no intermediates are identified the reaction is classified as interchange (I) (Langford and Gray, 1965). The A intermediate has a higher and the D intermediate a lower coordination number

than that of the reactant; in both cases there are two transition states along the reaction pathway. As no intermediate is formed in the interchange mechanism there is only one transition state. A rate constant k_{obs}, that is largely independent on the chemical nature of the entering ligand, indicates that the reaction mechanism is of dissociative type; the rate constant that depends strongly on the entering ligand is a characteristic of an associative mechanism. Szabó *et al.* (1996) have discussed fluoride exchange reactions in $UO_2F_n^{2-n}$ complexes using the Eigen–Wilkins mechanism.

The accessible coordination number at the metal center is often an important indicator when selecting the reaction mechanism. The characteristic coordination number for U(VI) and U(V) is five, but complexes with coordination numbers four and six are not uncommon; also U(IV) and U(III) have variable coordination numbers (9 ± 1). Hence, the coordination number is of little value as a mechanistic indicator in these cases, as neither associative nor dissociative mechanisms can be excluded. The size and charge of the metal ion and the ligand are also important for the mechanism; large ligands cannot enter the first coordination sphere until room is available through the dissociation of water. If water dissociation is rate determining, the intimate mechanism of the ligand exchange is dissociative; if the entry of the ligand from the second coordination sphere is rate determining the mechanism is associative.The simplest and most fundamental of the exchange reactions takes place between the aqua ions and the water solvent and this rate is often an important indicator for the mechanism of ligand substitution reactions of the Eigen–Wilkins type.

(b) Rates and mechanism of water exchange

The rate of water exchange has been studied both by proton NMR line-broadening at low temperature in mixed water–acetone solvents and in water containing 1 M $NaClO_4$. A complicating factor in experiments of this type is that it is not possible to vary the concentration of water in a pure water solvent; this is possible in the mixed water–acetone solvent. In the latter case, however, the concentration changes are often so large that the interpretation of the experimental data is ambiguous. Rate constants and activation parameters for the water exchange reactions are given in Table 5.38.

Because of the fast rate of exchange it is not possible to identify intermediates in these reactions and the rate equation alone is not sufficient to make a mechanistic assignment. This can be obtained by comparing the experimental activation energy with those for the D, A, and I mechanisms (Scheme 5.1), obtained using quantum chemical methods to identify the pathway of lowest activation energy; this value can then can be compared with the experimental data (Vallet *et al.*, 2001, 2004b). The theoretical activation energy of the pathways D, A, and I are 74, 19, and 21 kJ mol^{-1}, respectively; the dissociative pathway can be ruled out because of its high activation energy, while both the A and I mechanisms are consistent with the experimental value,

Table 5.39 *Experimental rate constants and activation parameters for some ligand substitution and ligand exchange reactions in aqueous uranyl(VI) systems studied by NMR and stopped-flow methods. The NMR experiments have been made in equilibrium systems where the rates of the forward reaction and the reverse reaction are equal. The stopped-flow experiments have been made under non-equilibrium conditions. The reactions in the table are in some cases elementary reactions; in other cases the mechanism is more complex and involves consecutive and/or parallel reactions. The ligand notation is: acetate ≡ ac; oxalate ≡ ox; picolinate ≡ pic; i-pentyl- picolinate ≡ i-pent-pic; 5-nitro-picolinate ≡ NO_2-pic; dipicolinate ≡ dipic; oxydiacetate ≡ oda. The following notation is used for the different fluoride ligands:* [a] *central fluoride,* [b,c] *edge fluorides. The rate constant in the forward and reverse directions is denoted +1 and –1, respectively; k_{ex} denotes an exchange reaction without net chemical change.*

Reaction	k_{obs} (s^{-1})	$\Delta H^{\neq}$ (kJ mol^{-1})	$\Delta S^{\neq}$ (J K^{-1} mol^{-1})	*References*
	NMR data at –5°C			
$UO_2(ac)F_3^{2-} + ac^{-*} \rightleftharpoons$ $UO_2(ac^*)F_3^{2-} + ac^-$	$k_1 = 2 \times 10^3$ s^{-1} $k_{-1} = 2.5 \times 10^4$ $M^{-1}s^{-1}$	–	–	Aas *et al.* (1999)
$UO_2(ac)_3^- \rightleftharpoons UO_2(ac)_2 + ac^-$	$k_1 = 2.7 \times 10^3$ s^{-1} $k_{-1} = 3.8 \times 10^5$ M^{-1} s^{-1}	22 ± 3	-61 ± 9	Aas *et al.* (1999)
$UO_2CO_3F_3^{3-} + F^{-*} \rightleftharpoons$ $UO_2CO_3F_3^{*3-} + F^-$	$k_{ex} = 14.2 \pm 2.1$[a,b,c] s^{-1}	53.7 ± 1.6	-15.7 ± 0.8	Szabó and Grenthe (1998)
$UO_2CO_3F_3^{3-} + C^*O_3^{2-} \rightleftharpoons$ $UOC^*O_3F_3^{3-} + CO_3^{2-}$	$k_{ex} = 8$ s^{-1} at pH 8.5	–	–	
$UO_2(pic)F_3^{3-} + F^{-*} \rightleftharpoons$ $UO_2(pic)F^{*3-}_3 + F^-$	$k_{ex} = 24.4 \pm 0.6$[a] s^{-1}; $k_{ex} = 12.8 \pm 0.3$[b,c] s^{-1}	61.4 ± 1.6	14.6 ± 0.5	Szabó and Grenthe (1998)
$UO_2(i\text{-pent-pic})F_3^{3-} + F^{-*} \rightleftharpoons$ $UO_2(i\text{-pent-pic})F^{*3-}_3 + F^-$	$k_{ex} = 18.2 \pm 1.8$[a] s^{-1} ; $k_{ex} = 13.9 \pm 1.1$[b,c] s^{-1}	59.7 ± 1.2	10.4 ± 0.8	
$UO_2(NO_2\text{-pic})F_3^{3-} + F^{-*} \rightleftharpoons$ $UO_2(NO_2\text{-pic})F^{*3-}_3 + F^-$	$k_{ex} = 16.0 \pm 1.2$[a,b,c] s^{-1}	60.3 ± 2.6	14.6 ± 0.6	
$UO_2(pic)F_3^{3-} + pic^{-*} \rightleftharpoons$ $UO_2(pic*)F_3^{3-} + pic^-$	$k_{ex} = 4.7 \pm 0.2$ s^{-1}	56.2 ± 4.2	-16.3 ± 1.2	
$UO_2(NO_2\text{-pic})F_3^{3-} + NO_{2-}$ $pic^{-*} \rightleftharpoons UO_2(NO_2\text{-}pic^*)F_3^{3-}$ $+NO_2\text{-}pic^-$	$k_{ex} = 55$ s^{-1}	59.4	11.3 ± 0.4	

	picolinate ring rotation			
pic	k_{ex}=300 s^{-1}	40.1 ± 2.4	–46.7 ± 2.8	Szabó and Grenthe (1998)
i-pent- pic	k_{ex} = 90 s^{-1}	46.8 ± 1.5	–32.8 ± 1.0	
NO_2-pic	k_{ex} = 2060 s^{-1}	49.6 ± 3.4	3.3 ± 1.2	
$UO_2(ox)F_3^{4-} + F^{-*} \rightleftharpoons$ $UO_2(ox)F^{*4-}_3 + F^-$	$k_{ex} = 21.6 \pm 2.4^{a,b,c}$ s^{-1}	58.9 ± 3.4	12.4 ± 1.0	Szabó and Grenthe (1998)
(In D_2O)	$k_{ex} = 14.1 \pm 0.8^{a,b,c}$ s^{-1}	60.4 ± 2.0	18.9 ± 0.6	
$UO_2(ox)F_3^{4-} + ox^{2-*} \rightleftharpoons$ $UO_2(ox^*)F_3^{4-} + ox^{2-}$	k_{ex} = 6.2 ± 0.2 s^{-1}	70.2 ± 5.6	23.1 ± 1.8	
$UO_2(ox)F(H_2O)_2^- + H_2O^* \rightleftharpoons$ $UO_2(ox)F(H_2O^*)_2^- + H_2O$	$k_{ex} = 1.6 \times 10^4$ s^{-1}	45.4 ± 3.8	–11.3 ± 0.5	Szabó *et al*. (1997) Farkas *et al*. (2000)
$UO_2(ox)F_2(H_2O)_2^- + H_2O^* \rightleftharpoons$ $UO_2(ox)F_2(H_2O^*)^{2-} + H_2O$	$k_{ex} = 1.6 \times 10^3$ s^{-1}			Szabó *et al*. (1997)
$UO_2(ox)_2F_3^- + F^{-*} \rightleftharpoons$ $UO_2(ox)_2F^{*3-} + F^-$	k_{ex} = 12.3 ± 1.0 s^{-1}	40.8 ± 2.0	–74.8 ± 3.6	Szabó and Grenthe (1998)
		47.1 ± 2.6	–56.3 ± 3.2	
(In D_2O)	8.7 ± 1.5 s^{-1}	42.0 ± 3.4	–73.3 ± 5.8	
$UO_2(ox)_2F^{3-} + ox^{2-*} \rightleftharpoons$ $UO_2(ox^*)_2F^{3-} + ox^{2-}$				
$UO_2(ox)_2(H_2O)^{2-} + ox^{2-*} \rightleftharpoons$ $UO_2(ox^*)_2(H_2O)^{2-} + ox^{2-*}$	$k_{ex} = 1.6 \times 10^3$ s^{-1}	31 ± 2	–56 ± 5	Aas *et al*. (1999)
$UO_2^{2+} + SO_4^{2-} \rightleftharpoons UO_2SO_4$	$k_1 = 3.4 \times 10^3$ M^{-1} s^{-1} $k_{-1} =$ 80 s^{-1}			Moll *et al*. (2000b)
$UO_2F_4(H_2O)^{2-} + F^- \rightleftharpoons UO_2F_5^{3-}$	$k_1 \approx 4 \times 10^3$ M^{-1} s^{-1} $k_{-1} = 6.5 \times 10^3$ s^{-1}			Vallet *et al*. (2002)
	stopped-flow data at 25°C μ = 0.10 M			
$UO_2^{2+} + dipic^{2-} \rightleftharpoons UO_2(dipic)$;		47.3 ± 2.6	–39 ± 9	Friese *et al*. (2001)
pH = 1.0	$k_1 = 0.94 \times 10^3$ M^{-1} s^{-1} $k_{-1} = 0.74$ s^{-1}	62.4 ± 1.6	–41 ± 6	
pH = 3.0	$k_1 = 3.21 \times 10^3$ M^{-1} s^{-1}	55.3 ± 1.3	6 ± 4	
	$k_{-1} = 0.38$ s^{-1}	57.1 ± 9.1	–61 ± 31	
$UO_2^{2+} + oda^{2-} \rightleftharpoons UO_2(oda)$;	$k_1 = 3.4$ M^{-1} s^{-1}	62.1 ± 2.8	–27 ± 9	Friese *et al*. (1998)
pH = 3.0	$k_{-1} = 0.43$ s^{-1}	58.0 ± 1.2	–57 ± 4	

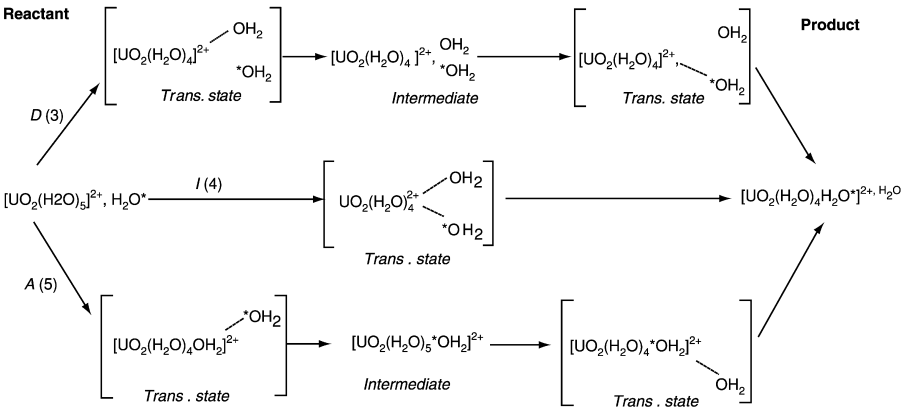

Scheme 5.1 *The scheme shows the dissociative* (*D*), *associative* (*A*) *and interchange* (*I*) *pathways for the water exchange between* $UO_2(OH_2)_5^{2+}$ *and water solvent from Vallet* et al. (2001) (*by permission of the American Chemical Society*).

$\Delta H^{\neq} = 26$ kJ mol^{-1}. The small difference in activation energy between these two pathways is understandable from the very similar structures of their transition states (Fig. 5.67a and b).

There are no experimental water exchange data for

$$UO_2(H_2O)_5^+ + H_2O^* \rightleftharpoons UO_2(H_2O^*)_5^+ + H_2O$$

However, the reaction has been studied using quantum chemical methods (Vallet *et al.* 2004a). In this system no stable intermediate $UO_2(H_2O)_6^+$ was found, hence the reaction cannot be associative. It was only possible to identify the reaction pathway for the dissociative mechanism with the electronic activation energy $\Delta E^{\neq} = 36.4$ kJ mol^{-1}. As judged by the activation energy one would expect the rate of water exchange to be slower in the uranyl(v) aquo-ion than that for the A/I mechanisms of the uranyl(vi) ion. However, the rate of reaction is determined by the Gibbs energy of activation, $\Delta G^{\neq} = \Delta H^{\neq} (\approx \Delta E^{\neq}) - T\,\Delta S^{\neq}$, where the activation entropy is larger for the D than for the A/I reactions (Wilkins, 1991, p. 202). Hence it is a reasonable assumption that the rate of water exchange in $UO_2(H_2O)_5^+$ is not too different from that in $UO_2(H_2O)_5^{2+}$.

The rate of water exchange and the activation energy for the reaction

$$U(H_2O)_n^{4+} + H_2O^* \rightleftharpoons U(H_2O^*)_n^{4+} + H_2O$$

has been determined experimentally (Farkas *et al.*, 2000b). The coordination number n is probably (9 ± 1), the rate constant 5.4×10^6 s^{-1} at 298 K and the activation enthalpy 34 kJ mol^{-1}. From the experimental data alone, it is not possible to determine the reaction mechanism. However, a quantum chemical study by Yang *et al.* (2003) of the water exchange in the corresponding thorium system indicates that the water exchange between $Th(H_2O)_9^{4+}$ and the water

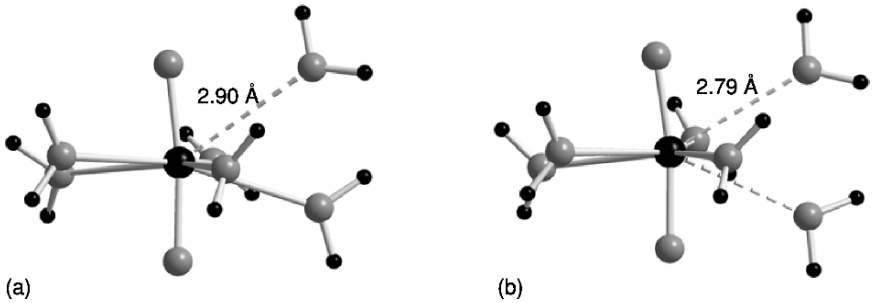

Fig. 5.67 (*a*) *Transition state in the A mechanism for the water exchange in the uranyl(VI) aqua ion. The geometry of the intermediate is very close to that of the I transition state*; *the bond distance in the entering and leaving water molecules are both* 2.65 Å. (*b*) *Transition state in the I mechanism. The U–H_2O distance for the two ligands above and below the equatorial plane in the I transition state is* 2.79 Å.

solvent takes place through an associative mechanism; from this we suggest that the mechanism is the same also for $U(H_2O)_9^{4+}$.

There are no experimental data for ligand exchange reactions in U(III) complexes, but Helm and Mehrbach (1999) have made extensive studies of the water exchange reactions of the trivalent lanthanides that are chemically very similar to the trivalent actinides. Based on these data, one expects the substitution mechanisms on U(III) to be similar to the nine-coordinated early lanthanides and to follow a dissociative mechanism.

(c) Water exchange in uranyl(VI) and uranium(IV) complexes

It is often assumed that the rate of water exchange at metal complexes is larger than that of the corresponding aqua ions. This does not seem to be the case for uranyl(VI) complexes as shown by the rate constant of water exchange in $UO_2(oxalate)F(H_2O)_2^-$ and $UO_2(oxalate)F_2(H_2O)^{2-}$, that are approximately 2×10^3 s^{-1} (Table 5.39); this is much smaller than that of $UO_2(H_2O)_5^{2+}$ ($k_{ex} = 1.3 \times 10^6$ s^{-1}; Szabó *et al.*, 1997). The rate constant of water exchange in $UF(H_2O)_8^{3+}$ is not significantly different from that in $U(H_2O)_9^{4+}$ (Farkas *et al.*, 2000b).

(d) Rates and mechanisms of complex formation reactions with inorganic and organic ligands

The rates and mechanisms of complex formation reactions have been studied both in equilibrium systems using NMR methods and in non-equilibrium systems using mainly stopped-flow and relaxation methods. In the former case the reactions are typically

$$ML_n + L^* \rightleftharpoons ML_n^* + L;$$

The rate constants in the forward and reverse directions are denoted k_1 and k_{-1}, respectively; as the system is in equilibrium the *rates* in the forward and reverse directions are the same. This is not the case in the non-equilibrium reactions where one often can arrange the experimental conditions so that the reverse reaction can be neglected; that is the reactions studied are of the type

$$ML_n + L \rightarrow ML_{n+1}$$

Some examples of experimental data, rate constants, and activation parameters are given in Table 5.39. The rate equations and reaction mechanisms have been deduced by investigating how the reaction rate depends on the concentration of reactants, products, and catalysts like H^+. The mechanistic deductions are complicated for multidentate ligands that in general are moderately strong bases; the rate of reaction is therefore often strongly dependent on the pH. Hines *et al*. (1993), Ekstrom and Johnson (1974), and Pippin and Sullivan (1989) give examples of such systems using the ligands diphosphonic acids and 4-(2-pyridylazo) resorcinol. However, the mechanisms of these reactions are far from clear. The rates of exchange for the ligands in Table 5.39 have been studied in more detail and some general comments about rate constants and mechanisms can therefore be made.

The rate of dissociation of coordinatively saturated complexes varies strongly with the strength of the complexes, e.g. from 2.7×10^3 s^{-1} for the acetate exchange in $UO_2(acetate)_3^-$ to 0.38 s^{-1} for the rate of dissociation of UO_2(dipicolinate); the latter ligand forms a very strong three-dentate chelate complex. The rate of formation and dissociation of UO_2(dipicolinate) and $UO_2(CO_3)F_3^{3-}$ are proton-catalyzed; the same is certainly the case for UO_2(oxydiacetate), but here there is only experimental data at one pH.

For multidentate ligands the mode of coordination is not always known and it is also unlikely that the formation or dissociation of such complexes takes place in one step. Hence, the experimental rate equation does not provide information on the rate-determining step. Some information may be obtained using the Eigen–Wilkins mechanism as exemplified by the rate constant for the formation of UO_2(dipicolinate) and UO_2SO_4. Both rate constants have nearly the same value (Table 5.39) indicating that the reaction is not strongly dependent on the entering ligand; this is a typical feature of dissociative reactions where the rate of water dissociation from the first coordination sphere is rate-determining. However, in the Eigen–Wilkins mechanism the experimental rate constant is a product of the rate of water exchange and the equilibrium constant for the formation of an outer-sphere complex with the entering ligand. A crude estimate of K_{os} for sulfate and dipicolinate is 5–50 M^{-1}, which would correspond to a rate constant for the water dissociation equal to $(0.7–0.07) \times 10^3$ s^{-1}. This is very different from the experimental value for the water exchange, indicating that the mechanism is more complex, suggesting that the rate of chelate ring closure/ring opening might have a significant effect on the rate of

formation/dissociation of the complexes. Hurwitz and Kustin (1967) have studied the rate and mechanism of reactions between UO_2^{2+} and SO_4^{2-}, SCN^-, CH_3COO^-, and $ClCH_2COO^-$ using the temperature jump method. The rate of complex formation with sulphate is 180 M^{-1} s^{-1} at 20°C, very different from the value obtained by Moll *et al.* (2000b) using NMR. This is not an ionic strength effect that would result in a larger rate constant at lower ionic strength (Wilkins, 1991, p. 110). The bimolecular rate constants for the formation of the 1:1 complex between UO_2^{2+} and actate and monochloracetate are 1050 and 110 M^{-1} s^{-1}. Hurwitz and Kustin (1967) note that the most significant feature of their observations is the relative slowness of the substitution reactions and their strong ligand dependence. This indicates that the substitution reactions are associative.

Jung *et al.* (1988) have determined the rate and mechanism of the formation and decomposition of the binuclear hydroxide complex $[(UO_2)_2(OH)_2]^{2+}$. The rate is sufficiently slow so that NMR line broadening of $U^{17}O_2^{2+}$ can be used. The rate equation is

$$\text{Rate} = k_2[UO_2^{2+}][UO_2OH^+] - k_{-2}K_a[H^+][(UO_2)_2(OH)_2^{2+}]/2$$

where K_a is the equilibrium constant for the reaction $(UO_2)_2(OH)_2^{2+} + H^+ \rightleftharpoons (UO_2)_2(OH)^{3+} + H_2O$. The suggested mechanism consists of two steps:

$$UO_2^{2+}UO_2OH^+ \rightleftharpoons (UO_2^{2+} \ldots UO_2(OH^+) \rightarrow [UO_2 - (OH) - UO_2]^{3+}$$

that are followed by the fast reaction

$$(UO_2)_2(OH)^{3+} + H_2O \rightleftharpoons (UO_2)_2(OH)_2^{2+} + H^+.$$

The first step is the formation of an outer-sphere ion pair and the second is rate determining. The estimated rate constant for this step is 7.6×10^5 s^{-1}, close to the rate of water exchange in the aqua ion. Frei and Wendt (1970) have studied the rate of dissociation of the binuclear complex using the stopped-flow method and also they suggested a mechanism where a single OH-bridged intermediate is formed.

Ligand exchange between a limiting complex (the complex with the largest number of coordinated ligands) and free ligand is most conveniently studied by using NMR methods. A typical example is the rate of ligand exchange for the reaction

$$UO_2F_5^{3-} + {}^*F^- \rightleftharpoons UO_2{}^*F_5^{3-} + F^-$$

As one reactant is a coordinatively saturated complex it is unlikely that the ligand exchange takes place according to an associative mechanism. It also turns out that the rate of ligand exchange for the above and many other reactions involving limiting complexes is independent on the concentration of free ligand, confirming that the exchange mechanism is dissociative (Vallet *et al.*, 2002). This result is supported by quantum chemical calculations, which

demonstrate that there is no stable intermediate $UO_2F_6^{4-}$ (Ikeda *et al.*, 1984; Szabó *et al.*, 1997; Vallet *et al.*, 2002).

(e) Mechanisms of intramolecular reactions

Important examples within this group are chelate ring opening/ring closure reactions, exemplified by the complex UO_2(picolinate)F_3^{2-}, (Fig. 5.68) (Szabó *et al.*, 1997; Vallet *et al.*, 2004b) and the experimental data in Table 5.39. In this complex there are three non-equivalent fluoride ligands, F_A, F_B and F_C, as shown in the ^{19}F NMR spectrum. The central peak, F_C, is narrow, indicating a slow exchange on the NMR time-scale while the other two peaks are broad, corresponding to a rate constant of 300 s^{-1} for the exchange between the F_A and F_B sites. This exchange is a result of an intramolecular process as the intermolecular exchange between coordinated and free fluoride is much slower, k_{obs} = 13 s^{-1} for F_A and F_B and 24 s^{-1} for F_C. The intramolecular exchange between F_A and F_B is the result of a a chelate ring opening/closure reaction that results in a rotation of the picolinate ligand and an exchange of the F_A and F_B sites The rate of exchange for the intermolecular exchange of picolinate is much slower, 4.7 s^{-1}.

The exchange between the different isomers of UO_2(picolinate)$_2F^-$ (Fig. 5.69) probably also takes place through a ring opening/ring closure reaction; a similar reaction mechanism has also been proposed for the kinetics of intra- and

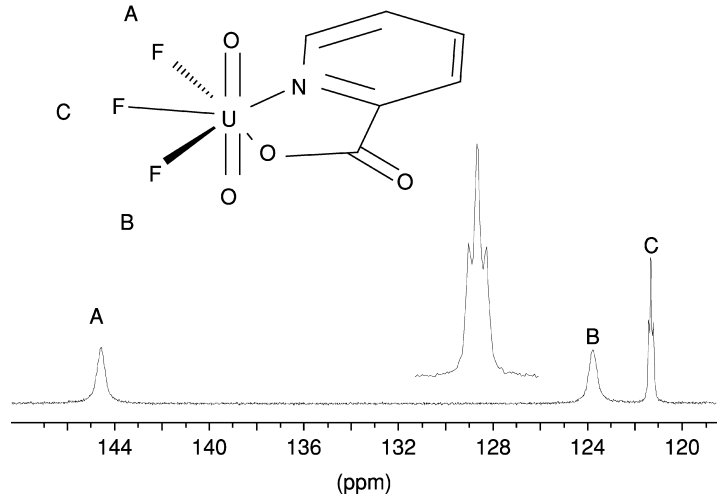

Fig. 5.68 *The ^{19}F NMR spectrum of UO_2(picolinate)F_3^{2-} at –5°C showing peaks for the three different fluorides (from Szabó* et al. *(1997), reproduced by the permission of American Chemical Society). There is no visible spin–spin coupling in the exchanged broadened peaks for fluorides A and B. Spin–spin coupling, a collapsed doublet of doublets, is evident in the narrow peak C, cf. the insert.*

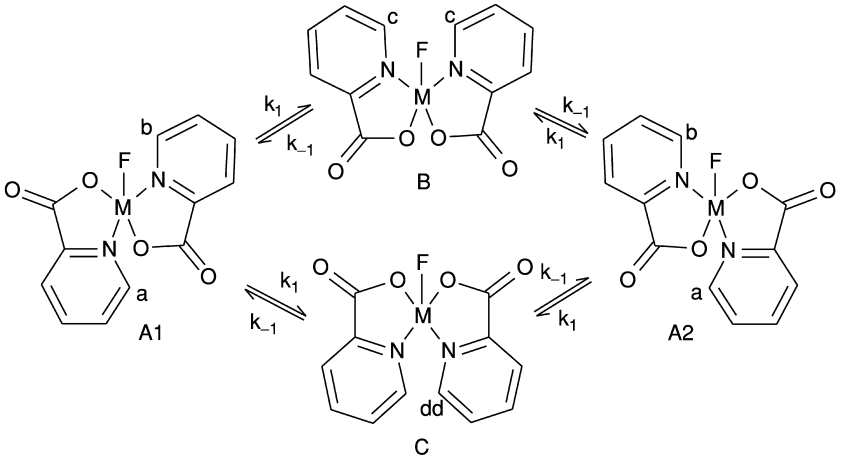

Fig. 5.69 *Different isomers of the complex* $UO_2(picolinate)_2^{F-}$ *and the possible exchange pathways between them* (*from Szabó* et al. (1997), *reproduced by the permission of American Chemical Society*). *The exchange presumably takes place through chelate ring opening/ring closure reactions.*

intermolecular exchange reactions of nonamethyl-imidodiphosphoramide (NIPA) in $UO_2(NIPA)_3^{2+}$ (Bokolo *et al.*, 1981).

Intramolecular reactions of the type encountered in $UO_2(picolinate)_2F^-$ do not necessarily proceed through chelate ring opening/ring closure as exemplified by $UO_2(acac)_2L$, in Fig. 5.70, where acac is a β-diketonate like acetylacetonate or dibenzoylmethanate and L an uncharged ligand such as dimethylsulfoxide (DMSO) (Ikeda *et al.*, 1984). The two methyl groups in the acetylacetone ^{13}C NMR spectrum are equivalent at room temperature due to fast exchange, but not at low temperature. The rate of intermolecular exchange between coordinated and free acac is slow and the fast exchange between the two methyl groups is therefore not the result of chelate ring opening/ring closure but of the fast dissociation/reentry of the ligand L that also results in exchange between the methyl groups (Fig. 5.70); the chelate ring opening is a very slow reaction.

Kramer and Maas (1981) have studied the fluxionality in U(VI) complexes of trifluoroacetylacetonate and various uncharged bases and suggest that the fluxionality of the complexes is a result of an intramolecular base migration; however, it is difficult to envisage that such a reaction is geometrically feasible.

(f) Rate and mechanism of ligand exchange in non-aqueous systems

The proposed mechanisms and activation parameters for ligand exchange in uranyl(VI) complexes between a number of uncharged ligands in non-aqueous systems are given in Table 5.40. The experimental rate constant k_{obs} for many of the reactions is given by

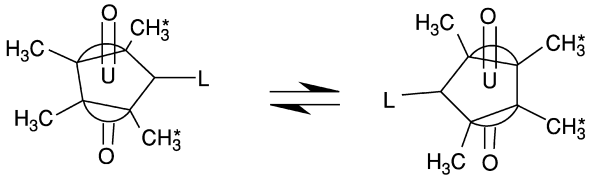

Fig. 5.70 *Ligand exchange in acetylacetonato complex $UO_2(acac)_2L$. The methyl groups in the coordinated acetylacetonate are non-equivalent as a result of their different chemical surroundings. The two sites are in fast exchange at room temperature as a result of the fast dissociation/re-entry of the ligand L.*

$$k_{obs} = k_1 + k_2[L],$$

where [L] is the free ligand concentration. In most systems k_2 is equal to zero, indicating a dissociative mechanism as seen in Table 5.40. When $k_2 \neq 0$ the rate of exchange depends on the ligand concentration, indicating an associative pathway. The difference in exchange mechanism for water (associative or associative interchange mechanism) and the dissociative pathway for the ligands in Table 5.40 is probably due to the larger steric constraints for the latter ligands. The occurrence of two parallel pathways, e.g. for DMSO indicates that the energy difference between complexes with four-, five-, and six-coordinated DMSO ligands is small. It is worth noting that there is no connection between the suggested mechanisms and the activation entropy for these reactions that all involve an uncharged ligand.

(g) Rate and mechanism of 'yl'-oxygen exchange in uranyl(VI) and uranyl(V) complexes: isotope exchange reactions

The rate of exchange between the 'yl'-oxygen atoms in $UO_2^{2+}(aq)$ and the water solvent is very slow, the half-life is 5000 to 10000 h as demonstrated by Gordon and Taube (1961a) using ^{18}O-enriched uranyl(VI). They noticed that the rate of exchange depends on the hydrogen ion concentration and that the reaction was photo-catalyzed. The fact that the exchange is very fast in the photo-excited state of the uranyl(VI) aqua ion (Bell and Buxton, 1974) has been used to prepare uranyl(VI) complexes where the 'yl'-oxygens are isotope-enriched in ^{17}O or ^{18}O (Howes *et al.*, 1988). The rate of exchange of the 'yl'-oxygens and the water solvent is strongly catalyzed by $UO_2^+(aq)$ (Gordon and Taube, 1961b). These two observations indicate that the exchange is related to the weakening of the $U–O_{yl}$ bond. In the photo-excited state, this is the result of transfer of a bonding electron to an empty f-orbital, and in $UO_2^+(aq)$ from the f-electron that is localized in a nonbonding f-orbital (Vallet *et al.*, 2004a). There are few precise and reproducible experimental observations and the mechanism for the exchange reaction has therefore not yet been clarified. Gordon and Taube (1961b) suggested that the rate law for the UO_2^+-catalyzed exchange

Table 5.40 *Mechanisms and activation parameters for the exchange of monodentate uncharged ligands, L, in the uranyl(VI) complexes $UO_2L_5^{2+}$ and $UO_2L_4^{2+}$. The solvent is deuterated acetone or dichloromethane. The ligands are: dimethylsulfoxide (DMSO), N,N,-dimethylacetamide (DMA), trimethylphosphate (TMP), triethylphosphate (TEP), N-methylacetamide (NMA), diethylphosphate (DEP), tetramethylurea (TMU), and hexamethylphosphoramide (HMPA).*

Complex	*Solvent*	*Mechanism*	$\Delta H^{\neq}$ (kJ mol^{-1})	$\Delta S^{\neq}$ (J K^{-1} mol^{-1})	*References*
$UO_2(DMSO)_5^{2+}$	CD_3COCD_3	D	39	–48	Honan *et al.* (1978); Ikeda *et al.* (1979b)
		D	54	6	
		A	39	–28	
$UO_2(DMA)_5^{2+}$	CD_2Cl_2	D	43	–44	Bowen *et al.* (1976)
$UO_2(TMP)_5^{2+}$	"	D or I_d	25	–110	Crea *et al.* (1977)
$UO_2(TEP)_5^{2+}$	"	D or I_d	44	–48	Crea *et al.* (1977)
$UO_2(NMA)_5^{2+}$	"	D	67	45	Honan *et al.* (1979)
$UO_2(DEP)_5^{2+}$	"	D	32	–54	Bowen *et al.* (1979)
$UO_2(TMU)_5^{2+}$	"	D	80	85	Ikeda *et al.* (1979b)
$UO_2(HMPA)_5^{2+}$	"	D	14	–172	Honan *et al.* (1978)
		A	22	–120	

$U^*O_2^{2+} + H_2O \rightleftharpoons UO_2^{2+} + H_2{}^*O$ is first order in $[UO_2^+]$ and suggest the mechanism

$$UO_2^+ + H_2{}^*O \rightleftharpoons U^*O_2^+ + H_2O$$

$$U^*O_2^+ + UO_2^{2+} \rightleftharpoons U^*O_2^{2+} + UO_2^+$$

where the first reaction is assumed to be fast, but the details of the oxygen exchange are not known and quantum chemical studies, similar to those of Schreckenbach *et al.* (1998) and Clark *et al.* (1999) on UO_2^{2+}, have not been made to our knowledge. Howes *et al.* (1988) have studied the second reaction and use the experimental data, in combination with the Marcus' cross-relations, to estimate the rate constant for the outer-sphere self-exchange to be in the range 1–15 M^{-1} s^{-1}, a value that is in good agreement with quantum chemical estimates by Privalov *et al.* (2004).

There are a number of other experimental studies of exchange between uranyl (VI) complexes and water, using ^{17}O-enriched uranyl(VI). This exchange is pH-dependent and much faster than in the $UO_2^{2+}(aq)$. The half-life is less than 1 h in the pH range where polynuclear complexes containing hydroxide/oxide bridges are present (Moll *et al.*, 2000b); the rate of exchange is much slower in $UO_2(OH)_4^{2-}$ and $UO_2(OH)_5^{3-}$ and very slow in limiting complexes that do not contain water or hydroxide in the first coordination sphere. Schreckenbach *et al.* (1998) and Clark *et al.* (1999) have discussed the mechanism, however the estimated activation energy seems large (160 kJ mol^{-1}).

(h) Isotopic exchange reactions involving uranium

Isotopic exchange using ^{233}U as a probe has been used to study the rate and mechanism of exchange reactions between UO_2^{2+}, UO_2^{+}, and U^{4+}. These studies have been made in acid solutions where the degree of hydrolysis is known. The exchange can take place either through bond breaking/bond formation or through electron transfer. The following exchange reaction is a typical example (Rona, 1950; Masters and Schwartz, 1961):

$$U^{4+}(aq) + {}^{*}UO_2^{2+}(aq) + 2H_2O \underset{k_r}{\overset{k_f}{\rightleftharpoons}} 2{}^{*}UO_2^{+}(aq) + 4H^{+}$$

where *U denotes uranium enriched in ^{233}U. The reaction follows two parallel pathways where the rate of exchange for the forward reaction at [U(IV)] < 0.01 M is equal to

$$\text{Rate} = k_f[U^{4+}][UO_2^{2+}][H^{+}]^{-3} \quad \text{with } k_f = 2.1 \times 10^{-7}\ \text{M}^{-1}\ \text{s}^{-1} \text{ at } 25^{\circ}\text{C}$$

Imai (1957) studied the rate for the reverse reaction and found

$$\text{Rate} = k_r[UO_2^{+}]^2[H^{+}] \quad \text{with } k_r = 436\ \text{M}^{-2}\ \text{s}^{-1} \text{ at } 25^{\circ}\text{C}$$

The ratio $k_r/k_f = 2 \times 10^9\ \text{M}^4$ is in good agreement with the experimental equilibrium constant $1 \times 10^9\ \text{M}^4$, indicating that both reactions have the same transition state. A slightly lower value of $k_r \approx 130$, was determined by Kern and Orleman (1949). The rate of exchange of the forward reaction is slow because it goes thermodynamically 'uphill', a result of the extensive bond breaking/bond formation during the exchange. The reverse reaction is fast because the reaction is now thermodynamically favored.

The intimate mechanism for most isotope exchange reactions is not known; for the U(IV)–U(V)–U(VI) reaction there is only information on the stoichiometry of the activated complex, $[HOUOUO_2^{3+}]^{\neq}$ and the activation energy 157 kJ mol^{-1}. At U(IV) concentrations higher than 0.01 M, there is a significant contribution from a second reaction pathway and the rate of exchange is now

$$\text{Rate} = k[U^{4+}]^2[UO_2^{2+}][H^{+}]^{-2}$$

but the mechanistic implications are not clear.

It is often difficult to decide if isotope exchange takes place through bond breaking/bond formation, or as a result of electron transfer; the isotope exchange between uranyl(VI) and uranyl(V) and other actinyl ions are typical examples. Kato *et al.* (1970) studied the exchange between UO_2^{2+} and U^{4+} by measuring the transfer of ^{18}O-enriched 'yl' oxygen to water. The rate constant was 6.5×10^{-4} M^{-1} s^{-1}, is very different from that of Masters and Schwartz (1961) that used different experimental conditions. Kato *et al.* suggested that the activated complex has the composition $[U(IV)U(VI)]^{\neq}$ and that the rate of oxygen exchange and electron exchange are of the same order of magnitude.

A number of the redox reactions to be discussed in the following section have been investigated experimentally using isotope exchange technique.

(i) Rate and mechanism of redox reactions

These reactions are in general studied using isotope exchange as exemplified by

$$U^*O_2^{2+}(aq) + UO_2^+(aq) \rightleftharpoons UO_2^{2+}(aq) + U^*O_2^+(aq)$$

The rate of exchange has been studied using ^{18}O-enriched UO_2^{2+} by following the isotope distribution using mass spectroscopy after separation of U(VI) and U(V) (Gordon and Taube, 1961b; Masters and Schwartz, 1961). The experimental rate of exchange is equal to

$$\text{Rate} = k_{obs}[UO_2^{2+}][UO_2^+]$$

with $k_{obs} \approx 50$ M^{-1} s^{-1} (Gordon and Taube, 1961b), close to the more accurate determination of the corresponding exchange reaction between Np(VI) and Np(V), $k_{obs} \approx 110$ M^{-1} s^{-1}, determined by Cohen *et al.* (1954). Howes *et al.* (1988) report rate constants in the range 1–15 M^{-1} s^{-1}. Privalov *et al.* (2004) have discussed the mechanism for the U(V)–U(VI) electron exchange between the aqua-ions, the fluoride, and the carbonate complexes using quantum chemical methods. Both outer-sphere and inner-sphere mechanisms were studied; the former for the aqua ions using the Marcus model and the latter using an inner-sphere model for binuclear complexes containing hydroxide, fluoride, and carbonate bridges. The calculated rate constant for the homogeneous electron exchange (outer-sphere) between $UO_2^{2+}(aq)$ and $UO_2^+(aq)$ is 26 M^{-1} s^{-1} in fair agreement with experimental data. The rate of electron transfer for the inner-sphere reactions is much faster, but here there are no experimental data that can be used for comparison. This study provides a model for the intimate reaction mechanisms as exemplified by the following structure of the precursor and transition state structures (Fig. 5.71).

The kinetics of redox reactions is also discussed in Chapter 23.

Rate constants and reaction mechanisms for a number of redox reactions involving uranium have been reported by Newton (1975) and in the second edition of this book (Katz *et al.*, 1986). It is not possible to discuss all this

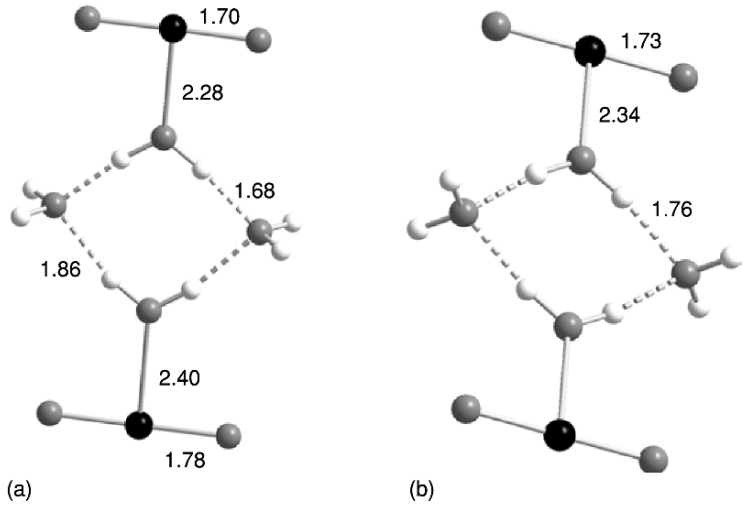

Fig. 5.71 *Quantum chemical model of the precursor* $[UO_2^{2+}\ldots UO_2^{+}]$ *in the outer-sphere electron transfer reaction* $U^*O_2^{2+}(aq) + UO_2^{+}(aq) \rightleftharpoons UO_2^{2+}(aq) + U^*O_2^{+}(aq)$ *from Privalov* et al. (2004). *The model is focused on the bridge between the two uranyl ions and their complete coordination spheres are therefore modeled using a continuum model.* (*a*) *shows the precursor with uranyl*(*v*) *and uranyl*(*vi*) *ions and* (*b*) *the transition state where the two uranyl ions are equivalent.*

information and we have accordingly selected a few examples that illustrate the interpretation of the experimental rate laws. A prerequisite for the mechanistic discussion is information on the equilibrium system, i.e. the complexes present in the test solutions under different experimental conditions. When determining the experimental rate law, care must be taken to identify possible parallel reaction pathways and possible catalysts. We will discuss the oxidation of U(IV) with Pu(VI) as this reaction is not only of scientific interest, but also important in nuclear reprocessing (Newton, 1958). In acid solutions of moderate concentration of the reactants, there is a complete reduction of Pu(VI) to Pu(III). When the reactant concentrations are about 10^{-4} M 96% of the U(IV) reacts according to

$$2\mathrm{Pu(VI)} + \mathrm{U(IV)} \rightleftharpoons 2\mathrm{Pu(V)} + \mathrm{U(VI)}$$

and the remaining 4% react according to

$$2/3\mathrm{Pu(VI)} + \mathrm{U(IV)} \rightleftharpoons 2/3\mathrm{Pu(III)} + \mathrm{U(VI)}$$

The latter two equations only represent the change in oxidation states of the actinides but do not account for the overall stoichiometry. At constant hydrogen ion concentration, the experimental rate law is

$$-\frac{\mathrm{d}[\mathrm{Pu(VI)}]}{\mathrm{d}t} = 2k''[\mathrm{Pu(VI)}][\mathrm{U(IV)}]$$

This rate equation requires that the activated complex has the composition $[\mathrm{Pu(VI)}^{\cdots}\mathrm{U(IV)}]^{\neq}$; as the hydrogen ion concentration is constant, there is no information of the hydrogen ion concentration dependence of the reaction rate. Based on this limited information, a possible reaction mechanism that involves the following two elementary reactions has been suggested (charges have been omitted):

$$\mathrm{Pu(VI)} + \mathrm{U(IV)} \rightleftharpoons \mathrm{Pu(V)} + \mathrm{U(V)}$$

$$\mathrm{Pu(VI)} + \mathrm{U(V)} \rightleftharpoons \mathrm{Pu(V)} + \mathrm{U(VI)}$$

The first reaction is rate-determining as it involves a major rearrangement between the coordination spheres of reactants and products, while the second is fast because these rearrangements are minor.

Additional mechanistic information is obtained by investigating how the rate of reaction depends in the hydrogen ion concentration. One finds that the rate is

$$-\frac{\mathrm{d}[\mathrm{Pu(VI)}]}{\mathrm{d}t} = 2k''\left(1 + \frac{K}{[\mathrm{H}^+]}\right)\left[\mathrm{PuO_2^{2+}}\right]\left[\mathrm{U^{4+}}\right]$$

This rate law suggests that there are two parallel pathways according to the following elementary reactions:

$\mathrm{U^{4+}} + \mathrm{H_2O} = \mathrm{UOH^{3+}} + \mathrm{H^+}$ (a fast equilibrium prior to the rate-determining step);

$\mathrm{UOH^{3+}} + \mathrm{PuO_2^{2+}} \rightleftharpoons \mathrm{HOUOPuO^{5+}}$ (rate-determining step in a reversible reaction);

$\mathrm{HOUOPuO^{5+}} = \mathrm{OUOPuO^{4+}} + \mathrm{H^+}$ (a fast equilibrium reaction);

$\mathrm{OUOPuO^{4+}} + \mathrm{H_2O} \rightleftharpoons \mathrm{UO_2^+} + \mathrm{PuO_2^+} + 2\mathrm{H^+}$ (a slow equilibrium reaction).

The elementary reactions above provide information on the stoichiometric mechanism, but not the details at the microscopic level, as that exemplified in Fig. 5.71 for the electron transfer reaction

$$\mathrm{U^*O_2^{2+}(aq)} + \mathrm{UO_2^+(aq)} \rightleftharpoons \mathrm{UO_2^{2+}(aq)} + \mathrm{U^*O_2^+(aq)}.$$

5.10.4 Fluorescence properties and photochemistry of uranyl(VI) complexes

Only light that is absorbed by a substance is effective in producing a photochemical change; Grotthuss and Draper stated this principle of photochemical activation in 1818, long before the quantum theory. According to quantum theory, the primary step of a photochemical reaction is the activation of *one* molecule by *one* absorbed quantum of radiation. The absorption of a photon leads to a transition from a singlet ground state to a singlet excited state; this is followed by a number of very fast processes with lifetimes in the picosecond

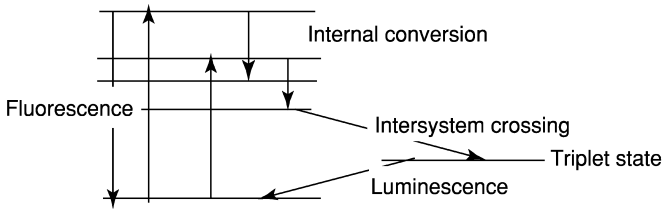

Fig. 5.72 *Molecular energy levels where the arrows denote the corresponding process for energy loss of the excited states. The ground state is a singlet, the excitation takes place without change of spin. The excited states can lose energy by fluorescence back to the ground state, via internal conversion from higher to lower excited states and by intersystem crossing to the triplet state. The typical fluorescence lifetime in the excited state is* 10^{-8} *to* 10^{-9} s *and for internal conversion* 10^{-12} s. *The energy loss from the triplet state to the ground state takes place either by luminescence/phosphorescence or thermally. In addition energy dissipation can take place through non-radiative decay and collisional quenching.*

range that take place before any photochemical reaction can occur. *Fluorescence* takes place from an excited singlet to the ground state, *internal conversion* between the excited singlet states, and *intersystem crossing* from the lowest excited singlet state to the triplet state (Fig. 5.72). The lifetime of the triplet state is long (micro to milliseconds) in comparison with that of the singlet states; the radiative emission from triplet to singlet is called phosphorescence. The long lifetime of the triplet also makes thermal energy dissipation possible.

There are other energy dissipation pathways than fluorescence from the excited states such as non-radiative transfer of the excitation energy to vibrational excitation in the coordinated ligands and the solvent and in collisional pathways, so called dynamic quenching; a more detailed discussion is given by Szabó *et al*. (2006). The intensity of fluorescence or phosphorescence depends on the competition between these physical and chemical processes. The quantum yield, Q_Y, is defined as the ratio between the number of photons emitted and absorbed and this quantity is accordingly strongly dependent on the different quenching mechanisms

$$Q_Y = \frac{1/\tau_n}{1/\tau_n + k_{nr}} = \frac{\tau}{\tau_n}$$

where τ_n is the lifetime in the absence of non-radiative processes and k_{nr} the rate constant for non-radiative decay; τ is the lifetime in the presence of non-radiative processes. In systems with dynamic quenching it is $1/\tau = 1/(1/\tau_n + k_{nr} + k_q)$, where k_q is the rate constant for collision quenching.

In addition to these quenching processes, the fluorescence intensity may also depend on static quenching that is the result of the formation of a non-fluorescent complex with a ligand, L, in the ground state. In order to understand and use information of fluorescence intensity and fluorescence lifetimes, it is essential to be able to distinguish and quantify all these mechanisms. Static and dynamic quenching can be distinguished by lifetime analysis (Toraishi *et al*., 2004).

In steady-state excitation the concentration of excited molecules and therefore the fluorescence intensity is constant. Hence, we have the following relations in the absence and presence of quenching:

$$\frac{\mathrm{d}I^*}{\mathrm{d}t} = f - (1/\tau_0)[I^*] = 0;$$

and

$$\frac{\mathrm{d}I^*}{\mathrm{d}t} = f - \left(1/\tau_0 + k_\mathrm{q}[L][I^*]\right) = 0$$

where f is the light flux, I^* is the concentration of the fluorescent species with a lifetime τ_0 in the absence of the quencher L. k_q is the rate constant for fluorescence decay in the presence of L. Hence

$$\left(\frac{I}{I_0}\right)^{-1} = \frac{1/\tau_0 + k_\mathrm{q}[\mathrm{L}]}{1/\tau_0} = 1 + k_\mathrm{q}\tau_0[\mathrm{L}]$$

where I and I_0 represent the measured fluorescence intensity in the presence and absence of L; this is the Stern–Volmer equation. The fraction of excited fluorophores relative to the total is equal to

$$\left(\frac{I}{I_0}\right) = \left(\frac{\tau}{\tau_0}\right)$$

which for the case of only static quenching in the ground state reduces to $(I/I_0) = 1$ because then $\tau = \tau_0$.

In uranyl(VI) systems where the ligand is a strong quencher, the rate constant k_q is very large; it is then not possible to detect the fluorescence spectrum for the complexes (e.g. Moll *et al*., 2003).

The photochemistry of uranium compounds is a 'classical' field of research that dates back to the Becquerels more than 100 years ago. The experimental quantities are the excitation and emission spectra and the lifetime(s) of the excited state(s) as a function of chemical parameters. The chemistry of photo-excited UO_2^{2+} has been extensively studied, both as a tool for synthesis, as a method to determine equilibrium constants in ground and excited states, and for elucidation of luminescence quenching mechanisms. Recent reviews by Baird and Kemp (1997), Fazekas *et al*. (1998), and Yusov and Shilov (2000) provide an introduction to the literature.

The photo-oxidation of oxalic acid was used in the first chemical actinometers to measure photon flux based on the reactions

$$UO_2^{2+} + h\nu \rightarrow (UO_2^{2+})^*;$$
$$(UO_2^{2+})^* + (COOH)_2 \rightarrow UO_2^{2+} + CO_2 + CO + H_2O$$

The actinometer must be calibrated to determine the quantum efficiency at the wavelength used.

The excited states responsible for luminescence emission have a charge-transfer character as a result of excitations from the σ_u or σ_g bonding U–O orbitals to an empty f-orbital via internal conversion and intersystem crossing as outlined in Fig. 5.72. The resulting triplet state is $^3\Delta_g$, or to be more precise the $\Omega = 1_g$ component of the relativistic $^3\Delta_g$ state (Zhang and Pitzer, 1999; Matsika *et al.*, 2001) and the transition to the ground state is accordingly spin forbidden, which accounts for the long lifetime. The very long lifetime in comparison with those from electronically excited states of organic molecules is the basis for the photo-reactivity of $(UO_2^{2+})^*$. The photo-excited state is a very strong oxidant with an estimated oxidation potential of 2.6 V. The probable deactivation pathways are (Fazekas *et al.*, 1998):

- intra-molecular radiationless deactivation via O-H stretch modes of coordinated water;
- intra-molecular energy transfer to vibrational modes of the water solvent as in rare-earth metal ions;
- electron transfer and radical formation

$$(UO_2^{2+})^* + H_2O \rightarrow UO_2^+ + (H_2O^+)^*;$$

or hydrogen abstraction

$$(UO_2^{2+})^* + H_2O \rightarrow UO_2H^+ + OH^*$$

The experimental basis for photochemical studies is provided by fluorescence spectroscopy and measurements of the decay of the fluorescence as a function of chemical parameters. The terminology is often misleading, the majority of the experimental 'fluorescence' spectra of uranyl(VI) systems refer to phosphorescence, often denoted luminescence. In the following we will use the luminescence terminology. Despite all experimental efforts there is no consensus about the primary deactivation processes. The luminescence properties of the uranyl(VI) ion in water solution can be used as an example. When the pH is increased in the UO_2^{2+}–water system, the peaks of the emission spectrum are displaced towards longer wavelength. At the same time, the luminescence lifetime is no longer mono-exponential; this is presumably a result of the formation of hydroxide complexes (Fazekas *et al.*, 1998). Moriyasu *et al.* (1977) made similar observations on other uranyl(VI) systems where complexes with fluoride and phosphate were formed, in particular they observed a strong enhancement of both the luminescence intensity and its lifetime that is the basis for an analytical method to determine uranium in low concentration. The increase of the lifetime of the triplet state is assumed to be a result of shielding of the uranyl ion from water that is an efficient quencher. Some authors explain the non-exponential luminescence decay by exciplex formation (Deschaux and Marcantanatos, 1979), other by a reversible crossing between two different excited uranyl states (Formosinho and Da Graca Miguel, 1984; Formosinho *et al.*, 1984). Billard and Lützenkirchen (2003) have discussed the problems encountered when analyzing experimental luminescence data in terms of elementary reactions as discussed below.

Laser-induced fluorescence spectroscopy is extensively used as a tool for the analytical determination of trace amounts of uranium as described in Chapter 30. The technique is also used to determine equilibrium constants and the speciation of uranium(VI) in aqueous solution both in laboratory and environmental systems. This raises the question if the measured equilibrium constant, K_{app}, refers to the ground or the excited state, a problem that has been discussed by Billard and Lützenkirchen (2003). Their starting point is the following mechanistic scheme (Scheme 5.2): where K is the equilibrium constant

$$\begin{array}{ccc} & \overset{k_1,\, k_{-1}}{} & \\ M^* + L & \rightleftharpoons & (ML)^* \\ \uparrow\downarrow \lambda_1 & & \uparrow\downarrow \lambda_2 \\ M + L & \rightleftharpoons & ML \\ & \underset{K}{} & \end{array}$$

Scheme 5.2 *Mechanistic scheme for the complex formation between M and L in ground and excited state. The notation is explained in the text.*

in the ground state, k_1 and k_{-1} the rate constants for the formation and dissociation of ML*, and λ_1 and λ_2 the rate constants for decay of M* and ML*.

In the experimental studies, time-resolved spectra are measured at different total concentrations of M and L, where the former is the fluorescence probe and the latter is assumed to be non-absorbing at the excitation wavelength. Scheme 5.2 has been used to deduce rate constants k_1 and k_{-1} and information on ground state and excited state chemistry from the amplitude of the emission spectra and ground state concentrations. In the case where there is no interac-

$$\begin{array}{ccc} M^* + L & & (ML)^* \\ \uparrow\downarrow \lambda_1 & & \uparrow\downarrow \lambda_2 \\ M + L & \rightleftharpoons & ML \\ & \underset{K}{} & \end{array}$$

Scheme 5.3 *Mechanistic scheme for reactions where the complex formation in the excited state can be neglected.*

tion between M* and L, or when the rate constants k_1 and $k_{-1} \ll \lambda_1$ and λ_2, Scheme 5.2 is reduced to Scheme 5.3 as follows:
where the measured lifetimes now represent M* and ML*. Billard and Lützenkirchen (2003) discuss the conditions under which K_{app} is a satisfactory approximation for the equilibrium constant K in the ground state. In their Model A, k_1 and $k_{-1} \ll \lambda_1$ and λ_2 and $K_{app} = K$ is then a good approximation. When k_1 and $k_{-1} \gg \lambda_1$, the chemistry in the excited state is dominating and the apparent equilibrium constant, K_{app} is then equal to

$$K_{app} = K^* \frac{\alpha\tau_1}{\beta\tau_2}$$

where α and β are the molar absorption coefficients and τ_1 and τ_2 the lifetimes of M* and ML* (Model C). In systems where k_1 and $k_{-1} \approx \lambda_1$ and λ_2, one has to use numerical simulations to deduce the rate constants from the experimental data (Model B). K^* is the equilibrium constant for the formation of ML*.

Billard and Lützenkirchen (2003) discuss a number of time-resolved laser fluorescence studies of uranyl complexes using the model outlined above. For example, in the uranyl–hydroxide system can be described by either Model A or B. Lopez and Birch (1997) observed two decay times that were independent of pH in the range 2.5–4.5, indicating that $K_{app} = K$.

(a) Quenching mechanisms of the uranyl ion

Quenching is in general described by the Stern–Volmer mechanism as described previously; it can proceed through a number of different reactions as outlined by Baird and Kemp (1997). Quenching by halide ions most likely takes place by electron transfer as indicated by the fact that the quenching efficiency depends on the oxidation potential, and decreases in the order $I^- > Br^- > Cl^- > F^-$; metal ions in low oxidation states like Ag^+, Fe^{2+}, and Mn^{2+} are also efficient quenchers that also act through an electron transfer mechanism.

Many organic compounds are very efficient quenchers and the mechanism involves either a process where the quencher forms a short-lived exciplex with the excited uranyl, or an electron transfer. In the latter case, the relative quenching rate depends on the ionization potential of the quencher (as for the halide ions). Burrows and Kemp (1974) have reviewed quenching reactions with different alcohols where hydrogen abstraction may be an important quenching mechanism as indicated by large primary hydrogen isotope effects.

The lifetime of the excited uranyl ion, $(UO_2^{2+})^*$ depends strongly on the total concentration of uranium (self-quenching), an observation that has been described by Deschaux and Marcantonatos (1979) and others as due to the formation of the binuclear exciplex

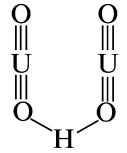

(b) Photochemistry of the uranyl(VI) ion

Rabinowitch and Belford (1964), Balzani and Carassiti (1970), and Güsten (1983) have reviewed the photochemistry of uranyl(VI) with organic substrates. The reactions involve oxidation of the substrate and reduction to uranyl(V); in

the absence of oxygen, a subsequent fast reaction leads to formation of uranyl (VI) and uranium(IV). In the presence of oxygen, uranyl(V) is rapidly oxidized to uranyl(VI) and accordingly the uranyl(VI) ion acts as a photo-catalyst, e.g. for the oxidation of alkanes, alkenes, alcohols, and aldehydes. The uranyl ion has also been used as a photo-catalyst for DNA footprinting as described in Section 5.11. All these reactions seem to take place by hydrogen abstraction from a C–H bond, followed by uranium-mediated product formation (Wang *et al.*, 1995). The mechanism can schematically be described by the following reactions, where SH_2 is the organic substrate, and S_{ox} the final oxidation product, an aldehyde or carboxylic acid.

$$SH_2 + (UO_2^{2+})^* \rightarrow SH^+ + UO_2^+ + H^+;$$
$$2SH^+ \rightarrow SH_2 + S_{ox};$$
$$2UO_2^+ \rightarrow UO_2^{2+} + U(IV).$$

5.11 ORGANOMETALLIC AND BIOCHEMISTRY OF URANIUM

There is an extensive organometallic chemistry for uranium(III) and uranium (IV); in fact, most of the organometallic chemistry as described in Chapters 25 and 26 deals with uranium and a detailed description of the synthesis and properties of organometallic uranium compounds can be found there. For historical reasons, we will here mention a few examples; the field was started by Wilkinson with the preparation of $(\eta^5\text{-cyclopentadienyl})_3UCl$ (Reynolds and Wilkinson, 1956), followed by reports from Fischer and Hristidu (1962) of additional cyclopentadienyl compounds, e.g. tetrakis(η^5-cyclopentadienyl)uranium(IV) (Fischer and Hristidu, 1962). The 'sandwich' compound uranocene, bis(π-cyclooctatetraene) uranium(IV), $U(C_5H_5)_2$ was prepared by Streitweiser and Müller-Westerhoff (1968). These compounds are π-complexes where uranium is coordinated by the cyclic ligands through their delocalized π-orbitals. Other complexes with the cyclopentadienyl ion $C_5H_5^-$ are $U(\eta^5\text{-}C_5H_5)_3$, $U(\eta^5\text{-}C_5H_5)_4X$, where X is an alkyl group, an alkoxy group, or BH_4. For description of these and other metal organic compounds the reader is referred to Chapter 25.

The biochemistry of uranium is totally dominated by investigations of the coordination of the uranyl(VI) ion to proteins, DNA/RNA and polysaccharide coatings in cell walls. In the proteins, the bonding takes place at the carboxylate and amino groups, in DNA/RNA at the phosphate groups, and in the polysaccharides at deprotonated OH groups. The strong binding of uranium has been used to make heavy-atom derivatives in protein crystallography (Tame, 2000) and as staining reagent in electron microscopy (Gray, 1994, 2001).

Photochemical oxidation of polydeoxynucleotides by UO_2^{2+} has been used for footprinting of DNA (Nielsen *et al.*, 1988). This is a technique used to identify the DNA region where a particular protein is bonded. It involves labeling of one

end of a DNA chain with ^{32}P; addition of UO_2^{2+} that binds to the phosphate groups and then irradiation with near-UV light to obtain photo-excited uranyl(VI) that abstracts a hydrogen from a nearby C–H group, resulting in cleavage of the DNA backbone diester chain both in single- and double-stranded DNA. The cleavage is random and not sensitive to the base sequence; it results in ^{32}P fragments of different lengths that can be identified through gel electrophoresis. When a protein is bonded to certain base sequences of DNA, these regions are not accessible to UO_2^{2+} and are therefore protected from cleavage; this results in a different fragmentation pattern and the base sequence where protein bonding takes place can therefore be identified. For details, see Stryer (1988). An important advantage of this method, as compared to the use of DNA-se enzymes as 'scissor', is the small size of the uranyl(VI) ion compared to the enzymes.

The uranyl ion has been used as a very efficient regioselective and stereoselective catalyst for the synthesis of oligonucleotides in solution (Sawai *et al.*, 1989, 1990, 1992, 1996; Shimazu *et al.*, 1993).

Uranium in the form of uranyl(VI) compounds is taken up by living organisms. In mammals the uranium is bonded to proteins, e.g. transferrin, with a residence time of several hours during which it is gradually transported and incorporated into bone tissue. The residence time is long and removal requires an extensive treatment with different sequestering agents (Scapolan, 1998). A detailed discussion of the behavior of uranium and other actinides is given in Chapter 31.

5.12 ANALYTICAL CHEMISTRY

There is wide array of options available for the determination of uranium including both classical wet chemical and instrument-based spectrometric techniques. The purpose of this section is to provide an overview of the analytical techniques and methods applicable to the determination of uranium in a variety of matrices with an emphasis on those techniques and methods useful for samples with uranium concentrations larger than 1 μg per gram of sample. An extensive review of the techniques and methods that are used for the determination of uranium at trace and ultra-trace (less than 1 μg per gram of sample) concentrations in geological, environmental, and biological matrices is given in Chapter 30.

5.12.1 Chemical techniques

(a) Sample preparation

Most bulk analytical techniques require that a stable, aqueous solution be prepared prior to analysis and element determination. The dissolution of uranium containing compounds and materials is typically performed either by fluxed fusion decomposition or acid dissolution. Fluxed fusion decomposition is the first step in many standard classical wet chemical procedures used for the determination of uranium at major and minor concentrations in uranium

containing ores. Ingamells and Pitard (1986) describe a chemical method for the determination of uranium in silicate minerals. In this method a several-gram quantity of silicate material is decomposed via fusion with Na_2O_2 in a platinum crucible. The fusion mass is dissolved in dilute HNO_3 and uranium is precipitated with a mixture of Na_2CO_3 and K_2CO_3 (Sandell, 1959). This precipitate is evaporated and redissolved in dilute HNO_3 before further purification or direct determination of uranium. Other fluxes that can be used for the fusion of uranium containing materials include hydroxides, carbonates, bisulfates, hydrosulfates, pyrosulfates, tetraborates, and metaborates (Dean, 1995).

Nearly all uranium compounds and uranium containing alloys can be dissolved in HNO_3. As briefly discussed in Section 5.6.4, uranium metal dissolves very rapidly in HCl, but a voluminous black residue is left unless a small amount of fluosilicate ion is present. uranium containing minerals, such as autunite, carnallite, gummite, phosphuranylite, torbernite, tyuyammite, uraninite, and uranophane will dissolve via open vessel digestion with HNO_3, HCl, and H_2SO_4 (Meites, 1963). Acid leaching with HNO_3, HCl, or H_2SO_4 has been used for industrial scale recovery of uranium from its ores. The various leaching processes for uranium ores are discussed in more detail in Section 5.4.3. A mixture of HF and HNO_3 can be employed when dissolution of silicates is required. When this mixture is used, complete recovery of uranium requires conversion of UF_4 to a soluble form by fuming with $HClO_4$ or H_2SO_4 or by complexation of F^- with H_3BO_3.

Separation and preconcentration of uranium can be achieved by most of the common chemical and physical separation methods: precipitation, coprecipitation, volatilization, electrolysis, liquid–liquid extraction, and ion-exchange chromatography. The simplest methods for the separation of uranium from solution are by precipitation or coprecipitation. Precipitation of uranium can be accomplished using inorganic and organic precipitants (Gindler, 1962). The formation of many precipitates in uranium containing solutions that also contain other anions and cations typically yields a group separation of uranium along with other elements. Uranium will coprecipitate from a carbonate-free solution with Fe(III) and Al(III) hydroxides. Carbonate is removed by heating the solution. Coprecipitation is accomplished by adding a macroscopic amount of Fe(III) or Al(III) to an acidified solution and adjusting the solution pH to basic with the addition of NH_4OH. Separation of uranium can also be accomplished by coprecipitation with $Ca(OH)_2$, $(NH_4)_2CO_3$, and $(NH_4)_2S$ (Rodden and Warf, 1950). Precipitation of uranium from acidic solutions can be performed fairly selectively as a peroxide or oxalate.

Electrochemical separation of uranium can be accomplished via Hg-cathode electrolysis and electrolytic deposition on a variety of solid metal electrodes (Casto, 1950) as well as electrodialysis and pyrometallurgical processes (Gindler, 1962). Electrodeposition from an electrolyte matrix adjusted to pH 3.5 onto a metal planchet is the most common method for the preparation of a thin sample for high-resolution alpha-spectrometric determination (Kressin, 1977

and references therein). Further discussion on sample preparation by electrodeposition for alpha spectrometry is given in Chapter 30, section 3.1.

Liquid–liquid extraction of uranium can be accomplished using organic acids, ketones, ethers, esters, alcohols, and phosphoric acid derivatives (Lally, 1992). In many cases, extraction of uranium can be greatly enhanced with the addition of nitrate salts to the solution (Gindler, 1962). Uranium(IV) can be extracted with ethyl acetate after treatment of an acidified solution with $Al(NO_3)_3 \cdot 9H_2O$ (Guest and Zimmerman, 1955). Uranium(VI) can be extracted with 25% TBP in toluene (Mair and Savage, 1986). Methyl isobutyl ketone has been used in large-scale uranium-separation processes. Recently, several uranium-specific exchange resins have been developed for the separation of uranium from acidic matrices. While these resins function by passing uranium-containing solution down an exchange column containing the material, the separation is based on liquid–liquid extraction. One of these extraction chromatographic resins, TRU Spec resin, consists of octyl(phenyl)-*N*,*N*-diisobutylcarbamoylmethylphosphine oxide in tri(*n*-butyl)phosphate supported by an inert polymeric substrate, Amberlite XAD-7 (Horwitz *et al.*, 1993). The second extraction chromatographic resin, U/TEVA Spec resin consists of diamylphosphonate sorbed on Amberlite XAD-7. This resin possesses tetravalent ion specificity.

Cation exchange is not a commonly used method for the separation of uranium due to the lack of selectivity of the UO_2^{2+} cation over other divalent metal ions. UO_2^{2+} forms strong anionic sulfate and weaker chloride complexes that can be the basis for uranium separation from other metals in solution via anion exchange. Uranium separations can be performed by use of basic anion-exchange resins such as Dowex-1, Dowex-2, Amberlite IRA-400, Amberlite IRA-410, and Bio-Rad AG1X8 from solutions of HCl, HF, HNO_3, H_2SO_4, $(NH_4)_2CO_3$, and H_3PO_4 (Gindler, 1962).

(b) Sample analysis

Total analysis techniques (also known as classical techniques) are the most accurate of all the available methods for uranium determination. Because these techniques provide definitive results, they are typically used as the basis for establishing primary uranium standards and are used extensively in the areas of material control, accountability, and safeguards. Volumetric and gravimetric techniques have both been applied for high accuracy determination of macroscopic quantities of uranium.

Volumetric techniques provide the highest precision and accuracy for uranium determination. Volumetric determination of uranium can be performed via complexation titration with ethylenediaminetetraacetic acid (EDTA). However, the most widely used method is a redox titration where U(VI) is first reduced (e.g. in a Jones reductor) and then back-titrated via oxidation with $KMnO_4$ or Ce(IV) using 1,10-phenanthroline as an indicator (Dean, 1995). The method of Davies and Gray (1964) utilizes excess Fe(II) to reduce U(VI) to U(IV) in a concentrated

H_3PO_4 solution containing H_2NSO_3H. The Fe(II) is selectively oxidized with the addition of HNO_3 in the presence of a Mo(IV) catalyst. After addition of H_2SO_4, U(IV) is titrated with standard Cr(VI) with Ba-diphenylaminesulfonate as an indicator. A modified version of this method has been developed in which the end point is determined potentiometrically (American Society for Testing and Materials, 1994, ASTM C1267–94). This method is exceptionally accurate (relative bias –0.042% and within laboratory variation 0.042%), but requires milligrams of uranium in the sample aliquot.

The necessity for the preparation of redox standard solutions can be circumvented by electrochemical titrations. Coulometric titration of uranium can be performed in both constant-current and controlled-potential titration. Procedures for oxidative coulometric titration of U(IV) and reductive coulometric titration of U(VI) in constant-current mode have been developed. Oxidative coulometric titration of U(IV) is performed via the electrogeneration of Ce(IV) subsequent to preparation of U(IV) by reduction with cadmium amalgam (Furman *et al.*, 1953). Reductive coulometric titration of U(VI) is performed with electrogenerated Ti(III) at a platinum cathode with amperometric endpoint detection (Kennedy and Lingane, 1958). Errors are as low as $\pm 0.3\%$. An improved version of this method has been developed that is capable of a precision of 0.008% (Marinenko *et al.*, 1983). Methods for oxidative controlled-potential titration of U(IV) and reductive controlled-potential titration of U(VI) have been developed. Oxidative controlled-potential titration of U(IV) can be performed in 1 M $HClO_4$ at a platinum electrode (Boyd and Menis, 1961). The most established controlled-potential coulometric titration of uranium utilizes a mercury pool for reduction of U(VI) (McEwen and DeVries, 1959). Experimental conditions have been established which enable uranium to be determined via controlled-potential coulometric titration at a platinum electrode (Davies *et al.*, 1970). Use of the platinum electrode has several advantages including the possibility of simultaneous consecutive determinations of Fe(III) and U(VI), or Pu(IV) and U(VI) in the same cell.

Gravimetric determination of the uranium content of uranium ores can be performed via the sulfide–carbonate–hydroxide method. In this method, the solid U-containing ore sample is dissolved with HNO_3 and H_2SO_4. Arsenic is first removed via addition of HBr. A treatment of the acidic solution with H_2S precipitates a large number of cations as sulfides; Co and Ni are precipitated with H_2S at low acidity; Al, Cr, and Fe are removed with subsequent addition of NH_4OH and $(NH_4)_2CO_3$;. The solution is then reacidified with HCl and U is precipitated with NH_4OH. The precipitate is filtered, washed, ignited, and determined gravimetrically as U_3O_8. Alternatively, the sample can be decomposed via fluxed fusion followed by dissolution in HCl and precipitation of U(IV) on the addition of 6% cupferron solution. The precipitate is filtered, washed, ignited, and determined gravimetrically as U_3O_8. This separation effectively removes Al, Cr, Mn, Zn, and PO_4^{3-} but the presence of Fe, Ti, V(V), and Zr would interfere with the uranium determination

(Dean, 1995). In general, the use of gravimetric methods is limited due to lack of specificity.

5.12.2 Nuclear techniques

The natural radioactivity inherent to uranium isotopes provides the means for their direct analysis by radiometric analytical techniques. While several radiometric techniques are amenable to the determination of uranium at concentrations higher than 1 μg per gram of sample, the most frequently used are high-resolution alpha and gamma spectrometries. Complete isotopic analysis of the naturally occurring isotopes ^{238}U, ^{235}U, and ^{234}U can be performed via high-resolution alpha spectrometry. Alpha-spectrometric determination requires complete sample dissolution, chemical separation of uranium, followed by preparation of a thin source, typically via electrodeposition or precipitation (Kressin, 1977 and references therein). Either ^{232}U or ^{236}U can be used as isotopic recovery spikes. Backgrounds and efficiencies of typical alpha spectrometers equipped with a 450-mm^2 ion-implanted Si detector would require a total of 0.4 μg of natural uranium to achieve 10% counting statistics for a 24-h sample count. Examples of several applications of alpha spectrometry for the determination of uranium and the measurement of U-series disequilibria are given in Ivanovich and Murray (1992).

High-resolution high-purity germanium (HPGe) detectors are capable of high-specificity measurement of individual radionuclide γ-rays and virtually eliminates the need for chemical treatment of samples. Due to its long half-life, the quantification of ^{238}U is usually based on the measurement of the 92.5 keV or the 63.3 keV γ-ray doublets produced by the short-lived daughter ^{234}Th provided secular equilibrium has been achieved (Harbottle and Evans, 1997). Determination of ^{238}U can also be performed by measurement of the 1001 keV γ-ray from the decay of ^{234m}Pa ($t_{1/2} = 1.175$ minutes). The low branching ratio for this γ-ray precludes its use for samples with uranium concentrations smaller than 10 μg per gram of sample. In the case of ^{235}U, direct quantification can be performed using its 185.7-keV γ-ray. A correction for interference from the 186.1 keV γ-ray, ^{226}Ra ($t_{1/2} = 1600$ years), is required for samples in secular equilibrium.

Radiometric determination of uranium can also be performed utilizing scintillation detection after chemical separation of uranium from interfering radionuclides. A standard test method for the determination of uranium in water by high-resolution alpha liquid-scintillation spectrometry utilizes a selective extractive scintillator solution containing dialkyl phosphoric acid (ASTM D6239–98, 1998).

Activation analysis of uranium is typically performed subsequent to irradiation with thermal neutrons. Uranium is essentially unique among naturally occurring elements in that neutron activation analysis (NAA) can be performed by detection of delayed neutrons (Parry, 1991). This method is highly

specific for uranium and has been used for many years in the exploration of uranium ores. NAA with delayed-neutron detection can be automated for online and unattended determination of uranium content in solid and liquid samples.

The coupling of NAA with high-resolution gamma spectrometric detection (instrumental neutron activation analysis, or INAA) yields a highly specific and sensitive method for the determination of uranium. At high concentrations, uranium can be determined by INAA via measurement of the 74 keV γ-ray photo peak from the decay of ^{239}U ($t_{1/2}$ = 23.5 minutes). Minor and trace quantities of uranium are typically determined by INAA via the $^{238}U(n,\gamma)^{239}U(\beta^-$, 23.5 minutes$)^{239}Np$ reaction with measurement of the 105 keV γ-ray photo peak from the decay of ^{239}Np (Parry, 1991). Enhanced sensitivity can be achieved by performing post-irradiation chemical separations (radiochemical neutron activation analysis, or RNAA) (Anders *et al.*, 1988). Both INAA and RNAA are applicable to the determination of trace and ultra trace concentrations of uranium and are further discussed in Chapter 30, section 3.3.

5.12.3 Spectrometric techniques

Uranium is amenable to determination by several fundamentally different spectrometric techniques including spectrophotometry, atomic absorption spectrometry (AAS), atomic emission spectrometry (AES), fluorometry, phosphorimetry, X-ray fluorescence (XRF), and mass spectrometry.

Spectrophotometric determination of uranium can be performed subsequent to sample dissolution, separation of uranium, complexation with an appropriate chromophore, and colorometric determination by comparison with prepared standards. For example, uranium can be determined colorimetrically in the aqueous phase after complexation with 4-(2-pyridylazo)recorcinol (PAR) (Pollard *et al.*, 1959) or as an organic-miscible complex with 4-(2- pyridylazo) napthol (PAN) (Pollock, 1977).

Selectivity of uranium spectrometric determination can be improved using techniques based on atomic absorption and emission. The determination of uranium via AAS techniques can be performed using flame sources (FAAS) or graphite furnace sources (GFAAS). FAAS determination of uranium is performed via the 358.5 nm absorption line using a nitrous oxide/acetylene flame. The detection limit for AAS is 40 $\mu g\ mL^{-1}$ for uranium in solution (Dean, 1995). GFAAS can achieve detection limits of 30 $ng\ mL^{-1}$ in much smaller sample volumes (20 μL). Both AAS and GFAAS are single-element methods that can achieve accuracies greater than $\pm 1\%$ if uranium concentrations are significantly higher than the detection limits.

Sensitivity of atomic spectrometric techniques can be improved via excitation in a high-temperature inductively coupled plasma (ICP) source followed by atomic emission spectrometric (AES) determination. The emission spectrum of U consists of thousands of resolvable lines. ICPAES determination of uranium

based on the 385.96 nm emission line can achieve detection limits of 20 ng mL^{-1} with accuracies of $\pm 1\%$ if concentrations are significantly higher than the detection limits (Dean, 1995). While all atomic spectrometric techniques generally determine total uranium concentration without isotopic selectivity, a high-resolution ICPAES has been developed for the determination of uranium isotopic ratios (Edelson, 1992).

Uranium is unique among most elements in that it can be determined directly via fluorometry without the addition of a fluorescent chelating agent. The fluorometric technique can determine uranium concentrations as low as 5 ng mL^{-1} (ASTM D2907–91, 1991a). Superior detection limits can be achieved by utilizing the ability of uranyl ions to phosphoresce when excited to a triplet state. The uranyl ion can be directly determined phosphorometrically in a H_3PO_4 or H_2SO_4 solution. The pulsed-laser phosphorometric technique can determine uranium concentrations as low as 50 pg mL^{-1} (ASTM D5174–91, 1991b). Further discussion of the fluorometric and phosphorometric techniques is given in Chapter 30 (Sections 30.4.1 and 30.4.2, respectively).

X-ray fluorescence (XRF) can provide qualitative identification and quantitative determination of uranium in a variety of matrices. A procedure for the determination of uranium in soils can be found in ASTM C1255-93 (1993). This procedure can be used to determine as little as 20 μg per gram of uranium.

Mass spectrometry is the most sensitive method for the determination of uranium. In contrast to most of the atomic spectrometric techniques outlined previously, mass spectrometry also provides the means for the determination of uranium isotopic composition. As such, mass spectrometry is an essential tool for the determination of uranium in nuclear fuel cycle applications, material control and accountability, environmental chemistry, geochemistry, and cosmo-chemistry. While a variety of mass spectrometric methodologies have been applied to the determination of uranium (Section 30.5; Wolf, 1999 and references therein), the most commonly used mass spectrometric methods for the determination of uranium are electron-impact gas source mass spectrometry, thermal ionization mass spectrometry (TIMS), and inductively coupled plasma mass spectrometry (ICPMS).

Electron-impact gas source mass spectrometry is used specifically for uranium isotopic analysis to monitor U-enrichment processes. Typically, UF_6 is analyzed in ultracentrifuge and thermal diffusion processes and uranium vapor is analyzed in laser enrichment processes (Platzner, 1997). Measurement by gas source mass spectrometry requires approximately 100 mg of sample. Such instruments are used in production line applications and can achieve a precision of $\pm 0.40\%$ for UF_6 with $>1\%$ ^{235}U enrichment (Nagatoro *et al.*, 1980). Highly portable quadrupole mass analyzers have been designed for UF_6 isotopic analysis in nuclear safeguard applications (Depaus *et al.*, 1987). A standard method for the isotopic analysis of UF_6 with an electron-impact gas source mass spectrometer utilizing a single standard has been developed for nuclear fuel cycle applications (ASTM C1344-97, 1997).

TIMS is one of the most precise and accurate methods for single element isotope ratio determination and is used when small masses of uranium are analyzed. Instruments configured with multiple Faraday detectors can routinely determine major uranium isotope ratios to a precision better than 0.05% (Walder, 1997) and require less than 1 μg of U. TIMS is a commonly used method in nuclear fuel cycle applications including the isotopic analysis of hydrolyzed UF_6 and uranyl nitrate solutions (ASTM C1413–99, 1999) and for the determination of atom percent fission in irradiated nuclear fuels (ASTM E244-80, 1980). Determination of uranium concentrations is performed via isotope dilution (ID) analysis typically using ^{233}U as an isotopic spike. The high sensitivity of TIMS makes this method suitable for the determination of uranium concentrations and isotopic composition at trace and ultra-trace concentrations such as in geological and cosmo-chemical materials. Procedures and applications of TIMS to uranium measurements in geological samples are summarized in Chen *et al*. (1992) and references therein. The TIMS methodology is capable of determining $^{234}U/^{238}U$ ratios with a precision of 0.5% (2σ) for a sample size of 5×10^9 ^{234}U atoms. The primary disadvantage of TIMS is that extensive sample preparation is required and only one element can be determined in a given prepared sample. Further discussion of the application of TIMS to trace and ultratrace analysis is given in Chapter 30, section 5.1.

A review of the trends of the techniques used for elemental determination indicates that ICPMS is one of the most commonly used methods today (Lipschutz *et al*., 2001). ICPMS has found applications for the determination of uranium in waters, soils, sludges, wastes, nuclear materials, biological, geological, and cosmo-chemical materials (Chapter 30, section 5.4 and references therein). The strength of ICPMS resides in its high sensitivity, multielement, high sample throughput capabilities. Quantification is typically performed based on external calibration using the most abundant uranium isotope ^{238}U. Solutions can be analyzed with minimal or no sample pre-treatment. Considering the sensitivities of modern state-of-the-art instruments, a minimum detection limit (MDL) of less than 100 fg in a 1 mL sample is readily attainable for uranium determination by ICPMS (Brenner *et al*., 1998). The combination of an ICP source with a high-precision, double-focusing, mass spectrometer in a single detector configuration (HR-ICPMS) results in an instrument capable of determining less than 1 fg uranium in 1mL solution (Wolf, 1999). This corresponds to a detection limit of approximately 3×10^6 atoms of uranium. Moens and Jakubowski (1998) have published a review of HR-ICPMS instrumentation and applications. Configuration of HR-ICPMS with multiple detectors (MC-ICPMS) yields a method possessing all the attributes of HR-ICPMS with enhanced precision. The routine use of MC-ICPMS in nuclear fuel cycle applications has the potential to dramatically decrease the cost of sample analysis by means of increased sample throughput while maintaining the high precision required for fuel fabrication. A five-fold improvement in sample throughput has been demonstrated for the analysis of

hydrolyzed UF_6 with accuracy and precision comparable to TIMS (Walder and Hodgeson, 1994). High sensitivity makes MC-ICPMS particularly attractive for uranium isotope determination in geo-chronological applications. A review of MC-ICPMS instrumentation and applications to uranium isotopic analysis in geological samples has been reported (Halliday *et al*., 1998). This paper reviews results of replicate analysis of NIST SRM-906 measured by TIMS and MC-ICPMS. Precisions comparable to the best achievable TIMS precisions were achieved. The external reproducibility of MC-ICPMS was superior to TIMS. Further discussion of the application of MC-ICPMS techniques to trace and ultratrace uranium analysis is given in Chapter 30, section 5.4, of this book.

REFERENCES

Aas, W., Moukhamet-Galeev, A., and Grenthe, I. (1998) *Radiochim. Acta*, **82**, 77–82.

Abazli, H., Cousson, A., Tabuteau, A., and Pagès, M. (1980) *Acta Cryst. B*, **36**, 2765–6.

Åberg, M. (1969) *Acta Chem. Scand.*, **23**, 791–810.

Åberg, M. (1971) *Acta Chem. Scand.*, **25**, 368–9.

Åberg, M. (1976) *Acta Chem. Scand. Series A*, **30**, 507–14.

Åberg, M. (1978) *Acta Chem. Scand.*, **A32**, 101–7.

Åberg, M., Ferri, D., Glaser, J., and Grenthe, I. (1983) *Inorg. Chem.*, **32**, 3986–9.

Abraham, B. M. Flotow, H. E. (1955) *J. Am. Chem. Soc.*, **77**, 1446–8.

Abraham, B. M., Osborne, D. W., Flotow, H. E., and Marcus, R. B. (1960) *J. Am. Chem. Soc.*, **82**, 1064–8.

Ackermann, R. J., Gilles, P. W., and Thorn, R. J. (1956) *J. Chem. Phys.*, **25**, 1089–97.

Ackermann, R. J., Thorn, R. J., Alexander, C., and Tetenbaum, M. (1960) *J. Phys. Chem.*, **64**, 350–5.

Ackermann, R. J. and Rauh, E. G. (1969) *J. Phys. Chem.*, **73**, 769–78.

Ackermann, R. J., Rauh, E. G., and Chandrasekharaiah, M. S. (1969) *J. Phys. Chem.*, **73**, 762–9.

Ackermann, R. J. and Rauh, E. G. (1972) *High Temp. Sci.*, **4**, 496–505.

Ackermann, R. J. and Chang, A. T. (1973) *J. Chem. Thermodyn.*, **5**, 873–90.

Ackermann, R. J. and Rauh, E. G. (1973) *J. Inorg. Nucl. Chem.*, **35**, 3787–94.

Ackermann, R. J., Rauh, E. G., and Rand, M. H. (1979) in *Thermodynamics of Nuclear Materials,* Proc. Symp. 1979, International Atomic Energy Agency, Vienna, pp. 11–27.

Addison, C. C. and Hodge, N. (1961) *J. Chem. Soc.*, 2490–6.

Addison, C. C. (1969) *J. Chem. Soc. A*, 2457–9.

Agron, P. A. (1958) in *The Chemistry of Uranium, Collected Papers* (eds. J. J. Katz and E. Rabinowitch), USAEC Technical Information Extension, Oak Ridge, TID-5290 Book 2, pp. 610–26.

Aitken, E. A., Bartram, S. F., and Juenke, E. F. (1964) *Inorg. Chem.*, **3**, 949–54.

Aitken, E. A. and Joseph, R. A. (1966) *J. Phys. Chem.*, **70**, 1090–7.

Akin, G. A., Kackenmaster, H. P., Schrader, R. J., and Strohecker, J. W., Tate, R. E. (1950) *Chemical Processing Plant Equipment: Electromagnetic Separation Process*, Nat. Nucl. En. Ser., Div. I, 12, TID-5232, Oak Ridge, TN.

Alberman, K. B., Blakey, R. C., and Anderson, J. S. (1951) *J. Chem. Soc.*, 1352–6.
Albrecht-Schmitt, T. E., Almond, P. M., Illies, A. J., Raymond, C. C., and Talley, C. E. (2000) *J. Solid State Chem.*, **46**, 87–100.
Alcock, C. B. and Grieveson, P. (1962) *J. Inst. Method.*, **90**, 304–10.
Alcock, C. B. and Grieveson, P. (1963) *Proc. Symp. Thermodyn. Nucl. Mater.*, 1962, International Atomic Energy Agency, Vienna, STI/PUB/58, pp. 563–79.
Alcock, N. W. (1968) *J. Chem. Soc.*, 1588–94.
Alcock, N. W. and Esperas, S. (1997) *J. Chem. Soc. Dalton Trans.*, 893–6.
Alcock, N. W., Kemp, T. J., Sostero, S., and Traverso, O. (1980) *J. Chem. Soc. Dalton Trans.*, 1182–5.
Alcock, N. W., Roberts, M. M., and Chakravorti, M. C. (1980) *Acta Cryst. B*, **36**, 687–90.
Aléonard, K. B., Le Fur, Y., Champarnaud-Mesjard, J. C., Frit, B., and Roux, M. T. (1983) *J. Cryst. Growth*, **217**, 250–4.
Alexander, C. A., and Ogden, J. S., Cunningham, G. C. (1967) Battelle Memorial Institute Report, BMI-1789.
Alibegoff, G. (1886) *Liebig's Ann.*, **233**, 117–43.
Allen, A. L., Anderson, R. W., and McGill, R. M., Powell, F. W. (1950) *Electrochemical Preparation of Uranium Tetrafluoride*, part I, Low Temperature Cell, K-680.
Allen, G. C. and Griffiths, G. C. (1977) *J. Chem. Soc. Dalton Trans.*, 1144–8.
Allen, G. C. Griffiths, A. J., and Suckling, C.W. (1978) *Chem. Phys. Lett.*, **53**, 309–12.
Allen, G. C., Tempest, P. A., and Tyler, J. W. (1982) *Nature*, **295**, 48–9.
Allen, G. C. and Tyler, J. W. (1986) *J. Chem. Soc., Faraday Trans. 1*, **82**, 1367–79.
Allen, G. C. and Holmes, N. R. (1995) *J. Nucl. Mater.*, **223**, 231–7.
Allen, P. G., Bucher, J. J., Clark, D. L., Edelstein, N. M., Ekberg, S. A., Gohdes, J. W., Hudson, E. A., Kaltsyoannis, N., Lukens, W. W., Neu, M. P., Palmer, P. P., Reich, T., Shuh, D. K., Tait, C. D., and Zwick, B. D. (1995) *Inorg. Chem.*, **34**, 4797–807.
Allen, P. G., Shuh, D. K., Bucher, J. J., Edelstein, N. M., Palmer, C. E. A., Silva, R. J., Nguyen, S. N., Marquez, L. N., and Hudson, E. A. (1996a) *Radiochim. Acta*, **75**, 47–53.
Allen, P. G., Shuh, D. K., Bucher, J. J., Edelstein, N. M., Reich, T., Denecke, M. A., and Nitsche, H. (1996b) *Inorg. Chem.*, **35**, 784–7.
Allen, P. G., Bucher, J. J., Shuh, D. K., and Edelstein, N. M. (2000) *Inorg. Chem.*, **39**, 595–601.
Allen, S., Barlow, S., Halasyamani, P. S., Mosselmans, J. F. W., O'Hare, D., Walker, S., and Walton, R. I. (2000) *Inorg. Chem.*, **39**, 3791–8.
Allpress, J. G. (1964) *J. Inorg. Nucl. Chem.*, **26**, 1847–51.
Allpress, J. G. and Wadsley, A. D. (1964) *Acta Cryst.*, **17**, 41–6.
Allpress, J. G. (1965) *J. Inorg. Nucl. Chem.*, **27**, 1521–7.
Allpress, J. G., Anderson, J. S., and Hambly, A. N. (1968) *J. Inorg. Nucl. Chem.*, **30**, 1195–208.
Almond, P. M. and Albrecht-Schmitt, T. E. (2002) *Inorg. Chem.*, **41**, 1177–83.
Almond, P. M., Peper, S. M., Bakker, E., and Albrecht-Schmitt, T. E. (2002) *J. Solid State Chem.*, **168**, 358–66.
Almond, P. M. and Albrecht-Schmitt, T. E. (2004) *Am. Miner.*, **89**, 976–80.
Amberger, H.-D., Grape, W., and Stumpp, E. (1983) *J. Less Common Metals*, **95**, 181–90.

American Society for Testing and Materials (1980) ASTM E244-80, Annual Book of ASTM Standards, vol. 12.01.
American Society for Testing and Materials (1991a) ASTM D2907-91, Annual Book of ASTM Standards, vol. 11.02.
American Society for Testing and Materials (1991b) ASTM D5174-91, Annual Book of ASTM Standards, vol. 11.02.
American Society for Testing and Materials (1993) ASTM C1255-93, Annual Book of ASTM Standards, vol. 12.01.
American Society for Testing and Materials (1994) ASTM D1267-94, Annual Book of ASTM Standards, vol. 12.01.
American Society for Testing and Materials (1997) ASTM C1344-97, Annual Book of ASTM Standards, vol. 12.01.
American Society for Testing and Materials (1998) ASTM D6239-98, Annual Book of ASTM Standards, vol. 11.02.
American Society for Testing and Materials (1999) ASTM C1413-99, Annual Book of ASTM Standards, vol. 12.01.
Amme, M. (2002) *Radiochim. Acta*, **90**, 399–406.
Anders, E., Wolf, R., Morgan, J. W., Ebihara, M., Woodrow, A. B., and Janssens, M.-J., Hertogen, J. (1988) NAS-NS-3117, Office of Scientific and Technical Information, USDOE.
Andersen, R. A. (1979) *Inorg. Chem.*, **18**, 1507–9.
Anderson, A., Chieh, C., Irish, D. E., and Tong, J. P. K. (1980) *Can. J. Chem.*, **58**, 1651–8.
Anderson, R. W., and Allen, A. L., Powell, E. W. (1950) *Electrochemical Preparation of Uranium Tetrafluoride*, Part II, High Temperature Cell, K-681.
Anderson, J. S. and Johnson, K. D. B. (1953) *J. Chem. Soc.*, 1731–7.
Anderson, J. S., Edgington, D. N., Roberts, L. E. J., and Wait, E. (1954) *J. Chem. Soc.*, 3324–31.
Anderson, J. S. and Barraclough, C. G. (1963) *Trans. Faraday Soc.*, **59**, 1572–9.
Anderson, J. S. (1969) *Chimia*, **23**, 438–44.
Anderson, J. S. (1970) in *Modern Aspects of Solid State Chemistry* (ed. C. N. R. Rao), Plenum Press, New York, pp. 29–105.
Andreev, A. V., Bartashevich, M. I., Deryagin, A. V., Havela, L., and Sechovský, V. (1986) *Phys. Status Solidi. A*, **98**, K47–K51.
Andreev, A. V., Zadvorkin, S. M., Bartashevich, M. I., Goto, T., Kamarád, J., Arnold, Z., and Drulis, H. (1998) *J. Alloys Compds*, **267**, 32–6.
Andres, H. P., Krämer, K., and Güdel, H.-U. (1996) *Phys. Rev B*, **54** (6), 3830–40.
Andresen, A. F. (1958) *Acta Crystallogr.*, **11**, 612–14.
Andrieux, L. (1948) *Rev. Met.*, **45**, 49–59.
Andrieux, L. and Blum, P. (1949) *C. R. Acad. Sci.*, **229**, 210–12.
Anonymous (1955) *Purex Technical Manual*, Chemical Development Subsection, Separations Technology Section, Engineering Department, Hanford Atomic Products Operation, declassified with deletion as HW-31000 DEL, ch.II, p. 202, fig. II-1.
Anson, C. E., Al-Jowder, O., Upali, A., Jayasooriya, U. A., and Powell, A. K. (1996) *Acta Cryst. C*, **52**, 279–81.
Anthony, A. M., Kiyoura, R., and Sata, T. (1963) *J. Nucl. Mater.*, **10**, 8–14.

Antill, J. E., Barnes, E., and Gardner, M. (1961) *Prog. Nucl. Energy, Div. V, Metallurgy and Fuels* (eds. H. H. Finniston and J. P. Howe), Pergamon Press, Oxford, vol. 1. pp. 9–18.
Appleman, D. E. and Evans, H. T. (1965) *Am. Miner.*, **50**, 825–42.
Arajs, S. and Colvin, R. V. (1964) *J. Less Common Metals*, 7, 54–66.
Arendt, J., Powell, E. W., and Saylor, H. (1957) A brief guide to UF_6-Handling, K-1323.
Arko, A. J. and Schirber, J. E. (1979) *J. Physique*, Suppl. 40, Coll. C4, 9–14.
Aronson, S. and Belle, J. (1958) *J. Chem. Phys.*, **29**, 151–8.
Aronson, S. and Clayton, J. C. (1960) *J. Chem. Phys.*, **32**, 749–54.
Aronson, S. and Clayton, J. C. (1961) *J. Chem. Phys.*, **35**, 1055–8.
Aronson, S., Rulli, J. E., and Schaner, B. E. (1961) *J. Chem. Phys.*, **35**, 1382–8.
Asami, N., Nishikawa, M., and Taguchi, M. (1975)in *Thermodynamics of Nuclear Materials,* Proc. Symp. 1974, vol. I, International Atomic Energy Agency, Vienna, pp. 287–94.
Atencio, D., Neumann, R., and Silva, A. J. G. C. (1991) *Can. Miner.*, **29**, 95–105.
Atencio, D., Carvalho, F. M. S., and Matioli, P. A. (2004) *Am. Miner.*, **89**, 721–4.
Atoji, M. and McDermott, M. J. (1970) *Acta Crysallogr. B*, **26**, 1540–4.
Aukrust, E., Førland, T., and Hagemark, K. (1962) in *Thermodynamics of Nuclear Materials,* Proc. Symp. 1962, International Atomic Energy Agency, Vienna, pp. 713–22.
Aurov, N. A. and Chirkst, D. E. (1983) *Radiokhimiya*, **25**, 468–73.
Aurov, N. A., Volkov, V. A., and Chirkst, D. E. (1983) *Radiokhimiya*, **25**, 366–72.
Auzel, F. and Malta, O. (1983) *J. Phys.(Paris)*, **44**, 201–6.
Avens, L. R., Bott, S. G., Clark, D. L., Sattelberger, A. P., Watkin, J. G., and Zwick, B. D. (1994) *Inorg. Chem.*, **33**, 2248–56.
Avignant, D. and Cousseins, J.-C. (1971) *Compt. Rend. C*, **272**, 2151–3.
Avignant, D., Vedrine, A., and Cousseins, J.-C. (1977) *Compt. Rend. C*, **284**, 651–4.
Avignant, D., Mansouri, I., Sabatier, R., and Cousseins, J.-C. (1980) *Acta Crystallogr. B*, **36**, 664–6.
Avignant, D., Mansouri, I., Sabatier, R., and Cousseins, J.-C. (1982) *Acta Crystallogr. B*, **24**, 1968–38.
Babelot, J. F., Brumme, G. D., Kinsman, P. R., and Ohse, R. W. (1977) *Atomwirtsch. Atomtech.*, **22**, 387–9.
Bacher, W. and Jacob, E. (1980) Verbindungen mit Fluor, in *Gmelin Handbuch der Anorganischen Chemie,* (1980) System no. 55, Uranium, Suppl. vol. C8, Springer, Berlin.
Bacher, W. and Jacob, E. (1982) *Chemiker-Zeitung*, **106** (3), 117–36.
Bacher, W. and Jacob, E (1986) Uranium hexafluoride, its chemistry related to its major applications, in *Handbook on the Physics and Chemistry of the Actinides* (eds. A. J. Freeman and C. Keller), Elsevier, Amsterdam, vol. 4, ch. 1, 1–38.
Bacmann, M. (1973) *Acta Crystallogr.*, **B29**, 1570–2.
Baes, C. F. Jr, Zingeno, R. A., and Coleman, C. F. (1958) *J. Phys. Chem.*, **62**, 129–35.
Baes, C. F. Jr and Mesmer, R. E. (1976) *The Hydrolysis of Cations,* John Wiley, New York.
Baer, Y. (1984) Electronic spectroscopy studies, in *Handbook on the Physics and Chemistry of the Actinides,* vol. 1, ch. 4, (eds. J. P. Desclaux and A. J. Freeman), Elsevier, Amsterdam, 271–340.

Bagnall, K. W., Brown, D., and Deane, A. M. (1962) *J. Chem. Soc.*, 1655–7.
Bagnall, K. W., Brown, D., and du Preez, J. G. H. (1964) *J. Chem. Soc.*, 2603–8.
Bagnall, K. W., Brown, D., Jones, P. J., and du Preez, J. G. H. (1965) *J. Chem. Soc.*, 350–3.
Bagnall, K. W. (1967) in *Halogen Chemistry of the Actinides,* (ed. V. Gutman), Academic Press, London, vol. 3, ch. 7.
Bagnall, K. W., Brown D., and Easey, J. F. (1968) *J. Chem. Soc. A*, 288–92.
Bagnall, K. W. and Wakerley, M. W. (1974) *J. Less Common Metals*, **35**, 267–74.
Bagnall, K. W., du Preez. J. G. H., Gellatly, B. J., and Holloway, J. H. (1975) *J. Chem. Soc. Dalton Trans.*, 1963–8.
Bagnall, K. W. (1979) Complex compounds of uranium, in *Gmelin Handbook of Inorganic Chemistry*, E 1 Suppl., 1–223.
Bagnall, K. W. (1987) The actinides, in *Comprehensive Coordination Chemistry* vol. 3, ch. 40 (eds. G. Wilkinson, R. D. Gillard, and J. A. McCleverty), Pergamon Press, New York, 1129–228.
Baïchi, M., Chattillon, C., and Guéneau, Le Ny, J. (2002) *J. Nucl. Mater.*, **303**, 196–9.
Baird, C. P. and Kemp, T. J. (1997) *Prog. Reaction Kinetics*, **22**, 87–139.
Bakakin, V. V. (1965) *Zh. Strukt. Khim.*, **6**, 563–6; *J. Struct. Chem.* (*USSR*), **6**, 536–9.
Baker, R. D., Hayward, B. R., Hull, G., Raich, B., and Weiss, A. R. (1946) *Preparation of Uranium Metal by the Bomb Method*, LA-472.
Balzani, V. and Carassiti, V. (1970) *Photochemistry of Coordination Compounds,* Academic Press, London, ch. 15.
Bannister, M. J. (1967) *J. Nucl. Mater.*, **24**, 340–2.
Bannister, M. J. and Taylor, J. C. (1970) *Acta Crystallogr.*, **B26**, 1775–81.
Bannister, M. J. and Buykx, W. J. (1974) *J. Nucl. Mater.*, **55**, 345–51.
Barash, Y. B., Barak, J., and Mintz, M. H. (1984) *Phys. Rev. B*, **29**, 6096–104.
Bard, A. J. and Parsons, R. (1985) *Standard Potentials in Aqueous Solution,* Marcel Dekker, New York.
Bardin, N., Rubini, P., and Madic, C. (1998) *Radiochim. Acta*, **83**, 189–94.
Barnard, R., Bullock, J. I., and Larkworthy, L. F. (1967) *Chem. Comm.*, 1270–2.
Barnard, R., Bullock, J. I., and Larkworthy, L. F. (1972a) *J. Chem. Soc. Dalton Trans.*, 964–70.
Barnard, R., Bullock, J. I., Gellatly, B. J., and Larkworthy, L. F. (1972b) *J. Chem. Soc. Dalton Trans.*, 1932–8.
Barnard, R., Bullock, J. I., Gellatly, B. J., and Larkworthy, L. F. (1973) *J. Chem. Soc. Dalton Trans.*, **6**, 604–7.
Barrett, C. S., Mueller, M. H., Hitterman, R. L. (1963) *Phys. Rev.* **129**, 625–9.
Barton, C. J., Friedman, H. A., Grimes, W. R., Insley, H., Moore, R. E., and Thoma, R. E. (1958) *J. Am. Ceram. Soc.*, **41**, 63–9.
Bartram, S. F., Juenke, E. F., and Aitken, E. A. (1964) *J. Am. Ceram. Soc.*, **47**, 171–5.
Bartram, S. F. (1966) *Inorg. Chem.*, **5**, 749–54.
Bartram, S. F. and Fryxell, R. E. (1970) *J. Inorg. Nucl. Chem.*, **32**, 3701–6.
Bartscher, W. and Sari, C. (1983) *J. Nucl. Mater.*, **118**, 220–3.
Bartscher, W., Boeuf, A., Caciuffo, R., Fournier, J. M., Kuhs, W. F., Rebizant, J., and Rustichelli, F. (1985) *Solid State Commun.*, **53**, 423–6.
Baskin, Y. and Shalek, P. D. (1964) *J. Inorg. Nucl. Chem.*, **26**, 1679–84.
Baskin, Y. (1969) *J. Inorg. Nucl. Chem.*, **29**, 2480–2.

Basnakova, G., Spencer, A. J., Palsgard, E., Grime, G. W., and Macaskie, L. E. (1998) *Environ. Sci. Technol.*, **32**, 760–5.
Bates, J. L. (1964) USAEC Hanford Report, HW-81603.
Bates, J. L. (1966) *J. Am. Ceram. Soc.*, **49**, 395–6.
Bates, J. L., Hinman, C. A., and Kawada, K. (1967) *J. Am. Ceram. Soc.*, **50**, 652–6.
Bates, J. K., Bradley, J. P., Teetsov, A., Bradley, C. R., and Buchholtz ten Brink, M. (1992) *Science*, **256**, 469–71.
Battles, J. E., Shinn, W. A., and Blackburn, P. E. (1972) *J. Chem. Thermodyn.*, **4**, 425–39.
Bayliss, P., Mazzi, F., Munno, R., and White, T. J. (1989) *Miner. Mag.*, **53**, 565–9.
Bayovlu, A. S. and Lorenzelli, R. (1984) *Solid State Ionics*, **12**, 53–66.
Beals, R. J. and Handwerk, J. H. (1965) *J. Am. Ceram. Soc.*, **48**, 271–4.
Bean, A. C., Campana, C. F., Kwon, O., and Albrecht-Schmitt, T. E. (2001a) *J. Am. Chem. Soc.*, **123**, 8806–10.
Bean, A. C., Ruf, M., and Albrecht-Schmitt, T. E. (2001b) *Inorg. Chem.*, **40**, 3959–63.
Beaudry, B. J. and Daane, A. H. (1959) *Trans. Met. Soc. (AIME)*, **215**, 199–203.
Beck, H. P. and Kuehn, F. (1995) *Z. Anorg. Allg. Chem.*, **621**, 1659–62.
Beck, M. T. and Nagypál, I. (1990) *Chemistry of Complex Equilibria,* Harwood Ltd. Publishers, New York.
Becker, E. W. (1979) in *Uranium Enrichment* (ed. S. Villani), Springer, Berlin, p. 245.
Becker, J. S. and Dietze, H.-J. (1998) *Spectrochim. Acta*, **52B**, 177–87.
Becquerel, H. (1896) *C.R. Acad. Sci.*, **122**, 501–3.
Belbeoch, B., Boivineau, J. C., and Pério, P. (1967) *J. Phys. Chem. Solids*, **28**, 1267–75.
Bell, J. T. (1969) *J. Inorg. Nucl. Chem.*, **31**, 703–10.
Bell, J. T. and Buxton, S. R. (1974) *J. Inorg. Nucl. Chem.*, **36**, 1575–9.
Bellamy, R. G. and Hill, N. A. (1963) *The Extraction and Metallurgy of Uranium, Thorium, and Beryllium,* Pergamon Press, Oxford.
Belle, J. (1961) *Uranium Dioxide, Properties and Nuclear Applications,* U.S. Atomic Energy Commission Division of Reactors, U.S. Government Printing Office, Washington, DC.
Belle, J. (1969) *J. Nucl. Mater.*, **30**, 3–15.
Benard-Rocherulle, P., Louer, M., Louer, D., Dacheux, N., Brandel, V., and Genet, M. (1997) *J. Solid State Chem.*, **132**, 315–22.
Bendall, P. J., Fitch, A. N., and Fender, B. E. F. (1983) *J. Appl. Cryst.* **16**, 164–70.
Benedict, U. (1987) *J. Less Common Metals*, **128**, 7–45.
Ben Salem, A., Meerschaut, A., and Rouxel, J. (1984) *Compt. Rend. Hebd. Séances. Acad. Sci. Ser. 2*, **299**, 617–19.
Benson, D. A. (1977) Sandia National Laboratories Report, SAND-77–0429.
Benz, R., Douglas, R. M., Kruse, F. H., and Penneman, R. A. (1963) *Inorg. Chem.*, **2**, 799–803.
Bereznikova, I. A., Ippolitova, E. A., Simanov, Yu. P., and Kovba, L. M. (1961) Argonne National Laboratory Report, ANL-trans-33, p. 176.
Berger, M. and Sienko, M. J. (1967) *Inorg. Chem.*, **6**, 324–6.
Berlincourt, T. G. (1959) *Phys. Rev.*, **114**, 969–77.
Berndt, U. and Erdman, B. (1973) *Radiochim. Acta*, **19**, 45–6.
Berndt, U., Tanamas, R., and Keller, C. (1976) *J. Solid State Chem.*, **17**, 113–20.
Bernstein, E. R., Keiderling, T. A., Lippard, S. J., and Mayerle, J. J. (1972a) *J. Am. Chem. Soc.*, **94**, 2552–3.

Bernstein, E. R., Hamilton, W. C., Keiderling, T. A., LaPlaca, S. J., Lippard, S. J., and Mayerle, J. J. (1972b). *Inorg. Chem.*, **11**, 3009–16.
Bernstein, E. R. and Keiderling, T. A. (1973) *J. Chem. Phys.*, **59**, 2105–22.
Berry, J. A., Poole, R. T., Prescott, A., Sharp, D. W. A., and Winfield, J. M. (1976) *J. Chem. Soc. Dalton Trans.*, 272–4.
Berry, J. A., Prescott, A., Sharp, D. W. A., and Winfield, J. M. (1977) *J. Fluorine Chem.*, **10**, 247–54.
Berthet J.-C., Rivière, C., Miquel, Y., Nierlich, M., Madic, C., and Ephritikhine, M. (2002) *Eur. J. Inorg. Chem.*, 14390–46.
Berthet, J.-C., Nierlich, M., and Ephritikhine, M. (2003) *Chem. Commun.*, 1660–1.
Berthold, H. J., Hien, H. G., and Reuter, H. (1957) *Ber. Dtsch. Keram. Ges.*, **50**, 111–14.
Berthold, H. J. and Knecht, H. (1965a) *Angew. Chem.*, **77**, 428.
Berthold, H. J. and Knecht, H. (1965b) *Angew. Chem.*, **72**, 453.
Berthold, H. J. and Delliehausen, C. (1966) *Angew. Chem.*, **78**, 750–1.
Berthold, H. J. and Knecht, H. (1966) *Z. Anorg. Allg. Chem.*, **348**, 50–7.
Berthold, H. J. and Knecht, H. (1968) *Z. Anorg. Allg. Chem.*, **356**, 151–62.
Bertino, J. P. and Kirchner, J. A. (1945) *U^{233} Purification and Metal Production*, LA-245.
Bertsch, P. M., Hunter, D. B., Sutton, S. R., Bajt, S., and Rivers, M. L. (1994) *Environ. Sci. Technol.*, **28**, 980–4.
Besson, J. and Chevallier, J. (1964) *Compt. Rend. Hebd. Séances Acad. Sci.*, **258**, 5888–91.
Bevan, D. J. M., Grey, I. E., and Willis, B. T. M. (1986) *J. Solid State Chem.*, **61**, 1–7.
Bevz, A. S., Kapshukov, I. I., Vorobei, M. P., and Skiba, O. V. (1970) *Zh. Strukt. Khim.*, **11**, 936; *J. Struct. Chem.* (*USSR*), **11**, 872.
Biennewies, M. and Schäfer, H. (1974) *Z. Anorg. Allg. Chem.*, **407**, 7–44.
Billard, I. and Lützenkirchen, K. (2003) *Radiochim. Acta*, **91**, 285–94.
Birch, W. D., Mumme, W. G., and Segnit, E. R. (1988) *Aust. Miner.*, **3**, 125–31.
Bittel, J. T., Sjodahl, L. H., and White, J. F. (1969) *J. Am. Ceram. Soc.*, **52**, 446–51.
Bjerrum, J., Schwarzenbach, G., and Sillén, L. G. (1956) *Stability Constants. Part I Organic Ligands,* The Chemical Society, London.
Bjerrum, J., Schwarzenbach, G., and Sillén, L. G. (1957) *Stability Constants. Part II Inorganic Ligands,* The Chemical Society, London.
Blackburn, P. E. (1958) *J. Phys. Chem.*, **62**, 897–902.
Blake, C. A., Baes, C. F. Jr, Brown, K. B., Coleman, C. F., and White, J. C. (1958) *Proc. Second Int. Conf. on Peaceful Uses of Atomic Energy*, **vol. 28**, pp. 289–98. Geneva, 1958,
Blank, H. and Ronchi, C. (1968) *Acta Crystallogr.*, **A24**, 657–66.
Blasse, G. (1964) *Z. Anorg. Allg. Chem.*, **331**, 44–50.
Blaton, N., Vochten, R., Peters, O. M., and van Springel, K. (1999) *Neues Jahrb. Miner. Monatsschr.*, pp. 253–64.
Blatov, V. A., Serezhkina, L. B., Serezhkin, V. N., and Trunov, V. K. (1989) *Zh. Neorg. Khim.*, **34**, 162–4; *Russian J. Inorg. Chem.*, **34**, 91–2.
Blum, P. L., Guinet, P., and Vaugoyeau, H. (1963) *C.R. Acad. Sci.(Paris)*, **257**, 3401–3.
Blumenthal, B. and Noland, R. A. (1956) *Progress in Nuclear Energy, Div. V, Metallurgy and Fuels* (eds. H. H. Finniston and J. P. Howe), Pergamon Press, Oxford, vol. 1 pp. 62–80.
Bober, M., Karow, H. U., and Schretzmann, K. (1975) in *Thermodynamics of Nuclear Materials,* Proc. Symp. 1974, vol. I, , International Atomic Energy Agency, Vienna, pp. 295–305.

Boehme, D. R., Nichols, M. C., Snyder, R. L., and Matheis, D. P. (1992) *J. Alloys Compds*, **179**, 37–59.
Boeyens, J. C. A. and Haegele, R. (1976) *Inorg. Chim. Acta*, **20**, L7.
Bogacz, A., Bros, J. P., Gaune-Escard, M., Hewat, A. W., and Taylor, J. C. (1980) *J. Phys. C*, **13**, 5273–8.
Bohrer, R., Conradi, E., and Müller, U. (1988) *Z. Anorg. Allg. Chem.*, **558**, 119–27.
Bohres, E. W., Krasser, W., Schenk, H.-J., and Schwochau, K. (1974) *J. Inorg. Nucl. Chem.*, **36**, 809–13.
Bois, C., Dao, N. Q., and Rodier, N. (1976a) *Acta Crystallogr. B*, **32**, 1541–9.
Bois, C., Dao, N. Q., and Rodier, N. (1976b) *J. Inorg. Nucl. Chem.*, **38**, 755–7.
Bokolo, K., Delpuech, J.-J., Rodehüser, L. R., and Rubini, P. R. (1981) *Inorg. Chem.*, **20**, 992–7.
Bommer, H. (1941) *Z. Anorg. Allg. Chem.*, **247**, 249–58.
Boraopkova, M. N., Kanetsova, G. N., and Novoselova, A. B. (1971) *Izvestia A.N. SSSR, Ser. Neorgan. Mater.*, **7**, 242.
Borène, J. and Cesbron, F. (1971) *Bull. Soc. Fr. Minér. Crystallogr.*, **94**, 8–14.
Borisov, S. K. and Zadneporovskii, G. M. (1971) *At. Energy (USSR)*, **31**, 63–5; Sov. At. Energy, **31**, 761–73.
Boroujerdi, A. (1971) Research Center Karlsruhe Report, KFK-1330.
Bougon, R. and Plurien, P. (1965) *Compt. Rend.*, **260**, 4217–18.
Bougon, R., Charpin, P., Desmoulin, J. P., and Malm, J. G. (1976a) *Inorg. Chem.*, **15**, 2532–40.
Bougon, R., Costes, R. M., Desmoulin, J. P., and Michel, J., Person, J. L. (1976b) *J. Inorg. Nucl. Chem.*, Suppl., 99–105.
Bougon, R., Joubert, P., Weulersse, J.-M., and Gaudreau, B. (1978) *Can. J. Chem.*, **56**, 2546–9.
Bougon, R., Fawcett, J., Holloway, J. H., and Russell, D. R. (1979) *J. Chem. Soc. Dalton Trans.*, 1881–5.
Boulet, P., Daoudi, A., Potel, M., Noël, H., Gross, G. M., Andre, G., and Bouree, F. (1997a) *J. Alloys Compds*, **247**, 104–8.
Boulet, P., Daoudi, A., Potel, M., and Noël, H. (1997b) *J. Solid State Chem.*, **129**, 113–16.
Boulet, P., Potel, M., Levet, J. C., and Noël, H. (1997c) *J. Alloys Compds*, **262–3**, 229–34.
Bowen, R. B., Lincoln, S. F., and Williams, E. H. (1976) *Inorg. Chem.*, **15**, 2126–9.
Bowen, R. B., Honan, G. J., Lincoln, S. F., Spotswood, T. M., and Williams, E. H. (1979) *Inorg. Chim. Acta*, **33**, 235–9.
Boyd, C. M. and Menis, O. (1961) *Anal. Chem.*, **33**, 1016–18.
Bradley, M. J. and Ferris, L. M. (1962) *Inorg. Chem.*, **1**, 683–7.
Bradley, M. J. and Ferris, L. M. (1964) *Inorg. Chem.*, **3**, 189–95.
Brandel, V., Dacheux, N., and Genet, M. (1996) *J. Solid State Chem.*, **121**, 467–72.
Branstätter, F. (1981) *Tschermaks Miner. Petrogr. Mitt.*, **29**, 1–8.
Brater, D. C. and Smiley, S. H. (1958) Structural transitions in UCl_4 anticipating melting, in *Progress in Nuclear Chemistry,* Ser. III, *Process Chemistry* vol. 2 (eds. F. R. Bruce, J. M. Fletcher, and H. H. Hyman), Pergamon Press, London, pp. 136–48.
Brauer, G. (1981) *Handbuch der Präparativen Anorganischen Chemie*, 3rd edn, Ferdinand Elke Verlag, Stuttgart.

Braun, R., Kemmler-Sack, S., Roller, H., Seemann, I., and Wall, I. (1975) *Z. Anorg. Allg. Chem.*, **415**, 133–55.
Bredig, M. A. (1972) in *Proc. CNRS Conf. in Odeillo, 1971*, CNRS, Paris, p. 183.
Breeze, E. W., Brett, N. H., and White, J. (1971) *J. Nucl. Mater.*, **39**, 157–65.
Breeze, E. W. and Brett, N. H. (1971) *J. Nucl. Mater.*, **40**, 113–15.
Breeze, E. W. and Brett, N. H. (1972) volume date1972/1973, *J. Nucl. Mater.*, **45**, 131–8.
Breitung, W. (1978) *J. Nucl. Mater.*, **74**, 10–18.
Brendt, U. and Erdman, B. (1973) *Radiochim. Acta*, **19**, 45–6.
Brenner, I. B., Liezers, M., Godfrey, J., Nelms, S., and Cantle, J. (1998) *Spectrochim. Acta*, **53**, 1087–107.
Brisi, C. (1960) *Ric. Sci.*, **30**, 2376–81.
Brisi, C. (1969) *Ann. Chim. (Rome)*, **59**, 400–11.
Brisi, C. (1971) *Rev. Int. Hautes Temp. Réfract.*, **8**, 37–41.
Brisi, C., Montorsi, M., and Burlando, G. A. (1972) *Atti. Acad. Sci. Torino, Cl. Sci. Fis. Mater. Nat.*, **106**, 257.
Brit, D. W. and Anderson, H. J. (1962) USAEC Technical Information Service, TID-7637, p. 408.
Brochu, R. and Lucas, J. (1967) *Bull. Soc. Chim. France*, 4764–7.
Brodsky, M. B., Griffin, N. J., and Odie, M. D. (1969) *J. Appl. Phys.*, **8**, 895–7.
Brookins, D. G. (1990) *Waste Manage.*, **10**, 285–96.
Bros, J. P., Gaune-Escard, M., Szczepaniak, W., Bogacz, A., and Hewat, A. W. (1987) *Acta Crystallogr. B*, **43**, 113–16.
Brown, D. (1966) *J. Chem. Soc.* (*A*), 766–9.
Brown, D. (1968) *The Halides of the Lanthanides and Actinides,* Wiley Interscience, New York.
Brown, D., Fletcher, S., and Holah, D. G. (1968) *J. Chem. Soc. A*, 1889–94.
Brown, D., Hill, J., and Rickard, C. E. F. (1970) *J. Chem. Soc. A*, 476–80.
Brown, D. (1972) The actinide halides and their complexes, in MTP (*Med. Tech. Publ. Co.*) *Intern. Rev. Sci. Inorg. Chem. Ser. One*, 7, 87–137.
Brown, D. and Edwards, J. (1972) *J. Chem. Soc. Dalton Trans.*, 1757–62.
Brown, D. (1973) in *Comprehensive Inorganic Chemistry,* vol. 5, Pergamon Press, Oxford, pp. 151–208.
Brown, D., Whittaker, B., and Lidster, P. E. (1975) Atomic Energy Research Establishment (UK) Report, AERE-R-8035, p. 16.
Brown, D., Lidster, P., Whittaker, B., and Edelstein, N. (1976) *Inorg. Chem.*, **15**, 511–51.
Brown, D. (1979) Compounds of Uranium with Chlorine, Bromine and Iodine, in *Gmelin Handbook of Inorganic Chemistry,* System no. 55, Uranium, Suppl., vol. C9, Springer, Berlin, pp. 1–186.
Brown, D., Berry, J. A., Holloway, J. H., Holland, R. F., and Staunton, G. M. (1983) *J. Less Common Metals*, **92**, 149–53.
Brown, D. R. and Denning, R. G. (1996) *Inorg. Chem.*, **35**, 6158–63.
Brown, G. M. and Walker, L. A. (1966) *Acta Crystallogr.*, **20**, 220–9.
Brown, K. B., Coleman, C. F., Crouse, D. J., Blake, C. A., and Ryan, A. D. (1958) *Proc. Second Int. Conf. on Peaceful Uses of Atomic Energy*, Geneva, 1958, vol. 3, pp. 472–87.
Browning, P., Gillan, M. J., and Potter, P. E. (1978) *Rev. Int. Hautes Tempér. Réfract. Fr.*, **15**, 333–46.

Browning, P. (1981) *J. Nucl. Mater.*, **98**, 345–56.
Browning, P., Hyland, G. J., and Ralph, J. (1983) Oak Ridge National Laboratory Report, *High Temp.-High Press.*, **15**, 169–78.
Brugger, J., Burns, P. C., and Meisser, N. (2003) *Am. Miner.*, **88**, 676–85.
Brugger, J., Krivovichev, S. V., Berlepsch, P., Meisser, N., Ansermet, S., and Armbruster, T. (2004) *Am. Mineral.*, **89**, 339–47.
Brunton, G. D. (1965) Oak Ridge National Laboratory Report, ORNL-3913, p. 10.
Brunton, G. D., Insley, H., and McVay, T. N., Thoma, R. E. (1965) Oak Ridge National Laboratory Report, ORNL-3761, p. 212; (1965) N.S.A. 19, no. 15416.
Brunton, G. D. (1966) *Acta Crystallogr.*, **21**, 814–17.
Brunton, G. D. (1967) *J. Inorg. Nucl. Chem.*, **29**, 1631–6; Oak Ridge National Laboratory Report, ORNL-4076; (1967) N.S.A. 21.
Brunton, G. D. (1969a) *Acta Crystallogr. B*, **25**, 2163–4; **26B**, 2519.
Brunton, G. D. (1969b) *Acta Crystallogr. B*, **25**, 1919–21.
Brunton, G. D. (1971) *Acta Crystallogr. B*, **27**, 245–7.
Brusset, H., Gillier-Pandraut, H., and Dao, N. Q. (1969) *Acta Crystallogr.*, **25B**, 67–73.
Brusset, H. and Dao, N. Q. (1971) *J. Inorg. Nucl. Chem.*, **33**, 1365–72.
Brusset, H., Dao, N. Q., and Rubinstein-Auban, A. (1972) *Acta Cryst. B*, **28**, 2617–19.
Brusset, H., Dao, N. Q., and Chourou, S. (1974) *Acta Cryst.*, **30B**, 768–73.
Buck, E. C., Brown, N. R., and Dietz, N. L. (1996) *Environ. Sci. Technol.*, **30**, 81–8.
Buck, E. C., Wronkiewicz, D. J., Finn, P. A., and Bates, J. K. (1997) *J. Nucl. Mater.*, **249**, 70–6.
Buck, E. C. and Bates, J. K. (1999) *Appl. Geochem.*, **14**, 635–53.
Buck, E. C., Finn, P. A., and Bates, J. K. (2004) *Micron*, **35**, 235–43.
Budnikov, P. P., Tresvyatsky, S. G., and Kushakovsky, V. I. (1958) in *Proc. Second Int. Conf. on Peaceful Uses of Atomic Energy*, Geneva, 1958, vol. 6, United Nations, Geneva, pp. 124–31.
Bugl, J. and Bauer, A. A. (1964) in Waber *et al.* (1964), pp. 215–24.
Buhrer, C. F. (1969) *J. Phys. Chem. Solids*, **30**, 1273–6.
Bullock, J. I. (1969) *J. Chem. Soc. A*, 781– 4.
Bunnell, L. R., Chikalla, T. D., and Woodley, R. E. (1975) *Hydrolysis of Uranium Carbide Fuel Beads*, BNWL-SA-5513.
Burk, W. (1967) *Z. Anorg. Allg. Chem.*, **350**, 92–6.
Burk, W. and Naumann, D. (1969) *Z. Chem. (Leipzig)*, **9**, 189.
Burns, J. H., Osborne, D. W., and Westrum, E. F. Jr (1960) *J. Chem. Phys.*, **33**, 387–94.
Burns, J. H. and Duchamp, D. J. (1962) Oak Ridge National Laboratory Report, ORNL-3262, pp. 14–16; N.S.A. 16, no. 17553.
Burns, J. H., Ellison, R. D., and Levy, H. A. (1968) *Acta Crystallogr. B*, **24**, 230–7.
Burns, P. C., Miller, M. L., and Ewing, R. C. (1996) *Can. Miner.*, **34**, 845–80.
Burns, P. C. (1997) *Am. Miner.*, **82**, 1176–86.
Burns, P. C., Ewing, R. C., and Miller, M. L. (1997a) *J. Nucl. Mater.*, **245**, 1–9.
Burns, P. C., Finch, R. J., Hawthorne, F. C., Miller, M. L., and Ewing, R. C. (1997b) *J. Nucl. Mater.*, **249**, 199–206.
Burns, P. C. (1998a) *Can. Miner.*, **36**, 847–53.
Burns, P. C. (1998b) *Can. Miner.*, **36**, 187–99.
Burns, P. C. (1998c) *Can. Miner.*, **36**, 1061–7.
Burns, P. C. (1998d) *Can. Miner.*, **36**, 1069–75.

Burns, P. C. (1999a) *Rev. Miner.*, **38**, 23–90.
Burns, P. C. (1999b) *Am. Miner.*, **84**, 1661–73.
Burns, P. C. and Finch, R. J. (1999) *Am. Miner.*, **84**, 1456–60.
Burns, P. C. and Hanchar, J. M. (1999) *Can. Miner.*, **37**, 1483–91.
Burns, P. C. (2000) *Am. Miner.*, **85**, 801–5.
Burns, P. C. and Hill, F. C. (2000a) *Can. Miner.*, **38**, 163–73.
Burns, P. C. and Hill, F. C. (2000b) *Can. Miner.*, **38**, 175–82.
Burns, P. C., Olson, R. A., Finch, R. J., Hanchar, J. M., and Thibault, Y. (2000) *J. Nucl. Mater.*, **278**, 290–300.
Burns, P. C. (2001a) *Can. Miner.*, **39**, 1139–46.
Burns, P. C. (2001b) *Can. Miner.*, **39**, 1153–60.
Burns, P. C. and Hayden, L. A. (2002) *Acta Crystallogr. C*, **58**, 121–2.
Burns, P. C. and Li, Y. (2002) *Am. Miner.*, **87**, 550–7.
Burns, P. C. and Hughes, K.-A. (2003) *Am. Mineralogist*, **88**, 1165–8.
Burns, P. C., Deely, K. M., and Hayden, L. A. (2003) *Can. Miner.*, **41**, 687–706.
Burns, P. C., Deely, K. M., and Skanthakumar, S. (2004a) *Radiochim. Acta*, **92**, 151–60.
Burns, C. J., Neu, M. P., Boukhalfa, H., Gutowski, K. E., Bridges, N. J., and Rogers, R. D. (2004) *The Actinides* in *Comprehensive Coordination Chemistry II*, vol. 3, 3.3, 189–345, Elsevier Ltd, Amsterdam.
Burns, P. C., Kubatko, K.-A., Sigmon, G., Fryer, B. J., Gagnon, J. E. Antonio, M. R. and Soderholm, L. (2005) *Angew. Chem. Int. Ed.,* **44**, 2135.
Burrows, H. D. and Kemp, T. J. (1974) *Chem. Soc. Rev.*, **3**, 139–65.
Bursten, B. E. and Strittmatter, R. J. (1987) *J. Am. Chem. Soc.*, **109**, 6606–9.
Busch, G., Hulliger, F., and Vogt, O. (1979a) *J. Physique Colloq.*, **40**, C4 62–3.
Busch, G., Vogt, O., and Bartolin, H. (1979b) *J. Physique Colloq.*, **40**, C4 64–5.
Cahill, C. L. and Burns, P. C. (2000) *Am. Miner.*, **85**, 1294–7.
Caillat, R., Coriou, H., and Perio, P. (1953) *Compt. Rend. Hebd. Séances Acad. Sci.*, **237**, 812–13.
Caillat, R. (1961) in *P. Pascal, Nouveau Traité de Chimie Minérale, Masson et Cie., Paris 1967*, vol. **XV** (2), 59–121; (1967) vol. **XV** (4), 497–517.
Caira, M. R., de Wet, J. F., du Preez, J. G. H., and Gellatly, B. J. (1978) *Acta Crystallogr. B*, **34**, 1116–20.
Caley, E. R. (1948) *Isis*, **38**, 190–3.
Caneiro, A. and Abriata, J. P. (1984) *J. Nucl. Mater.*, **126**, 255–67.
Carbajo, J. J., Yoder, G. L., Popov, S. G., and Ivanov, V. K. (2001) *J. Nucl. Mater.*, **299**, 181–98.
Carlson, E. H. (1969) *Phys. Lett.*, **29A**, 696–7.
Carlson, R. S. (1975) in *Proc. Int. Conf. on Radiation Effects and Tritium Technology for Fusion Reactors*, Gatlinburg, TN, 1975, vol. 4, p. 361.
Carnall, W. T., Neufeldt, S. J., and Walker, A. (1965) *Inorg. Chem.*, **4**, 1808–13.
Carnall, W. T., Walker, A., and Neufeldt, S. J. (1966) *Inorg. Chem.*, **5**, 2135–40.
Carnall, W. T. (1970) Unpublished results.
Carnall, W. T. (1982) in *Gmelin Handbuch der Anorganischen Chemie,* 8th edn, Uranium Suppl., vol. A5, , Springer Verlag, New York, pp. 69–161.
Carnall, W. T. and Crosswhite, H. M. (1985) Argonne National Laboratory Report, ANL 84–90.
Carnall, W. T. (1989) Argonne National Laboratory Report, ANL-89/39.

Carnall, W. T., Liu, G. K., Williams, C. W., and Reid, M. F. (1991) *J. Chem. Phys.*, **95**, 7194–203.
Carter, R. E. and Lay, K. W. (1970) *J. Nucl. Mater.*, **36**, 77–86.
Casto, C. C. (1950) in *Analytical Chemistry of the Manhattan Project* (ed. C. J. Rodden), McGraw-Hill, New York, pp. 511–36.
Catalano, J. G. and Brown, G. E. (2004) *Am. Miner.*, **89**, 1004–21.
Catlow, C. R. A. and Pyper, N. C. (1979) *J. Nucl. Mater.*, **80**, 110–14.
Caville, C. and Poulet, H. (1974) *J. Inorg. Nucl. Chem.*, **36**, 1581–7.
Čejka, J. (1999) *Rev. Miner.*, **38**, 521–622.
Cesbron, F., Ildefonse, P., and Sichere, M.-C. (1993) *Miner. Mag.*, **57**, 301–8.
Chakravorti, M. C., Bharadwaj, P. K., Pandit, S. C., and Mathur, B. K. (1978) *J. Inorg. Nucl. Chem.*, **40**, 1365–7.
Champarnaud-Mesjard, J.-C. and Gaudreau, B. (1976) *Comp. Rend. C*, **282**, 745–7.
Chapman, A. T. and Clark, G. W. (1965) *J. Am. Ceram. Soc.*, **48**, 494–5.
Charpin, P. (1965) *Compt. Rend.*, **260**, 1914–16.
Charpin, P., Montoloy, F., and Nierlich, M. (1968) *Compt. Rend. C*, **266**, 1685–7.
Charpin, P., Montoloy, F., and Nierlich, M. (1969) *Compt. Rend. C*, **268**, 156–8.
Charvillat, J. P., Baud, G., and Besse, J. P. (1970) *Mater. Res. Bull.*, **5**, 933–8.
Chatalet, J. (1967) in *P. Pascal, Nouveau Traité de Chimie Minérale, Masson et Cie.,* Paris (1967) vol. 4, 508–13.
Chen, F., Burns. P. C., and Ewing, R. C. (1999) *J. Nucl. Mater.*, **275**, 81–94.
Chen, F., Burns. P. C., and Ewing, R. C. (2000) *J. Nucl. Mater.*, **278**, 225–32.
Chen, J. H., Edwards, R. L., and Wasserburg, G. J. (1992) in *Uranium Series Disequilibrium Applications to Earth, Marine, and Environmental Sciences* (eds. M. Ivanovich and R. S. Harmon), Clarendon Press, Oxford, pp. 174–206.
Chen, Z., Luo, K., Tan, F., Zhang, Y., and Gu, X. (1986) *Kexue Tongbao*, **31**, 396–401.
Chernyayev, I. I. (1966) *Complex Compounds of Uranium* (translated from Russian by L. Mandel, eds. M. Govre and IPST staff), Israel Program for Scientific Translation, Jerusalem.
Chervet, J. (1960) *Nouveau Traité de Chimie Minérale* (ed. P. Pascal), XV (1), Masson et Cie, Paris., 52–94,
Chevalier, P.-Y., Fischer, E., and Cheynet, B. (2002) *J. Nucl. Mater.*, **303**, 1–28.
Chilton, J. M. (1963) *Proc. First Protactinium Chemistry Symp*., Gatlinburg, TN, April 25–26, TID-7675, p. 157.
Chiotti, P. (1980) *Bull. Alloy Phase Diagrams*, **1**, 99.
Chiotti, P., Akhachinskij, V. V., Ansara, I., and Rand, M. H. (1981) *The Chemical Thermodynamics of Actinide Elements and Compounds*, part 5, *The Actinide Binary Alloys*, IAEA, Vienna, STI/PUB/424/5.
Chirkst, D. E. (1981) *Koord. Khimiya*, **7**, 3–17.
Chisholm-Brause, C. J., Berg, J. M., Matzner, R. A., and Morris, D. E. (2001) *J. Colloid Interface Sci.*, **233**, 38–49.
Chodos, S. L. (1972) *J. Chem. Phys.*, **57**, 2712–14.
Choppin, G. R., Bokelund, H., and Valkiers, S. (1983) *Radiochim. Acta*, **33**, 229–32.
Christ, C. L., Clark, J. R., and Evans, H. T. Jr (1955) *Science*, **121**, 472–2.
Chukanov, N. V., Pushcharovsky, D. Y., Pasero, M., Merlino, S., Barinova, A. V., Mockel, S., Pekov, I. V., Zadov, A. E., and Dubinchuk, V. T. (2004) *Eur. J. Miner.*, **16**, 367–74.
Cinader, G., Peretz, M., Damir, D., and Hadari, Z. (1973) *Phys. Rev. B*, **8**, 4063–8.

Clark, D. L., Conradson, S. D., Ekberg, S. A., Hess, N. J., Neu, M. P., Palmer, P. D., Runde, W., and Tait, C. D. (1996) *J. Am. Chem. Soc.*, **118**, 2089–90.
Clark, D. L., Conradson, S. D., Donohue, R. J., Keogh, W. D., Morris, D. E., Palmer, P. D., Rogers, R. D., and Tait, C. D. (1999) *Inorg. Chem.*, **38**, 1456–66.
Clausen, K., Hayes, W., Hutchings, M. T., Kjems, J. K., Macdonald, J. E., and Osborn, R. (1985) *High Temp. Sci.*, **19**, 189–96.
Cleaves, H. E., Cron, M. M., and Sterling, J. T. (1945) AEC Report CT2–618.
Clegg, J. W. and Foley, D. D. (1958) *Uranium Ore Processing,* Addison-Wesley, Reading, MA.
Clemente, D. A., Bandoli, G., Benetollo, F., and Marzotto, A. (1974) *J. Cryst. Mol. Struct.*, **4**, 1–14.
Clifton, J. R., Gruen, D. M., and Ron, A. (1969) *J. Chem. Phys.*, **51**, 224–32.
Clusius, K. and Dickel, G. (1938) *Naturwissenschaften*, **26**, 546.
Cody, J. A. and Ibers, J. A. (1995) *Inorg. Chem.*, **34**, 3165–72.
Cody, J. A., Mansuetto, M. F., Pell, M. A., Chien, S., and Ibers, J. A. (1995) *J. Alloys Compds*, **219**, 1239–45.
Cohen, D. and Carnall, W. T. (1960) *J. Phys. Chem.*, **64**, 1933.
Cohen, I. and Schaner, B. E. (1963) *J. Nucl. Mater.*, **9**, 18–52.
Cohen, I. and Berman, R. M. (1966) *J. Nucl. Mater.*, **18**, 77–107.
Colella, M., Lumpkin, G. R., Zhang, Z., Buck, E. C., and Smith, K. L. (2005) *J. Phys. Chem. Miner.*, **32**, 52–64.
Condon, J. B. and Larson, E. A. (1973) *J. Chem. Phys.*, **59**, 855–65.
Contamin, P., Bacmann, J. J., and Marin, J. F. (1972) *J. Nucl. Mater.*, **42**, 54–64.
Conway, J. G. (1959) *J. Chem. Phys.*, **31**, 1002–4.
Cooper, M. A. and Hawthorne, F. C. (1995) *Can. Miner.*, **33**, 1103–9.
Cooper, M. A. and Hawthorne, F. C. (2001) *Can. Miner.*, **39**, 797–807.
Cordfunke, E. H. P. (1961) *J. Inorg. Nucl. Chem.*, **23**, 285–6.
Cordfunke, E. H. P. and Debets, P. C. (1964) *J. Inorg. Nucl. Chem.*, **26**, 1671.
Cordfunke, E. H. P. and Aling, P. (1965) *Trans. Faraday Soc.*, **61**, 50–3.
Cordfunke, E. H. P. and Loopstra, B. O. (1967) *J. Inorg. Nucl. Chem.*, **29**, 51–7.
Cordfunke, E. H. P. (1969) *The Chemistry of Uranium,* Elsevier, Amsterdam.
Cordfunke, E. H. P. and Loopstra, B. O. (1971) *J. Inorg. Nucl. Chem.*, **33**, 2427–36.
Cordfunke, E. H. P. (1975) in *Thermodynamics of Nuclear Materials,* Proc. Symp. 1974, vol. II, International Atomic Energy Agency, Vienna, pp. 185–92.
Cordfunke, E. H. P., van Egmond, A. B., and van Voorst, G. (1975) *J. Inorg. Nucl. Chem.*, **37**, 1433–6.
Cordfunke, E. H. P., Oweltjes, W., and Prins, G. (1976) *J. Chem. Thermodyn.*, **8**, 241–50.
Cordfunke, E. H. P., Prins, G., and van Vlaanderen, P. (1977) *J. Inorg. Nucl. Chem.*, **39**, 2189–90.
Cordfunke, E. H. P. and Westrum, E. F. Jr. (1979) in *Thermodynamics of Nuclear Materials,* Proc. Symp. 1979, vol. II, International Atomic Energy Agency, Vienna, pp. 125–41.
Cordfunke, E. H. P., Oweltjes, W., and van Vlaanderen, P. (1983) *J. Chem. Thermodyn.*, **15**, 237–43.
Cordfunke, E. H. P., van Vlaanderen, P., Goubitz, K., and Loopstra, B. O. (1985) *J. Solid State Chem.*, **56**, 166–70.
Cordier, S., Perrin, C., and Sergent, M. (1997) *Mater. Res. Bull.*, **32**, 25–33.

Cotton, F. A., Marler, D. O., and Schwotzer, W. (1984) *Acta Crystallogr.*, **40C**, 1186–8.
Cousson, A., Pagès, M., Cousseins, J.-C., and Vedrine, A. (1977) *J. Crystal Growth*, **40**, 157–60.
Cousson, A., Tabuteau, A., Pagès, M., and Gasperin, M. (1979) *Acta Crystallogr. B*, **35**, 1198–2000.
Cox, J. D., Wagman, D. D., and Medvedev, V. A. (1989) *CODATA Key Values for Thermodynamics,* Hemisphere, New York.
Crawford, M.-J., Ellern, A., and Mayer, P. (2005) *Angew. Chem. Int. Ed.* 1–5.
Crea, J., Diguisto, R., Lincoln, S. F., and Williams, E. H. (1977) *Inorg. Chem.*, **16**, 2825.
Crosswhite, H. M., Crosswhite, H., Carnall, W. T., and Paszek, A. P. (1980) *J. Chem. Phys.*, **72**, 5103–17.
Cunningham, J. E. and Adams, R. E. (1957) *Fuel Elements Conference*, Paris, November 18–23, TID-7546, Book 1, pp.102–19.
Dao, N. Q. (1972) *Acta Crystallogr. B*, **288**, 2011–15.
Dao, N. Q. and Chourou, S. (1972) *C. R. Acad. Sci. (Paris)*, **275C**, 745–8.
Dao, N. Q. and Chourou, S. (1974) *C. R. Acad. Sci. (Paris)*, **278C**, 879–81.
Dao, N. Q., Chourou, S., Rodier, N., and Bastein, P. (1979) *Compt. Rend. Serie C, Sciences Chimiques*, **289**, 405–8.
Dao, N. Q., Chourou, S., and Heckly, J. (1981) *J. Inorg. Nucl. Chem.*, **43**, 1835–9.
Daoudi, A., Levet, J. C., Potel, M., and Noël, H. (1996) *Mater. Res. Bull.*, **31**, 1213–18.
Davies, W. and Gray, W (1964) *Talanta*, **11**, 1203–11.
Davies, W., Gray, W., and McLeod, K. C. (1970) *Talanta*, **17**, 937–44.
Dawson, J. K. (1951) *J. Chem. Soc.*, 429–31.
Dawson, J. K., D'Eye, R. W. M., and Truswell, A. E. (1954) *J. Chem. Soc.*, 3922–9.
Dawson, J. K., Wait, E., Alcock, K., and Chilton, D. R. (1956) *J. Chem. Soc.*, 3531.
Day, J. P. and Venanzi, L. M. (1966) *J. Chem. Soc. A*, 1365–7.
D'Eye, R. W. M. and Martin, F. S. (1957) N.S.A. 11, no. 3372.
de Alleluia, I. B., Hoshi, M., Jocher, W. G., and Keller, C. (1981) *J. Inorg. Nucl. Chem.*, **43**, 1831–4.
Dean, J. A. (1995) *Analytical Chemistry Handbook,* McGraw-Hill, New York.
Debets, P. C. and Loopstra, B. O. (1963) *J. Inorg. Nucl. Chem.*, **25**, 945–53.
Debets, P. C. (1966) *Acta Crystallogr.*, **21**, 589–93.
Debets, P. C. (1968) *Acta Crystallogr.*, **24B**, 400–2.
de Coninck, R. and Devreese, J. (1969) *Phys. Status Solidi*, **32**, 823–9.
De Jong, W. A., Visscher, L., and Nieupoort, W. C. (1999) *Theochemistry*, **458**, 41–52.
Delamoye, P., Rajnak, K., Genet, M., and Edelstein, N. (1983) *Phys. Rev. B*, **28**, 4923–30.
Deleon, A. and Lazarević, M. (1971) in *The Recovery of Uranium,* Proc. Symp. Sao Paulo, Brazil, August 17–21, 1970, International Atomic Energy Agency, Vienna, STI/PUB/262, pp. 351–61.
Deliens, M. and Piret, P. (1981) *Can. Miner.*, **19**, 553–7.
Deliens, M. and Piret, P. (1982) *Can. Miner.*, **20**, 231–8.
Deliens, M. and Piret, P. (1983a) *Am. Miner.*, **68**, 456–8.
Deliens, M. and Piret, P. (1983b) *Bull. Minér.*, **106**, 305–8.
Deliens, M. and Piret, P. (1984a) *Bull. Minér.*, **107**, 21–4.
Deliens, M. and Piret, P. (1984b) *Bull. Minér.*, **107**, 15–19.
Deliens, M. and Piret, P. (1990a) *Eur. J. Miner.*, **1**, 85–8.
Deliens, M. and Piret, P. (1990b) *Eur. J. Miner.*, **2**, 407–11.

Dell, R. M. and Wheeler, V. I. (1963) *Trans. Faraday Soc.*, **59**, 485.
Della Ventura, G., Bonazzi, P., Oberti, R., and Ottolini, L. (2002) *Am. Miner.*, **87**, 739–44.
Demartin, F., Diella, V., Donzelli, S., Gramaccioli, C. M., and Pilati, T. (1991) *Acta Crystallogr.*, **B47**, 439–46.
Demartin, F., Gramaccioli, C. M., and Pilati, T. (1992) *Acta Crystallogr.*, **C48**, 1–4.
Dempster, A. J. (1935) *Nature*, **136**, 180.
Denes, G., Fonteneau, G., and Lucas, J. (1973) *Compt. Rend. C.*, **276**, 1553–6.
Denning, R. G., Snellgrove, T. R., and Woodwark, D. R. (1976) *Mol. Phys.*, **31**, 419–42.
Dent, A. J., Ramsey, J. D. F., and Swanton, S. W. (1992) *J. Colloid Interface Sci.*, **150**, 45–60.
Depaus, R., Guzzi, G., and Federico, A. (1987) *Proc. Int. Symp. Nuclear Material Safeguards*, Vienna, Austria, IAEA, vol. 2, p. 116.
Dereń, P., Karbowiak, M., Krupa, J. P., and Drożdżyński, J. (1998) *J. Alloys Compds*, **275–7**, 863–6.
Deschaux, M. and Marcantonatos, M. D. (1979) *Chem. Phys. Lett.*, **63**, 283–8.
Destriau, M. and Sériot, J. (1962) *Compt. Rend. Hebd. Séances Acad. Sci.*, **254**, 2982–4.
Deutsch, W. J., Krupka, K. M., Lindberg, M. J., Cantrell, K. J., Brown, C. F., and Schaef, H. F. (2004) *Hanford Tanks 241-C-203 and 241-C-204: Residual Waste Contaminant Release Model and Supporting Data,* PNNL-14903, Pacific Northwest National Laboratory, Richland, Washington.
de Wet, J. F., Caira, M. R., and Gellatly, B. J. (1978) *Acta Crystallogr. B*, **34**, 1121–4.
de Wet, J. F. and du Preez, J. G. H. (1978) *J. Chem. Soc., Dalton Trans.*, 592–7.
Dhar, S. K., Kimura, Y., Kouzaki, M., Sugiyama, K., Settai, R., Onuki, Y., Takeuchi, T., Kindo, K., Manfrinetti, P., and Palenzona, A. (1998) *Physica B* (*Amsterdam, Neth*), **245**, 210–18.
Dharwadkar, S. R., Chandrasekharaiah, M. S., and Karkhanavala, M. D. (1975) *J. Thermal Anal.*, **7**, 219–21.
Dharwadkar, S. R., Chandrasekharaiah, M. S., and Karkhanavala, M. D. (1978) *J. Nucl. Mater.*, **71**, 268–76.
Di Bella, S., Lanza, G., Fragalà, I. L., and Marks, T. J. (1996) *Organometallics*, **15**, 205–7.
Dickens, P. G., Stuttard, G. P., Dueber, R. E., Woodall, M. J., and Patat, S. (1993) *Solid State Ionics*, **63–5**, 417–23.
Diehl, H. G. and Keller, C. (1971) *J. Solid State Chem.*, **3**, 621–36.
Dion, C., Obbade, S., Raekelboom, E., Abraham, F., and Saadi, M. (2000) *J. Solid State Chem.*, **155**, 342–53.
Di Sipio, L., Tondello, E., Pellizzi, G., Ingletto, G., and Montenero, A. (1974a) *Crystal Struct. Commun.*, **3**, 297–300.
Di Sipio, L., Tondello, E., Pellizzi, G., Ingletto, G., and Montenero, A. (1974b) *Crystal Struct. Commun.*, **3**, 731–4.
Di Sipio, L., Tondello, E., Pellizzi, G., Ingletto, G., and Montenero, A. (1974c) *Crystal Struct. Commun.*, **3**, 527–30.
Di Sipio, L., Tondello, E., Pellizzi, G., Ingletto, G., and Montenero, A. (1974d) *Crystal Struct. Commun.*, **3**, 301–3.
Di Sipio, L., Tondello, E., Pellizzi, G., Ingletto, G., and Montenero, A. (1977) *Crystal Struct. Commun.*, **6**, 723–6.

Djogic, R. and Branica, M. (1992) *Electroanalysis*, **4**, 151–9.
Docrat, T. I., Mosselmans, J. F. W., Charnock, J. M., Whitley, M. W., Collison, D., Livens, F. R., Jones, C., and Edmiston, M. J. (1999) *Inorg. Chem.*, **38**, 1879–82.
Dodé, M. and Touzelin, B. (1972) *Rev. Chim. Minér.*, **9**, 139.
Donohue, J. and Einspahr, H. (1971) *Acta Crystallogr. B*, **27**, 1740–3.
Douglas, R. M. and Staritzky, E. (1957) *Anal. Chem.*, **29**, 459.
Douglass, R. M. (1962) *Acta Crystallogr.*, **15**, 505–6.
Downs, A. J. and Gardner, C. J. (1986) *J. Chem. Soc. Dalton Trans.*, 1289–96.
Doyle, G. A., Goodgame, D. M. L., Sinden, A., and Williams, D. L. (1993) *J. Chem. Soc. Chem. Commun.*, 1170–2.
Drożdżyński, J. and Conway, J. G. (1972) *J. Chem. Phys.*, **56**, 883–91.
Drożdżyński, J. (1978) *J. Inorg. Nucl. Chem.*, **40**, 319–23.
Drożdżynski, J. and Kamenskaya, A. N. (1978) *Chem. Phys. Lett.*, **56**, 549–53.
Drożdżyński, J. and Miernik, D. (1978) *Inorg. Chim. Acta*, **30**, 185–8.
Drożdżyński, J. (1979) *Inorg. Chim. Acta.*, **32**, L83–5.
Drożdżyński, J. (1984) *J. Mol. Struct.*, **114**, 449–56.
Drożdżyński, J. (1985) *Inorg. Chim. Acta*, **109**, 79–81.
Drożdżyński, J. (1988a) *Polyhedron*, **7**, 167–8.
Drożdżyński, J. (1988b) *J. Less Common Metals*, **138**, 271–9.
Drożdżyński, J. (1991) Chemistry of tervalent uranium, in *Handbook on the Physics and Chemistry of the Actinides* vol. 6, ch. 5 (eds. A. J. Freeman and C. Keller), North-Holland, Amsterdam, pp. 281–336.
Drożdżyński, J. and du Preez, J. G. H. (1994) *Inorg. Chim. Acta*, **218**, 203–5. no.1–2,
Drożdżyński, J., and Karbowiak, M. (2005) unpublished results.
Drulis, H., Petryński, W., Staliński, B., and Zigmunt, A. (1982) *J. Less Common Metals*, **83**, 87–93.
Ducroux, R. and Baptiste, Ph. J. (1981) *J. Nucl. Mater.*, **97**, 333–6.
Dudney, N. J., Coble, R. L., and Tuller, H. L. (1981) *J. Am. Ceram. Soc.*, **64**, 627–31.
Duff, M. C., Amrhein, C., Bertsch, P. M., and Hunter, D. B. (1997) *Geochim. Cosmochim. Acta*, **61**, 73–81.
Duff, M. C., Coughlin, J. U., and Hunter, D. B. (2002) *Geochim Cosmochim. Acta*, **66**, 3533–47.
du Preez, J. G. H., Gonsalves, J. W., and Steenkamp, P. J. (1977a) *Inorg. Chim. Acta*, **21**, 167–72.
du Preez, J. G. H., Gellatly, B. J., and Gibson, M. L. (1977b) *J. Chem. Soc. Dalton Trans.*, 1062–8.
du Preez, J. G. H. and Zeelie, B. (1987) *Inorg. Chim. Acta*, **134**, 303–8.
du Preez, J. G. H. and Zeelie, B. (1989) *Inorg. Chim. Acta*, **161**, 187–92.
Dusausoy, Y., Ghermain, N.-E., Podor, R., and Chuney, M. (1996) *Eur. J. Miner.*, **8**, 667–73.
Dyall, K. G. (1999) *Mol. Phys.*, **96**, 511–18.
Eastman, E. D., Brewer, L., Bromley, L. A., Gilles, P. W., and Lofgren, N. A. (1950) *J. Am. Chem. Soc.*, **72**, 2248–850; 4019–23.
Eastman, E. D. and Fontana, B. I. (1958) in *Chemistry of Uranium* (*TID –5290*), *Paper 30* (eds. J. Katz and E. Rabinowitch), Oak Ridge, TN, pp. 206–13.
Eastman, M. P., Eller, P. G., and Halstead, G. W. (1981) *J. Inorg. Nucl. Chem.*, **43**, 2839–42.

Ebert, W. L., Bates, J. K., and Bourcier, W. L. (1991) *Waste Manage.*, **11**, 205–21.
Edelson, M. C. (1992) in *Inductively Coupled Plasmas in Analytical Atomic Spectrometry,* 2nd edn (eds. A. Montaser and D. W. Golightly), VCH Publishers, New York, pp. 341–72.
Edelstein, N., Brown, D., and Whittaker, B. (1974) *Inorg. Chem.*, **13**, 563–7.
Edghill, R. (1991) *Radiochim. Acta*, **32**, 381–6.
Eding, H. J. and Carr, E. M. (1961) *High-Purity Uranium Compounds – Final Report*, ANL-6339.
Edwards, R. K. and Martin, A. E. (1966) in *Thermodynamics,* Proc. Symp. 1965, vol. 2, International Atomic Energy Agency, Vienna, pp. 423–9.
Edwards, R. K., Chandrasekharaiah, M. S., and Danielson, P. M. (1969) *High Temp. Sci.*, **1**, 98–113.
Efremova, K. M., Ippolitova, E. A., Simanov, Yu. P., and Spitsyn, V. I. (1959) *Dokl. Akad. Nauk. SSSR*, **124**, 1057–60.
Efremova, K. M., Ippolitova, E. A., and Simanov, Yu. P. (1961a) Argonne National Laboratory Report, ANL-trans-33, p. 44.
Efremova, K. M., Ippolitova, E. A., and Simanov, Yu. P. (1961b) Argonne National Laboratory Report, ANL-trans-33, p. 59.
Efremova, K. M., Ippolitova, E. A., and Simanov, Yu. P. (1961c) Argonne National Laboratory Report, ANL-trans-33, p. 65.
Ehrfeld, W. and Ehrfeld, U. (1980) in *Gmelin Handbuch der Anorganischen Chemie,* Uranium Suppl., vol. A2, Springer, Berlin, p. 57.
Eichberger, K. (1979) *Dissertation,* T.U. Munich, Germany.
Eichberger, K. and Lux, F. (1980) *Ber. Bunsenges. Phys. Chem.*, **84**, 800–7.
Eick, H. A. (1994) Lanthanide and actinide halides, in *Handbook on the Physics and Chemistry of Rare Earths* (eds. K. A. Gschneidner Jr, L. Eyring, G. R. Choppin, and G. H. Lander), Elsevier Science B. V., vol. 18, ch. 124, 365–411.
Ekeroth, E. and Jonsson, M. (2003) *J. Nucl. Mater.*, **322**, 242–8.
Ekstrom, A., Batley, G. E., and Johnson, D. A. (1974) *J. Catalysis*, **34**, 106–16.
Ekstrom, A. and Johnson, D. A. (1974) *J. Inorg. Nucl. Chem.*, **36**, 2549–56.
Eliseev, S. S., Glukhov, I. A., and Vozhdaeva, E. E. (1972) *Zh. Neorg. Khim.*, **17**, 1203–8; *Russ. J. Inorg. Chem.*, **17**, 627–9.
Ellens, A., Krämer, K., and Güdel, H. U. (1998) *J. Lumin.*, **76/77**, 548.
Eller, P. G., Larson, A. C., Peterson, J. R., Ensor, D. D., and Young, J. P. (1979) *Inorg. Chim. Acta*, **37**, 129–33.
Ellert, G. V., Tsapkin, V. V., Mikhailov, Yu. N., and Kuznetsov, V. G. (1965) *Zh. Neorg. Khim.*, **10**, 1572–80; (1965) *Russ. J. Inorg. Chem.*, **10**, 858–62.
Ellert, G. V., Eliseev, A. A., and Slovyanskikh, V. K. (1971) *Zh. Neorg. Khim.*, **16**, 1451; *Russ. J. Inorg. Chem.*, **16**, 768.
Ellert, G. V., Sevast'yanov, V. G., and Slovyanskikh, V. K. (1975) *Zh. Neorg. Khim.*, **20**, 221–7; *Russ. J. Inorg. Chem.*, **20**, 120–3.
Elliot, R. P. (1965) *Constitution of Binary Alloys,* 1st Suppl., McGraw-Hill, New York.
Ellison, A. J. G., Mazer, J. J., and Ebert, W. L. (1994) *Effect of Glass Composition on Waste Form Durability: A Critical Review*, Argonne National Laboratory Report, ANL-94/28, Argonne, IL, USA.
Engmann, R. and de Wolff, P. W. (1963) *Acta Crystallogr.*, **16**, 993–6.
Esch, U. and Schneider, A. (1948) *Z. Anorg. Allg. Chem.*, **257**, 254–66.

Espenson, J. H. (ed.) (1995) *Chemical Kinetics and Reaction Mechanisms,* McGraw-Hill, New York.
Evers, E. C. and Reynolds, M. B. (1954) U.S. Patent 2674518.
Ewing, R. C. (1999) *Proc. Nat. Acad. Sci.*, **96**, 3432–29.
Faber, J. Jr. and Lander, G. H. (1976) *Phys. Rev.*, **B14**, 1151–64.
Faile, S. P. (1978) *J. Crystal Growth*, **43**, 133–4.
Farges, F., Ponader, C. W., Calas, G., and Brown, G. E. (1992) *Geochim. Cosmochim. Acta*, **56**, 4205–20.
Farkas, I., Bányai, I., Szabó, Z., Wahlgren, U., and Grenthe, I. (2000a) *Inorg. Chem.*, **39**, 799–805.
Farkas, I., Grenthe, I., and Bányai, I. (2000b) *J. Phys. Chem. A*, **104**, 1201–6.
Faucher, M. D., Moune, O. K., Garcia, D., and Tanner, P. (1996) *Phys. Rev. B*, **53**, 9501–4.
Fawcett, J., Holloway, J. H., Laycock, D., and Russell, D. R. (1982) *J. Chem. Soc. Dalton Trans.*, 1355–60.
Fazekas, Z., Tomiyasu, H., Park, I.-L., Yamamura, T., and Harada, M. (1998) *Models in Chemistry*, **135** (5), 783–97, Akademiai,Kiadó, Budapest.
Fee, D. C. and Johnson, C. E. (1978) *J. Inorg. Nucl. Chem.*, **40**, 1375–81.
Feng, X., Buck, E. C., Mertz, C., Bates, J. K., Cunnane, J. C., and Chaiko, D. J. (1994) *Radiochim. Acta*, **66/67**, 197–205.
Ferguson, I. F. and Fogg, P. G. T. (1957) *J. Chem. Soc.*, 3679–81.
Ferguson, I. F. and Street, R. S. (1963) AERE Harwell Report, AERE-M 1192.
Fernandes, J. C., Continentino, M. A., and Guimarães, A. P. (1985) *Solid State Commun.*, **55**, 1011–15.
Figgins, P. E. and Bernardinelli, R. J. (1966) *J. Inorg. Nucl. Chem.*, **28**, 2193.
Finch, R. J. and Ewing, R. C. (1992) *J. Nucl. Mater.*, **190**, 133–56.
Finch, R. J., Suksi, J., Rasilainen, K., and Ewing, R. C. (1995) *Mater. Res. Soc. Symp. Proc.*, **353**, 647–52.
Finch, W. I. (1996) *Uranium Provinces of North America – Their Definition, Distribution, and Models*, U.S. Geological Survey Bulletin, 2141.
Finch, R. J., Cooper, M. A., Hawthorne, F. C., and Ewing, R. C. (1996a) *Can. Miner.*, **34**, 1071–88.
Finch, R. J., Suksi, J., Rasilainen, K., and Ewing, R. C. (1996b) *Mater. Res. Soc. Symp. Proc.*, **412**, 823–30.
Finch, R. J. and Ewing, R. C. (1997) *Am. Miner.*, **82**, 607–19.
Finch, R. J., Hawthorne, F. C., and Ewing, R. C. (1998) *Can. Miner.*, **36**, 831–45.
Finch, R. J. and Murakami, T. (1999) *Rev. Miner.*, **38**, 91–180.
Finch, R. J., Buck, E. C., Finn, P. A., and Bates, J. K. (1999a) *Mater. Res. Soc. Symp. Proc.*, **556**, 431–8.
Finch, R. J., Cooper, M. A., Hawthorne, F. C., and Ewing, R. C. (1999b) *Can. Miner.*, **37**, 929–38.
Findley, J. R., Gregory, J. N., and Weldrick, G. (1955) AERE Report, AERE-C/M-265.
Fine, M. A., Mendelson, A., and Schwartz, D. F. (1945) *Purification of Tuballoy by the Thermal Decomposition of Tuballoy Iodide*, CT-2695.
Fink, J. K. (2001) *World Wide Web, INSC Materials Properties Database*, http://www.insc.anl.gov/matprop/

Finnie, K. S., Zhang, Z., Vance, E. R., and Carter. M. L. (2003) *J. Nucl. Mater.*, **317**, 46–53.
Fischer, E. A., Kinsman, P. R., and Ohse, R. W. (1976) *J. Nucl. Mater.*, **59**, 125–36.
Fischer, E. O. and Hristidu, Y. (1962) *Z. Naturforsch.*, **17b**, 275–6.
Fisk, Z., Moreno, N. O., and Thompson, J. D. (2003) *J. Phys. Condensed Matter*, **15**, S1917–21.
Fitzmaurice, J. C. and Parkin, I. P. (1994) *New J. Chem.*, **18**, 825–32.
Flotow, H. E. and Abraham, B. M. (1951) Argonne National Laboratory, IL, Report AEDP-3074.
Flotow, H. E., Lohr, H. R., Abraham, B. M., and Osborne, D. W. (1959) *J. Am. Chem. Soc.*, **81**, 3529–33.
Flotow, H. E. and Osborne, D. W. (1967) *Phys. Rev.*, **164**, 755–8.
Flotow, H. E., Haschke, J. M., and Yamauchi, S. (1984) in *The Chemical Thermodynamics of Actinide Elements and Compounds, part 9, The Actinide Hydrides* (ed. F. L. Oetting), International Atomic Energy Agency, Vienna, pp. 32–44.
Fonteneau, G. and Lucas, J. (1974) *J. Inorg. Nucl. Chem.*, **36**, 1515–19.
Foote, F. (1956) *Proc. Int. Conf. on Peaceful Uses of Atomic Energy*, Geneva, 1955, vol. 9, p. 33.
Formosinho, S. J., Da Graca, M., and Miguel, M. (1984) *J. Chem. Soc., Faraday Trans. I*, **80**, 1745–56.
Formosinho, S. J., Da Graca, M., Miguel, M., and Burrows, H. D. (1984) *J. Chem. Soc., Faraday Trans. I*, **80**, 1717–33.
Fortner, J. A., Kropf, A. J., Finch, R. J., Bakel, A. J., Hash, M. C., and Chamberlain, D. B. (2002) *J. Nucl. Mater.*, **304**, 56–62.
Fournier, J.-M. and Troć, R. (1985) in *Handbook on the Physics and Chemistry of the Actinides* (eds. A. J. Freeman and G. H. Lander), vol. 2, North-Holland, Amsterdam, pp. 29–173.
Fredrickson, D. R. and Chasanov, M. G. (1970) *J. Chem. Thermodyn.*, **2**, 623–9.
Fredrickson, D. R. and Chasanov, M. G. (1972) *J. Chem. Thermodyn.*, **4**, 419–23.
Fredrickson, J. K., Zachara, J. M., Kennedy, D. W., Liu, C., Duff, M. C., Hunter, D. B., and Dohnalkova, A. (2002) *Geochim. Cosmochim. Acta*, **66**, 3247–62.
Freeman, A. J. and Darby, J. B. Jr (1974) *The Actinides: Electronic Structure and Related Properties,* Academic Press, New York.
Freestone, N. P. and Holloway, J. H. (1991) Actinide fluorides, in *Synthesis of Lanthanide and Actinide Compounds* (eds. G. Meyer and L. R. Morss), Kluwer, Dordrecht, pp. 67–133.
Frei, V. and Wendt, H. (1970) *Ber. Bunsenges. Phys. Chem.*, **74**, 593.
Friedman, H. A., Weaver, C. F., and Grimes, W. R. (1970) *J. Inorg. Nucl. Chem.*, **32**, 3131–3.
Friese, J. I., Nash, K. L., Jensen, M. P., and Sullivan, J. C. (1998) *Radiochim. Acta*, **83**, 175–81.
Friese, J. I., Nash, K. L., Jensen, M. P., and Sullivan, J. C. (2001) *Radiochim. Acta*, **89**, 35–41.
Frlec, B., Brčič, B. S., and Slivnik, J. (1966) *Inorg. Chem.*, **5**, 542–6.
Frlec, B. and Hyman, H. H. (1967) *Inorg. Chem.*, **6**, 2233–9.
Frolov, A. A. and Rykov, A. G. (1979) *Radiokhimiya*, **21**, 329–42; *Sov. Radiochem.*, **21**, 281–92.

Frondel, C. (1951a) *Am. Miner.*, **36**, 671–9.
Frondel, C. (1951b) *Am. Miner.*, **36**, 680–6.
Fuchs, L. H. and Gebert, E. (1958) *Am. Miner.*, **43**, 243–8.
Fuger, J. and Brown, D. (1973) *J. Chem. Soc. Dalton Trans.*, 428–34.
Fuger, J., Parker, V. B., Hubbard, W. N., and Oetting, F. L. (1983) *The Chemical Thermodynamics of Actinide Elements and Compounds,* part 8, The Actinide Halides, IAEA, Vienna, STI/PUB/424–8.
Fuji, K., Miyake, C., and Imoto, S. (1979) *J. Nucl. Sci. Technol.*, **16**, 207–13.
Fujino, T. and Naito, K. (1969) *J. Am. Ceram. Soc.*, **52**, 574–7.
Fujino, T. and Naito, K. (1970) *J. Inorg. Nucl. Chem.*, **32**, 627–36.
Fujino, T. (1972) *J. Inorg. Nucl. Chem.*, **34**, 1563–74.
Fujino, T., Masaki, N., and Tagawa, H. (1977) *Z. Kristallogr.*, **145**, 299–309.
Fujino, T., Tateno, J., and Tagawa, H. (1978a) *J. Solid State Chem.*, **24**, 11–19.
Fujino, T., Tagawa, H., Adachi, T., and Hashitani, H. (1978b) *Anal. Chim. Acta*, **98**, 373–83.
Fujino, T., Tagawa, H., and Adachi, T. (1981) *J. Nucl. Mater.*, **97**, 93–103.
Fujino, T., Ouchi, K., Yamashita, T., and Natsume, H. (1983) *J. Nucl. Mater.*, **116**, 157–65.
Fujino, T., Yamashita, T., and Tagawa, H. (1988) *J. Solid State Chem.*, **73**, 544–55.
Fujino, T. and Miyake, C. (1991) in *Handbook on the Physics and Chemistry of the Actinides* vol. 6 (eds. A. J. Freeman and C. Keller), North-Holland, Amsterdam, pp. 155–240.
Fujino, T., Ouchi, K., Mozumi, Y., Ueda, R., and Tagawa, H. (1990) *J. Nucl. Mater.*, **174**, 92–101.
Fujino, T. and Sato, N. (1992) *J. Nucl. Mater.*, **189**, 103–15.
Fujino, T., Sato, N., and Yamada, K. (1995) *J. Nucl. Mater.*, **223**, 6–19.
Fujino, T., Nakama, S., Sato, N., Yamada, K., Fukuda, K., Serizawa, H., and Shiratori, T. (1997a) *J. Nucl. Mater.*, **246**, 150–7.
Fujino, T., Sato, N., and Yamada, K. (1997b) *J. Nucl. Mater.*, **247**, 265–72.
Fujino, T., Sato, N., Yamada, K., Nakama, S., Fukuda, K., Serizawa, H., and Shiratori, T. (1999) *J. Nucl. Mater.*, **265**, 154–60.
Fujino, T., Sato, N., Yamada, K., Okazaki, M., Fukuda, K., Serizawa, H., and Shiratori, T. (2001a) *J. Nucl. Mater.*, **289**, 270–80.
Fujino, T., Park, K., Sato, N., and Yamada, M. (2001b) *J. Nucl. Mater.*, **294**, 104–11.
Fukushima, S., Ohmichi, T., Maeda, A., and Watanabe, H. (1981) *J. Nucl. Mater.*, **102**, 30–9.
Fukushima, S., Ohmichi, T., Maeda, A., and Watanabe, H (1982) *J. Nucl. Mater.*, **105**, 201–10.
Fukushima, S., Ohmichi, T., Maeda, A., and Handa, M. (1983) *J. Nucl. Mater.*, **114**, 312–25.
Fuoss, R. M. (1958) *J. Am. Chem. Soc.*, **80**, 5059–61.
Furman, N. H., Bricker, C. E., and Ditts, R. V. (1953) *Anal. Chem.*, **25**, 482–6.
Furman, S. C. (1957) Knolls Atomic Power Laboratory Report, KAPL-1664.
Gabuda, S. P., Matsutsin, A. A., and Zadneprovskii, G. M. (1969) *Zh. Strukt. Khimii*, **10**, 1115–16; (1969) *J. Struct. Chem.* (*USSR*), **10**, 996–8.
Gagarinskii, Yu. V., Khanaev, E. I., Galkin, N. P., Ananeva, L. A., and Gabuda, S. P. (1965) *At. Energy* (*USSR*)*, 18, 40–5;* (*1965*) *Sov. At. Energy*, **31**, 43–8.

Gagliardi, L., Grenthe, I., and Roos, B. O. (2001) *Inorg. Chem.*, **40**, 2976–8.
Gagliardi, L., Pyykkö, I., and Roos, B. O. (2005) *Phys. Chem. Chem. Phys.* **17**, 2415–17.
Gagliardi, L. and Roos, B. O. (2005a) *Nature*, **433**, 848–51.
Gagliardi, L. and Roos, B. O. (2005b) *Inorg. Chem. Prepublication, ASAP*, Dec. 15.
Gaines, R. V., Skinner, C. W., Foord, E. E., Mason, B., and Rosenzweig, A. (1997) *Dana's New Mineralogy: The System of Mineralogy of James Dwight Dana and Edward Salisbury Dana,* 8th edn, John Wiley, New York.
Gale, W. F. and Totemeier, T. C. (2003) *Smithells Metals Reference Book,* 8th edn, Elsevier, Amsterdam.
Galkin, N. P. and Sudarikov, B. N. (eds.) (1966) *Technology of Uranium*, Israel Program for Scientific Translations, Jerusalem; translated from Tekhnologiya Urana, Atomizdat, Moscow (1964).
Gamp, E., Edelstein, N., Khan Malek, C., Hubert, S., and Genet, M. (1983) *J. Chem. Phys.*, **79**, 2023–6.
Garg, S. P. and Ackermann, R. J. (1977) *Met. Trans.*, **8A**, 239–44.
Garg, S. P. and Ackermann, R. J. (1980) *J. Nucl. Mater.*, **88**, 309–11.
Garrido, F., Ibberson, R. M., Nowicki, L., and Willis, B. T. M. (2003) *J. Nucl. Mater.*, **322**, 87–9.
Gatehouse, B. M., Grey, I. E., and Kelly, P. R. (1979) *Am. Miner.*, **64**, 1010–17.
Gebert, E., Hoekstra, H. R., Reis, A. H. Jr, and Peterson, S. W. (1978) *J. Inorg. Nucl. Chem.*, **40**, 65–8.
Geichman, J. R., Smith, E. A. Trond, S. S., and Ogle, P. R. (1962) *Inorg. Chem.*, **2**, 1012–15.
Geichman, J. R., Smith, E. A., and Ogle, P. R. (1963) *Inorg. Chem.*, **1**, 661–5.
George, A. M. and Karkhanavala, M. D. (1963) *J. Phys. Chem. Solids*, **24**, 1207–12.
Gerdanian, P. (1964) CEA Report, CEA-R 2438.
Gerdanian, P. and Dodé, M. (1965) *J. Chim. Phys. Phys. Chim. Biol.*, **62**, 171–84.
Gerdanian, P. and Dodé, M. (1968) in *Thermodynamics of Nuclear Materials,* Proc. Symp. 1967, International Atomic Energy Agency, Vienna, pp. 41–54.
Gerdanian, P. (1974) *J. Phys. Chem. Solids*, **35**, 163–70.
Gerding, H., Prins, G., and Gabes, W. (1975) *Rev. Chim. Miner.*, **12**, 303–15.
Gesing, T. M. and Jeitschko, W. (1995) *Z. Naturforsch. B: Chem. Sci.*, **50**, 196–200.
Giammar, D. E. and Hering, J. G. (2002) *Geochim. Cosmochim. Acta.*, **66**, 3235–45.
Gibson, G. and Katz, J. J. (1951) *J. Am. Chem. Soc.*, **73**, 5436–8.
Gibson, G., Beintema, C. D., and Katz, J. J. (1960) *J. Inorg. Nucl. Chem.*, **15**, 110–14.
Gieré, R., Williams, C. T., and Lumpkin, G. R. (1998) *Schweiz Miner. Petrogr. Mitt.*, **78**, 433–59.
Gieré, R., Hatcher, C., Reusser, E., and Buck, E. C. (2002) *Mater. Res. Soc. Symp. Proc.*, **713**, 303–10.
Gillan, M. J. (1975) in *Thermodynamics of Nuclear Materials,* Proc. Symp. 1974, vol. I, International Atomic Energy Agency, Vienna, pp. 269.
Gilpatrick, L. O., Stone, H. H., and Secoy, C. H. (1964) Oak Ridge National Laboratory Report, ORNL-3591.
Ginderow, D. and Cesbron, F. (1983a) *Acta Crystallogr.*, **C39**, 1605–7.
Ginderow, D. and Cesbron, F. (1983b) *Acta Crystallogr.*, **C39**, 824–7.
Ginderow, D. and Cesbron, F. (1985) *Acta Crystallogr.*, **C41**, 654–7.

Ginderow, D. (1988) *Acta Crystallogr.*, **C44**, 421–4.
Gindler, G. E. (1962) *Radiochemistry of Uranium*, NAS-NS-3050, Technical Information Center, USAEC.
Gingerich, K. A. (1970) *J. Chem. Phys.*, **53**, 746–8.
Girdhar, H. L. and Westrum, E. F. Jr (1968) *J. Chem. Eng. Data*, **13**, 531–3.
Gittus, J. H. (1963) *Uranium,* Butterworths, Washington.
Gleichman, J. R., Ogle, P. R., and Swaney, L. R. (1961) *Reactions of Molybdenium, Tungsten and Uranium Hexafluoride with Nitrogen Compounds,* III, *Reactions with Nitrogen Dioxide and Nitrogen Oxyhalides*, GAT-T-809.
Gmelin, Handbook of Inorganic, chemistry, System no. 55, *Uran und Isotope mit einem Anhang über Transurane.* (1936) *Main volume,* Verlag Chemie, Berlin.
Gmelin Handbook of Inorganic Chemistry, Suppl. Ser., *Uranium*, Springer-Verlag, Berlin, Heidelberg, and New York.
(1979a) vol. Al, Uranium Deposits.
(1979b) vol. C9, Compounds with Chlorine, Bromine, and Iodine.
(1979c) vol. E1, Coordination Compounds.
(1980a) vol. A2, Isotopes.
(1980b) vol. C8, Compounds with Fluorine.
(1980c) vol. E2, Coordination Compounds (including Organouranium Compounds).
(1981a) vol. A3, Technology Uses.
(1981b) vol. C7, Compounds with Nitrogen.
(1981c) vol. C11, Compounds with Selenium, Tellurium, and Boron.
vol. C12, Carbides.
(1981d) vol. C14, Compounds with P, As, Sb, Bi, Ge.
(1982a) vol. A4, Irradiated Fuel Reprocessing.
(1982b) vol. A5, Spectra.
(1982c) vol. A7, Analytical Chemistry. Determination of the Isotope Composition. Biological Behavior. Health Protection and Safety Control.
vol. B2, Alloys with Alkali metals, Alkaline Earths, and Elements of Main Groups III and IV.
vol. B3, Alloys with Transition Metals of Groups IB to IVB.
(1983a) vol. A6, General Properties – Criticality.
(1983b) vol. C13, Carbonates, Cyanides, Thiocyanates, Alkoxides, Carboxylates, Compounds with Si.
(1983c) vol. D4, Cation Exchange and Chromatography.
(1984a) vol. C4, Uranium Dioxide. Preparation and Crystallographic Properties.
vol. C5, Uranium Dioxide. Physical Properties. Electrochemical Behavior.
(1984b) vol. C10, Compounds with Sulfur.
(1984c) vol. D1, Properties of U ions in Solutions and Melts.
(1982d) vol. D2, Solvent Extraction.
(1982e) vol. D3, Anion Exchange.
(1995a) vol. B4, Alloys with Transition Metals of Groups VB to VIIB.
vol. C1, Compounds with Rare Gases, and Hydrogen.System Uranium-Oxygen.
vol. C2, Oxides U_3O_8 and UO_3. Hydroxides. Oxide Hydrides. Peroxides.
vol. C3, Ternary and Polynary Oxides.
(1995b) vol. D5, Chemistry in Nonaqueous Solutions (Conductivity, Molecular weight, Solubility)

(1996a) vol. C6, Uranium Dioxide. Chemical Behavior.
(1996b) vol. D6, Chemistry in Nonaqueous Solutions (Formation of Complexes and Redox Reactions).
Gnandi, K. and Tobschall, H. J. (2003) *J. African Earth Sci.*, **37**, 1–10.
Gonsalves, J. W., Steenkamp, P. J., and du Preez, J. G. H. (1977) *Inorg. Chim. Acta*, **21**, 167–72.
Gorban, Yu. A., Pavlinov, L. V., and Bykov, V. N. (1967) *Sov. At. Energy*, **22**, 580–4.
Gordon, G. and Taube, H. (1961a) *J. Inorg. Nucl. Chem.*, **16**, 189–91.
Gordon, G. and Taube, H. (1961b) *J. Inorg. Nucl. Chem.*, **16**, 272–8.
Gorokhov, L. N., Emelyanov, A. M., and Khodeev, Y. S. (1974) *Teplofiz. Vyz. Temp.,* **12**, 1307–09.
Gotoo, K. and Naito, K. (1965) *J. Phys. Chem. Solids*, **26**, 1673–7.
Gray, C. W. (1994) *Methods Mol. Biol.*, **22**, 1–12.
Gray, C. W. (2001) *Methods Mol. Biol.*, **148**, 579–87.
Graziani, R., Bombieri, G., Forsellini, E., and Paolucci, G. (1975) *J. Crystal Mol. Struct.*, **5**, 1–14.
Greaves, C. and Fender, B. E. F. (1972) *Acta Crystallogr.*, **B28**, 3609–14.
Greaves, C., Cheetham, A. K., and Fender, B. E. F. (1973) *Inorg. Chem.*, **12**, 3003–7.
Greegor, R. B., Lytle, F. W., Chakoumakos, B. C., Lumpkin, G. R., Warner, J. K., and Ewing, R. C. (1989) *Mater. Res. Soc. Symp. Proc.*, **127**, 261–8.
Greek, B. F., Allen, O. W., and Tynan, D. E. (1957) *Ind. Eng. Chem.*, **49**, 628.
Greenberg, E. and Westrum, E. F. Jr (1956) *J. Am. Chem.Soc.*, **78**, 5144–7.
Gregory, N. W. (1958) in *The Chemistry of Uranium, Collected Papers.* TID-5290 (eds. J. J. Katz and E. Rabinowitch), USA EC Technical Information Extension, Oak Ridge, TN, pp. 465–510.
Grenthe, I., Ferri, D., Salvatore, F., and Diego, F. (1984) *J. Chem. Soc. Dalton Trans.*, 2439–43.
Grenthe, I., Fuger, J., Konings, R. J. M., Lemire, R. J., Muller, A. B., Nguyen-Trung, C., and Wanner, H. (1992) *Chemical Thermodynamics of Uranium,* NEA/OECD, North Holland.
Grenthe, I., Sandino, M. C. A., Puigdomenech, L., and Rand, M. H. (1995) *Corrections to the Uranium NEA-TDB Review. Appendix D in vol. 2. Chemical Thermodynamics of Americium*. By R. J. Silva *et al*. Nuclear Energy Agency, OECD, p. 347–74. Elsevier, Amsterdam.
Grenthe, I., Hummel, W., and Puigdomenech, I. (1997) in *Modelling in Aquatic Chemistry* (eds. I. Grenthe and I. Puigdomenech), Nuclear Energy Agency, OECD, Paris, ch. III.
Griffiths, T. R. and Volkovich, V. A. (1999) *J. Nucl. Mater.*, **274**, 229–51.
Grimes, W. R. (1978) Report CONF-780571-1; *Energy Res. Abstr.*, **3** (22), no. 52726.
Grimes, W. R. and Cuneo, D. R. (1960) in *Reactor Handbook,* vol. 1 (ed. R. Tripton), Interscience Publishers, New York.
Grønvold, F. (1955) *J. Inorg. Nucl. Chem.*, **1**, 357–70.
Grønvold, F., Kveseth, N. J., Sveen, A., and Tichý, J. (1970) *J. Chem. Thermodyn.*, **2**, 665–79.
Gross, E. B., Corey, A. S., Mitchell, R. S., and Walenta, K. (1958) *Am. Miner.*, **43**, 1134–43.
Grossman, L. N. and Priceman, S. (1954) *Nucleonics*, **12 (6)**, 68–9.

Grossman, L. N., Lewis, J. E., and Rooney, D. M. (1967) *J. Nucl. Mater.*, **21**, 302–9.
Gruen, D. M., Koehler, W. C., and Katz, J. J. (1951) *J. Am. Chem. Soc.*, **73**, 1475–9.
Gruen, D. M. (1955) *J. Chem. Phys.*, **23**, 1708–10.
Gruen, D. M. and McBeth, R. L. (1968) *Inorg. Nucl. Chem. Letters*, **4**, 294–8.
Gruen, D. M. and McBeth, R. L. (1969) *Inorg. Chem.*, **8**, 2625–33.
Grunzweig-Genossar, J., Kuznietz, M., and Meerovici, B. (1970) *Phys. Rev. B*, **1**, 1958–77.
Gueguin, M. M. (1964) *Bull. Soc. Chim. France*, 1184–7.
Guéneau, C., Dauvois, V., Pérodeaud, P., Gonella, C., and Dugne, O. (1998) *J. Nucl. Mater.*, **254**, 158–74.
Guéneau, C., Baichi, M., Labroche, D., Chatillon, C., and Sundman, B. (2002) *J. Nucl. Mater.*, **304**, 161–75.
Guest, R. J. and Zimmerman, J. B. (1955) *Anal. Chem.*, **27**, 931–6.
Guilbaud, P. and Wipff, G. (1993) *J. Phys. Chem. A*, **97**, 5685–92.
Guillaumont, R., Fanghänel, T., Fuger, J., Grenthe, I., Palmer, D., Rand, M., and Neck, V. (2003) *Chemical Thermodynamics of Uranium, Neptunium, Plutonium, Americium and Technetium,* NEA/OECD, North Holland.
Guinet, P., Vaugoyeau, H., and Blum, P. L. (1966) *C.R. Acad. Sci.* (*Paris*), **C263**, 17–20.
Gurevich, A. M., Polozhenskaya, L. P., Osicheva, N. P., and Solntseva, L. F. (1971a) *Radiokhimiya*, **13**, 688–692; *Sov. Radiochem.*, **13**, 706–9.
Gurevich, A. M., Polozhenskaya, L. P., and Osicheva, N. P. (1971b) *Radiokhimiya*, **13**, 588–92; *Sov. Radiochem.*, **13**, 604–7.
Gusev, Yu. K., Lychev, A. A., Mashirov, L. G., and Suglobov, D. N. (1985) *Radiokhimiya*, **27**, 412–15.
Güsten, H. (1983) in *Gmelin Handbook of Inorganic Chemistry,* Suppl., vol. A6, Springer-Verlag, Berlin-Heidelberg. ch. 3,
Haas, W. O. Jr and Smith, D. J. (1956) *Thorex Process Development at KAPL,* KAPL-1306 (declassified with deletions).
Habenschuss, A. and Spedding, F. H. (1980) *Crystal Struct. Commun.*, **9**, 71–6.
Haegele, R. and Boeyens, J. C. A. (1977) Nat. Inst. Met. Repub. S. Africa Res. Rep. no 1856.
Hagberg, D., Karlström, G., Roos, B. O., and Gagliardi, L. (2005) *J. Am. Chem. Soc.* **127**, 14250–6.
Hagemark, K. and Broli, M. (1966) *J. Inorg. Nucl. Chem.*, **28**, 2837–50.
Hagemark, K. and Broli, M. (1967) *J. Am. Ceram. Soc.*, **50**, 563–7.
Hagrman, D. T. (1995) SCADAP/RELAP5/MOD 3.1 Code Manual vol. 4, MATPRO, NUREG/CR-6150.
Hahn, O. (1925) *Z. Anorg. Chem.*, **147**, 16–23.
Hahn, O., Meitner, L., and Strassmann, F. (1937) *Ber. Dtsch. Chem. Ges.*, **70**, 1374–92.
Hahn, O. and Strassmann, F. (1939) *Naturwissenschaften*, **27**, 11–12.
Hall, D. A., Rae, A. D., and Waters, T. N. (1966) *Acta Crystallogr.*, **20**, 160–2.
Halliday, A. N., Lee, D.-C., Christensen, J. N., Rehkämper, M., Yi, W., Luo, X., Hall, C. M., Ballentine, C. J., Pettke, T., and Stirling, C. (1998) *Geochim. Cosmochim. Acta*, **62**, 919–40.
Halstead, G. W., Eller, P. G., and Eastman, P. (1979) *Inorg. Chem.*, **18**, 2867–72.
Handler, P. and Hutchison, C. A. (1956) *J. Chem. Phys.*, **25**, 1210–15.

Hansen, M. and Anderko, K. (1958) *Constitution of Binary Alloys,* McGraw-Hill, New York.
Hanson, S. L., Simmons, W. B., Falster, A. U., Foord, E. E., and Lichte, F. E. (1999) *Min. Mag.*, **63**, 27–36.
Hanuza, J., Hermanowicz, K., Macalik, L., Drożdżyński, J., Zych, E., and Meyer, G. (1999) *Vibrational Spectrosc.*, **21**, 111–26.
Harbottle, G. and Evans, C. V. (1997) *Radioact. Radiochem.*, **8**, 38–46.
Harrington, C. D. and Ruehle, A. E. (1959) *Uranium Production Technology,* Van Nostrand, Princeton, p. 461.
Harris, L. A. and Taylor, A. J. (1962) *J. Am. Ceram. Soc.*, **45**, 25.
Hart, F. A. and Tajik, M. (1983) *Inorg. Chim. Acta*, **71**, 169–73.
Haschke, J. M. (1991) in *Synthesis of Lanthanide and Actinide Compounds* (eds. G. Meyer and L. R. Morss), Kluwer Academic Publishers, Dordrecht, pp. 1–53.
Hauck, J. (1969) *Z. Naturforsch.*, **24b**, 1067–8.
Hauck, J. (1973) *Z. Naturforsch.*, **28b**, 215–16.
Hauck, J. (1974) *J. Inorg. Nucl. Chem.*, **36**, 2291–8.
Haug, H. and Weigel, F. (1963) *J. Nucl. Mater.*, **9**, 355–9.
Hay, P. J., Martin, R. L., and Schreckenbach, G. (2000) *J. Phys. Chem. A*, **104**, 6259–70.
Hayden, L. A. and Burns, P. C. (2002) *J. Solid State Chem.*, **163**, 313–18.
Hecht, H. G. and Gruber, J. B. (1974) *J. Chem. Phys.*, **60**, 4872–9.
Hecht, H. G., Malm, J. G., Foropoulos, J., and Carnall, W. T. (1986a) *J. Chem. Phys.*, **84**, 3653–62.
Hecht, H. G., Malm, J. G., and Carnall, W. T. (1986b) *J. Less Common Metals*, **115**, 79–89.
Heckers, U., Jacobs, H., and Kockelmann, W. (2003) *Z. Anorg. Allg. Chem.*, **629**, 2431–2.
Heidt, L. J. and Moon, K. A. (1953) *J. Am. Chem. Soc.*, **75**, 5808–9.
Hein, R. A. and Flagella, P. N. (1968) General Electric Report, GEMP-578.
Hein, R. A., Sjodahl, L. H., and Szwarc, R. (1968) *J. Nucl. Mater.*, **25**, 99–102.
Hellberg, K.-H. and Schneider, H. (1981) in *Gmelin Handbuch der Anorganischen Chemie*, System no. 55, Uranium, Suppl., vol. A3, Springer, Berlin, *Technology*, pp. 121–47.
Helm, L. and Mehrbach, A. E. (1999) *Coord. Chem. Rev.*, **187**, 151–81.
Helm, L. and Mehrbach, A. E. (2002) *J. Chem. Soc. Dalton Trans.*, 633–41.
Henche, G., Fiedler, K., and Gruehn, R. (1993) *Z. Anorg. Allg. Chem.*, **619**, 77–87.
Hendricks, M. E. (1971) DP-MS-71-46, p. 195.
Hendricks, M. E., Jones, E.R. Jr, Stone, J. A., and Karraker, D. G. (1971) *J. Chem. Phys.*, **55**, 2993–7.
Hendricks, M. E., Jones, E. R. Jr, Stone, J. A., and Karraker, D. G. (1974) *J. Chem. Phys.*, **60**, 2095–103.
Henkie, Z., Johanson, W. R., Crabtree, G. W., Dye, D. H., and Arko, A. J., Bazan, C. (1981) *Actinides*, Abstracts of September 1981 Asilomar Conf., Pacific Grove, CA, LBL-12441, pp. 176–8.
Henry, W. E. (1958) *Phys. Rev.*, **109**, 1976–80.
Hermann, J. A. and Suttle, J. F. (1957) *Inorg. Synth.*, **5**, 143–5.
Herrmann, H. (1861) *Uber verschiedene Uranverbindungen,* Dissertation, Göttingen.
Hidaka, H. and Holliger, P. (1998) *Geochim. Cosmochim. Acta*, **62**, 89–108.

Hiernaut, J. P., Hyland, G. J., and Ronchi, C. (1993) *Int. J. Thermophys.*, **14**, 259–83.
Higgins, L. R. and Roberts, J. T. (1956) *Development of the EXCER Process*, Part I, ORNL-1696.
Hildenbrand, D. (1977) *J. Chem. Phys.*, **66**, 4788.
Hill, D. C., Handwerk, J. H., and Beals, R. J. (1963) Argonne National Laboratory Report, ANL-6711.
Hill, F. C. (1999) *Rev. Miner.*, **38**, 635–79.
Hill, F. C. and Burns, P.C. (1999) *Can. Miner.*, **37**, 1283–8.
Hinatsu, Y. and Fujino, T. (1985) *J. Solid State Chem.*, **60**, 244–51.
Hinatsu, Y. and Fujino, T. (1986) *J. Solid State Chem.*, **62**, 342–50.
Hinatsu, Y. and Fujino, T. (1987) *J. Solid State Chem.*, **68**, 255–65.
Hinatsu, Y. and Fujino, T. (1988a) *J. Solid State Chem.*, **73**, 348–55.
Hinatsu, Y. and Fujino, T. (1988b) *J. Solid State Chem.*, **73**, 388–97.
Hinatsu, Y. and Fujino, T. (1988c) *J. Solid State Chem.*, **74**, 163–70.
Hinatsu, Y. and Fujino, T. (1988d) *J. Solid State Chem.*, **74**, 393–400.
Hinatsu, Y., Masaki, N., and Fujino, T. (1988) *J. Solid State Chem.*, **73**, 567–71.
Hinatsu, Y., Fujino, T., and Edelstein, N. (1992a) *J. Solid State Chem.*, **99**, 95–102.
Hinatsu, Y., Fujino, T., and Edelstein, N. (1992b) *J. Solid State Chem.*, **99**, 182–8.
Hines, M. A., Sullivan, J. C., and Nash, K. L. (1993) *Inorg Chem.*, **32**, 1820–3.
Ho, C. I., Powell, R. W., and Liley, P. E. (1972) *J. Phys. Chem. Ref. Data*, **1**, 279–421.
Hoard, J. L. and Stroupe, J. D. (1959) in *The Chemistry of Uranium – Collected Papers*, TID-5290, vol. 1, 325–49.
Hoch, M. and Furman, F. J. (1966) in *Thermodynamics*, Proc. Symp. 1965, International Atomic Energy Agency, Vienna, vol. 2, pp. 517–32.
Hodge, M. (l960) *Advances in Inorganic Chemistry and Radiochemistry,* vol. 2, Academic Press, New York, ch. 7.
Hoekstra, H. R. and Katz, J. J. (1952) *J. Am. Chem. Soc.*, **74**, 1683–90.
Hoekstra, H. R., Siegel, S., Fuchs, L. H., and Katz, J. J. (1955) *J. Phys. Chem.*, **59**, 136–8.
Hoekstra, H. and Siegel, S. (1956) in *Proc. First Int. Conf. on Peaceful Uses of Atomic Energy*, Geneva, vol. 7, P/737, 394–400.
Hoekstra, H. R. and Siegel, S. (1958) in *Proc. Second Int. Conf. on Peaceful Uses of Atomic Energy*, Geneva, paper 15/P/1548.
Hoekstra, H. R., Santoro, A., and Siegel, S. (1961) *J. Inorg. Nucl. Chem.*, **18**, 166–78.
Hoekstra, H. R. and Siegel, S. (1961) *J. Inorg. Nucl. Chem.*, **18**, 154–65.
Hoekstra, H. R. and Siegel, S. (1964) *J. Inorg. Nucl. Chem.*, **26**, 693–700.
Hoekstra, H. R. (1965) *J. Inorg. Nucl. Chem.*, **27**, 801–8.
Hoekstra, H. R. and Marshall, R. H. (1967) in *Lanthanide/Actinide Chemistry* (eds. P. Fields and T. Moeller), (ACS Advan. Chem. Ser. 71), American Chemical Society, Washington, DC, ch. 16, pp. 211–27.
Hoekstra, H. R., Siegel, S., and Charpin, P. (1968) *J. Inorg. Nucl. Chem.*, **30**, 519–23.
Hoekstra, H. R., Siegel, S., and Gallagher, F. X. (1970) *J. Inorg. Nucl. Chem.*, **32**, 3237–48.
Hoekstra, H. R. and Siegel, S. (1973) *J. Inorg. Nucl. Chem.*, **35**, 761–79.
Högfeldt, E. (1982) *Stability Constants of Metal-Ion Complexes. Part A Inorganic Ligands,* IUPAC Chemical Data Series no. 21, Pergamon Press, New York.
Holc, J. and Kolar, D. (1983) *J. Solid State Chem.*, **47**, 98–102.
Holden, A. N. (1958) *Physical Metallurgy of Uranium,* Addison-Wesley, London.

Holden, N. E. (1977) *Isotopic Composition of the Elements and Their Variation in Nature – A Preliminary Report, BNL-NCS-50605; (1979) Pure Appl. Chem.*, **52**, 2371.
Horwitz, E. P., Dietz, M. L., Chiarizia, R., Diamond, H., and Nelson, D. M. (1993) *Anal. Chim. Acta*, **281**, 361–72.
Hoskins, P. W. O. and Burns, P. C. (2003) *Miner. Mag.*, **67**, 689–96.
Howard, C. J., Taylor, J. C., and Waugh, A. B. (1982) *J. Solid State Chem.*, **45**, 396–8.
Howes, K. R., Bakac, A., and Espenson, J. H. (1988) *Inorg. Chem.*, **27**, 791–4.
Howlett, B. (1959/1960) *J. Inst. Met.*, **88**, 91–2.
Hsini, S., Caignol, E., Metin, J., Avignant, D., and Cousseins, J. C. (1986) *Rev. Chim. Minér.*, **23**, 35–47.
Hughes, K.-A. and Burns, P. C. (2003) *Am. Miner.*, **88**, 962–6.
Hughes, K.-A., Burns, P. C., and Kolitsch, U. (2003) *Can. Miner.*, **41**, 677–85.
Hughes-Kubatko, K.-A., Helean, K., Navrotsky, A., and Burns, P. C. (2003) *Science*, **302**, 1191–3.
Hughes-Kubatko, K. A., Helean, K., Navrotsky, A., and Burns, P. C. (2005) *Am. Miner.*, **90**, 1284–90.
Huie, R. E., Clifton, C. L., and Neta, P. (1991) *Radiat. Phys. Chem.*, **38**, 477–81.
Hummel, P., Winkler, J. R., and Gray, H. B. (2006) *J. Chem. Soc. Dalton Trans*. 168–71.
Hund, F., Peetz, U., and Kottenhahn, G. (1965) *Z. Anorg. Allg. Chem.*, **278**, 184–91.
Huntzicker, J. J. and Westrum, E. F. Jr (1971) *J. Chem. Thermodyn.*, **3**, 67–76.
Hutchings, M. T., Clausen, K., Dickens, M. H., Hayes, W., Kjems, J. K., Schnabel, P. G., and Smith, C. (1984) *J. Phys. C*, **17**, 3903–40.
Hutchings, M. T., Clausen, K., Hayes, W., Macdonald, J. E., Osborn, R., and Schnabel, P. (1985) *High Temp. Sci.*, **20**, 97–108.
Hyeon, J.-Y., Gottfriedsen, J., and Edelman, F. T. (2005) *Coord. Chem. Rev.* **249(24)** 2787–844.
Hyman, H. H., Sheft, I., and Katz, J. J. (1955) *Nuclear Engineering and Science Congress,* Cleveland, OH, Preprint 1997.
IAEA (1965) *Thermodynamic and Transport Properties of Uranium Dioxide and Related Phases*, Technical Report Series 39, IAEA, Vienna, STI/DOC/10/39 (1965).
IAEA (1966) *Processing of Low Grade Uranium Ores*, Proc. Panel convened by the International Atomic Energy Agency, Vienna, June 27–July 1, 1966, IAEA, Vienna, STI/PUB/146.
IAEA (1970) *The Recovery of Uranium*, Proc. Symp. Sao Paulo, Brazil, August 17–21, 1970, International Atomic Energy Agency, Vienna, STI/PUB/262.
IAEA (1978) *IWGFR Meeting on Equation of State of Materials of Relevance to the Analysis of Hypothetical Fast Breeder Reactor Accidents*, Harwell, UK, International Atomic Energy Agency,Vienna.
IAEA (1980) *Production of Yellow Cake and Uranium Fluorides*, Proc. Advisory Group Meeting organized by the IAEA, Paris, June 5–8, 1979, International Atomic Energy Agency, Vienna, STI/PUB/553.
Iandelli, A. (1952) *Atti Acad. Lincei, Class. Sci. Fiz. Mat. Nat. Rend.*, **13**, 138–44.
Ifill, R. O., Cooper, W. C., and Clark, A. H. (1996) *CIM Bull.*, **89**, 93–103.
Ikeda, Y., Soya, S., Fukutomi, H., and Tomiyasu, H. (1979a) *J. Inorg. Nucl. Chem.*, **41**, 1333–7.
Ikeda, Y., Tomiyasu, H., and Fukutomi, H. (1979b) *Bull. Res. Lab. Nucl. Reactors*, **4**, 47–59.

Ikeda, Y., Tomiyasu, H., and Fukutomi, H. (1984) *Inorg. Chem.*, **23**, 1356–60.
Imai, H. (1957) *Bull. Chem. Soc. Japan*, **30**, 873.
Inaba, H. and Naito, K. (1973) *J. Nucl. Mater.*, **49**, 181–8.
Inaba, H., Shimizu, H., and Naito, K. (1977) *J. Nucl. Mater.*, **64**, 66–70.
Inada, Y., Wisniewski, P., Murakawa, M., Aoki, D., Miyake, K., Watanabe, N., Haga, Y., Yamamoto, E., and Onuki, Y. (2001) *J. Phys. Soc. Japan*, **70**, 558–68.
Ingamells, C. O. and Pitard, F. (1986) *Applied Geochemical Analysis,* John Wiley, New York.
Ippolitova, E. A., Simanov, Yu. P., Kovba, L. M., Polunina, G. P., and Berznikova, N. A. (1959) *Radiokhimiya*, **1**, 660–4.
Ippolitova, E. A. and Kovba, L. M. (1961) *Dokl. Akad. Nauk. SSSR*, **138**, 377–80.
Ippolitova, E. A., Efremova, K. M., Orlinkova, O. L., and Simanov, Yu. P. (1961a) Argonne National Laboratory Report, ANL-trans-33, p. 52.
Ippolitova, E. A., Bereznikova, I. A., Kosynkin, V. D., Simanov, Yu. P., and Kovba, L. M. (1961b) Argonne National Laboratory Report, ANL-trans-33, p. 180.
Ippolitova, E. A., Bereznikova, I. A., Leonidov, V. Y., and Kovba, L. M. (1961c) Argonne National Laboratory Report, ANL-trans-33, p. 186.
Ippolitova, E. A., Simanov, Yu. P., Kovba, L. M., Murav'eva, I. A., and Krasnoyarskaya, A. A. (1961d) Argonne National Laboratory Report, ANL-trans-33, p. 153.
Ippolitova, E. A., Polunina, G. P., Kovba, L. M., and Simanov, Yu. P. (1961e) Argonne National Laboratory Report, ANL-trans-33, p. 213.
Ishii, T., Naito, K., and Oshima, K. (1970a) *J. Solid State Chem.*, **8**, 677–83.
Ishii, T., Naito, K., and Oshima, K. (1970b) *J. Nucl. Mater.*, **35**, 335–44.
Ishii, T., Naito, K., and Oshima, K. (1970c) *J. Nucl. Mater.*, **36**, 288–96.
Ivanov, V. E., Krugich, A. A., Pavlov, V. C., Kovtun, G. P., and Amonenko, V. M. (1962) in *Thermodynamics of Nuclear Materials,* Proc. Symp. 1962, International Atomic Energy Agency, Vienna, pp. 735–47.
Ivanov, S. B., Mikhailov, Yu. N., Kuznetsov, V. G., and Davidovich, R. L. (1980) *Koord. Khim.* [*Coord. Chem. (USSR)*], **6**, 1746–50.
Ivanov, S. B., Mikhailov, Yu. N., Kusnetsov, V. G., and Davidovich, R. L. (1981) *Zh. Strukt. Khim.*, **22**, 188–91.
Ivanov, S. B., Mikhailov, Yu. N., and Davidovich, R. L. (1982) *Koord. Khim.* (*Coord. Chemistry, USSR*), **8**, 1250–5.
Ivanovich, M. and Murray, A. (1992) in *Uranium Series Disequilibrium Applications to Earth, Marine, and Environmental Sciences* (eds. M. Ivanovich and R. S. Harmon), Clarendon Press, Oxford, pp. 127–73.
Iwasaki, M., Ishikawa, N., Ohwada, K., and Fujino, T. (1981) *Inorg. Chim. Acta*, **54**, L193–4.
Jackson, J. M. and Burns, P. C. (2001) *Can. Miner.*, **39**, 187–95.
Jackson, R. A., Murray, A. D., Harding, J. H., and Catlow, C. R. A. (1986) *Phil. Mag.*, **A53**, 27–50.
Jacob, I., Hadari, Z., and Reilly, J. J. (1984) *J. Less Common Metals*, **103**, 123–7.
Jacobs, H., Heckers, U., Zachwieja, U., and Kockelmann, W. (2003) *Z. Anorg. Allg. Chem.*, **629**, 2240–3.
Jakeš, D., Moravec, J., Křivý, I., and Sedláková, L. (1966) *Z. Anorg. Allg. Chem.*, **347**, 218–22.
Jakeš, D. and Schauer, V. (1967) *Proc. Brit. Ceram. Soc.*, **8**, 123–5.

Jakeš, D. (1973) *Colloq. Czech. Chem. Commun.*, **38**, 1–6.
Jakeš, D. and Křivý, I. (1974) *J. Inorg. Nucl. Chem.*, **36**, pp. 3885.
Jacob, E. and Polligkeit, W. (1973) *Z. Naturforsch.*, **28b**, 120–4.
Jacob, E. (1982) *Angew. Chem. Int. Ed. Engl.*, **21**, 142–3; (1982) *Angew. Chem.*, Suppl., 317.
Janeczek, J. and Ewing, R. C. (1991) *J. Nucl. Mater.*, **185**, 66–77.
Janeczek, J. and Ewing, R. C. (1992) *J. Nucl. Mater.*, **190**, 128–32.
Janeczek, J. (1999) *Rev. Miner.*, **38**, 321–92.
Jayadevan, N. G., Singh Mudher, K. D., and Chackraburtty, D. M. (1974) Bhabha Atomic Research Center Report, BARC-726.
Jensen, K. A., Palenik, C. S., and Ewing, R. C. (2002) *Radiochim. Acta*, **90**, 761–70.
Jerden, J. L. and Sinha, A. K. (2003) *Appl. Geochem.*, **18**, 823–43.
Jiang, J., Sarsfield, M. J., Renshaw, J. C., Livens, F. R., Collison, D., Charnock, J. M., Helliwell, M., and Eccles, H. (2002) *Inorg. Chem.*, **41**, 2799–806.
Jocher, W. G. (1978) Research Center Karlsruhe Report, KFK-2518.
Johansson, G. (1992) Structures of complexes in solution derived from X-ray diffraction measurements, in *Advances in Inorganic Chemistry* (ed. A. G. Sykes), Academic Press, Londonvol. 39.
Johnson, O., Powell, T., and Nottorf, R. (1974) *A Summary, of the Properties, Preparation and Purification of the Anhydrous Chlorides and Bromides of Uranium*, part A, Uranium Chlorides, part B, Uranium Bromides, CC-1974.
Johnson, Q., Biel, T. J., and Leider, H. R. (1976) *J. Nucl. Mater.*, **60**, 231–3.
Johnston, D. R., Satten, R. A., Schreiber, C. L., and Wong. E. (1966) *J. Chem. Phys.*, **44**, 3141–3.
Jones, E. R. Jr, Hendricks, M. E., Stone, J. A., and Karraker, D. G. (1974) *J. Chem. Phys.*, **60**, 2088–94.
Jones, L. H. (1958) *Spectrochim. Acta*, **10**, 395–403.
Jones, L. H. (1959) *Spectrochim. Acta*, **15**, 409–11.
Jones, L. V., Etter, D. E., Hudgens, C. R., Huffman, A. A., Rhinehammer, T. B., Rogers, N. E., and Wittenberg, L. J. (1959) Phase Equilibria in the LiF-BeF_2-UF_4 Ternary Fused Salt System, MLM-1080.
Jones, W. M., Gordon, J., and Long, E. A. (1952) *J. Chem. Phys.*, **20**, 695–9.
Joubert, P. and Bougon, R. (1975) *Compt. Rend.*, **C280**, 193–5.
Joubert, P., Bougon, R., and Gandreau, B. (1978a) *Can. J. Chem.*, **56**, 1874–80.
Joubert, P., Weulersse, J. M., Bougon, R., and Gaudreau, B. (1978b) *Can. J. Chem.*, **56**, 2546–9.
Jove, J. and Cousson, A. (1977) *Radiochim. Acta*, **24**, 73–5.
Jung, W.-S. and Juza, R. (1973) *Z. Anorg. Allg. Chem.*, **399**, 148–62.
Jung, W.-S., Harada, M., Tomiyasu, H., and Fukutomi, H. (1988) *Bull. Chem. Soc. Jpn.*, **61**, 3895–900.
Juza, R. and Sievers, R. (1965) *Naturwissenschaften*, **52**, 538–8.
Juza, R. and Meyer, W. (1966) *Naturwissenschaften*, **53**, 552.
Juza, R. and Meyer, W. (1969) *Z. Anorg. Allg. Chem.*, **366**, 43–50.
Kaltsyoannis, N. (2000) *Inorg. Chem.*, **39**, 6009–17.
Kanellakopulos, B., Henrich, E., Keller, C., Baumgärtner, F., König, E., and Desai, V. P. (1980) *Chem. Phys.*, **53**, 197–213.

Kanellakopulos, B. (1983) Electron paramagnetic resonance, in *Gmelin Handbook of Inorganic Chemistry*, System no. 55, Uranium, Suppl., vol. A6, Springer, Berlin, pp. 241–50.
Karabulut, M., Marasinghe, G. K., Ray, C. S., Day, D. E., Waddill, G. D., Allen, P. G., Booth, C. H., Bucher, J. J., Caulder, D. L., Shuh, D. K., Grimsditch, M., and Saboungi, M.-L. (2000) *J. Mater. Res.*, **15**, 1972–84.
Karbowiak, M. and Drożdżyński, J. (1990) *J.Less Common Metals*, **164**, 159–64.
Karbowiak, M. and Drożdżyński, J. (1993) *J. Alloys Compds*, **190**, 291–4.
Karbowiak, M., Drożdżyński, J., and Hanuza, J. (1996a) *Eur. J. Solid State Inorg. Chem.*, **33**, 1071–8.
Karbowiak, M., Hanuza, J., Drożdżyński, J., and Hermanowicz, K. (1996b) *J. Solid State Chem.*, **121**, 312–18.
Karbowiak, M., Drożdżyński, J., and Janczak, J. (1996c) *Polyhedron*, **15 (2)**, 241–4.
Karbowiak, M., Murdoch, K., Drożdżyński, J., Edelstein, N., and Hubert, S. (1996d) *Acta Phys. Polon.*, **90 (2)**, 371–6.
Karbowiak, M., Simoni, E., Drożdżyński, J., and Hubert, S. (1996e) *Acta Phys. Polon.*, **90 (2)**, 367–70.
Karbowiak, M., Drożdżyński, J., Murdoch, K. M., Edelstein, N. M., and Hubert, S. (1997) *J. Chem. Phys.*, **106**, 3067–77.
Karbowiak, M. and Drożdżyński, J. (1998a) *J. Alloys Compds*, **275–7**, 848–51.
Karbowiak, M. and Drożdżyński, J. (1998b) *J. Alloys Compds*, **271–3**, 863–6.
Karbowiak, M., Edelstein, N., Gajek, Z., and Drożdżyński, J. (1998a) *Spectrochim. Acta A*, **54**, 2035–44.
Karbowiak, M., Drożdżyński, J., Hubert, S., Simoni, E., and Streçk, W. (1998b) *J. Chem. Phys.*, **108**, 10181–8.
Karbowiak, M., Edelstein, N., Gajek, Z., and Drożdżyński, J. (1998c) *Spectrochim. Acta A*, **54**, 2035–44.
Karbowiak, M., Drożdżyński, J., Hubert, S., Simoni, E., and Stręk, W. (1998d) *J. Chem. Phys.*, **108**, 10181–8.
Karbowiak, M., Gajek, Z., and Drożdżyński, J. (2000) *Chem. Phys.*, **261**, 301–15.
Karbowiak, M., Drożdżyński, J., and Gajek, Z. (2001) *J. Alloys.Compds*, **323–4**, 678–82.
Karbowiak, M., Drożdżyński, J., and Sobczyk, M. (2002a) *J. Chem. Phys.*, **117**, 2800–8.
Karbowiak, M. A., Mech, A., Drożdżyński, J., Gajek, Z., and Edelstein, N. M. (2002b) *New. J. Chem.*, **26**, 1651–7.
Karbowiak, M. and Drożdżyński, J. (2003) *Mol. Phys.*, **101**, 971–5.
Karbowiak, M., Zych, E., Dereń, P., and Drożdżyński, J. (2003a) *Chem. Phys.*, **287**, 365–75.
Karbowiak, M., Mech, A., Drożdżyński, J., Edelstein, N. M., and Hubert, S. (2003b) *J. Phys. Chem. B*, **108**, 160–70.
Karbowiak, M., Sobczyk, M., and Drożdżynski, J. (2003c) *J. Solid State Chem.*, **173**, 59–68.
Karbowiak, M., Mech, A., Drożdżyński, J., and Edelstein, N. M. (2003d) *Phys. Rev. B*, **67**, 195108 (1–17).
Karbowiak, M., and Drożdżyński, J. (2004) *J. Phys. Chem. A.* **108**, 6397–406.
Karbowiak, M. (2005a) *J. Phys. chem. A*., **109**, 3569–77.
Karbowiak, M. (2005b) *Chem. Phys*., **314**, 189–97.

Karbowiak, M., Mech, A., Drozdzynski, J., Ryba-Romanowski, W., and Reid, M. F. (2005a) *J. Phys. Chem. B*, **109**, 155–66.
Karbowiak, M., Mech, A., and Drożdźński, J. (2005b) *Chem. Phys*., **308**, 135–45.
Karchevskĭ, A. I. and Buryak, E. M. (1962) *Sov. Phys. JETP*, **15**, 260–5.
Karmazin, L., Mazzanti, M., Gateau, C., Hill, C., and Pecaut, J. (2002) *Chem. Commun.* (*Cambridge, UK*), **23**, 2892–3.
Karraker, D. G. (1964) *Inorg. Chem.*, **3**, 1618–22.
Katakis, D. and Gordon, G. (1987) *Mechanism of Inorganic Reactions,* Wiley-Interscience, New York.
Kato, Y., Suzuki, K., Fukutomi, H., Tomiyasu, H., and Gordon, G. (1970) *Bull. Tokyo Inst Technol.*, **96**, 133–6.
Katz, J. J. and Rabinowitch, E. (1951) *The Chemistry of Uranium,* Natl. Nucl. En. Ser., Div. VIII, vol. 5, McGraw-Hill, New York.
Katz, J. J. and Rabinowitch, E. (1958) *The Chemistry of Uranium – Collected Papers*, TID-5290, Books I and 2, USAEC Technical Information Service, Oak Ridge, TN.
Katz, J. J. and Sheft, I. (l960) *Advances in Inorganic Chemistry and Radiochemistry,* vol. 2, Academic Press, New York, ch. 5.
Katz, J. J., Seaborg, G. T., and Morss, L. R. (1986) *The Chemistry of the Actinide Elements,* 2nd edn, vol. 1, Chapman and Hall, London, Table 5.68.
Katz, S. (1964) *Inorg. Chem.*, **3**, 1598–600.
Katzin, L. 1. (1952) *Production and Separation of* U^{233} *– Collected Papers*, Natl Nucl. En. Ser., Div. IV, 17B, Books 1 and 2, USAEC Technical Information Service, Oak Ridge, TN (declassified with deletions as TID-5223, Books 1 and 2).
Katzin, L. I. (1958) *J. Am. Chem. Soc.*, **80**, 5908–10.
Katzin, L. I., Kaplan, L., and Steitz, T. (1962) *Inorg. Chem.*, **1**, 963–4.
Kaufman, A. R., Cullity, B., and Brisianes, G. (1957) *Trans. AIME, J. Met.*, **209**, 23.
Keenan, T. K. (1966) *Inorg. Nucl Chem. Lett.*, **2**, 153–6.
Keenan, T. K. and Asprey, L. B. (1969) *Inorg. Chem.*, **8**, 235–8.
Keller, C. (1962a) *Nukleonik*, **4**, 271–7.
Keller, C. (1962b) *Z. Anorg. Allg. Chem.*, **317**, 241–4.
Keller, C. (1964) KFK Reports, KFK-225.
Keller, C., Koch, L., and Walter, K. H. (1965) *J. Inorg. Nucl. Chem.*, **27**, 1225–32.
Keller, C. and Salzer, M. (1967) *J. Inorg. Nucl. Chem.*, **29**, 2925–34.
Keller, C., Engerer, H., Leitner, L., and Sriyotha, U. (1969) *J. Inorg. Nucl. Chem.*, **31**, 965–80.
Keller, C. (1972) in *MTP International Review of Science, Inorganic Chemistry*, ser. 1, vol. 7 (ed. K. W. Bagnall), Butterworths, London; University Park Press, Baltimore, ch. 2, pp. 47–85.
Keller, C., Berndt, U., Debbabi, M., and Engerer, H. (1972) *J. Nucl. Mater.*, **42**, 23–31.
Keller, C. and Boroujerdi, A. (1972) *J. Inorg. Nucl. Chem.*, **34**, 1187–93.
Keller, C. (1975) in *Gmelin Handbuch der Anorganischen Chemie*, Suppl. Ser., Uranium, part C3, System no. 55, Springer-Verlag, Berlin, Heidelberg, and New York; *Ternäre und Polynäre Oxide des Urans*, pp. 295–359.
Keller, C. (1985) Heptavalent actinides, in *Handbook on the Physics and Chemistry of the Actinides* vol. 3, ch. 3 (eds. A. J. Freeman and G. H. Lander), North-Holland, Amsterdam, 143.

Keller, E. L. (compiler.) (1956) Uranium Hexafluoride Handling Procedures and Container Criteria, ORO-651; Revised Edition, ORO-651.
Keller, E. L., Furrer, A., Fischer, P., Allemspach, P., Krämer, K., Güdel, H. U., Doni, A., and Suzuki, T. (1995) *Phys. Rev. B*, **51** (5), 2881–90.
Kelley, W. E. (1955) *Nucleonics* **13**, 68–71.
Kelly, S. D., Newville, M. G., Cheng, L., Kemner, K. M., Sutton, S. R., Fenter, P., Sturchio, N. C., and Spötl, C. (2003) *Environ. Sci. Technol.*, **37**, 1284–7.
Kemmler-Sack, S. (1965) *Z. Anorg. Allg. Chem.*, **338**, 9–14.
Kemmler-Sack, S. and Rüdorff, W. (1966) *Z. Anorg. Allg. Chem.*, **344**, 23–40.
Kemmler-Sack, S. (1967) *Z. Naturforsch.*, **22B**, 597–79.
Kemmler-Sack, S. and Rüdorff, W. (1967) *Z. Anorg. Allg. Chem.*, **354**, 255–72.
Kemmler-Sack, S., Stumpp, E., Rüdorff, W., and Erfurth, H. (1967) *Z. Anorg. Allg. Chem.*, **354**, 287–300.
Kemmler-Sack, S. (1968a) *Z. Naturforsch. B*, **23**, 1260.
Kemmler-Sack, S. (1968b) *Z. Anorg. Allg. Chem.*, **363**, 295–304.
Kemmler-Sack, S. (1968c) *Z. Anorg. Allg. Chem.*, **363**, 282–94.
Kemmler-Sack, S. (1969) *Z. Anorg. Allg. Chem.*, **364**, 88–99.
Kemmler-Sack, S. and Wall, I. (1971) *Z. Naturforsch.*, **26b**, 1229–31.
Kemmler-Sack, S. (1973) *Z. Anorg. Allg. Chem.*, **402**, 255–78.
Kemmler-Sack, S. and Seemann, I. (1974) *Z. Anorg. Allg. Chem.*, **409**, 23–34.
Kemmler-Sack, S. and Seemann, I. (1975) *Z. Anorg. Allg. Chem.*, **411**, 61–78.
Kennedy, J. H. and Lingane, J. J. (1958) *Anal. Chim. Acta*, **18**, 240–4.
Kepert, D. L. (1982) *Inorganic Stereochemistry,* Springer-Verlag, Berlin.
Kern, D. M. H. and Orleman, E. F. (1949) *J. Am. Chem. Soc.*, **71**, 2102–6.
Kern, S., Hayward, J., Roberts, S., Richardson, J. W. Jr, Rotella, F. J., Soderholm, L., Cort, B., Tinkle, M., West, M., Hoisington, D., and Lander, G. H. (1994) *J. Chem. Phys.*, **101**, 9333–7.
Khanaev, E. I., Teterin, E. G., and Lukyanova, L. A. (1967) *Zh. Prikl. Spektrosk.*, **6**, 789–96; *J. Appl. Spectrosc.* (USSR), **6**, 533–8.
Kharitonov, Yu. Ya., Knyazeva, N. A., Tsapkin, V. V., and Ellert, G. V. (1967) *Radiokhimiya*, **9**, 322–30; (1967) *Sov. Radiochem.*, **9**, 316–23.
Khodadad, P. (1959) *C.R. Acad. Sci.*, **249**, 694–46.
Khodadad, P. (1960) *C.R. Acad. Sci.*, **250**, 3998–4000.
Khodadad, P. (1961) *Bull. Soc. Chim. Fr.*, 133–6.
Khosrawan-Sazedj, F. (1982) *Tschermaks Miner. Petrogr. Mitt.*, **30**, 111–15.
Killeen, J. C. (1980) *J. Nucl. Mater.*, **88**, 185–92.
Kim, K. C. and Olander, D. R. (1981) *J. Nucl. Mater.*, **102**, 192–9.
King, E. G. (1971) Quat. Met. Progr. Rep., no. 51.
Kirslis, S. S., McMillan, T. S., and Bernhardt, H. A. (1950) U.S. Report K-567, 1–36; (1956) N.S.A. Report **10**, no. 7198.
Kiukkola, K. (1962) *Acta Chem. Scand.*, **16**, 327–45.
Kjaerheim, G. and Rolstad, E. (1969) Halden Report, HPR-107.
Klaproth, M. H. (1789) *Chem. Ann.* (*Crell*), **11**, 387–403.
Klein-Haneveld, A. J. and Jellinek, F. (1964) *J. Inorg. Nucl. Chem.*, **26**, 1127–8.
Klein-Haneveld, A. J. and Jellinek, F. (1969) *J. Less Common Metals*, **18**, 123–9.
Klein-Haneveld, A. J. and Jellinek, F. (1970) *J. Less Common Metals*, **21**, 45–9.

Klepfer, H. H. and Chiotti, P. (1957) *Characteristics of the Solid State Transformations in Uranium*, ISC-893.
Kleykamp, H. (1985) *J. Nucl. Mater.*, **131**, 221–46.
Klíma, J., Jakeš, D., and Moravec, J. (1966) *J. Inorg. Nucl. Chem.*, **28**, 1861–9.
Koch, F. and Cohen, J. B. (1969) *Acta Crystallogr.*, **B25**, 275–87.
Kohlmann, H. and Beck, H. P. (1997) *Z. Anorg. Allg. Chem.*, **623**, 785–90.
Kohlmann, H. and Beck, H. P. (2000) *J. Solid State Chem.*, **150**, 336–41.
Kolitsch, U. and Giester, G. (2001) *Min. Mag.*, **65**, 717–24.
Kolitsch, W. and Müller, U. (1974) *Z. Anorg. Allg. Chem.*, **410**, 21–31.
Kolitsch, W. and Müller, U. (1975) *Z. Anorg. Allg. Chem.*, **418**, 235–42.
Kolomiets, A. V., Havela, L., Rafaja, D., Bordallo, H. N., Nakotte, H., Yartys, V. A., Hauback, B. C., Drulis, H., Iwasieczko, W., and De Long, L. E. (2000) *J. Appl. Phys.*, **87**, 6815–17.
Konrad, T. and Jeitschko, W. (1996) *J. Alloys Compds*, **233**, L3–7.
Korba, V. M. (1983) *Zh. Strukt. Khim.*, **24**, 172.
Kotlar, A., Gerdanian, P., and Dodé, M. (1967a) *J. Chim. Phys. Phys. Chim. Biol.*, **64**, 862–8.
Kotlar, A., Gerdanian, P., and Dodé, M. (1967b) *J. Chim. Phys. Phys. Chim. Biol.*, **64**, 1135–44.
Kotlar, A., Gerdanian, P., and Dodé, M. (1968) *J. Chim. Phys. Phys. Chim. Biol.*, **65**, 687–91.
Kovba, L. M., Ippolitova, E. A., Simanov, Yu . P., and Spitsyn, V. I. (1958) *Dokl. Akad. Nauk. SSSR*, **120**, 1042–4.
Kovba, L. M. (1960) *Zh. Strukt. Khim.*, **1**, 390.
Kovba, L. M. (1961) *Zh. Strukt. Khim.*, **2**, 585.
Kovba, L. M., Polunina, G. P., Simanov, Yu. P., and Ippolitova, E. A. (1961a) Argonne National Laboratory Report, ANL-trans-33, p. 17.
Kovba, L. M., Simanov, Yu. P., Ippolitova, E. A., and Spitsyn, V. I. (1961b) Argonne National Laboratory Report, ANL.trans-33, p. 24.
Kovba, L. M. (1962) *Zh. Strukt. Khim.*, **3**, 159.
Kovba, L. M., Vidanskii, L. M., and Lavut, E. G. (1963) *Zh. Strukt. Khim.*, **4**, 627.
Kovba, L. M. (1970) *Sov. Radiochem.*, **12**, 486–7.
Kovba, L. M. (1971a) *Sov. Radiochem.*, **13**, 319–20.
Kovba, L. M. (1971b) *Zh. Neorg. Khim.*, **16**, 3089–91.
Kovba, L. M. and Trunova, V. I. (1971) *Sov. Radiochem.*, **13**, 796–7.
Kovba, L. M. (1972a) *Sov. Radiochem.*, **14**, 746–9.
Kovba, L. M. (1972b) *Zh. Strukt. Khim.*, **13**, 256–9.
Kovba, L. M. (1972c) *Zh. Strukt. Khim.*, **13**, 458–60.
Kovba, L. M., Tsigunov, A. N., Kuz'micheva, E. U., and Kamaratseva, N. I. (1972) *Radiokhimiya*, **14**, 921–3.
Kovba, L. M., Murav'eva, I. A., and Orlova, A. S. (1974) *Sov. Radiochem.*, **16**, 638–9.
Krämer, K. and Meyer, G. (1989) (unpublished results).
Krämer, K., Meyer, G., Karbowiak, M., and Drożdżyński, J. (1991) *J. Less Common Metals*, **175**, 347–52.
Krämer, K., Keller, L., Fischer, P., Jung, B., Edelstein, N. M., Güdel, H. U., and Meyer, G. (1993) *J. Solid State Chem.*, **103**, 152–9.

Krämer, K., Güdel, H. U., Meyer, G., Heuer, T., Edelstein, N., Jung, B., Keller, L., Fischer, P., Zych, E., and Drożdżyński, J. (1994) *Z. Anorg. Allg. Chem.*, **620**, 1339–45.
Kramer, G. M. and Maas, E. T. Jr (1981) *Inorg. Chem.*, **20**, 3514–16.
Krause, W., Effenberger, H., and Brandstätter, F. (1995) *Eur. J. Miner.*, **7**, 1313–24.
Kressin, I. K. (1977) *Anal. Chem.*, **49**, 842–5.
Krol, D. M. (1981) *J. Chem. Soc., Dalton Trans.*, 687–93.
Krivovichev, S. V. and Burns, P. C. (2000a) *Can. Miner.*, **38**, 847–51.
Krivovichev, S. V. and Burns, P. C. (2000b) *Can. Miner.*, **38**, 717–26.
Krivovichev, S. V. and Burns, P. C. (2002a) *J. Solid State Chem.*, **168**, 245–58.
Krivovichev, S. V. and Burns, P. C. (2002b) *Can. Miner.*, **40**, 201–9.
Krivovichev, S. V. and Burns, P. C. (2002c) *Inorg. Chem.*, **41**, 4108–10.
Krivovichev, S. V. and Burns, P. C. (2003) *Can. Miner.*, **41**, 707–19.
Kruger, O. L. and Moser, J. B. (1967) *J. Phys. Chem. Solids*, **28**, 2321–5.
Krupa, J .C. (1987) *Inorg. Chim. Acta*, **139**, 223–41.
Kruse, F. H. (1962) *Inorg. Chem.*, **1**, 137–9.
Kruse, F. H. and Asprey, L. B. (1962a) *J. Inorg. Nucl. Chem.*, **33**, 1625–27.
Kruse, F. H. and Asprey, L. B. (1962b) *Inorg. Chem.*, **1**, 137–9.
Kruse, F. H. (1971) *J. Inorg. Nucl. Chem.*, **33**, 1625–7.
Kubaschewski, O. and Alcock, C. B. (1979) *International Series of Material Science and Technology*, Metallurgical Thermochemistry, vol. 24, 5th edn, Pergamon Press, Oxford.
Kudryashov, V. L., Suglobova, I. G., and Chirkst, D. E. (1978) *Radiokhimiya*, **20**, 366–72.
Kumar, N. and Tuck, D. G. (1984) *Inorg. Chim. Acta*, **95**, 211–15.
Labroche, D., Dugne, O., and Chatillon, C. (2003a) *J. Nucl. Mater.*, **312**, 21–49.
Labroche, D., Dugne, O., and Chatillon, C. (2003b) *J. Nucl. Mater.*, **312**, 50–66.
Lakner, J. F. (1978) University of California, Livermore, Lawrence Livermore National Laboratory, Report UCRL-52518.
Lally, A. E. (1992) in *Uranium Series Disequilibrium Applications to Earth, Marine, and Environmental Sciences* (eds. M. Ivanovich and R. S. Harmon), Clarendon Press, Oxford., pp. 94–126.
Lambertson, W. H. and Mueller, M. H. (1954) Argonne National Laboratory Report, ANL-5312.
Lander, G. H. and Müller, M. H. (1970) *Acta Crystallogr. B*, **26**, 129–36.
Lander, G. H., Fisher, E. S., and Bader, S. D. (1994) *Adv. Phys.*, **43**, 1–111.
Lang, S. M., Knudsen, F. P., Fillmore, C. L., and Roth, R. S. (1956) NBS Circ., no. 568, 32 pp.
Langford, C. H. and Gray, H. B. (1965) *Ligand Substitution Processes*, W. A. Benjamin, New York.
Larson, A. C., Roof, R. B., and Cromer, D. T. (1964) *Acta Crystallogr.*, **17**, 555.
Latta, R. E. and Fryxell, R. E. (1970) *J. Nucl. Mater.*, **35**, 195–210.
Lau, K. H. and Hildenbrand, D. L. (1982) *J. Chem. Phys.*, **76**, 2646.
Lau, K. H. and Hildenbrand, D. L. (1984) *J. Chem. Phys.*, **80**, 1312–17.
Laugier, J., Blum, P. L., and Detourminé, R. J. (1971) *J. Nucl. Mater.*, **41**, 106–8.
Laval, J. P., Mikou, A., Frit, B., Roult, G., and Pannetier, J. (1987) *Rev. Chim. Minér.*, **24**, 165–82.

Laveissière, J. (1967) *Bull. Soc. Franc. Minér. Crist.*, **90**, 308–10.
Lawson, A. C., Severing, A., Ward, J. W., Olsen, C. E., Goldstone, J. A., and Williams, A. (1990) *J. Less Common Metals*, **158**, 267–74.
Lawson, A. C., Goldstone, J. A., Huber, J. G., Giorgi, A. L., Conant, J. W., Severing, A., Cort, B., and Robinson, R. A. (1991) *J. Appl. Phys.*, **69**, 5112–16.
Lay, K. W. (1970) *J. Am. Ceram. Soc.*, **53**, 369–73.
Leask, M. J. M., Roberts, L. E. J., Walker, A. J., and Wolf, W. P. (1963) *J. Chem. Soc.*, 4788–94.
Lebeau, P. and Damien, A. (1913) *C.R. Acad. Sci.*, **156**, 1987–9.
Le Bihan, T., Rogl, P., and Noël, H. (2000) *J. Nucl. Mater.*, **277**, 82–90.
Lederer, C. M. and Shirley, V. S. (1978) *Table of Isotopes*, 7th edn, John Wiley, New York.
Lee, H. M. (1974) *J. Nucl. Mater.*, **50**, 25–30.
Leibowitz, L., Mishler, L. W., and Chasanov, M. G. (1969) *J. Nucl. Mater.*, **29**, 356–8.
Leonidov, V. Y. (1960) *Zh. Fiz. Khim.*, **34**, 1862.
Leroy, J. M. and Tridot, G. (1966) *C.R. Acad. Sci.* (*Paris*), **C262**, 1376–9.
Leslie, B. W., Pearcy, E. C., and Prikryl, J. D. (1993) *Mater. Res. Soc. Symp. Proc.*, **294**, 505–12.
Leung, A. F. and Poon, Y.-M. (1977) *Can. J. Phys.*, **55**, 937–42.
Leuze, R. E., Clinton, S. O., Chilton, J. M. and Vaughen, V. C. A. (1962) in *Transuranium Quarterly Progress Report for period ending Feb. 28, 1962* (compiler D. E. Ferguson), ORNL-3290, p. 79.
Leuze, R. E., Clinton, S. D., Chilton, J. M., and Vaughen, V. C. A. (1963) in *Transuranium Quarterly Progress Report for period ending Aug. 31, 1962* (compiler D. E. Ferguson), ORNL-3375, p. 51.
Levet, J. C. (1965) *Compt. Rend. C*, **260**, 4775–6.
Levet, J. C. (1969) *Compt. Rend. C*, **268**, 703–5.
Levet, J. C., Potel, M., and Le Marouille, J. Y. (1977) *Acta Crystallogr. B*, **33**, 2542–6.
Levet, J. C. and Noël, H. (1979) *J. Solid State Chem.*, **28**, 67–73.
Levet, J. C., Potel, M., and Le Marouille, J. Y. (1980) *J. Solid State Chem.*, **32**, 297–301.
Levet, J. C. and Noël, H. (1981) *J. Inorg. Nucl. Chem.*, **43**, 1841–3.
Levy, J. H., Taylor, J. C., and Wilson, P. W. (1975) *J. Less Common Metals*, **39**, 265–70.
Levy, J. H., Taylor, J. C., and Wilson, P. W. (1976) *J. Chem. Soc. Dalton Trans.*, 219–24.
Levy, J. H., Taylor, J. C., and Wilson, P. W. (1977) *J. Inorg. Nucl. Chem.*, **39**, 1989–91.
Levy, J. H., Taylor, J. C., and Wilson, P. W. (1978) *J Inorg. Nucl. Chem.*, **40**, 1055–7.
Levy, J. H., Taylor, J. C., and Waugh, A. B. (1980) *Inorg. Chem.*, **19**, 672–4.
Levy, J. H., Taylor, J. C., and Waugh, A. B. (1983) *J. Fluorine Chem.*, **23**, 29–36.
Lewis, W. B., Asprey, L. B., Jones, L. H., McDowell, R. S., Rabideau, S. W. Zeltman, A. H., and Levet, J. C. (1965) *Compt. Rend. C*, **260**, 4775–6.
Lewis, W. B., Hecht, H. G., and Eastman, M. P. (1973) *Inorg. Chem.*, **12**, 1634–9.
Lewis, W. B., Asprey, L. B., Jones, L. H., McDowell, R. S., Rabideau, S. W., Zeltman, A. H., and Paine, R. T. (1976) *J. Chem. Phys.*, **65**, 2707–14.
Li, J., Bursten, B. E., Liang, B., and Andrews, L. (2002) *Science*, **295**, 2242–5.
Li, Y.-P. and Burns, P. C. (2000a) *Can. Miner.*, **38**, 737–49.
Li, Y.-P. and Burns, P. C. (2000b) *Can. Miner.*, **38**, 727–35.
Li, Y.-P., Burns, P. C., and Gault, R. A. (2000) *Can. Miner.*, **38**, 153–62.
Li, Y.-P. and Burns, P. C. (2001a) *J. Nucl. Mater.*, **299**, 219–26.

Li, Y.-P. and Burns, P. C. (2001b) *Can. Miner.*, **39**, 1147–51.
Li, Y.-P., Krivovichev, S. V., and Burns, P. C. (2001a) *Miner. Mag.*, **65**, 285–92.
Li, Y.-P., Cahill, C. L., and Burns, P. C. (2001b) *Chem. Mater.*, **13**, 4026–31.
Libowitz, G. G. and Gibb, T. R. P. Jr (1957) *J. Phys. Chem.*, **61**, 793–5.
Libowitz, G. G. (1968) in *Metal Hydrides* (eds. W. Mueller, J. P. Blackledge, and G. G. Libowitz), Academic Press, New York., ch. 11
Lin, S. T. and Kaufmann, A. R. (1956) *Phys. Rev.*, **102**, 640–6.
Lincoln, S. F. (1979) *Pure Appl. Chem.*, **51**, 2059–65.
Lindemann, F. and Aston, F. W. (1919) *Phil. Mag.*, **6(37)**, 523.
Lindemer, T. B. and Besmann, T. M. (1985) *J. Nucl. Mater.*, **130**, 473–88.
Lindemer, T. B. and Brynestad, J. (1986) *J. Am Ceram. Soc.*, **69**, 867–76.
Lindemer, T. B. and Sutton, A. L. Jr (1988) *J. Am. Ceram. Soc.*, **71**, 553–61.
Lipschutz, M. E., Wolf, S. F., Hanchar, J. M., and Culp, F. B. (2001) *Anal. Chem.*, **73**, 2687–700.
Litz, L. M. (1948) *Uranium Carbides – Preparation, Structure and Hydrolysis*, Thesis, Ohio State University, NP-1453.
Litz, L. M., Garrett, A. B., and Croxton, E. C. (1948) *J. Am. Chem. Soc.*, **70**, 1718–22.
Locock, A. J. and Burns, P. C. (2003a) *Am. Miner.*, **88**, 240–4.
Locock, A. J. and Burns, P. C. (2003b) *Min. Mag.*, **67**, 1109–20.
Locock, A. J. and Burns, P. C. (2003c) *Can. Miner.*, **41**, 91–101.
Locock, A. J. and Burns, P. C. (2003d) *Can. Miner.*, **41**, 489–502.
Locock, A. J., Burns, P. C., and Flynn, T. M. (2005a) *Am. Miner.*, **90**, 240–6.
Locock, A. J., Burns, P. C., Flynn, T. M. (2005b) *Can. Miner*., **43**, 721–33.
Locock, A. J., Kinman, W. S., and Burns, P. C. (2005c) *Can. Miner.* **43**, 989–1003.
Lopez, M. and Birch, D. S. J. (1997) *Chem. Phys. Lett.*, **268**, 125–32.
Loopstra, B. O. (1962) *Acta Crystallogr.*, **17**, 651–4.
Loopstra, B. O. and Cordfunke, E. H. P. (1966) *Rec. Trav. Chim. Pays-Bas*, **58**, 135–42.
Loopstra, B. O. and Rietveld, H. M. (1969) *Acta Crystallogr.*, **B25**, 787–91.
Loopstra, B. O. (1970a) *J. Appl. Crystallogr.*, **3**, 94–6.
Loopstra, B. O. (1970b) *Acta Crystallogr.*, **B26**, 656–7.
Lorenzelli, R. and Touzelin, B. (1980) *J. Nucl. Mater.*, **95**, 290–302.
Lu, W. C., Ree, T., Gerard, V., and Eyring, H. (1968) *J. Chem. Phys.*, **49**, 797.
Lucas, J. (1964) *Rev. Chim. Minér.*, **1**, 479–517.
Lumpkin, G. R., Eyal, Y., and Ewing, R. C. (1988) *J. Mater. Res.*, **3**, 357–68.
Lumpkin, G. R. and Ewing, R. C. (1995) *Am. Miner.*, **80**, 732–43.
Lumpkin, G. R., Hart, K. P., McGlinn, P., Gieré, R., and Williams, C. T. (1995) *Radiochim. Acta*, 469–74.
Lumpkin, G. R., Payne, T. E., Fenton, B. R., and Waite, T. D. (1999) *Mater. Res. Soc. Symp. Proc.*, **556**, 1067–74.
Lundgren, G. (1952) *Arkiv Kemi*, 421–8.
Lupinetti, A. J., Fife, J. L., Garcia, E., Dorhout, P. K., and Abney, K. D. (2002) *Inorg. Chem.*, **41**, 2316–18.
Lychev, A. A., Mashirov, L. G., Smolin, Yu. I., and Shepelev, Yu. F. (1986) *Radiokhimiya*, **28**, 682–5.
Lyon, W. G., Osborne, D. W., Flotow, H. E., and Hoekstra, H. R. (1977) *J. Chem. Thermodyn.*, **9**, 201–10.
Lynch, E. D. (1965) Argonne National Laboratory Report, ANL-6894.

Łyżwa, R. and Erdös, P. (1987) *Phys. Rev. B*, **36**, 8570.
Macaskie, L. E., Bonthrone, K. M., Yong, P., and Goddard, D. T. (2000) *Microbiology*, **146**, 1855–67.
Mac Cordick, J. and Brun, C. (1970) *Compt. Rend. Acad. Sci. Ser. C.*, **270**, 620–3.
Mac Leod, A. C. (1972) *J. Chem. Thermodyn.*, **4**, 699–708.
Mac Wood, G. E. (1958) TID-5290, pp. 543–609.
Maglic, K. and Herak, R. (1970) *Rev. Int. Hautes Tempér. Réfract. Fr.*, **7**, 247.
Mair, M. A. and Savage, D. J. (1986) UK Atomic Energy Agency Report, ND-R-134.
Malek, C. K., Krupa, J.-C., Delamoye, P., and Genet, M. (1986a) *J. Phys.* (*Paris*), **47**, 1763–73.
Malek, C. K., Krupa, J.-C., and Genet, M. (1986b) *Spectrochim. Acta* part A, **42**, 907–12.
Malek, C. K. and Krupa, J.-C. (1994) *J. Chem. Phys.*, **84**, 6584–90.
Maletka, K., Fischer, P., Murasik, A., and Szczepaniak, W. (1992) *J. Appl. Cryst.*, **25**, 1–5.
Maletka, K., Murasik, A., Szczepaniak, W., Rundloef, H., and Tellgren, R. (1995) *Solid State Ionics*, **76**, 115–20.
Maletka, K., Tellgren, R., Rundloef, H., Szczepaniak, W., and Rycerz, L. (1996a) *Solid State Ionics*, **90**, 67–74.
Maletka, K., Ressouche, E., Szczepaniak, W., Rycerz, L., and Murasik, A. (1996b) *Mater. Sci. Forum*, **228**, 711–16.
Maletka, K., Ressouche, E., Rundloef, H., Tellgren, R., Delaplane, R., Szczepaniak, W., and Zablocka-Malicka, M. (1998) *Solid State Ionics*, **106**, 55–69.
Mallett, M. W., Gerds, A. F., and Nelson, H. R. (1952) *J. Electrochem. Soc.*, **99**, 197–204.
Mallett, M. W. and Gerds, A. F. (1955) *J. Electrochem. Soc.*, **102**, 292–6.
Mallett, M. W., Trzeciak, M. J., and Griffith, C. B. (1955) *Nuclear Engineering and Science Congress*, Cleveland, OH, Preprint 334.
Mallett, M. W. and Trzeciak, M. J. (1958) *Trans. Am. Soc. Met.*, **50**, 981–93.
Malm, J. G., Selig, H., and Siegel, S. (1966) *Inorg. Chem.*, **5**, 130–2.
Malm, J. G. (1980) *J. Inorg. Nucl. Chem.*, **42**, 993–4.
Manes, L. (ed.) (1985) *Struct. Bonding*, **59/60**; *Actinide-Chemistry and Physical Properties*, Springer Verlag, New York.
Marakov, E. S. and Bykov, V. N. (1959) *Kristallographica*, **4**, 183–5.
Marchidan, D. I. and Matei-Tanasescu, S. (1972) *Rev. Roum. Chim.*, **17**, 195–202.
Marchidan, D. I. and Matei-Tanasescu, S. (1974) *Rev. Roum. Chim.*, **19**, 1435.
Marchidan, D. I. and Matei-Tanasescu, S. (1975) *Rev. Roum. Chim.*, **20**, 1365.
Marcon, J.-P. (1969) *Contribution à l'Etude des Sulfures d'Actinides*, Thesis, University of Paris, CEA-3919.
Marcon, J. P. (1972) *Rev. Int. Hautes Temp. Réfract.*, **9**, 193.
Marin, J. F. (1968) CEA Report, CEA-N-883.
Marin, J. F. and Contamin, P. (1969) *J. Nucl. Mater.*, **30**, 16–25.
Marinenko, G., Koch, W. F., and Etz, E. S. (1983) *J. Res. Natl. Bur. Stand.*, **88**, 117–24.
Marinsky, J. A. (1956) Development of the EXCER Process, part II, ORNL-1979.
Markin, T. L. and Bones, R. J. (1962a) UKAEA Harwell Report, AERE-R 4178.
Markin, T. L. and Bones, R. J. (1962b) UKAEA Report, AERE-R 4042.
Markin, T. L. and Crough, E. C. (1970) *J. Inorg. Nucl. Chem.*, **32**, 77–82.
Markin, T. L., Street, R. S., and Crough, E. C. (1970) *J. Inorg. Nucl. Chem.*, **32**, 59–75.

Marples, J. A. C. (1976) in *Plutonium 1975 and Other Actinides*, Proc. Fifth Int. Conf. on Plutonium and Other Actinides, Baden-Baden, Germany (eds. H. Blank and R. Lindner), North-Holland, Amsterdam, pp. 353–9.
Martin, A. E. and Edwards, R. K. (1965) *J. Phys. Chem.*, **69**, 1788.
Martin, A. E. and Shinn, W. A. (1971) Argonne National Laboratory Report, ANL-7877.
Martin, P., Ripert, M., Petit, T., Reich, T., Hennig, C., D'Acapito, F., Hazemann, J. L., and Proux, O. (2003) *J. Nucl. Mater.*, **312**, 103–10.
Martinot, L. (1984) Uranium in molten in molten salts and melts, in *Gmelin Handbook of Inorganic Chemistry*, Uranium Suppl., vol. D1, 332–78.
Martinot, L. (1991) Molten-salt chemistry of the actinides, in *Handbook on the Physics and Chemistry of the Actinides* , vol. 6, ch. 4 (eds. A. J. Freeman and C. Keller), North-Holland, Amsterdam, 241–79.
Marzotto, A., Bandoli, G., Clemente, D. A., Benetollo, F., and Galzigna, L. (1973) *J. Inorg. Nucl. Chem.*, **35**, 2769–74.
Marzotto, A., Grazotto, R., Bombieri, G., and Forsellini, E. (1974) *J. Cryst. Mol. Struct.*, **4**, 253–62.
Masaki, N. and Tagawa, H. (1975) *J. Nucl. Mater.*, **58**, 241–3.
Mass, E. T. (1979) *J. Inorg. Nucl. Chem.*, **41**, 991.
Masson, J. P., Desmoulin, R., Charpin, P., and Bougon, R. (1976) *Inorg. Chem.*, **15**, 2529–31.
Masson, J. P., Naulin, C., Charpin, P., and Bougon, R. (1978) *Inorg. Chem.*, **17**, 1858–61.
Masters, B. J. and Schwartz, L. L. (1961) *J. Am. Chem. Soc.*, **83**, 2620–24.
Matonic, J. H., Scott, B. L., and Neu, M. P. (2001) *Inorg. Chem.*, **40**, 2638–9.
Matsika, S., Zhang, Z., Brozell, S. R., Bladeau, J.-P., Wang, Q., and Pitzer, R. M. (2001) *J. Phys. Chem. A*, **105**, 3825–8.
Matson, L. K., Moody, J. W., and Himes, R. C. (1963) *J. Inorg. Nucl. Chem.*, **25**, 795–800.
Matsui, T., Tsuji, T., and Naito, K. (1974) *J. Nucl. Sci. Technol.*, **11**, 216–22.
Matsui, T. and Naito, K. (1975) *J. Nucl. Mater.*, **56**, 327–35.
Matsui, T. and Naito, K. (1985a) *J. Nucl. Mater.*, **132**, 212–21.
Matsui, T. and Naito, K. (1985b) *J. Nucl. Mater.*, **136**, 59–68.
Matsui, T. and Naito, K. (1986) *J. Nucl. Mater.*, **138**, 19–26.
Matzke, Hj. (1981) in *Non-Stoichiometric Oxides* (ed. O. T. Sørensen), Academic Press, New York, ch. 4, pp. 156–232.
Matzke, Hj. (1987) *J. Chem. Soc., Faraday Trans. 2*, **83**, 1121–42.
Maximov, V. (compiler.) (1963) *Uranium Carbides, Nitrides, and Silicides*, vol. I (1961/1963), IAEA Bibliographical Series 14, International Atomic Energy Agency, Vienna, STI/PUB/21/14.
Maximov, V. (compiler.) (1965) *Uranium Carbides, Nitrides, and Silicides*, vol. II (1963/1965), IAEA Bibliographical Series 21, International Atomic Energy Agency, Vienna, STI/PUB/21/21.
Maximov, V. (compiler.) (1967) *Uranium Carbides, Nitrides, and Silicides*, vol. III (1965/1967), IAEA Bibliographical Series 33, International Atomic Energy Agency, Vienna, STI/PUB/21/33.
Mayer, H. and Mereiter, K. (1986) *Tschermaks Miner. Petrogr. Mitt.*, **35**, 133–46.
Mazurak, M., Drożdżyński, J., and Hanuza, J. (1988) *J.Mol. Struct.*, **174**, 443–8.

Mazzi, F. and Munno, R. (1983) *Am. Miner.*, **68**, 262–76.
McDowell, R. S., Asprey, L. B., and Paine, R. T. (1974) *J. Chem. Phys.*, **61**, 3571–80.
McEachern, R. J. and Taylor, P. (1998) *J. Nucl. Mater.*, **254**, 87–121.
McEwen, D. J. and De Vries, T. (1959) *Anal. Chem.*, **31**, 1672–2.
McLaughlin, R. (1962) *J. Chem. Phys.*, **36**, 2699–705.
McNamara, B. K., Buck, E. C., and Hanson, B. D. (2003) *Mater. Res. Soc. Symp. Proc.*, **757**, 401–6.
Mech, A., Karbowiak, M., Lis, T., and Drożdżyński, J. (2005) Polyhedron, in press.
Meinrath, G., Lis, S., Stryla, S., and Noubactep, C. (2000) *J. Alloys Compds.*, **300/301**, 107–12.
Meites, L. (ed.) (1963) *Handbook of Analytical Chemistry*, McGraw-Hill, New York.
Meitner, L., Hahn, O., and Strassmann, F. (1937) *Z. Phys.*, **106**, 249–70.
Mellor, J. W. (1932) *Comprehensive Treatise on Inorganic and Theoretical Chemistry*, vol. XII, , Longmans, Green and Co., London.
Mentink, S. A. M., Mason, T. E., Buyers, W. J. L., and Clausen, K. N. (1998) *Physica B.* (*Amsterdam, Neth.*), **241–243**, 669–71.
Menzies, C. (1966) UKAEA Report, TRG-1119(D).
Mereiter, K. (1982a) *Tschermaks Miner. Petrogr. Mitt.*, **30**, 277–88.
Mereiter, K. (1982b) *Tschermaks Miner. Petrogr. Mitt.*, **30**, 129–39.
Mereiter, K. (1982c) *Tschermaks Miner. Petrogr. Mitt.*, **30**, 47–51.
Mereiter, K. (1984) *Acta Crystallogr.*, **A40**, Suppl. C-247.
Mereiter, K. (1986) *Tschermaks Miner. Petrogr. Mitt.*, **35**, 1–18.
Merritt, R. C. (1971) *The Extractive Metallurgy of Uranium*, Colorado School of Mines Research Institute and USAEC, Golden, CO.
Meunier, G. and Galy, J. (1973) *Acta Crystallogr.*, **B29**, 1251–5.
Meusemann, H. and von Erichsen, L. (1973) *Bundesministerium für Forschung und Technologie*, Report no. BMFT-FBK-73–18.
Meyer, G., Gaebell, H.-Chr., and Hoppe, R. (1983) *J. Less Common. Metals*, **93**, 347–51.
Meyer, H. C., McDonald, P. F., and Settler, J. D. (1967) *Phys. Lett.*, **24A**, 569.
Meyer, R. A. and Wolfe, B. E. (1964) *Trans. Am. Nucl. Soc.*, **7**, 111–12.
Mighell, A. D. and Ondik, H. M. (1977) *J. Phys. Chem. Ref. Data*, **6**, 675–829.
Mignanelli, M. A. and Potter, P. E. (1983) *J. Nucl. Mater.*, **118**, 150–8.
Mignanelli, M. A. and Potter, P. E. (1986) *J. Less Common Metals*, **121**, 605–13.
Miguta, A. K. (1997) *Geol. Ore Deposits*, **39**, 275–93.
Mikhailov, Yu. N. and Kuznetsov, V. G. (1971) *Russ. J. Inorg. Chem.*, **16**, 1340–2.
Mikhailov, Yu. N., Udovenko, A. A., Kuznetsov, V. G., and Davidovich, R. L. (1972a) *Zh. Strukt. Khim.*, **13**, 942–3; (1972) *J. Strukt. Chem.* (*USSR*), **13**, 879–80.
Mikhailov, Yu. N., Udovenko, A. A., Kuznetsov, V. G., and Davidovich, R. L. (1972b) *Zh. Strukt. Khim.*, **13**, 741.
Mikhailov, Yu. N., Ivanov, S. B., Orlova, I. M., Podnebesnova, G. V., Kuznetsov, V. G., and Shchelokov, R. N. (1976a) *Koord. Khim.* [*Coord. Chem.* (*USSR*)], **2**, 1570–3.
Mikhailov, Yu. N., Ivanov, S. B., Kuznetsov, V. G., and Davidovich, R. L. (1976b) *Koord. Khim.* [*Coord. Chem.* (*USSR*)], **2**, 95–8.
Mikhailov, Yu. N., Ivanov, S. B., and Sadikov, G. G. (1979) *Koord. Khim.* [*Coord. Chem.* (*USSR*)], **5**, 1702–5.
Miller, D. (1965) Argonne National Laboratory Report, ANL-7120, p. 641.

Miller, M. L., Finch, R. J., Burns, P. C., and Ewing, R. C. (1996) *J. Mater. Res.*, **11**, 3048–56.
Miller, S. A. and Taylor, J. C. (1986) *Z. Kristallogr.*, **177**, 247–53.
Mills, K. C. (1974) *Thermodynamic Data for Inorganic Sulphides, Selenides, and Tellurides*, Butterworths, London.
Misaelides, P., Godelitsas, A., Filippidis, A., Charistos, D., and Anousis, I. (1995) *Sci. Total Environ.*, **173–174**, 237–46.
Miyake, C., Fuji, K., and Imoto, S. (1977) *Chem. Phys. Lett.*, **46**, 349–51.
Miyake, C., Fuji, K., and Imoto, S. (1979) *Chem. Phys. Lett.*, **61**, 124–6.
Miyake, C., Takeuchi, H., Ohya-Nishiguchi, H., and Imoto, S. (1982) *Phys. Status Solidi*, **A74**, 173–80.
Miyake, C., Kanamaru, M., Imoto, S., and Taniguchi, K. (1986) *J. Nucl. Mater.*, **138**, 36–9.
Miyake, C. (1991) Magnetochemistry of U(V) complexes and compounds, in *Handbook on the Physics and Chemistry of the Actinides* (eds. A. J. Freeman and C. Keller), Elsevier, vol. 6, ch. 5, 337–66.
Miyake, C., Kawasaki, O., Gotoh, K., and Nakatani, A. (1993) *J. Alloys Compds*, **200**, 187–90.
Miyake, C. and Fujino, T. (1998) *J. Alloys Compds*, **271–273**, 479–81.
Moens, L. and Jakubowski, N. (1998) *Anal. Chem.*, **70**, 251A–6A.
Moll, H., Denecke, M. A., Jalilehvand, F., Sandström, M., and Grenthe, I. (1999) *Inorg. Chem.*, **38**, 1795–99.
Moll, H., Reich, T., and Szabó, Z. (2000a) *Radiochim. Acta*, **88**, 411–15.
Moll, H., Reich, T., Hennig, C., Rossberg, A., Szabó, Z., and Grenthe, I. (2000b) *Radiochim. Acta*, **88**, 559–66.
Moll, H., Geipel, G., Reich, T., Bernhard, D., and Grenthe, I. (2003) *Radiochim. Acta*, **91**, 11–20.
Montignie, E. (1947) *Bull. Soc. Chim. Fr.*, 748–49.
Montoloy, F. and Plurien, P. (1968) *C. R. Acad. Sci.*, **267**, 1036.
Moody, D. C. and Odom, J. D. (1979) *J. Inorg. Nucl. Chem.*, **41**, 533–5.
Moody, D. C., Penneman, R. A., and Salazar, K. V. (1979) *Inorg. Chem.*, **18**, 208–9.
Moody, D. C., Zozulin, A. J., and Salazar, K. V. (1982) *Inorg. Chem.*, **21**, 3856–7.
Moore, G. E. and Kelley, K. K. (1947) *J. Am. Chem. Soc.*, **69**, 2105–7.
Morris, D. E., Allen, P. G., Berg, J. M., Chisolm-Brause, C. J., Conradson, S. D., Hess, N. J., Musgrave, J. A., and Tait, C. D. (1996) *Environ. Sci. Technol.*, **30**, 2322–31.
Morss, L. R. (1982) in *Actinides in Perspective* (ed. N. M. Edelstein), Pergamon Press, Oxford, pp. 381–407.
Morss, L. R. (1991) in *Synthesis of Lanthanide and Actinide Compounds* (eds. G. Meyer and L. R. Morss), Kluwer Academic Publishers, Dordrecht., pp. 237–58.
Moriyasu, M., Yokoyama, Y., and Ikeda, S. (1977) *J. Inorg. Nucl. Chem.*, **39**, 2199–203.
Moskvin, A. I. and Zaitseva, V. P. (1962) *Radiokhimiya*, **4**, 73–82; *Sov. Radiochem.*, **4**, 63–9.
Moskvin, A. I. (1968) *Radiokhimiya*, **10**, 13–21; *Sov. Radiochem*, **10**, 10–13.
Mucke, A. and Strunz, H. (1978) *Am. Miner.*, **63**, 941–6.
Mulak, J. and Żołnierek, Z. (1972) *Bull. Acad. Pol. Sci. Ser. Sci. Chim.*, **20**, 1081.
Mulak, J. and Żołnierek, Z. (1977) *Proc. Second Int. Conf. Electron. Struct. Actinides*, Wrocław, Poland., 1976, pp. 125–31.

Mulford, R. N. R., Ellinger, F. H., and Zachariasen, W. H. (1954) *J. Am. Chem. Soc.*, **76**, 297–8.
Müller, U. and Kolitsch, W. (1974) *Z. Anorg. Allgem. Chem.*, **410**, 32–8.
Murakami, T., Ohnuki, T., Isobe, H., and Sato, T. (1997) *Am. Miner.*, **82**, 888–99.
Murasik, A., Suski, W., Troć, R., and Leciewicz, L. (1968) *Phys. Status Solidi*, **30**, 61–6.
Murasik, A., Furrer, A., and Szczepaniak, W. (1980) *Solid State Commun.*, **33**, 1217.
Murasik, A., Fischer, P., and Szczepaniak, W. (1981) *J. Phys. C., Solid State Phys.*, **14**, 1847.
Murasik, A., Fischer, P., Furrer, A., and Szczepaniak, W. (1985) *J. Phys. C, Solid State Phys.*, **18**, 2909–21.
Murasik, A., Fischer, P., Furrer, A., Schmid, B., and Szczepaniak, W. (1986) *J. Less Common Metals*, **121**, 151–5.
Murch, G. E. and Catlow, C. R. A. (1987) *J. Chem. Soc., Faraday Trans. 2*, **83**, 1157–69.
Nagarajan, K., Saha, R., Yadav, R. B., Rajagopalan, S., Kutty, K. V. G., Saibaba, M., Rao, P. R. V., and Matthews, C. K. (1985) *J. Nucl. Mater.*, **130**, 242–9.
Nagatoro, Y., Ochiai, K., and Kaya, A. (1980) *J. Nucl. Sci. Technol.*, **17**, 687–93.
Nagels, P., Devreese, J., and Denayer, M. (1964) *J. Appl. Phys.*, **35**, 1175–80.
Naito, K., Ishii, T., Hamaguchi, Y., and Oshima, K. (1967) *Solid State Commun.*, **5**, 349–52.
Naito, K., Kamagashira, N., and Nomura, Y. (1971) *J. Crystal Growth*, **8**, 219–20.
Naito, K., Tsuji, T., and Matsui, T. (1973) *J. Nucl. Mater.*, **48**, 58–66.
Naito, K. and Kamegashira, N. (1976) in *Advances in Nuclear Science and Technology*, vol. 9, pp. 99–180.
Naito, K., Inaba, H., and Takahashi, S. (1982) *J. Nucl. Mater.*, **110**, 317–23.
Naito, K., Tsuji, T., and Ohya, F. (1983) *J. Nucl. Mater.*, **114**, 136–42.
Naito, K. (1989) *J. Nucl. Mater.*, **167**, 30–5.
Nakagawa, T., Matsuoka, H., Sawa, M., Hirota, M., Miyake, M., and Katsura, M. (1997) *J. Nucl. Mater.*, **247**, 127–30.
Nakajima, K., Ohmichi, T., and Arai, Y. (2002) *J. Nucl. Mater.*, **304**, 176–81.
Nakamura, A. and Fujino, T. (1986) *J. Nucl. Mater.*, **140**, 113–30.
Nakamura, A. and Fujino, T. (1987) *J. Nucl. Mater.*, **149**, 80–100.
Narducci, A. A. and Ibers, J. A. (1998) *Chem. Mater.*, **10**, 2811–23.
Nash, K. L. and Sullivan, J. C. (1998) *J. Alloys Compds*, **271–273**, 712–18.
Nassimbeni, L. R. and Rodgers, A. L. (1976) *Crystal Struct. Commun.*, **5**, 301–8.
Nasu, S. (1964) *Japan. J. Appl. Phys.*, **3**, 664–5.
Navaza, A., Charpin, P., Vigner, D., and Heger, G. (1991) *Acta Crystallogr. C*, **47**, 1842–5.
Neuefeind, J., Skanthakumar, S., and Soderholm, L. (2004a) *Inorg. Chem.*, **43**, 2422–6.
Neuefeind, J., Soderholm, L., and Skanthakumar, S. (2004b) *J. Phys. Chem. A*, **108**, 2733–9.
Neuhaus, A. (1958) *Fortschr. Miner.*, **35**, 151–4.
Neuhaus, A. and Recker, K. (1959) *Z. Elektrochem.*, **63**, 89–97.
Newton, A. S., Warf, J. C., Spedding, F. H., Johnson, O., Johns, I. B., Nottorf, R. W., Ayres, J. A., Fisher, R. W., and Kant, A. (1949) *Nucleonics*, **4** (2), 17–25.
Newton, T. W. and Baker, F. B. (1965) *Inorg. Chem.*, **4**, 1166–70.
Newton, T. W. (1975) *The Kinetics of the Oxidation-Reduction Reactions of Uranium, Neptunium, Plutonium and Americium in Aqueous Solution*, Report TID-26506,

Technical Information Center, Office of Public Affairs, US Energy and Development Administration.
Nguyen-Nghi, H., Dianoux, A.-J., and Marquet-Ellis, H. (1964) *Compt. Rend. Acad. Sci.* (*Paris*), **259**, 4683.
Nguyen-Nghi, H., Dianoux, A.-J., Marquet-Ellis, H., and Plurien, P. (1965) *Compt. Rend. Acad. Sci.* (*Paris*), **260**, Group 8, 1963–6.
Niedrach, C. W. and Glamm, A. (1954) *Electrorefining of Uranium – A New Approach*, KAPL-1154.
Nielsen, P. E., Jeppesen, C., and Buchardt, O. (1988) *FEBS Lett.*, **235**, 122–4.
Niinistö, L., Toivonen, J., and Valkonen, J. (1979) *Acta Chem. Scand.*, **33**, 621–4.
Nishioka, T., Motoyama, G., Nakamura, S., Kadoya, H., and Sato, N. K. (2002) *Phys. Rev. Lett.*, **88**, 237203/1–237203/4.
NIST (2004) *NIST Critically Selected Stability Constants of Metal Complexes: version 8.0. NIST Standard Reference Database 46,* National Institute of Standards and Technology, Gaithersburg, MD.
Noël, H. and Prigent, J. (1980) *Physica B+C: Phys. Condensed Matter + Atom Mol. Plasma Phys., Optics*, **102**, 372–9.
Noël, H. and Le Marouille, J. Y. (1984) *J. Solid State Chem.*, **52**, 197–202.
Noël, H. (1985a) *Inorg. Chim. Acta*, **109**, 205–7.
Noël, H. (1985b) *Physica B and C*, **130**, 499–500.
Noël, H. and Levet, J. C. (1989) *J. Solid State Chem.*, **79**, 28–33.
Noël, H., Potel, M., Troć, R., and Shlyk, L. (1996) *J. Solid State Chem.*, **126**, 22–6.
Noland, R. A. and Marzano, C. (1953) *The Electrolytic Refining of Uranium*, ANL-5102.
Norris, D. I. R. and Kay, P. (1983) *J. Nucl. Mater.*, **116**, 184–94.
Northrup, C. J. M. Jr (1975) *J. Phys. Chem.*, **79**, 726–31.
Nowicki, L., Garrido, F., Turos, A., and Thomé, L. (2000) *J. Phys. Chem. Solids*, **61**, 1789–804.
Nriagu, J. O. (1984) Formation and stability of base metal phosphates in soils and sediments, in *Phosphate Minerals* (eds. J. O. Nriagu and P. B. Moore), Springer Verlag, London, pp. 318–29.
Obbade, S., Dion, C., Saadi, M., and Abraham, F. (2004) *J. Solid State Chem.*, **177**, 1567–74.
O'Donnell, T. A., Stewart, D. F., and Wilson, P. W. (1966) *Inorg. Chem.*, **5**, 1438–41.
O'Donnell, T. A. (1983) *J. Fluorine Chem.*, **23**, 97.
OECD-NEA (1982) *Uranium–Resources, Production and Demand*, Paris.
Oetting, F. H., Rand, M. H., and Ackerman, R. J. (1976) *The Chemical Thermodynamics of Actinide Elements and Compounds*, part 1, The Actinide Elements, IAEA, Vienna, STI/PUB/421/1.
Ogard, A. E. and Leary, J. A. (1968) in *Thermodynamics of Nuclear Materials*, Proc. Symp. 1967, International Atomic Energy Agency, Vienna, pp. 651–65.
Ogliaro, F., Cordier, S., Halet, J.-F., Perrin, C., Saillard, J.-Y., and Sergent, M. (1998) *Inorg. Chem.*, **37**, 6199–207.
O'Hare, P. A. G., Shinn, W. A., Mrazek, F. C., and Martin, A. E. (1972) *J. Chem. Thermodyn.*, **4**, 401–9.
O'Hare, P. A. G. and Hoekstra, H. R. (1973) *J. Chem. Thermodyn.*, **5**, 769–75.
O'Hare, P. A. G. and Hoekstra, H. R. (1974a) *J. Chem. Thermodyn.*, **6**, 251–8.
O'Hare, P. A. G. and Hoekstra, H. R. (1974b) *J. Chem. Thermodyn.*, **6**, 1161–9.

O'Hare, P. A. G., Boerio, J., Fredrickson, D. R., and Hoekstra, H. R. (1977) *J. Chem. Thermodyn.*, **9**, 963–72.
Ohmichi, T., Fukushima, S., Maeda, A., and Watanabe, H. (1981) *J. Nucl. Mater.*, **102**, 40–6.
Ohnuki, T., Kozai, N., Samadfam, M., Yasuda, R., Yamamato, S., Narumi, K., Naramoto, H., and Murakami, T. (2004) *Chem. Geol.*, **211**, 1–14.
Ohse, R.W. (1966) *J. Chem. Phys.*, **44**, 1375–8.
Ohse, R. W., Babelot, J. F., Cercignani, C., Kinsman, P. R., Long, K. A., Magill, J., and Scotti, A. (1979) *J. Nucl. Mater.*, **80**, 232–48.
Ohwada, K. (1970a) *J. Inorg. Nucl. Chem.*, **32**, 1209–18.
Ohwada, K. (1970b) *Spectochim. Acta*, **26A**, 1723–30.
Ohwada, K. (1971) *Inorg. Chem.*, **10**, 2281–5.
Ohwada, K. (1972) *J. Chem. Phys.*, **56**, 4951–6.
Ohwada, K., Soga, T., and Iwasaki, M. (1972) *J. Inorg. Nucl. Chem.*, **34**, 363–5.
Ohwada, K. (1976) *J. Inorg. Nucl. Chem.*, **38**, 741–5.
Oikawa, K., Kamiyama, T., Asano, H., Onuki, Y., and Kohgi, M. (1996) *J. Phys. Soc. Japan*, **65**, 3229–32.
Ollier, N., Guittet, M.-J., Gautier-Soyer, M., Panczer, G., Champagnon, B., and Jollivet, P. (2003) *Opt. Mater.*, **24**, 63–8.
Olsen, T., Gerwald, L., and Benedict, U. (1985) *J. Appl. Crystallogr.*, **18**, 37–41.
Olsen, T., Gerwald, L., Benedict, U., Dabos, S., and Vogt, O. (1988) *Phys. Rev. B*, **37**, 8713–8.
Ondruš, P., Veslovský, F., and Rybka, R. (1990) *Neues Jahrb. Miner., Monatsschr.*, **9**, 393–400.
Ondruš, P., Skála, P., Veselovský, F., Sejkora, J., and Vitti, C. (2003) *Am. Miner.*, **88**, 686–93.
Onoe, J., Takeuchi, K., Nakamatsu, H., Mukoyama, T., Sekine, R., Kim, B.-I., and Adachi, H. (1993) *J. Chem. Phys.*, **99**, 6810–17.
Onoe, J., Nakamatsu, H., Mukoyama, T., Sekine, R., Adachi, H., and Takeuchi, K. (1997) *Inorg. Chem.*, **36**, 1934–8.
Onuki, Y., Ukon, I., Komatsubara, T., Takayanagi, S., Wada, N., and Watanabe, T. (1990) *Physica B* (*Amsterdam, Neth.*), **163**, 368–70.
Onuki, Y., Ukon, I., Yun, S. W., Umehara, I., Satoh, K., Fukuhara, T., Sato, H., Takayanagi, S., Shikama, M., and Ochiai, A. (1992) *J. Phys. Soc. Japan*, **61**, 293–9.
Orlandi, P., Pasero, M., Duchi, G., and Olmi, F. (1997) *Am. Miner.*, **82**, 807–11.
Osborne, D. W., Westrum, E. F. Jr, and Lohr, H. R. (1955) *J. Am. Chem. Soc.*, **77**, 2737–9.
Osborne, D. W. and Flotow, H. E. (1972) *J. Chem. Thermodyn.*, **4**, 411–18.
Osborne, D. W., Flotow, H. E., Dallinger, R. P., and Hoekstra, H. R. (1974) *J. Chem. Thermodyn.*, **6**, 751–6.
Otey, M. G. and Le Doux, R. A. (1967) *J. Inorg. Nucl. Chem.*, **29**, 2249–56.
Outebridge, W. F., Staatz, M. H., Meyrowitz, R., and Pommer, A. M. (1960) *Am. Miner.*, **45**, 39–52.
Pabalan, R. T., Prikryl, J. D., Muller, P. M., and Dietrich, T. B. (1993) *Mater. Res. Soc. Symp. Proc.*, **294**, 777–82.
Pabst, A. (1954) *Am. Miner.*, **37**, 137–57.
Pagoaga, M. K., Appleman, D. E., and Stewart, J. M. (1987) *Am. Miner.*, **72**, 1230–8.

Paine, R. T., Ryan, R. R., and Asprey, L. B. (1975) *Inorg. Chem.*, **14**, 1113–17.
Paine, R. T., McDowell, R. S., Asprey, L. B., and Jones, L. H. (1976) *J. Chem. Phys.*, **64**, 3081–3.
Paixão, J. A., Rebizant, J., Blaise, A., Delapalme, A., Sanchez, J. P., Lander, G. H., Nakotte, H., Burlet, P., and Bonnet, M. (1994) *Physica B* (*Amsterdam, Neth.*), **203**, 137–46.
Palenzona, A. and Manfrinetti, P. (1995) *J. Alloys Compds*, **221**, 157–60.
Panlener, R. J., Blumenthal, R. N., and Garnier, J. E. (1975) *J. Phys. Chem. Solids*, **36**, 1213–22.
Papiernik, R., Mercurio, D., and Frit, B. (1980) *Acta Crystallogr. B*, **36**, 1769–74.
Papiernik, R., Mercurio, D., Frit, B., and Baernighausen, H. (1983) *Acta Cryst. C*, **39**, 667–8.
Parks, S. I. and Moulton, W. G. (1968) *Phys. Rev.*, **1973**, 333–7.
Parry, S. J. (1991) in *Activation Spectrometry in Chemical Analysis* (eds. J. D. Winefordner, and I. M. Kolthoff), John Wiley, New York, pp. 206–7.
Partington, J. R. (1949) in *Treatise on Physical Chemistry*, vol. I, Longman, Green, p. 639.
Pascal, P. (ed.) (1962–1970) *Nouveau, Traité de Chimie, Minérale*, vols. VII (1962), IX (1963), XV (2) (1961), XV (3) (1962), XV (4) (1967), and XV (5) (1970), Masson et Cie, Paris.
Pascal, J., Morin, J., and Lacombe, P. (1964) *J. Nucl. Mater.*, **13**, 28–32.
Paszek, A. P. (1978) Ph.D. Dissertation, The John Hopkins University, Baltimore.
Patton, F. S., Googin, J. M., and Griffith, W. L. (1963) *Enriched Uranium Processing*, Int. Ser. Monogr. Nucl. En. Div. IX, vol. 2, Pergamon Press, New York.
Pattoret, A., Drowart, J., and Smoes, S. (1964) *Trans. Faraday Soc.*, **65**, 98.
Pattoret, A., Drowart, J., and Smoes, S. (1968) in *Thermodynamics of Nuclear Materials*, Proc. Symp. 1967, International Atomic Energy Agency, Vienna, pp. 613–36.
Paul, R. (1970) Research Center Karlsruhe Report, KFK-1297.
Paul, R. and Keller, C. (1971) *J. Nucl. Mater.*, **41**, 133–42.
Pearcy, E. C., Prokryl, J. D., Murphy, W. M., and Leslie, B. W. (1994) *Appl. Geochem.*, **9**, 713–32.
Pé1igot, E. (1841a) *J. Prakt. Chem.*, **1** (24), 442–51.
Pé1igot, E. (1841b) *C. R. Acad. Sci.*, **12**, 735–7; **13**, 417–26.
Péligot, E. (1842) *Ann. Chim. Phys.*, Series 3, **5**, 5–47.
Péligot, E. (1844) *Ann. Chim. Phys.*, Series 3, **12**, 549–74.
Penneman, R. A., Kruse, F. H., George, R. S., and Coleman, J. S. (1964a) *Inorg. Chem.*, **3**, 309–15.
Penneman, R. A., Sturgeon, G. D., and Asprey, L. B. (1964b) *Inorg. Chem.*, **3**, 126–9.
Penneman, R. A., Keenan, K., and Asprey, L. B. (1967) *Adv. Chem. Ser.*, **71**, 248–55.
Penneman, R. A., Ryan, R. R., and Rosenzweig, A. (1973) *Struct. Bonding*, Berlin, Heidelberg, New York, **13**, 1–52.
Penneman, R. A., Ryan, R. R., and Rosenzweig, A. (1974) *Acta Crystallogr.*, **B30**, 1966–70.
Pepper, R. T. (1964) *Appl. Mater. Res.*, **3**, 203.
Pério, P. (1953a) *Bull. Soc. Chim. Fr*, 256–63.
Pério, P. (1953b) *Bull. Soc. Chim. Fr*, 840–1.
Perrin, A. (1970) *Compt. Rend. C*, **270**, 319–22.

Perrin, A. and Caillet, P. (1976) *Compt. Rend. C*, **282**, 721–4.
Perrin, A. (1977a) *J. Inorg. Nucl. Chem.*, **39**, 1169–72.
Perrin, A. (1977b) *J. Appl. Crystallogr.*, **10**, 359–60.
Perrin, A. and Le Marouille, J. Y. (1977) *Acta Crystallogr. B*, **33**, 2477–81.
Perrin, D. D. (1979) *Stability Constants of Metal-Ion Complexes. Part B Organic Ligands*, IUPAC Chemical Data Series no. 22, , Pergamon Press, New York.
Perron, P. O. (1968) Atomic Energy of Canada Ltd Report, AECL-3072.
Peterson, S. (1961) *J. Inorg. Nucl. Chem.*, **17**, 135–7.
Pfeil, P. C. L. (1956) *Proc. Int. Conf. on Peaceful Uses of Atomic Energy*, Geneva 1955, vol. 9, p. 117.
Picard, C. and Gerdanian, P. (1981) *J. Nucl. Mater.*, **99**, 184–9.
Picon, M. and Flahaut, J. (1968) *Bull. Soc. Chim. Fr.*, 772–80.
Piekarski, C. and Morfeld, P. (1997) *Appl. Occup. Environ. Hyg.*, **12**, 915–18.
Pippin, C. G. and Sullivan, J. C. (1989) *Radiochim. Acta*, **48**, 37–8.
Piret, P., Declerq, J.-P., and Piret-Meunier, J. (1979) *Acta. Crystallogr.*, **B35**, 1880–2.
Piret, P., Declerq, J.-P., and Wauters-Stoop, D. (1980) *Bull. Minér.*, **103**, 176–8.
Piret, P. and Deliens, M. (1982) *Bull. Minér.*, **105**, 125–8.
Piret, P. and Declerq, J.-P. (1983) *Bull. Minér.*, **106**, 383–9.
Piret, P., Deliens, M., Piret-Meunier, J., and Germain, G. (1983) *Bull. Minér.*, **106**, 299–304.
Piret, P. (1985) *Bull. Minér.*, **108**, 659–66.
Piret, P. and Deliens, M. (1987) *Bull. Minér.*, **110**, 65–7.
Piret, P., Deliens, M., Piret-Meunier, J., and Germain, G. (1988) *Bull. Minér.*, **111**, 443–9.
Piret, P., Piret-Meunier, J., and Deliens, M. (1990) *Eur. J. Miner.*, **2**, 399–405.
Plaine, R. T., Ryan, R. R., and Asprey, L. B. (1975) *Inorg. Chem.*, **14**, 1113–17.
Plant, J., Simpson, P. R., Smith, B., and Windley, B. F. (1999) *Rev. Miner.*, **38**, 255–319.
Platzner, I. T. (1997) in *Modern Isotope Ratio Mass Spectrometry* (ed. I. T. Platzner), John Wiley, New York, pp. 363–77.
Plesko, E. P., Scheetz, B. E., and White, W. B. (1992) *Am. Miner.*, **77**, 431–7.
Plumer, M. L. and Caillé, A. (1989) *Phys. Rev. B*, **40**, 396–8.
Pollard, F. H., Hanson, P., and Geary, W. J. (1959) *Anal. Chim. Acta*, **20**, 26–31.
Pollock, E. N. (1977) *Anal. Chim. Acta*, **88**, 399–401.
Polunina, G. P., Kovba, L. M., and Ippolitova, E. A. (1961) Argonne National Laboratory Report, ANL-trans-33, p. 224.
Potol, M., Brochu, R., Padiou, J., and Grandjean, D. (1972) *C.R. Acad. Sci. C*, **275**, 1419–21.
Prescott, C. H., Reynolds, F. L., and Holmes, J. A. (1946) *The Preparation of Uranium Metal by Thermal Dissociation of the Iodide*, MDDC-437.
Prigent, J. (1958) *Compt. Rend. Hebd. Séances Acad. Sci.*, **247**, 1737–9.
Prigent, J. and Lucas, J. (1965) *Bull. Soc. Chim. Fr.*, **4**, 1129–31.
Prins, G. and Cordfunke, E. P. H. (1975) *J. Inorg. Nucl. Chem.*, **37**, 119–27.
Prins, G., Cordfunke, E. P. H., and Ouweltjes, W. (1978) *J. Chem. Thermodyn.*, **10**, 1003–10.
Prins, G. and Cordfunke, E. H. P. (1983) *J. Less Common Metals*, **91**, 177–80.
Privalov, T., Schimmelpfennig, B., Wahlgren, U., and Grenthe, I. (2002) *J. Phys. Chem.*, **106**, 11277–82.

Privalov, T., Macak, P., Schimmelpfennig, B., Fromager, E., Grenthe, I., and Wahlgren, U. (2004) *J. Am. Chem. Soc.*, **124**, 9801–8.
Proceedings (1960a) *Proc. Uranium Carbide Meeting*, Oak Ridge National Laboratory, December 1–2, 1960, TID-7603.
Proceedings (1960b) *Prog. Carbide Fuels, Notes from the Second AEC Uranium Carbide Meeting*, Battelle Memorial Institute, March 22 and 23, 1960, TID-7589.
Proceedings (1961) *Proc. Symp. on Uranium Carbides as Reactor Fuel Materials*, USAEC, April 4, 1961, AEC Headquarters, Germantown, MD, TID-7614.
Proceedings (1963) *Proc. Fourth Uranium Carbide Conf.*, East Hartfield, CT, May 20–21, 1963, TID-7676.
Proceedings (1966) *Proc. Second Int. Thorium Fuel Cycle Symp.*, Gatlinburg, TN, May 3–6, 1966, CONF-660524.
Pushcharovsky, D. Y., Rastsvetaeva, R. K., and Sarp, H. (1996) *J. Alloys Compds.*, **239**, 23–6.
Pyykkö, P., Li, J., and Runeberg, N. J. (1994) *J. Phys. Chem.*, **98**, 4809–13.
Rabinovich, D., Schimek, G. L., Pennington, W. T., Nielsen, J. B., and Abney, K. D. (1998) *Acta Crystallogr. C*, **54**, 1740–2.
Rabinowitch., E. and Belford, R. L. (1964) *Spectroscopy and Photochemistry of Uranyl Compounds*, Pergamon Press, Oxford.
Raetsky, V. M. (1967) *J. Nucl. Mater.*, **21**, 105–8.
Raj, P., Sathyamoorthy, A., Shashikala, K., Kumar, N. H., Rao, C. R. V., and Malik, S. K. (2000) *J. Alloys Compds.*, **296**, 20–6.
Rajnak, K., Gamp, E., Shinomoto, R., and Edelstein, N. M. (1998) *J. Chem. Phys.*, **80**, 5942–50.
Ralph, J. and Hyland, G. J. (1985) *J. Nucl. Mater.*, **132**, 76–9.
Rand, M. H. and Kubaschewski, O. (1963) *The Thermochemical Properties of Uranium Compounds*, Olivier&Boyd, Edinbourgh.
Rand, M. H., Ackermann, R. J., Grønvold, F., Oetting, F. L., and Pattoret, A. (1978) *Rev. Int. Hautes Tempér. Réfract. Fr.*, **15**, 355–65.
Ratho, T. and Patel, T. (1968) *Indian J. Phys.*, **42**, 240–2.
Ratho, T., Patel, T., and Sahoo, B. (1969) *Indian J. Phys.*, **43**, 164–6.
Rebenko, A. N., Brusentsev, F. A., and Opalovskii, A. A. (1968) *Izv. Sib. Otd. Nauk. SSSR, Ser. Khim. Nauk*, **1**, 136–8.
Rebizant, J., Van den Bossche, G., Spirlet, M. R., and Goffart, J. (1987) *Acta Crystallogr.*, **C43**, 1298–300.
Rediess, K. and Sawodny, W. (1982) *Z. Naturforsch.*, **37B**, 524–5.
Reeder, R. J., Nugent, M., Lamble, G. M., Tait, C. D., and Morris, D. E. (2000) *Environ. Sci. Technol.*, **34**, 638–44.
Reeder, R. J., Nugent, M., Drew Tait, C., Morris, D. E., Heald, S. M., Beck, K. M., Hess, W. P., and Lanzirotti. A. (2001) *Geochim. Cosmochim. Acta*, **65**, 3491–503.
Reedy, G. T. and Chasanov, M. G. (1972) *J. Nucl. Mater.*, **42**, 341–4.
Reis, A. H. Jr, Hoekstra, H. R., Gebert, E., and Peterson, S. W. (1976) *J. Inorg. Nucl. Chem.*, **38**, 1481–5.
Reshetov, K. V. and Kovba, L. M. (1966) *Zh. Strukt. Khim.*, **7**, 625–6.
Reynolds, L. T. and Wilkinson, G. (1956) *J. Inorg. Nucl. Chem.*, **2**, 246–53.
Rietveld, H. M. (1966) *Acta Crystallogr.*, **20**, 508–13.
Rigny, P. (1965) CEA Report CEA-R2827, pp. 1–30.

Rigny, P. (1966) N.S.A. 20, no. 1807.
Rigny, P. and Plurien, P. (1967) *J. Phys. Chem. Solids*, **28**, 2589–95.
Rigny, P., Dianoux, A.-J., and Plurien, P. (1971) *J. Chem. Phys. Solids*, **32**, 1175–80.
Rizzo da Rocha, S. M., Rodrigues de Aquino, A., and Abrao, A. (1995) *An. Assoc. Brasil. Quimica*, **44**, 33–40.
Roberts, L. E. J. and Walter, A. J. (1961) *J. Inorg. Nucl. Chem.*, **22**, 213–29.
Roberts, L. E. J. and Walter, A. J. (1966) in *Physico-Chimie du Protactinium* (eds. G. Bouissières and R. Muxart), Colloq. Int. 154, Centre National de la Recherche Scientifique, Paris, pp. 51–9.
Roberts, W. L., Campbell, T. J., and Rapp, G. R. (1990) in *Encyclopedia of Minerals*, Kluwer Academic Publishers, 2nd edn, February 1990.
Robins, R. G. (1961) *J. Nucl. Mater.*, **3**, 294–301.
Rodden, C. J. and Warf, J. C. (1950) in *Analytical Chemistry of the Manhattan Project* (ed. C. J. Rodden), McGraw-Hill, New York, pp. 3–159.
Rodriguez de Sastre, M. S., Philippot, J., and Moreau, C. (1967) CEA Report, CEA-R 3218.
Rogova, V. P., Belova, L. N., Kiziyarov, G. P., Kuznetsova, N. N. (1973) *Zap. Uses. Miner. Obshch.*, **102**, 75–81.
Rona, E. (1950) *J. Am. Chem. Soc.*, **72**, 4339–43.
Ronchi, C. and Hyland, G. J. (1994) *J. Alloys Compds.*, **213/214**, 159–68.
Ronchi, C., Sheindlin, M., Musella, M., and Hyland, G. J. (1999) *J. Appl. Phys.*, **85**, 776–89.
Rosén, A. and Fricke, B. (1979) *Chem. Phys. Lett.*, **61**, 75–8.
Rosenthal, M. W., Briggs, R. B., and Kasten, P. R. (1969) *Molten Salt Reactor Program Semiannual Progress Report for Period Ending August 31, 1968*, ORNL-4344, p. IX.
Rosenthal, M. W., Haubenreich, P. N., and Briggs, R. B. (1972) ORNL-4812, pp. 1–416.
Rosenzweig, A. and Cromer, D. T. (1970) *Acta Crystallogr.*, **B26**, 38–44.
Rosenzweig, A., Ryan, R. R., and Cromer, D. T. (1973) *Acta Crystallogr.*, **B29**, 460–2.
Rosenzweig, A. and Ryan, R. R. (1975) *Am. Miner.*, **60**, 448–53.
Rosenzweig, A. and Ryan, R. R. (1977) *Crystal Struct. Commun.*, **6**, 53–6.
Ross, M. and Evans, H. T. (1964) *Am. Miner.*, **49**, 1578–602.
Ross, J. W. and Lam, D. W. (1968) *Phys. Rev.*, **165**, 617.
Rossetto, G., Zanella, P., Paolucci, G., and de Paoli, G. (1982) *Inorg. Chim. Acta*, **61**, 39–42.
Rossotti, F. J. R. and Rossotti, H. (1961) *The Determination of Stability Constants and Other Equilibrium Constants in Solution*, McGraw-Hill, New York.
Roth, W. L. (1960) *Acta Crystallogr.*, **13**, 140–9.
Rough, F. A. and Bauer, A. A. (1958) *Constitution of Uranium and Thorium Alloys*, BMI-1300.
Roussel, P. and Scott, P. (1998) *J. Am. Chem. Soc.*, **1998**, 1070–1.
Ruch, W. C., Peterson, D. A., Gaskill, E. A., and Tepp, H. G. (1959) *Nuclear Engineering and Science Conf.*, Am. Inst. Chem. Eng., April 6–9, 1959, Cleveland, OH, Preprint V-52.
Rundle, R. E. (1947) *J. Am. Chem. Soc.*, **69**, 1719–23.
Rundle, R. E., Baenziger, N. C., Wilson, A. S., and McDonald, R. A. (1948) *J. Am. Chem. Soc.*, **70**, 99–105.
Rundle, R. E. (1951) *J. Am. Chem. Soc.*, **78**, 4172–4.

Runnals, O. J. C. (1953) *Can. J. Chem.*, **3**, 694.
Rutledge, G. P., Jarry, R. L., and Davis, W. Jr (1953) *J. Phys. Chem.*, **57**, 541–4.
Rüdorff, W. and Pfitzer, F. (1954) *Z. Naturforsch.*, **9b**, 568–9.
Rüdorff, W. and Leutner, H. (1957) *Z. Anorg. Allg. Chem.*, **292**, 193–6.
Rüdorff, W. and Menzer, W. (1957) *Z. Anorg. Allg. Chem.*, **292**, 197–202.
Rüdorff, W., Kemmler, S., and Leutner, H. (1962) *Angew. Chem.*, **74**, p. 429.
Rüdorff, W., Erfurth, H., and Kemmler-Sack, S. (1967) *Z. Anorg. Allg. Chem.*, **354**, 273–85.
Ryan, J. L. (1962) *Proc. Seventh Int. Conf. Coordination Chemistry*, pp. 367–9; and Ryan, J. L. and Keder, W. E., unpublished work.
Ryan, R. R. (1971) *J. Inorg. Nucl.Chem.*, **33**, 153–77.
Ryan, R. R. (1972) *Med. Tech. Pub. Co. Int. Rev. Sci. Inorg. Chem., Ser.1*, **7**, 323–67.
Ryan, R. R. (1974) *Inorg. Synth.*, **15**, 235–43.
Ryan, R. R., Cleveland, J. M., and Bryan, G. H. (1974) *Inorg. Chem.*, **13**, 214–18.
Ryan, R. R., Penneman, R. A., Asprey, L. B., and Paine, R. T. (1976) *Acta Crystallogr. B*, **32**, 3311–13.
Ryan, R. R. and Rosenzweig, A. (1977) *Crystal Struct. Commun.*, **6**, 611–15.
Saito, Y. (1974) *J. Nucl. Mater.*, **51**, 112–25.
Sakurai, T., Kameda, O., and Ishigame, M. (1968) *J. Crystal Growth*, **2**, 236–7.
Saller, H. A. and Rough, F. A. (1954) *Chem. Eng. Prog. Symp. Ser.* 11, **50**, 63–7.
Saller, H. A. and Rough, F. H. (1955) *Compilation of U.S. and U.K. Uranium and Thorium Constitutional Diagrams*, 1st edn, BMI-1000.
Samson, S. and Sillén, L. G. (1947) *Ark. Kemi. Min. Geol.*, **25A** (21), 1–16.
Samsonov, G. V. (1968) *Handbook of the Physicochemical Properties of the Elements*, IFI/Plenum, New York-Washington, p. 437.
Sandell, E. B. (1959) *Colorimetric Determination of Traces of Metals*, 3rd edn, Interscience, New York.
Sandino, A. and Bruno, J. (1992) *Geochim. Cosmochim. Acta.*, **56**, 4135–45.
Santini, P., Lémanski, R., and Erdös, P. (1999) *Adv. Phys.*, **48** (5), 538–653.
Santos, I. G. and Abram, U. (2004) *Inorg. Chem. Commun.*, **7**, 440–2.
Sara, K. H. (1970) *J. Indian Chem. Soc.*, **47**, 88.
Sarp, H., Bertrand, J., and Deferne, J. (1983) *Neues Jahrb. Miner., Monatsschr.*, **6**, 417–23.
Sarsfield, M. J. and Helliwell, M. (2003) *J. Am. Chem. Soc.*, **126**, 1036–7.
Satonnay, G., Ardois, C., Corbel, C., Lucchini, J. F., Barthe, M. F., Garrido, F., and Gosset, D. (2001) *J. Nucl. Mater.*, **288**, 11–19.
Satten, R. A., Schreiber, C. L., and Wong, E. Y. (1983) *J. Chem. Phys.*, **78**, 79–87.
Savage, A. W. (1956) *J. Am. Chem. Soc.*, **78**, 2700–2.
Sawai, H., Kuroda, K., and Hojo, T. (1989) *Bull. Chem. Soc. Japan*, **62**, 2018–23.
Sawai, H., Shibusawa, T., and Kuroda, K. (1990) *Bull. Chem. Soc. Japan*, **63**, 1776–80.
Sawai, H., Higa, K., and Kuroda, K. (1992) *J. Chem. Soc. Dalton Trans.*, 505–8.
Sawai, H., Ito, T., Kokaji, K., Shimazu, M., Shinozuka, K., and Taira, H. (1996) *Biorg Med. Chem. Lett.*, **6**, 1785–90.
Sawodny, W., Rediess, K., and Thewalt, U. (1980) *Z. Anorg. Allg. Chem.*, **469**, 81–6.
Sawodny, W., Rediess, K., and Thewalt, U. (1983) *Z. Anorg. Allg. Chem.*, **499**, 81–8.
Sawyer, J. O. (1963) *J. Inorg. Nucl. Chem.*, **25**, 899–902.
Sawyer, J. O. (1972) *J. Inorg. Nucl. Chem.*, **34**, 3268–71.

Saxena, S. S., Agarwal, P., Ahilan, K., Grosche, F. M., Haselwimmer, R. K. W., Steiner, J. J., Pugh, E., Walker, I. R., Julian, S. R., Monthoux, P., Lonzarich, G. G., Huxley, A., and Shalek, P. D. (1963) *J. Am. Ceram. Soc.*, **46**, 155–61.
Scapolan, S. (1998) *Mise au Point et Evaluation de Techniques de Spéciation pour L'Etudes des Especes Biologiques Circulantes de L'Uranium* (*VI*), Thesis, Université de Paris Sud.
Schaner, B. E. (1960) *J. Nucl. Mater.*, **2**, 110–20.
Schäfer, H. (1975) *Z. Anorg. Allg. Chem.*, **414**, 151–9.
Schindler, M. and Hawthorne, F. C. (2004) *Can. Miner.*, **42**, 1601–27.
Schindler, M., Mutter, A., Hawthorne, F. C., and Putnis, A. (2004) *Can. Miner.*, **42**, 1651–66.
Schirber, J. E., Arko, A. J., and Fischer, E. S. (1975) *Solid State Commun.*, **17**, 553.
Schleid, T., Meyer, G., and Morss, L. R. (1987) *J. Less Common Metals*, **132**, 69–77; Schleid, T. and Meyer, G. (1988) unpublished results.
Schleid, T. and Meyer, G. (1989) *Naturwissenschaften*, **76**, 118.
Schlesinger, H. I. and Brown, H. C. (1953) *J. Am. Chem. Soc.*, **75**, 219–21.
Schlyter, K. (1953) *Ark. Khemi*, **5**, 73.
Schmieder, H., Dornberger, E., and Kanelakopulos, B. (1970) *Appl. Spectrosc.*, **24**, 499.
Schmitz-Dumont, O., Füchtenbusch, F., and Schneiders, H. (1954) *Z. Anorg. Allg. Chem.*, **277**, 315–28.
Schmitz, F., Dean, G., and Halachmy, M. (1971) *J. Nucl. Mater.*, **40**, 325–37.
Schoebrechts, J.-P., Gens, R., Fuger, J., and Morss, L. R. (1989) *Thermochim. Acta*, **139**, 49–66.
Scholder, R. and Brixner, L. (1955) *Z. Naturforsch.*, **10b**, 178–9.
Scholder, R. (1958) *Angew. Chem.*, **70**, 583–94.
Scholder, R. (1960) *Angew. Chem.*, **72**, pp. 120.
Scholder, R. and Gläser, H. (1964) *Z. Anorg. Allg. Chem.*, **327**, 15–27.
Schreckenbach, G., Hay, P. J., and Martin, R. L. (1998) *Inorg. Chem.*, **37**, 4442–51.
Seaborg, G. T. and Katzin, L. 1. (1951) *Production and Separation of U^{233} – Survey*, Natl. Nucl. En. Ser. Div. IV, 17A, USAEC Technical Information Service, Oak Ridge, TN (declassified as TID-5222).
Seijo, L. and Barandiaran, Z. (2001) *J. Chem. Phys.*, **115**, 5554.
Sejkora, J., Čejka, J., Hloušek, J., Novák, M., and Šrein, V. (2004) *Can. Miner.*, **42**, 963–72.
Selbin, J. and Ortego, J. (1969) *Chem. Rev.*, **69**, 657–71.
Selbin, J., Ortego, J. D., and Gritzner, N. (1968) *Inorg. Chem.*, **7**, 976–82.
Selbin, J., Ballhausen, C. J., and Durrett, D. G. (1972a) *Inorg. Chem.*, **11**, 510–15.
Selbin, J., Durret, D. G., Sherrill, H. J., Newkome, G. R., and Wharton, J. H. (1972b) *J. Chem. Soc. Chem. Comm.*, 380–1.
Selbin, J., Durret, D. G., Sherrill, H. J., Newkome, G. R., and Collins, M. (1973) *J. Inorg. Nucl. Chem.*, **35**, 3467–80.
Selbin, J. and Sherrill, H. J. (1974) *Inorg. Chem.*, **13**, 1235–9.
Sémon, L., Boeme, C., Billard, I., Hennig, C., Lützenkirchen, K., Reich, T., Rossberg, A., Rossini, I., and Wipff, G. (2001) *Chem. Phys. Chem.*, **2**, 591–8.
Seppelt, K. and Hwang, I.-C. (2000) *J. Fluorine Chem.*, **102**, 69–72.

Sessler, J. L., Vivian, A. E., Seidel, D., Burrel, A. K., Hoehner, M., Mody, T. D., Gebauer, A., Weghorn, S. J., and Lynch, V. (2001) *Coord. Chem. Rev.*, **216–217**, 411–34.
Seta, K., Matsui, T., Inaba, H., and Naito, K. (1982) *J. Nucl. Mater.*, **110**, 47–54.
Shamir, J. and Silberstein, A. (1975) *J. Inorg. Nucl. Chem.*, **37**, 1173–5.
Shamir, J., Silberstein, A., Ferraro, J. B., and Choca, M. (1975) *J. Inorg. Nucl. Chem.*, **37**, 1429–32.
Shchelokov, R. N. and Belomestnykh, V. I. (1968a) *Zh. Neorg. Khim.*, **13**, 1398–1403; *Russ. J. Inorg. Chem.*, **13**, 733–6.
Shchelokov, R. N. and Belomestnykh, V. I. (1968b) *Zhur. Neorg. Khim.*, **13**, 3386–891; *Russ. J. Inorg. Chem.*, **13**, 1744–7.
Shchelokov, R. N., Tsivadze, A. Yu., Orlova, I. M., and Podnebesnova, G. V. (1977) *Inorg. Nucl. Chem. Lett.*, **13**, 367–74.
Shchukarev, S. A., Vasil'kova, I. V., Drozdova, V. M., and Frantseva, K. E. (1959a) *Zh. Neorg. Khim.*, **4**, 39–41; (1959) *Russ. J. Inorg. Chem.*, **4**, 15–16.
Shchukarev, S. A., Vasilkova, I. V., Drozdova, V. M., and Martynova, N. S. (1959b) *Zh. Neorg. Khim.*, **4**, 33–8; (1959) *Russ. J. Inorg. Chem.*, **4**, 13–15.
Sheikin, I., Braithwaite, D., and Flouquet, J. (2000) *Nature*, **406**, 587–92.
Shen, J. and Peny, Z. (1981) *Acta Crystallogr.*, **A37**, Suppl. C-186.
Shimazu, M., Shinozuka, K., and Sawai, H. (1993) *Angew. Chem. Int. Ed. Engl.*, **32**, 870–2.
Shoesmith, D. W. and Sunder, S. (1994) in *The Electrochemistry of Novel Materials* (eds. J. Lipkowski and P. N. Ross), VCH, New York, p. 297.
Shull, C. G. and Wilkinson, M. K. (1955) *Oak Ridge National Laboratory Report*, *ORNL*-1879, p. 24.
Shunk, F. A. (1969) *Constitution of Binary Alloys*, 2nd Suppl., McGraw-Hill, New York.
Siegel, S. (1956) *Acta Crystallogr.*, **9**, 827.
Siegel, S., Hoekstra, H. R., and Sherry, E. (1966) *Acta Crystallogr.*, **20**, 292–5.
Siegel, S. and Hoekstra, H. R. (1968) *Acta Crystallogr.*, **B24**, 967–70.
Siegel, S. and Hoekstra, H. R. (1971a) *Inorg. Nucl. Chem. Lett.*, **7**, 497–504.
Siegel, S. and Hoekstra, H. R. (1971b) *Inorg. Nucl. Chem. Lett.*, **7**, 455–9.
Siegel, S., Viste, A., Hoekstra, H. R., and Tani, B. (1972) *Acta Crystallogr.*, **B28**, 117.
Silberstein, A. (1972) INIS-mf-36, p. 46.
Sillén, L. G. and Martell, A. E. (1964) *Stability Constants of Metal-Ion Complexes*, The Chemical Society, London.
Sillén, L. G. and Martell, A. E. (1971) *Stability Constants of Metal-Ion Complexes*, Suppl. no. 1, The Chemical Society, London.
Silverman, L. and Sallach, R. A. (1961) *J. Phys. Chem.*, **65**, 370.
Simoni, E., Hubert, S., and Genet, M. (1988) *J. Phys.* (*France*), **49**, 1425–34.
Simoni, E., Louis, M., Gesland, J. Y., and Hubert, S. (1995) *J. Lumin.*, **65**, 153–61.
Simpson, K. A. and Wood, P. (1983) in *Proc. NRC Workshop on Spent Fuel/Cladding Reaction during Dry Storage*, Gaithersburg, MD, NUREG/CP-0049, p. 70.
Singh, R. N. and Coble, R. L. (1974) *J. Crystal Growth*, **21**, 261–6.
Sjkora, J., Čejka, J., Hloušek, J., Šrein, V., Novotná M. (2002) *Neu. Jahr. Miner. Monat.*, **8**, 353–67.
Slain, H. (1950) *Production of Uranium by Electrolysis of Fused Salts*, LA-1056.
Sleight, A. W. and Ward, R. (1962) *Inorg. Chem.*, **1**, 790–3.

Slovyanskikh, V. K., Ellert, G. V., and Yarembash, E. L. (1967) *Izv. Akad. Nauk SSSR, Neorg. Mater.*, **3**, 1088–90; *Inorg. Mater.* (*USSR*), **3**, 969–71.
Slovyanskikh, V. K., Rozanov, I. A., and Gracheva, N. V. (1977) *Zh. Neorg. Khim.*, **22**, 1645–50; *Russ. J. Inorg. Chem.*, **22**, 893–6.
Smiley, S. H. and Brater, D. C. (1956) Current Commission Methods for producing UO_3, UF_4 and UF_6, TID-5295, pp. 245–89.
Smiley, S. H. and Brater, D. C. (1958) K-1379 Del., pp. 1–18.
Smiley, S. H. and Brater, D. C. (1960) N.S.A, **16**, no.1573.
Smith, G. S., Johnson, O., and Elson, R. E. (1967) *Acta Crystallogr.*, **22**, 300–3.
Smith, R. M. and Martell, A. E. (1989) *Critical Stability Constants*, vol. 6, Second Suppl., Plenum Press, New York.
Sobczyk, M., Karbowiak, M., and Drożdżyński, J. (2003) *J. Solid State Chem.*, **170**, 443–9.
Sobczyk, M., Drożdżyński, J., and Karbowiak, M. (2005) *J. Solid. State Chem.*, **178/2**, 536–44.
Soga, T., Ohwada, K., and Iwasaki, M. (1972) *Appl. Spectrosc.*, **26**, 482–3.
Soga, T., Ohwada, K., and Iwasaki, M. (1973) *J. Inorg. Nucl. Chem.*, **35**, 2069–74.
Soulié, E. (1978) *J. Inorg. Nucl. Chem.*, **40**, 351–2.
Souter, P. F., Kushto, G. P., Andrews, L., and Neurock, M. J. (1997) *J. Am. Chem. Soc.*, **119**, 1682–87.
Spedding, F. H., Newton, A. S., Warf, J. C., Johnson, O., Nottorf, R. W., Johns, I. B., and Daane, A. H. (1949) *Nucleonics*, **4** (1), 4–15.
Speer, J. A. (1982) *Rev. Miner.*, **5**, 113–35.
Spencer, S., Gagliardi, L., Handy, N. C., Ioannou, A. G., Skylaris, C.-K., and Willets, A. (1999) *J. Phys. Chem. A*, **103**, 1831–7.
Spirlet, J. C. (1979) *J. Phys. Colloq.*, C4, **40**, 87–94.
Spirlet, J. C., Bednarczyk, E., and Müller, W. (1979) *J. Phys. Colloq.*, **40**, C4, 108–10.
Spirlet, M. R., Rebizant, J., Fuger, J., and Schoebrechts, J. P. (1988) *Acta Crystallogr. C*, **44**, 1300.
Spitsyn, V. I., Ippolitova, E. A., Simanov, Yu. P., and Kovba, L. M. (1961a) Argonne National Laboratory Report, ANL-trans-33, p. 4.
Spitsyn, V. I., Ippolitova, E. A., Efremova, K. M., and Simanov, Yu. P. (1961b) Argonne National Laboratory Report, ANL-trans-33, p. 142.
Spitsyn, V. I., Ippolitova, E. A., Efremova, K. M., and Simanov, Yu. P. (1961c) Argonne National Laboratory Report, ANL-trans-33, p. 148.
Spitsyn, V. I., Tshigunov, A. N., Kovba, L. M., and Kuz'micheva, E. U. (1972) *Dokl. Akad. Nauk SSSR*, **204**, 604–43.
Srirama Murti, P., Yadav, R. B., Nawada, H. P., Vasudeva Rao, P. R., and Mathews, C. K. (1989) *Thermochim. Acta*, **140**, 299–303.
Stadlbauer, E., Wichmann, U., Lott, U., and Keller, C. (1974) *J. Solid State Chem.*, **10**, 341–50.
Staritzky, E. and Singer, J. (1952) *Acta Crystallogr.*, **5**, 536–40.
Staritzky, E., and Douglass, R. M. (1956) *Anal. Chem.*, **28**, 1210–11.
Steinitz, M. O., Burleson, C. E., and Marcus, J. A. (1970) *J. Appl. Phys.*, **41**, 5057.
Stephens, F. M. Jr and McDonald, R. O. (1956) *Proc. First Int. Conf. on Peaceful Uses of Atomic Energy*, Geneva, 1955, vol. 8, pp. 18–25.
Sterns, M. (1967) *Acta Crystallogr.*, **23**, 264–72.

Stoewe, K. (1996a) *Z. Anorg. Allg. Chem.*, **622**, 1419–22.
Stoewe, K. (1996b) *Z. Anorg. Allg. Chem.*, **622**, 1423–7.
Stoewe, K. (1997a) *Z. Anorg. Allg. Chem.*, **623**, 749–54.
Stoewe, K. (1997b) *J. Alloys Compds*, **246**, 111–23.
Stohl, F. V. and Smith, D. K. (1981) *Am. Miner.*, **66**, 610–25.
Stoller, S. M. and Richards, R. B. (1961) *Reactor Handbook*, 2nd edn, vol. II, Fuel Processing, Interscience, New York.
Storms, E. K. (1985) *J. Nucl. Mater.*, **132**, 231–43.
Straka, M., Dyall, K. G., and Pyykkö, P. (2001) *Theor. Chem. Acc.*, **106**, 393–403.
Streitweiser, A. and Müller-Westerhoff, U. (1968) *J. Am. Chem. Soc.*, **90**, 7364.
Strotzer, E. F., Schneider, O., and Biltz, W. (1943) *Z. Anorg. Allg. Chem.*, **243**, 307–21.
Stryer, L. (1988) *Biochemistry*, 3rd edn, W. H. Freeman and Co, New York, p. 705.
Stumpp, E. (1969) *Naturwissenschaften*, **56**, 370.
Stumpp, E. and Piltz, G. (1974) *Z. Anorg Allg. Chem.*, **409**, 53–9.
Sturchio, N. C., Antonio, M. R., Soderholm, L., Sutton, S. R., and Brannon, J. C. (1998) *Science*, **281**, 971–3.
Sugisaki, M., Hirashima, K., Yoshihara, S., and Oishi, Y. (1973) *J. Nucl. Sci. Technol.*, **10**, 387–9.
Sugisaki, M. and Sueyoshi, T. (1978) *J. Inorg. Nucl. Chem.*, **40**, 1543–9.
Sugiyama, K. and Onuki, Y. (2003) *High Magn. Fields*, **2**, 139–70.
Suglobova, I. G. and Chirkst, D. E. (1978a) *Radiokhimiya*, **20**, 361–5; *Sov. Radiochem.*, **20**, 310–14.
Suglobova, I. G. and Chirkst, D. E. (1978b) *Radiokhimiya*, **20**, 352–60; (1978) *Sov. Radiochem.*, **20**, 302–9.
Suglobova, I. G. and Chirkst, D. E. (1981) *Koord. Khimiya*, **7**, 97–102.
Sullivan, J. C., Hindman, J. C., and Zielen, A. J. (1961) *J. Am. Chem. Soc.*, **83**, 3373–8.
Sunder, S., Cramer, J. J., and Miller, N. H. (1996) *Radiochim. Acta*, **74**, 303–7.
Sunder, S., Miller, N. H., and Shoesmith, D. W. (2004) *Corrosion Sci.*, **46**, 1095–111.
Suski, W., Gibifiski, T., Wojakowski, A., and Czaynik, A. (1972) *Phys. Status Solidi*, **9**, 653–8.
Suski, W., Wojakowski, A., Blaise, A., Salmon, P., Fournier, J., and Mydlarz, T. (1976) *J. Magn. Mater.*, **3**, 195–200.
Sutton, S. (1955) *J. Inorg. Nucl. Chem.*, **1**, 68–74.
Swihart, G. H., Sen Gupta, P. K., Schlemper, E. O., Bach, M. E., and Gaines, R. V. (1993) *Am. Miner.*, **78**, 835–9.
Sylwester, E. R., Hudson, E. A., and Allen, P. G. (2000) *Geochim. Cosmochim. Acta*, **64**, 2431–8.
Szabó, Z., Glaser, J., and Grenthe, I. (1996) *Inorg. Chem.*, **35**, 2036–44.
Szabó, Z., Aas, W., and Grenthe, I. (1997) *Inorg. Chem.*, **36**, 5369–75.
Szabó, Z., Moll, H., and Grenthe, I. (2000) *J. Chem. Soc., Dalton Trans.*, 3158–161.
Szabó, Z. and Grenthe, I. (2000) *Inorg. Chem.*, **39**, 5036–43.
Szabó, Z. (2002) *J. Chem. Soc., Dalton Trans.*, 4242–7.
Szabó, Z. Toraishi, T., Vallet, V., and Grenthe, I. (2006) *Coord. Chem. Rev.*, In print.
Szwarc, R. and Latta, R. E. (1968) *J. Am. Ceram. Soc.*, **51**, 264–8.
Tabuteau, A., Jové, J., Pagès, M., and de Novion, C. H. (1984) *Solid State Commun.*, **50**, 357–61.

Tachibana, T., Ohmori, T., Yamanouchi, S., and Itaki, T. (1985) *J. Nucl. Sci. Technol.*, **22**, 155–7.
Tagawa, H. (1975) *J. Inorg. Nucl. Chem.*, **37**, 731–3.
Tagawa, H., Fujino, T., and Tateno, J. (1975) Japan Atomic Research Institute Report, JAERI-M 6180.
Tagawa, H. and Fujino, T. (1977) *Inorg. Nucl. Chem. Lett.*, **13**, 489–93.
Tagawa, H., Fujino, T., and Tateno, J. (1977) *Bull. Chem. Soc. Japan*, **50**, 2940–4.
Tagawa, H. and Fujino, T. (1978) *J. Inorg. Nucl. Chem.*, **40**, 2033–6.
Tagawa, H. and Fujino, T. (1980) *Inorg. Nucl. Chem. Lett.*, **16**, 91–6.
Tagawa, H., Fujino, T., Watanabe, K., Nakagawa, Y., and Saita, K. (1981a) *Bull. Chem. Soc. Japan*, **54**, 138–42.
Tagawa, H., Fujino, T., Ouchi, K., Watanabe, K., and Morimoto, T. (1981b) *J. Nucl Sci. Technol.*, **18**, 811–16.
Tagawa, H., Fujino, T., Ouchi, K., Watanabe, K., Saita, K., and Morimoto, T. (1983) *J. Nucl. Sci. Technol.*, **20**, 467–74.
Takano, Y. (1961) *Am. Miner.*, **46**, 812–22.
Tame, J. R. H. (2000) *Acta Crystallogr.*, **D56**, 1554–9.
Tanaka, H., Kimura, E., Yamaguchi, A., and Moriyama, J. (1972) *J. Jpn. Inst. Metals*, **36**, 633–7.
Tanamas, R. (1974) Research Center Karlsruhe Report, KFK-1910.
Tanner, P. A., Hung, S.-T., Mak, T. C. W., and Wang, R.-J. (1992) *Polyhedron*, **11**, 817–22.
Tanner, P. A., Silvestre, J. P. F., and Dao, N. Q. (1993) *New J. Chem.*, **17**, 263–6.
Tasker, I. R., O'Hare, P. A. G., Lewis, B. M., Johnson, G. K., and Cordfunke, E. H. P. (1988) *Can. J. Chem.*, **66**, 620–5.
Tateno, J., Fujino, T., and Tagawa, H. (1979) *J. Solid State Chem.*, **30**, 265–73.
Tatsumi, K. and Hoffmann, R. (1980) *Inorg. Chem.*, **19**, 2656–8.
Taylor, J. C. (1971) *Acta Crystallogr.*, **B27**, 1088–91.
Taylor, J. C. and Wilson, P. W. (1973a) *Acta Crystallogr. B*, **29**, 1942–4.
Taylor, J. C. and Wilson, P. W. (1973b) *Acta Crystallogr. B*, **29**, 1073–6.
Taylor, J. C. and Wilson, P. W. (1974a) *Acta Crystallogr. B*, **30**, 175–7.
Taylor, J. C. and Wilson, P. W. (1974b) *Acta Crystallogr. B*, **30**, 1481–4.
Taylor, J. C. and Wilson, P. W. (1974c) *Acta Crystallogr. B*, **30**, 169–75.
Taylor, J. C. and Wilson, P. W. (1974d) *J. Chem. Soc. Chem. Commun.*, pp. 598–5.
Taylor, J. C. and Wilson, P. W. (1974e) *Acta Crystallogr. B*, **30**, 2664–7.
Taylor, J. C. and Wilson, P. W. (1974f) *Acta Crystallogr. B*, **30**, 2803–5.
Taylor, J. C. and Wilson, P. W. (1975a) *J. Inorg. Nucl. Chem.*, **39**, 1989–91.
Taylor, J. C., and Wilson, P. W. (1975b) *J. Solid State Chem.*, **14**, 378–82.
Taylor, J. C. (1976a) *Coord. Chem. Rev.*, **20**, 197–273.
Taylor, J. C. (1976b) *Inorg. Nucl. Chem. Lett.*, **12**, 725–8.
Taylor, J. C. and Waugh, A. B. (1980) *J. Solid State Chem.*, **35**, 137–40.
Taylor, J. C., Stuart, W. I., and Mumme, I. A., (1981) *J. Inorg. Nucl. Chem.*, **43**, 2719–23.
Taylor, J. C. and Waugh, A. B. (1983) *Polyhedron*, **2**, 211–16.
Taylor, J. C. (1987) *Z. Kristallogr.*, **181**, 151–60.
Tempest, P. A., Tucker, P. M., and Tyler, J. W. (1988) *J. Nucl. Mater.*, **151**, 251–68.
Templeton, L. K., Templeton, D. H., Bartlett, N., and Seppelt, K. (1976) *Inorg. Chem.*, **15**, 2720–2.

Tetenbaum, M. and Hunt, P. D. (1968) *J. Chem. Phys.*, **49**, 4739–44.
Tetenbaum, M. and Hunt, P. D. (1970) *J. Nucl. Mater.*, **34**, 86–91.
Thibaut, E., Boutique, J.-P., Verbist, J. J., Levet, J.-C., and Noël, H. (1982) *J. Am. Chem. Soc.*, **104**, 5266–73.
Thoma, R. E. and Grimes, W. R. (1957) Phase Equilibria Diagrams for Fused Salt Systems, ORNL-2295.
Thoma, R. E., Insley, H., Landau, B. S., Friedman, H. A., and Grimes, W. R. (1958) *J. Am. Ceram. Soc.*, **41**, 538–44.
Thoma, R.E. (1959) Phase diagrams of Nuclear Reactor Materials, ORNL-2548.
Thoma, R. E. and Penneman, R. A. (1965) ORNL-3789, 33–35; (1965) N.S.A. 19, no. 30066.
Thoma, R. E., Insley, H., Hebert, G. M., Friedman, H. A., and Weaver, C. F. (1963) *J. Am. Ceram. Soc.*, **46**, 37–42.
Thoma, R. E., Friedman, H. A., and Penneman, R. A. (1966) *J. Am. Chem. Soc.*, **88**, 2046–7.
Thoma, R. E. (1971) ORNL-4812, pp. 1–416.
Thoma, R. E. (1972) N.S.A. 26, no. 24796.
Tomiyasu, H. and Fukutomi, H. (1982) *Bull. Res. Lab. Nucl. Reactors*, **7**, 57–80.
Tougait, O., Potel, M., Padiou, J., and Noël, H. (1997) *J. Alloys Compds*, **262**, 320–4.
Tougait, O., Potel, M., and Noël, H. (1998a) *J. Solid State Chem.*, **139**, 356–61.
Tougait, O., Potel, M., Levet, J. C., and Noël, H. (1998b) *Eur. J. Solid State Inorg. Chem.*, **35**, 67–76.
Tougait, O., Potel, M., and Noël, H. (1998c) *Inorg. Chem.*, **37**, 5088–91.
Toussaint, C. J. and Avogadro, A. (1974) *J. Inorg. Nucl. Chem.*, **36**, 781–4.
Toraishi, T., Farkas, I., Szabó, Z., and Grenthe, I. (2002) *J. Chem. Soc. Dalton Trans.*, 3805–12.
Toraishi, T., Aoyagi, N., Nagasaki, S., and Tanaka, S. (2004) *J. Chem. Soc. Dalton Trans.*, 3495–502.
Totemeier, T. C. (1995) *A Review of the Corrosion and Pyrophoricity Behavior of Uranium and Plutonium*, ANL/ED/95–2.
Traverso, O., Portanova, R., and Carassiti, V. (1974) *Inorg. Nucl. Chem. Lett.*, **10**, 771–5.
Troć, R. (1992) *Proc. 22èmes Journées des Actinides*, Méribel, France, p. 97.
Troć, R. and Suski, W. (1995) *J. Alloys Compds*, **219**, 1–5.
Trzebiatowski, W., Śliwa, A., and Staliński, B. (1954) *Rocz. Chem.*, **28**, 12–20.
Trzebiatowski, W. and Jabloński, A. (1960) *Nukleonika*, **5**, 587–96.
Trzebiatowski, W. and Mulak, J. (1970) *Bull. Acad., Polon. Sci. Ser. Sci. Chim.*, **18**, 121–6.
Tsai, H. C., Corington, A., and Olander, D. R. (1975) Lawrence Berkeley Laboratory Report, LBL-6016, p. 188.
Tso, T. C., Brown, D., Judge, A. I., Holloway, J. H., and Fuger, J. (1985) *J. Chem. Soc. Dalton Trans.*, 1853–8.
Tsushima, S., Yang, T., and Suzuki, A. (2001) *Chem. Phys. Lett.*, **334**, 365–73.
Tuller, H. L. (1981) in *Nonstoichiometric Oxides* (ed. O. T. Sørensen), Academic Press, New York, ch. 6. pp. 271–335.
Tutov, A. G., Plakhtii, V. P., Usov, O. A., Bublyaev, R. A., and Chernenkov, Yu. P. (1991) *Kristallografiya*, **36**, 1135–8.
Ugajin, M. (1982) *J. Nucl. Mater.*, **110**, 140–6.

Ugajin, M. (1983) *J. Nucl. Sci. Technol.*, **20**, 228–36.
Ugajin, M., Shiratori, T., and Shiba, K. (1983) *J. Nucl. Mater.*, **116**, 172–7.
Une, K. and Oguma, M. (1982) *J. Nucl. Mater.*, **110**, 215–22.
Une, K. and Oguma, M. (1983a) *J. Am. Ceram. Soc.*, **66**, C179–80.
Une, K. and Oguma, M. (1983b) *J. Nucl. Mater.*, **115**, 84–90.
Une, K. and Oguma, M. (1983c) *J. Nucl. Mater.*, **118**, 189–94.
United Nations, (1955) *Proc. First Int. Conf. on Peaceful Uses of Atomic Energy*, Geneva, 1955, vol. 8, pp. 3–145.
United Nations, (1958) *Proc. Second Int. Conf. on Peaceful Uses of Atomic Energy*, Geneva, 1958, vol. 4, pp. 3–68.
United Nations, (1964) *Proc. Third Int. Conf. on Peaceful Uses of Atomic Energy*, Geneva, 1964, vol. 12, pp. 119–325.
Uvarova, Y. A., Sokolova, E., Hawthorne, F. C., Agakhanov, A. A., and Pautov, L. A. (2004) *Can. Miner.*, **42**, 1005–11.
Vallet, V., Maron, L., Schimmelpfennig, B., Leininger, T., Teichteil, C., Gropen, O., Grenthe, I., and Wahlgren, U. (1999) *J. Phys. Chem. A*, **103**, 9285–9.
Vallet, V., Wahlgren, U., Schimmelpfennig, B., Szabó, Z., and Grenthe, I. (2001) *J. Am. Chem. Soc.*, **123**, 11999–2008.
Vallet, V., Wahlgren, U., Szabó, Z., and Grenthe, I. (2002) *Inorg. Chem.*, **41**, 5626–33.
Vallet, V., Moll, H., Wahlgren, U., Szabó, Z., and Grenthe, I. (2003) *Inorg. Chem.*, **42**, 1982–93.
Vallet, V., Privalov, T., Wahlgren, U., and Grenthe, I. (2004a) *J. Am. Chem. Soc.*, **124**, 7766–7.
Vallet, V., Szabó, Z., and Grenthe, I. (2004b) *J. Chem. Soc. Dalton Trans.*, 3799–807.
Van Axeel Castelli, V., Dalla Cort, A., Mandolini, L., Reinhoudt, D. N., and Schiaffino, L. (2000) *Chem. Eur. J.*, **7**, 1193–8.
Van den Bossche, G., Rebizant, J. G., Spirlet, M. R., and Goffart, J. (1986) *Acta Crystallogr. C*, **42**, 1478–80.
Van den Bossche, G., Spirlet, M. R., Rebizant, J., and Goffart, J. (1987) *Acta Crystallogr. C*, **43**, 383–4.
van Egmond, A. B. (1975) *J. Inorg. Nucl. Chem.*, **37**, 1929–31.
van Egmond, A. B. (1976a) *J. Inorg. Nucl. Chem.*, **38**, 1645–7.
van Egmond, A. B. (1976b) *J. Inorg. Nucl. Chem.*, **38**, 1649–51.
van Egmond, A. B. (1976c) *J. Inorg. Nucl. Chem.*, **38**, 2105–7.
Van Impe, J. (1954) *Chem. Eng. Prog.*, **50**, 230–4.
van Lierde, W., Strumane, R., Smets, E., and Amelinckx, S. (1962) *J. Nucl. Mater.*, **5**, 250–3.
van Lierde, W., Pelsmaekers, J., and Lecocq-Robert, A. (1970) *J. Nucl. Mater.*, **37**, 276–85.
Vance, E. R., Watson, J. N., Carter, M. L., Day, R. A., and Begg, B. D. (2001) *J. Am. Ceram. Soc.*, **84**, 141–4.
Vance, J. E. and Warner, J. C. (1951) *Uranium Technology-General Survey*, Natl. Nucl. En. Ser., Div. VII, 2A, TID-5231, USAEC Technical Information Service, Oak Ridge, TN.
Vaugoyeau, H., Lombard, L., and Morterat, J. P. (1971) *J. Nucl. Mater.*, **39**, 323–9.
Vdovenko, V. M., Mashirov, L. G., Blokhima, V. K., Suglobova, I. G., and Suglobov, D. N. (1963) *Sov. Radiochem.*, **5**, 67–75.

Vdovenko, V. M., Mashirov, L. G., and Suglobov, D. N. (1964) *Radiokhimiya*, **6**, 299–305; *Sov. Radiochem.*, **6**, 289–94.
Vdovenko, V. M., Skoblo, A. I., Suglobov, D. N., Shcherbakova, L. L., and Scherbakov, V. A. (1969) *Zh. Neorg. Khim.*, **12**, 2863–5; *Russ. J. Inorg. Chem.*, **12**, 1513–15.
Vdovenko, V. M., Volkov, V. A., Kozhina, I. I., and Suglobova, I. G. (1972a) *Sov. Radiochem.*, **14**, 492–3.
Vdovenko, V. M., Volkov, V. A., Kozhina, I. I., and Suglobova, I. G. (1972b) *Sov. Radiochem.*, **14**, 489–91.
Vdovenko, V. M., Suglobova, I. G., and Chirkst, D. E. (1973a) *Radiokhimiya*, **15**, 58–61; (1973a) *Sov. Radiochem.*, **15**, 53–5.
Vdovenko, V. M., Kozhina, I. I., Suglobova, I. G., and Chirkst, D. E. (1973b) *Radiokhimiya*, **15**, 172–127; *Soviet Radiochem.*, **15**, 168–72.
Vdovenko, V. M., Kozhina, I. I., Suglobova, I. G., and Chirkst, D. E. (1974a) *Radiokhimiya*, **16**, 369–77; (1974) *Sov. Radiochem.*, **16**, 369–76.
Vdovenko, V. M., Volkov, V. A., and Suglobova, I. G. (1974b) *Radiokhimiya*, **16**, 363–8.
Vdovenko, V. M., Suglobova, I. G., and Chirkst, D. E. (1974c) *Radiokhimiya*, **16**, 203–8.
Védrine, A., Baraduc, L., and Cousseins, J.-C. (1973) *Mater. Res. Bull.*, **8**, 581–8.
Védrine, A., Trottier, D., Cousseins, J.-C., and Chevalier, R. (1979) *Mater. Res. Bull.*, **14**, 583–7.
Vilcu, R. and Misdolea, C. (1967) *J. Chem. Phys.*, **46**, 906.
Viswanathan, K. and Harnett, O. (1986) *Am. Miner.*, **71**, 1489–93.
Vita, O. A., Walker, C. R., and Litteral, E. (1973) *Anal. Chim. Acta*, **64**, 249–57.
Vochten, R. and Deliens, M. (1980) *Phys. Chem. Miner.*, **6**, 129–43.
Vochten, R., Blaton, N., Peeters, O., and Deliens, M. (1996) *Can. Miner.*, **34**, 1317–22.
Vochten, R., Blaton, N., and Peeters. O. (1997) *Can. Miner.*, **35**, 1021–5.
Vochten, R. and Deliens, M. (1998) *Can. Miner.*, **36**, 1077–81.
Vochten, R., Deliens, M., and Medenbach, O. (2001) *Can. Miner.*, **39**, 1685–9.
Vodovatov, V. A., Gorshkov, N. G., Lychev, A. A., Mashirov, L. G., and Leikena, E. V. (1984) *Radiokhimiya*, **26**, 261–4.
Vogt, O. (1982) *Actinides in Perspective* (ed. N. M. Edelstein), Pergamon Press, Oxford, pp. 289–307.
Voliotis, S. and Rimsky, A. (1975) *Acta Crystalogr. B*, **34**, 2612–15.
Volkov, V. A., Suglobova, I. G., and Chirkst, D. E. (1979) *At. Energy.*, **47** (2), 110–12.
Volkov, V. A., Suglobova, I. G., and Chirkst, D. E. (1987) *Radiokhimiya*, **29** (3), 273–6.
Volkovich, V. A., Griffiths, T. R., Fray, D. J., and Fields, M. (1998) *Vibr. Spectrosc.*, **17**, 83–91.
Vorobei, M. P., Siba, O. V., Bevz, A. S., and Kapshukov, I. I. (1971) *Zh. Fiz. Khim.*, **45**, 22–5.
Voronov, N. M., Danilin, A. S., and Kovalev, I. T. (1962) in *Thermodynamics of Nuclear Materials*, Proc. Symp. 1962, International Atomic Energy Agency, Vienna, pp. 789–800.
Voronov, N. M. and Sofronova, R. M. (1972) in *Physical Chemistry of Alloys and Refractory Compounds of Thorium and Uranium* (ed. O. S. Ivanov), Academy of Sciences of the USSR, Israel Program for Scientific Translations, Ltd., Jerusalem, pp. 204–14.
Voronov, N. M., Sofrononova, R. M., and Voitekhova, E. A. (1972) in *Physical Chemistry of Alloys and Refractory Compounds of Thorium and Uranium* (ed. O. S. Ivanov),

Academy of Sciences of the USSR, Israel Program for Scientific Translations, Ltd., Jerusalem, pp. 222–8.
Waber, J. T., Chiotti, P., and Miner, W. N. (1964) *Compounds of Interest to Reactor Technology*, IMD Special Report 13, Metallurgical Society of AIME.
Wachter, P. (ed.) (1980) *Proc. Int. Conf. on the Physics of Actinides and Related 4f Materials*, North-Holland, Amsterdam; *Physica*, 102B and 102C.
Wadier, J. F. (1973) CEA Report, CEA-R 4507.
Wadt, W. R. and Hay, P. J. (1979) *J. Am. Chem. Soc.*, **101**, 5198–206.
Wadt, W. R. (1981) *J. Am. Chem. Soc.*, **103**, 6053–7.
Wagner, W., Edelstein, N. M., Whittaker, B., and Brown, D. (1977) *Inorg. Chem.*, **16**, 1021–6.
Wahlgren, U., Moll, H., Grenthe, I., Schimmelpfennig, B., Maron, L., Vallet, V., and Gropen, O. (1999) *J. Phys. Chem. A*, **103**, 8257–64.
Wait, E. (1955) *J. Inorg. Nucl. Chem.*, **1**, 309–12.
Walder, A. J. and Hodgeson, T. (1994) in *DOE-ORNL 1994 Conf. Analytical Chemistry in Energy Technology* (eds. R. W. Morrow and J. S. Crain), ASTM Spec. Tech. Publ. 1291.
Walder, A. J. (1997) in *Modern Isotope Ratio Mass Spectrometry* (ed. I. T. Platzner), John Wiley, New York, pp. 83–108.
Walenta, K. (1965) *Am. Miner.*, **50**, 1143–57.
Walenta, K. (1974) *Am. Miner.*, **59**, 166–71.
Walenta, K. (1976) *Schweiz. Miner. Petrogr. Mitt.*, **56**, 167–85.
Walenta, K. (1983) *Neues Jahrb. Miner. Monatsschr.*, **6**, 259–69.
Walenta, K. (1985) *Tschermaks Miner. Petrogr. Mitt.*, **34**, 25–34.
Walenta, K. (1998) *Aufschluss*, **49**, 253–7.
Wang, W.-D., Bakac, A., and Espenson, J. H. (1995) *Inorg. Chem.*, **34**, 6034–9.
Ward, J. W., Cox, L. E., Smith, J. L., Stewart, G. R., and Wood, J. H. (1979) *J. Phys.* (*Paris*), **40**, C4, 15–17.
Ward, J. W. (1985) in *Handbook on the Physics and Chemistry of the Actinides,* vol. 3 (eds. A. J. Freeman and C. Keller) Elsevier, Amsterdam, pp, 1–74.
Wardman, P. (1989) *J. Phys. Chem. Ref. Data*, **18**, 1637.
Warf, J. C. (1958) in *The Chemistry of Uranium, Collected Papers*, TID-5290 (eds. J. J. Katz and E. Rabinowitch), Oak Ridge, TN, p. 81.
Warner, J. C. (1953) *Metallurgy of Uranium*, Natl Nucl. En. Ser., Div. IV, 12A, , USAEC Technical Information Service, Oak Ridge, TN.
Warner, J. K. and Ewing, R. C. (1993) *Am. Miner.*, **62**, 403–10.
Watkin, D. J., Denning, R. G., and Prout, K. (1991) *Acta Crystallogr. C*, **47**, 2517–19.
Watt, G. W., Baugh, D. W., and Gadd, K. F. (1974) *Inorg Nucl. Chem. Lett.*, **10**, 987–9.
Wedekind, E. and Jochem, O. (1913) *Ber. Dtsch. Chem. Ges.*, **46**, 1204–5.
Wedermeyer, H. (1984) in *Gmelin Handbuch der Anorganischen Chemie*, Suppl. Ser. Uranium, C4, pp. 1–64.
Weeks, J. L. (1955) *AIME, J. Metals*, **203**, 192.
Weigel, F. (1958) in *Handbuch der Präparativen Anorganischen Chemie* (ed. G. Brauer), Enke, Stutttgart, pp. 1197–203.
Weigel, F. and Neufeldt, S. (1961) *Angew. Chem.*, **73**, 468.
Weitzel, H. and Keller, C. (1975) *J. Solid State Chem.*, **13**, 136–41.

Weller, M. T., Light, M. E., and Gelbrich, T. (2000) *Acta Crystallogr.*, **B56**, 577–83.
Wells, A. F. (1990) in *Structural Inorganic Chemistry*, Oxford University Press.
Westrum, E. F. Jr and Grønvold, F. (1959) *J. Am. Chem. Soc.*, **81**, 1777–80.
Westrum, E. F. Jr and Grønvold, F. (1962) in *Thermodynamics of Nuclear Materials*, Proc. Symp. 1962, International Atomic Energy Agency, Vienna, pp. 3–37.
Westrum, E. F. Jr, Takahashi, Y., and Grønvold, F. (1965) *J. Phys. Chem.*, **69**, 3192–3.
White, T. J. (1984) *Am. Miner.*, **69**, 1156–72.
Whitman, C. I., Compton, V., and Holden, R. B. (1955) *Zone Melting of Uranium*, TID-10098.
Wicke, E. and Otto, K. (1962) *Z. Phys. Chem.* (NF), **31**, 222–48.
Wilhelm, H. A., Chiotti, P., Snow, A. I., and Daane, A. H. (1949) *J. Chem. Soc.*, Suppl. 2, 318–21.
Wilhelm, H. A. (1956) *Proc. First Int. Conf. on Peaceful Uses of Atomic Energy*, Geneva, 1955, vol. 8, pp. 162–74.
Wilkins, R. G. (1991) *Kinetics and Mechanism of Reactions of Transition Metal Complexes*, 2nd edn, VCH Publishers, Weinheim, Germany.
Wilkinson, M. K., Shull, C. G., and Rundle, R. E. (1955) *Phys. Rev.*, **99**, 627.
Wilkinson, W. D. and Murphy, W. F. (1958) *Nuclear Reactor Metallurgy*, van Nostrand.
Wilkinson, W. D. (1962) *Uranium Metallurgy*, vol. I, *Uranium Process Metallurgy*, vol. II, *Uranium Corrosion and Alloys*, Interscience, New York.
Williams, C. W., Morss, L. R., and Choi, I.-K. (1984) in *Geochemical Behavior of Disposed Radiochemical Waste* (eds. G. S. Barney, J. D. Navratil, and W. W. Schulz), Am. Chem. Soc. Symp. Ser. 246, American Chemical Society, Washington, DC, pp. 323–34.
Willis, B. T. M. (1964a) *J. Phys.* (*Paris*), **29**, 431–40.
Willis, B. T. M. (1964b) *Proc. Brit. Ceram. Soc.*, **1**, 9–19.
Willis, B. T. M. (1978) *Acta Crystallogr.*, **A34**, 88–90.
Willis, B. T. M. (1987) *J. Chem. Soc., Faraday Trans. 2*, **83**, 1073–81.
Wilmarth, W. R. and Peterson, J. R. (1981) Characterization of selected solid-state actinide (and related) compounds via Raman and absorption spectroscopy, in *Handbook on the Physics and Chemistry of the Actinides*, vol. 6 (eds. A. J. Freeman and C. Keller), North-Holland, Amsterdam, pp. 1–39.
Wilson, W. B., Alexander, C. A., and Gerds, A. F. (1961) *J. Inorg. Nucl. Chem.*, **20**, 242–51.
Wilson, W. W., Naulin, C., and Bougon, R. (1977) *Inorg. Chem.*, **16**, 2252–7.
Winslow, G. H. (1971) *High Temp. Sci.*, **3**, 361–80.
Winslow, G. H. (1973) *High Temp. Sci.*, **5**, 176–91.
Winter, P. W. (1989) *J. Nucl. Mater.*, **161**, 38–43.
Wisnyi, L. G. and Pijunowski, S. W. (1957) USAEC Technical Information Service, TID-7530.
Wolf, A. S., Posey, J. C., and Rapp, K. E. (1965) *Inorg. Chem.*, **4**, 751–4.
Wolf, S. F. (1999) in *Reviews in Mineralogy*, vol. 38 (eds. P. C. Burns and R. Finch), Mineralogical Society of America, Washington, DC, pp. 623–53.
Woodley, R. E. (1981) *J. Nucl. Mater.*, **96**, 5–14.
Woodward, L. A. and Ware, M. J. (1968) *Spectrochim. Acta A*, **24**, 921–5.
Woody, R. J. and George, D. R. (1955) *Nucl. Eng. Sci. Congr.*, Cleveland, OH, Preprint 329.

Wronkiewicz, D. J., Bates, J. K., Gerding, T. J., Veleckis, E., and Tani, B. S. (1992) *J. Nucl. Mater.*, **190**, 107–27.
Wronkiewicz, D. J., Bates, J. K., Wolf. S. F., and Buck, E. C. (1996) *J. Nucl. Mater.*, **238**, 78–95.
Wronkiewicz, D. J. and Buck, E. C. (1999) *Rev. Miner.*, **38**, 475–97.
Yamamoto, T., Kayano, H., Sinaga, S., Ono, S., Tanaka, S., and Yamawaki, M. (1991) *J. Less Common Metals*, **172–174**, 71–8.
Yamamoto, T., Kayano, H., and Yamawaki, M. (1994) *J. Alloys Compds*, **213–214**, 533–5.
Yamamoto, T., Teshigawara, M., Kayano, H., Minakawa, N., and Funahashi, S. (1995) *J. Alloys Compds*, **224**, 36–8.
Yamamoto, T., Ishii, Y., and Kayano, H. (1998) *J. Alloys Compds*, **269**, 162–5.
Yamanaka, S., Iguchi, T., Fujita, Y., Uno, M., Katsura, M., Hoshino, Y., and Saiki, W. (1999) *J. Alloys Compds*, **293–295**, 52–6.
Yamashita, T. and Fujino, T. (1985) *J. Nucl. Mater.*, **136**, 117–23.
Yamashita, T., Fujino, T., and Tagawa, H. (1985) *J. Nucl. Mater.*, **132**, 192–201.
Yang, T., Tsushima, S., and Suzuki, A. (2003) *J. Solid State Chem.*, **171**, 235–41.
Yoshihara, K., Yamagami, S., Kanno, M., and Mukaibo, T. (1971) *J. Inorg. Nucl. Chem.*, **33**, 3323–9.
Young, A. P. and Schwartz, C. M. (1962) Battelle Memorial Institute Report, BMI-1585.
Young, A. P. and Schwartz, C. M. (1963) *J. Inorg. Nucl. Chem.*, **25**, 1133–7.
Young, E. J., Weeks, A. D., and Meyrowitz, R. (1966) *Am. Miner.*, **51**, 651–63.
Young, G. A. (1955) *Feed Materials. A Bibliography of Classified Report Literature*, TID-3081.
Yusov, A. B. and Shilov, V. P. (2000) *Russ. Chem. Bull. Int. Ed.* **49**, 1925–53.
Zachariasen, W. H. (1945) Manhattan Project Report, CP-2611, p. 14.
Zachariasen, W. H. (1946) University of Chicago Metallurgical Laboratory Report, MDDC-1152.
Zachariasen, W. H. (1948a) *Acta Crystallogr.*, **1**, 265–8.
Zachariasen, W. H. (1948b) *Acta Crystallogr.*, **1**, 281–5.
Zachariasen, W. H. (1948c) *J. Chem. Phys.*, **16**, 254.
Zachariasen, W. H. (1948d) *J. Am. Chem. Soc.*, **70**, 2147–51.
Zachariasen, W. H. (1948e) *Acta Crystallogr.*, **1**, 277–81.
Zachariasen, W. H. (1948f) *Acta Crystallogr.*, **1**, 285–7.
Zachariasen, W. H. (1949a) *Acta Crystallogr.*, **2**, 94–9.
Zachariasen, W. H. (1949b) *Acta Crystallogr.*, **2**, 291–6.
Zachariasen, W. H. (1949c) *Acta Crystallogr.*, **2**, 296–8.
Zachariasen, W. H. (1949d) *Acta Crystallogr.*, **2**, 390–3.
Zachariasen, W. H. (1954a) *Acta Crystallogr.*, **7**, 788–91.
Zachariasen, W. H. (1954b) *Acta Crystallogr.*, **7**, 795–9.
Zachariasen, W. H. (1954c) *Acta Crystallogr.*, **7**, 783–7; 792–4.
Zachariasen, W. H. (1954d) *Acta Crystallogr.*, **7**, 783–7.
Zachariasen, W. H. (1975) LA-UR-75–1364, 1977, INIS Atomindex 8, no. 283142.
Zadneporovskii, G. M. and Borisov, S. V. (1971) *Zh. Strukt. Khim.*, **12**, 831–9; *J. Strukt. Chem.*, **12**, 761–9.
Zalkin, A., Templeton, D. H., and Hopkins, T. E. (1967) *Inorg. Chem.*, **5**, 1466–70.
Zalkin, A., Templeton, L. K., and Templeton, D. H. (1989) *Acta Cryst. C*, **45**, 810–11.

Zhang, J., Wan, A., and Gong, W. (1992) *Acta Petrol. Miner.*, **11**, 178–84. (in Chinese).
Zhang, Z. and Pitzer, R. M. (1999) *J. Phys. Chem. A*, **103**, 6880–6.
Zhangru, C., Keding, L., Falan, T., Yi, Z., and Xiaofa, G. (1986) *Kexue Tongbao* (*Chinese Science Bulletin*), **31**, 396–401.
Zhao, D. and Ewing, R. C. (2000) *Radiochim. Acta.*, **88**, 739–49.
Zimmermann, J. I. C. (1882) *Ber. Dtsch. Chem. Ges.*, **15**, 847–51; *Liebig's Ann. Chem.*, **213**, 285–319.
Zogal, O. J., Lam, D. J., Zygmunt, A., Drulis, H., Petryński, W., and Staliński, S. (1984) *Phys. Rev. B*, **29**, 4837–42.
Żołnierek, Z., Gajek, Z., and Khan Malek, Ch. (1984) *Physica B+C* (*Amsterdam, Neth.*), **125**, 199–214.
Zych, E. and Drożdżyński, J. (1986) *Inorg. Chim. Acta, f-Block Elements*, **115**, 219–22.
Zych, E. and Drożdżyński, J. (1990a) *Polyhedron*, **9** (17), 2175–6.
Zych, E. and Drożdżyński, J. (1990b) *J. Less Common Metals*, **164**, 233–8.
Zych, E. and Drożdżyński, J. (1991) *Eur. J. Solid State Inorg. Chem.*, **28**, 575–80.
Zych, E., Starynowicz, P., Lis, T., and Drożdżyński, J. (1993) *Polyhedron*, **12** (13), 1661–6.

SUBJECT INDEX

Vol. 1: 1–698, Vol. 2: 699–1395, Vol. 3: 1397–2111, Vol. 4: 2113–2798, Vol. 5: 2799–3440.

Page numbers suffixed by t and f refer to Tables and Figures respectively.

AUTHOR INDEX

Vol. 1: 1–698, Vol. 2: 699–1395, Vol. 3: 1397–2111, Vol. 4: 2113–2798, Vol. 5: 2799–3440.

Page numbers suffixed by t and f refer to Tables and Figures respectively.

CHAPTER SIX

NEPTUNIUM

Zenko Yoshida, Stephen G. Johnson, Takaumi Kimura, and John R. Krsul

6.1 HISTORICAL

The first report on the discovery of neptunium was in 1940 by McMillan and Abelson (1940), although McMillan did the preliminary work in 1939 and published his findings (McMillan, 1939). He did not claim that a new element had been discovered until confirmatory measurements had been undertaken in the following year. The production of neptunium was accomplished by placing a layer of uranium trioxide on paper with several aluminum or paper foils and then exposing this to neutrons from a cyclotron. Examination of the uranium paper sample containing the non-recoiling fraction displayed that two new radioactive components had been created. One component displayed a 23 min half-life, later identified as U-239, while the second exhibited a 2.3 day half-life. Both components decayed via β particle emission. Preliminary chemical analysis was performed to determine the behavior of the 2.3 day component and resulted in the contradictory assignment of this component as that exhibiting an atomic number of 93, but not being transuranic in nature (Segrè, 1939). Segrè noted in his paper that his conclusions were contradictory. However, the following quotation is from his paper, "The necessary conclusion seems to be that the 23 minute uranium decays into a very long-lived 93 and that transuranic elements have not yet been observed." The primary stumbling block to the proper assignment of the material as transuranic in nature was the lack of

observation of any alpha decay activity that would emanate from the daughter product of the beta decay of this new material with an atomic number 93. It was this work by Segrè (1939) that led McMillan and Abelson to revisit the chemical analysis and determine its properties in greater depth.

To initiate their work they first had to generate more material. In doing this they were able to confirm the 'linked' nature of the 23 min and 2.3 day half-life materials observed. The ratio of these two materials was observed to remain constant. This also confirmed the earlier suggestion by Hahn *et al.* (Quill, 1938) that the following reaction was possible when uranium underwent neutron bombardment:

$$\mathrm{U} + \text{neutron} \rightarrow \mathrm{U}(23\,\text{minute}) \rightarrow \text{Eka-Re} \tag{6.1a}$$

$$^{238}\mathrm{U}(\mathrm{n},\gamma)^{239}\mathrm{U}(\beta^-, 23\ \text{min}) \rightarrow {}^{239}\mathrm{Np}(\beta^-, 2.3\ \text{day}) \rightarrow {}^{239}\mathrm{Pu} \tag{6.1b}$$

Differences between the rare earths and this element were observed immediately by McMillan and Abelson (1940) because it did not form a precipitate when exposed to HF in the presence of bromate, an oxidizing agent, in a strong acid. It did form a precipitate with HF in the presence of SO_2, a reducing agent. This bifurcated behavior in the presence of HF was thought to explain the incorrect assignment of this element as a rare earth by Segrè (1939) since the oxidizing potential of the solution had not been well controlled in earlier experiments (Segrè, 1939). Further evidence strongly suggested that the material was indeed an actinide, such as, precipitation in the reduced state with a thorium carrier by iodate and in the oxidized state with a uranium carrier by acetate. Also the precipitation with thorium carrier in the presence of H_2O_2 and precipitation in a carbonate-free basic solution indicated actinide-like behavior. Careful confirmatory measurements, which involved uranium that had undergone neutron bombardment and subsequent purification via fluoride precipitation in the presence of SO_2, showed the in-growth of the new element with a 2.3 day half-life. The new material was observed to exhibit a beta particle of energy approximately 470 keV. Further speculation by McMillan and Abelson regarding the daughter product, which would have atomic number 94 and a mass number of 239, was also recorded but will be discussed in Chapter 7 of this work. The element discovered by McMillan and Abelson was named after the planet Neptune, which is the first planet beyond Uranus in our solar system. This system was likewise followed for naming plutonium as its orbit was beyond Neptune.

6.2 NUCLEAR PROPERTIES

Twenty-two isotopes of neptunium are now known (Table 6.1). The isotope ^{237}Np has a sufficiently long half-life ($t_{1/2} = 2.144 \times 10^6$ years) that can be handled at weighable quantities. It is the most significant neptunium

Table 6.1 *Nuclear properties of neptunium isotopes.*

Mass number	*Half-life*	*Mode of decay*	*Main radiations* (MeV)	*Method of production*
226	31 ms	EC, α	α 8.044	^{209}Bi(^{22}Ne,5n)
227	0.51 s	EC, α	α 7.677	^{209}Bi(^{22}Ne,4n)
228	61.4 s	EC, α		^{209}Bi(^{22}Ne,3n)
229	4.0 min	α ≥ 50% EC ≤ 50%	α 6.890	^{233}U(p,5n)
230	4.6 min	α > 99% EC ≤ 0.97%	α 6.66	^{233}U(p,4n)
231	48.8 min	EC < 99% α > 1%	α 6.28 γ 0.371	^{233}U(d,4n) ^{235}U(d,6n)
232	14.7 min	EC	γ 0.327	^{233}U(d,3n)
233	36.2 min	EC < 99% α ∼ 10^{-3}%	α 5.54 γ 0.312	^{233}U(d,2n) ^{235}U(d,4n)
234	4.4 d	EC 99.95% β$^+$ 0.05%	γ 1.559	^{235}U(d,3n)
235	396.1 d	EC > 99% α 1.6 × 10^{-3}%	α 5.022 (53%) 5.004 (24%)	^{235}U(p,2n)
236[a]	22.5 h	β$^-$ 50% EC 50%	β$^-$ 0.54 γ 0.642	^{235}U(d,n)
236[a]	1.54 × 10^5 yr	EC 87% β$^-$ 13%	γ 0.163	^{235}U(d,n)
237	2.144 × 10^6 yr >1 × 10^{18} yr	α SF	α 4.788 (51%) 4.770 (19%) γ 0.086	^{237}U daughter ^{241}Am daughter
238	2.117 d	β$^-$	β$^-$ 1.29 γ 0.984	^{237}Np(n,γ)
239	2.3565 d	β$^-$	β$^-$ 0.72 γ 0.106	^{243}Am daughter ^{239}U daughter
240	1.032 h	β$^-$	β$^-$ 2.09 γ 0.566	^{238}U(α,pn)
240 m	7.22 min	β$^-$	β$^-$ 2.05 γ 0.555	^{240}U daughter ^{238}U(α,pn)
241	13.9 min	β$^-$	β$^-$ 1.31 γ 0.175	^{238}U(α,p) ^{244}Pu(n,p3n)
242 g or m	5.5 min	β$^-$	β$^-$ 2.7 γ 0.786	^{244}Pu(n,p2n) ^{242}Pu(n,p)
242 g or m	2.2 min	β$^-$	β$^-$ 2.7 γ 0.736	^{242}U daughter
243	1.85 min	β$^-$	γ 0.288	^{136}Xe + ^{238}U
244	2.29 min	β$^-$	γ 0.681	^{136}Xe + ^{238}U

[a] Not known whether ground-state nuclide or isomer.

isotope for chemists. ^{237}Np is synthesized by neutron irradiation of uranium according to the reactions (6.2) to (6.4). In conventional nuclear reactors ^{237}Np is generated as a by-product mainly through reactions (6.2) and (6.3). The latter reaction predominates in reactors with fuels of enriched ^{235}U.

$$^{238}\mathrm{U}(n,2n)\,^{237}\mathrm{U}\underset{6.75\,\mathrm{d}}{\overset{\beta^-}{\rightarrow}}\,^{237}\mathrm{Np} \tag{6.2}$$

$$^{235}\mathrm{U}(n,\gamma)\,^{236}\mathrm{U}(n,\gamma)^{237}\mathrm{U}\overset{\beta^-}{\rightarrow}\,^{237}\mathrm{Np} \tag{6.3}$$

$$^{238}\mathrm{U}(n,\gamma)\,^{239}\mathrm{U}\overset{\beta^-}{\rightarrow}\,^{239}\mathrm{Np}\overset{\beta^-}{\rightarrow}\,^{239}\mathrm{Pu}(n,\gamma)^{240}\mathrm{Pu}\overset{\beta^-}{\rightarrow}\,^{240}\mathrm{Am}(n,\gamma)^{241}\mathrm{Am}\overset{\alpha}{\rightarrow}\,^{237}\mathrm{Np} \tag{6.4}$$

The isotopes ^{238}Np and ^{239}Np have relatively short half-lives and are useful as radioactive tracers for analytical applications or for fundamental chemistry research. They are synthesized by neutron irradiation of ^{237}Np and ^{238}U, respectively, through the following reactions:

$$^{237}\mathrm{Np}(n,\gamma)^{238}\mathrm{Np} \tag{6.5}$$

$$^{238}\mathrm{U}(n,\gamma)^{239}\mathrm{U}\overset{\beta^-}{\rightarrow}\,^{239}\mathrm{Np} \tag{6.6}$$

The isotopes ^{235}Np and ^{236}Np are synthesized by cyclotron irradiation of ^{235}U according the following reactions:

$$^{235}\mathrm{U}(d,n)^{236}\mathrm{Np} \tag{6.7}$$

$$^{235}\mathrm{U}(p,n)^{235}\mathrm{Np} \tag{6.8}$$

The isotopes heavier than ^{237}Np are unstable with respect to β^- decay. Isotopes lighter than ^{237}Np decay by electron capture and also are unstable with respect to alpha decay.

6.3 PRODUCTION OF PRINCIPAL NEPTUNIUM ISOTOPES

The principal isotopes of neptunium are generated by irradiation of uranium with neutrons. Of the 22 isotopes listed in Table 6.1, only ^{235}Np, ^{236}Np and ^{237}Np have half-lives long enough to permit accumulation. Neptunium-237 is generated by reactions (6.2), (6.3) and (6.4). However, by irradiating uranium, only ^{237}Np is capable of accumulating. Neptunium-239 is produced from irradiation of ^{238}U and the decay of the resulting ^{239}U, however, the half-life of ^{239}Np, 2.3565 days, is too short for accumulation. Irradiation of uranium by neutrons is unsuitable for the generation of ^{235}Np and ^{236}Np. Therefore only ^{237}Np is produced in any significant quantities. Currently, the production of plutonium is the source of ^{237}Np where the isotope is a by-product of the process. Significant quantities also reside in spent fuel, in high-level waste (HLW), and in solutions containing ^{237}Np stored at various reprocessing

facilities. There are no known commercial uses for neptunium. The need for ^{238}Pu as a heat source for radioisotope thermoelectric generators (RTGs) and radioisotope heater units (RHUs) is the main reason to separate and purify ^{237}Np. RTGs are used to supply electricity to space vehicles used in the Galileo, Ulysses, and Cassini NASA missions (see Chapter 7). RHUs are used to provide heat for delicate instruments on space missions. Future needs to separate ^{237}Np and the other actinides from spent fuel and HLW may be required by the proposed transmutation of actinides residing in these materials. Removal of the transuranics, including especially ^{237}Np, has the advantage of eliminating concerns for the long-term storage of radioactive waste. A recent and rather novel use of ^{237}Np is to produce pure ^{236}Pu tracer to assess the amount of plutonium in the environment. Yamana *et al.* (2001) demonstrated that the irradiation of ^{237}Np with bremsstrahlung of an electron beam of 23 and 30 MeV produced ^{236}Pu with low ^{238}Pu impurity. Neptunium-237 could also be used in nuclear weapons; its critical mass is approximately 73 kg.

Plutonium-238 is generated by the reaction shown below:

$$^{237}\mathrm{Np}(\mathrm{n},\gamma)\ ^{238}\mathrm{Np} \xrightarrow{\beta^-} {}^{238}\mathrm{Pu} \tag{6.9}$$

To obtain ^{238}Pu, ^{237}Np is separated from spent fuel by various modifications of the well-known plutonium and uranium recovery by extraction (Purex) process. After dissolution, neptunium is separated from the spent fuel by solvent extraction and ion exchange by careful adjustments of acid concentrations, oxidations states, and volume percent of tributyl phosphate (TBP). The separated neptunium is precipitated as neptunium oxalate, calcined to neptunium oxide, and fabricated into targets. Targets of the separated isotope are irradiated in a high neutron flux. After irradiation, the targets are cooled for a specific amount of time to allow for fission product decay and then dissolved. ^{238}Pu is then separated from ^{237}Np by taking advantage of the differences in the characteristic oxidation states of the resulting fission products, neptunium, and plutonium.

To date, the reprocessing of irradiated nuclear fuel has focused on the separation of plutonium and uranium from fission products and other actinides. Proposed transmutation and advanced nuclear fuel cycles will require the development of separations that include the actinides and are safe, efficient, and environmentally acceptable. The need for these new technologies will create significant opportunities for research and development activities in the field of actinide chemistry.

6.4 NEPTUNIUM IN NATURE

^{237}Np ($t_{1/2} = 2.144 \times 10^6$ years) has the longest half-life of neptunium isotopes. Because this half-life is considerably shorter than the age of the Earth, which is about 4.5×10^9 years, primordial ^{237}Np no longer exists on Earth.

Neptunium isotopes can be formed by nuclear reactions continuously taking place in the Earth's crust, resulting in a dynamic equilibrium between the rate of formation and the rate of decay. Neutron capture by ^{238}U produces ^{239}Np (see reaction (6.6)), and an (n,2n) reaction on ^{238}U forms ^{237}Np (see reaction (6.2)). The neutrons originate from the spontaneous fission of ^{238}U, the neutron-induced fission of ^{235}U, (α,n) reactions on elements of low atomic number, and/or fission or spallation reactions induced by cosmic rays. Small amounts of ^{239}Np are expected to occur in uranium minerals by continuous formation from ^{238}U, but its half-life of 2.36 days is too short to permit any significant equilibrium concentration to be reached (Garner *et al.*, 1948; Seaborg and Perlman, 1948; Levine and Seaborg, 1951). The isolation of microgram amounts of ^{239}Pu by Peppard *et al.* (1951) from Belgian Congo (now Democratic Republic of the Congo) uranium undoubtedly establishes the existence of ^{239}Np in nature. The isotope ^{237}Np itself has been identified in and isolated from a uranium ore concentrate from Belgian Congo and in other minerals (Peppard *et al.*, 1952). The maximum ratio of ^{237}Np to uranium in such minerals is about 10^{-12}.

The primary sources of neptunium in the biosphere, as with the other transuranium elements, are atmospheric nuclear explosions. On the basis of the analyzed results on global fallout, it was calculated that 2500 kg of ^{237}Np had been generated, which is comparable in mass with the quantity of plutonium (4200 kg of ^{239}Pu and 700 kg of ^{240}Pu) (Efurd *et al.*, 1984). There is little information about the man-made neptunium content of various natural materials, because of the low specific radioactivity of the long-lived ^{237}Np and the systematic difficulties in its determination (Novikov *et al.*, 1989). For global fallout, the ^{237}Np/^{239,240}Pu ratio lies within one order of magnitude (1–10) $\times$ 10^{-3}. When 5×10^{-3} is taken as an average value of the ratio, the concentration of ^{239,240}Pu in seawater is 13×10^{-3} mBq L^{-1}, and the ^{237}Np concentration comprises 6.5×10^{-5} mBq L^{-1} (Holm *et al.*, 1987).

6.5 SEPARATION AND PURIFICATION

Reprocessing of spent nuclear fuels to recover reusable uranium and plutonium and the partitioning of high-level radioactive liquid wastes (HLW) constitute the main processes of the nuclear fuel cycle. ^{237}Np, α emitter with a 2.144×10^6 years half-life, is one of the major nuclides to be separated from Purex process solutions and HLW. Several separation methods satisfying requirements for process-scale operation have been developed. At the same time, separation methods suitable for relatively small-scale operations are necessary to prepare pure neptunium as a source material in the synthesis of neptunium metal or its compounds, and to isolate or preconcentrate neptunium in analytical samples before determination.

Solvent extraction, ion-exchange chromatography, extraction chromatography, coprecipitation, and electrolytic deposition methods are used for the separation of neptunium ions. Most of the wet-chemical methods involve the control of neptunium ion oxidation states which varies between 3+ and 6+ or even 7+ and utilization of specific chemical behavior of the ion in each oxidation state. Well-established separation methods are reviewed by Burney and Harbour (1974). Choppin and Nash (1995) and Nash and Choppin (1997) recently evaluated separation methods. A report published by OECD/NEA (1997) reviewed separation chemistry of actinides in nuclear waste streams and materials.

6.5.1 Solvent extraction

Many extractants have been employed for the solvent extraction of neptunium ion (cf. reviews by Laskorin *et al.* (1985) and Rozen and Nikolotova (1988)). Multi-dentate β-diketone derivatives, organophosphorus compounds, and amine compounds are commonly used. Mathur *et al.* (2001) reviewed solvent extraction technology from the viewpoints of engineering the management of nuclear spent fuels and radioactive wastes.

Typical β-diketone, 2-thenoyltrifluoroacetone (HTTA, $pK_a = 6.23$), is most widely used for the extraction of neptunium ions. The separation scheme as shown in Fig. 6.1, which is for the analysis of ^{237}Np in sediments and soils by alpha-counting, inductively coupled plasma-mass spectrometry (ICP-MS), or neutron activation analysis, was proposed by Hursthouse *et al.* (1992) and is based on HTTA extraction and anion-exchange chromatography. In this procedure, Np(VI) and Np(V) in the sample solution are reduced to Np(IV), which is extracted from 1 M HNO_3 to 0.5 M HTTA (toluene) phase ($D_{Np(IV)} \geq 10^3$). Here, D denotes the distribution ratio of a metal ion, which is a ratio of the concentration of the metal in the organic phase to that in the aqueous phase under the extraction equilibrium condition. Coexisting U(VI) and Pu(III) are not extracted ($D_{U(VI)} \leq 5 \times 10^{-5}$ and $D_{Pu(III)} \leq 10^{-5}$), which enables the separation of neptunium from plutonium and uranium. Np(IV) in the toluene phase is back-extracted into 8 M HNO_3 solution. Alternatively, Np(IV) in toluene is reduced to Np(V) and back-extracted to 1 M HNO_3 ($D_{Np(V)} \leq 5 \times 10^{-4}$).

1-Phenyl-3-methyl-4-benzoyl-pyrazol-5-one (HPMBP, cf. Fig. 6.2) and its derivatives are useful extractants for actinide ions. The pK_a of HPMBP (4.11), which is smaller than the pK_a of HTTA, extracts Np(IV) from highly acidic solution, e.g. 1–4 M HNO_3. The ability of HPMBP to extract Np(IV) from such an acidic solution avoids an interference by hydrolysis of Np(IV). Np(VI) and Np(V) are not extracted under this condition.

The synergistic extraction with HPMBP and tri-*n*-octylphosphine oxide (TOPO) was employed to separate Np(V) from Am(III), Cm(III), U(VI), Pu(IV), and lanthanide(III) ions (Pribylova *et al.*, 1987). Zantuti *et al.* (1990) developed a

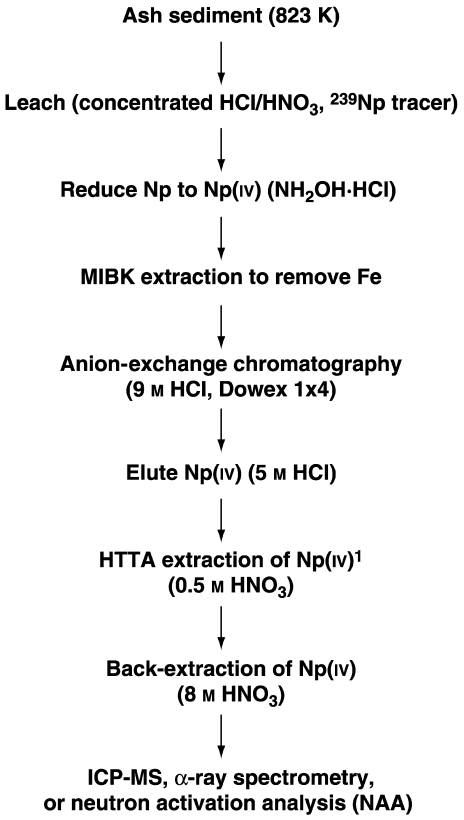

Fig. 6.1 *Procedure for the determination of* ^{237}*Np in sediment samples* (*Hursthouse* et al., 1992). [1]*HTTA extraction is repeated for* α*-ray spectrometry or NAA.*

method for the separation of a trace amount of neptunium from nitric acid solution containing a large quantity of uranium using the synergistic extraction with HPMBP and di-2-ethylhexylphosphoric acid. Tochiyama *et al.* (1989) showed that Np(v) was extracted efficiently with HPMBP in the presence of methyltrioctylammonium chloride. The 3-phenyl-4-bezoyl-5-isoxazolone was demonstrated to be powerful to extract Np(IV) and the procedure was developed for the separation of ^{237}Np from ^{236}Pu and ^{235}U in the irradiated sample of uranium target (Mohapatra and Manchanda, 1993).

Takeishi *et al.* (2001) studied the extraction behavior of actinide ions using bis (1-phenyl-3-methyl-4-acylpyrazol-5-one) derivatives H_2BPn, where n denotes the number of methylenes in a chain, having a structure as shown in Fig. 6.2. The log D vs $-\log[H^+]$ plots for the extraction of Np(IV) with various derivatives of HBPn (n = 3, 4, 5, 6, 7, 8, 10, 22) are shown in Fig. 6.3. The slopes of

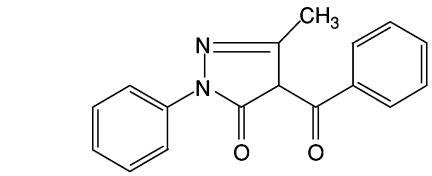

1-Phenyl-3-methyl-4-benzoyl-5-pyrazolone (HPMBP)

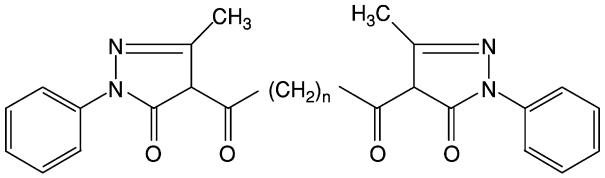

Bis(1-phenyl-3-methyl-4-acylpyrazol-5-one)
(H_2BPn; n = 3, 4, 5, 6, 7, 8, 10, 22, etc)

Fig. 6.2 *Structure of pyrazolone derivatives.*

log D vs $-\log[H^+]$ plot as well as slopes of log D vs $\log[H_2BPn]$ plot suggest Np $(BPn)_2$ as the extracted species. The H_2BPn derivatives are a stronger extractant than HPMBP, which is one of the remarkable characteristics of quadridentate H_2BPn compared with bidentate HPMBP. H_2BP7 and H_2BP8 exhibit higher extractability than the other H_2BPn derivatives examined. Based on their data a procedure for the separation of actinide ions of various oxidation states using H_2BP7 or H_2BP8 was developed.

TBP is the most useful extractant for the separation of actinide ions at the process scale. The early works with TBP are summarized in the reviews by Geary (1955) and Schneider and Harmon (1961), which provide a wide scope of TBP extraction chemistry and engineering. Np(VI) and Np(IV) are extracted as $NpO_2(NO_3)_2(TBP)_2$ and $Np(NO_3)_4(TBP)_2$, respectively, and the extraction efficiency increases with increasing concentrations of TBP and HNO_3 (1–10 M). The distribution ratios of Np(IV) and Np(VI) are 3.0 and 12.0, respectively, between 4 M HNO_3 and 30% TBP(dodecane) at 298 K. The procedure for the separation of neptunium from uranium and plutonium consists in the adjustment of the oxidation state to Np(VI), co-extraction with U(VI) and Pu(IV) and back-extraction of Np(V) by the reduction of Np(VI) to Np(V).

The *n*-octyl(phenyl)-*N*,*N*-diisobutyl-carbamoyl methylphosphine oxide (CMPO) is an effective extractant for the separation of actinide ions from acidic solutions (Kolarik and Horwitz, 1988). The mixed organic solvent of (0.1–0.2) M CMPO + (1.2–1.4) M TBP in dodecane is usually employed. Distribution ratios for Np(IV), Pu(IV), and Pu(III) between nitric acid solution and 0.1 M

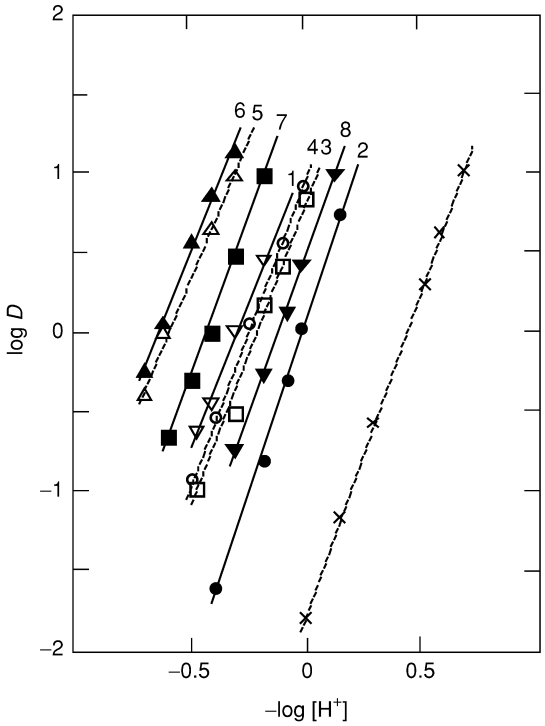

Fig. 6.3 *Log D vs −log* $[H^+]$ *plots for the extraction of* Np^{4+} *in* HNO_3 *solution with* 1×10^{-3} M H_2BPn *and HPMBP in chloroform solution.* (*From Takeishi* et al., 2001, *with permission from Elsevier*). (1) H_2BP_3, (2) H_2BP_4, (3) H_2BP_5, (4) H_2BP_6, (5) H_2BP_7, (6) H_2BP_8, (7) H_2BP_{10}, (8) H_2BP_{22}; *dotted line, HPMBP.*

CMPO + 1.4 M TBP + dodecane are shown in Table 6.2 (Mincher, 1989). For the separation of neptunium and plutonium, the oxidation states are adjusted to Np(IV) and Pu(III) with 0.1 M Fe(II) sulfamate and Np(IV) is then extracted into the CMPO/TBP phase. Pu(III) is removed by stripping with 0.01 M HNO_3 in the presence of 3% hydroxylamine nitrate. Neptunium is removed from the organic phase by an aqueous solution containing complexing agents such as $(COOH)_2$, CO_3^{2-}, or ethylenediaminetetraacetic acid (EDTA). Mathur *et al.* (1996c) compared the extraction behavior of Np(IV), Np(VI), Pu(IV), and U(VI) from nitric acid solutions with CMPO, dibutyldecanamide (DBDA), dihexyldecanamide (DHDA), and bis-2-ethylhexylsulfoxide (BEHSO) in dodecane. The extraction ability is in the order of CMPO > BEHSO > DHDA > DBDA.

Bis(2-ethylhexyl)phosphoric acid (HDEHP), which shows distinguished capability for the extraction of trivalent actinides and lanthanides ions, is also utilized for the separation of neptunium from uranium, plutonium, and

Table 6.2 *Distribution ratios of neptunium and plutonium ions between HNO_3 solution and* 0.1 M *CMPO* + 1.4 M *TBP* (*dodecane*) *at* (278 ± 1) K (*data cited from Mincher,* 1989).

	Concentration of HNO_3 (M)					
Ions	0.5	1.0	2.0	3.0	4.0	5.0
NpO_2^{2+}	43	100	114	133	150	150
NpO_2^{+}	10^{-2}	2×10^{-2}	4×10^{-2}	7×10^{-2}	0.12	0.18
Np^{4+}	0.55	6	113	670	1500	2200
Pu^{4+}	16	40	76	110	144	174
Pu^{3+}	1.6	3.0	5.2	7.1	10	14

americium. After the oxidation state of the actinide ions are adjusted to Np(V), U(VI), Pu(IV), and Am(III) in 1 M HNO_3 by adding $NaNO_2$, all actinide ions except Np(V) are extracted with HDEHP. Np(V) is then oxidized to Np(VI) and extracted with HDEHP. Np(VI) is reduced to Np(V) and back-extracted with 0.1 M HNO_3.

The extraction behavior of Np(IV) and Pu(IV) was investigated using eight kinds of multi-dentate organophosphorus compounds such as dioxides of diphosphine and carbamoyl phosphoryl compounds (Rozen *et al*., 1988). The extraction behavior of Np(V) was studied systematically with TBP, TOPO, and phosphine oxide derivatives (Rozen *et al.*, 1992). The results of K_{ex} suggested that the stability of the complex between Np(V) and the bidentate extractant was remarkably enhanced in the organic solution.

Solvent extraction with tri-*n*-octylamine (TnOA) has been extensively employed for the separation of ^{237}Np from environmental analytical samples. The separation scheme for ^{237}Np in soils and sediments, which was recommended by Yamamoto *et al*. (1994), is shown in Fig. 6.6 (see Section 6.10). Np(IV) in 10 M HCl is extracted with 10% TnOA (xylene) ($D_{Np(IV)} = 300$). Np(IV) is then back-extracted with a solution of 1 M HCl + 0.1 M HF.

Heptavalent neptunium ion as a form of $NpO_4(OH)_2^{3-}$ produced in 0.1–2 M LiOH (KOH) solution is extracted with various extractants such as TBP, TOPO, crown ether derivatives, HDEHP, etc. (Rozen *et al*., 1990). The most effective extractant is dicyclohexyl-18-crown-6 ether (in TBP) or HDEHP. Karalova *et al*. (1992a,b) studied the solvent extraction of Np(VII) from alkaline solutions with HPMBP, bis(2-oxy-4-alkyl-benzoyl)amine, bis(2-hydroxy-5-octylbenzyl) amine, and 2-hydroxy-5-*tert*-butylphenyl disulfide. The highest extraction efficiency is obtained when Np(VII) exists as $NpO_4(OH)_2^{3-}$, suggesting that the extraction process involves removal of OH^- from $NpO_4(OH)_2^{3-}$ and H^+ from the OH groups of the extractant molecules. During the extraction process the reduction of Np(VII) to Np(VI) or the oxidation of the extractant is possible, which must be taken into account for the practical use of the Np(VII) extraction procedure.

(a) Neptunium control in advanced Purex process

Currently operated commercial reprocessing plants are based on the Purex process consisting of the solvent extraction of uranium and plutonium with TBP. In principle, all neptunium is rejected into the HLW as a form of inextractable Np(V). The oxidation state of neptunium ion in the process solution, however, varies significantly depending on the chemical environment. Np(V) is oxidized to Np(VI) in the presence of HNO_2 which coexists in nitric acid solution of high concentration; the Np(V) slowly disproportionates generating Np(VI) and Np(IV) in highly acidic solution. Thus, the neptunium behavior is not fully controlled in the Purex process and neptunium distributes in different fractions of the process. Fig. 6.4 shows possible oxidation states of neptunium ions in the main stream of the Purex process. Experimental results at the THORP miniature pilot plant indicated that only 30% of the total neptunium was found in the

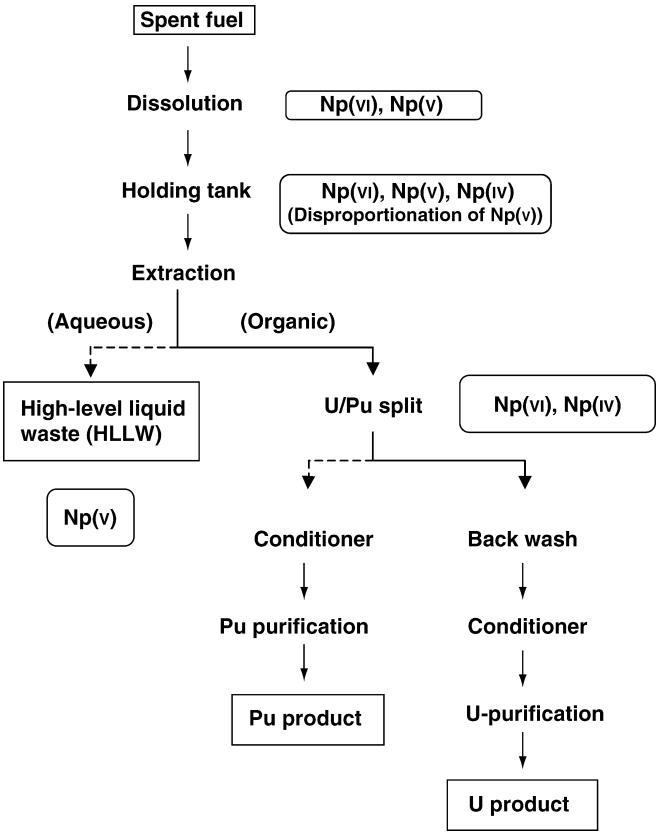

Fig. 6.4 *Flowsheet of the Purex process and the probable oxidation state of neptunium ion in the process solution.*

HLW (Taylor *et al*., 1997). The remaining neptunium was extracted with uranium and plutonium in the solvent product.

Many attempts have been done to design an advanced Purex process. Taylor *et al*. (1997) summarized the chemical behavior of neptunium in the reprocessing plant. Recent R&D activities at BNFL (UK) attempt to control neptunium in the advanced Purex process. The advanced Purex process is required to satisfy criteria including cost and environmental impact. Reducing the size and complexity of the process and minimizing the secondary waste generation assist in fulfilling these requirements. Efficient control of neptunium within the flowsheet is an important goal assigned to the advanced Purex process. Several scenarios for the control of neptunium in the flowsheet are recommended, i.e. all neptunium is led to: (1) the HLW stream; (2) the Pu fraction; or (3) the U fraction followed by the isolation from uranium, or (4) the recovery in the Np fraction before the U/Pu split process. In all cases, the method to control neptunium behavior is based on precise control of the oxidation state of the ion. Such appropriate redox reagents must be chosen to fulfill all criteria including (1) kinetics of redox reaction, (2) decomposability after the use and (3) stability toward high acidity and radiation.

The back-extraction of Np(V) is an effective way to separate neptunium from Pu(IV) and U(VI) that remain in the organic phase. Many studies have been carried out to select suitable salt-free organic reagents to reduce Np(VI) to Np(V). Taylor *et al.* (1998a) confirmed the selectivity between the reduction of Np(VI) to Np(V) and Pu(IV) to Pu(III) by comparing reduction rates with a wide range of potential reductants such as carboxylic acids, aldehydes, ketones, guanidines, and hydrazine derivatives. The hydrazine derivatives, i.e. *tert*-butyl hydrazine and 1,1-dimethyl hydrazine, are most promising from both viewpoints of the selectivity in the reduction of Np(VI) toward that of Pu(IV) and the reduction kinetics. The results of demonstration solvent extraction tests show that the reduction of Pu(IV) is accelerated by the presence of U(VI).

Uchiyama *et al.* (1998a) studied the reduction kinetics of Np(VI) and Pu(IV) with aldehyde derivatives and concluded that *n*-butyraldehyde was promising as a selective reductant of Np(VI). They proposed an advanced Purex process for the separation of neptunium, technetium, plutonium, and uranium, which consisted of five steps for (1) co-decontamination of these elements, (2) Np oxidation with V(V) and TBP extraction of Np(VI), (3) Np separation by the reduction of Np(VI) to Np(V) with *n*-butyraldehyde, (4) Tc separation using highly acidic scrubbing solution, and (5) U/Pu partitioning by the selective reduction of Pu (IV) to Pu(III) with iso-butyraldehyde.

Taylor *et al*. (1998b) employed hydroxamic acids such as formohydroxamic acid and acetohydroxamic acid, and found that they selectively and rapidly reduced Np(VI) to Np(V). The investigators also reported that the reagent preferentially complexed Np(IV) and Pu(IV) in the aqueous solution. These characteristics may offer advantages in the control of neptunium in the advanced Purex process.

One way to control neptunium separation in the Purex process flowsheet is to extract all neptunium as Np(VI) together with U(VI) and Pu(IV) and then to separate neptunium from U(VI) as the reduced form, Np(V), along with Pu(III). A suitable reductant to reduce Np(VI) to Np(V) and Pu(IV) to Pu(III) efficiently and rapidly must be used. Hydroxylamine derivatives such as hydroxylamine and methyl-, dimethyl-, diethyl-, isopropyl-, and dibutyl-hydroxylamines, have been extensively examined for this purpose (Koltunov and Baranov, 1987). Koltunov *et al.* (1999) performed a kinetic study on the reduction of Np(VI) and Pu(IV) with the recently synthesized reductants *N*,*N*-ethyl(hydroxyethyl) hydroxylamine (EHEH). The reduction rates of Np(VI) and Pu(IV) with EHEH are among the highest of the salt-free reductants examined. This rapidity of the reduction makes EHEH particularly suitable for solvent extraction contactors such as centrifugal contactors of very short residence time in the advanced Purex process. A recent study by Koltunov *et al.* (2000) provides data on the rate of the reduction of Np(VI) and Pu(IV) with acetaldoxime in nitric acid solution, and suggests that Np(VI) and Pu(IV) are reductively stripped from 30% TBP (dodecane) phase in the presence of U(VI).

A photochemical procedure for the control of the oxidation state of the neptunium ion in the process solution is attractive due to its potential for minimization of secondary waste generation and simplicity of process design. Enokida and Suzuki (1989) used a KrF excimer laser to induce the reduction of Np(VI) to Np(V) in a 30% TBP (dodecane) phase, which was then stripped into the aqueous solution. Uchiyama *et al.* (1998b) studied the selective reduction of Np(VI) to Np(V) indirectly by nitrous acid produced photochemically with a low-pressure mercury lamp. Using a mixer-settler equipped with a photochemical reactor they demonstrated the applicability of this technique to the selective reduction and stripping of Np(V), leaving Pu(IV) and U(VI) in the 30% TBP (dodecane) phase. Photochemical processes were proposed (Wada *et al.*, 1996) for the selective extraction of Pu(VI) and Pu(IV) from Np(V), the oxidation states of which were controlled by 2 M HNO_3 + 10^{-2} M hydroxylamine nitrate + hydrazine under photoirradiation. A similar photochemical process was used for the coextraction of Pu(VI), Pu(IV), and Np(VI) prepared in 3 M HNO_3 + 10^{-2} M urea solution under irradiation.

(b) Partitioning of neptunium from high-level liquid wastes

The α emitters with a long half-life, such as ^{237}Np and other transplutonium nuclides contained in the HLW from the Purex process, are of great environmental concern. A considerable amount of work has been performed to develop methods for the partitioning of the actinides from the HLW. Several partitioning processes based on the solvent extraction technique using different extractants have been proposed as follows. Mathur *et al.* (1996a) proposed a method based on the TBP extraction for the removal of neptunium and plutonium

together with U(VI). Quantitative extraction of Np(VI) and Pu(VI) from various kinds of simulated and real HLW was attained with 30% TBP (dodecane) after oxidizing neptunium and plutonium using 0.01 M $K_2Cr_2O_7$. More than 99% of neptunium and plutonium was stripped from the organic phase by reducing neptunium to Np(V) and plutonium to Pu(III) with 0.01 M ascorbic acid + 0.1 M H_2O_2 + 2 M HNO_3 solution, leaving most of the uranium in the organic phase. Feasibility of this method was confirmed by counter-current experiments using mixer-settlers with simulated HLW (Chitnis *et al.*, 1998). Pentavalent vanadium ion, VO_2^+, is also effective to adjust the oxidation state at Np(VI) and Pu(VI).

CMPO has been evaluated to be one of the best reagents for the partitioning strategy because of its high ability to extract hexavalent, tetravalent, and trivalent actinide ions from an acidic solution of relatively wide range of acid concentrations. The well-known TRUEX process for the recovery of all actinides from various types of nuclear waste solutions is based on CMPO extraction. Kolarik and Horwitz (1988), Wisnubroto *et al.* (1991), and Mathur *et al.* (1996b) accumulated the extraction data of neptunium ion of various oxidation states using TRUEX solvent. Np(V) is inextractable and must be oxidized to Np(VI) with $K_2Cr_2O_7$ or HNO_2 or reduced to Np(IV) with Fe(II) sulfamate or H_2O_2. Wisnubroto *et al.* (1991) showed that Np(V) readily disproportionated to Np(VI) and Np(IV) and the extraction efficiency of neptunium present initially as Np(V) in the sample solution increased, when the acid concentration of the aqueous solution was high enough, e.g. >4 M HNO_3. Np(IV) extracted in the TRUEX solvent was stripped quantitatively into the diluted HNO_3 solution containing complexing agents such as HF, $(COOH)_2$, carbonate, or EDTA. Np(VI) in the organic phase was easily stripped with diluted HNO_3 in the presence of H_2O_2 through the reduction of Np(VI) to Np(V).

The solvent extraction with diisodecylphosphoric acid (DIDPA) was applied to the partitioning of actinides in HLW (Morita *et al.*, 1996). The DIDPA extraction exhibits an advantage in that trivalent actinide ions, Am(III) and Cm(III), can be extracted from an aqueous solution of fairly low acidity, e.g. 0.5 M HNO_3, together with tetravalent and hexavalent ions. Even Np(V) in the sample solution is extracted by DIDPA. The addition of H_2O_2 enhances the rate of the extraction of Np(V) (Morita and Kubota, 1988). Rapid reduction of Np(V) to Np(IV) occurs during the DIDPA extraction in the presence of H_2O_2. The back-extraction of Np(IV) is achieved with 1 M $(COOH)_2$.

Trialkyl(C_6–C_8) phosphine oxides (TRPO) have been studied as an appropriate class of extractants for the recovery of Np, Pu, and Am from HLW (Zhu and Song, 1992). The optimum organic phase is 30 vol% TRPO (kerosene), and >99% of Np(IV) and Np(VI) with U(VI), Pu(VI), and Pu(IV) and >95% of trivalent actinide and lanthanide ions were extracted from 0.2 to 1 M HNO_3. The neptunium ion extracted is stripped with the plutonium ions into 0.5 M $(COOH)_2$ solution. In the recommended flowsheet, the oxidation state of neptunium is adjusted at 4+ by electrolytic reduction.

6.5.2 Chromatography using various resins

(a) Chromatography with ion-exchange resin

Various methods based on ion-exchange chromatography have been used for the separation of neptunium ions (Burney and Harbour, 1974). Cation-exchange chromatography of NpO_2^{2+}, NpO_2^{+}, and Np^{4+} with dilute acid solutions has been developed. The adsorption of ions of different oxidation states differ from each other so that the distribution ratio follows the order $Np^{4+} \gg NpO_2^{2+} \gg NpO_2^{+}$, which enables the mutual separation of neptunium ions of different oxidation states. Utilization of cation-exchange methods is limited because NpO_2^{2+} and NpO_2^{+} are often reduced to Np^{4+} when in contact with the resin; the adsorption behavior of Np^{4+} is not so selective from other coexisting cations.

Np(VI) and Np(IV) form anionic chloride or nitrate complexes in aqueous solutions containing high concentration of chloride or nitrate ions, and the anionic complexes formed are strongly adsorbed on anion-exchange resins. Well-established anion-exchange chromatographic methods are available and have been utilized for the isolation of neptunium from other actinides and fission product elements. From the viewpoint of the selectivity among neptunium ions and the other ions, nitrate media are preferable to chloride media. One such example is the procedure shown in Fig. 6.1 for the separation of ^{237}Np from environmental analytical samples, which consists of anion-exchange chromatography after solvent extraction with HTTA. The common procedure consists of the adjustment of neptunium ion at Np(IV) and the adsorption of Np(IV) nitrate complex, i.e. $Np(NO_3)_6^{2-}$, on the anion-exchange resin from 7 to 8 M HNO_3 solution. The anionic nitrate complexes of Pu(IV) and Th(IV) are also adsorbed on the resin. Pu(IV) is eluted as Pu(III) with a mixture of 6 M HNO_3 + 0.05 M Fe(II) sulfamate + 0.05 M hydrazine. Th(IV) is eluted with 8 M HCl. Np(IV) is then recovered by elution with 0.3 M HNO_3. Maiti *et al.* (1992) developed another method for the sequential separation of actinides by anion-exchange chromatography. Np(IV), Pu(IV), and U(VI) in 9 M HCl–0.05 M HNO_3 solution are adsorbed on the anion-exchange resin and Am(III) is not adsorbed under these conditions. Pu(IV), Np(IV), and U(VI) are eluted successively using 9 M HCl–0.05 M NH_4I, 4 M HCl–0.1 M HF, and 0.5 M HCl–1 M HF, respectively. The Pu(IV) is eluted by the reduction of Pu(IV) to Pu(III).

(b) Chromatography using chelate resins

Extraction chromatography using porous chelate resin loaded with an extractant is useful for the separation of actinides. A large number of theoretical plates of solvent extraction process is achieved during the column operation, which leads to an improvement of the selectivity in the separation. Maxwell (1997) developed a rapid method for the separation of neptunium using a resin loaded

with Aliquat™ 336, which is called TEVA resin. Flowsheet is shown in Fig. 6.5. The oxidation states of neptunium and plutonium are adjusted to Np(IV) and Pu(III) by reducing them in a solution of Fe(II) sulfamate and ascorbic acid. Np(IV) is retained on the resin while >99.9% Pu(III) is eluted and removed. This method can be applied to such samples as nuclear materials process samples, waste solutions, and environmental samples.

TnOA-loaded Teflon resin was used for the rapid and simple separation of ^{237}Np from environmental samples (Ji *et al*., 2001). Np(IV) in 2 M HNO_3 solution was adsorbed on the resin and eluted with 0.02 M $(COOH)_2$ + 0.16 M HNO_3 at 368 K. The decontamination factor for U(VI) was $>10^5$, allowing direct determination of ^{237}Np by ICP-MS.

Kimura (1990b) and Seranno and Kimura (1993) developed an extraction chromatographic method with TBP-loaded Amberlite XAD-4 resin for the

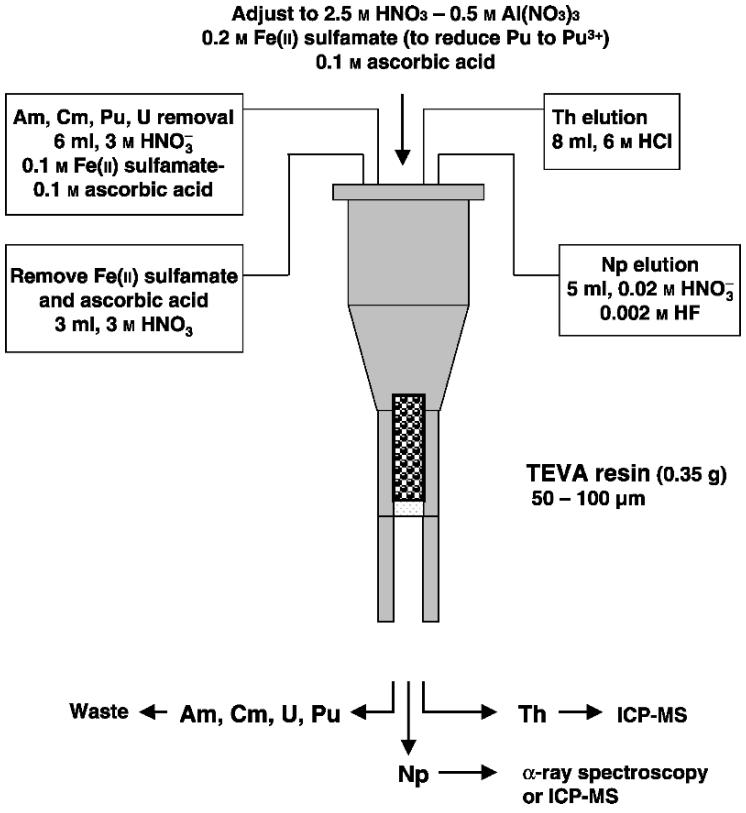

Fig. 6.5 *Procedure for the separation of neptunium ion from other actinide ions using TEVA resin.*

sequential separation of uranium, neptunium, plutonium, and americium. Np(VI) prepared by oxidizing neptunium ion in 3 M HNO_3 with 0.001 M $KBrO_3$ adsorbs on the resin and is eluted as Np(V) with the reductive effluent of 3 M HNO_3 + 0.05 M $NaNO_2$.

Heinrich and Klaus (1999) developed an automatic separation system, that is based on the extraction chromatography with silica gel particles loaded by TOPO, for the pretreatment of samples for nuclear material safeguards analysis. Np(IV), U(VI), and Pu(IV) in 3 M HNO_3 solution adsorb on the resin and are separated from Am(III), Cm(III), and fission products. Neptunium is eluted from the column as Np(V) with 0.1 M HNO_3 + 0.3 M H_2O_2 solution, plutonium is then eluted as Pu(III) with formic acid + ascorbic acid, and finally U(VI) is eluted with $(NH_4)_2CO_3$ solution.

Diphonix resin combines methylenediphosphonate, carboxylate, and sulfonate functional groups in a cross-linked polystyrene resin. This resin has strong affinity toward actinide and lanthanide ions of various oxidation states (Chiarizia *et al.*, 1994). Horwitz *et al.* (1994) obtained data of the adsorption of Np(IV), U(VI), and Am(III). One of the most distinguished features of this resin is its high adsorption ability of actinide ions from aqueous solutions even of high acidity.

6.5.3 Coprecipitation

Coprecipitation methods are traditional, well-established, and widely used for the separation of trace amounts of radioactive elements and the recovery of actinides such as neptunium. A typical example is the coprecipitation method for the preconcentration of ^{237}Np from a large volume of seawater for analytical purposes. Simplicity, rapidness, and applicability to treat large volumes of sample solution are the main advantages of this method. On the other hand, poor selectivity of coprecipitation often requires additional separation processes by solvent extraction or ion-exchange chromatography for the isolation of neptunium ions.

Several kinds of precipitates such as LaF_3, $BiPO_4$, $BaSO_4$, $Fe(OH)_3$, and MnO_2 have been used as a matrix. Np(IV) coprecipitates quantitatively with LaF_3 together with Pu(III), Pu(IV), Th(IV), and lanthanide (III). Because Np(VI) as well as Np(V) do not coprecipitate on LaF_3, neptunium can be separated from these metal ions by adjusting the oxidation state at Np(VI) or Np(V) before the coprecipitation procedure. U(VI) does not coprecipitate on LaF_3 from sulfate medium; therefore, U(VI) can be removed from the coprecipitated ions. Np(IV), Ce(III), Ba(II), and lanthanides (III) coprecipitate on $BiPO_4$ very efficiently. Kimura *et al.* (1986) developed a sequential separation procedure utilizing the coprecipitation of neptunium, plutonium, and americium ions with $BiPO_4$. Hoelgye (1998) employed the $BiPO_4$ coprecipitation method for the separation of neptunium from urine samples.

6.5.4 Electrodeposition methods

The electrodeposition reaction of a metallic actinide at a cathode in a eutectic mixture of LiCl + KCl (ca. 700–900 K) was applied as the separation method for the actinide. This method has been expected to be a novel technology for pyrometallurgical reprocessing of nuclear spent fuels or partitioning of the HLW. Electrolytic reaction reduces an actinide (III) to actinide (0) in LiCl + KCl melt and deposits the metallic actinide at the surface of the solid cathode such as tungsten or dissolves the actinide in the liquid cathode such as bismuth or cadmium melt. There have been fundamental studies on the electrode process between Np(III) and Np(0) to obtain thermodynamic data including the equilibrium redox potential of Np(III)/Np(0), the activity coefficient and the diffusion coefficient of Np(III) in LiCl + KCl (Roy *et al.*, 1996; Sakamura *et al.*, 1998, 2000; Shirai *et al.*, 2001). Martinot (1991) developed a method for the preparation of metallic neptunium of high purity by electrodeposition in LiCl + KCl (723 K). The metal product contained a total of 500 ppm impurities.

6.5.5 Biotechnology

Biotechnological methods exhibit the potential of removal of neptunium from the solution. Lloyd *et al.* (2000) proposed a procedure utilizing a combination of two microbial activities that reduce Np(V) in the sample solution to Np(IV) using the reductive capability of *Shewanella putrefaciens* followed by the formation of Np(IV) precipitate with a phosphate ligand enzymatically liberated by *Citrobacter species*. Immobilized cells of a *Citrobacter species* were prepared and employed for the removal of neptunium and plutonium ions from the sample solution (Macaskie and Basnakova, 1998).

6.6 THE METALLIC STATE

6.6.1 Neptunium metal

Although tracer quantities of neptunium were first produced by McMillan and Abelson (1940), it was not until 1945 that microgram quantities of metallic neptunium were synthesized by Magnusson and LaChapelle (1948). Their method reacted NpF_3 with barium at 1473 K. Several methods are currently used to produce gram-sized quantities of metallic neptunium. The first of these reacts NpF_4 with a stoichiometric excess of calcium and 0.15 mol of iodine 'booster' per mole of neptunium (Haire, 1986). A second method uses NpO_2 as a starting material, although other compounds such as $Cs_2NpO_2Cl_4$ and $Cs_3NpO_2Cl_4$ can be used as starting materials, and applies molten salt electrochemistry (Reavis *et al.*, 1985). A salt of LiCl/KCl is used as the electrolyte maintained at 723 K and the material is subjected to stream of HCl and H_2 gas

(Martinot, 1984). The neptunium produced can be collected either as a solid cathodic deposit on a tungsten mandrel or through use of a vitreous magnesia crucible suspended in the salt and positioned around the tungsten cathode to harvest the drops of neptunium from the cathode. The second method of collection is more challenging due to a higher operating temperature of 1023 K but can yield gram-sized quantities. A third method for producing neptunium is the reduction of NpC using tantalum followed by distillation of the neptunium metal (Spirlet and Vogt, 1984). The purity of the neptunium produced from the methods mentioned above is high, typically 99.95%, although the method involving calcium may require further electrorefining to obtain such an elevated level of purity. Recently, Hasegawa *et al.* (1998) developed a new method for the preparation of metallic neptunium based on the electrodeposition from aqueous solution. Neptunium is amalgamated by electrolysis at a mercury cathode with electrolyte solution of 1 M CH_3COOH + 0.3 M CH_3COONa (pH = 3.5) containing 0.05 M neptunium and then separated from mercury by evaporation at 1523 K.

Metallic neptunium is silvery in appearance and forms a thin oxide layer when exposed to air at ordinary temperatures. The reaction to form oxide is more pronounced at higher temperatures. The metallic form is similar to uranium in physical workability. The accepted values for melting point and density are (912 ± 3) K and 19.38 $cm^3\ g^{-1}$ (Lemire *et al.*, 2001, pp 85–87), respectively. Boiling point has not been determined experimentally; however, a value of 4447 K has been obtained via extrapolation of vapor pressure results (Eick and Mulford, 1964).

The thermodynamic properties of neptunium have been compiled by Oetting *et al.* (1976). Metallic neptunium exists in three crystalline forms (allotropes): α-form (orthorhombic), β-form (tetragonal), and γ-form (body-centered cubic (bcc)). The accepted transition temperatures, obtained by several independent groups (Zachariasen, 1952; Lee *et al.*, 1959; Wittenberg *et al.*, 1970), for the transitions are: α → β (553 ± 5 K) and β → γ (849 ± 5 K). The enthalpies and entropies of transition for the three allotropes are: (1) for the α → β transition, 5607 J mol^{-1} (ΔH°) and 10.1 J $K^{-1}mol^{-1}$ (ΔS°) and (2) for β → γ transition, 5272 J mol^{-1} (ΔH°) and 6.23 J $K^{-1}mol^{-1}$ (ΔS°). A later determination of these temperatures and enthalpies of transition using differential thermal analysis has yielded slightly different values: (1) for the α→β transition (555 K), 4730 J mol^{-1} (ΔH°) and (2) for β → γ transition (856 K), 2990 J mol^{-1} (ΔH°) (Foltyn, 1990). The largest difference between the latter values and earlier set are in the enthalpies of transition. It is reasonable to state that improvement in methods and instrumental techniques could account for this 'refinement' of the values of ΔH°. Some mention of a possible fourth allotrope has been advanced in the literature but without conclusive proof at this time (Foltyn, 1990).

The pertinent thermodynamic values at 298 K for metallic neptunium are: entropy, 50.5 J K^{-1} mol^{-1}, heat capacity, 29.6 J $K^{-1}mol^{-1}$, and the enthalpy component, $\{H^\circ(298) - H^\circ(0)\}$ 6.60 kJ mol^{-1}. The enthalpy and entropy of

Table 6.3 *Lattice parameters and space groups for allotropes of neptunium.* (*Lemire* et al., 2001)

Allotrope	*Symmetry*	*Space group*	a_0 (Å)	b_0 (Å)	c_0 (Å)
α-Np	orthorhombic	*Pnma*	6.663	4.723	4.887
β-Np[a]	tetragonal	*P*42	4.897	–	3.388
γ-Np[b]	Body-centered cubic	*Im3m*	3.518	–	–

[a] at 586 K.
[b] at 873 K.

fusion for neptunium are 5.19 kJ mol^{-1} and 5.69 J $K^{-1}mol^{-1}$, respectively (Wittenberg, 1970).

The fundamental studies of the crystallography of metallic neptunium were performed by Zachariasen (1952). This work was repeated, to a certain extent and with a different emphasis, by Mardon and Pearce (1959) as a portion of their study of the neptunium–uranium equilibrium diagram. The complete phase diagram for the allotropes of neptunium was first published by Stephens (1966). The lattice parameters for the allotropes are listed in Table 6.3.

The α allotrope of Np is orthorhombic and resembles a highly deformed bcc cell (Zachariasen, 1952). The coordination in this configuration has been reduced from 8 to 4 with a bond length of approximately 2.60 Å. The β allotrope of neptunium is a distorted tetragonal close-packed cell with 4 atoms per unit cell and a bond length of 2.76 Å. The bond length in the γ allotrope of neptunium is 2.97 Å. The phase diagram, fully developed by Stephens (1966), allows for several observations. The region of γ allotrope stability diminishes as the pressure is increased. The melting point of neptunium increases as the pressure is increased. The triple point of β-phase/γ-phase/liquid occurs at 998 K and 3200 MPa.

6.6.2 Neptunium alloys and intermetallic compounds

The past two decades have seen a resurgence of interest in the basic chemistry of neptunium in the area of alloys and intermetallic compounds (Hill, 1971; Aldred *et al.*, 1975; Elliot and Giessen, 1982; Potzel *et al.*, 1983, 1993; Gal *et al.*, 1987; Spitsyn and Ionova, 1987; Schafer *et al.*, 1989; Foltyn, 1990; Kalvius *et al.*, 1992, 1994; Yaar *et al.*, 1992; Gibson and Haire, 1993; Kitazawa *et al.*, 1993; Ogawa, 1993; Sanchez *et al.*, 1993, 1995; Wastin *et al.*, 1993; Zwirner *et al.*, 1993; Gibson *et al.*, 1994, 1996, 1999; Oddou *et al.*, 1994; Rodriguez *et al.*, 1994; Stewart *et al.*, 1994; Seret *et al.*, 1995; Jeandey *et al.*, 1996; Akabori *et al.*, 1997; Keiser *et al.*, 2000; Meresse *et al.*, 2000). The interest in intermetallic compounds in particular has been keen with the focus being the interesting and complex behavior observed due to the presence of f-shell electrons. The actinides and their intermetallic compounds exhibit magnetic behavior ranging from itinerant, band-like character, similar to transition metals, to local moment behavior, similar to the rare earths. The variety of behavior stems from either the overlap

of the 5f wave functions or the hybridization of f electrons with the ligand orbitals. For contrasting example, $NpAl_3$ is a ferromagnet, no ordering was found in $NpGe_3$, and $NpSn_3$ was thought to exhibit heavy fermion behavior (Sanchez *et al.*, 1993). The observation of heavy fermion behavior for compounds of several actinides (U, Np, Pu) has been reported by several groups (Potzel *et al.*, 1983, 1993; Gal *et al.*, 1987; Spitsyn and Ionova, 1987; Schafer *et al.*, 1989; Kalvius *et al.*, 1992, 1994; Yaar *et al.*, 1992; Sanchez *et al.*, 1993, 1995; Wastin *et al.*, 1993; Zwirner *et al.*, 1993; Gibson *et al.*, 1994; Oddou *et al.*, 1994; Rodirguez *et al.*, 1994; Seret *et al.*, 1995; Jeandey *et al.*, 1996; Meresse *et al.*, 2000). To restate this unusual behavior in other (more chemical) terms, the 5f electrons of neptunium are relatively unshielded from the crystalline electric field interaction, unlike the rare earths where the 4f electrons are very well shielded thus quenching the angular momentum term leading J to be a good quantum number. In metallic neptunium and other actinides, the spin–orbit coupling is on the same order as the crystalline electric field interaction, leading to possible mixing of the J multiplet and a metallic solid that does not strictly adhere to Hund's rule (Potzel, 1983).

The primary instrumental methods for investigating the various neptunium intermetallics have been: specific heat measurements (Stewart *et al.*, 1994), Mössbauer spectroscopy (Gal *et al.*, 1987; Yaar *et al.*, 1992; Potzel *et al.*, 1993; Sanchez *et al.*, 1993, 1995; Kalvius *et al.*, 1994; Oddou *et al.*, 1994; Jeandey *et al.*, 1996), electrical conductivity (Seret *et al.*, 1995), X-ray diffraction (Wastin *et al.*, 1993; Meresse *et al.*, 2000), magnetization measurements (Yaar *et al.*, 1992; Kitazawa *et al.*, 1993; Sanchez *et al.*, 1993), and neutron diffraction (Oddou *et al.*, 1994).

The investigations of magnetic properties of the intermetallic compounds of neptunium has primarily focused on crystalline compounds, however, some early work was also performed on metallic glasses by Elliott and Giessen (1982). They conducted a study of some 13 metallic glasses containing Np, U, and Pu using X-ray diffraction to determine the interatomic distances. The primary experimental focus has been in the area of crystalline compounds of several types: (1) ternary compounds of composition RMt_2X_2 (R is either Th, Np or Pu, Mt is a 3d, 4d, or 5d transition metal, and X is Si or Ge) (Potzel *et al.*, 1993; Wastin *et al.*, 1993; Jeandey *et al.*, 1996); (2) ternary compounds such as AnT_2Al_3 (where An is either Np or Pu and T is Ni or Pd) or Np_2T_2Sn (where T is Ni, Pd, or Pt) (Zwirner *et al.*, 1993; Sanchez *et al.*, 1995; Seret *et al.*, 1995); (3) binary compounds of composition NpX_3 (where X is Al, Ga, Ge, In, or Sn) (Sanchez *et al.*, 1993; Kalvius *et al.*, 1994; Oddou *et al.*, 1994; Meresse *et al.*, 2000); (4) binary compounds of composition $NpCd_{11}$ (Stewart *et al.*, 1994); (5) binary compounds such as $NpBe_{13}$, $NpRu_2$, $NpOs_2$, and $NpIr_2$ (Gal *et al.*, 1987); (6) ternary compounds of the composition $AnFe_4Al_8$ (where An is Th, U, or Np) (Schafer *et al.*, 1989); and (7) binary compounds of the composition NpM_2 (where M is Al, Cr, Mn, Fe, Co, Ni, Cu, Os, Ir, Ru, or Zn) (Spitsyn and Ionova, 1987).

The effort in the nuclear industry to minimize the amount of the long-lived heavy isotopes of Np, Am, and Pu present in spent fuel so as to make the disposal of the spent fuel more environmentally and economically palatable has led to the efforts in the field of alloying Np with Zr, U, Am, and Pu (Gibson and Haire, 1993; Rodriguez *et al*., 1994). Modeling efforts have also been employed to better understand the alloying behavior of neptunium with U, Am, Pu, Zr, and Fe (Ogawa, 1993; Gibson *et al*., 1999). The intent of these efforts is to take long-lived actinides that have been separated from light water reactor spent fuel and recast them into fuel for irradiation in either an accelerator or a breeder reactor and thus transform the long-lived heavy isotopes into shorter-lived isotopes. This work is still underway and the success or failure of these efforts may play a pivotal role in the needed capacity of future geologic repositories for spent fuel in the world.

The formation of binary compounds with stainless steel components such as Fe, Ni, Mn, and Co has been studied from two distinct vantage points. There has been some interest in their magnetic properties (Aldred *et al*., 1975). More recently intermetallic neptunium compounds (with Fe, Cr, Ni, and Zr) have been formed in a HLW produced from cladding hulls of spent breeder reactor fuel (Keiser *et al*., 2000). Some neptunium is left in the cladding hulls after electrometallurgical processing for recovery of the uranium. The neptunium that is left forms Laves-type intermetallics with iron, from the stainless steel cladding, and the zirconium, from the metallic alloy fuel, U/10 wt% Zr. More extensive investigations in the general behavior of neptunium with a variety of transition metals have been undertaken by Gibson *et al*. (1994) and Akabori *et al*. (1997).

With the continued interest in making the most economic and environmentally conscious use of the geologic repository for spent fuel and the focus on materials that exhibit possible superconducting properties this area of neptunium chemistry promises to be a lively one for years to come.

6.7 IMPORTANT CLASSES OF COMPOUNDS

Since the discovery of neptunium in 1940 several important activities have directed the synthesis and characterization of neptunium compounds. These activities include the importance of neptunium compounds to fundamental research, as source material for producing Pu-238, and recently neptunium's role as an environmental concern in waste disposal or as a 'burnable' component in future nuclear reactor fuels. As a result of these activities numerous publications are found in the open literature. Synthetic methods, crystal structure, chemical behavior, and thermodynamic properties have been reviewed in a number of books and publications as follows: *The Chemistry of the Transuranium Elements*, Verlag Chemie, Weinheim, Keller (1971); *Gemlin Handbuck der Anorganischen Chemie*, Suppl. Work 8th edn, Transuranium, Verlag Chemie,

Weinheim, vol. 4 part C, Compounds (1972); *The Chemical Thermodynamics of Actinide Elements and Compounds*, Part 4, Part 6, Part 8, Part 9 (ed. F. L. Oetting), International Atomic Energy Agency, Vienna, *Comprehensive Inorganic Chemistry* (ed. A. F. Trotman-Dichinson), Pergamon Press, Oxford, vol. 10, pp. 141–429 (1975); *Handbook on the Physics and Chemistry of the Actinides*, vol. 3 (eds. A. J. Freeman and C. Keller), Elsevier Science Publishers B.V., Amsterdam; (1985); *Handbook on the Physics and Chemistry of the Actinides*, vol. 6 (eds. A. J. Freeman and C. Keller), Elsevier Science Publishers B.V., Amsterdam; (1991); *Synthesis of Lanthanide and Actinide Compounds* (eds G. Meyer and L. R. Morss), Kluwer Academic Publishers, Dordrecht, The Netherlands (1991); and *Chemical Thermodynamics of Neptunium and Plutonium* (Lemire, R. J. *et al.*), Elsevier, Amsterdam (2001).

6.7.1 Hydrides

The reaction of neptunium with hydrogen results in the formation of hydrides similar to those produced by the reaction of hydrogen with plutonium (Fried and Davidson, 1948). Two hydrides, NpH_{2+x} and NpH_3, were synthesized and characterized by Mulford and Wiewandt (1965). Mintz *et al.* (1976) and recently Ward *et al.* (1987) confirmed the existence of these phases. A phase diagram proposed by Ward *et al.* (1987) for the neptunium–hydrogen system is shown in Fig. 6.6.

Mulford and Wiewandt (1965) found NpH_{2+x} to be face-centered cubic (fcc) and isostructural with PuH_{2+x} but with increasing lattice constants as hydrogen content increases. This trend is opposite of that expected when compared to the lattice constants for the plutonium–hydrogen system (Mulford and Wiewandt, 1965). Ward *et al.* (1987) confirmed this trend in neptunium–hydrogen lattice constants. A comparison of the lattice constants from the two investigations is given in Table 6.4. Both studies show the NpH_3 phase is hexagonal and isostructural with PuH_3. The lattice parameters found by Ward *et al.* (1987) are $a_0 = 6.5338$ Å and $c_0 = 6.7204$ Å.

Pressure–composition isotherms generated by Mulford and Wiewandt (1965) and later by Mintz *et al.* (1976) show flat plateaus to a [H]/[Np] value of approximately 2.16 in contrast to other actinides and lanthanides that show a phase boundary at 1.90. Another anomalous behavior found by Mulford and Wiewandt (1965) is increasing hydrogen content with increasing temperature as opposed to decreasing hydrogen with increasing temperature in the plutonium–hydrogen system. In addition to the anomalous behaviors described above, a comparison of the two reports show contrasting and conflicting thermodynamic values calculated from the pressure–composition isotherms. Ward *et al.* (1987) gives a detailed review of the two studies.

Thermodynamic data taken from Ward *et al.* (1987) are presented here. These data are selected for reporting because Ward re-examined the neptunium–hydrogen system using ultrapure, double-refined neptunium metal, and a

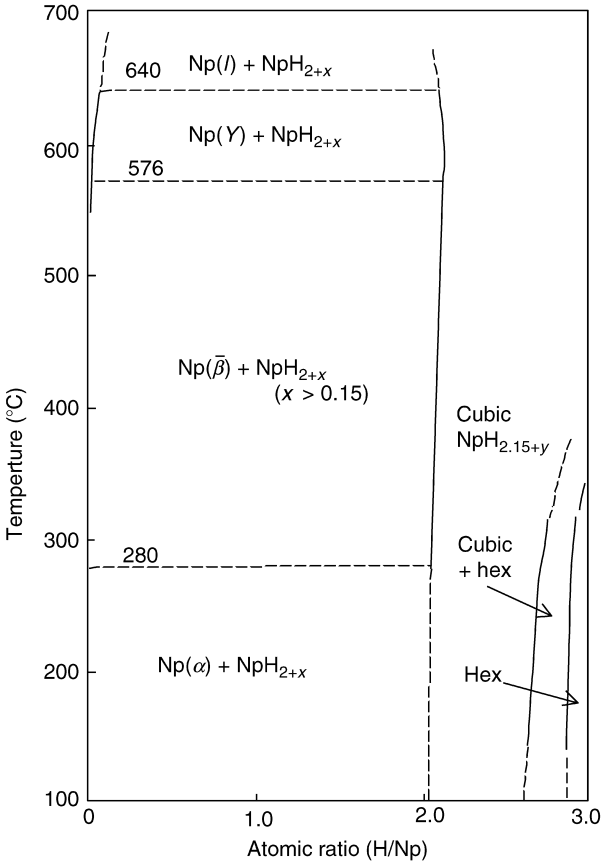

Fig. 6.6 *Partial phase diagram for the neptunium–hydrogen system. Reprinted from Ward* et al. (1987) *with permission from Elsevier Science.*

sophisticated Sievert's type apparatus. The pressure for hydrogen above $NpH_{2.13}$ below 849 K is given by:

$$\ln p\,(\text{pascals}) = 25.043 - 13421\,T^{-1} \tag{6.10}$$

From this equation enthalpies and entropies of formation for the reaction 0.94 $Np + H_2 = 0.94\ NpH_{2.13}$ are -118.8 kJ mol^{-1} (-28.38 kcal mol^{-1}) and -119.7 J K^{-1} mol^{-1} (-28.6 cal K^{-1} mol^{-1}), respectively. Ward calculated the enthalpy and entropy of formation for NpH_3 to be -153.9 kJ mol^{-1} (-36.78 kcal mol^{-1}) and -174.0 J K^{-1}mol^{-1} (-41.63 cal K^{-1} mol^{-1}), respectively. Ward tabulated calculated partial and integral enthalpies and entropies and compared the data vs the data of Mulford and Wiewandt (1965) and Mintz *et al.* (1976).

There are no known heat capacity data for neptunium hydrides. Flotow *et al.* (1984) estimated the heat capacity of NpH_2(s) from the data of Mulford and

Table 6.4 *Comparison of lattice parameters for cubic neptunium hydride.*

[*H*]/[*Np*]	*Mulford* et al. a_0 (Å)	*Space group*	*Ward* et al.
0.5	5.343	*Fm*3*m*	
1.5		*Fm*3*m*	5.3565
1.78	5.3428	*Fm*3*m*	
2		*Fm*3*m*	5.3475
2.15		*Fm*3*m*	5.3481
2.18	5.3431	*Fm*3*m*	
2.3		*Fm*3*m*	5.349
2.36	5.3463	*Fm*3*m*	
2.42	5.3478	*Fm*3*m*	
2.5	5.36	*Fm*3*m*	5.3516
2.8	5.355	*Fm*3*m*	5.3578

Wiewandt (1965) and Mintz *et al.* (1976). The estimated C_p° at 298 K is 47.279 J K^{-1} mol^{-1}. Flotow *et al.* (1984) lists estimated heat capacities from 298 to 900 K in tabular form.

There are few published data describing chemical behavior of neptunium hydrides. Haschke (1991) reviews the practical aspects of actinide hydrides focusing on safety, compound purity, reaction rates, and preparatory procedures. Recognizing the well-known pyrophoricity of both plutonium and uranium and the fact that neptunium hydride decomposes above 573 K in vacuum, yielding finely divided pyrophoric elemental neptunium, one must take great care in handling neptunium hydrides.

6.7.2 Oxides, hydrated oxides, and hydroxides

Given that neptunium has five oxidation states, it is surprising that there are only two known anhydrous oxides, NpO_2 and Np_2O_5. Attempts to synthesize higher oxides have not been successful (Katz and Gruen, 1949) and the early reported existence of Np_3O_8 has been shown to be the neptunium pentoxide (Sudakov *et al.*, 1972; Fahey *et al.*, 1976a,b). Richter and Sari (1987) on the basis of their work and recent new information on the two-phase boundaries between Np and NpO_{2-x} experimentally determined by Bartscher and Sari (1986) proposed modifications to the partial phase diagram constructed by Belyaev (1983). Their phase diagram, shown in Fig. 6.7, shows the effects of the three metal phases and the substoichiometric range, NpO_{2-x}, first noted by Ackerman *et al.* (1966). However much important work remains to be done to fully understand the neptunium–oxygen system. Recently, Beauvy *et al.* (1998) did not find neptunium metal in their investigation of the preparation of actinide compounds for actinide transmutation, contrary to the data shown in the neptunium–oxygen phase diagram.

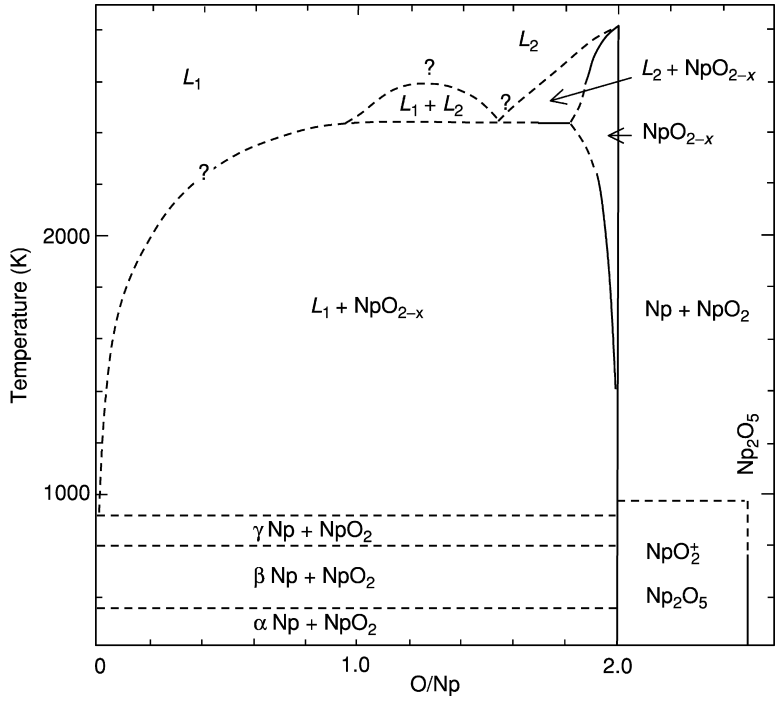

Fig. 6.7 *Phase relation of the neptunium–oxygen system. Reprinted from Richer and Sari* (1987), *with permission from Elsevier Science.*

NpO_2 is synthesized by the thermal decomposition of many neptunium compounds of any oxidation state. The oxide has a fluorite structure with a lattice parameter of (5.4334 ± 0.0003) Å and is isostructural with other actinide oxides (Fahey *et al.*, 1974). Martinot *et al.* (1970) grew single crystals of NpO_2 electrochemically. Spirlet *et al.* (1980) prepared single crystals of NpO_2 by means of a chemical transport reaction using tellurium tetrachloride as a transporting agent in a quartz ampoule at 1233 to 1323 K. X-ray diffraction characterization of the single crystals showed a fluorite lattice parameter of (5.433 ± 0.001) and (5.434 ± 0.001) Å, respectively, in relatively good agreement with literature data of Fahey *et al.* (1974, 1976a,b). Recently, Finch (2002) reported the crystallization of NpO_2 during corrosion experiments in which neptunium-doped U_3O_8 is reacted with humid air at 423 K for several weeks.

NpO_2 is extremely stable over a wide range of temperatures and pressures. The compound does not show a phase transition at low temperatures (Marples, 1975). Benedict *et al.* (1986) studied NpO_2 at pressures up to 50 GPa. Their study shows a phase transition from the fluorite fcc structure to orthorhombic

between 33 and 37 GPa. The phase returned to the fcc structure on releasing pressure. The compound is stable at oxygen pressures and temperatures to 2.84 MPa and 673 K (Fahey, 1986). Non-destructive assay standards require materials of known purity for calibration and certification of instruments. Starting with impure NpO_2 and metal, Yarbro *et al.* (1991) synthesized rather pure NpO_2 and metal using two different procedures. Following dissolution, double peroxide precipitations, ion exchange, and an oxalate precipitation of the impurities in the resulting oxides were below 100 ppm each.

The identification of Np_2O_5 and its position in the neptunium–oxygen system result from several investigations of earlier contradictory information (Fahey *et al.*, 1976a,b; Richter and Sari, 1987). Cohen (1963) and Cohen and Walter (1964) obtained Np_2O_5 by precipitation of the compound by bubbling ozone through molten $LiClO_4$ containing NpO_2^+. Bagnall and Laidler (1964) prepared the compound by the thermal decomposition of $NpO_3 \cdot H_2O$ and Sudakov *et al.* (1972) prepared the compound by the decomposition of NpO_2OH(am). Investigations by Fahey *et al.* (1976a,b) and Sudakov *et al.* (1972) provided clarification of early reported contradictory information. Bessonov *et al.* (1989a) reported the synthesis of Np_2O_5 from neptunium(IV) peroxide, double nitrate, and oxalate, apparently contradicting previously published reports. Neptunium peroxide was quantitatively converted to the pentoxide by heating at 573 to 623 K for 2 to 3 h or by heating in an ampoule at 453 to 473 K under a layer of water. The preparation of Np_2O_5 from the double nitrate and oxalate was complex involving several steps for the double nitrate. Attempts to prepare Np_2O_5 by oxidation of NpO_2 at temperatures between 700 and 970 K and oxygen pressures at 0.3 MPa were not successful (Richter and Sari, 1987). Brown Np_2O_5 is monoclinic with the following lattice parameters: $a_0 = (4.183 \pm 0.003)$ Å, $b_0 = (6.584 \pm 0.005)$ Å, and $c_0 = (4.086 \pm 0.003)$ Å, and $\beta = (90.32 \pm 0.03)^\circ$ (Fahey *et al.*, 1976a,b). Np_2O_5 is not very stable decomposing to NpO_2 and O_2 at 693 to 970 K (Bagnall and Laidler, 1964; Richter and Sari, 1987).

Neptunium hydrated oxides and hydroxides are very important in the context of the disposition of nuclear waste. Considerable interest has been devoted to Np(V) since it is the most stable valence of neptunium in the environment. Recent publications reporting the results of studies particularly on chemical thermodynamics have been exhaustively reviewed and summarized by Lemire *et al.* (2001), pp 105–29.

Heptavalent neptunium hydroxide has been precipitated from acidic solutions containing Np(VII) by addition of NaOH or LiOH to a pH at approximately 10 (Krot *et al.*, 1968a; Chaikhorskii and Leikina, 1972). Both studies reported a formula of $NpO_2(OH)_3$. Later, Musikas *et al.* (1974) reported the formula to be $NpO_3(OH)$ based on a titration study showing one hydroxyl ion per Np(VII) ion. Chaikhorskii *et al.* (1972) obtained Np(VII) hydroxide by passing ozone through a suspension of Np(V) hydroxide. The reaction was carried on at 363 K for 5 h or by passing ozone over dried Np(V) hydroxide at 368 to 373 K for 5 h. Nikonov *et al.* (1994) investigated the oxidation of Np(V)

hydroxide to form a compound containing Np(VII). The investigators reported the preparation of $(NpO_2OH)(NpO_4) \cdot 4H_2O$.

Several preparations for the synthesis of neptunium(VI) hydrates and hydroxides have been developed. LaChapelle *et al.* (1947) reported the precipitation of neptunium(VI) hydroxide by the addition of ammonia and sodium hydroxide to sulfuric acid solutions containing Np(VI). Cohen (1963) reported the preparation of $NpO_3 \cdot 2H_2O$ by oxidation of Np(V) in a molten $LiNO_3/KNO_3$ eutectic at 423 K with ozone. Bagnall and Laidler (1964), Chaikhorskii *et al.* (1974), and Belyaev *et al.* (1975) precipitated $NpO_3 \cdot H_2O$ and $NpO_3 \cdot 2H_2O$ by adding ozone to aqueous suspensions of neptunium(V) hydroxide. $NpO_2(OH)_2$ was prepared by bubbling ozone into an aqueous solution of NpO_2ClO_4 at pH = 5 and 363 K (Belyaev *et al.*, 1979). Kato *et al.* (1996) prepared $NpO_3 \cdot H_2O$ from an acidic solution. The X-ray diffraction pattern and infrared spectrum for their compound was different from that found by Bagnall and Laidler (1964). Recently, Saito *et al.* (1999), to prevent the formation of Np(VII), developed several methods to prepare neptunyl hydroxides. The authors prepared a starting solution containing $NpO_2(NO_3)_2 \cdot xH_2O$. Anhydrous $NpO_2(OH)_2$ and $NpO_2(OH) \cdot H_2O$ (orthorhombic) were precipitated by the addition of pyridine at 373 and 343 K, respectively. $NpO_2(OH) \cdot H_2O$ (hexagonal) and $NpO_2(OH)_2 \cdot xH_2O \cdot yNH_3$ ($x + y = 1$) were prepared by the addition of LiOH and ammonia water, respectively. The formula reported for the monohydrate has been reported variously as $NpO_3 \cdot H_2O$ and $NpO_2(OH)_2$ (Bagnall and Laidler, 1964; Kato *et al.*, 1996; Saito *et al.*, 1999). The recent review by Lemire *et al.* (2001), p 118 assigns the formula, $NpO_2(OH)_2$, to the dried solid of Bagnall and Laidler (1964) and the formula, $NpO_3 \cdot H_2O$, to the solid of Kato *et al.* (1996). In summary, Lemire *et al.* (2001), p 118 and Saito *et al.* (1999) describe the chemistry of the hydrated oxides and hydroxides of hexavalent neptunium to be a complicated system.

Interest in the solubility and hydrolysis reactions of Np(V) results from the stability and mobility of this oxidation state in the natural environment, the relatively long half-life of ^{237}Np (2.144×10^6 years), and its abundance in nuclear waste (Lierse *et al.*, 1985). Investigators obtained neptunium(V) hydroxide by adding ammonia, NaOH, or LiOH to slightly acidic or basic solutions containing Np(V) (LaChapelle *et al.*, 1947; Chaikhorskii *et al.*, 1974; Neck, 1992; Merli and Fuger, 1994). Neck *et al.* (1992) reported that freshly prepared green NpO_2OH in 1 M $NaClO_4$ turned to a gray-white precipitate with a lower solubility upon aging. The aged precipitate has a lower solubility than that obtained by the addition of ammonia water to a slightly acidic nitrate and $NaClO_4$ solutions containing NpO_2^+. Their preparations did not show any diffraction lines.

Neptunium(IV) hydroxides are formed in the manner of LaChapelle *et al.* (1947). There are apparently very few data on the hydrates/hydroxides of Np(IV) and Np(III) oxides. Keller (1975) reported that hydrous oxides, $MO_2(aq)$ have varying amounts of absorbed water rather than forming distinct compounds

such as $M(OH)_4$. In contrast, Rai *et al.* (1987), studying the solubility of $NpO_2 \cdot xH_2O$(am), reported that hydrous oxides are thermodynamically reproducible material over a period of 2 days to several months when maintained at 298 K. Lemire *et al.* (2001), pp 114–5 however, suggests that the compound is not thermodynamically stable representing a reproducible compound formed under different experimental conditions. Further research is required to fully characterize neptunium oxide hydrates.

Available thermodynamic data for the oxides, hydrates, and hydroxides have been extensively reviewed (Lemire *et al.*, 2001, pp 105–29). Table 6.5 lists the entropies, enthalpies, and Gibbs energies selected from the review Lemire *et al.* (2001).

Ternary oxides are primarily obtained by the reaction of NpO_2 with oxides of many different elements or by precipitation from alkaline solutions. The syntheses and characterization of these oxides have been extensively reviewed (Keller, 1972; Morss, 1982; Tabuteau and Pagès, 1985). Recently Morss *et al.* (1994) reviewed the pioneering work of Keller and co-workers in the synthesis and characterization of alkali neptunates and the importance of these compounds because of their bonding and electronic properties.

The known alkali and alkaline earth Np(VII) ternary oxides include: Li_5NpO_6, $Ba_3(NpO_5)_2$, Ba_2LiNpO_6, Rb_3NpO_5, K_3NpO_5, Cs_3NpO_5, $RbNpO_4$, $KNpO_4$, and $CsNpO_4$ (Keller and Seiffert, 1969; Awasthi *et al.*, 1971; Pages *et al.*, 1971; Mefod'eva *et al.*, 1976). Keller and Seiffert (1969) prepared Li_5NpO_6 by reacting Li_2O with NpO_2 at 673 K for 16 h. Awathi *et al.* (1971) reacted Li_2O_2 with $NpO_3 \cdot H_2O$ at 673 K for 16 h in a quartz tube in flowing oxygen at ambient pressure to obtain the compound. The compound was reported to be Li_5ReO_6 hexagonal structure with lattice parameters: $a_0 = (5.21 \pm 0.03)$ Å and $c_0 = (14.61 \pm 0.05)$ Å, the results of Awasthi *et al.* (1971) differing only slightly from those of Keller and Sieffert (1969). Recently Morss *et al.* (1994) reinvestigated the compound using X-ray and neutron diffractions. The objective of their

Table 6.5 *Thermodynamic properties of neptunium oxides and hydrated oxides at* 298.15 K.

	$\Delta_f H^\circ_m$ (kJ mol^{-1})	S°_m (J K^{-1} mol^{-1})	$\Delta_f G^\circ_m$ (kJ mol^{-1})	C°_{pm} (J K^{-1} mol^{-1})
NpO_2	-1074.0 ± 2.5	80.3 ± 0.4	-1021.731 ± 2.514	66.24 ± 0.5
Np_2O_5	-02162.7 ± 9.5	174 ± 20	-2031.6 ± 11.2	128.6 ± 5
$NpO_3 \cdot H_2O$	-1377 ± 5	129 ± 27	-1239.0 ± 6.1	120 ± 20
$NpO_2 \cdot OH$ (am, fresh)	-1222.9 ± 5.5	60 ± 27	-1114.7 ± 5.7	86 ± 20
$NpO_2 \cdot OH$ (am, aged)		70 ± 28	-1118.1 ± 6.3	
$NpO_2 \cdot$ (hyd,am)			-957.3 ± 8.0	

investigation was the redetermination of the structure based on the earlier finding that Li_5ReO_6 was monoclinic and not in the *R*3*m* space group (Betz and Hoppe, 1984). The investigators found the X-ray diffraction patterns to be consistent with past data. However, they did not confirm the originally suggested space group, *R*3*m*, or any other structure using any plausible model.

$Ba_3(NpO_5)_2$, Ba_2NaNpO_6, and Ba_2LiNpO_6 were obtained by solid state reactions of alkali and alkaline peroxides with $NpO_3 \cdot H_2O$ at temperatures between 673 and 873 K for 15 to 30 h (Awasthi *et al.*, 1971). Interestingly, the reaction between Na_2O_2 and $NpO_3 \cdot H_2O$ was incomplete under the conditions of the experiment. The authors reported the presence of both Np(VI) and Np(VII) absorption spectra in dilute NaOH solution of the dissolved product. Furthermore, X-ray examination of the product showed evidence of unreacted Na_2O_2. Attempts to produce K_5NpO_6 and Ba_2KNpO_6 using the appropriate reactants under similar conditions were not successful. Pagès *et al.* (1971) obtained K_3NpO_5, Rb_3NpO_5, and Cs_3NpO_5 by the general reaction:

$$NpO_2 + 3MO_2 \rightarrow M_3NpO_5(M = K, Cs, Rb) \tag{6.11}$$

Mefod'eva *et al.* (1976) precipitated $KNpO_4$, $RbNpO_4$, and $CsNpO_4$ from alkaline solutions containing the appropriate alkali metal nitrate, ozone, and Np(VII). Alkali metal to neptunium ratios for these compounds ranged from 1.07 to 1.19. The overestimation of the alkali metal content was explained by an admixture of nitrates.

A large number of hexavalent neptunium ternary oxides are obtained by solid state reactions of NpO_2 and alkali or alkaline earth oxides in a stream of oxygen. These oxides, generally isostructural, with uranates of the same chemical formula include: rhombohedral $Na_2Np_2O_7$, orthorhombic α-Na_2NpO_4 and β-Na_2NpO_4, tetragonal Li_4NpO_5 and α-Na_4NpO_5, orthorhombic β-Na_4NpO_5, Li_6NpO_6, and Na_6NpO_6 (Keller *et al.*, 1965a). Heating a 2:1 mixture of NpO_2 and Na_2O at temperature >673 K results in the formation of $Na_2Np_2O_7$. The heating of $Na_2Np_2O_7$ at >773 K gives α-Na_2NpO_4, which if heated to 1073 K results in the formation of β-Na_2NpO_4. Heating a 1:2 mixture of NpO_2 and Na_2O in an oxygen atmosphere at 673 K produces cubic α-Na_4NpO_5. Heating to >773 K may result in the formation of β-Na_4NpO_5. Further heating to 1073 K β-Na_4NpO_5 decomposes to β-Na_2NpO_4. When a 1:3 mixture of NpO_2 to Na_2O is heated to 773 K Na_6NpO_6 results. Heating a 1:2 mixture of NpO_2 and Li_2O at 673 to 773 K results in Li_4NpO_5 and heating a 1:3 mixture to 673 to 773 K results in Li_6NpO_6. $NaNp_2O_7$ is precipitated from molten salts containing either Np(V) or Np(VI) by reaction with BrO_3^- (Carnall *et al.*, 1965). Keller (1963) synthesized and characterized the following hexavalent Np(VI) alkaline earth oxides: $MNpO_4$ and M_3NpO_6 (where M = Ba, Ca, Sr). Appel *et al.* (1990) using crystallographic and spectroscopic techniques as well as magnetic susceptibility measurement and Mössbauer spectroscopy investigated the structure of $BaNpO_4$. The authors reported that structure to be isostructural with $BaUO_4$ with the lattice contants $a_0 = 5.726$ Å, $b_0 = 8.072$ Å, and $c_0 = 8.165$ Å. Hoekstra

and Gebert (1977) synthesized M_2NpO_4 and M_2NpO_7 (where M = K, Rb, and Cs), $Cs_4Np_5O_{17}$, $Cs_2Np_3O_{10}$, and Li_2NpO_4. The researchers obtained the compound by two methods: (1) thermal decomposition of coprecipitated alkali-actinide nitrates and (2) reaction of alkali hydroxides with Np_2O_5.

Compounds of the types $K_2Np_2O_7$, K_2NpO_4, and $BaNpO_4$ have crystal structures made up of linear NpO_2^{2+} groups arranged in layers. By contrast, no NpO_2^{2+} groups are found in the crystal lattice of Li_6NpO_6 (Morss, 1982). Coordination, crystal chemistry, and thermochemistry of these oxides have been reviewed by Morss (1982) and Mössbauer studies have been reported by Jovè *et al.* (1988a,b).

Ternary oxides containing pentavalent neptunium include: Li_3NpO_4, Na_3NpO_4, and Li_7NpO_6 (Keller *et al.*, 1965b). Li_3NpO_4 is obtained by heating Li_6NpO_6 at 1173 to 1273 K apparently in a stream of argon. Na_3NpO_4 results from the heating of a mixture of Na_6NpO_6 and NpO_2 in vacuum at 773 K for 8 h. Li_3NpO_4 is obtained by heating Li_6NpO_6 in vacuum at 1173 to 1273 K for 4 h.

Ternary oxides with Np(IV) compounds with the formula $BaNpO_3$ and $SrNpO_3$ are prepared by reacting NpO_2 with BaO and SrO in an inert and reducing atmosphere between 1373 and 1573 K (Keller, 1963). Mössbauer spectra and magnetic susceptibility of these compounds have been investigated by Kanellakopulos *et al.* (1980a,b), Konig *et al.* (1983), and Bickel and Kanellakopulos (1986).

Neptunium forms a number of ternary oxides with the oxides of group III through group VII elements. Synthesis conditions, structural properties, and phase diagrams have been reviewed by Tabuteau and Pagès (1985). Self-assembled uranyl peroxide nanosphere clusters of 24, 28, and 32 polyhedra (some containing neptunyl) that crystallize from alkaline solution have been characterized (Burns *et al.*, 2005).

6.7.3 Halides, halide complexes, and oxyhalides

The preparation and characterization of neptunium binary halides, oxyhalides, and complex halides have not been as extensively studied with respect to other actinides such as uranium and plutonium and more attention has been given to neptunium–fluorine compounds.

(a) Fluorides, fluoride complexes, and oxyfluorides

There are four known neptunium binary fluorides: NpF_3, NpF_4, NpF_5, and NpF_6. The lower valent neptunium fluorides can be prepared by the following reactions as initially reported by Fried and Davidson (1947):

$$NpO_2 + 1/2H_2 + 3HF \rightarrow NpF_3 + 2H_2O\,(773\,K) \tag{6.12}$$

$$NpF_3 + 1/4O_2 + HF \rightarrow NpF_4 + 1/2H_2O\,(773\,K) \tag{6.13}$$

The tetravalent fluoride can also be prepared by the reaction of HF directly with the oxide by the following reaction:

$$NpO_2 + 4HF \rightarrow NpF_4 + 2H_2O \tag{6.14}$$

Trevorrow *et al.* (1968) prepared NpF_4 by treating NpO_2 with a gaseous mixture of HF(75 v/o) and oxygen (25 v/o) at 773 K at approximatetly 101.3 kPa pressure. More recently, Kleinschmidt *et al.* (1992a) prepared NpF_4 by heating NpO_2 between 553 and 603 K in flowing fluorine. Neptunium is apparently transported downstream as NpF_6 and collected as NpF_4. An amorphous NpF_4 can be precipitated from a solution of Np(IV). Fried and Davidson (1947) did report that NpF_4 was not attacked by concentrated HNO_3. The crystal structures for NpF_3 and NpF_4 are shown in Table 6.6.

The preparation of NpF_5 has proved to be difficult. A number of preparations of NpF_5 are reported in the earlier literature (Cohen *et al.*, 1970; Drobyshevskii *et al.*, 1975, 1978; Baluka *et al.*, 1980). These preparations depend on the reaction of I_2 in IF_5 and KrF_2 or PF_3 in anhydrous HF with NpF_6, NpF_4, and NpF_6, respectively. Recently there have been two investigations searching for simpler alternatives to obtain NpF_5 in a pure form. Brown *et al.* (1982) reinvestigated the use of I_2 in IF_5 medium to reduce Np(VI) as shown in the following equation:

$$10NpF_6 + I_2 \rightarrow 10NpF_5 + 2IF_5 \tag{6.15}$$

The authors reported the precipitation of a cream-white precipitate which was determined to be 70.25 wt% Np. NpF_5 is 71.35 wt% Np. There was no evidence of Np(IV) in contrast to the reported contaminant by a similar method employed by Cohen *et al.* (1970). Malm *et al.* (1993) investigated several preparations for NpF_5. NpF_5 is prepared from the reaction of $NONpF_6$ with LiF

Table 6.6 *Crystal structures of neptunium halides.*

			Lattice constants			
Halide	*Symmetry*	*Color*	a_0 (Å)	b_0 (Å)	c_0 (Å)	*Angle (deg)*
NpF_3	trigonal	purple	7.129		7.288	
NpF_4	monoclinic	green	12.68	10.66	8.34	126.3
NpF_5	tetragonal	bluish-white	6.53		4.45	
NpF_6	orthorhombic	orange	9.909	8.997	5.202	
$NpOF_3$	rhombohedral	green	4.185		15.799	
NpO_2F_2	rhombohedral	pink	4.185		15.790	
$NpOF_4$	hexagonal	brown	13.17		5.70	
$NpCl_3$	hexagonal	green	7.413		4.282	
$NpCl_4$	tetragonal	red-orange	8.266		7.475	
$NpOCl_2$	orthorhombic	orange	15.209	17.670	3.948	
$NpBr_3$	hexagonal	green	7.919		4.392	
$NpBr_3$	orthorhombic	green	4.109	12.618	9.153	
$NpBr_4$	monoclinic	dark red	10.89	8.74	7.05	94.19
NpI_3	orthorhombic	brown	4.30	14.03	9.95	
NpOI	tetragonal	?	4.051		9.193	

and BF_3. NpF_6 reacts with CO and light to produce a fine white powder presumed to be a mixture of NpF_5 and unidentified material. NpF_5 did not result from the reaction of NpF_6 with PF_3 in anhydrous HF in contrast to an earlier report (Baluka *et al.*, 1980). Both investigators studied some of the chemical behavior of NpF_5. In summary, NpF_5 does not react with BCl_3 in contrast to UF_5, NpF_5 hydrolyzes in $HClO_4$, NpF_5 reacts with LiF in anhydrous hydrogen fluoride to produce $LiNpF_6$, and NpF_5 thermally decomposes at 591 K to produce NpF_4 and NpF_6. Interestingly, UF_5 decomposes at 423 K into UF_6 and then in a orderly fashion to U_2F_9, U_4F_{17}, and UF_4. The product of both investigations were examined by X-ray diffraction and the patterns were similar to those in the literature (Baluku *et al.*, 1980) and similar to α-UF_5. From the study by Malm *et al.* (1993) the lattice parameters for the tetragonal compound are $a_0 = 6.5358$ Å and $c_0 = 4.4562$ Å (see Table 6.6). Significant differences in the IR data reported by Brown *et al.* (1982) and IR data reported by Drobyshevskii *et al.* (1975, 1978) have apparently not been resolved.

The volatility of NpF_6, presenting possible separation schemes to recover Np from spent nuclear fuel, led to early interest in preparations and characterization of NpF_6 (Malm *et al.*, 1958; Seaborg and Brown, 1961; Trevorrow *et al.*, 1968). The volatility of NpF_6 is similar to that of UF_6 and PuF_6. Florin (1943) first prepared NpF_6 by reacting NpF_3 with fluorine at high temperatures. Malm *et al.* (1958) achieved the preparation of gram quantities of NpF_6 in specially designed fluorination reactors which dripped liquid fluorine onto heated NpF_4. Convection currents moved NpF_6 to a condenser. Trevorrow *et al.* (1968) studied the fluorination of NpF_4 and NpO_2 with fluorine, BrF_3, and BrF_5. The reaction of both BrF_3 and BrF_5 with NpF_4 produced NpF_6 and bromine. The reaction of fluorine with NpF_4 confirmed the production of NpF_6. The researchers identified an intermediate solid, NpF_4, in the preparations of NpF_6 from NpO_2. Similar reactions with UO_2 show an intermediate as UO_2F_2. Later, Henrion and Leurs (1971) reported NpO_2F_2 as an intermediate in the fluorination of NpO_2 with fluorine. The investigators suggest that the NpF_4 identified by Trevorrow *et al.* (1968) was the result of a secondary reaction.

The use of KrF_2 as a fluorinating agent to prepare NpF_6 at low temperatures has been reported by several investigators (Drobyshevskii *et al.*, 1975, 1978; Peacock and Edelstein, 1976; Asprey *et al.*, 1986). Low-temperature fluorinations avoid the safety and material concerns intrinsic to high-temperature fluorinations with F_2. Peacock and Edelstein (1976) reported that NpF_6 resulted when $NpOF_4$ was contacted with KrF_2 at 213 K. Asprey *et al.* (1986) showed that NpF_6 is prepared by the reaction of gaseous KrF_2 and as well KrF_2 dissolved in anhydrous hydrogen fluoride with neptunium substrates.

Eller *et al.* (1998a) investigated the reaction of O_2F_2 with neptunium oxides and fluorides. NpF_6 is prepared by gas–solid reactions as shown below:

$$NpF_4(s) + xO_2F_2(g) \rightarrow NpF_6(g) + xO_2 + (x-1)F_2(g) \tag{6.16}$$

$$NpO_2(s) + xO_2F_2 \rightarrow NpF_6(g) + (x+1)O_2(g) + (x-3)F_2(g) \tag{6.17}$$

Both reactions proceed almost quantitatively at ambient temperatures. Reaction (6.16) is >95% complete after 45 min and reaction (6.17) is >95% complete after 30 min. Neptunium hexafluoride is produced by reaction with excess O_2F_2 in anhydrous hydrogen fluoride at 195 K with both NpO_2 and NpF_4, but the reactions are much slower. Reaction with NpF_4 was >95% complete after 2 h and reaction with NpO_2 was >95% complete after 3 h. Under both conditions, NpO_2 is converted to NpF_6 with NpO_2F_2 as one of the intermediates. The investigators attempted to study the reaction of the two substrates by condensing O_2F_2 directly on the solid and allowing the mixture to warm to 195 K. Using this procedure, the reaction became uncontrollable with total decomposition of the O_2F_2 and no detectable NpF_6 was produced.

Neptunium hexafluoride is an orange solid melting at 327.8 K to a liquid. Both solid and liquid evaporate to reddish-brown gas. The crystal structure of NpF_6(s) is orthorhombic and the lattice parameters are given in Table 6.6. The vapor pressure is given by the following:

$$\log p(\text{torr}) = A - B(T(\text{K})) + \text{C}\ \log(T(\text{K})) \tag{6.18}$$

For the temperature range 273–328.1 K, $A = 18.48130$, $B = 2892.0$, and $C = -2.6990$. For the temperature range 328.1–349.82 K, $A = 0.01023$, $B = 1191.1$, and $C = 2.5825$ (Keller, 1982). Keller (1982) pointed out that NpF_6 has a higher vapor pressure than either UF_6 or PuF_6. As with other volatile radionuclides and radionuclide-containing compounds, $^{237}NpF_6$ is a radiological as well as a chemical hazard and engineered safety precautions are required.

NpF_6 like UF_6 and PuF_6 is a very reactive compound. The chemical behavior has been studied by a number of investigators (Malm *et al.*, 1958; Trevorrow *et al.*, 1968; Peacock and Edelstein, 1976; Eller *et al.*, 1998b). Malm *et al.* (1958) studied the reaction of NpF_6 with both BrF_3 and water. The reaction of NpF_6 with BrF_3 was very slow resulting in a non-volatile product presumed to be NpF_4 in contrast to PuF_6 which reacts very rapidly with BrF_3. Similar to UF_6 and PuF_6, the authors report that NpF_6 reacts vigorously with water to form NpO_2^{2+}. Trevorrow *et al.* (1968) studied the reaction of NpF_6 with sodium fluoride. In this reaction, NpF_6 reacts reversibly with sodium fluoride at 523 to 673 K according to the following reaction:

$$Na_3NpF_8(s) + 1/2F_2(g) \leftrightarrow 3NaF(s) + NpF_6(g) \tag{6.19}$$

This investigaton shows that hexavalent Np is reduced to pentavalent Np; in contrast hexavalent U reacted with NaF under the same conditions results in a hexavalent compound Na_2UF_8. Peacock and Edelstein (1976) investigated the hydrolysis of NpF_6 in anhydrous hydrogen fluoride to form $NpOF_4$. Attempts to oxidize $NpOF_4$ to Np(VII) with KrF_2 were not successful. In the same study, the investigators attempted to produce higher chlorides by an exchange reaction with BCl_3 similar to exchange reactions with uranium and tungsten. In their study, Np(VI) was reduced to Np(IV) by the following reaction:

$$3NpF_6 + 2BCl_3 \rightarrow 3NpF_4 + 3Cl_2 + 2BF_3 \tag{6.20}$$

The investigators reported that NpF_6 reacts with CsF at 298 K to produce $CsNpF_6$. Recently Eller *et al.* (1998b) studied the reactions of neptunium hexafluorides with nitrogen oxides and oxyfluorides. NpF_6 reacts with excess NO. X-ray powder diffraction pattern of a resulting green product indicated NpF_4. NpF_6 reacts with FNO under a UV lamp to produce $(NO)[NpF_6]$ confirming the earlier work of Malm *et al.* (1993). The authors did not observe any reaction between NpF_6 and FNO_2 and F_3NO even when the reaction was carried out under irradiation by UV lamp.

Np(IV), (V), (VI), and (VII) form a number of fluoro complexes. Tetravalent fluoro complexes with Li, Na, K, Rb, NH_3, Ca, Sr, and Ba have all been prepared and are well-characterized. Brown (1972) reviewed and summarized a number of preparatory methods. Examples of these compounds are shown in Table 6.7. Known pentavalent fluoro hexavalent complexes include $CsNpF_6$, Rb_2NpF_7, Na_3NpF_8, and $K_3NpO_2F_5$. Reduction of NpF_6 in contact with alkali metal fluorides or fluorination of tetravalent compounds mixed with the appropriate univalent fluoride leads to the pentavalent compounds. A selection of typical compounds of this class taken in part from a table by Brown (1972) is shown in Table 6.8. Additional information on these complexes is given by Keller (1971) and Penneman *et al.* (1973).

The known or inferred neptunium oxyfluorides are NpO_2F, $NpOF_3$, NpO_2F_2, and $NpOF_4$ (Bagnall *et al.*, 1968a; Henrion and Leurs, 1971; Drobyshevskii *et al.*, 1975, 1978; Peacock and Edelstein, 1976; Holloway and Laycock, 1984; Asprey *et al.*, 1986; Kleinschmidt *et al.*, 1992b; Eller *et al.*, 1998a). These compounds have not been extensively studied and characterized. Fried (1954) first reported the preparation of NpO_2F_2 by reacting $NaNpO_2Ac_3$ with anhydrous hydrogen fluoride at 573 to 625 K. Bagnall *et al.* (1968a) reported the preparation of the compound by reacting $NpO_3 \cdot H_2O$ and Np_2F_5 with anhydrous hydrogen fluoride at 523 to 548 K and fluorine at 603 K, respectively. The authors also reported the preparation of NpO_2F_2 by the reaction of $NpO_3 \cdot H_2O$ with fluorine at 603 K and BrF_3 at 298 K. Henrion and Leurs (1971) reported that NpO_2F_2 was an intermediate compound in the fluorination of NpO_2 with fluorine to produce NpF_6. Kleinschmidt *et al.* (1992b) prepared NpO_2F_2 by reacting NpO_2 with fluorine at 603 K and by the controlled hydrolysis of NpF_6 with trace H_2O in anhydrous hydrogen fluoride. Recently, Eller *et al.* (1998a) inferred that NpO_2F_2 was a dominant intermediate species in the preparation of NpF_6 by the reaction of O_2F_2 with NpO_2 at ambient temperature. NpO_2F_2 is a pink solid that is soluble in water and mineral acid. The crystal structure is rhombohedral and the lattice constants are shown in Table 6.6.

Peacock and Edelstein (1976) investigated the preparation of $NpOF_4$ by hydrolysis of NpF_6 with water in anhydrous hydrogen fluoride. Drobyshevskii *et al.* (1975) prepared $NpOF_4$ by reacting NpO_2 with KrF_2 in anhydrous hydrogen fluoride at ambient temperatures. Malm *et al.* (1993) reported that $NpOF_4$ was an impurity in all reported preparations of Np_2O_5.

Table 6.7 *Crystal structure and lattice constants of selected neptunium halide complexes.*

Compound	*Symmetry*	*Lattice constants*			*References*
		a_0 (Å)	b_0 (Å)	c_0 (Å)	
Cs_2NpCl_6	trigonal	7.46		6.03	Bagnall and Laidler (1966)
Li_4NpF_8	orthorhombic	9.91 ± 0.01	9.83 ± 0.01	5.98 ± 0.01	Jove and Cousson (1977)
Cs_2NpBr_6	cubic	11.082 ± 0.01			Magette and Fuger (1977)
$(NH_4)Np_3F_{13}$	orthorhombic	7.298 ± 0.005	7.942 ± 0.005	8.392 ± 0.005	Abazli *et al.* (1979)
$CsNpO_2Cl_2(H_2O)$	monoclinic	11.71 ± 0.02	6.99 ± 0.02	8.76 ± 0.02	Tomilin *et al.* (1986)
$Cs_2NaNpCl_6$	cubic	10.9065			Schoebrechts *et al.* (1989)

Table 6.8 *Thermodynamic Properties of Solid Neptunium Halides, Oxyhalides, and Halide Complexes at* 298.15 K.

	$\Delta_f H^\circ_m$ (kJ mol^{-1})	S°_m (J K^{-1} mol^{-1})	$\Delta_f G^\circ_m$ (kJ mol^{-1})	$C^\circ_{p,m}$ (J K^{-1} mol^{-1})
NpF_3	-1529.0 ± 8.3	130.6 ± 3.0	-1460.5 ± 8.3	94.2 ± 3.0
NpF_4	-1874.0 ± 16	148 ± 3	-1783.8 ± 16.0	116.1 ± 4.0
NpF_5	-1941.0 ± 25.0	200.0 ± 15.0	-1834.4 ± 25.4	132.8 ± 8.0
NpF_6	-1970.0 ± 20.0	229.1 ± 0.5	-1841.9 ± 20.0	167.4 ± 0.4
NpO_2F_2				103.2
Na_3NpF_8	-3514.0 ± 21.0	369.0 ± 12.0	-3521.2 ± 21.3	272.3 ± 12.0
$NpCl_3$	-896.8 ± 3.0	165.2 ± 6.0	-829.8 ± 3.0	101.9 ± 4.0
$NpCl_4$	-984.0 ± 1.8	196 ± 5	-895.6 ± 3.0	122.0 ± 6.0
$NpOCl_2$	-1030.0 ± 8.0	143.5 ± 5.0	-960.6 ± 8.1	95.0 ± 4.0
Cs_2NpCl_6	-1976.2 ± 1.9	410.0 ± 15.0	-1833.0 ± 4.9	
$Cs_3NpO_2Cl_4$	-2449.1 ± 4.8			
$Cs_2NpO_2Cl_4$	-2056.1 ± 5.4			
$Cs_2NaNpCl_6$	-2217.2 ± 3.1			
$NpBr_3$	-730.2 ± 2.9	200 ± 6	-705.5 ± 3.8	103.8 ± 6.0
$NpBr_4$	-771.2 ± 1.8	233 ± 5	-737.8 ± 3.5	128.0 ± 4.0
$NpOBr_2$	-950.0 ± 11.0	160.8 ± 4.0	-906.9 ± 11.1	98.2 ± 4.0
Cs_2NpBr_6	-1682.3 ± 2.0	469.0 ± 10.0	-1620.1 ± 3.6	
NpI_3	-512.4 ± 2.2	218 ± 5	-512.5 ± 3.7	110.0 ± 8.0

$NpOF_3$ has been prepared by reacting Np_2O_5 with anhydrous hydrogen fluoride at 313 to 333 K and dehydrating the resulting $NpOF_3$ hydrate at 373 to 423 K or by treating NpO_2 with KrF_2 in anhydrous HF (Bagnall *et al.*, 1968a; Drobyshevskii *et al.*, 1978). Compounds similar to NpO_2F have been obtained by reduction of NpO_2F_2 in hydrogen or the existence of the compound has been inferred as an intermediate in the reaction of NpO_2 with KrF_2 in anhydrous HF, respectively (Bagnall *et al.*, 1968a; Drobyshevskii *et al.*, 1975).

Neptunium tetrachloride has been prepared by at least two methods. One method is to react either neptunium oxalate or neptunium dioxide with CCl_4 at approximately 773 K (Fried and Davidson, 1951). Under these conditions, $NpCl_4$ forms and sublimes and is collected by condensation. Using a modification of this method Choporov and Chudinov (1968) reacted NpO_2 with a stream of CCl_4 vapor at lower temperatures, 553 to 673 K, to obtain $NpCl_4$. Apparently sublimation is minimal at these temperatures. Sublimation under vacuum at 633 to 653 K was used to purify their product. In the second method Bagnall and Laidler (1966) reacted $NpO_2 \cdot OH$ with hexachloropropene to obtain $NpCl_4$. They purified their product by sublimation at 923 K. $NpCl_4$(g) condenses as a dark red or orange red deposit.

There is still uncertainty in the melting point of $NpCl_4$. Several melting points for $NpCl_4$ have been reported. Fried and Davidson (1951) reported that $NpCl_4$

melts sharply at 811 K. Later, Choporov and Chudinov (1968) using both air and salt baths reported the melting point to be (790.5 ± 2.5) K. More recently, Gruen *et al.* (1976) reinvestigated the melting point of $NpCl_4$. Using data obtained from the spectroscopically measured vapor pressures, the investigators determined that 802.9 K is the best value.

As with most of the early man-made element investigations, $NpCl_4$ was initially identified by X-ray powder diffraction. Fried and Davidson (1951) reported that the crystal structure was tetragonal with lattice parameters $a_0 =$ (8.25 ± 0.01) Å and $c_0 =$ (7.46 ± 0.01) Å. Recently, Spirlet *et al.* (1994) performed a complete X-ray examination of single crystals of $NpCl_4$. They confirmed that the crystal structure is tetragonal and the lattice parameters are $a_0 = 8.229$ Å and $c_0 = 7.437$ Å in reasonably close agreement with the earliest work and the crystal structure data shown in Table 6.6.

Neptunium trichloride is prepared by several methods. Fried and Davidson (1951) obtained $NpCl_3$ by reduction of NpO_2 with a mixture of hydrogen and CCl_4 at 623 to 673 K. Brown and Edwards (1972) reported the quantitative synthesis of $NpCl_3$ by reducing $NpCl_4$ with an excess of zinc. In this method, $NpCl_4$ and zinc are sealed under vacuum in a quartz tube. The reactants are heated at 823 to 873 K for 12 to 24 h. After conversion, excess zinc and $ZnCl_2$ are purified by sublimation under high vacuum away from the $NpCl_3$. $NpCl_3$ is sublimed into a clean quartz tube at 1223 to 1273 K. Attempts by Brown and Edwards (1972) to reduce $NpCl_4$ with aluminum were not successful; conversions ranged from 15 to 60%. Recently, Foropoulus *et al.* (1992) prepared anhydrous $NpCl_3$ from aqueous solutions. In their patented method, neptunium is reduced to Np(III) in a chloride solution. The solution is evaporated and the resulting residue, $NpCl_3$ hydrate, is dehydrated by contacting with thionyl chloride. The authors report that an essentially pure $NpCl_3$, ca. 98%, is obtained by their method.

Efforts to prepare higher neptunium chlorides have been unsuccessful. Heating $NpCl_4$ in chlorine at 101.3 kPa does not result in the formation of $NpCl_5$. Efforts were also made to observe the possible formation of $NpCl_5$ spectroscopically in the vapor phase by heating $NpCl_4$ in a chlorine atmosphere. At temperatures up to 1273 K no new features in the absorption spectrum were found (Fried and Davidson, 1951).

Fried and Davidson (1948) reported the preparation of neptunium tetrabromide by reaction of NpO_2 with aluminum bromide at 623 K:

$$3NpO_2 + 4AlBr_3 \rightarrow 3NpBr_4 + 2Al_2O_3 \qquad (6.21)$$

Brown and Edwards (1972) in a method identical to the method described above for the synthesis of $NpCl_3$ reported the quantitative synthesis of $NpBr_3$ by reacting $NpBr_4$ with excess zinc. Brown *et al.* (1970) prepared $NpBr_4$ by direct action of metallic neptunium and bromine. Neptunium metal and bromine were vacuum-sealed in a quartz tube. One end of the tube containing neptunium metal was heated between 673 and 698 K. $NpBr_4$ sublimed and condensed in a cooler section of the tube.

Brown *et al.* (1968) investigated the preparation of $NpBr_3$ by dehydration of $NpBr_3$ hydrates. The authors prepared the hydrates by exposing the anhydrous tribromide to oxygen-free water vapor resulting in $NpBr_3$ hexahydrate. By controlling the temperature and vacuum, the hydrate was easily converted to the anhydrous form. Previously unknown $NpBr_3$ hexahydrate was characterized using X-ray powder diffraction, radioanalytical, and gravimetric methods.

Neptunium triiodide was prepared by Fried and Davidson (1951) with aluminum iodide. Another, perhaps more convenient, method for the preparation of these halides is the direct action of hydrogen bromide/hydrogen iodide on NpO_2 at 773 K. Because the anhydrous gases (HBr and HI) are available in small, easily handled cylinders, this reaction is advantageous for laboratory preparations. The reaction products can be readily purified from unreacted NpO_2 by sublimation at the appropriate temperature. Brown and Edwards (1972) prepared the triiodide by reacting neptunium metal with excess iodine. The reactants were sealed in a tube under vacuum. The reactants were then heated at 773 K. Excess iodine was sublimed from the product, which was identified as NpI_3. Neptunium tetraiodide is predicted to be unstable (Brewer *et al.*, 1949). NpI_3 has been studied by X-ray powder diffraction and the crystal structure and lattice paramters are shown in Table 6.6.

For the synthesis of $NpBr_3$ and NpI_3 described above using aluminum halide, the aluminum halide required for these syntheses is conveniently prepared *in situ* from the elements. This method has the convenience that on the laboratory scale it is unnecessary to handle small amounts of the extremely hygroscopic aluminum halides. In this method, however, if excess aluminum is present, $NpBr_3$ is formed rather than $NpBr_4$. The reaction between NpO_2 and aluminum halide is best carried out in a sealed vessel at 623 to 673 K. Any excess aluminum halide is easily sublimed away at about 523 K. The crystal structures and lattice parameters of neptunium bromides are shown in Table 6.6.

Neptunium oxyhalides have been prepared and characterized. Fried and Davidson (1951) reported $NpOCl_2$ results when $NpCl_4$ was heated in sealed and evacuated capillary. They hypothesized that the compound was the product of the reactions of the tetrachloride with either oxygen or water impurities. The compound was investigated by X-ray powder diffraction and reported to be isostructural with $UOCl_2$. The crystal structure is shown in Table 6.6. Bagnall *et al.* (1968b) reported the synthesis of $NpOCl_2$ by reacting $NpCl_4$ and antimony sesquioxide at 673 K in a vacuum. $NpOCl_2$ can be sublimed at 823 K in vacuum. The synthesis of NpOCl has been observed during efforts to prepare $NpCl_3$ (Brown and Edwards, 1972). Pentavalent neptunium oxychlorides, $NpOCl_2$ and NpO_2Cl, are prepared by the dehydration of a solution containing chloride ions and Np(v) (LaChapelle, 1964). Brown *et al.* (1977) prepared and characterized NpOI. The oxyhalide was prepared by reacting Sb_2O_3 and NpI_3 stoichiometrically in a sealed and evacuated tube at 573 to 773 K. Product SbI_3 was sublimed away from NpOI. The crystal structure is shown in Table 6.6.

Np(III), (IV), (V), and (VI) halide complexes with both alkali metal and alkaline earth elements and ammonia are known and have been characterized (Bagnall and Laidler, 1966; Fuger and Brown, 1971; Jove and Cousson, 1977; Magette and Fuger, 1977; Abazli *et al.*, 1979; Fuger, 1979; Tomilin *et al.*, 1986; Schoebrechts *et al.*, 1989). A selection of compounds collected from the above references is shown in Table 6.7. More recently, Lemire *et al.* (2001, pp 148–53) reviewed the available chemical and thermodynamic data of the following neptunium halide complexes: Na_3NpF_8, Cs_2NpCl_6, $Cs_3NpO_2Cl_4$, $Cs_2NpO_2Cl_4$, $Cs_2NaNpCl_4$, and Cs_2NpBr_6. The information and references therein should be consulted for additional information.

Measured thermodynamic data for the halides is limited. Recently the Nuclear Energy Agency (NEA) published the exhaustive review of the published thermodynamic data (Lemire *et al.* (2001), pp 131–53) and Table 6.8 gives some of the data. In summary much of the thermodynamic data are interpolated from those of the corresponding thorium, uranium, and plutonium compounds. The thermodynamic data are collected from the recommended values in Lemire *et al.* (2001) and those adopted in Chapter 19.

6.7.4 Chalcogenides, pnictides, and carbides

Neptunium pnictides and chalcogenides have been extensively investigated primarily to understand their electronic and magnetic properties. These properties have been studied by magnetic susceptibility, Mössbauer spectroscopy, electrical resistivity, neutron and low-temperature X-ray diffraction experiments (Aldred *et al.*, 1974; Rossat-Mignod *et al.*, 1984, 1989; Burlet *et al.*, 1989; Vogt and Mattenberger, 1994; Lander and Burlet, 1995). The rock salt-type monopnictides and monochalcogenides form ideal models for studying the magnetic properties of the 5f electrons.

(a) Chalcogenides

The known sulfides and oxysulfides are NpS, NpS_3, Np_2S_5, Np_3S_5, Np_2S_3 (α-, β-, and γ-) Np_3S_4, NpOS, Np_4O_4S, and Np_2O_2S (Marcon, 1967, 1969).

NpS has been synthesized by several methods. The compound can be prepared by heating Np_2S_3 and neptunium metal at 1873 K (Marcon, 1967, 1969; Charvillat *et al.*, 1976). Bihan *et al.* (1997) prepared NpS by reacting stoichiometric amounts of the pure elements by vapor reaction in a sealed tube. Details of this method are described by Spirlet and Vogt (1984). A more facile method for preparing the compound was patented by Van Der Sluys *et al.* (1992). In their method NpS was synthesized by heating an admixture of an organometallic precursor, a suitable solvent, and a protic Lewis acid at temperature and for sufficient time to form an intermediate neptunium complex. The complex is then heated at a specific temperature and time to form the monosulfide. NpS is isostructural with PuS and US, exhibiting the NaCl-type structure with lattice parameter $a_0 = (5.532 \pm 0.001)$ Å. Bihan *et al.* (1997)

investigated the compressibility of NpS up to 60 GPa. The authors reported no phase transformation from NaCl to CsCl over the pressure range investigated.

Np_2S_3 was first prepared by treating NpO_2 with a mixture of hydrogen sulfide and carbon disulfide at 1278 K (Fried and Davidson, 1948, 1951). This compound was reported to be isostructural with U_2S_3 with lattice parameters $a_0 = (10.3 \pm 0.1)$ Å, $b_0 = (10.6 \pm 0.1)$ Å, $c_0 = (3.86 \pm 0.5)$ Å (Zachariasen, 1949a, b). Marcon (1967) obtained α-Np_2S_3 by thermal dissociation of Np_3S_5 at 1200 K. The compound is orthorhombic and isotypic with α-Pu_2S_3 and α-Ce_2S_3 with lattice parameters $a_0 = (3.98 \pm 0.01)$ Å, $b_0 = (7.39 \pm 0.02)$ Å, $c_0 = (15.50 \pm 0.03)$ Å. At about 1500 K, α-Np_2S_3 transforms into tetragonal β-Np_2S_3, isotypic with β-Pu_2S_3 and Ce_5S_7, $a_0 = (14.94 \pm 0.02)$ Å, $c_0 = (19.84 \pm 0.02)$ Å. Finally, around 1800 K, change to the cubic Np_2S_3 (γ) with the structure of the Th_3P_4-type occurred ($a_0 = 8.440 \pm 0.001$ Å) (Marcon, 1967). The γ-form can also have the composition of Np_3S_4 (Damien and Berger, 1976). Np_3S_4 was obtained after the heat treatment described above by Charvillat *et al.* (1976). Np_3S_4 is cubic with a lattice parameter of $a_0 = 8.440$ Å.

Np_3S_5 was obtained by thermal decomposition of NpS_3 at 773 K (Marcon, 1967, 1969; Marcon and Pascard, 1968). Blaise *et al.* (1982) reported the preparation of Np_3S_5 by reaction of the appropriate chalcogen and neptunium hydride at 923 K. Np_3S_5 is isostructural with U_3S_5 with lattice parameters $a_0 = (7.42 \pm 0.01)$ Å, $b_0 = (8.07 \pm 0.01)$ Å, $c_0 = (11.71 \pm 0.02)$ Å.

Np_2S_5 is prepared by heating mixtures of Np_3S_5 and sulfur at 773 K (Marcon, 1967, 1969). The crystal structure is tetragonal ($a_0 = (10.48 \pm 0.01)$ Å, $c_0 = (9.84 \pm 0.1)$ Å), and isotypic with Th_2S_5, Th_2Se_5, and U_2S_5.

NpS_3 was prepared from the elements at 773 K by Marcon (1967, 1969). NpS_3 is monoclinic with lattice parameters $a_0 = (5.36 \pm 0.01)$ Å, $b_0 = (3.87 \pm 0.01)$ Å, $c_0 = (18.10 \pm 0.05)$ Å, $\beta = 99.5°$ and isostructural with US_3, USe_3, UTe_3, $NpSe_3$, and $NpTe_3$.

The three oxysulfides NpOS, Np_2O_2S, and $Np_4O_4S_3$ have been reported (Zachariasen, 1949b; Marcon, 1969). Only NpOS has been extensively studied (Thevenin *et al.*, 1985; Collard *et al.*, 1986). Thevenin *et al.* (1985) prepared NpOS by vacuum sealing and heating NpO_2, Np_3S_5, and sulfur in a quartz tube to 1073 K for 1 week. NpOS is tetragonal with lattice parameters $a_0 = b_0 = 3.808$ Å and $c_0 = 6.627$ Å. $Np_4O_4S_3$ and Np_2O_2S were prepared and characterized by Marcon (1969) and Zachariasen (1949b). Hexagonal Np_2O_2S is isostructural with the actinide and lanthanide oxysulfides of the same composition (Zachariasen, 1949b; Haire and Fahey, 1977). Hoffman and Kleykamp (1972) have presented an extensive review of the preparation and properties of these sulfides and oxysulfides.

Known neptunium selenides and oxyselenides are NpSe, Np_3Se_4, γ-Np_2Se_3, Np_2Se_5, Np_3Se_5, $NpSe_3$, NpOSe, and Np_2O_2Se. These compounds have been prepared and characterized by Mitchell and Lam (1971), Damien and Wojakowski (1975), Damien *et al.* (1973), Charvillat *et al.* (1976), and Thevenin and Pagès (1982).

Damien and Wojakowski (1975) and Charvillat *et al.* (1976) obtained NpSe by reacting neptunium hydride with a stoichiometric amount of selenium metal. The reactants, sealed in a quartz tube under vacuum, were heated at 800 K for 24 h. The investigators reported that NpSe crystallizes in the NaCl-type structure with lattice constant $a_0 = (5.804 \pm 0.002)$ Å for samples heated between 1593 and 1783 K. Gensini *et al.* (1993) reported that the selenide transforms from the NaCl to CsCl structure at 23 GPa.

Mitchell and Lam (1971) investigated the alloying behavior of neptunium and selenium and obtained Np_3Se_4. Neptunium and selenium were sealed, in vacuum, in a quartz ampoule. The reactants were heated to the melting point of selenium, 494 K, then heated to and maintained at 1273 K for 5 to 24 h. The final steps in the procedure held the ampoule at 773 K for 15 to 22 days followed by furnace cooling and X-ray diffraction analysis. Damien *et al.* (1973) obtained this phase by decomposition of Np_3Se_5 at 1123 K at high vacuum. After heating at 1323 K and apparently cooling, the lattice parameter decreased from $a_0 = (8.8242 \pm 0.0002)$ to (8.8223 ± 0.0003) Å similar to the cubic structure lattice constant $a_0 = (8.8261 \pm 0.00\ 02)$ Å reported by Mitchell and Lam (1971). Damien *et al.* (1973) could not determine if the composition of their product was γ-Np_2Se_3 or Np_3Se_4.

Damien *et al.* (1973) obtained Np_3Se_5 by thermal dissociation of $NpSe_3$ at 693 K in vacuum. Blaise *et al.* (1982) prepared Np_3Se_5 by heating the appropriate amounts of chalcogen with neptunium hydride at 923 K. The crystal structure is orthorhombic and the lattice parameters are $a_0 = (7.75 \pm 0.01)$ Å, $b_0 = (8.43 \pm 0.01)$ Å, and $c_0 = (12.24 \pm 0.02)$ Å. The compound is isostructural with U_3S_5, U_3Se_5, and Np_3S_5.

Np_2Se_5 is prepared either by thermal decomposition of $NpSe_3$ at 823 K for 2 weeks or by reaction of neptunium hydride and selenium metal at 753 K. Both preparations are performed in sealed and evacuated quartz tubes (Thevenin and Pagaès, 1982). The compound has an orthorhombic (pseudo-tetragonal) crystal structure with lattice parameters $a_0 = b_0 = 7.725$ Å and $c_0 = 10.6225$ Å.

$NpSe_3$ was synthesized by Damien *et al.* (1973) by reaction of neptunium hydride with excess selenium sealed in a quartz tube under vacuum and heating at 620 K for 1 week. Blaise *et al.* (1982) prepared $NpSe_3$ by reacting chalcogen with neptunium hydride at 1273 K. The investigators identified $NpSe_3$ by X-ray powder diffraction pattern to be analogous to that of USe_3. The triselenide crystal structure is monoclinic with lattice constants: $a_0 = (5.64 \pm 0.02)$ Å, $b_0 = (4.01 \pm 0.01)$ Å, $c_0 = (19.06 \pm 0.07)$ Å, $\beta = (79.60 \pm 20)^\circ$.

The known oxyselenides are NpOSe and Np_2O_2Se (Marcon, 1969). Only NpOSe has been investigated (Thevenin *et al.*, 1985). Thevenin *et al.* (1985) prepared NpOSe by vacuum sealing and heating NpO_2 and Np_2Se_5 to 1073 K for 1 week. NpOSe is tetragonal with lattice parameters $a_0 = b_0 = 3.869$ Å and $c_0 = 6.911$ Å. The known neptunium tellurides and oxytellurides are NpTe, Np_3Te_4, $NpTe_3$, $NpTe_{2-x}$, $\eta\gamma$-Np_2Te_3, and Np_2O_2Te.

Damien and Wojakowski (1975) and Charvillat *et al.* (1976) obtained a two-phase NpTe product by reacting neptunium hydride with a stoichiometric amount of tellurium metal sealed in a quartz tube under vacuum at 800 K for 24 h. The product formed was made into a pellet, heated at 1563 K for 4 h in a sealed quartz tube under vacuum, cooled, and examined by X-ray diffraction. Under these circumstances the investigators determined that NpTe crystallizes in the NaCl-type structure with lattice constant $a_0 = (6.197 \pm 0.0001)$ Å. Dabos-Seignon *et al.* (1990) investigated X-ray diffraction patterns of NpTe at pressures up to 51 GPa. The investigators reported that NpTe maintains the NaCl structure to 12 GPa where CsCl-type structure began to appear. Only the CsCl-type structure exists above 20 GPa.

Mitchell and Lam (1971), investigating the alloying behavior of neptunium and tellurium, obtained Np_3Te_4. Neptunium and tellurium were vacuum-sealed in a quartz ampoule. The reactants were heated to the melting point of tellurium, 494 K, then heated to and maintained at 1273 K for 5 to 24 h. The final step in the procedure held the ampoule at 772 K for 15 to 22 days. The lattice constant for the cubic structure was reported to be $a_0 = (8.8261 \pm 0.0002)$ Å (Mitchell and Lam, 1971).

Blaise *et al.* (1976), investigating magnetic properties of some neptunium chalcogenides, prepared $NpTe_3$ by reacting tellurium with neptunium hydride at 628 K. $NpTe_3$ is isostructural with rare earth tritellurides with the lattice parameters $a_0 = b_0 = 4.355$ Å and $c_0 = 25.40$ Å in agreement with literature values (Damien and Berger, 1976).

Thevenin *et al.* (1985) investigated the preparation and crystal structure of Np_2O_2Te. The investigators obtained Np_2O_2Te by reacting Np_2Te_3 and NpO_2 in a vacuum-sealed quartz tube at 1273 K for 1 week. The black compound is tetragonal with lattice constants $a_0 = b_0 = 4.003$ Å, $c_0 = 12.73$ Å and is isostructural with U_2O_2 Te and Pu_2O_2Te.

(b) Pnictides

Neptunium pnictides have been studied because of their solid state properties and relationship to advanced reactor fuels. Neptunium nitride, NpN, was prepared by Sheft and Fried (1953) who reacted ammonia gas and neptunium hydride at 1023 to 1048 K in a quartz X-ray capillary tube. Later preparations by Olson and Mulford (1966), De Novion and Lorenzelli (1968), and Aldred *et al.* (1974) reacted neptunium metal with a mixture of nitrogen and hydrogen at temperatures to 1773 K, NpH_{2+x} with nitrogen at temperatures to 1873 K, and NpH_3 with nitrogen at temperatures between 573 and 623 K, respectively.

In the method of Olson and Mulford (1966) neptunium filings were heated in a tungsten vee with nitrogen 0.5% in hydrogen as a catalyst. The reaction started at 873 K and upon apparent completion the temperature was brought to 1783 K. Gaseous neptunium hydride and neptunium were removed by pumping. De Novion and Lorezelli (1968) directly reacted nitrogen with NpH_{2+x} at 673 K,

while Aldred *et al.* (1974) reacted NpH_3 with nitrogen at 573 to 623 K for 5 h. The powder product was formed into pellets and heated at 1273 K for 2.5 h. More recently, Suzuki *et al.* (1994) synthesized NpN by a high temperature, 1823 K, carbothermic reduction of NpO_2 in a stream of N_2 gas. The crystal structure is NaCl-type (fcc) and the lattice parameter is $a = (4.8968 \pm 0.005)$ Å which agrees well with values reported in the literature (Olson and Mulford, 1966; De Novion and Lorenzelli, 1968). NpN is isomorphous with UN and PuN, reacts slowly with dilute hydrochloric and nitric acids, and appears to be relatively inert toward water (Sheft and Fried, 1953). The melting point of NpN has been determined to be 3103 K under a nitrogen pressure of ca. 1 MPa (Olson and Mulford, 1966). There is very little thermodynamic data reported for NpN. Arai *et al.* (1994) derived the following equation for the heat capacity of NpN: C_p (J mol^{-1} K) $= 52.85 + 2.55 \times 10^{-3}T - 8.37 \times 10^{5}T^{-2}$. Suzuki and Arai (1998) reviewed and investigated some thermal and thermodynamic properties of NpN. They reported the free energy of formation to be ΔG_f (J mol^{-1}) $=$ $427\,000 - 98.88T$(1700–2100 K).

Lander *et al.* (1973) prepared neptunium monophosphide by a hydriding, dehydriding, and nitriding technique. First the metal is converted to powder by hydriding and dehydriding. Then the powder reacted with phosphine gas at 623 K. NpP is single-phase fcc. The lattice parameter is (5.614 ± 0.001) Å. A compound with the formula, Np_3P_4, is formed by reacting an excess of red phosphorus with neptunium metal at 1013 K in an evacuated and sealed quartz tube (Sheft and Fried, 1953). Excess phosphorus is removed by sublimation in vacuo at 1073 K. The compound does not react with water but does react with 6 M HNO_3 to yield dark-green Np(IV) solution.

$NpAs_2$ and NpAs are prepared by reacting stoichiometrically arsenic and neptunium hydride in a vacuum-sealed tube for 1 week (Charvillat and Damien, 1973; Blaise *et al.*, 1981). In this method NpAs was synthesized at 923 K and $NpAs_2$ synthesized at 723 K. Dabos *et al.* (1986) synthesized NpAs by reacting arsenic vapor and neptunium metal turnings in a vacuum-sealed quartz tube. In this method, the reactants are separated by a quartz membrane and heated to just below the melting point of neptunium metal: arsenic sublimes at 886 K and the melting point of neptunium is 903 K. X-ray studies show that NpAs has the cubic NaCl structure with the lattice parameter $a_0 = (5.8338 \pm 0.0002)$ Å (Charvillat and Damien, 1973). $NpAs_2$ is tetragonal, anti-Fe_2As type with lattice parameter $a_0 = (3.962 \pm 0.001)$ Å, $b_0 = (8.115 \pm 0.002)$ Å (Charvillat and Damien, 1973; Blaise *et al.*, 1981). Wojakowski and Damien (1982) reported the preparation of single crystals of both $NpAs_2$ and Np_3As_4 using iodine as a transporting agent in a transport reaction process in sealed quartz tubes. The investigators reported that $NpAs_2$ single crystals are more stable in air than powder material. $NpAs_2$ crystals are brown to gold and Np_3A_4 are black in color. The reported lattice parameters are in agreement with literature values.

NpSb was prepared by an isothermal annealing technique (Mitchell and Lam, 1971). In this technique, equal atomic percentages of neptunium and 99.999%

pure antimony were sealed in a quartz tube under vacuum, and the mixture was heated at the melting temperature of antimony. The temperature was then raised to 1000°C, held at this temperature for 16 days, and then cooled. In all samples, traces of Np_3Sb_4 were present (Aldred *et al.*, 1974).

There are limited reports for the preparation and characterization of NpBi. Aldred *et al.* (1974) attempted to prepare the compound by reaction of the elements at 1273 K for 16 days and was not successful. Attempts to prepare single crystals of NpBi by Burlet *et al.* (1992) using the mineralization method described by Spirlet and Vogt (1984) were successful.

(c) Carbides

The neptunium compounds NpC, Np_2C_3 and NpC_2 have been reported in the literature with limited characterization. This is unfortunate because of the importance of carbides as advanced reactor fuels. Holley *et al.* (1984) reviewed the earlier literature and determined that two phases had been identified and that the identification of NpC_2 was tentative. Nevitt (1963) reported that the monocarbide exists in the range of $NpC_{0.82}$ to $NpC_{0.96}$. De Novion and Lorenzelli (1968) prepared $NpC_{0.95}$ by heating a mixture of neptunium hydride and graphite to 1673 K. Sandenaw *et al.* (1973) prepared $NpC_{0.91}$ by arc melting the elements using a tungsten electrode. Sheft and Fried (1953) reported the syntheses of NpC_2 by heating NpO_2 at various temperatures between 2933 and 3073 K in a graphite crucible. When an attempt is made to prepare neptunium metal by reaction of lithium vapor on NpF_3 in a graphite crucible at 1373 K, the reaction yields a mixture of NpC and Np_2C_3. When NpC reacts with excess carbon it forms a pure phase with the composition of Np_2C_3 (Lorenzelli, 1968). Sandenaw *et al.* (1973) measured the heat capacity of $NpC_{0.91}$. Holley *et al.* (1984) and Lemire *et al.* (2001), pp 201–2 reviewed the very limited thermodynamic properties of neptunium carbides.

6.7.5 Other inorganic compounds

Many other inorganic neptunium compounds have been synthesized and characterized. Interest has been shown in the preparation and characterization of phosphates, sulfates, and carbonates. The stability of phosphates makes them a candidate for immobilizing radioactive waste (Bamberger *et al.*, 1984; Volkov *et al.*, 1994). Bamberger *et al.* (1984) reported the preparation of green neptunium pyrophosphate, α-NpP_2O_7, by reacting NpO_2 and BPO_4 at 1373 K. The lattice parameter for the cubic compound was (8.593 ± 0.002) Å. Attempts to prepare $Np_3(PO_4)_4$ by a similar reaction were unsuccessful. Volkov *et al.* (1994) studied a series of double phosphate of neptunium with the formula $NpA_2(PO_4)_3$ where A = Li, Na, K, Rb, Cs. The compounds were synthesized by heating the appropriate mixtures of NpO_2, LiOH, $N(K)H_2PO_4$, $Rb(Cs)NO_3$, and H_3PO_4 at 373 to 573 K for 5 h followed by annealing in air from 773 to

1923 K. Monoclinic and trigonal crystalline structures were identified for the double phosphates containing the cations Li^+, Na^+, and K^+. Transitions from the monoclinic to trigonal phases for $NaLi_2(PO_4)_3$, $NaNa_2(PO_4)_3$, and $NaK_2(PO_4)_3$ occurred at 1723, 1623, and 1423 K, respectively. Only the trigonal phase was reported for both $NpRb_2(PO_4)_3$ and $NpCs_2(PO_4)_3$ and the latter compound formed an unidentified high-temperature phase.

A number of neptunium sulfates have been synthesized and characterized. The most recent studies of solid neptunium sulfates are by Weigel and Hellmann (1986) and Budantseva *et al.* (1988). Neptunium hydroxysulfate was synthesized and characterized by Wester *et al.* (1982).

Preparation and characterization of neptunium carbonates is essential to research conducted to understand neptunium behavior in geologic repositories and the environment. Radionuclides placed in repository, particularly the long-lived radiotoxic actinides, may contact carbonate and bicarbonate containing water, forming soluble complexes. Recognizing this concern and the need for research, Clark *et al.* (1995) and Lemire *et al.* (2001, pp 203–83) have exhaustively reviewed the available literature on neptunium carbonates.

6.7.6 Coordination compounds

Interest in the coordination chemistry of neptunium compounds is enhanced by the unique properties of each of the five oxidation states of neptunium and by the changes in coordination chemistry caused by decreasing ionic size across the actinide series. Therefore a number of compounds of neptunium and various ligands have been prepared to characterize neptunium coordination chemistry. A selected listing of these compounds and some reported crystal structures and lattice parameters are given in Table 6.9.

There is little published information of Np(III) coordination compounds. According to Mefod'eva and Gel'man (1971) the reason is in the instability of Np(III) in aqueous solutions to atmospheric oxygen. These investigators, however, reported the reduction of Np(IV) to Np(III) by sodium formaldehyde sulfoxylate, $NaHSO_2 \cdot CH_2O \cdot 2H_2O$. Apparently this compound stabilizes Np(III) and allows the formation of sparingly soluble compounds such as $Np_2(C_2O_4)_3 \cdot nH_2O (n = 11)$, $Np_2(C_6H_5AsO_3)_3 \cdot H_2O$ and $Np_2[C_6H_4(OH)COO]_3$. These compounds were formed by the addition of oxalic acid, phenylarsonic acid, or ammonium salicylate to solutions containing Np(III) reduced by $NaHSO_2 \cdot Ch_2O \cdot 2H_2O$. Atmospheric oxygen was removed from reagent solutions by argon purges and/or covering solutions with benzene. The precipitates were dried with ether and/or acetone and streams of argon.

A number of Np(IV) coordination compounds have been reported. Al-Kazzaz *et al.* (1972) prepared $(Et_4N)Np(NCS)_8$, where Et_4N = tetraethyl ammonium, which is isostructural with the uranium analog. Cousson *et al.* (1985) obtained $CoNp_2F_{10} \cdot 8H_2O$ and $CuNp_2F_{10} \cdot 6H_2O$. The investigators, using the method of Abazli *et al.* (1984), mixed and powdered transition metal cobalt or copper

Table 6.9 *Lattice parameters of selected neptunium coordination compounds.*

Compound	*Symmetry*	*Space group*	*Lattice constants*			Angle (deg)	*References*
			a_0 (Å)	b_0 (Å)	c_0 (Å)		
Np(III)							
$Np_2(C_2O_4)_3 \cdot nH_2O$							Mefod'eva and Gel'man (1971)
$Np_2(C_6H_5A_5O_3)_3 \cdot nH_2O$							Mefod'eva and Gel'man (1971)
$Np_2[C_6H_4(OH)COO]_3$							Mefod'eva and Gel'man (1971)
Np(IV)							
$(Net_4)Np(NCS)_8$			11.6		22.89		Al-Kazzaz *et al.* (1972)
$CoNp_2F_{10} \cdot 8H_2O$		$P2_1/a$	8.803	7.04	11.066	94.12	Cousson *et al.* (1985)
$CuNp_2F_{10} \cdot 6H_2O$		C_2/c	19.043	7.128	8.593	96.63	Cousson *et al.* (1985)
$NpCl_2 \cdot P(i\text{-}C_4H_9)_3O$							Bagnall *et al.* (1985)
$NpCl_4CH_3CON(i\text{-}C_3H_7)_2$							Bagnall *et al.* (1985)
$NpCl_4 \cdot 2.5HCON(CH_3)$							Bagnall *et al.* (1985)
$NpCl_4 \cdot 3.5P(CH_3)(C_6H_5)_2O$							Bagnall *et al.* (1985)
$Np(NO_3) \cdot C_{10}H_{10}N_2(NO_3) \cdot 2H_2O$		$P1/2$	8.445	9.013	11.87	102.56	Grigor'ev *et al.* (1986a)
$(C_{10}H_{10}N_2)[NP(NO_3)] \cdot 2H_2O$		$Pna2_1$	15.61	10.19	14.799		Grigor'ev *et al.* (1987)
Np(V)							
$Na_4(NpO_4)_2C_{12}O_{12} \cdot 8H_2O$		C_2/c	12.53	11.58	17.81	105.79	Cousson *et al.* (1984)
$(NpO_2)_2CH_2(CO_2)_2 \cdot 1H_2O$							
$(NpO_2)_2CH_2(CO_2)_2 \cdot 3H_2O$		$P2_1$	6.596	8.32	10.308	90.24	Grigor'ev *et al.* (1993b)

$(NpO_2)_2CH_2(CO_2)_2{\cdot}4H_2O$	monoclinic	$P2_1/n$	8.84	15.475	9.07	114.51	Krot *et al.* (1993)
$NH_4NpO_2CH_2(CO_2)_2$		$P2_1/c$	7.703	13.02	7.704	111.08	Krot *et al.* (1993)
$CsNpO_2CH_2(CO_2)_2$		$P2_1/m$	9.184	13.636	7.45	101.97	Krot *et al.* (1993)
$NaNpO_2CH_2(CO_2){\cdot}2H_2O$	monoclinic	$P2_1/n$	12.935	7.645	7.968	97.09	Krot *et al.* (1993)
$NpO_2OOCH{\cdot}H_2O$							
$NpO_2OOCCH_3{\cdot}H_2O$							
$NpO_2SO_3NH_2{\cdot}H_2O$			9.067	5.439	12.184		Budantseva *et al.* (1989)
$Cs[NpO_2(SO_4)_2]{\cdot}2H_2O$		$P1$	7.522	9.954	10.71	82.24	Grigor'ev *et al.* (1991c)
$[Co(NH_3)_6][NpO_2(SO_4)_2]{\cdot}2H_2O$		*Pnma*	17.48	7.143	12.515		Grigor'ev *et al.* (1991b)
$[Co(NH_3)_6]H_8O_3[NpO_2(SO_4)_3]$		*Pbca*	19.437	14.595	12.744		Grigor'ev *et al.* (1991b)
$(NpO_2)_2SO_4{\cdot}H_2O$		*Pnma*	15.79	6.932	6.714		Grigor'ev *et al.* (1993c)
$Cs_4(NpO_2)_3Cl_6(NO_3){\cdot}H_2O$		$Cmc2_1$	19.6	13.26	8.54		Tomilin *et al.* (1986)
Np(VI)							
$NpO_2C_2O_4$							Mefod'eva *et al.* (1969)
$(NH_4)NpO_2(CO_3)_3$							Marquart *et al.* (1983)
Np(VII)							
$LiCo(NH_3)_6Np_2O_8(OH)_2{\cdot}2H_2O$	monoclinic	C_2/c	10.739	10.45	15.013	116.38	Burns *et al.* (1973)
$NaCo(NH_3)_6Np_2O_8(OH_2){\cdot}2H_2O$			10.865	10.597	14.867	115.13	Burns *et al.* (1973)
$Co(NH_3)_6NpO_4(OH)_2{\cdot}2H_2O$		$P2_1/c$	6.778	8.449	12.448	119.3	Burns *et al.* (1973)
$CsNpO_2Cl_2(H_2O)$	monoclinic	$P2_1(P2_1/n)$	11.71	6.99	8.76	93.1	Tomilin *et al.* (1986)

difluorides and NpF_4. The mixtures were placed into gold tubes with a few drops of 40% HF. The tubes were sealed, placed in an autoclave, the pressure was adjusted to 152 MPa, and temperature increased to the desired reaction temperatures. The cobalt- and copper-containing compounds are reportedly formed at 400 and 600 K, respectively. Bagnall *et al.* (1985) reported the preparation of $NpCl_2 \cdot P(i\text{-}C_4H_9)_3O$, $NpCl_4 \cdot CH_3CON(i\text{-}C_3H_7)_2$, $NpCl_4 \cdot 2.5HCON(CH_3)$, and $NpCl_4 \cdot 3.5P(CH_3)(C_6H_5)_2O$. These compounds were obtained by mixing suspensions of Cs_2NpCl_6 in dichloromethane with the appropriate phosphine oxides and amides by stirring for 7 days and evaporating the solution to dryness. Complex nitrate compounds have been formed. Grigor'ev *et al.* (1986a) prepared $Np(NO_3)_4 \cdot 2C_{10}H_{10}N_2(NO_3)_2 \cdot 2H_2O$ with the intent of investigating the separation of Np(IV) as a more complicated compound. Grigor'ev *et al.* (1987) also prepared the Np(IV) coordination compound $(C_{10}H_{10}N_2)[Np(NO_3)_6] \cdot 2H_2O$. In both nitrate complex studies, the investigators formed single crystals by slow ambient temperature evaporation of solutions of Np(IV) in concentrated HNO_3 and excess 2,2′-pyridine.

The coordination chemistry of Np(V) compounds was stimulated by the discovery of the so-called cation–cation interaction in the solid state by Cousson *et al.* (1984). Interestingly, cation–cation interactions with actinyl ions in solution have been known since 1961 (Sullivan *et al.*, 1961). Cousson *et al.* (1984) obtained the neptunyl dimer, $Na_4(NpO_4)_2C_{12}O_{12} \cdot 8H_2O$, by dissolving neptunyl hydroxide in an aqueous solution of benzenehexacarboxylic acid (mellitic acid). The resulting solution was adjusted with NaOH to a pH of approximately 6.5 and was slowly evaporated, producing green crystals. The investigators reported, based on diffraction studies, the distance between the two neptunium atoms to be 3.4824 Å. Krot *et al.* (1993) and Grigor'ev *et al.* (1993a,b) synthesized and characterized Np(V) malonates and neptunyl malonate hydrates; $(NpO_2)_2CH_2(CO_2)_2 \cdot xH_2O$ where $x = 1$, 3, 4 and $MNpO_2CH_2(CO_2)_2$ where $M = NH_4$ or Cs and $NaNpO_2CH_2(CO_2) \cdot 2H_2O$. Grigor'ev *et al.* (1989) and Logvis' *et al.* (1994) prepared neptunyl formate, $NpO_2OOCH \cdot H_2O$, by reacting NH_4OOCH and HCOOH with a neptunyl(V) nitrate solution. Charushnikova *et al.* (1995) and Grigor'ev *et al.* (1995) prepared neptunyl glycolate by dissolving freshly prepared neptunyl hydroxide into excess glycolic acid and evaporation of the resulting solution until green crystals formed. In the same study Charushnikova *et al.* (1995) precipitated neptunyl trichloroacetate by dissolving the freshly prepared neptunyl hydroxide in equimolar amounts of trichloroacetic acid. The acetate, $NpO_2OOCCH_3 \cdot H_2O$, was obtained either by dissolving freshly prepared neptunyl(V) hydroxide in excess glacial acetic acid and collection of a resulting green precipitate by filtration or by the addition of $NaOOCH_3$ to a solution of Np(V) which had been adjusted to a pH of 4 to 5 with ammonia and collection of the resulting precipitate by filtration (Bessonov *et al.*, 1989b). Charushnikova *et al.* (1992) obtained neptunyl benzoate in a similar manner to the acetate. Ammonium benzoate was added to a solution of Np(V) which had been adjusted to a pH of 4 to 5 with ammonia water. Several

oxalate compounds have been prepared and characterized (Jones and Stone, 1972; Tomilin *et al.*, 1984). Grigor'ev *et al.* (1991a) reported the results of their study on two complex neptunium(V) oxalates; $[Co(NH_3)_6][NpO_2(C_2O_4)_2]\cdot nH_2O$ where $n = 3$ and 4. Single crystals of each compound formed were a function of the concentrations of $C_2O_4^{2-}$ and Np(V). Budantseva *et al.* (1989) synthesized and studied some of the properties of neptunyl sulfamate monohydrate. The air-stable compound, $NpO_2SO_3NH_2\cdot H_2O$, was obtained by eluting Np(V) from a cation-exchange resin in the neptunyl form with sodium sulfamate. The eluent was evaporated in a stream of air at 298 K. Attempts to prepare single crystals were not successful. Simple and complex neptunyl sulfate complexes have been prepared and characterized (Grigor'ev *et al.*, 1991b,c, 1993c). The lattice parameter for these compounds are given in Table 6.9. Saeki *et al.* (1999) studied the correlation between isomer shifts of ^{237}Np Mössbauer spectra and coordination numbers of neptunium atoms in some Np(V) compounds.

Np(VI) coordination compounds include simple compounds such as $NpO_2C_2O_4$ (Mefod'eva *et al.*, 1969) and complex compounds such as $(NH_4)_4NpO_2(CO_3)_3$ (Marquart *et al.*, 1983). The oxalate was obtained by adding oxalic acid to a nitric acid solution of Np(VI) containing $KBrO_3$. The resulting compound is not stable, Np(VI) is reduced to Np(IV) after storage even at cold temperatures. Green $(NH_4)_4NpO_2(CO_3)_3$ was prepared by adding an excess of $(NH_4)_2CO_3$ to a nitric acid solution containing Np(VI). Hexavalent actinide complexes of the formula $M_4AnO_2(CO_3)_3$ (An=U, Np, Pu; M = single valent cation) have been extensively studied (Clark *et al.*, 1995).

Since the discovery of Np(VII) (Krot and Gel'man, 1967) several Np(VII) coordination compounds have been prepared and studied. Krot *et al.* (1968b,c) reported the preparation of a compound with the formulation $Co(NH_3)_6NpO_5\cdot nH_2O$. Later, Burns *et al.* (1973) suggested the formulation should be $[Co(NH_3)_6][NpO_4(OH)_2]\cdot 2H_2O$ following their efforts to experimentally demonstrate the existence of $[NpO_4(OH)_2]^{3-}$ as the form of Np(VII) in alkaline solution. The investigators, using the method proposed by Krot *et al.* (1968a), precipitated $[Co(NH_3)_6][NpO_4(OH)_2]\cdot 2H_2O$ by the simultaneous dropwise addition of solutions of $Co(NH_3)_6Cl_3$ and Np(VII) in LiOH to a stirred solution of LiOH. In the same study Burns *et al.* (1973) reported the preparation of $LiCo(NH_3)_6Np_2O_8(OH)_2\cdot 2H_2O$ by slowly diffusing a LiOH solution of Np (VII) into a solution of $Co(NH_3)_6Cl_3$. The investigators also prepared an analog containing sodium from NaOH solution of Np(VII) but attempts to prepare a potassium analog from Np(VII) in KOH was unsuccessful. Apparently, the formation of $[Co(NH_3)_6][NpO_4(OH)_2]\cdot 2H_2O$ or $LiCo(NH_3)_6Np_2O_8(OH)_2\cdot 2H_2O$ is dependent on rapid precipitation vs slow diffusion, respectively. Grigor'ev *et al.* (1986b) obtained large single crystals of $Co(NH_3)_6NpO_4(OH)_2\cdot 2H_2O$ by mixing a LiOH solution of Np(VII) with a LiOH solution containing small excess of $Co(NH_3)_6Cl_3$ and placing the mixture into a cooler for several hours. The resulting prismatic crystals were dark green and a

maximum length of the edge 0.15–0.4 mm. The crystal structure and lattice parameters are given in Table 6.9. Nakamoto *et al.* (1999) reported the ^{237}Np Mössbauer spectroscopic study of $Co(NH_3)_6NpO_4(OH)_2 \cdot 2H_2O$. The preparation and some properties of $[Pt(NH_3)_5Cl]NpO_5 \cdot nH_2O$ (where n = ca. 1) were reported by Krot *et al.* (1968b). Blackish-green $[Pt(NH_3)_5Cl]NpO_5 \cdot nH_2O$ was obtained by adding a saturated solution of $[Pt(NH_3)_5Cl]Cl_3$ to a basic solution of Np(VII). Mefod'eva *et al.* (1970a,b) synthesized $[CoEn_3]NpO_5 \cdot 3H_2O$ (where En = ethylenediamine) using a method similar to the preparation described above for the preparation of $[Co(NH_3)_6][NpO_4(OH)_2] \cdot 2H_2O$ modified to use more concentration solutions because of the solubility of $[CoEn_3]NpO_5 \cdot 3H_2O$. The precipitates formed are thin green plate-like crystals, which decompose to a brown-colored material after stored for 5 to 6 days in a dry desiccator.

6.7.7 Important organometallic compounds

Neptunium organometallic compounds have been prepared and characterized, but not nearly to the extent of uranium organometallics. A survey of the literature produced a limited number of well-characterized neptunium organometallics. The radioactive hazard associated with neptunium and its scarcity are two reasons for the scarcity of published information. Most investigations reported to date deal with the preparation of neptunium cyclopentadienyl and cyclooctatetraenyl compounds and derivatives of these compounds. These compounds have been extensively reviewed (Gysling and Tsutsui, 1970; Hayes and Thomas, 1971; Legin, 1979; Marks and Ernest, 1982; Mishin *et al.*, 1986). The synthesis, characterization, and catalytic processes of organometallic actinides are discussed in Chapters 25 and 26.

(a) Cyclopentadienyl compounds

A trivalent neptunium cyclopentadienyl complex was synthesized and characterized by Karraker and Stone (1972). The complex is formed by the reduction of $Np(C_5H_5)_3Cl$ with sodium:

$$Np(C_5H_5)_3Cl + Na \rightarrow Np(C_5H_5) \cdot 3THF + NaCl \qquad (6.22)$$

Attempts to obtain $Np(C_5H_5)$ by heating and vacuum to remove tetrahydrofuran (THF) were unsuccessful.

Tetravalent neptunium tetracyclopentadienyl was prepared and characterized by Baumgartner *et al.* (1968). The complex was prepared by reacting $NpCl_4$ with KC_5H_5 in benzene under reflux for 160 h:

$$NpCl_4 + 4KC_5H_5 \rightarrow Np(C_5H_5)_4 + 4KCl \qquad (6.23)$$

The reddish-brown complex dissolved in benzene and THF. The authors reported that the compound is less sensitive to oxygen and water than $Pu(C_5H_5)_3$ and $Am(C_5H_5)_3$.

Other Np(IV) cyclopentadienyl compounds have been prepared and characterized. Two reactions have been reported for the preparation of tricyclopentadienyl chloride, $(C_5H_5)_3NpCl$. Fischer *et al.* (1966) prepared the compound by reacting NpX_4 (X = Cl, F) with potassium cyclopentadienyl, $3K(C_5H_5)$, in THF. Later Karraker and Stone (1972) prepared the compound by reacting $NpCl_4$ with beryllium cyclopentadienyl. Equations describing the two reactions are:

$$NpX_4 + 3K(C_5H_5)_4 \rightarrow Np(C_5H_5)_3X + 3KX \tag{6.24}$$

$$2NpCl_4 + 3BeC_5H_5 \rightarrow 2Np(C_5H_5)_3Cl + 3BeCl_2 \tag{6.25}$$

A number of derivatives can be prepared starting with tetrakiscyclopentadienyl Np(IV), $Np(C_5H_5)_4$, and tris(cyclopentadienyl)Np(IV) chloride, $(C_5H_5)_3NpCl$. These compounds have the general formula $(C_5H_5)_3NpL$ with either inorganic ionic ($L = Br^-$, I^-, $1/2SO_4^{2-}$, NCS^-, $ALCl_4$) or organic ligands ($L = NC_4H_4^-$, $N_2C_3H_3^-$, $C = CH^-$, $1/2C = C_2^-$, $C_2H_5^-$, $C_6H_5^-$) (Bohlander, 1986). An interesting and unusual synthetic method was reported by Baumgartner *et al.* (1965). These authors obtained $Np(C_5H_5)_3Cl$ by (γ,n) reaction with U-238 in $U(C_5H_5)_3Cl$.

(b) Cyclooctatetraene compounds

Karraker *et al.* (1970) prepared bis(cyclooctatetraenyl) Np(IV) by reacting $NpCl_4$ with a THF solution of $K_2(C_8H_8)$:

$$NpCl_4 + 2K_2(C_8H_8) \rightarrow Np(C_8H_8)_2 + 4KCl \tag{6.26}$$

After 16 h of stirring, the compound was precipitated by the addition of deaerated water and recovered by evaporation. The authors report that X-ray diffraction patterns indicate that $Np(C_8H_8)_2$ is isomorphous with $U(C_8H_8)_2$ and $Pu(C_8H_8)_2$. The chemical behavior of the three compounds are identical: the compounds are not sensitive to water or dilute base, they are air-sensitive, reacting quickly to form oxides, and they are very slightly soluble in organic solvents such as benzene and toluene.

Karraker (1973) synthesized both neptunium bis(ethylcyclotetraene) and bis (*n*-butylcyclotetraene) complexes by reacting the alkyl substitued potassium complex in THF with $NpCl_4$ as shown below:

$$2K_2RC_8H_7 + NpCl_4 \rightarrow Np(RC_8H_7)_2 + 4KCl \tag{6.27}$$

where R = ethanol, butanol.

A trivalent neptunium cyclotetraene complex was prepared and characterized by Karraker and Stone (1974) by reacting stoichiometric amounts of NpX_3 (X = Cl, Br, I) and $K_2(C_8H_8)$ in THF:

$$NpXr_3 + 2K_2(C_8H_8) \rightarrow KNp(C_8H_8) \cdot 2THF + 3KX \tag{6.28}$$

The compound is isostructural with $KPu(C_8H_8)_2 \cdot 2THF$ with an orthorhombic unit cell. Both compounds are reported to be air- and water-sensitive, converting to $Np(C_8H_8)_2$ by air oxidation and other trace amounts of oxidizing agents. The compound is soluble in THF but slightly soluble in benzene and toluene.

(c) Other organometallic compounds

Hydrocarbyl compounds of neptunium have been reported. Karraker and Stone (1976) reported the preparation of $Np(C_5H_5)_3R$ where R = *n*-butyl by reacting $Np(C_5H_5)_3Cl$ with RLi.

Recent investigations of suitable precursors for organometallic and inorganometallic compounds suggested the usefulness of solvated triiodide complexes for this purpose (Karraker, 1987; Zwick *et al.*, 1992). Karraker (1987) investigated the reaction of neptunium with diiodoethane. The reaction in THF is:

$$Np + 3/2C_2H_4I_2 \rightarrow NpI_3 \cdot x\text{THF} + 3/2C_2H_4 \qquad (6.29)$$

The reaction was carried out in a dry argon. The mixture of reactants were stirred at ambient temperature at times up to 1 week. A yellow precipitate was mixed with thallous methylcyclopentadienide in THF. The reaction is complete in 5 to 10 min. Two pure products, $NpI_2(MeC_5H_5) \cdot 3THF$ and $NpI(MeC_5H_5)$ 2.3THF can be obtained by evaporation or precipitation with ether. Using $NpI_3(THF)_4$ Zwick *et al.* (1992) reported the preparation of $Np[N(SiMe)_2]_3$, $Np[O\text{-}2,6\text{-}(t\text{-}C_4H_9)_2C_6H_3]_3$, and $Np[CH(SiMe_3)_2]_3$, demonstrating that $NpI_3(THF)_4$ is a precursor to new and existing compounds.

6.8 NEPTUNIUM IN AQUEOUS SOLUTION

6.8.1 Oxidation states of neptunium ions

Neptunium exists in an aqueous solution as ions of oxidation states from 3+ to 7+. These oxidation states are liable to change through reduction and oxidation reactions and disproportionation reaction of Np(V). The stability of the oxidation state is strongly affected by factors such as oxidants or reductants, acidity of the solution, presence of a complex forming ligand, and the concentration of neptunium itself in the solution. The stability of each ion can be simply predicted from the redox potentials as described below.

Trivalent and tetravalent neptunium exist as hydrated Np^{3+} and Np^{4+} in acidic solutions without ligand, Np^{3+} is quickly oxidized to Np^{4+} by air. Even in moderately acidic solutions, Np^{4+} is significantly hydrolyzed. Np(III) and Np(IV) form insoluble hydroxides in aqueous solutions of low acidity and the hydroxide of Np(III) is readily oxidized to the hydroxide of Np(IV) by air. The pentavalent neptunium ion, which is the most stable oxidation state in solution,

and hexavalent neptunium ion behave as strong Lewis acids and these ions form dioxo species, NpO_2^+ and NpO_2^{2+}, in acidic solution. NpO_2^{2+} is stable in acidic solution but is relatively easily reduced to NpO_2^+. Np(V) and Np(VI) form hydroxides in neutral and basic solutions. The solubilities of these hydroxides in the aqueous solution are higher than that of Np(IV) hydroxide. Np(VII) was first prepared by Krot and Gelman (1967) in basic solution. The chemical forms of Np(VII) in acidic and basic media are described in Section 6.8.2. NpO_3^+ is quickly reduced to NpO_2^{2+} by water (Spitsyn *et al*., 1969).

(a) Redox potentials of neptunium ions

(*i*) *Acidic media*

Np(III), Np(IV), Np(V), and Np(VI) ions exist in solutions of sufficiently high acidity or solutions containing ligands. Standard redox potentials are estimated from experimentally determined formal redox potentials by precise correction for activity coefficients. Alternatively, the standard redox potentials are calculated from standard enthalpies of formation and entropies of the ions. Chapter 19 of this work provides recommended values of the standard potentials of actinide ions as the following potential diagram:

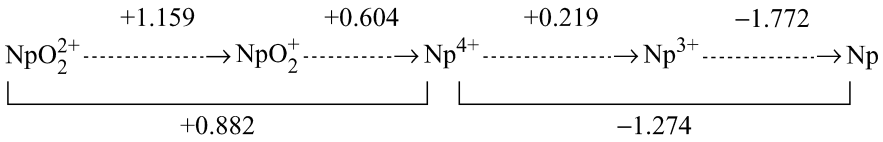

Recently, Kihara *et al*. (1999) critically evaluated the redox potentials of uranium, neptunium, and plutonium ions in acidic solutions by extrapolating the formal potentials to the state of zero ionic strength, referring mainly to the works by Riglet *et al*. (1987, 1989) and based on the Bronsted–Guggenheim–Scatchard specific ion-interaction theory (SIT) (Pitzer, 1979).

The E° for such reversible redox couples as NpO_2^{2+}/NpO_2^+ and Np^{4+}/Np^{3+} proposed by Riglet *et al.* (1987, 1989) are reliable and most of the experimental data are in good agreement with these E° if the activity coefficient is properly corrected in the conversion of the formal potential to E°. The formal potential for the redox couple between NpO_2^+ and Np^{4+} is difficult to determine by conventional voltammetry or polarography, because the electrode reaction between NpO_2^+ and Np^{4+} is slow or irreversible because Np–O bonds must be made or broken. The E° for NpO_2^+/Np^{4+} couple in the diagram was evaluated from data of Gibbs energy of formation (Martinot and Fuger, 1985). Kihara *et al*. (1999) re-estimated the electromotive force (EMF) data (Cohen and Hindman, 1952) by the activity coefficient correction based on the SIT and obtained +0.596 for NpO_2^+/NP^{4+} couple. The E° for NpO_3^+/NpO_2^{2+} estimated by Musikas *et al.* (1974) given in the diagram is recommended at the present time.

(*ii*) *Basic media*

Standard potentials or formal potentials for neptunium ions in basic media are less precise and less reliable than those in acidic media. For some redox reactions even chemical forms of hydrolytic species participating in the processes have not yet been fully understood. The potential diagram for neptunium ions in basic media by Martinot and Fuger (1985) is recommended:

$$NpO_5^{3-} \overset{+0.58}{\rightarrow} NpO_2(OH)_2 \overset{+0.6}{\rightarrow} NpO_2OH \overset{+0.3}{\rightarrow} NpO_2 \overset{-2.1}{\rightarrow} Np(OH)_3 \overset{-2.2}{\rightarrow} Np$$

Recently a new method for the determination of formal potentials by the use of *in situ* X-ray absorption near-edge structure (XANES) spectroscopy was applied to the redox couples of neptunium ions in 1 M $HClO_4$ (Soderholm *et al.*, 1999). The relative concentrations of Np(VI)/Np(V) or Np(IV)/Np(III) after the controlled potential electrolysis were determined from XANES spectra using the principal component analysis technique. XANES spectra specific for the hydrated neptunium ions of different oxidation states are shown in Fig. 6.8.

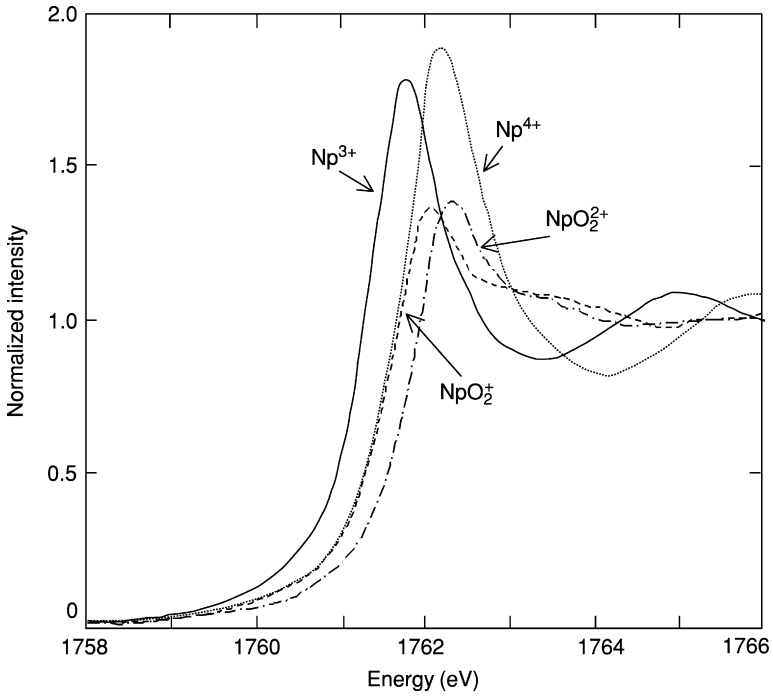

Fig. 6.8 *XANES spectra from the pure Np(III), Np(IV), Np(V), and Np(VI) ions in $HClO_4$; reprinted from Soderholm* et al. (1999) *with permission from American Chemical Society.*

The Nernstian plots between log([Np(VI)]/[Np(V)]) or log([Np(IV)]/[Np(III)]) and the applied potential lead to the precise determination of the formal potential, at which [Np(VI)]/[Np(V)] or [Np(IV)]/[Np(III)] equals unity. The formal potentials determined by this method are in good agreement with those determined by traditional voltammetry or polarography. An advantage of this method is that XANES is highly selective to the ion of interest that can interrogate a given redox couple in a complicated mixture such as the test solution containing multiple redox-active species.

(b) Electrolytic behavior of neptunium ions

(*i*) *Voltammetric behavior*

The measurements of current–potential relations by voltammetry, polarography, or related methods are important not only to elucidate the reaction mechanism and estimate the reaction rate but also to determine the formal potential for the evaluation of the standard redox potential. The voltammetric studies of the redox of neptunium ions, however, have not been conducted extensively enough.

Voltammetric data for the redox of neptunium ions in acidic media were provided by Niese and Vecernik (1981). The current–potential curves were recorded by cyclic voltammetry at a glassy carbon electrode with $HClO_4$, HNO_3, H_2SO_4, and acetate buffer solutions containing neptunium ion of a given oxidation state. Clear peaks due to one-electron redox reactions of NpO_2^{2+}/NpO_2^+ and Np^{4+}/Np^{3+} were observed. The peak potentials $E_{p,a}$ and $E_{p,c}$, at which the anodic and cathodic current peaks were observed, for the redox couples of NpO_2^{2+}/NpO_2^+ and Np^{4+}/Np^{3+} are summarized in Table 6.10. A difference between $E_{p,a}$ and $E_{p,c}$, ΔE_p, indicates that the redox processes of NpO_2^{2+}/NpO_2^+ and Np^{4+}/Np^{3+} in the 0.5 M $HClO_4$ or 1 M HNO_3 solutions are practically reversible and those in the H_2SO_4 or acetate buffer solutions are not reversible. The peak potential for NpO_2^{2+}/NpO_2^+ shifts more negatively with acetate buffer solution and the peak potential for Np^{4+}/Np^{3+} in HNO_3, H_2SO_4, and acetate buffer solution are more negative than that in $HClO_4$, which is due to stabilization of NpO_2^{2+} and Np^{4+} by the complex formation of NpO_2^{2+} with acetate ion and Np^{4+} with NO_3^-, SO_4^{2-}, and acetate ion.

The cathodic wave corresponding to further reduction of NpO_2^+ to Np^{4+} or Np^{3+} was not observed in the experiments by Niese and Vecernik (1981). The rate of the redox between Np^{4+} and NpO_2^+ as equation (6.30) is very slow, because the redox process involves formation or rupture of a Np–O bond which requires a large overpotential.

$$NpO_2^+ + 4H^+ + e^- \rightleftarrows Np^{4+} + 2H_2O \tag{6.30}$$

The potential for the reduction of NpO_2^+ to Np^{4+} is, therefore, more negative than that for the reduction of Np^{4+} to Np^{3+}, and the potential for the oxidation

Table 6.10 *Characteristics of voltammograms for redox of neptunium ions in $HClO_4$, HNO_3, H_2SO_4, or acetate buffer solutions.*

		Peak potentials (V vs SSE)		
Redox reactions	*Electrolyte*	*Anodic peak, $E_{p,a}$*	*Cathodic peak, $E_{p,c}$*	E_p
$NpO_2^{2+} + e^- = NpO_2^+$	0.5 M $HClO_4$	+1.01	+0.95	0.060
	1 M HNO_3	+1.04	+0.98	0.060
	0.5 M H_2SO_4	+1.02	+0.91	0.110
	0.5 M acetate buffer (pH = 4.2)	+0.84	+0.72	0.120
$Np^{4+} + e^- = Np^{3+}$	0.5 M $HClO_4$	+0.05	–0.02	0.070
	1 M HNO_3	–0.02	–0.08	0.070
	0.5 M H_2SO_4	–0.095	–0.23	0.135
	0.5 M acetate buffer (pH = 4.2)	–0.27	–1.06	0.790

of Np^{4+} to NpO_2^+ is more positive than that for the oxidation of NpO_2^+ to NpO_2^{2+} in $HClO_4$ and HNO_3 media.

Riglet *et al.* (1989) recorded voltammograms for the redox of Np(VI) and Np(V) in perchlorate media of various ionic strengths ($0.5 < I < 3$) for the precise determination of the formal redox potentials and re-evaluation of the standard redox potential at $I = 0$. The current–potential curves shown in Fig. 6.9 were recorded at rotating platinum disk electrode (2 mm in disk diameter) with rotation rate of 1500 rpm by scanning the potential at a rate of 0.002 V s^{-1}. The oxidation state of the neptunium ion in the test solution was controlled by the electrolysis so that NpO_2^+ initially present in the solution was partly oxidized to NpO_2^{2+} step by step (curves 2 to 5). The anodic wave developing at more positive potential and the cathodic wave at more negative potential than ca. +0.77 to +0.78 V correspond to the oxidation of NpO_2^+ and the reduction of NpO_2^{2+}, respectively. The redox reaction between NpO_2^+ and NpO_2^{2+} is not fully reversible at the platinum electrode because the slopes of the logarithmic analysis of the diffusion controlled waves are ca. 0.080 V per log unit, which are larger than the theoretical value.

Voltammetry using a rotating platinum electrode was applied to study the redox behavior of neptunium ions in 0.5– 4 M NaOH solution (Peretrukhin and Alekseeva, 1974). The successive reduction and oxidation among Np(VII), Np (VI), Np(V), and Np(IV) were investigated. The redox behavior of the neptunium ions strongly depends on the concentration of NaOH, which is interpreted as a change of the chemical form of Np(VI) during the electrolytic reduction and oxidation depending on the NaOH concentration.

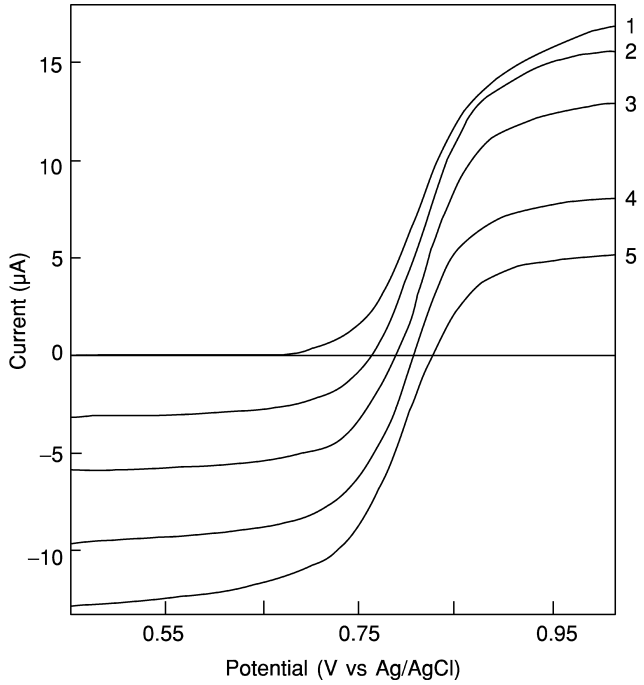

Fig. 6.9 *Current–potential curves for the redox couple of* NpO_2^{2+}/NpO_2^{+} *in* 1 M $HClO_4$ + 1 M $NaClO_4$ *at rotating platinum disk electrode* (1500 rpm). *Concentration of Np*; 10^{-3} M, *Potential;* V *vs Ag/AgCl electrode* ($E^\circ = 0.3329$ V *vs NHE*).

Electrochemical and spectroscopic studies of neptunium ions in concentrated aqueous carbonate and carbonate–hydroxide solutions were carried out by Varlashkin *et al.* (1984). The formal potential of the Np(VI)/Np(V) couple was determined as a function of pH of the solution. The redox reaction between Np(VI) and Np(V) was found to be quasi-reversible at a platinum electrode and the formal potential was estimated to be ($+0.23 \pm 0.01$) V vs saturated calomel electrode (SCE).

(*ii*) *Coulometric behavior*

Flow coulometry using multi-step column electrodes is a powerful technique to investigate a redox reaction even if the reaction is irreversible, because the surface area of the working electrode of the column electrode is very large comparing with a volume of the solution in the column and a quantitative electrolysis can be achieved very rapidly. The electrolysis method using column

electrode is also useful for the preparation of ions of a desired oxidation state as well as for the rapid determination or collection of various metals (Fujinaga and Kihara, 1977; Yoshida *et al.*, 1991).

Flow coulometry has been applied to the studies of overall redox behavior of the neptunium ions in acidic aqueous solution. Coulopotentiograms, which are current–potential curves observed by flow coulometry, were measured by using the multi-step column electrodes connected in series. Coulopotentiograms for the redox of neptunium ions of various oxidation states are shown in Fig. 6.10 after correction for the residual current. In the figure, the number of electrons involved in the redox reaction, *n*, converted from the current is plotted on the ordinate instead of the current.

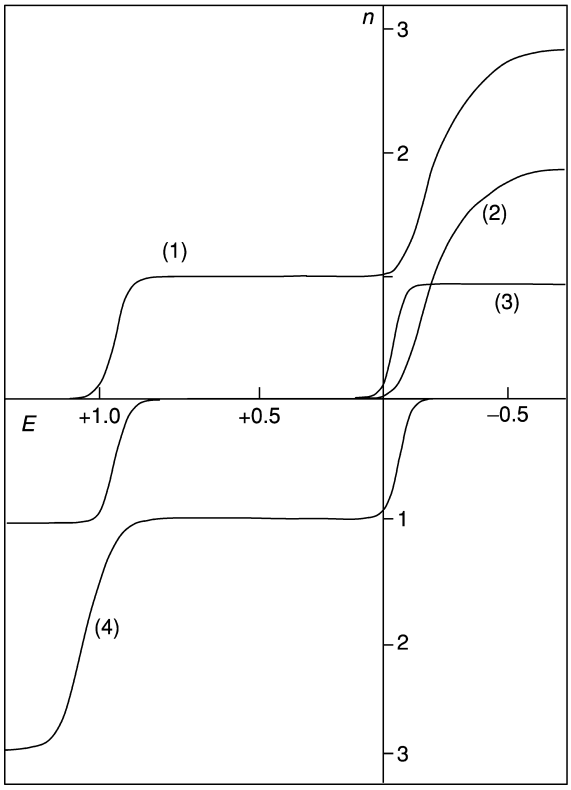

Fig. 6.10 *Coulopotentiograms for the redox of neptunium ions in* 1 M $HClO_4$ *solution*. n, *number of electrons involved in redox reaction;* E, *working electrode potential* (V *vs Ag–AgCl reference electrode*). (1) *Reduction of* NpO_2^{2+}, (2) *reduction and oxidation of* NpO_2^{+}, (3) *reduction of* Np^{4+}, (4) *oxidation of* Np^{3+}. *Sample solution;* 10^{-3} M *Np ion, flow rate,* 1.5 ml min^{-1}; *potential scan rate,* 0.002 V s^{-1}.

Coulopotentiogram 1 in Fig. 6.10 was recorded at a single column electrode with flowing 1 M $HClO_4$ solution containing 10^{-3} M NpO_2^{2+} and scanning the potential. The coulopotentiogram shows the reduction of NpO_2^{2+} to NpO_2^{+} at more negative potential than +0.85 V vs Ag–AgCl reference electrode (SSE) and further to Np^{3+} at more negative potential than −0.6 V. Coulopotentiogram 2 was recorded with a two-step column electrode system with the first column electrode kept at +0.5 V and the second column at the scanned potential. Here, NpO_2^{2+} in the test solution is converted to NpO_2^{+} quantitatively at the first column, and therefore, the redox behavior of NpO_2^{+} can be examined at the second column electrode. Coulopotentiogram 2 shows one-electron oxidation of NpO_2^{+} to NpO_2^{2+} at more positive potential than +1.1 V and two-electron reduction to Np^{3+} at more negative potential than −0.6 V. Coulopotentiograms 3 and 4 are recorded identically using two-step or three-step column electrode systems and show the reduction of Np^{4+} to Np^{3+} and the oxidation of Np^{3+} to Np^{4+} and further to NpO_2^{2+}.

(c) Disproportionation of NpO_2^{+}

NpO_2^{+} disproportionates to Np^{4+} and NpO_2^{2+} through the following reaction. The extent of the disproportionation is promoted when the acidity of the solution and the concentration of NpO_2^{+} are high:

$$2NpO_2^{+} + 4H^{+} \rightleftarrows Np^{4+} + NpO_2^{2+} + 2H_2O$$

$$K_{\text{dispro}} = [Np^{4+}][NpO_2^{2+}]/[NpO_2^{+}]^2[H^{+}]^4 \tag{6.31}$$

The equilibrium constant is increased by the addition of reagents that form complexes with Np^{4+} and $NpO_2^{2}+$ in the solution. For example, it was shown that $K_{\text{dispro}} = 4 \times 10^{-7}$ for Np(V) in 1 M $HClO_4$ and $K_{\text{dispro}} = 2.4 \times 10^{-2}$ for Np(V) 1 M H_2SO_4 solution (Keller, 1971). Hindman *et al.* (1954) suggested that the rate of the disproportionation reaction of equation (6.31) is expressed by equation (6.32).

$$-d[NpO_2^{+}]/dt = k[NpO_2^{+}][H^{+}]^2 \tag{6.32}$$

(d) Methods for the control of oxidation state of neptunium ions

(*i*) *Redox reagents*

The oxidation state of neptunium ions can be adjusted using various redox agents. The agent and chemical procedure feasible for the promotion of the redox between reversible couples such as NpO_2^{2+}/NpO_2^{+} or Np^{4+}/Np^{3+} are chosen properly by referring to the redox potentials for neptunium ions and those for the agent as well as a ligand coexisting in the solution. Typical procedures for the control of the oxidation state of neptunium ions are shown

Table 6.11 *Procedures for adjusting the oxidation state of neptunium ion in aqueous solutions using redox agents.*

Oxidation states of neptunium ion		*Procedures*	
Before treatment	*After treatment*	*Agents*	*Conditions*
Oxidative treatment			
Np(III), Np(IV), Np(V)	Np(VI)	Ce(IV)	HNO_3, H_2SO_4
		MnO_4^-	HNO_3, H_2SO_4
		Ag(II)	1 M $HClO_4$
		BrO_3^-	
		$HClO_4$	fuming
		Cl_2	1 M HCl (348 K)
Np(III)	Np(IV)	O_2 (air)	
Reductive treatment			
Np(V), Np(VI)	Np(IV)	Fe^{2+}	H_2SO_4
		I^-	5 M HCl (373 K)
Np(VI)	Np(V)	NH_2NH_2	1 M H^+
		NH_2OH	1 M H^+
		NO_2^-	1 M HNO_3
		H_2O_2	0.5 M HNO_3
		Sn^{2+}	HCl
		SO_2	H_2SO_4
Np(IV), Np(V), Np(VI)	Np(III)	Zn(Hg)	
		H_2 (Pt black)	

in Table 6.11. The kinetic factors are required to be evaluated to complete slow processes between NpO_2^{2+} and Np^{4+} or between NpO_2^+ and Np^{4+} involved in the procedure for the oxidation state control. The kinetics of the redox reactions for Np(VI)–H_2O_2, Np(V)–V(III), Np(V)–Cr(II), and Np(VII)–Hg(I) systems were summarized by Newton (1975). Nakamura *et al.* (1992) proposed a method for the rapid reduction of Np(V) to Np(IV) by hydroxylamine nitrate in the presence of platinum black catalyst.

Recently much attention has been paid to the kinetics of the redox of neptunium ions by various organic agents for the development of an advanced Purex process. These studies aim at screening of the most suitable 'salt-free' redox agent, which enables precise control of the oxidation state of the neptunium ion in the process flowsheet. Taylor *et al.* (1997) reviewed the redox chemistry of neptunium ion in the proposed procedures.

Aldehyde derivatives such as *n*- and isobutyraldehydes are effective reductants for Np(VI) and Pu(IV) as reported by Kolarik and Dressler (1984) and Uchiyama *et al.* (1993). Hydroxylamine- and hydrazine derivatives have been suggested as effective reducing agents for Np(VI) and Pu(IV). Koltunov *et al.* (1993, 1999) investigated the reduction kinetics of Np(VI) by *N*,*N*-ethyl

(hydroethyl)hydroxylamine ($HOC_2H_4(C_2H_5)NHOH^+$, EHEH) and *N*,*N*-diethyl hydroxylamine ($(C_2H_5)_2NHOH^+$, DEH) in nitric acid solution. The reduction reactions are expressed as follows.

$$4NpO_2^{2+} + HOC_2H_4(C_2H_5)NHOH^+ + 3H_2O \rightarrow 4NpO_2^+ + 2C_2H_5OH + HNO_3 + 9H^+ \quad (6.33)$$

$$8NpO_2^{2+} + (C_2H_5)_2NHOH^+ + 4H_2O \rightarrow 8NpO_2^+ + CH_3CHO + C_2H_5OH + HNO_3 + 5H^+ \quad (6.34)$$

The different characteristics of reactions by EHEH and DEH are explained by their different structures providing an availability of a hydroxyl group in the EHEH molecule. The kinetics of reactions (6.33) and (6.34) were studied in 0.3 – 2.0 M HNO_3 at ionic strength of 2.0. It was concluded that the reaction is first order relative to Np(VI) with excess reductants. The rate equations of reaction (6.33) and (6.34) are

$$-d[Np(VI)]/dt = k[Np(VI)][EHEH][H^+]^{-0.8} \quad (6.35)$$

where $k = (334 \pm 12)\ L^{0.2}\ mol^{-0.2}\ min^{-1}$ (298.6 K), and activation energy (E_A) = (42.3 ± 2.7) kJ mol^{-1}, and

$$-d[Np(VI)]/dt = k[Np(VI)][DEH][H^+]^{-0.84} \quad (6.36)$$

where $k = (22.6 \pm 0.8)\ L^{0.16}\ mol^{-0.16}\ min^{-1}$ (298 K), and $E_A = (68.5 \pm 0.9)$ kJ mol^{-1}. Np(VI) and Pu(IV) are reduced faster by EHEH than by DEH, which suggests that the introduction of the hydroxyl group into the reductant molecule enhances the kinetics.

A comprehensive study on the reduction kinetics of Np(VI) and Pu(IV) by Taylor *et al.* (1998a) suggests that 1,1-dimethylhydrazine (DMHz) and *tert*-butylhydrazine (*tert*-BHz) are the most promising agents for the rapid reduction of Np(VI) with high selectivity over Pu(IV) reduction. For example, 99% of Np(VI) (initial concentration (1–2) × 10^{-4} M) in 1 M HNO_3 solution was reduced to Np(V) at 298 K by the addition of 0.1 M DMHz or *tert*-BHz within 1 or 8.7 min, respectively, and only 0.23 or 0.11% of Pu(IV) (initial concentration (2–10) × 10^{-3} M) was reduced to Pu(III) during 99% reduction of Np(VI) under the equivalent condition. It was found that formohydroxamic acid (Taylor *et al.*, 1998b) and acetaldoxime (Koltunov *et al.*, 2000) were also effective reductants for the rapid reduction of Np(VI) to Np(V) in acid solution.

(*ii*) *Electrochemical methods*

Controlled potential electrolysis is available to control the oxidation state of neptunium ions. For example, Np(V) in acidic solutions such as 1 M $HClO_4$ solution is oxidized to Np(VI) completely at +1.20 V vs Ag–AgCl

(saturated KCl) reference electrode, Np(V) is quantitatively reduced to Np(III) at −0.20 V, and Np(III) is oxidized to Np(IV) at +0.40 V by controlled potential electrolysis using carbon or platinum working electrodes. Controlled potential electrolysis was applied to the preparation of carbonate complexes of neptunium ion of a given oxidation state in neutral or basic solutions (Li *et al.*, 1993).

The electrolytic technique using multi-step column electrodes of glassy carbon fiber working electrode as described in Section 6.8.1b is also useful to adjust the oxidation state of the neptunium ion in the flowing sample solution. The applied potential and the other electrolytic conditions can be chosen consulting with the current–potential relationship as shown in Fig. 6.10.

(*iii*) *Miscellaneous*

A sonochemical technique was applied to oxidize Np(V) efficiently (Nikitenko *et al.*, 1999). Np(V) in HNO_3 solution was found to be oxidized to Np(VI) in the presence of argon under the effect of power ultrasound (20 kHz, 1 W cm^{-2}). The addition of urea which exerts a buffering effect related to nitrous acid concentration helps to stabilize Np(VI) formed under sonification. The oxidation mechanism is related to the formation of HNO_2 by sonolysis of HNO_3, followed by the oxidation of Np(V) with HNO_3 catalyzed by HNO_2.

Photochemical reaction is feasible to oxidize and reduce Np(V) and Np(VI) in nitric acid solution (Fukasawa *et al.*, 1991). Np(VI) is reduced to Np(V) by HNO_2 generated by the photolysis of HNO_3 and is shown in reactions (6.37) to (6.39).

$$HNO_3(\text{photo irradiation}) \rightarrow OH + NO_2 \tag{6.37}$$

$$2NO_2 + H_2O \rightarrow HNO_2 + HNO_3 \tag{6.38}$$

$$NpO_2^{2+} + HNO_2 + H_2O \rightarrow 2NpO_2^{+} + 3H^{+} + NO_3^{-} \tag{6.39}$$

Addition of a scavenger for HNO_2, such as urea, allows the oxidation of Np(V) to Np(VI) by the action of OH radical as given by reactions (6.40) and (6.41).

$$2HNO_2 + CO(NH_2)_2 \rightarrow 2N_2 + CO_2 + 3H_2O \tag{6.40}$$

$$NpO_2^{+} + OH + H^{+} \rightarrow NpO_2^{2+} + H_2O \tag{6.41}$$

The kinetics of the photochemical reduction of Np(VI) to Np(V) in HNO_3 solution were investigated (Wada *et al.*, 1995) as a function of irradiation wavelength, the acidity of nitric acid, and the nature of the coexisting agents. It was concluded that the higher the irradiation rate and the HNO_3 concentration, the easier the oxidation reaction of Np(V) progressed.

6.8.2 Optical spectroscopy of neptunium

Optical spectroscopy has been extensively applied to neptunium to better understand the electronic structure of the aquo ions Np(III) through Np(VII), and of coordination complexes that occur in solution (Gruen, 1952; Waggener, 1958; Dukes and Shuler, 1960; Krot *et al.*, 1968a; Stafsudd *et al.*, 1969; Varga *et al.*, 1970; Chaikhorskii, 1971; Chaikhorskii and Leikina, 1972; Rykov and Frolov, 1972; Tsivadze and Krot, 1972; Kharitonov and Moskvin, 1973; Rykov *et al.*, 1973; Hessler *et al.*, 1980; Kanellakopulos *et al.*, 1980a,b; Lahalle *et al.*, 1986; Carnall *et al.*, 1987; Tait *et al.*, 1995; Matsika and Pitzer, 2000; Neck *et al.*, 2001). An excellent review article has been published by Gruen (1992) describing the development of the knowledge base for the f-electron elements, especially neptunium. Fig. 6.11 shows the visible absorption spectra for the neptunium ions (III, IV, V, and VI) in 2 M perchloric acid. Optical spectroscopy has been applied in both the visible and infrared portions of the spectrum with a wealth of information being gathered.

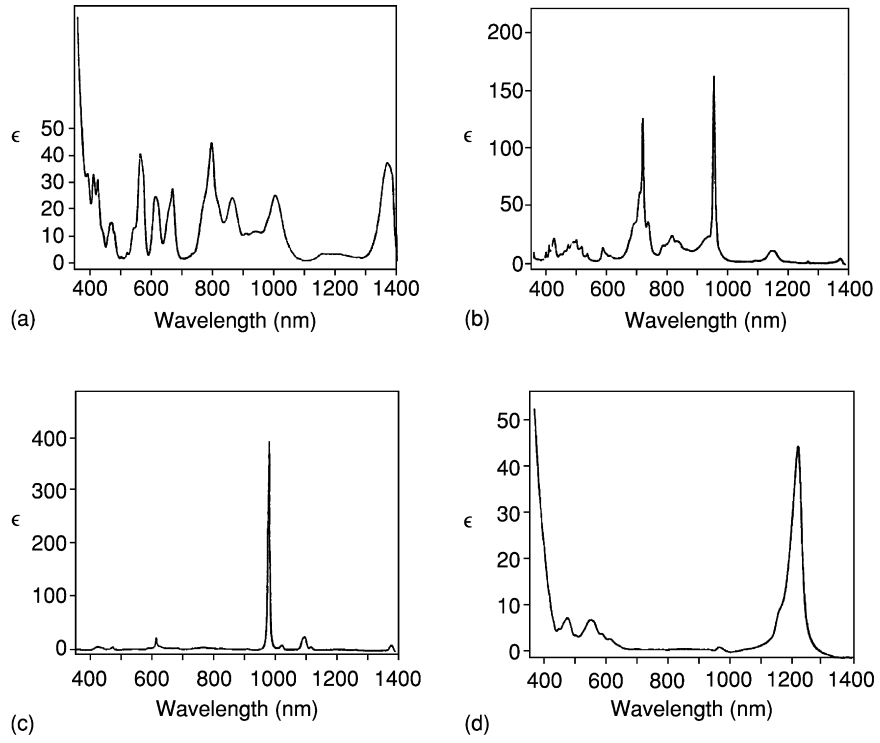

Fig. 6.11 *The absorption spectra of neptunium ions in* 2 M $HClO_4$ *solution:* (*a*)*Np*(III); (*b*) *Np*(IV); (*c*) *Np*(V); (*d*) *Np*(VI).

One of the earliest studies on the subject (Gruen, 1952) used optical means to obtain information on the spin–orbit coupling for NpO_2^{2+} species. A value of 950 cm^{-1} for the spin–orbit coupling energy provided the best agreement between calculated and experimentally observed results for the $5f^2$ configuration. This 'best fit' was obtained by using the intermediate case of mixing the pure spin–orbit coupling and the pure electrostatic case.

The absorption spectrum of neptunium has often been measured in nitric acid solution. This provides straightforward identification of what valence states are present as was shown by Dukes and Shuler (1960). Np(IV) displays a strong absorption band at 715 nm, while Np(V) displays a somewhat weaker band at 617 nm and Np(VI) displays a strong band in the region below 400 nm. The concentration of nitric acid was determined not to be a significant factor in the absorption spectrum from 1 to 6 M.

Absorption spectroscopy of the Np(VII) species is somewhat more difficult in that it can be observed only under basic conditions (Krot *et al*., 1968a; Williams *et al*., 2001) in a steady-state manner. The actual form of the Np(VII) in solution is as NpO_6^{5-} in basic solutions and NpO_2^{3+} in acidic solutions. The tetraoxo Np(VII) compound exhibits four 'short' bonded oxygen (~1.85 Å) and two 'long' bonded oxygen (~2.2 Å) in basic solutions. The acidic form can only be observed at room temperature for a matter of minutes before it is reduced to the Np(VI) state. The hydroxide, $NpO_2(OH)_3$ is assumed to have amphoteric properties in solution.

The absorption spectrum for Np(VII) in solution was investigated in more detail by Chaikhorskii (1971). They prepared Np(VII) species in the cationic form and then precipitated it for their study. It was determined that fine structure could be observed in the visible absorption bands (412 and 620 nm). This fine structure was attributed to two causes, electron transfer (oxygen $\pi \rightarrow$ 5f) and vibrational states. Several vibrational states were identified with energies between 681 and 2338 cm^{-1}. The vibrational bands identified were consistent with the predicted symmetry of a compound involving the NpO_2^{3+} species.

The infrared spectroscopy study by Chaikhorskii (1971) was extended by Tsivadze and Krot (1972) to include several compounds of Np in the Np(VII) state. Their work validated the earlier work of Chaikhorskii (1971) and furthered the knowledge base in that they determined the neptunium in the solid compounds that contained no isolated NpO_2 groups but that there were chains of 'infinite' length which connected the NpO_6 octahedra.

Stafsudd *et al.* (1969) studied Np(VI) by doping NpO_2^{2+} into a matrix of $Cs_2UO_2Cl_4$ and applying infrared and visible spectroscopies. They identified several pure electronic levels at 6880, 13 277, 15 426, 17 478, and 19 358 cm^{-1}. The ground state and the 6880 cm^{-1} state belong to the $5f^1$ configuration, whereas the other energy levels were thought to likely belong to an excited configuration involving electrons in the non-bonding 5f shell.

A more recent theoretical effort sought to improve the assignments of the electronic states for both Np(VI) and Np(V) species (Matsika and Pitzer, 2000).

This work is more complete than the much earlier effort of Eisenstein and Pryce (1965, 1966). Their work resulted in the calculation of the energy levels of 15 excited states for NpO_2^{2+} and 19 for NpO_2^{+}, as well as their respective wave functions. Their methods used relativistic spin–orbit coupling configuration interactions based on effective core potentials.

Work on the Np(V) species with a focus on its interaction with polyvalent species in different solvents was reported by Rykov and Frolov (1972). Visible spectroscopy of solutions of NpO_2^{+} in several different mixed solvents (water–methanol, water–ethanol, water–acetone) were obtained at room temperature in the presence of Fe^{3+}. The interaction of Fe^{3+} with Np^{5+} ion in mixed solvents was studied and it was reported that the formation of a complex involving both ions mirrored that of the electron exchange for Fe^{2+} and Fe^{3+} for aqueous solutions kinetically. The degree of interaction between the two ions being inversely dependent on the effective dielectric constant of the solvent.

Varga *et al*. (1970) performed an extensive spectroscopic study of the Np(IV) species from 300 to 1800 nm using NpF_4 either dissolved in $CsF \cdot 2HF$ (300–1300 nm) and in a fluorocarbon mull (1300–1800 nm). This study allowed for the assignment of 17 excited-state transitions for Np^{4+}. The experimental values for these transitions were compared to calculated values with good agreement. Infrared spectroscopy was also applied to a Np(IV) species in the form of several oxalate compounds formed with neptunium in the 4+ state (Kharitonov and Moskvin, 1973). This work identified several vibrational bands and their respective force constants and bond lengths (Np–O). The bond length was reported as 1.78 Å, which agreed well with the literature value for this quantity based on the vibrational band of approximately 825 cm^{-1} (Kharitonov and Moskvin, 1973).

Rykov *et al*. (1973) investigated the complexation behavior of Np(IV) in nitrate solutions of varying concentrations. A total of three types (A–B–C) of complexes were observed depending on whether there was very little nitrate present (type 'A' spectra observed) or nitrate solutions with very little free water present (type 'C' spectra observed). Type 'B' spectra were considered as intermediate to 'A' and 'C'. The fundamental distinction between the three types of complexes was assigned to the structure of the first coordination sphere. The type 'A' were thought to be of the M_{aq}^{4+} formula whereas the type 'C' were assigned to be a neptunium ion coordinated with six nitrates. The type 'B' complex had been thought to be an intermediate nitrate complex (less than six coordination) but their results were shown to be consistent with change in the aqueous coordinated complex and did not involve complexation by nitrate at all.

A later study of Np(IV) utilized low temperature spectroscopy (4.2 K) and two different crystalline hosts, $ThSiO_4$ and ThO_2 (Lahalle *et al*., 1986). The latter of the two crystalline hosts had been used in an earlier study by Gruber and Menzel (1969) and was used for comparison purposes. Their study identified 29 excited-state transitions in the $ThSiO_4$ host and 19 in the ThO_2 host for

Np(IV) using both absorption and fluorescence spectroscopies over the temperature range of 4.2–300 K. Work of a similar nature on alkali and alkaline earth neptunates involving Np(VI) was performed by Kanellakopulos *et al.* (1980a,b).

A spectroscopic investigation of Np(III) was undertaken by Hessler *et al.* (1980) using low-temperature, high-resolution absorption, and fluorescence spectroscopies. A crystalline host of $LaCl_3$ was used. The temperature dependence of the homogeneous linewidth of D_1 to Z_1 (671.51 nm) and the D_1 to Z_2 (677.18 nm) transitions were obtained.

Carnall *et al.* (1987) investigated the interpretation of the spectra of neptunium obtained in silicate glasses with a focus on determining the valence state of the neptunium present. This work was undertaken to assist in the understanding of the local environment of neptunium in waste glasses bound for disposal in a geologic repository. Another spectroscopic investigation that has ramifications in the nuclear waste community is that of Neck *et al.* (2001) which utilized absorption spectroscopy, laser-induced photoacoustic spectroscopy (LIPAS), and laser-induced breakdown spectroscopy to study the colloids formed by neptunium in solution. An aqueous solution of $HClO_4$–$NaClO_4$ with Np(IV) present was used to obtain the solubility product constant of $Np(OH)_4$ at a wide range of pH. Kihara *et al.* (1996) also applied LIPAS to the study of neptunium species in Purex solutions.

A rather extensive study of Np(IV) and Np(V) in hydrolysis and carbonate reactions using optical and NMR spectroscopies was performed by Tait *et al.* (1995). Chaikhorskii and Leikina (1972) had earlier performed a similar study on Np(VII) during hydrolysis using optical spectroscopy.

With the relative importance of neptunium in the field of nuclear waste disposal, due to its long half-life, it is anticipated that the field of optical spectroscopy will continue to be an active one for many years with a particular emphasis on determining its local environment *in situ*.

6.8.3 Hydrolysis behavior

The hydrolysis reaction as a particular case of complex formation is the primary common property of all actinide ions in aqueous solution. The tendency for neptunium ions to undergo hydrolysis is in the order of $Np^{4+} > NpO_2^{2+} > Np^{3+} > NpO_2^{+}$, following the effective charge of the ions. The pentavalent NpO_2^{+} ion is the most stable ion in solution and is not hydrolyzed appreciably at pH below 7. The trivalent Np^{3+} and hexavalent NpO_2^{2+} ions are the predominant species in solution at pH below 4–5 and 3–4, respectively, reflecting that the NpO_2^{2+} ion has an effective charge greater than the Np^{3+} ion. The tetravalent Np^{4+} ion shows a strong tendency towards hydrolysis and considerable hydrolysis is expected at pH 1 or above. Representative equilibrium constants for hydrolysis of neptunium ions, Np^{3+}, Np^{4+}, NpO_2^{+}, and NpO_2^{2+}, are listed in Table 6.12, together with some solubility products of the oxide or hydroxide.

Table 6.12 *Experimental equilibrium constants for hydrolysis of neptunium ion.*

Ion	*Method*	*Temp.* (°C)	*Medium*	*Equilibrium constants*	*References*
Np^{3+}	pot	25	0.3 M $NaClO_4$	$\log^*K_{11} = -7.43 \pm 0.11$	Mefod'eva *et al.* (1974)
Np^{4+}	sp	25	1.0 M	$\log^*K_{11} = -1.90$	Paul (1970)
	sol	25	0.0	$\log^*K_{14} = -9.8 \pm 0.11$	Rai *et al.* (1987)
				$\log^*K_s = 1.5 \pm 1.0$;	Lemire *et al.* (2001)
				$NpO_2(s) + 4H^+ \rightleftarrows Np^{4+} + 2H_2O$	
NpO_2^+	sol	25	0.1 M $NaClO_4$	$\log^*K_{11} = -11.36 \pm 0.16$	Neck *et al.* (1992)
				$\log^*K_{12} = -23.50 \pm 0.12$	
			1.0 M $NaClO_4$	$\log^*K_{11} = -11.13 \pm 0.20$	
				$\log^*K_{12} = -23.19 \pm 0.14$	
				$\log^*K_s = 4.50 \pm 0.06$;	
				$NpO_2OH(s) + H^+ \rightleftarrows NpO_2^+ + H_2O$	
NpO_2^{2+}	pot	25	1.0 M $NaClO_4$	$\log^*K_{11} = -5.17 \pm 0.03$	Cassol *et al.* (1972a)
				$\log^*K_{22} = -6.68 \pm 0.02$	
				$\log^*K_{35} = -18.25 \pm 0.02$	
	sol	25	0.1 M $NaClO_4$	$\log^*K_s = 5.87 \pm 0.17$;	Kato *et al.* (1996)
				$NpO_3H_2O(s) + 2H^+ \rightleftarrows NpO_2^{2+} + 2H_2O$	

* K_{mn} is the hydrolysis constant for the equilibrium: $mM^{a+} + nH_2O \rightleftarrows M_m(OH)_n^{am-n} + nH^+$.

(a) Neptunium(III)

The trivalent Np^{3+} ion is sufficiently stable in acidic solution to allow spectrophotometric studies, but it is rapidly oxidized by air to the tetravalent state. Therefore, Np^{3+} will be stable in the presence of strong reductants and/or in an oxygen-free atmosphere. The tendency of an ion to undergo hydrolysis increases with charge and with decreasing ionic radius. The order of the trivalent actinide ions for ease of hydrolysis should be as follows: $U^{3+} < Np^{3+} < Pu^{3+} < Am^{3+}$, because the stability of hydrolyzed ions increases as z/r_{ion} increases.

As only one experimental study for the equilibrium,

$$Np^{3+} + H_2O \leftrightarrows NpOH^{2+} + H^+ \tag{6.42}$$

Mefod'eva *et al.* (1974) determined $\log^*K_{11} = -7.43$ for 298 K and 0.3 M $NaClO_4$ from potentiometric measurements in the pH range 6–8. The Np^{3+} ion was produced by electrolysis of 0.022 M Cs_2NpCl_6(aq) in 0.1 M HCl using a mercury cathode in an inert atmosphere. The titration curves of Np^{3+} were compared with those of Pr^{3+} and Nd^{3+} under the similar conditions to obtain the ratios of the hydrolysis constants.

There has been no systematic study to determine the solubility product for Np(III) and no usable experimental data for $Np(OH)_3$(s) is available.

(b) Neptunium(IV)

From the same reasons as in the case of the trivalent state, the tendency of the tetravalent actinide ions to undergo hydrolysis follows the order: $Th^{4+} < U^{4+} < Np^{4+} < Pu^{4+}$. There are three reports of the first hydrolysis step of Np^{4+}.

$$Np^{4+} + H_2O \leftrightarrows NpOH^{3+} + H^+ \tag{6.43}$$

Sullivan and Hindman (1959) and Paul (1970) reported $\log^*K_{11} = -2.30$ ($I = 2.0$ M) and -1.90 ($I = 1.0$ M), respectively, in aqueous perchlorate solutions by spectrophotometry. From extraction experiments, Duplessis and Guillaumont (1977) reported $\log^*K_{11} = -0.50$ in 1.0 M $LiClO_4$. Two values $\log^*K_{12}$ for $Np(OH)_2^{2+}$ have been reported with a large discrepancy (three order of magnitude) (Duplessis and Guillaumont, 1977; Schmidt *et al.*, 1980), while there is no experimental evidence for the formation of $Np(OH)_3^+$.

Several groups (Ewart *et al.*, 1985; Rai and Ryan, 1985; Pratopo *et al.*, 1989; Eriksen *et al.*, 1993) measured the solubility of Np(IV) hydrated oxide or hydroxide in neutral to basic solutions at room temperature in the presence of reducing agents, e.g. $Na_2S_2O_4$, Fe, or Zn, and reported a limiting neptunium concentration of $10^{-8.5}$ to $10^{-8.1}$ M. The pH-independence of the solubility indicates that the main species in equilibrium with Np(IV) solids is uncharged $Np(OH)_4^0$ and that $Np(OH)_5^-$ is not an important species for Np(IV)

hydrolysis. Rai *et al.* (1987) studied the solubility of $NpO_2 \cdot xH_2O$ in the presence of Cu(I)/Cu(II) buffer and in the pH range from 1.5 to 2.5. Based on the measured redox potentials, pH, and calculated activities of Np^{4+} and NpO_2^+, the thermodynamic equilibrium constants were determined. After recalculation of the results in the NEA/TDB neptunium and plutonium volume (Lemire *et al.*, 2001), $\log^* K_s = 1.5$ and $\log^* K_{14} = -9.8$ were reported for the following reactions, respectively:

$$NpO_2(s) + 4H^+ \leftrightarrows Np^{4+} + 2H_2O \tag{6.44}$$

$$Np^{4+} + 4H_2O \leftrightarrows Np(OH)_4^0 + 4H^+ \tag{6.45}$$

The experimental $\log^* K_s$ values of Th(IV) (Ryan and Rai, 1987), Np(IV) (Rai *et al.*, 1987), and Pu(IV) (Rai, 1984) hydrous oxides show a linear relationship with the inverse square of the M^{4+} ionic radii.

(c) Neptunium(V)

The pentavalent NpO_2^+ ion is stable and disproportionates only at rather high acidities. Many groups have reported the formation constants of the hydroxo species by using various experimental methods (see Lemire *et al.*, 2001). The recent hydrolysis studies by solubility measurements (Lierse *et al.*, 1985; Itagaki *et al.*, 1992; Neck *et al.*, 1992) show smaller constants than found in earlier studies (Kraus and Nelson, 1948; Moskvin, 1971; Sevost'yanova and Khalturin, 1976; Schmidt *et al.*, 1980; Maya, 1983; Bidoglio *et al.*, 1985), which is probably due to the effect of carbonate complexation.

Neck *et al.* (1992) studied the hydrolysis behavior of the NpO_2^+ ion at 298 K by solubility experiments in the pH range 7–14 in 0.1, 1.0, and 3.0 M $NaClO_4$ solutions under CO_2-free argon atmosphere. In 0.1 M $NaClO_4$ Np(V) hydroxide precipitate remained amorphous (green) over several months, while in 1.0 M $NaClO_4$ the precipitate changed from an amorphous to a more stable-aged state (white) within a relatively short time. In 3.0 M $NaClO_4$ the aged modification of $NpO_2OH(s)$ is formed from the beginning. As shown in Table 6.12, the hydrolysis constants and solubility product for aged $NpO_2OH(s)$ were reported for the following reactions:

$$NpO_2^+ + H_2O \leftrightarrows NpO_2OH^0 + H^+ \tag{6.46}$$

$$NpO_2^+ + 2H_2O \leftrightarrows NpO_2(OH)_2^- + 2H^+ \tag{6.47}$$

$$NpO_2OH(s) + H^+ \leftrightarrows NpO_2^+ + H_2O \tag{6.48}$$

The solids (fresh and aged NpO_2OH) were not analyzed for possible incorporation of sodium ions, however the parallel solubility curves obtained

for the two solids in 1.0 M $NaClO_4$ strongly suggest that they have similar stoichiometries.

(d) Neptunium(VI)

The hexavalent NpO_2^{2+} ion is not as stable as the UO_2^{2+} and PuO_2^{2+} ions. Cassol *et al.* (1972a) studied the hydrolysis of the NpO_2^{2+} ion in 1 M $NaClO_4$ at 298 K by potentiometric titrations. The NpO_2^{2+} solution was prepared by electrolytic oxidation of a NpO_2^{+} solution. The hydrolysis constants shown in Table 6.12 were reported for the following equilibria:

$$NpO_2^{2+} + H_2O \leftrightarrows NpO_2OH^{+} + H^{+} \tag{6.49}$$

$$2NpO_2^{2+} + 2H_2O \leftrightarrows (NpO_2)_2(OH)_2^{2+} + 2H^{+} \tag{6.50}$$

$$3NpO_2^{2+} + 5H_2O \leftrightarrows (NpO_2)_3(OH)_5^{+} + 5H^{+} \tag{6.51}$$

The value $\log^*K_{11} = -5.17$ is consistent with the value ($\log^*K_{11} = -5.45$) reported by Schmidt *et al.* (1983), while the hydrolysis scheme proposed by Moskvin (1971) based on solubility measurements is rather different. Comparison of the results (Cassol *et al.*, 1972a) with some available data on the hydrolysis of U(VI) (Rush *et al.*, 1962; Rush and Johnson, 1963) and Pu(VI) (Cassol *et al.*, 1972b) indicates a close analogy in hydrolysis behavior for the three ions. The tendency in acidity with increasing atomic number is in the order of $UO_2^{2+} > NpO_2^{2+} > PuO_2^{2+}$.

Kato *et al.* (1996) have determined the solubility product of neptunium trioxide monohydrate at 298 K in acidic 0.1 M $NaClO_4$ solution prepared with ozone in air.

$$NpO_3H_2O(s) + 2H^{+} \leftrightarrows NpO_2^{2+} + 2H_2O \tag{6.52}$$

The solid was characterized to be $NpO_3 \cdot H_2O$, not $NpO_2(OH)_2$, by X-ray diffraction and Fourier transform infrared spectroscopy (FTIR).

(e) Neptunium(VII)

A cationic Np(VII) species in acidic solutions (Shilov *et al.*, 1991) and an anionic species in strongly alkaline solutions (Chaikhorskii *et al.*, 1975) have been reported, but no thermodynamic data are available. Np(VII) hydroxide or hydrated oxide has been prepared by several groups (Chaikhorskii *et al.*, 1974; Nikonov *et al.*, 1994) using different methods. No thermodynamic data for Np(VII) hydroxide and oxide are available.

6.9 COORDINATION COMPLEXES IN SOLUTION

Representative equilibrium constants and the experimental conditions at which they were determined are collected in Tables 6.13 and 6.14 for neptunium complexes with inorganic and organic ligands, respectively. Data on complex formation of neptunium and of other actinides have been compiled in the literature, e.g. Gel'man *et al.* (1962), Degischer and Choppin (1975), Fuger *et al.* (1992), Lemire *et al.* (2001), Smith and Martell (2002), etc., and are reviewed in Chapters 19 and 23.

In Tables 6.13 and 6.14, the following abbreviations are used in experimental methods: cix, cation exchange; dis, distribution between two phases; em, electromigration; emf, electromotive force; ise, ion selective electrode; pot, potentiometry; red, emf with redox electrode; sol, solubility; sp, spectrophotometry. The stepwise stability constants K_i and overall constants β_i are defined for the reaction of a cation M with a ligand L as follows:

$$K_1 = \beta_1 = [ML]/[M][L], K_2 = [ML_2]/[ML][L], K_3 = [ML_3]/[ML_2][L], \text{etc.}$$
$$\beta_2 = [ML_2]/[M][L]^2, \beta_3 = [ML_3]/[M][L]^3, \text{etc.}$$

Therefore

$$\beta_2 = K_1K_2, \beta_3 = K_1K_2K_3, \text{ etc.} \tag{6.53}$$

The other equilibrium constants are indicated in Tables 6.13 and 6.14.

6.9.1 Complexation with inorganic ligands

All of the equilibrium constants listed in Table 6.13 are for complexes of Np (IV), Np(V), and Np(VI). Only a few studies have been carried out on complexes of Np(III) and Np(VII). Shiloh and Marcus (1966) studied the Np^{3+}–halide system quantitatively by measurement of the absorption spectra. The stability constants for NpX^{2+} and NpX_2^+ ($X = Cl^-$, Br^-) were obtained in concentrated LiCl and LiBr solutions, respectively. Mefod'eva *et al.* (1970a,b) reported the complex formation of Np(VII)(NpO_2^{3+}) with sulfate ion in acid solution. The stability constants obtained for $NpO_2SO_4^+$ and $NpO_2(SO_4)_2^-$ were greater than those of NpO_2^{2+}.

The tendency of a neptunium ion for complex formation, as well as the hydrolysis reaction, depends on its ionic potential, i.e. its formal charge divided by its ionic radius. In analogy with neighboring uranium and plutonium, the order of decreasing ability for complex formation is

$$Np^{4+} > NpO_2^{2+} \geq Np^{3+} > NpO_2^+$$

The relative complex-forming ability of Np^{3+} and NpO_2^{2+} may depend on the ligand and/or the solvent with which these ions are associated. It is difficult to

Table 6.13 *Experimental equilibrium constants for neptunium complexes with inorganic ligands.*

Anion	*Ion*	*Method*	*Temp.* (°C)	*Medium*	*Equilibrium constants*	*References*
Fluoride, F^-						
	Np^{4+}	dis	25	1.0 M $HClO_4$	$\log^*\beta_1 = 4.60 \pm 0.20$	Choppin and Unrein (1976)
		dis	25	2.0 M $HClO_4$	$\log^*\beta_1 = 4.70 \pm 0.15$	Bagawde *et al.* (1976)
		cix, red	20	4.0 M $HClO_4$	$\log^*\beta_1 = 4.82 \pm 0.02$ $\log^*\beta_2 = 7.57 \pm 0.15$ $\log^*\beta_3 = 9.85$ $\log^*\beta_4 = 11.15$ $\log^*\beta_n$; $Np^{4+} + nHL \rightleftarrows NpL_n^{4-n} + nH^+$	Ahrland and Brandt (1966)
	NpO_2^+	dis	23	1.0 M $NaClO_4$	$\log K_1 = 1.26 \pm 0.30$	Choppin and Rao (1984)
		dis	25	2.0 M $NaClO_4$	$\log K_1 = 0.99 \pm 0.10$	Rao *et al.* (1979)
	NpO_2^{2+}	ise	20	0.1 M $NaClO_4$	$\log K_1 = 4.18 \pm 0.15$ $\log \beta_2 = 6.96 \pm 0.15$ $\log \beta_3 = 9.64$	Sawant *et al.* (1985)
		emf	25	0.5 M $HClO_4$	$\log^*\beta_1 = 1.11 \pm 0.20$ $\log^*\beta_2 = 1.14 \pm 0.40$	Al-Niaimi *et al.* (1970a)
		dis	20	1.0 M $HClO_4$	$\log^*\beta_1 = 0.93 \pm 0.11$ $\log^*\beta_2 = 1.11 \pm 0.10$ $\log^*\beta_n$; $NpO_2^{2+} + nHL \rightleftarrows NpO_2L_n^{2-n} + nH^+$	Ahland and Brandt (1968a)
Chloride, Cl^-						
	Np^{4+}	dis	20	0.5 M $HClO_4$	$\log K_1 = 0.15 \pm 0.20$	Shilin and Nazarov (1966)
				1.0 M $HClO_4$	$\log K_1 = -0.04 \pm 0.20$	
				2.0 M $HClO_4$	$\log K_1 = 0.04 \pm 0.20$	
		dis	25	2.0 M $HClO_4$	$\log K_1 = -0.05 \pm 0.05$	Patil and Ramakrishna (1975)
	NpO_2^+	dis	25	2.0 M $NaClO_4$	$\log K_1 = -0.42 \pm 0.04$	Rao *et al.* (1979)
	NpO_2^{2+}	emf	25	0.5 M $HClO_4$	$\log K_1 = -0.35 \pm 0.40$	Al-Niaimi *et al.* (1970b)
Bromide, Br^-						
	Np^{4+}	dis	25	2.0 M $HClO_4$	$\log K_1 = -0.21 \pm 0.01$	Raghavan *et al.* (1975)

Iodide, I^-					
Np^{4+}	dis	25	2.0 M $HClO_4$	$\log K_1 = 0.04 \pm 0.30$	Patil *et al.* (1981)
Iodate, IO_3^-					
NpO_2^+	dis	25	2.0 M $HClO_4$	$\log K_1 = 0.32 \pm 0.30$	Rao *et al.* (1979)
NpO_2^{2+}	sp	25	0.3 M $HClO_4$	$\log K_1 = 0.61 \pm 0.02$	Blokhin *et al.* (1972)
Azide, N_3^-					
NpO_2^+	sp	25	5.0 M $NaClO_4$	$\log K_1 = 1.08$ $\log K_2 = 0.77$ $\log K_3 = 0.38$	Musikas and Marteau (1978)
Nitrite, NO_2^-					
NpO_2^+	dis	25	2.0 M $NaClO_4$	$\log K_1 = -0.05 \pm 0.05$	Rao *et al.* (1979)
Nitrate, NO_3^-					
Np^{4+}	dis	20	1.0 M $HClO_4$	$\log K_1 = 0.34 \pm 0.10$ $\log \beta_2 = 0.08$ $\log \beta_3 = -0.26$	Shilin and Nazarov (1966)
	dis	25	4.0 M $NaClO_4$	$\log K_1 = -0.15 \pm 0.12$ $\log \beta_2 = -0.74 \pm 0.15$	Danesi *et al.* (1971)
NpO_2^+	dis	20	2.0 M $NaClO_4$	$\log K_1 = -0.55 \pm 0.09$	Rao *et al.* (1979)
NpO_2^{2+}	pot	25	0.5 M $HClO_4$	$\log K_1 = -0.96 \pm 0.02$	Al-Niaimi *et al.* (1970b)
	dis	25	4.0 M $NaClO_4$	$\log K_1 = -0.68 \pm 0.06$	Danesi *et al.* (1971)
Thiocyanate, SCN^-					
Np^{4+}	dis	25	2.0 M $HClO_4$	$\log K_1 = 1.49 \pm 0.07$ $\log \beta_2 = 2.06 \pm 0.08$ $\log \beta_3 = 2.53 \pm 0.02$	Rao *et al.* (1978)
NpO_2^+	dis	25	2.0 M $NaClO_4$	$\log K_1 = 0.32 \pm 0.02$	Rao *et al.* (1979)
	sp	25	5.0 M $NaClO_4$	$\log K_1 = 0.86$ $\log \beta_2 = 1.05$	Cuillerdier *et al.* (1977)

Table 6.13 (*Contd.*)

Anion	*Ion*	*Method*	*Temp.* (°C)	*Medium*	*Equilibrium constants*	*References*
Sulfate, SO_4^{2-}						
	Np^{4+}	dis	25	2.0 M $HClO_4$	$\log^*\beta_1 = 2.49 \pm 0.03$ $\log^*\beta_2 = 4.06 \pm 0.02$	Patil and Ramakrishna (1973)
		pol	25	3.0 M $NaClO_4$	$\log^*\beta_1 = 2.49 \pm 0.03$ $\log^*\beta_2 = 3.57 \pm 0.09$	Musikas (1963)
		cix	20	4.0 M $HClO_4$	$\log^*\beta_1 = 2.70 \pm 0.04$ $\log^*\beta_2 = 4.26 \pm 0.05$ $\log^*\beta_n$; $Np^{4+} + nHL^- \rightleftarrows NpL_n^{4-2n} + nH^+$	Ahrland and Brandt (1966)
	NpO_2^+	dis	25	1.0 M $NaClO_4$	$\log K_1 = 0.06 \pm 0.04$	Halperin and Oliver (1983)
		dis	25	2.0 M $NaClO_4$	$\log K_1 = 0.44 \pm 0.09$	Rao *et al.* (1979)
	NpO_2^{2+}	pot	25	0.1 M $HClO_4$	$\log^*\beta_1 = 0.88 \pm 0.01$	Al-Niaimi *et al.* (1970a)
				0.5 M $HClO_4$	$\log^*\beta_1 = 0.75 \pm 0.01$	
		dis	21	1.0 M $NaClO_4$	$\log^*\beta_1 = 0.79 \pm 0.13$ $\log^*\beta_2 = 0.55 \pm 0.31$	Ahrland and Brandt (1968b)
		dis	25	2.0 M $HClO_4$	$\log^*\beta_1 = 1.07 \pm 0.05$ $\log^*\beta_2 = 0.60 \pm 0.15$ $\log^*\beta_n$; $NpO_2^{2+} + nHL^- \rightleftarrows NpO_2L_n^{2-2n} + nH^+$	Patil and Ramakrishna (1976)
Carbonate, CO_3^{2-}						
	NpO_2^+	dis	25	0.1 M $NaClO_4$	$\log K_1 = 4.13 \pm 0.03$ $\log K_2 = 2.93$	Bidoglio *et al.* (1985)
		sol	25	1.0 M $NaClO_4$	$\log K_1 = 4.49 \pm 0.06$ $\log K_2 = 2.62 \pm 0.09$ $\log K_3 = 1.42 \pm 0.11$	Maya (1983)

				$\log K_{sp} = -10.14 \pm 0.04$; $NaNpO_2L(s) \rightleftarrows Na^+ + NpO_2^+ + L^{2-}$	
NpO_2^{2+}	sol	25	0.1 M $NaClO_4$	$\log K_1 = 9.02 \pm 0.10$ $\log \beta_3 = 20.41 \pm 0.09$	Kato *et al.* (1998)
				$\log K_{sp} = -14.04 \pm 0.07$; $NpO_2L(s) \rightleftarrows NpO_2^{2+} + L^{2-}$	
	pot	25	1.0 M $NaClO_4$	$\log \beta_2 = 16.51 \pm 0.14$ $\log \beta_3 = 21.15 \pm 0.12$	Maya (1984)
				$\log \beta_{213} = -1.49 \pm 0.14$; $2NpO_2^{2+} + L^{2-} + 3H_2O \rightleftarrows (NpO_2)_2L(OH_3^-) + 3H^+$	
	sp	22	3.0 M $NaClO_4$	$\log \beta_{36} = -10.1 \pm 0.1$; $3NpO_2L_3^{4-} \rightleftarrows (NpO_2)_3L_6^{6-} + 3L^{2-}$	Grenthe *et al.* (1986)
Chromate, CrO_4^{2-}					
Np^{4+}	sp	25	0.2 M $LiClO_4$	$\log \beta = 1.81 \pm 0.17$; $Np^{4+} + HL^- \rightleftarrows NpL^{2+} + H^+$	Burkhart and Thompson (1972)
Phosphate, PO_4^{3-}					
NpO_2+	cix	20	0.2 M NH_4ClO_4	$\log \beta = 2.85 \pm 0.15$; $NpO_2^+ + HL^{2-} \rightleftarrows NpO_2HL^-$	Moskvin and Peretrukhin (1964)
NpO_2^{2+}	dis	25	1.0 M $NaClO_4$	$\log \beta = 2.52 \pm 0.50$; $NpO_2^{2+} + H_2L^- \rightleftarrows NpO_2H_2L^+$	Mathur and Choppin (1994)
				$\log \beta = 4.54 \pm 0.70$; $NpO_2^{2+} + HL^{2-} \rightleftarrows NpO_2HL$	
				$\log \beta = 7.5 \pm 1.0$; $NpO_2^{2+} + 2HL^{2-} = NpO_2(HL)_2^{2-}$	

Table 6.14 *Experimental equilibrium constants for neptunium complexes with organic ligands.*

Anion	*Ion*	*Method*	*Temp.* (°C)	*Medium*	*Equilibrium constants*	*References*
Acetate, CH_3COO^-						
	NpO_2^+	em	25	0.3 M $NaClO_4$	$\log K_1 = 0.96$ $\log K_2 = 0.61$	Rösch *et al.* (1990)
		spec	25	2.0 M $NaClO_4$	$\log K_1 = 0.87 \pm 0.03$	Rizkalla *et al.* (1990a)
	NpO_2^{2+}	pot	20	1.0 M $NaClO_4$	$\log K_1 = 2.31 \pm 0.02$ $\log \beta_2 = 4.23 \pm 0.05$ $\log \beta_3 = 6.00 \pm 0.19$	Portanova *et al.* (1970)
Propionate, $C_2H_5COO^-$						
	NpO_2^{2+}	pot	20	1.0 M $NaClO_4$	$\log K_1 = 2.44 \pm 0.03$ $\log \beta_2 = 4.45 \pm 0.03$ $\log \beta_3 = 6.49 \pm 0.08$	Cassol *et al.* (1969)
Monochloroacetate, CH_2ClCOO^-						
	NpO_2^+	spec	25	2.0 M $NaClO_4$	$\log K_1 = 0.00 \pm 0.05$	Rizkalla *et al.* (1990a)
	NpO_2^{2+}	pot	20	1.0 M $NaClO_4$	$\log K_1 = 1.33 \pm 0.02$ $\log \beta_2 = 2.10 \pm 0.07$ $\log \beta_3 = 2.78 \pm 0.34$	Cassol *et al.* (1969)
β-Chloropropionate, $CH_2ClCH_2COO^-$						
	NpO_2^{2+}	pot	20	1.0 M $NaClO_4$	$\log K_1 = 1.88 \pm 0.03$ $\log \beta_2 = 3.30 \pm 0.04$ $\log \beta_3 = 3.60 \pm 0.32$	Cassol *et al.* (1969)
Glycolate, $CH_2(OH)COO^-$						
	NpO_2^+	spec	25	0.1 M $NaClO_4$	$\log K_1 = 1.51 \pm 0.03$	Eberle and Schaefer (1969)
		spec	25	2.0 M $NaClO_4$	$\log K_1 = 1.43 \pm 0.02$ $\log \beta_2 = 1.90 \pm 0.03$	Rizkalla *et al.* (1990a)
		dis	25	1.0 M $NaClO_4$	$\log K_1 = 1.31 \pm 0.04$ $\log \beta_2 = 2.06 \pm 0.03$	Tochiyama *et al.* (1992)
	NpO_2^{2+}	pot	20	1.0 M $NaClO_4$	$\log K_1 = 2.42 \pm 0.03$ $\log \beta_2 = 3.96 \pm 0.03$ $\log \beta_3 = 5.00 \pm 0.10$	Portanova *et al.* (1972)

Lactate, $CH_3CH(OH)COO^-$					
NpO_2^+	spec	25	0.1 M $NaClO_4$	$\log K_1 = 1.75 \pm 0.02$	Eberle and Schaefer (1969)
	dis	25	1.0 M $NaClO_4$	$\log K_1 = 1.40 \pm 0.02$	Tochiyama *et al.* (1992)
				$\log \beta_2 = 2.01 \pm 0.02$	
α-Hydroxybutyrate, $C_2H_5CH(OH)COO^-$					
NpO_2^+	spec	25	0.1 M $NaClO_4$	$\log K_1 = 1.62 \pm 0.02$	Eberle and Schaefer (1969)
	dis	25	1.0 M $NaClO_4$	$\log K_1 = 1.64 \pm 0.02$	Tochiyama *et al.* (1992)
				$\log \beta_2 = 2.13 \pm 0.03$	
α-Hydroxyvalerate, $C_3H_7CH(OH)COO^-$					
NpO_2^+	spec	25	0.1 M $NaClO_4$	$\log K_1 = 1.59 \pm 0.03$	Eberle and Schaefer (1969)
α-Hydroxycapronate, $C_4H_9CH(OH)COO^-$					
NpO_2^+	spec	25	0.1 M $NaClO_4$	$\log K_1 = 1.63 \pm 0.02$	Eberle and Schaefer (1969)
α-Hydroxyisobutyrate, $(CH_3)_2C(OH)COO^-$					
NpO_2^+	spec	25	2.0 M $NaClO_4$	$\log K_1 = 1.80 \pm 0.01$	Rizkalla *et al.* (1990a)
	dis	25	1.0 M $NaClO_4$	$\log K_1 = 1.73 \pm 0.02$	Tochiyama *et al.* (1992)
				$\log \beta_2 = 2.46 \pm 0.02$	
NpO_2^{2+}	pot	20	1.0 M $NaClO_4$	$\log K_1 = 3.15 \pm 0.04$	Magon *et al.* (1974)
				$\log K_2 = 2.10 \pm 0.10$	
Glycinate, $NH_2CH_2COO^-$					
NpO_2^+	spec	25	0.1 M $NaClO_4$	$\log K_1 = 3.31 \pm 0.02$	Eberle and Wede (1968)
				$\log \beta_2 = 5.44 \pm 0.07$	
α-Picolinate, $NC_5H_4COO^-$					
Np^{4+}	spec	25	1.0 M $NaClO_4$	$\log K_1 = 6.50 \pm 0.01$	Paul (1970)
NpO_2^+	dis	25	1.0 M $NaClO_4$	$\log K_1 = 3.53 \pm 0.03$	Tochiyama *et al.* (1992)
				$\log \beta_2 = 6.01 \pm 0.03$	
Salicylate, $C_6H_4(OH)COO^-$					
NpO_2^+	spec	25	2.0 M $NaClO_4$	$\log \beta_H = 0.20 \pm 0.01$	Rizkalla *et al.* (1990a)
Oxalate, $(COO^-)_2$ $(=L^{2-})$					
NpO_2^+	pot	20	1.0 M $NaClO_4$	$\log K_1 = 3.74 \pm 0.05$	Magon *et al.* (1972)
				$\log \beta_2 = 6.31 \pm 0.10$	
	dis	25	1.0 M $NaClO_4$	$\log K_1 = 3.71 \pm 0.02$	Tochiyama *et al.* (1992)

Table 6.14 (*Contd.*)

Anion	*Ion*	*Method*	*Temp.* (°C)	*Medium*	*Equilibrium constants*	*References*
					$\log \beta_2 = 6.15 \pm 0.02$	
Malonate, $^{-}OOCCH_2COO^{-}$ ($=L^{2-}$)						
	NpO_2^+	pot	20	1.0 M $NaClO_4$	$\log K_1 = 2.75 \pm 0.02$	Magon *et al.* (1972)
		dis	25	1.0 M $NaClO_4$	$\log K_1 = 2.62 \pm 0.02$	Tochiyama *et al.* (1992)
					$\log \beta_2 = 4.22 \pm 0.02$	
Succinate, $^{-}OOC(CH_2)_2COO^{-}$ ($=L^{2-}$)						
	NpO_2^+	pot	20	1.0 M $NaClO_4$	$\log K_1 = 1.72 \pm 0.03$	Magon *et al.* (1972)
		dis	25	1.0 M $NaClO_4$	$\log K_1 = 1.45 \pm 0.06$	Tochiyama *et al.* (1992)
					$\log \beta_2 = 2.43 \pm 0.05$	
Maleate, $^{-}OOC(CH)_2COO^{-}$ ($=L^{2-}$)						
	NpO_2^+	pot	20	1.0 M $NaClO_4$	$\log K_1 = 2.20 \pm 0.02$	Magon *et al.* (1972)
Phthalate, $C_6H_4(COO^{-})_2$ ($=L^{2-}$)						
	NpO_2^+	pot	20	1.0 M $NaClO_4$	$\log K_1 = 2.22 \pm 0.02$	Magon *et al.* (1972)
		spec	25	1.0 M $NaClO_4$	$\log K_1 = 1.62 \pm 0.02$	Choppin *et al.* (1998)
Trimellitate, $C_6H_3(COO^{-})_3$ ($=L^{3-}$)						
	NpO_2^+	spec	25	1.0 M $NaClO_4$	$\log K_1 = 1.57 \pm 0.02$	Choppin *et al.* (1998)
Hemimellitate, $C_6H_3(COO^{-})_3$ ($=L^{3-}$)						
	NpO_2^+	spec	25	1.0 M $NaClO_4$	$\log K_1 = 2.44 \pm 0.02$	Choppin *et al.* (1998)
Pyromellitate, $C_6H_2(COO^{-})_4$ ($=L^{4-}$)						
	NpO_2^+	spec	25	1.0 M $NaClO_4$	$\log K_1 = 1.80 \pm 0.01$	Choppin *et al.* (1998)
Mellitate, $C_6(COO^{-})_6$ ($=L^{6-}$)						
	NpO_2^+	spec	25	1.0 M $NaClO_4$	$\log K_1 = 2.34 \pm 0.01$	Choppin *et al.* (1998)
Oxydiacetate, $O(CH_2COO^{-})_2$ ($=L^{2-}$)						
	NpO_2^+	spec	25	0.5 M $NaClO_4$	$\log K_1 = 3.72 \pm 0.01$	Rizkalla *et al.* (1990b)
	NpO_2^{2+}	pot	20	1.0 M $NaClO_4$	$\log K_1 = 5.16 \pm 0.01$	Cassol *et al.* (1973)
Thiodiacetate, $S(CH_2COO^{-})_2$ ($=L^{2-}$)						
	NpO_2^+	spec	25	0.5 M $NaClO_4$	$\log K_1 = 1.18 \pm 0.04$	Rizkalla *et al.* (1990b)

Citrate, $^{-}OOCCH_2C(OH)(COO^{-})CH_2COO^{-}$ ($=L^{3-}$)

NpO_2^+	spec	25	2.0 M $NaClO_4$	$\log K_1 = 2.49 \pm 0.01$	Rizkalla *et al.* (1990a)
	spec	25	0.5 M $NaClO_4$	$\log K_1 = 2.73 \pm 0.02$	Palade (1997)
			1.0 M $NaClO_4$	$\log K_1 = 2.74 \pm 0.02$	
			2.0 M $NaClO_4$	$\log K_1 = 2.81 \pm 0.02$	

Iminodiacetate, $^{-}OOCCH_2NHCH_2COO^{-}$ ($=L^{2-}$)

NpO_2^+	spec	25	0.1 M $NaClO_4$	$\log K_1 = 6.27 \pm 0.11$	Eberle and Wede (1970)
				$\log \beta_H = 1.35 \pm 0.52$;	
				$NpO_2^+ + HL^- \rightleftarrows NpO_2HL$	
NpO_2^{2+}	pot	20	1.0 M $NaClO_4$	$\log K_1 = 8.72 \pm 0.02$	Cassol *et al.* (1973)

N-Methyliminodiacetate, $^{-}OOCCH_2N(CH_3)CH_2COO^{-}$ ($=L^{2-}$)

NpO_2^+	spec	25	0.1 M $NaClO_4$	$\log K_1 = 7.37 \pm 0.05$	Eberle and Wede (1970)
				$\log \beta_H = 1.28 \pm 0.48$;	
				$NpO_2^+ + HL^- \rightleftarrows NpO_2HL$	

N-(2-Hydroxyethyl)iminodiacetate, $^{-}OOCCH_2N(C_2H_4OH)CH_2COO^{-}$ ($=L^{2-}$)

Np^{4+}	spec	25	1.0 M $NaClO_4$	$\log K_1 = 12.97 \pm 0.04$	Eberle and Paul (1971)
				$\log K_2 = 10.75 \pm 0.11$	
NpO_2^+	spec	25	0.1 M $NaClO_4$	$\log K_1 = 6.08 \pm 0.05$	Eberle and Wede (1970)
				$\log \beta_H = 1.45 \pm 0.25$;	
				$NpO_2^+ + HL^- \rightleftarrows NpO_2HL$	
				$-\log \beta_{OH} = 11.42 \pm 0.03$;	
				$NpO_2L^- + H_2O \rightleftarrows NpO_2(OH)L^{2-} + H^+$	

Nitrilotriacetate, $NH(CH_2COO^{-})_3$ ($=L^{3-}$)

Np^{4+}	spec	25	1.0 M $NaClO_4$	$\log K_1 = 17.28 \pm 0.02$	Eberle and Paul (1971)
				$\log K_2 = 14.78 \pm 0.07$	
NpO_2^+	spec	25	0.1 M $NaClO_4$	$\log K_1 = 6.80 \pm 0.10$	Eberle and Wede (1970)
				$\log \beta_H = 1.77 \pm 0.37$;	
				$NpO_2^+ + HL^{2-} \rightleftarrows NpO_2HL^-$	
				$-\log \beta_{OH} = 11.46 \pm 0.11$;	
				$NpO_2L^{2-} + H_2O \rightleftarrows NpO_2(OH)L^{3-} + H^+$	

Table 6.14 (*Contd.*)

Anion	*Ion*	*Method*	*Temp.* (°C)	*Medium*	*Equilibrium constants*	*References*
Nitrilodiacetate mono-*n*-propionate, $-OOC(CH_2)_2N(CH_2COO^-)_2$ ($=L^{3-}$)						
	NpO_2^+	spec	25	0.1 M $NaClO_4$	$\log K_1 = 7.00 \pm 0.09$ $\log \beta_H = 2.35 \pm 0.12$; $NpO_2^+ + HL^{2-} \rightleftarrows NpO_2HL^-$ $-\log \beta_{OH} = 11.57 \pm 0.09$; $NpO_2L^{2-} + H_2O \rightleftarrows NpO_2(OH)L^{3-} + H^+$	Eberle and Wede (1970)
N-(2-Hydroxyethyl)ethylenediamine-*N*,*N*′,*N*′-triacetate, $(HOC_2H_4)(^-OOCCH_2)N(CH_2)_2N(CH_2COO^-)_2$ ($=L^{3-}$)						
	Np^{4+}	spec	25	1.0 M $NaClO_4$	$\log K_1 = 20.82 \pm 0.13$ $\log K_2 = 12.77 \pm 0.16$	Eberle and Paul (1971)
	NpO_2^+	spec	25	0.1 M $NaClO_4$	$\log K_1 = 6.87 \pm 0.11$ $\log \beta_H = 4.06 \pm 0.01$; $NpO_2^+ + HL^{2-} \rightleftarrows NpO_2HL^-$ $-\log \beta_{OH} = 11.37 \pm 0.10$; $NpO_2L^{2-} + H_2O \rightleftarrows NpO_2(OH)L^{3-} + H^+$	Eberle and Wede (1970)
Ethylenediamine-*N*,*N*,*N*′,*N*′,-tetraacetate, $(^-OOCCH_2)_2N(CH_2)_2N(CH_2COO^-)_2$ ($=L^{4-}$)						
	Np^{4+}	spec	25	1.0 M $NaClO_4$	$\log K_1 = 24.55 \pm 0.03$	Eberle and Paul (1971)
	NpO_2^+	spec	25	0.1 M $NaClO_4$	$\log K_1 = 7.33 \pm 0.06$ $\log \beta_H = 5.30 \pm 0.08$; $NpO_2^+ + HL^{3-} \rightleftarrows NpO_2HL^{2-}$ $-\log \beta_{OH} = 11.51 \pm 0.08$; $NpO_2L^{3-} + H_2O \rightleftarrows NpO_2(OH)L^{4-} + H^+$	Eberle and Wede (1970)
Diethylenetriamine-N,N,*N*′,*N*″,*N*″-pentaacetate, $^-OOCCH_2N[(CH_2)_2N(CH_2COO^-)_2]_2$ ($=L^{5-}$)						
	Np^{4+}	spec	20	0.5 M $NaClO_4$	$\log K_1 = 29.29 \pm 0.02$	Piskunov and Rykov (1972)
		spec	25	1.0 M $NaClO_4$	$\log K_1 = 30.33 \pm 0.12$	Eberle and Paul (1971)

compare the data listed in Table 6.13 because of the wide range of experimental conditions used and the lack of data for a given oxidation state of the ions with some ligands. However, the stability sequence for complexes of Np(IV), Np(V), or Np(VI) with monovalent inorganic ligands is seen to be

$$F^- > H_2PO_4^- > SCN^- > NO_3^- > Cl^- > ClO_4^-$$

For divalent inorganic ligands, the sequence is

$$CO_3^{2-} > HPO_4^{2-} > SO_4^{2-}$$

as would be expected from the relative strengths of the corresponding acids. Divalent ligands are more strongly complexing than monovalent ligands.

In addition to the data in Table 6.13, Np(V) (NpO_2^+) is known to form 'cation–cation' complexes with some multiply charged cations. The dioxo cation NpO_2^+ in perchloric acid solution forms complex ions with trivalent cations of Al, Ga, Sc, In, Fe, Cr, and Rh (Sullivan, 1962, 1964). The relative strength of the interaction between NpO_2^+ and M^{3+} was found to follow the following order: Fe > In > Sc > Ga > Al. Some of these polynuclear complexes such as $[NpO_2^+Cr^{3+}]$ and $[NpO_2^+Rh^{3+}]$ have been isolated by using an ion-exchange method, while the others were detected by spectrophotometry. The $[NpO_2^+Cr^{3+}]$ complex is also formed by the reduction of NpO_2^{2+} with Cr^{2+}. The formation of the complex between NpO_2^+ and UO_2^{2+} has extensively been studied by the use of potentiometry, spectrophotometry, Raman spectroscopy, and large-angle X-ray scattering (Sullivan *et al.*, 1961; Guillaume *et al.*, 1982, 1983; Stout *et al.*, 1993).

6.9.2 Complexation with organic ligands

With some exceptions, most of the data in Table 6.14 are for complexes of Np(V) with organic ligands. The following presents the results on several selected systems.

Stability data for complexes of M(VI) ions MO_2^{2+} (M = U, Np, and Pu) with monocarboxylic ligands L (L = acetate, propionate, monochloroacetate, and β-chloropropionate) have been reported and discussed by Cassol *et al.* (1969) and Portanova *et al.* (1970). In the range of ligand concentrations examined, complexes are formed in which the highest average ligand number is three. The stability order of complexes of the various ligands examined is $UO_2^{2+} > NpO_2^{2+} > PuO_2^{2+}$. The stability of complexes of a given MO_2^{2+} ion increases with increasing ligand basicity (pK_a), which suggests a strong 'hard' ionic character of these oxycations.

The stability constants of Np(V) complexes with a series of α-hydroxycarboxylates (e.g. glycolate and lactate) have been obtained by spectrophotometry (Eberle and Schaefer, 1969; Rizkalla *et al.*, 1990a) and solvent extraction (Tochiyama *et al.*, 1992). The stability of the α-hydroxycarboxylate complexes appears to increase a little with pK_a of the ligand, although the stability of these complexes is not much different. The stability of Np(V) complexes with

aliphatic dicarboxylates (e.g. oxalate and malonate) has also been studied by potentiometry (Magon *et al*., 1972), spectrophotometry (Stout *et al*., 1989), and solvent extraction (Tochiyama *et al*., 1992). The stability of the complexes is controlled mainly by the size of the chelate ring. In spite of the increase in the basicity of the ligand, the stability of the complexes decreases with increasing the number of carbon atoms between two carboxylate groups in the ligand.

The complexation of Np(v) with aromatic polycarboxylates has been studied by spectrophotometry (Choppin *et al*., 1998). The stability constants of the 1:1 complexes decreases in the order: hemimellitate > mellitate > pyromellitate > trimellitate≃phthalate. After correction for the number of chelating binding (bidentate) sites, the stability constants with all ligands except hemimellitate are approximately the same. The greater strength of hemimellitate complexation is attributed to an increase in electron density at the binding site through induction from the non-chelating carboxylate group.

With aliphatic aminopolycarboxylate ligands, the complexation of Np(IV) or Np(v) has been studied by spectrophotometry (Eberle and Paul, 1971; Eberle and Wede, 1970). The logarithms of the stability constants of the Np(IV) complexes increase linearly with the number of bound donor atoms of the ligands. On the other hand, the Np(v) ion forms protonated and normal chelates of 1:1 stoichiometry. In addition, at high pH chelate hydroxides with one ligand molecule and one hydroxyl group per NpO_2^+ are formed. The nature of the ligand has only slight or no influence on the stability constants of normal chelates or chelate hydroxides, respectively, suggesting that not more than two carboxylic groups and one amine-nitrogen are bound from one ligand to the central neptunium.

6.10 ANALYTICAL CHEMISTRY AND SPECTROSCOPIC TECHNIQUES

The concentration of ^{237}Np and the radioactivity arising from this nuclide in the environment is extremely low compared to most other α emitters. The background concentration of ^{237}Np in seawater due to global fallout was estimated to be at a level of 10^{-15} to 10^{-14} g L^{-1} (Novikov *et al*., 1989; Jha and Bhat, 1994). However, with the increase in nuclear power generation, this nuclide has become one of the most important from the viewpoint of long-term disposal of the radioactive waste. In fact, the analytical results showing contamination of ^{237}Np in seawater from nuclear fuel reprocessing plants have been reported, e.g. the concentrations of ^{237}Np were $3 \times 10^{-12} - 5.5 \times 10^{-11}$ g kg^{-1} in some samples from Irish sea (Pentreath and Harvey, 1981), 3×10^{-12} g kg^{-1} from Goury near La Hague, France (Germain *et al.*, 1987), $(2.3 \pm 0.4) \times 10^{-11}$ g kg^{-1} from English disposal area (May *et al*., 1987), and $2 \times 10^{-12} \sim 2 \times 10^{-11}$ g L^{-1} in a waste discharge point at Trombay, India (Jha and Bhat, 1994). More sensitive methods for measuring such low levels of ^{237}Np must be developed and applied. Novikov *et al*. (1989) reviewed the analytical methods to be applied to

^{237}Np in the environmental samples. Hursthouse *et al*. (1992) performed a comparative study to evaluate the practical advantages and disadvantages of the methods. Lee *et al*. (1995) reported the result of an intercomparison study by eight laboratories of low-level ^{237}Np determination in artificial urine samples in order to evaluate and establish the optimal method for a routine *in vivo* radioassay program. In addition, precise determination of the ^{237}Np in the nuclear spent fuel or HLW from the reprocessing process is still a major concern in the field of nuclear engineering as well as the related research and development works.

6.10.1 Radiometric methods

Radiometric methods that are based on counting of alpha particles from ^{237}Np and neutron activation of ^{237}Np have been widely employed for the quantitative analysis of trace amount of ^{237}Np in environmental samples. The alpha-particle counting method is useful for the rapid and low-cost determination of trace quantity of ^{237}Np (specific radioactivity $= 2.6 \times 10^7$ Bq g^{-1}). A recent report by Pavlotskaya (1997) reviewed critically the radiochemical analysis methods for the determination of a trace quantity of neptunium in environmental samples.

(a) Alpha- and gamma-ray spectrometry

Alpha spectroscopy with solid state detectors enables the determination of ^{237}Np in a thin sample of a mixture with other α emitters such as ^{239}Pu and ^{241}Am. A preparation of sufficiently thin counting source is a key in the measurement of a reproducible spectrum without a disturbance from the self-absorption of alpha particles in the source. A simple method adopting an evaporation of the sample solution on the source substrate such as a plate of stainless steel or platinum is typically employed. Methods based on the electrodeposition of neptunium directly on the source substrate are useful to prepare thinner sources. Coprecipitation methods are simple and feasible for the preparation of counting sources but may not yield a sufficiently thin source for energy discrimination. Kimura (1990a) utilized $BiPO_4$ precipitate for the quantitative recovery and the preparation of alpha-counting sources for the simultaneous determination of Np, Pu, Am, and Cm.

Holm *et al*. (1987) applied alpha spectroscopy to the determination of the fallout level of ^{237}Np in large volume samples of seawater. They employed a method for the isolation of ^{237}Np by a hydroxide coprecipitation, ion-exchange chromatography, a LaF_3 coprecipitation, and a solvent extraction with HTTA. Yamamoto *et al*. (1989) developed a method for determination of low levels of ^{237}Np in soil and sediment samples. The separation scheme they developed is shown in Fig. 6.12 and consists of leaching of neptunium by aqua regia, separation and purification by TnOA extraction, LaF_3 coprecipitation, and

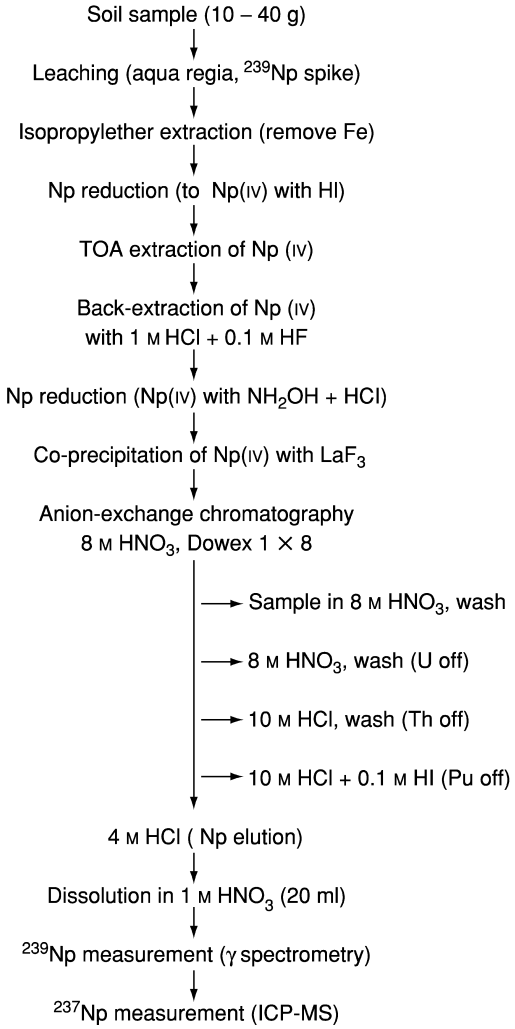

Fig. 6.12 *Chemical separation scheme for the determination of ^{237}Np by high-resolution ICP-MS.* (*Yamamoto* et al., 1994, *with permission from Elsevier Science*).

two steps of anion-exchange chromatography. ^{239}Np was used as a chemical yield monitor. The chemical yield of neptunium ranged from 50 to 84%. The detection limit for ^{237}Np was about 0.1 mBq per sample.

A method for the simultaneous determination of ^{237}Np and ^{239}Np in air, total deposition and sediment samples in ocean was developed (Rosner *et al.*, 1993). Alpha- and gamma-ray spectroscopies were used.

Alpha- and gamma-ray spectroscopies were applied to the determination of ^{237}Np in spent nuclear fuels (Shinohara *et al.*, 1989). After ion-exchange

separation of the dissolved fuel solution, the content of ^{237}Np was determined from the activity of ^{237}Np or ^{233}Pa, which is in radioactive equilibrium with ^{237}Np. The chemical yield was determined using inherent ^{239}Np. The proposed method does not require quantitative separation of neptunium and can be applied to routine analyses of burnup for the nuclear spent fuel.

One of the few uses of gamma spectroscopy for Np radioanalysis was that of isotope dilution gamma-ray spectroscopy method using ^{239}Np as a spike for the determination of ^{237}Np in uranium, plutonium, and mixed oxide samples (Sus *et al.*, 1996). Extraction chromatography with trialaurylamine fixed on a SGX-C18 support was used for the isolation of neptunium. A pair of γ-rays of 86.53 keV (^{237}Np) and 106.13 keV (^{239}Np) was employed for the detection. The detection limit was evaluated to be 5×10^{-8} g ^{237}Np.

(b) Liquid scintillation counting method

Liquid scintillation counting method does not require extensive sample preparation and is very sensitive for alpha-decaying radionuclides such as ^{237}Np. The alpha liquid scintillation method with rejection of γ emitters (PERALS spectrometer) is useful because of its high sensitivity, selectivity, and rapid sample preparation. Aupiais *et al.* (1999) developed a method for the determination of ^{237}Np which consists of (1) oxidation of Np(V) to Np(VI) with Ag(II), (2) extraction of Np(VI) from 0.5 to 0.75 M HNO_3 solution into the extractive scintillation cocktail of TOPO, and (3) gamma liquid scintillation counting with rejection of γ emitters. The method was applied to the biological samples.

The pulse shape discrimination (PSD) technique was introduced to liquid scintillation counting by Yang *et al.* (1994) for the determination of ^{237}Np coexisting with plutonium and americium. Np(IV) was separated from Pu(III), Am(III), and fission product elements by two steps of solvent extraction using TTA–xylene and triisooctylamine(TIOA)–xylene. The PDS technique enabled the alpha counting with an efficiency of higher than 99% and a beta discrimination factor of higher than 99.95%. The proposed method was applied to the determination of neptunium, plutonium, and americium in the HLW.

(c) Activation analysis

Neutron activation analysis based on ^{237}Np(n,γ)^{238}Np ($t_{1/2}$ of ^{238}Np = 2.117 days) reaction, for which the activation cross section is large and 170 barns, is one of the most sensitive methods for the determination of ^{237}Np. In general, neutron activation analysis is ca. 500 times more sensitive than the alpha-counting method. The procedure consists of (1) pretreatment of the sample, i.e. the leaching of ^{237}Np from the solid sample and the oxidation state adjustment at Np(IV), (2) the separation and preconcentration of Np(IV), (3) neutron irradiation, (4) separation of Np(IV) from the irradiated sample, and (5) the

determination of ^{238}Np by gamma-ray spectroscopy. May *et al.* (1987) applied this method to irradiated nuclear fuels, radioactive waste solutions, and environmental samples such as seawater and submarine fauna and flora of disposal areas. Cation-exchange chromatography with Dowex 1 × 8 was employed to separate Np(IV) both before and after the irradiation. They determined the detection limit to be 5×10^{-13} g ^{237}Np. A similar procedure was applied to the sediment samples around Sellafield, Cumbria (Bryne, 1986) and the samples taken from the marine environment of coastal nuclear sites in India (Jha and Bhat, 1994). Depending on the nature of the sample, the removal of the bulk of the iron is required, and they employed solvent extraction with methylisobutylketone (MIBK) or isopropyl ether. After the irradiation, ^{238}Np purified by solvent extraction of Np(IV) with HTTA (cf. Fig. 6.12). If necessary, neptunium ions in a large volume of the sample solution such as seawater sample was preconcentrated by coprecipitation with iron(III) hydroxide precipitate, and Na^+ (^{24}Na) was removed from the irradiated sample using the flow-through column of the hydrated antimony pentoxide. The chemical yield was monitored, usually with ^{239}Np tracer. Bryne (1986) evaluated the detection limit by this method to be 0.1 to 0.5 mBq ^{237}Np.

Neutron activation analysis using epithermal neutron was applied to the determination of ^{237}Np for the purpose of an environmental monitoring of Yucca Mountain area (Riggle, 1992). The sensitivity obtained by the activation analysis using epithermal neutrons was found to be similar to that by using thermal neutrons. The neutron activation analysis method is also feasible for the determination of ^{235}Np and Zhao *et al.* (1991) applied this method to the determination of ^{235}Np in silicate samples.

Maslov *et al.* (1997) developed a highly sensitive method based on the (γ,f) reaction of ^{237}Np followed by the fission track counting. The proposed method was feasible for the determination of ultra-trace amount of ^{237}Np, e.g. in environmental water, and the detection limit was estimated to be 1×10^{-14} g ^{237}Np.

6.10.2 Spectrophotometric method

Several spectrophotometric methods are available: (1) absorption spectrophotometry of Np ions (direct absorption spectrophotometry); (2) absorption spectrometry of the colored complexes formed by Np ions and a chelating reagent; and (3) fluorescence spectrophotometry. A report by Burney and Harbour (1974) summarized and evaluated traditional spectrophotometric methods.

The direct absorption spectrophotometry is useful for the speciation of the Np ions in a solution by a simple procedure, though the sensitivity is not high. The most appropriate wavelengths for the determination of Np^{3+}, Np^{4+}, NpO_2^+, and NpO_2^{2+} in 2 M $HClO_4$ are 786 nm (molar extinction coefficient ε is approximately 45 $mol^{-1}\ dm^3\ cm^{-1}$), 960 nm ($\varepsilon = 160\ mol^{-1}\ dm^3\ cm^{-1}$), 980 nm

($\varepsilon = 395$ mol^{-1} dm^3 cm^{-1}), and 1223 nm ($\varepsilon = 45$ mol^{-1} dm^3 cm^{-1}), respectively (cf. Fig. 6.11). This method is useful for rapid and non-destructive speciation of the Np ions in acidic solution. The detection limits are approximately 5×10^{-4} M Np^{3+}, 1×10^{-4} M Np^{4+}, 5×10^{-5} M NpO_2^+, and 5×10^{-4} M NpO_2^{2+} simply assuming that the lowest detectable absorption is 0.02.

LIPAS enables the direct detection of the ions of relatively low concentration in the solution (Schrepp *et al.*, 1983; Klenze and Kim, 1988). An utilization of LIPAS leads to an enhancement of the sensitivity by a factor of ten or more compared with traditional absorption spectrophotometry. Pollard *et al.* (1988) realized the sensitivity in the measurement of Np(IV), Np(V), and Np(VI) of ca. 10^{-7} M in acidic solution using a dual beam LIPAS system equipped in Harwell. The LIPAS was applied to the monitoring of Np(V) in the nitric acid solution of the Purex process condition (Kihara *et al.*, 1996).

Colored complexes of neptunium with high absorption ability have been utilized for the sensitive determination of neptunium (Burney and Harbour, 1974). A method using the complex of Np(IV) and 1,8-dihydroxy–3,6-disulfonicnaphthalene–2,7diazo, commonly referred to as arsenazo-III, is one of the most sensitive with a molar extinction coefficient of 10^5 mol^{-1} dm^3 cm^{-1} at 665 nm, when the complex is formed in 4–6 M HNO_3. Uranium, thorium, plutonium, and other ions also form complexes with arsenazo-III, and therefore these ions should be removed from the sample solution before the color formation reaction. Solvent extraction with HDEHP acid or TIOA was used to separate neptunium from these interfering ions. The detection limit obtained by arsenazo-III method is approximately 4×10^{-8} g ml^{-1} of neptunium. Thorin, xylenol orange, and chlorophosphonazo III are other common color-forming reagents for use in the determination of neptunium.

6.10.3 Luminescence methods

Measurement of the luminescence intensity from a phosphor such as CaF_2- or $PbMpO_4$-based crystal that is doped with neptunium makes the sensitive determination of neptunium possible. Aleksandruk *et al.* (1990, 1991a) developed a method that consisted of the leaching of neptunium from solid samples such as soil, the isolation of the neptunium by solvent extraction and extraction chromatography, and counting the luminescence intensity at 651 or 663 nm from a CaF_2(Np) crystal at 77 K using a nitrogen pulsed laser (337 nm) as the excitation source. Neptunium was concentrated on the surface layer of a CaF_2 pellet, which resulted as a remarkable improvement of the sensitivity (Aleksandruk *et al.*, 1990). The detection limit of the absolute amount of neptunium was approximately 10^{-12} to 5×10^{-13} g. The proposed method was applied to the determination of Np in soil samples taken from the 30 km zone of the Chernobyl area.

Several attempts have been made to improve the reliability or the sensitivity of the luminescence method. Stepanov *et al.* (1997) proposed a method using

uranium as an internal standard to enhance the reliability of determination of neptunium with CaF_2 phosphor. The procedure was applied to the neptunium analysis of nuclear materials. Ivanova *et al.* (1994) utilized a novel method for the preconcentration of neptunium with high concentrating efficiency by the use of a solid-supported liquid membrane containing trioctylmethylammonium nitrate, which was directly subjected to the preparation of the CaF_2 or $PbMoO_4$ phosphor. The detection limit was 1×10^{-13} g ml^{-1} in pure water and 5×10^{-13} g g^{-1} in soil sample. An alternative membrane technique, which is chemically compatible with the preparation of $PbMoO_4$ phosphor, was utilized by Novikov *et al.* (1997) for the preconcentration of neptunium and plutonium. The elaborate procedure for the determination of neptunium and plutonium consists of the HDEHP solvent extraction of Np(IV) and Pu(IV) from the soil leach and accumulation of these ions on the solid-supported aqueous membrane with $K_{10}P_2W_{17}O_{61}$.

Time-resolved laser-induced fluorescence spectroscopy (TRLFS) was applied for the analysis of Np in plutonium samples (Aleksandruk *et al.*, 1991b) to attain a detection limit of 2×10^{-12} g Np.

6.10.4 X-ray fluorescence spectroscopy (XRF)

The XRF technique, which is essentially a non-destructive method, does not require the removal of uranium, plutonium, and other elements, and can be applied to solid and liquid samples. This technique was utilized to monitor the neptunium content in the products of nuclear spent fuel reprocessing (Akopov *et al.*, 1988). It was found that neptunium of more than 4 mg L^{-1} could be determined by XRF using a high intensity X-ray source and Si:Li detector, when the Np/U and Np/Pu ratios were higher than 1/80 and 1/40, respectively. If the sample contained higher concentration of U or Pu, extraction chromatography was employed to remove these elements from neptunium and the detection limit was lowered to 0.1 mg L^{-1}.

A gamma-ray induced energy-dispersive K-line XRF was applied to the determination of heavy metals such as neptunium, uranium, and plutonium in the Purex process solution using a gamma-ray excitation source of ^{57}Co ($t_{1/2}$ = 27.1 days, 10 mCi), ^{133}Ba ($t_{1/2}$ = 10.7 years, 10 mCi), or ^{192}Ir ($t_{1/2}$ = 74 days, 10 Ci) (Pilz *et al.*, 1989). One of the most distinct advantages of this method is the wide dynamic concentration range from ppm level to 400 g L^{-1}.

6.10.5 Mass spectrometry

(a) Surface ionization mass spectrometry (SIMS)

Isotope dilution mass spectrometry using ^{235}Np or ^{239}Np as a spike is a useful method for the sensitive and precise determination of ^{237}Np. An ion source of surface ionization diffusion (SID)-type, which is prepared by electroplating

neptunium and overplating the sample with rhenium or platinum metal film, was applied to the detection of neptunium (Efurd *et al.*, 1986). This technique was applicable to ^{237}Np amounts ranging from 10^{-17} to 10^{-8} g.

(b) ICP-MS

ICP-MS has become one of the most powerful methods for the determination of ultra-trace levels of ^{237}Np in many kinds of samples such as environmental and biological samples, uranium fuels, and Purex process solutions. Distinct advantages of this method are a capability of a simultaneous multi-element analysis providing information on the isotopic composition for a large number of elements with high precision and accuracy, as well as a rapid analysis compared with traditional alpha spectrometry and neutron activation analysis, which require tedious pretreatment and measurement procedures. Interfering elements such as uranium and other heavy elements must be removed from the sample solution using optimum chemical separation methods. The separation of uranium, in particular, is important to avoid the interference from the downmass tailing of ^{238}U.

Kim *et al.* (1989) recommended a separation scheme for the ICP-MS analysis of ^{237}Np in a soil:solvent extraction with isopropyl ether to remove iron, solvent extraction with TOA to recover neptunium, and three-step anion-exchange chromatography. They obtained a detection limit of 0.02 mBq ml^{-1} (ca. 8×10^{-13} g ml^{-1}) of ^{237}Np. Yamamoto *et al.* (1994) conducted ICP-MS analysis of ^{237}Np in paddy field soil samples in Japan using high-resolution ICP-MS equipped with a double-focusing mass spectrometer in order to elucidate the temporal feature of global fallout of ^{237}Np deposition.

Riglet *et al.* (1992) applied ICP-MS to the determination of ^{237}Np in enriched uranium solutions. After extracting neptunium as Np(IV) from 1 M HNO_3 solution into 0.5 M HTTA xylene solution and back-extracting in 10 M HNO_3, the ICP-MS signal of ^{237}Np was recorded. Concentrations of ^{237}Np of more than 5 ng in a 1 g uranium sample could be determined. Fig. 6.13 shows a typical ICP-MS spectrum for ^{237}Np in uranium samples.

Barrero Moreno *et al.* (1997) developed a method for the online separation of neptunium, plutonium, and uranium by ion chromatography using a high-capacity cation-exchange column followed by the direct injection of the effluent to the ICP-MS system to determine neptunium and plutonium in the presence of a high concentration of uranium. The method was applied to various kinds of irradiated UO_2 and MOX fuels.

(c) Other methods based on mass spectrometry

Resonance-ionization mass spectroscopy (RIMS) is expected to be powerful for the ultra-trace analysis of long-lived radioactive elements such as neptunium because of its extremely high sensitivity and selectivity. Riegel *et al.* (1993)

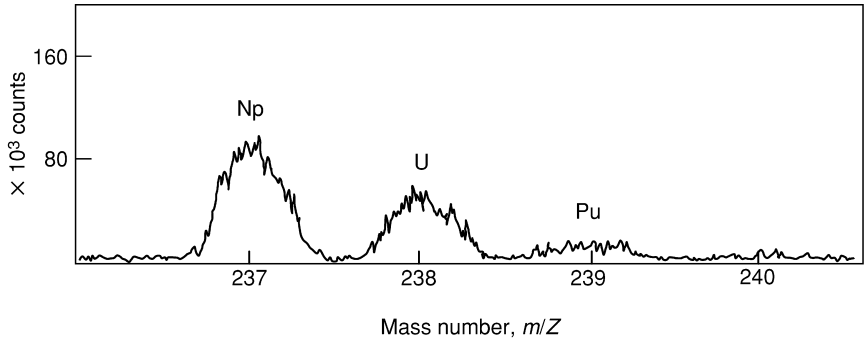

Fig. 6.13 *ICP mass spectrum for ^{237}Np in environmental samples. The mean value of the concentration of ^{237}Np was obtained to be* 6.2×0.1 Bq kg^{-1} *based on intercomparison analysis using spectrometry by seven laboratories. Reprinted from Kim* et al. (1989), *with permission from Elsevier Sequoia S. A.*

carried out the ^{237}Np detection by RIMS and estimated the detection limit as 4×10^8 atoms (1.6×10^{-13} g) which is almost two orders of magnitude more sensitive than that by alpha spectrometry.

Accelerator mass spectrometry (AMS) was applied to the detection of ^{237}Np in environmental samples such as mud, sediment, and pore water (Fifield *et al.*, 1997). It was estimated that sensitivity by AMS approached 10^5 atoms (4×10^{-17} g) of ^{237}Np. The results obtained by such a highly sensitive method make it possible to elucidate a distribution behavior of neptunium in natural environment and therefore to conclude that neptunium is more mobile than plutonium in the environment.

6.10.6 Electrochemical methods

Electrochemical methods are feasible for the determination of the total concentration and redox speciation of neptunium ions. The reduction–oxidation processes between Np(VI) and Np(V) and between Np(IV) and Np(III) are practically reversible and of simple one-electron transfer characteristics, which enables various electroanalytical performance based on these electrode reactions. The electroanalytical data of neptunium mainly obtained by voltammetry and polarography were reviewed by Kihara *et al.* (1999).

(a) Potentiometric titration and coulometry

Titration methods based on the reduction–oxidation of neptunium ions have been widely used for the accurate and precise determination of 1–10 mg quantities of neptunium. A method proposed by Godbole and Patil (1979) consists of the oxidation of neptunium ions to Np(VI) with Ag(II), destruction of excess

Ag(II) with sulfonic acid, reduction of Np(VI) to Np(IV) by a slight excess of Fe(II) in 2 M H_2SO_4, and potentiometric titration of the excess Fe(II) with standard Ce(IV) solution. The end point was detected potentiometrically using a platinum indicator electrode. Cao *et al.* (1994) proposed an alternative amperometric titration method by the use of Cr(VI) instead of Ce(IV) to titrate Fe(II). They attained less than 0.3% relative standard deviation in the determination of 2 mg of neptunium.

Controlled-potential coulometry is the standard method based on a primary theory, which enables an accurate and precise determination of neptunium. Stromatt (1959) recommended the procedure that consists of the oxidation of neptunium ion to Np(VI) with Ce(IV), the electrolytic reduction of Np(VI) and the excess Ce(IV) to Np(V) and Ce(III), and coulometric determination of Np(V) by the oxidation of Np(V) to Np(VI).

Kasar *et al.* (1991) determined 2–5 mg of neptunium with a relative standard deviation of $\pm 0.25\%$ by controlled-potential coulometry consisting of oxidation to Np(VI) with Ce(IV), decomposition of the excess Ce(IV) with $NaNO_2$, and titration based on the reduction of Np(VI) to Np(IV) with internally and electrolytically generated Fe(II). Karelin *et al.* (1991) developed constant current coulometry adopting amperometric end point detection, which enabled the determination of neptunium in the solution coexisting with uranium, plutonium, cerium, chromium, iron, and manganese. Chemists at the Savannah River Plant, USA, developed an automatically controlled apparatus for coulometry that was applied to the determination of neptunium. Measurement precision within 0.1% was achieved (Holland and Cordaro, 1988). Narrow span controlled-potential coulometry, which can minimize the interference from ions of formal redox potential close to that of the ion to be determined, was developed (Kalsi *et al.*, 1994) and applied to the determination of neptunium with enough high reproducibility, e.g. with relative standard deviation of 0.2%, even in the presence of five times the concentration of plutonium. Kihara *et al.* (1999) proposed a flow-coulometry method using multi-step column electrodes of glassy carbon fibers working electrode for the determination and speciation of neptunium ions in acidic solutions. (The redox behavior of neptunium ions observed by flow-coulometry is described in detail in Section 6.8.1b.)

(b) Voltammetry and polarography

Polarography was applied to the simultaneous determination of Np(V) and U(VI) in samples from the spent nuclear fuel reprocessing process based on the fluoride vaporization (Li *et al.*, 1988). The reduction currents of Np(V) and U(VI) were recorded with the electrolyte solution of a mixture of 2 M acetic acid and 2 M ammonium acetate. Kuperman *et al.* (1988) developed potentiostatic voltammetry for the determination of 2×10^{-8} to 1×10^{-5} M of neptunium and plutonium ions. Yakovlev and Kosyakov (1991) developed anodic stripping voltammetry method for the determination of neptunium using column

electrode of carbon fibers as a working electrode whose surface was modified by bis(2-ethylhexyl) phosphate. The recommended procedure consists of the electrolytic preconcentration of Np(VI) at the electrode surface and the measurement of the current peak due to the oxidation of Np(V) to Np(VI). The detection limit was ca. 10^{-7} M.

6.10.7 Mössbauer spectroscopy of ^{237}Np materials

Neptunium–237 is one of the best Mössbauer nuclei in the periodic table. ^{237}Np has the following characteristics which allow the Mössbauer spectroscopic measurement successful: (1) the lifetime of the excited state for Mössbauer transition is long enough, 68 ns, to obtain a sharp resonance line; (2) the spread range of the isomer shift is large enough to differentiate nature of chemical bonds from the shift; and (3) the radiation from a ^{237}Np absorber is low enough to record a spectrum in a standard transmission geometry. The most useful Mössbauer measurement system is the 60 keV radiation from ^{237}Np excited in the alpha decay of ^{241}Am. Nakada *et al.* (1998) developed a source assembly with small sources of ^{241}Am metal and designed the sealed holders to encapsulate the sample without the seepage of liquid helium.

Kalvius (1989) summarized basics and the power of Mössbauer spectroscopy of ^{237}Np in his review article demonstrating examples of study on 5f-electron structure of antiferromagnetic NpAs compounds and various Np(VI) and (VII) compounds. Jovè *et al*. (1991) reviewed applications of Mössbauer spectroscopy to the study of insulating neptunium compounds and discussed correlations between isomer shift, electric field gradient, and bonding or crystallographic structure of neptunium in crystallized or amorphous compounds of Np(III–VII).

Each oxidation state has a characteristic isomer shift range that is correlated with the number of 5f electrons present, and thus the isomer shift is a good indicator of the coordination number as well as the oxidation state of Np in a compound. The isomer shift increases regularly with decreasing oxidation state. Systematic trend of the isomer shift of ^{237}Np in various metal coordination complexes was studied and a linear dependence was found between the isomer shift and the mean neptunium–ligand distance in a series of Np(VI) compounds, which were summarized by Jovè *et al*. (1988a,b, 1991). Ionova and Jovè (1989) proposed a model, which correlated the population of the 5f orbital of ^{237}Np with the isomer shift, for the estimation of covalent effect in neptunium compounds based on the isomer shift. Bickel *et al*. (1987) studied the Mössbauer spectra of such oxoneptunates as $Li_5Np^{(VII)}O_6$, $Li_6Np^{(VI)}O_6$, $BaNp^{(VI)}O_4$, $Np^{(IV)}GeO_4$, $SrNp^{(IV)}O_3$, and $BaNp^{(IV)}O_3$. The isomer shifts were more negative or positive for the bond of ionic or covalent characteristics, respectively.

Sanchez *et al.* (1988) studied the electronic and magnetic properties of a novel intermetallic $NpRh_2Si_2$ by ^{237}Np Mössbauer spectroscopy. The isomer shift ranging from 5.3 (at 4.2 K) to 4.8 mm s^{-1} (at 77 K) with respect to $NpAl_2$ suggested a Np^{4+} electronic configuration in conducting materials.

Nakamoto *et al.* (1998) and Saeki *et al.* (1999) measured Mössbauer spectra of Np(V) compounds such as formate, $NpO_2OOCH \cdot H_2O$, and $NH_4NpO_2(OOCH)_2$, glycolate, $NpO_2OOCCH_2OH \cdot H_2O$, malonate $(NpO_2)_2C_3H_2O_4 \cdot 4H_2O$, and phthalate $(NpO_2)_2(OOC)_2C_6H_4 \cdot 4H_2O$, and found a good correlation between coordination numbers of Np atoms and isomer shifts in the range from –18.6 to –19.1 mm s^{-1} for the compounds with Np atoms surrounded by seven oxygen atoms, i.e. coordination number = 7. The isomer shift for Np of coordination number 8 in the compound is larger than that of coordination number 7. Isomer shifts of Np(IV) to (VII) with different coordination numbers in the compounds are summarized in Fig. 6.14 (Saeki, 2003).

Heptavalent neptunium compounds have been studied by Mössbauer spectroscopy. The characteristic isomer shift of Np(VII) has been reported to be from –64 to –75 mm s^{-1} with respect to $NpAl_2$ (Stone *et al.* 1969; Fröhlich *et al.* 1972; Ilyatov *et al.* 1975; Grigor'ev *et al.* 1979; Ananyev *et al.* 1980). Recently Nakamoto *et al.* (1999) reinvestigated the Mössbauer spectra for Np(VII) in $[Co(NH_3)_6][NpO_4(OH)_2] \cdot 2H_2O$ at 4.2 K. They pointed out that the fitting by using two quadrupole-split peaks did not give a good agreement with the previous data by Stone *et al.* (1969), although the spectrum observed by Nakamoto *et al.* (1999) consisted of two quadrupole-split peaks.

Filin *et al.* (1989, 1990) studied ^{237}Np Mössbauer emission spectra resulting from the alpha decay of ^{241}Am in various solid solutions of actinide dioxides. The oxidation state of ^{237}Np in ^{241}Am(0.6 and 11 at%) + PuO_2 was determined from the isomer shifts of –5.8 and 18.5 mm s^{-1} relative to $NpAl_2$ to be Np^{4+} and Np^{5+}, respectively. They found that the oxidation state strongly depended on the matrix stoichiometry of PuO_2 as well as on the content of the impurity in the sample.

6.10.8 Miscellaneous methods

Speciation of neptunium in samples has been a strong analytical interest and requirement, because the ions of five oxidation states from (III) to (VII) are stable under certain conditions and the ions form complexes differently with many kinds of ligands. The methods for the speciation were evaluated recently by OECD/NEA (2001).

The redox speciation of neptunium ion of relatively high concentration can be performed by direct absorption spectrophotometry (see Section 6.10.2) or electrochemical methods (see Section 6.10.6). For the redox speciation of neptunium ion at lower concentration, e.g. in environmental samples, a method utilizing chemical separation between ions of different oxidation states followed by the determination of the ions using sensitive methods such as radiometric methods and ICP-MS is employed. Coprecipitation with such precipitates as LaF_3, followed by solvent extraction with, e.g. HTTA, can be used for the separation. It is essential that the separation method does not disturb the

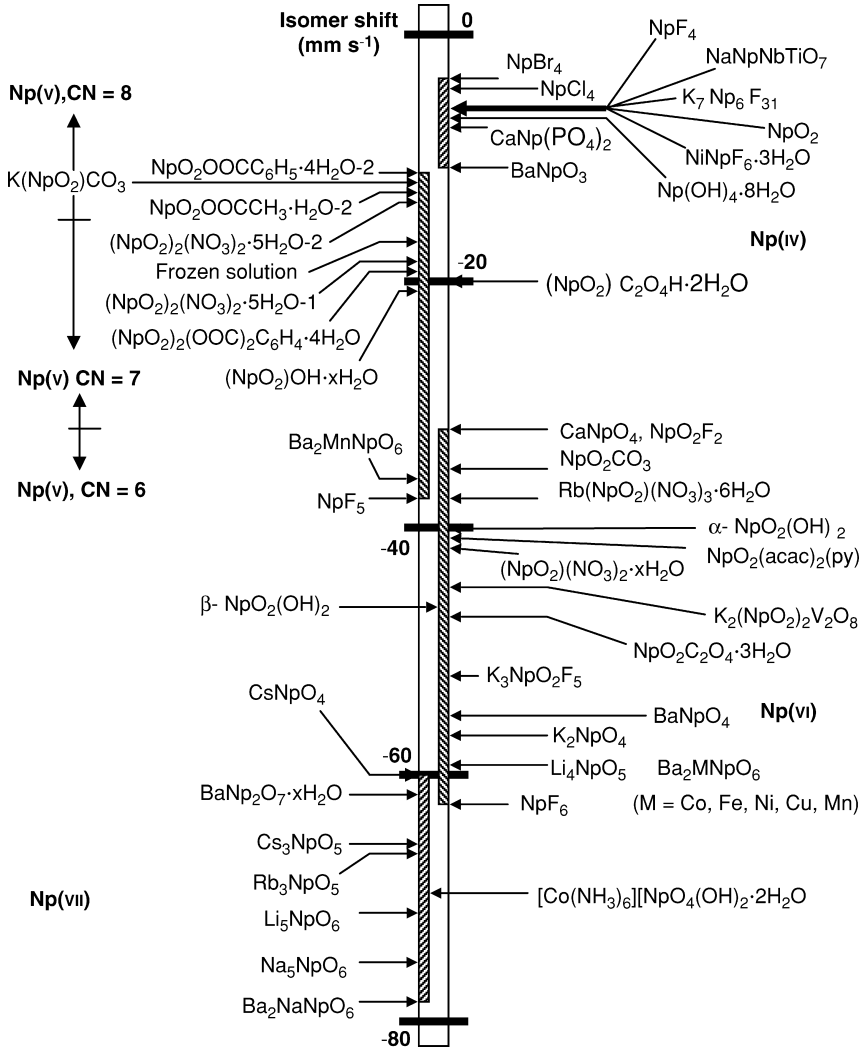

Fig. 6.14 *Isomer shifts of Np(IV), (V), (VI), and (VII) compounds.*

redox equilibrium during the treatment of the sample. Mang *et al.* (1993) investigated a continuous electrophoretic ion focusing method for the separation of Np(VI) from Np(V) at a trace concentration level, e.g. 10^{-14} M level using ^{239}Np tracer. Np(VI) was not stable enough under the recommended conditions. The Np(IV) and Np(V) species were well focused and separated with very reproducible peaks by continuous ion focusing with glycolic acid and tartaric acid.

Chen *et al.* (1992) employed traditional solvent extraction with HTTA and TOPO for the separation of Np(VI), Np(V), and Np(IV). Enokida and Suzuki (1987) employed extraction chromatography with TBP-impregnated resin for the separation of 10^{-5} M levels of neptunium ions of different oxidation states. Nagasaki *et al.* (1988) recommended a paper electrophoresis method for the redox speciation of neptunium ions.

X-ray absorption fine structure (XAFS) was applied to the speciation of Np(V) in an aqueous solution containing high concentration of chloride salt (Allen *et al.*, 1997), and adsorbed at the interface between alpha-Fe hydroxide solid and aqueous solution (Combes *et al.*, 1992).

High-resolution ultraviolet and X-ray photoelectron spectroscopy (UPS and XPS) were applied to characterize the surface of neptunium metal (Naegele *et al.*, 1987). An oxide layer of Np(III), i.e. Np_2O_3, was found in the near surface of about 10 Å in thickness of the sample.

REFERENCES

Abazli, H., Jovè, J., and Pagès, M. (1979) *C. R. Acad. Sc. Paris C*, **288**, 157–9.

Abazli, H., Cousson, J., Jovè, J., Pagès, M., and Gasperin, M. (1984) *J. Less Common Metals*, **96**, 23–33.

Ackermann, R. J., Faircloth, R. L., Rauh, E. G., and Thorn, R. J. (1966) *J. Inorg. Nucl. Chem.*, **28**, 111–18.

Ahrland, S. and Brandt, L. (1966) *Acta Chem. Scand.*, **20**, 328–46.

Ahrland, S. and Brandt, L. (1968a) *Acta Chem. Scand.*, **22**, 106–14.

Ahrland, S. and Brandt, L. (1968b) *Acta Chem. Scand.*, **22**, 1579–89.

Akabori, M., Haire, R. G., Gibson, J. K., Okamoto, Y., and Ogawa, T. (1997) *J. Nucl. Mater.*, **247**, 240–3.

Akopov, G. A., Krinitsyn, A. P., and Tikhonova, A. E. (1988) *Radiokhimiya*, **30**, 578–83.

Aldred, A. T., Dunlap, B. D., Harvey, A. R., Lam, D. J., Lander, G. H., and Mueller, M. H. (1974) *Phys. Rev. B*, **9**, 3766–78.

Aldred, A. T., Dunlap, B. D., Lam, D. J., Lander, G. H., Mueller, M. H., and Nowik, I. (1975) *Phys. Rev. B*, **11**, 530–44.

Aleksandruk, V. M., Babaev, A. S., Dem'yanova, T. A., and Stepanov, A. V. (1990) *Radiokhimiya*, **32**, 132–8.

Aleksandruk, V. M., Babaev, A. S., Dem'yanova, T. A., and Stepanov, A. V. (1991a) *Radiokhimiya*, **33**, 203–8.

Aleksandruk, V. M., Babaev, A. S., Dem'yanova, T. A., and Stepanov, A. V. (1991b) EUR-13686, pp. 215–18.

Al-Kazzaz, Z. M. S., Bagnall, K. W., Brown, D., and Whittaker, B. (1972) *J. Chem. Soc. Dalton Trans.*, **20**, 2273–7.

Allen, P. G., Bucher, J. J., Shuh, D. K., Edelstein, N. M., and Reich, T. (1997) *Inorg. Chem.*, **36**, 4676–83.

Al-Niaimi, N. S., Wain, A. G., and McKay, H. A. C. (1970a) *J. Inorg. Nucl. Chem.*, **32**, 2331–42.

Al- Niaimi, N. S., Wain, A. G., and McKay, H. A. C. (1970b) *J. Inorg. Nucl. Chem.*, **32**, 977–86.
Ananyev, A. V., Grigoryev, M. S., and Krot, N. N. (1980) *Radiochem. Radioanal. Lett.*, **44**, 217–26.
Appel, H., Bickel, M., Melchior, S., Kanellakopulos, B., and Keller, C. (1990) *J. Less Common Metals*, **162**, 323–34.
Arai, Y., Okamoto, Y., and Suzuki, Y. (1994) *J. Nucl. Mater.*, **211**, 248–50.
Asprey, L. B., Eller, P. G., and Kinkead, S. A. (1986) *Inorg. Chem.*, **25**, 670–2.
Aupiais, J., Dacheux, N., Thomas, A. C., and Matton, S. (1999) *Anal. Chim. Acta*, **398**, 205–18.
Awasthi, S. K., Martinot, L., Fuger, J., and Duyckaerts, G. (1971) *Inorg. Nucl. Chem. Lett.*, **7**, 145–51.
Bagawde, S. V., Ramakrishna, V. V., and Patil, S. K. (1976) *J. Inorg. Nucl. Chem.*, **38**, 2085–9.
Bagnall, K. W. and Laidler, J. B. (1964) *J. Chem. Soc.*, 2693–6.
Bagnall, K. W. and Laidler, J. B. (1966) *J. Chem. Soc. A*, 516–20.
Bagnall, K. W., Brown, D., and Easey, J. F. (1968a) *J. Chem. Soc. A*, 2223–7.
Bagnall, K. W., Brown, D., and Easey, J. F. (1968b) *J. Chem. Soc. A*, 286–91.
Bagnall, K. W., Payne, G. F., and Brown, D. (1985) *J. Less Common Metals*, **109**, 31–6.
Baluka, M., Yeh, S., Banks, R., and Edelstein, N. (1980) *Inorg. Nucl. Chem. Lett.*, **16**, 75–7.
Bamberger, C. E., Haire, R. G., Begun, G. M., and Hellwege, H. E. (1984) *J. Less Common Metals*, **102**, 179–86.
Barrero Moreno, J. M., Betti, M., and Garcia Alonso, J. I. (1997) *J. Anal. Atom. Spectrom.*, **12**, 355–61.
Bartscher, W. and Sari, C. (1986) *J. Nucl. Mater.*, **140**, 91–3.
Baumgartner, F., Fischer, E. O., and Laubereau, P. (1965) *Naturwissenschaften*, **52**, 560
Baumgartner, F., Fischer, E. O., Kanellakopulos, B., and Laubereau, P. (1968) *Angew. Chem. Int. Edn.*, **7**, 634
Beauvy, M., Duverneix, T., Berlanga, C., Mazoyer, R., and Duriez, C. (1998) *J. Alloys Compds.*, **271/273**, 557–62.
Belyaev, Y. I., Il'inskaya, T. A., Kudryavtsev, A. N., Smirnov, N. L., and Tolmachev, Y. M. (1975) *Sov. Radiochem.*, **17**, 847–60.
Belyaev, Y. I., Smirnov, N. L., and Taranov, A. P. (1979) *Radiokhimiya*, **21**, 682–6.
Belyaev, Y. I. (1983) *Radiokhimiya*, **25**, 791–4.
Benedict, U., Dabos, S., Dufour, C., and Spirelet, J. C. (1986) *J. Less Common Metals*, **121**, 461–8.
Bessonov, A. A., Afonas'eva, T. V., and Krot, N. N. (1989a) *Radiokhimiya*, **31**, 9–13.
Bessonov, A. A., Grigor'eva, M. S., Afonas'eva, T. V., and Krot, N. N. (1989b) *Sov. Radiochem.*, **31**, 393–6.
Betz, T. and Hoppe, R. (1984) *Z. Anorg. Allg. Chem.*, **512**, 19.
Bickel, M. and Kanellakopulos, B. (1986) *J. Less Common Metals*, **121**, 291–9.
Bickel, M., Adrian, G., Kanellakopulos, B., Haffner, H., Geggus, G., and Appel, H. (1987) *Inorg. Chim. Acta*, **140**, 101–3.
Bidoglio, G., Tanet, G., and Chatt, A. (1985) *Radiochim. Acta*, **38**, 21–6.
Bihan, T. L., Heathman, S., and Rebizant, J. (1997) *High Press. Res.*, **15**, 387–92.
Blaise, A., Fournier, J. M., Salmon, P., and Wojakowski, A. (1976) *Magnetic Properties of Some Neptunium and Plutonium Compounds. Plutonium and other Actinides.* in (eds. H. Blank and R. Linder), North-Holland, Amsterdam, pp. 635–40.

Blaise, A., Damien, D., and Suski, W. (1981) *Solid State Commun.*, **37**, 659–62.
Blaise, A., Damien, D., and Mulak, J. (1982) *Phys. Stat. Sol.*, **72**, K145–8.
Blokhin, V. I., Bukhtiyarova, T. N., Krot, N. N., and Gel'man, A. D. (1972) *Russ. J. Inorg. Chem.*, **17**, 1742–6.
Bohlander, R. (1986) *Zur Metallorganischen Kompleschemie Des Neptunium*, Dissertation, Kernforshcungszentrum Karlsruhe GmbH, KfK 4152.
Brewer, L., Bromely, L., Gilles, P. W., and Lofgren, N. (1949) in *The Transuranium Elements* (eds. G. T. Seaborg, J. J. Katz, and W. M. Manning), *Natl. Nucl. En. Ser.,* Div. IV, 14B, McGraw-Hill, New York, pp. 1111–18.
Brown, D., Fletcher, S., and Holah, D. G. (1968) *J. Chem. Soc. A*, 1889–94.
Brown, D., Hill, J., and Richard, C. E. F. (1970) *J. Chem. Soc. A*, 476–80.
Brown, D. (1972) in *Gmelin Handbuck der Anorganischen Chemie*, Suppl. Work, 8th edn, *Transuranium*, Verlag Chemie, Weinheim, vol. 4, part C, Compounds.
Brown, D. and Edwards, J. (1972) *J. Chem. Soc. Dalton Trans.*, 1757–62.
Brown, D., Hall, L., Hurtgen, C., and Moseley, P. T. (1977) *J. Inorg. Nucl. Chem.*, **39**, 1464–6.
Brown, W., Whittaker, B., Berry, J. A., and Holloway, J. H. (1982) *J. Less Common Metals*, **86**, 75–84.
Bryne, A. R. (1986) *J. Environ. Radioact.*, **4**, 133–44.
Budantseva, N. A., Fedoseev, M. S., Grigor'ev, M. S., Potemkina, T. I., Afonas'ev, T. V., and Krot, N. N. (1988) *Radiokhimiya*, **30**, 607–10.
Budantseva, N. A., Potemkina, T. I., Grigor'ev, M. S., Fedoseev, A. M., and Krot, N. N. (1989) *Radiokhimiya*, **31**, 5–8.
Burkhart, M. J. and Thompson, R. C. (1972) *J. Am. Chem. Soc.*, **94**, 2999–3002.
Burlet, P., Quezel, J., Rossat- Mignod, J., Spirlet, J. C., Rebizant, J., and Vogt, O. (1989) *Physica B*, **159**, 129–36.
Burlet, P., Bourdarot, F., Rossat- Mignod, J., Sanchez, J. P., Spirlet, J. C., Rebizant, J., and Vogt, O. (1992) *Physica B*, **180&181**, 131–2.
Burney, G. A. and Harbour, R. M. (1974) in *Radiochemistry of Neptunium*, NAS-NS-3060, Technical Information Center, USAEC.
Burns, J. H., Baldwin, W. H., and Stokely, J. R. (1973) *Inorg. Chem.*, **12**, 466–9.
Burns, P. C., Kubatko, K.-A., Sigmon, G., Fryer, B. J., Gagnon, J. E., Antonio, M. R., and Soderholm, L. (2005) *Angew. Chem. Int. Ed.,* **44**, 2135.
Cao, X., Xu, S., Wu, P., and Wen, Z. (1994) *He Huaxue Yu Fangshe Huaxue*, **16**, 43–8.
Carnall, W. T., Neufeldt, S. J., and Walker, A. (1965) *Inorg. Chem.*, **4**, 1808–13.
Carnall, W. T., Goodman, G. L., Veal, B. W., and Lam, D. J. (1987) *J. Less Common Metals*, **133**, 178–9.
Cassol, A., Magon, L., Tomat, G., and Portanova, R. (1969) *Inorg. Chim. Acta*, **3**, 639–43.
Cassol, A., Magon, L., Tomat, G., and Portanova, R. (1972a) *Inorg. Chem.*, **11**, 515–19.
Cassol, A., Magon, L., Portanova, R., and Tondello, E. (1972b) *Radiochim. Acta*, **17**, 28–32.
Cassol, A., Bernardo, P. D., Portanova, R., and Magon, L. (1973) *Inorg. Chim. Acta*, **7**, 353–8.
Chaikhorskii, A. A. (1971) *Radiokimiya* **13**, 320–5.
Chaikhorskii, A. A. and Leikina, E. V. (1972) *Radiokimiya*, **14**, 378–84.
Chaikhorskii, A. A., Zelentov, S. S., and Leikina, E. V. (1972) *Sov. Radiochem.*, **14**, 636.
Chaikhorskii, A. A., Matuzenko, M. Y., and Belyaev, Y. I. (1974) *Radiokhimiya*, **16**, 850–3.

Chaikhorskii, A. A., Matuzenko, M. Y., and Leikina, E. V. (1975) *Sov. Radiochem.*, **17**, 803–11.
Charushnikova, I. A., Afonas'eva, T. V., Perminov, V. P., and Krot, N. N. (1992) *Sov. Radiochem.*, **34**, 648–54.
Charushnikova, I. A., Afonas'eva, T. V., and Krot, N. N. (1995) *Radiochemistry*, **37**, 6–11.
Charvillat, J. P. and Damien, D. (1973) *Inorg. Nucl. Chem. Lett.*, **9**, 337–42.
Charvillat, J. P., Benedict, U., Damien, D., Novion, D., Wojakowski, A., and Muller, W. (1976) in *Tranplutonium Elements* (eds. W. Muller and R. Linder), North-Holland, Amsterdam, p. 79.
Chen, Y., Zhong, J., Zhao, Y., Tan, B., and Lin, Z. (1992) *Yuanzineng Kexue Jishu*, **26**, 63–7.
Chiarizia, R., Horwitz, E. P., and Alexandratos, S. D. (1994) *Solvent Extr. Ion Exch.*, **12**, 211–37.
Chitnis, R. R., Wattal, P. K., Ramanujam, A., Dhami, P. S., Gopalakrishnan, V., Mathur, J. N., and Murali, M. S. (1998) *Sep. Sci. Technol.*, **33**, 1877–87.
Choporov, D. Y. and Chudinov, E. T. (1968) *Radiokhimiya*, **10**, 221–7.
Choppin, G. R. and Unrein, P. J. (1976) in *Transuranium Elements 1975* (eds. W. Müller and R. Lindner), North-Holland, Amsterdam, pp. 97–107.
Choppin, G. R. and Rao, L. F. (1984) *Radiochim. Acta*, **37**, 143–6.
Choppin, G. R. and Nash, K. L. (1995) *Radiochim. Acta*, **70/71**, 225–36.
Choppin, G. R., Stout, B. E., and Pagès, M. (1998) *J. Alloys Compds.*, **271–273**, 774–7.
Clark, D. L., Hobart, D. E., and Neu, M. P. (1995) *Chem. Rev.*, **95**, 25–48.
Cohen, D. and Hindman, J. C. (1952) *J. Am. Chem. Soc.*, **74**, 4682–5.
Cohen, D. (1963) *Inorg. Chem.*, **2**, 866–7.
Cohen, D. and Walter, A. J. (1964) *J. Chem. Soc.*, 2696–9.
Cohen, D., Fried, S., Holloway, J. H., and Selig, H. (1970) Unpublished work at Argonne National Laboratory, Argonne, IL, Quoted by Brown, W., Whittaker, B., Berry, J. A., and Holloway, J. H. (1982). *J. Less Common Metals*, **86**, 75–84.
Collard, J. M., Blaise, A., Boge, M., Bonnisseau, D., Burlet, P., and Fournier, J. M. (1986) *J. Less Common Metals*, **121**, 313–8.
Combes, J-M., Chishoim- Brause, C. J., Brown, G. E., and Parks, G. A. (1992) *Environ. Sci. Technol.*, **26**, 376–82.
Cousson, A., Dabos, S., Abazli, H., Nectoux, F., Pagès, M., and Choppin, G. (1984) *J. Less Common Metals*, **99**, 233–40.
Cousson, A., Abazli, H., and Jovè, J. (1985) *J. Less Common Metals*, **109**, 155–68.
Cuillerdier, C., Musikas, C., and Mateau, M. (1977) Report CEA-CONF-3944.
Dabos, S., Dufour, C., Benedict, U., Spirlet, J. C., and Pagès, M. (1986) *Physica*, **144B**, 79–83.
Dabos-Seignon, S., Benedict, U., Heathman, S., and Spirlet, J. C. (1990) *J. Less Common Metals*, **160**, 35–51.
Damien, D., Damien, N., Jovè, J., and Chavrillat, J. P. (1973) *Inorg. Nucl. Chem. Lett.*, **9**, 649–55.
Damien, D. and Wojakowski, W. (1975) *Radiochem. Radioanal. Lett.*, **23**, 145–54.
Damien, D. and Berger, R. (1976) in Supplement to *J. Inorg. Nucl. Chem.* Proc. Moscow Symp. On the Chemistry of Transuranium Element, 1976 (eds. Spitsyn, V. I. and Katz, J. J.), Pergamon Press, Oxford, pp. 109–16.

Danesi, P. R., Chiarizia, R., Scibona, G., and D'Alessandro, G. (1971) *J. Inorg. Nucl. Chem.*, **33**, 3503–10.
De Novion, C. H. and Lorenzelli, R. (1968) *J. Phys. Chem. Solids*, **29**, 1901–5.
Degischer, G. and Choppin, G. R. (1975) in *Gmelin Handbuch der Anorganischen Chemie*, *Transurane*, Springer-Verlag, Berlin-Heidelberg, part D1, pp. 129–76.
Drobyshevskii, Y. V., Serik, V. F., and Sokotov, V. B. (1975) *Dokl. Akad. Nauk SSSR*, **225**, 1079–81.
Drobyshevskii, Y. V., Serik, V. F., Sokotov, V. B., and Tul'skii, M. N. (1978) *Radiokhimiya*, **20**, 238–43.
Dukes, E. K. and Shuler, W. E. (1960) Report DP-543, Dupont de Nemours Co.
Duplessis, J. and Guillaumont, R. (1977) *Radiochem. Radioanal. Lett.*, **31**, 293–302.
Eberle, S. H. and Wede, U. (1968) *Inorg. Nucl. Chem. Lett.*, **4**, 661–4.
Eberle, S. H. and Schaefer, J. B. (1969) *J. Inorg. Nucl. Chem.*, **31**, 1523–7.
Eberle, S. H. and Wede, U. (1970) *J. Inorg. Nucl. Chem.*, **32**, 109–17.
Eberle, S. H. and Paul, M. T. (1971) *J. Inorg. Nucl. Chem.*, **33**, 3067–75.
Efurd, D. W., Knobeloch, G. W., Perrin, R. E., and Barr, D. W. (1984) *Health Phys.*, **47**, 786–7.
Efurd, D. W., Drake, J., Roensch, F. R., Cappis, J. H., and Perrin, R. E. (1986) *Int. J. Mass Spectrom. Ion Processes*, **74**, 309–15.
Eick, H. A. and Mulford, R. (1964) *J. Chem. Phys.*, **41**, 1475–8.
Eisenstein, J. C. and Pryce, M. H. L. J. Re. (1965) *Natl. Bur. Stand.*, **A 69**, 217.
Eisenstein, J. C. and Pryce, M. H. L. J. Re. (1966) *Natl. Bur. Stand.*, **A 70**, 165.
Eller, P. G., Asprey, L. B., Kinkead, S. A., Swanson, B. I., and Kissane, R. J. (1998a) *J. Alloys Compds.*, **269**, 63–6.
Eller, P. G., Malm, J. G., Swanson, B. I., and Morss, L. R. (1998b) *J. Alloys Compds.*, **269**, 50–6.
Elliott, R. O. and Giessen, B. C. (1982) *Acta Metall.*, **30**, 785–9.
Enokida, Y. and Suzuki, A. (1987) *J. Nucl. Sci. Technol.*, **24**, 859–61.
Enokida, Y. and Suzuki, A. (1989) *Nucl. Technol.*, **88**, 47–54.
Eriksen, T. E., Ndalamba, P., Cui, D., Bruno, J., Caceci, M., and Spahiu, K. (1993) SKB Report TR-93–18.
Ewart, F. T., Gore, S. J. M., and Williams, S. J. (1985) Report AERE-R11975.
Fahey, J. A., Turcotte, R. P., and Chikalla, T. D. (1974) *Inorg. Nucl. Chem. Lett.*, **10**, 459–65.
Fahey, J. A., Turcotte, R. P., and Chikalla, T. D. (1976a) *Inorg. Nucl. Chem. Lett.*, **10**, 459–65.
Fahey, J. A., Turcotte, R. P., and Chikalla, T. D. (1976b) *J. Inorg. Nucl. Chem.*, **38**, 495–500.
Fahey, J. A. (1986) in *The Chemistry of the Actinide Elements, vol. 1* (eds. J. J. Katz, G. T. Seaborg, L. R. Morss), Chapman & Hall, New York, p. 456.
Fifield, L. K., Clacher, A. P., Morris, K., King, S. J., Cresswell, R. G., Day, J. P., and Livens, F. R. (1997) *Nucl. Instrum. Methods Phys. Res. Sect. B*, **123**, 400–4.
Filin, V. M., Gorbunov, V. F., and Ulanov, S. A. (1989) *Radiokhimiya*, **31**, 13–9.
Filin, V. M., Gorbunov, V. F., and Ulanov, S. A. (1990) *J. Radioanal. Nucl. Chem. Art.*, **143**, 125–34.
Finch, R. J. (2002) in *Scientific Basis for Nuclear Waste Management XXV* (eds. B. P. McGrail and G. A. Cragnolino), Materials Research Society Symp., 2001. The Materials Research Society, Warrendale, Pennsylvania, p. 713, JJ11.60.W.

Fischer, E. O., Laubereau, P., Baumgartner, F., and Kanellakopulos, B. (1966) *J. Organomet. Chem.*, **5**, 583–4.
Florin, A. E. (1943) Report MUC-GTS 2165.
Flotow, H. E., Haschke, J. M., and Yamauchi, S. (1984) in *The Chemical Thermodynamics of Actinide Elements and Compounds* part 9, *The Actinide Hydrides* (ed. F. L. Oetting), International Atomic Energy Agency, Vienna.
Foltyn, E. (1990) *J. Nucl. Mater.*, **172**, 180–3.
Foropoulus, J., Avens, L. R., and Trujillo, E. A. (1992) US Patent No. 5,098,682.
Fried, S. and Davidson, N. R. (1947) MDDC-1332, Argonne National Laboratory, Date Declassified: July 18, 1947.
Fried, S. and Davidson, N. R. (1948) *J. Am. Chem. Soc.*, **70**, 3539–47.
Fried, S. and Davidson, N. R. (1951) US Patent 2,578,416.
Fried, S. (1954) *The Actinide Elements,* Natl. Nucl. En. Ser., Div. IV, 14A (eds. G. T. Seaborg and J. J. Katz), McGraw-Hill, New York, p. 471.
Fröhlich, K., Gütlich, P., and Keller, C. (1972) *Angew. Chem.*, **84**, 26–7.
Fuger, J. and Brown, D. (1971) *J. Chem. Soc. A*, 842–6.
Fuger, J. (1979) *J. de physique, C4 (Suppl. 4)* **40**, 207–13.
Fuger, J., Khodakovsky, I. L., Sergeyeva, E. I., Medvedev, V. A., and Navratil, J. D. (1992) in *The Chemical Thermodynamics of Actinide Elements and Compounds*, part 12, *The Actinide Aqueous Inorganic Complexes*, International Atomic Energy Agency, Vienna.
Fujinaga, T. and Kihara, S. (1977) *CRC Crit. Rev. Anal. Chem.*, **6**, 223–54.
Fukasawa, T., Ikeda, T., and Kawamura, F. (1991) *Eur. J. Solid State Inorg. Chem.*, **28**, 73–6.
Gal, J., Litterst, J., Potzel, W., Moser, J., Potzel, U., Kalvius, G. M., Fredo, S., and Tapuchi, S. (1987) *Phys. Rev. B*, **36**, 2457–60.
Garner, C. S., Bonner, N. A., and Seaborg, G. T. (1948) *J. Am. Chem. Soc.*, **70**, 3453–4.
Geary, N. R. (1955) UKAEA, Risley-5142.
Gel'man, A. D., Moskvin, A. I., Zaitsev, L. M., and Mefod'eva, M. P. (1962) in *Complex Compounds of Transuranium Elements*. Consultants Bureau Enterprises, New York.
Gensini, M., Benedict, U., and Rebizant, J. (1993) *J. Alloys Compds.*, **201**, L19–20.
Germain, P., Guegueniat, P., May, S., and Pinte, G. (1987) *J. Environ. Radioact.*, **5**, 319–31.
Gibson, J. K. and Haire, R. G. (1993) *J. Nucl. Mater.*, **201**, 225–30.
Gibson, J. K., Haire, R. G., Gensini, M. M., and Ogawa, T. (1994) *J. Alloys Compds*, **213/4**, 106–10.
Gibson, J. K., Haire, R. G., Okamoto, Y., and Ogawa, T. (1996) *J. Alloys Compds*, **234**, 34–9.
Gibson, J. K., Haire, R. G., and Ogawa, T. (1999) *J. Nucl. Mater.*, **273**, 139–45.
Godbole, A. G. and Patil, S. K. (1979) *Talanta*, **26**, 330–2.
Grenthe, I., Riglet, C., and Vitorge, P. (1986) *Inorg. Chem.*, **25**, 1679–84.
Grigor'ev, M. S., Glauzunov, M. P., Mefod'eva, M. P., Krot, N. N., Makarov, E. F., Permyakov, Yu. V., and Zemskov, B. G. (1979) *Radiokhimiya*, **21**, 659–64.
Grigor'ev, M. S., Gulev, B. F., and Krot, N. N. (1986a) *Radiokhimiya*, **28**, 685–90.
Grigor'ev, M. S., Gulev, B. F., and Krot, N. N. (1986b) *Radiokhimiya*, **28**, 690–4.
Grigor'ev, M. S., Yanovskii, A. I., Krot, N. N., and Struchkov, Y. T. (1987) *Radiokhimiya*, **29**, 574–9.

Grigor'ev, M. S., Yanovskii, A. I., Struchkov, Y. T., Bessnov, A. A., Afonas'eva, T. V., and Krot, N. N. (1989) *Radiokhimiya*, **31**, 37–44.
Grigor'ev, M. S., Baturin, N. A., Regel', L. L., and Krot, N. N. (1991a) *Radiokhimiya*, **33**, 19–25.
Grigor'ev, M. S., Fedoseev, N. A., Budantseva, N. A., Yanovskii, A. I., Struchkov, Y. T., and Krot, N. N. (1991b) *Radiokhimiya*, **33**, 54–61.
Grigor'ev, M. S., Yanovskii, A. I., Fedoseev, A. M., Budantseva, N. A., Struchkov, Y. T., and Krot, N. N. (1991c) *Radiokhimiya*, **33**, 17–9.
Grigor'ev, M. S., Charushnikova, N. N., Krot, N. N., Yanovskii, A. I., and Struchkov, Y. T. (1993a) *Radiokhimiya*, **35**, 24–30.
Grigor'ev, M. S., Charushnikova, N. N., Krot, N. N., Yanovskii, A. I., and Struchkov, Y. T. (1993b) *Radiokhimiya*, **35**, 31–7.
Grigor'ev, M. S., Baturin, N. A., Budantseva, N. A., and Fedoseev, A. M. (1993c) *Radiokhimiya*, **35**, 29–38.
Grigor'ev, M. S., Charushnikova, I. A., Baturin, N. A., and Krot, N. N. (1995) *Russ. J. Inorg. Chem.*, **40**, 709–12.
Gruber, J. B. and Menzel, E. R. (1969) *J. Chem. Phys.*, **50**, 3772–9.
Gruen, D. M. (1952) *J. Chem. Phys.*, **20**, 1818–9.
Gruen, D. M., McBeth, R. L., and Fried, S. M. (1976) *J. Inorg. Nucl. Chem.*, (Suppl. 2), 27–30.
Gruen, D. M. (1992) in *Transuranium Elements; A Half Century* (eds. L. R. Morss and J. Fuger), American Chemical Society, Washington DC, pp. 63–77.
Guillaume, B., Begun, G. M., and Hahn, R. L. (1982) *Inorg. Chem.*, **21**, 1159–66.
Guillaume, B., Hahn, R. L., and Narten, A. H. (1983) *Inorg. Chem.*, **22**, 109–11.
Gysling, H. and Tsutsui, M. (1970) *Adv. Organomet. Chem.*, **9**, 361–93.
Haire, R. G. and Fahey, J. A. (1977) *J. Inorg. Nucl. Chem.*, **39**, 837–41.
Haire, R. G. (1986) *J. Less Common Metals*, **121**, 379–98.
Halperin, J. and Oliver, J. H. (1983) *Radiochim. Acta*, **33**, 29–33.
Haschke, J. M. (1991) in *Synthesis of Lanthanides and Actinide Compounds* (eds. G. Meyer and L. R. Morss), Kluwer Academic Publishers, The Netherlands, pp. 1–53.
Hasegawa, K., Shiokawa, Y., Akabori, M., Suzuki, Y., and Suzuki, K. (1998) *J. Alloys Compds.*, **271–273**, 680–4.
Hayes, R. G. and Thomas, J. L. (1971) *Organomet. Chem. Rev.*, **7**, 1–50.
Heinrich, Z. and Klaus, M. (1999) *Radiochim. Acta*, **86**, 123–8.
Henrion, P. N. and Leurs, L. (1971) *J. Nucl. Mater.*, **41**, 1–22.
Hessler, J. P., Brundage, R. T., Hegarty, J., and Yen, W. M. (1980) *Optics Lett.*, **5**, 348–50.
Hill, H. (1971) in *Plutonium 1970 and Other Actinide* (ed. W. N. Miner), The Metallurgical Society of AIME, New York, part 2.
Hindman, J. C., Sullivan, J. C., and Cohen, D. (1954) *J. Am. Chem. Soc.*, **76**, 3278–80.
Hoekstra, H. R. and Gebert, E. (1977) *J. Inorg. Nucl. Chem.*, **39**, 2219–21.
Hoelgye, Z. (1998) *J. Radioanal. Nucl. Chem.*, **227**, 127–8.
Hoffman, P. and Kleykamp, H. (1972) in *Gmelin Handbuch der Anorganischen Chemie*, Suppl. Work, 8th edn, *Transuranium*, Verlag Chemie, Weinheim, vol. 4, part C, Compounds.
Holland, M. K. and Cordaro, J. V. (1988) DP-1751.

Holley, C. E. Jr, Rand, M. H., and Storms, E. K. (1984) in *The Chemical Thermodynamics of Actinide Elements and Compounds*, part 6. The Actinide Carbides, International Atomic Energy Agency, Vienna, pp. 49–51.
Holloway, J. H. and Laycock, D. (1984) *Adv. Inorg. Chem. Radiochem.*, **28**, 73–99.
Holm, E., Aarkrog, A., and Ballestra, S. (1987) *J. Radioanal. Nucl. Chem. Art.*, **115**, 5–11.
Horwitz, E. P., Chiarizia, R., and Alexandratos, S. D. (1994) *Solvent Extr. Ion Exch.*, **12**, 831–45.
Hursthouse, A. S. A., Baxter, M. S., McKay, K., and Livens, F. R. (1992) *J. Radioanal. Nucl. Chem. Art.*, **157**, 281–94.
Ilyatov, K. V., Matuzenko, M. Y., Krizhanskii, L. M., and Chaikhorskii, A. A. (1975) *Radiokhimiya*, **17**, 905–9.
Ionova, G. V. and Jovè, J. (1989) *Radiokhimiya*, **31**, 31–6.
Itagaki, H., Nakayama, S., Tanaka, S., and Yamawaki, M. (1992) *Radiochim. Acta*, **58/59**, 61–6.
Ivanova, S. A., Mikheeva, M. N., Novikov, A. P., and Myasoedov, B. F. (1994) *J. Radioanal. Nucl. Chem. Lett.*, **186**, 341–52.
Jeandey, C., Sanchez, J. P., Oddou, J. L., Rebizant, J., Spirlet, J. C., and Wastin, F. (1996) *J. Phys.: Condens. Matter*, **8**, 4259–68.
Jha, S. K. and Bhat, I. S. (1994) *J. Radioanal. Nucl. Chem. Art.*, **182**, 5–10.
Ji, Y. Q., Li, J. Y., Luo, S. G., Wu, Y., and Liu, J. L. (2001) *Fresenius J. Anal. Chem.*, **371**, 49–53.
Jones, E. R. and Stone, J. A. (1972) *J. Chem. Phys.*, **56**, 1343–7.
Jovè, J. and Cousson, A. (1977) *Radiochim. Acta*, **24**, 73–5.
Jovè, J., Cousson, A., and Gasperien, M. (1988a) *J. Less Common Metals*, **139**, 345–50.
Jovè, J., Cousson, H., Abazli, H., Tabuteau, A., Thévenin, T., and Pagès, M. (1988b) *Hyperfine Interact.*, **39**, 1–16.
Jovè, J., He, L., Proust, J., Pagès, M., and Pyykkö, P. (1991) *J. Alloys Compds.*, **177**, 285–310.
Kalsi, P. K., Sawant, L. R., Sharma, R. C., and Vaidyanathan, S. (1994) *J. Radioanal. Nucl. Chem. Lett.*, **187**, 265–75.
Kalvius, G. M. (1989) *J. Nucl. Mater.*, **166**, 5–21.
Kalvius, G. M., Gal, J., Asch, L., and Potzel, W. (1992) *Hyperfine Interact.*, **72**, 77–95.
Kalvius, G. M., Potzel, W., Zwirner, S., Gal, J., and Nowik, I. (1994) *J. Alloys Compds.*, **213/214**, 138–47.
Kanellakopulos, B., Henrich, E., Keller, C., Baumgartner, F., Konig, E., and Desai, V. P. (1980a) *Chem. Phys.*, **53**, 109–213.
Kanellakopulos, B., Keller, C., Klenze, R., and Stollenwerk, A. H. (1980b) *Physica*, **102B**, 221–5.
Karalova, Z. I., Lavrinovich, E. A., and Myasoedov, B. F. (1992a) *J. Radioanal. Nucl. Chem.*, **159**, 259–66.
Karalova, Z. K., Lavrinovich, E. A., Ivanova, S. A., Myasoedov, B. F., Fedorov, L. A., and Sokolovskii, S. A. (1992b) *Radiokhimiya*, **34**, 132–8.
Karelin, A. I., Semenov, E. N., and Mikhailova, N. A. (1991) *J. Radioanal. Nucl. Chem.*, **147**, 33–40.
Karraker, D. G., Stone, J. A., Jones, E. R., Jr, and Edelstein, N. (1970) *J. Amer. Chem. Soc.*, **92**, 4841–5.

Karraker, D. G. and Stone, J. A. (1972) *Inorg. Chem.*, **11**, 1742–6.
Karraker, D. G. (1973) *Inorg. Chem.*, **12**, 1105–8.
Karraker, D. G. and Stone, J. A. (1974) *J. Amer. Chem. Soc.*, **96**, 6885–8.
Karraker, D. G. and Stone, J. A. (1976) *Abstracts*, *172nd National Meeting of the American Chemical Society*, San Francisco, CA, No. INOR 184.
Karraker, D. G. (1987) *Inorg. Chim. Acta*, **139**, 189–91.
Kasar, U. M., Joshi, A. R., and Patil, S. K. (1991) *J. Radioanal. Nucl. Chem. Art.*, **150**, 369–76.
Kato, Y., Kimura, T., Yoshida, Z., and Nitani, N. (1996) *Radiochim. Acta*, **74**, 21–5.
Kato, Y., Kimura, T., Yoshida, Z., and Nitani, N. (1998) *Radiochim. Acta*, **82**, 63–8.
Katz, J. J. and Gruen, D. M. (1949) *J. Amer. Chem. Soc.*, **71**, 2106–12.
Keiser, D. D., Abraham, D. P., Sinkler, W., Richardson, J. W., and McDeavitt, S. M. (2000) *J. Nucl. Mater.*, **279**, 234–44.
Keller, C. (1963) *Nukleonick*, **5**, 89–93.
Keller, C., Kock, L., and Walter, K. H. (1965a) *J. Inorg. Nucl. Chem.*, **27**, 1205–23.
Keller, C., Kock, L., and Walter, K. H. (1965b) *J. Inorg. Nucl. Chem.*, **27**, 1225–32.
Keller, C. and Seiffert, H., (1969) *Inorg. Nucl. Chem. Lett.*, **5**, 51–7.
Keller, C. (1971) *The Chemistry of the Transuranium Elements,* Verlog Chemie, Weinheim.
Keller, C. (1972) in *MTP International Review of Science, Inorganic Chemistry,* ser. 1, 7 (ed. K. W. Bagnall), Butterworths, London.
Keller, C. (1975) in *Comprehensive Inorganic Chemistry,* vol. 10 (ed. A. F. Trotman-Dickinson), Pergamon Press, Oxford, 248 pp.
Keller, C. (1982) *Chemiker-Zeitung*, **106**, 137–42.
Kharitonov, Y. Y. and Moskvin, A.I. (1973) *Radiokimiya*, **15**, 608–12.
Kihara, T., Fujine, S., Fukasawa, T., Matsui, T., Maeda, M., and Ikeda, T. (1996) *J. Nucl. Sci. Technol.*, **33**, 409–13.
Kihara, S., Yoshida, Z., Apyagi, H., Maeda, K., Shirai, O., Kitatsuji, Y., and Yoshida, Y. (1999) *Pure Appl. Chem.*, **71**, 1771–807.
Kim, C., Takaku, Y., Yamamoto, M., Kawamura, H., Shiraishi, K., Igarashi, Y., Igarashi, S., Takayama, H., and Ikeda, N. (1989) *J. Radioanal. Nucl. Chem. Art.*, **132**, 131–7.
Kimura, T., Kobayashi, Y., and Akatsu, J. (1986) *Radiochim. Acta*, **39**, 179–83.
Kimura, T. (1990a) *J. Radioanal. Nucl. Chem. Art.*, **130**, 297–305.
Kimura, T. (1990b) *J. Radioanal. Nucl. Chem. Art.*, **141**, 307–16.
Kitazawa, H., Kwon, Y., Ohe, Y., Amanowicz, M., Ayache, C., Rossat- Mignod, J., Rebizant, J., Sprilet, J. C., Suzuki, T., and Kasuya, T. (1993) *Physica B*, **186/188**, 694–6.
Kleinschmidt, P. D., Lau, K. H., and Hildenbrand, D. L. (1992a) *J. Chem. Phys.*, **97**, 1950–3.
Kleinschmidt, P. D., Lau, K. H., and Hildenbrand, D. L. (1992b) *J. Chem. Phys.*, **97**, 2417–21.
Klenze, R. and Kim, J. I. (1988) *Radiochim. Acta*, **44/45**, 77–85.
Kolarik, Z. and Dressler, P. (1984) *Extraction '84*, *Proc. Symp. On Liquid–Liquid Extraction Science*, Institute of Chemical Engineers Symp. Ser., **88**, 83–90.
Kolarik, Z. J. and Horwitz, E. P. (1988) *Solvent Extr. Ion Exch.*, **6**, 247–63.
Koltunov, V. S. and Baranov, S. M. (1987) *Inorg. Chim. Acta*, **140**, 31–4.

Koltunov, V. S., Baranov, S. M., Zharova, T. P., and Abramina, E. V. (1993) *Radiokhimiya*, **35**, 79–84.
Koltunov, V. S., Taylor, R. J., Baranov, S. M., Mezhov, E. A., and May, I. (1999) *Radiochim. Acta*, **86**, 115–21.
Koltunov, V. S., Taylor, R. J., Baranov, S. M., Mezhov, E. A., Pastuschak, V. G., and May, I. (2000) *Radiochim. Acta*, **88**, 65–70.
Konig, E., Rudowicz, C., and Desai, V. P. (1983) *J. Chem. Phys.*, **78**, 5764–71.
Kraus, K. A. and Nelson, F. (1948) Report AECD-1864.
Krot, N. N. and Gel'man, A. D. (1967) *Dokl. Akad, Nauk SSSR*, **177**, 124–6.
Krot, N. N., Mefodeva, M. P., and Gelman, A. D. (1968a) *Radiokhimiya*, **10**, 634–8.
Krot, N. N., Mefod'eva, M. P., Smirnova, T. V., and Gel'man, A. D. (1968b) *Radiokhimiya*, **10**, 412–8.
Krot, N. N., Mefod'eva, M. P., Zakharova, F. A., Smirnova, T. V., and Gel'man, A. D. (1968c) *Radiokhimiya*, **10**, 630–4.
Krot, N. N., Charushnikova, I. A., Afonas'eva, T. V., and Grigor'eva, M. S. (1993) *Radiokhimiya*, **35**, 14–29.
Kuperman, A. Y., Smirnov, Yu. A., Fedotov, S. N., Nikol'skaya, T. L., and Efimova, N. S. (1988) *Zh. Struk. Khim.*, **30**, 791–7.
LaChapelle, T. J., Magnusson, L. B., and Hindman, J. C. (1947) ANL-4065.
LaChapelle, T. J. (1964) US Patent 3,149,908.
Lahalle, M. P., Krupa, J. C., Guillaumont, R., and Rizzoli, C. (1986) *J. Less -Common Metals*, **122**, 65–73.
Lander, G. H., Dunlap, B. D., Mueller, M. H., Nowik, I., and Reddy, J. F. (1973) *Int. J. Magn.*, **4**, 99–104.
Lander, G. H. and Burlet, P. (1995) *Physica B*, **214**, 7–21.
Laskorin, B. N., Skorovarov, D. I., Filippov, E. A., and Yakshin, V. V. (1985) *Radiokhimiya*, **27**, 156–69.
Lee, A. J., Mardon, P. G., Pearce, J. H., and Hall, R. O. A. (1959) *J. Phys. Chem. Solids*, **11**, 177–81.
Lee, S. C., Hutchinson, J. M. R., Inn, K. G. W., and Thein, M. (1995) *Health Phys.*, **68**, 350–8.
Legin, E. K. (1979) *Radiokhimiya*, **21**, 565–78.
Lemire, R. J., Fuger, J., Nitsche, H., Potter, P., Rand, M. H., Rydberg, J., Spahiu, K., Sullivan, J. C., Ullman, W. J., Vitorge, P., and Wanner, H. (2001) *Chemical Thermodynamics of Neptunium and Plutonium*, Elsevier, Amsterdam.
Levine, C. A. and Seaborg, G. T. (1951) *J. Am. Chem. Soc.*, **73**, 3278–83.
Li, K., Zhang, X., and Dong, W. (1988) *He Huaxue Yu Fangshe Huaxue*, **10**, 107–12.
Li, Y., Kato, Y., and Yoshida, Z. (1993) *Radiochim. Acta*, **60**, 115–9.
Lierse, C., Treiber, W., and Kim, J. I. (1985) *Radiochim. Acta*, **38**, 27–8.
Lloyd, J. R., Yong, P., Macaskie, L. E. (2000) *Environ. Sci. Technol.*, **34**, 1297–301.
Logvis', A. I., Bessonov, A. A., and Krot, N. N. (1994) *Radiokhimiya*, **36**, 6–9.
Lorenzelli, R. (1968) *C. R. Acad. Sci. Paris C*, **226**, 900–2.
Macaskie, L. E. and Basnakova, G. (1998) *Environ. Sci. Technol.*, **32**, 184–7.
Magette, M. and Fuger, J. (1977) *Inorg. Nucl. Chem. Lett.*, **13**, 529–36.
Magnusson, L. B. and La Chapelle, T. J. (1948) *J. Am. Chem. Soc.*, **70**, 3534–8.
Magon, L., Bismondo, A., Tomat, G., and Cassol, A. (1972) *Radiochim. Acta*, **17**, 164–7.

Magon, L., Tomat, G., Bismondo, A., Portanova, R., and Croatto, U. (1974) *Gazz. Chim. Ital.*, **104**, 967.
Maiti, T. C., Kaye, J. H., and Kozelisky, A. E. (1992) *J. Radioanal. Nucl. Chem.*, **161**, 533–40.
Malm, J. G., Weinstock, B., and Weaver, E. E. (1958) *J. Phys. Chem.*, **62**, 1506–8.
Malm, J. G., Williams, C. W., Soderholm, L., and Morss, L. R. (1993) *J. Alloys Compds.*, **194**, 133–7.
Mang, M., Gehmecker, H., Trautmenn, N., and Herrmann, G. (1993) *Radiochim. Acta*, **62**, 49–54.
Marcon, J. P. (1967) *C. R. Acad. Sci. Paris* 265 Series C 235.
Marcon, J. P. and Pascard, R. (1968) *Rev. Int. Hautes Temp. Refract.*, **5**, 51–4.
Marcon, J. P. (1969) Rapport CEA-R 3319.
Mardon, P. G. and Pearce, J. H. (1959) *J. Less Common Metals*, **1**, 467–75.
Marks, T. J. and Ernst, R. D. (1982) in *Comp. Organomet. Chem.* (eds. G. Wilkinson, F. G. A. Stone, and E. W. Abel) Pergamon, Oxford, pp. 211–70.
Marples, J. A. C. (1975) in *Plutonium and Other Actinides* (eds. H. Blank and R. Lindner), North-Holland, Amsterdam, pp. 353–60.
Marquart, R., Hoffman, G., and Weigel, F. (1983) *J. Less Common Metals*, **91**, 119–27.
Martinot, L., Machiels, A., Fuger, J., and Duyckaerts, G. (1970) *Bull. Soc. Chim. Belg.*, **79**, 125–31.
Martinot, L. (1984) Journee d'etude des sels fondus, May 23–25, 1984, Societe Chimie de Belgique, Brussels.
Martinot, L. and Fuger, J. (1985) in *Standard Potentials in Aqueous Solutions* (eds. A. J. Bard, R. Parsons, and J. Jordan), Marcel Dekker, New York.
Martinot, L. (1991) *J. Less Common Metals*, **170**, 121–6.
Maslov, O. D., Dmitriev, S. N., Molokanova, L. G., and Tolmachyov, S. Y. (1997) *J. Radioanal. Nucl. Chem.*, **226**, 181–3.
Mathur, J. N. and Choppin, G. R. (1994) *Radiochim. Acta*, **64**, 175–7.
Mathur, J. N., Murali, M. S., Balarama Krishna, M. V., Iyer, R. H., Chitnis, R. R., Wattal, P. K., Theyyunni, T. K., Ramanujam, A., Dhami, P. S., and Gopalakrishnan, V. (1996a) *Sep. Sci. Technol.*, **31**, 2045–63.
Mathur, J. N., Murali, M. S., Balarama Krishna, M. V., Iyer, R. H., Chitnis, R. R., Wattal, P. K., Bauri, A. K., and Banerji, A. (1996b) *J. Radioanal. Nucl. Chem. Lett.*, **213**, 419–29.
Mathur, J. N., Ruikar, P. B., Balarama Krishna, M. V., Murali, M. S., Nagar, M. S., and Iyer, R. H. (1996c) *Radiochim. Acta*, **73**, 100–206.
Mathur, J. N., Murali, M. S., and Nash, K. L. (2001) *Solv. Extr. Ion Exch.*, **19**, 357–90.
Matsika, S. and Pitzer, R. M. (2000) *J. Phys. Chem.*, **A104**, 4064–8.
Maxwell, S.L., III (1997) *Radioact. Radiochem.*, **8**(4), 36–44.
May, S., Engelmann, Ch., and Pinte, G. (1987) *J. Radioanal. Nucl. Chem. Art.*, **113**, 343–50.
Maya, L. (1983) *Inorg. Chem.*, **22**, 2093–5.
Maya, L. (1984) *Inorg. Chem.*, **23**, 3926–30.
McMillan, E. (1939) *Phys. Rev.*, **55**, 510.
McMillan, E. and Abelson, P. H. (1940) *Phys. Rev.*, **57**, 1185–6.
Mefod'eva, M. P., Krot, N. N., Smirnova, T. V., and Gel'man, A. D. (1969) *Radiokhimiya*, **11**, 193–200.

Mefod'eva, M. P., Krot, N. N., and Gel'man, A. D. (1970a) *Radiokhimiya*, **12**, 232–7.
Mefod'eva, M. P., Krot, N. N., and Gel'man, A. D. (1970b) *Sov. Radiochem.*, **12**, 210–4.
Mefod'eva, M. P. and Gel'man, A. D. (1971) *Radiokhimiya*, **13**, 597–603.
Mefod'eva, M. P., Krot, N. N., Afanas'eva, T. V., and Gel'man, A. D. (1974) *Russ. Chem. Bull.*, **23**, 2285–7.
Mefod'eva, M. P., Krot, N. N., and Gel'man, A. D. (1976) *Radiokhimiya*, **18**, 93–5.
Meresse, Y., Heathman, S., Le Bihan, T., Rebizant, J., Brooks, M. S. S., and Ahuja, R. (2000) *J. Alloys and Compds.*, **296**, 27–32.
Merli, L. and Fuger, J. (1994) *Radiochim. Acta*, **66/67**, 109–13.
Mincher, B. J. (1989) *Solvent Extr. Ion Exch.*, **7**, 45–54.
Mintz, M. H., Hadari, Z., and Bixon, M. (1976) *J. Less Common Metals*, **48**, 183–6.
Mishin, V. Y., Sidorenko, G. V., and Suglobov, D. N. (1986) *Radiokhimiya*, **28**, 292–300.
Mitchell, A. W. and Lam, D. J. (1971) *J. Nucl. Mater.*, **39**, 219–23.
Mohapatra, P. K. and Manchanda, V. K. (1993) *Radiochim. Acta*, **61**, 69–72.
Morita, Y. and Kubota, M. (1988) *Solvent Extr. Ion Exch.*, **6**, 233–46.
Morita, Y., Glatz, J.-P., Kubota, M., Koch, L., Pagliosa, G., Roemer, K., and Nicholl, A. (1996) *Solvent Extr. Ion Exch.*, **14**, 385–400.
Morss, L. R. (1982) in *Actinides – 1981* (ed. N. Edelstein), Pergamon, Oxford, pp. 381–407.
Morss, L. R., Appelman, E. H., Gerz, R. R., and Martin-Rovet, D. (1994) *J. Alloys Compds.*, **203**, 289–95.
Moskvin, A. I. and Peretrukhin, V. F. (1964) *Sov. Radiochem.*, **6**, 198–205.
Moskvin, A. I. (1971) *Sov. Radiochem.*, **13**, 700–5.
Mulford, R. N. R. and Wiewandt, T. A. (1965) *J. Phys. Chem.*, **69**, 1641–4.
Musikas, C. (1963) *Radiochim. Acta*, **1**, 92–8.
Musikas, C., Couffin, F., and Marteau, M. (1974) *J. Chim. Phys.*, **71**, 641–8.
Musikas, G. and Marteau, M. (1978) *Sov. Radiochem.*, **20**, 213–6.
Naegele, J. R., Cox, L. E., and Ward, J. W. (1987) *Inorg. Chim. Acta*, **139**, 327–9.
Nagasaki, S., Tanaka, S., and Takahashi, Y. (1988) *J. Radioanal. Nucl. Chem. Art.*, **124**, 383–95.
Nakada, M., Saeki, M., Masaki, N. M., and Tsutsui, S. (1998) *J. Radioanal. Nucl. Chem.*, **232**, 201–7.
Nakamoto, T., Nakada, M., Masaki, N. M., Saeki, M., and Yamashita, T. (1998) *J. Radioanal. Nucl. Chem.*, **227**, 137–41.
Nakamoto, T., Nakada, M., Masaki, N. M., Saeki, M., Yamashita, T., and Krot, N. N. (1999) *J. Radioanal. Nucl. Chem.*, **239**, 257–61.
Nakamura, T., Takahashi, M., Fukasawa, T., and Utamura, M. (1992) *J. Nucl. Sci. Technol.*, **29**, 393–5.
Nash, K. L. and Choppin, G. R. (1997) *Sep. Sci. Technol.*, **32**, 255–74.
Neck, V., Kim, J. I., and Kanellakopulos, B. (1992) *Radiochim. Acta*, **56**, 25–30.
Neck, V., Kim, J. I., Seidel, B. S., Marquardt, C. M., Dardenne, K., Jensen, M. P., and Hauser, W. (2001) *Radiochim. Acta*, **89**, 439–46.
Nevitt, M. V. (1963) Argonne National Laboratory Report ANL-6868, p. 314.
Newton, T. W. (1975) TID-26506, National Technical Information Service, US Department of Commerce, Springfield, VA.
Niese, U. and Vecernik, J. (1981) *Isotopenpraxis*, **18**, 91–2.
Nikitenko, S. I., Moisy, Ph., and Madic, C. (1999) *Radiochim. Acta*, **86**, 23–31.

Nikonov, M. V., Bessonov, A. A., Krot, N. N., and Perminov, V. P. (1994) *Radiochemistry* (*Moscow*), **36**, 262–3.
Novikov, Y. P., Pavlotskaya, F. I., and Myasoedov, B. F. (1989) *Radiokhimiya*, **31**, 134–42.
Novikov, A. P., Mikheeva, M. N., Gracheva, O. I., and Myasoedov, B. F. (1997) *J. Radioanal. Nucl. Chem.*, **223**, 163–6.
Oddou, J. L., Arons, R. R., Blaise, A., Burlet, P., Colineau, E., Jeandey, C., Ressouche, E., Sanchez, J. P., Larroque, J., Rebizant, J., and Spirlet, J. C. (1994) *J. Magn. and Magn. Mater.*, **135**, 183–90.
OECD/NEA Report (1997) *Actinide Separation Chemistry in Nuclear Waste Streams and Materials*.
OECD/NEA Report (2001) *Evaluation of Speciation Technology*.
Oetting, F. L., Rand, M. H., and Ackermann, R. J. (1976) in *The Chemical Thermodynamics of Actinide Elements and Compounds*, part 1, IAEA, Vienna, pp. 20–3.
Ogawa, T. (1993) *J. Alloys Compds.*, **194**, 1–7.
Olson, W.M. and Mulford, R. N. R. (1966) *J. Phys. Chem. Solids*, **70**, 2932–4.
Pagès, M., Nectoux, F., and Freundlich, W. (1971) *Radiochem. Radioanal. Lett.*, **7**, 155–62.
Palade, D. M. (1997) *Russ. J. Coord. Chem.*, **23**, 636.
Patil, S. K. and Ramakrishna, V. V. (1973) *Radiochim. Acta*, **19**, 27–30.
Patil, S. K. and Ramakrishna, V. V. (1975) *Inorg. Nucl. Chem. Lett.*, **11**, 421–8.
Patil, S. K. and Ramakrishna, V. V. (1976) *J. Inorg. Nucl. Chem.*, **38**, 1075–8.
Patil, S. K., Ramakrishna, V. V., and Gudi, N. M. (1981) in *Proc. Nucl. Chem. Radiochem. Symp. 1980*, Indian Department of Atomic Energy, pp. 388–90.
Paul, M. T. (1970) Report KFK-1210.
Pavlotskaya, F. I. (1997) *J. Anal. Chem.*, **52**, 110–26.
Peacock, R. D. and Edelstein, N. (1976) *J. Inorg. Nucl. Chem.*, **38**, 771–3.
Penneman, R. A., Ryan, R. R., and Rosenzweig, A. (1973) *Struct. Bond*, **13**, 1–52.
Pentreath, R. J. and Harvey, B. R. (1981) *Mar. Ecol. Prog. Ser.* **6**, 243–7.
Peppard, D. F., Studier, M. H., Gergel, M. V., Mason, G. W., Sullivan, J. C., and Mech, J. F. (1951) *J. Am. Chem. Soc.*, **73**, 2529–31.
Peppard, D. F., Mason, G. W., Gray, P. R., and Mech, J. F. (1952) *J. Am. Chem. Soc.*, **74**, 6081–7.
Peretrukhin, V. F. and Alekseeva, D. P. (1974) *Radiokhimiya* **16**, 836–43.
Pilz, N., Hoffmann, P., and Lieser, K. H. (1989) *J. Radioanal. Nucl. Chem. Art.*, **130**, 141–53.
Piskunov, E. M. and Rykov, A. G. (1972) *Sov. Radiochem.*, **14**, 342–4.
Pitzer, K. S. (1979) in *Activity CoeYcients in Electrolyte Solutions,* vol. 1 (ed. R. M. Pytkowicz), CRC Press, Boca Raton, p. 157.
Pollard, P. M., Liezers, M., McMillan, J. M., Phillips, G., Thomason, H. P., and Ewart, F. T. (1988) *Radiochim. Acta*, **44/45**, 95–101.
Portanova, R., Tomat, G., Magon, L., and Cassol, A. (1970) *J. Inorg. Nucl. Chem.*, **32**, 2343–8.
Portanova, R., Tomat, G., Magon, L., and Cassol, A. (1972) *J. Inorg. Nucl. Chem.*, **34**, 1768–70.
Potzel, W., Moser, J., Asch, L., and Kalvius, G. M. (1983) *Hyperfine Interact.*, **13**, 175–98.

Potzel, W., Gleisner, A., Moser, J., Zwirner, S., Potzel, U., Gal, J., and Kalvius, G. M. (1993) *Physica B*, **190**, 98–106.
Pratopo, M. I., Moriyama, H., and Higashi, K. (1989) *Joint Int. Waste Manage. Conf.*, vol. 2, 309–12.
Pribylova, G. A., Chmutova, M. K., and Myasoedov, B. F. (1987) *Radiokhimiya*, **29**, 621–5.
Quill, L. L. (1938) *Chem. Rev.*, **23**, 87–155.
Raghavan, R., Ramakrishna, V. V., and Patil, S. K. (1975) *J. Inorg. Nucl. Chem.*, **37**, 1540–1.
Rai, D. (1984) *Radiochim. Acta*, **35**, 97–106.
Rai, D. and Ryan, J. L. (1985) *Inorg. Chim.*, **24**, 247–51.
Rai, D., Swanson, J. L., and Ryan, J. L. (1987) *Radiochim. Acta*, **42**, 35–41.
Rao, P. R. V., Bagawde, S. V., Ramakrishna, V. V., and Patil, S. K. (1978) *J. Inorg. Nucl. Chem.*, **40**, 339–43.
Rao, P. R. V., Gudi, N. M., Bagawde, S. V., and Patil, S. K. (1979) *J. Inorg. Nucl. Chem.*, **41**, 235–9.
Reavis, J. G., Bowersox, D. F., Christensen, D. C., and Mullins, L. J. (1985) *Radiochim Acta*, **38**, 135–9.
Richter, K. and Sari, C. (1987) *J. Nucl. Mater.*, **148**, 266–71.
Riegel, J., Deissenberger, R., Herrmann, G., Koehler, S., Sattelberger, P., Trautmann, N., Wendeler, H., Ames, F., Kluge, H.-J., Scheerer, F., and Urban, F -J. (1993) *Appl. Phys.*, **B56**, 275–80.
Riggle, K. (1992) DOE/OR/00033-T487.
Riglet, Ch., Vitorge, P., and Grenthe, I. (1987) *Inorg. Chim. Acta*, **133**, 323–9.
Riglet, Ch., Robouch, P., and Vitorge, P. (1989) *Radiochim. Acta*, **46**, 85–94.
Riglet, C., Provitina, O., Dautheribes, J., and Revy, D. (1992) *J. Anal. At. Spectrom.*, **7**, 923–7.
Rizkalla, E. N., Nectoux, F., Dabos-Seignor, S., and Pagès, M. (1990a) *Radiochim. Acta*, **51**, 113–7.
Rizkalla, E. N., Nectoux, F., Dabos-Seignor, S., and Pagès, M. (1990b) *Radiochim. Acta*, **51**, 151–5.
Rodriguez, R. J., Sari, C., and Portal, A. J. C. (1994) *J. Alloys Compds.*, **209**, 263–8.
Rösch, F., Dittrich, S., Buklanov, G. V., Milanov, M., Khalkin, V. A., and Dreyer, R. (1990) *Radiochim. Acta*, **49**, 29–34.
Rosner, G., Winkler, R., and Yamamoto, M. (1993) *J. Radioanal. Nucl. Chem.*, **173**, 273–81.
Rossat-Mignod, J., Lander, G. H., and Burlet, P. (1984) in *Handbook on the Physics and Chemistry of the Actinides,* vol. 1 (eds. A. J. Freeman and G. H. Lander), North-Holland, Amsterdam, pp. 415–500.
Rossat-Mignod, J., Burlet, P., Fournier, J. M., Pleska, E., and Quezel, S. (1989) *J. Nucl. Mater.*, **166**, 56–8.
Roy, J. J., Grantham, L. F., Grimmett, D. L., Fusselman, S. P., Krueger, C. L., Storvick, T. S., Inoue, T., Sakamura, Y., and Takahashi, N. (1996) *J. Electrochem. Soc.*, **143**, 2487–92.
Rozen, A. M. and Nikolotova, Z. I. (1988) *Radiokhimiya*, **30**, 594–606.
Rozen, A. M., Nikolotova, Z. I., and Kartasheva, N. A. (1988) *Radiokhimiya*, **30**, 614–8.

Rozen, A. M., Nikoforov, A. S., Kartasheva, N. A., Nikolotova, Z. I., and Tananaev, I. G. (1990) *Dokl. Akad. Nauk SSSR*, **312**, 897–900.
Rozen, A. M., Nikolotova, Z. I., Kartasheve, N. A., and Tananaev, I. G. (1992) *Radiokhimiya*, **34**, 54–7.
Rush, R. M., Johnson, J. S., and Kraus, K. A. (1962) *Inorg. Chem.*, **1**, 378–86.
Rush, R. M. and Johnson, J. S. (1963) *J. Phys. Chem.*, **67**, 821–5.
Ryan, J. L. and Rai, D. (1987) *Inorg. Chem.*, **26**, 4140–2.
Rykov, A. G. and Frolov, A. A. (1972) *Radiokimiya*, **14**, 717–21.
Rykov, A. G., Blokhin, N. B., and Vasilev, V. Y. (1973) *Radiokimiya*, **15**, 341–7.
Saeki, M., Nakada, M., Nakamoto, T., Yamashita, T., Masaki, N. M., and Krot, N. N. (1999) *J. Radioanal. Nucl. Chem.*, **239**, 221–5.
Saeki, M. (2003) unpublished work, provided for this chapter after revision of the figure in Saeki *et al.* (1999).
Saito, T., Wang, J., Kitazawa, T., Takahashi, M., Takeda, M., Nakada, M., Nakamoto, T., Masaki, N. M., Yamashita, T., and Saeki, M. (1999) *J. Radioanal. Nucl. Chem.*, **239**, 319–23.
Sakamura, Y., Hijikata, T., Kinoshita, K., Inoue, T., Storvick, T. S., Krueger, C. L., Roy, J. J., Grimmett, D. L., Fusselman, S. P., and Gay, R. L. (1998) *J. Alloys Compds.*, **271–273**, 592–6.
Sakamura, Y., Shirai, O., Iwai, T., and Suzuki, Y. (2000) *J. Electrochem. Soc.*, **147**, 642–9.
Sanchez, J. P., Rebizant, J., and Spirlet, J. C. (1988) *Phys. Lett. A*, **128**, 297–301.
Sanchez, J. P., Bouillet, M. N., Colineau, E., Blaise, A., Amanowicz, M., Burlet, P., Fournier, J. M., Charvolin, T., and Larroque, J. (1993) *Physica B*, **186/188**, 675–7.
Sanchez, J. P., Colineau, E., Jeandey, C., Oddou, J. L., Rebizant, J., Seret, A., and Spirlet, J. C. (1995) *Physica B*, **206/7**, 531–3.
Sandenaw, T. A., Gibney, R. B., and Holley, C. E. (1973) *J. Chem. Thermodyn.*, **5**, 41–7.
Sawant, R. M., Chaudhuri, N. K., Rizvi, G. H., and Patil, S. K. (1985) *J. Radioanal. Nucl. Chem.*, **91**, 41–58.
Schafer, W., Will, G., Gal, J., and Suski, W. (1989) *J. Less Common Metals*, **149**, 237–41.
Schmidt, K. H., Gordon, S., Thompson, R. C., and Sullivan, J. C. (1980) *J. Inorg. Nucl. Chem.*, **42**, 611–5.
Schmidt, K. H., Gordon, S., Thompson, M. C., and Sullivan, J. C. (1983) *Radiat. Phys. Chem.*, **21**, 321–8.
Schneider, R. A. and Harmon, K. M. (1961) USAEC Report HW-53368.
Schoebrechts, J. P., Gens, R., Fuger, J., and Morss, L. R. (1989) *Thermochim. Acta*, **139**, 49–66.
Schrepp, W., Stumpe, R., Kim, J. I., and Walther, H. (1983) *Appl. Phys.*, **B32**, 207–9.
Seaborg, G. T. and Perlman, M. L. (1948) *J. Am. Chem. Soc.*, **70**, 1571–3.
Seaborg, G. T. and Brown, H. S. (1961) US Patent No. 2,982,604.
Segrè, E. (1939) *Phys. Rev.*, **55**, 1104–5.
Seranno, J. G. and Kimura, T. (1993) *J. Radioanal. Nucl. Chem. Art.*, **172**, 97–105.
Seret, A., Wastin, F., Waerenborgh, J. C., Zwirner, S., Spirlet, J. C., and Rebizant, J. (1995) *Physica B*, **206/7**, 525–7.
Sevost'yanova, E. P. and Khalturin, G. V. (1976) *Sov. Radiochem.*, **18**, 738–43.
Sheft, I. and Fried, S. (1953) *J. Am. Chem. Soc.*, **75**, 1236–7.
Shilin, I. V. and Nazarov, V. K. (1966) *Sov. Radiochem.*, **8**, 474–8.

Shiloh, M. and Marcus, Y. (1966) *J. Inorg. Nucl. Chem.*, **28**, 2725–32.
Shilov, V. P., Tananaev, I. G., and Krot, N. N. (1991) *Sov. Radiochem.*, **33**, 250–1.
Shinohara, N., Kohno, N., Suzuki, S., and Usuda, S. (1989) *J. Radioanal. Nucl. Chem.*, **130**, 3–12.
Shirai, O., Iizuka, M., Iwai, T., and Arai, Y. (2001) *J. Appl. Electrochem.*, **31**, 1055–60.
Smith, R. M. and Martell, A. E. (2002) in *NIST Critically Selected Stability Constants of Metal Complexes: Version 6.0*, National Institute of Standards and Technology, Geithersburg.
Soderholm, L., Antonio, M. R., Williams, C., and Wasserman, S. R. (1999) *Anal. Chem.*, **71**, 4622–8.
Spirlet, T. E., Bednarcyk, J., Rebizant, J., and Walker, C. T. (1980) *J. Crystal Growth*, **49**, 171–2.
Spirlet, J. C. and Vogt, O. (1984) in *Handbook on the Physics and Chemistry of the Actindes* (eds. A. J. Freeman and G. H. Landers), Elsevier, Amsterdam, pp. 79–151.
Spirlet, M-R., Jemine, X., and Goffart, J. (1994) *J. Alloys Compds.*, **216**, 269–72.
Spitsyn, V. I., Gelman, A. D., Krot, N. N., Mefodiyeva, M. P., Zakharova, F. A., Komkov, Yu. A., Shilov, V. P., and Smirnova, I. V. (1969) *J. Inorg. Nucl. Chem.*, **31**, 2733–45.
Spitsyn, V. I. and Ionova, G. V. (1987) *Dokl. Akad. Nauk SSSR*, **292**, 412–5.
Stafsudd, O. M., Leung, A. F., and Wong, E. Y. (1969) *Phys. Rev.*, **180**, 339–43.
Stepanov, A. V., Nikitina, S. A., Karasev, V. T., Stepanov, D. A., Karmanova, V. Yu., Aleksandruk, V. M., and Dem'yanova, T. A. (1997) *Z. Anal. Khim.*, **52**, 144–9.
Stephens, W. R. (1966) *J. Phys. Chem. Solids*, **27**, 1201–4.
Stewart, G. R., Andraka, B., and Haire, R. G. (1994) *J. Alloys Compds.*, **213/214**, 111–3.
Stone, J. A., Pillinger, W. L., and Karraker, D. G. (1969) *Inorg. Chem.*, **8**, 2519–20.
Stout, B. E., Cacceci, M. S., Nectoux, F., and Pagès, M. (1989) *Radiochim. Acta*, **46**, 181–4.
Stout, B. E., Choppin, G. R., Nectoux, F., and Pagès, M. (1993) *Radiochim. Acta*, **61**, 65–7.
Stromatt, R. W. (1959) USAEC Report HW-59447.
Sudakov, L. V., Solnstsev, V. M., Kapshukov, I. I., Belyaev, Y. I., and Chistyakov, V. M. (1972) V. I. Lenin Scientific Research Institute for Atomic Reactors, Report NIIAR-P-138, Dimitrovgrad, Argonne National Laboratory Trans-935.
Sullivan, J. C. and Hindman, J. C. (1959) *J. Phys. Chem.*, **63**, 1332–3.
Sullivan, J. C., Hindman, J. C., and Zielen, A. J. (1961) *J. Am. Chem. Soc.*, **83**, 3373–8.
Sullivan, J. C. (1962) *J. Am. Chem. Soc.*, **84**, 4256–8.
Sullivan, J. C. (1964) *Inorg. Chem.*, **3**, 315–9.
Sus, F., Parus, J. L., and Raab, W. (1996) *J. Radioanal. Nucl. Chem. Art.*, **211**, 363–74.
Suzuki, Y., Arai, Y., Okamoto, Y., and Ohmichi, T. (1994) *J. Nucl. Sci. Tech.*, **31**, 677–80.
Suzuki, Y. and Arai, Y. (1998) *J. Alloys Compds.*, **271–273**, 577–82.
Tabuteau, A. and Pagès, M. (1985) in *Handbook on the Physics and Chemistry of the Actinides,* vol. 3 (eds. A. J. Freeman and C. Keller), North-Holland, Amsterdam, pp. 184–241.
Tait, C. D., Palmer, P. D., Ekberg, S. A., and Clark, D. L. (1995) Los Alamos National Laboratory Report LA-13012-MS.

Takeishi, H., Kitatsuji, Y., Kimura, T., Meguro, Y., Yoshida, Z., and Kihara, S. (2001) *Anal. Chim. Acta*, **431**, 69–80.
Taylor, R. J., Denniss, I. S., and Wallwork, A. L. (1997) *Nucl. Energy*, **36**, 39–46.
Taylor, R. J., May, I., Koltunov, V. S., Baranov, S. M., Marchenko, V. I., Mezhov, E. A., Pastuschak, V. G., Zhuravleva, G. I., and Savilova, O. A. (1998a) *Radiochim. Acta*, **81**, 149–56.
Taylor, R. J., May, I., Wallwork, A. L., Denniss, I. S., Hill, N. J., Galkin, B. Ya., Zilberman, B. Ya., and Fedorov, Yu. S. (1998b) *J. Alloys Compds.*, **271–273**, 534–7.
Thévenin, T. and Pagès, M. (1982) *J. Less Common Metals*, **84**, 133–7.
Thévenin, T., Jovè, J., and Pagès, M. (1985) *Mat. Res. Bull.*, **20**, 723–30.
Tochiyama, O., Inoue, Y., and Kuroki, Y. (1989) *Solvent Extr. Ion Exch.*, **7**, 289–314.
Tochiyama, O., Inoue, Y., and Narita, S. (1992) *Radiochim. Acta*, **58/59**, 129–36.
Tomilin, S. V., Volkov, Y. F., Visyashcheva, G. I., and Kapshukov, I. I. (1984) *Radiokhimiya*, **26**, 734–9.
Tomilin, S. V., Volkov, Y. F., Melkaya, R. F., Spiryakov, V. I., and Kapshukov, I. I. (1986) *Radiokhimiya*, **28**, 696–700.
Trevorrow, L. E., Gerding, T. J., and Steindler, M. J. (1968) *J. Inorg. Nucl. Chem.*, **30**, 2671–7.
Tsivadze, A. Y. and Krot, N. N. (1972) *Radiokimiya*, **14**, 629–33.
Uchiyama, G., Fujine, S., Hotoku, S., and Maeda, M. (1993) *Nucl. Technol.*, **102**, 341–51.
Uchiyama, G., Asakura, T., Hotoku, S., and Fujine, S. (1998a) *Solvent Extr. Ion Exch.*, **16**, 1191–213.
Uchiyama, G., Kihara, T., Hotoku, S., Fujine, S., and Maeda, M. (1998b) *Radiochim. Acta*, **81**, 29–32.
Van Der Sluys, W. G., Burns, C. J., and Smith, D. C. (1992) Patent No. 67487.
Varga, L. P., Reisfeld, M. J., and Asprey, L. B. (1970) *J. Chem. Phys.*, **53**, 250–5.
Varlashkin, P. G., Hobart, D. E., Begun, G. M., and Peterson, J. R. (1984) *Radiochim. Acta*, **35**, 91–6.
Vogt, O. and Mattenberger, K. (1994) *J. Alloys Compds.*, **213/214**, 248–53.
Volkov, Y. F., Melkaya, R. F., Spiryakov, V. I., and Timofeev, G. A. (1994) *Radiokhimiya*, **36**, 205–8.
Wada, Y., Morimoto, K., Goibuchi, T., and Tomiyasu, H. (1995) *J. Nucl. Sci. Technol.*, **32**, 1018–26.
Wada, Y., Morimoto, K., and Tomiyasu, H. (1996) *Radiochim. Acta*, **72**, 195–204.
Waggener, W. C. (1958) *J. Phys. Chem.*, **62**, 382–3.
Ward, J. W., Bartscher, W., and Rebizant, J. (1987) *J. Less Common Metals*, **130**, 431–89.
Wastin, F., Rebizant, J., Sprilet, J. C., Sari, C., Walker, C. T., and Fuger, J. (1993) *J. Alloys Compds.*, **196**, 87–92.
Weigel, F. and Hellmann, H. (1986) *J. Less Common Metals*, **121**, 415–23.
Wester, D. W., Mulak, J., Banks, R., and Carnall, W. T. (1982) *J. Solid State Chem.*, **45**, 235–40.
Williams, C. W., Blauden, J.-P., Sullivan, J. C., Antonio, M. R., Bursten, B., and Soderholm, L. (2001) *J. Amer. Chem. Soc.*, **123**, 4346–7.
Wisnubroto, D. S., Ikeda, H., and Suzuki, A. (1991) *J. Nucl. Sci. Technol.*, **28**, 1100–06.

Wittenberg, L. J., Vaughn, G. A., and De Witt, R. (1970) *Nucl. Metall. Met. Soc. AIME*, **17**, 659–68.
Wojakowski, A. and Damien, D. (1982) *J. Less Common Metals*, **83**, 263–7.
Yaar, I., Gal, J., Potzel, W., Kalvius, G. M., Will, G., and Schafer, W. (1992) *J. Magn. Magn. Mater.*, **104/7**, 63–4.
Yakovlev, N. G. and Kosyakov, V. N. (1991) *Radiokhimiya*, **33**, 82–7.
Yamamoto, M., Chatani, K., Komura, K., and Ueno, K. (1989) *Radiochim. Acta*, **47**, 63–8.
Yamamoto, M., Kofuji, H., Tsumura, A., Yamasaki, S., Yuita, K., Komamura, M., Komura, K., and Ueno, K. (1994) *Radiochim. Acta*, **64**, 217–24.
Yamana, H., Yamamoto, T., Kobayashi, K., Mitsugashira, T., and Moriyama, H. (2001) *J. Nucl. Sci. Tech.*, **38**, 859–65.
Yang, D., Zhu, Y., and Jiao, R. (1994) *J. Radioanal. Nucl. Chem Art.*, **183**, 245–60.
Yarbo, S. L., Dunn, S. L., and Schreiber, S. B. (1991) LA-11890.
Yoshida, Z., Aoyagi, H., and Kihara, S. (1991) *Fresenius J. Anal. Chem.*, **340**, 403–9.
Zachariasen, W. H. (1949a) *Acta Crystallogr.*, **2**, 291–6.
Zachariasen, W. H. (1949b) *Acta Crystallogr.*, **2**, 60–2.
Zachariasen, W. H. (1952) *Acta Crystallogr.*, **5**, 644–67.
Zantuti, F., Ivanova, S. A., Novikov, Y. P., and Myasoedov, B. F. (1990) *J. Radioanal. Nucl. Chem.*, **143**, 397–401.
Zhao, J., Mao, X., Jin, X., Guo, G., and Fu, Y. (1991) *Microchem. J.*, **44**, 59–62.
Zhu, Y. and Song, C. (1992) in *Transuranium Elements, A Half Century* (eds. L. R. Morss and J. Fuger), American Chemical Society Books, Washington DC, ch. 32.
Zwick, B. D., Sattelberger, A. P., and Avens, L. R. (1992) in *Transuranium Elements* (eds. L. R. Morss and J. Fuger), American Chemical Society, pp. 240–6.
Zwirner, S., Spirlet, J. C., Rebizant, J., Potzel, W., Kalvius, G. M., Geibel, C., and Steglich, F. (1993) *Physica B*, **186/8**, 681–3.

CHAPTER SEVEN

PLUTONIUM

David L. Clark, Siegfried S. Hecker, Gordon D. Jarvinen, and Mary P. Neu

7.1 INTRODUCTION

The element plutonium occupies a unique place in the history of chemistry, physics, technology, and international relations. After the initial discovery based on submicrogram amounts, it is now generated by transmutation of uranium in nuclear reactors on a large scale, and has been separated in ton quantities in large industrial facilities. The intense interest in plutonium resulted from the dual-use scenario of domestic power production and nuclear weapons – drawing energy from an atomic nucleus that can produce a factor of millions in energy output relative to chemical energy sources. Indeed, within 5 years of its original synthesis, the primary use of plutonium was for the release of nuclear energy in weapons of unprecedented power, and it seemed that the new element might lead the human race to the brink of self-annihilation. Instead, it has forced the human race to govern itself without resorting to nuclear war over the past 60 years. Plutonium evokes the entire gamut of human emotions, from good to evil, from hope to despair, from the salvation of humanity to its utter destruction. There is no other element in the periodic table that has had such a profound impact on the consciousness of mankind.

In 2005, approximately 2000 metric tons of plutonium exist throughout the world in the form of used nuclear fuel, nuclear weapons components, various nuclear inventories, legacy materials, and wastes (Albright and Kramer, 2004). This number grows every year by 70 to 75 metric tons through production in

irradiated nuclear fuels (Albright and Kramer, 2004). It is clear that the large inventories of plutonium must be prudently managed for many centuries. A complex blend of global political, socioeconomic, and technological challenges must be dealt with to manage these inventories efficiently and safely.

From physical, chemical, and technological perspectives, plutonium is one of the most complex and fascinating elements in the periodic table. The metal exhibits six solid allotropes at ambient pressure and its phases are notoriously unstable with temperature, pressure, chemical additions, and time. With little provocation, the metal can change its density by as much as 25%. It can be as brittle as glass or as malleable as aluminum; it expands when it solidifies, and its freshly machined surface will tarnish in minutes. It is highly reactive in air, has five chemical oxidation states (six if the metal is included), and can form numerous compounds and complexes in the environment and during chemical processing. Plutonium's continuous radioactive decay causes self-irradiation damage of the metal lattice, or modification of solutions containing plutonium ions. Plutonium sits near the middle of the actinide series, which marks the emergence of 5f electrons in the valence shell. Elements to the left of plutonium have delocalized (bonding) electrons, while elements to the right of plutonium exhibit more localized (nonbonding) character. Plutonium is poised in the middle, and in the δ-phase metal, the electrons seem to be in a unique state of being neither fully bonding nor localized, a property that leads to novel electronic interactions and unusual physical and chemical behavior. This position in the periodic table challenges our understanding of relativistic electronic interactions and the nature of chemical bonding in heavy element metals, compounds, and complexes. When the unique nuclear properties are also considered, the study of plutonium is inherently multidisciplinary in nature. The present discussion will be confined to the most recent aspects of the subject. Reviews describing aspects of the chemistry and physics of plutonium can be found by Keller (1971), Cleveland (1979), Wick (1980), Cooper and Schecker (2000), Hecker (2003), Hecker *et al.* (2004), and in the *Gmelin Handbook of Inorganic Chemistry* (Koch, 1972, 1976a,b).

7.2 HISTORICAL

When the first of the transuranium elements, neptunium (Chapter 6) was discovered, it was realized that the radioactive β decay of $^{239}_{93}$Np should lead to the formation of element 94. The scale of the experiments at that time, however, precluded its identification. Plutonium was first produced late in 1940 by Seaborg, McMillan, Kennedy, and Wahl (Seaborg *et al.*, 1946, 1949a) by bombarding uranium with deuterons to produce the isotope ^{238}Pu:

$$^{238}_{92}\mathrm{U} + {}^{2}_{1}\mathrm{H} \rightarrow {}^{238}_{93}\mathrm{Np} + 2\,{}^{1}_{0}\mathrm{n} \tag{7.1}$$

$$^{238}_{93}\mathrm{Np} \xrightarrow[2.1\mathrm{d}]{\beta^-} {}^{238}_{94}\mathrm{Pu}\ (t_{1/2} = 87.7\,\text{years}) \tag{7.2}$$

The short half-life of ^{238}Pu was conducive to tracer studies, and allowed Seaborg, Wahl, and Kennedy to obtain enough chemical information for subsequent separation and isolation of other plutonium isotopes. The isotope of major importance, ^{239}Pu, was discovered in 1941. Bombardment of $^{238}_{92}$U by neutrons produced $^{239}_{92}$U, which decayed to $^{239}_{93}$Np, and ultimately to $^{239}_{94}$Pu:

$$^{238}_{92}\mathrm{U} + {}^{1}_{0}\mathrm{n} \rightarrow {}^{239}_{92}\mathrm{U} + \gamma \tag{7.3}$$

$$^{239}_{92}\mathrm{U} \xrightarrow[23.5\ \mathrm{min}]{\beta^-} {}^{239}_{93}\mathrm{Np} \xrightarrow[2.36\,\mathrm{days}]{\beta^-} {}^{239}_{94}\mathrm{Pu}\,(t_{1/2} = 24,110\ \text{years}) \tag{7.4}$$

In 1941 Kennedy, Seaborg, Segré, and Wahl established the fissionability of ^{239}Pu with slow neutrons (Kennedy *et al.*, 1941). This crucial experiment revealed the potential of ^{239}Pu as a nuclear energy source. In March 1942, element 94 was christened 'plutonium' with the chemical symbol 'Pu' (Seaborg and Wahl, 1948a). Plutonium was named after the planet Pluto, following the pattern used in naming neptunium.

In August 1942, Cunningham and Werner, working at the wartime Metallurgical Laboratory at the University of Chicago, succeeded in isolating about 1 μg of $^{239}_{94}$Pu, which was prepared by cyclotron irradiation of 90 kg of uranyl nitrate (Cunningham and Werner, 1949a). This experiment made plutonium the first man-made element to be obtained (as Pu(IV) iodate) in a visible quantity. These same investigators carried out the first weighing of this man-made element using a larger sample size of 2.77 μg, on September 10, 1942.

Plutonium is now produced in much larger quantities than any other synthetic element. The large wartime chemical separation plant at Hanford, Washington, was constructed on the basis of investigations performed on the ultramicro chemical scale of investigation. The scale-up between ultramicro chemical experiments and the final Hanford plant corresponds to a factor of about 10^{10} (Seaborg, 1958). Seaborg and Cunningham give detailed first-hand accounts of the early history of plutonium in the *Proceedings of the 1963 Plutonium Chemistry Symposium* (1963). More recent descriptions of this fascinating history have been given by Seaborg (1977, 1978, 1979, 1980, 1983, 1992, 1995), Seaborg and Katz (1990), Seaborg and Loveland (1990), and by Hoffman *et al.* (2000).

7.3 NUCLEAR PROPERTIES

Numerous isotopes of plutonium have been synthesized, all of which are radioactive. These are listed in Table 7.l. The most recent isotope to be discovered is ^{231}Pu, which was reported in 1999 (Laue *et al.*, 1999). For data on nuclear masses the reader is referred to the compilation by Audi and Wapstra (1995),

Table 7.1 *Radioactive decay properties of plutonium isotopes*[a].

Mass number	*Half-life*	*Mode of decay*	*Main radiations* (MeV)	*Method of production*
228	1.1 s	α	α 7.772	^{198}Pt(^{34}S,4n)
229	–	α	α 7.460	^{207}Pb(^{26}Mg,4n)
230	2.6 min	EC, α	α 7.055	^{208}Pb(^{26}Mg,4n)
231	8.6 min	EC 90% α 10%	α 6.72	^{233}U(^{3}He,5n)
232	33.1 min	EC ≥80% α ≤20%	α 6.600 (62%) 6.542 (38%)	^{233}U(α,5n)
233	20.9 min	EC 99.88% α 0.12%	α 6.30 γ 0.235	^{233}U(α,4n)
234	8.8 h	EC 94% α 6%	α 6.202 (68%) 6.151 (32%)	^{233}U(α,3n)
235	25.3 min	EC >99.99% α 3×10^{-3}%	α 5.850 (80%) γ 0.049	^{235}U(α,4n)
236	2.858 yr 1.5×10^{9} yr	α SF 1.37×10^{-7}%	α 5.768 (69%) 5.721 (31%)	^{235}U(α,3n) ^{236}Np daughter
237	45.2 d	EC >99.99% α 4.24×10^{-3}%	5.356 (∼17.2%) 5.334 (∼43.5%)18 γ 0.059	^{235}U(α,2n) ^{237}Np(d,2n)
238	87.7 yr 4.77×10^{10} yr	α SF 1.85×10^{-7}%	α 5.499 (70.9%) 5.456 (29.0%)	^{242}Cm daughter ^{238}Np daughter
239	2.411×10^{4} yr 8×10^{15} yr	α SF 3.0×10^{-10}%	α 5.157 (70.77%) 5.144 (17.11%) 5.106 (11.94%) γ 0.129	^{239}Np daughter
240	6.561×10^{3} yr 1.15×10^{11} yr	α SF 5.75×10^{-6}%	α 5.168 (72.8%) 5.124 (27.1%)	multiple n capture
241	14.35 yr	β$^-$ >99.99% α 2.45×10^{-3}% SF 2.4×10^{-14}%	α 4.896 (83.2%) 4.853 (12.2%) β$^-$ 0.021 γ 0.149	multiple n capture
242	3.75×10^{5} yr 6.77×10^{10} yr	α SF 5.54×10^{-4}%	α 4.902 (76.49%) 4.856 (23.48%)	multiple n capture
243	4.956 h	β$^-$	β$^-$ 0.582 (59%) γ 0.084 (23%)	multiple n capture
244	8.08×10^{7} yr 6.6×10^{10} yr	α 99.88% SF 0.1214%	α 4.589 (81%) 4.546 (19%)	multiple n capture
245	10.5 h	β$^-$	β$^-$ 0.878 (51%) γ 0.327 (25.4%)	^{244}Pu(n,γ)
246	10.84 d	β$^-$	β$^-$ 0.15 (91%) γ 0.224 (25%)	^{245}Pu(n,γ)
247	2.27 d	β$^-$		multiple n capture

[a] See Appendix II.

and the update by Audi *et al.* (1997). A more detailed description of the nuclear properties of the individual plutonium isotopes may be found in the book by Hyde *et al*. (1964), in the *Table of Isotopes* (Firestone *et al.*, 1996, 1998), and in *Nuclear Data Sheets* (Tuli, 2004). As mentioned above, ^{238}Pu was the first of the plutonium isotopes discovered. Because of its relatively short half-life, it is a particularly useful tracer for plutonium. ^{238}Pu is readily obtained by neutron bombardment of ^{237}Np in the reaction:

$$^{237}\mathrm{Np}(\mathrm{n},\gamma)^{238}\mathrm{Np} \xrightarrow{\beta^-} {}^{238}\mathrm{Pu} \tag{7.5}$$

The ^{238}Pu is chemically separated from unreacted ^{237}Np by ion-exchange techniques (Burney, 1962; Tetzlaff, 1962; Coogler *et al.*, 1963; Burney and Thompson, 1972, 1974). ^{238}Pu may also be obtained from the α decay of ^{242}Cm and subsequent chemical separation from undecayed curium (Thompson, 1972). Because of its power density of 6.8–7.3 W cm^{-3} (specific power 0.57 W g^{-1}), ^{238}Pu has found important applications in radioisotope power systems – nuclear power systems that derive their energy from the spontaneous decay of radionuclides as distinguished from nuclear fission energy created in a nuclear reactor. Most radioisotope power systems utilize ^{238}Pu as an isotope heat source and an energy conversion system to partially transform the heat produced from ^{238}Pu radioactive decay into electricity (Lange and Mastal, 1994).

In the late 1960s, cardiac pacemakers suffered from early battery exhaustion, and the use of nuclear pacemakers whose battery life could outlive the patient was examined (Boucher and Quere, 1981; Pustovalov *et al.*, 1986). The first implantation of a ^{238}Pu-powered nuclear pacemaker was performed in France on April 27, 1970. Since that time, nuclear pacemakers powered by ^{238}Pu were implanted in patients in a number of countries. The overall results of these studies indicated that nuclear pacemakers required fewer follow-up operations and less maintenance, and were found to be safe and reliable. Subsequent advances in electronics in the intervening years rendered the plutonium-powered devices obsolete, and their use was discontinued. In 2004, there were still a number of living patients with ^{238}Pu pacemakers that had been functioning for over 30 years (Parsonnet *et al.*, 1990; Freedberg *et al.*, 1992; Parsonnet, 2004).

The most prevalent application for ^{238}Pu is as an important fuel for heat and power sources for space exploration (Lange and Mastal, 1994; Rinehart, 2001). For space exploration, heat source fuel is normally enriched to 83.5% in the ^{238}Pu isotope, and the oxygen atoms in $^{238}PuO_2$ are enriched in ^{16}O to reduce the neutron emission rate to as low as 6000 n s^{-1} g^{-1} ^{238}Pu. In freshly prepared fuel, the specific power is 0.4743 W g^{-1} Pu or 0.4181 W g^{-1} PuO_2. The ^{238}Pu isotope provides 99.9% of the thermal power in heat source fuel. Radioisotope thermoelectric generators (RTGs) have been used in the United States to provide electrical power for spacecraft since 1961 (Angelo and Buden, 1985). Early ^{238}Pu-fueled power sources employed Space Nuclear Auxiliary Power (SNAP) units to power satellites and remote instrument packages (DOE, 1987;

Lange and Mastal, 1994). SNAP units served as power sources for instrument packages on the five Apollo missions to the Moon, the Viking unmanned Mars Lander, and the Pioneer and Voyager probes to the outer planets (Jupiter, Saturn, Uranus, Neptune and beyond). The SNAP-3B and SNAP-9A systems were fueled with plutonium metal, the SNAP-19 and Transit systems were fueled with $^{238}PuO_2$–molybdenum cermets, and the SNAP-27 unit was fueled with $^{238}PuO_2$ microspheres (Rinehart, 2001). Voyager missions employed Multihundred Watt Radioisotope Thermoelectric Generators (MHW-RTGs) that consisted of 24 100-W heat sources of $^{238}PuO_2$ (Fig. 7.1) each enclosed in an iridium shell, a graphitic impact material, an ablative heat shield, and a thermoelectric material to convert the decay heat to electrical power at a design voltage of 30 V (Kelly, 1975; De Winter *et al.*, 1999).

The current systems employ General Purpose Heat Source-Radioisotope Thermoelectric Generators (GPHS-RTGs) fueled by $^{238}PuO_2$ pellets. Each GPHS consists of a hot-pressed 150 g pellet of $^{238}PuO_2$ encapsulated in an iridium alloy (iridium-0.3% tungsten) container or clad (Fig. 7.2). Each iridium

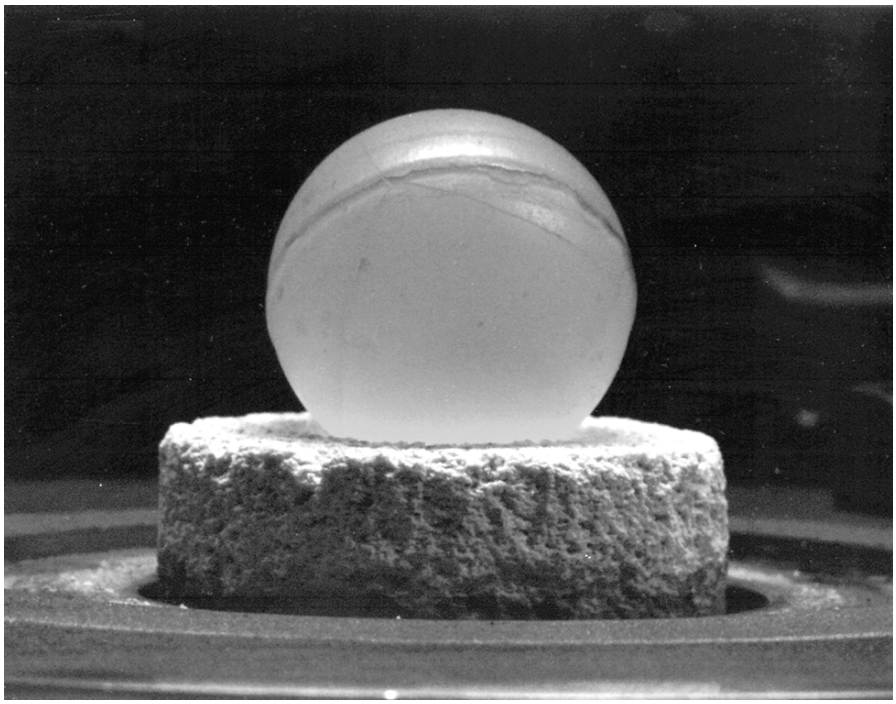

Fig. 7.1 *A* 100 W ^{238}*Pu heat source used in multihundred watt radioisotope thermoelectric generators* (*MHW-RTGs*) *employed in the Voyager space missions. The source contains* 250 g *of* $^{238}PuO_2$ *and was approximately* 3 cm *in diameter. The oxide glowed at red heat after being covered with an insulating ceramic blanket that was removed just before the photograph was taken* (*photograph courtesy of Los Alamos National Laboratory*).

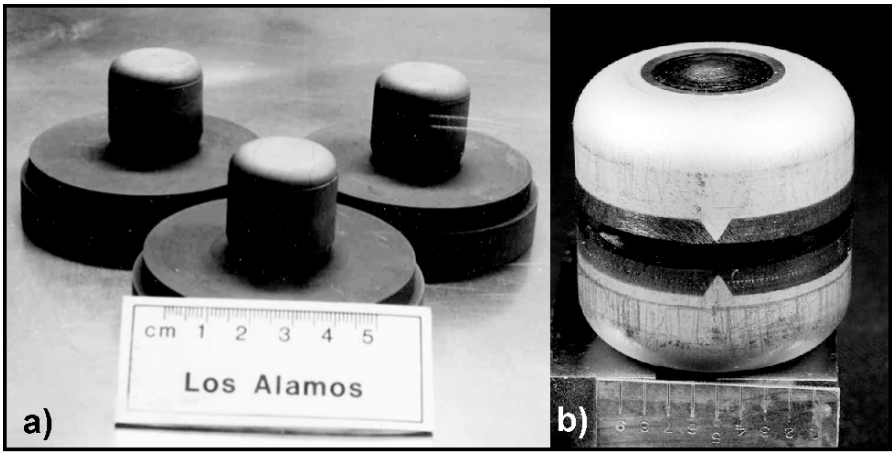

Fig. 7.2 *A modern* ^{238}*Pu general purpose heat source* (*GPHS*). *Hot pressed* 150 g *pellets of* $^{238}PuO_2$ *are* (*a*) *encapsulated in an iridium*-0.3% *tungsten alloy container, which is then encapsulated in* (*b*) *an iridium clad. Each iridium clad contains a sintered iridium powder frit vent designed to release the helium generated by the* α*-particle decay of the fuel. The iridium is compatible with plutonium dioxide at temperatures greater than* 1773 K, *and melts at* 2698 K. *Each GPHS produces* 62.5 *thermal watts* (*photographs courtesy of Los Alamos National Laboratory*).

clad contains a sintered iridium powder frit vent designed to release the helium generated by the α-particle decay of the $^{238}PuO_2$. The heat sources are packed in a tightly woven pierced fabric™ graphite aeroshell assembly that protects the fuel from impact, fire, or atmospheric reentry. The RTG consists of 72 GPHS pellets and a thermoelectric converter. The GPHS-RTGs flown on the Galileo, Ulysses, and Cassini spacecraft (3 RTGs per spacecraft) had a mass of 54 kg of PuO_2 and supplied 285 W of electrical power at the beginning of the mission from 4300 W of ^{238}Pu decay heat (Rinehart, 2001). These plutonium power sources have enabled huge advances in our scientific understanding of the solar system. The Cassini–Huygens spacecraft arrived at Saturn on June 30, 2004, and will provide vast amounts of new scientific data on the Saturnian system in the years to come.

Smaller Light Weight Radioisotope Heater Units (LWRHUs) are also used to maintain spacecraft equipment within their normal operating temperature range (Rinehart, 1992). The LWRHUs are cylindrical fueled clads consisting of a hot-pressed, 2.67 g pellet of $^{238}PuO_2$ encapsulated in a Pt-30%Rh container with a sintered platinum powder frit vent to release helium as shown in Fig. 7.3. As in the GPHS, the capsules are contained in a pyrolytic graphite insulator and aeroshell assembly (Rinehart, 2001). These smaller heater units have been employed on the Pioneer 10 and 11, Galileo, Mars Pathfinder, Mars Exploration Rovers (Spirit and Opportunity), and Cassini spacecraft, and are planned for use in many future missions.

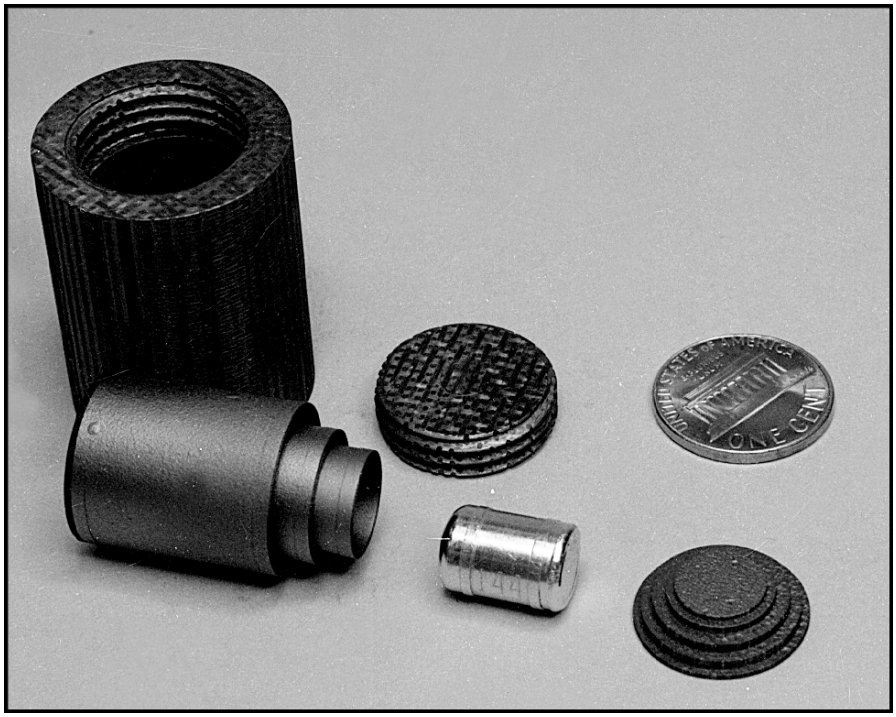

Fig. 7.3 *A* ^{238}*Pu lightweight radioisotope heater unit* (*LWRHU*) *before final assembly. The heat source consists of a fine weave pierced fabric graphite aeroshell, three inner layers of pyrolytic graphite thermal insulators, and a Pt-30% Rh-fueled clad containing a hot pressed* 2.67 g *pellet of* $^{238}PuO_2$ *that produces* 1 *thermal watt. The aeroshell serves as the primary heat shield to protect the interior components from aerodynamic forces and thermal heating during accidental atmospheric reentry as well as protecting the fueled clad from mechanical loads during ground impact. The pyrolytic graphite sleeves and plugs serve as thermal shields to keep the fueled clad from melting during an accidental reentry in the atmosphere* (*photograph courtesy of Los Alamos National Laboratory*).

Plutonium-239 is the most important isotope of plutonium. Its half-life (24,110 years) is sufficiently long to permit the preparation of this isotope in large-scale amounts, and to make it feasible to carry out conventional scientific studies. ^{239}Pu has a high cross-section for fission with slow neutrons, and is the isotope that serves as nuclear fuel for both nuclear power and nuclear weapons. By far the greatest portion of the knowledge of the chemical and physical properties of plutonium has been acquired by the use of ^{239}Pu. While its half-life is long enough to permit chemical studies, it is still short enough to present serious problems in handling. These difficulties are discussed in some detail below (Section 7.6). ^{239}Pu has a specific power of 2.2×10^{-3} W g^{-1}. In handling large quantities of ^{239}Pu, the criticality hazard caused by its fissionability becomes an additional problem. Amounts as small as 500 g may become critical

Table 7.2 *Minimum critical parameters of common forms of pure ^{239}Pu (Clark, 1981).*

metal	mass plutonium (kg)	5.0
	cylinder diameter (cm)	4.4
	slab thickness (cm)	0.65
oxide	mass plutonium (kg)	10.2
	mass PuO_2 (kg)	11.5
	cylinder diameter (cm)	7.2
	slab thickness (cm)	1.4
aqueous plutonium nitrate solution		
	plutonium mass (kg)	0.480
	concentration (g Pu L^{-1})	7.3
	H/Pu atomic ratio	3630
	cylinder diameter (cm)	15.4
	volume (L)	7.3

under certain conditions. In Table 7.2 some minimum critical parameters for pure ^{239}Pu obtained in various configurations have been summarized (Clark, 1981). Additional safety and criticality data are available in the compilations by Paxton (1975), Clark (1981), Knief (1985), and Paxton and Pruvost (1987).

The higher plutonium isotopes are formed as a result of successive neutron capture by the various plutonium isotopes:

$$^{239}\mathrm{Pu}(\mathrm{n},\gamma)^{240}\mathrm{Pu}(\mathrm{n},\gamma)^{241}\mathrm{Pu}(\mathrm{n},\gamma)\ \text{etc.} \tag{7.6}$$

The isotopic composition of plutonium produced in a nuclear reactor will therefore vary according to the length of time the plutonium formed is allowed to remain in the neutron flux. From this perspective it is noteworthy that the heavier isotopes ^{244}Pu, ^{245}Pu, and ^{246}Pu were originally discovered in the coral debris of the Mike thermonuclear test conducted in 1952, due to the extremely high neutron fluxes of the event. Hoffman, Ghiorso, and Seaborg described the events that led to the discoveries of these isotopes (Hoffman *et al.*, 2000). When ^{239}Pu targets were irradiated in a high-flux reactor to more than 90% burn-up, the residual plutonium was found to consist mainly of the higher isotopes ^{242}Pu and some ^{244}Pu. Many of the complications arising from the use of the relatively short-lived ^{239}Pu can be greatly ameliorated by the use of these long-lived isotopes of plutonium for fundamental scientific study.

Isotopically pure ^{240}Pu, ^{241}Pu, ^{242}Pu, and ^{244}Pu have become available from various sources. ^{240}Pu may readily be obtained by chemical separation from old ^{244}Cm samples. All the heavier plutonium isotopes have also been isotopically separated by electromagnetic separation in the Y-12 calutron plant in Oak Ridge (Love *et al.*, 1961; Love, 1973), but presently these calutrons have been placed in a standby condition. Gram quantities of these isotopes with isotopic purity above 99% were available from such separations. Russian scientists have

also been very successful in producing research quantities of higher plutonium isotopes using electromagnetic mass separation. Ultrapure ^{236}Pu and ^{237}Pu have been produced by Dmitriev and coworkers at the Joint Institute for Nuclear Research in Moscow (Dmitriev *et al.*, 1993, 1995, 1997), and Vesnovskii and Polynov at the Institute of Experimental Physics in Arzamas have been able to produce milligram to gram quantities of ^{240}Pu, ^{241}Pu, ^{242}Pu, and ^{244}Pu at greater than 99% isotopic purity (Vesnovskii and Polynov, 1992a,b). Milligram quantities of ^{244}Pu have been prepared at the IAEA Safeguards Analytical Laboratory in Austria using electromagnetic separation (Deron and Vesnovskii, 1999) and by selective ionization using a pulsed laser beam in Japan (Sasao and Yamaguchi, 1991).

The higher isotopes of plutonium possess interesting nuclear properties, which cannot be discussed in detail here. For further information see Hyde *et al.* (1964).

7.4 PLUTONIUM IN NATURE

Traces of plutonium are found all over the world, predominantly due to 'man-made' plutonium. In addition, two isotopes of plutonium (^{239}Pu and ^{244}Pu) can be found that are 'natural' in origin. Natural ^{239}Pu is produced in nature by nuclear processes occurring in uranium ore bodies, and minute traces of ^{244}Pu exist in nature as remnants of primordial stellar nucleosynthesis.

The presence of small amounts of plutonium in uranium of natural origin was first established in 1942 by Seaborg and Perlman (1948) and by Garner *et al.* (1948). These researchers were able to show that Canadian pitchblende and Colorado carnotite both contain a small amount of alpha activity due to a plutonium isotope, presumed to be ^{239}Pu at the time. Peppard *et al.* (1951) and Levine and Seaborg (1951) conclusively demonstrated the existence of ^{239}Pu in nature. Levine and Seaborg determined the plutonium content of a number of uranium ores, and Peppard and coworkers isolated microgram amounts of ^{239}Pu from uranium process wastes. Recent high-resolution thermal ionization mass spectrometry analyses of plutonium in uranium ore bodies have been described by Curtis *et al.* (1999) and by Dixon *et al.* (1997). The concentrations of plutonium in uranium ore bodies are collected in Table 7.3. No plutonium isotopes other than ^{239}Pu have been conclusively found in any of these experiments. More recently, ^{239}Pu has also been detected in granites from deep boreholes in Germany, and in salt brines from deep boreholes in the United States (Ganz *et al.*, 1991). Alpha pulse analysis and high-resolution mass spectrometry have been the experimental methods of choice for characterization of the isotopic composition of plutonium isolated from natural sources.

With the exception of the very long-lived ^{244}Pu, the half-lives of plutonium isotopes are so short that it is most unlikely that any plutonium except ^{244}Pu

Table 7.3 *Content of plutonium in natural uranium ore deposits.*

Ore	*Uranium content* (wt.%)	*Ratio* ^{239}Pu/U ($\times 10^{12}$)	*References*
Cigar Lake U deposit	31	6.4	Curtis *et al.* (1999)
Beaverlodge U deposit	7.09	14.3	Dixon *et al.* (1997)
Canadian pitchblende	13.5	7.1	Levine and Seaborg (1951)
Belgian Congo pitchblende	38	12	Levine and Seaborg (1951)
Colorado pitchblende	50	7.7	Levine and Seaborg (1951)
Brazilian monazite	0.24	8.3	Levine and Seaborg (1951)
N. Carolina monazite	1.64	3.6	Levine and Seaborg (1951)
Colorado furgusonite	0.25	<4	Levine and Seaborg (1951)
Colorado carnotite	10	<0.4	Levine and Seaborg (1951)

could have survived in nature from primordial times. It is overwhelmingly likely that ^{239}Pu arises in nature by nuclear reactions with ^{238}U and represents a steady-state concentration:

$$^{238}\mathrm{U}(\mathrm{n},\gamma)^{239}\mathrm{U} \xrightarrow{\beta^-} {}^{239}\mathrm{Np} \xrightarrow{\beta^-} {}^{239}\mathrm{Pu} \tag{7.7}$$

Neutrons necessary for the formation of ^{239}Pu from ^{238}U may arise from spontaneous fission of ^{238}U; by neutron multiplication in ^{235}U; from (α,n) reactions caused by the action of α particles (from the radioactive decay of uranium and daughters) on the nuclei of light elements in the ore (Li, B, Be, F, O, Si, Mg); and neutrons produced by cosmic rays. The neutrons from cosmic rays appear to be of negligible importance, since the neutron production from uranium by the capture of μ mesons is considerably less than 0.1% of the neutrons arising from spontaneous fission (Littler, 1952). Spontaneous fission in uranium occurs at the rate of (24.2 ± 0.5) fissions per gram per hour, which produces a neutron flux insufficient to account for the observed plutonium concentration. Neutron multiplication by capture of thermalized neutrons in ^{235}U and the production of fission neutrons will contribute to overcoming the deficiency. The contribution from this source will clearly depend on the uranium concentration, on the composition of the ore, and on the probability that a fission neutron will be slowed down to thermal energies. In all probability, the neutrons produced in (α,n) reactions account for a major portion of the neutrons required for ^{239}Pu formation. Fleming and Thode (1953a,b) found evidence that (α,n) and (α,p) reactions occur to a considerable extent in uranium minerals. This conclusion was reached from a study of the isotopic composition of argon obtained from uranium minerals. In thorium ores containing small amounts of uranium, the neutrons from (α,n) reactions predominate. The amount of plutonium created depends not only on the number of neutrons produced but also on their subsequent fate. Elements with high neutron-capture

cross-sections will compete for neutrons and decrease plutonium formation. In carnotite, potassium and vanadium atoms, and in fergusonite, tantalum atoms capture most of the available neutrons, thus accounting for the unusually low plutonium content found in these minerals (Table 7.3).

A fascinating example of the formation of ^{239}Pu by neutron multiplication in ^{235}U was found by French scientists in the uranium deposit at Oklo in the Gabon, Africa. From anomalies in the isotopic composition of rare earths (especially neodymium) and anomalies in the ^{235}U content, it was concluded that, in at least six different locations of this deposit, a self-sustaining nuclear chain reaction must have occurred (Bodu *et al.*, 1972; Neuilly *et al.*, 1972). It was found that, in these locations, a burn-up of part of the original ^{235}U had occurred, but the depletion found was not as great as one would have expected from the observed anomalies in the isotope composition of other elements. It is generally agreed that ^{239}Pu is formed through resonant capture of epithermal neutrons by the ^{238}U present in the matrix, and that subsequent radioactive decay of the ^{239}Pu again regenerates a fraction of the ^{235}U (Holliger and Devillers, 1981; Hidaka and Holliger, 1998; Hidaka, 1999). Since no plutonium has been found in the Oklo deposit, one may conclude that the self-sustaining chain reaction must have taken place around 1.9×10^9 years ago (Cowan, 1976).

A different situation exists with regard to ^{244}Pu, which is sufficiently long-lived to have survived from primordial times. In 1960, Kuroda postulated the existence of ^{244}Pu in the early solar system based on the Xe isotope ratios found in chondritic meteorites (Kuroda, 1960). In 1971, Alexander and coworkers measured the ratios of the Xe isotopes formed by spontaneous fission (SF) of ^{244}Pu and found they agreed with those found in chondritic meteorites, thus strongly supporting this hypothesis and SF decay of ^{244}Pu (Alexander *et al.*, 1971). The discovery of ^{244}Pu fission xenon in extraterrestrial samples such as the Moon (Kuroda and Myers, 1998), Martian (Marty and Marti, 2002), and other meteorites demonstrated that the transuranium elements were synthesized in exploding (supernovae) stars (Kuroda and Myers, 1998).

Conclusive proof for the occurrence of natural ^{244}Pu in a pre-Cambrian bastnasite ore was provided by Hoffman and coworkers (Hoffman *et al.*, 1971). Starting from approximately 85 kg of ore containing 10% bastnasite, these workers isolated 2×10^7 atoms (8×10^{-15} g) of ^{244}Pu corresponding to about 10^{-18} g of ^{244}Pu per gram of pure bastnasite. The presence of ^{244}Pu was conclusively identified using high-resolution mass spectrometry. Thus it seems most probable that this ^{244}Pu sample is a remnant of the stellar debris that coalesced to form the solar system.

That even the richest uranium deposits are not likely to supersede synthetic methods as a source of plutonium can be appreciated from the fact that the microgram amounts of plutonium isolated by Peppard and coworkers (Peppard *et al.*, 1951) required the residues of 100 metric tons of ore concentrate for each microgram of plutonium recovered.

7.5 SEPARATION AND PURIFICATION

7.5.1 Introduction

At the end of 2003, a little more than 60 years after the discovery of the first plutonium isotope in 1940, about 1855 metric tons of plutonium existed, principally within irradiated fuel from nuclear power plants (Albright and Kramer, 2004). About 225 metric tons of plutonium that had been separated and purified for recycling in commercial nuclear fuel cycles was in the unirradiated form. Roughly 260 metric tons of plutonium with a high ^{239}Pu content has been separated for use in nuclear weapons programs worldwide. Some of this weapons plutonium has been declared excess to military needs and will be incorporated into the commercial nuclear power system. Production of plutonium for military use had greatly decreased by early in the 21st century, but the total plutonium inventory will continue to increase as a consequence of nuclear power production for the foreseeable future. The rate of plutonium production in fuel of operating reactors was estimated at 70–75 metric tons per year at the end of 2003. Clearly, the separation of plutonium has been carried out on a large scale. The management of the separated plutonium and the large quantities of highly radioactive by-products of this production will continue to be a challenge in the decades to come.

Plutonium isotopes are produced mainly from neutron absorption by ^{238}U and the subsequent product nuclei as shown in the simplified scheme in Fig. 7.4. The major pathway to plutonium proceeds through absorption of a neutron to give ^{239}U followed by two successive β^- decays to give ^{239}Np and then ^{239}Pu. Neutron absorption by ^{239}Pu produces higher isotopes of plutonium and other transuranic elements, in competition with neutron-induced fission. Beta decay by ^{241}Pu and ^{243}Pu and further neutron absorption leads to the production of higher actinides, americium, curium, etc., but these steps are not shown in the diagram for the sake of clarity. As the scheme for the production of plutonium isotopes suggests, the isotopic composition of plutonium produced in a

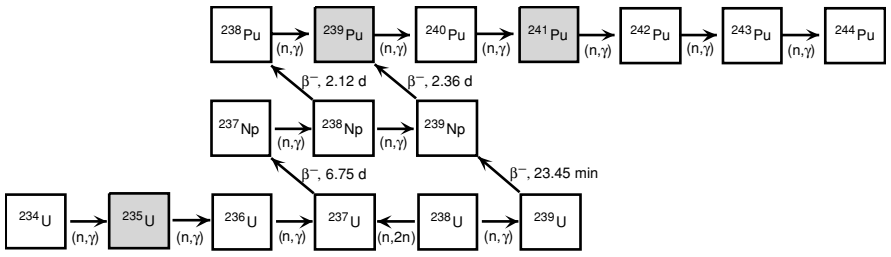

Fig. 7.4 *Major pathways for formation of plutonium isotopes by neutron absorption* (n, γ) *and beta decay* (β^-) *in uranium fuels or targets. Shaded boxes indicate most important isotopes undergoing neutron-induced fission in competition with neutron absorption.*

particular portion of the reactor fuel will be a complex function of the total flux and energy distribution of the neutrons that irradiate that fuel segment. The neutron flux and energy distribution will vary with irradiation time and the location of the fuel in the reactor.

The majority of nuclear power reactors around the world use low-enrichment uranium oxide fuels (^{235}U content of 3–5%) and light water (H_2O) to moderate the neutrons and act as the coolant for the system (Neeb, 1997). The uranium oxide fuel is fabricated into cylindrical pellets that are stacked inside a sealed container made of a cladding material such as a zirconium alloy to make a fuel pin. The plutonium content after 'burning' of these fuels amounts to about 1% of the mass of heavy metal content of the used fuel from a 'typical' light water reactor (LWR). Neutron-induced fission of the plutonium generated from neutron absorption by ^{238}U adds substantially to the total power production in commercial nuclear power plants (~40% of the total). The remaining mass of the used fuel consists of about 95% uranium, 4% fission products, and 0.1% all other transuranic actinides. It is the plutonium content in these 'spent' reactor fuels that provides most of the global plutonium inventory.

The build-up of the plutonium isotopes is accompanied by the production of a great variety of fission product elements. The fission process leads mostly to two product nuclei (only 0.2 to 0.3% of the fission events yield three fragments) that have an asymmetric statistical mass distribution with peaks at mass numbers of 95 and 138 for ^{235}U thermal (low energy) neutron-induced fission. The fission product nuclei commonly have excess neutrons relative to stable nuclei with the same atomic number and thus most are radioactive. The fission products decay primarily by beta/gamma chains to more stable nuclei. A calculation of the principal actinide and fission product isotopes present at the end of irradiation followed by 10 years of storage of a commercial reactor-type fuel is shown in Table 7.4. The burn-up of this fuel is higher than that used in most commercial plants to date, but the nuclear power industry trend is toward such higher burn-ups in the future. The list of fission product masses in Table 7.4 illustrates the two peaks in the fission product yield among the elements Zr through Pd and Xe through Nd. While the fission product masses do not change dramatically for most of the elements in the used fuel after 10 years of storage, the radioactivity has dropped more than two orders of magnitude and the ^{90}Sr and ^{137}Cs decay chains dominate the radioactivity of the used fuel from 10 years out to a few hundred years.

Inspection of Table 7.4 also illustrates that the fission products include elements from all the families of the periodic table. This considerably complicates the chemical problem of separation and purification of plutonium from the irradiated fuel. Additionally, the intense radioactivity requires facilities that use heavy shielding and remotely operated equipment to perform the separation processes. The mixture of plutonium isotopes present in the spent fuel is not so intensely radioactive and can be handled in a gloved box system once the fission products are removed. The term 'decontamination' is often applied to the

Table 7.4 *Actinide and fission product content of neutron-irradiated UO_2 fuel calculated using ORIGEN 2 code (Croff, 1980, 1983)*[a].

Element	*Weight at discharge* (g)	*Weight after* 10 yr *cooling* (g)	*Activity at discharge* (C_i)	*Activity after* 10 yr *cooling* (C_i)	*Major radioactive isotopes after* 10 yr *cooling and half-lives*
U-234	123	142	0.76	0.88	α, 2.46×10^5 yr
U-235	6 370	6 370	0.01	0.01	α, 7.04×10^8 yr
U-236	5 520	5 520	0.35	0.35	α, 2.34×10^7 yr
U-237	18	<0.1	1.47×10^6	2.76	β^-, 6.75 d
U-238	923 900	923 900	0.31	0.31	α, 4.47×10^9 yr
Np-237	1 020	1 050	0.72	0.74	α, 2.14×10^6 yr
Np-238	2	<0.1	5.23×10^5	0	β^-, 2.34 d
Np-239	100	<0.1	2.32×10^7	1.04×10^2	β^-, 2.34 d
Pu-238	236	242	3.99×10^3	4.09×10^3	α, 87.7 yr
Pu-239	4 900	5 000	3.01×10^2	3.07×10^2	α, 2.41×10^4 yr
Pu-240	2 070	2 130	4.57×10^2	4.70×10^2	α, 6.56×10^3 yr
Pu-241	1 820	1 130	1.85×10^5	1.15×10^5	β^-, 14.4 yr
Pu-242	579	579	2.3	2.3	α, 3.73×10^5 yr
Am-241	48	728	1.64×10^2	2.50×10^3	α, 432 yr
Am-242m	2	2	16.6	15.8	IT, 141 yr
Am-243	538	538	1.04×10^2	1.04×10^2	α, 7.37×10^3 yr
Cm-242	23	<0.1	7.75×10^4	13.0	α, 163 d
Cm-243	2	2	89.3	71.9	α, 29.1 yr
Cm-244	200	136	1.62×10^4	1.10×10^4	α, 18.1 yr
Cm-245	20	20	3.5	3.5	α, 8.5×10^3 yr
Cm-246	4	4	1.2	1.2	α, 4.76×10^3 yr
total An	**947 495**	**947 493**	**2.55×10^7**	**1.32×10^5**	
Se	85	85	9.6×10^5	0.58	Se-79 6.5×10^4 yr
Br	33	33	0	0	–
Kr	546	529	3.8×10^6	7.3×10^3	Kr-85 10.7 yr
Rb	520	537	5.4×10^6	<0.01	–
Sr	1 390	1 180	8.6×10^6	8.9×10^4	Sr-90 28.5 yr
Y	722	704	1.2×10^7	8.9×10^4	Y-90 64.1 h
Zr	5 480	5 630	1.0×10^7	2.8	Zr-93 1.5×10^6 yr
Nb	44	<0.01	1.5×10^7	1.1	Nb-93m 13.6 yr
Mo	5 090	5 210	0	0	–
Tc	1 220	1 230	1.2×10^7	21	Tc-99 2.1×10^5 yr
Ru	3 630	3 360	5.6×10^6	757	Ru-106 373 d
Rh	446	504	8.0×10^6	757	Rh-106 2.2 h
Pd	2 140	2 360	7.1×10^5	0.16	Pd-107 6.5×10^6 yr
Ag	73	71	9.4×10^5	0.33	Ag-110m 250 d
Cd	157	159	8.5×10^4	39	Cd-113m 13.7 yr
In	1	1	2.6×10^5	<0.01	–
Sn	76	75	1.5×10^6	1.1	Sn-126 2.5×10^5 yr
Sb	26	14	3.8×10^6	1.2×10^3	Sb-125 2.76 yr
Te	714	717	8.0×10^6	285	Te-125m 58 d
I	363	357	1.2×10^7	0.05	I-129 1.6×10^7 yr
Xe	8 190	8 190	9.0×10^6	<0.01	–
Cs	4 140	3 340	8.6×10^6	1.5×10^5	Cs-137 30.2 yr, Cs-135 2.3×10^6, Cs-134 2.07 yr

Table 7.4 (*Contd.*)

Element	*Weight at discharge* (g)	*Weight after* 10 yr *cooling* (g)	*Activity at discharge* (C_i)	*Activity after* 10 yr *cooling* (C_i)	*Major radioactive isotopes after* 10 yr *cooling and half-lives*
Ba	2 310	3 100	1.0×10^7	1.2×10^5	Ba-137m 2.5 mo
La	1 880	1 870	1.0×10^7	<0.01	–
Ce	4 170	3 690	8.1×10^6	190	Ce-144 284 d
Pr	1 690	1 730	7.0×10^6	193	Pr-144 17.3 mo
Nd	5 770	6 220	1.7×10^6	<0.01	–
Pm	100	7	1.8×10^6	6.9×10^3	Pm-147 2.63 yr
Sm	1 150	1 240	9.6×10^5	1.4×10^3	Sm-151 90 yr
Eu	309	243	6.2×10^5	1.3×10^4	Eu-155 4.73 yr, Eu-154 8.5 yr
Gd	237	309	8.1×10^3	<0.01	–
Tb	3	2	4.8×10^3	<0.01	–
Dy	2	2	1.4×10^3	<0.01	–
total FP	**52 700**	**52 700**	$\mathbf{1.8 \times 10^8}$	$\mathbf{4.8 \times 10^5}$	

[a] Based on an initial uranium loading of 4.25% ^{235}U enrichment (957.5 kg ^{238}U, 42.5 kg ^{235}U, 0.293 kg ^{234}U), burn-up of 50 000 MW-days (metric ton)$^{-1}$ (Hill, 2005).

process of removing the fission products from the plutonium, uranium, or other actinides of interest in the irradiated fuel or target material. The decontamination factor measures the extent to which the concentration of fission products has been removed relative to the original level in the spent fuel at the time processing begins. To allow the product plutonium to be handled by personnel using a gloved box without undue exposure to fission product radioactivity, the decontamination factor required for some fission products is on the order of 10^8. Clearly, the required decontamination factors will vary with the cooling time of the fuel before processing begins.

The fission products and actinides produced from the irradiated uranium fuel are dispersed intimately in the fuel matrix (Neeb, 1997). The fission product nuclei dissipate their kinetic energy after traveling on average 5–10 μm through the uranium oxide matrix, leaving an ionization track and displacement cascade that ultimately generates most of the heat that is used to generate electricity. Atomic mixing occurs from both radiation-induced and thermal mass transport processes. In a typical LWR fuel each atom of the fuel is displaced from its lattice site an average of once a day. Some segregation of the fission product elements occurs under reactor conditions (Neeb, 1997). For example, inert gases such as xenon and krypton can form bubbles in the fuel matrix and even escape into the gas space inside a fuel pin, and some transition elements (Mo, Ru, Rh, Pd, Tc) form small metal inclusions in the uranium oxide. However, the bulk of the fission products and transuranic elements are

dispersed fairly homogeneously within the uranium fuel. The uranium matrix must be dissolved into a suitable solution or converted into a volatile compound to allow the fission product and actinide 'impurities' to be separated from the uranium.

The methods used to recover plutonium (and other actinides) from irradiated fuels or targets can be divided into two major groups, aqueous and nonaqueous processes, depending on the primary phase used for the separation process. The major classes of aqueous processes are liquid–liquid extraction (solvent extraction), ion exchange, and precipitation. Examples of nonaqueous processes are electrorefining (ER) in molten salts and fluoride volatility. The separation methods use differences in the chemical properties of the various elements present to segregate some components preferentially between the primary phase and a secondary phase that can be a solid, liquid, or gas. Separation of the two phases partitions the components of the original single phase for further processing steps. These next steps can be additional stages of the same separation method (e.g., a bank of centrifugal contactors for extraction) or a different method (e.g., ion exchange followed by precipitation).

Nearly all of the separation methods take advantage of the multiple oxidation states that plutonium can adopt in its various chemical forms. The chemical properties of plutonium (and other metal ions) change to a large extent depending on the oxidation state. If conditions can be adjusted to obtain various metal ions in a mixture in different oxidation states, the separation of these metals is often straightforward. For example, in aqueous acid solutions it is possible to have uranium in the hexavalent oxidation state (as UO_2^{2+}), neptunium in the pentavalent state (as NpO_2^{+}), plutonium in the tetravalent state, and americium in the trivalent state. The complexes formed by ions in these different oxidation states in solution are quite different, so that separation by a number of methods is possible. In the case of an irradiated fuel with fission products present, if the chemical behavior of a fission product resembles that of plutonium in one oxidation state, it can be quite different when the plutonium oxidation state or the fission product element oxidation state is changed. The use of oxidation state changes to improve separations will be illustrated in the discussion of specific separation methods below.

The large-scale separation and purification of plutonium has been primarily accomplished using the Plutonium, Uranium, Reduction, EXtraction (PUREX) liquid–liquid extraction process. This process was first developed for separating plutonium from metallic uranium fuels irradiated to produce plutonium for nuclear weapons applications, but has since been adapted to separate uranium and plutonium from many kinds of fuels and targets, including commercial power reactor fuels. While a variety of other processes have been used to separate and purify plutonium from irradiated fuels, many of these are now of only historical interest. More detailed information on the separation technology for plutonium and the other actinides can be found in Chapter 24 of this work, *Actinide Separation Science and Technology*, including extensive

documentation of the separation literature. The goal in this chapter is to present the main features of selected separation methods of particular importance to plutonium and to illustrate major factors guiding development of plutonium separation processes. Only brief references to the history of plutonium separations will be made here.

Processes for separation of plutonium from neutron-irradiated uranium metal, uranium oxide, or other irradiated target materials are one important group of plutonium separation and purification methods, but there are additional separation needs. Separated plutonium must be converted into the forms required for various applications, for example, purification of PuO_2 to meet all the specifications for mixed oxide (MOX) fuel fabrication. Recovery and recycle of plutonium from the process and waste streams of these conversion operations constitute another important group of separation processes. A wider variety of separation methods can be employed to accomplish these separations because the high radiation levels of the fission products are not present and the amount of material to be processed is typically much smaller. There is also a need for separation processes to remove plutonium from items that have been contaminated by plutonium-containing materials resulting from normal operations or accidental release to the environment, e.g. equipment, concrete, soils, etc. These types of operations are commonly referred to as decontamination methods; the radioactive contaminant is plutonium in this case rather than a fission product. Finally, a large number of separation methods and reagents have been used to preconcentrate or remove interfering components in analytical procedures for plutonium-containing samples to improve detection limits and accuracy of the results.

As the above discussion indicates, many processes have been developed for separating plutonium from a variety of matrices. There are often variations for a particular method and many combinations of methods possible for accomplishing a specific separation goal. The chosen process can be a result of many factors at a particular facility including available equipment and expertise, safety and operational limits, product specifications, national regulatory requirements, waste management, cost, and schedule. It is possible in some processes to vary operating conditions over a wide range and still obtain a desired result. In the discussion of separation methods that follow, variations in process conditions are common. Defining an 'optimum' process depends on factors like those mentioned above, which can vary even at a single facility over its lifetime. Operational details of this kind are beyond the scope of this chapter.

7.5.2 Introduction to aqueous-based separation methods

Before discussing aqueous separation processes for plutonium in more detail, a brief overview of actinide chemistry in aqueous solution is useful because most actinide separations have been performed using aqueous acid solutions.

The separation of actinides from basic aqueous solutions has been employed less often because the low solubilities of the hydroxides or oxyhydroxides of the high-valent actinide metal ions greatly limit the amount of material that can be processed in a given volume except where strongly complexing ligands, such as carbonate or peroxide, are present. More detailed information on the solution chemistry of plutonium (see Section 7.9) and the other actinide metal ions can be found in the appropriate sections of the chapters for each element and in other chapters of this work.

As noted above, the separation of plutonium and the other early actinides (Th–Am) from fission products and from each other is generally accomplished by adjusting the oxidation state of the actinide ion in aqueous solution to make the coordination chemistry of the actinide ion substantially different from the other species to be separated. The actinides are highly electropositive metals and form cationic species in aqueous solutions. These cations are 'hard' Lewis acids and form strong complexes in solution with hard anions such as hydroxide and fluoride. The oxidation states from III to VI are accessible in aqueous acid solutions of uranium, neptunium, and plutonium. After plutonium the actinides become more lanthanide-like with the coordination chemistry of the trivalent metal ion dominating. The pentavalent and hexavalent actinide ions are found in aqueous solutions as linear dioxo cations, e.g. NpO_2^+ and PuO_2^{2+}. These 'actinyl' species have no close analogs in transition metal oxo complexes and are also hard Lewis acids. Water and other ligands bind to these linear cations in a ring-shaped equatorial region around the metal ion between the two tightly bound oxoanions. The coordination numbers and geometries for the actinide ions are highly variable and reflect the largely ionic bonding in these complexes: generally, 6–12 for An(IV), 6–9 for An(III), and 4–6 in the equatorial ring of AnO_2^+ or AnO_2^{2+}. The trivalent actinides exhibit a slightly stronger bonding to ligands containing soft donor atoms (e.g. sulfur, nitrogen, chloride) than the corresponding lanthanides and this property can be used as a basis for separating these groups of elements.

For plutonium the oxidation states from III to VII are accessible in aqueous solution. The species Pu(III), Pu(IV), and Pu(VI) (PuO_2^{2+}) are most important in acidic aqueous solution. The pentavalent ion PuO_2^+ disproportionates rapidly in acidic solution at moderate plutonium concentrations and is usually a very minor species in acidic aqueous separation systems. Stabilizing Pu(VII) requires strongly complexing ligands such as hydroxide, fluoride, or carbonate in basic solution and, thus, Pu(VII) has not been used in any separation systems.

7.5.3 Precipitation and crystallization methods

As noted above, the oxidation states of the actinide ions in solution produce large differences in coordination chemistry facilitating separation by a variety of methods. An example of this is shown in Table 7.5 which lists the qualitative solubility behavior of the actinides in oxidation states III–VI with some common

Table 7.5 *Precipitation reactions characteristic of various actinide oxidation states* (*aqueous solution,* 1 M H^+)[a].

Anion	M^{3+}	M^{4+}	MO_2^+	MO_2^{2+}
OH^-	I	I	I	I
F^-	I	I	I[b]	S
IO_3^-	I	I	S	S
O_2^{2-}	–	I	–	–
$C_2O_4^{2-}$	I	I	I	I
CO_3^{2-}	(I)[c]	I[c]	I[d]	S
$CH_3CO_2^-$	S	S	S	I[e]
PO_4^{3-}	I	I	I[f]	I[g]
$Fe(CN)_6^{4-}$	I	I	S	I

I = insoluble, S = soluble.
[a] Unless otherwise stated (the OH^- and CO_3^{2-} precipitations occur in alkaline solution).
[b] At pH = 6, $RbPuO_2F_2$ and $NH_4PuO_2F_2$ may be precipitated by addition of RbF or NH_4F, respectively.
[c] Complex carbonates are formed.
[d] Solid $KPuO_2CO_3$ precipitates on addition of K_2CO_3 to Pu(V) solution.
[e] From solution of Pu(VI) in CH_3CO_2H, $NaPuO_2(CH_3CO_2)_3$ precipitates on addition of Na^+.
[f] Addition of $(NH_4)_2HPO_4$ to Pu(V) solution yields $(NH_4)HPuO_2PO_4$.
[g] On addition of H_3PO_4, $HPuO_2PO_4{\cdot}xH_2O$ precipitates.

anions. These precipitations are very useful for separating mixtures of the actinides and for recovery of solid products from an aqueous stream after using another separation process such as ion exchange or solvent extraction. They are generally not selective enough to be used as the primary process for separation of plutonium or other actinides from all the fission products in irradiated fuel or targets. This is illustrated by a study (Winchester and Maraman, 1958) that used precipitation of Pu(III) oxalate, Pu(IV) oxalate, Pu(III) fluoride, and Pu(IV) peroxide to recover plutonium directly from an irradiated plutonium-rich alloy dissolved in nitric acid. The decontamination factors reported in Table 7.6 indicate that none of the precipitation processes achieved high enough fission product or corrosion product (Fe and Co) removal for use as a primary separation process. However, as will be described below, coprecipitations with other metal ion species such as bismuth phosphate were used in the first large-scale separations of plutonium from irradiated uranium. These processes were replaced in time by more efficient solvent extraction processes.

The distinction between crystallization and precipitation is quite often based on the speed of the process and the size of the solid particles produced. The term precipitation commonly refers to a rapid crystallization that gives small crystals that may not appear crystalline to the eye, but still may give very distinct X-ray diffraction (XRD) peaks. Precipitation often involves a relatively irreversible reaction between an added reagent and other species in solution whereas

Table 7.6 *Decontamination factors for plutonium using various precipitation methods.*

Element	*Pu(III) oxalate*	*Pu(IV) oxalate*	*Pu(IV) peroxide*	*Pu(III) fluoride*
Fe	33	10	50	1.4
Co	47	>95	30	8.6
Zr	3.5	>44	1	1.1
Mo	>13	>15	>140	1.1
Ru	>38	33	>14	36
Ce	1	1	6	1.1

crystallization products can usually be redissolved using relatively simple means such as heating or dilution. The details of the precipitation or crystallization process can be very important to produce a pure product and one that separates well from the liquid phase. Thus, the order and speed of reagent addition, the temperature, and the 'aging' time before filtration or centrifugation can all be important parameters in a precipitation or a crystallization process. The Pu(IV) oxyhydroxide 'polymer' that readily forms in relatively low acid solutions of Pu(IV) is an infamous example of a 'difficult' precipitate that can complicate the processing of plutonium aqueous solutions. The characteristics of this polymer will be described in more detail in Section 7.9.1.d.

(a) Coprecipitation methods

Coprecipitation processes were the first to be used for the recovery of plutonium. The tiny amounts of plutonium present in the first preparations were too small to be precipitated directly, so coprecipitation or 'carrier' precipitations were used to purify and deduce the chemical properties of plutonium and many other radioactive elements. In general, plutonium will coprecipitate if the anion contained in the bulk precipitate forms an insoluble salt with plutonium in the same oxidation state or states present in the solution. Useful carrier precipitation methods for plutonium have been reviewed (Sorantin, 1975). Coprecipitation methods have also been used to purify plutonium in microgram amounts and for recovery on a production scale.

(*i*) *Lanthanum fluoride*

Precipitation of lanthanum fluoride or other lanthanide fluorides from acid solutions carries trivalent and tetravalent actinides, but not the pentavalent and hexavalent ions. The lanthanide and yttrium fission products coprecipitate, but most of the other fission products remain in solution. The behavior of

neptunium and plutonium in lanthanum fluoride precipitation was used to establish the existence of two oxidation states of these elements before weighable quantities were available (Seaborg and Wahl, 1948b). The lanthanum fluoride carrier precipitation was also a key step in the first isolation of a weighable plutonium compound to be described below.

Cunningham and Werner isolated a PuO_2 sample that weighed 2.77 μg, the first weighable quantity of any synthetic element, on September 10, 1942 at the Metallurgical Laboratory of the University of Chicago (Cunningham and Werner, 1949b). The plutonium had been separated from about 90 kg of uranyl nitrate hexahydrate that had been irradiated for 1 to 2 months with neutrons produced by bombarding a beryllium target with deuterons at the cyclotron facility at Washington University in St. Louis. The separation of plutonium was accomplished through oxidation state adjustments and a series of LaF_3 precipitations that carried Pu(IV) and Np(IV) but not Pu(VI) or Np(VI). The brief overview that follows provides an example of a coprecipitation separation method and also illustrates the painstaking effort required in these first explorations of plutonium chemistry.

About 90 kg of irradiated $UO_2(NO_3)_2 \cdot 6H_2O$ was mixed with 100 L of diethyl ether to yield about 120 L of ether solution containing uranyl nitrate solvate, $UO_2(NO_3)_2[O(CH_2CH_3)_2]_2$, and a small amount of fission products and 8 L of an aqueous phase that consisted of about 50 wt % uranyl nitrate hydrate with most of the fission products and transuranic elements, principally neptunium and plutonium. This was essentially a solvent extraction step that partitioned most of the U(VI) to the ether phase along with a small amount of the fission products.

The aqueous phase was diluted to 20 L, made 2 M in nitric acid and 0.014 M in La(III) and then HF was added to give a solution 4 M in HF. The resulting 40 g of LaF_3 precipitate contained the transuranium elements and about 25% of the original fission product activity (mostly the lanthanide and yttrium fission products). The separated LaF_3 precipitate was heated in concentrated sulfuric acid to distill HF and then dissolved in and diluted to 5 L with 2 M nitric acid. The Pu(IV) was oxidized to Pu(VI) by using $K_2S_2O_8$ and Ag(I) as a catalyst. The solution was then made 4 M in HF which produced about 40 g of LaF_3 precipitate that was separated by filtration. The LaF_3 precipitate contained most of the remaining fission product activity, while the solution contained the Pu(VI) and Np(VI). The addition of a 6% SO_2 solution to the filtrate and washings reduced the Pu(VI) and Np(VI) and the excess peroxydisulfate. Addition of 2 g of $La(NO_3)_3$ in solution precipitated LaF_3 that carried the tetravalent plutonium and neptunium. Repeated cycles of precipitation with progressively smaller amounts of LaF_3 were used to further decontaminate the plutonium and neptunium. For two of the LaF_3 precipitation cycles, $KBrO_3$ was employed as the oxidizer to selectively oxidize neptunium, but not plutonium. This allowed the separation of the neptunium into the filtrate solutions while plutonium was carried with the LaF_3. These additional cycles of smaller

precipitations eventually yielded a 120 μL solution of 1.7 M HNO_3 and 5 M HF that was fumed in a platinum crucible and treated with 10 M ammonium hydroxide to precipitate Pu(VI) hydroxide. The washed precipitate of plutonium hydroxide contained about 40 μg of plutonium. The microliter-scale solution manipulations were performed in a specially designed glass apparatus viewed with a microscope. Additional purification steps yielded a 50 μL solution of plutonium in nitric acid. Ten μL of this solution were placed on a platinum weighing pan, dried, and heated to give the oxide. This sample provided the first weighable quantity of plutonium that is now displayed in the Lawrence Hall of Science at Berkeley, California.

(*ii*) *Bismuth phosphate process*

The bismuth phosphate process was used for the first large-scale purification of plutonium from neutron-irradiated uranium at the Hanford site during the Manhattan Project, and after the war until the 1950s when it was replaced by solvent extraction processes. More detail on the bismuth phosphate process and its replacement by solvent extraction processes can be found in Chapter 24. The precipitation of $BiPO_4$ from acid solutions carries the trivalent and tetravalent actinides, and especially Pu(IV), but not the pentavalent and hexavalent ions. Bismuth phosphate is quite insoluble in moderately concentrated nitric and sulfuric acids. This is an important property because addition of sulfuric acid to a nitric acid solution of neutron-irradiated uranium could be used to keep the relatively large quantity of U(VI) in solution as a sulfate complex while bismuth phosphate was precipitated and carried the plutonium. The $BiPO_4$ precipitate carried only small amounts of the fission products, and could be redissolved in concentrated nitric acid; thus simplifying the process relative to use of a lanthanum fluoride carrier that is difficult to redissolve. A series of oxidation state adjustments and precipitations of $BiPO_4$ from solutions of neutron-irradiated uranium in nitric acid separated the plutonium from the uranium, neptunium and fission products in a scheme that resembles the lanthanum fluoride process described above. In fact, cycles of lanthanum fluoride precipitation from nitric acid were incorporated into the bismuth phosphate process to concentrate and further purify plutonium.

Thompson and Seaborg first developed the bismuth phosphate process (Thompson and Seaborg, 1956). The scale-up of the process from the laboratory to an operating plant by a factor of 10^8 in a short time is a remarkable story (Hill and Cooper, 1958). An overall decontamination factor from the fission products of 10^7 was obtained at Hanford for the plutonium. The disadvantages of the process included discarding the uranium with the fission products, generation of large volumes of high salt wastes, and batch operation. Continuous solvent extraction processes based on extraction of uranium and plutonium from nitric acid solutions of dissolved fuel have replaced the bismuth phosphate process.

(b) Precipitation and crystallization methods for conversion chemistry of plutonium

Solvent extraction processes have displaced the original bismuth phosphate coprecipitation method for production scale plutonium separation from neutron-irradiated uranium fuels and targets. However, precipitation and crystallization from aqueous solutions have always been important processes for preparing and purifying solid compounds for the various applications of plutonium. The major products are plutonium metal for irradiation targets and fuels, weapons components, or storage and PuO_2 for MOX fuels, heat sources (when the ^{238}Pu content is high), and storage.

The bulk of the aqueous processing of plutonium takes place in nitric or hydrochloric acid solutions and most plutonium solids are precipitated from these solutions (Cleveland, 1980; Christensen *et al.*, 1988). The most common precipitations use oxalate, peroxide, hydroxide, and fluoride. The typical reasons for using these precipitations are:

- Good recovery of plutonium can be obtained in the solid in a form suitable for preparing metal or oxide.
- Relatively concentrated plutonium nitrate or chloride solutions can be largely or partially purified from many cationic impurities.
- Precipitation from relatively dilute solutions provides a very quick and convenient method for concentrating plutonium.
- Calcination at 500–800°C readily converts properly precipitated Pu(III) and Pu(IV) oxalates to PuO_2 that is suitable for direct oxide reduction (DOR) with calcium to the metal, or hydrofluorination to PuF_4 that is then reduced to metal (see Section 7.7.2).
- Precipitation of plutonium or americium hydroxides from waste solutions such as oxalate or peroxide filtrates generally provides an effective method to recycle the plutonium and americium in the separated precipitate and to dispose of the alkaline filtrate to low-level waste treatment operations.

This group of common precipitation methods will be briefly reviewed. The detailed procedures used at different facilities vary widely because of the many facility-specific factors that enter into the process design as discussed briefly in Section 7.5.1. Both batch and continuous processes have been developed for these precipitations.

(*i*) *Plutonium(III) oxalate precipitation*

Since the time of the Manhattan Project, researchers have found it useful to precipitate the easily filterable turquoise-blue $Pu_2(C_2O_4)_3 \cdot 10H_2O$ by reducing plutonium to the trivalent state in low acid solution and carefully adding an oxalic acid solution. Directly adding solid oxalic acid will produce a crystalline precipitate with a smaller average particle size (Christensen *et al.*, 1988). The solubility of $Pu_2(C_2O_4)_3 \cdot 10H_2O$ can be approximated by the expression

$[Pu(mg\,L^{-1})] = 3.24[H^+]^3[H_2C_2O_4]^{-3/2}$ (Harmon and Reas, 1957). However, the typical filtrate from a production run will have somewhat higher concentrations of plutonium (0.1–0.5 g L^{-1}) left in solution than that calculated from this equation. The precipitation is useful over a wide range of conditions when the Pu(III) concentration is more than 1 g L^{-1} and with less than 4 M acid. The Pu(III) oxalate precipitation gives good decontamination factors from such impurities as Al(III), Fe(III), and U(VI). There is less decontamination from sodium, potassium, and calcium and none from Am(III). Plutonium(III and IV) can be scavenged from very dilute solutions using Ca(II) or Pb(II) oxalates as carriers (Maraman *et al.*, 1954; Akatsu, 1982; Akatsu *et al.*, 1983).

(*ii*) *Plutonium*(*IV*) *oxalate precipitation*

Plutonium(IV) precipitates as the tan solid $Pu(C_2O_4)_2 \cdot 6H_2O$ from low acid solutions upon addition of oxalic acid, but it is usually a very fine tacky solid at room temperature (Christensen *et al.*, 1988). Precipitation at elevated temperatures can greatly improve the filterability of the solid. Typical losses of plutonium to the filtrate in practical operations are 0.2–0.5 g L^{-1}. The precipitation is used over a wide range of conditions with Pu(IV) concentrations greater than 1 g L^{-1} and acid concentrations between 1 and 5 M. The decontamination factors for impurities such as Al(III), Fe(III), and U(VI) are typically higher than for the Pu(III) oxalate method. There is no decontamination from Am(III).

(*iii*) *Plutonium*(*IV*) *peroxide precipitation*

Plutonium(IV) peroxide is an olive-green solid formed by the addition of hydrogen peroxide solutions to acid solutions of Pu(IV). The typical range of acid concentration is 2.5–5.5 M. The solutions are often cooled to 10–15°C to reduce the decomposition of hydrogen peroxide. High levels of iron, copper, manganese, or nickel catalyze the decomposition of the H_2O_2 and interfere with precipitation. At higher acid concentrations and with careful H_2O_2 addition, a very filterable hexagonal form of plutonium(IV) peroxide precipitates. At lower acidities a gelatinous cubic form precipitates that is difficult to filter. Plutonium(IV) peroxide is not a stoichiometric compound and its O:Pu ratio may approach 3.5 (Cleveland, 1979, 1980), but does not reach 4.0 as is suggested by the formula $Pu(O_2)_2$. Anions such as nitrate, chloride, and sulfate, if present in the solution, are incorporated into the solid. Indeed, sulfate is added in some processes at a concentration of 0.1–0.3 M to nitric acid solutions to improve the filterability of the peroxide precipitate.

The Pu(IV) peroxide precipitation is a powerful method for purification of plutonium from many impurity elements except those such as thorium, neptunium, and uranium that form similar peroxides under these conditions. Unlike the oxalate precipitations, Am(III) is removed to a high degree. The excellent

decontamination factors obtained for many elements and the use of one reagent that is easily decomposed to water and oxygen in subsequent operations are the major advantages of using this process. The disadvantages are greater losses of plutonium in the filtrate (typically 0.1–0.5%) and violent decomposition of H_2O_2 that can occur during precipitations in the presence of high concentrations of iron and other metal ion catalysts for the decomposition reaction.

(*iv*) *Plutonium*(III) *fluoride precipitation*

Addition of aqueous HF to a solution of Pu(III) in nitric or hydrochloric acid precipitates blue-violet $PuF_3 \cdot xH_2O(x \sim 0.75)$ (Christensen *et al.*, 1988). The Pu(IV) concentration should be kept low because the hydrated PuF_4 precipitate is very gelatinous and much more soluble than the trifluoride. Significant Pu(IV) content will thus increase filtering time and plutonium losses to the filtrate. Reducing agents such as hydroxylamine, sulfamic acid, or ascorbic acid are commonly used. With careful oxidation state control, losses of plutonium to the filtrate are very low (0.05–0.1%). A disadvantage of preparing any fluorine-containing compound of plutonium is increased production of neutrons from α-n reactions relative to the oxygen-, carbon-, and nitrogen-based precipitants. The trifluoride precipitation does not give decontamination factors from cationic impurities that are as high as the oxalate or especially the peroxide precipitations. It gives moderate decontamination from many impurities including iron, but not from aluminum, zirconium, and uranium. Dried PuF_3 can be roasted in oxygen to produce a mixture of PuF_4 and PuO_2 that can be directly reduced with calcium metal to give 95–97% yields of plutonium metal (See Sections 7.7.1 and 7.7.2).

(*v*) *Plutonium hydroxide precipitation*

Hydroxide precipitation is quite useful to produce a filtrate with very low levels of plutonium. Sodium or potassium hydroxide solutions are commonly added to precipitate the gelatinous green Pu(IV) hydroxide (Christensen *et al.*, 1988). If Pu(III) is present, it will slowly oxidize to Pu(IV). Many other metal ions will precipitate as hydroxides as well or be carried by the plutonium hydroxide so that this is not a useful purification procedure. The hydroxide is generally difficult to filter. If large amounts of magnesium or calcium are present, the voluminous hydroxide precipitates of these metal ions make filtration especially difficult, unless they are avoided by carefully controlling the pH. The dried hydroxide cake can be recycled for plutonium recovery by dissolving it in acid. The formation of the Pu(IV) oxyhydroxide polymer should be avoided because this material behaves quite differently from the hydroxide precipitate and can be quite difficult to redissolve in acid. The formation and properties of the polymer are described in more detail in Section 7.9.1.d.

(*vi*) *Miscellaneous precipitations*

Other precipitation methods have been tested for plutonium processing operations, but have not been deployed or as widely used as those reviewed above. These include $CaPuF_6$ and Cs_2PuCl_6 from acid solutions for metal production operations (Christensen *et al.*, 1988; Muscatello and Killion, 1990) and $(NH_4)_4PuO_2(CO_3)_3$ or mixed $(NH_4)_4(Pu, U)O_2(CO_3)_3$ from alkaline solution for the preparation of MOX fuels (Roepenack *et al.*, 1984).

7.5.4 Solvent extraction separation processes

Liquid–liquid (or solvent) extraction partitions solutes between two immiscible liquid phases. The two phases are generally intimately mixed to improve the rate of transfer of solutes between them. The use of a laboratory separatory funnel by a synthetic chemist illustrates the operation of a single stage of liquid–liquid extraction. The two immiscible phases, commonly an organic and an aqueous phase, are shaken vigorously for some time to approach the equilibrium distribution of solutes between the phases and then the phases are allowed to coalesce and reform layers that can be separated. On an industrial scale, the labor-intensive separatory funnel is replaced by a wide variety of equipment that pumps, mixes and separates the phases in a continuous operation so that multiple stages of extraction and back-extraction can be accomplished in an efficient manner. Solvent extraction is a very versatile and useful industrial separation method and has proven to be very important for the recovery and purification of plutonium and other actinides. In fact, as discussed in Chapter 24 of these volumes, the industrial practice of solvent extraction advanced considerably because of the new development work needed to solve the separation challenges of processing neutron-irradiated fuels and targets for military and industrial applications.

In the case of plutonium and other actinide metal ions, the two immiscible phases used in solvent extraction processes are usually an aqueous acid solution and an organic solvent containing components that stabilize certain metal ion complexes in the organic phase. Nitric acid is the most common acidic solution used; hydrochloric acid has seen more limited application. Acids with more strongly complexing anions such as sulfuric, phosphoric, or hydrofluoric acids can have problems with limited solubilities of actinide ions (see Table 7.5) and also some fission product metal ions and are used less commonly. In some cases, these acids with more strongly complexing anions are used in controlled amounts in the acidic aqueous phase as 'masking agents' to hold certain metal ions in the aqueous phase and to improve the selectivity of the extraction into the organic phase. They can also be deployed in an aqueous phase to 'strip' or back-extract metal ions from an organic phase that has been 'loaded' with metal ions in a previous step of the process.

The organic phases used for actinide extractions comprise a wide range of solvents (or diluents) and organic-soluble compounds (extractants) that stabilize metal complexes in an organic phase. Aliphatic and aromatic hydrocarbons, chlorinated hydrocarbons, ethers, and ketones represent some of the major solvent groups. In some cases the solvent and the extractant are the same. For example, chemists used diethyl ether to extract uranyl nitrate from aqueous solutions long before the nuclear age dawned. The influence of the solvent on the extraction system is manifested in various ways such as the solubility of the extractant and metal ion species, the overall thermodynamic activity of the extractant, and the concentration of water in the organic phase (Cox and Flett, 1983).

Metal ions can be stabilized in the organic phase in a variety of structures. While uncharged individual metal ion complexes are solvated in the organic phase in many cases, ion-pairs, reverse micelles, and other aggregated structures are observed, especially as higher concentrations of metal ions are loaded into the organic phase (Borkowski *et al.*, 2003; Chiarizia *et al.*, 2003). For many extraction systems, a third phase can form if the metal ion concentration becomes too high in the organic phase (Rao and Kolarik, 1996). This is a situation to be avoided because the extraction equipment is designed to separate two liquid phases, not three, and any solid phase is particularly troublesome. Phase-modifying reagents are sometimes added to the organic solvent to inhibit third-phase formation and to allow higher levels of metal loading.

When two or more extractant compounds are combined in a single solvent they may act independently or the extraction equilibrium for a metal ion can be enhanced over what each extractant would give independently. This effect is referred to as synergism. It is most typically observed when an acidic extractant is combined with a neutral donor extractant and the major extractant complex contains both extractants bound to the metal ion (Cox and Flett, 1983).

The range and combinations of compounds that have been used in organic solvents to extract plutonium is very extensive and cannot be reviewed here. The extractant compounds can be generally divided into two large groups: compounds with donor atoms that form organic-soluble complexes with the metal ion, and ion-pair reagents that stabilize a charged metal ion complex in the organic phase. Given the hard Lewis acid character of the actinide metal ions, it is not surprising that most of the ligand-type extractants have one or more oxygen donor atom sites that coordinate to the metal ion in the organic phase. The major actinide extractant classes are alkyl and aryl phosphates, $(RO)_3P{=}O$, phosphonates, $(RO)_2RP{=}O$, phosphinates, $(RO)R_2P{=}O$, and phosphine oxides, $R_3P{=}O$; alkyl and aryl phosphoric, $(RO)_2PO_2H$, phosphonic, $(RO)RPO_2H$, and phosphinic acids, R_2PO_2H; ethers, R_2O; ketones, $R_2C{=}O$; 1,3-diketones, $RC(O)CH_2C(O)R$; amides, $RC(O)NR_2$, malonamides, $R_2NC(O)CHRC(O)NR_2$, and carbamoylmethylphosphine oxides, $(RO)_2P(O)CH_2C(O)NR_2$ (the R groups in the formulas can all have different or identical alkyl or aryl functionality). The major ion-pair extractant classes

for actinides are tetraalkylammonium salts, $R_4N^+X^-$, and protonated tertiary amines, $R_3NH^+X^-$. More detail on the classes of solvent extraction systems and their use for actinide separations is found in Chapter 24. Tri(*n*-butyl) phosphate (TBP), $(n\text{-BuO})_3P{=}O$, is of particular importance for plutonium separations as the key component of the PUREX process and will be discussed below.

(a) The PUREX process

As mentioned previously, nearly all of the roughly 500 metric tons of plutonium that has been separated to date has been recovered using the PUREX solvent extraction process. The use of TBP to extract nitrate complexes of uranium and other actinides was examined as early as 1944 during the Manhattan Project (Orlemann, 1944; Spedding *et al.*, 1945; Warf, 1945) and a patent application for a solvent extraction process for plutonium based on TBP and other trialkylphosphates was submitted in 1947 – the patent was not issued until 1960 because of security concerns (Anderson and Asprey, 1960). The development work leading to deployment of the process started in the late 1940s principally at Oak Ridge National Laboratory (Coleman and Leuze, 1978). The PUREX process was first used in 1954 at the Savannah River site of the U.S. Atomic Energy Commission and then in 1956 at the Hanford site (Swanson, 1990). With many variations in operational details, the process has since been used around the world as the principal method to separate plutonium and uranium from used reactor fuel and neutron-irradiated actinide materials (McKay *et al.*, 1990). The key to this process is the selective extraction of U(VI) and Pu(IV) from a nitric acid solution of dissolved irradiated fuel into an aliphatic hydrocarbon solvent containing TBP while leaving most of the fission products in the acid solution. The plutonium and then the uranium can be back-extracted separately from the loaded organic solvent into an aqueous strip phase. Additional solvent extraction stages with TBP can be used to further purify the uranium and plutonium or another method such as ion exchange can be used. Most PUREX operations target very pure uranium and plutonium products with high decontamination factors from the fission products of about 10^8 and high recovery (typically about 99.9%).

The following equilibrium equations represent the major separation steps of the PUREX process:

$$Pu^{4+}_{(aq)} + 4NO^-_{3\,(aq)} + 2TBP_{(org)} \rightleftharpoons Pu(NO_3)_4(TBP)_{2\,(org)} \tag{7.8}$$

$$UO^{2+}_{2\,(aq)} + 2NO^-_{3\,(aq)} + 2TBP_{(org)} \rightleftharpoons UO_2(NO_3)_2(TBP)_{2\,(org)} \tag{7.9}$$

$$HNO_{3\,(aq)} + TBP_{(org)} \rightleftharpoons TBP \cdot HNO_{3\,(org)} \tag{7.10}$$

The subscripts (aq) and (org) refer to species present in the aqueous and organic phases, respectively. The distribution coefficient (D) in liquid–liquid

extraction is defined as the ratio of the concentration of the solute in the organic phase to that in aqueous phase under a particular set of conditions, e.g. volume ratio of the aqueous to organic phase, temperature, extractant concentration, pH, metal ion concentration. Tetravalent and hexavalent actinide ions are selectively extracted under the PUREX conditions (typically 1–3 M nitric acid and 20–30 vol % TBP in an aliphatic hydrocarbon diluent) but the trivalent and pentavalent oxidation states of the actinides and most of the fission products are poorly extracted. This is illustrated by the data in Table 7.7 that lists the single-stage distribution coefficients for U(VI), Pu(VI), Pu(IV), Pu(III), and a group of fission products for TBP and two other compounds, hexone [$CH_3C(O)CH_2CH(CH_3)_2$] and dibutylcarbitol [$CH_3(CH_2)_3O(CH_2)_2O(CH_2)_2O(CH_2)_3CH_3$] that were the basis for two other competing solvent extraction processes, REDOX and BUTEX (Peterson and Wymer, 1963). The REDOX and BUTEX processes were used for a time at Hanford and in the United Kingdom, respectively, but eventually were replaced by the PUREX process. The data in Table 7.7 illustrate that the modest D values like those for uranium of 1.5–8.1 can be exploited for high recovery by using multiple stages of extraction. The data in the table also show that the bulk of the fission product have very low D values, but there are exceptions (Zr, Ru, and Tc). These fission product contaminants can be removed in various ways during the additional uranium and plutonium purification operations.

The equations shown above for Pu(IV) and U(VI) extraction indicate that higher nitrate concentrations in the aqueous phase and higher TBP concentrations in the organic phase should increase the D values for these metal ions. This is indeed observed as long as the activities of the various species are taken into account and metal ion concentrations are low. However, the extraction of nitric acid by TBP indicated in (7.10) competes with metal ion extraction for the TBP and limits the increase in the D value with increasing nitric acid concentration. The D values will continue to increase at a low fixed nitric acid concentration if nitrate salts are added to the aqueous phase rather than nitric acid. Pure TBP is

Table 7.7 *Distribution coefficients of uranium, plutonium, and some fission products using TBP, hexone, and Butex extractants.*

Solvent	*U(VI)*	*Pu(VI)*	*Pu(IV)*	*Pu(III)*	*Fission products*[a]
hexone[b]	1.6	2.9	0.84	4.5×10^{-4}	0.03
TBP[c]	8.1	0.62	1.55	0.008	0.001
Butex[d]	1.5	1.8	7	<0.01	~ 0.02

[a] Combined β emitters (without Zr, Ru, Ca).
[b] From 0.3 M HNO_3/1.0 M $Al(NO_3)_3$/(U,Pu) into hexone at 25°C, or from 0.25 M HNO_3/1.5 M $Al(NO_3)_3$/ΣFP into hexone at 25°C.
[c] From 3.0 M HNO_3 into 30 vol.% TBP in kerosene at 25°C.
[d] From 4 M HNO_3 into dibutylcarbitol (Butex).

a liquid and can be used as the organic phase in an extraction, but it is quite viscous. PUREX plants typically operate with 20–30 vol % TBP in an aliphatic hydrocarbon diluent (Swanson, 1990).

Adjusting the oxidation state of plutonium from Pu(IV) to Pu(III) is the most commonly used way of selectively stripping plutonium from the loaded organic phase. As shown in Table 7.7, the D value of Pu(III) is quite low and it will preferentially distribute to the aqueous nitric acid phase. Reducing agents that have been used to strip plutonium from the TBP phase are Fe(II), hydroxylamine, and U(IV). The addition of ferrous sulfamate in the aqueous acid solution used to strip the plutonium has given some of the best results as indicated by the purity of the uranium and plutonium products that result (Miles *et al.*, 1990). The overall equation for the Fe(II) reduction and stripping reaction is:

$$Pu(NO_3)_4(TBP)_{2\,(org)} + Fe^{2+}_{(aq)} \rightarrow Pu^{3+}_{(aq)} + 4NO^{-}_{3\,(aq)} + Fe^{3+}_{(aq)} + 2TBP_{(org)} \tag{7.11}$$

After the removal of plutonium, the uranium can be stripped from the TBP phase with a dilute acid solution. The TBP solution can then be reused to extract more uranium and plutonium. A generalized PUREX flow sheet is shown in Fig. 7.5.

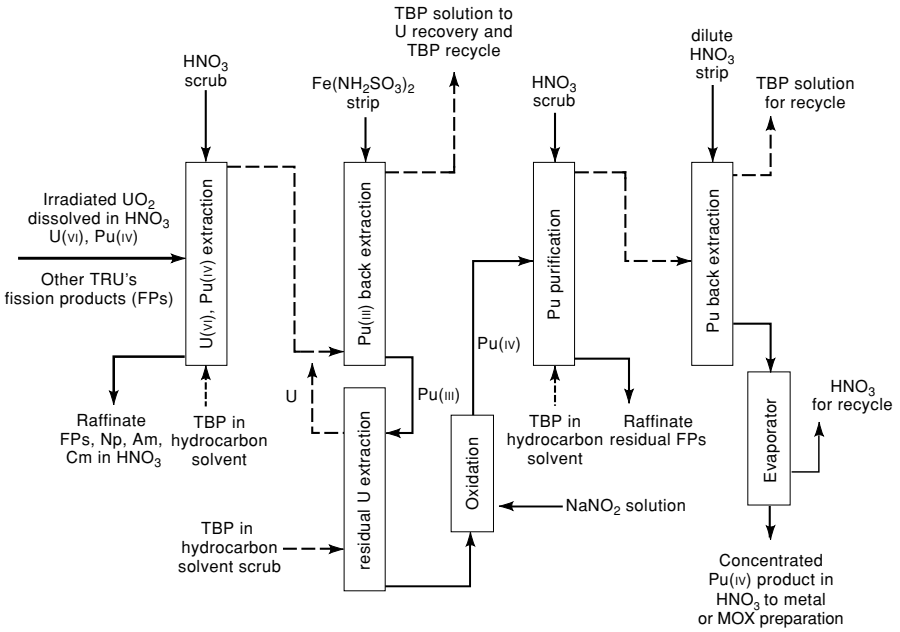

Fig. 7.5 *A generalized PUREX flow sheet where the dashed line indicates the organic stream.*

Of course, there are many other operations needed for running an actual PUREX plant that are not indicated by the simple extraction equations above. A few will be mentioned here and the references can be consulted for more detail. The decladding and dissolution of the fuel in nitric acid in a highly shielded facility are major operations that prepare the feed for the PUREX process. During the extraction process, the organic solvent and TBP undergo degradation reactions because of reactive species produced by the high level of ionizing radiation, particularly in the first extraction cycle where all the fission products are present. Some of the degradation products of TBP, dibutylphosphoric and monobutylphosphoric acids can cause problems by forming solids and modifying the D values for certain metal ions. This is dealt with by adding a washing operation to keep the concentration of these compounds below certain levels. The slight solubility of TBP and any entrainment of organic phase droplets in the aqueous phase also cause losses that must be replaced. Maintaining the oxidation states of various actinide and fission product metal ions in the intense radiation field requires careful adjustments at various points in the process. To improve process efficiency and to minimize wastes, evaporators are used to recover nitric acid and concentrate solutions at various points in the process. Finally, the products and wastes from all the operations must be handled properly and transported to their next destination.

During more than 50 years of use around the world, the PUREX process has undergone many improvements. Enhancements continue to be made at operating plants and new plants that will begin operations in the future. As options are considered for advanced nuclear fuel cycles, additional separations operations are under development for potential deployment in PUREX-type plants (see Chapter 24, section 4). Among these operations are solvent extraction processes for recovery of neptunium, americium, and curium to allow their transmutation in advanced reactor systems and for technetium, cesium, and strontium to allow these fission products to be disposed of more efficiently. Solvent extraction systems are certainly the most developed separation processes to accomplish these goals in the near future. The use of other separation approaches to augment or replace solvent extraction in advanced nuclear fuel cycles will require large technology development efforts.

(b) Extraction chromatography and supported liquid membranes

Liquid–liquid extraction can be deployed in forms other than the typical methods of mixing and separating the immiscible liquid phases. In extraction chromatography, the extractant and solvent (in some cases) are prepared in a thin layer on a solid support that usually consists of small spherical particles of a polymer or inorganic material. Inorganic materials such as silica require a surface treatment to generate a relatively hydrophobic surface that will be compatible with the organic extraction components. Aqueous solutions are contacted with the solid and metal ions are extracted into the thin surface

layer much as occurs in a liquid–liquid extraction system. However, the composition of the surface layer can be quite different from that of the liquid–liquid system and this must be taken into account when predicting extraction behavior. Extraction chromatography materials are used most commonly for analytical separations of plutonium and other actinides and have been deployed for a limited number of gloved box scale process operations. These materials generally do not have the radiation stability or capacity for use in large-scale processing of irradiated fuels. However, such an approach has been proposed and tested at a small scale with a spent fuel solution using some silica-based extraction materials by Wei and coworkers (Wei *et al.*, 2002).

Supported liquid membranes consist of a liquid phase that separates two fluid phases: two gases, two liquids, or a gas and a liquid. Components in the fluid phases can be separated by differential transport through the liquid membrane phase driven by the chemical potential gradients. For metal ion separations, the fluid phases on each side of the membrane are usually aqueous solutions and the membrane consists of a porous solid support with an organic extractant solution filling the pores. Supported liquid membranes have been demonstrated on the laboratory scale to be an efficient separation method for metal ions, but have seen relatively few industrial applications because of long-term stability problems. With time, the components of the liquid membrane are lost to the aqueous phases and the membrane fails. Many approaches have been considered to overcome this problem, but none have yet seen widespread industrial use (Sastre *et al.*, 1998).

In the extraction chromatography and supported liquid membrane systems the active extractant is not chemically bound to the support. Solids that do contain such chemically bound groups that can selectively bind plutonium and other actinides will be discussed under ion-exchange processes (see Section 7.5.5).

7.5.5 Ion-exchange processes

Ion-exchange materials are insoluble solid materials with groups of one charge fixed in a three-dimensional solid matrix and mobile or exchangeable ions of the opposite charge associated with these fixed sites that balance the charge in the solid. In contact with a liquid phase that contains dissolved ions, the mobile ions will be exchanged for ions of like charge in the solution if the overall free energy of the system is lowered after the exchange. The relative affinity of the ion-exchange material for various cations or anions can be used to separate particular ions from solution. By using a regeneration solution under different conditions, it is usually possible to recover the adsorbed ions from the ion-exchange material (often in more concentrated and pure form) and prepare the ion-exchanger for additional cycles of exchange and regeneration. Both inorganic solids and organic polymers, including natural materials such as clays and zeolites, can function as ion exchangers. Ion exchange has long been an important process for water treatment. One of the first industrial

applications of ion exchange described in 1905 was the use of synthetic sodium aluminosilicates (zeolites) to exchange Ca^{2+} from hard water with Na^{+} (Simon, 1991).

Ion exchangers are commonly deployed in industrial processes as a packed bed of small particles to obtain a high surface area and accessible exchange sites with minimal diffusion path lengths to the sites. In the loading phase, liquid feed solution is passed through the bed until the mobile ions in the solution have been exchanged for mobile ions in the solid to the extent that the target ion or ions are no longer being removed from solution to the required level. If the ions loaded on the exchanger are to be recovered as a product (e.g. plutonium), one or more wash solutions may be passed through the bed to improve the final purity by removing residual feed solution and exchanging more weakly held ions. In the elution phase a different solution is passed through the column to recover the product ions. The conditions during the elution phase are changed (pH, ion concentration or type, temperature, etc.) so that the target ions bound during the loading phase are exchanged back into the solution. After elution the ion exchanger may be ready for reuse directly or may require an additional regeneration step. Most ion-exchange processes are operated in such a batch mode with separate loading and elution or regeneration steps. Continuous ion-exchange processes have also been developed, but are not as widely used as batch operations (Simon, 1991).

Ion-exchange processes for metal ion separation most commonly use an organic polymer solid phase (often referred to as an ion-exchange 'resin') containing charged functional groups fixed to the polymer structure to selectively bind metal ions or complexes of metal ions with a net opposite charge from an aqueous solution. The organic polymer is usually prepared in the form of small spherical particles or beads with a large internal porosity. The structure of the polymer greatly affects the final ion-exchange properties and the synthetic conditions are adjusted to control properties such as the degree of crosslinking, the number of ion-exchange sites, the size distribution of the pores, and the bead size. The polymer structure in most commercial ion-exchange materials is formed from styrene (vinyl benzene)–divinylbenzene copolymers with the fixed charged groups attached to the phenyl rings. The most common functional groups are sulfonic acid and carboxylic acid groups with protons that exchange for cations (cation exchangers) and alkylamine, alkanolamine, and tetraalkylammonium groups that act as anion exchangers. Other polymer structures have been used to make ion exchangers including polyacrylates and polyvinylpyridines (Simon, 1991; Harland, 1994).

(a) Plutonium ion-exchange separations

Both cation- and anion-exchange processes have been used for concentrating and purifying plutonium from aqueous solutions that result from processing operations ranging from solvent extraction (e.g. PUREX) to recovery of

plutonium leached from scrap or debris material. Ion exchange is generally not used as the primary step to separate plutonium and other actinides from fission products in nuclear fuel or neutron-irradiated targets because the intense radiation field degrades the polymer matrix too rapidly. However, organic ion exchangers are very useful for separations in acidic solutions where the radiation dose comes mostly from plutonium and other actinides. Inorganic ion exchangers are generally more radiation-resistant than organic exchangers, but have other problems for large-scale processing such as limited stability over wide pH ranges, difficulty in obtaining reproducible behavior from batch to batch, and the greater difficulty of preparing particles of suitable size and shape for processing (Pekarek and Marhol, 1991).

Plutonium in any of its oxidation states can be taken up onto cation exchangers from dilute acid solutions with weakly binding anions such as nitric, hydrochloric, or perchloric acids. The strength of the binding of the oxidation state decreases in the order $Pu^{4+} > Pu^{3+} > PuO_2^{2+} > PuO_2^{+}$ as expected with the decreasing net charge on the cation. The ion-exchange process on a strong acid cation exchanger can be represented by the reaction:

$$Pu^{n+}_{(aq)} + nRH_{(org)} \rightarrow Pu(R)_{n\,(org)} + nH^{+}_{(aq)} \tag{7.12}$$

where RH represents a proton exchange site on the organic resin (usually a sulfonic acid site) and $n+$ is the net charge on the plutonium species. Separations can be made based on the ionic charge alone, but the greater utility of ion exchange results from using the exchange material in combination with complexants in the aqueous solution that bind the various oxidation states of plutonium and other metal ions differently. For example, in dilute hydrofluoric acid, Pu(III) will bind to a cation-exchange resin more strongly than Np(IV), in apparent disagreement with the expected order based on oxidation state alone. This is because Np(IV) forms complexes with fluoride to a greater extent than Pu(III) thereby reducing its overall net charge, e.g. NpF_3^{+} and NpF_2^{2+} (Zagrai and Sel'chenkov, 1962). Measuring the change in the ion-exchange equilibrium as a function of metal ion binding in the aqueous phase is one method for determining stability constants and can be particularly useful for radioactive metal ions like plutonium that can be analyzed at low concentrations.

The formation of anionic complexes of plutonium, especially by Pu(IV) and Pu(VI), is the basis for separations using anion-exchange resins. For example, in moderate concentrations of hydrochloric acid (~6 M) both Pu(IV) and Pu(VI) absorb strongly on a Dowex 1 resin (quaternary ammonium exchange sites), but Pu(III) shows no significant uptake even in concentrated HCl. Spectroscopic and ion-exchange capacity data indicate that the anionic species bound in the resin are $PuCl_6^{2-}$ and $PuO_2Cl_4^{2-}$ (Ryan, 1975). If high concentrations of chloride salts (e.g. 10 M LiCl) are used with a relatively low acid concentration, Pu(III) can also be taken up on Dowex 1 as an anionic complex. The absorbed plutonium species can be eluted from the resin by using low concentrations of HCl.

Anion exchange of Pu(IV) from moderate concentrations of nitric acid or nitrate salts is a particularly useful separation method for plutonium and has been applied from the process scale to the analytical scale. Applications range from concentrating and purifying the plutonium product stream from PUREX plants, to recovering and purifying plutonium dissolved from a wide range of scrap, residue, and debris materials, to preparation of analytical samples. The basis for the separation is the strong adsorption of Pu(IV) onto the anion-exchange resin from moderate concentrations of nitric acid or nitrate salts. Few other elements are significantly retained under these conditions by an anion exchanger and large separation factors can be obtained (Faris and Buchanan, 1964). The III, V, and VI oxidation states of plutonium and other actinides are also not bound strongly. Fig. 7.6 shows the Pu(IV) distribution coefficients (K_d) onto Dowex 1×4 resin plotted as a function of nitrate concentration for HNO_3 and $Ca(NO_3)_2$ solutions at 25 and 60°C (Ryan, 1959). The high distribution coefficients for Pu(IV) near 7 M nitric acid when combined with

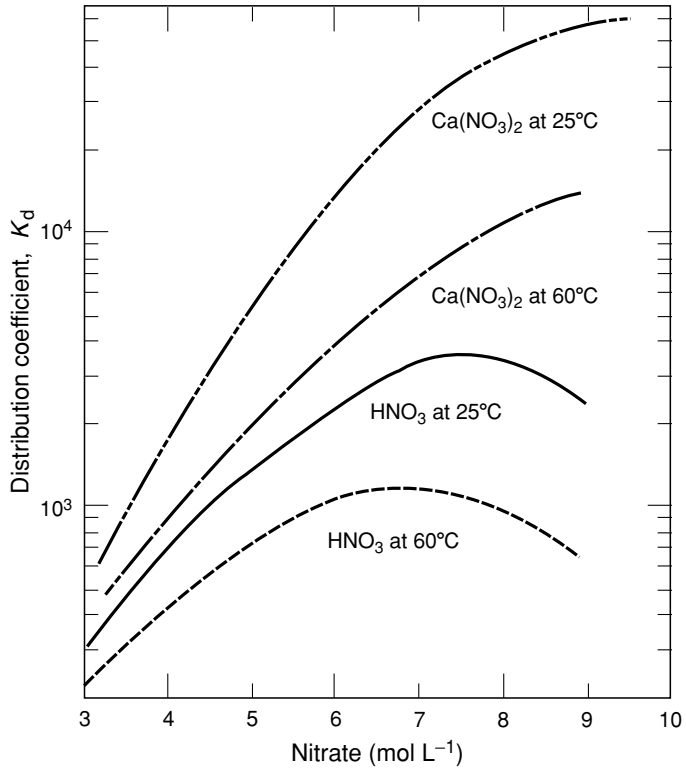

Fig. 7.6 *Plutonium(IV) distribution coefficients from nitric acid and calcium nitrate onto Dowex* 1 × 4 *anion-exchange resin* (*Ryan*, 1959).

an efficient elution method make large concentration factors possible. Elution of the plutonium is usually accomplished using a low nitric acid concentration alone or a low concentration of nitric acid and a reducing agent that generates Pu(III). The data in Fig. 7.6 show that the K_d values are lower at higher temperature, however, the kinetics of loading and elution are faster at higher temperature and this factor can be used as an advantage in process design (Ryan, 1975).

Visible absorption spectroscopy and resin capacity data show that Pu(IV) is absorbed on anion exchangers from nitric acid or nitrate salt solutions as the hexanitrato complex, $Pu(NO_3)_6^{2-}$ (Ryan, 1960, 1975). This has been confirmed by recent extended X-ray absorption fine structure (EXAFS) studies of anion exchange resins loaded with plutonium (Marsh *et al.*, 2000). Visible absorption, nuclear magnetic resonance (NMR), and EXAFS spectra of Pu(IV) and Th(IV) in nitric acid have also refined the information on the complexes formed in nitric acid solution (Veirs *et al.*, 1994; Allen *et al.*, 1996b; Berg *et al.*, 1998, 2000). At low nitric acid concentrations (~0.1 to 3 M) Pu^{4+}, $Pu(NO_3)^{3+}$, and $Pu(NO_3)_2^{2+}$ are the major species present (water molecules fill the rest of the plutonium coordination sphere in these complexes). At high nitric acid concentrations (>10 M), $Pu(NO_3)_6^{2-}$ is the dominant complex. At intermediate nitric acid concentration, in addition to $Pu(NO_3)_2^{2+}$ and $Pu(NO_3)_6^{2-}$, one major additional species is present that has been assigned as $Pu(NO_3)_4$. The trinitrato and pentanitrato complexes do not appear to be present at levels that can be easily observed (See Section 7.9.1.e). The concentration profile of the putative $Pu(NO_3)_4$ complex peaks at about 7 M nitric acid and correlates well with the distribution coefficient profile for Pu(IV) on anion-exchange resins from nitric acid (Marsh *et al.*, 1991). This observation suggests that the uncharged $Pu(NO_3)_4$ species might be important to the mechanism of uptake for Pu(IV) on an anion exchanger, but further work will be needed to verify this.

A general flow sheet for the operation of an anion-exchange process for plutonium recovery is illustrated in Fig. 7.7 (Christensen *et al.*, 1988). The oxidation state of plutonium dissolved in the nitric acid feed solution is carefully adjusted to maximize the amount of Pu(IV) because plutonium in other oxidation states is not retained on the exchanger. A variety of methods can be used for the oxidation state adjustment based on the composition of the feed. If fluoride is present in the feed solution, aluminum may be added to preferentially complex the fluoride and improve plutonium recovery. The nitric acid concentration is adjusted to 7 M and the solution is pumped through the packed bed of anion exchange beads so that $Pu(NO_3)_6^{2-}$ binds to the exchanger. The loaded resin is washed with 7 M nitric acid to remove impurities. Nitric acid at low concentration (0.35–0.6 M) is then pumped through the bed to elute the Pu(IV), or a solution of hydroxylammonium nitrate (or another suitable reducing agent) in dilute nitric acid is used to elute Pu(III). The plutonium in the eluate is commonly precipitated as an oxalate complex of either Pu(III) or Pu(IV) and the washed and dried oxalate solid is calcined to give a PuO_2 product.

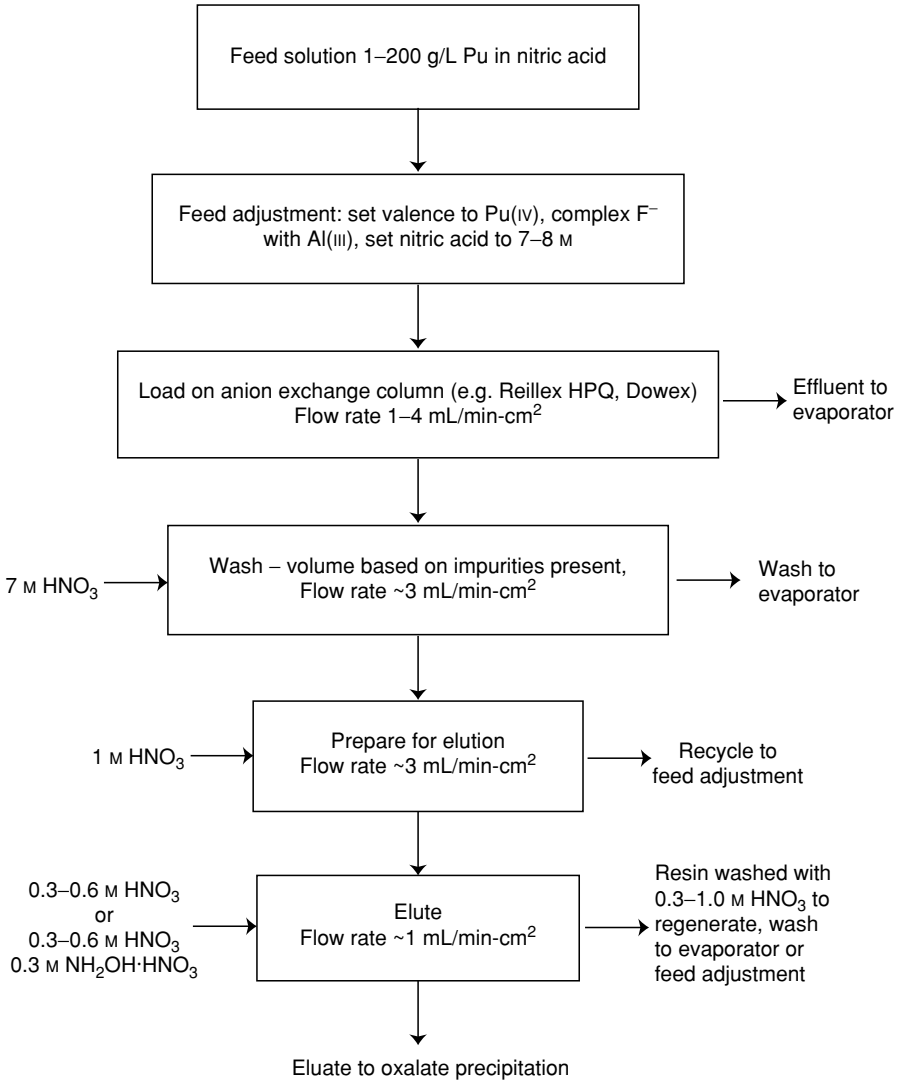

Fig. 7.7 *General flow sheet for operation of Pu(IV) anion-exchange purification process in nitric acid.*

There are a number of important features that must be controlled to safely and efficiently operate such an anion-exchange process for plutonium purification. Some of these features will be mentioned here. More detail can be found in the references (Cleveland, 1980; Christensen *et al.*, 1988). The batch size and the geometry of the packed bed are set up so that criticality cannot occur during

normal operation. During elution of plutonium from the column, the nitric acid concentration should not drop so low as to allow the formation of the Pu(IV) polymer (see Section 7.9.1.d) as this material can clog the column and can be difficult to redissolve. The nitric acid–organic resin system can undergo a runaway oxidation reaction if temperatures are allowed to reach an initiation point around 160–180°C. A variety of safety devices and operating procedures are used to avoid this situation. For example, in using anion exchange to purify plutonium with a high percentage of the ^{238}Pu isotope for radioisotope heat sources, smaller batch sizes and columns are used to allow removal of the additional heat generated by decay of ^{238}Pu in comparison to 'regular' plutonium with a high ^{239}Pu content (Pansoy-Hjelvik *et al.*, 2001).

Ion exchange has been employed for separating plutonium and studying its chemistry since its discovery of more than 60 years ago. Considerable advances have been made in the processes used to manufacture ion-exchange materials during this time, partly driven by the need to separate plutonium and other actinides more efficiently. Highly uniform ion-exchange beads with reproducible behavior are now standard. The development of methods to synthesize macroporous polymer structures in the beads has reduced swelling and shrinkage of the bed as a function of changing solution conditions while retaining good kinetics of absorption (Simon, 1991). The organic ion-exchange polymers are degraded by radiation-induced reactions as noted above, including the alpha-induced radiolysis reactions of plutonium solutions in nitric acid. Anion exchange polymers made from 4-vinylpyridine crosslinked with divinylbenzene (e.g. Reillex HPQ) were demonstrated to be substantially more resistant to radiation-induced degradation than related polystyrene-based anion exchangers while maintaining excellent properties for plutonium processing (Marsh *et al.*, 1991; Buscher *et al.*, 1999). Reillex HPQ has thus replaced the polystyrene-based materials for plutonium recovery operations at some facilities.

Of course, improvements in ion-exchange technology will continue. Exchange columns that consist of a microporous polymer monolith with uniform flow paths and relatively short diffusion pathways compared to packed beds of beads have been developed. These materials could greatly improve future ion-exchange processes (Buchmeiser, 2001; Viklund *et al.*, 2001). Inorganic ion exchangers are continuing to become more versatile and should see wider applications. Membrane-based ion-exchange processes are also seeing wider application and offer potentially very efficient separation operations, but generally will require membrane materials with better long-term stability, including radiation stability, to replace the more common column method.

(b) Liquid ion exchangers and chelating ion exchangers

The solvent extraction processes discussed in Section 7.5.4 that use organic-soluble tetraalkylammonium salts or trialkylamines to extract anionic metal ion complexes as ion pairs are ion-exchange processes as well. These extractants

are sometimes referred to as 'liquid anion exchangers.' Liquid cation exchangers are also used, for example, aliphatic and aromatic sulfonic acid compounds. Also, many types of functional groups have been placed on polystyrene and other polymer supports that can bind directly to the inner coordination sphere of a metal ion and help to stabilize a complex of the metal ion on the solid phases. This includes essentially all of the oxygen donor functionalities that were discussed in Section 7.5.4 (e.g. phosphates, phosphonates, phosphinates, and phosphine oxides). These polymers containing fixed ligand sites resemble solid versions of solvent extraction systems. However, fixing of the ligand to the polymer structure can considerably alter the metal ion-binding properties relative to an analogous ligand in solution. These kinds of materials are often referred to as 'chelating ion-exchange polymers' or resins, but it must be recognized that more than exchange of ion pairs is occurring in such materials and the thermodynamics of complex formation must be included in determining the selectivity and strength of the metal ion binding in these polymers. The use of chelating ion-exchange materials for separations of actinides is reviewed in Chapter 24 and a more general review for metal ion separations was published by Beauvais and Alexandratos (1998).

7.5.6 Separations in aqueous alkaline solutions

As noted in the brief discussion of aqueous actinide chemistry above, alkaline solutions are generally not used for actinide processing because the hydroxide complexes are quite insoluble. Large amounts of high-level caustic waste containing small amounts of actinides have been generated at Hanford and Savannah River as a result of neutralizing nitric acid solutions from PUREX recovery operations. A large body of work has been performed to better define the speciation of the actinides and to examine some potential processes for removing actinides from highly caustic tank wastes, including plutonium removal with various precipitants and absorbents. An overview of this work with references to the extensive literature has been published (Clark and Delegard, 2002).

Alkaline solutions containing strong ligands that can compete with hydroxide such as carbonate, fluoride, and peroxide can give high solubility to actinides in some oxidation states and even stabilize unusual oxidation states such as Pu(VII). The relatively small amount of work that has been done on extraction of actinides from alkaline solutions is reviewed in Chapter 24 (Section 3.7). One method to produce MOX fuels uses crystallization of Pu(VI) and U(VI) from ammonium carbonate solutions as $(NH_4)_4PuO_2(CO_3)_3$ or $(NH_4)_4UO_2(CO_3)_3$, respectively. The ammonium plutonyl and uranyl carbonates can be crystallized separately and blended or coprecipitated as the mixed carbonate (Roepenack *et al.*, 1984). An alkaline processing scheme for separation of the components of spent fuel in sodium carbonate/bicarbonate has been proposed and tested at a small scale on uranium and nonradioactive fission product elements (Asanuma *et al.*, 2001).

7.5.7 Nonaqueous separation processes

As noted above, the recovery of plutonium from irradiated uranium fuels has been dominated by the PUREX process, which requires dissolution of the fuel matrix in nitric acid. Alternative fluid media have been used or are under study to dissolve the uranium matrix and allow separation of the fission products from uranium, plutonium, and the other actinides, but none of these methods have been deployed on a large scale. The types of fluid media used include molten salts, molten metals, volatile halide compounds, ionic liquids, and supercritical fluids. The potential advantages for separation processes using these types of media compared to aqueous-based separations include: (1) greater resistance to radiation damage relative to water and organic solvents, (2) fewer and sometimes less complex steps to obtain products, (3) smaller highly shielded processing area, (4) smaller waste volumes that may also allow ready preparation for disposal, (5) simpler criticality control with reduced amounts of neutron moderating and reflecting materials, and (6) new separation selectivity. The separation selectivity for some of the nonaqueous processes are lower on a per stage basis relative to some of the aqueous technology, but that is not always a disadvantage when considering that more impurities may be acceptable in future reactor fuels and that safeguards benefits may result from keeping some components of the original mixture together. The advantages listed above do not apply to every process, but serve to give an indication of why there is continuing interest around the world in nonaqueous processing for advanced nuclear power systems.

The nonaqueous separation methods have disadvantages as well. The major disadvantage has already been mentioned, in that these processes have not been developed as extensively as the aqueous methods and thus have less well-defined costs, safety envelopes, and operational experience. The chemistry of these nonaqueous separation methods is presented in more detail in Chapter 24, especially as they apply to advanced methods for partitioning of spent nuclear fuel. In this chapter, we will briefly review the nonaqueous separation methods most relevant to plutonium processing.

(a) Pyrochemical separation and conversion processes

After plutonium has been separated from the fission products, pyrometallurgical operations have been used since the days of the Manhattan Project to prepare and purify metallic plutonium from various compounds (Hammel, 1998). Plutonium is a very electropositive and reactive metal, and preparation and purification methods based on molten salts and molten metals under inert atmospheres were adapted from industrial practice with adjustments required for actinide-specific factors such as radioactivity and criticality. The major pyrochemical processes used to prepare and purify plutonium metal (bomb

reduction of PuF_4, direct oxide reduction (DOR) of PuO_2, molten salt extraction (MSE) of americium, electrorefining (ER), and pyroredox) are discussed in Sections 7.7.1 and 7.7.2. The pyrochemical operations occur in mixtures of molten Group 1 or 2 chloride or fluoride salts at temperatures of 700–900°C, although temperature spikes near 2000°C may occur during the bomb reduction of PuF_4 with calcium metal. Preparing the feed materials for these pyrochemical operations using aqueous processing operations is reviewed in Section 7.5.3(b).

A wide variety of pyrochemical processes have been considered to separate the components of spent nuclear fuels in advanced nuclear fuel cycles. The processes range from early work on use of molten metals such as silver, cadmium, zinc, and magnesium that are immiscible with molten uranium as extractants for plutonium (Dwyer *et al.*, 1959; Wiswall *et al.*, 1959) to recent work on the pyroelectrochemical deposition of PuO_2 and UO_2 from molten chloride salts for direct fabrication by vibropacking into fast reactor fuel elements (Grachev *et al.*, 2004). An entire reactor system, the Molten Salt Reactor Experiment, based on a molten BeF_2 and ^7LiF core containing fissile UF_4 and fertile ThF_4 was studied at Oak Ridge National Laboratory in the 1960s. Reviews of these processes, both historical and those under development, have been published (Long, 1978; Bychkov and Skiba, 1999).

(b) Room temperature ionic liquids

Room temperature ionic liquids (RTILs) are salts that are liquid at or near room temperature. The RTILs currently under study consist of an organic cation (e.g. quaternary ammonium, $R_1R_2R_3R_4N^+$, or alkylpyridinium) paired with a wide variety of inorganic and organic anions (e.g. $AlCl_4^-$, PF_6^-, $CF_3CO_2^-$). The RTILs are under study for a wide array of applications, such as organic synthesis, battery electrolytes, catalyst systems, and metal ion separations (Rogers and Seddon, 2002). It should be noted that the RTILs and the inorganic molten salts discussed above under pyrochemistry are part of the larger class of ionic liquids. The inorganic salts generally have much higher melting points, but that situation may change to some extent as new classes of ionic liquids are investigated. For example, the sodium/potassium nitrate eutectic has a melting point near 170°C.

Potential applications of RTILs to plutonium and actinide separations are under development in two main areas: use as low temperature ionic liquid solvents for electrochemical deposition of metal or oxide and as liquid–liquid extractants for actinide metal ions from aqueous solutions. A research team led by the Queen's University of Belfast and British Nuclear Fuels, Ltd. has also proposed using RTILs to process spent nuclear fuel (Baston *et al.*, 2002; Pitner *et al.*, 2003). It is not yet known if the present generation of organic-containing RTILS is sufficiently radiation resistant for the processing of spent fuel.

(c) Halide volatility processes

The isotopic separation of volatile UF_6 using processes such as gaseous diffusion or gas centrifugation has been practiced at a large scale since the 1940s. In 1949, Sheft, Andrews, and Katz proposed a separation process for irradiated nuclear fuel based on fluorination using liquid interhalogen compounds. This was the beginning of an extensive research and development program into what is commonly called the fluoride volatility process (Sheft *et al.*, 1949). In this type of process, the irradiated fuel (uranium oxide, uranium alloys, even fuel assemblies with cladding intact) is dissolved in a liquid fluorinating solution, a molten salt sparged with fluorine, or fluorinated directly in a fluidized bed. The volatile UF_6 (along with NpF_6 and PuF_6 depending on the process details) and fission product fluorides such as TcO_3F, RuF_6, NbF_6, and MoF_6 are collected and separated using volatility differences and differences in reactivity of the fluorides with beds of solid reagents. In some proposed fluoride volatility processes, neptunium and plutonium are left with the nonvolatile fission product fluorides and separated by another method such as solvent extraction (Amano *et al.*, 2004).

The major advantages of the fluoride volatility process are relatively simple chemistry, radiation resistance of the reagents, high decontamination factors, and separation of uranium in a form suitable for re-enrichment. The disadvantages are the use of extremely corrosive reagents and the attendant corrosion of materials of construction, the criticality concerns associated with the high reactivity of hexafluorides, especially PuF_6, and controlling their deposition in the process equipment. Investigations of variants of fluoride volatility continue today, but these processes have not yet been deployed on a large scale. A fluoride volatility process for recovery of plutonium from certain scrap materials was demonstrated at the Rocky Flats Plant on a pilot scale, but was never deployed as a regular plant operation (Standifer, 1968).

Chloride volatility processes for separating the components of spent fuels have also been investigated (Bohe *et al.*, 1997). In general, this appears to be a less selective process because of the greater number of volatile fission product chlorides that could accompany the volatile actinide species, but the separation of the various volatile chloride species has not received as much effort as the fluoride system. The removal of zirconium alloy cladding materials by chlorination with HCl or Cl_2 and collection of the volatile $ZrCl_4$ has also been examined (Gens, 1961). This process could potentially provide an attractive alternative to mechanical decladding methods and could allow recycling of the slightly radioactive zirconium.

(d) Supercritical fluid extraction processes

Supercritical fluids, principally carbon dioxide, have been investigated to extract actinides from waste materials, for separating actinides and fission products from spent nuclear fuels, and as an alternative to conventional

liquid–liquid extraction. Reagents required for forming metal ion complexes (which include complexing agents, acids, and/or redox reagents) such as 1,3-diketones or TBP · HNO_3 are dissolved in supercritical carbon dioxide and this fluid phase is contacted with a solid material (e.g. uranium oxides or a waste solid) or an aqueous phase. The extracted metal ions can be recovered by a number of methods: changing the pressure to modify solubility and filtering a solid product, removing the carbon dioxide as a gas to leave a solid or liquid product, or back-extracting the metal ions into an aqueous phase. The bulk of the studies in this area with actinides have used uranium and thorium, but some work with plutonium and other transuranic elements has appeared. Extraction of U(VI) and Pu(IV) from aqueous nitric acid solutions into supercritical CO_2 solutions of TBP has been studied as a function of temperature and pressure (Iso *et al.*, 2000). Some data on the dissolution of oxides with TBP · HNO_3 dissolved in supercritical CO_2 have been reported for PuO_2 and solid solutions of $(Pu,U)O_2$ and $(Pu,Am,U)O_2/Eu_2O_3$ (Trofimov *et al.*, 2004). The use of chelating agents dissolved in supercritical CO_2 or liquid CO_2 with modifiers such as pyridine or water for decontamination of various solid materials including stainless steel, rubber, cotton, plastic, and soil from plutonium and other radionuclides has been studied (Murzin *et al.*, 2002b). The solubility of some 1,3-diketone complexes of U(VI), Np(IV), Pu(IV), and Am(III) in supercritical CO_2 has been measured (Murzin *et al.*, 2002a,b). Removal of plutonium and americium from soil using TBP and thenoyltrifluoroacetone (TTA) or hexafluoroacetone in supercritical CO_2 has been investigated (Mincher *et al.*, 2001; Fox and Mincher, 2002). The studies of supercritical fluid extraction for actinides are reviewed extensively in Chapter 24 (section 3.10).

(e) Combination processes

A great variety of aqueous, nonaqueous, and combined aqueous and nonaqueous processes have been proposed for partitioning of spent fuel. As described above, to prepare and purify plutonium metal, a combination of aqueous (PUREX and precipitation-crystallization methods) and nonaqueous (pyrochemical) processes has been used. A few recent examples proposed in the literature will be briefly described to indicate that combination processes are being considered in future separation facilities for processing used nuclear fuels. Amano and coworkers proposed the use of fluoride volatility on irradiated fuel to separate uranium for re-enrichment. Some volatile fission product fluorides such as technetium would also be collected separate from the uranium. The residual solid would then be dissolved in nitric acid for PUREX-type solvent extraction to separate plutonium and other transuranic actinides from the fission products to recycle the actinides to a fast reactor system, the so-called FLUOREX process (Amano *et al.*, 2004). Another group in Japan has proposed separating uranium, neptunium, and plutonium from spent fuel dissolved in nitric acid by oxidizing the neptunium and plutonium to the hexavalent state

and then cooling the nitric acid solution to crystallize out the mixed nitrate complex $(U, Np, Pu)O_2(NO_3)_2 \cdot xH_2O$ (Kikuchi *et al.*, 2003). A variety of other combined aqueous/nonaqueous processes that have been proposed for processing irradiated fuels are reviewed in Chapter 24.

7.6 ATOMIC PROPERTIES

Plutonium, like all of the heaviest elements, has a very complex electronic structure. The free atom and free ion spectra of plutonium are among the richest and most thoroughly studied of any chemical element. The complexity of the electronic structure is apparent in the spectral properties, such as X-ray absorption and emission spectra, and arc, spark, and discharge emission spectra. Early measurements were made with electrodeless discharge lamps and large grating spectrographs such as the 9.15 m Paschen–Runge spectrograph at Argonne National Laboratory (ANL). Very high-resolution grating spectrographs have been replaced by Fourier transform (FT) spectrometers such as those at the Laboratoire Aimé Cotton (LAC) (built in 1970) and at the Kitt Peak National Solar Observatory. The plutonium free atom, Pu^0, designated Pu I, has 94 electrons of which 86 electrons are in filled shells as found in the radon atom. It is customary in discussing the actinide series to only list the electrons in shells outside the radon core. The outermost electrons of the free actinide atoms and ions outside the radon core are found in the 7s, 7p, 6d, and 5f shells. For example, the ground state (lowest energy) configuration for Pu I is $5f^67s^2$. Identified excited configurations of Pu I within the first 3 eV ($\sim$24,000 cm^{-1}) of the ground state include $5f^56d7s^2$, $5f^66d7s$, $5f^56d^27s$, $5f^67s7p$, $5f^57s^27p$, and $5f^56d7s7p$. In the free atoms and ions, many low-lying configurations interact strongly with each other, giving rise to a large number of electronic states, and tens of thousands of spectral lines. A detailed discussion and review of the spectra of actinide free atoms and ions can be found in Chapter 16, and in reviews by Blaise *et al.* (1983a, 1986), Reader and Corliss (1980), and Blaise and Wyart (1992).

7.6.1 Optical emission spectra of Pu I and Pu II

The emission spectrum of neutral (Pu I) and singly ionized (Pu II) plutonium, which can be excited by arc, spark, hollow cathode, or inductively coupled plasmas, has been extensively studied. The first measurements of plutonium were conducted in 1943 by Rollefson and coworkers (Rollefson and Dodgen, 1943; Dodgen *et al.*, 1944, 1949) who measured the wavelengths and intensities of about 125 spectral lines. In the initial publications of plutonium spectra, only the wavelengths and intensities of unidentified transitions were reported. In 1959, McNally and Griffin reported the first energy level analysis

for Pu II, where seven levels of the lowest terms of the $5f^6 7s$ (^8F and ^6F) electronic configuration were determined (McNally and Griffin, 1959). In 1961, Bovey and Gerstenkorn determined the five lowest levels of $5f^6 7s^2$ (^7F) for Pu I (Bovey and Gerstenkorn, 1961). In 1961, a collaboration was formed between scientists at ANL, LAC, and Lawrence Livermore National Laboratory (LLNL) to continue studies of the term analyses of Pu I and Pu II spectra. In 1970, the FT spectrometry at LAC was used to record the spectra of ^{240}Pu and of a mixture of ^{240}Pu, ^{242}Pu, and ^{244}Pu isotopes up to 3.59 μm. A portion of one of these spectra is shown in Fig. 7.8. The high resolution and extension into the infrared spectral region greatly enhanced the spectral analysis and allowed the connection between the lowest odd and even levels (Blaise *et al.*, 1983a).

The first comprehensive description of Pu I and Pu II spectra became available in 1983, when Blaise, Fred, and Gutmacher collected wavelengths, wavenumbers, intensities, classifications, and isotope shift data in a 612 page ANL report (Blaise, 1983b). In 1992, Blaise and Wyart published all known energy levels of the actinide elements that had been analyzed up to that time and listed ionization stage, energies, intensities, *J*-values, and level assignments of selected lines (Blaise and Wyart, 1992). The contents of that compilation are available on an updated database at LACs website (www.lac.u-psud.fr).

At the time of this writing (2005), 9500 isotope shifts have been measured, and half of them are in the IR region. More than 31,000 lines of the Pu I and Pu II spectra have been observed, of which 52% have been classified as transitions between pairs of levels (Blaise *et al.*, 1983a, 1986; Blaise and Wyart, 1992). With the aid of Zeeman and isotope-shift data, a total of 606 even and 589 odd levels for Pu I, and 252 even and 746 odd levels for Pu II, have been identified. For all

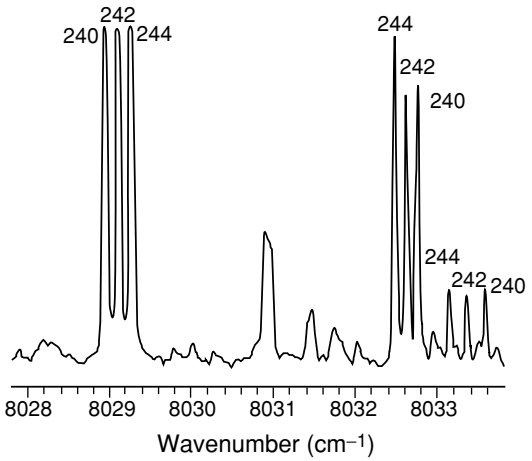

Fig. 7.8 *Fourier transform spectrum of a mixture of ^{240}Pu, ^{242}Pu, and ^{244}Pu isotopes* (*Blaise* et al., 1983a).

these levels the quantum number J has been assigned, and for many levels Landé g-factors are given. To date, levels belonging to 14 different electronic configurations in Pu I, and 9 electronic configurations in Pu II have been identified. The lowest levels of these configurations are given in Table 7.8 along with the Landé g-factors and experimental isotope shifts (Blaise *et al.*, 1983a; Blaise and Wyart, 1992).

The full-term analysis of plutonium spectra is still not yet complete because, even in 2005, a detailed quantum-mechanical treatment is hindered by the extreme complexity of the spectra. Even though the emission spectra of plutonium are still not completely assigned, they are among the best-understood spectra of the heavy elements.

7.6.2 Ionization potentials

The first ionization potential (IP) is a fundamental physical and chemical property of an element, and it is directly connected to the atomic spectra. Its accurate determination is important for identifying systematic trends within the actinide series of elements. In 1973 and 1974, Sugar derived values for the ionization energies of neutral plutonium and other actinides by using interpolated spectral properties of the atoms (Sugar, 1973, 1974). For neutral plutonium, the first IP was calculated to be 6.06(2) eV or 48,890(200) cm^{-1}. Worden *et al.* (1993) measured the first IP of ^{239}Pu by laser resonance techniques requiring as much as 2 g of ^{239}Pu. The photoionization threshold value for the ^{239}Pu I IP was determined to be 48,582(30) cm^{-1}, and the more accurate value from the Rydberg series measurements was 48,604(1) cm^{-1} or 6.0262(1) eV. In 1998, Erdmann and coworkers reported the first IP of ^{239}Pu using resonance ionization mass spectrometry (RIMS), a technique that requires only a few hundred picograms of material. In this approach, one- or two-step resonant laser excitation in a well-defined electric field promotes the atoms to a highly excited state, and ionization is obtained by scanning the wavelength of an additional tunable laser across the threshold, and extrapolation to zero field strength. From RIMS data, the first IP was found to be 48,601(2) cm^{-1} or 6.0258(2) eV (Erdmann *et al.*, 1998; Waldek *et al.*, 2001).

7.6.3 X-ray spectra

Plutonium X-ray spectra have been studied in detail by several authors (Cauchois *et al.*, 1954; Cauchois and Manescu, 1956; Shacklett and DuMond, 1957; Merrill and DuMond, 1958, 1961; Nelson *et al.*, 1969, 1970), and detailed wavelength and energy tables have been published by Bearden (Bearden, 1967; Bearden and Burr, 1967). The reader is also referred to the *Gmelin Handbook* (Koch, 1973c). The K and L series of the Pu X-ray spectra are known, and a few lines of the M and N series have been measured (Cauchois *et al.*, 1963a,b; Bonnelle, 1976). The L edges of the X-ray absorption spectra have been used

Table 7.8 *The lowest energy level of each electronic configuration of neutral Pu I and monovalent Pu II with their corresponding term symbol, energy, Landé g-values, and isotope shifts* (*Blaise and Wyart*, 1992).

Configuration	*Parity*	*Term*	*Energy* (cm^{-1})	*g*	*IS* (240–239) (10^{-3} cm^{-1})	*References*
Pu I						
$5f^6 7s^2$	even	$^7F_0$	0.000	–	465	Bovey and Gerstenkorn (1961)
$5f^5 6d 7s^2$	odd	$^7K_4$	6 313.886	0.487	653	Bauche *et al.* (1963b)
$5f^6 6d 7s$	even	$^9H_1$	13 528.246	−0.59	253	Bauche *et al.* (1963b)
$5f^5 6d^2 7s$	odd	$^9L_4$	14 912.011	0.496	488	Bauche *et al.* (1963b)
$5f^6 7s 7p$	odd	$^9G_0$	15 449.472	–	336	Brewer (1971a)
$5f^5 7s^2 7p$	even	$^7I_3$	17 897.119	0.450	698	Bauche *et al.* (1963b) and Blaise *et al.* (1983a)
$5f^5 6d 7s 7p$	even	$^9L_4$	20 828.477	0.352	467	Bauche *et al.* (1963b)
$5f^7 7s$	odd	$^9S_4$	25 192.231	1.768	273	Blaise *et al.* (1983a,b)
$5f^6 7s 8s$	even	$^9F_1$	31 572.610	2.403	446	Bauche *et al.* (1963b)
$5f^6 6d^2$	even	$^9I_2$	31 710.912	0.200	115	Blaise *et al.* (1983a)
$5f^6 7s 7p$	odd	$^9I_2$	33 070.58	0.673	293	Blaise *et al.* (1983a, unpublished)
$5f^4 6d^2 7s^2$	even	$^7M_6$	36 050.562	0.83	535	Brewer (1971a)
$5f^5 6d^2 7p$	even	$^9M_5$	37 415.524	0.980	403	Blaise *et al.* (1983a, unpublished)
$5f^5 6d 7s 8s$	odd	$^9K_3$	39 618.16	0.27	503	Blaise *et al.* (1986)
Pu II						
$5f^6 7s$	even	$^8F_{1/2}$	0.000	3.150	381	McNally and Griffin (1959)
$5f^5 7s^2$	odd	$^6H_{5/2}$	8 198.665	0.415	896	Fred *et al.* (1966)
$5f^5 6d 7s$	odd	$^8K_{7/2}$	8 709.640	0.310	555	Brewer (1971b) and Blaise *et al.* (1983a)
$5f^6 6d$	even	$^8H_{3/2}$	12 007.520	−0.019	77	Bauche *et al.* (1963b)
$5f^5 6d^2$	odd	$^8L_{9/2}$	17 296.88	0.494	242	Brewer (1971b) and Blaise *et al.* (1983a)
$5f^6 7p$	odd	$^8G_{1/2}$	22 038.95	0.345	287	McNally and Griffin (1959) and Brewer (1971b)
$5f^5 7s 7p$	even	$^8I_{5/2}$	30 956.36	0.650	424	Brewer (1971b) and Blaise *et al.* (1983a)
$5f^5 7s 7p$	even	$^8L_{9/2}$	33 793.30	0.795	208	Blaise *et al.* (1983a)
$5f^4 6d^2 7s$	even	$^8M_{11/2}$	37 640.78	0.70	813	Brewer (1971b) and Blaise *et al.* (1983a)

for plutonium oxidation state determination through the X-ray absorption near edge structure (XANES) in a variety of matrices (Conradson *et al.*, 1998, 2004a; Duff *et al.*, 1999; Richmann *et al.*, 1999; Fortner *et al.*, 2002; Antonio *et al.*, 2004; Lechelle *et al.*, 2004).

7.6.4 Core-level spectra

A few core-level spectra on plutonium compounds have been measured and comprehensively reviewed by Teterin and Teterin (2004). Core-level spectra that probe plutonium 4d, 4p, 4f, 5d, 5p, 6s, and 6p levels have been applied to determination of oxidation states and local environment, the magnetic properties of compounds, the nature of the chemical bonding, and secondary electronic processes that accompany photoemission. The use of fine structure spectral parameters, together with the electron binding energies and line intensities, significantly extends the scope of application of the X-ray photoelectron spectroscopy (XPS) method in structural studies. We mention only a few recent applications of core-level spectra.

Kotani and coworkers examined 4f core XPS of PuO_2 and other actinide dioxides and employed the Anderson impurity model to show that PuO_2 is a strongly mixed-valent compound and that a crossover between Mott–Hubbard and charge-transfer insulators occurs near NpO_2 (Kotani and Ogasawara, 1993; Kotani *et al.*, 1993). Allen and coworkers examined Pu 4f XPS of the α, β, γ, and δ phases of plutonium metal. They found that the 4f core-level spectra display features that vary systematically for the α, β, γ, and δ phases. For all phases they observed a sharp feature at binding energy 422 eV and a much broader shoulder that is approximately 2.5 eV higher. Application of an Anderson impurity model indicates that these features represent well-screened ($5f^6$) and poorly screened ($5f^5$) final states, respectively (Allen *et al.*, 1996a; Cox *et al.*, 1999). More recently, Gouder *et al.* (2002) employed 4f core-level spectroscopy to demonstrate dramatic changes in the electronic structure of ultrathin layers of α-Pu, and suggest that the surface of α-Pu should have δ-Pu character.

7.6.5 Mössbauer spectra

It is possible to obtain Mössbauer spectra on plutonium using excited states of ^{238}Pu, ^{239}Pu, and ^{240}Pu. In the case of ^{238}Pu, the β decay of ^{238}Np yields the 44 keV excited state of ^{238}Pu, which decays to the ground state with $T_{1/2} = 183$ ps and E2 dipole radiation. The 44 keV γ-ray may be used in resonance absorption measurements. A disadvantage is the short half-life of the 44 keV level (170 ps), which causes line broadening, and the relatively short half-life (2.1 days) of the source nuclide ^{238}Np, which makes it difficult to prepare sufficient amounts of the latter for a Mössbauer spectroscopy source.

For ^{239}Pu, the β decay of ^{239}Np produces a 57.3 keV state of ^{239}Pu, which decays through E2 γ radiation, which may be used in resonance fluorescence

spectroscopy. Gal *et al.* (1972) studied the resonance fluorescence of the 57.3 keV γ ray using a $^{239}NpO_2$–ThO_2 source and ^{239}Pu as the absorber. At 4.2 K, a resonance with a half-width of (5.13 $\pm$ 0.10) cm s^{-1} was observed. Assuming a Debye temperature of (250 $\pm$ 50) K for PuO_2, they calculated a natural linewidth of (473 $\pm$ 0.25) cm s^{-1}. This corresponds to a half-life of (101 $\pm$ 5) ps, in agreement with the lifetime of rotational levels, which decay by E2 transitions.

For ^{240}Pu, the α decay of ^{244}Cm yields a 42.9 keV state in ^{240}Pu in 23.3% of all occurring α decays. This state decays to the ground state with $T_{1/2} = 164$ ps. The 42.9 keV transition has an internal conversion coefficient of $\alpha_T = 920$. The use of this transition for Mössbauer spectroscopy was first demonstrated by Kalvius *et al.* (1978), who studied tetravalent $^{240}PuO_2$ and hexavalent $^{240}PuO_2C_2O_4$. In the tetravalent system, at 4.2 and 77 K, a single resonance line was found with a width of about 20% larger than the natural width of about 40 mm s^{-1}. In the hexavalent plutonyl oxalate, $PuO_2C_2O_4$, at 4.2 K a quadrupole interaction $|e^2qQ| = 95$ mm s^{-1} was found, but no isomer shifts were detected.

7.7 PLUTONIUM METAL AND INTERMETALLIC COMPOUNDS

Plutonium metal, alloys, and intermetallic compounds have important technological applications principally because of the nuclear properties of isotope 239. Plutonium metals and alloys are the materials of choice for the nuclear explosive in nuclear weapons and for fuel elements for some advanced reactor designs. The metallic properties of plutonium are important not only for nuclear weapons design, but also for the safe storage and disposition of excess weapons-grade plutonium. Plutonium alloys were used in some early reactor concepts (Anderson *et al.*, 1960; Kiehn, 1961; Burwell *et al.*, 1962) and are under development for advanced designs such as the Integral Fast Reactor (Keiser *et al.*, 2003). Much of the early work on plutonium metal and alloys was done in secrecy in the declared nuclear weapons states (mostly in the United States, Soviet Union, U.K., and France). President Eisenhower's Atoms for Peace initiative, which was launched with his December 8, 1953 speech to the United Nations brought most of the scientific work and many of the engineering properties into the open through a series of international conferences, starting with the first Atoms for Peace Conference in Geneva in 1955. Today, the threats of proliferation and terrorism cause concern about the amount of practical information regarding the construction of nuclear devices available in the open literature. Over the years, the U.S. government has taken the position that the fundamental scientific and engineering properties of plutonium be treated as open information. However, practical manufacturing methods, including those specific to weapons manufacture and the performance of nuclear weapons, remain classified. These guidelines are followed in this chapter.

In addition to its technological importance, plutonium in condensed matter also proves to be fascinating scientifically. The unusual nature of plutonium in the solid state is the result of its peculiar electronic structure. It lies near the middle of the actinide series – precisely at a transition point between the 5f electrons participating in bonding or being localized and chemically inert. Exploring the properties of plutonium and its compounds is an area of great interest in condensed matter physics. From a metallurgical perspective, the peculiarities associated with plutonium's electronic structure cause plutonium to defy most conventional metallurgical wisdom. These peculiarities, along with much of the interesting chemistry of plutonium, have been the subject of several recent reviews (Guerin, 1996; Cooper and Schecker, 2000; Terminello *et al.*, 2001; Hanrahan *et al.*, 2003; Jarvinen, 2003). In this section, we focus on the basic properties of plutonium, but we also explore properties of the neighboring actinides to better understand plutonium within the context of the entire actinide series.

Although our focus is on properties, we state at the outset that to delineate plutonium's metallic behavior it is imperative to understand what is called in the materials science community the processing–structure–properties relationship. Metallurgical practitioners routinely adjust properties by tailoring structure through careful control of chemistry and processing of metals and alloys. By structure we mean crystal structure, grain structure, and defect structure on the nano- and microscale. Plutonium is notoriously unstable with respect to temperature, pressure, and chemical additions, and its surface is reactive, especially in the presence of hydrogen or water. The synthesis and processing of plutonium are quite complex. There is considerable concern over lot-to-lot variations in processing and structure because criticality considerations limit the production of plutonium metal and alloys to small lots (at most on the order of kilograms). Also, microcracks, surface reactions, inclusions from impurities, and retained second phases can affect sample properties. In addition, the self-irradiation of plutonium (especially the prevalent isotopes ^{239}Pu and ^{238}Pu) causes microstructural changes that may affect its properties as it ages. Hence, the age of plutonium samples, or the time elapsed since the material was last molten or heat treated, can affect the properties. Unfortunately, most publications on plutonium properties provide little structural information, and detailed descriptions of processing conditions or sample age are typically limited.

We will draw attention to those cases for which the properties are especially sensitive to structure, processing, and age. The reader is also advised to examine reported density data and X-ray crystal structure information as both provide a good indication of what phases were present in the samples studied.

7.7.1 Preparation of plutonium metal

Plutonium metal may be obtained by a number of reduction reactions of plutonium compounds. Summaries of the various reactions have been given by Harmon *et al.* (1961), Leary and Mullins (1966), McCreary (1955),

Christensen and coworkers (Christensen and Mullins, 1983; Christensen *et al.*, 1988), Coops *et al.* (1983), and Baldwin and Navratil (1983). Not all of the reactions that produce plutonium metal are ideally suited for metal preparation in production work. For production processes, the chemical reactions must (a) produce a dense, coherent mass of pure plutonium in high yield; (b) generate sufficient heat to melt both the metal and the resulting slag; (c) result in a slag that stays molten and nonviscous long enough to allow the plutonium to coalesce; and (d) work on the scale desired (a reaction suitable for microgram-scale reductions might be less useful for gram- or multigram-scale reductions and vice versa). In reactions where one of the conditions (a–d) is not initially fulfilled, modified process conditions may still make the technique usable. For example, if the heat of reaction for a Ca reduction is insufficient (condition b), then addition of an iodine booster or use of a laser can provide sufficient heat to make the overall process usable. The resulting CaI_2 in turn helps to improve condition (c).

The pyrochemical preparation of plutonium metal is best carried out by reduction of PuF_4, PuF_3, $PuCl_3$, PuO_2, or a PuO_2–PuF_4 mixture with calcium metal in a high-temperature molten salt. Quite often a booster (such as iodine) initiates the reaction and provides sufficient energy to ensure the complete reaction:

$$PuF_4 + 2Ca^0 \rightarrow Pu^0 + 2CaF_2 \tag{7.13}$$

$$2PuCl_3 + 3Ca^0 \rightarrow 2Pu^0 + 3CaCl_2 \tag{7.14}$$

$$PuO_2 + 2Ca^0 \rightarrow Pu^0 + 2CaO \tag{7.15}$$

These methods of preparation do not produce any purification (Leary and Mullins, 1966); they simply produce metallic plutonium. Of these approaches, the reduction of PuO_2 has become the preferred route for preparation of plutonium metal. $PuCl_3$ is extremely hygroscopic, which poses handling difficulties, particularly for large quantities of material. The plutonium fluorides (PuF_4, PuF_3) are neutron emitters (due to α-n reactions), and working with plutonium fluorides requires considerable protective shielding. A related lithium reduction of PuO_2 has been developed as a pyrochemical process for the recycle of oxide fuels (Usami *et al.*, 2002).

Hydriding and dehydriding or hydriding followed by oxidation can recover plutonium metal scraps adhering to other metal surfaces (Haschke, 1991; Flamm *et al.*, 1998). Even at room temperature, plutonium metal reacts reversibly with hydrogen to form a metallic PuH_x powder (see Section 7.8.1).

$$2Pu^0 + xH_2 \rightleftharpoons 2PuH_x \tag{7.16}$$

The hydride spalls off the inert substrate and subsequent heating of the hydride product in a vacuum recovers the plutonium metal.

7.7.2 Modern pyrochemical preparation and refining

Over time, the general process for obtaining, preparing, and refining plutonium has evolved based on the kinds of feed materials available. Historically, plutonium was first produced in production reactors; extracted, concentrated, and converted to either an oxide or fluoride; and then reduced to metal. The resulting metal was used for fabrication of various parts and components. The fabrication process itself generates major quantities of waste and scrap plutonium that must then be recovered and recycled. In modern times, the feed material for preparation and refining of metallic plutonium has evolved to recovery and recycle of residues and scrap material. This in turn drives the current technology selection for metal preparation and refining. In addition, the technology selection must take nuclear material safeguards, accountability, criticality safety, and radiation exposure into consideration. The major pyrochemical processes that are currently employed in large facilities are bomb reduction of PuF_4, DOR, MSE, anode casting, ER, and pyroredox, and these techniques are integrated into a general processing flow diagram, such as the Los Alamos approach indicated in Fig. 7.9. As the figure shows, each operation produces residues that are treated either by pyrochemical or aqueous means to recover plutonium. We will discuss these pyrochemical processes in some detail.

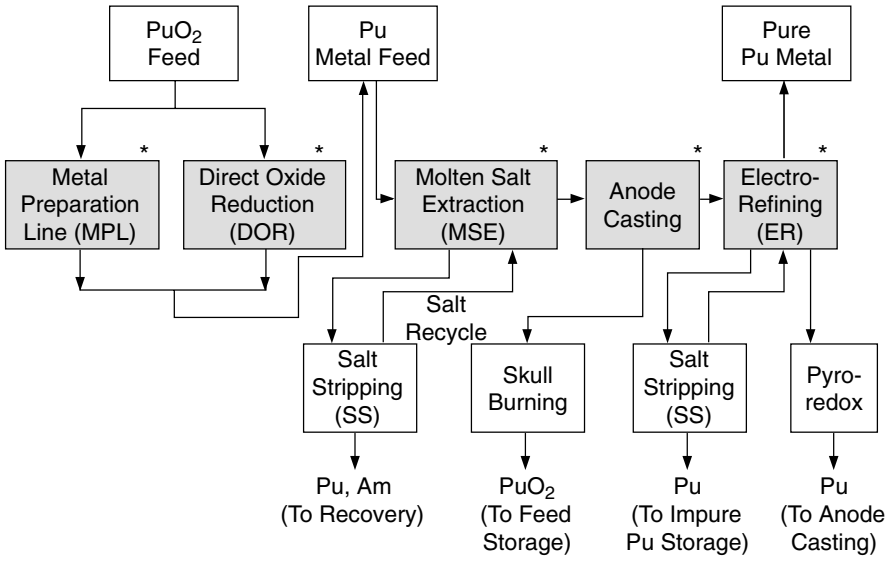

Fig. 7.9 *A general integrated pyrochemical processing system for plutonium metal preparation* (*Christensen* et al., 1988).

(a) Fluorination and reduction

The fluorination and reduction process produces plutonium metal from PuF_4 by the high-pressure reaction between the fluoride and calcium metal (Baker, 1946). Plutonium dioxide is converted to PuF_4 with HF in a hydrofluorination reaction, or by direct fluorination with F_2 (see Section 7.8.6.a). After fluorination of oxide, a chemical booster, such as iodine, initiates the reduction reaction:

$$PuO_2 + 4HF \rightarrow PuF_4 + 2H_2O \tag{7.17}$$

$$PuO_2 + 2F_2 \rightarrow PuF_4 + O_2 \tag{7.18}$$

$$PuF_4 + 3Ca^0 + I_2 \rightarrow Pu^0 + 2CaF_2 + CaI_2 \tag{7.19}$$

An illustration of a typical bomb reduction furnace is shown in Fig. 7.10. The PuF_4, calcium metal, and MgO (magnesia) slag are thoroughly mixed in a molded, open-porosity magnesia crucible. Iodine, added before the equipment is assembled and heated, acts as an initiator and reaction booster. At approximately 325°C, calcium and iodine react exothermically to rapidly raise the temperature. At 600°C, the PuF_4 reduction reaction begins and the system temperature rises rapidly to nearly 2000°C. The slag remains molten while the liquid plutonium sinks to the bottom of the crucible and solidifies. After the equipment has cooled, the crucible is broken to recover the metal button, which is mechanically separated from the slag (Christensen *et al.*, 1988). Little or no purification occurs during the process, and the metal purity is similar to that of the feed material. If the reagents are of high purity, and sufficiently pure plutonium feed is used, then the resulting metal is satisfactory for high-purity applications. Yields usually range from 97 to 99% (Baker and Maraman, 1960). This reaction can be carried out on a relatively large scale, and up to 6 kg batches of plutonium metal are not uncommon.

(b) Direct oxide reduction (DOR)

In the DOR process, plutonium dioxide is reduced with calcium metal to produce plutonium metal and calcium oxide (Mullins *et al.*, 1982; Mullins and Foxx, 1982; Christensen and Mullins, 1983). The reaction takes place in a molten $CaCl_2$ or $CaCl_2$–CaF_2 solvent, which dissolves the resulting CaO and allows the plutonium metal to coalesce in the bottom of the crucible to form a metal button. The PuO_2, calcium metal, and fused $CaCl_2$ are loaded into a vitrified magnesia crucible. The $CaCl_2$ is cast before use and contains no detectable water. The generic DOR apparatus is shown in Fig. 7.11 (Christensen and Mullins, 1983). The crucible is heated in a resistance furnace to 800°C. Once the $CaCl_2$ is molten, a Ta stirrer and a Ta–Ni thermocouple sheath are lowered in the melt. The reaction typically begins at about 820°C with a temperature

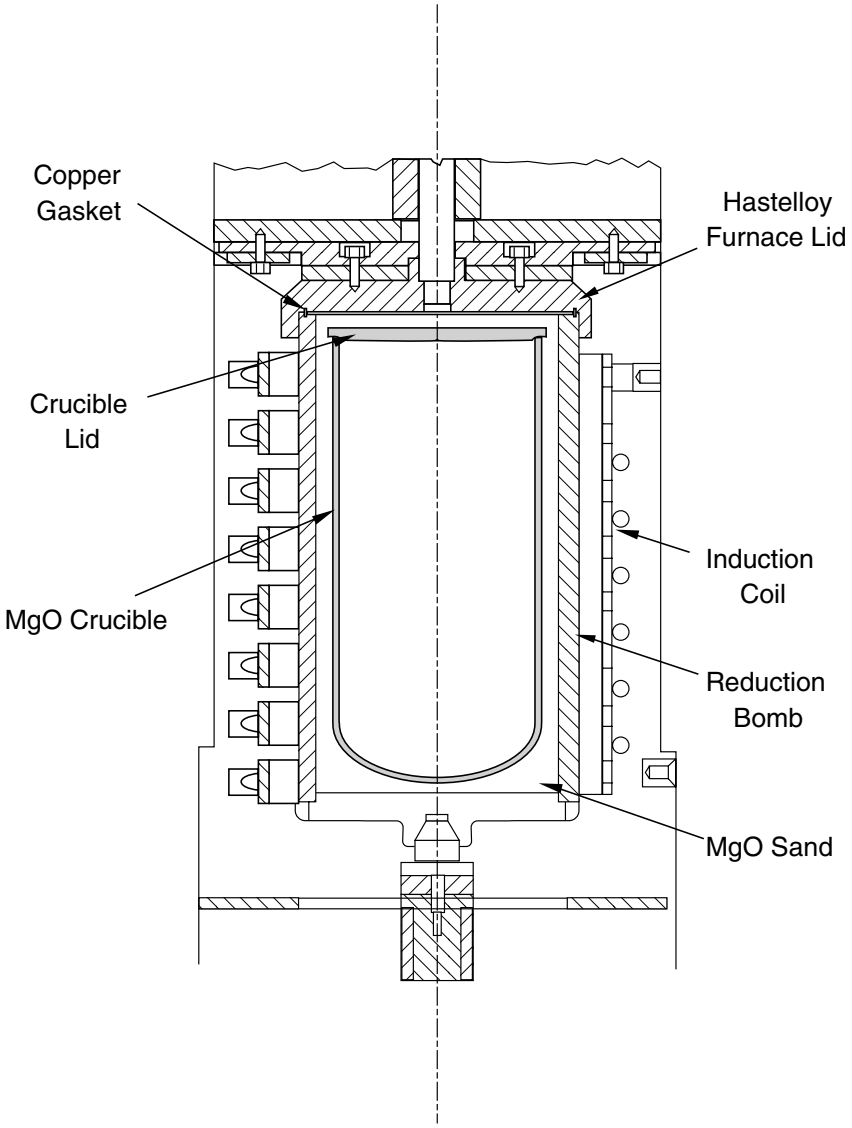

Fig. 7.10 *A furnace assembly for plutonium metal production by reduction of* PuF_4 (*Christensen* et al., 1988).

spike to 875°C. The reaction is complete within 15 min. The reaction proceeds to completion when excess calcium is present, sufficient $CaCl_2$ is available to dissolve the CaO that is produced, and rapid stirring is applied. While stirring, the reaction is monitored with a thermocouple. After completion of the

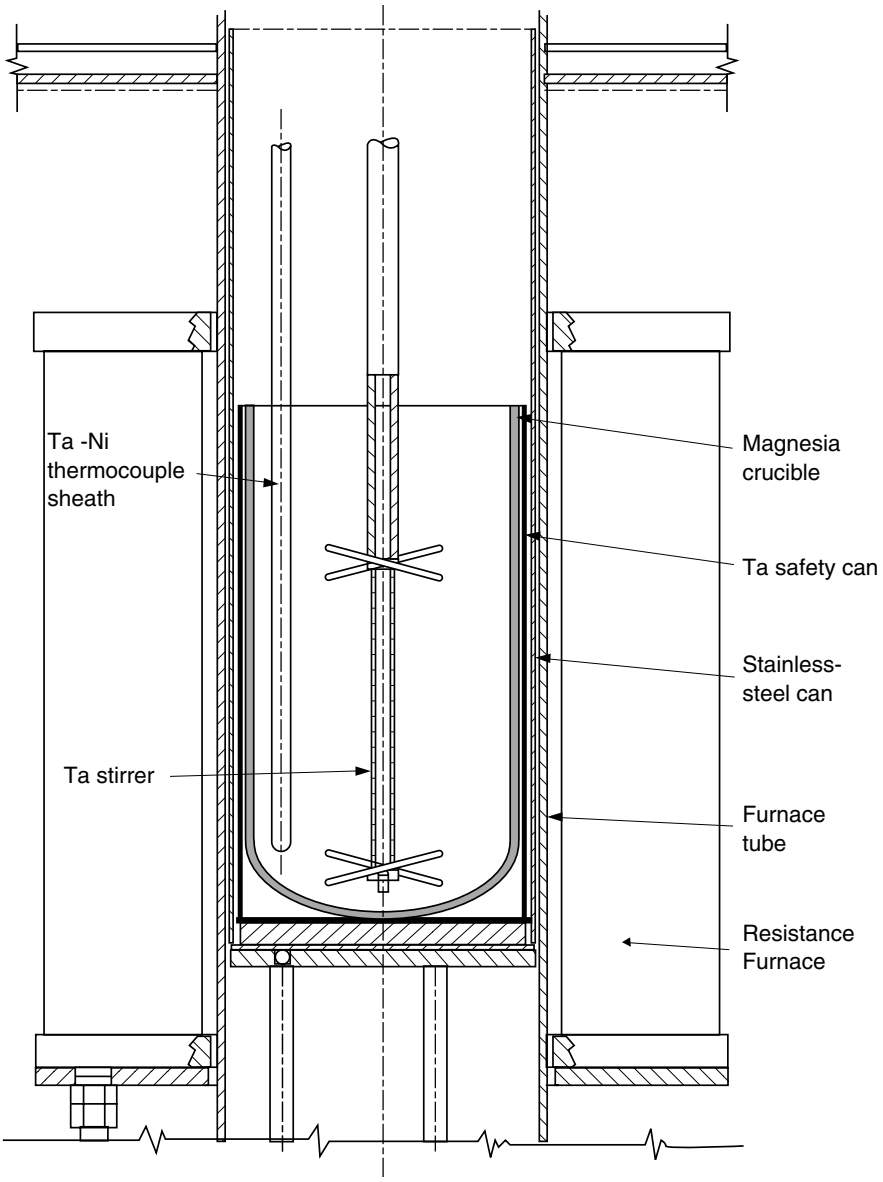

Fig. 7.11 *A general furnace assembly for direct oxide reduction* (*DOR*), *molten salt extraction of americium* (*MSE*) *and pyroredox operations* (*Christensen* et al., 1988).

reaction, the thermocouple well and stirrer are retracted, and the melt is allowed to settle and cool. Almost all the plutonium forms a metal button at the bottom of the crucible, and a typical DOR reaction product is shown in Fig. 7.12. The salt immediately above the button contains a layer of metal shot, and the bulk of

Fig. 7.12 (*a*) *A photograph of a DOR breakout showing the MgO crucible, residues, and metal product at the bottom.* (*b*) *The DOR metal button* (*top*) *and residues* (*photographs courtesy of Los Alamos National Laboratory*).

the salt solidifies above the metal. The plutonium button is mechanically separated, and the shot is recovered by reheating the shot-rich (usually with calcium present) material above the melting point to consolidate the metal. Product yields are greater than 95% (Mullins *et al.*, 1982).

(c) Molten salt extraction (MSE)

The plutonium metal produced in PuF_4 and PuO_2 reduction is impure and needs to be refined. The MSE process is specifically designed to reduce the americium content of plutonium metal (^{241}Am spontaneously grows into plutonium as a result of ^{241}Pu β-decay), but it also separates the more reactive elements, such as rare-earths, alkali-metals, and alkaline-earth metals (Knighton and Steunenberg, 1965; Knighton *et al.*, 1976; Coops *et al.*, 1983). The general principle of MSE is to oxidize the americium to Am(III) to extract it into the salt phase, leaving plutonium in the metallic phase. The extraction procedure is identical to the DOR process and uses essentially the same apparatus shown in Fig. 7.11, with the exception that a reusable tantalum vessel replaces the magnesia crucible, an oxidant is added, and the stirring time is typically 30 min instead of only a few minutes. To run the reaction, workers place impure plutonium metal in contact with a ternary salt, consisting of

$MgCl_2$ as the oxidizing agent in a NaCl/KCl eutectic. The major reactions are (Mullins *et al.*, 1968; Leary and Mullins, 1974):

$$2Am^0 + 3MgCl_2 \rightarrow 2AmCl_3 + 3Mg^0 \tag{7.20}$$

$$2Pu^0 + 3MgCl_2 \rightarrow 2PuCl_3 + 3Mg^0 \tag{7.21}$$

$$Am^0 + PuCl_3 \rightarrow AmCl_3 + Pu^0 \tag{7.22}$$

A typical batch size is 4.5 kg with a 12-h temperature cycle to 750°C. (The actual reaction time is only 30 min.) After the equipment has cooled to room temperature, the fused salt containing the americium and other impurities is separated from the plutonium metal button and crucible. Usually, each feed button goes through two batch extractions. In a typical 4.5-kg run containing 3000 ppm americium, 90% of the americium is oxidized at the expense of ca. 100 g plutonium. A typical product weighs 4.4 kg and contains 98% of the feed plutonium (Christensen and Mullins, 1983; Christensen *et al.*, 1988).

(d) Vacuum melting and casting

After the americium is extracted from the impure metal, the plutonium metal must be cast into a cylindrical geometry that is compatible with the ER cell (Anderson and Maraman, 1962). The ER operation is typically carried out with 6 kg of plutonium, in which case the high-density α phase must be avoided due to nuclear criticality concerns. This requires alloying with sufficient gallium to bring the density from >19 to <16.5 g cm^{-3}. Casting is accomplished by mixing about 6 kg of impure metal with an appropriate amount of gallium in a tantalum pour crucible as shown in Fig. 7.13 (Christensen *et al.*, 1988). The metal and gallium mix upon melting and are bottom-poured from the tantalum crucible into a graphite mold. A casting residue, or "skull", always forms and contains light element impurities, oxide films (thorium, americium, alkali metals, alkaline-earth, and rare-earth metals) or other high melting contaminants. A typical ingot is shown in Fig. 7.14 with yields generally averaging more than 90%.

(e) Electrorefining (ER)

In the ER process, liquid plutonium oxidizes from the anode ingot into a molten-salt electrolyte (Mullins *et al.*, 1960, 1963a,b, 1982; Mullins and Leary, 1965; Mullins and Morgan, 1981). The resulting Pu(III) ion is transported through the salt to the cathode, where it is reduced back to metal. The process is carried out at 740°C in a molten salt consisting of an equimolar mixture of NaCl/KCl containing a small amount of $MgCl_2$ as an oxidizing agent. The $MgCl_2$ reacts with the impure plutonium metal to charge the electrolyte with Pu(III) before a current is passed and ensures the initial reduction of plutonium at the cathode.

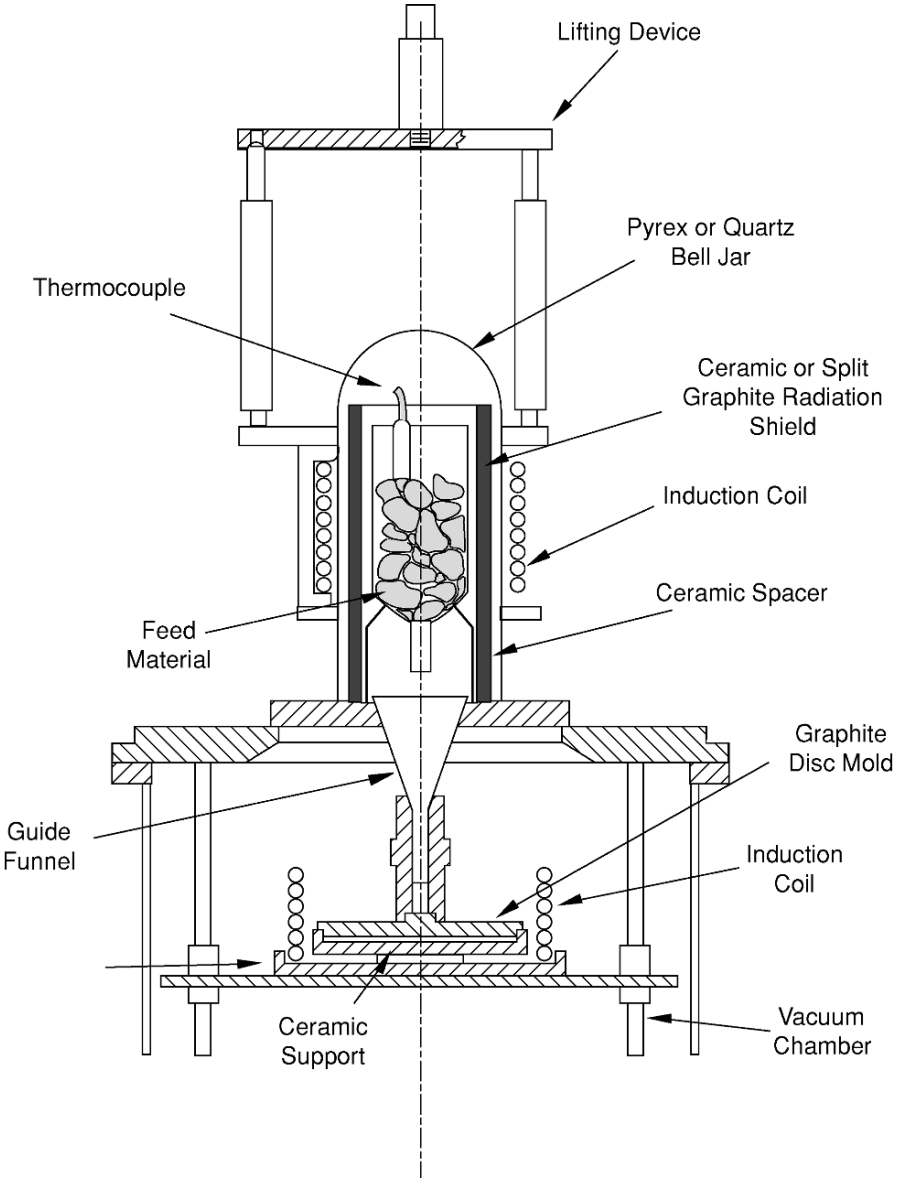

Fig. 7.13 *A general furnace assembly for vacuum casting of plutonium metal* (*Christensen* et al., 1988).

The process is performed in a double-cupped, vitrified magnesia crucible as shown in Fig. 7.15 (Mullins and Morgan, 1981). The inner cup contains the impure metal ingot that serves as the anode material. The electrolyte salt casting is placed on top of the ingot. The crucible is placed inside a tantalum safety can

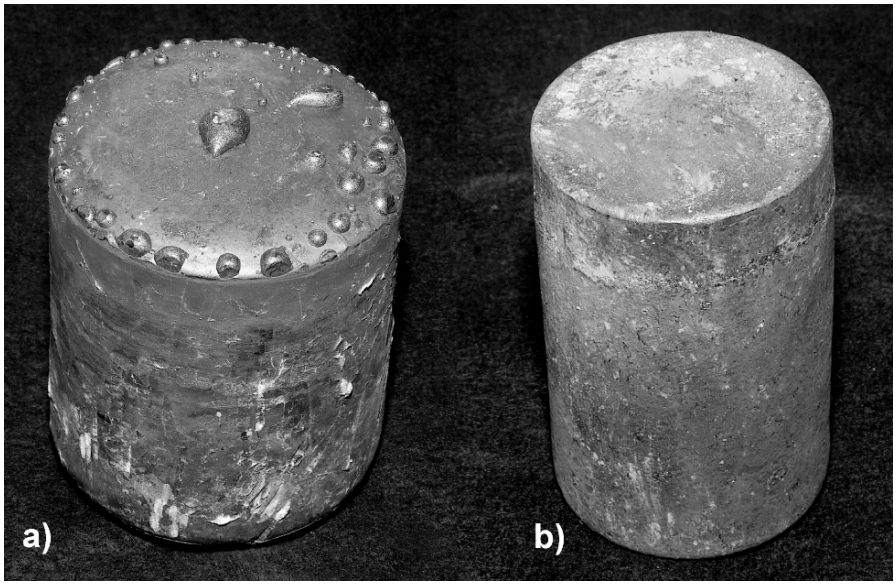

Fig. 7.14 *Photographs of plutonium ingots from vacuum casting.* (*a*) *Metal feed for electrorefining, and* (*b*) *for double electrorefining* (*photographs courtesy of Los Alamos National Laboratory*).

and placed inside the furnace. The assembly is heated using a resistance furnace (the entire assembly is shown in Fig. 7.16). A tantalum or vitrified magnesia stirrer stirs both the impure metal and the molten salt electrolyte. A tungsten rod is suspended in the impure metal pool to serve as the anode rod, and electrically insulated from the salt by a magnesia sleeve. A cylindrically shaped sheet of tungsten is suspended in the annular space between the two cups and serves as the cathode. Stirring and passing a dc current between the anode and cathode accomplish the process. Plutonium oxidizes at the anode and reduces back to metal at the cathode. The liquid metal drips off the cathode and into the annular space. After cooling to room temperature, the cell is broken apart and the plutonium recovered as an annular metal casting, or 'ER ring,' as shown in Fig. 7.17. The product yield from a Pu-1 wt % Ga alloy is greater than 80%. Approximately 10% of the residual plutonium remains in the anode as a very impure anode heel. The rest of the plutonium remains in the salt either as uncoalesced metal shot or as Pu(III), both of which can be recovered and recycled.

(f) Pyroredox or anode recovery

The pyroredox process recovers the plutonium from impure scrap materials and has found application in recovering plutonium from the spent anode heels from

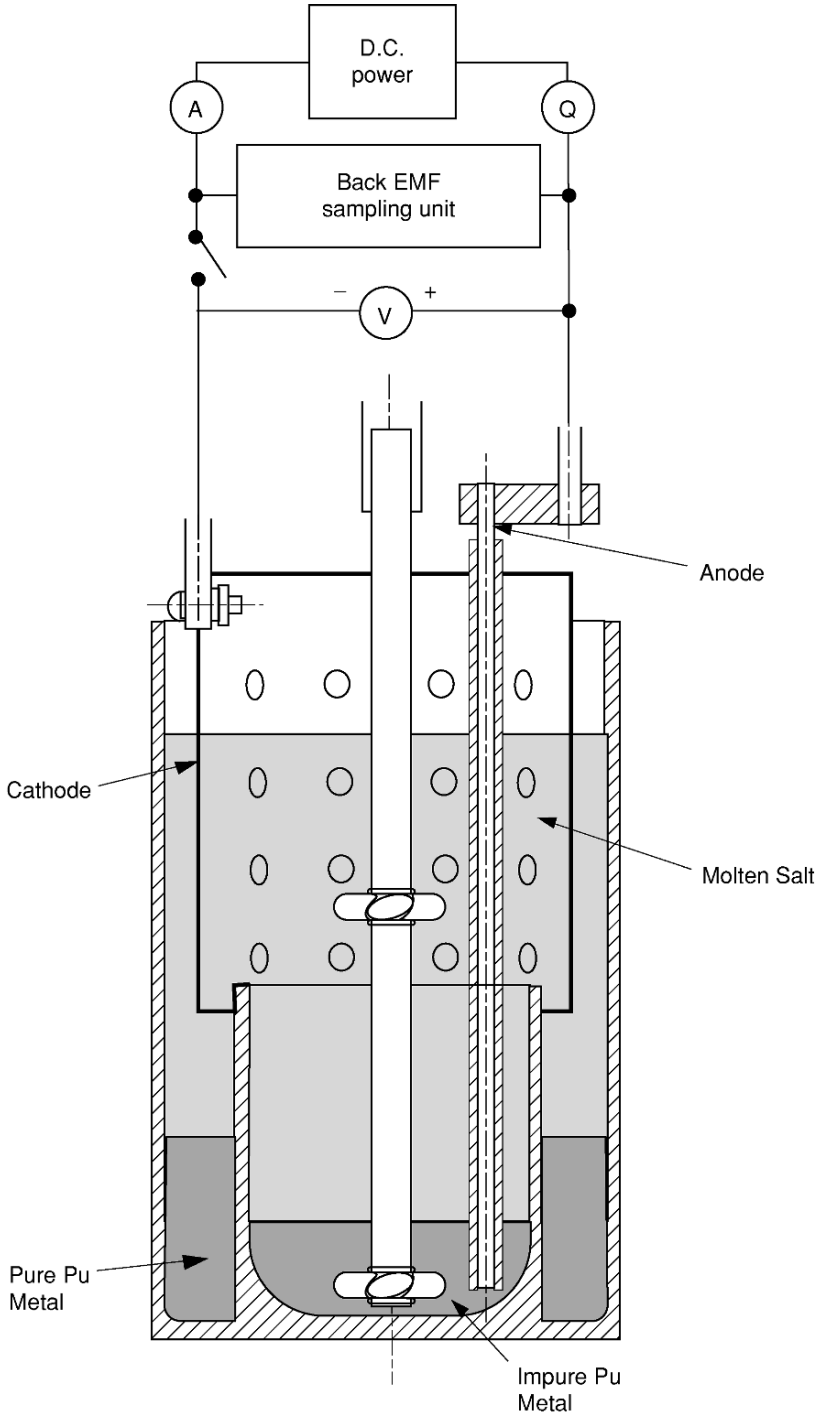

Fig. 7.15 *A general schematic of an electrorefining* (*ER*) *cell showing major features* (*Christensen* et al., 1988).

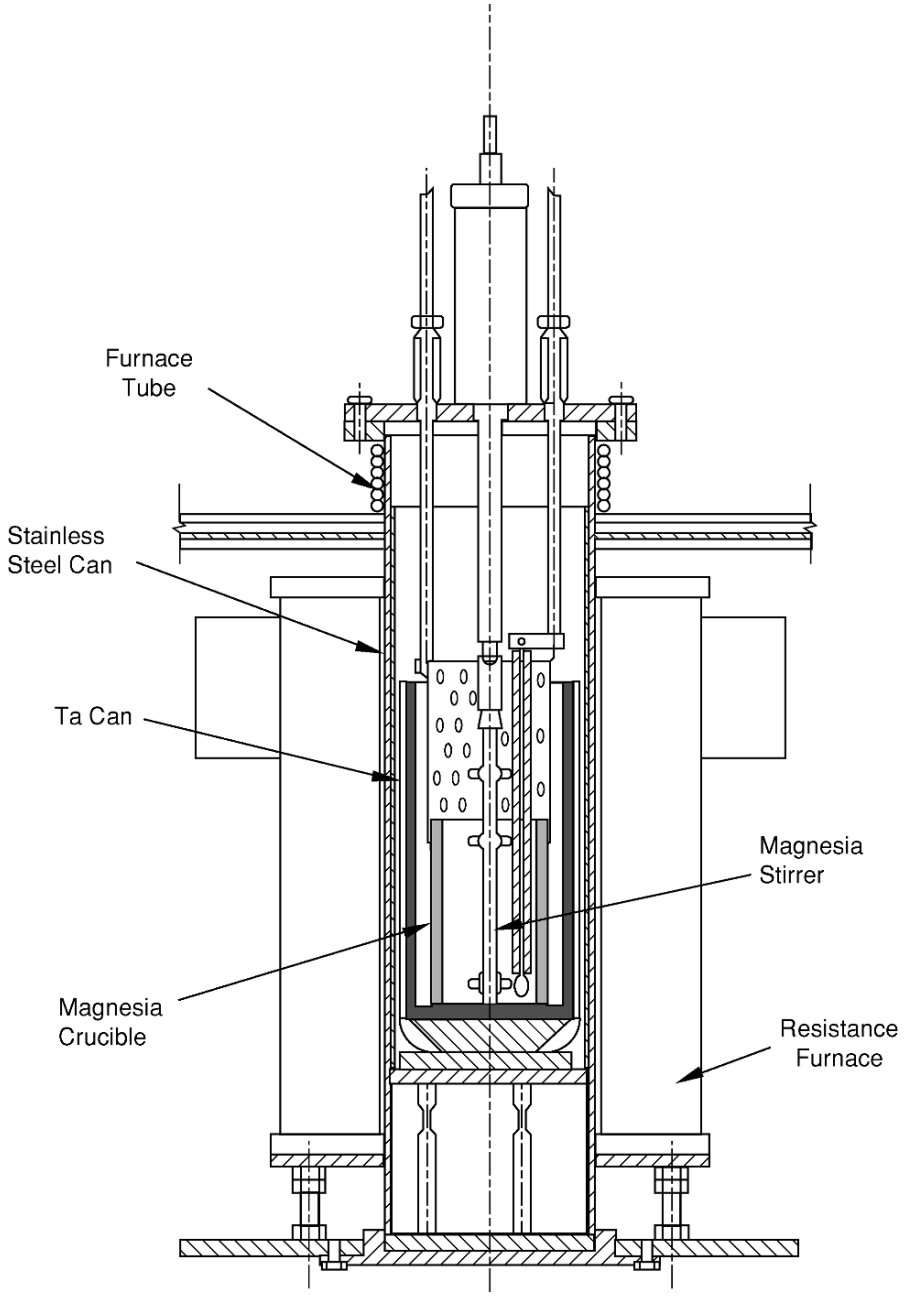

Fig. 7.16 *A general schematic of an electrorefining (ER) furnace apparatus showing major features* (*Christensen* et al., 1988).

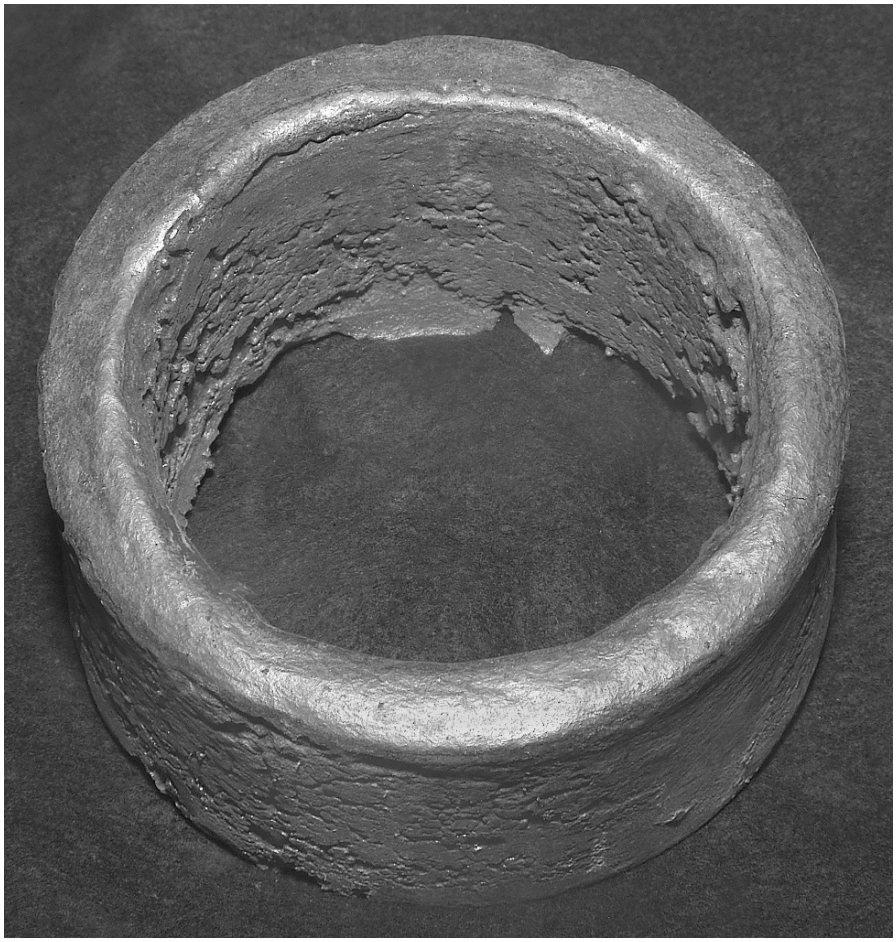

Fig. 7.17 *Photograph of a plutonium product ring from electrorefining* (*ER*) (*photograph courtesy of Los Alamos National Laboratory*).

the ER process (Baldwin and Navratil, 1983; Coops *et al*., 1983; McNeese *et al*., 1986; Christensen *et al*., 1988). The process equipment is identical to that used in DOR (Fig. 7.11). In the pyroredox process, workers initially polish the spent anode with calcium to ensure that all the plutonium is present as metal. The metal is then oxidized to Pu(III) with $ZnCl_2$ dissolved in KCl at 750°C with stirring. After an hour, the mixture is heated to 850°C to promote phase separation. In addition to plutonium, all other elements more active than zinc are oxidized into the salt phase. This process forms a zinc button that may be mechanically separated from the salt and discarded. For the reduction step, the salt containing $PuCl_3$ is crushed and mixed with a $Ca/CaCl_2$ mixture, pressed into an ingot, and placed back into a magnesia crucible and inserted into the

furnace assembly. The vessel is heated to 850°C with stirring, and then allowed to cool after removing the stirrer. The chemical reactions are:

$$2Pu^0 + 3ZnCl_2 \rightarrow 2PuCl_3 + 3Zn^0 \tag{7.23}$$

$$2PuCl_3 + 3Ca^0 \rightarrow 2Pu^0 + 3CaCl_2 \tag{7.24}$$

The reaction product is a salt phase above a two-phase metal button. The salt phase is mechanically separated and discarded. The bottom, denser metal phase is composed of plutonium and small quantities of calcium and zinc. The upper phase is typically 50% plutonium with the remainder being primarily zinc. Several buttons are allowed to coalesce at 850°C for 6 h to separate the ingots into a plutonium-rich lower phase suitable for ER and a less-pure upper phase that is recycled back to the oxidation step.

(g) Zone-refining of small research samples

Plutonium metal that has been doubly electrorefined is considered of high purity for most applications but still contains small amounts of Fe, U, Mg, Ca, Ni, Al, K, Si, O, C, and H. For small-scale research applications, it can be further purified via levitation zone-refining using a floating molten zone to minimize introduction of impurities from crucible materials. Tate and Anderson (1960) originally observed the phenomenon when they reported that zone melting promoted a reduction of impurity elements within a plutonium rod. Spriet (1965) conducted a more detailed investigation to include quantification of rates and impurity analyses. In more recent work, levitation zone-refining in concert with levitation distillation at reduced pressure has proven to be quite successful at producing ultrahigh purity specimens (Blau, 1998; Lashley *et al.*, 1999). Levitation zone-refining targets metals and metalloids while levitation vacuum-distillation targets daughter products and gases. In the levitation apparatus, radio frequency (rf) power-induced electric current flows into a crucible while the crucible acts as a transformer, inducing a current in the opposite direction to the current in the crucible. Magnetic fields in the crucible and the plutonium are opposed, causing repulsion and levitation of the plutonium a small distance from the crucible walls. Magnetic levitation of plutonium metal rods between 700 and 1000°C enables purification while eliminating plutonium-crucible interactions and minimizing the contact with other elements. The magnetic levitation is the fundamental operating basis for both the zone-refining apparatus and the distillation apparatus.

The zone-refining process involves casting a rod of unalloyed plutonium and then serially passing a molten zone through the rod in one direction at a slow rate. Impurities travel in the same or opposite direction to the direction of motion of the zone, depending on whether it lowers or raises the melting point of the plutonium. Consequently, impurities are swept and become concentrated in the ends of the rod, thereby leaving the remainder purified. The degree of

separation approaches an infinitesimal limit as the number of passes increases. Recent work has shown that ten passes through a molten zone can result in the reduction of impurities in double-electrorefined and vacuum-cast unalloyed plutonium from 727 to 184 ppm through levitation zone-refining (Blau, 1998; Lashley *et al.*, 1999).

Since americium exhibits a high vapor pressure relative to plutonium it is possible to remove ^{241}Am daughters from plutonium samples via vaccum distillation. The ^{241}Am is separated when plutonium metal is heated to the liquid state under reduced pressure (10^{-7} Torr). The molten plutonium is levitated while ^{241}Am is distilled off and condensed onto a cold finger. The plutonium is cooled and solidifies. Recent results from levitation distillation show that the concentration of ^{241}Am was reduced from 1100 to 500 ppm (Lashley *et al.*, 1999). These general principles have been combined into a floating zone refining followed by an *in situ* distillation, alloying, and casting technique for high-purity research samples of δ-Pu. In the procedure, a mixture of α-Pu is first levitation zone-refined. The α-Pu and gallium are then added to a levitation crucible. The mixture is heated to the melt while suspended in a magnetic levitation field. As the gallium mixes with the plutonium in the melt, it will stabilize the δ phase upon solidification. While in the melt, ^{241}Am is distilled from the plutonium and collected on a water-cooled condenser. Next, the furnace power is reduced, and plutonium is cast directly from the electromagnetic field into a ceramic mold. The apparatus is illustrated in Fig. 7.18.

7.7.3 Phase stability – allotropes, crystal structures, and transformations

It is important to understand the different allotropic phases of plutonium and the limits of stability with temperature, pressure, chemical additions, and time. We describe the stability of unalloyed plutonium along with the characteristics of its phases as a function of temperature and pressure in this section. We deal with the effects of chemical additions and time subsequently.

C. S. Smith and his Manhattan Project team of metallurgists and chemists were the first to come to grips with the unstable nature of this enigmatic element (Hammel, 1998). During their initial work in 1944, they routinely found the densities of their freshly prepared plutonium samples to vary by more than a factor of two. They quickly determined that unalloyed plutonium has at least five allotropes (a sixth was eventually found) over a very narrow temperature range and that it exhibits large volume changes at the various phase transitions during cooling from the melt, making it difficult to cast. Smith soon found that most of the transformations and the large volume changes could be avoided by alloying pure plutonium with a few atomic percent aluminum or gallium. Such alloying additions retained the high-temperature face-centered cubic (fcc) δ-phase, which is less dense, weak, and ductile, in contrast to the typical room temperature α-phase, which is very dense, strong, and brittle. The profound influence of chemical additions to plutonium on phase stability and the

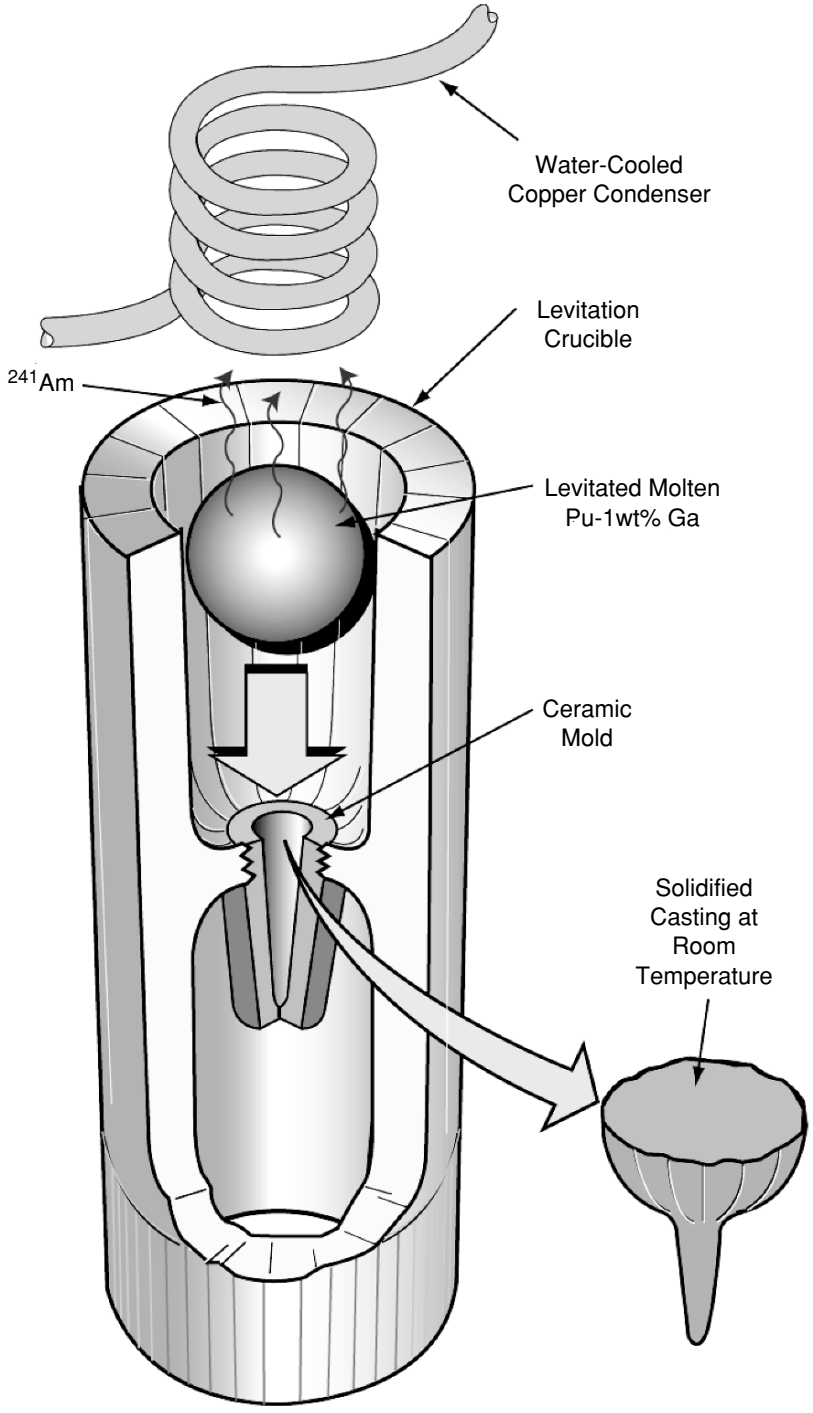

Fig. 7.18 In situ *americium distillation, alloying, and chill casting apparatus* (*Lashley* et al., 1999).

dramatic differences in properties exhibited by the different plutonium allotropes must be kept firmly in mind when considering plutonium and its properties. Moreover, phase transformations between the different allotropes are difficult to avoid during sample preparation, especially if samples are heated, cooled, worked, ground, or polished.

Zachariasen (1944) was the first to suggest that the large density and property variations in the early separated plutonium samples were due to crystallographic modifications of plutonium. Five solid allotropes designated by the Greek symbols α, β, γ, δ, and ϵ were identified during the early studies. A sixth, designated by the symbol δ', was discovered in 1954 by Cramer (Cramer *et al.*, 1961) in high-purity plutonium. An idealized thermal expansion curve is shown for pure plutonium in Fig. 7.19 (Miner and Schonfeld, 1980), along with the crystal structures and densities of the solid phases and the liquid phase. The stability ranges and crystal structure data for the individual allotropes are shown in Table 7.9. The transformation temperatures of the α, β, and γ phases are only approximate because the transformations are kinetically sluggish. The limits represent the approximate transformation temperatures as obtained by dilatometry and thermal analysis at slow heating or cooling rates of 1 to 1.5°C min^{-1}. The actual heating and cooling curves show significant hysteresis.

The data shown in Fig. 7.19 and Table 7.9 demonstrate the idiosyncratic behavior of plutonium. The six solid allotropes at ambient pressure (a seventh was found under pressure by Morgan (1970)) are the most of any element in the periodic table. Plutonium has an unusually low melting point of 640°C, and it contracts upon melting. The maximum density difference between the phases is a very large 20%. Moreover, the classical close-packed fcc phase is the least dense (less dense than the liquid). The two low-temperature phases are low-symmetry monoclinic structures, atypical of metals. The thermal expansion coefficients of these phases are very large and positive, whereas that of the fcc phase is negative.

The low-density, high-temperature phases of plutonium are easily transformed to the higher density phases under hydrostatic pressure as shown in Fig. 7.20 (Liptai and Friddle, 1967). Morgan (1970) clearly demonstrated the existence of a seventh phase at high pressure, designated ζ phase, as shown in Fig. 7.21. Its structure has yet to be determined. Elliott (1980) pointed out the similarity of the new ζ phase to the η phase in the Pu–U and Pu–Np systems. As shown in Fig. 7.20, at 3.0 GPa the ζ phase and all other high-volume phases collapse to the two low-temperature α and β allotropes.

The low-symmetry monoclinic ground-state α phase of plutonium results from the peculiar nature of the 5f electron bonding in plutonium as discussed below. Zachariasen and Ellinger (1957, 1963a) and Zachariasen (1961a) demonstrated that the α phase is a simple monoclinic crystal structure ($P2_1/m$) with 16 atoms per unit cell and eight unique atom positions. All 16 atoms lie in the reflection planes with coordinates $\pm$ (x,¼,z). Several views of the crystal structure of α plutonium are shown in Fig. 7.22. The 16 structural parameter values

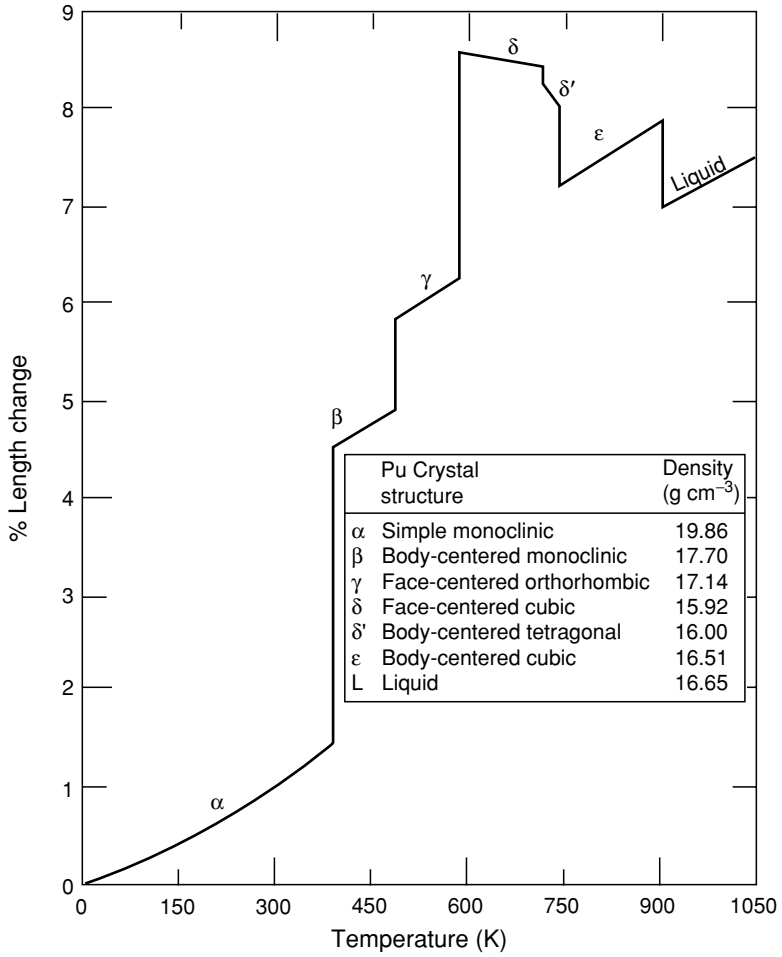

Fig. 7.19 *Thermal expansion of unalloyed plutonium. This idealized curve was generated by Schonfeld and Tate* (1996) *based on the best available expansion data. Of particular relevance is the correction to the α-Pu thermal expansion, as detailed in Fig.* 7.44.

are listed in Table 7.10 along with the bond lengths. The monoclinic structure of α plutonium is a slight distortion from a hexagonal lattice. This similarity was used by Crocker (1971) in modeling the crystallographic relationships of phase transformations involving the α phase. In addition, the bonding characteristics of the eight atom positions are markedly different. Position 1 has the greatest number of short bonds, whereas position 8 has the fewest short bonds (as shown in Table 7.11). All positions have the same point symmetry. The bonding characteristics are important in determining how the α phase accommodates

Table 7.9 *Crystal structure data for plutonium.*

Phase	*Stability range* (K)	*Crystal lattice and space group*	*Unit cell dimensions* (Å)	*Atoms per unit cell*	*X-ray density* ($g\ cm^{-3}$)	*Transformation temperature* (K)[b]
α	below 397.6	simple monoclinic $P2_1/m$	at 294 K $a = 6.183(1)$ $b = 4.822(1)$ $c = 10.963(1)$ $\beta = 101.79°(1)$	16	19.85	
β	397.6 – 487.9	body-centered monoclinic $I2/m$[a]	at 463 K $a = 9.284(3)$ $b = 10.463(4)$ $c = 7.859(3)$ $\beta = 93.13°(3)$	34	17.71 (α→β)	397.6
γ	487.9 – 593.1	face-centered orthorhombic F*ddd*	at 508 K $a = 3.159(1)$ $b = 5.768(1)$ $c = 10.162(2)$	8	17.15 (β→γ)	487.9
δ	593.1 – 736.0	face-centered cubic F*m*3*m*	at 593 K $a = 4.6371(4)$	4	15.92 (γ→δ)	593.1
δ′	736.0 – 755.7	body-centered tetragonal I4/*mmm*	at 738 K $a = 3.34(1)$ $c = 4.44(4)$	2	16.03 (δ→δ′)	736.0
ϵ	755.7 – 913.0	body-centered cubic I*m*3*m*	at 763 K $a = 3.6361(4)$	2	16.51 (δ′→ϵ) m.p.	755.7 913.0

[a] Although space group $I2/m$ is not one of the 'standard' space groups tabulated in the International Union of Crystallography, *International Tables for X-ray Crystallography,* vol. 1, Kynoch Press, Birmingham, its notation is retained to obtain a β angle of approximately 90° (data from Miner and Schonfeld, 1980).
[b] Data from Lemire *et al.* (2001). The reader is cautioned that the transformation temperatures vary between sources, and are sensitive to heating and cooling rates and metal purity.

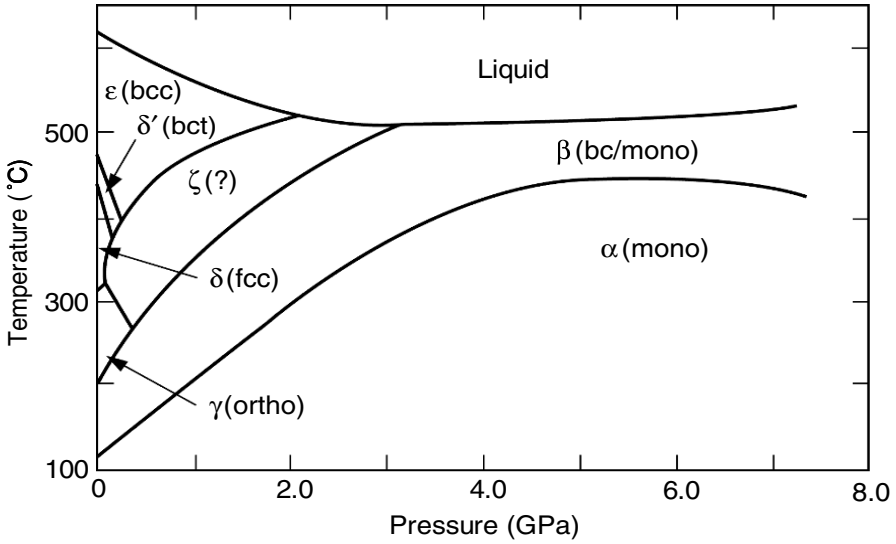

Fig. 7.20 *Pressure–temperature phase diagram of unalloyed plutonium from Liptai and Friddle* (1967).

impurity atoms. Lawson *et al.* (1996) pointed out that with eight unique atom positions, α plutonium looks like a self-intermetallic, much like α manganese. The low-symmetry monoclinic structure of the α phase has a profound influence on its properties; it has no macroscopic ductility, and most properties are highly directional.

The β phase is a body-centered monoclinic (*I2/m*) and equally complex. The atomic coordinates, the structural parameters, and the bond lengths are shown in Table 7.12 (Zachariasen and Ellinger, 1963b). It is considerably less dense than the α phase (17.7 g cm^{-3} compared to 19.85 g cm^{-3}), and it has 34 atoms per unit cell with seven unique atom positions. Properties are also quite anisotropic. The crystal structure of the β phase is compared to the other five allotropes in Fig. 7.23.

The γ phase is a face-centered orthorhombic (*Fddd*) with eight equivalent atoms per unit cell and a density of 17.14 g cm^{-3} (Zachariasen and Ellinger, 1955, 1959; Crocker, 1971). Each atom has four neighbors at 3.026 Å, two at 3.159 Å, and four at 3.228 Å. Roof (cited by Miner and Schonfeld, 1980) pointed out that placing the origin at the center of symmetry places the positions of the eight atoms of the unit cell at ± (1/8,1/8,1/8) + (0,0,0; 0,½, ½; ½,0, ½; ½,½,0). The crystal structure of the γ phase is shown along with the other allotropes in Fig. 7.23.

The δ phase is fcc (*Fm3m*) with four equivalent atoms per unit cell as shown in Fig. 7.23. It is the least dense of the plutonium allotropes at 15.92 g cm^{-3}. Each

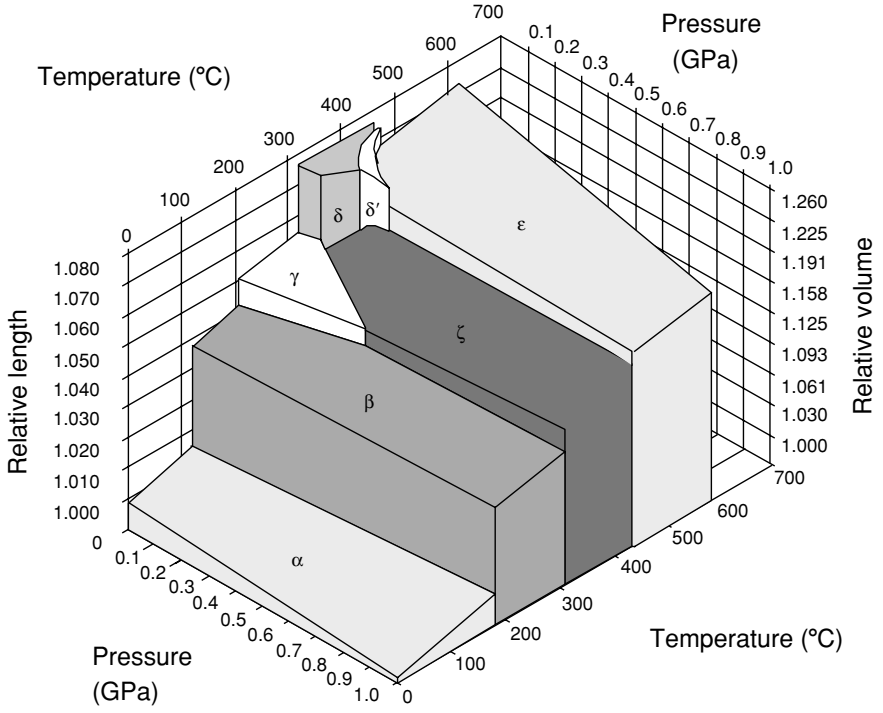

Fig. 7.21 *Pressure–temperature phase diagram from Morgan* (1970) *showing the existence of a seventh phase,* ζ.

atom has 12 neighbors at 3.279 Å in the standard fcc arrangement (0,0,0; 0,½,½; ½,0,½; ½,½,0). The δ′ phase is described by Ellinger (1956) as body-centered tetragonal (*I4/mmm*) with two atoms per unit cell at (0,0,0) and (½,½,½), with a density of 16.00 g cm^{-3}. He pointed out that the structure can be alternatively described as a face-centered tetragonal cell containing four atoms per unit cell, derived from the close-packed arrangement by a slight compression along the [001] direction. The ϵ phase is body-centered cubic (bcc) (*Im3m*) with two equivalent atoms per unit cell at (0,0,0) and (½,½,½). Each atom has eight neighbors at 3.149 Å.

As shown in Figs. 7.20 and 7.21, a seventh solid allotrope, the ζ phase, appears with the application of hydrostatic pressure at elevated temperatures. Very little is known about the precise crystal structure of this phase. However, Elliott (1980) suggested a similarity of this structure with the η phase of the PuU and PuNp systems.

The local coordination and interatomic distances for the four higher-temperature allotropes are shown in Table 7.13. Based on the crystal structure

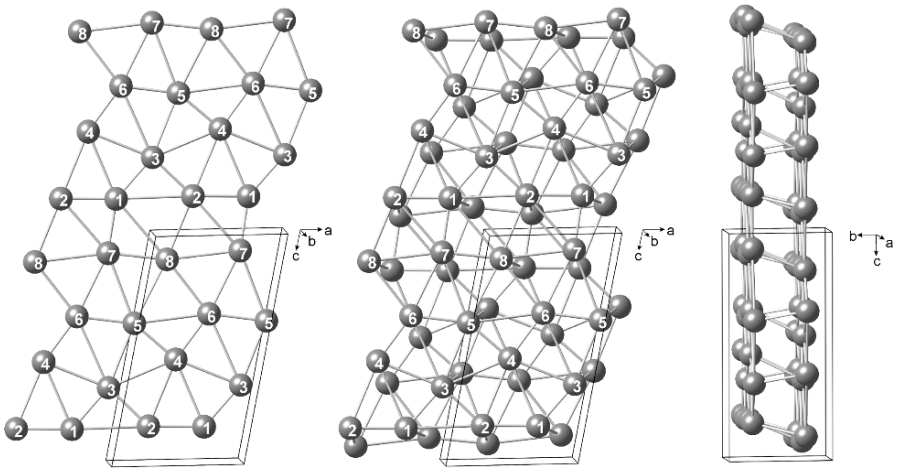

Fig. 7.22 *Several views of the monoclinic α-phase structure of plutonium with* 16 *atoms per unit cell and eight different atom positions.*

Table 7.10 *Structural parameters and bond lengths for α plutonium* (*Miner and Schonfeld*, 1980).

			Short bonds (Å)		*Long bonds* (Å)		*All bonds* (Å)	
Atom	*x*	*z*	*No.*	*Range*	*No.*	*Range*	*No.*	*Mean*
1	0.345(4)	0.162(2)	5	2.57–2.76	7	3.21–3.71	12	3.10
2	0.767(4)	0.168(2)	4	2.60–2.64	10	3.19–3.62	14	3.21
3	0.128(4)	0.340(3)	4	2.58–2.66	10	3.24–3.65	14	3.18
4	0.657(5)	0.457(3)	4	2.58–2.74	10	3.26–3.42	14	3.13
5	0.025(5)	0.618(3)	4	2.58–2.72	10	3.24–3.51	14	3.19
6	0.473(4)	0.653(2)	4	2.64–2.74	10	3.21–3.65	14	3.22
7	0.328(4)	0.926(2)	4	2.57–2.78	10	3.30–3.51	14	3.15
8	0.869(4)	0.894(2)	3	2.76–2.78	13	3.19–3.71	16	3.32

Table 7.11 *Bond characteristics for the eight different atom positions in the α-plutonium structure.*

Atom	*Short bonds*[a]	*Average length* (Å)
1	5	2.67
2–7	4	2.64
8	3	2.77

[a] The short bonds range from 2.57 to 2.78 Å and the long bonds from 3.19 to 3.71 Å. The point symmetry is the same for all eight atom positions.

Table 7.12 *Structural parameters for β plutonium* (*Zachariasen and Ellinger*, 1963*b*).

			Crystallographic parameters			*Bond lengths*			
Type	*No.*	*General atom positions*	*x*	*y*	*z*	*No.*	*Short bonds* (Å)	*No.*	*Long bonds* (Å)
1	2	(0, 0, 0)	0	0	0	4	2.97	8	3.15–3.26
2	4	±(x, 0, z)	0.146(4)	0	0.387(5)	3	3.03–3.10	11	3.26–3.55
3	4	±(x, 0, z)	0.337(4)	0	0.082(5)	4	2.79–3.03	9	3.15–3.43
4	4	±(x, 0, z)	0.434(4)	0	0.672(5)	4	2.79–3.01	8	3.16–3.48
5	4	±(1/2, y, 0)	0.500	0.220(3)	0	4	2.80–2.84	10	3.36–3.63
6	8	±(x, y, z), (x, $\bar{y}$, z)	0.145(3)	0.268(2)	0.108(3)	4	2.91–3.10	10	3.16–3.55
7	8	±(x, y, z), (x, $\bar{y}$, z)	0.167(3)	0.150(2)	0.753(4)	5	2.59–3.05	7	3.14–3.63

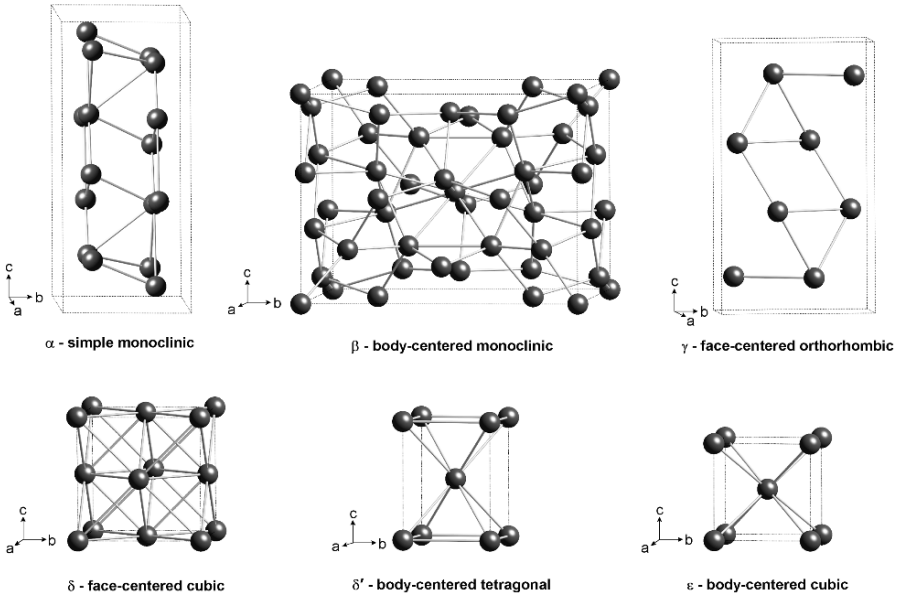

Fig. 7.23 *Crystal structures of all six solid phases of plutonium.*

information presented above, Zachariasen (1961b, 1973) derived metallic radii by normalizing the radii to coordination number 12 and extrapolating the high-temperature data to room temperature. His results are shown in Table 7.14. Zachariasen and others also calculated the valences for the plutonium allotropes. We do not present these here because we do not consider these estimates to be useful in considering the complexity of the f-electron bonding. We also list Dormeval's (2001) compilation of atomic volumes for the various allotropes in Table 7.14.

The liquid phase of plutonium is denser than the three highest-temperature solid phases. Density as a function of temperature is listed in Table 7.15, based on the work of Herrick *et al.* (1959) and Serpan and Wittenberg (1961). Extrapolation of the data in Table 7.15 yields a density of 16.65 g cm^{-3} at the melting point of 640°C. Hence, plutonium contracts approximately 2.5% upon melting. Plutonium liquid has a high surface tension and high viscosity.

The transitions (or, in metallurgical terms, phase transformations) between the various allotropes are important. Most studies of such transformations in unalloyed plutonium were conducted before 1970. A typical thermal expansion curve from Goldberg and Massalski (1970) for high-purity, electrorefined plutonium heated and cooled at 4.5°C min^{-1} is shown in Fig. 7.24. The sluggish nature of the transformation among the lower temperature phases results in

Table 7.13 *Coordination and interatomic distances of the higher plutonium allotropes* (*Ellinger* et al., 1956).

Phase	*Symmetry*	*Coordination*	*Distance* (Å)	*Effective coordination number*	*Average distance* (Å)	*Temperature* (°C)
γ	orthorhombic	Pu–4Pu Pu–2Pu Pu–4Pu	3.021 3.160 3.286	10	3.155	210
		Pu–4Pu Pu–2Pu Pu–4Pu	3.026 3.159 3.288	10	3.157	235
		Pu–4Pu Pu–2Pu Pu–4Pu	3.041 3.154 3.294	10	3.165	310
δ	face-centered cubic	Pu–12Pu	3.279	12	3.279	320
		Pu–12Pu	3.275	12	3.275	440
δ′	body-centered tetragonal	Pu–8Pu Pu–4Pu	3.249 3.327	12	3.275	465
		Pu–8Pu Pu–4Pu	3.239 3.347	12	3.275	485
ϵ	body-centered cubic	Pu–8Pu	3.149	8	3.149	490
		Pu–8Pu	3.156	8	3.156	550

Table 7.14 *Metallic radii* (*Zachariasen*, 1961*b; Zachariasen and Ellinger*, 1963*b*) *and volumes* (*Dormeval*, 2001) *of plutonium atoms.*

Phase	*Temperature* (°C)	*Radius* (Å)	*Radius at* 25°C (Å)	*Atomic volume* (Å^3)
α	25	1.580	1.580	20.00
β	93	1.600	1.590	22.43
γ	235	1.601	1.589	23.14
δ	320	1.640	1.644	24.93
δ′	465	1.638	1.644	24.69
ϵ	490	1.622	1.594	24.00

significant hysteresis, compared with the idealized curve shown in Fig. 7.19, and makes it difficult to conclusively determine the transformation temperatures. These temperatures depend on metal purity, microstructural variables (such as grain size and dislocation density), heating or cooling rates, applied stress,

Table 7.15 *Density of liquid plutonium* (g cm^{-3}).

Temperature (°C)	*Serpan and Wittenberg* (1961)[a]	*Olsen* et al. (1955)[b]
664	16.62	16.604
691	16.58	16.554
728	16.52	16.511
746	16.50	16.485
752	16.49	16.476
771	16.46	16.488
788	16.43	16.424

[a] Density equation $\rho = (17.63 - 1.52 \times 10^{-3}\ T) \pm 0.04$; temperature in °C
[b] Density equation $\rho = (17.567 - 0.001451\ T) \pm 0.021$; temperature in °C

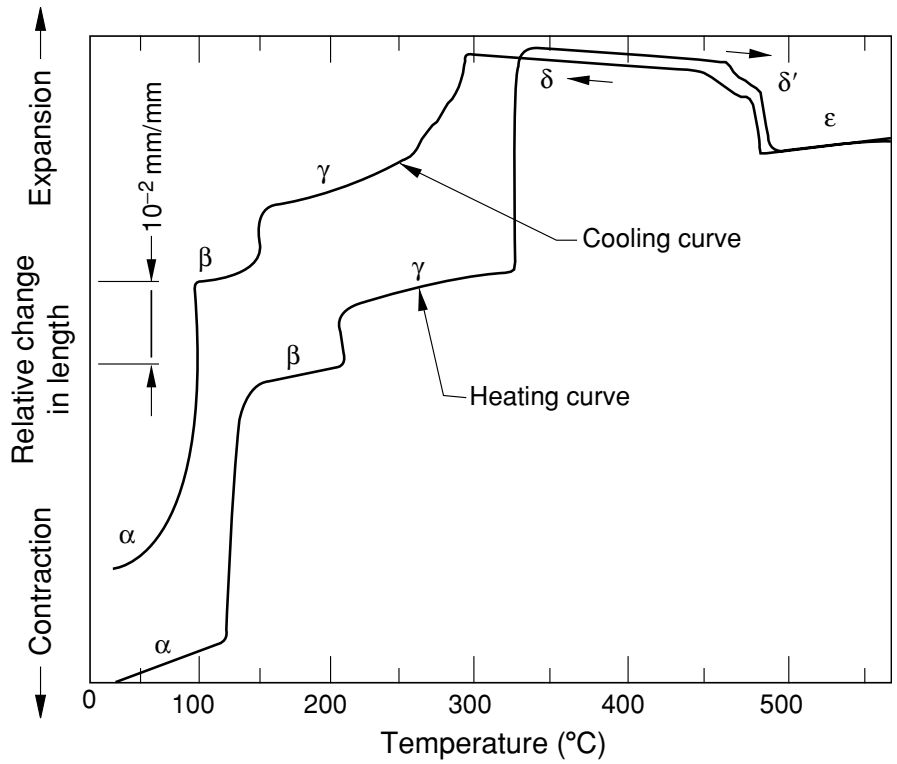

Fig. 7.24 *Experimental thermal expansion curve for heating and cooling of unalloyed plutonium showing typical hysteresis* (*after Goldberg and Massalski,* 1970).

sample size and shapes (resulting in stress effects), and prior transformation history.

Lemire *et al.* (2001) compared various phase transformation studies and compiled the best estimates of transformation temperatures and stability ranges

for the various allotropes listed in Table 7.9. Precise transformation temperatures are difficult to measure not only because they depend on the variables mentioned above, but also because all transformations exhibit significant time dependence. The isothermal (as opposed to athermal, where no thermal activation is needed) nature of the $\alpha \rightarrow \beta$ and $\beta \rightarrow \alpha$ transformations is best illustrated by the so-called time–temperature–transformation (TTT) diagram shown in Fig. 7.25 (after Nelson (1980)). The 'C-curve' shape of the transformation demonstrates how the temperature for the onset of transformation depends on the cooling rate. By determining the curves for both transformations, Nelson was able to establish the equilibrium transformation temperature as 112°C (compared with the average transformation temperature of 122°C during heating at relatively slow rates reported in Table 7.9).

Significant uncertainty still exists about the nature of the transformation mechanisms among the allotropes of plutonium (Hecker, 2000). The transformations among the high-temperature allotropes (δ, δ', and ϵ) are generally considered to be of a diffusion-controlled (diffusive) nature. However,

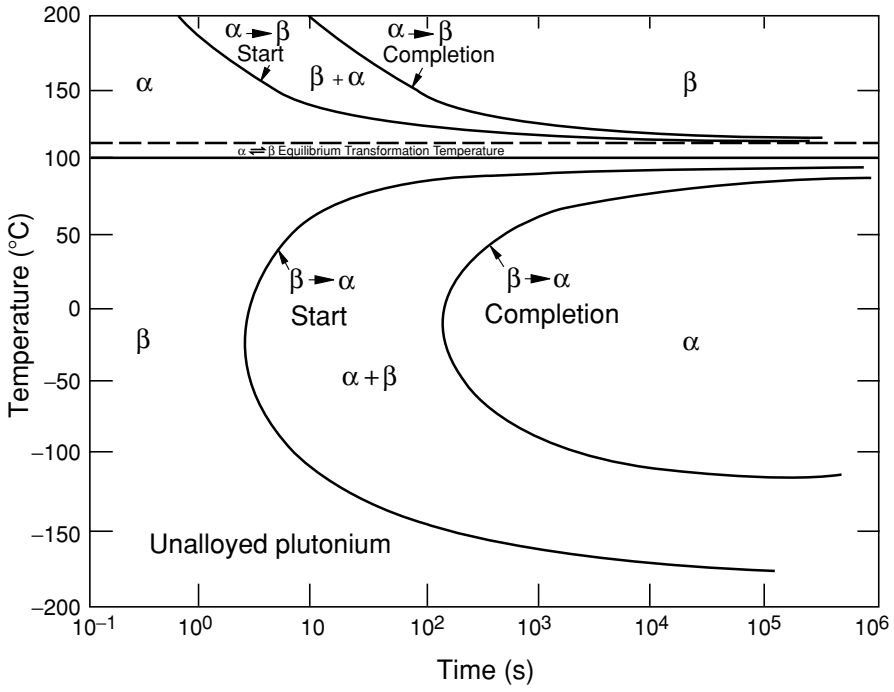

Fig. 7.25 *Representative time–temperature-transformation (TTT) curves of the $\beta \rightarrow \alpha$ and $\alpha \rightarrow \beta$ transformations in high-purity, electrorefined plutonium. The sample was taken to the β phase for* 45 min *at* 170°C (*from Nelson*, 1980).

transformations at lower temperatures among the δ, γ, β, and α phases show signs of diffusive and diffusionless, shear-type transformations. Shear transformations (of a martensitic nature) involve cooperative shear motion of the atoms and typically result in specific crystallographic relationships between the parent and the transformed phases. The evidence for such relationships was reviewed by Nelson (1980) and by Goldberg and Massalski (1970), who described the highly textured α-phase transformation product that can be formed when the β→α transformation is induced by cooling under applied stress.

Microcracking is difficult to avoid in most unalloyed plutonium as it cools from the melt or from annealing at elevated temperatures. The volume fraction of microcracks can range from 0.1 to 3%. High purity, large sample size, and slow cooling rates result in more extensive microcracking. Thermal cycling between the α and β allotropes greatly exacerbates the microcracking problem and results in sample distortion and surface rumpling (Hecker, 2000). On the other hand, quenching samples from the β phase to –80°C minimizes microcracking. Nelson pointed out that α-phase densities greater than 19.65 g cm^{-3} are generally considered to be good-quality plutonium. Densities around 19.8 g cm^{-3} have been achieved by cooling through the β→α transformation under pressure or by hydrostatic extrusion and concurrent recrystallization (Merz, 1970).

Another important consideration in sample preparation and subsequent property determination is the amount of retained high-temperature phases at ambient temperature. As noted in Figs. 7.24 and 7.25, the transformation from β→α is time-dependent and, hence, not necessarily complete at room temperature, resulting in retained β phase (or sometimes retained γ or δ phases). Impurities generally shift the onset of transformation (the 'C-curve' in Fig. 7.25) to the right. Spriet (1967) demonstrated that the onset of transformation was retarded by a factor of ten as the purity level changed from 200 to 400–1000 ppm. The impurities Ti, Hf, Zr, and U retard the β→α transformation and lead to greater β-phase retention at ambient temperature (Oetting *et al.*, 1976; Hecker, 2000). The impurities Ga, Al, and Si favor retention of the δ phase (Hecker, 2000). The most convenient method to determine the presence of retained high-temperature phases in α plutonium is to measure the density. The best way to identify the retained phases is by XRD; however, by using XRD it is difficult to identify retained phases at the level of less than a few volume percent.

Thermodynamic properties related to phase transformations can be measured directly by calorimetry or estimated from phase diagrams. Such properties are summarized in Table 7.16 along with the best estimates of the equilibrium transformation temperatures and volume changes. The scatter is quite large for reasons mentioned above. Nevertheless, these values are important to help guide the theory and modeling activities. Transformation enthalpies for the pressure-induced ζ phase are shown in Fig. 7.26, as derived from the data of Morgan (1970).

Table 7.16 *Entropies and enthalpies of transformations of the plutonium allotropes.*

Phase transformation	ΔS^a (J K^{-1} mol^{-1})	ΔS^b (J K^{-1} mol^{-1})	ΔH^c (J mol^{-1})	ΔH^d (J mol^{-1})	ΔH^e (J mol^{-1})
$\alpha \rightarrow \beta$	9.55	8.66	3430	3600	3706 ± 100
$\beta \rightarrow \gamma$	1.38	1.34	565	586	478 ± 20
$\gamma \rightarrow \delta$	1.05	0.88	586	649	713 ± 40
$\delta \rightarrow \delta'$	0.04	0.04	84	41	84 ± 20
$\delta' \rightarrow \epsilon$	2.47	2.46	1841	1859	1841 ± 100
$\epsilon \rightarrow$liquid	3.09	3.18	2824	2847	2824 ± 100

[a] Wick (1980); [b] Wittenberg *et al.* (1970); [c] Oetting *et al.* (1976); [d] Deloffre (1997); [e] Lemire *et al.* (2001).

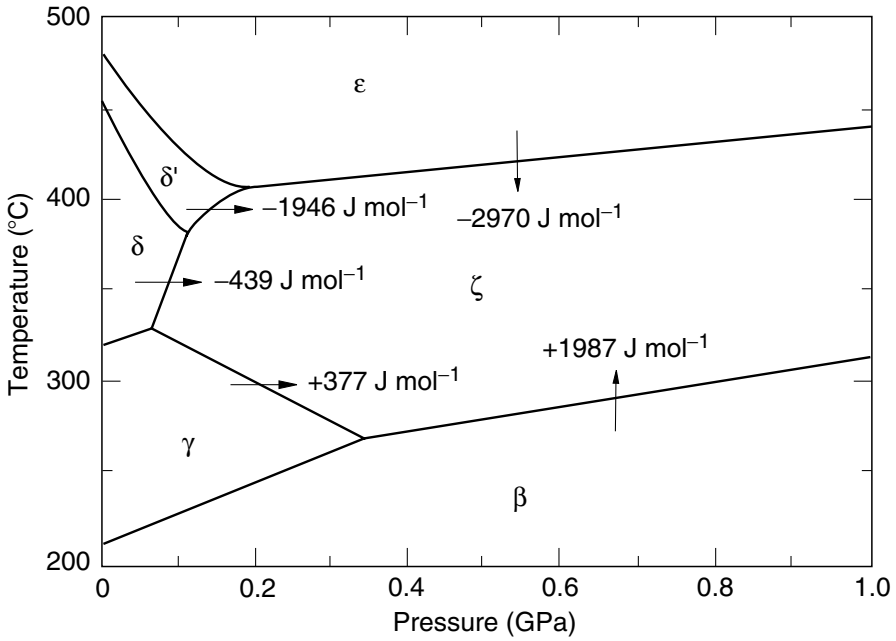

Fig. 7.26 *Transformation enthalpies of ζ plutonium calculated from the Clapeyron equation and slopes from Fig.* 7.21 (*Morgan*, 1970).

7.7.4 Alloys and phase transformations

Equilibrium phase diagrams provide a map of phase stability as a function of chemical concentration and temperature (most of the work of this nature has been done at ambient pressure and for binary alloy systems). All of the early work on phase diagrams of plutonium done during and after the Manhattan Project was classified. It was not until President Eisenhower launched the

'Atoms for Peace' initiative that much of that work was declassified and published. The Russian research group associated with A. A. Bochvar (Konobeevsky, 1955) published the first series of plutonium phase diagrams (with elements Be, Pb, V, Mn, Fe, Ni, and Os, as well as the ternary Pu–U–Fe) at a Moscow conference during the summer of 1955 in the preface to the first Conference on Peaceful Uses of Atomic Energy held in Geneva that fall. The U.S., U.K., and France rapidly followed suit. The Russian group added the Pu–Cu, Pu–Al, Pu–Bi, Pu–Zr, Pu–Mo, Pu–Th, and Pu–U systems at the second Geneva conference held in 1958 (Bochvar *et al.*, 1958). Coffinberry *et al.* (1958), and Schonfeld *et al.* (1959) published plutonium phase diagrams based on their work at Los Alamos Scientific Laboratory. Waldron *et al.* (1958) and Cope *et al.* (1960) published the U.K. results and Hocheid *et al.* (1967) the French results.

By 1968, most of the binary phase diagrams of plutonium were determined and published in the classic report of Ellinger *et al.* (1968b). Additional compilations were published in the *Plutonium Handbook*, edited by Wick (1980) and in the *Plutonium Metallurgy Handbook* (Hasbrouk and Burns, 1965). The most recent compilation is presented by Peterson and Kassner (1988). We review the salient features of binary plutonium phase diagrams below. The reader is referred to the reviews mentioned above for a discussion of available ternary plutonium diagrams. We also note that Blank provides a comprehensive compilation of phase diagram data in Table 2/1 of the *Gmelin Handbook of Inorganic Chemistry* (Blank, 1976). In addition, Blank (1976, 1977) provides a comprehensive treatment of the properties of plutonium alloys.

(a) Elements that expand the δ-phase field

Chemical additions (or alloying) significantly affect plutonium phase stability with temperature and pressure. The dramatic effects of the addition of a few atomic percent gallium to plutonium on its thermal behavior are demonstrated in Fig. 7.27. The addition of gallium retains the attractive feature of expansion during solidification while avoiding all of the large volume perturbations during cooling because the addition of gallium retains the fcc δ phase to room temperature. The thermal expansion is essentially zero, or 'Invar-like,' (Hecker, 2004) making Pu–Ga alloys much easier to cast. Moreover, the soft and ductile nature of the fcc δ phase makes these alloys much easier to shape than unalloyed plutonium. Consequently, most of the detailed work on properties of plutonium alloys has focused on systems that retain the δ phase. However, interest in metallic reactor fuels (Keiser *et al.*, 2003) has also resulted in work on β-phase retainers and on lean plutonium alloys involving uranium.

The complexity of chemical alloying is demonstrated in Fig. 7.28 for the Pu–Ga system. In addition to the six allotropes of plutonium, several new binary phases and 11 intermetallic compounds are formed. The fcc δ phase is retained to room temperature over a substantial range of gallium concentrations.

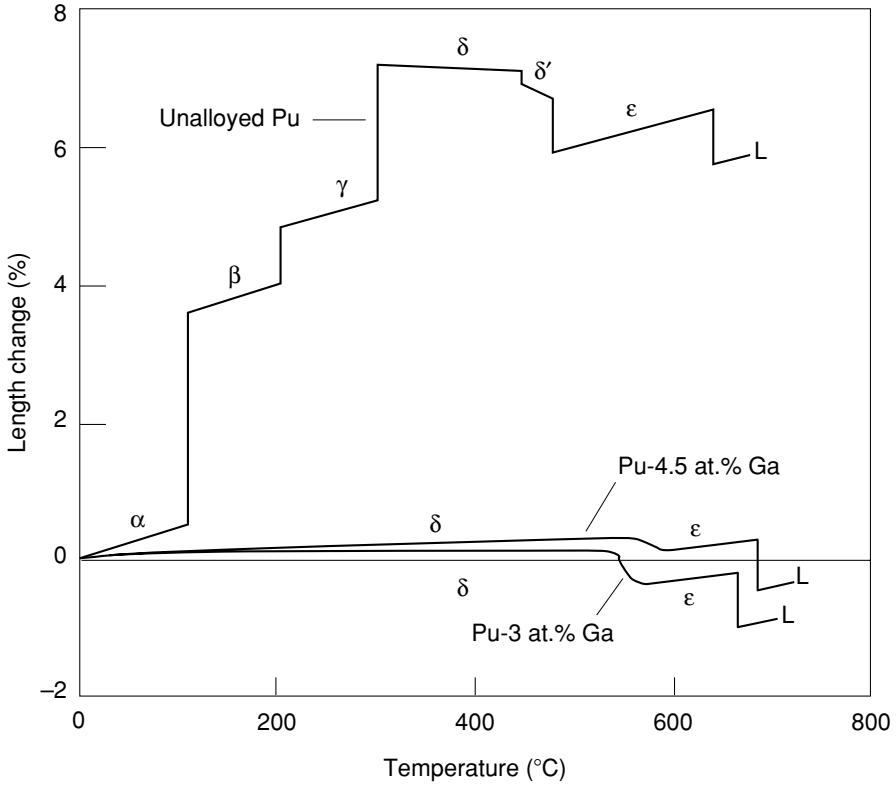

Fig. 7.27 *Length changes for unalloyed plutonium compared to Pu*-3.0 at.% *Ga and Pu*-4.5 at.% *Ga alloys.*

The question of whether the retained δ phase is stable or metastable was resolved only recently when Hecker and Timofeeva (2000) reconciled the U.S. (as well as the U.K. and French) and Russian versions of the Pu–Ga phase diagram. A comparison of the two versions of this fundamental phase diagram is shown in Fig. 7.29. They now believe that the Russian diagram (Fig. 7.29b), which shows an eutectoid point at 97°C and 7.9 at.% Ga, is the true equilibrium phase diagram (or as close a representation as possible, recognizing that radioactive decay in plutonium precludes true equilibrium). This diagram indicates that the δ phase should decompose below 97°C into α-Pu + Pu_3Ga. Such decomposition has never been observed because the kinetics are too slow. Timofeeva (2001) built her case on a clever set of experiments that demonstrated conclusively that the phase boundaries just above the eutectoid temperature clearly point to a decomposition (Hecker and Timofeeva, 2000). In fact, Timofeeva (2001) estimated that such decomposition requires more than 10,000 years at room temperature because the kinetics of the decomposition are exceedingly slow.

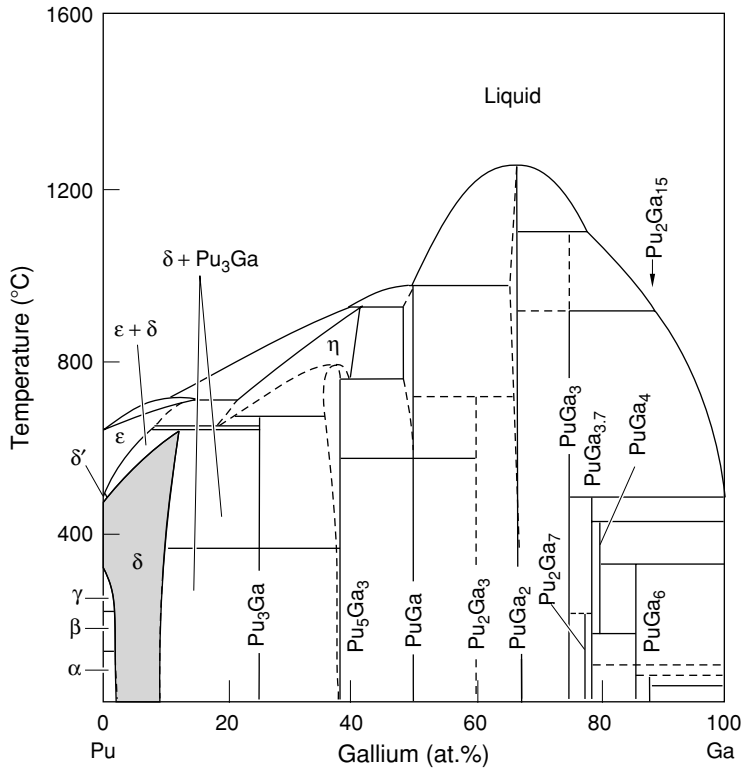

Fig. 7.28 *The Pu–Ga phase diagram at ambient pressure (from Peterson and Kassner*, 1988).

Therefore, the U.S. version (Fig. 7.29a), in which the δ phase is retained at least down to room temperature, represents an adequate 'working' diagram. Blank (1977), in his Table 2/105, presented the most complete table of crystal structures, atom positions, and atomic distances.

Timofeeva (2001) also demonstrated that the Pu–Al system undergoes a similar eutectoid decomposition near 100°C. The plutonium-rich end of the U.S. and Russian diagrams are shown in Fig. 7.30. In addition to the difference in findings related to the stability of the δ phase, Timofeeva also concluded that the intermetallic compound Pu_3Al does not extend to room temperature at thermodynamic equilibrium but rather only to 380°C. The eutectoid decomposition below 93°C is to α-Pu + PuAl (Timofeeva, 2001, 2003a). This finding differs from the conclusions of both the prior U.S. work reported by Ellinger *et al.* (1968b) and the prior Russian work reported by Bochvar *et al.* (1958). Timofeeva (2001) pointed out that the differences result because of slow kinetics. Her experiments allowed for sufficient time to demonstrate that PuAl is the intermetallic compound stable at room temperature.

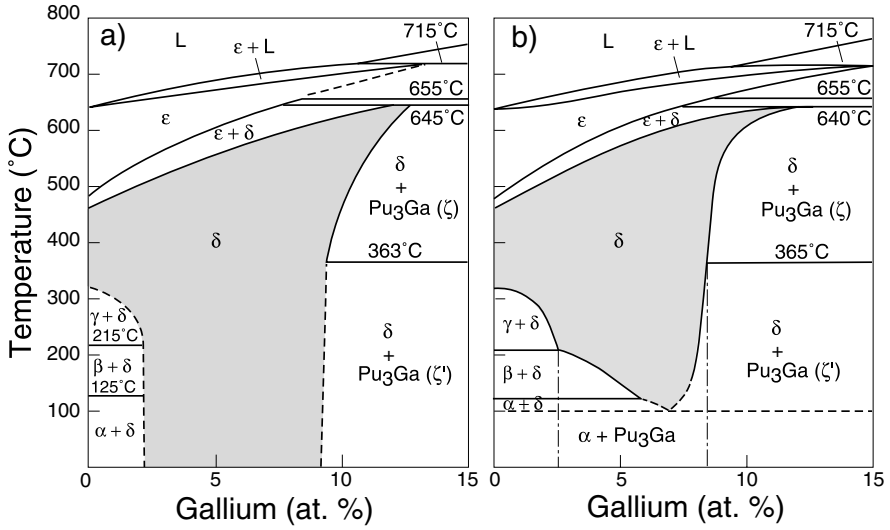

Fig. 7.29 *Comparison of* (*a*) *US and* (*b*) *Russian Pu–Ga phase diagrams from Hecker and Timofeeva* (2000).

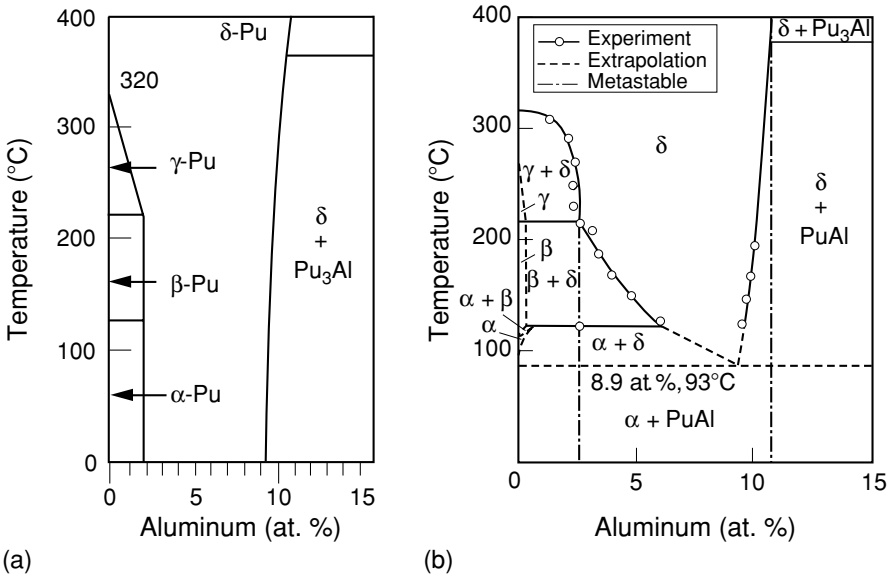

Fig. 7.30 *US* (*a*) *and Russian* (*b*) *versions of the Pu-rich side of the Pu–Al phase diagram. The US version is from Ellinger* et al. (1962*b*), *and the Russian version is from Hecker and Timofeeva* (2000).

Timofeeva (2003a) recently published data on 53 eutectoid transformations found in 30 binary plutonium phase diagrams. Eutectoid transformations are observed in binary systems of plutonium with transition metal elements (12), lanthanides (7), actinides, and elements of group IIIB (4 each). Only one eutectoid transformation exists with the elements of groups II, IV, and V. An interesting set of results is shown in Fig. 7.31 for four elements that expand the δ-phase field, Al, Ga, In, and Tl. Timofeeva demonstrated that the compositional range of the δ-phase field decreases and the eutectoid temperature increases monotonically with increasing atomic number of the alloying element. Additions of most trivalent elements expand the δ-phase field (Hecker, 2000), and in addition to Al, Ga, In, and Tl listed above, Ellinger *et al.* (1968b) showed that Sc, Ce, and Am also retain the δ phase. However, as discussed above, the retention appears to be metastable for most of these elements. It is likely that only Am results in a thermodynamically stable δ phase at room temperature. Timofeeva (2003a) reports a eutectoid transformation in Pu–Ce, and Pu–Sc systems that appears not to have received the same scrutiny as the other elements, so its status remains inconclusive.

In addition to the elements that readily retain the δ phase to room temperature (Al, Ga, Ce, Am, Sc, In, and Tl), there is a second class of elements (Si, Zn, Zr, and Hf) that retain the δ phase in a metastable state under conditions of rapid cooling. There are also some indications that the δ phase in Pu–Th alloys can be retained by rapid quenching (Gschneidner *et al.*, 1960).

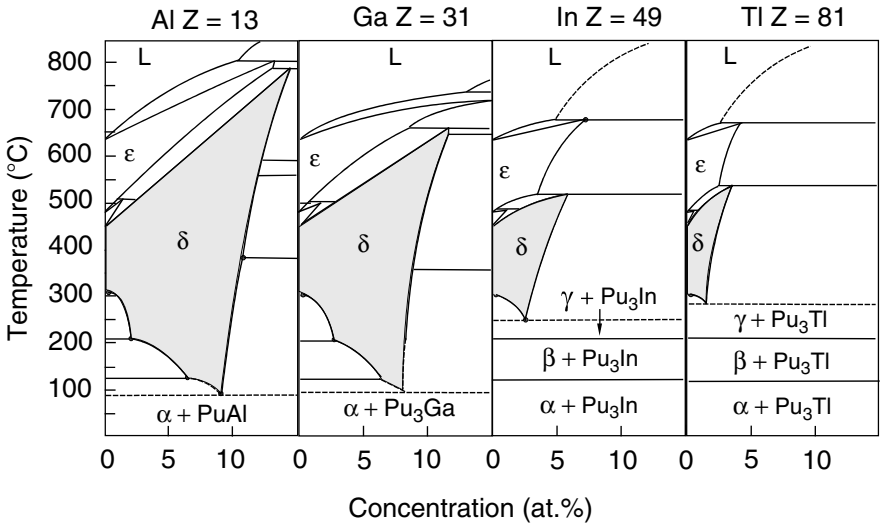

Fig. 7.31 *Phase diagrams of plutonium with several group* III*B elements show the eutectoid parameters and δ-phase region dependence* (*from Timofeeva,* 2003b).

Gschneidner *et al.* (1960) also found a number of the trivalent lanthanides (Dy, Er, Tm, Lu, and possibly Tb) to favor δ-phase retention, but their phase diagrams exhibit no δ-phase stability. Elliott and coworkers (Elliott and Giessen, 1975; Giessen *et al.*, 1975) demonstrated that retention of the δ phase and the bcc ϵ-phase can be extended in a metastable manner by splat cooling (rates from 10^6 to 10^8 s^{-1}). For example, both of these phases can be retained in splat-cooled Pu–Ti alloys. In Pu–Ga alloys, the maximum solubility of gallium in plutonium at room temperature is extended from 12.5 to 20 at.%. In Pu–Ce alloys, fcc δ phases can be retained across the entire range of cerium additions by splat cooling.

(b) α-Phase and β-phase stabilizers

Only neptunium has been found to expand the α-phase field. No other element is known to have any equilibrium solubility in the monoclinic α phase. Neptunium is also the only element that significantly expands the β-phase region. However, limited solubility of U, Hf, and Zr has been found in the β phase. Also, additions of Ti, Hf, and Zr will retain the β phase to room temperature and below by rapid quenching. Neptunium and uranium lower the melting point of plutonium slightly. The elements Hf, Zr, and Ti raise it significantly, even with small additions.

(c) Eutectic-forming elements

Additions of Mn, Fe, Co, or Ni lower the melting point of plutonium substantially. These elements form a low-melting eutectic much as does lead alloyed with tin to make solder. For example, the Pu–Fe phase diagram, shown in Fig. 7.32, exhibits the eutectic decomposition at 410°C and close to 10 at.% Fe from the liquid to δ-Pu + Pu_6Fe. This eutectic alloy was used in the first metallic plutonium fuel elements in the Los Alamos Molten Plutonium Reactor (LAMPRE) in the late 1940s (Kiehn, 1961; Burwell *et al.*, 1962). The elements Mn, Co, and Ni exhibit eutectic temperatures at approximately, 525°C, 405°C, and 465°C, respectively. These elements decompose to the intermetallic compounds $PuMn_2$, Pu_6Co, and PuNi, respectively. Other elements form eutectics but at somewhat higher temperatures. These include Si, Mn, Os, Ru, Rh, and Th. Eutectic-forming elements such as Mn, Fe, Ni, or Co are of special significance because they limit the useful temperature range of plutonium and its alloys. For example, plutonium metal heated above 410°C contained in steel will melt through the steel by forming the eutectic. Even when present in small amounts in plutonium, the alloying elements can segregate to grain boundaries, enriching the local alloying concentration and causing local melting or embrittlement at temperatures close to the eutectic temperature. Blank (1977) presented a thorough review of the properties of plutonium alloys and intermetallics with the eutectic-forming elements.

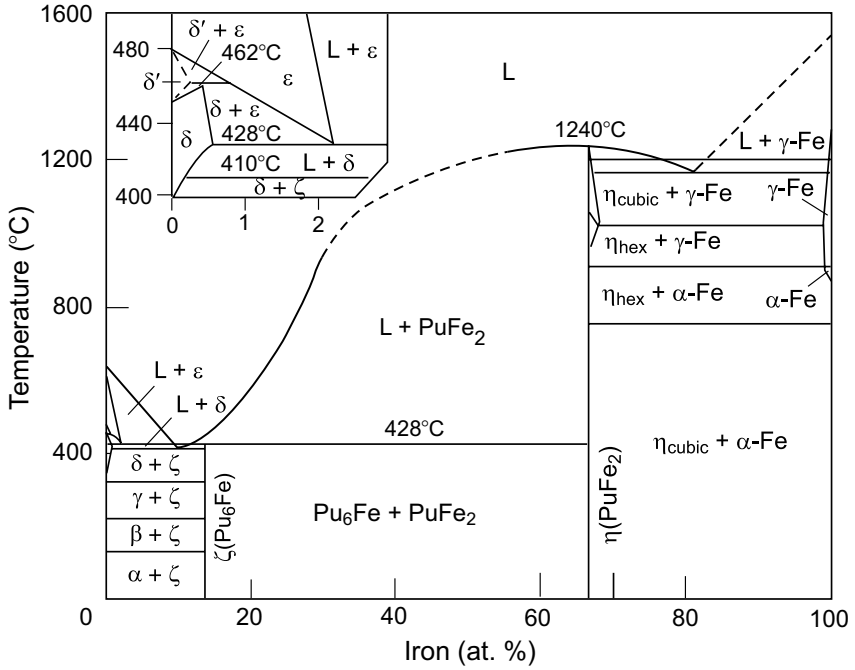

Fig. 7.32 *The Pu–Fe phase diagram at ambient pressure from Ellinger* et al. (1968*b*) *and first reported by Schonfeld* (1961).

(d) Interstitial compounds

When nonmetallic elements with very small radii are alloyed with metals, they tend to form interstitial solid solutions. A general rule of thumb is that if the radius of the nonmetallic element is <0.59 that of the metallic element, then an intermetallic compound with a simple structure (often fcc or hcp) forms. If the ratio is greater, then compounds with complex structures form. The most important nonmetallic elements for plutonium in the solid state are O, C, N, and H. None of these elements shows any solubility in the equilibrium phase diagrams. The Pu–O phase diagram is shown in Fig. 7.90. The elements O, C, and N all form several high-melting, refractory ceramic compounds. The structure and properties of these ceramic compounds will be discussed in greater detail in Section 7.8. Hydrogen also has a tendency to form compounds, but these readily decompose, rather than being refractory.

(e) The rest of the elements

Most other elements show only limited solubility in the δ phase, while some elements such as Ba, Sr, and Ca are immiscible. Most elements increase the

melting point. Some have shallow eutectics before the melting point increases. More than half of the elements, namely Th, Np, U, Ti, Ru, Rh, Pt, Os, and most lanthanides, show solubility in the ϵ phase.

Detailed X-ray crystal structure data are presented for many intermetallic compounds of plutonium in Table 7.17.

(f) Microsegregation in δ-phase alloys

Since alloys in which the fcc δ phase is retained to room temperature are of particular interest, we discuss the problem of microsegregation, which can dramatically influence the properties of δ-phase alloys. We use the Pu–Ga system shown in Fig. 7.33 for the purpose of illustration. During solidification and cooling, alloys within the range of gallium content to 13 at.% must cool through the liquid + ϵ and ϵ + δ two-phase regions. In a two-phase region, assuming gallium diffusivity is infinite in both phases, the composition of each phase is given by the phase boundaries at that temperature (the lever rule), giving rise to possible microsegregation. We track the gallium content through the ϵ + δ two-phase field in Fig. 7.33a. As the temperature reaches point A, the first δ phase to form has the gallium concentration shown at point B. As the temperature is lowered, the gallium concentration in the δ phase moves along the line BD, whereas the gallium concentration in ϵ moves along the line AC – if diffusion is sufficiently rapid to allow migration of gallium consistent with the imposed cooling rate. (Of course, the average gallium concentration in the alloy must be the initial concentration.) The diffusion rate of gallium is approximately 10^4 faster in the ϵ phase (because of its open bcc structure) than the δ phase, thereby not allowing equilibration in the δ phase for typical cooling rates. As a consequence, the gallium concentration of the remaining ϵ phase is pushed to lower values as cooling proceeds, resulting in increased segregation over that expected from equilibrium conditions.

As a result, the microstructure of a typical as-cast δ-phase alloy exhibits a range of gallium concentrations between points B and C. The interior of the δ-phase grains reflects the gallium concentration at point B and the grain boundaries may have very little gallium because they are the last ϵ-phase areas to transform with gallium at or below point C. The resulting microstructure appears heavily 'cored' or segregated as shown in Fig. 7.33b. It consists of gallium-rich δ phase in the center, a gallium-lean δ-phase shell (dark areas) at the core boundaries, and a gallium-lean intercore region that transformed to the α phase during cooling because of insufficient gallium. This type of microsegregation typically occurs during cooling through liquid + solid two-phase regions because diffusion in the liquid is so much faster than in the solid. However, the anomalously high diffusion rate in ϵ-plutonium avoids the problem in the liquid + ϵ region, only to have it reappear in the ϵ + δ two-phase region. Equilibrating the gallium concentration requires a sustained return to temperatures high in the δ-phase region, typically hundreds of hours, to achieve

Table 7.17 *X-ray crystal structure data for selected intermetallic compounds of plutonium.*

Phase	*Structure type*	*Symmetry*	*Space group*	*Lattice parameters* a_0(Å)	b_0(Å)	c_0(Å)	*Angle* (deg)	*Units per cell*	*X-ray density* (g cm^{-3})	*References*
$PuAg_3(\zeta)$		hexagonal	P6/*m*	12.730(3)		9.402(5)		16	11.33	Ellinger *et al.* (1968b), Miner (1970), Kutaitsev *et al.* (1967), and Runnalls (1956)
				12.72(5)		9.39(3)				Freeman and Darby (1974) and Blank *et al.* (1962)
$PuAg_{3.6}$	$GdAg_{3.6}$	hexagonal	P6/*m*	12.727(6)		9.392(4)			11.15	Ellinger *et al.* (1968b) and Miner (1970)
$PuAg_2$										Miner (1970)
Pu–Ag phase diagram										Ellinger *et al.* (1968b) and Kutaitsev *et al.* (1967)
$Pu_3Al(\zeta)$	$SrPb_3$	tetragonal	P4/*mmm*	4.499(1)		4.536(1)		1	13.45	Ellinger *et al.* (1968b), Freeman and Darby (1974), Blank *et al.* (1962), and Bochvar *et al.* (1958)
	Ti_3Cu			4.499(2)		4.538(2)			13.45	Coffinberry and Miner (1961)
		cubic		4.500						Ellinger *et al.* (1962b)
				4.530		4.575				
$PuAl(\eta)$	related to CsCl	bcc		10.769(1)				29	10.25	Ellinger *et al.* (1968b), Freeman and Darby (1974), Blank *et al.* (1962), and Bochvar *et al.* (1958)
				10.769					10.253	Kay and Waldron (1967)
$PuAl_2(\theta)$	Cu_2Mg	cubic	F*d*3*m*	7.831(5)				8	8.09	Ellinger *et al.* (1968b), Freeman and Darby (1974), Blank *et al.* (1962), and Runnalls (1956)
				7.840(1)(Pu-rich)						Bochvar *et al.* (1958)
				7.836(1)(Al-rich)						Bochvar *et al.* (1958)
				7.874						Ellinger *et al.* (1962b)
				7.838(1)(Pu-rich)					8.06	Coffinberry and Miner (1961)
				7.848(1)(Al-rich)						Coffinberry and Miner (1961)

				7.833				8.095	Kay and Waldron (1967)
$PuAl_3(\iota)$	$PuAl_3$	hexagonal(6H)	$P6_3/mmc$	6.08(1)		14.40(3)			Ellinger *et al.* (1968b), Freeman and Darby (1974), Blank *et al.* (1962), and Runnalls (1956)
				6.084(1)		14.427(2)	6	6.8	Bochvar *et al.* (1958)
				6.10(2)		14.47(4)		6.84	Larson *et al.* (1957)
		hexagonal		6.083		14.410		6.643	Kay and Waldron (1967)
		cubic(3H)	$Pm3m$	4.262				6.604	Kay and Waldron (1967)
		rhomb($9H_\beta$)	$R\bar{3}m$	7.879			$\alpha = 45.94$	6.657	Kay and Waldron (1967)
		rhomb($9H_\alpha$)		7.901			$\alpha = 45.81$	6.634	Kay and Waldron (1967)
$PuAl_4(\kappa)$	UAl_4	orthorhombic	*Imma*	4.42(2)	6.26(2)	13.66(3)			Ellinger *et al.* (1968b), Freeman and Darby (1974), and Blank *et al.* (1962)
				4.387(2)	6.262(2)	13.714(4)	4	6.02–6.11	Bochvar *et al.* (1958)
				4.41	6.29	13.79			Ellinger *et al.* (1968b)
α-$PuAl_4$		orthorhombic	*Imma*	4.396(1)	6.266(1)	13.708(2)	3.6	5.680	Kay and Waldron (1967)
β-$PuAl_4$		orthorhombic	*Imma*	4.396(1)	6.266(1)	13.708(2)		5.680	Kay and Waldron (1967)
(α- and β-$PuAl_4$ differ by the distribution of lattice vacancies)									
Pu–Al phase diagram, see Fig. 7.30									Kay and Waldron (1967), Bochvar *et al.* (1958), Waldron *et al.* (1958), Ellinger *et al.* (1962b), and Moeller and Schonfeld (1950)
Pu–Am system, no compounds, phase diagram known									Ellinger *et al.* (1966)
Pu–As system, see Section 7.8, Table 7.33									
$Pu_xAu_y(\eta)$									Ellinger *et al.* (1968b) and Kay and Waldron (1967)
$PuAu(\zeta)$									Ellinger *et al.* (1968b) and Kay and Waldron (1967)

Table 7.17 (*Contd.*)

Phase	*Structure type*	*Symmetry*	*Space group*	*Lattice parameters* a_0(Å)	b_0(Å)	c_0(Å)	*Angle* (deg)	*Units per cell*	*X-ray density* (g cm^{-3})	*References*
$PuAu_2$(ι)										Ellinger *et al.* (1968b) and Kay and Waldron (1967)
Pu_xAu_y(κ)										Ellinger *et al.* (1968b) and Kay and Waldron (1967)
$PuAu_3$(λ)		hexagonal	P6/*m*	12.710		9.210		16	17.11	Ellinger *et al.* (1968b), Kay and Waldron (1967), and Kutaitsev *et al.* (1967)
$PuAu_4$(μ)										Ellinger *et al.* (1968b) and Kay and Waldron (1967)
$PuAu_5$(ν)										Ellinger *et al.* (1968b) and Kay and Waldron (1967)
Pu–Au phase diagram										Ellinger *et al.* (1968b), Kay and Waldron (1967), and Kutaitsev *et al.* (1967)
Pu–B system, see Section 7.8, Table 7.28										
Pu–Ba system, no compounds										(Seaborg *et al.* 1946, 1949b), Ellinger *et al.* (1968b), and Bochvar *et al.* (1958)
$PuBe_{13}$	$NaZn_{13}$	cubic	F*m*3*c*	10.284(1)(Be-rich)				8	4.35	Runnalls (1956)
				10.278(1)(Pu-rich)						Runnalls (1956)
				10.274(2)					4.36	Seaborg *et al.* (1946) and Bochvar *et al.* (1958)
				10.282(1)(Be-rich)					4.35	Coffinberry and Miner (1961)
Pu–Be phase diagram										Seaborg *et al.* (1946, 1949b), Konobeevsky (1955), Ellinger *et al.* (1968b), and Bochvar *et al.* (1958)

Pu–Bi system, see Section 7.8, Table 7.33									
Pu–Bi phase diagram									Seaborg *et al.* (1946, 1949b), Ellinger *et al.* (1968b), and Bochvar *et al.* (1958)
Pu–C system, see Section 7.8, Table 7.29									
Pu–Ca system, no compounds									Seaborg *et al.* (1946, 1949b), Ellinger *et al.* (1968b), and Bochvar *et al.* (1958)
$PuCd_2(\zeta)$									Etter *et al.* (1965)
$PuCd_4(\eta)$									Etter *et al.* (1965)
$PuCd_6(\theta)$	$CeCd_6$	cubic	I*m*3	15.59(1)				9.61	Etter *et al.* (1965) and Johnson *et al.* (1965)
$PuCd_{11}(\iota)$	$BaHg_{11}$	cubic	P*m*3*m*	9.282(2)			3	10.25	Etter *et al.* (1965) and Johnson *et al.* (1965)
Pu–Cd phase diagram									Ellinger *et al.* (1968b), Etter *et al.* (1965), and Johnson *et al.* (1965)
Pu–Ce system, no compounds, phase diagram known									Wilkinson (1960), Ellinger *et al.* (1968b), and Selle and Etter (1964)
$Pu_6Co(\zeta)$	U_6Mn	tetragonal	I4/*mcm*	10.45(1)		5.32(1)	4	17.6	Bochvar *et al.* (1958)
				10.46(2)		5.33(1)	4	17.00	Coffinberry and Miner (1961)
$Pu_3Co(\eta)$	Al_2CuMg	orthorhombic	C*mcm*	3.501(3)	11.03(3)	9.23(15)(Pu-rich)		14.7	Poole and Nichols (1961)
				3.477(3)	10.99(3)	9.20(15)(Co-rich)			Poole and Nichols (1961)
				3.470	10.939	9.196		14.76	Coffinberry and Miner (1961)
				3.475(4)	10.976(10)	9.220(8)		14.65	Larson *et al.* (1963)
$Pu_2Co(\theta)$	Fe_2P	hexagonal	P321	7.902(4)(Pu-rich)		3.549(2)	3	14.0	Coffinberry and Miner (1961)
				7.763(2)(Co-rich)		3.648(3)			Coffinberry and Miner (1961)
				7.803(8)(Pu-rich)		3.606(5)			Poole and Nichols (1961)
				7.732(8)(Co-rich)		3.654(5)			Poole and Nichols (1961)
$PuCo_2(\iota)$	Cu_2Mg	cubic	F*d*3*m*	7.075(5)			8	13.39	Runnalls (1956)
				7.083(10)(Pu-rich)					Bochvar *et al.* (1958)
				7.066(10)(Co-rich)					Bochvar *et al.* (1958)
				7.081(1)(Pu-rich)					Coffinberry and Miner (1961)
				7.095(5)(Pu-rich)					Poole and Nichols (1961)

Table 7.17 (*Contd.*)

Phase	*Structure type*	*Symmetry*	*Space group*	*Lattice parameters* a_0(Å)	b_0(Å)	c_0(Å)	*Angle* (deg)	*Units per cell*	*X-ray density* (g cm^{-3})	*References*
				7.023(5)(Co-rich)						Poole and Nichols (1961)
$PuCo_3(\kappa)$	$PuNi_3$	rhombohedral (hexagonal setting)		8.635(10) 8.327(5)			$\alpha = 33°40'$	3	11.74	Poole and Nichols (1961)
$Pu_2Co_{17}(\lambda)$	Th_2Ni_{17}	hexagonal	$P6_3/mmc$	8.325(2) 8.327(5)	8.104(3) 8.107(5)			2	10.10	Bochvar *et al.* (1958) Poole and Nichols (1961)
Pu–Co phase diagram										Seaborg *et al.* (1946, 1949b) and Poole and Nichols (1961)
Pu–Cr system, no compounds, phase diagram known										Ellinger *et al.* (1968b), Bochvar *et al.* (1958), and Bowersox and Leary (1968)
Pu–Cs system, no compounds										Seaborg *et al.* (1946, 1949b) and Bochvar *et al.* (1958)
$PuCu_2(\zeta)$	$CeCu_2$	orthorhombic	*Imma*	4.332(2) 4.32(2)	6.686(1) 6.69(2)	7.376(1) 7.38(2)		4	11.20	Pons *et al.* (1972) Lataillade *et al.* (1971)
$PuCu_4(\eta)$		orthorhombic		4.320(1) 4.37(2)	8.264(3) 8.37(2)	9.226(3) 9.32(2)		4	10.12	Pons *et al.* (1972) Lataillade *et al.* (1971)
$Pu_4Cu_{17}(\theta)$										Lataillade *et al.* (1971)
$PuCu_6(\iota)$	$CeCu_6$	orthorhombic	*Pnma*	8.50(3) 8.16	5.025(3) 5.14	10.059(6) 10.06		4	10.12	Kutaitsev *et al.* (1967) Wittenberg and Grove (1964)
Pu–Cu phase diagram										Ellinger *et al.* (1968b), Grison *et al.* (1960), and Kutaitsev *et al.* (1967)
Pu–Dy system, miscibility gap, no compounds										Ellinger *et al.* (1968b)
Pu–Er system, miscibility gap, no compounds										Ellinger *et al.* (1968b)
Pu–Eu system, immiscibility, no compounds										Ellinger *et al.* (1968b)
$Pu_6Fe(\zeta)$	U_6Mn	tetragonal	$I4/mcm$	10.41(1)		5.359(4)		4		Mardon *et al.* (1957)

				10.404(4)	5.355(2)	4	17.07	Coffinberry and Miner (1961)
				10.403	5.347		17.10	Konobeevsky (1955)
				10.405(5)	5.349(3)			Bowersox and Leary (1966)
				10.40(2)	5.345(5)			Coffinberry and Waldron (1956)
$PuFe_2(\eta_{cub})$	Cu_2Mg	cubic	F*d*3*m*	7.150(5)('preparation a')			12.74	Runnalls (1956)
				7.190(5)('preparation b')			12.53	Runnalls (1956)
				7.191(1)(Pu-rich)		4	12.53	Coffinberry and Miner (1961)
				7.178			12.59	Konobeevsky (1955)
				7.189				Mardon *et al.* (1957)
$PuFe_2(\eta_{hex})$	$MgNi_2$	hexagonal		5.64	18.37			Avivi (1964)
Pu–Fe phase diagram								Ellinger *et al.* (1968b) and Grove (1966)[f]
Pu–Ga(η)		cubic	$I2_13$	7.207(18%Ga)			16	Blank and Lindner (1976)
			$I2_1$	7.167(41.6%Ga)				Chebotarev (1976)
		bcc pseudo-cell		3.58				Ellinger *et al.* (1964)
α-$Pu_3Ga(\zeta')$	$SrPb_3$	tetragonal	P4/*mmm*	4.470	4.523	1	14.45	Blank and Lindner (1976)
				4.469(1)	4.527(2)	1	14.45	Ellinger *et al.* (1964)
				4.492	4.555			Hocheid *et al.* (1965)
β-$Pu_3Ga(\zeta)$	$AuCu_3$	cubic	P*m*3*m*	4.514(Pu-rich)		1	14.27	Blank and Lindner (1976)
				4.497(Ga-rich)				
				4.507(2)		1	14.27	Ellinger *et al.* (1964)
				4.500				Hocheid *et al.* (1965)
$Pu_5Ga_3(\theta)$	W_5Si_3	tetragonal	I4/*mcm*	11.736	5.559	4	12.29	Blank and Lindner (1976)
		tetragonal	I4/*mcm*	11.735(3)	5.511(2)	4	12.29	Ellinger *et al.* (1964)
		fcc		5.570				Hocheid *et al.* (1965)
α-PuGa		cubic	I*m*3*m*	3.53		2		Hocheid *et al.* (1965)
β-PuGa(ι)		tetragonal	I4/*mm*	6.641	8.069	8	11.52	Blank and Lindner (1976)
				6.666	7.985(Pu-rich)			Blank and Lindner (1976)
				6.640(1)	8.066(1)	8	11.53	Ellinger *et al.* (1964)
Pu_2Ga_3 (κ)		hexagonal		4.378	3.792			Blank and Lindner (1976)
$PuGa_2(\lambda)$	AlB_2	hexagonal	P6/*mmm*	4.248(1)	4.120	1	9.76	Ellinger *et al.* (1964)
				4.258	4.120			Hocheid *et al.* (1965)
				4.248	4.107(Pu-rich)	1	9.77	Blank and Lindner (1976)
				4.258	4.139(Ga-rich)			Blank and Lindner (1976)
α-$PuGa_3(\mu)$	Ni_3Sn	rhombohedral	$R\bar{3}m$	6.173	27.99	12	9.66	Blank and Lindner (1976)

Table 7.17 (*Contd.*)

Phase	*Structure type*	*Symmetry*	*Space group*	*Lattice parameters* a_0(Å)	b_0(Å)	c_0(Å)	*Angle* (deg)	*Units per cell*	*X-ray density* (g cm^{-3})	*References*
				6.178(1)		28.031(4)				Larson *et al.* (1965)
				(10.001)			($\alpha = 35°59'$)	12	9.63	Larson *et al.* (1965)
β-$PuGa_3$(μ′)	Mg_3Cd	hexagonal	$P6_3/mmc$	6.299		4.513		2	9.61	Blank and Lindner (1976)
	Ni_3Sn	hexagonal	$P6_3/mmc$	6.300(1)		4.514(1)		2	9.59	Ellinger *et al.* (1964)
~Pu_2Ga_7(?)		tetragonal		4.253		9.695				Blank and Lindner (1976)
Pu_3Ga_{11}–Pu_4Ga_{15}										Blank and Lindner (1976)
$PuGa_4$(ν)	UAl_4	orthorhombic	*Imma*	4.380(1)	6.290(1)	13.673(4)		4	9.13	Land *et al.* (1965a) and Ellinger and Zachariasen (1965)
			Imma	4.387	6.297	13.663		4	9.11	Blank and Lindner (1976)
α-$PuGa_6$										Blank and Lindner (1976)
β-$PuGa_6$(ζ)	$PuGa_6$	tetragonal	P4/*nbm*	5.942(1)		7.617(1)		2	8.11	Land *et al.* (1965a) and Ellinger and Zachariasen (1965)
			P4/*mbm*	5.941		7.621		2	8.12	Blank and Lindner (1976)
~Pu_2Ga_{15}		tetragonal		6.206		8.332		1	7.88	Blank and Lindner (1976)
Pu–Ga phase diagram										Ellinger *et al.* (1964), Hocheid *et al.* (1965), and Akhachinskii and Bashlykov (1970)
Pu–Al–Ga phase diagram										Blank and Lindner (1976)
Pu–Gd system, miscibility gap, no compounds										Kutaitsev *et al.* (1967)
Pu_3Ge										Coffinberry and Miner (1961)
Pu_3Ge_2										Coffinberry and Miner (1961)
Pu_2Ge_3	AlB_2	hexagonal	P6/*mmm*	3.975(2)		4.198(2)		0.5	10.16	Coffinberry and Miner (1961)
$PuGe_2$	$ThSi_2$	bc tetragonal	I4/*amd*	4.102(2)		13.81(1)		4	10.98	Coffinberry and Miner (1961)
$PuGe_3$	$AuCu_3$	cubic	P*m*3*m*	4.223(1)				1	10.07	Coffinberry and Miner (1961)
Pu–Ge phase diagram unknown										Ellinger *et al.* (1968b)
Pu–H system, see Section 7.8, Table 7.26										

$Pu_{28}Hf(\zeta)$	$Pu_{28}Zr$	bc tetragonal	$I4_1/a$	18.19		7.851	4	17.57	Zachariasen and Ellinger (1970)
									Ellinger and Land (1968)
$\sim Pu_{15.7}Hf(\theta)$									
$\sim Pu_{10}Hf(\zeta)$		hexagonal		3.205(1)	5.100(1)			17.07	Kutaitsev *et al.* (1967)
$\sim Pu_9Hf(\theta)$		orthorhombic		10.415(5)	10.428(5)	11.245(5)		17.7	Kutaitsev *et al.* (1967)
Pu–Hf phase diagram									Ellinger *et al.* (1968b), Kutaitsev *et al.* (1967), and Ellinger and Land (1968)
$PuHg_3(?)$	$UHg_3(?)$								Coffinberry and Miner (1961)
$PuHg_4$		pseudo-cubic		3.61(1)					Coffinberry and Miner (1961)
Pu_5Hg_{21}	γ-brass	distorted bcc	$D8_{1-3}$	21.78(1)			16	13.90	Berndt (1966)
Pu–Hg phase diagram									Seaborg *et al.* (1946, 1949b) and Ellinger *et al.* (1968b)
Pu–Ho system, no compounds									Ellinger *et al.* (1968b)
$Pu_3In(\zeta)$	$AuCu_3$	cubic	P*m*3*m*	4.702(1)(Pu-rich)			1		Bochvar *et al.* (1958)
				4.705(Pu-rich)				13.34	Ellinger *et al.* (1965)
				4.722(In-rich)				12.96	Ellinger *et al.* (1965)
				4.750					Hocheid *et al.* (1965)
				4.703(2)			1	13.3	Coffinberry and Miner (1961)
η phase									Ellinger *et al.* (1965)
PuIn(θ)	AuCu	tetragonal	P4/*mmm*	4.811(1)		4.538(1)	2	11.19	Ellinger *et al.* (1965)
$Pu_3In_5(\iota)$									Ellinger *et al.* (1965)
$PuIn_3(\kappa)$	$AuCu_3$	cubic	P*m*3*m*	4.607(1)					Bochvar *et al.* (1958)
				4.6096(2)				9.22	Ellinger *et al.* (1965)
				4.6185(Pu-rich)					Ellinger *et al.* (1965)
				4.6088(In-rich)					Ellinger *et al.* (1965)
Pu–In phase diagram									Hocheid *et al.* (1965) and Ellinger *et al.* (1965)
Pu_5Ir_3	W_5Si_3	tetragonal	I4/*mcm*	11.0438		5.6115	4	17.18	Beznosikova *et al.* (1974)
				11.043		5.611			Beznosikova *et al.* (1974)
				11.012(3)		5.727(2)	4	16.94	Cromer (1977a)
				11.015		5.621(Ir-rich)			Beznosikova *et al.* (1974)
Pu_5Ir_4	Pu_5Ir_4	orthorhombic	P*nma*	7.245	14.60	7.455	4	16.54	Blank and Lindner (1976)
$PuIr_2$	Cu_2Mg	fcc	F*d*3*m*	7.512(1)–7.528(1)			8		Kutaitsev *et al.* (1967)
				7.518					Erdmann and Keller (1973)

Table 7.17 (*Contd.*)

Phase	*Structure type*	*Symmetry*	*Space group*	*Lattice parameters* a_0(Å)	b_0(Å)	c_0(Å)	*Angle* (deg)	*Units per cell*	*X-ray density* (g cm^{-3})	*References*
Pu–Ir phase diagram, no information										Erdmann and Keller (1973)
Pu–K system, no compounds										Ellinger *et al.* (1968b)
Pu–La system, miscibility gap, no compounds										Grison *et al.* (1960), Kutaitsev *et al.* (1967), and Ellinger *et al.* (1967)
Pu–Li system, no compounds										Ellinger *et al.* (1968b)
Pu–Lu system, no information										
$PuMg_2(\zeta)$	CaF_2	fcc	F*m*3*m*	7.34(1)				4	4.83	Coffinberry and Miner (1961) and Ellinger *et al.* (1968b)
$PuMg_{2+x}$		hexagonal		13.8(1)		9.7(1)				Coffinberry and Miner (1961) and Ellinger *et al.* (1968b)
Pu–Mg phase diagram										Ellinger *et al.* (1968b) and Knoch *et al.* (1969)
$PuMn_2$	Cu_2Mg	fcc	F*d*3*m*	7.290(5)(Pu-rich)				8	11.96	Runnalls (1956)
				7.292(1)(Pu-rich)					11.95	Coffinberry and Miner (1961)
				7.29(Pu-rich)						Konobeevsky (1955)
				7.26(Mn-rich)						Konobeevsky (1955)
Pu–Mn phase diagram										Konobeevsky (1955), Ellinger *et al.* (1968b), Bochvar *et al.* (1958), and Grove (1966)
Pu–Mo system, no compounds, phase diagram established										Ellinger *et al.* (1968b), Grison *et al.* (1960), and Bochvar *et al.* (1958)
Pu–N system, see Section 7.8, Table 7.33										
Pu–Na system, no compounds										Ellinger *et al.* (1968b)
Pu–Nb system, no compounds, phase diagram established										Ellinger *et al.* (1968b) and Bochvar *et al.* (1958)
Pu–Nd system, miscibility gap, no compounds, phase diagram established										Ellinger *et al.* (1968a,b) and Kutaitsev *et al.* (1967)

PuNi(ζ)	TlI	orthorhombic	C*mcm*	3.59(1)	10.21(2)	4.22(1)		4	12.78	Cromer and Roof (1959)
$PuNi_2$(η)	Cu_2Mg	fcc	F*d*3*m*	7.16(1)				8	13.1	Runnalls (1956)
				7.141(1)(Pu-rich)						Coffinberry and Miner (1961)
				7.115(1)(Ni-rich)						
				7.14						
$PuNi_3$(θ)	$PuNi_3$	rhombohedral	R$\bar{3}$*m*	8.615			$\alpha = 33°44'$	3	11.8	Cromer and Olsen (1959)
$PuNi_4$(ι)	$PuNi_4$	monoclinic	C2/*m*	4.87(1)	8.46(2)	10.27(2)	$\beta = 100°$	6	11.33	Ellinger *et al.* (1968b) and Cromer and Larson (1960)
$PuNi_5$(κ)	$CaZn_5$	hexagonal	P6/*mmm*	4.875(5)		3.970(5)		1	10.8	Runnalls (1956)
				4.872(2)(Pu-rich)		3.980(1)				Coffinberry and Miner (1961)
				4.861(2)(Ni-rich)		3.982(1)				Coffinberry and Miner (1961)
Pu_2Ni_{17}(λ)	Th_2Ni_{17}	hexagonal	P6_3/*mmc*	8.30(1)		8.00(1)				Runnalls (1956)
				8.29(2)		8.01(2)		2	10.3	Coffinberry and Miner (1961)
Pu–Ni phase diagram										Ellinger *et al.* (1968b) and Wensch and Whyte (1951)
Pu–Np										
η phase		orthorhombic		10.86	10.67	10.43		54		Mardon *et al.* (1961) and Cope *et al.* (1960)
Pu–Np phase diagram										Mardon *et al.* (1961) and Cope *et al.* (1960)
Pu–O system, see Section 7.8, Table 7.37										
$Pu_{19}Os$(ζ)	related to β-Pu	orthorhombic	P*nna*	15.839(5)	7.819(3)	9.151(3)		52	18.02	Cromer (1979b)
$Pu_{19}Os$(η)		orthorhombic	C*mca*	5.345(5)	14.884(14)	10.898(15)		2	18.12	Cromer (1978)
Pu_3Os										Konobeevsky (1955)
Pu_3Os(η′)										Ellinger *et al.* (1968b)
Pu_5Os_3(θ)	W_5Si_3	tetragonal	I4/*mcm*	10.8818		5.6645		4	17.48	Beznosikova *et al.* (1974) and Cromer *et al.* (1975)
$PuOs_2$(ι)	$MbZn_2$	hexagonal	P6_3/*mmc*	5.337		8.683		4	19.2	Konobeevsky (1955)
Pu–Os phase diagram										Konobeevsky (1955), Ellinger *et al.* (1968b), and Miner (1970)

Table 7.17 (*Contd.*)

Phase	*Structure type*	*Symmetry*	*Space group*	*Lattice parameters* a_0(Å)	b_0(Å)	c_0(Å)	*Angle* (deg)	*Units per cell*	*X-ray density* (g cm^{-3})	*References*
Pu–P system, see Section 7.8, Table 7.33										
$Pu_3Pb(\zeta)$	Cu_3Au	cubic	P*m*3*m*[a]	4.737(1)				1	14.56	Wood *et al.* (1969)
$Pu_5Pb_3(\eta)$	W_5Si_3	tetragonal	I4/*mcm*	12.310(2)		6.084(1)			13.07	Wood *et al.* (1969)
$Pu_5Pb_4(\theta)$	Ti_5Ga_4	hexagonal	$P6_3/mcm$	9.523(4)		6.482(3)			13.31	Wood *et al.* (1969)
$Pu_4Pb_5(\iota)$	Pu_4Pb_5(?)[b]	hexagonal	$P6_322$	16.52(1)		6.440(3)				Wood *et al.* (1969)
$PuPb_2(\kappa)$[c]	$HfGa_2$	tetragonal	$I4_1/amd$	4.621(5)		31.29(3)			12.99	Wood *et al.* (1969)
$PuPb_3(\lambda)$	Cu_3Au	cubic	P*m*3*m*	4.8084(Pu-rich)				1		Wood *et al.* (1969)
				4.8077(Pb-rich)					12.86	Wood *et al.* (1969)
				4.808(1)				1	12.86	Bochvar *et al.* (1958) and Wood *et al.* (1969)
				4.81						Coffinberry and Miner (1961), Konobeevsky (1955), and Bochvar *et al.* (1958)
Pu–Pb phase diagram										Bochvar *et al.* (1958) and Wood *et al.* (1969)
Pu_5Pd_4 (probably identical with PuPd)										Kutaitsev *et al.* (1967)
PuPd	FeB	orthorhombic	P*nma*	7.036(4)	4.550(2)	5.663(2)		4	12.65	Cromer (1975)
				7.028(5)	4.571(1)	5.658(2)		4	12.6	
Pu_3Pd_4	Pu_3Pd_4	rhombohedral	$R\bar{3}$	7.916			$\alpha = 114.2$			Kutaitsev *et al.* (1967)
		(hexagonal setting)		13.304		5.783		2	12.8	Kutaitsev *et al.* (1967)
				13.344(2)		5.744(2)			12.85	Cromer *et al.* (1973)
Pu_3Pd_5	Ga_5Zr_3	orthorhombic	C*mcm*	9.201	7.159	9.771		4	12.89	Cromer (1976)
$PuPd_3$	$AuCu_3$	cubic	P*m*3*m*	4.077–4.119				1	13.41[d]	Kutaitsev *et al.* (1967)
				4.095						Erdmann and Keller (1973)
Pu–Pd phase diagram										Ellinger *et al.* (1968b) and Kutaitsev *et al.* (1967)

Pu–Pr system, no compounds, miscibility gap, phase diagram established									Ellinger *et al.* (1968a,b) and Kutaitsev *et al.* (1967)
$Pu_5Pt_3(\zeta)$	Mn_5Si_3	hexagonal	P$6_3/mcm$	8.490		6.094	2		Beznosikova *et al.* (1974)
				8.490(2)		6.084(2)	2	15.57	Cromer and Larson (1975)
$Pu_{31}Pt_{20}(\eta)$	$Pu_{31}Pt_{20}$	tetragonal	I4/*mcm*	11.302(5)		37.388(23)	4	15.73	Cromer and Larson (1977)
PuPt(θ)	TaB	orthorhombic	C*mcm*	3.816	10.694	4.428		15.95	Kutaitsev *et al.* (1967), Cromer and Roof (1959)
$PuPt_2(\iota)$	Cu_2Mg	fcc	F$d3m$	7.633			8	18.69	Erdmann and Keller (1973)
				7.631–7.653					Kutaitsev *et al.* (1967)
α-$PuPt_3(\kappa)$	$AuCu_3$	cubic	P$m3m$	4.107			1	19.75	Kutaitsev *et al.* (1967)
				4.105					Erdmann and Keller (1973)
β-$PuPt_3(\kappa')$	PNi_3	bc tetragonal	$I\bar{4}$	10.39(1)		4.60(3)			Land *et al.* (1978)
$PuPt_4(\lambda)$	defect $PuPt_5$	orthorhombic	C*mmm*	5.258(15)	8.759(29)	4.563(13)			Land *et al.* (1978)
$PuPt_5(\mu)$	$CaCu_5$	hexagonal	P6/*mmm*	5.262(8)		4.393(8)			Land *et al.* (1978)
	$SmPt_5$	orthorhombic		5.314	9.100	26.51			Erdmann and Keller (1973)
Pu–Pt phase diagram									Kutaitsev *et al.* (1967) and Land *et al.* (1978)[f]
Pu–Rb system, no compounds									Ellinger *et al.* (1968b)
$PuRe_2$	$MgZn_2$	hexagonal	P$6_3/mmc$	5.396(1)		8.729(1)	4	18.45	Coffinberry and Miner (1961)
Pu–Re phase diagram unknown									
$Pu_2Rh(\zeta)$									Kutaitsev *et al.* (1967)
$Pu_5Rh_3(\eta)$		tetragonal	P4/*ncc*	10.94		6.020	4		Kutaitsev *et al.* (1967) and Beznosikova *et al.* (1974)
$Pu_{31}Rh_{20}(\theta)$	$Pu_{31}Pt_{20}$	tetragonal	I4/*mcm*	11.076(1)		36.933(12)	4	13.87	Cromer and Larson (1977)
$Pu_5Rh_4(\iota)$		orthorhombic	P*nma*	7.276(2)	14.332(4)	7.419(2)	4	13.79	Cromer (1977b)
				7.263	14.48	7.464	4	13.59	Blank and Lindner (1976)
PuRh(κ)									Kutaitsev *et al.* (1967)
$Pu_3Rh_4(\lambda)$									Kutaitsev *et al.* (1967)
$PuRh_2(\mu)$	Cu_2Mg	fcc	F$d3m$	7.488			8	14.07	Kutaitsev *et al.* (1967) and Erdmann and Keller (1973)
$PuRh_3(\nu)$	$AuCu_3$	cubic	P$m3m$	4.009–4.040			1	13.95	Kutaitsev *et al.* (1967)
				4.042					Erdmann and Keller (1973)
Pu–Rh phase diagram									Kutaitsev *et al.* (1967) and Land *et al.* (1978)

Table 7.17 (*Contd.*)

Phase	*Structure type*	*Symmetry*	*Space group*	*Lattice parameters* a_0(Å)	b_0(Å)	c_0(Å)	*Angle* (deg)	*Units per cell*	*X-ray density* (g cm^{-3})	*References*
$Pu_{19}Ru(\zeta_2)$	$Pu_{19}Os$(?)									Ellinger *et al.* (1968b) and Miner (1970)
$Pu_3Ru(\eta)$		(ortho?)		(6.216)	(6.924)	(8.093)		(4)	(15.60)	Berndt (1962)
$Pu_5Ru_3(\theta)$	W_5Si_3	tetragonal	I4/*mcm*	10.7685		5.7473		4	14.93	Beznosikova *et al.* (1974)
				10.745(3)		5.719(2)		4	15.07	Cromer *et al.* (1975)
$PuRu(\iota)$	CsCl	cubic	P*m*3*m*	3.363(1)				1	14.87	Coffinberry and Miner (1961)
				3.3635(6)					14.84	Kutaitsev *et al.* (1967)
$PuRu_2(\kappa)$	Cu_2Mg	fcc	F*d*3*m*	7.476(1)				8	14.06	Coffinberry and Miner (1961)
				7.472(1)–7.476(1)					14.03	Coffinberry and Miner (1961)
				7.4737(1)(Ru-rich)						Kutaitsev *et al.* (1967)
Pu–Ru phase diagram										Seaborg *et al.* (1946, 1949b), Kutaitsev *et al.* (1967), and Cope (1960)
Pu–S system, see Section 7.8, Table 7.39										
'$Pu_{11}Sc_9$'(ζ)		hexagonal	P6_3/*mmc*	3.310(Pu-rich)		10.717		4	10.5	Kutaitsev *et al.* (1967)
				3.308(Sc-rich)		10.709				
'Pu_5Sc_4'										Kutaitsev *et al.* (1967)
Pu–Sc phase diagram										Ellinger *et al.* (1968b), Miner (1970), and Kutaitsev *et al.* (1967)
Pu–Se system, see Section 7.8, Table 7.39										
Pu–Si system, see Section 7.8, Table 7.32										
Pu–Sm phase diagram										Ellinger *et al.* (1968a,b)[f]
Pu_3Sn	$AuCu_3$(?)	fcc		4.680						Ellinger *et al.* (1968b)
$PuSn_2$	$HfGa_2$	tetragonal	I4_1/*amd*	4.43(2)		31.0(1)				Wallace and Harvey (1974)
$PuSn_3$	$AuCu_3$	fcc	P*m*3*m*	4.630(1)				1	9.96	Coffinberry and Miner (1961)
				4.654(2)						Akhachinskii and Bashlykov (1970)

Pu–Sn phase diagram unknown								
Pu–Sr system, no compounds								Ellinger *et al.* (1968b)
Pu–Ta system, no compounds, phase diagram established								Ellinger *et al.* (1968b)
Pu–Tc system, no information								
Pu–Tb system, no compounds								Ellinger *et al.* (1968b)
Pu–Te system, see Section 7.8								
$Pu_{13}Th_6$		orthorhombic	9.820	8.164	6.681	6		Poole *et al.* (1957)
			7.90	8.43	9.79	8		Bochvar *et al.* (1958)
Pu–Th phase diagram								Seaborg *et al.* (1946, 1949b), Ellinger *et al.* (1968b), Bochvar *et al.* (1958), and Poole *et al.* (1957)
Pu–Ti system, no compounds, phase diagram established								Ellinger *et al.* (1968b) Grison *et al.* (1960) Kutaitsev *et al.* (1967)
Pu_3Tl	$AuCu_3$	cubic	4.723				14.5	Bochvar *et al.* (1958)
$PuTl_3$	disordered							
	Mg	hexagonal	3.458		5.519		12.4	Bochvar *et al.* (1958)
Pu–Tl system, phase diagram not yet established								
Pu–Tm system, no compounds								Bowersox and Leary (1966)
Pu–U(ζ)		primitive cubic						
35 at.%U			10.60(2)					Waldron *et al.* (1958)
35 at.%U			10.692				18.5	Ellinger *et al.* (1959)
50 at.%U			10.61(1)					Waldron *et al.* (1958)
50 at.%U			10.664					Ellinger *et al.* (1959)
65 at.%U			10.65(1)					Waldron *et al.* (1958)
70 at.%U			10.651			58	18.8	Waldron *et al.* (1958)
Pu–U(η)		tetragonal						
25 at.%U			10.57(5)		10.76(5)	52	17.3	Ellinger *et al.* (1959)
20 at.%U			10.44		10.73	56	18.5	Bochvar *et al.* (1958)
Pu–U phase diagram								Coffinberry and Miner (1961) and Ellinger *et al.* (1959)

Table 7.17 (*Contd.*)

Phase	*Structure type*	*Symmetry*	*Space group*	*Lattice parameters* a_0(Å)	b_0(Å)	c_0(Å)	*Angle* (deg)	*Units per cell*	*X-ray density* (g cm^{-3})	*References*
Pu–V system, no compounds, phase diagram established										Konobeevsky (1955), Ellinger *et al.* (1968b), and Bowersox and Leary (1967)
Pu–W system, no compounds, phase diagram established										Ellinger *et al.* (1968b)
PuY system, no compounds, phase diagram established										Ellinger *et al.* (1968b), Kutaitsev *et al.* (1967), and Wittenberg and Grove (1963)
Pu–Yb system, no compounds										Ellinger *et al.* (1968b)
$PuZn_2(\zeta)$	Cu_2Mg	bc tetragonal	F*d*3*m*	7.760(1)(Pu-rich) 7.747(1)(Zn-rich)				8	10.54 10.5	Cramer *et al.* (1960)
$Pu_2Zn_{\sim 9}(\eta)$		hexagonal	$P6_3/mmc$ (?)	28.86(2)		14.14(1)			9.05	Larson and Cromer (1967)
$Pu_{13}Zn_{58}$	subcell of $Pu_2Zn_{\sim 9}$	hexagonal	$P6_3/mmc$ or $P6_3mc$	(14.43)		(14.14)		2	8.98	Larson and Cromer (1967)
$Pu_3Zn_{22}(\theta)$		bc tetragonal	$I4_1/amd$	8.85		21.18		4	8.71	Johnson *et al.* (1967)
$Pu_2Zn_{17}(\iota)$	Th_2Zn_{17}	rhombohedral (hexagonal setting)	$R\bar{3}m$	8.95		13.1			8.5	Cramer and Wood (1967)
'Pu_2Zn_{17}'(κ)[e]		hexagonal	P6/*mmm*	8.9		17.7				Cramer and Wood (1967)

'Pu_2Zn_{17}'(κ')[e]		hexagonal	$P6_3/mmc$	8.98		8.85			Cramer and Wood (1967)
'Pu_2Zn_{17}'(λ)[e]		hexagonal	$P6_322$	8.98		8.85			Cramer and Wood (1967)
Pu–Zn phase diagram									Cramer *et al.* (1960) and Albrecht (1964)
$Pu_{28}Zr(\zeta)$	related to β-Pu	bc tetragonal	$I4_1/a$	18.1899(3)		7.8576(2)	4		Cromer (1979a)
				18.19(1)		7.851(3)		17.444	Zachariasen and Ellinger (1970)
$\sim Pu_6Zr$		orthorhombic		10.39	10.44	11.18	8	16.7	
$Pu_4Zr(\iota)$		tetragonal	$P4/ncc$	10.893(3)		14.889(7)	16	15.76	Berndt (1967)
$PuZr_{2-3}(\kappa)$	UZr_2	hexagonal	$P6/mmm$	5.060		3.119	1		Bochvar *et al.* (1958)
				5.055		3.123			Marples (1960)
Pu–Zr phase diagram									Bochvar *et al.* (1958) and Johnson (1954)

[a] No superstructure observed (Pu_3Pb).
[b] Preliminary analysis (Pu_4Pb_5).
[c] Low-temperature modification($PuPb_2$).
[d] For 75 at.% Pu ($PuPd_3$).
[e] Assignments to phase regions at the zinc-rich end of the phase diagram (Pu_2Zn_{17}).
[f] Also, F. H. Ellinger, C. C. Land, and K. A. Johnson, unpublished work, Los Alamos Scientific Laboratory.

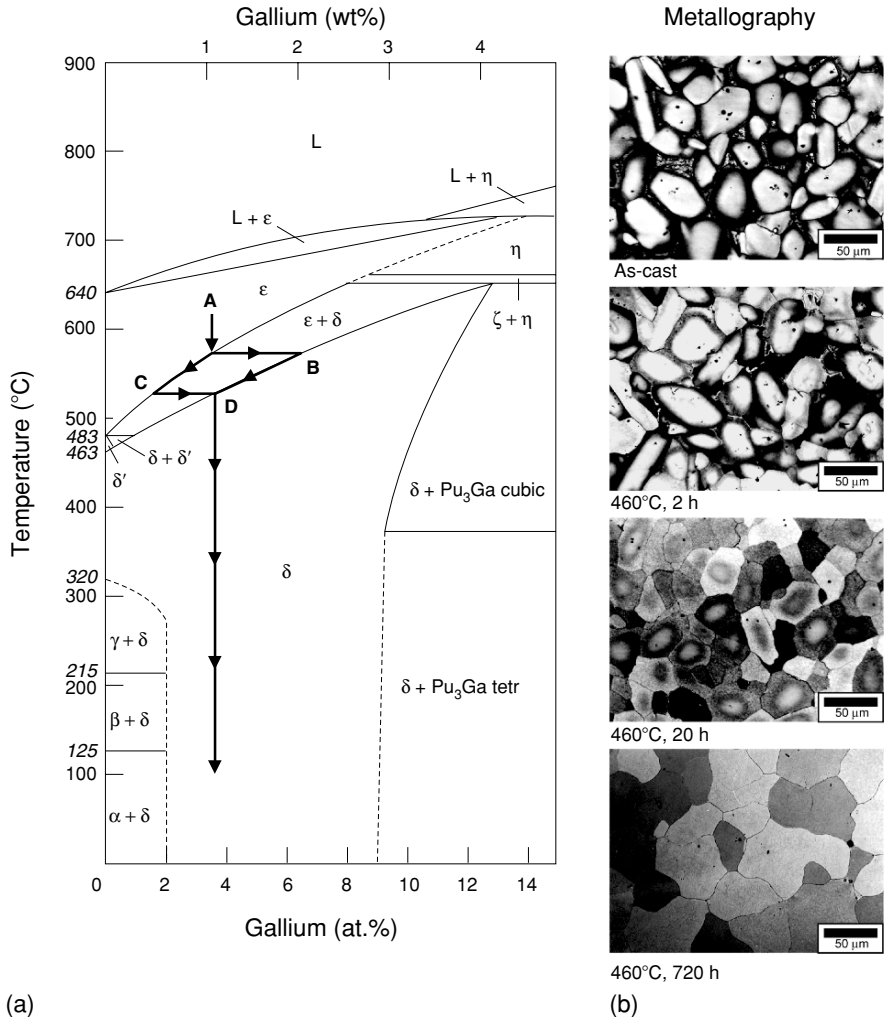

Fig. 7.33 (*a*) *The Pu-rich side of the Pu–Ga phase diagram depicting a typical gallium segregation path.* (*b*) *Typical optical microstructures of a Pu*-3.4 at. *% Ga alloy for various conditions* (*from as-cast to annealed at* 460°C *for* 720 h) (*Mitchell* et al., 2001).

a uniform gallium concentration. The progression of gallium 'homogenization' and consequent change in microstructure are also shown for a homogenization temperature of 460°C in Fig. 7.33(b).

Such microsegregation can occur with any of the alloying elements that retain the δ phase to room temperature. The extent of microsegregation depends on the cooling rate and on the shape of the two-phase field. A typical gallium

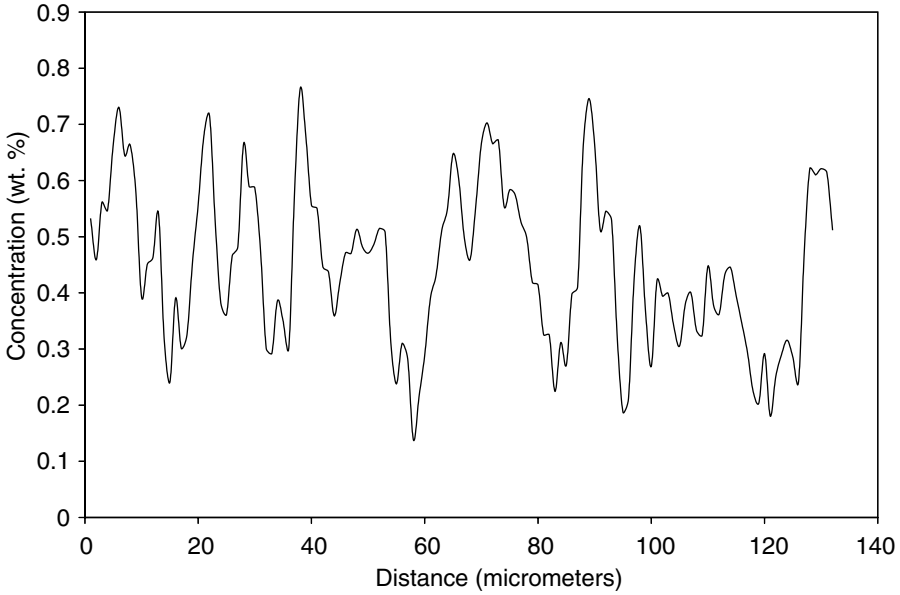

Fig. 7.34 *A typical gallium concentration profile for a nominal Pu*-1.7 at. *% Ga* (0.5 wt. *% Ga*) *alloy by electron microprobe. The grain size was roughly* 30 μm (*from unpublished work of one of the authors, S. S. Hecker*).

profile taken with an electron microprobe is shown in Fig. 7.34 for Pu–1.8 at.% Ga cooled at a rate of $\sim$5°C min^{-1}. At such rates, all areas with $<$1.4 at.% Ga transform to the α phase upon cooling to room temperature. If initial cooling rates are rapid, and homogenization times of hundreds of hours at 460°C are employed, then the δ phase can be retained to room temperature with as little as 1 at.% Ga. However, the retained δ phase is metastable and will transform at low temperatures and/or hydrostatic compression. Hence, proper homogenization treatments for δ-phase alloys are important in studying plutonium alloys. If not properly homogenized, such alloys exhibit continuously varying gallium gradients (on the scale of the grain size as shown in Fig. 7.34), or they may consist of two-phase mixtures. Either one of these conditions can significantly affect the properties of the alloy.

(g) Phase transformations in δ-phase alloys

Hecker *et al.* (2004) and Deloffre (1997) presented comprehensive overviews of phase transformations in δ-phase plutonium alloys. During cooling the retained fcc δ phase transforms to the monoclinic α phase (sometimes through an intermediate phase such as the β phase or γ phase). The transformation behavior as monitored in a dilatometer is shown for a constant cooling rate for several

Pu–Ga alloys (Hecker *et al.*, 2004) in Fig. 7.35. The transformation is martensitic, that is, diffusionless and displacive (shear). The transformation start temperature depends strongly on the gallium concentration (all three alloys shown were thoroughly homogenized before cooling) as shown in Fig. 7.35. The transformation behavior depends on cooling rate and is, therefore, characterized as an isothermal martensitic transformation. Orme *et al.* (1976) determined the TTT kinetics for Pu–Ga alloys as illustrated by the double C-curves shown in Fig. 7.36. Thermal activation appears to be necessary to nucleate the transformation before the martensite transformation product grows by a shear mechanism at sonic velocities. The C-curve kinetics result from insufficient

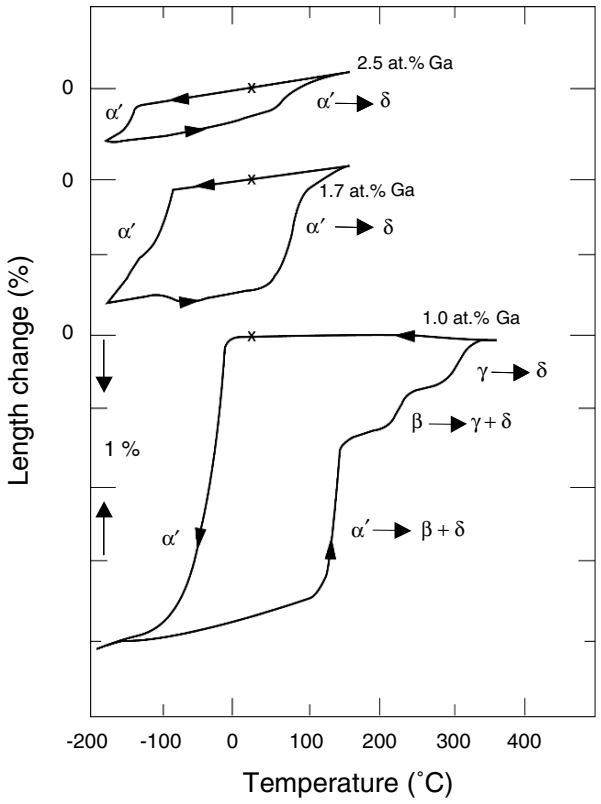

Fig. 7.35 *Thermally induced δ→α′ and reverse transformations for Pu–Ga alloys during cooling and heating. The zero is offset for the three curves as shown. The α′ phase in the* 2.4 *and* 1.7 at. *% Ga alloys revert back to the δ phase. The α′ phase in the Pu-*1 at. *% Ga alloy reverts along a more complex path to mostly β, then γ and finally to the δ phase with a small amount of the α′ phase reverting directly to the δ phase as the rest transforms to the β phase. The x in each of the three figures denotes the onset of the cooling and the end point after heating and cooling* (*Hecker* et al., 2004).

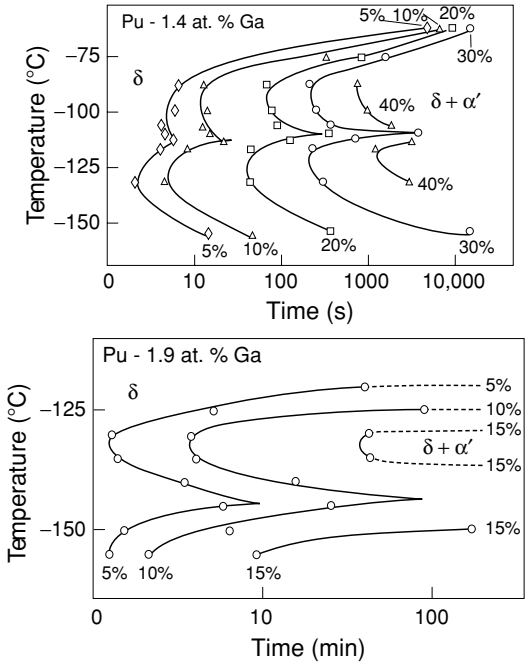

Fig. 7.36 *Time–temperature-transformation curves for* (*top*) *Pu*-1.4 at. *% Ga and* (*bottom*) *Pu*-1.9 at. *% Ga alloys* (*Orme* et al., 1976). *Transformation curves are shown for* 5, 10, 20, *and* 30% *transformation in* (*top*) *and for* 5, 10, *and* 15% *transformation in* (*bottom*) (*from Hecker* et al., 2004).

driving force at the higher temperatures and insufficient thermal activation at the lower temperatures. The overall kinetics is shown to be dependent on gallium concentration.

Similar transformation behavior is observed for δ-phase Pu–Al alloys as demonstrated by Hecker *et al.* (2004) and shown in Fig. 7.37. The well-homogenized Pu–2 at.% Al alloys begin to transform at approximately –130°C during cooling. After cooling to liquid nitrogen temperature and heating back to room temperature, metallographic and X-ray examination showed that the resulting microstructure (shown in Fig. 7.37) consisted of 25% α′ phase (in the form of martensite platelets) and 75% residual δ phase. The α′-phase designation is used here to indicate that the aluminum or gallium atoms, which have no equilibrium solubility in the α phase, are trapped by the martensitic transformation and expand the lattice of the α phase (Hecker *et al.*, 2004). During hydrostatic compression at room temperature, the δ phase collapses just below 0.4 GPa (as shown in Fig. 7.37), transforming martensitically first to the β′ followed by the α′ phase. The microstructure is more complex as shown in Fig. 7.37. If such

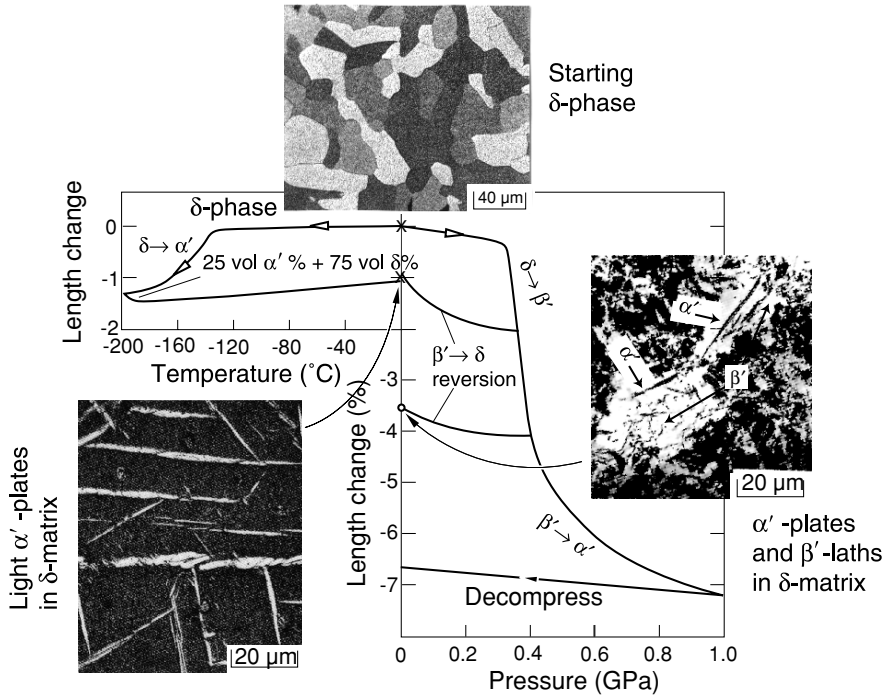

Fig. 7.37 *Temperature and pressure-induced transformations in Pu*-2.0 at. *% Al alloys* (*Zukas* et al., 1981*; Hecker* et al., 1982). *The starting δ-phase microstructure is shown on top and the transformed microstructures on the left and right for temperature and pressure-induced transformations, respectively.*

samples are compressed only partially, then both product phases appear in the residual δ-phase matrix.

Adler and coworkers (Olson and Adler, 1984; Adler *et al.*, 1986) modeled the crystallography of the δ→α′ transformation during cooling. Zocco *et al.* (1990) subsequently confirmed their predictions by transmission electron microscopy (TEM) and determined the lattice correspondence between the parent and product phases and the α′-phase habit plane. The details of the experimental and theoretical results are reviewed by Hecker *et al.* (2004). Heating the transformed α′ phase above room temperature for Pu–Ga alloys results in the transformation behavior shown in Fig. 7.35. The low-gallium alloys transform from α′→β→γ, whereas the higher-gallium alloys transform directly from α′→δ at temperatures significantly lower than the α→β transformation temperature.

Complex stress states such as those found during cold rolling, machining, or mechanical polishing all trigger the δ→α′ transformation. Machining most likely produces a complex mixture of α′ and α-phases (that is, expanded and

unexpanded) because of the heat generated. Mechanical polishing is especially effective in promoting the γ'-phase as an intermediary phase (Zukas *et al.*, 1983). These authors also observed that samples that had previously undergone a $\delta \rightarrow \alpha$ transformation were susceptible to the reverse $\alpha' \rightarrow \delta$ transformation at the crack tip of tensile specimens. Hydrostatic tension favors the larger volume δ phase. Hecker and Stevens (2000) reported this behavior for both transformed samples and for unalloyed α plutonium. The reversion results reinforce the importance of the sign and magnitude of the hydrostatic stress component in triggering martensitic transformations in plutonium.

The complex nature of the transformation behavior for plutonium and its alloys must be taken into account during sample synthesis and preparation. In plutonium alloys, the slightest mechanical polishing or machining procedures can leave a layer of transformation product that may influence the properties to be measured. Such transformation products can be avoided or removed, but only if sufficient care is taken. For example, electropolishing is quite effective to remove surface products. Heating is also effective but must be done with care so as to not introduce new artifacts or changes in structure (this is especially true for aged samples in which helium has been generated by self-irradiation damage).

7.7.5 Electronic structure, theory, and modeling

The complex electronic structure of plutonium has been a subject of intense study for theorists and modelers for more than 50 years. Arko *et al.* (2006) present the most recent review of electronic structure in the actinides, including plutonium, in Chapter 21 of this work. As mentioned above, the actinides mark the filling of the 5f atomic subshell much like the rare earths mark the filling of the 4f subshell. Yet, the 5f electrons of the light actinides behave more like the 5d electrons of the transition metals than the 4f electrons of the rare earths. The peculiar properties described in Section 7.7.3, and shown in Fig. 7.19, are telltale signs of novel interactions and correlations among electrons, which result in behavior that cannot be explained by the one-electron band theory of metals. Boring and Smith (2000) point out that such novel interactions typically result from a competition between itinerancy (bonding electrons that form bands in metals) and localization (electrons with local moments that magnetically order at low temperature). In these elements, we find that such novel interactions occur in the d- and f-electron metals near iron, at cerium, and near plutonium. Based on these considerations, Smith and Kmetko (1983) rearranged the periodic table for the transition metals, the rare earths, and the actinides as shown in Fig. 7.38. This representation shows that most transition metals, lanthanides, and actinides have predictable ground states and become either superconducting or magnetic as the temperature is lowered. The elements along the diagonal have two or more partially filled bands that are close in energy. One of the bands is typically relatively narrow with a high density of states (DOS) at the Fermi

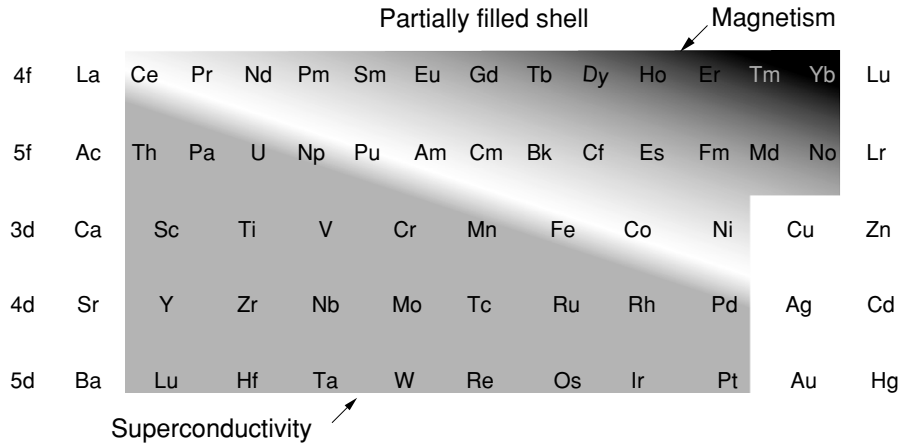

Fig. 7.38 *Smith and Kmetko* (1983) *rearranged periodic table that highlights the transition in electronic behavior from localized electrons* (*resulting in magnetism*) *to itinerant electrons* (*resulting in superconductivity*).

energy (the f-bands are 2 to 4 eV wide and the d-bands span 5 to 10 eV). Narrow bands tend to mix or hybridize with other bands close in energy. The electrons in these narrow bands can be strongly correlated, but still bonding. They spend much more of their time close to their atomic cores than do the 'free' (valence) s-electrons. The electrons in the narrow bands are highly sensitive to small perturbations, which enhances polymorphism and causes instability in the solid state. Smith and Boring point out that in addition to exhibiting multiple crystal structures, the elements along the diagonal also exhibit strong catalytic activity, have a great affinity for hydrogen, and spark easily when struck. Moreover, the behavior of the elements can easily be moved across the diagonal by changes in temperature, pressure, or by alloying.

The electronic configuration of isolated plutonium atoms is $7s^2 5f^6$ (see Section 7.6). In the metallic state the electronic configuration is $7s^2 6d^1 5f^5$. The atomic volumes in the solid state change abruptly across the actinide series at plutonium, as shown in Fig. 7.39. This change indicates a major electronic transition between the light and the heavy actinides. In the light actinides up to plutonium, each additional 5f electron (like each d-electron in the transition metals) goes into the conduction band, where it increases the chemical bonding forces, pulling the atoms closer together and resulting in a decrease in atomic volume. Beginning at americium, the 5f electrons behave like the 4f electrons of the rare earths, localizing at each lattice site and becoming chemically inert. With no 5f contribution to bonding, the atomic volume suddenly increases at americium, and contracts only slightly with increasing atomic number because the 5f electrons remain localized in the remainder of the series. As shown in

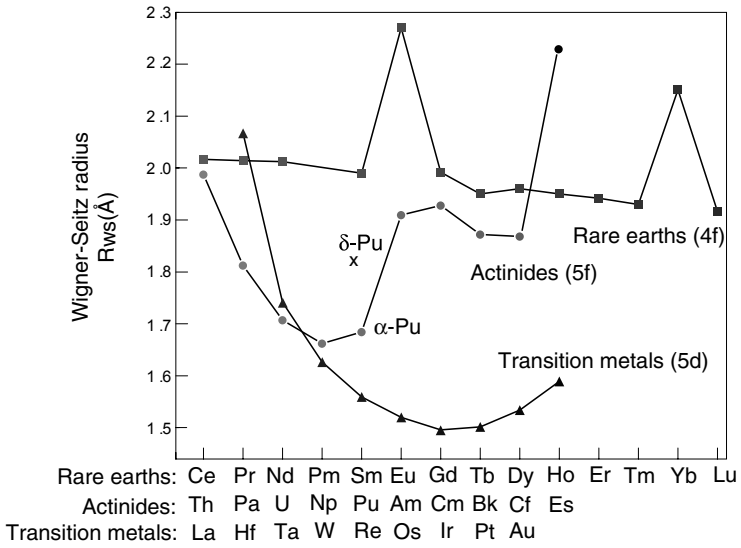

Fig. 7.39 *Wigner–Seitz radii for the actinides compared to the lanthanides and 5d transition metals. The actinides include the data for Es* (*Haire* et al., 2004), *which is divalent with a large volume, much like Eu in the lanthanides.*

Fig. 7.39, this behavior is similar to the lanthanides. The large jump in atomic volume at Es is due to divalent behavior similar to that for Eu and Yb for the lanthanides. The pattern of local moments, another strong indicator of what the electrons are doing, confirms this general picture. The light actinides show no local moments, as expected if all the valence electrons are in the conduction band, whereas the heavy actinides and the lanthanides generally exhibit local moments.

In the α phase, the 5f electrons appear to be bonding (although Savrasov *et al.* (2001) claim that the f-electrons are already strongly correlated in the α phase), whereas in americium the 5f electrons are clearly localized. It is interesting to note here that americium was found to be an ordinary superconductor with no hint of a magnetic moment although it is on the 'magnetic' side of the diagonal in Fig. 7.38 (Smith and Haire, 1978). This is a consequence of the $5f^6$ electronic configuration resulting in a total angular momentum $J = 0$, so that no moment is present even in the free ion limit. As shown by the atomic volumes in Fig. 7.39, the δ phase in pure plutonium falls between the plutonium α phase and the americium dhcp phase. The plutonium δ phase is a state that appears to be unique among the elements. Before addressing the δ phase, we will first consider the α phase ground state.

First-principles total-energy calculations based on density-functional theory (DFT) successfully predict electronic structure and bonding properties of simple

metals and the transition metals (Skriver, 1985). With the advent of high-performance computing, it has become possible during the past 10 to 15 years to extend such calculations to the actinides by incorporating low-symmetry crystal structures, relativistic effects, and electron–electron correlations. The complicated electron–electron exchange term arising from the Pauli exclusion principle and electron–electron electrostatic interactions are incorporated through a local density approximation (LDA) or a generalized gradient approximation (GGA), which incorporates the local electron density and the density gradient. Wills and Eriksson (2000), who summarized their efforts and those of their colleagues, successfully predicted the structures and volumes of the low-symmetry ground states of the light actinides, including plutonium. These calculations show that in α plutonium all eight valence electrons are in the conduction band. However, the 5f bands are very narrow – that is, each 5f electron is nearly localized on an atomic site and, hence, spends a long time near this site before it jumps to the next site. Because the bands are narrow, they exhibit a very high DOS. As the number of 5f electrons populating the band increases across the actinide series, the specific properties of the band begin to dominate the bonding properties of the metal.

Wills and Eriksson demonstrated that the α phase is the stable ground state of plutonium because special conditions favor lattice distortions. Specifically, the very narrow band of the 5f electrons with a high DOS at or very near the Fermi energy split the band in certain regions, thereby lowering the total energy through a Jahn–Teller/Peierls-like distortion. We recall that in iron the degeneracy of the d-conduction band is lifted by the electron spins causing the d-band to split spontaneously into spin-up and spin-down bands. In plutonium the degeneracy of the f-band is lifted by a lattice distortion leading to lower energy. Also, because the narrow 5f band overlaps the s, p, and d bands, a number of electronic configurations have nearly equal energy, leading to multiple allotropes in the light actinides and to their great sensitivity to external influences such as temperature, pressure, and chemical additions. Before the insight gained from the calculations of Wills and Eriksson, the low-symmetry ground state in metallic plutonium was attributed to directional or covalent-like bonding, resulting from the angular characteristics of f-electron orbitals (somewhat analogous to molecular bonding, see Section 7.9.3) (Boring and Smith, 2000; Hecker, 2000). Although total-energy electronic structure calculations apply only at zero temperature, they have been remarkably successful in predicting the ground-state properties of the actinides, both at ambient and elevated pressures. In addition, energy differences for various structures can be calculated to give an indication of whether these are thermally accessible. Wills and Eriksson (2000) point out that including temperature effects is not a simple task. One possibility is to integrate existing molecular dynamics or Monte Carlo simulations with electronic structure calculations. It may also be possible that accurate calculations of the phonon spectra of different allotropes may enable reliable calculations of the free energy as a function of temperature.

We now turn to the fcc δ phase, which is the most desirable from an engineering standpoint but the least understood from a physics standpoint. As shown in Fig. 7.39, the volume (the Wigner–Seitz radius is actually plotted) of the δ phase falls between that of α plutonium and americium. The 5f electrons appear to be in some mixed state, neither fully itinerant nor fully localized. Above, we pointed out that the δ phase has other unusual properties, such as a negative thermal expansion coefficient and an unusually large low-temperature electronic specific heat. Unfortunately, even the best calculations based on standard DFT with some LDA do not adequately predict the δ-phase volume or elastic constants in unalloyed plutonium. This failure has spawned numerous attempts to go beyond the LDA. Wills and Eriksson (2000) found that they had to 'constrain' their calculations by localizing four of the five 5f electrons in the δ phase to predict the correct atomic volume using the same formalism as for the ground state of the light actinides. The constrained 5f electrons cannot hop from site to site and do not hybridize with other electrons. In essence, the constrained calculations combine knowledge of DFT and atomic theory. Hecker *et al.* (2004) review other recent attempts to explain the peculiarities of the δ phase. However, none of them currently provide an adequate explanation. The approach of Wills and Eriksson provides the best current guidance for understanding the δ phase and the alloying behavior of plutonium. This is clearly an area where we can expect significant advances in our understanding over the coming decade.

(a) Alloy theory and modeling

Before discussing the alloying behavior, it is instructive to view the behavior of plutonium in context of the other actinides. Fig. 7.40 shows the connected binary alloy phase diagrams of the actinides through curium. At the beginning of the actinides, there is little f-electron influence and, hence, one finds typical metallic crystal structures, few allotropes, and high melting points. As more f-electrons are added (up to plutonium) and participate in bonding (that is, they are itinerant), the crystal structures become less symmetric, the number of allotropes increases, and the melting points decrease. At americium and beyond, crystal structures typical of metals return, the number of allotropes decrease, and the melting points rise – all indications of the f-electrons becoming localized or inert. So we see that the peculiar properties of plutonium are not a single anomaly, but rather the culmination of a systematic trend across the actinides. And, the transition occurs not between plutonium and americium, but right at plutonium – between the ground-state α phase and the elevated-temperature δ phase.

To predict plutonium alloy phase diagrams, we need to know the Gibbs free energy of all the phases and compounds as a function of alloy concentration and temperature. We must calculate the internal energy and the entropy (electronic, vibrational, and configurational). To predict δ-phase stability, we must be able

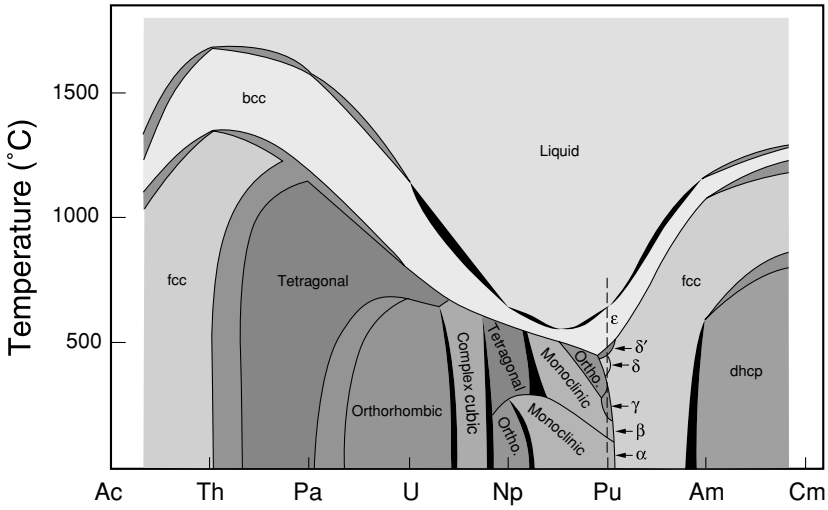

Fig. 7.40 *The experimentally determined, connected binary alloy phase diagram of adjacent actinide elements* (*Smith and Kmetko,* 1983).

to calculate the internal energy of a random substitutional alloy from first principles, which is an immense challenge. So, it is not surprising that semiempirical and phenomenological approaches have guided metallurgical practitioners for many decades. The Hume–Rothery rules, recently reviewed by Massalski (1996) and Gschneidner (1980), relate limits of solid solubility as well as the stability and extent of transition element intermediate phases to three factors:

1. If the atomic size differences of A and B are greater than 15%, solid solubility will be restricted. Significant experimental data support this rule. From a theoretical point of view, large size differences result in large elastic strain energies. The atomic size rule is primarily a 'negative' rule stressing that size differences will restrict solid solution formation. Within favorable size ranges, size differences become only of secondary importance.
2. High chemical affinity of A for B (usually denoted by large differences in electronegativity) helps promote intermetallic compounds and, therefore, limits solid solubility.
3. The relative valence rule stresses the importance of electron concentration, which is typically taken as the ratio of all valence electrons to the number of atoms (e/a).

Darken and Gurry (1953) developed a map that predicts solubility for size differences less than 15% and electronegativity differences of less than 0.4.

Gschneidner (1980) achieved best overall agreement on a large number of known binary alloys by relating solubility to size and similar electronic structures (for which he used the crystal structure as a first approximation) of the constituents. The Darken and Gurry maps for plutonium alloys have been discussed by Blank (1977).

We have not found any of these approaches, or the more sophisticated methods developed by Pettifor (1996) (using tight-binding approximation models) or by Miedema and coworkers (Miedema, 1973, 1976) (using a two-parameter model based on the work function, which is closely related to electronegativity, and on electron density) helpful in predicting solid solubility in δ-phase plutonium. Given the complex electronic structure of plutonium, especially the δ phase, this is not surprising. It is difficult to imagine that these simple approaches would capture the essence of how the electronic structure of plutonium changes with the addition of other elements. However, the Hume–Rothery size rule appears to set a reasonable upper limit on solubility.

Brewer (1965, 2000) developed models based on chemical binding insight to relate phase stability primarily to the total number of valence electrons per atom. Ferro and Cacciamani (2002) recently reviewed the work of Brewer and colleagues on the classification and mapping of alloying patterns. Brewer (1970, 1983) provided some useful insights and general guidance on solubility, melting points, and thermodynamic properties of plutonium and the actinides. For example, he predicted little mutual solubility between plutonium and the alkali metals, the alkaline-earth metals from calcium through radium, and europium and ytterbium. Also, he predicted little solubility of the 4d and 5d transition metals in plutonium, but somewhat greater solubility of the 3d transition metals. He also offered an explanation of the low melting point of plutonium based on the unusually stable liquid phase. He pointed out that plutonium exhibits four or more electronic configurations of comparable energy in the metal. Consequently, atoms of plutonium have different sizes that are readily accommodated in the liquid and pack to very high density. The strain energy resulting from trying to accommodate different-sized atoms into structures such as bcc and fcc with equivalent atom sites destabilizes these structures compared to the liquid. The stability of the liquid, according to Brewer, results from the increased entropy of mixed valence in the liquid state.

A more quantitative, phenomenological approach to predicting phase diagrams was developed by Kaufman and coworkers (Kaufman and Bernstein, 1970; Chang *et al.*, 2002; Kaufman, 2002). The success of CALPHAD (calculation of phase diagrams), a computational thermodynamics approach to predicting phase diagrams of multicomponent alloy systems based on the work of Kaufman and coworkers, was recently reviewed by Turchi *et al.* (2002). Applications of computational thermodynamic modeling to plutonium and its alloys is being developed, but is limited by the lack of good thermodynamic data on plutonium, its alloys, and its compounds. Adler (1991) assessed the Pu–Ga diagram with a calculation using FACT (Facility for the Analysis of Chemical

Thermodynamics, A. Pelton) and retrieved the excess free energy consistent with the Russian phase diagram. Turchi *et al.* (2004) applied the CALPHAD methodology to study the stability and the kinetics of phase transformation and evolution in plutonium-based alloys. They report very good agreement with the thermodynamic properties of pure, unalloyed plutonium. They also predict eutectoid decompositions for both the Pu–Ga and Pu–Al alloy systems.

This brings us back to the first-principles calculations for random alloy systems. In pure materials and perfectly ordered systems, the solution of the many-body Schrödinger equation is simplified by Bloch's theorem that allows us to solve the equation for one cell and use translational symmetry. Random substitutional alloys are disordered by definition and, hence, require some short-range order approximation, typically using an Ising-like cluster expansion. Colinet (2002) recently reviewed the state of the art of deriving phase diagrams by combining quantum mechanics and statistical thermodynamics contributions. Local chemistry affects both the internal energy and the configurational entropy. Statistical treatments of short- or long-range order in solid solutions can use the cluster variation method (CVM) or Monte Carlo simulations. The cluster interactions are either derived experimentally or from first-principles calculations. Local relaxations around the solute atoms are important but also difficult to treat theoretically (Zunger *et al.*, 1990; Abrikosov *et al.*, 1998). Although significant progress has been made in some of the well-studied alloy systems, first-principles calculations of phase stability or phase diagrams are still beyond our grasp. For plutonium, the difficulty is exacerbated by the fact that the parent δ phase is not well understood theoretically and key experimental measurements are sparse.

Baskes (2000) recently extended his semiempirical atomistic embedded-atom method (which is based on DFT) to plutonium. He found reasonable agreement of the calculated energetics and volumes of the phases of plutonium with experimental data. With this method, it is possible to calculate the properties of perfect and defect-containing bulk metal as a function of temperature and pressure. Baskes *et al.* (2003) extended the modified embedded-atom method to model the Pu–Ga phase diagram. They found that a subregular solid solution model is required to describe the properties of the δ phase. They were able to predict the eutectoid decomposition of the δ phase, in qualitative agreement with the Russian phase diagram. However, the accuracy of the calculated temperature and composition of the eutectoid point is limited by inadequate thermodynamic data on Pu_3Ga.

For now, the calculations of Wills and Eriksson (2000) provide good insight into δ-phase stability and alloying. They demonstrated that the low-symmetry ground states in plutonium and the other light actinides require the special conditions of narrow bands and high DOS at or very near the Fermi energy (a natural consequence of the oddity of an f-electron conduction band). It seems reasonable then that anything that destroys these special conditions favors the retention of high-symmetry structures. Their calculations show that energy can

be gained (that is, the total energy lowered) either through bonding energy gained from a structural distortion, or through correlation energy gained by localization of the electrons. Plutonium is exactly at that position in the periodic table where either process leads to about the same energy gain. However, alloying or defects disturb the coherence of the 5f bands, thus reducing the bonding energy and leading to at least partial localization of the 5f electrons. Hence, we believe that the fcc δ phase is favored at high temperature in unalloyed plutonium because of 'bond stretching' (in addition to entropy considerations) and in alloys because of 'bond breaking.' Hence, we may expect any alloy addition without bonding 5f electrons to favor the δ phase, assuming it can be dissolved in plutonium. Likewise, defects such as vacancies, vacancy clusters, dislocations, and grain boundaries may favor the retention of the δ phase locally.

Sadigh and Wolfer (2005) recently suggested another mechanism based on their DFT calculations, which showed that the volume decrease that occurs with gallium additions to the δ phase is primarily the result of the reduction in size of the plutonium host atoms. This reduction accounts for roughly two-thirds of the experimentally measured value. The other third is split between the misfit of the gallium in the δ-phase lattice and the elastic strains. The large volume reduction of the plutonium is accompanied by a negative heat of mixing. Their calculations showed that the enthalpy of transformation from the δ→α phase at absolute zero decreases substantially with the addition of gallium solutes. They conclude this reduction accounts for the retention of the δ phase. Clearly one must then invoke a different mechanism for the existence of the δ phase in unalloyed plutonium at high temperature. For example, it could be a combination of entropy effects and possible changes in electronic structure, such as those observed by Manley *et al.* (2001) for uranium. The calculations of Sadigh and Wolfer (as those of Söderlind (2001)) require large local spin moments in the δ phase to get the volume correct.

Considerable debate still exists over these calculational techniques because no local moments have been found experimentally (as recently reviewed by Lashley (2005). The search for magnetic moments has been so elusive, Söderlind explains, because his calculations predict a near zero-ordered moment as the spin and orbital moments are close in magnitude but antiparallel. However, Shick *et al.* (2005), using the *around-the-mean-field* version of the LDA+U method, predict a nonmagnetic ground state for the δ phase. They claim the nonmagnetic character results from $S = 0$ and $L = 0$, rather than the cancellation of spin and orbital parts of the momentum. They claim good agreement with experimental measurements of δ-phase plutonium properties. Shorikov *et al.* (2005) used the LDA+U+SO method to predict nonmagnetic ground states with zero values of spin, orbital, and total moments in both δ-phase and α-phase plutonium. We look forward to future advances in electronic structure theory that provide satisfactory explanations to the enigma surrounding plutonium.

(b) Lattice effects and local structure

We now examine in greater detail some of the interesting electronic structure effects observed in binary plutonium alloys. Binary alloys of plutonium with Am, Ce, Ga, and Al solutes were studied recently by Dormeval *et al.* (2003). Fig. 7.41 shows the approximate range of the δ-phase fields at room temperature for these solutes and the variation in the δ-phase plutonium lattice parameters. The addition of americium or cerium expands the plutonium lattice, whereas gallium and aluminum shrink it. All of them show some deviation from the ideal solution behavior described by Vegard's law, which is not surprising considering the complex electronic interactions expected in plutonium alloys.

In americium, the 5f electrons are completely localized. Substituting large americium atoms into the smaller δ-phase lattice expands the plutonium lattice and causes the 5f electrons in plutonium to become more localized, thereby stabilizing the δ phase over the entire range of americium concentrations. Also,

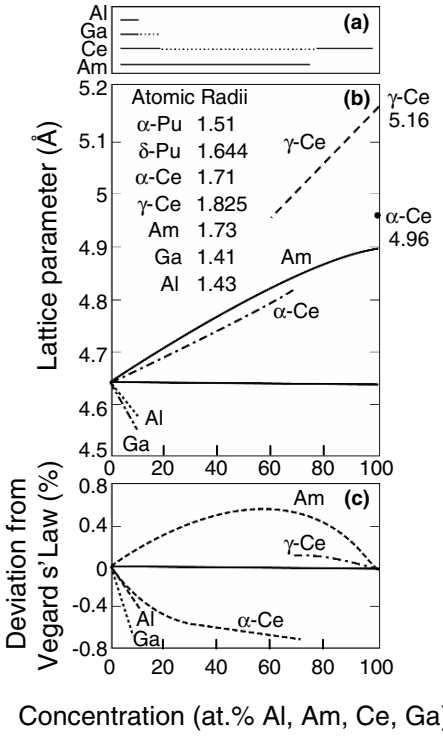

Fig. 7.41 (*a*) *Approximate solubility ranges at room temperature for the δ phase alloyed with Al, Ga, Ce, and Am.* (*b*) *Lattice parameters for these alloys.* (*c*) *Deviation from Vegard's Law* (*Dormeval,* 2001*; Hecker* et al., 2004).

the increased localization of the 5f electrons in plutonium causes the plutonium atoms themselves to increase in size, resulting in a positive deviation from Vegard's law. If a transition from itinerant (bonding) 5f electrons to localized 5f electrons were to suddenly occur in plutonium atoms as the americium concentration is increased, then we would expect a sudden increase in lattice parameter. As seen in Fig. 7.41, no discontinuities in lattice parameters are observed across the entire americium concentration range. This behavior demonstrates that the limited stability of the δ phase in unalloyed plutonium is just the tip of the iceberg for δ-phase stability upon alloying. This is shown most convincingly by looking more closely at the connected binary Np–Pu–Am phase diagrams shown in Fig. 7.42.

In contrast to additions of americium, neptunium stabilizes the α phase of plutonium. In fact, the Pu–Np phase diagram looks strikingly like the plutonium temperature–pressure phase diagram also shown for comparison in Fig. 7.42. Hence, adding neptunium has the same effect as applying pressure to the plutonium lattice, whereas adding americium is equivalent to applying hydrostatic tension.

As shown in Fig. 7.41, the addition of cerium also expands the δ-phase plutonium lattice. The range of stability for the fcc phase was extended across the entire concentration range of cerium by splat cooling (as indicated by the

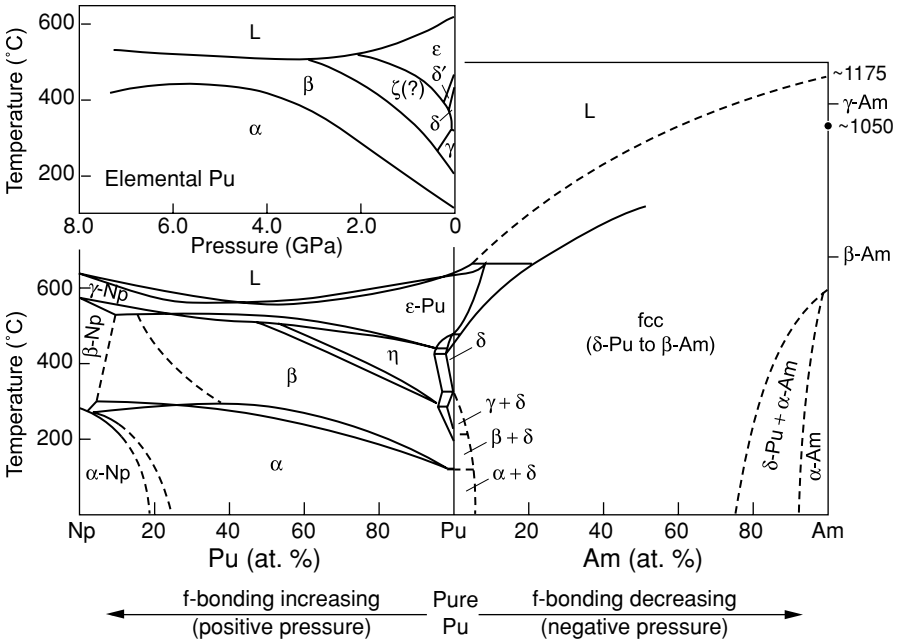

Fig. 7.42 *Plutonium pressure–temperature phase diagram compared to connected Np–Pu–Am binary ambient-pressure phase diagrams* (*Hecker,* 2004).

dotted lines in Fig. 7.41a). In addition to retaining the stable fcc phases of δ plutonium and γ cerium, Giessen *et al.* (1975) were able to retain the metastable fcc α-cerium phase at intermediate concentrations. Unlike americium, which behaves as a rigid sphere because the 5f electrons are well-localized, cerium is a 'soft' sphere, whose diameter adapts to its surroundings. When squeezed into the smaller δ-phase plutonium lattice at the plutonium-rich end, cerium's 4f electrons become delocalized and it takes on the α-phase radius ($r = 1.71$ Å). At 75 at.% Ce, an abrupt transition is observed to γ-cerium (with $r = 1.825$ Å). When viewed from the cerium end, the smaller plutonium atoms substitute in the γ-cerium lattice, until at 25 at.% Pu the pressure is sufficient to collapse the unstable cerium atom to its α-phase radius. Using EXAFS spectroscopy, Conradson (2003) showed that the cerium solute atom was accommodating in the plutonium lattices. It readily adapted its size to fit either into the δ-phase lattice or the even smaller α-plutonium lattice (when trapped in the α lattice under metastable conditions).

Dormeval *et al.* (2003) calculated the deviation of lattice constants from Vegard's law by considering two different limits in the law. As a result of the pressure imposed by the δ-plutonium lattice, cerium is α-like at concentrations below 75 at.% Ce and γ-like above that level. Hence, on the cerium end, there are two different limits corresponding to α-cerium and γ-cerium extrapolated to room temperature and pressure. Following this approach, Dormeval *et al.* found the deviation from Vegard's law to be negative on the plutonium-rich end, while slightly positive at the cerium-rich end as shown in Fig. 7.41c. Based on measurements of lattice constants, electrical resistivity, and magnetic susceptibility, Dormeval *et al.* suggested that the principal cause of the complex alloying behavior of cerium in plutonium is not the plutonium itself but the unstable nature of the cerium atom.

The addition of aluminum or gallium shrinks the δ-phase plutonium lattice (Fig. 7.41). Both show negative deviations from Vegard's law, with the gallium deviation being more than twice that of aluminum. As mentioned above, several investigators have probed the local structure of Pu–Ga alloys using EXAFS (Cox *et al.*, 1995; Faure *et al.*, 1996; Conradson, 2000; Allen *et al.*, 2002). These EXAFS results show that the first-neighbor Pu–Ga bond is 0.13 Å, or 3.7% (the experimental measurements vary from 3.5 to 4%) shorter than the Pu–Pu bond in dilute alloys. Scheuer and Lengeler (1991) and Massalski (1996) pointed out that local distortions in substitutional alloys may bear little or no relation to macroscopic distortions of the unit cell. The local distortions can vary greatly in magnitude and in sign compared to the average change in lattice parameters. The contraction in Pu–Ga is at the upper end of that found in substitutional alloys. Scheuer and Lengeler reported that the change in the next-nearest-neighbor and more distant shells is typically small for substitutional alloys. Conradson (2000) found contractions in the second and third nearest-neighbor shells in Pu–Ga to be almost negligible (0.05 and 0.01 Å, respectively). He also reported a significant change in local order in Pu–Ga alloys as the gallium

concentration increases beyond roughly 3.5 at.% Ga. He found the Pu–Ga distance to remain constant with gallium addition, whereas Faure *et al.* (1996) found it to first increase and then decrease. Resolution of the differences in local Pu–Ga arrangements must await additional experiments. However, Ravat *et al.* (2003) recently reported results similar to those of Conradson; that is, the first shell distance for the Pu–Ga bond is 0.1 Å shorter than the Pu–Pu bond, and the second shell bonds are close to the Pu–Pu bond length. We must also heed the caution expressed by Scheuer and Lengeler that alloy additions of roughly 2% or more typically cause complex local ordering effects.

A lattice contraction with the addition of gallium or aluminum to plutonium is expected from purely elastic considerations because the atomic radii of aluminum and gallium are considerably smaller than the radius of δ-phase plutonium. The atoms tend to relax toward their natural bond length rather than retain their average spacing. Harrison (2001) pointed out that each solute atom eliminates 12 f–f bonds in δ-phase plutonium. The f–f bond cutting should counter the elastic contraction of the solutes. However, Harrison's calculations for Pu–Ga alloys showed that the experimentally observed negative deviation from Vegard's law results from a coupling between the core d-states in gallium and the unoccupied d-states in plutonium. Faure *et al.* (1996) suggested that negative deviation to Vegard's law is proof of delocalization. They assume that this negative deviation results from the f–p bonding between Pu 5f and Ga 4p electrons. Thus, in the Pu–Ga alloys the solutes delocalize some of the 5f electrons in alloyed δ plutonium compared to the pure δ plutonium, which, in turn, promotes more bonding and smaller atomic volumes. As pointed out above, using DFT (with spin polarization for the δ phase), Sadigh and Wolfer (2005) predicted that the δ-lattice volume decrease results primarily from the reduction in size of the plutonium host atoms. All of these analyses indicate that electronic effects play a major role in determining the alloying characteristics of plutonium.

Another interesting electronic effect in plutonium is the behavior of alloying elements such as gallium and aluminum in α-phase plutonium. Ellinger *et al.* (1968b) showed that there is no measurable equilibrium solubility of these elements in the α phase. However, as pointed out by Hecker *et al.* (2004), lean δ-phase Pu–Ga and Pu–Al alloys transform to the α phase upon cooling below 0°C or with hydrostatic pressure at ambient temperature and below. Adler *et al.* (1986) and Olson and Adler (1984) concluded that the temperature-induced δ→α transformations are martensitic. Zukas *et al.* (1981) concluded that the pressure-induced δ→α transformations are also martensitic – that is, displacive with no compositional change. Hence, the solute atoms are trapped in the monoclinic α lattice. The crystal structure, as shown in Fig. 7.22, has 16 atoms per unit cell, with eight unique lattice sites and with variable bond lengths.

Hecker *et al.* (2004) reported that XRD measurements and immersion-density measurements of the transformed α phase clearly showed that the gallium is in substitutional lattice positions in the monoclinic lattice, but that

it expanded the α lattice (the expanded lattice is called the α′ phase). All three-crystal axes expand, whereas the monoclinic angle remains nearly constant. The volume expansions in the α′ phase with the addition of gallium or aluminum are shown in Fig. 7.43 and contrasted with the volume contractions in the δ phase with alloying additions. With the addition of gallium, the α-phase volume expands ~0.9% per at.% Ga, whereas the δ-phase volume decreases by ~0.6% per at.% Ga.

These results are a most interesting manifestation of the peculiar electronic effects in plutonium. As explained above, the gallium atom, which is 14.2% smaller than the δ-plutonium atom, contracts the lattice significantly more than expected because it is believed to make the plutonium atoms contract in its presence. In other words, the addition of gallium causes more of the 5f electrons in plutonium to bond. This result is conceptually consistent with the calculations of Wills and Eriksson (2000), which indicated that only one of the five 5f electrons appears to be bonding in the unalloyed δ phase. Also, Sadigh and Wolfer (2005) predict the decrease in the size of the plutonium atoms quantitatively.

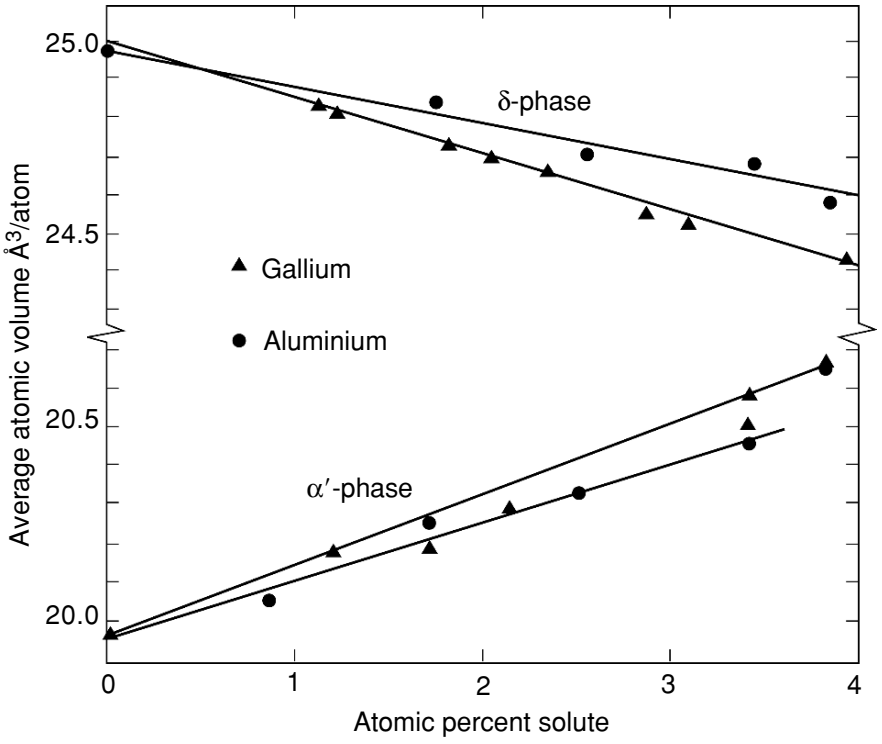

Fig. 7.43 *Atomic volumes of Pu–Ga and Pu–Al alloys in the δ and α′ phases.*

On the other hand, the gallium atom, although 7% smaller than the α-plutonium atom, expands the α lattice, indicating that in the α phase the presence of gallium localizes more of the 5f electrons. The calculations of Wills and Eriksson (2000) showed that all five 5f electrons bond in the α phase, hence it is quite likely that the solute additions disrupt the bonding, causing the volume to expand. Hecker *et al.* (2004) also showed that the lattice expansion in the α′ phase disappears slowly with time at ambient temperature and quite rapidly at slightly elevated temperatures. During the martensitic transformation, the solute atoms are trapped randomly in the α′ lattice, causing it to expand.

However, the eight different lattice sites have different bond lengths as shown in Fig. 7.22. Hecker *et al.* (2004) suggested that there is a strong driving force to rearrange the solute atoms into preferred sites, namely lattice site 8, because it has the fewest number of short bonds (Table 7.l0). Based on their recent calculations, Sadigh and Wolfer (2005) showed that site 8 is by far the most favorable substitutional position for gallium. Furthermore, they found that the unit cell of the α phase is not expanded when gallium occupies site 8, while significant expansions are exhibited when gallium is substituted in other sites, with the largest expansion for site 1 occupancy. The energies for gallium substitution correlate with this volume expansion, with a maximum difference of 1.5 eV between site 1 and site 8, confirming the suggestion of Hecker *et al.* (2004) that gallium entrapped in sites other than site 8 will tend to order to this site and in the process contract the unit cell of the α′ phase.

These results demonstrate that plutonium atoms, like cerium atoms, readily change their electronic configurations and adjust their size as their lattice environment changes. It is no surprise then that alloying of plutonium is so complex.

7.7.6 Physical and thermodynamic properties

The physical and thermodynamic properties of plutonium are of great practical interest and present significant engineering challenges; they also represent some of the most puzzling features of solid-state behavior.

(a) Densities and lattice parameters

The densities of the six solid plutonium allotropes and liquid plutonium are summarized in Table 7.18. Of particular note is the fact that the density of liquid plutonium exceeds that of the three high-temperature allotropes and that the δ phase, which is also the closest-packed crystal structure, exhibits a particularly low density compared to the other allotropes. As pointed out above, full density is difficult to achieve in the α phase of unalloyed plutonium because of the propensity for microcracking during cooling and the retention

Table 7.18 *Typical densities for plutonium allotropes, alloys, and compounds.*

Material	*Density* (g cm^{-3}); *References calculated*[a]		*Density* (g cm^{-3}); *References experimental*	
α-Pu	19.86;	Zachariasen and Ellinger (1963a)	19.82;	Merz (1974)
β-Pu	17.69;	Zachariasen and Ellinger (1963b)		
γ-Pu	17.15;	Zachariasen and Ellinger (1955)		
δ-Pu	15.92;	Ellinger (1956)		
δ′-Pu	16.00;	Ellinger (1956)		
ϵ-Pu	16.51;	Ellinger (1956)		
liquid Pu	16.65;	Miner and Schonfeld (1980)		
Pu-1.24 at.% Ga	15.86		15.83;	Gardner (1965)
Pu-1.7 at.% Ga	15.85		15.82;	Hecker (unpublished)
Pu-2.61 at.% Ga	15.827		15.78;	Gardner (1965)
Pu-3.35 at.% Ga	15.806		15.76;	Hecker (unpublished)
Pu-4.22 at.% Ga	15.787		15.73;	Gardner (1965)
Pu-5.0 at.% Ga	15.77		15.69;	Hecker (unpublished)
Pu-1.2 at.% Al	15.82		15.80;	Elliott *et al.* (1962)
Pu-2 at.% Al	15.76		15.70;	Hecker *et al.* (1982)
Pu-3.4 at.% Al	15.66		15.56;	Elliott *et al.* (1962)
Pu-5 at.% Al	15.55		15.50;	Rosen *et al.* (1969)
Pu-11 at.% Al	15.135		15.19;	Rosen *et al.* (1969)
Pu-5 at.% Ce	15.47		15.45;	Elliott *et al.* (1962)
Pu-10 at.% Ce	15.03		14.93;	Elliott *et al.* (1962)
Pu-18 at.% Ce	14.34		14.24;	Elliott *et al.* (1962)
Pu-5 at.% Am	15.75;	Ellinger *et al.* (1966)		
Pu-10 at.% Am	15.61;	Ellinger *et al.* (1966)		
Pu-15 at.% Am	15.45;	Ellinger *et al.* (1966)		
Pu_6Fe	17.10;	Ellinger *et al.* (1968b)		
Pu_3Ga (cubic)	14.27;	Ellinger *et al.* (1968b)		
Pu_3Ga (tetragonal)	14.45;	Ellinger *et al.* (1968b)		
PuO_2	11.46;	Ellinger *et al.* (1968b)		
Pu_2O_3 (hexagonal)	11.47;	Ellinger *et al.* (1968b)		
PuC_{1-x}	13.6;	Ellinger *et al.* (1968b)		
PuN	14.22;	Ellinger *et al.* (1968b)		

[a] From X-ray data.

of lower-density phases during processing. Merz (1974) achieved exceptionally high density (19.82 g cm^{-3}) in α-phase plutonium by extrusion and concurrent recrystallization, which resulted in very fine grain size (on the order of micrometers). Alpha phase plutonium samples with densities >19.7 g cm^{-3} are typically considered as sound samples.

Alloying plutonium with elements such as aluminum and gallium, which promote δ-phase retention to room temperature, yields densities close to that of the unalloyed high-temperature δ phase. The densities of some δ-phase alloys are also compared to that of the plutonium allotropes and common plutonium compounds in Table 7.18. The densities reported in the middle column were calculated by the authors from the lattice parameters measured by XRD by a number of investigators. Experimental densities are typically measured by liquid immersion techniques. The experimental densities for the δ-phase alloys are usually lower than the calculated densities from X-ray measurements because of impurities and inclusions. Experimental densities higher than X-ray densities are almost always the result of transforming the surfaces of test samples from the δ phase to the α phase during sample preparation (such as punching, machining, filing, or polishing). The compounds Pu_6Fe, PuO_2, PuC, and PuN are common inclusions found in plutonium metal and alloys of typical purity. PuO_2, PuC, and PuN have also been considered for reactor fuels. The compound Pu_3Ga is the most plutonium-rich compound in the Pu–Ga system. Figs. 7.41 and 7.43 show how the lattice parameters of δ-phase plutonium alloys decrease with increasing alloy content.

(b) Thermal expansion

Thermal expansion of the unalloyed α, β, and γ phases of plutonium is large and positive. Thermal expansion of these allotropes is also anisotropic because of their low-symmetry crystal structures. Table 7.19 lists the coefficients of thermal expansion for all allotropes, including coefficients for different lattice directions for the low-symmetry allotropes. The values shown in Table 7.19 were taken primarily from X-ray measurements because of the variability of dilatometric results. Schonfeld and Tate (1996) recently reviewed available thermal expansion results for unalloyed plutonium. We have chosen to present their best fits to the available dilatometric data, as shown in Fig. 7.19. The low-temperature behavior of α-phase plutonium is quite nonlinear, as reported by Cramer *et al.* (1961) and Lallement (1963). On page 37 of the *Plutonium Handbook*, Miner and Schonfeld (1980) show an inflection in thermal expansion near 60 K. However, more recently, Schonfeld and Tate (1996) argued convincingly that the slight lattice expansion in α-phase plutonium reported below 60 K results from self-irradiation damage. Schonfeld and Tate replotted all available thermal expansion data for α-phase plutonium, as shown in Fig. 7.44. They list the average thermal expansion coefficient between 0 and 393 K as 37.8×10^{-6} K^{-1} and that between 294 and 377 K as 53.8×10^{-6} K^{-1} (by dilatometry) and 54×10^{-6} K^{-1}

Table 7.19 *Linear thermal expansion of plutonium.*[a]

Phase	*Principal coefficient*	*Temperature range* (°C)	*Mean coefficient* (10^{-6}°C^{-1})	*Method*	*References*
α	$\bar{\alpha}_p$ (average)	−186 to 101	42.3	dilatometry	Cramer *et al.* (1961)
	$\bar{\alpha}_1 \perp c$-axis	21 to 104	60	X-ray	Zachariasen and Ellinger (1963a)
	$\bar{\alpha}_2 = \bar{\alpha}_b$		75		
	$\bar{\alpha}_3 = \bar{\alpha}_c$		29		
	$\bar{\alpha}_p$ (average)		54		
β	$\bar{\alpha}_1$	93 to 190	94	X-ray	Zachariasen and Ellinger (1963b)
	$\bar{\alpha}_2 = \bar{\alpha}_b$		14		
	$\bar{\alpha}_3 \perp (10\bar{1})$		19		
	$\bar{\alpha}_p$ (average)		42		
γ	$\bar{\alpha}_a$	210 to 310	-19.7 ± 1.0	X-ray	Zachariasen and Ellinger (1955)
	$\bar{\alpha}_b$		39.5 ± 0.6		
	$\bar{\alpha}_c$		84.3 ± 1.6		
	$\bar{\alpha}_p$ (average)		34.6 ± 0.7		
δ	$\bar{\alpha}$	320 to 440	-8.6 ± 0.3	X-ray	Ellinger (1956)
δ′	$\bar{\alpha}_a$	452 to 480	444.8 ± 12.1	X-ray	Elliott and Larson (1961)
	$\bar{\alpha}_c$		-1063.5 ± 18.2		
	$\bar{\alpha}_p$ (average)		-65.6 ± 10.1		
ϵ	$\bar{\alpha}$	490 to 550	36.5 ± 1.1	X-ray	Ellinger (1956)
liquid	$\bar{\alpha}_v$	664 to 788	93[b]	pycnometry	Serpan and Wittenberg (1961)

[a] For low symmetry allotropes, coefficients are given for different lattice directions.
[b] Mean coefficient of volume expansion.

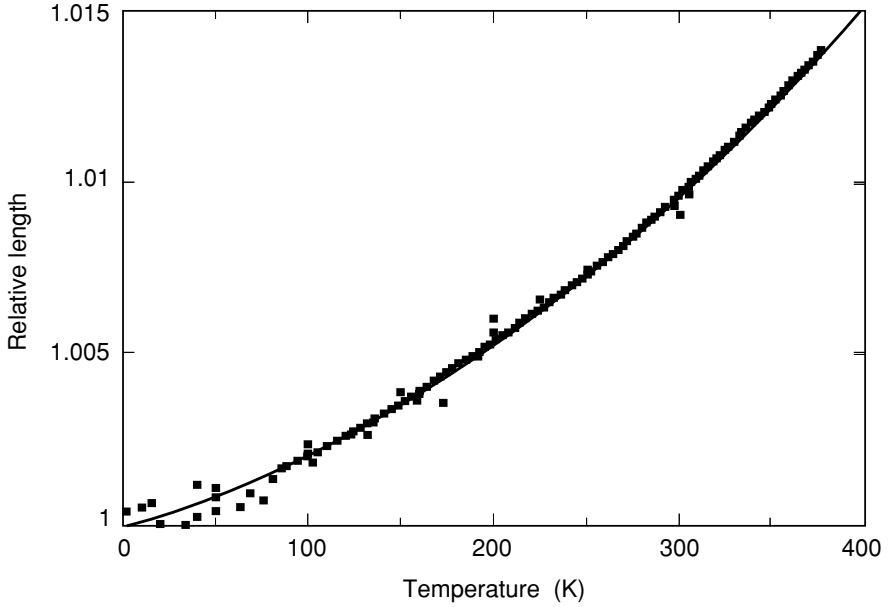

Fig. 7.44 *Thermal expansion of unalloyed α-phase plutonium over most of its temperature region of stability. The curve is a composite generated by Schonfeld and Tate* (1996) *based on data from several references* (*Sandenaw,* 1960*b; Cramer* et al., 1961*; Lee* et al., 1965*a; Lallement and Solente,* 1967*; Miner and Schonfeld,* 1980*; Lawson* et al., 1994).

(by X-ray measurements). The low-temperature results of Schonfeld and Tate are incorporated into the overall thermal expansion curve shown in Fig. 7.19.

The expansion of the high-temperature δ and ϵ phases is isotropic. However, the δ and δ′ phases exhibit negative thermal expansion. Thermal expansion of the δ′ phase is also highly anisotropic. The explanation of this unusual behavior has been a contentious issue since the late 1950s. In δ-phase alloys, the thermal expansion coefficient varies from slightly negative to positive, depending on the amount of alloying addition. A graphic example of this behavior is shown for Pu–Ga alloys in Fig. 7.45 (Goldberg *et al.*, 1970). We also show the thermal expansion behavior of various δ-phase plutonium alloys in Fig. 7.46 (taken mostly from the work of Elliott *et al.* (1960) and Lawson *et al.* (2002)). All alloying additions move the coefficient of thermal expansion to more positive values from that of the unalloyed δ phase; that is, alloying results in thermal expansion behavior closer to that observed in normal metals. As shown in Fig. 7.46, significantly less aluminum or gallium is required to increase the coefficient compared to cerium. The properties of Pu–Am alloys were estimated from the measurements of Shumakov *et al.* (1990).

The peculiar thermal expansion behavior of δ-phase plutonium alloys was reviewed by Lawson *et al.* (2002). A negative thermal expansion is associated

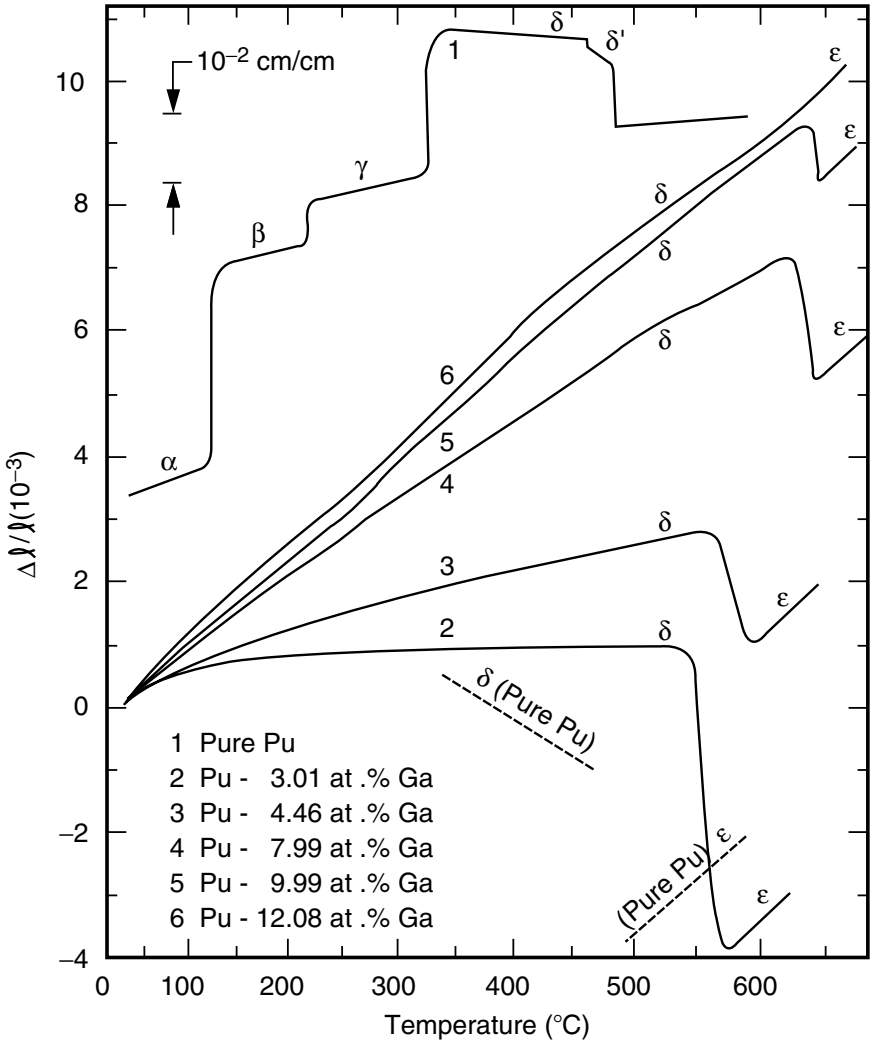

Fig. 7.45 *Corrected dilatometric heating curve* (*at* 4.5°C min^{-1}) *for a series of δ-phase Pu–Ga alloys. The curve for unalloyed* (*pure*) *plutonium is based on a scale of one-tenth* (*as shown in insert*) *that used for the alloys. The dashed curves for unalloyed* (*pure*) *plutonium are portions redrawn on the same scale used for the alloys. The scale on the ordinate refers only to the alloys* (*Goldberg* et al., 1970).

with increasing disorder (higher entropy) at higher pressures according to the Maxwell relation $(\partial V/\partial T)_p = -(\partial S/\partial P)_T$, in contrast with the behavior found in ordinary metals. However, for some complex solids with negative thermal expansion, such as the recently discovered ZrW_2O_8, increasing pressure has

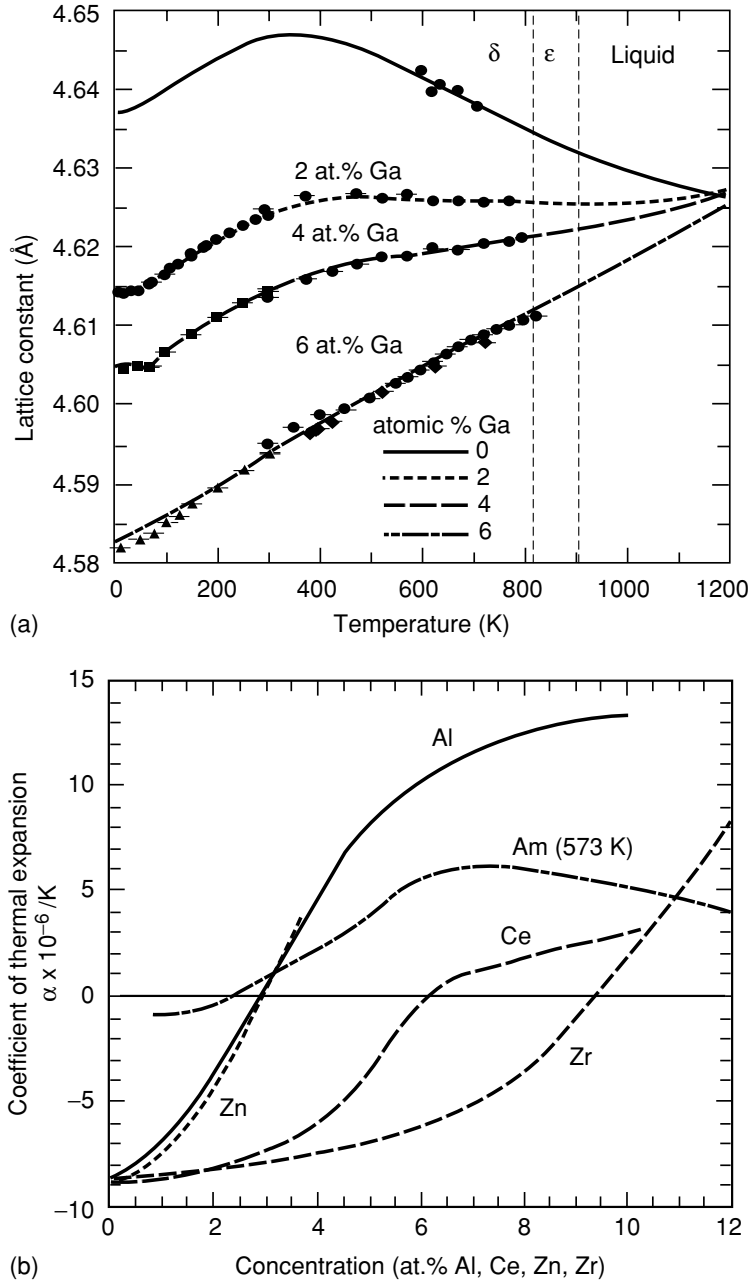

Fig. 7.46 (*a*) *Lattice constants of δ-phase Pu–Ga alloys measured by neutron diffraction by Lawson* et al. (2002). *The line through the data is a fit by the 'Invar' model proposed by Lawson* et al. (*b*) *Coefficient of thermal expansion as a function of solute content for δ-phase plutonium alloys* (*Elliott* et al., 1960). *The results for Pu–Am alloys were estimated from the measurements of Shumakov* et al. (1990) *taken at* 573 K, *where the range of solid solution across the Pu–Am diagram is complete.*

been shown to increase the vibrational entropy of the molecular modes (Evans *et al.*, 1996; Mary *et al.*, 1996; Mittal *et al.*, 2001). For fcc δ plutonium there are no internal vibrational modes, so Lawson *et al.* looked for an electronic degree of freedom whose entropy variation with pressure determines the thermal expansion. They believe zero thermal expansion (Invar-like behavior) of some of the alloys results from a thermal transfer of plutonium atoms from a lower-energy, higher-volume δ_1 state to a higher-energy, lower-volume δ_2 state, comparable to the Weiss two-level model used to explain the Invar behavior in Fe–Ni alloys (Weiss, 1963).

For ordinary metals that follow Grüneisen's law, the thermal expansion behavior can be used to estimate the temperature dependence of the bulk modulus (or the sound speed or Debye temperature); namely, $dB/dT = -\gamma\beta B$, where B is the bulk modulus, γ the Grüneisen parameter, and β the volume thermal expansion. The δ-phase plutonium alloys, however, do not follow this relationship since the thermal expansion is small – or even negative – and dB/dT is large. For these alloys it is necessary to assume that the elastic stiffness is intrinsically temperature dependent, independent of volume. For unalloyed α-phase plutonium, a recent review by Ledbetter (2004) and by Ledbetter and Migliori (2005) of Grüneisen parameters shows large variations from values of 3.1 to 7.0. They believe the best value is ~3.5. We also note that Hasbrouk and Burns (1965) provide additional listings of thermal expansion in various plutonium allotropes and in several alloys.

(c) Elastic constants and sound velocities

Early elastic constant measurements for unalloyed plutonium and several plutonium alloys by various investigators were compiled by Hasbrouk and Burns (1965). As pointed out by Fisher (1974) in a later compilation, reported elastic constant measurements (particularly the bulk modulus) exhibit significant scatter because of difficulties in fabricating quality samples. Acoustic measurements typically yield the most reliable elastic constants. Calder *et al.* (1981) reported elastic constants of α plutonium and δ-phase Pu–3.4 at.% Ga alloys at elevated temperatures. Migliori *et al.* (2004, 2006) and Ledbetter *et al.* (2004, 2005) recently performed the most accurate acoustic measurements to date on high-quality, high-purity, unalloyed plutonium (with a density >19.7 g cm^{-3}), and Pu–Ga alloys using the resonant ultrasound technique (Migliori *et al.*, 2000). Their room-temperature results are summarized in Table 7.20. Unalloyed α plutonium is soft elastically – its bulk modulus is nearly 50% less than that of α uranium. As shown in Table 7.20, the δ-phase Pu–Ga alloys exhibit substantially reduced elastic constants compared to α plutonium. Typical sound velocities are also listed in Table 7.20.

The temperature dependence of the elastic modulus (Young's modulus), the shear modulus, bulk modulus, and Poisson's ratio is shown for unalloyed

plutonium in Fig. 7.47. All but Poisson's ratio are quite sensitive to temperature. The ratio of the bulk modulus at 0 K to the bulk modulus at 300 K for α plutonium is 1.303, compared to 1.104 for lead, 1.03 for iron, and 1.075 for aluminum. There are no single-crystal elastic constant measurements in the literature for α plutonium because of the difficulty of making single crystals of unalloyed plutonium. In addition, making elastic constant measurements of the monoclinic structure of the α phase with 13 independent elastic constants is a daunting task. Moment (2000) and Lashley *et al.* (2000) describe techniques used to prepare single crystals of δ-phase plutonium alloys. Ledbetter and Moment (1976) reported elastic constant measurements on a single crystal δ-phase Pu–3.4 at.% Ga alloy. As shown in Fig. 7.48, the elastic constants are highly anisotropic. The single crystals are stiff in tension and compression and soft in shear in the [111] direction and vice versa in the [100] direction. In fact, the Zener anisotropy ($Z = 2c_{44}/c_{11}–c_{12}$), where c_{ij} are the typical elastic constants is 7.03; whereas lead, the next elastically most anisotropic fcc metal, is roughly 4 and aluminum is nearly isotropic at slightly over 1.0. The elastic constants for a polycrystalline δ-phase Pu–3.35 at.% Ga alloy reported by Calder *et al.* (1981) and shown in Fig. 7.49, exhibit a greater reduction in elastic constants with temperature than that for unalloyed α plutonium. Poisson's ratio for the δ-phase alloy increases monotonically with temperature as is typical for fcc metals.

In addition to providing stiffness data, elastic constants also play an important role in determining the overall mechanical response of materials (Hecker and Stevens, 2000). The Debye temperature at 0 K can be determined by correcting for the temperature dependence of the elastic constants. We will compare these results to the Debye temperatures from specific heat measurements in a subsequent section. Sound velocities provide a convenient way to determine elastic constants. They are also important in dynamic and shock responses of materials. The sound velocities for α plutonium and Pu–Ga alloys are presented in Table 7.20. We also note that Rosen *et al.* (1969) measured elastic properties ultrasonically at low temperatures and found no discontinuities in the elastic constants at low temperature (at the time they were looking for a possible magnetic transition) for α plutonium, and δ-phase Pu–Al and Pu–Ce alloys. However, they observed a sharp peak in the longitudinal wave attenuation accompanied by a normal temperature dependence of the transverse attenuation. Cornet and Bouchet (1968) measured the elastic properties of unalloyed plutonium with temperature, including the bcc ϵ phase (the room-temperature density was 19.1 g cm^{-3}, indicating that the samples contained many microcracks). They reported detailed results for Young's modulus for the δ, δ′, and ϵ phases. They found the ϵ phase to exhibit a large compressibility (0.16 GPa^{-1} at 758 K) and a low Young's modulus (11 GPa at 703 K). As indicated above, however, the sample quality was questionable because of its low density.

Table 7.20 *Elastic constants and sound velocities for plutonium and plutonium alloys at room temperature.*

Material	*Temperature* (°C)	*Density* (g cm^{-3}) *at* 25°C	*Bulk modulus* (GPa)	*Shear modulus* (GPa)	*Young's modulus* (GPa)	*Poisson's ratio*	*Sound speed* (km s^{-1}) (*longitudinal*)	*Sound speed* (km s^{-1}) (*transverse*)	*References*
unalloyed α Pu (high purity)	27	>19.70	54.4	43.7	103.4	0.183	2.39	1.49	Migliori *et al.* (2004) and Ledbetter *et al.* (2005)
unalloyed α Pu (high purity)	~25	19.71	53.43	42.26	100.66	0.186	–	–	Linford quoted in Gardner (1980)
Pu-2.36 at.% Ga	27	15.795	31.2 ± 0.1	16.6 ± 0.01	42.4	0.274	1.86	1.04	Migliori *et al.* (2004)
Pu-2.4 at.% Ga	25	15.75	30.6 ± 0.1	16.3 ± 0.05	41.8 ± 0.1	0.272	–	–	Migliori *et al.* (2006)
Pu-3.3 at.% Ga	27	15.76	29.7 ± 0.4	16.74 ± 0.02	42.3	0.263	1.82	1.03	Migliori *et al.* (2004)
Pu-3.35 at.% Ga	25[a]	15.9	–	15.7	40.5	~0.295	–	–	Calder *et al.* (1981)
Pu-4.64 at.% Ga	27	15.70	30.9	17.1	43.0	0.267	1.86	1.04	Migliori *et al.* (2004)
Pu-5 at.% Al	~25	15.5	–	18.28	45.4	0.24	–	–	Rosen *et al.* (1969)
Pu-6 at.% Al	20	–	–	18.5	46.8	0.264	–	–	Taylor *et al.* (1965)

[a] Extrapolated.

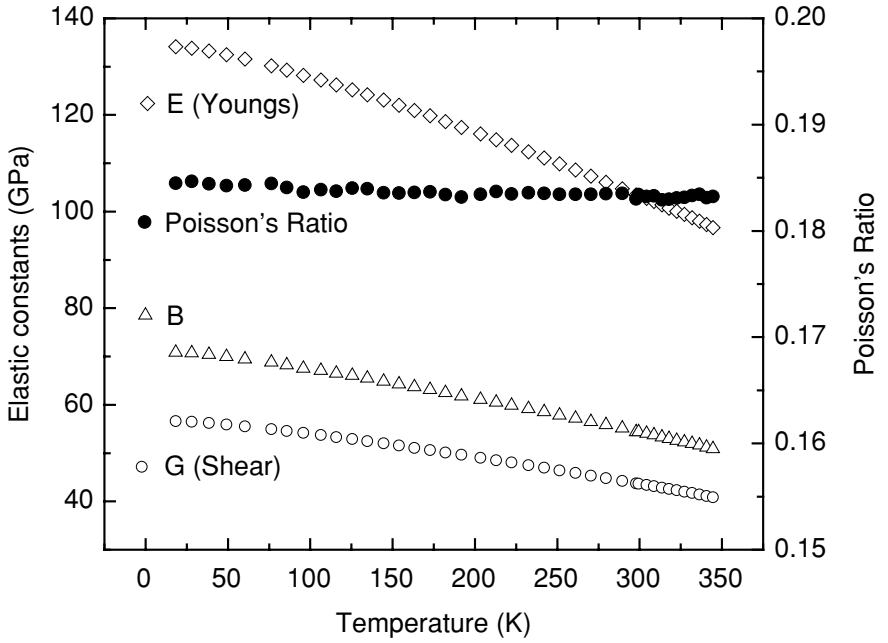

Fig. 7.47 *Elastic moduli of a high-purity, unalloyed α-plutonium polycrystal. Error bars are much smaller than the data points. The primary error is in the determination of density, computed from the dimensions and mass. E denotes Young's modulus, G, the shear modulus, and B, the bulk modulus* (*data from Ledbetter* et al., 2004; *Migliori* et al., 2004).

(d) Heat capacity

In 1976, Oetting *et al.* (1976) reviewed the early heat capacity measurements on plutonium. Low-temperature measurements of the heat capacity in ^{239}Pu, the most readily available plutonium isotope, have been plagued by self-heating (typically 2.2×10^{-3} W g^{-1} for ^{239}Pu) and by self-irradiation damage, which is especially pronounced at low temperatures where little if any healing of lattice damage occurs (Hecker and Martz, 2001). Although several investigators (Sandenaw and Gibney, 1971; Gordon *et al.*, 1976) minimized the effects of self-irradiation damage by using ^{242}Pu, they still had difficulty in obtaining sufficiently low temperatures to accurately measure the electronic specific heat. Lashley *et al.* (2003b) also reviewed previous low-temperature measurements and extended the measurements to ~2 K on ^{242}Pu using a thermal relaxation method and a specially designed sample mount (Lashley, 2003).

Lashley *et al.* demonstrated conclusively that previously reported anomalies in the heat capacity of plutonium resulted from the effects of self-irradiation damage. They also showed that anomalies in some of the δ-phase plutonium

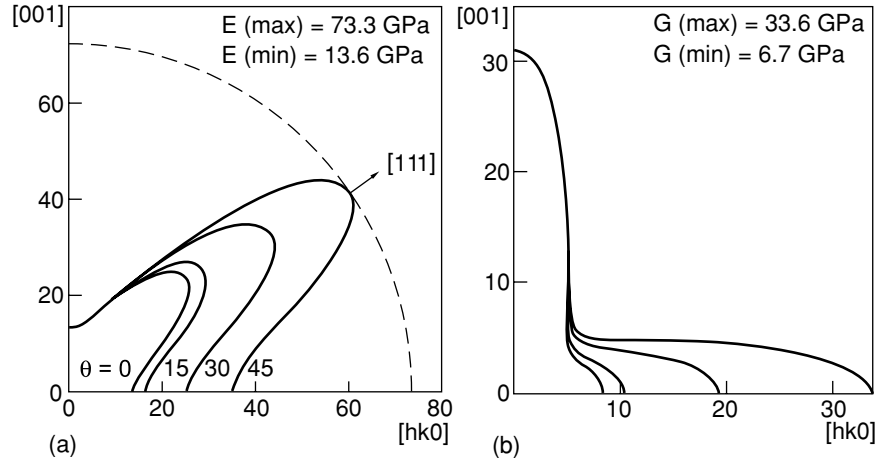

Fig. 7.48 *Elastic constants measured by Ledbetter and Moment* (1976) *on a δ-phase Pu*-3.4 at. *% Ga single crystal.* (*a*) *Young's modulus, E, as a function of crystal direction and* (*b*) *torsion modulus, G, as a function of direction.*

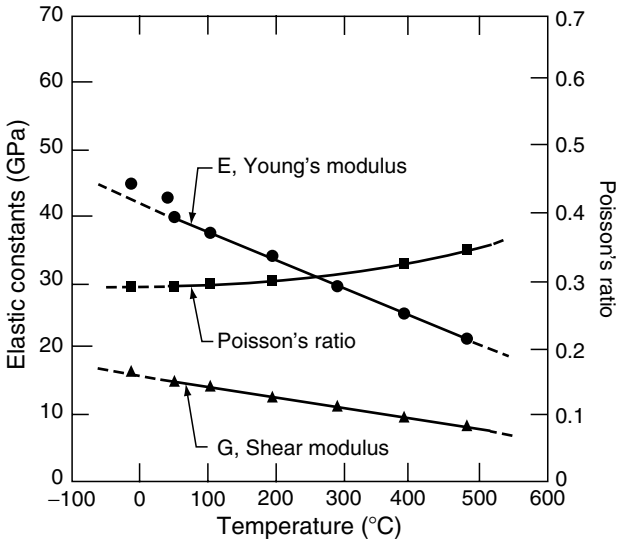

Fig. 7.49 *Elastic moduli of polycrystalline δ-phase Pu*-3.35 at. *% Ga as a function of temperature* (*after Calder* et al., 1981).

alloys at low temperatures resulted from martensitic transformations incurred in such samples when cooled to cryogenic temperatures. The results of Lashley *et al.* for very pure, zone-refined α-phase ^{242}Pu (<200 ppm impurities) are shown in Fig. 7.50 and compared to those reported by Gordon *et al.* (1976).

The electronic contribution to the specific heat can be measured at low temperatures where the phonon contribution is small. It is represented by equation (7.25)

$$(C_p/T) = \gamma + \alpha T^2 + \delta T^4 + \ldots \tag{7.25}$$

where γT and $\alpha T^3 = (12\pi^4 RT^3)/(5\theta_D{}^3)$ are the electronic and phonon contributions to C_p and θ_D is the Debye temperature. The results of Lashley *et al.* (2003b) for low-temperature heat capacity measurements on high-purity ^{242}Pu and a ^{242}Pu–5 at.% Ga alloy are shown in Fig. 7.51. The intercept at $T = 0$, γ, is a measure of the electronic DOS. The low-temperature fit yields $\gamma = (17 \pm 1)$ mJ K^{-2} mol^{-1}, which is within the range of 16 to 23 reported by Gordon *et al.* (1976), but less than the values of 22 to 25 reported by Stewart and Elliott (1981).

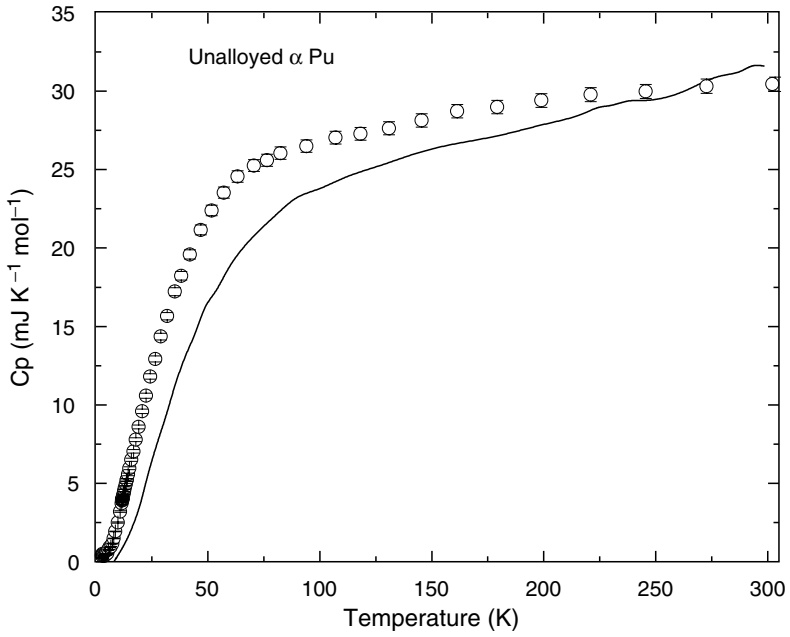

Fig. 7.50 *Heat capacity of unalloyed ^{242}Pu (solid line from Gordon* et al., 1976) *and high-purity, unalloyed ^{239}Pu (symbols) from Lashley* et al. (2003*b*) *who took extraordinary care to avoid self-irradiation damage at low temperatures.*

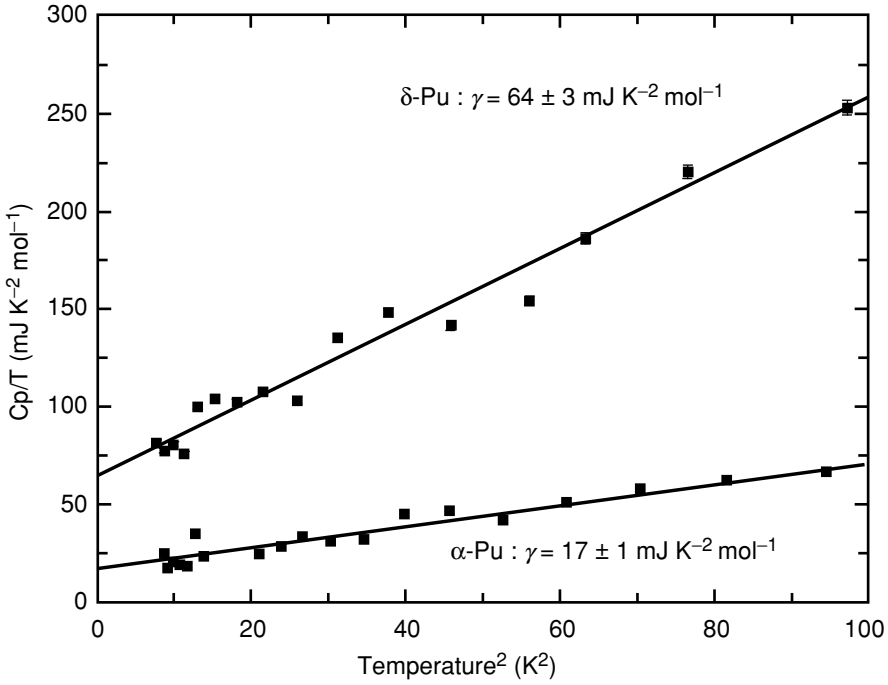

Fig. 7.51 *The low-temperature specific heat of unalloyed α plutonium and a δ-phase Pu-*5.1 at. *% Al alloy. These data represent the lowest temperature specific heat measurements reported on plutonium* (*after Lashley* et al., 2003*a,b*).

Since Lashley *et al.* reached the lowest temperatures, it is likely that their values are the most accurate. In any case, γ for plutonium is larger than that of any other element (Kittel and Kroemer, 1980). The δ-phase Pu–Al alloy has an even more remarkable γ of (64 ± 3) mJ K^{-2} mol^{-1}. Stewart and Elliott measured γ for Pu–Al alloys of varying aluminum concentration and found γ to vary from 44 to 63 mJ K^{-2} mol^{-1}. Extrapolation of the alloy data to zero alloy content yields $\gamma = 53$ mJ K^{-2} mol^{-1} for pure plutonium in the δ phase. Hence, the δ phase of plutonium, which is known to have less participation by the 5f electrons in bonding than the α phase, nevertheless has three times the electronic DOS at the Fermi energy.

Lashley *et al.* (2003b) calculated a Debye temperature, θ_D, of 153 K for α plutonium. On the other hand, Migliori *et al.* (2004, 2005) report the Debye temperature ($T = 0$ K) as 205 K based on the extrapolation of their elastic constant measurements to absolute zero. This method typically yields more accurate estimates of the Debye temperatures because it is less susceptible to the effects of self-irradiation damage. The literature values for α plutonium as determined from heat capacity, elastic constant, EXAFS, and neutron

scattering Debye–Waller measurements (Sandenaw, 1961, 1962; Taylor *et al.*, 1965; Lee *et al.*, 1965b; Gordon *et al.*, 1976; Stewart and Elliott, 1981; Lawson *et al.*, 1994; Lashley *et al.*, 2003b) vary from 118 to 205 K. On the other hand, the Debye temperature for the δ-phase plutonium alloys are reported to vary much less; namely, from 100 to 130 K (Ledbetter and Moment, 1976; Stewart and Elliott, 1981; Lashley *et al.*, 2003b).

Heat capacity measurements below and above room temperature as reported by Oetting and Adams (1983), Taylor *et al.* (1968), and Lashley (2005) for unalloyed plutonium, and by Lashley *et al.* (2003a), Lashley (2005), and Rose *et al.* (1970) are shown in Table 7.21. The heat capacity measurements above room temperature are not affected by self-irradiation damage because defects are sufficiently mobile to heal the damage. As pointed out by Oetting *et al.* (1976) and others, no anomalies in the paramagnetic susceptibility with temperature have been observed, thus the magnetic contribution to heat capacity is negligible, as confirmed by Lashley (2005).

Oetting and coworkers (Oetting *et al.*, 1976) present a comprehensive listing of the thermodynamic functions – enthalpy and entropy – along with the enthalpies of transformation between the various plutonium allotropes. The heat capacity of unalloyed plutonium as a function of temperature taken from Lashley *et al.* (2003b) and Kay and Loasby (1964) is shown in Fig. 7.52. The enthalpies and entropies of transformation are listed for unalloyed plutonium in Table 7.16.

(e) Magnetic behavior

Fig. 7.53 shows the molar magnetic susceptibilities of unalloyed plutonium and a Pu–6 at.% Ga alloy as a function of temperature. The plots are taken from Lashley (2005). The data for unalloyed plutonium above 300 K are those of Comstock, published by Sandenaw (1961) with additional details provided by Olsen *et al.* (1992). These data were obtained by the Gouy method on large samples of ^{239}Pu with a purity of 99.9%. The low-temperature data for the unalloyed α plutonium and all of the data for the alloy is that of Méot-Reymond and Fournier (1996). Their plutonium alloy samples were of high purity, electrorefined, with ferromagnetic impurities constituting <10 ppm. In the plot shown in Fig. 7.53, Lashley *et al.* align Méot-Reymond and Fournier's high- and low-temperature alloy data at 300 K because of the concerns expressed by Méot-Reymond and Fournier about their high-temperature technique.

We note that the susceptibilities of unalloyed plutonium and the alloy are similar – both are quite large, similar to the magnetic susceptibility of manganese. Unlike manganese, which orders antiferromagnetically at 95 K, plutonium shows no anomaly in its susceptibility at low temperatures. Magnetic susceptibilities on the order of those exhibited by plutonium are characteristic of metals with relatively strong paramagnetism caused by electronic band magnetism (such as that for palladium). Lashley *et al.* (2004) recently concluded that a

Table 7.21 *Experimental heat capacities (C_p) at various temperatures for α plutonium and δ-phase Pu–Ga alloys.*

	C_p (*unalloyed α-Pu*) (mJ K^{-1} mol^{-1})			C_p (δ-*Pu alloys*) (mJ K^{-1} mol^{-1})	
				Pu-1.7 at.% *Ga*	*Pu*-3.3 at.% *Ga*
T (K)	*Oetting and Adams* (1983)	*Lashley* (2005)	*Taylor* et al. (1968)	*Lashley* et al. (2003b) *and Lashley* (2005)	*Rose* et al. (1970)
2.78		0.227			
3		0.236			
3.5		0.317			
3.7				0.3201	
4		0.414		0.36968	
4.5		0.477		0.46436	
5		0.52		0.58135	
5.5		0.714		0.71759	
6		0.87049		0.87265	
6.5		0.93806		1.05475	
7		1.02		1.24524	
8		1.5		1.70936	
10		2.6		2.81808	
12		4.02757		4.15583	
15		5.92989		6.41797	
20		9.14411	3.65	10.37966	
22		10.36358		11.90103	
25		12.16125		14.26709	
30		14.80288		17.8891	
35		17.10077		21.10807	

40		18.85255		23.92317	
45		20.5505		25.89824	
50		21.95556	16.68	27.62289	
65		24.72443		31.5921	
70		25.19762		32.49775	
75		25.51758		33.19174	
80		25.86718		33.63288	
90		26.33692		34.84199	
100		26.73917	24.09	35.84115	
125		27.46718		34.99518	
150		28.3027		34.62373	
200		29.42604	28.66	33.40867	
250		30.04106		30.59754	
300	31.57	30.43499	32.18	30.80206	31.97
340	33.66				
380	35.16				32.43 (373 K)
400	32.64				
440	33.16				
480	33.69				33.81 (473 K)
500	33.50				
540	34.42				
580	35.34				36.12 (573 K)
600	34.96				
640	35.40				
680	35.83				39.30 (673 K)
700	36.04				
773					43.41
863					33.94
903					33.94

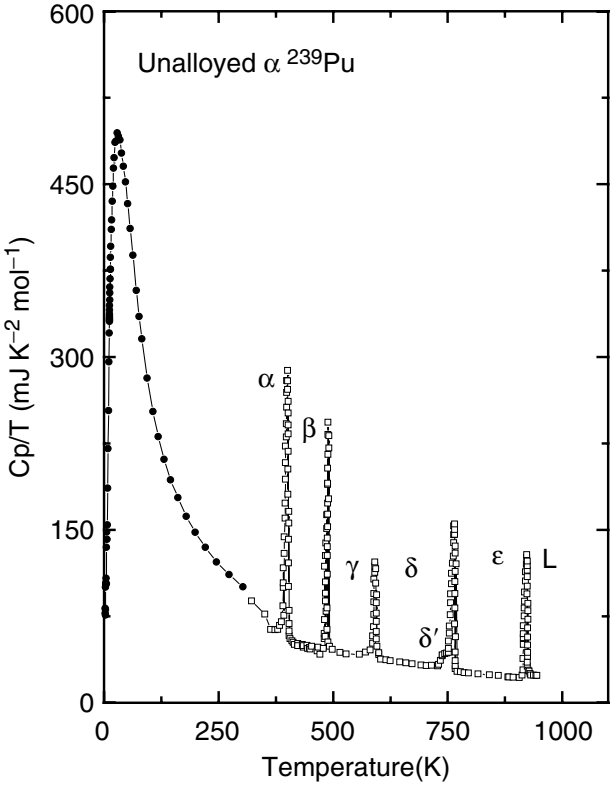

Fig. 7.52 *Heat capacity divided by temperature for high-purity, unalloyed α-phase plutonium. Open symbols are from Kay and Loasby* (1964) *and the solid symbols are unpublished work from Lashley* (2004).

thorough review of experimental data for plutonium (both in the unalloyed α phase and in the alloyed δ phase) provides no evidence for localized magnetic moments. They concluded that neither temperature nor magnetic-field dependencies of measured susceptibilities show evidence for ordered or disordered moments. They reinforce their conclusions with the results of other experimental probes, such as specific heat and NMR.

Magnetic moments and atomic volume are indicators of what the electrons are doing. As shown in Fig. 7.39, the atomic volumes of the actinides exhibit a huge expansion right at plutonium (between the α and δ phases, with an additional expansion at americium). In their review of actinide theory related to magnetic behavior, Lashley *et al.* (2004) show that the consensus among theorists is that a localization of the 5f electrons is required to explain the large volume expansion between the α phase and the δ phase, which leads inexorably

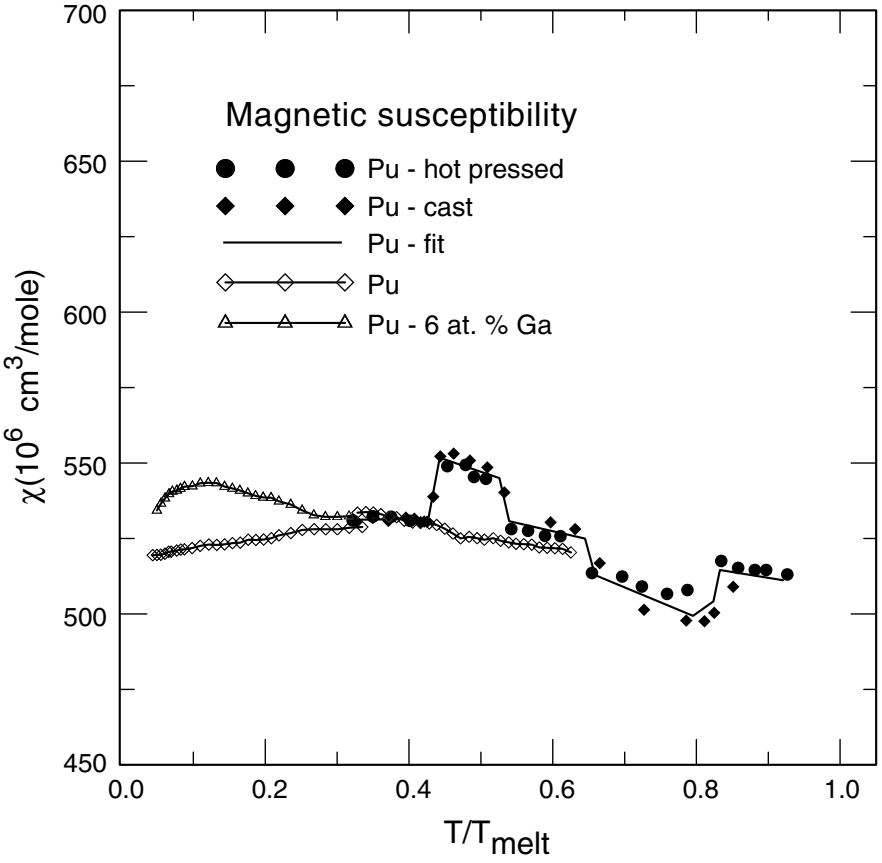

Fig. 7.53 *Molar susceptibility of unalloyed plutonium and δ-phase Pu-*6 at. *% Al alloy plotted as a function of temperature scaled by the melting point* (*from Lashley* et al., 2004). *See text for details of data.*

to magnetic ordering in the δ phase. Some theorists also predict magnetic order in the α phase. The magnetic moments are predicted to be large in both cases. Some of the theoretical treatments have suggested a partial cancellation between the spin and the orbital parts of the moments. However, even with such cancellation, magnetic moments of the order of 1 to $2\mu_B$ are predicted. Yet, the experimental evidence points overwhelmingly to the conclusion reached by Lashley *et al.* namely, neither ordered nor disordered local moments exist. Recent theoretical treatments by Shick *et al.* (2005) and Shorikov *et al.* (2005) predict reasonable volumes without any magnetic moments.

The reader is referred to the *Plutonium Handbook* (Miner and Schonfeld, 1980) and the *Gmelin Handbook of Inorganic Chemistry* (Lesser and Peterson,

1976; Blank, 1977) for additional references to magnetic susceptibility measurements and to the Hall effect in plutonium and its alloys. Recent magnetic susceptibility measurements on plutonium alloys, including Pu–Am and Pu–Ce, are also reported by Dormeval (2001) and Dormeval *et al.* (2000, 2003).

(f) Electrical resistivity, thermal conductivity, thermal diffusivity, and thermoelectric power

The unusual electrical resistivity of unalloyed plutonium is shown in Fig. 7.54 from Sandenaw and Gibney (1958). Unlike most normal metals that exhibit a linear decrease in resistivity at low temperatures, plutonium exhibits an increase and a maximum in resistivity at ~105 K. This low-temperature anomaly was initially believed to result from antiferromagnetic ordering. However, as pointed out above, no magnetic ordering has been found in plutonium or its alloys. Méot-Reymond and Fournier (1996) and Dormeval *et al.* (2000) suggest that the resistivity maximum is an indication of a Kondo effect in plutonium and its alloys. Boring and Smith (2000) make a convincing argument that the resistivity behavior along with other properties (such as the enhanced low-temperature specific heat) is an indication of strong electron–electron correlations involving spin and charge interactions. The resistivity maximum in plutonium is at the level of 150 μΩ cm, which means that an electron is scattered by roughly every atom in the lattice. As pointed out by Boring and Smith (2000), this type of scattering is considered the highest possible simple resistance that a

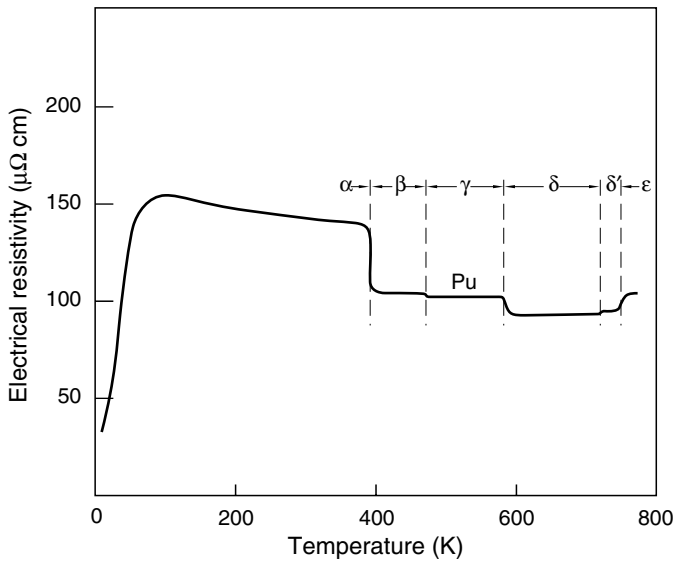

Fig. 7.54 *Electrical resistivity of unalloyed plutonium* (*from Sandenaw and Gibney,* 1958).

simple metal can exhibit; it is called the unitary limit. We also note that Lee *et al.* (1961) and Smith (1980) showed that plutonium does not become superconducting down to 0.75 K. Boivineau (2001) has extended resistivity measurements into the liquid phase using very high heating rates. He found the resistivity to remain nearly constant over the whole liquid range at a value of approximately 108 μΩ cm.

The resistivity of the δ-phase alloys has been measured by a number of investigators. The room-temperature values typically fall between 105 and 125 μΩ cm, depending on the alloying element and concentration. Extensive measurements have been reported on Pu–Ce alloys (Elliott *et al.*, 1962), Pu–Al alloys (Sandenaw, 1960a; Lee *et al.*, 1961; Elliott *et al.*, 1962), and Pu–Ga alloys (Joel *et al.*, 1971). The low-temperature results of Joel *et al.* (1971) for Pu–Ga alloys with gallium concentrations from 3 to 10 at.% are shown in Fig. 7.55. The results of Elliott *et al.* for Pu–Al alloys are very similar. We do not show the results for Pu–Ga alloys with gallium concentrations <3 at.% because they transform to the α′ phase upon cooling. The resistivities of all alloys are lower than that for unalloyed plutonium shown in Fig. 7.54. They also increase with decreasing temperature and exhibit a broad maximum. Increasing gallium concentration moves the maximum to lower temperatures and leads to higher

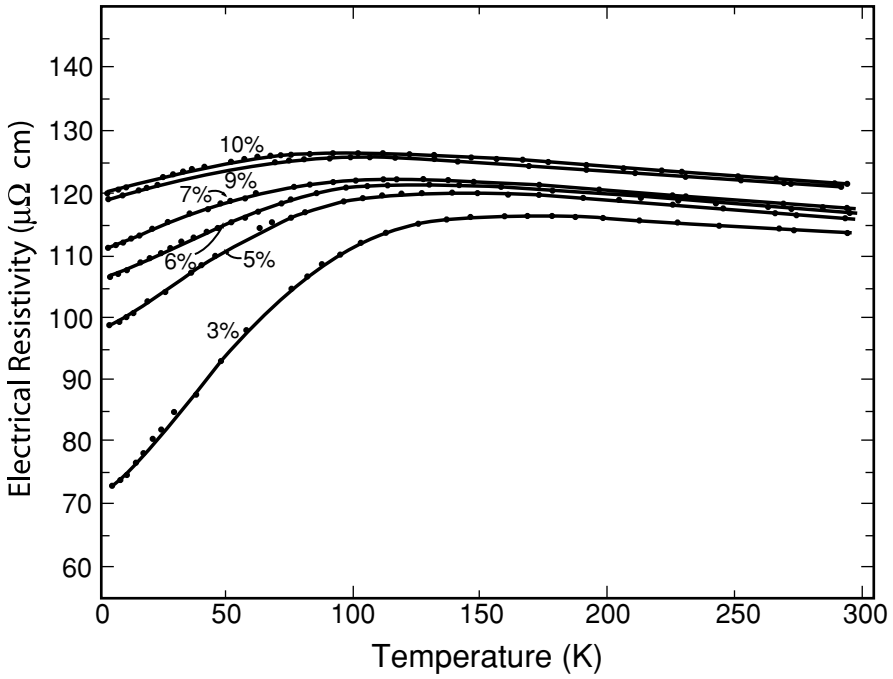

Fig. 7.55 *Electrical resistivity of various δ-phase Pu–Ga alloys* (*after Joel* et al., 1971).

resistivity. However, the increase with alloy concentration is less than what is typically observed for other metals. The low- and high-temperature regimes are shown together in Fig. 7.56 (taken from Blank (1977) and based on the work of Gibney and Sandenaw (1954)).

Gomez Marin (1997) and Dormeval (2001) recently measured resistivities of Pu–Am alloys across the entire range of δ-phase solubility at low temperatures. The resistivities for the entire range of alloys were considerably higher than any other plutonium alloy system. For example, the values for a Pu–15 at.% Am alloy was reported by Dormeval to be 370 μΩ cm at 293 K and 170 μΩ cm at 4 K. This alloy exhibited a slight maximum at 200 K. Alloys with higher americium contents were shown by Gomez Marin to decrease monotonically although not as rapidly as pure americium. Dormeval also reported resistivities of Pu–Ce alloys and of a number of ternary Pu–Ce–Ga and Pu–Am–Ga alloys. Blank (1977) reported the results of Mortimer and Adamson on Pu_3Al and Pu_6Fe. The resistivities at room temperature were 150 and 140 μΩ cm, respectively, and showed a maximum at lower temperatures. The resistivity for Pu_3Al remained unusually high (142 μΩ cm) at 4 K.

The literature shows large variations in low-temperature electrical resistivities measured in unalloyed plutonium. Much of this problem was a result of impurities. In addition, low-temperature measurements in plutonium are plagued by self-irradiation damage (see Section 7.7.9), which increases the resistivity

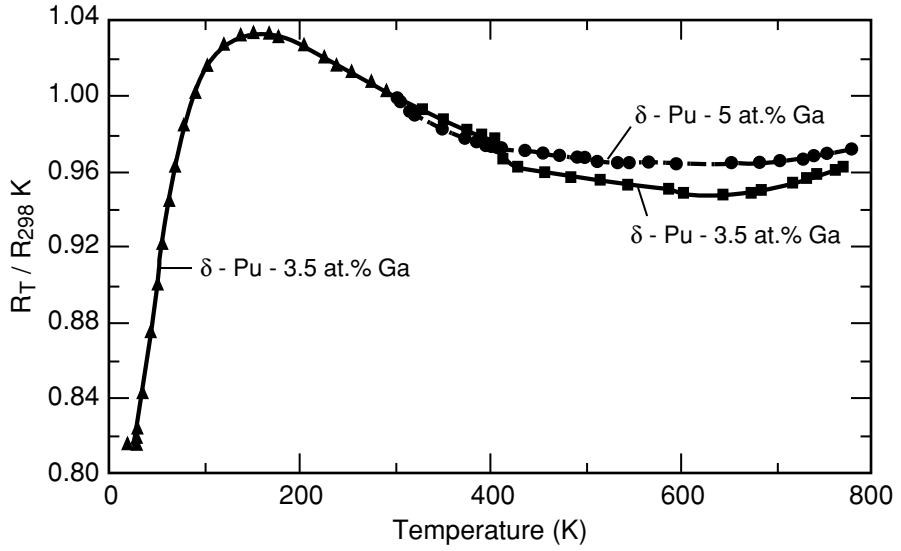

Fig. 7.56 *Electrical resistivity of a δ-phase Pu-*3.5 at. *% Ga alloy between* 25 *and* 750 K *and a δ-phase Pu-*5 at. *% Ga alloy between* 298 *and* 750 K. *The curves were normalized at* 298 K (*taken from Blank,* 1977 *with reference to Gibney and Sandenaw,* 1954).

because there is insufficient mobility of the defects generated to move and heal the lattice (Hecker and Martz, 2001). Olsen and Elliott (1962) reported some of the earliest measurements on the effects of impurities and self-irradiation on the resistivity of α-phase plutonium at low temperatures.

Thermal conductivity measurements on unalloyed plutonium were reported by Sandenaw and Gibney (1958), Lee and Mardon (1961), and Powell (1960). Andrew (1967) measured thermal conductivity of high-purity (99.98%) plutonium, chill-cast to minimize microcracking (density of 19.77 g cm^{-3}), and of preferentially oriented α-phase plutonium (by cooling from the β phase under pressure). The thermal conductivity decreases smoothly from a value of 0.0155 cal s^{-1} cm^{-1} K^{-1} at 300 K to 0.0075 cal s^{-1} cm^{-1} K^{-1} at 80 K for the chill-cast sample. Hence, the mechanisms that cause the increase in electrical resistivity and resistivity maximum at ~100 K do not seem to play a role in the thermal conductivity. Andrew found the thermal conductivity perpendicular to the [020] planes to be about 3 mW cm^{-1} K^{-1} higher than the thermal conductivity parallel to the [020] planes. He also reported a Lorenz number of 3.11×10^{-8} WΩ K^{-2} at 300 K and 5.95×10^{-8} WΩ K^{-2} at 80 K.

Andrew (1969) also reported thermal conductivities for high-purity, well-homogenized δ-phase Pu alloys. The conductivity of the Pu–3.35 at.% Ga alloy varied smoothly from 0.022 cal s^{-1} cm^{-1} K^{-1} at 300 K to 0.0098 cal s^{-1} cm^{-1} K^{-1} at 80 K. The conductivities of a Pu–7 at.% Ga alloy was approximately 10% lower and that of a Pu–10 at.% Ce alloy, approximately 20% higher. As was the case for the unalloyed plutonium, the thermal conductivities do not exhibit the anomalous low-temperature behavior found in resistivity measurements. Lewis *et al.* (1976) reported thermal conductivities calculated from thermal diffusivity measurements on high-purity Pu–3.35 at.% Ga alloys at high temperatures. Their calculated room-temperature value of 0.0205 cal s^{-1} cm^{-1} K^{-1} at 300 K increased to 0.04 cal s^{-1} cm^{-1} K^{-1} at 673 K.

Lewis *et al*. (1976) reported that the thermal diffusivity of high-purity plutonium (<200 ppm impurities) increased approximately linearly from about 0.011 cm^2 s^{-1} at 293 K (α phase) to 0.057 cm^2 s^{-1} at 843 K (ϵ phase). The thermal diffusivities of the δ-phase Pu–3.35 at.% Ga alloy increased smoothly from 0.04 cm^2 s^{-1} at 293 K to 0.065 cm^2 s^{-1} at 673 K.

The thermoelectric power of plutonium at room temperature is large and positive, and it decreases after each allotropic transformation as the temperature is increased, except for the δ′ to ϵ transformation, which shows an increase. The average value and ranges measured are shown in Table 7.22, taken from Wick (1980) and based on the work of Lee and Hall (1959), Costa (1960), Meadon and Lee (1962), and Lallement (1963). The thermoelectric power decreases rapidly at low temperatures with a slight rise at 80 K before falling very rapidly to 4 K. Blank (1977) reviewed thermoelectric power measurements for plutonium alloys. Lee *et al.* (1961) and Brodsky (1961) showed that the thermoelectric power in Pu–Al alloys exhibited an increase with decreasing temperature with a maximum at ~80 K for a δ-phase Pu–6 at.% Al alloy.

Table 7.22 *Thermoelectric power of plutonium* (*Wick*, 1980).

Phase	*Temperature* (K)	*Thermoelectric power, averaged values* ($\mu V\ K^{-1}$)	$\mu V\ K^{-1}$, *range*
α	~20	1.75	~1.5–~2
	~80	10.1	8.6–11.6
	~100	9.8	8.2–11.5
	~293	~13	11.2–15.6
	300	11.5	7–15.5
β	400	9.1	7–10.7
γ	500	8.4	7.4–9.4
δ	600	3.0	2.3–3.7
δ'	725	2.32	–
ϵ	800	3.5	3.2–3.8

The value of the thermoelectric power at room temperature was approximately 4 $\mu V\ K^{-1}$, about one third the value of unalloyed plutonium in the α phase.

(g) Diffusion

Diffusion rates in solids depend principally on crystal structure and homologous temperature (T/T_m), that is, how close the temperature is to the melting point (Sherby and Simnad, 1961). Plutonium, of course, has multiple allotropes and a very low melting point. Sherby and Simnad (1961) showed that the Arrhenius-like rate equation for self-diffusion, $D = D_0 \exp(-Q/k_B T)$, where D_0 is a constant and Q is the activation energy for self-diffusion (vacancy formation and migration), fits the diffusion data for most solids. The activation energy, Q, was found to depend primarily on the homologous temperature and the crystal structure. Experimental data for plutonium are summarized by Lesser and Peterson (1976), Blank (1977), and Deloffre (1997). The diffusion data presented in Table 7.23 are based on Deloffre's summary (1997) of the work of Tate and coworkers (Tate and Cramer, 1964; Tate and Edwards, 1966), Johnson (1964), Edwards *et al.* (1968), Rafalski and coworkers (Rafalski *et al.*, 1967; Harvey *et al.*, 1971), Dupuy and Calais (1968), Wade (1971), and Wade *et al.* (1978).

The data presented in Table 7.23 contrast self-diffusion rates in the various phases of plutonium. There are no data available for α-phase plutonium because it is stable only below 395 K where diffusion rates are extremely slow. Wade *et al.* (1978) showed that the large variations in diffusion rates in the β and γ phases were a result of short-circuit diffusion along paths such as dislocations or grain boundaries. The diffusion rates in ϵ plutonium are anomalously high even for the open bcc crystal structure. In fact, Cornet (1971) showed that the rate of self-diffusion decreased under pressure, similar to what was previously found for white phosphorus (Nachtrieb and Lawson, 1955). He calculated the

Table 7.23 *Diffusion constants in plutonium and Pu–Ga alloys.*

Pu phase method	*Temperature range* (K)	*Diffusion mechanism*	*Frequency factor* D_0 ($cm^2\ s^{-1}$)	*Activation energy* Q ($J\ mol^{-1}$)	*References*
(a) Self-diffusion in unalloyed plutonium					
ϵ Pu diffusion couple ^{238}Pu tracer	773–893	lattice	2×10^{-2} $3 \times 10^{-3} < D_0 < 9 \times 10^{-2}$	$77\,400 \pm 10\,500$	Dupuy and Calais (1968)
ϵ Pu thin film ^{238}Pu tracer	765–886	lattice	$(4.5 \pm 1) \times 10^{-3}$	$66\,940 \pm 1\,675$	Wade (1971)
δ Pu diffusion couple ^{238}Pu tracer	623–713	lattice	4.5×10^{-3}	99 600	Tate and Cramer (1964)
δ Pu thin film ^{238}Pu tracer	594–715	lattice	$(5.17 \pm 0.7) \times 10^{-1}$	$126\,370 \pm 800$	Wade *et al.* (1978)
γ Pu diffusion couple ^{238}Pu tracer	488–580	lattice	2.1×10^{-5}	69 870	Tate and Edwards (1966)
γ Pu thin film ^{238}Pu tracer	484–544	lattice	$(3.8 \pm 10) \times 10^{-1}$	$118\,410 \pm 7\,500$	Wade *et al.* (1978)
	504–564	short circuit	$(1.76 \pm 0.7) \times 10^{-5}$	$69\,040 \pm 1\,670$	
β Pu thin film ^{238}Pu tracer	409–454	lattice	$(1.69 \pm 0.5) \times 10^{-2}$	$108\,000 \pm 1\,200$	Wade *et al.* (1978)
		short circuit	$(3.9 \pm 0.05) \times 10^{-7}$	$56\,070 \pm 60$	
(b) Self- and interdiffusion in Pu–Ga alloys					
δ phase, thin film ^{238}Pu tracer, self-diffusion	613–781	lattice	76.0	152 000	Wade (1971)
	513–613	grain boundary	1.6×10^{-2}	110 000	
ϵ phase, thin film ^{238}Pu tracer, self-diffusion	847–917	lattice	7×10^{-4}	56 070	Wade (1971)
ϵ phase, diffusion couple, interdiffusion	833–909	lattice	5.3×10^{-4}	55 230	Harvey *et al.* (1971)
δ phase, homogenization interdiffusion	698–798	lattice	65	168 000	Johnson (1964)
δ phase, diffusion couple, interdiffusion	673–807	lattice	9.8×10^{-2}	139 300	Rafalski *et al.* (1967)
δ phase, diffusion couple, interdiffusion	688–790	lattice	1.3×10^{-2}	156 000	Edwards *et al.* (1968)

activation volume to be –4.9 cm^3, which is one-third of the molar volume of plutonium. He suggested an interstitial diffusion mechanism instead of the vacancy mechanism typically associated with lattice diffusion. Hill and Kmetko (1976) agreed with the proposed interstitial mechanism and suggested that the high self-diffusivity in the ϵ phase results from the nature of the 5f electron bonding in plutonium.

As shown in Table 7.23, the frequency factor, D_0, in plutonium is higher for self-diffusion than for interdiffusion. This behavior is shown graphically by the work of Edwards *et al.* (1968) in Fig. 7.57. It also agrees with the general observation that diffusion rates decrease with the addition of elements that raise the melting point of the host metal (Shewmon, 1963). Hilliard *et al.* (1959) showed that diffusion rates decrease significantly with increasing solute concentrations in typical alloy systems. Dupuy and Calais (1968) and Wade (1971) reported decreases in D_0 with additional solute additions. However, as reported by Mitchell *et al.* (2001), Edwards *et al.* (1968), and Rafalski *et al.* (1967) all concluded that the interdiffusion of gallium in plutonium did not vary with concentration over the range studied. Likewise, Tate and Edwards (1966) found no concentration dependence of diffusion rates in a series of δ-phase Pu–Al alloys. They reported values of $D_0 = 2.25 \times 10^{-4}$ and $Q = 106{,}690$ J mol^{-1} in the range of 623 to 790 K.

The large differences in interdiffusion rates of gallium between the δ and ϵ phases are particularly important because they lead to microsegregation of gallium in δ-phase plutonium alloys, as discussed in Section 7.7.4. The diffusion data for such alloys were recently summarized by Mitchell *et al.* (2001). Hecker *et al.* (2004) showed that interdiffusion of gallium in the α' phase of plutonium (an expanded α phase resulting from the entrapment of gallium atoms in a martensitically transformed δ-phase plutonium alloy) appears to be quite rapid even at room temperature.

Irradiation enhances both self-diffusion and interdiffusion rates in solids and can lead to phase instability or radiation-enhanced segregation. Such effects are particularly important in plutonium since the radiation is self-induced. Smirnov and Shmakov (1999) provide experimental and theoretical results for the actinides including plutonium and also present a rich Russian literature on this topic.

(h) Liquid plutonium, surface tension, viscosity, and vapor pressure

Liquid plutonium is highly corrosive and easily oxidized. Early measurements of its properties, including compatibility with container materials, were made as part of the LAMPRE program. Comstock (1952) reported some of the first direct measurements on liquid plutonium. There is general agreement today that the melting point of plutonium is (913 ± 2) K. The low melting point (with respect to its position in the periodic table) has many consequences on the practical properties of plutonium. In addition to restricting the temperature

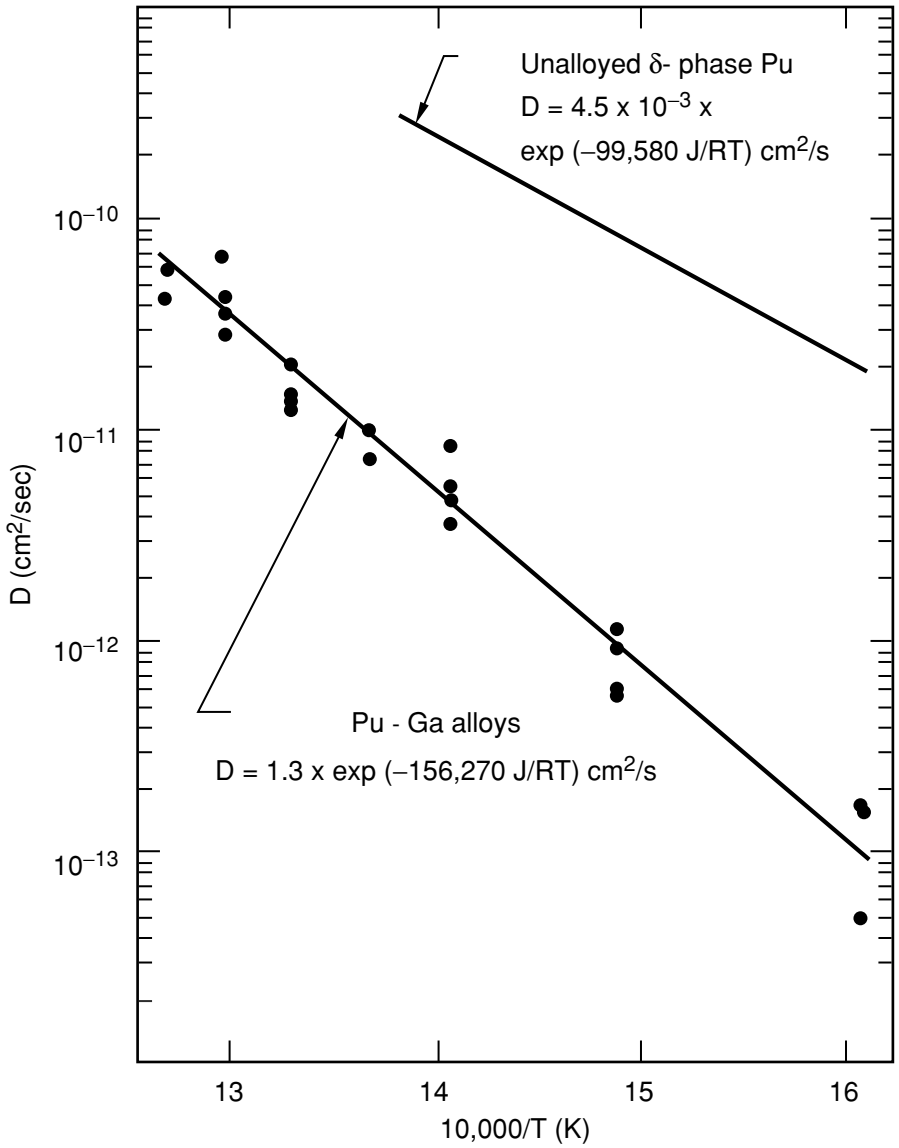

Fig. 7.57 *Diffusion coefficient, D, as a function of temperature for unalloyed plutonium and a δ-phase Pu*-3 at. *% Ga alloy plotted on a customary Arrhenius plot* (*Edwards* et al., 1968).

range of applications, it also affects all thermally activated processes, which scale with the melting point (Hecker, 2000). For example, room temperature represents a homologous temperature of 0.33, a temperature at which many defects become quite mobile. In addition, as pointed out by Nelson *et al.* (1965),

the effective melting point of the α phase is significantly lower than that of the ϵ phase, increasing the homologous temperature at room temperature to 0.53 for the α phase (see Hecker *et al.* (2004) for a discussion of the metallurgical consequences).

Liquid plutonium has many peculiarities, including a density greater than the last three solid allotropes, and its heat of fusion (~2800 J mol^{-1} as shown in Table 7.16) is unusually small. The stability of liquid plutonium has been attributed to the nature of 5f electron bonding in plutonium by Hill and Kmetko (1976) and Brewer (1983). Its melting point decreases with increasing pressure up to 3 GPa (Liptai and Friddle, 1967; Morgan, 1970) consistent with the volume contraction on melting. Other materials such as gallium, bismuth, antimony, germanium, silicon, tellurium, and water show similar behavior. Merz *et al.* (1974) and Boivineau (2001) also reported an increase in sound speed in liquid plutonium with increasing temperature, with a slope of 0.08 to 0.1 m s^{-1} K^{-1}. Using a rapid heating technique, Boivineau showed that the sound speed increases to 2000 K before undergoing a rapid change in slope to a negative value from 2000 to 3600 K. Similar results have been reported for cerium (McAlister and Crozier, 1981), in which 4f electrons also play a role in bonding under pressure. Lawson *et al.* (2000) and Lawson (2001) modified Lindemann's rule for melting to include the temperature dependence of the elastic properties. Lawson *et al.* explain the anomalously low melting point of plutonium and the trend across the light actinides by temperature-induced elastic softening.

The viscosity of liquid plutonium was measured by Wittenberg and coworkers at the Mound Laboratory (Eichelsberger, 1961; Jones *et al.*, 1962; Wittenberg, 1963; Ofte and Rohr, 1965; Ofte *et al.*, 1966). Jones *et al.* (1962) reported the viscosity of liquid plutonium to follow the relation:

$$\log \eta = 672/T + 0.037 \text{ (in centipoise)} \tag{7.26}$$

which yields a viscosity of 6 cP at the melting point. This is one of the highest viscosities measured for metals and is similar to the melting point viscosity of 6.53 cP for uranium (Wittenberg, 1975) and 5.8 cP for iron (Ofte *et al.*, 1966). Ofte *et al.* pointed out that the viscosity of plutonium and its fluid flow properties place it in a class of metals whose melting points are substantially higher than that of plutonium. However, if one accounts for its high mass and low Debye temperature, then plutonium falls only somewhat above the correlation established by Iida *et al.* (1988) for most liquid metals.

Blank (1977) reviewed the measurements of viscosity on liquid Pu–Fe alloys by Ofte and coworkers (Wittenberg *et al.*, 1960; Ofte and Wittenberg, 1964; Wittenberg *et al.*, 1968). The Pu–Fe system is of practical importance because it forms the low-melting eutectic compound, Pu_6Fe. The viscosities of Pu–Fe alloys were uniformly high. That of a Pu–9.5 at.% Fe eutectic alloy (near the compound Pu_6Fe) was a remarkable 25.2 cP at 684 K (and decreased to 6.14 cP at 1081 K). Blank (1977) provides great detail in his summary of the Pu–Fe

system. Wittenberg *et al.* (1960) found the activation energy for viscous flow for the eutectic alloy to be 21.9 kJ mol^{-1}. Ofte *et al.* (1966) reported viscosities for Pu–Ce and Pu–Ce–Co alloys in excess of that for plutonium. The viscosity of Pu–28.4 at.% Ce–23.7 at.% Co was reported as 23 cP at its melting point, nearly matching the viscosity of the Pu–Fe eutectic alloy. The Debye temperatures for these alloys are not available, so it is not possible to check if the viscosities fit the correlation established by Iida *et al.* (1988).

The accepted value for the surface tension of unalloyed liquid plutonium is that reported by Spriet (1963), namely 0.55 N m^{-1}. Wittenberg (1975) also reported 0.55 N m^{-1} for plutonium and 1.5 N m^{-1} for uranium. The value for plutonium fits the correlation of surface tension with melting point and molar volume proposed by Iida *et al.* (1988) for most elements in the periodic table. That of uranium appears to be anomalously high.

The optical properties and normal spectral emissivity of liquid Pu–3.4 at.% Ga at 632.8 nm were measured over the temperature range of 2016 to 2189 K using rotating analyzer ellipsometry by Sheldon *et al.* (2001). The temperature dependence of three optical properties ϵ_λ (emissivity), n_λ (index of refraction), and k_λ (extinction coefficient) were reported as:

$$\varepsilon_\lambda = 5.38 \times 10^{-5} + 0.250$$

$$n_\lambda = -1.29 \times 10^{-4}\ \mathrm{T} + 3.82$$

$$k_\lambda = -7.04 \times 10^{-4} + 5.77$$

The value for ϵ_λ is almost a third higher than that measured for uranium by Krishnan *et al.* (1993), demonstrating that the light actinides exhibit significant variations in emissivity.

Phipps *et al.* (1955) reported the vapor pressure of liquid plutonium. Subsequently, Mulford (1965), Kent and Leary (1968), and Kent (1969) added to these measurements, and reported the vapor pressure to be described by the following equation with T in K and P in atmospheres:

$$\log P = (4.924 \pm 0.120) - (17,420 \pm 184)/T \qquad (7.27)$$

This relationship extrapolates to a boiling point of (3573 ± 100) K. Hence, the boiling point is quite high, in keeping with the position of plutonium in the periodic table. The combination of a high boiling point and a low melting point results in a wide range of liquid stability. Kent and Leary (1968) also reported the standard enthalpy of vaporization (H°_{298}) as (347.7 ± 2.1) kJ mol^{-1} and the standard entropy of vaporization (S°_{298}) as 123.2 J mol^{-1} K^{-1}. Oetting *et al.* (1976) reviewed the available data and recommended the best average for the enthalpy of vaporization as (345.2 ± 0.4) kJ mol^{-1}. A detailed listing of the thermodynamic properties of plutonium gas is given in Oetting *et al.* The data for the Pu_6Fe intermetallic reported by Sandenaw and Harbur (1973) were summarized by Blank (1977).

(i) New tools, new measurements of physical properties

Arko *et al.* (2006) reviewed the properties of actinides in the metallic state in Chapter 21 of this work. Their emphasis is on those properties that are unique or predominantly found in the metallic solid state. Such properties include magnetism, superconductivity, enhanced mass, spin, and charge density waves as well as quantum critical points. We refer the reader to this chapter for discussion of how plutonium fits into the trends across the actinides. They also provide detailed results of photoemission spectroscopy measurements on plutonium and its alloys.

There has been a revival of experimental work (along with a great increase in theoretical activity) in plutonium over the past 5 years. Some of the modern tools of materials science developed during the past couple of decades are being used to make measurements on plutonium and its alloys. We summarize a few salient ones in this section. One of the key barriers to many of the techniques remains the difficulty in synthesizing single crystals of the various phases of plutonium. No single crystals of α plutonium have been fabricated since the pioneering work in the 1960s by Liptai *et al.* (1967), who grew very large grains by a high-pressure technique. However, Lashley *et al.* (2000, 2001) have refined the strain-anneal technique developed in the 1960s by Moment (1968) to grow large grains of δ-phase plutonium alloys, which are suitable for many of the single-crystal measurements. These large-grained, very high-purity plutonium samples have been used for many recent physics experiments.

Zocco and Schwartz (2003) provide a history of the development of TEM techniques and their application to plutonium and its alloys. This technique is an essential tool for metallurgical studies, first demonstrated for plutonium around 1980 and revived in 2000. Zocco and Schwartz show examples of how TEM has helped answer key questions about phase transformations in plutonium alloys, as well as study the effects of self-irradiation damage. Boehlert *et al.* (2001) demonstrated how electron backscattered diffraction can be used to examine the grain structures in Pu–Ga alloys.

Ledbetter and Moment (1976) raised interest in the phonon spectrum of plutonium with their results nearly 30 years ago on the unusual elastic anisotropy of δ-phase plutonium. In a pioneering paper, Wong *et al.* (2003b) recently reported the first complete phonon dispersion curves of plutonium using inelastic X-ray scattering from a third-generation synchrotron facility (the European Synchrotron Radiation Facility in Grenoble, France). Their results are shown in Fig. 7.58 for a Pu–2 at.% Ga δ-phase alloy large-grained polycrystal grown by the techniques developed by Lashley *et al.* (2001). Wong *et al.* confirmed the large elastic anisotropy found by Ledbetter and Moment. They also found a small shear elastic modulus, C', a Kohn-like anomaly in the T_1 [011] branch, and a pronounced softening of the [111] transverse modes. They relate these findings to a strong coupling between the lattice structure and the 5f valence instabilities in plutonium. Dai *et al.* (2003) predicted the phonon dispersion

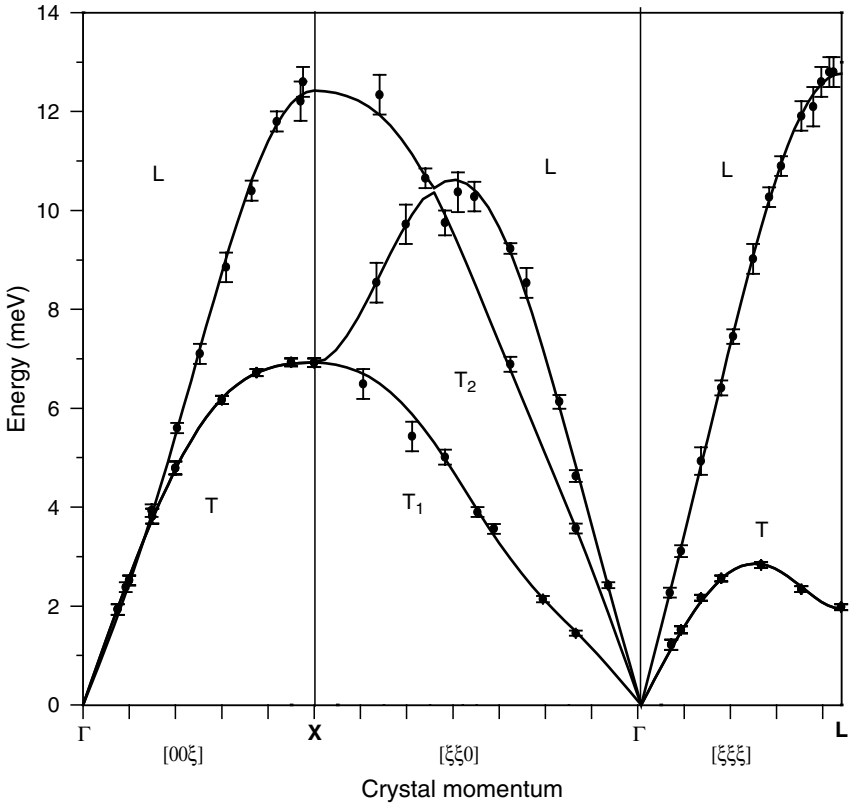

Fig. 7.58 *Phonon dispersion along high-symmetry directions in δ-phase Pu*-2 at. *% Ga alloy. The longitudinal and transverse modes are denoted L and T, respectively. The experimental data are shown with error bars. Along the* [0ξξ] *direction, there are two transverse branches,* [011]<011>(T_1) *and* [011]<100>(T_2). *The softening of the TA* (*transverse acoustic*) [111] *branch toward the L point is apparent. The curves represent the fourth-nearest neighbor Born–von Kármán model fit* (*Wong* et al., 2003*b*).

curves using dynamical mean-field theory (DMFT), which includes electron correlations that are so important in plutonium. Wong *et al.* point out that although the qualitative agreement between theory and experiment is quite good, there are important quantitative differences. Wong *et al.* (2003a) also developed a thermal diffuse scattering technique to complement their inelastic scattering technique.

McQueeney *et al.* (2004) reported the temperature dependence of the phonon spectrum, as observed from measurements of the phonon DOS and sound velocities as shown in Fig. 7.59. The DOS was measured with inelastic neutron scattering on a polycrystalline ^{242}Pu–5 at.% Al δ-phase alloy. The ^{242}Pu isotope was used because the absorption of thermal neutrons is low compared to the

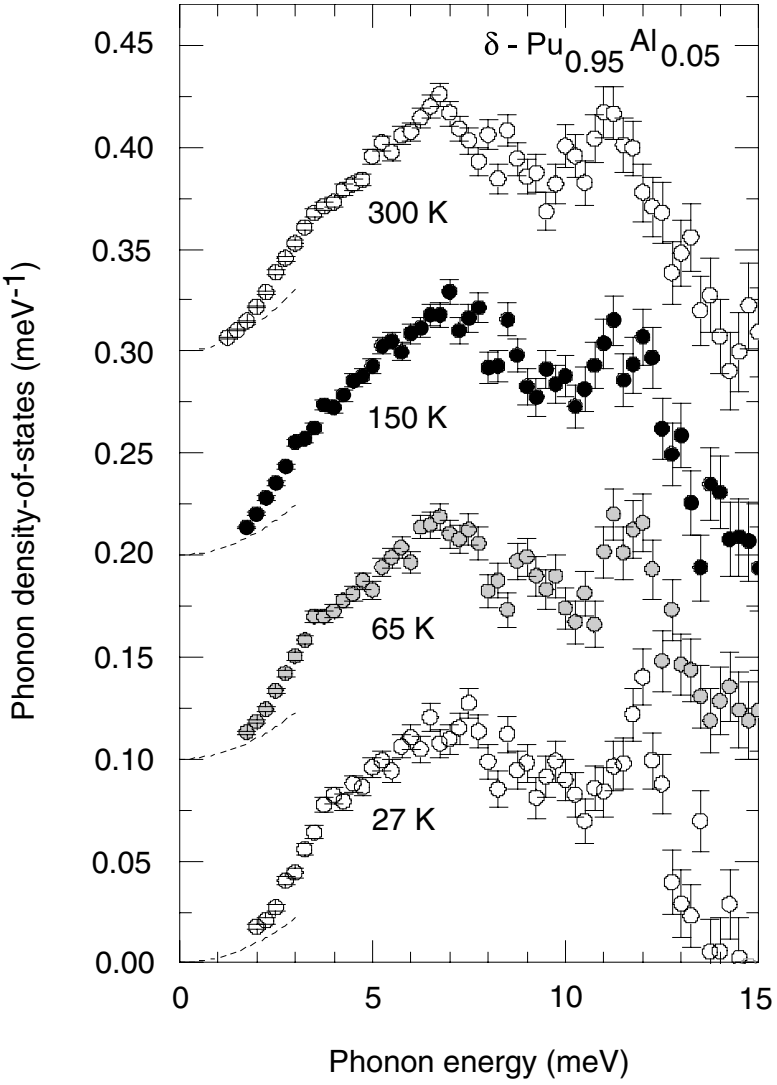

Fig. 7.59 *Phonon density of states of δ-phase Pu*-5 at. *% Al at four temperatures. The dashed line represents the quadratic part of the DOS at each temperature, as estimated by the average sound velocity obtained from resonant ultrasound measurements* (*from McQueeney* et al., 2004).

standard ^{239}Pu isotope. The phonon frequencies and sound velocities soften considerably with increasing temperature in spite of nearly zero thermal expansion over this temperature range. The frequency softening of the transverse branch along the [111] direction is anomalously large (~30%) and sensitive to

alloy composition. Based on a comparison to the results of Wong *et al.*, McQueeney *et al.* concluded that the interatomic potential is extremely sensitive to alloy composition, pressure, and temperature, unlike any other metal. They suggest that this behavior may arise from an unusual temperature dependence of the electronic structure.

We referred to local structure measurements at the modern synchrotron sources earlier using EXAFS along with conventional XRD in Section 7.7.5. Allen *et al.* (2002) reported temperature-dependent EXAFS measurements over the temperature range of 20–300 K of the vibrational properties of a Pu–3.3 at. % Ga δ-phase alloy as a means of discerning differences in the vibrational character of the gallium and plutonium sites. They obtained pair-specific, correlated Debye temperatures, θ_{cD}, of (110.7 ± 1.7) K for the Pu–Pu pairs and (202.6 ± 3.7) K for the Pu–Ga pairs. Allen *et al.* concluded that these results indicate that Ga–Pu bonds are significantly stronger than the Pu–Pu bonds. Lynn *et al.* (1998) previously reported a Pu-specific value of $\theta_D = 127$ K and a Ga-specific $\theta_D = 255$ K using neutron-resonance Doppler spectroscopy on a Pu–3.6 at.% Ga alloy. Nelson *et al.* (2003a,b) reported EXAFS measurements on the vibrational properties of both the δ phase and the α′ phase of a Pu–1.9 at. % Ga alloy (in the δ-phase and mixed, α′ + δ, phase conditions). They found a bond-length contraction for the Pu–Ga bond of 0.11 Å in the δ phase, but only 0.03 Å in the α′ phase. They reported correlated Debye temperatures of θ_{cD} (δ) = (120.4 ± 2.6) K and θ_{cD} (α′) = 159.1 ± 12.5 K.

Moore *et al.* (2003) used high-energy electron energy loss spectroscopy (HE-EELS) in a TEM and synchrotron-radiation-based X-ray absorption spectroscopy to determine phase-specific electronic structure information on plutonium. The sample was a dilute Pu–Ga alloy treated to produce a mixture of the α + δ phases. The TEM examination allowed individual grains of each phase to be examined. Moore *et al.* conclude that Russell–Saunders coupling fails for the 5f states of plutonium, and that only the use of JJ or intermediate coupling is appropriate. In addition, they conclude that their results confirm calculations that there is considerable spin–orbit splitting of the occupied and unoccupied 5f states of plutonium, indicating that spin–orbit splitting cannot be neglected in the Hamiltonian for the 5f states of plutonium.

Superconductivity has recently been discovered above 18 K in a plutonium-based nearly magnetic compound, $PuCoGa_5$ by Sarrao *et al.* (2002, 2003a,b). At the same temperature, this compound exhibits a step-like transition in heat capacity, from which they inferred the electronic specific heat, γ, to be 77 mJ mol^{-1} K^{-2}, which points to strong electron–electron correlations. In addition, field-dependent resistivity data gave an upper critical field of 74 T, a surprisingly large value. Other actinide-based superconductors have transition temperatures below a few K. The cerium-based isostructural compounds $CeCoIn_5$ and $CeIrIn_5$ are also superconducting but only in the 1-K range, and for $CeRhIn_5$ only under pressure. The T_c of $PuCoGa_5$ can be further enhanced to about 22 K by applying pressure (Griveau *et al.*, 2004). $PuRhGa_5$ is superconducting, as

well, with $T_c = 8.6$ K (Bauer *et al.*, 2004). The properties of these plutonium-based superconductors are indicative of an unconventional, most likely magnetically mediated, superconductivity (Sarrao *et al.*, 2003b).

7.7.7 Mechanical properties of plutonium metal and alloys

Mechanical properties of metals and alloys depend to first order on their crystal structure and melting point, which indirectly affects all thermally activated processes. The multiple allotropes of plutonium lead to a rich spectrum of mechanical properties as reviewed recently by Hecker and Stevens (2000). The low melting point allows for relatively easy mobility of defects near and above room temperature. Consequently, the mechanical properties of plutonium are especially sensitive to temperature and strain rate. They are also sensitive to chemistry (both intentional alloying and unintentional impurities) and processing, which, in turn, control the microstructure (phases present, their structure and distribution, and the nature and number of defects). Therefore, it is necessary to know the chemistry and the processing history to compare the properties of plutonium.

Gardner (1980) presented the most comprehensive review of the mechanical properties of plutonium and its alloys. His results for the yield and ultimate tensile strengths of unalloyed plutonium (for a range of purities and processing histories) are summarized in Fig. 7.60. These data demonstrate the dramatic temperature and crystal-structure dependence of the strength properties of plutonium. As reported by Gardner, the monoclinic crystal structure of plutonium (the only element in the periodic table with this low-symmetry structure) precludes the necessary conditions for plastic slip (by dislocation glide) in polycrystalline material for extended plastic flow. Consequently, the α phase of plutonium is brittle at and near room temperature. As shown in Fig. 7.60, it is quite strong. However, the tendency for α plutonium to microcrack during typical processing causes significant scatter in the properties. Moreover, certain impurities lead to the retention of second phases (typically the δ or β phases) or the presence of inclusions (such as oxides, nitrides, carbides, or the eutectic intermetallic, Pu_6Fe), which can have a significant effect on the mechanical properties.

Another important variable in determining the mechanical behavior of α plutonium is the grain size. Merz (1970, 1971) demonstrated that in α plutonium with decreasing grain size the mechanism for plastic flow changes. He fabricated very fine-grained α plutonium (1–3 μm) by extrusion and concurrent recrystallization of electrorefined, high-purity plutonium. He demonstrated that the strength decreased substantially with grain size and the ductility increased. At room temperature, he found surprising plastic elongation of 8% at low strain rates. On the high-temperature end of α-phase stability, he found extended plasticity, that is, elongations in excess of 100% (Merz and Allen, 1973;

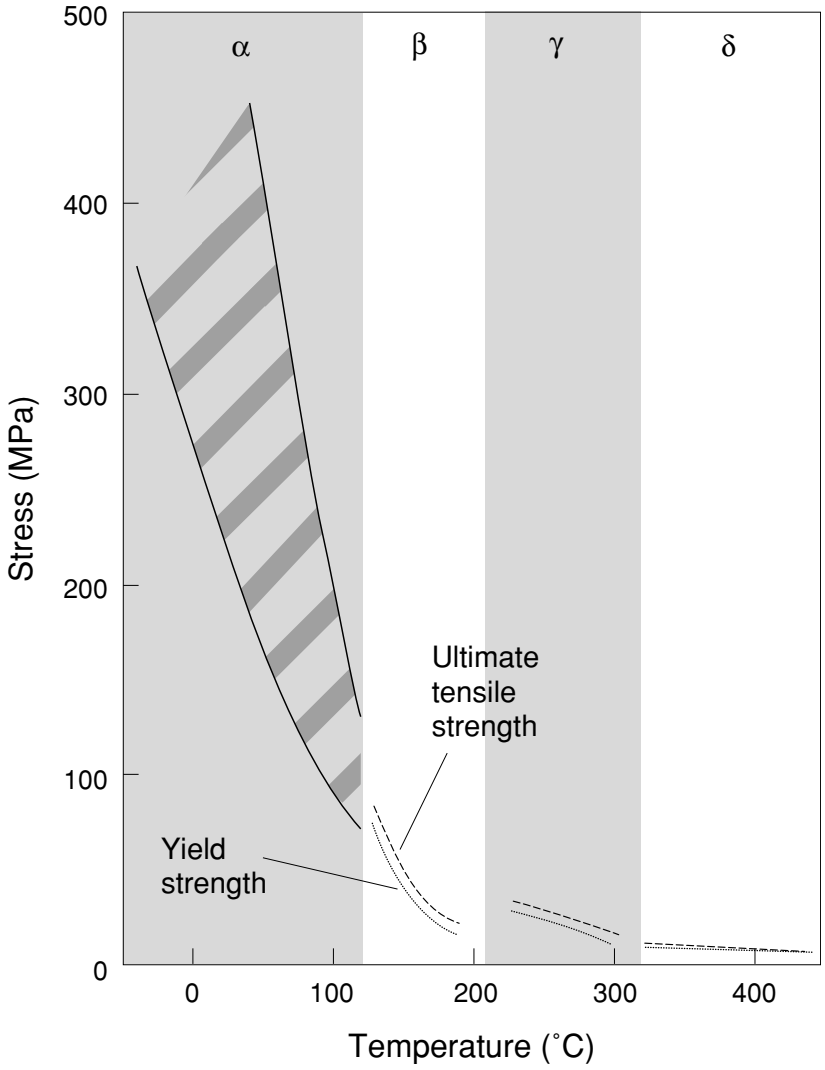

Fig. 7.60 *Strength as a function of temperature for unalloyed plutonium tested in uniaxial tension at nominal strain rates of* 10^{-3} s^{-1} (*after Gardner,* 1980).

Merz, 1974). In the β phase, he found the fine-grained plutonium to exhibit classical superplasticity with several 100% elongation. He explained that the deformation mechanism changed from dislocation glide to grain boundary sliding because of the small grain size and the high homologous temperature

of 0.53 at room temperature for the α phase of plutonium. Fig. 7.61 shows the change in Vickers Microhardness with temperature for several grain sizes in α plutonium (Merz and Nelson, 1970). Hecker and Morgan (1976) found that the strength of coarse-grained α plutonium increased moderately at intermediate strain rates. Hecker and Stevens (2000) pointed out several other interesting features about the mechanical behavior of α plutonium in their review.

As shown in Fig. 7.60, the other phases of unalloyed plutonium are relatively weak compared to the α phase. Gardner shows no data for the ϵ phase. Cornet and Bouchet (1968) showed that the elastic moduli of the ϵ phase is approximately two-thirds that of the δ phase, and we also expect its strength properties to be lower. The other phases of plutonium are also considerably more ductile than the α phase. As pointed out earlier, a few atom percent of alloying

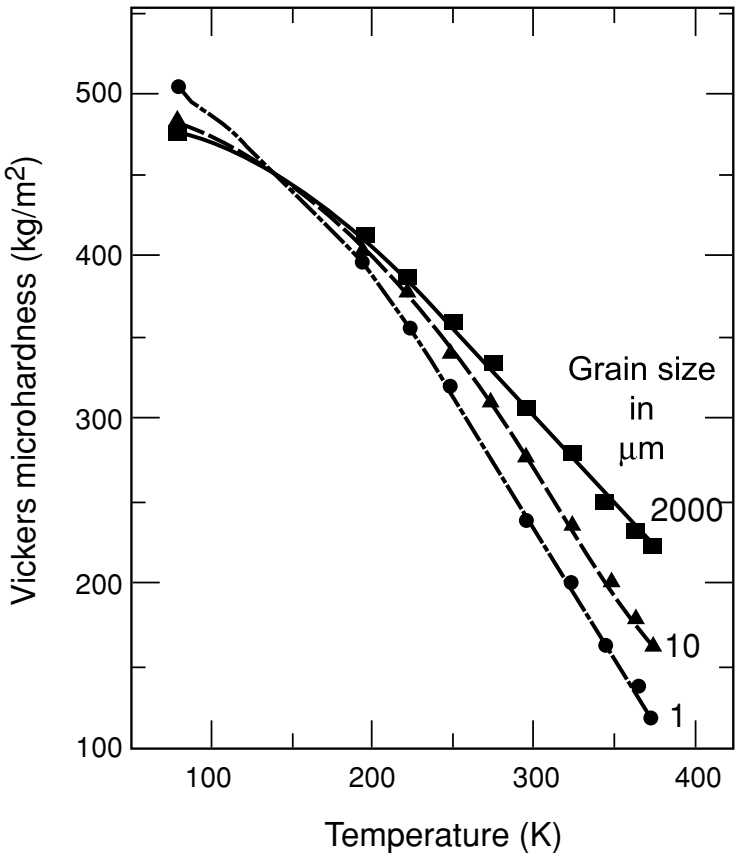

Fig. 7.61 *Vickers microhardness as a function of temperature for unalloyed α plutonium at various grain sizes* (*after Merz and Nelson,* 1970).

additions of elements such as gallium or aluminum retain the fcc δ phase to room temperature. As expected the δ phase alloys are considerably more ductile than the monoclinic α phase. A comparison of room temperature mechanical behavior is shown in Fig. 7.62 (Hecker and Stevens, 2000). The α phase is shown to be strong and brittle (like cast iron), whereas the δ-phase Pu–Ga alloy is weak and ductile (like commercially pure aluminum). Processing of the δ-phase alloys strongly influences the mechanical properties. Particularly important are gallium segregation, which can be minimized by elevated-temperature annealing treatments and thermo-mechanical treatments (see Fig. 7.33). Robbins (2004) recently reported an extensive compilation of the mechanical properties of Pu–3.4 at.% Ga δ-phase alloys. The compression behavior of a typical, well-homogenized alloy is shown in Fig. 7.63 (from the work of Barmore and Uribe (1970)). We should note that the mechanical properties of δ-phase Pu–Al alloys are similar to Pu–Ga alloys with similar atomic concentrations of the alloying element.

Detailed mechanical properties of plutonium and various alloys, including strength, hardness, ductility, creep, impact strength, and fatigue strength are presented by Gardner (1980), by Lesser and Peterson (1976) for unalloyed

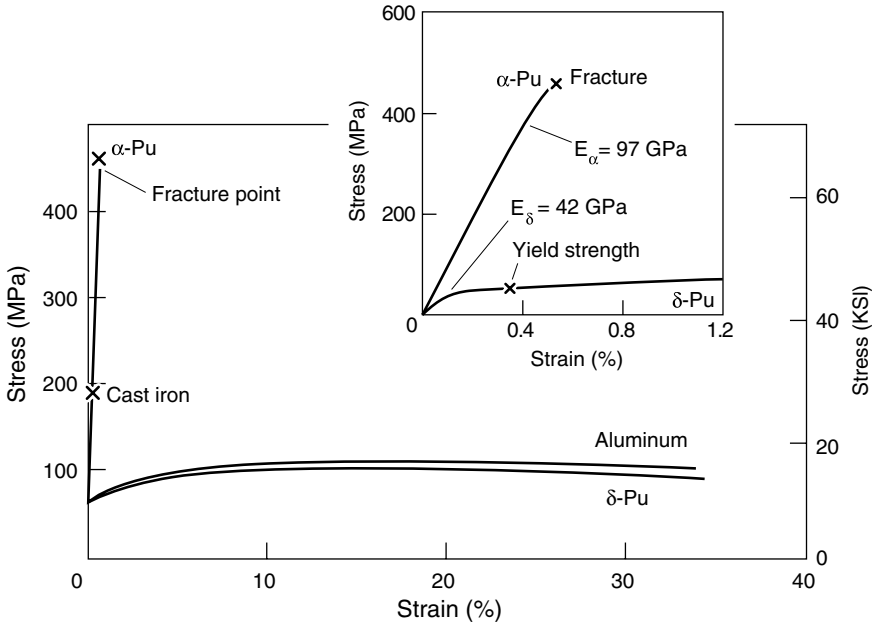

Fig. 7.62 *Typical uniaxial tensile stress–strain curves for unalloyed α plutonium compared to a δ-phase Pu–Ga alloy at a nominal strain rate of* 10^{-3} s^{-1}. *The insert shows the initial stress–strain curve at higher resolution* (*after Hecker and Stevens,* 2000).

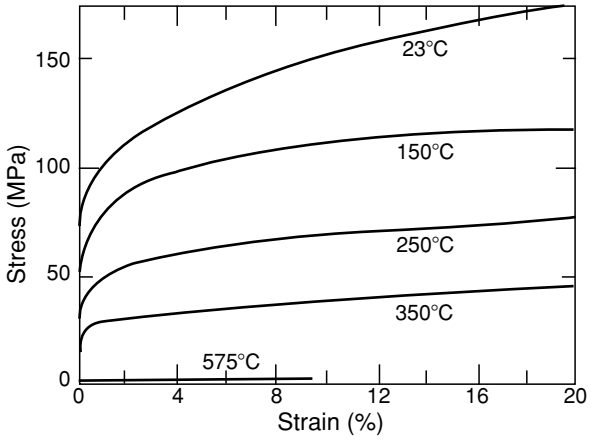

Fig. 7.63 *Uniaxial stress–strain curves in compression for a δ-phase Pu*-3.4 at. *% Ga alloy at different temperatures and a nominal strain rate of* 10^{-2} s^{-1} (*after Barmore and Uribe,* 1970).

plutonium (on pp. 29–33 of their review), and by Blank (1977) for Pu–Al alloys (pp. 180–183) and for Pu–Ga alloys (pp. 221–232). Blank (1976, 1977) also provides mechanical properties for additional alloy systems, with a particularly extensive discussion of the Pu–Fe system (Blank, 1976). Care must be taken during low-temperature experiments on δ-phase alloys to avoid transformation of the retained δ phase to the α′ phase. Since the α′ phase is so much harder than the δ phase, even small amounts of α′ result in significant strengthening.

There are few theoretical treatments of mechanical behavior of plutonium in the literature. The principal problem stems from the fact that the mechanical properties are controlled by microstructure and defects, which are still beyond the reach of *ab initio* calculations for all practical metals. Stout *et al.* (2002) developed a physically based constitutive model to predict the mechanical behavior of fcc δ-phase plutonium alloys. The input to the model was based on previous work with other fcc metals and the published test results on Pu–Ga alloys referenced above. The model is able to predict the temperature and strain-rate effects on the yield and ultimate strengths of Pu–Ga alloys. It also allowed the authors to isolate the effects of microstructural variables such as grain size, alloy content, and impurity content. The effect of gallium solutes has the largest strengthening effect. The yield strength increases by 50% with an increase in gallium from 1 to 6 atomic percent. The grain size effect follows the classical Hall–Petch relationship:

$$\sigma_y = \sigma_0 + \kappa/\sqrt{d} \tag{7.28}$$

where σ_y is the yield strength for a grain diameter d in μm, and σ_0 and κ are measured constants. Hence, decreasing grain size leads to increased strength in

the deformation regime controlled by dislocation glide. (We note that in the deformation regime dominated by grain boundary sliding, the relationship is inverted – small grain size leads to lower strength.) The parameters for Pu–Ga alloys are given by Stout *et al.* (2002). The model allowed them to demonstrate that the typical impurities (such as C, O, N, and Fe form hard inclusions of μm to tens of μm in diameter) in these alloys have little effect on strength values at ambient temperature. However, the fracture behavior will be affected negatively by higher impurity contents. In addition, Beitscher (1970) showed that iron impurities at the level >300 ppm lead to dramatic high-temperature embrittlement (at 683 K and low strain rates) because the Pu_6Fe intermetallic inclusions melt and lead to brittle behavior known as 'hot shortness.'

7.7.8 Oxidation and corrosion in plutonium metal and alloys

Degradation of plutonium surfaces under various atmospheric conditions is of concern during handling and for all considerations that require storage of plutonium, its alloys, or its compounds. Although plutonium is a reactive metal as suggested by a standard reduction potential of –2.02 V for the Pu^{3+}/Pu^0 couple (see Fig. 7.116a), its oxidation rate in very dry air (<0.5 ppm H_2O) is a minuscule 20 pm h^{-1} (Haschke *et al.*, 1996). Clean plutonium surfaces have a silvery, metallic sheen, similar to clean iron or nickel. Plutonium loses its metallic sheen quite rapidly in most atmospheres. It takes on a darker appearance and exhibits interference colors before it begins to develop a loose, olive-green powder of PuO_2 'rust' (see Section 7.8.5.a). Although this process occurs quite slowly in most of the protective atmospheres in which plutonium is handled, experience over the years has yielded many surprises, including pyrophoric behavior and anomalous corrosion rates catalyzed under complex atmospheric conditions of hydrogen or moist air that can increase surface corrosion rates by a staggering 13 orders of magnitude. The enhanced oxidation rates in the presence of moisture were already discovered at Los Alamos during the Manhattan Project by Covert and Kolodney (1945). Uncontrolled surface reactions are one of the greatest risks during storage or use of plutonium metal. Not only do these reactions change the geometry of the material, they typically result in finely powdered forms that are more readily dispersed, and hence, increase the health risk of inadvertent release and uptake of plutonium, a safety hazard of paramount importance for long-term plutonium storage (Haschke *et al.*, 1998).

Waber (1980) summarized the available knowledge on corrosion and oxidation of plutonium up to 1964. Subsequent results to 1976 were summarized by Lesser and Peterson (1976). More recently, Haschke *et al.* (2000a) presented a current understanding of corrosion and oxidation, and Hecker and Martz (2001) summarized current understanding and presented practical examples of plutonium corrosion problems. Much of the discussion here is based on the

report of Hecker and Martz. We refer the reader to Lesser and Peterson (1976) for a description of the reaction of plutonium with other gases such as nitrogen and ammonia at higher temperatures as well as surface reactions of plutonium with acids and other solvents.

(a) Oxidation in air

Corrosion rates depend greatly on plutonium surface chemistry. Hence, it is crucial to understand the specific surface chemistry for different plutonium substrates and for different atmospheric conditions. In dry air, the reactive plutonium metal surface is passivated by a layer of protective $PuO_{2\pm x}$ that forms rapidly over the entire surface. In the Pu–O system, Pu(IV) is a stable oxidation state and forms a classic fluorite-type crystal structure, with four plutonium cations per unit cell arranged in an fcc lattice, and eight oxygen anions at the tetrahedral interstices in a simple cubic packing (as discussed in Section 7.8.5.a, and shown in Fig. 7.90).

The oxidation rate is controlled by the diffusion of oxygen through the oxide surface to the oxide–metal interface, yielding classic parabolic growth rates. Significant stresses build up at the interface because the density of the oxide is 11.46 g cm^{-3} compared to pure α plutonium at 19.86 g cm^{-3}. The oxide layer reaches a steady-state thickness of 4 to 5 μm because at this thickness the oxide begins to spall, leading to a balance between spalling of the oxide and re-oxidation of the surface (Martz *et al.*, 1994). A constant isothermal oxidation rate is maintained by diffusion of oxygen through an oxide layer of constant average thickness. Fig. 7.64 also shows that corrosion rates depend strongly on temperature and atmospheric conditions. The details of this behavior are presented by Haschke *et al.* (1998) and discussed by Hecker and Martz (2001). Activation energies of oxidation in unalloyed plutonium are reported by Blank (1977), based on the work of Thompson (1965), to be 96.2 kJ mol^{-1} for the α phase, 50.2 kJ mol^{-1} for the β phase, and 58.6 kJ mol^{-1} for the γ phase, each in their temperature range of phase stability. However, Blank points out that significantly different results have been cited by other authors because of the substantial influence of microcracks, impurities, and crystallographic textures. The reader is referred to Haschke *et al.* (1998) for a more detailed discussion of the thermodynamics and kinetics of the oxidation process.

(b) Moisture-enhanced oxidation

Corrosion of plutonium metal in moist air occurs at a rate 200 times greater than in dry air at room temperature and five orders of magnitude greater at 100°C. The mechanisms of water-catalyzed corrosion of plutonium have only recently been elucidated (Haschke *et al.*, 1996). It had been generally accepted that the greatest oxygen concentration possible in plutonium oxide was in the

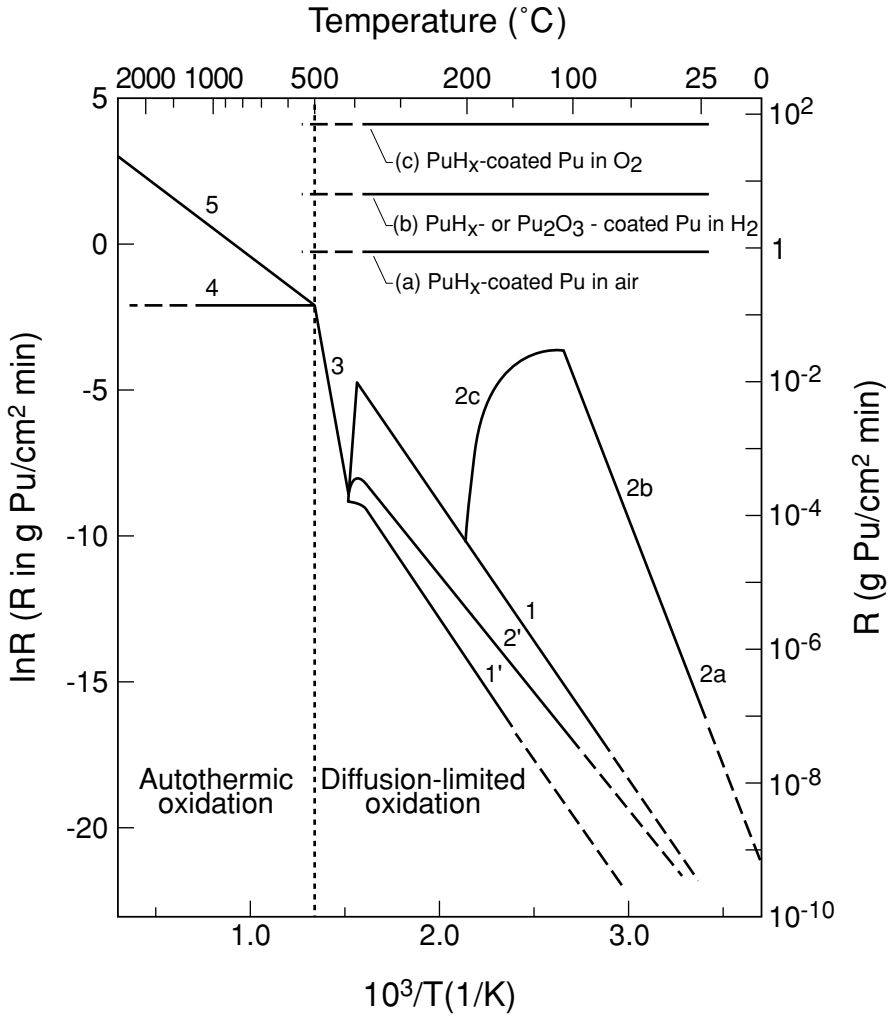

Fig. 7.64 *Oxidation rates of plutonium vs temperature. Curve* 1 *shows the oxidation rate for pure plutonium exposed to dry air or oxygen at an* O_2 *pressure of* 21.3 kPa. *Curve* 2*a presents the oxidation rate when the same, dry Pu samples are exposed to water vapor at the same pressure* (21.3 kPa). *Note the increase of four orders of magnitude in oxidation rate. Curves* 2*b and* 2*c extend the water-exposed oxidation rate to the temperature ranges of* 61–110°C *and* 110–200°C, *respectively. The drop in oxidation rate at higher temperatures is not fully understood, but may be related to the lack of spallation of product oxide at higher temperatures. Curves* 1′ *and* 2′ *present oxidation data for Ga-stabilized δ Pu in dry and moist air, respectively. Distinctions in oxidation rates for various alloys and conditions disappear at high temperatures as shown by curve* 3. *Curve* 4 *shows the constant oxidation rate observed under static conditions, while curve* 5 *shows recent data extrapolated from ignited Pu droplets oxidizing during free-fall in air. The reactions of hydride-coated Pu are shown in curves a–c. Curve a shows the constant reaction rate for hydride-coated Pu exposed to dry air. This represents an increase in reaction rate of over* 10^9 *compared to pure Pu. Curve c shows the same material exposed to pure oxygen. This reaction is* 10^{13} *times faster than pure Pu exposed to* O_2. *Finally, curve b shows the constant reaction rate of either hydride- or cubic sesquioxide-coated Pu to hydrogen* (*at* 101 kPa) (*Martz and Haschke,* 1998*; Haschke* et al., 2000*a*).

dioxide, namely $PuO_{2.0}$. However, Stakebake *et al.* (1993) and Haschke *et al.* (2000a, 2001) demonstrated that hyperstoichiometric plutonium oxide, PuO_{2+x}, forms in the presence of either gaseous or liquid water. The largest value they measured for x was 0.26. Rapid oxidation by adsorbed water produces hydrogen at the gas–solid interface and forms a higher oxide as Pu(IV) cations in PuO_2 are replaced by Pu(V) and an equal number of O^{2-} or OH^- ions in interstitial defect sites (see Section 7.8.5). In moist air, product hydrogen combines with disassociatively adsorbed oxygen to reform water on the surface. A water-catalyzed cycle is propagated as Pu and O_2 are transformed into oxide at the rapid rate characteristic of the metal–water reaction. This change in the composition of the oxide is also accompanied by a dull yellow to a khaki-to-green color change.

(c) Oxidation behavior of plutonium alloys

The overall rate of oxidation is less for alloyed plutonium in the fcc δ phase than it is for unalloyed plutonium (shown in Fig. 7.64) because the lowered stresses upon oxide formation (the δ-phase density is 15.8 g cm^{-3} compared to 19.86 g cm^{-3} for the α phase). Haschke (1999) has also speculated that gallium is not incorporated in the PuO_2 lattice and resides in octahedral sites of the fluorite structure. Consequently, since oxygen diffusion occurs via these sites, he suggested transport of oxygen through the oxide layer may be inhibited. Blank (1977) summarized the work of Raynor and Sakman (1965) and Waber (1980) on oxidation of plutonium δ-phase alloys. Pu–Ga alloys were found to oxidize at a lower rate than unalloyed plutonium at all temperatures in moist air. The oxidation rates were found to be greater in moist argon. However, the protection afforded by alloying was less for the case of moist argon than for moist air. Blank (1977) also summarized oxidation results for Pu–Al alloys. A partial summary, presented in Table 7.24, shows that the addition of aluminum lowers the oxidation rate, but that the behavior depends strongly on temperature and relative humidity. As examples of actual weight gain through oxidation, Blank cites the results of Waber *et al.* (1961): 0.1 mg cm^{-2} for Pu–9 to 12 at.% Al alloys after 500 h at 75°C and 50% relative humidity and 0.5 mg cm^{-2} for Pu–8 at.% Al after 8700 h at 35°C and 20% relative humidity. Blank (1977) also provided a summary of the oxidation behavior of Pu–Fe and other alloys.

(d) Pyrophoricity of plutonium metal in air

Fig. 7.64 also shows that at elevated temperatures, plutonium exhibits an autothermic reaction, igniting spontaneously in air when the temperature reaches 500°C. Studies of pyrophoricity of plutonium by Martz *et al.* (1994) helped to elucidate the role of another oxide of plutonium, namely the cubic (bcc) sesquioxide, Pu_2O_3. The revised view of the plutonium–oxygen interface is shown in Fig. 7.65. Although the dioxide is the one observed when plutonium

Table 7.24 *The relative merit given by the merit ratio (MR) as defined by weight increase of unalloyed α-phase plutonium divided by the weight increase of a δ-phase Pu–Al alloy after the oxidation of the samples by water vapor as compiled by Blank* (1977).

Al content at.%	*T* (°C)	*Relative humidity* (%)	*Time* 12 h	*Time* 50 h	*Time* 1000 h	*Time* 4300 h	*Time* 8700 h	*References*
3.5	30	95			8			Sackman (1960)
3.5	90	95	130					Sackman (1960)
3.5	90	55	50	100	120			Sackman (1960)
3.5	100	0			6			Sackman (1960)
3.0	55	50					~17	Waber (1958)
9	75	50			666			Waber *et al.* (1961)
8	35	20			~19	42.5	51	Waber (1958)

metal is exposed to oxygen or air, there is always a layer of the cubic sesquioxide present at the metal-oxide interface. However, at room temperature, its thickness is small compared to that of the dioxide. The cubic sesquioxide acts as a layer that separates the oxide-rich surface from the plutonium-rich substrate, being simultaneously consumed and formed by competing reactions. The thickness of these various oxides depends upon a variety of factors including temperature and oxygen concentration. At temperatures exceeding 150°C and in oxygen-poor environments, the cubic sesquioxide becomes the predominant phase, appearing as a surface product under oxygen-free environments.

Martz *et al.* (1994) explained the apparent paradox that plutonium metal with low specific surface areas ignites at temperatures above 500°C, whereas metal with large specific surface areas (turnings, chips, and powder) spontaneously ignites in air at temperatures between 150 and 200°C. In such cases, Martz *et al.* concluded that heating metal to 150–200°C in air transforms a large fraction of the surface oxide to cubic sesquioxide. Rapid oxidation of the sesquioxide back to dioxide produces a thermal spike sufficient to heat high-surface-area chips and turnings to the autothermic reaction temperature of 500°C.

(e) Hydrogen- and hydride-catalyzed corrosion

Plutonium reacts readily with hydrogen at rates unprecedented for other metals. It forms an fcc solid solution of PuH_x hydrides with a fluorite structure similar to plutonium oxides (Haschke, 1991; Bartscher, 1996) as discussed in Section 7.8.1 and shown in Fig. 7.72. The hydrogen mole ratio, x, varies from 1.9 to 3.0. As the hydrogen content increases, the hydride exhibits a transition from metallic material near $x = 2$ to a semiconductor near $x = 3$. The electronic structure of the hydride is complex, with electrons apparently being removed from the conduction band and bound as H^- on octahedral sites as the hydrogen concentration is increased in the hydride.

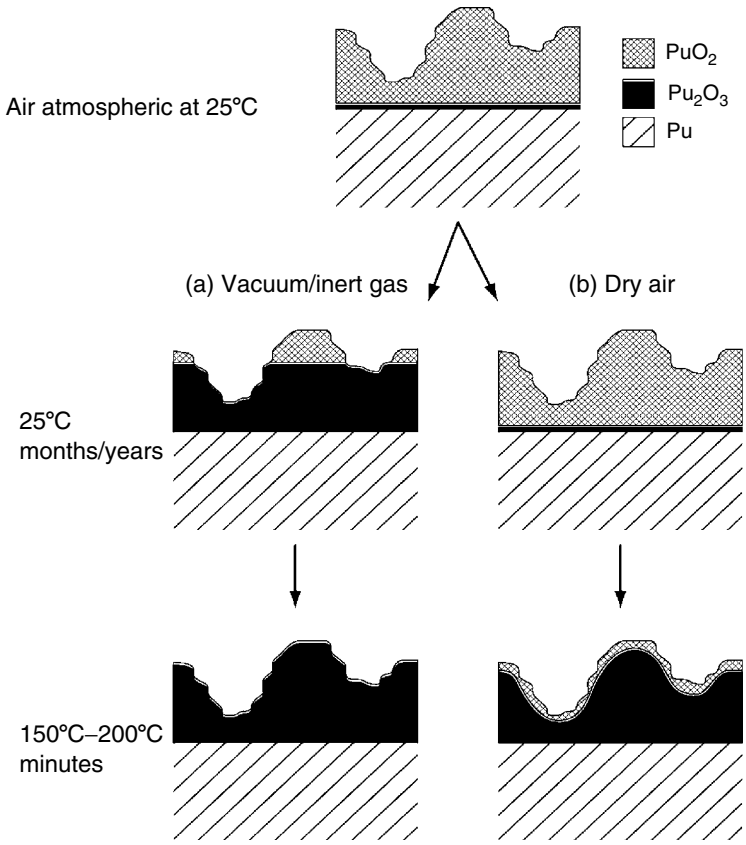

Fig. 7.65 *Evolution of the oxide layer on metallic plutonium. These simplified sketches present the structure of the oxide on Pu. In air, a constant thickness of PuO_2 is present on a thin layer of cubic Pu_2O_3. If this surface is exposed to inert conditions (vacuum or inert gas), the PuO_2 autoreduces to a thicker layer of Pu_2O_3. At elevated temperatures, the rate of the autoreduction reaction increases, increasing the thickness of the internal Pu_2O_3 layer under all conditions. Oxidation of this layer and its subsequent heat evolution is the attributed cause for the pyrophoric behavior of thin films and small particles (Martz* et al., 1994). *In addition, the growth of Pu_2O_3 under inert conditions at elevated temperatures will activate the surface to the hydride reaction, a fact exploited in the hydride–dehydride recovery process for metallic plutonium.*

Reactions of hydrogen on metallic plutonium are complicated by the ever-present layer of plutonium dioxide. Hydrogen gains access to the metal surface only after the dioxide layer is penetrated at cracks or spallation sites, making the nucleation of the hydride reaction heterogeneous. The hydriding rate increases exponentially as nucleation sites grow. Once the entire metal surface is covered with hydride, the reaction occurs very rapidly at rates of 20 cm h^{-1} linear

penetration for H_2 at 1 bar compared to the rate of the oxidation reaction of 20 pm h^{-1} in dry air (10^{11} times faster). Haschke (1991) has suggested that this catastrophic enhancement occurs by one of two mechanisms. First, if PuH_x forms, it catalyzes the dissociation of adsorbed H_2 and promotes transport of atomic hydrogen to the hydride–metal interface. Or alternatively, if cubic Pu_2O_3 is exposed to H_2, then the hydride reaction begins instantaneously because Pu_2O_3 also catalyzes the dissociation of H_2 and becomes the medium for hydrogen transport. In either case, rapid dissociation of adsorbed H_2 results in a dramatic enhancement of the reaction rate. Further, the transport of anions in the fluorite structures of PuH_x or cubic Pu_2O_3 is potentially very rapid because in these anion-deficient fluorite structures both tetrahedral and octahedral sites may be vacant and able to participate in the transport of anions such as hydrogen and oxygen (see Sections 7.8.1 and 7.8.5). Another factor is the high self-diffusivity of oxygen in nonstoichiometric PuO_{2-x}, which increases dramatically from PuO_2 to Pu_2O_3.

If a hydride-coated plutonium surface is exposed to oxygen, it has been proposed that PuH_x will promote a dramatic catalytic enhancement of the corrosion rate (Haschke and Martz, 1998a). In this proposed mechanism, oxygen reacts with the pyrophoric plutonium hydride to produce heat and an oxide layer. The temperature is raised sufficiently that the cubic sesquioxide is preferentially formed. The hydrogen produced at the oxide–hydride interface moves through the PuH_x layer increasing the stoichiometry of the hydride. Excess hydrogen is continuously produced at the oxide–hydride interface and consumed at the hydride–metal interface. Thus, hydrogen is involved in a classic catalytic cycle to enhance the oxidation rate. This hydride-catalyzed reaction continues until all the metal is consumed. The rate for reaction of hydride-coated metal with pure oxygen (Fig. 7.64) is 10^{13} times greater than oxidation rates in dry air. Hydride-coated plutonium also reacts rapidly in air. However, the rate is 100 times slower than that in oxygen, apparently due to additional steps involving reaction or transport of nitrogen in air (Haschke, 1991). These fast reactions generate large amounts of heat (approximately 836.8 kJ mol^{-1} of plutonium), which can produce thermal hazards as well. Of additional concern is the possibility of plutonium nitride formation when the temperature exceeds 200–250°C and hydride is exposed to the nitrogen in air. This reaction results in a consumption of all of the major gases in air, preventing the formation of an inert nitrogen 'blanket' and allowing the reaction to proceed to completion within many storage environments. Hecker and Martz (2001) describe some of the practical consequences of enhanced corrosion problems in the storage of plutonium.

7.7.9 Aging and self-irradiation damage in plutonium

The aging of plutonium and its alloys has received increased attention during the past decade because of interest in extending the lifetimes of plutonium components and in the long-term storage of excess weapons-grade plutonium.

Several reviews of the salient aging issues have been reported by Hecker and Martz (2000, 2001), Wolfer (2000), Martz and Schwartz (2003), and Wirth *et al.* (2001). The complexities of plutonium materials are compounded by changes that occur with age. Phase stability is of concern because the various allotropic phases of plutonium are very close in energy and, hence, sensitive to any changes, including kinetic changes, that can occur with time at temperatures close to ambient. The differences in U.S. and Russian phase diagrams for Pu–Ga (Fig. 7.29) demonstrate that we lack definitive information on some basic characteristics of plutonium alloys such as thermodynamic steady-state phase stability. In addition, the very reactive nature of plutonium just described makes it especially susceptible to surface-induced modifications resulting from different atmospheric environments. If that were not sufficient, the most perplexing change is caused by the radioactive decay of the plutonium nucleus in its various isotopic forms. Moreover, in most practical applications the effects of these three types of aging-induced changes occur simultaneously and in synergy causing significant changes in plutonium and its alloys over time. The phase stability and surface behavior were described in some detail above. We will provide additional details of the salient consequences of self-irradiation damage and transmutation resulting from radioactive decay in plutonium and its alloys.

The two primary consequences of plutonium radioactive decay are the displacement damage in the lattice induced by the self-irradiation, and the transmutation of plutonium into its decay products. Displacement damage can cause changes in lattice parameters, the accumulation of defects and, potentially, void swelling. Transmutation may upset the delicate balance of phase stability and lead to phase changes. One of the decay products, helium, is of particular concern because it can form helium bubbles if self-irradiation occurs at temperatures at which helium is mobile. Schwartz *et al.* (2005) provided an excellent overview of the effects of self-irradiation in plutonium. They identified three self-irradiation-related effects that could cause dimensional changes: lattice damage resulting in an initial transient, helium accumulation, and void swelling.

The unstable plutonium nucleus decays principally by α-particle decay. Two primary energetic nuclear particles are produced by α decay – an α particle and a recoil nucleus. These primary particles are created in much less than a femtosecond (10^{-15} s). The range of the 5 MeV α particle is approximately 10 μm within the crystal lattice. The α particle captures two electrons from the plutonium metal and comes to rest in the lattice as a helium atom. The light α particle loses nearly 99.9% of its energy to electrons, heating the plutonium lattice. Some atomic displacements occur near the end of range, producing ~265 Frenkel pairs (vacancies and self-interstitial atoms). Wolfer (2000) calculated the helium generation to be ~41 atomic ppm per year.

The 86 keV ^{235}U recoil nucleus has a range of ~12 nm and creates roughly 2300 Frenkel pairs. Calculations by Wolfer (2000) showed that there are 3×10^9 α events g^{-1} s^{-1} for a typical ^{239}Pu isotopic mix, resulting in a lattice

displacement rate of roughly 0.1 displacements per atom (dpa) per year. Wolfer (2000) and Wirth *et al.* (2001) used molecular-dynamics simulations showing that in the first 200 ns, 90% of the Frenkel pairs return to their original lattice sites, whereas the other 10% remain as free interstitials and vacancies or interstitial/vacancy clusters. In reactor applications, it was shown that these types of microstructural changes ultimately result in property changes that include void swelling, mechanical hardening, and embrittlement. Wirth *et al.* pointed out that although the damage produced by the α particle and the uranium recoil atom are different, it is the eventual interaction and evolution of these spatially uncorrelated primary defects that may, over time, drive materials evolution and the aging process, thus producing microstructural changes over time scales as long as many decades.

(a) Self-irradiation lattice damage

Studies of self-irradiation lattice damage in plutonium at low temperatures (at which little or no annealing of nonequilibrium defect structures is expected) were reported as early as 1962 by American researchers (Olsen and Elliott, 1962) and British researchers (Lee *et al.*, 1962; Wigley, 1964, 1965), and in 1965 by French researchers (Lallement and Solente, 1967). However, more than 40 years later, we still understand little about the mechanisms of defect migration and agglomeration in plutonium. Few measurements and direct observations of the defect structures in plutonium have been made compared to the vast body of literature that exists for irradiation-induced defect structures in other metals and alloys; see Ehrhart *et al.* (1991) for an excellent review. The early work showed that plutonium undergoes substantial lattice damage as determined by increases in electrical resistivity and by length changes. As shown in Fig. 7.66, the α phase in unalloyed plutonium expands during self-irradiation at 4.2 K. Retained β-phase and retained δ-phase plutonium alloys contract. As discussed below, self-irradiation damage of δ-phase plutonium at room temperature results in a volume expansion. All three phases exhibit increases in electrical resistivity with self-irradiation at this temperature; see Hecker and Martz (2001) for more detailed discussions.

Marples and Hall found that if low-temperature irradiation was allowed to proceed sufficiently long, lattice expansion in the α phase saturated at approximately 10.5 vol %. In the δ-phase alloy, lattice contraction saturated at –15 vol %. Their results on all three phases examined are summarized in Table 7.25. Interestingly, all three phases appear to converge to the same density, 18.4 g cm^{-3}. These results may indicate that all three phases are becoming increasingly disordered, approaching an amorphous state. It would not be surprising to create local amorphous regions as a result of the collision cascades following α-decay events. At sufficiently low temperatures, in the absence of significant defect rearrangement, these regions could eventually consume the entire sample. However, the XRD work done at low temperatures showed that

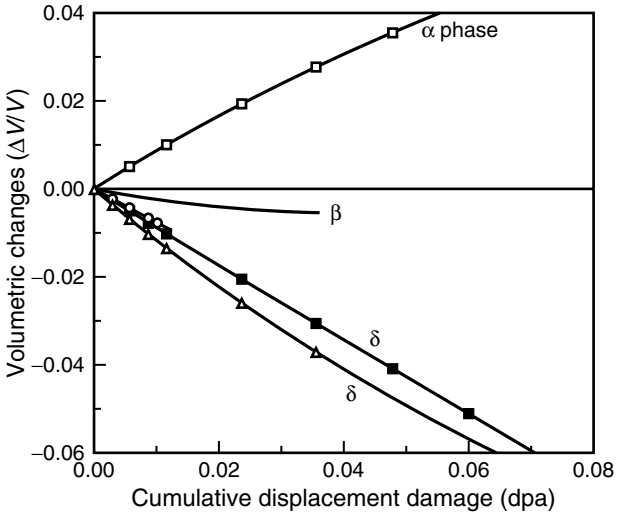

Fig. 7.66 *Volume change vs damage in* dpa (*displacements per atom*) *during self-irradiation of plutonium at* 4.2 K. *The α-Pu data is from Marples* et al. (1970), *as are the data for the δ-phase Pu-*6 at. *% Al alloy* (*solid squares*). *The triangles represent data from Jacquemin and Lallement* (1970) *on a δ-phase Pu-*6 at. *% Al alloy. The β phase was retained by the addition of* 4 at. *% Ti as reported also by Jacquemin and Lallement. Marples* et al. *reported a calculated saturation in volume change of* 10.5% *for the α phase and* –15% *for the δ phase.*

Table 7.25 *Initial and final densities for plutonium self-irradiated at* 4 K (*Marples and Hall,* 1972).

Phase	*Initial density* (g cm^{-3})	*Final density* (g cm^{-3})
α	20.3	18.4
β	18.2	18.4
δ	15.6	17.4
		18.3 after correction for presence of 6 at.% Al

the initial crystal structures were retained, although significant line broadening was observed.

At ambient temperature, damage from self-irradiation of plutonium is partially annealed out by thermally activated recovery. Lattice damage created at low temperatures is also annealed out as the temperature is raised. Some of the early experiments of Wigley (1964, 1965) are summarized by Hecker and Martz (2001). Typical damage recovery (based on electrical resistivity measurements)

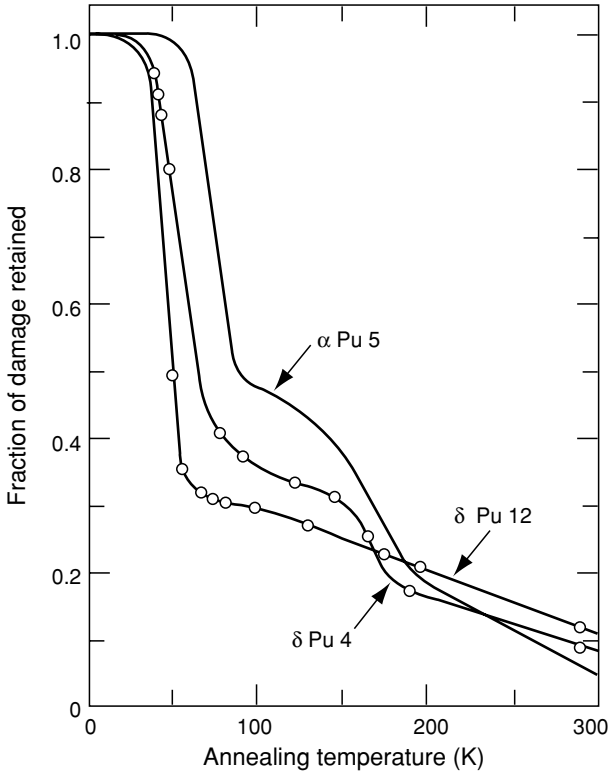

Fig. 7.67 *Damage recovery during isochronal annealing after self-irradiation at* 4.5 K. *δPu*4 *is for an alloy of Pu-*4 at. *% Al with* 920 h *at* 4.5 K. *δPu*12 *is for an alloy of* Pu-12 at. *% Al with* 665 h *at* 4.5 K. *The α-Pu sample, αPu*5, *was self-irradiated for* 640 h *at* 4.5 K (*from Hecker and Martz,* 2001 *based on original data from Wigley,* 1965*; King* et al., 1965).

during isochronal annealing of self-irradiated unalloyed plutonium and δ-phase Pu–Al alloys is shown in Fig. 7.67, based on the work of Wigley (1965) and King *et al.* (1965). Based on comparison to a vast literature of irradiation damage in metals (Ehrhart *et al.*, 1991), Hecker and Martz estimated the following temperatures for the key recovery stages in plutonium alloys: ~18 K for Stage I (recombination and migration of self-interstitials); ~180 K for Stage III (vacancy migration and annihilation); and 410 K for Stage V (thermal dissociation of vacancy and/or interstitial clusters). Unfortunately, the data on plutonium are limited and difficult to interpret quantitatively because of incomplete information about precise isotopic contents, purity levels, prior age, and processing conditions. Wirth *et al.* (2001) reported on recent self-irradiation and isochronal annealing experiments. They found the onset of Stage I to be diffuse and difficult to determine. Their best estimates for the temperatures for the onset

of Stage III and Stage V were 190 K and slightly above 320 K. Hence, the defect mobility in plutonium alloys at ambient temperature is substantial. Although much of the damage is healed at room temperature, some of it remains.

For self-irradiation at ambient temperature, we would then expect lattice damage to compete with recovery resulting from the defect mobility. Chebotarev and Utkina (1975) reported a lattice expansion in δ-phase plutonium alloys. Wolfer (2000) showed that the initial transient results in the formation of dislocation loops that lead to expanded lattice parameters, which tend to saturate within approximately 2 years. Unlike at low temperatures, both the unalloyed α-phase plutonium and alloyed δ-phase plutonium exhibit lattice expansion with age. Ellinger *et al.* (1962a) reported that X-ray samples of typical plutonium in the δ phase (alloyed with 12.8 at.% Al) retained their fcc crystal structure with a 0.1% expansion of the lattice constant (0.3% volume change) after 10 years at ambient temperature. Chebotarev and Utkina (1975) also reported slight lattice expansion in δ-phase Pu–Al alloys, with the expansion increasing with increasing aluminum content. For aluminum contents slightly below 10 at.%, they found an expansion of the lattice parameter of 0.25% after 2.5 years at ambient temperature. They also reported that all changes were recovered after a long-term anneal at 423 K.

Morales *et al.* (2003) confirmed that δ-phase alloys expand at ambient temperature and possibly undergo an orthorhombic distortion at long aging times. In recent TEM studies of aged δ-phase plutonium alloys, Schwartz and coworkers observed nanometer-size helium bubbles (see Wirth *et al.*, 2001; Martz and Schwartz, 2003; Schwartz *et al.*, 2005). These will be discussed in greater detail below.

We report one additional important aspect of self-irradiation damage in plutonium described in recent presentations and abstracts by Russian researchers Gorbunov and Seleznev (2001). They studied unalloyed plutonium consisting mostly of ^{238}Pu, which increased the α-decay damage rate by a factor of 240 over the typical ^{239}Pu. They used thin films to keep the temperature close to room temperature. Starting with a sample of α-phase plutonium, their XRD measurements demonstrated that the sample experienced numerous crystallographic transformations over the period of 1 year (equivalent to 240 years of aging for the typical mix of isotopes in plutonium). Specifically, they claim to find evidence that all six phases of plutonium coexisted at 40 to 50 days of age, and that after roughly 1 year, the sample consisted mostly of the α and δ phases. They suggest that the vacancies and vacancy clusters resulting from the intense self-irradiation affect the delicate balance between bonding and localized 5f electrons and, hence, affect phase stability.

(b) Actinide transmutation products and radiogenic helium

In addition to the lattice damage described above, α decay also results in transmutation products. The decay products for plutonium isotopes and

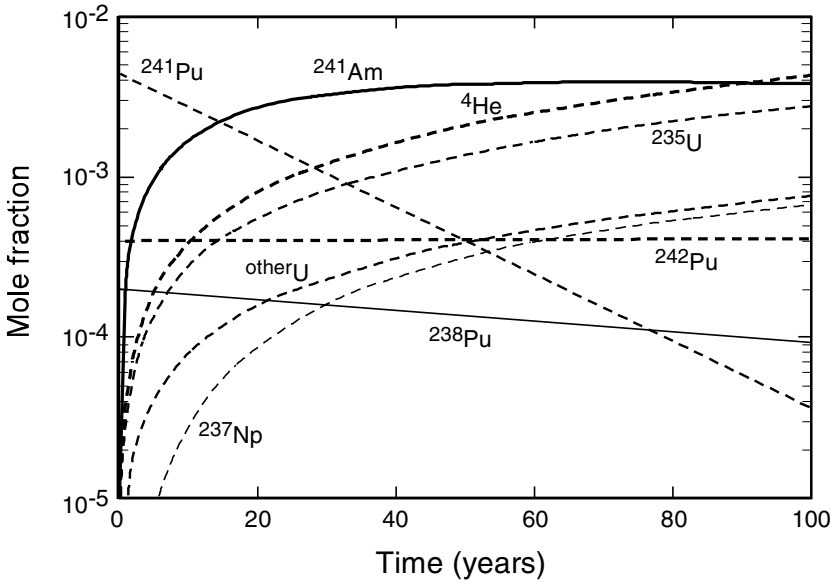

Fig. 7.68 *Transmutation products in typical* ^{239}*Pu metal* (*from Hecker and Martz,* 2001) *as a function of time. For typical* ^{239}*Pu,* 10 years *results in* 1 dpa.

its transmutation products are shown in Fig. 7.68. Helium grows in at the rate of 41.1 atomic ppm per year (based on the assumption made by Wolfer (2000) for typical plutonium). Hence, after 50 years of storage, approximately 2000 ppm helium, 3700 ppm americium, 1700 ppm uranium, and 300 ppm neptunium have grown into plutonium metal. After that length of time, a 1 kg piece of plutonium will contain nearly two-tenths of a liter of helium (measured at standard conditions). Several thousand ppm of americium should help to further stabilize δ-phase alloys. For pure plutonium it is conceivable that the in-growth of americium could stabilize microscopic regions of higher-temperature phases in the monoclinic α phase. However, in both cases, the nonequilibrium conditions that exist immediately following the decay event may further complicate the effects of the transmutation products. Under equilibrium conditions, uranium and neptunium reduce δ-phase stability. As in the case of americium, however, the effect of their presence associated with decay products under the nonequilibrium conditions is not well understood. Our best estimate is that the in-growth of actinides, other than americium, over a time frame of decades should have no major macroscopic effects, but their presence as atomic impurities may influence some microscopic processes. In addition, one must take account of the heat generated during the decay process. For the typical isotopic mixtures discussed above,

the heat is a rather modest 2 W kg^{-1}, making kilogram quantities of plutonium warm to the touch. On the other hand, ^{238}Pu used in radioisotope heat sources is roughly 250 times more radioactive.

The accumulation of radiogenic helium, on the other hand, could potentially affect the properties of plutonium significantly. It is well known that less than 100 ppm of helium in fcc stainless steel can cause swelling or dramatic embrittlement. Once helium atoms are generated in the plutonium lattice, they quickly fill nearby vacancies and diffuse through the lattice as helium-filled vacancies (Howell *et al.*, 1999). Wirth *et al.* (2001) calculated that at relatively high helium generation rates, a critical helium bubble nucleus consists of just two helium atoms and one or two vacancies. Russian researchers (Filin *et al.*, 1989) used angle-resolved positron annihilation to study self-irradiation-induced defects in aged δ-phase Pu–3.6 at.% Ga with 800 ppm helium. They concluded that elementary complexes of helium and vacancies are energetically favorable. Their results showed that pores with radii of 0.4–0.8 nm and 17–23 nm formed at temperatures above 200°C. They concluded that the small pores are probably simple helium-vacancy complexes and the larger pores are complex helium-vacancy clusters, possibly also associated with solute atoms. They observed groups of small bubbles with diameters <1 μm by optical metallography after heating the aged plutonium alloy above 425°C. Using TEM, Zocco and Rohr (1988) observed helium bubbles of 3–7 nm and 10–15 nm in diameter in a 10-year-old δ-phase Pu–Ga alloy after annealing at 400°C. Decades-old plutonium will not only swell substantially after heating to such temperatures, but may also suffer major microstructural void damage under these conditions.

Schwartz and coworkers recently observed nanometer-sized helium bubbles using a Fresnel fringe imaging technique in TEM. Schwartz *et al.* (2005) examined Pu–Ga δ-phase alloys ranging in age from 6 months to 42 years. Their observations revealed that the dominant defects attributable to self-irradiation damage at ambient temperature are nanometer-sized, homogeneously distributed helium bubbles as shown in Fig. 7.69. They found no bubbles in the 6-month-old sample above their resolution limit of 0.7 nm. For samples 16–42 years old, they reported a number density of bubbles in the range of $0.6–2.0 \times 10^{17}$ cm^{-3}, which increases at a steady rate with time. The average diameter of the bubbles in this age range varies from 1.3 to 1.6 nm and is observed to change little with age beyond 16 years. The volume fraction of bubbles increased from roughly 0.01 to 0.03% within the age range of 16–42 years. Based on positron annihilation spectroscopy by Howell and Sterne (personal communications to Schwartz) (Howell and Sterne, 2002), Schwartz *et al.* concluded that helium bubbles containing two to three helium atoms per vacant site must already be present in 6-month old plutonium. Moreover, the characteristic positron lifetime of 180–190 ps remains remarkably constant for

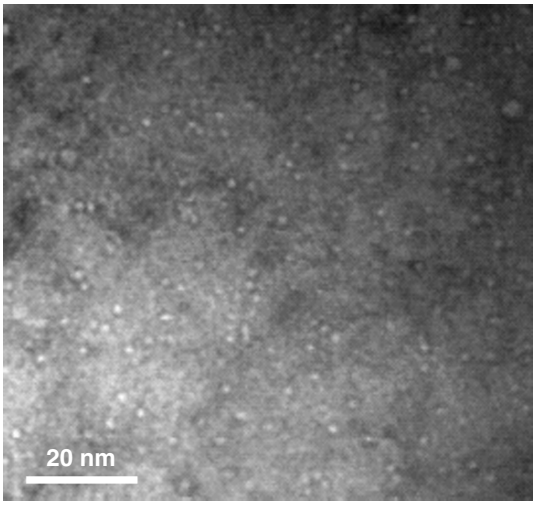

Fig. 7.69 *Transmission electron micrograph of nanometer-scale helium bubbles in a* 30+-year-*old δ-phase Pu*-3.4 at.% *Ga alloy* (*from Martz and Schwartz,* 2003; *Zocco and Schwartz,* 2003; *Schwartz* et al., 2005).

all aged material, implying a constant helium density within the bubbles of 2 to 3 helium atoms per vacant site.

The combination of irradiation-induced lattice damage and the presence of helium can cause void growth and bulk swelling at much lower temperatures without the presence of helium bubbles. Void growth is an obvious potential consequence of vacancy migration and clustering. Sustained void growth requires both the presence of biased defect sinks and the presence of neutral sinks. Wolfer (2000) estimated that for δ-phase plutonium alloys this may vary from 1 to 10 dpa (lifetimes from 10 to 100 years for typical ^{239}Pu). No experimental evidence for void swelling in plutonium has been found to date. In addition, our experience at Los Alamos shows that δ-phase plutonium aged at ambient temperature for 30–40 years retains structural integrity and exhibits no discernable microstructural changes. The influence of aging on the full range of plutonium properties remains to be assessed.

7.8 COMPOUNDS OF PLUTONIUM

From an historical perspective, the early study of plutonium compounds was plagued with difficulties. In addition to the fact that only very small amounts of

plutonium were available for early experimentation, there were also special problems associated with the handling and manipulation due to radioactivity.

The problem of handling very small amounts of plutonium was overcome through the introduction of ultramicroscale experimental methods (Cunningham, 1949; Cefola, 1958; Fried *et al.*, 1958), and characterization of small quantities of compounds was masterfully performed by X-ray crystallography by Zachariasen (1954b), who made a major contributions to the structural chemistry of plutonium, almost entirely with Debye–Scherrer X-ray films of polycrystalline samples.

In more modern times, the available quantities of plutonium are large enough that the study of plutonium compounds can be conducted on the milligram and gram scale, and occasionally even on the multigram or kilogram scale. In the latter case, however, special safeguards to prevent criticality have to be taken (cf. Table 7.2) (Clayton, 1965; Thomas, 1969; Hunt and Boss, 1971; Hunt and Rothe, 1974; Paxton and Pruvost, 1987).

The evolution of modern techniques for handling plutonium has taken advantage of specialized high-efficiency particulate air (HEPA) filtered hoods, gloved boxes, and inert atmosphere dry boxes (Maraman *et al.*, 1975; Louwrier and Richter, 1976; Oi, 1995) that make it possible to work with plutonium with confidence, and the health and safety records of laboratories engaged in research with plutonium are very good. It cannot be denied, however, that laboratory work with plutonium and other actinide elements requires more than ordinary foresight and laboratory experience for the investigator. Laboratory safety guides (Peddicord *et al.*, 1998; *Health Physics Manual of Good Practices for Plutonium Facilities*, 1988) have been published that describe handling techniques and operational procedures in plutonium laboratories.

A considerable body of information on the compounds of plutonium has been amassed over the past 65 years, and the sheer volume of data is a testimony to the intense interest in the chemistry of plutonium. Several thorough monographs, conference proceedings, and reviews of the chemistry of plutonium before 1970 are available, and provide fascinating and often personal accounts of the many individual achievements that defined much of our current understanding in this field (Katzin, 1944; Thomas, 1944; Harvey *et al.*, 1947; Seaborg *et al.*, 1949b; Connick, 1954; Cunningham, 1954; Hindman, 1954; Seaborg, 1958; Grison *et al.*, 1960; Taube, 1964; Kay and Waldron, 1967; Miner, 1970; Blank and Lindner, 1976). Since 1970 there have been a number of comprehensive reviews (Keller, 1971; Cleveland, 1979; Wick, 1980; Carnall and Choppin, 1983; Hoffman, 2000) and finally, there are a series of modern reviews concerning a wide range of more specific topics such as chemistry in marine environments (Choppin and Wong, 1998), colloids in groundwater (Kim, 1991, 1994), bioinorganic chemistry in blood (Taylor, 1998), environmental behavior (Guillaumont and Adloff, 1992; Graf, 1994; Silva and Nitsche, 1995), behavior in carbonate media (Clark *et al.*, 1995), behavior in alkaline media (Shilov, 1998; Shilov and Yusov, 2002), actinide–lanthanide separations (Nash, 1993),

synthetic methodologies for compounds (Meyer and Morss, 1991; Morss and Fuger, 1992), and a comprehensive compendium of XRD data for plutonium compounds (Roof, 1989).

7.8.1 Plutonium hydrides and deuterides

Plutonium hydrides were first observed in 1944 (Johns, 1944) when Johns found that elemental plutonium would react rapidly with H_2 to form a continuous solid solution of varying stoichiometry, PuH_x, with $1.9 \leq x \leq 3$ according to the equation:

$$Pu(s) + x/2H_2(g) \rightarrow PuH_x(s) \tag{7.29}$$

The reaction proceeds at a range of H_2 pressures. Heating is often required to initiate and sustain the process (Haschke, 1991). The chemical reaction is facile and reversible, making hydride–dehydride cycles a convenient route for preparing powdered plutonium metal samples. It is important to emphasize that stoichiometric compounds such as PuH_2 or PuH_3 do not exist as distinct phases apart from the PuH_x solid solution, though many authors describe reactions in terms of the stoichiometry PuH_2 or PuH_3 to facilitate the balancing of equations (Haschke, 1991).

Recent interest in plutonium hydrides has emerged due to considerations of long-term storage and safe handling of plutonium metal and compounds (Haschke and Allen, 2001) and the application of the plutonium–hydrogen reaction for pyrochemical processing of excess weapons plutonium (Flamm *et al.*, 1998; Mashirev *et al.*, 2001). Several excellent reviews have appeared on the synthesis and kinetics (Haschke, 1991), the thermodynamics (Flotow *et al.*, 1984; Lemire *et al.*, 2001), and the physicochemical characteristics of plutonium and other actinide hydrides (Flotow *et al.*, 1984; Ward, 1985; Ward *et al.*, 1992; Ward and Haschke, 1994; Bartscher, 1996; Haschke and Haire, 2000).

(a) Preparation and reactivity

The only practical method for preparing plutonium hydrides is the direct reaction of plutonium metal with gaseous H_2. In general, there are no good procedures for purification of PuH_x once it is formed, so purity is generally controlled through the use of high-purity metal and gaseous reagents. Plutonium metal must be cleaned to remove surface oxide and other impurities, and this is most conveniently conducted inside a secondary positive pressure chamber within an inert atmosphere gloved box to maintain proper H_2 partial pressures and temperatures. A Sieverts apparatus, and pressure–volume–temperature (PVT) relationships are commonly employed to determine the exact Pu–H stoichiometry, which is crucial because of the stoichiometric variability in the PuH_x product ($1.9 \leq x \leq 3$). Even when the stoichiometry is carefully controlled, differences in preparation or storage can result in differences in homogeneity,

morphology, and even crystal structure (see below). Desorption of H_2 is a common problem encountered in working with plutonium hydrides, even under ambient conditions.

Plutonium hydrides are hard, typically black metallic-appearing materials that show different behaviors based on particle size and composition. The color ranges from silver near $x = 2$ to black at higher values of x. Small particles can be extremely reactive towards O_2 and H_2O, and powders near composition PuH_2 can be pyrophoric or ignite spontaneously in air (Flotow *et al.*, 1984; Haschke *et al.*, 1987; Haschke, 1991; Haschke and Allen, 2001). The hydrides can also react with N_2 and CO_2, although these reactions are quite slow. Hence all manipulations and storage should be carried out under inert atmospheres. An excellent and thorough discussion of the practical considerations necessary for preparing plutonium hydrides has appeared (Haschke, 1991).

The kinetics of the Pu–H_2 reaction have been well studied, and the highly complex reaction proceeds through induction, acceleration, parabolic, linear, and terminal stages. Detailed discussions of reaction rates and the role of catalysis are available (Haschke, 1991; Haschke and Allen, 2001). Moreover, hydride stoichiometry and composition changes induced by the addition or removal of H_2 from PuH_x are important in determining plutonium hydride reactivity.

(b) Stoichiometry and phase relationships

The PuH_x phase relationships are remarkably complex. A broad range of nonstoichiometric phases is exhibited that extends from $PuH_{1.9}$ to near stoichiometric PuH_3. Equilibrium data indicate that the hydride composition near the gas–surface interface may also vary from $PuH_{2.3}$ to $PuH_{2.7}$ while the composition at the plutonium metal–plutonium hydride interface remains close to $PuH_{1.95}$ (Ward and Haschke, 1994). The resulting stoichiometry and phase can differ between studies conducted at low temperatures and low pressures, or at high temperatures and high pressures. As a result, two notional phase diagrams, one for slow reaction at low pressure and one for rapid reaction at high pressure, have been proposed and discussed in detail by Haschke and coworkers (Haschke *et al.*, 1987) and by Bartscher (1996). These complex stoichiometry and phase relationships are best understood from consideration of the solid-state structures of the PuH_x system.

The phase relationships in the plutonium–hydrogen system are shown in the phase diagrams of Fig. 7.70 (slow reaction at low pressure) and Fig. 7.71 (rapid reaction at high pressure) (Flotow *et al.*, 1984). Hydrogen dissolves in solid and liquid plutonium (melting point 640°C) to form plutonium metal that is essentially saturated in hydrogen. This is denoted as PuH_s in the figures. Hydrogen-saturated plutonium (PuH_s) coexists with the cubic PuH_x solid solution up to composition $x \approx 1.9$. Between composition $PuH_{1.9}$ and PuH_3, a continuous solid solution forms. The exact value of x is highly dependent upon the

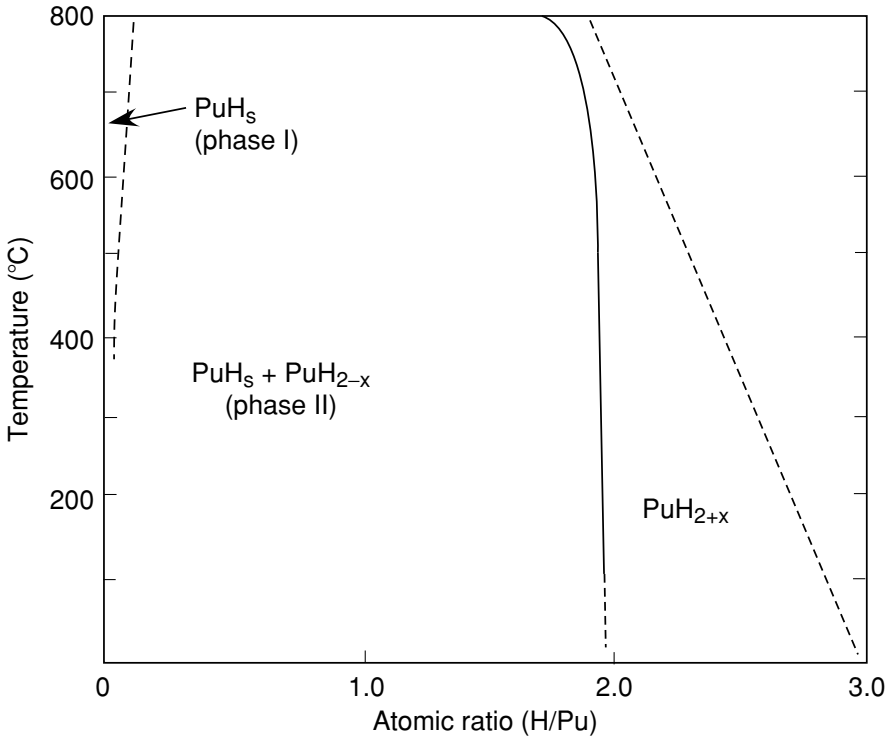

Fig. 7.70 *A plutonium–hydrogen phase diagram depicting equilibrium relationships based on Wick* (1980) *and Flotow* et al. (1984).

conditions of formation (Haschke *et al.*, 1987). The variable composition arises because the hydride reacts reversibly with H_2 between 25 and 500°C and pressures less than 1 bar (Johns, 1944; Haschke *et al.*, 1987). Extrapolation of 25°C data suggests that at 1 bar H_2 pressure, a composition $PuH_{2.93}$ is attained, while at 25 bar H_2, composition PuH_3 is attained. These observations are consistent with the phase diagram for slow reaction at low pressure shown in Fig. 7.70. An alternative phase diagram based on data generated at high pressures and rapid reaction is shown in Fig. 7.71 (Haschke *et al.*, 1987). This diagram is based on measurement of partial molar free energy isotherms that suggest the existence of five hydride phases (indicated as II–VI in Fig. 7.71) in addition to PuH_s (phase I). These data suggest the coexistence of a cubic $PuH_{2.70}$ and a hexagonal $PuH_{2.88}$ in the III + IV two-phase region. Hexagonal phase IV is thought to have a structure similar to that of disordered tysonite (LaF_3), while phase V is thought to be similar to that of orthorhombic YF_3 with a composition near $PuH_{2.95}$. The properties of phase VI are unknown. For a detailed discussion of the plutonium–hydrogen phase equilibria, the reader is

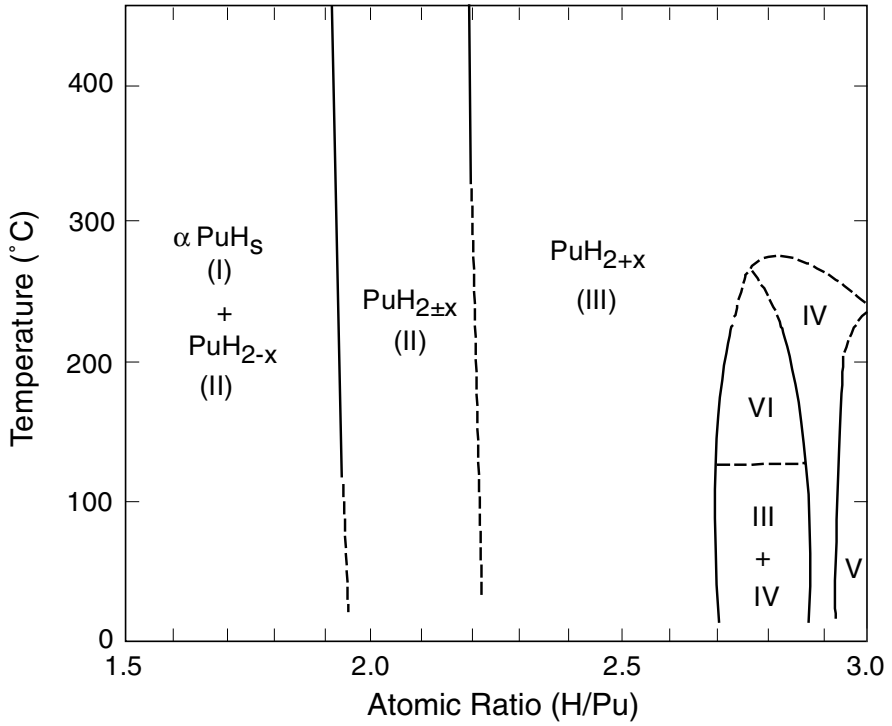

Fig. 7.71 *A plutonium–hydrogen phase diagram for rapid high-pressure reaction conditions, based on Haschke* et al. (1987).

referred to reviews by Flotow *et al.* (1984), Bartscher (1996), and Haschke and Haire (2000).

(c) Solid-state structures

The solid-state crystal structures of plutonium hydrides possess many similarities to those of the lanthanide hydrides, and Haschke and coworkers have suggested a similarity and analogy to the lanthanide trifluoride system (Haschke *et al.*, 1987). A summary of crystallographic data for plutonium hydrides is given in Table 7.26. Plutonium hydride forms a cubic fluorite-type phase over the composition range of PuH_x, where $1.9 < x < 2.7$, and a lanthanum trifluoride-related hexagonal phase beyond $x = 2.9$. The cubic fluorite-type structure based upon CaF_2 is illustrated in Fig. 7.72. As the composition of the fcc PuH_x varies between $1.9 < x < 2.7$, the lattice parameter decreases from 5.360(1) Å at $x = 1.9$ to 5.34(1) Å at $x = 2.7$. Within this fcc arrangement of plutonium metal cations are tetrahedral (t) and octahedral (o) interstices that may be occupied by the H^- ion. For an idealized PuH_2 structure with lattice

Table 7.26 *Crystal structure data for plutonium hydrides.*

Formula	*Symmetry*	*Space group*	*Lattice parameter* a_0 (Å)	c_0 (Å)	*Formula units per cell*	*Calculated density* (g cm^{-3})	*References*
$PuH_{2.0}$	fcc	F*m*3*m*	5.359(1)		4	10.40	Ellinger (1961)
$PuH_{2.51}$[a]	fcc	F*m*3*m*	5.342(4)		4		Muromura *et al.* (1972)
PuH_3	hexagonal	$P6_3/mmc$ or $P\bar{3}c1$	3.78(1)[b] 6.55(1)	6.76(1)	2	9.608	Ellinger (1961)

[a] The values of x between 2.15 and 2.70 are represented by the equation a_0 (Å) = 5.4337 – 0.003575 (H/Pu) (Bartscher, 1996).
[b] Hexagonal LaF_3 (tysonite) has space group $P\bar{3}c1$, which is the same as observed in hexagonal lanthanide hydrides, and is the likely space group for PuH_3. To transform from $P6_3/mmc$ to $P\bar{3}c1$, one would use $a_0 = a'\sqrt{3}$, or $a_0 = 6.55$ (Å) for PuH_3.

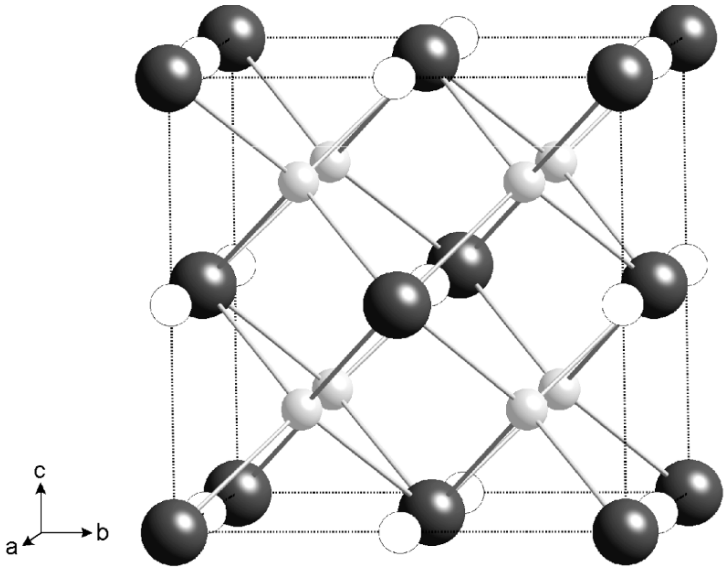

Fig. 7.72 *The cubic* (*Fm*3*m*) *fluorite-like solid-state structure of* PuH_x *showing the fcc arrangement of Pu atoms* (*black*) *with tetrahedral H atoms* (*gray*). *Octahedral vacancies are indicated with white circles, and the unit cell is indicated as a dashed line. For lattice parameter,* $a = 5.336$ Å, *Pu–H* = 2.31 Å, *Pu–Pu* = 3.77 Å, *and Pu-vacancy* = 2.67 Å (*Ellinger,* 1961).

parameter $a = 5.34$ Å, there is eight-fold (cubic) coordination of each plutonium atom by 8 hydrogen atoms, and four-fold tetrahedral (t) coordination of hydrogen atoms by 4 plutonium atoms with a Pu–H distance of 2.31 Å. The six-fold octahedral (o) sites in this model are vacant. Compositions of PuH_x, where $x < 2$, are likely formed by the creation of hydrogen atom vacancies in the normal t sites. At low temperatures, low pressures, and slow reaction times, an extended metastable cubic solid solution can exist all the way up to the PuH_3 phase boundary, and a simplistic model (see discussion below) would have additional hydrogen atoms randomly filling the o sites, with a concomitant decrease in lattice parameter.

The simple model of random occupancy of o sites in the fluorite lattice by additional hydrogen atoms when H–Pu is greater than two is overly simplistic. Since hydrogen mobility can occur at fairly low temperatures, the hydrogen atom can be disordered between t and o sites in the lattice (Muromura *et al.*, 1972; Flotow *et al.*, 1984; Haschke *et al.*, 1987; Ward and Haschke, 1994). Bartscher and coworkers employed elastic neutron scattering on deuterated samples of composition $PuD_{2.25}$, $PuD_{2.33}$, and $PuD_{2.65}$ and demonstrated a progressive depletion of t sites and occupation of o sites relative to PuD_2 (Bartscher *et al.*, 1985). Deuterium atoms in the o sites are displaced by 0.4 Å in the [111] direction (body diagonal) toward the t sites, in analogy with that observed in lanthanide systems (Ward and Haschke, 1994). In lanthanides, this low-temperature ordering of octahedral hydrogen atoms appears with a concomitant doubling of the c-axis of the unit cell. The 'freezing in' of the hydrogen atoms in this structure can be observed by NMR and by heat-capacity measurements (see below) (Cinader *et al.*, 1976; Flotow *et al.*, 1984). Haschke has proposed a conceptual model based on vacancy clusters for interpreting the relative t- and o-site occupancy factors in this structural model (Haschke *et al.*, 1987).

The structural behavior of the Pu–H system near the PuH_3 phase boundary is complex, and this region remains to be fully characterized. At low temperatures and for compositions above $PuH_{2.7}$, a cubic (fcc) form has been identified (Fig. 7.72). Under the appropriate conditions of rapid (high-temperature and high-pressure) reaction, both hexagonal and orthorhombic phases can also be formed near the PuH_3 boundary. In the range $PuH_{2.9}$–$PuH_{3.0}$, there is a hexagonal, nonstoichiometric phase in which the proposed structure is based on a disordered LaF_3 (tysonite) hexagonal structure ($P\bar{3}c1$), and an orthorhombic phase thought to be based on the YF_3 structure (Haschke *et al.*, 1987). The hexagonal phase was originally reported by Ellinger and assigned space group $P6_3/mmc$ (Ellinger, 1961), but more recent studies of the related lanthanide hydrides and fluorides reveal that trigonal space group $P\bar{3}c1$ is more likely the correct choice (Cheetham *et al.*, 1976). According to Haschke, the two-phase regions separating cubic (fcc) and hexagonal hydrides close in on themselves at 200–400°C, and only the cubic phases exist at higher temperatures (Haschke *et al.*, 1987). For more detailed discussion of these phase relationships, the reader is referred to the recent review by Haschke and Haire (2000).

(d) Physical properties and electronic structure

Trends in electronic properties as a function of x in PuH_x systems are crucial for understanding the nature of chemical bonding in plutonium hydrides. All data are consistent with the general description of cubic plutonium hydrides consisting of a localized 5f shell with a trivalent Pu(III) ion, best formulated as $Pu^{3+}(H^-)_x(e^-)_{3-x}$. Plutonium is trivalent for all compositions and exhibits 'rare-earth like' behavior. For nominal composition PuH_2, XPS shows a 4f intensity at the same 4f binding energy as a Pu(III) standard (Willis *et al.*, 1985). Neutron scattering data display an ordered magnetic moment of $0.71\mu_B$ per plutonium atom, which is the same as the trivalent free ion value (Bartscher *et al.*, 1985). Electrical conductivity decreases with increasing x, indicating that electrons are progressively removed from the conduction band and bound as H^- as the value of x increases (Willis *et al.*, 1985). Moreover, as the conductivity decreases, the hydride color changes from silver to black. Valence band XPS recorded on a (nominal composition) PuH_2 film reveal a large 5f peak consistent with a localized 5f shell, while core-level XPS on the same sample shows $4f^{5/2}$ and $4f^{7/2}$ peaks characteristic of Pu(III) (Ward *et al.*, 1992). Recent XPS data on a thin film of nominal composition PuH_3 shows the disappearance of the 5f peak (Gouder, 2005). Cinader and coworkers studied ^1H NMR spectroscopy on cubic PuH_x (where $x = 1.78$, 2.35, 2.65, and 2.78) between 77 and 300°C (Cinader *et al.*, 1976). Evaluation of line shapes, Knight shifts, and relaxation times are consistent with paramagnetic phases with localized 5f moments. Different line shapes and shifts were observed for t and o sites, and they were able to observe the 'freeze in' of the hydrogen atoms at low temperature. Enthalpies and entropies of formation for the extended cubic phase composition are given in Table 7.27.

(e) Applications

The hydriding reaction may be used to prepare plutonium metal powder. Compact pieces of plutonium metal can be converted to one of the hydrides and then powdered under an H_2 atmosphere by a magnet hammer. Subsequent

Table 7.27 *Enthalpies and entropies of formation for cubic plutonium hydrides at* 550 K[a].

Product	$\Delta_f H$ (kJ mol^{-1})	$\Delta_f S$ (J K^{-1} mol^{-1})
$PuH_{1.90}$	-155.6 ± 10.9	-138.5 ± 10.9
$PuH_{2.50}$	-190.4 ± 5.0	-175.7 ± 8.4
$PuH_{3.00}$[b]	-205.9 ± 4.6	-211.7 ± 11.7
$PuD_{1.90}$	-141.8 ± 1.7	-125.1 ± 3.8
$PuD_{2.50}$	-174.5 ± 4.2	-160.2 ± 7.5
$PuD_{3.00}$[b]	-189.1 ± 11.7	-188.3 ± 8.4

[a] Data from (Ward and Haschke, 1994).
[b] Based on extrapolated partial molar Gibbs energy data.

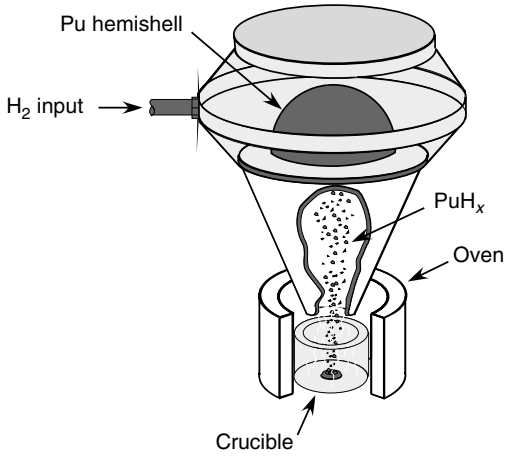

Fig. 7.73 *A schematic representation of the hydride–dehydride or hydride-oxidation chamber for conversion of surplus weapons plutonium. A weapon hemishell sits in the upper chamber, PuH_x spalls off and falls into the lower crucible, where it can be converted to the metal, a nitride or oxide* (*Toevs,* 1997).

decomposition *in vacuo* at more than 400°C leaves finely divided, highly reactive plutonium powder (Stiffler and Curtis, 1960). Both the U.S. and Russian technology for disassembly and conversion of excess plutonium from nuclear weapons employs a hydride–dehydride, or hydride–oxidation process for conversion into an unclassified form that can be examined by inspectors from other nations (Cremers *et al.*, 1995; Toevs, 1997; Nelson, 1998; Mashirev *et al.*, 2001). The U.S. process uses continuous H_2 recycle where the hydride falls into a crucible that is heated, driving off H_2 gas, leaving molten plutonium in the crucible. The H_2 refluxes to the top of the chamber, where it removes additional plutonium from the component. A schematic representation of the reaction chamber employed in this process is shown in Fig. 7.73. For conversion to an oxide, the crucible is not heated, and either O_2 is admitted and the hydride burned to release H_2 and leave an oxide powder, or N_2 is used and burned to a nitride powder. The nitride can then be converted to the oxide by burning with O_2. The three-step process of converting the hydride to the nitride and then the oxide avoids having an H_2–O_2 atmosphere in a glove box (Toevs, 1997). The hydride–dehydride approach to weapons conversion avoids the generation of large volumes of liquid waste from wet chemical methods.

7.8.2 Plutonium borides

Plutonium borides form at stoichiometric compositions PuB_2, PuB_4, PuB_6, PuB_{12}, and PuB_{66}, and at a very restricted solid solution of less than 0.5 at.% Pu in β-rhombohedral boron. These five compounds have high melting points,

and with the exception of the preparation and identification of the compounds, very little experimental work is available. Recent detailed reviews describing the plutonium–boron system have appeared (Potter, 1991; Rogl and Potter, 1997).

Plutonium borides were first reported in 1960 (McDonald and Stuart, 1960), when the crystal structures of 'PuB,' PuB_2, PuB_4, and PuB_6 were described. Additional studies of the plutonium boron phase relationships were reported shortly thereafter (Skavdahl, 1963; Skavdahl and Chikalla, 1964; Skavdahl *et al.*, 1964; Weber *et al.*, 1964). Careful structural investigations employing XRD and metallography demonstrated that cubic samples of 'PuB' were contaminated with cubic PuN, and that 'PuB' was not actually a real phase in the Pu–B system (Eick, 1965; Chipaux *et al.*, 1989). Two additional compounds, plutonium dodecaboride, PuB_{12}, and the hectoboride, PuB_{66} were also discovered (Eick, 1965). The hectoboride was originally reported as having composition PuB_{100} (Eick, 1965), but based on analogy with rare-earth elements, which show a YB_{66}-type structure (Kasper, 1976), Rogl and Potter (1997) suggest that PuB_{66} represents a more-likely composition. Using the similarities between rare-earth and actinide boride systems, Rogl and Potter have provided a cautious assessment of the plutonium–boron phase diagram, shown in Fig. 7.74 (Rogl and Potter, 1997).

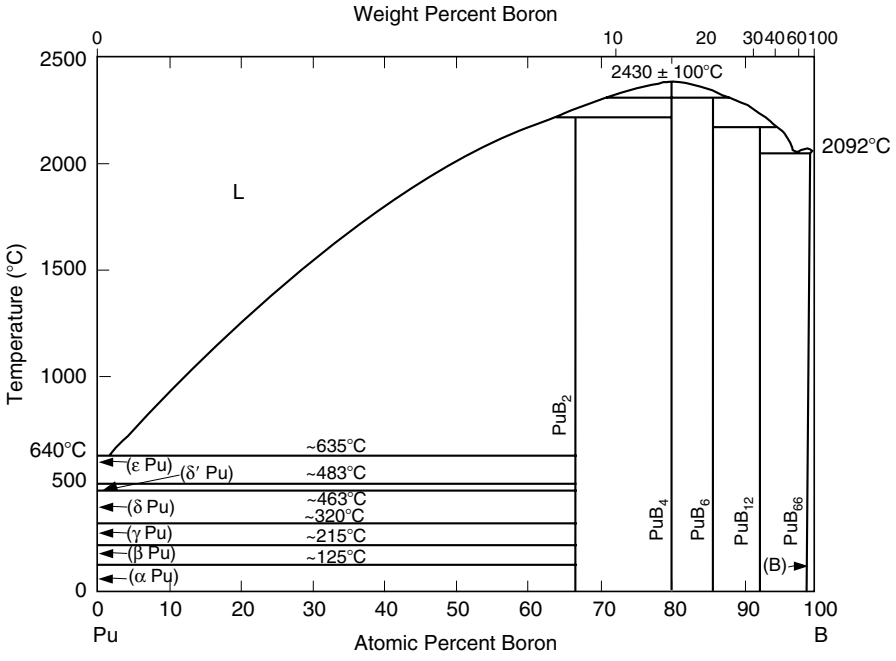

Fig. 7.74 *The plutonium–boron phase diagram* (*redrawn from Rogl and Potter,* 1997).

(a) Preparation

Plutonium borides can be prepared by a variety of methods: heating mixtures of pressed powders of elemental plutonium and boron under vacuum between 900 and 1200°C (McDonald and Stuart, 1960; Weber *et al.*, 1964), arc-melting pure plutonium with crystalline boron under a purified argon atmosphere followed by heat treatment (Eick, 1965), reaction of plutonium hydride with elemental boron at 900°C (Chipaux *et al.*, 1988, 1990), or reduction of PuO_2 by elemental boron and carbon (Skavdahl, 1963; Skavdahl and Chikalla, 1964; Skavdahl *et al.*, 1964; Larroque *et al.*, 1986). All of these reactions are carried out at high temperature (800–1500°C) under Ar or *in vacuo*. A comprehensive listing of preparative methods has been reported (Rogl and Potter, 1997). In view of the recent advances in the low-temperature synthesis of highly refractory materials (Rice, 1983; Wynne and Rice, 1984), and a possible application of actinide borides as an alternative storage form for actinide elements (Lupinetti *et al.*, 2002), it seems likely that this area will grow in interest and importance over the coming decades.

(b) Solid-state structures

The solid-state structures of plutonium borides (as in most metal borides) are dominated by B–B bonding, and the structures are made up of three-dimensional boron atom networks or clusters in which the plutonium atoms occupy otherwise vacant sites (Greenwood and Earnshaw, 1997). The B–B distances in all the plutonium borides are within the same range as those found in elemental boron and other boride complexes, and span 1.73–1.92 Å. The basic structural units in actinide borides, as in all metal borides, are readily described in terms of the B–B bonding configuration, followed by the actinide atom coordination (Potter, 1991; Greenwood and Earnshaw, 1997). Boron bonding units can be conveniently described as belonging to B_2-sp^2, B_6-octahedral, or B_{12}-cubeoctahedral boron atom cluster configurations as shown schematically in **1**, **2**, and **3** below (Potter, 1991; Greenwood and Earnshaw, 1997). To date, the structural characterization of plutonium borides has been performed exclusively by X-ray powder diffraction techniques, and a summary of crystallographic parameters of plutonium borides is given in Table 7.28. No single crystal diffraction studies have been reported.

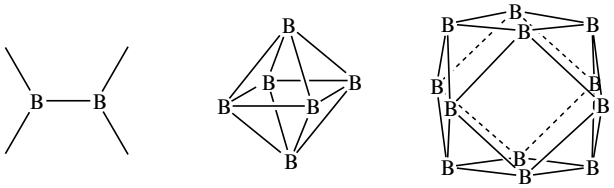

B_2-sp^2 **B_6** **B_{12}**

1 **2** **3**

Table 7.28 *X-ray crystallographic data for plutonium borides.*

Compound	*Structure type*	*Symmetry*	*Space group*	*Unit cell dimensions* (Å)	*Formula units per cell*	*X-ray density* ($g\ cm^{-3}$)[a]	*References*
PuB_2	AlB_2	hexagonal	P6/*mmm*	$a = 3.1857(2)$ $c = 3.9485(4)$	1	12.470	Eick (1965)
PuB_4	ThB_4	tetragonal	P4/*mbm*	$a = 7.1018(3)$ $c = 4.0028(1)$	4	9.285	Eick (1965)
PuB_6	CaB_6	cubic	P$m\bar{3}m$	$a = 4.1134(3)$	1	7.249	Eick (1965)
PuB_{12}	UB_{12}	cubic	F$m\bar{3}m$	$a = 7.4843(3)$	4	5.842	Eick (1965)
PuB_{66} ('PuB_{100}')	YB_{66}	cubic	P$n\bar{3}n$	$a = 23.43(4)3$	24	2.485	Eick (1965)

[a] Calculated for ^{239}Pu.

Plutonium diboride (PuB_2) exhibits the hexagonal AlB_2 structure in space group *P6/mmm* containing one formula unit per unit cell (McDonald and Stuart, 1960; Eick, 1965). The AlB_2 structure is by far the most common phase displayed by metal borides (Spear, 1976). The solid-state structure (Fig. 7.75) consists of graphite-like hexagonal layers of catenated boron atoms with a close B–B contact of 1.84 Å. These hexagonal boron layers are separated by a hexagonal close packed (hcp) layer of plutonium atoms, positioned so that the centroid of a hexagonal ring of boron atoms lies directly above and below each plutonium atom. The closest Pu–B contact in this structure is 2.70 Å, with a closest Pu–Pu separation of 3.19 Å.

Plutonium tetraboride (PuB_4) has a tetragonal lattice (space group *P4/mbm*) formed by chains of B_6 octahedra along the *c*-axis and linked in the lateral direction by pairs of B_2 units in the *ab* plane (McDonald and Stuart, 1960;

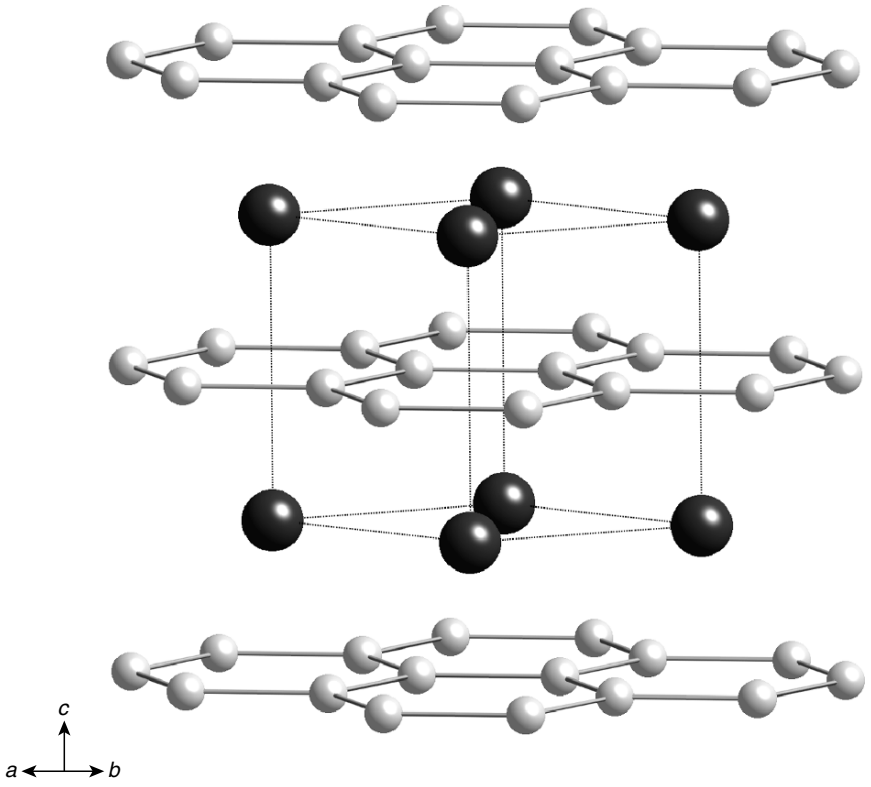

Fig. 7.75 *The solid-state structure of PuB_2 shown perpendicular to the c-axis, and emphasizing the hexagonal graphite-like layers of boron atoms (gray) separated by layers of plutonium atoms (black). The unit cell is indicated as dashed lines.*

Eick, 1965). This forms a three-dimensional network with channels along the *c*-axis that are filled by plutonium atoms. B–B contacts span a narrow range between 1.70 and 1.76 Å, with the shortest Pu–Pu contact of 3.66 Å between chains, and a longer contact of 4.00 Å along the chains. The closest Pu–B contact is 2.72 Å between Pu atoms and B_6 units. This structure type is shown in Fig. 7.76.

Plutonium hexaboride (PuB_6) has a cubic CsCl-type lattice (*Pm3m*) in which the plutonium atom and B_6 octahedra occupy the metal and halogen sites, respectively, as shown in Fig. 7.77(a) (McDonald and Stuart, 1960; Eick, 1965). In this structure, the B_6 octahedra are linked together in all six orthogonal directions. Within this framework, plutonium atoms occupy the corner

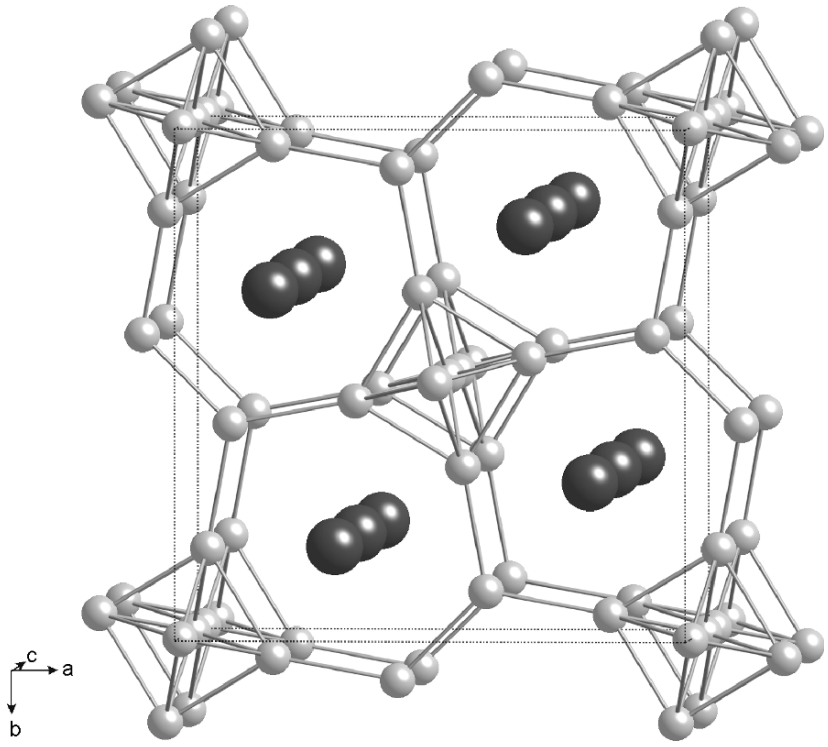

Fig. 7.76 *The solid-state structure of PuB_4 shown looking down the c-axis and emphasizing the open channels filled with plutonium ions* (*black*). *Boron atoms* (*gray*) *comprise octahedral B_6 units linked by bridging B_2 units within the ab plane. The unit cell is indicated as dashed lines.*

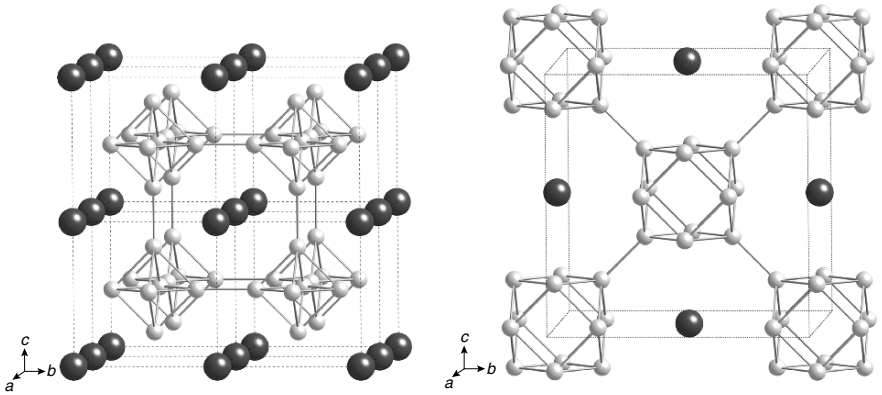

Fig. 7.77 *The solid-state structure of PuB_6 (a), and PuB_{12} (b). PuB_6 has alternating plutonium (black) and B_6 octahedra (gray) in a 'CsCl-type' lattice. PuB_{12} has alternating plutonium (black) and B_{12} cubeoctahedra (gray) in a 'NaCl-type' lattice.*

positions of an interpenetrating cubic sublattice. B–B contacts within the B_6 unit, and linking adjoining B_6 units, are 1.70 Å, Pu–B contacts are 3.03 Å, and the Pu–Pu nonbonding contact is 4.11Å. Plutonium dodecaboride (PuB_{12}) has a cubic NaCl-type fcc lattice (*Fm3m*) in which the plutonium atoms and B_{12} cubeoctahedral clusters occupy the metal and halogen sites, respectively, as shown in Fig. 7.77(b) (Eick, 1965). B–B distances within the B_{12} unit are 1.76 Å, Pu–B distances between plutonium and B_{12} units are 2.79 Å, and the Pu–Pu nonbonding contact is 5.29 Å.

Plutonium hectoboride was originally formulated as 'PuB_{100}' (Eick, 1965), but this phase is most likely of composition PuB_{66}, belonging to a family of metal hectoborides based on the structure of YB_{66} (Potter, 1991; Rogl and Potter, 1997). This structure is exceedingly complicated, and the reader is referred to Richards and Kasper for a detailed description (Richards and Kasper, 1969). A simplified description is that of a well-known 13-icosahedron unit (156 boron atoms) found in β-rhombohedral boron, comprised of 12 B_{12} icosahedra grouped around a 13th central B_{12} unit. The yttrium atoms in YB_{66} are distributed in channels and coordinate to the cage boron atoms.

(c) Properties

Very little is known about the physicochemical properties of plutonium borides. It seems well established that PuB_4 and PuB_{66} are the only congruently melting plutonium borides (Rogl and Potter, 1997). Magnetic susceptibility measurements of PuB_2 and magnetic susceptibility and Mössbauer measurements on solid solutions of $Np_{1-x}Pu_xB_2$ and NpB_2 suggest a tetravalent oxidation state

for neptunium, and presumably plutonium in the diborides. PuB_2 was found to be a weak paramagnet, and the data were fit by a modified Curie–Weiss law with and effective paramagnetic moment of $\mu^*_{eff} = 0.32\mu_B$ and $\theta_p = -30$ K. Renormalization led to $\mu_{eff} = 0.75\mu_B$ (Chipaux *et al.*, 1990). Smith and Fisk (1982) reported little temperature dependence in magnetic susceptibility of PuB_6.

7.8.3 Plutonium carbides and silicides

(a) The plutonium–carbon system

Four compounds are known in the plutonium–carbon system: Pu_3C_2, PuC_{1-x}, Pu_2C_3, and PuC_2. All these compounds undergo peritectic decomposition at high temperatures. The Pu–C phase diagram according to Green and Leary (1970), and assessed by Kassner and Peterson (1995), is shown in Fig. 7.78. Pu_3C_2 decomposes between 558 (Rosen *et al.*, 1963) and 575°C (Mulford *et al.*, 1960) to ϵ-Pu + PuC_{1-x} and may be unstable at lower temperatures

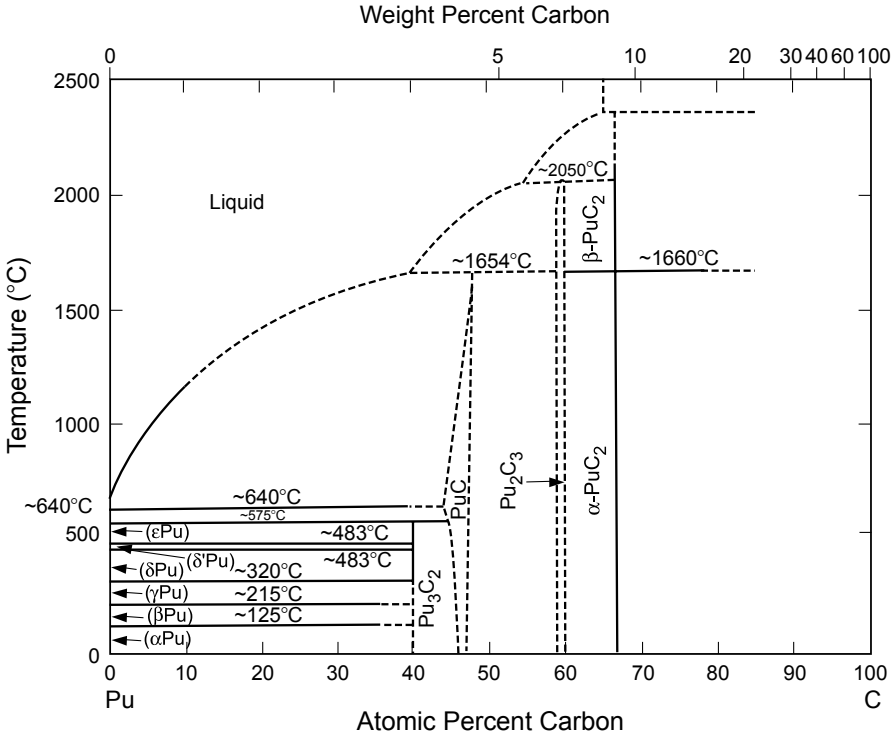

Fig. 7.78 *The plutonium–carbon phase diagram (redrawn from Green and Leary,* 1970*; Kassner and Peterson,* 1995*). See text for discussion of stability of PuC_2 below* 1660°C.

(Pascard, 1962). Plutonium monocarbide 'PuC' exists only as substoichiometric PuC_{1-x}, with a stoichiometry ranging from $PuC_{0.6}$ to $PuC_{0.92}$. At 1654°C, PuC_{1-x} decomposes into Pu_2C_3 plus liquid. Plutonium sesquicarbide Pu_2C_3 occurs in a rather narrow phase region around 60 at.% C. It decomposes at 2050°C into the high-temperature cubic phase PuC_2 and liquid (Mulford *et al.*, 1960). Plutonium dicarbide PuC_2 is only stable between 1660 ± 10 and 2230 ± 20°C (Reavis and Leary, 1970). The polymorphic transformation of PuC_2 below 1660°C to give the metastable tetragonal phase was added to the phase diagram in Fig. 7.78 by Kassner and Peterson (1995).

An extensive literature on plutonium carbides exists because actinide carbides have been considered as advanced nuclear fuels. Topical reviews can be found on general behavior (Storms, 1964, 1967; Ogard and Leary, 1970; Potter, 1975), thermodynamics (Holley, 1974; Holley *et al.*, 1984), thermal expansion and density (Andrew and Latimer, 1975), defect and transport properties (Matzke, 1984), and use as nuclear fuel (Russell, 1964; Andrew and Latimer, 1975; Herbst and Matthews, 1982; Handa and Suzuki, 1984).

(*i*) *Preparation*

Quite a few different preparation methods have been used to synthesize plutonium carbides. Carbides of plutonium can be formed by reaction between plutonium metal, plutonium hydrides, or plutonium oxides with elemental carbon at high temperature using furnace or arc-melting techniques (Drummond *et al.*, 1957; Ogard *et al.*, 1962; Pascard, 1962; Kruger, 1963; Chackraburtty and Jayadevan, 1965; Ogard and Leary, 1970). Plutonium oxide reductions using carbon can leave oxygen impurities in the products, and this is particularly true for the cubic monocarbides PuC_{1-x}. The products depend strongly on the temperature of reaction and reaction time. For example, PuC_{1-x} can be prepared by sintering or arc-melting a plutonium carbon mixture at 1000°C for 5 h, by direct reaction of PuO_2 with elemental carbon between 800 and 1350°C, by sintering $PuH_{2.7}$ with carbon in an inert atmosphere between 880 and 1650°C, or by reaction of PuH_2 with Pu_2C_3 at 650–750°C. The sesquicarbide can be obtained by reaction of PuO_2 with carbon under an argon atmosphere between 1250 and 1450°C at 6 h, 1350°C for 2 h or 1300–1400°C under vacuum. Pu_2C_3 can also be obtained by reaction of plutonium hydride with propane at 650–750°C.

(*ii*) *Crystal structures*

The crystal structures of all plutonium carbides, with the exception of Pu_3C_2 have been determined, and crystallographic data are summarized in Table 7.29. The lattice constants depend on the composition and the history of the individual sample. Plutonium monocarbide 'PuC' exists only as substoichiometric PuC_{1-x}, and adopts the cubic NaCl structure with defects in the carbon

Table 7.29 *X-ray crystallographic data for plutonium carbides.*

Compound	*Symmetry*	*Space group*	*Lattice parameters*			*Formula units per cell*	*Calculated density* (g cm^{-3})	*References*
			a_0 (Å)	b_0 (Å)	c_0 (Å)			
PuC_{1-x}	fcc	F*m*3*m*	4.9582(3) (C-poor)			4	13.6	Mulford *et al.* (1960)
			4.9737(3) (C-rich)					Mulford *et al.* (1960)
Pu_2C_3	bcc	I$\bar{4}$3*d*	8.1258(3) (C-poor)			8	12.70	Mulford *et al.* (1960)
			8.1317(3) (C-rich)					Mulford *et al.* (1960)
PuC_2	tetragonal	I4/*mmm*	3.63	3.63	6.094	2	10.88	Chackraburtty and Jayadevan (1965)

sublattice (Zachariasen, 1949c; Mulford *et al.*, 1960). As the carbon content increases, all the carbide carbon atoms are replaced by acetylide C_2 units adopting a stoichiometry $Pu_4(C_2)_3$ (equivalent to Pu_2C_3) and PuC_2. Pu_2C_3 is cubic with 12 C_2 groups in the unit cell, with each plutonium atom bonded to nine carbon atoms, three at 2.48 Å, three at 2.51 Å, and three at 2.84 Å (Zachariasen, 1952). This structure is illustrated in Fig. 7.79, where only the shortest set of three Pu–C bonds are indicated. Due to the difficulty in accurately locating carbon atoms in the presence of the larger plutonium atoms by XRD, the carbon atoms were placed in assumed locations with a C–C single bond distance of 1.54 Å. Neutron diffraction studies on the isostructural U_2C_3 revealed a much shorter C–C distance of 1.295 Å (Austin, 1959), which is considerably lengthened relative to C_2 unit in acetylene at 1.20 Å.

Plutonium dicarbide, PuC_2 is a high-temperature compound that is not stable below ~1750°C (Mulford *et al.*, 1960) and decomposes to Pu_2C_3 and carbon. High temperature XRD revealed an fcc structure at 1710°C with a lattice parameter $a_0 = 5.70(1)$ Å (Harper *et al.*, 1968) which is consistent with

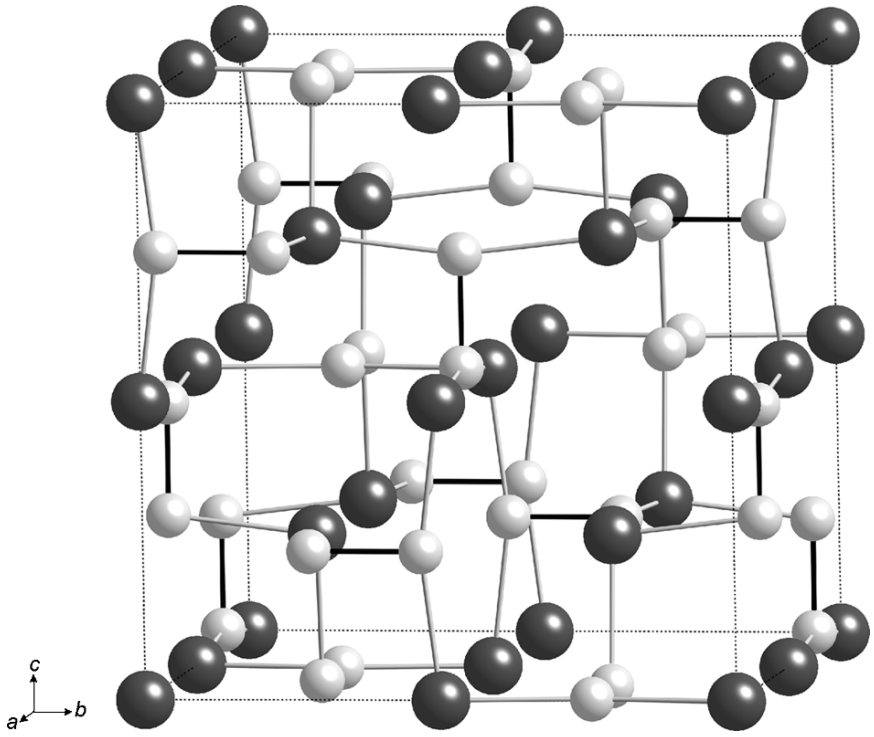

Fig. 7.79 *The solid-state structure of Pu_2C_3 shown looking down the a-axis. Plutonium atoms are black and carbon atoms are gray. The unit cell is indicated as dashed lines. The bold lines between C atoms indicates the* 12 C_2 *groups in the unit cell* (*Zachariasen,* 1952).

the CaC_2 structure that has a NaCl arrangement of Ca atoms and C_2 units (Wells, 1984). A room-temperature structure of what must be considered metastable PuC_2 was found to contain a tetragonal cell, probably due to martensitic transformation on quenching fcc PuC_2 to room temperature (Chackraburtty and Jayadevan, 1965). The tetragonal structure of PuC_2 and its similarity to the NaCl structural unit is shown in Fig. 7.80. For tetragonal PuC_2, the short Pu–C distance is found to be 2.48 Å with Pu–Pu = 3.63 and 3.98 Å (Chackraburtty and Jayadevan, 1965). As in the case of Pu_2C_3, the carbon atom positions are not accurately determined, but a neutron diffraction study on the isostructural tetragonal UC_2 revealed a C–C distance of 1.34 Å (Austin, 1959).

(*iii*) *Chemical properties*

The chemical properties of the plutonium carbides have been studied in some detail (Cleveland, 1979; Wick, 1980). Plutonium monocarbide oxidizes in air at temperatures as low as 200–300°C. It ignites at 400°C in an O_2 atmosphere (Drummond *et al.*, 1957). Compact PuC_{1-x}, kept in air at room temperature, did not show any sign of reaction after 2 months. However, PuC_{1-x} powder was found to be reactive, and sometimes pyrophoric (Ogard *et al.*, 1962). With N_2, PuC_{1-x} reacts more slowly than UC. A PuC_{1-x} sample, kept at 0.5 atm N_2, contains 1 ppm N_2 after 12 h at 200°C and 16 ppm after 12 h at 500°C. If heated

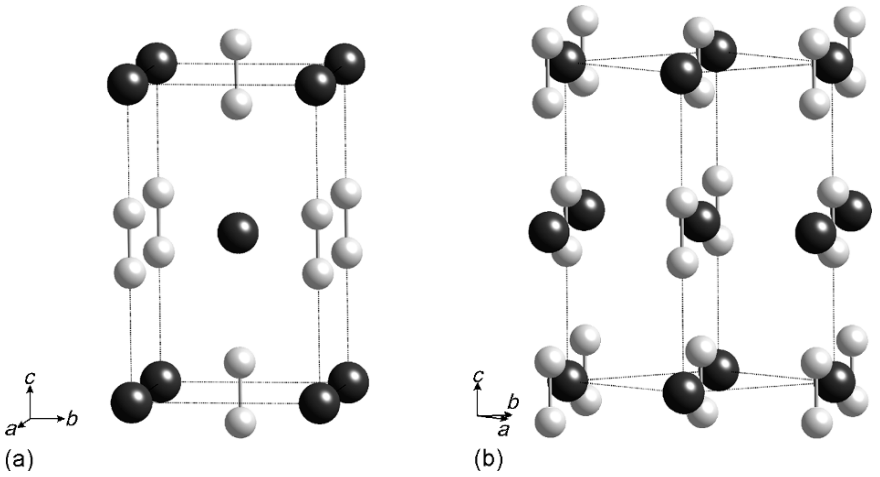

Fig. 7.80 (*a*) *The metastable tetragonal structure of* PuC_2 *shown looking perpendicular to the c-axis, and emphasizing the discrete* C_2 *units within the structure. Plutonium atoms are black and carbon atoms are gray.* (*b*) *The same structure rotated by* 45° *and emphasizing the relationship to the cubic NaCl structure with alternating Pu and* C_2 *units. At high temperature of* 1710°C, $a = b = c = 5.70(1)$ Å.

to 1400°C, the PuC_{1-x} reacts more rapidly to PuN and Pu_2C_3 (Lorenzelli *et al.*, 1966). Plutonium sesquicarbide, Pu_2C_3, shows chemical behavior similar to the monocarbide. It is slightly more stable to oxidation at higher temperatures (Drummond *et al.*, 1957). If heated to 1000°C in H_2, Pu_2C_3 is reduced to $PuC_{0.85}$ (Russell, 1964). PuC_{1-x} reacts with hot water to form $Pu(OH)_3$ and a mixture of H_2 and hydrocarbons. Pu_2C_3 appears to be more stable to hydrolysis in boiling water, but less stable to atmospheric hydrolysis (Drummond *et al.*, 1957).

All the plutonium carbides dissolve in HNO_3–HF mixtures (Storms, 1967). With oxidizing acids, CO_2 is formed. By the dissolution of lower carbides, carbon may be liberated along with hydrocarbons (Storms, 1967) along with organic acids such as mellitic and oxalic acids (Bokelund and Glatz, 1984).

(*iv*) *Thermodynamic properties*

Because of the importance of the plutonium carbides as potential high-temperature reactor fuels, the mechanical, thermal, electrical, magnetic, and thermodynamic properties of these compounds have been determined. For details about these properties and for additional references to the literature, the reader is referred to Holley *et al.* (1984), who reviewed the literature in the 1980s. The 2001 evaluation of plutonium thermodynamic data by the Nuclear Energy Agency (NEA) concludes that little significant thermodynamic information has been published since that time (Lemire *et al.*, 2001) but offers some reassessment of earlier data and provides recommended values for key thermodynamic constants. These are given in Table 7.30.

Monatomic plutonium is the only species that evaporates on heating from Pu–C phases. The equilibria in the solids have been inferred from vapor-pressure measurements (Mulford *et al.*, 1963; Olson and Mulford, 1967; Campbell *et al.*, 1970; Holley *et al.*, 1984). A general survey of the thermal decomposition behavior observed in the plutonium–carbon system has been given by Storms (1967). Specific-heat measurements of plutonium carbides have been reported by numerous authors and reviewed by Holley *et al.* (1984). The NEA review recommends the following temperature dependences (Lemire *et al.*, 2001):

Table 7.30 *Thermodynamic parameters for plutonium carbides.* (*Lemire* et al., 2001).

Compound	$\Delta_f G^\circ_{298}$ (kJ mol^{-1})	$\Delta_f H^\circ_{298}$ (kJ mol^{-1})	S°_{298} (J K^{-1} mol^{-1})	$C^\circ_{p^{298}}$ (J K^{-1} mol^{-1})
$PuC_{0.84}$	-49.8 ± 8.0	-45.2 ± 8.0	74.8 ± 2.1	47.1 ± 1.0
Pu_2C_3	-156.5 ± 16.7	-149.4 ± 16.7	150.0 ± 2.9	114.0 ± 0.4
Pu_3C_2	-123.5 ± 30.0	-113 ± 30	210.0 ± 50	136.8 ± 2.5

$PuC_{0.84}$ ($298.15 \leq T \leq 1875$ K)

$$C_p^o = 71.5910 - 5.95042 \times 10^{-2}T + 4.94346 \times 10^{-5}T^2 - 9.9320 \times 10^5 T^{-2}\text{JK}^{-1}\text{mol}^{-1} \quad (7.30)$$

Pu_2C_3 ($298.15 \leq T \leq 2285$ K)

$$C_p^o = 156.000 - 7.9726 \times 10^{-2}T + 7.04170 \times 10^{-5}T^2 - 2.1757 \times 10^6 T^{-2}\text{JK}^{-1}\text{mol}^{-1} \quad (7.31)$$

Pu_3C_2 ($298.15 \leq T \leq 850$ K)

$$C_p^o = 120.67 + 4.686 \times 10^{-2}T + 1.9456 \times 10^5 T^{-2}\text{JK}^{-1}\text{mol}^{-1} \quad (7.32)$$

(*v*) *Ternary phases*

Several ternary plutonium carbides have been prepared. Of particular importance are the phases formed in the systems Pu–U–C and Pu–Th–C, which may be used in high-temperature reactors and thorium breeders, respectively. The Pu–U–C ternary phase diagram has been reported by Mardon and Potter (1970) and by Rosen *et al.* (1963, 1964). In this system, compounds M_3C_2, MC_{1-x}, M_2C_3, and MC_2 are all observed, where M = (U, Pu), in a wide range of compositions. The Pu–Th–C system has been studied by Reavis and Leary (1970), who reported a partial-phase diagram, and by Dalton *et al.* (1967) and Dalton and Griffin (1964).

A few ternary plutonium carbide phases with transition elements have been prepared by arc melting from the components and have been characterized by their XRD data. These compounds are compiled in Table 7.31. An attempt to estimate ternary phase diagrams for a number of ternary plutonium carbide systems was reported by Holleck (1975). A few mixed carbonitrides, carbide oxides, and carbide hydrides, all of them nonstoichiometric, have been prepared.

(b) The plutonium–silicon system

Five compounds are known in the plutonium–silicon system: Pu_5Si_3, Pu_3Si_2, PuSi, Pu_3Si_5, and $PuSi_2$, melting at 1377, 1441, 1576, 1646, and 1638°C, respectively. The phase diagram determined by Land *et al.* (1965b) and redrawn by Kassner and Peterson (1995) is shown in Fig. 7.81. A recent XRD study by Boulet and coworkers found no new compounds other than the five listed above and confirms the phase diagram (Boulet *et al.*, 2003).

The literature of plutonium silicides is relatively sparse, but there are a few detailed reports on exchange reactions and enthalpies of formation (Krikorian and Hagerty, 1990), physical properties (Taylor, 1966), magnetic properties (Boulet *et al.*, 2003), and the phase diagram (Land *et al.*, 1965b); and an excellent overall review (Potter, 1975).

Table 7.31 *X-ray crystallographic data for selected plutonium ternary carbide phases.*

Compound	*Structure type*	*Space group*	*Lattice parameters*			*Formula units per cell*	*Calculated density* (g cm^{-3})	*References*
			a_0 (Å)	b_0 (Å)	c_0 (Å)			
$PuWC_2$	orthorhombic	P*nma*	5.621(3)	3.245(2)	10.896(7)	4	14.93	Ugajin and Abe (1973)
$PuRh_3C$	cubic	P*m3m*	4.098			1	13.50	Haines and Potter (1975)
$PuRu_3C$	cubic	P*m3m*	4.124			1	13.12	Haines and Potter (1975)

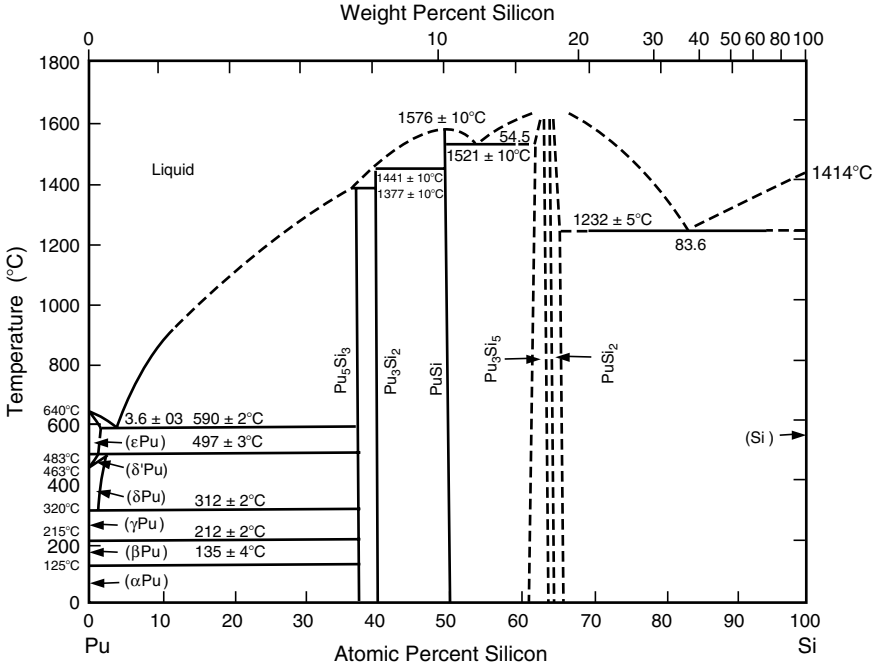

Fig. 7.81 *The plutonium–silicon phase diagram from Land* et al. (1965*b*) *and redrawn from Kassner and Peterson* (1995).

(*i*) *Preparation*

The preparation of plutonium–silicon phases is best carried out by reduction *in vacuo* of plutonium trifluoride with elemental silicon at temperatures above 1200°C in a BeO crucible (Runnalls, 1958):

$$4PuF_3 + (3 + 4x)Si \rightarrow 4PuSi_x + 3SiF_4 \qquad (7.33)$$

Volatile SiF_4 is pumped off, and the plutonium silicide remains. The silicides may also be prepared by arc melting of silicon with plutonium metal or plutonium hydride in an argon atmosphere (Pardue *et al.*, 1964b; Land *et al.*, 1965b; Krikorian and Hagerty, 1990), by reduction of PuO_2 with Si or SiC *in vacuo* at 1400°C (Pardue *et al.*, 1964b), and by fluidized-bed reduction of PuO_2 in the presence of SiO_2 with silane (Fletcher *et al.*, 1967).

(*ii*) *Crystal structures*

The crystal structures of all plutonium silicides have been determined. The basic crystallographic data are listed in Table 7.32. Silicon, like boron, is more electropositive than carbon; thus silicides are more closely related structurally to the borides than the carbides. With increasing silicon content, there is an

Table 7.32 *X-ray crystallographic data for plutonium silicides.*

Compound	*Structure type*	*Space group*	*Lattice parameters*			*Formula units per cell*	*Calculated density* ($g\ cm^{-3}$)	*References*
			a_0 (Å)	b_0 (Å)	c_0 (Å)			
Pu_5Si_3	W_5Si_3	I4/*mcm*	11.409(3)		5.448(2)	2	11.98	Cromer *et al.* (1964)
			11.407(5)		5.444(3)	2		Land *et al.* (1965b)
			11.4035(8)		5.448(3)	2		Boulet *et al.* (2003)
Pu_3Si_2	U_3Si_2	P4/*mbm*	7.483(2)		4.048(2)	2	11.33	Land *et al.* (1965b)
			7.5061(3)		4.0642(3)	2		Boulet *et al.* (2003)
PuSi	FeB	P*nma*	7.933(3)	3.847(1)	5.727(5)	4	10.15	Land *et al.* (1965b)
			7.9360(1)	3.8510(1)	5.7336(1)	4		Boulet *et al.* (2003)
Pu_3Si_5	AlB_2	P6/*mmm*	3.875(4)		4.102(7)	0.5	8.96	Land *et al.* (1965b)
($PuSi_{2-x}$)			3.884(3)		4.082(3)	0.5		Runnalls and Boucher (1955)
			3.8793(6)		4.0860(8)	0.5		Boulet *et al.* (2003)
$PuSi_2$	$ThSi_2$	I4/*amd*	3.967(1)		13.72(3)	4	9.08	Ellinger (1961)
			3.98(1)		13.58(5)	4		Zachariasen (1949b)
			3.9707(3)		13.6809(5)	4		Boulet *et al.* (2003)

increasing tendency to catenate into isolated Si_2 units, or into chains, layers or three-dimensional networks of silicon atoms. Plutonium silicides adopt examples of all these structure types.

The plutonium-rich compound Pu_5Si_3 adopts the tetragonal W_5Si_3 structure, and this structural unit is shown in Fig. 7.82 (Cromer *et al.*, 1964). In this structure, there is a silicon chain composed of columns of alternating $SiPu_8$ square antiprisms with Pu–Si = 3.025 Å. The linear silicon chain runs parallel to the *c*-axis with a Si–Si distance of 2.72 Å. Interspersed between the square antiprisms is another chain of edge-shared $PuSi_4$ tetrahedra that also runs parallel to the *c*-axis, with Pu–Pu = 2.72 Å. In the linear plutonium chain, each plutonium atom in the $PuSi_4$ tetrahedra shows a Pu–Si distance of 2.89 Å. The silicon atoms in the $PuSi_4$ tetrahedra bridge to the plutonium atoms in the $SiPu_8$ antiprisms with a Si–Pu distance of 3.01 Å. These bridges are omitted

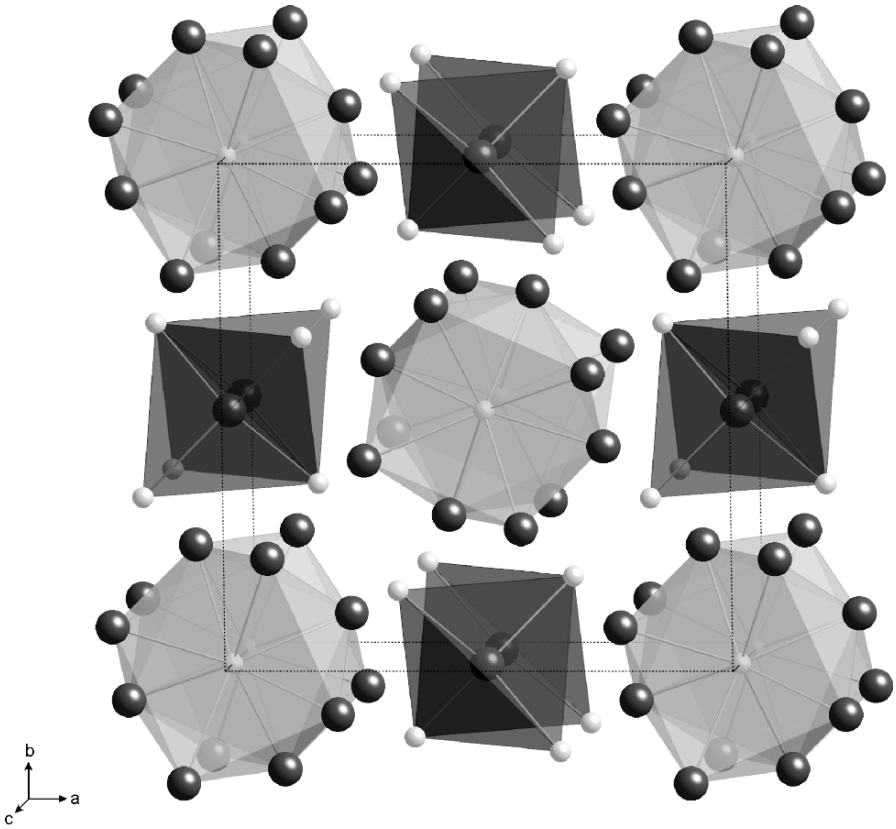

Fig. 7.82 *A polyhedral representation of the solid-state structure of Pu_5Si_3 shown looking down the c-axis, and emphasizing the alternating columns of $SiPu_8$ antiprisms and $PuSi_4$ tetrahedra within the structure. Plutonium atoms are black and silicon atoms are gray.*

from Fig. 7.82 for clarity. Pu_3Si_2 adopts the U_3Si_2 structure, and the basic structural unit is shown in Fig. 7.83. This structure contains a network of Si_2 pairs that are perpendicular to the four-fold axis with Si–Si = 2.35 Å, identical to the Si–Si distance observed in elementary silicon. The plutonium atoms form a puckered cage with Pu–Pu distances of 3.41 Å. The Pu–Si distances range from 2.99 to 3.03 Å.

Plutonium monosilicide is isostructural with ThSi and USi, adopting the FeB structure with infinite one-dimensional zig-zag chains of silicon atoms (Si–Si = 2.35 Å) (Land *et al.*, 1965b). Each silicon atom in the chain is also surrounded by six plutonium atoms at the apices of a trigonal prism with Pu–Si distances spanning the range 2.95–3.03 Å. The PuSi structure is shown in Fig. 7.84. There are four Pu–Pu distances of 3.62 Å, and two Pu–Pu distances of 3.73 Å.

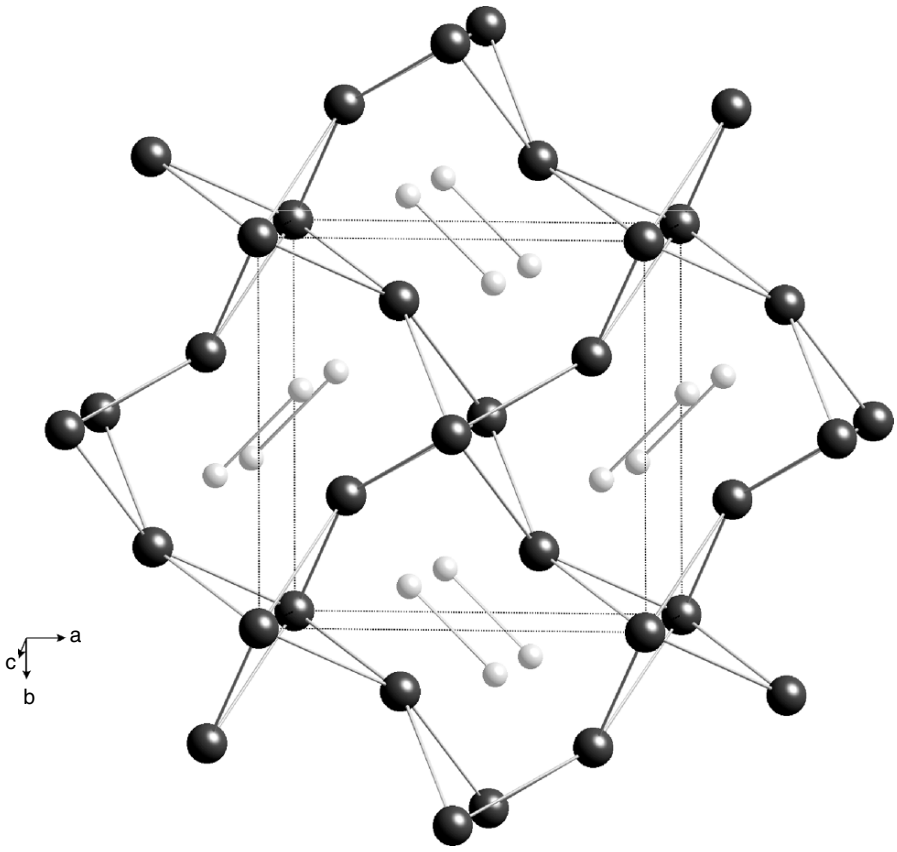

Fig. 7.83 *The solid-state structure of Pu_3Si_2 shown looking down the c-axis, and emphasizing the discrete Si_2 units within the structure. Plutonium atoms are black and silicon atoms are gray.*

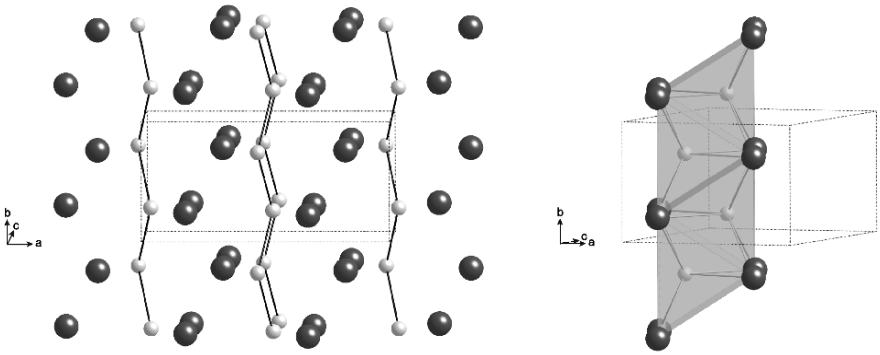

Fig. 7.84 (*left*) *The solid-state structure of PuSi shown looking down the c-axis, and emphasizing the zig-zag chains of Si atoms that run perpendicular to the c-axis. Plutonium atoms are black and silicon atoms are gray.* (*right*) *The same structure rotated by* 45° *and emphasizing the trigonal prismatic* $SiPu_6$ *coordination polyhedra.*

The disilicides form two different structural types that are best considered as defect structures of $PuSi_{2-x}$. There is a hexagonal form of nominal formula Pu_3Si_5 (Runnalls and Boucher, 1955; Ellinger, 1961; Boulet *et al.*, 2003), that adopts the hexagonal AlB_2 structure (discussed for PuB_2, and shown in Fig. 7.75), but the solid is silicon deficient, with vacancies in the silicon sublattice. In this structure there are hexagonal (graphitic) layers of silicon atoms (Si–Si = 2.23 Å) with plutonium atoms interleaved between them (see Fig. 7.75). There is also a tetragonal form that adopts the three-dimensional $ThSi_2$ network structure as shown in Fig. 7.85 (Zachariasen, 1949a,b). In this structure, the silicon atoms form an open, three-coordinated, three-dimensional network. The Si–Si bond lengths are 2.35 and 2.29 Å, which are slightly shorter than that observed in elementary silicon. In the large spaces in this network are the plutonium atoms, each bonded to 12 silicon neighbors with Pu–Si = 3.02 Å. The next nearest neighbors to silicon are six plutonium atoms at this same distance.

(*iii*) *Properties*

The plutonium silicides are hard, brittle, and pyrophoric, with a metallic appearance. They oxidize in air to form PuO_2 (Westrum, 1949b) and are rapidly attacked by water (Pardue and Keller, 1964). Due to their high melting points and high Pu densities, plutonium silicides have been considered as reactor fuels, but the difficulty of preparing them as pure phases has hampered their development for this purpose (Pardue and Keller, 1964; Potter, 1975).

A recent determination of the magnetic properties of PuSi and tetragonal ($ThSi_2$-type) $PuSi_2$ revealed that PuSi orders ferromagnetically around 72 K,

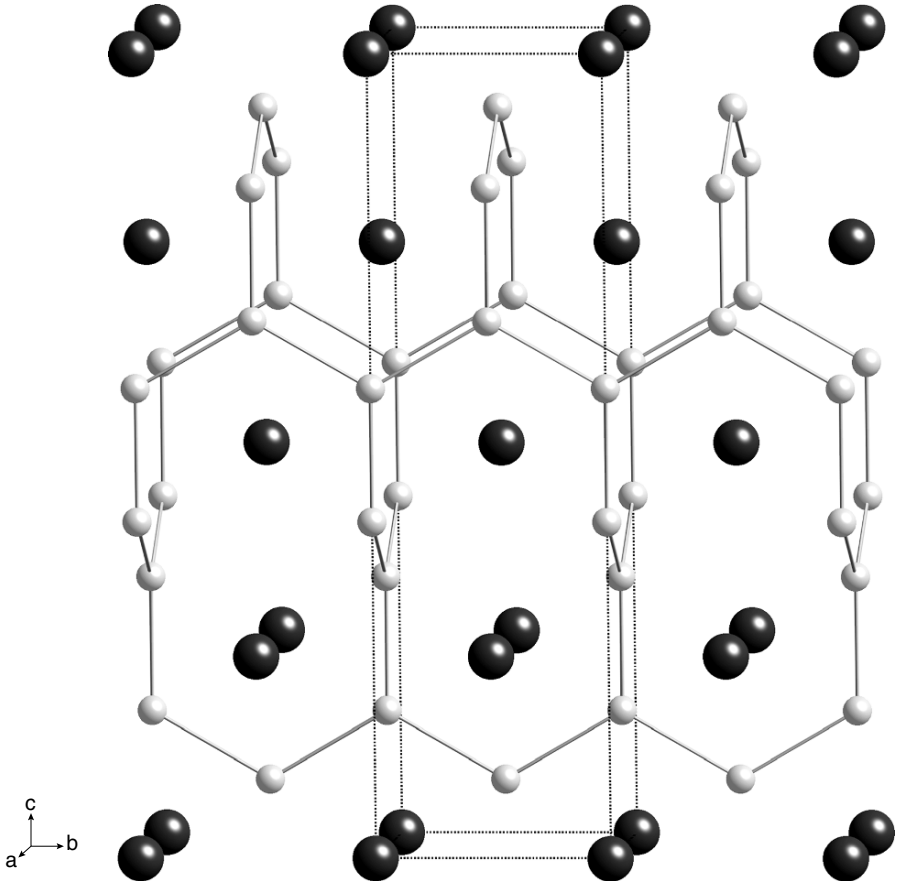

Fig. 7.85 *The solid-state structure of tetragonal $PuSi_2$ shown looking down the a-axis, and emphasizing the three-dimensional network structure of the silicon atoms. Plutonium atoms are black and silicon atoms are gray.*

whereas $PuSi_2$ shows no magnetic ordering (Boulet *et al.*, 2003). The values of the effective moments of PuSi (μ_{eff} ca. $0.72\mu_B$) and $PuSi_2$ (μ_{eff} ca. $0.54\mu_B$) are consistent with a $5f^5$ electronic configuration and a Pu^{3+} oxidation state.

7.8.4 Plutonium pnictides

With pnictogen elements, plutonium forms compounds in three basic families with the highest order composition being PuX_2 that is only found for the heaviest pnictogen elements (X = Sb and Bi). With antimony, thermal dissociation permits the preparation of an intermediate composition Pu_4Sb_3. By far, the most important class of compounds are the monopnictides PuX (N, P,

As, Sb, Bi), which form an isostructural series that has played an important role in understanding the degree of localized versus delocalized bonding with 5f electrons.

Plutonium pnictides are generally prepared by reaction of plutonium metal or hydride with the pnictogen in evacuated sealed quartz tubes that are heated to 400–750°C. The monopnictides can be prepared by thermal dissociation of a higher pnictide. Reviews of synthesis (Spirlet, 1991) and structural properties are available (Damien *et al.*, 1986).

(a) The plutonium–nitrogen system

There is only one compound in the plutonium–nitrogen system that is known with certainty: the cubic mononitride PuN. The Pu–N phase diagram has recently been assessed (Wriedt, 1989; Kassner and Peterson, 1995) and is illustrated in Fig. 7.86. The locations of the boundaries on the Pu-rich and N-rich sides of PuN have not been evaluated in detail, but the composition range of PuN is probably quite narrow. PuN decomposes under 1 bar of N_2 pressure at 2570°C into N_2-saturated liquid plutonium and N_2. Liquid plutonium is formed

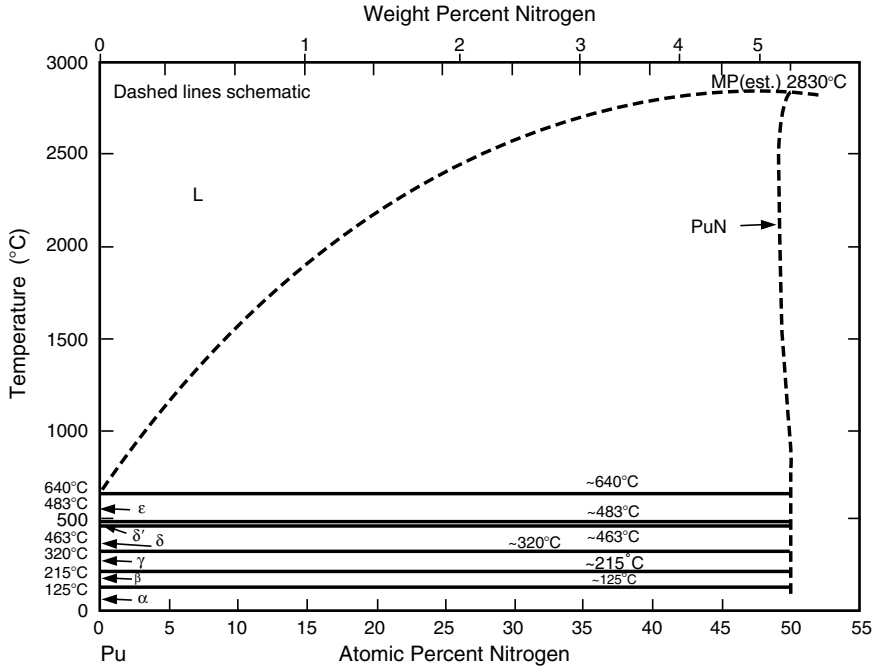

Fig. 7.86 *The plutonium–nitrogen phase diagram* (*Wriedt,* 1989*; Kassner and Peterson,* 1995).

above 1500°C due to incongruent evaporation of PuN. Because of problems associated with sample vaporization, the melting point of PuN has not been observed.

There is a fascinating report by Green and Reedy (1978a) of the observation of matrix isolated PuN_2 containing a molecular N_2 unit and characterized using IR spectroscopy. Theoretical studies discussing the existence, and the nature of chemical bonding in PuN_2 have subsequently appeared (Archibong and Ray, 2000; Tan, 2003).

(*i*) *Preparation*

Cubic PuN can be prepared most conveniently by reaction of metal with H_2 (150–200°C) to produce plutonium hydride, followed by heating the hydride under N_2 at temperatures between 500 and 1000°C (Pardue *et al.*, 1964a, 1967). The preparation can also be accomplished by reaction of plutonium metal with N_2 containing small amounts of H_2 at 250°C (Anselin, 1963a,b; Bridger and Dell, 1967). In view of the facile reactivity of plutonium metal with H_2 (see Section 7.7.1) it is likely that this reaction is catalyzed by surface hydriding of the plutonium metal at 200°C. In the absence of H_2, the direct reaction of pure plutonium metal with N_2, even over a period of 150 h at 1000°C, does not ensure complete conversion to PuN (Brown *et al.*, 1955). The nitride can also be prepared by the carbothermic reduction of PuO_2 under N_2 (Muromura, 1982; Suzuki *et al.*, 1983; Bardelle and Bernard, 1989; Takano *et al.*, 2001), though care must be taken to avoid product contamination with carbon and oxygen impurities. This is a common approach for making nitride fuels as it avoids making large quantities of plutonium hydride in a nuclear facility. The nitride can also be prepared by the reaction of plutonium hydride with ammonia between 600 and 650°C (Abraham *et al.*, 1949c). An interesting low-temperature route to PuN is the reaction of PuI_3 with sodium or potassium metal in liquid ammonia:

$$PuI_3 + NH_{3(l)} + 3M \rightarrow PuN + 3MI + 1.5H_2, \quad M = Na, K \tag{7.34}$$

In this approach, PuI_3 is dissolved in liquid ammonia, followed by reduction with a stoichiometric amount of sodium or potassium metal. The reaction likely proceeds through the *in situ* formation of the active metal amide, MNH_2 (M = Na, K), which undergoes subsequent metathesis with PuI_3. PuN precipitates from liquid ammonia as a black powder, which is washed with liquid ammonia and annealed at 700°C for 24 h (Cleveland *et al.*, 1974, 1975).

Freshly prepared PuN is black, turning brown in moist air due to hydrolysis (Storms, 1964). Formulations of (U, Pu, Zr)N that contain only a few percent of plutonium are golden-yellow. Because of problems with sample vaporization, the melting point of PuN has not been observed, but it has been estimated that congruent melting occurs at 2830 ± 50°C for an N_2 pressure of 50 ± 20 atm (Spear and Leitnaker, 1968).

(*ii*) *Crystal structure*

The crystal structure of PuN was first studied by Zachariasen and shown to exhibit the cubic NaCl structure (Zachariasen, 1949c,d). In cubic PuN, the plutonium and nitrogen atoms alternate in a fcc sphere packing arrangement, with both Pu and N having regular octahedral coordination. Using a lattice parameter of 4.905 Å, the Pu–N and Pu–Pu distances are 2.45 and 3.47 Å, respectively. Many lattice parameter studies of PuN have been reported and recently were summarized (Wriedt, 1989). The rather large variation in lattice parameter is most likely due to the effects of impurities, self-irradiation damage, or nitrogen concentration. A lattice parameter value of 4.918 Å was reported from the results of neutron diffraction on ^{239}PuN at –213°C (Boeuf *et al.*, 1984). Crystallographic properties of PuN and other plutonium pnictides are given in Table 7.33.

(*iii*) *Properties*

Plutonium mononitride is a refractory material with great potential for use as a nuclear reactor fuel (Matzke, 1986; Blank, 1994). It has a high melting point, high density, and high thermal conductivity. Moreover, it is compatible with austenitic steels up to 600°C and with sodium up to its boiling point of 890°C. One drawback is that PuN has a high volatility (due to release of N_2) at the high temperatures possible in a reactor accident. Due to the potential use of PuN in reactor fuels (Sano *et al.*, 1971; Bernard, 1989; Ogawa *et al.*, 1998; Albiol and Arai, 2001), there is an extensive literature on PuN, and topical reviews can be found on the physical and chemical properties (Spear and Leitnaker, 1968; Benedict, 1979), thermodynamic properties (Matsui and Ohse, 1987; Lemire *et al.*, 2001), phase equilibria (Wriedt, 1989), and synthesis (Spirlet, 1991). Selected physical properties of PuN are given in Table 7.34 (Holleck and Kleykamp, 1972; Kleykamp, 1999), and thermodynamic properties of PuN and other plutonium pnictides can be found in Table 7.35.

Powdered PuN reacts with O_2 at 200°C and ignites at 280–300°C to form PuO_2 (Kruger and Moser, 1967a). In moist O_2, the oxidation rate is increased: in the presence of 500 ppm water vapor, the reaction rate at 279°C is three times that without H_2O vapor. In air at room temperature, PuN powder is converted to PuO_2 within 3 days, but compact PuN is oxidized rather slowly (Pardue *et al.*, 1967).

PuN reacts slowly with cold water, but readily with hot water (Bridger *et al.*, 1969). In moist air, PuN decomposes within a few hours at 80–90°C, and within days at room temperature (Storms, 1964). The hydrolysis of PuN was determined in a stream of Ar–H_2O as a function of temperature to give hydrated PuO_2 (Bridger and Dell, 1967). Concentrated mineral acids will decompose PuN with decreasing violence of reaction in the order $HNO_3 > HCl > H_3PO_4 > H_2SO_4 > HF$ (Pardue *et al.*, 1964a).

Table 7.33 *X-ray crystallographic data for plutonium pnictides.*

Compound	*Symmetry*	*Space group*	*Lattice parameter,* a_0 (Å)	*Formula units per cell*	*Calculated density* (g cm^{-3})	*References*
PuN	fcc	F*m*3*m*	4.9055(3)	4	14.22	Ellinger (1961)
			4.9053–4.9056 (N-rich)			Olson and Mulford (1964)
			4.9051 (N-deficient)			Olson and Mulford (1964)
			4.9053 (O-free)			Bridger and Dell (1967)
			4.908 (O-saturated)			Bridger and Dell (1967)
PuP	fcc	F*m*3*m*	5.664(4)	4	9.87	Kruger and Moser (1966a)
			5.6582(1)–5.6613(1)		9.89	Kruger and Moser (1967a)
PuAs	fcc	F*m*3*m*	5.855(4)	4	10.39	Kruger and Moser (1966a)
			5.8586(1)		10.34	Kruger and Moser (1967a)
PuSb	fcc	F*m*3*m*	6.241(1)	4	9.86	Kruger and Moser (1967a)
			6.2396(1)	4		Mitchell and Lam (1971)
Pu_4Sb_3	cubic	I$\bar{4}$3*d*	9.2406[a]	4		Mitchell and Lam (1974)
			9.2370(5)			Charvillat (1978)
$PuSb_2$	orthorhombic	C*mca*	$a = 6.19(1)$	8	9.735	Charvillat *et al.* (1977)
			$b = 6.05(1)$			
			$c = 17.58(4)$			
PuBi	fcc	F*m*3*m*	6.350(1)	4	11.62	Ellinger (1961)

[a] Labeled as Pu_3Sb_4.

Table 7.34 *Selected properties of PuN of relevance to nuclear fuel.*

Property	*Value*	*References*
Decomposition temperature, 1 bar N_2	2570°C	Oetting (1967)
Nitrogen partial pressure at		
1500°C	2×10^{-7} bar	Alexander *et al.* (1969)
2000°C	1×10^{-4} bar	Alexander *et al.* (1969)
Metal partial pressure at		
1500°C	1×10^{-6} bar	Alexander *et al.* (1969)
2000°C	6×10^{-4} bar	Alexander *et al.* (1969)
Thermal conductivity at		
1000°C	13 W K^{-1} m^{-1}	Alexander *et al.* (1976)
1500°C	14 W K^{-1} m^{-1}	Alexander *et al.* (1976)
2000°C	15 W K^{-1} m^{-1}	Alexander *et al.* (1976)

Table 7.35 *Selected thermodynamic properties of plutonium pnictides, PuX (X = N, P, As, Sb, Bi)* (*Lemire* et al., 2001).

Compound	$\Delta_f G^\circ_{298}$ (kJ mol^{-1})	$\Delta_f H^\circ_{298}$ (kJ mol^{-1})	S°_{298} (J K^{-1} mol^{-1})	$C^\circ_{p_{298}}$ (J K^{-1} mol^{-1})
PuN	-273.7 ± 2.6	-299.2 ± 2.5	64.8 ± 1.5	49.6 ± 1.0
PuP	-313.8 ± 21.1	-318 ± 21	81.3 ± 6.0	50.20 ± 4.00
PuAs	-241.4 ± 20.1	-240 ± 20	94.3 ± 7.0	51.6 ± 4.0
PuSb	-152.1 ± 20.1	-150 ± 20	106.9 ± 7.5	52.8 ± 3.5
PuBi	-119.6 ± 20.2	-117 ± 20	120 ± 10	

(b) The plutonium–phosphorus system

Plutonium monophosphide, PuP, is the only well-defined binary plutonium–phosphorus compound known. Cubic PuP can be prepared by reaction of metal with H_2 (150–200°C) to produce plutonium hydride, followed by heating the hydride with PH_3 (Kruger *et al.*, 1966; Kruger and Moser, 1966b). By employing a stepwise reaction consisting of alternate hydride decomposition and reaction of the decomposition product with PH_3, one can obtain very pure PuP product. At least two cycles of alternate hydride decomposition and reaction with phosphine are required. The conversion cycles are followed by 4 h annealing at 1400°C. The preparation can also be accomplished by reaction of powdered plutonium hydride with excess (100–150%) red phosphorus in tantalum-lined pressure vessels at 600–800°C in an argon atmosphere (Moser and Kruger, 1966). After completion of the reaction, excess phosphorus is removed by distillation at 300°C. Alternatively, the phosphide can be prepared by induction melting of plutonium chips with elemental phosphorus *in vacuo* or under pressure of 1 atm of helium. The exothermal reaction goes to completion

at 1400°C (Gorum, 1957). Another method involves the reaction of sol–gel prepared PuO_2 with a stream of PH_3 at temperatures of 1000°C or greater (Cogliati *et al.*, 1969).

PuP has a dark-gray color and melts with decomposition at 2600°C under argon. It exhibits the NaCl structure (see Table 7.33) (Gorum, 1957; Kruger *et al.*, 1966), with lattice constants that depend on sample history. Below 125 K, a tetragonal distortion is observed (Mueller *et al.*, 1979). A number of physical properties (microhardness, thermal expansion, thermoelectric power, temperature conductivity, and heat capacity) have been measured (Hall *et al.*, 1985).

PuP is ferromagnetic below a Curie temperature of $T_c = 126 \pm 1$ K. Above this temperature, the magnetic susceptibility has a temperature dependence given by $\chi_m = 190 \times 10^{-6} + N_L\mu^2/[3k(T–126)]$ cm^3 mol^{-1} where $\mu = 1.06\mu_B$ (Lam *et al.*, 1969). The ferromagnetic moment obtained by extrapolation to 0 K was found to be $0.42/\mu_B$ (Lam *et al.*, 1969). The Landé *g*-factor obtained by a correlation between Knight shift and χ_m is $g = 2/7$ (Fradin, 1970). Thermodynamic and magnetic properties have been discussed (Arai and Ohmichi, 1995).

(c) The plutonium–arsenic system

Plutonium arsenide, PuAs, may be prepared by reaction of plutonium metal with excess arsenic under 1 atm of helium or *in vacuo* at 500–1200 K (Gorum, 1957; Pardue *et al.*, 1964b; Mitchell and Lam, 1974) for a period of 3–7 h. It can also be prepared by reaction of PuH_3 with As *in vacuo* (0.02 Torr, 2.6×10^{-5} atm) at temperatures above 400°C, which are slowly increased to 700°C. The product is homogenized *in vacuo* at a still higher temperature (Kruger and Moser, 1967b; Fradin, 1970; Handwerk and Kruger, 1971; Charvillat and Damien, 1973). Finally, it can be prepared by reaction of plutonium partially converted to the hydride with AsH_3 at 250°C and subsequent recycling at 400, 500, 600, and 700°C in a similar manner as just described for PuP in Section 7.8.4(b) (Anselin, 1963b; Lam *et al.*, 1969). Because of the low decomposition temperature of AsH_3 (300°C), the primary reaction is done at 250°C, and only the annealing cycles are carried out at the higher temperatures mentioned above. Plutonium arsenide is a gray, metallic-looking material, black in finely divided form. Its crystallographic properties are listed in Table 7.33.

(d) The plutonium–antimony system

Arc melting of mixtures of plutonium and antimony yields PuSb (Kruger and Moser, 1966a). In addition to the monopnictide, plutonium also forms a dipnictide $PuSb_2$ (Charvillat *et al.*, 1977), and an intermediate composition, Pu_4Sb_3 (Damien *et al.*, 1986). Cubic PuSb melts at 1980 ± 30°C under 3 atm of argon (Mitchell and Lam, 1974).

The diantimonide exhibits an unusual orthorhombic structure formed by ten layers of atoms, and this structure is shown in Fig. 7.87. Each plutonium atom has four nearest antimony atoms ranging 3.15–3.30 Å away forming a distorted Sb_4 square just below, and another just above but rotated by 45 degrees. The local coordination polyhedron about plutonium is that of a distorted square antiprism. The Sb–Sb distances within the square are 3.095 Å, and the Sb–Sb distances linking the two groups of antiprisms are 2.755 Å. The structure is described in more detail for AB_2 rare-earth compounds by Wang and Steinfink (1967).

(e) Valency and electronic structure in PuX compounds

Plutonium monopnictides show moderately delocalized 5f electrons. The degree of localization increases with atomic number of the pnictogen, with delocalization being largely dominated by plutonium–pnictogen interactions. The lattice parameter is affected by this partial delocalization, making it hard to deduce plutonium valence from the crystal structure or lattice parameter value.

Magnetic susceptibility measurements of plutonium monopnictides show high-temperature Curie–Weiss-like behavior that gives effective moments close to the value of $1.24\mu_B$, consistent with an f^5 ion, and trivalent plutonium (Vogt and Mattenberger, 1993, 1995). The ordered magnetic moments are significantly smaller, and the experimental data suggest partial f-electron localization. For example, X-ray photoemission studies of PuSb clearly indicate localized f-electrons (Gouder *et al.*, 2000), while resistivity measurements show a semimetallic Kondo-like behavior (Blaise *et al.*, 1985). Magnetism experiments show a very strong anisotropy in all PuX compounds, with magnetic moments oriented along the [100] direction (Mattenberger *et al.*, 1986). Neutron scattering experiments (Lander *et al.*, 1984, 1985) support Cooper's interpretation of moderate f-electron delocalization being responsible for the reduction in the ordered moment and strong anisotropy in plutonium monopnictides (Cooper *et al.*, 1983). Recent electronic structure calculations of PuX compounds based upon a self-interaction correlated local spin density (SIC-LSD) approach support the interpretation that the plutonium 5f-electron manifold is best described in a mixed picture of localized and delocalized states (Petit *et al.*, 2002).

7.8.5 Plutonium chalcogenides

(a) The plutonium–oxygen system

Binary plutonium oxides, especially PuO_2, are of tremendous technological importance. They find widespread application as nuclear fuels, as long-term storage forms for both spent nuclear fuels and surplus weapons materials, and

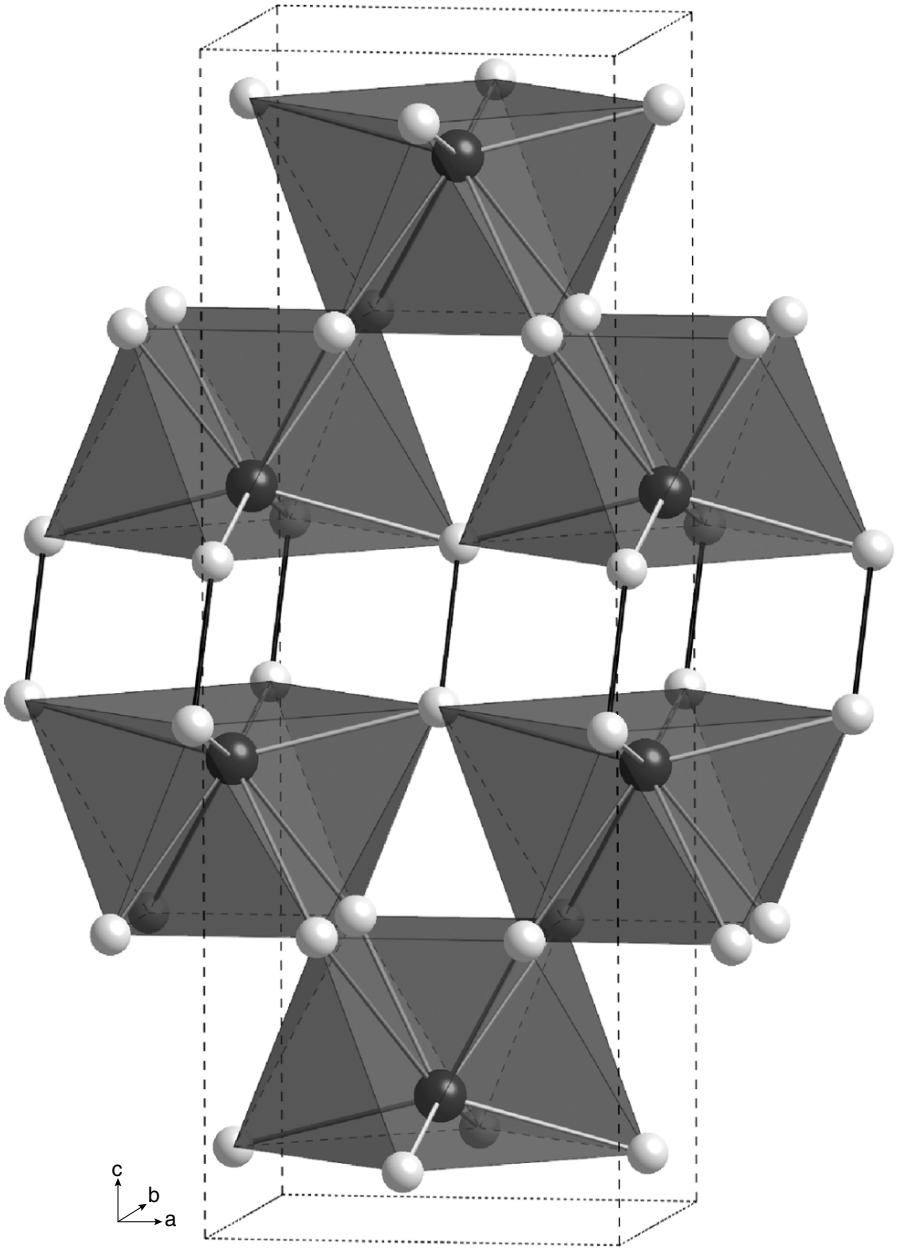

Fig. 7.87 *The solid-state structure of $PuSb_2$ shown looking perpendicular to the c-axis, and emphasizing the antiprismatic $PuSb_8$ polyhedral layers. Plutonium atoms are black and antimony atoms are gray.*

as heat and power generators (^{238}Pu) for interplanetary exploration. Their properties are also important because oxide particulates contribute to environmental actinide migration, participate in corrosion reactions in nuclear weapons, and exist as chemical intermediates in the purification and preparation of other actinide compounds. This same family of oxides is also of fundamental scientific interest. Even though plutonium oxides were among the first compounds of plutonium to be studied, it is astonishing to consider how much remains unknown about plutonium oxides. A number of reviews on the plutonium–oxygen system have appeared (Chikalla *et al.*, 1962; IAEA, 1967; Wriedt, 1990; Naito *et al.*, 1992).

(*i*) *Phase equilibria*

A good deal of discussion has appeared in the literature regarding the phase diagram for the plutonium–oxygen system, and there are conflicting sets of data for some phases (IAEA, 1967; Wriedt, 1990; Naito *et al.*, 1992; Haschke *et al.*, 2000a). The system is complex, and additional study is still needed to resolve certain issues surrounding the phase diagram. To adequately describe the issues associated with the plutonium–oxygen system, Haschke and Haire (2000) chose to present two diagrams, one based on the most recent assessment with modifications, and another, more pedagogical diagram based upon analogy with the more well-studied and better understood lanthanide oxide systems. There is great utility in this approach, and we have adopted it for our discussion. The proposed phase diagram based on the most recent assessments is shown in Fig. 7.88, and a table of crystallographic data for plutonium oxides is given in Table 7.36.

There are four fundamental equilibrium solid phases in the plutonium–oxygen system. The first of these is the stoichiometric hexagonal sesquioxide of formula Pu_2O_3 with a very small composition range near 60 at.% oxygen and with an ideal stoichiometry of $PuO_{1.5}$. This phase is also commonly known in the literature as hexagonal A-Pu_2O_3, or β-Pu_2O_3, and other designations have also been used (Wriedt, 1990; Haschke and Haire, 2000). We will use the designation A-Pu_2O_3. There is a bcc sesquioxide of composition $PuO_{1.52}$, reported to have only a small composition range near 60.3 at.% oxygen, but this narrow stoichiometry range is not supported by all the available data (Haschke and Haire, 2000). This phase has been commonly referred to as cubic C-Pu_2O_3, α-Pu_2O_3, and α-$Pu_2O_{3+\delta}$, but again, other designations have also appeared in the literature. We will use the designation C-Pu_2O_3.

There is a bcc oxide of intermediate composition $PuO_{1.61}$ with a composition range between 61.7 and 63.0 at.% oxygen that is commonly referred to as C′-Pu_2O_3, α′-Pu_2O_3, $PuO_{1.6+\delta}$, and others. This cubic phase is not stable at room temperature but exists above 335°C. Due to its broad composition range, Haschke and Haire referred to this phase as $PuO_{1.6+\delta}$ to help distinguish this bcc phase from the oxygen-deficient fcc PuO_{2-x}. We will use the designation

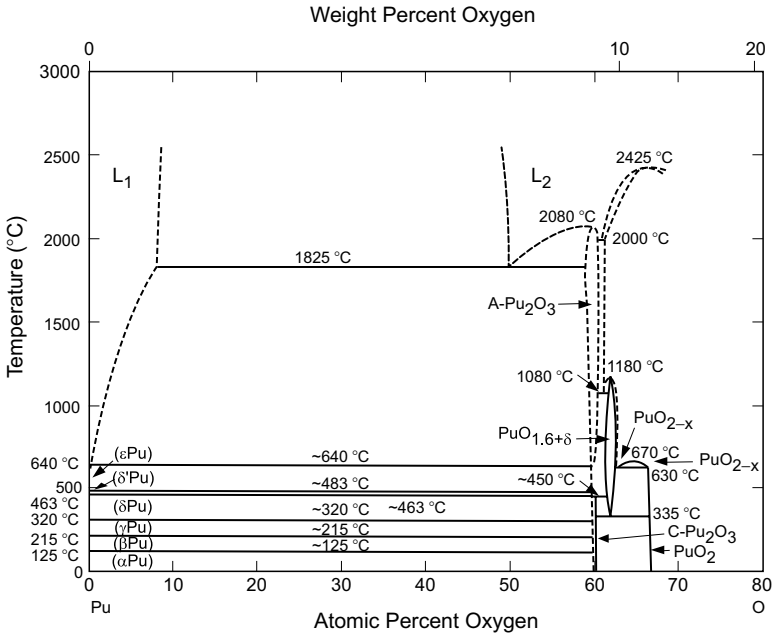

Fig. 7.88 *The plutonium–oxygen phase diagram* (*Wriedt,* 1990*; Naito* et al., 1992*; Haschke* et al., 2000*a*).

$PuO_{1.6+\delta}$. There is a fcc dioxide PuO_2 with a wide composition range that runs from $PuO_{1.6}$ to PuO_2, and sometimes referred to as substoichiometric PuO_2 or PuO_{2-x}. At room temperature, PuO_{2-x} has a fairly narrow composition range between $PuO_{1.98}$ and $PuO_{2.03}$, while at higher temperatures the homogeneity range widens to $PuO_{1.6}$ and PuO_2 as indicated in the phase diagram. Note that the oxygen-deficient fcc $PuO_{1.6}$ (PuO_{2-x}) is not the same as the bcc $PuO_{1.61}$ described above; this is why we prefer the nomenclature $PuO_{1.6+\delta}$ for the bcc phase. On the plutonium-rich side, cubic $PuO_{1.6+\delta}$ coexists with cubic C-Pu_2O_3 until it undergoes a peritectoid decomposition into hexagonal A-Pu_2O_3 and cubic $PuO_{1.6+\delta}$ above 450°C. On the oxygen-rich side of this composition range, C-Pu_2O_3 coexists with PuO_{2-x} below 630°C, and with metal-rich PuO_{2-x} at higher temperatures until it congruently transforms into PuO_{2-x} at 1180°C. Hexagonal A-Pu_2O_3 coexists with oxygen-saturated metal and displays an increasing extent of nonstoichiometry until the congruent melting point of 2080°C is reached. PuO_2 undergoes congruent melting at 2425°C. Only recently has there been enough new data to suggest the addition of a hyperstoichiometric fcc oxide, PuO_{2+x} with composition that runs from stoichiometric PuO_2 to $PuO_{2.27}$ between room temperature and 350°C (Haschke *et al.*, 2000b). This is not shown in Fig. 7.88, but is included in the notional phase diagram shown in Fig. 7.92.

Table 7.36 *X-ray crystallographic data for plutonium oxides.*

Compound or phase	*Structure type*	*Symmetry*	*Space group*	*Unit cell dimensions* (Å)	*Formula units per cell*	*X-ray density* ($g\ cm^{-3}$)	*References*
PuO	NaCl	fcc	F*m*3*m*	$a = 4.96(1)$	4	13.88	Ellinger (1961)
$PuO_{1.5}$ ($A\text{-}Pu_2O_3$, $\beta\text{-}Pu_2O_3$)	La_2O_3	hexagonal	P$\bar{3}$*m*1	$a = 3.841(6)$ $c = 5.958(5)$	1	11.47	Ellinger (1961)
$PuO_{1.51}$ ($C\text{-}Pu_2O_3$, $\alpha\text{-}Pu_2O_3$)	Mn_2O_3	bcc	I*a*3	$a = 11.02(2)$	16	10.44	Ellinger (1961)
$PuO_{1.61}$ ($PuO_{1.6+\delta}$, $C'\text{-}Pu_2O_3$, $\alpha'\text{-}Pu_2O_3$)	Mn_2O_3	bcc	I*a*3	$a = 10.95 - 11.01$			Gardner *et al.* (1965)
PuO_2	CaF_2	fcc	F*m*3*m*	$a = 5.3960(3)$ for stoichiometric composition	4	11.46	Ellinger (1961)
$^{238}PuO_2$	CaF_2	fcc	F*m*3*m*	$a = 5.4141(1)$	4		Roof (1973)
$PuO_{2.26}$	CaF_2	fcc	F*m*3*m*	$a = 5.404$	4		Haschke *et al.* (2000b)

(*ii*) *Preparation*

Plutonium monoxide, PuO

While it has been reported on numerous occasions, the existence of a *stable* condensed oxide of formula PuO is still uncertain and is therefore not indicated in the phase diagram of Fig. 7.88. The material that has been described by many authors is most likely a disordered oxide–carbide $Pu(O_x,C_{1-x})$. Mooney and coworkers (Mooney and Zachariasen, 1949; Zachariasen, 1949d) described powder patterns that could be attributed to cubic PuO, and Holley *et al.* reported a NaCl-type fcc phase with $a_0 = 4.96(1)$ Å as a surface film formed on plutonium metal. Westrum (1949a) describes the material as a semimetallic substance with an almost metallic luster. This surface material has also been observed upon heating oxide-coated plutonium metal *in vacuo* at 250–500°C (Terada *et al.*, 1969). Other reports on the preparation of PuO include the reaction of molten plutonium (microgram quantities) with stoichiometric oxygen generated by thermal decomposition of Ag_2O (Akimoto, 1960), by reduction of PuO_2 with carbon at 1500–1800°C (Skavdahl, 1964), or by reduction of PuOCl or PuO_2 with Ba vapor at 1250°C (Westrum, 1949a). Reshetnikov (2003) has recently claimed to prepare pure PuO by heating PuOCl with calcium at 1200°C, but no characterization data are provided to substantiate the claim. Haschke and Haire (2000) point out that plutonium oxide that results from metal oxidation may be covered with a layer of unbound carbon formed as a result of interaction of the oxide with hydrocarbons or CO_2, and that experiments by Forbes *et al.* (1966) indicate that all products thus obtained contain carbon. The observed lattice parameter is nearly identical to that found for oxide–carbide solid solutions (Mulford *et al.*, 1965; Oetting, 1967). Work on the Pu–O–C phase diagram has shown conclusively that the oxygen-rich limit of the $Pu(O_x,C_{1-x})$ phase lies at a composition of approximately $PuC_{0.3}O_{0.7}$ (Forbes *et al.*, 1966; Taylor *et al.*, 1967; Larson, 1980; Larson and Haschke, 1981). Larson and Haschke (1981) used XPS data to demonstrate that a material believed to be PuO was in fact $PuO_{0.65\pm0.15}C_{0.45\pm0.15}$.

Although the above paragraph argues that most materials that were thought to be PuO were likely contaminated with carbon, and therefore likely to be $Pu(O_xC_{1-x})$ there are several intriguing reports about an unstable, metallic-gray, pyrophoric product that deserve additional study. Reshetnikov (2003) describes an explosion that occurred in 1949 upon grinding a sample thought to be plutonium with a glass rod. Similarly, Haschke described a steel-gray product formed upon the thermal decomposition of PuOH (Haschke *et al.*, 1983; Haschke, 1992). This material underwent a violent exothermic reaction with oxygen, destroying a quartz microbalance container. Such behavior would not be expected for PuO_xC_{1-x}. Thus there may be some instances where a metastable form of solid PuO has indeed been prepared. The full characterization of the material produced by Haschke was not undertaken due its pyrophoric nature (Haschke, 1992), and characterization of the material prepared by Reshetinikov

was not provided. We will need to wait for additional characterization data to resolve this issue.

While the existence of solid-phase PuO is unresolved, there is little doubt that gaseous PuO is one of the major species of plutonium oxides in the vaporization process (Green and Reedy, 1978b; Capone *et al.*, 1999; Ronchi *et al.*, 2000). PuO is observed in both the mass spectrum of effusing vapors over PuO_2 (Capone *et al.*, 1999; Ronchi *et al.*, 2000), and in the IR absorption spectra of vapors trapped in argon and krypton matrixes. $Pu^{16}O$ trapped in an argon matrix displays an infrared vibrational frequency of 822.28 cm^{-1} (Green and Reedy, 1978b).

Plutonium sesquioxide phases, Pu_2O_3

There is a good deal of confusion about both the preparative methods and the phase relationships between hexagonal (A-Pu_2O_3) and cubic (C-Pu_2O_3) forms of plutonium sesquioxide. The methods of preparation of hexagonal and cubic forms are very similar, yet these oxides are described as separate and distinct phases at low temperature. As outlined in recent reviews (Wriedt, 1990; Haschke and Haire, 2000), these compounds are thought to be distinct phases because (i) both cubic and hexagonal phases have been observed to coexist; (ii) the transformation between hexagonal and cubic forms has not been observed; and (iii) their regions of composition do not overlap. It has been suggested that kinetic factors may favor the formation of the cubic sesquioxide at low temperature in the presence of plutonium metal (Haschke and Haire, 2000). For example, cubic C-Pu_2O_3 readily forms as a surface layer when PuO_2-coated δ-stabilized plutonium metal is heated to 150–200°C under vacuum (Terada *et al.*, 1969). This observation is highly suggestive that the preexisting fcc lattice of metal atoms in either the underlying metal, the fcc dioxide, or both, imparts some control over the nature of the product in the reaction, and that once the cubic sesquioxide is formed, this phase cannot transform into the hexagonal form unless the temperature exceeds 450°C. The hexagonal form apparently does not transform back into the cubic form at this temperature, suggesting perhaps that more kinetic energy is necessary to rearrange the metal atoms in the lattice. This behavior is not consistent with the known behavior of the isomorphic lanthanide oxides, where hexagonal Nd_2O_3 will transform reversibly to cubic Nd_2O_3 near 600°C (Haire and Eyring, 1994). Thus cubic C-Pu_2O_3 may be only metastable at low temperatures.

Several methods of preparation have been reported for the hexagonal A-Pu_2O_3 sesquioxide. Plutonium dioxide can be reduced with plutonium metal (Holley *et al.*, 1958), dry hydrogen (Flotow and Tetenbaum, 1981), or carbon (Skavdahl, 1964) to form A-Pu_2O_3. Pure hexagonal A-Pu_2O_3 has been prepared by reducing pure PuO_2 with a 20% excess of plutonium turnings or chips in a closed tantalum crucible at 1500°C according to the stoichiometry (Holley *et al.*, 1958):

$$3PuO_2 + Pu \rightarrow 2Pu_2O_3 \qquad (7.35)$$

After a reaction period of 3 h, the excess plutonium metal was removed by sublimation from the open crucible at 1800–1900°C *in vacuo* (Holley *et al.*, 1958; Chikalla *et al.*, 1962, 1964). At higher reaction temperatures, large, flat crystals of hexagonal A-Pu_2O_3 were obtained. In another procedure, Gardner *et al.* (1965) reduced pure PuO_2 powder with a 20% excess of hydride-powdered plutonium metal in a ThO_2 crucible at 1500°C for 3 h in a stream of purified dry hydrogen.

Hydrogen reduction of PuO_2 to produce hexagonal A-Pu_2O_3 can be accomplished at 1550°C in very dry hydrogen purified over titanium turnings (Gardner *et al.*, 1965). Complete reduction of PuO_2 by hydrogen has also been reported to occur in the temperature range 1700–2000°C (Dayton and Tipton, 1961; Flotow and Tetenbaum, 1981). Pure hexagonal A-Pu_2O_3 may be prepared by the stoichiometric reduction of PuO_2 with carbon at (1800 ± 50)°C for 5.5 h in a pure helium atmosphere (Skavdahl, 1964; Forbes *et al.*, 1966) according to the reaction:

$$2PuO_2 + C \rightarrow Pu_2O_3 + CO \tag{7.36}$$

Chikalla and coworkers reported a large-scale preparation (ca. 110 g Pu) of hexagonal A-Pu_2O_3 by sintering pressed compacts of PuO_2 and carbon *in vacuo*, followed by melting under an inert atmosphere (Chikalla *et al.*, 1962, 1964; Skavdahl, 1964). Reaction of PuO_2 with a slight excess of carbon at 1650°C *in vacuo* produced a mixture of hexagonal A-Pu_2O_3 and a small amount of $Pu(O_x,C_{1-x})$. The latter, being more volatile than the Pu_2O_3, could be removed by heating *in vacuo*. Final arc melting resulted in hexagonal A-Pu_2O_3 with an O:Pu ratio of (1.500 ± 0.015), with 175 ppm carbon impurity and 93% theoretical density.

The cubic C-Pu_2O_3 sesquioxide is a silvery, metallic, lustrous solid, which is difficult to prepare by high-temperature methods. Haschke and Haire point out that reports of its preparation by simply heating PuO_2 *in vacuo* to temperatures between 1650 and 1800°C (Westrum, 1949a; Dayton and Tipton, 1961) are suspect because the O:Pu ratio of congruently vaporizing PuO_{2-x} is 1.85–1.90 in this temperature range (Ackermann *et al.*, 1966). The best means of preparation seems to be the heating of PuO_2 coated δ-stabilized plutonium metal to 150–200°C under vacuum (Terada *et al.*, 1969).

Hyperstoichiometric sesquioxide, $PuO_{1.6+\delta}$ (C'-Pu_2O_3, α'-Pu_2O_3, $PuO_{1.61}$)

When PuO_2 is melted, there is an evolution of oxygen resulting in a melt composition of $PuO_{1.62}$, which is the approximate composition of cubic C-Pu_2O_3 (Chikalla *et al.*, 1964). This phase can only be retained with extremely fast quenching. Since it is a high-temperature form of C-Pu_2O_3, it has been given the designation C'-Pu_2O_3 (or α'-Pu_2O_3, $PuO_{1.61}$, $PuO_{1.6+\delta}$). It is likely bcc. Slow cooling of the melt yields a mixture of C-Pu_2O_3 and PuO_{2-x} even in the absence of oxygen. Sari *et al.* (1968) reported that this compound has a composition range from $PuO_{1.62}$ to $PuO_{1.63}$ at 350°C, which extends to a range of $PuO_{1.62}$ to

$PuO_{1.69}$ at 600°C. Because of this broad composition range, we prefer the designation $PuO_{1.6+\delta}$.

Substoichiometric plutonium dioxide, PuO_{2-x}

The oxides between compositions $PuO_{1.61}$ to $PuO_{1.98}$ are mainly single-phase materials at temperatures above about 650°C. They may be prepared by heating PuO_2 at high temperature with carbon, hydrogen, or *in vacuo* (IAEA, 1967). The crystal lattice expands with decreasing oxygen composition (Gardner *et al.*, 1965; IAEA, 1967). Some annealing may be required, but prolonged heating *in vacuo* will cause a change in composition due to incongruent vaporization. This olive-green phase exists in the stoichiometry range $PuO_{1.61}$ to $PuO_{1.98}$ and is closely related to the stoichiometric oxide $PuO_{2.00}$. Its exact composition depends on the temperature and the oxygen partial pressure over the plutonium oxide solid (Drummond and Welch, 1957). Atlas and coworkers performed density measurements at 750°C that are consistent with the formation of oxygen vacancies in the crystal lattice (Atlas *et al.*, 1966). Atlas and Schlehman (1967) conducted a detailed study of the variation in oxygen content, x, with oxygen pressure. The composition–pressure–temperature relationship is shown in Fig. 7.89.

Stoichiometric plutonium dioxide, $PuO_{2.00}$

Plutonium dioxide is formed when metallic plutonium is ignited in air or by calcination of a number of plutonium compounds (except phosphates). Plutonium dioxide often forms when oxygen-containing compounds are heated *in vacuo* or in an inert atmosphere to 1000°C. The most widely used approach to prepare pure, crystalline PuO_2 is by heating Pu(III) or Pu(IV) oxalate to

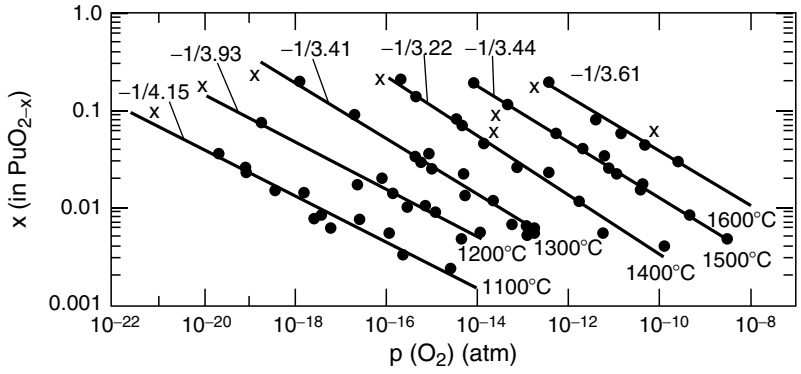

Fig. 7.89 *Variation of x in PuO_{2-x} with temperature and oxygen pressure (Atlas and Schlehman,* 1967). *Slopes (i.e.* –1/4.15, *etc.) of the log–log plots are shown above the lines. Experimental data points marked in x represent values derived from weight change measurements, whereas the circles represent gas-analysis results.*

1000°C in air. The Pu(III) oxalate is often preferred because it forms a powder that is easy to manipulate, while the Pu(IV) oxalate forms a tacky solid (see Section 7.9.1(e)i). The heating rate must be kept slow up to about 700°C to avoid rapid decomposition and gas evolution, followed by heating to 1000°C to remove any residual carbon. Drummond and Welch (1957) studied the stoichiometry of PuO_2 as a function of preparative history, and found that many materials need to be heated to 1250°C to produce reproducible stoichiometric PuO_2.

The method of preparation and process details have a significant influence on the PuO_2 product characteristics, which affect all subsequent uses of the material, such as fabrication and sintering properties of fuel materials containing PuO_2 or its behavior in long-term storage. PuO_2 is normally olive green, but it's observed color is a function of purity, particle size, method of preparation, stoichiometry, and possible reactions with water. The observed colors range from dull yellow, to green, khaki, buff, slate or black. Many of these samples are most likely hyperstoichiometric PuO_{2+x} (see section PuO_{2+x}). All samples turned to a darker, khaki color upon ignition to 1200°C. The qualitative characteristics of various PuO_{2+x} preparations obtained from different starting materials are summarized in Table 7.37 (Drummond and Welch, 1957).

Special preparations of PuO_2

Plutonium dioxide may be pressed and sintered to form pellets or compacts, which may be used in reactor technology or (in the case of $^{238}PuO_2$) in heat- and power-source technology for space exploration. For detailed descriptions, the reader is referred to the *Plutonium Handbook* (Wick, 1980). As an illustrative example of the general pellet-forming process, $^{238}PuO_2$ used to fabricate GPHS and LWRHU fuel pellets (see Section 7.3) for the Cassini mission was subjected to ^{16}O isotope exchange (to reduce neutron emission), ball milling, granulation and seasoning at 1100 and 1600°C to produce $^{238}PuO_2$ granules with <210 μm sized particles. The granules were then blended using those seasoned at

Table 7.37 *Qualitative characteristics of PuO_{2+x} from decomposition of selected materials at* 870°C (*Drummond and Welch,* 1957).

Material	*Color*	*Appearance*
metal	dull yellow	powder
sulfate	yellow-green to green	bulky powder
nitrate	dull yellow	bulky solid
chloride	dull yellow	powder
fluoride	khaki with black traces	granular solid
oxalate	yellow-buff	bulky powder
iodate	buff	very bulky
hydroxide	black with yellow traces	dense, shiny particles

1100°C (60 wt %) with those seasoned at 1600°C (40 wt %) by rolling the granules in a ball-mill jar without balls. After blending, the fuel charges were loaded into a hot press graphite die, placed under vacuum, and heated to 1530°C under a force of 11.8 kN. During hot pressing, the PuO_2 is reduced by the graphite die. After the pellets sat overnight, the PuO_{2-x} stoichiometry was about $PuO_{1.93}$. To oxidize the pellets back to a stoichiometry of PuO_2 and increase their density to meet mission specifications, the pellets were sintered in flowing Ar–$H_2{}^{16}O$ for 6 h at 1000°C, followed by 6 h at 1527°C (Rinehart, 1992, 2001).

Two other forms of PuO_2 also deserve a more detailed description: PuO_2 microspheres and single crystals. Plutonium dioxide microspheres with 10–250 μm diameter may be prepared by the sol-gel process for ^{239}Pu (Wymer and Coobs, 1967; Lloyd and Haire, 1968; Louwrier *et al.*, 1968; Wymer, 1968), ^{238}Pu (Grove *et al.*, 1965; Hass *et al.*, 1966; Hincks and McKinley, 1966), or MOX (U, Pu)O_2 (Vaidya *et al.*, 1983; Smolders and Gilissen, 1987; Stratton *et al.*, 1987). In this process, a stable Pu(IV) hydroxide sol is prepared by extraction or evaporation of HNO_3 from HNO_3–$Pu(NO_3)_4$ solution, injection of the resulting sol into a dehydrating organic solvent (for instance, 2-ethylcyclohexanol), and firing the resulting gel to form PuO_2 microspheres (Hass *et al.*, 1966; Lloyd and Haire, 1968; Wymer, 1968).

Very dense microspheres, which have a remarkable freedom from loose α-particle contamination, may be prepared by plasma spheroidization (Jones *et al.*, 1964). In this method, plutonium oxide is first compacted into pellets, which are fired at 1500°C for 1 h in an oxygen-enriched plasma to inhibit loss of oxygen during melting. The resulting compacts are ground to the desired mesh size, and are then fed into an induction-coupled plasma torch, which uses argon, oxygen, or Ar–O_2 mixtures as feed gas. In the high temperature of the plasma torch (up to 20,000°C), each plutonium oxide particle immediately melts to a small spherical droplet, which, upon leaving the plasma zone, immediately solidifies into a small sphere with a smooth surface. Depending on the particle size of the feed particles, microspheres from 10 to 250 μm may be obtained (Jones *et al.*, 1964).

Spheres with less than 50 μm diameter are amber-colored and have a clear, vitreous appearance. Those of more than 50 μm diameter do not transmit light and appear opaque black (Jones *et al.*, 1964). If prepared in an O_2 plasma, they have the lattice constants of stoichiometric PuO_2. Each individual sphere usually consists of a single crystal (Jones *et al.*, 1964).

Plutonium dioxide single crystals of considerable size have been prepared by several authors (Phipps and Sullenger, 1964; Schlechter, 1970; Finch and Clark, 1972; Rebizant *et al.*, 2000). Finch and Clark (1972) obtained PuO_2 single crystals from Li_2O–$2MoO_3$ melt in a temperature gradient ranging from 1270 to 1300°C in a tightly closed platinum vessel over a 2 week period. Crystals of $2 \times 3 \times 3$ mm have been obtained in this fashion. Schlechter (1970) grew single crystals of approximately the same size by slow thermal decomposition of

$Pu(SO_4)_2$ either in LiCl–KCl eutectic or in $PbCl_2$–KCl melt at 600–800°C and subsequent cooling at a rate of 2.2°C h^{-1} from 715°C to room temperature. Phipps and Sullenger (1964) obtained PuO_2 single crystals with well-defined faces and edges up to 60 μm long when they prepared plutonium-bearing glass fibers by drawing the molten glass (90% SiO_2–30% Na_2O) from a platinum–rhodium bushing at 1300°C. $(U,Pu)O_2$ single crystals have been grown through a chemical transport reaction (Rebizant *et al.*, 2000).

Higher oxides, PuO_{2+x}, PuO_3, and PuO_4

While plutonium is capable of forming molecular compounds of oxidation state VI and VII, most practitioners have been of the opinion that in the plutonium–oxygen system, the stoichiometric tetravalent oxide $PuO_{2.0}$ represents the highest obtainable binary oxide. The historical basis for this opinion began in 1944, when Moulton (1944) observed that during ignition of plutonyl nitrate, only PuO_2 was formed, but no PuO_3 or any other higher oxide was produced. Moulton took this as evidence for the nonexistence of any oxide of composition higher than PuO_2. In 1953, Brewer (1953) predicted from thermodynamic calculations that any solid anhydrous oxide of plutonium higher than PuO_2 would probably not be stable. This view seemed to be confirmed by the work of Westrum (1949a), who used strongly oxidizing conditions (O_2 at 400°C and 70 atm pressure; ozone at 600–1000°C; atomic oxygen) but failed to oxidize PuO_2. Katz and Gruen (1949) also reported that PuO_2 is not oxidized to a higher oxide with NO_2 or atomic oxygen at 500°C. Moreover, Weigel and coworkers (Marquart *et al.*, 1983) attempted to prepare anhydrous PuO_3 by careful decomposition of PuO_2CO_3, $(NH_4)_2PuO_2(CO_3)_2$, and $PuO_3 \cdot 0.8H_2O$, but did not succeed in preparing any higher oxide. Gouder has attempted to prepare thin films of PuO_3 by reacting PuO_2 with oxygen atoms, and found no evidence for its formation (Gouder, 2005).

A number of recent reports on higher-valent oxides such as $PuO_{2.26}$ in the solid state, and PuO_3 and PuO_4 in the gas phase have challenged these traditional views. While not all of the data are consistent, and there are still disagreements among practitioners, these recent reports strongly suggest that the established views on the oxidation behavior of plutonium are worth reconsideration, and that additional detailed study is appropriate.

PuO_{2+x} As early as 1957, Drummond and Welch (1957) had prepared compositions of PuO_2–$PuO_{2.09}$, and concluded that compounds with O:Pu ratios higher than 2.0 were the result of low temperature ignition of plutonium compounds. Oxygen-rich PuO_2 can also be prepared by heating cubic C-Pu_2O_3 in oxygen at 1000°C, and the material formed in this manner displayed a slightly reduced lattice constant (a_0) of 5.382 Å as compared to 5.396 Å for stoichiometric PuO_2. It was possible that the higher O:Pu ratio in these preparations was attributed to excess oxygen dissolved in the crystal lattice. In other studies, mass changes indicating the formation of $PuO_{2.1}$ during

atmospheric corrosion of plutonium metal had been attributed to adsorption of water (Sackman, 1960).

These views remained widely held until Stakebake and coworkers found evidence for a new fluorite-related phase of composition $PuO_{2.17}$ formed as a surface layer by plutonium metal reaction with water vapor at 200–350°C (Stakebake *et al.*, 1993). XPS data were consistent with the presence of Pu(VI). Confirmatory evidence for the formation of a higher oxide was reported by Haschke *et al.* (2000a,b), who studied the reaction of PuO_2 with water vapor between 25 and 350°C. Mass spectroscopic analysis of the gases produced in this reaction showed that H_2 and H_2O were the only gaseous products and indicated that the reaction proceeds according to the reaction:

$$PuO_2(s) + xH_2O(g) \rightarrow PuO_{2+x}(s) + xH_2(g) \qquad (7.37)$$

The final product approached a composition of $PuO_{2.3}$. XRD analyses of the reaction products revealed a single fcc phase with a fluorite-related structure and a slightly expanded lattice. The lattice expansion was accompanied by a linear increase in the O:Pu ratio, consistent with the formation of a solid-solution of PuO_{2+x} in analogy with UO_{2+x} (Allen and Tempest, 1986). Isothermal measurements showed that hydrogen is generated at linear, temperature-dependent rates from which the authors derived an activation energy (E_a) for the reaction of (39 ± 3) kJ mol^{-1}. This was interpreted as being consistent with a chemical reaction, and not with radiolysis, which is expected to be temperature-independent. It should be noted, however, that the rates observed for hydrogen evolution in the reaction of PuO_2 with water vapor at 25°C are in close agreement to the rate of hydrogen evolution observed during exposure of PuO_2 to aqueous salt solutions (Haschke *et al.*, 1983). The report of H_2 being the only gaseous product is not consistent with the observations of Vladimirova and Kulikov (2002), who reported the observation of both H_2 and O_2 in the gas phase during their study of the reaction of PuO_2 with sorbed water using high- and low-burnup plutonium, and therefore different radiolytic dose rates. Their data are consistent with the rates of formation of H_2 and O_2 being in direct proportion to the dose rate. They followed their reactions for 600 days, but did not report on the characterization of the oxide at the end of the experiment.

There is good agreement that water vapor reacts with PuO_2 to generate hydrogen. The generation of hydrogen in storage containers represents a significant safety concern (Haschke and Martz, 1998b), and has led to use of strict standards for stabilization, packaging, and storage of plutonium residue materials that require thermal stabilization using calcinations in air, followed by sealing the materials in nested welded stainless steel containers before storage or transport (Paffett *et al.*, 2003b).

Haschke and coworkers have suggested that the formation of explosive H_2–O_2 mixtures by reaction of water vapor with PuO_2 in air-filled containers is not possible because moisture-enhanced corrosion proceeds via a water-catalyzed cycle (Haschke *et al.*, 2001). In their proposed mechanism, water

absorbs strongly on the oxide below 120°C and desorbs as the temperature is increased to 200°C. Dissociative adsorption of water forms surface OH^-, promotes the formation of PuO_{2+x}, and releases H_2. When O_2 is present, they propose a surface catalyzed H_2–O_2 recombination to form surface adsorbed water that then reacts to form PuO_{2+x}, and atomic H on the surface. In the absence of O_2, H atoms associate as H_2 as indicated in equation 7.37 above. Association of H atoms with dissociatively adsorbed oxygen reforms H_2O and prevents the accumulation of H_2 whenever O_2 is present. H_2 appears only after O_2 is depleted.

While this proposed mechanism is plausible, it remains speculative until more data are produced to confirm the proposed mechanisms or to establish an alternative mechanism. What is clear from the above discussion is that our understanding of plutonium oxide chemistry, particularly the associated surface reactions is clearly inadequate.

Gas phase PuO_3 and PuO_4 By analyzing data on transpiration experiments of plutonium oxide, Krikorian and coworkers found that the observed oxygen pressure could only be explained by the presence of a PuO_3 molecule in the gas phase (Krikorian *et al.*, 1997). The presence of gas-phase PuO_3 was confirmed by Ronchi and coworkers a few years later (Ronchi *et al.*, 2000). Knudsen-effusion experiments in combination with mass spectrometry were used to show that PuO_2(s) exposure to oxygen above 1800–1900°C produces gas-phase molecules of PuO_3, along with the expected PuO and PuO_2 gas-phase molecules. These workers concluded that formation of PuO_3(g) was not formed from a gas-phase reaction of PuO_2(g) with oxygen or carbon dioxide gases, but rather the product of a reaction of gaseous oxygen with the surface of the solid PuO_2. In another recent report, Domanov *et al.* (2002) heated PuO_2 in a stream of helium–oxygen and employed a thermogradient tube furnace to separate and condense the volatile components that were subsequently analyzed by α-detection. The data were interpreted as producing volatile or gas-phase PuO_3 and PuO_4. The latter species was expected to have an abnormally high volatility, close to that of OsO_4. As the partial pressure of oxygen was decreased, the yield of the proposed PuO_4 species decreased. These data, while indirect, are quite intriguing. The relationship between the volatile species observed by Domanov *et al.* to those reported by Krikorian *et al.* and Ronchi *et al.* is uncertain. Further study using mass spectrometry as a function of oxygen partial pressure would help to clarify whether gas phase PuO_4 really exists. The clear finding from these studies, however, is that plutonium oxides can exist in oxidation states higher than IV, at least in the gas phase. These findings clearly challenge the traditional view that PuO_2 is the terminal species.

(*iii*) *Solid-state structures*

A summary of crystallographic data for plutonium oxides is given in Table 7.36. The majority of solid-state structures of plutonium oxides are structurally

related to the fluorite structure displayed by PuO_2. As a result of these structural similarities, we discuss the fluorite structure first to make the comparison with other oxide structures more understandable.

Cubic PuO_{2-x}

Plutonium dioxide forms a cubic fluorite phase over the composition range of PuO_{2-x}, where $0.4 < x < 0$. The cubic fluorite-type unit cell based upon CaF_2 is illustrated in Fig. 7.72. The lattice consists of an fcc arrangement of plutonium metal cations with O anions occupying most or all the four-fold tetrahedral sites, while the six-fold octahedral sites are vacant. In this structure, when $x = 0$, each plutonium atom is surrounded by eight oxygen atoms at the corners of a cube. Each cubic PuO_8 coordination polyhedron shares an edge with each of 12 neighboring PuO_8 polyhedra as shown in Fig. 7.90a. In this high-symmetry environment, all the Pu–O distances are the same. For a lattice parameter $a_0 = 5.396$ Å, this corresponds to a Pu–O distance of 2.337 Å, and a Pu–Pu distance of 3.816 Å. When $x > 0$, there are disordered oxygen vacancies.

Cubic C-Pu_2O_3

The C-Pu_2O_3 form of the sesquioxide displays the bcc Mn_2O_3 structure that is related to the fluorite structure with a doubled unit cell. The unit cell of the C-type sesquioxide can be considered as consisting of eight fluorite unit cells [a_0(bcc) = $2a_0$(fcc)] from which one-fourth of the oxygen atoms have been removed in an ordered way, and with the metal positions remaining almost unchanged from their fcc positions. The local coordination of the plutonium atom decreases from eight to six, and the PuO_8 cubes become PuO_6 octahedra but now with two types of plutonium atom. For one-fourth of the plutonium atoms, these missing oxygen atoms are at the ends of a body diagonal of the original PuO_8 cube, and for the other three-fourths they are at the ends of a face diagonal. Both PuO_6 coordination groups may be described as distorted octahedral, and each oxygen atom is four-coordinate and approximately tetrahedral. For cubic Pu_2O_3 with $a = 11.02$ Å, one plutonium atom has six equidistant Pu–O distances of 2.367 Å, and another plutonium atom has three pairs of Pu–O distances of 2.342, 2.360, and 2.383 Å. A comparison of the cubic PuO_2 and Pu_2O_3 structures is shown in Fig. 7.90.

Hexagonal A-Pu_2O_3

The A-type hexagonal sesquioxide formed at elevated temperatures displays the A-La_2O_3 crystal structure, typical of light lanthanide sesquioxides (Haire and Eyring, 1994). A striking feature of the hexagonal A-Pu_2O_3 structure is the highly unusual seven-coordination of the plutonium atoms. This gives three different Pu–O distances, three at 2.359, one at 2.353, and three at 2.623 Å. The local PuO_7 geometry is that of a mono-capped octahedron. Actually, there is also an eighth oxygen atom below the opposite face, but a much greater distance of 3.605 Å. This last oxygen atom, together with the seven in the PuO_7

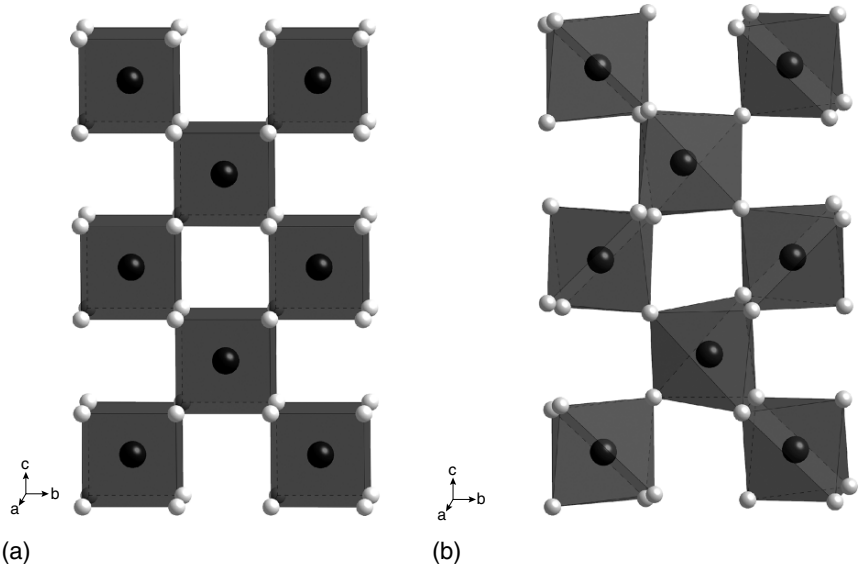

Fig. 7.90 (*a*) *A polyhedral representation of a layer of the fluorite-type structure of stoichiometric* PuO_2*, emphasizing the alternating cubic* PuO_8 *coordination polyhedra and vacancy sites within the structure, and illustrating the overall face-centered cubic arrangement of Pu metal atoms.* (*b*) *A polyhedral representation of a layer of the cubic C-type* Pu_2O_3 *structure drawn on the same scale and orientation, emphasizing the similarity in the fcc arrangement of Pu metal atoms between the cubic structures of* PuO_2 *and C-*Pu_2O_3*. The local coordination environment around Pu is now reduced to six near neighbors, with alternating* PuO_6 *distorted octahedra. Plutonium atoms are black and oxygen atoms are gray.*

polyhedron forms a distorted cube. These distorted cubes form the basis of the representation given for the A-type lattice given in Fig. 7.91.

Intermediate oxide structures, PuO_{2-x}

Intermediate oxides that display O:Pu stoichiometries between 1.5 and 2.0 (or those with stoichiometry between Pu_2O_3 and PuO_2) are not well characterized for plutonium. In general, intermediate oxides are common to both lanthanides and actinides, although their properties are much better established for the lanthanides. Since both sesquioxides and dioxides are known for plutonium, it is reasonable to assume that plutonium can form a homologous series of intermediate mixed-valent oxide phases Pu_nO_{2n-2} in analogy with the lanthanides. Unfortunately, very few data exist in this stoichiometry region for plutonium, though it is known that heavier actinides, americium, curium, berkelium, and californium form some members of an intermediate An_nO_{2n-2} series

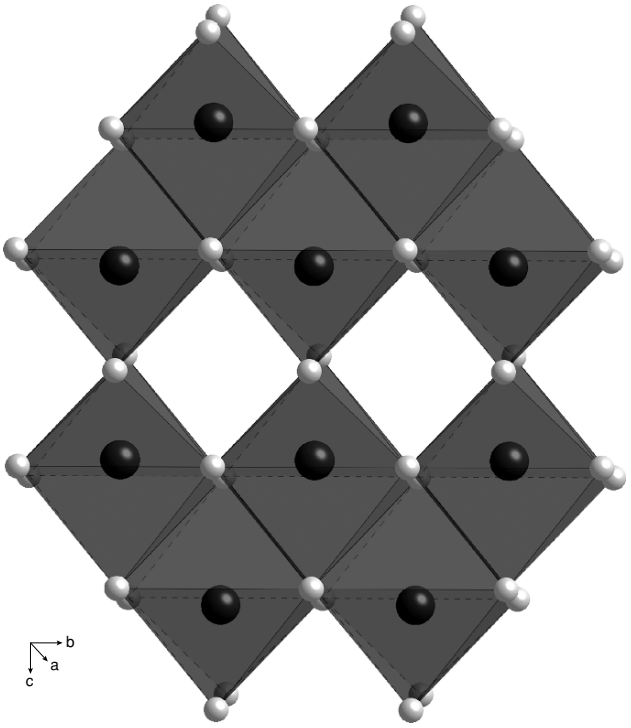

Fig. 7.91 *A polyhedral representation of a layer of the hexagonal A-type Pu_2O_3 emphasizing the hexagonal arrangement of Pu atoms. The local coordination environment around Pu has eight near neighbors, giving a highly distorted PuO_8 cube. Plutonium atoms are black and oxygen atoms are gray.*

(Haire and Eyring, 1994). Since Pu_2O_3 will take up oxygen to yield a hyperstoichiometric sesquioxide, and PuO_2 will lose oxygen to give a substoichiometric dioxide, the potential for such a series is most intriguing. Upon comparison of the ionic radii and relative free energies of the trivalent and tetravalent oxidation states of plutonium with those of cerium and praseodymium, Haschke concluded that such a mixed-valence series should be stable, and reported data from oxygen titration experiments in which the existence of a series Pu_nO_{2n-2} with $n = 5$, 7, 9, 10, and 12 was inferred (Haschke, 1992). Since the solid phases were not identified, the existence of the Pu_nO_{2n-2} series is not definitive, but clearly this is another area in which more detailed study is warranted.

The possibility of the existence of an intermediate oxide series of formula Pu_nO_{2n-2} is strongly suggested by structural principles established for the more well-studied cerium and praseodymium systems, and forms the basis of the

pedagogical phase diagram introduced by Hashke and coworkers (Haschke *et al.*, 2000a), shown in Fig. 7.92. In the structural model upon which this phase diagram is based, there is an fcc array of plutonium atoms in which all (and only) the tetrahedral interstices are occupied with oxygen atoms to form the end-member PuO_2. The intermediate phase compositions and structures are realized by omission of oxygen atoms in a regular way. Except for small shifts away from the vacant oxygen sites, the metal atoms maintain their fcc positions, and this leads to a homologous series Pu_nO_{2n-2} where Pu_2O_3 is the other end-member. Since Pu_2O_3 has a bcc structure, this end-member corresponds to $n = 4$ (Pu_4O_6). With this understanding, it is easy to rationalize the phase diagram of Fig. 7.92. There is a stoichiometric hexagonal sesquioxide (O:Pu = 1.5); a cubic sesquioxide with some vacancies occupied by oxygen (O:Pu = 1.5–1.7), showing variable lattice parameters; an oxide phase corresponding to the Pu_nO_{2n-2} homologous series (rhombohedral, narrow stoichiometry range); a substoichiometric fcc dioxide (O:Pu = 1.8–2.0) with variable and larger lattice parameter than the stoichiometric dioxide; and the stoichiometric and hyperstoichiometric dioxide. Like in the lanthanide systems, the intermediate oxides merge into a continuous PuO_{2-x} solid solution above 700°C. Whether the plutonium oxide system actually contains all of these

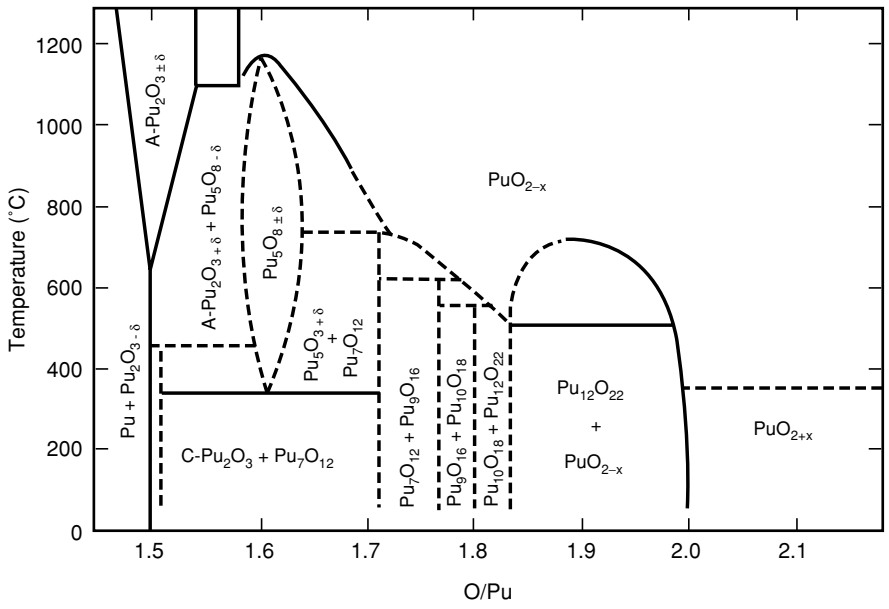

Fig. 7.92 *A pedagogical plutonium–oxygen phase diagram introduced by Hashke and Haire* (2000), *and based upon structural principles established for the more well-studied Ce and Pr oxide systems* (*Haschke* et al., 2000*a*).

features and closely resembles the lanthanide system will require more extensive study.

PuO_{2+x} structural studies

XRD analysis of the products of reaction between PuO_2 and water vapor show a single fcc phase with a fluorite-related structure with an expanded lattice. After reaching a minimum of 5.3975 Å at $PuO_{2.00}$, the lattice parameter increases over a narrow stoichiometry range, consistent with an initial stepwise expansion of the lattice and then a gradual increase with increasing oxygen composition. Results for O:Pu in the 2.016–2.169 range follow Vegard's law, implying that the oxide is a continuous PuO_{2+x} solid solution with a lattice constant given by:

$$a_0 = 5.3643 + 0.01764\ \mathrm{O:Pu} \tag{7.38}$$

Once the PuO_2 stoichiometry is reached, the lattice parameter is not very sensitive to composition, as shown in Fig. 7.93. Haschke and coworkers proposed that the additional oxygen atoms are accommodated in the vacant octahedral sites in the fluorite lattice, and that charge balance is maintained by replacing Pu(IV) with a higher oxidation state plutonium cation. Initial XPS data were interpreted as being consistent with Pu(VI), but more recent XANES spectroscopy has been interpreted as indicating the presence of Pu(V) (Conradson *et al.*, 2003). Recent EXAFS studies indicate that the original proposal of oxygen atoms in octahedral sites is far too simplistic (Conradson *et al.*, 2004b), and warrants further discussion.

Conradson and coworkers investigated 24 PuO_{2+x} samples prepared by a variety of methods including heterogeneous oxidation of plutonium metal and PuO_2 with gaseous H_2O and/or O_2, and by the hydrolysis and precipitation of the aqueous Pu(IV) ion (Conradson *et al.*, 2003, 2004b). Fourier transforms (FT) of the EXAFS data for selected plutonium oxide compounds are shown in Fig. 7.94. For stoichiometric, ordered $PuO_{2.0}$ the first peak in the Fourier transform is the contribution of the eight nearest neighbor oxygen atoms at 2.33 Å, well separated from the more distant second nearest neighbor peak of 12 plutonium atoms at 3.80 Å (the peaks in Fig. 7.94 are all phase-shifted to lower R). Regular features from the well-ordered extended structure subsequently continue to a very high distance from the central absorbing atom. This spectrum is therefore consistent with the crystal structure of stoichiometric PuO_2 shown in Fig. 7.90a.

However, as x increases from $PuO_{2.00}$ to $PuO_{2.26}$, the amplitudes of all of the peaks in the Fourier transform decrease monotonically, indicative of diminished order via displacements of the plutonium and oxygen atoms from their lattice sites coupled to the incorporation of the nonstoichiometric oxygen atoms into interstitial, essentially defect sites. What contradicts the current models in this process is the splitting of the first oxygen shell in the EXAFS (clearly evident

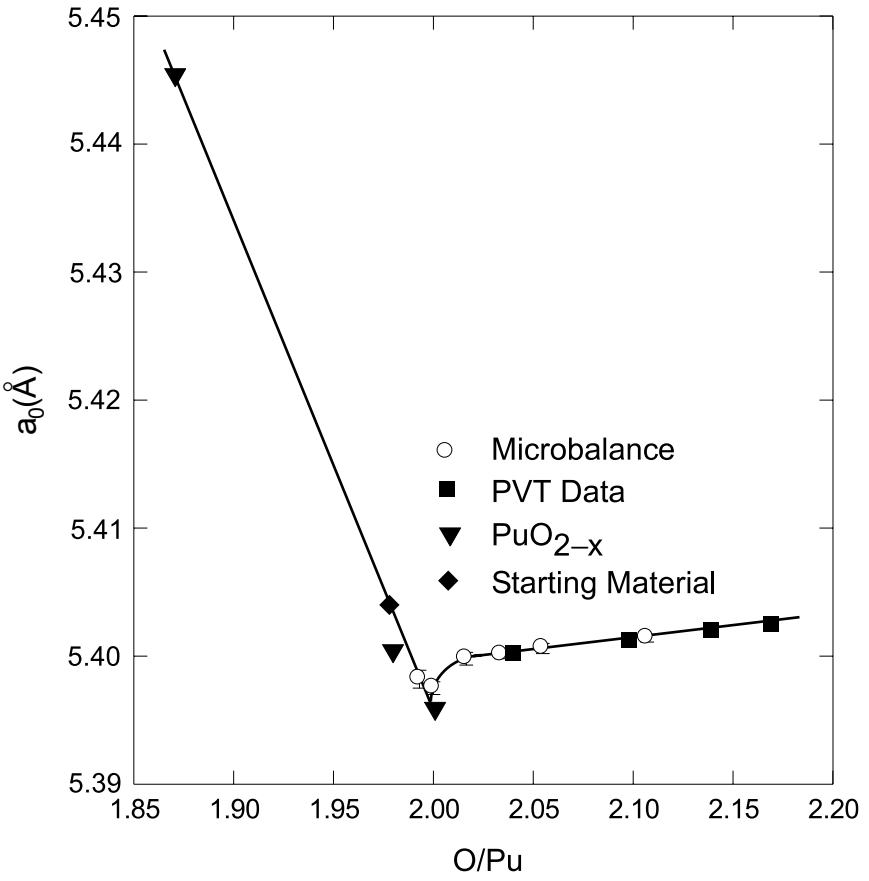

Fig. 7.93 *Variation of the cubic lattice parameter* (a_0) *of* $PuO_{2\pm x}$ *with O*:*Pu ratio at* 25°C. *Data for* PuO_{2-x} *are shown by gray triangles, microbalance data by open circles, and PVT data by solid squares* (*Haschke* et al., 2000*b*).

in Fig. 7.94) and the appearance of a short Pu–O bond distance of 1.84 Å. Traditional diffraction techniques that probe long-range order have never observed this phenomenon, but the bond distance is similar to the 1.85 Å distance found in axial Pu=O bonds in molecular Pu(V) compounds. Indeed, XANES results were interpreted as being consistent with a mixture of Pu(IV) and Pu(V). Combined, these data suggest that as the plutonium center becomes partially oxidized in PuO_{2+x}, there is a strong driving force to form short, strong, covalent Pu=O bonds.

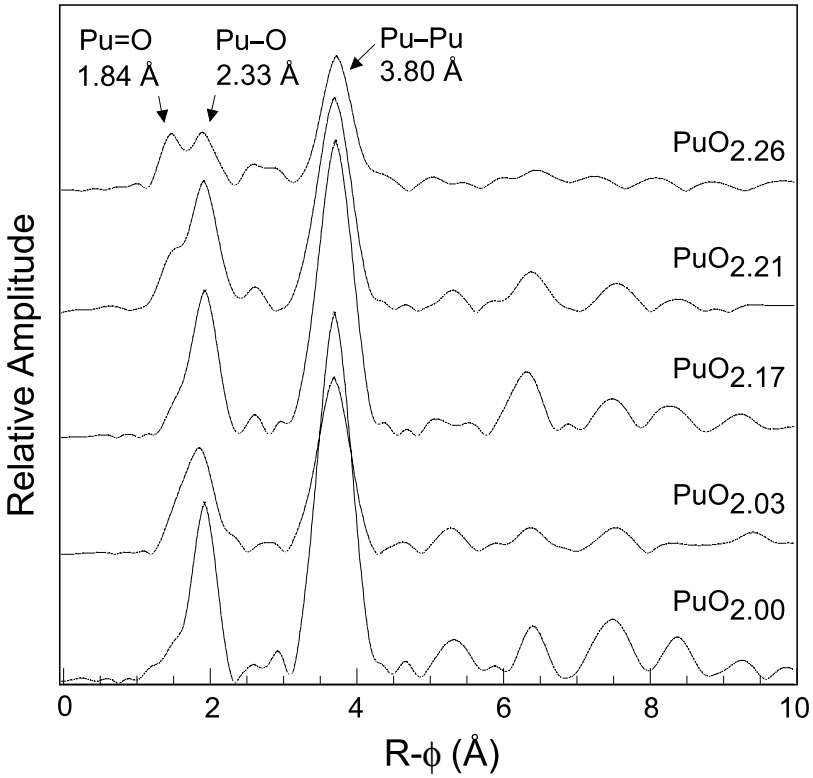

Fig. 7.94 *A comparison of k^3-weighted EXAFS moduli of PuO_{2+x} samples as indicated, and all data are taken from Conradson* et al. (2004*b*). *The peak positions are phase-shifted to lower distance from the actual Pu–O or Pu–Pu distances.*

These data also show that the plutonium atoms retain their essentially fcc positions, and while the plutonium sublattice retains its order through the progression of $PuO_{2.00}$ to $PuO_{2.26}$, the nearest-neighbor oxygen atoms are found in a multisite distribution. In addition to Pu–O distances of 2.33 Å, the additional oxygen atom in PuO_{2+x} generates new bonds both shorter and longer than the 2.33 Å value. These new Pu–O distances were tentatively assigned to bridging O^{2-}/OH^- (2.13, 2.28 Å) and possibly H_2O (2.41 Å) ligands. Based on these observations, Conradson *et al.* suggest that the oxidation produces linear PuO_2^+ moieties that are aperiodically distributed through the lattice, and suggest several structural models that would be consistent with all the observations (Conradson *et al.*, 2004b). Finally, recent XPS results indicate a hydroxylated surface in PuO_{2+x} samples whose thickness depends on exposure conditions (temperature, partial pressure of H_2O) (Paffett *et al.*, 2003a). Much more study in this area is expected in the coming years.

The original report of PuO_{2+x} and its relevance to long-term storage of plutonium through H_2 gas generation has prompted several theoretical studies of this material. To study the electronic structure of PuO_{2+x} with $x = 0.25$, a periodic supercell consisting of four PuO_2 formula units has been used, constituting the conventional fluorite cubic cell of Pu_4O_8 (as shown in Fig. 7.71 for PuH_2). The additional oxygen atom was placed on the octahedral interstitial site, giving rise to a hypothetical Pu_4O_9 compound. Employing a self-interaction correction local spin density method, Petit *et al*. (2003) concluded that stoichiometric PuO_2 displays Pu(IV) with a localized f^4 shell. When oxygen is introduced into the octahedral interstitial site, the nearby plutonium atoms turn into Pu(V) (f^3) by transferring electrons to the oxygen. Oxygen vacancies cause Pu(III) (f^5) to form by taking up electrons released by oxygen (Petit *et al.*, 2003). In another DFT study, Korzhavyi *et al.* (2004) find a similar result, and calculate the thermodynamics for reactions of PuO_2 with either O_2 or H_2O to form PuO_{2+x}. In both cases the reactions are endothermic, i.e. to occur they require a supply of energy. However, the calculations also show that PuO_{2+x} can be formed as an intermediate product by reaction with H_2O radiolysis products such as H_2O_2. While the placement of the interstitial oxygen atom in the octahedral hole of a hypothetical Pu_4O_9 system is not consistent with the experimental findings for PuO_{2+x}, they are consistent with the formation of Pu(V), and offer insights to guide further experimental study.

Penneman and Paffet applied Zachariasen's classic bond strength–bond length relationships (Zachariasen, 1954a,b) to the Pu_4O_9 ($PuO_{2.25}$) entity to suggest that a better description is Pu_4O_8OH containing Pu(V) ions (Penneman and Paffett, 2004, 2005). Bond strength–bond length arguments justify the location of a hydroxide ion, rather than a central oxide ion, in a plutonium dioxide structure, providing an alternative interpretation for the experimental data on plutonium dioxide oxidation by water.

(*iv*) *Properties of plutonium oxides*

Oxygen diffusion

Fluorite-related lanthanide oxides exhibit unusual diffusional properties in that the oxygen substructure (excess interstitial oxygen ions and oxygen vacancies) is mobile below 300°C, which places them in the category of fast-ion conductors (Haire and Eyring, 1994). In actinide oxides of the fluorite structure, interstitial excess oxygen ions and oxygen vacancies are extremely mobile with diffusion rates similar to those of other fluorite-type superionic conductors (Matzke, 1982). Chemical diffusion measurements on PuO_{2-x} reveal relatively high values for diffusion coefficients (Bayoglu and Lorenzelli, 1984), and activation energies in the vicinity of 46 kJ mol^{-1}, which is very close to the migration energy of anion vacancies in UO_{2-x} (49 kJ mol^{-1}) (Chereau and Wadier, 1973; Bayoglu and Lorenzelli, 1979).

For stoichiometric PuO_2, oxygen diffusion has been studied by gas-phase isotope exchange by Bayoglu and coworkers, and by Deaton and Wiedenheft who obtained activation energies of 177 and 187 kJ mol^{-1}, respectively (Deaton and Wiedenheft, 1973; Bayoglu *et al.*, 1983). Murch and Catlow (1987) have suggested that since oxygen interstitials in PuO_2 are almost certainly less mobile than oxygen vacancies, one can assume that the activation energy for oxygen diffusion in stoichiometric PuO_2 can be partitioned into two parts, given by

$$Q = H_F/2 + H_v^m \tag{7.39}$$

where H_v^m is the anion vacancy migration enthalpy and H_F is the enthalpy for anion Frenkel defect formation. With H_v^m given by 46 kJ mol^{-1}, the Frenkel energy is given by 262–282 kJ mol^{-1}.

Melting behavior

The melting behavior of the individual plutonium oxides has been studied by many authors (Holley *et al.*, 1958; Pijanowski and DeLucas, 1960; Chikalla *et al.*, 1962, 1964; Lyon and Baily, 1965, 1967; Chikalla, 1968; Riley, 1970), and has been thoroughly reviewed (IAEA, 1967; Wriedt, 1990; Lemire *et al.*, 2001).

Stoichiometric hexagonal A-Pu_2O_3 ($PuO_{1.50}$) was found to have a melting point of 2085 ± 25°C (Chikalla *et al.*, 1962, 1964), which agrees well with the value of 2075°C reported by Riley (1970). The value of 2080°C was adopted by the IAEA review panel (IAEA, 1967), and by Wriedt (1990) in their reviews.

No melting point can be reported for cubic C-Pu_2O_3 ($PuO_{1.52}$), since this compound undergoes a solid-state peritectoid decomposition to A-Pu_2O_3 ($PuO_{1.5}$) and C′-Pu_2O_3 ($PuO_{1.6+\delta}$) at 450°C (Wriedt, 1990). No melting point for C′-Pu_2O_3 ($PuO_{1.6+\delta}$) can be reported as it transforms congruently to PuO_{2-x} above a temperature of about 1180°C (Wriedt, 1990).

The melting point of PuO_{2-x} depends on the O:Pu ratio. For stoichiometric $PuO_{2.00}$, a number of values have been reported; however, the best values are thought to be those reported by Lyon and Baily (1965, 1967), who found 2390 ± 20°C, or Aitken and Evans (1968) who found a value of 2445°C. These experiments were performed on specimens sealed in tungsten capsules to prevent loss of oxygen. Wriedt (1990) proposed a value of 2445°C, and Adamson *et al.* (1985) recommend the intermediate value of 2428°C.

Vaporization behavior

The plutonium oxide vaporization process is extremely complicated because the solid undergoing vaporization changes its composition during the process. The majority of vapor pressure measurements of plutonium oxides have been carried out by the Knudsen-effusion method (Phipps *et al.*, 1950b; Mulford and Lamar, 1961; Paprocki *et al.*, 1962a; Pardue and Keller, 1964; Ackermann *et al.*, 1966; IAEA, 1967; Capone *et al.*, 1999), with the notable exception of a few

mass spectrometry reports (Battles *et al.*, 1968, 1969; Battles and Blackburn, 1969; Kent, 1973). All these data have been reviewed (Wriedt, 1990). The results of these measurements are often conflicting because the condensed oxide phase PuO_{2-x} is at its congruent vaporizing composition, which varies with temperature. When inert containers are used, solid PuO_2 that has a higher O:Pu ratio than the congruent composition will produce vapor with relatively high concentrations of $PuO_2(g)$, $O_2(g)$, and O(g). In contrast, compositions with a lower O:Pu ratio than the congruent composition will produce relatively high concentrations of PuO(g) (Wriedt, 1990). Thus, the early Knudsen measurements yield insufficient information to explain the vaporization behavior of PuO_2 and PuO_{2-x} in detail.

Battles and coworkers (Battles *et al.*, 1968, 1969; Battles and Blackburn, 1969) have determined the species that occur in the vapor of PuO_{2-x} and in the vapor over the binary condensed phase mixture of Pu_2O_3 and $PuO_{1.61}$ over a period of 20 hours. A typical set of data is shown in Fig. 7.95.

In the case of single-phase material, it was found that initially stoichiometric $PuO_{2.00}$ slowly turns into $PuO_{1.831}$ and retains the latter composition. In the vapor, the species PuO_2^+ (g) and PuO^+(g) were observed. At 2219 K the partial pressures of Pu(g) and of O(g) were calculated to be 2.6×10^{-9} and 2.6×10^{-7} atm, respectively. The mass spectrometry results (Battles *et al.*, 1968, 1969; Battles and Blackburn, 1969; Kent, 1973) are in good agreement with those measured by effusion in open containers by Ackermann and coworkers (Ackermann *et al.*, 1966). Partial pressures of O(g), $O_2(g)$, Pu(g), PuO(g) and $PuO_2(g)$ have been tabulated for various PuO_{2-x} compositions and temperatures (Kent and Zocher, 1976; Green *et al.*, 1983).

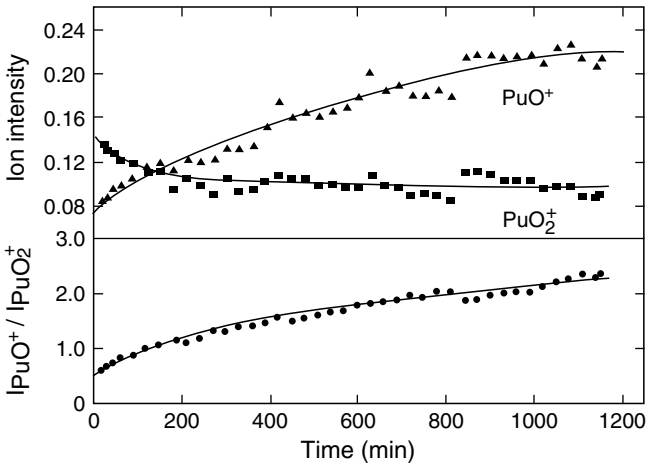

Fig. 7.95 *Mass spectroscopic intensities of gaseous* PuO_2^+ *and* PuO^+, *and the ratio of intensities* $I_{PuO^+}/I_{PuO_2^+}$ *as a function of time at* 2225 K (*Battles* et al., 1968, 1969).

More recently, Krikorian and coworkers suggested that heating PuO_2 in the presence of oxygen produced the PuO_3 molecule in the gas phase (Krikorian *et al.*, 1997), and this was definitively proven by Ronchi and coworkers who used Knudsen-effusion experiments in combination with mass spectrometry to show that PuO_2 exposure to oxygen above 1800–1900°C produces a gas phase molecule PuO_3, along with the expected PuO and PuO_2 gas phase molecules (Ronchi *et al.*, 2000).

Thermodynamic properties of plutonium oxides

The thermodynamic properties of the plutonium oxides have been studied and assessed by numerous authors, and the reader is directed to extensive compilations by Rand (1966), IAEA (1967), Wriedt (1990), and the recent OECD-NEA review of plutonium and neptunium thermodynamics (Lemire et al., 2001). A summary of the most recent OECD-NEA selected thermodynamic data for plutonium oxides is given in Table 7.38.

Stoichiometric Pu_2O_3 ($PuO_{1.5}$) Flotow and Tetenbaum (1981) measured the low-temperature heat capacity from –265 to 77°C on a sample of $^{242}Pu_2O_3$. The heat capacity (C_p°) and entropy (S°) at standard conditions derived from their data were selected by the OECD-NEA reviewers, and are given in Table 7.38 (Lemire *et al.*, 2001). Estimates of the heat capacity of Pu_2O_3 at higher temperatures have been given by IAEA (1967), Glushko (1982), and Besmann and Lindemer (1983). The NEA reviewers recommended the following expressions for heat capacity of Pu_2O_3 over two separate temperature ranges.

$$(298.15 - 350\text{K})$$
$$C_p^\circ = 169.466 - 79.98 \times 10^{-3}T - 25.459 \times 10^5 T^{-2}\ \text{J K}^{-1}\text{mol}^{-1} \qquad (7.40)$$

$$(350 - 2358\text{K})$$
$$C_p^\circ = 122.953 + 28.548 \times 10^{-3}T - 15.012 \times 10^5 T^{-2}\ \text{J K}^{-1}\text{mol}^{-1} \qquad (7.41)$$

There are no direct measurements of the enthalpy of formation of Pu_2O_3. The value has been derived indirectly from the partial molar Gibbs energies and enthalpies of oxygen in the single-phase oxides Pu_2O_3 and PuO_2, and the two-phase fields between these phases. A thorough discussion of the data and measurement techniques is available in the most recent reviews (IAEA, 1967;

Table 7.38 *Thermodynamic parameters for plutonium oxides* (*Lemire* et al., 2001).

Compound	$\Delta_f G^\circ_{298}$ (kJ mol^{-1})	$\Delta_f H^\circ_{298}$ (kJ mol^{-1})	S°_{298} (J K^{-1} mol^{-1})	C°_{p298} (J K^{-1} mol^{-1})
Pu_2O_3	−1580.4 ± 10.1	−1656.0 ± 10.0	163.0 ± 0.6	117.0 ± 0.5
$PuO_{1.61}$	−834.8 ± 10.1	−875.5 ± 10.0	83.0 ± 5.0	61.2 ± 5.0
PuO_2	−998.1 ± 1.0	−1055.8 ± 1.0	66.13 ± 0.26	66.25 ± 0.26

Wriedt, 1990; Lemire *et al.*, 2001). The recommended values for the enthalpy and Gibbs energy of formation are listed in Table 7.38.

Hyperstoichiometric $PuO_{1.52}$ (C-Pu_2O_3) The only thermodynamic data for this phase are the enthalpies of combustion reported by Chereau *et al.* (1977). Their values correspond to an enthalpy of formation of –845 kJ mol^{-1} (Lemire *et al.*, 2001).

Hyperstoichiometric $PuO_{1.6+\delta}$ No experimental data are available. Thermodynamic functions were estimated by NEA reviewers (Lemire *et al.*, 2001).

Stoichiometric $PuO_{2.00}$ The thermodynamic properties of stoichiometric $PuO_{2.00}$ have been the subject of a large number of studies (Sandenaw, 1963; Pardue and Keller, 1964; Ackermann *et al.*, 1966; Rand, 1966; Kruger and Savage, 1968; Engel, 1969; Ogard, 1970; Flotow *et al.*, 1976), and have been extensively reviewed (IAEA, 1967; Cordfunke *et al.*, 1990; Wriedt, 1990; Carbajo *et al.*, 2001; Lemire *et al.*, 2001).

To overcome difficulties performing low-temperature heat capacity measurements on $^{239}PuO_2$, Flotow *et al.* (1976) performed studies with the less radio active isotopes $^{242}PuO_2$ and $^{244}PuO_2$ to avoid problems associated with radiation damage of the solid for low temperatures up to 350 K. These measurements are thought to provide the most reliable values for standard heat capacity (C_p°) and entropy (S°). Their values were selected by the NEA review, and are listed in Table 7.38. High-temperature measurements of enthalpy were measured by Kruger and Savage (1968), Engel (1969), Ogard (1970), and Oetting (1982). Fink (1982) used these data to derive a complex expression for heat capacity, and these were refit to polynomials by Cordfunke *et al.* (1990). The Fink expressions were recently modified by the NEA review to give the following polynomial expression over the temperature range 298.15–2500 K (Lemire *et al.*, 2001):

$$C_p^\circ = 84.495 + 10.639 \times 10^{-3} T - 6.1136 \times 10^5 T^2 - 19.00564 \times 10^5 T^{-2} \text{ J K}^{-1}\text{mol}^{-1} \quad (7.42)$$

The original polynomial functions derived by Fink are far more complex than the NEA modification, and for more information the reader is referred to the original Fink citation (Fink, 1982) or a recent review by Carbajo *et al.* (2001).

There is good agreement between authors on the values for the enthalpy and Gibbs free energy (Holley *et al.*, 1958; Glushko, 1982). The values accepted by the NEA review are given in Table 7.38 (Lemire *et al.*, 2001).

Chemical properties of plutonium oxides

Dissolution of PuO_2 PuO_2 that has been ignited at high temperatures is difficult to dissolve. Christensen and Maraman (1969), Gilman (1965, 1968),

Ryan and Bray (1980), and Nikitina *et al.* (1997a,b), have reviewed the methods reported. In general, the rate of dissolution for each reagent often depends on the ignition temperature used to prepare the oxide and on the previous history of the sample. The reagent most frequently used is a boiling mixture of 16 M HNO_3 with 1 M HF as a fluoride complexant. Instead of HF, H_2SiF_6, or Na_2SiF_6 may also be used. High-temperature fired PuO_2 is dissolved only slowly. Irradiated PuO_2 dissolves better, the rate of dissolution being higher, the higher the burnup.

The difficulty in dissolving PuO_2 has led to the search for aggressive approaches to achieve dissolution, such as the use of fused salts (Harvey *et al.*, 1947; Feldman, 1960; Crocker, 1961), dioxygen difluoride, O_2F_2 (Malm *et al.*, 1984), or krypton difluoride, KrF_2 (Asprey *et al.*, 1986). Dioxygen difluoride, and krypton difluoride react readily with PuO_2 to form PuF_6 and/or PuO_2F_2, but this approach has not been pursued on a large scale because of the extreme difficulty in handling KrF_2 and O_2F_2. Two major improvements to the dissolution of PuO_2 have recently appeared. They are based on the electrochemical oxidative dissolution in HNO_3 with Ag(II) as a catalyst (Bourges *et al.*, 1986; Sakurai *et al.*, 1989, 1993; Madic *et al.*, 1992), and oxidative dissolution catalyzed by Ce(IV) in the presence of anions of oxygen-containing acids of group IV–VII elements (Horner *et al.*, 1977; Scheitlin and Bond, 1980). The kinetics and mechanism of these processes and their use for dissolving plutonium from recycled products and wastes have been reviewed (Nikitina *et al.*, 1997a).

Compatibility with Container Materials Because of its importance as a nuclear reactor and heat source fuel, the compatibility of PuO_2 with refractory materials (both metals and ceramics) has been extensively studied. Paprocki *et al.* (1962b) studied the chemical reactions of plutonium dioxide with reactor materials.

An extensive study of the compatibility of $^{238}PuO_2$ with container materials has been reported by Selle *et al.* (1970a,b). They studied the reactions of $^{238}PuO_2$ with container materials such as tantalum, molybdenum, tungsten, rhenium, platinum, rhodium, and their alloys in the temperature range 1000–2500°C and for time periods up to 532 days. For the results, the reader is referred to the comprehensive original reports. Such studies have led to the use of iridium–0.3% tungsten alloys for encapsulation of $^{238}PuO_2$ general-purpose heat sources, and Pt–30%Rh alloys for encapsulation of $^{238}PuO_2$ light weight radioisotope heater units (see Section 7.3).

(b) The plutonium–sulfur, -selenium, and -tellurium systems

With heavier chalcogen elements (X = S, Se, and Te), plutonium forms binary compounds in four basic families (Table 7.39) with the highest-order composition being PuX_3 that is only found for tellurium. All the heavy chalcogen

Table 7.39 *Crystallographic properties of binary plutonium chalcogenides.*

Compound	*Symmetry*	*Space group*	*Lattice parameters*			*Density* ($g\ cm^{-3}$)	*References*
			a_0 (Å)	b_0 (Å)	c_0 (Å)		
PuX							
$PuS_{0.95}$	fcc	F*m*3*m*	5.5280(5)				Marcon (1969)
PuS	fcc	F*m*3*m*	5.5400(5)			10.60	Marcon (1969)
PuS	fcc	F*m*3*m*	5.5437(3)				Wastin *et al*. (1995)
PuSe	fcc	F*m*3*m*	5.79334(1)			10.86	Kruger and Moser (1967a)
PuSe	fcc	F*m*3*m*	5.7992(5)				Wastin *et al*. (1995)
PuSe	fcc	F*m*3*m*	5.773(3)				Damien (1976)
PuSe	fcc	F*m*3*m*	5.776(1)				Marcon (1969)
PuTe	fcc	F*m*3*m*	6.183(4)			10.32	Gorum (1957)
PuTe	fcc	F*m*3*m*	6.151(3)				Allbutt *et al*. (1970)
PuTe	fcc	F*m*3*m*	6.1900(6)				Wastin *et al*. (1995)
Pu_2X_3							
Pu_3S_4	bcc	I$\bar{4}$3*d*	8.395			9.41	Damien (1976)
γ-Pu_3S_{4+x}	bcc	I$\bar{4}$3*d*	8.4155(5)			8.53	Marcon (1969)
γ-Pu_3S_{3-x}	bcc	I$\bar{4}$3*d*	8.4590(5)			8.41	Marcon (1969)
α-Pu_2S_3	orthorhombic	P*nmm*	3.97(1)	7.37(2)	15.45(3)	8.31	Marcon (1969)
γ-Pu_2S_3	bcc	I$\bar{4}$3*d*	8.4585				Damien (1976)
γ-Pu_2Se_3	bcc	I$\bar{4}$3*d*	8.7965(5)				Marcon (1969)

γ-Pu_2Se_3	bcc	I$\bar{4}$3*d*	8.802				Damien (1976)
Pu_3Se_4	bcc	I$\bar{4}$3*d*	8.768				Damien (1976)
η-Pu_2Se_3	orthorhombic	P*bnm*	4.10(1)	11.10(2)	11.32(2)		Marcon (1969)
γ-Pu_2Te_3	bcc	I$\bar{4}$3*d*	9.355				Damien (1976)
η-Pu_2Te_3	orthorhombic	P*bnm*	11.94(2)	12.10(2)	4.339(6)		Damien (1976)
***PuX*$_{2-x}$**							
$PuS_{1.76}$	tetragonal	P4/*nmm*	3.936		7.958		Allbutt and Dell (1967) and Damien (1976)
$PuS_{1.9}$	tetragonal	P4/*nmm*	3.943(3)		7.962(5)		Marcon (1969)
$PuS_{2.0}$	monoclinic	P2_1/*a*	7.962(10)	3.981(5)	7.962(10)		Marcon (1969)
$PuS_{2.0}$	tetragonal	P4/*nmm*	3.974		7.947	8.0	Allbutt and Dell (1967)
$PuSe_{1.8}$	tetragonal	P4/*nmm*	4.100(5)		8.364(5)		Marcon (1969)
$PuSe_{1.814}$	tetragonal	P4/*nmm*	4.088		8.539		Allbutt and Dell (1967) and Damien (1976)
$PuSe_{1.9}$	tetragonal	P4/*nmm*	4.165		8.41(1)		Marcon (1969)
$PuSe_{1.987}$	tetragonal	P4/*nmm*	4.132		8.343		Allbutt and Dell (1967) and Damien (1976)
$PuTe_{1.81}$	tetragonal	P4/*nmm*	4.334		8.984		Damien (1976)
$PuTe_{2.02}$	tetragonal	P4/*nmm*	4.391		8.938		Damien (1976)
***PuX*$_3$**							
$PuTe_3$	pseudo-tetragonal	B*mmb*	4.338(5) 6.151(3)	4.338(5)	25.60(9)		Damien (1973) Damien (1976)

elements form the series of substoichiometric complexes PuX_{2-x}. For the sesquichalcogenides of formula Pu_2X_3, sulfur forms an α-phase, all the chalcogenides form a γ-phase, while selenium and tellurium form an η-phase. All the heavier chalcogenides form the simple binary PuX.

(*i*) *Preparation*

All of the heavier chalcogenide compounds of plutonium can be prepared by gas–solid reaction between the appropriate stoichiometry of plutonium hydride (PuH_x) and chalcogen element in quartz tubes sealed under secondary vacuum (Damien, 1973, 1976; Damien and De Novion, 1981; Damien *et al.*, 1986). After a typical reaction time of 1 week at 350–750°C, the dichalcogenide, PuX_{2-x} is formed. Compounds with lower X/Pu ratio can be prepared by thermal decomposition of PuX_{2-x} in a sealed tube where one end is kept outside the furnace to allow for the deposition of the chalcogen element. The monochalcogenide, PuX requires much-higher temperature for formation. Typically the quartz tube is heated to 800°C, and the products are pressed into pellets and sintered at 1200–1600°C. This approach works for all the chalcogenide elements except tellurium. Reaction of plutonium hydride with excess tellurium under high vacuum at 350°C for 1 week produces $PuTe_3$ (Damien, 1973). The plutonium tritelluride undergoes decomposition in a stepwise fashion to produce $PuTe_{2-x}$ at 400°C, η-Pu_2Te_3 at 700°C, and γ-Pu_2Te_3 at 900°C (Allbutt *et al.*, 1970; Damien, 1973).

In addition to preparation using plutonium hydride, all the plutonium chalcogenides (sulfur, selenium, tellurium) may be prepared by direct synthesis from the elements (Gorum, 1957; Marcon and Pascard, 1966a,b; Kruger and Moser, 1967a; Marcon, 1969; Wastin *et al.*, 1995). For volatile compounds, the reactions may be carried out in two- or three-zone vacuum-sealed quartz tubes that are placed in a temperature gradient resistance furnace (Spirlet, 1982; Spirlet and Vogt, 1982). The product stoichiometry and phase is controlled by the reaction temperature and stoichiometry of reactants. For compounds that are not highly volatile, excellent results have been obtained when using levitation melting in an induction coil or in a Hukin magnetic levitation cold crucible, by semilevitation melting on a pedestal, or by arc melting (Wastin *et al.*, 1995).

There are other methods for preparation of a few specific plutonium chalcogenide. In the early work of Abraham *et al.* (1949b), PuS was accidentally obtained when PuF_3 was reduced with Ca vapor in a BaS crucible at 1250°C. High-purity PuS may also be obtained when compact plutonium metal is first reacted to give the hydride, the hydride is ground to powder in an inert-gas atmosphere, and, after decomposition to the metal, is reacted with H_2S. A similar reaction of the plutonium hydride with H_2S may also be used to prepare α-Pu_2S_3. Finally, PuSe can be obtained by reacting a higher selenide with plutonium metal (Marcon, 1969).

(*ii*) *Solid-state structures*

Crystallographic properties of binary plutonium chalcogenides are summarized in Table 7.39.

Plutonium tritelluride crystallizes in the orthorhombic $NdTe_3$ structure type (Norling and Steinfink, 1966; Damien, 1973). In this structure, the unit cell contains 12 planar layers each consisting of a single type of atom. Since the separation between the plutonium and tellurium layers is about 0.9 Å, the two layers can be considered as a single puckered layer. In this way, the structure can be described as consisting of four puckered Pu–Te layers and four densely packed tellurium layers. Each plutonium atom is surrounded by nine near-neighbor tellurium atoms, and the $PuTe_9$ coordination polyhedron approximates a capped square antiprism with a distortion of the plutonium atom out of the center of the tellurium prism, as depicted in Fig. 7.96.

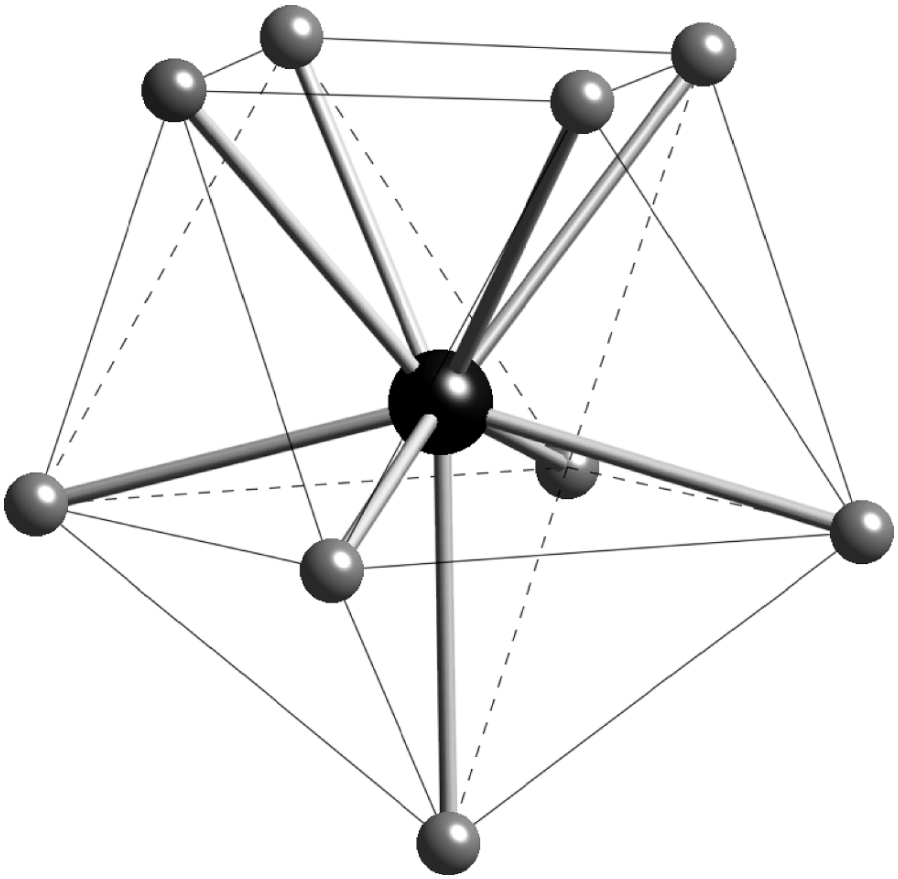

Fig. 7.96 *Local coordination sphere around plutonium in $PuTe_3$ and PuX_2. The plutonium atom is black and tellurium atoms are gray.*

The ideal structure of plutonium dichalcogenides, PuX_2 is the anti-Fe_2As in space group $P4/nmm$ ($Z = 2$) (Damien *et al.*, 1986). In this structure, layers of five chalcogen atoms in the basal face-centered square plane are separated by two slabs of alternating Pu^{3+} (nine-fold coordination) and X^{2-} ions. The local PuX_9 coordination polyhedron is identical to that seen in $PuTe_3$, depicted in Fig. 7.96. All the PuX_{2-x} compounds are distorted from this idealized structure due to the formation of X–X bonding pairs within the basal planes. A typical structure is shown in Fig. 7.97. This distortion gives rise to a number of pseudo-cubic, tetragonal, orthorhombic, and monoclinic ($\beta = 90°$) anti-Fe_2As superstructures (Flahaut, 1979; Rolland *et al.*, 1994). From Table 7.39, it can be seen that all PuX_{2-x} (X = S, Se, and Te) compounds display the pseudo-tetragonal cell of the anti-Fe_2As structure, with the exception of PuS_2, which displays the monoclinic ($\beta = 90°$) $CeSe_2$ variant of the structure (Marcon and Pascard, 1968).

The sesquichalcogenides of plutonium are isostructural with the rare-earth analogs (Damien *et al.*, 1986). The low-temperature stoichiometric phase,

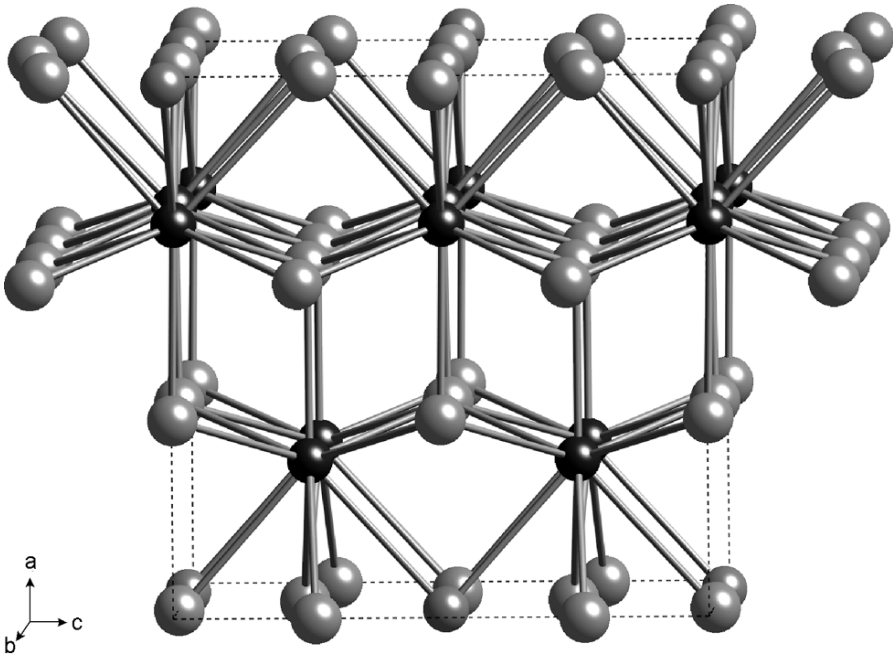

Fig. 7.97 *Solid-state crystal structure of plutonium dichalcogenides, PuX_2, emphasizing the local PuX_9 coordination. The X–X bonding pairs are not indicated for clarity. The distortions in the chalcogen layers due to X–X bonding are clearly evident in this model, based on monoclinic $LaTe_2$ (Stöwe,* 2000). *Plutonium atoms are black and chalcogen atoms are gray.*

referred to as α-Pu_2X_3 only exists for the sulfide, and has the orthorhombic La_2S_3-type structure, with two plutonium sites displaying local PuS_7 and PuS_8 coordination. The high-temperature γ-Pu_2X_3 phase is not a stoichiometric phase, and exists over a range of compositions varying from Pu_2X_3 to Pu_3X_4. This phase displays the cubic Th_3P_4 structure, where the coordination number of the plutonium atom is eight. For selenium and tellurium, there is a η-Pu_2X_3 phase that displays the orthorhombic U_2S_3 structure. The η-Pu_2Se_3 is thermally unstable and transform near 800°C into the cubic γ-Pu_2Se_3 of the Th_3P_4 structure. Early reports of a β-phase for Pu_2S_3 have been shown to be incorrect, as the material is now known to be a ternary oxychalcogenide (Carre *et al.*, 1970). All monochalcogenides of plutonium (PuX) have the cubic NaCl crystal structure.

(*iii*) *Properties*

The monochalcogenides have a metallic luster that can be described as gold, copper, and black for the sulfide, selenide, and telluride, respectively. The monochalcogenides have been the subject of extensive study directed towards understanding valency and the itinerant or localized nature of their 5f electrons. Several excellent overviews are available (Rossat-Mignod *et al.*, 1984; Buyers and Holden, 1985; Dunlap and Kalvius, 1985; Fournier and Troc, 1985; Santini *et al.*, 1999; Wachter, 2003).

Single crystal samples of PuX have been examined by neutron scattering, magnetic susceptibility, and electrical resistivity. All of the PuX compounds (X = S, Se, Te) are nonmagnetic with magnetic susceptibilities that are almost temperature independent for temperatures above 50 K (Lander *et al.*, 1987). Electrical resistivity increases continuously from room temperature with two changes of thermal behavior around 200 and 30 K, confirming the hypothesis that the PuX compounds are semiconductors with small energy gaps. Fournier *et al.* (1990) suggest that the ground state of the monochalcogenides is a weak magnetic nonconducting $6d^1$–$5f^5$ Kondo state with a high Kondo temperature of ca. 400 K.

Wachter and coworkers proposed that these properties of PuX compounds can be consistently explained by the assumption that the plutonium chalcogenides are related to the high-pressure intermediate-valent form of the isoelectronic samarium chalcogenides. Pressure in the divalent SmX serves to enhance f–d hybridization to achieve an intermediate valence state, whereas in PuX, f–d hybridization is achieved without pressure because of the larger radial extension of the 5f wave functions relative to the 4f wave functions. Using PuTe as an example, they conclude that SmTe achieves the same state under a pressure of 58 kbars, and achieves an intermediate valence of 2.75 (Wachter *et al.*, 1991). The intermediate valence model is supported by experimental measurement of elastic constants and observation of a negative value for c_{12} (–39 GPa) (Mendik *et al.*, 1993; Wachter *et al.*, 2001). Photoemission measurements on PuSe films

(Gouder *et al.*, 2000) were interpreted as a 5f localization and not an intermediate valent configuration where 5f and 6d states hybridize. Wachter suggested that the existence of a strong Pauli paramagnetism gives a high DOS near the Fermi level, complicating the interpretation. Recent photoemission studies on PuTe single crystals confirm the presence of a strong three-peak structure near the Fermi level in agreement with of an intermediate valence state in PuTe (Durakiewicz *et al.*, 2004).

(c) Ternary and polynary plutonium chalcogenides

A large number of ternary and polynary plutonium/metal chalcogenides have been described in the literature. The majority of these compounds are ternary and quaternary oxide phases, some of which have gained technological importance. The term 'ternary oxide phases' in this context includes two general classes of material. The first are oxoplutonate compounds with PuO_x^{n-} polyhedral anions and mono-, di-, or trivalent metal cations. A typical example would be Ba_3PuO_6. The second general class are oxometallate compounds with MO_x^{n-} polyhedral anions of main group or transition metal elements in which the plutonium serves as the tri- or tetravalent counter cation. A typical example of this class of compound would be $PuCrO_3$.

Ternary and polynary sulfides, selenides, and tellurides are few, generally not well characterized and will not be discussed.

(*i*) *Preparation of alkali metal oxoplutonates*

When plutonium dioxide and alkali metal oxides, hydroxides, peroxides, or carbonates are intimately mixed and heated in a stream of oxygen, inert gas, or vacuum, they react to form ternary oxide phases in which the plutonium is the central atom of an oxoplutonate anion $\left(PuO_x^{n-}\right)$ and may assume any of the oxidation states from IV to VII. Alkali metal oxoplutonates have been prepared with all the alkali metals with the exception of francium.

Pu(IV). The only alkali oxoplutonate(IV) known at the time of writing is greenish brown Li_8PuO_6, which is obtained by heating a Li_2O–PuO_2 mixture (4.2:1) in a sealed evacuated tube at 600°C (Keller *et al.*, 1965b).

Pu(V). For pentavalent plutonium, Li_7PuO_6, Li_3PuO_4, and Na_3PuO_4 have been reported. These compounds may be obtained by reaction of Li_2O or Na_2O with PuO_2 in an oxidizing atmosphere for 8 h at 700–900°C, respectively. Li_3PuO_4 may be prepared by heating a 3:1 mixture of $LiOH \cdot H_2O$ and PuO_2 in an oxygen stream at 900°C for 24 h (Yamashita *et al.*, 1992). M_3PuO_4 compounds are also reportedly obtained by thermal decomposition of hexavalent M_6PuO_6 for 4 h in an argon atmosphere to give the M_3PuO_4 product and PuO_2 (1100°C, M = Li; 1000°C, M = Na) (Keller, 1964). Brownish-green Li_7PuO_6 was prepared by reacting Li_3PuO_4 with two equivalents of Li_2O at 600°C for 6 h in an evacuated quartz tube (Koch, 1964).

Pu(VI). For hexavalent plutonium, M_6PuO_6, M_4PuO_5, (M = Li, Na), and M_2PuO_4 (M = K, Rb, Cs) compounds have been prepared. These compounds may be either dark green (M_6PuO_6) or brown (M_4PuO_5 and M_2PuO_4). The compounds M_4PuO_5 and M_6PuO_6 dissolve in dilute acids to form yellow-brown or yellow-green aqueous solutions (respectively) and show characteristic Pu(VI) absorption spectra (Koch, 1964).

Li_6PuO_6 is obtained by heating a 3:1 mixture of Li_2O and PuO_2 at 400–500°C in an oxygen atmosphere. If a 2:1 mixture is used, Li_4PuO_5 is formed. When Li_4PuO_5 is heated at 900–1000°C, Li_3PuO_4 is formed. Li_4PuO_5 may also be prepared by heating a 4:1 mixture of $LiOH \cdot H_2O$ and PuO_2 under an oxygen stream at 600°C for 24 h (Yamashita *et al.*, 1992).

Heating a 2:1 mixture of Na_2O and PuO_2 in an oxygen atmosphere at 400°C results in the formation of cubic α-Na_4PuO_5, which may be converted to tetragonal β-Na_4PuO_5 by raising the temperature to 500°C. At 900°C, β-Na_4PuO_5 decomposes to Na_3PuO_4. When a 3:1 mixture of Na_2O and PuO_2 is used, α-Na_4PuO_5 is produced at 400°C; and Na_6PuO_6 is produced at 500°C. Upon heating Na_6PuO_6 to 750°C, it is converted to β-Na_4PuO_5 (Koch, 1964; Keller *et al.*, 1965a).

The M_2PuO_4 class of compounds (M = K, Rb, Cs) may be conveniently prepared by reaction of a 2:1 mixture of MOH with PuO_2 in gold crucibles under an oxygen atmosphere, and heated to at least 450°C (Hoekstra and Gebert, 1977). These compounds decompose in air above 650°C. The rubidium and cesium analogs may also be prepared by heating the corresponding oxoplutonates (VII), M_3PuO_5 to temperatures above 320°C (Pagès *et al.*, 1971a,b).

Pu(VII). For heptavalent plutonium, M_5PuO_6 (M = Li, Na) and M_3PuO_5 (M = Rb, Cs) have been reported. Greenish-black Li_5PuO_6 is formed when a 3:1 mixture of Li_2O and PuO_2 is heated in a stream of oxygen at 430°C (Keller and Seiffert, 1969). The corresponding sodium compound, Na_5PuO_6, has not yet been isolated in the pure state. However, the reaction product of Na_2O_2 and PuO_2 in O_2 atmosphere at 400°C, yields a green aqueous solution upon dissolution in dilute aqueous hydroxide, which shows the characteristic absorption spectrum of Pu(VII) (Keller and Seiffert, 1969).

The black compounds M_3PuO_5 (M = Rb, Cs) have been obtained by heating 3:1 mixtures of the corresponding superoxide MO_2 with PuO_2 at 250°C for more than 6 h. These compounds are reportedly less sensitive to air than the corresponding Np compounds, but have a lower thermal stability. At 320°C, they reportedly decompose to M_2PuO_4 and M_2O_2 (Pagès *et al.*, 1971a,b).

(*ii*) *Preparation of ternary and quaternary alkaline-earth oxoplutonates*

The oxoplutonates of the alkaline-earth elements can be prepared in a manner similar to the alkali-metal oxoplutonates. The alkaline-earth oxides, peroxides

or carbonates react with PuO_2 to form alkaline-earth oxoplutonates, in which the plutonium may occur in oxidation states III, IV, V, VI, and VII.

Pu(III). The only alkaline-earth oxoplutonate(III) that has been reported is $BaPu_2O_4$, which is formed by reacting a 1:3:2 mixture of BaO, elemental Pu and PuO_2 (Keller, 1962). An intimate mixture of Pu, PuO_2, and BaO is first heated in a stream of hydrogen to convert plutonium metal to hydride (PuH_x). The resulting mixture of PuH_x, PuO_2, and BaO is powdered in an inert-gas atmosphere and then heated in a stream of argon at 600°C for 2 h and at 1200°C for 8 h. At 600°C, the plutonium hydride decomposes, and the resulting finely divided metal reacts with PuO_2 to give Pu_2O_3. The Pu_2O_3 in turn reacts with BaO to form $BaPu_2O_4$, which may be isostructural with the lanthanide compounds $BaPr_2O_4$ and $BaNd_2O_4$ (Keller, 1962). No lattice constants of $BaPu_2O_4$ have been reported.

Pu(IV). Discrete alkaline-earth oxoplutonates(IV) can be prepared with the heavy alkaline-earth elements strontium and barium but not for the lighter alkaline-earth elements beryllium and magnesium. Beryllium and magnesium oxides react with PuO_2 to form solid solutions rather than stoichiometric compounds. The mutual solubilities of MO–PuO_2 systems (M = Be, Mg) have been determined by Hough and Marples (1965) and by Carroll (1964). With the heavier alkaline-earth elements, heating stoichiometric mixtures of MO (M = Sr, Ba) with PuO_2 gives $MPuO_3$ (Chackraburtty *et al.*, 1963; Chackraburtty and Jayadevan, 1964). Chackraburtty and coworkers have recommended the use of excess alkaline-earth oxide (3:1 mixtures) to ensure complete conversion of PuO_2 to oxoplutonate. The excess alkaline-earth oxide may be subsequently removed by extraction with methanol (Russell *et al.*, 1960; Keller, 1962, 1964; Chackraburtty and Jayadevan, 1964). $BaPuO_3$ has also been prepared by ball-milling a stoichiometric mixture of $BaCO_3$ and PuO_2, followed by heating under argon at 1197°C for 24 h (Christoph *et al.*, 1988). $SrPuO_3$ and $BaPuO_3$ can also be prepared by reduction of Sr_3PuO_6 or Ba_3PuO_6 in a stream of hydrogen at 1600–1800°C.

Pu(V). Deep black $Ba_3PuO_{5.5}$ is obtained by reacting a mixture of Ba_3PuO_6, PuO_2, and BaO in a stream of argon at 1100–1200°C. It is uncertain whether this compound contains Pu(V) or a mixture of Pu(IV) and Pu(VI) (Keller, 1962, 1964). There are a few quaternary compounds of general formula Ba_2MPuO_6, where M is a trivalent metal ion (M = La, Nd, In). These compounds are prepared by heating a 4:1:1:1 mixture of PuO_2, $PuO_2(NO_3)_2{\cdot}nH_2O$, M_2O_3, and BaO_2 in a platinum crucible at 750–950°C for 8–10 h (Awasthi *et al.*, 1968).

Pu(VI). For hexavalent plutonium, there are ternary alkaline-earth oxoplutonates (VI) of formula $MPuO_4$ and M_3PuO_6 (M = Ca, Sr, Ba) and quaternary compounds of general formula Ba_2MPuO_6, where M is a divalent metal ion (M = Sr, Mn, Pb, Mg, Ca). It is uncertain whether the manganese compound, Ba_2MnPuO_6, contains Mn(II)/Pu(VI) or Mn(III)/Pu(V).

M_3PuO_6 compounds have been prepared by heating 3:1 to 5:1 mixtures of MO (M = Ca, Sr, Ba) with PuO_2 in a stream of oxygen at 950–1050°C

(M = Ca) (Chackraburtty *et al.*, 1963; Awasthi *et al.*, 1968), 900–1200°C (M = Sr), or 800–1300°C (M = Ba) (Keller, 1962, 1964). Sr_3PuO_6 and Ba_3PuO_6 form solid solutions, which range in composition from Ba_3PuO_6 to $Ba_{0.75}Sr_{2.25}PuO_6$.

The reaction of a 1:1 mixture of SrO and PuO_2 in an oxidizing atmosphere at 900–1000°C yields $SrPuO_4$ (Keller, 1962, 1964). $BaPuO_4$ appears to be produced by shaking Ba_3PuO_6 with excess, CO_2-free water for 15–30 min. BaO dissolves and leaves $BaPuO_4$ as the residue (Keller, 1962, 1964).

Pu(VII). Alkaline-earth oxoplutonates(VII) have not yet been prepared by solid-state reactions at elevated temperatures, as has been done with alkali oxoplutonates (VII). However, the compound $Ba_3(PuO_5)_2 \cdot xH_2O$ was obtained by precipitation with $Ba(OH)_2$ from aqueous solutions of Pu(VII) (Komkov *et al.*, 1968).

(*iii*) *Solid-state structures*

Characterization of most alkali and alkaline-earth oxoplutonates are limited to X-ray powder diffraction data. These data have been summarized in Table 7.40. All of the oxoplutonate compounds contain PuO_6^{n-} polyhedra that are octahedral with six equidistant Pu–O bonds, or tetragonally distorted with two short (plutonyl-like) and four long, or four short and two long Pu–O bonds. Representative examples of these structure types will be discussed.

Perovskites – $MPuO_3$

Plutonium (and other light actinides) form an extensive class of complex oxides that are related to the perovskite ($CaTiO_3$) structure in which Pu(IV), Pu(VI), or Pu(VII) ions exist in octahedral PuO_6^{n-} coordination. General structural classifications of perovskites have been discussed (Galasso, 1968; Wells, 1984; Zhou and Goodenough, 2005). The idealized ABO_3 perovskite structure consists of a simple cubic lattice with apex-shared, BO_6 octahedra with large A cations at the center of the unit cell, bonded to 12 oxygen atoms situated at the centers of the cell edges. In this ideal ABO_3 structure, all atomic positions are fixed by symmetry and the packing is very dense. In most perovskites, the actual unit cell symmetry is lower than cubic, which can be accomplished by rotation of the BO_6 octahedra allowing a lengthening of the B–O bonds and lowering the effective A-site coordination number (typically to eight).

Through rotation of a BO_6 unit, the perovskite structure can accommodate a large range of A:B:O radius ratios. Barium plutonate ($BaPuO_3$) is an excellent example of how a 5f element is accommodated into this important structure type. The structure of $BaPuO_3$ had been somewhat controversial, the cell symmetry being reported variously as cubic or orthorhombic (Russell *et al.*, 1960; Keller, 1962; Chackraburtty *et al.*, 1963; Christoph *et al.*, 1988). Christoph and coworkers utilized Zachariasen's bond-length–bond-strength relationships to predict that in the structure of $BaPuO_3$ the PuO_6 octahedra

Table 7.40 *Crystallographic data of alkali and alkaline-earth oxoplutonates.*

Compound	*Symmetry*	*Space group*	*Lattice constants*			*Density* ($g\ cm^{-1}$)	*References*
			a_0 (Å)	b_0 (Å)	c_0 (Å)		
Pu(IV)							
α-$BaPuO_3$	cubic	F*m*3*m*	4.357(7)			8.34	Keller (1962)
α-$BaPuO_3$	cubic	F*m*3*m*	4.373(3)				Chackraburtty *et al.* (1963)
α-$BaPuO_3$	cubic	P*m*3*m*	4.391 (4.385)				Russell *et al.* (1960)
β-$BaPuO_3$	orthorhombic	P*nma*[a]	5.982(4)	5.976(11)	5.847(4)		Chackraburtty *et al.* (1963)
β-$BaPuO_3$	orthorhombic	P*nma*[b]	6.193(1)	8.744(1)	6.219(1)	8.37	Christoph *et al.* (1988)
$SrPuO_3$	cubic	F*m*3*m*	4.28(3)				Keller (1962)
$SrPuO_3$	orthorhombic	A*mm*2[c]	4.273(4)	5.981(5)	6.124	7.94	Chackraburtty and Jayadevan (1964)
Li_8PuO_6	hexagonal		5.64(2)		15.95(5)		Walter (1965)
Ba_2CePuO_6	cubic	F*m*3*m*	8.72(2)				Awasthi *et al.* (1968)
Ba_2TiPuO_6	cubic	F*m*3*m*	8.06(2)				Awasthi *et al.* (1968)
Pu(V)							
Li_3PuO_4	tetragonal	I4/*mmm*	4.464(2)		8.367(5)	6.45	Keller *et al.* (1965b)
$Ba_3PuO_{5.5}$	cubic	F*m*3*m*	8.813(7)				Keller (1962)
Ba_2LaPuO_6	pseudo-cubic	F*m*3*m*	8.63(2)				Awasthi *et al.* (1968)
Ba_2NdPuO_6	cubic	F*m*3*m*	8.66(2)				Awasthi *et al.* (1968)
Ba_2InPuO_6	cubic	F*m*3*m*	8.50(2)				Awasthi *et al.* (1968)
Pu(VI)							
K_2PuO_4	tetragonal	I4/*mmm*	4.298(3)		13.07(1)	5.22	Hoekstra and Gebert (1977)

Rb_2PuO_4	tetragonal	I4/*mmm*	4.323(3)		13.74(1)		Hoekstra and Gebert (1977)
Cs_2PuO_4	tetragonal	I4/*mmm*	4.368(3)		14.71(1)		Hoekstra and Gebert (1977)
$SrPuO_4$	rhombohedral	$R\bar{3}$	6.51(2)			7.72	Keller (1962)
Li_4PuO_5	tetragonal	I4/*m*	6.677(2)		4.421(3)	5.84	Keller *et al*. (1965a)
α-Na_4PuO_5	cubic	F*m*3*m*	4.718(5)			5.20	Keller *et al*. (1965a)
β-Na_4PuO_5	tetragonal	I4/*m*	7.449(5)		4.590(5)	5.36	Keller *et al*. (1965a)
Li_6PuO_6	hexagonal	$R\bar{3}$	5.184(2)		14.59(5)	5.35	Keller *et al*. (1965a)
Na_6PuO_6	hexagonal	$R\bar{3}$	5.76(2)		15.9(1)	5.16	Keller *et al*. (1965a)
Ba_3PuO_6	cubic	F*m*3*m*	8.844(6)			7.17	Keller (1962)
Ba_2SrPuO_6	cubic	F*m*3*m*	8.780(2)				Keller (1962)
Ba_2SrPuO_6	orthorhombic		6.204(42)	6.188(62)	8.822(32)		Gens *et al*. (1985)
$BaSr_2PuO_6$	cubic	F*m*3*m*	8.717(8)				Keller (1962)
Ba_2MnPuO_6	cubic	F*m*3*m*	8.32(2)				Awasthi *et al*. (1968)
Ba_2ZnPuO_6	pseudo-cubic	F*m*3*m*	8.38(2)				Awasthi *et al*. (1968)
Ba_2PbPuO_6	cubic	F*m*3*m*	8.58(2)				Awasthi *et al*. (1968)
Ba_2MgPuO_6	cubic	F*m*3*m*	8.332(6)				Gens *et al*. (1985)
Ba_2CaPuO_6	cubic	F*m*3*m*	8.611(4)				Gens *et al*. (1985)
***Pu*(*VII*)**							
Li_5PuO_6	hexagonal	$R\bar{3}$	5.19(2)		14.48(2)	3.53	Keller and Seiffert (1969a)
Li_5PuO_6	monoclinic[d]	C2/*m*	5.0679(6)	8.7315(8)	5.0293(6)	5.88	Keller *et al*. (1965a)
Na_5PuO_6	monoclinic[d]	C2/*m*	5.6877(8)	8.7314(13)	5.6074(9)	5.75	Keller *et al*. (1965a)

[a] Original space group P*mcm*, recalculated by Roof (1989) in standard setting P*nma*.
[b] Neutron diffraction data; original space group P*bnm*, recalculated by Roof (1989) in standard setting P*nma*.
[c] Original space group B centered, recalculated by Roof (1989) in standard setting A*mm*2.
[d] Keller *et al*. (1965a) reported that Li_5PuO_6 and Na_5PuO_6 are hexagonal and isotypic with rhenium analogs Li_5ReO_6 and Na_5ReO_6. Betz and Hoppe (1984) described the structures of Li_5ReO_6 and Na_5ReO_6 as being monoclinic. Roof (1989) recalculated both Pu structures using the data from Betz and Hoppe, and these are the cell constants reported here with $\beta = 110.24°$ for Li_5PuO_6 and $\beta = 111.01(1)°$ for Na_5PuO_6.

should rotate by about 11 degrees to give the theoretical Pu–O distance predicted by Zachariasen's relationship. This prediction was tested by performing a low-temperature neutron diffraction study on $Ba^{242}PuO_3$ which confirmed the expectations of a distortion away from the cubic perovskite structure (Christoph *et al.*, 1988). The idealized cubic and experimentally confirmed orthorhombic solid-state structures are illustrated in Fig. 7.98. In the low-temperature neutron structure, the PuO_6 octahedra are rotated by about 15 degrees from the idealized position in the cubic perovskite, and this is indicated in Fig. 7.98(b). The PuO_6 rotation gives Pu–O–Pu angles of 157.07 (8) and 160.53(5) degrees. The plutonium atom coordination is only slightly distorted from octahedral with Pu–O distances of 2.2306(5), 2.2295(12), and 2.2230(12) Å. The mean Pu–O distance is 2.228 Å.

Double perovskites M_3PuO_6 and Ba_2MPuO_6

Another important class of plutonium perovskite oxide is the so-called 'double perovskite' typified by M_3PuO_6 (M = Ba, Sr) and Ba_2MPuO_6 (M = Mg, Ca, Sr, Mn, Zn). The double perovskite can be considered as an ideal perovskite with M^{2+} and Pu^{6+} ions occupying alternating octahedral sites in a cubic unit cell with doubled cell edges. The ordered fcc structure (*Fm*3*m*) has the elpasolite (K_2NaAlF_6) structure, and the basic structural unit is shown in Fig. 7.99. This figure maintains the same orientation as Fig. 7.98, and emphasizes the alternating PuO_6 and MO_6 octahedra in the double perovskite structure. As in the ideal

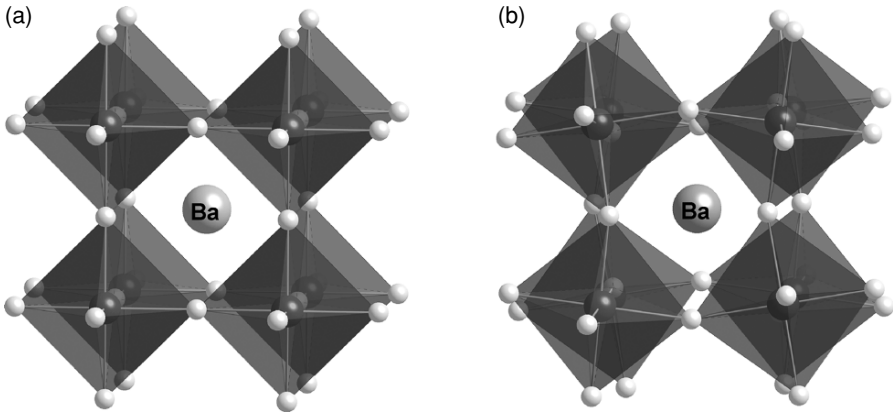

Fig. 7.98 *Idealized cubic* (*a*) *and experimental orthorhombic* (*b*) *crystal structures of $BaPuO_3$, emphasizing the rotation of the local PuO_6 octahedra between cubic and orthorhombic symmetries. The cubic structure is based on the original report by* (*Russell* et al., 1960), *and the orthorhombic structure is based on the low-temperature neutron diffraction study* (*Christoph* et al., 1988). *In this polyhedral representation, the plutonium atoms are dark gray* (*center of octahedra*), *oxygen atoms are white, and the central barium atom is light gray.*

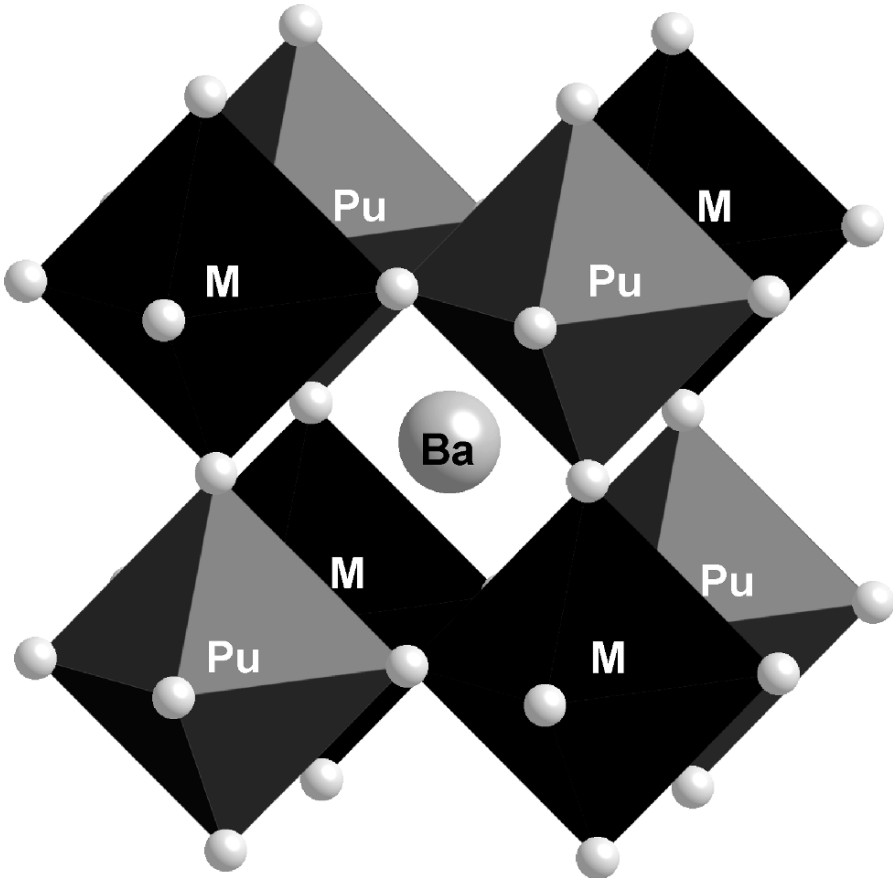

Fig. 7.99 *Polyhedral representation of the idealized double perovskite structure of Ba_2MPuO_6 compounds. This polyhedral representation emphasizes the alternating octahedral PuO_6 (gray) and MO_6 (black) sites in the structure. The central barium ion is light gray.*

perovskite structure, many of these compounds are distorted away from ideal cubic symmetry, and this is often observed as the presence of extra, weak diffraction lines (Gens *et al.*, 1985).

M_4PuO_5

These hexavalent compounds are isostructural with M_4UO_5 (M = Li, Na) and crystallize in tetragonal space group I4/*m*. The solid-state structure of Li_4PuO_5 displays an extended pseudo-octahedral chain of $PuO_4(\mu\text{-}O)_2$ units with a square-planar arrangement of four short equatorial Pu–O bonds of 1.98 Å,

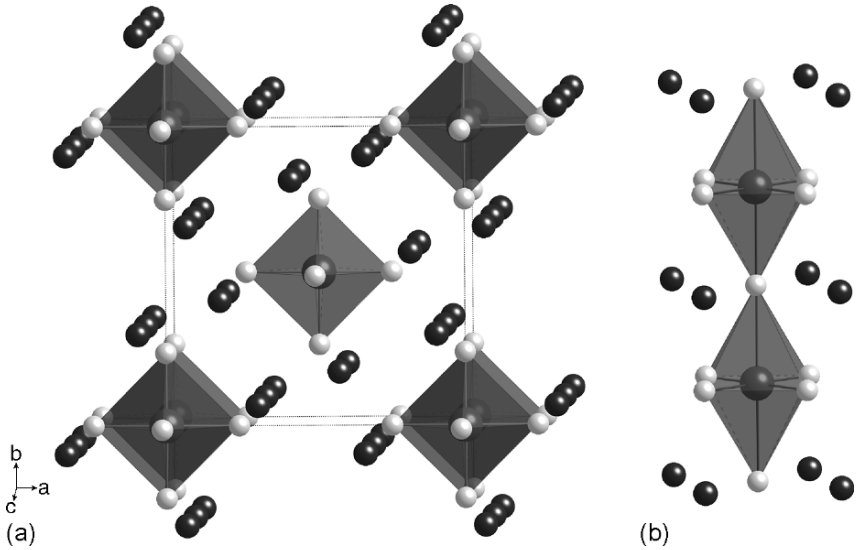

Fig. 7.100 *Polyhedral representation of the solid-state structure of M_4PuO_5 compounds. (a) A view looking down the crystallographic c-axis, and (b) a view perpendicular to the c-axis. The view in (b) emphasizes the distorted PuO_6 polyhedra (gray) surrounded by Li or Na ions (black).*

and two longer axial Pu–O bridging bonds of 2.21 Å that link the planar PuO_4 units together (Keller *et al.*, 1965a). The basic structural unit is shown in Fig. 7.100. This compound is isostructural with β-Na_4PuO_5 that has four short Pu–O bonds of 2.09 Å and two longer Pu–O bonds of 2.29 Å (Keller *et al.*, 1965a). This class of compound is significant in that it demonstrates that hexavalent complex actinide oxides do not necessarily retain actinyl (AnO_2^{2+}) ions with two short metal–oxygen bonds in the solid state.

M_5PuO_6

For heptavalent actinides, Keller reported that M_5PuO_6 (M = Li, Na) compounds were hexagonal and isotypic with rhenium analogs M_5ReO_6 (M = Li, Na) (Keller *et al.*, 1965a). Since Keller's original report, Betz and Hoppe (1984) determined that the structures of M_5ReO_6 were monoclinic and characterized by tetragonally distorted MO_6^{5-} units. In 1994, Morss and coworkers reexamined the structures of both Li_5NpO_6 and Li_5ReO_6 by neutron diffraction and confirmed the monoclinic structure for Li_5ReO_6, but in contrast to the original report, the structure of Li_5NpO_6 was not identifiable (Morss *et al.*, 1994). Thus the actual solid-state structure of M_5PuO_6 compounds remains unresolved.

(*iv*) *Ternary and quaternary oxides of plutonium with main group and transition elements*

A number of ternary oxides of plutonium with the oxides of metallic and semimetallic elements have been prepared. In these compounds plutonium occurs as Pu(III) or Pu(IV), and the tendency for plutonium to assume the role of the cation increases as one proceeds from group III toward group VII elements. A wide variety of compositions are observed, with stoichiometric compounds and nonstoichiometric phases being formed. The crystallographic properties of those compounds having a stoichiometric composition are summarized in Table 7.41. Compounds of the type $PuXO_4$, containing Pu(III) and X = P or As, as well as the phosphates and arsenates of Pu(IV) and Pu(VI) will be discussed in Section 7.8.5.c(i).

Trivalent compounds

Ternary and quaternary oxides containing trivalent plutonium range from simple compounds of the types $PuMO_3$ and $PuMO_4$, to more complex formulae such as $Pu(ReO_4)_3$, or to complicated silicate structures such as $Ba_2Pu_8(SiO_4)_6O_2$ related to apatite.

$PuMO_3$. This class of compound displays the perovskite structure (Fig. 7.98), but with Pu(III) now serving the role of the cation. These compounds have been prepared by Russell *et al.* (1960) for M = Al(III), V(III), Cr(III), and Mn(III), and by Keller *et al.* (1972) for M = Sc(III) by heating mixtures of PuO_2 with the appropriate metal oxide (Al_2O_3, V_2O_5, CrO_3) or carbonate ($MnCO_3$) under argon or hydrogen atmospheres between 1500 and 1600°C for several hours (Russell *et al.*, 1960). Attempts to prepare analogous compounds with M = Fe (III) and Ga(III) were unsuccessful (Chackraburtty and Jayadevan, 1964).

Ba_2PuPaO_6. This is the only known compound in this class, and it shows a double perovskite structure (Fig. 7.99). This compound is prepared as a white powder by heating a 4:1:1 mixture of $BaCO_3$, Pa_2O_5, and Pu_2O_3 at 1350–1400°C *in vacuo* (Keller, 1965b). It is unknown whether this compound contains Pu(III)/Pa(V) or Pu(IV)/Pa(IV).

$PuMO_4$. A few such compounds have been prepared with M = Nb(V) or Ta(V), and contain trivalent plutonium. They are obtained by heating intimate mixtures of Pu_2O_3 and M_2O_3 and M_2O_5 *in vacuo* at 1200°C (Keller and Walter, 1965).

$Pu(ReO_4)_3$. Reaction of plutonium(III) oxalate with Re_2O_7 yields green plutonium(III) perrhenate, $Pu(ReO_4)_3$. This salt-like compound is also obtained by solid-state reaction of PuO_2 with Re_2O_7. $Pu(ReO_4)_3$, is deliquescent in air, and forms hydrates with 1, 2, or $3H_2O$. $Pu(ReO_4)_3$ decomposes at 700°C to PuO_2 and Re_2O_7 (Silvestre *et al.*, 1977). The X-ray powder pattern of anhydrous $Pu(ReO_4)_3$ has not yet been interpreted.

Pu(III) silicates. No simple plutonium(III) silicates are known. However, De Alleluia and coworkers (De Alleluia *et al.*, 1983) have prepared a number of

Table 7.41 *Crystallographic data of ternary oxides of plutonium with main group and transition elements.*

Compound	*Symmetry*	*Space group*	*Lattice constants*			*Density* ($g\ cm^{-1}$)	*References*
			a_0 (Å)	b_0 (Å)	c_0 (Å)		
Pu(III)							
$PuAlO_3$	orthorhombic	A*mm*2	3.750	5.314	5.350	9.78	Runnalls (1965)
$PuScO_3$	orthorhombic	P*bnm*	5.654	5.839	8.104		Keller *et al.* (1972)
$PuVO_3$	orthorhombic[a]	P*nma*	5.61	7.78	5.48	9.38	Russell *et al.* (1960)
$PuCrO_3$	orthorhombic[a]	P*nma*	5.51	7.76	5.46	9.65	Russell *et al.* (1960)
$PuMnO_3$	orthorhombic[b]	P*nma*	5.497(3)	7.730(4)	5.450(3)	9.72	Russell *et al.* (1960)
$PuAsO_4$	monoclinic[c]	$P2_1/n$	6.92(2)	7.09(2)	6.66(2)		Keller and Walter (1965)
$PuNbO_4$	monoclinic[d]	I2/*a*	5.46	11.27	5.17	8.29	Keller and Walter (1965)
$PuTaO_4$	monoclinic[e]	$C2_1/c$	7.618(1)	5.531(1)	7.767(1)	10.0	Keller and Walter (1965)
$Ba(Pu_{0.5}Pa_{0.5})O_3$	cubic		8.748	5.17			Keller (1965b)
$Pu_{9.33}(SiO_4)_6O_2$	hexagonal	$P6_3m$	9.589(5)		7.019(5)		De Alleluia *et al.* (1983)
$Pu_8(SiO_4)_6$	hexagonal	$P6_3m$	9.595(5)		7.037(5)		De Alleluia *et al.* (1983)
$LiPu_9(SiO_4)_6O_2$	hexagonal	$P6_3m$	9.566(5)		6.999(5)		De Alleluia *et al.* (1983)
$NaPu_9(SiO_4)_6O_2$	hexagonal	$P6_3m$	9.594(5)		7.025(5)		De Alleluia *et al.* (1983)
$Mg_2Pu_8(SiO_4)_6O_2$	hexagonal	$P6_3m$	9.559(5)		6.973(5)		De Alleluia *et al.* (1983)
$Ca_2Pu_8(SiO_4)_6O_2$	hexagonal	$P6_3m$	9.570(5)		7.043(5)		De Alleluia *et al.* (1983)
$Sr_2Pu_8(SiO_4)_6O_2$	hexagonal	$P6_3m$	9.604(5)		7.122(5)		De Alleluia *et al.* (1983)
$Ba_2Pu_8(SiO_4)_6O_2$	hexagonal	$P6_3m$	9.701(5)		7.198(5)		De Alleluia *et al.* (1983)
$Sr_3Pu_6(SiO_4)_6$	hexagonal	$P6_3m$	9.619(5)		7.131(5)		De Alleluia *et al.* (1983)
Pu(IV)							
$PuSiO_4$	tetragonal	$I4_1/amd$	6.906(6)		6.221(6)	7.37	Keller (1963)
$PuGeO_4$	tetragonal	$I4_1/a$	5.040(2)		11.11(1)	8.82	Keller (1963)
$Pu(TeO_3)_2$	orthorhombic		5.60	10.46	11.76		Wroblewska *et al.* (1979)
$Pu(NbO_3)_4$	tetragonal[f]	I4/*mmm*	7.67(1)		7.74(1)	5.85	Keller (1965a)

$Pu(TaO_3)_4$	tetragonal[f]	I4/*mmm*	7.654(5)		7.731(5)	Keller (1965a)
$Pu(MoO_4)_2$	orthorhombic[g]	P*mna*	9.422(8)	13.993(10)	10.039(11)	Tabuteau *et al.* (1972)
$Pu(ReO_4)_4{\cdot}4H_2O$	monoclinic[h]		32.4	6.69	16.85	Silvestre *et al.* (1977)
$LiPu_2(VO_4)_3$	tetragonal		7.09		6.35	Pagès and Freundlich (1976)
$NaPu_2(VO_4)_3$	tetragonal		7.14		6.37	Pagès and Freundlich (1976)
$AgPu_2(VO_4)_3$	tetragonal		5.06		11.32	Pagès and Freundlich (1976)
$CdPu(VO_4)_2$	tetragonal		7.04		6.33	Pagès and Freundlich (1976)
$CaPu(VO_4)_2$	tetragonal		7.16		6.33	Pagès and Freundlich (1976)
$SrPu(VO_4)_2$	tetragonal		7.29		6.47	Pagès and Freundlich (1976)
$Na_2Pu(MoO_4)_3$	tetragonal		5.198		11.280	Tabuteau *et al.* (1972)
$Li_4Pu(MoO_4)_4$	tetragonal		11.085		10.600	Tabuteau *et al.* (1972)
$Na_4Pu(MoO_4)_4$	tetragonal		11.20		11.69	Tabuteau *et al.* (1972)
$K_2Pu(MoO_4)_3$	monoclinic[i]	*Cc* or *C*2/*c*	17.538(9)	11.992(6)	5.243(4)	Tabuteau and Pagès, 1980)
$K_8Pu(MoO_4)_6$	monoclinic[j]	*Cc* or *C*2/*c*	10.416(4)	10.416(4)	7.748(4)	Tabuteau and Pagès (1980)
$Rb_2Pu(MoO_4)_3$	monoclinic[k]	*Cc* or *C*2/*c*	17.77(3)	12.068(13)	5.282(7)	Tabuteau and Pagès (1980)
$Rb_8Pu(MoO_4)_6$	monoclinic[l]	*Cc* or *C*2/*c*	10.67(2)	17.71(5)	7.99(12)	Tabuteau and Pagès (1980)
$Cs_2Pu(MoO_4)_3$	orthorhombic		26.516(31)	9.702(25)	5.178(9)	Tabuteau and Pagès (1980)

[a] Original space group P*bnm*, atomic positions transformed to standard setting P*nma* by Roof (1989).
[b] Russell *et al.* indicated that $PuMnO_3$ is orthorhombic and perhaps isomorphic with $PuCrO_3$. The structure was refined by Roof using original d-spacings and transformed into standard space group P*nma* (Roof, 1989).
[c] $\beta = 105.45°$.
[d] $\beta = 94.58°$. Keller and coworkers reported lattice constants and suggested that the structure was of the β-fergusonite type (Keller and Walter, 1965). The latter structure was refined in I2/*a* by Santoro *et al.* (1980).
[e] $\beta = 100.94°$. Keller and coworkers reported the structure to be of the $CeTaO_4$ type, whose structure was refined by Santoro *et al.* (1980). Lattice constants, atomic positions and thermal parameters refined by Roof (1989).
[f] Space group assignment described by Roof (1989).
[g] Lattice constants refined by Roof and transformed into standard space group *Pmna* (Roof, 1989).
[h] $\beta = 110.07°$.
[i] $\beta = 104.80(6)°$.
[j] $\beta = 116.59(4)°$.
[k] $\beta = 107.78(10)°$.
[l] $\beta = 116.3(1)°$.

complex silicates of the types $Pu_8(SiO_4)_6$; $Pu_{9.33}(SiO_4)_6O_2$; $M_2Pu_9(SiO_4)_6O_2$ (M = Li, Na), $M_2Pu_8(SiO_4)_6O_2$ (M = Mg, Ca, Sr, Ba), and $Sr_3Pu_6(SiO_4)_6$. All these compounds have hexagonal apatite-type structures, some with lattice defects. All these compounds, which show the blue color of Pu(III), are prepared by reducing mixtures of PuO_2, SiO_2, and the respective alkali or alkaline-earth oxides in ultrapure H_2 at temperatures between 1100 and 1400°C in alumina or iridium vessels for periods up to 3 days. In these systems, the reduction to Pu(III) is accomplished much more readily than the reduction to Pu(III) in other mixed oxide systems.

Tetravalent compounds

$PuMO_4$. Compounds of this type containing M = Si or Ge can be obtained by hydrothermal synthesis from 1:1 mixtures of PuO_2 and MO_2 at 250°C. They may also be prepared by solid-state reactions at 1200°C from the same components (Keller, 1963). $PuSiO_4$ is green; $PuGeO_4$ is pale brown or olive brown.

$Pu(MO_3)_4$. These compounds contain Pu(IV) and M(V) (M = Nb, Ta) and may be obtained by solid-state reaction of a 2:1 mixture of M_2O_5 and PuO_2 (Keller, 1965a).

$Pu(MO_3)_2$. The only representative of this type of compound is white plutonium(IV) tellurite, $Pu(TeO_3)_2$, which is prepared by heating a 1:2 mixture of PuO_2 and TeO_2 for 24 h at 700°C (Wroblewska *et al.*, 1979).

$Pu(MO_4)_2$. The only compound of this type known now is brown-red plutonium(IV) molybdate, $Pu(MoO_4)_2$. This compound may be prepared by heating a stoichiometric mixture of PuO_2 and MoO_3 for 2 h at 500°C, followed by 4 h at 800°C (Tabuteau *et al.*, 1972).

A number of quaternary plutonium(IV) molybdates have been obtained by reaction of $Pu(MoO_4)_2$ with M_2MoO_4 (M = Li, Na, K, Rb, Cs) compounds at high temperature (Tabuteau *et al.*, 1972). Reaction of Li_2MoO_4 with $Pu(MoO_4)_2$ at 500°C gives $Li_4Pu(MoO_4)_4$. $Li_4Pu(MoO_4)_4$ melts congruently at 630°C and has a reversible solid-state transformation at 510°C. Solid-state reaction of Na_2MoO_4 with $Pu(MoO_4)_2$ at 600°C gives $Na_2Pu(MoO_4)_3$ and $Na_4Pu(MoO_4)_4$. Both compounds show peritectic decomposition, $Na_2Pu(MoO_4)_3$ at 714°C and $Na_4Pu(MoO_4)_4$ at 708°C. Similarly, $M_2Pu(MoO_4)_3$ and $M_8Pu(MoO_4)_6$ have been prepared by solid-state reactions between M_2MoO_4 and $Pu(MoO_4)_2$ (M = K, Rb). With Cs_2MoO_4, only $Cs_2Pu(MoO_4)_3$ has been prepared by solid-state reaction with $Pu(MoO_4)_2$ (Tabuteau *et al.*, 1972).

Pu(IV) perrhenates. Plutonium(IV) perrhenate tetrahydrate, $Pu(ReO_4)_4 \cdot 4H_2O$, is obtained as a red powder by dissolving the oxalate $Pu(C_2O_4)_2 \cdot 6H_2O$ in 0.5 M perrhenic acid solution, evaporating the resulting solution to dryness, and heating the residue to a temperature below 100°C. So far, the anhydrous compound has not been prepared. At 250°C, $Pu(ReO_4)_4 \cdot 4H_2O$ decomposes partially to $Pu(ReO_4)_3$ (Silvestre *et al.*, 1977).

Pu(IV) vanadates. No simple plutonium(IV) vanadate has been prepared. However, Pagès and Freundlich (1976) prepared a number of quaternary plutonium(IV) vanadates of the types $MPu_2(VO_4)_3$ (M = Li, Na, Ag) and $M'Pu(VO_4)_2$, (M′ = Ca, Sr, Cd). Heating a 4:3:1 mixture of PuO_2, V_2O_5, and Ag_2O at 500°C produces $AgPu_2(VO_4)_3$. The corresponding alkali compounds (M = Li, Na) are prepared by heating 1:1:3 mixtures of M_2CO_3, PuO_2, and V_2O_5 at 700–750°C. The alkaline-earth compounds are obtained in the same manner from a mixture of $M'CO_3$, PuO_2, and V_2O_5. The compounds $MPu_2(VO_4)_3$ and $M'Pu(VO_4)_2$ have the zircon structure, while $AgPu_2(VO_4)_2$ has the scheelite structure.

(d) Ternary oxides of plutonium with lanthanide oxides

No stoichiometric compounds of plutonium oxides with lanthanide oxides have been observed. The following systems have been studied in some detail: PuO_2–CeO_2 (Farkas, 1966), PuO_{2+x}–$YO_{1.5}$ (Jackson and Rand, 1963), PuO_2–$EuO_{1.5}$ (Haug, 1963; Haug and Weigel, 1963), PuO_2–$HoO_{1.5}$ (Engerer, 1967), PuO_2–$TmO_{1.5}$ (Leitner, 1967), and PuO_2–$LuO_{1.5}$ (Sriyotha, 1968). Preliminary data are available for the systems PuO_{2+x}–$YO_{1.5}$ (Jackson and Rand, 1963) and PuO_{2+x}–$EuO_{1.5}$ (Haug, 1963; Haug and Weigel, 1963), while pseudo-binary phase diagrams have been established for the systems PuO_{2+x}–$HoO_{1.5}$ (Engerer, 1967), PuO_{2+x}–$TmO_{1.5}$ (Leitner, 1967), and PuO_{2+x}–$LuO_{1.5}$ (Sriyotha, 1968) up to temperatures of 1700°C in oxygen-free atmosphere (argon) and in 1 atm O_2. A detailed discussion of all these systems is beyond the scope of this work.

From these phase diagrams, it may be concluded that $PuO_{2\pm x}$ may dissolve considerable amounts of $LnO_{1.5}$ to form a solid solution. For instance, in the system $PuO_{2\pm x}$–$HoO_{1.5}$, 46.0 mol% $HoO_{1.5}$ at 1250°C, and 72.0 mol% at 1700°C. The anion defects formed by inclusion of $LnO_{1.5}$ into the PuO_2 lattice may be partially compensated by oxidation of Pu(IV) to Pu(>IV). For instance, the average oxidation number $\overline{W}$ of plutonium in the system PuO_{2+x}–$HoO_{1.5}$ at $p(O_2) = 1$ atm for a composition of 50 mol% $HoO_{1.5}$ and 1400°C was found to be $\overline{W} = 4.36$ at an O:(Pu + Ho) ratio of 1.84 (Engerer, 1967). At a composition of 70 mol% $HoO_{1.5}$ and 1100°C, it was found to be $\overline{W} = 4.51$ at an O:(Pu + Ho) ratio of 1.68. In general, the average oxidation number of the plutonium in the fluorite phases containing lanthanide elements is lower than the corresponding oxidation number in the uranium or neptunium systems at approximately the same composition in the fluorite phases.

The solubility of $PuO_{2\pm x}$ in $LnO_{1.5}$ (Ln = Ho, Tm, Lu) is considerably larger than the solubility of uranium or neptunium oxides. In the system PuO_{2+x}–$HoO_{1.5}$ and at $p(O_2) = 1$ atm, it is 18.5 mol% PuO_2 at 1100°C, and 25 mol% at 1550°C (Engerer, 1967).

A different situation exists in the system $PuO_{2(+x)}$–CeO_2. At 1000°C, the compositions PuO_2–CeO_2 form a series of solid solutions throughout the whole range of concentrations. Microspheres of PuO_2–CeO_2 have been prepared by

the sol-gel process (Farkas, 1966). A detailed X-ray study of the lattice constants of various compositions demonstrates that the solid solutions obey Vegard's law (Mulford and Ellinger, 1958).

(e) Ternary oxides of plutonium with actinides

Ternary oxides of plutonium with actinides have been prepared with thorium, protactinium, uranium, and curium.

(*i*) *The plutonium–thorium system*

At 1000°C the PuO_2–ThO_2 system, forms a series of solid solutions throughout the whole composition range (Mulford and Ellinger, 1958) and these follow Vegard's law. Above 1650°C, under an argon atmosphere, a partial phase separation with formation of C-Pu_2O_3 takes place. The melting points of $(Th,Pu)O_2$ solid solutions are practically constant up to 25 wt % Th and show a linear increase at higher Th contents. $(Pu,Th)O_2$ microspheres have been prepared by the sol–gel process and in the induction-coupled plasma torch.

(*ii*) *The plutonium–uranium–oxygen system*

The plutonium–uranium–oxygen system is one of the best-understood plutonium–actinide oxide systems due to its widespread application in nuclear reactor fuel. For this reason, the mixed plutonium–uranium oxide system has been extensively studied. In spite of this great technological importance, only relatively limited data have been reported in the open literature. There is much more information in the proprietary literature of fuel manufacturing organizations. Plutonium–uranium oxides of general formula $(U,Pu)O_2$ are often referred to as 'mixed oxide' or MOX, and can refer to fuels containing 2–30% PuO_2. These fuels behave very differently depending on the percentage of PuO_2. Fuels for light water reactors (LWR) only contain a small percentage of plutonium (2–6%), and will therefore behave like UO_2 with a small amount of impurity, while fuels for fast breeder reactors (FBR) have a higher percentage of plutonium (15–35%), and behave very differently (Schneider and Roepenack, 1986). Four plants currently produce commercial quantities of MOX fuel. Two are in France, one in Belgium, and one in the United Kingdom. In 2000, about 190 metric tons per year of MOX was produced, incorporating 10–12 metric tons of plutonium. MOX production capacity is presently around 300 metric tons per year, using 18–22 metric tons of plutonium. Since 1963 about 400 metric tons of plutonium have been used in MOX. We only cover the fundamental aspects of the plutonium–uranium–oxygen system; for further details, the reader is referred to part C of the *Gmelin Handbook* (Koch, 1972), to the *Plutonium Handbook* (Wick, 1980), and to a number of original papers (Russell *et al.*, 1962; Markin and Street, 1967; Thuemmler *et al.*, 1967; Benedict and Sari, 1969; Dean

et al., 1970; Sari *et al.*, 1970), and reviews (IAEA, 1967; Matzke, 1982; Schneider and Roepenack, 1986; Matthews, 1987; Baily *et al.*, 1989; Bernard, 1989; Bairiot and Deramaix, 1992; Carbajo *et al.*, 2001; Bairiot *et al.*, 2003).

The plutonium–uranium–oxygen phase diagram

The details of the Pu–U–O phase diagram up to 1000°C have been obtained primarily through lattice constant measurements at high temperature and on quenched samples. It is well established that mixed uranium–plutonium oxides with stoichiometric compositions form a continuous solid solution from UO_2 to PuO_2, and the lattice parameters follow Vegard's law (see Fig. 7.101) so long as the stoichiometry is carefully controlled (Markin and Street, 1967; Thuemmler *et al.*, 1967).

The room-temperature phase diagram of the ternary U–Pu–O system is shown in Fig. 7.102 (IAEA, 1967; Markin and Street, 1967; Benedict and Sari, 1969; Koch, 1972). The system is characterized by four single-phase regions: orthorhombic U_3O_8; a cubic fluorite phase, $MO_{2\pm x}$, which occupies the largest area of the single-phase region; a cubic superstructure, M_4O_9; and a fcc C-M_2O_3 phase.

The orthorhombic U_3O_8 phase includes plutonium in its lattice to form $(U,Pu)_3O_{8-x}$ (Benedict, 1970). The maximum amount of plutonium accommodated at 1000°C corresponds to a Pu:(U + Pu) ratio of 0.06, which decreases to 0.02 at 1400°C. It is assumed that the plutonium ions introduced into the lattice occupy the U_{II} positions in U_3O_8.

The fluorite phase $(U,Pu)O_{2\pm x}$ may be hyperstoichiometric, stoichiometric, or substoichiometric with regard to the O:(U + Pu) ratio. The stoichiometric region corresponds to the pseudo-binary system UO_2–PuO_2, in which the lattice constants obey Vegard's law (see Fig. 7.101). Since PuO_2 loses oxygen at high temperature, deviations from Vegard's law can be observed. At room temperature, the range of the single-phase substoichiometric fluorite structure goes up to the ratio Pu:(U + Pu) = 0.17. A large region with two cubic phases extends from Pu:(U + Pu) ~0.20 up to the binary Pu–O system. One of these two cubic phases is an fcc phase with O:(U + Pu) = 1.985. In the range $0.2 \leq$ Pu:(U + Pu) ≤ 0.5, this phase is in equilibrium with a second fcc phase; and for higher plutonium contents, in equilibrium with a bcc phase of the C-Pu_2O_3 type. In the region Pu:(U + Pu) > 0.5 with low O:(U + Pu) ratios, there exists a bcc single-phase region, which extends up to Pu:(U + Pu) = 0.95 and contracts for Pu:(U + Pu) = 0.97 to a single line at O:(U + Pu) ~1.51. In the region Pu:(U + Pu) ≥ 0.97, a hexagonal phase of A-Pu_2O_3 type exists.

Oxidation of $(U,Pu)O_2$ mixtures yields one- or two-phase products, depending on conditions (Brett and Fox, 1966). In the hyperstoichiometric fluorite phase $(U,Pu)O_{2+x}$, only U is oxidized to U (>IV). At room temperature, for a ratio Pu:(U + Pu) ≤ 0.30 and for O:(U + Pu) ≤ 2.20, a two-phase region $M_4O_9 + MO_{2+x}$ is observed. The M_4O_9 phase exists in the range $2.20 \leq$ O:(U + Pu) ≤ 2.27. For O:(U + Pu) > 2.27 and Pu:(U + Pu) < 0.5, a Pu-rich

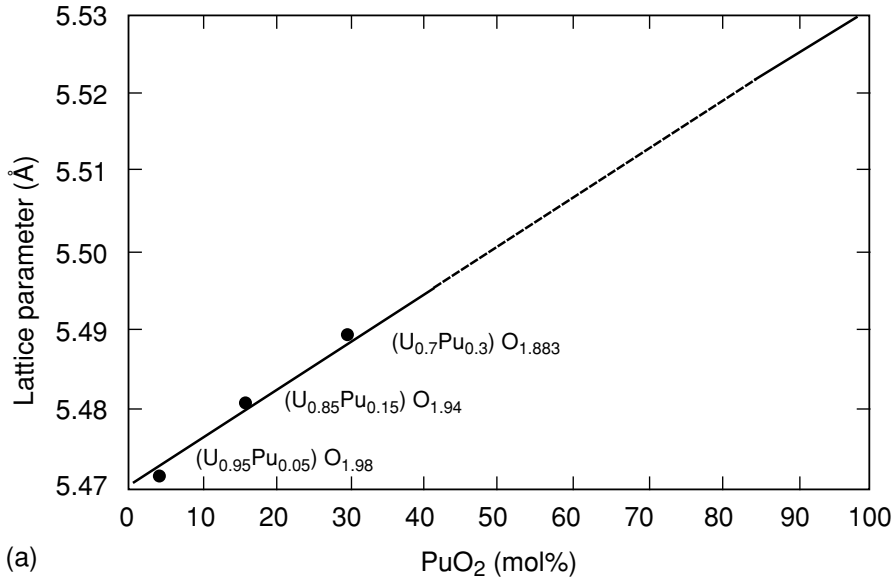

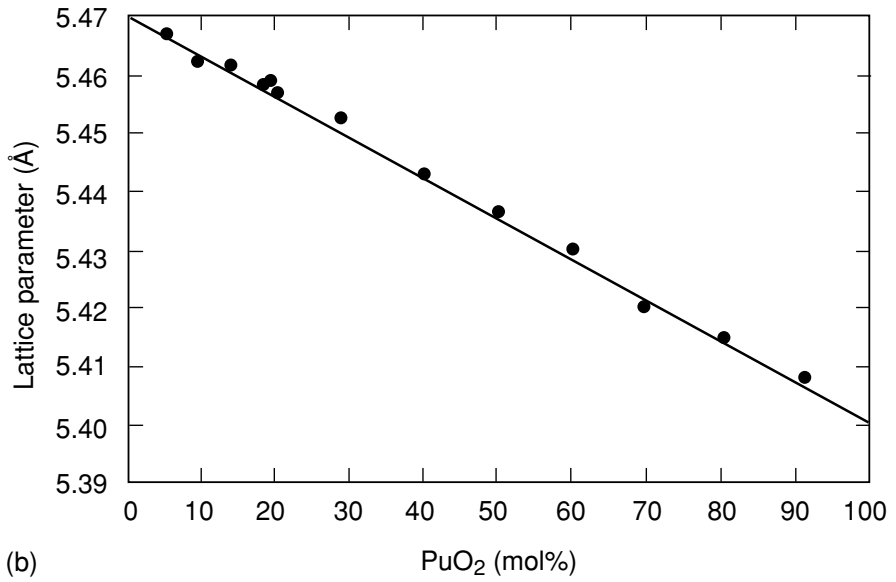

Fig. 7.101 *Lattice parameters of UO_2–PuO_2 mixed oxides that show* (*a*) *the dependence on O*:*M ratio, and* (*b*) *the dependence on PuO_2 concentration* (*Thuemmler* et al., 1967).

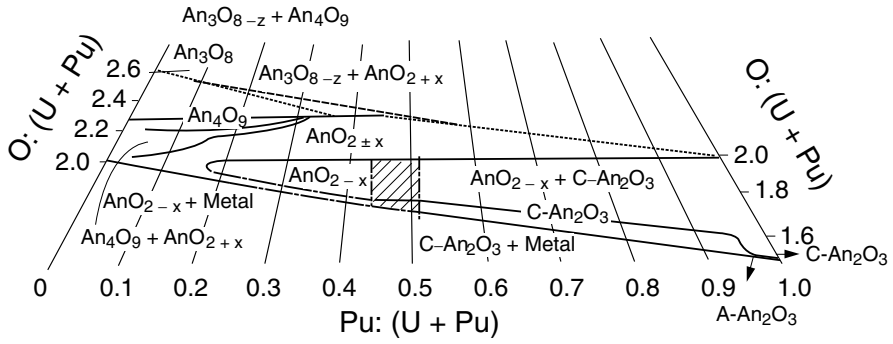

Fig. 7.102 *The phase diagram for the ternary U–Pu–O system in the composition range* $(U,Pu)O_2$–$(U,Pu)O_{2.67}$ *at room temperature* (*Benedict and Sari,* 1969).

fluorite phase is in equilibrium with uranium-rich M_3O_8. The oxidation of $(U,Pu)O_2$ at 600°C yields a metastable U_3O_7 type phase for Pu:(U+Pu) <0.25 and O:(U+Pu) = 2.28. Dean and Boivineau (1970) postulate a rhombohedral phase at composition M_7O_{12} for up to 60 at.% plutonium. According to Nakayama (1971), the phase relationships in the U–O system apply to $0.8 > y > 0.7$ in the MOX system $(U_yPu_{1-y})O_{2+x}$. For $y > 0.7$ there exists the tetragonal phase $(U_yPu_{1-y})O_{2+0.36y}$, which is stable up to 600°C.

Preparation

The preparation of well-defined uranium–plutonium mixed oxides is of particular importance because it is applied to the industrial production of nuclear fuel element materials. The majority of all work reported deals with oxides that contain up to 30% PuO_2, the type commonly encountered in fuel element fabrication. Oxides with more than 30% PuO_2 are much less-frequently studied. A large body of literature has been accumulated on the production of $(U,Pu)O_2$ ceramics for use in nuclear reactors, and a detailed account of all of this work is beyond our scope. The reader is referred to the reviews given in the *Plutonium Handbook* (Wick, 1980), the *Gmelin Handbook* (Koch, 1973c), and the peer-review literature (Schneider and Roepenack, 1986; Baily *et al.*, 1989; Bernard, 1989).

The major technical challenge in preparing $(U,Pu)O_2$ for fuel applications is to produce a product with the maximum degree of homogeneity. There are two main routes to deliver the required properties: comilling of UO_2 and PuO_2 and coprecipitation of UO_2 and PuO_2. Once the $(U,Pu)O_2$ material is formed, both processes entail mixing, pressing, sintering, and grinding operations (Schneider and Roepenack, 1986; Baily *et al.*, 1989; Bernard, 1989; Güldner and Schmidt, 1991). Hundreds of tons of mixed oxide (MOX) fuel have been produced using these processes.

Coprecipitation Processes The main process is the ammonium/uranyl/plutonyl/carbonate process (AUPuC) that produces a powder that is soluble in nitric acid. In this approach, gaseous NH_3 and CO_2 are dissolved into a mixed uranyl/plutonyl nitrate aqueous solution (<40% Pu) to generate an AUPuC of formula $[NH_4]_4[(U,Pu)O_2(CO_3)_3]$. The AUPuC precipitates as a coarse green crystalline product. These crystals are calcined into a $(U,Pu)O_2$ powder by firing at 800°C under a reducing atmosphere of N_2/H_2. The resulting $(U,Pu)O_2$ shows good flowability and sinterability (Schneider and Roepenack, 1986).

Comilling Processes Comilling generally involves mechanical grinding of UO_2 and PuO_2 powders followed by a granulation step before pressing into pellets. This process has been employed extensively at the CEA (Commissariat à l'Energie Atomique) plant in Cadarache, France. An alternate comilling approach designed by Belgonucleaire, and practiced at the French MELOX plant is referred to as the micronized master blend (MIMAS) process. In this process, plutonium and uranium oxides are mixed into a master blend that is 30% PuO_2. The master blend is homogenized and micronized in a dry ball mill, and then blended with free-flowing UO_2 powder to achieve the desired plutonium enrichment, and then pellitized (Schneider and Roepenack, 1986; Baily *et al.*, 1989; Bernard, 1989).

Properties

Due to their technological importance, the thermophysical properties of mixed uranium–plutonium oxide phases have been studied in detail. Unfortunately, most of these data are not available in the open literature. The data that are available have been critically reviewed by Fink (1982) and by Carbajo *et al.* (2001). Much of the discussion that follows has been summarized from those critical reviews.

Vaporization Behavior Vapor pressure measurements on the $(U,Pu)O_2$ system were carried out by Dean *et al.* (1970) with a Knudsen-effusion cell using ^{239}Pu and ^{233}U. Mass spectroscopy studies of vaporization of the $(U,Pu)O_2$ system were carried out by Ohse and Olson (1970), Battles *et al.* (1970), and Raj *et al.* (1999) to evaluate the effect of O:M ratio on the nature of gaseous species. These workers found that the total vapor pressure varies with O:M ratio and goes through a minimum value, suggesting there is no congruently vaporizing composition.

Solidus and Liquidus Temperatures There is an extensive literature on melting behavior. UO_2 melts at a higher temperature (2730–2876°C) than PuO_2 (2238–2445°C), and the $(U,Pu)O_2$ solid solution melts at a temperature between that of pure UO_2 and pure PuO_2. The liquidus and solidus curves of the PuO_2–UO_2 system are shown in Fig. 7.103 for the stoichiometric

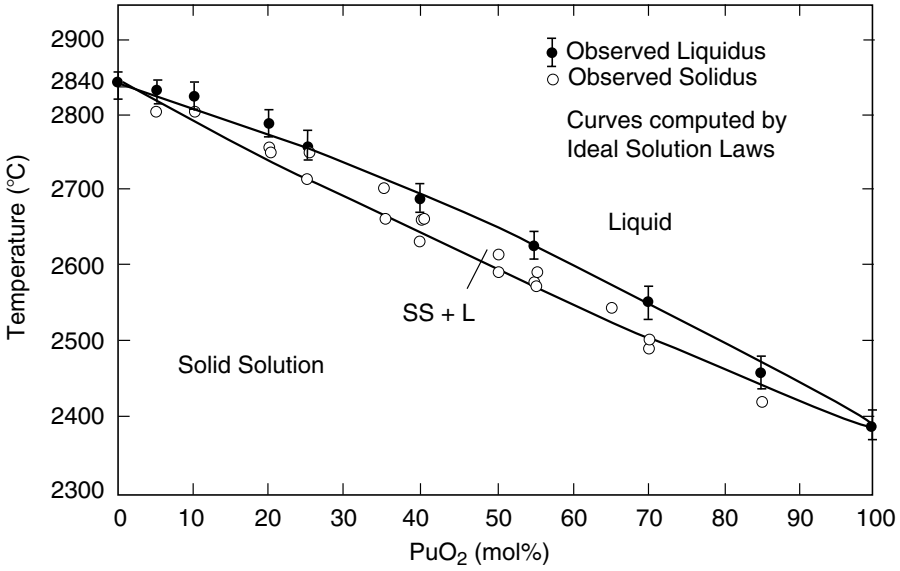

Fig. 7.103 *The solid–liquid phase diagram for the UO_2–PuO_2 system at stoichiometric composition AnO_2 (Lyon and Baily,* 1967).

compositions (Lyon and Baily, 1967). In MOX fuel, the actual melting temperature decreases with increasing PuO_2 content of the fuel as shown in Fig. 7.103 and with burnup (Carbajo *et al.*, 2001). Adamson has developed the following equations that predict the liquidus $[T_L(y)]$ and solidus $[T_S(y)]$ temperatures (in K), where y is the mole fraction of PuO_2 in $(U,Pu)O_2$ (Adamson *et al.*, 1985).

$$T_L(y) = 3120 - 388.1y - 30.4y^2 \tag{7.43}$$

$$T_S(y) = 3120 - 655.3y + 336.4y^2 - 99.9y^3 \tag{7.44}$$

Thermal Expansion and Density MOX fuel density is a function of the fuel composition, temperature, porosity, burnup, and O:M ratio (Carbajo *et al.*, 2001). The $(U,Pu)O_2$ is slightly heavier than UO_2. The density decreases with temperature due to thermal expansion. Fuel burnup changes the porosity and hence the density. At low burnup, the density increases by densification, and at higher burnup the density decreases due to swelling (Carbajo *et al.*, 2001). Martin (1988) developed equations to describe the thermal expansion and density of stoichiometric $(U,Pu)O_2$ compositions. The densities of UO_2 and PuO_2 at 273 K are 10.97 and 11.46 g cm^{-3}, respectively. The density of the solid

solution $(U_{1-y}Pu_y)O_2$ changes according to the linear scaling law below, with y being the mole fraction of PuO_2 (Carbajo *et al.*, 2001).

$$\rho_s(273) = 10970 + 490y(\text{kg m}^{-3}) \tag{7.45}$$

Enthalpy and Heat Capacity Enthalpy and heat capacity are functions of the temperature, fuel composition (fractions of UO_2 and PuO_2), gadolinium content (added as a burnable neutron "poison"), O:M ratio, and burnup. The heat capacity is an important thermodynamic property that is necessary for understanding the various chemical interactions likely to occur during the irradiation of the fuel as well for modeling fuel behavior. Temperature and composition are the main influences on both enthalpy and heat capacity. Both enthalpy and heat capacity increase with temperature. The heat capacity reaches a maximum at the melting point, and then decreases. The heat capacity of UO_2 is lower than that of PuO_2. Carbajo *et al.* (2001) recommended the calculation of enthalpy and heat capacity of solid MOX fuel $U_{1-y}Pu_yO_2$ by using the Neumann–Kopp molar additivity rule, since the $(U,Pu)O_2$ system is an almost ideal solid solution. For example, to calculate the specific heat, one would use:

$$\text{Cp}(\text{T}, \text{MOX}) = (1 - y)\text{Cp}(\text{T}, \text{UO}_2) + y\text{Cp}(\text{T}, \text{PuO}_2) \tag{7.46}$$

where the heat capacity values for UO_2 and PuO_2 are calculated using polynomial expressions developed by Fink (2000) for UO_2, and Cordfunke *et al.* (1990) for PuO_2. Enthalpy polynomials were derived by integrating the Cp equations. For a detailed discussion, listings of the polynomial expressions, and tables of the necessary constants used in these equations, the reader is referred to the original publications (Cordfunke *et al.*, 1990; Fink, 2000; Carbajo *et al.*, 2001). A recent study by Kandan and coworkers experimentally verified that the enthalpies of $(U,Pu)O_2$ solid solutions does obey the Neumann–Kopp molar additivity rule (Kandan *et al.*, 2004).

Enthalpy of Fusion There is only one experimental value for the enthalpy of fusion of a MOX fuel of composition $U_{0.8}Pu_{0.2}O_2$, where Leibowitz *et al.* (1974) obtained a value of 67(3) kJ mol^{-1}.

Thermal Conductivity The thermal conductivity of MOX fuels is a function of the temperature, fuel composition, porosity, burnup, and deviation from stoichiometric composition. Thermal conductivity is a property that does not follow the law of mixtures. The existing data have been reviewed by Carbajo *et al.* (2001). The thermal conductivity decreases with temperature up to approximately 2000 K and then increases with temperature. Addition of PuO_2 to the fuel or increasing porosities reduces the thermal conductivity. Burnup, and/or deviations from stoichiometry significantly decrease the thermal conductivity. For fully dense MOX fuel, Carbajo *et al.* recommended an equation that is a combination of that proposed by Dureiz *et al.* (2000) and

that of Ronchi *et al.* (1999). For full details and discussion, the reader is referred to the review by Carbajo *et al.* (2001).

7.8.6 Plutonium halides and oxyhalides

The decreasing stability of the higher actinide oxidation states in progressing from uranium through neptunium to plutonium is perhaps most clearly revealed in the halogen compounds of plutonium. With the significant and most important exception of fluorine (and, to a minor degree, chlorine), all the halogens form solid binary trihalides of general formula PuX_3 (X = F, Cl, Br, I). For tetrahalides, the only stable solid is the tetrafluoride, PuF_4, while the binary tetrachloride is only marginally stable in the high temperature gas phase as $PuCl_4(g)$. Gas phase data have been interpreted in terms of PuF_5, but there are no known pentahalides, PuX_5, in the solid state (Jouniaux, 1979; Jouniaux *et al.*, 1979; Kleinschmidt, 1988). Fluorine forms the only binary PuX_6, the technologically important hexafluoride, PuF_6. All the halogens form trivalent oxyhalides PuOX (X = F, Cl, Br, I), while fluorine forms a number of oxyfluorides that include pentavalent $PuOF_3$, and hexavalent $PuOF_4$ and PuO_2F_2.

Complex tetrahalide salts of formula M_2PuX_6 are known for X = F, Cl, Br, where M is a monovalent cation. The fluoride ion forms a range of complex salts of general formula $MPuF_5$, $MPuF_6$, M_2PuF_6, M_3PuF_7, M_4PuF_8, and $M_7Pu_6F_{31}$ for the appropriate choice of monovalent cation, M.

Plutonium hexafluoride is by far the most volatile compound of plutonium and is of extraordinary interest in that it makes possible the study of a gaseous binary compound with a rare-earth-like f^2 electron configuration.

A number of reviews have been published in which the properties of the halides have been discussed in detail (Katz and Sheft, 1960; Hodge, 1961; Bagnall, 1967a,b; Brown, 1968; Peterson, 1995).

(a) Plutonium fluorides

(*i*) *Preparation*

Because of their importance in the preparation of plutonium metal (see Sections 7.7.1 and 7.7.2), the binary plutonium fluorides have received a fair amount of attention. Their preparation has been discussed in detail by Johns and Moulton (1944), Reavis *et al.* (1960), Dawson *et al.* (1951), and Dawson and Truswell (1951). The most common procedures involve hydrofluorination of plutonium dioxide or oxalates to generate PuF_3 and PuF_4, while stronger oxidizing conditions such as F_2 will generate PuF_6.

$$2PuO_2 + H_2 + 6HF \xrightarrow{600^\circ C} 2PuF_3 + 4H_2O \tag{7.47}$$

$$Pu_2(C_2O_4)_3 + 6HF \xrightarrow{600^\circ C} 2PuF_3 + 3CO + 3CO_2 + 3H_2O \tag{7.48}$$

$$2Pu(C_2O_4)_2 + 6HF \xrightarrow{600^\circ C} 2PuF_3 + 3CO + 5CO_2 + 3H_2O \tag{7.49}$$

$$PuO_2 + 4HF \xrightarrow[O_2]{550^\circ C} PuF_4 + 2H_2O \tag{7.50}$$

$$PuO_2 + 3F_2 \overset{300^\circ C}{\rightleftharpoons} PuF_6 + O_2 \tag{7.51}$$

$$PuF_4 + F_2 \overset{300^\circ C}{\rightleftharpoons} PuF_6 \tag{7.52}$$

Hydrogen fluoride stored in iron cylinders contains hydrogen, which forms on reaction with the container. Occasionally sulfur dioxide is present. Under reducing conditions like these, PuF_3 results. To secure positive results, either hydrogen may be added, or the absence of reducing agents can be ensured by the addition of oxygen. Between room temperature and 150°C, hydroxyfluorides of the type $Pu(OH)_2F_2$ or $Pu(OH)F_3$ are produced by reaction of PuO_2 with HF. These intermediate compounds are readily converted either to PuF_3 by HF and H_2, or to PuF_4 by HF and O_2 by raising the temperature above 200°C. Instead of plutonium dioxide or one of the oxalates, various other plutonium(III) or plutonium(IV) compounds may also be used as starting materials for fluoride preparations, such as plutonium(IV) nitrate or plutonium peroxide.

Plutonium trifluoride

Plutonium trifluoride is insoluble in water and may therefore be prepared as a hydrate by precipitation from aqueous solution by addition of hydrofluoric acid to an aqueous Pu(III) solution. The preparation of PuF_3 from solution is best accomplished by first reducing Pu(IV) with hydroxylamine (Dawson *et al.*, 1954b) or with SO_2 (Jones, 1953; Weigel, 1965). The purple crystals of the hydrated trifluoride, $PuF_3 \cdot nH_2O$, appear to contain less than one water molecule of hydration. According to Jones (1953), the exact composition of the hydrated compound is $PuF_3 \cdot (0.40 \pm 0.05)H_2O$.

Anhydrous PuF_3 may be obtained by heating $PuF_3 \cdot nH_2O$ in a stream of hydrogen fluoride gas at 200–300°C, or by first heating plutonium(III) oxalate in a stream of hydrogen at 150 to 600°C, followed by hydrogen fluoride at 200 to 300°C (Dawson and Truswell, 1951). The latter method has been used on the 100–350 g scale. PuF_4 may be reduced directly to anhydrous PuF_3 by heating in a stream of hydrogen at 600°C (Garner, 1950).

Plutonium tetrafluoride

Addition of hydrofluoric acid to aqueous plutonium(IV) solutions precipitates pale pink plutonium tetrafluoride hydrate, $PuF_4 \cdot 2.5H_2O$. Attempts to dehydrate this substance by heating *in vacuo* did not yield anhydrous plutonium

tetrafluoride, but rather the trifluoride. According to Dawson *et al.* (1954b), this rather surprising result may be accounted for by the following reaction scheme:

$$PuF_4 + H_2O \rightleftharpoons PuO_2 + 4HF \tag{7.53}$$

$$3PuF_4 + PuO_2 \rightleftharpoons 4PuF_3 + O_2 \tag{7.54}$$

with a net reaction of:

$$4PuF_4 + 2H_2O \rightleftharpoons 4PuF_3 + 4HF + O_2 \tag{7.55}$$

Increasing temperature and high vacuum displaces the equilibrium toward the right and aids in the production of the trivalent fluoride. Both plutonium trifluoride and tetrafluoride hydrates are insoluble in water and will dissolve in acid only sparingly. By contrast, they may be dissolved with comparative ease in aqueous solutions of ions that form stable complexes with fluoride ions, such as Zr(IV), Fe(III), and Al(III), or with BO_3^{3-} which forms BF_4^-. Solutions of 0.1 M HNO_3 saturated with boric acid or aluminum nitrate are therefore especially well suited for the dissolution of PuF_3 or PuF_4. Detailed procedures for the dissolution of PuF_4 with nitric acid have been summarized by Navratil (1969a–c).

Plutonium tetrafluoride hydrate, $PuF_4 \cdot 2.5H_2O$, may be dehydrated in a stream of HF gas to anhydrous PuF_4. According to Khanaev *et al.* (1967), the dehydration of $PuF_4 \cdot 2.5H_2O$ proceeds through the successive formation of $PuF_4 \cdot 2.5H_2O$, and ultimately anhydrous PuF_4.

Both plutonium trifluoride and plutonium tetrafluoride react with oxygen at elevated temperatures. Fried and Davidson (1949) concluded that the reaction of plutonium trifluoride with oxygen proceeds according to the equation:

$$4PuF_3 + O_2 \xrightarrow{600^\circ C} 3PuF_4 + PuO_2 \tag{7.56}$$

This conclusion was confirmed by Dawson and Truswell (1951), who measured the oxygen partial pressure for the reverse reaction of PuF_4 with PuO_2. In the presence of water vapor and oxygen, the reaction product is PuO_2 (Dawson and Elliott, 1953). Plutonium tetrafluoride is stable in oxygen at 600°C and *in vacuo* at 900°C. On heating PuF_4 *in vacuo*, some material sublimes and the residue is found to be PuF_3. Fried and Davidson (1949) interpreted this as a disproportionation of PuF_4 into PuF_3 and PuF_5. Dawson *et al.* (1951) confirmed these conclusions but were able to show that the sublimate is probably not PuF_5. It is possible that the compound formed in this process is an oxyfluoride, as observed by Jouniaux *et al.* (1979) for the reaction of PuO_2 with F_2.

Intermediate fluoride and plutonium pentafluoride

During the preparation of plutonium hexafluoride (see below), a brick-red solid residue has been observed. This solid was identified by X-ray powder diffraction and fluorine analysis by pyrohydrolysis to be the mixed-valent compound

Pu_4F_{17} (Mandleberg *et al.*, 1956). Hawkins (1956) and Gendre (1962) have also reported evidence for the existence of this compound, but it has not been isolated in the pure state. Jouniaux and coworkers proposed the formation of gas-phase PuF_5 in their thermochromatographic study (Jouniaux *et al.*, 1979), and Kleinschmidt (1988) also interpreted his mass spectroscopy results on PuF_6 in the presence of alumina in terms of formation of this gas-phase species.

Plutonium hexafluoride

It is well known that fluorine oxidizes transition metals to their highest oxidation states. This general characteristic also holds true for plutonium. The high volatility of PuF_6 has made this compound of great technological importance, and therefore a considerable amount of information about PuF_6 is available.

Plutonium hexafluoride was first prepared at Los Alamos by Florin and coworkers (Florin, 1950a,b, 1953; Florin and Tannenbaum, 1952; Florin *et al.*, 1956). The preparation and determination of some fundamental properties was carried out at Harwell by Mandleberg and colleagues (Hurst *et al.*, 1953; Mandleberg *et al.*, 1953, 1956), while Malm and coworkers (Malm and Weinstock, 1954; Weinstock and Malm, 1956a,b) performed extensive research on the basic properties of PuF_6 at Argonne National Laboratory. Scientists at Argonne (Chemical Engineering Division) performed extensive research on PuF_6 in connection with the development of the fluoride volatility process (Adams *et al.*, 1957; Steindler *et al.*, 1958, 1959; Steindler, 1963). The review by Steindler (1963) gives an excellent summary on the preparation and properties of plutonium hexafluoride.

Plutonium hexafluoride is most easily prepared by using elemental fluorine as an oxidizing–fluorinating agent with PuF_4 or PuO_2, typically at 600°C according to the following reactions:

$$PuO_2 + 3F_2 \rightleftharpoons PuF_6 + O_2 \tag{7.57}$$

$$PuF_4 + F_2 \rightleftharpoons PuF_6 \tag{7.58}$$

The fluorination of plutonium dioxide produces oxygen, which accumulates in any apparatus in which the gases are recirculated over the unreacted solid, and periodic removal of oxygen is required to avoid dilution of fluorine. Since plutonium tetrafluoride is always formed in the fluorination of plutonium dioxide, the preferred method of preparing PuF_6 is the fluorination of PuF_4.

The preparation of PuF_6 from PuF_4 and F_2 proceeds at a reasonable rate only at fairly high temperatures, typically at 300°C. Passage of fluorine over PuF_4, in a conventional tube furnace is possible, but is not very efficient. In order to prevent thermal decomposition of the PuF_6 product, special reaction vessels are employed to permit rapid condensation of the volatile products close to the point of their preparation. Fluorination reactor vessels of this type were first used by Florin and coworkers (Florin, 1950a,b, 1953; Florin and Tannenbaum, 1952; Florin *et al.*, 1956), and by Weinstock and coworkers (Malm and

Weinstock, 1954; Weinstock and Malm, 1956b). Two of these reactor designs are shown in Fig. 7.104. The starting charge of PuF_4 is placed in a nickel dish, which is heated in a fluorine atmosphere by an induction coil. The induction coil consists of copper tubing, through which liquid nitrogen is circulated, such that the coil serves as both the heating element and the product condenser. Once formed, the PuF_6 product collects on the surface of the coil in crystalline form. This type of reactor works very well for gram-quantity preparations. For larger quantities, fluidized-bed fluorination is the preferred method. Quantities up to 500 g of Pu have been volatilized in the fluidized-bed fluorination of PuF_4. For details of the technique, see Levitz *et al.* (1968).

The use of elemental fluorine at elevated temperature is the only known method of economically producing PuF_6. Los Alamos researchers evaluated

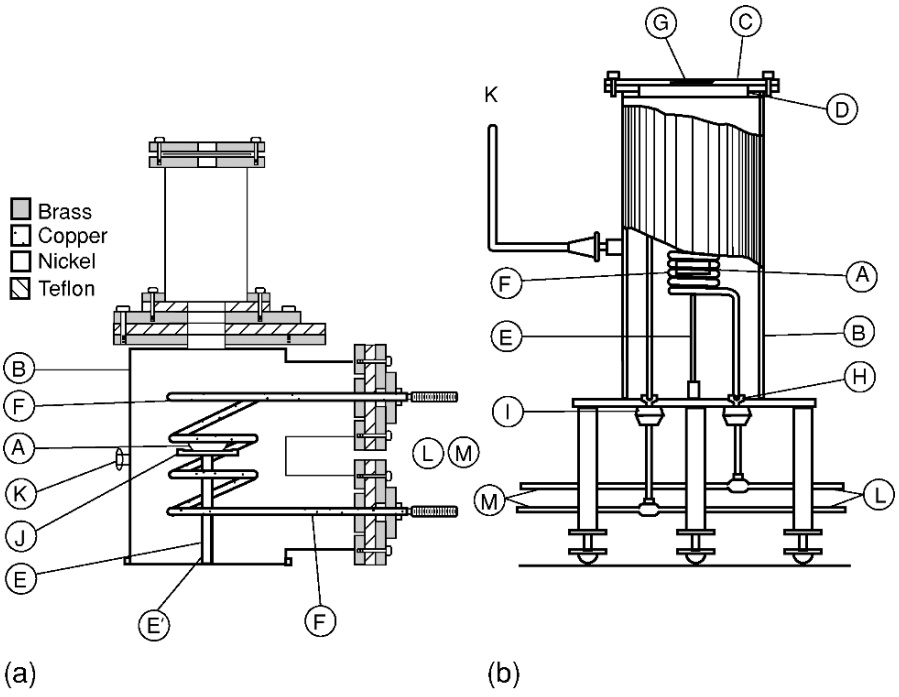

Fig. 7.104 *Two fluorination reactors for the preparation of plutonium hexafluoride. (a) The reactor used by Florin, Tannenbaum and Lemons, and (b) the reactor used by Weinstock and Malm. The legend for both reactors is as follows: A, nickel dish filled with PuF_4; B, brass reactor can; C, removable cover for loading the reactor; D, tongue and groove Teflon gasket for closure; E, nickel supporting rod for nickel dish; E', nickel supporting tube; F, copper tubing induction coil that also serves as cooling coil; G, Fluorothene window; H, Teflon seal and insulator; I, Micalox insulator; J, support for nickel dish; K, connecting line to fluorine source, storage vessels and pumping systems; L, RF connection; M, liquid nitrogen circulation.*

the use of alternative oxidation fluorinating agents that proved capable of producing PuF_6 at or below room temperature (Eller *et al.*, 1992). Plutonium tetrafluoride, oxide, and oxyfluorides are all readily converted to PuF_6 by reaction with gaseous dioxygen difluoride O_2F_2 or O_2F_2/HF solutions at or below room temperature (Malm *et al.*, 1984; Erilov *et al.*, 2002). In a similar fashion, gaseous krypton difluoride, KrF_2 will also produce PuF_6 at ambient or low temperatures (Asprey *et al.*, 1986). The ability of both O_2F_2 and KrF_2 to volatilize plutonium at ambient temperature at moderate rates could have practical applications for recovery of plutonium as volatile PuF_6 from solid wastes.

Plutonium hexafluoride, when rigorously freed from traces of hydrogen fluoride, can be handled in glass equipment. Samples of PuF_6 can be purified by trap-to-trap distillation at cryogenic temperatures to remove HF, F_2, and other impurities. The handling and manipulation of PuF_6 is a very hazardous operation. A broken container means the spreading of hazardous plutonium through the air by the volatile and hydrolytically reactive hexafluoride. An actual multigram release of plutonium from a ruptured container has occurred and has been described by Trevorrow *et al.* (1965). Kessie and Ramaswami (1965) have described methods to prevent the spread of PuF_6 vapor through the ventilation system by operating the vacuum line containing the compound in a moist atmosphere. This hydrolyzes any escaped PuF_6 and converts it to PuO_2F_2, which is a filterable solid.

The rate of formation of plutonium hexafluoride by fluorination of the dioxide and the tetrafluoride was studied by Steindler (1963), who derived activation energies between 43.5 and 52.3 kJ mol^{-1}. These activation energies were found to be greater, the smaller the specific surface area. In the case of a PuF_4 sample having a bulk density of 1.3 g cm^{-3}, the rate of reaction with fluorine was found to follow the relationship

$$\log_{10}(\text{rate/mg PuF}_4\ \text{cm}^{-2}\text{h}^{-1}) = 5.917 - 2719/T \qquad (7.59)$$

The dependence of the reaction rate on the F_2 partial pressure is shown in Fig. 7.105 (Steindler, 1963).

(*ii*) *Solid-state structures*

Crystallographic data for plutonium halide and oxyhalide compounds are given in Table 7.42.

PuF_3. Plutonium trifluoride crystallizes in hexagonal (trigonal) symmetry and adopts the LaF_3 (tysonite) structure. Zachariasen (1949d) indexed the powder pattern based on hexagonal symmetry in space group $P6_3/mmc$. Subsequent work has shown that the tysonite structure has the larger trigonal cell ($P\bar{3}c1$), where $a_0 = a_0'/\sqrt{3}$ (Cheetham *et al.*, 1976). The polymeric structure is complicated, but the simple description is that each plutonium atom is surrounded by nine fluorine atoms, and the plutonium atoms lie on a two-fold axis of symmetry.

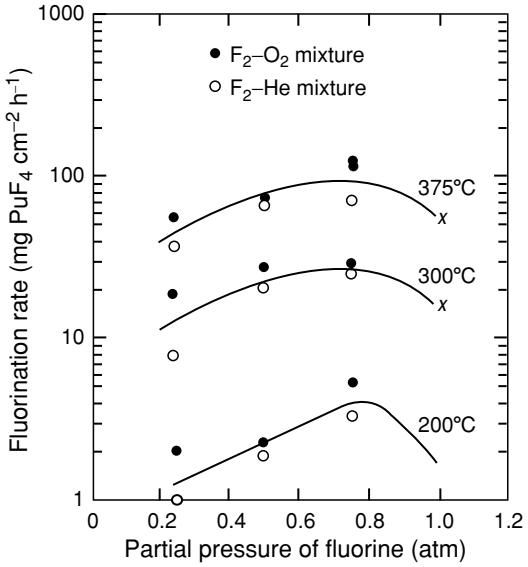

Fig. 7.105 *Fluorination of PuF_4 by fluorine diluted with He/O_2 mixtures to produce PuF_6* (*Steindler,* 1963).

PuF_4. Plutonium tetrafluoride has the ZrF_4 structure and is isostructural with all the lanthanide and actinide tetrafluorides (Wells, 1984). It possesses monoclinic symmetry, space group C2/*c*, with 12 molecules per unit cell (Zachariasen, 1949d). The basic repeating unit contains five plutonium atoms arranged in a distorted pyramid with four plutonium atoms forming a distorted base, and the fifth occupying the apex of the pyramid. Both types of nonequivalent plutonium atom are surrounded by eight fluorine atoms forming a slightly distorted square antiprism that shares vertices with eight other antiprisms. The local PuF_8 pseudo-antiprismatic coordination geometry in PuF_4 is illustrated in Fig. 7.106.

PuF_6. The solid-state structure of PuF_6 was determined by XRD by Florin and coworkers (Florin *et al.*, 1956). Crystalline PuF_6 possesses orthorhombic symmetry with four molecules per unit cell, with Pu–F distances spanning a range from 2.01 to 2.13 Å. The individual PuF_6 molecules in the crystal do not exhibit perfect octahedral symmetry, but spectroscopic studies clearly show that the compound retains octahedral symmetry in the gas phase (see below).

(*iii*) *Properties*

The plutonium trihalides have a small but finite volatility at elevated temperatures. Phipps *et al.* (1949, 1950a) were the first to measure the vapor pressures of the trihalides PuX_3, where X = F, Cl, and Br. In the case of PuF_3, the results are

Table 7.42 *Some physical constants and X-ray crystal structure data for plutonium halides and oxyhalides.*

Compound	*Color*	*Symmetry*	*Space group*	*Lattice parameters*			*Density* (g cm^{-3})	*References*
				a_0 (Å)	b_0 (Å)	c_0 (Å)		
PuF_3	violet-blue	trigonal	$P\bar{3}c1$[a]	7.092		7.254(1)	9.32	Zachariasen (1949d)
PuF_4	pale brown	monoclinic	$C2/c$[b]	12.59(3)	10.69(2)	8.29(4)	7.04	Keenan and Asprey (1969)
$PuF_4{\cdot}2.5H_2O$	pink	orthorhombic	*Pnam*	12.66(3)	11.03(5)	6.99(5)	4.89	Dawson *et al.* (1954a)
PuF_6	reddish brown	orthorhombic	*Pnma*[c]	9.888(9)	8.961(8)	5.203(5)	5.085	Florin *et al.* (1956)
$PuCl_3$	emerald green	hexagonal	$P6_3/m$	7.394(1)		4.243(1)	5.708	Burns *et al.* (1975)
$PuBr_3$	green	orthorhombic	*Cmcm*[d]	4.097(8)	12.617(10)	9.147(10)	6.71	Brown and Edwards (1972)
$PuBr_3{\cdot}6H_2O$	blue	monoclinic	$P2/n$[e]	10.022(5)	6.798(3)	8.181(4)		Brown *et al.* (1968)
PuI_3	bright green	orthorhombic	*Cmcm*[d]	4.326(6)	13.962(20)	9.974(20)	6.92	Brown and Edwards (1972)
PuOF	metallic	tetragonal	*P4/nmm*	4.05(1)		5.71(1)	8.20	Zachariasen (1951)
PuOCl	blue-green	tetragonal	*P4/nmm*	4.012(2)		6.792(10)	8.82	Zachariasen (1949d)
PuOBr	dark green	tetragonal	*P4/nmm*	4.022(4)		7.571(11)	9.08	Zachariasen (1949d)
PuOI	green	tetragonal	*P4/nmm*	4.042(2)		9.169(15)	8.47	Zachariasen (1949d)
PuO_2F_2	white	rhombohedral	$R\bar{3}m$	4.154		15.84	6.50	Wyckoff (1963)
$PuOF_4$	chocolate brown	trigonal	*R3m*	12.90(2)		5.56(2)		Burns and O'Donnell (1977)

[a] Originally reported by Zachariasen in hexagonal space group $P6_3/mmc$. The hexagonal LaF_3 (tysonite) has trigonal space group $P\bar{3}c1$, which is the likely space group for PuF_3. To transform from $P6_3/mmc$ to $P\bar{3}c1$, one would use $a_0 = a'\sqrt{3}$ to derive $a_0 = 7.092$ (Å), which is the value reported above.
[b] $\beta = 126.0(2)$.
[c] Lattice constants refined from original data by Roof (1989).
[d] Original space group *Ccmm*, changed to standard setting *Cmcm* by Roof (1989).
[e] $\beta = 92.97(3)$.

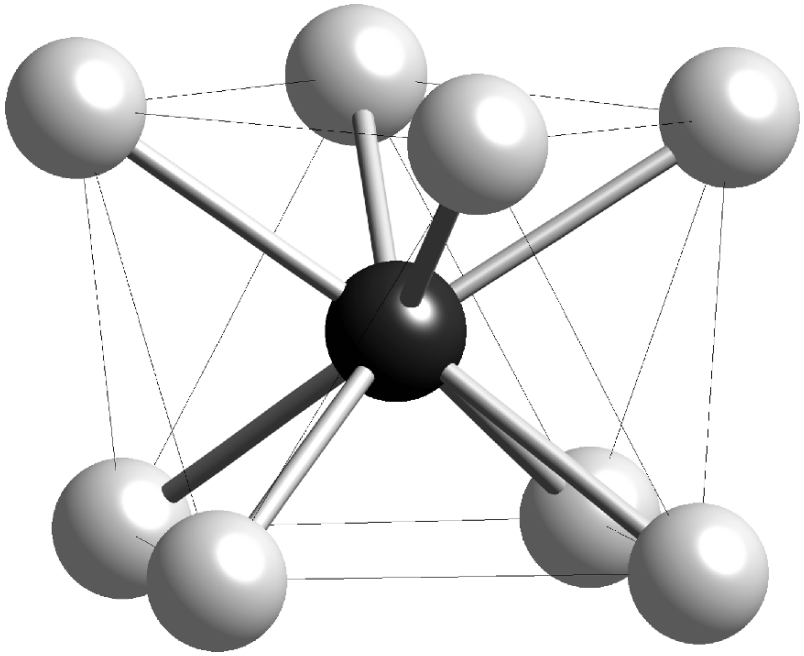

Fig. 7.106 *A view of the local coordination geometry of PuF_4 that emphasizes the local PuF_8 pseudo-antiprismatic coordination environment. The plutonium atoms are black and fluorine atoms gray.*

somewhat conflicting. In the work of Phipps *et al.* (1949, 1950a), an apparent inflection in the vapor–pressure curve implied an improbably low value for the melting point of 1447 K. A direct measurement by Westrum and Wallmann (1951) yielded values of (1698 ± 2) K for the melting point and (1699 ± 2) K for the solidification point, leading these authors to a different interpretation of the data and thus to a vapor–pressure equation that was different from the equation(s) given by Phipps *et al.* (1949, 1950a). Carniglia and coworkers (Carniglia, 1953; Carniglia and Cunningham, 1955) also measured the PuF_3 vapor pressure. Their data, agreed in general with the results of Phipps *et al.* (1949, 1950a), but the calculated enthalpies and entropies are both somewhat smaller. Kent (1968) reinvestigated the PuF_3 vapor pressure in the range 1243–1475 K by evaporating a mixture of PuF_3 and plutonium metal from a tantalum Knudsen cell attached to a mass spectrometer. He observed the species PuF_2^+, PuF^+, and Pu^+, but very little PuF_3^+. Kent used these data to obtain several important thermodynamic quantities, and have been reviewed by Lemire *et al.* (see Table 7.43).

The vapor pressure of PuF_4 has been measured by Mandleberg and Davies (1954, 1961), Chudinov and Choporov (1970), and Berger and Gäumann

(1961). Rand (1966) and Lemire *et al.* (2001) critically assessed these data. They prefer the results of Chudinov and Choporov to the data reported by the two other groups of authors. Chudinov and Choporov used a modified Knudsen method employing a nickel effusion cell, which is not attacked by fluorides. Rand discounts the measurements reported by Mandleberg and Davies because the tantalum effusion cell used by these authors would have reduced PuF_4 to PuF_3. On the basis of the known instability of PuF_5, there is also reason to believe that the disproportionation of PuF_4 into PuF_3 and PuF_5 postulated by Mandleberg and Davies is unlikely to occur, because the calculated pressure of PuF_6 in equilibrium with PuF_4 at 1200 K is 10^{-11} Torr, and because PuF_5 is less stable than PuF_6. The data of Berger and Gäumann (1961) yield too small an entropy change for a sublimation process, suggesting some reduction in their platinum effusion vessel. Another serious objection to these results is the implication that PuF_4 appears to be less volatile than UF_4, something that is not consistent with general trends in vapor pressures of other actinide halides.

In the case of $PuCl_3$ and $PuBr_3$, the only measurements reported are those by Phipps *et al.* (1949, 1950a) and, for $PuCl_3$, those by Weinstock (1944). No other recent measurements are reported. The vapor–pressure equations for PuI_3 were reported by Katz and Sheft (1960).

A detailed assessment and review of the important thermodynamic quantities such as the enthalpy of formation, standard entropy, heat capacity, and fusion data have been given by Lemire *et al.* (2001). Selected thermodynamic constants are given in Table 7.43.

Plutonium hexafluoride is a low-melting, highly volatile solid, whose vapor has the brown color of nitrogen dioxide, and which melts to a deep brown, transparent liquid. The following melting points have been reported: 325 K (52°C), 327 K (54°C), 323.7 K (50.5°C), and 324.74 K (51.59°C), the most-accurate value being the last, measured at $p = 533$ Torr. The boiling point was reported as 335.3 K (62.15°C).

The vapor pressure of PuF_6 has been measured by several authors (Hurst *et al.*, 1953; Mandleberg *et al.*, 1953, 1956; Florin *et al.*, 1956 Adams *et al.*, 1957). The most careful determination and description is that of Weinstock *et al.* (1959), who fit their data to a three-term function of temperature to derive a number of important thermochemical properties. A refit of their data by Lemire *et al.* (2001) gives $\Delta_{\text{subl}}H^\circ = (48.65 \pm 1.00)$ kJ mol^{-1} and $\Delta_f H^\circ = -(1861.35 \pm 20.17)$ kJ mol^{-1}.

Additional thermodynamic data for PuF_6 have been assessed and compiled by Rand (1966), Fuger *et al.* (1983), and Lemire *et al.* (2001). Thermodynamic data calculated from spectroscopic measurements were reported by Sundaram (1962), Nagarajan (1962), and Hawkins *et al.* (1954).

The PuF_6 molecule has 15 fundamental modes of vibration. These vibrations fall into two groups according to their predominant Pu–F stretching (ν_1, ν_2, ν_3) or bending (ν_4, ν_5, ν_6) modes. The symmetries of these modes indicate that ν_3, ν_4, ν_5, and ν_6 are all triply degenerate, ν_2 doubly degenerate, and ν_1 nondegenerate.

Table 7.43 *Thermodynamic parameters for plutonium halides* (*Lemire* et al., 2001).

Compound	$\Delta_f G^\circ_{298}$ (kJ mol^{-1})	$\Delta_f H^\circ_{298}$ (kJ mol^{-1})	S°_{298} (J K^{-1} mol^{-1})	C°_{p298} (J K^{-1} mol^{-1})[a]
Solids				
PuF_3 (cr)	−1517.4 ± 3.7	−1586.7 ± 3.7	126.1 ± 0.4	92.6 ± 0.3
PuF_4 (cr)	−1756.7 ± 20.0	−1850 ± 20	147.3 ± 0.4	116.2 ± 0.3
PuF_6 (cr)	−1729.9 ± 20.2	−1861.3 ± 20.2	221.8 ± 1.1	168.1 ± 2.0
PuOF (cr)	−1091.6 ± 20.2	−1140 ± 20	96 ± 10	69.4 ± 10
$PuCl_3$ (cr)	−891.8 ± 2.0	−959.6 ± 1.8	161.7 ± 3.0	101.2 ± 4.0
$PuCl_4$ (cr)	−879.4 ± 5.8	−968.7 ± 5.0	201 ± 10	121.4 ± 4.0
$PuBr_3$ (cr)	−767.3 ± 2.7	−792.6 ± 2.0	198 ± 6	101.8 ± 6.0
PuOBr (cr)	−838.4 ± 8.5	−870 ± 8	127 ± 10	73 ± 8
PuI_3 (cr)	−579 ± 4.5	−579.2 ± 2.8	228 ± 12	110 ± 8
PuOI (cr)	−776.6 ± 20.5	−802 ± 20	130 ± 15	75.6 ± 10.0
Cs_2PuCl_6 (cr)	−1838.2 ± 6.7	−1982 ± 5	412 ± 15	
Cs_3PuCl_6 (cr)	−2208.0 ± 9.5	−2364.4 ± 9.0	545.9 ± 11.0	258.6 ± 10.0
$CsPu_2Cl_7$ (cr)	−2235.1 ± 5.3	−2399.4 ± 5.7	424 ± 7.3	254.9 ± 10.0
Cs_2PuBr_6 (cr)	−1636.3 ± 6.1	−1697.4 ± 4.2	470 ± 15	
$Cs_2NaPuCl_6$ (cr)	−2143.5 ± 5.2	−2294.2 ± 2.6	440 ± 15	
Gases				
PuF (g)	−141 ± 10.1	−112.6 ± 10.0	251 ± 5	33.5 ± 3.0
PuF_2 (g)	−626.1 ± 6.7	−614.3 ± 6.0	297 ± 10	51.5 ± 5.0
PuF_3 (g)	−1161.1 ± 4.8	−1167.8 ± 3.7	336.1 ± 10.0	72.2 ± 5.0
PuF_4 (g)	−1517.9 ± 22.2	−1548 ± 22	359 ± 10	92.4 ± 5.0
PuF_6 (g)	−1725.1 ± 20.1	−1812.7 ± 20.1	368.9 ± 1.0	129.3 ± 1.0
$PuCl_3$ (g)	−641.3 ± 3.6	−647.4 ± 2.0	368.6 ± 10.0	78.5 ± 5.0
$PuCl_4$ (g)	−764.7 ± 10.4	−792 ± 10	409 ± 10	103.4 ± 5.0
$PuBr_3$ (g)	−529.8 ± 15.7	−488 ± 15	423 ± 15	81.6 ± 10.0
PuI_3 (g)	−366.5 ± 15.7	−305 ± 15	435 ± 15	82 ± 5

[a] Temperature coefficients of this function are tabulated by Lemire *et al.* (2001) in their Table 4.3.

Only ν_3 (stretching) and ν_4 (bending) are infrared active. The first comprehensive gas-phase absorption spectrum covering 4,000–20,000 cm^{-1} was reported by Steindler and Gunther in 1964 (Steindler and Gunther, 1964a,b). The observed spectrum is shown in Fig. 7.107. These measurements were refined in the wavelength region between 3000 and 9000 cm^{-1} by Walters and Briesmeister (1984) using a very long pathlength cell. In both of these early studies, the spectrometers gave spectral resolutions of several wavenumbers so that vibrational components of the spectra were not resolved. Kugel *et al.* (1976) studied PuF_6 at much higher resolution using an intracavity laser quenching technique. Analysis of the room-temperature absorption spectrum is rendered difficult by the clustering of electronic transitions as well as number of hot bands that result from the low-energy bending vibrations (ν_4, ν_5, ν_6). In a low-temperature matrix, the elimination of rotations and hot bands greatly simplifies the spectral analysis. Dewey *et al.* (1986) studied the absorption and emission of matrix-isolated PuF_6 at 8 K and were able to assign transitions below 17,000 cm^{-1}. From these data, all the vibrational frequencies have been determined from the fundamental or combination bands, and they are compiled in Table 7.44 (Dewey *et al.*, 1986).

Kim and coworkers studied the fine structure in the vibronic band near 800 nm, resolving Coriolis fine structure at the Doppler-limited resolution (Kim *et al.*, 1987). Finally, David and Kim (1988) reported the entire absorption spectrum of PuF_6 in the near IR and visible regions at high sensitivity and high resolution. They measured isotope shifts between $^{239}PuF_6$ and $^{242}PuF_6$ to identify the specific vibrational modes. The Raman spectrum of PuF_6 has not yet been observed, because of the rapid photochemical decomposition at 5641 Å (Hawkins *et al.*, 1954).

The magnetic susceptibility of plutonium hexafluoride was measured at several temperatures by Gruen *et al.* (1956). Molar susceptibilities of 131×10^{-6} cgs units at 81 K and of 173×10^{-6} cgs units at 131 K were observed. Gruen *et al.* indicated that, based on the small susceptibilities observed compared with the susceptibility of isoelectronic compounds of U(IV), Np(V), and PuO_2^{2+}, which show larger, strongly temperature-dependent values, the ground electronic state of plutonium hexafluoride is nondegenerate (see Section 7.9.3). Furthermore, the first excited state of plutonium hexafluoride must be at least 1000 cm^{-1} (0.12 eV) above the ground state, which means that there is a much greater splitting than required for the isoelectronic U(IV) compounds.

Florin *et al.* (1956) studied the equilibrium system

$$PuF_6(g) \rightleftharpoons PuF_4(s) + F_2(g) \tag{7.60}$$

and obtained the equilibrium constant in the range 160–600°C. Their data showed a significant break at 308°C, suggesting a phase change. Weinstock and coworkers (Malm and Weinstock, 1954; Weinstock and Malm, 1956a) reported a measurement of the equilibrium constant at 220°C. Trevorrow and coworkers (Trevorrow and Shinn, 1960; Trevorrow *et al.*, 1961) reexamined this system and made a careful determination of the equilibrium constant in the

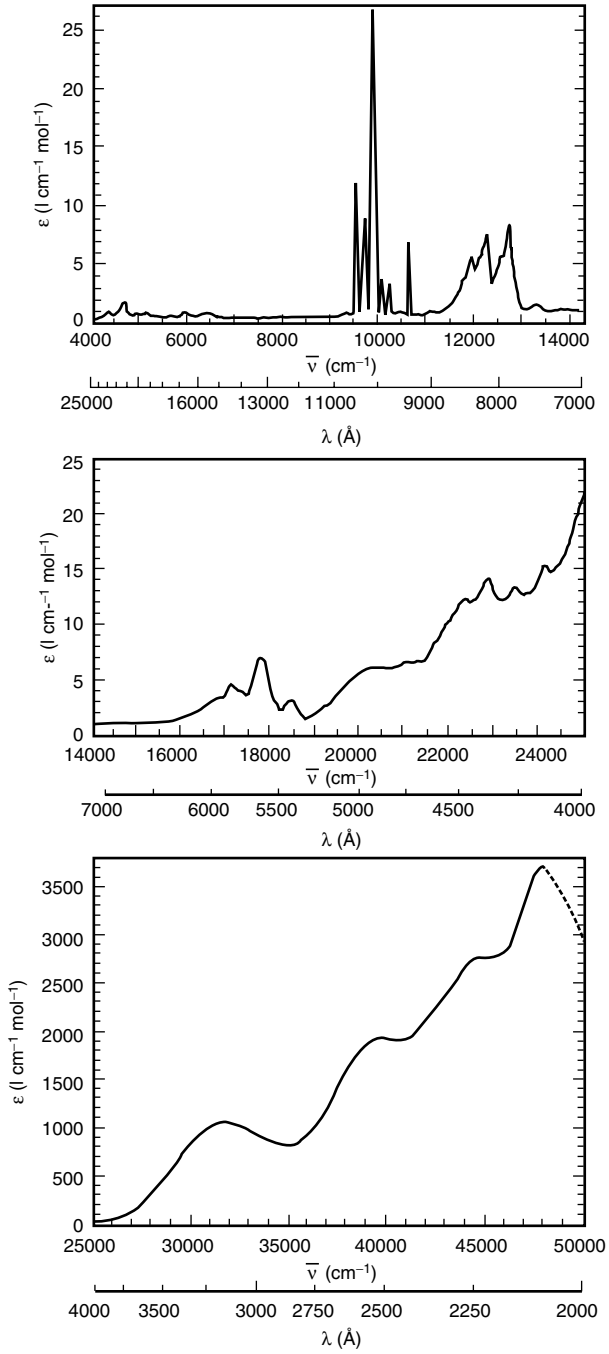

Fig. 7.107 *The absorption spectrum of gaseous PuF_6 from Steindler and Gunther* (1964*a*).

Table 7.44 *Vibrational frequencies of the PuF_6 molecule.*

Mode	*Matrix frequency* (cm^{-1})[a]	*Gas phase frequency* (cm^{-1})[b]
ν_1	(625)	(628)
ν_2	(519)	(523)
ν_3	612	616
ν_4	200[b]	(203)
ν_5	(209)	(211)
ν_6	(177)	(173)
$\nu_1 + \nu_3$	1236	1244
$\nu_2 + \nu_3$	1130	1139
$\nu_3 + \nu_5$	821	827
$\nu_1 + \nu_4$	–	831
$\nu_2 + \nu_4$	–	726
$\nu_4 + \nu_5$	–	414
$\nu_2 + \nu_6$	696	696

[a] From matrix isolation experiments by Dewey *et al.* (1986).
[b] From fluorescence measurements by Weinstock and Goodman (1965).

temperature range 150–400°C. Fig. 7.108 shows a plot of the log of the equilibrium constant K_p versus inverse temperature using the data of various authors (Florin *et al.*, 1956; Trevorrow and Shinn, 1960; Trevorrow *et al.*, 1961). Trevorrow and Shinn (1960) measured the equilibrium constant of the reverse reaction in the temperature range 170–395 K. This equilibrium has been measured at high pressures of fluorine (up to 825 bar) (Steindler *et al.*, 1958) and found to be pressure-independent. The free energy of the reaction

$$PuF_4(s) + F_2(g) \rightarrow PuF_6(g) \tag{7.61}$$

can be calculated from the equation

$$\Delta G^\circ = -RT\ \ln K = 2.55 \times 10^4 + 5.27T(\mathrm{K})\mathrm{J\ mol^{-1}} \tag{7.62}$$

The calculated value of ΔG° at 275°C is (28.36 ± 0.38) kJ mol^{-1}. The mean value of ΔH° for the reaction is (25.48 ± 0.59) kJ mol^{-1} and the mean value of ΔS° for the reaction is $-(5.44 \pm 0.84)$ J K^{-1} mol^{-1}.

Radiation decomposition

The α radioactivity of ^{239}Pu (Table 7.l) causes a continuous decomposition of PuF_6 (Steindler *et al.*, 1963; Wagner *et al.*, 1965). As the emitted α particle travels through the crystal lattice, bonds are ruptured and decomposition of PuF_6 to F_2 and lower plutonium fluorides occurs. The observed rate of decomposition (Gruen *et al.*, 1956) of gaseous PuF_6 is not a linear function of time but decreases with time from 1.78 to 0.064% of the initial PuF_6 (100 Torr) per day in the range from 0.5 to 571 days at 26°C. The initial high decomposition rate of 1.78% per day may be partly attributed to the reaction of the PuF_6 with the

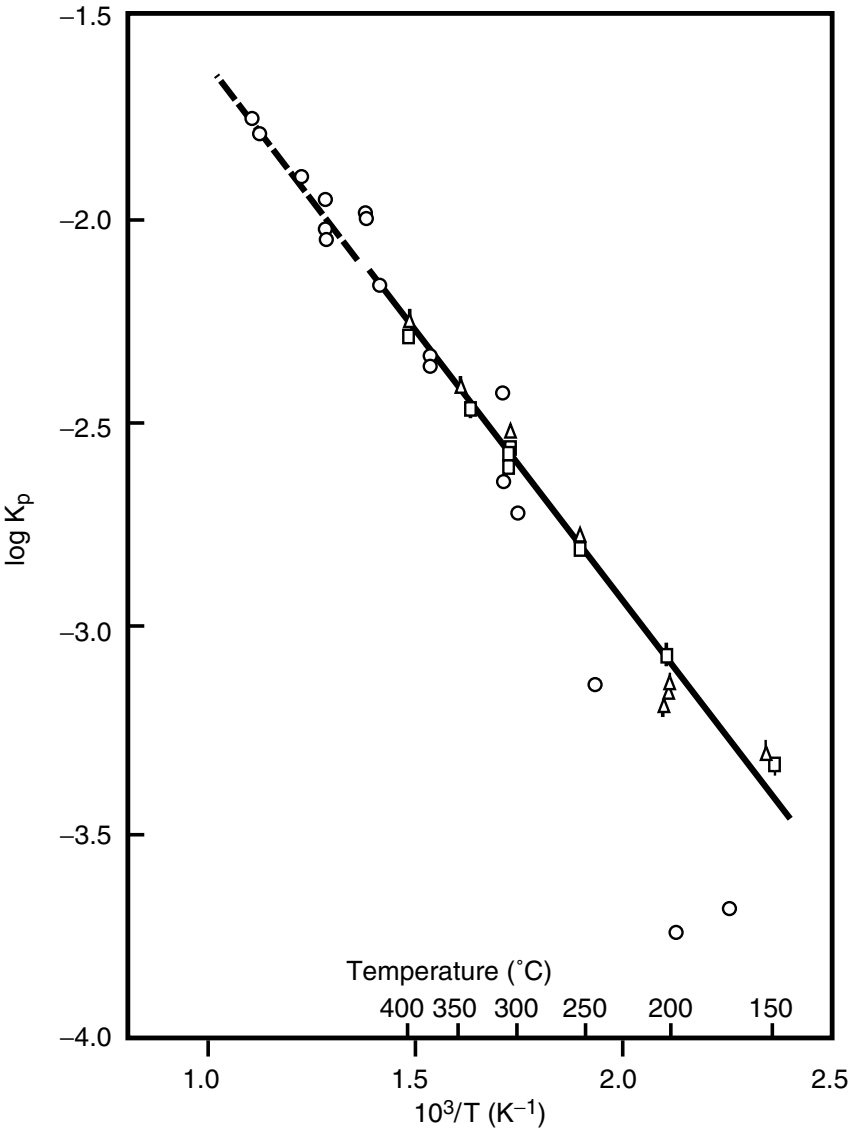

Fig. 7.108 *The relationship between the equilibrium constant and temperature for reaction* 7.60 (*Trevorrow and Shinn,* 1960). *Open circles are data from Florin* et al. (1956), *triangles are from Trevorrow* et al. *with heating to equilibrium, and squares are from Trevorrow* et al. *with cooling to equilibrium* (*Trevorrow* et al., 1961).

container material. If the pressure of the PuF_6 is lowered from 100 to 50 Torr, a lower decomposition rate is observed. Malm measured surprisingly low gas pressure in decades-old, sealed PuF_6 cylinders at ANL, and it was believed to be the result of recombination, probably involving F atoms (Morss, 2005).

Increase of the temperature introduces some thermal decomposition besides radiation decomposition. Observed rates after 77 days were $(0.64 \pm 0.66)\%$ per day at 82°C, but only $(0.18 \pm 0.03)\%$ per day at 26°C. Other factors influencing the decomposition of PuF_6 include the initial pressure and presence or absence of PuF_4, and presence or absence and partial pressure of He, Kr, O_2, N_2, or F_2. The exact mechanism of PuF_6 decomposition is still not completely known.

Steindler *et al.* (1963) studied the decomposition of PuF_6 under the influence of γ radiation. This is important because of the possible use of PuF_6 in the fluoride volatility process (see Section 7.5.7(c)). It was observed that PuF_6, if exposed to fission-product radiation, decomposes to form PuF_4 and F_2 with a *G*-value of (7.5 ± 1.7). Addition of 1 atm of He does not significantly change the *G*-value (number of molecules decomposed per 100 eV of radiation absorbed). Krypton, on the other hand, causes a marked enhancement of PuF_6 decomposition by γ radiation. The *G*-value observed in the presence of F_2 or O_2 is less than that observed with pure PuF_6. On the other hand, irradiation of mixtures of $PuF_4 + F_2$ produced larger quantities of PuF_6 than those calculated from the thermodynamic equilibrium constant at the temperature of the irradiation.

Because of the decomposition of PuF_6 by its own α radiation, the compound is best stored in the gaseous state under reduced pressure.

Chemical properties

Because plutonium hexafluoride tends to decompose into PuF_4 and F_2, it is a highly reactive fluorinating agent. The majority of its chemical properties are due to this reactivity.

(b) Plutonium chlorides, bromides, and iodides

In the plutonium–chlorine system, the only stable solid compound is $PuCl_3$, which has been prepared and characterized in large quantities. The only stable higher valent chloride is $PuCl_4$, which is not stable as a solid, and only known as a gaseous species that decomposes upon condensation. For the plutonium–bromine and plutonium–iodine systems, the only stable binary compounds are the trihalides, $PuBr_3$ and PuI_3.

(*i*) *Preparation*

Plutonium trichloride

This was one of the first plutonium compounds to have been prepared and characterized in detail following the initial discovery of the element (Abraham *et al.*, 1949a). Abraham *et al.* (1949a) and Garner (1950) have provided detailed

discussions on the fundamental methods for its preparation. Of the various preparative methods, the hydrochlorination of plutonium(III) oxalate hydrate was found to work best on medium-scale reactions (1–10 g) according to the general reaction:

$$Pu_2(C_2O_4)_3 \cdot 10H_2O + 6HCl \rightarrow 2PuCl_3 + 3CO_2 + 3CO + 13H_2O \qquad (7.63)$$

The direct chlorination of plutonium metal at 303–500°C and subsequent sublimation at 600–800°C yields emerald green crystals of $PuCl_3$ on the 500 mg scale (Baumgärtner *et al.*, 1965). If metallic plutonium in 100 g quantities is available, this may be converted to the hydride, which is then reacted with HCl gas at 450°C in a fluid-bed reaction. The resulting $PuCl_3$ is fused at 800°C and sparged with HCl for 45 min to remove oxychlorides. The molten $PuCl_3$ may be purified by filtering through a fritted silica disk (Bjorklund *et al.*, 1959; Reavis *et al.*, 1960).

Chlorination of PuO_2 with either phosgene or carbon tetrachloride at temperatures above 500°C can produce analytically pure samples of $PuCl_3$ (Tolley, 1953; Boreham *et al.*, 1960). This process has been used at Los Alamos to convert large quantities of PuO_2 to anhydrous $PuCl_3$ (West *et al.*, 1988).

Christensen and Mullens (1952) developed a very straightforward procedure that is applicable in most transuranium chemistry laboratories, in which plutonium(III) oxalate is reacted with hexachloropropene at 180–190°C:

$$Pu_2(C_2O_4)_3 \cdot 10H_2O + 3C_3Cl_6 \rightarrow 2PuCl_3 + 3C_3Cl_4O + 3CO_2 + 3CO + 10H_2O \qquad (7.64)$$

The oxalate is refluxed with excess hexachloropropene for 18 h, yielding $PuCl_3$ of 96–98% purity, which is separated by filtration and further purified by sublimation. The method has been applied for preparations on the 100 g scale.

A method for continuous production of 98% $PuCl_3$ at a rate of 250 g h^{-1} was reported by Rasmussen and Hopkins (1961). In this process, $Pu(C_2O_4)_2 \cdot 6H_2O$ is first precipitated from Pu(IV) solution, dried on a filter drum, and calcined to reactive PuO_2. The PuO_2 is chlorinated to $PuCl_3$ with phosgene in a vibrating Hastelloy tube furnace at 500°C.

Plutonium(III) chloride, which is obtained by evaporation of a plutonium(III) solution in HCl, followed by dehydration of the $PuCl_3 \cdot 6H_2O$ residue in a stream of HCl, is a slate-blue solid. $PuCl_3$ prepared by one of the anhydrous methods is a blue-green solid or an emerald green, fine crystalline powder. Emerald green single crystals are obtained by condensation from the vapor phase (Burns *et al.*, 1975). As for other lanthanide and actinide trihalides, sublimation in evacuated, sealed quartz tubes is advisable for purification of $PuCl_3$ (Fuger and Cunningham, 1963).

Plutonium tetrachloride

As early as 1945, Brewer *et al.* (1949) predicted that no solid binary plutonium(IV) chloride should exist. However, from their calculations, the possible existence of

gaseous $PuCl_4$ in an atmosphere of Cl_2 over $PuCl_3$ was inferred. Abraham *et al.* (1949a) were the first to observe an enhanced volatility of $PuCl_3$ in a stream of chlorine. This increase in volatility was ascribed to the formation of $PuCl_4$ by the equilibrium

$$PuCl_3 + 0.5\,Cl_2 \rightleftharpoons PuCl_4 \tag{7.65}$$

The $PuCl_4$ gas, on condensation, decomposes again to form solid $PuCl_3$ and Cl_2 gas. Abraham *et al.* (1949a) made the first calculations of the $PuCl_4$ partial pressure over $PuCl_3$ in an atmosphere of Cl_2 and predicted values in the range 10^{-5} mmHg at 500°C to 0.3 mmHg at 800°C. Benz (1962) employed a transpiration technique to determine the equilibrium constant and free energy for the above reaction.

Gruen and deKock (1967) measured the absorption spectrum of the gas phase over solid $PuCl_3$ in 1 atm of Cl_2. The absorption spectrum observed at 928°C is shown in Fig. 7.109, and shows unequivocally the presence of a new species, which is different from Cl_2 and $PuCl_3$. This spectrum is regarded as proof of the existence of gaseous $PuCl_4$.

Even though solid $PuCl_4$ has never been prepared, a number of tetravalent chloro complexes derived from $PuCl_4$, such as Cs_2PuCl_6, have been obtained, and are stable.

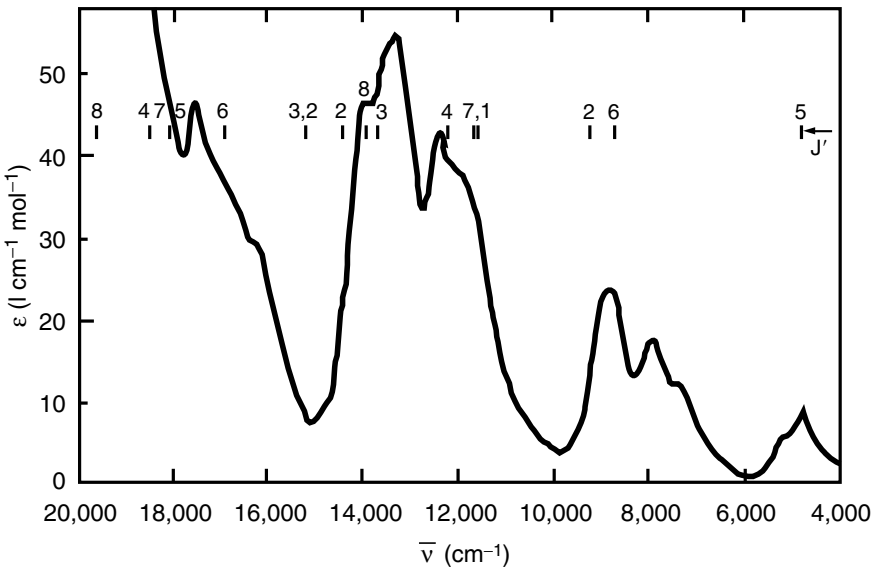

Fig. 7.109 *The absorption spectrum of gaseous $PuCl_4$ at* 928°C (*Gruen and deKock*, 1967).

Plutonium tribromide

This compound was first prepared by Hyde *et al.* (1944), and is a light-green solid. The methods for the preparation of $PuBr_3$ have been summarized by Bluestein and Garner (1944) and by Davidson *et al.* (1949). The two best methods for the preparation of $PuBr_3$ are the direct synthesis from the elements (Davidson *et al.*, 1949; Gruen and deKock, 1967), and the hydrobromination of the hydride at 600°C in a stream of HBr (Reavis *et al.*, 1960).

$$2Pu + 3Br_2 \rightarrow 2PuBr_3 \tag{7.66}$$

$$PuH_x + xHBr \xrightarrow{600°C} PuBr_3 + xH_2 \tag{7.67}$$

Other satisfactory methods for the preparation of $PuBr_3$ include the dehydration of $PuBr_3 \cdot 6H_2O$ by controlled vacuum thermal decomposition (Brown *et al.*, 1968) and the hydrobromination of plutonium(III) oxalate at 400–600°C (Bluestein and Garner, 1944; Davidson *et al.*, 1949; Weigel *et al.*, 1982), either with pure HBr (Bluestein and Garner, 1944; Davidson *et al.*, 1949) or an HBr/H_2 mixture (Weigel *et al.*, 1982). These methods have the advantage that they do not require plutonium metal as the starting material, but make use of starting materials such as $Pu_2(C_2O_4)_3 \cdot 10H_2O$, which can be prepared from aqueous solutions (see Section 7.9.1.e.(i)).

Another method involves bromination of $Pu(OH)_4$ (dried at 70°C). This reaction proceeds satisfactorily above 600°C with HBr gas (Davidson *et al.*, 1949; Fomin *et al.*, 1958), and at 800°C with bromine and sulfur dibromide (Davidson *et al.*, 1949; Davidson and Katz, 1958). Plutonium(IV) oxalate or the tribromide hexahydrate react with HBr at 500°C and at 30–300°C, respectively, but the product of the latter reaction is usually contaminated with PuOBr. NH_4Br addition minimizes the PuOBr formation. Finally, one may convert $PuCl_3$ with HBr at 750°C (Davidson *et al.*, 1949; Bonnelle, 1976) and react PuO_2 mixed with carbon, sulfur, or phosphorus with Br_2 at elevated temperatures. Plutonium tribromide is a light green solid.

Plutonium triodide

The first attempts to prepare this compound were made by Hagemann *et al.* (1949). After initial failures, in which the oxyiodide was the reaction product, they finally succeeded in preparing PuI_3 by reacting plutonium metal with HI at 400°C. A more straightforward approach is the redox transmetallation reaction between plutonium metal and mercuric iodide, according to the reaction:

$$2Pu + 3HgI_2 \rightarrow 2PuI_3 + 3Hg \tag{7.68}$$

The plutonium metal and HgI_2 are sealed in a silica tube, and heated for 2 hours at 500°C (Asprey *et al.*, 1964). The mercury byproduct is conveniently separated by distillation away from the product. PuI_3 is extremely sensitive to moisture. Its properties have not been well characterized.

(*ii*) *Solid-state structures*

Crystallographic data on plutonium halides are summarized in Table 7.42.

$PuCl_3$. The crystal structure of $PuCl_3$ was first determined by Zachariasen (1948a) and later refined by Burns *et al.* (1975). Plutonium(III) chloride crystallizes in the hexagonal UCl_3 structure with two formula units per cell. Each plutonium atom has nine-fold coordination with a local tricapped trigonal prismatic coordination environment. Six chlorine atoms form a trigonal prism with Pu–Cl bonds of 2.886(1) Å, and the other three chlorine atoms cap the rectangular faces with Pu–Cl distances of 2.919 (1) Å (Burns *et al.*, 1975). The trigonal prisms share their triangular bases to form infinite chains along the crystallographic *c*-axis. These basic structural features are shown in Fig. 7.110.

$PuBr_3$ and PuI_3. Plutonium tribromide and triiodide are isostructural and display an orthorhombic structure known as the $PuBr_3$ structure. The structures

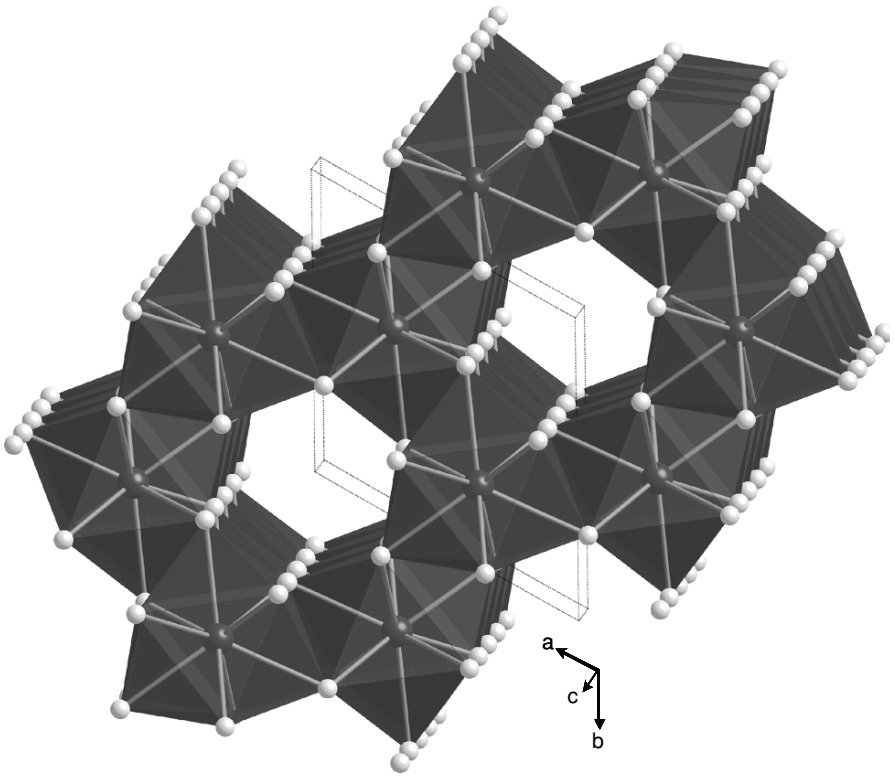

Fig. 7.110 *The solid-state crystal structure of $PuCl_3$ viewed down the c-axis and emphasizing both the hexagonal cell, and the infinite chains of tricapped trigonal prisms. Plutonium atoms are black, and chlorine atoms are light gray.*

of both $PuBr_3$ and PuI_3 were originally determined by Zachariasen (1948a), with subsequent refinements of the iodide reported by Asprey and coworkers (Asprey *et al.*, 1964). For $PuBr_3$, there are six Pu–Br bonds of 3.08 Å that form a trigonal prismatic geometry. There are two additional Pu–Br bonds that cap two of the three rectangular faces with Pu–Br distances of 3.06 Å. As in the $PuCl_3$ structure, these capped trigonal prisms stack in an infinite chain (this time along the *a*-axis) by sharing triangular bases as illustrated in Fig. 7.111. The infinite columns are now separated from each other such that the ninth bromine atom that would complete the tricapped trigonal prism is 4.03 Å away, and outside the bonding radius.

The main difference between the $PuCl_3$ and $PuBr_3$ structures is that in the $PuCl_3$ structure, each plutonium atom is nine-coordinate, while in the $PuBr_3$ structure, each plutonium atom is eight coordinate. This is surprising because the ninth bromine atom in the $PuBr_3$ structure is essentially in the correct position. The change in structure is thought to be due to the larger size of bromine and iodine (Brown, 1968), and the associated electron–electron repulsion between halogen atoms. A comparison of the column stacking between $PuBr_3$ and $PuCl_3$ structures is shown in Fig. 7.112.

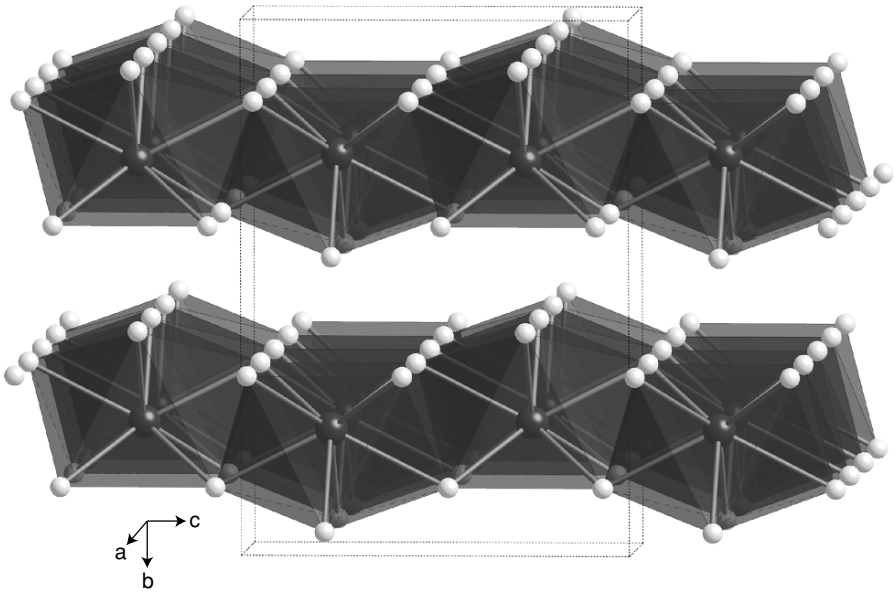

Fig. 7.111 *The solid-state crystal structure of $PuBr_3$ viewed down the a-axis and emphasizing the infinite chains of bicapped trigonal prisms. Plutonium atoms are black, and bromine atoms are light gray.*

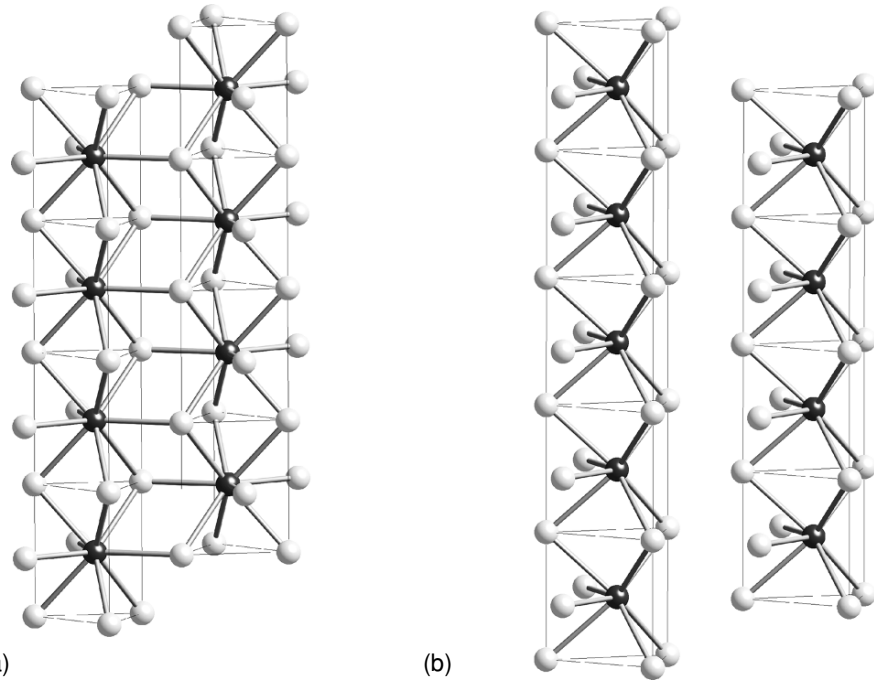

Fig. 7.112 *A comparison of the column stacking of $PuCl_3$ and $PuBr_3$ units.* (*a*) *The column arrangement of $PuCl_3$ units showing how tricapped trigonal prisms are formed by linking adjacent trigonal prismatic columns.* (*b*) *The column arrangement of trigonal prismatic units in the $PuBr_3$ structure, illustrating the vacant coordination site.*

(*iii*) *Properties*

The more important physical properties of plutonium(III) chloride are well known. Thermodynamic data are given in Table 7.43. The enthalpy of formation was first measured by Westrum and Robinson (1949a), then by Fuger and Cunningham (1963) and has been assessed by Fuger *et al*. (1983), and by Lemire *et al.* (2001). The standard free energy of formation as a function of T(K) was determined by Benz (1961), who found the following temperature dependence (958–1014 K):

$$\Delta G = -924.7 + 0.222\ 92T(\text{kJ mol}^{-1}) \tag{7.69}$$

By electromotive force (EMF) measurements in fused PuCl–NaCl, Benz and Leary (1961) found the standard free energy and entropy of formation of pure solid $PuCl_3$ at 700°C to be 711 kJ mol^{-1} and 215.9 J K^{-1} mol^{-1}, respectively. From potentiometric measurements based on the $Pu/PuCl_3$ electrode, the free

energy of formation of solid $PuCl_3$ in the 755–916 K temperature range was found to fit the expression

$$\Delta G = -909.6 + 0.175T(\text{kJ mol}^{-1}) \tag{7.70}$$

The optical properties of solid and gaseous $PuCl_3$ have been studied. Lipis and Pozharskii (1960) measured the absorption spectrum of $PuCl_3$ in the range 340–1000 nm. This spectrum is altered by water of crystallization, but not by absorbed or occluded water.

Conway and coworkers (Lammermann and Conway, 1963; Conway and Rajnak, 1966) measured the absorption spectrum of Pu^{3+} in an anhydrous $LaCl_3$ matrix and calculated the electrostatic, spin–orbit, and configuration-interaction parameters from these data.

The absorption spectrum of gaseous $PuCl_3$ was measured by Gruen and deKock (1967). Its energies and intensities are summarized in Table 7.45.

The magnetic susceptibility of $PuCl_3$ was measured in the range 90–600 K by Dawson *et al.* (1951). The temperature dependence of χ suggested a $5f^5$ electronic configuration for the Pu^{3+} ion.

The chemical properties of plutonium trichloride have been studied in great detail because of its application in molten-salt chemistry and metal production. $PuCl_3$ may be readily reduced to the metal by Ca, Mg, or La. The phase diagram

Table 7.45 *Energies and intensities of $PuBr_3(g)$ and $PuCl_3(g)$ transitions* (*Gruen and deKock,* 1967).

	$\bar{\nu}$ (cm^{-1})	ϵ (L cm^{-1} mol^{-1})	$\bar{\nu}$ (cm^{-1})	ϵ (L cm^{-1} mol^{-1})
$PuBr_3(g)$	5 810	2.2	17 390	20
	6 290	3.3	17 600	17 sh
	7 720	2.2 sh	17 860	19
	7 870	7	18 660	25 sh
	8 060	4.8	22 220	170 sh
	8 400	7.5 sh	22 730	210
	8 500	14	23 040	220
	8 930	4.0	23 360	230
	9 520	3.3 sh	23 580	230
	9 710	3.7	23 810	215
	10 870	4.0	24 510	180 sh
	14 490	3.7 sh	24 750	175 sh
	15 380	6 sh	25 000	165 sh
	16 390	9.5 sh	27 500	290 sh
	16 830	16	29 500	420 sh
	17 140	16	31 500	800
$PuCl_3(g)$	22 990	310	24 450	200
	23 360	330	24 940	160
	23 750	290	31 750	1 900

of the system $PuCl_3$–Pu has been studied by Johnson and Leary (1964). The metal solubility at the monotectic (740°C) was found to be 7%, but there was no indication of the formation of divalent plutonium. For the reaction of $PuCl_3$ melts with Am metal, see Mullins *et al.* (1966).

With water, $PuCl_3$ reacts to form several hydrates with 1, 2, or 6 H_2O, depending on the H_2O partial pressure (Abraham *et al.*, 1949a).

Sheft and Davidson (1949b) and Weigel *et al.* (1977) have measured the vapor-phase hydrolysis of $PuCl_3$ by determining the equilibrium constant of the reaction

$$PuCl_3(s) + H_2O(g) \rightleftharpoons PuOCl(s) + 2HCl(g) \tag{7.71}$$

as a function of temperature. The two groups obtained nearly identical results with regard to the thermodynamic parameters of the above reaction.

With alkaline or alkaline-earth chlorides, a number of ternary chloro complexes are formed. For the individual compounds, see Section 7.8.6(d).

The optical properties of gaseous $PuBr_3$ have been studied by Gruen and deKock (1967). The energies and intensities are summarized in Table 7.45. The absorption spectrum of solid $PuBr_3$ was determined by Lipis and Pozharskii (1960) in the 340–1000 nm range. It was found to be similar to that of aqueous $PuBr_3$, but differed considerably from that of solid $PuCl_3$. This difference, together with the structural difference between $PuCl_3$ and $PuBr_3$, has been interpreted by Fomin *et al.* (1958) to indicate a change in the nature of bonding from predominantly ionic in $PuCl_3$ to predominantly covalent in $PuBr_3$.

The enthalpy of formation of $PuBr_3$ was first determined by Westrum (1949c) from its enthalpy of solution in 6 M HCl. The enthalpy of solution in O_2-free 0.1 and 1.0 M HCl, was also measured by Brown *et al.* (1977).

Sheft and Davidson (1949a) and Weigel *et al.* (1982) have measured the vapor-phase hydrolysis of plutonium(III) bromide by determining the equilibrium constant of the reaction

$$PuBr_3 + H_2O \rightleftharpoons PuOBr + 2HBr \tag{7.72}$$

as a function of temperature. The results of both groups are in close agreement. The enthalpies of formation derived from these measurements, and reviewed by Lemire *et al.* (2001), are listed in Table 7.43.

$PuBr_3$ reacts with moisture to form the hexahydrate $PuBr_3 \cdot 6H_2O$ (Mullins *et al.*, 1966). The structural data of $PuBr_3 \cdot 6H_2O$ are listed in Table 7.42.

The enthalpy of formation of PuI_3 is reported by Brown *et al.* (1977).

(c) Oxyhalides of plutonium

Plutonium forms a number of oxyhalides in the valence states III and VI. So far, no oxyhalides of Pu(IV) or Pu(V) have been prepared. With Pu(III), the oxyhalides, PuOF, PuOCl, PuOBr, and PuOI are known.

(*i*) *Preparation and properties*

For plutonium(III) oxyfluoride, no direct method of preparation has been reported. Rather, PuOF was accidentally obtained in the attempted reduction of PuF_3 by hydrogen (Cunningham, 1954), and in an attempt to measure the melting point of plutonium metal.

Plutonium(III) oxychloride, PuOCl, was first prepared by Abraham *et al.* (1949a) by heating $PuCl_3 \cdot 6H_2O$ in a sealed tube at 400°C. The resulting preparation contained 60% PuOCl and 40% $PuCl_3$. In another similar preparation, a product containing 60–65% PuOCl and 40–35% $PuCl_3$ was obtained, which could be converted to pure PuOCl by heating in a sealed tube with 95 Torr H_2 and 55 Torr HCl at 675°C.

A preparation method yielding pure PuOCl in a one-step reaction was reported by Westrum and Robinson (1949b). They also made the first determination of the enthalpy of formation using the reaction of $PuCl_3$ with a stream of H_2, HCl and water vapor at 675°C.

The formation of PuOCl in the vapor-phase hydrolysis of $PuCl_3$ (see Section 7.8.6.b.(iii)) has been studied by several authors (Abraham and Davidson, 1949; Sheft and Davidson, 1949b; Weigel *et al.*, 1977), who have also determined the enthalpy of formation. The best values at the time of writing are given in Table 7.43.

Plutonium(III) oxybromide, PuOBr, was first observed by Davidson *et al.* (1949) as a residue from the sublimation of small amounts of $PuBr_3$ in a silica tube. It can be obtained in a pure state by treating gently heated Pu(IV) hydroxide (70°C) with moist hydrogen bromide at 750°C (Davidson *et al.*, 1949; Sheft and Davidson, 1949a), or by vapor-phase hydrolysis (Weigel *et al.*, 1982).

The enthalpy of formation of PuOBr was determined by Weigel *et al.* (1982) by measurement of the equilibrium constant of the vapor-phase hydrolysis of $PuBr_3$. Rand (1966), Fuger *et al.* (1983), and Lemire *et al.* (2001) have assessed previous values of the enthalpy of formation and the recommendations of the latter are listed in Table 7.43.

Plutonium(III) oxyiodide, PuOI, was observed to form in attempts to prepare PuI_3 (Hagemann *et al.*, 1949). In all reactions in which even traces of water are present, or are being formed in the course of the reaction, the bright-green PuOI is formed.

So far, no oxyhalides of tetravalent or pentavalent plutonium have been prepared. However, there is thermochromatographic evidence for the existence of $PuOF_3$ (Jouniaux, 1979; Jouniaux *et al.*, 1979), but this compound has not yet been isolated.

The only oxyhalides of hexavalent plutonium that have been isolated and prepared in substantial quantities are plutonyl fluoride, PuO_2F_2 (Alenchikova *et al.*, 1961a), plutonium(VI) oxytetrafluoride, $PuOF_4$ (Burns and O'Donnell, 1977), and plutonyl chloride, $PuO_2Cl_2 \cdot 6H_2O$ (Alenchikova *et al.*, 1959). $PuOF_4$ is formed when an excess of PuF_6 is condensed on a 0.23% solution of

deionized water in HF, and the mixture is warmed to room temperature. After evaporation of unreacted HF and PuF_6, the $PuOF_4$ separates as a chocolate-brown solid. PuO_2F_2 is prepared by slow, low-temperature hydrolysis of PuF_6:

$$PuF_6 + 2H_2O \rightarrow PuO_2F_2 + 4HF \tag{7.73}$$

Alenchikova *et al.* (1961a) studied the system PuO_2F_2–HF–H_2O and observed $PuO_2F_2 \cdot H_2O$, $PuO_2F_2 \cdot HF \cdot 4H_2O$, and anhydrous PuO_2F_2 solids in equilibrium with the solution for 0–1.3% HF, 1.9–0.85% HF, and 87–100% HF, respectively.

Plutonyl chloride hexahydrate, $PuO_2Cl_2 \cdot 6H_2O$, has been prepared by vacuum evaporation at room temperature of Pu(VI) chloride solutions (Alenchikova *et al.*, 1959) formed by oxidation of Pu(IV) chloride solutions with chlorine. The greenish-yellow $PuO_2Cl_2 \cdot 6H_2O$ was identified by chemical and spectrophotometric analysis. $PuO_2Cl_2 \cdot 6H_2O$ is not stable, and gradually decomposes to a Pu(IV) compound.

(*ii*) *Solid-state structures*

All the PuOX compounds with heavier halides (Cl, Br, I) have the well-known PbClF structure type, and were first characterized by Zachariasen (1949d). This basic structure is built up of layers of different atom types. Each complex layer in the PuOX structure consists of a central sheet of coplanar oxygen atoms with a sheet of halogen atoms on each side, and plutonium atoms sandwiched in between. The basic layer structure is shown in Fig. 7.113(a). Within one of these complex layers, the plutonium atoms are coordinated by four oxygen and four chlorine atoms, making a local square antiprismatic coordination geometry. A view of the structure that emphasizes the square antiprismatic geometry is shown in Fig. 7.113(a).

The crystal structure of PuOF was originally reported to be cubic by Zachariasen (1949d), but a subsequent study of powder diffraction data showed that the compound was actually tetragonal (Zachariasen, 1951). In the tetragonal form, the structure fits into a class of MOF structures that display a superstructure that is related to the fluorite structure. In the tetragonal superstructure, the oxygen and fluorine atoms arrange themselves in sheets separated by a layer of plutonium atoms. The local coordination around plutonium is that of cube, with four fluorine atoms on one side, and four oxygen atoms on the opposite side. This cubic PuF_4O_4 coordination environment is compared with the square antiprismatic coordination environment found in PuOX (X = Cl, Br, I) in Fig. 7.113(b).

(d) Ternary halogenoplutonates

With ammonium, alkali, and alkaline-earth halides, and, in a few cases, with transition-metal halides, plutonium(III), (IV), (V), and (VI) halides form a large number of ternary halogenoplutonates.

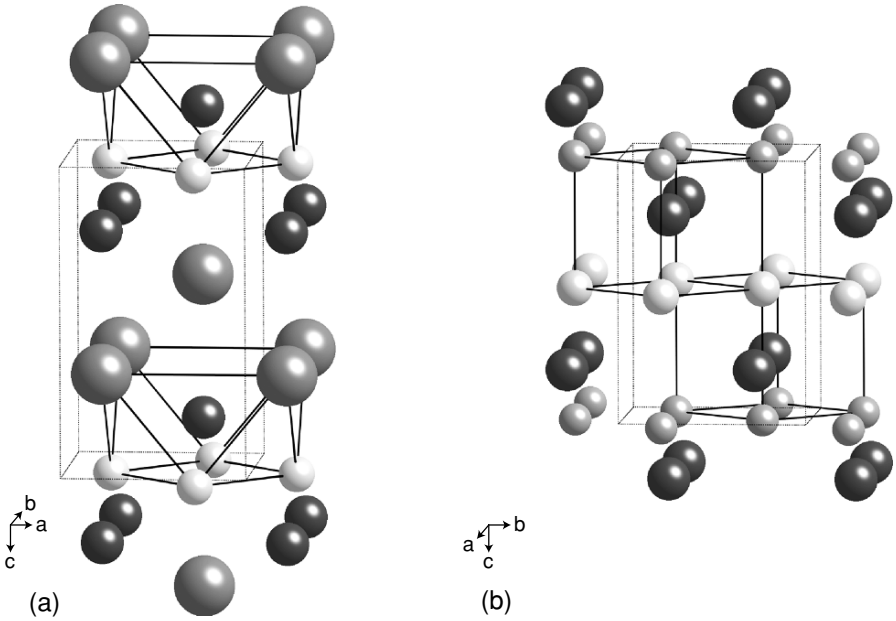

Fig. 7.113 *Comparison of PuOX solid-state structures.* (*a*) *The basic structural unit for PuOX* ($X = Cl, Br, I$) *illustrating the layered nature of the repeat units, and the local* PuO_4X_4 *square antiprismatic local coordination geometry.* (*b*) *The basic structural unit for tetragonal PuOF showing the layered nature of repeat units, and the local cubic* PuO_4F_4 *coordination geometry.*

The fluoroplutonates and pseudo-binary systems containing plutonium fluorides are of major interest as potential materials for molten-salt fuels in high-temperature reactors. Therefore, much work has been devoted to the individual compounds and, in some cases, to pseudo-binary phase diagrams. Leary (1962) has summarized the phase diagram work done up to 1962.

The preparation of individual fluoroplutonates depends on the nature of the compound to be prepared. The following methods are the ones usually employed.

1. A compound is precipitated from aqueous solution, and dried below 100°C.
2. Stoichiometric amounts of alkali halide and plutonium(III) or plutonium(IV) halide in HCl or HF solution(s) are evaporated to dryness. The residue is heated in a platinum boat or a sapphire dish at 300°C in a stream of HF.
3. Stoichiometric amounts of PuF_4 or PuO_2 and alkali or alkaline-earth fluoride are intimately mixed and heated at 300–600°C in a stream of HF, $HF + O_2$, or $HF + H_2$ (the latter for preparation of Pu(III) complexes).
4. Stoichiometric amounts of PuF_4 or PuO_2 and NH_4F are heated together in a closed vessel at 70–100°C. The product is pulverized and heated again in

the same manner. This procedure is repeated until a homogeneous product has been obtained.

5. Thermal decomposition of a higher complex, or treatment of another plutonium fluoro complex with elemental fluorine.
6. PuF_6 and alkali or alkaline-earth fluoride are reacted.
7. Alkali carbonate is added to plutonium nitrate solution, the solution evaporated with HF and treated with F_2.
8. PuF_4 is fused with the stoichiometric amount of the corresponding alkali fluoride.
9. PuF_4 is fused with the stoichiometric amount of alkali or metal fluoride.
10. Cooled solution of Pu(v) in dilute acid is added to ice-cold saturated RbF solution.

The known fluoroplutonate complexes have been compiled in Table 7.46. The phase diagrams of the systems LiF–PuF_3 and NaF–PuF_3 have been reported by Barton *et al.* (1961). These two systems are the only ones based on PuF_3 for which phase diagrams have been determined. No other systems, neither based on PuF_3 nor based on PuF_4, have been reported.

With the chloride systems, a different situation exists. Even though only very few compounds have been characterized as individual entities, several phase diagrams have been determined. Most of the compounds occurring in these phase diagrams have never been studied in great detail. Phase diagrams have been reported for solid–liquid equilibria in the binary systems $PuCl_3$–MCl, where M = Li (Bjorklund *et al.*, 1959), Na (Bjorklund *et al.*, 1959), K (Benz *et al.*, 1959), Rb (Benz and Douglass, 1961b), Cs (Benz and Douglass, 1961b), and $PuCl_3$–$M'Cl_2$, where M′ = Mg, Ca, Sr, and Ba (Johnson *et al.*, 1961). An excellent summary of these phase diagrams was reported by Leary (1962). Some of the systems based on $PuCl_3$ have become of practical importance in fused-salt ER of plutonium, and in the DOR and pyroredox processes (see Section 7.7.2). As a representative phase diagram of such a system, the diagram of the system KCl–$PuCl_3$ is shown in Fig. 7.114 (Benz *et al.*, 1959). In these systems based on $PuCl_3$, compounds such as $RbPu_2Cl_7$ (light blue), $CsPu_2Cl_7$ (greenish blue to deep green), $RbPuCl_5$ (brownish to greenish yellow), Cs_3PuCl_6 (green), or M_3PuCl_9 (M = Sr, Ba) (no color given) have been observed, but none of these compounds have been studied in detail.

The hexachloroplutonates M_2PuCl_6, where M = Na, Rb, Cs, $(CH_3)_4N^+$, or $(C_2H_5)_4N^+$, are obtained as pale greenish yellow (alkali compounds) or orange-yellow (alkylammonium compounds) crystals by precipitation from concentrated HCl solution. Except for Cs_2PuCl_6, the properties of these compounds are not known in detail. Cs_2PuCl_6 is sufficiently stable to be useful as a primary plutonium standard (Miner *et al.*, 1963). No bromo or iodo complexes of plutonium(IV) are known, with the sole exception of the red bromo complex, $[(C_2H_5)_4N]_2PuBr_6$, which was prepared by Ryan and Joergensen (1964) by precipitation from ethanolic HBr solution on the addition of acetone.

Table 7.46 *X-ray crystal structure data for plutonium double fluorides.*

Plutonium valence	*Compound*	*Color*	*Symmetry*	*Space group*	*Lattice parameters*			*Angle* (deg)	*Density* ($g\ cm^{-3}$)	*References*
					a_0 (Å)	b_0 (Å)	c_0 (Å)			
Pu(III)	$NaPuF_4$	blue	hexagonal	P321	6.129(6)		3.753(4)			Zachariasen (1948a)
					6.13(2)		3.76(1)		6.87	Keller and Schmutz (1964)
	$KPuF_4$		orthorhombic	P*nma*	6.23	3.75	15.42		6.53	Jove and Pagès (1977)
	$RbPuF_4$		orthorhombic	P*nma*	6.39	3.80	15.86		6.91	Jove and Pagès (1977)
	KPu_2F_7	blue	cubic	F*m*3*m*	5.880				5.31	Schmutz (1966)
Pu(IV)	$LiPu_4F_{17}$		tetragonal		8.84(1)		11.31(2)		7.25	Jove and Cousson (1977)
	KPu_2F_9	red-brown	orthorhombic[a]	P*nma*	8.58(4)	11.35(6)	6.96(4)		6.74	Zachariasen (1948b)
	$LiPuF_5$	brown	tetragonal	$I4_1/a$	14.67(2)		6.479(5)			Keenan (1966)
			tetragonal	$I4_1/a$	14.65(1)		6.486(5)		6.51	Keller and Schmutz (1966)
	$NaPuF_5$	green	rhombohedral	$R\bar{3}$	8.93(3)			$\alpha = 107.48(16)$	6.03	Zachariasen (1948b)
	$KPuF_5$	green	rhombohedral	$R\bar{3}$	9.27(3)			$\alpha = 107.03(08)$	5.66	Zachariasen (1948b)
	$RbPuF_5$	green	rhombohedral	$R\bar{3}$	9.46(3)			$\alpha = 106.93(16)$	5.88	Zachariasen (1948b)
	α-NH_4PuF_5	light brown	rhombohedral	$R\bar{3}$	9.42					Benz *et al.* (1963)
	β-NH_4PuF_5	yellow-green	orthorhombic		9.83	6.98	6.27			Benz *et al.* (1963)
	$Li_7Pu_6F_{31}$	brown	tetragonal		14.650(1)		6.468(5)		4.96	Schmutz (1966)
	$Na_7Pu_6F_{31}$	brown/green	rhombohedral	$R\bar{3}$	9.006			$\alpha = 107.75$	6.14	Schmutz (1966)
			(hexagonal)		14.52(2)		9.704(3)		6.14	Keller and Schmutz (1966)
	$K_7Pu_6F_{31}$	green/brown	rhombohedral	$R\bar{3}$	9.275(5)			$\alpha = 107.17$	5.77	Schmutz (1966)
			(hexagonal)		14.93(2)		10.28(1)		5.76	Keller and Schmutz (1966)
	$Rb_7Pu_6F_{31}$	green/brown	rhombohedral	$R\bar{3}$	9.466(5)			$\alpha = 106.90(1)$	6.14	Schmutz (1966)
			(hexagonal)		15.21(2)		10.61(1)			Keller and Schmutz (1966)

Table 7.46 (*Contd.*)

Plutonium valence	*Compound*	*Color*	*Symmetry*	*Space group*	*Lattice parameters* a_0 (Å)	b_0 (Å)	c_0 (Å)	*Angle* (deg)	*Density* (g cm^{-3})	*References*
	$(NH_4)_7Pu_6F_{31}$	orange	rhombohedral	$R\bar{3}$	9.42			$\alpha = 107.33$		Benz *et al.* (1963)
	$Tl_7Pu_6F_{31}$		(hexagonal)		15.08		10.40			Jove *et al.* (1976)
	Na_2PuF_6	pink	hexagonal	P321	6.059(5)	7.130(5)			5.84	Keller and Schmutz (1966)
		pink-brown	hexagonal	P321	6.055(3)		3.571(5)			Alenchikova *et al.* (1958)
	Rb_2PuF_6		orthorhombic	*Cmcm*	6.971(18)	12.033(16)	7.602(10)			Keenan (1967)
	Cs_2PuF_6		orthorhombic		12.145	7.156	4.056			Riha and Trevorrow (1965)
	$(NH_4)_2PuF_6$	pink								Benz *et al.* (1963)
	Tl_2PuF_6		orthorhombic	*Pmma*[b]	11.35(2)	6.89(1)	4.05(1)			Jove *et al.* (1974)
	$CaPuF_6$	red-brown	hexagonal	$P\bar{3}c1$[c]	3.997		7.097		6.65	Keller and Salzer (1967)
	$SrPuF_6$	red-brown	hexagonal	$P\bar{3}c1$[c]	7.091		7.255		6.95	Keller and Salzer (1967)
	Na_3PuF_7		tetragonal	I4/*mmm*	5.460		10.920		3.98	Riha and Trevorrow (1965)

	Tl_3PuF_7		cubic	F$m3m$[d]	9.30				8.13	Jove *et al.* (1974)
	$(NH_4)_4PuF_8$	pink-red								Benz *et al.* (1963)
Pu(v)	Rb_2PuF_7	green	monoclinic	P$2_1/c$	6.270(8)	13.416(8)	8.844(8)	$\beta = 90$		Penneman *et al.* (1965)
	$CsPuF_6$	green	rhombohedral	R$\bar{3}$	8.036(3)		8.388(4)		5.16	Penneman *et al.* (1965)
	$RbPuO_2F_2$	lavender	rhombohedral	R$\bar{3}m$	6.796(8)			$\alpha = 36.28$		Keenan (1965)
	$(NH_4)PuO_2F_2$	lavender	rhombohedral	R$\bar{3}m$	6.817(6)			$\alpha = 36.27$		Keenan (1965)
Pu(vi)	$KPuO_2F_3{\cdot}H_2O$		cubic		8.126					Alenchikova *et al.* (1961b)
	$RbPuO_2F_3{\cdot}H_2O$		cubic		8.458					Alenchikova *et al.* (1961b)
	$CsPuO_2F_3{\cdot}H_2O$		cubic		8.916					Alenchikova *et al.* (1961b)

[a] Space group reported as P*nam*, changed to standard setting P*nma* by Roof (1989).
[b] Original lattice constant reported in space group P*mcm*. Changed to standard setting P*mma* by Roof (1989).
[c] Roof (1989) suggests that the original space group P$6_3/mmc$ is likely the trigonal space group P$\bar{3}c1$, hence the *a*-axis lattice constant has been divided by $\sqrt{3}$ to derive the value reported above.
[d] Jove reports the lattice constants, Avignant describes that the structure is isotypic of $(NH_4)_3ZrF_7$ (Avignant and Cousseins, 1971), and this structure is described by Hurst (Hurst and Taylor, 1970).

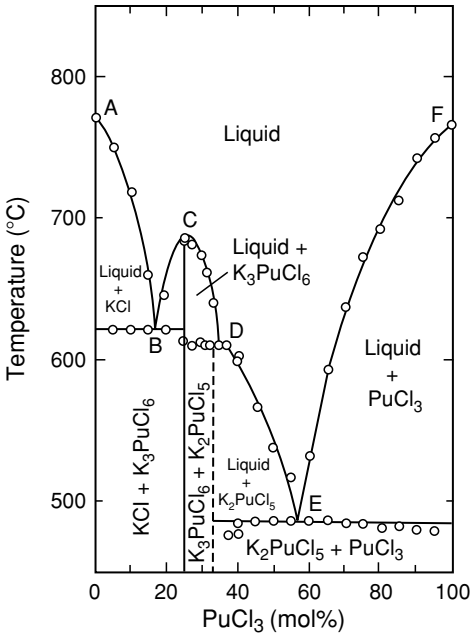

Fig. 7.114 *The phase diagram of the KCl–$PuCl_3$ system* (*Benz* et al., 1959). *Key points in the diagram include A, the KCl melting point at* 771°C*; B, eutectic point at* 621°C *corresponding to* 17% *$PuCl_3$; C, K_3PuCl_6 melting point at* 685°C*; D, peritectic point at* 611°C *and* 35% *$PuCl_3$; E, eutectic point at* 486°C *and* 57% *$PuCl_3$;and F, $PuCl_3$ melting point at* 769°C.

A number of derivatives of plutonyl chloride, PuO_2Cl_2, which is known as the hexahydrate $PuO_2Cl_2 \cdot 6H_2O$ (Alenchikova *et al.*, 1959), have been prepared. These compounds contain the anion $[PuO_2Cl_4]^{2-}$. Probably the best-known compounds of this type are the rubidium salt, $Rb_2PuO_2Cl_4$, and the cesium salt, $Cs_2PuO_2Cl_4$, which form orange-yellow crystals. The lattice constants of both compounds have been determined by Werner (1982) and are listed in Table 7.47. The lattice constants and other crystallographic properties determined for halo complexes of plutonium are listed in Table. 7.47.

7.9 SOLUTION CHEMISTRY

Descriptive solution and coordination chemistry played a key role in the discovery of plutonium and in the formulation of the actinide series concept (Seaborg and Loveland, 1990). The need to separate and purify plutonium from nuclear fuel during the Manhattan Project drove much of the early solution chemistry and included the extraction of plutonium coordinated by organic ligands, pyrochemical processing in molten salts, and the distillation or

Table 7.47 *X-ray crystal structure data for plutonium double chlorides*[a].

Compound	*Color*	*Symmetry*	*Space group*	*Lattice parameters*			*Density* ($g\ cm^{-3}$)	*References*
				a_0 (Å)	b_0 (Å)	c_0 (Å)		
Pu(III)								
K_2PuCl_5		orthorhombic	P*nma*	12.626(12)	8.674(7)	7.953(5)		Axler *et al.* (1992)
K_2PuCl_5		orthorhombic	P*nma*	12.674(3)	8.727(2)	7.969(2)	3.73	Morss and Fujino (1988b)
Rb_2PuCl_5		orthorhombic	P*nma*	13.093(8)	8.909(5)	8.178(5)	4.09	Morss and Fujino (1988b)
Pu(IV)								
K_2PuCl_6		monoclinic[b]	P2/*m*	7.218(5)	7.611(6)	10.208(7)	3.14	Morss and Fujino (1988a)
Rb_2PuCl_6		hexagonal	$P6_3mc$	7.377(2)		11.880(7)	3.69	Morss and Fujino (1988a)
Cs_2PuCl_6	pale yellow	trigonal	$P\bar{3}m$	7.44(1)		6.04(1)	4.10	Zachariasen (1948c)
$[(CH_3)_4N]_2PuCl_6$	orange-yellow	fcc	F*m*3*m*	12.96(5)			1.330	Staritzky and Singer (1952)
$[(C_2H_5)_4N]_2PuCl_6$	yellow	orthorhombic	F*mmm*	14.23(1)	14.53(3)	13.53(5)	1.691	Staritzky and Singer (1952)
Pu(VI)								
$Rb_2PuO_2Cl_4$	orange	monoclinic[c]	I2/*c*	11.60(3)	7.42(5)	5.50(3)		Werner (1982)
$Cs_2PuO_2Cl_4$	orange	monoclinic[d]	I2/*c*	11.879(6)	7.693(6)	11.533(7)		Werner (1982)
$[(CH_3)_4N]_2PuO_2Cl_4$	yellow	tetragonal	I4/*m*	10.00(5)		12.90(5)		Staritzky and Singer (1952)
$[(C_2H_5)_4N]_2PuO_2Cl_4$	yellow	tetragonal	I4/*m*	9.20(5)		11.90(5)		Staritzky and Singer (1952)

[a] All oxidation states Pu(III) through Pu(VI) have been observed in molten salts of the alkali chlorides (Gruen *et al.*, 1960; Benz and Douglass, 1961a; Swanson, 1964).
[b] $\beta = 91.59(4)°$.
[c] $\beta = 100.1(6)°$.
[d] $\beta = 96.99(5)°$.

centrifugation of volatile halide, alkoxide, and borohydride complexes (Koch, 1972, 1973a–c, 1976a,b). Solution and coordination chemistry continues to play a role in modern plutonium processing and separations, and for recycle of plutonium in closed nuclear fuel cycles. More recently, interest has grown in the chemistry of plutonium under biologically and environmentally relevant conditions, as attention has turned to understanding the long-term fate and transport of plutonium stored in geological repositories (Clark *et al.*, 1995; Neu *et al.*, 2002; Silva and Nitsche, 2002). Selected aspects of plutonium coordination chemistry have been reviewed by Cleveland (1979) and Carnall and Choppin (1983), and within broader reviews on actinide elements (Lemire *et al.*, 2001; Burns *et al.*, 2004). In this section we describe the preparation, stability, structure, and spectroscopy, of aqueous and nonaqueous molecular complexes of plutonium.

7.9.1 Aqueous solution chemistry

The chemistry of plutonium in aqueous solution is unique and rich. It is also complicated, primarily due to the small energy separations between the various oxidation states and the extreme oxophilicity of plutonium cations. Five oxidation states, Pu(III), Pu(IV), Pu(V), Pu(VI), and Pu(VII), can be readily prepared and stabilized in aqueous solution under the appropriate conditions. The lower oxidation states, Pu(III) and Pu(IV), are generally more stable in acid solution while the higher oxidation states, Pu(VI) and Pu(VII), are favored under alkaline conditions. Tetravalent plutonium is the most stable and consequently the most studied, followed by plutonium in the trivalent and hexavalent states. In the decades following the discovery of plutonium, its solution chemistry was motivated by the need to separate plutonium from mixtures of actinides and fission products in multiple oxidation states under highly acidic conditions. Processes that used oxidation and/or reduction steps in solution and condensed phases bolstered the study and understanding of aqueous Pu(III) and Pu(VI). In contrast, pentavalent plutonium is most stable in near-neutral pH solutions that are dilute in both plutonium and other ions. Although Pu(V) was identified along with the other common oxidation states, research on the solution complexes of this oxidation state was not widely pursued until the 1990s when the behavior of plutonium in environmental matrices gained importance. Heptavalent plutonium was the last oxidation state to be discovered, and it was first reported in 1967 (Krot and Gel'man, 1967). Plutonium in this oxidation state is stable only in highly alkaline solution and in the presence of strong oxidizing agents, and is therefore the least well studied. There are very recent spectroscopic studies that suggest the possibility of the existence of Pu(VIII) in alkaline solution (Nikonov *et al.*, 2004, 2005). The existence of this oxidation state is equivocal, and we look forward to future research in this area.

Under noncomplexing strongly acidic conditions, such as in perchloric or triflic acid solutions, both Pu(III) and Pu(IV) exist as the simple hydrated (or

aquo) ions, $Pu^{3+}_{(aq)}$ or $Pu^{4+}_{(aq)}$, retaining their overall formal charge. In the sections that follow, we refer to the $Pu^{3+}_{(aq)}$ or $Pu^{4+}_{(aq)}$ species as simply Pu^{3+} and Pu^{4+}, or Pu(III) and Pu(IV), respectively. Pentavalent and hexavalent plutonium cations have such large positive charges that in aqueous solution they immediately hydrolyze to form a unique class of trans dioxo cations, $PuO^{+}_{2(aq)}$ and $PuO^{2+}_{2\,(aq)}$, which are commonly referred to as plutonyl ions. Under noncomplexing acid conditions (such as perchloric or triflic acid), both ions exist as the simple hydrated (or aquo) ions, $PuO^{+}_{2(aq)}$ and $PuO^{2+}_{2(aq)}$, and we refer to these as simply PuO^{+}_{2} and PuO^{2+}_{2}, or Pu(V) and Pu(VI), respectively. These plutonyl cations have estimated effective charges of 2.2 and 3.3, respectively (Choppin, 1983). Heptavalent plutonium is not stable in acid solution, and can only be prepared under highly alkaline solution conditions. Under alkaline conditions, the heptavalent ion forms a tetra-oxo species PuO^{-}_{4}, which is always coordinated with hydroxide ions to give $PuO_4(OH)^{3-}_{2}$. We will refer to this species as Pu(VII). The OECD-NEA has evaluated thermodynamic properties for plutonium ions in aqueous solution, and a selected set of their recommended values is given in Table 7.48 (Lemire *et al.*, 2001).

(a) Stoichiometry and structure of plutonium ions

From an historical perspective, the charge and composition of plutonium ions in acid solution were inferred from solvent extraction studies. For example, plutonium(III) and plutonium(IV) are written as Pu^{3+} and Pu^{4+} in part from an interpretation of charge balances in solvent extraction studies with thenoyltrifluoroacetone (Poskanzer and Foreman, 1961), and also from the lack of hydrogen-ion dependence of the reversible Pu(IV)/Pu(III) redox couple (Rabideau, 1956). The Pu(V)/Pu(IV) redox couple on the other hand, is not rapidly reversible, nor independent of hydrogen-ion concentration, indicating that the two ions differ in degree of oxygenation. The existence of the trans dioxo ions in Pu(V) and Pu(VI) (PuO^{+}_{2} and PuO^{2+}_{2}, respectively) was originally based on crystallographic data on solid compounds. For Pu(VI), XRD data for $NaPuO_2(O_2CCH_3)_3$ and $Cs_2PuO_2Cl_4$ confirmed that the compounds were isostructural with the corresponding uranium, neptunium, and americium analogs, and contained the linear PuO^{2+}_{2} unit (Werner, 1982). Similar structural

Table 7.48 *Selected chemical thermodynamic values for plutonium aquo ions* (*Lemire* et al., 2001).

Formula	$\Delta_f G^\circ$ (kJ mol^{-1})	$\Delta_f H^\circ$ (kJ mol^{-1})	S° (J K^{-1} mol^{-1})
Pu^{3+}	-579.0 ± 2.7	-591.8 ± 2.0	-184.5 ± 6.2
Pu^{4+}	-478.0 ± 2.7	-539.9 ± 3.1	-414.5 ± 10.2
PuO^{+}_{2}	-852.6 ± 2.9	-910.1 ± 8.9	$+1 \pm 30$
PuO^{2+}_{2}	-762.4 ± 2.8	-822.0 ± 6.6	-71 ± 22

comparisons were found for other Pu(VI) compounds, and helped to assign the basic formula PuO_2^{2+} to Pu(VI) in solution. Plutonium(V), likewise, was assigned the formula PuO_2^{+} because of the existence of the PuO_2^{+} unit in the solid-state structure of $KPuO_2CO_3$ (Ellinger and Zachariasen, 1954), and in part because the oxidation–reduction couple Pu(VI)/Pu(V) is reversible and independent of the hydrogen-ion concentration (except for the shift in potential due to hydrolysis). This argued that there was no structural rearrangement during redox, and therefore that the oxygen content was identical in both ions.

Recent X-ray absorption and vibrational spectroscopic studies provide more direct characterization of the solution forms of the ions in all oxidation states. Under noncomplexing acid conditions, Pu(III), Pu(IV), Pu(V), and Pu(VI) are coordinated by water molecules, resulting in hydrated cations of general formula $Pu(OH_2)_n^{3+}$, $Pu(OH_2)_n^{4+}$, $PuO_2(OH_2)_n^{+}$, and $PuO_2(OH_2)_n^{2+}$, respectively. Structural analysis in solution using EXAFS spectroscopy has been recently employed to determine the number of coordinated water molecules (n) and the Pu–O distances in the aquo ions (Allen *et al.*, 1997; Conradson *et al.*, 2004a). For the Pu(III) aquo ion, $Pu(OH_2)_n^{3+}$, EXAFS studies report coordination numbers of 9 (Conradson *et al.*, 2004a) and 10 (Allen *et al.*, 1997), with Pu–O distances of 2.48(1) and 2.51(1) Å, respectively. These coordination number estimates are consistent with previous estimates of 9 that were based upon comparison with Cm(III) from luminescence lifetime measurements (Kimura and Choppin, 1994), and Am(III) determined from optical absorption spectroscopy (Carnall, 1989). Relativistic DFT calculations suggest eight or possibly nine water molecules for the Pu(III) aquo ion, $Pu(OH_2)_9^{3+}$ (Blaudeau and Bursten, 2000). A recent single crystal XRD study of a salt containing the $Pu(OH_2)_9^{3+}$ unit substantiates the coordination number of 9 for the Pu(III) aquo ion (Matonic *et al.*, 2001) in the solid state. In this compound, the $Pu(OH_2)_9^{3+}$ ion adopts a tricapped trigonal prismatic coordination environment, where all nine coordinated water molecules show a similar Pu–O distance that averages 2.51 Å (Matonic *et al.*, 2001) comparable to the values observed by EXAFS. For Pu(IV), EXAFS analysis indicates the presence of eight water molecules at a shorter Pu–O distance of 2.39(1) Å (Conradson *et al.*, 2004a). For Pu(V) and Pu(VI) aquo ions, EXAFS data reveal two short plutonyl Pu=O bonds at 1.81(1) and 1.75(1) Å (respectively) consistent with expectations for trans dioxo ions. Each plutonyl unit is coordinated by four or five water molecules with Pu–O bond distances of 2.47(1) and 2.41(1) Å, respectively (Conradson *et al.*, 2004a). Similar analyses on the aquo ions of UO_2^{2+}, NpO_2^{2+}, and NpO_2^{+} indicate that a coordination number of 5 is the most common, but that this value will be affected by changes in the ionic strength of solution (Antonio *et al.*, 2001). Theoretical analysis of XANES, coupled with experimental measurements, have provided new insights on the electronic structure of these ions, especially the nature of the bonding interactions between plutonium and axial oxygen atoms in the PuO_2^{+}, and PuO_2^{2+} aquo ions (Ankudinov *et al.*, 1998).

Ions of Pu(VII) also contain Pu=O multiple bonds, and the preponderance of evidence indicates the presence of polyoxo ions with four or more oxo groups depending on solution conditions. The reversibility of the Pu(VII/VI) reduction, similar to the Pu(VI/V) reversible reduction supports the formulation of a polyoxo ion. A series of anionic polyoxo species that form between 0.5 and 18 molar hydroxide has been proposed and includes $PuO_4(OH_2)_2^-$, $PuO_4(OH)(OH_2)^{2-}$, $PuO_4(OH)_2^{3-}$, $PuO_5(OH)^{4-}$, or PuO_6^{5-}, depending on hydroxide concentrations (Spitsyn *et al.*, 1969; Krot, 1975; Tananaev *et al.*, 1992). Of the proposed species, only $PuO_4(OH)_2^{3-}$ has a known analog in neptunium chemistry (Grigor'ev *et al.*, 1986). The neptunium analog, $NpO_4(OH)_2^{3-}$, has a highly unusual geometry with four short Np=O bonds in a square plane, with two axial OH^- ligands (Grigor'ev *et al.*, 1986; Bolvin *et al.*, 2001; Williams *et al.*, 2001). Current research is aimed at defining conditions that favor the various forms, and at identifying their exact structure and reactivity.

Structural representations of the simple aquo ions of plutonium are given in **4**, **5**, **6,** and **7** below.

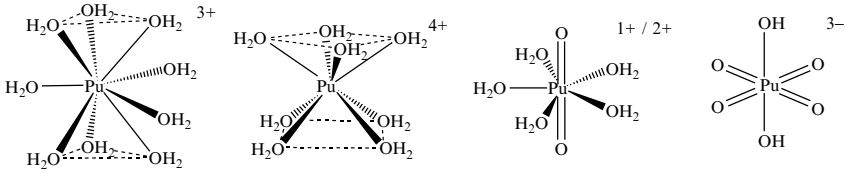

4 **5** **6** **7**

(b) Spectroscopic properties of plutonium ions

The electronic absorption spectra of plutonium ions, like those of most other actinide elements, are characterized by the presence of a few very sharp bands with relatively low molar absorptivities compared to those of d-block metal ions. The very sharp bands are strongly reminiscent of spectra of the rare-earth ions, which are attributed to electronic transitions within the shielded 4f–4f manifold of states (Edelstein, 1991). In the actinide elements, similar but relatively less shielded transitions are attributed to the 5f shell (Carnall *et al.*, 1991; Carnall, 1992; Denning, 1992, 1999). The 5f–5f transitions are more intense than the 4f–4f transitions of the lanthanides, due in part to relativistic effects that generate larger spin–orbit coupling. Energy levels for trivalent actinide ions calculated using 5f transitions compare well with experimental spectra, supporting this representation of electronic structure in plutonium (Mikheev *et al.*, 1983; Carnall, 1992). Since these transitions are forbidden by the selection rules, the absorption bands are narrow, but still not very intense.

Internal 5f–5f transitions of the plutonium ions give absorption bands in the visible and near-IR region of the electronic absorption spectrum. These

absorption features are characteristic for each oxidation state and therefore frequently used for identification and quantitative analysis of plutonium ions in solution (Cohen, 1961a). Representative electronic absorption spectra of plutonium ions of common oxidation states are given in Fig. 7.115 and molar absorptivities for distinctive bands are given in Table 7.49. Plutonium ions of all oxidation states have strong absorbance in the UV region of the optical spectrum (Stewart, 1956; Cohen, 1961b). In addition to conventional electronic absorption spectroscopy, two-photon optical absorption spectroscopy has also been used to probe the electronic structure of plutonium ions isolated in host matrices and these data have provided useful extrapolations for interpreting the spectra of the solvated ions (Denning, 1991).

Photothermal spectroscopic techniques have been applied to increase the sensitivity and selectivity of the optical absorption method of plutonium analysis. For example, photoacoustic spectroscopy, in which the pressure pulse generated from absorbed light heating the solution is transduced to an electronic signal, generally has 10 to 100 times greater sensitivity (depending on the spectral region) than conventional spectrophotometry (Stumpe *et al*., 1984; Neu *et al*., 1994). Thermal-lensing spectroscopy has sensitivities similar to photoacoustic spectroscopy and also uses the heating of the solution due to the absorption of small amounts of energy to detect and quantify analytes. This method optically probes the gradient in the refractive index, which is generated from solution heating, as a 'thermal lens' (Moulin *et al*., 1988). The use of fiber optics and pulsed laser diode excitation sources with either of these techniques allows for remote or in-process detection and quantification of plutonium ions (Neu *et al*., 1994; Wruck *et al*., 1994) in micromolar concentrations or lower. Both methods have been used in solution thermodynamic studies aimed at quantitatively evaluating complexation of plutonyl ions by chelating ligands and even by the oxo ligands of other actinyl ions (Bennett *et al*., 1992; Stoyer *et al*., 2000).

Vibrational spectroscopy, both infrared absorption and Raman scattering, are useful for 'fingerprint' comparisons, for structure determination, for analyzing intramolecular bond strength, and for understanding the electronic structure of plutonium ions. Comparison of infrared and Raman spectra of actinyl ions across the actinide series were used to establish that higher valent plutonium (V, VI) species in aqueous solution exist as linear trans dioxo ions with strong covalent Pu=O bonds. The hexavalent actinide ions all show an asymmetric O=An=O stretching frequency (ν_3) in the energy region 930–970 cm^{-1}, with the Pu(VI) aquo ion in noncomplexing perchlorate solution observed at 962 cm^{-1} (Jones and Penneman, 1953). These studies confirmed the symmetric and linear, or nearly linear, structures of both PuO_2^+, and PuO_2^{2+} in a more compelling way than do arguments based on similarities in the fine structure of the visible absorption spectrum. Infrared spectroscopic studies of plutonyl species in condensed phases, using very long pathlengths, powerful excitation sources, and sensitive detectors also contributed to vibrational band assignments for

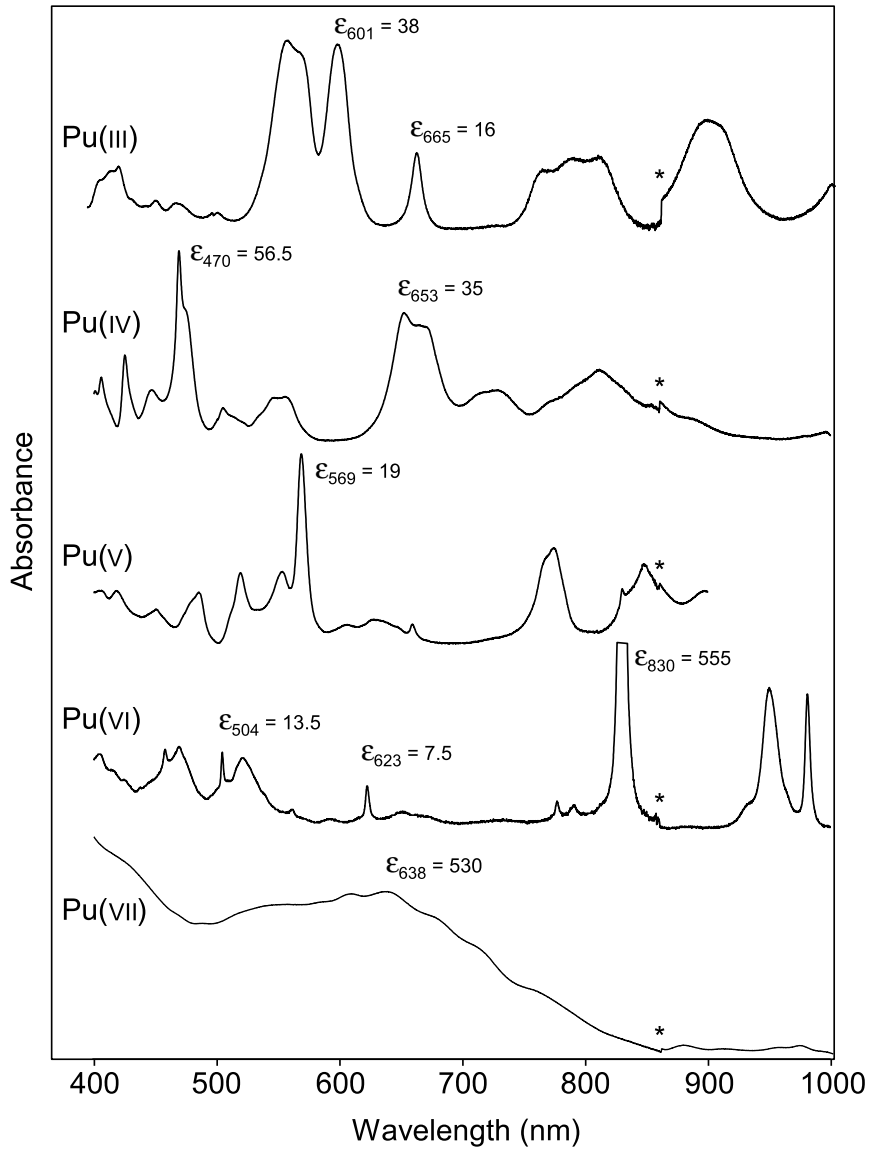

Fig. 7.115 *Electronic absorption spectra of major plutonium aqua ions recorded at* 25°C. *The asterisk marks a spectrophotometer grating change. Plutonium*(III) *recorded on* 1.89 mM *solution in* 1 M $HClO_4$ *using* 1 cm *cell. Plutonium*(IV) *recorded on* 2.91 mM *solution in* 1 M $HClO_4$ *using* 1 cm *cell. Plutonium*(V) *recorded on* 10.2 mM *solution in* 1 M $(Na,H)ClO_4$ *solution at pH* 3.14 *using* 1 cm *cell. Plutonium*(VI) *recorded on* 0.89 mM *solution in* 1 M $HClO_4$ *using* 1 cm *cell. Plutonium*(VII) *recorded on* 20 mM *solution in* 2.5 M *NaOH using* 1 cm *cell* (*spectra courtesy of Phillip D. Palmer of Los Alamos National Laboratory*).

Table 7.49 *Characteristic optical absorption bands of plutonium aquo ions in* 1 M (*H,Na*) ClO_4 *at* 25°C *unless noted otherwise* (*Cohen*, 1961*b*).

Species	*Peak max.* (nm)	*Full width at half height* (nm)[a]	*Molar absorption,* ϵ (L mol^{-1} cm^{-1})
Pu^{3+}	244	broad	1500
	561	broad	38
	601	21.7	38
	665	10.9	16
Pu^{4+}	470	13.6 (shoulder)	56.5
	653	42.7 (shoulder)	35
PuO_2^{+}[b]	569	8.6	19
	1131	32	22
PuO_2^{2+}	504	3.0	13.5
	623	3.8	7.5
	830	2.5	555
$PuO_4(OH)_4^{3-}$[c]	638	broad	530

[a] FWHM estimated from Cohen (1961b).
[b] 10°C, 0.2 M $HClO_4$.
[c] Pu(VII) spectrum from Krot and Gel'man (1967).

ions in solution (Bovey and Steers, 1960; Vdovenko *et al.*, 1973; Kim and Campbell, 1985). Complementary Raman studies assigned the symmetric O=Pu=O stretching frequency (ν_1) for PuO_2^{2+} in 1.0 M (H,Na)ClO_4 at (834 ± 3) cm^{-1}, which compares well with ν_1 for the analogous NpO_2^{2+} and UO_2^{2+} ions at (855 ± 2) cm^{-1} and (865 ± 5) cm^{-1}, respectively. These ν_1 frequencies were assigned to ground state vibrations from both fluorescence spectra intervals and Raman shifts (Madic *et al.*, 1984; Tait *et al.*, 2004). This Raman shift also agrees with the prediction of 830 cm^{-1} based on the visible spectrum of plutonium(VI) in HCl that contains a 708 cm^{-1} frequency interval in the fine structure within the wavelength region 390–430 nm. The Raman shift of PuO_2^{+} in 1.0 M ClO_4^{-} was observed at 748 cm^{-1}. Disproportionation of PuO_2^{+} was evidenced by the decrease of the intensity of the 748 cm^{-1} PuO_2^{+} band and the increase of bands located at 833 and 817 cm^{-1} assigned to PuO_2^{2+} and $(PuO_2)_2(OH)_2^{2+}$, respectively (Madic *et al.*, 1984).

Correlations of vibrational frequencies to bond strength and molecular structure of the linear O=An=O moiety have been made. Recent X-ray absorption spectroscopy studies of solution and polycrystalline actinide samples allow for correlation of the energy of the symmetric ν_1 Raman frequency with measured An=O bond lengths. Clear trends can be seen within a particular oxidation state of an actinide and a general trend of heavier actinyl ions having weaker bonds has emerged. The Raman frequency for Pu(VI) is sensitive to complexation environment, showing shifts in ν_1 greater than 40 cm^{-1} between solution species for which the measured changes in the Pu=O bond length are only minimal.

Comparisons of Pu(V) with Np(V), and Pu(VI) with U(VI) and Np(VI) aquo complexes show that as nuclear charge increases across the series uranium to plutonium, the stretching frequencies actually decrease with decreasing An=O bond length. The bond shortening is clearly a result of the actinide contraction, and the weaker bonding is an indication of 5f orbital contraction across the actinide series (Tait *et al.*, 2004). The nature of chemical bonding in the plutonyl ions is discussed in Section 7.9.3 and in Chapter 17.

(c) Oxidation and reduction reactions

(*i*) *Oxidation–reduction equilibria between plutonium ions*

The oxidation–reduction (redox) relationships of the plutonium ions present one of the most complex and fascinating aspects of the aqueous solution chemistry of plutonium. The redox potentials that couple the four common oxidation states (III, IV, V, VI) of plutonium in acid solution are all of comparable magnitude and very close to 1 V. Moreover, the kinetics of the reactions among oxidation states creates a unique situation where finite amounts of multiple oxidation states can coexist in solution under the appropriate conditions. This situation is unique for plutonium among all the elements in the periodic table. The complications arising from this unusual behavior are responsible for a considerable amount of research devoted to understanding the kinetics and mechanisms of these important reactions. We will discuss these reactions independently, and then discuss several examples to illustrate the complexity of the system. Much of this discussion follows from the excellent reviews by Cleveland (1979) and by Newton (1975, 2002).

The equilibrium concentrations of species involved in these reactions are usually determined from the potentials and the pertinent complex formation constants. Calculating standard potential values for the various couples is challenging since nearly all the data were acquired at high ionic strength, requiring extrapolation to infinite dilution. It is particularly difficult to study tetravalent plutonium independently of its hydrolysis and disproportionation. Redox reactions and corresponding electrochemical potentials that are useful for making predictions of plutonium chemistry in solution are given in Table 7.50. The constants listed for reactions in acid and some of those in base are from direct measurements, while those at pH 8 were estimated from hydrolysis data and standard potentials in acid for Pu(III), Pu(IV), and Pu(VI) and related ions (Allard *et al.*, 1980). Electrochemical studies and reported potentials have been reviewed in recent publications (Mikheev and Myasoedov, 1985; Capdevila and Vitorge, 1995; Peretrukhin *et al.*, 1995; Lemire *et al.*, 2001) and in Chapter 19 of this work. Formal redox potential schemes for selected plutonium couples at 25°C have been derived for 1 M $HClO_4$ (Lemire *et al.*, 2001), 1 M HCl (Rabideau and Cowan, 1955; Rabideau *et al.*, 1959), and 1 M HNO_3 (Artyukhin *et al.*, 1958), and are shown in Fig. 7.116.

Table 7.50 *Formal electrochemical potentials for redox couples relating the plutonium ions in acidic, neutral, and basic aqueous solution versus the standard hydrogen electrode (SHE).*

Couple	*Acidic*[a]	*Neutral*[b]	*Basic*[c]
Pu(IV)/Pu(III)	+0.982	−0.39	−0.96
Pu(V)/Pu(IV)	+1.170	+0.70	−0.67; +0.52[d]
Pu(VI)/Pu(V)	+0.913	+0.60	+0.12
Pu(VI)/Pu(IV)	+1.043	+0.65	+0.34
Pu(V)/Pu(III)		+1.076	
Pu(VII)/Pu(VI)			+0.85
Pu(V)/Pu(IV)	+1.17		

[a] Formal potential in 1 M $HClO_4$ solution (Lemire *et al.*, 2001).
[b] pH 8 (Allard *et al.*, 1980).
[c] Determined in 1 M NaOH solution (Peretrukhin *et al.*, 1995).
[d] Formal oxidation potential (Allard *et al.*, 1980).

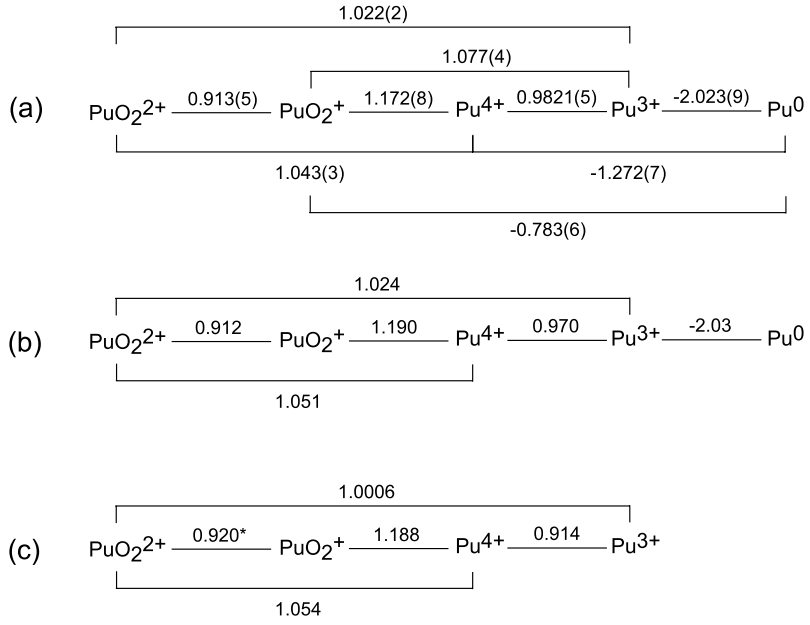

Fig. 7.116 *Formal redox potentials for selected plutonium couples at* 25°C *in V vs SHE* (*a*) *in* 1 M $HClO_4$ (*Lemire* et al., 2001), (*b*) *in* 1 M *HCl* (*Rabideau and Cowan*, 1955*; Rabideau* et al., 1959), *and* (*c*) 1 M HNO_3 (*Artyukhin* et al., 1958).

The formal potential of the Pu(VII)/Pu(VI) couple depends upon the square of the hydroxide ion concentration, and is about 0.85 V in 1 M NaOH, corresponding to the reaction (Spitsyn *et al.*, 1969; Musante and Ganivet, 1974; Krot, 1975):

$$PuO_4(OH)_2^{3-} + 2H_2O \rightleftarrows PuO_2(OH)_4^{2-} + 2OH^- + e^- \qquad (7.74)$$

In voltammetric studies performed at lower hydroxide concentration (with a different proposed reaction), the Pu(VII/VI) reduction in 0.01 M hydroxide ion was observed at +1.20 V vs standard hydrogen electrode (Musante and Ganivet, 1974). Due to the instability of Pu(VII) at low hydroxide concentration (and therefore low ionic strength) it is not possible to extrapolate the potential to estimate a standard potential and other standard thermodynamic values.

The redox couples between Pu(V)/Pu(III), Pu(VI)/Pu(III), Pu(V)/Pu(IV), and Pu(VI)/Pu(IV), are quasireversible or irreversible because they involve the breaking or forming of Pu=O multiple bonds. In contrast, the redox couples between species where no Pu=O bond forming or breaking occurs, such as Pu(IV)/Pu(III), Pu(VI)/Pu(V), and Pu(VII)/Pu(VI) couples are reversible. Experimental, standard, and predicted reduction and oxidation potentials have been reported under a wide range of conditions, with the exception of those for Pu(VII). Standard redox potentials in acidic solution are described in greater detail in Chapter 19. Since the redox couples that connect the four main oxidation states (III, IV, V, VI) are relatively similar, it is possible for all four oxidation states to coexist under the appropriate solution conditions. The ability to have multiple oxidation states in solution at the same time will depend upon several key factors. The most important of these are the tendency of Pu(IV) and Pu(V) to disproportionate, and the relatively slow kinetics of reactions that involve the making or breaking of Pu=O bonds in plutonyl ions (PuO_2^+ and PuO_2^{2+}). Other factors are plutonium ion concentration, ionic strength, pH, temperature, and presence or absence of complexing ligands. Thermodynamic and activation data for redox reactions between plutonium ions are summarized in Table 7.51.

(*ii*) *Disproportionation of Pu(IV)*

In acid solution in the absence of complexing ligands, the disproportionation of Pu(IV) proceeds according to the following equation:

$$3Pu^{4+} + 2H_2O \rightleftharpoons 2Pu^{3+} + PuO_2^{2+} + 4H^+ \qquad (7.75)$$

From this equation one can derive the equilibrium constant expression as:

$$K = \frac{[Pu^{3+}]^2[PuO_2^{2+}][H^+]^4}{[Pu^{4+}]^3} \qquad (7.76)$$

Rabideau carefully determined the equilibrium constant for this reaction in $HClO_4/NaClO_4$ solution under a constant ionic strength of 1.0 M (Rabideau, 1953). Rabideau's work on this system is seminal in that it takes into account the plutonium self-reduction by α particle radiolysis, and the hydrolysis of Pu(IV) at low pH. The concentration of Pu(IV) in the equilibrium constant expression above has been corrected for both effects. The equilibrium constant, K, was determined to have a weighted average value of 0.0089 for 1.0 M ionic

Table. 7.51 *Thermodynamics and activation data for plutonium redox reactions* (*Newton,* 2002).

Process	I (M)	ΔG (kJ mol^{-1})	ΔH (kJ mol^{-1})	ΔS (J K^{-1} mol^{-1})	*S* complex* (J K^{-1} mol^{-1})	*References*
$Pu^{3+} + {}^*Pu^{4+} = Pu^{4+} + {}^*Pu^{3+}$		0.0	0.0	0.0	0.0	
$Pu^{3+} + Pu^{4+} + H_2O = [Pu(Pu)OH^*]^{6+} + H^+$	2	56.1	31.0	-84.2 ± 17	-485	Keenan (1957)
$Pu^{3+} + PuO_2^+ + 4H^+ = 2Pu^{4+} + 2H_2O$		-18.2	-120.9	-344		
$Pu^{3+} + PuO_2^+ + H^+ = [Pu(PuO_2)H^*]^{5+}$	1	82.5	33.5	-164 ± 2	-332	Lavallee and Newton (1972)
	2	78.3	43.1	-117 ± 3	-289	Koltunov *et al.* (1980b)
$Pu^{3+} + PuO_2^{2+} = Pu^{4+} + PuO_2^+$		6.3	-35.6	-140		
$Pu^{3+} + PuO_2^{2+} = [Pu(PuO_2)^*]^{5+}$	1	70.7	20.1	-169 ± 1	-416	Rabideau and Kline (1958)

strength. Rabideau and Cowan (1955) subsequently studied this same disproportion reaction in HCl solution and found the same fourth order dependence on hydrogen ion concentration. It was concluded that the mechanism of Pu(IV) disproportion was identical in both media. The fourth order dependence on hydrogen ion concentration is consistent with experimental observations of essentially no disproportionation of Pu(IV) in strongly acidic solutions. The study in HCl solution is somewhat more straightforward in that α particle reduction was essentially absent. In addition, the value of the equilibrium constant is somewhat smaller ($K = 0.00192$ in 1 M HCl) than observed in perchloric acid ($K = 0.0084$ in 1 M $HClO_4$) and this difference is attributed to stabilization of Pu(IV) ions by complexation with chloride ions in HCl solution. Rabideau and Cowan (1955) also examined the temperature dependence of the equilibria in HCl, and found that raising the temperature from 25 to 45°C increased the value of the equilibrium constant by a factor of 70 ($K = 0.00142$ at 25°C; $K = 0.0967$ at 45.16°C).

Connick studied the kinetics of the disproportionation reaction and found that the overall reaction takes place in two separate steps with a transient Pu(V) intermediate (Connick, 1949). In the first slow step (equation (7.77)), two equivalents of Pu(IV) combine to generate Pu(III) and Pu(V). This reaction is slow because it involves the formation of a Pu=O bond in forming Pu(V). In the second step (equation (7.78)), the Pu(V) produced in the first step reacts with Pu(IV) in a rapid equilibrium.

$$2Pu^{4+} + 2H_2O \rightleftharpoons Pu^{3+} + PuO_2^+ + 4H^+ \text{ (slow)} \tag{7.77}$$

$$PuO_2^+ + Pu^{4+} \rightleftharpoons Pu^{3+} + PuO_2^{2+} \text{ (fast)} \tag{7.78}$$

Thus, the disproportionation is complete when both reactions (7.77) and (7.78) have reached equilibrium. The addition of equations (7.77) and (7.78) yields the common representation of the Pu(IV) disproportionation reaction that was given in equation (7.75). Equation (7.75) represents a reaction that comes to equilibrium in any plutonium solution, but equation (7.75) does not adequately represent the disproportionation of tetravalent plutonium because it fails to include Pu(V), even as an infinitesimally small intermediate. Silver (1971, 2003) has shown that a linear combination of equations (7.77) and (7.78) produces a new equation for the dissociation of Pu(IV) and is shown in equation (7.79), where the parameter M represents the equilibrium ratio for $[PuO_2^{2+}]/[PuO_2^+]$.

$$\begin{aligned}(2 + 3M)[Pu^{4+}] + (2M + 2)[H_2O] \rightleftharpoons (1 + 2M)[Pu^{3+}] \\ + [PuO_2^+] + M[PuO_2^{2+}] + (4M + 4)[H^+]\end{aligned} \tag{7.79}$$

The value of M was found as the root of the cubic equation (7.80) where $K_{(7.77)}$ and $K_{(7.78)}$ are the equilibrium constants for equations (7.77) and (7.78), respectively.

$$K^2_{(7.78)}[H^+]^4 - K_{(7.77)}(M^2 + 2M^3) = 0 \tag{7.80}$$

As the value of the ratio M increases, the coefficient of Pu(v) decreases and the stoichiometry of equation (7.79) approaches the stoichiometry of equation (7.75). In 1 M perchloric acid, the value of M is about 50.

(*iii*) *Disproportionation of Pu*(*v*)

In moderately acidic solutions Pu(v) is unstable towards disproportionation reactions. The disproportionation of Pu(v) into Pu(vi) and Pu(iv) or Pu(iii) is expected to proceed by either of two possible mechanisms. From a study of the rate of the disproportionation of Pu(v) in 0.5 M HCl, Connick (1949) has shown that the actual mechanism consists of the slow reaction (7.81) coupled with the rapid equilibrium (7.78).

$$PuO_2^+ + Pu^{3+} + 4H^+ \rightleftharpoons 2Pu^{4+} + 2H_2O \text{ (slow)} \tag{7.81}$$

$$PuO_2^+ + Pu^{4+} \rightleftharpoons Pu^{3+} + PuO_2^{2+} \text{ (fast)} \tag{7.78}$$

with an overall reaction

$$3PuO_2^+ + 4H^+ \rightleftharpoons Pu^{3+} + 2PuO_2^{2+} + 2H_2O \tag{7.82}$$

Connick (1949) pointed out that the disproportionation of Pu(v) proceeded by the mechanism of equation (7.82) under the conditions of his experiment, but that this mechanism cannot be true under all circumstances. At very low concentrations of Pu(iii) the mechanism must necessarily change to that represented by equation (7.83).

$$2PuO_2^+ + 4H^+ \rightleftharpoons Pu^{4+} + PuO_2^{2+} + 2H_2O \tag{7.83}$$

Thus equations (7.82) and (7.83) are limiting cases for Pu(v) disproportionation, and the actual reaction path depends on the plutonium species present in solution (Connick, 1949). The use of equations (7.82) or (7.83) have been widely cited in the literature, but Connick's original caveats on their intimate connection to solution conditions has not always been kept in mind. Without this understanding, equations (7.82) and (7.83) would appear to be contradictory because they do not predict the same reaction products (Pu^{3+} in (7.82), and Pu^{4+} in (7.83)). Under many solution conditions encountered in the laboratory, Pu(v) disproportionation may follow both mechanisms, in which case neither equation 7.82 or 7.83 by itself adequately describes Pu(v) disproportionation. This apparent discrepancy has been discussed in detail by Silver (1971, 1997, 2002, 2004) who has shown that the disproportionation reaction under any particular solution condition can be expressed as a linear combination of these two limiting cases. In this manner Pu(v) disproportionates in accordance with

the stoichiometry of equation (7.84), where the parameter M represents the equilibrium ratio for $[PuO_2^{2+}]/[PuO_2^{+}]$.

$$\begin{aligned}(3 + 2M/K_{(7.78)})[PuO_2^{+}] + (4 + 4M/K_{(7.78)})[H^{+}] \rightleftharpoons \\ [Pu^{3+}] + (M/K_{(7.78)})[Pu^{4+}] + (2 + M/K_{(7.78)})[PuO_2^{2+}] \\ + (2 + 2M/K_{(7.78)})[H_2O]\end{aligned} \tag{7.84}$$

The value of M was found as the positive, real root of equation (7.85) where $K_{(7.78)}$ and $K_{(7.77)}$ are the equilibrium constants for equations (7.78) and (7.77), respectively.

$$2K_{(7.78)}^2[H^{+}]^4 + (K_{(7.78)}[H^{+}]^4 M - K_{(7.77)}M^3) = 0 \tag{7.85}$$

The mathematical details are beyond the scope of this discussion, and the interested reader should see the works of Silver (1971, 1997, 2002, 2004) for more detail.

It is noteworthy that both reactions 7.82 and 7.83 for the disproportionation of Pu(v) have equilibrium constants with a fourth order dependence on the hydrogen ion concentration. This illustrates why Pu(v) solutions are only stable at near-neutral pH where the hydrogen ion concentration is low. Many workers have used this observation to prepare solutions of Pu(v) in the absence of other oxidation states (Gevantman and Kraus, 1949; Markin and McKay, 1958; Gel'man and Zaitseva, 1965a,b; Newton, Hobart *et al.*, 1986a).

Rabideau studied the kinetics and mechanism of the Pu(v)-Pu(v) reaction in the absence of Pu(iii) (Rabideau, 1957).

(*iv*) *Equilibrium between Pu*(*iii*), (*iv*), (*v*), *and* (*vi*)

The reaction that describes the equilibrium between all four oxidation states has been used in the discussion of the disproportionation of Pu(iv) and Pu(v). The equilibrium constant for this reaction is given by:

$$K = \frac{[\text{Pu(III)}][\text{Pu(VI)}]}{[\text{Pu(IV)}][\text{Pu(V)}]} \tag{7.84}$$

This equilibrium constant has been determined in various media, but not all studies have corrected for the hydrolysis of Pu(iv). Rabideau and Kline (1958) determined this equilibrium constant in unit ionic strength $HClO_4/NaClO_4$ solution for various hydrogen ion concentrations. They obtained a value of $K = (13.1 \pm 0.08)$ at 25°C that is corrected for hydrolysis and is independent of H^+ concentration over the range $0.1 \leq H^+ \leq 1.0$ M. In D_2O solution, the corresponding hydrolysis-corrected value was determined to be (40.6 ± 1.0). Rabideau and Kline studied the kinetics of the reaction in both H_2O and D_2O solution, and determined that a hydrogen atom transfer process is not

involved in the reaction. In complexing acids such as HCl and HNO_3, the equilibrium was found to shift to favor higher concentrations of Pu^{4+}.

Because this system is rather complicated, it is instructive to examine a series of figures that describe the system under various conditions. Equilibrium oxidation state distribution diagrams are useful for predicting the behavior of various plutonium stock solutions made up in the laboratory. Equilibrium diagrams showing the predominant oxidation state as a function of pH and average oxidation state for 1.0 M ionic strength are given in Fig. 7.117.

Fig. 7.117(a) shows the distribution for a solution with average oxidation state IV. It is seen that a solution which is initially pure Pu(IV) will contain significant concentrations of Pu(III) and Pu(VI) at equilibrium in 1 M acid. At pH 1 Pu(III) predominates and at pH 2 the solution is primarily a mixture of Pu(III) and Pu(V). The calculations that produced these plots took the first hydrolysis constant for Pu(IV) into account. It should be pointed out that the distribution in the region between pH 1 and 2 is less certain as the second hydrolysis constant was not taken into account. A small amount of irreversible hydrolysis to give colloidal Pu(IV) hydroxide is also expected at very low concentrations. Fig. 7.117(b) shows a distribution for a solution with average oxidation state V, for example an equimolar mixture of Pu(IV) and Pu(VI). Here, Pu(VI) predominates until a pH of about 1.2 is reached. At higher values, Pu(V) becomes predominant.

It is also important to know how rapidly redox equilibria will be reached in plutonium solutions. The rate constants and hydrogen ion dependences for the reactions above are known for solutions at 25°C and unit ionic strength. The kinetics of the system are somewhat complicated in that the forward and reverse

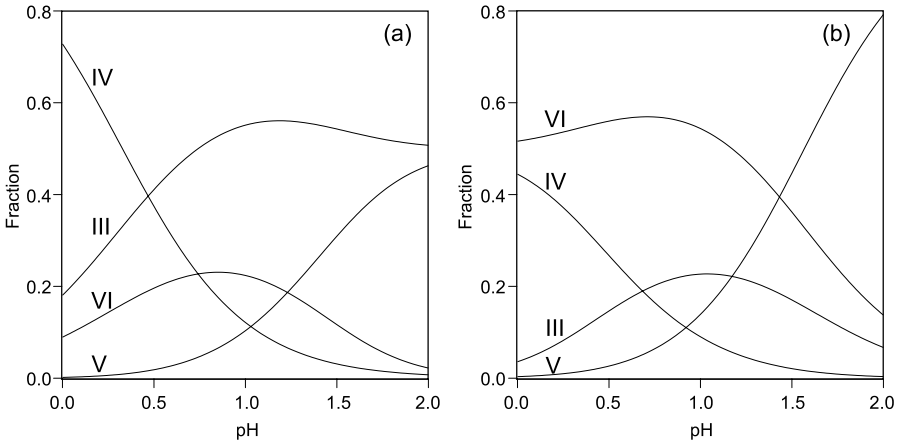

Fig. 7.117 *Oxidation state distribution diagram showing the predominant oxidation state of plutonium in* 1 M *(H,Na)*ClO_4 *solution as a function of pH and* (*a*) *average oxidation state Pu(IV), and* (*b*) *average oxidation state Pu(V)* (*calculations courtesy of T. W. Newton*).

rates of all three of the reactions listed above must be considered. The disproportionation of Pu(IV) in 0.1 M acid has been calculated and the results for 1.0 M ionic strength at pH 1.0 are shown in Fig. 7.118(a). Appreciable concentrations of the other oxidation states appear after relatively short periods of time. The rates depend on the total plutonium concentration, so the time scale is given in units of M s (molar second). The time required to reach any particular distribution is found by dividing the total concentration. For example, Fig. 7.118(a) indicates that if the concentration of Pu(IV) is 0.002 M, then half of the Pu(IV) will be gone in about 3 hours. In a similar fashion, Pu(V) is quite stable at pH 3 and can be formed, for example, by mixing Pu(III) and Pu(VI). The course of this reaction at unit ionic strength is shown in Fig. 7.118(b). For a concentration of 0.001 M, equilibrium is reached in about a day and within about 10% of equilibrium within about 5 hours. Reducing the ionic strength decreases the rate. Selected oxidation and reduction rate data for different plutonium oxidation states are given in Table 7.52.

(*v*) *Preparation and stability of pure oxidation states*

Newton and coworkers have provided excellent experimental procedures for the preparation of oxidation state pure plutonium solutions. The following discussion comes essentially from Newton *et al.* (1986a).

Pu(III). Acidic solutions of Pu(III) are conveniently prepared by dissolving weighed samples of pure α-phase metal in 6 M HCl or $HClO_4$, with cooling, followed by dilution to the desired concentration. Corrosion products on the

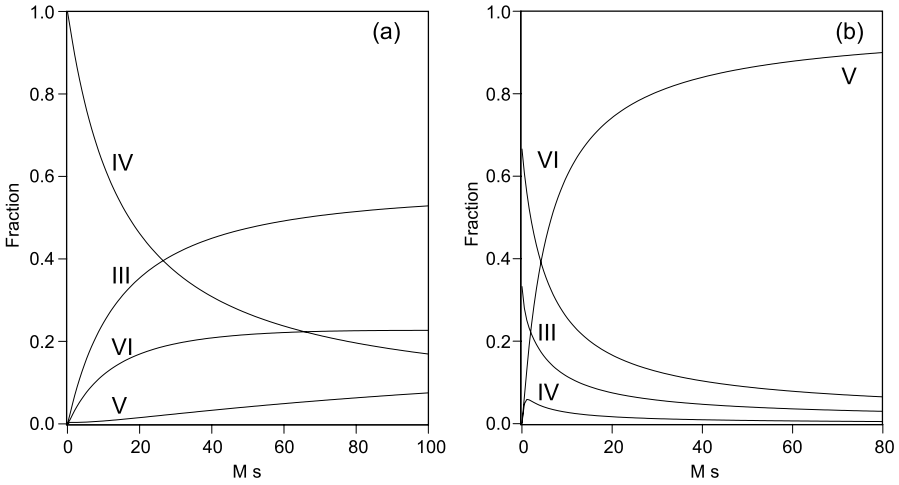

Fig. 7.118 *Kinetics for disproportionation of plutonium in* 1 M $(H,Na)ClO_4$ *solution at* (*a*) *pH 1 and average oxidation state Pu*(IV), *and* (*b*) *pH 3 and average oxidation state Pu*(V) (*calculations courtesy of T. W. Newton of Los Alamos*).

Table 7.52 *Selected plutonium oxidation and reduction rate as compiled by data Newton* (2002).

Agent	*Concentration* (M)	*Solution*	*Temperature* (°C)	*Results*	*References*
Pu(III) oxidation					
NO_3^-	0.2 ($NaNO_3$)	0.5 M HCl	room	$t_{1/2} \approx 600$ h; autocatalytic; rapid in 16 M HNO_3	Connick (1954)
HNO_2	~0.05	2 M HNO_3	16	$k'' = (0.88 \pm 0.03)$ $[HNO_2]^{0.5}[H^+]^{0.5}[NO_3^-]^{0.4}$ M^{-1} min^{-1} E_a (16–32°) = (55.8 ± 3.4) kJ mol^{-1} net reaction is the HNO_2 catalyzed oxidation of Pu(III) by HNO_3	Koltunov and Marchenko (1973) and Newton (2002)
Pu(IV)	3×10^{-6}	2 M (H,Li)ClO_4	25	$k'' = 6.4 \times 10^4$ $[H^+]^{-1}$ M^{-1} s^{-1} $E_a = (31 \pm 5)$ kJ mol^{-1} also studied in Cl^- and SO_4^{2-} solutions	Keenan (1957) Nikitenko and Ponomareva (1989)
Pu(V)	1.3×10^{-3}	2 M (H,Na)NO_3	38	$k'' = (k + k_1[NO_3^-][H^+])$ M^{-1} s^{-1} $k_o = (0.21 \pm 0.09)$ M^{-2} s^{-1} $k_1 = (0.59 \pm 0.07)$ M^{-3} s^{-1}	Koltunov and Mikhailova (1977) and Newton (2002)
Pu(VI)	10^{-4}	1 M $HClO_4$	25	$k'' = 2.68[H^+]^0$ M^{-1} s^{-1} $\Delta H^* = (20.2 \pm 0.4)$ kJ mol^{-1}	Rabideau and Kline (1958) Alei *et al.* (1967)
Pu(IV) oxidation					
HNO_3	1–5	HNO_3	90	steady-state Pu(IV)–Pu(VI) concentrations reached in about 1 d. Fraction Pu(VI) at the steady state is given by $0.11([Pu(IV)]_0)^{-0.61}$ $([HNO_3])^{-0.74}$	Glazyrin *et al.* (1989)

O_3		1 M $(H,Na)NO_3$	20	$k = (1.32 \pm 0.13) \times 10^{-2}\ [O_3]^0[H^+]^{-1}\ min^{-1}$ $[Pu(IV)] = 10^{-6}$–10^{-5} M $E_a = (19 \pm 5)$ kJ mol^{-1}	Vyatkin *et al.* (1972)
Pu(V) oxidation					
Ce(IV)	6×10^{-5}	2 M $HClO_4$	23	very rapid; $k'' > 7 \times 10^5\ M^{-1}\ s^{-1}$	Newton and Burkhart (1971)
O_2	1 atm	4 M NaOH	25 ± 2	$k = 4.5 \times 10^{-4}\ min^{-1}$	Budantseva *et al.* (1998)
Pu(IV) reduction					
Fe(II)	2×10^{-3}	2 M $(H,Li)ClO_4$	20	$k'' = 27[H^+]^{-1}\ M^{-1}\ s^{-1}$ $E_a = (82 \pm 2.5)$ kJ mol^{-1}	Newton and Cowan (1960)
$H_2C_2O_4$ oxalic acid	0.04 excess Pu(IV)	5 M $(H,Na)NO_3$	98	$k'' = \dfrac{0.215}{[Pu(IV)] + [H^+]^2/K}\ M^{-1}\ min^{-1}$ $K = 86.8$ M $= [PuC_2O_4^{2+}][H^+]^2/[Pu^{4+}][H_2C_2O_4]$ (recalculated from the original data)	Newton (2002)
H_2O_2	~0.01	2 M $(H,Na)NO_3$	25	$k'' = (11.9 \pm 1.0)[H^+]^{-1}[NO_3^-]^{-1}$ E_a (15–45°) $= (95.5 \pm 3.8)$ kJ mol^{-1}	Koltunov *et al.* (1981a)
H_2O_2	7.9×10^{-4}	0.5 M HCl	25	$t_{1/2} = 64$ min (excess H_2O_2) complicated by rapid formation of Pu(IV)–H_2O_2	Mazumdar *et al.* (1970)
NH_3OH^+	~0.1	2.5 M $(H,Na)(NO_3,ClO_4)$	25	$k'' = 13.7/[[H^+]^2\ (1 + [NO_3^-]/0.35)]\ M^{-1}\ s^{-1}$ E_a (25–45°) $= (120 \pm 8)$ kJ mol^{-1} for approach to equilibrium in the reaction: $Pu(IV) + NH_3OH^+ = Pu(III) + NHOH\bullet + 2H^+$	Barney (1976)

Table 7.52 (*Contd.*)

Agent	*Concentration* (M)	*Solution*	*Temperature* (°C)	*Results*	*References*
			30	$-d[Pu(IV)]/dt = (0.27 \pm 0.07)\left(\frac{[Pu(IV)][NH_3OH^+]}{[Pu(III)][H^+]^2(1+[NO_3^-]/0.33)}\right)^2$ M min^{-1} E_a (30–45°) = (186 ± 8) kJ mol^{-1} after equilibrium established	
NH_3OH^+ oxidized to N_2	0.2	3 M HNO_3	30	$-d[Pu(IV)]/dt = (0.195 \pm 0.013)\left(\frac{[Pu(IV)][NH_3OH^+]}{[Pu(III)][H^+]^2(1+[NO_3^-]/0.33)}\right)^2$ M min^{-1} E_a (30–45°) = (205 ± 3) kJ mol^{-1} after equilibrium established	Koltunov and Zhuravleva (1978)
Pu(IV) (disproportionation)	1×10^{-2}	1 M (H,Na)ClO_4	25	$-d[Pu(IV)]/3dt = [Pu^{4+}]^2(2.56 \times 10^{-5}\,[H^+]^{-3} + 3.9 \times 10^{-6}\,[H^+]^{-4})$ M s^{-1} also studied in HNO_3 solutions	Rabideau (1953) Artyukhin *et al.* (1959)
Pu(V) reduction					
ascorbic acid $C_6H_8O_6$	0.02	2 M (H,Na)ClO_4	25	$k' = (4.2 \pm 0.4)10^{-2}[H^+]^{1.2}$ M^{-1} min^{-1} E_a (25.1–44.9°) = (57.3 ± 6.3) kJ mol^{-1}	Koltunov *et al.* (1980a)
		4 M (H,Na)ClO_4	25	$k' = (7.4 \pm 0.5)10^{-2}[H^+]^{2.2}$ M^{-1} min^{-1} *note*: the reaction studied occurs in parallel with the reduction of Pu(V) by Pu(III). Pu(III) is the final product	

Pu(V)	$\sim 10^{-3}$	1 M $(H,Na)ClO_4$	25	$k'' = 3.6 \times 10^{-3}\ [H^+]\ M^{-1}\ s^{-1}$ $\Delta H^* = (79 \pm 4)$ kJ mol^{-1}	Rabideau (1957)
	5.3×10^{-4}	3.3 M NaOH	22	$k'' = 0.024\ M^{-1}\ s^{-1}$ E_a (10–30°) = 88 kJ mol^{-1}	Shilov (1997)
Pu(VI) reduction					
EDTA	2×10^{-3}	1 M $NaClO_4$ pH 3–5	room	$k'' = 4.3 \pm 1.6\ M^{-1}\ s^{-1}$	Kabanova *et al.* (1960)
Fe(II)	4×10^{-5}	2 M $(H,Li)ClO_4$	25	$k'' = 1000 + (2 \times 10^{-4} + 1.3 \times 10^{-3}\ [H^+])^{-1}\ M^{-1}\ s^{-1}$ evidence for a binuclear intermediate $E_a = (22.6 \pm 0.8)$ kJ mol^{-1} for first rate constant	Newton and Baker (1963) and Beitz *et al.* (1986)
HNO_2	0.027	0.55 M $(H,Na)NO_3$	20	$k'' = (2.4 \pm 0.2)/[H^+]\ M^{-1}\ min^{-1}$	Koltunov and Zhuravleva (1968)
	0.02	2 M $(H,Na)NO_3$	22	(a) forward reaction $k'' = (10.55 \pm 0.86)/[H^+]\ M^{-1}\ min^{-1}$ E_a (8–30°) = (111 ± 2) kJ mol^{-1} (b) reverse reaction $k'' = (9.63 \pm 0.42)\ \dfrac{[NO_3^-]^{0.4}[H^+]^{0.6}}{[HNO_2]^{0.5}}\ M^{-1}\ min^{-1}$ E_a (8–30°) = (92 ± 3) kJ mol^{-1}	Koltunov and Ryabova (1980)
NH_3OH^+	0.016	3 M $(H,Na)ClO_4$	60	$k'' = (4.22 \pm 0.12)/[H^+]\ M^{-1}\ min^{-1}$ $E_a = (78 \pm 2)$ kJ mol^{-1}	Koltunov *et al.* (1981b)

Table 7.52 (*Contd.*)

Agent	*Concentration* (M)	*Solution*	*Temperature* (°C)	*Results*	*References*
$N_2H_5^+$	0.02	2 M (H,Na) (NO_3,ClO_4)	40	$k'' = (0.314 \pm 0.042)$ $[H^+]^{-1}[NO_3^-]^0$ M^{-1} min^{-1} $-d[Pu(VI)]/dt = k_a[Pu(VI)]\left(\frac{[N_2H_5^+]}{[H^+]}\right)^{0.85}$ $k_a = (0.243 + 0.024)$ min^{-1} $E_a = (67.4 \pm 0.8)$ kJ mol^{-1} for either rate law	Koltunov and Zhuravleva (1973) and Newton (2002)
EDTA	2×10^{-3}	1 M $NaClO_4$; pH 3–5	room	$k'' = 4.3 \pm 1.6$ M^{-1} s^{-1}	Kabanova *et al.* (1960)

surface of the metal may be removed electrochemically (Bergstresser, 1950) or mechanically. The standard potential for the three-electron oxidation of α-Pu metal is –(2.000 ± 0.009) V (Lemire *et al.*, 2001). Alternatively, plutonium in higher oxidation states in acid solutions may be reduced electrolytically using either a mercury or platinum cathode. The potential should be about 0.75 V (vs NHE) or less (Cohen, 1961a). Chemical reductants such as hydroxylamine or hydrazine may also be used, but these are generally less satisfactory because the oxidized form of the reducing agent is often left in the solution. The Pu(III) aquo ion imparts a blue or blue-violet color to aqueous acidic solutions and exhibits hydrolysis, complexation, and solubility properties similar to the rare-earth ion neodymium(III).

In solutions of noncomplexing acids, Pu(III) is stable with respect to reaction with the oxygen in air. However, in dilute sulfuric acid, for example, the reaction occurs at a conveniently measurable rate (Newton and Baker, 1956). At a pH of 4, Pu(III) is slowly oxidized but at pH values greater than about 4 or 5, or in 0.4 M $NaHCO_3$, Pu(III) is rapidly oxidized by atmospheric oxygen (Newton *et al.*, 1986a). For ^{239}Pu, α-particle induced oxidation occurs in $HClO_4$ solutions at a rate of about 1.5% per day, approaching a steady state containing about 10% Pu(IV) and 90% Pu(III) (Rabideau *et al.*, 1958). In HCl solutions the α-particle induced oxidation proceeds to nearly pure Pu(IV) (Newton *et al.*, 1986a).

Pu(IV). Solutions of Pu(IV) are conveniently prepared by the electrolytic oxidation of Pu(III) at about 1.2 V. At this potential Pu(VI) is thermodynamically stable, but its rate of formation is insignificant due to the slow kinetics of forming the Pu=O bond (Cohen, 1961a). Alternatively, Pu(IV) may be prepared by reacting Pu(III) with Pu(VI) according to the equation:

$$2Pu^{3+} + PuO_2^{2+} + 4H^+ \rightleftharpoons 3Pu^{4+} + 2H_2O \qquad (7.86)$$

This reaction is the reverse of the Pu(IV) disproportionation reaction (equation 7.75), and the equilibrium constant is approximately 112 in 1 M $HClO_4$ solution at 25°C (Rabideau, 1953), so at equilibrium under these conditions as much as 28% of the plutonium will be in other oxidation states. Higher acid concentrations or the presence of complexing anions such as chloride will give larger fractions of Pu(IV). This is why it is a common practice to prepare and store Pu(IV) solutions in 3 M HCl (Newton *et al.*, 1986a). Acidic solutions of Pu^{4+} that are free of complexing agents are orange-brown or tan in color.

In acid solutions Pu(IV) is thermodynamically unstable with respect to reaction with oxygen, but the rate of this reaction is negligible. In $HClO_4$, α-particle induced reduction occurs to give the same steady state as described for Pu(III). In HCl solutions, however, Pu(IV) is significantly stabilized (Rabideau *et al.*, 1958). Newton *et al.* (1986a) found that stock solutions of Pu(IV) in about 3 M HCl are stable for many months. Even in 1 M acid, Pu(IV) hydrolyzes appreciably, and, at pH values greater than about 1, significant formation of green colloidal Pu(IV) hydroxide occurs. The rate of colloid formation depends on the plutonium concentration as well as the pH. Rates under specific conditions

have been described (Costanzo *et al.*, 1973; Toth *et al.*, 1981; Newton and Rundberg, 1984). Complexation constants for tetravalent plutonium are among the highest for any cation of any element, being most similar to those of Th(IV), U(IV), and Np(IV).

Pu(V). Solutions of Pu(V) are conveniently prepared by the electrolytic reduction of 0.02 M Pu(VI) in $HClO_4$ solution at pH near 3. A potential close to 0.54 V (vs SCE) is suitable (Cohen, 1961a). In most preparations it is necessary to readjust the pH during electrolysis because hydrogen ions are transported from the counter electrode compartment (Newton *et al.*, 1986a). The use of a photochemically produced reducing agent in a two-phase system has also been described (Choppin and Saito, 1984). The PuO_2^+ ion imparts a pink or light purple color to aqueous solutions, has a low effective charge and undergoes hydrolysis only at higher pH (approximately pH = 9 for millimolar plutonium).

In acid solution Pu(V) disproportionates with the reaction rate proportional to the fourth power of the hydrogen ion concentration and the square of the Pu(V) concentration (Rabideau, 1957). Thus both the thermodynamics and the kinetics favor Pu(V) at low acidities. However, α-radiolysis effects, even at pH values greater than 3, cause fairly rapid formation of colloidal Pu(IV) and Pu(VI) (Newton *et al.*, 1986b). These effects are more pronounced at higher Pu(V) concentrations, and less pronounced at low concentrations. Pu(V) can persist in near-neutral pH solutions when the total plutonium concentration is very low ($<10^{-6}$ M), as may be the case in slightly-contaminated natural waters and some waste solutions.

Pu(VI). Solutions of Pu(VI) are conveniently prepared by oxidation with hot, concentrated $HClO_4$ (Newton *et al.*, 1986a). Plutonium ions in lower oxidation states, in the absence of coordinating anions are oxidized to Pu(VI) by fuming strongly with $HClO_4$. The remaining free acid may be estimated gravimetrically and traces of chlorine oxides can be removed by boiling the diluted solutions. Acidic solutions of PuO_2^{2+} in the absence of complexing agents are yellow or orange in color. Hexavalent plutonium nitrate can also be generated by heating nitric acid solutions of plutonium almost to dryness at about 170°C. A glassy solid results after cooling the nitrate melt that is a very stable storage form for Pu(VI) and is readily soluble in aqueous solutions (Stoll *et al.*, 1982).

In $HClO_4$ solutions Pu(VI) is unstable with respect to α-particle induced reduction. With millimolar or greater plutonium concentrations, at pH values between about 0 and 2, the rate of reduction is about 1.2 to 2% of the total plutonium per day (Rabideau *et al.*, 1958; Newton *et al.*, 1986b). At very low plutonium concentrations (2.2×10^{-5} M) the rates are much slower. It has also been reported that chloride ions inhibit the α-reduction of Pu(VI) in analogy with Pu(IV) (Rabideau *et al.*, 1958).

Pu(VII). Blue-black heptavalent plutonium is the least stable oxidation state, prepared by vigorous oxidation of highly alkaline solutions of hexavalent plutonium. In alkali solutions, ozonization, anodic oxidation or treatment with peroxydisulfate, or other strong oxidants can produce the heptavalent form (Komkov

et al., 1969; Krot *et al.*, 1976; Tananaev *et al.*, 1992). The high formal potential of Pu(VII) puts it outside the region of thermodynamic stability of water for hydroxide concentrations less than about 7 M, and heptavalent plutonium is instantly reduced in acid solutions. This plutonium ion is less stable than the heptavalent neptunium analog (Varlashkin *et al.*, 1984; Tananaev *et al.*, 1992).

(*vi*) *Pu(VI) oxygen exchange with solvent water*

Masters and Rabideau (1963) measured the rate of exchange between PuO_2^{2+} and ^{18}O-enriched water in dilute $HClO_4$ solution. The studies were conducted under chlorine atmosphere to ensure that Pu(VI) was the only oxidation state present. This was done because the rate of exchange was found to be accelerated by the presence of lower oxidation states of plutonium in the solutions (Rabideau and Masters, 1963). Like the exchange for the uranyl ion (Gordon and Taube, 1961), the exchange rate was found to be extremely slow with a half-time of 4.55×10^4 h at 23°C. The exchange rate was found to be the sum of the rates of two separate reaction paths that include the intrinsic $PuO_2^{2+} - H_2^{18}O$ exchange reaction and the exchange induced by the breaking of Pu=O bonds by α-particle reduction. Studies employing ^{238}Pu demonstrated that the exchange rate was much faster than with ^{239}Pu, and extrapolation of the rates to the flux conditions of ^{239}Pu solutions suggested a half-time for radiation-induced exchange of about the same order of magnitude (approximately 10^4 h). This was interpreted as indicating that in 0.15 M Pu(VI) solution, the major contribution to the exchange is from radiation-induced reaction, and that the rate of the intrinsic exchange reaction is even slower.

(*vii*) *Oxidation and reduction by actinide ions*

These reactions have been studied primarily in acidic solutions because hydrolysis and precipitation of these high-valent metal ions limit their solubility at higher pH values. Most of the actinide separations and processing technology has been developed in acid solutions motivating much of the quantitative study of plutonium redox reactions. An important subset of these reactions has been described by Newton (2002) and is given in Table 7.53. The use of catalysts to enhance the rate of reactions has also been studied for plutonium both to accomplish process steps more rapidly on an industrial scale and to determine rate constants that are otherwise difficult to determine because of back reactions, competing reactions, or other complications (Newton, 1975).

The redox reactions between plutonium and other actinides are important because they are applicable to many aqueous solutions used in separation processes and waste operations. These reactions are also useful because the reactions involving ions with similar structures but different reduction potentials can be compared. For example, the rates of reactions (reaction 3 through

Table 7.53 *Thermodynamic constants for plutonium-actinide redox reactions at* 25°C (*Newton,* 2002).

	ΔG (kJ mol^{-1})	ΔH (kJ mol^{-1})	ΔS (J K^{-1} mol^{-1})	k'' (M^{-1} s^{-1})	I (M)	ΔG^* (kJ mol^{-1})	ΔH^* (kJ mol^{-1})	ΔS^* (J K^{-1} mol^{-1})	*References*
1. $Pu^{3+} + NpO_2^{2+} \rightleftarrows Pu^{4+} + NpO_2^+$									
	−15.1	−60.7	−153	$35.5 + 3.1\ [H^+]^{-1}$	1.0	64.2	14.6	−166	Fulton and Newton (1970)
2. $Pu^{3+} + PuO_2^{2+} \rightleftarrows Pu^{4+} + PuO_2^+$									
	6.3	−35.6	−140	2.7	1.0	70.5	20.2	−169	Rabideau and Kline (1958)
3. $2Pu^{4+} + 2H_2O \rightleftarrows Pu^{3+} + PuO_2^+ + 4H^+$									
	18.2	121	344	$2.9 \times 10^{-5}\ [H^+]^{-3}$	1.0	101.0	154.5 ± 0.5	180 ± 2	Lavallee and Newton (1972)
				$4.4 \times 10^{-2}\ [H^+]$[a]	1.0	80.8	33.5 ± 0.5	-158 ± 2	
4. $Np^{4+} + Pu^{4+} + 2H_2O \rightleftarrows NpO_2^+ + Pu^{3+} + 4H^+$									
	−23.4	92	387	$0.253\ [H^+]^{-3}$	2.0	76.6	142 ± 6	218 ± 21	Rykov *et al.* (1969)[b]
				$2.2 \times 10^{-5}[H^+]$	1.0	99.6	50	-167 ± 21	
5. $U^{4+} + Pu^{4+} + 2H_2O \rightleftarrows UO_2^+ + Pu^{3+} + 4H^+$									
	−36.4	68.5	352	$34.4\ [H^+]^{-2}$	2.0	64.3	102 ± 2.5	126 ± 8	Newton (1959)
				$1.9 \times 10^{-5}\ [H^+]^2$	1.0	100	33.1	-216 ± 8	

6. $U^{4+} + PuO_2^{2+} + 2H_2O = UO_2^{+} + PuO_2^{+} + 4H^{+}$								
	−30.0	33	213	$[(4.35[H^+]^{-1})^{-1} + (11.25[H^+]^{-2})^{-1}]^{-1}$	2	69.5	73.6 ± 0.4	15 ± 2	Newton (1958)
						66.9	88.8 ± 1.2	74 ± 5	
6a. $PuO_2^{2+} + U^{4+} + H_2O = [PuO_2(UOH)^{*}]^{5+} + H^{+}$									
	69.5	73.6	14 ± 2		2			−368	Newton (1958)
6b. $PuO_2^{2+} + U^{4+} + H_2O = [PuO_2(UO)^{*}]^{4+} + 2H^{+}$									
	66.9	89.1	75 ± 5		2			−303	Newton (1958)
7. $Np^{4+} + PuO_2^{2+} + 2H_2O \rightleftarrows NpO_2^{+} + PuO_2^{+} + 4H^{+}$									
	−17.1	56.5	247	$3.5 \times 10^{-4}\,[H^+]^{-2}$	1.0	92.76	130 ± 4	126 ± 13	Newton and Montag (1976)
				$8.8 \times 10^{-6}\,[H^+]^{-3}$	1.0	102	168 ± 8	222 ± 25	
8. $Pu^{4+} + PuO_2^{2+} + 2H_2O \rightleftarrows PuO_2^{+} + 4H^{+}$									
	24.5	85.3	204	$1.2 \times 10^{-7}\,[H^+]^{-3}$	2	112.5	164	172	Rabideau (1957)[c]
				$3.6 \times 10^{-3}\,[H^+]$[a]		87.0	79 ± 11	25 ± 38	

[a] The reaction was measured in the opposite direction, with the result given here.
[b] An estimate for the reverse reaction.
[c] Calculated from the reverse reaction.

8 in Table 7.53) that involve the making of An=O bonds as An^{4+} is oxidized to AnO_2^+ differ by orders of magnitude for the different elements. Four hydrogen ions are produced in the overall reaction, but only two or three are given up in the activation processes. The rate laws for oxidation of U^{4+} and Np^{4+} by PuO_2^{2+} show consecutive rate-determining steps of which only one or two can be redox reactions. This reaction is described below for U^{4+}, as an illustration of the importance of considering multiple intermediates and pathways.

The reaction between U^{4+} and PuO_2^{2+} proceeds through AnO_2^+ intermediates, and in acid solution leads eventually to Pu^{3+} (Newton, 1958, 1975). In dilute solutions (1.8×10^{-4} M Pu(VI) and 0.62×10^{-4} M U(IV) in 1 M $HClO_4$), approximately 96% of the U(IV) reacts according to the following equation:

$$2\text{Pu(VI)} + \text{U(IV)} \rightarrow 2\text{Pu(V)} + \text{U(VI)} \tag{7.87}$$

The remaining U(IV) reacts according to

$$\frac{2}{3}\text{Pu(VI)} + \text{U(IV)} \rightarrow \frac{2}{3}\text{Pu(III)} + \text{U(VI)} \tag{7.88}$$

Equations 7.87 and 7.88 only represent the change in oxidation states of the actinides but do not account for the overall stoichiometry. The reaction rates, as studied by spectrophotometric monitoring of the concentration of Pu(VI), are consistent with the rate law:

$$-\frac{\text{d[Pu(VI)]}}{\text{d}t} = 2k''[\text{Pu(VI)}][\text{U(IV)}] \tag{7.89}$$

This requires that the activated complexes be formed from one Pu(VI) and one U(IV), probably according to the reaction

$$\text{Pu(VI)} + \text{U(IV)} \rightarrow \text{Pu(V)} + \text{U(V)} \tag{7.90}$$

followed by the rapid reaction

$$\text{Pu(VI)} + \text{U(V)} \rightarrow \text{Pu(V)} + \text{U(VI)} \tag{7.91}$$

Steady-state calculations show that U(V) disproportionation into U(VI) and U(IV)

$$2\text{U(V)} \rightarrow \text{U(IV)} + \text{U(VI)} \tag{7.92}$$

is too slow to account for the disappearance of U(V) and is unimportant with respect to reaction (7.91). Under these conditions (1 M $HClO_4$) the U(IV) undergoes hydrolysis, while Pu(VI) does not. Thus

$$[\text{U(IV)}] = [U^{4+}](1 + K/[H^+]) \tag{7.93}$$

and

$$[\text{Pu(VI)}] = [PuO_2^{2+}] \tag{7.94}$$

where K is the first hydrolysis constant for U(IV). In terms of the species present, the rate law (7.89) becomes

$$-\frac{\mathrm{d}[\mathrm{Pu(VI)}]}{\mathrm{d}t} = 2k''\left(1+\frac{K}{[\mathrm{H^+}]}\right)[\mathrm{PuO_2^{2+}}][\mathrm{U^{4+}}] \tag{7.95}$$

The hydrogen-ion dependence as a function of temperature suggests that the most important activated complex is that formed by the prior loss of H^+, and that a second activated complex resulting from the loss of two H^+ ions may also be involved. The decrease in the apparent H^+ dependence with decreasing $[H^+]$ is not consistent with parallel rate-determining steps, but suggests consecutive reactions (6a and 6b in Table 7.53) instead.

From the linearity of $\{k''([H^+] + K)\}^{-1}$ vs $[H^+]$ for the data at each temperature (k_1 and k_2 are rate constants distinct from k' or k''). Newton arrived at the following rate law:

$$-\frac{\mathrm{d}[\mathrm{Pu(VI)}]}{\mathrm{d}t} = \frac{2[\mathrm{Pu(VI)}][\mathrm{U(IV)}]}{1+K/[\mathrm{H^+}]}\left(\frac{1}{k_1[\mathrm{H^+}]^{-1}}+\frac{1}{k_2[\mathrm{H^+}]^{-2}}\right)^{-1} \tag{7.96}$$

The rate law (7.96) governs many detailed mechanisms, all of which require a binuclear intermediate that can react to give products or dissociate to give reactants at rates that depend on $[H^+]$. A simple mechanism consistent with the rate law is:

$$\mathrm{U^{4+}} + \mathrm{H_2O} \rightarrow \mathrm{UOH^{3+}} + \mathrm{H^+} \quad \text{(rapid equilibrium)} \tag{7.97}$$

$$\mathrm{UOH^{3+}} + \mathrm{PuO_2^{2+}} \rightleftarrows \mathrm{PuO_2(UOH)^{5+}} \quad \text{(rate-determining, reversible)} \tag{7.98}$$

$$\mathrm{PuO_2(UOH)^{5+}} \rightarrow \mathrm{PuO_2(UO)^{4+}} + \mathrm{H^+} \quad \text{(rapid equilibrium)} \tag{7.99}$$

$$\mathrm{PuO_2(UO)^{4+}} + \mathrm{H_2O} \rightarrow \mathrm{UO_2^+} + \mathrm{PuO_2^+} + 2\mathrm{H^+} \quad \text{(rate-determining)} \tag{7.100}$$

The two net activation processes required by the rate law do not depend on the details of the mechanism. The activation parameters ΔG^*, ΔH^*, and ΔS^* for these processes as determined from simultaneous treatment of the hydrogen ion and temperature data are listed in Table 7.53 under reactions 6a and 6b. For a more detailed discussion of redox reactions between plutonium and other actinide ions, the reader is referred to Newton (2002).

(*viii*) *Oxidation and reduction by nonactinide species*

Plutonium ions are well known to undergo redox reactions with ions of almost every element in the periodic table and many inorganic and organic redox reagents. Almost all of the redox reactions of aqueous plutonium ions are first order in the oxidizing or reducing agent, but some are either inhibited or catalyzed by the reaction products. The rates are often strongly influenced by

the concentration of H^+ and of complexing ligands. For example, reductions using synthetic and natural organic acids, such as oxalic, ascorbic, hydroxamic, and humic acids are pH dependent with rates that generally increase with increasing [H^+] (Cleveland, 1979; Choppin *et al.*, 1986; Nikitenko, 1988; Czerwinski and Kim, 1997; Ruggiero *et al.*, 2000; Moulin and Moulin, 2001; Taylor *et al.*, 2002). Common strong oxidizing agents that are relatively poor ligands for the actinides, such as dichromate, bromate, and iodate, have comparatively rapid plutonium oxidation rates (Newton, 1975). A large body of empirical observations has been accumulated on the oxidation–reduction behavior of plutonium with various reagents, while quantitative data are available for a relatively small subset. Since among plutonium ions, Pu(IV) forms the strongest complexes, redox reactions of the other ions can be interpreted using similar but simplified reactions and rate laws.

There is a broad qualitative relation between the rates of redox processes and the particular plutonium ions involved. Generally, the reactions of Pu^{4+} with single-electron reductants, such as Fe^{2+}, are rapid. The oxidation of Pu^{3+} or the reduction of Pu^{4+} with two-electron reagents is expected to be slower, although the variation in rate for different reagents varies from slow to a rate too fast to measure. A similar situation exists for one-electron reduction of PuO_2^{2+} to PuO_2^{+}. In contrast, reactions that make or break Pu=O multiple bonds are inherently slower. Multielectron processes, such as Pu^{4+} oxidation to PuO_2^{2+}, can proceed in one two-electron step or two one-electron steps. Oxidation of Pu^{4+} or reduction of PuO_2^{+} can generally proceed by direct reaction with the oxidizing or reducing agent, or by oxidation or reduction through the disproportionation reaction. Reactions of plutonium ions are further complicated in that slight changes in solution conditions can profoundly affect the rate and even the direction of the reaction, particularly for Pu^{4+}, owing to its tendency to form multiple stable molecular complexes. For example, reactions in sulfuric acid or carbonate media may take a different course or proceed at a different rate compared to those in perchlorate solutions. Early observations on the redox behavior of plutonium that were made on tracer level concentrations before all of the oxidation states had been well established cannot be applied directly to higher concentrations without reservations. Many of those experiments were qualitative, designed to determine whether reactions were complete or not, and will not be discussed here. A few important systems that relate to plutonium processing and also illustrate particular details of plutonium chemistry will be described here, including reactions with ferrous ion, nitrate, nitrite, hydroxylamine, and hydrogen peroxide. For additional detailed information or lists of reactions and rates, the reader is directed to reviews by Newton (2002) and Cleveland (1979), and general references that contain oxidation and reduction potentials (Wick, 1980).

The multistep reduction of Pu(VI) by Fe(II) is important in fuel reprocessing and has complicated mechanisms and rate laws that were described by Newton (1958, 2002).

When Fe(II) is added to an excess of Pu(VI), the predominant reaction is

$$PuO_2^{2+} + Fe^{2+} \rightarrow PuO_2^{+} + Fe^{3+} \tag{7.101}$$

Using a 60% excess of Pu(VI), Newton (1958) found that for each mole of Fe(II) oxidized approximately one mole of Pu(VI) was reduced as the acid concentration was varied from 2.0 to 0.05 M. Although Fe(II) is capable of reducing Pu(VI) all the way to Pu(III), appreciable amounts of Pu(IV) are observed, even if an excess of Fe(II) is used.

In addition to Pu^{4+} disproportionation, the following reactions were found to be important:

$$PuO_2^{+} + Fe^{2+} + 4H^{+} \rightarrow Pu^{4+} + Fe^{3+} + 2H_2O \tag{7.102}$$

$$Pu^{4+} + Fe^{2+} \rightarrow Pu^{3+} + Fe^{3+} \tag{7.103}$$

From sets of individual reactions in which the pH, then ionic strength, then metal ion concentrations were varied, Newton and Baker (1963) found the following rate law:

$$-\frac{d[PuO_2^{2+}]}{dt} = \{A + (B + C[H^{+}])^{-1}\}[PuO_2^{2+}][Fe^{2+}] \tag{7.104}$$

The necessity of three parameters in the rate law equation indicates three rate-determining steps and three important activated complexes. The above three-parameter equation may be rearranged to give

$$-\frac{d[PuO_2^{2+}]}{dt} = A[PuO_2^{2+}][Fe^{2+}] + \left(\frac{1}{B^{-1}[PuO_2^{2+}][Fe^{2+}]} + \frac{1}{C^{-1}[PuO_2^{2+}][Fe^{2+}]/[H^{+}]}\right)^{-1} \tag{7.105}$$

In this equation, parameter A is associated with the path that leads directly to products, and the B and C terms involve consecutive reactions that parallel the direct reaction. Newton and Baker found several mechanisms that were consistent with the data. All involve the same three activated complexes formed in both consecutive and parallel paths, as well as PuO_2^{2+} hydrolysis.

Plutonium reduction and oxidation reactions in nitric acid solutions have been extensively studied. Descriptions of Pu(IV) oxidation and reduction in nitrate solutions benefited from recent spectroscopic studies that measured the formation constants for two Pu(IV) nitrate species, $Pu(NO_3)_n^{4-n} (n = 1, 2)$ (Berg *et al.*, 2000). Complexation of Pu(IV) by nitrate can decrease the concentration of aquo Pu^{4+}, and thereby slow down the rates of some reactions, or it can provide additional reaction pathways for other reactions. For example,

reactions involving Pu(IV) either as a reactant or product with pentavalent metal ions are much faster in nitrate solutions than in perchlorate solutions. Conversely, oxidation of Pu(IV) by Ce(IV) or Np(VI) are both slower in HNO_3. Reductions of Pu(IV) are also generally slower in HNO_3 than in $HClO_4$ (Newton, 2002).

A great deal of information is available for Pu(IV) redox involving nitrous acid, hydroxylamine, and hydrazine in HNO_3, systems that are important for processing applications. Nitrous acid is commonly used to adjust the oxidation state of plutonium, both as a pure reagent and inadvertently as a contaminant in nitric acid. The key to understanding plutonium redox reactions in nitric and nitrous acid is that small equilibrium concentrations of NO_2 are present in HNO_2–HNO_3 mixtures. For example, although Pu(III) is quite stable in dilute nitric acid solutions, in the presence of HNO_2 it is readily oxidized to Pu(IV) by the following reaction:

$$2Pu^{3+} + 3H^+ + NO_3^- \rightleftarrows 2Pu^{4+} + HNO_2 + H_2O \qquad (7.106)$$

An empirical rate law and a plausible mechanism for the reaction were derived by Koltunov and Marchenko (1973). The oxidation may be retarded by the addition of a "holding reductant" to react with the HNO_2 as soon as it is formed. Effective reductants include sulfamic acid, ferrous sulfamate or hydrazine (Cleveland, 1979).

Plutonium(V) is reduced very slowly by nitrous acid (Koltunov *et al.*, 1982b). These studies consistently show that NO_2, formed by reaction of HNO_2 with HNO_3, is the important oxidant in the Pu(III) or Pu(V) oxidation by HNO_3. The rate of the following equilibrium reaction involving Pu(V) and Pu(VI) has been measured in both directions (Koltunov and Ryabova, 1980).

$$2PuO_2^{2+} + HNO_2 + H_2O \rightleftarrows 2PuO_2^+ + NO_3^- + 3H^+ \qquad (7.107)$$

Hydroxylamine and hydrazine are very useful reducing agents for all of plutonium's higher oxidation states, because they are nonmetallic, yield volatile oxidation products, and tend to react rapidly. These reactants are two-electron reducing agents, so one-electron oxidation leads to radical intermediates that can either decompose to stable products or be oxidized by plutonium and therefore influence the overall stoichiometry and the rate law. If the two one-electron oxidations occur at approximately the same rates, the stoichiometry will change during the course of the overall reaction and the rate laws will be very complicated. Additional redox agents and mechanistic complexity are added when the reduction of plutonium by these reagents is conducted in nitric acid solutions.

When hydroxylamine is oxidized by plutonium(IV), the two limiting overall reactions are (Barney, 1976):

$$2Pu^{4+} + 2NH_3OH^+ \rightleftarrows 2Pu^{3+} + N_2 + 4H^+ + 2H_2O \qquad (7.108)$$

and

$$2Pu^{4+} + NH_3OH^+ \rightleftarrows 2Pu^{3+} + 3H^+ + 0.5N_2O + 0.5H_2O \qquad (7.109)$$

The empirical rate law for the plutonium reduction by hydroxylamine in 2.5 M [(H, Na) (NO_3, ClO_4)] was found to be

$$-\mathrm{d}[\mathrm{Pu(IV)}]/\mathrm{d}t = [\mathrm{Pu}^{4+}]^2[\mathrm{NH_3OH}^+]^2/[\mathrm{Pu}^{3+}]^2[\mathrm{H}^+]^4(1+\beta_1[\mathrm{NO_3^-}])^2 \quad (7.110)$$

The factor $(1+\beta_1[\mathrm{NO_3^-}])$ is consistent with the formation of a nitrate complex. An independent investigation using 3 M (H,Na)NO_3 and large excess amounts of NH_3OH^+ gave results at 30°C that agreed reasonably well with the rate law and stoichiometries (Koltunov and Zhuravleva, 1978), yet the rate law does not account for higher nitrate complexes that are known to form when the $[NO_3^-]$ is greater than ~2–3 M (Berg *et al.*, 1998).

Yarbro *et al.* (1998) recently summarized past studies of Pu(IV) reduction by hydroxylamine and reported results with hydroxylamine nitrate (HAN) in the presence of excess plutonium. Rather than define the kinetic expression in terms of concentrations (although plausible mechanisms and complex stoichiometries were discussed), the following fractional conversion was defined:

$$X = 1 - (N_\mathrm{A}/N_{\mathrm{A}^0}) \quad (7.111)$$

where X is the fraction of compound reacted, N_{A^0} is the initial number of moles of the reactant A and N_A is the number of moles of reactant A at some time t. If acid and nitrate concentrations are constant, then the fractional conversion of HAN can be described as follows:

$$\begin{aligned} -\mathrm{d}X/\mathrm{d}t = {} & (kk_\mathrm{H}^{0.44}/C_{\mathrm{Pu}^0}[\mathrm{H}^+]^{0.56})([\mathrm{H}^+]^{0.65} \\ & + k_\mathrm{a}[\mathrm{NO_3^-}])[(1-X)/X]^2([\mathrm{HAN}_0] - C_{\mathrm{Pu}^0}X)^{0.44} \end{aligned} \quad (7.112)$$

where k is the kinetic constant; k_H is the dissociation constant for HAN; k_a is the dissociation constant for HNO_3; C_{Pu^0} is the initial plutonium molar concentration and $[\mathrm{HAN}_0]$ is the initial HAN molar concentration. This expression is useful at low HAN to plutonium molar ratios.

An improved understanding of this system and more broadly applicable rate law requires additional research, including quantitative evaluation of multiple plutonium nitrate complexes (beyond the 1:1 complex), the oxidation of HAN by nitric acid, the reoxidation of Pu(III) by nitrous acid, the disproportionation of Pu(IV), and, for solutions concentrated in Pu, radiolytic oxidation of Pu(III) and reduction of Pu(IV). The Pu(IV) hydroxylamine reaction has also been studied in perchlorate solutions using relatively high $[\mathrm{Pu(IV)}]_o/[\mathrm{NH_3OH}^+]_o$ ratios (Koltunov and Zhuravleva, 1978). These conditions favor the path in which the radical intermediate is oxidized to N_2O. Kinetic studies of Pu(IV) reduction by a derivatized hydroxylamine, where the reducing agent was present in molar excess of plutonium, showed similar dependencies on hydrogen ion and hydroxylamine concentrations (Anyun *et al.*, 2002).

The reduction of Pu(VI) by NH_3OH^+ has been studied in 3 M perchlorate solutions at temperatures near 60°C (Koltunov *et al.*, 1981b). When $[H^+]$ is

<0.55 M, the disproportionation of Pu(V) is relatively slow and the net reaction is probably as follows:

$$2PuO_2^{2+} + NH_3OH^+ \rightleftarrows 2PuO_2^+ + 3H^+ + 1/2N_2O + 1/2H_2O \qquad (7.113)$$

This reaction requires that a radical intermediate be oxidized by Pu(VI). The rate law was found to be

$$-d[Pu(VI)]/dt = 2k_0[PuO_2^{2+}][NH_3OH^+]/[H^+] \qquad (7.114)$$

This rate law is much simpler than the one for the reduction of Pu(IV), and shows that the rate-determining step is the initial formation of the radical intermediate. At higher $[H^+]$, the disproportionation of Pu(V) becomes important. The Pu(IV) formed is rapidly reduced by NH_3OH^+ to Pu(III), which in turn reacts rapidly with Pu(VI). These steps lead to the catalytic reduction of Pu(VI) by Pu(III). Thus, during the course of the reaction, the concentration of Pu(V) will increase to a maximum, then decrease as the concentration of Pu(III) increases. The complex rate laws for this system have been integrated numerically and give concentrations that are in good agreement with the experimental results (Koltunov *et al.*, 1981b).

The reduction of Pu(IV) by hydrazine has been studied in 2 M $(H,Na)NO_3$ (Koltunov and Zhuravleva, 1974). The limiting overall reactions are probably the following:

$$Pu^{4+} + N_2H_5^+ \rightleftarrows Pu^{3+} + NH_4^+ + H^+ + 1/2N_2 \qquad (7.115)$$

and

$$4Pu^{4+} + N_2H_5^+ \rightleftarrows 4Pu^{3+} + N_2 + 5H^+ \qquad (7.116)$$

The stoichiometric ratio was found to depend on the initial reactant concentrations, just as with hydroxylamine. At 50°C with a $[H^+]$ range between 0.5 and 1.9 M, the rate law for the Pu(IV)–hydrazine reaction was found to be

$$-d[Pu(IV)]/dt = k[Pu^{4+}][N_2H_5^+]/(K_h + [H^+]) \qquad (7.117)$$

This rate law shows that the rate-determining step is the formation of the radical intermediate ($N_2H_4\cdot$), not its subsequent reaction. The parameter K_h was interpreted as the hydrolysis constant for Pu(IV), but the 1:1 Pu(IV)–nitrate complex should be included in the rate law. An alternative explanation involves the formation of low steady-state concentrations of a plutonium–hydrazine intermediate (Newton, 2002). Additional kinetic studies of the reduction of Pu(IV) have been reported for substituted hydrazines, with similar overall reactions and small changes in reaction rates (Koltunov *et al.*, 1989).

The reduction of Pu(VI) by $N_2H_5^+$ was shown to have features similar to the reduction of Pu(IV) (Koltunov and Zhuravleva, 1973). The initial reaction is most probably

$$PuO_2^{2+} + N_2H_5^+ \rightleftarrows PuO_2^+ + NH_4^+ + 1/2N_2 + H^+ \qquad (7.118)$$

The final reaction product is Pu(III), which arises from the reduction of Pu(IV) described above. The reduction of Pu(V) to Pu(IV) occurs by two parallel pathways: direct reaction of Pu(V) with hydrazine, and comproportionation of Pu(VI) with Pu(III) to give Pu(IV). The kinetics of the reduction of Pu(V) by hydrazine as well as the use of the overall reductions in the nuclear fuel cycle have been described (Koltunov and Baranov, 1993). The rate law in 2 M Na (NO_3,ClO_4) was found to be approximately

$$-\mathrm{d}[\mathrm{Pu(VI)}]/\mathrm{d}t = k[\mathrm{PuO_2^{2+}}][\mathrm{N_2H_5^+}]/[\mathrm{H^+}] \tag{7.119}$$

The nitrate dependence was found to be zero in the range from 0.15 to 2 M at constant ionic strength. The reduction of Pu(VI) by substituted hydrazines has been shown to proceed with similar overall reactions, some differences in the exponents of the reactants in the rate equation, and small changes in reaction rates (Koltunov *et al.*, 2004).

Both fundamental research and process application of plutonium redox reactions with hydrogen peroxide are complicated by the incomplete characterization of molecular Pu(IV) and Pu(VI) complexes that form with peroxide, and the chemical and radiolytic complexities of plutonium–hydrogen peroxide mixtures. Recent studies indicate the utility of hydrogen peroxide reduction of Pu(VI) and mixtures of Pu(VI) and Pu(IV) on the mM scale by 0.3% H_2O_2 in the presence of extraction resins (Morgenstern *et al.*, 2002). Hydrogen peroxide is more commonly used to reduce Pu(VI) in nitrate solutions. Maillard and Adnet (2001) studied effects of acidity and plutonium and H_2O_2 concentrations on the kinetics of Pu(VI) reduction. The kinetics results generally showed an induction period where the [Pu(VI)] does not change, followed by a linear decrease of [Pu(VI)]. The length of the induction period depends on temperature, [HNO_3], and [H_2O_2], but not on the H_2O_2/Pu(VI) ratio. Total reduction time decreases with increasing [Pu(VI)] and [HNO_3] from 0.5 to 6 M [HNO_3], but increases when [HNO_3] varies from 6 to 8 M. Red-brown peroxo complexes were observed and PuO_2^+ was an intermediate in these reductions.

The kinetics of the reduction of ~1 mM PuO_2^+ by [H_2O_2] has been studied in 1.0 M NaCl solutions at near-neutral pH. The reduction was found to be first order with respect to [H_2O_2] and inverse first order with respect to [H^+] and described by the rate equation (7.119) with $k = 3.59$ to 1.79×10^{-9} $\mathrm{min^{-1}}$ (Morgenstern and Choppin, 1999).

$$\mathrm{d}[\mathrm{Pu(V)}]/\mathrm{d}t = k\,[\mathrm{PuO_2^+}][\mathrm{H_2O_2}]/[\mathrm{H^+}] \tag{7.120}$$

(*ix*) *Autoradiolysis*

When plutonium isotopes undergo radioactive decay in aqueous solution they deposit a great deal of energy (approximately 5 MeV per α particle) in α particle tracks that both heat the solution and produce ions, radicals, and solvated electrons. The predominant products generated by water radiolysis in the bulk

solution are H, OH, HO_2, and H_2O_2 (Spinks and Woods, 1990; Vladimirova and Kulikov, 2002). Under plutonium process conditions α radiation generates concentrations of these reactive species that can significantly affect individual stages of reactions as well as the final products. If solute concentrations (most commonly plutonium and nitrate) are less than approximately 1 M, then there will be little direct reaction between the α particles or the transient species and the solute within the tracks.

Reactive species that diffuse out of the alpha-tracks can act as either oxidizing or reducing agents for plutonium and other solutes. For example, in 0.4 M H_2SO_4, 0.53 μmol of Fe(II) is oxidized to Fe(III) per joule of deposited energy (Spinks and Woods, 1990), expressed as $G[\text{Fe(III)}] = 0.53$ μmol J^{-1}; whereas Ce(IV) is reduced with $G[\text{Ce(III)}] = 0.33$ μmol J^{-1} (Spinks and Woods, 1990). The G-values for the reduction of Pu(IV) or Pu(VI) in 1 M $HClO_4$, 0.36 – 0.03 μmol J^{-1}, are similar (for either oxidation state) to those for Fe(II) or Ce(IV) (Kasha, 1949; Newton, 2002). The reduction of Pu(IV) reaches a steady state in which its rate equals the rate of oxidation of Pu(III). At 4°C, the mean oxidation number was found to depend slightly on the total plutonium concentration and/or the dose rate, e.g. 3.05 in 0.022 M Pu, which corresponds to an energy deposition rate of 0.01 Sv L^{-1} (Rabideau *et al.*, 1958).

Plutonium radiolysis in nitrate solution was reviewed by Miner and Seed (1967). Recent research has emphasized the behavior of plutonium in HNO_3 solutions that have much higher dose rates. The results are complicated due to the formation of HNO_2, volatile NO_x, and H_2O_2. Andreichuk *et al.* (1990) studied the oxidation of Pu(III) to Pu(IV) in HNO_3 solutions by using radiation from *in situ* ^{244}Cm. This group first studied the formation of HNO_2 from HNO_3 by ^{244}Cm irradiation in the absence of plutonium (Andreichuk *et al.*, 1984b). These studies, where nitric acid concentrations and dose rates ranged up to 8.6 M and 11.5 W L^{-1}, respectively, showed initial rates of HNO_2 formation to be closely proportional to dose rate, with a yield of 0.21 μmol J^{-1} in 1.89 M HNO_3. A steady-state concentration of 6 mM HNO_2 was reached after 30 h with a dose rate of 3.2 W L^{-1}. In subsequent measurements of Pu(III) oxidation from a dose rate of 3.2 Gy s^{-1}, where $[\text{Pu(III)}]_0 = 10$ mM, and $[HNO_3] < 0.5$ M, steady state was reached within 1 h and approximately 15% of the plutonium had been oxidized. Small concentrations of a $\text{Pu(IV)} \cdot H_2O_2$ complex were observed. At higher acid concentrations, the peroxide complex was not detected and oxidation to Pu(IV) was complete. The reaction was observed to be autocatalytic; that is, initial rates were low but increased to a maximum when approximately one-half the Pu(III) had been oxidized. The corresponding radiation yields of Pu(IV) ranged up to approximately 5 μmol J^{-1} in 2.9 M acid. These yields were relatively high because Pu(III) is readily oxidized in the presence of HNO_2. Plutonium was oxidized further to Pu(VI), but only after no Pu(III) remained. The initial rates for the alpha-radiolytic oxidation of Pu(IV) were similarly found to be proportional to the concentration of the Pu(IV) multiplied by the dose rate

(Andreichuk *et al.*, 1979). For example, for 0.01 M $[Pu(IV)]_0$, the yield in 6 M HNO_3 is 0.00044 μmol W^{-1}.

The alpha-radiolytic reduction of Pu(VI) is much more complicated. Small steady-state concentrations of Pu(V) are formed initially, followed by the formation of HNO_2. Further reaction is autocatalytic because the Pu(V) disproportionation is catalyzed by both HNO_2 and Pu(IV) (Vladimirova, 1982). The Pu(VI)/Pu(IV) steady-state ratios were found to vary widely, depending on total plutonium concentration, HNO_3 concentration, and dose rate (Andreichuk *et al.*, 1979, 1984a,b). For example, a dose rate of 3.46 W L^{-1} in 1 M HNO_3 for plutonium concentrations of 2.1 and 14.8 mM yielded Pu(VI)/Pu(IV) ratios of 5.1 and 0.047, respectively. For 10 mM Pu in 6 M HNO_3, the dose rates of 1.4 and 13.8 W L^{-1} yielded Pu(VI)/Pu(IV) ratios of 0.76 and 3.15, respectively. Kinetic models for the rates of the radiolytic oxidation of Pu(IV) and the reduction of Pu(VI) have been presented by Vladimirova (1990, 1998) and Frolov *et al.* (1990). In a study designed to mimic conditions of dissolved nuclear fuel in nitric acid, Rance and Zilberman (2002) found that the addition of U and fission products to Pu(VI) solutions eliminates the induction periods for reduction. This study reported *G*-values of 0.6–1.1 for 3 g L^{-1} ^{239}Pu solutions that contained from 0.12 to 9.2% ^{238}Pu.

Haschke and Oversby have proposed an alternate disproportion reaction to explain the instability of Pu(VI) in aqueous solution that does not require water radiolysis (Haschke and Oversby, 2002; Haschke, 2005):

$$PuO_2^{2+} + 1/2H_2O \rightleftarrows PuO_2^{+} + H^{+} + 1/4O_2 \qquad (7.121)$$

Their proposed mechanism invokes the disproportionation of PuO_2^{2+} to produce PuO_2^{+} and heptavalent PuO_2^{3+}, followed by the water oxidation by PuO_2^{3+} to produce oxygen. The fact that PuO_2^{3+} has never been observed makes this mechanism doubtful. In a subsequent report, Newton and Hobart (2004) reiterate that below pH 6 the instability of Pu(VI) clearly results from reactions with reducing species produced by alpha radiolysis of water.

Chlorine is formed by radiolysis of HCl solutions, counteracting the processes that reduce plutonium, such that neither Pu(IV) nor Pu(VI) appear to be reduced in 1 M HCl (see discussion in Section 7.9.1.c(ii)). However, at lower chloride concentrations, alpha-reduction of $^{239}Pu(IV)$ does take place. Rabideau and Kline (1958) showed that *G*[Pu(III)] decreases from 0.36 in 1 M $HClO_4$ μmol J^{-1} to approximately 0.077 in 0.5 M HCl–0.5 M $HClO_4$. More recent experiments by Büppelmann *et al.* (1988) using higher chloride concentrations, more nearly neutral acid concentrations, and ^{238}Pu to give higher dose rates, show that Pu(IV) can be oxidized to Pu(V) or Pu(VI). With NaCl concentrations less than 3 M and dose rates of 0.15 W L^{-1}, the product is primarily Pu(V). Higher concentrations of NaCl and/or higher dose rates give Pu(VI). These reactions involve the oxidation of Pu(IV) hydroxide by HClO or ClO^{-}. The effect of dose rate on the reduction of Pu(VI) in $HClO_4$ is illustrated by the

Table 7.54 *Alpha-induced reduction of Pu(VI)* (*Newton,* 2002).

Pu(VI) (mM)	*Dose rate* (W L^{-1})	*Yield* (μeq J^{-1})	*Radiation source*	*References*
<2	<0.002	0.33–0.38	^{239}Pu	Rabideau *et al.* (1958)
1.1	0.15	0.04	^{238}Pu	Büppelmann *et al.* (1988)
1.4	4.16	0.0024	^{244}Cm and ^{239}Pu	Frolov *et al.* (1990)

results of experiments using ^{239}Pu, ^{238}Pu, and ^{239}Pu–^{244}Cm mixtures as summarized in Table 7.54. From the Table it is clear that the yield decreases as the dose rate increases.

(d) Hydrolytic stability of plutonium ions

The hydrolytic behavior of the plutonium ions has been the subject of many studies. This interest has been intensified by the practical importance of hydrolysis in the manipulation of plutonium solutions. This class of solution phenomena is as important in the chemistry of plutonium as it is for the actinide elements generally because of the existence of highly charged positive ions in aqueous solution. Hydrolysis leads to the formation of ionic species or precipitates by the action of water as illustrated in equation (7.122) for trivalent plutonium. While hydrolysis reactions are often written as in equation (7.122), hydrolysis is actually a complexation reaction with the hydroxide ion. Therefore, it is also common to express hydrolysis as a complex formation as indicated in equation (7.123). The hydrolysis constant $^*\beta$ (corresponding to equation (7.122)) is related to the formation constant β (equation (7.123)) by the ion product of water, K_w (Grenthe *et al.*, 1997).

$$Pu^{3+} + H_2O \rightleftharpoons Pu(OH)^{2+} + H^+ \tag{7.122}$$

$$Pu^{3+} + OH^- \rightleftharpoons Pu(OH)^{2+} \tag{7.123}$$

Characterization of the hydrolysis behavior of plutonium is the cornerstone of understanding its aqueous coordination chemistry, particularly the thermodynamic stability of complexes. The tendency to undergo hydrolysis increases with the charge/size ratio of the ion. Therefore hydrolysis is most pronounced for Pu^{4+}, and the least pronounced for PuO_2^+. The tendency for hydrolysis follows the general order

$$Pu^{4+} > PuO_2^{2+} \approx Pu^{3+} > PuO_2^+$$

Plutonium ions hydrolyze readily and thereby limit both the stability fields of individual aquo ions and the overall solubility of plutonium ions in aqueous

solution. At the extreme end of the spectrum, Pu(IV) hydrolyzes even in pH 1 solutions and can form complicated polymeric (or colloidal) hydroxides and precipitates (Lemire *et al.*, 2001; Neck and Kim, 2001; Rothe *et al.*, 2004), making even the first hydrolysis product of Pu(IV) difficult to characterize. Each of the other common oxidation states forms more soluble and discrete hydroxide species, although Pu(VI) also forms both monomeric and polymeric hydroxide species. The coordination numbers and structures of all of the pure hydroxides can be inferred from the hydration numbers, the stoichiometry of the hydroxo species, and X-ray structures of corresponding solids. X-ray absorption spectroscopy has been used to determine the bond lengths and coordination numbers more directly. Selected hydrolysis constants for plutonium ions are given in Table 7.55 and follow the usual hydrolysis equilibrium expression and associated hydrolysis constant, $^*\beta_n$ (Lemire *et al.*, 2001).

$$Pu^{x+} + nH_2O \rightleftharpoons Pu(OH)_n^{(x-n)+} + nH^+ \tag{7.124}$$

$$^*\beta_n = \frac{[Pu(OH)_n^{(x-n)+}][H^+]^n}{[Pu^{x+}]} \tag{7.125}$$

A complete review of hydrolysis products and the solubility of plutonium hydroxides is available in the NEA compilation of the chemical thermodynamics of neptunium and plutonium (Lemire *et al.*, 2001) and its most recent update (Guillaumont *et al.*, 2003). Hydration and hydrolysis of plutonium are compared with that of the other actinide elements in Chapter 23.

Pu(III) The tendency of an ion to displace a proton from water increases with charge and, for a given charge, with decreasing ionic radius. The acidity of the tripositive actinide ions, then, should follow the order

$$Pu^{3+} > Np^{3+} > U^{3+}$$

with Pu^{3+} being the strongest acid and therefore the trivalent actinide ion of this triad that undergoes the most extensive hydrolysis. On the basis of its ionic radius, Pu^{3+} should have an acidity similar to the lanthanide ions, and should have a first hydrolysis constant lying between those of Ce^{3+} and Pr^{3+}.

The hydrolysis of Pu^{3+} can be studied only with careful control of the plutonium solubility and maintenance of an inert or reducing atmosphere to avoid oxidation to Pu^{4+}, which is increasingly favored as the solution pH is raised. The first hydrolysis product, $Pu(OH)^{2+}$, has been inferred from solvent extraction, potentiometric and spectrophotometric titration studies in acid solutions up to pH ~3 (where it accounts for ca. 70% of plutonium present). Kraus and Dam (1949) have studied the hydrolysis of trivalent plutonium according to equation (7.122). From titration curves of plutonium(III) chloride and perchlorate solutions with alkali, Kraus and Dam (1949) identified the first hydrolysis species $Pu(OH)^{2+}$ and reported the first hydrolysis constant $^*\beta_1$.

Table 7.55 *Hydrolysis constants for plutonium ions.*

Reaction stoichiometry	I (M)	$\log_{10}{}^{*}\beta_{mn}$	$\log_{10}{}^{*}\beta^{\circ}_{mn}$	*References*
$Pu^{3+} + H_2O \rightleftarrows Pu(OH)^{2+} + H^+$	0.1	−6.9	−6.9 ± 0.3	Baes and Mesmer (1976) and Lemire *et al.* (2001)
$Pu^{3+} + 2H_2O \rightleftarrows Pu(OH)_2^+ + 2H^+$	–	−15.0	–	Fuger (1992)
$Pu^{4+} + H_2O \rightleftarrows Pu(OH)^{3+} + H^+$	1.0	−0.45	0.6 ± 0.2	Metivier and Guillaumont (1972) and Guillaumont *et al.* (2003)
$Pu^{4+} + 2H_2O \rightleftarrows Pu(OH)_2^{2+} + 2H^+$	1.0	−0.75	0.6 ± 0.3	Metivier and Guillaumont (1972) and Guillaumont *et al.* (2003)
$Pu^{4+} + 3H_2O \rightleftarrows Pu(OH)_3^+ + 3H^+$	1.0	−0.33	−2.3 ± 0.4	Metivier and Guillaumont (1972) and Guillaumont *et al.* (2003)
$Pu^{4+} + 4H_2O \rightleftarrows Pu(OH)_{4(aq)} + 4H^+$	1.0	−0.63	−8.5 ± 0.5	Metivier and Guillaumont (1972) and Guillaumont *et al.* (2003)
$PuO_2^+ + H_2O \rightleftarrows PuO_2(OH)_{(aq)} + H^+$	0.1	−9.73	≤−11.3 ± 1.5	Bennett *et al.* (1992) and Lemire *et al.* (2001)
$PuO_2^{2+} + H_2O \rightleftarrows PuO_2(OH)^+ + H^+$	0		−5.5 ± 0.5[a]	Guillaumont *et al.* (2003)
$PuO_2^{2+} + 2H_2O \rightleftarrows PuO_2(OH)_{2(aq)} + 2H^+$	0		−13.2 ± 0.5[a]	Guillaumont *et al.* (2003)
$2PuO_2^{2+} + 2H_2O \rightleftarrows (PuO_2)_2(OH)_2^{2+} + 2H^+$	0.1	−7.8	−7.5 ± 0.5[a]	Okajima and Reed (1993), Guillaumont *et al.* (2003), Reilly *et al.* (2000), and Madic *et al.* (1984)
$2PuO_2^{2+} + 4H_2O \rightleftarrows (PuO_2)_2(OH)_4 + 4H^+$	0.1	−19.3	–	Okajima and Reed (1993) and Reilly *et al.* (2000)

[a] Asymmetric uncertainties (+0.5, −1.5).

Later studies reported the same species stoichiometry and contributed to the recommended hydrolysis constant of $\log_{10} {}^*\beta_1 = -7.0$ (Baes and Mesmer, 1976; Lemire *et al.*, 2001). The overall formula for $Pu(OH)^{2+}$ is likely to be $Pu(OH)(OH_2)_8^{2+}$ based upon the coordination number 9 observed for the Pu^{3+} aquo ion (see Section 7.9.1(a)) (Matonic *et al.*, 2001). Quantitative evaluation of the formation of higher hydrolysis products is inhibited by oxidation and precipitation of Pu(III/IV) hydroxides. Based on the hydrolysis of other trivalent actinides the second hydrolysis constant for formation of $Pu(OH)_2^+$ via equation (7.122) is approximately $\log_{10} {}^*\beta_2 = -15.0$ (Baes and Mesmer, 1976; Fuger, 1992).

The solid trivalent plutonium hydroxide that precipitates from aqueous solutions is presumed to be $Pu(OH)_3 \cdot nH_2O$, by analogy with the known Am^{3+} hydroxide. Solubility studies that were performed as a function of ionic strength provide a solubility product of $\log_{10} K_{sp} = -(15.8 \pm 1.5)$ under standard conditions (Felmy *et al.*, 1989).

Pu(IV). On the basis of size and charge, the plutonium(IV) ion should undergo much more extensive hydrolysis than does plutonium(III). For the same reasons as in the case of the III state, the tendency to undergo hydrolysis should be greater in plutonium than for its predecessors in the actinide series:

$$Pu^{4+} > Np^{4+} > U^{4+} > Pa^{4+} > Th^{4+}$$

In the early stages of hydrolysis, only monomeric species such as $Pu(OH)^{3+}$ are important. It is likely that Pu^{4+} hydrolyzes in a stepwise manner to yield monomeric $Pu(OH)_n^{4-n}$ ($n = 1, 2, 3, 4$); however, the intermediate hydrolysis products ($2 \leq n \leq 4$) undergo irreversible polymerization with the formation of large colloidal aggregates (see below).

The first hydrolysis product for the formation of $Pu(OH)^{3+}$, has been determined from solution complex formation studies.

$$Pu^{4+} + H_2O \rightleftharpoons Pu(OH)^{3+} + H^+ \qquad (7.126)$$

Reported hydrolysis constants for this reaction vary widely, with limited correlation between the experimental technique used and the resulting value of the hydrolysis constant (Baes and Mesmer, 1976; Lemire *et al.*, 2001; Guillaumont *et al.*, 2003). From the many reported values, several are considered the most accurate. Rabideau (1957) carefully measured the pH dependence of the Pu^{4+}/Pu^{3+} redox couple and calculated a hydrolysis constant of $\log_{10} {}^*\beta_1 = -1.41$ at $I = 0.1$ M using the Nernst equation. Compared with directly measuring the formation of the hydrolysis product, for example, by quantifying the shift in the optical absorption bands for Pu^{4+} as the hydroxide forms, or calculating a constant to best model the solubility of (oxy)hydroxide solids, this approach explicitly considers the formation and subsequent hydrolysis of Pu^{3+} at low pH. The 2003 NEA review recommended the value of $\log_{10} {}^*\beta_1 = (0.60 \pm 0.20)$ under standard conditions ($I = 0$) (Guillaumont *et al.*, 2003), which is based on

values proposed in recent studies by Knopp *et al.* (1999) and Neck and Kim (2001). The constant for the second hydrolysis product was originally estimated to be $\log_{10} {}^*\beta_2 = -3.7$ at $I = 0.1$ M (Kraus and Nelson, 1950). The 2003 NEA review recommended $\log_{10} {}^*\beta_2 = (0.60 \pm 0.30)$ for $I = 0$ based on the most recent studies (Guillaumont *et al.*, 2003). The overall formulae for $Pu(OH)^{3+}$ and $Pu(OH)_2^{2+}$ are likely to be $Pu(OH)(OH_2)_7^{3+}$ and $Pu(OH)_2(OH_2)_6^{2+}$ based upon the coordination number 8 observed for the Pu^{4+} aquo ion (see Section 7.9.1(a)).

$$Pu^{4+} + 2H_2O \rightleftharpoons Pu(OH)_2^{2+} + 2H^+ \tag{7.127}$$

Characterization of subsequent third and fourth hydrolysis species [$Pu(OH)_3^+$ and $Pu(OH)_4$] is frustrated by the propensity of these hydroxides to polymerize, as discussed below. The direct observation of the solution species and definitive determination of the constants are prevented by the detection limits of current techniques coupled with the sparing solubility of the (hydr)oxide phases. Attempts to accurately determine these constants from solubility data are focused on the following: identifying discrete solution ion and colloidal species, improving the quantification of the Pu^{4+} ion, refining the operational definitions of the solid/solution phase (commonly delineated by the phase separation method), and better characterizing and controlling the solid phase [crystalline PuO_2, hydrated PuO_2, crystalline or amorphous $Pu(OH)_4$]. Based on the most recent work by Knopp *et al.* (1999), and by Neck and Kim (2001), the 2003 NEA review proposed the value of $\log_{10} {}^*\beta_3 = -(2.3 \pm 0.4)$, and $\log_{10} {}^*\beta_4 = -(8.5 \pm 0.5)$ for the third and fourth hydrolysis constants at $I = 0$, respectively (Guillaumont *et al.*, 2003).

The published solubility product of amorphous Pu(IV) hydroxide, $Pu(OH)_4(s)$, is $\log_{10} K_{sp} = -(58 \pm 1)$ (Capdevila and Vitorge, 1998; Lemire *et al.*, 2001; Neck and Kim, 2001). This value gives a calculated Pu(IV) solution concentration near pH 7 of 10^{-11} M, while observed solubilities span a range of 10^{-8}–10^{-13} M due to interactions with other simple ligands, formation of other hydroxide species, redox instability, and the formation of colloidal species (Neck and Kim, 2001; Rothe *et al.*, 2004).

Pu(IV) polymerization. It has been known for half a century that aqueous solutions of Pu(IV) will form colloidal polymers under the appropriate solution conditions (Kraus and Nelson, 1950; Kraus, 1956). Early emphasis focused on avoiding Pu(IV) polymer because of its intractability and potential for interference in plutonium process chemistry. Newer concerns involve retention of plutonium in nuclear waste repositories where radioactive heating and low acidity of ground waters favor Pu(IV) colloid formation and thus could provide a potential transport pathway for migration of plutonium away from the repository. Radiocolloids are very fine, well-dispersed, intrinsic particles of radioactive compounds, whose formation in the case of the actinides is intimately connected to their hydrolysis chemistry.

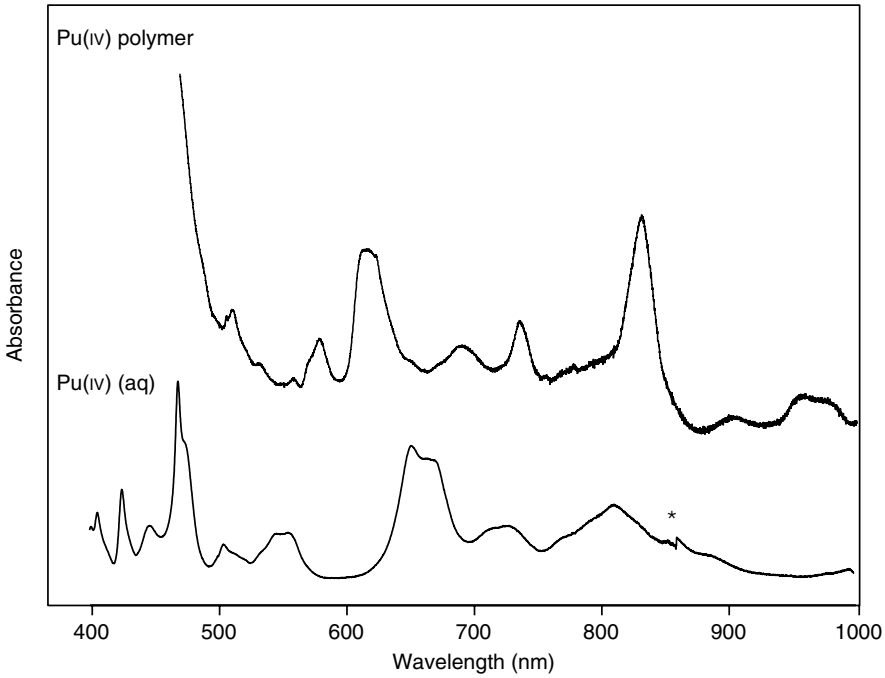

Fig. 7.119 *Electronic absorption spectra of Pu(IV) polymer compared to the Pu(IV) aquo ion. Plutonium(IV) polymer recorded on* 9.0 mM *solution; plutonium(IV) aquo ion recorded on* 2.91 mM *solution in* 1 M $HClO_4$ *using* 1 cm *cell. The asterisk indicated a spectrometer grating change* (*spectra courtesy of P. D. Palmer of Los Alamos*).

For plutonium (IV) the colloid can form green solution-like sols that are optically clear, display a characteristic absorption spectrum (Fig. 7.119), and do not settle on long-standing (Ockenden and Welch, 1956; Lloyd and Haire, 1978). Under the appropriate conditions, these colloids may decompose or disaggregate into soluble ionic species, or age into relatively insoluble materials (Newton *et al.*, 1986b).

The formation of colloidal Pu(IV) polymer was first reported by Kraus, and much of the early information on it is based on the work of Kraus and his coworkers (Kraus and Nelson, 1950; Kraus, 1956). Pu(IV) polymer can be prepared by a number of methods (Hobart *et al.*, 1989). Precipitation methods include the partial neutralization of Pu(IV) solutions, addition of water to 'dried' acid samples, or precipitation with alkali followed by peptization in dilute acid (90°C). Redox methods include slow oxidation of Pu(III) by oxygen and/or alpha irradiation products, or the reduction of Pu(V). The polymer formation depends on acidity, Pu(IV) concentration, presence of other ions, and temperature (Rainey, 1959). Solutions of Pu(IV) polymer can be very readily obtained when plutonium(IV) hydroxide is treated with less than four equivalents of

hydrogen ion per mole of plutonium; when plutonium(IV) hydroxide is dissolved in dilute acid, plutonium polymer forms. Likewise, if a solution of plutonium(IV) in moderately concentrated acid is poured slowly into boiling water, polymeric plutonium is obtained. It is also formed when a plutonium nitrate solution is depleted of nitric acid by extraction with *n*-hexanol. The colloid polymer is ideally formed in nitrate solution in about 0.8 mole per mole of plutonium(IV) (Lloyd and Haire, 1978). This colloidal polymer may be isolated as a solid, which shows the electron diffraction pattern typical of an amorphous substance and has a practical size of up to 20 Å. This colloid can easily be redissolved. On standing or artificial aging, the particle size increases, and the solid becomes finely crystalline and exhibits the XRD pattern of PuO_2. The colloidal character of plutonium(IV) polymer is manifested by the strong absorption of the polymer on glass and on substances such as paper, cotton, and silica, which acquire a negative surface charge when immersed in water.

Until recently, the characterization of plutonium(IV) colloid has met with only limited success. Thiyagarajan *et al.* (1990) measured the structures of Pu(IV) hydrous polymers by small-angle neutron scattering (SANS) in aqueous media and after solvent extraction into an organic phase. The SANS data indicate long, thin, rod-like particles that measured (4.7 ± 0.2) by (190.0 ± 20.0) nm. XRD was consistent with a fcc crystal system similar to that found in crystalline PuO_2 (see Section 7.8.5.a(iii)).

Light scattering methods have also be used to characterize macromolecular Pu(IV) hydroxide solutions. Rundberg *et al.* (1988) and Triay *et al.* (1991) employed autocorrelation photon spectroscopy (APS) to determine the size distribution of Pu(IV) colloidal suspensions that were prepared by dilution, peptization, and autoxidation of Pu(III). The plutonium(IV) colloids measured by APS were assumed to be spherical particles in order to utilize the Stokes–Einstein relationship to calculate a particle diameter. In the initial study by Rundberg *et al.* (1988) the average size of the colloid diameter was measured to be (2.9 ± 0.2) nm. The diameter of a plutonium colloid sample measured over a period of 2 years resulted in reproducible diameters of 180 nm. Subsequently, Triay *et al.* (1991) examined colloid diameters as a function of preparation method, and found that the size of the colloids varied from 1 to 370 nm depending on method of preparation. Small colloid diameters on the order of 1.5 nm were found when the colloid was prepared by the method of Savage and Kyffin (1986) by heating a plutonium nitrate solution with hydrogen peroxide, neutralizing most of the free acid with sodium hydroxide, and diluting to known volume to give 2.5 g L^{-1} solutions. Dilution of a well-characterized Pu(IV) stock solution using distilled water yields colloids in the range of 2–6 nm in diameter (Triay *et al.*, 1991). Peptization gave a mixture of two different sizes (14 and 370 nm). Autoxidation of Pu(III) yielded the largest single-sized colloid.

More recently, Rothe *et al.* (2004) investigated Pu(IV) colloid growth using a combination of laser-induced breakdown detection (LIBD) and X-ray absorption fine structure (XAFS) spectroscopy. LIBD measurements gave colloid sizes ranging from 12 to 25 nm depending on solution conditions.

Rothe *et al.* proposed a model for colloid formation that is consistent with their XAFS, LIBD, and UV-Vis spectroscopic data, based on the stepwise buildup of polynuclear species and loss of water, in analogy to a mechanism proposed by Fujiwara and coworkers (Fujiwara *et al.*, 2001). In this model, they propose hydrolysis of aquo Pu^{4+} to form an eight coordinate monomer $Pu(OH)_2(OH_2)_6^{2+}$ followed by condensation of two monomers to form a dimer of cubic units connected at their edges. The condensation of $Pu(OH)_2^{2+}$ units as reactants satisfies a –2 slope dependency on LIBD data, and the eight coordinate monomer $Pu(OH)_2(OH_2)_6^{2+}$ satisfies the coordination environment from XAFS data. This basic condensation model is described in equation (7.128), and the structural model for the resulting dimer is illustrated in **8**.

$$2Pu(OH)_2(H_2O)_6^{2+} + xH_2O \rightleftharpoons Pu_2O_p(OH)_{8-2p}(OH_2)_{6+p} + 4H^+ + (2+x)H_2O \quad (7.128)$$

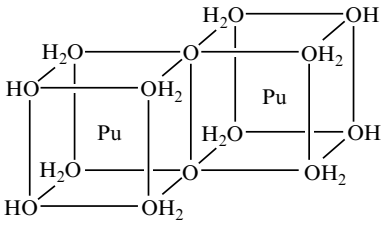

8

In rationalizing the formation of higher order polymers, a trimeric species could be envisioned as forming through the subsequent condensation of monomeric $Pu(OH)_2(OH_2)_6^{2+}$ with the dimer **8**. To be consistent with XAFS data, the new trimer must retain an essentially fcc Pu sublattice with an approximately 3.87 Å distance between Pu centers. This is possible through condensation of the third monomeric $Pu(OH)_2(OH_2)_6^{2+}$ unit along cube edges to form a chain, or by condensing a third monomeric unit along two edges of neighboring cubes of the dimer to form a trimer of cubes sharing one common corner. Examples of these proposed trimeric units are shown in **9** and **10**.

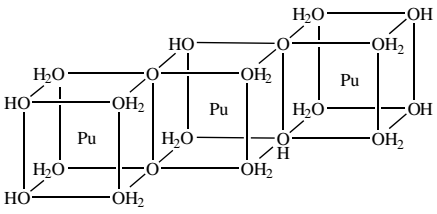

9

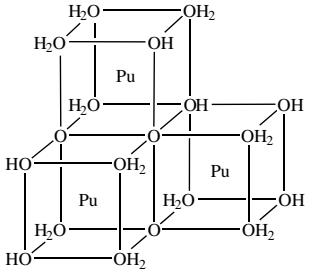

10

The fundamental components of this polymerization mechanism are to grow oligomeric units that maintain a Pu–Pu separation near 3.87 Å, maintain a Pu:OH ratio of 2, and keep the overall cluster size small enough to be consistent with UV-Vis results. Polymerization to larger units can proceed by subsequent condensation of dimers or trimers with each other, or with monomeric units.

The XAFS data from Rothe *et al.* reveal the presence of several different Pu–O distances between 2.20 and 2.42 Å consistent with different coordinating oxygen atoms (–O, –OH, and OH_2). Similarly, the XAFS data show a Pu–Pu distance between 3.86 and 3.89 Å. The fcc cubic environment and the 3.8 Å Pu–Pu separation gives a basic structural unit that is similar to that observed in fcc PuO_2 (see Section 7.8.5(a)). These workers also observed a small feature in their XAFS data near 1.9 Å, and they argued that this feature was too short to be reconcilable with a Pu(IV)–O bond. As this feature had also been observed in ThO_2 XAFS spectra (Rothe *et al.*, 2002), and in XAFS reported by other workers, it was concluded that this feature was most consistent with multiple electron excitation. Essentially identical structural features were observed in XAFS data of Pu(IV) colloid samples reported by Conradson and coworkers (Conradson *et al.*, 2004b). The primary focus of the Conradson study was to examine the structural features of solid PuO_{2+x} materials (see Section 7.8.5(a)). The XAFS data from PuO_{2+x} solids show many remarkable structural similarities to the Pu(IV) colloid samples studied by Rothe *et al.* (2004) and Conradson *et al.* (2004b). Both studies show a range of Pu–O distances consistent with different coordinating oxygen atoms (–O, –OH, and OH_2). In the oxide of stoichiometry of $PuO_{2.26}$, the short interatomic distance near 1.9 Å is no longer a small feature, but has become a dominant spectroscopic feature (see Fig. 7.94). Conradson also reported XAFS data on a number of Pu(IV) colloid samples whose XAFS spectra vary as a function of preparation and aging. Conradson's data show that both Pu(IV) polymers and solid PuO_{2+x} compounds share structural features, and are consistent with an fcc arrangement of plutonium atoms with a 3.8 Å separation. The difference between the two studies is that in solid PuO_{2+x} compounds, the XANES data were consistent with a mixture of Pu(IV) and Pu(V). Conradson *et al.* suggested that the short internuclear distance that averaged 1.86 Å was consistent with the presence of Pu(V), where solution measurements show a distance of 1.85 Å for PuO_2^+. In the freshly prepared samples studied by Rothe *et al.* (2004) this feature was quite small. In the aged samples studied by Conradson *et al.* (2004b) this feature was quite pronounced. These two XAFS studies remind us of the complex nature of the Pu(IV) polymer, and suggest that the elegant polymerization mechanism proposed by Rothe *et al.* may need to be expanded. We look forward to future advances in this area.

Pu(V). Of the common oxidation states of plutonium only Pu(V) is not hydrolyzed until the solution pH becomes basic. Because of the tendency of pentavalent plutonium to disproportionate or be reduced by even weak agents there are very few studies on the hydrolysis of this plutonium ion. Similarly, the

presence of inorganic and organic ligands will generally favor the formation of Pu(IV)–ligand complexes in accordance with their relative formation constants. Early conventional spectrophotometric studies showed that Pu(V) hydrolyses above pH 9 to form stepwise products, $PuO_2(OH)$ and $PuO_2(OH)_2^-$ (Baes and Mesmer, 1976; Madic *et al.*, 1984; Fuger, 1992). By analogy with Np(V) hydroxides, which have been studied in detail by optical absorption and Raman spectroscopy (Madic *et al.*, 1984; Sullivan *et al.*, 1991), Pu(V) hydroxide complexes $PuO_2(OH)$ and $PuO_2(OH)_2^+$ likely have two or three inner-sphere water molecules in the equatorial plane and pentagonal bipyramidal coordination geometry. The monohydroxide hydrate solid is amorphous and has not been structurally characterized. Attempts to increase the crystallinity of the $NpO_2(OH)$ analog have produced Np_2O_5 (Runde *et al.*, 2002). Bennett and coworkers used photoacoustic spectroscopy to perform spectrophotometric titrations of millimolar and submillimolar PuO_2^+, which provided a formation constant for the first hydrolysis product of $\log_{10} {}^*\beta_1 = -(9.73 \pm 0.10)$ (Bennett *et al.*, 1992). Mixed hydroxo carbonato complexes, such as $PuO_2(OH)(CO_3)_2^{4-}$ or $PuO_2(OH)_2(CO_3)^{3-}$ may form (by analogy with Np(V) chemistry) but they have not been characterized. In addition, there is some evidence that the super-stoichiometric Pu(IV) oxide (PuO_{2+x}) contains Pu(V) (Conradson *et al.*, 2003, 2004b). Thus, Pu(V) hydroxides may be much more important in plutonium chemistry and material science than was previously thought.

Pu(VI). Plutonium(VI) hydrolysis is intermediate between that of Pu(III) and Pu(IV), corresponding to its effective charge of ~3.2. Similar to Pu(IV), low solubility and polymerization challenge the characterization of products above neutral pH. The first hydrolysis products, $PuO_2(OH)^+$ and $PuO_2(OH)_2$ have hydrolysis constants of $\log_{10} {}^*\beta_1 = -(5.5 \pm 0.5)$ and $\log_{10} {}^*\beta_2 = -(13.2 \pm 1.5)$ at $I = 0$, respectively (Lemire *et al.*, 2001), comparable to the analogous U(VI) species (Grenthe *et al.*, 1992). Structurally, these monomeric species likely have three or four water molecules in addition to hydroxide in the equatorial plane and a pentagonal bipyramidal geometry with respect to inner-sphere oxygen atoms as indicated in **11**. There is substantial data from potentiometric, optical absorption, and Raman studies that indicates that at higher plutonium concentrations (estimated to be $\sim 5 \times 10^{-4}$ M) the first hydrolysis product is the dimer, $(PuO_2)_2(OH)_2^{2+}$, with two bridging hydroxides and pseudo-pentagonal bipyramidal coordination as shown in **12** (Madic *et al.*, 1984; Okajima and Reed, 1993; Reilly *et al.*, 2000). The hydrolysis constant for the dimer is estimated to be $\log_{10} {}^*\beta_{22} = -(7.5 \pm 1.5)$ at $I = 0$ (Lemire *et al.*, 2001). Polymerization is less pronounced for Pu(VI) than for U(VI) and there is no evidence for the trimeric hydroxide complexes that have been well characterized for uranyl, e.g. $(UO_2)_3(OH)_5^+$, (Grenthe *et al.*, 1992; Palmer and Nguyen-Trung, 1995). Solids precipitated from these systems have been formulated based on stoichiometry as $PuO_2(OH)_2$ or various hydrated phases, but neither their structures nor solubility products have been determined.

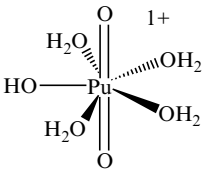

11

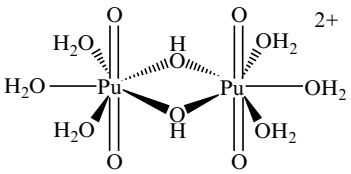

12

Under alkaline solution conditions of 1 M LiOH, Tananaev (1989) presented data to suggest the formation of $PuO_2(OH)_4^{2-}$ that converts to $PuO_2(OH)_3^-$ upon lowering the hydroxide concentration. The single crystal XRD structures (Clark *et al.*, 1999a) and solution XAFS data (Wahlgren *et al.*, 1999; Clark *et al.*, 1999a; Moll *et al.*, 2000; Bolvin *et al.*, 2001) have been reported on the $UO_2(OH)_4^{2-}$ and $NpO_2(OH)_4^{2-}$ analogs.

Pu(VII). Heptavalent plutonium has only been studied in strongly alkaline solutions, given its immediate reduction to Pu(VI) under all other conditions. Interest in the coordination environment of Pu(VII) in solution has been renewed because highly alkaline conditions could be technologically useful in nuclear waste processing, and because Pu(VII) hydroxides provide an opportunity to examine structure/bonding relationships in actinide systems with an unusual number of Pu–O multiple bonds. Pu(VII) appears to be analogous to Np(VII) for which many more studies have been reported. A series of anionic polyoxo species that form between 0.5 and 18 M hydroxide has been proposed and includes the following, $PuO_4(OH_2)_2^-$, $PuO_4(OH)(OH_2)^{2-}$, $PuO_4(OH)_2^{3-}$, $PuO_5(OH)^{4-}$, or PuO_6^{5-}, depending on hydroxide concentrations (Spitsyn *et al.*, 1969; Krot, 1975; Tananaev *et al.*, 1992). Of the proposed species, only $PuO_4(OH)_2^{3-}$ has a proven analog in neptunium chemistry, and its likely structure is shown in **7** (see Section 7.9.1.a) (Grigor'ev *et al.*, 1986). No hydrolysis constants are known. Crystalline samples of analogous Pu(VII) compounds have been prepared (Zakharova *et al.*, 1972).

(e) Complex ions

In this section we describe the preparation, stability, structure, and in selected cases the spectroscopy and solid-state forms, of molecular complexes of plutonium in aqueous solution. The little information that is available on the non-aqueous coordination and organometallic chemistry of plutonium will be described in Section 7.9.2. The stoichiometry and stability of aqueous plutonium complexes has generally been determined indirectly from proton, ligand, and metal titrations, including the following approaches: measured plutonium extraction efficiencies as a function of extractant ligand concentrations, pH titrations of protic ligands in the absence and presence of plutonium, pH/ligand/plutonium titrations monitored by optical spectroscopy, and less

frequently from multinuclear NMR and vibrational spectroscopic analysis. The structures of solution species have also been inferred from the characterization of corresponding solids. More direct methods, including electrospray mass spectroscopy and X-ray absorption spectroscopy, are increasingly being applied to characterize molecular plutonium complexes. Fluorescence spectroscopy has the potential to be used to characterize plutonium species, similar to its application in uranyl chemistry, as emission from plutonium ions has been observed, albeit under very special conditions.

The coordination chemistry of plutonium ions is generally characteristic of exceptionally 'hard' Lewis acids, those that show preference for complexation by hard (i.e. first row donor atom) ligands. Weak Lewis bases, such as HS^- form weak complexes with plutonium and strong Lewis bases, such as CO_3^{2-}, F^-, and PO_4^{3-} form very stable complexes. Plutonium ions have relatively large ionic radii and therefore form complexes with high coordination numbers (8–14). For a given ligand the strength of complexation (the stability of the Pu–ligand complex) and the tendency of ions to hydrolyze decrease following the effective charges:

$$Pu^{4+} > PuO_2^{2+} \approx Pu^{3+} > PuO_2^{+}$$

Overall, the bonding in plutonium complexes can generally be described as ionic, where the geometry of coordination complexes is primarily governed by steric considerations (ligand–ligand repulsions). Plutonium–ligand orbital overlap is considered to be important in some types of complexes, and comparatively more important than in corresponding complexes of lanthanides and lighter actinides with similar ionic radii. Ligand exchange in plutonium complexes is facile, and reaction rates are generally fast.

Complexation in this chapter generally refers to inner-sphere coordination, where the ligand is directly bonded to plutonium and displaces more weakly bound ligands and/or solvent water. Outer sphere complexation and ion pairing are also important interactions, particularly in high ionic strength and otherwise complicated solutions. Equilibrium constants for the reactions of plutonium ions with ligands reflect the competition between protons and plutonium for ligand atom bonding and are experimentally determined. Formation constants are pH independent values calculated from equilibrium constants, ligand pK_as, and plutonium hydrolysis constants and therefore more directly reflect the strength of interaction between the plutonium ion and the deprotonated ligand. For weaker ligands it is important to note that this interaction may be on the order of plutonium–solvent interactions, a factor not easily separated out to provide a quantitative pure plutonium–ligand interaction constant. In the text that follows, we will use K for the consecutive or stepwise formation constants, and β for the cumulative or overall formation constants (Lemire *et al.*, 2001). In cases where complex formation involves a deprotonation of a ligand, the equilibrium constant (K) or formation constant (β) will be denoted by an asterisk as indicated below.

$$PuL_{n-1} + L \rightleftharpoons PuL_n, \quad K_n = \frac{[PuL_n]}{[PuL_{n-1}][L]} \tag{7.129}$$

$$PuL_{n-1} + HL \rightleftharpoons PuL_n + H^+, \quad {}^*K_n = \frac{[PuL_n][H^+]}{[PuL_{n-1}][HL]} \tag{7.130}$$

$$Pu + nL \rightleftharpoons PuL_n, \quad \beta_n = \frac{[PuL_n]}{[Pu][L]^n} \tag{7.131}$$

$$Pu + nHL \rightleftharpoons PuL_n + nH^+, \quad {}^*\beta_n = \frac{[PuL_n][H^+]^n}{[Pu][HL]^n} \tag{7.132}$$

Selected formation constants and equilibrium constants will be defined and conditions specified in summary tables. The emphasis is on describing the types of molecular plutonium complexes that form and highlighting specific chemical, structural, and physical properties. For a more comprehensive discussion of stability constant determinations and analysis done to compute thermodynamic constants under standard conditions the reader is referred to specialized critical reviews (Grenthe *et al.*, 1997; Lemire *et al.*, 2001; Guillaumont *et al.*, 2003). Comparisons across the actinide series and a fine description of the details of plutonium complexation in solution are given in Chapter 23. Selected formation and equilibrium constants for plutonium complexes are given in Table 7.56.

(*i*) *Oxoanions*

Plutonium ions are oxophilic and therefore readily form complexes with oxo ligands, as exemplified by high hydration numbers and extreme hydrolysis described in Section 7.9.1(d). Anionic inorganic oxo ligands effectively complex plutonium to form complexes whose stability depends on the charge and basicity of the ligand. For a given plutonium ion the order of complexation strength for common oxoanions is: $ClO_4^- < IO_3^- < NO_3^- < SO_4^{2-} << CO_3^{2-} < PO_4^{3-}$. Perchlorate is often referred to as a noninteracting counter ion, but does coordinate to plutonium at very high concentrations. Nitrate complexes are much more stable than analogous perchlorate species and slightly more stable than chloride complexes of the same stoichiometry. Phosphate is an exceptionally strong ligand for plutonium. These ions usually chelate plutonium ions in a bidentate fashion. The stability of plutonium oxoanionic complexes follow the general trends of Pu(IV) being the strongest and Pu(V) being the weakest.

The coordination numbers of plutonium oxoanion complexes ranges from 7 for PuO_2^+ to up to 12 for Pu^{4+}, where water is successively displaced from the inner coordination sphere by chelating ligands. Water that remains bonded to the Pu center can hydrolyze to form mixed-ligand complexes that contain one or more bidentate oxoanion and one or more hydroxide ligand. These species are favored at near-neutral pH and lower oxoanion concentrations. Solution

complex formation constants and solid-state structures are known for relatively few of these species, such as Pu(IV) hydroxo oxalates. It is difficult to distinguish mixed-ligand complexes from the coexistence of individual complexes, which explains the uncertainty in, for example, plutonium(IV) carbonate speciation and thermodynamic stability.

Carbonate

Plutonium carbonates are of interest because of their fundamental chemistry and environmental behavior, including aspects of actinide mineralogy and nuclear waste isolation. Separation schemes based on carbonate that utilize the pH-dependent complexing properties of this ligand have been proposed as alternatives to acid-based or organic extraction processes for used nuclear fuels (Asanuma *et al.*, 2001). Some features are common to the carbonate complexation of plutonium ions. Carbonate binds plutonium in a bidentate fashion and has a small bite angle so that coordination numbers of resulting complexes are generally quite high, 7–10. The actinyl ions, PuO_2^+ and PuO_2^{2+} have pentagonal and hexagonal bipyramidal structures in which the linear triatomic O=An=O unit forms the axis of a pentagonal or hexagonal bipyramidal coordination polyhedron with respect to carbonato and aquo oxygen atoms bound to the metal center. In addition to chelating the plutonium ion, carbonate ligands often hydrogen bond to outer sphere waters or counter ions to produce chains and layers and other less regular hydrogen bond networks in the solid-state structures. For all of the oxidation states the stability constant for the initial monocarbonato complex is known with the greatest accuracy and precision because they can be determined spectrophotometrically from the reduction/shift in the characteristic absorption band for the aquo ion. Thermodynamic constants of the limiting carbonato complexes are better known from the solubility and carbonate titration studies than are those corresponding to intermediate species because the former usually have large stability fields. And the limiting molecular complexes are usually isostructural with the solution species from which they are precipitated. Intermediate carbonate complexes are not well characterized for any of the oxidation states. Several reviews on actinide carbonate and environmental chemistry describe plutonium carbonato complexes in detail (Grenthe *et al.*, 1986b; Newton and Sullivan, 1986; Fuger, 1992; Clark *et al.*, 1995; Choppin and Wong, 1998).

Trivalent plutonium carbonato complexes generally oxidize rapidly to tetravalent species. In aqueous Pu(III) solutions there is evidence for the stepwise formation of the carbonato complexes, $Pu(CO_3)^+$ and $Pu(CO_3)_2^-$. Additional carbonato and hydroxocarbonato complexes may form, but are immediately oxidized to Pu(IV) species. Formation constants of $\log_{10}\beta_1 = 7.5$ and $\log_{10}\beta_2 = 12.4$ have been estimated at low ionic strength (0.1–0.5 M) (Cantrell, 1988). These values have not been verified, but are consistent with well-known constants of Am(III) carbonato complexes (Silva *et al.*, 1995).

Table 7.56 *Formation constants for plutonium oxo anions.*

Reaction stoichiometry	*I* (M)	$\log_{10}\beta_n$	$\log_{10}\beta_n^\circ$	*References*
carbonate				
$Pu^{3+} + CO_3^{2-} \rightleftarrows PuCO_3^+$	0.1–0.5	7.5		Cantrell (1988)
$Pu^{3+} + 2CO_3^{2-} \rightleftarrows Pu(CO_3)_2^-$	0.1–0.5	12.4		Cantrell (1988)
$Pu^{4+} + CO_3^{2-} \rightleftarrows PuCO_3^{2+}$	0.3	17.0 ± 0.7		Nitsche and Silva (1996) and Rai *et al.* (1999)
$Pu^{4+} + 4CO_3^{2-} \rightleftarrows Pu(CO_3)_4^{4-}$	1.5	44.5	37.0 ± 1.1[a]	Capdevila *et al.* (1996) and Guillaumont *et al.* (2003)
$Pu^{4+} + 5CO_3^{2-} \rightleftarrows Pu(CO_3)_5^{6-}$	0		36.65 ± 1.13[a]	Guillaumont *et al.* (2003)
$Pu(CO_3)_4^{4-} + CO_3^{2-} \rightleftarrows Pu(CO_3)_5^{6-}$	3.0	-1.36 ± 0.09	–	Capdevila *et al.* (1996)
$Pu^{4+} + 2CO_3^{2-} + 4OH^- \rightleftarrows Pu(CO_3)_2(OH)_4^{4-}$	~ 0.1	46.4 ± 0.7[b]		Yamaguchi *et al.* (1994)
$Pu^{4+} + 2CO_3^{2-} + 2OH^- \rightleftarrows Pu(CO_3)_2(OH)_4^{2-}$		44.8[b]		Rai *et al.* (1999)
$PuO_2^+ + CO_3^{2-} \rightleftarrows PuO_2CO_3^-$	0.5	4.60 ± 0.04	5.12 ± 0.14[a]	Bennett *et al.* (1992) and Guillaumont *et al.* (2003)
$PuO_2^+ + 3CO_3^{2-} \rightleftarrows PuO_2(CO_3)_3^{5-}$		7.5	5.025 ± 0.92[a]	Wester and Sullivan (1983), Capdevila *et al.* (1992), and Guillaumont *et al.* (2003)
$PuO_2^{2+} + CO_3^{2-} \rightleftarrows PuO_2CO_3$	3.5	8.6 ± 0.3	9.5 ± 0.5[a]	Robouch and Vitorge (1987) and Guillaumont *et al.* (2003)
	0.1	8.7 ± 0.3		Pashalidis *et al.* (1997)
$PuO_2^{2+} + 2CO_3^{2-} \rightleftarrows PuO_2(CO_3)_2^{2-}$	0.1	13.1 ± 0.1	14.7 ± 0.5[a]	Sullivan *et al.* (1982)
	3.5	13.6 ± 0.7		Robouch and Vitorge (1987) and Guillaumont *et al.* (2003)

$PuO_2^{2+} + 3CO_3^{2-} \rightleftarrows PuO_2(CO_3)_3^{4-}$	0.1	18.2 ± 0.4	18.0 ± 0.5[a]	Ullman and Schreiner (1988), Robouch and Vitorge (1987), and Guillaumont *et al.* (2003)
$3PuO_2(CO_3)_3^{4-} \rightleftarrows (PuO_2)_3(CO_3)_6^{6-} + 3CO_3^{2-}$	3.0	-7.4 ± 0.2		Grenthe *et al.* (1986a)
nitrate				
$Pu^{4+} + NO_3^- \rightleftarrows PuNO_3^{3+}$	2	0.51 ± 0.05	1.95 ± 0.15[a]	Berg *et al.* (2000) and Guillaumont *et al.* (2003)
$Pu^{4+} + 2NO_3^- \rightleftarrows Pu(NO_3)_2^{2+}$	2	1.05 ± 0.08		Berg *et al.* (2000)
phosphate				
$Pu^{4+} + H_3PO_4 \rightleftarrows PuH_3PO_4^{4+}$	2	2.3	2.4 ± 0.3[a]	Denotkina *et al.* (1960) and Guillaumont *et al.* (2003)
$PuO_2^+ + HPO_4^{2-} \rightleftarrows PuO_2HPO_4^-$	1	2.39 ± 0.04		Moskvin and Poznyakov (1979)
sulfate				
$Pu^{3+} + HSO_4^- \rightleftarrows PuSO_4^+ + H^+$			1.93 ± 0.614[a]	Guillaumont *et al.* (2003)
$Pu^{3+} + 2HSO_4^- \rightleftarrows Pu(SO_4)_2^- + 2H^+$			1.74 ± 0.76[a]	Guillaumont *et al.* (2003)
$Pu^{4+} + HSO_4^- \rightleftarrows PuSO_4^{2+} + H^+$			4.91 ± 0.22[a]	Guillaumont *et al.* (2003)
$Pu^{4+} + 2HSO_4^- \rightleftarrows Pu(SO_4)_4 + 2H^+$			7.18 ± 0.32[a]	Guillaumont *et al.* (2003)
$PuO_2^{2+} + SO_4^{2-} \rightleftarrows PuO_2SO_4$			3.38 ± 0.20[a]	Guillaumont *et al.* (2003)
$PuO_2^{2+} + 2SO_4^{2-} \rightleftarrows PuO_2(SO_4)_2^{2-}$			4.4 ± 0.2[a]	Guillaumont *et al.* (2003)

[a] NEA Update Vol 5 (Guillaumont *et al.*, 2003).
[b] Species may not exist, based on later studies of Pu(IV) carbonates (Capdevila *et al.*, 1996).

Tetravalent plutonium probably forms stepwise complexes, $Pu(CO_3)_n^{4-2n}$, $n = 1$–5, with increasing solution pH and carbonate concentration (Newton and Sullivan, 1986; Clark *et al.*, 1995). The end members of this series and the tetracarbonato complex have been characterized, while the bis- and tris-species are inferred from studies of other actinide(IV) carbonates. Monocarbonato Pu(IV) of formula $Pu(CO_3)^{2+}$ is prepared by addition of carbonate to acidic solutions of the ion or from carbonate-mediated dissolution of hydroxide or oxide solids. The formation constant for $Pu(CO_3)^{2+}$ is reported to be $\log_{10} \beta_1 = (17.0 \pm 0.7)$ (Nitsche and Silva, 1996; Rai *et al.*, 1999). Given the generally accepted hydration number of eight for Pu(IV), this complex likely has six additional water molecules in the inner coordination sphere. In concentrated carbonate solutions, $Pu(CO_3)_4^{4-}$ is in equilibrium with $Pu(CO_3)_5^{6-}$. The formation constants for these individual species are highly correlated with each other and with the lower carbonate species.

Capdevila *et al.* (1996) studied the formation of the limiting carbonato complex of formula $Pu(CO_3)_5^{6-}$ by electronic absorption spectroscopy with varying ionic strength. From the study of the equilibrium in equation (7.133), they were able to determine an equilibrium constant for the reaction of $\log_{10} K_5 = -(1.36 \pm 0.09)$, and the formation constant for the limiting complex of $\log_{10} \beta_5 = (35.8 \pm 1.3)$ in 3 M $NaClO_4$ solution. The NEA review recommended a zero ionic strength value of $\log_{10} \beta_5 = (36.65 \pm 1.13)$ (Lemire *et al.*, 2001). By combining the value for β_5 with the equilibrium constant K_5 for equation (7.133), the formation constant for $Pu(CO_3)_4^{4-}$ at zero ionic strength was recommended to be $\log_{10} \beta_4 = (37.0 \pm 1.1)$ (Lemire *et al.*, 2001).

$$Pu(CO_3)_4^{4-} + CO_3^{2-} \rightleftarrows Pu(CO_3)_5^{6-} \tag{7.133}$$

Recent conventional spectrophotometric and electrochemical studies have focused on refining the thermodynamic constants for the carbonato species and determining the stability field and stoichiometry of mixed hydroxo/carbonato Pu(IV) complexes (Capdevila and Vitorge, 1999). The NEA critical review of thermodynamic data suggests that spectroscopic signatures and solubility characteristics that have been attributed to mixed hydroxo/carbonato complexes are in fact explained by the simultaneous and independent formation of hydrolysis products and carbonato complexes (Lemire *et al.*, 2001). Counter arguments are that colloidal Pu(IV) polymer formation is suppressed by carbonate complexation, and that absorption spectra of Pu(IV) in carbonate solutions over the entire pH range are wholly reproduced by linear combinations of known individual hydroxide and carbonate spectra.

Plutonium(IV) carbonato solids of general formula $M_xAn(CO_3)_y \cdot nH_2O$ have been prepared with a variety of cations ($M = Na^+, K^+, NH_4^+, C(NH_2)_3^+$; $y = 4$, 5, 6, 8) by precipitating or crystallizing the solution species. For example, $[Na_6Pu(CO_3)_5]_2 \cdot Na_2CO_3 \cdot 33H_2O$ was crystallized from 2.5 M Na_2CO_3 solution and characterized by single-crystal XRD (Clark *et al.*, 1998). The structure

contains the discrete $Pu(CO_3)_5^{6-}$ ion, which can be viewed as a pseudo-hexagonal bipyramid with three CO_3^{2-} ligands in an equatorial plane and two in axial positions as shown in **13**. Solution XAFS data for Pu(IV) in 2.5 M Na_2CO_3 solution gave bond distances and coordination numbers that corresponded extremely well with the average Pu–O, nonbonding Pu– –C, and distal Pu– –O distances of 2.42(1), 2.87(1), and 4.12(1) Å, respectively, found in the solid-state structure for the $Pu(CO_3)_5^{6-}$ ion. A peak-by-peak correspondence of the optical absorption spectra of the solution and diffuse reflectance spectrum of the ground crystalline solid, together with the solution XAFS data provide conclusive evidence that the $Pu(CO_3)_5^{6-}$ ion is the limiting species in high carbonate solutions. Depending on reaction conditions, green amorphous powders of compositions $K_4Pu(CO_3)_4{\cdot}nH_2O$, $K_6Pu(CO_3)_5{\cdot}nH_2O$, $K_8Pu(CO_3)_6{\cdot}nH_2O$, and $K_{12}Pu(CO_3)_8{\cdot}nH_2O$ have all been reported (Gel'man and Zaitsev, 1958). Since Clark *et al.* identified the $Pu(CO_3)_5^{6-}$ ion as the limiting species, it is reasonable to assume that the latter two solids are more realistically formulated as $[K_6Pu(CO_3)_5][K_2CO_3]{\cdot}nH_2O$ and $[K_6Pu(CO_3)_5][K_2CO_3]_3{\cdot}nH_2O$. Sodium salts of formula $Na_4Pu(CO_3)_4{\cdot}3H_2O$, $Na_6Pu(CO_3)_5{\cdot}2H_2O$, and $Na_6Pu(CO_3)_5{\cdot}4H_2O$ have also been claimed as light green crystalline compounds that appear to dehydrate in air (Gel'man and Zaitsev, 1958). Similarly, the $(NH_4)_4Pu(CO_3)_4{\cdot}4H_2O$ and $[Co(NH_3)_6]_2Pu(CO_3)_5{\cdot}5H_2O$ salts have been reported (Ueno and Hoshi, 1970).

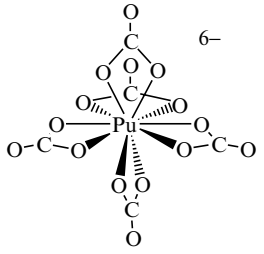

13

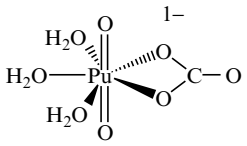

14

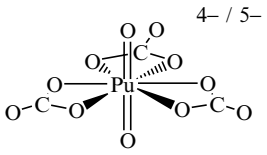

15

Pentavalent plutonium carbonato complexes are prepared by addition of alkali metal carbonate solutions to mildly acidic solutions of PuO_2^+, or by the one-electron reduction of Pu(VI) carbonato complexes. The mono- and triscarbonato complexes, $PuO_2(CO_3)^-$ and $PuO_2(CO_3)_3^{5-}$, have been observed directly by optical absorption spectroscopy, and their formation constants have been determined. In contrast, the biscarbonato complex $PuO_2(CO_3)_2^{3-}$ has not been observed directly, and is only inferred. Sensitive laser photoacoustic spectroscopy was used to determine the formation constant of $\log_{10}\beta_1 = (4.6 \pm 0.04)$ for $PuO_2(CO_3)^-$ (Bennett *et al.*, 1992). Using the Nernst equation, the measured reversible reduction of hexavalent $PuO_2(CO_3)_3^{4-}$ at 339 mV vs SHE in 1 M Na_2CO_3 and comparisons with Np(V) carbonato formation constants, the formation constant for $PuO_2(CO_3)_3^{5-}$ can be estimated to be $\log_{10}\beta_3 = 7.5$

(Wester and Sullivan, 1983; Capdevila *et al.*, 1992). These solution species are likely isostructural with the corresponding $NpO_2(CO_3)(OH_2)_3^-$, and $NpO_2(CO_3)_3^{5-}$ complexes which have been characterized by EXAFS spectroscopy, and illustrated in **14** and **15** (Clark *et al.*, 1996). These complexes have the general actinyl carbonate structure with axial O=An=O units at a bond distance of 1.85 Å and bidentate carbonato and water oxygen atoms arrayed about the equatorial plane to form a pentagonal or hexagonal bipyramidal coordination polyhedron at average bond distances of 2.45 and 2.42 Å, respectively. Optical absorption spectra do not suggest that the biscarbonato complex $PuO_2(CO_3)_2^{3-}$ is ever a predominant solution species, consistent with the small difference between the stability constants for the mono- and tris-species that suggest a very small stability field for this intermediate species. Mixed hydroxo carbonato complexes have been proposed for Np(v) (Sullivan *et al.*, 1991), but the identification and existence of analogous Pu(v) species is questionable.

Solids corresponding to the Pu(v) carbonate solution species have been prepared as microcrystalline powders via precipitation and the orthorhombic solid-state structure of $KPuO_2CO_3$ has been determined (Ellinger and Zachariasen, 1954). Much more data is available for analogous salts of Np(v) carbonates, $MNpO_2CO_3$, and $M_3NpO_2(CO_3)_2$, where M is an alkali metal or ammonium ion (Simakin *et al.*, 1974; Volkov *et al.*, 1974a,b, 1981). These structure types have been reviewed by Clark *et al.* (1995). These compounds show interesting structural changes due to the size similarity of hydrated ions such as K^+ and NpO_2^+, and the extent of hydration. For example, for $MNpO_2CO_3$ where M = Cs^+, Rb^+, NH_4^+, K^+, Na^+, and Li^+, a hexagonal-to-orthorhombic phase change is observed within the NpO_2CO_3 layer at the potassium–sodium boundary. The solids both contain actinyl carbonate layers and the hexagonal and orthorhombic sheets are related by displacement of the chains of actinyl units through half a translation along the crystallographic *a*-axis. These basic layers are illustrated qualitatively in **16** and **17**. The orthorhombic structure **17** is more open than the hexagonal structure **16**, which appears to allow for the closer contacts necessary for the smaller sodium and lithium cations.

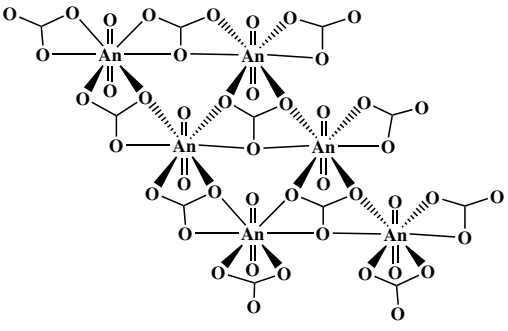

16

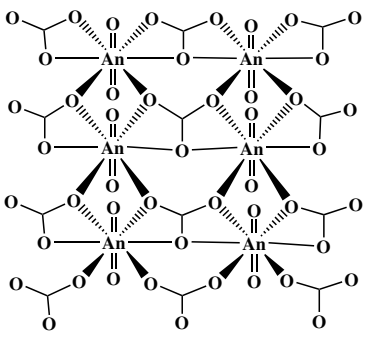

17

The biscarbonato solid $M_3NpO_2(CO_3)_2$ displays an overall orthorhombic structure, but exhibits a pseudo-hexagonal layer similar to **16**, except that one half of the AnO_2^+ ions in the anionic carbonate layer have been replaced by alkali metal cations. One can envision that M^+ and AnO_2^+ cations form alternating chains within the hexagonal sheet and give rise to the approximate composition $[M_{0.5}(AnO_2)_{0.5}(CO_3)]$ within the layer. This arrangement is illustrated qualitatively in **18**. The cation and anion layers are oriented such that an alkali metal cation, M^+, lies directly above and below the linear AnO_2^+ ion of adjacent sheets. The anionic carbonate layer and the cationic potassium layers line up such that they are parallel to the crystallographic *c*-axis, and this allows for an M–O=An interaction between layers and yields a maximally ordered structure (Clark *et al.*, 1995).

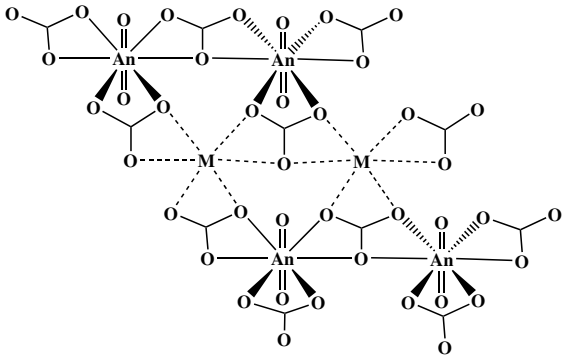

18

Hexavalent plutonium carbonato complexes have been studied primarily as an extension of uranyl carbonate chemistry. Uranyl carbonato complexes are very important in uranium geochemistry actinide contaminant environmental transport, uranium mining, and nuclear fuel production and reprocessing, owing to their high solubility and stability in aqueous solution. Substitution of the plutonyl ion in uranyl phases has the potential to form solid solutions.

Carbonate complexation of Pu(VI) increases with pH and carbonate concentration. Pashalidis *et al.* (1997) studied the solubility of both UO_2CO_3 and PuO_2CO_3 in aqueous carbonate solutions and determined equilibrium constants for the formation of $PuO_2(CO_3)$, $PuO_2(CO_3)_2^{2-}$, and $PuO_2(CO_3)_3^{4-}$. These results are in good agreement with earlier studies on $AnO_2(CO_3)$ solids of uranium, neptunium, and plutonium by Ullman and Schreiner (1988), and $PuO_2(CO_3)$ solids by Robouch and Vitorge (1987). The most recent NEA review recommends $\log_{10}\beta_1 = (9.5 \pm 0.5)$, $\log_{10}\beta_2 = (14.7 \pm 0.5)$, and $\log_{10}\beta_3 = (18.0 \pm 0.5)$ for the corresponding formation constants (Guillaumont *et al.*, 2003).

Both $PuO_2(CO_3)_{(aq)}$ and $PuO_2(CO_3)_3^{4-}$ have been spectroscopically observed. In contrast, while the $AnO_2(CO_3)_2^{2-}$ species has been spectroscopically observed for U(VI) and Np(VI), the stability field of the corresponding $PuO_2(CO_3)_2^{2-}$ analog appears to be so small that it has not been directly observed. Spectrophotometric and calorimetric studies of the formation of the monocarbonato complex from the Pu(VI) hydroxide illustrated that carbonate can outcompete hydroxide to coordinate to plutonium, and provided the first formation constants (Sullivan *et al.*, 1982). Subsequent solubility studies and additional spectrophotometric data provide a formation constant of $\log_{10}\beta_1 = (8.7 \pm 0.3)$ for $PuO_2(CO_3)$ in 0.1 M $NaClO_4$ (Pashalidis *et al.*, 1997). X-ray powder diffraction and XAFS studies of the corresponding $PuO_2(CO_3)$ solid show that it is isostructural with rutherfordine, $UO_2(CO_3)$ (Reilly *et al.*, 2000). This solid has a layered structure where the local coordination environment of the plutonyl ion is a hexagonal bipyramidal arrangement of oxygen atoms with the plutonyl units perpendicular to the orthorhombic plane (Clark *et al.*, 1995). Each plutonium atom forms six equatorial bonds with the oxygen atoms of four carbonate ligands, two in a bidentate manner and two in a monodentate manner. The orthorhombic plane is identical to that shown in **17**. The orthorhombic plane of hexagonal bipyramidal plutonyl units forms infinite, two-dimensional layers.

Solution EXAFS and single crystal XRD studies show the limiting $PuO_2(CO_3)_3^{4-}$ is isostructural with the uranyl analog, which has pseudo-hexagonal pyramidal coordination geometry as illustrated in **15**. The Pu=O distance was found to be 1.74 Å with an average Pu–O distance to carbonate ligands of 2.45 Å (Clark *et al.*, 1999b; Neu *et al.*, 2000; Conradson *et al.*, 2004a). The stability constant for $PuO_2(CO_3)_3^{4-}$ has been determined from solubility, calorimetry, and spectrophotometric studies to be $\log_{10}\beta_3 = (18.2 \pm 0.4)$ in 0.1 M electrolytes (Robouch and Vitorge, 1987; Ullman and Schreiner, 1988). Pashalidis *et al.* determined a value of (17.8 ± 0.2) in 0.1 M $NaClO_4$ solution, and the recent NEA assessment recalculated their value to correct for a systematic error and obtained (18.4 ± 0.2) (Guillaumont *et al.*, 2003). This species can be readily precipitated to form salts with monovalent cations.

In contrast with uranyl carbonate chemistry where the bis carbonato $UO_2(CO_3)_2^{2-}$ and its trimeric oligomer $(UO_2)_3(CO_3)_6^{6-}$ are major species (Allen *et al.*, 1995; Banyai *et al.*, 1995), the bis carbonato plutonyl complex, $PuO_2(CO_3)_2^{2-}$, has a small stability field and neither it nor the trimer $(PuO_2)_3(CO_3)_6^{6-}$ have been characterized. Similar to the hexavalent hydroxides, oligomerization reactions appear to decrease dramatically across the series from uranium to plutonium. Mixed actinyl trimers, $(UO_2)_2(PuO_2)(CO_3)_6^{6-}$ and $(UO_2)(PuO_2)_2(CO_3)_6^{6-}$ have been proposed based on optical absorption and emf studies (Grenthe *et al.*, 1986b). Similarly, additional polymeric species known for uranyl $(UO_2)_2(CO_3)(OH)_3^-$, $(UO_2)_3O(OH)_2(HCO_3)^+$, and $(UO_2)_{11}(CO_3)_6(OH)_{12}^{2-}$ under conditions of high metal ion concentration or high ionic strength (Grenthe *et al.*, 1992) have not been observed for plutonyl.

Nitrate

Nitrates were among the first complexes studied for plutonium and are very important in plutonium processing (Cleveland, 1979). The effectiveness of solvent extraction and ion-exchange processes in nitric acid, for example, depends strongly on the stoichiometry, stability, molecular geometry and molecular charge of nitrate complexes. Nitrate tends to bind plutonium in a bidentate fashion and to retain its planar molecular geometry, similar to carbonate. But it is a much weaker ligand. Because nitric acid solutions of plutonium and nitrate solids of Pu(IV) and Pu(VI) are both prevalent forms in process and synthetic chemistry, a tremendous number of mixed-ligand complexes are known that contain one or more mono- or bidentate nitrates in the inner coordination sphere.

Trivalent nitrate species have been prepared in nitric acid solution, but they are unstable with respect to oxidation.

Aqueous Pu(IV) nitrate complexes are very well studied because of their use in solvent extraction methods and ion-exchange chromatography. The solution species, $Pu(NO_3)_n^{4-n}$ ($n = 1$–6), have been studied in detail. There is evidence from numerous ion exchange and extraction studies and more recent NMR and EXAFS experiments that the mono-, bis-, tetra, and the hexanitrato complexes are significant, but the tris- and pentanitrato complexes are not (Veirs *et al.*, 1994). X-ray absorption data for the system suggest aquo ligation decreases in the inner sphere even before sequential bidentate nitrates bind the metal center. Solution EXAFS data gives coordination numbers of 11–12 for the first coordination sphere, with average Pu–O bond distances of 2.49 and 2.38 Å for nitrate and water ligands, respectively (Allen *et al.*, 1996b). Formation constants measured for the mononitrato complex, $Pu(NO_3)^{3+}$, were critically evaluated by the NEA reviewers, who recommend the constant $\log_{10}\beta_1 = (1.95 \pm 0.15)$ at $I = 0$ (Lemire *et al.*, 2001). A recent spectrophotometric study in 2 molal $HClO_4$ and extensive analysis by Monte Carlo methods sheds new light on the relative importance of the $Pu(NO_3)^{3+}$ and $Pu(NO_3)_2^{2+}$ complexes, and reported the constants $\log_{10}\beta_1 = (0.51 \pm 0.05)$ and $\log_{10}\beta_2 = (1.05 \pm 0.08)$ (Berg *et al.*, 2000).

Cation exchange resins have a strong affinity for the hexanitrato species, $Pu(NO_3)_6^{6-}$. This nitrate-based purification method is used to separate plutonium from most of the elements in the periodic table, and is used on an industrial scale (Section 7.5.5). There has been some discussion over whether the limiting Pu(IV) nitrate in solution is the penta- or hexanitrato species and some experiments suggest that the hexanitrate is only a major species in the presence of resins or in concentrated salt solutions that favor ion pairing (Veirs *et al.*, 1994; Clark and Delegard, 2002).

Plutonium(IV) nitrate solids are readily formed in nitric acid by dissolution of hydroxides or carbonates followed by precipitation or crystallization. Crystalline orthorhombic $Pu(NO_3)_4{\cdot}5H_2O$ can be obtained in this way and

also by heating a Pu(VI) nitrate salt (Staritzky, 1956). Hexanitrato complexes, $M_2Pu(NO_3)_6{\cdot}2H_2O$, where M = Rb, Cs, NH_4, and pyridinium, are obtained from moderately concentrated (8 to 14 M) nitric acid. A single crystal XRD study was performed on $(NH_4)_2Pu(NO_3)_6$ by Spirlet *et al.* (1992). In the solid state the icosohedral $Pu(NO_3)_6^{2-}$ unit is characterized by three mutually perpendicular planes formed by the trans NO_3^- ligands giving virtual T_h symmetry as illustrated in **19**. The 12 Pu–O bond distances average 2.487(6) Å.

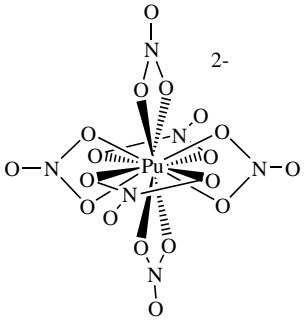

19

Numerous additional solution studies on Pu(IV) mixed ligand-nitrate complexes have been performed in the development and performance testing of extractants. Most notably these include TBP and phosphine oxides. As other examples, a variety of mixed amide-nitrate complexes have been proposed based upon NMR, IR, and extraction behavior (Berthon and Chachaty, 1995; Preston and du Preez, 1995; Romanovski *et al.*, 1999).

No inner-sphere Pu(V) nitrate complexes have been characterized. The existence of the solid nitrates of Np(V) and Pa(V), $NpO_2(NO_3){\cdot}xH_2O$ (x = 1, 5), $RbNpO_2(NO_3)_2{\cdot}H_2O$, and $PaO(NO_3)_3{\cdot}xH_2O$ (x = 1–4) suggests that it might be possible to isolate solid Pu(V) nitrates if the oxidation state could be stabilized in nitrate solution. Pu(VI) nitrates are weak complexes and only the mononitrate, $PuO_2(NO_3)^+$, species is significant in solution. Mixed TBP-nitrate complexes have been widely studied, including a recent EXAFS study of the structural changes as the actinyl species are reduced to An(IV) (Den Auwer *et al.*, 1999). The hydrated solid, $PuO_2(NO_3)_2{\cdot}xH_2O$, x = 3,6, has been characterized.

Sulfate

Trivalent plutonium forms at least two stepwise complexes, $PuSO_4^+$ and $Pu(SO_4)_2^-$ in acid solutions according to equations below (Fardy and Buchanan, 1976; Rao *et al.*, 1978; Nash and Cleveland, 1983).

$$Pu^{3+} + HSO_4^- \rightleftharpoons PuSO_4^+ + H^+ \quad (7.134)$$

$$Pu^{3+} + 2HSO_4^- \rightleftharpoons Pu(SO_4)_2^- + 2H^+ \quad (7.135)$$

The NEA reviewers recalculated the formation constants for these species according to the reactions above, extrapolated to zero ionic strength and recommended $\log_{10} {}^*\beta_1 = (1.93 \pm 0.61)$ and $\log_{10} {}^*\beta_2 = (1.74 \pm 0.76)$ (Lemire *et al.*, 2001). The fact that higher order anions such as $Pu(SO_4)_4^{5-}$ are found in solids such as $K_5Pu(SO_4)_4{\cdot}4H_2O$ suggests that higher order ions of formula $Pu(SO_4)_n^{3-2n}$ must form to a small extent in solution (Mudher *et al.*, 1995). There is some evidence for the formation of solid $Pu_2(SO_4)_3{\cdot}xH_2O$. The Pu(III) solid is likely isostructural with $Am_2(SO_4)_3{\cdot}8H_2O$, which is comprised of eight coordinate Am(III) (Bullock *et al.*, 1980). The ternary salts of $MPu(SO_4)_2{\cdot}H_2O$, where M is an alkali metal, are isostructural with the Nd(III) analog (Iyer and Natarajan, 1989, 1990). Similarly, the $(NH_4)Pu(SO_4)_2{\cdot}4H_2O$ is isomorphous with the corresponding Sm(III) compounds; and all of these structures contain nine coordinate metal centers containing water and bidentate sulfate ligands. Salts of other complex anions, such as $K_5Pu(SO_4)_4$, which is isostructural with $K_5La(SO_4)_4$, are also known (Mudher *et al.*, 1995).

Sulfate has high affinity for plutonium(IV). The stability of the complexes has been studied both to understand the properties of the complexes themselves and to evaluate how sulfate competes with extractants (Laxminarayanan *et al.*, 1964; Sokhina *et al.*, 1978; Solovkin and Rubisov, 1983). As for Pu(III), formation constants for Pu(IV) sulfato complexes are accurately expressed as solution reaction constants from bisulfate addition to Pu^{4+} according to reactions (7.136) and (7.137).

$$Pu^{4+} + HSO_4^- \rightleftharpoons PuSO_4^{2+} + H^+ \quad (7.136)$$

$$Pu^{4+} + 2HSO_4^- \rightleftharpoons Pu(SO_4)_{2\,(aq)} + 2H^+ \quad (7.137)$$

The data are most consistent with the formation of two complexes, $PuSO_4^{2+}$ and $Pu(SO_4)_2$, but higher order species $Pu(SO_4)_n^{4-2n}$ are implied by the existence of salts such as $K_4Pu(SO_4)_4{\cdot}2H_2O$. The NEA review recommends the constants $\log_{10} {}^*\beta_1 = (2.75 \pm 0.01)$ and $\log_{10} {}^*\beta_2 = (4.43 \pm 0.01)$ in 2.2 molal $(H, Na)_2SO_4$ solutions (Lemire *et al.*, 2001). Extrapolation to zero ionic strength gives $\log_{10} {}^*\beta_1 = (4.91 \pm 0.22)$ and $\log_{10} {}^*\beta_2 = (7.18 \pm 0.32)$ (Lemire *et al.*, 2001). Based upon the crystal structure of $Pu_2(OH)_2(SO_4)_3(H_2O)_4$, mixed hydroxo sulfato complexes are also thought to form in solution at higher pH (Wester, 1983).

The neutral hydrates can be precipitated as $Pu(SO_4)_2{\cdot}nH_2O$ ($n = 9, 8, 6, 4$), and subsequently dehydrated up to 400°C. The red tetrahydrate Pu(IV) phase is noteworthy because of its high purity (Cleveland, 1979). The common bicapped square antiprismatic geometry of four sulfates and four waters is adopted by the

Pu(IV) centers in the tetra- and octahydrates. Each sulfate group is shared by two Pu(IV) ions, and sulfates not bonded to plutonium are hydrogen bonded to water molecules (Kierkegaard, 1956; Jayadevan *et al.*, 1982). Two orthorhombic polymorphs of the tetrahydrate differ only by hydrogen bonding in the structures (Jayadevan *et al.*, 1982). The octahydrate loses four water molecules at relatively low temperature, and can be fully dehydrated. Ternary salts have also been characterized, such as the green Pu(IV) compounds $M_4Pu(SO_4)_4{\cdot}xH_2O$ and $M_6Pu(SO_4)_5{\cdot}xH_2O$ (M = K, NH_4) (Sood *et al.*, 1992). The structure of the anion in $K_4Pu(SO_4)_4{\cdot}2H_2O$ consists of chains of plutonium atoms linked by pairs of bridging sulfate groups, and the plutonium atom exhibits a tricapped trigonal prismatic coordination geometry. The structure of the Pu(IV) mixed hydroxo-sulfato complex, $Pu_2(OH)_2(SO_4)_3(H_2O)_4$, has been determined and is isomorphous with the hydroxosulfates of Zr, Hf, and Ce (Wester, 1983).

Sulfate complexes of Pu(V) have not been characterized, but they may be important environmental species since sulfate can be a major component of natural waters and minerals. Therefore research on these types of complexes is merited.

Mono- and bis-sulfato complexes of plutonyl(VI), $PuO_2(SO_4)$ and $PuO_2(SO_4)_2^{2-}$, are generally prepared from acidic solutions. Solution equilibrium constants derived in terms of formation constants for the reactions listed below have been measured (Patil and Ramakrishna, 1976; Ullman and Schreiner, 1986).

$$PuO_2^{2+} + SO_4^{2-} \rightleftharpoons PuO_2SO_4(aq) \tag{7.138}$$

$$PuO_2^{2+} + 2SO_4^{2-} \rightleftharpoons PuO_2(SO_4)_2^{2-} \tag{7.139}$$

The NEA reviewers evaluated these results and recommended the zero ionic strength formation constants of $\log_{10}\beta_1 = (3.38 \pm 0.20)$ and $\log_{10}\beta_2 = (4.4 \pm 0.2)$ (Lemire *et al.*, 2001). Changes in the electronic structure of hexavalent plutonium and neptunium as a function of sulfate, selenate, and chromate complexation have been studied by optical and IR spectroscopy and attributed to covalence variation in An=O bonding or distortions in the ligand arrangement (Budantseva *et al.*, 2000).

Plutonyl sulfate solids of formula $M_2PuO_2(SO_4)_2$ have been prepared and are likely isostructural with the neptunyl analogs. The solid state layered structure of $Cs_2NpO_2(SO_4)_2$ is built up by anionic layers $[NpO_2(SO_4)_2]_n^{2n-}$, linked together by Cs^+ ions. Each NpO_2^{2+} ion in the anionic layer is linked via the sulfate ions to three other atoms to form an hexagonal net similar to the actinyl(V) carbonate structures (Fedosseev *et al.*, 1999).

Phosphate

Because of their very low solubility as exemplified by stable minerals and ore bodies, actinide phosphates have been proposed as potential radioactive waste

forms (Boatner and Sales, 1988). Phosphate has multiple protonation states, PO_4^{3-}, HPO_4^{2-} and $H_2PO_4^-$, and related condensed phosphate anions such as $P_2O_7^{4-}$ and $(PO_3)_n^{n-}$ with many coordination modes that can lead to intricate three-dimensional structures in the solid state, making the plutonium phosphate compounds particularly challenging to characterize. The limited information that is available for plutonium phosphate solution species comes from solubility studies and X-ray and optical absorption spectroscopic studies. In the solid state, the major classes of actinide phosphate are phosphates, hydrogenphosphates, dihydrogen phosphates, diphosphates (pyrophosphates), and polytrioxophosphates (metaphosphates). In addition there are numerous ternary compounds, mixed valent uranium phosphates, halophosphates, organophosphates, and more recently, open framework and templated phases.

Plutonium(III) phosphate solution species are proposed to have the formula $Pu(H_2PO_4)_n^{3-n}$ ($n = 1$–4), but they have not been spectroscopically or structurally characterized (Moskvin, 1971a). For Pu(III), the blue, hexagonal $PuPO_4{\cdot}0.5H_2O$ has been prepared by precipitation from relatively dilute HNO_3/H_3PO_4 solution, then heated to yield the anhydrous compound (Bamberger, 1985). Anhydrous plutonium pyrophosphate PuP_2O_7 has been prepared by the thermal decomposition of plutonium oxolatophosphates (Bjorklund, 1957; Bamberger, 1985).

By considering the protonation behavior of phosphoric acid (Grenthe *et al.*, 1992) the following plutonium(IV) complexes may form: $Pu(H_3PO_4)_x(H_2PO_4)_y^{(4-y)+}$ ($x = 0$, 1; $y = 0$, 1, 2) under acidic conditions; $Pu(HPO_4)_3(H_2PO_4)_x^{(2+x)-}$ ($x = 1$, 2) at neutral pH; and $Pu(HPO_4)_x^{4-2x}$ ($x = 1$–3) under basic conditions. All of the known Pu(IV) solids have such low solubilities that only experiments with $Pu(HPO_4)_2{\cdot}xH_2O$ have yielded solution speciation information. The solution complex in equilibrium with the solids, $Pu(H_3PO_4)^{4+}$, has a formation constant of $\log_{10}\beta_1 = 2.3$ in 2 M (H,Na)NO_3 (Denotkina *et al.*, 1960), and the NEA reviewers recommended the value $\log_{10}\beta_1 = (2.4 \pm 0.3)$ at zero ionic strength (Lemire *et al.*, 2001).

The chemistry of tetravalent actinide phosphates has been recently reviewed and a new classification system proposed for these compounds (Brandel and Dacheux, 2004a,b). New characterization data indicates that a number of previously reported actinide phosphate phases appear to be polyphase mixtures, particularly the "$M_3(PO_4)_4$" group of compounds. Solid Pu(IV) phosphates can be considered a subset of known Th(IV) and U(IV) compounds. Plutonium(IV) polytrioxophosphate, $Pu(PO_3)_4$, can be crystallized by dissolving PuO_2 in polyphosphoric acid (Douglass, 1962). The hydrogenphosphate, $Pu(HPO_4)_2{\bullet}xH_2O$, is reported to precipitate as a gelatinous solid upon addition of phosphoric acid to nitric acid solutions of Pu(IV) and can be used as precursor for other phosphate phases. Anhydrous plutonium diphosphate PuP_2O_7, has been prepared by the thermal decomposition of plutonium oxolatophosphates or by heating a mixture of PuO_2 and BPO_4 (Bjorklund, 1957; Bamberger, 1985). Additonal Pu(IV) phosphates and diphosphates are likely

based on the growing list of thorium and uranium phosphate phases reported. For example, Bénard *et al.* reported two distinct thorium types in $Th_4(PO_4)_4(P_2O_7)$, one eight-coordinate with oxygen from five phosphate and one diphosphate group and around the thorium atom (Bénard, Brandel *et al.*, 1996). Thorium(IV) can be replaced by Pu(IV) up to a maximum value of x = 1.67 for $Th_{4-x}M_x(PO_4)_4(P_2O_7)$ (Dacheux, Brandel *et al.*, 1998). Ternary compounds of the general formula $M(I)Th_2(PO_4)_3$ and $M(II)Th(PO_4)_2$ with M(I) = alkali cation, Tl, Ag, Cu, (Louer, Brochu *et al.*, 1995; Bénard, Brandel *et al.*, 1996) and M(II) = Ca, Sr, Cd, Pb, (Merigou, Genet *et al.*, 1995) are also known for U(IV).

Plutonium(V) phosphate, $NH_4PuO_2HPO_4{\cdot}4H_2O$, was precipitated from solutions of PuO_2^+ in nitric acid with the addition of $(NH_4)_2HPO_4$ (Gel'man and Zaitseva, 1964). There is evidence for $PuO_2HPO_4^-$ from adsorption studies of PuO_2^+ on iron oxides in phosphoric acid, but it has not been fully characterized (Moskvin and Poznyakov, 1979; Morgenstern and Kim, 1996). Its formation constant has been reported to be $\log_{10}\beta_1 = (2.39 \pm 0.04)$ in 1 M NH_4Cl (Moskvin and Poznyakov, 1979). It is likely that additional complexes are formed, but their stoichiometries are not certain.

Denotkina *et al.* reported the first studies of Pu(VI) phosphates (Denotkina, Shevchenko *et al.*, 1965; Denotkina and Shevchenko, 1967). This work was later revised and augmented by Fischer *et al.* who prepared a series of compounds of Pu(VI) with phosphates and arsenates with the general formulas, $MPuO_2XO_4{\bullet}yH_2O$ and $M'(PuO_2XO_4)_2{\bullet}zH_2O$ (X = P, As; M = H^+, K^+, Rb^+, NH_4^+; M′ = Ca^{2+}, Sr^{2+}), and compared the characterization data with analogous uranium and neptunium compounds (Fischer, Werner *et al.*, 1981). The hydrogenphosphate compounds, $PuO_2(HXO_4){\bullet}yH_2O$ (X = P, As), were prepared by reacting Pu(VI) hydroxide with aqueous solutions of H_3PO_4 and H_3AsO_4. The compounds $MPuO_2(PO_4){\bullet}yH_2O$ (M = K^+, NH_4^+) precipitated from aqueous solutions of Pu(VI) in dilute nitric acid upon addition of K_2PO_4 and $(NH_4)_2PO_4$. The acidic proton in the solid arsenate hydrogenarsenate complex was partially exchanged by mixing the solid with a solution of the Group 1 or 2 metal chloride. Weger *et al.* reported preliminary data on the solubility and speciation of Pu(VI) in phosphate solutions and observed evidence for colloid formation from filtration data and for three complexes between pH 2.7 to 12 in the visible–near infrared absorption spectra (Weger, Okajima *et al.*, 1993). Further work is needed to determine if the absorption features are due to soluble or colloidal species.

Iodate

The precipitate of Pu(IV) iodate, $Pu(IO_3)_4$, was one of the first forms of ^{239}Pu isolated and is a common end product in low pH actinide/lanthanide separations (Cleveland, 1979). This useful solid has not been characterized, but likely has the same stoichiometry as the thorium perchlorate analog that forms upon reaction of thorium hydroxide with perchloric acid, $Th(ClO_4)_4{\cdot}4H_2O$. Attempts

to prepare Pu(IV) iodates by hydrothermal methods have produced Pu(VI) phases (described below).

Similarly, most conditions that would be used to attempt to prepare Pu(V) iodates have yielded Pu(VI) or Pu(IV) solids. The solid-state structure of $NpO_2(IO_3)$ was recently determined by single crystal XRD (Albrecht-Schmitt *et al.*, 2003). Its structure consists of neptunyl(V) cations linked to one another by $O_2Np{-}O{=}Np{=}O$ bonds and bridging iodate anions, creating a pentagonal bipyramidal NpO_7 unit.

The binary plutonyl(VI) iodate, $PuO_2(IO_3)_2{\cdot}H_2O$, has been prepared under hydrothermal conditions and has a layered structure with PuO_7 pentagonal bipyramids linked by iodate anions. By contrast, $UO_2(IO_3)_2$ is one-dimensional, and contains chains of edge-sharing UO_8 hexagonal pyramids. A second actinyl (VI) compound with water in the inner coordination sphere, $AnO_2(IO_3)_2(H_2O)$, has been characterized for uranyl and neptunyl, but not for the slightly smaller plutonyl ion (Bean *et al.*, 2001; Runde *et al.*, 2003b). The addition of cations to the starting solution for these hydrothermal preparations produces ternary phases where the cations are located between chains and layers in the three-dimensional structure (Shvareva *et al.*, 2005). A dimeric plutonyl hydoxo iodate $(PuO_2)_2(IO_3)(\mu\text{-}OH)_3$ was isolated from a hydrothermal reaction of Pu(IV) in a mixed hydroxide, H_5IO_6 solution. In this structure hydroxide bridges are the primary structural element and seven-coordinate plutonium atoms are bridged by iodate and hydroxide (Bean *et al.*, 2005).

Perchlorate

Because perchlorates and perchloric acid solutions (similar to nitrates) are very common starting materials in actinide chemistry there are numerous examples of perchlorate containing plutonium compounds. However, pure binary plutonium perchlorates have not been characterized in the solution or solid state. Perchlorate is such a weak ligand that it most likely does not form inner-sphere complexes in aqueous solution, but acts as a simple counter ion. For comparison, crystals of uranyl perchlorate, $UO_2(ClO_4)_2{\cdot}nH_2O$ have been obtained with 6 and 7 hydration water molecules. The uranyl is coordinated with 5 water molecules in the equatorial plane with a distance of U–O(aquo) of 2.45 Å. The complex is best formulated as $[UO_2(H_2O)_5][ClO_4]_2{\cdot}nH_2O$ (Alcock and Esperas, 1977).

Oxalate

Oxalates have been widely used in plutonium separations and processing (Cleveland, 1979; Wick, 1980). The rapid formation of microcrystalline phases that are easily filtered from solution is the basis for the large-scale recovery of plutonium from concentrated solutions. In addition, the low solubility of the oxalates makes them useful in 'polishing' or 'finishing' steps where minor amounts of material are recovered. Plutonium oxalates may also be important in environmental chemistry since oxalate is a major byproduct of plant

metabolism and can be concentrated in some soils. The stoichiometry for the oxalate complexes has been determined from a combination of thermogravimetric analyses and XRD on solid compounds. The oxalate ligand $\left(C_2O_4^{2-}\right)$ generally binds actinide ions in a mono- or bidentate fashion, and can also bridge metal centers to produce a variety of chains, layers, and intricate three-dimensional structures with high coordination numbers. Solution species are only poorly studied, as expected given their low solubilities.

The solid trivalent plutonium oxalate system is dominated by two hydrates of formula $Pu_2(C_2O_4)_3{\cdot}10H_2O$ and $Pu_2(C_2O_4)_3{\cdot}6H_2O$ that are readily precipitated from solution in the presence of reducing agents, such as hydroxylamine. The blue, monoclinic decahydrate $Pu_2(C_2O_4)_3{\cdot}10H_2O$ forms in concentrated solutions and can be dehydrated or fired to produce highly pure finely divided PuO_2 (Rao *et al.*, 1963). This stoichiometric oxalate is isostructural with lanthanide (III) oxalate decahydrate, which includes nine-coordinate metal centers (Jenkins *et al.*, 1965). A single crystal XRD structure of a nonahydrate $Pu_2(C_2O_4)_3{\cdot}9H_2O$ has been recently reported (Runde *et al.*, 2005a). This two-dimensional solid consists of tricapped trigonal prismatic PuO_9 units that are linked by $C_2O_4^{2-}$ groups and a network of interstitial water molecules. The plutonium atom is coordinated to six oxygen atoms from three bidentate oxalate ligands and three oxygen atoms from coordinated water. The Pu–O distances range from 2.47 to 2.56 Å (Runde *et al.*, 2003a). Complex plutonium(III) oxalates of general formula $MPu(C_2O_4)_2{\cdot}xH_2O$ (M = Na, K, Cs, NH_4) have also been prepared (Runde *et al.*, 2005a).

Solution oxalate complexes are mainly of the form, $Pu(C_2O_4)_n^{3-2n}$, $n = 2$–4. The bis-oxalate species is the most important, while the latter complexes have very narrow ranges of stability (Cleveland, 1979; Hasilkar *et al.*, 1994). Numerous mixed-ligand Pu(III) oxalate complexes have been postulated to form but have not been studied in detail.

Tetravalent plutonium oxalates have been prepared with 2, 4, and 5 oxalate ligands bound to plutonium. The binary oxalate hydrates, $Pu(C_2O_4)_2{\cdot}xH_2O$ ($x = 0$, 1, 2, or 6), can be prepared from Pu(III) solutions in the presence of peroxide or other mild oxidizing agents, or precipitated directly from Pu(IV) solutions. Detailed structural analyses of these solids have not been reported. They are likely isostructural with the related binary Th(IV) and U(IV) oxalates, which generally have a coordination number of eight, comprised of bidentate and bridging oxalate and water molecules in the inner sphere arranged in irregular cubic and square antiprismatic coordination geometries. Complex salts of the tetra- and pentaoxalates, including $Na_4[Pu(C_2O_4)_4]{\cdot}5H_2O$, $(NH_4)_6[Pu(C_2O_4)_5]{\cdot}5H_2O$, and $K_6[Pu(C_2O_4)_5]{\cdot}5H_2O$ have been prepared. Uranium and thorium analogs of the tetraoxalate contain a ten-coordinate actinide (IV) atom in an irregular bicapped square antiprism linked to other metal centers by oxalato or aquo bridges (Favas *et al.*, 1983; Harrowfield *et al.*, 1983). Hydrothermal synthesis produced single crystals of $KPu(C_2O_4)_2(OH){\cdot}2H_2O$ (Runde, 2005a). The single-crystal structure of $KPu(C_2O_4)_2(OH){\cdot}2H_2O$ shows

a three-dimensional framework built up from oxalate-linked PuO_9 polyhedra. Each PuO_9 polyhedron consists of eight oxygen atoms from four chelating oxalate ligands and one hydroxide ligand. This finding is suggestive that $Pu(C_2O_4)_4(OH)^{5-}$ may be the limiting Pu(IV) solution complex under high oxalate concentrations (Runde, 2005a).

Plutonium(V) in the presence of oxalate disproportionates to a mixture of oxidation states under most conditions (Nikitenko, 1988). Plutonium(V) oxalates (such as $NH_4PuO_2(C_2O_4) \cdot xH_2O$) can be isolated by rapid precipitation from neutral pH solutions and have been identified by optical absorption spectroscopy and chemical analyses (Zaitseva *et al.*, 1973). Plutonium(VI) oxalates that are isostructural with uranyl oxalates have been prepared (Jenkins *et al.*, 1965; Bessonov *et al.*, 1996). The simple binary, $PuO_2(C_2O_4) \cdot 3H_2O$, is the most studied and was recently employed in an EPR study to show the evidence for the participation of 5f electrons in plutonium chemical bonding (Bhide *et al.*, 2000).

Peroxide

Hydrogen peroxide is commonly used to reduce Pu(V) or Pu(VI) to Pu(IV) and to precipitate Pu(IV) from acidic solution, often in the presence of other anions (Balakrishnan and Ghosh Mazumdar, 1964; Hagan and Miner, 1980). Efficient separation and purification processes have been developed from this chemistry (see Section 7.5.3(b)) even though the exact nature of species in solution is not definitively known (Cleveland, 1979; Wick, 1980). Plutonium(IV) can also be reduced by hydrogen peroxide to form Pu(III) or Pu(III)/Pu(IV) mixtures, depending upon the acidity, presence of sulfate, and total plutonium concentration (Balakrishnan and Ghosh Mazumdar, 1964; Koltunov, 1982a).

Connick and McVey (1949) spectroscopically identified two Pu(IV) peroxide complexes in acidic solution. Small amounts of peroxide produced a brown complex with absorption bands at 495 ($\epsilon = 266$ L mol^{-1}cm^{-1}) and 540 nm, with a suggested peroxo-bridged formula of $[Pu(O_2)(OH)Pu]^{5+}$ and corresponding formation constant of 8.8×10^6 in 0.5 M HCl. As more peroxide is added, the brown complex converts to a red complex with an absorption maximum at 513 nm. The equilibrium between these two solution complexes (equilibrium constant of 145 in 0.5 M HCl) suggests intermediates of general composition $[Pu(\mu\text{-}O_2)_2Pu]^{4+}$. While there is no structural information to confirm the proposed solution complex stoichiometries, Runde (2005b) has recently isolated single crystals containing the $Pu_2(\mu\text{-}O_2)_2(CO_3)_6^{8-}$ ion, that confirms the presence of a doubly bridged $Pu_2(\mu\text{-}O_2)_2$ core as illustrated in **20**. When the peroxide concentration is increased, two green precipitates form with different oxygen to plutonium ratios that also incorporate other anions present in the solution, e.g. sulfate, nitrate, and chloride (Leary *et al.*, 1959). The hexagonal form ($a = 4.00$ Å) precipitates preferentially at high acidity and high ionic strength and has an oxygen to plutonium ratio of 3.0–3.4 depending on whether the solid is dry or wet, respectively. At less than 2 M acidity a fcc

form ($a = 16.5$ Å) of higher purity and with an oxygen to plutonium ratio of 3.0 is obtained (Hagan and Miner, 1980) regardless of whether the solid is wet or dry.

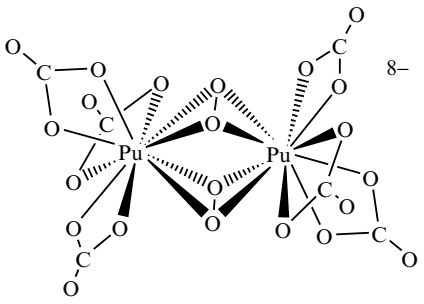

20

Less is known about the complexation of plutonyl ions by peroxide in alkaline media. Nash *et al.* (1980) reported that Pu(VI) in a 3 mM H_2O_2/0.05 M $NaHCO_3$ solution is reduced to Pu(V) via an intermediate reddish-brown colored complex, which was assumed to be a 1:1 Pu(VI) peroxo complex. The rate of formation of this complex was determined to be $(6.9 \pm 0.8) \times 10^3$ M^{-1} s^{-1} in 0.05 M $NaHCO_3$ (Nash *et al.*, 1980).

(*ii*) *Carboxylate and polyaminocarboxylate complexes*

Plutonium complexes with carboxylates and polyaminocarboxylic acids are important in separations, decontamination, and environmental migration. They have also been studied to achieve a better understanding of fundamental aqueous actinide chemistry. Owing to their multiple anionic chelating oxygen donor atoms, these ligands form highly stable and soluble complexes with plutonium ions. Solution complex formation constants for the plutonium species follow the usual trend where Pu(IV) complexes are the most stable and Pu(V) complexes the least stable. These ligands and other multidentate chelating organic acids stabilize Pu(IV) complexes to such a great extent, that under most conditions plutonium ions of the other oxidation states are rapidly oxidized/reduced to the tetravalent state.

Many studies have been reported for plutonium complexes with citrate, tartrate, malonate, glycine, and other carboxylates and amino acids, most recently by researchers at the Russian Academy of Sciences. Among these the acetate complexes are arguably the most comprehensively studied. The solution chemistry of plutonium complexes of other similar ligands can be inferred by considering the acetate complexes and the comparative basicity of the ligands; hence, only the acetate complexes will be discussed in this section. Among plutonium complexes of the amino polyacetates, iminodiacetate (IDA), nitrilotriacetate (NTA), ethylenediaminetetraacetate (EDTA), diethylenetriamine pentaacetate (DTPA), and derivatives, the EDTA complexes have been studied

most extensively and used most broadly in applications. The pentaacetate analog, DTPA, has special application for treatment of internal human plutonium contamination through chelation therapy. The stoichiometry and stability of plutonium polyacetate solution complexes are generally known from spectrophotometric and potentiometric titration experiments. Solution and solid-state structures have been proposed by inference. The chemistry of the lower valent ions, Pu^{3+} and Pu^{4+} is comparative and will be described first, followed by that of the higher oxidation state ions, PuO_2^+ and PuO_2^{2+}. Formation constants for selected carboxylate and aminocarboxylate ligands are given in Table 7.57.

Pu(III) and (IV). Acetate complexes of Pu(III) have been studied primarily for stabilization with respect to oxidation to Pu(IV). Each of the stepwise complexation species from the mono- to pentaacetate has been reported. The formation constants for the first two species are $\log_{10}\beta_1 = 2.02$ and $\log_{10}\beta_2 = 3.34$ in 0.3 M $NaClO_4$ (Moskvin, 1969; Nair and Joshi, 1981). These constants have been reported from independent studies and compare well with values reported for acetate complexes of trivalent lanthanides. The limiting pentaacetate complex has an estimated formation constant of $\log_{10}\beta_5 = 16.7$ (Cleveland, 1979), which is high relative to the formation constants for the mono- and bis complexes and may therefore be considered an upper limit. Similarly, stepwise constants for Pu(IV) have been reported. Values for the first and limiting (penta) species are known with the greatest certainty, $\log_{10}\beta_1 = 5.31$ and $\log_{10}\beta_5 = 22.6$ (Cleveland, 1979). Solid-state structures of the lower valent plutonium acetate complexes are not known.

Plutonium(III) complexes of NTA^{3-} and $EDTA^{4-}$ have been studied directly by optical spectroscopy, voltammetry, and cation exchange, as well as indirectly in the study of Pu(IV) EDTA complexes at very low pH. Multiple species have been identified from pH and ligand titration experiments. In solutions with pH > 5, Pu(III) complexes are rapidly oxidized to Pu(IV). Studies at low pH have yielded the formation constant for the Pu(NTA) complex of $\log_{10}\beta_1 = 10.26$ (Merciny *et al.*, 1978; Anderegg, 1982). The protonated species Pu(EDTA)H forms in strong acid solutions and is deprotonated to $Pu(EDTA)^-$ above pH 3, and then to the mixed EDTA hydroxo complex, $Pu(EDTA)(OH)^{2-}$. Solution formation constants for the first complex and protonated forms have been reported from multiple independent studies (Cauchetier and Guichard, 1973; Merciny *et al.*, 1978). A value for the stability constant of the binary, deprotonated species, $Pu(EDTA)^-$, $\log_{10}\beta_1 = 16.1$ is reported in a critical review of EDTA thermodynamic data (Anderegg, 1977). $DTPA^{5-}$, with an additional bidentate acetate group, forms a more stable 1:1 complex with Pu^{3+}, $\log_{10}\beta_1 = 21.5$ (Merciny *et al.*, 1978).

Tetravalent plutonium–EDTA complexes are important because EDTA stabilizes Pu^{4+} over all other oxidation states sufficient for use in chemical processing, and because the complexes may promote the transport of plutonium contamination in the environment. Studies of Pu–EDTA complexation are challenging because of the extreme hydrolysis of Pu^{4+} and low solubility of

Table 7.57 *Formation constants for selected organic acids and aminopolycarboxylates.*

Ligand	*Complex*	Pu^{+3}	Pu^{+4}	PuO_2^+	PuO_2^{2+}	*References*
acetate, Ac^-	[ML]/[M][L]	2.02	5.31		2.2	Moskvin (1969), Nair and Joshi (1981), Cleveland (1979), Magon *et al.* (1968), and Eberle and Wade (1970)
	$[ML_2]/[M][L]^2$	3.34			3.6	Moskvin (1969) and Nair and Joshi (1981)
	$[ML_5]/[M][L]^5$	16.7	22.6			Cleveland (1979)
IDA^{2-}	[ML]/[M][L]			6.2	8.5	Eberle and Wade (1970) and Cassol *et al.* (1973)
NTA^{3-}	[ML]/[M][L]	10.3	12.9	6.8		Merciny *et al.* (1978), Anderegg (1982), and AlMahamid *et al.* (1996)
$EDTA^{4-}$	[ML]/[M][L]	16.1	26.4	12.3	14.6	Anderegg (1977), Boukhalfa *et al.* (2004), and Cauchetier and Guichard (1975)
	$[ML_2]/[M][L]^2$		35.39			Boukhalfa *et al.* (2004)
$DTPA^{5-}$	[ML]/[M][L]	21.5	29.5			Merciny *et al.* (1978), Anderegg (1982), Moskvin (1969), and Nair and Joshi (1981)
$citrate^{2-}$	[ML]/[M][L]	8.9	15.6			Martell and Smith (2001)
	$[ML_2]/[M][L]^2$		29.8			
$lactate^-$	$[ML_4]/[M][L]^4$		16.2			Martell and Smith (2001)
$oxalate^{2-}$	[ML]/[M][L]		8.30		6.6	Martell and Smith (2001) and Rogozina *et al.* (1973)
	$[ML_2]/[M][L]^2$	9.3	14.9		9.4	
	$[ML_3]/[M][L]^3$	9.4	23.4			
	$[ML_4]/[M][L]^4$	9.9	27.5			
$malonate^{2-}$	[ML]/[M][L]				4.8	Martell and Smith (2001) and Rogozina *et al.* (1973)
$succinate^{2-}$	[ML]/[M][L]				3.4	Martell and Smith (2001)
$glutamate^{2-}$	[ML]/[M][L]	4.7				Martell and Smith (2001) and Rogozina *et al.* (1973)
$aspartate^{2-}$	[ML]/[M][L]	4.8				Martell and Smith (2001) and Rogozina *et al.* (1973)
$glycinate^-$	[ML]/[M][L]	3.2				Martell and Smith (2001) and Rogozina *et al.* (1973)

plutonium hydroxides, inherent limits of analytical and spectrophotometric techniques, large number of potential species, precipitation of EDTA in strong acid solution, and uncertainties in experimental proton concentrations. Despite these limitations, solubility, potentiometric, spectrophotometric, and electrochemical studies provide species formulations that are consistent between techniques (Cauchetier and Guichard, 1973; Rai *et al.*, 2001; Boukhalfa *et al.*, 2004).

In acidic solution (pH < 4) and at 1:1 ligand to metal ratio, Pu(EDTA) is the predominant species, with an overall formation constant of $\log_{10}\beta_1 = 26.44$ in 1 M (Na,H)ClO_4. The absorption maximum of the binary complex is at 496 nm. At higher pH the hydrolysis species Pu(EDTA)$(OH)^-$ and Pu(EDTA)$(OH)_2^{2-}$ form with the corresponding overall stability constants of $\log_{10}\beta = 21.95$ and 15.29, respectively. The reduction potential of the complex Pu(EDTA) at pH = 2.3 is reported to be $E_{1/2} = 342$ mV (vs SHE). It was recently determined that under conditions of neutral pH and excess EDTA relative to Pu^{4+}, a second ligand coordinates to the ion. The formation of such species, as well as mixed-ligand EDTA complexes, can be anticipated knowing that the Pu^{4+} ions may accommodate up to 12 ligand donor atoms in their inner coordination sphere as in the hexanitrato structure, **19**. The bis chelate complex, Pu$(EDTA)_2^{4-}$, forms with an overall formation constant of $\log_{10}\beta = 35.39$ (Boukhalfa *et al.*, 2004). In the presence of ancillary ligands, mixed-ligand complexes form, as exemplified by the citrate and carbonate complexes Pu(EDTA)$(citrate)^{3-}$ and Pu$(EDTA)(CO_3)^{2-}$ (Boukhalfa *et al.*, 2004).

Dissolution of Pu(IV) hydrous oxides, PuO_2, $PuO_2{\cdot}xH_2O$, and '$Pu(OH)_4$' in the presence of EDTA has been studied both to understand how EDTA may promote plutonium solubility in waste and the environment and as a method to determine the thermodynamic stability of the resulting Pu–EDTA solution complexes. Dissolution rates of 0.0074 and 0.42 μmol g^{-1} day^{-1} Pu in the presence of 10 mM EDTA were measured for the oxide and hydroxide, respectively, in a study that measured the solubility over months (Ruggiero *et al.*, 2002). A faster dissolution rate for the oxide has been reported in a study of shorter duration (Rai *et al.*, 2001).

DTPA solution complexes have been studied in pure solutions using the same methods as those employed for the EDTA and NTA complexes. The formation constants are less accurately known because they have been studied by fewer researchers, but mostly because they form in highly acidic solutions where there is uncertainty in the proton concentration and the protonation state of DTPA. The constant, $\log_{10}\beta_1 = 29.5$, can be considered a best estimate (Moskvin, 1971b). Given the high stability constant and positive results from plutonium complexation in aqueous solution, DTPA has been studied as a plutonium decontamination agent (Stradling *et al.*, 1989). It is highly effective in chelating plutonium in complex media that mimic physiological environments, and is the standard against which other potential therapeutic agents are measured. The efficacy of plutonium solubilization and complexation by DTPA has been studied in blood, urine, and cells (Rosenthal *et al.*, 1975). Most mammalian studies are

done with Zn and Ca salts ($CaNa_3DTPA$ or $ZnNa_3DTPA$) since early chelation therapy studies indicated that these essential metals were scavenged and depleted in the body. For a more detailed account of *in vivo* actinide chelation, the reader is referred to chapter 31 of this work.

Pu(V) and (VI). Plutonium(VI) acetate complexes have been well studied in solution, and characterized in detail in the solid state. Plutonium(V) acetate complexes are not stable with respect to oxidation or reduction, depending on the solution conditions. Spectrophotometric and potentiometric studies have yielded the following average formation constants for plutonium(VI) acetates $\log_{10}\beta_1 = 2.2$, $\log_{10}\beta_2 = 3.6$, and $\log_{10}\beta_3 = 5.0$, in 1.0 M $(Na,H)ClO_4$ (Magon *et al.*, 1968; Moskvin, 1969; Eberle and Wade, 1970; Cleveland, 1979). In the presence of alkali ions, triacetate complexes of the form $MAnO_2(CH_3COO)_3$ precipitate from solutions containing Pu(VI). The cubic pink sodium plutonyl acetate and the analogous cesium salt are the most studied (Jones, 1955).

Plutonium(V) and plutonium(VI) aminocarboxylate complexes have been identified in electrochemical and pH titration studies (Cauchetier and Guichard, 1975). A stability constant for the complex of Pu(V) with NTA^{3-} was reported to be $\log_{10}\beta_1 = 6.8$ in 0.1 M $(Na,H)ClO_4$ (AlMahamid *et al.*, 1996) consistent with a number of previous studies (Eberle and Wade, 1970). The related iminodiacetate (IDA^{2-}) complex has a reported formation constant $\log_{10}\beta_1 = 6.2$ (Eberle and Wade, 1970), which as expected is somewhat lower than the constant for the Pu(V) complex with NTA^{3-}. A stability constant for a Pu(V) complex with $EDTA^{4-}$ has been estimated to be $\log_{10}\beta_1 = 12.3$ from spectrophotometric titrations (Cauchetier and Guichard, 1975). The reduction to Pu(IV) proceeds at a rate that depends on pH, plutonium concentration, and the ligand to metal ratio. At neutral pH and submicromolar plutonium

Table 7.58 *Formation constants and Gibbs energies for selected aqueous plutonium halides.*[a]

Species	*Reaction*	$\log_{10}\beta_n^\circ$	$\Delta_r G_m^\circ$ (kJ mol^{-1})
PuF^{3+}	$F^- + Pu^{4+} \rightleftarrows PuF^{3+}$	8.84 ± 0.10	-50.46 ± 0.57
PuF_2^{2+}	$2F^- + Pu^{4+} \rightleftarrows PuF_2^{2+}$	15.7 ± 0.2	-89.62 ± 1.14
PuO_2F^+	$F^- + PuO_2^{2+} \rightleftarrows PuO_2F^+$	4.56 ± 0.20	-26.03 ± 1.14
PuO_2F_2 (aq)	$2F^- + PuO_2^{2+} \rightleftarrows PuO_2F_2(aq)$	7.25 ± 0.45	-41.38 ± 2.57
$PuCl^{2+}$	$Cl^- + Pu^{3+} \rightleftarrows PuCl^{2+}$	1.2 ± 0.2	-6.85 ± 1.14
$PuCl^{3+}$	$Cl^- + Pu^{4+} \rightleftarrows PuCl^{3+}$	1.8 ± 0.3	-10.27 ± 1.71
PuO_2Cl^+	$Cl^- + PuO_2^{2+} \rightleftarrows PuO_2Cl^+$	0.23 ± 0.03	-1.31 ± 0.17
PuO_2Cl_2 (aq)	$2Cl^- + PuO_2^{2+} \rightleftarrows PuO_2Cl_2(aq)$	-1.15 ± 0.30	6.56 ± 1.71
$PuBr^{3+}$	$Br^- + Pu^{4+} \rightleftarrows PuBr^{3+}$	1.6 ± 0.3	-9.13 ± 1.71
PuI^{2+}	$I^- + Pu^{3+} \rightleftarrows PuI^{2+}$	1.1 ± 0.4	-6.28 ± 2.28

[a] Data from Lemire *et al.* (2001).

concentrations, the higher oxidation states can persist in the presence of excess NTA and EDTA for weeks (AlMahamid *et al.*, 1996). For Pu(VI), stability constants have been reported for the complexes with IDA^{2-} and $EDTA^{4-}$, $\log_{10}\beta_1 = 8.5$ (Cassol *et al.*, 1973), $\log_{10}\beta_1 = 14.6$ (Cauchetier and Guichard, 1975), respectively. Comparable constants reported for uranyl aminocarboxylates and for other ligand complexes of Pu(VI), suggest that these constants, while not yet confirmed by multiple independent studies, accurately describe the stability of the solution species.

(*iii*) *Halides*

Halide complexes were among the first complexes studied for plutonium and the fluorides and chlorides are of particular importance in plutonium purification and metal production as discussed in Sections 7.5 and 7.7.1. The formation constants for aqueous halide complexes of plutonium(III, IV, and VI) that have been critically evaluated by the NEA reviewers are listed in Table 7.58 (Lemire *et al.*, 2001; Guillaumont *et al.*, 2003). Only the addition of one or two halide ligands to any plutonium aqueous species is considered reliably established by these reviewers.

Many double salts of plutonium(III–VI) fluorides and chlorides have been reported (see Tables 7.46 and 7.47) and these salts have been prepared by aqueous or high temperature methods or combinations of these methods as described in Section 7.8.6(d). Where XRD data are available, the plutonium salts are usually observed to be isostructural with analogous compounds for thorium, uranium, neptunium, or the early lanthanides. For example, K_2PuCl_5 is isostructural with K_2PrCl_5 (Axler *et al.*, 1992) and $[K(18\text{-Crown-6})]_2PuO_2Cl_4$ is isostructural with $[K(18\text{-Crown-6})]_2UO_2Cl_4$ (Danis *et al.*, 2001; Clark, in preparation).

(*iv*) *Cation–cation complexes*

Owing to the linear structure and primary ionic bonding in the equatorial plane of actinyl ions AnO_2^{2+} and AnO_2^{+} (see Section 7.9.3), the oxygen atoms within these ions have a negative charge and can form bonds with a second metal center to produce 'cation–cation' complexes. This type of interaction was first characterized for UO_2^{2+} and NpO_2^{+} (Sullivan *et al.*, 1961), and is most well known for NpO_2^{+} (Stout *et al.*, 1993). For example, the structure of $NpO_2(ClO_4)\cdot 4H_2O$ consists of layers of NpO_2^{+} cations where axial O=Np=O units link to the equatorial plane of adjacent NpO_2^{+} units (Grigor'ev *et al.*, 1995). Interactions of this type have also been observed for the plutonyl ions. Newton and Burkhart (1971) oxidized Pu(IV) with Cr(VI) in dilute $HClO_4$ solution to form a $CrOPuO^{4+}$ cation, and recovered the complex by ion exchange. Photoacoustic spectroscopy was used to estimate an equilibrium

constant of $K = (2.2 \pm 1.5)$ L mol^{-1} for the interaction between UO_2^{2+} and PuO_2^+ in a 6.0 M perchlorate solution (Stoyer *et al.*, 2000).

7.9.2 Nonaqueous and organometallic chemistry

There is an extensive literature on the nonaqueous and organometallic coordination chemistry of the light actinide elements thorium and uranium. A good deal of this chemistry should, in principle, be accessible to plutonium. Extending this chemistry to plutonium and other transuranium elements would be of great value in elucidating trends in structure and bonding across the actinide series. Unfortunately, the corresponding plutonium chemistry is virtually unexplored, clearly due to the extreme difficulty associated with handling plutonium isotopes, the paucity of synthetic laboratories equipped to conduct this kind of chemical research, and the scarcity of suitable starting materials. The known chemistry has been summarized in several excellent reviews by Ephritikhine (1992), Burns and Sattelberger (2002), Burns *et al.* (2005), and Burns and Eisen in Chapter 25 of this work.

(a) Sigma-bonded ligands

(*i*) *Organic-solvent soluble halides*

As discussed in Section 7.8.6(b), the binary trihalides, PuX_3 (X = F, Cl, Br, I) are polymeric solids that are insoluble in polar organic solvents. Therefore, the PuX_3 compounds have not been particularly useful starting materials for the nonaqueous preparation of other inorganic or organometallic complexes. Over the last two decades, there has been considerable effort to develop organic-solvent soluble forms of plutonium trihalides. Karraker (1987) reported the reaction between alpha plutonium metal and 1,2-diiodoethane in tetrahydrofuran (THF) solvent to give the solvated triiodide complex $PuI_3(THF)_x$, and suggested that such complexes would be useful synthetic starting materials for preparation of nonaqueous inorganic and organometallic compounds. Zwick, Avens and coworkers subsequently reported that stoichiometric amounts of elemental iodine would oxidize plutonium metal in aprotic, coordinating solvents such as THF, pyridine (Py), or dimethylsulfoxide (DMSO) to give hydrocarbon soluble Lewis base adducts of formula PuI_3L_4 in extremely high yields (Zwick *et al.*, 1992; Avens *et al.*, 1994). Unlike the corresponding reaction between uranium metal and iodine, there is no need to rigorously remove any oxide coating from the surface of plutonium metal. The reaction is exothermic, however, and will cause the solvent to boil if the rate of iodine addition is too rapid.

$$2Pu + 3ICH_2CH_2I \xrightarrow[THF]{} 2PuI_3(THF)_x + 3C_2H_4 \qquad (7.140)$$

$$2Pu + 3I_2 \xrightarrow[L]{} 2PuI_3L_4, \quad (L = THF, Py, DMSO) \tag{7.141}$$

Infrared spectra of PuI_3L_4 compounds are virtually identical to their UI_3L_4 counterparts, and show vibrational bands characteristic of coordinated ligands. Thermogravimetric analysis demonstrated that upon heating PuI_3L_4, all four coordinated solvent molecules are displaced between 56 and 180°C to give anhydrous PuI_3. Room temperature ^{1}H NMR spectra of $PuI_3(THF)_4$ in $CDCl_3$ solution shows a single THF ligand environment, consistent with the spectra of the $NpI_3(THF)_4$ and $UI_3(THF)_4$ analogs (Avens *et al.*, 1994). Unlike the uranium and neptunium analog spectra, $PuI_3(THF)_4$ shows reasonably sharp ^{1}H NMR resonances ($\Delta\nu_{1/2} = 11.4$ Hz). Subsequent variable temperature ^{1}H NMR experiments in CD_2Cl_2 solution revealed a dynamic solution process that generates equivalent THF ligand resonances at room temperature, but freezes out a static structure at –90°C with two types of coordinated THF ligand consistent with the solid-state structure of $UI_3(THF)_4$ (**21**). The NMR data were interpreted in terms of the dynamic equilibrium between **21** and **22** shown below. Therefore, while no crystallographic data have been presented for $PuI_3(THF)_4$, the detailed characterization of the series of $AnI_3(THF)_4$ complexes (An = U, Np, Pu) leaves little doubt that in the solid state, the molecule displays the pentagonal bipyramidal coordination geometry, with two trans iodide ligands occupying apical coordination sites, and the third iodide and four THF ligands lying in the equatorial plane as shown in **21** below.

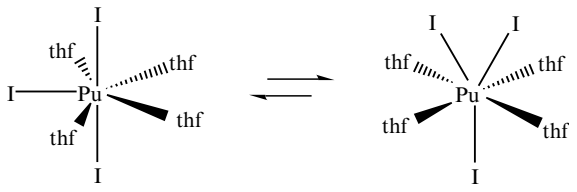

21 **22**

In a variation of the oxidative dissolution of plutonium metal, Enriquez *et al.* (2003) found that plutonium metal will also dissolve in acetonitrile solvent in the presence of three equivalents of thallium or silver hexafluorophosphate as the oxidant to give a blue solution containing $Pu(NCMe)_9^{3+}$. Filtration and cooling gives crystals of $[Pu(NCMe)_9][PF_6]_3 \cdot MeCN$.

$$Pu \xrightarrow[MeCN]{3MPF_6} [Pu(NCMe)_9][PF_6]_3 \cdot MeCN, \quad (M = Ag, T1) \tag{7.142}$$

The solid-state crystal structure reveals a $Pu(NCMe)_9^{3+}$ cation surrounded by three noncoordinating PF_6^- anions. The $Pu(NCMe)_9^{3+}$ ion displays a nine-coordinate tricapped trigonal prismatic coordination environment as

shown in **23**. There is little variation in the Pu–N bond distances between apical and capping ligands, which span the narrow range between 2.554(4) and 2.579(5) Å.

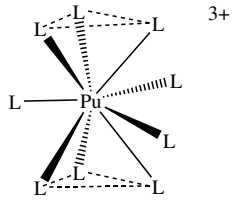

23

While binary $PuCl_4$ is unstable in the solid state (see Section 7.8.6(b)), it can be stabilized by formation of Lewis base adducts. Bagnall and coworkers showed that the reaction of Cs_2PuCl_6 with amide ($RCONR'_2$) or phosphine oxide (R_3PO) ligands in dichloromethane or acetonitrile solvent gives the Lewis base adducts $PuCl_4L_2$ or $PuCl_4L_3$, depending on the steric demands of the Lewis base (Bagnall *et al.*, 1961, 1985a). These adducts were characterized by IR, diffuse reflectance, and X-ray powder diffraction. In many cases, the solids were reported to be isostructural with thorium or uranium counterparts. The $PuCl_4L_2$ complexes were presumed to contain a pseudo-octahedral plutonium center, with trans Lewis base ligands. These Lewis base adducts have the potential to serve as good synthetic starting materials, though their general utility has yet to be explored.

(*ii*) *Amides*

The Lewis base adducts of plutonium triiodide have proven to be useful starting materials for the preparation of a number of trivalent organometallic and nonaqueous coordination compounds. A THF slurry of $PuI_3(THF)_4$ reacts smoothly at room temperature with three equivalents of $NaN(SiMe_3)_2$ to give an air-sensitive yellow-orange $Pu[N(SiMe_3)_2]_3$ in 93–95% yield (Zwick *et al.*, 1992; Avens *et al.*, 1994).

$$PuI_3(THF)_4 + 3NaN(SiMe_3)_2 \xrightarrow{THF} Pu[N(SiMe_3)_2]_3 + 3NaI \qquad (7.143)$$

The tris silylamide complex sublimes at 60°C under reduced pressure, gives an elemental analysis consistent with the formulation of $Pu[N(SiMe_3)_2]_3$, and shows a single ^1H NMR resonance at $\delta = 0.7$ ppm. The infrared spectra display vibrational features nearly identical to the uranium counterpart, and reveal the asymmetric $\nu(PuNSi_2)$ stretch at 986 cm^{-1}. Based on the similarity in spectroscopic properties, it is presumed that this compound will display the

well-established pyramidal structure that is shared by the uranium and lanthanide analogs as indicated in **24**.

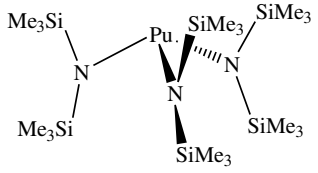

24

(*iii*) *Alkoxides*

Zwick and coworkers reported that the alcoholysis of $Pu[N(SiMe_3)_2]_3$ with the sterically demanding 2,6-$Bu^t_2C_6H_3(OH)$ gives the tan, air-sensitive tris aryloxide derivative $Pu(O\text{-}2,6\text{-}Bu^t_2C_6H_3)_3$ in 70% yield (Zwick *et al.*, 1992). The structural formulation as a monomeric compound is based on the similarity of spectroscopic data (^1H NMR and IR) to the well-characterized uranium analog which shows a monomeric structure in the solid state (Van der Sluys *et al.*, 1988).

$$Pu[N(SiMe_3)_2]_3 + 3HO\text{-}2,6\text{-}Bu^t_2C_6H_3 \xrightarrow{\text{hexane}} Pu(O\text{-}2,6\text{-}Bu^t_2C_6H_3)_3 + 3HN(SiMe_3)_2 \quad (7.144)$$

The tris aryloxide complex will coordinate Lewis bases to form $LPu(O\text{-}2,6\text{-}Bu^t_2C_6H_3)_3$ complexes (shown in **25**), where L is triphenylphosphine oxide, 4,4′-dimethoxybenzophenone, or *N*,*N*-di-isopropyl-benzamide (Oldham *et al.*, 2000). The relative binding affinities were found to correspond with that observed in process extraction chemistry (see Section 7.5.4), with the phosphine oxide and benzamide showing similar binding affinities, which were much larger than that of the benzophenone. Kinetic investigations of the self-exchange process probed by ^{31}P NMR spectroscopy yielded activation parameters indicative of an associative process, with a five-coordinate $L_2Pu(O\text{-}2,6\text{-}Bu^t_2C_6H_3)_3$ intermediate (**26**).

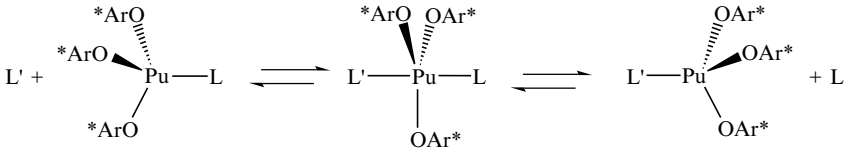

25 **26** **25**

Bradley and coworkers prepared aliphatic alkoxide complexes of general formula $Pu(OR)_4$ using $(Hpy)_2PuCl_6$ and benzene/alcohol solutions containing ammonia (Bradley *et al.*, 1957). With excess isopropanol, the reaction mixture was stirred with NH_3 at room temperature, and then the NH_4Cl and C_5H_6NCl salts removed by filtration. Solvent removal produced a mixture of grass-green $Pu(OPr^i)_4$ and $(Py)Pu(OPr^i)_4$. Recrystallization from isopropanol gives emerald green $Pu(OPr^i)_4(Pr^iOH)$. The base-free, homoleptic $Pu(OPr^i)_4$ compound sublimes at 220°C (0.05 mmHg). A similar reaction employing a large excess of *t*-butanol/benzene gave pale green $Pu(OBu^t)_4$, which sublimes at 112°C (0.05 mmHg). These aliphatic alkoxides were extremely sensitive to moisture, but appeared to be unaffected by dry air. No other characterization data have been reported.

$$(Hpy)_2PuCl_6 + xsPr^iOH \xrightarrow[NH_3/C_6H_6]{} Pu(OPr^i)_4(HOPr^i) + 4(NH_4)Cl + 2HpyCl \quad (7.145)$$

Very little is known about the trivalent isopropoxide, $Pu(OPr^i)_3$, although its use in catalytic reduction of ketones by isopropanol has been reported. Warner and coworkers examined the ability of trivalent and tetravalent lanthanide and actinide isopropoxides to facilitate the Meerwein–Ponndorf–Verley reduction of ketones (Warner *et al.*, 2000). Tetravalent $Pu(OPr^i)_4$ was found to be inactive in ketone reduction, but *in situ* production of $Pu(OPr^i)_3$ by dissolution of $Pu[N(SiMe_3)_2]_3$ in neat isopropanol generated an effective catalyst for the reduction of a range of substituted aryl-alkyl ketones, with yields that were equal or higher than similar reactions employing lanthanides.

(*iv*) *Alkyls*

There is only one example in the literature of an alkyl complex of plutonium, but its characterization data is limited to IR spectroscopy. Zwick and coworkers reported that the reaction of $Pu(O\text{-}2,6\text{-}Bu^t_2C_6H_3)_3$ with three equivalents of $LiCH(SiMe_3)_2$ in hexane solution yields yellow-brown $Pu[CH(SiMe_3)_2]_3$ as an oily solid (Zwick *et al.*, 1992). The IR spectrum was virtually identical to the well-characterized $U[CH(SiMe_3)_2]_3$ analog (Van der Sluys *et al.*, 1989). Other chemical characteristics, such as extreme sensitivity to air, rapid decomposition in solution, and thermal instability are consistent with this formulation. If the formulation is correct, then this complex would be an extremely rare example of a true organometallic complex of plutonium containing metal–carbon sigma bonds.

(*v*) *Borohydrides*

The first attempt to prepare plutonium borohydride was made by Schlesinger and Brown at the University of Chicago Metallurgical Laboratory in 1942 (Schlesinger and Brown, 1943). These authors tried to prepare plutonium borohydride in tracer quantities by reaction of uranium tetrafluoride containing trace amounts of plutonium with aluminum borohydride. Excess aluminum borohydride was removed and the reaction products that were volatile at 60°C were condensed at 20, 0, –23, –80, and –190°C. Only a few percent of the plutonium was recovered from the volatile fractions, the bulk of the plutonium remaining in the nonvolatile residue in the reaction vessel. It was therefore concluded that plutonium borohydride was either not formed or was not volatile at 60°C.

The first unequivocal preparation of plutonium(IV) borohydride was accomplished by Banks, Edelstein and coworkers (Banks *et al.*, 1978; Banks, 1979; Banks and Edelstein, 1980) at the Lawrence Berkeley Laboratory. Treatment of anhydrous PuF_4 with $Al(BH_4)_3$ at 0°C for 4 h in a solvent-free sealed tube reaction gives $Pu(BH_4)_4$ according to the reaction below.

$$PuF_4 + 2Al(BH_4)_3 \rightarrow Pu(BH_4)_4 + 2Al(BH_4)F_2 \qquad (7.146)$$

The unreacted $Al(BH_4)_3$ passes through a dry-ice trap and is collected in a liquid nitrogen trap. The $Pu(BH_4)_4$ is not as volatile and can be collected in the dry-ice trap. By intermolecular exchange in the gas phase with D_2, the deuterated compound $Pu(BD_4)_4$ may also be prepared. $Pu(BH_4)_4$ is a pyrophoric bluish-black liquid that melts at approximately 14°C. Infrared spectroscopy indicates that the compound adopts a monomeric pseudo-tetrahedral coordination geometry similar to $Zr(BH_4)_4$ and $Hf(BH_4)_4$ in the gas phase. Low temperature X-ray powder diffraction was consistent with this assessment, and suggests that the monomeric compound consists of a tetrahedral arrangement of four BH_4^- units coordinated by three B–H bridges per borohydride, giving the 12-coordinate structure shown in **27** below.

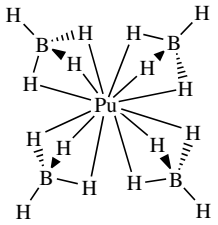

27

(b) Pi-bonded ligands

(*i*) *Cyclooctatetraene complexes*

The synthesis and characterization of the uranium(IV) sandwich complex, U(η-$C_8H_8)_2$, uranocene, was an important milestone in the history of organometallic chemistry, as it represented the logical extension of the bonding concepts that were developing for organotransition metal complexes (Seyferth, 2004). It was only a few years later when the plutonium analog was reported.

Bis(cyclooctatetraenyl)plutonium, or 'plutonocene' has been prepared by metathesis of $[NEt_4]_2[PuCl_6]$ with two equivalents of $K_2(C_8H_8)$ in THF solution to give a bright red product (Karraker *et al.*, 1970). Alternatively, $Pu(C_8H_8)_2$ may be prepared by reaction of degassed cyclooctatetraene, C_8H_8, with finely divided plutonium metal (prepared through hydride–dehydride cycles) in a sealed glass tube. The reaction mixture was heated at 160°C for 15 min, producing a red sublimate of $Pu(C_8H_8)_2$ (Starks and Streitwieser, 1973). Plutonocene reacts rapidly with air, and is only sparingly soluble in aromatic and chlorinated hydrocarbon solvents.

$$(NEt_4)_2PuCl_6 + 2K_2C_8H_8 \rightarrow Pu(\eta\text{-}C_8H_8)_2 + 2(NEt_4)Cl + 4KCl \quad (7.147)$$

$$Pu + 2C_8H_8 \rightarrow Pu(\eta\text{-}C_8H_8)_2 \quad (7.148)$$

The hydrocarbon solution solubility of plutonocene is enhanced by adding alkyl groups to the C_8H_8 rings. A number of alkyl substituted derivatives have been prepared, including $Pu(EtC_8H_7)_2$, $Pu(Bu^nC_8H_7)_2$, and $Pu(Bu^tC_8H_7)_2$ using the metathesis route employing $[NEt_4]_2[PuCl_6]$ and the potassium salt of the annulene dianion (Karraker, 1973; Eisenberg *et al.*, 1990). The tetramethyl-substituted complex Pu(1,3,5,7-$Me_4C_8H_4)_2$ was originally claimed (Solar *et al.*, 1980), but subsequent studies on other alkyl substituted complexes led Streitwieser to conclude that this compound was almost certainly the trivalent complex $[K(THF)_2][Pu(1,3,5,7\text{-}Me_4C_8H_4)_2]$ (Eisenberg *et al.*, 1990).

Single crystal XRD studies on $U(C_8H_8)_2$ shows that this molecule adopts a sandwich-type structure with the uranium center sandwiched between two planar C_8H_8 rings in rigorous D_{8h} symmetry (Zalkin and Raymond, 1969; Avdeef *et al.*, 1972). X-ray powder diffraction, infrared, electronic absorption, solution NMR, and Mössbauer spectroscopy reveal that the neptunium and plutonium analogs maintain the identical D_{8h} structure as shown in **28** (Karraker *et al.*, 1970; Karraker, 1973; Eisenberg *et al.*, 1990). Plutonocene is unique in that it has a $J = 0$ ground state with temperature-independent paramagnetism. Optical spectroscopy shows electronic transitions with intensities approaching 1000 (L mol^{-1} cm^{-1}), which argued against the assignment as 5f–5f transitions, and suggested an unusual 5f–6d orbital mixing with appreciable covalency in the bonding (Karraker *et al.*, 1970; Hayes and Edelstein, 1972).

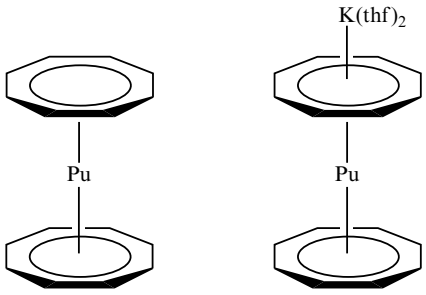

28 **29**

A number of trivalent plutonocene complexes of the type $[K(THF)_2][Pu(RC_8H_7)_2]$ have been prepared, where R = an alkyl group or H. These are prepared by reaction of $PuBr_3$ or PuI_3 with $K_2(RC_8H_7)$ in THF solution at –10 to –20°C (Karraker and Stone, 1974). These complexes may also be prepared by the direct reaction of potassium metal with $Pu(RC_8H_7)_2$ in THF solution (Eisenberg *et al.*, 1990).

$$PuX_3 + 2K_2C_8H_8 \xrightarrow[THF]{} [K(THF)_2][Pu(\eta\text{-}C_8H_8)_2] + 3KX \ (X = Br, I) \quad (7.149)$$

$$Pu(\eta\text{-}C_8H_8)_2 + K \xrightarrow[THF]{} [K(THF)_2][Pu(\eta\text{-}C_8H_8)_2] \quad (7.150)$$

The trivalent $[K(THF)_2][Pu(C_8H_8)_2]$ complex was described as turquoise-green, and it has been characterized by elemental analysis, X-ray powder diffraction, and magnetic susceptibility measurements (Karraker and Stone, 1974). The lime green $[K(THF)_2][Pu(Bu^tC_8H_7)_2]$ was not isolated, but was produced *in situ* in deuterated THF solvent, and characterized by ^1H NMR (Eisenberg *et al.*, 1990). The change in chemical shifts in the NMR spectrum with temperature was indicative of paramagnetic behavior expected for Pu(III). The solid-state structure of the uranium analog, $[K(diglyme)][U(C_8H_8)_2]$ has been determined by single crystal XRD revealing that the potassium ion is also involved in a multihapto interaction with a C_8H_8 ring. The X-ray powder diffraction data on the plutonium analogs indicate similar structures, as shown in **29** (Karraker and Stone, 1974).

(*ii*) *Cyclopentadienyl complexes*

Cylcopentadienyl ligands (C_5H_5, Cp) have played a central role in the development of the field of organometallic chemistry. The same is true in the field of organoactinide chemistry that was inaugurated with Reynolds and Wilkinson's seminal report on the preparation of $(C_5H_5)_3UCl$ in 1956 (Reynolds and Wilkinson, 1956). The first plutonium compounds containing cyclopentadienyl

ligands were reported by Baumgärtner and coworkers in 1965 (Baumgärtner *et al.*, 1965).

The microscale reaction between anhydrous $PuCl_3$ and molten $(C_5H_5)_2Be$ at around 70°C produces tris(cyclopentadienyl)plutonium, $(C_5H_5)_3Pu$, (or Cp_3Pu) (Baumgärtner *et al.*, 1965). Fractional sublimation first removes unreacted $(C_5H_5)_2Be$, and allows the moss green $(C_5H_5)_3Pu$ product to be isolated at a sublimation temperature of approximately 170°C. The transmetallation using $(C_5H_5)_2Be$ has been very useful for preparing transplutonium tris(cyclopentadienyl) complexes, but the nuisance of α-n reactions between the plutonium and beryllium nuclei limit the scale of the reaction. To prepare larger quantities of $(C_5H_5)_3Pu$, Crisler and Eggerman (1974) turned to the reaction between plutonium chloride starting materials with sodium or magnesium metathesis reagents. Both $PuCl_3$ and Cs_2PuCl_6 react with $(C_5H_5)_2Mg$ in THF solution to yield an emerald green product. In THF solution the first product is most likely $(C_5H_5)_3Pu(THF)$, which loses the THF ligand during sublimation to yield $(C_5H_5)_3Pu$ at 140°C under reduced pressure. The reaction is over within minutes when Cs_2PuCl_6 is employed as compared to hours for the reaction with $PuCl_3$. This is most likely because Cs_2PuCl_6 contains discrete $PuCl_6^{2-}$ ions, while $PuCl_3$ displays an extended three-dimensional structure (see Section 7.8.6(b)). Tris (cyclopentadienyl)plutonium can also be prepared from the reaction of $PuCl_3$ with $(C_5H_5)Na$ in THF solution, but the reaction requires 10 days. Zwick and coworkers found that a very convenient way to circumvent this solubility problem is to react $PuI_3(THF)_4$ with three equivalents of $(C_5H_5)Li$ in THF solution (Zwick *et al.*, 1992).

$$2PuCl_3 + 3Be(C_5H_5)_2 \xrightarrow[\text{melt}]{70^\circ} 2(\eta\text{-}C_5H_5)_3Pu + 3BeCl_2 \tag{7.151}$$

$$PuCl_3 + 3Na(C_5H_5) \xrightarrow[\text{THF}]{} (\eta\text{-}C_5H_5)_3Pu(THF) + 3NaCl \tag{7.152}$$

$$2PuCl_3 + 3Mg(C_5H_5)_2 \xrightarrow[\text{THF}]{} 2(\eta\text{-}C_5H_5)_3Pu(THF) + 3MgCl_2 \tag{7.153}$$

$$PuI_3(THF)_4 + 3Li(C_5H_5) \xrightarrow[\text{THF}]{} (\eta\text{-}C_5H_5)_3Pu(THF) + 3LiI \tag{7.154}$$

X-ray powder diffraction data suggest that $(C_5H_5)_3Pu$ is isostructural with $(C_5H_5)_3Ln$ compounds. The lanthanide analogs have been shown to contain polymeric zigzag chains of distinct $(C_5H_5)_2Ln(\mu\text{-}\eta^2\text{-}\eta^5\text{-}C_5H_5)$ units (Hinrichs *et al.*, 1983).

Bagnall and coworkers reported that the reaction between $(C_5H_5)Tl$ and Cs_2PuCl_6 in acetonitrile solution does not give an overall reduction to trivalent plutonium as discussed above, but produces tetravalent $(C_5H_5)_3PuCl$ (Bagnall *et al.*, 1982a). The chloride can be replaced with thiocyanate via a simple metathesis reaction with stirring in a THF solution of K(NCS) for 16 h (Bagnall *et al.*, 1982a). Both the chloride and thiocyanate complexes are dark brown and

moisture sensitive, and both are soluble in THF and acetonitrile solution. The anionic analog, $(C_5H_5)_3Pu(NCS)_2^-$, is also reported as a tetraphenylarsonium salt, but little characterization data have been reported (Bagnall *et al.*, 1982b).

$$Cs_2PuCl_6 + 3Tl(C_5H_5) \xrightarrow[CH_3CN]{} (\eta\text{-}C_5H_5)_3PuCl + 2CsCl \tag{7.155}$$

$$(\eta\text{-}C_5H_5)_3PuCl + K(NCS) \xrightarrow[THF]{} (\eta\text{-}C_5H_5)_3Pu(NCS) + KCl \tag{7.156}$$

The chloride compound, $(C_5H_5)_3PuCl$, was found to be isostructural with its uranium counterpart (Bagnall *et al.*, 1982a), which contains a pseudo-tetrahedral unit in which the centroids of the Cp rings occupy three vertices, and the chloride takes up the fourth as illustrated in **30**.

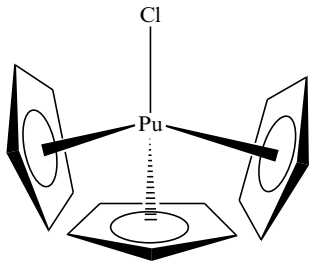

30

Bagnall and coworkers have prepared several examples of mono(cyclopentadienyl) plutonium complexes (Bagnall *et al.*, 1985b). Room temperature reaction of $(C_5H_5)Tl$ with $PuCl_4L_2$ or Cs_2PuCl_6 in dry acetonitrile for 48 h gave $(C_5H_5)PuCl_3L_2$ in 50–85% yield depending on the nature of the Lewis base, L. Neutral Lewis base ligands (L) included a number of phosphine oxide (R_3PO) and amide ($RCONR'_2$) derivatives. Similar reactions employing $(C_5H_5)Tl$ and $Pu(NCS)_4L_2$ produced the analogous $(C_5H_5)Pu(NCS)_3L_2$ complexes (Bagnall *et al.*, 1986). All of these materials have been characterized by infrared and Vis-NIR spectroscopy. It is assumed that these complexes adopt a structure similar to their uranium analogs.

7.9.3 Electronic structure and bonding

(a) Ionic and covalent bonding models

The nature of metal–ligand bonding in light actinide compounds and complexes is quite complicated. In general, the actinides are best viewed as being intermediate between the strongly ionic bonding observed in lanthanide elements, and the more covalent bonding observed in d-block transition elements. There are clearly cases that show ionic behavior, and there are just as clearly cases that show considerable covalency.

Many plutonium–ligand bonds are nondirectional, and determined largely by electrostatic attraction to the metal, electrostatic repulsion between ligands, and steric demands around the metal center. These metal–ligand bonds are relatively weak, and kinetically labile in solution. There are also examples of metal–ligand bonds that are incredibly strong, show a stereochemical orientation, and are kinetically inert. The former situation is often taken as evidence for ionic behavior, while the latter is clearly consistent with covalent interactions. The view that plutonium complexes are generally ionic is supported by the premise that the 5f orbitals are core-like in that they are so contracted they cannot interact in bonding with the ligands. This is generally what is observed, especially for the heavier actinide elements. However, the 5f orbitals of the lighter actinides are much less contracted, and there are certain classes of compounds where the 5f orbitals have been shown to play a significant role in covalent metal–ligand bonding. By consideration of the behavior of the 5f orbitals alone, it is difficult to reconcile these stark differences in chemical behavior.

This is an area where electronic structure calculations have taught us a great deal about how to think about the nature of chemical bonding in molecular plutonium complexes. Electronic structure calculations have demonstrated that for metal–ligand bonding in plutonium (and all light actinides) one cannot consider the 5f orbitals alone, but must consider the relative roles of both the virtual 5f and 6d orbitals as well as the 'semicore' 6s and 6p orbitals. The radial distributions of the plutonium 6s and 6p semicore orbitals lie in the valence region, and they must be considered as active in chemical bonding. In addition, the virtual 6d orbitals are relatively low-lying, and have far larger radial extent than the 5f orbitals. This is illustrated in the radial distribution function for a Pu^{3+} ion shown in Fig. 7.120 (Schreckenbach *et al.*, 1999). Most modern quantum chemical calculations find evidence of mixing of the 6p semicore orbital into metal–ligand bonding combinations. Moreover, there is now a general consensus that the dominant metal–ligand bonding takes place through ligand interactions with the 6d orbitals. The 6d orbitals are strongly split by the presence of a ligand field (as in transition element complexes), but the more contracted 5f orbitals show only weak splitting. The ground state electron configurations are therefore generally governed by the occupation of these closely spaced 5f orbitals, which leads to many open shell states. Spin–orbit coupling and electron correlation effects are extremely important, particularly for understanding spectroscopic properties. In addition to Chapter 17, several excellent reviews exist that describe trends and views on the electronic structure of actinide molecular complexes (Bursten and Strittmatter, 1991; Pepper and Bursten, 1991; Denning, 1992; Schreckenbach *et al.*, 1999; Matsika *et al.*, 2001).

(b) Specific examples

There are a number of specific examples in plutonium chemistry where covalency in metal–ligand bonding plays an important role in the observed chemical

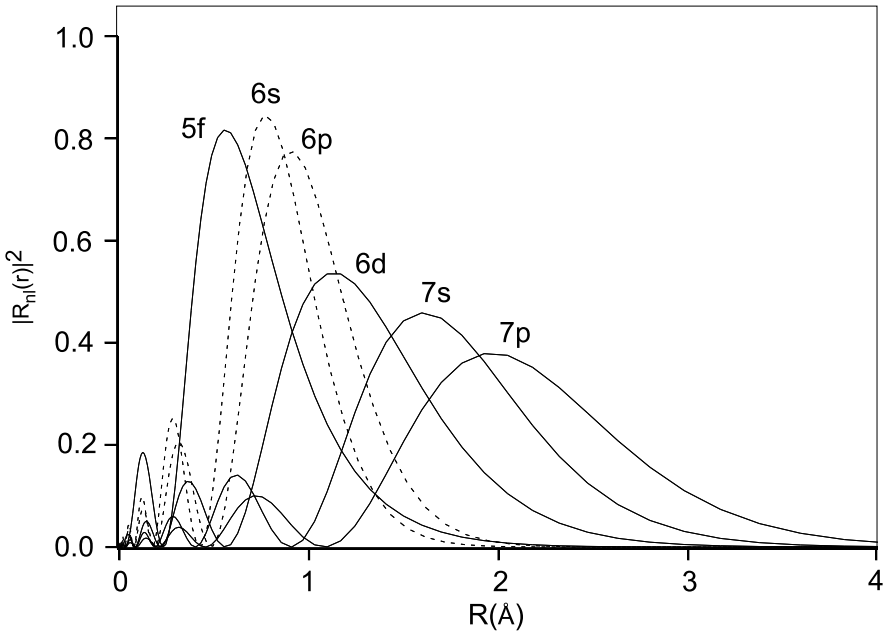

Fig. 7.120 *Radial probability densities of* Pu^{3+} *valence orbitals from relativistic Hartree–Fock orbitals* $\Phi_{nl}(r)$ (*Schreckenbach* et al., 1999). *The authors are grateful to P.J. Hay of Los Alamos for providing the raw data used to prepare this figure.*

behavior. These are plutonium hexafluoride, PuF_6, the linear plutonyl cation, PuO_2^{2+}, and the organoplutonium sandwich compound plutonocene, $Pu(\eta\text{-}C_8H_8)_2$. We provide a qualitative discussion of the bonding in these systems, illustrate the main 6d and 5f orbital interactions, and highlight the 'strong field-weak field' differences in 6d and 5f interactions that make spin–orbit splitting important for understanding spectroscopic properties. Before discussing the examples, we remind the reader that unlike p- or d-orbitals, there is no unique way of representing the angular dependence functions of all seven f-orbitals. In high symmetry cubic point groups, a cubic set of orbitals is used, while in systems containing a high order axis of symmetry, a general set can be used. These two common sets of f-orbital depictions are simply linear combinations of each other, and they are illustrated qualitatively in Fig. 7.121. We will use both the general and cubic orbital sets in describing the bonding in our examples.

(*i*) *PuF_6*

As discussed in Section 7.8.6(a), plutonium hexafluoride is a stable molecule in the gas-phase. In view of the electronegativity difference between hexavalent plutonium and the fluoride anion, this observation might seem somewhat surprising in that one might expect Pu–F bonds to show the greatest ionic

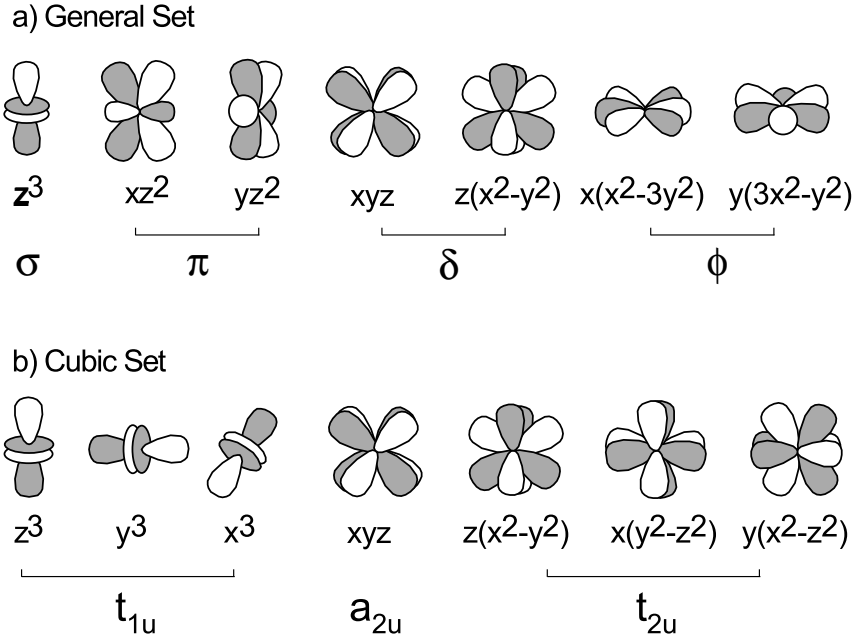

Fig. 7.121 *Qualitative representations of the general (a) and cubic (b) sets of valence f orbitals.*

behavior. Spectroscopic properties show that this is clearly not the case. Electronic structure calculations have provided some valuable insights into the nature of Pu–F bonding in this system.

A number of high-level electronic structure calculations have been performed on AnF_6 systems, with the majority of calculations performed on uranium. Calculations on PuF_6 have been reported by Kugel *et al.* (1976), Koelling *et al.* (1976), Boring and Hecht (1978), Wadt (1987), Hay and Martin (1998), Schreckenbach *et al.* (1999), and Onoe (1997). It is clear from all the theoretical calculations that the purely ionic bonding model is an inadequate description of PuF_6. A qualitative molecular orbital diagram for PuF_6 based on an octahedral ligand field that contains the basic features of these calculations is shown in Fig. 7.122. The octahedral point group is relatively straightforward as the 5f and 6d orbitals cannot mix by symmetry. The set of σ lone pairs on the six F atoms transform as $a_{1g} + e_g + t_{1u}$ symmetry under O_h symmetry. The 12 π lone pairs transform as $t_{1u} + t_{1g} + t_{2u} + t_{2g}$ under O_h symmetry. As expected, the set of σ lone pairs interacts most strongly with the Pu atom, resulting in molecular orbitals of a_{1g}, e_g, and t_{1u} symmetry which are lower-lying that the π symmetry orbitals. Of the four triply degenerate sets of F ligand π orbitals, the t_{2g} is of appropriate symmetry to interact with the 6d orbitals of the plutonium atom,

the t_{2u} can interact with the 5f orbitals, and the t_{1g} orbital cannot interact with any low-lying metal orbitals, and should remain as an noninteracting set of lone pairs. The t_{1u} orbital can interact with the 5f orbitals of the plutonium atom, but it can also mix with the t_{1u} set of σ orbitals derived from mixing between the semicore 6p and valence 7p orbitals. From simple overlap considerations, one would expect the F lone pair t_{2u} and t_{2g} orbitals to be the most stabilized by donation to the metal, the t_{1g} will be entirely nonbonding, and the t_{1u} will stabilized by π bonding from above, but destabilized by mixing with the σ interaction from below. In all the calculations, appreciable covalency with both 5f and 6d orbitals is present. The covalent interactions are found in Pu–F σ- and π-bonding that takes place through t_{2g} and e_g interactions with Pu 6d orbitals, and σ bonding that takes place through t_{1u} interactions with the 5f and 6p/7p orbitals. These metal–ligand bonding interactions are illustrated qualitatively in the molecular orbital diagram of Fig. 7.122. Wadt employed a Mulliken population analysis to determine the relative amount of plutonium 5f and 6d contribution to bonding (Wadt, 1987). The σ and π components of the t_{1u} interactions are mixed, but the virtual $5t_{1u}$ orbital (the $3t_{1u}$ orbital in Fig. 7.122) was calculated to comprise 71% Pu f, 3% Pu p, and 26% F p character

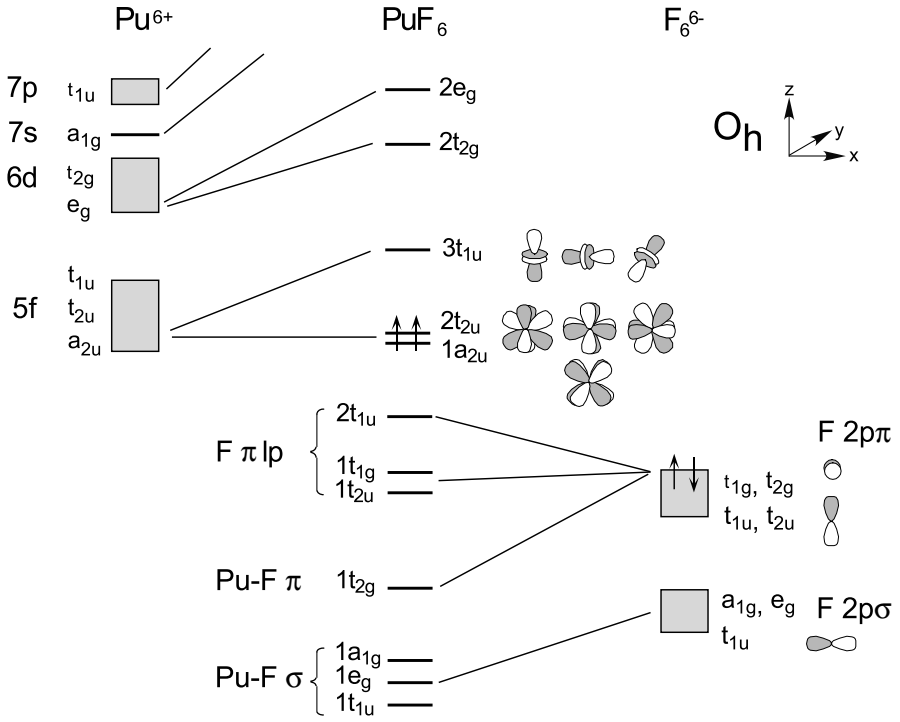

Fig. 7.122 *A qualitative molecular orbital interaction diagram for PuF_6.*

indicating a significant amount of covalency involving Pu 5f orbital interaction with the F ligands. It also shows the importance of mixing 'semicore' 6p character into a f–p σ hybrid orbital that enhances σ bonding. The total population of the Pu 5f orbitals was calculated to be 4.24. Since this system is nominally $5f^2$, the extra 2.24 electrons in 5f orbitals come from σ and π donation from occupied F ligand orbitals into Pu 5f orbitals.

For octahedral PuF_6, a simple filling of this qualitative MO scheme with the 16 valence electrons would give a valence electronic configuration $(1a_{2u})^2$ or $(1a_{2u})^1(2t_{2u})^1$ corresponding to $^1A_{1g}$ or $^3T_{1g}$ ground states, respectively. The 5f ordering in an octahedral ligand field is $a_{2u} < t_{2u} < t_{1u}$, and the calculations indicate that the $1a_{2u}$ and $2t_{2u}$ 5f orbitals are nearly degenerate, suggesting that the $^3T_{1g}$ state would be the likely ground state. This one-electron picture is oversimplistic, because the ligand field splitting of the 5f orbitals is so weak that spin–orbit effects must also be considered. Spin–orbit coupling splits the 5f manifold and gives a $^1\Gamma_{1g}$ (in O_h double group symmetry) ground state. The inclusion of spin–orbit coupling is necessary to understand the stabilization of a singlet ground state, and is in agreement with experiment that shows an absence of temperature-dependent contributions to the magnetic susceptibility, and indicates a nondegenerate ground state. Sophisticated electronic structure calculations are needed to quantify these spin–orbit effects. Wadt employed spin–orbit configuration interaction (CI) calculations that examined all possible arrangements of two electrons in seven 5f levels (Wadt, 1987). Wadt found that the ground $^1\Gamma_{1g}$ state in the octahedral double group representation was comprised of 78% $^3T_{1g}$ and 18% $^1A_{1g}$. More recently, Hay and Martin (1998) performed hybrid DFT calculations on both the $^1A_{1g}$ and $^3T_{1g}$ states and found the $^3T_{1g}$ state to lie lower in energy, consistent with Wadt's study, but did not include the spin–orbit coupling.

(*ii*) PuO_2^{n+}

The linear trans dioxo cations of light actinide elements are among the most well-studied actinide molecular systems. Electronic structure calculations on actinyl ions have revealed a great deal about covalency in metal–oxygen bonds and the relative roles of the valence 5f, 6d, and semicore 6p orbitals. The majority of theoretical studies have been devoted to UO_2^{2+}, but the smaller subset of calculations on PuO_2^{2+} reveals that much of the basic bonding description is essentially the same. The most thorough review on the subject is Denning's 1992 examination of experimental and theoretical work performed up to that time (Denning, 1992). Subsequent reviews build upon that work, and the reader is referred to discussions by Pepper and Bursten (1991), Dyall (1999), Denning *et al.* (2002), and Chapter 17 of this work for additional information.

The trans dioxo cations, AnO_2^{n+}, are invariably linear, regardless of the number of valence 5f electrons. The metal–oxygen bonds are unusually short, strong, and chemically inert. Based on all the experimental and theoretical

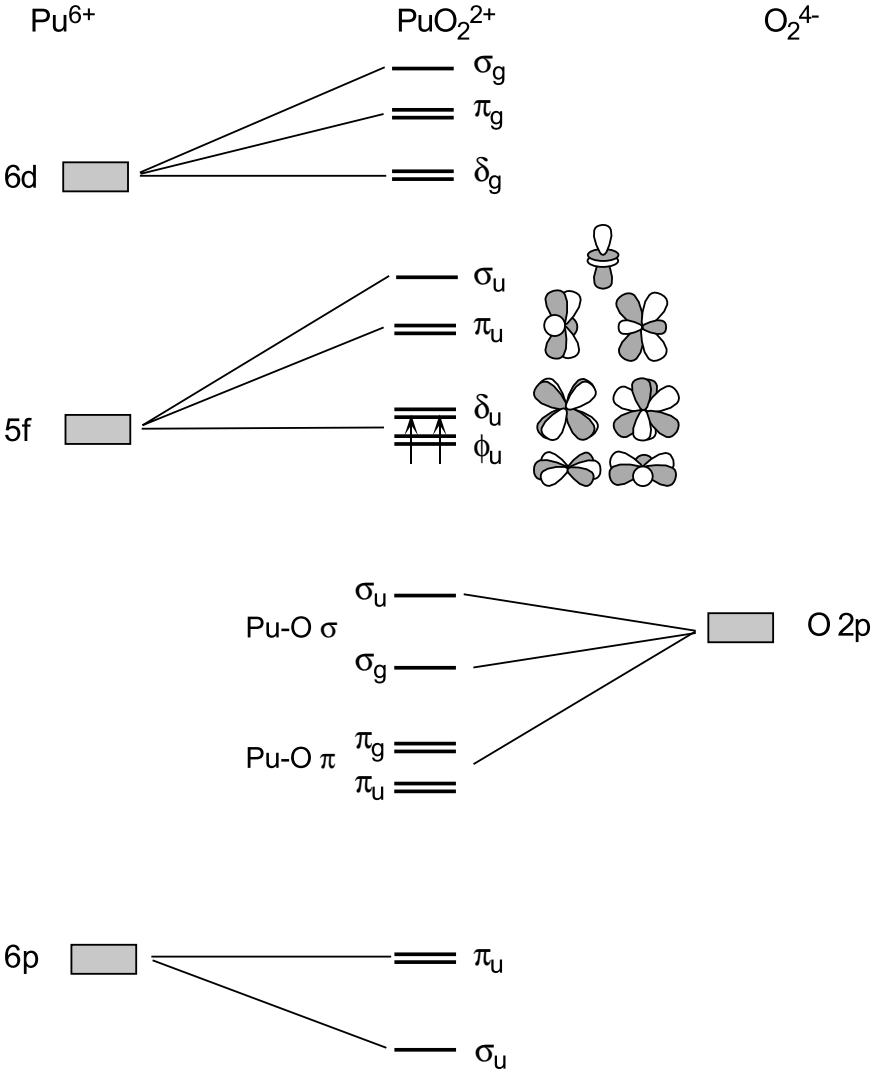

Fig. 7.123 *A qualitative molecular orbital interaction diagram for a linear triatomic* PuO_2^{2+} *ion.*

studies, there is uniform agreement on the molecular orbital description of bonding in these systems. A qualitative molecular orbital diagram for the linear triatomic PuO_2^{2+} ion that contains the basic features of the calculations is given in Fig. 7.123. In centrosymmetric $D_{\infty h}$ symmetry, the molecular orbitals are

conveniently labeled according to their axial symmetry, and the 5f and 6d orbitals cannot mix. The in-phase and out-of-phase combinations of the two O 2p σ orbitals span σ_u and σ_g symmetry, while the corresponding O 2p π orbitals span π_u and π_g symmetry. The metal 6d orbitals span σ_g, π_g, and δ_g symmetry, while the 5f orbitals span σ_u, π_u, δ_u, and φ_u symmetry. Metal–oxygen σ bonds are formed by interaction of the O 2p σ orbitals with metal $6d_{z^2}$ (σ_g) and a hybrid metal orbital formed by mixing $5f_{z^3}$ with the semicore $6p_z$ (σ_u). Metal–oxygen π bonds are formed by interaction of O 2pπ orbitals with metal $6d_\pi$ (π_g) and $5f_\pi$ (π_u) orbitals. The 5f δ_u and φ_u orbitals have no symmetry match with the ligands, and they remain as unperturbed, essentially degenerate, nonbonding 5f orbitals as indicated in Fig. 7.123.

In this qualitative diagram, the 14 valence electrons occupy the molecular orbitals to give a ground state electron configuration of $(\sigma_g^2\pi_g^4\sigma_u^2\pi_u^4)(\delta_u^2)$. Since the δ_u orbital is a nonbonding 5f orbital on the metal, this gives rise to formal Pu–O triple bonds in the linear PuO_2^{2+} unit. These four metal–ligand bonding orbitals are shown qualitatively in **31–34** below.

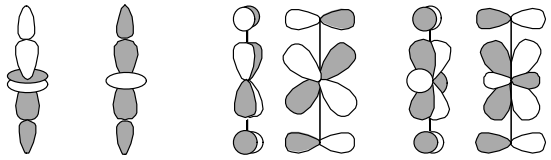

σ_u σ_g π_g π_u

31 **32** **33** **34**

Much discussion and debate has centered around the ordering of the four occupied metal–oxygen bonding orbitals σ_g, π_g, σ_u, and π_u. It is now generally accepted that a filled–filled interaction takes place between the σ_u Pu–O bonding orbital and the lower-lying (semicore) metal $6p_z$ orbital that also has σ_u symmetry. This repulsive interaction keeps the metal–oxygen bonding σ_u at high energy, and this now classical picture has been verified experimentally by Denning and coworkers using polarized oxygen Kα X-ray absorption and emission spectroscopy on a uranyl sample (Denning *et al.*, 2002). The linear trans dioxo cations were the first systems where theoretical calculations revealed that the closed shell (semicore) 6p orbitals were active in chemical bonding. Several studies have focused on the role of semicore 6p involvement, and have shown that $5f_{z^3}$–$6p_z$ hybridization forms an unusually strong metal–oxygen σ bond, and stabilizes the linear geometry (Dyall, 1999; Kaltsoyannis, 2000).

This basic bonding picture holds for all the trans dioxo cations from uranium through plutonium (Hay *et al.*, 2000) and americium. For the 5f orbitals, the overall ordering of levels is $\delta_u \sim \varphi_u < \pi_u << \sigma_u$ because the π_u and σ_u orbitals are destabilized by bonding interactions at lower energy. This basic orbital ordering scheme makes it easy to understand why the AnO_2^{n+} ions remain linear regardless of the number of 5f electrons. As the 5f electron count increases from UO_2^{2+} (f^0) to AmO_2^{2+} (f^3), each successive 5f electron is added to the nonbonding

5f orbitals of δ_u or φ_u symmetry. This is in contrast to transition element complexes where d^0 dioxo complexes are invariably cis, while d^2 dioxo complexes are invariably trans in order to maximize metal–oxygen π bonding. For the actinyl ions, the trans geometry maximizes σ bonding, and the formal metal–oxygen triple bond is retained regardless of the metal 5f electron count.

From this basic molecular orbital description, it is also easy to understand why most equatorial ligands show only a weak interaction with the highly covalent linear AnO_2^{2+} core. Let us consider the D_{4h} symmetry case of four equatorial ligands that only interact via σ bonding to form $PuO_2L_4^{2+}$. The four lone-pair orbitals of the equatorial ligands span a_{1g}, b_{1g}, and e_u symmetry, and these correspond to the $D_{\infty h}$ σ_g, δ_g, and π_u orbitals of the linear PuO_2^{2+} ion. The σ_g orbital has already been significantly destabilized by formation of the axial PuO_2^{2+} σ bonds, and the π_u orbital has very little overlap with incoming ligands in the equatorial plane. This leaves only one component of the degenerate δ_g orbital $\left(d_{x^2-y^2}, d_{xy}\right)$ that is directed towards the incoming ligands. In D_{4h} symmetry, the δ_g orbital $\left(d_{x^2-y^2}, d_{xy}\right)$ transforms as $b_{1g} + b_{2g}$, and only the b_{1g} orbital has the appropriate symmetry to interact. Overall, this gives only one molecular orbital (b_{1g}) that is bonding to all four equatorial bonds with a formal bond order of one quarter. The $PuO_2L_4^{2+}$ molecule therefore has two strong covalent Pu–O triple bonds in the axial direction, and four weak, relatively ionic bonds in the equatorial plane. This qualitative molecular orbital interaction diagram is illustrated in Fig. 7.124.

As in the PuF_6 example, the weak ligand field splitting of the 5f manifold, particularly the δ_u and φ_u orbitals mandates that electron repulsion and spin–orbit interactions be taken into account in order to understand the complexity of molecular electronic spectra. In the actinyl ions, Matsika and coworkers concluded that after consideration of the axial ligand field, electron repulsion was generally larger than spin–orbit coupling, leading them to the use of a Russell–Saunders-like Λ-S coupling scheme to calculate electronic states and optical transitions (Matsika *et al.*, 2001). For the $5f^2$ PuO_2^{2+} system, the $(\delta_u,\varphi_u)^2$ configuration gives two $^3\sum_g^-$ states, $^3\Pi_g$, ^3H_g and several higher energy singlets when only considering electron repulsion. When spin–orbit interaction is taken into account, the ^3H_g is lowered considerably, giving a ground state of $^3H_{4g}$ in agreement with spectroscopic data (Bleaney, 1955; Denning, 1992). Hay *et al.* (2000) obtain the same $^3H_{4g}$ ground state using spin–orbit configuration interaction (CI) calculations.

(*iii*) *Pu*(C_8H_8)$_2$

Following the discovery of the transition metal sandwich complex ferrocene, Fe(η-C_5H_5)$_2$, R. D. Fischer predicted the existence of the U(η-C_8H_8)$_2$ sandwich complex based on the recognition that the nodal properties of f-orbitals would require an expanded C_8H_8 ring (Fischer, 1963). Five years later uranocene, U(η-C_8H_8)$_2$, was synthesized and only shortly thereafter the plutonium

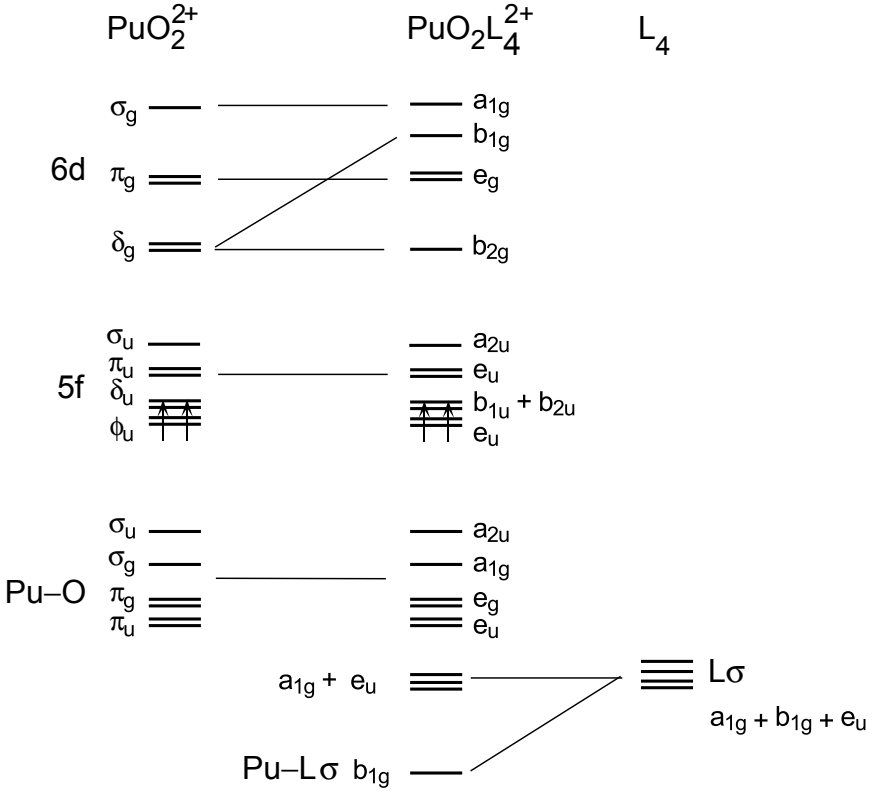

Fig. 7.124 *A qualitative molecular orbital interaction diagram for a linear triatomic PuO_2^{2+} ion interacting with four equatorial ligands, L, to form $PuO_2L_4^{2+}$.*

analog was prepared. As one of the first organometallic actinide complexes, the actinocene system has been the topic of much study aimed at understanding the relative roles of 5f and 6d orbitals in bonding (Boerrigter *et al.*, 1988; Brennan *et al.*, 1989; Kaltsoyannis and Bursten, 1997; Li and Bursten, 1998). A qualitative molecular orbital interaction diagram for Pu(η-C_8H_8)$_2$ under D_{8h} symmetry that contains the basic features of the electronic structure calculations is given in Fig. 7.125. The eight carbon $2p_\pi$ orbitals of the planar $C_8H_8^{2-}$ ring transform as a_{2u}, e_{1g}, e_{2u}, e_{3g}, and b_{1u} symmetry in D_{8h}, and these are often referred to as π_0, π_1, π_2, π_3, and π_4. This π_n nomenclature is convenient for visualization because the value of n refers to the number of nodes in the Hückel p_π orbitals of the $C_8H_8^{2-}$ ring. When two $C_8H_8^{2-}$ rings are brought together in D_{8h} symmetry, the in-phase and out-of-phase combinations of these π_n orbitals give rise to 16 orbitals as indicated in Fig. 7.125. These orbitals retain their π_n parentage as π_0 ($a_{1g} + a_{2u}$), π_1 ($e_{1g} + e_{1u}$), π_2 ($e_{2g} + e_{2u}$), π_3 ($e_{3g} + e_{3u}$), and π_4 ($b_{1u} + b_{2g}$). Interaction of these 16 π orbital combinations with Pu 6d atomic

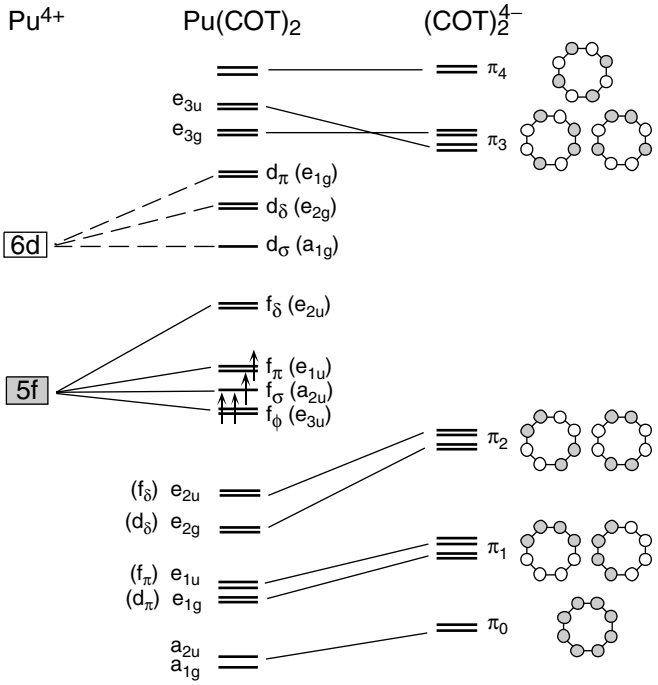

Fig. 7.125 *A qualitative molecular orbital interaction diagram for plutonocene, Pu(η-C_8H_8)$_2$.*

orbitals of d_σ, d_π, and d_δ symmetry gives rise to metal–ligand bonding molecular orbitals of a_{1g}, e_{1g}, and e_{2g} symmetry, respectively. Both the d_π (e_{1g}) and d_δ (e_{2g}) molecular orbitals are significantly destabilized due to strong interactions that occur with ligand orbitals at lower energy. The Pu 5f orbitals are split into the f_σ, f_π, f_δ, and f_φ molecular orbitals of a_{2u}, e_{1u}, e_{2u}, and e_{3u} symmetry, respectively. The lobes of the f_δ orbital are directed towards the $C_8H_8^{2-}$ rings, and interaction with the ligands strongly destabilizes this orbital and moves it significantly higher in energy than the remaining f_σ, f_π, and f_φ orbitals. Ligand interactions with the remaining f_σ, f_π, and f_φ orbitals are significantly weaker, giving rise to an f-orbital splitting pattern where one degenerate set is removed from the 5f manifold, leaving the other five orbitals clustered at lower energy (Boerrigter *et al.*, 1988). These general interactions are illustrated in Fig. 7.125.

As seen in the other examples, the 6d orbital interactions with the ligands are significantly stronger than the 5f interactions. The δ-type interactions have significant metal–ligand overlap and give rise to appreciable covalency through both 6d and 5f orbital interactions. A Mulliken population analysis for nonrelativistic orbitals showed that the $6d_\delta$ orbital is approximately 88% ligand and

11% 6d in character, while the $5f_\delta$ orbital is 48% ligand and 49% 5f in character (Boerrigter *et al.*, 1988). The latter represents significant 5f covalency. In addition, these calculations reveal that the semicore 6p orbitals also have a considerable amplitude at the position of the rings, and that this permits a strong interaction with deeper lying ring orbitals of the appropriate symmetry (Boerrigter *et al.*, 1988). These $6d_\delta$ (e_{2g}) and $5f_\delta$ (e_{2u}) metal–ligand bonding orbitals are illustrated qualitatively in **35** and **36**.

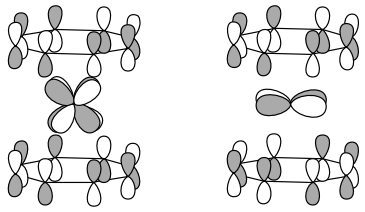

f_δ **d_δ**

35 **36**

This general bonding scheme has been experimentally confirmed by Brennan and coworkers who performed variable energy photoelectron spectroscopy on $U(\eta\text{-}C_8H_8)_2$ over a photon energy range of 24–125 eV (Brennan *et al.*, 1989). A mapping of the intensity changes in the ionization from the $5f_\delta$ (e_{2u}) orbital

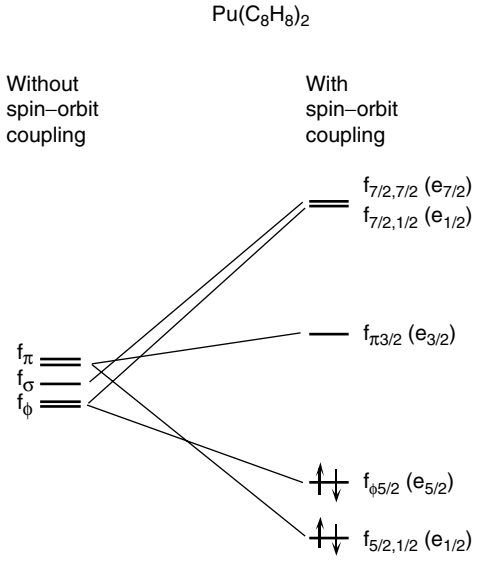

Fig. 7.126 *The effect of spin–orbit coupling on the 5f orbitals of Pu(η-C_8H_8)$_2$ adapted from Boerrigter* et al. (1988). *For consistency with Chapter* 17, *the D_{8h}* double group notation is given in parentheses.*

provided conclusive spectroscopic evidence for substantial 5f orbital covalency in $U(\eta\text{-}C_8H_8)_2$.

Relativistic calculations employing the HFS LCAO method conclude that the f_σ, f_π, and f_φ orbitals are nearly degenerate, and that they are equally populated with the four valence electrons in $Pu(\eta\text{-}C_8H_8)_2$ (Boerrigter *et al.*, 1988). This is not consistent with the experimental observation of a $M_j = 0$ ground state. As in our other examples, spin–orbit coupling must be taken into account in order to understand spectroscopic data. Boerrigter and coworkers have shown that strong ligand field splitting effectively removes the $5f_\delta$ orbital from the 5f orbital manifold, and this simplifies the discussion of spin–orbit coupling. The spin–orbit interaction on a degenerate set of f_σ, f_π, and f_φ orbitals gives a four-level pattern with two low-lying orbitals, the $f_{5/2,1/2}$ and $f_{\varphi 5/2}$, and three high-lying orbitals, the $f_{\pi 3/2}$, and the degenerate $f_{7/2,7/2}$ and $f_{7/2,1/2}$, as shown in Fig. 7.126. After inclusion of spin–orbit coupling, it is easy to see that $Pu(\eta\text{-}C_8H_8)_2$ is closed shell as both the low-lying $f_{5/2,1/2}$ and $f_{\varphi 5/2}$ are fully occupied leading to a $M_j = 0$ ground state in agreement with the measured magnetic properties.

ACKNOWLEDGMENTS

The authors acknowledge expert assistance from Karen Kippen, Leonard Martinez, Meredith Coonley, Ed Lorusso, and Susan Ramsay in preparing the manuscript. The authors are grateful to Thomas W. Newton and Phillip D. Palmer for electronic absorption spectra and calculations. DLC and MPN acknowledge the Division of Chemical Sciences, Geosciences, and Biosciences, Office of Basic Energy Research, U.S. Department of Energy for their support of actinide chemistry research at Los Alamos National Laboratory.

REFERENCES

(1963) *Plutonium Chemistry Symposium*, Report TID-7683, Argonne National Laboratory, 44 pp.

Abraham, B. M. and Davidson, N. R. (1949) High-temperature Hydrolysis of Plutonium Oxychloride, in *Natl. Nucl. Energy Ser.,* Div IV **14B**(Transuranium Elements, Pt. I) (eds. G. T. Seaborg, J. J. Katz, and W. M. Manning), McGraw-Hill, New York, pp. 779–83.

Abraham, B. M., Brody, B. B., Davidson, N. R., Hagemann, F., Karle, I., Katz, J. J., and Wolf, M. J. (1949a) Preparation and Properties of Plutonium Chlorides and Oxychlorides, in *Natl. Nucl. Energy Ser.,* Div IV **14B**(Transuranium Elements, Pt. I) (eds. G. T. Seaborg, J. J. Katz, and W. M. Manning), McGraw-Hill, New York, pp. 740–58.

Abraham, B. M., Davidson, N. R., and Westrum, E. F., Jr (1949b) Preparation and Properties of Some Plutonium Sulfides and Oxysulfides, in *Natl. Nucl. Energy Ser.,*

Div IV **14B**(Transuranium Elements, Pt. I) (eds. G. T. Seaborg, J. J. Katz, and W. M. Manning), McGraw-Hill, New York, pp. 814–17.

Abraham, B. M., Davidson, N. R., and Westrum, E. F., Jr (1949c) Preparation of Plutonium Nitride, in *Natl. Nucl. Energy Ser.,* Div IV **14B**(Transuranium Elements, Pt. I) (eds. G. T. Seaborg, J. J. Katz, and W. M. Manning), McGraw-Hill, New York, pp. 945–8.

Abrikosov, I. A., Ruban, A. V., Johansson, B., and Skriver, H. L. (1998) *Comput. Mater. Sci.,* **10**(1–4), 302–5.

Ackermann, R. J., Faircloth, R. L., and Rand, M. H. (1966) *J. Phys. Chem.,* **70**(11), 3698–706.

Adams, M. D., Steunenberg, R. K., and Vogel, R. C. (1957) *The Transfer of Plutonium Hexafluoride in the Vapor Phase*, Report ANL-5796, Argonne National Laboratory, 14 pp.

Adamson, M. G., Aitken, E. A., and Caputi, R. W. (1985) *J. Nucl. Mater.,* **130**, 349–65.

Adler, P. H. (1991) *Metall. Trans. A,* **22A**(10), 2237–46.

Adler, P. H., Olson, G. B., and Margolies, D. S. (1986) *Acta Metall.,* **34**(10), 2053–64.

Aitken, E. A. and Evans, S. K. (1968) *A Thermodynamic Data Program Involving Plutonium and Urania at High Temperatures*, Report GEAP-5672, General Electric Company, Vallecitos Nucleonics Laboratory, 10 pp.

Akatsu, J. (1982) *Sep. Sci. Technol.,* **17**(12), 1433–42.

Akatsu, J., Moriyama, N., Dojiri, S., Matsuzuru, H., and Kobayashi, Y. (1983) *Sep. Sci. Technol.,* **18**(2), 177–86.

Akhachinskii, V. V. and Bashlykov, S. N. (1970) *Atomnaya Energiya,* **29**(6), 439–47.

Akimoto, Y. (1960) *Chemistry Division Semi-annual Report - June through November 1959*, USAEC Report UCRL-9093, Lawrence Radiation Laboratory.

Albiol, T. and Arai, Y. (2001) *Review of Actinide Nitride Properties with Focus on Safety Aspects*, Report JAERI-Review, Department of Nuclear Energy System, Tokai Research Establishment, Japan Atomic Energy Research Institute, i–vi, pp. 1–50.

Albrecht, E. D. (1964) *J. Nucl. Mater,* **12**(2), 125–130.

Albrecht-Schmitt, T. E., Almond, P. M., and Sykora, R. E. (2003) *Inorg. Chem.,* **42**(12), 3788–95.

Albright, D. and Kramer, K. (2004) *B. Atom. Sci.,* **60**(6), 14–16.

Alcock, N. W. and Esperas, S. (1977) *J. Chem. Soc. Dalton Trans.,* **9**, 893–6.

Alei, M., Johnson, Q. C., Cowan, H. D., and Lemons, J. F. (1967) *J. Inorg. Nucl. Chem.,* **29**, 2327.

Alenchikova, I. F., Zaitseva, L. L., Lipis, L. V., Fomin, V. V., and Chebotarev, N. T. (1958) *Proc. Second UN Int. Conf. Peaceful Uses Atomic Energy*, vol. 28, Geneva, 1958, pp. 309–15.

Alenchikova, I. F., Zaitseva, L. L., Lipis, L. V., and Fomin, V. V. (1959) *Zh. Neorg. Khim.,* **4**, 961–2.

Alenchikova, I. F., Lipis, L. V., and Nikolaev, N. S. (1961a) *Atomnaya Energiya,* **10**, 592–6.

Alenchikova, I. F., Zaitseva, L. L., Lipis, L. V., Nikolaev, N. S., Fomin, V. V., and Chebotarev, N. T. (1961b) *Zh. Neorg. Khim.,* **6**, 1513–19.

Alexander, C. A., Ogden, J. S., and Pardue, W. M. (1969) Report BMI-1862, A7, Batelle Memorial Institute, Columbus, OH.

Alexander, E. C., Jr., Lewis, R. S., Reynolds, J. H., and Michel, M. C. (1971) *Science* **172**(3985), 837–40.

Alexander, C. A., Clark, R. B., Kruger, O. L., and Robbins, J. L. (1976) Fabrication and High-temperature Thermodynamic and Transport Properties of Plutonium Mononitride. *Plutonium 1975 and Other Actinides*, *Proc. Conf. in Baden-Baden,* Sept. 10–13, 1975/*Proc. Fifth Int. Conf. on Plutonium and Other Actinides*, 1975 (eds. H. R. Blank and R. Lindner), pp. 277–86.

Allard, B., Kipatsi, H., and Lilijenzin, J. O. (1980) *J. Inorg. Nucl. Chem.,* **42**(7), 1015–27.

Allbutt, M. and Dell, R. M. (1967) *J. Nucl. Mater.,* **24**(1), 1–20.

Allbutt, M., Dell, R. M., and Junkison, A. R. (1970) Plutonium Chalcogenides, in *Chem. Extended Defects Non-Metal. Solids,* (eds. L. Eyring and M. O'Keefe), Proc. Inst. Advan. Study. Scottsdale, AZ, pp. 124–47.

Allen, G. C. and Tempest, P. A. (1986) *Proc. R. Soc. Lon. Ser. A,* **406**(1831), 325–44.

Allen, P. G., Bucher, J. J., Clark, D. L., Edelstein, N. M., Ekberg, S. A., Gohdes, J. W., Hudson, E. A., Kaltsoyannis, N., Lukens, W. W., Neu, M. P., Palmer, P.D., Reich, T., Shuh, D. K., Tait, C. D., and Zwick, B. D. (1995) *Inorg. Chem.,* **34**(19), 4797–807.

Allen, J. W., Zhang, Y. X., Tjeng, L. H., Cox, L. E., Maple, M. B., and Chen, C. T. (1996a) *J. Electron Spectro. Rel. Phenom.,* **78**, 57–62.

Allen, P. G., Veirs, D. K., Conradson, S. D., Smith, C. A., and Marsh, S. F. (1996b) *Inorg. Chem.,* **35**(10), 2841–5.

Allen, P. G., Bucher, J. J., Shuh, D. K., Edelstein, N. M., and Reich, T. (1997) *Inorg. Chem.,* **36**(21), 4676–83.

Allen, P. G., Henderson, A. L., Sylwester, E. R., Turchi, P. E. A., Shen, T. H., Gallegos, G. F., and Booth, C. H. (2002) *Phys. Rev. B.,* **65**(21), 214107/1–214107/7.

Al Mahamid, I., Becraft, K. A., Hakem, N. L., Gatti, R. C., and Nitsche, H. (1996) *Radiochim. Acta,* **74**, 129–34.

Amano, O., Sasahira, A., Kani, Y., Hoshino, K., Aoi, M., and Kawamura, F. (2004) *J. Nucl. Sci. Technol.,* **41**(1), 55–60.

Anderegg, G. (1977) *Critical Survey of Stability Constants of EDTA Complexes,* Pergamon Press, Oxford.

Anderegg, G. (1982) *Pure Appl. Chem.,* **54**, 2693.

Anderson, H. H. and Asprey, L. B. (1960) *Solvent-extraction Process for Plutonium*. US Patent no. 2924 506. (U.S. Atomic Energy Commission).

Anderson, J. W. and Maraman, W. J. (1962) *Trans. Am. Foundrymen's Soc.,* **70**, 1057–72.

Anderson, J. W., Leary, J. A., and McNeese, W. D. (1960) *Preparation and Fabrication of Plutonium Fuel Alloy for Los Alamos Molten Plutonium Reactor Experiment No. 1*, Report LA-2439, Los Alamos Scientific Laboratory, 30 pp.

Andreichuk, N. N., Vasil'ev, V. Y., Rykova, A. G., Osipov, S. V., Kalashnikov, V. M., and Vysokoostrovskaya, N. B. (1979) *Sov. Radiochem.,* **21**(6), 727–36.

Andreichuk, N. N., Rotmanov, K. V., Frolov, A. A., and Vasil'ev, V. Y. (1984a) *Sov. Radiochem.,* **26**(1), 90–4.

Andreichuk, N. N., Rotmanov, K. V., Frolov, A. A., and Vasil'ev, V. Y. (1984b) *Sov. Radiochem.,* **26**(6), 701–6.

Andreichuk, N. N., Frolov, A. A., Rotmanov, K. V., and Vasil'ev, V. Y. (1990) *J. Radioanal. Nucl. Chem. Lett.,* **143**(2), 427–32.

Andrew, J. F. (1967) *J. Phys. Chem. Solids,* **28**(4), 577–80.

Andrew, J. F. (1969) *J. Nucl. Mater.,* **30**(3), 343–5.
Andrew, J. F. and Latimer, T. W. (1975) *Review of Thermal Expansion and Density of Uranium and Plutonium Carbides*, Report LA-6037-MS, Los Alamos Science Laboratory, Los Alamos, NM, 17 pp.
Angelo, J. A., Jr, and Buden, D. (1985) *Space Nuclear Power,* Orbit Book Company, Malabar, FL, 286 pp.
Ankudinov, A. L., Conradson, S. D., Mustre de Leon, J., and Rehr, J. J. (1998) *Phys. Rev. B,* **57**(13), 7518–25.
Anselin, F. (1963a) *J. Nucl. Mater.,* **10**(4), 301–220.
Anselin, F. (1963b) *Compt. Rend.,* **256**, 2616–19.
Antonio, M. R., Soderholm, L., Williams, C. W., Blaudeau, J.-P., and Bursten, B. E. (2001) *Radiochim. Acta,* **89**(1), 17–25.
Antonio, M. R., Chiang, M.-H., Williams, C. W., and Soderholm, L. (2004) *Mater. Res. Soc. Symp. Proc*., **802**, 157–68.
Anyun, Z., Jingxin, H., Xianye, Z., and Fangding, W. (2002) *J. Radioanal. Nucl. Chem.,* **252**(3), 565–71.
Arai, Y. and Ohmichi, T. (1995) *J. Solid State Chem.,* **115**(1), 66–70.
Archibong, E. F. and Ray, A. K. (2000) *Theochem,* **530**(1,2), 165–70.
Arko, A. J., Joyce, J. J., and Havela, L. (2006) *The Chemistry of the Actinide and Transactinide Elements,* (eds. L. R. Morss, N. M. Edelstein, and J. Fuger), Springer Publishing, New York, ch. 21.
Artyukhin, P. I., Gel'man, A. D., and Medvedovskii, V. I. (1958) *Doklady Akad. Nauk SSSR,* **120**, 98–100.
Artyukhin, P. I., Medvedovskii, V. I., and Gel'man, A. D. (1959) *Zh. Neorg. Khim.,* **4**, 1324–31.
Asanuma, N., Harada, M., Ikeda, Y., and Tomiyasu, H. (2001) *J. Nucl. Sci. Technol.,* **38**(10), 866–71.
Asprey, L. B., Keenan, T. K., and Kruse, F. H. (1964) *Inorg. Chem.,* **3**(8), 1137–240.
Asprey, L. B., Eller, P. G., and Kinkead, S. A. (1986) *Inorg. Chem.,* **25**(5), 670–2.
Atlas, L. M. and Schlehman, G. J. (1967) Defect Equilibria of Nonstoichiometric Plutonium dioxide 1045 to 1505 Deg. *Plutonium 1965, Proc. Third Int. Conf. on Plutonium* (eds. A. E. Kay and M. B. Waldron), Chapman and Hall, London, pp. 838–44.
Atlas, L. M., Schlehman, G. J., and Readey, D. W. (1966) *J. Am. Ceram. Soc.,* **49**(11), 624–5.
Audi, G. and Wapstra, A. H. (1995) *Nucl. Phys. A,* **595**(4), 409–80.
Audi, G., Bersillon, O., Blachot, J., and Wapstra, A. H. (1997) *Nucl. Phys. A,* **624**(1), 1–124.
Austin, A. E. (1959) *Acta Crystallogr.,* **12**, 159–61.
Avdeef, A., Raymond, K. N., Hodgson, K. O., and Zalkin, A. (1972) *Inorg. Chem.,* **11**(5), 1083–8.
Avens, L. R., Bott, S. G., Clark, D. L., Sattelberger, A. P., Watkin, J. G., and Zwick, B. D. (1994) *Inorg. Chem.,* **33**(10), 2248–56.
Avignant, D. and Cousseins, J. C. (1971) *Compt. Rend.,* **272**(26), 2151–3.
Avivi, E. (1964) *Etudes d'Alliages Plutonium - Fer at d'Alliages Uranium - Plutonium-Fer*, Thesis, Universite de Paris, 72 pp.
Awasthi, S. K., Chackraburtty, D. M., and Tondon, V. K. (1968) *J. Inorg. Nucl. Chem.,* **30**(3), 819–21.

Axler, K. M., Roof, R. B., and Foltyn, E. M. (1992) *J. Nucl. Mater.,* **189**(2), 231–2.
Baes, C. F. and Mesmer, R. E. (1976) *The Hydrolysis of Cations,* Wiley, New York, 489 pp.
Baglan, N., Fourest, B., Guillaumont, R., Blain, G., Le Du, J.-F., and Genet, M. (1994) *New J. Chem.,* **18**(7), 809–16.
Bagnall, K. W. (1967a) *Coord. Chem. Rev.,* **2**(2), 145–62.
Bagnall, K. W. (1967b) *Halogen Chem.,* **3**, 303–82.
Bagnall, K. W., Deane, A. M., Markin, T. L., Robinson, P. S., and Stewart, M. A. A. (1961) *J. Chem. Soc., Abstracts*: 1611–17.
Bagnall, K. W., Plews, M. J., and Brown, D. (1982a) *J. Organomet. Chem.,* **224**(3), 263–6.
Bagnall, K. W., Plews, M. J., Brown, D., Fischer, R. D., Klaehne, E., Landgraf, G. W., and Sienel, G. R. (1982b) *J. Chem. Soc., Dalton Trans.*, (10), 1999–2007.
Bagnall, K. W., Payne, G. F., and Brown, D. (1985a) *J. Less-Common Met.,* **109**(1), 31–6.
Bagnall, K. W., Payne, G. F., and Brown, D. (1985b) *J. Less-Common Met.,* **113**(2), 325–9.
Bagnall, K. W., Payne, G. F., and Brown, D. (1986) *J. Less-Common Met.,* **116**(2), 333–9.
Baily, H., Bernard, H., and Mansard, B. (1989) *Mater. Sci. Forum,* **48–49**(Nucl. Fuel Fabr.), 175–83.
Bairiot, H. and Deramaix, P. (1992) *J. Nucl. Mater.,* **188**, 10–18.
Bairiot, H., Blanpain, P., Farrant, D., Ohtani, T., Onoufriev, V., Porsch, D., Stratton, R., Brown, C., Deramaix, P., Golovnin, I., Haas, E., Laraia, M., Nagai, S., Pope, R., Sanchis, H., Shea, T., and Weston, R. (2003) *Status and Advances in MOX Fuel Technology*, Technical Report Series - International Atomic Energy Agency (415), Report 1-179.
Baker, R. D. (1946) *Preparation of Plutonium Metal by the Bomb Method*, Report LA-473, Los Alamos Scientific Laboratory, 65 pp.
Baker, R. D. and Maraman, W. J. (1960) *Extract. Phys. Met. Plutonium and Alloys, Symp.,* San Francisco, California, 43–59.
Balakrishnan, P. V. and Ghosh Mazumdar, A. S. (1964) *J. Inorg. Nucl. Chem.,* **26**(5), 759–63.
Baldwin, C. E. and Navratil, J. D. (1983) *ACS Symp. Ser.* **216** (Plutonium Chem.) (eds. W. T. Carnall and G. R. Choppin), American Chemcial Society, Washington, DC. pp. 369–80.
Bamberger, C. E. (1985) in *Handbook on the Physics and Chemistry of the Actinides* (eds. A. J. Freeman and C. Keller), Elsevier Science, New York, ch. 6, pp. 289–303.
Banks, R. H. (1979) *Preparation and Spectroscopic Properties of Three New Actinide(IV) Borohydrides*, Thesis, Report LBL-10292, Lawrence Berkeley Laboratory, University of California, 209 pp.
Banks, R. H. and Edelstein, N. M. (1980) *ACS Symp. Ser.* **131**(Lanthanide Actinide Chem. Spectrosc.), American Chemcial Society, Washington, DC. 331–48.
Banks, R. H., Edelstein, N. M., Rietz, R. R., Templeton, D. H., and Zalkin, A. (1978) *J. Am. Chem. Soc.,* **100**(6), 1957–8.
Banyai, I., Glaser, J., Micskei, K., Toth, I., and Zekany, L. (1995) *Inorg. Chem.,* **34**(14), 3785–96.

Bardelle, P. and Bernard, H. (1989) *Preparation of Uranium and/or Plutonium Nitride for Use as a Nuclear Reactor Fuel*, (Commissariat a l'Energie Atomique, France). Ep Patent 307311, 5 pp.

Barmore, W. L. and Uribe, F. S. (1970) *Mechanical Behavior of Pu-Ga, Proc. Fourth Int. Conf. on Plutonium and Other Actinides* (ed. W. N. Miner), Santa Fe, NM, The Metallurgical Society of AIME, 1, 414 pp.

Barney, G. S. (1976) *J. Inorg. Nucl. Chem.,* **38**(9), 1677–81.

Barton, C. J., Redman, J. D., and Strehlow, R. A. (1961) *J. Inorg. Nucl. Chem.,* **20**, 45–52.

Bartscher, W. (1996) *Diffusion and Defect Data–Solid State Data, Pt. B. Solid State Phenomena,* **49–50**(Hydrogen Metal Systems I), 159–238.

Bartscher, W., Boeuf, A., Caciuffo, R., Fournier, J. M., Haschke, J. M., Manes, L., Rebizant, J., Rustichelli, F., and Ward, J. W. (1985) *Physica B & C,* **130**(1–3), 530–2.

Baskes, M. I. (2000) *Phys. Rev. B: Condens. Matter,* **62**(23), 15532–7.

Baskes, M. I., Muralidharan, K., Stan, M., Valone, S. M., and Cherne, F. J. (2003) *JOM,* **55**(9), 41–50.

Baston, G. M. N., Bradley, A. E., Gorman, T., Hamblett, I., Hardacre, C., Hatter, J. E., Healy, M. J. F., Hodgson, B., Lewin, R., Lovell, K. V., Newton, G. W. A., Nieuwenhuyzen, M., Pitner, W. R., Rooney, D. W., Sanders, D., Seddon, K. R., Simms, H. E., and Thied, R. C. (2002) Ionic Liquids for the Nuclear Industry: A Radiochemical, Structural and Electrochemical Investigation, in *Ionic Liquids - Industrial Applications to Green Chemistry* (eds. R. D. Rogers and K. R. Seddon), American Chemical Society, Washington, DC, pp. 162–77.

Battles, J. E. and Blackburn, P. E. (1969) *Reactor Development Program Progress Report September 1969*, Report ANL-7618, Argonne National Laboratory, 141 pp.

Battles, J. E., Reishus, J. W., and Shinn, W. A. (1968) *Am. Ceram. Soc. Bull.,* **47**(4), 414.

Battles, J. E., Reishus, J. W., and Shinn, W. A. (1969) *Volatilization Studies of Plutonium Compounds by Mass Spectrometry, in Chemical Engineering Division, Annual Report 1968*, Report ANL-7575, Argonne National Laboratory, pp. 77–82.

Battles, J. E., Shinn, W. A., Blackburn, P. E., and Edwards, R. K. (1970) *Plutonium 1970 and Other Actinides, Proc. Fourth Int. Conf. on Plutonium and Other Actinides,* Santa Fe, NM, Oct. 5–9, 1970 (ed. W. N. Miner), AIME, New York, 733 pp.

Bauche, J., Blaise, J., and Fred, M. (1963) *Compt. Rend.,* **257**(16), 2260–3.

Bauer, E. D., Thompson, J. D., Sarrao, J. L., Morales, L. A., Wastin, F., Rebizant, J., Griveau, J. C., Javorsky, P., Boulet, P., Colineau, E., Lander, G. H., and Stewart, G. R. (2004) *Phys. Rev. Lett.,* **93**(14), 147005/1–4.

Baumgärtner, F., Fischer, E. O., Kanellakopulos, B., and Laubereau, P. (1965) *Angew. Chem.,* **77**(19), 866–7.

Bayoglu, A. S. and Lorenzelli, R. (1979) *J. Nucl. Mater.,* **79**(2), 437–8.

Bayoglu, A. S. and Lorenzelli, R. (1984) *Solid State Ionics,* **12**, 53–66.

Bayoglu, A. S., Giordano, A., and Lorenzelli, R. (1983) *J. Nucl. Mater.,* **113**(1), 71–4.

Bean, A. C., Campana, C. F., Kwon, O., and Albrecht-Schmitt, T. E. (2001) *J. Am. Chem. Soc.,* **123**(36), 8806–10.

Bean, A. C., Abney, K., Scott, B. L., and Runde, W. (2005) *Inorg. Chem.,* **44**(15), 5209–11.

Bearden, J. A. (1967) *Rev. Mod. Phys.,* **39**, 78–124.

Bearden, J. A. and Burr, A. F. (1967) *Rev. Mod. Phys.,* **39**, 125–42.

Beauvais, R. A. and Alexandratos, S. D. (1998) *React. Funct. Polym.,* **36**(2), 113–23.

Beitscher, S. (1970) *Hot Shortness in Plutonium-1 Weight Percent Gallium*, *Proc. Fourth Int. Conf. Plutonium - Other Actinides*, Santa Fe, NM (ed. W. N. Miner), The Metallurgical Society of AIME, 1, pp. 449–56.
Beitz, J., Jonah, C., Sullivan, J. C., and Woods, M. (1986) *Radiochim. Acta,* **40**(1), 7–9.
Benard, P., Brandel, V., Dacheux, N., Jaulmes, S., Launay, S., Lindecker, C., Genet, M., Louer, D., and Quarton, M. (1996) *Chem. Mater.,* **8**(1), 181–8.
Benedict, U. (1970) *J. Nucl. Mater.,* **35**(3), 356–61.
Benedict, U. (1979) *Solid Solubility of Fission Product and Other Transition Elements in Carbides and Nitrides of Uranium and Plutonium*, European Institute for Transuranium Elements, Report 6 pp.
Benedict, U. and Sari, C. (1969) *Ternary System Uranium dioxide-Uranium oxide (U_3O_8)-Plutonium dioxide*, Report EUR-4136, Transuranium Institute, European Atomic Energy Community, Karlsruhe, Germany, 38 pp.
Bennett, D. A., Hoffman, D., Nitsche, H., Russo, R. E., Torres, R. A., Baisden, P. A., Andrews, J. E., Palmer, C. E. A., and Silva, R. J. (1992) *Radiochim. Acta,* **56**(1), 15–19.
Benz, R., Kahn, M., and Leary, J. A. (1959) *J. Phys. Chem.,* **63**, 1983–4.
Benz, R. (1961) *J. Phys. Chem.,* **65**(1), 81–4.
Benz, R. (1962) *J. Inorg. Nucl. Chem.,* **24**(Dec), 1191–5.
Benz, R. and Douglass, R. M. (1961a) *J. Inorg. Nucl. Chem.,* **23**, 134–6.
Benz, R. and Douglass, R. M. (1961b) *J. Phys. Chem.,* **65**, 1461–3.
Benz, R. and Leary, J. A. (1961) *J. Phys. Chem.,* **65**(6), 1056–8.
Benz, R., Douglass, R. M., Kruse, F. H., and Penneman, R. A. (1963) *Inorg. Chem.,* **2**(4), 799–803.
Berg, J. M., Smith, C. A., Cisneros, M. A., Vaughn, R. B., and Veirs, D. K. (1998) *J. Radioanal. Nucl. Chem. Lett.,* **235**(1–2), 25–9.
Berg, J. M., Veirs, D. K., Vaughn, R. B., Cisneros, M. R., and Smith, C. A. (2000) *Appl. Spectrosc.,* **54**(6), 812–23.
Berger, R. and Gäumann, T. (1961) *Helv. Chim. Acta,* **44**(4), 1084–8.
Bergstresser, K. S. (1950) *Plutonium Electropolishing Cell*, Report LA-1106, Los Alamos Scientific Laboratory, 10 pp.
Bernard, H. (1989) *J. Nucl. Mater.,* **166**(1–2), 105–11.
Berndt, A. F. (1962) *On the Use of a Modified Radial Distribution Analysis for Indexing Powder Patterns*, Report ANL-FGF-360, Argonne National Laboratory, 12 pp.
Berndt, A. F. (1966) *J. Less-Common Met.,* **11**(3), 216–19.
Berndt, A. F. (1967) *J. Less-Common Met.,* **12**(1), 82–3.
Berthon, C. and Chachaty, C. (1995) *Solvent Extr. Ion Exc.,* **13**(5), 781–812.
Besmann, T. M. and Lindemer, T. B. (1983) *J. Am. Ceram. Soc.,* **66**(11), 782–5.
Bessonov, A. A., Krot, N. N., Budantseva, N. A., and Afonas'eva, T. V. (1996) *Radiokhimiya,* **38**(3), 223–5.
Betz, T. and Hoppe, R. (1984) *Z. Anorg. Allg. Chem.,* **512**, 19–33.
Beznosikova, A. V., Chebotarev, N. T., Luk'yanov, A. S., Chernyi, A. V., and Smirnova, E. A. (1974) *Sov. At. Energy,* **37**(2), 842–6.
Bhide, M. K., Kadam, R. M., Babu, Y., Natarajan, V., and Sastry, M. D. (2000) *Chem. Phys. Lett.,* **332**(1,2), 98–104.
Bjorklund, C. W. (1957) *J. Am. Chem. Soc.,* **79**, 6347–50.
Bjorklund, C. W., Reavis, J. G., Leary, J. A., and Walsh, K. A. (1959) *J. Phys. Chem.,* **63**(10), 1774–7.

Blaise, A., Collard, J. M., Fournier, J. M., Rebizant, J., Spirlet, J. C., and Vogt, O. (1985) *Physica B & C,* **130**(1–3), 99–101.

Blaise, J., Fred, M. S., Carnall, W. T., Crosswhite, H. M., and Crosswhite, H. (1983a) Measurement and Interpretation of Plutonium Spectra (ACS Symp. Ser. no. 216), (eds. W. T. Carnall and G. R. Choppin), American Chemical Society, Washington, DC, pp. 173–98.

Blaise, J., Fred, M., and Gutmacher, R. G. (1983b) *The Atomic Spectrum of Plutonium*, Report ANL-83-95, Argonne National Laboratory, 612 pp.

Blaise, J., Fred, M., and Gutmacher, R. G. (1986) *J. Opt. Soc. Am.,* **B3**(3), 403–18.

Blaise, J., Fred, M., and Gutmacher, R. G., unpublished results.

Blaise, J. and Wyart, J.-F. (1992) *Energy levels and atomic spectra of actinides,* Tables Internationales de Constantes, Paris, France, ISBN 2-9506414-0-7.

Blank, H. (1976) Transurane: Binare Legierungsysteme 1, in *Gmelin Handbuch der Anorganische Chemie* (ed. K.-C. Buschbeck), Springer-Verlag, Berlin, 38 pp.

Blank, H. (1977) Binary Alloys, in *Gmelin Handbuch der Anorganische Chemie Transurane: The Alloys* (ed. K.-C. Buschbeck), Springer-Verlag, Berlin, pp. 1–275.**39, B3:**

Blank, H. (1994) in *Nuclear Materials* (ed. B. R. T. Frost), VCH publishers, Weinheim, 203 pp.

Blank, H., Brossman, G., Kemmerich, M., and Weitzenmiller, F. (1962) *Zwei- und mehrstoffsysteme mit plutonium. Literaturubersicht, phasendiagramme und daten, teil 1, Pu-Ag bis Pu-Sn.* Karlsruhe, Kernreaktor Bau- und Betriebs-Gesellschaft, 243 pp.

Blank, H. R. and Lindner, R. (eds.) (1976a) *Plutonium 1975 and Other Actinides: Proc. Conf. in Baden-Baden*, Sept. 10–13, 1975/*Proc. Fifth Int. Conf. on Plutonium and Other Actinides*, 1975, American Elsevier Publication, New York; North-Holland, Amsterdam.

Blau, M. S. (1998) *J. Radioanal. Nucl. Chem.,* **235**(1–2), 41–5.

Blaudeau, J.-P. and Bursten, B. E. (2000) *Abstracts of Papers, 220th ACS National Meeting*, Aug. 20–24, 2000, Washington, DC, INOR-419.

Bleaney, B. (1955) *Discuss. Faraday Soc.,* **19**, 112–18.

Bluestein, B. A. and Garner, C. S. (1944) *The Preparation of Plutonium Tribromide*, Report LA-116, Los Alamos Scientific Laboratory, 7 pp.

Boatner, L. A. and Sales, B. C. (1988) in *Monazite,* (eds. W. Lutze and R. C. Ewing), Radioactive Waste Forms for the Future North-Holland, Amsterdam.

Bochvar, A. A., Konobeevsky, S. T., Kutaitsev, V. I., Menshikova, T. S., and Chebotarev, N. T. (1958) *Interaction of Plutonium and Other Metals in Connection with the Arrangement in Mendeleev's Periodic Table, Proc. Second UN Int. Conf. on the Peaceful Uses of Atomic Energy,* Geneva, Switzerland, 6, pp. 184–93.

Bodu, R., Bouzigues, H., Morin, N., and Pfiffelmann, J. P. (1972) *C. R. Acad. Sci., Ser. D,* **275**(16), 1731–2.

Boehlert, C. J., Schulze, R. K., Mitchell, J. N., Zocco, T. G., and Pereyra, R. A. (2001) *Scr. Mater.,* **45**(9), 1107–15.

Boerrigter, P. M., Baerends, E. J., and Snijders, J. G. (1988) *Chem. Phys.,* **122**(3), 357–74.

Boeuf, A., Caciuffo, R., Fournier, J. M., Manes, L., Rebizant, J., Roudaut, E., and Rustichelli, F. (1984) *Solid State Commun.,* **52**(4), 451–3.

Bohe, A. E., Nassini, H. E., Bevilacqua, A. M., and Pasquevich, D. M. (1997) *Chlorination Reactions Applied to Reprocessing of Aluminum–Uranium Spent Nuclear Fuels,*

1997 *Symp. on Scientific Basis for Nuclear Waste Management XXI* (eds. I. G. McKinley and C. McCombie), Materials Research Society, Davos, Switzterland, 506, pp. 535–42.
Boivineau, M. (2001) *J. Nucl. Mater.,* **297**, 97–106.
Bokelund, H. and Glatz, J. P. (1984) *Inorg. Chim. Acta,* **94**(1–3), 131–132.
Bolvin, H., Wahlgren, U., Moll, H., Reich, T., Geipel, G., Fanghaenel, T., and Grenthe, I. (2001) *J. Phys. Chem. A,* **105**(51), 11441–5.
Bonnelle, C. (1976) *Struct. Bond. I,* **31**, 23–48.
Boreham, D., Freeman, J. H., Hooper, E. W., Jenkins, I. L., and Woodhead, J. L. (1960) *J. Inorg. Nucl. Chem.,* **16**, 154–6.
Boring, M. and Hecht, H. G. (1978) *J. Chem. Phys.,* **69**(1), 112–16.
Boring, A. M. and Smith, J. L. (2000) *Los Alamos Science,* **26**(1), 90.
Borkowski, M., Chiarizia, R., Jensen, M. P., Ferraro, J. R., Thiyagarajan, P., and Littrell, K. C. (2003) *Separ. Sci. Technol.,* **38**(12–13), 3333–51.
Boucher, R. and Quere, Y. (1981) *J. Nucl. Mater.,* **100**(1–3), 132–6.
Boukhalfa, H., Reilly, S. D., Smith, W. H., and Neu, M. P. (2004) *Inorg. Chem.,* **43**(19), 5816–23.
Boulet, P., Wastin, F., Colineau, E., Griveau, J. C., and Rebizant, J. (2003) *J. Phys. Condens. Mat.,* **15**(28), S2305–S2308.
Bourges, J., Madic, C., Koehly, G., and Lecomte, M. (1986) *J. Less-Common Met.,* **122**, 303–11.
Bovey, L. and Gerstenkorn, S. (1961) *J. Opt. Soc. Am.,* **51**, 522–5.
Bovey, L. and Steers, E. B. M. (1960) *Spectrochim. Acta,* **16**, 1184–99.
Bowersox, D. F. and Leary, J. A. (1966) *The Solubilities of Selected Elements in Liquid Plutonium. X. Thulium*, Report LA-3623, Los Alamos Scientific Laboratory, 10 pp.
Bowersox, D. F. and Leary, J. A. (1967) *Trans. Amer. Nucl. Soc.,* **10**(1), 106.
Bowersox, D. F. and Leary, J. A. (1968) *The Solubilities of Selected Elements in Liquid Plutonium. XII Chromium*, Report LA-3850, Los Alamos Scientific Laboratory, 5 pp.
Bradley, D. C., Harder, B., and Hudswell, F. (1957) *J. Chem. Soc.*, *Abstracts*: 3318.
Brandel, V. and Dacheux, N. (2004a) *J. Solid State Chem.,* **177**, 4743–54.
Brandel, V. and Dacheux, N. (2004b) *J. Solid State Chem.,* **177**, 4755–67.
Brennan, J. G., Green, J. C., and Redfern, C. M. (1989) *J. Am. Chem. Soc.,* **111**(7), 2373–7.
Brett, N. H. and Fox, A. C. (1966) *J. Inorg. Nucl. Chem.,* **28**(5), 1191–203.
Brewer, L. (1953) *Chem. Rev.,* **52**, 1–75.
Brewer, L. (1965) in *High-strength Materials* (ed. V. F. Zackay), John Wiley, New York, 12.
Brewer, L. (1970) *Proc. Fourth Int. Conf. on Plutonium and Other Actinides,* (ed. W. N. Miner), The Metallurgical Society of AIME, Warrendale, PA, 650 pp.
Brewer, L. (1971a) *J. Opt. Soc. Am.,* **61**(8), 1101–11.
Brewer, L. (1971b) *J. Opt. Soc. Am.,* **61**(12), 1666–82.
Brewer, L. (1983) Systematics of the Properties of the Lanthanides, in *Systematics and the Properties of the Lanthanides* (eds. S. P. Sinha, D. Reidel), Hingham, MA, pp. 17–69.
Brewer, L. (2000) *Metall. Mater. Trans.,* **31B**(4), 603–7.

Brewer, L., Bromley, L., Gilles, P. W., and Lofgren, N. L. (1949) *Natl. Nucl. En. Ser.*, Div IV **14B**(Transuranium Elements, Pt. II) (eds. G. T. Seaborg, J. J. Katz and W. M. Manning), McGraw-Hill, New York, pp. 861–86.

Bridger, N. J. and Dell, R. M. (1967) *Research on Plutonium Nitride*, Report AERE-R-5441, UK Atomic Energy Research Group, Atomic Energy Research Establishment, 14 pp.

Bridger, N. J., Dell, R. M., and Wheeler, V. J. (1969) *Reactivity Solids, Proc. Sixth Int. Symp.*, pp. 389–400.

Brodsky, M. B. (1961) *Comment on J. Friedel Paper, Plutonium 1960,* Grenoble, France (eds. E. Grison, W. B. H. Lord, and R. D. Fowler), Cleaver-Hume Press, London, 1, 210 pp.

Brown, D. (1968) *Halides of the Lanthanides and Actinides.* Wiley-Interscience, New York, 290 pp.

Brown, F., Ockenden, H. M., and Welch, G. A. (1955) *J. Chem. Soc.*, *Abstracts*: 4196–201.

Brown, D., Fletcher, S., and Holah, D. G. (1968) *J. Chem. Soc.*, *(London)* (8), 1889–94.

Brown, D., and Edwards, J. (1972) *J. Chem. Soc., Dalton Trans.: Inorg. Chem.* (1972–1999) (16), 1757–1762.

Brown, D., Hurtgen, C., and Fuger, J. (1977) *Rev. Chim. Miner.,* **14**(2), 189–98.

Buchmeiser, M. R. (2001) *Macromol. Rapid Commun.,* **22**(14), 1081–94.

Budantseva, N. A., Shilov, V. P., and Krot, N. N. (1998) *Radiochemistry,* **40**(6), 565–7.

Budantseva, N. A., Fedosseev, A. M., Bessonov, A. A., Grigoriev, M. S., and Krupa, J. C. (2000) *Radiochim. Acta,* **88**(5), 291–5.

Bullock, J. I., Ladd, M. F. C., Povey, D. C., and Storey, A. E. (1980) *Inorg. Chim. Acta,* **43**(1), 101–8.

Büppelmann, L., Kim, J. I., and Lierse, C. (1988) *Radiochim. Acta,* **44–45**(Pt. 1), 65–70.

Burney, G. A. (1962) *Separation of Neptunium and Plutonium by Anion Exchange*, Report DP-689, E. I. du Pont de Nemours & Co., Aiken, SC, 33 pp.

Burney, G. A. and Thompson, G. H. (1972) *Radiochem. Radioanal. Lett.,* **12**(4–5), 207–14.

Burney, G. A. and Thompson, G. H. (1974) *Separation of Plutonium-238 from Neptunium-237 by Pressurized Anion Exchange*, Report DP-1331, Savannah River Laboratory, E. I. DuPont de Nemours and Co., Aiken, SC, 21 pp.

Burns, C. J. and Sattelberger, A. P. (2002) Organometallic and Nonaqueous Coordination Chemistry, in *Advances in Plutonium Chemistry 1967–2000* (ed. D. C. Hoffman), American Nuclear Society, La Grange Park, IL, pp. 61–76.

Burns, C. J., Neu, M. P., Boukhalfa, H., Gutowski, K. E., Bridges, N. J., and Rogers, R. D. (2004) *Comprehensive Coord. Chem. II,* **3**, 189–345.

Burns, C. J., Clark, D. L., and Sattelberger, A. P. (2005) Actinides: Organometallic Chemistry, in *Encyclopedia of Inorganic Chemistry 2nd Ed.* (ed. R. B. King), Wiley Interscience, New York, 33–59.

Burns, J. H., Peterson, J. R., and Stevenson, J. N. (1975) *J. Inorg. Nucl. Chem.,* **37**(3), 743–9.

Burns, R. C. and O'Donnell, T. A. (1977) *Inorg. Nucl. Chem. Lett.,* **13**(12), 657–60.

Bursten, B. E. and Strittmatter, R. J. (1991) *Angew. Chem., Int. Ed. Engl.,* **30**(9), 1069–85.

Burwell, C. C., Bidwell, R. M., Hammond, R. P., Kemme, J. E., and Thamer, B. J. (1962) *Nucl. Sci. Eng.,* **14**, 123–34.

Buscher, C. T., Donohoe, R. J., Mecklenburg, S. L., Berg, J. M., Tait, C. D., Huchton, K. M., and Morris, D. E. (1999) *Appl. Spectrosc.,* **53**(8), 943–53.

Buyers, W. J. L. and Holden, T. M. (1985) in *Handbook on the Physics and Chemistry of Actinides,* vol. 2, (eds. A. J. Freeman and G. H. Lander), North-Holland, Amsterdam, 239 pp.

Bychkov, A. V. and Skiba, O. V. (1999) Review of Non-aqueous Nuclear Fuel Reprocessing and Separation Methods, in *Chemical Separation Technologies and Related Methods of Nuclear Waste Management* (eds. G. R. Choppin and M. K. Khankhasayev), Kluwer Academic Publishers, Boston, MA, pp. 71–98.

Calder, C. A., Draney, E. C., and Wilcox, W. W. (1981) *J. Nucl. Mater.,* **97**, 126–36.

Campbell, G. M., Kent, R. A., and Leary, J. A. (1970) *Plutonium 1970 and Other Actinides, Proc. Fourth Int. Conf. on Plutonium and Other Actinides,* (ed. W. N. Miner), Santa Fe, NM, Oct. 5–9, 1970 Metallurgical Society of AIME, New York, 781 pp.

Cantrell, K. J. (1988) *Polyhedron,* **7**(7), 573–4.

Capdevila, H. and Vitorge, P. (1995) *Radiochim. Acta,* **68**(1), 51–62.

Capdevila, H. and Vitorge, P. (1998) *Radiochim. Acta,* **82**, 11–16.

Capdevila, H. and Vitorge, P. (1999) *Czech. J. Phys. Sect. B,* **49**(Suppl. 1, Pt. 2, 13th Radiochemical Conference, 1998, 603–9.

Capdevila, H., Vitorge, P., and Giffaut, E. (1992) *Radiochim. Acta,* **58/59**(Pt. 1), 45–52.

Capdevila, H., Vitorge, P., Giffaut, E., and Delmau, L. (1996) *Radiochim. Acta,* **74**, 93–8.

Capone, F., Colle, Y., Hiernaut, J. P., and Ronchi, C. (1999) *J. Phys. Chem. A,* **103**(50), 10899–906.

Carbajo, J. J., Yoder, G. L., Popov, S. G., and Ivanov, V. K. (2001) *J. Nucl. Mater.,* **299** (3), 181–98.

Carnall, W. T. (1989) *J. Less-Common Met.,* **156**, 221–35.

Carnall, W. T. (1992) *J. Chem. Phys.,* **96**(12), 8713–26.

Carnall, W. T., and Choppin, G. R. (eds.) (1983) *ACS Symp. Ser.*, **216**(Plutonium Chem.), American Chemical Society, Washington, DC. 484 pp.

Carnall, W. T., Liu, G. K., Williams, C. W., and Reid, M. F. (1991) *J. Chem. Phys.,* **95** (10), 7194–203.

Carniglia, S. C. (1953) *Vapor-pressures of Americium Trifluoride and Americium Metal*. Thesis, Report UCRL-2389, University of California, Berkeley, 76 pp.

Carniglia, S. C., and Cunningham, B. B. (1955) *J. Am. Chem. Soc.,* **77**(6), 1451–3.

Carre, D., Laruelle, P., and Besancon, P. (1970) *Cr. Acad. Sci. C Chim.,* **270**(6), 537–9.

Carroll, D. F. (1964) *J. Am. Ceram. Soc.,* **47**(12), 650.

Cassol, A., Di Bernardo, P., Portanova, R., and Magon, L. (1973) *Inorg. Chim. Acta,* **7**, 353.

Cauchetier, P. and Guichard, C. (1973) *Radiochim. Acta,* **19**(3), 137–46.

Cauchetier, P. and Guichard, C. (1975) *J. Inorg. Nucl. Chem.,* **37**(7–8), 1771–8.

Cauchois, Y. and Manescu, I. (1956) *Compt. Rend.,* **242**, 1433–6.

Cauchois, Y., Manescu, I., and Le Berquier, F. (1954) *Compt. Rend.,* **239**, 1780–2.

Cauchois, Y., Bonnelle, C., and Bersuder, L. (1963a) *Compt. Rend.,* **257**(20), 2980–3.

Cauchois, Y., Bonnelle, C., and de Bersuder, L. (1963b) *Compt. Rend.,* **256**, 112–14.

Cefola, M. (1958) *Microchem. J.,* **2**, 205–17.

Chackraburtty, D. M. and Jayadevan, N. C. (1964) *Indian J. Phys.,* **38**(11), 585–6.

Chackraburtty, D. M. and Jayadevan, N. C. (1965) *Acta Crystallogr.,* **18**, 811.

Chackraburtty, D. M., Jayadevan, N. C., and Swaramakrishnan, C. K. (1963) *Acta Crystallogr.,* **16**(Pt. 10), 1060–1.

Chang, Y. A., Chen, S. L., Zhang, F., and Oates, W. A. (2002) Improving Multicomponent Phase Diagram Calculations, in *CALPHAD and Alloy Thermodynamics* (eds. P. E. A. Turchi, A. Gonis and R. D. Shull), TMS-Minerals, Metals & Material Society, Warrendale, PA, 53 pp.

Charvillat, J. P. (1978) *Crystal Chemistry of Transuranium Pnictides*, Report CEA-R-4933, CEA, CEN, Fontenay-aux-Roses, France, 364 pp.

Charvillat, J. P. and Damien, D. (1973) *Inorg. Nucl. Chem. Lett.,* **9**(5), 559–63.

Charvillat, J. P., Damien, D., and Wojakowski, A. (1977) *Rev. Chim. Miner.,* **14**(2), 178–88.

Chebotarev, N. T. and Utkina, O. N. (1975) Relation between Structure and Some Properties of δ-plutonium and γ-uranium Alloys. *Plutonium 1975 and Other Actinides*, *Proc. Fifth Int. Conf.*, Baden-Baden, Germany (eds. H. Blank and R. Lindner), North-Holland Publishing Company, New York, pp. 559–66.

Cheetham, A. K., Fender, B. E. F., Fuess, H., and Wright, A. F. (1976) *Acta Crystallogr. B,* **B32**(1), 94–7.

Chereau, P. and Wadier, J. F. (1973) *J. Nucl. Mater.,* **46**(1), 1–8.

Chereau, P., Dean, G., De Franco, M., and Gerdanian, P. (1977) *J. Chem. Thermodyn.,* **9** (3), 211–19.

Chiarizia, R., Jensen, M. P., Borkowski, M., Ferraro, J. R., Thiyagarajan, P., and Little, K. C. (2003) *Separ. Sci. Technol.,* **38**(12–13), 3313–31.

Chikalla, T. D. (1968) *J. Am. Ceram. Soc.,* **46**(7), 328.

Chikalla, T. D., McNeilly, C. E., and Skavdahl, R. E. (1962) *The Plutonium-Oxygen System*, Report HW-74802, General Electric Company, Hanford Atomic Products Operation, 30 pp.

Chikalla, T. D., McNeilly, C. E., and Skavdahl, R. E. (1964) *J. Nucl. Mater.,* **12**(2), 131–41.

Chipaux, R., Bonnisseau, D., Boge, M., and Larroque, J. (1988) *J. Magn. Magn. Mater.,* **74**(1), 67–73.

Chipaux, R., Larroque, J., and Beauvy, M. (1989) *J. Less-Common Met.,* **153**(1), 1–7.

Chipaux, R., Blaise, A., and Fournier, J. M. (1990) *J. Magn. Magn. Mater.,* **84**(1–2), 132–42.

Choppin, G. R. (1983) *Radiochim. Acta,* **32**(1–3), 43–53.

Choppin, G. R. and Saito, A. (1984) *Radiochim. Acta,* **35**(3), 149–54.

Choppin, G. R. and Wong, P. J. (1998) *Aquat. Geochem.,* **4**(1), 77–101.

Choppin, G. R., Roberts, R. A., and Morse, J. W. (1986) *ACS Symp. Ser.* **305** (Org. Mar. Geochem.), American Chemical Society, Washington, D.C. 382–8.

Christensen, E. L. and Maraman, W. J. (1969) *Plutonium Processing at the Los Alamos Scientific Laboratory*, Report LA-3542, Los Alamos Scientific Laboratory, 85 pp.

Christensen, E. L. and Mullens, L. J. (1952) *Preparation of Anhydrous Plutonium trichloride*, Report LA-1431, Los Alamos Scientific Laboratory, Los Alamos, NM, 8 pp.

Christensen, D. C. and Mullins, L. J. (1983) *ACS Symp. Ser.* **216**(Plutonium Chem.) (eds. W. T. Carnall and G. R. Choppin), American Chemical Society, Washington, DC. pp. 409–31.

Christensen, D. C., Bowersox, D. F., McKerley, B. J., and Nance, R. L. (1988) *Wastes from Plutonium Conversion and Scrap Recovery Operations*, Report LA-11069-MS, Los Alamos National Laboratory, Los Alamos, NM, 96 pp.

Christoph, G. G., Larson, A. C., Eller, P. G., Purson, J. D., Zahrt, J. D., Penneman, R. A., and Rinehart, G. H. (1988) *Acta Crystallogr. B,* **B44**(6), 575–80.

Chudinov, E. G. and Choporov, D., Ya. (1970) *At. Energiya,* **28**(2), 151–3.
Cinader, G., Zamir, D., and Hadari, Z. (1976) *Phys. Rev. B,* **14**(3), 912–20.
Clark, H. K. (1981) *Nucl. Sci. Eng.,* **79**(1), 65–84.
Clark, D. L. (in preparation) Crystal structures of K(18-crown-6)$_2$AnO$_2$Cl$_4$, (An = Np, Pu), Los Alamos National Laboratory, for publication.
Clark, S. B. and Delegard, C. (2002) Plutonium in Concentrated Solutions, in *Advances in Plutonium Chemistry 1967–2000* (ed. D. C. Hoffman), American Nuclear Society, La Grange Park, IL, pp. 118–68.
Clark, D. L., Hobart, D. E., and Neu, M. P. (1995) *Chem. Rev.,* **95**(1), 25–48.
Clark, D. L., Conradson, S. D., Ekberg, S. A., Hess, N. J., Neu, M. P., Palmer, P. D., Runde, W., and Tait, C. D. (1996) *J. Am. Chem. Soc.,* **118**(8), 2089–90.
Clark, D. L., Conradson, S. D., Keogh, D. W., Palmer, P. D., Scott, B. L., and Tait, C. D. (1998) *Inorg. Chem.,* **37**(12), 2893–9.
Clark, D. L., Conradson, S. D., Donohoe, R. J., Keogh, D. W., Morris, D. E., Palmer, P. D., Rogers, R. D., and Tait, C. D. (1999a) *Inorg. Chem.,* **38**(7), 1456–66.
Clark, D. L., Conradson, S. D., Keogh, D. W., Neu, M. P., Palmer, P. D., Runde, W., Scott, B. L., and Tait, C. D. (1999b) *X-ray Absorption and Diffraction Studies of Monomeric Actinide Tetra-, Penta-, and Hexa-Valent Carbonato Complexes*. Speciation, Techniques and Facilities for Radioactive Materials at Synchrotron Light Sources, OECD Nuclear Energy Agency, pp. 121–33.
Clayton, E. D. (1965) *Phys. Today,* **18**(9), 46–8, 50–2.
Cleveland, J. M. (1979) *The Chemistry of Plutonium,* American Nuclear Society, La Grange Park, IL, 680 pp.
Cleveland, J. M. (1980) Section IV: Chemical Processing, in *Plutonium Handbook: A Guide to the Technology,* vol. 2, (ed. O. J. Wick), American Nuclear Society, LaGrange Park, IL, 966 pp.
Cleveland, J. M., Bryan, G. H., Heiple, C. R., and Sironen, R. J. (1974) *J. Am. Chem. Soc.,* **96**(7), 2285–6.
Cleveland, J. M., Bryan, G. H., Heiple, C. R., and Sironen, R. J. (1975) *Nucl. Technol.,* **25**(3), 541–5.
Coffinberry, A. S. and Miner, W. N. (eds.) (1961) *The Metal Plutonium,* University of Chicago Press, Chicago, 446 pp
Coffinberry, A. S. and Waldron, M. B. (1956) Metallurgy and Fuels in *Progress in Nuclear Energy,* (eds. J. P. Howe and H.M. Finniston), ser. V, vol. 1, Pergamon Press, London, pp. 354–410.
Coffinberry, A. S., Schonfeld, F. W., Cramer, E. M., Miner, W. N., Ellinger, F. H., Elliott, R. O., and Struebing, V. O. (1958) *The Physical Metallurgy of Plutonium and its Alloys*. Second United Nations International Conference on the Peaceful Uses of Atomic Energy, Geneva, Switzerland, United Nations, 6, 681 pp.
Cogliati, G., Recrosio, A., and Lanz, R. (1969) *Plutonium Compounds*, (Comitato Nazionale per l'Energia Nucleare) De Patent 1801682, 14 pp.
Cohen, D. (1961a) *J. Inorg. Nucl. Chem.,* **18**, 207–10.
Cohen, D. (1961b) *J. Inorg. Nucl. Chem.,* **18**, 211–18.
Coleman, C. F. and Leuze, R. E. (1978) *J. Tenn. Acad. Sci.,* **53**(3), 102–7.
Colinet, C. (2002) Phase Diagram Calculations: Contribution of *Ab initio* and Cluster Variation Methods, in *CALPHAD and Alloy Thermodynamics.* (eds. P. E. A. Turchi, A. Gonis and R. D. Shull), TMS-Minerals, Metals & Material Society, Warrendale, PA, 21 pp.

Comstock, A. A. (1952) *Measurement of Plutonium Liquid Density*, Report LA-1348, Los Alamos Scientific Laboratory, 23 pp.
Connick, R. E. (1949) *J. Am. Chem. Soc.,* **71**, 1528–33.
Connick, R. E. (1954) Oxidation States, Potentials, Equilibria, and Oxidation–Reduction Reactions of Plutonium, in *The Actinide Elements* (eds. G. T. Seaborg and J. J. Katz), McGraw-Hill, New York, pp. 221–300.
Connick, R. E. and McVey, W. H. (1949) *J. Am. Chem. Soc.,* **71**(5), 1534–42.
Conradson, S. D. (2000) *Los Alamos Science,* **26**(2), 356.
Conradson, S. D. (2003) personal communication, S. S. Hecker, Los Alamos, NM.
Conradson, S. D., Mahamid, I. A., Clark, D. L., Hess, N. J., Hudson, E. A., Neu, M. P., Palmer, P. D., Runde, W. H., and Tait, C. D. (1998) *Polyhedron,* **17**(4), 599–602.
Conradson, S. D., Begg, B. D., Clark, D. L., Den Auwer, C., Espinosa- Faller, F. J., Gordon, P. L., Hess, N. J., Hess, R., Keogh, D. W., Morales, L. A., Neu, M. P., Runde, W., Tait, C. D., Veirs, D. K., and Villella, P. M. (2003) *Inorg. Chem.,* **42**(12), 3715–17.
Conradson, S. D., Abney, K. D., Begg, B. D., Brady, E. D., Clark, D. L., Den Auwer, C., Ding, M., Dorhout, P. K., Espinosa- Faller, F. J., Gordon, P. L., Haire, R. G., Hess, N. J., Hess, R. F., Keogh, D. W., Lander, G. H., Lupinetti, A. J., Morales, L. A., Neu, M. P., Palmer, P. D., Paviet- Hartmann, P., Reilly, S. D., Runde, W. H., Tait, C. D., Veirs, D. K., and Wastin, F. (2004a) *Inorg. Chem.,* **43**(1), 116–31.
Conradson, S. D., Begg, B. D., Clark, D. L., Den Auwer, C., Ding, M., Dorhout, P. K., Espinosa- Faller, F. J., Gordon, P. L., Haire, R. G., Hess, N. J., Hess, R. F., Keogh, D. W., Morales, L. A., Neu, M. P., Paviet- Hartmann, P., Runde, W., Tait, C. D., Veirs, D. K., and Villella, P. M. (2004b) *J. Am. Chem. Soc.,* **126**(41), 13443–58.
Conway, J. G. and Rajnak, K. (1966) *J. Chem. Phys.,* **44**, 348–54.
Coogler, A. L., Craft, R. C., and Tetzlaff, R. N. (1963) *Proc. Conf. on Hot Laboratory Equipment*, vol. 11, pp. 75–87.
Cooper, B. R., Thayamballi, P., Spirlet, J. C., Mueller, W., and Vogt, O. (1983) *Phys. Rev. Lett.,* **51**(26), 2418–21.
Cooper, N. G. and Schecker, J. A. (eds.) (2000) *Los Alamos Science,* Vol. 26, Los Alamos Science, Los Alamos National Laboratory, 493 pp
Coops, M. S., Knighton, J. B., and Mullins, L. J. (1983) *ACS Symp. Ser.* **216**(Plutonium Chem.) (eds. W. T. Carnall and G. R. Choppin), American Chemical Society, Washington, DC. pp. 381–408.
Cope, R. G., Hughes, D. G., Loasby, R. G., and Miller, D. C. (1960) The Plutonium–Ruthenium and Plutonium–Neptunium Binary Phase Diagrams, in *Plutonium 1960,* Grenoble, France (eds. E. Grison, W. B. H. Lord and R. D. Fowler), Cleaver-Hume Publishing, London, 280 pp.
Cordfunke, E. H. P., and Konings, R. J. M., Editors (1990) *Thermochemical Data for Reactor Materials and Fission Products,* North-Holland, Amsterdam, 696 pp.
Cornet, J. A. (1971) *J. Phys. Chem. Solids,* **32**, 1489–506.
Cornet, J. A. and Bouchet, J. M. (1968) *J Nucl. Mater.,* **28**, 303–10.
Costa, P. (1960) *J. Nucl. Mater.,* **2**, 75.
Costanzo, D. A., Biggers, R. E., and Bell, J. T. (1973) *J. Inorg. Nucl. Chem.,* **35**(2), 609–22.
Covert, A. S. and Kolodney, M. (1945) *Protection of Plutonium against Atmospheric Oxidation*, Report LA-314, Los Alamos Scientific Laboratory, 38 pp.

Cowan, G. A. (1976) *Sci. Am.,* **235**(1), 36–47.
Cox, M. and Flett, D. S. (1983) Metal Extractant Chemistry, in *Handbook of Solvent Extraction* (eds. T. C. Lo, M. H. I. Baird, and C. Hanson), Wiley, New York, 980 pp.
Cox, L. E., Martinez, R., Nickel, J. H., Conradson, S. D., and Allen, P. G. (1995) *Phys. Rev. B,* **51**(2), 751–5.
Cox, L. E., Peek, J. M., and Allen, J. W. (1999) *Physica B,* **259–261**, 1147–8.
Cramer, E. M. and Wood, D. H. (1967) *J. Less-Common Met.,* **13**(1), 112–21.
Cramer, E. M., Ellinger, F. H., and Land, C. C. (1960) *Extractive and Physical Metallurgy of Plutonium and its Alloys* (ed. W. D. Wilkinson), Interscience Publishers, New York, 169 pp.
Cramer, E. M., Hawes, L. L., Miner, W. N., and Schonfeld, F. W. (1961) *The Dilatometry and Thermal Analysis of Plutonium Metal,* in *The Metal Plutonium.* (eds. A. S. Coffinberry and W. N. Miner), University of Chicago Press, Chicago, IL, pp. 112–22.
Cremers, T. L., Dworzak, W. R., Brown, W. G., Flamm, B. F., Sampson, T. E., Bronisz, L. E., Nelson, T. O., Bronson, M. C., Colmenares, C. A., and Merrill, R. D. (1995) *Proc. Fifth Int. Conf. on Radioactive Waste Management and Environmental Remediation*, vol. 1, Berlin, Sept. 3–7, 1995, pp. 553–6.
Crisler, L. R. and Eggerman, W. G. (1974) *J. Inorg. Nucl. Chem.,* **36**(6), 1424–6.
Crocker, A. G. (1971) *J. Nucl. Mat.,* **41**(2), 167.
Crocker, H. W. (1961) *Ammonium bifluoride Fusion of Ignited Plutonium dioxide*, Report HW-68655, General Electrical Company, Richland, Washington, 5 pp.
Croff, A. G. (1980) ORIGEN2: *A Revised and Updated Version of the Oak Ridge Isotope Generation and Depletion Code*, Report ORNL-5621, Oak Ridge National Laboratory, 62 pp.
Croff, A. G. (1983) *Nucl. Technol.,* **62**(3), 335–52.
Cromer, D. T. (1975) *Acta Crystallogr.* **B31**, 1760.
Cromer, D. T. (1976) *Acta Crystallogr.* **B32**, 1930.
Cromer, D. T. (1977a) *Acta Crystallogr.* **B33**, 1993.
Cromer, D. T. (1977b) *Acta Crystallogr.* **B33**, 1996.
Cromer, D. T. (1978) *Acta Crystallogr.* **B34**, 913.
Cromer, D. T. (1979a) *Acta Crystallogr.* **B35**, 14.
Cromer, D. T. (1979b) *Acta Crystallogr.* **B35**, 1945.
Cromer, D. T. and Larson, A. C. (1960) *Acta Crystallogr.,* **13**(11), 909–12.
Cromer, D. T. and Larson, A. C. (1975) *Acta Crystallogr.* **B31**, 1758.
Cromer, D. T. and Larson, A. C. (1977) *Acta Crystallogr.* **B33**, 2620.
Cromer, D. T. and Olsen, C. E. (1959) *Acta Crystallogr.,* **12**(9), 689–94.
Cromer, D. T. and Roof, R. B. (1959) *Acta Crystallogr.,* **12**(11), 942–3.
Cromer, D. T., Larson, A. C., and Roof, R. B. Jr., (1964) *Acta Crystallogr.,* **17**(8), 947–50.
Cromer, D. T., Larson, A. C., and Roof, R. B. (1973) *Acta Crystallogr.* **B29**, 564–7.
Cromer, D. T., Larson, A. C., and Roof, R. B. (1975) *Acta Crystallogr.* **B31**, 1756.
Cunningham, B. B. (1949) *Nucleonics,* **5**(No. 5), 62–85.
Cunningham, B. B. (1954) Preparation and Properties of the Compounds of Plutonium, in *The Actinide Elements* (eds. G. T. Seaborg and J. J. Katz), McGraw-Hill, New York, pp. 371–434.
Cunningham, B. B. and Werner, L. B. (1949a) *J. Am. Chem. Soc.,* **71**, 1521–8.
Cunningham, B. B. and Werner, L. B. (1949b) The First Isolation of a Synthetic Element 94Pu239, in *Natl. Nucl. Energy Serv.*, Div IV **14B**(Transuranium Elements,

Pt. I) (eds. G. T. Seaborg, J. J. Katz and W. M. Manning), McGraw-Hill, New York, 51–78.

Curtis, D., Fabryka- Martin, J., Dixon, P., and Cramer, J. (1999) *Geochim. Cosmochim. Acta,* **63**(2), 275–85.

Czerwinski, K. and Kim, J.-I. (1997) *Mater. Res. Soc. Symp. Proc.,* **465**(Scientific Basis for Nuclear Waste Management XX), 743–50.

Dacheux, N., Podor, R., Brandel, V. and Genet, C. R. (1998) *J. Nucl. Mater.,* **252,** 179–86.

Dai, X., Savrasov, S. Y., Kotliar, G., Migliori, A., Ledbetter, H., and Abrahams, E. (2003) *Science,* **300**(5621), 953–5.

Dalton, J. T. and Griffin, R. M. (1964) *The Thorium–Plutonium–Carbon System*, Report AERE-R-4742, Atomic Energy Reseach Establishment, Harwell, UK, 20 pp.

Dalton, J. T., Potter, P. E., and Shaw, J. L. (1967) *Plutonium 1965, Proc. Third Int. Conf.*, pp. 775–805.

Damien, D. (1973) *Inorg. Nucl. Chem. Lett.,* **9**(4), 453–6.

Damien, D. (1976) *Synthesis and Crystal Chemistry of Transuranium Element Chalcogenides. Contribution to the Study of the 5f Electron Localization*, Report CEA-R-4783, CEN, CEA, Fontenay-aux-Roses, France, 161 pp.

Damien, D. and De Novion, C. H. (1981) *J. Nucl. Mater.,* **100**(1–3), 167–77.

Damien, D., de Novion, C. H., and Thevenin, T. (1986) Crystal Chemistry of Actinide Chalcogenides and Pnictides, in *Handbook on the Physics and Chemistry of the Actinides* (eds. A. J. Freeman and C. Keller), Elsevier Science, Amsterdam, pp. 39–96.

Danis, J. A., Lin, M. R., Scott, B. L., Eichhorn, B. W., and Runde, W. H. (2001) *Inorg. Chem.,* **40**(14), 3389–94.

Darken, L. S. and Gurry, R. W. (1953) *Physical Chemistry of Metals,* McGraw-Hill, New York, 535 pp.

David, S. J. and Kim, K. C. (1988) *J. Chem. Phys.,* **89**(4), 1780–6.

Davidson, N. R. and Katz, J. J. (1958) *Plutonium halides*. US Patent no. 2859 097. (U.S. Atomic Energy Commission)

Davidson, N. R., Hagemann, F., Hyde, E. K., Katz, J. J., and Sheft, I. (1949) The Preparation and Properties of Plutonium Tribromide and Oxybromide. *Natl. Nucl. Energy Ser.*, Div IV **14B**(Transuranium Element, Pt. I) (eds. G. T. Seaborg, J. J. Katz and W. M. Manning), McGraw Hill, New York, 759–74.

Dawson, J. K. and Elliott, R. M. (1953) *The Thermogravimetry of Some Plutonium Compounds*, Report AERE-C/R-1207, Great Britain Atomic Energy Research Establishment, 20 pp.

Dawson, J. K. and Truswell, A. E. (1951) *The Preparation of Plutonium Trifluoride and Tetrafluoride by the Use of Hydrogen Fluoride*, Report AERE-C/R-662, Great Britain Atomic Energy Research Establishment, 6 pp.

Dawson, J. K., Mandleberg, C. J., and Davies, D. (1951) *J. Chem. Soc.*, 2047–50.

Dawson, J. K., D'Eye, R. W. N., and Truswell, A. E. (1954a) *J. Chem. Soc., Abstracts*: 3922–9.

Dawson, J. K., Elliott, R. M., Hurst, R., and Truswell, A. E. (1954b) *J. Chem. Soc.*, 558–64.

Dayton, R. W. and Tipton, C. R., Jr (1961) *Progress Relating to Civilian Applications during June 1961*, Report BMI-1524(Del.), Battelle Memorial Institute, 104 pp.

De Alleluia, I. B., Berndt, U., and Keller, C. (1983) *Rev. Chim. Miner.,* **20**(4–5), 441–8.

De Winter, F., Stapfer, G., and Medina, E. (1999) *The Design of a Nuclear Power Supply with a 50 Year Life Expectancy: the JPL Voyager's SiGe MHW RTG. Proc. 34th Intersociety Energy Conversion Engineering Conf.*, pp. 433–40.

Dean, G. and Boivineau, J. C. (1970b) *Plutonium 1970 and Other Actinides, Proc. Fourth Int. Conf. on Plutonium and Other Actinides*, Santa Fe, NM, Oct. 5–9, 1970 (ed. W. N. Miner), AIME, New York.

Dean, G., Boivineau, J. C., Chereau, P., and Marcon, J. P. (1970a) *Plutonium 1970 and Other Actinides, Proc. Fourth Int. Conf. on Plutonium and Other Actinides*, Santa Fe, NM, Oct. 5–9, 1970 (ed. W. N. Miner), AIME, New York, 753 pp.

Deaton, R. L. and Wiedenheft, C. J. (1973) *J. Inorg. Nucl. Chem.,* **35**(2), 649–50.

Deloffre, P. (1997) *Etude de la Stabilite de la Phase Delta des Alliages de Plutonium Obtenue par Additions d'elements Deltagenes,* Thesis, Universite de Paris-Sud, Department d'Etudes et Technologies Nucleaires, Paris, 152 pp.

Den Auwer, C., Revel, R., Charbonnel, M. C., Presson, M. T., Conradson, S. D., Simoni, E., Le Du, J. F., and Madic, C. (1999) *J. Synchrotron Radiat.,* **6**(2), 101–04.

Denning, R. G. (1991) *Eur. J. Solid State Inorg.,* **28**(Suppl.), 33–45.

Denning, R. G. (1992) *Structure and Bonding,* **79**(Complexes, Clusters Cryst. Chem.), 215–76.

Denning, R. G. (1999) *Spectrochim. Acta. A,* **55**(9), 1757–65.

Denning, R. G., Green, J. C., Hutchings, T. E., Dallera, C., Tagliaferri, A., Giarda, K., Brookes, N. B., and Braicovich, L. (2002) *J. Chem. Phys.,* **117**(17), 8008–20.

Denotkina, R. G., Moskvin, A. I., and Shevchenko, V. B. (1960) *Russ. J. Inorg. Chem.,* **5**, 387–9.

Denotkina, R. G., Shevchenko, V. B., and Moskvin, A. I. (1965) *Russ. J. Inorg. Chem.,* **10**, 1333–35.

Denotkina, R. G., and Shevchenko, V. B. (1967) *Russ. J. Inorg. Chem.,* **12**, 42–45.

Deron, S. and Vesnovskii, S. (1999) *Nucl. Instrum. Meth. A,* **438**(1), 20–2.

Dewey, H. J., Barefield, II, J. E., and Rice, W. W. (1986) *J. Chem. Phys.,* **84**(2), 684–91.

Dixon, P., Curtis, D. B., Musgrave, J., Roensch, F., Roach, J., and Rokop, D. (1997) *Anal. Chem.,* **69**(9), 1692–9.

Dmitriev, S. N., Oganessian, Y. T., Buklanov, G. V., Kharitinov, Y. P., Novgorodov, A. F., Salamatin, L. I., Starodub, G. Y., Shishkin, S. V., Yushkevich, Y. V., and Newton, D. (1993) *Appl. Radiat. Isot.,* **44**(8), 1097–100.

Dmitriev, S. N., Oganessian, Y. T., Starodub, G. Y., Shishkin, S. V., Bulanov, G. V., Kharitonov, Y. P., Novgorodov, A. F., Yushkevich, Y. V., Newton, D., and Talbot, R. J. (1995) *Appl. Radiat. Isot.,* **46**(5), 307–9.

Dmitriev, S. N., Zaitseva, N. G., Starodub, G. Y., Maslov, O. D., Shishkin, S. V., Shishkina, T. V., Buklanov, G. V., and Sabelnikov, A. V. (1997) *Nucl. Instrum. Methods Phys. Res., Sect. A,* **397**(1), 125–30.

Dodgen, H. W., Chrisney, J., and Rollefson, G. K. (1944) *The Spectrum of Plutonium*, Report ANL-JJK-14B-24, Argonne National Laboratory, 17 pp.

Dodgen, H. W., Chrisney, J., and Rollefson, G. K. (1949) *Natl. Nucl. Energy Ser.*, Div IV **14B**(Transuranium Elements, Pt. II) (eds. G. T. Seaborg, J. J. Katz and W. M. Manning), McGraw Hill, New York, 1327–36.

DOE (1987) *Atomic Power in Space: A History*, Report DOE/NE/32117-H1; DE87010618 (Mar. 1987), 189 pp.

Domanov, V. P., Buklanov, G. V., and Lobanov, Y. V. (2002) *Radiochemistry,* **44**(2), 114–20.

Dormeval, M. (2001) *Structure Electronique d'alliages Pu-Ce(-Ga) et Pu-Am(-Ga) Stabilises en Phase Delta*, Thesis, Chimie - Physique, Dijon, L'Universite de Bourgogne, 194 pp.
Dormeval, M., Baclet, N., and Fournier, J. M. (2000) *AIP Conf. Proc.* **532**(Plutonium Futures–The Science) (eds. K. K. S. Pillay and K. C. Kim), p. 33.
Dormeval, M., Baclet, N., Valot, C., Rofidal, P., and Fournier, J. M. (2003) *J. Alloys Compd.,* **350**(1–2), 86–94.
Douglass, R. M. (1962) *Acta Cryst.,* **15**, 505–6.
Drummond, J. L. and Welch, G. A. (1957) *J. Chem. Soc., Abstracts*: 4781–5.
Drummond, J. L., McDonald, B. J., Ockenden, H. M., and Welch, G. A. (1957) *J. Chem. Soc.*, 4785–9.
Duff, M. C., Newville, M., Hunter, D. B., Bertsch, P. M., Sutton, S. R., Triay, I. R., Vaniman, D. T., Eng, P., and Rivers, M. L. (1999) *J. Synch. Rad.,* **6**(3), 350–2.
Dunlap, B. D. and Kalvius, G. M. (1985) in *Handbook on the Physics and Chemistry of Actinides,* vol. 2, (eds. A. J. Freeman and G. H. Lander), North-Holland, Amsterdam, 329 pp.
Dupuy, M. and Calais, D. (1968) *T. Am. I. Min. Met. Eng.,* **242**, 1679.
Durakiewicz, T., Joyce, J. J., Lander, G. H., Olson, C. G., Butterfield, M. T., Guziewicz, E., Arko, A. J., Morales, L., Rebizant, J., Mattenberger, K., and Vogt, O. (2004) *Phys. Rev. B,* **70**(20), 205103/1–205103/11.
Duriez, C., Alessandri, J. P., Gervais, T., and Philipponneau, Y. (2000) *J. Nucl. Mater.,* **277**(2,3), 143–58.
Dwyer, O. E., Eshaya, A. M., and Hill, F. B. (1959) *Continuous Removal of Fission Products from Uranium-Bismuth Fuels*, *Proc. Second Int. Conf. on the Peaceful Uses of Atomic Energy*, 1958, Geneva, United Nations, New York, 17, pp. 428–37.
Dyall, K. G. (1999) *Mol. Phys.,* **96**(4), 511–18.
Eberle, S. H. and Wade, U. (1970) *J. Inorg. Nucl. Chem.,* **32**, 109.
Edelstein, N. M. (1991) *Eur. J. Solid State Inorg. Chem.,* **28**(Suppl.), 47–55.
Edwards, G. R., Tate, R. E., and Hakkila, E. A. (1968) *J. Nucl. Mater.,* **25**(3), 304–9.
Ehrhart, P., Jung, P., Schultz, H., and Ullmaier, H. (1991) *Atomic Defects in Metals,* vol. 25, (ed. H. Ullmaier), Springer-Verlag, Berlin, 437 pp.
Eichelsberger, J. F. (1961) *Mound Laboratory Progress Report for December 1960*, Report MLM-1108, Mound Laboratory, 16 pp.
Eick, H. A. (1965) *Inorg. Chem.,* **4**(8), 1237–9.
Eisenberg, D. C., Streitwieser, A., and Kot, W. K. (1990) *Inorg. Chem.,* **29**(1), 10–14.
Eller, P. G., Kinkead, S. A., and Nielsen, J. B. (1992) in *Transuranium Elements: A Half Century* (eds. L. R. Morss and J. Fuger), 202–12.
Ellinger, F. H. (1956) *J. Metals,* **8**(AIME Trans. 206), 1256–9.
Ellinger, F. H. (1961) A Review of the Intermetallic Compounds of Plutonium, in *The Metal Plutonium* (eds. A. S. Coffinberry and W. N. Miner), University of Chicago Press, Chicago.
Ellinger, F. H. and Land, C. C. (1968) *J. Nucl. Mater.,* **28**(3), 291–6.
Ellinger, F. H. and Zachariasen, W. H. (1954) *J. Phys. Chem.,* **58**, 405–8.
Ellinger, F. H. and Zachariasen, W. H. (1965) *Acta Crystallogr.,* **19**, 281–3.
Ellinger, F. H., Elliott, R. O., and Cramer, E. M. (1959) *J. Nucl. Mater.,* **1**(3), 233–43.
Ellinger, F. H., Land, C. C., and Miner, W. N. (1962a) *J. Nucl. Mater.,* **1**, 115.
Ellinger, F. H., Land, C. C., and Miner, W. N. (1962b) *J. Nucl. Mater.,* **5**(2), 165–72.

Ellinger, F. H., Land, C. C., and Struebing, V. O. (1964) *J. Nucl. Mater.,* **12**(2), 226–36.
Ellinger, F. H., Land, C. C., and Johnson, K. A. (1965) *Trans. Metall. Soc. AIME,* **233** (7), 1252–8.
Ellinger, F. H., Johnson, K. A., and Struebing, V. O. (1966) *J. Nucl. Mater.,* **20**(1), 83–6.
Ellinger, F. H., Land, C. C., and Johnson, K. A. (1967) *Trans. Metall. Soc. AIME,* **239**(6), 895.
Ellinger, F. H., Land, C. C., and Johnson, K. A., unpublished work, Los Alamos Scientific Laboratory.
Ellinger, F. H., Land, C. C., and Johnson, K. A. (1968a) *J. Nucl. Mater.,* **29**(2), 178–83.
Ellinger, F. H., Miner, W. N., O'Boyle, D. R., and Schonfeld, F. W. (1968b) *Constitution of Plutonium Alloys*, Report LA-3870, Los Alamos Scientific Laboratory, 185 pp.
Elliott, R. O. (1980) personal communication, S. S. Hecker, Los Alamos, NM.
Elliott, R. O. and Giessen, B. C. (1975) Splat Cooling, in *Plutonium and Other Actinides* (eds. H. Blank and R. Lindner), North-Holland, Amsterdam, p. 47.
Elliott, R. O. and Larson, A. C. (1961) Delta-prime Plutonium, in *The Metal Plutonium* (eds. A. S. Coffinberry and W. N. Miner), University of Chicago Press, Chicago, pp. 265–80.
Elliott, R. O., Gschneidner, K. A., and Kempter, C. P. (1960) Thermal Expansion. *Plutonium 1960, Proc. Second Int. Conf. on Plutonium and Other Actinides* (eds. E. Grison, W. B. H. Lord, and R. D. Fowler), Cleaver-Hume Press, London, 142 pp.
Elliott, R. O., Olsen, C. E., and Louie, J. (1962) *J. Phys. Chem. Solids,* **23**(AUG), 1029–44.
Engel, T. K. (1969) *J. Nucl. Mater.,* **31**(2), 211–14.
Engerer, H. (1967) *Phase Equilibrium in the Systems* ThO_2–$HoO_{1.5}$($LuO_{1.5}$, $ScO_{1.5}$) *and* $HoO_{1.5}$–UO_2, UO_{2+x}, NpO_{2+x}, PuO_{2+x}), Thesis, Report KFK-597, Kernforschungszentrum, Karlsruhe, Federal Republic of Germany, 59 pp.
Enriquez, A. E., Matonic, J. H., Scott, B. L., and Neu, M. P. (2003) *Chem. Commun.*, (15), 1892–3.
Ephritikhine, M. (1992) *New J. Chem.,* **16**(4), 451–69.
Erdmann, B. and Keller, C. (1973) *J. Solid State Chem.,* **7**(1), 40–8.
Erdmann, N., Nunnemann, M., Eberhardt, K., Herrmann, G., Huber, G., Kohler, S., Kratz, J. V., Passler, G., Peterson, J. R., Trautmann, N., and Waldek, A. (1998) *J. Alloys Compd.,* **271–273**, 837–40.
Erilov, P. E., Titov, V. V., Serik, V. F., and Sokolov, V. B. (2002) *Atomic Energy (Translation of Atomnaya Energiya),* **92**(1), 57–63.
Etter, D. E., Martin, D. B., Roesch, D. L., Hudgens, C. R., and Tucker, P. A. (1965) *Trans. Metall. Soc. AIME,* **233**(11), 2011–13.
Evans, J. S. O., Mary, T. A., Vogt, T., Subramanian, M. A., and Sleight, A. W. (1996) *Chem. Mater.,* **8**, 2809.
Fardy, J. J. and Buchanan, J. M. (1976) *J. Inorg. Nucl. Chem.,* **38**(3), 579–83.
Faris, J. P. and Buchanan, R. F. (1964) *Anal. Chem.,* **36**(6), 1157.
Farkas, M. S. (1966) *Preparation and Heat Content of Uranium-, Plutonium-, and Neptunium-Containing Microspheres for Use as Intrinsic Thermocouple Flux Probes*, Report BMI-X-10175, Battelle Memorial Institute, Columbus, OH, 19 pp.
Faure, P., Deslandes, B., Bazin, D., Tailland, C., Doukhan, R., Fournier, J. M., and Falanga, A. (1996) *J. Alloys Compd.,* **244**(1–2), 131–9.

Faust, L. G., Brackenbush, L. W., Heid, K. R., Herrington, W. N., Kenoyer, J. L., Munson, L. F., Munson, L. H., Selby, J. M., Soldat, K. L., Stoetzel, G. A., Traub, R. J. and Vallario, E. J. (1988) *Health Physics Manual of Good Practices for Plutonium Facilities*, Report PNL-6534, Pacific Northwest Laboratory, 251 pp.

Favas, M. C., Kepert, D. L., Patrick, J. M., and White, A. H. (1983) *J. Chem. Soc. Dalton Trans.*, (**3**), 571–81.

Fedosseev, A. M., Budantseva, N. A., Grigoriev, M. S., Bessonov, A. A., Astafurova, L. N., Lapitskaya, T. S., and Krupa, J. C. (1999) *Radiochim. Acta,* **86**(1–2), 17–22.

Feldman, C. (1960) *Anal. Chem.,* **32**, 1727–8.

Felmy, A. R., Rai, D., Schramke, J. A., and Ryan, J. L. (1989) *Radiochim. Acta,* **48**(1–2), 29–35.

Ferro, R. and Cacciamani, G. (2002) Chemical Criteria in the Assessment of Alloy Constitutional Properties, in *CALPHAD and Alloy Thermodynamics* (eds. P. E. A. Turchi, A. Gonis and R. D. Shull), TMS, Warrendale, PA, 177 pp.

Filin, V. M., Bulkin, V. I., Timofeeva, L. F., and Polyakova, M. Y. (1989) *Sov. Radiochem.,* **30**, 683–721.

Finch, C. B. and Clark, G. W. (1972) *J. Cryst. Growth,* **12**(2), 181–2.

Fink, J. K. (1982) *Int. J. Thermophys.,* **3**(2), 165–200.

Fink, J. K. (2000) *J. Nucl. Mater.,* **279**(1), 1–18.

Firestone, R. B., Shirley, V. S., Baglin, C. M., Chu, S. Y. F., and Zipkin, J. (eds.) (1996) *Table of Isotopes,* John Wiley & Sons, New York.

Firestone, R. B., Shirley, V. S., Baglin, C. M., Chu, S. Y. F., and Zipkin, J. (eds.) (1998) *Table of Isotopes,* 8th edn, John Wiley & Sons, New York.

Fischer, R. D. (1963) *Theor. Chim. Acta,* **1**(5), 418–31.

Fischer, R., Werner, G.-D., Lehmann, T., Hoffmann, G. and Weigel, F. (1981) *J. Less-Comm. Met.,* **80**, 121–32.

Fisher, E. S. (1974) Ultrasonic Waves in Actinide Metals and Compounds, in *The Actinides: Electronic Structure and Related Properties,* part II, vol. 2 (eds. A. J. Freeman and J. B. Darby), Academic Press, New York, pp. 289–343.

Flahaut, J. (1979) in *Handbook on the Physics and Chemistry of Rare Earths* (eds. K. A. Gschneidner, Jr., and L. Eyring), North-Holland, Amsterdam, p. 2.

Flamm, B. F., Isom, G. M., and Nelson, T. O. (1998) *Proc. Third Topical Meeting on DOE Spent Nuclear Fuel and Fissile Materials Management*, vol. 1, Sept. 8–11, 1998, Charleston, SC, pp. 191–2.

Fleming, W. H. and Thode, H. G. (1953a) *Phys. Rev.,* **90**, 857–8.

Fleming, W. H. and Thode, H. G. (1953b) *Phys. Rev.,* **92**, 378–82.

Fletcher, J. M., Hyde, K. R., and Roberts, F. P. (1967) Germany Patent no. 108 4338.

Florin, A. E. (1950a) *Plutonium Hexafluoride, Plutonium (VI) Oxyfluoride: Preparation, Identification, and Some Properties*, Report LAMS-1118, Los Alamos Scientific Laboratory, Los Alamos, NM, US, 24 pp.

Florin, A. E. (1950b) *Plutonium Hexafluoride: Second Report on the Preparation and Properties*, Report LA-1168, Los Alamos Scientific Laboratory, 18 pp.

Florin, A. E. (1953) *Thermodynamic Properties of Plutonium Hexafluoride: A Preliminary Report*, Report LAMS-1587, Los Alamos Scientific Laboratory, 9 pp.

Florin, A. E. and Tannenbaum, I. R. (1952) *An Improved Apparatus for the Preparation of Plutonium Hexafluoride*, Report LA-1580, Los Alamos Scientific Laboratory, 12 pp.

Florin, A. E., Tannenbaum, I. R., and Lemons, J. F. (1956) *J. Inorg. Nucl. Chem.,* **2**, 368–79.

Flotow, H. E. and Tetenbaum, M. (1981) *J. Chem. Phys.,* **74**(9), 5269–77.

Flotow, H. E., Osborne, D. W., Fried, S. M., and Malm, J. G. (1976) *J. Chem. Phys.,* **65**(3), 1124–9.

Flotow, H. E., Haschke, J. M., and Yamauchi, S. (1984) *The Chemical Thermodynamics of Actinide Elements and Compounds,* part 9, *The Actinide Hydrides,* International Atomic Energy Agency, Vienna, Austria, 115 pp.

Fomin, V. V., Reznikova, V. E., and Zaitseva, L. L. (1958) *Zh. Neorg. Khim.,* **3**, 2231–5.

Forbes, R. L., Fuhrman, N., Andersen, J. C., and Taylor, K. M. (1966) *Uranium-Plutonium Monoxides*, Report UNC-5144, United Nuclear Corporation, Elmsford, New York, 81 pp.

Fortner, J. A., Kropf, A. J., Finch, R. J., Bakel, A. J., Hash, M. C., and Chamberlain, D. B. (2002) *J. Nucl. Mater.,* **304**(1), 56–62.

Fournier, J. M. and Troc, R. (1985) in *Handbook on the Physics and Chemistry of Actinides,* vol. 2 (eds. A. J. Freeman and G. H. Lander), North-Holland, Amsterdam, 29 pp.

Fournier, J. M., Pleska, E., Chiapusio, J., Rossat- Mignod, J., Rebizant, J., Spirlet, J. C., and Vogt, O. (1990) *Physica B,* **163**(1–3), 493–5.

Fox, R. V. and Mincher, B. J. (2002) *ACS Symp. Ser.* **860**(Separ. Processes Using Supercritical Carbon Dioxide) (eds. A. S. Gopalan, C. M. Wai and H. K. Jacobs), American Chemical Society, Washington, DC, pp. 36–49.

Fradin, F. Y. (1970) *Plutonium 1970 and Other Actinides, Proc. Fourth Int. Conf. on Plutonium and Other Actinides*, Santa Fe, NM, Oct. 5–9, 1970 (eds. W. N. Miner), New York, 264 pp.

Fred, M., Blaise, J., and Gutmacher, R. (1966) *J. Opt. Soc. Am.,* **56**, 1416A.

Freedberg, N. A., Antonelli, D., Bloch, L., and Rosenfeld, T. (1992) *Pacing Clin. Electrophysiol.,* **15**(11), 1639–41.

Freeman, A. J. and J. B. Darby, J. (eds.) (1974) *The Actinides, Electronic Structure and Related Properties*, Academic Press, New York.

Fried, S. and Davidson, N. R. (1949) *Nat'l. Nucl. Energy Ser.,* Div IV **14B**(Transuranium Elements, Pt. I) (eds. G. T. Seaborg, J. J. Katz and W. M. Manning), McGraw-Hill, New York, pp. 784–92.

Fried, S., Westrum, Jr, E. F., Baumbach, H. L., and Kirk, P. L. (1958) *J. Inorg. Nucl. Chem.,* **5**, 182–9.

Frolov, A. A., Andreichuk, N. N., Ratmanov, K. V., Frolova, I. M., and Vasiliev, V. Y. (1990) *J. Radioanal. Nucl. Ch. Le.,* **143**(2), 433–44.

Fuger, J. (1992) *Radiochim. Acta,* **58–59**(1), 81–91.

Fuger, J. and Cunningham, B. B. (1963) *J. Inorg. Nucl. Chem.,* **25**(11), 1423–9.

Fuger, J., Oetting, F. L., Hubbard, W. N., and Parker, V. B. (1983) *Chemical Thermodynamics of Actinide Elements and Compounds. Pt. 8. The Actinide Halides.* IAEA, Vienna, Austria, 267 pp.

Fujiwara, K., Yamana, H., Fujii, T., and Moriyama, H. (2001) *Genshiryoku Bakkuendo Kenkyu (J. Nucl. Fuel Cycle Environ. (Japan)),* **7**(1), 17–23.

Fulton, R. B. and Newton, T. W. (1970) *J. Phys. Chem.,* **74**(8), 1661–9.

Gal, J., Hadari, Z., Bauminger, E. R., and Ofer, S. (1972) *Phys. Lett. B,* **41**(1), 53–4.

Galasso, F. S. (1968) *Structure, Properties, and Preparation of Perovskite-type Compounds,* Pergamon Press, Oxford, England.

Ganz, M., Barth, H., Fuest, M., Molzahn, D., and Brandt, R. (1991) *Radiochim. Acta,* **52–53**(Pt. 2), 403–4.
Gardner, H. (1965) Mechanical Properties *Plutonium 1965, Proc. Third Int. Conf.* (eds. A. E. Kay and M. B. Waldron), Chapman and Hall, London, 118 pp.
Gardner, H. R. (1980) Mechanical Properties *The Plutonium Handbook,* vol. 1, (ed. O. J. Wick), American Nuclear Society, La Grange Park, IL, pp. 59–100.
Gardner, E. R., Markin, T. L., and Street, R. S. (1965) *J. Inorg. Nucl. Chem.,* **27**(3), 541–51.
Garner, C. S. (1950) *Los Alamos Technical Series, Chemistry of Uranium and Plutonium*, Report LA-1100, Los Alamos Scientific Laboratory, Los Alamos, NM, pp. 110–16.
Garner, C. S., Bonner, N. A., and Seaborg, G. T. (1948) *J. Am. Chem. Soc.,* **70**, 3453–4.
Gel'man, A. D. and Zaitsev, L. M. (1958) *Zh. Neorg. Khim.,* **3**, 1304–11.
Gel'man, A. D. and Zaitseva, V. P. (1964) *Dokl. Akad. Nauk SSSR,* **157**(6), 1403–5.
Gel'man, A. D. and Zaitseva, V. P. (1965a) *Radiokhimiya,* **7**(1), 49–55.
Gel'man, A. D. and Zaitseva, V. P. (1965b) *Radiokhimiya,* **7**(1), 56–68.
Gendre, R. (1962) *Preparation of Plutonium hexafluoride: Recovery of Plutonium from Waste Dross*, Report CEA-2161, Commissariat a l'Energie Atomique, 109 pp.
Gens, T. A. (1961) *Nucl. Sci. Eng.,* **9**(4), 488–94.
Gens, R., Fuger, J., Morss, L. R., and Williams, C. W. (1985) *J. Chem.Thermodyn.,* **17**(6), 561–73.
Gevantman, L. H. and Kraus, K. A. (1949) *Natl. Nucl. Energy Ser.*, Div IV, **14B** (Transuranium Elements, Pt. I), (eds. G. T. Seaborg, J. J. Katz, and W. M. Manning), pp. 500–18.
Gibney, R. B. and Sandenaw, T. A. (1954) *Electrical Resistivity of Plutonium Metal and of Gallium–Plutonium Alloys over the Temperature Range of 26 K to ~773 K*, Report LA-1883, Los Alamos Scientific Laboratory, 26 pp.
Giessen, B. C., Elliott, R. O., and Struebing, V. O. (1975) *Mat. Sci. Eng.,* **18**(2), 239–43.
Gilman, W. S. (1965) *A Review of the Dissolution of Plutonium Dioxide*, Report MLM-1264, Mound Laboratory, Miamisburg, OH, 12 pp.
Gilman, W. S. (1968) *Review of the Dissolution of Plutonium Dioxide. II*, Report MLM-1513, Mound Laboratory, Miamisburg, OH, 12 pp.
Glazyrin, S. A., Rodchenko, P. Y., and Sokina, L. P. (1989) *Radiokhimiya,* **31**(4), 48–52 (pp 407–410 in English translation).
Glushko, V. P. (ed.) (1982) *Thermodynamic Properties of Individual Substances,* vol. 4, Nauka, Moscow, 623 pp.
Goldberg, A. and Massalski, T. (1970a) *Phase Transformations in the Actinides, Proc. Fourth Int. Conf. on Plutonium and Other Actinides,* Santa Fe, NM (ed. W. N. Miner), The Metallurgical Society of AIME, pp. 875–945.
Goldberg, A., Rose, R. L., and Matlock, D. K. (1970b) *The Delta and Epsilon Thermal Expansion Coefficients and the Delta-to-epsilon Contraction for Some Plutonium-rich Alloys, Proc. Fourth Int. Conf. on Plutonium and Other Actinides 1970, vol. 2,* (ed. W. N. Miner), The Metallurgical Society of AIME, Warrendale, PA, pp. 1056–68.
Gomez Marin, E. (1997) *Etude du Comportement de la Resistivite Electrique des Mono-Chalcogenures de Plutonium et des Alliages de Plutonium et Americium*, Thesis, l'Universite Grenoble, Grenoble.
Gorbunov, S. I. and Seleznev, A. G. (2001) *Radiochemistry,* **43**(2), 111–117.
Gordon, G. and Taube, H. (1961) *J. Inorg. Nucl. Chem.,* **19**, 189–91.

Gordon, J. E., Hall, R. O., Lee, J. A., and Mortimer, M. J. (1976) *Proc. R. Soc. London, Ser. A,* **351**(1665), 179–96.
Gorum, A. E. (1957) *Acta Crystallogr.,* **10**, 144.
Gouder, T., Wastin, F., Rebizant, J., and Havela, L. (2000) *Phys. Rev. Lett.,* **84**(15), 3378–81.
Gouder, T., Havela, L., Wastin, F., and Rebizant, J. (2002) *J. Nucl. Sci. Tech.*, (Suppl. 3), 49–55.
Gouder, T., (2005) *XPS studies of PuH_3 thin films, personal communication*, D. L. Clark, Los Alamos, NM.
Grachev, A. F., Maershin, A. A., Skiba, O. V., Tsykanov, V. A., Bychkov, A. V., Kormilitsyn, M. V., and Sokolvskii, Y. S. (2004) *At. Energ.,* **96**(5), 320–6.
Graf, W. L. (1994) *Plutonium and the Rio Grande: Environmental Change and Contamination in the Nuclear Age,* Oxford University Press, New York, 329 pp.
Green, J. L. and Leary, J. A. (1970) *J. Appl. Phys.,* **41**(13), 5121–4.
Green, D. W. and Reedy, G. T. (1978a) *J. Chem. Phys.,* **69**(2), 552–5.
Green, D. W. and Reedy, G. T. (1978b) *J. Chem. Phys.,* **69**(2), 544–51.
Green, D. W., Fink, J. K., and Leibowitz, L. (1983) *ACS Symp. Ser.* **216**(Plutonium Chem.) (eds. W. T. Carnall and G. R. Choppin), American Chemical Society, Washington, DC, pp. 123–43.
Greenwood, N. N. and Earnshaw, A. (1997) *Chemistry of the Elements,* Butterworth-Heinemann, Oxford, England, 1341 pp.
Grenthe, I., Riglet, C., and Vitorge, P. (1986a) *Inorg. Chem.,* **25**(10), 1679–84.
Grenthe, I., Robouch, P., and Vitorge, P. (1986b) *J. Less-Common Met.,* **122**, 225–31.
Grenthe, I., Fuger, J., Konigs, R. J. M., Lemire, R. J., Muller, A. B., Nguyen- Trung, C., and Wanner, H. (1992) *Chemical Thermodynamics of Uranium,* Elsevier Science Publishing Company, New York, 676 pp.
Grenthe, I., Puigdomenech, I., and Allard, B. (1997) *Modelling in Aquatic Chemistry,* Nuclear Energy Agency, OECD, Washington, DC, 724 pp.
Grigor'ev, M. S., Gulyaev, B. F., and Krot, N. N. (1986) *Sov. Radiochem.,* **28**(6), 630–4.
Grigor'ev, M. S., Baturin, N. A., Bessonov, A. A., and Krot, N. N. (1995) *Radiokhimiya,* **37**(1), 15–18.
Grison, E., Lord, W. B. H., and Fowler, R. D. (eds.) (1960) *Plutonium 1960, Proc. Second Int. Conf. on Plutonium Metallurgy,* Grenoble, France, Apr. 19–22, 1960, Cleaver Hume, London.
Griveau, J. C., Pfleiderer, C., Boulet, P., Rebizant, J., and Wastin, F. (2004) *J. Magn. Magn. Mater.,* **272/276**, 154–5.
Grove, G. R. (1966) *Reactor Fuels and Materials Development. Plutonium Research. April–Sept.*, Report MLM-1347, Mound Laboratory, pp. 11–18.
Grove, G. R., Goldenberg, J. A., Kelly, D. P., and Prosser, D. L. (1965) *Plutonium-238 Isotopic Power Sources, a Summary Report*, Report MLM-1270, Mound Laborabory, Miamisburg, OH, 234 pp.
Gruen, D. M. and deKock, C. W. (1967) *J. Inorg. Nucl. Chem.,* **29**(10), 2569–75.
Gruen, D. M., Malm, J. G., and Weinstock, B. (1956) *J. Chem. Phys.,* **24**(4), 905–6.
Gruen, D. M., McBeth, R. L., Kooi, J., and Carnall, W. T. (1960) *Ann. N.Y. Acad. Sci.,* **79**(11), 941–9.
Gschneidner, K. A., Jr (1980) Theory Alloy Phase Form., Proc. Symp, Meeting Date 1979, Metall. Soc. AIME, Warrendale, PA, 1–39.

Gschneidner, Jr, K. A., Elliott, R. O., and Struebing, V. O. (1960) *Pu Phase Diagrams Discussion, Proc. Second Int. Conf. on Plutonium and Other Actinides,* Grenoble, France (eds. E. Grison, W. B. H. Lord, and R. D. Fowler), Cleaver-Hume Press, London, 1, 166 pp.

Guerin, G. (1996) Research on Actinides. CLEFS/CEA. **31**, 1–71.

Guillaumont, R. and Adloff, J. P. (1992) *Radiochim. Acta,* **58–59**(Pt. 1), 53–60.

Guillaumont, R., Fanghaenel, T., Fuger, J., Grenthe, I., Neck, V., Palmer, D. A., and Rand, M. H. (2003) *Update on the Chemical Thermodynamics of Uranium, Neptunium, Plutonium, Americium, and Technetium,* Elsevier, Amsterdam, The Netherlands, 919 pp.

Güldner, R. and Schmidt, H. (1991) *J. Nucl. Mater.,* **178**(2–3), 152–7.

Hagan, P. G. and Miner, F. J. (1980) *ACS Symp. Ser.,* **117**(Actinide Sep.), 51–67.

Hagemann, F., Abraham, B. M., Davidson, N. R., Katz, J. J., and Sheft, I. (1949) The Preparation and Properties of Plutonium Iodide and Plutonium Oxyiodide, in *Natl. Nucl. Energy Ser.,* Div IV **14B**(*Transuranium Elements*, Pt. II), (eds. G. T. Seaborg, J. J. Katz, and W. M. Manning), McGraw-Hill, New York, pp. 957–63.

Haines, H. R. and Potter, P. E. (1975) *Thermodyn. Nucl. Mater*., Proc. Symp., 4th, Meeting Date 1974, **2,** pp. 145–73.

Haire, R. G. and Eyring, L. (1994) Comparison of the Binary Oxides, in *Handbook on the Physics and Chemistry of Rare Earths,* vol. 18, (eds. K. A. J. Gschneidner, L. Eyring, G. R. Choppin, and G. H. Lander), Elsevier Science, New York, pp. 413–505.

Haire, R. G., Heathman, S., Le Bihan, T., Lindbaum, A., and Iridi, M. (2004) *Mater. Res. Soc. Symp. Proc.,* **802**, (Actinides–Basic Science Technol.), 15–20.

Hall, R. O. A., Jeffery, A. J., Lee, J. A., Mortimer, M. J., and Lander, G. H. (1985) *Heat Capacity Measurements on Plutonium Phosphide*, Report AERE-R-11075, Atomic Energy Research Establishment, Harwell, UK, 24 pp.

Hammel, E. F. (1998) *Plutonium Metallurgy at Los Alamos, 1943–1945: Recollections of Edward F. Hammel,* Los Alamos National Laboratory, Los Alamos, NM, 173 pp.

Handa, M. and Suzuki, Y. (1984) *Nihon Genshiryoku Gakkaishi,* **26**(1), 2–7.

Handwerk, J. H. and Kruger, O. L. (1971) *Nucl. Eng. Des.,* **17**(3), 397–408.

Hanrahan, R. J., Boehlert, C., and McDeavitt, S. (2003) *J. Metals*, **55**(9).

Harland, C. E. (1994) *Ion Exchange: Theory and Practice*, 2nd Ed., The Royal Society of Chemistry, Cambridge.

Harmon, K. M. and Reas, W. H. (1957) *Conversion Chemistry of Plutonium Nitrate*, Report HW-49597 A, 15 pp.

Harmon, K. M., Judson, B. F., Lyon, W. L., Pugh, R. A., and Smith, R. C. (1961) in *Reactor Handbook,* 2nd edn, vol. II, (eds. S. M. Stoller and R. B. Richard), Interscience Publishers, New York, 680 pp.

Harper, E. A., Hedger, H. J., and Dalton, J. T. (1968) *Nature,* **219**(5150), 151.

Harrison, W. A. (2001) *Phys. Rev. B,* **64**(23), 235112/1–10.

Harrowfield, J. M. B., Kepert, D. L., Patrick, J. M., White, A. H., and Lincoln, S. F. (1983) *J. Chem. Soc. Dalton Trans.*, (2), 393–6.

Harvey, B. G., Heal, H. G., Maddock, A. G., and Rowley, E. L. (1947) *J. Chem. Soc.*, 1010–21.

Harvey, M. R., Doyle, J. H., Rafalski, A. L., and Riefenberg, D. H. (1971) *J. Less-Common Met.,* **23**, 446.

Hasbrouk, M. E. and Burns, M. P. (1965) *Plutonium Metallurgy Handbook*, Report BNWL-37, Pacific Northwest Laboratory.

Haschke, J. M. (1991) Actinide Hydrides, in *Topics in f-element Chemistry,* vol. 2 (eds. G. Meyer and L. R. Morss), Kluwer Academic Publishers, Boston, MA, pp. 1–53.

Haschke, J. M. (1992) *Hydrolysis of Plutonium. Plutonium–Oxygen Phase Diagram* in *Transuranium Elements: A Half Century* (eds. L. R. Morss and J. Fuger), pp. 416–25.

Haschke, J. M. (1999) Pu Oxidation, personal communication, J. C. Martz, Los Alamos, NM.

Haschke, J. M. (2005) *J. Nucl. Mater.,* **340**(2–3), 299–306.

Haschke, J. M. and Allen, T. H. (2001) *J. Alloys Compd.,* **320**(1), 58–71.

Haschke, J. M. and Haire, R. G. (2000) Crystalline Solids and Corrosion Chemistry, in *Advances in Plutonium Chemistry 1967–2000* (ed. D. C. Hoffman), The American Nuclear Society, La Grange Park, IL, pp. 212–59.

Haschke, J. M. and Martz, J. C. (1998a) *J. Alloys Compd.,* **266**(1–2), 81–9.

Haschke, J. M. and Martz, J. C. (1998b) *Encyclopedia of Environmental Analysis and Remediation, Plutonium Storage,* vol. 6, John Wiley, New York, pp. 3740–55.

Haschke, J. M. and Oversby, V. M. (2002) *J. Nucl. Mater.,* **305**(2–3), 187–201.

Haschke, J. M., Hodges, A. E., III, Bixby, G. E., and Lucas, R. L. (1983) *Reaction of Plutonium with Water. Kinetic and Equilibrium Behavior of Binary and Ternary Phases in the Plutonium + Oxygen + Hydrogen System*, Report RFP-3416, Rockwell International Corporation, Rocky Flats Plant, Golden, CO, 24 pp.

Haschke, J. M., Hodges, III, A. E., and Lucas, R. L. (1987) *J. Less-Common Met.,* **133**(1), 155–66.

Haschke, J. M., Allen, T. H., and Stakebake, J. L. (1996) *J. Alloys Compd.,* **243**(1–2), 23–35.

Haschke, J. M., Allen, T. H., and Martz, J. C. (1998) *J. Alloys Compd.,* **271**, 211–15.

Haschke, J. M., Allen, T. H., and Morales, L. A. (2000a) *Los Alamos Science,* **26**(1), 252–73.

Haschke, J. M., Allen, T. H., and Morales, L. A. (2000b) *Science,* **287**(5451), 285–7.

Haschke, J. M., Allen, T. H., and Morales, L. A. (2001) *J. Alloys Compd.,* **314**(1–2), 78–91.

Hasilkar, S. P., Khedekar, N. B., Chander, K., Jadhav, A. V., and Jain, H. C. (1994) *J. Radioanal. Nucl. Chem.,* **185**(1), 119–25.

Hass, P. A., Lloyd, M. H., Band, W. D., and McBride, J. P. (1966) *Sol-Gel Process Development and Microsphere Preparation*, Report ORNL-P-2159, Oak Ridge National Laboratory, 42 pp.

Haug, H. (1963) *The Systems Uranium Oxide–Europium Oxide and Plutonium Oxide–Europium Oxide*, Thesis, Report NP-13003, University of Munich, Germany, 97 pp.

Haug, H. and Weigel, F. (1963) *J. Nucl. Mater.,* **9**(3), 160–3.

Hawkins, N. J. (1956) *Report of the Chemistry and Engineering Section for February, March, April, 1956*, Report KAPL-1536, Knolls Atomic Power Laboratory, Schenectady, New York, 98 pp.

Hawkins, N. J., Mattraw, H. C., and Sabol, W. W. (1954) *Infrared Spectrum and Thermodynamic Properties of PuF_6*, Report KAPL-1007, Knolls Atomic Power Laboratory, 21 pp.

Hay, P. J. and Martin, R. L. (1998) *J. Chem. Phys.,* **109**(10), 3875–81.

Hay, P. J., Martin, R. L., and Schreckenbach, G. (2000) *J. Phys. Chem. A,* **104**(26), 6259–70.

Hayes, R. G. and Edelstein, N. (1972) *J. Am. Chem. Soc.,* **94**(25), 8688–91.
Hecker, S. S. unpublished work, Los Alamos National Laboratory.
Hecker, S. S. (2000) *Los Alamos Science,* **26**(2), 290.
Hecker, S. S. (2003) *JOM* **55**(9), 13–50.
Hecker, S. S. (2004) *Metall. Mater. Trans. A,* **35 A**(8), 2207–22.
Hecker, S. S. and Martz, J. C. (2000) *Los Alamos Science* **26**(1), 238–43.
Hecker, S. S. and Martz, J. C. (2001) Plutonium Aging: from Mystery to Enigma, in *Aging Studies and Lifetime Extension of Materials* (ed. L. G. Mallinson), Kluwer Academic, New York, pp. 23–52.
Hecker, S. S. and Morgan, J. R. (1976) *Effect of Strain Rate on the Tensile Properties of Alpha - and Delta - Stabilized Plutonium, Proc. Fifth Int. Conf. on Plutonium and Other Actinides 1975, Sept. 10–13, 1975,* Baden-Baden, West Germany, (eds. H. Blank and R. Linder), North-Holland, Amsterdam, The Netherlands, pp. 697–709.
Hecker, S. S. and Stevens, M. F. (2000) *Los Alamos Science* **26**(2), 336–55.
Hecker, S. S. and Timofeeva, L. F. (2000) *Los Alamos Science* **26**(1), 244–51.
Hecker, S. S., Zukas, E. G., Morgan, J. R., and Pereyra, R. A. (1982) *Temperature-Induced Transformation in a Pu-2 at.% Al Alloy. Proc. Int. Conf. on Solid to Solid Phase Transformations;* Pittsburgh, PA, Metallurgical Society of AIME, 1982, Warrendale, PA, pp. 1339–43.
Hecker, S. S., Harbur, D. R., and Zocco, T. G. (2004b) *Prog. Mater. Sci.,* **49**(3–4), 429–85.
Herbst, R. J. and Matthews, R. B. (1982) *Uranium–Plutonium Carbide as an LMFBR Advanced Fuel*, Report LA-9259-MS, Los Alamos National Laboratory, Los Alamos, NM, 24 pp.
Herrick, C. C., Olsen, C. E., and Sandenaw, T. A. (1959) *The Density of Liquid Plutonium Metal*, Report LA-2358, Los Alamos Scientific Laboratory, 17 pp.
Hidaka, H. (1999) *J. Radioanal. Nucl. Chem.,* **239**(1), 53–8.
Hidaka, H. and Holliger, P. (1998) *Geochim. Cosmochim. Acta,* **62**(1), 89–108.
Hill, O. F. and Cooper, V. R. (1958) *Ind. Eng. Chem.,* **50**(4), 599–602.
Hill, H. H. and Kmetko, E. A. (1976) *J. Phys. F: Me. Phys.,* **6**(6), 1025–37.
Hill, R. N. (2005), personal communication, G. Jarvinen.
Hilliard, J. E., Averbach, B. B., and Cohen, M. (1959) *Acta Met.,* **7**, 86.
Hincks, J. A. and McKinley, L. C. (1966) *Heat Source Fabrication*, Report MLM-1365, Mound Laboratory, 35 pp.
Hindman, J. C. (1954) Ionic and Molecular Species of Plutonium in Solution, in *The Actinide Elements* (eds. G. T. Seaborg and J. J. Katz), McGraw-Hill, New York, pp. 301–70.
Hinrichs, W., Melzer, D., Rehwoldt, M., Jahn, W., and Fischer, R. D. (1983) *J. Organomet. Chem.,* **251**(3), 299–305.
Hobart, D. E., Morris, D. E., Palmer, P. D., and Newton, T. W. (1989) *Formation, Characterization, and Stability of Plutonium (IV) Colloid: A Progress Report*, Report LA-UR-89-2541, Los Alamos National Laboratory, 9 pp.
Hocheid, B., Tanon, A., and Despres, J. (1965) *J. Nucl. Mater.,* **15**(3), 241–4.
Hocheid, B., Tanon, A., Bedere, S., Despres, J., Hay, S., and Miard, F. (1967) *Pu-Ga Phase Diagram,* Plutonium 1965, Proc. Third Int. Conf. on Plutonium (eds. A. E. Kay, and M. B. Waldron), Chapman-Hall, London, 321 pp.
Hodge, N. (1961) in *Advances in Fluorine Chemistry,* vol. 2 (eds. M. Stacey, J. C. Tatlow, and A. G. Sharpe), Butterworths, London, England, 138 pp.

Hoekstra, H. R. and Gebert, E. (1977) *J. Inorg. Nucl. Chem.,* **39**(12), 2219–21.
Hoffman, D. C. (ed.) (2000) *Advances in Plutonium Chemistry 1967–2000,* The American Nuclear Society, La Grange Park, IL, 320 pp.
Hoffman, D. C., Lawrence, F. O., Mewherter, J. L., and Rourke, F. M. (1971) *Nature,* **234**(5325), 132–4.
Hoffman, D. C., Ghiorso, A., and Seaborg, G. T. (2000) *The Transuranium People: The Inside Story,* Imperial College Press, London, England, 467 pp.
Holleck, H. (1975) *Proc. Fourth Symp. on Thermodyn. Nucl. Mater.,* vol. 2, pp. 213–64.
Holleck, H. and Kleykamp, H. (1972) *Gmelin Handbook of Inorganic Chemistry, Transuranium Elements, part C,* Verlag Chemie, Weinheim, 83 pp.
Holley, C. E., Jr (1974) *J. Nucl. Mater.,* **51**(1), 36–46.
Holley, C. E., Jr, Mulford, R. N. R., Huber, E. J., Jr, Head, E. L., Ellinger, F. H., and Bjorklund, C. W. (1958) *Proc. Second UN Int. Conf. Peaceful Uses Atomic Energy*, Geneva, 1958, vol. 6, pp. 215–20.
Holley, C. E., Rand, M. H., and Storms, E. K. (1984) The Actinide Carbides, in *Chemical Thermodynamics of Actinide Elements and Compounds: Part. 6,* IAEA, Vienna, Austria, 101 pp.
Holliger, P. and Devillers, C. (1981) *Earth Planet. Sc. Lett.,* **52**(1), 76–84.
Horner, D. E., Crouse, D. J., and Mailen, J. C. (1977) *Cerium-promoted Dissolution of Plutonium dioxide and Plutonium dioxide–Uranium dioxide in Nitric Acid*, Report ORNL/TM-4716, Oak Ridge National Laboratory, TN, 41 pp.
Hough, A. and Marples, J. A. C. (1965) *J. Nucl. Mater.,* **15**(4), 298–309.
Howell, R. H. and Sterne, P. A. (2002) Positron Annihilation Spectroscopy, personal communication, A. J. Schwartz, Livermore, CA.
Howell, R. H., Sterne, P. A., Hartley, J., and Cawan, T. E. (1999) *Appl. Surf. Sci.,* **149**, 103–5.
Hunt, D. C. and Boss, M. R. (1971) *J. Nucl. Energy,* **25**(6), 241–51.
Hunt, D. C. and Rothe, R. E. (1974) *Nucl. Sci. Eng.,* **53**(1), 79–92.
Hurst, H. J. and Taylor, J. C. (1970) *Acta Crystallogr.,* **B26**(Pt. 4), 417–21.
Hurst, R., Mandleberg, C. J., Rae, H. K., Davies, D., Francis, K. E., and Brooks, R. (1953) *Plutonium Hexafluoride*, part II, *Preparation and Some Physical Properties*, Report AERE-C/R-1312, Great Britain Atomic Energy Research Establishment.
Hyde, E. K., Davidson, N. R., Katz, J. J., and Wolf, M. J. (1944) *Chemical Research - Special Chemistry of Plutonium. Report for Month Ending April 1, 1944*, Report CK-1512, Metallurgical Laboratory, pp. 5–7.
Hyde, E. K., Perlman, I., and Seaborg, G. T. (1964) *The Nuclear Properties of the Heavy Elements Vol. I: Systematics of Nuclear Structure and Radioactivity. Vol. II: Detailed Radioactivity Properties*, Prentice-Hall, Englewood Cliffs, NJ, 400 pp.;36 pp.
IAEA (1967) *The Plutonium–Oxygen and the Uranium–Plutonium–Oxygen Systems. A Themochemical Assessment*, Report Tech. Rep Ser. No. 79, STI\DOC-10\79, International Atomic Energy Agency, 86 pp.
Iida, T., Guthrei, R. I. L., and Morita, Z. (1988) *Can. Metall. Quart.,* **27**(1), 1–5.
Iso, S., Uno, S., Yoshihiro, M., Sasaki, T., and Yoshida, Z. (2000) *Prog. Nucl. Energ.,* **37** (1–4), 423–8.
Iyer, P. N. and Natarajan, P. R. (1989) *J. Less-Common Met.,* **146**(1–2), 161–6.
Iyer, P. N. and Natarajan, P. R. (1990) *J. Less-Common Met.,* **159**(1–2), 1–11.

Jackson, E. F. and Rand, M. H. (1963) *Oxidation Behaviour of Plutonium Dioxide and Solid Solutions Containing Plutonium Dioxide*, Report AERE-R-3636, Atomic Energy Research Establishment, Harwell, UK, 13 pp.

Jacquemin, J. and Lallement, R. (1970) *Self-irrad Damage*, *Proc. Int. Conf. on Plutonium and Other Actinides 1970* (ed. W. N. Miner), The Metallurgical Society of AIME, pp. 616–22.

Jarvinen, G. D. (ed.) (2003) *AIP Conf. Proc.*, **673**(Plutonium Futures – The Science). 421 pp.

Jayadevan, N. C., Mudher, K. D. S., and Chackraburtty, D. M. (1982) *Z. Kristallogr.,* **161**(1–2), 7–13.

Jenkins, I. L., Moore, F. H., and Waterman, M. J. (1965) *J. Inorg. Nucl. Chem.,* **27**(1), 77–80.

Joel, J., Roux, C., and Rapin, M. (1971) *J. Nucl. Mater.,* **40**, 297–304.

Johns, I. B. (1944) *Plutonium Hydride And Deuteride*, Report LA-137, Los Alamos Scientific Laboratory, 12 pp.

Johns, I. B. and Moulton, G. H. (1944) *Large-scale Preparation of the Anhydrous Fluorides of Plutonium*, Report LA-193, Los Alamos Scientific Laboratory, Los Alamos, NM, 20 pp.

Johnson, K. W. R. (1954) *Preparation of High-purity Plutonium Metal*, Report LA-1680, Los Alamos Scientific Laboratory.

Johnson, K. A. (1964) *Homogenization of Gallium-stabilized Delta-phase Plutonium*, Report LA-2989, Los Alamos Scientific Laboratory, 43 pp.

Johnson, K. W. R. and Leary, J. A. (1964) *J. Inorg. Nucl. Chem.,* **26**(1), 103–5.

Johnson, K. W. R., Kahn, M., and Leary, J. A. (1961) *J. Phys. Chem.,* **65**, 2226–9.

Johnson, I., Chasanov, M. G., and Yonco, R. M. (1965) *Trans. Metall. Soc. AIME,* **233** (7), 1408–14.

Johnson, Q. C., Wood, D. H., and Smith, G. S. (1967) *The Crystal Structure of Pu_3Zn_{22}*, Report UCRL-70500.

Jones, M. M. (1953) *A Study of Plutonium Trifluoride Precipitated from Aqueous Solution*, Report HW-30384, Hanford Atomic Products Operation, 15 pp.

Jones, L. H. (1955) *J. Chem. Phys.,* **23**, 2105–7.

Jones, L. H. and Penneman, R. A. (1953) *J. Chem. Phys.,* **21**(3), 542–4.

Jones, L. V., Ofte, D., Rohr, L. J., and Wittenberg, L. J. (1962) *Am. Soc. Metals, Trans. Quart.,* **55**, 819–25.

Jones, L. V., Ofte, D., Phipps, K. D., and Tucker, P. A. (1964) *Ind. Eng. Chem. Prod. R. D.,* **3**(2), 78–82.

Jouniaux, B. (1979) *Study by Thermochromatography of Fluorides of Transuranium Elements*, Thesis, Report IPNO-T-79-05, Paris-6 Univ. 75; Paris-11 Univ. 91, Inst. de Physique Nucleaire, Orsay, France, 99 pp.

Jouniaux, B., Legoux, Y., Merinis, J., and Bouissieres, G. (1979) *Radiochem. Radioanal. Lett.,* **39**(2), 129–40.

Jove, J. and Cousson, A. (1977) *Radiochim. Acta,* **24**(2–3), 73–5.

Jove, J. and Pagès, M. (1977) *Inorg. Nucl. Chem. Lett.,* **13**(7), 329–34.

Jove, J., Pagès, M., and Freundlich, W. (1974) *Compt. Rend.,* **278**(12), 873–4.

Jove, J., Pagès, M., and Freundlich, W. (1976) *Inorg. Nucl. Chem. - Herbert H. Hyman Mem. Vol.*, 189–92.

Kabanova, O. L., Danuschenkova, M. A., and Paley, P. N. (1960) *Anal. Chim. Acta,* **22**, 66.

Kaltsoyannis, N. (2000) *Inorg. Chem.,* **39**(26), 6009–17.
Kaltsoyannis, N. and Bursten, B. E. (1997) *J. Organomet. Chem.,* **528**(1–2), 19–33.
Kalvius, G. M., Cohen, D., Dunlap, B. D., and Shenoy, G. K. (1978) *Phys. Rev. B,* **18**(9), 4581–7.
Kandan, R., Babu, R., Nagarajan, K., and Rao, P. R. V. (2004) *J. Nucl. Mater.,* **324**(2–3), 215–19.
Karraker, D. G. (1973) *Inorg. Chem.,* **12**(5), 1105–8.
Karraker, D. G. (1987) *Inorg. Chim. Acta,* **139**(1–2), 189–91.
Karraker, D. G. and Stone, J. A. (1974) *J. Am. Chem. Soc.,* **96**(22), 6885–8.
Karraker, D. G., Stone, J. A., Jones, E. R., Jr, and Edelstein, N. (1970) *J. Am. Chem. Soc.,* **92**(16), 4841–5.
Kasha, M. (1949) Reactions between Plutonium Ions in Perchloric Acid Solutions. Rates, Mechanisms, and Equilibria, in *Natl. Nucl. Energy Ser.*, Div IV **14B**(Transuranium Element, Pt. I) (eds. G. T. Seaborg, J. J. Katz, and W. M. Manning), McGraw-Hill, New York, ch. 3, 295–334.
Kasper, J. S. (1976) *J. Less-Common Met.,* **47**, 17–21.
Kassner, M. E. and Peterson, D. E. (1995) *Phase Diagrams of Binary Actinide Alloys.* ASM International, Materials Park, OH, 489 pp.
Katz, J. J. and Gruen, D. M. (1949) *J. Am. Chem. Soc.,* **71**, 2106–12.
Katz, J. J. and Sheft, I. (1960) Halides of the Actinide Elements, in *Advances in Inorganic Chemistry and Radiochemistry,* vol. 2, (eds. H. J. Emeleus and A. G. Sharpe), Academic Press, San Diego, pp. 195–236.
Katzin, L. I. (1944) *Survey of the Chemistry of Plutonium*, Report CK-2240(Del.), Chicago University Metallurgical Laboratory, 46 pp.
Kaufman, L. (2002) Keynote: Humerothery and Calphad Thermodynamics, in *CALPHAD and Alloy Thermodynamics* (eds. P. E. A. Turchi, A. Gonis and R. D. Shull), TMS, Warrendale, PA, 3 pp.
Kaufman, L. and Bernstein, H. (1970) *Computer Calculation of Phase Diagrams with Special Reference to Refractory Metals.* Academic Press, New York, 334 pp.
Kay, A. E. and Loasby, R. G. (1964) *Philos. Mag.,* **9**(97), 37–49.
Kay, A. E. and Waldron, W. B. (1967) *Plutonium 1965,* Proc. Third Int. Conf. on Plutonium, Institute of Metals, Chapman and Hall, London, 1114 pp.
Keenan, T. K. (1957) *J. Phys. Chem.,* **61**, 1117.
Keenan, T. K. (1965) *Inorg. Chem.,* **4**(10), 1500–1.
Keenan, T. K. (1966) *Inorg. Nucl. Chem. Lett.,* **2**(6), 153–6.
Keenan, T. K. (1967) *Inorg. Nucl. Chem. Lett.,* **3**(10), 463–7.
Keenan, T. K. and Asprey, L. B. (1969) *Inorg. Chem.,* **8**(2), 235–238.
Keiser, D. L. J., Hayes, S. L., Meyer, M. K., and Clark, C. R. (2003) *J. Metals,* **55**(9), 55.
Keller, C. (1962) *Nukleonik,* **4**, 271–7.
Keller, C. (1963) *Nukleonik,* **5**, 41–8.
Keller, C. (1964) *Solid-state Chemistry of the Actinide Oxides*, Thesis, Report KFK-225, Kernforschungszentrum, Karlsruhe, 261 pp.
Keller, C. (1965a) *J. Inorg. Nucl. Chem.,* **27**(6), 1233–46.
Keller, C. (1965b) *J. Inorg. Nucl. Chem.,* **27**(2), 321–7.
Keller, C. (1971) *The Chemistry of the Transuranium Elements* (*Nuclear Chemistry in Monographs,* vol. 3). Verlag Chemie, Weinheim, 675 pp.
Keller, C. and Salzer, M. (1967) *J. Inorg. Nucl. Chem.,* **29**(12), 2925–34.

Keller, C. and Schmutz, H. (1964) *Zeitschr. Naturfors.,* **19b**(11), 1080.
Keller, C. and Schmutz, H. (1966) *Inorg. Nucl. Chem. Lett.,* **2**(11), 355–8.
Keller, C. and Seiffert, H. (1969) *Angew. Chem., Int. Ed. Engl.,* **8**(4), 279–80.
Keller, C. and Walter, K. H. (1965) *J. Inorg. Nucl. Chem.,* **27**(6), 1253–60.
Keller, C., Koch, L., and Walter, K. H. (1965a) *J. Inorg. Nucl. Chem.,* **27**(6), 1205–23.
Keller, C., Koch, L., and Walter, K. H. (1965b) *J. Inorg. Nucl. Chem.,* **27**(6), 1225–32.
Keller, C., Berndt, U., Debbabi, M., and Engerer, H. (1972) *J. Nucl. Mater.,* **42**(1), 23–31.
Kelly, C. E. (1975) MHW [Multihundred Watt] converter (RTG) [radioisotope thermoelectric generator]. *Rec. Intersoc. Energy Convers. Eng. Conf*., 10, 880–6.
Kennedy, J. W., Seaborg, G. T., Segre, E., and Wahl, A. C. (1941) *Phys. Rev.,* **70**, 555–6.
Kent, R. A. (1968) *J. Am. Chem. Soc.,* **90**(21), 5657–9.
Kent, R. A. (1969) *High Temp. Sci.,* **1**, 169.
Kent, R. A. (1973) *Thermodynamic Analysis of MHW Space Electric Power Generator*, Report LA-5202-MS, Los Alamos Scientific Laboratory, Los Alamos, NM, 108 pp.
Kent, R. A. and Leary, J. A. (1968) *Mass Spectrometric Studies of Plutonium Compounds at High Temperatures, I: the Heats of Vaporization of Gold and Plutonium and the Heat of Decomposition of Plutonium Mononitride*, Report LA-3902, Los Alamos Scientific Laboratory, Los Alamos, NM, 20 pp.
Kent, R. A. and Zocher, R. W. (1976) *Reduction of Plutonia by Carbon Monoxide and Equilibrium Partial Pressures above Plutonia*, Report LA-6534, Los Alamos Scientific Laboratory, Los Alamos, NM, 27 pp.
Kessie, R. W. and Ramaswami, D. (1965) *Removal of Plutonium Hexafluoride from Cell Exhaust Air by Hydrolysis Filtration*, Report ANL-7066, Argonne National Laboratory, Argonne, IL,70 pp.
Khanaev, E. I., Teterin, E. G., and Luk'yanova, L. A. (1967) *Zh. Prikl. Spektrosk.,* **6**(6), 789–96.
Kiehn, R. M. (1961) Pu LAMPRE, in *The Metal Plutonium* (eds. A. S. Coffinberry and W. M. Miner), University of Chicago Press, Chicago, IL, 333 pp.
Kierkegaard, P. (1956) *Acta Chem. Scand.,* **10**(4), 599–616.
Kikuchi, T., Koyama, T., and Homma, S. (2003) *AIP Conf. Proc.,* **673**(Plutonium Futures – The Science), 42–4.
Kim, J. I. (1991) *Radiochim. Acta,* **52–53**(Pt. 1), 71–81.
Kim, J. I. (1994) *MRS Bull.,* **19**(12), 47–53.
Kim, K. C. and Campbell, G. M. (1985) *Appl. Spectrosc.,* **39**(4), 625–8.
Kim, K. C., Krohn, B. J., Briesmeister, R. A., and Rabideau, S. (1987) *J. Chem. Phys.,* **87**, 1538.
Kimura, T. and Choppin, G. R. (1994) *J. Alloys Compd.,* **213–214**, 313–17.
King, E., Lee, J. A., Mendelssohn, K., and Wigley, D. A. (1965) *Proc. R. Soc. Lond. Ser. A,* **284**(1398), 325–43.
Kittel, C. and Kroemer, H. (1980) *Thermal Physics,* Freeman and Company, San Francisco, CA, p. 196.
Kleinschmidt, P. D. (1988) *J. Chem. Phys.,* **89**(11), 6897–904.
Kleykamp, H. (1999) *J. Nucl. Mater.,* **275**, 1–11.
Knief, R. A. (1985) *Nuclear Criticality Safety: Theory and Practice,* American Nuclear Society, La Grange Park, IL, 233 pp.
Knighton, J. B., Auge, R. G., Berry, J. W., and Franchini, R. C. (1976) *Molten Salt Extraction of Americium from Molten Plutonium Metal*, Report RFP-2365, Rocky Flats Plant, Rockwell International, Golden, CO, 24 pp.

Knighton, J. B. and Steunenberg, R. K. (1965) *J. Inorg. Nucl. Chem.,* **27**(7), 1457–62.
Knoch, W., Knighton, J. B., and Steunenberg, R. K. (1969) *Nucl. Metall. Met. Soc. AIME,* **15**, 535–46.
Knopp, R., Neck, V., and Kim, J. I. (1999) *Radiochim. Acta,* **86**(3–4), 101–8.
Koch, L. (1964) *The Ternary oxide of Quinque- and Sexivalent Neptunium and Plutonium with Lithium and Sodium*, Thesis, Report KFK-196, Institute fur Radiochemie, Kernforschungszentrum, Karlsruhe, Germany, 74 pp.
Koch, G. (ed.) (1972) *Gmelin Handbook of Inorganic Chemistry*, vol. 4*: Transuranium Elements, C*, Verlag Chemie, Weinheim, 279 pp.
Koch, G. (ed.) (1973a) *Gmelin Handbook of Inorganic Chemistry*, vol. 7a, *Transuranium Elements, A1, I, The Elements*, Verlag Chemie, Weinheim.
Koch, G. (ed.) (1973b) *Gmelin Handbook of Inorganic Chemistry*, vol. 7b, *Transuranium Elements, A1, II, The Elements*, Verlag Chemie, Weinheim.
Koch, G. (ed.) (1973c) *Gmelin Handbook of Inorganic Chemistry*, vol. 8, *Transuranium Elements, A2, The Elements*, Verlag Chemie, Weinheim.
Koch, G. (ed.) (1976a) *Gmelin Handbook of Inorganic Chemistry, Supplementary Work*, vol. 31, *Transuranium Elements, B1, The Metals*, 8th edn, Springer-Verlag, Berlin.
Koch, G., Ed. (1976b) *Gmelin Handbook of Inorganic Chemistry. Supplementary Work,* vol. 38, *Transuranium Elements, B2: Binary Alloy Systems 1*, 8th edn, Springer-Verlag, Berlin.
Koelling, D. D., Ellis, D. E., and Bartlett, R. J. (1976) *J. Chem. Phys.,* **65**(8), 3331–40.
Koltunov, V. S. (1982a) *Radiokhimiya,* **23**(3), 462.
Koltunov, V. S., Frolov, K. M., Marchenko, V. I., Tikhonov, M. F., Zhuravleva, G. I., Kulikov, I. A., and Ryabova, A. A. (1982b) *Radiokhimiya,* **24**(5), 607–14 (508 pp. in English translation).
Koltunov, V. S. and Baranov, S. M. (1993) *Radiokhimiya,* **35**(6), 11–21.
Koltunov, V. S. and Marchenko, V. I. (1973) *Sov. Radiochem.,* **15**(6), 787–95.
Koltunov, V. S. and Mikhailova, N. A. (1977) *Radiokhimiya,* **19**(3), 342–8 (pp. 282–8 in English translation).
Koltunov, V. S. and Ryabova, A. A. (1980) *Sov. Radiochem.,* **22**(5), 481–7.
Koltunov, V. S. and Zhuravleva, G. I. (1968) *Radiokhimiya,* **10**(6), 662–9 (pp. 648–54 in English translation).
Koltunov, V. S. and Zhuravleva, G. I. (1973) *Sov. Radiochem.,* **15**(1), 73–6.
Koltunov, V. S. and Zhuravleva, G. I. (1974) *Sov. Radiochem.,* **16**(1), 80–3.
Koltunov, V. S. and Zhuravleva, G. I. (1978) *Sov. Radiochem.,* **20**(1), 73–80.
Koltunov, V. S., Frolov, K. M., Tikhonov, M. F., and Shapovalov, M. P. (1980a) *Radiokhimiya,* **22**(4), 491–8 (pp. 386–93 in English translation).
Koltunov, V. S., Tikhonov, M. F., Frolov, K. M., and Shapovalov, M. P. (1980b) *Radiokhimiya,* **22 (1)**, 65–74 (pp. 45–53 in English translation).
Koltunov, V. S., Kulikov, I. A., Kermanova, N. V., and Nikishova, L. K. (1981a) *Radiokhimiya,* **23**(3), 462–5 (pp. 384–6 in English translation).
Koltunov, V. S., Zhuravleva, G. I., and Shapovalov, M. P. (1981b) *Sov. Radiochem.,* **23** (4), 449–553.
Koltunov, V. S., Baranov, S. M., and Zhuravleva, G. I. (1989) *Sov. Radiochem.,* **31**(1), 47–52.
Koltunov, V. S., Pastushchak, V. G., Mezhov, E. A., and Koltunov, G. V. (2004) *Radiochemistry,* **46**(2), 125–30.

Komkov, Y. A., Krot, N. N., and Gel'man, A. D. (1968) *Radiokhimiya,* **10**(6), 625–9.
Komkov, Y. A., Peretrukhin, V. F., Krot, N. N., and Gel'man, A. D. (1969) *Radiokhimiya,* **11**(4), 407–12.
Konobeevsky, S. T. (1955) *Conf. Acad. Sci. USSR, Peaceful Uses of Atomic Energy*, vol. 4, Consultants Bureau, 207.
Korzhavyi, P. A., Vitos, L., Andersson, D. A., and Johansson, B. (2004) *Nat. Mater.,* **3** (4), 225–8.
Kotani, A. and Ogasawara, H. (1993) *Physica B,* **186–188**, 16–20.
Kotani, A., Ogasawara, H., and Yamazaki, T. (1993) *JJAP Series* **8**(Physical Properties of Actinide and Rare Earth Compounds), 117–28.
Kraus, K. A. (1956) *Proc. Int. Conf. Peaceful Uses Atomic Energy,* vol. 7, Geneva, pp. 245–57.
Kraus, K. A. and Dam, J. R. (1949) *in Natl. Nucl. Energy Ser.,* Div IV **14B**(*Transuranium Elements, Pt. I*) (eds. G. T. Seaborg, J. J. Katz, and W. M. Manning), McGraw-Hill, New York, 466.
Kraus, K. A. and Nelson, F. (1950) *J. Am. Chem. Soc.,* **72**(9), 3901–6.
Krikorian, O. H. and Hagerty, D. C. (1990) *J. Nucl. Mater.,* **171**(2–3), 237–44.
Krikorian, O. H., Fontes, A. S., Jr, Ebbinghaus, B. B., and Adamson, M. G. (1997) *J. Nucl. Mater.,* **247**, 161–71.
Krishnan, S., Weber, J. K. R., Anderson, C. D., Nordine, P. C., and Sheldon, R. I. (1993) *J. Nucl. Mater.,* **203**(2), 112–21.
Krot, N. N. (1975) *Radiokhimiya,* **17**(5), 677–83.
Krot, N. N. and Gel'man, A. D. (1967) *Dokl. Akad. Nauk SSSR,* **177**(1), 124–5; see also (1968) Chem. Abstr., **68,** 26372b.
Krott, N. N., Gel'man, A. D., Mefodeva, M. P., Shilov, V. P., Peretrukhin, V. F., and Zakharova, F. A. (1976) *Moscow Symp. on the Chemistry of the Transuranium Elements*, *V* (eds. I. Spitsyn and J. J. Katz), pp. 249–52.
Kruger, O. L. (1963) *J. Am. Ceram. Soc.,* **46**, 80–5.
Kruger, O. L. and Moser, J. B. (1966a) *J. Am. Ceram. Soc.,* **49**(12), 661–7.
Kruger, O. L. and Moser, J. B. (1966b) *J. Inorg. Nucl. Chem.,* **28**(3), 825–32.
Kruger, O. L. and Moser, J. B. (1967a) *J. Phys. Chem. Solids,* **28**(11), 2321–5.
Kruger, O. L. and Moser, J. B. (1967b) *Chem. Eng. Prog., Symp. Ser.,* **63**(80), 1–10.
Kruger, O. L. and Savage, H. (1968) *J. Chem. Phys.,* **49**(10), 4540–4.
Kruger, O. L., Moser, J. B., and Wrona, B. J. (1966a) *Preparation of Plutonium Monosulfide or Monophosphide*, (United States Atomic Energy Commission). US Patent no. 3282 656, 2 pp.
Kugel, R., Williams, C., Fred, M., Malm, J. G., Carnall, W. T., Hindman, J. C., Childs, W. J., and Goodman, L. S. (1976) *J. Chem. Phys.,* **65**(9), 3486–92.
Kuroda, P. K. (1960) *Nature,* **187**, 36–8.
Kuroda, P. K. and Myers, W. A. (1998) *J. Radioanal. Nucl. Chem.,* **230**(1–2), 175–95.
Kutaitsev, V. I., Chebotarev, N. I., Lebedev, I. G., Adrianov, M. A., Konev, V. N., and Menchikova, T. S. (1967) *Proc. Third Int. Conf. on Plutonium, Plutonium 1965,* (eds. A. E. Kay and M. B. Waldron), Chapman & Hall, London, England, pp. 429–30.
Lallement, R. (1963) *Phys. Chem. Solids* **24**, 1617.
Lallement, R. and Solente, P. (1967) *Low-Temperature Irradiation, Proc. Third Int. Conf. on Plutonium 1965* (eds. A. I. Kay and M. B. Waldron), Chapman and Hall for Institute of Metals, London, pp. 147–61.

Lam, D. J., Fradin, F. Y., and Kruger, O. L. (1969) *Phys. Rev.,* **187**(2), 606–10.
Lammermann, H. and Conway, J. G. (1963) *J. Chem. Phys.,* **38**(1), 259.
Land, C. C., Ellinger, F. H., and Johnson, K. A. (1965a) *J. Nucl. Mater.,* **16**(1), 87.
Land, C. C., Johnson, K. A., and Ellinger, F. H. (1965b) *J. Nucl. Mater.,* **15**(1), 23–32.
Land, C. C., Peterson, D. E., and Roof, R. B. (1978) *J. Nucl. Mater.,* **75**(2), 262–73.
Lander, G. H., Delapalme, A., Brown, P. J., Spirlet, J. C., Rebizant, J., and Vogt, O. (1984) *Phys. Rev. Lett.,* **53**(23), 2262–5.
Lander, G. H., Delapalme, A., Brown, P. J., Spirlet, J. C., Rebizant, J., and Vogt, O. (1985) *J. Appl. Phys.,* **57**(8, Pt. 2B), 3748–50.
Lander, G. H., Rebizant, J., Spirlet, J. C., Delapalme, A., Brown, P. J., Vogt, O., and Mattenberger, K. (1987) *Physica B & C,* **146**(3), 341–50.
Lange, R. G. and Mastal, E. F. (1994) A Tutorial Review of Radioisotope Power Systems, in *A Critical Review of Space Nuclear Power and Propulsion 1984–1993* (ed. M. S. El-Genk), American Institute of Physics, AIP Press, New York, pp. 1–20.
Larroque, J., Chipaux, R., and Beauvy, M. (1986) *J. Less-Common Met.,* **121**, 487–96.
Larson, D. T. (1980) *Effect of Vacuum Heat Treatment on Plutonium Oxide Surfaces as Studied by XPS and AES*, Report RFP-3108, Energy Systems Group, Rockwell International Corporation, Canoga Park, CA, 10 pp.
Larson, A. C. and Cromer, D. T. (1967) *Acta Crystallogr.,* **23**(1), 70–7.
Larson, D. T. and Haschke, J. M. (1981) *Inorg. Chem.,* **20**(7), 1945–50.
Larson, A. C., Cromer, D. T., and Stambaugh, C. K. (1957) *Acta Crystallogr.,* **10**(7), 443–6.
Larson, A. C., Roof, R. B., and Cromer, D. T. (1963) *Acta Crystallogr.,* **16**(8), 835–6.
Larson, A. C., Cromer, D. T., and Roof, R. B. (1965) *Acta Crystallogr.,* **18**(2), 294–5.
Lashley, J. C. (2003) *Cryogenics,* **43**, 369.
Lashley, J. C. (2004) Heat capacity, personal communication, S. S. Hecker, Los Alamos, NM.
Lashley, J. (2005) *Phys. Rev. B: Condens. Matter.*, **71**(17).
Lashley, J. C., Blau, M. S., Staudhammer, K. P., and Pereyra, R. A. (1999) *J. Nucl. Mater.,* **274**(3), 315–19.
Lashley, J. C., Moment, R. L., and Blau, M. S. (2000) *Los Alamos Science,* **26**(1), 226–32.
Lashley, J. C., Stout, M. G., Pereyra, R. A., Blau, M. S., and Embury, J. D. (2001) *Scripta. Mater.,* **44**(12), 2815–20.
Lashley, J. C., Migliori, A., Singleton, J., McQueeney, R. J., Blau, M. S., Pereyra, R. A., and Smith, J. L. (2003a) *J. Metals,* **55**(9), 34.
Lashley, J. C., Singleton, J., Migliori, A., Betts, J. B., Fisher, R. A., Smith, J. L., and McQueeney, R. J. (2003b) *Phys. Rev. Lett.,* **91**(20), 205901/1.
Lashley, J. C., Lawson, A. C., McQueeney, R. J., and Lander, G. H. (2004) *Absence of Magnetic Moments in Plutonium*, Report LA-UR-04-3439 Preprint Archive, Condensed Matter (2004), Los Alamos National Laboratory, pp. 1–30.
Lataillade, F., Pons, F., and Rapin, M. (1971) *J. Nucl. Mater.,* **40**(3), 284–8.
Laue, C. A., Gregorich, K. E., Sudowe, R., Hendricks, M. B., Adams, J. L., Lane, M. R., Lee, D. M., McGrath, C. A., Shaughnessy, D. A., Strellis, D. A., Sylwester, E. R., Wilk, P. A., and Hoffman, D. C. (1999) *Phys. Rev. C,* **59**(6), 3086–92.
Lavallee, C. and Newton, T. W. (1972) *Inorg. Chem.,* **11**, 2616.
Lawson, A. C. (2001) *Philos. Mag. B,* **81**(3), 255–66.
Lawson, A. C., Goldstone, J. A., Cort, B., Sheldon, R. I., and Foltyn, E. M. (1994) *J. Alloys Compd.,* **213/214**, 426–8.

Lawson, A. C., Goldstone, J. A., Cort, B., Martinez, R. J., Vigil, F. A., Zocco, T. G., Richardson, J. W., Jr, and Mueller, M. H. (1996) *Acta Crystallogr.,* **B52**, 32–7.

Lawson, A. C., Martinez, B., Roberts, J. A., and Bennett, B. I. (2000) *Philos. Mag. B,* **80** (1), 53–9.

Lawson, A. C., Roberts, J. A., Martinez, B., and Richardson, J. W. (2002) *Philos. Mag. B,* **82**(18), 1837–45.

Laxminarayanan, T. S., Patil, S. K., and Sharma, H. D. (1964) *J. Inorg. Nucl. Chem.,* **26** (6), 1001–9.

Leary, J. A. (1962) *Temperature-composition Diagrams of Pseudo-binary Systems Containing Plutonium (III) Halides*, Report LA-2661, Los Alamos Scientific Laboratory, Los Alamos, NM, 16 pp.

Leary, J. A. and Mullins, L. J. (1966) *Int. Atomic Energy Agency - Proc. Ser. Thermodynamics*, vol. 1, pp. 459–71.

Leary, J. A. and Mullins, L. J. (1974) *J. Chem.Thermodyn.,* **6**(1), 103–4.

Leary, J. A., Morgan, A. N., and Maraman, W. J. (1959) *Ind. Eng. Chem.,* **51**(1), 27–31.

Lechelle, J., Bleuet, P., Martin, P., Girard, E., Bruguier, F., Martinez, M. A., Somogyi, A., Simionovici, A., Ripert, M., Valdivieso, F., and Goeuriot, P. (2004) *IEEE Trans. Nucl. Sci.,* **51**(4, Pt. 1), 1657–61.

Ledbetter, H. (2004) Grüneisen constants, personal communication, S. S. Hecker, Los Alamos, NM.

Ledbetter, H. M. and Moment, R. L. (1976) *Acta Metall. Mater.,* **24**, 891–9.

Ledbetter, H., Migliori, A., Betts, J., Harrington, S., and El-Khatib, S. (2004) *Elastic Constant Measurements*, Report LA-UR-04-6980, Los Alamos National Laboratory.

Ledbetter, H., Migliori, A., Betts, J., Harrington, S., and El-Khatib, S. (2005) *Phys. Rev. B.*, **71**, 172101/1–4.

Ledbetter, H., and Migliori, A., (2005) Report LA-UR-05-1800, Los Alamos National Laboratory.

Lee, J. A. and Hall, R. O. A. (1959) *J. Less-Common Met.,* **1**, 356.

Lee, J. A. and Mardon, P. G. (1961) Thermal Conductivity, in *The Metal Plutonium* (ed. A. S. Coffinberry), Chicago University Press, Chicago, IL.

Lee, J. A., Hall, R. O. A., King, E., and Meaden, G. T. (1961) Electrical Resistivity, in *Plutonium 1960,* vol. 1, (eds. E. Grison, W. B. H. Lord, and R. D. Fowler), Cleaver-Hume Press Ltd., London, pp. 39–50.

Lee, J. A., Mendelssohn, K., and Wigley, D. A. (1962) *Phys. Lett.,* **1**(8), 325–7.

Lee, J. A., Marples, J. A. C., Mendelssohn, K., and Sutcliffe, P. W. (1965a) Thermal Expansion, in *Plutonium 1965* (eds. K. A. E. and R. G. Loasby), Chapman-Hall Publishers, London, England, pp. 176–88.

Lee, J., Mendelssohn, K., and Sutcliffe, P. (1965b) *Cryogenics,* **5**, 227.

Leibowitz, L., Fischer, D. F., and Chasanov, M. G. (1974) *Enthalpy of Molten Uranium–Plutonium Oxides*, Report ANL-8082, Argonne National Laboratory, Argonne, IL, 19 pp.

Leitner, L. (1967) *Quasibinary Phase Diagrams of the System Thulium Oxide–Actinide Oxide (ThO_2, UO_2, NpO_2, PuO_2) below 1700 deg*, Report KFK-521, Kernforschungszentrum, Karlsruhe, Germany, 86 pp.

Lemire, R. J., Fuger, J., Nitsche, H., Potter, P., Rand, M. H., Rydberg, J., Spahiu, K., Sullivan, J. C., Ullman, W. J., Vitorge, P., and Warner, H. (2001) *Chemical*

Thermodynamics of Neptunium and Plutonium, Elsevier, Amsterdam, The Netherlands, 845 pp.
Lesser, R. and Peterson, J. R. (1976) *Transurane: Die Metalle*, part B1, in *Transurane,* vol. 31, (ed. K.-C. Buschbeck), Springer-Verlag, Berlin, Germany, pp. 40–1.
Levine, C. A. and Seaborg, G. T. (1951) *J. Am. Chem. Soc.,* **73**, 3278–83.
Levitz, N. M., Vogel, G. J., Carls, E. L., Grosvenor, D. E., Murphy, W. F., Kullen, B. J., and Raue, D. J. (1968) *Engineering Development of Fluid-bed Fluoride Volatility Processes*, part 15, *Material Balance Demonstrations, Production Rates, and Fluorine Utilizations in Fluorination of Kilogram Quantities of PuF_4 to PuF_6 with Elemental Fluorine in a Fluid-bed Reactor*, Report ANL-7568, Argonne National Laboratory, Argonne, IL, 28 pp.
Lewis, H. D., Kerrisk, J. F., and Johnson, K. W. (1976) *Effect of a Delta-phase Stabilizer on the Thermal Diffusivity of Plutonium, Proc. 14th Int. Conf. on Therm Conduct,* Jun. 2–4, 1975, University of Connecticut, Storrs, Plenum Press, New York, pp. 201–8.
Li, J. and Bursten, B. E. (1998) *J. Am. Chem. Soc.,* **120**(44), 11456–66.
Lipis, L. V. and Pozharskii, B. G. (1960) *Zh. Neorg. Khim.,* **5**, 2162–6.
Liptai, R. G. and Friddle, R. J. (1967) *J. Nucl. Mater.,* **21**(1), 114.
Liptai, R. G., Lloyd, L. T., and Friddle, R. J. (1967) *J. Phys. Chem. Solids,* **1**, 573.
Littler, D. J. (1952) *Proc. Phys. Soc.,* **65A**, 203–8.
Lloyd, M. H. and Haire, R. G. (1968) *Nucl. Appl. Technol.,* **5**(3), 114–22.
Lloyd, M. H. and Haire, R. G. (1978) *Radiochim. Acta,* **25**(3–4), 139–48.
Long, J. T. (1978) *Engineering for Nuclear Fuel Reprocessing*, American Nuclear Society, La Grange Park, IL, 1025 pp.
Lorenzelli, R., Martin, A., and Schickel, R. (1966) *Reaction of Uranium and Plutonium Carbides with Nitrogen*, Report CEA-R 2997, 21 pp.
Louer, M., Brochu, R., Louer, D., Arsalane, S., and Ziyad, M. (1995) *Acta Crystallogr. B,* **51**(6), 908–13.
Louwrier, K. P. and Richter, K. (1976) *Des. Equip. Hot Lab.*, *Proc. Symp.*, pp. 3–12.
Louwrier, K. P., Ronchi, C., Steemers, T., and Zamorani, E. (1968) *Sol-gel Processes for Ceramic Nuclear Fuels*, *Proc. Panel on Sol-gel Processes for Ceramic Nuclear Fuels*, Report STI/PUB/207, International Atomic Agency, pp. 97–106.
Love, L. O. (1973) *Science,* **182**(4110), 343–52.
Love, L. O., Banic, G. M., Bell, W. A., and Prater, W. K. (1961) *Electromagnetic Separation Radioactive Isotopes, Proc. Int. Symp.,* Vienna, Austria, pp. 141–54.
Lupinetti, A. J., Fife, J. L., Garcia, E., Dorhout, P. K., and Abney, K. D. (2002) *Inorg. Chem.,* **41**(9), 2316–18.
Lynn, J., Kwei, G., Trela, W. J., Yuan, V. W., Cort, B., Martinez, R. J., and Vigil, F. (1998) *Phys. Rev. B,* **65**, 214107–1.
Lyon, W. L. and Baily, W. E. (1965) *Solid-liquid Phase Diagram for the Uranium Oxide–Plutonium Oxide System*, Report GEAP-4878, General Electric Company, 17 pp.
Lyon, W. L. and Baily, W. E. (1967) *J. Nucl. Mater.,* **22**(3), 332–9.
Madic, C., Begun, G. M., Hobart, D. E., and Hahn, R. L. (1984) *Inorg. Chem.,* **23**(13), 1914–21.
Madic, C., Berger, P., and Machuron-Mandard, X. (1992) in *Transuranium Elements: A Half Century*, American Chemical Society, Washington, DC, pp. 457–68.
Magon, L., Portanova, R., and Cassol, A. (1968) *Inorg. Chim. Acta,* **2**, 237.
Maillard, C. and Adnet, J.-M. (2001) *Radiochim. Acta,* **89**(8), 485–90.

Malm, J. G. and Weinstock, B. (1954) *Argonne Plutonium Hexafluoride Program*, Report ANL-5366, Argonne National Laboratory, 14 pp.
Malm, J. G., Eller, P. G., and Asprey, L. B. (1984) *J. Am. Chem. Soc.,* **106**(9), 2726–7.
Mandleberg, C. J. and Davies, D. (1954) *The Vapour Pressure of Plutonium Tetrafluoride*, Report AERE-C/R-1321, Great Britain Atomic Energy Research Establishment, 18 pp.
Mandleberg, C. J. and Davies, D. (1961) *J. Chem. Soc., Abstracts*: 2031–7.
Mandleberg, C. J., Rae, H. K., Hurst, R., Long, G., Davies, D., and Francis, K. E. (1953) *Plutonium Hexafluoride*, part I, *Preparation and Some Physical Properties*, Report AERE-C/R-1172, Great Britain Atomic Energy Research Establishment.
Mandleberg, C. J., Rae, H. K., Hurst, R., Long, G., Davies, D., and Francis, K. E. (1956) *J. Inorg. Nucl. Chem.,* **2**(5–6), 358–67.
Manley, M. E., Fultz, B., McQueeney, R. J., Brown, C. M., Hults, W. L., Smith, J. L., Thoma, D. J., Osborn, R., and Robertson, J. L. (2001) *Phys. Rev. Lett.,* **86**(14), 3076–9.
Maraman, W. J., Beaumont, A. J., Christensen, E. l., Henrickson, A. V., Hermann, J. A., Johnson, K. W. R., Mullins, L. J., and Winchester, R. S. (1954) *Calcium Oxalate Carrier Precipitation of Plutonium*, Report LA-1692, Los Alamos Scientific Laboratory, Los Alamos, NM, 10 pp.
Maraman, W. J., McNeese, W. D., and Stafford, R. G. (1975) *Health Phys.,* **29**(4), 469–80.
Marcon, J. P. (1969) *Actinide Sulfides*, Report CEA-R-3919, Commissariat al'Energie Atomique, France, 99 pp.
Marcon, J. P. and Pascard, R. (1966a) *J. Inorg. Nucl. Chem.,* **28**(11), 2551–60.
Marcon, J. P. and Pascard, R. (1966b) *CR Acad. Sci. C. Chim.,* **262**(24), 1679–81.
Marcon, J. P. and Pascard, R. (1968) *CR Acad. Sci. C. Chim.,* **266**(4), 270–2.
Mardon, P. G. and Potter, P. E. (1970) *Plutonium 1970 and Other Actinides, Proc. Fifth Int. Conf. on Plutonium and Other Actinides,* Baden-Baden, West Germany, (ed. W. N. Miner), North-Holland, New York, 809 pp.
Mardon, P. G., Haines, H. R., Pearce, J. H., and Waldron, M. B. (1957) *J. I. Met.,* **86** (Part 4), 166–71.
Mardon, P. G., Pearce, J. H., and Marples, J. A. C. (1961) *J. Less-Common Met.,* **3**(4), 281–92.
Markin, T. L. and McKay, H. A. C. (1958) *J. Inorg. Nucl. Chem.,* **7**, 298–999.
Markin, T. L. and Street, R. S. (1967) *J. Inorg. Nucl. Chem.,* **29**(9), 2265–80.
Marples, J. A. C. (1960) *J. Less-Common Met.,* **2**(5), 331–51.
Marples, J. A. C. and Hall, R. O. A. (1972) *J. Nucl. Mater.,* **42**(2), 212–16.
Marples, J. A. C., Hough, A., Mortimer, M. J., Smith, A., and Lee, J. A. (1970) *Self-irrad Damage*, in *Proc. Fourth Int. Conf. on Plutonium and Other Actinides 1970* (ed. W. N. Miner), The Metallurgical Society of AIME, pp. 623–34.
Marquart, R., Hoffmann, G., and Weigel, F. (1983) *J. Less-Common Met.,* **91**(1), 119–27.
Marsh, S. F., Day, R. S., and Veirs, D. K. (1991) *Spectrophotometric Investigation of the Pu(IV) Nitrate Complex Sorbed by Ion Exchange Resins*, Report LA-12070, Los Alamos National Laboratory, Los Alamos, NM, 22 pp.
Marsh, S. F., Veirs, D. K., Jarvinen, G. D., Barr, M. E., and Moody, E. W. (2000) *Los Alamos Science,* **26**(2), 454–63.

Martell, A. E. and Smith, R. M. (2001) *Critical Stability Constants,* Standard Reference Database 46, Version 6.0., National Institute of Standards, Gaithersburg, MD.
Martin, D. G. (1988) *J. Nucl. Mater.,* **152**(2–3), 94–101.
Marty, B. and Marti, K. (2002) *Earth Planet. Sc. Lett.,* **196**(3–4), 251–63.
Martz, J. and Haschke, J. (1998) *J. Alloys Compd.,* **266**(1–2), 90–103.
Martz, J. C. and Schwartz, A. J. (2003) *J. Metals,* **55**(9), 19–23.
Martz, J. C., Haschke, J. M., and Stakebake, J. L. (1994) *J. Nucl. Mater.,* **210**(1–2), 130–42.
Mary, T. A., Evans, J. S. O., Vogt, T., and Sleight, A. W. (1996) *Science,* **272**, 90.
Mashirev, V. P., Shatalov, V. V., Grebenkin, K. F., Zuev, Y. N., Panov, A. V., Subbotin, V. G., and Chuvilin, D. Y. (2001) *At. Energ.,* **90**(3), 235–42.
Massalski, T. B. (1996) *Physical Metallurgy* (eds. R. W. Cahn and P. Haasen), Elsevier Science, Amsterdam, The Netherlands, 136 pp.
Masters, B. J. and Rabideau, S. W. (1963) *Inorg. Chem.,* **2**, 1–5.
Matonic, J. H., Scott, B. L., and Neu, M. P. (2001) *Inorg. Chem.,* **40**(12), 2638–9.
Matsika, S., Zhang, Z., Brozell, S. R., Blaudeau, J. P., Wang, Q., and Pitzer, R. M. (2001) *J. Phys. Chem. A,* **105**(15), 3825–8.
Matsui, T. and Ohse, R. W. (1987) *High Temp.-High Press.,* **19**(1), 1–17.
Mattenberger, K., Vogt, O., Spirlet, J. C., and Rebizant, J. (1986) *J. Magn. Magn. Mater.,* **54–57**(1), 539–40.
Matthews, J. R. (1987) *J. Chem. Soc., Faraday Trans., 2,* **83**(7), 1273–85.
Matzke, H. (1982) *Mater. Sci. Monogr.,* **15**(Transp. Non-Stoichiom. Compd.), 203–31.
Matzke, H. (1984) *Solid State Ionics,* **12**, 25–45.
Matzke, H. (1986) *Science of Advanced LMFBR Fuels: Solid State Physics, Chemistry, and Technology of Carbides, Nitrides, and Carbonitrides of Uranium and Plutonium,* North-Holland, New York, 740 pp.
Mazumdar, A. S. G., Natarajan, P. R., and Vaidyanathan, S. (1970) *J. Inorg. Nucl. Chem.,* **32**, 3363.
McAlister, S. P. and Crozier, E. D. (1981) *Solid State Commun.,* **40**, 375.
McCreary, W. J. (1955) *J. Am. Chem. Soc.,* **77**, 2113–14.
McDonald, B. J. and Stuart, W. I. (1960) *Acta Crystallogr.,* **13**, 447.
McKay, H. A. C., Schulz, W. W., Navratil, J. D., Burger, L. L., and Bender, K. P. (1990) The PUREX Process. Part 1: Introduction. Science and Technology of Tributyl Phosphate, vol. 3, *Applications of Tributyl Phosphate in Nuclear Fuel Processing,* CRC Press, Boca Raton, FL, pp. 1–9.
McNally, Jr J. R., and Griffin, P. M. (1959) *J. Opt. Soc. Am.,* **49**, 162–6.
McNeese, J. A., Bowersox, D. F., and Christensen, D. C. (1986) *Proc. Electrochem. Soc.,* **86-1**(Molten Salts), 474–84.
McQueeney, R. J., Lawson, A. C., Migliori, A., Kelley, T. M., Fultz, B., Ramos, M., Martinez, B., Lashley, J. C., and Vogel, S. C. (2004) *Phys. Rev. Lett.,* **92**(14), 146401.
Meadon, G. T. and Lee, J. A. (1962) *Cryogenics,* **2**, 182.
Mendik, M., Wachter, P., Spirlet, J. C., and Rebizant, J. (1993) *Physica B,* **186–188**, 678–80.
Méot-Reymond, S. and Fournier, J. M. (1996) *J. Alloys Compd.,* **232**(1–2), 119–25.
Merciny, E., Gatez, J. M., and Duyckaerts, G. (1978) *Anal. Chim. Acta,* **100**, 329–42.
Merigou, C., Genet, M., Ouillon, N., and Chopin, T. (1995) *New J. Chem.,* **19**(3), 275–85.
Merrill, J. J. and Du Mond, J. W. M. (1958) *Phys. Rev.,* **110**, 79–84.

Merrill, J. J. and Du Mond, J. W. M. (1961) *Ann. Phys. (N.Y.)* **14**, 166–228.
Merz, M. D. (1970) *J. Nucl. Mater.,* **34**, 108–10.
Merz, M. D. (1971) *J. Nucl. Mater.,* **41**, 348–50.
Merz, M. D. (1974) *J. Nucl. Mater.,* **50**, 31–9.
Merz, M. D. and Allen, R. P. (1973) *J. Nucl. Mater.,* **46**, 110.
Merz, M. D. and Nelson, R. D. (1970) Alpha Plutonium, in *Plutonium 1970 and Other Actinides,* vol. 1 (ed. W. N. Miner), The Metallurgical Society of the AIME, Santa Fe, NM, 387 pp.
Merz, M. D., Hammer, J. H., and Kjarmo, H. E. (1974) *J. Nucl. Mater.,* **51**(3), 357–8.
Metivier, H. and Guillaumont, R. (1972) *Radiochem. Radioanal. Lett.,* **10**(1), 27–35.
Meyer, G. and Morss, L. R. (eds.) (1991) Synthesis of Lanthanide and Actinide Compounds, in *Topics in f-element Chemistry*, Kluwer Academic, Boston, MA.
Miedema, A. R. (1973) *J. Less-Common Met.,* **32**(1), 117–36.
Miedema, A. R. (1976) On the Heat of Formation of Plutonium Alloys. *Plutonium 1975 Other Actinides, Proc. Fifth Int. Conf.* (eds. H. Blank and R. Lindner), North-Holland, Amsterdam, The Netherlands, pp. 3–20.
Migliori, A., Baiardo, J. P., and Darling, T. W. (2000) *Los Alamos Science,* **26**(1), 209–25.
Migliori, A., Ledbetter, H., Betts, J., Ramos, M., Harrington, S., and El-Khatib, S. (2004) *Elastic Constants of Plutonium*, Report LA-UR-04-7419, Los Alamos National Laboratory.
Migliori, A., Ledbetter, H., Lawson, A. C., Ramirez, A. P., Miller, D. A., Betts, J. B., Ramos, M., and Lashley, J. C. (2006) *Phys. Rev. B.*, **73**, 052101/1–4.
Mikheev, N. B. and Myasoedov, B. F. (1985) Lower and Higher Oxidation States of Transplutonium Elements in Solutions and Melts, in *Handbook on the Physics and Chemistry of the Actinides* (eds. A. J. Freeman and C. Keller), Elsevier Science, New York, pp. 347–86.
Mikheev, N. B., Rumer, I. A., and Auerman, L. N. (1983) *Radiochem. Radioanal. Lett.,* **59**(5–6), 317–28.
Miles, J. H., Schulz, W. W., Navratil, J. D., Burger, L. L., and Bender, K. P. (1990) The PUREX Process. Part 2: Separation of Plutonium and Uranium. Science and Technology of Tributyl Phosphate, vol. 3. *Applications of Tributyl Phosphate in Nuclear Fuel Processing* (eds. W. W. Schulz and J. D. Navratil), CRC Press, Boca Raton, FL, pp. 11–54.
Mincher, B. J., Fox, R. V., Holmes, R. G. G., Robbins, R. A., and Boardman, C. (2001) *Radiochim. Acta,* **89**(10), 613–17.
Miner, W. N. (1970) *Plutonium 1970 and Other Actinides, Proc. Fourth Int. Conf. on Plutonium and Other Actinides,* Santa Fe, NM (ed. W. N. Miner), Metallurgical Society of AIME, New York, 2 v.
Miner, W. N. and Schonfeld, F. W. (1980) Physical Properties, in *Plutonium Handbook,* vol. 1 (ed. O. J. Wick), American Nuclear Society, La Grange Park, IL, pp. 31–59.
Miner, F. J. and Seed, J. R. (1967) *Chem. Rev.,* **67**, 299–315.
Miner, F. J., De Grazio, R. P., and Byrne, J. T. (1963) *Anal. Chem.,* **35**(9), 1218–23.
Mitchell, A. W. and Lam, D. J. (1971) *J. Nucl. Mater.,* **39**(2), 219–23.
Mitchell, A. W. and Lam, D. J. (1974) *The Actinides: Electronic Structure and Related Properties,* vol. II (eds. A. J. Freeman and J. B. J. Darby), Academic Press, New York, 139 pp.

Mitchell, J. N., Gibbs, F. E., Zocco, T. G., and Pereyra, R. A. (2001) *Metall. Mater. Trans. A,* **32**(3A), 649–59.
Mittal, R., Chaplot, S. L., Schober, H., and Mary, T. A. (2001) *Phys. Rev. Lett.,* **86**, 4692.
Moeller, R. D. and Schonfeld, F. W. (1950) *Alloys of Plutonium with Aluminum*, Report LA-1000, Los Alamos Scientific Laboratory, Los Alamos, NM, 87 pp.
Moll, H., Reich, T., and Szabo, Z. (2000) *Radiochim. Acta,* **88**(7), 411–15.
Moment, R. L. (1968) *J. Cryst. Growth,* **2**(1), 15–25.
Moment, R. (2000) *Los Alamos Science,* **26**(1), 233–7.
Mooney, R. C. L. and Zachariasen, W. H. (1949) *Natl. Nucl. Energy Ser.*, Div IV **14B** (Transuranium Elements, Pt. II) (eds. G. T. Seaborg, J. J. Katz and W. M. Manning), pp. 1442–7.
Moore, K. T., Wall, M. A., Schwartz, A. J., Chung, B. W., Shuh, D. K., Schulze, R. K., and Tobin, J. G. (2003) *Phys. Rev. Lett.,* **90**(19), 196404.
Morales, L. A., Lawson, A. C., Conradson, S., Butler, E. N., Moore, D. P., Ramos, M., Roberts, J. A., and Martinez, B. (2003) *AIP Conf. Proc.,* **673**(Plutonium Futures – The Science), 174–5.
Morgan, J. R. (1970) *Plutonium 1970 and Other Actinides, Proc. Fourth Int. Conf. on Plutonium and Other Actinides,* Santa Fe, NM (ed. W. N. Miner), Metallurgical Society of AIME, 669 pp.
Morgenstern, A. and Choppin, G. R. (1999) *Radiochim. Acta,* **86**(3–4), 109–13.
Morgenstern, A. and Kim, J. I. (1996) *Radiochim. Acta,* **72**(2), 73–7.
Morgenstern, A., Apostolidis, C., Carlos-Marquez, R., Mayer, K., and Molinet, R. (2002) *Radiochim. Acta,* **90**(2), 81–5.
Morss, L. R. (2005) PuF_6 gas pressure in aged cylinders, personal communication, D. L. Clark, Los Alamos, NM.
Morss, L. R. and Fuger, J. (eds.) (1992) *Transuranium Elements: A Half Century,* American Chemical Society, Washington, DC, 562 pp.
Morss, L. R. and Fujino, T. (1988a) *J. Solid State Chem.,* **72**(2), 338–52.
Morss, L. R. and Fujino, T. (1988b) *J. Solid State Chem.,* **72**(2), 353–62.
Morss, L. R., Appelman, E. H., Gerz, R. R., and Martin-Rovet, D. (1994) *J. Alloys Compd.,* **203**(1–2), 289–95.
Moser, J. B. and Kruger, O. L. (1966) *J. Less-Common Met.,* **10**(6), 402–7.
Moskvin, A. I. (1969) *Radiokhimiya,* **11**, 447.
Moskvin, A. I. (1971a) *Sov. Radiochemistry,* **13**, 688–93.
Moskvin, A. I. (1971b) *Radiokhimiya,* **13**, 641.
Moskvin, A. I. and Poznyakov, A. N. (1979) *Russ. J. Inorg. Chem.,* **24**, 1357–62.
Moulin, V. and Moulin, C. (2001) *Radiochim. Acta,* **89**(11–12), 773–8.
Moulin, C., Delorme, N., Berthoud, T., and Mauchien, P. (1988) *Radiochim. Acta,* **44–45**(1), 103–6.
Moulton, G. H. (1944) *Decomposition Products of Plutonyl Nitrate and Plutonium Oxalate*, Report LA-172, Los Alamos Scientific Laboratory, Los Alamos, NM, 10 pp.
Mudher, K. D. S., Krishnan, K., and Iyer, P. N. (1995) *NUCAR 95*, *Proc. Nuclear and Radiochemistry Symp.*, Feb. 21–24, 1995, Kalpakkam, India, pp. 228–9.
Mueller, M. H., Lander, G. H., Hoff, H. A., Knott, H. W., and Reddy, J. F. (1979) *J. Phys. Colloq.*, (4), 68–9.
Mulford, R. N. R. (1965) *Vapor Pressure, Joint Symp. of IUPAC and IAEA on Thermodynamics,* IAEA, Vienna, Austria 231 pp.

Mulford, R. N. R. and Ellinger, F. H. (1958) *J. Phys. Chem.,* **62**, 1466–7.
Mulford, R. N. R., Ellinger, F. H., Hendrix, G. S., and Albrecht, E. D. (1960) The Plutonium–Carbon System. *Plutonium 1960*, *Proc. Int. Conf. on Plutonium Metal*, Grenoble, France (eds. E. Grison, W. B. H. Lord and R. D. Fowler), pp. 301–11.
Mulford, R. N. R., Ellinger, F. H., and Johnson, K. A. (1965) *J. Nucl. Mater.,* **17**(4), 324–9.
Mulford, R. N. R., Ford, J. O., and Hoffman, J. J. (1963) *Thermodynamics of Nuclear Materials, Proc. Symp. on Thermodynamics of Nuclear Materials* 1962, pp.517–25.
Mulford, R. N. R. and Lamar, L. E. (1961) Volatility of Plutonium Oxide. *Plutonium 1960*, *Proc. Int. Conf. on Plutonium Metal*, Grenoble, France (eds. E. Grison, W. B. H. Lord and R. D. Fowler), pp. 411–21.
Mullins, L. J. and Foxx, C. L. (1982) *Direct Reduction of Plutonium-238 Dioxide and Plutonium-239 Dioxide to Metal*, Report LA-9073, Los Alamos National Laboratory, Los Alamos, NM, 19 pp.
Mullins, L. J. and Leary, J. A. (1965) *Ind. Eng. Chem., Process Design Develop.,* **4**(4), 394–400.
Mullins, L. J. and Morgan, A. N. (1981) *Review of Operating Experience at the Los Alamos Plutonium Electrorefining Facility, 1963–1977*, Report LA-8943, Los Alamos National Laboratory, Los Alamos, NM, 24 pp.
Mullins, L. J., Leary, J. A., and Bjorklund, C. W. (1960) *Large-Scale Preparation of High-purity Plutonium Metal by Electrorefining*, Report LAMS-2441, Los Alamos Scientific Laboratory, Los Alamos, NM, 16 pp.
Mullins, L. J., Leary, J. A., and Morgan, A. N. (1963a) *Large Scale Electrorefining of Plutonium from Plutonium–Iron Alloys*, Report LA-3029, Los Alamos Scientific Laboratory, Los Alamos, NM, 35 pp.
Mullins, L. J., Leary, J. A., Morgan, A. N., and Maraman, W. J. (1963b) *Ind. Eng. Chem., Process Design Develop.,* **2**, 20–4.
Mullins, L. J., Beaumont, A. J., and Leary, J. A. (1966) *Distribution of Americium between Liquid Plutonium and a Fused Salt: Evidence for Divalent Americium*, Report LA-3562, Los Alamos Scientific Laboratory, Los Alamos, NM, 26 pp.
Mullins, L. J., Beaumont, A. J., and Leary, J. A. (1968) *J. Inorg. Nucl. Chem.,* **30**(1), 147–56.
Mullins, L. J., Christensen, D. C., and Babcock, B. R. (1982) *Fused Salt Processing of Impure Plutonium dioxide to High-purity Plutonium Metal*, Report LA-9154-MS, Los Alamos National Laboratory, Los Alamos, NM, 26 pp.
Murch, G. E. and Catlow, C. R. A. (1987) *J. Chem. Soc. Faraday Trans. 2,* **83**(7), 1157–69.
Muromura, T. (1982) *J. Nucl. Sci. Technol.,* **19**(8), 638–45.
Muromura, T., Yahata, T., Ouchi, K., and Iseki, M. (1972) *J. Inorg. Nucl. Chem.,* **34**(1), 171–3.
Murzin, A. A., Babain, V. A., Shadrin, A. Y., Kamachev, V. A., Romanovskii, V. N., Starchenko, V. A., Podoinitsyn, S. V., Revenko, Y. A., Logunov, M. V., and Smart, N. G. (2002a) *Radiochemistry,* **44**(4), 410–15.
Murzin, A. A., Babain, V. A., Shadrin, A. Y., Smirnov, I. V., Lumpov, A. A., Gorshkov, N. I., Miroslavov, A. E., and Muradymov, M. A. (2002b) *Radiochemistry,* **44**(5), 467–71.
Musante, Y. and Ganivet, M. (1974) *J. Electroanal. Chem.,* **57**(2), 225–30.

Muscatello, A. C. and Killion, M. E. (1990) *Chloride Anion Exchange Coprocessing for Recovery of Plutonium from Pyrochemical Residues and Cs_2PuCl_6 Filtrate*, Report RFP–4325, EG & G Rocky Flats, Golden, CO, 19 pp.
Nachtrieb, N. H. and Lawson, A. W. (1955) *J. Chem. Phys.,* **23**(7), 1193–5.
Nagarajan, G. (1962) *Bull. Soc. Chim. Belg.,* **71**(1–2), 88–1.
Nair, G. M., and Joshi, J. K. (1981) *J. Indian Chem. Soc.,* **58**, 311.
Naito, K., Tsuji, T., Matsui, T., Fujino, T., Yamashita, T., and Ohuchi, K. (1992) *Defect Chemistry of Plutonium Oxides*, in *Transuranium Elem. Symp.* (eds. L. R. Morss and J. Fuger), American Chemical Society, Washington, DC, pp. 440–50.
Nakayama, Y. (1971) *J. Inorg. Nucl. Chem.,* **33**(12), 4077–84.
Nash, K., Noon, M. E., Fried, S., and Sullivan, J. C. (1980) *Inorg. Nucl. Chem. Lett.,* **16**(1), 33–5.
Nash, K. L. (1993) *Solvent Extr. Ion Exc.,* **11**(4), 729–68.
Nash, K. L. and Cleveland, J. M. (1983) *ACS Symp. Ser.,* **216**(Plutonium Chem.), 251–62.
Navratil, J. D. (1969a) *Dissolution of Impure Plutonium Tetrafluoride in Nitric Acid*, Report RFP-1118, Dow Chemical Company, Rocky Flats Division, Golden, CO, 4 pp.
Navratil, J. D. (1969b) *Dissolution of Plutonium Tetrafluoride in Nitric Acid*, Report RFP-1151, Dow Chemical Company, Rocky Flats Division, Golden, CO, 5 pp.
Navratil, J. D. (1969c) *J. Inorg. Nucl. Chem.,* **31**(11), 3676–80.
Neck, V. and Kim, J. I. (2001) *Radiochim. Acta,* **89**(1), 1–16.
Neeb, K.-H. (1997) *The Radiochemistry of Nuclear Power Plants with Light Water Reactors,* Walter de Gruyter, Berlin, New York, 725 pp.
Nelson, R. D. (1980) Solid State Reactions, in *Plutonium Handbook,* vol. 2, (ed. O. J. Wick), American Nuclear Society, La Grange Park, IL, 101 pp.
Nelson, T. O. (1998) *WM'98 Proc.*, Tucson, AZ, Mar. 1–5, 1998, pp. 1234–9.
Nelson, R. D., Bierlein, T. K., and Bowman, F. E. (1965) *The Steady-State Creep of High-Purity Plutonium*, Report BNWL-32, Battelle Pacific Northwest National Laboratory, 20 pp.
Nelson, G. C., Saunders, B. G., and John, W. (1969) *Phys. Rev.,* **188**(1), 4–6.
Nelson, G. C., Saunders, B. G., and Salem, S. I. (1970) *Z. Phys.,* **235**(4), 308–12.
Nelson, E. J., Blobaum, J. M., Wall, M. A., Allen, P. G., Schwartz, A. J., and Booth, C. H. (2003a) *AIP Conf. Proc.,* **673**(Plutonium Futures – The Science), 187–9.
Nelson, E. J., Blobaum, K. J. M., Wall, M. A., Allen, P. G., Schwartz, A. J., and Booth, C. H. (2003b) *Phys. Rev. B,* **67**(22), 224206.
Neu, M. P., Hoffman, D. C., Roberts, K. E., Nitsche, H., and Silva, R. J. (1994) *Radiochim. Acta,* **66–67**, 251–8.
Neu, M. P., Matonic, J. H., Smith, D. M., and Scott, B. L. (2000) *AIP Conf. Proc.,* **532** (Plutonium Futures – The Science), 381–2.
Neu, M., P., Ruggiero, C. E., and Francis, A. J. (2002) Bioinorganic Chemistry of Plutonium and Interactions of Plutonium with Microorganisms and Plants, in *Advances in Plutonium Chemistry 1967–2000* (ed. D. C. Hoffman), American Nuclear Society and the University Research Alliance, La Grange Park, IL, pp. 169–203.
Neuilly, M., Bussac, J., Frejacques, C., Nief, G., Vendryes, G., and Yvon, J. (1972) *C. R. Acad. Sci., Ser. D,* **275**(17), 1847–9.
Newton, T. W. (1958) *J. Phys. Chem.,* **62**, 943–7.
Newton, T. W. (1959) *J. Phys. Chem.,* **63**, 1493.

Newton, T. W. (1975) *Kinetics of the Oxidation–Reduction Reactions of Uranium, Neptunium, Plutonium, and Americium in Aqueous Solutions*, Los Alamos Scientific Laboratory, Report ERDA Critical Review Series, TID 26506, 131 pp.
Newton, T. W. (2002) Redox Reactions of Plutonium Ions in Aqueous Solutions, in *Advances in Plutonium Chemistry 1967–2000* (ed. D. C. Hoffman), American Nuclear Society and the University Research Alliance, La Grange Park, IL, pp. 24–60.
Newton, T. W. and Baker, F. B. (1956) *J. Phys. Chem.,* **60**, 1417–21.
Newton, T. W. and Baker, F. B. (1963) *J. Phys. Chem.,* **67**, 1425.
Newton, T. W. and Burkhart, M. J. (1971) *Inorg. Chem.,* **10**(10), 2323–6.
Newton, T. W. and Cowan, G. A. (1960) *J. Phys. Chem.,* **64**, 244.
Newton, T. W. and Hobart, D. E. (2004) *J. Nucl. Mater.,* **334**(2–3), 222–4.
Newton, T. W. and Montag, T. (1976) *Inorg. Chem.,* **15(11)**, 2856–61.
Newton, T. W. and Rundberg, V. L. (1984) *Mater. Res. Soc. Symp. Proc.,* **26**(Sci. Basis Nucl. Waste Manage. 7), 867–73.
Newton, T. W. and Sullivan, J. C. (1986) in *Handbook on the Physics and Chemistry of the Actinides* (eds. A. J. Freeman and C. Keller), Elsevier Science Publishers, Amsterdam, p. 387.ch. 10,
Newton, T. W., Hobart, D. E., and Palmer, P. D. (1986a) *The Preparation and Stability of Pure Oxidation States of Neptunium, Plutonium, and Americium*, Report LA-UR-86-967, Los Alamos National Laboratory, Los Alamos, NM, 11 pp.
Newton, T. W., Hobart, D. E., and Palmer, P. D. (1986b) *Radiochim. Acta,* **39**(3), 139–47.
Nikitenko, S. I. (1988) *Radiokhimiya,* **30**(4), 448–52.
Nikitenko, S. I. and Ponomareva, O. G. (1989) *Radiokhimiya,* **31**(2), 58–63 (pp 195–9 in English translation).
Nikitina, G. P., Ivanov, Y. E., Listopadov, A. A., and Shpunt, L. B. (1997a) *Radiochemistry,* **39**(2), 109–22.
Nikitina, G. P., Ivanov, Y. E., Listopadov, A. A., and Shpunt, L. B. (1997b) *Radiochemistry,* **39**(1), 12–25.
Nikonov, M. V., Gogolev, A. V., Tananaev, I. G., and Myasoedov, B. F. (2004) *Radiochemistry,* **46**(4), 340–2.
Nikonov, M. V., Gogolev, A. V., Tananaev, I. G., and Myasoedov, B. F. (2005) *Mendeleev Commun.,* **Mar–Apr 2005**(2), 50–2.
Nitsche, H. and Silva, R. J. (1996) *Radiochim. Acta,* **72**, 65–72.
Norling, B. K. and Steinfink, H. (1966) *Inorg. Chem.,* **5**(9), 1488–91.
Ockenden, D. W. and Welch, G. A. (1956) *J. Chem. Soc., Abstracts*: 3358–63.
Oetting, F. L. (1967) *Chem. Rev.,* **67**(3), 261–97.
Oetting, F. L. (1982) *J. Nucl. Mater.,* **105**(2–3), 257–61.
Oetting, F. L. and Adams, J. B. (1983) *J. Chem. Thermodyn.,* **15**(6), 537–54.
Oetting, F. L., Rand, M. H., and Ackerman, R. J. (1976) *The Chemical Thermodynamics of Actinide Elements and Compounds,* part 1, The Actinide Elements, IAEA, Vienna, Austria, 111 pp.
Ofte, D. and Rohr, W. G. (1965) *J. Nucl. Mater.,* **15**(3), 231.
Ofte, D. and Wittenberg, L. J. (1964) *Am. Soc. Metals, Trans. Quart.,* **57**(4), 916–23.
Ofte, D., Rohr, W. G., and Wittenberg, L. J. (1966) *Trans. Amer. Nucl. Soc.,* **9**, 5–6.
Ogard, A. E. (1970) High-Temperature Heat Content of Plutonium Dioxide. *Plutonium 1970, Proc. Fourth Int. Conf. on Plutonium and Other Actinides*, Santa Fe, NM (ed. W. N. Miner), pp. 78–83.

Ogard, A. E. and Leary, J. A. (1970) *Plutonium Carbides*, Report LA-4415, Los Alamos Scientific Laboratory, Los Alamos, NM, 6 pp.

Ogard, A. E., Pritchard, W. C., Douglass, R. M., and Leary, J. A. (1962) *J. Inorg. Nucl. Chem.,* **24**, 29–34.

Ogawa, T., Kobayashi, F., Sato, T., and Haire, R. G. (1998) *J. Alloys Compd.,* **271–273**, 347–54.

Ohse, R. W. and Olson, W. M. (1970) *Plutonium 1970 and Other Actinides, Proc. Fourth Int. Conf. on Plutonium and Other Actinides,* Santa Fe, NM, Oct. 5–9, 1970 (ed. W. N. Miner), AIME, New York, 743.

Oi, N. (1995) *Proc. Fifth Int. Conf. on Radioactive Waste Management and Environmental Remediation,* vol. 1, Berlin, Sept. 3–7, 1995, pp. 469–70.

Okajima, S. and Reed, D. T. (1993) *Radiochim. Acta,* **60**(4), 173–84.

Oldham, S. M., Schake, A. R., Burns, C. J., Morgan, III, A. N., Schnabel, R. C., Warner, B. P., Costa, D. A., and Smith, W. H. (2000) *AIP Conf. Proc.,* **532**(Plutonium Futures – The Science), 230–1.

Olsen, C. E. and Elliott, R. O. (1962) *J. Phys. Chem. Solids,* **23**, 1225.

Olsen, C. E., Sandenaw, T. A., and Herrick, C. C. (1955) *The Density of Liquid Plutonium Metal*, Report LA-2358, Los Alamos Scientific Laboratory, Los Alamos, NM, 17 pp.

Olsen, C. E., Comstock, A. C., and Sandenaw, T. A. (1992) *J. Nucl. Mater.,* **195**, 312.

Olson, G. B. and Adler, P. H. (1984) *Scripta Met.,* **18**(4), 401–6.

Olson, W. M. and Mulford, R. N. R. (1964) *J. Phys. Chem.,* **68**(5), 1048–51.

Olson, W. M. and Mulford, R. N. R. (1967) *Thermodynamics of the Plutonium Carbides*, Report LA-DC-8012, Los Alamos Scientific Laboratory, Los Alamos, NM, 19 pp.

Onoe, J. (1997) *J. Phys. Soc. Jpn.,* **66**(8), 2328–36.

Orlemann, E. F. (1944) *Distribution of 49 [Pu-239] between Aqueous and Non-Aqueous Phases*. Fundamental Chemistry of 49.

Orme, J. T., Faiers, M. E., and Ward, B. J. (1976) The Kinetics of the Delta to Alpha Transformation in Plutonium Rich Pu-Ga Alloys, *5th Int. Conf. on Plutonium and Other Actinides 1975,* Sept. 10–13, 1975, Baden-Baden, West Germany (eds. H. Blank and R. Linder), 1976, North-Holland, Amsterdam, The Netherlands, pp.761–73.

Paffett, M. T., Farr, D., and Kelly, D. (2003a) *AIP Conf. Proc.,* **673**(Plutonium Futures – The Science), 193–5.

Paffett, M. T., Kelly, D., Joyce, S. A., Morris, J., and Veirs, K. (2003b) *J. Nucl. Mater.,* **322**(1), 45–56.

Pagès, M. and Freundlich, W. (1976) Some Actinides Double Orthovanadates and Orthoarsenates: Structural "Evolution" Due to Cationic and Anionic Substitutions. *Plutonium 1975 Other Actinides*, *Proc. Fifth Int. Conf.* (eds. H. Blank and R. Lindner), North-Holland, Amsterdam, pp. 205–7.

Pagès, M., Nectoux, F., and Freundlich, W. (1971a) *Radiochem. Radioanal. Lett.,* **8**(3), 147–50.

Pagès, M., Nectoux, F., and Freundlich, W. (1971b) *CR Acad. Sci. C. Chim.,* **273**(16), 978–80.

Palmer, D. A. and Nguyen- Trung, C. (1995) *J. Solution Chem.,* **24**(12), 1281–91.

Pansoy-Hjelvik, M. E., Brock, J., Nixon, J. Z., Moniz, P., Silver, G., and Ramsey, K. B. (2001) Purification and Neutron Emission Reduction of Plutonium-238 Oxide by Nitrate Anion Exchange Processing. *Space Technology and Applications International Forum (STAIF-2001)*, Albuquerque, NM, American Institute of Physics, *AIP Conf. Proc.*, **52,** 770–3.

Paprocki, S. J., Keller, D. L., Alexander, C. A., and Pardue, W. M. (1962a) *Volatility of Plutonium Dioxide in Nonreducing Atmospheres*, Report BMI-1591, Battelle Memorial Institute, Columbus, OH, 16 pp.

Paprocki, S. J., Keller, D. L., and Purdue, W. M. (1962b) *The Chemical Reactions of Plutonium Dioxide with Reactor Materials*, Report BMI-1580, Battelle Memorial Institute, Columbus, OH, 12 pp.

Pardue, W. M. and Keller, D. L. (1964) *J. Am. Ceram. Soc.,* **47**(12), 610–14.

Pardue, W. M., Storhok, V. W., Smith, R. A., Bonnell, P. H., Gates, J. E., and Keller, D. L. (1964a) *Synthesis, Fabrication, and Chemical Reactivity of Pu Mononitride*, Report BMI-1693, Battelle Memorial Institute, Columbus, OH, 38 pp.

Pardue, W. M., Storhok, V. W., Smith, R. A., and Keller, D. L. (1964b) *An Evaluation of Plutonium Compounds as Nuclear Fuels*, Report BMI-1698, Battelle Memorial Institute, Columbus, OH, 22 pp.

Pardue, W. M., Storhok, V. W., and Smith, R. A. (1967) *Chemical Engineering Progress, Symposium Series,* **63**(80), 142–6.

Parsonnet, V. (2004) personal communication, L. R. Morss.

Parsonnet, V., Berstein, A. D., and Perry, G. Y. (1990) *Am. J. Cardiol.,* **66**(10), 837–42.

Pascard, R. (1962) *Plansee Proc.,* **1961**, 387–419.

Pashalidis, I., Czerwinski, K. R., Fanghanel, T., and Kim, J. I. (1997) *Radiochim. Acta,* **76**(1–2), 55–62.

Patil, S. K. and Ramakrishna, V. V. (1976) *J. Inorg. Nucl. Chem.,* **38**(5), 1075–8.

Paxton, H. C. (1975) *Los Alamos Critical-Mass Data*, Report LA-3067-MS, Los Alamos Scientific Laboratory, Los Alamos, NM, 57 pp.

Paxton, H. C. and Pruvost, N. L. (1987) *Critical Dimensions of Systems Containing Uranium-235, Plutonium-239 and Uranium-233: 1986 Revision*, Report LA-10860-MS, Los Alamos National Laboratory, Los Alamos, NM, 205 pp.

Peddicord, K. L., Lazarev, L. N., and Jardine, L. J. (eds.) (1998) *Nuclear Materials Safety Management, NATO Advanced Research Workshop on Nuclear Materials Safety Management* (*1997: Amarillo, TX*). NATO ASI series. Partnership sub-series 1, Disarmament technologies; vol. 20. Kluwer Academic, Boston, MA, 378 pp.

Pekarek, V. and Marhol, M. (1991) Historical Background of Inorganic Ion Exchangers, their Classification, and Present Status, in *Inorganic Ion Exchangers in Chemical Analysis* (eds. M. Qureshi and K. G. Varshney), CRC Press, Boca Raton, FL, pp. 1–32.

Penneman, R. A. and Paffett, M. T. (2004) personal communication, D. L. Clark.

Penneman, R. A. and Paffett, M. T. (2005) *J. Solid State Chem.,* **178**(2), 563–6.

Penneman, R. A., Sturgeon, G. D., Asprey, L. B., and Kruse, F. H. (1965) *J. Am. Chem. Soc.,* **87**(24), 5803–4.

Peppard, D. F., Studier, N. H., Gergel, N. V., Mason, G. W., Sullivan, J. C., and Mech, J. F. (1951) *J. Am. Chem. Soc.,* **73**, 2529–31.

Pepper, M. and Bursten, B. E. (1991) *Chem. Rev.,* **91**(5), 719–41.

Peretrukhin, V. F., Shilov, V. P., Pikaev, A. K., and Delegard, C. H. (1995) *Alkaline Chemistry of Transuranium Elements and Technetium Elements and Technetium and the Treatment of Alkaline Radioactive Wastes*, Report WHC-EP-0817, Westinghouse Hanford Company, 172 pp.

Peterson, J. R. (1995) *J. Alloys Compd.,* **223**, 180–4.

Peterson, D. E. and Kassner, M. E. (1988) *Bull. Alloy Phase Diagr.,* **9**, 261.

Peterson, S. and Wymer, R. G. (1963) *Chemistry in Nuclear Technology,* Pergamon Press, Oxford, England.
Petit, L., Svane, A., Szotek, Z., and Temmerman, W. M. (2003) *Science,* **301**(5632), 498–501.
Petit, L., Svane, A., Temmerman, W. M., and Szotek, Z. (2002) *Eur. Phys. J. B,* **25**(2), 139–46.
Pettifor, D. G. (1996) in *Physical Metallurgy* (eds. R. W. Cahn and P. Haasen), Elsevier Science, Amsterdam, The Netherlands, 47 pp.
Phipps, K. D. and Sullenger, D. B. (1964) *Science,* **145**(3636), 1048–9.
Phipps, T. E., Sears, G. W., Seifert, R. L., and Simpson, O. C. (1949) *Natl. Nucl. Energy Ser.*, Div. IV, **14B**(Transuranium Elements, Pt. I), (eds. G. T. Seaborg, J. J. Katz, and W. M. Manning), McGraw-Hill, New York, 682–703.
Phipps, T. E., Sears, G. W., Seifert, R. L., and Simpson, O. C. (1950a) *J. Chem. Phys.,* **18**(5), 713–23.
Phipps, T. E., Sears, G. W., and Simpson, O. C. (1950b) *J. Chem. Phys.,* **18**, 724–34.
Phipps, T. E., Sears, G. W., Seifert, R. L., and Simpson, O. C. (1955) *Vapor Pressure of Liquid Plutonium*, *Proc. Int. Conf. on the Peaceful Uses of Atomic Energy*, Geneva, 7, pp. 382–5.
Pijanowski, S. W. and DeLucas, L. S. (1960) *Melting Points in the System PuO_2-UO_2*, Report KAPL-1937, KAPL General Electric Co., Schenectady, N.Y., pp. 1–5.
Pitner, W. R., Bradley, A. E., Rooney, D. W., Sanders, D., Seddon, K. R., Thied, R. C., and Hatter, J. E. (2003) *NATO Sci. Ser. II: Math. Phys. Chem.,* **92**(Green Industrial Applications of Ionic Liquids), 209–26.
Pons, F., Barbe, B., and Roux, C. (1972) *J. Appl. Crystallogr.,* **5**, 47.
Poole, D. M. and Nichols, J. L. (1961) *The Plutonium Cobalt System*, Report AERE-R-3609, UK Atomic Energy Authority Research Group.
Poole, D. M., Williamson, G. K., and Marples, J. A. C. (1957) *J. I. Met.,* **86**(4), 172–6.
Poskanzer, A. M. and Foreman, B. M. (1961) *J. Inorg. Nucl. Chem.,* **16**(3–4), 323–36 and references therein.
Potter, P. E. (1975) *MTP Int. Rev. Sci.: Inorg. Chem., Ser.2,* **7**, 257–315.
Potter, P. E. (1991) The Actinide Borides, in *Handbook on the Physics and Chemistry of the Actinides,* (eds. A. J. Freeman and C. Keller), vol. 6, North-Holland, Amsterdam, The Netherlands, 39 pp.
Powell, R. F. (1960) Thermal Conductivity of Plutonium, in *Plutonium 1960,* (eds. E. Grison, W. B. H. Lord and R. D. Fowler), vol. 1, Cleaver-Hume Press, London, 107 pp.
Preston, J. S. and du Preez, A. C. (1995) *Solvent Extr. Ion Exch.,* **13**(3), 391–413.
Pustovalov, A. A., Shapovalov, V. P., Bovin, A. V., and Fedorets, V. I. (1986) *At. Energ.,* **60**(2), 125–9.
Rabideau, S. W. (1953) *J. Am. Chem. Soc.,* **75**, 798–801.
Rabideau, S. W. (1956) *J. Am. Chem. Soc.,* **78**(12), 2705–7.
Rabideau, S. W. (1957) *J. Am. Chem. Soc.,* **79**(24), 6350–3.
Rabideau, S. W. and Cowan, H. D. (1955) *J. Am. Chem. Soc.,* **77**(23), 6145–8.
Rabideau, S. W. and Kline, R. J. (1958) *J. Phys. Chem. A,* **62**, 617–20.
Rabideau, S. W. and Masters, B. J. (1963) *J. Phys. Chem.,* **67**, 318–23.

Rabideau, S. W., Bradley, M. J., and Cowan, H. D. (1958) *Alpha-particle Oxidation and Reduction in Aqueous Plutonium Solutions*, Report USAEC-LAMS-2236, Los Alamos Scientific Laboratory, 28 pp.

Rabideau, S. W., Asprey, L. B., Keenan, T. K., and Newton, T. W. (1959) *Proc. Second Int. Conf. Peaceful Uses of Atomic Energy,* vol. 28, Geneva, pp. 361–72.

Rafalski, A. L., Harvey, M. R., and Riefenberg, D. H. (1967) *ASM Trans. Q,* **60**(4), 721.

Rai, D., Hess, N. J., Felmy, A. R., Moore, D. A., Yui, M., and Vitorge, P. (1999) *Radiochim. Acta,* **86**(3–4), 89–99.

Rai, D., Bolton, Jr, H., Moore, D. A., Hess, N. J., and Choppin, G. R. (2001) *Radiochim. Acta,* **89**(2), 67–74.

Rainey, R. H. (1959) *Chemistry of Plutonium(IV) Polymer*, Report CF-59-12-95, Oak Ridge National Laboratory, 4.

Raj, D. D. A., Nalini, S., Viswanathan, R., and Balasubramanian, R. (1999) *Proc. Eighth ISMAS Symp. on Mass Spectrometry,* vol. II, Dec. 7–9, 1999 (ed. S. K. Aggarwal), Indian Institute of Chemical Technology, Hyderabad, Indian Society for Mass Spectrometry, Mumbai, p. 847.

Rance, P. and Zilberman, B. (2002) *J. Nucl. Sci. Technol.*, (Suppl. 3), 375–8.

Rand, M. H. (1966) *Atom. Energy Rev.,* **4**(1), 7–51.

Rao, P. R. V. and Kolarik, Z. (1996) *Solvent Extr. Ion. Exch.,* **14**(6), 955–93.

Rao, G. S., Subramanian, M. S., and Welch, G. A. (1963) *J. Inorg. Nucl. Chem.,* **25**(10), 1293–5.

Rao, P. R. V., Bagawde, S. V., Ramakrishna, V. V., and Patil, S. K. (1978) *J. Inorg. Nucl. Chem.,* **40**(1), 123–7.

Rasmussen, M. J. and Hopkins, H. H., Jr (1961) *J. Ind. Eng. Chem.,* **53**, 453–7.

Ravat, B., Jolly, L., Valot, C., and Baclet, N. (2003) *AIP Conf. Proc.,* **673**(Plutonium Futures – The Science), 7–8.

Raynor, J. B. and Sakman, J. F. (1965) Oxidation, in *Proc. Third Int. Conf. on Plutonium 1965* (eds. A. E. Kay and M. B. Waldron), Cleaver - Hume, London, England, 575 pp.

Reader, J. and Corliss, C. H. (1980) *Wavelengths and Transition Probabilities for Atoms and Atomic Ions*, part I, *Wavelengths*, Report NSRDS-NBS 68, Natl. Meas. Lab., Natl. Bur. Stand., Washington, DC, pp. 1–357.

Reavis, J. G. and Leary, J. A. (1970) *Plutonium 1970 and Other Actinides, Proc. Fifth Int. Conf. on Plutonium and Other Actinides,* Baden-Baden, West Germany (ed. W. N. Miner), North-Holland, New York, 809 pp.

Reavis, J. G., Johnson, K. W. R., Leary, J. A., Morgan, A. N., Ogard, A. E., and Walsh, K. A. (1960) *The Preparation of Plutonium Halides for Fused Salt Studies, Extractive and Physical Metallurgy of Plutonium and its Alloys, Symp.,* San Francisco, CA (ed. W. D. Wilkinson), Interscience Publishers, New York, pp. 89–100.

Rebizant, J., Bednarczyk, E., Boulet, P., Fuchs, C., and Wastin, F. (2000) *Single Crystal Growth of* $(U_{1-x}Pu_x)O_2$ *Mixed Oxides. AIP Conf. Proc.,* **532**(Plutonium Futures–The Science), 355–6.

Reilly, S. D., Neu, M. P., and Runde, W. (2000) *AIP Conf. Proc.,* **532**(Plutonium Futures – The Science), 269–71.

Reshetnikov, F. G. (2003) *Mendeleev Commun.*, (4), 155–6.

Reynolds, L. T. and Wilkinson, G. (1956) *J. Inorg. Nucl. Chem.,* **2**, 246.

Rice, R. W. (1983) *Am. Ceram. Soc. Bull.,* **62**(8), 889–92.

Richards, S. M. and Kasper, J. S. (1969) *Acta Crystallogr. B,* **B25**, 237.
Richmann, M. K., Reed, D. T., Kropf, A. J., Aase, S. B., and Lewis, M. A. (1999) *XAFS/XANES Studies of Plutonium-loaded Sodalite/glass Waste Forms*, *Annual Meeting Proc. Institute of Nuclear Materials Management*, 40, pp. 668–75.
Riha, J. and Trevorrow, L. (1965) *Chemical Engineering Division Semiannual Report, January – June 1967*, Report ANL-7375, Argonne National Laboratory, pp. 54–6.
Riley, B. (1970) *Sci. Ceram.,* **5**, 83–109.
Rinehart, G. H. (1992) *Space Nucl. Power Syst.,* **10**, 39–43.
Rinehart, G. H. (2001) *Prog. Nucl. Energ.,* **39**(3–4), 305–19.
Robbins, J. L. (2004) *J. Nucl. Mater.,* **324**(2/3), 125–33.
Robouch, P. and Vitorge, P. (1987) *Inorg. Chim. Acta,* **140**, 239–42.
Roepenack, H., Schneider, V. W., and Druckenbrodt, W. G. (1984) *Am. Ceram. Soc. Bull.,* **63**(8), 1051–3.
Rogers, R. D. and Seddon, K. R., Eds. (2002) *ACS Symp. Ser.* **118**(Ionic Liquids – Industrial Applications for Green Chemistry), American Chemical Society, Washington, DC.
Rogl, P. and Potter, P. E. (1997) *J. Phase Equilib,* **18**(5), 467–73.
Rogozina, E. M., Konkina, L. F., and Popov, D. K. (1973) *Radiokhimiya,* **15**(1), 61–3.
Rolland, B. L., Molinie, P., Colombet, P., and McMillan, P. F. (1994) *J. Solid State Chem.,* **113**(2), 312–19.
Rollefson, G. K. and Dodgen, H. W. (1943) *Report on Spectrographic Analysis Work*, Report CK-812.
Romanovski, V. V., White, D. J., Xu, J., Hoffman, D. C., and Raymond, K. N. (1999) *Solvent Extr. Ion Exch.,* **17**(1), 55–71.
Ronchi, C., Sheindlin, M., Musella, M., and Hyland, G. J. (1999) *J. Appl. Phys.,* **85**(2), 776–89.
Ronchi, C., Capone, F., Colle, J. Y., and Hiernaut, J. P. (2000) *J. Nucl. Mater.,* **280**(1), 111–15.
Roof, R. B., Jr. (1973) *Adv. X. Ray Anal.,* **16**, 396–400.
Roof, R. B. (1989) *X-ray Diffraction Data for Plutonium Compounds: Plutonium and Plutonium Binary Compounds*, Los Alamos National Laboratory, Report LA-11619, 3 volumes.
Rose, R. L., Robbins, J. L., and Massalski, T. B. (1970) *J Nucl. Mater.,* **36**(1), 99–107.
Rosen, S., Nevitt, M. V., and Mitchell, A. W. (1963) *J. Nucl. Mater.,* **10**(2), 90–8.
Rosen, S., Nevitt, M. V., and Mitchell, A. W. (1964) *U-Pu-C Ternary Phase Diagram Below 50 Atomic Percent Carbon*, Report ANL-6435, Argonne National Laboratory, Argonne, IL, 107 pp.
Rosen, M., Erez, G., and Shtrikman, S. (1969) *J. Phys. Chem. Solids,* **30**(5), 1063–70.
Rosenthal, M. W., Rahman, Y. E., Moretti, E. S., and Cerny, E. A. (1975) *Radiat. Res.,* **63**(2), 262–74.
Rossat-Mignod, J., Lander, G. H., and Burlet, P. (1984) in *Handbook on the Physics and Chemistry of Actinides,* vol. 1 (eds. A. J. Freeman and G. H. Lander), North-Holland, Amsterdam, 415 pp.
Rothe, J., Denecke, M. A., Neck, V., Mueller, R., and Kim, J. I. (2002) *Inorg. Chem.,* **41**(2), 249–58.
Rothe, J., Walther, C., Denecke, M. A., and Fanghaenel, T. (2004) *Inorg. Chem.,* **43**(15), 4708–18.

Ruggiero, C. E., Matonic, J. H., Neu, M. P., and Reilly, S. P. (2000) *AIP Conf. Proc.,* **532**(Plutonium Futures – The Science), 284–5.

Ruggiero, C. E., Matonic, J. H., Reilly, S. D., and Neu, M. P. (2002) *Inorg. Chem.,* **41**(14), 3593–5.

Rundberg, R. S., Mitchell, A. J., Triay, I. R., and Torstenfelt, N. B. (1988) *Mater. Res. Soc. Symp. Proc.,* **112**(Sci. Basis Nucl. Waste Manage. 11), 243–8.

Runde, W. (2005a) Preparation and characterization of tetravalent plutonium oxalate compounds, personal communication, D. L. Clark, Los Alamos, NM.

Runde, W. (2005b) Preparation and characterization of peroxocarbonato complexes of tetravalent plutonium, personal communication, D. L. Clark, Los Alamos, NM.

Runde, W., Conradson, S. D., Wes Efurd, D., Lu, N., Van Pelt, C. E., and Tait, C. D. (2002) *Appl. Geochem.,* **17**(6), 837–53.

Runde, W., Bean, A., and Scott, B. L. (2003a) *AIP Conf. Proc.,* **673**(Plutonium Futures – The Science), 23–5.

Runde, W., Bean, A. C., Albrecht-Schmitt, T. E., and Scott, B. L. (2003b) *Chem. Commun.*, 478.

Runnalls, O. J. C. (1956) *Can. J. Chem.,* **34**(2), 133–45.

Runnalls, O. J. C. (1958) *The Preparation of Plutonium–Aluminum and Other Plutonium Alloys*, Report AECL-543, Atomic Energy Canada Ltd., Chalk River, 25 pp.

Runnalls, O. J. C. (1965) *Phase-equilibrium Studies on the Aluminum–Plutonium System*, Report AECL-2275, Atomic Energy Canada Ltd., Chalk River, 20 pp.

Runnalls, O. J. C. and Boucher, R. R. (1955) *Acta Crystallogr.,* **9**, 592.

Russell, L. E., Harrison, J. D. L., and Brett, N. H. (1960) *J. Nucl. Mater.,* **2**, 310–20.

Russell, L. E., Brett, N. H., Harrison, J. D. L., and Williams, J. (1962) *J. Nucl. Mater.,* **5**, 216–27.

Russell, L. E. (1964) *Carbides in Nuclear Energy*, vol. 1, *Physical and Chemical Properties; Phase Diagrams;* vol. 2, *Preparation and Fabrication; Irradiation Behavior*, 966 pp.

Ryan, J. L. (1959) *Concentration and Final Purification of Neptunium by Anion Exchange*, Report HW-59193 Rev, Hanford Works, 22 pp.

Ryan, J. L. (1960) *J. Phys. Chem.,* **64**(10), 1375–85.

Ryan, J. L. (1975) Anion Exchange Reactions, in *Gmelin Handbook of Inorganic Chemistry, Transuranic Elements* (ed. G. Koch), Springer-Verlag, New York. [D2 Chemistry in Solution: 418 and 432.]

Ryan, J. L. and Bray, L. A. (1980) *ACS Symp. Ser.* **117**(Actinide Sep.), American Chemical Society, Washington, DC, 499–514.

Ryan, J. L. and Joergensen, C. K. (1964) *Mol. Phys.,* **7**(1), 17–29.

Rykov, A. G., Timofeev, G. A., and Yakovlev, C. N. (1969) *Radiokhimiya,* **11(4)**, 413–18 (pp 403–407 in English translation).

Sackman, J. F. (1960) The Atmospheric Oxidation of Plutonium Metal. *Plutonium 1960*, *Proc. Int. Conf. Plutonium Met.*, Grenoble, France (ed. E. Grison, W. B. H. Lord and R. D. Fowler), pp. 222–9.

Sadigh, B. and Wolfer, W. G. (2005) *Phys. Rev. B.* **70**(20), 205122/1–12.

Sakurai, S., Tachimori, S., Akatsu, J., Kimura, T., Yoshida, Z., Mutoh, H., Yamashita, T., and Ohuchi, K. (1989) *Nihon Genshiryoku Gakkaishi,* **31**(11), 1243–50.

Sakurai, S., Usuda, S., Ami, N., Hirata, M., Wakamatsu, S., and Tachimori, S. (1993) *Nihon Genshiryoku Gakkaishi,* **35**(2), 147–54.

Sandenaw, T. A. (1960a) *Phys. Chem. Solids,* **16**, 329.

Sandenaw, T. A. (1960b) *The Thermal Expansion of Plutonium Metal below 300 K, Proc. Second Int. Conf. on Plutonium Metallurgy: Plutonium 1960,* Grenoble, France vol. 1, (eds. E. Grison, W. B. H. Lord, and R. D. Fowler), Cleaver-Hume Press, London, pp. 79–90.

Sandenaw, T. A. (1961) *Results of Measurements of Physical Properties of Plutonium metal*. in *The Metal Plutonium* (eds. A. S. Coffinberry and W. N. Miner), University of Chicago Press Chicago, IL, 154 pp.

Sandenaw, T. A. (1962) *Phys. Chem. Solids,* **23**(Sep), 1241–8.

Sandenaw, T. A. (1963) *J. Nucl. Mater.,* **10**(3), 165–72.

Sandenaw, T. A. and Gibney, R. B. (1958) *Phys. Chem. Solids,* **6**, 81.

Sandenaw, T. A. and Gibney, R. B. (1971) *J. Chem. Thermodyn.,* **3**, 85.

Sandenaw, T. A. and Harbur, D. R. (1973) *J. Phys. Chem. Solids,* **34**(9), 1487–95.

Sano, T., Tanaka, O., Akimoto, I., Imoto, S., Kikuchi, T., Ichikawa, M., Watanabe, H., Nishio, G., and Shimokawa, J. (1971) *Nihon Genshiryoku Gakkaishi,* **13**(11), 642–67.

Santini, P., Lemanski, R., and Erdos, P. (1999) *Adv. Phys.,* **48**(5), 537–653.

Santoro, A., Marezio, M., Roth, R. S., and Minor, D. (1980) *J. Solid State Chem.,* **35**(2), 167–75.

Sari, C., Benedict, U., and Blank, H. (1968) *Metallographic and X-ray Investigations in the Plutonium–Oxygen and Uranium–Plutonium–Oxygen Systems*, *Proc. Symp. on Thermodynamics of Nuclear Materials*, Vienna, Austria, pp. 587–611.

Sari, C., Benedict, U., and Blank, H. (1970) *J. Nucl. Mater.,* **35**(3), 267–77.

Sarrao, J. L., Morales, L. A., Thompson, J. D., Scott, B. L., Stewart, G. R., Wastin, F., Rebizant, J., Boulet, P., Colineau, E., and Lander, G. H. (2002) *Nature,* **420**(6913), 297–9.

Sarrao, J. L., Morales, L. A., Thompson, J. D., Scott, B. L., Stewart, G. R., Wastin, F., Rebizant, J., Boulet, P., Colineau, E., and Lander, G. H. (2003a) *AIP Conf. Proc.,* **673** (Plutonium Futures – The Science), 12–14.

Sarrao, J. L., Morales, L. A., and Thompson, J. D. (2003b) *J. Metals,* **55**(9), 38–40.

Sasao, N. and Yamaguchi, H. (1991) *Apparatus for Laser Isotope Separation*, (Power Reactor and Nuclear Fuel Development Corp., Japan). Jpn. Patent 03068420, 10 pp.

Sastre, A. M., Kumar, A., Shukla, J. P., and Singh, R. K. (1998) *Sep. Purif. Methods,* **27**(2), 213–98.

Savage, D. J. and Kyffin, T. W. (1986) *Polyhedron,* **5**(3), 743–52.

Savrasov, S. Y., Kotliar, G., and Abrahams, E. (2001) *Nature,* **410**(6830), 793–5.

Scheitlin, F. M. and Bond, W. D. (1980) *Recovery of Plutonium from HEPA Filters by Cerium(IV)*, *Promoted Dissolution of Plutonium Dioxide and Recycle of the Cerium Promoter*, Report ORNL/TM-6802, Oak Ridge National Laboratory, Oak Ridge, TN, 58 pp.

Scheuer, U. and Lengeler, B. (1991) *Phys. Rev. B,* **44**(18), 9883–94.

Schlechter, M. (1970) *J. Nucl. Mater.,* **37**(1), 82–8.

Schlesinger, H. I. and Brown, H. (1943) *Chemical Separation of 94 from Uranium on the Basis of the Volatility of the Borohydrides*, Report CN-441, University of Chicago.

Schmutz, H. (1966) *System Alkali Fluoride–Lanthanide/Actinide Fluoride (Lithium, Sodium, Potassium, Rubidium–Lanthanum, Rare Earths, Yttrium/Neptunium, Americium)*, Report KFK-431, Kernforschungszentrum, Karlsruhe, Germany, 73 pp.

Schneider, V. W. and Roepenack, H. (1986) Fabrication of (U/Pu)O_2-mixed oxide Fuel Elements, in *Handbook on the Physics and Chemistry of the Actinides* (eds. A. J. Freeman and C. Keller), Elsevier Science, New York, 531–55.

Schonfeld, F. W. (1961) Pu Phase Diagrams, in *The Metal Plutonium* (eds. A. S. Coffinberry and W. N. Miner), University of Chicago Press, Chicago, 243.

Schonfeld, F. W. and Tate, R. E. (1996) *The Thermal Expansion Behavior of Unalloyed Plutonium*, Report LA-13034-MS, Los Alamos National Laboratory, pp. 1–34.

Schonfeld, F. W., Cramer, E. M., Miner, W. N., Ellinger, F. H., and Coffinberry, A. S. (1959) *Prog. Nucl. Energy* (eds. H. M. Finniston, and J. P. Howe, Pergamon Press) *Ser. V,* **2**, 579–99.

Schreckenbach, G., Hay, P. J., and Martin, R. L. (1999) *J. Comput. Chem.,* **20**(1), 70–90.

Schwartz, A. J., Wall, M. A., Zocco, T. G., and Wolfer, W. G. (2005) *Philos. Mag.,* **85**, 479–88.

Seaborg, G. T. (1958) *The Transuranium Elements*, Addison-Wesley, Reading, MA, 348 pp.

Seaborg, G. T. (1977) *History of Met Lab section C-I, April 1942 – April 1943*, Report PUB-112(vol.1), Lawrence Berkeley Laboratory, University of California, Berkeley, CA, 708 pp.

Seaborg, G. T. (1978) *History of Met Lab section C-I, May 1943 – April 1944*, Report PUB-112(vol.2), Lawrence Berkeley Laboratory, University of California, Berkeley, CA, 581 pp.

Seaborg, G. T. (1979) *History of Met Lab section C-I, May 1944 – April 1945*, Report PUB-112(Vol.3), Lawrence Berkeley Laboratory, University of California, Berkeley, CA, 625 pp.

Seaborg, G. T. (1980) *History of Met Lab section C-I, May 1945 – May 1946*, Report PUB-112(vol. 4), Lawrence Berkeley Laboratory, University of California, Berkeley, CA, 657 pp.

Seaborg, G. T. (1983) *ACS Symp. Ser.* **216**(Plutonium Chem.) (eds. W. T. Carnall and G. R. Choppin), American Chemical Society, Washington, DC, pp. 1–22.

Seaborg, G. T. (1992) *Transuranium Elements. A Half Century* (eds. L. R. Morss and J. Fuger), American Chemical Society, Washington, DC, pp. 10–49.

Seaborg, G. T. (1995) *Radiochim. Acta,* **70/71**, 69–90.

Seaborg, G. T. and Katz, J. J. (1990) *Proc. Robert A. Welch Found. Conf. Chem. Res.,* **34**, 224–51.

Seaborg, G. T. and Loveland, W. D. (1990) *The Elements beyond Uranium,* John Wiley & Sons, New York, 359 pp.

Seaborg, G. T. and Perlman, M. L. (1948) *J. Am. Chem. Soc.,* **70**, 1571–3.

Seaborg, G. T. and Wahl, A. C. (1948a) *J. Am. Chem. Soc.,* **70**, 1128–34.

Seaborg, G. T. and Wahl, A. C. (1948b) *J. Am. Chem. Soc.,* **70**(3), 1128–34.

Seaborg, G. T., Wahl, A. C., and Kennedy, J. W. (1946) *Phys. Rev.,* **69**, 367.

Seaborg, G. T., Wahl, A. C., and Kennedy, J. W. (1949a) *Natl. Nucl. Energy Ser.,* Div. IV **14B**(Transuranium Elements, Pt. I), (eds. G. T. Seaborg, J. J. Katz and W. M. Manning), McGraw-Hill, New York, 13–20.

Seaborg, G. T., Katz, J. J., and Manning, W. M. (eds.) (1949b) *Natl. Nucl. Energy Ser.,* Div IV **14**B (Transuranium Elements Pt. I), McGraw-Hill, New York.

Selle, J. E. and Etter, D. E. (1964) *Trans. Metall. Soc. AIME,* **230**(5), 1000–5.
Selle, J. E., English, J. J., Teaney, P. E., and McDougal, J. R. (1970a) *Compatibility of Plutonium-238 Dioxide with Various Refractory Metals and Alloys: Interim Report*, Report MLM-1706, Mound Laboratoary, Miamisburg, OH, 214 pp.
Selle, J. E., McDougal, J. R., and Schaeffer, D. R. (1970b) *Compatibility of Plutonium-238 Dioxide with Platinum and Platinum–Rhodium Alloys*, Report MLM-1684, Mound Laboratory, Miamisburg, OH, 124 pp.
Serpan, C. Z. and Wittenberg, L. J. (1961) *Trans. Metall. Soc. AIME,* **221**(5), 1017–20.
Seyferth, D. (2004) *Organometallics,* **23**(15), 3562–83.
Shacklett, R. L. and Du Mond, J. W. M. (1957) *Phys. Rev.,* **106**, 501–12.
Sheft, I. and Davidson, N. R. (1949a) Equilibrium in the Vapor-phase Hydrolysis of Plutonium Tribromide, in *Natl. Nucl. Energy Ser.,* Div **14**B, (Transuranium Elements Pt. I) (eds. G. T. Seaborg, J. J. Katz, and W. M. Manning), McGraw-Hill, New York, pp. 831–40.
Sheft, I. and Davidson, N. R. (1949b) Equilibrium in the Vapor-phase Hydrolysis of Plutonium Trichloride, in *Natl. Nucl. Energy Ser.,* Div **14**B, (Transuranium Elements Pt. I) (eds. G. T. Seaborg, J. J. Katz, and W. M. Manning), McGraw-Hill, New York, pp. 841–7.
Sheft, I., Andrews, H. and Katz, J. J. (1949) *Summary Report for July, August, and September 1949*, Report ANL-4379, Chemistry Division, Section C1, Argonne National Laboratory, Argonne National Laboratory, pp. 43–50.
Sheldon, R. I., Rinehart, G. H., Krishnan, S., and Nordine, P. C. (2001) *Mater. Sci. Eng.,* **B79**, 113–22.
Sherby, O. D. and Simnad, M. T. (1961) *Am. Soc. Metals, Trans. Quart.,* **54**, 227–40.
Shewmon, P. G. (1963) *Diffusion in Solids,* McGraw-Hill, New York, 134 pp.
Shick, A. B., Drchal, V., and Havela, L. (2005) *Europhys. Lett.,* **69**(4), 588–94.
Shilov, V. P. (1997) *Radiokhimiya,* **39**(4), 330–2 (pp. 328–31 in English translation.).
Shilov, V. P. (1998) *Radiochemistry,* **40**(1), 11–16.
Shilov, V. P. and Yusov, A. B. (2002) *Russ. Chem. Rev.,* **71**(6), 465–88.
Shorikov, A. O., Lukoyanov, A. V., Korotin, M. A., and Anisimov, V. I. (2005) *Los Alamos National Laboratory, Preprint Archive, Condensed Matter*: 1–21, arXiv:cond-mat/0412724 v2.
Shumakov, V. D., Kosulin, N. S., and Chebotarev, N. T. (1990) *Phys. Metal Metalloved (Russian),* **37**, 14.
Shvareva, T. Y., Almond, P. M., and Albrecht- Schmitt, T. E. (2005) *J. Solid State Chem.,* **178**(2), 499–504.
Silva, R. J. and Nitsche, H. (1995) *Radiochim. Acta,* **70/71**, 377–96.
Silva, R. J. and Nitsche, H. (2002) *Environmental Chemistry*, in *Advances in Plutonium Chemistry 1967–2000* (ed. D. C. Hoffman), American Nuclear Society and the University Research Alliance, La Grange Park, IL, pp. 89–111.
Silva, R. J., Bidoglio, G., Rand, M. H., Robouch, P. B., Wanner, H., and Puigdomenech, I. (1995) *Chemical Thermodynamics of Americium,* Elsevier Science Publishers, Amsterdam, Netherlands, 392 pp.
Silver, G. L. (1971) *J. Inorg. Nucl. Chem.,* **33,** 577–583.
Silver, G. L. (1997) *Radiochim. Acta,* **77**, 189.
Silver, G. L. (2002) *Appl. Radiat. Isot.* **57,** 1–5.
Silver, G. L. (2003) *Appl. Radiat. Isot.* **59,** 217–20.

Silver, G. L. (2004) *J. Radioanal. Nucl. Chem.* **262**(3), 779–781.
Silvestre, J. P., Freundlich, W., and Pagès, M. (1977) *Rev. Chim. Miner.,* **14**(2), 225–9.
Simakin, G. A., Volkov, Y. F., Visyashcheva, G. I., Kapshukov, I. I., Baklanova, P. F., and Yakovlev, G. N. (1974) *Sov. Radiochem.,* **16**(6), 838–41.
Simon, G. P. (1991) *Ion Exchange Training Manual.* Van Nostrand Reinhold, New York, pp. 1–47.
Skavdahl, R. E. (1963) *Plutonium–Boron System*, Report HW-76302, Article 2.4, US Atomic Energy Commission.
Skavdahl, R. E. (1964) *The Reactions between PuO_2 and Carbon*, Report HW-77906 12 pp.
Skavdahl, R. E. and Chikalla, T. D. (1964) *The Plutonium–Boron System*, Report HW-81602, Article 2.1, US Atomic Energy Commission.
Skavdahl, R. E., Chikalla, T. D., and McNeilly, C. E. (1964) *Trans. Am. Nucl. Soc.,* **7**, 403–4.
Skriver, H. L. (1985) *Phys. Rev. B,* **31**, 1909.
Smirnov, E. A. and Shmakov, A. A. (1999) *Defect Diffus. Forum,* **166**, 63–7.
Smith, J. L. (1980) No superconductivity in plutonium, personal communication, S. S. Hecker, Los Alamos, NM.
Smith, J. L. and Fisk, Z. (1982a) *J. Appl. Phys.,* **53(11)**, 7883–6.
Smith, J. L. and Haire, R. G. (1978) *Science,* **200**(4341), 535–7.
Smith, J. L. and Kmetko, E. A. (1983) *J. Less-Common Met.,* **90**(1), 83–8.
Smolders, A. and Gilissen, R. (1987) *Mater. Sci. Monogr.,* **38C**(High Tech Ceram., Pt. C), 2849–60.
Soderlind, P. (2001) *Europhys. Lett.,* **55**(4), 525–31.
Sokhina, L. P., Solovkin, A. S., Teterin, E. G., Bogdanov, F. A., and Shesterikov, N. N. (1978) *Radiokhimiya,* **20**(1), 28–34.
Solar, J. P., Burghard, H. P. G., Banks, R. H., Streitwieser, A., Jr, and Brown, D. (1980) *Inorg. Chem.,* **19**(7), 2186–8.
Solovkin, A. S. and Rubisov, V. N. (1983) *Radiokhimiya,* **25**(5), 625–8.
Sood, D. D., Jayadevan, N. C., Mudher, K. D. S., Khandekar, R. R., and Krishnan, K. (1992) *Transuranium Elements: A Half Century* (eds. L. R. Morss and J. Fuger), American Chemical Society, Washington, DC, pp. 524–32.
Sorantin, H. (1975) *Determination of Uranium and Plutonium in Nuclear Fuels,* Verlag Chemie, Weinheim, Germany, 285 pp.
Spear, K. E. (1976) *J. Less-Common Met.,* **47**, 195–201.
Spear, K. E. and Leitnaker, J. M. (1968) *Review and Analysis of Phase Behavior and Thermodynamic Properties of the Plutonium–Nitrogen System*, Report ORNL-TM-2106, Oak Ridge National Laboratory, Oak Ridge, TN, 24 pp.
Spedding, F. H., Kant, A., Wright, J. M., Warf, J. C., Powell, J. E., and Newton, A. S. (1945) *Extraction Purification of Thorium Nitrate*, Report CC-2393.
Spinks, J. W. T. and Woods, R. J. (1990) *An Introduction to Radiation Chemistry,* 3rd ed, John Wiley & Sons, New York, Ch. 7, 574 pp.
Spirlet, J. C. (1982) *Nucl. Instrum. Methods,* **200**(1), 45–53.
Spirlet, J. C. (1991) Synthesis of f-element Pnictides, in *Topics in f-element Chemistry,* vol. 2, (eds. G. Meyer and L. R. Morss), Kluwer Academic Publishers, Boston, pp. 353–67.

Spirlet, J. C. and Vogt, O. (1982) *J. Magn. Magn. Mater.,* **29**(1–3), 31–8.

Spirlet, M. R., Rebizant, J., Apostolidis, C., Kanellakopulos, B. K., and Dornberger, E. (1992) *Acta Crystallogr.,* **C48**(7), 1161–4.

Spitsyn, V. I., Gel'man, A. D., Krot, N. N., Mefod'eva, M. P., Zakharova, F. A., Komkov, Y. A., Shilov, V. P., and Smirnova, I. V. (1969) *J. Inorg. Nucl. Chem.,* **31**(9), 2733–45.

Spriet, B. (1963) *Mem. Etud. Sci. Rev. Met.,* **60**, 531.

Spriet, B. (1965) *J. Nucl. Mater.,* **15**(3), 220–30.

Spriet, B. (1967) Study of Allotropic Transformation of Plutonium, in *Plutonium 1965* (eds. A. E. Kay and M. B. Waldron), Chapman and Hall, London, England, pp. 88–117.

Sriyotha, U. (1968) *Phase Equilibrium in the UO_{2+x}-$LuO_{1.5}$($ErO_{1.5}$) and $LuO_{1.5}$-UO_2(NpO_2,NpO_{2+x},PuO_2,PuO_{2+x}) Systems*, Thesis, Report KFK-737, Kernforschungszentrum, Karlsruhe, Germany, 61 pp.

Stakebake, J. L., Larson, D. T., and Haschke, J. M. (1993) *J. Alloys Compd.,* **202**(1–2), 251–63.

Standifer, R. L. (1968) *Fluoride Volatility 1968, Proc. Rocky Flats Fluoride Volatility Conf.,* Jun. 24–25, 1968, (eds. J. M. Cleveland and M. A. Thompson), Dow Chemical Company, pp. 79–98.

Staritzky, E. (1956) *Anal. Chem.,* **28**(12), 2021–2.

Staritzky, E. and Singer, J. (1952) *Acta Crystallogr.,* **5**, 536–40.

Starks, D. F. and Streitwieser, A., Jr (1973) *J. Am. Chem. Soc.,* **95**(10), 3423–4.

Steindler, M. J. (1963a) *Laboratory Investigations in Support of Fluid-bed Fluoride Volatility Processes*, part II, *The Properties of Plutonium Hexafluoride*, Report ANL-6753, Argonne National Laboratory, 83 pp.

Steindler, M. J. and Gunther, W. H. (1964a) *Laboratory Investigations in Support of Fluid-bed Fluoride Volatility Processes*, part VI, *A. The Absorption Spectrum of Plutonium Hexafluoride. B. Analysis of Mixtures of Plutonium Hexafluoride and Uranium Hexafluoride by Absorption Spectrometry*, Report ANL-6817, Argonne National Laboratory, 16 pp.

Steindler, M. J. and Gunther, W. H. (1964b) *Spectrochim. Acta,* **20**(8), 1319–22.

Steindler, M. J., Steidl, D. V., and Steunenberg, R. K. (1958) *The Fluorination of Plutonium Tetrafluoride*, Report ANL-5875, Argonne National Laboratory, 29 pp.

Steindler, M. J., Steidl, D. V., and Steunenberg, R. K. (1959) *Nucl. Sci. Eng.,* **6**(4), 333–40.

Steindler, M. J., Steidl, D. V., and Fischer, J. (1963) *Laboratory Investigations in Support of Fluid-bed Fluoride Volatility Processes*, part V, *The Radiation Chemistry of Plutonium Hexafluoride*, Report ANL-6812, Argonne National Laboratory, 24 pp.

Stewart, D. C. (1956) *Absorption Spectra of Lanthanide and Actinide Rare Earths. III. Heavier Lanthanide Elements in Aqueous Perchloric Acid Solution*, Report ANL-5624, US Atomic Energy Commission, 16 pp.

Stewart, G. R. and Elliott, R. O. (1981) *Specific Heat Studies of Alpha and Delta Plutonium. Actinides - 1981*, Report LBL-12441, Lawrence Berkeley Laboratory, Berkeley, CA.

Stiffler, G. L. and Curtis, M. H. (1960) *The Preparation of Plutonium Powder by a Hydriding Process: Initial Studies*, Report HW-64, 289, US Atomic Energy Commission, 17 pp.
Stoll, W., Scheider, V., and Ost, C. (1982) German Patent 3, **101**, 505 A.
Storms, E. K. (1964) *A Critical Review of Refractories*, Report LA-2942, US Atomic Energy Commission, 245 pp.
Storms, E. K. (1967) *The Refractory Carbides,* vol. 2 (*Refractory materials series*) Academic Press, New York, 284 pp.
Stout, B. E., Choppin, G. R., Nectoux, F., and Pagès, M. (1993) *Radiochim. Acta,* **61**, 65.
Stout, M. G., Kachner, G. C., and Hecker, S. S. (2002) *Mechanical Behavior of Delta-Phase Plutonium–Gallium Alloys*, Report LA-994458-PR-Revised, Los Alamos National Laboratory, pp. 1–38.
Stöwe, K. (2000) *J. Solid State Chem.,* **149**, 155–66.
Stoyer, N. J., Hoffman, D. C., and Silva, R. J. (2000) *Radiochim. Acta,* **88**(5), 279–82.
Stradling, G. N., Stather, J. W., Gray, S. A., Moody, J. C., Ellender, M., Hodgson, A., Volf, V., Taylor, D. M., Wirth, P., and Gaskin, P. W. (1989) *Int. J. Radiat. Biol.,* **56**(4), 503–14.
Stratton, R. W., Ledergerber, G., Ingold, F., Nicolet, M., and Botta, F. (1987) *Improv. Water React. Fuel Technol. Util., Proc. Int. Symp.*, pp. 353–62.
Stumpe, R., Kim, J. I., Schrepp, W., and Walther, H. (1984) *Appl. Phys. B-Photo,* **34**(4), 203–6.
Sugar, J. (1973) *J. Chem. Phys.,* **59**(2), 788–91.
Sugar, J. (1974) *J. Chem. Phys.,* **60**(10), 4103.
Sullivan, J. C., Hindman, J. C., and Zielen, A. J. (1961) *J. Am. Chem. Soc.,* **83**(16), 3373–8.
Sullivan, J. C., Woods, M., Bertrand, P. A., and Choppin, G. R. (1982) *Radiochim. Acta,* **31**(1–2), 45–50.
Sullivan, J. C., Choppin, G. R., and Rao, L. F. (1991) *Radiochim. Acta,* **54**(1), 17–20.
Sundaram, S. (1962) *Z. Phys. Chem.,* **34**, 225–32.
Suzuki, Y., Arai, Y., and Sasayama, T. (1983) *J. Nucl. Mater.,* **115**(2–3), 331–3.
Swanson, J. L. (1964) *J. Phys. Chem.,* **68**(2), 438–9.
Swanson, J. L. (1990) The PUREX Process. Part 3: PUREX Process Flowsheets. Science and Technology of Tributyl Phosphate, vol. 3, *Applications of Tributyl Phosphate in Nuclear Fuel Processing* (eds. W. W. Schulz, J. D. Navratil, L. L. Burger and K. P. Bender), CRC Press, Boca Raton, FL, pp. 55–79.
Tabuteau, A. and Pagès, M. (1980) *J. Inorg. Nucl. Chem.,* **42**(3), 401–3.
Tabuteau, A., Pagès, M., and Freundlich, W. (1972) *Mater. Res. Bull.,* **7**(7), 691–7.
Tait, C. D., Donohoe, R. J., Clark, D. L., Conradson, S. D., Ekberg, S. A., Keogh, D. W., Neu, M. P., Reilly, S. R., Runde, W. H., and Scott, B. L. (2004) *Actinide Research Quarterly,* Report LA-LP-04-60, Los Alamos National Laboratory, **1,** 20–2.
Takano, M., Itoh, A., Akabori, M., Ogawa, T., Numata, M., and Okamoto, H. (2001) *J. Nucl. Mater.,* **294**(1,2), 24–7.
Tan, J.-h. (2003) *Sichuan Shifan Daxue Xuebao, Ziran Kexueban,* **26**(3), 297–9.
Tananaev, I. G. (1989) *Radiokhimiya,* **31**(3), 46–51.
Tananaev, I. G., Rozov, S. P., and Mironov, V. S. (1992) *Radiokhimiya,* **34**(3), 88–92.

Tate, R. E. and Anderson, R. W. (1960) Some experiments in zone refining plutonium, *Extract. Phys. Met. Plutonium and Alloys, Symposium,* San Francisco, CA, Interscience, New York, pp. 231–42.

Tate, R. E. and Cramer, E. M. (1964) *Trans AIME,* **230**, 639.

Tate, R. E. and Edwards, G. R. (1966) *Diffusion*. Symposium on thermodynamics with emphasis on nuclear materials and atomic transport, Vienna, Austria, 2, 105 pp.

Taube, M. (1964) *Plutonium,* Macmillan Publishing, New York, 258 pp.

Taylor, J. M. (1966) *Physical Properties of Several Pu-base Intermetallic Compounds*, Report BNWLSA-385, Pacific Northwest Laboratory, Battelle Memorial Institute, Richland, WA, 7 pp.

Taylor, D. M. (1998) *J. Alloys Compd.,* **271–273**, 6–10.

Taylor, J. C., Loasby, R. G., Dean, D. J., and Linford, P. F. (1965) Elastic Constants, *Plutonium 1965, Proc. Third Int. Conf.,* London, England (eds. A. E. Kay and M. B. Waldron), Chapman and Hall, New York, 162 pp.

Taylor, J. C., Linford, P. F. T., and Dean, D. J. (1968) *J. Inst. Metals,* **96**(Part 6), 178–82.

Taylor, K. M., Andersen, J. C., Strasser, A., Stahl, D., and Forbes, R. L. (1967) *J. Am. Ceram. Soc.,* **50**(6), 321–5.

Taylor, R. J., Mason, C., Cooke, R., and Boxall, C. (2002) *J. Nucl. Sci. Technol.* (Suppl. 3), 278–81.

Terada, K., Meisel, R. L., and Dringman, M. R. (1969) *J. Nucl. Mater.,* **30**(3), 340–2.

Terminello, L. J., Caturla, M. J., Fluss, M. J., Gouder, T., Haire, R. G., Haschke, J. M., Hecker, S. S., Lander, G. H., Muller, I., Nitsche, H., Rebizant, J., Schwartz, A. J., Silva, R. J., Wall, M. A., Wastin, F., Weber, W. J., Wirth, B. D., and Wolfer, W. G. (2001) *Mater. Res. Soc. Bull.,* **26**(9), 667–71.

Teterin, Y. A. and Teterin, A. Y. (2004) *Russ. Chem. Rev.,* **73**(6), 541–80.

Tetzlaff, R. N. (1962) *Chemical Processing of 238Pu*, E. I. du Pont de Nemours & Co., Aiken, SC, Report DP-729, US Atomic Energy Commission, 30 pp.

Thiyagarajan, P., Diamond, H., Soderholm, L., Horwitz, E. P., Toth, L. M., and Felker, L. K. (1990) *Inorg. Chem.,* **29**(10), 1902–7.

Thomas, C. A. (1944) *The Chemistry, Purification and Metallurgy of Plutonium*, Report MUC-JCW-223 (Books 1 and 2) (Dec. 1944).

Thomas, W. (1969) *Critical and Safe Parameters for Plutonium and Plutonium Compounds*, Report MRR-56, Inst Mess- Regelungstech., Tech. Hochsch. Muenchen, Munich, Germany, 40 pp.

Thompson, M. A. (1965) Plutonium Oxidation, in *Plutonium 1965* (eds. A. E. Kay and R. G. Loasby), London, England, 592 pp.

Thompson, G. H. (1972) *Radiochem. Radioanal. Let.,* **10**(4), 223–30.

Thompson, S. G. and Seaborg, G. T. (1956) First use of bismuth phosphate for separating plutonium from uranium and fission products, *Progress in nuclear energy-Series 3*, *Process chemistry* (eds. F. R. Bruce, J. M. Fletcher, H. H. Hyman, and J. J. Katz), pp. 163–71.

Thuemmler, F., Theisen, R., and Patrussi, E. (1967) *Phase Relations, Production, and Characteristics of Substoichiometric Uranium and Plutonium oxide Fuels* (UO_{2-x} *and* (*Uranium, Plutonium Uranium*)O_{2-x}), Report KFK-543, Kernforschungszentrum, Karlsruhe, Germany, 44 pp.

Timofeeva, L. F. (2001) Phase Diagrams, in *Ageing Studies and Lifetime Extension of Materials* (ed. L. G. Mallinson), Kluwer Academic Publishers, New York, 191 pp.
Timofeeva, L. F. (2003a) *J. Metals*, (September 2003), 51–4.
Timofeeva, L. F. (2003b) *At.Energ.,* **95**(2), 540–5.
Toevs, J. W. (1997) *Surplus Weapons Plutonium: Technologies for Pit Disassembly/ Conversion and MOX Fuel Fabrication*, Report LA-UR-97-4113, Los Alamos National Laboratory, 8 pp.
Tolley, W. B. (1953) *Plutonium Trichloride: Preparation by Reaction with Phosgene or Carbon Tetrachloride, and Bomb Reduction to Metal*, Report HW-30121, General Electric Company, Richland, WA, 28 pp.
Toth, L. M., Friedman, H. A., and Osborne, M. M. (1981) *J. Inorg. Nucl. Chem.,* **43**(11), 2929–34.
Trevorrow, L. E. and Shinn, W. A. (1960) *in Chemical Engineering Division Summary Report for October, November, December 1959* (eds. Lawroski, S, Roedge, W. A., Vogel, R. C., Munnecke, V. H.), Report ANL-6101, Argonne National Laboratory, 80 pp.
Trevorrow, L., Shinn, W. A., and Steunenberg, R. K. (1961) *J. Phys. Chem.,* **65**(3), 398–403.
Trevorrow, L. E., Kessie, R. W., and Steindler, M. J. (1965) *Laboratory Investigations in Support of Fluid-bed Fluoride Volatility Process*, part VIII, *Analysis of an Accidental Multigram Release of Plutonium Hexafluoride in a Glovebox*, Report ANL-7068, Argonne National Laboratory, 20 pp.
Triay, I. R., Hobart, D. E., Mitchell, A. J., Newton, T. W., Ott, M. A., Palmer, P. D., Rundberg, R. S., and Thompson, J. L. (1991) *Radiochim. Acta,* **52–53**(Pt. 1), 127–31.
Trofimov, T. I., Samsonov, M. D., Kulyako, Y. M., and Myasoedov, B. F. (2004) *CR Chim,* **7**(12), 1209–13.
Tuli, J. K. (ed.) (2004) *Nuclear Data Sheets,* Academic Press, San Diego.
Turchi, E. A., Gonis, A., and Shull, R. D. (eds.) (2002) *CALPHAD and Alloy Thermodynamics,* TMS-Minerals, Metals & Materials Society, Warrendale, PA, 281 pp.
Turchi, P. E. A., Kaufman, L., Lui, Z.-K., and Zhou, S. (2004) *Thermodynamics and Kinetics of Phase Transformations in Plutonium Alloys* - part I, Report UCRL-TR-206658, Lawrence Livermore National Laboratory,
Ueno, K. and Hoshi, M. (1970) *J. Inorg. Nucl. Chem.,* **32**, 381.
Ugajin, M. and Abe, J. (1973) *J. Nucl. Mater.,* **47**(1), 117–20.
Ullman, W. J. and Schreiner, F. (1986) *Radiochim. Acta,* **40**(4), 179–83.
Ullman, W. J. and Schreiner, F. (1988) *Radiochim. Acta,* **43**(1), 37–44.
Usami, T., Kurata, M., Inoue, T., Sims, H. E., Beetham, S. A., and Jenkins, J. A. (2002) *J. Nucl. Mater.,* **300**(1), 15–26.
Vaidya, V. N., Kamat, R. V., Joshi, J. K., Iyer, V. S., Suryanarayana, S., Srinivasan, N. L., Pillai, K. T., and Sood, D. D. (1983) *Proc. Nucl. Chem. Radiochem. Symp.*, pp. 549–51.
Van der Sluys, W. G., Burns, C. J., Huffman, J. C., and Sattelberger, A. P. (1988) *J. Am. Chem. Soc.,* **110**(17), 5924–5.
Van der Sluys, W. G., Burns, C. J., and Sattelberger, A. P. (1989) *Organometallics,* **8**(3), 855–7.

Varlashkin, P. G., Begun, G. M., and Peterson, J. R. (1984) *Radiochim. Acta,* **35**(4), 211–18.

Vdovenko, V. M., Vodovatov, V. A., Mashirov, L. G., and Suglobov, D. N. (1973) *Dokl. Akad. Nauk SSSR,* **209**(2), 352–5.

Veirs, D. K., Smith, C. A., Berg, J. M., Zwick, B. D., Marsh, S. F., Allen, P., and Conradson, S. D. (1994) *J. Alloys Compd.,* **213–214**, 328–32.

Vesnovskii, S. P. and Polynov, V. N. (1992a) in *Transuranium Elements: A Half Century* (eds. L. R. Morss and J. Fuger), American Chemical Society, Washington, DC, 131–6.

Vesnovskii, S. P. and Polynov, V. N. (1992b) *Nucl. Instrum. Methods Phys. Res., Sect. B,* **b70**(1–4), 9–11.

Viklund, C., Nordstrom, A., Irgum, K., Svec, F., and Frechet, J. M. J. (2001) *Macromolecules,* **34**(13), 4361–9.

Vladimirova, M. V. (1982) *Sov. Radiochem.,* **24**(4), 393–401.

Vladimirova, M. V. (1990) *J. Radioanal. Nucl. Chem.,* **143**(2), 445–54.

Vladimirova, M. V. (1998) *Sov. Radiochem.,* **40**(5), 395–404.

Vladimirova, M. V. and Kulikov, I. A. (2002) *Radiochemistry (Moscow, Russian Federation) (Translation of Radiokhimiya),* **44**(1), 86–90.

Vogt, O. and Mattenberger, K. (1993) *Handbook on the Physics and Chemistry of Rare Earths,* vol. 17 (eds. K. A. J. Gschneidner, L. Eyring, G. R. Choppin, and G. H. Lander), Elsevier Science, New York, 301 pp.

Vogt, O. and Mattenberger, K. (1995) *J. Alloys Compd.,* **223**(2), 226–36.

Volkov, Y. F., Kapshukov, I. I., Visyashcheva, G. I., and Yakovlev, G. N. (1974a) *Radiokhimiya,* **16**(6), 863–7.

Volkov, Y. F., Kapshukov, I. I., Visyashcheva, G. I., and Yakovlev, G. N. (1974b) *Radiokhimiya,* **16**(6), 868–73.

Volkov, Y. F., Visyashcheva, G. I., Tomilin, S. V., Kapshukov, I. I., and Rykov, A. G. (1981) *Radiokhimiya,* **23**(2), 254–8.

Vyatkin, V. E., Davidov, Y. P., and Shashukov, E. A. (1972) *Radiokhimiya,* **14**(2), 289–93 (pp 299–303 in English translation).

Waber, J. T. (1958) *Plutonium Oxidation*, *Proc. Second UN Int. Conf. Peaceful Uses Atomic Energy*, Geneva, Switzerland, United Nations, 6, 204 pp.

Waber, J. T. (1980) Corrosion and Oxidation, in *Plutonium Handbook,* vol. 1 (ed. O. J. Wick), American Nuclear Society, La Grange, IL, pp. 145–89.

Waber, J. T., Olson, W. M., and Roof, R. B. (1961) *J. Nucl. Mater.,* **3**, 205.

Wachter, P. (2003) *Solid State Commun.,* **127**(9–10), 599–603.

Wachter, P., Marabelli, F., and Bucher, B. (1991) *Phys. Rev. B,* **43**(13-B), 11136–44.

Wachter, P., Filzmoser, M., and Rebizant, J. (2001) *Physica B,* **293**(3&4), 199–223.

Wade, W. Z. (1971) *J. Nucl. Mater.,* **38**, 292.

Wade, W. Z., Short, D. W., Walden, J. C., and Magana, J. W. (1978) *Metall. Trans. A,* **9A**, 965.

Wadt, W. R. (1987) *J. Chem. Phys.,* **86**(1), 339–46.

Wagner, R. P., Shinn, W. A., Fischer, J., and Steindler, M. J. (1965) *Laboratory Investigations in Support of Fluid-bed Fluoride Volatility Processes*, part VII, *The Decomposition of Gaseous Plutonium Hexafluoride by Alpha Radiation*, Report ANL-7013, Argonne National Laboratory, 32 pp.

Wahlgren, U., Moll, H., Grenthe, I., Schimmelpfennig, B., Maron, L., Vallet, V., and Gropen, O. (1999) *J. Phys. Chem. A,* **103**(41), 8257–64.

Waldek, A., Erdmann, N., Gruning, C., Huber, G., Kunz, P., Kratz, J. V., Lassen, J., Passler, G. and Trautmann, N. (2001) *RIMS Measurements for the Determination of the First Ionization Potential of the Actinides Actinium up to Einsteinium.* Melville, NY, American Institute of Physics, *AIP Conf. Proc.,* **584**, 219–24.

Waldron, M. B., Garstone, J., Lee, J. A., Mardon, P. G., Marples, J. A. C., Poole, O. M., and Williamson, G. K. (1958) *Proc. Second Int. Conf. Peaceful Uses of Atomic Energy*, vol. 6, Geneva, United Nations, 162 pp.

Wallace, P. L. and Harvey, M. R. (1974) *J. Nucl. Mater.,* **54**(2), 171–4.

Walter, K. H. (1965) *Ternary oxides of Tri- to Sexivalent Americium. Thesis*, Report KFK-280, Kernforschungszentrum, Karlsruhe, 76 pp.

Walters, R. T. and Briesmeister, R. A. (1984) *Spectrochim. Acta,* **40A**, 587.

Wang, R. and Steinfink, H. (1967) *Inorg. Chem.,* **6**(9), 1685–92.

Ward, J. W. (1985) *Physica B & C,* **130**(1–3), 510–15.

Ward, J. W. and Haschke, J. M. (1994) Comparison of 4f and 5f Element Hydride Properties, in *Handbook on the Physics and Chemistry of Rare Earths,* vol. 18 (eds. K. A. J. Gschneidner, E. L., G. R. Choppin, and G. H. Lander), Elsevier Science, New York, pp. 293–363.

Ward, J. W., Cort, B., Goldstone, J. A., Lawson, A. C., Cox, L. E., and Haire, R. G. (1992) in *Transuranium Elements: A Half Century* (eds. L. R. Morss and J. Fuger), American Chemical Society, Washington, DC, 404–15.

Warf, J. C. (1945) *The Extraction Purification of Cerium*, Report CC-2402.

Warner, B. P., D'Alessio, J. A., Morgan, A. N., III, Burns, C. J., Schake, A. R., and Watkin, J. G. (2000) *Inorg. Chim. Acta,* **309**(1–2), 45–8.

Wastin, F., Spirlet, J. C., and Rebizant, J. (1995) *J. Alloys Compd.,* **219**(1–2), 232–7.

Weber, E. T., Chikalla, T. D., and McNeilly, C. E. (1964) *The Plutonium–Boron System*, Report HW-81603, Article 2.9, US Atomic Energy Commission, 80 pp.

Weger, H. T., Okajima, S., Cunnane, J. C., and Reed, D. T. (1993) *Mater. Res. Soc. Symp. Proc.*, **294**(Scientific Basis Nucl. Waste Manag.), 739–45.

Wei, Y. Z., Arai, T., Hoshi, H., Kumagai, M., Bruggeman, A., Gysemans, M., and Sawa, T. (2002) *JAERI-Conf* **2002–004**(Proc. Int. Symp. NUCEF 2001), 225–36.

Weigel, F. (1965) *Preparation and Roentgenographic Study of Highly Radioactive Material*, Thesis, Report NP-15826, Munich University, 301 pp.

Weigel, F., Wishnevsky, V., and Hauske, H. (1977) *J. Less-Common Met.,* **56**(1), 113–23.

Weigel, F., Güldner, R., and Wishnevsky, V. (1982) *J. Less-Common Met.,* **84**(1), 147–55.

Weinstock, B. (1944) *Vapor Pressure of Plutonium Trichloride*, Report LA-122, Los Alamos Scientific Laboratory, 9 pp.

Weinstock, B. and Goodman, G. L. (1965) *Adv. Chem. Phys.,* **9**, 169–316.

Weinstock, B. and Malm, J. G. (1956a) *J. Inorg. Nucl. Chem.,* **2**(5–6), 380–94.

Weinstock, B. and Malm, J. G. (1956b) *Proc. First Int. Conf. on the Peaceful Uses of Atomic Energy*, vol. 2, New York, pp. 380–94.

Weinstock, B., Weaver, E. E., and Malm, J. G. (1959) *J. Inorg. Nucl. Chem.,* **11**(2), 104–14.

Weiss, R. J. (1963) *Proc. Phys. Soc.,* **62**, 28.

Wells, A. F. (1984) *Structural Inorganic Chemistry,* Oxford University Press, Oxford, England, 1382 pp.
Wensch, G. W. and Whyte, D. D. (1951) *The Nickel Plutonium System*, Report LA-1304, Los Alamos Scientific Laboratory, 29 pp.
Werner, G. D. (1982) *Doctoral Dissertation*, Report, University of Munich.
West, M. H., Ferran, M. D., and Fife, K. W. (1988) *The Chlorination of Plutonium Dioxide*, Report LA-11256, Los Alamos National Laboratory, Los Alamos, NM, 13 pp.
Wester, D. W. (1983) *ACS Symp. Ser.,* **216**(Plutonium Chem.), (eds. W. T. Carnall and G. R. Choppin) American Chemical Society, Washington, DC 49–63.
Wester, D. W. and Sullivan, J. C. (1983) *Radiochem. Radioanal. Lett.,* **57**, 35.
Westrum, E. F., Jr (1949a) Preparation and Properties of Plutonium Oxides, in *Natl. Nucl. Energy Ser.*, Div IV **14**B (Transuranium Elements Pt. II) (eds. G. T. Seaborg, J. J. Katz, and W. M. Manning), McGraw-Hill, New York, pp. 936–44.
Westrum, E. F., Jr (1949b) Preparation and Properties of Plutonium Silicides, in *Natl. Nucl. Energy Ser.*, Div IV **14**B (Transuranium Elements Pt. I) (eds. G. T. Seaborg, J. J. Katz, and W. M. Manning), McGraw-Hill, New York, pp. 729–30.
Westrum, E. F., Jr (1949c) Heat of Formation of Plutonium Tribromide, in *Natl. Nucl. Energy Ser.*, Div IV **14**B (Transuranium Elements Pt. II) (eds. G. T. Seaborg, J. J. Katz and W. M. Manning), McGraw-Hill, New York, pp. 926–9.
Westrum, E. F., Jr and Robinson, H. P. (1949a) Heat of Formation of Plutonium Trichloride, in *Natl. Nucl. Energy Ser.*, Div IV **14**B (Transuranium Elements Pt. II) (eds. G. T. Seaborg, J. J. Katz, and W. M. Manning), McGraw-Hill, New York, pp. 914–21.
Westrum, E. F., Jr and Robinson, H. P. (1949b) Heat of Formation of Plutonium Oxychloride, in *Natl. Nucl. Energy Ser.*, Div IV **14**B (Transuranium Elements Pt. II) (eds. G. T. Seaborg, J. J. Katz, and W. M. Manning), McGraw-Hill, New York, pp. 930–5.
Westrum, E. F., Jr and Wallmann, J. C. (1951) *J. Am. Chem. Soc.,* **73**, 3530–1.
Wick, O. J. (ed.) (1980) *Plutonium Handbook: A Guide to the Technology,* American Nuclear Society, La Grange Park, IL, 992 pp.
Wigley, D. A. (1964) PhD thesis, Oxford University, Oxford, UK.
Wigley, D. A. (1965) *Proc. Roy. Soc. Lond. Ser. A,* **284**(1398), 344–53.
Wilkinson, W. D. (ed.) (1960) *Extractive and Physical Metallurgy of Plutonium and its Alloys,* Interscience Publishers, New York.
Williams, C. W., Blaudeau, J. P., Sullivan, J. C., Antonio, M. R., Bursten, B., and Soderholm, L. (2001) *J. Am. Chem. Soc.,* **123**(18), 4346–7.
Willis, J. O., Ward, J. W., Smith, J. L., Kosiewicz, S. T., Haschke, J. M., and Hodges, A. E., III (1985) *Physica B & C,* **130**(1–3), 527–9.
Wills, J. M. and Eriksson, O. (2000) *Los Alamos Sci.,* **26**(1), 128.
Winchester, R. S. and Maraman, W. J. (1958) *Proc. Second UN Int. Conf. Peaceful Uses Atomic Energy*, vol. 17,Geneva, pp. 168–71.
Wirth, B. D., Schwartz, A. J., Fluss, M. J., Cartula, M. J., Wall, M. A., and Wolfer, W. G. (2001) *Mat. Res. Soc. Bull.,* **26**(9), 679–84.
Wiswall, R. J., Jr, Egan, J. J., Ginell, W. S., Miles, F. T., and Powell, J. R. (1959) *Recent Advances in the Chemistry of Liquid Metal Fuel Reactors*, *Proc. Second Int. Conf. Peaceful Uses of Atomic Energy*, 1958, Geneva, Switzerland, 17, pp. 421–7.

Wittenberg, L. J. (1963) *Symp. on Research at Mound Laboratory,* June 6–7, 1963, Report MLM-1163, Mound Laboratory, 157 pp.

Wittenberg, L. J. (1975) A Model for Liquid Uranium and Plutonium with Implications on the Adjacent Solid Phases, in *Plutonium and Other Actinides,* Baden-Baden, Germany (eds. H. Blank and R. Lindner), North-Holland, New York, pp. 71–83.

Wittenberg, L. J. and Grove, G. R. (1963) *Reactor Fuels and Materials Development. Plutonium Research*, Report MLM-1184, Mound Laboratory, pp. 12–16.

Wittenberg, L. J. and Grove, G. R. (1964) *Reactor Fuels and Materials Development. Plutonium Research*, Report MLM-1244, Mound Laboratory, 56 pp.

Wittenberg, L. J., Jones, L.V., and Ofte, D. (1960) *The Viscosity of a Liquid Pu-Fe Eutectic Alloy, Proc. Second Int. Conf. Plutonium,* Grenoble, France (eds. E. Grison, W. B. H. Lord, and R. D. Fowler), Cleaver-Hume Press, London, 1, pp. 671–83.

Wittenberg, L. J., Ofte, D., and Curtiss, C. F. (1968) *J. Chem. Phys.,* **48**(7), 3253–60.

Wittenberg, L. J., Vaughn, G. A., and DeWitt, R. (1970) *Phase Relationships in Uranium, Neptunium and Plutonium, Proc. Fourth Int. Conf. on Plutonium and Other Actinides,* Santa Fe, NM (ed. W. N. Miner), The Metallurgical Society of the AIME, II, 659–68.

Wolfer, W. G. (2000) *Los Alamos Sci.,* **26**(2), 274–85.

Wong, J., Holt, M., Hong, H., Schwartz, A. J., Zschack, P., Chiang, T. C., and Wall, M. (2003a) *AIP Conf. Proc.,* **673**(Plutonium Futures – The Science), 221–3.

Wong, J., Krisch, M., Farber, D. L., Occelli, F., Schwartz, A. J., Chiang, T. C., Wall, M., Boro, C., and Xu, R. Q. (2003b) *Science,* **301**(5636), 1078–80.

Wood, D. H., Cramer, E. M., Wallace, P. L., and Ramsey, W. J. (1969) *J. Nucl. Mater.,* **32**(2), 193–207.

Worden, E. F., Carlson, L. R., Johnson, S. A., Paisner, J. A., and Solarz, R. W. (1993) *J. Opt. Soc. Am.,* **B10**(11), 1998–2005.

Wriedt, H. A. (1989) *Bull. Alloy Phase Diagr.,* **10**(5), 593–602, 615–16.

Wriedt, H. A. (1990) *Bull. Alloy Phase Diagr.,* **11**(2), 184–202.

Wroblewska, J., Dobrowolski, J., Pages, M., and Freundlich, W. (1979) *Radiochem. Radioanal. Lett.,* **39**(3), 241–6.

Wruck, D. A., Russo, R. E., and Silva, R. J. (1994) *J. Alloys Compd.,* **213–214**, 481–3.

Wyckoff, R. W. G. (1963) *Crystal Structures,* Interscience, New York, 289 pp.

Wymer, R. G. (1968) *Sol-gel Processes for Ceramic Nuclear Fuels*, *Proc. Panel on Sol-gel Processes for Ceramic Nuclear Fuels*, Report STI/PUB–207;CONF-680532, International Atomic Energy Agency, pp. 131–72.

Wymer, R. G. and Coobs, J. H. (1967) *P. Brit. Ceramic Soc.,* **7**, 61–79.

Wynne, K. J. and Rice, R. W. (1984) *Annu. Rev. Mater. Sci.,* **14**, 297–334.

Yamaguchi, T., Sakamoto, Y., and Ohnuki, T. (1994) *Radiochim. Acta,* **66/67**, 9–14.

Yamashita, T., Ohuchi, K., Takahashi, K., and Fujino, T. (1992) Formation of Lithium Plutonates by the Reaction of Lithium Nitrate and Lithium Hydroxide with Plutonium dioxide, in *Transuranium Elements, A Half Century* (eds. L. R. Morss and J. Fuger), American Chemical Society, Washington, DC, pp. 451–6.

Yarbro, S. L., Schreiber, S. B., Ortiz, E. M., and Ames, R. L. (1998) *J. Radioanal. Nucl. Chem.,* **235**(1–2), 21–4.

Zachariasen, W. H. (1944) *X-ray Diffraction Results for Uranium and Plutonium Compounds*, Report CK-1367, Report USAEC Manhattan Project, Metallurgical Laboratory.
Zachariasen, W. H. (1948a) *Acta Crystallogr.,* **1**, 265–8.
Zachariasen, W. H. (1948b) *J. Am. Chem. Soc.,* **70**, 2147–51.
Zachariasen, W. H. (1948c) *Acta Crystallogr.,* **1**, 268–9.
Zachariasen, W. H. (1949a) in *Natl. Nucl. Energy Ser., Div. IV,* **14B**(Transuranium Elements Pt. II), (eds. G. T. Seaborg, J. J. Katz, and W. M. Manning), McGraw-Hill, New York, 1451–3.
Zachariasen, W. H. (1949b) *Acta Crystallogr.,* **2**, 94–9.
Zachariasen, W. H. (1949c) in *Natl. Nucl. Energy Ser., Div. IV,* **14B**(Transuranium Elements Pt. II), (eds. G. T. Seaborg, J. J. Katz, and W. M. Manning), 1448–50.
Zachariasen, W. H. (1949d) *Acta Crystallogr.,* **2**, 388–90.
Zachariasen, W. H. (1951) *Acta Crystallogr.,* **4**, 231–6.
Zachariasen, W. H. (1952) *Acta Crystallogr.,* **5**, 17–19.
Zachariasen, W. H. (1954a) *Acta Crystallogr.,* **7**, 795–9.
Zachariasen, W. H. (1954b) Crystal Chemistry of the 5f Elements, in *The actinide elements* (eds. G. T. Seaborg and J. J. Katz), McGraw-Hill, New York, pp. 769–96.
Zacharaisen, W. H. (1961a) Crystal-structure Studies of Plutonium Metal, in *The Metal Plutonium* (eds. A. S. Coffinberry and W. N. Miner), University of Chicago Press, Chicago, IL, pp. 99–107.
Zachariasen, W. H. (1961b) Crystal-structure Studies of Plutonium Metal, in *The Metal Plutonium* (eds. A. S. Coffinberry and W. N. Miner), University of Chicago Press, Chicago, IL, pp. 104–7.
Zachariasen, W. H. (1973) *J. Inorg. Nucl. Chem.,* **35**(10), 3487–97.
Zachariasen, W. H. and Ellinger, F. H. (1955) *Acta Crystallogr.,* **8**(7), 431–3.
Zachariasen, W. H. and Ellinger, F. H. (1957) *J. Chem. Phys.,* **27**(3), 811–12.
Zachariasen, W. H. and Ellinger, F. H. (1959) *Acta Crystallogr.,* **12**, 175–6.
Zachariasen, W. H. and Ellinger, F. H. (1963a) *Acta Crystallogr.,* **16**(8), 777–84.
Zachariasen, W. H. and Ellinger, F. H. (1963b) *Acta Crystallogr.,* **16**(5), 369–75.
Zachariasen, W. H. and Ellinger, F. H. (1970) *Unit Cell of the Zeta Phase of the Plutonium Zirconium and the Plutonium Hafnium Systems*, Report LA-4367, Los Alamos Scientific Laboratory, 4 pp.
Zagrai, V. D. and Sel'chenkov, L. I. (1962) *Radiokhimiya,* **4**, 181–4.
Zaitseva, V. P., Alekseeva, D. P., and Gel'man, A. D. (1973) *Radiokhimiya,* **15**(3), 385–90.
Zakharova, F. A., Orlova, M. M., and Gel'man, A. D. (1972) *Sov. Radiochem.,* **14**(1), 121–22.
Zalkin, A. and Raymond, K. N. (1969) *J. Am. Chem. Soc.,* **91**(20), 5667–8.
Zhou, J. S. and Goodenough, J. B. (2005) *Phys. Rev. Lett.,* **94**(6), 065501/1–065501/4.
Zocco, T. G. and Schwartz, A. J. (2003) *JOM,* **55**(9), 24–7.
Zocco, T. G., Stevens, M. F., Adler, P. H., Sheldon, R. I., and Olson, G. B. (1990) *Acta Met. Mater.,* **38**(11), 2275–82.
Zocco, T. T. and Rohr, D. L. (1988) *Mater. Res. Soc. Symp. Proc.*, **115** (Specimen Prep. Transm. Electron Mircosc. Mater.), 259–64.

Zubarev, V. G. and Krot, N. N. (1984) *Radiokhimiya,* **26**(2), 176–80.
Zukas, E. G., Hecker, S. S., Morgan, J. R., and Pereyra, R. A. (1981) *Pressure-induced Transformation in a Pu-2.0 at.% Al Alloy*, *Proc. Int. Conf. Solid-Solid Phase Transform*., Pittsburgh, AIME, 1, 1333–7.
Zukas, E. G., Hecker, S. S., and Pereyra, R. A. (1983) *J. Nucl. Mater.,* **115**(1), 63–8.
Zunger, A., Wei, S. H., Ferreira, L. G., and Bernard, J. E. (1990) *Phys. Rev. Lett.,* **65**(3), 353–6.
Zwick, B. D., Sattelberger, A. P., and Avens, L. R. (1992) in *Transuranium Elements: A Half Century* (eds. L. R. Morss and J. Fuger), American Chemical Society, Washington, DC, 239–46.

CHAPTER EIGHT

AMERICIUM

Wolfgang H. Runde and Wallace W. Schulz

8.1 HISTORICAL

Americium, element 95, was discovered in 1944–45 by Seaborg *et al.* (1950) at the Metallurgical Laboratory of the University of Chicago as a product of the irradiation of plutonium with neutrons:

$$^{239}\mathrm{Pu}(\mathrm{n},\gamma)^{240}\mathrm{Pu}(\mathrm{n},\gamma)^{241}\mathrm{Pu} \xrightarrow{-\beta^-} {}^{241}\mathrm{Am}$$

This reaction is still the best method for the production of pure ^{241}Am. In post-World War II work at the University of Chicago, Cunningham isolated $Am(OH)_3$ and measured the first absorption spectrum of the Am^{3+} aquo ion (Cunningham, 1948). By the 1950s, the major center for americium chemistry research in the world was at Los Alamos. Since the 1970s, the majority of publications on americium have come from researchers in the former USSR and West Germany. Extensive reviews of americium chemistry can be found in Freeman and Keller (1985), Gmelin (1979), Penneman and Asprey (1955), and Schulz (1976).

8.2 NUCLEAR PROPERTIES OF ISOTOPES

To date, 13 americium isotopes with mass numbers 232–247 and half-lives ranging from 55 s to 7370 years are known (Table 8.1). While the isotopes with mass numbers 232, 234, and 237–247 have been known for some time, the neutron-deficient isotopes Am-233, Am-235, and Am-236 have only recently

Table 8.1 *Nuclear properties of americium isotopes.*

Mass number	*Half-life*	*Mode of decay*	*Main radiations* (MeV)	*Method of production*
232	1.4 min	SF isomer		^{230}Th(^{10}B, 8n)
233	3.2 min	α	α 0.00678	^{238}U(^{6}Li, 6n)
234	2.6 min	EC		^{230}Th(^{10}B, 6n)
235	15 min	EC		^{238}Pu(^{1}H, 4n)
236	4.4 min[a]	EC		^{235}U(^{6}Li, 5n)
	3.7 min[b]	EC		^{237}Np(^{6}He, 4n)
237	1.22 h	EC > 99%	α 6.042	^{237}Np(α, 4n)
		α 0.025%	γ 0.280 (47%)	^{237}Np(^{3}He, 3n)
238	1.63 h	EC > 99%	α 5.94	^{237}Np(α, 3n)
		α 1.0×10^{-4}%	γ 0.963 (29%)	
239	11.9 h	EC > 99%	α 5.776 (84%)	^{237}Np(α, 2n)
			5.734 (13.8%)	
		α 0.010%	γ 0.278 (15%)	^{239}Pu(d, 2n)
240	50.8 h	EC > 99%	α 5.378 (87%)	^{237}Np(α, n)
		α 1.9×10^{-4}%	5.337 (12%)	^{239}Pu(d, n)
			γ 0.988 (73%)	
241	432.7 yr	α	α 5.486 (84%)	^{241}Pu daughter
	1.15×10^{14} yr	SF	5.443 (13.1%)	multiple n capture
			γ 0.059 (35.7%)	
242	16.01 h	β^- 82.7%	β^- 0.667	^{241}Am(n, γ)
		EC 17.3%	γ 0.042 weak	
242 m	141 yr	IT 99.5%	α 5.207 (89%)	^{241}Am(n, γ)
	9.5×10^{11} yr	SF α (0.45%)	5.141 (6.0%)	^{241}Am(n, γ)
			γ 0.0493 (41%)	
243	7.38×10^{3} yr	α	α 5.277 (88%)	multiple
	2.0×10^{14} yr	SF	5.234 (10.6%)	n capture
			γ 0.075 (68%)	
244	10.1 h	β^-	β^- 0.387	^{243}Am(n, γ)
			γ 0.746 (67%)	
244 m	26 min	β^- > 99%	β^- 1.50	^{243}Am(n, γ)
		EC 0.041%		
245	2.05 h	β^-	β^- 0.895	^{245}Pu daughter
			γ 0.253 (6.1%)	
246[c]	25.0 min	β^-	β^- 2.38	^{246}Pu daughter
		γ	0.799 (25%)	
246[c]	39 min	β^-	γ 0.679 (52%)	^{244}Pu(α, d)
				^{244}Pu(^{3}He, p)
247	24 min	β^-	γ 0.285 (23%)	^{244}Pu(α, p)

SF, spontaneous fission; EC, electron capture; IT, isomeric transition.
[a] Hall (1989).
[b] Tsukada *et al.* (1998).
[c] Not known whether ground-state nuclide or isomer.

been produced and characterized (Hall, 1989; Tsukada *et al.*, 1998; Weifan *et al.*, 1999; Sakama *et al.*, 2000). The light isotopes up to ^{243}Am mainly decay by electron capture, emission of alpha particles, and spontaneous fission; the isotopes beyond ^{243}Am are short-lived β^--emitters. Data in Table 8.1 are taken primarily from the comprehensive compilation in Gmelin (1973) and others (Hyde *et al.*, 1971; Wapstra and Gove, 1971; Skobelev, 1972; Natowitz, 1973; Schulz, 1976; Lederer and Shirley, 1978; Kuznetsov and Skobelev, 1966). Although not noted in Table 8.1, literature references (e.g. Schulz, 1976) indicate that some of the identified americium isotopes exist in more than one isomeric energy state.

8.3 PRODUCTION OF PRINCIPAL ISOTOPES

The most important isotopes of americium are ^{241}Am and ^{243}Am due to their long half-lives of 433 and 7380 years, respectively. These isotopes have been made in kilogram quantities with high purity. ^{242}Am ($t_{1/2}$ = 141 years) can be produced to the extent of only a few percent in ^{241}Am by neutron capture.

Americium-241 is superior to all competing radionuclides as a low-energy gamma source because of its cost, convenience, spectral purity, and half-life (Crandall, 1971) and its application as a low-energy gamma source may well be the largest of any actinide nuclide (Seaborg, 1970; LeVert and Helminski, 1973). The major use for ^{241}Am is in smoke-detector alarms and in neutron sources to furnish alpha particles for the (α,n) reaction on beryllium. As a source of nearly monoenergetic alpha (5.44 and 5.49 MeV) and gamma (59.6 keV) radiation, ^{241}Am is also widely used in thickness gauging and density and radiographic measurements, and is utilized to produce ^{242}Cm (up to 0.65 g ^{242}Cm per gram of ^{241}Am (Hennelly, 1972)) by thermal neutron capture. The thermal neutron capture sequence involved in producing ^{242}Cm from ^{241}Am is:

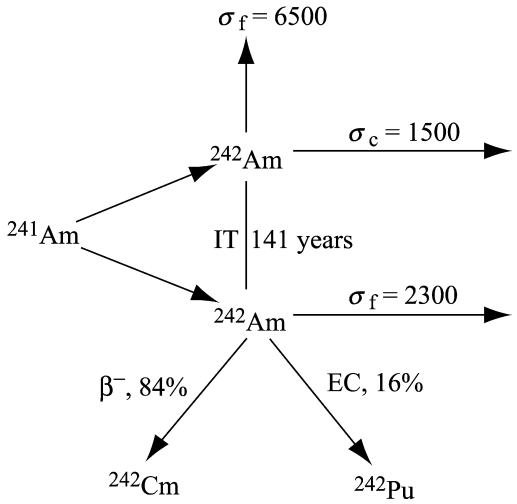

The lower specific activity of ^{243}Am compared to ^{241}Am makes it particularly useful in chemical studies. It is also used in the production of ^{244}Cm, ^{249}Bk/Cf, ^{252}Cf, and other transcurium elements in high neutron-flux reactors.

8.3.1 Production of ^{241}Am by irradiation of ^{239}Pu

Neutron irradiation of ^{239}Pu yields ^{241}Pu, which decays by beta emission with a half-life of 14.4 ± 0.3 years to ^{241}Am. In 1977, more than 1.5 kg of ^{241}Am was isolated from reprocessing aged plutonium at the US Department of Energy (DOE) Rocky Flats site. In 1980, a similar amount was isolated at the DOE Los Alamos site.

8.3.2 Production of ^{243}Am by irradiation of ^{242}Pu

Nearly isotopically pure ^{243}Am results from irradiation of ^{242}Pu with thermal neutrons:

$$^{242}\mathrm{Pu}(\mathrm{n},\gamma)^{243}\mathrm{Pu} \xrightarrow[5\mathrm{h}]{\beta^-} {}^{243}\mathrm{Am}$$

8.3.3 Availability of ^{241}Am and ^{243}Am from power reactor fuel

Commercial nuclear power reactors produce kilogram quantities of both ^{241}Am and ^{243}Am with an isotopic composition dependent on reactor burn-up. The US DOE Savannah River site reactors produced about 9 kg of a ^{243}Am–^{244}Cm mixture over a period of 10 years (Baybarz, 1970). About 1 kg of mixed ^{241}Am and ^{243}Am was recovered at the US DOE Hanford site during reprocessing of the Shippingport reactor blanket fuel (Wheelwright *et al.*, 1968). Approximately 30 kg of americium is reported to remain in the US DOE Hanford site waste tanks (Agnew *et al.*, 1997). But, no industrial reprocessor of commercial nuclear reactor fuel anywhere in the world has opted to pursue systematic recovery of americium. However, a potentially large source of americium is the high-level Purex-process liquid waste from plutonium processing; indeed, future waste storage may require separation of americium.

8.3.4 Critical mass

The calculated minimum critical mass of ^{242}Am in aqueous solution is 23 g at a concentration of 5 g L^{-1} (Bierman and Clayton, 1969). Note that mass separation of ^{242}Am from ^{241}Am is required to obtain pure ^{242}Am.

8.4 SEPARATION AND PURIFICATION OF PRINCIPAL ISOTOPES

Most of the standard methods, aqueous and non-aqueous, for separating and purifying americium from all kinds of sources and materials were developed in the 1950s, 1960s, and 1970s; progress made in this time frame was summarized

in the second edition of this work. In contrast to the earlier time period, in the 1980s and 1990s research efforts to develop new or improved technology for recovery and/or purification of americium were largely confined to development and testing of new and improved solvent extraction processes. Worldwide, aside from purely academic investigations mainly in Russia and India, scientists and engineers were motivated by one of two main goals:

(1) In the USA, principally, to find new or modified practicable ways of removing minor amounts of neptunium, plutonium, and americium from various stored defense wastes to convert such wastes from so-called TRU (transuranium) wastes to non-TRU wastes, thus requiring less expensive final disposal procedures and facilities.
(2) To develop and demonstrate practicable technology for removal (partitioning) of long-lived actinides as well as certain long-lived and mobile fission products, e.g. ^{99}Tc, ^{129}I from the high-level aqueous waste (HLW) generated in reprocessing of irradiated commercial nuclear power reactor fuel. Partitioning of these species from the HLW, it is believed, would greatly facilitate and simplify the many current technical and legal obstacles to final geologic disposal of the HLW. Recovered, purified, and concentrated actinides and fission products can, it is further believed, be converted (transmuted) to stable or short-lived radioisotopes by suitable neutron irradiation. Because irradiated commercial nuclear reactor fuel is being reprocessed in Japan, France, and China, investigators in these countries have been active in pursuing partitioning technology options. Several references (ANS, 1993; Prunier *et al.*, 1997; Cohen, 2000; NN, 2002) provide much additional detail concerning the incentives for and status of the development of partitioning and transmutation technology. Particular attention is called to an excellent summary article on actinide partitioning technology (Mathur *et al.*, 2001).

Americium separation technology is presented and discussed here in the same order used in the second edition of this monograph. Significant separation technology developments that have occurred since the second edition was published are incorporated and discussed at appropriate places in the text. (The knowledgeable reader will appreciate that when this text was prepared (early 2002) all the americium separations technologies described in the subsequent parts of Section 8.4 was essentially only of academic and/or historic interest. The present authors are not aware of any current significant effort in any country to actually separate and/or purify americium isotopes from any source.)

8.4.1 Pyrochemical processes

A two-stage, countercurrent molten-salt extraction process was used to extract ^{241}Am from many kilograms of aged plutonium, in which ^{241}Am had grown-in by beta decay of ^{241}Pu. The purification scheme removed about 90% of the

americium from plutonium metal, typically containing 200–2000 ppm ^{241}Am (Schulz, 1976).

Mullins and Leary (1969) patented a method of separating americium from plutonium that involves bubbling a mixture of oxygen and argon gas into a molten salt containing both elements. Plutonium precipitates as PuO_2, whereas americium remains in solution.

Ferris *et al.* (1972) determined the equilibrium distribution of americium (and other transuranium elements) between liquid bismuth and molten LiCl, LiBr, and several LiF–BeF_2–ThF_4 solutions at temperatures of 600–750°C. Some of the americium appeared to be in the divalent state in the Am/$PuCl_3$ system (Mullins and Leary, 1969). The distribution coefficient, $D =$ (g Am per g metal phase)/(g Am per g salt phase), of americium between molten aluminum metal and molten $AlCl_3$–KCl is 1.96 (Moore and Lyon, 1959). Mills and Reese (1994) demonstrated that ^{241}Am in aged PuF_4 can be cleanly separated from plutonium by low-temperature reaction with O_2F to generate volatile PuF_6. Americium remains in the fluorination residue from which it can be recovered and concentrated by any of the several aqueous methods.

As part of their comprehensive experimental and theoretical studies of the partitioning of actinides from high-level radioactive fuel reprocessing aqueous waste, Japanese scientists, in collaboration with some US investigators, have been developing a pyrometallurgical partition process (Sakamura *et al.*, 1998). The process consists of four main steps: (1) denitration of the HLW; (2) chlorination to convert oxides to chlorides; (3) reductive extraction to reduce actinides in a molten salt by lithium metal and to extract them into liquid cadmium; and (4) electrorefining in LiCl–KCl eutectic to separate actinides from the liquid cadmium anode. Preliminary experimental tests of the entire process show that uranium, plutonium, and neptunium are relatively easily separated from fission product rare earths but that americium is accompanied by some rare earth elements. In related theoretical studies of actinide partitioning technology, Yamana and Moriyama (1996) concluded that it may be feasible to separate americium and curium from lanthanide elements by electrolytic amalgamation techniques.

8.4.2 Precipitation processes

Initially, only precipitation processes were available for recovery and purification of americium. Later, new ion-exchange and solvent extraction processes largely, but not completely, supplanted the early precipitation recovery/purification processes. Because of their insolubility and other special properties precipitation of certain compounds of americium, e.g. AmF_3, $K_8Am_2(SO_4)_7$, $Am_2(C_2O_4)_3$, $K_3AmO_2(CO_3)_3$, is routinely considered for recovery or purification of a batch of americium. The latter two compounds are useful because oxalate ion prevents certain impurities from accompanying americium in the

precipitate and, also, because americium oxalate is a convenient starting point for preparation of AmO_2. The insoluble Am(V) carbonate complex is particularly useful for the large-scale separation of americium from curium (Buijs *et al.*, 1973; King *et al.*, 1973).

Hermann (1956) demonstrated that a substantial separation of americium from lanthanum can be obtained by fractional precipitation of americium and lanthanum oxalates. The precipitation is effected in homogeneous solution; the precipitant is generated by slow hydrolysis of dimethyl oxalate. The oxalate precipitate is greatly enriched in americium; about 50% of the lanthanum can be rejected at each stage with only about 4% of the americium.

Stephanou and Penneman (1952) found that Cm(III) could be separated from americium by oxidizing the latter to Am(VI) with potassium persulfate and precipitating CmF_3; Am(VI) is soluble under these conditions. Proctor and Connor (1970) at the US DOE Rocky Flats site used precipitation of cerium peroxide to separate gram quantities of americium from cerium. Proctor (1976) also separated Am(VI) from large quantities of rare earths by precipitation of their trifluorides.

Bhanushali *et al.* (1999) have recently proposed a new application of oxalate precipitation technology for separation of americium. Based on some experimental data, these workers suggest that traces of americium and plutonium remaining in the aqueous waste generated during plant-scale precipitation of plutonium oxalate can be effectively removed by simple coprecipitation with thorium oxalate. It is not known if such a coprecipitation step has been incorporated into routine processing of plutonium in India.

8.4.3 Solvent extraction processes

Solvent extraction processes and systems using amine and organophosphorus compounds are extensively used for the initial recovery and separation of gram to kilogram amounts of americium. Excellent reviews of the solvent extraction chemistry of trivalent americium have been published by Weaver (1974) and Shoun and McDowell (1980). Myasoedov *et al.* (1974a) discussed solvent extraction systems useful for the analysis of americium.

(a) Organophosphorus extractants (Gureev *et al.*, 1970)

(*i*) *Tri*-n-*butyl phosphate* (*TBP*)

TBP is the extractant in widest use for nuclear fuel processing. Extraction of Am^{3+} from nitrate media by TBP conforms to the reaction (Weaver, 1974):

$$Am^{3+}(aq) + 3\,NO_3^-(aq) + 3\,TBP(org) \rightarrow Am(NO_3)_3 + 3\,TBP(org)$$

The equilibrium constant, $K_{ex} = [Am(NO_3)_3 \cdot 3TBP]/[Am^{3+}][NO_3^+]^3[TBP]^3$, has the value of 0.4 at zero ionic strength (Zemlyanukhin *et al.*, 1962). While

TBP, even undiluted, extracts americium only weakly from strong nitric acid solutions, americium is extracted by TBP quite strongly from neutral (or low-acid), highly salted nitrate solutions.

As part of their intensive effort to develop feasible partitioning–transmutation technologies, Kamashida and his coworkers investigated TBP extraction of Am(VI) from nuclear reactor fuel reprocessing solutions (Kamashida and Fukasawa, 1996; Kamashida *et al.*, 1998) as a means of removal of americium while separating it from associated trivalent rare earths (good separation of americium from rare earth elements is desirable/necessary to make efficient use of neutrons in the transmutation process). In these studies, Am(VI) was produced by oxidation of Am(III) with silver-catalyzed peroxydisulfate, both in the presence and absence of $(NH_4)_{10}P_2W_{17}O_{61}$ added to stabilize americium in the hexavalent oxidation state. By use of neat TBP to extract Am(VI) from 1 M HNO_3, an americium distribution ratio as high as 4 was realized; the separation factor from Nd(III) was 50.

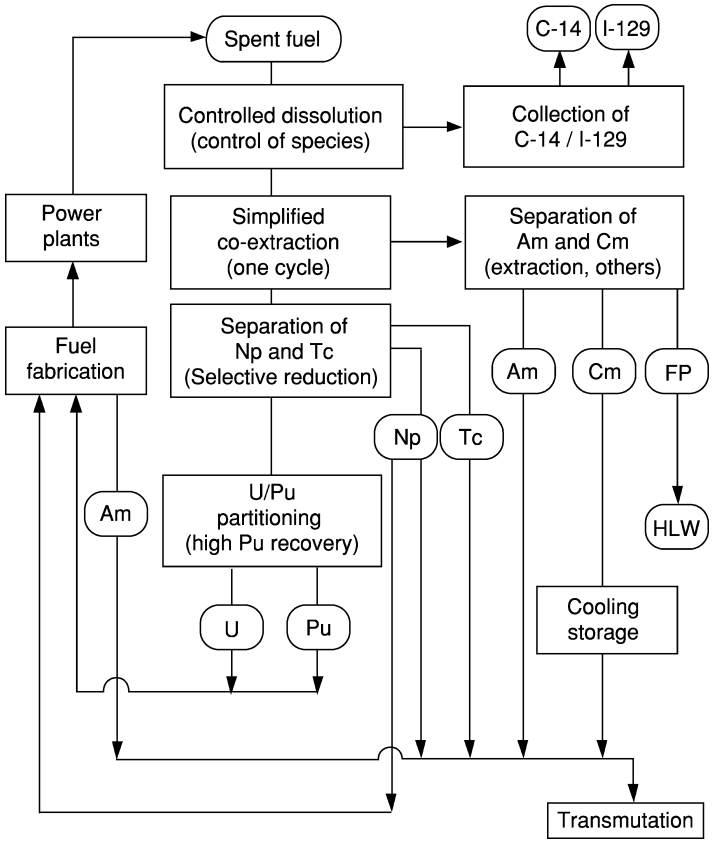

Fig. 8.1 *Schematic of Japanese PARC process* (*Uchiyama* et al., 2000).

In other recent studies, Japanese scientists have developed an advanced Purex process, the PARtitioning Conundrum Key (PARC) process (Uchiyama *et al.*, 2000). Fig. 8.1 shows a schematic diagram of the PARC process concept where americium is not separated in the mainline Purex process, but from HLW generated in the Purex process. The PARC process thus provides for use of certain organic compounds to provide effective Purex process recovery and separation of uranium, neptunium, plutonium, and technetium. Uchiyama *et al.* (2000) conducted tests of parts of the PARC process with aqueous feeds resulting from nitric acid dissolution of highly irradiated (8000 MWD/tU) fuel. Important findings were:

- Np(VI) was reduced to Np(V) by *n*-butyraldehyde selectively in the presence of U(VI), Pu(VI), and Tc(VII);
- high acid scrubbing was effective for separation of technetium;
- isobutyraldehyde reduced Pu(IV) to Pu(III) very effectively;
- *N*-butylamine compounds (carbonate and oxalate) were effective solvent-washing agents.

The French, as stated earlier, are energetically pursuing the partitioning–transmutation alternative for their Purex process HLW. Apparently for proprietary reasons, they have not widely publicized their progress. However, a recent article (NN, 2002) states: "... the Marcoule team have been able to push the current Purex processing technique to enable about 99% of uranium, plutonium, and the minor actinides of most concern, which are neptunium, americium, and curium to be isolated. The separation levels of the main long-lived fission products, which include iodine-129, technetium-99, and cesium-135, are equally impressive. The yields of iodine and technetium extracted are 95 and 90%, respectively. The process for separating cesium is nearing fruition, and technical feasibility is also expected by 2005. These levels of separation provide important benefits as the resulting vitrified waste contains fewer long-lived isotopes. According to the CEA, the radioisotopes of the advanced vitrified product – referred to as 'light glass' – will drop to the level of natural uranium in less than 300 years. This compares to more than 10000 years for the current vitrified HLW and hundreds of thousands for spent fuel." The article in *Nuclear News* does not provide any detail as to the Purex process modifications used to separate americium; it may be, just as in the Japanese PARC process, that the French plan to recover americium from the Purex process HLW by any of several available procedures.

It should be noted that formation constants of complexes formed by Am(III) with aminopolycarboxylic acids are larger than for the comparable complexes of the light lanthanides ($Z = 57$–61). Thus, addition of an aminopolycarboxylic acid to a lithium or aluminum nitrate solution containing Am(III) and rare earth enhances TBP extraction of the lanthanides relative to americium (Koehly and Hoffert, 1967). Americium can be separated from rare earths by TBP extraction from 1 M ammonium thiocyanate solution (Penneman and Keenan, 1960).

The mechanism of Am(III) and Eu(III) extraction from 1 M ammonium thiocyanate media by TBP in both the presence and the absence of a quaternary ammonium thiocyanate compound was investigated by Indian scientists (Khopkar and Narayankutty, 1971).

(*ii*) *Dibutyl butylphosphonate* (*DBBP*)

DBBP, $(C_4H_9O)_2(C_4H_9)PO$, extracts Am(III) from nitrate media more strongly than TBP and was used in a production-scale process at the US DOE Hanford site for several years (Schulz, 1976).

(*iii*) *Trialkylphosphine oxides* (*TRPO*)

It is well known that the basicity of the P–O functionality increases in going from alkyl phosphates (e.g. TBP) to alkyl phosphonates (e.g. DBBP) to alkylphosphine oxides (e.g. TRPO). Corresponding to the increased basicity is increased extractive power for trivalent actinides, e.g. Am(III) and Cm(III) from aqueous 1–2 M HNO_3 solutions. Chinese investigators have made use of the extractive power of TRPOs to develop a process for partitioning actinides, including americium and curium, from acidic Purex process HLW (Zhu and Jiao, 1994). Most of the results of Zhu *et al.* have been published in Chinese language journals, which, apparently, have not been translated into readily available English versions. Zhu and Jiao (1994) presented an admirable English language summary of their work up to 1994. They used a 30 vol% TRPO–kerosene solvent to extract trivalent (Am, Cm, lanthanides), tetravalent (Np, Pu), and hexavalent (U) actinides from both synthetic and actual Purex process HLW adjusted to about 1 M HNO_3. These experimenters used a mixture of C_6–C_8 alkylphosphine oxides available commercially (at least in the early 1990s) from operation of a fertilizer manufacturing plant. Zhu and coworkers found their particular 30% TRPO reagent to be very effective in extracting over 99% of all the actinides and lanthanides from the adjusted HLW. Extracted actinides could be stripped successively with 5.5 M HNO_3, 0.6 M oxalic acid, and 5% Na_2CO_3 solution to yield Am + rare earth, Np + Pu, and U fractions, respectively. Auxiliary experiments showed the TRPO solvent to have excellent actinide extraction kinetics and to be quite resistant to radiolytic degradation. Their highly successful batch and continuous countercurrent extraction–stripping tests led the Chinese to believe (at least in 1994) that their TRPO extractant was eminently suited for use in plant-scale partitioning of actinides from Chinese defense HLW. We, the authors, were not able to establish the present status of development/utilization of the Chinese TRPO extraction process.

Very recently, Murali and Mathur in India revisited use of TRPO for partitioning actinides from Purex process HLW (Murali and Mathur, 2001). They used a 30 vol% solution of a commercially available mixture of alkyl TRPOs (Cyanex-923) in dodecane. Cyanex-923 (Cytec Canada, Inc.) is a mixture of

four alkylphosphine oxides, $R_3PO, R'_3PO, R_2R'PO, RR'_2PO$; R = hexyl and R′ = octyl. (Murali and Mathur point out that Cyanex-923 is not the same mixture of alkylphosphine oxides used earlier by the Chinese investigators.) With dodecane as the diluent, the Indian investigators found it necessary to add TBP (5–20 vol%) to the Cyanex-923-dodecane solvent to avoid formation of a third phase even after adjusting the HLW acidity to 1 M HNO_3. Under the latter conditions, Murali and Mathur were able to both successfully extract and strip actinides, including americium, from synthetic Purex process HLW. Despite this successful performance, Murali and Mathur judged, "... the TRUEX solvent (0.2 M CMPO + 1.2 M TBP in dodecane) seems to be a superior extractant for partitioning of minor actinides from HLW solutions as there is no need for any feed adjustment and it tolerates significant amounts of sulfate, fluoride, and oxalate anions." (The TRUEX process is discussed in the later part of Section 8.4.3.)

(*iv*) *Bis*(*2-ethylhexyl*)*phosphoric acid* (*HDEHP*)

HDEHP is an excellent extractant for Am(III) from certain aqueous solutions. This extractant is commercially available in large quantities, can be readily purified, and has been widely used for both analytical purposes and plant-scale recovery and purification of americium (Peppard *et al.*, 1958, 1962; Gureev *et al.*, 1964). A countercurrent HDEHP extraction process was used at the DOE Hanford site in the late 1960s as part of the processing sequence for recovering and purifying 1 kg of americium and 50 g of curium from irradiated Shipping-port reactor fuel (Boldt and Ritter, 1969). An HDEHP batch extraction–strip process (Cleanex process) was routinely used in the Transuranium Processing Plant at the DOE Oak Ridge National Laboratory to reclaim americium, curium, and other transuranium elements from rework solution and/or to convert from nitrate to chloride media (Bigelow *et al.*, 1980). The Talspeak HDEHP processes are based upon the results of Weaver and Kappelmann (1964) who were the first to show that HDEHP extracts lanthanides much more strongly than actinides from aqueous carboxylic acid solutions containing an aminopolycarboxylic acid chelating agent. Lactic acid is used to avoid precipitation of solids when the concentration of lanthanides is high. HDEHP solutions have been used to selectively extract Am(VI) from Cm(III) (Musikas *et al.*, 1980a); in such systems rapid reduction of Am(VI) to lower oxidation states is a problem.

Extraction of Am(III) is very sensitive to the nature of compounds used to dilute the HDEHP (Gureev *et al.*, 1964). The kinetics of Am(III) extraction by HDEHP solutions were studied by Choppin and Nash (1977). In 1998, Indian scientists (Mapara *et al.*, 1998) studied solvent extraction of Am(III) from aqueous 0.1–1.0 M HNO_3 solutions using both HDEHP and 2-ethylhexyl phosphonic acid (PC88a in their notation). Before use, 1 M solutions of both extractants in kerosene were partially neutralized (saponified) to varying degrees with NaOH. In agreement with previously well-known chemistry of

HDEHP and PC88a, Am(III) extraction increased as more and more of the acidic extractant was converted to the sodium form.

(*v*) *Diisodecylphosphoric acid* (*DIDPA*)

Morita, Kubota, and other Japanese scientists (Morita and Kubota, 1988; Morita *et al.*, 1993) closely examined properties of solutions of DIDPA for extraction of actinides from acidic Purex process HLW. DIDPA solutions extract hexavalent (U) and tetravalent (Pu,Np) actinides quite efficiently from 1 to 3 M HNO_3 media. (Before extraction of ^{237}Np, however, it must be first reduced to Np(IV) by reduction of Np(V) and Np(VI) with hydrogen peroxide.) But, a disadvantage of the DIDPA extraction technique is that trivalent americium and curium do not extract well at feed acidities much above about 0.5 M HNO_3. Once extracted, Am(III) and Cm(III) can be selectively stripped with a diethylenetriaminepentaacetic acid (DTPA) solution; lanthanides can be easily stripped with 4 M HNO_3; and plutonium and neptunium can be removed from the organic phase by stripping with an aqueous oxalic acid solution. Japanese tests, both batch and countercurrent, of the DIDPA process with simulated Purex process HLW were generally regarded as successful.

(*vi*) *Neutral multifunctional organophosphorus and carbamoylphosphonate reagents*

Monofunctional organophosphorus extractants, e.g. TBP, DBBP, tri-*n*-octylphosphine oxide (TOPO), do not extract Am(III) from strongly acidic (>1 M HNO_3) aqueous solutions. Such behavior is desirable when the goal decades ago was to separate and purify plutonium and uranium from nitric acid solutions of irradiated nuclear fuel, e.g. the Purex process. But, evolving nuclear waste management strategies and policies have driven an urgent need for liquid–liquid extraction agents and processes capable of effective recovery and/or removal of Am(III) and Cm(III) as well as actinides in the +4 and +6 oxidation states from strong nitric acid medium. Thus, in the USA in the 1970s and 1980s there was an economic incentive to convert so-called transuranic acidic waste solutions containing ^{241}Am and various other actinides, chiefly plutonium, to low-level waste, which could be disposed of inexpensively. And, of course, the emergence of the partitioning–transmutation philosophy for advanced nuclear waste management and disposal places a premium on solvent extraction technology for efficient removal of trivalent actinides from acidic HLW solutions.

In the early 1960s, Siddall (1963, 1964) opened the door to the desired practical solvent extraction schemes for extraction of trivalent americium and curium from concentrated nitric acid solutions. Siddall in his papers noted that certain bifunctional organophosphorus reagents, e.g. diphosphonates and carbamoylmethylphosphonates (CMPs), i.e. compounds of the type $(R_1O)_2P(O)$—$(CH_2)_n$—(O)C—N—$(R_2)_2$, were especially effective in extracting trivalent actinides and lanthanides from strong nitric acid solutions.

Siddall's highly significant work lay buried in the literature until resurrected by Schulz and coworkers (Schulz, 1974, 1975; McIsaac and Schulz, 1976; Schulz and Navratil, 1982) in the early and middle 1970s. Both Schulz at the US DOE Hanford site and McIsaac at the US DOE Idaho site were motivated to develop solvent extraction processes for removing Am(III) and Pu(IV) from certain site acid waste solutions to convert the large volumes of these wastes to more easily managed and disposed of low-level wastes.

Based upon Siddall's data, both Schulz and McIsaac elected to use dihexyl-*N*,*N*-diethylcarbamoylmethyl phosphonate (DHDECMP) as the extractant for Am(III) and 4+ and 6+ actinides. Siddall's results indicated that CMPs were better extracting agents for 3+ actinides than diphosphonates. Another candidate, dibutyl-*N*,*N*-diethylcarbamoylmethylphosphonate, was rejected for use because of its high solubility in aqueous phases. Finally, of considerable significance, DHDECMP was available in liter quantities, albeit in a highly impure state (50–70% DHDECMP), from the Wateree Chemical Co. in South Carolina.

Batch tests with the impure DHDECMP solvent at both the Hanford and the Idaho sites quickly confirmed Siddall's results and demonstrated that this particular reagent would indeed permit efficient removal of all actinides from actual candidate acidic wastes. Auxiliary tests soon showed DHDECMP were sufficiently resistant to radiolysis, both alpha and gamma, to have a long useful life in plant-scale continuous countercurrent operations, especially in short residence time contacting equipment. Kinetics of actinide extraction and stripping were sufficiently rapid for satisfactory operation of continuous countercurrent contactors. The propensity of 20–30 vol% DHDECMP–NPH (normal paraffin hydrocarbon) solvents to form a third phase (second organic phase) when contacted with some acidic (HNO_3) waste solutions was overcome by either changing to an aromatic diluent, e.g. tetrachlorobenzene or decalin, or substituting TBP for a large portion of the NPH diluent. All the batch contact experiments culminated in chemical flowsheets (extraction–scrub–strip) that were very successfully demonstrated with both actual Idaho and Hanford sites acid waste solutions.

The only serious discordant note observed in tests with the impure Wateree Chemical Co. DHDECMP arose in attempts to use very dilute, e.g. ~0.01 M HNO_3 solutions to selectively strip 3+ actinides and lanthanides from pregnant organic phases. With as-received DHDECMP extractant D_{Am} instead of decreasing regularly upon successive strip contacts actually increased, resulting in a certain fraction of unstrippable americium. Such behavior is very symptomatic of the presence of an acidic organic compound in an otherwise neutral extractant. To overcome the deleterious effects of the acidic organic impurity, the 20–30 vol% DHDECMP solvent, before use, was subjected to various empirical chemical treatments designed to remove or at least reduce the concentration of the impurity, e.g. washing with ethylene glycol or alternate washing with HCl and NaOH solutions to hydrolyze the organic impurity. These

chemical treatments, although cumbersome, removed enough of the offending impurity to allow successful selective stripping of americium in continuous countercurrent flowsheet tests.

Tetravalent actinides and, if not previously removed, trivalent actinides were easily and effectively stripped from the DHDECMP phase with aqueous solutions containing fluoride or oxalate ions. And, as would be expected, dilute NaOH solutions effectively removed all 3+, 4+, and 6+ actinides from the DHDECMP solvent.

Following publication of the Schulz and McIsaac work, many other investigators, both in and outside the USA, conducted comprehensive experimental studies with DHDECMP and various other CMP-type reagents (Martella and Navratil, 1979; Petrzilova *et al.*, 1979; Horwitz *et al.*, 1981; Kalina *et al.*, 1981b; Hugen *et al.*, 1982; McIsaac, 1982; McIsaac and Baker, 1983; Kalina and Horwitz, 1985; Mathur *et al.*, 1991, 1992b). Indeed, as late as 1994, long after the TRUEX process had been proposed (cf. Section 8.4.3a(vi)), Rapko and Lumetta (1994) were still investigating use of a 0.75 M DHDECMP–1.05 M TBP/NPH solvent for extracting U(VI), Pu(IV), and Am(III), as well as competing metal ions, e.g. Fe(III), Zr(IV), from nitric acid solutions. And, in the late 1980s DHDECMP-based flowsheets were still under consideration for removal of all actinides from the DOE Idaho site sodium-bearing waste. Most of the work with CMP-based reagents after the early Schulz and McIsaac studies were done with DHDECMP; some investigators, however, synthesized various other CMP-type compounds to investigate their capability for extracting 3+ as well as 4+ and 6+ actinides from various acid waste solutions.

As discussed in the next section, CMP processes for efficient extraction of Am(III) and other actinides from acidic media have been supplanted and superseded by advanced organophosphorus reagent technology. Even so, the significance of the pioneering work of Schulz and McIsaac cannot be overstated. Through their efforts, scientists and engineers throughout the world became aware of Siddall's papers and the great potential of multifunctional organophosphorus reagents in actinide separation and recovery from many other sources.

Carbamoylphosphine oxide reagents

"CMPO" is a generic acronym for any carbamoylmethylenephosphine oxide. CMPO is also used here and elsewhere in the literature to denote one particular compound, namely, octylphenyl-*N*,*N*-diisobutylmethylenecarbamoylphosphine oxide, $(C_8H_{17})(C_6H_5)P(O)–CH_2–(O)C–N–N–(iC_4H_9)_2$. The actinide separation community is indebted to Dr E. P. Horwitz and his colleagues for their innovative efforts in initially synthesizing this particular CMPO and in evaluating many of its outstanding properties.

Being familiar with the Schulz and McIsaac results with DHDECMP (Section 8.4.3a(vi)), and having worked with this carbamoylphosphonate, Horwitz was motivated to find an improved trivalent actinide extractant with the following highly desirable attributes:

- Greatly increased capability for extracting 3+ actinides.
- Ease of synthesis of high-purity reagent.
- Increased solubility/compatibility with straight-chain hydrocarbon diluents.
- Excellent chemical and radiolytic stability.
- Suitability of extractant-diluent(s) solution for use in centrifugal contactors.
- Satisfactory selectivity for actinide and lanthanide extraction from aqueous media.

Horwitz's aspirations were essentially realized with the synthesis of the octylphenyl CMPO compound and the many successful tests of this reagent.

Gatrone and coworkers (Gatrone and Rickert, 1987; Gatrone *et al.*, 1987, 1989) published complete details of the synthesis of CMPO via a Grignard reaction. The crude CMPO product from the Grignard synthesis contains one or more acidic organophosphorus impurities that seriously interfere with the use of dilute nitric acid solutions to strip trivalent actinides and lanthanides. After testing various purification schemes, Gatrone and coworkers concluded that the most effective way to remove the offending acidic compounds was to first contact a heptane solution of the CMPO with 50 g L^{-1} of a macroporous cation-exchange resin at 50°C and then, without removing the cation resin, contact the heptane–CMPO solution with 50 g L^{-1} of a macroporous anion-exchange resin. This procedure, which Gatrone and his collaborators believe is generic and applicable to removal of acidic compounds from anyneutral organophosphorus extractant, yields solvent extraction-grade CMPO, i.e. $D_{Am} = <0.02$ in 0.01 M HNO_3/CMPO.

Many different diluents have been used in bench-scale studies of the extraction properties of solvent extraction-grade CMPO. Candidate diluents used at one time or another include aromatic (decalin), chlorinated (tetrachloroethylene), and aliphatic (dodecane) commercially available mixtures of C_{10}–C_{12} NPHs. For plant-scale application of CMPO a mixture of NPHs is the preferred diluent. However, HNO_3 and metal nitrates, e.g. lanthanide nitrates, have only a very limited solubility in CMPO/NPH solutions; once the solubility limit is exceeded, the organic phase splits into two phases (familiar third-phase formation phenomenon). Horwitz *et al.* (1985b) found that a simple and highly effective way to avoid the complications of a third-phase formation is to dilute the CMPO extractant with Purex process solvent to yield, for example, a 0.2 M CMPO/1.2 M TBP/dodecane solution. This solvent composition allows the CMPO fraction to be loaded to near theoretical capacity with trivalent lanthanides without causing a second organic phase to form. And, of course, an added advantage of the latter solvent composition is that its physical properties are little changed from those of familiar Purex process solvent and, therefore, no mechanical difficulties are encountered in operating centrifugal (or other) contactors with the CMPO/TBP/dodecane (or NPH) solvent. Horwitz and

coworkers (Kalina *et al.*, 1981a; Horwitz *et al.*, 1982, 1985b, 1986; Horwitz and Kalina, 1984; Kolarik and Horwitz, 1988), as well as many other investigators (Liansheng *et al.*, 1991; Mathur *et al.*, 1992a; Rapko, 1995), conducted comprehensive bench-scale studies to establish the extractive properties of CMPO/TBP/diluent solvents for many different metal ions over a wide range of conditions. Most of these studies were concerned with the extraction of actinides and other metal ions from nitrate-based aqueous media with CMPO/TBP/dodecane (or NPH) solvent, but some work has been done with aqueous HCl solutions (Horwitz *et al.*, 1987). All these bench-scale studies confirmed that the CMPO/TBP/diluent mixture would efficiently extract trivalent actinides and lanthanides as well as 4+ and 6+ actinides from almost any strong, i.e. ca. 1 M, nitric acid solution. Indeed, the more or less constant distribution ratio values for Am(III), Pu(IV), and U(VI) between 1 and 6 M HNO_3 is a very valuable and unique aspect of the CMPO/TBP system.

While the lanthanides and actinides are extracted almost quantitatively by CMPO/TBP/diluent solutions, with only a few exceptions most common metal ions in nuclear waste solutions are not extracted by the CMPO reagent (Horwitz *et al.*, 1985b). Not unexpectedly, Zr(IV) is significantly extracted ($D_{Zr} = \sim 1$–3) by CMPO/TBP/diluent solution from aqueous 1 M HNO_3. Zirconium is one of the major constituents of the DOE Idaho site waste; this particular waste also contains large concentrations of fluoride ion, which, fortunately, greatly inhibits CMPO extraction of inert zirconium (McIsaac and Baker, 1983). Paralleling known Purex process experience, ^{99}Tc, if present, is also well extracted ($D_{Tc} =$ 1–3) from nitric acid feed solutions as the $HTcO_4$ species. (Technetium largely remains in the CMPO phase during actinide scrubbing and stripping stages and is removed when the CMPO phase is washed with alkaline carbonate solutions to remove degradation and other species.) Other metallic contaminants of some interest ($D_M = 0.1$–0.6) include Mo, Ru, Pd, Ag, and Fe; these constituents are present in nearly all nuclear waste solutions that contain Am and other actinides. Adequate separation of actinides from the latter metal ions in CMPO extraction systems can be controlled by adding oxalic acid to the feed solution and/or by scrubbing the CMPO extract with a dilute oxalic solution before stripping of actinides.

To strip actinides from the CMPO/diluent or, more commonly, CMPO/TBP/NPH phase, conventional practice is to selectively strip, in order, 3+ actinides and lanthanides, 4+, and, if present, 6+ actinides. For this order of actinide stripping, preferred reagents (Mathur *et al.*, 2001) are, respectively, dilute nitric acid, e.g. <0.05 M HNO_3; a dilute oxalic acid, dilute ammonium oxalate, or a mixture of HF and HNO_3, e.g. 0.05 M HNO_3/0.05 M HF; and dilute sodium carbonate, e.g. 0.25 M Na_2CO_3. Sodium carbonate solutions do double duty and also act as a solvent cleanup reagent to remove solvent degradation products. But, in the case where it is desired to strip all the 3+, 4+, and 6+ actinides and lanthanides into a single aqueous phase, Horwitz and Schulz (1990) recommended use of a solution of either vinylidene-1,1-diphosphonic acid (VDPA)

or 1-hydroxyethylene-1,1-diphosphonic acid (HEDPA). Also, in a novel approach, Rizvi and Mathur (1997) utilized the ferrocyanide ion to co-strip actinides and lanthanides from CMPO phases. Other stripping agent studies of interest are those of Chitnis *et al.* (1998, 1999) who used a mixture of formic acid, hydrazine hydrate, and citric acid to remove Am(III) and Pu(IV) from CMPO solutions. Finally, Ozawa *et al.* (1998) reported that a mixture of hydrazine oxalate, hydrazine carbonate, and tetramethylammonium hydroxide will selectively strip 3+, 4+, and 6+ actinides from CMPO extractants.

A matter of concern for any liquid–liquid extraction process, especially one dealing with radionuclides, is the resistance of the extractant and its diluents to chemical and radiolytic degradation. Five separate studies (Chiarizia and Horwitz, 1986, 1990; Nash *et al.*, 1988, 1989; Mathur *et al.*, 1998) addressed this concern for CMPO extraction systems. Three of these investigations were concerned only with CMPO/TBP/dodecane solvents while two (Chiarizia and Horwitz, 1986; Nash *et al.*, 1988) also addressed radiolysis of CMPO diluted with decalin or tetrachloroethylene. Test solvents were irradiated both neat and while in contact with aqueous nitric acid solutions. Although results varied to some degree with the reagent used to dilute the CMPO and TBP, the general degradation behavior of CMPO/TBP/diluent solvent was independent of the nature of the diluent. Thus, the general degradation behavior is that chemical hydrolysis produces only acidic degradation products while radiolysis generates both neutral and acidic organophosphorus compounds.

The neutral organophosphorus degradation products of CMPO serve only as diluents for CMPO and TBP. But the acidic radiolytic degradation products are highly troublesome because they seriously interfere with stripping of Am(III) by dilute (<0.05 M HNO_3) solutions. Mathur *et al.* (2001) have published an excellent table, based on data obtained by Mathur *et al.* (1998) that illustrates very markedly the increase in the distribution ratio for Am(III) at 0.04 M nitric acid upon irradiation of a 0.2 M CMPO/1.2 M TBP/dodecane solvent to a total absorbed dose of 26–28 Mrad. According to these data, up to a dose of about 20 Mrad the distribution ratio of Am(III) at 0.04 M nitric acid is less than 1 and, hence, stripping with 0.04 M nitric acid should still be possible. Also, up to a dose of about 20 Mrad washing the spent solvent with a dilute sodium carbonate solution will remove most of the acidic degradation products. But, at higher absorbed radiation doses, in addition to sodium carbonate washing, it is necessary to provide a secondary solvent cleanup step, i.e. treatment with macroporous anion and cation-exchange resins or treatment with basic alumina.

In 1985, Horwitz and his collaborators (Horwitz and Schulz, 1985, 1986, 1990, 1999; Horwitz *et al.*, 1985a,b; Schulz and Horwitz, 1988) proposed a generic actinide solvent extraction process, the TRUEX process (Table 8.2) based on the superior properties of CMPO to remove all 3+, 4+, and 6+ actinides from any nitrate-based aqueous nuclear waste solution. The generic

Table 8.2 *Applications of the TRUEX process.*

Year	*Country*	*References*	*TRUEX process application/demonstration*
1985	USA	[1]	Removal of Am and Pu from Hanford complexant concentrate waste
1985	USA	[1]	Removal of Am and other actinides from Hanford single-shell tank sludges
1985–1991	USA	[2]	Removal of Am and other actinides from Hanford neutralized cladding removal waste
1988	USA	[3]	Removal Am and Pu from Hanford plutonium finishing plant waste
1988–1989	Italy	[4]	Removal of actinides from MOX fuel fabrication waste and waste from analytical laboratories
1992–1998	Japan	[5]	Removal of actinides from actual Purex process high-level waste
1993–1998	India	[6]	Removal of actinides (Am, Cm, Pu, Np, U) from synthetic pressurized water reactor reprocessing Purex process waste
1993–1998	India	[6]	Removal of actinides (Am, Cm, Pu, Np, U) from synthetic Purex process sulfate-bearing high-level waste (SBHLW)
1994–2000	India	[7]	Recovery of Pu and U from oxalate precipitation process waste
1997	USA	[8]	Removal of actinides from actual Argonne National Laboratory analytical wastes
1998	USA	[9]	Removal of actinides from Idaho site actual sodium-bearing waste
1998	USA	[10]	Removal of actinides from actual dissolved Idaho site calcine waste

[1] (Horwitz *et al.*, 1985b); [2] (Swanson, 1991; Lumetta and Swanson, 1993a,b); [3] (Schulz and Horwitz, 1988); [4] (Casarci *et al.*, 1988, 1989); [5] (Ozawa *et al.*, 1992, 1998); [6] (Deshingkar *et al.*, 1993, 1994; Chitnis *et al.*, 1998); [7] (Mathur *et al.*, 1994; Michael *et al.*, 2000); [8] (Chamberlain *et al.*, 1997); [9] (Law *et al.*, 1998a); [10] (Law *et al.*, 1998b).

TRUEX process, which utilizes a nominal 0.2 M CMPO/1.05 M TBP/dodecane (or other NPH-type diluent) solvent, is intended for use in short residence time centrifugal contactors. It typically comprises four separate operations: extraction, scrubbing of the organic phase, one or more stripping steps, and solvent cleanup. The users of the TRUEX process are free to specify whatever the number of extraction stages and organic-to-aqueous phase flow ratios are required to provide the required degree of removal of Am(III) and other actinides. Similarly, the TRUEX process operator is responsible for choosing the number of scrub stages (if any) and the composition of scrub solution(s) needed to adequately remove any co-extracted impurities, e.g. Zr(IV). The generic TRUEX process allows, by choosing particular aqueous phase strip

compositions, either selective stripping of 3+, 4+, and 6+ actinides or stripping of combinations of actinides, e.g. 3+ and 4+ or 4+ and 6+. One or two contactor stages for washing the stripped TRUEX process solvent with a dilute sodium carbonate solution are typically included to remove solvent degradation products and any traces of metal ions. Investigators in several countries have conducted continuous countercurrent demonstrations of variations of the TRUEX process with actual radioactive waste solutions of interest to them: references cited in the following list should be consulted for further details:

For various reasons, including the prolonged Cold War syndrome, Russian scientists, largely independent of Western world progress, conducted extensive studies of the actinide extraction properties of multifunctional organophosphorus reagents (Myasoedov *et al.*, 1980, 1986; Chmutova *et al.*, 1983, 1989; Myasoedov and Lebedev, 1991). A recent review paper by Myasoedov (1994) is of special interest. The Russian version of the American TRUEX process utilizes diphenyl-*N*,*N*-dibutylcarbamoylmethylenephosphine oxide dissolved in a commercially available (at least in Russia) fluoroether diluent (Fluoropol 732). According to Russian investigators, use of the fluoroether diluent eliminates any need to dilute the diphenyl CMPO with TBP to avoid third-phase formation; but others (Horwitz and Schulz, 1999) have expressed concern that diluent degradation under plant-scale conditions could lead to undue formation of corrosive HF. The Russian transuranium element extraction process behaves very similarly (Myasoedov, 1994) to the TRUEX process in its efficiency for extracting trivalent americium; in continuous countercurrent tests of the process in centrifugal extractors greater than 99.5% of the actinide elements in the aqueous feed were removed. In addition to the possibility of excessive generation of HF, other possible limitations to the Russian process include difficult americium stripping because of the need to use a very low concentration of nitric acid in the aqueous strip solution and complex solvent cleanup before reuse of the solvent (Horwitz and Schulz, 1999). In addition to the americium extraction results discussed earlier in Section 8.4.3a, certain other, more academically oriented studies of the extraction characteristics of novel phosphate-based reagents are of interest. For example, Paine and his research group (Bond *et al.*, 1997, 1998) investigated the extraction of Am(III) by 1,6-bis(diphenylphosphino)methyl-pyridine-*N*,*P*,*P*′-trioxide solutions from both hydrochloric and nitric acid media. And, Mishra *et al.* (1996) investigated the synergistic extraction of Am(III) by a mixture of Aliquat 336 and TOPO from acidic nitrate medium.

Rais and Tachimori (1994) studied the synergism in extraction and separation of Am(III) and Eu(III) in two systems: (1) dicarbollide anion and dibutyldiethylcarbamoylmethylenephosphonate (DBDECMP) and (2) dicarbollide anion and CMPO. Synergism was observed in both systems at low aqueous phase acidities but the effect was lower with CMPO than with DBDECMP.

Mohapatra and Manchanda (1995, 1999) reported on the unusual extraction behavior of Am(III) and UO_2^{2+} from aqueous picric acid solutions by TBP and TOPO extractants. Surprisingly, under these conditions, the organophosphorus compounds extract Am(III) better than the uranyl ion. Of course, from aqueous nitrate media, TBP and TOPO both extract U(VI) much better than Am(III). Mohapatra and Manchanda attribute the different extraction order from picric acid media to the formation of outer sphere rather than inner-sphere coordination complexes.

(b) Amine extractants

Nitrogen-based extractants, especially tertiary amines and quaternary ammonium compounds, are particularly effective in separating and recovering americium and other actinide elements from aqueous media.

(*i*) *Tertiary amine salts*

Tertiary amine salts extract Am^{3+} poorly from concentrated nitric or hydrochloric acids but extract it very strongly from concentrated nitrate or chloride solutions of low acidity (Myasoedov *et al.*, 1974a). Marcus *et al.* (1963) and Horwitz *et al.* (1966) found that Am^{3+} is extracted from nitrate media as complex $(R_3NH)_2Am(NO_3)_5$. A much more detailed account of the application of tertiary amine salts to extract americium is provided in Schulz (1976); indeed, essentially all the reported results obtained with tertiary amine salts in extraction of americium have been summarized in Schulz (1976).

(*ii*) *Quaternary ammonium salts*

Quaternary alkylammonium nitrate salts were shown by Horwitz *et al.* (1966) to extract Am^{3+} considerably more efficiently from low-acid, highly salted aqueous nitrate solutions than do tertiary alkylamines. The extraction sequence for trivalent actinides into either Aliquat 336 (a mixture of trioctylmethylammonium and tridecylmethylammonium salts made by General Mills, Inc.) nitrate or trilaurylmethylammonium nitrate is Cm<Cf<Am<Es. Horwitz *et al.* (1969) included an extraction step with Aliquat 336 in the preparation of 20–30 Ci of high-purity ^{242}Cm. Koch and Schoen (Koch and Schoen, 1968; Koch, 1969) devised and tested on a laboratory scale a quaternary ammonium extraction process for the isolation of ^{241}Am from aged plutonium scrap. Advantages of a quaternary ammonium nitrate extraction process over other schemes, e.g. Tramex process, for isolating trivalent lanthanides and actinides were discussed by Moore (1966a). Finally, Moore (1964, 1966b) and later Gerontopulos *et al.* (1965) found that the thiocyanate salt of Aliquat 336 preferentially extracts actinides over lanthanides in moderately concentrated NH_4SCN solutions.

(c) Amide extraction reagents

Diamide extractants are generally organic compounds with the generic formula $(R_1,R_2)N–C(O)–CR_3H–C(O)–N(R_1,R_2)$ where R_1, R_2, and R_3 are (typically) alkyl substituents. For various reasons, including doubtlessly their well-recognized nationalistic pride, French investigators have chosen to focus on diamides for possible application in partitioning of americium and other actinides from aqueous Purex process HLW vis-à-vis one of the more well-known and tested carbamoylphosphonates or phosphine oxides. Interestingly, various researchers including the French repeatedly extol the virtues of the carbon, hydrogen, oxygen, nitrogen (CHON) principle, i.e. design and use of liquid–liquid extraction reagents that contain neither sulfur nor phosphorus. Supposedly, degraded CHON-type extractants would be easier to dispose of, e.g. incinerate, than spent extractants that contain phosphorus or sulfur; there are no economic or technical data and/or experience to support the latter claim.

Between 1987 and 2002, numerous diamide compounds have been synthesized and examined for their ability to extract actinides in various oxidation states from aqueous nitric acid solutions. Details and results of these studies were reported (Musikas and Hubert, 1983; Musikas, 1987, 1995; Charbonnel and Musikas, 1988; Cuillerdier *et al.*, 1991a,b, 1993; Musikas *et al.*, 1991; Baudin *et al.*, 1993; Madic *et al.*, 1994; Nigond *et al.*, 1994; Shen *et al.*, 1996; Tan *et al.*, 1999).

Currently, one diamide, namely, *N*,*N*′-dimethyl-*N*,*N*′-dibutyl-2-tetradecylmalonamide (DMDBTDMA) appears particularly suitable for use in plant-scale removal of actinides from Purex process HLW. In France DMDBTDMA has been chosen as the extractant in their DIAMEX process for partitioning of actinides from Purex process HLW. Experiments show that DMDBTDMA is soluble in dodecane and does not produce a third phase when dodecane solutions are contacted with 3–4 M HNO_3. Indian scientists (Mahajan *et al.*, 1998) have also studied DMDBTDMA extraction of Am(III), U(VI), Np(IV), Fe(III), Sr(II), and Cs(I) from various nitric acid solutions and also from a simulated HLW, which would result from reprocessing of commercial pressurized water reactor fuel. These latter experiments confirm that DMDBTDMA is very promising for extraction of Am(III) and other actinides from 3 to 4 M HNO_3, particularly under high solvent loadings of neodymium or neodymium plus uranium.

Even after two decades, diamide extraction of actinides from nitric acid media is a continuing fertile research area. For example, Spjuth *et al.* (2000) have recently prepared seven new malonamide extractants by placing phenyl substituents on the nitrogen atoms in the malonamide or an ether oxygen into the bridging chain. The basicity of such compounds is reported to be less than that of DMDBTDMA, which makes them slightly better extractants for Am(III).

Sasaki and Tachimori (2002) have recently synthesized diamide extractants that they term 'structurally tailored diamides.' The diamides investigated include $(CH_2)_n$–$(CONR_1R_2)_2$ (n = 0, 1, 2, and 3); O–$((CH_2)_{n'}$–$CONR_1R_2)_2$; S–$((CH_2)_{n''}$–$CONR_1R_2)_2$; and SS–$((CH_2)_{n'''}$–$CONR_1R_2)_2$, (n', n'', n''' = 1, 2). The diglycolamide introducing an ether oxygen into the main structure, O–$(CH_2$–$CONR_1R_2)_2$, exhibits the highest extractability for An(III), An(IV), and An(VI) compared with the other bidentate diamides. The results of Sasaki and Tachimori also demonstrated that the thiaglycolamide, which substitutes an ether sulfur atom or oxygen in the molecule also enhances the extraction of actinides.

(d) Separation of americium from lanthanides

The challenge of separating Am(III) from trivalent lanthanides was first addressed and resolved by Weaver and Kappelmann (1964) as early as 1964. These investigators devised the Talspeak process that is based upon the fact that HDEHP solutions extract trivalent lanthanides much more strongly than trivalent actinides from aqueous carboxylic acid solutions containing an aminopolycarboxylic acid chelating agent.

A reverse Talspeak process involves, naturally, using an aqueous solution of an aminopolycarboxylic acid (e.g. DTPA) to preferentially strip Am(III) (and Cm(III) also if present) from an organic phase containing both trivalent actinides and lanthanides. In the DIDPA extraction process (Section 8.4.3a(v)) an aqueous lactic acid solution containing DTPA is used to strip trivalent americium and curium (Persson *et al.*, 1984); lanthanides remaining in the DIDPA phase are subsequently stripped with 4 M HNO_3.

In yet another application of the Talspeak process technology, the Japanese SETFICS (Solvent Extraction for Trivalent f elements Intragroup separation in CMPO-complexant System), a typical TRUEX process extraction stage, utilizes an aqueous 0.4 M $NaNO_3$ solution containing DTPA (Koma *et al.*, 1998). In a countercurrent test of the SETFICS process with radioactive feed, the reported $^{144}Ce/^{241}Am$ decontamination factor was 72.

The renewed focus on partitioning–transmutation technology that began in the 1980s (and continues unabated to this day) prompted many new studies of technology for separation of trivalent actinides from trivalent lanthanides. (See the review of the subject of lanthanide/actinide separations (Nash, 1994).) The breakthrough to more efficient lanthanide/actinide separation technology originated with Musikas in France who pointed out that soft-donor extractant molecules containing nitrogen or sulfur functionalities offered great potential to achieve the desired separation (Musikas *et al.*, 1980b; Musikas, 1984). In work published in the late 1970s and mid-1980s, Musikas reported that an extractant consisting of tripyridyltriazene (TPTZ) and dinonylnapthalene sulfonic acid (HDNNS) in carbon tetrachloride preferentially extracted Am(III) from a dilute nitric acid solution containing Am(III) and trivalent

lanthanides. In 1985, Musikas in his paper noted that the HDNNS could be replaced by bromocapric acid in an aliphatic hydrocarbon diluent.

Musikas' seminal work in the mid-1980s has triggered a cascade of studies of the ability of other nitrogen (and also sulfur)-containing extractants to provide separation of trivalent actinides from trivalent lanthanides. Noteworthy examples of such research efforts, not in chronological order, include work by Ensor and coworkers (Ensor *et al.*, 1988; Smith *et al.*, 1989), who used the synergistic combination of 4-benzoyl-2,3-dihydro-5-methyl-2-phenyl-3H-pyrazol-3-thione and 4,7-diphenyl-1,10-phenanthroline as an extractant to separate trivalent americium and europium, in the USA; Ensor *et al.* reported Am/Eu separation factors of greater than 10 with this synergistic combination of reagents. In Germany, Kolarik *et al.* (1999) investigated an extraction system based on polyaza ligands, e.g. 2,6-di-(5,6-dipropyl-1,2,4-triazin-3-yl) pyridenes for selective extraction of trivalent actinides from 1.9 M NH_4NO_3/HNO_3 solutions. Kolarik *et al.* reported Am/Eu separation factors in the range 100–120. And, of course Madic and Hudson (1998) as late as 1998 were still investigating TPTZ extraction systems for separating trivalent actinides from associated lanthanides in France. Madic's latest efforts center around attempts to suppress the solubility of TPTZ in aqueous phases by placing alkyl substituents at the 2-pyridyl rings and in replacing bromocapric acid by other anion sources.

An effective nitrogen-based soft-donor extractant for separation of trivalent actinides and lanthanides clearly would adhere to the CHON principle. But, unfortunately, to date at least, research efforts from 1987 to 2002 do not appear to have yielded a nitrogen-based 3+ actinide extractant suitably effective and stable for use on a plant scale with radioactive aqueous nitrate media. Conversely, because of recent breakthrough research results obtained by Zhu and his coworkers, prospects for developing a sulfur-based soft-donor extractant (non-CHON-type) suitable for plant-scale application appear to be reasonably good. In 1996, Zhu and coworkers reported that the compound bis(2,3,4-trimethylpentyl)-dithiophosphinic acid dissolved in a suitable diluent, e.g. heptane, preferentially extracted Am(III) from Eu(III) in aqueous nitrate media (Zhu, 1995; Zhu *et al.*, 1996b, 1998); Zhu and his collaborators found a separation factor as high as 5900 in favor of Am(III). Of particular interest and advantage, bis(2,3,4-trimethylpentyl)-dithiophosphinic acid is marketed commercially by Cyanamide Canada, Inc. under the trade name Cyanex 301; Cyanex 301 contains 77.2% of the dithiophosphinic acid compound. The primary impurities in Cyanex 301 are 14.6% R_3PS, 3.5% R_2POOH, and 0.8% R_2PSOH (Zhu *et al.*, 1996b). Chen *et al.* (1996) developed a scheme for upgrading commercially supplied Cyanex 301 to >99% bis(2,3,4-trimethylpentyl)-dithiophosphinic acid.

The excellent results obtained by Zhu and his coworkers with as-received Cyanex 301 were quickly confirmed in work at Florida State University by Zhu *et al.* (1996a). Data in Fig. 8.2 clearly illustrate the propensity of Cyanex 301 solutions to provide clean separation of Am(III) from trivalent lanthanides in

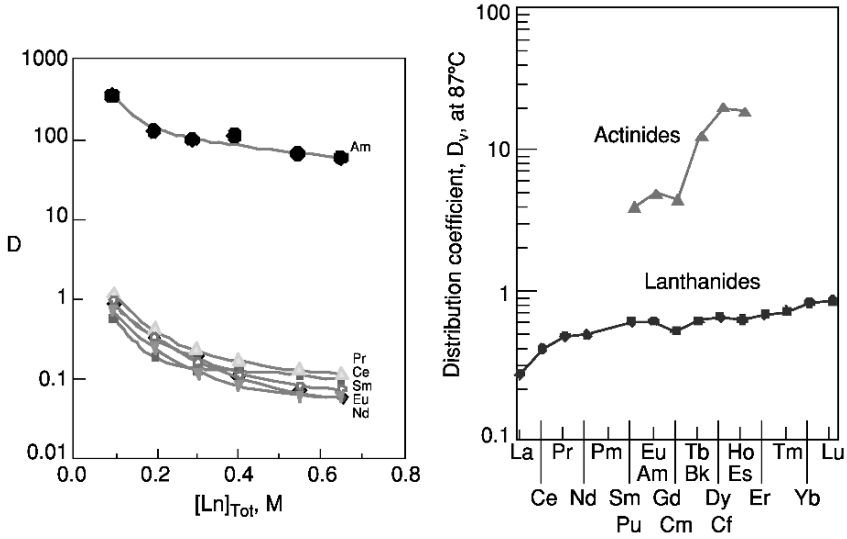

Fig. 8.2 *Distribution ratios of Am(III) and Ln(III) in* 1.0 M *Cyanex* 301-*heptane* (16 mol% *of Cyanex* 301 *neutralized before extraction contacts*) (*left*) (*Zhu* et al., 1996a). *Distribution coefficients of actinides and lanthanides into Dowex* 1 × 8 *resin from* 10 M *LiCl* (*right*) (*Hulet* et al., 1961).

pH 3 aqueous media. In later work, Modolo and Odoj (1998) also confirmed the initial results of Zhu and his collaborators with Cyanex 301. One very successful continuous countercurrent test of a Cyanex 301-based trivalent actinide/lanthanide separation flowsheet was made; using three extraction and two scrub stages >99.9% of Am(III) was separated from a trace amount of Eu with <0.1% extraction of Eu (Modolo and Odoj, 1998).

An immediate and continuing concern about plant-scale use of Cyanex 301 (or for that matter, any sulfur-based extractant) in a rather hostile environment, e.g. high nitrate concentration–high radiation zone, is its chemical and radiolytic stability. With respect to chemical stability, Sole *et al.* (1993) found that Cyanex 301 exhibits satisfactory resistance to chemical degradation when in contact with aqueous sulfuric acid, hydrochloric acid, and nitric acid solutions provided that the nitric acid concentration is maintained at (or less) than 2 M. With respect to radiolytic stability, one study found that irradiation of Cyanex 301 produces dialkylmonothiophosphonic acid, dialkylphosphinic acid, and other phosphorus compounds (Chen *et al.*, 1996). Purified Cyanex 301 separates tracer amounts of Am(III) from tracer amounts of Eu(III) even after irradiation to a cumulative dose of 10^5 gray; commercially available Cyanex 301 only performs satisfactorily at radiation doses up to 10^4 gray. The practical plant-scale consequences of the relatively poor resistance of Cyanex 301, even purified, to radiolysis would be reflected in the need to conduct countercurrent

extraction operations in short residence time equipment, e.g. centrifugal contactors, and, likely, frequent extractant inventory change-outs.

In addition to its relatively poor resistance to radiolytic degradation, Modolo and Odoj (1999) note another serious disadvantage to the use of Cyanex 301 to separate trivalent lanthanides and actinides, namely, the need to conduct extraction operations at an aqueous feed pH of 3 or higher. This latter need derives directly from the mechanism whereby Cyanex 301 humic acid (HA) extracts Am(III) and Eu(III):

$$M^{3+}_{aq} + 2(HA)_{2\ org} \rightarrow MA_3(HA)_{org} + 3H^{+}_{aq} \text{ where } M = Am, Eu$$

Three protons are released during the extraction operation; thus, Cyanex 301 only becomes an effective extractant at aqueous phase pH of 3 or more.

Modolo and Odoj (1999) recently synthesized and tested a new class of aromatic dithiophosphinic acids as separating agents for trivalent actinides and lanthanides. These compounds are conveniently represented as R_2PSSH with R = C_6H_5, ClC_6H_4, FC_6H_4, and $CH_3C_6H_4$. Modolo and Odoj achieved high separation factors (>20) with $D_{Am} > 1$ in the range 0.1–1.0 M HNO_3 by means of synergistic mixtures of $(C_6H_4Cl)_2PSSH$ with either TBP, TOPO, or tributylphosphine oxide. (Interestingly, none of the R_2PSSH compounds by itself has any capacity to extract trivalent actinides.) Not only do the aromatic dithiophosphinic acids achieve satisfactory separation of trivalent actinides from trivalent lanthanides from low pH (0.1–1.0 M HNO_3) aqueous solutions but they are also reported to be considerably more resistant to radiation degradation than is Cyanex 301. Thus, Modolo and Odoj demonstrated that the selectivity and capacity of all the R_2PSSH–synergist combinations remained intact even at an absorbed dose as high as 10^6 gray. The capability of aromatic compounds to act as radiation 'sinks' is, of course, well known. Finally, it should be noted that none of the R_2PSSH compounds synthesized and studied by Modolo and Odoj are commercially available in large amounts.

Hence, when and if any country commits to plant-scale execution of a partitioning–transmutation approach to nuclear waste management and disposal, it seems quite likely that past and ongoing research and development efforts by many investigators will have culminated in a new solvent extraction process for separation of Am(III) and Cm(III) from lanthanides that operates satisfactorily under plant-scale conditions. The usable fallback technology, even though it may be considered cumbersome, is the Talspeak process.

8.4.4 Ion-exchange processes

The combination of chromatographic elution techniques with cation-exchange resins provides a powerful and sophisticated tool to purify americium from lanthanides and other trivalent actinides. Elution chromatography involves the use of organic chelating agents to produce the largest possible difference in the

distribution coefficients of the metal ions to be separated. Both elution-development and displacement-development (also known as barrier-ion or retaining-ion) chromatography have been used in cation-exchange separation and purification of americium. Ryan (1974) points out that displacement-development chromatography is capable of separating macroquantities only, whereas, unless very large columns are used, elution-development chromatography is applicable only to the separation of tracer amounts. Jenkins and Wain (1972) listed publications covering the use of ion exchange to recover and purify ^{241}Am and ^{243}Am.

(a) Cation-exchange resin systems

Cation-exchange resins sorb Am^{3+} very strongly from dilute nitric acid solutions. An important application is to concentrate Am^{3+} and other trivalent and tetravalent ions from dilute acid solutions to separate them, at least partially, from many impurities (Hale and Lowe, 1969; Gmelin, 1979). Before production operations ceased at the US DOE Rocky Flats site, a cation–anion exchange process had replaced the hydroxide precipitation and thiocyanate ion-exchange system formerly used for recovering ^{241}Am from solutions of spent NaCl–KCl–$MgCl_2$ salt residues generated at the site (Proctor, 1975).

(*i*) *Distribution coefficients: separation factors*

Data for the distribution of Am^{3+} between cation-exchange resins and many aqueous solutions were analyzed in a comprehensive review by Ryan (1974). Solutions of α-hydroxycarboxylic acid and aminopolycarboxylic acids are commonly used to elute americium from cation-exchange resins. When these reagents are used in a displacement elution system, they provide excellent separation of americium from trivalent lanthanides and other trivalent actinides. For example, the separation factor for americium from curium ranges from 1.2 to 1.4 for α-hydroxycarboxylic acids and from 1.2 to 2 for aminopolycarboxylic acids (Schulz, 1976).

(*ii*) *Chromatographic elution schemes*

Although citric acid has found use, both lactic and α-hydroxyisobutyric acids provide better separation of americium from curium. Using chromatographic elution from Dowex 50-X12 resin with α-hydroxyisobutyric acid, Campbell (1970) demonstrated the effective use of high-pressure ion-exchange methods for the rapid separation of americium from curium. Highly efficient displacement chromatographic separation schemes that use nitrilotriacetic acid (NTA) and/or DTPA as eluents have been applied at the US DOE Hanford and at Savannah River sites to purify kilogram amounts of americium from curium and lanthanides (Wheelwright *et al.*, 1968; Harbour *et al.*, 1972). Wheelwright

et al. (1968) successfully used a two-cycle cation-exchange process to separate and purify 1 kg of ^{241}Am and ^{243}Am, about 60 g of ^{244}Cm, and 140 g of ^{147}Pm extracted from 13.5 tons of blanket fuel elements from the Shippingport nuclear reactor. Highly purified americium and curium fractions were obtained by americium–curium displacement elution at 60°C through a series of four Zn^{2+}-form Dowex 50 resins beds with a 0.105 M NTA solution buffered to pH 6.5 with NH_4OH. Harbour *et al.* (1972) adapted the displacement elution scheme to pressurized columns at the Savannah River site.

Nearly 20 years after Wheelwright's work, Chuveleva and some of his colleagues at the Institute of Physical Chemistry in Moscow revisited, as recently as 1999, displacement chromatography for separation of traces of americium and curium (Chuveleva *et al.*, 1999) (interestingly, in these papers Chuveleva *et al.* did not make any reference to Wheelwright's earlier work). The basic system used by the Russian scientists in 1999 utilized their KU-2 cation-exchange resin previously converted to the Ni- (or Zn) form; a NTA solution for elution, and Cd^{2+} as the separating ion. Performance of the Russian system was quite satisfactory; indeed, their results appeared to be in full accord with expectations from Wheelwright's earlier studies.

(b) Anion-exchange resin systems

For routine, large-scale purification of americium, application of anion-exchange resins is limited to sorption from thiocyanate, chloride, and, to a limited extent, nitrate solutions (Hermann, 1956).

(*i*) *Thiocyanate solutions*

Am(III) forms relatively strong complexes, e.g. $AmSCN^{2+}$, $Am(SCN)_2^+$, and $Am(SCN)_3$ in concentrated aqueous thiocyanate solutions, and its thiocyanate species are sorbed on anion-exchange resins considerably more strongly than are the corresponding lanthanide thiocyanate complexes (Coleman *et al.*, 1955, 1957; Surls and Choppin, 1957). Thiocyanate anion-exchange systems have been used to purify americium from rare earths. For example, a plant-scale thiocyanate ion-exchange process has long been used (1960–75) at the US DOE Rocky Flats plant for routine purification of ^{241}Am recovered from aged plutonium metal (Schulz, 1976).

(*ii*) *Chloride solutions*

Am(III) is sorbed much more strongly onto anion-exchange resins from concentrated lithium chloride solutions than are the lanthanides (Hulet *et al.*, 1961). Americium distribution ratios increase with increased lithium chloride concentration whereas increased temperature enhances the separation of americium from rare earths. A lithium chloride-based anion-exchange process

for separating milligram amounts of americium and curium from lanthanide fission products and to isolate an Am–Cm fraction free of heavier actinides was routinely operated at the US DOE Oak Ridge facility (Baybarz, 1970).

(c) Inorganic exchangers

Most studies concerned with sorption of Am^{3+} from aqueous solutions have used zirconium phosphate. The order of the distribution coefficients of trivalent actinides and lanthanides on zirconium phosphate is the reverse of the order observed with a typical strong-base cation-exchange resin (Horwitz, 1966). Both American (Moore, 1973) and Russian (Shafiev *et al.*, 1971) scientists utilized the fact that the singly charged AmO_2^+ is not sorbed by zirconium phosphate from dilute acid media to separate americium from curium and other metal ions.

Inorganic exchangers formed by hydrolysis of the alkoxides of titanium, niobium, or zirconium were developed for actinide/lanthanide separation (Lynch *et al.*, 1975) and possible disposal. Schulz *et al.* (1980) investigated the use of sodium titanate [$Na(Ti_2O_5H)$] and bone char (a form of calcium hydroxyapatite) to decontaminate alkaline nuclear waste streams containing minor amounts of americium and other actinides and to separate trivalent curium from trivalent americium.

More recently, as part of the overall Japanese partitioning–transmutation program, Yamagishi *et al.* (1996) reported results of experiments to use the inorganic cation exchanger titanium antimonate 'TiSb' to separate Am(III) from trivalent lanthanides. Before Yamagishi *et al.*'s work the TiSb exchanger had been reported (Kaneko *et al.*, 1992, 1993) to have a high selectivity for Pu^{4+} and trivalent americium and a low selectivity for trivalent lanthanides from concentrated HNO_3 solutions. Yamagishi *et al.* prepared TiSb according to conditions reported by Abe and coworkers (Abe and Tsujii, 1983; Abe *et al.*, 1985) and found that the TiSb exchanger exhibited superior selectivity toward trivalent americium over trivalent europium and other rare earths. The Japanese investigators concluded that TiSb is a promising material particularly for preconcentration of Am^{3+} from HNO_3 solutions containing Am^{3+} and large amounts of La^{3+} without the need for complexing or oxidizing agents.

Ritter (Ebner *et al.*, 1999) and his coworkers synthesized a new magnetic adsorbent material that combines the properties of both organic resin and inorganic material for use in actinide removal from nuclear waste solutions. This new material is called magnetic polyamine–epichlorohydrin (MPE) resin. MPE resin consists of spherical beads of polyamine–epichlorohydrin that have activated iron ferrite (magnetite) particles attached to their outer surfaces. Ferrites have been shown in previous work (Boyd *et al.*, 1986; Kochen, 1987; Kochen and Navratil, 1987; Boyd and Kochen, 1993) to be excellent adsorbents for actinide elements (including Am^{3+}) in wastewaters at relatively low alkaline conditions (pH $>$ 9) and independent of a magnetic field. Results obtained by Ritter and his colleagues demonstrated that MPE resin has a significantly

enhanced capacity for actinides over conventional-based ferrite surface complexation adsorption processes (where no field is applied) and over traditional high-gradient magnetic separation processes that remove suspended particles.

8.4.5 Extraction chromatographic processes

Extraction chromatography combines the best features of liquid–liquid solvent extraction and chromatographic separation techniques. Extraction chromatographic systems consist of a mobile liquid phase and a stationary liquid phase on an inert support. Separations are achieved by taking advantage of the difference in the distribution of ions between the two liquid phases.

Many systems using either HDEHP or Aliquat 336 as the stationary phase have been studied for extraction chromatographic separation of americium at tracer-level concentrations. An Aliquat 336 (nitrate-form)–kieselguhr system was used both in the USA and in Europe to separate milligram to gram amounts of americium from curium (Horwitz *et al.*, 1967; Müller, 1971).

In the two decades since the publication of the second edition of this monograph extraction chromatographic techniques for separating Am(III) and small amounts of other actinides from various aqueous media have been pursued for routine analytical purposes and for specialized process purposes. Thus far, the analytical applications have met with much greater acceptance and success than the proposed process applications.

Horwitz and his colleagues at the U.S. Argonne National Laboratory have been the prime movers in developing practical extraction chromatographic materials and procedures for analytical-scale separations and determination of Am(III) and other actinides. (Materials developed by Horwitz *et al.* are commercially manufactured and marketed by Eichrom Industries, Darien, Illinois.) Horwitz *et al.* (1990, 1993) initially developed an extraction chromatographic material, which was marketed under the name TRU^{TM} resin; the TRU^{TM} resin, which consisted of a solution of CMPO adsorbed on Amberchrom-CG 71 (Rohm & Haas Co.), had a number of attractive features including offering the possibility of sequential elution of individual sorbed actinide elements. However, a major weakness of the TRU^{TM} resin was that it would not effectively sorb actinides from solutions containing significant concentrations of complexing anions such as fluoride, oxalate, or phosphate. Extraction chromatographic analytical applications of the TRU^{TM} resin for the separation and determination of Th, U, Pu, Am, and Cm have been described in a series of papers (PilvVo and Bichel, 1998, 2000; PilvVo *et al.*, 1999).

In follow-on development work by Horwitz *et al.* the Diphonix^{TM} resin, containing geminally substituted diphosphonic acid groups chemically bonded to a styrene-based polymer matrix, was shown to exhibit extraordinarily strong affinity for the actinides particularly the 4+ and 6+ ions. Because of its strong retention of actinides, the Diphonix^{TM} resin found application in the characterization of mixed and transuranic waste (Chiarizia *et al.*, 1997) and in analytical

pre-concentration of actinides from a variety of biological and environmental samples (Smith *et al.*, 1995). Further tests revealed two important weaknesses of the Diphonix^{TM} resin in extraction chromatographic applications, namely (i) insufficient uptake and retention of trivalent actinides and (ii) difficult stripping/recovery of actinides from the loaded resin.

The final important contribution to actinide element extraction chromatography of the Horwitz group at the Argonne National Laboratory was the development and introduction of the DIPEX^{TM} resin (Horwitz *et al.*, 1997). The DIPEX^{TM} resin consists of a new compound, bis(2-ethylhexyl)methanediphosphonic acid (H_2DEH[MDP]) supported on an inert polymeric substrate. Horwitz and his coworkers state that this compound contains the same diphosphonic acid functional group as the Diphonix^{TM} resin but two of the four ionizable hydrogen atoms have been replaced by a C_8 alkyl group to make the molecule more lipophilic. According to the experimental evidence of Horwitz and colleagues, the DIPEX^{TM} resin exhibits stronger affinity for 3+, 4+, and 6+ actinides from acidic chloride media and superior selectivity for Am(III) over Al(III) and Fe(III) than the Diphonix^{TM} resin. Indeed, so strongly does the DIPEX material sorb actinides that the only convenient way to strip sorbed actinides appears to be to wash the resin with isopropanol to completely solubilize the H_2DEH[MDP] for subsequent wet oxidation to liberate the actinides for further treatment and analysis. Despite what appears to be a cumbersome procedure for stripping sorbed actinides, the DIPEX^{TM} resin is considered to be eminently suited for separation and pre-concentration of actinides from complex soil and bioassay matrices.

Nowadays, extraction chromatographic materials and techniques are generally considered to be most suited for analytical aims. But, some process-scale applications of such materials and techniques continue to be proposed from time to time. For example, Akatsu and Kimura (1990) reported on the use of extraction chromatography in the DHDECMP–(XAD-4) HNO_3 system. Also, several investigators (Barney and Cowan, 1992; Lumetta *et al.*, 1993) studied the feasibility of using TRU^{TM} resin and other types of extraction chromatographic supports impregnated with CMPO to separate actinide elements from stored US DOE Hanford site tank wastes including actual neutralized decladding waste and also other acidic waste solutions. Scientists in India (Gopalakrishnan *et al.*, 1995; Mathur *et al.*, 1995) have reported good success in applying an extraction chromatographic material consisting of CMPO adsorbed on Chromosorb-102 to selectively take up U(VI), Pu(IV), and Am(III) from neat nitric acid media, from synthetic sulfate-bearing high-level waste (SBHLW) and actual Purex process oxalate supernatant liquors.

Two other extraction chromatographic process-scale applications for separation of americium and other actinides are noteworthy. Mohapatra *et al.* (2000) found that the diamide DMDBTDMA adsorbed on an inert support was very efficient in taking up tracer concentrations of Am(III) and other actinide ions from 3 to 5 M HNO_3 solutions. Wei and his coworkers (Wei, 2000a,b) prepared

and investigated the actinide sorption properties of several novel silica-based extraction chromatographic resins by impregnating organic extractants such as CMPO, HDEHP, and Cyanex 301 into a styrene–divinylbenzene copolymer, which is immobilized in porous silica particles. Recently, these scientists have synthesized 2,6-bis-((5,6-dialkyl)-1,2–4-triazene-3-yl)-pyridine and impregnated such compounds into styrene–divinylbenzene copolymers immobilized in porous silica particles (Wei *et al.*, 2000a,b). The resulting extraction chromatographic material preferentially sorbed Am(III) over trivalent lanthanides.

A most unusual and intriguing type of extraction chromatographic separation scheme for Am(III) and other actinides was prepared by Nunez *et al.* (1996). These researchers adsorbed a layer of CMPO/TBP onto polymeric-coated ferromagnetic particles. The CMPO/TBP was very efficient in taking up actinides from 0.01 to 6 M HNO_3 nuclear waste solutions as expected from the results with the TRUEX process (see Section 8.4.3a(vi)). Once loaded with actinides, the ferromagnetic particles could be readily recovered from the waste solutions with a magnet.

8.5 ATOMIC PROPERTIES

8.5.1 Electron configuration

Americium is the sixth member of the actinide series, with electron configurations in its ground and ionized states analogous to those of its lanthanide homolog, europium. Note, however, that the solution chemistries of these two elements show substantial differences, with the major ones being the difficulties in preparing Am(II) and the absence of Eu(IV), Eu(V), and Eu(VI). Electronic configurations of gaseous americium species as determined from spectroscopic and atomic-beam experiments showed a $5f^7 7s^2$ ground state for Am(g) and $(5f^7)^{2+}$ state for Am^{2+} (Tomkins and Fred, 1949).

8.5.2 Atomic and ionic radii

Metallic, covalent, and ionic radii of americium in various oxidation states were first calculated by Zachariasen (1948a, 1954). The radius of americium metal with a coordination number (CN) of 12 was reported to be 1.73 Å (McWhan *et al.*, 1960). On the basis of a refined single-crystal structure for $AmCl_3$, Burns and Peterson (1970, 1971) calculated the ionic radius of Am^{3+} (CN 6) in $AmCl_3$ to be 0.984 ± 0.003 Å. Zachariasen (1978) has also deduced some highly useful bond length–bond strength relationships that provide, as a function of americium valence and coordination number, a condensation of many americium–oxygen and americium–halogen distances derived from the best-known structures. For the Am^{3+} and Am^{4+} ions, Zachariasen (1948a) reported crystal

radii of 1.00 and 0.85 Å, respectively. Shannon (1976) provided a list of revised effective ionic radii and reported 1.21 Å (CN 6) and 1.26 Å (CN 8) for Am^{2+}, 0.975 Å (CN 6) and 1.09 Å (CN 8) for Am^{3+}, 0.85 Å (CN 6) and 0.95 Å (CN 8) for Am^{4+}. No data are available on Am(v) and Am(vi). David (1986) reported an ionic radius for Am^{3+} of 0.980 Å (CN 6) and 1.106 Å (CN 8).

8.5.3 Ionization potentials

Trautmann and colleagues (Trautmann, 1994; Deissenberger *et al.*, 1995) experimentally determined the first ionization potential of americium to be 5.9738 (2) eV. This determination was made with only 10^{12} atoms of americium using a newly developed method based on resonance ionization mass spectroscopy in the presence of an external electric field. Before the work of Trautmann and colleagues, Carlson *et al.* (1970) calculated the ionization potential values for Am^0 (5.66 eV), Am^+ (12.15 eV), and Am^{2+} (18.8 eV). Penneman and Mann (1976) also estimated the same potentials based on *jj* coupling; these investigators underestimated the first ionization potential but were in good agreement on the potentials for higher ionizations.

8.5.4 Emission spectra

Studies of the arc and spark spectra of americium have been summarized by Carnall (1973a) in *Gmelin's Handbook of Inorganic Chemistry*. Corresponding to the absolute term value (48767 cm^{-1}) of the ground state, the ionization potential of Am(i) is 6.0 eV (Carlson *et al.*, 1970). As noted above Deissenberger *et al.* (1995) refined the ionization potential to 5.9738(2) eV.

8.5.5 X-ray spectrum

Atomic energy levels (binding energies) of americium have been calculated from experimental measurements of X-ray emission wavelengths; for example, the value for $K–M_{III}$ is 120.319 and 102.041 keV for the $K–L_{II}$ transition (Carnall, 1973b). All K X-ray energies of americium correspond to electric dipole transitions. A critical literature evaluation and a listing of atomic energy levels of americium are given in Bearden (1967).

8.5.6 Photoelectron spectrum

In a highly important experimental measurement, Naegele and coworkers (Naegele *et al.*, 1984) at the European Institute for Transuranium Elements were able in 1984 to directly conduct X-ray and high-resolution ultraviolet photoemission spectroscopy of the conduction band of americium metal. These measurements, parallel to those successfully performed earlier with uranium metal, directly revealed that the 5f electrons in americium metal are

localized. Naegele *et al.* state that the final-state multiplet structure arises from a trivalent $5f^6$ Am ground state. In later work, Naegele *et al.* (Martensson *et al.*, 1987) attempted an interpretation of the valence band photoelectron spectrum for americium metal.

8.5.7 Mössbauer spectrum

Beta decay of ^{243}Pu ($t_{1/2} = 4.98$ h) to the 83.9 keV level of ^{243}Am produces an excited nuclear state ($t_{1/2} = 2.34$ ns) of ^{243}Am that is suitable for Mössbauer spectroscopy (Kalvius *et al.*, 1969; Bode *et al.*, 1976). Data obtained with a $^{243}PuO_2$ source at 4.2 K showed the shift of the $^{243}AmF_3$ resonance line relative to $^{243}AmO_2$ to have an unusually large value of 55 mm s^{-1} (Kalvius *et al.*, 1969; Bode *et al.*, 1976).

8.6 METAL AND ALLOYS

8.6.1 Metal preparation

Americium metal has been prepared by the following methods: (1) reduction of AmF_3 with barium (or lithium) metal; (2) reduction of AmO_2 with lanthanum metal; (3) bomb reduction of AmF_4 with calcium metal; and (4) thermal decomposition of Pt_5Am. Lanthanum metal (or thorium metal) reduction of AmO_2 in tantalum equipment and subsequent distillation of the americium metal from the reaction mixture yields americium of very high (>99.9%) purity. Americium is about a factor of 10^4 more volatile than lanthanum. Extensive applications of this technique by the Euratom group led to important new measurements of the physical and thermodynamic properties of americium metal (Oetting *et al.*, 1976). Workers at the U.S. DOE Rocky Flats site also reported similar success with vacuum distillation techniques (Berry *et al.*, 1982).

Preparation of americium metal by thermal decomposition of the intermetallic compound Pt_5Am is a more recent development. Müller *et al.* (1972) produced high-purity americium metal by thermal decomposition of the intermetallic compound at 1550°C and 10^{-6} Torr, followed by further distillation.

8.6.2 Properties

Americium metal is silvery, ductile, non-magnetic, and very malleable. Selected physical properties are listed in Table 8.3. There are two well-established crystalline forms of americium metal, a double hexagonal close-packed (dhcp, $P6_3/mmc$) phase, stable at room temperature, and a face-centered cubic (fcc, $Fm3m$) phase (McWhan *et al.*, 1960; Stephens *et al.*, 1968; Oetting *et al.*, 1976). Differential thermal analysis and dilatometric experiments on americium metal have presented (Rose *et al.*, 1979) evidence for at least three phases existing between room temperature and the melting point (1170°C): an alpha phase

Table 8.3 *Selected properties of americium metal* (*adopted from Schulz* (1976) *and Oetting* et al. (1976); *see also Chapter* 19).

Property	*Values*[a]
Crystallographic data	
symmetry	<658°C, dhcp (α) 793–1004°C, fcc (β) ~1050–1173°C, bcc (?)
space group	$P6_3/mmc$ and $Fm\bar{3}m$
lattice parameters	dhcp: $a = 3.4681$ Å, $c = 11.241$ Å fcc: $a = 4.894$ Å
density	13.671 g cm^{-3} (calc.); 13.671 g cm^{-3} (obs.)[b]
high-pressure structures[c]	0–5 GPa Am (I): dhcp; 5 to 8–10 GPa Am(II): fcc; 8 to 15–23 GPa Am(III): double body-centered monoclinic, or trigonal distortion of fcc, or monoclinic α-Pu; >15–23 GPa Am(IV): orthorhombic α-U or monoclinic (α-U alloys)
metallic radius (CN 12)	1.73 Å
melting point	(1149 ± 5) K
boiling point	2067°C (calc.)
coefficient of thermal expansion	$\alpha_a = 7.5 \pm 0.2 \times 10^{-6}$ K^{-1} and $\alpha_c = 6.2 \pm 0.2 \times 10^{-6}$ K^{-1}
compressibility at 1 atm	0.00277 $kbar^{-1}$ at 23°C
vapor pressure[d]	$\log (p/\text{atm}) = (6.578 \pm 0.046) - (14315 \pm 55)/T$ at 990–1358 K
magnetic susceptibility	$\chi_{20°C} = (881 \pm 46) \times 10^{-6}$ cm^3 mol^{-1}
magnetic moment	~0
microhardness (Vickers) at 25°C	800 MN m^{-2}
electrical resistivity	68 μΩ cm (300 K), 71 μΩ cm (298 K)
crystal entropy, $S°298$	55 J K^{-1} mol^{-1}
heat capacity, $(C_P)_{298}$	25.5 J K^{-1} mol^{-1}
heat of vaporization at boiling point	230.2 kJ mol^{-1} (calc.)
entropy of vaporization at boiling point	100.8 J K^{-1} mol^{-1} (calc.)
heat of transformation	5.9 kJ mol^{-1}
heat of fusion	14.4 kJ mol^{-1}
heat of dissolution in aqueous HCl	1 M HCl: −616.3 kJ mol^{-1} 1.5 M HCl: −615.5 kJ mol^{-1} 6 M HCl: −618.0 kJ mol^{-1}

[a] For the dhcp-form unless otherwise indicated.
[b] By immersion in monobromobenzene.
[c] Refer to Section 8.6.2.
[d] Ward *et al.* (1975) give the following equation for americium above its melting point: $\log(p/\text{atm}) = 5.185–13191/T$.

existing up to 658°C; a beta phase existing between 793 and 1004°C; and a gamma phase which forms at 1050°C. In studies with high-purity americium metal, Sari *et al.* (1972/73) concluded that there is no phase transition between 600 and 700°C. But, Russian scientists (Seleznev *et al.*, 1979) put forth evidence that the transition from the dhcp structure to the fcc structure occurs at 771 ± 15°C; their observation is in agreement with the conclusions reached from dilatometric and differential thermal analysis measurements.

Smith and Haire (1978) found that americium metal with the dhcp structure became superconducting between 0.55 and 0.75 K; observation of the onset of superconductivity in americium metal confirmed an earlier prediction made from theoretical considerations. In later work, Link *et al.* (1994) found that the superconductivity transition temperature of dhcp americium increases considerably with pressure, reaching a maximum value of 2.3 K at 6.6 GPa. Müller *et al.* (1978), at several laboratories in Europe and in USA, recently measured the electrical resistivity and specific heat of americium metal. These latter investigators observed binding in americium metal to be reduced compared to that in lighter actinide metals and attributed this result to the importance of 5f electrons in electrical conduction. In a later paper, Hall *et al.* (1980) used their data to generate 'best values' for the heat capacity, crystal entropy, and electrical resistivity of americium metal; these 'best values' are shown in Table 8.3.

Owing to its unique position and properties in the actinide series of elements, americium metal has proven to be, over the last quarter of a century, a material of great interest to both theoreticians and experimentalists. In the light actinide metals (Ac–Pu) the 5f electrons are known to be itinerant and not localized. But, there is much evidence, e.g. cohesive properties, magnetic properties, atomic volume, etc. to indicate that the 5f electrons in americium metal at atmospheric pressure are localized and chemically inert. (Indeed, results of recent photoemission spectral studies cited in Section 8.4 essentially prove that 5f electrons in americium metal are localized.) Once the 5f electron localization behavior was noted for americium metal, Johannson (1978) also posited that americium metal under compression will transform to a dense phase where the 5f electrons are itinerant and not localized.

The first experimental study of the behavior and some properties of americium metal above atmospheric pressure was conducted by Stephens *et al.* (1968). These investigators determined the compressibility and electrical resistance of americium metal at room temperature over the range 3.5–12 GPa. They also made an attempt to determine the phase diagram of americium metal over this range of pressures.

Following Johannson's 1978 paper several groups of scientists in the early 1980s determined structural properties from X-ray diffraction data for americium metal at various pressures. The overall goal of these studies was to determine the number and type of different crystalline structures formed as a function of applied pressure and, thereby, obtain experimental evidence for delocalization of the 5f electrons. Thus, Akella and coworkers (Akella *et al.*, 1980;

Roof *et al.*, 1980; Smith *et al.*, 1981; Roof, 1982) established four different crystalline structures in americium metal over the pressure range from 100 kPa (1 atm) to 18 GPa: Am(I)-dhcp; Am(II)-fcc (at 5 ± 1 GPa); Am(III)-not indexed (10 ± 1 GPa); and Am(IV)-not indexed (15 ± 1 GPa). Later Roof (1982) repeated and extended the pressure experiments of Akella and coworkers up to 20 GPa. Roof and his collaborators noted the same four crystalline phases as observed by Akella and coworkers. But, Roof and his collaborators indexed the Am(III) phase (10–15 GPa) as a double-body centered monoclinic structure and the Am(IV) phase (10–20 GPa) as an orthorhombic structure similar to that of alpha uranium metal.

The latest experimental studies of delocalization of 5f electrons in americium metal under pressure were performed by Benedict and colleagues (Benedict *et al.*, 1985, 1986). Benedict *et al.* conducted their experiments over the pressure range 3 to 52 GPa, and, under these conditions, also noted the Am(I)–Am(II)–Am(III)–Am(IV) phase transformation sequence. Benedict *et al.* however, state that the transitions between phases occur at higher pressures than noted by previous workers; in particular, Benedict and his fellow authors state that the Am(III) to Am(IV) transition occurs at 23 GPa, not at 15 GPa. Benedict *et al.* claim that the Am(III) phase is not a monoclinic structure, as previously indexed, but is really a trigonal distortion of the Am(II) fcc structure. Finally Benedict *et al.* state that according to their results, 5f electron delocalization occurs only at a pressure of 23 GPa or above. Lindbaum *et al.* (2001) observed the transition of the normal-pressure double hexagonal close packed ($P6_3/mmc$) structure transforms at 6.1 GPa to the face centered cubic (*Fm3m*) form, which converts at 10.0 GPa to a face centered orthorhombic (*Fddd*) structure. This orthorhombic form converts at 16 GPa to a primitive orthorhombic (*Pnma*) form, which is stable up to at least 100 GPa. Based on the data of americium's pressure behavior the authors concluded that Am f-electrons are involved in the metallic bonding of the AmIII and IV phases.

Coincident with experiments conducted to ascertain the response of americium metal to increasing pressure, theoreticians in several countries have mounted a sustained effort to apply first-principles calculations to deduce the state of 5f electrons both in the presence and absence of applied pressure (Skriver *et al.*, 1980; Johannson, 1984; Nikolaev and Ionova, 1991; Eriksson and Wills, 1992; Eriksson *et al.*, 1993, 1995, 2000; Soderland *et al.*, 2000). The present state of the theoretical calculations is best discussed in a recent paper by Soderland *et al.* (2000). The latter investigators used density functional electronic calculations to study the high-pressure behavior of americium metal. At about 8 GPa, such calculations revealed a phase transition from the fcc structure Am(II) to a dense phase of lower symmetry that Johannson *et al.* were convinced is a monoclinic form similar to the structure of α-plutonium (Fig. 8.3); they state emphatically that it does not have the orthorhombic structure called out by Roof and Benedict *et al.* According to Johannson and collaborators, their calculation results are consistent with a Mott transition;

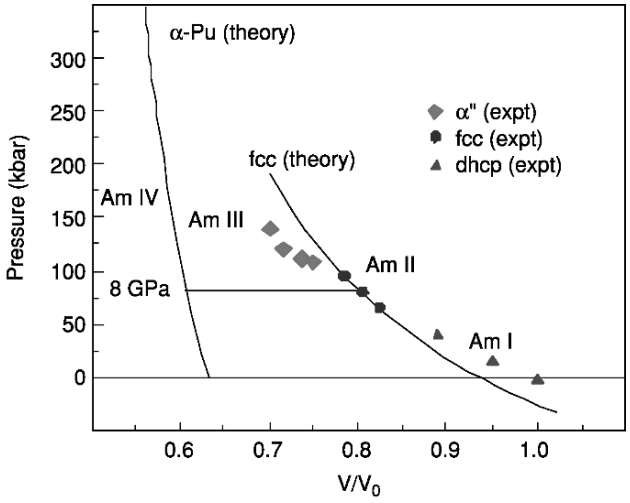

Fig. 8.3 *Calculated equations of state for americium metal from fits to total energies* (*Soderland* et al., 2000)*; equations indicate a volume decrease of* 25% *at* 8 GPa.

the 5f electrons are delocalized and bonding on the high-density side of the transition and chemically inert and non-bonding (localized) on the low-density (fcc phase) side of the transition.

Even at this advanced time in the chemistry of americium, there are still some serious disagreements between experimentally determined and calculated (from theoretical considerations) effects of compression of americium metal. To be sure, both approaches offer strong support for the contention that upon compression the 5f electrons in americium delocalize. Both the experimentalists and the theoreticians concur that at moderate applied pressure, the dhcp structure converts to the fcc phase. And, both groups concur that at some threshold applied pressure the fcc structure transforms to a more dense phase, i.e. Am(III) and, possibly, Am(IV), in which the 5f electrons are delocalized. But, certainly the parties involved do not agree on exactly how many different dense phases (one or two) eventually form on further application of pressure or on the exact pressure of phase transformations and certainly not on the crystal structure of the new dense phase(s). (The data shown in Table 8.3 are listed so as to capture much of the present uncertainty concerning transition pressures and crystalline structures.) Another important point of disagreement and uncertainty, long known and troublesome to theoreticians, is that the experimentally observed volume decreases when the 5f electrons in americium metal are delocalized only to about 6% compared to the 30–35% decrease predicted from theory. The present disagreement between experimental and calculated results point to flaws and deficiencies in both approaches, e.g. difficulties in obtaining and accurately deciphering X-ray diffraction data from a pressurized radioactive system and

inadequacies of present calculational tools. It is hoped that future research will resolve the discrepancies between calculation and experiment.

8.6.3 Alloys and intermetallic compounds

Presently, alloy systems involving interaction of americium metal with some 23 different elements have been investigated. One or more intermetallic compounds of definite composition are known to exist in 16 of these systems; Table 8.4 summarizes the significant stoichiometry, structure, and synthesis information for these 16 systems and also provides relevant literature references.

No definite compounds have been observed in the Am–Ce, Am–Hg, Am–La, Am–Np, Am–Pu, Am–Th, or Am–U systems. Phase diagrams for the Am–Np, Am–Pu, and Am–U systems have recently been summarized and published by Okamoto (1998). Okamoto took careful note of the phase diagram for the Am–Pu system constructed earlier by Ellinger *et al.* (1966). Gibson and Haire (1992a) have reported phase relations in the Am–Np system while Adair (1970) prepared alloys of thorium with 0.54–5.0 wt% americium by both levitation and arc melting of prepared mixtures of americium and thorium metal.

Interaction of americium metal with two rare earth metals, lanthanum and cerium, has been investigated, respectively, by Hill and coworkers (Hill and Ellinger, 1971; Hill *et al.*, 1971) and by Connor (1982). Lanthanum–americium alloys containing 0.92–2.37 at% americium dissolved in fcc-beta lanthanum were produced by arc melting the constituent elements. Connor used both co-melting (arc) and co-reduction techniques in his studies of the Am–Ce system. Co-reduction alloy preparation involved calcium metal reduction of an appropriate mixture of AmF_4 and CeF_3 in a sealed vessel.

The Am–Hg system has been studied by Bouissières and Legoux (1965), David and Bouissières (1968), Maly (1969), and Tikhonov *et al.* (1988). A dilute americium amalgam may be prepared either by reduction of Am(III) ions with a sodium amalgam or by electroreduction of Am(III) ions on a mercury electrode. Tikhonov *et al.* also investigated some properties of a concentrated americium amalgam that was prepared electrolytically; their results indicated the formation of an Am–Hg intermetallic compound but no information on the stoichiometry or structure of such a compound was reported. Guminski (1995) recently reviewed and evaluated the equilibrium and thermodynamics of the Am–Hg system.

8.7 IMPORTANT COMPOUNDS

Inorganic compounds containing halides or oxygen-donor ligands are far more numerous than simple oxides, hydroxides, or other binary or ternary compounds. The structures and references to the preparation of about 180 compounds of americium with anionic inorganic ligands are listed in alphabetical order in Table 8.5; compounds of americium with organic ligand coordination are listed

in Table 8.6. A group of compounds in which americium could be considered as part of the anionic constituent appears under the heading oxides, ternary.

8.7.1 Inorganic compounds

(a) Oxides and hydroxides

The binary americium oxides are limited to AmO, Am_2O_3, AmO_2, and non-stoichiometric phases between Am_2O_3 and AmO_2. Although the AmO (fcc) phase has been reported twice (Zachariasen, 1949a,c; Akimoto, 1967), the corresponding lattice parameters, 4.95 Å (Zachariasen, 1949a,c) and 5.045 Å (Akimoto, 1967), are not consistent. Accidental exposure of AmH_{2+x} to air at 300°C yielded a fcc phase (Roddy, 1973), which agrees with Akimoto's AmO (Akimoto, 1967) but may in fact be an oxynitride similar to the corresponding 'PuO' (Larson and Haschke, 1981). The difficulty in achieving Am(II) in solution and in solid compounds makes it likely that the monoxide can only be synthesized under high pressure by conproportionation of Am metal and Am_2O_3, analogous to the preparation of the lanthanide monoxide SmO (Leger *et al.*, 1981). Recent evidence that PuO and surface-layer lanthanide monoxides are really oxycarbides or nitrides (Larson and Haschke, 1981) reinforces the uncertainty of whether any claim for AmO is valid.

Phase relationships and thermodynamic data in the $AmO_{1.5}$–AmO_2 systems are well established. The red-brown ('persimmon') sesquioxide, Am_2O_3, is easily prepared in H_2 at temperatures as low as 600°C but it oxidizes very readily in air, even at room temperature. Baybarz (1973a) summarized the transition temperatures of the low-temperature (body-centered cubic (bcc), C-phase) to medium-temperature (monoclinic, B-phase) to high-temperature (hexagonal, A-phase) sesquioxides. The C→B transition temperature appears to be sluggish, occurring between 460 and 650°C and the B→A transition occurs between 800 and 900°C (Chikalla and Eyring, 1968; Hurtgen and Fuger, 1977). The pale tan hexagonal sesquioxide phase undergoes slight swelling with time and self-irradiation causes cubic Am_2O_3 to transform to the hexagonal phase at room temperature within about 3 years (Hurtgen and Fuger, 1977). It is possible that the monoclinic Am_2O_3 is stabilized by small amounts of rare earth impurities (Berndt *et al.*, 1974; Keller and Berndt, 1975) and that pure Am_2O_3 passes directly from the C- to the A-phase; it is also possible that the C→B transition occurs well below 650°C. The hexagonal sesquioxide is stoichiometric but the cubic form may have a lower oxygen limit of $AmO_{1.513}$ (Chikalla and Eyring, 1968). Studies on americium oxides include the measurement of the melting point of Am_2O_3, 2205 ± 15°C (Chikalla *et al.*, 1973), and the enthalpy of formation of AmO_2, -932.2 ± 3.0 kJ mol^{-1} (Morss and Fuger, 1981).

The dioxide AmO_2 was the first reported compound of americium (Zachariasen, 1949a,c). It can be prepared by heating a variety of americium compounds, e.g. hydroxides, carbonates, oxalate, or nitrate, in air or oxygen at

Table 8.4 *Intermetallic compounds in the americium alloy system.*

Class	*Formula*	*Symmetry*	*Structure type*	*Lattice constants* a_0 (Å)	c_0 (Å)	*Comments*	*References*
aluminide	$AmAl_2$	cubic	$MgCu_2$	7.861		arc melt	[1]
antimonides	AmSb	fcc		6.239		Am/Sb/heat	[2]
	$AmSb_2$		$LaSb_2$				
	Am_4Sb_3	bcc	anti-Th_3	9.239		AmH_3/Sb/heat	[3]
arsenide	AmS	fcc	F*m*3*m*	5.880		Am/As/heat	[4]
				5.875		AmH_3/As/heat	
beryllide	$AmBe_{13}$	fcc	F*m*3*c*	10.283		AmF_3/Be/vac/heat	[6]
						AmO_2/Be/vac/heat	[7]
bismuthide	AmBi	fcc	F*m*3*c*	6.338		Am/Bi/heat	[8]
						AmH_3/Bi/heat	[8]
cobaltide	$AmCo_2$	$MgCu_2$				arc melt	[9]
iridium	Ir_2Am	cubic	F*d*3*m*, Cu_2Mg	7.55		AmO_2/H_2/Ir/1550°C	[10]
iron	Fe_2Am	cubic	Cu_2Mg	7.30		arc melt, ferromagnetic	[9]
lead	Pb_3Am	not reported				PbF_2/AmF_3/Ca/heat	[11]
nickel	Ni_2Am	cubic	F*d*3*m*,Cu_2Mg	6.99		Am/Ni/arc melt	[12]
osmium	Os_2Am	hexagonal	P6_3/*mmc*	5.320	8.849	Am/Os/arc melt	[12]
palladium	Pd_3Am	cubic	P*m*/3*m*	4.158		$Am_2O_3/Pd/H_2$/heat	[13]
platinum	Pt_2Am	cubic	F*d*3*m*	7.615		$AmO_2/Pt/H_2$/heat	[13]
	Pt_5Am		$CaCu_5$	5.312	4.411	$Am_2O_3/Pt/H_2$/heat	[13]
rhodium	Rh_2Am	cubic	F*d*3*m*,Cu_2Mg	7.548		$AmO_2/Rh/H_2$/heat	[13]
	Rh_3Am	cubic	P*m*3*m*,Cu_3A	4.098		$Am_2O_3/Rh/H_2$/heat	[14]
ruthenium	Ru_2Am	hexagonal	$MgZn_2$	5.26	8.73	arc melt	[9]
tin	Am_2Ni_2Sn	tetragonal	P4/*mbm*,U_3Si_2				[15]
	Am_2Pd_2Sn	tetragonal					[15]

[1] (Hyde *et al.*, 1971; Aldred *et al.*, 1975); [2] (Mitchell and Lam, 1970a; Roddy, 1974; Charvillat *et al.*, 1975a, 1977); [3] (Charvillat *et al.*, 1975b); [4] (Roddy, 1974); [5] (Charvillat and Damien, 1973); [6] (Runnals and Boucher, 1955, 1956; Benedict *et al.*, 1975); [7] (Brachet and Vasseur, 1969); [8] (Roddy, 1974); [9] (Hyde *et al.*, 1971; Aldred *et al.*, 1975); [10] (Erdmann, 1971; Erdmann and Keller, 1971, 1973; Rebizant and Benedikt, 1978); [11] (Connor, 1982); [12] (Lam and Mitchell, 1972); [13] (Erdmann, 1971; Rebizant and Benedikt, 1978); [14] (Erdmann and Keller, 1971); [15] (Pereira *et al.*, 1997).

Table 8.5 *Inorganic compounds of americium.*

Class	*Structural formula*	*Symmetry*	*Type*	*Lattice constants* a_0 (Å)	b_0 (Å)	c_0 (Å)	*Angle* (deg)	*Comments*	*References*
Aluminates									
	$AmAlO_3$	hexagonal	$R\bar{3}m$, $LaAlO_3$	5.336		12.91		$Am(OH)_3/Al(OH)_3/H_2$/heat	[1,2]
Arsenates									
	$AmAsO_4$	monoclinic	$P2_1/n$	6.89	7.06	6.62	$\beta = 105.5$		[2]
	NH_4AmO_2 $AsO_4 \cdot nH_2O$	tetragonal	$P4/nmn$ or $I4/mmm$	7.11		8.93		Am(VI)/0.1 M H_3AsO_4/pH 3.5, lemon yellow	[3]
	$KAmO_2$ $AsO_4 \cdot nH_2O$	tetragonal	$P4/nmn$ or $I4/mmm$	7.10		9.09		Am(VI)/0.1 M H_3AsO_4/pH 3.5, lemon yellow	[3]
	$RbAmO_2$ $AsO_4 \cdot nH_2O$	tetragonal	$P4/nmn$ or $I4/mmm$	7.15		17.73		Am(VI)/0.1 M H_3AsO_4/pH 3.5, lemon yellow	[3]
	$CsAmO_2$ $AsO_4 \cdot vnH_2O$	tetragonal	$P4/nmn$ or $I4/mmm$	7.09		17.72		Am(VI)/0.1 M H_3AsO_4/pH 3.5, lemon yellow	[3]
Borates									
	$AmBO_3$	orthorhombic	$Pnam$	5.053	8.092	5.738		AmO_2/B_2O_3/heat	[1,2]
Borides									
	AmB_4	tetragonal	$P4/mbm$	7.105		4.006		vac. heat Am/B 1:2	[4]
	AmB_6	simple cubic	$Pm3m$	4.115				arc melt Am/B	[4]
Bromides									
	$AmBr_2$	*tetragonal*	$P4/n$, $EuBr_2$	11.59		7.121		Am/$HgBr_2$/vac./heat	[5,6]
	$AmBr_3$	orthorhombic	$Cmcm$, $PuBr_3$	4.064	12.66	9.144			[7,8,9]
	$AmBr_3 \cdot 6H_2O$	monoclinic	$P2/n$	9.955	6.783	8.166	$\beta = 91.75$	$AmBr_3$, H_2O vapor	[9]
	$[(C_6H_5)_3PH]_3$ $AmBr_6$							ethanol pptn.	[10]
	AmOBr	tetragonal	$P4/nmm$	3.982		7.644			[11]
Carbides									
	Am_2C_3	bcc	$I\bar{4}3d$	8.276				Am/C arc melt	[12]
Carbonates									
	$AmOHCO_3$	orthorhombic						Am(III)/$NaHCO_3$/0.03% CO_2	[13]
	$Am_2(CO_3)_3 \cdot 2H_2O$							Am(III)/trichloroacetate	[14]
	$Am_2(CO_3)_3 \cdot 4H_2O$							Am(III)/$NaHCO_3/CO_2$	[15]
	$NaAm(CO_3)_2 \cdot nH_2O$	tetragonal	$NaNdO_2CO_3$	13.07		9.93		Am(III)/Na_2CO_3/5 M NaCl	[16]

Table 8.5 (*Contd.*)

Class	*Structural formula*	*Symmetry*	*Type*	*Lattice constants*			*Angle* (deg)	*Comments*	*References*
				a_0 (Å)	b_0 (Å)	c_0 (Å)			
	$NH_4AmO_2CO_3$	hexagonal	*C*6/*mmc*					Am(III)/$(NH_4)_2CO_3/O_3$	[17]
	$Na_{2x+1}AmO_2(CO_3)_{1+x}$							Am(VI)/Na_2CO_3/heat	[17,18]
	$KAmO_2CO_3 \cdot nH_2O$	hexagonal	*C*6/*mmc*	5.112		9.740		*n* is variable with H_2O	[18–20]
	$RbAmO_2CO_3$	hexagonal	*C*6/*mmc*	5.12		10.46		Am(III)/10 M Rb_2CO_3/O_3	[17,21]
	$CsAmO_2CO_3$	hexagonal	*C*6/*mmc*	5.123		11.538		Am(III)/$CsHCO_3/O_3$	[22]
	$K_3AmO_2(CO_3)_2 \cdot nH_2O$	rhombic (a,b)	*C*6/*mmc*	5.32	9.21	8.76		(a) 4.7 M, (b) 2.3 M K_2CO_3	[20]
				5.29	9.11	8.83		Am(III)/3.5 M K_2CO_3	[23]
	$K_5AmO_2(CO_3)_3$	orthorhombic						Am(III)/>5 M K_2CO_3/O_3	[17,24]
	$(NH_4)_5AmO_2(CO_3)_3$							Am(VI)/NH_4CO_3	[3]
	$(NH_4)_4AmO_2(CO_3)_3$							Am(VI)/$NaHCO_3/(NH_4)_2CO_3$	[25]
	$Cs_4AmO_2(CO_3)_3$							Am(VI)/$NaHCO_3/Cs_2CO_3$	[25]
Chlorides									
	$AmCl_2$	orthorhombic	*Pbnm*	8.963	7.573	4.532		Am/$HgCl_2$/heat	[5,6]
	$AmCl_3$	hexagonal	P_{63}/m	7.382		4.214		AmO_2/HCl	[7–9,26]
	$AmCl_3 \cdot 6H_2O$	monoclinic	*P*2/*n*	9.702	6.567	8.009	$\beta = 93.62$		[26,27]
	AmOCl	tetragonal	*P*4/*nmm*	4.00		6.78			[28]
	$CsAmCl_4$							Am(III)/HCl/CsCl	[29]
	$CsAmCl_4 \cdot 4H_2O$							Am(III)/HCl/CsCl	[29,30]
	Cs_3AmCl_6							Am(III)/HCl/CsCl	[31]
	$Cs_2NaAmCl_6$	fcc	*Fm*3*m*	10.8548(8)				Am(V)/HCl/CsCl/NaCl	[29,30,32]
	$[(C_6H_5)_3PH]_3$ $AmCl_6$		$Cs_3NpO_2Cl_4$					ethanol pptn.	[10,33]
	$Rb_2AmO_2Cl_4$	monoclinic	*C*2/*c*	11.53	7.48	5.65	$\beta = 99.19$	Am(V)/HCl/RbCl	[3]
	$Cs_2AmO_2Cl_4$	monoclinic	*C*2/*c*	11.92	7.61	1167	$\beta = 99.56$	Am(V)/HCl/CsCl	[3]
Chromate									
	$(AmO_2)_2CrO_4 \cdot nH_2O$							20–80°C	[34]
Fluorides									
	AmF_3	hexagonal	$P\bar{3}c1$, LaF_3	7.044		7.225		m.p. 1400°C/v.p.	[35]
	AmF_4	monoclinic	*C*2/*c*, UF_4	12.538	10.516	8.204	$\beta = 126.8$	AmF_3/F_2/v.p.	[36,37]
	AmO_2F_2	hexagonal	*R*3*m*	4.136		15.85			[38]
	AmF_6							KrF_2/HF(li); dark brown	[39]

	$NaAmF_4$	hexagonal	*P*6	6.109		3.731		AmO_2/HF–H_2/NaF	[40,41]
	$KAmF_4$	orthorhombic	*Pnma*	6.13	3.71	15.2			[42]
	K_3AmF_6	hexagonal	K_3LaF_6	22.75		7.56		AmO_2/HF–H_2/KF/650°C	[42]
	K_2AmF_5		K_2PrF_5						[42]
	KAm_2F_7	cubic	KEu_2F_7	5.857					[41,42]
	$(NH_4)_4AmF_8$	monoclinic	C2/*c*, $(NH_4)_4UF_8$					$Am(OH)_4$/NH_4F	[43]
	$LiAmF_5$	tetragonal	$I4_1/a$	14.63		6.449			[44]
	$K_7Am_6F_{31}$	hexagonal	*R*3	14.938		10.293		Am(III)/KF	[44,45]
	$Na_7Am_6F_{31}$	hexagonal	*R*3	14.48		9.665			[45]
	$RbAmF_4$	orthorhombic	*Pnma*	6.43	3.76	16.0			[42]
	Rb_2AmF_6	orthorhombic	*Cmcm*	6.962	12.001	7.579			[45,46]
	$KAmO_2F_2$	rhombohedral	*R*3*m*,$CaUO_4$	6.78			$\alpha = 36.25$	AmO_2+/KF	[47]
	$RbAmO_2F_2$	rhombohedral	*R*3*m*	6.789			$\alpha = 36.25$	AmO_2+/RbF	[48]
Germanate									
	$AmGeO_4$	Tetragonal	$I4_1/a$	5.04		11.03			[49]
Hydrides									
	AmH_2	fcc	*Fm*3*m*	5.348				AmH_{2+x}, $x = 0$–0.7	[50,51]
	AmH_3	trigonal	*P*3*c*1	6.68		6.75			[51]
Hydroxide									
	$Am(OH)_3$(am)	hexagonal	$Nd(OH)_3$	6.426		3.745		Am(III)/NaOH, Ksp $\sim 3 \times 10^{-18}$	[52]
	$Am(OH)_3$(cr)							Am_2O_3(s)/H_2O(g)	[53]
	$Am(OH)_4$							$Am(OH)_3$/NaOCl	[54]
	$LiAmO_2(OH)_2 \cdot xH_2O$							Am(V)/0.1–2 M LiOH	[55]
	$NaAmO_2(OH)_2 \cdot xH_2O$							Am(V)/0.1–0.5 M NaOH	[55]
	$KAmO_2(OH)_2 \cdot xH_2O$							Am(V)/0.1–0.5 M KOH	[55]
	$RbAmO_2(OH)_2 \cdot xH_2O$							Am(V)/0.1–0.5 M RbOH	[56]
	$CsAmO_2(OH)_2 \cdot xH_2O$							Am(V)/0.1–0.5 M CsOH	[56]
	$Na_2AmO_2(OH)_3 \cdot xH_2O$							Am(V)/2 M NaOH	[55]
	$K_2AmO_2(OH)_3 \cdot xH_2O$							Am(V)/2 M KOH	[55]
	$Rb_2AmO_2(OH)_3 \cdot xH_2O$							Am(V)/>2 M RbOH	[56]
	$Cs_2AmO_2(OH)_3 \cdot xH_2O$							Am(V)/>2 M CsOH	[56]
Iodides									
	AmI_2	monoclinic		7.677	8.311	7.925	$\beta = 98.46$	Am/H_2/I_2/vac.	[57]
	α-AmI_3	orthorhombic	*Ccmm*	4.31	14.03	9.92		AmO_2/AlI_3	[8,58]
	β-AmI_3	hexagonal	*R*3	7.42		20.55			[8,58]
	AmOI	tetragonal		4.011		9.204			[8,58]
Iodates									
	$Am(IO_3)_3$	monoclinic	$P2_1/c$	7.243	8.538	13.513	$\beta = 100.123$	Am/HCl/KIO_4/180°C	[59]
	K_3Am_3 $(IO_3)_{12} \cdot HIO_3$	triclinic		22.096	22.096	13.436	$\gamma = 120$	Am/KIO_4/180°C	[59]

Table 8.5 (*Contd.*)

Class	*Structural formula*	*Symmetry*	*Type*	*Lattice constants* a_0 (Å)	b_0 (Å)	c_0 (Å)	*Angle* (deg)	*Comments*	*References*
Molybdates									
	α-$Am_2(MoO_4)_3$	tetragonal	$I4_1/a$	5.24		11.52		$AmO_2/MoO_3/\sim 825°C$	[60,61]
	β-$Am_2(MoO_4)_3$	orthorhombic		9.095	10.527	10.820		$AmO_2/MoO_3/>850°C$	[60,61]
	$LiAm(MoO_4)_2$	tetragonal	$I4_1/a$, $LiGd(MoO_4)_2$	5.20		11.39		$Am_2(MoO_4)_3/Li_2MoO_4$	[61]
	$Am_2(MoO_4)_3$	tetragonal	scheelite						[60]
	$NaAm(MoO_4)_2$	tetragonal	scheelite	5.25		11.55			[61]
	$Na_5Am(MoO_4)_4$		$Na_5La(WoO_4)_4$	11.515		11.429		solid-state reaction	[61]
	$K_2Am(MoO_4)_4$							solid-state reaction	[61]
	$K_{10}Am(MoO_4)_8$							solid-state reaction	[61]
	K_3AmO_2							$AmO_2NO_3/K_6Mo_7O_{24}$	[62]
	$(Mo_2O_7)_2 \cdot nH_2O$								
	$(NH_4)_3AmO_2$							$AmO_2NO_3/(NH_4)_6$	[62]
	$(Mo_2O_7)_2 \cdot nH_2O$							Mo_7O_{24}	
	$AmO_2Mo_2O_7$							AmO_2SO_4/Na_2MoO_4, <100°C	[62]
Nitride									
	AmN	fcc	*Fm*3*m*,NaCl	5.000				$Am(AmH_3)/N_2$	[63,64]
Nitrate									
	$CsAmO_2(NO_3)_3$							$Cs_4AmO_2(CO_3)_3/2M$ HNO_3/O_3; evap	[25]
Oxides									
	AmO(?)	fcc	*Fm*3*m*	5.045				Am/Ag_2O	[63,65]
	A-Am_2O_3	hexagonal	*P*3*m*1	3.817		5.971		$AmO_2/H_2/800°C$	[66,70]
	B-Am_2O_3	monoclinic	*C*2/*m*	14.38	3.52	8.92	$\beta = 100.4$		[67,68]
	C-Am_2O_3	cubic	*Ia*3	11.03				600°C	[66,69,70]
	AmO_2	fcc	*Fm*3*m*	5.374				$^{241}AmO_2$, $^{243}AmO_2$	[70,71]
	AmO_{2-x}								[67,74]
	$LiAmO_2$								[1,72,73]
	Li_2AmO_3								[1,72,73]
	Li_8AmO_6	hexagonal	Li_8PbO_6	5.62		15.96			[1,72,73]
	Li_3AmO_4	tetragonal	Li_3UO4	4.459		8.355			[1,72,73]

Li_7AmO_6	hexagonal	*R*3	5.54		15.65			[1,72,73]
Li_4AmO_5	tetragonal	*I*4/*m*	6.666		4.415			[1,72,73]
Li_6AmO_6	hexagonal	Li_6ReO_6	5.174		14.59			[1,72,73]
K_2AmO_4	tetragonal	*I*4/*mmm*	4.286		13.05			[73]
Na_2AmO_3	monoclinic	*C*2/*c*	5.92	10.26	11.23	$\beta = 100.12$		[1,72,73]
Na_3AmO_4	fcc	*Fm*3*m*	4.757					[1,72,73]
Na_4AmO_5	fcc	*Fm*3*m*	4.70					[1,72,73]
Na_6AmO_6	hexagonal	Li_6ReO_6	4.76		16.10			[1,72,73]
$BaAm_2O_4$								[1,75]
$BaAmO_3$	cubic	perovskite	4.356					[1,75]
Ba_3AmO_6	cubic	*F*43*m*	8.81					[1,75]
$SrAm_2O_4$								[1,75]
$SrAmO_3$	cubic	perovskite	4.23					[1,75]
Sr_3AmO_6	cubic	Ba_3WO_6						[1,75]
Cs_2AmO_4	tetragonal	*I*4/*mmm*	4.364		14.65		$AmO_2/CsOH/O_2/$ 250°C	[76]
Rb_2AmO_4	tetragonal	*I*4/*mmm*	4.316		13.71		$AmO_2/RbOH/O_2/$ 250°C	[76]
$(Am_{0.30},Cm_{0.70})O_{2.00}$	fcc		5.368				350°C in O_2	[77]
$(Am_{0.30},Cm_{0.70})O_{1.83}$	fcc		5.433				550°C in O_2	[77]
$(Am_{0.30},Cm_{0.70})O_{1.685}$	rhombohedral		6.687			$\alpha = 99.47$	760°C in He	[77]
$(Am_{0.30},Cm_{0.70})O_x$	bcc		10.935				900°C in He	[77]
$(Am_{0.64},Cm_{0.36})O_{1.5}$	monoclinic		14.321	3.665	8.926	$\beta = 100.17$	1100°C in H_2/He	[77]
$(Am_{0.64},Cm_{0.36})O_{1.5}$	hexagonal		3.812		5.980		1500°C in H_2/He	[77]
$AmO–ZrO_2$	cubic	fluorite					18–100% $AmO_2/$ ZrO_2, SS	[1,78]
$AmO–HfO_2$							SS, extent unknown	[1,78]
$AmO–ThO_2$	cubic	fluorite					ThO_2/AmO_2, complete SS	[1]
α-$AmNbO_4$	monoclinic	I2	5.444	11.25	5.141	$\beta = 94.95$	AmO_2/Nb_2O_5	[1,2]
β-$AmNbO_4$	tetragonal	$I4_1/a$	5.30		11.34		α→β ~ 600°C	[1,2]
$Am_{0.33}NbO_3$	pseudo-tetragonal	*P*4/*mm*, $La_{0.33}TaO_3$	3.819		7.835			[1,2]
Ba_2AmNbO_6	cubic	*F*43*m*	8.520				$AmNbO_4/BaO$	[1,2]
$AmNbTiO_6$	orthorhombic	*Pnam*	5.34	11.00	7.53		$AmNbO_4/TiO_2$	[1,2]
$AmTaO_4$	monoclinic	*I*2	5.489	11.21	5.115	95.37	AmO_2/Ta_2O_5	[1,2]
$Am_{0.33}TaO_3$	tetragonal	*I*41/*a*	3.889		7.820		AmO_2/Ta_2O_5	[1,2]
Ba_2AmTaO_6	cubic	*F*43*m*	8.518					[1,2]
$AmTaTiO_6$	orthorhombic	*Pnam*	5.33	10.95	7.49			[2]
$AmPaO_4$	fcc	*Fm*3*m*	5.458				AmO_2/Pa_2O_5	[1,2]
Ba_2AmPaO_6	cubic	*F*43*m*	8.793				$(Am_{0.5}Pa_{0.5})$ O_2/BaO	[1,2,79]

Table 8.5 (*Contd.*)

Class	*Structural formula*	*Symmetry*	*Type*	*Lattice constants* a_0 (Å)	b_0 (Å)	c_0 (Å)	*Angle* (deg)	*Comments*	*References*
Phosphates									
	$AmPO_4$	monoclinic	$P2_1/n$	6.73	6.93	6.41	103.5	stable to 1000°C	[2]
	$AmPO_4 \cdot 0.5H_2O$	Hexagonal		6.99		6.39		pptn. dried at 200°C	[2]
	$NH_4AmO_2PO_4 \cdot 3H_2O$							Am(VI)/$NaHCO_3$/ $NH_4H_2PO_4$	[25]
	$NH_4AmO_2PO_4 \cdot zH_2O$	tetragonal	*P4/nmm* or *I4/mmm*	6.99		9.06		Am(VI)/0.1 M H_3PO_4/ pH 3.5, lemon yellow	[3]
	$KAmO_2PO_4 \cdot zH_2O$	tetragonal	*P4/nmm* or *I4/mmm*	6.91		9.00		Am(VI)/0.1 M H_3PO_4/ pH 3.5, lemon yellow	[3]
	$RbAmO_2PO_4 \cdot zH_2O$	tetragonal	*P4/nmm* or *I4/mmm*	6.94		9.02		Am(VI)/0.1 M H_3PO_4/ pH 3.5, lemon yellow	[3]
	$CsAmO_2PO_4 \cdot zH_2O$	tetragonal	*P4/nmm* or *I4/mmm*	6.94		8.82		Am(VI)/0.1 M H_3PO_4/ pH 3.5, lemon yellow	[3]
Phosphide									
	AmP	cubic	NaCl	5.711				AmH_3/P/580°C	[63,80]
Rhenate									
	$Am(ReO_4)_3$	hexagonal		10.11		6.26		AmO_2/aq $HReO_4$	[81]
								AmO_2/Re_2O_7/850°C	[81]
Scandate									
	$AmScO_3$	orthorhombic	*P6mm*, $GdFeO_3$	5.540	5.785	8.005		$AmO_2/H_2/Sc_2O_3$ oxidation yields fluorite	[82] [68]
Selenates									
	AmSe	cubic	NaCl	5.821				AmH_3/Se	[63]
	$AmSe_{2-x}$	tetragonal		4.096		8.347			[83]
	Am_3Se_4	bcc	*I43d*, Th_3P_4	8.799					[63,80,86]
Silicate									
	$AmSiO_4$	tetragonal	zircon	6.87		6.20		hydrothermal	[49]
Silicide									
	Am_5Si_3			11.419		5.538		AmF_3/Si/1050°C	[84]
	AmSi	orthorhombic		8.39	4.09	6.01		AmF_3/Si/1050°C	[85]
	Am_3Si_5. . .Am_2Si_3	hexagonal	Pu_3Si_5	3.871		4.120		AmF_3/Si/1050°C	[84]
	$AmSi_x$ ($x < 2$)	tetragonal	α-$ThSi_2$	4.02		13.7			[85]

Sulfates								
	$Am_2(SO_4)_3 \cdot 8H_2O$							[37]
	$Am_2O_2SO_4$							[37]
	$Am_2(SO_4)_3 \cdot 5H_2O$							[37]
	$KAm(SO_4)_2$							[37]
	$NaAm(SO_4)_2 \cdot H_2O$							[37]
	$KAm(SO_4)_2 \cdot 2H_2O$							[37]
	$RbAm(SO_4)_2 \cdot 4H_2O$							[37]
	$CsAm(SO_4)_2 \cdot 4H_2O$							[37]
	$TlAm(SO_4)_2 \cdot 4H_2O$							[37]
	$K_3Am(SO_4)_3 \cdot H_2O$							[37]
	$K_8Am_2(SO_4)_7$							[37]
	$Cs_8Am_2(SO_4)_7$							[37]
	$Tl_8Am(SO_4)_7$							[37]
	$\{[Co(NH_3)_6](HSO_4)_2[AmO_2(SO_4)_3]\} \cdot nH_2O$	cubic						[87]
	$(AmO_2)_2SO_4 \cdot nH_2O$						AmO_2OH/aqH_2SO_4/evap	[88]
	$CsAmO_2SO_4 \cdot nH_2O$						aq. Cs_2SO_4/$(AmO_2)_2SO_4$/evap	[88]
	$Co(NH_3)_6AmO_2(SO_4)_2 \cdot 2H_2O$							[88]
Sulfides								
	AmS	fcc	*Fm*3*m*	5.592				[89]
	Am_2O_2S	trigonal	*P*3*m*	3.91		6.772		[52]
	$AmS_{1.9}$	tetragonal		3.938		7.981		[52]
	α-Am_2S_3	orthorhombic	*Pnma*	3.98	6.39	15.36	α→γ ~ 1300°C	[89,90]
	β-Am_2S_3							[91]
	γ-Am_2S_3	bcc	*I*43*m*	8.434				[91]
	$Am_{10}S_{14}O_3$							[91]
Tellurides								
	$AmTe_2$	tetragonal		4.366		8.969	AmH_3/Te/heat	[63,92]
	$AmTe_3$	orthorhombic	*Bmmb*	4.399	4.339	25.57		[92]
	Am_2Te_3	orthorhombic	*Pbnm*	11.93	12.12	4.33		[93]
	Am_3Te_4	bcc	I43*d*	9.394				[93,96]
Titanates								
	$Am_2Ti_2O_7$	monoclinic		13.07		7.69	AmO_2/TiO_2/1200–1300°C	[94]
	$SrAm_2Ti_4O_{12}$	tetragonal		3.89		7.75	$SrCO_3$/AmO_2/TiO_2/1215°C	[94]
Tungstate								
	$Am_2(WO_4)_3$	tetragonal	$I4_1/a$					[60]

Table 8.5 (*Contd.*)

Class	*Structural formula*	*Symmetry*	*Type*	*Lattice constants* a_0 (Å)	b_0 (Å)	c_0 (Å)	*Angle* (deg)	*Comments*	*References*
Vanadates									
	$AmVO_3$	orthorhombic	*Pbnm*, $GdFeO_3$	5.45	5.58	7.76		AmO_2/V_2O_5	[1,2]
	$AmVO_4$	tetragonal	zircon	7.31		6.42			[1,2]
Xenate									
	$Am_4(XeO_6)_3 \cdot 40H_2O$								[95]

[1] (Keller and Walter, 1965); [2] (Keller, 1967); [3] (Lawaldt *et al.*, 1982); [4] (Eick and Mulford, 1969); [5] (Peterson, 1973); [6] (Baybarz, 1973b); [7] (Zachariasen, 1948b; Fried, 1951; Brown *et al.*, 1968; Pappalardo *et al.*, 1969b); [8] (Asprey *et al.*, 1965); [9] (Brown *et al.*, 1968); [10] (Ryan, 1967); [11] (Weigel *et al.*, 1979); [12] (Mitchell and Lam, 1970b); [13] (Runde *et al.*, 1992); [14] (Weigel and ter Meer, 1967); [15] (Fang and Keller, 1969); [16] (Runde and Kim, 1994); [17] (Nigon *et al.*, 1954); [18] (Coleman *et al.*, 1963); [19] (Keenan and Kruse, 1964); [20] (Volkov *et al.*, 1974); [21] (Ellinger and Zachariasen, 1954); [22] (Keenan, 1965); [23] (Burney, 1968); [24] (Yakovlev and Gorbenko-Germanov, 1955); [25] (Fedoseev and Perminov, 1983); [26] (Burns and Peterson, 1970, 1971); [27] (Lohr and Cunningham, 1951; Fuger and Cunningham, 1963); [28] (Weigel *et al.*, 1975); [29] (Bagnall *et al.*, 1968; Morss *et al.*, 1970); [30] (Bagnall *et al.*, 1967); [31] (Marcus and Shiloh, 1969); [32] (Schoebrechts *et al.*, 1989); [33] (Marcus and Bomse, 1970); [34] (Fedoseev *et al.*, 1991); [35] (Jones, 1951; Carniglia and Cunningham, 1955; Burnett, 1965, 1966); [36] (Asprey, 1954; Asprey and Keenan, 1958; Chudinov and Choporov, 1970; Connor, 1971); [37] (Yakovlev and Kosyakov, 1958a,b); [38] (Keenan, 1968); [39] (Drobyshevskii *et al.*, 1980); [40] (Keller and Schmutz, 1964); [41] (Schmutz, 1966); [42] (Jove and Pages, 1977); [43] (Asprey and Penneman, 1962); [44] (Keenan, 1966); [45] (Keenan, 1967); [46] (Kruse and Asprey, 1962); [47] (Asprey *et al.*, 1954a); [48] (Keenan, 1965); [49] (Keller, 1963); [50] (Katz and Seaborg, 1957); [51] (Olson and Mulford, 1966); [52] (Weaver and Shoun, 1971; Haire *et al.*, 1977); [53] (Morss and Williams, 1994); [54] (Cunningham, 1949; Penneman *et al.*, 1961); [55] (Tananaev, 1990b); [56] (Tananaev, 1991); [57] (Baybarz and Asprey, 1972); [58] (Asprey *et al.*, 1964); [59] (Bean *et al.*, 2003b); [60] (Freundlich and Pages, 1969; Tabuteau and Pages, 1978); [61] (Tabuteau *et al.*, 1972); [62] (Fedoseev and Budantseva, 1990); [63] (UCRL, 1959; Akimoto, 1967); [63] (Charvillat *et al.*, 1975a); [64] (Charvillat and Zachariasen, 1977); [65] (Zachariasen, 1949a); [66] (Templeton and Dauben, 1953); [67] (Chikalla and Eyring, 1968; Chikalla *et al.*, 1973); [68] (Berndt *et al.*, 1974; Keller and Berndt, 1975); [69] (Eyring *et al.*, 1949, 1952); [70] (Hurtgen and Fuger, 1977); [71] (Fahey *et al.*, 1974); [72] (Keller *et al.*, 1965b); [73] (Hoekstra and Gebert, 1978); [74] (Chikalla and Eyring, 1967); [75] (Keller, 1964); [76] (Hoekstra and Gebert, 1978); [77] (Mosley, 1970); [78] (Radzewitz, 1966); [79] (Keller, 1965); [80] (Charvillat *et al.*, 1975b); [81] (Silvestre *et al.*, 1977); [82] (Keller *et al.*, 1972); [83] (Damien and Jove, 1971); [84] (Wittmann, 1980); [85] (Burns and Baybarz, 1972; Weigel *et al.*, 1977); [86] (Mitchell and Lam, 1970a; Roddy, 1974); [87] (Ueno and Hoshi, 1971); [88] (Fedoseev and Budentseva, 1989); [89] (Damien, 1971); [90] (Zachariasen, 1949d); [91] (Damien *et al.*, 1972, 1975, 1976); [92] (Burns *et al.*, 1979); [93] (Damien and Charvillat, 1972); [94] (Shoup and Bamberger, 1997); [95] (Marcus and Cohen, 1966).

temperatures of 600–800°C (Eyring *et al.*, 1952; Baybarz, 1960; Chikalla and Eyring, 1967; Hurtgen and Fuger, 1977; Morss and Fuger, 1981). This stoichiometry of the black oxide is believed to be $AmO_{2.00}$ (Chikalla and Eyring, 1967, 1968) and is better than $AmO_{1.99}$ even at 1000°C in oxygen (Chikalla and Eyring, 1967). It undergoes an expansion of its fcc lattice constant due to radiation damage, which reversibly broadens the diffraction lines at low temperatures in both $^{241}AmO_2$ and $^{243}AmO_2$ (Hurtgen and Fuger, 1977; Benedict and Dufour, 1980). Benedict and Dufour (1980) studied the variation of the lattice parameter, of the thermal linear expansion, and of the coefficient of thermal linear expansion for AmO_2 in the range 38–300 K. Upon cooling, AmO_2 contracts more strongly than the dioxides of the lower actinides. The lattice parameters quoted in Table 8.3 represent an extrapolation to zero time for both $^{241}AmO_2$ and $^{243}AmO_2$ (Fahey *et al.*, 1974; Hurtgen and Fuger, 1977).

There is no evidence for any binary oxide of americium higher than AmO_2 (Katz and Gruen, 1949; Templeton and Dauben, 1953). However, ternary oxides are known for Am(III) through Am(VI) (Keller, 1964, 1965; Keller *et al.*, 1965b; Radzewitz, 1966; Mosley, 1970; Keller *et al.*, 1972; Keller and Berndt, 1975; Hoekstra and Gebert, 1978). Stabilization of high oxidation states in complex oxides is frequently observed (Keller, 1964, 1967; Morss, 1982); excellent examples are the thermally stable Am(VI) compounds Cs_2AmO_4 and Ba_3AmO_6. Most complex oxides of americium have been prepared by Keller and Hoekstra and their coworkers (Keller, 1964, 1967; Keller *et al.*, 1965b; Hoekstra and Gebert, 1978).

Initially, americium was prepared in significant quantities as $Am(OH)_3$ and to date hydroxide phases are known for the oxidation states III–VI. Isostructural to its chemical analog $Nd(OH)_3$, the Am(III) hydroxide is by far the most important americium hydroxide for separation and purification purposes and its solubility has been widely studied. The pinkish amorphous hydroxide precipitates by addition of dilute hydroxide to Am(III) solutions under ambient conditions. Rod-like microcrystalline $Am(OH)_3$, similar to $Nd(OH)_3$, is obtained in water after heating at 80°C for about 90 min (Milligan and Beasley, 1968). The transformation rate depends on various experimental parameters, such as solution composition, basicity, temperature, radiolysis, and the (pre)treatment of the precipitate. The crystalline phase can also be obtained by boiling a $^{241}Am(OH)_3$ suspension in 5 M NaOH (Silva, 1982) or hydration of Am_2O_3 with steam at 225°C (Morss and Williams, 1994). The destruction of the crystalline phase by its own alpha-radiation depends strongly on the specific activity of the isotope used: complete degradation is obtained within 1 day using ^{244}Cm(III) (specific activity 3000 MBq mg^{-1}) and 5 months with ^{241}Am(III) (specific activity 120 MBq mg^{-1}) (Haire *et al.*, 1977). The complex aging behavior of $Am(OH)_3$ in aqueous solutions and the changes in particle size result in large differences in its solubility. Nevertheless, two thermodynamic solubility products for the reaction

$$Am(OH)_3 + 3H^+ = Am^{3+} + 3H_2O$$

have been recommended: $\log K^\circ = 15.2 \pm 0.6$ for crystalline $Am(OH)_3$ and 17.0 ± 0.6 for amorphous $Am(OH)_3$ (Silva *et al.*, 1995).

Few attempts to prepare and characterize $Am(OH)_4$ were reported, probably due to the instability of Am(IV). A black precipitate of $Am(OH)_4$ was obtained by heating $Am(OH)_3$ at 90°C in 0.2 M NaOH with NaOCl or in 7 M KOH with peroxydisulfate (Penneman *et al.*, 1961). The dissolution of this precipitate in sulfuric or nitric acid leads to a mixture of Am(III), Am(V), and Am(VI). Structural and thermodynamic data on $Am(OH)_4$ are not known. $AmO_2(OH)$ has been suggested to precipitate in slightly basic concentrated NaCl solutions under inert atmosphere but the amorphous character of the solid phase inhibited characterization (Magirius *et al.*, 1985; Stadler and Kim, 1988; Giffaut and Vitorge, 1993; Runde and Kim, 1994; Runde *et al.*, 1996). In more concentrated hydroxide solutions ternary Am(V) hydroxides, yellow $MAmO_2(OH)_2 \cdot nH_2O$ at 0.1–0.5 M OH^- and rose-colored $M_2AmO_2(OH)_3 \cdot nH_2O$ (M = Na, K, Rb, Cs) at 0.5–2.0 M OH^- (Tananaev, 1990b, 1991), form, and were characterized by X-ray diffraction. Only the lithium compound appeared to be stable over the entire range of hydroxide concentrations. No information on Am(VI) hydroxides is available.

(b) Hydrides

Olson and Mulford (1966) characterized the ^{241}Am–hydrogen system and found parallels to the lanthanides. The reported AmH_{2+x} (fcc) phase is isostructural with NpH_{2+x}, PuH_{2+x}, and most of the rare earth dihydrides (Roddy, 1973). There is also a phase that approximates hexagonal AmH_3. Although the lattice parameters were reported to be $a_0 = 3.77$ Å and $c_0 = 6.75$ Å (Olson and Mulford, 1966), Keller (1971) has pointed out that recent data on HoD_3 makes the most probable space group $P3c1$ (lattice parameters are given in Table 8.3). A study by Roddy (1973) with ^{243}Am essentially confirms this conclusion.

(c) Halides

A number of americium halides have been synthesized with americium in oxidation states II–VI and the halide systems have been studied extensively. Most remarkable are the halides of americium in extreme oxidation states, i.e. divalent and hexavalent. While solid structures are rare for divalent americium compounds, the black halides, $AmCl_2$ and $AmBr_2$ (Baybarz, 1973b), and AmI_2 (Figure 8.8) (Baybarz and Asprey, 1972) were prepared by reacting metallic americium with the corresponding mercuric halides at 300–400°C. The dihalides cannot be prepared by hydrogen reduction of the Am(III) halides, although

hydrogen reduction is successful for the chemical analog lanthanides Sm, Eu, and Yb. Interestingly, all three compounds crystallize in different lattices: orthorhombic $AmCl_2$, tetragonal $AmBr_2$, and monoclinic AmI_2.

(1) Am(III): A number of Am(III) halides have been synthesized and their compositions range from binary AmX_3 adducts such as $AmCl_3 \cdot MCl$ where MCl is LiCl, CsCl, $(C_4H_9)_4NCl$, or $(C_2H_5)_4NCl$, to ternary complexes, i.e. $MAmX_4$, M_2AmX_5, KAm_2F_7, and M_2AmX_6 and M_3AmX_3. In addition, Bagnall *et al.* (1968) and Morss *et al.* (1970) made the cubic derivative $Cs_2NaAmCl_6$, in which the americium atoms are surrounded by six chlorides in an octahedral environment. The iodide AmI_3 is the only actinide triiodide known to be dimorphic; spectrophotometric observations indicate a pressure-induced phase transition from the rhombohedral to the orthorhombic structure (Haire *et al.*, 1985). The compound $(NH_4)_2AmCl_5$ decomposes at 300°C under vacuum to form $AmCl_3$ (Schleid *et al.*, 1987). Crystal structures have been reported for AmF_3 (Templeton and Dauben, 1953), $AmCl_3$ (Burns and Peterson, 1970) and $AmCl_3 \cdot 6H_2O$ (Burns and Peterson, 1971), $AmBr_3$ and AmI_3 (Zachariasen, 1948b; Baybarz and Asprey, 1972), and AmOX (X = Cl Figure 8.8 (Templeton and Dauben, 1953), Br (Weigel *et al.*, 1979) and I (Baybarz and Asprey, 1972)). Octahedral $AmCl_6^{3-}$ and $AmBr_6^{3-}$ can be prepared as triphenyl phosphonium salts in anhydrous ethanol (Ryan, 1967; Marcus and Bomse, 1970).

(2) Am(IV): Orange-pink crystals of orthorhombic Rb_2AmF_6 form in concentrated aqueous fluoride solutions with $RbAmO_2F_2$ or $Am(OH)_4$ (Kruse and Asprey, 1962).

(3) Am(V): The ternary Am(V) fluorides, $KAmO_2F_2$ (Asprey *et al.*, 1954a) and $RbAmO_2F_2$, precipitate from concentrated aqueous fluoride solutions of Am(V) and consist of $AmO_2F_2^-$ connected by K^+ or Rb^+ cations. In contact with acidic RbF solution, $RbAmO_2F_2$ reduces overnight to Rb_2AmF_6 (Kruse and Asprey, 1962). The green chloride $Cs_3AmO_2Cl_4$ precipitates with ethanol from 6 M HCl containing Am(V) hydroxide and CsCl (Bagnall *et al.*, 1968) and is isostructural with the analogous Np(V) compound (Bagnall *et al.*, 1967).

(4) Am(VI): The binary Am(VI) fluoride AmO_2F_2 was prepared by reacting solid sodium Am(VI) acetate with anhydrous HF containing a small amount of F_2 at −196°C (Keenan, 1968). The compound is isostructural with other actinyl(VI) fluorides. Dark-red $Cs_2AmO_2Cl_4$ is obtained by the unusual oxidation of $Cs_3AmO_2Cl_4$ in concentrated HCl (Bagnall *et al.*, 1967). The cubic form of $Cs_2AmO_2Cl_4$ appears to transform to a monoclinic form when washed with small volumes of concentrated HCl (Bagnall *et al.*, 1968). It is suggested that the cubic form is probably a mixed oxidation state compound of formula $Cs_7(AmO_2)(AmO_2)_2Cl_{12}$ (Melkaya *et al.*, 1982).

Conflicting claims have been put forth concerning the existence of AmF_6. Drobyshevskii *et al.* (1980) reported generating a solid by reaction of AmF_3

with KrF_2 in anhydrous HF and inferred its composition to be AmF_6 based upon its volatility, IR spectrum, and hydrolysis to AmO_2^{2+}; the IR absorption band at $604 \pm 3\ cm^{-1}$ is expected for the ν_3 mode of AmF_6. Fargeas *et al.* (1986) also inferred the existence of AmF_6 in their experiments from thermochromatography data. Most recently, Gibson and Haire (1992b) report that they were not able to confirm the existence of AmF_6; in their words, "... but have not been able to identify or provide evidence for the elusive and controversial AmF_6 species, despite having invoked several synthetic approaches and the sensitive analytical tool of mass spectrometry." Given these latest results, we have elected not to list AmF_6 among the identified inorganic compounds of americium in Table 8.5. It is interesting to note, however, that the proposed hexachloro compound of Am(VI) appears to be sufficiently stable to permit X-ray crystallographic studies.

(d) Chalcogenides and pnictides

The chalcogenides of americium comprise a number of compounds with the general formula AmX (X = S, Se, Te), $AmTe_2$, Am_3X_4 (X = S, Se, Te), AmX_3 (X = S, Se, Te), Am_2X_3 (X = S, Se, Te), and substoichiometric compounds AmX_{2-n} (X = S, Se). Some structural and synthetic properties of these chalcogenides, insofar as they have been determined, are briefly listed in Table 8.5; additional details concerning these compounds are provided in this section. The authors of this chapter are not aware that the chalcogenides are of any but academic interest.

The reaction of AmH_3 with stoichiometric amounts of selenium or telluride metal at 800°C in a vacuum yields the monochalcogenides AmSe and AmTe, respectively (Charvillat *et al.*, 1975a, 1977). Further heating of the monochalcogenides at 1100–1200°C produces Am_3X_4 and a second phase that was identified as (probably unreacted) AmX (Charvillat *et al.*, 1975a, 1977). In contrast, α-Am_2S_3 and not AmS is obtained when AmH_3 is heated with elemental sulfur at 500°C; it decomposes to γ-Am_2S_3 and AmS when heated in a vacuum above 650°C (Damien, 1971).

Americium sesquisulfide exhibits a complex structural chemistry and apparently exists in three different crystalline forms. α-Am_2S_3 is obtained by vapor-phase reaction for 4 days of a stoichiometric amount of sulfur with AmH_3 in a quartz and Pyrex tube sealed under high vacuum (Damien, 1971). The quartz end of the tube is heated at 500°C and the Pyrex part is maintained at 300°C to prevent sulfur from condensing. According to Damien *et al.* (1972), α-Am_2S_3 transforms into β-Am_2S_3 when heated at 1100°C. However, the existence of the β-form of americium sesquisulfide is seriously in doubt since the same French scientists believe that β-Am_2S_3 is better considered an oxysulfide, namely $Am_{10}S_{14}O$. When heated in a vacuum at 1300°C, α-Am_2S_3 changes to pure γ-Am_2S_3 (Damien, 1971). The pure γ-Am_2S_3 can also be prepared by passing a mixture of H_2S and CS_2 over heated (1400–1500°C) AmO_2 for 5 min

(Fried, 1951). Zachariasen (1949d) determined the crystal structure of γ-Am_2S_3. Am_2Te_3 is formed by dissociation of $AmTe_2$ at 600°C and is isostructural with the rare earth sesquitellurides (η-form) (Damien and Charvillat, 1972). The Am_2Te_3 phase is stable up to around 850°C and transforms into Am_3Te_4 above 900°C. No sesquiselenide of americium has been reported.

The only americium trichalcogenide yet reported, $AmTe_3$, is prepared by vapor-phase reaction of AmH_3 with excess tellurium for 120 h at 350°C (Damien, 1972; Burns *et al.*, 1979). Orthorhombic $AmTe_3$ is isostructural with the corresponding rare earth tritellurides and is used as a precursor for the synthesis of a number of americium/tellurium compounds. In a high vacuum at 400°C, $AmTe_3$ dissociates to tetragonal $AmTe_2$, which is the only stoichiometric americium dichalcogenide. $AmTe_2$ is isostructural with the rare earth ditellurides and most likely has the Fe_2As-type structure. Roddy (1974) prepared what appeared to be tetragonal $AmSe_2$ by heating ^{243}Am metal or hydride with selenium metal for 24 h at 950°C. However, although two research groups (Charvillat *et al.*, 1977; Burns *et al.*, 1979) reported the preparation and properties of $AmTe_2$, Damien and Jove (1971) state that the $AmTe_2$ prepared as described above is rather a tellurium-deficient compound $AmTe_{2-x}$ with a large homogeneity range between 400 and 600°C. The same homogeneity range seems to exist in the Am–S and Am–Se system and the dichalcogenides actually have a composition near $AmS_{1.9}$ and $AmSe_{1.8}$. The black non-stoichiometric compounds are prepared by heating an excess of sulfur or selenium metal with AmH_3 for 1 week at 400°C under high vacuum (Damien and Jove, 1971).

The americium chalcogenides Am_3Se_4 and Am_3Te_4 are isostructural (bcc) with Th_3P_4 and are without magnetic ordering down to 4.2 K (Dunlap *et al.*, 1972). Both compounds can be prepared by heating ^{243}Am metal with elemental selenium or tellurium for 24 h at 950°C (Roddy, 1974). However, X-ray diffraction measurements show that this synthesis contains at least one other phase (Dunlap *et al.*, 1972). Am_3Se_4 (bcc) is also formed when a mixture of 50 mass% americium metal and 50 mass% elemental selenium is heated for 1 h at 217°C and then for 7 h at 850°C before cooling to room temperature (Mitchell and Lam, 1970a). Am_3Te_4 also forms by decomposition of η-Am_2Te_3 at 900°C (Damien and Charvillat, 1972).

Compounds of americium with all group VB elements N, P, As, Sb, and Bi have been prepared. While AmN is of most interest due to its potential use as nuclear reactor fuel, the americium pnictides are mainly of academic interest. Ogawa *et al.* (1997) note that certain actinide nitrides, e.g. UN, NpN, PuN, can be fabricated by carbothermic reduction of their oxides in a nitrogen atmosphere. Based upon the thermodynamics of the carbothermic synthesis of AmN, calculations indicate that the carbothermic preparation of AmN would be much more difficult than preparation of either UN or PuN.

Americium nitride, AmN, was first prepared by reacting AmH_3 (above 800°C) or americium metal (at 750°C) with nitrogen (Akimoto, 1967; Tagawa, 1971) or in a 99.9% N_2/0.1% H_2 atmosphere (Radchenko *et al.*, 1982). Potter

and Tennery (1973) disclosed a cyclic process to prepare finely divided AmN, which consists of incrementally dehydriding AmH_3 and nitriding the metal. Charvillat *et al.* (1975a, 1977) prepared milligram quantities of AmN by heating AmH_3 at 550°C under high-purity nitrogen in a sealed tube. A review of the phase behavior and crystal structure of actinide nitrides has been published (Tagawa, 1971).

The only reported synthesis of AmP was published a quarter of a century ago. Charvillat *et al.* (1975a,b, 1977) synthesized AmP by reacting red phosphorus with AmH_3 in a sealed quartz tube at 580°C.

The product of the vapor-phase reaction of excess elemental arsenic with $^{241}AmH_3$ at 330°C contains both unreacted elemental arsenic and a cubic phase that was assigned as AmAs by analogy with the corresponding NpAs and PuAs (Charvillat and Damien, 1973). Heating ^{243}Am metal and elemental arsenic for 24 h at 675°C and then 7 days at 400°C produces AmAs with slightly higher lattice parameters (Roddy, 1974). However, a slight decrease in the lattice parameters is observed after heating AmAs for 10 h at 1000°C. Weak lines that correspond to AmO are observed in the X-ray diffraction pattern of the resulting product indicating the existence of a solid solution between AmAs and AmO. The slight difference in lattice parameters may have been the result of an isotope effect or may be attributed to other minor americium oxide impurities.

The reaction of ^{243}Am metal with elemental antimony for 23 h at 775–900°C in an evacuated quartz bulb yielded cubic AmSb (Roddy, 1974). Cubic AmSb with almost the same lattice parameters was obtained by heating equimolar amounts of ^{241}Am metal and high-purity elemental antimony under vacuum for 1 h at 630°C (Mitchell and Lam, 1970a). The temperature was gradually raised to 850°C and held at this temperature for 7 h before cooling to room temperature. Finally, the resulting AmSb was heated at 1000°C for 24 h, cooled, and then heated again at 400°C for 10 days. The reaction of a 4:3 stoichiometric ratio of $^{241}AmH_3$: elemental antimony in a Pyrex tube at 550°C produced two phases, AmSb and a second phase with the bcc structure of anti-Th_3P_4-type (Charvillat *et al.*, 1975b).

Like AmP, AmBi has also been investigated. Roddy (1974) produced AmBi by reaction of metallic bismuth vapor with either americium metal or americium hydride in a sealed, evacuated quartz tube for 48 h at 975°C.

The magnetic susceptibilities of actinide chalcogenides and pnictides can be fit by the modified Curie–Weiss law:

$$\chi_{\text{measured}} = \chi_{\text{Curie+Weiss}} + \chi_0 = (C/(T - \theta_{\text{para}})) + \chi_0$$

where C is the Curie constant, θ_{para} is the paramagnetic Curie temperature, and χ_0 is a generally temperature-independent additional term. For the americium compounds, the Curie–Weiss term vanishes and experimentally determined values for χ_0 are reported to be 777 for AmN, 550 for AmAs, 1250 for AmSb, and 500 for AmBi (Kanellakopulos *et al.*, 1975; Vogt *et al.*, 1998).

The effective magnetic moment of AmN is 136 Bohr magnetons (Nellis and Brodsky, 1974; Kanellakopulos *et al.*, 1975) and that of AmAs is 1.14 Bohr magnetons (Kanellakopulos *et al.*, 1975). Kanellakopulos measured the magnetic susceptibility of AmAs between liquid helium and room temperature and observed an antiferromagnetic transition at 13 K. Magnetic susceptibility measurements on AmSb show a temperature-independent value of $\chi_0 = (1250 \pm 100) \times 10^{-6}$ emu mol^{-1} for the range 4.2 K $< T <$ 320 K (Dunlap *et al.*, 1972).

(e) Carbides and carbonates

The binary Am(III) carbide, Am_2C_3, is the only known carbide of americium and is prepared by arc melting americium metal with high-purity graphite in an argon–helium atmosphere (Mitchell and Lam, 1970b). The compound is isostructural with Pu_2C_3.

Carbonate compounds of Am(III) and Am(V) have been synthesized and characterized. They are applied in separation processes and also may form under environmental conditions. No solid carbonates of Am(IV) or Am(VI) are known.

(1) Am(III): The binary Am(III) carbonate, $Am_2(CO_3)_3$, precipitates from a CO_2-saturated solution of $NaHCO_3$ (Meinrath and Kim, 1991b; Runde and Kim, 1994). Thermogravimetric analysis of the precipitated binary compound suggests the formula $Am_2(CO_3)_3 \cdot 2H_2O$ (Weigel and ter Meer, 1967) or $Am_2(CO_3)_3 \cdot 4H_2O$ (Keller and Fang, 1969). The ternary compounds $NaAm(CO_3)_2 \cdot 4H_2O$ and $Na_3Am(CO_3)_3 \cdot 3H_2O$ precipitate from 0.5 M $NaHCO_3$ and 1.5 M Na_2CO_3 solutions, respectively (Keller and Fang, 1969). In analogy to neodymium and europium hydroxycarbonates, orthorhombic $AmOHCO_3$ was characterized by X-ray powder diffraction data (Meinrath and Kim, 1991b; Runde *et al.*, 1992), but the formation of its hexagonal form (Standifer and Nitsche, 1988) could not be confirmed.

(2) Am(V): A number of 'double carbonates' of general formula $MAmO_2CO_3$ where M = K (Nigon *et al.*, 1954; Volkov *et al.*, 1974), Na (Nigon *et al.*, 1954; Runde and Kim, 1994), Rb, Cs, NH_4 (Nigon *et al.*, 1954) have been synthesized by precipitation of Am(V) in dilute bicarbonate solutions of the corresponding cation. The use of large excess of alkali carbonate yields the $K_3AmO_2(CO_3)_2$ and $K_5AmO_2(CO_3)_3$ solids (Yakovlev and Gorbenko-Germanov, 1955; Volkov *et al.*, 1981).

(f) Phosphates and sulfates

Light pink $AmPO_4 \cdot xH_2O$ precipitates by adding dilute solutions of H_3PO_4, Na_2HPO_4, or $(NH_4)_2HPO_4$ to a weakly acidic Am^{3+} solution (Lawaldt *et al.*, 1982; Fedoseev and Perminov, 1983; Rai *et al.*, 1992). Rai and coworkers

suggest the precipitation of $AmPO_4 \cdot xH_2O$ from dilute acidic solution but the study lacks characterization of the solid phase. Dehydration of the hydrous precipitate yields hexagonal $AmPO_4 \cdot 0.5H_2O$ at 200°C and $AmPO_4$ at higher temperatures up to 1000°C. The anhydrous compound can also be obtained by reacting AmO_2 with stoichiometric amounts of $(NH_4)_2HPO_4$ at 600–1000°C.

Because of the tendency of Am(VI) towards reduction to Am(V) at near-neutral pH, Am(VI) phosphates can be precipitated only in the narrow pH range of 3.5–4. Four ternary Am(VI) phosphates $MAmPO_4 \cdot xH_2O$ with M = NH_4, K, Rb, Cs have been prepared by Lawaldt *et al.* (1982) by precipitating Am(VI) in 0.1 M H_3PO_4 after adjusting the pH with the corresponding carbonate solution.

Binary sulfate compounds are known for Am(III), Am(V), and Am(VI), especially a large number of double sulfates of Am(III).

(1) Am(III): Evaporation of a neutral solution of ^{243}Am(III) sulfate yields thick, up to 0.5 mm long, tabular, pale yellow-pink crystals of $Am_2(SO_4)_3 \cdot 8H_2O$ (Burns and Baybarz, 1972). Crystals of the octahydrate, after being dried in air, are stable to change in their degree of hydration for several days. On the basis of analyses for americium, sulfate, and water, Yakovlev *et al.* (1958) assign the formula $Am_2(SO_4)_3 \cdot 5H_2O$ to the precipitate obtained by adding ethanol to a solution of Am(III) in 0.5 M H_2SO_4. The white anhydrous Am(III) sulfate, $Am_2(SO_4)_3$, is prepared by heating the hydrate to a temperature of 500–600°C in air (Hall and Markin, 1957). Anhydrous americium sulfate does not take up water when cooled to room temperature in air.

A number of double sulfates of Am(III) with formulas $MAm(SO_4)_2 \cdot xH_2O$ (M = K, Na, Rb, Cs, Tl; x = 0, 1, 2, 4), $K_3Am(SO_4)_3 \cdot xH_2O$, and $M_8Am_2(SO_4)_7$ (M = K, Cs, Tl) have been prepared by adding a metal sulfate solution to a solution of Am^{3+} in 0.5 M H_2SO_4. The concentration ratios M^+/Am^{3+} for the preparation of the various double sulfates as well as the absorption spectra of some Am(III) double sulfates at 80, 200, and 300 K are given by Yakovlev *et al.* (1958). Surprisingly, no X-ray diffraction data were reported for these double sulfates. Coprecipitation of trace amounts of Am(III) with K_2SO_4 and $La_2(SO_4)_3$ has also been published (Grebenshschikova and Babrova, 1958, 1961; Grebenshschikova and Cheinyavskaya, 1962).

(2) Am(V): Fedoseev and Budentseva (1989) claimed the preparation of three solid sulfates of Am(V). $(AmO_2)_2(SO_4) \cdot xH_2O$ crystallizes upon evaporation of an Am(V)-containing sulfuric acid solution. Am(V) sulfate also crystallizes from an ozonated solution of $Am(OH)_3$ after addition of sulfuric acid and subsequent evaporation. Two double salts have been reported: Large light green crystals of $CsAmO_2SO_4 \cdot xH_2O$ were obtained by evaporating a solution containing $(AmO_2)_2(SO_4)$ and Cs_2SO_4 in a 3:1 ratio. According to Fedoseev and Budentseva $Co(NH_3)_6AmO_2(SO_4)_2 \cdot 2H_2O$ can be easily

made by simply including Am(V) among the reagents used to prepare $Co(NH_3)_6(SO_4)_2$.

(3) Am(VI): Addition of hexamine cobalt(III) ions to an aqueous sulfate solution containing hexavalent americium yields orange cubic crystals of $Co(NH_3)_6(HSO_4)_2(AmO_2(SO_4)_3) \cdot nH_2O$ (Ueno and Hoshi, 1971). The compound is isostructural with the corresponding uranyl and neptunyl compounds. No precipitate forms, however, in an ammonium sulfate solution containing Am(III) and hexamine cobalt(III) ions.

(g) Other inorganic compounds

Shirokova *et al.* (2001) reported the complexation of Am(III) with *N*,*N*-dimethylacetamide and the Keggin-type heteropolyanion $PW_{12}O_{40}^{3+}$. Lawaldt *et al.* (1982) applied the same procedures as used to prepare Am(VI) phosphates for the precipitation of Am(VI) arsenates. The obtained compounds were isostructural to the analogous Am(VI) phosphates.

Only two phases, AmB_4 and AmB_6, have been reported in the boride system in contrast to the richer Np–B system with four phases (Eick and Mulford, 1969).

Weigel *et al.* (1977, 1984) reported the formation of several silicide phases upon reacting AmF_3 with elemental Si at different temperatures. Up to 950°C, the phases Am_5Si_3, AmSi, Am_2Si_3, and $AmSi_2$ have been characterized by X-ray powder diffraction. Orthorhombic AmSi is also prepared at 1050°C and the substoichiometric tetragonal phase $AmSi_x$ ($1.87 < x < 2.0$) forms at 1150–1200°C.

The only silicate known to date, $AmSiO_4$, is obtained as a brown solid by reacting $Am(OH)_4$ with excess SiO_2 in 1 M $NaHCO_3$ solution at 230°C for 1 week (Katz and Seaborg, 1957). $^{241}AmSiO_4$ is patented for the use in manufactured alpha sources.

Large orange needle-like crystals thought to be $AmO_2CrO_4 \cdot H_2O$ were prepared by slowly evaporating a chromic acid (H_2CrO_4) solution containing Am(V) (Fedoseev *et al.*, 1991). Although there is some spectroscopic evidence for the presence of Am(V) in the solid chromate (electronic absorbances at about 518 and 728 nm) the suggested formula of $AmO_2CrO_4 \cdot H_2O$ appears to be erroneous and should rather be $(AmO_2)_2CrO_4 \cdot H_2O$.

Tabuteau and coworkers (Tabuteau *et al.*, 1972; Tabuteau and Pages, 1978) investigated the Am–molybdate and Am–tungstate systems. The solid state reaction of stoichiometric amounts of AmO_2 and MoO_3 or WO_3 at 1080°C resulted in the formation of monoclinic $Am_2(MoO_4)_3$ and $Am_2(WO_4)_3$. Two ternary phases, $KAm(MoO_4)_2$ and $K_5Am(MoO_4)_4$, were found to form at 650°C in the presence of potassium. Fedoseev and Budantseva (1990) report the synthesis of $AmO_2Mo_2O_7 \cdot 3H_2O$ at 100°C, however, no information on the phase characterization was provided.

8.7.2 Compounds of americium with organic ligands

Relatively few solid compounds of americium with organic ligands have been prepared; these are listed in Table 8.6. For detailed reviews of this chemistry see Kanellakopulos (1979) and also Chapters 23 and 25.

(a) Oxalate

Because of its importance for americium separation chemistry $Am_2(C_2O_4)_3 \cdot xH_2O$ (Weigel and ter Meer, 1967) is the most important organic compound of americium. The pink solid precipitates from slightly acidic or neutral solutions of Am^{3+} on addition of oxalic acid or alkali oxalate solution. The hydration number x was previously thought to vary with conditions of preparation and drying and values of 7 (Markin, 1958), 9 (Yakovlev and Kosyakov, 1958a), and 11 (Staritzky and Truitt, 1954) have been reported. Based on their X-ray diffraction studies and in analogy to Nd(III), Pu(III), and Cm(III), Weigel and ter Meer (1967) concluded that the hydration number x is 10. The decahydrate decomposes to the anhydrous form at 340°C through several hydrates and further decomposes to carbonate $Am_2(CO_3)_3$ at about 430°C. The oxalate complexes with general formula $MAm(C_2O_4)_2 \cdot xH_2O$ have been prepared from Am(III) oxalate and $M_2C_2O_4$ ($M = NH_4$, Na, K, Cs) in neutral solution (Zubarev and Krot, 1982, 1983a,b).

(b) Formate

Pink crystals of hexagonal $Am(HCOO) \cdot 0.2H_2O$ form upon evaporation of a concentrated formic acid solution (Weigel and ter Meer, 1967). The formate decomposes at 300–350°C to AmO(HCOO), and at 400–500°C to the oxycarbonate $Am_2O_3CO_3$, which forms at 520°C the sesquioxide Am_2O_3 (Weigel and ter Meer, 1971).

(c) Acetate

Addition of sodium acetate to an acidic Am(VI) solution precipitates lemon-yellow cubic crystals of $NaAmO_2(OOCCH_3)_3$ (Asprey *et al.*, 1950, 1951). The force constant of the Am–O bond in $NaAmO_2(OOCCH_3)_3$ is determined to be 6.12 megadynes/Å (Jones, 1953). The refractive index is 1.528 ± 0.002 (Asprey *et al.*, 1951).

(d) Acetone derivate compounds

Addition of ammonia to aqueous Am^{3+} solution that contains a small amount of acetylacetone precipitates pale-rose $Am(C_5H_7O_2)_3 \cdot H_2O$ at pH 6. The precipitate can be recrystallized in ethanol and dried in air over silica gel or P_2O_5 (Keller and Schreck, 1969). Dropwise addition of aqueous Am^{3+} (pH 4.5) to warm, slightly less than stoichiometric amounts of ammonium benzoylacetone yields pale-rose $Am(C_{10}H_6F_3O_2)_3 \cdot 3H_2O$. Both compounds decompose in air at

Table 8.6 *Organic compounds of americium.*

Organic ligand	*Formula of compound*	*Comments*	*References*
Acetate	$NaAmO_2(OOCCH_3)_3$	lemon yellow	[1]
acetylacetone	$Am(C_5H_7O_2)_3 \cdot H_2O$	pale rose	[2]
benzoyltrifluoroacetone	$Am(C_{10}H_6F_3O_2)_3 \cdot 3H_2O$	pale rose	[2]
cyclooctatetraene	$KAm(C_8H_8)_2 \cdot 2THF$[a]	yellow	[3]
cyclopentadiene	$Am(C_5H_5)_3$	flesh	[4]
dipivalomethane	$Am(C_{11}H_{19}O_2)_3$		[5]
formate	$Am(HCOO)_3 \cdot 0.2H_2O$	pink	[6]
hexafluoroacetylacetone	$CsAm(C_5HF_6O_2)_4 \cdot H_2O$	yellow	[7]
hexafluoroacetyl-acetone/TBP	$Am(C_5HF_6O_2)_3 \cdot 2(C_4H_9O)_3PO$	volatile, 175°C	[8]
8-hydroxyquinoline	$Am(C_9H_6NO)_3$	yellow-green	[9]
5-chloro-8-hydroxyquinoline	$Am(C_9H_5ClNO)_3$	dark green	[9]
5,7-dichloro-8-hydroxyquinoline	$Am(C_9H_4Cl_2NO)_3$	green	[9]
oxalate	$Am_2(C_2O_4)_3 \cdot 10H_2O$	pink	[10]
	$KAmO_2C_2O_4 \cdot xH_2O$	color varies from pink to brick red depending on preparation conditions	[11]
	$CsAmO_2C_2O_4 \cdot xH_2O$	green, cubic ($a = 12.5$ Å)	[11]
	$MAmO_2C_2O_4 \cdot xH_2O$	M = NH_4, Na	[11]
phthalocyanine	$Am(C_{32}H_{16}N_2)_2$	dark violet	[12]
pyridine-2-carboxylate	$AmO_2(C_5H_4NCOO)_2$	red-brown	[13]
	$HAmO_2(C_5H_4NCOO)_3$	red-brown	[13]
pyridine-*N*-oxo-carboxylate	$AmO_2[C_5H_4N(O)COO]_2$		[14]
salicylate	$Am(C_7H_5O_3)_3 \cdot H_2O$		[15]
thenoyltrifluoroacetate	$Am(C_5H_4F_3O_2S)_3 \cdot 3H_2O$	pale rose	[2]

[a] THF, tetrahydrofuran.

[1] (Asprey *et al.*, 1950, 1951, 1954b); [2] (Keller and Schreck, 1969); [3] (Karraker, 1975, 1977); [4] (Baumgärtner *et al.*, 1966a, 1977; Kanellakopoulos *et al.*, 1970, 1978; Seaborg, 1972); [5] (Danford *et al.*, 1970; Moore, 1970; Sakanoue and Amano, 1975); [6] (Lebedev *et al.*, 1960b, 1962); [7] (Burns and Danford, 1969; Danford *et al.*, 1970; Bagnall, 1972; Sakanoue and Amano, 1975); [8] (Davydov *et al.*, 1975); [9] (Keller *et al.*, 1965a, 1966); [10] (Eyring *et al.*, 1952; Yakovlev and Kosyakov, 1958b; Lebedev *et al.*, 1960a; Weigel *et al.*, 1966; Burney and Porter, 1967; Chikalla and Eyring, 1967; Weigel and ter Meer, 1967, 1971); [11] (Zubarev and Krot, 1982, 1983a); [12] (Kirin *et al.*, 1967; Lux, 1973); [13] (Eberle and Robel, 1970; Robel, 1970); [14] (Robel, 1970); [15] (Burns and Baldwin, 1977).

above 200°C to AmO_2. Yellow $CsAm(C_5HF_6O_2)_4 \cdot H_2O$ crystallizes from $AmCl_3$ solution after addition of excess cesium hexafluoroacetylacetone in 50 vol% ethanol (Burns and Danford, 1969; Danford *et al.*, 1970).

(e) Cyclooctatetraene and cyclopentadiene

Reaction of $^{241}AmI_3$ with $K_2C_8H_8$ in tetrahydrofuran (THF) solution yields the adduct $KAm(C_8H_8)_2 \cdot 2THF$, which is isostructural with its plutonium analog $KPu(C_8H_8)_2 \cdot 2THF$ (Karraker, 1975). The compound decomposes in water and burns in air. Reacting the halides AmF_3 (Moore, 1970) or $AmCl_3$ (Baumgärtner *et al.*, 1966a,b; Kanellakopoulos *et al.*, 1970; Seaborg, 1972) with molten $Be(C_5H_5)_2$ at 65–70°C produces $Am(C_5H_5)_3$ (Moore, 1970). The pure compound can be obtained by fractional sublimation at 10^{-5} Torr and 160–205°C (Baumgärtner *et al.*, 1966a,b). Unlike $Pu(C_5H_5)_3$, $Am(C_5H_5)_3$ is not pyrophoric and decomposes only slowly in air. The IR and absorption spectra of $Am(C_5H_5)_3$ have been reported (Pappalardo *et al.*, 1969a; Kanellakopoulos *et al.*, 1970).

(f) Others

Reaction of AmI_3 at 200°C with phthalodinitride in 1-chloronaphthalene yields the dark violet phthalocyanine compound $Am(C_{32}H_{16}N_8)_2$, which was the first synthesized Am(IV) compound with an organic ligand (Lux, 1973). There is evidence that americium also forms the monophthalocyaninato complex.

Danford *et al.* (1970) precipitated the dipivaloylmethane compound $Am(C_{11}H_{19}O_2)_3$ by adding aqueous Am(III) sulfate to a solution of dipivaloylmethane and NaOH in 70% aqueous ethanol. Sakanoue and Amano (1975) determined the volatility of $Am(C_{11}H_{19}O_2)_3$ and several lanthanide and actinide analog complexes at 180°C and 10^{-3} torr and observed that $Am(C_{11}H_{19}O_2)_3$ is less volatile than its analog compounds of Th, Pu, Cf, or Eu, Gd, or Sc.

The only recorded aliphatic compounds of americium appear to be the citrates $Am(C_6H_5O_7) \cdot xH_2O$ and $[Co(NH_3)_6][Am(C_6H_5O_7)_2] \cdot xH_2O$ (Bouhlassa, 1983), and the salicylate $Am(C_7H_5O_3)_3 \cdot H_2O$ (Burns and Baldwin, 1976); its structure is described in Section 8.9.2.

Hölgye (1982) studied the coprecipitation of Am(III) with various metal cupferrates. With cupferrates of lanthanides and Sc(III), Am(III) coprecipitated quantitatively. But Am(III) coprecipitated only partially with cupferrates of Fe(III), Cu(II), Al(III), In(III), Pb(II), and Bi(III).

8.8 AQUEOUS SOLUTION CHEMISTRY

8.8.1 Oxidation states

In aqueous solutions, americium exhibits the III, IV, V, and VI oxidation states. All four oxidation states can coexist under certain conditions in carbonate media (Bourges *et al.*, 1983). In dilute acid, only the aquo ions Am^{3+} and

AmO_2^{2+} ions are stable, whereas in alkaline solution, americium can exist in all four valence states. In the III and IV oxidation states, americium forms Am^{3+} and Am^{4+} ions in solution, respectively. The highly charged ions in the V and VI states are unstable and hydrolyze instantly to form the linear *trans*-dioxo americyl cations, AmO_2^+ and AmO_2^{2+}, respectively. Analogous to Np(VII) and Pu(VII), americium reportedly can be oxidized to the VII oxidation state in highly alkaline media (Krot *et al.*, 1974a,b; Myasoedov and Kremliakova, 1985).

(a) Preparation

(1) Am(II): In contrast to its chemical analog of the lanthanide series, europium, the divalent state of Am is unstable in aqueous solution. Conditions that stabilize Yb^{2+}, Eu^{2+}, or Sm^{2+} do not reduce Am^{3+} to Am^{2+} (Keenan, 1959). Milyukova *et al.* (1980) claimed electrochemical evidence for unstable Am(II) in acetonitrile; they found that Am(II) was rapidly oxidized to Am(III) by water in the solvent. Sullivan *et al.* (1976, 1978) formed transient Am(II) by pulse radiolysis with an absorption maximum at 313 nm and $t_{1/2} \sim 5 \times 10^{-6}$ s for disappearance. Am(II) can be accessed in the solid state and as dilute solution in CaF_2 (Zachariasen, 1948b; Fried, 1951; Pappalardo *et al.*, 1969b; Baybarz, 1973b; Peterson, 1973). The solid compounds $AmCl_2$ (Baybarz, 1973b), $AmBr_2$ (Baybarz, 1973b), and AmI_2 (Baybarz and Asprey, 1972) have been prepared and characterized.

(2) Am(III): Trivalent americium is the most common and stable oxidation state in aqueous solution. It can be easily prepared by dissolving the metal in acid, dissolving AmO_2 in hot HCl, or by reducing higher valent americium compounds with most common reducing agents, such as NH_2OH, SO_2, or KI (Coleman *et al.*, 1963). Acidic solutions of Am^{3+} are pink in mineral acids but are yellow in concentrated $HClO_4$ or when the Am^{3+} concentration exceeds 0.1 M. Numerous solid compounds of Am(III) have been prepared and characterized.

(3) Am(IV): Tetravalent americium is unstable in non-complexing solutions and is reduced spontaneously to its more stable III oxidation state. Stable Am(IV) can be prepared by dissolving $Am(OH)_4$ in concentrated NH_4F solutions (Asprey and Penneman, 1962). Yanir *et al.* (1969) demonstrated that Am(IV) remains stable in phosphoric and pyrophosphate media. Myasoedov *et al.* (1977) reported that pure Am(IV) is obtained in 8–15 M phosphoric acid by anodic oxidation, while at lower phosphoric acid concentrations impurities of Am(VI) are formed. Similar stability of Am(IV) was reported in an oxidizing mixture of Ag_3PO_4 and $(NH_4)_2S_2O_8$. Electrolytic oxidation of ^{243}Am(III) (<1 V) in 2–5.5 M carbonate solutions resulted in the formation of a golden-yellow Am(IV) carbonate species, which was slowly reduced to Am(III) (Hobart *et al.*, 1982). At potentials exceeding 1.1 V, Am(IV) is oxidized to Am(V) and Am(VI). Am(IV) can be stabilized with heteropolyanions and reduction to Am(III) is caused solely by radiolytic effects

(Saprykin *et al.*, 1976; Kosyakov *et al.*, 1977; Erin *et al.*, 1979). Transient Am(IV) has been observed by pulse radiolysis (Sullivan *et al.*, 1976, 1978).

(4) Am(V): Am(III) can be oxidized to Am(V) in near-neutral and alkaline solution. In acidic media, oxidation of Am(III) yields only Am(VI) because Am(V) is more easily oxidized to Am(VI) than Am(III) is oxidized to Am(V). Solutions of Am(V) can be prepared by oxidation of Am(III) with ozone (Keenan, 1965), hypochlorite (Yakovlev and Gorbenko-Germanov, 1955), and peroxydisulfate (Nigon *et al.*, 1954), or by reduction of Am(VI) with bromide, or by electrolysis (Hobart *et al.*, 1983b). Solid sodium Am(V) carbonate can be precipitated by heating a 2 M Na_2CO_3 Am(VI) solution for 60 min to 60°C (Coleman *et al.*, 1963). Dissolution of the solid in near-neutral solutions yields pure Am(V) solution free of Am(III) and Am(VI). AmO_2^+ solutions free of Am^{3+} can be prepared by first extracting AmO_2^+ from buffered 1 M acetate (pH 3) solutions into 0.1 M thenoyltrifluoroacetone in isobutanol and back-extraction into an aqueous phase (Hara, 1970). More exotic methods include the dissolution of solid Li_3AmO_4 in dilute perchloric acid or the electrolytic oxidation of Am(III) in 2 M $LiIO_3$/0.7 M HIO_3 solutions (pH 1.5) (Keller, 1971).

(5) Am(VI): Powerful oxidants, i.e. peroxydisulfate or Ag(II), oxidize Am(III) and Am(V) in dilute, non-reducing acidic solution to Am(VI) (Myasoedov and Kremliakova, 1985). At acidities above 0.5 M, peroxydisulfate will not oxidize Am(III) completely to Am(VI) because of the interference of acid hydrolysis of $S_2O_8^{2+}$ (Penneman and Asprey, 1955). Ce(IV) oxidizes Am(V) to Am(VI) but only partially oxidizes Am(III) to Am(VI) (Penneman and Asprey, 1955). Electrolytic oxidation of Am(III) in 2 M H_3PO_4 and 6 M $HClO_4$ leads to Am(VI) (Myasoedov *et al.*, 1977) while ozone does not oxidize Am(III) to Am(VI) in acidic medium. In aqueous 2 M carbonate solutions oxidation of Am(III), Am(IV), or Am(V) with ozone or oxidation with $Na_2S_2O_8$ yields an intensely colored red-brown carbonate complex of Am(VI) (Coleman *et al.*, 1963). This complex is also obtained electrolytically at a potential of 1.3 V vs NHE in sodium carbonate solutions (Hobart *et al.*, 1982) or by dissolution of sodium americyl(VI) acetate in sodium carbonate solutions. Ozone oxidation in carbonate solution yields Am(VI) only at 25°C or below while at 90°C oxidation does not proceed past Am(V). Ozone does not oxidize $Am(OH)_3$ or $KAmO_2CO_3$ in 0.1–0.5 M $KHCO_3$ and $K_2S_2O_8$ does not oxidize $Am(OH)_3$ or $NaAmO_2CO_3$ in 0.1 M $NaHCO_3$ (Coleman *et al.*, 1963). This difference to the easy oxidation by $Na_2S_2O_8$ is attributed to the lower solubility of $KAmO_2CO_3$ compared to $NaAmO_2CO_3$. In 0.1–0.5 M $NaHCO_3$, Am(VI) is stable at 90°C to reduction by H_2O, Cl^-, or Br^-, but is easily reduced by I^-, N_2H_4, H_2O_2, NO_2^-, and NH_2OH. Very slow reduction of Am(VI) occurs in 2 M Na_2CO_3. Yellow-colored solutions of Am(VI) in any alkali hydroxide solutions can be prepared by oxidation of solid $Am(OH)_3$ with ozone (Cohen, 1972). Am(VI) in alkali hydroxide solutions undergoes

gradual reduction to form a light-tan solid, which yields Am(V) when dissolved in mineral acid. It is claimed that Am(VI) disproportionates into Am(VII) and Am(V) in >10 M NaOH (Nikolaevskii *et al.*, 1975).

The reaction of KrF_2 with AmF_3 in anhydrous HF yields a dark-brown solid of AmF_6 with a vapor pressure that is similar to that of UF_6 (Drobyshevskii *et al.*, 1980).

(6) Am(VII): While attempts to synthesize Am(VII) from Li_2O–AmO_2 mixtures at 300–400°C failed, oxidation of 3–4 M NaOH solutions containing 0.001–0.002 M Am(VI) with ozone at 0–7°C yields a green-colored solution of Am(VII) (Krot *et al.*, 1974a,b; Myasoedov and Kremliakova, 1985). A similar green-colored solution can be obtained by ^{60}Co gamma irradiation at 0°C of a N_2O-saturated 3 M NaOH solution. (N_2O scavenges hydrated electrons by the reaction $N_2O + e^-(aq) \rightarrow N_2 + O^-$; $S_2O_8^{2-}$ may be substituted for N_2O.) Spectrophotometric studies showed the oxidation of Np(VI) to Np(VII) and Pu(VI) to Pu(VII) under similar conditions, which provides strong evidence that the green solutions indeed contain a powerful oxidant such as Am(VII) (Krot *et al.*, 1974a,b).

(b) Hydration and coordination numbers

Information on the structure of the $Am^{3+}(aq)$ ion has been obtained indirectly from a variety of spectroscopic techniques. From the similar absorption spectra of Am^{3+} in aqueous solution, $AmCl_3$, and Am^{3+} doped into $LaCl_3$, Carnall (1989) concluded that there were nine inner-sphere water molecules associated in $Am^{3+}(aq)$. Horrocks and Sudnick (1979, 1981) and Choppin and coworkers (Barthelemy and Choppin, 1989; Choppin and Peterman, 1998) developed a linear relationship between the decay rate of the lanthanide(III) and the Am(III) fluorescence and the number of inner-sphere water molecules: $n_{H_2O} = (x/\tau) - y$. Kimura and Kato (Kimura and Kato, 1998) determined $x = 2.56 \times 10^{-7}$ s and $y = 1.43$ for Am(III) by measuring the fluorescence lifetime of Am^{3+} in H_2O and D_2O and using Carnall's proposed nine hydration waters. Runde *et al.* (2000) used Kimura's parameters and calculated from the fluorescence lifetime 11 coordinated water molecules for the Am^{3+} ion. Allen *et al.* (2000) determined ten coordinated water molecules around the Am^{3+} aquo ion in dilute aqueous chloride solution using X-ray absorption fine structure (XAFS) spectroscopy. Recently, Matonic *et al.* (2001) crystallized the isostructural Am(III) and Pu(III) triflate (trifluoromethanesulfonic acid) salts where the Am^{3+} ion bonds to nine water molecules in a tricapped, trigonal prismatic geometry (Fig. 8.4).

Shilov and Yusov (1999) analyzed reported variations in the Am(V)/Am(VI) potentials and the stability constants of the actinyl(V) oxalate complexes and proposed that the $NpO_2^+(aq)$ and $AmO_2^+(aq)$ ions are coordinated with five water molecules in the equatorial plane, in contrast to the coordination of four waters by $PuO_2^+(aq)$ and $UO_2^+(aq)$.

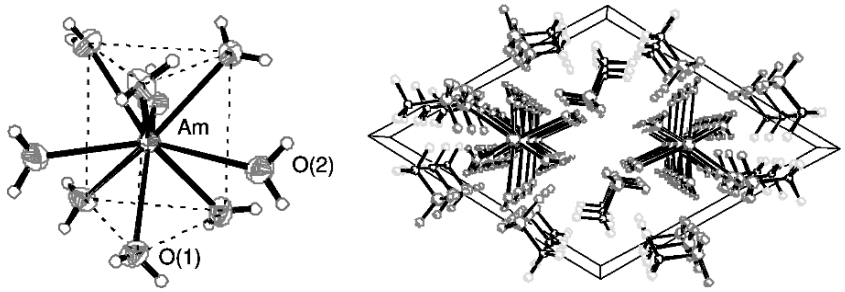

Fig. 8.4 *Coordination environment of* Am^{3+} *and crystal packing in* $[Am(H_2O)_9][CF_3SO_3]$ (*Matonic* et al., 2001).

(c) Electrode potentials and thermodynamic properties

A critical evaluation of available enthalpy and electromotive force (EMF) data were reported (Musikas, 1973b; Fuger and Oetting, 1976; Schulz, 1976; Fuger *et al.*, 1992; Silva *et al.*, 1995). Table 8.7 lists the electrode potentials for americium couples in various aqueous media. The diagram reflects the latest values and data evaluation of Martinot and Fuger (1985), which were accepted with minor changes by the recent Nuclear Energy Agency (NEA) review (Silva *et al.*, 1995). Except for the standard electrode potential (E°) of the Am(VI/V) couple, the electrode potentials of all redox couples were measured indirectly.

(1) Am(III)/(0): Fuger *et al.* (1972) measured the enthalpy of dissolution of Am metal (dhcp) in hydrogen-saturated HCl solutions and, using the estimated entropy of Am^{3+}(aq), estimated E° to be -2.06 ± 0.01 V in 1 M $HClO_4$; later Martinot and Fuger (1985) recommended -2.07 V.
(2) Am(III)/(II): Nugent *et al.* (1973a) estimated the potential to be -2.3 V as a best value by comparing the properties of lanthanide and actinide chloro complexes in relation to their M(II)/M(III) potentials. The estimated value is close to the -2.4 V estimated by Bratsch and Lagowski (1986).
(3) Am(IV)/(III): Due to the difficulties in preparing Am(IV) in appreciable amounts, estimating its thermodynamic properties is difficult. The originally estimated 2.44 V in 1 M $HClO_4$ appeared to be too small compared to data on the reduction of $Am(OH)_4$ to $Am(OH)_3$ (Penneman *et al.*, 1961). While the reported electrode potentials in concentrated H_3PO_4 are in agreement, 1.75 ± 0.03 V (Marcus *et al.*, 1972) and 1.78 V in 10 M H_3PO_4 (Nugent *et al.*, 1971a), their extrapolated values, $E^\circ = 2.50 \pm 0.06$ and 2.34 ± 0.22 V, respectively, differ significantly, most likely due to uncertainties in solution speciation. A value of 2.6 ± 0.09 V has been calculated from enthalpy measurements (Morss and Fuger, 1981), and has been confirmed by electrochemical data in carbonate solutions (Hobart *et al.*, 1982). Stabilization by carbonate and phosphotungstate decreases the electrode

Table 8.7 *Electrode potentials of americium redox couples.*

(a) 1 M $HClO_4$ (Schulz, 1976; Silva *et al.*, 1995):

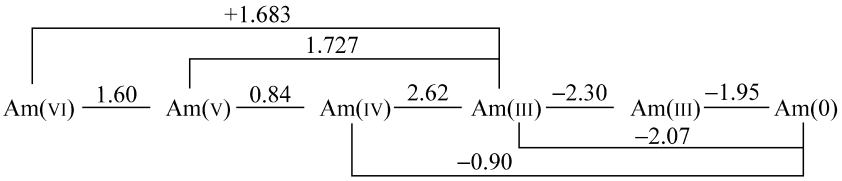

(b) Phosphoric Acid (Yanir *et al.*, 1959; Nugent *et al.*, 1971a; Myasoedov *et al.*, 1977):

$$\mathrm{Am(VI)} \xrightarrow[0.54\ \mathrm{M}\ H_3PO_4]{1.43} \mathrm{Am(V)} \quad \text{and} \quad \mathrm{Am(VI)} \xrightarrow[4.34\ \mathrm{M}\ H_3PO_4]{1.32} \mathrm{Am(V)}$$

$$\mathrm{Am(IV)} \xrightarrow[10\text{–}14.5\ \mathrm{M}\ H_3PO_4]{1.75\text{–}1.78} \mathrm{Am(III)}$$

(c) 1 M NaOH (Standard potentials were calculated based on the solubility products of $K_{sp}(Am(OH)_3) = 10^{23.3}$ and $K_{sp}(Am(OH)_4) = 10^{64}$) (Penneman *et al.*, 1961; Musikas, 1973b; Schulz, 1976):

$$\mathrm{Am(VI)} \xrightarrow{0.9} \mathrm{Am(V)} \xrightarrow{0.7} \mathrm{Am(IV)} \xrightarrow{0.5} \mathrm{Am(III)} \xrightarrow{-2.5} \mathrm{Am(0)}$$

(d) Carbonate media (Bourges *et al.*, 1983; Hobart *et al.*, 1983b; Berger *et al.*, 1988):

$$\mathrm{Am(VI)} \xrightarrow[2\ \mathrm{M}\ Na_2CO_3]{0.975} \mathrm{Am(V)} \quad \text{and} \quad \mathrm{Am(IV)} \xrightarrow[2\ \mathrm{M}\ Na_2CO_3]{0.92} \mathrm{Am(III)}$$

potential to 0.92 V (Hobart *et al.*, 1982; Bourges *et al.*, 1983) and 1.52 V (Kosyakov *et al.*, 1977), respectively.

(4) Am(VI)/(V): Penneman and Asprey (1950) measured directly the potential of the AmO_2^{2+}/AmO_2^{+} couple to be 1.600 ± 0.0005 V in 1 M $HClO_4$ and 1.614 ± 0.001 V in 0.3 M $HClO_4$. From studies of Am(VI) with Pu(VI) in NaOH, Nikolaevskii *et al.* (1974) estimated that the potential for the Am(IV)/Am(V) couple is about 0.65 V rather than 1.1 V.

(5) Am(VII)/(VI): Shilov (1976) reported a value of 1.05 V for the Am(VII)/Am(VI) couple in 1 M NaOH, while Peretrukhin and Spitsyn (1982) reported 0.78 V for this couple in 10 M hydroxide.

The heat of dissolution of americium metal in HCl at 298 ± 0.05 K was redetermined by Fuger *et al.* (1972) with pure americium metal prepared by distillation. Combined with earlier results, Fuger and Oetting (1976) calculated a standard enthalpy of formation of $Am^{3+}(aq)$ at 198 K of -616.7 ± 1.3 kJ mol^{-1}.

The following enthalpies of formation, free Gibbs energies of formation, and standard entropies for the americium aquo ions have been accepted by the NEA review (Silva *et al.*, 1995):

	$\Delta_f H_m^\circ$(298.15 K) (kJ mol^{-1})	$\Delta_f G_m^\circ$(298.15 K) (kJ mol^{-1})	S_m°(298.15 K) (kJ mol^{-1})
Am^{2+}(aq)	-355 ± 16	-377 ± 15	-1 ± 15
Am^{3+}(aq)	-616.7 ± 1.5	-598.7 ± 4.8	-201 ± 15
Am^{4+}(aq)	-406 ± 6	-346 ± 9	-406 ± 21
AmO_2^+(aq)	-804.3 ± 5.4	-739.8 ± 6.2	-21 ± 10
AmO_2^{2+}(aq)	-650.8 ± 4.8	-585 ± 5.7	-88 ± 10

A correlation function of P(M) that connects the trivalent gaseous lanthanide atoms with their aqueous ions changes systematically as a function of atomic number (Nugent *et al.*, 1973b). The same property is moderately well-behaved for trivalent actinides (Nugent *et al.*, 1973b; David *et al.*, 1978; Morss, 1983). The calculated P(Am) is about 20 kJ greater than expected from neighboring actinides. This anomaly was attributed to the large positive change in entropy of vaporization of Am (Ward and Hill, 1976).

(d) Autoreduction

Radiolytically produced species in aqueous solution, e.g. H_2O_2 and HO_2 radicals, reduce the higher oxidation states of americium to Am(III). Because of its lower specific activity, the rates of autoreduction of ^{243}Am species are much less than those of ^{241}Am. Zaitsev *et al.* (1960b) account for the autoreduction kinetics of aqueous AmO_2^{2+} and AmO_2^+ ions by assuming that H_2O_2 is consumed only in reducing Am(VI) and Am(V) is reduced only by HO_2 radicals, but that Am(V) may be oxidized to Am(VI) by OH radicals.

All investigators concur that autoreduction is kinetically zero order with respect to the AmO_2^{2+} ion and first order with respect to the total americium concentration:

$$-\mathrm{d}[\mathrm{Am(VI)}]/\mathrm{d}t = \mathrm{d}[\mathrm{Am(V)}]/\mathrm{d}t = k_1[\mathrm{Am_{total}}]$$

In both perchloric and sulfuric acid media, the value of the rate constant k_1 decreases with increasing acid concentration, 0.04 h^{-1} in dilute acid to zero in 12 M $HClO_4$ (Zaitsev *et al.*, 1960b). The autoreduction rate of ^{241}Am(VI) approaches 10% per hour in 9 M HNO_3 (Zaitsev *et al.*, 1960b); a slower rate was found in a later study (Myasoedov *et al.*, 1974b). The rate of autoreduction of ^{243}Am(VI) in 2 M $HClO_4$ solution at 76°C is about six times greater than that at room temperature (Zaitsev *et al.*, 1960b).

The autoreduction of Am(V) to Am(III) is usually stated to depend only on the total americium concentration but to be independent of the Am(V) concentration.

Zaitsev *et al.* (1960b) disagreed and found that under some conditions the rate of autoreduction of Am(V) to Am(III) does depend on the Am(V) concentration. The autoreduction of $^{241}AmO_2^+$ proceeds more slowly in 0.5 M HCl than in 0.2 M $HClO_4$. The maximum reduction rate of AmO_2^+ is about 1% per hour in 0.5 M HNO_3 and 0.8% per hour in 3 M HNO_3 (Zaitsev *et al.*, 1960b).

In 13 M NH_4F, ^{241}Am(IV) is autoreduced at a rate of about 4% per hour (Asprey and Penneman, 1962), increasing to 10% per hour in 3 M fluoride solution (Yanir *et al.*, 1969). Self-reduction of Am(IV) to Am(III) in phosphoric acid solution follows first-order reaction kinetics (Yanir *et al.*, 1969; Myasoedov *et al.*, 1973, 1975;). In acidic peroxydisulfate solution, no Am(III) is observed until all Am(VI) is reduced to Am(V). In the presence of $S_2O_8^{2-}$ ions, the radiolytic reduction of Am(V) proceeds more slowly than that of Am(VI) (Rykov *et al.*, 1970).

(e) Disproportionation

1. Am(IV): Tetravalent americium rapidly disproportionates in nitric and perchloric acid solutions according to the following reaction (Penneman *et al.*, 1961):

$$2\text{Am(IV)} \rightarrow \text{Am(III)} + \text{Am(V)}.$$

Assuming a reaction that is second order in Am(IV) concentration, Penneman *et al.* (1961) estimated k_1 in the equation

$$-\text{d[Am(IV)]}/\text{d}t = k_1[\text{Am(IV)}]^2$$

to be greater than $3.7 \times 10^{+4}$ L mol^{-1} h^{-1} in 0.05 M HNO_3 at 0°C. The dissolution of $Am(OH)_4$ in 0.05–2 M H_2SO_4 at either 0 or 25°C or of AmO_2 in 1 M H_2SO_4 yields solutions containing Am^{3+} and AmO_2^{2+} (Yakovlev and Kosyakov, 1958b; Penneman *et al.*, 1961). These results are explained by the following mechanism:

$$\text{Disproportionation of Am(IV)}: \quad 2\text{Am(IV)} \rightarrow \text{Am(III)} + \text{Am(V)}$$

and

$$\text{Redox Reaction}: \quad \text{Am}^{4+} + \text{AmO}_2^+ \rightarrow \text{Am}^{3+} + \text{AmO}_2^{2+}$$

The AmO_2^{2+} fraction increases with SO_4^{2-} and HSO_4^- concentrations at constant H^+ concentration, possibly as a result of SO_4^{2-} (or HSO_4^-) stabilization of an Am(IV) complex. Am(IV) is stable only in concentrated H_3PO_4, $K_4P_2O_7$, phosphotungstate, and fluoride (NH_4F, KF) solutions. The average oxidation number of americium remains IV when $Am(OH)_4$ is dissolved in either perchloric, nitric, or sulfuric acids (Penneman *et al.*, 1961), indicating no significant reduction by water, in contrast to the reduction of Cm(IV) (Kosyakov *et al.*, 1977).

2. Am(V): The most thorough study of the disproportionation kinetics of Am(V) was performed by Coleman (1963), who used ^{243}Am to minimize the radiolytically induced redox reactions associated with ^{241}Am. Coleman investigated the disproportionation of Am(V) in 3–8 M $HClO_4$ at 25°C, in 1–2 M $HClO_4$ at 75.7°C, and in about 2 M HCl, H_2SO_4, and HNO_3 solutions at 75.7°C. The disproportionation of Am(V) in 5 M $HClO_4$ and 5 M HCl at 25°C is shown in Fig. 8.5. The disproportionation of Am(V) in all media except HCl follows the reaction

$$3\ AmO_2^+ + 4H^+ \rightarrow Am^{3+} + 2AmO_2^{2+} + 2H_2O,$$

reflecting the fourth power dependence on the H^+ concentration. The rate law for this disproportionation reaction is

$$-d[Am(V)]/dt = k_1\,[AmO_2^+]^2[H^+]^4 = k_2\,[AmO_2^+]^2[H^+]^2 + k_3\,[AmO_2^+]^2[H^+]^3,$$

with $k_2 = (6.94 \pm 1.01) \times 10^{-4}\ L^3\,mol^{-3}\,s^{-1}$ and $k_3 = (4.63 \pm 0.71) \times 10^{-4}\ L^3 mol^{-3} s^{-1}$. The disproportionation rates at 75.7°C in 2 M HNO_3, HCl, and H_2SO_4 are, respectively, 4.0, 4.6, and 24 times greater than in 1 M $HClO_4$, whereas at 25°C the reaction rate increased 450 times in going from 3 to 8 M $HClO_4$. Using the temperature-dependence data from Coleman, Newton (1975) estimated thermodynamic quantities of activation for the disproportionation of Am(V). Note that the formation of Am(VI) in $HClO_4$ reaches a maximum after 5–6 h and then decreases successively with the main end product being Am(III). In 0.5 and 5 M HCl, Am(V) disappears much faster than in the non-complexing perchlorate medium. The formation of Am(VI) has not been observed in HCl media, indicating a fast reduction of Am(VI) by chloride (Hall and Herniman, 1954; Runde and Kim, 1994).

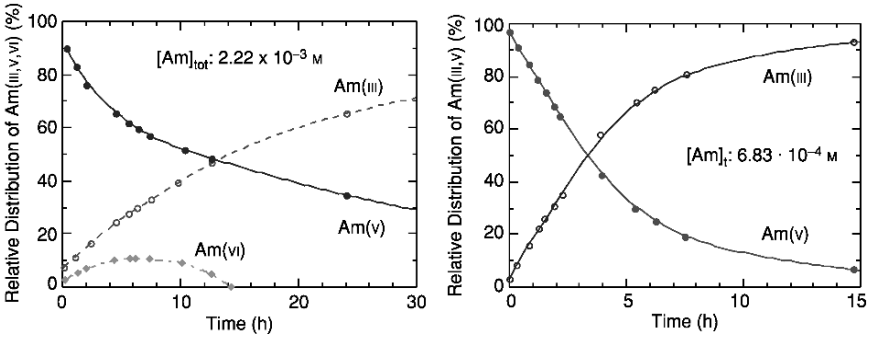

Fig. 8.5 *Disproportionation of Am(V) in 5 M $HClO_4$ (left) and 5 M HCl (right) (Runde and Kim, 1994).*

(f) Kinetics of oxidation–reduction reactions

Data for the few oxidation–reduction reactions that have been studied in detail can now be summarized. This summary supplements information presented by Hindman (1958), Newton and Baker (1967), and Gourisse (1966). An important recent reference on this subject is the critical review by Newton (1975).

(*i*) *Peroxydisulfate oxidation of Am(III) in acid media*

Early exploratory work by Asprey *et al.* (1950), the discoverers of the reaction between $S_2O_8^{2-}$ and Am(III) that produces Am(VI), established that the reaction proceeded in the concentration range from 10^{-8} to 10^{-1} M Am(III), implying a low-order dependence of the rate on Am(III) concentration. They further found that acidities greater than a few tenths molar were deleterious, presumably due to the acid-catalyzed decomposition path of $S_2O_8^{2-}$ (Penneman and Asprey, 1955). The general pattern of the oxidation (Fig. 8.6) represents an induction period and a linear region of constant rate followed by a region of gradually decreasing rate at high nitric acid concentrations. Reaction rates are dependent on temperature and on the concentration of HNO_3, $S_2O_8^{2-}$, and, when present, Ag^+. Newton (1975) states that the stoichiometry of the oxidation reaction is

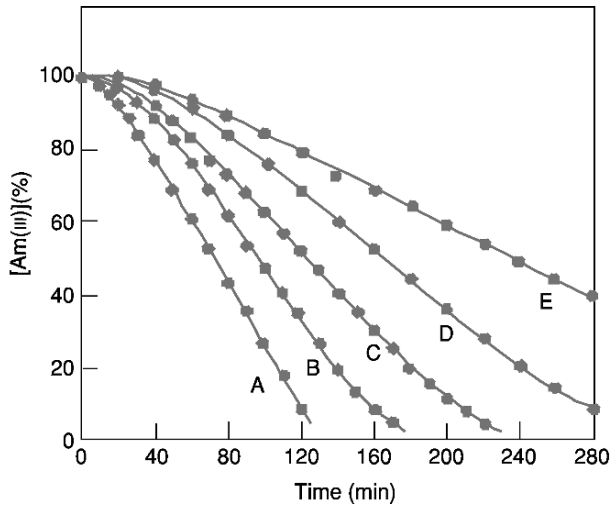

Fig. 8.6 *Kinetics of Am(III) oxidation by peroxydisulfate in nitric acid at* 50.6°C ($[S_2O_8^{2+}]_0 = 0.40$ M (*Ermakov* et al., 1971a, 1973, 1974)). *HNO_3 concentrations: A,* 0.09 M*; B,* 0.14 M*; C,* 0.19 M*; D,* 0.24 M*; E,* 0.28 M.

$$3/2S_2O_8^{2-} + Am^{3+} + 2H_2O \rightarrow 3SO_4^{2-} + AmO_2^{2+} + 4H^+$$

All researchers concur that the oxidizing agent is not the $S_2O_8^{2-}$ ion itself but its thermal decomposition products (e.g. $SO_4^{\bullet-}$ or $HS_2O_8^-$).

In contrast to conclusions from studies using micromolar Am(III), Ermakov *et al.* (1971a, 1973, 1974), on the basis of studies with millimolar amounts of ^{243}Am(III), claim that (in the absence of Ag^+) the rate of oxidation of Am(III) in the linear portion of kinetic curves does not depend on the Am(III) concentration and that the rate is given by:

$$-d[Am(III)]/dt = (a + b[H^+])[S_2O_8^{2-}][Am(III)]_0$$
$$= 2/3k_1 - (k_4[H^+]/(1 + x))[S_2O_8^{2-}]_0 = k_{III}$$

At 50.6°C, $a = 4.9 \times 10^{-5}$ min^{-1} and $b = 0.9 \times 10^{-4}$ L mol^{-1} min^{-1}. In this equation $[S_2O_8^{2-}]_0$ is the initial concentration of the peroxydisulfate ion, $x = k_5/k_6[H_2O]$, and k_1, k_4–k_6 are rate constants for the following reactions:

$$S_2O_8^{2-} \xrightarrow{k_1} 2SO_4^{\bullet-}$$

$$S_2O_8^{2-} + H^+ \xrightarrow{k_4} HSO_4^- + SO_4^{\bullet}$$

$$SO_4^{\bullet} \xrightarrow{k_5} SO_3 + O$$

$$SO_4^{\bullet} + H_2O \xrightarrow{k_6} H_2O_2 + SO_3$$

(*ii*) *Peroxydisulfate oxidation of Am(v) in HNO_3*

Ermakov *et al.* (1971a, 1973, 1974) also investigated the kinetics of the oxidation of Am(V) by $S_2O_8^{2-}$ ion in 0.09–0.6 M HNO_3 media at 45.6–60°C. According to Newton (1975) the stoichiometry of this reaction is

$$1/2\ S_2O_8^{2-} + AmO_2^+ \rightarrow SO_4^{2-} + AmO_2^{2+}$$

Ermakov gives the law:

$$-d[Am(v)]/dt = (a' + b'[H^+])[S_2O_8^{2-}][Am(v)]_0$$

At 50.6°C, $a' = 15 \times 10^{-5}$ min^{-1} and $b' = 2.7 \times 10^{-4}$ L mol^{-1} min^{-1}. It follows from this result and the rate data given in the preceding section that

$$-d[Am(III)]/dt = -(1/3)d[Am(v)]/dt$$

The results of Rykov *et al.* (1970) indicate that the mechanism of reduction of Am(VI) in the presence of $S_2O_8^{2-}$ ions is identical with that proposed for the oxidation of Am(V).

(*iii*) *Peroxydisulfate oxidation of Am(III) in carbonate media*

Peroxydisulfate oxidation of Am(III) in carbonate solutions proceeds through the intermediate formation of Am(V). Ermakov *et al.* (1971a, 1973, 1974) found that the rate of oxidation of Am(III) to Am(V) is independent of the total Am and K_2CO_3 concentrations and is equal to the rate of decomposition of $S_2O_8^{2-}$ ions. However, the rate of oxidation of Am(V) to Am(VI) is directly proportional to both the total americium concentration and the $S_2O_8^{2-}$ concentration, and is inversely proportional to the K_2CO_3 concentration. The effective activation energy of the $S_2O_8^{2-}$ oxidation of Am(III) to Am(V) in K_2CO_3 solutions is close to the activation energy (140 kJ mol^{-1}) of the thermal decomposition of $S_2O_8^{2-}$ ions. Recall that $Na_2S_2O_8$ will oxidize either Am(III) or Am(V) to Am(VI) in Na_2CO_3 or $NaHCO_3$.

(*iv*) *Reduction of Am(VI) by hydrogen peroxide*

Using ^{243}Am in $LiClO_4$–$HClO_4$ media, Woods *et al.* (1974) studied the kinetics of the reaction of AmO_2^{2+} with H_2O_2 and found the reduction of Am(VI) to be first order in both Am(VI) and H_2O_2 concentrations:

$$2AmO_2^{2+} + H_2O_2 \rightarrow 2AmO_2^{+} + 2H_2$$

(*v*) *Reduction of Am(VI) by other reductants*

Woods and Sullivan (1974) studied the reaction between AmO_2^{2+} and NpO_2^{+} in 1 M (H,Li)ClO_4. The rate law is:

$$-d[Am(VI)]/dt = k[Am(VI)][Np(V)]$$

At 25°C, k is $(2.45 \pm 0.4) \times 10^4$ L mol^{-1} s^{-1}; for this reaction, $\Delta H^* = 27.87 \pm 0.33$ kJ mol^{-1} and $\Delta S^* = -67.8 \pm 1.3$ J K^{-1} mol^{-1}. Oxalic acid reduces Am(VI) rapidly to approximately equal mixtures of Am(III) and Am(V), whereas reagents such as H_2O_2, HCl, HCOOH, HCHO, etc., reduce Am(VI) initially only to Am(V). The reduction of Am(VI) by nitrous acid is first order in each (Woods *et al.*, 1976).

(*vi*) *Reduction of Am(V) by H_2O_2*

From studies of the reduction of AmO_2^{+} to Am^{3+} by H_2O_2 in 0.1 M $HClO_4$, Zaitsev *et al.* (1960a) deduced the rate law:

$$-d[AmO_2^{+}]/dt = k[AmO_2^{+}][H_2O_2]$$

where $k = 14.8 \pm 1.5$, 21.6 ± 2.2, and 30.3 ± 3.01 mol^{-1} h^{-1} at 25, 30, and 35°C, respectively. The activation energy deduced for the reduction reaction is 55.2 kJ mol^{-1}. The only other reported studies of the Am(III)–Am(V)–H_2O_2–$HClO_4$ system have been made by Damien and Pages (1969, 1970). They reported

that the rate at which AmO_2^+ is reduced is inversely proportional to the perchloric acid concentration and is also strongly dependent on the initial $[Am^{3+}]_0/[AmO_2^+]_0$ and $[H_2O_2]_0/[AmO_2^+]_0$ concentration ratios.

(*vii*) *Reduction of Am(v) in NaOH solutions*

Shilov *et al.* (1997) investigated the reduction rate of Am(V) in 1.5 and 3 M NaOH at room temperature. Slow reduction of Am(V) is observed in the presence of 0.005–0.4 M of dithionite ($Na_2S_2O_4$), sulfite (Na_2SO_3), or thiourea dioxide ($(NH_2)_2CSO_2$) with a half-reduction time ranging between 0.2 and 9 h. The reduction of Am(V) in 3–14 M NaOH with about 0.01 M hydrazinium nitrate or hydroxylamine is accelerated with reductant concentration and temperature.

(*viii*) *Reduction of Am(v) by Np(iv) in perchloric acid media*

Blokhin *et al.* (1973) used spectrophotometry to study the kinetics of the Np(IV)–Am(V) reaction in 0.23–1.97 M $HClO_4$ at temperatures in the range 35.0–54.6°C. Depending on the initial concentrations of Np(IV) and Am(V), the reaction products are either Np(V) and Am(III) or Np(VI) and Am(III). The reaction rate falls rapidly with increasing acidity. Under the assumption of constant Am(IV) concentration, the kinetic data follow the rate law:

$$d[Am^{3+}]/dt - k'1[Np^{4+}][AmO_2^+] + k'2[NpO_2^+][AmO_2^+]$$

The authors report the following thermodynamic activation parameters: $\Delta H^* = 126 \pm 4$ kJ mol^{-1}, $\Delta G^* = 87 \pm 4$ kJ mol^{-1}, and $\Delta S^* = 130 \pm 13$ J K^{-1} mol^{-1}.

(*ix*) *Reduction of Am(v) by Np(v) in perchloric acid*

Rykov *et al.* (1973) determined spectrophotometrically the rate of the reaction:

$$2NpO_2^+ + AmO_2^+ + 4H^+ \rightarrow 2NpO_2^{2+} + Am^{3+} + 2H_2O$$

Kinetic data were collected in perchlorate ($\mu = 2.0$ M) at temperatures in the range 24.7–44.1°C. These researchers claim that reduction of Am(V) by Np(V) is an irreversible second-order reaction.

(*x*) *Reduction of Am(v) by Np(v) in Na_2CO_3*

Kinetics of the reduction of Am(V) by Np(V) in Na_2CO_3 solutions were investigated spectrophotometrically (Chistyakov *et al.*, 1974). The stoichiometry of the reduction is

$$4H^+ + AmO_2^+ + 2NpO_2^+ \rightarrow Am^{3+} + 2NpO_2^{2+} + 2H_2O$$

The kinetics of the Am(V) reactions in aqueous Na_2CO_3 follow the same rate law as in $HClO_4$ media.

(*xi*) *Reduction of Am(V) by U(IV) in perchloric acid*

At 11.2 and 3.60°C in 0.51–2.60 M $HClO_4$, the reaction between Am(V) and U(IV) proceeds according to the equation:

$$AmO_2^+ + U^{4+} \rightarrow Am^{3+} + UO_2^{2+}$$

Blokhin *et al.* (1974) derived the following rate law:

$$d[Am^{3+}]/dt = k[AmO_2^{2+}][U^{4+}]$$

In 2.0 M $HClO_4$ at 9.5°C, $k = 725 \pm 30$ L mol^{-1} min^{-1}. Standard thermodynamic activation parameters are $\Delta H^* = 75 \pm 4$ kJ mol^{-1}, $\Delta G^* = 63.6 \pm 0.8$ kJ mol^{-1}, and $\Delta S^* = 37.7 \pm 12.5$ J K^{-1} mol^{-1}.

(*xii*) *Oxidation of Am(II) by water*

In an elegant experiment carried out at the U.S. Argonne National Laboratory, the absorption spectra of both divalent americium and tetravalent americium were obtained (Sullivan *et al.*, 1976, 1978). This technique involved irradiation of Am(III) solutions with single electron pulses and recording the spectra with a streak camera at postirradiation times of 50 μs for Am(II) and 100 μs for Am(IV). Am(II) disappeared via reaction with water, while the Am(IV) species disproportionated to yield Am(III) and Am(V).

(g) Radiolysis

The most commonly used americium isotopes, ^{241}Am and ^{243}Am, decay primarily by emitting high-energy alpha particles of about 5.4 and 5.2 MeV, respectively (see Table 8.1). In solution, the energy (1 mg ^{241}Am releases about 7×10^{14} eV s^{-1}) is released in dense tracks producing radicals, ions, and electrons; thus can impact the stability of americium oxidation states in aqueous solutions. There are numerous reports on the effect of the intense alpha radiation of transuranium elements on their chemical behavior in acidic, basic, and highly concentrated chloride solutions. In acidic media, Am(III) is the most stable oxidation state and Am(V) and Am(VI) are rather rapidly reduced (Vladimirova *et al.*, 1977; Kornilov *et al.*, 1986). The reduction rate is closely related to the dose rate and electrolyte concentration. Vladimirova and coworkers (Vladimirova *et al.*, 1977; Vladimirova, 1986) suggested that Am(V) and Am(VI) reduction in nitric acid solutions cannot be explained by involving only radiolytically produced radicals but also require consideration of chemical reactions with radiolytically produced H_2O_2 and HNO_2:

$$2AmO_2^{2+} + HNO_2 + H_2O \rightarrow 2AmO_2^{+} + 3H^{+} + NO_3^{-}$$

$$2AmO_2^{+} + HNO_2 + 6H^{+} \rightarrow 2Am^{4+} + 3H_2O + HNO_3$$

In perchlorate solutions, alpha-radiolysis produces multiple species, such as Cl_2, ClO_2, or Cl^- that are effective reductants for Am(VI) (Kornilov *et al.*, 1986). A radiolytically enhanced chemical oxidation of Am(III) to Am(V) and Am(VI) (at large gamma doses) is observed in perchlorate solutions at pH 3–6 in the presence of excess of N_2O, $S_2O_8^{2-}$, or XeO_3 (Pikaev *et al.*, 1977). As expected the stability of higher oxidation states increases with pH and Am(III) is radiolytically oxidized to Am(V) in carbonate solutions under the exposure of intense alpha-radiation from ^{244}Cm (3–8 KCi L^{-1}) (Osipov *et al.*, 1977). The formation of oxidizing species in concentrated chloride solutions, i.e. Cl_2 and ClO^-, leads to the autoradiolytical oxidation of Am(III) to Am(V) (Magirius *et al.*, 1985; Runde and Kim, 1994). The radiolytical formation of hypochlorite in basic 5 M NaCl is directly correlated with the alpha-specific activity of ^{241}Am.

8.8.2 Complexation reactions

A critical review of the chemical thermodynamics of experimental data and chemical thermodynamics for americium inorganic compounds was recently published by the NEA (Silva *et al.*, 1995). Nearly all formation constants listed in Table 8.8 are for complexes formed by Am(III), as little work has been done on complexes with Am in higher oxidations states. Color changes of Am(III)-containing solutions indicate existence of Am(VI) nitrate, sulfate, and fluoride complexes. Some spectroscopic evidence exists for a Am(V) peroxide complex in 1 M NaOH (Musikas, 1973a). In agreement with the behavior of other actinide (III) and (IV) ions, the stability of Am(III) complexes with monovalent inorganic ligands follows the sequence:

$$F^- > H_2PO_4^- > SCN^- > NO_3^- > Cl^- > ClO_4^-.$$

As a Chatt–Ahrland 'A' type or Pearson 'hard' cation, Am^{3+} association with inorganic ligands proceeds initially through electrostatic interactions to form outer-sphere complexes, such as chlorides or perchlorates. Spectrophotometric results suggested the inner-sphere formation of chloride and nitrate ions in concentrated Na/LiCl and $LiNO_3$ solutions (Marcus and Shiloh, 1969; Allen *et al.*, 2000). Inner-sphere complexes are also found to form with harder ligands, such as fluoride or sulfate. In most cases, the stability of Am(III) complexes is similar to those that contain lanthanide ions with similar ionic radii, e.g. Nd(III) and Eu(III). In some cases, the stability of the Am(III) complex is slightly greater than that of the corresponding lanthanide complex presumably because of the participation of f-electrons in the bonding (Moskvin, 1967, 1971, 1973). As discussed earlier, this difference in stability can be used to separate Am(III) effectively from lanthanide elements.

Table 8.8 *Selected formation constants and solubility products of inorganic americium complexes* (*Silva* et al., 1995).

Complex	*log* β° *or* *log* K°_{sp}	$\Delta_f G^o_m$(298.15K) (kJ mol^{-1})	$\Delta_f H^o_m$(298.15K) (kJ mol^{-1})
Solution species			
$AmOH^{2+}$	–6.4 ± 0.7	–799.31 ± 6.21	
$Am(OH)_2^+$	–14.1 ± 0.6	–992.49 ± 5.86	
$Am(OH)_3$(aq)	–25.7 ± 0.5	–1163.42 ± 5.55	
$Am(CO_3)^+$	7.8 ± 0.3	–1171.12 ± 5.07	
$Am(CO_3)_2^-$	12.3 ± 0.4	–1724.71 ± 5.33	
$Am(CO_3)_3^{3-}$	15.2 ± 0.6	–2269.16 ± 5.98	
$AmSCN^{2+}$	1.3 ± 0.3	–513.42 ± 6.45	
AmF^{2+}	3.4 ± 0.4	–899.63 ± 5.32	
AmF_2^+	5.8 ± 0.2	–1194.85 ± 5.08	
$AmCl^{2+}$	1.05 ± 0.1	–735.91 ± 4.77	
$AmSO_4^+$	3.85 ± 0.03	–1364.68 ± 4.78	
$Am(SO_4)_2^-$	5.4 ± 0.8	–2117.53 ± 6.27	
$AmNO_3^{2+}$	1.33 ± 0.2	–717.08 ± 4.91	
$AmH_2PO_4^{2+}$		–1752.97 ± 5.76	
Solid phases			
$Am(OH)_3$(am)	–17.0 ± 0.6		
$Am(OH)_3$(cr)	–15.2 ± 0.6		
AmO_2(cr)		–874.49 ± 4.27	–932.20 ± 3.00
Am_2O_3 (cr)		–1613.32 ± 9.24	–1690.40 ± 8.00
AmF_3 (cr)		–1518.83 ± 13.10	–1588.00 ± 13.00
AmF_4 (cr)		–1616.83 ± 20.06	–1710 ± 20.00
$Am_2(CO_3)_3$ (cr)	16.7 ± 1.1	–2971.74 ± 15.79	
$Am(OH)CO_3$ (cr)	21.2 ± 1.4	–1404.83 ± 9.31	
$AmPO_4$ (am)	24.8 ± 0.6	–1752.97 ± 5.76	

(a) Hydrolysis

(1) Am(III): The hydrolysis of Am(III) has been studied extensively, partly because the hydrolysis reactions are strongly favored in aqueous systems. It is established that Am(III) is complexed by hydroxide above pH 5 to form complexes of general formula $Am(OH)_n^{3-n}$ where $n = 1$–3. Thermodynamic stabilities of these complexes were calculated from data obtained by a variety of methods, such as solubility studies, solvent extraction, and potentiometric and electromigration measurements. Spectroscopic characterization or structural information of these complexes is absent because of their low solubilities. The existence of the anionic species $Am(OH)_4^-$ has been postulated, which would increase the Am(III) solubility at high pH. However, an increase in solubility is not observed at pH > 13 and contamination of the solution by carbonate may have produced anionic carbonate complexes that increase

the overall Am(III) solubility. There is substantial uncertainty about the formation of polynuclear complexes, as common in the U(VI) hydrolysis system.

(2) Am(V): Kim and coworkers (Magirius *et al.*, 1985; Stadler and Kim, 1988) measured the solubility of autoradiolytically formed $^{241}AmO_2(OH)$(s) in 3 and 5 M NaCl. Runde and coworkers (Runde and Kim, 1994; Runde *et al.*, 1996) reported an increased solubility of $^{241}AmO_2(OH)$(s) over $^{237}NpO_2(OH)$(s) in 5 M NaCl. Slope analysis of the solubility data indicated formation of only two americyl(V) hydrolysis products in solution, $AmO_2(OH)$(aq) and $AmO_2(OH)_2^-$. Tananaev (1990a) suggested the formation of $AmO_2(OH)_3^{2-}$ (with an absorption peak at 750 nm) and $AmO_2(OH)_4^{3-}$ in highly alkaline media based on spectroscopic measurements of Am(V) in 0.001–1 M LiOH solutions. Because of the radiolytic formation of oxidizing species (such as OCl^-) and the subsequently increased stability of Am(V), the few solubility studies of Am(V) were performed in concentrated chloride solutions. The reported apparent stability constants for $AmO_2(OH)$(aq) and $AmO_2(OH)_2^-$ are close to those for the analogous Np(V) species (Runde *et al.*, 1996). However, the solubility of $^{241}AmO_2OH$ appears to be higher than that of $^{237}NpO_2OH$, probably due to higher alpha-radiation damage of the Am(V) solid.

(3) Am(IV) and Am(VI): The hydrolysis of Am(IV) and Am(VI) remains rather unexplored because of the instabilities of these oxidation states in aqueous solutions under ambient conditions. There is spectroscopic evidence for the formation of Am(VI) hydrolysis species of general formula $AmO_2(OH)_n^{2-n}$ where $n = 1$–4.

(b) Carbonate complexation

(1) Am(III): The carbonate complexation of Am(III) has been widely investigated using a variety of methods, such as solvent extraction, spectrophotometry, electromigration, and solubility. Meinrath and Kim (1991a) monitored the solubility and complexation reactions of Am(III) in carbonate-containing solutions spectroscopically. Three solution species, $Am(CO_3)_n^{3-2n}$ with $n = 1$–3, were characterized by their distinct absorbances at 505.4 nm ($\varepsilon = 385$ L mol^{-1} cm^{-1}), 506.5 nm ($\varepsilon = 350$ L mol^{-1} cm^{-1}), and 507.8 nm ($\varepsilon = 330$ L mol^{-1} cm^{-1}), respectively. Wruck *et al.* (1999) determined the formation constant of the monocarbonato complex, $Am(CO_3)^+$, at 25, 50, and 75°C at 0.1 m ionic strength using laser-induced photoacoustic spectroscopy. There is no experimental or spectroscopic proof for the proposed formation of bicarbonato complexes, $Am(HCO_3)_n^{3-2n}$, and mixed hydroxocarbonato species, $Am(OH)_m(CO_3)_n^{3-m-2n}$ (Bernkopf and Kim, 1984). These complexes were used to explain extraction and solubility data although the experimental data can be explained by pure carbonato

and hydroxo species. The solid phases $AmOHCO_3$ and $Am_2(CO_3)_3$ were found as solubility-controlling phases in aqueous carbonate solutions (Meinrath and Kim, 1991b; Runde *et al.*, 1992). The double carbonate $NaAm(CO_3)_2 \cdot nH_2O$ was identified by X-ray diffraction to form at increased NaCl concentrations (Runde and Kim, 1994; Rao *et al.*, 1996).

(2) Am(IV): There is only one carbonato complex of Am(IV) discussed in the literature. From combined spectroscopy and cyclic voltammetry data in bicarbonate/carbonate solutions (Bourges *et al.*, 1983), it was concluded that $Am(CO_3)_5^{6-}$ is the limiting carbonate complex of Am(IV). Its logarithmic stability constant, $\log \beta_5^o = 39.3 \pm 2.1$ (Silva *et al.*, 1995), is comparable to those of the analogous U(IV) (34.0 ± 0.9 (Grenthe *et al.*, 1992)) and Np(IV) complexes (33.9 ± 2.6 (Kaszuba and Runde, 1999)).

(3) Am(V): Giffaut and Vitorge (1993) studied the solubility of $NaAmO_2CO_3$ in carbonate-containing 4 M NaCl solution and claimed the formation of two Am(V) carbonate complexes, $AmO_2(CO_3)^-$ and $AmO_2(CO_3)_2^{3-}$. Runde and coworkers (Runde and Kim, 1994; Runde *et al.*, 1996) reported identical solubility and speciation behavior of Am(V) and Np(V) in carbonated 3 and 5 M NaCl solutions. In analogy to the well-characterized Np(V) system in 5 M NaCl, the solubility data were interpreted with the formation of $AmO_2(CO_3)_n^{1-2n}$ ($n = 1$–3) in solution and $NaAmO_2CO_3 \cdot nH_2O$ as the solid equilibrium phases.

Spectroscopic evidence suggests that an Am(V) carbonate complex in $NaHCO_3$, presumably the triscarbonato complex $AmO_2(CO_3)_3^{5-}$, has an absorbance at 727 nm (Tananaev, 1990a).

(4) Am(VI): The appearance of a burgundy-red color upon introducing Am(VI) into carbonate-containing solutions indicates the coordination of AmO_2^{2+} with carbonate ions. However, spectroscopic studies of the carbonate complexation of Am(VI) are few. Based on electrochemical measurements, it is assumed that the limiting complex is the $AmO_2(CO_3)_3^{4-}$ anion (Bourges *et al.*, 1983; Silva *et al.*, 1995).

(c) Organic ligands

With few exceptions, the data in Table 8.9 are for complexes of Am(III). Generally, the higher oxidation states of americium are reduced by organic complexing agents. Aminopolycarboxylic acids complex Am(III) more strongly than either hydroxycarboxylic or aminoalkylpolyphosphoric acids (e.g. ethylenediamine bis(methylene)phosphonic acid). Keller (1971) observed that in the series of α-hydroxycarboxylic acids (e.g. glycolic and lactic), the stability of the Am(III) complex decreases with increasing number of carbon atoms. The logarithm of the stability constant of the Am(III) complexes with aminopolycarboxylic acids increases linearly (Fig. 8.7) with the number of bound donor atoms of the ligand.

Table 8.9 *Complexes of Am(III) with organic ligands (unless otherwise noted, see the compilation by Schulz (1976) and references therein).*

Ligand	*Method*	*Temp.* (°C)	*Ionic strength, medium* μ (mol L^{-1})	*Log of formation constants* β_1	β_2	*Other constants*	*References*
acetic acid (HAc)	IX	20	9.0 M HAc	2.28 ($AmAc^{2+}$)	3.84($AmAc_2^+$)	$\beta_3 = 4.78$ ($AmAc_3$)	[1]
						$\beta_4 = 5.7$ ($AmAc_4^+$)	[1]
						$\beta_5 = 6.66$ ($AmAc_5^{2+}$)	[1]
						$\beta_6 = 7.62$ ($AmAc_3^{6+}$)	[1]
	PT	20	1.0 M NH_4ClO_4	1.81	3.20	$\beta_3 = 4.57$; $\beta_4 = 5.7$	[1]
						$\beta_5 = 6.73$; $\beta_6 = 7.73$	[1]
	SX	25 ± 0.1	2.0 M NH_4ClO_4	1.95 ± 0.11			[2]
	IX	20	0.5 M NaClO4	1.99 ± 0.01	3.27 ± 0.07	$\beta_3 = 3.9$	[3]
	IX	25	$\mu = 0.2$	2.15	3.83		[4]
		25	$\mu = 0.5$	2.30	3.81		[4]
		25	$\mu = 1.0$	2.08	3.62		[4]
	SX	~25	0.1–1.0 M Ac	1.40 (AmO_2Ac)	2.51($AmO_2Ac_2^-$)		[5]
	SX	25 ± 0.5	0.5 M NH_4ClO_4	2.39 ± 0.05			[6]
α-alanine	SX	25	2.0 M $NaClO_4$	0.79 ($AmAla^{2+}$)			[7]
(Ala)	Spec	18 ± 2	1.0 M KCl	3.9 ± 0.2			[8]
anthranil-*N*,*N*-diacetic acid (H_3ADA)							
	IX	25	0.1 M NH_4ClO_4	8.92 (AmADA)	14.5($Am(ADA)_2^{3-}$		[26,52]
arginine				3.8 ± 0.3			[8]
aspartic acid	Spec	18 ± 2	1.0 M KCl	5.1 ± 0.02			[8]
Benzoyltrifluoroacetone (HBTA)							
	SX	25	0.1 M NH_4ClO_4			$\beta_3 = 14.84$ ($Am(BTA)_3$)	[9]
citric acid (H_3Cit)	Spec	25	1.0 M $NaClO_4$	6.96 (AmCit)	10.3($Am(Cit)_2^{3-}$)	$\beta_1' = 4.53$ ($AmHCit^+$)	[10,11]
	SX	25	0.1 M(H,Li)ClO_4		12.15	$\Delta G° = 44.98$ kJ mol^{-1} ($AmHCit^{2-}$)	[12]
	IX	25	0.1 M $NaClO_4$	9.16 ± 0.03		$\beta_1' = 7.00$	[11]
			0.5 M $NaClO_4$	8.73 ± 0.066		$\beta_1' = 6.29$	[11]
			1.0 M $NaClO_4$	6.72 ± 0.05		$\beta_1' = 4.24$	[11]
	IX	25	0.1 M NaH_2 Cit	6.74	11.55	$\beta_1' = 5.31$	[13]
						$\beta_2' = 8.23$ ($Am(HCit)_2^-$)	[13]
	IX		1.0 M NH_4Cl	7.11	14.0	$\beta_3''3 = 8.29$ ($Am(H_2Cit)_3$)	[14]
	PEP		0.04 M		9.66		[15]
	SX		0.1 M $LiClO_4$	10.1 ($Am(HCit)^+$)			[16]

				8.0 (Am(Cit))			[16]
				20 ($Am(HcCit)_2^-$)			[16]
				16.3 ($Am(HCit)(Cit)^{2-}$)			[16]
				12.1 ($Am(Cit)_2^{3-}$)			[16]
	PT		0.1 M $LiClO_4$	11.36 ($Am(HCit)^+$)			[16]
				8.69 (Am(Cit))			[16]
				18.97 ($Am(HCit)(Cit)^{2-}$)			[16]
				14.29($Am(Cit)_2^{3-}$)			[16]
				10.53 ($Am(OH)(Cit)^-$)			[16]
				22.80 ($Am(OH)(Cit)_2^{2-}$)			[16]
	SX	25	0.3 M NaCl	5.9 ± 0.1			[17]
			1.0 M NaCl	5.2 ± 0.1			[17]
			2.0 M NaCl	5.0 ± 0.1			[17]
			3.0 M NaCl	4.84 ± 0.04			[17]
			4.0 M NaCl	5.38 ± 0.06			[17]
			5.0 M NaCl	5.10 ± 0.15			[17]
15-crown-5	SX	25	0.1 M	0.21 ± 0.02			[18]
18-crown-6	SX	25	0.1 M	0.55 ± 0.06			[18]
cysteine	Spec	18 ± 2	1.0 M KCl		4.3 ± 0.3		[8]
1,2-diaminocyclohexanetetraacetic acid (H_4DCTA)							
	EM	20 ± 0.5	0.1 M KCl/HCl	18.34 ($AmDCTA^-$)		$\beta_1' = 2.87$ ($AmHDCTA^-$)	[19]
	IX	25 ± 1	0.1 M NH_4ClO_4	18.79			[20]
	IX	80	0.001 M H_4DCTA +0.02 M ammonium-α-hydroxyisobutyrate	18.79[e]			[21]
	SX	20	0.1 M NH_4Cl	18.21		$\beta_1'' = 2.85 \pm 0.04$ $(AmO_{22}DTPA)^{2-}$	[22]
1,2-diaminopropanetetraacetic acid (H_4DTPrA^-)							
	IX	25	0.1 M $NaClO_4$	17.69 ($AmDTPrA^-$)		$\beta_1' = 9.79$ (AmHDTPrA)	[11]
1,10-diaza-4,7,13,16-tetraoxacyclooctadecane (diaza-crown ether; kryptofix 22; K22)							
	SX	25	1.0 M NaCl	6.05 ± 0.3			[23]
dibutyl-P,P′-ethane-1,2-diphosphonic acid (H_2B_2EDP)							
	SX	25	1.0 M $NaClO_4$			$\beta_1' = 14.52$ $(Am(HB_2EDP)_3)$	[24]
5,7-dichloro-8-hydroxyquinoline (HDCO)							
	SX	25 ± 0.5	0.1 M $(NH_4, H)ClO_4$			$\beta_3 = 21.93$ (Am(DCO)3)	[25]

Table 8.9 (*Contd.*)

Ligand	*Method*	*Temp.* (°C)	*Ionic strength, medium* μ (mol L^{-1})	*Log of formation constants* β_1	β_2	*Other constants*	*References*
diethylenetriaminepentaacetic acid (H_5DTPA)							
	IX	25	0.1 M NH_4ClO_4	23.07 ($AmDTPA^{2-}$)		$\beta'_1 = 14.06$ ($AmHDTPA^{+}$)	[26]
	IX	25	0.1 M NH_4ClO_4	22.92			[27]
	EM	25 ± 0.2	0.1 M KNO_3	22.74		$\beta'_1 = 14.3$	[28]
	SX		$\mu = 0.1$	23.2			[29]
	Spec	25	$\mu = 0.1$	23.2			[30]
	Spec	25	0.1 M NH_4ClO_4	24.03			[31]
	Spec	20 ± 0.1	0.5 M $HClO_4/HNO_3$	22.09			[32]
	IX	25	0.1 M NH_4ClO_4	23.32			[33]
	IX	25	1.0 M NH_4ClO_4	21.3		$\beta'_1 = 15.46$	[1]
diethylphosphinylpropionic acid (HDEPP)							
	IX	25	0.5 M NH_4ClO_4; $HClO_4$	1.76 ($AmDEPP^{2+}$)	3.16 ($Am(DEPP)_2^{+}$)		[34]
diglycolic acid (H_2DGA)							
	Spec	25.2	0.1 M NH_4ClO_4	6.47 ($AmDGA^{+}$)	10.96 ($Am(DGA)_2^{-}$)	$\beta_3 = 13.83$ ($Am(DGA)_3^{3-}$)	[35]
dioctyl-P,P′-ethane-1,2-diphosphonic acid (H_2O_2 EDP)							
	SX	25	1.0 M NaClO4			$\beta'_1 = 19.53$ ($Am(HO_2EDP)_3$)	[24]
diphosphine dioxides (1,1-DiPO=$(C_6H_{13})_2P(O)CH_2(O)P(C_6H_{13})_2$; 1,4-DiPO=$(C_6H_{11})_2P(O)(CH_2)_4(O)P(C_6H_{11})_2$; 1,5-DiPO=$(C_6H_{11})_2P(O)(CH_2)_5(O)P(C_6H_{11})_2$)							
	SX	2.0	2.0 M $NaNO_3$	1.43 ($Am(NO_3)_3 \cdot$ (1,1-DiPO))			[36]
				6.56 ($Am(NO_3)_3 \cdot$ 2(1,4-DiPO))			[36]
				5.92 ($Am(NO_3)_3 \cdot$ 2(1,5-DiPO))			[36]
ethylenediaminebis(isopropyl)phosphonic acid (H_4EDIP)							
	EM	25	0.1 M KNO_3	18.00 ($AmEDIP^{-}$)		$\beta'_1 = 6.26$ (AmH_3EDIP^{2+})	[28]
						$\beta'_1 = 8.94$ (AmH_2EDIP^{+})	[28]
						$\beta'_1 = 13.95$ (AmHEDIP)	[28]

ethylenediaminebis(methyl)phosphonic acid (H_4EDMP)							
	EM	25	0.1 M KNO_3	16.52 ($AmEDMP^-$)		$\beta'_1 = 6.3$ (AmH_3EDMP^{2+})	[37]
						$\beta'_1 = 8.48$ (AmH_2EDMP^+)	[37]
						$\beta'_1 = 12.3$ (AmHEDMP)	[37]
	IX	25	0.5 M NH_4ClO_4			$\beta'_1 = 6.12$ (AmH_2EDMP^+)	[38]
ethylenediaminetetraacetic acid (H_4EDTA)							
	IX	25	0.1 M $NaClO_4$	18.15 ($AmEDTA^-$)			[11]
			0.5 M $NaClO_4$	16.36		$\beta'_1 = 9.68$ (AmHEDTA)	[11]
			1.0 M $NaClO_4$	15.72			[11]
	Spec	25 ± 0.2	1.0 M $NaClO_4/HClO_4$	15.33	22.10 ($Am(EDTA)_2^{5+}$	$\beta'_1 = 8.94$ (AmHEDTA)	[11]
	SX	20	0.1 M NH_4Cl	16.91 ± 0.04			[39]
	Spec	25	0.1 M NH_4ClO_4	18.06			[31]
	IX	25 ± 0.02	0.1 M NH_4ClO_4	18.16 ± 0.10			[40]
	IX		1.0 M NH_4ClO_4	18.03 ± 0.13		$\beta'_1 = 10.29$ (AmHEDTA)	[41]
	EM	25 ± 0.5	0.1 M HCl/KCl	17.0		$\beta'_1 = 9.21$ (AmHEDTA)	[42]
	IX	80	0.001 M H_4EDTA + 0.2 M α-hydroxyisobutyrate	17.14			[43]
	EM	25 ± 0.1	0.1 M KNO_3	17.00 ± 0.09		$\beta'_1 = 9.21$ (AmHEDTA)	[22,44]
	Spec	25	$\mu = 0.1$			$\beta = 19.98$ (AmO_2HEDTA^{2+})	[22,44]
						$\beta''_1 = 4.88 \pm 0.05$ (AmO_2HEDTA^{2+})	[22,44]
ethylenediaminetetramethylphosphonic acid (H_8EDTMP)							
	EM	25 ± 0.1	0.1 M KNO_3	22.47 ± 0.08 ($AmEDTMP^{5-}$)		$\beta'_1 = 4.8 \pm 0.6$ (AmH_5EDTMP)	[44]
						$\beta''_1 = 7.33 \pm 0.09$ (AmH_4EDTMP)	[44]
						$\beta'''_1 = 11.17 \pm 0.07$ (AmH_3EDTMP)	[44]
						$\beta''''_1 = 14.90 \pm 0.06$ (AmH_2EDTMP)	[44]
						$\beta'''''_1 = 18.45 \pm 0.08$ (AmHEDTMP)	[44]

Table 8.9 (*Contd.*)

Ligand	*Method*	*Temp.* (°C)	*Ionic strength, medium* μ (mol L^{-1})	*Log of formation constants* β_1	β_2	*Other constants*	*References*
ethylenediaminetetrapropionic acid (H_4EDTP)							
	Spec	25 ± 0.2	1.0 M $NaClO_4/HClO_4$	18.84 ± 0.02 ($AmEDTP^-$)	$\beta'_1 = 12.31$ (AmHEDTP)		[11]
ethyleneglycol*bis*(2-aminoethyl)tetraacetic acid (H_4EGTA)							
	IX	25	0.1 M NH_4ClO_4	18.22 (AmEGTA)			[26]
formate	Sol	25	2.0 M $NaClO_4$	2.54 (lg β_1)	4.02 (lg β_2)	log $\beta_3 = 4.64$ log $\beta_4 = 4.5$	[45]
formate (Am(v))	Spec	25	2.0 M $NaClO_4$	1.22 ± 0.3			[46]
fulvic acid	Spec	25	0.1 M $NaClO_4$	5.78 ± 0.07			[22]
	SX	25	3 M NaCl	4.7 ± 0.1			[13]
			6 M NaCl	6.0 ± 0.7			
glutamic acid	Spec	18 ± 2	1.0 M KCl	5.6 ± 0.1			[8]
glycine (HGlyn)	SX	25	2.0 M $NaClO_4$	0.69 ± 0.02 ($AmGlyn^{2+}$)			[47]
	Spec	18 ± 2	1.0 M KCl	4.1 ± 0.02			[8]
glycolic acid (HGlyc)							
	IX	0.5	0.5 M $NaClO_4$	2.82 ($AmGlyc^{2+}$)	4.85($Am(Glyc)_2^+$)	$\beta_3 = 6.30$ ($Am(Glyc)_3$)	[3]
	SX	25	2.0 M $NaClO_4$	2.59			[48]
	Spec	25 ± 0.2	1.0 M $NaClO_4/HClO_4$	2.44 ± 0.02	4.29 ± 0.2	$\beta_3 = 5.20$	[11]
	IX	25	0.5 M $NaClO_4$	2.57 ± 0.02	4.01 ± 0.1		[11]
histadine	Spec	18 ± 2	1.0 M KCl	4.8 ± 0.2			[8]
hydrazine-*N,N*-diacetic acid (H_2HyDA)							
	IX	25	0.1 M $NaClO_4$	10.74 ($AmHyDA^+$)	20.20 ($Am(HyDA)_2^+$)		[11]
	EM	25	$\mu = 0.1$	11.01	19.78		[37]
hydrazineiminodiacetic acid (H_2HyIDA)							
	EM	25	0.1 M KNO_3	10.98 ($AmHyIDA^+$)	19.97 ($(AmHyIDA)_2^-$)	$\beta'_1 = 4.13$ ($AmHHyIDA^{2+}$)	[49]
2-hydroxycyclohexylethlenediaminetriacetic acid (H_3HCEDTA)							
	IX	25	0.1 M $NaClO_4$	16.09 (AmHCEDTA)		$\beta'_1 = 7.44$ ($AmHHCEDTA^+$)	[11]

N (2-hydroxyethyl)ethylene-*N,N,N'*-triacetic acid (H_3NHEDTA)						
	IX	25	0.1 M $HClO_4/NH_4ClO_4$	15.72 (AmNHEDTA)	22.47 $(Am(NHEDTA)_2^{3-})$	[26,50]
	Spec	25 ± 0.2	1.0 M $HClO_4/NH_4ClO_4$	14.84	22.18	[13]
	Spec	25	0.1 M NH_4ClO_4	16.18		[31]
	IX	22	0.15 M HCl/KCl	15.34		[51]
N' (2-hydroxyethyl)iminodiacetic acid (H_2NHIDA)						
	IX	25	0.1 M NH_4ClO_4	9.14 (\rm $Am(NHIDA^+)$	17.04 $(Am(NHIDA)_2^-)$	[26,52]
	Spec	25	0.1 M NH_4ClO_4	9.80	17.01	[31]
	SX			9.3 ± 0.1		[53]
	EM	25	0.1 M KNO_3	9.3 ± 0.13	16.5 ± 0.2	[54]
α-hydroxyisobutyric acid (HIBA)						
	Spec	25 ± 0.2	1.0 M $HClO_4/NaClO_4$	2.68 ($AmIBA^{2+}$)	4.38 $(Am(IBA)_2^+)$	[11]
	IX	25 ± 0.2	0.5 M NH_4ClO_4	2.88 ± 0.01	4.03 ± 0.02	[11]
	IX		0.5 M NH_4ClO_4/NH_4IBA	2.38	4.67	$\beta_3 = 5.12$ (Am(IBA)3) [55]
	IX			2.72	4.69	$\beta_3 = 5.64$ [56]
	SX					$\beta_3 = 6.1$ [57]
bis(hydroxymethyl)phosphonic acid (HMP′A)						
	IX	25		1.76 ± 0.06 ($AmMPA^{2+}$)	2.48 ± 0.02 $(Am(MPA)_2^+)$	[58]
hydroxymethylphosphonic acid (HMP′A)						
	IX	25	0.2 M NH_4ClO_4	1.55 $AmMP'A^{2+}$)	3.18 $(Am(MP'A)_2^+)$	[59]
o-hydroxyphenyliminodiacetic acid (H_2HPIDA)						
	SX	25 ± 0.1	0.1 M NH_4ClO_4	6.80 $(Am(HPIDA)^{2+})$	11.9 $(Am(HPIDA_2^+)$	[60]
8-hydroxyquinoline-5-sulfonic acid (H_2OXSA)						
	IX	25 ± 0.2	0.1 M NH_4ClO_4	8.64 ± 0.09 ($AmOXSA^+$)		[61]
iminodiacetic acid (H_2IDA)						
	IX	25	0.1 M NH_4ClO_4	7.37 ($AmIDA^+$)	12.39 $(Am(IDA)_2)$	[26]
	Spec	25 ± 0.2	1.0 M $HClO_4/NaClO_4$	6.14		$\beta_5 = 3.34$ $(Am(IDA)_5^{7-})$ [11]
	Spec	25	0.1 M NH_4ClO_4	6.94		[31]
7-iodo-8-hydroxyquinoline-5-sulfonic acid (H_2IOXSA)						
	IX	25 ± 0.2	0.1 M NH_4ClO_4	6.92 ($AmIOXSA^+$)		[61]
β-isopropyltropolone (HIPT)						
	IX		0.1 M NH_4ClO_4			$\beta_3 = 22.22 \pm 0.15$ (Am(IPT)3) [9]
	SX	25	0.1 M NH_4ClO_4			$\beta_3 = 21.37$ [9,62]

Table 8.9 (*Contd.*)

Ligand	*Method*	*Temp.* (°C)	*Ionic strength, medium* μ (mol L^{-1})	*Log of formation constants* β_1	β_2	*Other constants*	*References*
lactic acid (HLact)	SX	25	2.0 M NH_4ClO_4	2.52 ($AmLact^{2+}$)	4.77 ($Am(Lact)_2^+$)	$\beta_3 = 5.98$ (Am(Lact)3)	[63]
	IX		0.5 M NH_4ClO_4	2.77	4.64		[64]
	SX	20	0.5 M NH_4ClO_4			$\beta_3 = 5.71 \pm 0.03$	[65]
	IX	20	0.5 M NH_4ClO_4			$\beta_3 = 5.73$	[65]
	PEP	10	1.5 M KCl/HLact	2.57	4.21		[66]
methionine	Spec	18 ± 2	1.0 M KCl	4.8 ± 0.2			[8]
N-methyliminodiacetic acid (H_2MIDA)							
	IX	25	0.1 M NH_4ClO_4	7.01 ($AmMIDA^+$)	12.51 ($Am(MIDA)_2^-$)		[26]
6-methyl-2-picoline acid (HMAPS)							
	IX	25 ± 0.2	0.1 M NH_4ClO_4	4.26 ($AmMAPS^{2+}$)			[61]
6-methyl-2-picolyliminodiacetic acid (H_2MPIDA)							
	IX	25	0.1 M NH_4ClO_4	8.38 ($AmMPIDA^+$)			[26]
methylolethylphosporic acid (HMEPA)							
	IX	25	0.2 M NH_4ClO_4	1.79 ± 0.12 ($AmMEPA^{2+}$)			[59]
(methylphenylphosphinyl)methylphenylposphinic acid (HMPPA)							
	SX	25	0.2 M NH_4ClO_4	3.35 ($AmMPPA^{2+}$)			[59]
methylphosphinic acid (HMPA)							
	IX	25 ± 0.2	0.5 M NH_4ClO_4	2.79 ($AmMPA^{2+}$, at $\mu = 0$)			[67]
naphthoyltrifluoroacetone (HNTA)							
	SX	25	0.1 M NH_4ClO_4			$\beta_3 = 18.31$ ($Am(NTA)_3$)	[9]
nitrilodiacetomonobutyric acid (H_3NDMBA)							
	IX	25	0.1 M NH_4ClO_4			$\beta_1' = 3.53$ (AmHNDMBA)	[68,69]
nitrilodiacetomonopropionic acid (H_3NDAPA)							
	IX	25	0.1 M NH_4ClO_4	10.54 (AmNDAPA)	17.83 ($Am(NDAPA)_2^{3-}$)	$\beta_1' = 4.02$ (AmHNDAPA)	[68,69]
nitrilodiacetomonovaleric acid (H_3NDAVA)							
	IX	25	0.1 M NH_4ClO_4			$\beta_1' = 3.47$ (AmHNDAVA)	[68,69]

nitrilotriacetic acid (H_3NTA)							
	IX	25 ± 0.2	0.1 M $NaClO_4$	11.72 ± 0.02 (AmNTA)			[11]
			0.5 M $NaClO_4$	10.84 ± 0.06			[11]
	SX	20	0.1 M NH_4ClO_4	10.70	19.71($Am(NTA)_2^{3-}$)		[39]
	IX	20	1.0 M NH_4ClO_4	10.87			[1]
	IX	25.6	0.1 M NH_4ClO_4	11.91	20.18		[35]
	IX	25	0.1 M NH_4ClO_4–$HClO_4$	11.52	20.24		[68]
	IX	25	0.1 M (NH_4, $HClO_4$)	11.68	20.47		[69]
	Spec	24.6	0.1 M NH_4ClO_4	11.99	21.1		[70]
		20		11.65	19.52	$\beta_3 = 13.56$ ($AmNTA(HNTA)^{2-}$)	[71]
oxalic acid (H_2Ox)	SX	20	0.1 M NH_4Cl		8.3 ($Am(Ox)_2^-$)	$\beta_3 = 11.8$ ($Am(Ox)_3^{3-}$)	[39]
	IX		1.0 M NH_4Cl		9.95	$\beta_4' = 11.0$ ($Am(HOx)_4^-$)	[41]
	Sol	25	$HClO_4/H_2Ox$	7.10 ($AmOx^+$)	11.2	$\beta_3 = 12.3$	[72]
	IX	20–25	0.2 M NH_4ClO_4	5.99	10.1		[73]
	EM	25	0.1 M NH_4Cl/HCl	6.45	10.5		[73]
	SX	25	1.0 M $NaClO_4$	4.63	8.35	$\beta_3 = 11.2$	[74,75]
	IX	25	0.5 M $NaClO_4$	3.8 ± 0.02	8.61 ± 0.01		[28]
	Spec	25 ± 0.1	$\mu = 0.25$; oxalate,pH1–5	3.27 (AmO_2Ox^+)	2.09 ($AmO_2(Ox)_2^{3-}$)		[75]
	SX	21	0.7 M Na NaCl	4.58 ± 0.05 (pH 6.0)	7.91 ± 0.10 (pH 6.0)		[76]
				3.95 ± 0.15 (pH 8.05)	7.54 ± 0.20 (pH 8.05)		
	Sol	25 ± 0.2	I = 0	6.68	9.94	11.62	[77]
	EM	25	0 M $NaClO_4$		9.6		[78]
			0.01 M $NaClO_4$		9.0		[78]
			0.05 M $NaClO_4$		8.3		[78]
			0.1 M $NaClO_4$		8.2		[78]
	SX	25.0	1.0 M $NaClO_4$	4.61 ± 0.06	8.39 ± 0.12		[79]
			3.0 M $NaClO_4$	4.65 ± 0.04	8.67 ± 0.13		[79]
			5.0 M $NaClO_4$	4.83 ± 0.06	9.24 ± 0.09		[79]
			7.0 M $NaClO_4$	4.93 ± 0.11	9.42 ± 0.06		[79]
			9.0 M $NaClO_4$	4.54 ± 0.06	8.77 ± 0.05		[79]
phenylalanine	Spec	18 ± 2	1.0 M KCl	5.1 ± 0.3			[8]
1-phenyl-3-methyl-4-acetylpyrazolone-5 (HPMAP)							
	SX	25	0.1 M NH_4ClO_4			$\beta_3 = 12.23$ ($Am(PMAP)_3$)	[80]
1-phenyl-3-methyl-4-benzoylpyrazolone-5 (HPMBP)							
	SX	25	0.1 M NH_4ClO_4			$\beta_3 = 16.49$ ($Am(PMBP)_3$)	[80]
1-phenyl-3-methyl-4-trichloroacetylpyrazolone-5 (HPMTCP)							
	SX	25	0.1 M NH_4ClO_4			$\beta_3 = 7.47$ ($Am(PMTCP)_3$)	[80]

Table 8.9 (*Contd.*)

Ligand	*Method*	*Temp.* (°C)	*Ionic strength, medium* μ (mol L^{-1})	*Log of formation constants* β_1	β_2	*Other constants*	*References*
1-phenyl-3-methyl-4-trifluoroacetylpyrazolone-5 (HPMTFP)							
	SX	25	0.1 M NH_4ClO_4			$\beta_3 = 9.70$ ($Am(PMTFP)_3$)	[80]
phosphonoacetic acid (H_3PAA)							
	IX	0.2 M NH_4ClO_4				$\beta_1'' = 2.75$ ($Am(H_2PAA)^2$)	[81]
						$\beta_1''' = 5.15$ ($AmHPAA^+$)	[81]
						$\beta_2''' = 8.5$ ($Am(HPAA)_2^-$)	[81]
pyridine-2-carbonic acid (HAPS)							
	IX	25 ± 0.2	0.1 M NH_4ClO_4	4.28 ± 0.05 ($AmAPS^{2+}$)	7.99 ± 0.03 ($Am(APS)_2^+$)	$\beta_3 = 10.51 \pm 0.05$ (Am(APS)3)	[61]
α-picolinic acid-*N*-oxide (HAPSNO)							
	IX	25 ± 0.2	0.1 M NH_4ClO_4	3.09 ± 0.07 ($AmAPSNO^{2+}$)	5.49 ± 0.07 ($Am(APSNO)_2^+$)		[61]
2-picolyliminodiacetic acid (H_2PIDA)							
	IX	25	0.1 M NH_4ClO_4	8.96 ($Am(PIDA^+)$)	17.71 ($Am(PIDA)_2^+$)		[26,52]
	Spec	25	0.1 M	0.94 ± 0.01 ($Am(PIDA)^+$)			[82]
				1.24 ± 0.001 ($Am(PIDA)_2^-$)			[82]
propanetricarboxylic acid (H_3PTA)							
	Spec	25	1.0 M $NaClO_4$	5.61 ± 0.07 (AmPTA)		$\beta_1' = 4.96 \pm 0.02$ ($AmHPTA^+$)	[10,11]
α-pyridiylacetic acid (HAPAA)							
	IX	25 ± 0.2	0.1 M NH_4ClO_4	3.63 ± 0.07 ($AmAPPA^{2+}$)			[61]
pyridine-3-carboxylic acid (Nicotinic acid) (HNIC)							
	IX	25 ± 0.2	0.1 M NH_4ClO_4	3.18 ± 0.07 ($AmNIC^{2+}$)			[61]
pyridine-2,6-dicarboxylic acid (H_2PDA)							
	IX	25 ± 0.2	0.1 M NH_4ClO_4	9.33 ± 0.09 ($AmPDA^+$)	16.51 ± 0.09 ($Am(PDA)_2^-$)		[61]
pyruvic acid (HPruv)							
	SX	25	2.0 M $NaClO_4$	2.03 ($AmPruv^{2+}$)	3.34 ($Am(Pruv)_2^+$)	$\beta_3 = 3.87$ ($Am(Pruv)_3$)	[63]

bis(3-methoxysalicylidenaldehyde)ethylenediimine (B3MOXSEDI)							
	SX	25	0.3 M KNO_3			$\beta'_2 = 0.59$ (AmH(B3MoxSEDI)$_2$)	[83]
bis(salicylidenaldehyde)ethylenediimine (BSEDI)							
	SX	25	0.3 M KNO_3			$\beta'_2 = 4.94$(AmH(BSEDI)$_2$)	[83]
serine		Spec	18 ± 2	1.0 M KCl	4.3 ± 0.1		[8]
squaric acid (H_2Sq, Diketocyclobutenediol)							
	IX	25	1.0 M $(H,NH_4)ClO_4$	2.17($AmSq^+$)	3.10 ($Am(Sq)_2$)		[84]
5-sulphosalicylic acid							
	PT	25	1.0 M $NaClO_4$	8.06 ± 0.02	15.34 ± 0.02		[85]
tartaric acid (H_2Tart)							
	IX		1.0 M NH_4Cl		10.7 ($Am(Tart)_2^+$)		[14,86]
	SX	20	0.1 M NH_4Cl	3.9 ($AmTart^+$)	6.8		[39]
	PEP	(?)	(?)		7.88		[87]
	SX	25 ± 0.5	0.5 M NH_4ClO_4	4.20 ± 0.06	6.84 ± 0.07		[6]
taurine-*N,N*-diacetic acid (H_3TDA)							
	IX	25	0.1 M NH_4ClO_4	8.08 (AmTDA)		$\beta'_1 = 2.29$ ($AmHTDA^+$)	[26]
	Spec	25	0.1 M	0.89 ± 0.001 ($Am(H_3TDA)$)			[82]
				1.14 ± 0.005 ($Am(H_3TDA)_2^{3-}$)			[82]
N,N,N′,N′-tetrakis(2-pyridylmethyl)ethylenediamine (TPEN)							
	PT	25	0.1 M $NaClO_4$	6.69 ± 0.03 ($Am(TPEN)^{+3}$)			[88]
	Spec	25	0.1 M $NaClO_4$	6.77 ± 0.01 ($Am(TPEN)^{+3}$)			[88]
thenoyltrifluoroacetone (HTTA)							
	SX	25	0.1 M NH_4ClO_4	3.4 ($AmTTA^{2+}$)	8.5($Am(TTA)_2^+$)	$\beta_3 = 13.3$ ($Am(TTA)_3$)	[9]
	SX	10.40	0.1 M $HClO_4/ClO_4$			$\Delta G^\circ = 43.9$ kJ mol^{-1} (Am(TTA)3)	[12]
thiodiglycolic acid (H_2TDGA)							
	Spec	25.6	0.1 M NH_4ClO_4	3.52 ± 0.08 ($AmTDGA^+$)	5.66 ± 0.07 ($Am(TDGA)_2^+$)	$\beta'_1 = 2.06 \pm 0.08$ ($AmHTDGA^{2+}$)	[35]
thioglycolic acid (HTGlyc)							
	IX	20	0.5 M NH_4ClO_4	1.55 ($AmGlyc^{2+}$)	2.60($Am(TGlyc)_2^+$)		[3]
p-toluenesulfonic acid (pTSAH)							
	SX	25	2.0 M $HClO_4$/pTSAH	–0.028 ± 0.028 ($AmpTSA2^+$)			[89]
	SX	25	2.0 M HBF_4/pTSAH	0.075 ± 0.018			[89]

Table 8.9 (*Contd.*)

Ligand	*Method*	*Temp.* (°C)	*Ionic strength, medium* μ (mol L^{-1})	*Log of formation constants* β_1	β_2	*Other constants*	*References*
triethylenetetraaminehexaacetic acid (H_6TTHA)							
	IX	25	0.1 M NH_4ClO_4			$\beta'_1 = 18.13$ ($AmHTTHA^{2+}$)	[26]
						$\beta''_1 = 11.85$ (AmH_2TTHA^{-})	[26]
	Spec	25	0.1 M NH_4ClO_4	27.61 ($AmTTHA^{3-}$)		$\beta = 30.97$ (Am2TTHA)	[1,31]
						$\beta = 9.15(Am_2H_2(TTHA)_3^{10-})$	[1,31]
Tropolene	SX	25	0.1 M $HClO_4$			$\beta_3 = 16.17 \pm 0.08$	[62]
Tryptophan	Spec	18 ± 2	1.0 M KCl	4.7 ± 0.2			[8]

[1] (Moskvin, 1967, 1971, 1973); [2] (Choppin, 1965, 1970, 1975); [3] (Grenthe, 1962); [4] (Gureev *et al.*, 1970); [5] (Hara, 1970); [6] (Rao *et al.*, 1987); [7] (Aziz and Lyle, 1971); [8] (Rogozina *et al.*, 1974); [9] (Keller and Schreck, 1969); [10] (Eberle and Moattar, 1972); [11] (Moattar, 1971); [12] (Hubert *et al.*, 1974, 1975); [13] (Ohyoshi and Ohyoshi, 1971); [14] (Moskvin *et al.*, 1962); [15] (Marcu and Samochocka, 1966); [16] (Bouhlassa and Guillaumont, 1984); [17] (Wall *et al.*, 2002); [18] (Mohapatra and Manchanda, 1991); [19] (Stepanov *et al.*, 1967); [20] (Baybarz, 1966); [21] (Elesin and Zaitsev, 1971a); [22] (Shilov *et al.*, 1976); [23] (Mohapatra and Manchanda, 1995); [24] (Zur Nedden, 1969); [25] (Keller *et al.*, 1965a, 1966); [26] (Bayat, 1970); [27] (Baybarz, 1965); [28] (Lebedev and Shalinets, 1968; Lebedev *et al.*, 1968); [29] (Burch, 1964); [30] (Hafez, 1968); [31] (Delle Site and Baybarz, 1969); [32] (Piskunov and Rykov, 1972); [33] (Brandau, 1971); [34] (Elesin and Zaitsev, 1972); [35] (Grigorescu-Sabau, 1972); [36] (Goffart and Kuyckaerts, 1969; Vorob'eva *et al.*, 1973a); [37] (Shalinets and Stepanov, 1971, 1972); [38] (Elesin *et al.*, 1973); [39] (Stary, 1966); [40] (Fuger, 1958); [41] (Moskvin *et al.*, 1959); [42] (Lebedev *et al.*, 1967); [43] (Elesin and Zaitsev, 1971b); [44] (Shalinets, 1972a,c); [45] (Anan'ev and Krot, 1985; Anan'ev and Shilov, 1985); [46] (Buckau *et al.*, 1992); [47] (Tanner and Choppin, 1968); [48] (Choppin and Degischer, 1972); [49] (Levakov and Shalinets, 1971); [50] (Eberle and Bayat, 1967); [51] (Mercing and Duyckaerts, 1967); [52] (Eberle and Bayat, 1969); [53] (Ermakov *et al.*, 1971c); [54] (Shalinets, 1972b); [55] (Dedov *et al.*, 1961); [56] (Graus Odenheimer and Choppin, 1956); [57] (Stary, 1965); [58] (Vorob'eva *et al.*, 1973b); [59] (Elesin *et al.*, 1972a,b); [60] (Ermakov *et al.*, 1971b); [61] (Al Rifai, 1970); [62] (Cilindro and Keller, 1974); [63] (Aziz and Lyle, 1971); [64] (Lebedev and Yakovlev, 1961); [65] (Ermakov and Starπ, 1967); [66] (Sakanque and Nakatani, 1972); [67] (Borisov *et al.*, 1967); [68] (Eberle and Ali, 1968); [69] (Ali, 1968); [70] (Eberle and Sabau, 1972); [71] (Gedeonov *et al.*, 1967); [72] (Lebedev *et al.*, 1960a); [73] (Stepanov and Makarova, 1965; Stepanov, 1971); [74] (Sekine, 1965); [75] (Shilov *et al.*, 1974); [76] (Caceci and Choppin, 1983); [77] (Pazukhin *et al.*, 1987); [78] (Rosch *et al.*, 1989); [79] (Choppin and Chen, 1996); [80] (Backer and Keller, 1973); [81] (Elesin *et al.*, 1972c); [82] (Bayat and Moattar, 1982); [83] (Stronski and Rekas, 1973); [84] (Cilindro *et al.*, 1972); [85] (Nair and Chander, 1983); [86] (Gel'man *et al.*, 1967); [87] (Marcu and Samochocka, 1965); [88] (Jensen *et al.*, 2000); [89] (Baisden *et al.*, 1972).

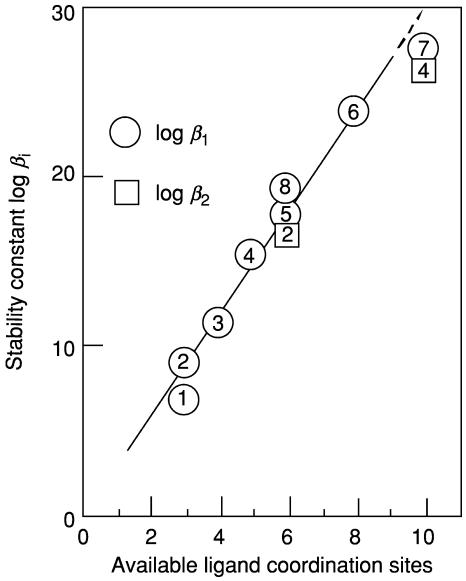

Fig. 8.7 *Correlation of stability constants with number of available coordination sites*. 1, *iminidiacetic acid;* 2, *N-hydroxy-ethyliminodiacetic acid;* 3, *nitrilotriacetic acid;* 4, *N-hydroxyethylenediaminetriacetic acid;* 5, *ethylenediaminetetraacetic acid;* 6, *diethylenetriaminepentaacetic acid;* 7, *triethylenetetraaminehexaacetic acid;* 8, *diaminocyclohexanetetraacetic acid* (*Keller*, 1971).

Methods are being sought to estimate and correlate the strengths of Am(III) complexes and other trivalent actinides and lanthanides with various organic ligands. Shalinets and Stepanov (1971, 1972) suggests a 'rule of additivity of the strength of rings' according to which, under similar conditions, the logarithm of the thermodynamic formation constant of the complex is proportional to the sum of the strengths of the individual rings. In a few cases, formation constants of americium chelates calculated by Shalinets are in good agreement with experimental data. For a more detailed discussion of the nature and stability of organic complexes of americium, refer to Chapters 23 and 25.

It is not surprising that a number of studies focus on the complexation of Am(III) with natural organic substances because of its importance for the assessment of nuclear waste disposal in geologic formations. The majority of naturally occurring organic materials derive from the decomposition of organic matter to soluble polymeric HA and fulvic acid (FA). The surfaces of these substances have a number of hydrophilic functional groups, such as amine, hydroxyl, carboxyl, and phenolic. As a hard cation, Am^{3+} interacts predominantly with the oxygen-donating phenolic and carboxylic groups. A large number of experimental data exist that are usually interpreted by the charge neutralization

model or a polyelectrolyte model (Choppin and Labonne-Wall, 1997). The charge neutralization model is based on the cation complexation by a number of carboxylate groups expressed as an experimentally determined loading capacity of the organic substance. The polyelectrolyte model can better accommodate the chemical behavior of the humic/fulvic acids and takes into account the nature of the binding functional group (carboxylate). The concentration of binding sites and the ionization degree is determined experimentally via pH titration. For a more detailed discussion of these two models and of the impact of humate and fulvate complexation on the environmental behavior of americium, refer to Chapters 27 and 29.

Choppin and coworkers (Bertha and Choppin, 1978) performed ion-exchange studies at pH 4.5 to determine $\log \beta_1 = 6.83$ and $\log \beta_2 = 10.58$ for a Lake Bradford, Florida (USA), humic substance. These results agree well with $\log \beta_1 = 6.4$ and $\log \beta_2 = 10.58$ determined for HA from Mount Kanmuri, Japan (Yamamoto and Sakanoue, 1982). Applying a degree of ionization of the HA, Choppin and coworkers (Torres and Choppin, 1984) reported $\log \beta_1 =$ 6.8–11.6 and $\log \beta_2 = 11.9$–14.3 for the Am(III)—HA (Lake Bradford) complex determined at pH 3.75–5.7. Using UV–VIS and laser-induced photoacoustic spectroscopy Kim *et al.* (1993) determined $\log \beta_1 = 6.4 \pm 0.1$ at pH = 6 ($I = 0.1$) for HAs obtained from natural water at the German Gorleben (Gohy-573) site and from a commercial HA (Aldrich Chemical Co.). For the calculation of the Am(III)–HA stability constant, Kim *et al.* determined a loading capacity of 62.2% for Gohy-573 HA and of 81.5% for Aldrich HA. The Am(III) absorption band at 506 nm was assigned to an Am(III)–HA complex and was used for data analysis. Moulin *et al.* (1987) spectroscopically monitored the complexation of Am(III) with Aldrich HA at pH 4.65 ($I = 0.1$) and calculated $\log \beta_1 = 7$–7.5.

The stability constants found for Am(III) fulvate are slightly smaller than those found for humate. Buckau *et al.* (1992) determined $\log \beta_1 = 5.9$ for FA extracted from the Gohy-573 groundwater using UV–VIS absorption spectroscopy. This FA is characterized by a proton exchange capacity of 5.7 meq g^{-1} and a loading capacity of 64.9% at pH 6.0. Interestingly, the stability constant of the Am(III)–FA complex is constant in the Am(III) concentration range of 4×10^{-5} to 5×10^{-8} mol L^{-1} at [HA] = 10^{-6} mol L^{-1}.

Complexation of Am(III) with the hexadentate ligand *N*,*N*,*N*′,*N*′-tetrakis (2-pyridylmethyl)ethylenediamine (TPEN) in 0.1 M $NaClO_4$ at 25°C to form $Am(TPEN)^{3+}$ is about two orders of magnitude higher than that of Sm(III), reflecting the stronger bonding of the trivalent actinide cations with softer ligands as compared to lanthanides (Jensen *et al.*, 2000).

(d) Others

The stability constants of Am(III) fluoride complexes are much larger than for the other halides (Silva *et al.*, 1995). Positive enthalpies for the reaction of Am^{3+} with F^- anions indicate that the AmF_n^{3-n} are inner-sphere complexes.

Two Am(III) fluoride solution species have been identified, AmF^{2+} and AmF_2^+, with recommended formation constants of $\log \beta_1^o = 3.4 \pm 0.4$ and $\log \beta_2^o = 5.8 \pm 0.2$, respectively. In contrast, the recommended formation constant for $AmCl^{2+}$, $\log \beta_1^o = 1.05 \pm 0.06$, suggests a very weak bonding of chloride ions.

Few reliable data have been reported for the sulfate complexation of Am(III). Stability constants for two complexes, $AmSO_4^+$ ($\log \beta_1^o = 3.85 \pm 0.03$) and $Am(SO_4)_2^-$ ($\log \beta_2^o = 5.4 \pm 0.7$), were recommended (Silva *et al.*, 1995). There is no evidence for the formation of $Am(III) - HSO_4^-$ complexes.

The formation of Am(III) thiocyanate complexes was studied intensively because of the use of such complexes in separation of lanthanide and actinide elements. Three complexes of general formula $Am(SCN)_n^{3-n}$ ($n = 1$–3) have been identified from spectroscopic and solvent extraction data. The complexation of Am(III) by thiocyanate is quite weak and the accepted thermodynamic constant for the 1:1 complex is $\log \beta_1^o = 1.3 \pm 0.3$ (Silva *et al.*, 1995).

Nitrate complexes of Am(III) are weak complexes and two complexes, $AmNO_3^{2+}$ and $Am(NO_3)_2^+$, have been used to interpret solvent extraction data in nitric acid media. The recommended formation constant of the 1:1 complex is $\log \beta_1^o = 1.33 \pm 0.20$ (Silva *et al.*, 1995).

A number of studies of Am(III) complexation in phosphate media have been reported with only a few reliable data interpretations and complex characterizations. The system is complicated by the presence of multiple (hydrogen) phosphate species in solution. The solution complexes $AmHPO_4^+$ and $Am(H_2PO_4)_n^{3-n}$ ($n = 1$–4) have been used to interpret cation exchange, solvent extraction, and spectroscopic data. Lebedev *et al.* (1979) attributed the changes of the characteristic absorption band of Am^{3+} at 503 nm to the formation of $Am(III) - H_2PO_4^-$ complexes. With increasing phosphoric acid concentration (up to 13 M), the absorbance maximum is shifted to about 502 nm and the characteristic shoulder in the Am^{3+} band at 506 nm almost disappears. It remains unclear if these changes are due to inner-sphere complexation with phosphate or to changes in the number of coordinated water molecules in these extreme experimental conditions. The NEA recommends a stability constant only for the complex $AmH_2PO_4^{2+}$, $\log \beta_1^o = 3.0 \pm 0.5$ (Silva *et al.*, 1995).

Am(IV) can be stabilized in acidic media by complexation with heteropolyanions. Chartier *et al.* (1999) reported spectroscopic evidence for the formation of $AmP_2W_{17}O_6^{16-}$ and $Am(P_2W_{17}O_{61})_2^{16-}$ via their absorbance bands at 789 and 560 nm, respectively. Chartier *et al.* reported $\log \beta_1 = 19.2 \pm 0.2$ and $\log \beta_2 = 22.8 \pm 0.2$ in 1 M HNO_3. The rate of autoradiolytic reduction of Am(IV) in these complexes is independent of the complex composition. Th(IV) causes the destruction of the complexes and subsequent disproportionation of free Am(IV) into Am(III) and Am(VI). Complex formation of Am(III) with $W_{10}O_{36}^{12-}$, $PW_{11}O_{39}^{7-}$, and $SiW_{11}O_{39}^{8-}$ was discussed qualitatively by Yusov (1989). Chartier *et al.* (1999) determined the apparent formation constants for $AmSiW_{11}O_{39}^{4-}$ and for $Am(SiW_{11}O_{39})_2^{12-}$ in 1 M HNO_3, $\log \beta_1 = 21.3 \pm 0.3$ and $\log \beta_2 = 26.2 \pm 0.2$,

respectively. In contrast, Williams *et al.* (2000) used extended X-ray absorption fine structure (EXAFS) to determine that the Am center cation is trivalent when integrated in the Preyssler anion, $AmP_5W_{30}O_{110}^{12-}$.

Sullivan *et al.* (1961) discovered cation–cation interaction between pentavalent and hexavalent actinides. Subsequently, Guillaume *et al.* (1981) found spectroscopic evidence for the Am(V)–U(VI) interaction in perchlorate medium where the interaction between AmO_2^+ and UO_2^{2+} shifts the main absorbance peak of AmO_2^+ at 716–733 nm and a new band appears at 765 nm. Both bands are close to the absorbances reported for the solid $KAmO_2CO_3$ (733 and 770 nm (Varga *et al.*, 1971)). Upon interaction of Am(V) with U(VI), the symmetrical stretching (Raman) frequency of AmO_2^+ at 732 cm^{-1} is shifted to 719 cm^{-1} (Guillaume *et al.*, 1982). The Am(V)–U(VI) ($K = 0.35 \pm 0.07$ at $I = 10$) and Am(V)–Np(VI) ($K = 0.095 \pm 0.03$ at $I = 6$) (Guillaume *et al.*, 1981, 1982) complexes appeared to be much weaker than the corresponding Np(V) complexes: Np(V)–U(VI) ($K = 3.7 \pm 0.1$ at $I = 7$) and Np(V)–Np(VI) ($K = 3.0 \pm 0.1$ at $I = 7$ (Madic *et al.*, 1979)).

8.9 COORDINATION CHEMISTRY AND COORDINATION COMPLEXES

Although over 250 compounds of americium have been synthesized and characterized, the coordination chemistry of americium is relatively unknown. As of 2001, the crystal structures of 39 americium compounds with inorganic ligands and only seven americium compounds with organic ligands have been structurally characterized. However, the majority of phase identification and characterization relied on X-ray powder diffraction and comparison to isostructural lanthanide, neptunium, or plutonium compounds. Certainly, the application of EXAFS provides useful insight into coordination and bonding of solution complexes and amorphous solid phases. As hard metal ions Am(III to VI) have a high affinity for hard donor atoms, such as O or N, and the light halides, and their coordination will be discussed in this section. Because of its high redox stability, trivalent americium coordination complexes are the most common. Generally, higher dimensional structures are found containing Am^{2+}, Am^{3+}, or Am^{4+} while the introduction of the linear americyl unit forces Am(V) and Am(VI) to form layered structures.

8.9.1 Compounds with inorganic ligands

(a) Halides

Americium exhibits different coordination environments in halide complexes with coordination numbers of 7, 8, 9, and 11. In the orthorhombic M_2AmCl_5 (M = K, NH_4, or Rb) trivalent americium is seven-coordinate in $AmCl_5^{2-}$ chains with two of the five chlorides bridging to adjacent Am atoms. In the monoclinic

hexahydrate, $AmCl_3 \cdot 6H_2O$, americium is coordinated to two chlorides and six water molecules forming $AmCl_2(H_2O)_6^+$ cations that are linked through chloride anions in the lattice and an extensive hydrogen bond network (Burns and Peterson, 1971). Considering the inner-sphere bonding of the water molecules, the formula of this compound is better represented by $AmCl_2(H_2O)_6 \cdot Cl$. Eight-coordinate americium is also found in the tetrafluoride AmF_4. $AmO_2F_2^-$ layers held together by K^+ ions form the rhombohedral $KAmO_2F_2$, in which americium is eight-coordinate with two axial oxygen atoms (Am–O = 1.936 Å) and six fluorides (Am–F = 2.473 Å) in the equatorial plane (Asprey *et al.*, 1954a). The isostructural oxyhalides AmOCl (Weigel *et al.*, 1975) and AmOI (Asprey *et al.*, 1964, 1965) also contain nine-coordinate americium that is surrounded by four oxygen (2.343 Å) and five iodine atoms (4 Am–I of 2.994 Å and 1 Am–I of 3.0035 Å). Interestingly, AmOBr (Weigel *et al.*, 1979) is reported to be built up from linear Br–Am–O units stacked along the *c*-axis with reported interatomic distances of 2.415 Å for Am–O and 3.21 and 3.36 Å for Am–Br. Using the atomic coordinates reported for AmOBr, we calculate 2.339 and 2.979 Å for Am–O and 3.145 and 3.801 Å for Am–Br bond distances. Considering the discrepancies in the bond distances and the structural anomaly within the AmOX series, there are serious doubts about the reported structure of AmOBr. The trifluoride AmF_3 crystallizes in the 11-coordinate LaF_3 structure (Templeton and Dauben, 1953). In the anhydrous $AmCl_3$, the americium atom is bonded to six chlorine atoms at 2.874 Å and three chlorine atoms at 2.915 Å (Burns and Peterson, 1970) (Fig. 8.8).

(b) Oxides

Several americium oxides of varying stoichiometry have been prepared and structural data rely principally on X-ray powder diffraction powder data. The binary oxide AmO (CN 6) crystallizes in a cubic structure with octahedral O and Am atoms (Zachariasen, 1949b). Interatomic distances are calculated to be 2.480 Å for Am–O and 3.507 Å for Am–Am. However, AmO may be an oxynitride, as discussed in Section 8.7.1. As discussed in Section 8.7.1, three Am_2O_3 phases are known. Templeton and Dauben (1953) report the lattice parameters $a = 11.03 \pm 0.01$ Å for the low-temperature cubic form and $a = 3.817 \pm 0.005$ Å, $c = 5.971 \pm 0.010$ Å for the high-temperature hexagonal form. In the cubic phase two crystallographically different americium atoms exist: distorted $[Am(1)O_6]$ octahedra with Am(1)–O bond lengths of 2.369 Å are bridged through their oxygens to six Am(2) atoms. The Am(2) atoms are centered within a distorted octahedral environment of six oxygen atoms with Am–O distances of 1.984, 2.678, and 2.774 Å. The Am(2)–O distances of 1.984 Å are unusually short for trivalent actinide–oxygen bonds and only slightly longer than the reported bond lengths of about 1.935 Å for the linear Am=O bonds in Am(v) compounds (Asprey *et al.*, 1954a; Ellinger and Zachariasen, 1954). The intermediate-temperature monoclinic AmO_2 is isostructural with

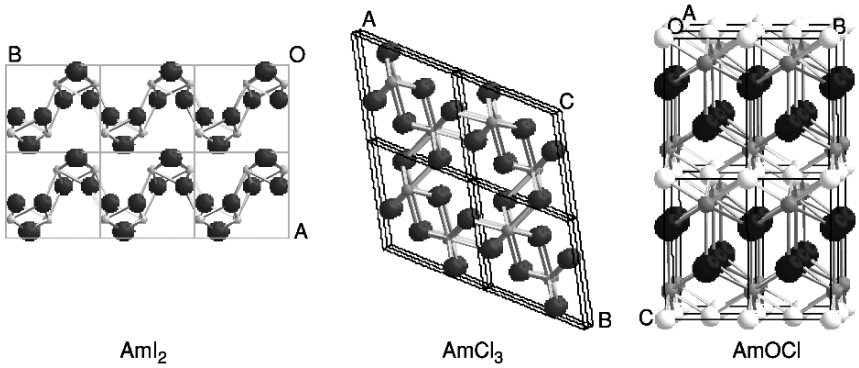

Fig. 8.8 *Structures of americium halide compounds: AmI_2 (Baybarz and Asprey,* 1972), *$AmCl_3$ (Burns and Peterson,* 1970), *and AmOCl (Templeton and Dauben,* 1953).

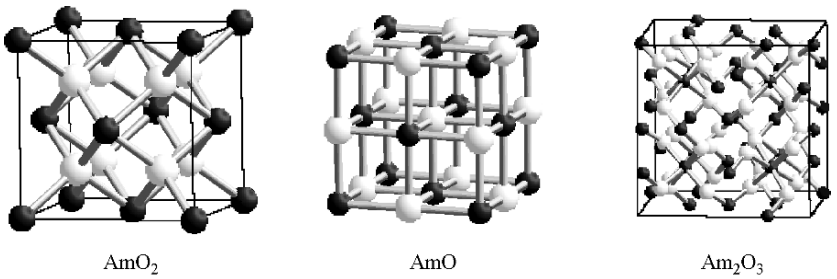

Fig. 8.9 *Unit cells of americium oxides: AmO_2 (Templeton and Dauben,* 1953; *Chikalla and Eyring* 1967, 1968), *AmO (Zachariasen,* 1949a,b), *and Am_2O_3, (Templeton and Dauben,* 1953).

PuO_2 with eight Am–Am distances of 3.803 Å and a tetrahedral arrangement of four Am atoms around each oxygen atom (Am–O is 2.480 Å) (Templeton and Dauben, 1953). The three-dimensional ternary oxide $BaAmO_3$ (cubic perovskite structure, $a = 4.35$ Å, although possibly distorted as are $BaPuO_3$ and $BaLnO_3$) is built from edge-sharing [AmO_6] octahedra with large Ba^{2+} cations in 12-coordinated sites (Keller, 1964). Each AmO_6 octahedron shares all oxygen atoms with six adjacent octahedra. The Am–O distances are calculated to be 2.175 Å (Fig. 8.9).

(c) Chalcogenides and pnictides

The americium monochalcogenides AmX (X = S, Se, Te) crystallize in the cubic NaCl-type structure (CN 6) with the lattice parameters increasing with chalcogen atomic number. Early work of Zachariasen (1949d) concluded from powder

X-ray diffraction data that the sesquisulfide Am_2S_3 is isostructural with cubic Ce_2S_3 and contains 16 sulfur atoms and $10^{2/3}$ americium atoms per unit cell. The calculated interatomic Am–S distances of 2.94 Å are indicative of an ionic bonding between Am^{3+} and S^{2-} and compare well with the value of 2.93 Å reported by Damien and Jove (1971) in the substoichiometric compound $AmS_{1.9}$. The substoichiometric ditelluride, $AmTe_{1.73}$ (CN 9), crystallizes in a tetragonal anti-Fe_2As-type structure (Burns *et al.*, 1979). Layers of Te atoms are interleaved with puckered double layers of AmTe. The bond length between Te atoms in the pure Te layer is much shorter than the Te^{2-} interionic distances, suggesting some covalency within the pure Te layer. Random vacancy at sites within the pure Te layers causes the variable stoichiometry in Am–Te_2. The Am–Te bond lengths within the AmTe layers are only slightly shorter (3.258 and 3.208 Å) than the 3.269 Å from the Am atoms to the nearest Te atoms in the pure Te layer.

The structural information on the known pnictides of general formula AmX (X = N, P, Sb, As) was obtained from X-ray powder diffraction data. All binary pnictides crystallize in the cubic NaCl-type structure; both lattice parameters and Am–X bond length increase along the series: in AmN ($a = 5.005$ Å) Am–N is 2.503 Å, in AmP ($a = 5.711$ Å) Am–P is 2.856 Å, in AmAs ($a = 5.875$ Å) Am–As is 2.938 Å, and in AmSb ($a = 5.6.24$ Å) Am–Sb is 3.120 Å.

(d) Silicides

Weigel *et al.* (1977, 1984) reported structural information of several silicide phases. The layered structure of the binary AmSi is built up from corner-sharing [$AmSi_3$] pyramids with μ_3-Si atoms and Am–Si distances of 2.56 and 2.66 Å. The tetragonal $AmSi_2$ is isostructural with α-$ThSi_2$ and Am–Si distances range between 2.01 and 2.70 Å. In the sesquisilicide Am_2Si_3 americium atoms are coordinated to Si atoms at Am–Si distances of 3.04 Å.

(e) Oxoanionic ligands

Six oxygen atoms from three bidentately bonded carbonate ligands in the equatorial plane and two axial americyl oxygens form the inner coordination sphere of Am(v) in $RbAmO_2CO_3$ (Ellinger and Zachariasen, 1954) (Fig. 8.10). The Am=O and Am–O_{eq} bond distances are calculated from X-ray powder diffraction data to be 1.935 and 2.568 Å, respectively. Both distances are significantly longer than those in the Np(v) compounds, i.e. 1.75 Å for Np=O and 2.46 Å for Np–O_{eq} in aqueous $NpO_2(CO_3)_n^{1-2n}$ complexes (Clark *et al.*, 1996).

In the pseudotetragonal molybdate $Am_2(MoO_4)_3$ one-third of the Am sites are replaced by ordered vacancies (Tabuteau and Pages, 1978). The molybdate is isostructural to several lanthanide molybdates that crystallize in the pseudo-scheelite structure. The Am(III) tungstate, $Am_2(WO_4)_3$, is structurally analogous to $Eu_2(WO_4)_3$ and is built up from [AmO_8] dodecahedra and [WO_4] tetrahedra.

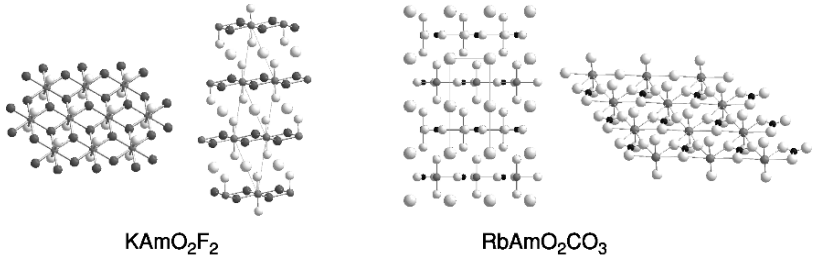

Fig. 8.10 *Sheet structures and crystal packing of the Am(v) compounds* $KAmO_2F_2$ (*Asprey* et al., 1954a) *and* $RbAmO_2CO_3$ (*Ellinger and Zachariasen*, 1954).

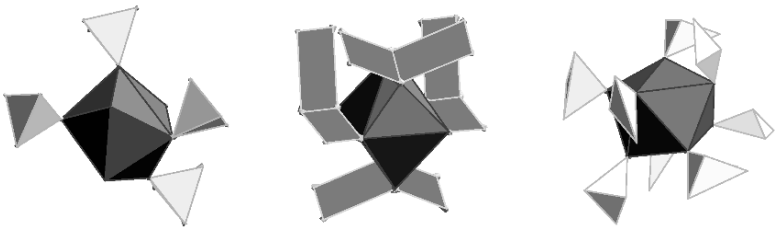

Fig. 8.11 *Coordination of oxyanions in the Am(III) compounds* $Am_2(SO_4)_3 \cdot 8H_2O$ (*Burns and Baybarz*, 1972), $Am_2(MoO_4)_3$ (*Tabuteau and Pages*, 1978), and α-$Am(IO_3)_3$ (*Bean* et al., 2003).

Burns and Baybarz (1972) reported the synthesis and single-crystal structure analysis of $Am_2(SO_4)_3 \cdot 8H_2O$. Eight-coordinate americium bonded to eight O atoms from four sulfate ligands (Am–O distances range from 2.381 to 2.951 Å) and four water molecules (Am–O range from 2.406 to 2.553 Å). The sulfate tetrahedra share edges and bridge americium atoms within the layers; extensive hydrogen bonding involving the lattice waters occurs between the layers.

Very recently, Bean *et al.* (2003) synthesized the anhydrous Am(III) iodate, α-$Am(IO_3)_3$, which is isostructural to the Gd(III) compound (Liminga *et al.*, 1977), and a new f-element iodate of composition $K_3Am_3(IO_3)_{12} \cdot HIO_3$ (Runde *et al.*, 2003) (Fig. 8.11). In both compounds, oxygens from eight iodate pyramids and Am^{3+} ions are located within a distorted $[AmO_8]$ dodecahedron that form a three-dimensional network with Am–O bond distances ranging from 2.34 to 2.60 Å and averaged I–O distances of 1.80 Å. Runde and coworkers also reported the synthesis of β-$Am(IO_3)_3$, that exhibits a novel two-dimensional architecture type within the f-element iodates. The nine-coordinate Am atoms are coordinated with only 7 iodate ligands via a combination of edge-sharing and corner-sharing $[IO_3]$ groups (Bean *et al.*, 2003).

(f) Others

The hydride AmH_3 crystallizes in a cubic structure with eight hydrogen atoms surrounding each Am atom and a tetrahedral arrangement of four Am atoms around each H atom. The bond lengths for Am–H and Am–Am are calculated to be 2.316 and 3.782 Å (Olson and Mulford, 1966).

8.9.2 Compounds with organic ligands

Only seven compounds of americium are listed in the Cambridge Structural Database (version 5.22, October 2001) that compiles complexes of metal cations with organic molecules. However, it is noteworthy that structures obtained from single crystal X-ray diffraction are reported only for two compounds. For the other five compounds, only cell constants and space groups were obtained from X-ray powder patterns and information on bond distances remains unavailable. Information on the overall structure was obtained by analogy to the corresponding compounds of rare earth elements. For a more detailed discussion of the preparation and reactivity of organic americium compounds, refer to Chapters 23 and 29.

(a) Oxygen-donor ligands

A wide variety of oxygen-donor ligands have been used to complex and separate americium. The most synthesized compounds of Am(III) are those with carboxylic acids, because of their applications in separation (Weigel and ter Meer, 1967). However, only the single-crystal structure of the hydrated Am(III) salicylate, $Am(C_7H_5O_3)_3(H_2O)$, has been reported. In this compound, americium is nine-coordinate to one water molecule and six salicylato ligands (Burns and Baldwin, 1976). The six salicylato ligands display three different coordination modes: (i) monodentate binding through the carboxylic oxygens of four ligands; (ii) bidentate binding through its carboxyl group; and (iii) and bidentate binding through a combination of carboxylic and phenolic oxygens. Salicylato complexes have been reported for rare earths and plutonium and are important because the ligands contain carboxylic and hydroxo functional groups, which are typical for the more complex natural humic materials.

The sodium acetate, $NaAmO_2(CH_3CO_2)_3$, is the only characterized complex of americyl(VI) (Jones, 1955). Lychev *et al.* (1980) synthesized the cesium salt of Am(V), $CsAmO_2(CH_3CO_2)_3$, but solved the crystal structure only of the isostructural analogous Np(V) compound. In both americyl acetate compounds, three carboxylates are coordinated bidentately in the equatorial planes of AmO_2^+ and AmO_2^{2+}. Burns and Danford (1969) obtained single crystals of orthorhombic $CsAm(hfa)_4$ (hfa = hexafluoro-acetylacetone) when recrystallizing monoclinic $CsAm(hfa)_4 \cdot H_2O$ (Danford *et al.*, 1970) in 1-butanol. The

compound is composed of Am(hfa)-chains that interact with Cs^+ ions. The Am^{3+} ion is chelated by the eight acetone–oxygen atoms of the four hfa ligands with Am–O bond distances between 2.36 and 2.45 Å. $CsAm(hfa)_4$ and $CsAm(hfa)_4 \cdot H_2O$ sublimes at about 135°C. Both hydrated and the anhydrous compounds are metastable and degrade after about 1 week with AmF_3 identified as one of the degradation products (Fig. 8.12).

EXAFS studies of the structure of the solvent-containing $Am(NO_3)_3(TEMA)_2$ complexes (TEMA = *N*,*N*,*N*′,*N*′-tetraethylmalonamide) resulted in Am–O distances of 2.52 ± 0.01 Å and a coordination polyhedron similar to that of the corresponding Nd compound, where Nd is ten-coordinate (DenAuwer *et al.*, 2000).

In recent years, the reactions of americium ions with a number of organic molecules were studied in the gas phase. As an example, the gas-phase reaction of laser-ablated americium ions with alcohols yields a mixture of hydroxides and alkoxides, i.e. $Am(OR)^+$ and $Am(OR)^{2+}$ (Gibson, 1999b). The reaction with dimethylether yields the methoxy ion $Am(OCH_3)^+$ as the primary product. Although these reactions do not reveal any structural details, they provide some understanding of potential interaction mechanisms in americium organometallic chemistry. Other products of laser-ablated Am^+ or AmO^+ ions reacting with polyimide, nitriles, or butylamines are AmC_2H^+, $AmC_2H_4^+$, $AmC_2H_2^+$, several cations of general formula $AmC_xH_yN_z^+$, and metal oxide clusters such as Am_2O^+ an $Am_2O_2^+$ (Gibson, 1998a, 1999a). An interesting anomaly was the observation of dimeric Am_2^+ clusters that were not formed by any other actinides studied (Gibson, 1999a).

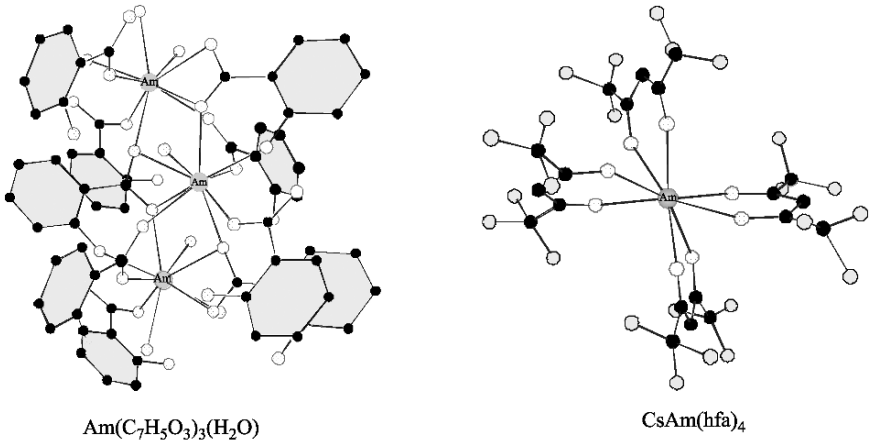

Fig. 8.12 *Nine-fold coordination of Am(III) in $Am(C_7H_5O_3)_3(H_2O)$ (Burns and Baldwin, 1976) and eight-coordinate Am(III) in $CsAm(hfa)_4$ (Burns and Danford, 1969).*

(b) Nitrogen donors

Only a few complexes of americium with N-donating ligands have been studied yet; structural details are limited. The bis-phthalocyanine complex has been synthesized and displays a sandwich-type complex with eight-coordinate americium (Moskalev *et al.*, 1979). Yaita *et al.* (2001) studied the Am(III) benzimidazole complex using XAFS spectroscopy and found a bidentate coordination of Am through two nitrogen atoms with the bond distance Am–N of 2.63 Å. The overall coordination number of Am(III) is reported to be close to 10.

(c) Sulfur donors

Only few structural studies are reported involving compounds with Am–S bonds. Gibson (1999b) observed SH abstraction from thiols and formation of the hydrosulfide $Am(SH)^+$ in the gas phase. The gas-phase reaction with propanethiol yielded the thiolate $Am(PrS)^+$. Tian *et al.* (2002) used EXAFS to study the structure of extraction complexes of Am(III) with di-*n*-octyldithiophosphinic acid and di(2,4,4-trimethylpentyl)dithiophosphinic acid in kerosene. The two extraction complexes appear to be similar in coordination with eight sulfur atoms in the inner sphere and four phosphorus atoms in the second shell with average Am–S and Am–P bond distances of 2.9 and 3.5 Å, respectively.

(d) Cyclopentadienyl and cyclooctatetraenyl compounds

The organometallic chemistry of americium remains essentially unstudied. The most studied compound is the cyclopentadiene complex, $Am(C_5H_5)_3$, which crystallizes in the orthorhombic *Pbcm* space group and is isostructural with, but not pyrophoric like $Pu(C_5H_5)_3$ (Baumgärtner *et al.*, 1966a). Pappalardo *et al.* (1969a) reported the absorbance spectrum of $Am(C_5H_5)_3$ films from which Nugent *et al.* (1971b) calculated a bond covalency of only $2.8 \pm 0.2\%$ (relative to the corresponding bands of $Am(aq)^{3+}$) indicating that the organometallic bonding in $Am(C_5H_5)_3$ is highly ionic. Consequently, Nugent *et al.* suggested that the compound should be designated as a tris-cyclopentadienide rather than a tricyclopentadienyl compound. Bursten and coworkers (Bursten *et al.*, 1989; Li and Bursten, 1997) calculated the electronic structure of $AnCl_3$, $An(C_7H_7)_2$, and $An(C_5H_5)_3$, and discussed the relative role of the 5f and 6d atom orbitals. Karraker (1975, 1977) reported the synthesis of the potassium salt of a bis-cyclooctatetraenyl Am(III) complex, $KAm(C_8H_8)_2$, and obtained the absorbance spectrum in THF. The compound $KAm(C_8H_8)_2 \cdot 2THF$ decomposes in water and burns when exposed to air. The X-ray powder diffraction data show that $Am(C_8H_8)_2$ is isostructural with the analogous Np and Pu compounds and the sandwich complex uranocene. The gas-phase reaction of Am^+ ions with 1.5-cyclooctadiene and cyclooctatetraene produced the dehydrogenation complexes $Am-C_8H_8^+$ and $Am-C_8H_6^+$ that were detected by mass spectrometry

(Gibson, 1998b). The gas-phase reaction of laser-ablated Am^+ with pentamethylcyclopentadiene (HCp^*) yielded the fragments $AmC_8H_{14}^+$, $AmC_9H_{12}^+$, and $AmC_{10}H_{14}^+$ (Gibson, 2000). In contrast to the multiple dehydrogenation reactions observed with Np^+ and Pu^+, the Am^+ ion appeared unreactive and induced exclusively single hydrogen loss. Gibson concludes from this finding that the valence 5f electrons of Am^+ are too inert to form σ-bonds with carbon or hydrogen atoms and therefore do not participate in the Am–HCp interaction.

8.10 ANALYTICAL CHEMISTRY AND SPECTROSCOPY

8.10.1 Radioanalytical chemistry

(a) Alpha spectroscopy

Common analytical procedures include alpha spectrometry for the detection of ^{241}Am and ^{243}Am. The typical alpha-spectrum of ^{241}Am exhibits a peak at 5.49 MeV. The energy of the main alpha particles of ^{243}Am (5.28 MeV) differs by only about 0.2 MeV, which can result in peak broadening and overlap with α-peaks of other radionuclides (Lin *et al.*, 2002). Quantitative analysis by alpha spectrometry requires extensive radiochemical purification, preparation of a high-quality americium source by a skilled radiochemist, and correction for absorption and backscattering from the planchet. Scintillation counting has largely replaced alpha spectrometry in many radioanalytical procedures.

(b) Gamma spectroscopy

Nuclide identification and analysis of biological and environmental samples mainly use high-sensitivity gamma counting in a germanium multichannel detector. ^{241}Am emits two main γ-rays at 59.5 (36%) and 26.3 keV (2.4%). Scintillation counting is also commonly used when only one γ-emitting isotope is in the sample.

8.10.2 Spectroscopy

(a) Solution absorption

(1) Am(III): UV–VIS–NIR absorption spectroscopy has been widely used to characterize americium solution species. The major absorbance that has been measured to speciate Am(III) corresponds to the transition $^7F_0 \rightarrow {}^5L_6$ with its maximum at 503.2 nm ($\varepsilon \sim 410$ L mol cm^{-1}) for Am^{3+}(aq). The molar absorptivity may change with spectral slit widths, temperature, and ionic strength of the solution. Shifts in the position of the absorbance bands

and changes in molar absorbance are evidence of changes in the number of inner-sphere coordinated water molecules and/or coordination of ligands, i.e. carbonate or sulfate. Theoretical calculations of the electronic energy bands in the Am^{3+} ion have been performed by a number of investigators (Conway, 1963, 1964; Carnall and Wybourne, 1964; Carnall *et al.*, 1964; Carnall and Fields, 1967). An unexpected predicted $^7F_0 \rightarrow {}^5D_1$ transition was found in more concentrated Am(III) solution. Carnall (1989) analyzed the energy levels of the Am^{3+} ion by comparing the absorption spectra of $AmCl_3$ and $LaCl_3$ that was doped with Am(III).

Barbanel *et al.* (1997, 2001) studied the transitions in the octahedral complexes AmX_6^{3+} in the Cs_2NaLuX_6 (X = Cl, Br) crystal. The absorption spectra showed excitation to the ground level states $^7F_2$, $^7F_4$, $^7F_6$ and to the exited states $^5L_6$, $^5G_2$, and $^5D_2$. Absorbance spectra have been recorded in H_2SO_4, H_3PO_4, HNO_3, HCl, $HClO_4$, and in carbonate media (Keenan, 1959; Marcus and Shiloh, 1969; Shiloh *et al.*, 1969; Stadler and Kim, 1988; Meinrath and Kim, 1991a; Runde and Kim, 1994) (Fig. 8.13).

(2) Am(IV): The spectrum of Am(IV) in acid media is characterized by broad absorption features and has been measured in 13 M HF (Asprey and Penneman, 1961, 1962), 12 M KF (Varga *et al.*, 1973), 12 M H_3PO_4 (Myasoedov *et al.*, 1977), and in 2 M Na_2CO_3 (Bourges *et al.*, 1983; Hobart *et al.*, 1983b). The spectrum of Am(IV) in concentrated fluoride solution resembles very closely that of solid AmF_4 (Fig. 8.14).

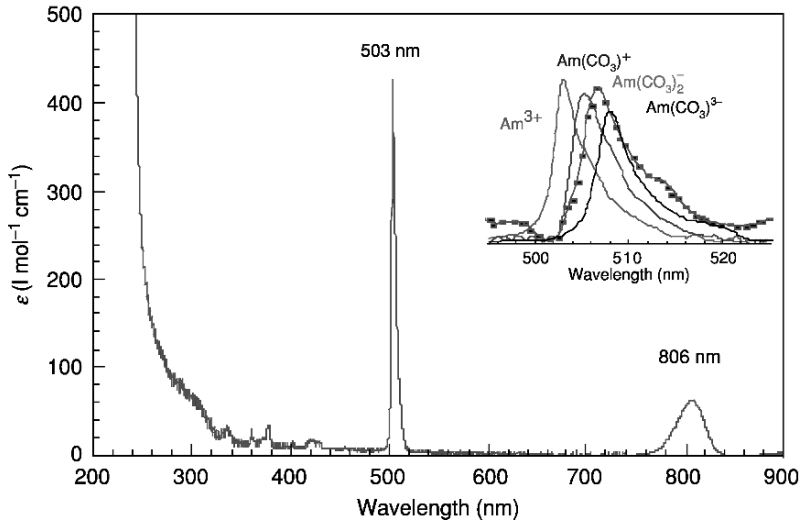

Fig. 8.13 *Electronic absorption spectra of* Am^{3+} *in* 1 M $HClO_4$ *and of the predominant Am*(III) *species in carbonate-containing solutions* (*inset*) (*Meinrath and Kim*, 1991a).

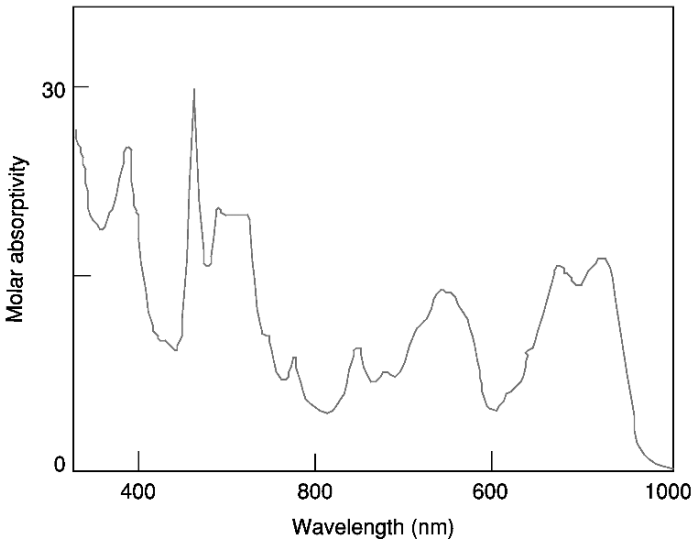

Fig. 8.14 *Absorption spectrum of Am(IV) in* 13 M NH_4F (*Asprey and Penneman*, 1962).

(3) Am(V): The Am(V) transitions $^5I_4 \rightarrow {}^3G_5$ and $^5I_4 \rightarrow {}^3I_7$ with their absorbance peaks at 513.7 nm ($\varepsilon \sim 45$ L mol cm^{-1}) and 716.7 nm ($\varepsilon \sim 60$ L mol cm^{-1}), respectively, are the main absorbance bands of the AmO_2^+ ion in aqueous solutions. Absorbance spectra of Am(V) have been recorded in H_2SO_4 (Werner and Perlman, 1950), HCl (Hall and Herniman, 1954; Stadler and Kim, 1988; Runde and Kim, 1994), $HClO_4$ (Asprey *et al.*, 1951; Stephanou *et al.*, 1953), NaCl (Stadler and Kim, 1988; Runde and Kim, 1994), and in 2 M Na_2CO_3 (Bourges *et al.*, 1983; Hobart *et al.*, 1983b) (Fig. 8.15).

(4) Am(VI): The spectrum of Am(VI) in acid media is characterized by the sharp absorption band at about 996 nm with $\varepsilon \sim 100$ L mol cm^{-1} in $HClO_4$ and $\sim$100 L mol cm^{-1} in H_3PO_4. A less intense absorbance appears at 666 nm. Bell (1969) has compared band positions of transuranium actinyl spectra, including those of AmO_2^+ and AmO_2^{2+}, with the spacings between positions of the UO_2^{2+} bands. His results indicate that a single molecular orbital model can represent any of the actinyl ions when the uranyl ion is assumed to have the bonding orbitals exactly filled; the transuranium actinyl ions are represented with the uranyl core and a progressive increase of electrons in the first two lowest unoccupied molecular orbitals (LUMOs). Although the Am(VI) absorbance appears when Am(V) disproportionates in $HClO_4$, the absorbance is absent in HCl media potentially because of the formation of chloride complexes of lower molar absorptivity or due to the instability of Am(VI) in acidic chloride media (Fig. 8.16).

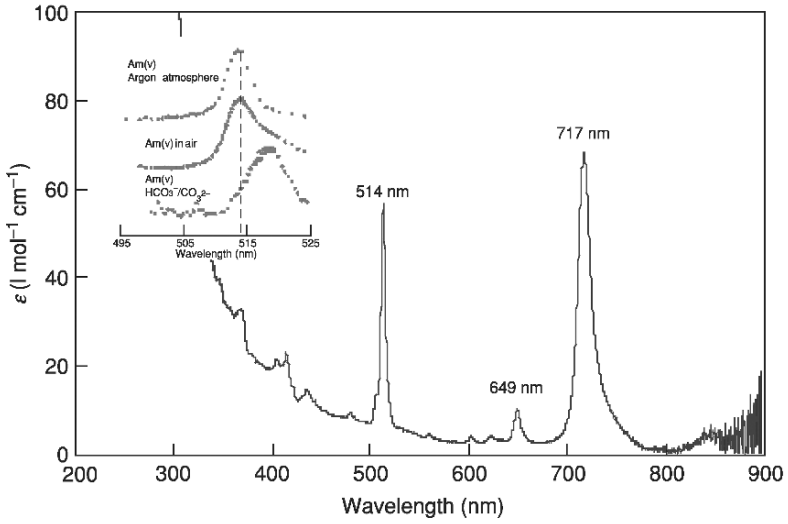

Fig. 8.15 *Electronic absorption spectra of* AmO_2^+ *in* 1 M $HClO_4$ *and in carbonate-containing solutions* (*inset*) (*Stadler and Kim*, 1988).

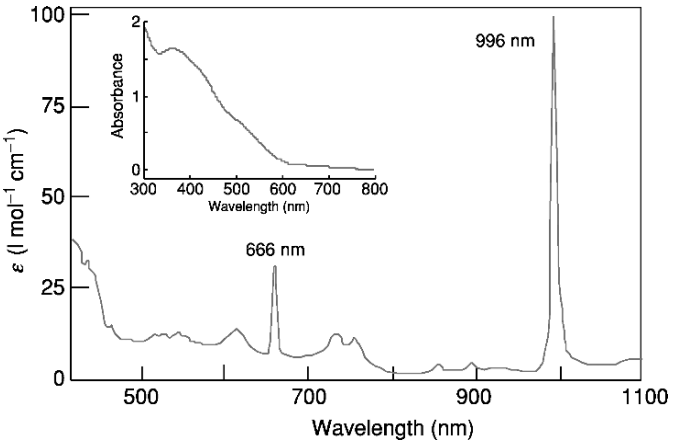

Fig. 8.16 *Absorption spectrum of Am*(VI) *in* 1 M $HClO_4$ *and in carbonate solution* (*inset*) (*Penneman and Asprey*, 1955).

(5) Am(VII): Green-colored solutions, believed to be Am(VII), are prepared by oxidation of Am(VI) in 3–5 M NaOH at 0–7°C with either ozone or the O^- radical. The spectrum of Am(VI) and Am(VII) was measured in 3.5 M NaOH solution by Krot *et al*. (1974a,b) and exhibited a broad absorbance

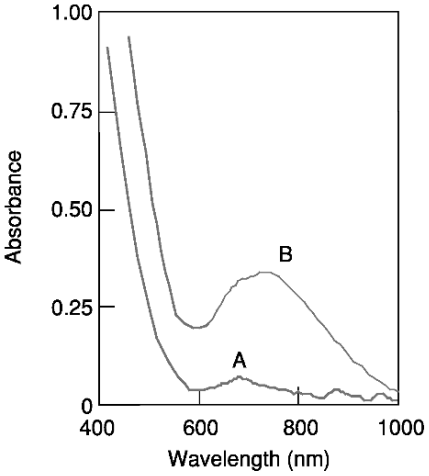

Fig. 8.17 *Absorption spectra of Am(VI) and Am(VII) in* 3.5 M *NaOH* (*Krot* et al., 1974a). *A*, 0.0194 M *Am(VI)*; *B*, 0.0194 M Am_{tot} *with* 50% *Am(VI) and* 50% *Am(VII)*.

at 740 nm (Fig. 8.17). Heptavalent americium is unstable and reduces to Am (VI) within minutes. It can be easily reduced by hydrogen peroxide, hydrazine, hydroxylamine, sulfite, and ferrocyanide ions, and Np(VI) and Pu(VI) (Shilov, 1976). A review on the chemistry of heptavalent transplutonium elements can be found in Mikheev and Myasoedov (1985).

(b) Luminescence

Luminescence has been observed only for Am(III). Reviews of Am(III) luminescence studies can be found in Beitz (1994) and Yusov (1993). The first study on the luminescence properties of Am(III) was reported by Beitz *et al.* (1989). Excitation of Am(III) from the $^7F_0$ ground state to the $^5L_6$ state at 503 nm results in the emission from the lowest luminescent level to the ^7F_J ground-state manifold. From seven expected transitions only two are experimentally accessible. The two most populated transitions are the $^5D_1 \rightarrow {}^7F_1$ band at 685 nm and the $^5D_1 \rightarrow {}^7F_2$ band at 836 nm. These transitions can be used for the determination of trace concentrations of Am(III) in solution or solid-state matrices (Thouvenot *et al.*, 1993). Beitz and coworkers (Liu *et al.*, 1997) investigated the crystal field splitting and hyperfine energy level structure in the $^5D_1$ level of $^{243}Am^{3+}$ in $LaCl_3$ and $CaWO_4$.

The fluorescence lifetime of the Am^{3+} ion(aq) is reported to be 20.4 ± 2.1 ns (Runde *et al.*, 2000), 24.6 ± 0.6 ns (Kimura and Kato, 1998), and 22 ± 3 ns (Beitz, 1994) in aqueous systems. The lifetime increases dramatically to 155 ± 4 ns (Beitz, 1994) in D_2O. Complexation of the Am^{3+} ion changes the position of the emission bands and the duration of the fluorescence lifetime; e.g. the

fluorescence of the triscarbonato complex, $Am(CO_3)_3^{3+}$, is observed at 693 nm with a lifetime of 34.5 ± 2.4 ns (Runde *et al.*, 2000). The luminescence spectra of Am^{3+} have been also measured in Am-doped powdered ThO_2 (Hubert and Thouvenot, 1992), $Cs_2NaLuCl_6$ (Barbanel *et al.*, 1998), $LiYF_4$ (Cavellec *et al.*, 1997), heavy metal fluoride glass containing AmF_3 (Beitz, 1994), and in fluorozirconate glass (Valenzuela and Brundage, 1990; Brundage, 1994) (Fig. 8.18) .

(c) Vibrational (IR and Raman)

There are few data on the IR spectra of americium compounds. Tananaev (1991) reported the antisymmetric vibration frequency of the AmO_2^+ group in $CsAmO_2(OH)_2 \cdot nH_2O$ at 802 cm^{-1}. Hobart *et al.* (1983a) reported the Raman spectra of $AmPO_4$ and $Am(PO_3)_3$ with the most intense Raman frequencies for the symmetric stretching mode of PO_4^{3-} at 973 cm^{-1} and of PO_3^- groups at 1195 cm^{-1}. Jones and Penneman (1953) studied the infrared absorption assigned to the infrared O–An–O asymmetric stretch of actinyl(v) and (vi) ions, concluding that these ions were linear or very nearly so. For the solid $NaAmO_2(CH_3COO)_2$ the vibrational frequencies $\nu_1 = 749$ and $\nu_2 = 914$ cm^{-1} were reported (Jones, 1955). Data on Raman scattering of americyl(v) and (vi) ions have been reported in non-complexing perchloric acid and complexing carbonate solutions (Basile *et al.*, 1974). The values for the polarized symmetric stretching frequencies (ν_1) of AmO_2^+ and AmO_2^{2+} were found to be 730 and 796 cm^{-1}, respectively (Basile *et al.*, 1974). The Raman scattering in carbonate solutions showed a shift of ν_1 to 747 cm^{-1} for Am(v) (Madic *et al.*, 1983) and to 760 cm^{-1} for Am(vi) (Basile *et al.*, 1978). A study of the correlation of the Raman spectra of actinyl(v) and (vi) ions in perchlorate and carbonate

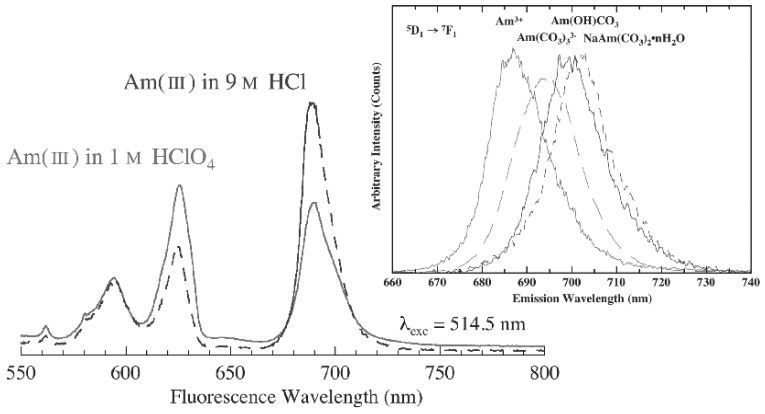

Fig. 8.18 *Luminescence spectrum of* Am^{3+} *in acidic media and of Am*(iii) *carbonate complexes*. (*Runde* et al., 2000, 2002).

solutions, as well as the spectra of solid actinide(V) double carbonate compounds, $Na_3AnO_2(CO_3)_2 \cdot H_2O$, was published by Madic *et al.* (1983).

(d) X-ray absorption

Although X-ray absorption spectroscopy (XAS, see Chapter 28) has been increasingly used since 1990 to obtain structural information of actinide compounds, only a small number of XAS studies on americium compounds have been reported. Bearden and Burr (1967) reported the edge energy of americium metal at 18504 eV. Soderholm *et al.* (1996) observed the Am edge energy at 18515 eV in the Am(IV) compound $Pb_2Sr_2AmCu_3O_8$, which is about 4 eV higher in energy compared to the solid Am(III) reference compounds AmF_3 and $Cs_2NaAmCl_6$. EXAFS has been used to study the coordination of americium in organic complexes (DenAuwer *et al.*, 2000; Yaita *et al.*, 2001) and inorganic complexes with $P_5W_{30}O_{110}^{15-}$ (Williams *et al.*, 2000), chloride (Allen *et al.*, 2000), and carbonate (Runde *et al.*, 2002).

REFERENCES

Abe, M. and Tsujii, M. (1983) *Chem. Lett.*, 1561.

Abe, M., Chitrakar, R., Tsujii, M., and Fukumoto, K. (1985) *Solvent Extr. Ion Exch.*, **3**, 149.

Adair, H. L. (1970) *J. Inorg. Nucl. Chem.*, **32**, 1170.

Agnew, S. F., Boyer, J., Corbin, R. A., Duran, T. B., Fitzpatrick, J. R., Jurgensen, K. A., Ortiz, T. P., and Young, B. L. (1997) *Hanford Tank Chemical and Radionuclide Inventories: HDW Model Rev. 4*, Los Alamos National Laboratory.

Akatsu, J. and Kimura, T. (1990) *J. Radioanal. Nucl. Chem.*, **140**, 195.

Akella, J., Johnson, Q., and Schock, R. N. (1980) *J. Geophys. Res.*, **85**, 7056–8.

Akimoto, Y. (1967) *J. Inorg. Nucl. Chem.*, **29**, 2650–2.

Al Rifai, S. (1970) *Complex Formation between Trivalent Transuranium Elements and Ligand which Contain the Pyridinie or Quinoline Ring*. German Report IRCH-10/70-2.

Aldred, A. T., Dunlap, B. D., Lam, D. J., and Shenoy, G. K. *Transplutonium 1975, Proc. 4th Int. Symp.,* Baden-Baden, Germany 1975; Ed. by W. Müller and R. Lindner, North-Holland, Amsterdam; p. 191–5.

Ali, S. (1968) *Chelatbildung der Dreiwertigen Transplutoniumelemente mit Nitrilotriessigsaeure und Ihren Derivaten*.

Allen, P. G., Bucher, J. J., Shuh, D. K., Edelstein, N. M., and Craig, I. (2000) *Inorg. Chem.*, **39**, 505–601.

Anan'ev, A. V. and Krot, N. N. (1985) *Sov. Radiochem.* (*Engl. Transl.*), **26**(6), 716–9.

Anan'ev, A. V. and Shilov, V. P. (1985) *Sov. Radiochem.* (*Engl. Transl.*), **26**(6), 768–70.

ANS (1993) *Int. Conf. and Tech. Exposition on Future Nuclear Systems: Emerging Fuel Cycles and Waste Disposal Options*, *Global '93*. Seattle, WA. 1993; Amer. Nucl. Soc., La Grange Park, IL. ISBN 0894481827.

Asprey, L. B., Stephanou, S. E., and Penneman, R. A. (1950) *J. Am. Chem. Soc.*, **72**, 1425–6.
Asprey, L. B., Stephanou, S. E., and Penneman, R. A. (1951) *J. Am. Chem. Soc.*, **73**, 5715–7.
Asprey, L. B. (1954) *J. Am. Chem. Soc.*, **76**, 2019–20.
Asprey, L. B., Ellinger, F. H., and Zachariasen, W. H. (1954a) *J. Am. Chem. Soc.*, **76**, 5235–7.
Asprey, L. B., Stephanou, S. E., and Penneman, R. A.: patent number 2681 923. US, (1954).
Asprey, L. B. and Keenan, T. K. (1958) *J. Inorg. Nucl. Chem.*, **7**, 27–31.
Asprey, L. B. and Penneman, R. A. (1961) *J. Am. Chem. Soc.*, **83**, 2200.
Asprey, L. B. and Penneman, R. A. (1962) *Inorg. Chem.*, **1**, 134–6.
Asprey, L. B., Keenan, T. K., and Kruse, F. H. (1964) *Inorg. Chem.*, **3**, 1137–40.
Asprey, L. B., Keenan, T. K., and Kruse, F. H. (1965) *Inorg. Chem.*, **4**, 985–6.
Aziz, A. and Lyle, S. J. (1971) *J. Inorg. Nucl. Chem.*, **33**, 3407.
Backer, W. and Keller, C. (1973) *J. Inorg. Nucl. Chem.*, **35**, 2945.
Bagnall, K. W., Laidler, J. B., and Stewart, M. A. A. (1967) *Chem. Commun.*, **1**, 24–5.
Bagnall, K. W., Laidler, J. B., and Stewart, M. A. A. (1968) *J. Chem. Soc.* **A**, 133–6.
Bagnall, K. W. (1972) *The Actinide Elements,* Elsevier, New York.
Baisden, P. A., Choppin, G. R., and Kinard, W. K. (1972) *J. Inorg. Nucl. Chem.*, **34**, 2029.
Barbanel, Y. A., Chudnovskaya, G. P., Dushin, R. B., Kolin, V. V., Kotlin, V. P., Nekhoroshkov, S. N., and Pen'kin, M. V. (1997) *Radiochim. Acta*, **78**, 69–72.
Barbanel, Y. A., Chudnovskaya, G. P., Dushin, R. B., Kolin, V. V., Kotlin, V. P., Nekhoroshkov, S. N., and Penkin, M. V. (1998) *J. Alloys Compd.*, **277**, 295–300.
Barbanel, Y. A., Dushin, R. B., Kolin, V. V., Kotlin, V. P., and Nekhoroshkov, S. N. (2001) *Radiochemistry*, **43**, 118–23.
Barney, G. S. and Cowan, R. G. (1992) Separation of actinide ions from radioactive waste solutions using extraction chromatography, *American Chemical Society National Meeting*, San Francisco, CA, USA, April 5–10, p. 77.
Barthelemy, P. and Choppin, G. R. (1989) *Inorg. Chem.*, **28**, 3354–7.
Basile, L. J., Sullivan, J. C., Ferrarro, J. R., and La Bonville, P. (1974) *Appl. Spectrosc.*, **28**, 142–5.
Basile, L. J., Ferrarro, J. R., Mitchell, M. L., and Sullivan, J. C. (1978) *Appl. Spectrosc.*, **32**, 535–7.
Baudin, G., Lefevre, J., Prunier, C., and Salvatore, M. (1993) IAEA Report TECDOC-783, p. 37.
Baumgärtner, F., Fischer, E. O., and Kanellakopulos, B. (1966a) *Angew. Chem. Int. Edn.*, **5**(1), 134–5.
Baumgärtner, F., Fisher, E. O., Kanellakopulos, B., and Laubereau, P. G. (1966b) *Angew. Chem. Int. Edn.*, **78**, 112–3.
Baumgärtner, F., Fisher, E. O., Kanellakopulos, B., and Laubereau, P. G. (1977) *J. Inorg. Nucl. Chem.*, **39**, 87–9.
Bayat, I. (1970) *Über Komplexe dreiwertiger Transurane mit Aminopolykarbonsäuren*, German Report, KFK-1291.
Bayat, I. and Moattar, F. (1982) *Radiochem. Radioanal. Lett.*, **51**(3), 171–9.

Baybarz, R. D. (1960) *Preparation of Americium Dioxide by Thermal Decomposition of Americium Oxalate in Air*, Oak Ridge National Laboratory.
Baybarz, R. D. (1965) *J. Inorg. Nucl. Chem.*, **27**, 1831.
Baybarz, R. D. (1966) *J. Inorg. Nucl. Chem.*, **28**, 1055.
Baybarz, R. D. (1970) *At. Energy Rev.*, **8**, 327–60.
Baybarz, R. D. and Asprey, L. B. (1972) *J. Inorg. Nucl. Chem.*, **34**, 3427–31.
Baybarz, R. D. (1973a) *J. Inorg. Nucl. Chem.*, **35**, 4149–58.
Baybarz, R. D. (1973b) *J. Inorg. Nucl. Chem.*, **35**, 483–7.
Bean, A. C., Scott, B. L., Albrecht- Schmitt, T., and Runde, W. (2003) *Plutonium Futures – the Science*, *Third Topical Conference on Plutonium and Actinides*, pp. 233–5.
Bearden, J. A. (1967) *Rev. Mod. Phys.*, **39**, 78.
Bearden, J. A. and Burr, A. F. (1967) *Rev. Mod. Phys.*, **39**, 125–42.
Beitz, J. V., Jursich, G., and Sullivan, J. C. (1989) Fluorescence studies of Am3+ in aqueous solution, in *Rare Earth 1988* (eds. L. R. M. H. B. Silber and L. E. Delony), Elsevier Sequoia, Amsterdam.
Beitz, J. V. (1994) *J. Alloys Compd.*, **207/208**, 41–50.
Bell, J. T. (1969) *J. Inorg. Nucl. Chem.*, **31**, 703–10.
Benedict, U., Bujis, K., Dufour, S., and Toussaint, J. C. (1975) *J. Less Common Metals*, **42**, 345–54.
Benedict, U. and Dufour, C. (1980) *Physica*, **102B**, 303–7.
Benedict, U., Itíe, J. P., Dufour, C., Dubos, S., and Spirlet, J. C. (1985) in *Americium and Curium Chemistry and Technology* (eds. N. Edelstein, J. Navratil, and W. Schulz), D. Reidel, The Netherlands.
Benedict, U., Itíe, J. P., Dufour, C., Dubos, S., and Spirlet, J. C. (1986) *Physica*, B&C, **139**, 284.
Berger, P., Blanc, P., and Bourges, J. (1988) *Radiochim. Acta*, **43**, 217–22.
Berndt, U., Tanamas, R., Maier, D., and Keller, C. (1974) *Inorg. Nucl. Chem. Lett.*, **10**, 315–21.
Bernkopf, M. F. and Kim, J. I. (1984) *Hydrolydsereaktionen und Karbonatkomplexierung von dreiwertigem Americium in natürlichen aquatischen Systemen*, Technische Universität München.
Berry, J. W., Knoghton, J. B., and Nannie, C. A. (1982) *Vacuum Distillation of Americium Metal*, US Department of Energy.
Bertha, E. I. and Choppin, G. R. (1978) *J. Inorg. Nucl. Chem.*, **40**, 655–8.
Bhanushali, R. D., Pius, I. C., Muherjee, S. K., and Vaidya, V. N. (1999) *J. Radioanal. Nucl. Chem.*, **240**, 977–9.
Bierman, S. R. and Clayton, E. D. (1969) *Trans. Am. Nucl. Soc.*, **12**, 887–8.
Bigelow, J. E., Collins, E. d., and King, L. J. (1980) *The Cleanex Process: A Versatile Solvent-Extraction Process for Recovery and Purification of Lanthanides*, *Americium*, *and Curium, Amer. Chem. Soc.* pp. 147–55.
Blokhin, N. B., Ermakov, V. A., and Rykov, A. G. (1973) *Radiokhimiya*, **16**, 189–92.
Blokhin, N. B., Ermakov, V. A., and Rykov, A. G. (1974) *Radiokhimiya*, **16**, 551–3.
Bode, D. D., Wild, J. F., and Hulet, E. K. (1976) *J. Inorg. Nucl. Chem.*, **38**, 1291–7.
Boldt, A. L. and Ritter, G. L. (1969) *Recovery of Am*, *Cm*, *and Pm from Shipping Port Reactor Fuel Reprocessing Wastes by Successive TBP and D2EHPA Extractions*, Atlantic Richfield Hanford Company.

Bond, E. M., Engelhardt, U., Deere, T. P., Rapko, B. M., Paine, R. T., and FitzPatrick, J. R. (1997) *Solvent Extr. Ion Exch.*, **15**, 381.
Bond, E. M., Engelhardt, U., Deere, T. P., Rapko, B. M., Paine, R. T., and Fitz Patrick, J. R. (1998) *Solvent Extr. Ion Exch.*, **16**, 967.
Borisov, M. S., Elesin, A. A., Lebedev, I. A., Piskunov, E. M., Filimonof, V. T., and Yakovlev, G. N. (1967) *Radiokhimiya*, **9**, 166.
Bouhlassa, S. (1983) *Chem. Abstr.*, **98**, 82730.
Bouhlassa, S. and Guillaumont, R. (1984) *J. Less Common Metals*, **99**(1), 157–71.
Bouissières, G. and Legoux, Y. (1965) *Bull. Soc. Chim. Fr.*, **2**, 386.
Bourges, J. Y., Guillaume, B., Koehly, G., Hobart, D. E., and Peterson, J. R. (1983) *Inorg. Chem.*, **22**, 1179–84.
Boyd, T. E., Cusick, M. J., and Navratil, J. D. (1986) *Recent Developments in Separation Science,* CRC Press, Boca Raton, FL.
Boyd, T. E. and Kochen, R. L. (1993) *Ferrite Treatment of Actinide Waste Solutions: Continuous Processing of Rocky Flats Process Waste,* Rockwell International, Golden, CO.
Brachet, G. and Vasseur, C. (1969) *Reduction of Americium Oxide by Beryllium for Neutron-Source Production,* CEA, France.
Brandau, E. (1971) *Inorg. Nucl. Chem. Lett.*, **7**, 1177.
Bratsch, S. G. and Lagowski, J. J. (1986) *J. Phys. Chem.*, **90**, 307–12.
Brown, D., Fletcher, S., and Holah, D. G. (1968) *J. Chem. Soc.* **A**, 1889–94.
Brundage, R. T. (1994) *J. Alloys Compd.*, **213**, 199–206.
Buckau, G., Kim, J. I., klenze, R., Rhee, D. S., and Wimmer, H. (1992) *Radiochim. Acta*, **57**(2–3), 105–11.
Buijs, K., Müller, W., Reul, J., and Toussaint, J. C. (1973) *Separation and Purification of Americium on the Multigram Scale*, Euratom.
Burch, W. D. (1964) *Transuranium Quarterly Progress Report for Period Ending February* 29, 1963, Oak Ridge National Laboratory.
Burnett, J. L. (1965) *Trans. Am. Nucl. Soc.*, **8**, 335.
Burnett, J. L. (1966) *J. Inorg. Nucl. Chem.*, **28**, 2454–6.
Burney, G. A. and Porter, J. A. (1967) *Inorg. Nucl. Chem. Lett.*, **3**, 79–85.
Burney, G. A. (1968) *Nucl. Appl.*, **4**, 217–21.
Burns, J. H. and Danford, M. D. (1969) *Inorg. Chem.*, **8**, 1780–4.
Burns, J. H. and Peterson, J. R. (1970) *Acta Crystallogr. B*, **26**, 1885–7.
Burns, J. H. and Peterson, J. R. (1971) *Inorg. Chem.*, **10**, 147–51.
Burns, J. H. and Baybarz, R. D. (1972) *Inorg. Chem.*, **11**, 2233–7.
Burns, J. H. and Baldwin, W. H. (1976) *Inorg. Chem.*, **16**(2), 289–94.
Burns, J. H. and Baldwin, W. H. (1977) *Inorg. Chem.*, **16**, 289–94.
Burns, J. H., Damien, D., and Haire, R. G. (1979) *Acta Crystallogr. B*, **35**, 143–4.
Bursten, B. E., Rhodes, L. F., and Strittmatter, R. J. (1989) *J. Less Common Metals*, **149**, 207–11.
Caceci, M. and Choppin, G. (1983) *Radiochim. Acta*, **33**(2/3), 101–4.
Campbell, D. O. (1970) *Ind. Eng. Chem. Process Des. Dev.*, **9**, 95–9.
Carlson, T. A., Nestor, C. W. J., Wasserman, N., and McDowell, J. D. (1970) *Comprehensive Calculations of Ionization Potentials and Binding Energies for Multiply-Charged Ions*, Oak Ridge National Laboratory.

Carnall, W. T. and Wybourne, B. G. (1964) *J. Chem. Phys.*, **40**, 3428–33.
Carnall, W. T., Fields, P. R., and Wybourne, B. G. (1964) *J. Chem. Phys.*, **41**, 2195–6.
Carnall, W. T. and Fields, P. R. (1967) in *Lanthanide/Actinide Chemistry* (ed. R. F. Gould), American Chemical Society, Washington, DC, pp. 86–101.
Carnall, W. T. (1979a) Emission Spectra, in *Gmelins Handbuch der Anorganischen Chemie*, Transurane, Teil A2, vol. 8, (ed. G. Koch), Verlag Chemie, Weinheim, Germany, p. 42.
Carnall, W. T. (1979b) X-ray spectra, in *Gmelins Handbuch der Anorganischen Chemie,* Transurane, Teil A2, vol. 8, (ed. G. Koch), Verlag Chemie, Weinheim, p. 80.
Carnall, W. T. (1989) *J. Less Common Metals*, **156**, 221–35.
Carniglia, S. C. and Cunningham, B. B. (1955) *J. Am. Chem. Soc.*, **77**, 1451–3.
Casarci, M., Chiarizia, R., Gasparini, G. M., Puzzuoli, G., and Valeriani, G. (1988) in *Proc. of ISEC '88,* Moscow, USSR.
Casarci, M., Gasparini, G. M., and Grossi, G. (1989) in *Proc. of Actinides – 89*, Tashkent, Russia.
Cavellec, R., Hubert, S., and Simoni, E. (1997) *J. Solid State Chem.*, **129**, 189–95.
Chamberlain, D. B., Conner, C., Hutter, J. C., Leonard, R. A., Wygmans, D. G., and Vandegrift, G. F. (1997) *Sep. Sci. Technol.*, **32**, 303.
Charbonnel, M. C. and Musikas, C. (1988) *Solvent Extr. Ion Exch.*, **6**, 461.
Chartier, D., Donnet, L., and Adnet, J. M. (1999) *Radiochim. Acta*, **85**, 25–31.
Charvillat, J. P., Benedict, U., Damien, D., de Novion, C., Wojakowski, A., and Müller, W. (1975a) in *Transplutonium 1975*, *Proc. 4th Int. Symp.*, pp. 79–93.
Charvillat, J. P., Benedict, U., Damien, D., and Müller, W. (1975b) *Radiochem. Radioanal. Lett.* **20**, 371–381.
Charvillat, J. P. and Damien, D. (1973) *Inorg. Nucl. Chem. Lett.*, **9**, 559–63.
Charvillat, J. P. and Zachariasen, W. H. (1977) *Inorg. Nucl. Chem. Lett.*, **13**, 161–3.
Charvillat, J. P., Benedict, U., Damien, D., de Novion, C., Wojakowski, A., and Müller, W. (1977) *Rev. Chim. Minér.*, **14**, 178–88.
Chen, J., Jiao, R., and Zhu, Y. (1996) *Solvent Extr. Ion Exch.*, **14**, 555.
Chiarizia, R. and Horwitz, E. P. (1986) *Solvent Extr. Ion Exch.*, **4**, 677.
Chiarizia, R. and Horwitz, E. P. (1990) *Solvent Extr. Ion Exch.*, **8**, 907.
Chiarizia, R., Horwitz, E. P., Alexandratos, S. D., and Gula, M. J. (1997) *Separation Science and Technology*, **32**(1–4), 1–35.
Chikalla, T. D. and Eyring, L. (1967) *J. Inorg. Nucl. Chem.*, **29**, 2281–93.
Chikalla, T. D. and Eyring, L. (1968) *J. Inorg. Nucl. Chem.*, **30**, 133–45.
Chikalla, T. D., McNeilly, C. E., Bates, J. L., and Rasmussen, J. J. (1973) in *Proc. Int. Colloq. on High Temp. Phase Transform.*, CNRS Publ. No. 205, pp. 351–60.
Chistyakov, V. M., Ermakov, V. A., and Rykov, A. G. (1974) *Radiokhimiya*, **16**, 553–5.
Chitnis, R. R., Wattal, P. K., Ramanujam, A., Dhami, P. S., Gopalakrishnan, V., Mathur, J. N., and Murali, M. S. (1998) *Sep. Sci. Technol.*, **33**, 1877.
Chitnis, R. R., Wattal, P. K., Ramanujam, A., Dhami, P. S., Gopalalkrishnan, V., Bauri, A. K., and Bannerji, A. (1999) *J. Radioanal. Nucl. Chem.*, **240**, 721.
Chmutova, M. K., Kochetkova, N. E., Koiro, O. E., Myasoedov, B. F., Medved, T. Y., Nesterova, N. P., and Kabachnik, M. I. (1983) *J. Radioanal. Chem.*, **80**, 63.
Chmutova, M. K., Kochetkova, N. E., and Myasoedov, B. G. (1989) *J. Inorg. Nucl. Chem.*, **42**, 897.
Choppin, G. R. (1965) *Inorg. Chem.*, **4**, 1250–4.

Choppin, G. R. (1970) *J. Inorg. Nucl. Chem.*, **32**, 3283–8.
Choppin, G. R. and Degischer, G. (1972) *J. Inorg. Nucl. Chem.*, **34**, 3473–7.
Choppin, G. R. and Unrein, P. J. (1975) in *Transplutonium 1975, Proc. 4th Int. Symp.*, Baden-Baden, Germany, Ed. by W. Müller and R. Lindner, North-Holland, Amsterdam, Netherlands, p. 97–107.
Choppin, G. R. and Nash, K. L. (1977) *Rev. Chim. Minér.*, **14**, 230–6.
Choppin, G. R. and Chen, J. F. (1996) *Radiochim. Acta*, **74**, 105–10.
Choppin, G. R. and Labonne-Wall, N. (1997) *J. Radioanal. Nucl. Chem.*, **221**(1–2), 67–71.
Choppin, G. R. and Peterman, D. R. (1998) *Coord. Chem. Rev.*, **174**, 283–99.
Chudinov, E. G. and Choporov, D. Y. (1970) *At. Energy (USSR)*, **28**, 62–4.
Chuveleva, E. A., Peshkov, A. S., Kharitonov, O. V., and Firosova, L. A. (1999) *Radiochemistry* (*Eng. Transl.*), **41**, 442–4, 445–7, and 465–7.
Cilindro, L. G., Stadlbauer, E., and Keller, C. (1972) *J. Inorg. Nucl. Chem.*, **34**, 2577.
Cilindro, L. G. and Keller, C. (1974) *Radiochim. Acta*, **21**, 29–32.
Clark, D. L., Conradson, S. D., Ekberg, S. A., Hess, N. J., Neu, M. P., Palmer, P. D., Runde, W., and Tait, C. D. (1996) *J. Am. Chem. Soc.*, **118**, 2089–90.
Cohen, D. (1972) *Inorg. Nucl. Chem.*, **8**, 533–5.
Cohen, K. P. (2000) *Nucl. News*, **43** (Nov), 45–6.
Coleman, J. S., Armstrong, D. E., Asprey, L. B., Keenan, T. K., La Mar, L. E., and Penneman, R. A. (1955) *Purification of Gram Amounts of Americium*, Los Alamos Scientific Laboratory.
Coleman, J. S., Armstrong, D. E., Asprey, L. B., Keenan, T. K., La Mar, L. E., and Penneman, R. A. (1957) *J. Inorg. Nucl. Chem.*, **3**, 327–8.
Coleman, J. S. (1963) *Inorg. Chem.*, **2**, 53–7.
Coleman, J. S., Keenan, T. K., Jones, L. H., Carnall, W. T., and Penneman, R. A. (1963) *Inorg. Chem.*, **2**, 58–61.
Conner, W. V. (1971) *J. Less Common Metals*, **25**, 379–84.
Connor, W. V. (1982) *Nucl. Instrum. Methods*, **200**, 55–66.
Conway, J. G. (1963) University of California, Lawrence Laboratory.
Conway, J. G. (1964) *J. Chem. Phys.*, **40**, 2504–7.
Crandall, J. L. (1971) *Applications of Transplutonium Elements*, Savannah River Laboratory.
Cuillerdier, C., Musikas, C., and Hoel, P. (1991a) in *New Separations Technology for Radioactive Waste and Other Specific Applications* (eds. L. Cecille, M. Cesarci, and L. Pietrelli), Elsevier Applied Science, p. 41.
Cuillerdier, C., Musikas, C., Hoel, P., Nigond, L., and Vitart, X. (1991b) *Sep. Sci. Technol.*, **26**, 1229.
Cuillerdier, C., Musikas, C., and Nigond, L. (1993) *Sep. Sci. Technol.*, **28**, 155.
Cunningham, B. B. (1948) *Isolation and Chemistry of Americium*, Argonne National Laboratory.
Cunningham, B. B. (1949) in *The Transuranium Elements* (eds. G. T. Seaborg and J. J. Katz), Natl. Nucl. En. Ser., Div. IV, 14B, McGraw-Hill, New York, pp. 1363–70.
Damien, D. and Pages, M. (1969) in *Rapport Semestriel du Department de Chimie No.* 6, *Juin* 1968–*Novembre*1968, CEA, p. 407.
Damien, D. and Pages, M. (1970) in *Rapport Semestriel du Department de Chimie No.* 8, *Juin* 1969–*Novembre*1969, CEA, p. 472.

Damien, D. (1971) *Inorg. Nucl Chem. Lett.*, **7**, 291–7.
Damien, D. and Jove, J. (1971) *Inorg. Nucl. Chem. Lett.*, **7**, 685–8.
Damien, D. (1972) *Inorg. Nucl Chem. Lett.*, **8**, 501.
Damien, D. and Charvillat, J. P. (1972) *Inorg. Nucl. Chem. Lett.*, **8**, 705–8.
Damien, D., Jove, J., and Marcon, J. P. (1972) *Inorg. Nucl. Chem. Lett.*, **8**, 317–20.
Damien, D., Marcon, J. P., and Jove, J. (1975) *Radiochem. Radioanal. Lett.*, **23**, 145–54.
Damien, D., Marcon, J. P., and Jove, J. (1976) *Bull. D'Inform. Sci. Tech. (fr.)*, **217**, 67–76.
Danford, M. D., Burns, J. H., Higgins, C. E., Stokeley, J. R. J., and Baldwin, W. H. (1970) *Inorg. Chem.*, **9**, 1953–5.
David, F. and Bouisissiéres, G. (1968) *Inorg. Nucl. Chem. Lett.*, **4**, 153–9.
David, F., Samhoun, K., Guillaumont, R., and Edelstein, N. (1978) *J. Inorg. Nucl. Chem.*, **40**, 69–74.
David, F. (1986) *J. Less Common Metals*, **121**, 27.
Davydov, A. V., Myasoedov, B. F., and Travnikov, S. S. (1975) *Dokl. Akad. Nauk SSSR*, **225**, 1075–8.
Dedov, V. B., Lebedev, I. A., Ryzhov, M. N., Trakhlyaev, P. S., and Yakovlev, G. N. (1961) *Radiokhimiya*, **3**, 701.
Deissenberger, R., Kohler, S., Ames, F., Eberhardt, K., Erdmann, N., Funk, H., Herrmann, G., Kluge, H., Nunnemann, M., Passler, G., Riegel, J., Scheerer, F., Trautmann, N., and Urban, F. J. (1995) *Angew. Chem. Int. Edn.*, **34**, 814–5.
Delle Site, A. and Baybarz, R. D. (1969) *J. Inorg. Nucl. Chem.*, **31**, 2201.
Den Auwer, C., Charbonnel, M. C., Drew, M. G. B., Grigoriev, M., Hudson, M. J., Iveson, P. B., Madic, C., Nierlich, M., Presson, M. T., Revel, R., Russell, M. L., and Thuery, P. (2000) *Inorg. Chem.*, **39**, 1487–95.
Deshingkar, D. S., Chitnis, R. R., Theyyunni, T. K., Wattal, P. K., Ramanujam, A., Dhami, P. S., Gopalakrishnan, V., Rao, M. K., Mathur, J. N., Murali, M. S., Iyer, R. H., Badheka, L. P., and Bannerji, A. (1993) Report BARC.
Deshingkar, D. S., Chitnis, R. R., Wattal, P. K., Theyyunni, T. K., Nair, M. K. T., Ramanujam, A., Dhami, P. S., Gopalakrishnan, V., Rao, M. K., Mathur, J. N., Murali, M. S., Iyer, R. H., Badheka, L. P., and Bannerji, A. (1994) Report BARC.
Drobyshevskii, I. V., Prusakov, V. N., Serik, V. F., and Sokolov, V. B. (1980) *Radiokhimiya*, **22**(44), 591–4.
Dunlap, B. D., Lam, D. J., Kalvius, G. M., and Shenoy, G. K. (1972) *J. Appl. Phys.*, **42**, 1419.
Eberle, S. H. and Bayat, I. (1967) *Radiochim. Acta*, **7**, 214.
Eberle, S. H. and Ali, S. (1968) *Z. Anorg. Allg. Chem.*, **361**, 1.
Eberle, S. H. and Bayat, I. (1969) *Inorg. Nucl. Chem. Lett.*, **5**, 229.
Eberle, S. H. and Robel, W. (1970) *Inorg. Nucl. Chem. Lett.*, **6**, 359–65.
Eberle, S. H. and Moattar, F. (1972) *Inorg. Nucl. Chem. Lett.*, **8**, 265.
Eberle, S. H. and Sabau, C. S. (1972) *Radiochem. Radioanal. Lett.*, **11**, 77.
Ebner, A. D., Ritter, J. A., Ploehn, H. J., Kochen, R. L., and Navratil, J. D. (1999) *Sep. Sci. Technol.*, **34**, 1277–300.
Eick, H. A. and Mulford, R. N. R. (1969) *J. Inorg. Nucl. Chem.*, **31**, 371–5.
Elesin, A. A. and Zaitsev, A. A. (1971a) *Radiokhimiya*, **13**, 902.
Elesin, A. A. and Zaitsev, A. A. (1971b) *Radiokhimiya*, **13**, 775.

Elesin, A. A. and Zaitsev, A. A. (1972) *Radiokhimiya*, **14**, 370.
Elesin, A. A., Zaitsev, A. A., Ivanovich, N. A., Karaseva, V. A., and Yakovlev, G. N. (1972a) *Radiokhimiya*, **14**, 546.
Elesin, A. A., Zaitsev, A. A., Karaseva, V. A., Nazarova, I. I., and Petukhova, I. V. (1972b) *Radiokhimiya*, **14**, 374.
Elesin, A. A., Zaitsev, A. A., Kazakova, S. S., and Yakovlev, G. N. (1972c) *Radiokhimiya*, **14**, 541.
Elesin, A. A., Zaitsev, A. A., Sergeev, G. M., and Nazarova, I. I. (1973) *Radiokhimiya*, **15**, 64.
Ellinger, F. H. and Zachariasen, W. H. (1954) *J. Phys. Chem.*, **58**, 405–8.
Ellinger, F. H., Johnson, K. A., and Struebing, V. O. (1966) *J. Nucl. Mater.*, **20**, 83–6.
Ensor, D. D., Jarvinen, G. D., and Smith, B. F. (1988) *Solvent Extr. Ion Exch.*, **6**, 439.
Erdmann, B. (1971) *Darstellung von Actiniden/Lanthaniden-Edelmetall (Pt, Pd, Ir, Rh)-Legierungsphasen durch gekoppelte Reduktion*, Kernforschungszentrum karlsruhe.
Erdmann, B. and Keller, C. (1971) *Inorg. Nucl. Chem. Lett.*, **7**, 675–83.
Erdmann, B. and Keller, C. (1973) *J. Solid State Chem.*, **7**, 40–8.
Eriksson, O. and Wills, J. M. (1992) *Phys. Rev. B*, **45**, 3198–203.
Eriksson, O., Soderland, J. M., Wills, J. M., and Boring, A. M. (1993) *Physica B*, **190**, 5–11.
Erin, E. A., Kopytov, V. V., Rykov, A. G., and Kosyakov, V. N. (1979) *Radiokhimiya*, **21**, 63–7.
Ermakov, V. A. and Star, I. (1967) *Radiokhim.*, **9**, 197.
Ermakov, V. A., Rykov, A. G., Timofeev, G. A., and Yakovlev, G. N. (1971a) *Radiokhimiya*, **13**, 826–32.
Ermakov, V. A., Vorob'eva, V. V., Zaitsev, A. A., and Yakovlev, G. N. (1971b) *Radiokhimiya*, **13**, 692.
Ermakov, V. A., Vorob'eva, V. V., Zaitsev, A. A., and Yakovlev, G. N. (1971c) *Radiokhimiya*, **13**, 840.
Ermakov, V. A., Rykov, A. G., Timofeev, G. A., and Yakovlev, G. N. (1973) *Radiokhimiya*, **15**, 380–5.
Ermakov, V. A., Rykov, A. G., Timofeev, G. A., and Yakovlev, G. N. (1974) *Radiokhimiya*, **16**, 810–17.
Eyring, L., Lohr, H. R., and Cunningham, B. B. (1949) University of California Radiation Laboratory.
Eyring, L., Lohr, H. R., and Cunningham, B. B. (1952) *J. Am. Chem. Soc.*, **74**, 1186–90.
Fahey, J. A., Turcotte, R. P., and Chikalla, T. D. (1974) *Inorg. Nucl. Chem. Lett.*, **10**, 459–65.
Fang, D. and Keller, C. (1969) *Radiochim. Acta*, **11**, 123–7.
Fargeas, M., Fremont- Lamouranne, R., Legoux, Y., and Morini, O. J. (1986) *J. Less Common Metals*, **121**, 439.
Fedoseev, A. M. and Perminov, V. F. (1983) *Sov. Radiochem.* (*Engl. Transl.*), **25**, 522–3.
Fedoseev, A. M. and Budentseva, N. A. (1989) *Sov. Radiochem.* (*Engl. Transl.*), **31**, 525–37.
Fedoseev, A. M. and Budantseva, N. A. (1990) *Radiokhimiya*, **32**, 14–18 and 19–24.
Fedoseev, A. M., Budantseva, N. A., Grigor'ev, M. S., and Perminov, V. P. (1991) *Radiokhimiya*, **33**, 7–19.

Ferris, L. M., Smith, F. J., Mailen, J. C., and Bell, M. J. (1972) *J. Inorg. Nucl. Chem.*, **34**, 2921–33.
Freeman, A. J. and Keller, C. (1985) in *Handbook on the Physics and Chemistry of Actinides*, Elsevier Science Publishers.
Freundlich, W. and Pages, M. (1969) *C. R. Acad. Sci. Ser. C*, **269**, 392–4.
Fried, S. (1951) *J. Am. Chem. Soc.*, **73**, 416–18.
Fuger, J. (1958) *J. Inorg. Nucl. Chem.*, **5**, 332.
Fuger, J. and Cunningham, B. B. (1963) *J. Inorg. Nucl. Chem.*, **25**, 1423–9.
Fuger, J., Spirlet, J. C., and Müller, W. (1972) *Inorg. Nucl. Chem. Lett.*, **8**, 709–23.
Fuger, J. and Oetting, F. L. (1976) *The Chemical Thermodynamics of Actinide Elements and Compounds,* part 2, *The Actinide Aqueous Ions*, IAEA, Vienna.
Fuger, J., Khodakovsky, I. L., Serfeyeva, E. I., Medvedev, V. A., and Navratil, J. D. (1992) *Part 12, The Actinide Aqueous Inorganic Complexes*, IAEA, Vienna.
Gatrone, R. C., Kaplan, L., and Horwitz, E. P. (1987) *Solvent Extr. Ion Exch.*, **5**, 1075.
Gatrone, R. C. and Rickert, P. G. (1987) *Solvent Extr. Ion Exch.*, **5**, 1117.
Gatrone, R. C., Horwitz, E. P., Rickert, P. G., and Diamond, H. (1989) *Solvent Extr. Ion. Exch.*, **7**, 793.
Gedeonov, L. I., Lebedev, I. A., Stepanov, A. V., Shalinets, A. B., and Yakovlev, G. N. (1967) *Chemistry of the Transuranium and Fission Elements*, Izd. Nauka, p. 140.
Gel'man, A. D., Moskvin, A. I., Zaitsev, L. M., and Medfod'eva, M. P. (1967) *Complex Compounds of Transuranides* (*Engl. transl.*), Israel Program for Scientific Translations, Jerusalem.
Gerontopulos, P. T., Rigali, L., and Barbano, P. G. (1965) *Radiochim Acta*, **4**, 75.
Gibson, J. K. and Haire, R. G. (1992a) *J. Nucl. Mater.*, **195**, 156–65.
Gibson, J. K. and Haire, R. G. (1992b) *J. Alloys Compd.*, **181**, 23–32.
Gibson, J. K. (1998a) *J. Phys. Chem. A*, **102**, 4501–8.
Gibson, J. K. (1998b) *Organometallics*, **17**, 2583–9.
Gibson, J. K. (1999a) *Inorg. Chem.*, **38**, 165–73.
Gibson, J. K. (1999b) *J. Mass Spectrom.,* **34**(11), 1166–77.
Gibson, J. K. (2000) *Int. J. Mass Spectrom.*, **202**, 19–29.
Giffaut, E. and Vitorge, P. (1993) *Mat. Res. Soc. Symp. Proc.*, **294**, 747–51.
Gmelin (1973) in *Gmelins Handbuch der Anorganischen Chemie*, Suppl. Work, 8th edition, Verlag Chemie, Weinheim, Germany: Vol. 4, Transurane, Teil C Verbindungen (Compounds); Vol. 7a, Die Elemente (The Elements), Teil A1 (1973); Vol. 8, Teil A2, Die Elemente (The Elements) (1973).
Gmelin (1979) in *Gmelin Handbook of Inorganic Chemistry*, vol. *Transuranium*, Parts A1, A2, B1–3, C, D1, D2, Verlag Chemie, Weinheim.
Goffart, J. and Kuyckaerts, G. (1969) *Anal. Chim. Acta.*, **43**, 99.
Gopalakrishnan, V., Dhami, P. S., Ramanujam, A., Balaramarkishna, M. V., Murali, M. S., Mathur, J. N., Iyer, R. H., Bauri, A. K., and Bannerji, A. (1995) *J. Radioanal. Nucl. Chem. Art.*, **191**, 279.
Gourisse, D. (1966) *Cinetique des Reactions D'Oxydo-Reduction des Elements Transuraniens en Solution*, CEA.
Graus Odenheimer, B. and Choppin, G. R. (1956) *Stability Constants of Alpha hydroxyisobutyric Acid Complexes with Actinide Elements*, University of California Radiation Laboratory, Berkeley.
Grebenshchikova, V. I. and Babrova, V. N. (1958) *Zhur. Neorg. Khim.*, **3**, 400.

Grebenshschikova, V. I. and Babrova, V. N. (1961) *Radiochemistry USSR* **3**, 32.
Grebenshschikova, V. I. and Cheinyavskaya, N. B. (1962) *Sov. Radiochem.* (*Engl. Transl*), **4**, 207.
Grenthe, I. (1962) *Acta. Chem. Scand.*, **16**, 1695.
Grenthe, I., Fuger, J., Konings, R. J. M., Lemire, R. J., Muller, A. B., Nguyen-Trung, C., and Wanner, H. (1992) *Chemical Thermodynamics of Uranium*, Elsevier Science Publishers, North-Holland.
Grigorescu-Sabau, C. S. (1972) *Über die Temperaturabhangigkeit von Komplexgleichgewichten der Transplutone*, Kernforschungszentrum Karlsruhe.
Guillaume, B., Hobart, D. E., and Bourges, J. Y. (1981) *J. Inorg. Nucl. Chem.,* **43**(12), 3295–9.
Guillaume, B., Begun, G. M., and Hahn, R. L. (1982) *Inorg. Chem.*, **21**, 1159–66.
Guminski, C. (1995) *J. Phase Equilib.*, **16**, 333.
Gureev, E. S., Kosyakov, V. N., and Yakovlev, G. N. (1964) *Sov. Radiochem.*, **6**, 639–47.
Gureev, E. S., Dedov, V. B., Karpacheva, S. M., Shvetsov, I. K., Ryzhov, M. N., Trukchlayev, P. S., Yakovlev, G. N., and Lebedev, I. A. (1970) in *Progress in Nuclear Energy, Process Chemistry*, ser. III, vol. 4, (eds. C. E. Stevenson, E. A. Mason, and A.T. Gresky), Pergamon Press, New York, p. 631.
Hafez, M. B. (1968) *Spectrophotometric Study of the Complexes of Cerium and Uranides with Diethylenetriaminepentaacetic Acid* (DTPA).
Haire, R. G., Lloyd, M. H., Milligan, W. O., and Beasley, M. L. (1977) *J. Inorg. Nucl. Chem.*, **39**(5), 837–41 and 843–7.
Haire, R. G., Benedict, U., Young, J. P., Peterson, J. R., and Begun, G. M. (1985) *J. Phys. C: Solid State Phys.*, **18**(24), 4595–601.
Hale, W. H. and Lowe, J. T. (1969) *Inorg. Nucl. Chem. Lett.*, **5**, 363–9.
Hall, G. R. Herniman, and P. D. (1954) *J. Chem. Soc.*, 2214–21.
Hall, G. R. and Markin, T. L. (1957) *J. Inorg. Nucl. Chem.*, **4**, 137–42.
Hall, R. O. A., Lee, J. A., Mortimer, M. J., McElroy, D. L., Müller, W., and Spirlet, J. C. (1980) *J. Low Temp. Phys.*, **41**, 397–403.
Hall, H. L. (1989) Report USDOE LBL-27878, University of California, Berkeley, USA.
Hara, M. (1970) *Bull. Chem. Soc. Jpn.*, **43**, 89–94.
Harbour, R. M., Hale, W. H., Burney, G. A., and Lowe, J. T. (1972) *At. Energy Rev.*, **10**, 379–99.
Hennelly, E. J. (1972) in *Radioisotope Engineering* (ed. G. G. Eichholz), Marcel Dekker, New York, pp. 44–134.
Hermann, J. A. (1956) *Coprecipitation of Am*(III) *with Lanthanum Oxalate*, Los Alamos Scientific Laboratory.
Hill, H. H. and Ellinger, F. H. (1971) *J. Less Common Metals*, **23**, 92.
Hill, H. H., Lindsey, J. D. G., White, R. W., Asprey, L. B., Streubing, V. O., and Matthias, B. T. (1971) *Physica*, **55**, 615.
Hindman, J. C. (1958) Proc. of the *Second Int. Conf. on the Peaceful Uses of Atomic Energy*, Geneva, United Nations, p. 349–60.
Hobart, D., Samhoun, K., and Peterson, J. R. (1982) *Radiochim. Acta*, **31**, 139–45.
Hobart, D. E., Begun, G. M., Haire, R. G., and Hellwege, H. E. (1983a) *J. Raman Spectrosc.,* **14**(1), 59–62.
Hobart, D. E., Samhoun, K., and Peterson, J. R. (1983b) *Radiochim. Acta*, **31**, 139–45.

Hoekstra, H. and Gebert, E. (1978) *Inorg. Nucl. Chem. Lett.*, **14**, 189–91.
Hölgye, Z. (1982) *Radiochem. Radioanal. Lett.*, **53**, 285–90.
Horrocks, W. D. Jr and Sudnick, D. R. (1979) *Science,* **206**(7), 1194–6.
Horrocks, W. D. Jr and Sudnick, D. R. (1981) *Acc. Chem. Res.*, **14**, 384–92.
Horwitz, E. P. (1966) *J. Inorg. Nucl. Chem.*, **28**, 1469–78.
Horwitz, E. P., Bloomquist, C. A. A., Sauro, L. J., and Henderson, D. J. (1966) *J. Inorg. Nucl. Chem.*, **28**, 2313–24.
Horwitz, E. P., Bloomquist, C. A. A., Orlandini, K. A., and Henderson, D. J. (1967) *Radiochim. Acta*, **8**, 127–32.
Horwitz, E. P., Bloomquist, C. A. A., and Griffin, H. E. (1969) Argonne National Laboratory.
Horwitz, E. P., Kalina, D. G., and Muscatello, A. C. (1981) *Sep. Sci. Technol.*, **16**, 403.
Horwitz, E. P., Kalina, D. G., Kaplan, L., Mason, G. W., and Diamond, H. (1982) *Sep. Sci. Technol.*, **17**, 1261.
Horwitz, E. P. and Kalina, D. G. (1984) *Solvent Extr. Ion Exch.*, **2**, 179.
Horwitz, E. P. and Schulz, W. W. (1985) in *Solvent Extraction and Ion Exchange in the Nuclear Fuel Cycle* (eds. D. H. Logsdail and A. L. Mills), Ellis Horwood, Chichester, p. 137.
Horwitz, E. P., Kalina, D. G., Diamond, H., Kaplan, L., Vandegrift, G. F., Leonard, R. A., Steindler, M. J., and Schulz, W. W. (1985a) in *Actinide/Lanthanide Separations* (eds. G. R. Choppin, J. D. Navratil, and W. W. Schulz), World Scientific, Singapore, p. 43.
Horwitz, E. P., Kalina, D. G., Diamond, H., Vandegrift, G. F., and Schulz, W. W. (1985b) *Solvent Extr. Ion Exch.*, **3**, 75.
Horwitz, E. P. and Schulz, W. W. (1986) in *Proc. ISEC '86.*
Horwitz, E. P., Martin, K. A., Diamond, H., and Kaplan, L. (1986) *Solvent Extr. Ion Exch.*, **4**, 449.
Horwitz, E. P., Diamond, H., Martin, K. A., and Chiarizia, R. (1987) *Solvent Extr. Ion Exch.*, **3**, 419 and 447.
Horwitz, E. P. and Schulz, W. W. (1990) *Symposium on New Separation Chemistry for Radioactive Waste and Other Specific Applications*.
Horwitz, E. P., Dietz, M. L., Nelson, D. M., La Rosa, J. J., and Fairman, W. B. (1990) *Anal. Chim. Acta.*, **238**, 263.
Horwitz, E. P., Chiarizia, R., Dietz, M. L., and Diamond, H. (1993) *Anal. Chem.*, **281**, 361.
Horwitz, E. P., Chiarizia, R., and Dietz, M. L. (1997) *React. Funct. Polym.*, **33**, 25.
Horwitz, E. P. and Schulz, W. W. (1999) in *Metal Ion Separation and Preconcentration: Progress and Opportunities* (eds. A. H. Bond, M. L. Dietz, and R. D. Rogers), American Chemical Society, Washington, DC, p. 20.
Hubert, S., Hussonnois, M., Brillard, L., Goby, G., and Guillaumont, R. (1974) *J. Inorg. Chem.*, **36**, 2361.
Hubert, S., Hussonois, M., Brillard, L., and Guillaumont, R. (1975) in *Transplutonium Elements, Proc. 4th Int. Symp.*, Baden-Baden, Sept. 13–17, Ed. by Müller, W. Lindner, R., North-Holland/Amer. Elsevier, p. 109–118.
Hubert, S. and Thouvenot, P. (1992) *J. Lumin.*, **54**, 103–11.
Hugen, Z., Yuxing, Y., and Xuexian, Y. (1982) *Actinide Recovery from Waste and Low-Grade Source*, Harwood Academic Publishers, New York, USA.

Hulet, E. K., Gutmacher, R. G., and Coops, M. S. (1961) *J. Inorg. Nucl. Chem.*, **17**, 350–60.
Hurtgen, C. and Fuger, J. (1977) *Inorg. Nucl. Chem. Lett.*, **13**, 1186–90.
Hyde, E. K., Perlman, I., and Seaborg, G. T. (1971) *The Nuclear Properties of the Heavy Elements*, Prentice-Hall, New York.
Jenkins, I. L. and Wain, A. G. (1972) *Rep. Prog. Appl. Chem.*, **57**, 308–19.
Jensen, M. P., Morss, L. R., Beitz, J. V., and Ensor, D. D. (2000) *J. Alloys Compd.*, **303**, 137–41.
Johannson, B. (1978) *J. Phys. Chem. Solids*, **39**, 467.
Johannson, B. (1984) *Phys. Rev B*, **30**, 3533–55.
Johannson, B. (1995) *J. Phys. Compds.*, **223**, 211–15.
Johannson, B. (2000) *Physics World*, 26–7.
Jones, M. E. (1951) *The Vapor Pressure of Americium Trifluoride* (Thesis), University of California Radiation Laboratory.
Jones, L. L. (1953) *J. Chem. Phys.*, **23**, 2105.
Jones, L. H. and Penneman, R. A. (1953) *J. Chem. Phys.*, **21**, 542–4.
Jones, L. H. (1955) *J. Chem. Phys.*, **23**, 2105–7.
Jove, J. and Pages, M. (1977) *Inorg. Nucl. Chem.*, **13**, 329–34.
Kalina, D. G., Horwitz, E. P., Kaplan, L., and Muscatello, A. C. (1981a) *Sep. Sci. Technol.*, **16**, 1127.
Kalina, D. G., Mason, G. W., and Horwitz, E. P. (1981b) *J. Inorg. Nucl. Chem.*, **43**, 159.
Kalina, D. G. and Horwitz, E. P. (1985) *Solvent Extr. Ion Exch.*, **3**, 235.
Kalvius, G. M., Ruby, S. L., Dunlap, B. D., Shenoy, G. K., Cohen, D., and Brodsky, M. B. (1969) *Phys. Lett. B*, **29**, 489–90.
Kamashida, M. and Fukasawa, T. (1996) *J. Nucl. Sci. Technol.*, **33**, 403–8.
Kamashida, M., Fukasawa, T., and Kawamura, F. (1998) *J. Nucl. Sci. Technol.*, **35**, 185–9.
Kaneko, H., Tsujii, M., Abe, M., Morita, Y., and Kubota, M. (1992) *J. Nucl. Sci. Technol.*, **29**, 988.
Kaneko, H., Tsujii, M., and Tamaura, Y. (1993) *Solvent Extr. Ion Exch.*, **11**, 693.
Kanellakopoulos, B., Fisher, E. O., Dornberger, E., and Baumgärtner, F. (1970) *J. Organomet. Chem.*, **24**, 507–14.
Kanellakopulos, B., Charvillat, J. P., Maino, F., and Müller, W. (1975) in *Transplutonium Elements*, *Proc. 4th Int. Symp.*, Baden-Baden, Sept. 13–17, Ed. by Müller, W. Linder, R., North-Holland/Amer. Elsevier.
Kanellakopulos, B., Aderhold, C., Dornberger, E., Müller, W., and Baybarz, R. D. (1978) *Radiochim. Acta* **25** (2), 89–92.
Kanellakopulos, B. (1979) in *Organometallics of the f-Elements* (eds. T. J. Marks and R. D. Fischer), Reidel, Dordrecht, pp. 1–35.
Karraker, D. G. Potassium Bis(Cyclooctatetraenyl) Americium(III). in *Transplutonium Elements, proc. 4th Int. Symp.,* Baden-Baden, Sept. 13–17, Ed. by Müller, W. Lindner, R., North-Holland/Amer. Elsevier, p. 131–5.
Karraker, D. G. (1977) *J. Inorg. Nucl. Chem.,* **39**(1), 87–9.
Kaszuba, J. P. and Runde, W. (1999) *Environ. Sci. Technol.*, **33**, 4427–33.
Katz, J. J. and Gruen, D. M. (1949) *J. Am. Chem. Soc.*, **71**, 2106–12.
Katz, J. J: Seaborg, G. T. (1957) *The Chemistry of the Actinide Elements*, Methuen, London, UK.

Keenan, T. K. (1959) *J. Chem. Educ.*, **36**, 27–31.
Keenan, T. K. and Kruse, F. H. (1964) *Inorg. Chem.*, **3**, 1231–2.
Keenan, T. K. (1965) *Inorg. Chem.*, **4**, 1500–1.
Keenan, T. K. (1966) *Inorg. Nucl. Chem. Lett.*, **2**, 153–6 and 211–14.
Keenan, T. K. (1967) *Inorg. Nucl Chem. Lett.*, **3**, 391–6 and 463–7.
Keenan, T. K. (1968) *Inorg. Nucl. Chem. Lett.*, **4**, 381–4.
Keller, C. (1963) *Nukleonik*, **5**, 41–8.
Keller, C. (1964) *Über die Festkörperchemie der Actiniden-Oxide*, Kernforschungszentrum Karlsruhe.
Keller, C. and Schmutz, H. (1964) *Z. Naturf. B*, **19**, 1080.
Keller, C. (1965) *J. Inorg. Nucl. Chem.*, **27**, 321–7.
Keller, C. and Walter, K. H. (1965) *J. Inorg. Nucl. Chem.*, **27**, 1247–51 and 1253–60.
Keller, C., Eberle, S. H., and Mosdzelewski, K. (1965a) *Radiochim. Acta*, **4**, 141–5.
Keller, C., Koch, L., and Walter, K. H. (1965b) *J. Inorg. Nucl. Chem.*, **27**, 1205–23 and 1225–32.
Keller, C., Eberle, S. H., and Mosdzelewski, K. (1966) *Radiochim. Acta*, **5**, 185–8.
Keller, C. (1967) in *Lanthanide/Actinide Chemistry* (ed. R. F. Gould), American Chemical Society, Washington, DC, , pp. 228–47.
Keller, C. and Fang, D. (1969) *Radiochim. Acta*, **11**, 123.
Keller, C. and Schreck, H. (1969) *J. Inorg. Nucl. Chem.*, **31**, 1121–32.
Keller, C. (1971) *Chemistry of the Transuranium Elements*, Verlag Chemie, Weinheim.
Keller, C., Berndt, U., Debbabi, M., and Engerer, H. (1972) *J. Nucl. Mater.*, **42**, 23–31.
Keller, C. and Berndt, U. (1975) in *Transplutonium, Proc. 4th Int. Symp.,* Baden-Baden, Sept. 13–17, Ed. by Müller, W. Lindner, R., North-Holland/Amer. Elsevier, p. 85–93.
Khopkar, P. K. and Narayankutty, P. (1971) *J. Inorg. Nucl. Chem.*, **33**, 495–502.
Kim, J. I., Rhee, D. S., Wimmer, H., Buckau, G., and Klenze, R. (1993) *Radiochim. Acta*, **62**, 35.
Kimura, T. and Kato, Y. (1998) *J. Alloys Compd*, **271**, 867–71.
King, L. J., Bigelow, J. E., and Collins, E. D. (1973) *Transuranium Processing Plant Semiannual Report of Production*, *Status*, *and Plans for Period Ending June* 30, 1972, Oak Ridge National Laboratory.
Kirin, I. S., Moskalev, P. N., and Mishin, V. Y. (1967) *Zh. Obshch. Khim.*, **37**, 1065–8.
Koch, G. and Schoen, J. (1968) German Report KFK-783, Kernforschungszentrum Karlsruhe, Germany.
Koch, G. (1969) Conf. Report CONF-690426, Liege, Belgium.
Kochen, R. L. (1987) *Actinide Removal from Aqueous Solution with Activated Magnetite*, Rockwell International, Golden, CO.
Kochen, R. L. and Navratil, J. D. (1987) *Lanthanide/Actinide Res.*, **2**, 9.
Koehly, G. and Hoffert, F. (1967) *Semiannual Report of the Chemistry Department*, *Center for Nuclear Studies at Fontenay-aux-Roses*, *December* 1966–*May* 1967, Argonne National Laboratory.
Kolarik, Z. J. and Horwitz, E. P. (1988) *Solvent Extr. Ion Exch.*, **6**, 247.
Kolarik, Z., Müllich, U., and Gassner, F. (1999) *Solvent Extr. Ion Exch.*, **17**, 23 and 1155.
Koma, Y., Watanabe, M., Nemoto, S., and Tanaka, Y. (1998) *Solvent Extr. Ion Exch.*, **16**, 1357.
Kornilov, A. S., Frolov, A. A., and Vasil'ev, V. Y. (1986) *Radiokhimiya*, **28**(5), 656–60.

Kosyakov, V. N., Timofeev, G. A., Erin, E. A., Andreev, V. I., Kopytov, V. V., and Simakin, G. A. (1977) *Radiokhimiya*, **19**, 511–7.

Krot, N. N., Shillov, V. P., Nikolaevskii, V. B., Nikaev, A. K., Gel'man, A. D.,and Spitsyn, V. I. (1974a) *Dokl. Acad. Sci. USSR*, **217**(3), 525–7.

Krot, N. N., Shillov, V. P., Nikolaevskii, V. B., Nikaev, A. K., Gel'man, A. D., and Spitsyn, V. I. (1974b). Oak Ridge National Laboratory.

Kruse, F. H. and Asprey, L. B. (1962) *Inorg. Chem.*, **1**(1), 137–9.

Kuznetsov, V. I. and Skobelev, N. K. (1966) ORO-tr-3346-15, Joint Inst. for Nuclear Research, Dubna (USSR), translation of Russian report JINR-p7-2984.

Lam, D. J. and Mitchell, A. W. (1972) *J. Nucl. Mater.*, **44**, 279–84.

Larson, D. T. and Haschke, J. M. (1981) *Inorg. Chem.*, **20**, 1945–50.

Law, J. D., Brewer, K. N., Herbst, R. S., Todd, T. A., and Olsen, L. G. (1998) Report INEL/EXT-98-00004, Idaho National Engineering and Environmental Laboratory, Idaho Falls, Idaho, USA.

Law, J. D., Brewer, K. N., Herbst, R. S., and Todd, T. A. (1998) Report INEL/EXT-97-00837, Idaho National Engineering and Environmental Laboratory, Idaho Falls, Idaho, USA.

Lawaldt, D., Marquart, R., Werner, G.-D., and Wigel, F. (1982) *J. Less Common Metals*, **85**, 37–41.

Lebedev, I. A., Pirozhkov, S. V., Razbitnoi, V. M., and Yakovlev, G. N. (1960a) *Radiokhimiya*, **2**, 351–6.

Lebedev, I. A., Pirozhkov, S. V., and Yakovlev, G. N. (1960b) *Radiokhimiya*, **2**, 549–58.

Lebedev, I. A. and Yakovlev, G. N. (1961) *Radiokhimiya*, **3**, 455.

Lebedev, I. A., Pirozhkov, S. V., and Yakovlev, G. N. (1962) *Radiokhimiya*, **4**, 304–8.

Lebedev, I. A., Maksimova, A. M., Stepanov, A. V., and Shalinets, A. B. (1967) *Radiokhimiya*, **9**, 707.

Lebedev, I. A. and Shalinets, A. B. (1968) *Radiokhimiya*, **10**, 233.

Lebedev, I. A., Filimonov, V. T., Shalinets, A. B., and Yakovlev, G. N. (1968) *Radiokhimiya*, **10**, 93.

Lebedev, I. A., Frenkel, V. Y., Kulyako, Y. M., and Myasoedov, B. F. (1979) *Radiokhimiya*, **21**(6), 809–16.

Lederer, C. M. and Shirley, V. S. (1978) in *Table of Radioactive Isotopes*, John Wiley, New York.

Leger, J. M., Yacoubi, N., and Loriers, J. (1981) *J. Solid State Chem.*, **36**, 261–70.

Levakov, B. I. and Shalinets, A. B. (1971) *Radiokhimiya*, **13**, 295.

Le Vert, F. E. and Helminski, E. L. (1973) *Literature Review and Commercial Source Evaluation of Americium-241*, Tuskegee Institute.

Li, J. and Bursten, B. E. (1997) *J. Am. Chem. Soc.,* **119**(38), 9021–32.

Liansheng, W., Casarci, M., and Gasparini, G. M. (1991) *Solvent Extr. Ion Exch.*, **8**, 49.

Liminga, R., Abrahams, S. C., and Bernstein, J. L. (1977) *J. Chem. Phys.*, **67**(3), 1015–23.

Lin, Z., Berne, A., Cummings, B., Filliben, J. J., and Inn, K. G. W. (2002) *Appl. Radiat. Isot.*, **56**, 57–63.

Lindbaum, A., Heathman, S., Litfin, K., Meresse, Y., Haire, R. G., Le Bihan, T., and Libotte, H. (2001) *Phys. Rev. B*, **63**, 214101 (1–10).

Link, P., Braithwaite, D., Wittig, J., Benedict, U., and Haire, R. G. (1994) *J. Alloys Compd.*, **213/214**, 148–52.

Liu, G. K., Beitz, J. V., Huang, J., Abraham, M. M., and Boatner, L. A. (1997) *J. Alloys Compd.*, **250**, 347–51.
Lohr, H. R. and Cunningham, B. B. (1951) *J. Am. Chem. Soc.*, **73**, 2025–8.
Lumetta, G. J. and Swanson, J. L. (1993a) *Sep. Sci. Technol.*, **28**, 43.
Lumetta, G. J. and Swanson, J. L. (1993b) Pacific Northwestern Laboratory.
Lumetta, G. J., Wester, D. W., Morrey, J. R., and Wagner, M. J. (1993) *Solvent Extr. Ion Exch.*, **11**, 663.
Lux, F. (1973) *Proc. Tenth Rare Earth Reasearch Conf.,* Carefree, Arizona, April 30-May 3, Ed. by Kevane, C. J. and Moeller, T., pp. 871–80.
Lychev, A. A., Mashirov, L. G., Smolin, Y. I., Suglobov, D. N., and Shepelev, Y. F. (1980) *Radiokhimiya*, **22**, 43–8.
Lynch, R. W., Dosch, R. G., Kenna, B. T., Johnstone, J. K., and Nowak, E. J. (1975) *The Sandia Solidification Process: A Broad Range Aqueous Waste Solidification Method.*
Madic, C., Guillaumont, B., Morisseau, J. C., and Moulin, J. P. (1979) *J. Inorg. Nucl. Chem.*, **83**, 3373.
Madic, C., Hobart, D. E., and Begun, G. M. (1983) *Inorg. Chem.*, **22**, 1494–503.
Madic, C., Blanc, P., Condamines, N., Baron, P., Berthon, L., Nicol, C., Pozo, C., Lecomte, M., Phillipe, M., Masson, M., Hequet, C., and Hudson, M. J. (1994) French Report CEA-CONF-12297.
Madic, C. and Hudson, M. J. (1998) Report EUR 18038 EN.
Magirius, S., Carnall, W. T., and Kim, J. I. (1985) *Radiochim. Acta*, **38**, 29–32.
Mahajan, G. R., Prabhu, D. R., Manchanda, V. K., and Badheka, L. P. (1998) *Waste Manage.*, **18**, 125.
Maly, J. (1969) *J. Inorg. Nucl. Chem.*, **31**, 1007–17.
Manchanda, V. K. and Mohapatra, P. K. (1995) *Radiochim. Acta*, **69**, 81.
Mapara, P. M., Godbole, A. G., Rajendra, S., and Thakur, N. V. (1998) *Hydrometallurgy*, **49**, 197–201.
Marcu, G. and Samochocka, K. (1965) *Stud. Univ. Babes-Bolyai, Ser. Chem.*, **10**, 71.
Marcu, G. and Samochocka, K. (1966) *Stud. Univ. Babes-Bolyai, Ser. Chem.*, **11**, 15.
Marcus, Y., Givon, M., and Choppin, G. R. (1963) *J. Inorg. Nucl. Chem.*, **25**, 1457–63.
Marcus, Y. and Cohen, D. (1966) *Inorg. Chem.*, **5**, 1740–3.
Marcus, Y. and Shiloh, M. (1969) *Israel J. Chem.*, **7**, 31–43.
Marcus, Y. and Bomse, M. (1970) *Israel J. Chem.*, **8**, 901–11.
Marcus, Y., Yanir, E., and Givon, M. (1972) The standard potential of the americium III/IV couple. An estimate from the formal potential and complex stabilities in phosphoric acid, in *Coordination Chemistry in Solution*, Vol. kungl. Tek. Högsk. Handl. Nr. 265 (ed. E. Högfeldt), Swedish Nat. Sci. Res. Council, pp. 227–38.
Markin, T. L. (1958) *J. Inorg. Nucl. Chem.* **7**, 290–2.
Martella, L. L. and Navratil, J. D. (1979) US Report.
Martensson, N., Johansson, B., and Naegele, J. R. (1987) *Phys. Rev. B*, **35**, 1437–9.
Martinot, L. and Fuger, J. (1985) *The Actinides* in *Standard Potentials in Aqueous Solution*, ed. by Bard, A. J., Parsons, R., Jordan, J., Dekker, New York, USA, p. 631–74.
Mathur, J. N., Murali, M. S., and Natarajan, R. R. (1991) *J. Radioanal. Nucl. Chem.*, **152**, 127.
Mathur, J. N., Murali, M. S., Natarajan, P. R., Bodheka, L. P., and Benerji, R. (1992a) *Talanta*, **39**, 493.

Mathur, J. N., Murali, M. S., and Natarajan, R. R. (1992b) *J. Radioanal. Nucl. Chem.*, **155**, 195.
Mathur, J. N., Murali, M. S., Rizvi, G. H., Iyer, R. H., Michael, K. M., Kapoor, S. C., Dhumwad, R. K., Badheka, L. P., and Bannerji, A., (1994) *Solvent Extr. Ion Exch.*, **12**, 745.
Mathur, J. N., Murali, M. S., Iyer, R. H., Ramanujam, A., Dhami, P. S., Gopalakrishnan, V., Badheka, L. P., and Bannerji, A. (1995) *Nucl. Technol.*, **109**, 216.
Mathur, J. N., Murali, M. S., Ruikar, P. B., Nagar, M. S., Sipahimalani, A. R., Bauri, A. K., and Bannerji, A. (1998) *Sep. Sci. Technol.*, **33**, 2179.
Mathur, J. N., Murali, M. S., and Nash, K. L. (2001) *Solvent Extr. Ion Exch.*, **19**, 357–90.
Matonic, J. H., Scott, B. L., and Neu, M. P. (2001). *Inorg. Chem.*, **40**, 2638.
McIsaac, L. D. and Schulz, W. W. (1976) *Transplutonium 1975*, North-Holland, Amsterdam.
McIsaac, L. D. (1982) *Sep. Sci. Technol.*, **17**, 387.
McIsaac, L. D. and Baker, J. D. (1983) *Solvent Extr. Ion Exch.*, **1**, 72.
McWhan, D. B., Wallmann, J. C., Cunningham, B. B., Asprey, L. B., Ellinger, F. H., and Zachariasen, W. H. (1960) *J. Inorg. Nucl. Chem.*, **15**, 185–7.
Meinrath, G. and Kim, J. I. (1991a) *Radiochim. Acta*, **52/53**, 29.
Meinrath, G. and Kim, J. I. (1991b) *Eur. J. Inorg. Solid State Chem.*, **28**, 383–8.
Melkaya, R. F., Volkov, Y. F., Sokolov, E. I., Kapshukov, I. I., and Rykov, A. G. (1982) *Dokl. Chem.* (*Engl. Transl.*), **262/7**, 42.
Mercing, E. and Duyckaerts, E. (1967) *Anal. Lett.*, **1**, 23.
Michael, K. M., Rizvi, G. H., Mathur, J. N., and Ramanujam, A. (2000) *J. Radioanal. Nucl. Chem.*, **246**, 355.
Mikheev, N. B. and Myasoedov, B. F. (1985) Lower and higher oxidation states of transplutonium elements in solutions and Metals, in *Handbook on the Physics and Chemistry of the Actinides*, ch. 9 (eds. J. A. Freeman and C. Keller), Elsevier Science Publishers, pp. 347–86.
Milligan, W. O. and Beasley, M. L. (1968) *Acta Crystallogr. B*, **24**, 979–81.
Mills, T. R. and Reese, L. W. (1994) *J. Alloys Compd.*, **213/214**, 360–2.
Milyukova, M. S., Litvina, M. N., and Myasoedov, B. F. (1980) *Radiochem. Radioanal. Lett.,* **44**(4), 259–68.
Mishra, S., Chakravortty, V., and Vasudeva Rao, P. R. (1996) *Radiochim. Acta*, **73**, 89.
Mitchell, A. W. and Lam, D. J. (1970a) *J. Nucl. Mater.*, **37**, 349–52.
Mitchell, A. W. and Lam, D. J. (1970b) *J. Nucl. Mater.*, **36**, 110–12.
Moattar, F. (1971) *Compounds of Trivalent Transuranium Compounds Appearing in Mixtures of Complexing Agents.* Report KFK-1416, Kernforschungszentrum Karlsruhe, Germany.
Modolo, G. and Odoj, R. (1998) *J. Radioanl. Nucl. Chem.*, **228**, 83.
Modolo, G. and Odoj, R. (1999) *Solvent Extr. Ion Exch.*, **17**, 33.
Mohapatra, P. K. and Manchanda, V. K. (1991) *Radiochim. Acta*, **55**(4), 193–7.
Mohapatra, P. K. and Manchanda, V. K. (1995) *Polyhedron,* **14**(13–14), 1993–7.
Mohapatra, P. K. and Manchanda, V. K. (1999) *J. Radioanal. Nucl. Chem.*, **240**, 259.
Mohapatra, P. K., Sriram, S., Manchanda, V. K., and Badheka, L. P. (2000) *Sep. Sci. Technol.*, **35**, 39.
Moore, R. H. and Lyon, W. L. (1959) *Distribution of Actinide Elements in Molten System KCl-$AlCl_3$-Al*, General Electric Company, Hanford Atomic Products Operation.

Moore, F. L. (1964) *Anal. Chem.*, **36**, 2158.
Moore, F. L. (1966a) *Anal. Chem.*, **38**, 510.
Moore, F. L. (1966b) US Patent 3 194 494.
Moore, G. E. (1970) *Chemistry Division Annual Progress Report for Period Ending May* 20, 1970, Oak Ridge National Laboratory.
Moore, F. L. (1973) US Patent 3 687 641.
Morita, Y. and Kubota, M. (1988) *Solvent Extr. Ion Exch.*, **6**, 233.
Morita, Y., Yamaguchi, L., Kondo, Y., Shirahashi, K., Yamagishi, I., Fugiwara, T., and Kubota, M. (1993) in Proc. of Technical Committee on *Safety and Environmental Aspects of Partitioning and Transmutation of Actinides and Fission Products*. Report IAEA-TECDOC-783, Vienna, Austria.
Morss, L. R., Siegal, M., Stenger, L., and Edelstein, N. (1970) *Inorg. Chem.*, **9**(7), 1771–5 .
Morss, L. R. and Fuger, J. (1981) *J. Inorg. Nucl. Chem.*, **43**(9), 2059–64.
Morss, L. R. (1982) in *Actinides in Perspective* (ed. N. Edelstein), Pergamon Press, New York, pp. 381–407.
Morss, L. R. (1983) *J. Less Common Metals*, **93**, 301–21.
Morss, L. R. and Williams, C. W. (1994) *Radiochim. Acta*, **66/67**, 99–103.
Moskalev, P. N., Shapkin, G. N., and Darovskikh, A. N. (1979) *Zh. Neorg. khim.*, **24**, 340–6.
Moskvin, A. I., Khalturin, G. V., and Gel'man, A. D. (1959) *Radiokhimiya*, **1**, 141.
Moskvin, A. I., Khalturin, G. V., and Gel'man, A. D. (1962) *Radiokhimiya*, **4**, 162.
Moskvin, A. I. (1967) *Radiokhimiya*, **9**, 718–20.
Moskvin, A. I. (1971) *Radiokhimiya*, **13**, 221–3, 224–30, 575–81, and 668–74.
Moskvin, A. I. (1973) *Radiokhimiya*, **15**, 504–13.
Mosley, W. C. (1970) in *Proc. 4th Internat. Conf. on Plutonium and other Actinides*, Santa Fe, NM, USA, USAEC CONF-701001, Parts II, pp 762–771.
Moulin, V., Robouch, P. B., Vitorge, P., and Allard, B. (1987) *Inorg. Chim. Acta*, **140**, 303.
Müller, W. (1971) *Angew. Chem.*, **83**, 625.
Müller, W., Reul, J., and Spirlet, J. C. (1972) *Atomwirtschaft*, **17**, 415.
Müller, W., Schenkel, R., Schmick, H. E., Spirlet, J. C., McElroy, D. L., Hall, R. O. A., and Mortimer, M. J. (1978) *J. Low Temp. Phys.*, **40**, 361–78.
Mullins, L. J. and Leary, J. A. (1969) US Patent 3420639.
Murali, M. S. and Mathur, J. N. (2001) *Solvent Extr. Ion Exch.*, **19**, 61–77.
Musikas, C. (1973a) *Radiochem. Radioanal. Lett.*, **13**, 255–8.
Musikas, C. C. (1973b) Electrochimie en solution aqueuse, in *Gmelin Handbook of Inorganic Chemistry*, vol. part D1, Verlag Chemie, Weinheim, pp. 5–23.
Musikas, C., Germain, M., and Bathelier, A. (1980a) in *Actinide Separations* (eds. J. D. Navratil and W. W. Schulz) (*ACS Symp. Ser. 117*), American Chemical Society, Washington, DC, pp. 157–73.
Musikas, C., Le Marois, G., Fitoussi, R., and Cuillerdier, C. (1980b). in *Actinide Separations* (eds. J. D. Navratil and W. W. Schulz), (*ACS Symp. Ser. 117*), American Chemical Society, Washington, DC, pp. 131–45.
Musikas, C. and Hubert, H. (1983) *Proc. ISEC '83*, p. 449.
Musikas, C. (1984) *Actinide/Lanthanide Separations, Proc., Int. Symp.*, 19–30.

Musikas, C. (1987) *Inorg. Chim. Acta*, **140**, 197.
Musikas, C., Condamines, C., Cuillerdier, C., and Nigond, L. (1991) *International Symposium on Radiochemistry and Radiation Chemistry*.
Musikas, C. (1995) *Nuclear and Radiochemistry Symposium*.
Myasoedov, B. F., Mikhailov, V. M., Lebedev, I. A., Litvina, M. N., and Frenkel, V. Y. (1973) *Radiochem. Radioanal. Lett.*, **14**, 17–24.
Myasoedov, B. F., Guseva, L. I., Lebedev, I. A., Milyukova, M. S., and Chmutova, M. S. (1974a) *Analytical Chemistry of the Transplutonium Elements,* John Wiley, New York.
Myasoedov, B. F., Lebedev, I. A., Frenkel, V. Y., and Vyatkina, I. I. (1974b) *Sov. Radiochem.*, **16**, 803–7.
Myasoedov, B. F., Milyukova, M. S., Lebedev, I. A., Livina, M. N., and Frenkel, V. Y. (1975) *J. Inorg. Nucl. Chem.*, **37**, 1475–8.
Myasoedov, B. F., Lebedev, I. A., and Milyukova, M. S. (1977) *Rev. Chem. Minér.*, **14**, 160–71.
Myasoedov, B. F., Chmutova, M. K., and Karalova, Z. K. (1980) in *Actinide Separations* (eds. J. D. Navratil and W. W. Schulz), American Chemical Society, Washington, DC, p. 101.
Myasoedov, B. F. and Kremliakova, N. Y. (1985) Studies of americium and curium solution chemistry in the USSR, in *Americium and Curium Chemistry and Technology* (ed. N. M. Edelstein), D. Reidel, Germany, pp. 53–79.
Myasoedov, B. F., Chmutova, M. K., Kochetkova, N. E., Koiro, O. E., Priibylova, G. A., Nesterova, N. P., Medved, T. Y., and Kabachnik, M. I. (1986) *Solvent Extr. Ion Exch.*, **4**, 61.
Myasoedov, B. F. and Lebedev, I. A. (1991) in *Handbook on the Physics and Chemistry of the Actinides* (eds. A. J. Freeman and C. Keller), Elsevier, New York, p. 551.
Myasoedov, B. F. (1994) *J. Alloys Compd.*, **290**, 213–14.
Naegele, J. R., Manes, L., Spirlet, J. C., and Müller, W. (1984) *Phys. Rev. Lett.*, **52**, 1834–7.
Nair, G. M. and Chander, K. (1983) *J. Less Common Metals*, **92**(1), 29–34.
Nash, K. L., Gatrone, R. C., Clark, G. A., Rickert, P. G., and Horwitz, E. P. (1988) *Sep. Sci. Technol.*, **23**, 1355.
Nash, K. L., Gatrone, R. C., Clark, G. A., Rickert, P. G., and Horwitz, E., (1989) *Solvent Extr. Ion Exch.*, **7**, 644.
Nash, K. L. (1994) in *Handbook on the Physics and Chemistry of Rare Earths*, *Gschneidner* (eds. K. A. Gschneidner, Jr, L. Eyring, G. R. Choppin, and G. H. Lander), New York, Elsevier North-Holland, pp. 197–235.
Natowitz, J. B. (1973) USAEC Report ORO-3924–14.
Nellis, W. and Brodsky, M. B. (1974) in *The Actinides: Electronic Structure and Related Properties*, Academic Press, New York.
Newton, T. W. and Baker, F. (1967) in *Lanthanide/Actinide Chemistry* (ed. R. F. Gould), ACS Adv. Chem. Ser., American Chemical Society, Washing DC, pp. 268–95.
Newton, T. W. (1975) *The Kinetics of the Oxidation–Reduction Reactions of Uranium*, *Neptunium*, *Plutonium*, *and Americium Ions in Aqueous Solutions.*
Nigon, J. P., Penneman, R. A., Staritzki, E., Keenan, T. K., and Asprey, L. B. (1954) *J. Phys. Chem.*, **58**, 403–4.

Nigond, L., Musikas, C., and Cuillerdier, C. (1994) *Solvent Extr. Ion Exch.*, **12**, 261 and 297.
Nikolaev, A. V. and Ionova, G. V. (1991) *Phys. Stat. Sol. (6)* **167**, 613–23.
Nikolaevskii, V. B., Shilov, V. P., and Krot, N. N. (1974) *Radiokhimiya*, **16**, 122–3.
Nikolaevskii, V. B., Shilov, V. P., Krot, N. N., and Peretrukhin, V. F. (1975) *Radiokhimiya*, **17**, 420–2 and 431–3.
NN (2002) *Nucl. News*, **45**(Jan), 58–60.
Nugent, L. J., Baybarz, R. D., Burnett, J. L., and Ryan, J. L. (1971a) *J. Inorg. Nucl. Chem.*, **33**, 2503–30.
Nugent, L. J., Laubereau, P. G., Werner, G. K., and Vander Sluis, K. L. (1971b) *J. Organomet. Chem.*, **27**(3), 365–72.
Nugent, L. J., Baybarz, R. D., Burnett, J. L., and Ryan, J. L. (1973a) *J. Phys. Chem.*, **77**, 1528–39.
Nugent, L. J., Burnett, J. L., and Morss, L. R. (1973b) *J. Chem. Thermodyn.*, **5**, 665–78.
Nunez, L., Buchholz, B. A., Kaminski, M., Aase, S. B., Brown, N. R., and Vandegrift, G. F. (1996) *Sep. Sci. Technol.*, **31**, 1393.
Oetting, F. L., Rand, M. H., and Ackermann, R. J. (1976) in *The Chemical Thermodynamics of Actinide Elements and Compounds*, *part 1*, *The Actinide Elements*. IAEA.
Ogawa, T., Shirasu, Y., Minato, K., and Serizawa, H. (1997) *J. Nucl. Mater.*, **247**, 151–7.
Ohyoshi, E. and Ohyoshi, A. (1971) *J. Inorg. Nucl. Chem.*, **33**, 4265.
Okamoto, H. (1998) *J. Phase Euilib.*, **20**, 450–2.
Olson, W. M. and Mulford, R. N. R. (1966) *J. Phys. Chem.*, **70**, 2934–7.
Osipov, S. V., Andreichuk, N. N., Vasil'ev, V. Y., and Rykov, A. G. (1977) *Radiokhimiya*, **19**(4), 522–4.
Ozawa, M., Nemoto, S., Togashi, A., Kawata, T., and Onishi, K. (1992) *Solvent Extr. Ion Exch.*, **10**, 829.
Ozawa, M., Koma, Y., Nomura, K., and Tanaka, Y. (1998) *J. Alloys Compd.*, **538**, 272–3.
Pappalardo, R., Carnall, W. T., and Fields, P. R. (1969a) *J. Chem. Phys.*, **51**(2), 842–3.
Pappalardo, R. G., Carnall, W. T., and Fields, P. R. (1969b) *J. Chem. Phys.*, **51**, 1182–2000.
Pazukhin, E. M., Krivokhatskii, A. S., and Kochergin, S. M. (1987) *Sov. Radiochem.*, **29**(1), 9–13.
Penneman, R. A. and Asprey, L. B. (1950) *The formal potential of the Am(V)-Am(VI) couple*, Los Alamos National Laboratory.
Penneman, R. A. and Asprey, L. B. (1955) *A Review of Americium and Curium Chemistry*, *Proc. First Int. Conf. on the Peaceful Uses of Atomic Energy*, pp. 355–62.
Penneman, R. A. and Keenan, T. K. (1960) *The Radiochemistry of Americium and Curium*, National Academy of Sciences.
Penneman, R. A., Coleman, J. S., and Keenan, T. K. (1961) *J. Inorg. Nucl. Chem.*, **17**, 138–45.
Penneman, R. A. and Mann, J. B. (1976) *J. Inorg. Nucl. Chem.*, Suppl., 257–63.
Peppard, D. F., Mason, G. W., Driscoll, W. J., and Sironen, R. J. (1958) *J. Inorg. Nucl. Chem.*, **7**, 276–85.
Peppard, D. F., Mason, G. W., Driscoll, W. J., and Sironen, R. J. (1962) *J. Inorg. Nucl. Chem.*, **24**, 881–8.

Pereira, L. C. J., Wastin, F., Winand, J. M., Kanellakopoulos, B., Rebizant, J., Spirlet, J. C., and Almeida, M. (1997) *J. Solid State Chem.*, **134**, 138–47.
Peretrukhin, V. F. and Spitsyn, V. I. (1982) *Izv. Akad. Nauk SSSR, Ser. Khim.*, **31**, 826–31.
Persson, G. E., Svantesson, S., Wingefors, S., and Liljenzin, J. O. (1984) *Solvent Extr. Ion Exch.*, **2**, 89.
Peterson, J. R. (1973) in *Proc. 10th Rare Earth Research Conf.* (eds. C. J. Kevane and T. Moeller), April 30-May 3, Carefree, Arizona.
Petrzilova, H., Binka, J., and Kuca, L. (1979) *J. Radioanal. Nucl. Chem.*, **51**, 107.
Pikaev, A. K., Shilov, V. N., Nikolaevskii, V. B., Krot, N. N., and Spitsyn, V. I. (1977) *Radiokhimiya*, **19**(5), 720–4.
Pilv Vo, R. and Bickel, M. (1998) *J. Alloys Compd.*, **49**, 271.
Pilv Vo, R., La Rosa, J. J., Mouchel, D., Nardel, R., Bichel, M., and Altzizaglau, T. (1999) *J. Environ. Radioact.*, **43**, 343.
Pilv Vo, R. and Bichel, M. (2000) *Appl. Radiat. Isot.*, **53**, 273.
Piskunov, E. M. and Rykov, A. G. (1972) *Radiokhimiya*, **14**, 638.
Potter, R. A. and Tennery, V. J. (1973) US Patent, 3,758, 669.
Proctor, S. G. and Connor, W. V. (1970) *J. Inorg. Nucl. Chem.*, **32**, 3699–701.
Proctor, S. G. (1975) *Cation Exchange Process for Molten Salt Extraction Residues*, Rocky Flats Plant, Dow Chemical Company.
Proctor, S. G. (1976) *J. Less Common Metals*, **44**, 195–9.
Prunier, C., Guérin, L., Faugére, J.-L., Cocuaud, N., and Pidnet, J.-M. (1997) *Nucl. Technol.*, **120**, 110–20.
Radchenko, V. M., Ryabinin, M. A., Selezenev, A. G., Shimbarev, E. V., Sudakov, L. V., Kapashukov, I. I., and Vasil'ev, V. Y. (1982) *Sov. Radiochem.* (*Engl. Trans.*), **24**, 144–6.
Radzewitz, H. (1966) *Festkörperchemische Untersuchungen über die Systeme* $SeO_{1.5}$–ZrO_2 (HfO_2, $AmO_{1.5}$–ZrO_2 (HfO_2, ThO_2)–O_2, und TiO_2–NpO_2 (PuO_2), Kernforschungszentrum Karlsruhe.
Rai, D., Felmy, A. R., and Fulton, R. W. (1992) *Radiochim. Acta*, **56**(1), 7–14.
Rais, J. and Tachimori, S. (1994) *J. Radioanal. Nucl. Chem. Lett.,***188**, 157.
Rao, V. K., Mahajan, G. R., and Natarajan, P. R. (1987) *Inorg. Chim. Acta*, **128**(1), 131–4.
Rao, L. F., Rai, D., Felmy, A. R., Fulton, R. W., and Novak, C. F. (1996) *Radiochim. Acta*, **75**(3), 141–7.
Rapko, B. M. and Lumetta, G. J. (1994) *Solvent Extr. Ion Exch.*, **12**, 967.
Rapko, B. M. (1995) in *Separations of Elements* (eds. K. L. Nash and G. R. Choppin), Plenum Press, New York, p. 99.
Rebizant, J. and Benedikt, U. (1978) *J. Less Common Metals*, **58**, 31–3.
Rizvi, G. H. and Mathur, J. N. (1997), Report BARC/P004, p. 56.
Robel, W. (1970) *Complex Compounds of Hexavalent Actinides with Pyridine Carboxylic Acids*. KFK.
Roddy, J. W. (1973) *J. Inorg. Nucl. Chem.*, **35**, 4141–8.
Roddy, J. W. (1974) *J. Inorg. Nucl. Chem.*, **36**, 2531–3.
Rogozina, E. M., Konkina, L. F., and Popov, D. K. (1974) *Radiokhimiya*, **16**, 383–6.
Roof, R. B., Haire, R. G., Schiferl, D., Schwalbe, L., Kmetko, E. A., and Smith, J. L. (1980) *Science*, **207**, 1353–5.

Roof, R. B. (1982) *Z. Kristallogr.*, **158**, 307–12.
Rosch, F., Reimann, T., Ludwig, R., Dreyer, R., Buklanov, G. V., Khalkhin, V. A., Milanov, M., and Tran Kim, H. (1989) in *Actinides-89 Abstracts*, Tashkent, USSR.
Rose, R. L., Kelly, R. E., and Lesuer, D. R. (1979) *J. Nucl. Mater.*, **79**, 414–16.
Runde, W., Meinrath, G., and Kim, J. I. (1992) *Radiochim. Acta*, **58/59**, 93–100.
Runde, W. and Kim, J. I. (1994) *Chemisches Verhalten von Drei- und Fünfwertigem Americium in Salinen NaCl-Lösungen*, Institut für Radiochemie, Technische Universität München.
Runde, W., Neu, M. P., and Clark, D. L. (1996) *Geochim. Cosmochim. Acta*, **60**(12), 2065–73.
Runde, W., Van Pelt, C., and Allen, P. G. (2000) *J. Alloys Compd.*, **303/304**, 182–90.
Runde, W., Neu, M. P., Conradson, S., and Tait, C. D. (2002) American Chemical Society Meeting ACS 2002, Orlando, Florida, USA.
Runde, W., Bean, A., and Scott, B. (2003) *Chem. Commun.*, 1848–9.
Runnals, O. J. C. and Boucher, R. R. (1955) *Nature*, **176**, 1019–20.
Runnals, O. J. C. and Boucher, R. R. (1956) *Can. J. Phys.*, **34**, 949–58; Great Britain Patent 741441 (1956); and US Patent 2809887 (1975).
Ryan, J. L. (1967) Octahedral complexes of trivalent actinides, in *Lanthanide/Actinide Chemistry* (ed. R. F. Gould), American Chemical Society, Washing DC, pp. 331–4.
Ryan, J. L. (1974) Ion exchange, in *Gmelins Handbuch der Anorganischen Chemie*, vol. 21, *Transurane*, part D2, Verlag Chemie, Weinheim.
Rykov, A. G., Ermakov, V. A., Timofeev, G. A., Chistyakov, V. M., and Yakovlev, G. N. (1970) *Sov. Radiochem.*, **13**, 858–61.
Rykov, A. G., Timofeev, G. A., and Chistyakov, V. M. (1973) *Radiokhimiya*, **15**, 872–4.
Sakama, M., Tsukada, K., Asai, M., Tchikawa, S., Haka, H., Gata, S., Oura, Y., Nishanaka, I., Nagama, Y., Shibata, M., Kojima, Y., Kawada, K., Ebihara, M., and Nikahara, H. (2000) *Eur. Phys. J. A*, **9**, 303–5.
Sakamura, Y., Hijkata, T., Kinoshita, K., Inoue, T., Storvik, T. S., Kreuger, C. L., Grantham, L. F., Fusselman, S. F., Grimmett, D. L., and Roy, J. J. (1998) *J. Nucl. Sci. Technol.*, **35**, 49–59.
Sakanoue, M. and Amano, R. (1975) in *Transplutonium 1975*, *Proc. 4th Int. Symp.*, pp. 123–9.
Sakanque, M. and Nakatani, M. (1972) *Bull. Chem. Soc. Jpn.*, **45**, 3429.
Saprykin, A. S., Spitsyn, V. I., and Krot, N. N. (1976) *Dokl. Akad. Nauk SSSR*, **228**, 649–51.
Sari, C., Müller, W., and Benedict, U. (1972/73) *J. Nucl. Mater.*, **45**, 73–5.
Sasaki, Y. and Tachimori, S. (2002) *Solvent Extr. Ion Exch.*, **20**, 21.
Schleid, T., Morss, L. R., and Meyer, G. (1987) *J. Less Common Metals*, **127**, 183–7.
Schmutz, H. (1966) *Untersuchungen in den Systemem Alkalifluorid-Lanthaniden/Actinidenfluorid* (*Li*, *Na*, *K*, *Rb-La*, *S. E.*, *Y/Np*, *Pu*, *Am*), KFK.
Schoebrechts, J. P., Gens, R., Fuger, J., and Morss, L. R. (1989) *Thermochim. Acta*, **139**, 49–66.
Schulz, W. W. (1974) *Bidentate Organophosphorus Extraction of Americium and Plutonium from Hanford Plutonium Reclamation Facility Waste*, Atlantic Richfield Hanford Company.
Schulz, W. W. (1975) *Trans. Am. Nucl. Soc.*, **21**, 262–3.

Schulz, W. W. (1976) *The Chemistry of Americium*, DOE Technical Information Center.
Schulz, W. W., Koenst, J. W., and Tallant, D. R. (1980) *Actinide Separations,* American Chemical Society, Washington, DC.
Schulz, W. W. and Navratil, J. D. (1982) in *Recent Developments in Separation Science*, vol. 7 (ed. Li, N.), CRC Press, Boca Raton, FL.
Schulz, W. W. and Horwitz, P. (1988) *Sep. Sci. Technol.*, **23**, 1191.
Seaborg, G. T., James, R. A., Ghiorso, A., and Morgan, L. O. (1950) *Phys. Rev.*, **78**, 472.
Seaborg, G. T. (1970) *Nucl. Appl. Technol.*, **9**, 830–50.
Seaborg, G. T. (1972) *Pure Appl. Chem.*, **30**, 539–49.
Sekine, T. (1965) *Acta Chem. Scand.*, **19**, 1476.
Seleznev, A. G., Shushakov, V. D., and Kosulin, N. S. (1979) *Phys. Met. Metall.* (*Engl. Transl.*), **46**, 193–4.
Shafiev, A. I., Efremov, Y. V., Nikolaev, V. M., and Yakovlev, G. N. (1971) *Sov. Radiochem.*, **13**, 123–5.
Shalinets, A. B. and Stepanov, A. V. (1971) *Radiokhimiya*, **13**, 566–70.
Shalinets, A. B. and Stepanov, A. V. (1972) *Radiokhimiya*, **14**, 280–3.
Shalinets, A. B. (1972a) *Radiokhimiya*, **14**, 275.
Shalinets, A. B. (1972b) *Radiokhimiya*, **14**, 33.
Shalinets, A. B. (1972c) *Radiokhimiya*, **14**, 269.
Shannon, R. D. (1976) *Acta Crystallogr. B*, **A32**, 751–67.
Shen, C., Bao, B., Zhu, J., Wang, Y., and Cao, Z. (1996) *J. Radioanal. Nucl. Chem. Art.*, **212**, 187.
Shiloh, M., Givon, M., and Marcus, Y. (1969) *J. Inorg. Nucl. Chem.*, **31**, 1807–14.
Shilov, V. P., Nikolaevskii, V. B., and Krot, N. N. (1974) *Zh. Neorg. Khim.*, **19**, 469.
Shilov, V. P. (1976) *Radiokhimiya*, **18**, 659–60.
Shilov, V. P., Nikalagevsky, V. B., and Krot, N. N. (1976) in *Chemistry of Transuranium Elements* (eds. V. I. Spitsyn and J. J. Katz), Pergamon Press, New York, pp. 225–8.
Shilov, V. P., Garnov, A. Y., Krot, N. N., and Yusov, A. B. (1997) *Radiochemistry* (*Eng. Transl.*), **39**(6), 504–7.
Shilov, V. P. and Yusov, A. B. (1999) *Radiochemiya* (*Moscow*), **41**(5), 445–7.
Shirokova, I. B., Grigor'ev, M. S., Makarenkov, V. I., Den Auwer, C., Fedoseev, A. M., Budantseva, N. A., and Bessonov, A. A. (2001) *Russ. J. Coord. Chem.*, **27**, 729–30.
Shoun, R. R. and McDowell, W. J. (1980) *Actinide Separation*, ch 6.
Shoup, S. and Bamberger, C. (1997) *Radiochim. Acta*, **76**, 63–9.
Siddall, T. H. I. (1963) *J. Inorg. Nucl. Chem.*, **25**, 883–92.
Siddall, T. H. J. (1964) *J. Inorg. Nucl. Chem.*, **26**, 1991.
Silva, R. J. (1982) *Thermodynamic Properties of Chemical Species in Nuclear Waste. Topical Report*: *The Solubilities of Crystalline Neodymium and Americium Trihydroxides*, Lawrence Berkeley National Laboratory, p. 57.
Silva, R. J., Bidoglio, G., Rand, M. H., Robouch, P. B., Wanner, H., and Puigdomenech, I. (1995) *Chemical Thermodynamics of Americium,* Elsevier, New York.
Silvestre, J. P., Freundlich, A., and Pages, M. (1977) *Rev. Chim. Minér.*, **14**, 225–9.
Skobelev, N. K. (1972) *Sov. J. Nucl. Phys.* (*Engl. Transl*), **15**, 249.
Skriver, H. L., Anderson, O. K., and Johannson, B. (1980) *Phys. Rev. Lett.*, **44**, 1230–3.
Smith, J. L. and Haire, R. G. (1978) *Science*, **200**, 535–7.
Smith, G. S., Akella, J., Reichlin, R., Johnson, Q., Schock, R. N., and Schwab, M. (1981) *Actinides – 1981*, Lawrence Berkeley Laboratory.

Smith, B. F., Jarvinen, G. D., Jones, M. M., and Hay, P. J. (1989) *Solvent Extr. Ion Exch.*, **7**, 749.
Smith, L. L., Crain, J. P., Yeager, J. P., Horwitz, E. P., Diamond, H., and Chiarizia, R. (1995) *J. Radioanal. Chem.*, **15**, 194.
Soderholm, L., Skanthakamur, S., Antonio, M. R., and Conradson, S. (1996) *Z. Phys. B*, **101**, 539–45.
Soderland, P., Ahuja, R., Eriksson, O., Johannson, B., and Wills, J. M. (2000) *Phys. Rev. B*, **61**, 8119–24.
Sole, K. C., Hiskey, J. B., and Ferguson, T. L. (1993) *Solvent Extr. Ion Exch.*, **11**, 1993.
Spjuth, L., Liljenzin, J. O., Hudson, M. I., Drew, M. G. B., Iveson, P. B., and Madic, C. (2000) *Solvent Extr. Ion Exch.*, **18**, 1.
Stadler, S. and Kim, J. I. (1988) *Radiochim. Acta*, **44/45**, 39–44.
Standifer, E. M. and Nitsche, H. (1988) *Lanthanide and Actinide Res.*, **2**, 383.
Staritzky, E. and Truitt, A. L. (1954) Optical properties of some compounds of Uranium, Plutonium, and related elements, in *The Actinide Elements* (eds. G. T. Seaborg and J. J. Katz), Natl. Nucl. En. Ser., Div. IV, Vol. 14A, McGraw-Hill, New York, chapter 9.
Stary, J. (1965) *Talanta*, **13**, 421.
Stary, I. (1966) *Radiokhimiya*, **8**, 504.
Stepanov, A. V. and Makarova, T. P. (1965) *Radiokhimiya*, **7**, 670.
Stepanov, A. V., Makarova, T. P., Maksimova, A. M., and Shalinets, A. B. (1967) *Radiokhimiya*, **9**, 710.
Stepanov, A. V. (1971) *Zh. Neorg. Khim.*, **16**, 2981.
Stephanou, S. E. and Penneman, R. A. (1952) *J. Am. Chem. Soc.*, **74**, 3701–2.
Stephanou, S. E., Nigon, J. P., and Penneman, R. A. (1953) *J. Chem. Phys.*, **21**, 42–5.
Stephens, D. R., Stromberg, H. D., and Lilley, E. M. (1968) *J. Phys. Chem. Solids*, **29**, 815–21.
Stronski, I. and Rekas, M. (1973) *Radiochem. Radioanal. Lett.*, **14**, 297.
Sullivan, J. C., Hindman, J. C., and Zielen, A. J. (1961) *J. Am. Chem. Soc.*, **83**, 3373.
Sullivan, J. C., Gordon, S., Mulac, W. A., Schmidt, K. M., Cohen, D., and Sjoblom, R. (1976) *Inorg. Nucl. Chem. Lett.*, **12**, 599–601.
Sullivan, J. C., Gordon, S., Mulac, W. A., Schmidt, K. M., Cohen, D., and Sjoblom, R. (1978) *Inorg. Chem.*, **17**, 294–6.
Surls, J. P. J. and Choppin, G. R. (1957) *J. Inorg. Nucl. Chem.*, **4**, 62–73.
Swanson, J. L. (1991) Reports PNL-7716, 7734, and 7780, Pacific Northwestern Laboratory, Richland, Washington, USA.
Tabuteau, A., Pages, M., and Freundlich, W. (1972) *Radiochem. Radioanal. Lett.*, **12**, 139–44.
Tabuteau, A. and Pages, M. (1978) *J. Solid State Chem.*, **26**(2), 153–8.
Tagawa, H. (1971) *Nippon Genshiryoku Gakkaishi*, **5**, 267.
Tan, X.-F., Wang, U.-S., Tan, T.-Z., Zhou, G.-F., and Bao, B.-R. (1999) *J. Radioanal. Nucl. Chem. Art.*, **242**, 123.
Tananaev, I. G. (1990a) *Radiokhimiya*, **32**(5), 53–7.
Tananaev, I. G. (1990b) *Radiokhimiya*, **32**(4), 4–6.
Tananev, I. G. (1991) *Sov. Radiochem.*, **33**, 224–30.
Tanner, S. P. and Choppin, G. R. (1968) *Inorg. Chem.*, **7**, 2046.

Templeton, D. H. and Dauben, C. H. (1953) *J. Am. Chem. Soc.*, **75**, 4560–2.
Thouvenot, P., Hubert, S., Moulin, C., Decambox, P., and Mauchien, P. (1993) *Radiochim. Acta*, **61**, 15–21.
Tian, G. X., Zhu, Y. J., Xu, J. M., Hu, T. D., and Xie, Y. N. (2002) *J. Alloys Compd.*, **334**, 86–91.
Tikhonov, M. F., Nepomnyaskeru, V. Z., Kalinina, S. V., Khokhlov, A. D., Bulkin, V. I., and Filin, B. M. (1988) *Radiokhimiya*, **28**, 804–9.
Tomkins, F. S. and Fred, M. (1949) *J. Opt. Soc. Am.*, **39**, 357–63.
Torres, R. A. and Choppin, G. R. (1984) *Radiochim. Acta*, **35**, 143.
Trautmann, N. (1994) *J. Alloys Compd.*, **213/214**, 28–32.
Tsukada, K., Ichikawa, Y., Hatsukawa, Y., Nishinaka, I., Hata, K., Nagame, Y., Oura, Y., Ohyama, T., Sueki, K., Nakahara, H., Asai, M., Kojima, Y., Hirose, T., Yamamoto, H., and Kawade, K. (1998) *Phys. Rev. C*, **57**, 2057–60.
Uchiyama, G., Mineo, H., Hataku, S., Asakura, T., Kansi, K., Watanabe, M., Nakano, Y., Kimura, S., and Fujine, S. (2000) *Prog. Nucl. Energy*, **35**, 151–6.
UCRL (1959) Chemistry Division Semiannual Report for December 1958 Through May 1959 and Chemistry Division Semiannual Report for June Through December 1959.
Ueno, K. and Hoshi, M. (1971) *J. Inorg. Nucl. Chem.*, **33**, 1765 and 2631–3.
Valenzuela, R. W. and Brundage, R. T. (1990) *J. Chem. Phys.*, **93**, 8469–73.
Varga, L. P., Mann, J. B., Asprey, L. B., and Reisfeld, M. J. (1971) *J. Chem. Phys.*, **55**(9), 4230..
Varga, L. P., Baybarz, R. D., Reisfeld, M. J., and Asprey, L. B. (1973) *J. Inorg. Nucl. Chem.*, **35**, 2775–85.
Vladimirova, M. V., Ryabova, A. A., ulikov, I. A., and Milovanova, A. S. (1977) *Radiokhimiya*, **19**(5), 725–31.
Vladimirova, M. V. (1986) *Radiokhimiya*, **28**(5), 649–56.
Vogt, O., Mattenberger, K., Löhle, J., and Rebizant, J. (1998) *J. Alloys Compd.*, **271–273**, 508–12.
Volkov, Y. F., Kapshukov, I. I., Visyasheva, G. I., and Yokovlev, G. N. (1974) *Radiokhimiya*, **16**, 859–63, 863–7, and 868–73.
Volkov, Y. F., Visyasheva, G. I., Tomilin, S. V., Kapshukov, I. I., and Rykov, A. G. (1981) *Sov. Radiochem.*, **23**, 195.
Vorob'eva, V. V., Elesin, A. A., and Zaitsev, A. A. (1973a) *Complexing of Trivalent Americium, Curium, Californium, Promethium, and Yttrium Ions with Dioxymethylphosphinic Acid.*
Vorob'eva, V. V., Elesin, A. A., and Zaitsev, A. A. (1973b) *Complexing Trivalent Americium, Curium, Californium, and Yttrium Ions with Bis(hydroxymethyl)phosphinic Acid.*
Wall, N., Borkowski, M., Chen, J., and Choppin, G. (2002) *Radiochim. Acta*, **90**(9–11), 563–8.
Wapstra, A. H. and Gove, N. B. (1971) *Nucl. Data Tables*, **9**, 265–468.
Ward, J. W., Müller, W., and Kramer, G. F. (1975), in *Transplutonium Elements, Proc. 4th Int. Symp.*, Baden-Baden, Sept. 13–17, (eds. W. Müller and R. Lindner), Elsevier, North-Holland/Amer. Elsevier, p. 161–71.
Ward, J. W. and Hill, H. H. (1976) *Heavy Elements Properties,* North-Holland, Amsterdam.

Weaver, B. and Kappelmann, F. A. (1964) *Talspeak: A New Method of Separating Americium and Curium from the Lanthanides by Extraction from and Aqueous Solution of an Aminopolyacetic Acid Complex with a Monoacidic Organophosphate or Phosphonate*, Oak Ridge National Laboratory.

Weaver, B. and Shoun, R. R. (1971) in *Proc. 9th Rare Earth Research Conf.*, p. 322.

Weaver, B. (1974) in *Ion Exchange and Solvent Extraction,* (eds. J. A. Marinsky and Y. Marcus), A Series of Advances, vol. 6 , Marcel Dekker, New York.

Wei, Y. Z., Kumagai, M., Takashima, Y., Modolo, G., and Odoj, R. (2000a) *Nucl. Tech.*, **132**, 413–23.

Wei, Y. Z., Sabharwal, K. N., Kumagi, M., Asakara, T., Uchiyama, G., and Fujine, S. (2000b) *J. Nucl. Sci. Technol.*, **37**, 1108–10.

Weifan, Y., Junsheng, G., Wantong, M., Keming, F., Zaiguo, G., Hongye, L., Lijun, S., Shuifa, S., Shuanggui, Y., Shuhong, W., Denming, K., and Jimin, Q. (1999) *J. Radioanal. Nucl. Chem.*, **240**, 379–81.

Weigel, F., Ollendorff, W., Scherer, V., and Hagenbruch, R. (1966) *Z. Anorg. Allg. Chem.*, **345**, 119–28.

Weigel, F. and Meer, ter N. (1967) *Inorg. Nucl. Chem. Lett.*, **3**, 403–8.

Weigel, F. and Meer, ter N. (1971) *Z. Naturf. B*, **26**, 504–12.

Weigel, F., Wishnevsky, V., and Hauske, H. (1975), in *Transplutonium Elements, Proc. 4th Int. Symp.*, Baden-Baden, Sept. 13–17, (eds. W. Müller and R. Lindner), Elsevier, North-Holland/Amer., p. 217–26.

Weigel, F., Wittmann, F. D., and Marquart, R. (1977) *J. Less Common Metals*, **56**, 47–53.

Weigel, F., Wishnevsky, V., and Wolf, M. (1979) *J. Less Common Metals*, **63**, 81–6.

Weigel, F., Wittmann, F. D., Schuster, W., and Marquart, R. (1984) *J. Less Common Metals*, **102**(2), 227–38.

Werner, L. B. and Perlman, I. (1950) *J. Am. Chem. Soc.*, **73**, 495–6.

Wheelwright, E. J., Roberts, F. P., and Bray, L. A. (1968) *Simultaneous Recovery and Purification of Pm, Am, and Cm by the Use of Alternating DTPA and NTA Cation-Exchange Flowsheets*, Pacific Northwest Laboratories.

Williams, C. W., Antonio, M. R., and Soderholm, L. (2000) *J. Alloys Compd.*, **303/304**, 509–13.

Wittmann, F. D. (1980) University of Munich.

Woods, M., Cain, A., and Sullivan, J. C. (1974) *J. Inorg. Nucl. Chem.*, **36**, 2605–7.

Woods, M. and Sullivan, J. C. (1974) *Inorg. Chem.*, **13**, 2774–5.

Woods, M., Montag, T. A., and Sullivan, J. C. (1976) *J. Inorg. Nucl. Chem.*, **38**, 2059–61.

Wruck, D. A., Palmer, C. E. A., and Silva, R. J. (1999) *Radiochim. Acta*, **85**, 21–4.

Yaita, T., Tachimori, S., Edelstein, N. M., Bucher, J. J., Rao, L., Shuh, D. K., and Allen, P. G. (2001) *J. Synchrotron Radiation*, **8**, 663–5.

Yakovlev, G. N. and Gorbenko- Germanov, D. S. (1955) in *Proc. Int. Conf. on the Peaceful Uses of Atomic Energy*, pp. 306–8.

Yakovlev, G. N., Gorbenko- Germanov, D. S., Zenkova, R. A., Razbitnoi, V. L., and Kazanski, K. S. (1958) *J. Gen. Chem. USSR*, **28**(2653).

Yakovlev, G. N. and Kosyakov, V. N. (1958a) *An Investigation of the Chemistry of Americium*, *Proc. 2nd Int. Conf. on the Peaceful Uses of Atomic Energy*, pp. 373–84.

Yakovlev, G. N. and Kosyakov, V. N. (1958b) *Spectrophotometric Studies of the Behaviour of Americium Ions in Solutions*, *Proc. 2nd Int. Conf. on the Peaceful Uses of Atomic Energy*, pp. 363–8.
Yamagishi, I., Morita, Y., and Kubota, M. (1996) *Radiochim. Acta*, **75**, 27–32.
Yamamoto, M. and Sakanoue, M. (1982) *J. Radiat. Res.*, **23**, 261.
Yamana, H. and Moriyama, H. (1996) *J. Nucl. Sci. Technol.*, **33**, 288–97.
Yanir, E., Givon, M., and Marcus, Y. (1959) *Inorg. Nucl. Chem. Lett.*, **6**, 415–9.
Yanir, E., Givon, M., and Marcus, Y. (1969) *Inorg. Nucl. Chem. Lett.*, **5**, 369–72.
Yusov, A. B. (1989) Photoluminescence of americium(III) in aqueous and organic solutions, in *Actinides '89*, p. 240 and pp. 241–2.
Yusov, A. B. (1993) *Radiochem. Radioanal. Lett.*, **35**, 1–14.
Zachariasen, W. H. (1948a) *Phys. Rev. B*, **73**, 1104–5.
Zachariasen, W. H. (1948b) *Acta Crystallogr.*, **1**, 265–9.
Zachariasen, W. H. (1949a) *Acta Crystallogr.*, **2**, 288–91.
Zachariasen, W. H. (1949b) *Acta Crystallogr.*, **2**, 388–90.
Zachariasen, W. H. (1949c) *Phys. Rev.*, **73**, 1104.
Zachariasen, W. H. (1949d) *Acta Crystallogr.*, **2**, 57–60.
Zachariasen, W. H. (1954) in *The Actinide Elements* (eds. G. T. Seaborg, L. R. Morss and J. J. Katz), McGraw-Hill, New York, pp. 769–95.
Zachariasen, W. H. (1978) *J. Less Common Metals*, **62**, 1–7.
Zaitsev, A. A., Kosyakov, V. N., Rykov, A. G., Sobolev, Y. B., and Yakovlev, G. N. (1960a) *Radiokhimiya*, **2**(3), 348–50.
Zaitsev, A. A., kosyakov, V. N., Rykov, A. G., Sobolov, Y. P., and Yakovlev, G. N. (1960b) *Sov. At. Energy*, **7**, 562–9.
Zemlyanukhin, V. I., Savoskina, G. P., and Pushlenkov, M. F. (1962) *Sov. Radiochem.*, **4**, 501–5.
Zhu, Y. (1995) *Radiochim. Acta*, **68**, 1995.
Zhu, Y., Chen, J., and Choppin, G. R. (1996a) *Solvent Extr. Ion Exch.*, **14**, 543.
Zhu, Y., Chen, J., and Jiao, R. (1996b) *Solvent Extr. Ion Exch.*, **14**, 61.
Zhu, Y. and Jiao, R. (1994) *Nucl. Technol.*, **108**, 361–9.
Zhu, Y., Xu, J., Chen, J., and Chen, Y. (1998) *J. Alloys Compd.*, **742**, 271–3.
Zubarev, V. G. and Krot, N. N. (1982) *Sov. Radiochem.* (*Engl. Transl.*), **24**, 264–7.
Zubarev, V. G. and Krot, N. N. (1983a) *Sov. Radiochem.*, **25**, 601.
Zubarev, V. G. and Krot, N. N. (1983b) *Sov. Radiochem.*, **25**, 594.
Zur Nedden, P. (1969) *Z. Anal. Chem.*, **247**, 236.

SUBJECT INDEX

Vol. 1: 1–698, Vol. 2: 699–1395, Vol. 3: 1397–2111, Vol. 4: 2113–2798, Vol. 5: 2799–3440.

Page numbers suffixed by t and f refer to Tables and Figures respectively.

AUTHOR INDEX

Vol. 1: 1–698, Vol. 2: 699–1395, Vol. 3: 1397–2111, Vol. 4: 2113–2798, Vol. 5: 2799–3440.

Page numbers suffixed by t and f refer to Tables and Figures respectively.

CHAPTER NINE

CURIUM

Gregg J. Lumetta, Major C. Thompson, Robert A. Penneman, and P. Gary Eller

9.1 HISTORICAL

Curium, element 96, is named after Pierre and Marie Curie, by analogy with its lanthanide congener, gadolinium (named after the Finnish chemist, J. Gadolin). Curium is not a naturally occurring terrestrial element.

The first curium isotope, ^{242}Cm, was prepared by Seaborg, James, and Ghiorso in mid-1944 by cyclotron helium ion (He^{2+}) bombardment of ^{239}Pu, and was identified by its characteristic alpha radiation (Seaborg *et al.*, 1949). The discovery of curium preceded that of americium (element 95). G. T. Seaborg described this discovery in a fascinating historical account (Seaborg, 1985). Werner and Perlman (1951) separated the first weighable quantity of curium (40 μg of impure ^{242}Cm oxide), which was prepared by prolonged neutron irradiation of ^{241}Am.

Curium is the element of highest atomic number that is available on the gram scale. However, chemical studies are typically done on the milligram scale using glove boxes, although microchemical techniques were originally used (Seaborg, 1972; Stevenson and Peterson, 1975). Larger scale work usually requires remote handling. Because of the limited availability of long-lived isotopes (especially ^{248}Cm), the high radioactivity of its most common isotopes (^{242}Cm and ^{244}Cm), and its general occurrence in aqueous systems as a 3+ ion, considerably less physical and chemical information about curium is available than for americium. Excellent reviews have been published on various aspects of

curium chemistry (Katz and Seaborg, 1957; Brown, 1968; Keller, 1971; Bagnall, 1972; Gmelin, 1972–74; Penneman *et al*., 1973; Edelstein *et al*., 1985; Navratil and Schulz, 1993).

This chapter provides an overview of curium chemistry, with emphasis on advances since the publication of the 1986 version of this chapter (Eller and Penneman, 1986). The technical literature indicates that chemical investigations during this period have focused on the following general areas:

- Separations chemistry related to high-level waste management: This topic is addressed in Section 9.5.
- High-temperature superconductivity studies of curium compounds: Soderholm (1992) has provided an excellent review in this area. Additional discussion can be found in Section 9.7 and in Chapter 20.
- Behavior of curium in the environment: This topic is addressed in Chapter 27.
- Use of curium isotopes as targets to prepare superheavy elements: Hoffman (1985) and Lobanov *et al*. (1997) provide examples. This subject is discussed in Chapter 14.
- Use of curium isotopes in analytical space applications: Radchenko *et al*. (1999, 2000), Abramychev *et al*. (1992), and Vesnovskii *et al*. (1996) provide illustrative examples of this type of work applied to alpha spectrometry analysis of extraterrestrial rocks and soils.
- Transmutation in reactors and accelerators: Artisyuk *et al*. (1999), Gerasimov *et al*. (2000), and Raison and Haire (2001) describe this topic.

9.2 NUCLEAR PROPERTIES

Properties of the known curium isotopes, which range in mass from 238 to 251, are summarized in Table 9.1. Additional information is available in the appendix. Electron binding energies, radiation energies, X-ray spectra, and L-shell fluorescence data are available, as well as both alpha and spontaneous fission data (see Chu, 1972; Kerrigan and Banick, 1975; Lederer and Shirley, 1978; Lougheed *et al*., 1978; Holden, 1989). Three isotopes (^{242}Cm, ^{244}Cm, and ^{248}Cm) are available in quantities sufficient for chemical study. Macroscopic studies with ^{242}Cm and ^{244}Cm are complicated by the high specific alpha activities of these isotopes (half-lives of 163 days and 18.1 years, respectively). The practical limit for chemical operations with ^{248}Cm in glove boxes is 10–20 mg because of the significant neutron exposure hazard from the 8% spontaneous fission yield of this isotope.

Both ^{242}Cm and ^{244}Cm have been used in power sources (thermal and electrical) for space and medical applications (Groh *et al*., 1965; Abramychev *et al*., 1992; Vesnovskii *et al*., 1996). The isotope ^{242}Cm has a specific heat output (122 W g^{-1}) about 43 times higher than that of ^{244}Cm (2.8 W g^{-1}),

Table 9.1 *Nuclear properties of curium isotopes.*

Mass number	*Half-life*	*Mode of decay*	*Main radiations* (MeV)	*Method of production*
237	–	EC, α	α 6.660	^{237}Np(^{6}Li,6n)
238	2.3 h	EC < 90%	α 6.52	^{239}Pu(α,5n)
		α > 10%		
239	2.9 h	EC	γ 0.188	^{239}Pu(α,4n)
240	27 d	α	α 6.291 (71%)	^{239}Pu(α,3n)
	1.9×10^6 yr	SF	6.248 (29%)	
241	32.8 d	EC 99.0%	α 5.939 (69%)	^{239}Pu(α,2n)
		α 1.0%	5.929 (18%)	
			γ 0.472 (71%)	
242	162.8 d	α	α 6.113 (74.0%)	^{239}Pu(α,n)
	7.0×10^6 yr	SF	6.070 (26.0%)	^{242}Am daughter
243	29.1 yr	α 99.76%	α 5.785 (73.5%)	^{242}Cm(n,γ)
		EC 0.24%	5.741 (10.6%)	
			γ 0.278 (14.0%)	
244	18.10 yr	α	α 5.805 (76.7%)	multiple n capture
	1.35×10^7 yr	SF	5.764 (23.3%)	^{244}Am daughter
245	8.5×10^3 yr	α	α 5.362 (93.2%)	multiple n capture
			5.304 (5.0%)	
			γ 0.175	
246	4.76×10^3 yr	α	α 5.386 (79%)	multiple n capture
	1.80×10^7 yr	SF	5.343 (21%)	
		β stable		
247	1.56×10^7 yr	α	α 5.266 (14%)	multiple n capture
			4.869 (71%)	
			γ 0.402 (72%)	
248	3.48×10^5 yr	α 91.61%	α 5.078 (82%)	multiple n capture
		SF 8.39%	5.034 (18%)	
249	64.15 min	β^-	β^- 0.9	^{248}Cm(n,γ)
			γ 0.634 (1.5%)	
250	$\sim 8.3 \times 10^3$ yr	SF		multiple n capture
251	16.8 min	β^-	β^- 1.42	^{250}Cm(n,γ)
			γ 0.543 (12%)	

This table is reproduced directly from the compilations in Appendix II of this volume by I. Ahmad.

and a cake of $^{242}Cm_2O_3$ weighing a few grams can be photographed using its own incandescence for illumination. These isotopes provide convenient energy sources for short-period/high-output and long-period/moderate-output applications. However, because of its greater availability and high-energy density, ^{238}Pu has supplanted both ^{242}Cm and ^{244}Cm for many such uses. The isotope ^{248}Cm has been a favored nuclide for accelerator studies attempting to form superheavy elements (Hoffman, 1985; Lobanov *et al.*, 1997).

9.3 PRODUCTION

Intense neutron exposure of ^{242}Pu and ^{243}Am in nuclear reactors forms significant quantities of the isotopes ^{244}Cm, ^{246}Cm, and ^{248}Cm, with lesser amounts of the odd-mass isotopes, ^{245}Cm and ^{247}Cm. Most curium isotopes heavier than ^{244}Cm have longer half-lives, but cannot be prepared isotopically pure by neutron capture. Except for ^{248}Cm, which is available as an essentially pure isotope from the decay of ^{252}Cf, curium isotope enrichment is accomplished in mass separators. The isotope ^{248}Cm is particularly desirable for chemical studies because of its long half-life (3.48×10^5 years). Approximately 100 mg of ^{248}Cm was produced in the 1970s and 1980s in the United States by purification from parent ^{252}Cf.

By far, the greatest quantity of curium exists as the isotope ^{244}Cm, which has been produced on the several kilogram scale at the Savannah River Site (Groh *et al.*, 1965; Baybarz, 1970; Gmelin, 1972–74). This isotope is produced by successive neutron capture starting with ^{239}Pu, ^{242}Pu, or ^{243}Am:

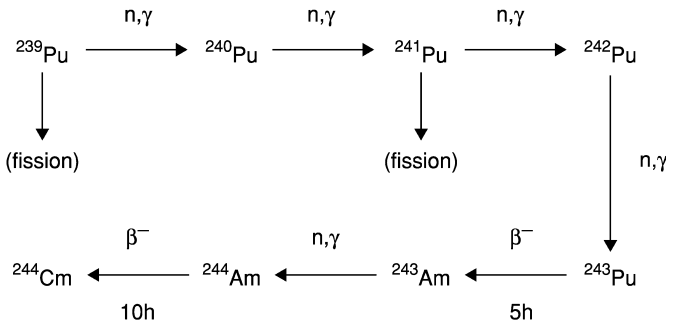

For 20 years following the discovery of curium, only milligram amounts of curium were available from the irradiation of ^{241}Am. It was not until Glenn T. Seaborg became Chairman of the US Atomic Energy Commission that a large-scale national program was instituted. Kilograms of ^{239}Pu were transferred from the weapons program for irradiation at Savannah River Site. This 'expenditure' of plutonium required a Presidential Directive. The authors note that, especially in 1960, this transfer from programmatic use was extraordinary and stands in striking contrast to current views regarding the disposition of many

tons of excess weapons-grade plutonium. The aim of the irradiation campaign was to produce major amounts of the higher-mass isotopes of plutonium and elements of higher atomic number for research. The demand for large quantities of higher isotopes has diminished, resulting in the disposal of 2–3 kg of Cm from the Savannah River Site in 2002 (Peters *et al.*, 2002).

Initially, 8.5, then 12.0 kg for a total of 20.5 kg of ^{239}Pu, was staged in a Savannah River reactor. This approach was necessary to remove the immense heat produced (3×10^6 Btu h^{-1} ft^{-2}) from ^{239}Pu and ^{241}Pu fission. The yield from 20.5 kg of initial ^{239}Pu was 930 g of ^{242}Pu and 630 g of ^{243}Am and ^{244}Cm combined (Penneman and Ferguson, 1971). The mixture was sent for separation to the Oak Ridge National Laboratory (ORNL), where the high-mass plutonium was fabricated into cermet targets for the High Flux Isotope Reactor (HFIR). A neutron flux of 5×10^{15} neutrons cm^{-2} s^{-1} was used for the specific purpose of creating higher-mass/higher-atomic-number isotopes. The plutonium feed composition was initially ^{238}Pu (0.43%), ^{239}Pu (1.12%), ^{240}Pu (1.8%), ^{241}Pu (0.91%), and ^{242}Pu (95.7%) (Bigelow, 2002).

At the height of production, about 1 g of ^{252}Cf was produced per year. Its short alpha decay half-life (2.6 years) yields ^{248}Cm. Production of ^{252}Cf has diminished, but continues because it is desirable for neutron irradiation in health applications. Its decay currently yields 35–50 mg of ^{248}Cm annually (Knauer, 2002).

The relatively stable isotope ^{248}Cm can be obtained in multi-milligram quantities by milking aged, prepurified ^{252}Cf materials that have undergone alpha decay. This method routinely yields milligram amounts of ^{248}Cm with an isotopic purity of 97%. Even so, 99.9% of the alpha activity arises from ^{244}Cm and ^{246}Cm impurities.

$$^{252}\mathrm{Cf} \xrightarrow[2.6\ \mathrm{y}]{\alpha} {}^{248}\mathrm{Cm}$$

Small (microgram) amounts of ^{245}Cm have been separated from alpha decay products of ^{249}Cf, itself a daughter of ^{249}Bk.

To isolate ^{244}Cm, irradiated material is dissolved in nitric acid and tetravalent plutonium is removed by solvent extraction (Groh *et al.*, 1965; Baybarz, 1970). The trivalent species (americium, curium, and the lanthanides) remaining in the aqueous phase are then extracted with 50% tributyl phosphate (TBP) in kerosene, and then back-extracted into dilute acid. For purification from lanthanides, Am/Cm chlorides are extracted with tertiary amines from slightly acidic 11 M LiCl (Tramex process), and then back-extracted into aqueous 7 M HCl. Subsequent precipitation of Am(V) as the potassium double carbonate effectively separates americium, leaving soluble Cm(III) in the K_2CO_3 medium.

The isotope ^{242}Cm is best obtained by neutron irradiation of ^{241}Am at an intermediate flux level. High neutron fluxes diminish the yield of ^{242}Cm because of the increased fission of ^{242}Am:

$$^{241}\mathrm{Am} \xrightarrow{\mathrm{n},\gamma} {}^{242}\mathrm{Am} \xrightarrow[16\ \mathrm{h}]{\beta^-} {}^{242}\mathrm{Cm}$$

Following irradiation of AmO_2/Al cermet targets, hot NaOH is used to dissolve the aluminum. Dissolution in HCl also can be used, in which case Al^{3+} must be removed before further processing. For small-scale separations, the Am/Cm/lanthanide fraction is dissolved in HCl; the solution is then made 11 M in LiCl, and passed through an anion-exchange column. Under these conditions, trivalent actinides (but not rare earth elements) are retained on the column. Alternatively, a tertiary amine extractant can be substituted for the anion-exchange resin to provide a group separation between actinides (extracted) and lanthanides (Baybarz, 1970). A subsequent americium/curium separation step is then required. A combination of anion and cation exchange was used successfully to separate about 1 g of ^{242}Cm from neutron-irradiated ^{241}Am (Thompson, 1972).

Numerous other techniques, including high-pressure ion exchange, extraction chromatography, and di(2-ethylhexyl)phosphoric acid (HDEHP) extraction also have been used for Cm separation and purification (Dedov *et al.*, 1965; Baybarz, 1970; Gmelin, 1972–74; Thompson, 1972; Buijs *et al.*, 1973; Haug, 1974; Lebedev *et al.*, 1974; Bigelow *et al.*, 1980; Bond and Leuze, 1980). Pressurized displacement ion-exchange chromatography has been applied to large-scale ^{244}Cm/^{243}Am separation and purification using Dowex® 50 resin in the Zn^{2+} form and diethylenetriaminepentaacetic acid (DTPA) as eluant (Stephanou and Penneman, 1952). Where sufficient quantities of Cm are present to give a substantial band, a pure curium cut can be obtained, since it leads the americium band.

9.4 ATOMIC PROPERTIES

Selected properties of curium-free atoms and ions are summarized in Table 9.2. A set of recommended thermodynamic parameters is available in the recent publication of Konings (2001b). Thermodynamic properties of actinides are addressed in Chapter 19.

The great stability of the $5f^7$ configuration of Cm(III) and its lanthanide congener Gd(III) is shown by the large M(III)–(IV) oxidation potentials (see Section 9.7.1). In contrast, it is noteworthy that the tendency of americium to attain the $5f^7$ configuration by assuming a divalent state is much weaker than that displayed by europium. Isolated Cm(II) compounds are unknown and a value of –2.78 V has been estimated for the Cm(III)/Cm(II) redox potential (Mikheev *et al.*, 1992).

The spectra of the Cm(III) aquo ion and of a metastable Cm(IV) aqueous fluoride solution complex ion are shown in Figs. 9.1 and 9.2, respectively. In contrast to solutions of Gd(III) (Moeller and Moss, 1951), aqueous solutions of

Table 9.2 *Selected properties and references of curium ions and metal.*

Property	*Value*	*Reference*	*Comment*
Cm(0) electronic configuration	$5f^7ds^2$ ($^9D_2$)	Keller (1971, p. 79)	
Cm(III) electronic configuration	$5f^7$	Katz and Seaborg (1957, Chapter 5)	
Metallic radius	1.743 Å	Reichlin *et al.* (1981); Zachariasen (1973)	dhcp form
Cm(III) ionic radius	0.97 Å	Shannon (1976)	six coordination
Cm(IV) ionic radius	0.85 Å	Shannon (1976)	six coordination
first ionization potential	5.99 eV	Deissenberger *et al.* (1995)	
Cm(0)–Cm(III) potential	−2.06 V	Fuger *et al.* (1975)	
Cm(II)–Cm(III) potential	−2.8 V	Mikheev (1983)	
Cm(III)–(IV) potential	−3.1 V	Keller (1971, p. 212)	1 M $HClO_4$
metal cell constants	dhcp, $a = 3.496(3)$ Å, $c = 11.331(5)$ Å; fcc, $a = 5.039$ (2) Å	Reichlin *et al.* (1981); Stevenson and Peterson (1979); Baybarz *et al.* (1976)	
melting point	1345 ± 50°C	Oetting *et al.* (1976); Fuger and Oetting (1976)	
boiling point	3110°C (calcd.)	Ward *et al.* (1975)	
ΔH_{fus}	13.85 kJ mol^{-1}	Ward *et al.* (1975)	
gaseous entropy	47.2 J K^{-1} mol	Edelstein *et al.* (1985, p. 139)	
density	13.5 g cm^{-3}	Reichlin *et al.* (1981)	dhcp form
magnetic moment	8.07 μ_B	Reichlin *et al.* (1981); Kanellakopulos *et al.* (1976)	100–550°K

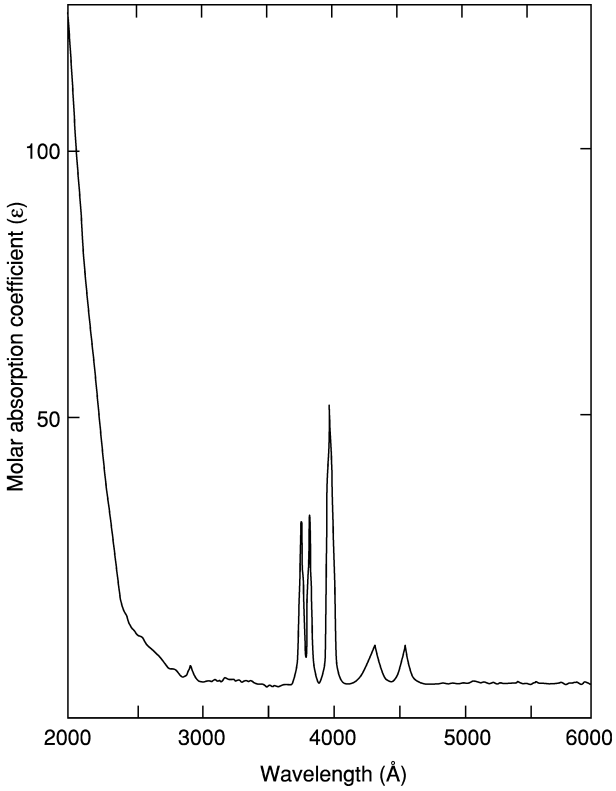

Fig. 9.1 *The absorption spectrum of Cm(III) in* 0.04 N $HClO_4$ (*aq*). (*Adapted from Carnall* et al., 1958.)

Cm(III) have weak absorption bands in the near-violet region, although intense absorptions are present in the ultraviolet region (Asprey and Keenan, 1958; Keenan, 1961; Barbanel *et al*., 1977). The absorption spectra of metastable Cm(IV) was measured at Los Alamos by dissolving CmF_4 prepared by fluorination of dry CmF_3, and that of Cm(III) was measured at both Los Alamos and Argonne using curium solutions carefully purified from rare earths and americium. The principal peaks of Cm(IV) strongly resemble those of Am(III), with which it is isoelectronic (Carnall *et al*., 1958).

Electronic transitions for Cm(III) solutions are shifted 20–30 Å to longer wavelengths compared to the solid state. The addition of complexing ions normally produces a diminution of intensities, and small changes in band positions. The transition energies for CmF_3 are considerably lower than those of GdF_3, due to smaller electrostatic repulsion terms and larger spin–orbit coupling in Cm(III). The spectra in both cases may be interpreted in terms of a $5f^7$ ground-state configuration. The spectrum of $Cs_2NaCmCl_6$, which

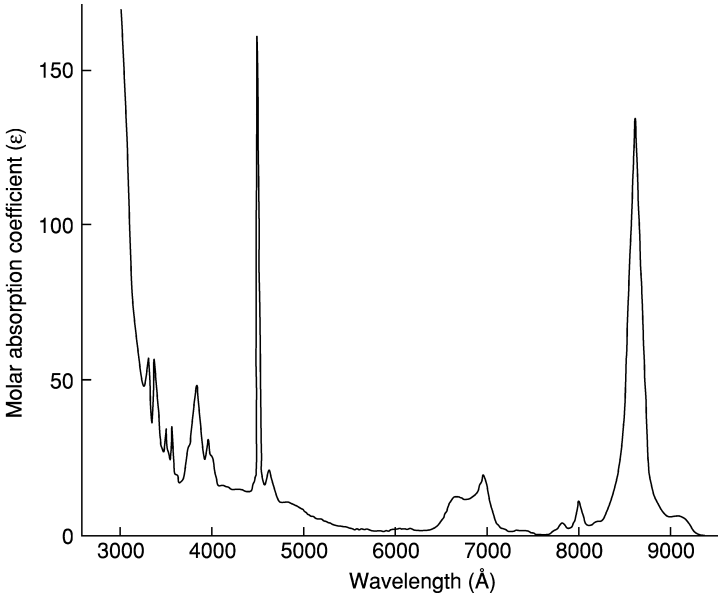

Fig. 9.2 *The absorption spectrum of Cm(IV) in* 15 M *CsF* (*aq*). (*Adapted from Keenan*, 1961.)

contains octahedrally coordinated Cm(III), was reported for both the solid and molten phases (Barbanel *et al.*, 1977). The most notable spectral effect is a sharp diminution in intensity compared to that of aqueous Cm(III) because of the highly symmetric curium coordination, which precludes observation of symmetry-forbidden f–f electronic transitions.

Time-resolved laser-induced fluorescence spectroscopy has been shown to be an especially valuable tool for determining curium concentration and speciation (Elesin *et al.*, 1973; Dem'yanova *et al.*, 1986; Yusov *et al.*, 1986b; Decambox *et al.*, 1989; Kim *et al.*, 1991; Myasoedov and Lebedev, 1991; Myasoedov, 1994; Moulin *et al.*, 1997; Dacheux and Aupais, 1998). Curium solutions have the unique property of strongly fluorescing in the range of 595–613 nm when irradiated with a laser or a mercury-discharge lamp (Myasoedov and Lebedev, 1991; Myasoedov, 1994). The broad unresolved fluorescence emission band is attributed to relaxation from the $^6D_{7/2}$ (*A*) state to the $^8S_{7/2}$ (*Z*) ground state (Kim *et al.*, 1991).

The energy of the emission band is dependent on the ligands attached to the curium ion. Taking advantage of this feature, time-resolved laser-induced fluorescence spectroscopy has been used extensively since the mid-1980s to investigate the fundamental solution chemistry of Cm (see Section 9.8). The method has been used to determine the hydration number for curium in solution (Kimura *et al.*, 1996) and complexation constants for a number of ligands. Furthermore,

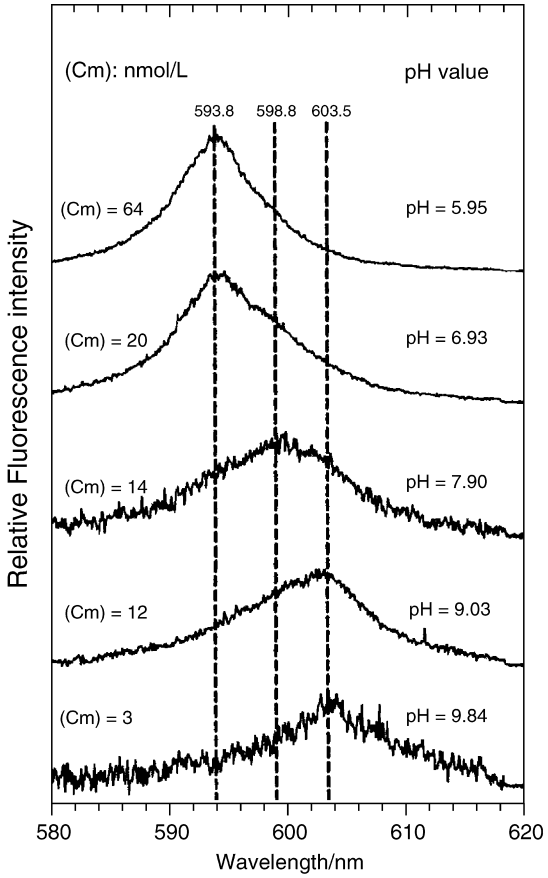

Fig. 9.3 *Curium*(III) *fluorescence emission spectra taken in the course of hydrolysis reaction in the pH range of* 5.05–9.84. *Used with permission from Wimmer* et al. (1992).

time-resolved laser-induced fluorescence spectroscopy has been used to characterize the Cm species present in groundwater taken from sites being considered for disposition of nuclear wastes (Wimmer *et al.*, 1992). Fig. 9.3 displays examples of fluorescence spectra for aqueous Cm species (Wimmer *et al.*, 1992). The examples presented are for Cm(III) as a function of pH and indicate the successive conversion of Cm(III) ion to $[Cm(OH)]^{2+}$ and $[Cm(OH)_2]^{+}$ (see Section 9.8 for a more detailed discussion of this topic).

For more thorough discussions of actinide ion absorption and luminescence spectra, see the sections on this subject by Carnall and Crosswhite (Gmelin, 1972–74). Chapter 18 of this work covers additional recent spectroscopic studies, including high-resolution spectra.

9.5 SEPARATION AND PURIFICATION OF PRINCIPAL ISOTOPES

The chemistry of curium in separation and purification is similar to that of other trivalent actinides and lanthanides and involves a series of steps, the number depending on the source of the curium. For example, separation of curium from irradiated uranium or plutonium materials requires more steps than separation of ^{248}Cm from decay of ^{252}Cf. Section 9.3 covers separation of curium from irradiated fuels and targets. This section covers separation and purification from high-level waste and other solutions, which has received more emphasis in recent years. In addition, Section 9.9 contains references to separations done for analysis of curium. Some of the analytical separations are also applicable to separation and purification.

9.5.1 Solvent extraction

Myasoedov and Kremliakova (1985) reviewed Russian literature up to the mid–1980s on americium and curium chemistry, including separations. A subsequent review has updated the work up to 1994 (Myasoedov, 1994). A recent book on separations for nuclear waste management contains reviews of work in the United States, France, and Russia (Choppin, 1999; Jarvinen, 1999; Musikas, 1999).

Extractions with organic phosphates (e.g. TBP, phosphine oxides, dialkylphosphoric acids, high-molecular-weight amines, β-diketones, and combinations of these) have been studied. Extraction by alkylphosphates depends on the structure and nature of the alkyl groups (Myasoedov, 1994; Zhu and Jiao, 1994). For example, mixed alkylphosphates with alkyl chains of six to eight carbons in length are reported to have properties superior to TBP (Zhu and Jiao, 1994). Extraction also depends on the salting agent present in solution. HDEHP has been widely studied for americium and curium extractions from both HNO_3 and LiCl solutions (Myasoedov and Kremliakova, 1985; Choppin, 1999). The latter solution has been used to separate the actinides from the lanthanides. Trioctylamine has been used to separate americium and curium from the lanthanides, with the salting agent and the diluent being important factors for extraction of curium, but not the lanthanides (Myasoedov and Kremliakova, 1985; Choppin, 1999). Russian researchers have studied the β-diketone, 1-phenyl-3-methyl-4-benzoyl-pyrazol-5-one, extensively (Myasoedov and Kremliakova, 1985). More recently, studies have been done with 1-phenyl-3-methyl-4-acylpyrazol-5-one in which the length of the carbon chain for the acyl group was varied from 2 to 22 (Takeishi *et al.*, 2001). A flowsheet was demonstrated with an acyl chain length of 8, which resulted in separate uranium, plutonium, and transplutonium fractions. All actinides were extracted from a 1 M HNO_3 solution and sequentially stripped by adjusting the pH with NaOH (Takeishi *et al.*, 2001).

Extensive studies have been done using bifunctional extractants, especially compounds such as octyl(phenyl)-*N*,*N*-diisobutyl carbamoylmethylphosphine

oxide (CMPO) to recover transuranium elements, including curium, from high-level waste solutions (Horwitz and Schulz, 1991; Ozawa *et al*., 1992; Myasoedov, 1994; Felker and Benker, 1995; Choppin, 1999; Musikas, 1999). This class of extractants can extract all the actinides from acid solutions, with separation of uranium, plutonium, and trivalent cations, by using selective stripping solutions. The separation results in a product with both the trivalent lanthanides and the actinides in the same solution, which requires further processing to isolate a pure curium stream.

French researchers have done extensive work on diamides for the extraction of trivalent actinides and lanthanides from plutonium and uranium recovery by extraction (Purex) waste solutions (Musikas, 1999). These bifunctional ligands are stronger extractants than monofunctional ligands and can be destroyed thermally without leaving a solid residue (phosphorus-containing ligands leave a solid residue when incinerated). They have also investigated nitrogen donor ligands for separation of actinides from lanthanides. The neutral tridentate ligand 2,4,6-tris-(2-pyridyl)-1,3,5-triazine has promise, but requires an additive to increase nitrate ion solubility in the organic phase (Musikas, 1999).

The largest separation factors for actinides and lanthanides have been shown with ligands containing sulfur, a 'soft' donor that forms stronger covalent bonds with the actinides than with lanthanides (Jarvinen, 1999; Musikas, 1999). Thio derivatives of acylpyrazolones containing both nitrogen and sulfur donor atoms are good extractants, but give best separation when combined with TBP or a phosphine oxide (Jarvinen, 1999). Dithiophosphoric or phosphinic acids have shown the highest separation factors for actinides and lanthanides (Jarvinen, 1999; Musikas, 1999).

Separation of actinides has also been done with salt mixtures and polyethylene glycol (Myasoedov and Kremliakova, 1985; Myasoedov, 1994). Cm(III) has been extracted from sulfate, carbonate, phosphate, and nitrate solutions. Extraction requires addition of complexants to the salt solutions, with arsenazo-III and xylenol orange being the most effective solution (Molochnikova *et al*., 1992). Potassium phosphotungstate in salt solution aids in the separation of neptunium from trivalent actinides (Myasoedov, 1994).

Recovery of curium from carbonate and hydroxide solutions has been demonstrated with quaternary ammonium bases, primary amines, alkylpyrocatechols, β-diketones, and *N*-alkyl derivatives of amino-alcohols or phenols (Myasoedov and Kremliakova, 1985; Bukina *et al*., 1988; Karalova *et al*., 1988; Novikov *et al*., 1988; Myasoedov, 1994). This method requires the addition of a complexant to the aqueous phase to maintain the solubility of the actinides in the solutions. The strength of the complexant must differ depending on the mechanism for extraction. Some extractants form ion pairs in the organic phase, while others extract the complexes. In the case of alkylpyrocatechols, the kinetics of extraction of lanthanides and actinides are significantly different, allowing group separation (Novikov *et al*., 1988).

Am(III) and Cm(III) have also been separated using supported liquid membranes with 1 M HDEHP in hexane (Novikov and Myasoedov, 1987). The separation factor between Am and Cm was increased from 1.1 for simple extraction to 5.0 with the membrane in which potassium phosphotungstate is added to one solution to increase the chemical potential of the membrane and speed the kinetics of the process (Novikov and Myasoedov, 1987).

9.5.2 Ion exchange

Ion exchange in almost all forms has been used for curium separation from americium and the lanthanides. Organic cation and anion resins, chelating resins, chromatographic columns, and inorganic sorbents have been used (Ryan, 1975; Myasoedov and Kremliakova, 1985; Bokelund *et al.*, 1989; Choppin, 1999).

A review in 1975 summarizes the work on ion exchange, with sections on cation, anion, and chelating resins as well as inorganic sorbents (Ryan, 1975). The trivalent actinides and lanthanides are strongly adsorbed from low concentrations of common monovalent acid solutions. Separation of lanthanides from actinides is accomplished by elution with a variety of organic complexants, such as α-hydroxyisobutyric acid, ethylenediaminetetracetic acid (EDTA), or DTPA. Such complexants can also be used to separate trivalent actinides from each other (Lebedev *et al.*, 1974; Ryan, 1975; Myasoedov and Kremliakova, 1985; Bokelund *et al.*, 1989). Extraction chromatography with Zn^{2+} and DTPA was used for separation of kilograms of curium from americium (Haug, 1974). Thiocyanate solutions are also useful in accomplishing similar separations.

Anion-exchange resins have been used with HCl, LiCl, and HNO_3 in both aqueous and aqueous–alcohol mixtures (Ryan, 1975; Myasoedov and Kremliakova, 1985; Bokelund *et al.*, 1989; Choppin, 1999). Solutions of LiCl have been used extensively (Ryan, 1975; Choppin, 1999). A time-resolved laser-induced fluorescence spectroscopic study of a $LiCl/H_2O/CH_3OH$ anion-exchange system suggested the primary Cm species in the solution phase (at 14 M LiCl) is $CmCl_4^-$, but the number of coordinated chloride ions is greater than 4 for the species sorbed to the anion-exchange resin (Arisaka *et al.*, 2002). Thiocyanate solutions have also been used for separation (Myasoedov and Kremliakova, 1985). Solvents that are a mixture of alcohols and acids have been widely used for curium separations (Ryan, 1975).

A variety of zirconium-based inorganic sorbents have been used for separation of Am(III) and Cm(III), either using solutions similar to those employed with organic cation-exchange resins, or by oxidizing Am(III) to Am(V), which does not adsorb (Moore, 1971; Ryan, 1975).

Extraction chromatography with CMPO on an organic support allows ready separation of an americium and curium fraction (Cunningham and Wallmann, 1964; Fuger and Oetting, 1976; Oetting *et al.*, 1976). A commercially available resin based on CMPO has been used in studies (Kaye *et al.*, 1995; Maxwell, 1996).

Different chelate groups have been tried to increase selectivity of resins for curium (Ryan, 1975; Myasoedov and Kremliakova, 1985). A column containing the tertiary amine base, Aliquat-336, was used in combination with a column of HDEHP to obtain 6 g of pure ^{244}Cm (Bokelund *et al.*, 1989). Curium was first loaded onto the Aliquat column from $LiNO_3$, eluted, loaded onto the HDEHP column, and finally eluted with 1 M lactic acid containing DTPA. Other ion-exchange methods are described in Section 9.9.2.

9.5.3 Precipitation

Precipitation has been used for the separation of Cm(III) from americium in its higher valence states of V and VI. Separation at Savannah River was achieved by adjusting the solution to an Am(Cm) concentration of 10 g L^{-1} and 3.5 M K_2CO_3, oxidizing the Am(III) to Am(V) with hypochlorite, peroxydisulfate, or ozone, and precipitating the double carbonate $K_5AmO_2(CO_3)_3$ at 85°C (Groh *et al.*, 1965). Am(III) has also been oxidized to Am(V) electrochemically (Myasoedov and Kremliakova, 1985). A second precipitation is sometimes used to remove residual Am from the Cm solution. This process is based on the original work of Stephanou and Penneman (1952). After precipitation of Am(V) as the complex carbonate, Cm(III) can be precipitated with oxalate, hydroxide, or fluoride. It is noteworthy that the choice of cation is critical; if sodium is used in place of potassium, oxidation of americium proceeds past Am(V) to form the magenta-colored Am(VI) carbonate complex, which is soluble. Based on this observation, and utilizing the insolubility of $Cm(OH)_3$ in $NaHCO_3$, the americium content in the $Cm(OH)_3$ precipitate can be reduced to low levels (Coleman *et al.*, 1963).

9.6 THE METALLIC STATE

9.6.1 Physical properties

Curium is a lustrous, malleable, silvery metal with many properties comparable to those of the lighter actinide elements. The melting point of Cm (dhcp form) is 1345 ± 50°C (Fuger and Oetting, 1976; Oetting *et al.*, 1976), much higher than for the immediately preceding actinide elements, Np–Am (639–1173°C), but very similar to that of gadolinium (1312°C), its lanthanide analog (Cunningham and Wallmann, 1964; Reichlin *et al.*, 1981).

Curium metal exists in two modifications, a double hexagonal close-packed (dhcp) structure (α-lanthanum type) and a high-temperature cubic close-packed (fcc) structure. Using ^{244}Cm, the dhcp form was found to have lattice constants $a = 3.496(3)$ and $c = 11.331(5)$ Å, giving a calculated density of 13.5 g cm^{-3} and a metallic radius of 1.74 Å (Stevenson and Peterson, 1979; Reichlin *et al.*, 1981). Baybarz and Adair (1972) and Baybarz *et al.* (1976) reported the high-temperature fcc phase with $a = 5.039(2)$ Å, prepared by metal volatilization at 1650°C.

Using ^{248}Cm, Stevenson and Peterson (1979) also obtained this phase with $a = 5.065$ Å. Other preparations of Cm metal using ^{248}Cm have been reported. They exhibit the dhcp structure with $a = 3.500 \pm 0.003$ Å and $c = 11.34 \pm 0.01$ Å, and with $a = 3.490 \pm 0.006$ Å and $c = 11.308 \pm 0.018$ Å (Reichlin *et al.*, 1981). Other X-ray diffraction studies of ^{248}Cm metal have yielded evidence for an orthorhombic form as well as delocalization and compressibility data (Benedict *et al.*, 1985; Haire *et al.*, 1985).

The entropy of vaporization for Cm metal is similar to that of gadolinium; its vapor pressure is about double that of gadolinium over the measured range. The vapor pressure of triply distilled ^{244}Cm metal has been measured between 1300 and 2000 K and obeys the following relations (Ward *et al.*, 1975):

$$\log_{10}(p/(\text{atm})) = (6.082 \pm 0.129) - (19\,618 \pm 193)/T(\text{K}) \quad (\text{solid}, 1327\text{–}1639\ \text{K})$$

$$\log_{10}(p/(\text{atm})) = (5.586 \pm 0.157) - (18\,894 \pm 275)/T(\text{K}) \quad (\text{liquid}, 1640 - 1972\ \text{K})$$

From the latter equation the calculated boiling point of Cm is 3110°C. The derived heat of fusion, entropy of fusion, and average second-law entropy are 13.85 kJ mol^{-1}, 9.16 J K^{-1} mol^{-1}, and 106.7 ± 3.0 J K^{-1} mol^{-1}, respectively. Determination of low-temperature condensed-phase thermodynamic parameters awaits the availability of long-lived isotopes. For excellent discussions of thermodynamic, electronic, and magnetic effects in curium and other actinide and lanthanide metals, the reader is referred to articles by Ward and Hill (1975) and Ward *et al.* (1980). Konings (2001b) has reevaluated the thermodynamic data for curium metal in the solid, liquid, and gaseous states and has reported a set of recommended values that are similar to values by Ward *et al.* (1980).

Metallic curium obeys a Curie–Weiss magnetic susceptibility relationship between 100 and 550 K with a magnetic moment of 8.07 μ_B (Kanellakopulos *et al.*, 1976; Nave *et al.*, 1981; Reichlin *et al.*, 1981), comparable to earlier values of 7.85–8.15 μ_B (Marei and Cunningham, 1972), although a lower value of 6.0 μ_B was reported recently (Fujita *et al.*, 1976). However, the form of the metal was not identified by X-ray diffraction in the latter case. Schenkel (1977) performed electrical resistance measurements on ^{244}Cm metal, and showed that curium is the first reported magnetically ordered actinide metal, with a Néel temperature of 52.5 K. A neutron diffraction study of the dhcp (α-La) form indicated no structural change down to 5 K and also showed antiferromagnetic ordering below 52 K (Fournier *et al.*, 1977). A careful susceptibility study with ^{248}Cm metal confirmed an antiferromagnetic transition at about 65 K, but the fcc phase reveals a ferrimagnetic transition near 200 K (Eubanks and Thompson, 1969).

9.6.2 Preparation of curium metal

Curium metal can be prepared from CmF_3 by reduction with barium or lithium metal. Dry, oxygen-free CmF_3 is required and the temperatures used (>1600 K) are well above the melting point of the metal. One to ten micrograms of

Cm metal was made using tungsten coils and tantalum crucibles (tantalum is reported to dissolve slightly in Cm) (Cunningham and Wallmann, 1964; Stevenson and Peterson, 1979; Reichlin *et al.*, 1981). Gram quantities of the metal have been prepared in 75–90% yield by reduction with a magnesium–zinc alloy of CmO_2 suspended in a $MgF_2/MgCl_2$ melt (Eubanks and Thompson, 1969). When CmO_2 or Cm_2O_3 and pure hydrogen are heated to temperatures between 1200 and 1500°C in the presence of Pt, Ir, or Rh, alloy phases result with compositions of Pt_5Cm, Pt_2Cm, Ir_2Cm, Pd_3Cm, and Rh_3Cm (Erdmann and Keller, 1971, 1973). Similar alloys with Ni (Radchenko *et al.*, 1995), Al (Radchenko *et al.*, 1996), and Si (Radchenko *et al.*, 1998) have also been reported. Reports on CmPd alloys showed formation of a solid solution of Cm in Pd, with the fcc lattice parameter increasing linearly with at.% Cm (Radchenko *et al.*, 1985, 1989). The Cm–Pu phase diagram has been reported, which indicates that α-Cm (dhcp) predominates at lower wt% Pu and temperature, with β-Cm (fcc) forming as the Pu concentration and temperature increase, ultimately leading to γ-Cm (space group *Im*3*m*) (Okamoto, 2000). Pure curium metal has been prepared by decomposition of these intermetallic compounds (Müller *et al.*, 1972, 1977). The dhcp form of curium has also been prepared by reducing the dioxide or sesquioxide with thorium metal, followed by volatilization and condensation of the curium metal vapor on a tantalum condenser (Baybarz and Adair, 1972; Damian *et al.*, 1975; Baybarz *et al.*, 1976).

9.6.3 Chemical properties of the metallic state

Metallic curium appears to be even more susceptible to corrosion than the earlier actinide elements, a property due at least in part to radioactive self-heating. The metal dissolves rapidly in dilute acid solutions. The metal surface rapidly oxidizes in air to form a film that may begin as CmO (Cunningham and Wallmann, 1964; Burney, 1980; Reichlin *et al.*, 1981), progresses to Cm_2O_3 at room temperature, and further to CmO_2 at elevated temperatures. The metal is pyrophoric when finely divided.

The direct reactions of curium metal with non-metals such as Bi, P, As, Sb, S, and Se have been reported, and binary compounds with N, P, As, and Sb have been prepared by reactions using curium hydride (see Sections 9.7.5 and 9.7.6) (Charvillat *et al.*, 1975, 1976; Gibson and Haire, 1987; Zhu and Jiao, 1994).

9.7 CLASSES OF COMPOUNDS

9.7.1 General

Because curium is available in macro quantities, a number of Cm compounds have been synthesized and structurally characterized. Table 9.3 lists crystallographic data for Cm metal, alloys, and compounds.

Table 9.3 *Crystallographic data for curium metal, alloys, and compounds.*

	References	*Lattice type*	*Crystal system-space group*	*Lattice constants*		
				a_0 (Å)	b_0 (Å)	c_0 (Å)
Metal						
α-Cm	Cunningham and Wallmann (1964 Müller *et al.* (1972, 1977)	α-La	hexagonal-$P6_3/mmc$	3.496		11.331
β-Cm	Baybarz and Adair (1972); Baybarz *et al.* (1976)		fcc	5.039		
Alloys						
Pd_3Cm	Erdmann and Keller (1973); Radchenko *et al.* (1985)	Cu_3Au	cubic-$Pm3m$	4.147		
Rh_3Cm	Erdmann and Keller (1973); Radchenko *et al.* (1985)	Cu_3Au	cubic-$Pm3m$	4.106		
Ir_2Cm	Erdmann and Keller (1973); Radchenko *et al.* (1985)	Cu_2Mg	cubic-$Fd3m$	7.561		
Pt_5Cm	Erdmann and Keller (1973); Radchenko *et al.* (1985)	Pt_5Sm	orthorhombic	5.329	9.108	26.38
Pt_2Cm	Erdmann and Keller (1973); Radchenko *et al.* (1985)	Cu_2Mg	cubic-$Fd3m$	7.625		
Ni_5Cm	Radchenko *et al.* (1995)	Cu_5Ca	hexagonal	4.871		4.018
$Ni_{15}Cm_2$	Radchenko *et al.* (1995)	$Ni_{17}Th_2$	hexagonal	8.348		8.071
Al_2Cm	Radchenko *et al.* (1996)	Cu_2Mg	cubic	7.878		
CmSi	Radchenko *et al.* (1998)		orthorhombic	8.288	3.912	5.966
Cm_2Si_3	Radchenko *et al.* (1998)		hexagonal	3.879		4.147
$CmSi_2$	Radchenko *et al.* (1998)		tetragonal	3.977		13.719
$CmSi_{1.88}$	Radchenko *et al.* (1998)		tetragonal	4.029		13.715
Oxides and chalcogenides						
α-Cm_2O_3	Noé *et al.* (1970)	α-La_2O_3	hexagonal- $P\bar{3}m1$	3.7952		5.985
β-Cm_2O_3	Noé *et al.* (1970); Morss *et al.* (1983)	β-La_2O_3	monoclinic	14.282	3.641 $\beta = 100.29$	8.883

Table 9.3 (*Contd.*)

	References	*Lattice type*	*Crystal system-space group*	*Lattice constants*		
				a_0 (Å)	b_0 (Å)	c_0 (Å)
γ-Cm_2O_3	Noé *et al.* (1970)	γ-Mn_2O_3	cubic-*Ia*3	11.002		
CmO_2	Wallmann (1964); Noé and Fuger (1971); Peterson and Fuger (1971); Mosley (1972)	fluorite	cubic-*Pm*3*m*	5.3584		
CmO	Cunningham and Wallmann (1964)		cubic-*Fm*3*m*	5.09		
CmS	Damien *et al.* (1979a,b)		fcc	5.5754		
CmSe	Damien *et al.* (1979a,b)		fcc	5.791		
CmTe	Damien *et al.* (1979a,b)		fcc	6.150		
Cm_2S_3	Damien *et al.* (1975)	Th_3P_4	bcc	8.452		
$CmS_{1.98}$	Damien *et al.* (1975)	Fe_2As	tetragonal	3.926		8.01
Cm_2Se_3	Damien *et al.* (1975)	Th_3P_4	bcc	8.788		
$CmSe_{1.98}$	Damien *et al.* (1975)	Fe_2As	tetragonal	4.096		8.396
$CmTe_3$	Damien *et al.* (1976)	$NdTe_3$	orthorhombic (pseudotetragonal)	4.34		25.7
$CmTe_2$	Damien *et al.* (1976)	Fe_2As	tetragonal	4.328		8.93
Cm_2Te_3	Damien *et al.* (1976)	η-U_2S_3	orthorhombic	11.94	12.13	4.330
Cm_2O_2S	Haire and Fahey (1977)	Pu_2O_2S	hexagonal	3.889		6.736
Cm_2O_2Te	Damien *et al.* (1976)	La_2O_2Te	tetragonal	3.98		12.58
$Cm_2O_2SO_4$	Haire and Fahey (1977)	$Nd_2O_2SO_4$	orthorhombic	4.209	4.087	13.270
$BaCmO_3$	Haire and Fahey (1977)	perovskite				
$CmAlO_3$	Haire and Fahey (1977)	perovskite				

Pnictides						
CmN	Charvillat *et al.* (1976)	NaCl	fcc	5.041		
CmP	Damien *et al.* (1979a,b)	NaCl	fcc	5.743		
CmAs	Damien *et al.* (1979a,b)	NaCl	fcc	5.887		
CmSb	Damien *et al.* (1979a,b)	NaCl	fcc	6.242		
Cm_2O_2Sb	Charvillat and Zachariasen (1977)	La_2O_2Te	tetragonal–14/*mmm*	3.920		13.41
Cm_2O_2Bi	Charvillat and Zachariasen (1977)	La_2O_2Te	tetragonal–14/*mmm*	3.957		13.359
Halides						
CmF_3	Stevenson (1973); Asprey *et al.* (1965)	LaF_3	trigonal- $P\bar{3}\,Cl$	7.019		7.198
$CmCl_3$	Asprey *et al.* (1965); Peterson and Burns (1973)	UCl_3	hexagonal-$P6_3/m$	7.3743		4.1850
$CmBr_3$	Asprey *et al.* (1965); Burns *et al.* (1975)	$PuBr_3$	orthorhombic-*Cmcm*	4.041	12.709	9.135
CmI_3	Asprey *et al.* (1965)	BiI_3	hexagonal-$R\bar{3}$	7.44		20.4
CmF_4	Asprey and Haire (1973); Haug and Baybarz, (1975)	UF_4	monoclinic-$C2/c$	12.500 $\beta = 126.10$	10.488	8.183
$LiCmF_5$	Keenan (1966a)	$LiUF_5$	tetragonal-$I14_1/a$	14.579		6.437
$K_7Cm_6F_{31}$	Keenan (1966b)	$Na_7Zr_6F_{31}$	hexagonal-$R\bar{3}$	14.41		9.661
$Na_7Cm_6F_{31}$	Keenan (1967a)	$Na_7Zr_6F_{31}$	hexagonal-$R\bar{3}$	14.89		10.254
Rb_2CmF_6	Keenan (1967b)	Rb_2UF_6	orthorhombic-*Cmcm*	6.931		7.56
CmOCl	Peterson (1972)	PbClF	hexagonal	3.98		6.75
Hydrides						
CmH_{2+x}	Gibson and Haire (1985)	fluorite	fcc	5.322		
$CmH_{3-\delta}$	Gibson and Haire (1985)	PuH_3	trigonal-$P\bar{3}\,ClCl$	3.769		6.732

The most important chemical characteristic that distinguishes curium from the lighter actinides is the great stability of the 3+ state with respect to oxidation or reduction. The stability of Cm(III) has been attributed to the relative stability of a half-filled ($5f^7$) configuration, and causes a chemical resemblance to lanthanides. All known Cm(IV) compounds are either fluorides or oxides.

In contrast to americium, the oxidation of Cm(III) to Cm(IV) is achieved only with the strongest oxidizing agents, and only two reports claim evidence for an oxidation state greater than IV (Peretrukhin *et al.*, 1978; Fargeas *et al.*, 1986). Transient divalent and tetravalent states have been observed in aqueous perchlorate media using pulse radiolysis techniques (Sullivan *et al.*, 1976). Attempts have been made to induce Cm(III)–Cm(IV) oxidation chemically (using ozone (Pages and Demichelis, 1966) and perxenate (Holcomb, 1967)) or electrochemically (Myasoedov *et al.*, 1973). These attempts have failed, an effect clearly not attributable solely to radiolytic reduction.

However, formation of a red Cm(IV) complex in phosphotungstate solution was achieved by the use of peroxydisulfate as the oxidant (Saprykin *et al.*, 1976). Kosyakov *et al.* (1977) demonstrated that, in such solutions, the Cm(IV) is reduced much more rapidly than can be accounted for by radiolytic effects, while Am(IV) in such solutions is much more stable, being reduced at a rate attributable to radiolytic effects alone. This behavior stands in contrast to the reduction of Cm(IV) in 15 M CsF, which does proceed at the slower radiolytic rate (Keenan, 1961). No value for the E°(Cm(IV)/Cm(III)) is known, but, from existing data, it is substantially more positive than $E^\circ(Am^{4+}/Am^{3+})$ and probably about as positive as $E^\circ(Pr^{4+}/Pr^{3+})$.

With the more common isotopes ^{242}Cm and ^{244}Cm, intense alpha self-irradiation and heating effects cause aqueous-solution instability (peroxide is always present) and solid-state instability (lattice changes and compound alteration). In some cases, these effects are sufficiently large that certain compounds may be identified in bulk only with the more stable isotopes, e.g. $^{244}CmF_4$ and $^{248}Cm(n\text{-}C_5H_5)_3$ (Asprey and Keenan, 1958; Laubereau and Burns, 1970b).

9.7.2 Hydrides

The hydrides of Cm are relatively little explored. The first Cm hydride was prepared by Bansal and Damien (1970) by reacting ^{244}Cm metal with hydrogen at 200–250°C. Based on its X-ray diffraction pattern, this hydride was characterized as the face-centered cubic (fcc) CmH_{2+x}, by analogy to NpH_{2+x}, PuH_{2+x}, and AmH_{2+x}. The existence of the dihydride was confirmed by Gibson and Haire (1985), who prepared the dihydride from ^{248}Cm metal. In the latter work, the hexagonal $CmH_{3-\delta}$ was also prepared. The trihydride was characterized from its x-ray diffraction pattern by analogy to those of known lanthanide and actinide trihydrides.

The dissociation enthalpy for CmH_2 has been reported to be 187 ± 14 kJ mol^{-1}, consistent with the trend in stability of the actinide dihydrides becoming more like that of the lanthanide dihydrides with increasing atomic number (Gibson and Haire, 1990). The order of stability of f-element dihydrides can be summarized as follows:

$$\text{Ln(most stable)} > \text{Cm} > \text{Am} > \text{Pu}$$

9.7.3 Halides

The halides represent by far the most extensively characterized class of curium compounds (see Table 9.3). The complete CmX_3 series (X = F, Cl, Br, I), as well as CmF_4 and several complex Cm(IV) fluorides, have been prepared and studied. Several reviews deal specifically with actinide halides; for further information (especially for cross-comparisons of Cm with other actinide halides) the reader is referred to these articles (Katz and Sheft, 1960; Bagnall, 1967; Brown, 1968; Penneman *et al.*, 1973).

Curium trifluoride is a white, sparingly soluble (~10 mg L^{-1}) compound (Cunningham, 1966) with the LaF_3 structure, which precipitates when fluoride ion is added to weakly acidic Cm(III) solutions, or HF to $Cm(OH)_3$. The anhydrous trifluoride is obtained by desiccation over P_2O_5 or by treatment with hot HF(g). The trifluoride melts at 1406 ± 20°C; its standard enthalpy and entropy of formation have been estimated to be 1660 kJ mol^{-1} (Ionova *et al.*, 1997) and 121 J K^{-1} mol^{-1} (Burnett, 1966; Cunningham, 1966) at 298 K, respectively. Curium has an irregular tricapped trigonal prismatic coordination in CmF_3 (Penneman *et al.*, 1973).

Curium trichloride is a white compound that can be obtained by treating curium oxides or CmOCl with anhydrous hydrogen chloride at 400–600°C (Wallmann *et al.*, 1967). The hydrate has been reported to be light green. A single-crystal study showed that $CmCl_3$ has the hexagonal UCl_3-type structure common among the actinide trichlorides. Based on the lattice constants for $CmCl_3$ (Table 9.3), a radius of 0.971 Å has been calculated for Cm(III) (Peterson and Burns, 1973). Curium has nine chloride neighbors in the form of a tricapped trigonal prism, with Cm–Cl lengths of 2.859 and 2.914 Å. A melting point of 695°C (Peterson and Burns, 1973) and an enthalpy of formation (298 K) of −974 ± 4 kJ mol^{-1} (Fuger *et al.*, 1975; Oetting *et al.*, 1976) have been reported. The entropy of formation of $CmCl_3$ at 298 K has been estimated to be 163 ± 6 J K^{-1} mol^{-1} (Konings, 2001a).

Curium tribromide has been prepared by heating the trichloride with NH_4Br at 400–450°C in a hydrogen atmosphere (Asprey *et al.*, 1965) and also by hydrogen bromide treatment of the calcined oxide at 600°C (Burns *et al.*, 1975). The compound melts at 625°C and has the $PuBr_3$ (orthorhombic) structure (Burns *et al.*, 1975). The metal ion is surrounded by eight bromide ions, two at 2.865 Å, four at 2.983 Å, and two at 3.137 Å. An analogous

procedure ($CmCl_3 + NH_4I$) has been used to prepare CmI_3, a colorless material having the BiI_3 structure (Asprey *et al.*, 1965). Preparation from elemental curium and iodine has also been reported (Seaborg *et al.*, 1949). The standard enthalpies of formation of $CmBr_3$ and CmI_3 are estimated to be 794 and 564 kJ mol^{-1}, respectively, at 298 K (Ionova *et al.*, 1997).

The halides of tetravalent curium include the simple fluoride CmF_4 (Keenan and Asprey, 1969; Asprey and Haire, 1973; Haug and Baybarz, 1975), and a series of complex fluorides of the type $M_7Cm_6F_{31}$ (Keenan, 1966b, 1967a), M_2CmF_6 (Keenan, 1967b), and $MCmF_5$ (Keenan, 1966a), where M is an alkali metal. As with terbium, the only reported method for preparing the tetrafluoride is by fluorine oxidation of the trifluoride. CmF_4 is a brownish-tan solid with a monoclinic ZrF_4-type structure, in which curium has an antiprismatic eight coordination (Asprey and Haire, 1973; Penneman *et al.*, 1973; Haug and Baybarz, 1975). Magnetic susceptibility measurements suggest a fluoride-deficient structure, CmF_{4-x} (Haire *et al.*, 1982; Nave *et al.*, 1983).

Evidence for the existence of CmF_6 and $CmOF_3$ (as well as $NpOF_3$, NpF_7, PuO_3F, AmF_5, AmF_6, and EsF_4) has been reported using thermochromatographic techniques (Fargeas *et al.*, 1986). These fluorides were claimed to form in low yield when a deposit of Cm (chemical form not reported) on Ni metal was treated with a mixture of BF_3 and F_2 at 800°C. However, there has been no independent confirmation of these species.

A prominent series of isostructural complex actinide(IV) fluorides, $M_7An_6F_{31}$, with the $Na_7Zr_6F_{31}$ structure have been prepared (Keenan, 1966b, 1967a). With curium, the Na and K salts are known. The compounds were prepared by direct fluorination of evaporated salt mixtures of MX and CmX_3 at about 300°C. This 7:6 type of compound predominates with the larger alkali cations. The basic coordination polyhedron is a square antiprism (Penneman *et al.*, 1973). In tetragonal $LiCmF_5$, the curium coordination is tricapped trigonal prismatic (Penneman *et al.*, 1973). The compound Rb_2CmF_6 is orthorhombic with the Rb_2UF_6 structure, which consists of chains of fluoride dodecahedra (Penneman *et al.*, 1973). The oxychloride CmOCl has been synthesized by treatment of $CmCl_3$ (or Cm_2O_3) at 500–600°C, with the vapor in equilibrium with a 10 M HCl solution (Peterson, 1972):

$$CmCl_3 + H_2O \leftrightarrow CmOCl + 2HCl$$

From the equilibrium and known heats of formation, ΔH°_{f298} for CmOCl was calculated (Weigel *et al.*, 1977, Table 17.4). Marei and Cunningham (1972) found that the magnetic susceptibility of CmOCl follows the Curie–Weiss law over the temperature range 77–298 K, with $\mu_{eff} \sim 7.58\ \mu_B$ and a Curie temperature of approximately 22 K. The structure of CmOCl is of the PbClF-type (hexagonal), with each metal surrounded by four oxides and five chlorides (Peterson, 1972).

9.7.4 Oxides

Konings (2001a,b) has recently reviewed the thermochemical and thermophysical properties of Cm oxides. Crystallographic data for the various oxides are compiled in Table 9.3.

The white to faint tan sesquioxide Cm_2O_3 (m.p. 2270 ± 25°C) (Konings, 2001b) was prepared by thermal decomposition of $^{244}CmO_2$ at 600°C and 10^{-4} torr pressure (Asprey *et al.*, 1955). This material has the Mn_2O_3-type cubic-C lattice, which gradually changes at room temperature to a hexagonal A-form because of self-irradiation effects (Wallmann, 1964; Noé *et al.*, 1970). Haug (1967) prepared monoclinic B-type Cm_2O_3 by reduction of $^{244}CmO_2$ with hydrogen. This study showed that the cubic form described by Asprey *et al.* (1955) predominates at reaction temperatures below 800°C, changing to the monoclinic B-form at higher temperatures (Haug, 1967). These three crystal modifications correspond to the three types observed for lanthanide sesquioxides. Structural data, enthalpy of formation, and magnetic susceptibility were obtained by Morss *et al.* (1983) with B-form $^{248}Cm_2O_3$. The enthalpy of formation at 25°C has been estimated as –1684 ± 14 kJ mol^{-1} for the monoclinic Cm_2O_3 (Konings, 2001b), with the corresponding entropy of formation estimated to be 167 ± 5 J K^{-1} mol^{-1} (Konings, 2001a).

Preparation of the black curium dioxide by ignition in air was first claimed by Asprey *et al.* (1955). The product had a cubic (fcc) structure. The compound is also formed by thermal decomposition of ^{244}Cm(III)-loaded resin (Hale and Mosley, 1973) and by heating $^{244}Cm_2O_3$ to 650°C in 1 atm of oxygen, followed by cooling in oxygen (Noé and Fuger, 1971; Peterson and Fuger, 1971). Others have shown that the dioxide is the stable oxide form in an oxygen atmosphere at temperatures below 400°C (Chikalla and Eyring, 1969). At temperatures between 380 and 420°C, CmO_2 is reduced to $CmO_{1.95}$; above 430°C, rapid decomposition occurs via various intermediate oxides to Cm_2O_3 (Mosley, 1972). The enthalpy of formation at 25°C has been estimated as −912 ± 7 kJ mol^{-1} for CmO_2 (Konings, 2001b).

Curium oxalate, $Cm_2(C_2O_4)_3$, is routinely used for calcination to CmO_2. For example, oxalate precipitation has been used to process kilograms of ^{244}Cm, with subsequent metathesis with 0.5 M hydroxide to $Cm(OH)_3$ (Scherer and Fochler, 1968; Bibler, 1972).

Morss *et al.* (1989) reported a neutron diffraction and magnetic susceptibility study of CmO_2 prepared by calcination of Cm(III) oxalate at 775°C in flowing O_2, followed by annealing for 4 days at 350°C in flowing O_2. Based on the lattice parameter (a_0 = 5.359 ± 0.002 Å), the stoichiometry of this material was reported to be $CmO_{1.99 \pm 0.01}$, indicating that the material essentially contained only Cm(IV). Nevertheless, the effective paramagnetic moment was found to be $(3.36 \pm 0.06)\mu_B$, a value which had previously been attributed to the presence of Cm(III). Based on these data, it has been suggested that the electronic ground states in actinide dioxides may need to be reexamined.

The curium–oxygen phase diagram studies show a great similarity to analogous Pu, Pr, and Tb systems, and indicate the possible existence of two additional Cm_2O_3 phases which have not yet been isolated (Eyring, 1967; Stevenson and Peterson, 1975). Two intermediate oxides, $CmO_{1.72}$ and $CmO_{1.82}$, and two other non-stoichiometric phases close to the composition of CmO_2 and $CmO_{1.5}$, have also been detected (Chikalla and Eyring, 1969). A cubic (fcc) phase, CmO, was reported in an early preparation of the metal (Cunningham and Wallmann, 1964).

The ternary oxides $BaCmO_3$ (Fuger *et al.*, 1993) and Cm_2CuO_4 (Soderholm *et al.*, 1999) have recently been reported. The latter is of interest by its analogy to M_2CuO_4 (M = La, Pr–Eu), which are parent compounds for high-temperature superconductors. When doped with Th^{4+}, the M_2CuO_4 (M = Pr–Eu) materials become superconducting, with T_c of ~32 K. Although Cm_2CuO_4 is isostructural with the M_2CuO_4 (M = Pr–Gd) series, its Th-doped analog is not superconducting. This effect may be due to its high magnetic ordering temperature relative to other M_2CuO_4.

Hale and Mosley (1973) have reported the preparation of curium oxysulfate, $^{244}Cm_2O_2SO_4$, by heating Cm(III)-loaded resin (sulfonate form) in a stream of oxygen at 900°C. The thermogravimetric analysis indicated that heating to 1175°C under otherwise similar conditions yielded Cm_2O_3, which on cooling formed CmO_2. Haire and Fahey (1977) have prepared $Cm_2O_2SO_4$ by calcination of the hydrated sulfate in air at about 750°C. The brown $Cm_2O_2SO_4$ has a body-centered orthorhombic structure, similar to $Nd_2O_2SO_4$ and $Cf_2O_2SO_4$. The computed Cm(III) radius in $Cm_2O_2SO_4$, 0.980 Å, agrees with the value of 0.979 Å derived from Cm_2O_3. The oxysulfide Cm_2O_2S is formed when the sulfate is heated to about 800°C in H_2/Ar (Haire and Fahey, 1977). Cell constants for Cm_2O_2Sb and Cm_2O_2Bi have been reported (Charvillat and Zachariasen, 1977).

9.7.5 Chalcogenides

Damien *et al.* (1975) prepared $^{244}CmS_2$ and $^{244}CmSe_2$ by slow reaction of excess sulfur or selenium vapor with curium hydride in vacuum. The resulting solids gave powder patterns indicating the tetragonal Fe_2As-type cell (isostructural with AmS_2 and $AmSe_2$) with lattice parameters (Table 9.3) showing the materials to be non-stoichiometric.

The sesquisulfide Cm_2S_3 forms a defect body-centered cubic (bcc) phase of the Th_3P_4-type (Damien *et al.*, 1975). The sesquiselenide was obtained by thermal dissociation of $CmSe_2$ at 620°C, again yielding a Th_3P_4-type phase (Damien *et al.*, 1975). Unlike gadolinium or plutonium, no other sesquiselenide forms were observed, even after thermal treatment at various temperatures.

The monochalcogenides were prepared by heating stoichiometric mixtures of chalcogen and curium metal at 700–750°C for 15 h, followed by heating at 1250–1500°C under high vacuum (Damien *et al.*, 1979a). The monochalcogenides

have fcc structures. In these preparations, accessory phases, possibly γ-Cm_2S_3, Cm_2O_2S, γ-Cm_2Se_3, and Cm_2O_2Te, were detected.

The oxysulfide Cm_2O_2S was prepared by partial oxidation of CmS_2 at 700°C (Damien *et al.*, 1975; Haire and Fahey, 1977). This compound has a hexagonal structure and is isostructural with the Np, Pu, and Cf analogs (Haire and Fahey, 1977).

Damien *et al.* (1976) have reported the preparation of $CmTe_3$ by the reaction of the hydride with tellurium at 400°C. At temperatures above 400°C, the tritelluride decomposes to form the successive lower tellurides $CmTe_2$ and Cm_2Te_3. At 1100°C in a quartz tube, the oxytelluride Cm_2O_2Te is formed.

9.7.6 Pnictides

The syntheses of the pnictide compounds CmX, where X = N, P, As, and Sb, have been reported (Charvillat *et al.*, 1975, 1976; Kanellakopulos *et al.*, 1976; Damien *et al.*, 1979a,b; Stevenson and Peterson, 1979; Nave *et al.*, 1981). The compounds were obtained by heating curium hydride or metal with the respective pnictide element in a sealed tube to temperatures of 350–950°C. The N, P, As, and Sb compounds all have the NaCl structure (Charvillat *et al.*, 1975, 1976; Kanellakopulos *et al.*, 1976; Damien *et al.*, 1979a,b; Nave *et al.*, 1981). Damien *et al.* (1979a,b) prepared the monopnictides (N, P, As, Sb) by directly heating stoichiometric mixtures of the elements. CmN and CmAs are ferromagnetic, with T_c of 109 and 88 K, respectively (Kanellakopulos *et al.*, 1976; Nave *et al.*, 1981). The calculated effective magnetic moments are 7.02 and 6.58 μ_B, lower than expected for a pure $5f^7$ configuration, probably because of strong spin–orbit coupling and crystal field effects (Kanellakopulos *et al.*, 1976; Nave *et al.*, 1981).

The possibility of using mixed nitride fuels for transmutation of minor actinides has gained recent attention because it is anticipated that the actinide nitrides are mutually miscible. The miscibility of CmN and PuN has been confirmed by the carbothermic synthesis of (Cm,Pu)N (Takano *et al.*, 2001). This was achieved by heating graphite and $(Cm_{0.4}Pu_{0.6})O_{2-x}$ at 1773 K in N_2. The lattice parameter of the resulting mixed nitride was close to that expected from the known lattice parameters for CmN and PuN.

9.7.7 Miscellaneous compounds

The trihydroxide, $Cm(OH)_3$, has been prepared from aqueous solution and crystallized by aging in water (Haire *et al.*, 1977). The compound has the lanthanide trihydroxide (hexagonal) structure. Although there have been no reports of Cm carbide, the silicides CmSi, $CmSi_2$, Cm_2Si_3, and Cm_5Si_3 have been reported (Weigel and Marquardt, 1983; Radchenko *et al.*, 2000).

The oxalate $Cm_2(C_2O_4)_3 \cdot 10H_2O$ forms when aqueous Cm(III) and oxalic acid are mixed. The compound dehydrates in a stepwise fashion when heated

in vacuo, yielding the anhydrous oxalate at 280°C, which then converts to a carbonate above 360°C (Scherer and Fochler, 1968). A differential thermal analysis (DTA) investigation of the hydrated Cm oxalate under helium revealed endothermic events centered at 145 and 400°C, corresponding to the release of water and the formation of $Cm_2O_2CO_3$, respectively. Above 500°C, the $Cm_2O_2CO_3$ converts to Cm_2O_3 (Vasil'ev *et al.*, 1989). The hydrated oxalate dissolves readily in aqueous alkali-metal carbonate solutions (Bibler, 1972; Burney and Porter, 1967). The compound has a solubility (~0.8 mg Cm per liter at 23°C) lower than that of the americium analog in 0.1 M $H_2C_2O_4$/0.2 M HNO_3. The solubility increases rapidly with temperature.

Curium nitrate can be isolated by evaporation of solutions formed by dissolving curium oxide in nitric acid. DTA analysis of the freshly prepared $^{244}Cm(NO_3)_3$ indicated the decomposition pathway is the same under an oxygen atmosphere as it is under helium (Vasil'ev *et al.*, 1990). The thermal decomposition is characterized by endothermic events centered at 90, 180, 400, and 450°C. By analogy to the thermal decomposition of lanthanide nitrates, the first two endotherms have been assigned to melting of the crystalline hydrated nitrate and its dehydration, respectively. The last two endotherms (which overlap) are associated with the decomposition of the anhydrous Cm nitrate. The final product of the thermal decomposition is CmO_2, indicating the Cm is oxidized to Cm(IV) during the decomposition process. The enthalpy of formation of the anhydrous crystalline $Cm(NO_3)_3$ was estimated to be -700 kJ mol^{-1} from the DTA data.

Complex sulfates of the type $MAn(SO_4)_2 \cdot xH_2O$, where M = alkali metal, have been precipitated from solutions of M_2SO_4 and the appropriate trivalent actinide ion in dilute HCl or H_2SO_4 (Dedov *et al.*, 1965). Structural characterization is lacking for these compounds.

A series of actinide phosphates having the formulation $AnPO_4 \cdot 0.5H_2O$ has been prepared (An = Pu, Am, Cm) (Weigel and Haug, 1965; Kazantsev *et al.*, 1982). These compounds form when aqueous Cm(III) solutions are mixed with Na_2HPO_4 or $(NH_4)_2HPO_4$. The structures of the $AnPO_4 \cdot 0.5H_2O$ compound are unknown. The hydrated phosphate of Cm(III) dehydrates at 300°C to $CmPO_4$, which has the monazite structure (Weigel and Haug, 1965; Kazantsev *et al.*, 1982).

The compound $Cm[Fe(CN)_6]$ forms as a dark red precipitate when $K_3[Fe(CN)_6]$ is added to a solution of Cm nitrate in 0.2 M HNO_3 (Kulyako *et al.*, 1993). This contrasts to the lanthanides (Eu, Ce, Pr) that do not form precipitates under identical conditions, but is similar to the behavior of Am.

The compounds $CmNbO_4$ and $CmTaO_4$ are isotypic with the corresponding lanthanide compounds and are obtained by heating the precipitated, mixed hydroxide/hydrous oxides at 1200°C (Keller and Walter, 1965).

Heating mixtures of curium oxide and alumina affords $CmAlO_3$, which gives either a rhombohedral or a cubic product depending upon the quenching conditions (Mosley, 1971). The rhombohedral phase transforms to the cubic

phase at room temperature. $BaCmO_3$ has also been reported (Haire, 1980; Nave *et al.*, 1983). The addition of K_2CO_3 to Cm(III) solution precipitates $Cm_2(CO_3)_3$ (Dedov *et al.*, 1965). The compound is soluble in 40% K_2CO_3.

The salt $CsCm(HFAA)_4 \cdot H_2O$, where HFAA = hexafluoroacetylacetone, has been studied in detail (Nugent *et al.*, 1969). This compound, as well as the Eu, Gd, Tb, Nd, Am, Bk, Cf, and Es analogs, forms readily when HFAA is added to ethanol solutions of Cm(III) in the presence of cesium ion. Of the actinides studied for possible laser properties, only Cm displayed UV-excited, sharp-line sensitized luminescence (Nugent *et al.*, 1969). Cm(III) was found to be a highly efficient emitter (resembling Eu(III)) in the crystalline state, in ethanol solution, and doped into a $CsGd(HFAA)_4$ crystal matrix; hence laser emission should be demonstrable. Strong luminescence has been observed from ^{244}Cm (III) on an anion-exchange resin and in solution (Gutmacher *et al.*, 1964; Beitz and Hessler, 1980).

A number of adducts of the type $CmL_3 \cdot nQ$ have been prepared, where L is a fluorinated β-diketonate and Q is TBP or trioctylphosphine oxide (Davydov, 1978). The volatility, thermal, and radiation stabilities were studied with consideration of such compounds for gas chromatographic separation of Am and Cm.

9.7.8 Organometallics

Despite substantial recent advances in the organometallic chemistry of other actinide elements, progress with curium has been slow. This lack of progress apparently results from the radiolytic properties of the element rather than an inherent chemical instability of the organometallic compounds. For more detailed discussion of actinide organometallic compounds, the reader is directed to Chapters 25 and 26.

The synthesis and spectroscopic characterization of milligram quantities of white, crystalline tris(η^5-cyclopentadienyl)curium, $Cm(C_5H_5)_3$, has been reported from the reaction of $^{248}CmCl_3$ with $Be(C_5H_5)_2$ (Baumgärtner *et al.*, 1970; Laubereau and Burns, 1970b). The compound can be sublimed in vacuum at 180°C and is isostructural with the Pr, Pm, Sm, Gd, Tb, Bk, and Cf analogs (Laubereau and Burns, 1970a,b). Mass spectrometric evidence for volatile $Cm(C_5H_5)_3$ using microgram amounts of ^{244}Cm was obtained (Baumgärtner *et al.*, 1970).

In terms of structural properties, volatility, thermal stability, and solubility, $Cm(C_5H_5)_3$ closely resembles other actinide and lanthanide tris(cyclopentadienide) compounds and hence the bonding must be similar. Nugent *et al.* (1971) studied the optical spectrum of $^{248}Cm(C_5H_5)_3$ and found weak bands, typical for Cm(III). These workers derived a value for the nephelauxetic parameter $d\beta$ of 0.050 ± 0.004, corresponding to very weak covalency in the organometallic bond. Thus, like the lanthanide analogs, the bonding in $Cm(C_5H_5)_3$ appears to have rather little covalent character. The ^{248}Cm compound fluoresces bright red under 360 nm irradiation (Nugent *et al.*, 1971).

Gas-phase reactions of Cm^+ and CmO^+ ions with small organic compounds have been investigated (Gibson and Haire, 1998, 1999). The gas-phase Cm ions used in these studies were generated by laser ablation of Cm_7O_{12} and the reaction products were characterized by mass spectroscopy. Using this methodology, a number of Cm organometallic fragments have been identified, including Cm_2^+, CmC_2H^+, $CmCN^+$, and a series of $CmC_xH_y^+$ species. The relative ability of Cm^+ to activate C–H bonds is less than that for U^+ or Tb^+ ions.

9.8 AQUEOUS CHEMISTRY

9.8.1 Inorganic

The aqueous solution chemistry of curium is almost exclusively that of Cm(III). Relatively little non-aqueous solution chemistry has been reported with curium other than that related to separations and environmental applications. Dilute Cm(III) solutions are normally colorless, but Cm(III) in concentrated HCl appears greenish. Curium-242 solutions with concentrations of about 1 g l^{-1} will boil unless cooled. The hydration number for the Cm(III) ion is estimated to be 9, based on fluorescence lifetimes (Kimura and Choppin, 1994; Kimura *et al.*, 1996). In HCl solution, the hydration number for the Cm(III) ion remains 9 up until 5 M HCl, then decreases with increasing HCl concentration (Kimura *et al.*, 1998). At 11 M HCl, the hydration number is 7. In contrast, the hydration number for Cm(III) drops steadily with increasing HNO_3 concentration from 0 to 13 M, with the hydration number being 5 at 13 M HNO_3. The differences between the HCl and HNO_3 systems are presumably simply due to the stronger binding affinity of the nitrate ion compared to chloride.

For dissolution of dhcp Cm metal in 1 M HCl, the value of ΔH is -615 ± 4 kJ mol^{-1} at 298.2 K, which, with an estimated $S^\circ = -194$ J mol^{-1} h^{-1} for the Cm^{3+} (aquo) ion, yields an estimated -2.06 ± 0.03 V for the Cm(III)/Cm(0) couple (Fuger *et al.*, 1975) (see Chapter 17). Raschella *et al.* (1981) found $\Delta H = -606.5 \pm 11.7$ kJ mol^{-1} for dissolution using ^{248}Cm metal. From electron-transfer spectra, the Cm(III)/Cm(II) couple was estimated at -4.4 V (Nugent *et al.*, 1973), but the results of the pulse radiolysis study and the potential of the hydrated electron place a lower value on this couple (Sullivan *et al.*, 1976). From studies in a melt, Mikheev (1983) obtained –2.8 V for E°(Cm(III)/Cm(II)). Fuger and Martinot (1985) report E°(Cm(III)/Cm(IV)) to be -3.1 V.

Solution reactions of Cm(III) resemble those of the trivalent lanthanides and other trivalent actinides. The fluoride, oxalate, phosphate, iodate, and hydroxide are essentially water-insoluble, and the chloride, iodide, perchlorate, nitrate, and sulfate are water-soluble. The first hydrolysis constant for Cm(III), i.e. for the reaction

$$Cm(III) + H_2O \rightarrow CmOH^{2+} + H^+$$

is 1.2×10^{-6} ($\mu = 0.1$; 23°C), which is within experimental error of the value for Am^{3+} but ten times greater than that for Pu^{3+} (Désiré *et al.*, 1969; Korotkin, 1974). The formation constants for $[Cm(OH)]^{2+}$ and $[Cm(OH)_2]^{+}$ have been determined by time-resolved laser-induced fluorescence spectroscopy (Fanghänel *et al.*, 1994). The measurements were made under high ionic strength (up to 6M NaCl). Extrapolation to zero ionic strength yielded values of $\log \beta_{11} = 6.44$ and $\log \beta_{12} = 12.3$. Ionic strength significantly affects the distribution of hydrolyzed species with the Cm(III) ion becoming more easily hydrolyzed as the ionic strength increases (Fig. 9.4).

Stability constants for Cm(III) complexes have been determined for a number of inorganic and organic liquids in aqueous solution (Table 9.4). Most recent stability constant measurements for Cm(III) have been performed using time-resolved laser-induced fluorescence spectroscopy; these studies provide the most self-consistent set of stability constant data for Cm(III). Cm(III) is a 'class A' or 'hard' metal ion, and thus complexes far more strongly to oxygen and fluoride donors than to more polarizable donors such as chloride or sulfur. This is reflected in the fact that β_1 for F^- is three orders-of-magnitude greater than that for Cl^-. The stability constants for oxygen donors (e.g. OH^- and CO_3^{2-}) are even higher than that for F^-.

Cm(III) forms complexes with a number of polytungstate and heteropolytungstate anions and the luminescence properties of these complexes have been extensively studied. Included in this class of compounds are $CmW_{10}O_{36}^{9-}$, $Cm(SiW_{11}O_{39})_2^{13-}$, $CmSiW_{11}O_{39}^{5-}$, $Cm(PW_{11}O_{39})_2^{11-}$, $CmPW_{11}O_{39}^{4-}$, $Cm(P_2W_{17}O_{61})_2^{17-}$, and $CmP_2W_{17}O_{61}^{7-}$ (Yusov and Fedoseev, 1989b, 1990). The polytungstate ligands quench the luminescence of Cm(III), evidently due to charge transfer between the excited Cm*(III) and W(VI). This effect is magnified when the solutions of these complexes are frozen, resulting in a sharp decrease in

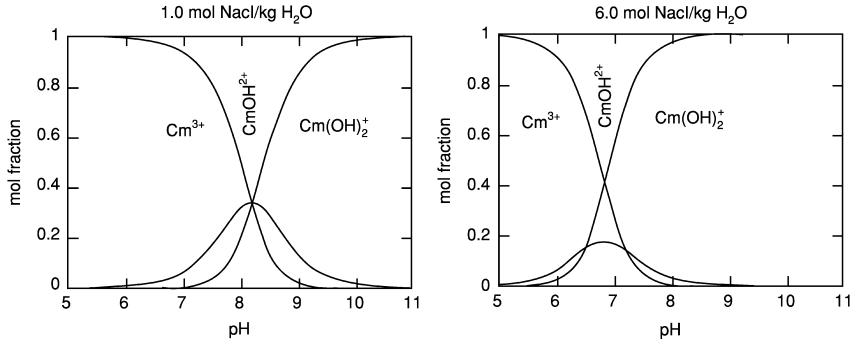

Fig. 9.4 *Comparison of Cm(III) species distribution as function of pH at two NaCl molalities. The speciation determination is based on Cm(III) fluorescence spectra. Used with permission from Fanghänel* et al. (1994).

Table 9.4 *Stability constants for selected Cm(III) complexes.*

Ligand	*Conditions*	*Stability constants*	*References*
OH^-	time-resolved laser fluorescence spectroscopy extrapolated to $\mu = 0$	$\beta_1 = 2.75 \times 10^6$; $\beta_2 = 2.00 \times 10^{12}$	Fanghänel *et al.* (1994)
F^-	time-resolved laser fluorescence spectroscopy, $\mu = 0$	$\beta_1 = 1.45 \times 10^3$	Aas *et al.* (1999)
F^-	extraction with di(2-ethylhexyl) phosphoric acid, pH = 3.6, $\mu = 0.50$	$\beta_1 = 2.21 \times 10^3$: $\beta_2 = 1.50 \times 10^6$: $\beta_3 = 1.2 \times 10^9$	Aziz and Lyle (1969)
F^-	extraction, $\mu = 1.0$	$\beta_1 = 4 \times 10^2$	Choppin and Unrein (1976)
Cl^-	extraction with dinonylnaphthalene sulfonic acid, $\mu = 1.0$	$\beta_1 = 1.6$; $\beta_2 = 0.9$	Khopkar and Mathur (1980a)
Cl^-	time-resolved laser fluorescence spectroscopy, $\mu = 6.8$ m, $T = 25°C$	$\beta_1 = 0.02$; $\beta_2 = 0.0007$	Fänghanel *et al.* (1995)
Cl^-	time-resolved laser fluorescence spectroscopy and Pitzer parameterization, $\mu = 0$ m, $T = 25°C$	$\beta_1 = 1.7$; $\beta_2 = 0.2$	Könnecke *et al.* (1997)
N_3^-	extraction with dinonylnaphthalene sulfonic acid pH = 5.9, $\mu = 0.5$, $T = 25°C$	$\beta_1 = 4.36$	Choppin and Barber (1989)
SCN^-	extraction with dinonylnaphthalene sulfonic acid pH = 2.8, $\mu = 1.0$	$\beta_1 = 1.53$; $\beta_2 = 4.08$	Khopkar and Mathur (1974, 1980b)

NO_2^-	extraction with dinonylnaphthalene sulfonic acid	$\beta_1 = 6.6$	Vasudeva Rao *et al.* (1978)
NO_3^-	extraction with dinonylnaphthalene sulfonic acid, $\mu = 1$, $T = 30°C$	$\beta_1 = 2.2$; $\beta_2 = 1.3$	Khopkar and Mathur (1980a)
CO_3^{2-}	time-resolved laser fluorescence spectroscopy and Pitzer parameterization, $\mu = 0$ m, $T = 25°C$	$\beta_1 = 1.3 \times 10^7$; $\beta_2 = 1.0 \times 10^{13}$; $\beta_3 = 1.6 \times 10^{15}$; $\beta_4 = 1.0 \times 10^{13}$	Fänghanel *et al.* (1999)
SO_4^{2-}	extraction, pH = 3.0, $\mu = 2.0$, $T = 25°C$	$\beta_1 = 22$; $\beta_2 = 73$	de Carvalho and Choppin (1967)
SO_4^{2-}	ion exchange	$\beta_1 = 32$; $\beta_2 = 241$	Khopkar and Mathur (1980a)
SO_4^{2-}	time-resolved laser fluorescence spectroscopy, $\mu = 3$ m	$\beta_1 = 8.5$; $\beta_2 = 4.1$	Paviet *et al.* (1996)
$P_3O_9^{3-}$	ion exchange	$\beta_1 = 4.4 \times 10^3$	Elesin *et al.* (1967)
$PW_{11}O_{39}^{7-}$	luminescence spectroscopy 0.1 M HNO_3	$\beta_1 = 5.0 \times 10^6$	Ioussov and Krupa (1997)
$SiW_{11}O_{39}^{8-}$	luminescence spectroscopy 0.1 M HNO_3	$\beta_1 = 3.2 \times 10^6$	Ioussov and Krupa (1997)
acetate	ion exchange, $\mu = 0.5$, $T = 20°C$	$\beta_1 = 114$; $\beta_2 = 1240$	Grenthe (1963)
glycolate	ion exchange, $\mu = 0.5$, $T = 20°C$	$\beta_1 = 700$; $\beta_2 = 5.6 \times 10^4$	Grenthe (1963)
glycinate	extraction, $\mu = 2.0$, $T = 25°C$	$\beta_1 = 6.4$	Tanner and Choppin (1968)
lactate	extraction, $\mu = 0.5$	$\beta_1 = 5.5 \times 10^2$; $\beta_2 = 3.0 \times 10^2$; $\beta_3 = 1.3 \times 10^6$	Nikolaev and Lebedev (1975)
2-hydroxyisobutyrate	cation exchange, $\mu = 0.5$	$\beta_1 = 2.7 \times 10^3$; $\beta_2 = 5.1 \times 10^4$; $\beta_3 = 1.7 \times 10^5$	Dedov *et al.* (1961)

Table 9.4 (*Contd.*)

Ligand	*Conditions*	*Stability constants*	*References*
5-sulfosalicylate	time-resolved laser fluorescence spectroscopy, $\mu = 0.05$	$\beta_1 = 2.8 \times 10^6$; $\beta_2 = 9.8 \times 10^8$	Klenze *et al.* (1998)
$C_4O_4^{2-}$	solubility ion exchange, $\mu = 0.2$	$\beta_1 = 9.1 \times 10^5$; $\beta_2 = 1.40 \times 10^{10}$	Lebedev *et al.* (1960, 1962)
citrate	extraction, $\mu = 0.1$	$\beta_1 = 4.9 \times 10^{10}$; $\beta_2 = 8.5 \times 10^{11}$	Hubert *et al.* (1974)
ethylenediaminetetraacetate	cation exchange, $\mu = 0.1$	$\beta_1 = 2.5 \times 10^{17}$	Elesin and Zaitsev (1971)
nitrilotriacetate	ion exchange, $\mu = 0.1$, $T = 25°C$	$\beta_1 = 6.3 \times 10^{11}$; $\beta_2 = 4.0 \times 10^{20}$	Eberle and Ali (1968)
ethylenediamine-bis(methyl) phosphonic acid	ion exchange, $\mu = 0.5$, $T = 25°C$	$\beta_1 = 2.5 \times 10^6$	Elesin *et al.* (1973)
thenoyltrifluoroacetone	extraction ($CHCl_3$), $\mu = 0.1$, $T = 25°C$	$\beta_3 = 2.5 \times 10^{13}$	Keller and Schreck (1969)

the luminescence lifetimes. However, upon further cooling, the luminescence quenching decreases and sharp luminescence bands are observed for these complexes at 77 K. The luminescence quenching is severe in Cm(III) complexes with $P_2W_{17}O_{61}^{10-}$ as these complexes do not luminesce in solution at 293 K. In contrast, $CmW_{10}O_{36}^{9-}$, $CmPW_{11}O_{39}^{4-}$, $CmSiW_{11}O_{39}^{5-}$, $Cm(SiW_{11}O_{39})_2^{13-}$, and $Cm(PW_{11}O_{39})_2^{11-}$ all display luminescence in D_2O at 293 K. At 77 K, the luminescence spectra of the $P_2W_{17}O_{61}^{10-}$ complexes are very similar to the other Cm(III) polytungstate complexes. Addition of molybdate to solutions of the Cm(III) polytungstate or heteropolytungstate complexes results in rapid quenching of the Cm(III) luminescence (Yusov and Fedoseev, 1992a,b). This behavior is the opposite of what is observed for the analogous Eu, Nd, and Yb systems.

The trends for the complexation of carboxylate ligands to Cm(III) are somewhat difficult to interpret. The β_1 values at $\mu = 0.5$ can be compared for acetate, glycolate, lactate, and 2-hydroxyisobutyrate (Table 9.4). The β_1 value increases from 114 to 700 in going from acetate to glycolate, which could be due to interaction of the hydroxyl group in glycolate with the Cm(III) center. One would expect that the inductive effect of an added methyl group would lead to a further increase in β_1 for complexation of lactate ion, but the β_1 value drops to 550 for lactate. On the other hand, addition of yet another methyl group does result in a significant increase in β_1 for 2-hydroxyisobutyrate ($\beta_1 = 2700$). The anomaly for lactate may simply reflect the differing experimental conditions under which the measurements were made. As would be expected, the chelating carboxylate ligands display substantially stronger binding to Cm(III) than the monocarboxylate ligands.

There are a limited number of reports concerning Cm(IV) in aqueous media. A fluoride complex of Cm(IV) was obtained when CmF_4 was dissolved in concentrated (15 M) MF solution (M = alkali–metal ion) (Asprey and Keenan, 1958; Keenan, 1961) (see Fig. 9.2). Even under these conditions, and using ^{244}Cm, the self-reduction rate because of alpha decay is about 1% per minute. When CmF_4 is added to aqueous NH_4F, an immediate oxidation–reduction reaction occurs, with deposition of CmF_3. This is in sharp contrast to the stability of Am(IV) in NH_4F solution (Asprey and Penneman, 1962).

Other than the CmF_4/MF system, the only claims for chemically generated Cm(IV) in solution are the reports that red solutions result when aqueous Cm(III) solutions are mixed with potassium peroxydisulfate and heteropolyanions such as $[P_2W_{17}O_{61}]^{10-}$ (Saprykin *et al.*, 1976; Kosyakov *et al.*, 1977). Cm(IV), produced by persulfate oxidation of Cm(III) in phosphotungstate solution, converts back to Cm(III) at a rate that suggests that the reduction involves both radiolytic mechanisms and direct reduction by water (Kosyakov *et al.*, 1977). In contrast, reduction of Am(IV) to Am(III) under similar conditions is dominated by radiolytic processes. Electrochemical generation of Cm(IV) in phosphate solutions was unsuccessful, owing to the large Cm(IV)/Cm(III) potential, estimated to be

greater than 2 V in these systems (Myasoedov *et al*., 1973, 1974). Other attempts to prepare Cm(IV) by oxidation of Cm(III) in solution have failed. These attempts include electrochemical methods (Myasoedov *et al*., 1973, 1974; Ionova and Spitsyn, 1978) and the use of sodium perxenate (Holcomb, 1967) and ozone (Pages and Demichelis, 1966), agents which readily oxidize Am(III) to Am(V) or Am(VI). $Cm(OH)_3$ in $NaHCO_3$ is not oxidized by ozone or $Na_2S_2O_8$, conditions which produce Am(VI) as a carbonate complex (Coleman *et al*., 1963).

The polytungstate Cm(IV) complexes – $CmW_{10}O_{36}^{8-}$, $Cm(SiW_{11}O_{39})^{12-}$, and $Cm(PW_{11}O_{39})_2^{10-}$ – display chemiluminescence upon reduction to Cm(III) (Yusov *et al*., 1986a,b). The brightest chemiluminescence was observed when the initial complexes were treated with 1–3 M alkali, in which case water in the system most probably served as reductant. Chemiluminescence has also been observed during dissolution of the Cm(IV) double oxide Li_xCmO_y in mineral acids (Yusov and Fedoseev, 1989a, 1991).

Despite the numerous unsuccessful attempts to oxidize Cm(III) and Cm(IV) compounds to higher oxidation states, some theoretical work suggests the possibility that Cm(VI) may be even more stable than Am(VI), and the lack of success in preparing Cm(VI) may result from the low stability of Cm(V) and the high Cm(IV)/Cm(III) potential (Ionova and Spitsyn, 1978; Spitsyn and Ionova, 1978). One report claims the synthesis of Cm(VI) by beta decay of $^{242}AmO_2^+$ (Peretrukhin *et al*., 1978).

$$^{242}AmO_2^+ \xrightarrow[16h]{\beta^-} CmO_2^{2+}$$

The $K_3AmO_2(CO_3)_2$ starting material was aged 18–40 h and then dissolved in 0.1 M $NaHCO_3$ in the presence of ozone, followed by addition of $Na_4UO_2(CO_3)_3/K_2CO_3$ solution to precipitate MO_2^{2+} species as $K_4MO_2(CO_3)_3$. From the enhancement of Cm in the precipitate over that expected for Cm(III), it was concluded that a 30–60% conversion to Cm(VI) had occurred.

Cm(II) is unknown other than as a transient aqueous species and a species coprecipitated from melts, and possibly in CmO. Pulse radiolysis, producing OH radicals as oxidant and the aquo electron as reductant, produced changes in aqueous americium and curium perchlorate solutions. The new absorbances were attributed to transient formation of Cm(II), A_{max} 240 nm, and Cm(IV), A_{max} 260 nm (Sullivan *et al*., 1976).

9.8.2 Organic

Studies of Cm chemistry in pure organic solvents are rare. The solvation of Cm(III) in non-aqueous and binary mixed solvents has been investigated by luminescence spectroscopy (Kimura *et al*., 2001). This study revealed that the relative preference for solvation of Cm(III) ion is dimethylsulfoxide > dimethylformamide > H_2O > methanol.

Very few curium compounds containing organic ligands have actually been isolated (see Section 9.7.8), although it seems likely that efforts to isolate such compounds would prove fruitful. Because of the interest in extraction schemes for treating radioactive wastes, a substantial number of studies have determined stability constants and distribution coefficients for solutions containing curium and various organic ligating agents. However, these experiments have often involved tracer amounts of curium and have employed a variety of experimental conditions (ionic strength, temperature, concentrations, etc.); therefore, quantitative comparisons of the determined values are difficult. As with the inorganic anions, values, and in some cases even trends, can vary markedly under seemingly similar conditions. Most studies do not involve isolation or definitive formulation of the actual species in solution, and it is possible that complicated structures occur, e.g. $CmF_3 \cdot (HDEHP)_x$ (Aziz and Lyle, 1969).

Furthermore, crystal structure determinations for a number of pertinent lanthanide and actinide extractant complexes illustrate that surprises may be expected when more definitive structural information becomes available (Burns, 1982; Bowen *et al*., 1984). Because of these complications, we have not tried to analyze the voluminous Cm extraction data that are available, but included in Table 9.4 the data for only a few of the more important extractants. The reader is referred to a more extensive compilation for additional data of this type (Jones and Choppin, 1969).

Keller and Schreck (1969) have shown that Cm(III), as well as Ac(III), Am(III), and Cf(III), are extracted with β-diketone ligands as 1:3 chelates only, with stability constants ($\log\beta_3$) decreasing in the series Cf > Cm ~ Am > Ac. Keller *et al*. (1966) have also shown that Am(III) and Cm(III) are extracted from aqueous solutions into chloroform solutions of 8-hydroxyquinoline ligands as AnL_2Y, where L is the 8-hydroxyquinolate anion and Y is probably OH^-, in contrast to the lanthanides, which are extracted as LnL_3 chelates.

Distribution ratios (chloroform–water) have been reported for curium complexes with 8-hydroxyquinoline, cupferron, and *N*-benzoylphenylhydroxylamine (Akatsu *et al*., 1968). Only 1:3 complexes with Cm(III) and Am(III) were reported, and extraction into the organic phase appears to be very high at pH values above 5. Solution interaction of Cm(III) with bis(salicylidene)ethylenediimine and derivatives has also been studied (Stroński and Rekas, 1973). With the reagent arsenazo-III, both Cm(III) and Am(III) form 1:1 and 1:2 complexes (Myasoedov *et al*., 1970).

During the last 20 years, the use of neutral bifunctional compounds as extractants for trivalent actinides has been extensively investigated. These compounds include carbamoylmethylphosphonates, CMPOs, and diamides. The mechanism by which these extractants operate is still open to debate. Slope analysis studies often give varied results. For example, Mincher (1992) has reported the extraction of trivalent actinides (including Cm) by CMPO to be due to formation of $M(NO_3)_3(CMPO)_4$ complexes, whereas most other studies indicate a stoichiometry of the type $M(NO_3)_3L_3$ (Horwitz *et al*.,

1981). Similar confusion can be cited for the diamide extractants, although mechanistic studies have not been performed specifically with Cm for this class of ligands.

9.9 ANALYTICAL CHEMISTRY

The analysis for curium has been done by the typical methods for metal ions and alpha-emitting actinides, such as alpha, gamma, and neutron spectroscopy, nuclear track detection, photon/electron-rejecting alpha liquid scintillation, mass spectrometry, spectrophotometry of highly colored complexes such as arsenazo, and time-resolved laser-induced fluorescence or luminescence spectroscopy (Buijs, 1973). In most cases, at least some separations are required before analysis of curium.

9.9.1 Analysis of curium

The curium isotopes, 242, 243, and 244, emit high-energy alpha particles (see Table 9.1) that are easily quantified in the presence of lower-energy α emitters without extensive separations. Curium isotopes 245–248 emit lower-energy alpha particles and generally require more extensive separations before alpha analysis. Alpha spectrometry is typically used for curium determination, although photon/electron-rejecting alpha liquid scintillation has been shown to have lower detection limits when combined with extractive scintillators (Metzger *et al*., 1995; Dacheux and Aupais, 1998). One extractive scintillator was a combination of HDEHP and CMPO, allowing the separation and analysis to occur in one step (Metzger *et al*., 1995). The key to alpha spectrometry is the preparation of counting plates with minimal solids to degrade the energy of the alpha particles. Various deposition techniques have been used, including electrodeposition, evaporation, and precipitation of insoluble compounds (Trautmann and Folger, 1989; Kaye *et al*., 1995; Gascon *et al*., 1996; Rameback and Skalberg, 1998; Diakov *et al*., 2001). Precipitation can involve addition of a lanthanide ion to act as a carrier for curium (Kaye *et al*., 1995). Nuclear track analysis has been shown to be useful for very low concentrations of curium, such as environmental samples and waste streams at nuclear power plants (Lancsarics *et al*., 1988; Espinosa *et al*., 1995). The alpha energies were determined by the size of the track after calibration with sources of known energy.

Spontaneous fission occurs for the even isotopes of curium, allowing neutron counting to be used for their determination, especially for ^{244}Cm and ^{248}Cm, but this method requires pure isotopes for quantification (Trautmann and Folger, 1989). Curium analyses have been done by inductively coupled mass spectrometry and isotope dilution thermal ionization mass spectrometry after separation

to obtain a pure curium solution (Kinard *et al.*, 1995; Niese and Gleisberg, 1995; Chartier and Aubert, 1999).

As has been mentioned previously, time-resolved laser-induced fluorescence spectroscopy has been shown to be an especially valuable tool for investigating Cm solution chemistry, but it has also proved useful for quantitative determination of Cm (Elesin *et al.*, 1973; Dem'yanova *et al.*, 1986; Yusov *et al.*, 1986a,b; Decambox *et al.*, 1989; Kim *et al.*, 1991; Myasoedov and Lebedev, 1991; Myasoedov, 1994; Moulin *et al.*, 1997; Dacheux and Aupais, 1998). The Cm fluorescence emission signal is strong enough that no separations from other transuranium or lanthanide elements are required to use this technique to quantify Cm ion in solution. Sensitivity for curium detection is about 5×10^{-11} M in carbonate solution without separation from matrix elements (Radchenko *et al.*, 1999). An even lower detection limit of 5×10^{-13}M has been observed at 612 nm (Moulin *et al.*, 1997).

9.9.2 Separations for analysis

Separations are a primary component of most analytical procedures. Initial separation is from non-radioactive elements and the large quantity of uranium that may be present in the sample. Plutonium is often separated to allow determination without interference from the higher actinides. Separation of curium from americium and the lanthanides is possible, but may not be necessary, depending on the method of final analysis. A variety of separation methods have been reported, including ion exchange, extraction chromatography, and solvent extraction, or combinations of several of these methods. Early work was summarized in Gmelin (Buijs, 1973). A more recent review summarizes many of the methods for analytical separations (Myasoedov, 1994).

Anion-exchange resins have been used with HCl and HNO_3 in both aqueous and aqueous–alcohol mixtures (Trautmann and Folger, 1989; Gascon *et al.*, 1996; Diakov *et al.*, 2001). Anion exchange alone usually results in a product containing all trivalent actinides and lanthanides. Cation exchange from HCl solutions has been used to separate lanthanides from actinides, or with α-hydroxyisobutyric acid to separate both lanthanides and actinides (Myasoedov, 1994). Anion exchange from HCl has also been used to remove uranium and plutonium, followed by a rapid separation of curium from americium by high-pressure liquid chromatography (HPLC) using 2-hydroxy-2-methylbutyric acid as the eluent (Trautmann and Folger, 1989). Americium–curium separation was rapid, with no overlap between curium and americium peaks. Anion exchange has been combined with HDEHP to separate an americium–curium product (Gascon *et al.*, 1996).

Another method involves a combination of extraction of plutonium with trioctylphosphine oxide in cyclohexane from HNO_3, then absorbing the metal ions onto Dowex® 50 resin from an HCl solution containing oxalic acid.

Washing the column with 2 M HCl removed impurities, followed by americium–curium elution in 6 M HNO_3 (Niese and Gleisberg, 1995).

Extraction chromatography with CMPO on an organic support allows ready separation of an americium and a curium fraction. A commercially available resin based on CMPO has been used (Kaye *et al*., 1995; Maxwell, 1996).

Separations by solvent extraction include extraction of all the actinides into HDEHP, with selective back-extraction of americium and curium into 5 M HNO_3 (Rameback and Skalberg, 1998). Another method used extraction of plutonium from HCl solution with triisooctylamine in xylene. Americium and curium were then extracted with dibutyl-*N*,*N*-diethylcarbamoyl phosphonate and stripped into dilute acid (Kimura *et al*., 1996). CMPO has been used extensively for solvent extraction separations of americium and curium (Myasoedov and Lebedev, 1991). Other separation methods are given in the review by Myasoedov (1994).

ACKNOWLEDGMENT

This work was performed under the auspices of the U.S. Department of Energy. The authors gratefully acknowledge the excellent editorial support of Paula Ložar and helpful suggestions by Calvin Delegard (Pacific Northwest National Laboratory) and anonymous peer reviewers.

REFERENCES

Aas, W., Steinle, E., Fanghänel, Th., and Kim, J. I. (1999) *Radiochim. Acta*, **84**, 85–8.

Abramychev, S. M., Balashov, N. V., Vesnovskii, S. P., Vjachin, V. N., Lapin, V. G., Nikitin, E. A., and Polynov, V. N. (1992) *Nucl. Instrum. Methods*, **B70**, 5–8.

Akatsu, E., Hoshi, M., Ono, R., and Ueno, K. (1968) *J. Nucl. Sci. Tech.*, **5**, 252–5.

Arisaka, M., Kimura, T., Suganuma, H., and Yoshida, Z. (2002) *Radiochim. Acta*, **90**, 193–7.

Artisyuk, V., Chmelev, A., Saito, M., Suzuki, M., and Fujii, E.Y. (1999) *J. Nucl. Sci. Tech.*, **36**, 1135–40.

Asprey, L. B., Ellinger, F. H., Fried, S., and Zachariasen, W. H. (1955) *J. Am. Chem. Soc.*, **77**, 1707–8.

Asprey, L. B. and Keenan, T. K. (1958) *J. Inorg. Nucl. Chem.*, **7**, 27–31.

Asprey, L. B. and Penneman, R. A. (1962) *Inorg. Chem.*, **1**, 134–6.

Asprey, L. B., Keenan, T. K., and Kruse, F. H. (1965) *Inorg. Chem.*, **4**, 985–6.

Asprey, L. B. and Haire, R. G. (1973) *Inorg. Nucl. Chem. Lett.*, **9**, 1121–8.

Aziz, A. and Lyle, S. J. (1969) *J. Inorg. Nucl. Chem.*, **31**, 3471–80.

Bagnall, K. W. (1967) *Coord. Chem. Rev.*, **2**, 145–62.

Bagnall, K. W. (1972) *The Actinide Elements,* Elsevier, New York.

Bansal, B. M. and Damien, D. (1970) *Inorg. Nucl. Chem. Lett.*, **6**, 603–6.

Barbanel, Yu. A., Kotlin, V. P., and Kolin, V. V. (1977) *Radiokhimiya*, **19**, 497–501; *Sov. Radiochem.*, **19**, 406–9.

Baumgärtner, F., Fischer, E. O., Billich, H., Dornberger, E., Kanellakopulos, B., Roth, W., and Stieglitz, L. (1970) *J. Organomet. Chem.*, **22**, C17–18.
Baybarz, R. D. (1970) *At. Energy Rev.*, **8**, 327–60.
Baybarz, R. D. and Adair, M. L. (1972) *J. lnorg. Nucl. Chem.*, **34**, 3127–30.
Baybarz, R. D., Bohet, J., Buijs, K., Colsen, L., Müller, W., Reul, J., Spirlet, J. C., and Toussaint, J. C. (1976) in *Transplutonium 1975* (eds. W. Müller and R. Lindner), North-Holland, Amsterdam, pp. 61–8.
Beitz, J. V. and Hessler, J. P. (1980) *Nucl. Tech.*, **51**, 169–77.
Benedict, U., Haire, R. G., Peterson, J. R., and Itié, J. P. (1985) *J. Phys. F*, **15**, L29–35.
Bibler, N. E. (1972) *Inorg. Nucl. Chem. Lett.*, **8**, 153–6.
Bigelow, J. E., Collins, E. D., and King, L. J. (1980) in *Actinide Separations* (ACS Symp. Ser. 117), American Chemical Society, Washington DC, pp. 147–55.
Bigelow, J. (2002) Oak Ridge National Laboratory, personal communication.
Bokelund, H., Apostolidis, C., and Glatz, J. P. (1989) *J. Nucl. Mater.*, **166**, 181–8.
Bond, W. D. and Leuze, R. E. (1980) in *Actinide Separations* (ACS Symp. Ser. 117), American Chemical Society, Washington DC, pp. 441–53.
Bowen, S. M., Dresler, E. N., and Paine, R. T. (1984) *Inorg. Chim. Acta*, **84**, 221; also see earlier articles by these authors.
Brown, D. (1968) *Halides of the Lanthanides and Actinides,* Wiley-Interscience, New York.
Buijs, K. (1973) in *Handbook of Inorganic Chemistry, Transuranics*, part A2 (ed. G. Koch), Verlag Chemie, Weinheim, pp. 164–73.
Buijs, K., Müller, W., Reul, J., and Toussaint, J. C. (1973) Euratom Report 5040. *Nucl. Sci. Abstr.*, **29**, 02573.
Bukina, T. I., Khizhnyak, P. L., Karalova, Z. K., and Myasoedov, B. F. (1988) *Radiokhimiya.*, **31**, 94–98; *Sov. Radiochem.*, **31**, 452–56.
Burnett, J. (1966) *J. Inorg. Nucl. Chem.*, **28**, 2454–6.
Burney, G. A. and Porter, J. A. (1967) *Inorg. Nucl. Chem. Lett.*, **3**, 79–85.
Burney, G. A. (1980) *Sep. Sci. Technol.*, **15**, 163–82.
Burns, J. H., Peterson, J. R., and Stevenson, J. N. (1975) *J. Inorg. Nucl. Chem.*, **37**, 743–9.
Burns, J. H. (1982) Oak Ridge National Laboratory Report, ORNL/TM–8221.
Carnall, W. T., Fields, P. R., Stewart, D. C., and Keenan, T. K. (1958) *J. Inorg. Nucl. Chem.*, **6**, 213–16.
Chartier, F. and Aubert, P. (1999) *Fresenius J. Anal. Chem.*, **364**, 320.
Charvillat, J. P., Benedict, U., Damien, D., and Müller, W. (1975) *Radiochem. Radioanal. Lett.*, **20**, 371–81.
Charvillat, J. P., Benedict, U., Damien, D., de Novion, C. H., Wojakowski, A., and Müller, W. (1976) in *Transplutonium 1975* (eds. W. Müller and R. Lindner), North-Holland, Amsterdam, , pp. 79–84.
Charvillat, J. P. and Zachariasen, W. H. (1977) *Inorg. Nucl. Chem. Lett.*, **13**, 161–3.
Chikalla, T. D. and Eyring, L. (1969) *J. Inorg. Nucl. Chem.*, **31**, 85–93.
Choppin, G. R. and Unrein, P. J. (1976) in *Transplutonium 1975* (eds. W. Müller and R. Lindner), North-Holland, Amsterdam, pp. 97–105.
Choppin, G. R. and Barber, D. W. (1989) *J. Less Common Metals*, **149**, 231–5.
Choppin, G. R. (1999) in *Chemical Separation Technologies and Related Methods of Nuclear Waste Management* (eds. G. R. Choppin and M. Kh. Khankhasayev), Kluwer Academic Publications, Dordrecht, pp. 1–16.

Chu, Y. Y. (1972) *Phys. Rev. A*, **5** (1), 67–72.
Coleman, J. S., Keenan, T. K., Jones, L. H., Carnall, W. T., and Penneman, R. A. (1963) *Inorg. Chem.*, **2**, 58–61.
Cunningham, B. B. and Wallmann, J. C. (1964) *J. Inorg. Nucl. Chem.*, **26**, 271–5.
Cunningham, B. B. (1966) *Prep. Inorg. Reactions*, **3**, 79–121.
Dacheux, N. and Aupais, J. (1998) *Anal. Chim. Acta* **363**, 279–94.
Damien, D., Charvillat, J. P., and Müller, W. (1975) *Inorg. Nucl. Chem. Lett.*, **11**, 451–7.
Damien, D., Wojakowski, W., and Müller, W. (1976) *Inorg. Nucl. Chem. Lett.*, **12**, 441–9.
Damien, D. A., Haire, R. G., and Peterson, J. R. (1979a) *J. Less Common Metals*, **68**, 159–65.
Damien, D. A., Haire, R. G., and Peterson, J. R. (1979b) *J. Phys. Colloq.*, 95–100.
Davydov, A. V., Myasoedov, B. F., Travnikov, S. S., and Fedoseev, E. V. (1978) *Radiokhimiya*, **20**, 257–64; *Sov. Radiochem.*, **20**, 217–24.
de Carvalho, R. G. and Choppin, G. R. (1967) *J. Inorg. Nucl. Chem.*, **29**, 725–35.
Decambox, P., Mauchien, P., and Moulin, C. (1989) *Radiochim. Acta*, **42**, 23–8.
Dedov, V. D., Lebedev, I. A., Ryzhov, M. N., Trukhlyaev, P. S., and Yakovlev, G. N. (1961) *Radiokhimiya*, **3**, 701–5; *Sov. Radiochem.*, **3**, 197–201.
Dedov, V. D., Volkov, V. V., Gvozdev, B. A., Ermakov, V. A., Lebedev, I. A., Razbitnoi, V. M., Trukhlyaev, P. S., Chuburkov, Yu. T., and Yakovlev, G. N. (1965) *Radiokhimiya*, **7**, 453–61; *Sov. Radiochem.*, 7, 452–8.
Deissenberger, R., Köhler, S., Ames, F., Eberhardt, K., Erdman, N., Funk, H., Herrmann, G., Kluge, H.-J., Munnemann, M., Passler, G., Riegel, J., Scheere, F., Trautmann, N., and Urban, F.-J. (1995) *Angew. Chem. Int. Ed. Engl.*, **34**, 814–15.
Dem'yanova, T. A., Stepanov, A. V., Babaev, A. S., and Aleksandruk, V. M. (1986) *Radiokhimiya*, **28**, 494–8; *Sov. Radiochem.*, **28**, 450–3.
Désiré, B., Hussonnois, M., and Guillaumont, R. (1969) *C. R. Acad. Sci. Paris C*, **269**, 448–51.
Diakov, A. A., Perekhozheva, T. N., and Zlokazova, E. I. (2001) *Rad. Meas.*, **34**, 463–6.
Eberle, S. H. and Ali, S. A. (1968) *Z. Anorg. Allg. Chem.*, **361**, 1–14.
Edelstein, N. M., Navratil, J. D., and Schulz, W. W. (eds.) (1985) *Americium and Curium Chemistry and Technology,* Reidel Publishing Co, Boston.
Elesin, A. A., Lebedev, I. A., Piskunov, E. M., and Yakovlev, G. N. (1967) *Radiokhimiya*, **9**, 161–6; *Sov. Radiochem.*, **9**, 159–63.
Elesin, A. A. and Zaitsev, A. A. (1971) *Radiokhimiya*, **13**, 775–8; *Sov. Radiochem.*, **13**, 798–801.
Elesin, A. A., Zaitsev, A. A., Sergeev, G. M., and Nazarova, I. I. (1973) *Radiokhimiya*, **15**, 64–8; *Sov. Radiochem.*, **15**, 62–6.
Eller, P. G. and Penneman, R. A. (1986) in *The Chemistry of the Actinide Elements*, Chapman and Hall, New York, ch. 9.
Erdmann, B. and Keller, C. (1971) *Inorg. Nucl. Chem. Lett.*, **7**, 675–83.
Erdmann, B. and Keller, C. (1973) *J. Solid State Chem.*, **7**, 40–8.
Espinosa, G., Gammage, R. B., Meyer, K., Wheeler, R. B., and Salasky, M. (1995) *Rad. Prot. Dos.*, **59**, 227–9.
Eubanks, I. D. and Thompson, M. C. (1969) *Inorg. Nucl. Chem. Lett.*, **5**, 187–91.
Eyring, L. (1967) in *Adv. Chem. Ser.*, **71**, pp. 67–85. American Chemical Society, Washington DC.

Fanghänel, Th., Kim, J. I., Paviet, P., Klenze, R., and Hauser, W. (1994) *Radiochim. Acta*, **66/67**, 81–7.
Fanghänel, Th., Kim, J. I., Klenze, R., and Kato, Y. (1995) *J. Alloys Compds*, **225**, 308–11.
Fanghänel, Th., Könnecke, Th., Weger, H., Paviet-Hartmann, P., Neck, V., and Kim, J. I. (1999) *J. Soln. Chem.*, **28**, 447–62.
Fargeas, M., Fremont- Lamouranne, R., Legoux, Y., and Merini, J. (1986) *J. Less Common Metals*, **121**, 439–44.
Felker, L. K. and Benker, D. E. (1995) *Application of the TRUEX Process to Highly Irradiated Targets*, USDOE Report ORNL/TM–12784.
Fournier, J. M., Blaise, A., Müller, W., and Spirlet, J. C. (1977) *Physica*, **87–88B**, 30–1.
Fuger, J., Reul, J., and Müller, W. (1975) *Inorg. Nucl. Chem. Lett.*, **11**, 265–75.
Fuger, J. and Oetting, F. L. (1976) in *The Chemical Thermodynamics of Actinide Elements and Compounds*, part 2, *The Actinide Aqueous Ions*, IAEA, Vienna, p. 48.
Fuger, J. and Martinot, L. (1985) The Actinides, Standard Potentials in Aqueous Solutions in (eds. A. J. Bard, R. Parsons, and J. Jordan), Marcel Dekker, New York, ch. 21, pp. 631–73.
Fuger, J., Haire, R. G., and Peterson, J. R. (1993) *J. Alloys Compds*, **200**, 181–5.
Fujita, D. K., Parsons, T. C., Edelstein, N., Noe, M., and Peterson, J. R. (1976) in *Transplutonium 1975* (eds. W. Müller and R. Lindner), North-Holland, Amsterdam, pp. 173–8.
Gascon, J. L., Rodriguez, M., and Suarez Del Rey, J. A. (1996) *J. Radioanal. Nucl. Chem.*, **207**, 63–9.
Gerasimov, A. S., Zaritskaya, T. S., Kiselev, G. V., and Myrtsymova, L. A. (2000) *At. Energy*, **89**, 663–7.
Gibson, J. K. and Haire, R. G. (1985) *J. Solid State Chem.*, **59**, 317–23.
Gibson, J. K. and Haire, R. G. (1987) *J. Less Common Metals*, **132**, 149–54.
Gibson, J. K. and Haire, R. G. (1990) *J. Phys. Chem.*, **94**, 935–9.
Gibson, J. K. and Haire, R. G. (1998) *J. Phys. Chem. A*, **102**, 10746–53.
Gibson, J. K. and Haire, R. G. (1999) *Organometallics*, **18**, 4471–7.
Gmelin Handbook of Chemistry Inorganic (1972–74) Suppl. Work, 8th edn, *Transuranium*, part A1, II (1973); part A1, II (1974); part A2 (1973); part C (1972),Verlag Chemie, Weinheim.
Grenthe, I. (1963) *Acta. Chem. Scand.*, **17**, 1814–15.
Groh, H. J., Huntoon, R. T., Schlea, C. S., Smith, J. A., and Springer, F. H. (1965) *Nucl. Appl.*, **1**, 327–36.
Gutmacher, R. G., Hulet, E. K., and Conway, J. G. (1964) *J. Opt. Soc. Am.*, **54**, 1403–4.
Haire, R. G. and Fahey, J. A. (1977) *J. Inorg. Nucl. Chem.*, **39**, 837–41.
Haire, R. G., Lloyd, M. H., Milligan, W. O., and Beasley, M. L. (1977) *J. Inorg. Nucl. Chem.* **39**, 843–7.
Haire, R. G. (1980) *Proc. 10th Journée des Actinides*, Stockholm, p. 19.
Haire, R. G., Nave, S. E., and Huray, P. G. (1982) *12th Journée des Actinides*, Orsay.
Haire, R. G., Benedict, U., Peterson, J. R., Dufour, C., and Itié, J. P. (1985) *J. Less Common Metals*, **109**, 71–8.
Hale, W. H. Jr and Mosley, W. C. (1973) *J. Inorg. Nucl. Chem.*, **35**, 165–71.
Haug, H. O. (1967) *J. Inorg. Nucl. Chem.*, **29**, 2753–8.
Haug, H. O. (1974) *J. Radioanal. Chem.*, **21**, 187–98.

Haug, H. O. and Baybarz, R. D. (1975) *Inorg. Nucl. Chem. Lett.*, **11**, 847–55.
Hoffman, D. C. (1985) in *Americium and Curium Chemistry and Technology* (eds. N. M. Edelstein, J. D. Navratil, and W. W. Schulz), Reidel Publishing, Boston, pp. 241–260.
Holcomb, H. P. (1967) *J. Inorg. Nucl. Chem.*, **29**, 2885–8.
Holden, N. E. (1989) *Pure Appl. Chem.*, **61**, 1483–504.
Horwitz, E. P., Muscatello, A. C., Kalina, D. G., and Kaplan, L. (1981) *Sep. Sci. Technol.*, **16**, 417–37.
Horwitz, E. P. and Schulz, W. W. (1991) The Truex process: A vital tool for disposal of U.S. defense nuclear waste, in *New Separation Chemistry Techniques for Radioactive Waste and Other Specific Applications*, Elsevier Applied Science, Amsterdam.
Hubert, S., Hussonnois, M., Brillard, L., Goby, G., and Guillaumont, R. (1974) *J. Inorg. Nucl. Chem.*, **36**, 2361–6.
Ionova, G. V. and Spitsyn, V. I. (1978) *Dokl. Akad. Nauk SSSR*, **241**, 590–1; *Dokl. Acad. Sci. USSR*, **241**, 348–9.
Ionova, G., Madic, C., and Guillaumont, R. (1997) *Radiochim. Acta*, **78**, 83–90.
Ioussov, A. and Krupa, J. C. (1997) *Radiochim. Acta*, **78**, 97–104.
Jarvinen, G. D. (1999) in *Chemical Separation Technologies and Related Methods of Nuclear Waste Management* (eds. G. R. Choppin and M. Kh. Khankhasayev), Kluwer Academic Publications, Dordrecht, pp. 53–70.
Jones, A. D. and Choppin, G. R. (1969) *Actinide Rev.*, **1**, 311–36.
Kanellakopulos, B., Charvillat, J. P., Maino, F., and Müller, W. (1976) in *Transplutonium 1975* (eds. W. Müller and R. Lindner), North-Holland, Amsterdam, pp. 181–90.
Karalova, Z. K., Myasoedov, B. F., Bukina, T. I., and Lavrinovich, E. A. (1988) *Solvent Extr. Ion Exch.*, **6**, 1109–35.
Katz, J. J. and Seaborg, G. T. (1957) *The Chemistry of the Actinide Elements,* Methuen, London.
Katz, J. J. and Sheft, I. (1960) *Adv. Inorg. Chem. Radiochem.*, **2**, 195–236.
Kaye, J. H., Strebin, R. S., and Orr, R. D. (1995) *J. Radioanal. and Nucl. Chem.*, **194**, 191–6.
Kazantsev, G. N., Skiba, O. V., Burnaevà, A. A., Kolesnikov, V. P., Volkov, Yu. F., Kryukova, A. I., and Korshunov, I. A. (1982) *Radiokhimiya*, **24**, 88–91.
Keenan, T. K. (1961) *J. Am. Chem. Soc.*, **83**, 3719–20.
Keenan, T. K. (1966a) *Inorg. Nucl. Chem. Lett.*, **2**, 153–6.
Keenan, T. K. (1966b) *Inorg. Nucl. Chem. Lett.*, **2**, 211–4.
Keenan, T. K. (1967a) *Inorg. Nucl. Chem. Lett.*, **3**, 391–6.
Keenan, T. K. (1967b) *Inorg. Nucl. Chem. Lett.*, **3**, 463–7.
Keenan, T. K. and Asprey, L. B. (1969) *Inorg. Chem.*, **8**, 235–8.
Keller, C. and Walter, K. H. (1965) *J. Inorg. Nucl. Chem.*, **27**, 1253–60.
Keller, C., Eberle, S. H., and Mosdzelewski, K. (1966) *Radiochim. Acta*, **5**, 185–8.
Keller, C. and Schreck, H. (1969) *J. Inorg. Nucl. Chem.*, **31**, 1121–32.
Keller, C. (1971) *The Chemistry of the Transuranium Elements,* Verlag Chemie, Weinheim.
Kerrigan, W. J. and Banick, C. J. (1975) *J. Inorg. Nucl. Chem.*, **37**, 641.
Khopkar, P. K. and Mathur, J. N. (1974) *J. Inorg. Nucl. Chem.*, **36**, 3819–25.
Khopkar, P. K. and Mathur, J. N. (1980a) *J. Inorg. Nucl. Chem.*, **42**, 109–13.

Khopkar, P. K. and Mathur, J. N. (1980b) *Thermochim. Acta*, **37**, 71–8.
Kim, J. I., Klenze, R., and Wimmer, H. (1991) *Eur. J. Solid State Inorg. Chem.*, **28**, 347–56.
Kimura, T. and Choppin, G. R. (1994) *J. Alloys Compds*, **213/214**, 313–17.
Kimura, T., Choppin, G. R., Kato, Y., and Yoshida, Z. (1996) *Radiochim. Acta*, **72**, 61–4.
Kimura, T., Kato, Y., Takeishi, H., and Choppin, G. R. (1998) *J. Alloys Compds*, **271/274**, 719–22.
Kimura, T., Nagaishi, R., Kato, Y., and Yosida, Z. (2001) *Radiochim. Acta*, **89**, 125–30.
Kinard, W. F., Bibler, N. E., Coleman, C. J., Dewberry, R. A., Boyce, W. T., and Wyrick, S. B. (1995) *ASTM Spec. Tech. Publ.*, STP **1291**, 48–58.
Klenze, R., Panak, P., and Kim, J. I. (1998) *J. Alloys Compds*, **271–273**, 746–50.
Knauer, J. B. (2002) Oak Ridge National Laboratory, personal communication.
Konings, R. J. M. (2001a) *J. Nucl. Mater.*, **295**, 57–63.
Konings, R. J. M. (2001b) *J. Nucl. Mater.*, **298**, 255–68.
Könnecke, Th., Fänghanel, Th., and Kim, J. I. (1997) *Radiochim. Acta*, **76**, 131–5.
Korotkin, Yu. S. (1974) *Radiokhimiya*, **16**, 221–5; *Sov. Radiochem.*, **16**, 223–6.
Kosyakov, V. N., Timofeev, G. A., Erin, E. A., Andreev, V. I., Kopytov, V. V., and Simakin, G. A. (1977) *Radiokhimiya*, **19**, 511–17; *Sov. Radiochem.*, **19**, 418–23.
Kulyako, Yu. M., Trofimov, T. I., Malikov, D. A., Lebedev, I. A., and Myasoedov, B. F. (1993) *Radiokhimiya*, **35**, 38–41; *Radiochemistry*, **35**, 399–401.
Lancsarics, G., Feher, I., Sagi, L., and Palfalvi, J. (1988) *Rad. Prot. Dos.*, **22**, 111–3.
Laubereau, P. G. and Burns, J. H. (1970a) *Inorg. Chem.*, **9**, 1091–5.
Laubereau, P. G. and Burns, J. H. (1970b) *Inorg. Nucl. Chem. Lett.*, **6**, 59–63.
Lebedev, I. A., Pirozhkov, S. V., and Yakovlev, G. N. (1960) *Radiokhimiya*, **2**, 549–58; *Sov. Radiochem.*, **2** (5), 39–47.
Lebedev, I. A., Pirozhkov, S. V., and Yakovlev, G. N. (1962) *Radiokhimiya*, **4**, 304–8; *Sov. Radiochem.*, **4**, 273–6.
Lebedev, I. A., Myasoedov, B. F., and Guseva, L. I. (1974) *J. Radioanal. Chem.*, **21**, 259–66.
Lederer, C. M. and Shirley, V. S. (eds.) (1978). *Table of Isotopes,* 7th edn, Wiley-Interscience, New York.
Lobanov, Yu. V., Buklanov, G. V., Abdullin, F. Sh., Polyakov, A. N., Shirokovsky, I. V., Tsyganov, Yu. S. and Utyonkov, V. K. (1997) *Nucl. Instrum. Methods*, **A397**, 26–29.
Lougheed, R. W., Wild, J. F., Hulet, E. K., Hoff, R. W., and Landrum, J. H. (1978) *J. Inorg. Nucl. Chem.*, **40**, 1865–9.
Marei, S. A. and Cunningham, B. B. (1972) *J. Inorg. Nucl. Chem.*, **34**, 1203–6.
Maxwell, S. L. (1996) *Nucl. Mater. Manage.*, **25**, 686–90.
Metzger, R. L., Jessop, B. H., and McDowell, B. L. (1995) *Radioact. Radiochem.*, **6**, 46–50.
Mikheev, N. B. (1983) *Radiochim. Acta*, **32**, 69.
Mikheev, N. B., Kazakevich, M. Z., and Rumer, I. A. (1992) *Radiokhimiya*, **34**, 31–4; *Radiochemistry*, **34**, 293–5.
Miles, J. H. (1965) *J. Inorg. Nucl. Chem.*, **27**, 1595–600.
Mincher, B. J. (1992) *Solvent Extr. Ion Exch.*, **10**, 615–22.
Moeller, T. and Moss, F. A. (1951) *J. Am. Chem. Soc.*, **73**, 3149–51.

Molochnikova, N. P., Shkinev, V. M., and Myasoedov, B. F. (1992) *Solvent Extr. Ion Exch.*, **10**, 679–712.
Moore, F. L. (1971) *Anal. Chem.*, **43**, 487–9.
Morss, L. R., Fuger, J., Goffart, J., and Haire, R. G. (1983) *Inorg. Chem.*, **22**, 1993.
Morss, L. R., Richardson, J. W., Williams, C. W., Lander, G. H., Lawson, A. C., Edelstein, N. M., and Shalimoff, G. V. (1989) *J. Less Common Metals*, **156**, 273–89.
Mosley, W. C. (1971) *J. Am. Ceram. Soc.*, **54**, 475–9.
Mosley, W. C. (1972) *J. Inorg. Nucl. Chem.*, **34**, 539–55.
Moulin, C., Decambox, P., and Mauchien, P. (1997) *J. Radioanal. Nucl. Chem.*, **226**, 135–8.
Müller, W., Reul, J., and Spirlet, J. C. (1972) *Atomwirt. Atomtech.*, **17**, 415–16.
Müller, W., Reul, J., and Spirlet, J. C. (1977) *Rev. Chim. Miner.*, **14**, 212–24.
Musikas, C. (1999) in *Chemical Separation Technologies and Related Methods of Nuclear Waste Management* (eds. G. R. Choppin and M. Kh. Khankhasayev), Kluwer Academic Publications, Dordrecht, pp. 99–122.
Myasoedov, B. F., Milyukova, M. S., and Ryzhova, L. V. (1970) *Radiochem. Radioanal. Lett.*, **5**, 19–23.
Myasoedov, B. F., Lebedev, I. A., Mikhailov, V. M., and Frenkel, V. Ya. (1973) *Radiochem. Radioanal. Lett.*, **14**, 131–4; (1974) *Radiochem. Radioanal. Lett.*, **17**, 359–65.
Myasoedov, B. F. and Kremliakova, N. Yu. (1985) in *Americium and Curium Chemistry and Technology* (eds. N. M. Edelstein, J. D. Navratil, and W. W. Schulz), Reidel Publishing Co, New York, pp. 53–79.
Myasoedov, B. F. and Lebedev, I. A. (1991) *Anal. Chem.*, **147**, 5–26.
Myasoedov, B. F. (1994) *J. Alloys Compds*, **213/214**, 290–9.
Nave, S. E., Huray, P. G., Peterson, J. R., Damien, D. A., and Haire, R. G. (1981) *Physica*, **107B**, 253–4.
Nave, S. F., Haire, R. G., and Huray, P. G. (1983) *Phys. Rev. B*, **28**, 2317–27.
Navratil, J. D. and Schulz, W. W. (1993) *J. Miner. Metals Mater.*, **45**, 32–4.
Niese, S. and Gleisberg, B. (1995) *J. Radioanal. Nucl. Chem. Lett.*, **200**, 31–41.
Nikolaev, V. M. and Lebedev, V. M. (1975) *Zh. Neorg. Khim.*, **20**, 1359–61; *Sov. J. Inorg. Chem.*, **20**, 765–7.
Noé, M., Fuger, J., and Duyckaerts, G. (1970) *Inorg. Nucl. Chem. Lett.*, **6**, 111–19.
Noé, M. and Fuger, J. (1971) *Inorg. Nucl. Chem. Lett.*, **7**, 421–30.
Novikov, A. P. and Myasoedov, B. F. (1987) *Solvent Extr. Ion Exch.*, **5**, 117–27.
Novikov, A. P., Bukina, T. I., Karalova, Z. K., and Myasoedov, B. F. (1988) *Radiokhimiya*, **29**, 184–9.
Nugent, L. J., Burnett, J. L., Baybarz, R. D., Werner, G. K., Tanner, J. P., Tarrant, J. R., and Keller, O. L. (1969) *J. Phys. Chem.*, **73**, 1540–9.
Nugent, L. J., Laubereau, P. G., Werner, G. K., and Vander Sluis, K. L. (1971) *J. Organomet. Chem.*, **27**, 365–72.
Nugent, L. J., Baybarz, R. D., Burnett, J. L., and Ryan, J. L. (1973) *J. Phys. Chem.*, **77**, 1528–39.
Oetting, F. L., Rand, M. H., and Ackermann, R. J. (1976) *The Chemical Thermodynamics of Actinide Elements and Compounds,* part 1, *The Actinide Elements*, IAEA, Vienna, p. 34.
Okamoto, H. (2000) *J. Phase Equil.*, **21**, 108.

Ozawa, M., Nemeto, S., Togashi, A., Kawata, T., and Onishi, K. (1992) *Solvent Extr. Ion Exch.*, **10**, 829–46.

Pages, M. and Demichelis, R. (1966) *C. R. Acad. Sci. Paris C*, **263**, 938–40.

Paviet, P., Fanghänel, Th., Klenze, R., and Kim, J. I. (1996) *Radiochim. Acta*, **74**, 99–103.

Penneman, R. A. and Ferguson, D. E. (1971) *Proc. Sem. Radiat. Prot. Problems Relating to Transuranium Elements,* Karlsruhe, West Germany, September 21–25, 1970, CID, Luxembourg, pp. 85–98.

Penneman, R. A., Ryan, R. R., and Rosenzweig, A. (1973) *Struct. Bonding*, **13**, 1–52.

Peretrukhin, V. F., Enin, E. A., Dzyubenko, V. I., Kopytov, V. V., Polyukhov, V. G., Vasil'ev, V. Ya., Timofeev, G. A., Rykov, A. G., Krot, N. N., and Spitsyn, V. I. (1978) *Dokl. Akad. Nauk SSSR*, **242**, 1359–62; *Dokl. Acad. Sci. USSR*, **242**, 503–6.

Peters, T. B., Hobbs, D. T., Diprete, D. P., Diprete, C. C., and Fink, S. D. (2002) *Final Report on the Demonstration of Disposal of Americium and Curium Legacy Material Through the High Level Waste System*, US Report WSRC-TR–2001–00503.

Peterson, J. R. and Fuger, J. (1971) *J. Inorg. Nucl. Chem.*, **33**, 4111–7.

Peterson, J. R. (1972) *J. Inorg. Nucl. Chem.*, **34**, 1603–7.

Peterson, J. R. and Burns, J. H. (1973) *J. Inorg. Nucl. Chem.*, **35**, 1525–30.

Radchenko, V. M., Seleznev, A. G., Shushakov, V. D., Ryabinin, M. A., Lebedeva, L. S., Karelin, E. A., and Vasil'ev, V. Ya. (1985) *Radiokhimiya*, **27**, 33–7; *Sov. Radiochem.*, **27**, 33–6.

Radchenko, V. M., Seleznev, A. G., Lebedeva, L. S., Droznik, R. R., Ryabinin, M. A., and Shushakov, V. D. (1989) *Radiokhimiya*, **31**, 1–7; *Sov. Radiochem.*, **31**, 145–50.

Radchenko, V. M., Seleznev, A. G., Ryabinin, M. A., Droznik, R. R., and Vasil'ev, V. Ya. (1995) *Radiokhimiya*, **37**, 317–321; *Radiochemistry*, **37**, 292–6.

Radchenko, V. M., Seleznev, A. G., Ryabinin, M. A., Droznik, R. R., and Vasil'ev, V. Ya. (1996) *Radiokhimiya*, **38**, 391–4; *Radiochemistry*, **38**, 369–72.

Radchenko, V. M., Seleznev, A. G., Droznik, R. R., and Ryabinin, M. A. (1998) *Radiokhimiya*, **40**, 6–8; *Radiochemistry*, **40**, 4–6.

Radchenko, V. M., Andreichikov, B. M., Wänke, H., Gavrilov, V. D., Korchuganov, B. N., Rieder, R., Ryabinin, M. A., and Economou, T. (1999) *Radiokhimiya*, **41**, 150–2; *Sov. Radiochem.*, **41**, 155–8.

Radchenko, V., Andreichikov, B., Wänke, H., Gavrilov, V., Korchuganov, B., Rieder, R., Ryabinin, M., and Economou, T. (2000) *Appl. Rad. Isot.*, **53**, 821–4.

Raison, P. E. and Haire, R. G. (2001) *Prog. Nucl. Energy*, **38**, 251–4.

Rameback, H. and Skalberg, M. (1998) *J. Radioanal. Nucl. Chem.*, **235**, 229–33.

Raschella, D. L., Fellows, R. L., and Peterson, J. R. (1981) *J. Chem. Thermodyn.*, **13**, 303–12.

Reichlin, R. L., Akella, J., Smith, G. S., and Schwab, M. (1981) in *Actinides – 1981*, Lawrence Berkeley Laboratory Report LBL-l2441.

Ryan, J. L. (1975) *Gmelin Handbook of Inorganic Chemistry, Transuranics,* part D2 (ed. G. Koch), Springer-Verlag, Berlin, pp. 373–436.

Saprykin, A. S., Shilov, V. P., Spitsyn, V. I., and Krot, N. N. (1976) *Dokl. Akad. Nauk SSSR*, **226**, 853–6; *Dokl. Acad. Sci. USSR*, **226**, 114–16.

Schenkel, R. (1977) *Solid State Commun.*, **23**, 389–92.

Scherer, V. and Fochler, M. (1968) *J. Inorg. Nucl. Chem.*, **30**, 1433–7.

Seaborg, G. T., James, R. A., and Ghiorso, A. (1949) in *The Transuranium Elements* (eds. G. T. Seaborg, J. J. Katz, and W. W. Manning), Natl. Nucl. En. Ser., Div. IV, 14B, McGraw-Hill, New York, pp. 1554–71.
Seaborg, G. T. (1972) *Pure Appl. Chem.*, **30**, 539–49.
Seaborg, G. T. (1985) The 40th Anniversary of the Discovery of Americium and Curium, in *Americium and Curium Chemistry and Technology* (eds. N. M. Edelstein, J. D. Navratil, and W. W.Schulz), Reidel Publishing, Boston, MA, pp. 3–17.
Shannon, R. D. (1976) *Acta Crystallogr.*, **A32**, 751–67.
Soderholm, L. (1992) *J. Alloys Compds*, **181**, 13–22.
Soderholm, L., Skanthakumar, S., and Williams, C. W. (1999) *Phys. Rev. B*, **60**, 4302–8.
Spitsyn, V. I. and Ionova, G. V. (1978) *Radiokhimiya*, **20**, 328–32; *Sov. Radiochem.*, **20**, 279–83.
Stephanou, S. E. and Penneman, R. A. (1952) *J. Am. Chem. Soc.*, **74**, 3701.
Stevenson, J. N. (1973) Oak Ridge National Laboratory Report TID–26453, 28, 30534.
Stevenson, J. N. and Peterson, J. R. (1975) *Microchem. J.*, **20**, 213–20.
Stevenson, J. N. and Peterson, J. R. (1979) *J. Less Common Metals*, **66**, 201–10.
Stroński, I. and Rekas, M. (1973) *Radiochem. Radioanal. Lett.*, **14**, 297–304.
Sullivan, J. C., Gordon, S., Mulac, W. A., Schmidt, K. M., Cohen, D., and Sjoblom, R. (1976) *Inorg. Nucl. Chem. Lett.*, **12**, 599–601.
Takano, M., Itoh, A., Akabori, M., Ogawa, T., Numata, M., and Okamoto, H. (2001) *J. Nucl. Mater.*, **294**, 24–7.
Takeishi, H., Kitatsuji, Y., Kimura, T., Meguro, Y., Yoshida, Z., and Kihara, S. (2001) *Anal. Chim. Acta*, **431**, 69–80.
Tanner, S. P. and Choppin, G. R. (1968) *Inorg. Chem.*, **7**, 2046–8.
Thompson, G. H. (1972) *Ion Exch. Membranes*, **1**, 87–9.
Trautmann, N. and Folger, H. (1989) *Nucl. Instrum. Methods*, **A282**, 102–6.
Tuli, J. K. (ed.) (2002) *Nucl. Data Sheets* 95.
Vasil'ev, V. I., Kalevich, E. S., Radchenko, V. M., Egunov, V. P., Izmalkov, A. N., Shimbarev, E. V., and Vasil'ev, V. Ya. (1989) *Radiokhimiya*, **31**, 35–7; *Sov. Radiochemistry*, **31**, 651–3.
Vasil'ev, V. I., Kalevich, E. S., Radchenko, V. M., Egunov, V. P., Izmalkov, A. N., Shimbarev, E. V., and Vasil'ev, V. Ya. (1990) *Radiokhimiya*, **32**, 6–8; *Sov. Radiochem.*, **32**, 141–3.
Vasudeva Rao, P. R., Kusumakumari, M., and Patil, S. K. (1978) *Radiochem. Radioanal. Lett.*, **33**, 305–14.
Vesnovskii, S. P., Vjachin, V. N., and Kavitov, P. N. (1996) *J. Radioanal. Nucl. Chem.*, 105–12.
Wallmann, J. C. (1964) *J. Inorg. Nucl. Chem.*, **26**, 2053–7.
Wallmann, J. C., Fuger, J., Peterson, J. R., and Green, J. L. (1967) *J. Inorg. Nucl. Chem.*, **29**, 2745–51.
Ward, J. W. and Hill, H. H. (1975) in *Heavy Element Properties* (eds. W. Müller and M. Blank), vol. I, North-Holland, Amsterdam, pp. 65–79.
Ward, J., Ohse, R. W., and Reul, R. (1975) *J. Chem. Phys.*, **62**, 2366–72.
Ward, J. W., Kleinschmidt, P. D., Haire, R. G., and Brown, D. (1980) in *Lanthanide and Actinide Chemistry and Spectroscopy* (ACS Symp. Ser. 131), American Chemical Society, Washington DC, pp. 199–220.
Weigel, F. and Haug, H. (1965) *Radiochim. Acta*, **4**, 227–8.

Weigel, F., Wishnevsky, V., and Hauske, H. (1977) *J. Less Common Metals*, **56**, 113–23.
Weigel, F. and Marquardt, R. (1983) *J. Less Common Metals*, **90**, 283–90.
Werner, L. B. and Perlman, I. (1951) *J. Am. Chem. Soc.*, **73**, 5215–17.
Wimmer, H., Klenze, R., and Kim, J. I. (1992) *Radiochim. Acta*, **56**, 79–83.
Wimmer, H., Kim, J. I., and Klenze, R. (1992) *Radiochim. Acta*, **58/59**, 165–71.
Yusov, A. B., Fedoseev, A. M., Spitsyn, V. I., and Krot, N. N. (1986a) *Dokl. Akad. Nauk SSSR*, **289**, 1441–4.
Yusov, A. B., Perminov, V. P., and Krot, N. N. (1986b) *Radiokhimiya*, **28**, 72–8; *Sov. Radiochem.*, **28**, 63–8.
Yusov, A. B. and Fedoseev, A. M. (1989a) *Radiokhimiya*, **31**, 16–19; *Sov. Radiochem.*, **31**, 538–41.
Yusov, A. B. and Fedoseev, A. M. (1989b) *Radiokhimiya*, **31**, 19–23; *Sov. Radiochem.*, **31**, 541–4.
Yusov, A. B. and Fedoseev, A. M. (1990) *Radiokhimiya*, **32**, 73–6; *Sov. Radiochem.*, **31**, 69–71.
Yusov, A. B. and Fedoseev, A. M. (1991) *J. Radioanal. Nucl. Chem. Articles*, **147**, 201–6.
Yusov, A. B. and Fedoseev, A. M. (1992a) *Radiokhimiya*, **34**, 61–70; *Sov. Radiochem.*, **34**, 314–20.
Yusov, A. B. and Fedoseev, A. M. (1992b) *Radiokhimiya*, **34**, 70–77; *Sov. Radiochem.*, **34**, 320–5.
Zachariasen, W. H. (1973) *J. Inorg. Nucl. Chem.*, **35**, 3487–97.
Zhu, Y. and Jiao, R. (1994) *Nucl. Tech.*, **1083**, 361–9.

CHAPTER TEN

BERKELIUM

David E. Hobart and Joseph R. Peterson

10.1 HISTORICAL

As was the case for the previously discovered transuranium elements, element 97 was first produced via a nuclear bombardment reaction. In December 1949 ion-exchange separation of the products formed by the bombardment of ^{241}Am with accelerated alpha particles provided a new electron-capture activity eluting just ahead of curium (Thompson *et al.*, 1950a,b). This activity was assigned to an isotope (mass number 243) of element 97. The new element was named berkelium after Berkeley, California, USA, the city of its discovery, in a manner parallel to the naming of its lanthanide analog, terbium, after Ytterby, Sweden. The initial investigations of the chemical properties of berkelium were limited to tracer experiments (ion exchange and coprecipitation), and these were sufficient to establish the stability of Bk(III) and the accessibility of Bk(IV) in aqueous solution and to estimate the electrochemical potential of the Bk(IV)/Bk(III) couple (Thompson *et al.*, 1950b,c). Because a complete study of the chemistry of an element is not possible by tracer methods alone, a program for long-term neutron irradiation of about 8 g of ^{239}Pu was initiated in 1952 in the Materials Testing Reactor (Arco, Idaho, USA) to provide macroquantities of berkelium (Cunningham, 1959). In 1958 about 0.6 μg of ^{249}Bk was separated, purified, and used in experiments to determine the absorption spectrum of Bk(III) in aqueous solution and to measure the magnetic susceptibility of Bk(III) (Cunningham, 1959). No Bk(III) absorption was observed over the wavelength range 450–750 nm, but an upper limit of about 20 was set for the molar absorptivity of any

Bk(III) absorption in this wavelength region. The magnetic susceptibility, measured from 77 to 298 K with the Bk(III) ions sorbed in a single bead of cation-exchange resin, was found to conform to the Curie–Weiss law with an effective moment of 8.7 μ_B, suggesting a $5f^8$ electronic configuration for the Bk(III) ion. The first structure determination of a compound of berkelium, the dioxide, was carried out in 1962 (Cunningham, 1963). Four X-ray diffraction lines were obtained from 4 ng of BkO_2 and indexed on the basis of a face-centered cubic (fcc) structure with $a_0 = (0.533 \pm 0.001)$ nm. In the intervening years since this initial work to characterize element 97, considerable information about the physicochemical properties of berkelium has been obtained in spite of the rather limited availability and the short half-life (330 days) of ^{249}Bk, the only isotope available in bulk quantities.

The authors have focused this review of the chemistry of berkelium on open literature references in English or English translation, except where it was deemed necessary to cite a research institution report or technical memorandum or personal communication. References to theses, dissertations, and patents are minimal. The biologic and metabolic effects of exposure to and/or ingestion of berkelium on humans and animals have not been reviewed here (see Chapter 31). Also excluded are references dealing with the determination and/or use of the nuclear properties of the various isotopes of berkelium, with the notable exception of a few modern references dealing with the use of ^{249}Bk as a target material for the production of transactinide elements. The references cited herein are not necessarily inclusive or always the original ones, yet they should be adequate to permit the interested reader to access easily the broader literature beyond.

Earlier reviews of the physicochemical properties of berkelium are available in Keller (1971), in several new supplement series volumes of the *Gmelin Handbuch der Anorganischen Chemie* (e.g. Peterson, 1976), Peterson and Hobart (1984), and in Hobart and Peterson (1986).

10.2 NUCLEAR PROPERTIES, AVAILABILITY, AND APPLICATIONS

Selected nuclear properties of the 14 known isotopes of berkelium, ranging from mass numbers 238 to 251, are listed in Table 10.1 (Appendix II). Included in this list are two neutron-deficient isotopes that have been identified since the publication of the second edition of this text in 1986. These are ^{238}Bk with an electron-capture decay half-life of 2.4 min (Kreek *et al.*, 1994) and ^{241}Bk with an electron-capture decay half-life of 4.6 min (Asai *et al.*, 2003). Only ^{249}Bk is available in bulk quantities for chemical studies, as a result of prolonged neutron irradiation of Pu, Am, or Cm (Bigelow *et al.*, 1981). About 1 g of this isotope has been isolated from target rods irradiated in the High Flux Isotope Reactor (HFIR) at Oak Ridge National Laboratory (ORNL) in east Tennessee, USA, over the period 1967–2001 (Knauer, 2002). The relative atomic mass of

Table 10.1 *Nuclear properties of berkelium isotopes.*[a]

Mass number	*Half-life*	*Mode of decay*	*Main radiations* (MeV)	*Method of production*
238	2.4 min	EC		^{241}Am(α,7n)
240	4.8 min	EC		^{232}Th(^{14}Ne,6n)
241	4.6 min	EC	γ 0.2623	^{239}Pu(^{6}Li,4n)
242	7.0 min	EC		^{232}Th(^{14}N,4n)
				^{232}Th(^{15}N,5n)
243	4.5 h	EC 99.85%	α 6.758 (15%)	^{243}Am(α,4n)
		α 0.15%	6.574 (26%)	
			γ 0.755	
244	4.35 h	EC > 99%	α 6.667 (∼50%)	^{243}Am(α,3n)
		α 6×10^{-3}%	6.625 (∼50%)	
			γ 0.218	
245	4.94 d	EC > 99.88%	α 6.349 (15.5%)	^{243}Am(α,2n)
		α 0.12%	6.145 (18.3%)	
			γ 0.253 (31%)	
246	1.80 d	EC	γ 0.799 (61%)	^{243}Am(α,n)
247	1.38×10^3 yr	α	α 5.712 (17%)	^{247}Cf daughter
			5.532 (45%)	^{244}Cm(α,p)
			γ 0.084 (40%)	
248[b]	23.7 h	β^- 70%	β^- 0.86	^{248}Cm(d,2n)
		EC 30%	γ 0.551	
248[b]	>9 yr	decay not observed		^{246}Cm(α,pn)
249	330 d	$\beta^- > 99\%$	α 5.417 (74.8%)	multiple n capture
		α 1.45×10^{-3}%	5.390 (16%)	
			β^- 0.125	
			γ 0.327 weak	
250	3.217 h	β^-	β^- 1.781	^{254}Es daughter
			γ 0.989 (45%)	^{249}Bk(n,γ)
251	55.6 min	β^-	$\beta^- \sim 1.1$	^{255}Es daughter
			γ 0.178	

[a] Appendix II.
[b] Not known whether ground state nuclide or isomer.

^{249}Bk was given as 249.075 (Audi and Wapstra, 1995), and the most recent determination of its half-life yielded a value of (330 ± 4) days (Popov and Timofeev, 1999).

Besides the research use of ^{249}Bk for the characterization of the chemical and physical properties of element 97, its relatively rapid decay to ^{249}Cf (ca. 0.22% per day) makes it a valuable source of this important isotope of californium for chemical study. This genetic relationship has been exploited in studies of the chemical consequences of beta (β^-) decay in the bulk-phase solid state (Young *et al.*, 1980; Ensor *et al.*, 1981; Young *et al.*, 1984; Peterson *et al.*, 1986).

As a consequence of recent interest in nuclear power reactors to increase fuel burn-up and in the areas of nuclear waste transmutation, nuclear deterrence, and astrophysics, more accurate data on the nuclear characteristics of heavier actinides, including berkelium, are in demand. A recent compilation of the decay characteristics of actinides, including ^{249}Bk and ^{250}Bk, has been published (Popov and Timofeev, 1999). Fission fragment angular distributions for the compound nucleus ^{246}Bk have been measured (Behera *et al.*, 2001). ^{246}Bk was produced via two nuclear reaction pathways, lying on either side of the Businaro–Gallone critical asymmetry parameter.

By combining measured fission probabilities for reactions such as ^{248}Cm(^{3}He, d)^{249}Bk$\rightarrow$fission (Gavron *et al.*, 1977) with calculated total neutron inelastic cross sections, empirical predictions for the neutron-induced fission cross sections for several actinides have been obtained (Britt and Wilhelmy, 1979). These predictions ignore differences in angular momentum distributions between the direct reaction products and the incident neutrons when populating the same energy levels in the compound nucleus. As demonstrated by Britt and Wilhelmy (1979), this assumption is reasonably good for equivalent neutron energies (energy of an incident neutron that would leave the identical residual nucleus at the same energy as is reached by the direct nuclear reaction) of greater than about 0.5 MeV. For Bk the equivalent (n,f) cross sections were extracted for the berkelium isotopes with mass numbers 244 to 248. Odd-mass-number Bk nuclei exhibit a strong reduction in the fission probability for excitation energies above the neutron-binding energy that is presumably caused by the opening of a large number of competing decay channels (Britt and Wilhelmy, 1979). Although no experimentally measured fission cross section for ^{248m}Bk has been determined, estimates of up to 1000 barns have been predicted based on correlations with other actinides having similar characteristics (Ronen, 1998).

The intrinsic single-particle states of ^{249}Bk have been studied by measuring the gamma radiations emitted after the alpha decay of ^{253}Es. The low spin states were studied by measuring gamma rays in the beta decay of ^{249}Cm. Levels in ^{249}Bk were also studied by the reaction ^{248}Cm(α,t)^{249}Bk. A diagram of the intrinsic states for ^{249}Bk, deduced from these decay studies, has been constructed. This well-established nuclear structure information, available only for the heaviest elements for which macro amounts are obtainable, can be used either to determine the parameters of a single-particle potential or to test the nuclear models of super-heavy elements (Ahmad, 2002).

Although currently there are no practical or commercial applications for any known berkelium isotopes, ^{249}Bk has been used extensively as a target material for the production of still heavier actinides such as lawrencium (Brüchle *et al.*, 1988; Scherer *et al.*, 1988) and transactinide elements such as element 104, rutherfordium, and element 107, bohrium (Gregorich *et al.*, 1988; Kratz *et al.*, 1992; Gobrecht *et al.*, 1999; Paulus *et al.*, 1999; Eichler *et al.*, 2000; Wilk *et al.*, 2000).

10.3 PRODUCTION

Methods of production for each of the isotopes of berkelium are listed in Table 10.1 (Appendix II). Only ^{249}Bk is available in bulk quantities for chemical studies, as a result of prolonged neutron irradiation of Pu, Am, or Cm (Bigelow *et al.*, 1981). About 0.73 g of this isotope was isolated from target rods irradiated with neutrons in the ORNL HFIR over the period 1967–1985 (Ferguson and Bigelow, 1969; King *et al.*, 1981; Bigelow, 1985). Toward the end of 1986, HFIR was shut down for an extended period of time for major maintenance and safety considerations. This action resulted from the nuclear reactor accident at Chernobyl (former USSR) earlier that year. After a 4+ year hiatus, HFIR was restarted with a power limit of 85 MW, down from the previous 100 MW level. Through the HFIR product campaign that started in late 2000, an additional 0.28 g of ^{249}Bk was recovered during the period 1986–2001. It is not known to the present authors how much ^{249}Bk has been produced elsewhere in the world, for instance, in the former USSR.

10.4 SEPARATION AND PURIFICATION

Berkelium may be purified by many methods that are also applicable to other actinide elements. Therefore, only those methods that apply specifically to berkelium separation and purification are treated here.

Because berkelium can be readily oxidized to Bk(IV), it can be separated from other, non-oxidizable transplutonium elements by combining oxidation–reduction (redox) methods with other separation techniques. The first application of this approach was performed by oxidizing Bk(III) with BrO_3^- in nitric acid solution (Peppard *et al.*, 1957). The resultant Bk(IV) was then extracted with bis(2-ethylhexyl)phosphoric acid (HDEHP) in heptane followed by back-extraction with nitric acid containing H_2O_2 as a reducing agent. In addition to other reports of the use of BrO_3^- as an oxidizing agent in berkelium purification procedures (Knauer and Weaver, 1968; Weaver, 1968; Fardy and Weaver, 1969; Overman, 1971; Erin *et al.*, 1979b), the use of CrO_4^{2-} (Knauer and Weaver, 1968; Milyukova *et al.*, 1980), $Cr_2O_7^{2-}$ (Moore, 1966; Shafiev *et al.*, 1974; Milyukova *et al.*, 1980), $Ag(I)/S_2O_8^{2-}$ (Milyukova *et al.*, 1978, 1980), PbO_2 (Myasoedov *et al.*, 1971; Myasoedov, 1974; Shafiev *et al.*, 1974), BiO_3^- (Shafiev *et al.*, 1974), O_3 (Myasoedov, 1974), and photochemical oxidation (Myasoedov, 1974) has also been reported.

Separation of the oxidized berkelium has been accomplished by the use of: (1) liquid–liquid extraction with HDEHP (Peppard *et al.*, 1957; Knauer and Weaver, 1968; Kosyakov *et al.*, 1977; Erin *et al.*, 1979b; Yakovlev and Kosyakov, 1983), trioctylphosphine oxide (Kosyakov and Yakovlev, 1983), alkylpyrocatechol (Karalova *et al.*, 1983), 2-thenoyltrifluoroacetone (TTA) (Moore 1966, 1969), primary, tertiary, or quaternary amines (Moore, 1969;

Milyukova and Myasoedov, 1978; Milyukova *et al*., 1978, 1980; Malikov *et al*., 1983), or tri(*n*-butyl)phosphate (TBP) (Milyukova *et al*., 1981; Yakovlev *et al*., 1982); (2) extraction chromatography with HDEHP (Kooi and Boden, 1964; Kooi *et al*., 1964; Overman, 1971; Erin *et al*., 1979a) or zirconium phosphate adsorbant (Myasoedov *et al*., 1971; Shafiev and Efremov, 1972; Myasoedov, 1974; Shafiev *et al*., 1974); (3) precipitation of the iodate (Weaver, 1968; Fardy and Weaver, 1969); or (4) ion-exchange methods (Moore, 1967; Overman, 1971; Shafiev and Efremov, 1972; Guseva and Stepushkina, 1987; Guseva *et al*., 1987, 1991; Firsova *et al*., 1996, 1998a,b). These techniques can be applied separately or in combination with one another.

The purification procedures outlined above provide separation of berkelium from all trivalent lanthanides and actinides with the notable exception of cerium. Because berkelium and cerium exhibit nearly identical redox behavior, most redox separation procedures include a Bk–Ce separation step (Moore, 1967; Horwitz *et al*., 1969; Guseva *et al*., 1971; Chudinov and Pirozhkov, 1972; Shafiev and Efremov, 1972; Shafiev *et al*., 1974). Separation of Bk(III) from Ce(III) and other trivalent lanthanide and actinide elements can also be accomplished without the use of redox procedures (Moore and Jurriaanse, 1967; Farrar *et al*., 1968; Horwitz *et al*., 1969; Aly and Latimer, 1970; Guseva *et al*., 1971; Chudinov and Pirozhkov, 1972; Harbour, 1972; Shafiev and Efremov, 1972; Horwitz and Bloomquist, 1973; Korpusov *et al*., 1975; Khopkar and Mathur, 1980; Mathur and Khopkar, 1982; Ensor and Shah, 1984).

During the period 1967–2001, personnel at ORNL isolated and purified a total of about 1 g of ^{249}Bk (King *et al*., 1981; Bigelow, 1985; Knauer, 2002) using the procedure outlined in Fig. 10.1.

The transcurium elements, partitioned by LiCl-based anion exchange, are precipitated as hydroxides, filtered, and dissolved in nitric acid. Initial isolation is accomplished by high-pressure elution from cation-exchange resins with α-hydroxyisobutyrate solution. The berkelium fraction is oxidized and extracted into HDEHP/dodecane from HNO_3–$NaBrO_3$ solution. The organic fraction containing Bk(IV) is treated with 2,5-di(*t*-butyl)hydroquinone (DBHQ) to reduce the Bk(IV) to Bk(III) before back-extracting (stripping) it into HNO_3–H_2O_2 solution. Then another oxidation/extraction, reduction/back-extraction cycle is carried out. The solution at this point is radiochemically pure except for the fission product cerium. After solvent cleanup and evaporation to dryness, the berkelium is dissolved in 0.1 M HCl for final ion-exchange purification steps including alcoholic HCl elution from cation-exchange resin and cation cleanup columns (Baybarz *et al*., 1973).

Procedures for the rapid separation of berkelium from other actinides, lanthanides, and fission products have been developed in order to measure the decay properties of short-lived isotopes. Berkelium and cerium were separated from other elements using solvent extraction with HDEHP followed by cation-exchange high-pressure liquid chromatography (HPLC) using α-hydroxyisobutyrate as the eluant (Liu *et al*., 1981). The elution curve, showing

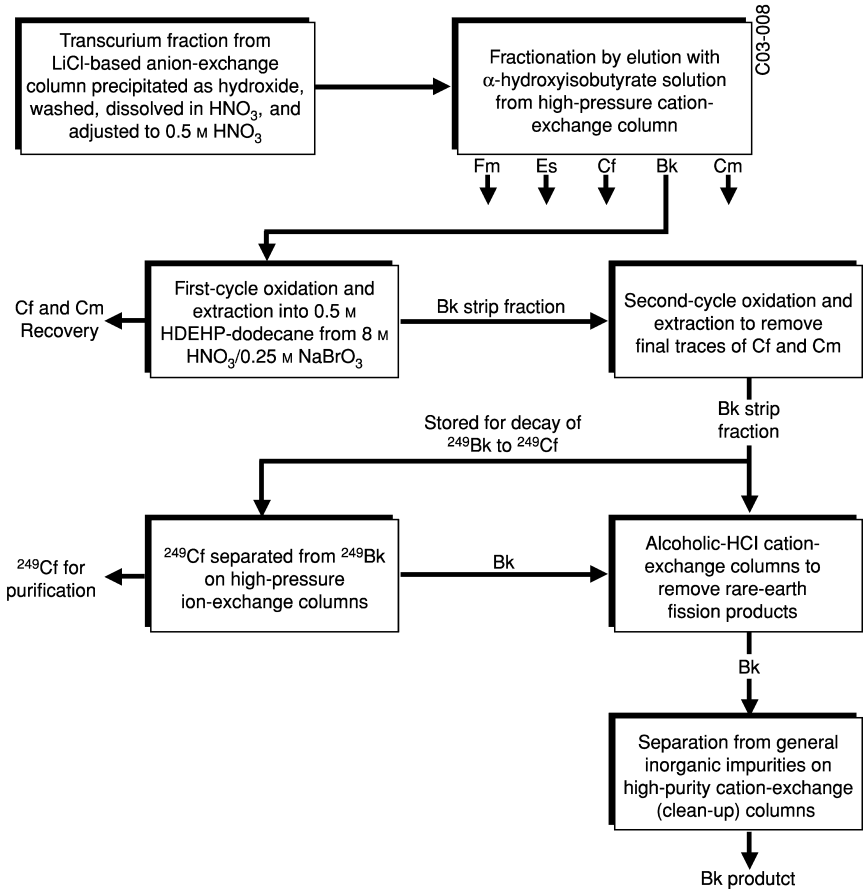

Fig. 10.1 *Schematic diagram of procedures used in the final isolation and purification of berkelium in the transuranium processing plant at the Oak Ridge National Laboratory.* (*Adapted from Baybarz* et al., 1973.)

a clean separation of Bk from Ce, is shown in Fig. 10.2. The total separation time was reported to be 8 min. (*Note*: A discrepancy exists in the drop number in the abscissa of Fig. 10.2; however, this figure is presented as it appeared in Liu *et al*. (1981).)

The fast separation of berkelium from beryllium foil targets and gold catcher foils has been published (Liu *et al*., 1983). New, fast separation techniques, involving volatile mineral acid–alcohol solvent systems used to isolate very short-lived isotopes, have been reported (Maruyama *et al*., 2002).

For additional discussion of berkelium separation procedures, the reader is referred to several reviews and comprehensive texts on the subject (Korkisch, 1966; Ulstrup, 1966; Müller, 1967; Bigelow, 1974; Myasoedov *et al*., 1974;

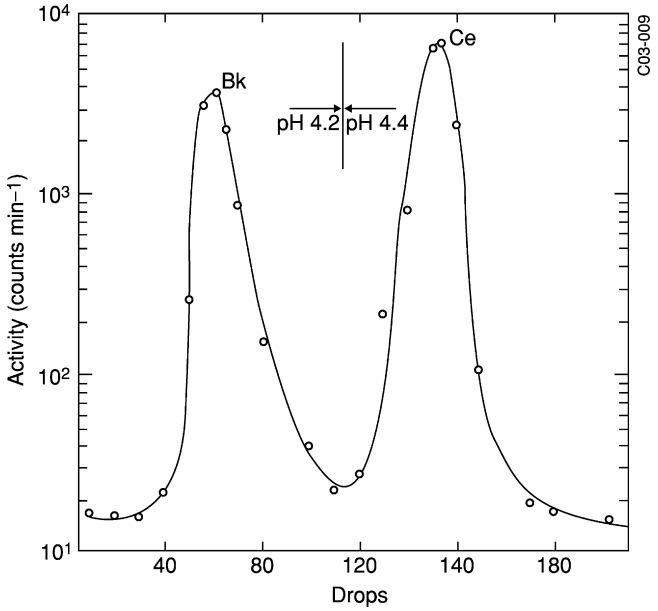

Fig. 10.2 *HPLC elution curve of Bk and Ce using* 0.5 M *ammonium α-hydroxyisobutyrate on a cation-exchange column* (*Liu* et al., 1981).

Campbell, 1981; Collins *et al.*, 1981; Myasoedov, 1987; Myasoedov and Lebedev, 1991).

10.5 PROPERTIES OF FREE ATOMS AND IONS

10.5.1 Thermochromatographic behavior of neutral atoms

The adsorption of ^{250}Bk atoms on niobium foils in a sapphire support tube has been studied (Hübener *et al.*, 2000). A deposition temperature of 1535 K was found in two separate experiments, and the enthalpy of adsorption was calculated to be –332 kJ mol^{-1}. A regular trend in the adsorption enthalpies of Bk–Fm and No is consistent with Bk adsorption on niobium in its trivalent $5f^8 6d^1 7s^2$ state (Taut *et al.*, 1998; Hübener *et al.*, 2000). In another approach by the same research group, the adsorption of elemental ^{248}Bk onto niobium was measured thermochromatographically (Taut *et al.*, 2000). The enthalpy of adsorption was determined to be $-(349 \pm 15)$ kJ mol^{-1}, in agreement with the above value, taking into account the experimental uncertainties.

10.5.2 Electronic energies

The ionization potential of neutral berkelium ($5f^97s^2$) was initially derived from spectroscopic data to be (6.229 ± 0.025) eV (Sugar, 1974). The changes in entropy associated with the stepwise ionization of gaseous berkelium atoms have also been calculated (Krestov, 1966). The energy interval between the ground level ($^7H_8$) and the first excited level ($^5H_7$) of singly ionized berkelium was determined from measurements done on plates using a high-resolution emission spectrograph and was found to be 1.48752×10^5 m^{-1} (Worden *et al.*, 1969). Several authors have calculated the energies of, and energy intervals between, the lowest-lying levels of the various electronic configurations of neutral berkelium (Nugent and Vander Sluis, 1971; Brewer, 1971a; Vander Sluis and Nugent, 1972, 1974) and of singly, doubly, and triply ionized berkelium (Brewer, 1971b; Vander Sluis and Nugent, 1974).

More recently, experimental determination of the first ionization potential of neutral berkelium was accomplished by resonance ionization mass spectroscopy (Erdmann *et al.*, 1998; Passler *et al.*, 1998; Waldek *et al.*, 2001). In this elegant approach (Kohler *et al.*, 1997) an atomic beam of Bk atoms was produced from heating a tantalum foil onto which Bk had been electrodeposited and then covered with a thin layer of titanium to reduce the Bk species to the metallic state. The Bk atoms were ionized in the presence of an electric field by multiple resonant laser excitation, and the Bk^+ ions were mass-selectively detected in a time-of-flight spectrometer. The first ionization potential was obtained by scanning the wavelength of the laser used for the last excitation step across the ionization threshold (indicated by a sudden increase in the Bk^+ count rate) at various electric field strengths. A linear plot of the ionization threshold against the square root of the electric field strength, extrapolated to zero field strength, yielded the first ionization potential of Bk to be (6.1979 ± 0.0002) eV. This value is just below the one derived from an extrapolation of spectral properties (Sugar, 1974). In addition the resonant excitation scheme used provided the energies of three of the excited energy levels of neutral Bk: 17666.0, 31541.3, and 32710.3 cm^{-1} (Kohler *et al.*, 1997; Erdmann *et al.*, 1998; Passler *et al.*, 1998).

From measurements of the energies of a number of internal conversion lines in ^{249}Bk (produced by the alpha decay of ^{253}Es), the atomic electron-binding energies in berkelium were calculated for the K through O shells (Hollander *et al.*, 1965). The K-series X-ray energies and intensities of berkelium were later measured, and the K-shell electron-binding energy was calculated (Dittner and Bemis, 1972). The measured energies and relative transition probabilities agreed well with theoretical predictions (Carlson *et al.*, 1969; Lu *et al.*, 1971). Also available are the results of relativistic relaxed-orbital *ab initio* calculations of L-shell Coster–Kronig transition energies for all possible transitions in berkelium atoms (Chen *et al.*, 1977), relativistic relaxed-orbital Hartree–Fock–Slater calculations of the neutral-atom electron binding energies in berkelium (Huang *et al.*, 1976), and calculations of the K- through O-shell

binding energies and K and L X-ray energies for berkelium (Carlson and Nestor, 1977). Relativistic Hartree–Slater values of the X-ray emission rates for the filling of K- and L-shell vacancies in berkelium have been tabulated (Scofield, 1974). X-ray emission rates for the filling of all possible single inner-shell vacancies in berkelium by electric dipole transitions have been calculated using nonrelativistic Hartree–Slater wave functions (Manson and Kennedy, 1974).

10.5.3 Emission spectra

Twenty emission lines, produced from 0.2 μg of berkelium in a high-voltage spark, were reported by Gutmacher *et al.* (1965). In 1967 between 3000 and 5000 lines were recorded in the wavelength region 250–900 nm from 38 μg of ^{249}Bk in an electrodeless discharge lamp (Worden *et al.*, 1967). Many of the emission lines exhibited a well-resolved eight-component hyperfine structure, which established the nuclear spin of ^{249}Bk to be 7/2 (Worden *et al.*, 1967). This value is in agreement with that derived from nuclear decay systematics.

The ground state electronic configurations (levels) of neutral and singly ionized berkelium were identified as $5f^97s^2$ ($^6H_{15/2}$) and $5f^97s^1$ ($^7H_8$), respectively (Worden *et al.*, 1970). A nuclear magnetic dipole moment of 1.5 μ_N (Worden *et al.*, 1969) and a quadrupole moment of 4.7 barns (Conway, 1976) were determined for ^{249}Bk, based on analysis of the hyperfine structure in the berkelium emission spectrum.

The wavenumbers, wavelengths, and relative intensities of 1930 of the stronger emission lines from ^{249}Bk in the 254–980 nm wavelength region are available (Worden and Conway, 1978). The infrared emission spectrum of ^{249}Bk from 830 to 2700 nm has been recorded (Conway *et al.*, 1977). The emission profile of ^{249}Bk(III) in a silicate matrix has been studied as a function of excitation power and temperature (Assefa *et al.*, 1998). With both experimental parameters it was found that the two primary emission bands (believed to originate from f→f transitions) decreased in intensity at different rates with increasing excitation power or temperature, such that the higher-energy band became dominant over the lower-energy one. Thermal quenching and/or energy transfer between neighboring ions are possible factors responsible for this behavior (Assefa *et al.*, 1998).

A preliminary report on the self-luminescence of ^{249}Bk(III) in a $LaCl_3$ host lattice was published by Gutmacher *et al.* (1963), and the self-luminescence spectra of ^{249}Bk-doped BaF_2 and $SrCl_2$ were reported by Finch *et al.* (1978). The fluorescence and excitation spectra of Bk^{3+} ions (<0.001 mol fraction) in single-crystal $LaCl_3$ were determined using dye laser techniques (Hessler *et al.*, 1978). Selective laser excitation was used to excite specific Bk^{3+} levels, and then the subsequent fluorescence spectrum was recorded. Determining fluorescence lifetimes of all fluorescing levels and grouping the lines by lifetimes precluded

confusion caused by transference of the excitation energy to a fluorescing level of another ion. The fluorescing manifolds of Bk^{3+} were found to be $J = 6$ at 1.540 μm^{-1} and $J = 4$ at 1.953 μm^{-1} (Hessler *et al.*, 1978). The absence of UV-excited sharp-line sensitized luminescence of ^{249}Bk-doped gadolinium hexafluoroacetyl acetonate has been observed (Nugent *et al.*, 1969, 1970). Such luminescence was absent also in cesium berkelium hexafluoroacetyl acetonate chelate in anhydrous ethanol (Nugent *et al.*, 1969). A study of Bk^{3+} fluorescence in H_2O and D_2O solutions has been reported, and a basis for assessing the use of fluorescence detection for transuranic ions established (Beitz *et al.*, 1981).

The first report of fluorescence from the Bk^{4+} ion included establishment of the total ground state splitting of this ion and probing the higher-lying electronic states of its $5f^7$ configuration (Jursich *et al.*, 1987). The Bk^{4+} ions were stabilized in CeF_4, where it is known that there are two distinct low-symmetry sites to accommodate them. Two Bk^{4+} bands were detected and assigned to transitions to the ground state. From laser excitation spectra taken at 4 K, a $5f^7$ energy-level diagram was proposed, which is consistent with the authors' assumption of a single average D_{4d} site symmetry. Mixing of higher lying states into the ground state caused the total ground state crystal-field splitting of Bk^{4+} in CeF_4 to be 58 cm^{-1} (Jursich *et al.*, 1987). The results of a detailed, systematic spectral analysis of these data, along with those obtained in additional site-selective laser excitation studies of another sample of Bk^{4+} in CeF_4, have been reported (Liu *et al.*, 1994a). A complete set of crystal-field parametric values was given and compared with those derived from the previous five tetravalent actinides. In addition an observed and calculated line list out to about 27 000 cm^{-1} was published (Liu *et al.*, 1994a). Another paper from the same research group focused on the use of fluorescence line narrowing spectra of 0.1 at% Bk^{4+} in CeF_4 to study emissions from the lowest energy component of $^6D_{7/2}$ at 16 375 cm^{-1} to the four components of the $^8S_{7/2}$ ground multiplet (Liu *et al.*, 1994b). A linear relationship was observed between the excitation-laser photon energy and the energies of the Bk^{4+} emission lines. A subsequent study of the influence of the crystal field on the $^8S_{7/2}$ ground state splitting of Bk^{4+} ion in CeF_4, based on the 24 energy levels observed in their earlier work (Liu *et al.*, 1994a), was carried out (Brito and Liu, 2000). The parametric model used a set of nine nonzero parameters (corresponding to C_{2v} point symmetry) and yielded a good correlation between the experimental and calculated energy levels in Bk^{4+} ion. Compared with the isoelectronic Cm^{3+} ion, the large ground state splitting of Bk^{4+} ion in CeF_4 is attributed to the smaller energy gap between the ground state and the low-lying excited states (Brito and Liu, 2000). Subsequently, a model that included relativistic effects in an effective way was used to improve the theoretical reproduction of the splitting of the energy levels for such S-state f-electron ions (Smentek *et al.*, 2001). It was concluded in this work that the fitting procedure applied for the determination of the crystal-field parameters had to be done within the parametrization scheme that included the relativistic weights of the various parameters.

10.5.4 Solid-state absorption spectra

The absorption spectrum of Bk(III) in a lanthanum chloride host matrix at 77 K was first obtained by Gutmacher (1964). A prediction of the energy-level structure of Bk(III) was made by others the same year (Fields *et al.*, 1964). Extensive, low-temperature spectroscopic studies of $BkCl_3$ showed the absence of transitions to excited $J = 0$ and $J = 1$ states (Carnall *et al.*, 1972, 1973). This provided good evidence for a $\mu = 0$ ground level for Bk(III), consistent with that of Tb(III):$LaCl_3$ (Carnall and Fried, 1976). Experimental and theoretical studies of the crystal-field parameters of Bk(III) in a $LaCl_3$ host lattice have also been reported (Carnall *et al.*, 1977).

Microscale spectrophotometric techniques, using 0.5–10 μg berkelium samples, have been applied for identification and characterization of berkelium halides and oxyhalides (Young *et al.*, 1978). The spectra of orthorhombic and hexagonal $BkCl_3$ have been recorded (Peterson *et al.*, 1986) and are shown in Fig. 10.3. Spectra of orthorhombic and monoclinic $BkBr_3$ (Peterson *et al.*, 1977a,b), trigonal and orthorhombic BkF_3 (Ensor *et al.*, 1981), and monoclinic BkF_4 (Ensor *et al.*, 1981) have been reported. This technique has also been applied to the study of the chemical consequences of radioactive decay in bulk-phase solid-state samples (Young *et al.*, 1980, 1981). It was found that the ^{249}Cf daughter growing into crystalline $^{249}BkBr_3$ exhibited the same oxidation state and crystal structure as its berkelium parent (Young *et al.*, 1980).

The absorption spectra of Bk(III) and Bk(IV) hydroxides as suspensions in 1 M NaOH have been reported (Cohen, 1976). The solid-state absorption spectrum (Haire *et al.*, 1983) and Raman spectrum (Hobart *et al.*, 1983) of berkelium(III) orthophosphate have been obtained, as well as those for berkelium(III) oxalate decahydrate, $Bk_2(C_2O_4)_3 \cdot 10H_2O$ (Morris *et al.*, 2005). Line lists of the absorption bands of two organoberkelium compounds, $Bk(C_5H_5)_3$ (Laubereau and Burns, 1970) and $[Bk(C_5H_5)_2Cl]_2$ (Laubereau, 1970), have been published.

For additional information (Carnall, 1973) and discussion of the development of the theoretical treatment of berkelium spectra, the reader is referred to other sources (Carnall and Fried, 1976; Conway, 1976; Carnall *et al.*, 1984; Liu *et al.*, 1994a) and to Chapters 16 and 18.

10.5.5 Ion–molecule reactions in the gas phase

Organoberkelium ions have been produced by laser ablation of Bk_2O_3 dispersed in polyimide (Gibson and Haire, 2001a). Characterization of the resulting products via time-of-flight spectrometry identified the primary species as $BkCH_3^+$, BkC_2^+, BkC_2H^+, $BkCN^+$, BkC_4H^+, $Bk(OH)(CN)^+$, $BkOCN^+$, $BkOH^+$, $Bk(OH)_2^+$, and BkO^+, as shown in Fig. 10.4. The product ion compositions and abundance distributions were reasonably explained in the context of the electronic structure and energetics of the Bk^+ ion. Several of these organoberkelium species incorporate direct metal ion–carbon bonding via a single

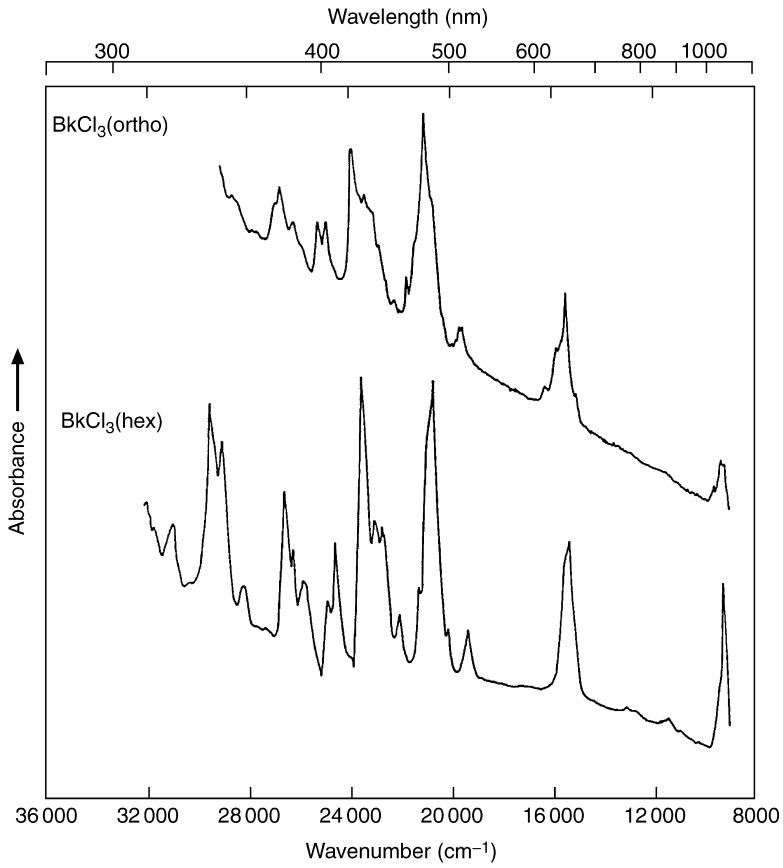

Fig. 10.3 *The solid-state absorption spectra of orthorhombic and hexagonal* $BkCl_3$ (*Peterson* et al., 1986).

σ-type covalent bond. Comparisons of the product ion compositions and abundance distributions of similarly produced organoactinide and lanthanide species provided correlations with the electronic promotion energies required to create a divalent or a monovalent state, capable of forming two or one covalent bonds, respectively (Gibson and Haire, 2001a). In an extension of the above work, gas-phase reactions of Bk^+ ion with several alkenes, butylamine, butyronitrile, and other reagents were studied in concert with similar reactions with Pu^+ ion or homologous Tb^+ ion to aid in the interpretation of the results in the context of the electronic structure and energetics of berkelium (Gibson and Haire, 2001b). A key result of this work was the finding that the efficiency of hydrocarbon, nitrile, and amine activation by Bk^+ ion directly reflected the energy required to excite the ion from its ground electronic state, $5f^97s^1$, to the lowest lying state with two spin-unpaired non-5f valence electrons, $5f^86d^17s^1$. Thus it appears that

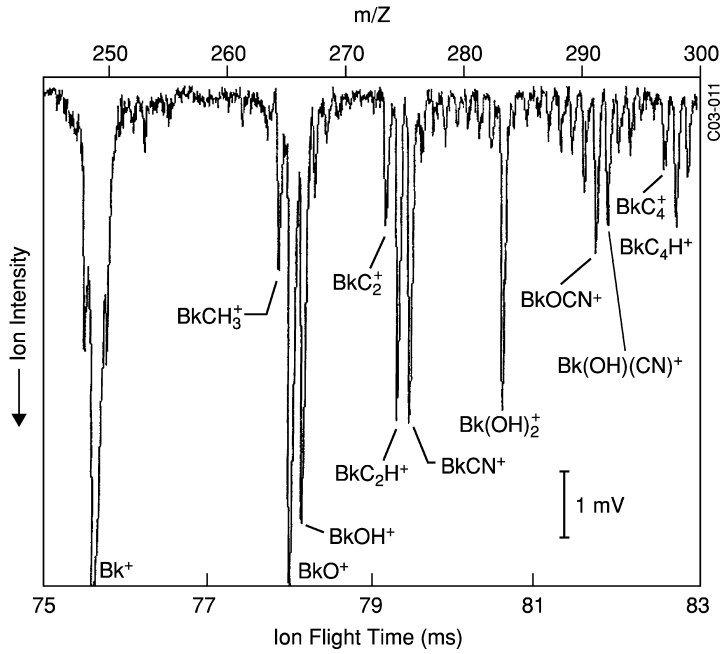

Fig. 10.4 *The mass spectrum of positive ions ablated from a Bk–polyimide target.* (*Reprinted figure with permission from Gibson and Haire* (2001*a*). *Copyright* 2001 *by Oldenbourg Verlag.*)

the 5f electrons in Bk^+ ions do not participate in organometallic bond activation. A variety of organoberkelium species were identified, as well as a few inorganic ones, e.g. BkF^+. A covalent bonding model was used to estimate the Bk^+–O bonding energy as (610 ± 40) kJ mol^{-1} (Gibson and Haire, 2001b).

10.6 THE METALLIC STATE

10.6.1 Pure metal

(a) Preparation

The first bulk (>1 μg) samples of berkelium metal were prepared in early 1969 by the reduction of BkF_3 with lithium metal vapor at about 1300 K (Peterson *et al.*, 1971). The BkF_3 samples were suspended in a tungsten wire spiral above a charge of Li metal in a tantalum crucible. Berkelium metal samples up to 0.5 mg each have been prepared via the same chemical procedure (Fuger *et al.*, 1975). Elemental berkelium can also be prepared by reduction of BkF_4 with lithium metal and by reduction of BkO_2 with either thorium or lanthanum metal

(Spirlet *et al.*, 1987). The latter reduction process is better suited to the preparation of thin metal foils unless multi-milligram quantities of berkelium are available.

(b) Physical properties

Berkelium metal exhibits two crystallographic modifications: double hexagonal close-packed (dhcp) and fcc. Thus, it is isostructural with the two preceding actinide elements, both of which also exhibit the fcc structure at high temperature. The room-temperature lattice constants of the dhcp (α) form are $a_0 = (0.3416 \pm 0.0003)$ nm and $c_0 = (1.1069 \pm 0.0007)$ nm, yielding a calculated density of 14.78 g cm^{-3} and a metallic radius (coordination number, CN 12) of 0.170 nm (Peterson *et al.*, 1971). The room-temperature metastable fcc (β) lattice parameter is $a_0 = (0.4997 \pm 0.0004)$ nm, from which the X-ray density and metallic radius (CN 12) are calculated to be 13.25 g cm^{-3} and 0.177 nm, respectively (Peterson *et al.*, 1971). The metallic radius of berkelium, assuming a metallic valence of 3- and 12-fold coordination, has been calculated to be 0.1739 nm (Sarkisov, 1966). On the other hand, the radii (CN 12) of berkelium were predicted to be 0.184 nm for a trivalent metal and 0.1704 nm for a tetravalent metal; so it was proposed that the observed dhcp form corresponds to tetravalent metal, while the fcc form represents a metallic valence of $\sim$3.5 (Zachariasen, 1973).

Although berkelium metal is dimorphic, the transformation temperature is not known with certainty. A change in the appearance of Bk metal samples at (1203 ± 30) K during the course of two melting point determinations might correspond to the dhcp$\rightarrow$fcc phase transformation, which should be accompanied by a 12% change in the volume of the sample (Fahey *et al.*, 1972). By analogy with the behavior of neodymium, a phase-transition temperature of (1250 ± 50) K was assigned by Ward *et al.* (1982), in agreement with the Fahey *et al.* (1972) observation. The melting point of berkelium metal was first determined to be (1259 ± 25) K from measurements on two samples (Fahey *et al.*, 1972). The melting and boiling points of elemental berkelium have been reported to be (1323 ± 50) K and (2900 ± 50) K, respectively (Ward *et al.*, 1982). These two melting-point determinations are in agreement, considering their experimental uncertainties.

The first studies of berkelium metal under pressure were performed with a diamond anvil pressure cell using energy-dispersive X-ray powder diffraction analysis (Haire *et al.*, 1984). Three different metallic phases were observed as the pressure was increased to 57 GPa. The normal-pressure dhcp form changed to an fcc form at about 8 GPa. Above 22 GPa (reported to be at about 32 GPa in later reports; Itié *et al.*, 1985; Peterson *et al.*, 1987), the fcc form was transformed to the alpha-uranium-type orthorhombic structure (Haire *et al.*, 1984). A 12% shrinkage in volume accompanied the latter transition. This collapse was associated with delocalization of the 5f electrons (Benedict *et al.*, 1984).

Below 22 GPa, a bulk modulus (compressibility) of (30 ± 10) GPa was estimated for berkelium metal (Haire *et al.*, 1984). This bulk modulus only for the normal-pressure dhcp phase of Bk metal was reported later to be 52 GPa (Itié *et al.*, 1985). Berkelium metal under pressure behaves similarly to americium, curium, and some light lanthanide metals and does not appear to undergo an isostructural phase transition corresponding to a change in metallic valence before delocalization of the 5f electrons (Johansson *et al.*, 1981).

Retention of the fcc phase in Bk metal after release of pressure (pressure quenched) allows comparison of the atomic volume of this cubic phase at room temperature and pressure (RTP) with the atomic volume of the same phase produced via thermal treatment and quenching to RTP (temperature quenched) (Haire *et al.*, 1986). The values obtained were 2.80×10^{-2} nm^3 for the pressure-quenched fcc phase and 3.12×10^{-2} nm^3 (Peterson *et al.*, 1971) for the temperature-quenched fcc phase. Similar results were found in the cases of Cm and Cf metals. In fact, for the three metals, the atomic volumes of their temperature-quenched fcc phases are all larger than those of their RTP dhcp phases. In contrast, the atomic volumes of their pressure-quenched fcc phases at RTP are in good agreement with those of their RTP dhcp phases (Haire *et al.*, 1986). The argument is made that the lattice parameter of the pressure-quenched fcc phase of these metals is preferred to that of the temperature-quenched fcc phase, in that it provides consistency with the atomic volumes of their RTP dhcp phases and the known trend in lattice parameters of their corresponding mononitrides (Haire *et al.*, 1986).

In the first experiments to measure the vapor pressure of metallic berkelium using Knudsen effusion target-collection techniques, the preliminary data were fitted with a least-squares line to give a provisional vaporization equation for the temperature range 1326–1582 K and $\Delta_v H^0_{298} = (382 \pm 18)$ kJ mol^{-1} (Ward *et al.*, 1980). Later measurements of the vapor pressure of Bk metal over the temperature range 1100–1500 K, using combined Knudsen effusion mass-spectrometric and target-collection techniques (Ward *et al.*, 1982), led to the vaporization equations:

$$\log p(\text{atm}) = (5.78 \pm 0.21) - (15718 \pm 253)/T(\text{K})$$

for solid Bk between 1107 and 1319 K, and

$$\log p(\text{atm}) = (5.14 \pm 0.17) - (14902 \pm 244)/T(\text{K})$$

for liquid Bk between 1345 and 1528 K. The enthalpy of fusion was calculated to be 7.92 kJ mol^{-1}, and the enthalpy associated with the dhcp→fcc transition was calculated to be 3.66 kJ mol^{-1} (Ward *et al.*, 1982). The crystal entropy, S^0_{298}, of berkelium was estimated to be (76.2 ± 1.3) J K^{-1} mol^{-1} (Ward and Hill, 1976) and then later to be (78.2 ± 1.3) J K^{-1} mol^{-1}, and the average of data according to the second and third law data analysis yielded (310 ± 6) kJ mol^{-1} for its enthalpy of vaporization, $\Delta_v H^0_{298}$ (Ward *et al.*, 1982). Earlier correlation systematics had suggested that the standard enthalpy of sublimation of berkelium

metal, $\Delta_f H^0$(Bk(g)), is 280 kJ mol^{-1}, and that the standard enthalpy of formation of aqueous Bk(III), $\Delta_f H^0$ (Bk^{3+}(aq)), is -615 kJ mol^{-1} (Nugent *et al.*, 1973a; Johansson and Rosengren, 1975). A later modification of the systematics (Nugent *et al.*, 1973a) led to values of (320 ± 8) kJ mol^{-1} and $-(590 \pm 21)$ kJ mol^{-1} for $\Delta_f H^0$ (Bk(g)) and $\Delta_f H^0$ (Bk^{3+}(aq)), respectively (David *et al.*, 1976). There is very good agreement between the value of (320 ± 8) kJ mol^{-1} for $\Delta_f H^0$ (Bk(g)) derived from systematics and the value of (310 ± 6) kJ mol^{-1} for $\Delta_v H^0_{298}$, which is the same thermodynamic quantity, derived from experiment.

The enthalpy of solution of Bk metal (dhcp) to Bk^{3+}(aq) in 1 M HCl at 298 K was determined from five measurements to be $-(576 \pm 25)$ kJ mol^{-1} (Fuger *et al.*, 1975). The error limits reported did not reflect the precision of the calorimetric measurements but rather the uncertainties in the purity of the berkelium metal. A new determination of the enthalpy of solution of Bk metal (dhcp) in 1 M HCl at (298.15 ± 0.05) K has yielded a value of $-(600.2 \pm 5.1)$ kJ mol^{-1} (Fuger *et al.*, 1981). From this value $\Delta_f H^0$ (Bk^{3+}(aq)) was derived to be $-(601 \pm 5)$ kJ mol^{-1}, in good agreement with the value from systematics (David *et al.*, 1976), and, using reasonable entropy estimates, the standard potential of the Bk(III)/Bk(0) couple was calculated to be $-(2.01 \pm 0.03)$ V (Fuger *et al.*, 1981).

Studies of the magnetic susceptibility of berkelium metal have been hampered by the difficulty in obtaining well-characterized, single-phase bulk samples containing minimal amounts of daughter californium. Recent results obtained from a 21 μg sample of dhcp Bk metal (~12 at% Cf) indicated a transition to antiferromagnetic behavior at about 34 K and paramagnetic behavior between 70 and 250 K (Nave *et al.*, 1980). Applying the Curie–Weiss susceptibility relationship to the berkelium data obtained at fields greater than 0.08 T (where the field dependency was saturated) yielded $\mu_{eff} = 9.69\ \mu_B$ and $\theta = 101.6$ K. The agreement of this value with the theoretical free-ion effective moment (9.72 μ_B) calculated for trivalent berkelium with LS coupling suggests that dhcp Bk metal exhibits high-temperature magnetic behavior like its lanthanide homolog, terbium. The results of earlier magnetic measurements on smaller samples of berkelium metal exhibiting mixed phases were reported by others (Fujita, 1969; Peterson *et al.*, 1970).

(c) Chemical properties

During the handling of microgram-sized samples of berkelium metal, it was observed that the rate of oxidation in air at room temperature is not extremely rapid, possibly due to the formation of a 'protective' oxide film on the metal surface (Peterson *et al.*, 1970). Berkelium is a chemically reactive metal, and berkelium hydride (Fahey *et al.*, 1972), some chalcogenides (Fahey *et al.*, 1972; Damien *et al.*, 1979, 1981), and pnictides (Stevenson and Peterson, 1979; Damien *et al.*, 1980) have been prepared directly from the reaction of Bk metal with the appropriate nonmetallic element. Berkelium metal dissolves

rapidly in aqueous mineral acids, liberating hydrogen gas and forming Bk(III) in solution.

(d) Theoretical treatment

A hybridized nondegenerate 6d and 5f virtual-bound-states model has been used to describe the properties of the actinide metals, including berkelium (Jullien *et al*., 1972). It accounted for the occurrence of localized magnetism in Bk metal. A review of the understanding of the electronic properties of berkelium metal as derived from electronic band theory was published shortly thereafter (Freeman and Koelling, 1974). Included was the relativistic energy band structure of fcc Bk metal ($5f^8 6d^1 7s^2$), and the conclusion was that berkelium is a rare earth-like metal with localized (ionic) 5f electrons resulting from less hybridization with the 6d and 7s itinerant bands than occurs in the lighter actinides.

A phenomenological model based on crystal structure, metallic radius, melting point, and enthalpy of sublimation has been used to arrive at the electronic configuration of berkelium metal (Fournier, 1976). An energy difference of 0.92 eV was calculated between the $5f^9 7s^2$ ground state and the $5f^8 6d^1 7s^2$ first excited state. The enthalpy of vaporization of trivalent Bk metal was calculated to be 2.99 eV (288 kJ mol^{-1}), reflecting the fact that berkelium metal is more volatile than curium metal. It was also concluded that the metallic valence of the fcc form of berkelium metal is less than that of its dhcp modification (Fournier, 1976).

A relativistic Hartree–Fock–Wigner–Seitz band calculation has been performed for Bk metal in order to estimate the Coulomb term U (the energy required for a 5f electron to hop from one atomic site to an adjacent one) and the 5f electron excitation energies (Herbst *et al*., 1976). The results for berkelium, in comparison to those for the lighter actinides, show increasing localization of the 5f states, i.e. the magnitude of the Coulomb term U increases through the first half of the actinide series with a concomitant decrease in the width of the 5f level.

10.6.2 Intermetallics

There have been no reports of berkelium intermetallics. Bk–Cf alloys formed from the natural decay of ^{249}Bk metal samples have been studied and are discussed in Section 10.6.3.

10.6.3 Alloys

^{249}Bk ($t_{1/2}$ = 330 days) decays by β^- emission to ^{249}Cf, and because this transition occurs on an atomic scale at randomly distributed lattice sites, truly homogeneous solid solutions (alloys) result. Two such alloys, one Bk-rich (65%)

and the other Cf-rich (60%), have been studied under pressure via energy-dispersive X-ray powder diffraction (Itié *et al*., 1985; Peterson *et al*., 1987). The Bk-rich alloy exhibited the same phases with increasing pressure as did pure Bk metal, and the Cf-rich alloy exhibited the same phases with increasing pressure as did pure Cf metal (Peterson *et al*., 1987). Continuity was observed between the values for pure Bk and Cf metals in the phase-transition pressures, the relative volume and volume decrease upon delocalization (point at which the α-uranium structure is first exhibited), and the bulk modulus. Thus one can consider these alloys as actinide metals with nonintegral atomic numbers (Itié *et al*., 1985).

Two ^{248}Cm–Bk alloys have been prepared by reduction of their mixed anhydrous trifluorides (precipitated from aqueous solution and treated with fluorine) with lithium metal (Heathman and Haire, 1998). One alloy contained 30% Bk and the other contained 54% Bk. The stated goal of this work was to understand the phase and relative volume behavior of both alloys in terms of chemical bonding, each element's electronic configuration, and the alloys' pressure behavior relative to that reported for the pure Am–Cf metals (Heathman and Haire, 1998). The structural behavior of these two alloys was monitored by energy-dispersive X-ray powder diffraction. Both exhibited the expected RTP dhcp phase that transformed to the fcc phase at 12 GPa (30% Bk) or 8 GPa (54% Bk). The fcc phase changed to a third, unidentified phase at 35 GPa (30% Bk) or at 24 GPa (54% Bk), which was retained up to the maximum pressure studied (53 GPa) (Heathman and Haire, 1998). These results are consistent with the phase-transition pressures in pure Cm and Bk metals, i.e. the greater the concentration of Bk in the alloy, the lower the corresponding phase transition pressure.

10.7 COMPOUNDS

10.7.1 General summary

The trivalent oxidation state of berkelium prevails in the known berkelium compounds, although the tetravalent state is exhibited in BkO_2, BkF_4, Cs_2BkCl_6, and $[N(CH_3)_4]_2BkCl_6$. Selected crystallographic data for a number of berkelium compounds are collected in Table 10.2. In cases where there have been multiple reports of lattice parameters for a particular compound, the ones considered more reliable by the present authors are given in Table 10.2. The interested reader is encouraged to refer to the citations given in the table and text for complete details. An inherent difficulty, not addressed here, in the determination of lattice constants of 'pure' ^{249}Bk compounds concerns the ingrowth of daughter ^{249}Cf at the rate of about 0.22% per day. Two experimental methods to address this problem are: (1) the determination of the lattice parameters of berkelium compounds as a function of californium content and

then extrapolation to zero californium content; and (2) the utilization of Vegard's law to correct measured berkelium lattice parameters for the presence of a known amount of californium (assuming, of course, that the lattice parameters of the isostructural 'pure' californium compound are known).

A summary and discussion of the structural aspects of solid-state actinide chemistry are presented in Chapter 22, so no attempt is made to do so here for the compounds of berkelium. Estimated thermochemical values for many compounds of berkelium can be found in Chapter 19. Only those values determined by direct experiment are discussed here.

An empirical set of 'effective' ionic radii in oxides and fluorides, taking into account the electronic spin state and coordination of both the cation and the anion, have been calculated (Shannon and Prewitt, 1969). For six-coordinate Bk(III), the radii values are 0.096 nm, based on a six-coordinate oxide ion radius of 0.140 nm, and 0.110 nm, based on a six-coordinate fluoride ion radius of 0.119 nm. For eight-coordinate Bk(IV), the corresponding values are 0.093 and 0.107 nm, respectively, based on the same anion radii (Shannon and Prewitt, 1969). Other self-consistent sets of trivalent and tetravalent lanthanide and actinide ionic radii, based on isomorphous series of oxides (Peterson and Cunningham, 1967a; Shannon, 1976) and fluorides (Peterson and Cunningham, 1968b; Shannon, 1976), have been published. Based on a crystal radius for Cf(III), the ionic radius of isoelectronic Bk(II) was calculated to be 0.114 nm (Ionova *et al.*, 1977). It is important to note, however, that meaningful comparisons of ionic radii can only be made if the values compared are calculated in like fashion from the same type of compound, with respect to both composition and crystal structure (Shannon, 1976).

The thermal decomposition of $Bk(NO_3)_3 \cdot 4H_2O$, $BkCl_3 \cdot 6H_2O$, $Bk_2(SO_4)_3 \cdot 12H_2O$, and $Bk_2(C_2O_4)_3 \cdot 4H_2O$ has been studied in air, argon, and H_2–Ar atmospheres and compared to that of the corresponding hydrates of cerium, gadolinium, and terbium (Haire, 1973). In air or Ar the final berkelium product was BkO_2; in H_2–Ar it was Bk_2O_3.

10.7.2 Hydrides

The preparation of berkelium hydride has been accomplished by treatment of berkelium metal at 500 K with H_2 gas derived from thermal decomposition of UH_3 (Fahey *et al.*, 1972). The product exhibited an fcc structure with lattice parameter $a_0 = (0.523 \pm 0.001)$ nm determined from nine observed X-ray diffraction lines. By analogy with the behavior of the lanthanide hydrides (Holley *et al.*, 1955), the stoichiometry BkH_{2+x} $(0 < x < 1)$ was assigned. Later studies of the berkelium–hydrogen system resulted in products with either fcc symmetry, identified as the dihydride, or hexagonal symmetry, which was taken to be berkelium trihydride, BkH_{3-x} $(0 < x < 1)$ (Gibson and Haire, 1985). Additional work is required to characterize fully the berkelium–hydrogen system.

Table 10.2 *Selected crystallographic data for berkelium compounds.*

Substance	*Structure type*	*Crystal system*	*Lattice parameters*[a]				*Other*[b]	*References*
			a_0 (nm)	b_0 (nm)	c_0 (nm)	β (degree)		
Hydrides								
BkH_{2+x}	CaF_2	cubic (fcc)	0.523					Fahey *et al.* (1972)
BkH_{2+x}	CaF_2	cubic (fcc)	0.5248					Gibson and Haire (1985)
BkH_{3-x}	LaF_3	trigonal	0.6454		0.6663			Gibson and Haire (1985)
Oxides								
BkO_2	CaF_2	cubic (fcc)	0.53315					Fahey *et al.* (1974)
Bk_2O_3	$(Fe,Mn)_2O_3$	cubic (bcc)	1.0887					Peterson and Cunningham (1967a)
Bk_2O_3	Sm_2O_3	monoclinic	1.4197	0.3606	0.8846	100.23		Baybarz (1973)
Bk_2O_3	La_2O_3	hexagonal	0.3754		0.5958		*V*72.7	Baybarz (1973)
Halides								
BkF_4	UF_4	monoclinic	1.2396	1.0466	0.8118	126.33	*V*70.7	Haug and Baybarz (1975)
BkF_3	LaF_3	trigonal	0.697		0.714		ρ10.15	Peterson and Cunningham (1968b)
BkF_3	YF_3	orthorhombic	0.670	0.709	0.441		ρ9.70	Peterson and Cunningham (1968b)
$BkCl_3$	UCl_3	hexagonal	0.7382		0.4127			Peterson and Cunningham (1968a)
Cs_2BkCl_6	Rb_2MnF_6	hexagonal	0.7451		1.2097		ρ4.155	Morss and Fuger (1969)
$Cs_2NaBkCl_6$	$(NH_4)_3AlF_6$	cubic (fcc)	1.0805				ρ3.952	Morss and Fuger (1969)
$BkCl_3 \cdot 6H_2O$	$GdCl_3 \cdot 6H_2O$	monoclinic	0.966	0.654	0.797	93.77	ρ3.06	Burns and Peterson (1971)
$BkBr_3$	$PuBr_3$	orthorhombic	0.403	1.271	0.912		*V*116.8	Burns *et al.* (1975)

$BkBr_3$	$AlCl_3$	monoclinic	0.723	1.253	0.683	110.6	V144.8	Burns *et al.* (1975)
BkI_3	BiI_3	hexagonal	0.7584		2.087			Fellows *et al.* (1977)
Chalcogenides								
BkS_{2-x}	anti-Fe_2As	tetragonal	0.3902		0.792			Damien *et al.* (1981)
Bk_2S_3	deficit Th_3P_4	cubic (bcc)	0.8358					Damien *et al.* (1981)
$BkSe_{2-x}$	anti-Fe_2As	tetragonal	0.404		0.828			Damien *et al.* (1981)
Bk_2Se_3	deficit Th_3P_4	cubic (bcc)	0.8712					Damien *et al.* (1981)
$BkTe_3$	$NdTe_3$	orthorhombic	0.4318	0.4319	2.5467			Damien *et al.* (1979, 1981)
$BkTe_{2-x}$	anti-Fe_2As	tetragonal	0.4314		0.8945			Damien *et al.* (1979)
Bk_2Te_3	Sc_2S_3	orthorhombic	1.226	0.8685	2.605			Damien *et al.* (1979)
Pnictides								
BkN	NaCl	cubic (fcc)	0.4951					Damien *et al.* (1980)
BkP	NaCl	cubic (fcc)	0.5669					Damien *et al.* (1980)
BkAs	NaCl	cubic (fcc)	0.5829					Damien *et al.* (1980)
BkSb	NaCl	cubic (fcc)	0.6191					Damien *et al.* (1980)
Other inorganic compounds								
BkOCl	PbFCl	tetragonal	0.3966		0.6710		ρ9.45	Peterson and Cunningham (1967b)
BkOBr	PbFCl	tetragonal	0.395		0.81			Cohen *et al.* (1968)
BkOI	PbFCl	tetragonal	0.3986		0.9149			Fellows *et al.* (1977)
$Bk_2O_2SO_4$	$La_2O_2SO_4$	orthorhombic	0.4195	0.4083	1.3110			Haire and Fahey (1977)
Bk_2O_2S	Pu_2O_2S	trigonal	0.3861		0.6686			Haire and Fahey (1977)
$Bk_2(C_2O_4)_3{\cdot}10H_2O$	$La_2(C_2O_4)_3{\cdot}10H_2O$	monoclinic	1.112	0.9746	0.987	114.1		Morris *et al.* (2005)
Coordination compounds								
$[Bk(C_5H_5)_2Cl]_2$	$[Sm(C_5H_5)_2Cl]_2$							Laubereau (1970)
$[N(CH_3)_4]_2BkCl_6$	K_2PtCl_6	cubic (fcc)	1.308					Morss *et al.* (1991)
Organometallic compounds								
$Bk(C_5H_5)_3$	$Pr(C_5H_5)_3$	orthorhombic	1.411	1.755	0.963		ρ2.47	Laubereau and Burns (1970)

[a] See original source for precision claimed on these room-temperature values and for information regarding sample purity.
[b] ρ = density in 10^3 kg m^{-3}(g cm^{-3}); V = formula volume in 10^6 pm^3(Å^3).

10.7.3 Oxides

The first compound of berkelium identified on the basis of its characteristic X-ray powder diffraction pattern was BkO_2 (Cunningham, 1963). Other researchers have since confirmed its CaF_2-type fcc structure with $a_0 = 0.533$ nm (Peterson and Cunningham, 1967a; Baybarz, 1968, 1973; Fahey *et al.*, 1974; Sudakov *et al.*, 1977). The thermal expansion of BkO_2 in 1 atm of oxygen was determined and shown to be reversible with temperature (Fahey *et al.*, 1974). The data were fitted by the expression

$$a_0(t) = 5.3304 + (4.32 \times 10^{-5})t + (15.00 \times 10^{-9})t^2,$$

where $a_0(t)$ is the unit cell edge (in Å) at temperature t (in °C). In addition, the instantaneous expansion coefficients at 25 and 900°C were calculated to be 8.25×10^{-6} °C^{-1} and 13.2×10^{-6} °C^{-1}, respectively (Fahey *et al.*, 1974).

The results of a preliminary study of a sample of berkelium oxide (BkO_2, Bk_2O_3, or a mixture of the two) via X-ray photoelectron spectroscopy (XPS) included measured core- and valence-electron-binding energies (Veal *et al.*, 1977). The valence-band XPS spectrum, which was limited in resolution by phonon broadening, was dominated by 5f electron emission. The photoelectron spectrum of the 4f lines of Bk in BkO_2 was recorded, and the binding energies of the $4f_{5/2}$ electrons determined to be 515.6(4) eV, and those of the $4f_{7/2}$ electrons, 499.6(4) eV (Krause *et al.*, 1988). These values were reported to be slightly lower than theoretical estimates, but the spin–orbit splitting of the 4f levels, 16.0 (3) eV, was in good agreement with the results of relativistic Hartree–Slater calculations (Krause *et al.*, 1988).

A capacitance manometer system was used to measure the equilibrium oxygen decomposition pressures over non-stoichiometric BkO_x ($1.5 < x < 2.0$) (Turcotte *et al.*, 1971). Three broad non-stoichiometric phases were defined: $BkO_{1.5–1.77}$; $BkO_{1.81–1.91}$; and BkO_{2-x} ($x \leq 0.07$). Later, an X-ray diffraction investigation of this BkO_x system under equilibrium conditions was undertaken to correlate the above data with structural behavior (Turcotte *et al.*, 1980). A phase diagram was suggested, showing above 673 K two widely non-stoichiometric phases: body-centered cubic (bcc) for $1.5 < O/Bk \leq 1.70$ and fcc for $1.78 \leq O/Bk < 2.00$. Interestingly, no evidence was found for the formation of Bk_7O_{12}, expected to exhibit a rhombohedral structure based on its common presence in other MO_x ($1.5 < x < 2.0$) systems. Using the data from the work of others (Peterson and Cunningham, 1967a; Baybarz, 1968, 1973; Turcotte *et al.*, 1980), a berkelium–oxygen phase diagram was constructed over the range from 59 to 67 at% oxygen and from 200 to 900°C (Okamoto, 1999). Also provided is a summary of Bk–O crystal structure data.

The stable room-temperature form of berkelium sesquioxide exhibits the bixbyite-type bcc structure with $a_0 = 1.0887$ nm (Peterson and Cunningham, 1967a). This has been corroborated by an independent study (Baybarz, 1968, 1973). The cubic sesquioxide has also been analyzed by electron diffraction

(Haire and Baybarz, 1973). The high-temperature behavior of Bk_2O_3 has been studied, with the finding that the cubic-to-monoclinic transition at (1473 ± 50) K is irreversible, while the monoclinic-to-hexagonal transition at about 2025 K is reversible (Baybarz, 1973). In addition, the melting point of Bk_2O_3 was determined to be (2193 ± 25) K. Thus berkelium continues the trend of actinide sesquioxides exhibiting trimorphism; with increasing temperature, the structure of Bk_2O_3 changes from bcc (C-form) to monoclinic (B-form) to hexagonal (A-form).

The possibility of the existence of BkO has been considered (Fahey *et al.*, 1972). The true identity of the brittle, gray material exhibiting an fcc structure with $a_0 = 0.4964$ nm is still in doubt. This phase might represent a nitride or an oxide nitride.

A preliminary report of the synthesis and structural characterization of polycrystalline $Bk_2M_2O_7$ and solid solutions of $(Bk,M)O_2$, where M = Zr or Hf, has been given, but no specifics were provided (Haire and Raison, 2000). In a later report the lattice parameter for $Bk_2Zr_2O_7$ was presented to be 1.058 nm in a graph (Haire *et al.*, 2002).

As part of an investigation of the fundamental chemistry and materials science of the 4f and several 5f elements in glass matrices, berkelium was put into two high-temperature (850 and 1450°C), silicate-based glasses and into one sol–gel glass (formed by the hydrolysis of a silicate ester) (Haire *et al.*, 1998). Berkelium (along with cerium and americium) provided an exception to the general observation that the oxidation state of the f element in the high-temperature glasses correlated with that in the element's usual binary oxide produced in air. The same correlation also applied to the f elements in the sol–gel glasses after they had been heated to 200–400°C. The authors only observed Bk(III) in the three glasses and reasoned that without the added stability afforded by the fluorite lattice in BkO_2, Bk(III) was the more stable oxidation state in these glasses (Haire *et al.*, 1998). The anomalous dependence on excitation power of the emission profile of Bk(III) in the 850°C silicate-based glass (Assefa *et al.*, 1998) has been discussed in Section 10.5.3.

10.7.4 Halides

The only reported binary Bk(IV) halide is BkF_4 (Asprey and Keenan, 1968; Keenan and Asprey, 1969; Asprey and Haire, 1973; Haug and Baybarz, 1975), prepared by fluorination of BkO_2 or BkF_3. Although these researchers agree that it exhibits the UF_4-type monoclinic structure, there is some variance in the reported lattice parameters. This could result from the complexity of the X-ray powder diffraction pattern of BkF_4. A molecular volume of 7.07×10^7 pm^3 is calculated from the lattice constants given in Table 10.2, in contrast to those of 7.148×10^7 pm^3 (Asprey and Haire, 1973) and 7.28×10^7 pm^3 (Asprey and Keenan, 1968; Keenan and Asprey, 1969) derived from the other reported lattice parameters. The solid-state absorption spectrum of BkF_4 was obtained

by Ensor *et al.* (1981). Mixed alkali metal (M)–Bk(IV) fluoride compounds of the types $MBkF_5$, M_2BkF_6, M_3BkF_7, and $M_7Bk_6F_{31}$, although at present unreported, should be readily prepared. The structural systematics of such actinide fluoride complexes have been discussed elsewhere (Thoma, 1962; Penneman *et al.*, 1973).

In addition to $[N(CH_3)_4]_2BkCl_6$ (discussed in Section 10.7.7), one other Bk(IV) halide compound, Cs_2BkCl_6, has been characterized by its crystallographic properties (Morss and Fuger, 1969). This orange compound precipitated upon dissolution of Bk(IV) hydroxide in chilled, concentrated HCl solution containing CsCl, and was found to crystallize in the Rb_2MnF_6-type hexagonal structure with $a_0 = 0.7451$ nm and $c_0 = 1.2097$ nm. Using a separated halogen atom model, the lattice energy of this compound has been calculated to be 1295 kJ mol^{-1} and the average radius of the $BkCl_6^{2-}$ ion to be 0.270 nm (Jenkins and Pratt, 1979).

The trihalides of berkelium can be prepared by hydrohalogenation of BkO_2, Bk_2O_3, or a lighter berkelium halide. BkF_3 (Peterson and Cunningham, 1968b; Ensor *et al.*, 1981), $BkCl_3$ (Peterson and Cunningham, 1968a; Young *et al.*, 1978; Peterson *et al.*, 1981, 1986), and $BkBr_3$ (Burns *et al.*, 1975; Peterson *et al.*, 1977b) have been shown by X-ray powder diffraction and absorption spectrophotometric studies to be dimorphic. Berkelium is the lightest actinide whose trifluoride exhibits the YF_3-type orthorhombic structure as the room-temperature alpha phase and the LaF_3-type trigonal structure as the high-temperature phase (Peterson and Cunningham, 1968b).

In the case of dimorphic $BkCl_3$, the UCl_3-type hexagonal structure (Peterson and Cunningham, 1968a) represents the low-temperature form, while the $PuBr_3$-type orthorhombic structure is exhibited by the high-temperature modification (Peterson *et al.*, 1981, 1986). The phase-transition temperature appears to be close (Peterson *et al.*, 1981, 1986) to the $BkCl_3$ melting point (876 K) (Peterson and Burns, 1973). The volatilization behavior of many of the binary actinide chlorides including $BkCl_3$ has been studied and correlated with the oxidation state and atomic number ($Z < 92$ or $Z \geq 92$) of the actinide (Merinis *et al.*, 1970). More recent thermochromatographic studies of berkelium chloride using ^{250}Bk confirmed these early results, in that under non-oxidizing conditions, only one deposition peak was observed, corresponding to $BkCl_3$ (Yakushev *et al.*, 2003). With oxidizing conditions (Cl_2 or $Cl_2/SOCl_2$), however, a lower temperature deposition peak grows slowly over time and was assigned to more volatile $BkCl_4$. The adsorption enthalpies were calculated via a Monte Carlo simulation method (Zvara, 1985) and found to be $-(201 \pm 6)$ and $-(154 \pm 6)$ kJ mol^{-1} for $BkCl_3$ and $BkCl_4$, respectively (Yakushev *et al.*, 2003). White $Cs_2NaBkCl_6$ was crystallized from aqueous CsCl–HCl solution by increasing the HCl concentration and cooling to $-23°C$, and it was found to exhibit an fcc structure in which the Bk(III) ions (O_h site symmetry) are octahedrally coordinated by chloride ions (Morss and Fuger, 1969). The unique properties of such compounds stimulated the synthesis and study of an

isostructural set of Cs_2NaMCl_6 compounds containing trivalent cations (including M = U, Np, Pu, Am, and Cf) whose ionic radii ranged from 0.065 to 0.106 nm (Morss *et al.*, 1970; Schoebrechts *et al.*, 1989).

X-ray diffraction from a powder sample of $BkCl_3 \cdot 6H_2O$ showed that it is isostructural with $AmCl_3 \cdot 6H_2O$, whose structure was refined by single-crystal diffraction methods (Burns and Peterson, 1971). By analogy, the basic units of the berkelium structure are $BkCl_2(OH_2)_6^+$ cations and Cl^- anions, the latter being octahedrally coordinated by water molecules.

From X-ray powder diffraction patterns of $BkBr_3$ obtained as a function of the sample's thermal treatment, it was concluded that the $PuBr_3$-type orthorhombic structure is the low-temperature form of $BkBr_3$, and the $AlCl_3$-type monoclinic structure is the high-temperature form (Burns *et al.*, 1975). Because these two crystallographic modifications differ by 2 in the Bk(III) CN, absorption spectrophotometric analysis easily distinguishes between them (Peterson *et al.*, 1977b). The possibility of a third polymorph of $BkBr_3$ has been suggested on the basis of eight lines of low intensity in one powder pattern (Burns *et al.*, 1975). If it does exist, it would be the form intermediate between the $PuBr_3$- and $AlCl_3$-type structures and would exhibit the $FeCl_3$-type rhombohedral structure with $a_0 = 0.766$ nm and $\alpha = 56.6°$ (Burns *et al.*, 1975). There is one additional report (Cohen *et al.*, 1968) with lattice parameters for the orthorhombic form of $BkBr_3$ and for BiI_3-type hexagonal BkI_3.

Samples of berkelium trifluoride, trichloride, tribromide, and triiodide have been studied over time to ascertain the physicochemical effects of beta decay in the bulk-phase solid state (Young *et al.*, 1984). In each case Bk^{3+} was found to transform to Cf^{3+}, and the crystal structure of the solid remained unchanged. Maintenance of oxidation state would seem to be a chemical effect of this transformation, whereas maintenance of crystal structure is more of a physical effect, the structure of the progeny being controlled by its environment. Details of the characterization and study of dimorphic $BkCl_3$, via X-ray powder diffraction and absorption spectrophotometry, have been published (Peterson *et al.*, 1986). The results of monitoring each of the crystal forms of $BkCl_3$ over a period of almost 3 years are included. Justification (and some limitations) for the use of electronic f→f absorption peaks in the spectra of berkelium (and other actinide) compounds for the elucidation of the crystal structures of these compounds (crystal-field effects) has been published (Peterson *et al.*, 1990). In addition to absorption spectrophotometry, phonon Raman spectroscopy has been shown to be an effective way to elucidate the structure of a solid-state compound. Each crystal type possesses a unique set of fundamental crystal vibrations resulting from the positions, coordinations, bonding, and masses of its atoms. A catalog of phonon Raman spectral data for selected actinide compounds, including both crystallographic and spectroscopic parameters for each individual crystal structure exhibited, is available (Wilmarth and Peterson, 1991). A discussion of the comparative science of the lanthanide and actinide halides, mainly focusing on the trivalent chlorides and

bromides, provides the systematics into which berkelium fits as expected (Peterson, 1995).

10.7.5 Chalcogenides and pnictides

The only other crystallographic result reported for a berkelium chalcogenide besides those summarized in Table 10.2 is a cubic lattice parameter of 0.844 nm for Bk_2S_3 (Cohen *et al.*, 1968). The microscale synthesis of the brownish-black sesquisulfide was carried out by treatment of berkelium oxide at 1400 K with a mixture of H_2S and CS_2 vapors. In a later work (Damien *et al.*, 1979, 1981), the higher chalcogenides were prepared on the 20–30 μg scale in quartz capillaries by direct combination of the elements. These were then thermally decomposed *in situ* to yield the lower chalcogenides. The stoichiometries of these compounds have not been determined directly.

The berkelium monopnictides have been prepared on the multi-microgram scale by direct combination of the elements (Damien *et al.*, 1980). In all cases the lattice constants of the NaCl-type cubic structures were smaller than those of the corresponding curium monopnictides but comparable to those of the corresponding terbium compounds. This supports the semimetallic classification for these compounds. One additional report of BkN has appeared (Stevenson and Peterson, 1979). The lattice parameter derived from the sample exhibiting a single phase was (0.5010 ± 0.0004) nm, whereas that extracted from the mixed-phase sample of BkN resulting from incomplete conversion of a hydride was (0.4948 ± 0.0003) nm. Additional samples of BkN should be prepared to establish more firmly its lattice constant.

10.7.6 Other inorganic compounds

BkOCl (Peterson and Cunningham, 1967b), BkOBr (Cohen *et al.*, 1968), and BkOI (Cohen *et al.*, 1968; Fellows *et al.*, 1977) have been synthesized and are found to exhibit the PbFCl-type tetragonal structure. Although presently unreported, BkOF certainly can be prepared and probably exhibits polymorphism.

Both the oxysulfate (body-centered orthorhombic) and the oxysulfide (trigonal) of Bk(III) have been studied by X-ray powder diffraction (Haire and Fahey, 1977). $Bk_2O_2SO_4$ resulted from the decomposition of $Bk_2(SO_4)_3 \cdot nH_2O$ in an argon atmosphere (to prevent oxidation to BkO_2) at about 875 K, whereas Bk_2O_2S was formed upon thermal decomposition of the sulfate hydrate in a 4% H_2/96% Ar atmosphere. No decomposition of the oxysulfide was observed up to 1300 K in the H_2/Ar gas mixture (Haire and Fahey, 1977). Both $Bk_2O_2SO_4$ and Bk_2O_2S are isostructural with the corresponding lanthanide and actinide compounds.

Berkelium(III) orthophosphate has been prepared and characterized by X-ray powder diffraction and solid-state absorption and Raman spectroscopies (Haire *et al.*, 1983; Hobart *et al.*, 1983). Analysis of the X-ray data has shown

this compound to be isostructural with samarium and europium orthophosphates and to exhibit similar lattice parameters (Haire *et al.*, 1983). The structure type was confirmed by the direct correlation of the Raman spectrum of $BkPO_4$ with those of the isostructural lanthanide orthophosphates (Hobart *et al.*, 1983).

The preparation of berkelium(III) sesquioxalate decahydrate has been reported, along with its monoclinic unit cell parameters and its absorption and Raman spectra. It was observed that the Bk(III) compound underwent oxidation in about 24 h to a non-stoichiometric Bk(IV) oxalate complex, presumably the result of its self-irradiation (Morris *et al.*, 2005).

10.7.7 Coordination compounds

A β-diketonate compound of Bk(III) has been prepared and reported to be stable when volatilized. The possibility of using this volatile compound in transport and subsequent separation of berkelium from other actinides has been proposed (Fedoseev *et al.*, 1983).

More recently $[N(CH_3)_4]_2BkCl_6$ samples were prepared from cold, concentrated HCl(aq) on the milligram scale and studied via X-ray powder diffraction and optical spectroscopy in KBr and KCl pellets (Morss *et al.*, 1991). The powder patterns were indexed on fcc symmetry, with $a_0 = 1.308(2)$ nm, although from systematics a smaller lattice parameter was expected. No fluorescence attributable to Bk^{4+} was found under several modes of excitation. Strong f-center absorptions, due to radiation damage, and several very weak absorptions, presumably due to transitions to the first excited state of Bk^{4+}, were noted (Morss *et al.*, 1991).

10.7.8 Organometallic compounds

Two cyclopentadienylberkelium(III) compounds have been reported, but only one of them, $Bk(C_5H_5)_3$, has been characterized crystallographically (Laubereau and Burns, 1970). In addition to the data given in Table 10.2, the formula volume of this compound is 2.98×10^8 pm^3. The amber-colored tris (cyclopentadienyl)berkelium(III) was isolated from a reaction mixture of $BkCl_3$ and molten $Be(C_5H_5)_2$ by sublimation in vacuum at 475–495 K. It decomposes to an orange melt at 610 K (Laubereau and Burns, 1970).

During vacuum sublimation from a mixture of $BkCl_3$ and molten $Be(C_5H_5)_2$ at temperatures above 500 K (up to 600 K), a second berkelium fraction was obtained (Laubereau, 1970). Its identity was established to be bis(cyclopentadienyl)berkelium(III) chloride dimer, $[Bk(C_5H_5)_2Cl]_2$, based on the similarities of its X-ray powder diffraction pattern and sublimation behavior to those of known $[Sm(C_5H_5)_2Cl]_2$. The solid-state absorption spectrum of $[Bk(C_5H_5)_2Cl]_2$ was obtained and noted to be very similar to that of $Bk(C_5H_5)_3$ (Laubereau, 1970).

10.7.9 Magnetic behavior of berkelium ions

In order to improve upon the precision (±10%) of the initial measurements of the magnetic susceptibility of Bk(III) ions (Cunningham, 1959) and to extend the range of measurements to lower temperatures, single beads of cation-exchange resin were saturated with Bk(III) and subjected to susceptibility measurements over the temperature range 9–298 K (Fujita, 1969). The magnetic behavior of Bk(III) over the entire temperature range was described well by the Curie–Weiss relationship with $\mu_{eff} = (9.40 \pm 0.06)\ \mu_B$ and $\Theta = (11.0 \pm 1.9)$ K. The magnetic susceptibility of Bk(III) in an octahedral environment of host matrix $Cs_2NaLuCl_6$ was measured; temperature-independent paramagnetism was observed over the temperature range 10–40 K, with the lowest level of Bk(III) determined to be Γ_1 and with a Γ_1–Γ_4 separation of $8.5 \times 10^3\ m^{-1}$ (Hendricks *et al.*, 1974).

Results of electron paramagnetic resonance (Boatner *et al.*, 1972) and magnetic susceptibility (Karraker, 1975) studies of Bk(IV) in ThO_2 have been reported. The eight-line hyperfine pattern confirmed that the nuclear spin of ^{249}Bk is 7/2; the estimated nuclear moment was $(2.2 \pm 0.4)\ \mu_N$ (Boatner *et al.*, 1972). Two regions of temperature-dependent paramagnetism of BkO_2 in ThO_2 were observed over the temperature range 10–220 K; the possibility of an antiferromagnetic transition at 3 K was noted (Karraker, 1975).

The first measurements of the magnetic susceptibilities of bulk-phase samples of some berkelium compounds (BkO_2, BkF_3, BkF_4, and BkN) were made in 1981. The effective moments were found to agree with the calculated free-ion values, assuming Bk(IV) or Bk(III) cores and LS coupling (Nave *et al.*, 1981). The paramagnetic effective moments for BkF_4 and BkO_2 were determined from a Curie–Weiss fit to the data displayed in Fig. 10.5. The experimentally determined μ_{eff} values for BkF_4 and BkO_2 of $(7.93 \pm 0.03)\ \mu_B$ and $(7.92 \pm 0.1)\ \mu_B$, respectively, are in good agreement with a localized $5f^7$ ionic model where μ_{eff} (theory) $= 7.94\ \mu_B$ (Nave *et al.*, 1983).

10.8 IONS IN SOLUTION

10.8.1 Oxidation states

Berkelium exhibits both III and IV oxidation states in solution, as would be expected from the oxidation states displayed by its lanthanide counterpart, terbium. Evidence has been offered for the existence of Bk(II), but there is only speculation on the possible existence of Bk(V). Bk(III) is the most stable oxidation state in non-complexing aqueous solutions. Bk(IV) is reasonably stable in solution in the absence of reducing agents because of the stabilizing influence of the half-filled $5f^7$ subshell. Bk(III) and Bk(IV) exist in aqueous solution as simple hydrated ions, Bk^{3+}(aq) and Bk^{4+}(aq), respectively, unless complexed by ligands. Bk(III) is green in most mineral acid solutions. Bk(IV) is yellow in HCl solution and orange-yellow in H_2SO_4 solution.

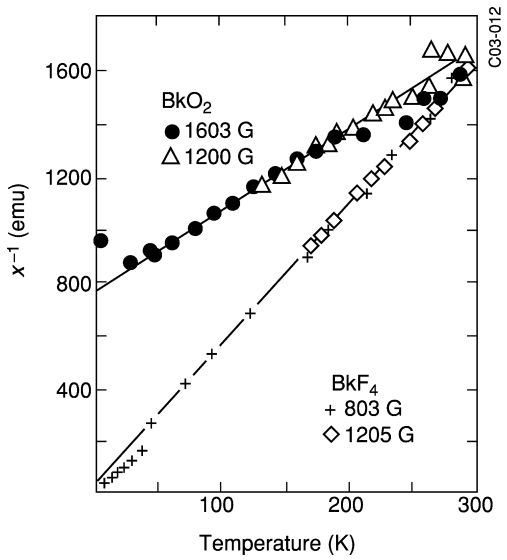

Fig. 10.5 *Inverse magnetic susceptibility of* BkF_4 *at* 803 *and* 1205 G *and* BkO_2 *at* 1200 *and* 1603 G *as a function of temperature*. (*The solid lines are least-squares fits of the data to the Curie–Weiss law*.) (*Reprinted figure with permission from Nave* et al. (1983). *Copyright* 1983 *by the American Physical Society*.)

The possible existence of divalent berkelium was studied by polarography in acetonitrile solution. Because of high background currents, caused by radiolysis products obscuring the polarographic wave, evidence for Bk(II) was not obtained (Friedman and Stokely, 1976). Divalent berkelium has been reported to exist in mixed lanthanide chloride–strontium chloride melts. The claim is based on the results of the distribution of trace amounts of berkelium between the melt and a solid crystalline phase (co-crystallization technique) (Mikheev *et al*., 1979; D'yachkova *et al*., 1980). As discussed in Section 10.8.2, additional evidence for the transient existence of Bk(II), generated via pulse radiolysis of an aqueous bicarbonate–ethanol solution, has been reported (Sullivan *et al*., 1988).

10.8.2 Spectra in solution

The first attempts to measure the absorption spectrum of Bk(III) involved the use of a single ion-exchange resin bead (Cunningham, 1959). Later the spectrum of a 3.6×10^{-3} M Bk(III) solution was recorded in a microcell (Gutmacher *et al*., 1967). Sixteen absorption bands of Bk(III) were identified in the solution spectrum recorded in a 'suspended-drop' microcell over the wavelength range 320–680 nm (Peterson, 1967, 1980). The results of additional observations identified a total of 23 absorption bands in the 280–1500 nm wavelength region (Fujita, 1969).

The first attempts to record the Bk(IV) solution absorption spectrum were hindered by the presence of cerium impurities (Gutmacher *et al.*, 1967). The positions of the Bk(IV) absorption bands, superimposed on the strong Ce(IV) bands, suggested the assignment of $5f^7$ for the electronic configuration of Bk(IV), which is in agreement with the actinide hypothesis.

The absorption spectra of Bk(III) and Bk(IV) have been recorded in a variety of solutions (Baybarz *et al.*, 1972). New absorption bands were reported as the result of using larger quantities of ^{249}Bk of higher purity. Observations of the spectrum of Bk(III) were extended further into the UV wavelength region (to 200 nm), and nine new absorption bands were reported (Gutmacher *et al.*, 1973). An interpretation of the low-energy bands in the solution absorption spectra of Bk(III) and Bk(IV) was published (Carnall *et al.*, 1971). Later experimental work using larger quantities of berkelium than had been available previously, coupled with a new technique for rapidly separating small quantities of daughter ^{249}Cf, has resulted in a Bk(III) solution absorption spectrum with minimal interference from radiolysis products and significantly higher resolution than those of previously published spectra (Carnall *et al.*, 1984). A parametric fit of the data was performed in order to obtain the energy-level structure of the Bk^{3+} aquo ion. The band intensities were analyzed using the Judd–Ofelt theory, and fluorescent branching ratios were computed from theoretical parameters (Carnall *et al.*, 1984).

The spectra of Bk(III) and Bk(IV) in complexing, concentrated aqueous carbonate solutions have been reported (Hobart *et al.*, 1990). Bk(III) rapidly oxidizes in strongly basic carbonate solutions, and thus the Bk(III) spectrum could only be obtained by electrochemically reducing Bk(IV) in such solutions in a semi-micro cell. The stable Bk(IV) carbonate solution spectrum exhibited a strong charge transfer band peaking at 282 nm in 2 M carbonate solution and at 274 nm in 5 M carbonate solution. The Bk(III) carbonate spectrum showed characteristic f–f transitions superimposed on remnants of the Bk(IV) spectrum. The spectra of Bk(III) in 0.1 M citrate solution at pH values of 1 and 4 have also been reported (Hobart *et al.*, 1990).

The solution absorption spectra of 1×10^{-4} M solutions of yellow Bk(IV) nitrate- and brown Bk(IV) perchlorate–triphenylarsine oxide adducts in acetonitrile were recorded as a result of ozonolysis of initial Bk(III) adduct solutions. Both Bk(IV) spectra exhibited a charge transfer UV cutoff around 300 nm (Payne and Peterson, 1987).

Fluorescence X-ray absorption near-edge spectra (XANES) and the L_3-edge fluorescence X-ray absorption fine structure (XAFS), and their Fourier transforms, of Bk(III) and Bk(IV) aquo ions have been published (Antonio *et al.*, 2002).

Although there have been a number of elegant solid-state studies that provided indirect evidence for the existence of the divalent state of berkelium (e.g. Young *et al.*, 1981), an attempt was made to generate Bk(II) in an aqueous bicarbonate–ethanol solution via pulse radiolysis (Sullivan *et al.*, 1988). The absorption

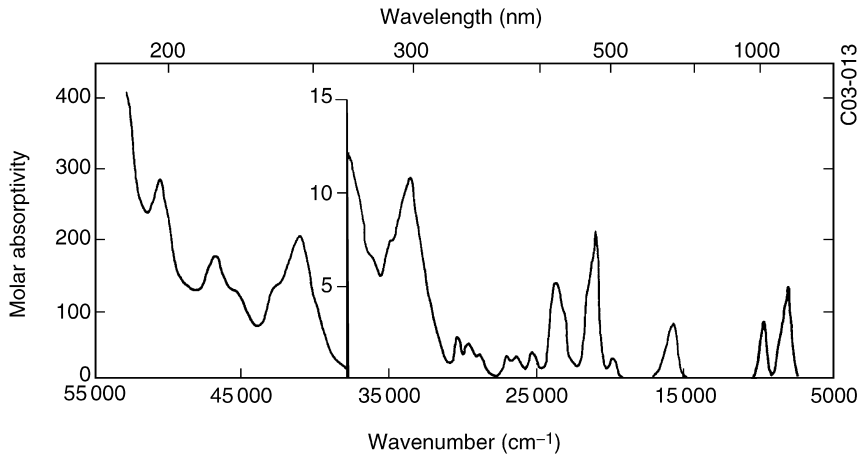

Fig. 10.6 *Solution absorption spectrum of Bk(III) in* 0.2 M $HClO_4$ (*DCl solutions were used for portions of the infrared spectrum*) (*Carnall* et al., 1984).

spectrum of Bk(II), obtained by subtracting out the contributions of the ethanol radical, yielded a peak with a maximum at 310 nm and a molar absorptivity of $(2.3 \pm 0.2) \times 10^3$ cm^{-1} M^{-1}. Bk(II) is unstable in this medium, and the rate of its disappearance was reported to be $(1.53 \pm 0.25) \times 10^5$ s^{-1} (Sullivan *et al.*, 1988).

The solution absorption spectrum of non-complexed Bk(III) is shown in Fig. 10.6. This spectrum is characterized by sharp absorption bands of low molar absorptivity attributed to 'Laporte-forbidden' f–f transitions and by intense absorption bands in the UV region attributed to f–d transitions (Gutmacher *et al.*, 1973). The spectra of Bk(IV) shown in Fig. 10.7 are dominated by a strong absorption band at 250–290 nm, the peak position of which is strongly dependent on the degree of complexation of Bk(IV) by the solvent medium. This dominant band is attributed to a charge transfer mechanism (Gutmacher *et al.*, 1973).

Electronic spectra of Bk(III) (Varga *et al.*, 1973b; Carnall *et al.*, 1984) and Bk(IV) (Varga *et al.*, 1973c) and a prediction of the electronic spectrum of Bk(II) (Varga *et al.*, 1973a) have been published. Spin–orbit coupling diagrams for these berkelium ions, based on a free-ion interpretation of the f–f spectra, were proposed. Further discussion of the absorption spectra of berkelium ions in solution can be found in Chapter 18.

10.8.3 Hydrolysis and complexation behavior

Although Bk(IV) is well known in solution, only stability constants of complexes with Bk(III) have been reported, most of which were determined during investigations of separation procedures. A compilation of the stability constants of Bk(III) complexes with various anions is given in Table 10.3. In most cases the

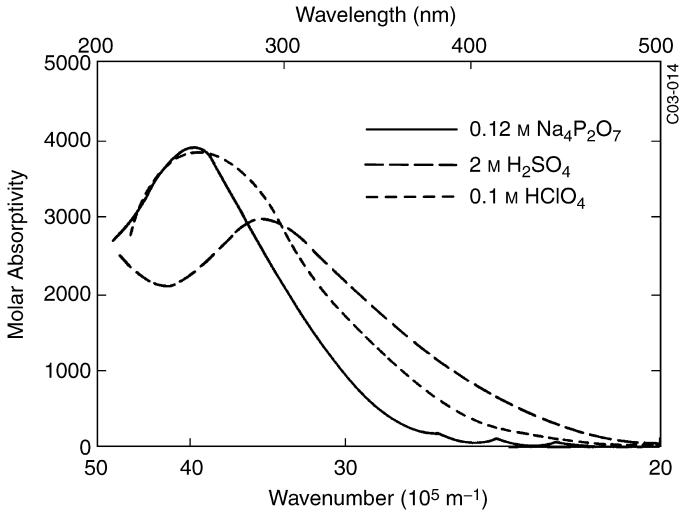

Fig. 10.7 *Solution absorption spectra of Bk(IV) in various media* (*Gutmacher* et al., 1973).

lack of replicate results precludes an assessment of the accuracy of the reported values. The reader should consult the original sources for any information regarding the precision of the stability constant values. Although the number of directly measured stability constants for complexes of Bk(III) is rather small, a number of additional, reasonably accurate values for other complexes of Bk(III) can be obtained by interpolation of the stability constant data for the corresponding complexes of Am(III), Cm(III), and Cf(III).

Attempts to obtain thermodynamic data for solvent extraction of Bk(III) by thenoyltrifluoroacetone (TTA) in benzene and for complexation of Bk(III) by hydroxide and citrate ions were unsuccessful (Hubert *et al.*, 1976). The high extractibility and complexibility of the easily accessible tetravalent state of berkelium probably accounts for the difficulty encountered in this study. However, TTA was used successfully to determine the first hydrolysis constant (Désiré *et al.*, 1969; Hussonnois *et al.*, 1973) and citrate complexation constants (Aly and Latimer, 1970; Stepanov, 1971) of Bk(III).

Although no complexation constant values have been reported for Bk(IV), one study is worth noting (Makarova *et al.*, 1979). The electromigration behavior of Bk(IV), Ce(IV), and other actinide(IV) ions was studied in perchloric and nitric acid solutions and mixtures of these acids. In pure 6 M $HClO_4$ both Bk(IV) and Ce(IV) have equal mobilities of $(13.0 \pm 1.0) \times 10^{-5}$ cm^2 V^{-1} s^{-1} and behave as free hydrated ions. As HNO_3 is added to $HClO_4$ solution, keeping the total acid concentration constant at 6 M, the mobility of both ions decreases, with the Bk(IV) mobility decreasing more sharply and then remaining constant (4×10^{-5} cm^2 V^{-1} s^{-1}) between 3 and 6 M HNO_3 (Makarova *et al.*, 1979). The decreased mobility is attributed to changes in the charge of the berkelium species, possibly

Table 10.3 *Stability constants of Bk(III) complexes with various anions.*

Ligand	*Conditions*[a]	*Stability constants*[b]	*References*
fluoride ion, F^-	solv. extrn., 298 K, $\mu = 1.0$, pH = 2.72	$\beta_1 = 7.8 \times 10^2$	Choppin and Unrein (1976)
chloride ion, Cl^-	solv. extrn., 298 K, $\mu = 1.0$ pH = 2	$\beta_1 = 0.96$	Harmon *et al.* (1972a)
	solv. extrn., ca. 293 K, $\mu = 3.0$, pH = 0.82	$\beta_1 = 0.59$ $\beta_2 = 0.25$	Fukasawa *et al.* (1982)
bromide ion, Br^-	solv. extrn., ca. 293 K, $\mu = 3.0$, pH = 0.82	$\beta_1 = 0.15$ $\beta_2 = 0.29$	Fukasawa *et al.* (1982)
hydroxide ion, OH^-	solv. extrn., 293 K, $\mu = 0.1$	$\beta_1 = 2.2 \times 10^8$	Désiré *et al.* (1969), Hussonnois *et al.* (1973)
sulfate ion, SO_4^{2-}	solv. extrn., 298 K, calc. values for $\mu = 0$ (meas. $\mu \leq 0.5$)	$\beta_1 = 5.1 \times 10^3$ $\beta_2 = 3.9 \times 10^5$ $\beta_3 = 1.1 \times 10^5$	McDowell and Coleman (1972)
thiocyanate ion, SCN^-	solv. extrn., 298 K, $\mu = 5.0$	$\beta_1 = 7.21$	Kinard and Choppin (1974)
	$\mu = 1.0$, pH = 2	$\beta_1 = 3.11$, $\beta_2 = 0.31$ $\beta_3 = 2.34$	Harmon *et al.* (1972b)
oxalate ion, $C_2O_4^{2-}$	electromigrn. rates, 298 K, $\mu = 0.1$, pH $\sim$ 1.8	$\beta_1 = 2.8 \times 10^5$ $\beta_2 = 1.4 \times 10^9$	Stepanov (1971)
acetate ion, CH_3COO^-	solv. extrn., 298 K, 2.0 M $NaClO_4$	$\beta_1 = 1.11 \times 10^2$	Choppin and Schneider (1970)
glycolate ion, $CH_2(OH)COO^-$	solv. extrn., 298 K, 2.0 M $NaClO_4$	$\beta_1 = 4.4 \times 10^2$ $\beta_2 = 5.0 \times 10^4$	Choppin and Degischer (1972)
lactate ion, $CH_3CH(OH)COO^-$	ion exch., $\mu = 0.5$	$\beta_3 = 7.9 \times 10^5$ (est.)	Stary (1966)
2-methyllactate ion, $(CH_3)_2C(OH)COO^-$	solv. extrn., 10^{-2} to 1 M	$\beta_1 = 6.39 \times 10^3$	Aly and Latimer (1970)
α-hydroxyisobutyrate ion, $CH_3CH_2CHOHCOO^-$	ion exch. $\mu = 0.5$	$\beta_3 = 4.0 \times 10^6$ (est.)	Stary (1966)

Table 10.3 (*Contd.*)

Ligand	*Conditions*[a]	*Stability constants*[b]	*References*
malate ion, $CH(OH)(COO)CH_2COO^{2-}$	solv. extrn., 10^{-2}–1 M	$\beta_1 = 1.07 \times 10^7$	Aly and Latimer (1970)
tartrate ion, $[CH(OH)COO]_2^{2-}$	solv. extrn., 10^{-2} to 1 M	$\beta_1 = 6.80 \times 10^5$	Aly and Latimer (1970)
citrate ion, $C(OH)(COO)(CH_2COO)_2^{3-}$	electromigrn. rates, 298K, $\mu = 0.1$	$\beta_1 = 7.8 \times 10^7$ $\beta_2 = 1.5 \times 10^{11}$	Stepanov (1971)
	solv. extrn., 10^{-2}–1 M	$\beta_1 = 3.00 \times 10^{11}$	Aly and Latimer (1970)
ethylenediamine-tetraacetate ion (EDTA) $C_2H_4N_2(CH_2COO)_4^{4-}$	ion exch., 298K, $\mu = 0.1$	$\beta_1 = 7.59 \times 10^{18}$	Fuger (1961)
trans-1,2-diaminecyclohexane-tetraacetate ion (DCTA) $C_6H_{10}N_2(CH_2COO)_4^{4-}$	ion exch., 298K, $\mu = 0.1$	$\beta_1 = 1.44 \times 10^{19}$	Baybarz (1966)
diethylenetriamine-pentaacetate ion (DTPA) $C_4H_8N_3(CH_2COO)_5^{5-}$	ion exch., 298K, $\mu = 0.1$	$\beta_1 = 6.2 \times 10^{22}$	Baybarz (1965)

[a] Solv. extrn. = solvent extraction; calc. = calculated; meas. = measured; electromigrn.= electromigration; exch.= exchange.
[b] Overall stability constants, e.g.

$$\beta_1 = \frac{\left[\mathrm{BkL}^{(3-n)+}\right]}{\left[\mathrm{Bk}^{3+}\right]\left[\mathrm{L}^{n-}\right]},\ \beta_2 = \frac{\left[\mathrm{BkL}_2^{(3-2n)+}\right]}{\left[\mathrm{Bk}^{3+}\right]\left[\mathrm{L}^{n-}\right]^2}, \text{ and } \beta_3 = \frac{\left[\mathrm{BkL}_3^{(3-3n)+}\right]}{\left[\mathrm{Bk}^{3+}\right]\left[\mathrm{L}^{n-}\right]^3}.$$

forming $[Bk(H_2O)_x(NO_3)_3]^+$ between 3 and 6 M HNO_3. It was also reported that Bk(IV) does not form negatively charged species up to 10 M HNO_3. This study provides an explanation for the differences observed in the ion-exchange and solvent extraction behavior of Bk(IV) as compared to that of Ce(IV), Th(IV), Np(IV), and Pu(IV) (Makarova *et al.*, 1979).

The extraction of Bk(III) by organophosphorus acids has been studied, and activity coefficients for Bk(III) in nitric acid solution were estimated (Chudinov *et al.*, 1976). In addition a mechanism for the extraction of Bk(IV) by HDEHP from nitric acid solution was proposed. The self-diffusion coefficients (D) of Bk(III) ion in perchloric acid media were measured using the open-end capillary method (Latrous and Oliver, 1999). The limiting value, D_0, at zero ionic strength was reported to be 5.95×10^{-6} cm^2 s^{-1}. This value is in good agreement with $D_0 = 5.81 \times 10^{-6}$ cm^2 s^{-1}, calculated by using a microscopic version of the Stokes–Einstein law (Mauerhofer *et al.*, 2003). Both reported values correlate well with experimentally determined values for neighboring trivalent actinide and analog lanthanide ions.

The kinetics of exchange of Bk(III) with $EuEDTA^-$ (EDTA = ethylenediaminetetraacetic acid) in aqueous acetate solutions of 0.1 M ionic strength has been studied (Williams and Choppin, 1974). The exchange was found to be first order with both acid-dependent and acid-independent rate terms. Rate values were calculated and compared to other actinide reaction rates.

The aqueous solubilities of Bk(III) oxalate and Bk(IV) iodate have been reported to be 1.5 and 10 mg L^{-1}, respectively (Erin *et al.*, 1977).

10.8.4 Redox behavior and potentials

Berkelium(III) in solution can be oxidized by strong oxidizing agents such as BrO_3^- (Knauer and Weaver, 1968; Weaver, 1968; Fardy and Weaver, 1969; Overman, 1971; Erin *et al.*, 1979b; Malikov *et al.*, 1980), AgO (Erin *et al.*, 1976), $Ag(I)S_2O_8^{2-}$ (Milyukova *et al.*, 1977, 1978, 1980), perxenate (Lebedev *et al.*, 1975), and ozone (Myasoedov *et al.*, 1973, 1974, 1975; Myasoedov, 1974).

Oxidation of green Bk(III) hydroxide as a suspension in 1 M NaOH to yellow Bk(IV) hydroxide was performed by bubbling ozone through the slurry (Cohen, 1976). In hydroxide solution, Bk(III) is unstable toward oxidation by radiolytically produced peroxide (Cohen, 1976). This 'self-oxidation' has also been observed in carbonate solutions (Baybarz *et al.*, 1972; Timofeev *et al.*, 1987; Hobart *et al.*, 1990; Morris *et al.*, 1990). Bk(III) can be stabilized in these solutions, however, by the presence of a reducing agent such as hydrazine hydrate (Cohen, 1976).

$BkCl_3$ is reported to be soluble in acetonitrile saturated with tetraethylammonium chloride (Nugent *et al.*, 1971). A colorless 7.6×10^{-4} M $BkCl_6^{3-}$ solution was formed that could be completely oxidized to red-orange $BkCl_6^{2-}$ by treatment with chlorine gas. The color of this Bk(IV) solution was quite similar to that observed for crystalline Cs_2BkCl_6 (Morss and Fuger, 1969).

Investigation of the amalgamation behavior of actinides in aqueous acetate and citrate solutions by treatment with sodium amalgam showed that berkelium and the lighter actinides do not readily form the amalgam. Those lanthanides that are known to exist only in the trivalent or the tetravalent state in solution also do not readily amalgamate. This behavior is in contrast to that of the heavier actinides californium, einsteinium, fermium, and mendelevium, and those lanthanides that exhibit stable divalent states, all of which readily amalgamate (Malý, 1967, 1969). This has been extensively studied as a basis for lanthanide/actinide and actinide/actinide separations and for determining redox reactions, kinetics, potentials, and other thermodynamic parameters (David *et al*., 1990).

Bk(IV) is a strong oxidizing agent, comparable to Ce(IV) (Weaver and Stevenson, 1971). It can be coprecipitated with cerium iodate (Weaver, 1968) or zirconium phosphate (Cunningham, 1959). The stability of Bk(IV) solutions is a function of the degree of complexation of Bk(IV) by the solvent medium (Baybarz *et al*., 1972). Bk(IV) is reduced by radiolytically generated peroxide in acidic and neutral solutions. The rate of reduction of Bk(IV) can be accelerated by the introduction of a reducing agent such as hydrogen peroxide (Peppard *et al*., 1957; Kazakova *et al*., 1975), hydroxylamine hydrochloride (Kazakova *et al*., 1975), or ascorbic acid (Kazakova *et al*., 1975).

Potentials of berkelium redox couples are summarized in Table 10.4. Replicate values for the Bk(IV)/Bk(III) couple under various conditions are in reasonable agreement with one another. The first estimate of the Bk(IV)/Bk(III) potential was made in 1950, only a short time after the discovery of the element. A value of 1.6 V was reported, based on tracer experiments (Thompson *et al*., 1950a). Later, a refined value of (1.62 $\pm$ 0.01) V was reported for the couple, based on the results of experiments with microgram quantities of berkelium (Cunningham, 1959). The potential of the Bk(IV)/Bk(III) couple has subsequently been determined by several workers using direct potentiometry (Stokely *et al*., 1969; Propst and Hyder, 1970; Nugent *et al*., 1973b; Simakin *et al*., 1977a; Kulyako *et al*., 1981) or indirect methods (Musikas and Berger, 1967; Weaver and Fardy, 1969; Weaver and Stevenson, 1971). A recent, novel determination of the Bk(IV)/Bk(III) potential in $HClO_4$ solution, using *in situ* X-ray absorption spectroelectrochemistry, was reported to be (1.595 $\pm$ 0.005) V (Antonio *et al*., 2002), in close agreement with some of the other values in perchloric acid solution listed in Table 10.4.

All of the above-mentioned determinations were performed in media of relatively low complexing capability. The potential of the Bk(IV)/Bk(III) couple is significantly shifted to less positive values in media containing anions that strongly complex Bk(IV). Values of 1.36 V (Stokely *et al*., 1969; Kulyako *et al*., 1981) and 1.12 V (Stokely *et al*., 1972) have been reported for the couple in sulfuric and phosphoric acid solutions, respectively. Carbonate ions, apparently forming the strongest complex with Bk(IV) of the anions listed in Table 10.4, provide conditions for the least positive potential, 0.26 V (Stokely *et al*., 1972), as compared to the potential of 1.6 V for the couple in non-complexing

Table 10.4 *Potentials of berkelium redox couples.*

Redox couple	*Potential* (V versus *NHE*)	*Conditions*[a]	*References*
Bk(IV)–Bk(III)	1.6 ± 0.2	calc.	Nugent *et al.* (1973b, 1976)
	1.664	calc.	Simakin *et al.* (1977b)
	1.54 ± 0.1	1 M $HClO_4$, dir. pot.	Stokely *et al.* (1972)
	1.597 ± 0.005	1 M $HClO_4$, dir. pot.	Simakin *et al.* (1977a)
	1.595 ± 0.005	1 M $HClO_4$, spectroelectro.	Antonio *et al.* (2002)
	1.735 ± 0.005	9 M $HClO_4$, dir. pot.	Simakin *et al.* (1977a)
	1.54 ± 0.1	1 M HNO_3, dir. pot.	Stokely *et al.* (1972)
	1.562 ± 0.005	1 M HNO_3, dir. pot.	Simakin *et al.* (1977a)
	1.56	6 M HNO_3, solv. extrn.	Musikas and Berger (1967)
	1.6	3–8 M HNO_3, coprecip.	Thompson *et al.* (1950a)
	1.543 ± 0.005	8 M HNO_3, dir. pot.	Simakin *et al.* (1977a)
	1.43	0.1 M H_2SO_4, dir. pot.	Propst and Hyder (1970)
	1.44	0.25 M H_2SO_4, solv. extrn.	Musikas and Berger (1967)
	1.38	0.5 M H_2SO_4, dir. pot.	Stokely *et al.* (1969)
	1.42	0.5 M H_2SO_4, solv. extrn.	Musikas and Berger (1967)
	1.37	1 M H_2SO_4, dir. pot.	Stokely *et al.* (1969), Kulyako *et al.* (1981)
	1.36	2 M H_2SO_4, dir. pot.	Stokely *et al.* (1969), Kulyako *et al.* (1981)
	1.12 ± 0.1	7.5 M H_3PO_4, dir. pot.	Stokely *et al.* (1972)
	0.85	0.006 M $K_{10}P_2W_{17}O_{61}$, pH = 0, dir. pot.	Baranov *et al.* (1981)
	0.65	0.006 M $K_{10}P_2W_{17}O_{61}$, pH > 4, dir. pot.	Baranov *et al.* (1981)
	0.24	1 M Na_2CO_3, dir. pot.	Timofeev *et al.* (1987)
	0.26 ± 0.1	2 M K_2CO_3, dir. pot.	Stokely *et al.* (1972)
Bk(III)–Bk(II)	–2.8 ± 0.2	calc.	Nugent *et al.* (1976)
	–2.75	calc.	Lebedev (1978)
Bk(III)–Bk(0)	–2.03 ± 0.05	calc.	Nugent (1975)
	–2.4	calc.	Krestov (1965)
	–1.99 ± 0.09	calc.	David *et al.* (1976)
	–2.18 ± 0.09	0.1 M LiCl, radiopol.	Samhoun and David (1976, 1979)
	–2.01 ± 0.03	calc.	Fuger *et al.* (1981)

[a] Calc. = calculated value; dir. pot. = direct potentiometry; spectroelectro. = spectroelectrochemistry; solv. extrn. = solvent extraction; coprecip. = coprecipitation; radiopol. = radiopolarography.

perchlorate solutions (Stokely *et al.*, 1972; Simakin *et al.*, 1977a). Other studies of the Bk(IV)/Bk(III) couple in complexing concentrated carbonate solutions also yielded potential values significantly shifted from those in non-complexing perchloric acid media (Timofeev *et al.*, 1987; Hobart *et al.*, 1990; Morris *et al.*, 1990). This behavior closely parallels that of the Ce(IV)/Ce(III) couple. In fact the

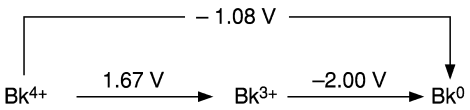

Fig. 10.8 *Standard reduction potential diagram for berkelium ions in acid solution* (*Chapter* 19).

Bk(IV)/Bk(III) couple markedly resembles the Ce(IV)/Ce(III) couple in its redox chemistry.

The overall thermodynamic and electrochemical data support a value of (1.67 ± 0.07) V for the standard potential (E°) of the Bk(IV)/Bk(III) couple (Fuger and Oetting, 1976; Martinot and Fuger, 1985), which is 0.05 V less positive than the accepted value of (1.72 ± 0.02) V for the corresponding cerium couple (Morss, 1985), though within the stated uncertainties.

The potential of the Bk(III)/Bk(0) couple has been investigated using radiopolarography (Samhoun and David, 1976, 1979) and theoretical calculations (Krestov, 1965), as well as by correlation with data concerning enthalpy of formation (David *et al*., 1976; Fuger *et al*., 1981). Estimates of the potentials of berkelium redox couples have also been made from correlation plots of electron-transfer and f–d absorption band energies versus redox potential and by theoretical calculations (Nugent *et al*., 1971, 1973b, 1976; Nugent, 1975). The overall data support a value of −(2.00 ± 0.02) V for the standard potential of the Bk(III)/Bk(0) couple.

Theoretical estimates of the potentials of the Bk(V)/Bk(0) and Bk(V)/Bk(IV) couples have been reported as 0.2 and 3.5 V, respectively (David *et al*., 1976). These estimates suggest that Bk(V) would be very unstable in aqueous solution.

The scatter in the potential values of the Bk(III)/Bk(II) and Bk(III)/Bk(0) couples in Table 10.4 reflects the necessary requirement of making estimates of thermodynamic quantities that have not been directly determined. A standard reduction potential diagram for berkelium ions is shown in Fig. 10.8. Additional information on the redox behavior of berkelium can be found in reviews by Martinot (1978) and Martinot and Fuger (1985).

10.8.5 Thermodynamic properties

Values of thermodynamic properties for the formation of berkelium ions in solution, according to the reactions:

$$\mathrm{Bk(cr, dhcp)} + 3\mathrm{H^+(aq)} \rightarrow \mathrm{Bk^{3+}(aq)} + 3/2\,\mathrm{H_2(g)}$$

and

$$\mathrm{Bk(cr, dhcp)} + 4\mathrm{H^+(aq)} \rightarrow \mathrm{Bk^{4+}(aq)} + 2\mathrm{H_2(g)},$$

are summarized in Table 10.5. These values result from the evaluation of experimental measurements on the enthalpy of formation of $Bk^{3+}(aq)$

Table 10.5 *Thermodynamic quantities for simple aqueous berkelium ions at* 298 K.[a]

Bk ion	$\Delta_f H^o$ (kJ mol^{-1})	$\Delta_f G^o$ (kJ mol^{-1})	S^o (J K^{-1} mol^{-1})
Bk^{3+}(aq)	–(601 ± 5)	–(578 ± 7)	–(194 ± 17)
Bk^{4+}(aq)	–(483 ± 5)	–(417 ± 7)	–(402 ± 17)

[a] Chapter 19.

(Fuger *et al*., 1981), on the temperature dependence of the Bk(IV)/Bk(III) couple (Simakin *et al*., 1977b), and on estimated entropies. These values are discussed in more detail in Chapter 19.

An electrostatic hydration model has been applied to the trivalent lanthanide and actinide ions in order to predict the standard Gibbs energy ($\Delta_{hydr}G_t^0$) and enthalpy ($\Delta_{hydr}H_t^0$) of hydration for these series. Assuming crystallographic and gas-phase radii for Bk(III) to be 0.096 and 0.1534 nm, respectively, and using 6.1 as the primary hydration number, $\Delta_{hydr}G_{298}^0$ was calculated to be –3357 kJ mol^{-1} and $\Delta_{hydr}H_{298}^0$ to be –3503 kJ mol^{-1} (Goldman and Morss, 1975). Later efforts to calculate semi-empirically entropy and enthalpy effects associated with hydration (David, 1986a,b), as well as an effort to intercorrelate non-complexed di-, tri-, and tetravalent actinide aquo ions based on crystallographic radii, have been published (David, 1986c). More recently the hydration enthalpy of Bk(III) has been derived by interpolation from data for the neighboring actinides attained by combining previously published thermodynamic and structural data with new data on high-symmetry elpasolites ($Cs_2NaAnCl_6$) using Born–Haber cycles (Schoebrechts *et al*., 1989). The value obtained for Bk(III), $\Delta_{hydr}H_{298}^0 = -3501$ kJ mol^{-1}, is in excellent agreement with that calculated by Goldman and Morss (1975). A more comprehensive treatment of the thermodynamic properties of berkelium, including correlations of berkelium hydration enthalpies and Gibbs hydration energies with those of other actinides, can be found in Chapter 19.

Activity coefficients for Bk(III) in aqueous $NaNO_3$ solutions have been calculated from distribution data for the ion between the aqueous phase and a tertiary alkylamine organic phase (Chudinov and Pirozhkov, 1973). The activity coefficient values were reported as a function of the $NaNO_3$ concentration. Additional discussion of, and derived thermochemical properties for, a number of compounds of berkelium can be found in Chapter 19.

10.9 ANALYTICAL CHEMISTRY

The analytical determination of berkelium is dominated by radioanalytical methods, usually after separation from other radionuclides by procedures outlined in Section 10.4. ^{249}Bk, the most common isotope available, emits primarily (>99%) beta (β^-) particles up to a maximum energy of 125 keV. A proportional flow or liquid scintillation counter is used to measure this

radiation. The use of scintillators for this determination is complicated by the fact that most substances quench the weak scintillations induced by the beta particles; however, a detection limit of ~0.1 Bq can be attained with an error of about 0.1% (Myasoedov, 1987). The beta decay of ^{249}Bk results in the ingrowth of daughter ^{249}Cf ($t_{1/2}$ = 351 years) at about 0.22% per day. This has been utilized for an analytical determination of the parent berkelium. After an initial Bk/Cf separation, the ingrowth decay product is measured over time (Propst and Hyder, 1970) to determine the original berkelium amount.

Methods other than radioanalytical techniques have been developed for berkelium determination. Coulometric determinations of berkelium utilizing the Bk(IV)/Bk(III) couple have been reported (Propst and Hyder, 1970; Timofeev *et al.*, 1986). A spectrophotometric titration method for determination of microgram amounts of berkelium has been proposed (Frolova *et al.*, 1986). Berkelium is electrolytically oxidized to Bk(IV) in nitric acid solution and titrated with H_2O_2 or $NaNO_2$ solution with the equivalence point determined by the disappearance of the high molar absorptivity peak of Bk(IV) at 350 nm. The error in the determination of >70 mg of Bk is reported to be 3–5% (Frolova *et al.*, 1986).

Mass spectrometric techniques that provide increased sensitivity for detection of lanthanides and other actinides in berkelium samples have been developed. In 0.1 μg of berkelium, californium can be determined at the 0.03% level with an error of 10–20% (Tikhomirov *et al.*, 1981). The ionization efficiency of ^{250}Bk has been investigated utilizing an on-line isotope separator, which may have valuable applications in analytical determinations (Asai *et al.*, 2002).

A sensitive neutron-activation method for Bk determination in mixtures of curium and californium has been developed (Ivanov *et al.*, 1979). Thermal neutron irradiation of ^{249}Bk produces ^{250}Bk ($t_{½}$ = 3.217 h) which emits intense gamma radiation at 989 keV that can be measured using a semiconductor detector. The absolute measurement error for Bk in a 2 μg sample was 1.8×10^{-4} %, and a detection limit for Bk of 4 pg was observed (Ivanov *et al.*, 1979).

The emission spectrum of berkelium over the range from 250 to 336 nm excited by an alternating current arc has been investigated in an effort to develop a semi-quantitative analysis method for berkelium in solutions containing large amounts of curium, cerium, and other elements. The reported detection limit for berkelium is 30 ng over the concentration range 1–100 μg of total metal per milliliter (Myasoedov, 1987).

10.10 CONCLUDING REMARKS

Berkelium is the first member of the second half of the actinide series of elements. Extended knowledge of the stability and accessibility of the various oxidation states of berkelium is important to the understanding and predictability

of its physicochemical behavior. In addition such information would enable more accurate extrapolations to the physicochemical behavior of the transberkelium elements for which experimental studies are severely limited by lack of material and/or by intense radioactivity.

Although berkelium oxidation states 0, III, and IV are known in bulk phase, further work is required to characterize more completely the solid-state and solution chemistries of this element. The synthesis of divalent berkelium in bulk should be possible via the metallothermic reduction of its trihalides, e.g.

$$Bk + 2BkBr_3 \rightarrow 3BkBr_2,$$

in an inert reaction vessel. It is quite possible that nature accomplishes this synthesis through alpha decay of the dihalides of ^{253}Es. A direct synthesis, however, would allow both absorption spectrophotometric and X-ray powder diffraction analyses, the results of which would aid in the identification of Bk(II) species in aged einsteinium dihalide samples that also contain Cf(II) (Peterson *et al.*, 1979; Young *et al.*, 1981).

Intermetallic compounds, various alloys, and additional semimetallic compounds of berkelium should be prepared and characterized to extend the knowledge of the physicochemical behavior of berkelium in these kinds of solids. Studies of such materials under pressure would be of interest in determining the effects of the non-berkelium component on physical properties such as bulk modulus (compressibility), pressure for the onset of 5f electron delocalization, and possible volume collapse associated with a change in the metallic valence of berkelium from three to four.

The range of oxidation states accessible to berkelium in solution should be further examined by using strong complexing agents in an effort to stabilize Bk(II), Bk(IV), and possibly Bk(V), produced chemically or electrochemically in nonaqueous or molten salt media. The complexation of Bk(III) with additional organic ligands should be studied to improve solvent extraction separation procedures. Also lacking to date, but experimentally obtainable, are stability constants of any complexes of Bk(IV). With an estimated potential of 3.5 V for the Bk(V)/Bk(IV) couple, it may be possible to prepare Bk(V) in a noncomplexing molten salt solution.

In the intervening years since the 1986 publication of the second edition of this work, a surprisingly large number of berkelium research reports have been published. This is significant because berkelium is quite rare and its longest-lived isotope has a half-life of a little less than 1 year. This continued interest must be attributed, in part, to the extensive use of ^{249}Bk as a nuclear target for creating still heavier elements. New research on this fascinating element will continue to contribute to the knowledge of the physicochemical properties of berkelium and will aid in elucidating the intricacies of the structure of the atom and in extending the limits of the periodic table.

ACKNOWLEDGMENTS

The authors gratefully acknowledge the assistance of Ms Kathy Garduno at the Los Alamos National Laboratory for gathering some of the references included herein and of Ms Annie Loweere and Mr Josh Smith for graphics support. The cooperation of numerous colleagues in supplying and/or verifying information, identifying oversights, and in commenting on the manuscript is greatly appreciated. J.R.P. acknowledges with gratitude Professor B. B. Cunningham (University of California, Berkeley; deceased), whose guidance, inspiration, and personal interest during the first systematic study of the physicochemical properties of berkelium are still fondly remembered. D.E.H. acknowledges with sincere appreciation his coauthor, Professor Emeritus J.R.P., for his dedication in the early education and mentoring of his young protégé and in his continued rewarding collaborations in the exciting area of actinide chemistry.

The preparation of this chapter was sponsored by the Division of Chemical Sciences, Geosciences, and Biosciences, Office of Basic Energy Sciences, U.S. Department of Energy, under contracts W-7405-ENG-36 with Los Alamos National Laboratory, operated by the University of California, and DE-ACO5-00OR22725 with Oak Ridge National Laboratory, managed and operated by UT-Battelle, LLC.

REFERENCES

[NOTE: In citations to *Sov. Radiochem.* and *Radiochem.*, both of which are English translations of *Radiokhimiya*, the year given herein is that of the original publication in Russian. This date is the same or one year later in the English translation.]

Ahmad, I. (2002) *J. Nucl. Radiochem. Sci.*, **3**, 179–82.

Aly, H. F. and Latimer, R. M. (1970) *Radiochim. Acta*, **14**, 27–31.

Antonio, M. R., Williams, C. W., and Soderholm, L. (2002) *Radiochim. Acta*, **90**, 851–6.

Asai, M., Sakama, M., Tsukada, K., Ichikawa, S., Haba, H., Nishinaka, I., Nagame, Y., Goto, S., Akiyama, K., Toyoshima, A., Kojima, Y., Oura, Y., Nakahara, H., Shibata, M., and Kawade, K. (2002) *J. Nucl. Radiochem. Sci.*, **3**, 187–90.

Asai, M., Tsukada, K., Ichikawa, S., Sakama, M., Haba, H., Nagame, Y., Nishinaka, K., Akiyama, K., Toyoshima, A., Kaneko, T., Oura, Y., Kojima, Y., Shibata, M. (2003) *Eur. Phys. J. A*, **16**, 17–19.

Asprey, L. B. and Keenan, T. K. (1968) *Inorg. Nucl. Chem. Lett.*, **4**, 537–41.

Asprey, L. B. and Haire, R. G. (1973) *Inorg. Nucl. Chem. Lett.*, **9**, 1121–8.

Assefa, Z., Haire, R. G., and Stump, N. A. (1998) *J. Alloys Compds*, **271–273**, 854–8.

Audi, G. and Wapstra, A. H. (1995) *Nucl. Phys. A*, **595**, 409–80.

Baranov, A. A., Simakin, G. A., Kosyakov, V. N., Erin, E. A., Kopytov, V. V., Timofeev, G. A., and Rykov, A. G. (1981) *Sov. Radiochem.*, **23**, 104–6.

Baybarz, R. D. (1965) *J. Inorg. Nucl. Chem.*, **27**, 1831–9.

Baybarz, R. D. (1966) *J. Inorg. Nucl. Chem.*, **28**, 1055–61.

Baybarz, R. D. (1968) *J. Inorg. Nucl. Chem.*, **30**, 1769–73.
Baybarz, R. D., Stokely, J. R., and Peterson, J. R. (1972) *J. Inorg. Nucl. Chem.*, **34**, 739–46.
Baybarz, R. D. (1973) *J. Inorg. Nucl. Chem.*, **35**, 4149–58.
Baybarz, R. D., Knauer, J. B., and Orr, P. B. (1973) *Final Isolation and Purification of the Transplutonium Elements from the Twelve Campaigns Conducted at TRU During the Period August 1967–December 1971*, U.S. Atomic Energy Commission Document ORNL-4672, Oak Ridge National Laboratory.
Behera, B. R., Jena, S., Satpathy, M., Kailas, S., Mahata, K., Shrivastava, A., Chatterjee, A., Roy, S., Basu, P., Sharan, M. K., and Datta, S. K. (2001) *Phys. Rev. C*, **64**, 041602 (R)1–3.
Beitz, J. V., Carnall, W. T., Wester, D. W., and Williams, C. W. (1981) in *Actinides – 1981*, Pacific Grove, California, September 1981, Abstracts Volume (ed. N. M. Edelstein), U.S. Department of Energy Document LBL-12441, University of California, Lawrence Berkeley Laboratory, pp. 108–9.
Benedict, U., Peterson, J. R., Haire, R. G., and Dufour, C. (1984) *J. Phys. F: Met. Phys.*, **14**, L43–7.
Bigelow, J. E. (1974) in *Gmelin Handbuch der Anorganischen Chemie*, System No. 71, *Transurane*, New Suppl. Ser., vol. 7b, part A1, II, *The Elements*, Springer-Verlag, New York, pp. 326–36.
Bigelow, J. E., Corbett, B. L., King, L. J., McGuire, S. C., and Sims, T. M. (1981) in *Transplutonium Elements – Production and Recovery* (eds. J. D. Navratil and W. W. Schulz) (ACS Symp. Ser. 161), American Chemical Society, Washington, DC, pp. 3–18.
Bigelow, J. E. (1985) Oak Ridge National Laboratory, personal communication.
Boatner, L. A., Reynolds, R. W., Finch, C. B., and Abraham, M. M. (1972) *Phys. Lett. A*, **42**, 93–4.
Brewer, L. (1971a) *J. Opt. Soc. Am.*, **61**, 1101–11.
Brewer, L. (1971b) *J. Opt. Soc. Am.*, **61**, 1666–82.
Brito, H. F. and Liu, G. K. (2000) *J. Chem. Phys.*, **112**, 4334–41.
Britt, H. C. and Wilhelmy, J. B. (1979) *Nucl. Sci. Eng.*, **72**, 222–9.
Brüchle, W., Schädel, M., Scherer, U. W., Kratz, J. V., Gregorich, K. E., Lee, D., Nurmia, M., Chasteler, R. M., Hall, H. L., Henderson, R. A., and Hoffman, D. C. (1988) *Inorg. Chim. Acta*, **146**, 267–76.
Burns, J. H. and Peterson, J. R. (1971) *Inorg. Chem.*, **10**, 147–51.
Burns, J. H., Peterson, J. R., and Stevenson, J. N. (1975) *J. Inorg. Nucl. Chem.*, **37**, 743–9.
Campbell, D. O. (1981) in *Transplutonium Elements – Production and Recovery* (eds. J. D. Navratil and W. W. Schulz) (ACS Symp. Ser. 161), American Chemical Society, Washington, DC, pp. 189–201.
Carlson, T. A., Nestor, C. W. Jr, Malik, F. B., and Tucker, T. C. (1969) *Nucl. Phys. A*, **135**, 57–64.
Carlson, T. A. and Nestor, C. W. Jr (1977) *At. Data Nucl. Data Tables*, **19**, 153–73.
Carnall, W. T., Sjoblom, R. K., Barnes, R. F., and Fields, P. R. (1971) *Inorg. Nucl. Chem. Lett.*, **7**, 651–7.
Carnall, W. T., Fried, S., Wagner, F. Jr, Barnes, R. F., Sjoblom, R. K., and Fields, P. R. (1972) *Inorg. Nucl. Chem. Lett.*, **8**, 773–4.
Carnall, W. T. (1973) in *Gmelin Handbuch der Anorganischen Chemie*, System No. 71, *Transurane*, New Suppl. Ser., vol. 8, part A2, *The Elements*, Springer-Verlag, New York, pp. 35–80.

Carnall, W. T., Fried, S., and Wagner, F. Jr (1973) *J. Chem. Phys.*, **58**, 3614–24.
Carnall, W. T. and Fried, S. (1976) in *Proc. Symp. Commemorating the 25th Anniversary of Elements 97 and 98*, January 20, 1975, U.S. Energy Research and Development Administration Document LBL–4366, University of California, Lawrence Berkeley Laboratory, pp. 61–9.
Carnall, W. T., Crosswhite, H. M., Crosswhite, H., Hessler, J. P., Aderhold, C., Caird, J. A., Paszek, A., and Wagner, F. W. (1977) in *Proc. 2nd Int. Conf. on the Electronic Structure of the Actinides,* Wrocław, Poland, September 1976 (eds. J. Mulak, W. Suski, and R. Troć), Ossolineum, Wrocław, pp. 105–10.
Carnall, W. T., Beitz, J. V., and Crosswhite, H. (1984) *J. Chem. Phys.*, **80**, 2301–8.
Chen, M. H., Crasemann, B., Huang, K., Aoyagi, M., and Mark, H. (1977) *At. Data Nucl. Data Tables*, **19**, 97–151.
Choppin, G. R. and Schneider, J. K. (1970) *J. Inorg. Nucl. Chem.*, **32**, 3283–8.
Choppin, G. R. and Degischer, G. (1972) *J. Inorg. Nucl. Chem.*, **34**, 3473–7.
Choppin, G. R. and Unrein, P. J. (1976) in *Transplutonium Elements 1975* (eds. W. Müller and R. Lindner), *Proc. 4th Int. Transplutonium Element Symp.*, Baden-Baden, September 1975, North-Holland, Amsterdam, pp. 97–107.
Chudinov, E. G. and Pirozhkov, S. V. (1972) *J. Radioanal. Chem.*, **10**, 41–6.
Chudinov, E. G. and Pirozhkov, S. V. (1973) *Sov. Radiochem.*, **15**, 195–9.
Chudinov, E. G., Kosyakov, V. N., Shvetsov, I. K., and Vereshchaguin, Yu. I. (1976) in *Transplutonium 1975* (eds. W. Müller and R. Lindner), *Proc. 4th Int. Transplutonium Element Symp.*, Baden-Baden, September 1975, North-Holland, Amsterdam, pp. 49–56.
Cohen, D., Fried, S., Siegel, S., and Tani, B. (1968) *Inorg. Nucl. Chem. Lett.*, **4**, 257–60.
Cohen, D. (1976) *J. Inorg. Nucl. Chem.*, Suppl., 41–9.
Collins, E. D., Benker, D. E., Chattin, F. R., Orr, P. B., and Ross, R. G. (1981) in *Transplutonium Elements – Production and Recovery* (eds. J. D. Navratil and W. W. Schulz) (ACS Symp. Ser. 161), American Chemical Society, Washington, DC, pp. 147–60.
Conway, J. G. (1976) in *Proc. Symp. Commemorating the 25th Anniversary of Elements 97 and 98*, January 20, 1975, U.S. Energy Research and Development Administration Document LBL-4366, University of California, Lawrence Berkeley Laboratory, pp. 70–5.
Conway, J. G., Worden, E. F., Blaise, J., Camus, P., and Vergès, J. (1977) *Spectrochim. Acta*, **32B**, 101–6.
Cunningham, B. B. (1959) *J. Chem. Edn.*, **36**, 32–7.
Cunningham, B. B. (1963) in *Proc. Robert A. Welch Foundation Conf. on Chemical Research*, vol. VI, *Topics in Modern Inorganic Chemistry*, Houston, Texas, November 1962, (ed. W. O. Milligan), The Robert A. Welch Foundation, Houston, pp. 237–59.
Damien, D. A., Haire, R. G., and Peterson, J. R. (1979) *J. Physique*, **40** (C4), 95–100.
Damien, D., Haire, R. G., and Peterson, J. R. (1980) *J. Inorg. Nucl. Chem.*, **42**, 995–8.
Damien, D., Haire, R. G., and Peterson, J. R. (1981) Oak Ridge National Laboratory, unpublished results.
David, F., Samhoun, K., Guillaumont, R., and Nugent, L. J. (1976) in *Heavy Element Properties* (eds. W. Müller and H. Blank), *Proc. Joint Session, 4th Int. Transplutonium Element Symp. & 5th Int. Conf. on Plutonium and Other Actinides*, Baden-Baden, September 1975, North-Holland, Amsterdam, pp. 97–104.
David, F. (1986a) *J. Less Common Metals*, **121**, 27–42.

David, F. (1986b) *J. Chim. Phys.*, **83**, 393–401.
David, F. (1986c) in *Handbook on the Physics and Chemistry of the Actinides*, vol. 4 (eds. A. J. Freeman and C. Keller), North-Holland, Amsterdam, pp. 97–128.
David, F., Maslennikov, A. G., and Peretrukhin, V. P. (1990) *J. Radioanal. Nucl. Chem.*, **143**, 415–26.
Désiré, B., Hussonnois, M., and Guillaumont, R. (1969) *C. R. Acad. Sci. Paris C*, **269**, 448–51.
Dittner, P. F. and Bemis, C. E. Jr (1972) *Phys. Rev. A*, **5**, 481–4.
D'yachkova, R. A., Auérman, L. N., Mikheev, N. B., and Spitsyn, V. I. (1980) *Sov. Radiochem.*, **22**, 234–8.
Eichler, R., Brüchle, W., Dressler, R., Düllmann, Ch. E., Eichler, B., Gäggler, H. W., Gregorich, K. E., Hoffman, D. C., Hübener, S., Jost, D. T., Kirbach, U. W., Laue, C. A., Lavanchy, V. M., Nitsche, H., Patin, J. B., Piguet, D., Schädel, M., Shaughnessy, D. A., Strellis, D. A., Taut, S., Tobler, L., Tsyganov, Y. S., Türler, A. Vahle, A., Wilk, P. A., and Yakushev, A. B. (2000) *Nature*, **407**, 63–5.
Ensor, D. D., Peterson, J. R., Haire, R. G., and Young, J. P. (1981) *J. Inorg. Nucl. Chem.*, **43**, 1001–3.
Ensor, D. D. and Shah, A. H. (1984) *Solvent Extr. Ion Exch.*, **2**, 591–605.
Erdmann, N., Nunnemann, M., Eberhardt, K., Herrmann, G., Huber, G., Köhler, S., Kratz, J. V., Passler, G., Peterson, J. R., Trautmann, N., and Waldek, A. (1998) *J. Alloys Compds*, **271–273**, 837–40.
Erin, E. A., Kopytov, V. V., and Vityutnev, V. M. (1976) *Sov. Radiochem.*, **18**, 446–8.
Erin, E. A., Kopytov, V. V., Vasil'ev, V. Ya., and Vityutnev, V. M. (1977) *Sov. Radiochem.*, **19**, 380–2.
Erin, E. A., Vityutnev, V. M., Kopytov, V. V., and Vasil'ev, V. Ya. (1979a) *Sov. Radiochem.*, **21**, 85–8.
Erin, E. A., Vityutnev, V. M., Kopytov, V. V., and Vasil'ev, V. Ya. (1979b) *Sov. Radiochem.*, **21**, 487–9.
Fahey, J. A., Peterson, J. R., and Baybarz, R. D. (1972) *Inorg. Nucl. Chem. Lett.*, **8**, 101–7.
Fahey, J. A., Turcotte, R. P., and Chikalla, T. D. (1974) *Inorg. Nucl. Chem. Lett.*, **10**, 459–65.
Fardy, J. J. and Weaver, B. (1969) *Anal. Chem.*, **41**, 1299–302.
Farrar, L. G., Cooper, J. H., and Moore, F. L. (1968) *Anal. Chem.*, **40**, 1602–4.
Fedoseev, E. V., Ivanova, L. A., Travnikov, S. S., Davidov, A. V., and Myasoedov, B. F. (1983) *Sov. Radiochem.*, **25**, 343–7.
Fellows, R. L., Young, J. P., and Haire, R. G. (1977) in *Physical–Chemical Studies of Transuranium Elements* (Progress Report April 1976–March 1977) (ed. J. R. Peterson), U.S. Energy Research and Development Administration Document ORO-4447-048, University of Tennessee, Knoxville, pp. 5–15.
Ferguson, D. E. and Bigelow, J. E. (1969) *Actinides Rev.*, **1**, 213–21.
Fields, P. R., Wybourne, B. G., and Carnall,W. T. (1964) *The Electronic Energy Levels of the Heavy Actinides* $Bk^{3+}(5f^8)$, $Cf^{3+}(5f^9)$, $Es^{3+}(5f^{10})$, and $Fm^{3+}(5f^{11})$, U.S. Atomic Energy Commission Document ANL-6911, Argonne National Laboratory.
Finch, C. B., Fellows, R. L., and Young, J. P. (1978) *J. Lumin.*, **16**, 109–15.
Firsova, L. A., Chuveleva, E. A., and Kharitonov, O. V. (1996) *Radiochemistry*, **38**, 407–9.

Firsova, L. A., Chuveleva, E. A., and Kharitonov, O. V. (1998a) *Radiochemistry*, **40**, 254–6.

Firsova, L. A., Chuveleva, E. A., and Kharitonov, O. V. (1998b) *Radiochemistry*, **40**, 257–61.

Fournier, J. M. (1976) *J. Phys. Chem. Solids*, **37**, 235–44.

Freeman, A. J. and Koelling, D. D. (1974) in *The Actinides: Electronic Structure and Related Properties,* vol. 1 (eds. A. J. Freeman and J. B. Darby Jr), Academic Press, New York, pp. 51–108.

Friedman, H. A. and Stokely, J. R. (1976) *Inorg. Nucl. Chem. Lett.*, **12**, 505–13.

Frolova, L. M., Vityutnev, V. M., Vasil'ev, V. Ya. (1986) *Sov. Radiochem.*, **28**, 349–53.

Fuger, J. (1961) *J. Inorg. Nucl. Chem.*, **18**, 263–9.

Fuger, J., Peterson, J. R., Stevenson, J. N., Noé, M., and Haire, R. G. (1975) *J. Inorg. Nucl. Chem.*, **37**, 1725–8.

Fuger, J. and Oetting, F. L. (1976) in *The Chemical Thermodynamics of Actinide Elements and Compounds,* part 2, *The Actinide Aqueous Ions.* (eds. V. Medvedev, M. H. Rand, E. F. Westrum Jr and F. L. Oetting), IAEA, Vienna, pp. 50–3.

Fuger, J., Haire, R. G., and Peterson, J. R. (1981) *J. Inorg. Nucl. Chem.*, **43**, 3209–12.

Fuger, J. (1982) in *Actinides in Perspective, Proc. Actinides – 1981*, Pacific Grove, California, September 1981 (ed. N. M. Edelstein), Pergamon Press, New York, pp. 409–31.

Fujita, D. K. (1969) *Some Magnetic*, *Spectroscopic*, *and Crystallographic Properties of Berkelium*, *Californium*, *and Einsteinium*, PhD Thesis, U.S. Atomic Energy Commission Document UCRL-19507, University of California, Lawrence Berkeley Radiation Laboratory.

Fukasawa, T., Kawasuji, I., Mitsugashira, T., Satô, A., and Suzuki, S. (1982) *Bull. Chem. Soc. Jpn.*, **55**, 726–9.

Gavron, A., Britt, H. C., Goldstone, P. D., Schoenmackers, R., Weber, J., and Wilhelmy, J. B. (1977) *Phys. Rev. C*, **15**, 2238–40.

Gibson, J. K. and Haire, R. G. (1985) *J. Less Common Metals*, **109**, 251–9.

Gibson, J. K. and Haire, R. G. (2001a) *Radiochim. Acta*, **89**, 363–9.

Gibson, J. K. and Haire, R. G. (2001b) *Radiochim. Acta*, **89**, 709–19.

Gobrecht, J., Zehnder, A., Kubik, P., Kettle, P.-R., Junker, K., Herlach, D., and Gaeggler, H. (1999) *Particles and Matter*, vol. 1, Paul Sherrer Institute Scientific Report INIS-CH-019.

Goldman, S. and Morss, L. R. (1975) *Can. J. Chem.*, **53**, 2695–700.

Gregorich, K. E., Henderson, R. A., Lee, D. M., Nurmia, M. J., Chasteler, R. M., Hall, H. L., Bennett, D. A., Gannet, C. M., Chadwick, R. B., Leyba, J. D., Hoffman, D. C., and Hermann, G. (1988) *Radiochim. Acta*, **43**, 223–31.

Guseva, L. I., Gregor'eva, S. I., and Tikhomirova, G. S. (1971) *Sov. Radiochem.*, **13**, 802–4.

Guseva, L. I. and Stepushkina, V. V. (1987) *Sov. Radiochem.*, **29**, 611–14.

Guseva, L. I., Tikhomirova, G. S., and Stepushkina, V. V. (1987) *Sov. Radiochem.*, **29**, 733–9.

Guseva, L. I., Tikhomirova, G. S., and Stepushkina, V. V. (1991) *Sov. Radiochem.*, **33**, 193–8.

Gutmacher, R. G., Hulet, E. K., Worden, E. F., and Conway, J. G. (1963) *J. Opt. Soc. Am.*, **53**, 506.

Gutmacher, R. G. (1964) *Atomic Spectroscopy of Berkelium* (Abstract), U.S. Atomic Energy Commission Document UCRL-12275-T, University of California, Lawrence Livermore Radiation Laboratory.
Gutmacher, R. G., Hulet, E. K., and Lougheed, R. (1965) *J. Opt. Soc. Am.*, **55**, 1029–30.
Gutmacher, R. G., Hulet, E. K., Lougheed, R., Conway, J. G., Carnall, W. T., Cohen, D., Keenan, T. K., and Baybarz, R. D. (1967) *J. Inorg. Nucl. Chem.*, **29**, 2341–5.
Gutmacher, R. G., Bodé, D. D., Lougheed, R. W., and Hulet, E. K. (1973) *J. Inorg. Nucl. Chem.*, **35**, 979–94.
Haire, R. G. (1973) in *Proc. 10th Rare Earth Research Conf.,* Carefree, AZ, April–May 1973, vol. II (eds. C. J. Kevane and T. Moeller), National Technical Information Service, U.S. Department of Commerce, Springfield, VA, pp. 882–91.
Haire, R. G. and Baybarz, R. D. (1973) *J. Inorg. Nucl. Chem.*, **35**, 489–96.
Haire, R. G. and Fahey, J. A. (1977) *J. Inorg. Nucl. Chem.*, **39**, 837–41.
Haire, R. G., Hellwege, H. E., Hobart, D. E., and Young, J. P. (1983) *J. Less Common Metals*, **93**, 358–9.
Haire, R. G., Peterson, J. R., Benedict, U., and Dufour, C. (1984) *J. Less Common Metals*, **102**, 119–26.
Haire, R. G., Benedict, U., Peterson, J. R., Dufour, C., and Dabos, S. (1986) *Physica*, **144B**, 19–22.
Haire, R. G., Assefa, Z., and Stump, N. (1998) *Mat. Res. Soc. Symp. Proc.*, **506**, 153–60.
Haire, R. G. and Raison, P. E. (2000) *AIP Conf. Proc.*, **532**, 173–4. (Plutonium Futures – The Science, Santa Fe, NM, July 10–13, 2000.)
Haire, R. G., Raison, P. E., and Assefa, Z. (2002) *J. Nucl. Sci. Technol.*, Suppl. 3, 616–19.
Harbour, R. M. (1972) *J. Inorg. Nucl. Chem.*, **34**, 2680–1.
Harmon, H. D., Peterson, J. R., and McDowell, W. J., (1972a) *Inorg. Nucl. Chem. Lett.*, **8**, 57–63.
Harmon, H. D., Peterson, J. R., McDowell, W. J., and Coleman, C. F. (1972b) *J. Inorg. Nucl. Chem.*, **34**, 1381–97.
Haug, H. O. and Baybarz, R. D. (1975) *Inorg. Nucl. Chem. Lett.*, **11**, 847–55.
Heathman, S. and Haire, R. G. (1998) *J. Alloys Compds*, **271–273**, 342–6.
Hendricks, M. E., Jones, E. R. Jr, Stone, J. A., and Karraker, D. G. (1974) *J. Chem. Phys.*, **60**, 2095–103.
Herbst, J. F., Watson, R. E., and Lindgren, I. (1976) *Phys. Rev. B*, **14**, 3265–72.
Hessler, J. P., Caird, J. A., Carnall, W. T., Crosswhite, H. M., Sjoblom, R. K., and Wagner, F. Jr (1978) in *The Rare Earths in Modern Science and Technology* (eds. G. J. McCarthy and J. J. Rhyne), Plenum, New York, pp. 507–12.
Hobart, D. E., Begun, G. M., Haire, R. G., and Hellwege, H. E. (1983) *J. Raman Spectrosc.*, **14**, 59–62.
Hobart, D. E. and Peterson, J. R. (1986) in *The Chemistry of the Actinide Elements,* 2nd edn (eds. J. J. Katz, G. T. Seaborg, and L. R. Morss), Chapman & Hall, London, pp. 989–1024.
Hobart, D. E., Morris, D. E., Palmer, P. D., Haire, R. G., and Peterson, J. R. (1990) *Radiochim. Acta*, **49**, 119–24.
Hollander, J. M., Holtz, M. D., Novakov, T., and Graham, R. L. (1965) *Ark. Fys.*, **28**, 375–9.
Holley, C. E. Jr, Mulford, R. N. R., Ellinger, F. H., Koehler, W. C., and Zachariasen, W. H. (1955) *J. Phys. Chem.*, **59**, 1226–8.

Horwitz, E. P., Bloomquist, C. A. A., Henderson, D. J., and Nelson, D. E. (1969) *J. Inorg. Nucl. Chem.*, **31**, 3255–71.

Horwitz, E. P. and Bloomquist, C. A. A. (1973) *J. Inorg. Nucl. Chem.*, **35**, 271–84.

Huang, K., Aoyagi, M., Chen, M. H., Crasemann, B., and Mark, H. (1976) *At. Data Nucl. Data Tables*, **18**, 243–91.

Hübener, S., Taut, S., Vahle, A., Eichler, B., Trautmann, N., and Peterson, J. R. (2000) in *Annual Report 1999*, Laboratory for Radio- and Environmental Chemistry, University of Bern and Paul Scherrer Institute, Switzerland, p. 16.

Hubert, S., Hussonnois, M., Brillard, L., and Guillaumont, R. (1976) in *Transplutonium 1975* (eds. W. Müller and R. Lindner), *Proc. 4th Int. Transplutonium Element Symp.*, Baden-Baden, September 1975, North-Holland, Amsterdam, pp. 109–18.

Hussonnois, M., Hubert, S., Brillard, L., and Guillaumont, R. (1973) *Radiochem. Radioanal. Lett.*, **15**, 47–56.

Ionova, G. V., Spitsyn, V. I., and Mikheev, N. B. (1977) in *Proc. 2nd Int. Conf. on the Electronic Structure of the Actinides,* Wrocław, Poland, September 1976 (eds. J. Mulak, W. Suski, and R. Troć), Ossolineum, Wrocław, pp. 39–47.

Itié, J. P., Peterson, J. R., Haire, R. G., Dufour, C., and Benedict, U. (1985) *J. Phys. F: Met. Phys.,***15**, L213–19.

Ivanov, O. I., Krainov, E. V., and Sviridov, A. F. (1979) *Sov. At. Energ.*, **45**, 924–6.

Jenkins, H. D. B. and Pratt, K. F. (1979) *Prog. Solid State Chem.*, **12**, 125–76.

Johansson, B. and Rosengren, A. (1975) *Phys. Rev. B*, **11**, 1367–73.

Johansson, B., Skriver, H. L., and Andersen, O. K. (1981) in *Physics of Solids Under High Pressure* (eds. J. S. Schilling and R. N. Shelton), North-Holland, Amsterdam, pp. 245–62.

Jullien, R., Galleani d'Agliano, E., and Coqblin, B. (1972) *Phys. Rev. B*, **6**, 2139–55.

Jursich, G. M., Beitz, J. V., Carnall, W. T., Goodman, G. L., Williams, C. W., and Morss, L. R. (1987) *Inorg. Chim. Acta*, **139**, 273–4.

Karalova, Z. K., Myasoedov, B. F., Rodionova, L. M., and Kuznetsov, V. S. (1983) *Sov. Radiochem*, **25**, 175–9.

Karraker, D. G. (1975) *J. Chem. Phys.*, **62**, 1444–6.

Kazakova, G. M., Kosyakov, V. N., and Erin, E. A. (1975) *Sov. Radiochem.*, **17**, 315–18.

Keenan, T. K. and Asprey, L. B. (1969) *Inorg. Chem.*, **8**, 235–8.

Keller, C. (1971) *The Chemistry of the Transuranium Elements,* Verlag Chemie, Weinheim, pp. 553–66.

Khopkar, P. K. and Mathur, J. N. (1980) *J. Radioanal. Chem.*, **60**, 131–40.

Kinard, W. F. and Choppin, G. R. (1974) *J. Inorg. Nucl. Chem.*, **36**, 1131–4.

King, L. J., Bigelow, J. E., and Collins, E. D. (1981) in *Transplutonium Elements – Production and Recovery* (eds. J. D. Navratil and W. W. Schulz) (ACS Symp. Ser. 161), American Chemical Society, Washington, DC, pp. 133–45.

Knauer, J. B. and Weaver, B. (1968) *Separation of Berkelium from Trivalent Actinides by Chromate Oxidation and HDEHP Extraction*, U.S. Atomic Energy Commission Document ORNL-TM-2428, Oak Ridge National Laboratory.

Knauer, J. B. Jr (2002) Oak Ridge National Laboratory, personal communication.

Kohler, S., Deissenberger, R., Eberhardt, K., Erdmann, N., Herrmann, G., Huber, G., Kratz, J. V., Nunnemann, M., Passler, G., Rao, P. M., Riegel, J., Trautmann, N., and Wendt, K. (1997) *Spectrochim. Acta Part B*, **52**, 717–26.

Kooi, J. and Boden, R. (1964) *Radiochim. Acta*, **3**, 226.

Kooi, J., Boden, R., and Wijkstra, J. (1964) *J. Inorg. Nucl. Chem.*, **26**, 2300–2.
Korkisch, J. (1966) *Oesterr. Chem. Ztg.*, **67**, 273–9.
Korpusov, G. V., Patrusheva, E. N., and Dolidze, M. S. (1975) *Sov. Radiochem.*, **17**, 230–6.
Kosyakov, V. N., Yakovlev, N. G., Kazakova, G. M., Erin, E. A., and Kopytov, V. V. (1977) *Sov. Radiochem.*, **19**, 397–400.
Kosyakov, V. N. and Yakovlev, N. G. (1983) *Sov. Radiochem.*, **25**, 172–5.
Kratz, J. V., Gober, M. K., Zimmerman, H. P., Schädel, M., Brüchle, W., Schimpf, E., Gregorich, K. E., Türler, A., Hannink, N. J., Czerwinski, K. R., Kadkhodayan, B., Lee, D. M., Nurmia, M. J., Hoffman, D. C., Gäggeler, H., Jost, D., Kovacs, J., Scherer, U. W., and Weber, A. (1992) *Phys. Rev. C*, **45**, 1064–9.
Krause, M. O., Haire, R. G., Keski-Rahkonen, O., and Peterson, J. R. (1988) *J. Electron. Spectrosc. Relat. Phenom.*, **47**, 215–26.
Kreek, S. A., Hall, H. L., Gregorich, K. E., Henderson, R. A., Leyba, J. D., Czerwinski, K. R., Kadkhodayan, B., Neu, M. P., Kacher, C. D., Hamilton, T. M., Lane, M. R., Sylwester, E. R., Türler, A., Lee, D. M., Nurmia, M. J., and Hoffman, D. C. (1994) *Phys. Rev. C,* **49**, 1859–66.
Krestov, G. A. (1965) *Sov. Radiochem.*, **7**, 69–77.
Krestov, G. A. (1966) *Sov. Radiochem.*, **8**, 200–3.
Kulyako, Yu. M., Frenkel, V. Ya., Lebedev, I. A., Trofimov, T. I., Myasoedov, B. F., and Mogilevskii, A. N. (1981) *Radiochim. Acta*, **28**, 119–22.
Latrous, H. and Oliver, J. (1999) *J. Mol. Liq.*, **81**, 115–21.
Laubereau, P. G. (1970) *Inorg. Nucl. Chem. Lett.*, **6**, 611–16.
Laubereau, P. G. and Burns, J. H. (1970) *Inorg. Chem.*, **9**, 1091–5.
Lebedev, I. A., Chepovoy, V. I., and Myasoedov, B. F. (1975) *Radiochem. Radioanal. Lett.*, **22**, 239–42.
Lebedev, I. A. (1978) *Sov. Radiochem.*, **20**, 556–62.
Liu, Y.-F., Luo, C., von Gunten, H. R., and Seaborg, G. T. (1981) *Inorg. Nucl. Chem. Lett.*, **17**, 257–9.
Liu, Y.-F., Luo, C., Moody, K. J., Lee, D., Seaborg, G. T., and von Gunten, H. R. (1983) *J. Radioanal. Chem.*, **76**, 119–24.
Liu, G. K., Carnall, W. T., Jursich, G., and Williams, C. W. (1994a) *J. Chem. Phys.*, **101**, 8277–89.
Liu, G. K., Jursich, G., Huang, J., Beitz, J. V., and Williams, C. W. (1994b) *J. Alloys Compds*, **213–214**, 207–11.
Lu, C. C., Malik, F. B., and Carlson, T. A. (1971) *Nucl. Phys. A*, **175**, 289–99.
Makarova, T. P., Fridkin, A. M., Kosyakov, V. N., and Erin, E. A. (1979) *J. Radioanal. Chem.*, **53**, 17–24.
Malikov, D. A., Almasova, E. V., Milyukova, M. S., and Myasoedov, B. F. (1980) *Radiochem. Radioanal. Lett.*, **44**, 297–305.
Malikov, D. A., Milyukova, M. S., Kuzovkina, E. V., and Myasoedov, B. F. (1983) *Sov. Radiochem.*, **25**, 293–6.
Malý, J. (1967) *Inorg. Nucl. Chem. Lett.*, **3**, 373–81.
Malý, J. (1969) *J. Inorg. Nucl. Chem.*, **31**, 1007–17.
Manson, S. T. and Kennedy, D. J. (1974) *At. Data Nucl. Data Tables*, **14**, 111–20.
Martinot, L. (1978) in *Encyclopedia of Electrochemistry of the Elements* (ed. A. J. Bard), Marcel Dekker, New York, ch. VIII-2, pp. 196–8.

Martinot, L. and Fuger, J. (1985) in *Standard Potentials in Aqueous Solution* (eds. A. J. Bard, R. Parsons, and J. Jordan), Marcel Dekker, New York, ch. 21, pp. 631–73.
Maruyama, T., Kaji, D., Kaneko, T., Goto, S., Tsukada, K., Haba, H., Asai, M., Ichikawa, S., Nagame, Y., and Kudo, H. (2002) *J. Nucl. Radiochem. Sci.*, **3**, 155–8.
Mathur, J. N. and Khopkar, P. K. (1982) *Sep. Sci. Technol.*, **17**, 985–1002.
Mauerhofer, E., Zhernosekov, K., and Rösch, F. (2003) *Radiochim. Acta*, **91**, 473–7.
McDowell, W. J. and Coleman, C. F. (1972) *J. Inorg. Nucl. Chem.*, **34**, 2837–50.
Merinis, J., Legoux, Y., and Bouissières, G. (1970) *Radiochem. Radioanal. Lett.*, **3**, 255–61.
Mikheev, N. B., D'yachkova, R. A., and Spitsyn, V. I. (1979) *Dokl. Chem.*, **244**, 18–20.
Milyukova, M. S., Malikov, D. A., and Myasoedov, B. F. (1977) *Radiochem. Radioanal. Lett.*, **29**, 93–101.
Milyukova, M. S. and Myasoedov, B. F. (1978) *Sov. Radiochem.*, **20**, 324–30.
Milyukova, M. S., Malikov, D. A., and Myasoedov, B. F. (1978) *Sov. Radiochem.*, **20**, 762–8.
Milyukova, M. S., Malikov, D. A., and Myasoedov, B. F. (1980) *Sov. Radiochem.*, **22**, 267–72.
Milyukova, M. S., Malikov, D. A., Kuzovkina, E. V., and Myasoedov, B. F. (1981) *Radiochem. Radioanal. Lett.*, **48**, 355–61.
Moore, F. L. (1966) *Anal. Chem.*, **38**, 1872–6.
Moore, F. L. (1967) *Anal. Chem.*, **39**, 1874–6.
Moore, F. L. and Jurriaanse, A. (1967) *Anal. Chem.*, **39**, 733–6.
Moore, F. L. (1969) *Anal. Chem.*, **41**, 1658–61.
Morris, D. E., Hobart, D. E., Palmer, P. D., Haire, R. G., and Peterson, J. R. (1990) *Radiochim. Acta*, **49**, 125–34.
Morris, D. E., Hobart, D. E., Palmer, P. D., Begun, G. M., Young, J. P., and Haire, R. G. (2005) *Structural characterization of berkelium and californium oxalates*, U.S. Department of Energy Document LA-UR-05-4597, University of California, Los Alamos National Laboratory.
Morss, L. R. and Fuger, J. (1969) *Inorg. Chem.*, **8**, 1433–9.
Morss, L. R., Siegal, M., Stenger, L., and Edelstein, N. (1970) *Inorg. Chem.*, **9**, 1771–5.
Morss, L. R. (1985) in *Standard Potentials in Aqueous Solution* (eds. A. J. Bard, R. Parsons, and J. Jordan), Marcel Dekker, New York, ch. 20, pp. 587–629.
Morss, L. R., Carnall, W. T., Williams, C. W., Fahey, J. A., Fuger, J., Meyer, G., and Irmler, M. (1991) *J. Less Common Metals*, **169**, 1–8.
Müller, W. (1967) *Actinides Rev.*, **1**, 71–119.
Musikas, C. and Berger, R. (1967) in *Lanthanide/Actinide Chemistry* (eds. P. R. Fields and T. Moeller) (ACS Adv. Chem. Ser. 71), American Chemical Society, Washington, DC, pp. 296–307.
Myasoedov, B. F., Barsukova, K. V., and Radionova, G. N. (1971) *Radiochem. Radioanal. Lett.*, **7**, 269–74.
Myasoedov, B. F., Chepovoy, V. I., and Lebedev, I. A. (1973) *Radiochem. Radioanal. Lett.*, **15**, 39–45.
Myasoedov, B. F. (1974) *Sov. Radiochem.*, **16**, 716–21.
Myasoedov, B. F., Guseva, L. I., Lebedev, I. A., Milyukova, M. S., and Chmutova, M. K. (1974) in *Analytical Chemistry of Transplutonium Elements* (ed. D. Slutzkin), John Wiley, New York, pp. 122–32.

Myasoedov, B. F., Chepovoy, V. I., and Lebedev, I. A. (1975) *Radiochem. Radioanal. Lett.*, **22**, 233–8.
Myasoedov, B. F. (1987) *Talanta*, **34**, 31–40.
Myasoedov, B. F. and Lebedev, I. A. (1991) *J. Radioanal. Nucl. Chem.*, **147**, 5–26.
Nave, S. E., Huray, P. G., and Haire, R. G. (1980) in *Crystalline Electric Field and Structural Effects in f-Electron Systems* (eds. J. E. Crow, R. P. Guertin, and T. W. Mihalisin), Plenum, New York, pp. 269–74.
Nave, S. E., Haire, R. G., and Huray, P. G. (1981) in *Actinides – 1981,* Pacific Grove, California, September 1981, Abstracts Volume (ed. N. M. Edelstein), U.S. Department of Energy Document LBL-12441, University of California, Lawrence Berkeley Laboratory, pp. 144–6.
Nave, S. E., Haire, R. G., and Huray, P. G. (1983) *Phys. Rev. B*, **28**, 2317–27.
Nugent, L. J., Burnett, J. L., Baybarz, R. D., Werner, G. K., Tanner, S. P., Tarrant, J. R., and Keller, O. L. Jr (1969) *J. Phys. Chem.*, **73**, 1540–9.
Nugent, L. J., Baybarz, R. D., Werner, G. K., and Friedman, H. A. (1970) *Chem. Phys. Lett.*, **7**, 179–82.
Nugent, L. J. and Vander Sluis, K. L. (1971) *J. Opt. Soc. Am.*, **61**, 1112–5.
Nugent, L. J., Baybarz, R. D., Burnett, J. L., and Ryan, J. L. (1971) *J. Inorg. Nucl. Chem.*, **33**, 2503–30.
Nugent, L. J., Burnett, J. L., and Morss, L. R. (1973a) *J. Chem. Thermodyn.*, **5**, 665–78.
Nugent, L. J., Baybarz, R. D., Burnett, J. L., and Ryan, J. L. (1973b) *J. Phys. Chem.*, **77**, 1528–39.
Nugent, L. J. (1975) *J. Inorg. Nucl. Chem.*, **37**, 1767–70.
Nugent, L. J., Baybarz, R. D., Burnett, J. L., and Ryan, J. L. (1976) *J. Inorg. Nucl. Chem.*, Suppl., 37–9.
Okamoto, H. (1999) *J. Phase Equilib.*, **20**, 351.
Overman, R. F. (1971) *Anal. Chem.*, **43**, 600–1.
Passler, G., Nunnemann, M., Huber, G., Deissenberger, R., Erdmann, N., Köhler, S., Kratz, J. V., Trautmann, N., Waldek, A., and Peterson, J. R. (1998) *AIP Conf. Proc.*, **454**, 183–8. (Resonance Ionization Spectroscopy, Manchester, UK, June 21–25, 1998)
Paulus, W., Kratz, J. V., Strub, E., Zauner, S., Brüchle, W., Pershina, V., Schädel, M., Schausten, B., Adams, J. L., Gregorich, K. E., Hoffman, D. C., Lane, M. R., Laue, C., Lee, D. M., McGrath, C. A., Shaughnessy, D. A., Strellis, D. A., and Sylwester, E. R. (1999) *Radiochim. Acta*, **84**, 69–77.
Payne, G. F. and Peterson, J. R. (1987) *Inorg. Chim. Acta*, **139**, 111–12.
Penneman, R. A., Ryan, R. R., and Rosenzweig, A. (1973) *Struct. Bond.*, **13**, 1–52.
Peppard, D. F., Moline, S. W., and Mason, G. W. (1957) *J. Inorg. Nucl. Chem.*, **4**, 344–8.
Peterson, J. R. (1967) *The Solution Absorption Spectrum of Bk^{3+} and the Crystallography of Berkelium Dioxide, Sesquioxide, Trichloride, Oxychloride, and Trifluoride*, PhD Thesis, U.S. Atomic Energy Commission Document UCRL-17875, University of California, Lawrence Berkeley Radiation Laboratory.
Peterson, J. R. and Cunningham, B. B. (1967a) *Inorg. Nucl. Chem. Lett.*, **3**, 327–36.
Peterson, J. R. and Cunningham, B. B. (1967b) *Inorg. Nucl. Chem. Lett.*, **3**, 579–83.
Peterson, J. R. and Cunningham, B. B. (1968a) *J. Inorg. Nucl. Chem.*, **30**, 823–8.
Peterson, J. R. and Cunningham, B. B. (1968b) *J. Inorg. Nucl. Chem.*, **30**, 1775–84.

Peterson, J. R., Fahey, J. A., and Baybarz, R. D. (1970) *Nucl. Metall.*, **17**, 20–34.
Peterson, J. R., Fahey, J. A., and Baybarz, R. D. (1971) *J. Inorg. Nucl. Chem.*, **33**, 3345–51.
Peterson, J. R. and Burns, J. H. (1973) *J. Inorg. Nucl. Chem.*, **35**, 1525–30.
Peterson, J. R. (1976) in *Gmelin Handbuch der Anorganischen Chemie,* New Suppl. Ser., vol. 31 (ed. G. Koch), Springer-Verlag, New York, pp. 72–6.
Peterson, J. R., Fellows, R. L., Young, J. P., and Haire, R. G. (1977a) in *Proc. 2nd Int. Conf. on the Electronic Structure of the Actinides,* Wrocław, Poland, September 1976 (eds. J. Mulak, W. Suski, and R. Troć), Ossolineum, Wrocław, pp. 111–16.
Peterson, J. R., Fellows, R. L., Young, J. P., and Haire, R. G. (1977b) *Rev. Chim. Minér.*, **14**, 172–7.
Peterson, J. R., Ensor, D. D., Fellows, R. L., Haire, R. G., and Young, J. P. (1979) *J. Physique*, **40**(C4), 111–13.
Peterson, J. R. (1980) in *Lanthanide and Actinide Chemistry and Spectroscopy* (ed. N. M. Edelstein) (ACS Symp. Ser. 131), American Chemical Society, Washington, DC, pp. 221–38.
Peterson, J. R., Young, J. P., Ensor, D. D., and Haire, R. G. (1981) in *Actinides – 1981,* Pacific Grove, California, September 1981, Abstracts Volume (ed. N. M. Edelstein), U.S. Department of Energy Document LBL-12441, University of California, Lawrence Berkeley Laboratory, pp. 118–20.
Peterson, J. R. and Hobart, D. E. (1984) in *Adv. Inorg. Chem. Radiochem.,* vol. 28 (eds. H. J. Emeléus and A. G. Sharpe), Academic Press, New York, pp. 29–72.
Peterson, J. R., Young, J. P., Ensor, D. D., and Haire, R. G. (1986) *Inorg. Chem.*, **25**, 3779–82.
Peterson, J. R., Haire, R. G., Benedict, U., and Young, J. P. (1987) *J. Less Common Metals*, **33**, 143–53.
Peterson, J. R., Young, J. P., Wilmarth, W. R., and Haire, R. G. (1990) *Appl. Spectrosc.*, **44**, 461–5.
Peterson, J. R. (1995) *J. Alloys Compds*, **223**, 180–4.
Popov, Yu. S. and Timofeev, G. A. (1999) *Radiochem.*, **41**, 26–30, and references therein.
Propst, R. C. and Hyder, M. L. (1970) *J. Inorg. Nucl. Chem.*, **32**, 2205–16.
Ronen, Y. (1998) *Ann. Nucl. Energy*, **25**, 983–5.
Samhoun, K. and David, F. (1976) in *Transplutonium Elements 1975* (eds. W. Müller and R. Lindner), *Proc. 4th Int. Transplutonium Element Symp.*, Baden-Baden, September 1975, North-Holland, Amsterdam, pp. 297–304.
Samhoun, K. and David, F. (1979) *J. Inorg. Nucl. Chem.*, **41**, 357–63.
Sarkisov, E. S. (1966) *Dokl. Akad. Nauk SSSR*, **166**, 627–30.
Scherer, U. W., Kratz, J. V., Schädel, M., Brüchle, W., Gregorich, K. E., Henderson, R. A., Lee, D., Nurmia, M., and Hoffman, D. C. (1988) *Inorg. Chim. Acta*, **146**, 249–54.
Schoebrechts, J.-P., Gens, R., Fuger, J., and Morss, L. R. (1989) *Thermochim. Acta*, **139**, 49–66.
Scofield, J. H. (1974) *At. Data Nucl. Data Tables*, **14**, 121–37.
Shafiev, A. I. and Efremov, Yu. V. (1972) *Sov. Radiochem.*, **14**, 754–6.
Shafiev, A. I., Efremov, Yu. V., and Yakovlev, G. N. (1974) *Sov. Radiochem.*, **16**, 31–4.
Shannon, R. D. and Prewitt, C. T. (1969) *Acta Crystallogr. B*, **25**, 925–46.
Shannon, R. D. (1976) *Acta Crystallogr. A*, **32**, 751–67.

Simakin, G. A., Kosyakov, V. N., Baranov, A. A., Erin, E. A., Kopytov, V. V., and Timofeev, G. A. (1977a) *Sov. Radiochem.*, **19**, 302–7.
Simakin, G. A., Baranov, A. A., Kosyakov, V. N., Timofeev, G. A., Erin, E. A., and Lebedev, I. A. (1977b) *Sov. Radiochem.*, **19**, 307–9.
Smentek, L., Wybourne, B. G., and Kobus, J. (2001) *J. Phys. B*, **34**, 1513–22.
Spirlet, J. C., Peterson, J. R., and Asprey, L. B. (1987) in *Advances in Inorganic Chemistry,* vol. 31 (eds. H. J. Emeléus and A. G. Sharpe), Academic Press, Orlando, FL, pp. 1–41.
Stary, J. (1966) *Talanta*, **13**, 421–37.
Stepanov, A. V. (1971) *Russ. J. Inorg. Chem.*, **16**, 1583–6.
Stevenson, J. N. and Peterson, J. R. (1979) *J. Less Common Metals*, **66**, 201–10.
Stokely, J. R., Baybarz, R. D., and Shults, W. D. (1969) *Inorg. Nucl. Chem. Lett.*, **5**, 877–84.
Stokely, J. R., Baybarz, R. D., and Peterson, J. R. (1972) *J. Inorg. Nucl. Chem.*, **34**, 392–3.
Sudakov, L. V., Erin, E. A., Kopytov, V. V., Baranov, A. Yu., Shimbarev, E. V., Vasil'ev, V. Ya., and Kapshukov, I. I. (1977) *Sov. Radiochem.*, **19**, 394–6.
Sugar, J. (1974) *J. Chem. Phys.*, **60**, 4103.
Sullivan, J. C., Schmidt, K. H., Morss, L. R., Pippin, C. G., and Williams, C. (1988) *Inorg. Chem.*, **27**, 598–9.
Taut, S., Hübener, S., Eichler, B., Türler, A., Gäggeler, H. W., Timokhin, S. N., and Zvara, I. (1998) *J. Alloys Compds*, **271–273**, 316–21.
Taut, S., Vahle, A., Hübener, S., Eichler, B., Jost, D., and Türler, A. (2000) in *Annual Report 1999,* Laboratory for Radio- and Environmental Chemistry, University of Bern and Paul Scherrer Institute, Switzerland, p. 17.
Thoma, R. E. (1962) *Inorg. Chem.*, **1**, 220–6.
Thompson, S. G., Cunningham, B. B., and Seaborg, G. T. (1950a) *J. Am. Chem. Soc.*, **72**, 2798–801.
Thompson, S. G., Ghiorso, A., and Seaborg, G. T. (1950b) *Phys. Rev.*, **77**, 838–9.
Thompson, S. G., Ghiorso, A., and Seaborg, G. T. (1950c) *Phys. Rev.*, **80**, 781–9.
Tikhomirov, V. V., Chetverikov, A. P., and Gabeskiriya, V. Ya. (1981) *Sov. Radiochem.*, **23**, 722–5.
Timofeev, G. A., Chistyakov, V. M., and Erin, E. A. (1986) *Sov. Radiochem.*, **28**, 454–8.
Timofeev, G. A., Chistyakov, V. M., Erin, E. A., and Baranov, A. A. (1987) *Sov. Radiochem.*, **29**, 147–51.
Turcotte, R. P., Chikalla, T. D., and Eyring, L. (1971) *J. Inorg. Nucl. Chem.*, **33**, 3749–63.
Turcotte, R. P., Chikalla, T. D., Haire, R. G., and Fahey, J. A. (1980) *J. Inorg. Nucl. Chem.*, **42**, 1729–33.
Ulstrup, J. (1966) *At. Energy Rev.*, **4**, 3–82.
Vander Sluis, K. L. and Nugent, L. J. (1972) *Phys. Rev. A*, **6**, 86–94.
Vander Sluis, K. L. and Nugent, L. J. (1974) *J. Opt. Soc. Am.*, **64**, 687–95.
Varga, L. P., Baybarz, R. D., Reisfeld, M. J., and Asprey, L. B. (1973a) *J. Inorg. Nucl. Chem.*, **35**, 2775–85.
Varga, L. P., Baybarz, R. D., Reisfeld, M. J., and Volz, W. B. (1973b) *J. Inorg. Nucl. Chem.*, **35**, 2787–94.
Varga, L. P., Baybarz, R. D., and Reisfeld, M. J. (1973c) *J. Inorg. Nucl. Chem.*, **35**, 4313–7.

Veal, B. W., Lam, D. J., Diamond, H., and Hoekstra, H. R. (1977) *Phys. Rev. B*, **15**, 2929–42.

Waldek, A., Erdmann, N., Grüning, C., Huber, G., Kunz, P., Kratz, J. V., Lassen, J., Passler, G., and Trautmann, N. (2001) *AIP Conf. Proc.*, **584**, 219–24. (Resonance Ionization Spectroscopy, Knoxville, TN, October 8–12, 2000.)

Ward, J. W. and Hill, H. H. (1976) in *Heavy Element Properties* (eds. W. Müller and H. Blank), *Proc. Joint Session, 4th Int. Transplutonium Element Symp. & 5th Int. Conf. on Plutonium and Other Actinides,* Baden-Baden, September 1975, North-Holland, Amsterdam, pp. 65–79.

Ward, J. W., Kleinschmidt, P. D., Haire, R. G., and Brown, D. (1980) in *Lanthanide and Actinide Chemistry and Spectroscopy* (ed. N. M. Edelstein) (ACS Symp. Ser. 131), American Chemical Society, Washington, DC, pp. 199–220.

Ward, J. W., Kleinschmidt, P. D., and Haire, R. G. (1982) *J. Chem. Phys.*, **77**, 1464–8.

Weaver, B. (1968) *Anal. Chem.*, **40**, 1894–6.

Weaver, B. and Fardy, J. J. (1969) *Inorg. Nucl. Chem. Lett.*, **5**, 145–6.

Weaver, B. and Stevenson, J. N. (1971) *J. Inorg. Nucl. Chem.*, **33**, 1877–81.

Wilk, P. A., Gregorich, K. E., Türler, A., Laue, C. A., Eichler, R., Ninov, V., Adams, J. L., Kirbach, U. W., Lane, M. R., Lee, D. M., Patin, J. B., Shaughnessy, D. A., Strellis, D. A., Nitsche, H., and Hoffman, D. C. (2000) *Phys. Rev. Lett.*, **85**, 2697–700.

Williams, K. R. and Choppin, G. R. (1974) *J. Inorg. Nucl. Chem.*, **36**, 1849–53.

Wilmarth, W. R. and Peterson, J. R. (1991) in *Handbook on the Physics and Chemistry of the Actinides,* vol. 6 (eds. A. J. Freeman and C. Keller), North-Holland, New York, pp. 1–38.

Worden, E. F., Hulet, E. K., Lougheed, R., and Conway, J. G. (1967) *J. Opt. Soc. Am.*, **57**, 550.

Worden, E. F., Gutmacher, R. G., Conway, J. G., and Mehlhorn, R. J. (1969) *J. Opt. Soc. Am.*, **59**, 1526.

Worden, E. F., Gutmacher, R. G., Lougheed, R. W., and Conway, J. G. (1970) *J. Opt. Soc. Am.*, **60**, 1555.

Worden, E. F. and Conway, J. G. (1978) *At. Data Nucl. Data Tables*, **22**, 329–66.

Yakovlev, N. G., Kosyakov, V. N., and Kazakova, G. M. (1982) *J. Radioanal. Chem.*, **75**, 113–20.

Yakovlev, N. G. and Kosyakov, V. N. (1983) *Sov. Radiochem.*, **25**, 687–92.

Yakushev, A., Eichler, B., Türler, A., Gäggeler, H. W., and Peterson, J. (2003) *Radiochim. Acta*, **91**, 123–6.

Young, J. P., Haire, R. G., Fellows, R. L., and Peterson, J. R. (1978) *J. Radioanal. Chem.*, **43**, 479–88.

Young, J. P., Haire, R. G., Peterson, J. R., Ensor, D. D., and Fellows, R. L. (1980) *Inorg. Chem.*, **19**, 2209–12.

Young, J. P., Haire, R. G., Peterson, J. R., Ensor, D. D., and Fellows, R. L. (1981) *Inorg. Chem.*, **20**, 3979–83.

Young, J. P., Haire, R. G., Peterson, J. R., and Ensor, D. D. (1984) in *Geochemical Behavior of Disposed Radioactive Waste* (eds. G. S. Barney, J. D. Navratil, and W. W. Schulz) (ACS Symp. Ser. 246), American Chemical Society, Washington, DC, pp. 335–46.

Zachariasen, W. H. (1973) *J. Inorg. Nucl. Chem.*, **35**, 3487–97.

Zvara, I. (1985) *Radiochim. Acta*, **38**, 95–101.

CHAPTER ELEVEN

CALIFORNIUM

Richard G. Haire

11.1 INTRODUCTION

The discovery of californium came in the era of the syntheses and identifications of other transplutonium elements, following the end of World War II. The discovery of the element californium, like many of the other actinide elements, hinged on the development of new experimental techniques in conjunction with predictions based on nuclear systematics. Californium was named after the University and State of California where many of the transuranium elements were first identified. This element was discovered by Thompson, Street, Ghiorso, and Seaborg (Hyde *et al.*, 1971; Seaborg and Loveland, 1990) in February, 1950. The discovery of californium came only 2 months after the preparation and identification of the first isotope of berkelium, element 97 (see Chapter 10). An account of the discovery and reminiscences about the early work on californium has been given by Ghiorso (1983).

The first preparative method for californium was to bombard microgram targets of ^{242}Cm with 35 MeV helium ions in a 60 in. cyclotron. This produced ^{244}Cf by a (α,2n), reaction which decayed primarily by alpha emission ($t_{1/2}$ = 19.4 min, with two different alpha energies having a 75% and 25% branching ratios; see Table 11.1). This isotope also has a small decay branch that proceeds via electron capture. Since element 98 ('eka-dysprosium') was expected to have a stable tripositive oxidation state in aqueous solution, its elution behavior in chromatographic separation schemes was predicted and this was used as a guide to estimate which collection fractions should be examined for the new element. In addition to acquire a high degree of decontamination

Table 11.1 *Nuclear properties of californium isotopes*.*

Mass number	*Half-life*	*Mode of decay*	*Main radiations* (MeV)	*Method of production*
237**	2.1 s	EC, SF		^{206}Pb(^{34}S,3n)
238**	21 ms	EC, SF		^{207}Pb(^{34}S,3n)
239	39 s	α	α 7.63	^{243}Fm daughter
240	1.06 min	α	α 7.59	^{233}U(^{12}C,5n)
241	3.8 min	α	α 7.335	^{233}U(^{12}C,4n)
242	3.7 min	α	α 7.385 (∼ 80%)	^{233}U(^{12}C,3n)
			7.351 (∼ 20%)	^{235}U(^{12}C,5n)
243	10.7 min	EC ∼ 86%	α 7.06	^{235}U(^{12}C,4n)
		α ∼ 14%		
244	19.4 min	α	α 7.210 (75%)	^{244}Cm(α,4n)
			7.168 (25%)	^{236}U(^{12}C,4n)
245	45.0 min	EC ∼ 70%	α 7.137	^{244}Cm(α,3n)
		α ∼ 30%		^{238}U(^{12}C,5n)
246	35.7 h	α	α 6.758 (78%)	^{244}Cm(α,2n)
	2.0×10^3 yr	SF	6.719 (22%)	^{246}Cm(α,4n)
		β stable		
247	3.11 h	EC 99.96%	α 6.296 (95%)	^{246}Cm(α,3n)
		α 0.035%	γ 0.294 (1.0%)	^{244}Cm(α,n)
248	334 d	α	α 6.258 (80.0%)	^{246}Cm(α,2n)
	3.2×10^4 yr	SF	6.217 (19.6%)	
		β stable		
249	351 yr	α	α 6.194 (2.2%)	^{249}Bk daughter
	6.9×10^{10} yr	SF	5.812 (84.4%)	
			γ 0.388 (66%)	
250	13.08 yr	α	α 6.031 (83%)	multiple n capture
	1.7×10^4 yr	SF	5.989 (17%)	
251	898 yr	α	α 5.851 (27%)	multiple n capture
			5.677 (35%)	
			γ 0.177 (17%)	
252	2.645 yr	α 96.91%	α 6.118 (84%)	multiple n capture
		SF 3.09%	6.076 (15.8%)	
253	17.81 d	β^- 99.69%	α 5.979 (95%)	multiple n capture
		α 0.31%	5.921 (5%)	
254	60.5 d	SF 99.69%	α 5.834 (83%)	multiple n capture
		α 0.31%	5.792 (17%)	
255	1.4 h	β^-		^{254}Cf(n,γ)
256	12.3 min	SF		^{254}Cf(t,p)

SF = spontaneous fission: EC = electron capture
* See Appendix II.
** The existence of these isotopes has been questioned but included for completeness.

from other radionuclides, it was also necessary that the chemical separations be completed rapidly (within about 1 h) due to the short half-life projected for this isotope of californium.

Californium, element 98, is in the second half of the actinide series, where its 5f electrons are further removed from the valence electrons than in the lighter

actinide elements. It is this effect that makes californium more 'lanthanide-like' in many compounds and in solutions. However, in progressing across this half of the actinide series, there is also an increasing tendency for a divalent metallic state and the formation of a divalent state in compounds, and several compounds containing Cf(II) are known. Thus, its comparison to the lanthanide elements has limitations, as seen from topics discussed throughout this chapter. Unlike members of the second half of the lanthanide series, which may exhibit either a divalent or tetravalent oxidation state in addition to their more common trivalent state, californium is known to exhibit a divalent, trivalent, and tetravalent state in compounds. In solution, the trivalent state is dominant, although the II, IV states, and a potential V state have been reported. In its elemental state, californium properties differ from those exhibited by its lanthanide homolog, dysprosium.

When the existence of californium was established, scientific interests and efforts progressed to prepare other isotopes of this element, to determine their nuclear properties, and to investigate the chemistry of the element. These initial studies were performed using only small numbers of atoms, but it is to the credit of the early investigators that considerable amounts of chemical and nuclear data were accumulated in their work. Tracer experiments were sufficient to establish the stability of Cf(III) in solution, as well as some of the element's basic chemistry. Additional information on the chemistry of californium was generated as microgram quantities became available, which also permitted the preparation and study of solid compounds. The first compound of californium of a definitive structure (the oxychloride by Cunningham and Wallmann) was determined a decade after the discovery of the element (Seaborg and Loveland, 1990).

Larger quantities of the transplutonium elements, including californium, subsequently became available by the development of a reactor irradiation program that was initiated in the mid-1960s by the former U.S. Atomic Energy Commission. The U.S. Department of Energy retains the ability to produce these transplutonium elements, including sub-gram amounts of the different californium isotopes yearly in the High-Flux Isotope Reactor (HFIR) at Oak Ridge National Laboratory, Oak Ridge, Tennessee. The continued production at HFIR may be limited in the future. Transplutonium elements are also produced in high-flux reactors at Dimitrovgrad in the Russian Federation, and potentially in other reactors. Smaller amounts of californium can be generated by irradiation of special targets in accelerators, but in the best case these smaller quantities only serve for chemical tracer studies or for determining their nuclear properties.

Reactor-produced californium consists of californium isotopes from ^{249}Cf through ^{254}Cf, with the major isotope produced being ^{252}Cf. Californium isotopes produced in accelerators normally have lower atomic masses and obtained in much smaller quantities. Considering these production schemes and the californium daughters formed as daughter products of other decaying isotopes, californium isotopes with masses as small as 237 and as large as 256

have been reported. An example of accelerator-produced californium is the generation of ^{242}Cf reported by Sikkeland and Ghiorso (1967), in the time frame when HFIR was producing californium isotopes through successive neutron capture processes.

This chapter focuses on the chemistry and physical properties of californium that are available in the open literature, and supplementing/evaluating this information when appropriate. An effort was made to minimize the number of references to technical reports, unpublished information, etc., except for cases when such a citation was warranted. The number of publications dealing with technological and medical applications of neutrons from ^{252}Cf is very large. There are numerous references to work done with californium covering biological studies, radiotherapy, neutron radiography, neutron activation analyses, dosimetry, etc. Some 70% of the work published during the last decade concerns efforts in these arenas using the ^{252}Cf isotope. The remaining reports deal with chemical studies and separation work, which normally employ the longer-lived ^{249}Cf isotope.

A significant amount of the basic chemical work on californium has been reported in different publications, but this should not be construed to interpret that additional chemical or physical studies are not needed! Indeed, given some of the recent advances in scientific techniques (i.e. those involving synchrotron sources, such as extended X-ray absorption fine structure (EXAFS), X-ray absorption near edge structure (XANES), photoelectron scattering, etc.), new studies should be pursued with californium and its compounds, and such investigations would be expected to yield even further insights into this element's science. Some of the more recent thrusts in the chemistry and physics of californium have involved its gas-phase chemistry, high-pressure studies of the metal and compounds, and new separation science. These topics are covered in the different sections of this chapter.

11.2 PREPARATION AND NUCLEAR PROPERTIES

It is unlikely that, nor have there been reports or evidence of, primordial californium in nature. Thus, isotopes of californium with mass numbers between 237 and 256 have been prepared as man-made isotopes. A summary of methods for the preparation of and nuclear data for these isotopes is given in Table 11.1, and in Appendix II. The lighter masses (neutron deficient) are produced by accelerator methods, (e.g. the helium bombardment of curium isotopes) which was the initial technique used to generate and discover californium. But californium isotopes can also be prepared by heavy-ion bombardment of elements other than curium. Examples of the latter are bombarding thorium with oxygen ions, and uranium with carbon or nitrogen ions. These preparations involve high-energy accelerators and produce only limited numbers of atoms of the product nucleus, and therefore are not useful for producing

weighable quantities (i.e. even micrograms quantities) of californium needed for the preparation of pure solid compounds. An excellent discussion on the history, preparation, and nuclear properties of californium isotopes is given by Hyde *et al.* (1971) and Seaborg and Loveland (1990).

Californium isotopes with larger neutron contents (higher mass numbers) are usually prepared by irradiation of targets (plutonium through curium) in nuclear reactors that have a high neutron flux ($>10^{15}$ neutrons cm^{-2} s^{-1}). These and even heavier californium isotopes are also generated in nuclear explosions, where for short periods of time the neutron flux is even higher (fluence $> 10^{29}$ neutrons cm^{-2}). In the latter case, the formation of higher-Z elements and heavier isotopes is favored due to the high density of neutrons and in time spans that are short relative to the various decay half-lives of the materials formed. In principle, the objective would be to favor the significant neutron capture by the uranium to plutonium atoms present in such devices over the decay process of the products formed. This builds very rapidly by capture beyond the particularly short-lived isotopes before they can decay appreciably. Although transplutonium elements have been intentionally produced in underground nuclear explosions, processing of large amounts of 'ore material' (rock debris) in reasonable time periods makes this preparation procedure for these elements impracticable. Thus, weighable quantities of californium are best obtained as direct or indirect products from irradiation of materials in nuclear reactors.

Since the mid-1960s californium has been produced in special nuclear reactors (i.e. the HFIR at Oak Ridge National Laboratory). Most recently the intial targets consist mainly of curium isotopes (^{244}Cm through ^{248}Cm isotopes), which are irradiated in the reactor by neutrons to produce californium isotopes from ^{249}Cf through ^{255}Cf with the major isotope being ^{252}Cf. The HFIR located at Oak Ridge National Laboratory can produce currently up to 0.5 g of ^{252}Cf (together with other californium isotopes) per year. By using larger reactors, this quantity could be conceivably be increased to produce several grams of ^{252}Cf per year, and at one time this was planned in the U.S. but the greater need for this isotope never materialized.

The ^{252}Cf isotope has a 2.6 year alpha decay half-life, and a 85 year spontaneous fission branching half-life, which is the source of the neutrons it emits. Neutrons from its fission offer the main use for this isotope (i.e. neutron activation analysis, medical treatments, neutron radiography, etc.), but it is also useful for chemical tracer work, given its high specific alpha activity and greater availability. However, the neutron field (3×10^6 neutrons s^{-1} $\mu g^{-1}$and the gamma radiation accompanying fission and/or the alpha decay of ^{252}Cf (up to 7 MeV gammas)) normally precludes its use for basic chemical/physical studies, as considerable shielding is required to protect personnel and equipment from even microgram amounts of it (gloved box limits are normally only a few micrograms). As a result, the mixture of californium isotopes obtained directly from reactors (which contains ^{252}Cf as the primary isotope) is not

generally considered when multiple micrograms or more of californium are needed for studies without extensive shielding. Instead, the ^{249}Cf isotope is used.

Although in principle, ^{251}Cf has the most desirable radiation characteristics with regard to performing research studies, and it could be isolated from mixed californium isotopes using a mass separator, the cost and low yields (10%) makes this process unattractive. This isotope is only formed at low concentrations, as a result of its high-neutron capture and fission cross sections.

Another isotope, ^{253}Cf, is important as a parent for obtaining isotopically pure ^{253}Es (see Chapter 12). If a chemically pure (i.e. free of einsteinium) fraction of mixed californium isotopes from a reactor is obtained, and the ^{253}Cf present is allowed to decay, then a subsequent chemical separation of this californium fraction allows recovery of its pure ^{253}Es daughter.

For the majority of basic studies, especially those requiring weighable quantities of californium, the ^{249}Cf isotope is desired. Its alpha half-life of 351 years makes it suitable for chemical/physical experiments in gloved boxes, although there is still significant gamma radiation associated with its decay, which may require some shielding for protection. Typically, gloved box studies are rather limited to less than 10 mg because of radiation levels.

Isotopically pure ^{249}Cf is best obtained form the decay of ^{249}Bk (beta emitter, half-life of 330 days; see Appendix II). This latter isotope is the major berkelium isotope obtained from reactor irradiations (^{250}Bk is also formed in reactors but it has a 3.217 h half-life and rapidly decays; see appendix II). Thus, to obtain ^{249}Cf free of other californium isotopes for research studies, it is necessary to generate berkelium in a reactor and then separate it chemically from the other transplutonium elements present. After sufficient decay of the ^{249}Bk to ^{249}Cf, the latter can be subsequently separated chemically from the berkelium fraction. It is possible to obtain multi-milligrams (up to 60 mg at the HFIR at Oak Ridge National Laboratory) per year in this manner. And, as the half-life of ^{249}Cf is 351 years, it is possible to accumulate larger amounts of it over time by recovery operations. The only other known production source of ^{249}Bk in significant quantities, and hence a source of isotopically pure ^{249}Cf by its decay, is in Russia but the quantity available there is often smaller. It is then possible to provide in relatively short time frames multi-milligram amounts of ^{249}Cf.

The half-life of ^{250}Cf (13.08 years), which is produced along with other californium isotopes in reactors, has been determined recently (Popov *et al*., 1996). The ^{238}Cf nuclide had been reported from bombardment of lead isotopes (^{207}Pb and ^{208}Pb) with ^{34}S and ^{36}S ions (Lazarev *et al*., 1995). Its mode of decay is suggested to occur by spontaneous fission.

The K series of X-rays generated form californium has been discussed by Dittner and Bemis (1972), and can be used for the identification of californium during its decay processes. The vibration states in californium nuclei have been discussed by Ahmad (1980).

11.3 APPLICATIONS

As mentioned in Section 11.2, californium produced in nuclear reactors is mainly comprised of ^{252}Cf, and only a small quantity of this isotope mixture can be employed for chemical/physical studies outside of heavy shielding or hot cells. Thus, the applications for this ^{252}Cf isotope are for: (1) neutron emissions; (2) a target material for producing transcalifornium elements; (3) a californium tracer, using its higher specific alpha activity; and/or (4) a parent for obtaining ^{248}Cm (^{248}Cm is the alpha-decay product of ^{252}Cf; see Chapter 9). This long-lived isotope of curium is very useful for basic studies of curium. In practice, a mixture of ^{246}Cm, ^{248}Cm, and small amounts of other curium isotopes are obtained from the decayed californium reactor products ($\sim$97% ^{248}Cm and 3% ^{246}Cm from the alpha decays of ^{252}Cf and ^{250}Cf isotopes present).

Although it is beyond the scope of this work to review such applications of ^{252}Cf fully, or mixtures where this is the main californium isotope, its potential usefulness warrants some coverage here. The reader is also referred to: the ^{252}Cf Information Center at the Savannah River Laboratory (USAEC Rept, 1969) , Georgia, U.S.A. or the ^{252}Cf User Facility located at Oak Ridge National Laboratory. More extensive information is also given by Martin *et al.* (1997, 2000) and by Osborne-Lee and Alexander (1995). When ^{252}Cf is used as a neutron source, the data listed in Table 11.2 may be useful. Martin *et al.* (1998; 2004) have discussed applications of ^{252}Cf.

Considering the spontaneous fission half-lives, ^{252}Cf has the shortest one (85 years), a 3.09% fission fraction and yields 3.767 neutrons per fission. One observes a range from 2 to 3.8 neutrons per event for other fissioning actinide isotopes. The calculated neutron emission rate for ^{252}Cf is 2.3×10^{12} neutrons s^{-1} g^{-1}, although one would rarely expect to have a gram. In contrast, high-flux reactors have fluxes of three orders of magnitude higher. But, this rate for ^{252}Cf is lower than that for ^{254}Cf (1.2×10^{15} neutrons s^{-1} g^{-1}) due to its 99.7% fission fraction and 3.83 neutrons per fission event. But, this later isotope is not readily available in any significant quantities. For comparison, the neutron emission for ^{248}Cm, which also undergoes spontaneous fission, is only 4.2×10^{7} neutrons s^{-1} g^{-1}. It has a long alpha decay having a half-life of 3×10^{5} years, 8.39% fission fraction, and 3.2 neutrons per fission event. Data are summarized in Table 11.2.

Applications of ^{252}Cf can be broadly classified as medical, analyses, and biological studies, where the majority of the work involves in one way or the other the spontaneous-fission neutrons emitted from ^{252}Cf (Karelin *et al.*, 1997). These sources have been useful in such areas as neutron activation analysis, neutron radiography (a technique that complements X-ray radiography), and medical therapy for treatment of cancer. They are most useful where access to nuclear reactors is not possible, or convenient, and/or where a lower neutron flux is adequate for the need at hand. An important application for ^{252}Cf is to

Table 11.2 *Data for ^{252}Cf and other selected neutron sources*.*

Isotope	*Half Life* (yrs)	*Specific Activity* (Ci g^{-1})	*Spontaneous Fission Half-Life* (yrs)	*Fission Fraction* (%)	*Neutrons per Fission*	*Neutron Rate* (n $s^{-1}g^{-1}$)
^{252}Cf	2.645	5.38×10^2	85	3.09	3.767	2.3×10^{12}
^{252}Cf alpha energies:			6.118 (84%) 6.076 (16%)			
Specific heat from decay of ^{252}Cf			38 W g^{-1}			
Neutrons from (α, n) reaction on Al metal: 1.3×10^7 n s^{-1} g^{-1}						
^{254}Cf	0.17	8.45×10^3	–	99.7	3.83	1.2×10^{15}
^{248}Cm	3.4×10^5	4.25×10^{-3}	41	8.39	3.16	4.2×10^7

**Sources*: The Health Physics and Radiological Health Handbook (1998); Osborne-Lee and Alexander (1995).

provide neutrons for the initial start-up of nuclear reactors (Osborne-Lee and Alexander, 1995).

Portable neutron activation analysis systems using ^{252}Cf have been designed for use in deep-sea exploration for minerals, or for space probes (Senftle *et al.*, 1969; Wiggins *et al.*, 1969; Filippov, 1979; Bakiev *et al.*, 1991).

Various sizes and forms of ^{252}Cf sources have been designed for medical applications, both for external irradiation and for internal implantation. How extensive the practical applications of ^{252}Cf can be determined by the success of experiments using this nuclide. The more extensive shielding hinders medical applications needed for the neutrons (greater thickness of paraffin for neutrons versus that of lead for shielding X-rays). Remote operation/delivery of the californium sources to the application site aids in this respect. A large number of such applications have been reported (Castro *et al.*, 1973; Poda and Hall, 1975; Zech *et al.*, 1976a,b; Maruyama *et al.*, 1978, 1980, 1991; Belenkll *et al.*, 1991; Yanch *et al.*, 1993; Patchell *et al.*, 1997; Knapp *et al.*, 1999; Rivard, 1999a,b, 2000a–c; Rivard *et al.*, 1999, 2002, 2004; Wanwilairat *et al.*, 2000; Tacev *et al.*, 2003a,b, 2004a,b).

Studies involving the injection of ^{252}Cf into beagles (Lloyd *et al.*, 1972a,b, 1976; Taylor *et al.*, 1972) and into swine (Mahony *et al.*, 1973; Beamer *et al.*, 1974) have also been reported. Investigations involving mouse mammary-carcinoma and bone were also reported (Fu and Phillips, 1973).

Several biological studies have used ^{252}Cf to examine the effects of neutron radiation. Work on DNA (Tacev *et al.*, 1998; Florjan *et al.*, 1999) has been done, as well as work on its bioefficiency (Cebulska-Wasilewska *et al.*, 1999). The biokinetics of it in marine isopods (Carvalho and Fowler, 1985) and the survival of human cells under irradiation (Todd *et al.*, 1984) have also been published. A solvent extraction/liquid scintillation counting method for determining ^{252}Cf in biological samples has been discussed (Miglio, 1978).

There is an extensive list of reports and publications dealing with the applications. The reader is referred to these for more extensive information. One useful source in this regard is an ORNL Report (Osborne-Lee and Alexander, 1995). Other sources of information involve the use of ^{252}Cf: for cervical carcinoma treatment (a 12 year review by Tacev *et al.*, 2004a,b); a review of other clinical applications (Mignano and Rivard, 2004); and advances in neutron radiographic techniques (Berger, 2004). Dullmann *et al.* (2003) also discuss fission fragment sources using ^{252}Cf.

11.4 SEPARATION AND PURIFICATION

The choice of a separation and purification scheme for californium depends on the nature of its source, the particular isotopes of californium involved, the amount of material, the impurities present, as well as several other factors. In short, the best procedure needs to be customized to the particular situation at

hand. Usually, ion exchange is involved either as the main separation technique, or at least in some secondary capacity. Since californium in aqueous solutions is normally stable only in its tripositive state, oxidation–reduction cycles are not useful for separation. Due to the very similar chemical behavior of the tripositive transplutonium elements, as well as lanthanide ions of comparable ionic radii (i.e. Sm–Tb), the separation chemistry for californium employed must often rely on small differences in chemical behaviors for the different materials to be separated.

The separation procedure most suitable for californium isotopes generated in accelerators may not be the same as that used for californium produced in reactor targets. In some accelerator experiments, the desired californium isotopes generated may be physically separated via recoil mechanisms from the targets, which simplifies the separations and shortens the time required for the shorter-lived isotopes. The need for nuclear or radioactive purity, as opposed to chemical purity, will also affect the particular separation processes to be used. A considerable amount of information on californium chemistry was determined using tracer levels of californium, usually using ^{252}Cf isotope. The major purification schemes for californium at tracer levels have frequently involved ion-exchange techniques to separate californium from other transcurium elements.

For purposes of separation, the transplutonium elements can be placed into two groups: (1) americium and curium and (2) the group of the next several transcurium elements, which includes californium. The separation of californium from its neighbors, especially einsteinium, is therefore more difficult than separating it from americium/curium or from the lighter actinides. Separation of californium from berkelium is simplified by the ability to oxidize berkelium in an aqueous medium, which then permits the solvent extraction of Bk(IV) away from Cf(III).

A number of procedures have been used for the separation/purification of californium. One of the early ion-exchange methods involved the use of cation-exchange resin (Dowex 50) and ammonium citrate or ammonium lactate as eluants. A superior eluant, ammonium α-hydroxyisobutyrate (α-HIBA), was first used over 30 years ago (Choppin *et al.*, 1956), and this reagent is still in use today for the separation of californium from other actinides. Thompson *et al.*, (1954). A very useful group separation between the lanthanides and actinides can be accomplished using concentrated hydrochloric acid as an eluant for the transcurium elements sorbed on cation resin; the separation is improved by using an ethanol–hydrochloric acid mixture as an eluant (Street and Seaborg, 1950). Another method for separation elements from the two groups, especially with smaller quantities has been the use of TEVA™ columns (Horwitz *et al.*, 1992, 1993, 1995; Porter *et al.*, 1997). These resin columns are available commercially (Eichrom Industries) and employ thiocyanate and formic acid solutions. The greater complexing ability of the transplutonium elements is evident as they desorb ahead of the lanthanide elements when using these separation approaches. The separation of californium from its actinide neighbors, using

cation- or anion-exchange resins, or elution with either hydrochloric or ethanol–hydrochloric acid mixture, alone is not feasible.

Anion-exchange separation procedures using slightly acidic $LiNO_3$ or $Al(NO_3)_3$ solutions (Surls and Choppin, 1957; Adar *et al.*, 1963; Marcus *et al.*, 1963) or ethylenediaminetetraacetic acid (EDTA; Baybarz, 1966a,b) as eluants have also been reported. Several extraction procedures have been used, such as the extraction of trivalent actinides from concentrated LiCl or $LiNO_3$ (slightly acidic) solutions and the use of trilaurylamine or other trialkylamines (Baybarz *et al.*, 1963) or quaternary ammonium salts (Moore, 1964, 1966; Horwitz *et al.*, 1966). Extraction chromatography using quaternary ammonium salts or bis(2-ethylhexyl)phosphoric acid (HDEHP) as a stationary phase has also been employed (Gavrilov *et al.*, 1966; Horwitz *et al.*, 1967, 1969a,b). Inorganic ion exchangers such as zirconium phosphate materials have limited applications for californium separations due to their lower selectivity as compared to organic-type extractant materials.

Several summaries of separation procedures have been discussed and can be found in: Miller (1967), Keller (1971), Myasoedov *et al.* (1974), Bigelow (1974), Ishimori (1980), King *et al.* (1981), Collins *et al.* (1981), Benker *et al.* (1981), and Campbell (1981).

Most extraction procedures are useful for separating californium from americium/curium or from lighter actinides, but are limited for separating it from other transcurium elements. For example, HDEHP dissolved in an aromatic diluent has been used to separate Cf and Cm providing a separation factor of about 50, but it is not useful for californium–einsteinium separations. Efforts continue to find new and better extractants with the aim of improving separation factors and selectivity. It is unlikely that a specific extractant for californium alone will be developed but new materials may provide improved separation factors over methods presently used or known. Reviews that discuss californium extraction chemistry are available (Bigelow *et al.*, 1980, 1981; Myasoedov *et al.*, 1980; Shoun and McDowell, 1980).

One application of HDEHP on an inert support material, such as porous glass (i.e. Bioglass), is worth noting. An excellent separation between curium and californium can be achieved using this approach, which is important process for recovering $^{248}Cm/^{246}Cm$ from their $^{252}Cf/^{250}Cf$ parents. In this procedure, the actinides are loaded onto a column with the agent, and then eluted with 0.1 M HNO_3. As the californium is retained more strongly due to complexation, the curium is eluted first.

It is also useful to note that berkelium and californium can be readily separated by solvent extraction of Bk(IV) away from Cf(III). This separation is important since isotopically pure ^{249}Cf is obtained from the beta decay of ^{249}Bk. The berkelium can be readily oxidized to Bk(IV) in aqueous solution with a strong oxidant (i.e. bromate ion) in nitric acid solution.

Since the majority of californium is produced in nuclear reactors, or obtained as a by-product from reactor-produced ^{249}Bk, it is appropriate to discuss briefly

a flowsheet for the separation techniques employed in recovering californium for reactor targets. If uranium or plutonium is present as the main target material, then these elements must also be separated from the transplutonium element group (containing the californium) in addition to fission products (lanthanide elements, transition metals, etc.) and other products (aluminum from target assemblies, etc.). If americium and curium, or pure curium, is the main starting material, then only small amounts (if any) of the lighter actinides may be present, which simplifies the situation.

The general separation scheme, Scheme A in Fig. 11.1, is for separating and purifying californium from the HFIR products containing uranium and plutonium at the Oak Ridge National Laboratory. Reports on different aspects of these purification processes are available (Baybarz *et al.*, 1973; King *et al.*, 1981; Bigelow *et al.*, 1981). The procedure begins with alkali dissolution of the aluminum target holders used for the reactor. This leaves the insoluble actinide oxides, which are subsequently dissolved in hydrochloric or nitric acid to generate a solution of the elements to be separated.

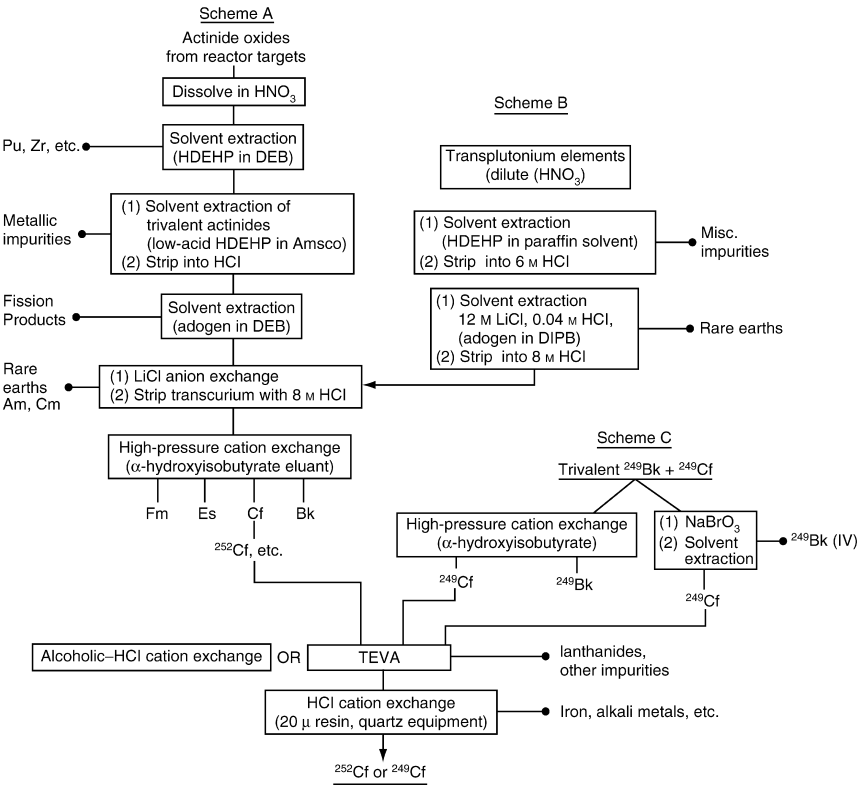

Fig. 11.1 *Separation and purification scheme for californium.*

Solvent extraction (HDEHP in an aromatic diluent as diethylbenzene) (DEB) removes plutonium and zirconium from the system. Scheme B is given for the situation where only the transplutonium elements are present (i.e. starting with americium and curium targets rather than plutonium).

In both cases, the transplutonium elements are then extracted with HDEHP in an aliphatic solvent, and a subsequent amine extraction (adogen) of these actinides removes them from most of the fission products. At this point, the product contains the transplutonium elements and any lanthanides present (fission products). A LiCl anion-exchange process partitions the transcurium elements from americium, curium, and the lanthanides, leaving the transcurium elements as a separate fraction. Scheme B in the figure considers only mixtures of the transplutonium elements.

The transcurium elements (Bk, Cf, Es, and some Fm) are then separated on high-pressure cation-exchange columns. Using a buffered α-hydroxyisobutyric acid solution as an eluant, californium is obtained as a separate fraction using a high-pressure ion-exchange process (very small resin particles, elevated temperature, at 80°C). The subsequent treatment of the different fractions obtained from this process depends on several factors, which include the final use of the material. The purification requirements for the californium isotopes produced directly in the reactor are based on whether Es or Cm daughters will be recovered, or the medical/industrial uses of the californium isotopes.

The californium fraction is further treated to remove residual lanthanide elements; this is especially important for nuclear studies where traces of radioactive lanthanide isotopes are detrimental, or for target materials, where unwanted reaction products may be generated from any impurities present. An ethanol–hydrochloric column is shown in Fig. 11.1, but it could also be replaced by a TEVA™ column. Horwitz *et al.*, (1992, 1993, 1995); Porter *et al.*, (1997).

Since most basic research studies involving milligram quantities of californium make use of ^{249}Cf obtained from the decay of ^{249}Bk, the purification requirements and processes for the californium produced in this manner is different, and shown in Scheme C in Fig. 11.1. Here, the material normally consists of only ^{249}Bk and ^{249}Cf isotopes plus any non-actinide impurities (i.e. accumulated from berkelium used in research studies). The objective is then to separate californium from its berkelium parent and any other impurities that may be present. To achieve the very high chemical purity desired for basic research work on californium, different things must be considered and the necessary separation processes must be addressed on an individual basis. The easiest situation is when the ^{249}Bk precursor for ^{249}Cf is already available in a highly pure state, and the separation of the californium involves only its separation from a relatively pure parent material. It this case, Scheme C in the figure could apply. For separating berkelium and californium, either a cation-exchange column (with α-hydroxyisobutyrate as the complexing agent) or the solvent extraction of berkelium as Bk(IV) away from trivalent californium (several different extracts schemes can be used). In the latter process, the

berkelium is first oxidized to Bk(IV) in solution with bromate ions, and the californium remains trivalent. An advantage with the ion-exchange process is that it avoids generating higher acid solutions and does not add bromide or bromate ions to the californium fraction.

In general, the purification of ^{249}Cf normally involves multiple pressurized cation-exchange columns with 0.25 M α-hydroxyisobutyric acid as an eluant (using solutions of variable pH from 3.8 to 4.2 at 80°C) to separate californium from other transplutonium elements, which also provides a general purification from other impurities than actinides. Then, a cation-exchange column with an ethanol–hydrochloric acid as an eluant, or a TEVA column, can remove lanthanide elements, alkaline earths, alkali metals, iron, nickel, etc. The columns, especially the final column and product receiver, are often constructed of acid-leached quartz. Special alpha detectors are used to determine the fractions that contain the californium. Using this process, a very pure californium chloride product is obtained, which can then be used for preparing compounds or the metal of californium for research.

Additional separation approaches have been reported in more recent publications. Firsova *et al.* (1998) have used bis(1-phenyl-3-methyl-4-acylpyrazolol-5-one) and its derivatives for solvent extraction, and other chromatographic separation methods (Firsova *et al.*, 1996) for separating berkelium and californium. Extractions using 4-benzoyl-2, 4-dichloro-5-methyl-2-phenyl-3H-pyrozol-3-thione, and tri-*n*-octylphosphine oxide (TOPO) have also been tested (Hannink *et al.*, 1992). Separation exclusion chromatography techniques have also been applied for separating californium from americium, curium, and lanthanides (Firsova *et al.*, 1990). The transplutonium elements have also been extracted from carbonate solutions using oligomers and alkylphenol derivatives (Karalova *et al.*, 1990), and extraction chromatography results with *DHDECMP* in nitric acid and characterization of DHDECMP/XAD-4 resins have been tested in the purification process (Kimura and Akatsu, 1991).

Extractions approaches for Cf(III) have also been done with aqueous pyrophosphates and lithium polyphosphate solutions with HDEHP (Chakravortty *et al.*, 1989). Extractions have also used HDEHP in nitric acid solutions (Kasimov and Skobelev, 1987). A modified ion-exchange procedure using α-hydroxyl-2-methyl butyrate was reported by Vobecky (1989). The separation of einsteinium from californium irradiation targets by ion exchange has been discussed by Elesin *et al.* (1986). The separation of californium using different salts of HDEHP was published by Dedov *et al.* (1986a,b). The extraction of magnesium and its influence on californium extraction via HDEHP for citric acid–magnesium nitrate systems has also been discussed (Kovantseva *et al.*, 1986). The effect of cations on exchange chromatography of curium and californium has been reported (Erin *et al.*, 1981) and the complexation of Cf(III) in perchlorates was also reported (Lebedev and Mazur, 1981). A simple separation approach for special applications has been suggested by Guseva *et al.* (1973), and a curium–californium extraction chromatography approach

was published by Aly and Abdelras (1972). The use of 8-hydroxyquinoline and 5,7-dichloro-8-hydroxyquinoline for extraction of californium was suggested by Feinauser and Keller (1969).

Three extraction studies involving californium were reported by Horwitz and coworkers. One study involved bis(2-ethyl)orthophosphoric acid (Horwitz *et al.*, 1969a); a second report was made on the same system (Horwitz *et al.*, 1969b); and the third effort was an extraction using high molecular weight quaternary amines in ammonium nitrate solutions (Horwitz *et al.*, 1967). The chelating and extraction of Cf(III) by acetylacetone and derivatives of it were also reported by Keller and Schreck (1969). Fused salt, molten metal processes have also been examined for separating californium (Knighton and Steunenberg, 1966; Mailen and Ferris, 1971). The analytical chemistry of the actinides has been reviewed by Myasoedov and Lebedev (1991), and several aspects of separation chemistry are also discussed in this work.

In principle, an alternative procedure for the separation of californium in special circumstances may be to reduce a mixture of actinide oxides with thorium metal under vacuum, and distill away the more volatile californium metal and then condense it on a suitable receiver (Haire, 1982). The separation of californium oxide from curium oxide using a vacuum sublimation procedure was also suggested (Aleksandrov *et al.*, 1972).

11.5 ELECTRONIC PROPERTIES AND STRUCTURE

A considerable amount of spectroscopic data has been obtained for californium and a number of theoretical calculations have been made concerning its energy levels. The californium neutral atom's ground state is assigned as $5f^{10}7s^2$ ($^5I_8$) and the Cf^+ ground state as $5f^{10}7s$ ($^6I_{17/2}$) (Worden and Conway, 1970; Martin *et al.*, 1974; Blaise and Wyart, 1992; for further details see Chapter 16). The ionization energy for the neutral californium atom has been calculated from spectroscopic data and were found to be 6.298 eV or 50800 (200) cm^{-1} (Sugar, 1973), respectively, but it now has been determined experimentally and found to be 6.2817(2) eV or 50665(200) cm^{-1}, respectively (Erdmann *et al.*, 1996, 1998) using resonance ionization mass spectrometry. Some of the lowest energy levels and the representative configurations are given in Tables 11.3 and 11.4, and experimental F^k(ff) and Hartree–Fock values are listed in Table 11.5. These values were determined using the ^{249}Cf isotope. Ionova *et al.* (1977) have also discussed the electronic levels of californium.

From limited absorption and self-luminescence spectra for californium, an early partial energy-level scheme was published for the $5f^9$ configuration (Conway *et al.*, 1962a,b). Predictions of the energy-level structure for Cf(III) appeared in 1964 (Fields *et al.*, 1964), and work on the triply ionized form of californium has also been published (Carnall *et al.*, 1973; Varga *et al.*, 1973a,b).

Table 11.3 *Lowest californium electronic levels for configurations listed.*

Species	*Configuration*	*Parity term*	*Level* (cm^{-1})	G_{obs}	*Hfs* (10^{-3} cm^{-1})
^{249}Cf(II)	$5f^{10}6s$	E $^6I_{17/2}$	0.00	1.28	
^{249}Cf(II)	$5f^{10}6d$	E $J = 15/2$	19 359.06		
^{249}Cf(II)	$5f^{9}6d7s$	O $J = 19/2$	24 213.34	1.27	
^{249}Cf(II)	$5f^{10}7p$	O $J = 15/2$	26 858.90	1.26	
^{249}Cf(I)	$5f^{10}7s^2$	E $^5I_8$	0.000	1.213	0
^{249}Cf(I)	$5f^{9}6d7s^2$	O $J = 8$	16 909.355	1.301	–40
^{249}Cf(I)	$5f^{10}7s7p$	O $J = 8$	17 459.210	1.277	–140
^{249}Cf(I)	$5f^{10}6d7s$	E $J = 8$	20 043.930		–210
^{249}Cf(I)	$5f^{9}7s^27p$	E $J = 7$	24 727.600		60
^{249}Cf(I)	$5f^{10}7s8s$	E $^7I_9$	32 983.180	1.300	–490
^{249}Cf(I)	$5f^{9}6d7s7p$	E $J = 8$	33 952.135		–200
^{249}Cf(I)	$5f^{10}7s8p$	O $J = 8$	38 225.945		–410
^{249}Cf(I)	5f107s7d	E $J = 8$	39 091.175	1.245	
^{249}Cf(I)	$5f^{9}7s^28s$	O $J = 8$	45 183.155		–150

Source: Chapter 16 and references therein.

Table 11.4 *Lowest electronic levels for neutral californium configurations.*

Configuration	*Level* (cm^{-1})
$5f^{9}6d7s^2$	16 909
$5f^{9}6d^27s$	31 500
$5f^{9}6s^27p$	24 728
$5f^{9}6d7s7p$	33 952
$5f^{10}7s^2$	0
$5f^{10}6d7s$	20 044
$5f^{10}6d^2$	50 000
$5f^{10}7s7p$	17 459

Source: Chapter 16 and references therein.

Table 11.5 *Selected experimental values of* F^k(ff), *Hartree–Fock values and* F^k/F^2 *ratios for californium.*

Configuration	*Element*	*Parameter* (r)	*Exp.*	*Hartree–Fock*	F^k/F^2 (exp.)	F^k/F^2 (calc.)	*Exp./H.F.*	*H.F.-exp.*
$5f^{10}7s^2$	Cf(I)	F^2	57 870	84 799	1.000	1.000	0.682	26 929
$5f^{10}7s^2$	Cf(I)	F^4	45 052	55 085	0.779	0.650	0.818	10 033
$5f^{10}7s^2$	Cf(I)	F^6	31 873	40 345	0.551	0.476	0.790	8472

Source: Chapter 16 and references therein.

Blaise and Wyart (1992) and Wyart *et al.* (2005) have more recently reported a comprehensive list of electron energy levels for californium, which are recommended values. Additional information is given in Chapter 15.

Absorption spectra of Cf(III) are mainly characteristic of f–f transitions (Laporte forbidden) within the $5f^{10}$ configuration. Spectra of Cf(III) in $DClO_4$–D_2O have been used to make term assignments and energy levels for californium (Varga *et al.*, 1973a). The electronic spectrum and estimated energies of the electronic configurations of Cf(IV) has also been predicted from spin–orbit coupling (Varga *et al.*, 1973b). Estimated energies of the electronic configurations for californium had appeared earlier (Brewer, 1971a,b), where values were given for singly, doubly, and triply charged californium ions.

A detailed theoretical interpretation of solid-state absorption spectra of $CfCl_3$ has also been published (Carnall *et al.*, 1973), and energy level assignments made for several californium absorption bands. The observed and calculated free-ion energy levels for Cf(III) have also been compared to the lower energy levels in californium's analog, Dy(III) (Carnall *et al.*, 1973). An attempt to correlate the electronic excitation energies for 4f and 5f elements suggested that the $f^n s^2 \rightarrow f^{n-1} d s^2$ excitation values for californium compare best with the lighter lanthanide elements (Mikheev *et al.*, 1979). A valence-band approach for high-coordination bonding in the californium compounds has also been suggested by Carter (1979); this approach implies d- and f-orbital splitting into bonding hybrids. From quantum chemistry considerations, the monopositive ion of californium should be more stable than monopositive lanthanide or lighter actinide ion, based on its lower calculated excitation energy. Calculations have also shown that, from berkelium to nobelium, the excitation (promotion) energies for the $f^n s^2 \rightarrow f^{n-1} d s^2$ configuration, which is taken as a measure of the stability of the divalent state, increases with the atomic number up to element 103 (Spitsyn, 1977). Thus, Cf(II) should be more stable than Bk(II) but less stable than Es(II). These promotion energies are discussed throughout this chapter and play an important role in the californium chemistry.

Predictions for excitation energies for $7s^2 \rightarrow 7s7p$ and $7s^2 6d$ levels have also been given (Carnall *et al.*, 1977). Experimental data were obtained and crystal field calculations have been made for Cf(III) in different crystal hosts (Carnall *et al.*, 1977). Relativistic Hartree–Fock–Slater calculations have yielded neutral-atom electron binding energies for californium (Haung *et al.*, 1976), and relativistic relaxed-orbital calculations of L-shell Coster–Kronig transition energies have been reported for californium (Chen *et al.*, 1977). An interpolation scheme for cohesive energies provides binding energies for electrons, which can correlate and compare the divalent nature of transplutonium elements; this approach has predicted a divalent metallic state for einsteinium rather than for californium (Johansson and Rosengren, 1975a,b). The divalent metallic state for einsteinium has been verified (see Chapter 12) but this state is less likely for bulk forms of californium (see Section 11.6).

Photoelectron spectrometry of californium has been performed on Cf_2O_3 and Cf_7O_{12}, using an MgKα excitation source (Krause *et al.*, 1988). Values for the

4f doublet ($4f_{5/2}$ and $4f_{7/2}$) of californium were determined in that work. The spin–orbit splitting for californium was estimated to be 17.5 eV.

The energy spectrum of electrons in ^{252}Cf has been given (Rykov and Yudin, 1998) and the energy levels of ^{249}Cf, both neutral Cf(I) and singly ionized Cf(Ii), are also available (Blaise and Wyart, 1992; Conway *et al.*, 1995; and Chapter 16). Ionova *et al.* (1989a,b) has reported computational results for the electronic structure of californium. Also see subsequent sections of this chapter regarding discussions of the absorption spectra of Cf(II) in solids and Cf(III) in solution, and californium's electronic behavior in the gas-phase studies (see Section 11.9). The nuclear magnetic moment of ^{249}Cf has been determined and found to be –0.28 nuclear magnetons, and its nuclear spin is accepted as being 9/2 (see Ahmad, Appendix I).

11.5.1 Emission spectra

The first emission spectrum for californium was reported by Conway *et al.* (1962a,b) and obtained via the copper-spark method. The majority of subsequent work on californium has been carried out using electrodeless lamps, where multi-microgram amounts of material are sealed in quartz envelopes and the californium is excited by external radiation. Emission spectra of californium have been observed from 2400 to 2.5 μm, with approximately 25000 lines having been recorded and accurately measured (Conway, 1976; Conway *et al.*, 1977). Fourier transform analyses of data obtained from californium lamps have been carried out with the goal of resolving the hyperfine structure (Blaise and Wyart, 1992; Wyart *et al.*, 2005). The $5f^{10}7s^2$ ground state, the $5f^{10}7s8s$, and $5f^{9}6d7s^2$ configurations have been established from californium spectra (Warden *et al.*, 1970; Conway, 1976; Conway *et al.*, 1977; for further details see Chapter 16).

11.5.2 X-ray emission spectroscopy

The characteristic X-rays resulting from atomic readjustment to inner shell vacancies provide a very useful means for identification of an element (see Dittner and Bemis, 1972). Several X-ray emissions for heavy elements and their bonding energies are known, and such data have been tabulated for californium (Carlson and Nestor, 1977).

Similar calculations using nonrelativistic Hartree–Slater wave functions (Manson and Kennedy, 1974) and relativistic Hartree–Slater theory (Scofield, 1974) have also provided data for californium. The atomic form factors, the incoherent scattering functions (Hubbell *et al.*, 1975), and a total Compton profile have been tabulated for californium (Biggs *et al.*, 1975).

Systematic X-ray photoelectron spectroscopy (XPS) studies have also been carried out on transplutonium oxides through californium, providing experimental binding energies for their electrons, which can be compared to the

calculated energies (Veal *et al.*, 1977). An interpolation scheme has also been reported for determining the binding energies of some lanthanides and actinides, including californium (Johansson and Rosengren, 1975a). The nature of the 5f electrons in the actinide series including californium has also been discussed (Johansson and Rosengren, 1975b).

11.6 THE METALLIC STATE

11.6.1 Preparation

The first attempt to prepare californium metal was made in the late 1960s (Fujita and Cunningham, 1969). Subsequently, several additional attempts have been made to prepare and study this metal. The relatively high volatility of californium metal has made its preparation and study on the microscale more difficult than the first three transplutonium metals. The possibility that the metal may exist in two different metallic valence states has also made it an interesting candidate for study, but it has also complicated the full understanding of californium's metallic state. The potential for californium to exist in two metallic valence states arises due to its f $\rightarrow$ d electron promotion or excitation energy (see subsequent discussion).

Two preparative approaches have been utilized for californium metal. The first approach utilizes the reduction of the trifluoride with lithium metal at elevated temperatures; the excess reductant and lithium fluoride are removed by vacuum distillation. The second preparative method employs thorium or lanthanum metal to reduce one of the californium oxides, permitting the distillation and subsequent condensation of the metal (Haire, 1982) and leaving the thorium or lanthanide metal and their oxides as residues. With thorium metal, the reaction is a solid–solid reaction and thorium has a lower vapor pressure, which should reduce the presence of the reductant in the vaporized product. With lanthanum, one encounters a liquid–solid reaction, as the lanthanum melts at 920°C; it also has a higher vapor pressure than thorium at high temperatures. The latter property must be considered to avoid incorporating lanthanum into the distilled californium product.

With the halide reduction process, where californium is to be retained as a solid residue, the volatility of californium is greater than that of lithium fluoride. This makes it difficult to volatilize the lithium fluoride completely from the californium product without simultaneously volatilizing away significant amounts of californium. In the oxide reduction procedure, the distillation of microgram quantities of metal yields thin films that are difficult to remove from the collection substrate. Also, a very good vacuum (free of residual materials such as hydrogen, oxygen, water or oil vapor, etc.) is required to avoid the formation of undesired compounds during the distillation of the reactive metal. With multi-milligram quantities, the distillation procedure is the best preparative route. The limited availability of the ^{249}Cf isotope and the radiation fields

encountered with this isotope do limit the amount of metal that can be prepared in an unshielded gloved box to 10–20 mg. There is little information about the preparation of ^{252}Cf metal using these procedures, and it is likely little if any has been made by this route.

Some work has been done on preparing californium–palladium alloys via hydrogen reduction of oxide–palladium metal mixtures in conjunction with medical applications of this isotope (Haire and Sato, 1998; Rivard *et al.*, 1999). The latter products are not pure alloys but sufficient for pressing or making extruded sources if the californium content is kept below 20 at%. The malleability of the products is found to decrease with higher californium contents. The reduction in this procedure is driven by the stability of actinide–noble metal alloys. Radchenko *et al.* (1986b) have discussed the formation of $CfPt_5$ on platinum surfaces.

The preparation of pure ^{249}Cf metal to date has been in the 2–10 mg range, with the largest known amount prepared at one time being about 10 mg (Haire, 1978, 1980, 1982). A picture of a 10 mg ^{249}Cf product is shown in Fig. 11.2, where it is compared to the head of a common safety pin. A more detailed account of the preparation of californium metal is available (Haire, 1982).

The limited quantities of californium metal have placed restrictions on the amount of analytical data that can be obtained for products; normally it is not possible to analyze for hydrogen, nitrogen, and oxygen contents. The quality of the metal has then been ascertained mainly by diffraction analysis, total metal impurities by mass spectrometry, its physical properties and appearance and its behavior (such as the rate and extent of dissolution for enthalpy-of-solution

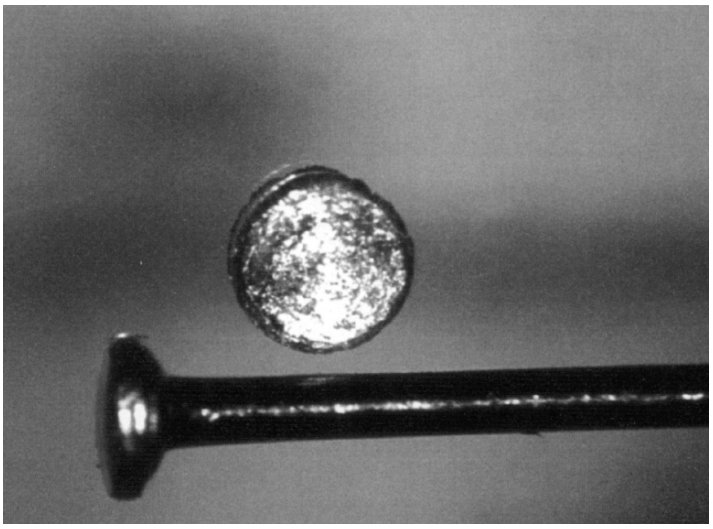

Fig. 11.2 *Ten milligram disc of californium compared to a straight pin.*

measurements) in experiments performed with the metal. Ideally, a larger quantity of metal would be prepared, characterized, and then used for a number of scientific measurements or experiments. But with californium (and some of the other transcurium metals), the preparation of the metal often becomes an integral part of a subsequent study, and either the major portion or the entire preparation is needed and often consumed in the study at hand (i.e. dissolved in acid in determining the enthalpy-of-solution of the metal) in an experiment.

11.6.2 Physical properties

There have been several different reports regarding the crystal data for californium over the years, and these are summarized in Table 11.6. Based on extrapolations from trivalent americium, curium, and berkelium metals, a double hexagonal close-packed structure with parameters on the order of $a_0 = 3.4$ Å and $c_0 = 11.0$ Å, and a face-centered cubic (fcc) high-temperature phase with $a_0 \sim 4.8$ Å would be expected for trivalent californium metal.

In earlier work, a face-centered structure with a parameter of 5.40 Å was reported, which was from a product obtained by the lithium reduction of its fluoride (Cunningham and Parsons, 1970). This is a difficult technique for preparing californium metal (see Section 11.6.1) and this work also involved very small quantities of californium. A potential explanation for this reported parameter is that it represents a poorly crystallized sesquioxide (body-centered cubic (bcc)), lattice parameter of 10.831 Å (see Section 11.7.4), which with the absence of weak diffraction lines in a diffraction pattern of marginal quality may be interpreted as arising from a face-centered material of 5.42 Å (10.831/2).

Subsequently, cubic and hexagonal structures were observed by Haire and Baybarz (1973a,b) in very thin films (<2.5 Å) of californium distilled onto electron microscopy grids and then analyzed by electron diffraction. These data suggested a metallic radius of slightly greater than 2.0 Å, suggesting californium may be a divalent metal. An extrapolation by Zachariasen (1975) also suggested that californium metal would be a cubic lattice and a larger radius than the trivalent metal. Subsequently, very small quantities of apparent metal were also analyzed by X-ray diffraction (Noé and Peterson, 1976) that duplicated the 5.747 Å cubic structure reported by Haire and Baybarz (1973a,b, 1974). Thus, these early data thus suggested californium may be a divalent metal.

With larger quantities of californium, its crystallographic data (Haire and Asprey, 1976; Noé and Peterson, 1976) independently showed that the metal was trivalent with a room temperature double hexagonal close-packed parameters of $a_0 = 3.384$ Å and $c_0 = 11.040$ Å, which suggests an atomic radius of 1.69 Å, which is in line with radii reported for americium, curium, and berkelium metals. The crystal forms of californium metal were also determined by Radchenko *et al.* (1986a) and Seleznev *et al.* (1989) for 1.5 mg of californium.

Table 11.6 *Crystallographic data reported for californium metal.*

Crystal System	*Lattice Parameters*		*Atomic Volume* (Å)^3	*Crystal Density* (g cm^{-3})	*Metallic Radius* (Å)	*References*
	a_0 (Å)	c_0 (Å)				
fcc	5.40	–	39.4	10.5	1.91	Cunningham and Parsons (1970)
fcc	5.743	–	47.4	8.72	2.03	Haire and Baybarz (1970)
hcp	3.988	6.887	47.4	8.72	2.07	Haire and Baybarz (1970)
dhcp	4.002	12.804	44.4	9.31	1.99	Haire and Asprey (1976)
dhcp	3.384	11.040	27.4	15.1	1.69	Haire and Asprey (1976)
fcc	4.94	–	30.1	13.7	1.75	Noé and Peterson (1976)
fcc	5.75	–	47.4	8.72	2.03	Noé and Peterson (1976)
dhcp	3.39	11.01	27.4	15.1	1.69	Noé and Peterson (1976)
fcc	4.78	–	27.4	15.1	1.69	Haire *et al.* (1986)
dhcp	3.380	11.025	27.3	15.0	1.69	Radchenko *et al.* (1986); Seleznyov *et al.* (1989)
fcc	4.994	–	30.1	13.7	1.75	Stevenson (1973)
CfN, fcc	4.94	–	30.1	13.7	–	Haire *et al.* (1986)

Recommended values for californium are: (a) dhcp 3.384(3) Å and 11.040(10) Å and (b) fcc = 4.78(1) Å. Both yield a metallic radius of 1.69 Å, a volume of 27.4 Å and a density of 15.1 g cm^{-3}.

From these efforts double hexagonal lattice parameters of: $a = 3.380(2)$ Å and $c = 11.025(2)$ Å were reported.

A fcc-form (high-temperature form and also a high-pressure form at modest pressures) have been observed for californium. This form of californium was reported to have a fcc structure with a parameter of 4.94 Å (Noé and Peterson, 1976), but this parameter gives an atomic radius for californium that is too large. It agrees better with the parameter for californium nitride ($a_0 = 4.94$ Å; Haire *et al.*, 1986), with an oxynitride (oxygen and nitrogen exchanged in the crystal sites), or could have represented an expanded lattice that was 'quenched in' at elevated temperatures. The proper lattice parameter (4.78 Å) for this cubic form of californium at room temperature and at a pressure 1 atm was observed both with pressure-quenched samples (Haire *et al.*, 1986) and also from larger quantities of californium obtained as foils prepared by distillation (Haire, 1978). The atomic radius derived from this smaller cubic parameter agrees well with that obtained from the ambient temperature, double hexagonal parameters. Pressure-quenched cubic parameters for curium, berkelium, and californium metals have also been found to give identical atomic radii and atomic volumes as obtained from their room temperature, double hexagonal forms, while earlier work with samples quenched from elevated temperatures also resulted in larger (expanded) parameters for curium and berkelium metals (Haire *et al.*, 1986). The preparation and lattice parameters for the californium metal have also been reported by Radchenko *et al.* (1986a) and by Seleznev *et al.* (1989). An alloy of californium and platinum ($CfPt_5$) was obtained when thin films of californium were vapor deposited on platinum surfaces. The products were analyzed as formed on the surfaces (Radchenko *et al.*, 1986b).

The transition temperature for the hexagonal to cubic phase of californium is not well-established, and only limited efforts have been made to determine it (Noé and Peterson, 1976). It is likely to be in the region of 600–800°C. The dhcp to fcc structural transition occurs under pressure at about 16 GPa (Peterson *et al.*, 1983; Benedict *et al.*, 1984). This cubic phase formed under pressure can be retained at atmospheric pressure and 25°C (Haire *et al.*, 1986), and provides a lattice parameter of 4.78 Å. This transition from a hexagonal to cubic state is a low-energy transition in the transplutonium metals. The different crystal data for californium that have been reported are summarized in Table 11.6.

Californium lies very close to the 'border' between a divalent and trivalent metal due to its f- to d-electron promotion energy (see Fig. 12.4 and discussion in Chapter 12). It is possible that in very thin films californium metal may retain a divalent state (i.e. a metastable state) under the conditions of preparation. A similar situation has been observed previously with very thin films of samarium metal (Allen *et al.*, 1978), where the surface atoms of samarium metal in these films remain divalent, although atoms in bulk metal are normally trivalent. Samarium also exhibits a unique rhombohedral crystal form in bulk form. The next element after samarium in the lanthanide series is europium, and it is a divalent metal. Thus, the situation with the californium structures may be

similar to the samarium case, as the next element after californium, einsteinium, is also a divalent metal (see Chapter 12). However, californium metal is correctly identified as being a trivalent metal in bulk forms, but does display aspects of this 'closeness' to being divalent (see discussion of its enthalpy of sublimation of the metal in section 11.6). The best lattice parameters for both the dhcp and fcc crystal forms of californium metal are those that give an atomic radius of about 1.69 Å.

There has been only one reported value for the melting point of californium metal, which is (900 ± 30)°C (Haire and Baybarz, 1973a,b). This value was obtained by observing the 'puddling' of metal particles in an electron microscope with thin films of californium metal. This melting point is lower than those reported for americium, curium, and berkelium metals, but is close to the melting point of einsteinium metal (Haire and Baybarz, 1979). Californium's lower melting point is also in accord with some of its physical properties, and the trend toward divalency (which would yield lower melting points) in going across the actinide series. The properties for californium and the other transplutonium metals are compared in an ASM report by Haire (1990).

Californium metal has been examined under high pressure using X-ray diffraction techniques. Early high-pressure studies showed that its dhcp form transformed to a fcc form at 16 GPa (Peterson *et al.*, 1983). A bulk modulus of (50 ± 5) GPa was derived from those data, which is similar to moduli for many of the trivalent lanthanide metals but much lower than those of the earlier actinides with itinerant 5f electrons (i.e. Pa–Pu). Subsequent work with californium metal under higher pressures up to 48 GPa showed a transition of the fcc structure to a new lower symmetry structure (reported to be orthorhombic, alpha-uranium structure; Benedict *et al.*, 1984). Formation of this structure was interpreted as reflecting the delocalization of californium's 5f electrons and their participation in the metal's bonding. Very recently californium metal has been reexamined under much higher pressures and with the use of synchrotron radiation (Haire *et al.*, 2004). These studies have provided much higher quality data, which have shown the occurrence of three structural transitions, and confirmed that the 5f electrons of californium do indeed delocalized and become involved in bonding at these higher pressures. But the new californium structures observed at higher pressures (after the fcc phase), are very similar to those noted in the behavior of americium metal under pressure (Heathman *et al.*, 2000). Work on the structures of californium observed at pressures above 40 GPa are being finalized and details will be published later. However, in this work on californium, it was very clear that when progressing across the actinide series, it takes higher and higher pressures to force the delocalization of the 5f electrons, as they become further withdrawn from the Fermi surface due to the greater nuclear charges (Haire *et al.*, 2004). Thus, californium requires much higher pressures to force the delocalization of its 5f electrons than do the first three transplutonium metals.

The vapor pressure and enthalpy of sublimation of californium metal have been measured using the Knudsen effusion technique (Ward *et al.*, 1979). The vaporization of californium metal, starting at 298 K with the dhcp crystal form, and over the temperature range of 733–973 K, is described by the following equation:

$$\log p(\text{atm}) = (5.675 \pm 0.0319) - (9895 \pm 34)\ \text{T}^{-1}$$

The $\Delta_{\text{sub}}H^{\text{o}}_{298.15\text{ K}}$ was calculated to be (196.23 ± 1.26) kJ mol^{-1}, and $\Delta_{\text{sub}}S^{\text{o}}_{298.15\text{ K}}$ was derived to be 120.6 J K^{-1} mol^{-1}. The estimated boiling point for the metal is 1745 K. Nugent *et al.* (1973b) had estimated the enthalpy of sublimation of californium to be 163 kJ mol^{-1} and David *et al.* (1976a,b) had predicted a value of 197 kJ mol^{-1}. By comparison, the vapor pressure behavior of californium is intermediate between that of samarium metal (a trivalent metal) and europium metal (a divalent metal), which is discussed by Ward *et al.* (1979).

The enthalpy of sublimation is an important bulk property of an element, and can be a measure of the metal's cohesive energy. From the magnitude of the enthalpy, the number of bonding electrons can be inferred from it, and this allows systematic comparisons to be made between the two f-electron elements series.

The experimental sublimation data for californium (Ward *et al.*, 1979) are in accord with it being a trivalent metal up to 1026 K, although it is one of the most volatile (has one of the lowest sublimation enthalpies) of the trivalent actinide metals; its high volatility precludes vaporization studies of it above 1073 K. Evidence for CfO was not obtained in this mass spectrometry study, and this finding is in accord with subsequent studies on californium oxides (Haire, 1994; see Section 11.7.3).

Thermochromatographic studies (involving sublimation and adsorption) of californium, einsteinium, and fermium using different metal columns (titanium, tantalum, etc.) were performed to yield enthalpies of adsorption for these actinides. Attempts have been made to relate these adsorption enthalpies to enthalpies of sublimation, but there is a significant difference in the actual numerical values, as they measure different properties. A comparison between the enthalpies of sublimation for the americium through californium trivalent actinide metals and their enthalpies of absorption is striking, and efforts have been made to compare them (Haire, 1997). Fig. 11.3 shows plots of these values for selected actinides. The enthalpies of sublimation range irregularly for the first four transplutonium elements with the values reflecting in part differences in 5f to 6d promotion energies – smaller promotion energies link with larger, more positive enthalpies of sublimation.

The enthalpy of sublimation for californium is 196 kJ mol^{-1} (Ward *et al.*, 1979, 1986). In contrast, the enthalpy of adsorption for californium ranges from –302 to –310 kJ mol^{-1} (Hübener, 1980; Hübener *et al.*, 1994). The exact value depends on the particular metal substrate used for its adsorption. A comparison between these enthalpies of vaporization and adsorption is shown

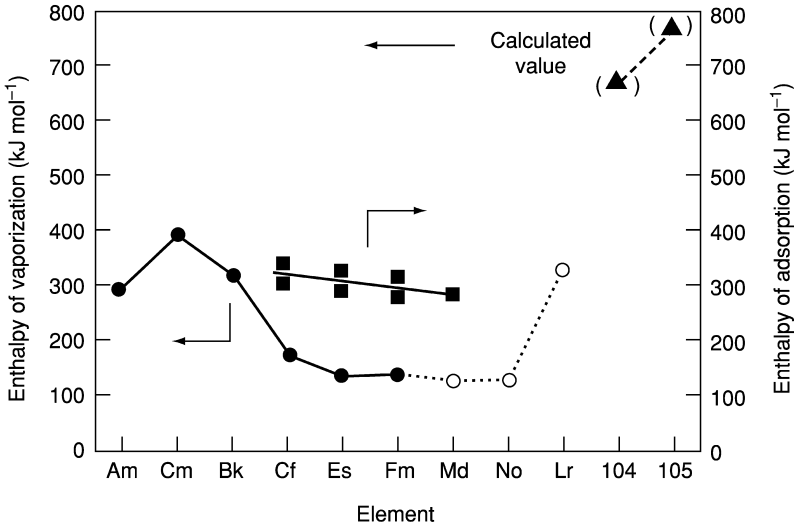

Fig. 11.3 *Vaporization and adsorption enthalpies for selected actinides.*

in Fig. 11.3 (Haire, 1997) for californium through mendelevium elements, and using some extrapolated values for sublimation of the two transfermium elements. The sublimation values for element 104 (Johnson and Fricke, 1991) and 105 (Pershina *et al.*, 1994) are calculated values, and are included here for comparison purposes. Their larger more positive enthalpies of sublimation reflect that greater bonding (i.e. greater than three electrons) is present in these latter two elements. One advantage of the adsorption technique versus the sublimation method is the former can be used for smaller quantities of materials (tracer levels).

It can be seen from Fig. 11.3 that the sublimation enthalpy for californium and the adsorption enthalpy are close to the comparable enthalpies for divalent einsteinium and fermium; the sublimation enthalpy for californium is considerably smaller (less positive, lower energy required) than values for americium, curium, and berkelium, which are trivalent metals.

Initially, the adsorption behavior (i.e. temperature of adsorption) of californium with different metal columns was taken as an indication of a metallic divalency (Hübener and Zvara, 1982) but more recent interpretations of adsorption enthalpies and the relative behavior of californium through nobelium elements suggests that californium is trivalent but close to the divalent–trivalent border Eichler *et al.* (1997). Using adsorption enthalpies, fermium is considered unquestionably as being divalent (Taut *et al.*, 1997), while californium is trivalent an atomic from source for actinide elements has been discussed (Eichler *et al.* 1997.)

The initial enthalpy of solution of californium metal (dhcp crystal form, trivalent metal) in 1.0 M HCl at 298 K is $-(617 \pm 11)$ kJ mol^{-1} (Raschella *et al.*, 1982).

This value was corrected in a subsequent determination of this important thermodynamic quantity using larger samples of well-characterized metal to yield an enthalpy of solution value of $-(576.1 \pm 3.1)$ kJ mol^{-1} for 1 M HCl (Fuger *et al.*, 1984; for further details see Chapter 19). This less-negative enthalpy value shows a trend among the transplutonium metals from americium through californium of less-negative enthalpies with increasing atomic numbers, and is in accord with an increasing trend toward metallic divalency in progressing across the series. This enthalpy of solution of the metal is important for providing the enthalpy of formation of the Cf(III) ion in solution and discussed in a subsequent section (see Section 11.8.3) on thermodynamic properties.

Several efforts have been made to obtain the magnetic susceptibility of californium metal. Magnetic information is valuable in ascertaining the metallic valence of metals and the bonding present. However, in the case of californium, such information is not useful and cannot differentiate between a divalent form (presumable a $5f^{10}$ state) that would have an effective moment of 10.22 μ_B, while the trivalent form (for an $5f^9$ state) would have an effective moment of 10.18 μ_B.

The first magnetic measurements were made by Fujita *et al.* (1976) using two samples believed to represent a fcc form of divalent californium metal from 22 to 298 K. Both samples followed a Curie–Weiss relationship, and the data produced an average moment of 9.75 μ_B. Subsequent magnetic measurements were made on well-characterized samples of the dhcp, trivalent form of californium from 4.2 to 350 K and in applied fields of up to 50 kG (Nave *et al.*, 1983, 1984). These data showed that californium exhibits at least two differing magnetic behaviors as a function of temperature. Below 51 K, the metal was either ferro- or ferrimagnetic; a distinction between the transition type could not be made owing to the inability to obtain a saturated moment of greater than 6.1 μ_B in the highest field of 50 kG. There was also evidence for antiferromagnetic behavior in the temperature range of 48–66 K. Additional magnetic studies of californium compounds (i.e. oxides and nitrides in particular) need to be done to rule out the possibility that their presence as impurities may be responsible for this latter behavior. Above 160 K, californium exhibits paramagnetic behavior. An average effective moment of (10.6 ± 0.2) μ_B was obtained for three different samples, whereas a fourth sample produced a moment of (9.7 ± 0.2) μ_B. Results from Nave *et al.* (1983) indicate that the magnetic behavior of californium is similar in some respects to that of its electronic homolog, dysprosium. Additional comments on magnetic behavior of californium and its compounds are given in Section 11.7.5 and in Table 11.11.

11.6.3 Chemical and mechanical properties

Californium is a fairly reactive metal, comparable to those of the lighter lanthanide metals but is less reactive than europium, which is considered as the most reactive lanthanide metal. This reactivity of europium is related to several factors but in part arises from it being a divalent metal. On standing to air or

when exposed to moisture at room temperature, small bulk pieces or foils of californium quickly form an oxide, but it is not a violent reaction. Moisture and temperature increase the rate of the reaction. One of the difficulties of preparing small quantities of californium metal is that it only takes small amounts of impurities to form reaction products with it. When the temperature is elevated, the reactivity of californium metal increases, and reactions occur readily with hydrogen, nitrogen, the chalcogen elements, etc. The silver colored, relatively soft californium metal quickly adopts a golden or bluish color on its surface when reacting with small amounts of other materials. Pure californium metal is easily cut with a 'razor' blade and is also malleable in its pure state.

When californium is sealed in evacuated quartz containers and when heated to 300°C, especially when it is a film on the quartz surface, the metal quickly deteriorates. Solid pieces of californium metal stored in quartz under vacuum and heated to moderate temperatures (i.e. 300°C) can vaporize sufficiently to form 'mirrors' on the quartz surface. Vaporization and reaction with the quartz worsens at higher temperatures. Products are usually oxides or silicates.

The metal reacts very rapidly with dry gaseous hydrogen halides and aqueous mineral acids to evolve hydrogen. In aqueous media, a Cf(III) solution is obtained, except with the case of hydrogen fluoride, where an insoluble californium trifluoride precipitate is formed.

Californium forms alloys when heated with the lanthanide metals but these products have not been well-characterized. When heated, it 'wets' tantalum, which usually limits the use of tantalum containers for high-temperature work with it. Tungsten containers are preferred, especially those made from single crystals, which prevents the metal from entering the grain boundaries of the containers.

11.6.4 Theoretical treatments

The chemistry of the actinide series can be complex and changes considerably when progressing across the actinide series. The development of a self-consistent model for these elements has had limited success in the past but more recent computational approaches have been more successful. However, even plutonium is still not completely understood, and total agreement on details of its fundamental science is not realized fully even after some 60 years of extensive studies. In comparison, far less effort has been done on californium, although its behavior is more lanthanide-like and has fewer complexities than plutonium, which has delocalized 5f electrons. However, the increased promotion energy for the 5f electrons of californium makes it close to being a divalent metal, and therefore its properties and behavior deviate somewhat from those of the americium through berkelium metals, as well as some of the trivalent lanthanide metals.

Efforts have been made to describe the overall fundamental aspects of these actinide metals, and be able to correlate them with other members of the periodic table (Brewer, 1971a,b; Nugent *et al.*, 1973a,b; Johansson and Rosengren, 1975a,b; Nugent, 1975; David *et al.*, 1976a,b, 1978; Samhoun and David, 1979;

Brooks *et al.*, 1984). These authors provide useful considerations for understanding the series in general and the changes that are observed when moving across it.

With respect to californium, the important questions often have to do with the role of its 5f electrons, their position with respect to the Fermi level, the narrowing of its 5f levels relative to earlier members of the series and the position of the 5f electrons with respect to the other outer electrons. The concept of promotion energy for the 5f electrons (f → d) is an important factor here. At 1 atm and room temperature, the 5f electrons in californium and its compounds are fully localized, much like the 4f electrons in the lanthanide series.

Several predictions for the properties of californium have been made with regard to its 5f electrons. One of the predictions was addressed by Brooks *et al.* (1984). It was accepted that californium was close to the divalent–trivalent metallic boundary. This pseudo-boundary considered that the crystal energy gained from acquiring three bonding electrons versus two in isolated atoms, had to be greater than the promotion energy needed for promoting a 5f electron to a d-state (to provide three bonding electrons). As with many of the other actinide metals, atomic californium in the vapor state has only two bonding electrons, but upon condensation, a third bonding electron can be acquired by promoting a 5f electron to a '6d' state. True divalency in the metallic state is believed to occur first in the higher members of the series, starting with einsteinium and fermium metals (see Chapters 12 and 13, and Johansson and Rosengren, 1975a,b; Brooks *et al.*, 1984). Additional discussions in this regard on the nature of californium can be found in the literature and in Section 11.9.

Correlation between crystal entropy and metallic radius, atomic weight, magnetic properties, and electronic structure have permitted an accurate calculation of unknown entropies for the actinide elements, including californium (Ward and Hill, 1976). This required a defined electronic structure to predict the entropy values. In addition, thermodynamics for the transplutonium metals have been summarized (Ward *et al.*, 1980; Ward, 1983). A pattern of superconductivity in f-band metals has also received attention over the years. It is unlikely that californium would show superconductivity, due to its large magnetic moment (see Section 11.6.2 on metal properties) and localized 5f electrons. Prospects for superconducting behavior in other actinides have been discussed (Smith, 1979, 1980; Baring and Smith, 2000). Of the first four transplutonium metals, ending with californium, only americium metal (Smith and Haire, 1978) is known to become superconducting at low temperature.

11.7 SOLID COMPOUNDS

11.7.1 General comments

A wide variety of californium compounds have been reported, even though only small amounts of this element (especially the ^{249}Cf isotope) have been available

an overview of Cf solid state chemistry is available (Haire & Gibson, 1989). Most of the expected halides and oxides for californium are established. It is accepted that californium exhibits three oxidation states, II, III, IV, in solids. There are reports that suggest the possibility of a Cf(V) state in solution (see Section 11.8); this state for californium is questionable. The II, III, and IV states are observed in different halides, and the III and IV states are found in oxides. The existence of stable, solid CfO is less probable and a minor product (see Section 11.9 on gas-phase behavior of californium). The trivalent state is the most prevalent state in both compounds and solutions, and the tetravalent state is only observed in the compounds, CfO_2, $BaCfO_3$, and CfF_4 and special solutions. The divalent state is found in the pure solids $CfCl_2$, $CfBr_2$, and CfI_2.

There are other compounds of californium where the oxidation state is less well-defined, such as in compounds with pnictogens, chalcogens, hydrides, etc. For example, in CfN, a formal state of Cf(III) can be assigned but it is not fully clear if this state is correct for a potentially more covalent material, as expected in its nitride. With hydrides, stoichiometries can range between a value of two (dihydride) and three (trihydride), in addition to intermediate hydrogen stoichiometries (i.e. CfH_{2+x} cubic materials and CfH_{3-y} hexagonal products). This suggests that the bonding in hydrides is other than purely ionic.

Ionic radii for each oxidation state of californium can be established from crystallographic data for these compounds, and some radii are provided in Table 11.7 for comparison. Many similarities in behavior between californium

Table 11.7 *Comparison of selected radii of californium and some lanthanides.*

Ion	*Compound*	*Radius* (Å)	*References*
Cf^{2+}	$CfBr_2$	1.08	Peterson and Baybarz (1972)
Eu^{2+}	$EuBr_2$	1.09	Peterson and Baybarz (1972)
Cf^{3+}	$CfCl_3$	0.932[a]	Burns *et al.* (1973)
Gd^{3+}	$GdCl_3$	0.938[a]	Burns *et al.* (1973)
Cf^{3+}	Cf_2O_3	0.942[b]	Baybarz *et al.* (1972)
Cf^{3+}	Cf_2O_3	0.95	Shannon (1976)
Gd^{3+}	Gd_2O_3	0.938[b]	Haire and Baybarz (1973a,b)
Eu^{3+}	Eu_2O_3	0.950[b]	Haire and Baybarz (1973a,b)
Cf^{4+}	CfO_2	0.859[c]	Baybarz *et al.* (1972)
Cf^{4+}	–	0.821[d]	Shannon (1976)
Ce^{4+}	CeO_2	0.898[c]	Haire and Eyring (1994)
Pr^{4+}	PrO_2	0.890[c]	Haire and Eyring (1994)
Tb^{4+}	TbO_2	0.817[c]	Haire and Eyring (1994)

[a] Derived from apical distances of hexagonal trichloride cells; six-coordinated metal atom.
[b] Derived from sesquioxide lattice parameters, using an oxygen radius of 1.46 Å and adding 0.08 Å for covalent M–O bond character; six-coordinate metal ion. (Lattice parameters for are taken from Haire and Eyring, 1994).
[c] Derived from dioxide lattice parameters, using an oxygen radius of 1.46 Å, correcting for covalent character of M–O bond (+0.10 Å) and for coordination number of 8 to 6 (−0.08 Å).
[d] Radius from plot of r^3 vs volume.

and other actinides and the lanthanides can be made based on ionic radii. It is important when making such comparisons that the radii were calculated in the same manner and perhaps even from the same compounds. In many cases, the transplutonium elements (i.e. californium specifically) with similar radii will likely form the same compounds, have the same structures, display similar phase behaviors, and may even have similar lattice parameters. This affords some predictability for properties of different californium compounds.

It must be recognized that a shift in radii is found between the lanthanide and actinide series, such that Cf(III) has a similar radius to Gd(III) rather than Dy(III), its apparent electronic homolog. Crystallographic data for a number of californium compounds are given in Table 11.8. This ionic radius relationship contrasts with the behaviors of the f-electron metals; metallic radii for the trivalent actinide metals are smaller than their lanthanide counterparts, and the metallic radius for californium is smaller than that of the smallest lanthanide metal, lutetium.

11.7.2 Halides and oxyhalides

Based on the estimated IV and III reduction potentials (Nugent *et al.*, 1971; David *et al.*, 1978) for californium, it would be expected that the only stable, bulk binary Cf(IV) halide would be its tetrafluoride. This compound can be prepared by fluorinating materials such as the oxides or CfF_3 with F_2 or ClF_3 (Asprey, 1970; Asprey and Haire, 1973; Haug and Baybarz, 1975). General preparative routes for the halides are summarized in Table 11.9 and their preparations have been summarized by Haire (1982).

The tetrafluoride has limited thermal stability and decomposes to CfF_3 (Haire and Asprey, 1973a,b) at 300–400°C. This temperature has limited the degree of crystallinity that can be obtained for it. There has been some variation in the lattice parameters reported for CfF_4, which arises mainly from indexing the monoclinic structure using powder diffraction data from samples of moderate crystallinity. A solid-state absorption spectrum has been obtained for the compound, its thermal stability examined and new X-ray data for the compound evaluated using small differences between the reported values (Haire *et al.*, 1980).

Ternary alkali-metal fluoride complexes of the types $MCfF_5$, M_2CfF_6, M_3CfF_7, and $M_7Cf_6F_{31}$ (M = Li through Cs) are expected to exist, and these complexes should provide added stability for the Cf(IV) state. These complex salts are well-established for the tetravalent state of lanthanides (Brown, 1968). The existence of CfF_4 in the vapor state has been claimed based on high-temperature (>500°C) chromatographic studies using tracer quantities of californium (Jouniaux, 1979; Bouissières *et al.*, 1980), which appears to conflict with the thermal decomposition of bulk CfF_4 at low temperatures (i.e. 300–400°C).

All of the trihalides and oxyhalides of Cf(III) are known (see Table 11.8), and many of these compounds were among the first prepared and reported for

Table 11.8 *Crystallographic data for californium compounds.*

Substance	*Structure Type*	*Crystal System*	*Lattice Parameters*				*References*
			a_0 (Å)	b_0 (Å)	c_0 (Å)	*Angle* (deg)	
Oxides							
Cf_2O_{Green}	Mn_2O_3	bcc	10.839			$\beta = 100.3$	Copeland and Cunningham (1969);
	Sm_2O_3	monoclinic	14.12	3.591	8.809		Green and Cunningham (1967)
	La_2O_3	hexagonal	3.72		5.96		Baybarz and Haire (1976)
Cf_7O_{12}	Tb_7O_{12}	rhombohedral	6.596			$\alpha = 99.40$	Turcotte and Haire (1976)
CfO_2	CaF_2	fcc	5.310				Baybarz *et al.* (1972); Haire (1976) [see also Haire and Eyring (1994) for oxides]
Halides							
CfF_3	LaF_3	trigonal	6.945		7.101		Stevenson and Peterson (1973)
CfC_3	YF_3	orthorhombic	6.653	7.039	4.393		Stevenson and Peterson (1973)
CfC_4	UF_4	monoclinic	12.42	10.47	8.126	$\beta = 126.0$	Haire and Asprey (1973)
	UF_4	monoclinic	12.33	10.40	8.113	$\beta = 126.44$	Haug and Baybarz (1975)
$CfCl_3$	UCl_3	hexagonal	7.379		4.090		Green and Cunningham (1967)
$CfCl_3$	$PuBr_3$	orthorhombic	3.859	11.748	8.561		Burns *et al.* (1973)
$CfBr_2$	$SrBr_2$	tetragonal	11.50		7.109		Peterson and Baybarz (1972)
$CfBr_3$	$AlCl_3$	monoclinic	7.215	12.423	6.825	$\beta = 110.7$	Fried *et al.* (1968)
$CfBr_3$	$FeCl_3$	rhombohedral	7.58			$\alpha = 56.2$	Burns *et al.* (1975)
CfI_2	$CdCl_2$	rhombohedral	7434			$\alpha = 35.83$	Wild *et al.* (1978)
	CdI_2	hexagonal	4.557		6.992		Wild *et al.* (1978)
CfI_3	BiI_3	hexagonal	7.587		20.814		Wild *et al.* (1978)
		rhombohedral	8.205			$\alpha = 55.08$	Wild *et al.* (1978)

Oxyhalides							
CfOF	CaF_2	cubic	5.561				Peterson and Burns (1968)
CfOCl	PbFCl	tetragonal	3.956		6.662		Copeland and Cunningham (1969)
CfOBr	PbFCl	tetragonal	3.90		8.		Fried *et al.* (1968)
CfOI	PbFCl	tetragonal	3.97		9.14		
$Cf(IO_3)_3$	$Bi(IO_3)_3$	monoclinic	8.7994(2)	5.9388(7)	15.157(2)	96.833(2)	Sykora *et al.* (2006)
pnictides							
CfN	NaCl	fcc	4.98				Haire (1974)
CfAs	NaCl	fcc	5.809				Damien *et al.* (1980)
CfSb	NaCl	fcc	6.165				Damien *et al.* (1980)
hydride							
CfH_{2+x}	NaCl	cubic	5.285				Gibson and Haire (1985)
oxysulfide and oxysulfate							
CfO_2S	La_2O_2S	trigonal	3.844		6.656		Barbarz *et al.* (1974)
$Cf_2I_2SO_4$	$La_2O_2SO_4$	orthorhombic	4.187	4.072	13.008		
cyclopentadienyl							Laubereau and Burns (1970)
$Cf(C_5H_5)_3$		orthorhombic	1.410	1.750	0.969		
pyrochlore							
$Cf_2Zr_2O_7$		cubic	10.55				Haire *et al.* (2002)

Table 11.9 *Preparation of californium halides.*

tetrafluoride
CfF_3 or Cf oxide + $F_2 \rightarrow CfF_4$
trihalides
Cf oxide + $HX \rightarrow CfX_3 (X = F, Cl, Br)$
$Cf^0 + HX \rightarrow CfX_3$
$Cf^0 + X_2 \rightarrow CfX_3$
$CfX_3 + 3HI \rightarrow CfI_3 + 3HX$
oxyhalides
Cf oxide or $CfX_3 + HX/H_2O \rightarrow CfOX$
dihalides (X = Cl, Br, I)
$CfX_3 + Cf^0 \rightarrow CfX_2$
$CfX_3 + H_2 \rightarrow CfX_2$

californium. Their crystal structures vary between the different compounds, but are often isostructural with the lanthanide trihalides for lanthanides having comparable ionic radii (i.e. Gd(III)).

The oxyhalides can be prepared by incomplete halide formation starting from oxides, careful hydrolysis of the anhydrous halides or thermal decomposition of hydrated halides. They are also prepared by hydrohalogenation of Cf_2O_3 or via treatment of a californium oxide with moist interhalogens at an elevated temperature. The anhydrous trihalides can be prepared by treating californium oxides with dry hydrogen halides or the metals with hydrogen halides or elemental halogens. However, the reaction of the oxide with hydrogen iodide does not give satisfactory results; the triiodide can be prepared by treating $CfBr_3$ or $CfCl_3$ with hydrogen iodide, or the metal with iodine. The trihalides have relatively low-melting temperatures and can be melted in inert atmospheres and/or in vacuum. Careful melting and cooling of such anhydrous halide melts have been used to create single crystals.

The trifluoride is dimorphic (orthorhombic, YF_3-type; high-temperature form, trigonal, LaF_3-type) with the transition temperature above 600°C (Cunningham and Ehrlich, 1970; Stevenson and Peterson, 1973). Treatment of CfF_3 with water vapor above 700°C or non-purified/moist HF produces CfOF (Peterson and Burns, 1968). The enthalpy of formation of CfF_3 at 298.15 K is accepted as being –1553(35) kJ mol^{-1} (see Chapter 19).

Californium trichloride is also dimorphic, exhibiting the UCl_3-type hexagonal structure (low-temperature form) and the $PuBr_3$-type orthorhombic structure (Green and Cunningham, 1967; Burns *et al.*, 1973). The melting point of $CfCl_3$ is 545°C (Burns *et al.*, 1973).

Treatment of Cf_2O_3 with moist hydrogen chloride, or $CfCl_3$ with water vapor, at elevated temperatures produces tetragonal CfOCl (Copeland and Cunningham, 1969). The preparation and measurement of the enthalpy of solution for CfOCl was also reported (Burns *et al.*, 1998). From the solution data, the enthalpy of formation ($\Delta_f H°(CfOCl_{cr})$) at 298 K was calculated to be –970(7) kJ mol^{-1}. This value is also discussed in Chapter 19.

Californium tribromide is trimorphic, but only two of these forms have been prepared by a direct synthetic route. The high-temperature form (>500°C) is an $AlCl_3$-type, monoclinic structure (Fried *et al.*, 1968; Burns *et al.*, 1975; Young *et al.*, 1976). A less well-characterized form, a $FeCl_3$-type rhombohedral structure, has also been reported (Burns *et al.*, 1975). A third form, a $PuBr_3$-type orthorhombic structure was acquired indirectly, aged (after a few half-lives of decay) from an orthorhombic form of its $BkBr_3$ parent (Young *et al.*, 1980). Interestingly, when mixed tribromides of californium–berkelium were synthesized, the orthorhombic structure did not form if the californium content exceeded 45 at%. And, when heating the orthorhombic $CfBr_3$ above 330°C, it immediately transforms into the monoclinic structure, which illustrates that the orthorhombic form is limited to the region of the ionic radius of californium (Young *et al.*, 1980). In contrast, applying pressure on monoclinic $CfBr_3$ (>3 GPa) transforms it to the orthorhombic structure (Peterson *et al.*, 1985). The oxybromide of californium, CfOBr (Fried *et al.*, 1968), is isostructural with CfOCl (Copeland and Cunningham, 1969), and both are prepared by the same methods (see Table 11.9). The molar enthalpy of formation of $CfBr_3$ has been reported to be –752.5 (3.2) kJ mol^{-1} at 298.15 K (Fuger *et al.*, 1990; see Chapter 19).

Californium triiodide is monophasic, and exhibits the BiI_3-type hexagonal structure (Fried *et al.*, 1968; Wild *et al.*, 1978). It is prepared by treating 'californium hydroxide' with hydrogen iodide at 800°C (Fried *et al.*, 1968), but a preferred synthetic route is to heat $CfBr_3$ or $CfCl_3$ with hydrogen iodide (Wild *et al.*, 1978). The CfOI is isostructural with CfOCl and CfOBr, and is prepared by the same procedure used for the latter two compounds (see Table 11.9).

The dichloride, dibromide, and diiodide of californium have all been prepared but the difluoride has not been reported. It would be expected that the Gibbs energy change between the di- and trivalent compounds would be the least for the iodides and hence the diiodide would be the most stable. The first compound of Cf(II) was $CfBr_2$ prepared by hydrogen reduction of $CfBr_3$ at elevated temperature (Peterson and Baybarz, 1972; Fried *et al.*, 1973). Subsequently, it was observed, and shown by absorption spectra, that lime-green $CfBr_3$ could also be reduced by thermal treatment alone (760°C) to produce an amber-colored $CfBr_2$ (Young *et al.*, 1975). The structure of $CfBr_2$ is tetragonal ($SrBr_2$-type; Peterson and Baybarz, 1972). Table 11.8 gives some crystallographic data for these compounds.

The first preparation of CfI_2 produced the high-temperature CdI_2-type hexagonal form (Young *et al.*, 1975); subsequently, a second structural form ($CdCl_2$-type rhombohedral structure) was reported (Wild *et al.*, 1978). The diiodide can be obtained via hydrogen or thermal reduction of the triiodide.

Of the three californium dihalides, $CfCl_2$ proved to be the most difficult to prepare, and many early attempts to prepare it were unsuccessful (Fujita and Cunningham, 1969; Young *et al.*, 1980). It was eventually prepared by hydrogen reduction of the trichloride at 700°C (Peterson *et al.*, 1977). The X-ray structure

of $CfCl_2$ still has not been resolved; the existence of this compound is based on its solid-state spectra. It is expected that $CfCl_2$ would exhibit either the $PbCl_2$-type orthorhombic or the $SrBr_2$-type tetragonal structure (Young *et al.*, 1975; Peterson *et al.*, 1977).

There is some evidence that californium halides may form so-called mixed-valence compounds (M_5X_{11}, $M_{11}X_{24}$ or M_6X_{13}, where M = metal ion and X = halide ion) like those reported for some of the lanthanide elements (Bärnighausen, 1976; Haschke, 1976; Luke and Eick, 1976). To avoid the necessity of carefully controlling reduction of californium to the proper stoichiometry, mixtures of gadolinium and californium (both have comparable III radii; see subsequent section) were used such that total reduction of the californium to Cf(II) would produce the desired cation II/III stoichiometry for formation of the structures, Cf_4GdCl_{11} and Cf_4GdBr_{11} (Haire *et al.*, 1978).

It has been reported that Cf(II) can be obtained in crystalline strontium tetraborate matrices (Peterson and Xu, 1996). It appears that this tetraborate matrix provides stability for the divalent state of the lanthanides and actinides. It was concluded from spectral data that Cf(II) existed in the material.

Except for the trifluoride, anhydrous californium trihalides are hygroscopic and must be protected from moisture. The dihalides are very sensitive to both moisture and oxygen. Normally, their syntheses are carried out in glass (except for the fluorides) so that products can be flame-sealed *in situ*, avoiding subsequent transfers of the products. Some preparative and experimental techniques for studying californium halides have been reviewed (Young *et al.*, 1978; Haire, 1982). In general, californium forms the same halide compounds and structures as lanthanide elements having a similar ionic radius.

11.7.3 Oxides

Oxides of californium have received a great deal of study, in part because they are primary compounds of interest and use, and were among the first compounds of this element that were investigated given their ease of formation. Oxides often serve as starting materials for preparing other compounds and can be obtained by calcining in air different materials (e.g. nitrates, oxalates, etc.) obtained from solutions. The stoichiometries (O/M ratios), crystal structures, and oxidation states of the californium oxide obtained, all depend on the experimental conditions employed. Haire *et al.* (1972) have discussed the californium-oxygen system.

Oxides of both Cf(III) and Cf(IV) (the sesquioxide and dioxide) are well known, as well as oxides with intermediate oxide compositions (i.e. between O/M of 1.5 and 2.00). The compound, Cf_7O_{12}, which is isostructural with Tb_7O_{12}, has also been established and its crystal structure and stability are known. It exists as a rhombohedral structure over a very narrow stoichiometry range (Turcotte and Haire, 1976). Although the monoxide has been observed in the vapor state, a true CfO solid has not been identified. This is in accord with the difficulty of preparing a true monoxide of ytterbium, although EuO is

known. It is likely that a oxynitride (i.e. Cf(O,N)) or oxycarbonitride (i.e. Cf(O, N,C)) may exist as a solid phase; if so, a variation of lattice parameter (likely fcc-type structure) would be expected for these compounds depending on the actual O/N/C ratios. The formation of californium monoxide may be possible by reacting stoichiometric quantities of the metal and sesquioxide under high pressure and at elevated temperatures. If formed, it would be expected to exhibit a fcc structure with a parameter of 4.8–5.0 Å. This high-pressure preparation of monoxides has been used with selected lanthanides to prepare their monoxides (Leger *et al.*, 1980), but often small residues of metal or oxides remain in the products.

Crystallographic data for the sesquioxides are listed in Table 11.8. Three structures are known for californium sesquioxide: a bcc, a monoclinic, and a hexagonal form. A phase diagram for the transneptunium sesquioxides is shown in Fig. 11.4, where it can be seen that the hexagonal form of californium sesquioxide exists only over a very narrow temperature range up to its melting point of about 1750°C (Haire and Eyring, 1994). There is a trend of decreasing melting point of the actinide sesquioxides with atomic number, which contrasts with the trend observed with the lanthanide compounds. The cubic sesquioxide exists below 1400°C but the monoclinic to cubic transition is very difficult to achieve and appears irreversible, whereas the reverse transition occurs readily. Fig. 11.5 shows the relationship in the molecular volumes for the sesquioxides of the f-elements, where it can be seen that the density for the three californium

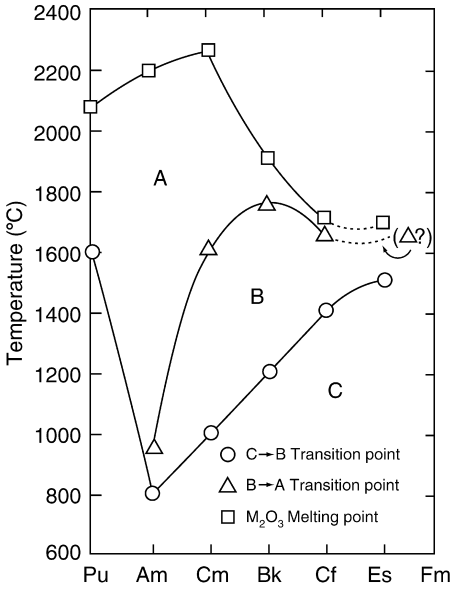

Fig. 11.4 *Phase diagram for the Pu through Es sesquioxides.*

forms increases in going from the cubic to the monoclinic to the hexagonal structures (Baybarz and Haire, 1976; Haire and Eyring, 1994). This trend for the californium compounds is in accord with those seen for the other f-element sesquioxides.

The monoclinic form of Cf_2O_3 (Sm_2O_3-structure type) was established early (Green and Cunningham, 1967) and the bcc (α-Mn_2O_3-type) was observed subsequently (Copeland and Cunningham, 1969). It was noted that slight oxidation of the bcc form may occur when it was heated in air. The hexagonal form of Cf_2O_3 was established later and was difficult to retain on cooling – it could be retained in samples quenched rapidly with helium from the melt (Baybarz, 1973; Baybarz and Haire, 1976; Haire and Eyring, 1994). One aspect of this monoclinic sesquioxide is its oxygen to metal ratio is 'fixed' at 1.5, whereas the cubic sesquioxide readily adds oxygen to its lattice up to a oxygen to metal ratio of 1.67.

As stated above, the hexagonal form of the californium sesquioxide exists over a narrow temperature region (Fig. 11.4). This structural form of berkelium sesquioxide is known and the hexagonal form of californium sesquioxide has also been observed in old samples of hexagonal Bk_2O_3 after berkelium has decayed to californium.

The transition temperature for the bcc to monoclinic form of californium sesquioxide was reported to be both 1100°C (Green and Cunningham, 1967) and 1400°C (Baybarz, 1973; Baybarz and Haire, 1976). The transition from the monoclinic to the hexagonal form was set at 1700°C, just 50°C below the oxide's melting point. While the monoclinic to cubic transition appears irreversible, the hexagonal to monoclinic form is readily reversible.

The fcc dioxide has been prepared by heating lower oxides of californium with atomic oxygen or under high-pressure molecular oxygen (Baybarz *et al.*, 1972; Haire, 1976). It usually appears as a black or dark-brown material, whereas the sesquioxide is very light green to light-tan color. With time, the dioxide's lattice parameter increases slightly, due to swelling and/or small losses of oxygen, both processes probably being due to self-irradiation. When heated in air above 200°C, the dioxide begins to lose oxygen and eventually forms Cf_7O_{12} or lower oxides at temperatures above 400°C (Haire, 1976).

A capacitance manometer system, capable of analyzing oxygen overpressures for samples as small as 1.4 mg of californium, together with X-ray diffraction analyses have established the californium–oxygen system between $1.50 < O/Cf < 1.72$ (Turcotte and Haire, 1976). In that work it was shown that Cf_7O_{12} (a rhombohedral structure) was the stable oxide in air or oxygen up to 750°C. At higher temperatures this compound loses oxygen to eventually form the sesquioxide. A stoichiometric bcc sesquioxide is obtained when these higher oxides of californium are heated in vacuum to 800–1000°C, or when an air-calcined oxide is subsequently treated in hydrogen or carbon monoxide at 850–1000°C.

Thus, the californium sesquioxide system is trimorphic, and there are also the established Cf_7O_{12} and CfO_2 compounds. The bcc sesquioxide lattice can also

accept additional oxygen, and this structure exists for an O/M ratio of 1.5 to 1.67. It is expected that californium oxides with O/M compositions between 1.8 and 2.0 would have fcc structures but this has not been well established. Both the bcc lattice parameters for the sesquioxides up to an O/M of 1.67, and the fcc lattice parameters for the oxides having an O/M of 1.8–2.0, decrease in magnitude with the addition of oxygen to the lattices. In many respects (e.g., stability, formation of specific oxides, structures with specific O/M ratios, etc.), the californium–oxygen system is similar to that of the terbium–oxygen system (Haire and Eyring, 1994).

One other aspect regarding californium oxides is the behavior of (Bk,Cf) oxides as a function of the californium content (Turcotte, 1980). It appears that with californium contents up to 25 at%, the actinides can be oxidized up to an O/M of 2.0 (behaving like pure berkelium oxide). When the californium content is 64 at% or greater, the californium now controls the behavior of berkelium and limits the stoichiometry of the products to M_7O_{12}.

Although the preparation of CfO_2 normally requires strong oxidizing conditions and moderate temperatures, under certain conditions lower oxides of californium stored in air or oxygen can 'self-oxidize,' presumably due to an active oxygen species (atomic oxygen?) generated by the alpha radiation field (Haire, 1976); in contrast, small (few micrograms) samples of CfO_2 may lose oxygen under these conditions. The exact composition of aged californium oxides is difficult to ascertain by X-ray analyses alone, as the lattice parameters measured reflect both radiation damage to the lattice (swelling, larger parameter) and/or oxidation that affects the O/M ratios (decrease in parameter with greater oxygen content). Both effects may be operational in these systems. There are reviews on the effects of radiation damage on actinide oxides (Fuger, 1975; Fuger and Matzke, 1991).

The high-temperature vaporization of californium oxides has been explored by Knudsen effusion studies (Haire, 1994). With californium, oxides with O/M ratios > 1.5 lose oxygen, especially in vacuum, when heated (see above discussion) so that vaporization studies at higher temperatures basically deal with the sesquioxide. From the phase behavior in Fig. 11.4, vaporization from solid Cf_2O_3 should involve its monoclinic or hexagonal phases. Vaporization products observed for Cf_2O_3 were atomic Cf and CfO, in a ratio of $\sim$1:10 at 1800 K. This low concentration of CfO (i.e. CfO is not a dominant species, even though CfO may be expected) is due to the relatively low dissociation energy of CfO (about 498 kJ mol^{-1}) as compared to CmO (about 728 kJ mol^{-1}; Cm/CmO < 0.1) (Haire, 1994). A value for the enthalpy of formation of the Cf_2O_3 from the vaporization studies was reported as between –1650 and –1700 kJ mol^{-1} (Haire, 1994), which compares to –1653(10) kJ mol^{-1} obtained from solution calorimetry experiments (see Chapter 19).

A systematic treatment of data for the lanthanide and actinide oxides has generated estimated thermochemical values for the oxides of californium (Morss, 1983). A comparison of the lanthanide and actinide oxygen systems

in detail, which includes discussions of the californium oxides, is also available (Haire and Eyring, 1994). In Section 11.9, discussions on the gas-phase behavior of californium are presented and include other chemical aspects of californium oxides. Both experimental and computational thermochemical data for californium oxides are given in Chapter 19.

There are a number of more complex oxide materials (i.e. ternary systems for one) that are outside the scope of the present chapter. However, one system, the zirconium–californium oxide pyrochlores, is discussed given its potential applications and systematic comparisons with other comparable actinide pyrochlores. The zirconium–californium–oxygen compound has the stoichiometry of $Cf_2Zr_2O_7$. These f-element materials are called pyrochlores given their similarity of their structures to that of the mineral, 'pyrochlore.' A related system to these pyrochlores involves solid solutions of zirconium and californium dioxides, which can be prepared from the pyrochlores by adding oxygen to their lattice.

Applications for the americium and curium pyrochlore counterparts include transmutation and nuclear waste matrices, although these uses are not considered for the californium products. The californium–zirconium oxide pyrochlore is cubic with a lattice parameter of 10.57 Å, and it is isostructural with comparable compounds formed with the trivalent actinides plutonium through presumable einsteinium and zirconium or hafnium (Haire *et al.*, 2002). The fit of the lattice parameter of the californium compound with the plutonium through californium and lanthanide zirconium pyrochlores is shown in Fig. 11.6, which can be used to generate a linear equation for the parameters of mixed f-elements or ascertain the oxygen content of a particular pure pyrochlore. This relationship is useful to analyze mixed actinide or lanthanide–actinide pyrochlores when encountered.

11.7.4 Other compounds of californium

In addition to the oxides and halides, several other compounds of californium have been prepared and their crystallographic data reported (see Table 11.8). Some of these data represent preliminary values or even results from a single experiment. In some cases (pnictides, chalcogenides, etc.), the limited supply of californium metal has precluded the preparation of specific compounds via the reaction of the metal, especially where close control of the stoichiometries is required (for example, the preparation of the potential compound, CfS). The general preparative techniques for the different pnictides and chalcogenides of the transuranium elements have been reviewed (Damien *et al.*, 1979).

Stoichiometries other than 1:1 ratio are not expected for the californium pnictides. These materials can be prepared by direct reaction of the elements, and exhibit a NaCl-type, cubic structure. From preparations of CfN, a fcc lattice constant of 4.94 Å has been derived (Haire, 1988). This parameter is only slightly different or the same as reported for samples of fcc californium metal (4.994 Å, Stevenson, 1973; or 4.94 Å, Noé and Peterson, 1976; see Section 11.6)

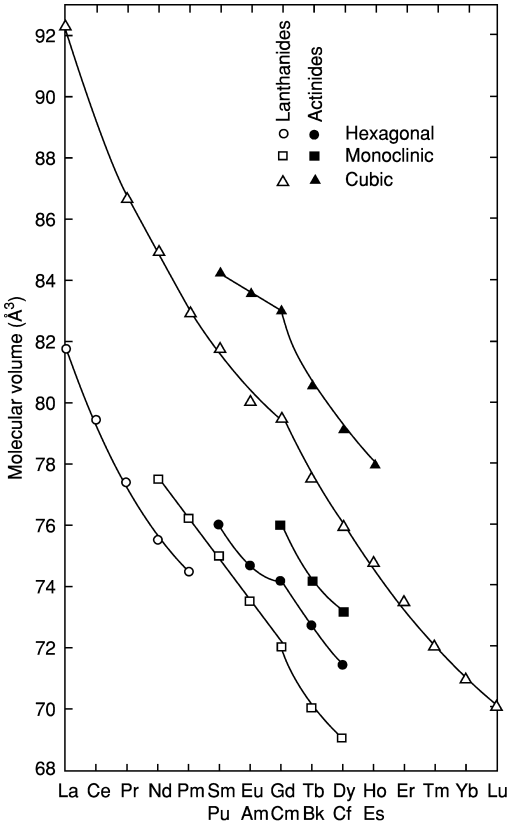

Fig. 11.5 *Molecular volumes of f-element sesquioxides.*

but much larger than the 4.78 Å parameter reported for the metal by Haire (1978) and Haire *et al.* (1986). It should be noted that carbon, nitrogen, and oxygen can replace one another in f-element, cubic NaCl-type compounds as the mononitride. The substitution going from carbon to nitrogen to oxygen increases the compound's parameter. For the remaining pnictogens, the monophosphide of californium has not been reported, but the monoarsenide and monoantimonide have been prepared (Damien *et al.*, 1980; see Table 11.8).

In contrast to the pnictides, californium chalcogenides of different stoichiometries can be prepared (Damien *et al.*, 1980). Preparation of the monochalcogenides requires close control of the reactant stoichiometries to avoid the formation of higher chalcogenides, and attempts to prepare californium monochalcogenides as single-phase products have not been successful to date. Another difficulty is that the monosulfide can convert to higher sulfides by volatilizing californium metal and driving the stoichiometry to a higher sulfide. The tritelluride, ditelluride, diselenide, disulfide, sesquiselenide, and sesquisulfide of

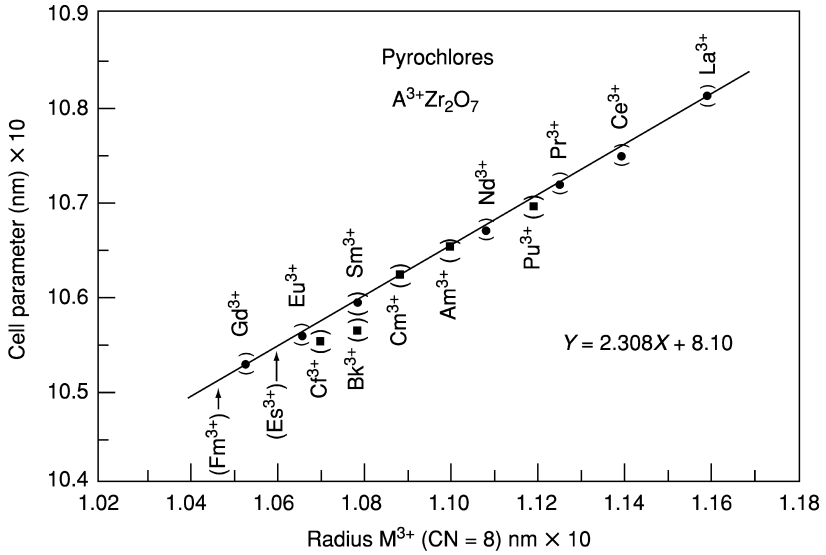

Fig. 11.6 *Relationship of lattice parameters and radii for f-element pyrochlore oxides.* (*units shown are equivalent to Ångströms*)

californium have all been prepared (Damien *et al.*, 1980). These higher chalcogenides are normally prepared by direct combination of the elements, and lower stoichiometries can be obtained by thermal decomposition of compounds having higher compositions. Lattice parameters for many of these californium compounds have not been reported. It is believed the tritelluride of californium has an orthorhombic structure isomorphous with the NdFe structure. All the dichalcogenide compounds crystallize in the anti-FeAs-type of tetragonal structure (as do the corresponding plutonium, americium, curium, and berkelium compounds). Four transuranium sesquichalcogenide structure types are known; but the sesquisulfide and sesquiselenide of californium have been obtained as the alpha form (bcc; anti-Th_3P_4 type of structure; Damien *et al.*, 1980).

There have been different reports on the preparation of californium hydrides (Gibson and Haire, 1985). The hydrides are generally prepared by reaction of californium metal with hydrogen at elevated temperatures. It was believed that the stoichiometries of the products were close to that for the dihydride (CfH_{2+x}). The products exhibited fcc structures with an average lattice parameter of $a = 5.285$ Å, which is slightly larger than expected for the compound based on extrapolations of parameters for preceding actinide dihydrides. This larger parameter and the inability to prepare a trihydride of californium in the initial efforts were believed to reflect a tendency for californium to be divalent. In the lanthanide–hydrogen system, the hydrides of divalent europium and

ytterbium metals also deviate from the behavior of the other lanthanide hydrides (Topp, 1965). Reports of californium hydrides up to trihydride were subsequently published, which also included stoichiometries intermediate to the dihydride and trihydride (Gibson and Haire, 1987).

The oxysulfate (orthorhombic) and the oxysulfide (trigonal) of californium have also been reported (see Table 11.8); Baybarz *et al.*, 1974). These compounds can be prepared by thermally decomposing either Dowex ion-exchange resin beads containing Cf(III) or hydrated $Cf_2(SO_4)_3$ salt. The oxysulfide is obtained by heating these materials in a vacuum or a reducing (hydrogen-containing) atmosphere. The oxysulfate does not decompose to the sesquioxide when heated in air until the temperature exceeds 860°C.

A solid organocalifornium compound, $Cf(C_5H_5)_3$, has been prepared and characterized crystallographically (Laubereau and Burns, 1970a,b; see Table 11.8). Both powder and single-crystal X-ray data were obtained for this orthorhombic, cyclopentadienyl compound, which was prepared by reacting anhydrous $CfCl_3$ and molten $Be(C_2H_5)_2$, and the crystalline product was isolated by vacuum sublimation (135–200°C). A solid-state absorption spectrum of Cf $(C_5H_5)_3$ was obtained from these crystals, which showed a broad absorption from 600 nm to lower wavelengths. This was accredited to the presence of an electron-transfer process in the system.

Some work has also been reported on a californium dipivaloylmethanato complex, where the volatility of the complex was compared to complexes of other lanthanides and actinides (Sakanoue and Amano, 1976). These tracer studies suggested that the californium complex deposited at lower temperatures than the americium or plutonium complexes. Other studies have been done on formation of californium β-diketonates, and their thermochromatography behavior has been described (Aizenberg *et al.*, 1988).

11.7.5 Magnetic properties of compounds

A limited amount of magnetic work has been reported for californium and its compounds. Magnetic data for the metallic state of californium have been described in Section 11.6. The transplutonium metals with localized 5f electrons behave as though they consist of ions embedded in a sea of conduction electrons. It is these 5f electrons that are then mainly responsible for the susceptibility. With this simple model, the effective moment for californium metal should be the same as that for a californium ion, where the same number of nonbonding 5f electrons is present.

In Table 11.10 magnetic data for some f-element metal ions are listed, including californium, and their calculated magnetic moments based on LS coupling and Hund's rule. On this basis, the moments of Cf(IV), Tb(III), or Bk(III) would be the same, the moments of Cf(III), Dy(III), or Es (IV) would be identical, and the moments of Cf(II), Es(III), or Ho(III) would be equal. It is unfortunate that the measured moments cannot differentiate between Cf(II) and Cf(III),

Table 11.10 *Electronic states* (3+) *and effective magnetic moments given by LS coupling and Hund's rule: expected moments of californium.*[a]

Lanthanide	*Actinide*	3+ *Ion configuration*	*Basic level*	*L*	*S*	*J*	g_J	$g_J[J(J+1)]^{1/2}$	μ^*_{eff}
Gd	Cm	f^7	$^8S_{7/2}$	0	7/2	7/2	2	7.94	7.66
Tb	Bk	f^8	$^9F_6$	3	3	6	3/2	9.7	9.40
Dy	Cf	f^9	$^6H_{15/2}$	5	5/2	15/.2	4/3	10.63	10.22
Ho	Es	f^{10}	$^5I_8$	6	2	8	5/4	10.60	10.18

Based on these assumptions: Cf(II) = 10.60 μ_B; Cf(III) = 10.63 μ_B; and Cf(IV) = 9.72 μ_B.

[a] Edelstein and Karraker (1976) and Huray and Nave (1987). Based on intermediate coupling as opposed to pure *LS* coupling.

and that the calculated difference between Cf(III) and Cf(IV) is only 0.9 Bohr magnetons (see Table 11.10). However, the magnetic behavior of these materials as a function of temperature and/or magnetic field can still provide very useful information, and by itself may be sufficient to differentiate between these states.

The first magnetic data reported for californium compounds were obtained from 56 ng of californium; this small quantity required a microscope to measure the deflections of a Faraday apparatus (Cunningham, 1959). The objective of this experiment was to confirm that californium, deposited on an ion-exchange resin bead, had a radon core plus $5f^9$ electrons. The results showed that the sample followed the Curie–Weiss law and produced a moment of 9.2 μ_B. A subsequent experiment with larger samples (0.3–1.2 μg) of californium on resin beads gave effective moments of 9.1–9.2 μ_B. Magnetic studies on oxides, Cf_2O_3, Cf_7O_{12}, CfO_2, and $BaCfO_3$, have been reported (Moore *et al.*, 1986). The magnetic moments obtained in these studies were in agreement with the charge states assigned to californium based on the stoichiometries in the materials. Magnetic studies have also been carried out on three monopnictides, CfN, CfAs, and CfSb (Nave *et al.*, 1985) and on the two structure types of $CfCl_3$ (Nave *et al.*, 1986).

In other studies, the moment of californium in a Cs_2NaYCl_6 host has been measured (Karraker and Dunlap, 1976). An electron paramagnetic resonance study on Cf(III) in a cubic $NaLuCl_4$ host (<1% Cf by weight) produced a 10-line spectrum to confirm the nuclear spin to be 9/2 (Edelstein and Karraker, 1976). The crystal field ground state was also identified in this work and the nuclear dipole moment of ^{249}Cf was determined to be –0.28 μ_n. The magnetic properties of californium compounds and metal are summarized and compared in Table 11.11.

11.7.6 Solid-state absorption spectra

The anhydrous transplutonium halides have been extensively studied by absorption spectrophotometry. The f–f and f–d transitions in californium spectra

Table 11.11 *Effective magnetic moments of californium metal and compounds.*

Material	*T range* (K)	θ (K)	μ_{eff} (μ_B)	T_N (K)	*References*
CfO_2	80–320	–70	9.1(2)	7(2)	Nave *et al.* (1981)
Cf_7O_{12}	80–320	95	9.5(2)	8(2)	Moore *et al.* (1986)
CfF_4	150–340	–51	9.4(1)		Chang *et al.* (1990)
CfF_4 (aged)	150–340	–33	9.1(1)	9–12	Chang *et al.* (1990)
Cf^{3+} (on a resin bead)	77–298	–5.6	9.14(6)		Fujita and Cunningham (1969)
$BaCfO_3$	80–320	–210	9.2(2)	7(2)	Moore *et al.* (1986)
Cf_2O_3 (monoclinic)	80–320	–80	10.1(2)	8(2)	Moore *et al.* (1986)
Cf_2O_3 (bcc)	80–320	–115	9.8(2)	19(2)	Moore *et al.* (1986)
Cf_2O_3 (bcc)	90–300	–80	9.7	–	Morss *et al.* (1987)
CfF_3	150–340	–20	10.2(1)	6–7	Chang *et al.* (1990)
$CfCl_3$	60–340	13	10.1(2)	7	Moore *et al.* (1988)
$Cs_2NaCfCl_6$	2–14	–2.8	7.36(20)	–	Karraker and Dunlap (1976)
$Cs_2NaCfCl_6$	20–100	–13.5	10.0(1)	–	Karraker and Dunlap (1976)
Cf metal	28–298	3.24	9.84		Fujita *et al.* (1976)
	22–298	–3.00	9.67		
Cf metal	100–340	40	9.7(2)		Nave *et al.* (1985)
CfN	4–340	41	10.3(2)	25	Nave *et al.* (1986)
CfAs	4–340	29	10.3(2)	25	Nave *et al.* (1986)
CfSb	4–340	18	10.3(2)	25	Nave *et al.* (1986)

can be utilized to ascertain the oxidation state and coordination number of californium in the compounds. A valuable technique in these spectroscopy studies was the use of a 'fingerprint' approach, where spectra of materials with known structures were used to compare with other compounds. Some of these experimental techniques employed for studying microgram quantities of californium halides have been reported (Green, 1965; Green and Cunningham, 1966; Fujita and Cunningham, 1969; Young *et al.*, 1978). One of the first absorption spectra for californium was obtained from a single crystal of anhydrous $CfCl_3$. Subsequently, other spectra have also been obtained for this compound (Carnall *et al.*, 1972; Peterson *et al.*, 1977) and for $CfCl_2$ (Peterson *et al.*, 1977). Absorption spectra have also been obtained for anhydrous $CfBr_3$ (Young *et al.*, 1975, 1980); $CfBr_2$ (Young *et al.*, 1980), CfI_3 and CfI_2 (Wild *et al.*, 1978), plus CfF_4 and CfF_3 (Haire *et al.*, 1980).

In Fig. 11.7 solid-state absorption spectrum for $CfCl_2$ is shown, which is compared with a spectrum for $CfCl_3$. There is a distinct difference between the absorption spectrum for Cf(III) and Cf(II) states. For a given oxidation state, differences in absorption spectra as well as emission spectra can be noted when the crystal structures are different. This arises from symmetry conditions and how they affect the splitting of electronic levels in the californium compounds. These spectra, once assigned to specific structures, may be used to identify the

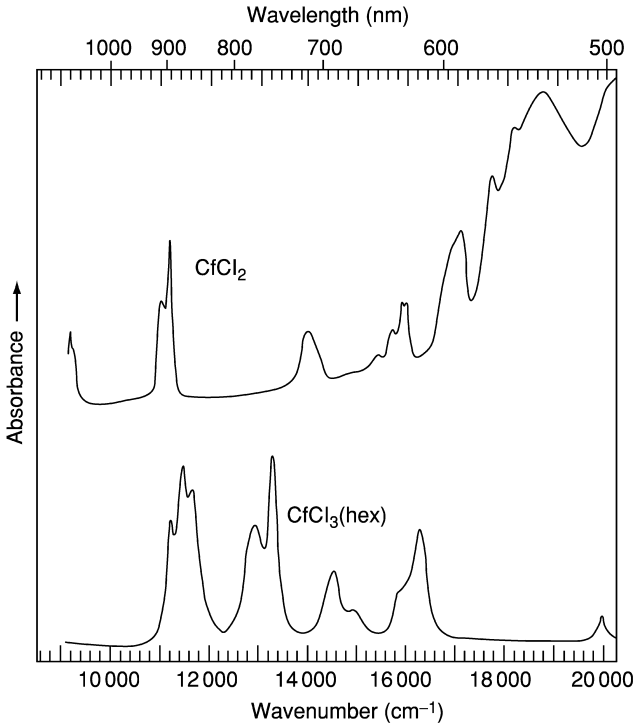

Fig. 11.7 *Solid-state spectra for $CfCl_2$ and $CfCl_3$.*

structure type by a 'fingerprint' technique. Thus, one finds the spectral envelops of the absorption spectrum for the hexagonal form of $CfCl_3$ differs from that of the orthorhombic form of this compound. A review of solid-state spectral studies on californium halides is available (Wilmarth and Peterson, 1991a,b). In this review the authors also give a discussion of Raman spectra obtained for californium.

Laser-induced fluorescence of Cf^{3+} in a $LaCl_3$ host has also been reported (Caird *et al.*, 1976; Hessler *et al.*, 1978). A limited amount of spectral information has been reported for the dicyclopentadienyl californium compound, where Cf exists as Cf(III) (Laubereau and Burns, 1970a,b). The spectra of Cf(IV) in CeF_4 matrices has also been discussed (Liu *et al.*, 1993) and information obtained was interpreted in terms of line broadening.

Infrared spectra for californium materials have also been obtained (Conway *et al.*, 1977). Crystal field calculations and parameters for the trivalent actinides in crystal hosts have been made and published (Carnall and Fried, 1976; Conway *et al.*, 1977; Crosswhite, 1977). The spectroscopic properties of californium compounds pertinent to potential laser applications have also been discussed, and the transition from the $J = 11/2$ state at 6500 cm to the $^6H_{15/2}$ ground

state appears to be a likely candidate in this regard (Weber, 1980). Free-ion energy levels and the optical properties for californium have also been published (Hessler and Carnall, 1980).

In addition, absorption spectra of californium halides have been obtained and examined as a function of time, looking at the daughter or granddaughter products in studies that examined the chemical and structural consequences of the radioactive decay processes (Young *et al.*, 1980, 1981, 1984). Following the chemistry and structural forms through radioactive decay processes by examining the californium granddaughter products produced from the decay of Es-253 halides (i.e.Es-253 $\rightarrow$ Bk-249 $\rightarrow$ Cf-249 $\rightarrow \cdots$) is an example. It is worthwhile to note that in the latter decay sequence, Cf(III) halide product was produced from an initial Es(III) halide product and a Cf(II) halide product when starting with a Es(II) halide. Essentially, the oxidation state was retained through two decay events, first an alpha and then a beta decay). This implies that a Bk(II) product was formed in the transition although Bk(II) has not been synthesized directly.

11.8 SOLUTION CHEMISTRY

11.8.1 General comments

Although californium exhibits oxidation states of II, III, and IV in the solid state, its solution chemistry is basically that of a trivalent ion. There has been only a couple of unsubstantiated reports of an oxidation state above Cf(IV) in solution even though formation of Cf(V) presumably would acquire some stabilizing influence by attaining a half-filled, 5f-orbital state ($5f^7$).

To retain the tetravalent state in solution is also more difficult than generating it in the solid state, and for solutions it requires a high degree of complexation to afford sufficient stabilization to maintain this state. It has been reported (Kosyakov *et al.*, 1977) that Cf(IV) was stabilized in phosphotungstate solutions, where M(IV)/M(III) couples can be shifted by as much as 1.0 V (Barnanov *et al.*, 1981). Another report for stabilizing Cf(IV) in solution involved the use of triphenylarsine oxide in acetonitrile (Payne and Peterson, 1987).

It is expected to be easier to stabilize Cf(II) than Cf(IV) in solutions. Nonaqueous solvents also offer some promise for obtaining both the II and IV oxidations states of californium. But in all cases, the effects of self-irradiation and the potential for generating oxidizing and/or reducing conditions must be considered and factored into the picture.

Although californium is the electronic homolog of dysprosium, its divalent–trivalent behavior in solution should be considered to be more similar to that of samarium, and its trivalent–tetravalent behavior may be comparable to that of terbium. Thus, samarium and terbium can be used as template elements for testing the oxidation behavior of californium.

Trivalent californium's behavior in solution is very similar to the behaviors of the trivalent lanthanide ions in solution, except californium has a greater tendency to form complexes (is more covalent). This arises from the somewhat extended 5f orbitals of actinides compared to the 4f orbitals, which provides a slightly greater degree of complexing ability to afford californium's greater covalent nature. The higher degree of complexation found with the transplutonium (III) ions in ethanol–HCl solution, as compared to the lanthanide (III) ions (see Section 11.4), has used this condition as one method for a group separation.

As with the lanthanides, both fluoride and oxalate ions will precipitate trivalent californium from dilute acid solutions. Addition of hydroxide to a Cf(III) solution produces a gelatinous, light green-tinted precipitate, which is presumably its trihydroxide. In non-complexing solutions (i.e. dilute acid solutions, 0.1 M perchloric or hydrochloric acids), Cf(III) exists as a hydrated cation; at higher acid concentrations (i.e. 6 M HCl), complexation is sufficient so that californium will not be held on cation-exchange resins but will elute as an anion complex. This difference in complexation forms the basis for a number of group separations between trivalent lanthanides and actinide ions. The greater complexing nature of the actinides allows them to be removed from cation-exchange resins with different reagents while the lanthanides are retained on the columns.

11.8.2 Oxidation–reduction reactions

Several reduction potentials for californium have been derived from both experimental data and from systematic calculations, and some of these values are given in Table 11.12. The calculated Cf(IV)/(III) couple of 3.2 V (Nugent *et al.*, 1971) is in accord with the inability to obtain Cf(IV) in most aqueous media. This value for californium can be compared to the Tb(IV)/Tb(III) couple of 3.1–3.3 V, the Am(IV)/Am(III) couple of 2.2–2.5 V, and the Cm(IV)/Cm(III) couple of 3.1–3.5 V (Nugent *et al.*, 1973a,b). It is difficult to maintain Am(IV) and essentially not feasible to produce Cm(IV) in most aqueous solutions. Preparation of these higher oxidation states for the actinides in general should be more favorable in alkaline than acidic media, but complexation can also offer stabilization. Thus, in principle, the ease of forming Cf(IV) should be comparable to forming Tb(IV) or Cm(IV) in solution, which are more difficult than forming Am(IV) in solution. This relative behavior of californium in solution may be likened to that in the solid state: the formation of californium dioxide is comparable to preparing terbium dioxide, with both being more difficult to prepare than americium or curium dioxide (see Section 11.7.3).

The ability to oxidize Cf(III) to Cf(IV) in a phosphotungstate solution has been summarized in a paper on the solution behavior of the transplutonium elements (Myasoedov, 1982). Both Tb(IV) and Am(IV) can be stabilized in strong carbonate; thus, it would appear possible to prepare Cf(IV) in a strong carbonate medium, utilizing the expected shift of 1.7 V in the Cf(IV)/Cf(III) couple arising from carbonate complexation of the Cf(IV). Two conflicting reports exist on the

Table 11.12 *Reduction potentials for californium.*

Couple	*Potential* (V vs NHE)	*Method*	*References*
Cf(IV)/Cf(III)	3.3; 3.2	calculated	Nugent *et al.* (1971, 1973a,b)
Cf(IV)/Cf(III)	3.2		Chapter 19
Cf(III)/Cf(II)	–2.0; –1.9	calculated; spectra	Nugent *et al.* (1969)
	–1.6		Chapter 19
	–1.4	calculated	David (1970a,b,c)
	–1.6	calculated; spectra	Friedman *et al.* (1972)
	–1.47	polarographic/voltammetric	Musikas *et al.* (1981)
	–1.6	polarographic (acetonitrile)	Friedman *et al.* (1972)
Cf(III)/Cf(0)	–2.32	calculated	David (1980)
	–2.01	radiopolarography	David *et al.* (1978) and Samhoun and David (1976)
	–2.06	calculated	Raschella *et al.* (1982)
	–1.93		Chapter 19
Cf(III)/Cf(Hg)	–1.61	Calculated	Musikas *et al.* (1981)
Cf(III)/Cf(Hg)	–1.503	radiopolarography	Samhoun and David (1976)
Cf(II)/Cf(Hg)	–1.68	polarographic/voltammetric	Samhoun and David (1976)
Cf(II)/Cf(0)	–2.1		Chapter 19

oxidation of Cf(III) in carbonate. One group (Hobart *et al.*, 1981, 1983) was unable to find evidence for Cf(IV) after chemical or electrical treatments, while a second team (Myasoedov *et al.*, 1986) reported that 20% of the Cf(III) present in a K_2CO_3 solution could be oxidized electrochemically.

The behavior of californium and the next two actinide elements in molten salts where strong reducing agents were present has been reported (Kulyukhin *et al.*, 1997). The ease of preparing the divalent state increases in going across the series to einsteinium.

A number of studies have supported the potential for the existence of Cf(II) in solution. In one study, the tendency for californium to form amalgams rapidly is compared to the behavior of the lanthanides known to acquire a divalent state (Maly, 1967; Maly and Cunningham, 1967; Nugent, 1975). In early work, the inability to reduce Cf(III) in 0.1 M NH_4Cl suggested a potential limit of -1.4 V for the Cf(III)/Cf(II) couple (Cunningham *et al.*, 1970). David (1970a–c) also proposed a value of –1.4 V from radiopolarographic and amalgamation behaviors using tracers.

Studies on the coprecipitation behavior of californium (Cohen *et al.*, 1968; Fried and Cohen, 1968; Mikheev *et al.*, 1972a,b) have also supported the existence for Cf(II) in solution. The difference in formal potentials between the Sm(III)/Sm(II) and Cf(III)/Cf(II) couples has been estimated to be 0.045 V (californium being more negative) by studies on coprecipitation of chloride salts in

aqueous ethanol solutions (Mikheev *et al*., 1972a,b). Another comparison between the reduction behavior of californium and samarium was made in anhydrous acetonitrile (Friedman *et al*., 1972), where the Cf(III)/Cf(II) and Sm(III)/Sm(II) couples were found to be nearly identical; a value of –1.58 V was proposed for the Cf(III)/Cf(II) couple. Essentially the same value (–1.60 V) for this couple was reported from co-crystallization studies (Mikheev *et al*., 1972a,b). Nugent *et al*. (1969, 1973a) have suggested the potential for the Cf(III)/Cf(II) couple is –1.6 V, based on systematic analyses of electron-transfer bands. Radiopolarographic experiments on californium have resulted in two reports regarding its behavior. The first report (David, 1970a) suggested two couples: –2.32 V for Cf(III)/Cf(0) and –1.4 V for Cf(III)/Cf(II). Subsequent work (Samhoun and David, 1976) concluded that the first radiopolarographic results were incorrect, and that Cf(III) is reduced directly to Cf(Hg) in one step ($E_{1/2}$ = 1.503 V): correcting for the amalgamation process yields a Cf(III)/Cf(0) couple of –2.01 V. Guminski (1996) has discussed the Hg-Cf system.

Subsequently, a polarographic and voltammetric study (Musikas *et al*., 1981) on larger amounts of californium concluded that californium is reduced via a two-step process as is found with samarium: (1) Cf(III) → Cf(II) and (2) Cf(II) → Cf(Hg). Potentials for these processes were given as –1.47 and –1.68 V, respectively. These data yield a calculated value of –1.61 V for Cf(III)/Cf(0). An evaluation of earlier amalgamation experiments has also led to a proposed value of –2.2 V for the Cf(II)/Cf(0) couple (Nugent, 1975).

These reported differences for californium have not been resolved and additional work needs to be done to resolve the system. Since Cf(II) can be prepared and maintained in the solid state, there still remains a good possibility that Cf(II) can be stabilized in aqueous and/or nonaqueous solvents. David *et al*. (1990a,b) and David and Bouissières (1968) discuss the electrochemical reduction in aqueous solution for separations, and for the formation of intermetallic compounds and amalgams. Other work on the radiopolarography of californium has also been published (Skiokawa and Suzuki, 1984).

Evidence for Cf(II) in molten-salt systems has also been reported (Ferris and Mailen, 1971). The distribution coefficient of californium between molten lithium chloride and lithium–bismuth metals at 640°C indicated that divalent californium was present in the salt phase. However, evidence for the existence of Cf(II) was not found in lithium fluoride–beryllium fluoride melts (Ferris and Mailen, 1970).

It is generally accepted that the stability of the divalent state increases for the second half of the actinide series of elements, and it has been accepted that californium metal is close to being a metal having only two bonding electrons (see earlier section). Starting with californium, the M(III)/M(II) couples increase regularly in the order: No > Md > Fm > Es > Cf, with values ranging from –1.45 V for nobelium to –1.60 V for californium (Myasoedov, 1982).

In discussing the oxidation states of californium in solution, the possibility of attaining Cf(V) could be enhanced by the attainment of a $5f^7$ electronic state.

Some early coulometric data obtained with a few micrograms of californium suggested that Cf(V) may have been attained in a 1 M H_2SO_4 solution (Propst and Hyder, 1969), but these results have not been confirmed and are likely to be incorrect. More recently, a claim for the generation of Cf(V) in a carbonate media was made based on results of coprecipitation experiments (Kosyakov *et al.*, 1982a,b). In this work, small amounts (<10%) of californium, generated from the decay of Bk(IV) in the solution, were found in $Na_4UO_2(CO_3)_3$ 'wet' solids precipitated from the solutions. The presence of 'co-precipitated' californium in these precipitates was interpreted as reflecting the presence of an oxidized form of californium (Cf(IV) or Cf(V) i.e. as the CfO^{2+} or CfO_2^+ ion) within the uranium precipitate. These results must be accepted with some caution, as other explanations for the behavior can be given. It is likely that Cf(IV) would accompany Bk(IV) in such situations. Thermodynamic (David *et al.*, 1978) and quantum-chemical calculations (Ionova *et al.*, 1980) have been made that indicate it may be possible to obtain Cf(V) state in the solid state, which could be considered for the solid phases mentioned above. However, it would seem most plausible that Cf(IV) or Cf(V) would be stabilized in alkaline conditions/materials, oxygenated complexes, complex polyanion materials (i.e. polytungstates), etc.

11.8.3 Complexation chemistry

A considerable portion of the published data dealing with californium concerns the complexation and solvent extraction chemistry of Cf(III). This is in part a consequence of the fact that a large amount of this information could be obtained using tracer quantities of the more abundant ^{252}Cf isotope, which also has a higher specific activity. In addition, there was an impetus to perform this type of study using the small quantities available during the investigation/development of californium's separation chemistry for processing. A compilation of stability constants for californium complexes and chelates is given in Table 11.13.

Some of the first data on californium complexes involved materials such as halides, citrates, lactates, α-hydroxyisobutyrate complex, etc., as these materials played a role in early separation/purification schemes (Katz and Seaborg, 1957; Keller, 1971) for californium (see Section 11.4). In general, it is expected that only small differences in stability would exist between Cf(III) and its two trivalent near neighbors, Bk(III) and Es(III), with potentially larger differences existing between Cf(III) and Am(III). A general discussion of actinide complexes (including californium) in aqueous solution is available (Jones and Choppin, 1969). Horwitz *et al.* (1997) discuss complexer in solution.

From the initial studies on Cf(III) and sulfate ions (De Carvalho and Choppin, 1967) it was concluded that 1:1 and 1:2 complexes $Cf(SO_4)^+$ and $Cf(SO_4)_2^-$ were formed, but subsequent work in the sulfate system suggested that mono-, di-, and trisulfate species were formed (McDowell and Coleman, 1972).

Table 11.13 *Stability constants of Cf(III) complexes and chelates.*

Ligand	*Experimental method*	*Log of stability constants*[a] *at* 25°C	*References*
fluoride ion	solv. extract.	$\beta_1 = 3.03$ $\mu = 1.0$	Choppin and Unrein (1976)
hydroxide ion	solv. extract	$\beta_1 = 5.62$ $\beta_1 = 5.05$ $\mu = 2.00$	Desiré *et al.* (1969)
sulfate ion	solv. extract.	$\beta_1 = 1.36$ $\beta_2 = 2.07$ $\mu = 2.0$ $K_{01} = -3.73$ $K_{02} = -5.58$ $K_{03} = -5.09$ $\mu = 0$	De Carvalho and Choppin (1967)
thiocyanate ion	solv. extract. solv. extract.	$\beta_1 = 3.06$ $\beta_1 = 3.71$ $\beta_2 = 0.28$ $\beta_3 = 2.65$	Choppin and Ketels (1965) Coleman (1972)
acetate ion	solv. extract.	$\beta_1 = 2.11$ $\mu = 1.0$	Choppin and Schneider (1970)
oxalate ion	–	$\beta_3 = 12.5$ $\mu = 0.1$	Stary (1966)
	electromigr.	$\beta_1 = 5.50$ $\beta_2 = 3.87$ $\mu = 0.1$	Stepanov (1971)
lactic acid	–	$\beta_3 = 6.08$ $\mu = 0.15$	Stary (1966)
	solv. extract.	$\beta_3 = 6.09$ $\mu = 0.5$	Ermakov and Stary (1967)
	ion exchange	$\beta_3 = 6.08$ $\mu = 0.5$	Ermakov and Stary (1967)

α-hydroxyiso-butyric acid	ion exchange	$\beta_3 = 6.9$ $\mu = 0.5$	Desiré *et al*. (1969)
tartaric acid	–	$\beta_2 = 6.8$ $\mu = 0.1$	Desiré *et al*. (1969)
	solv. extract.	$\beta_2 = 5.86$	Aly and Latimer (1970)
ethylenediaminetetraacetic acid	ion exchange	$\beta_1 = 19.09$	Fuger (1958)
1,2-diaminocyclohexane-tetraacetic acid	ion exchange	$\beta_1 = 19.42$	Baybarz (1966a,b)
diethylenetriaminepentaacetic acid	–	$\beta_1 = 22.6$	Stary (1966)
	ion exchange	$\beta_1 = 22.57$	Baybarz (1965)
	ion exchange	$\beta_1 = 25.19$	Brandau (1971)
glycolate ion	solv. extract.	$\beta_1 = 2.63$ $\beta_2 = 1.97$ $\mu = 2.0$ (53°C)	Choppin and Degischer (1972)
2-methyllactic acid	solv. extract.	$\beta_1 = 4.10$ $\mu = 0.1$	Aly and Latimer (1970)
malic acid	solv. extract.	$\beta_1 = 7.02$ $\mu = 0.1$	Aly and Latimer (1970)
citric acid	solv. extract.	$\beta_1 = 11.61$ $\mu = 0.1$	Aly and Latimer (1970)
	electromigr.	$\beta_1 = 7.93$ $\beta_2 = 3.3$ $\mu = 0.1$	Stepanov (1971)
	solv. extract.	$\beta\left(C\frac{2-}{2}\right) = 10.90$ $\mu = 0.1$ $\beta\left(C\frac{3-}{2}\right) = 12.26$ $\mu = 0.1$	Hubert *et al*. (1974)
	solv. extract.	$\beta(\mathrm{M(HCit^-)_2} = 5.8;$ $\mu = 0.1$ $\beta(\mathrm{M(HCit)(Cit^{2-})} = 9.9;$ $\mu = 0.1$	Guillaumont and Bourderie (1971)

Table 11.13 (*Contd.*)

Ligand	*Experimental method*	*Log of stability constants*[a] *at* 25°C	*References*
thenoyltrifluoroacetone	solv. extract.	$\beta_3 = 14.94$ $\mu = 0.1$	Keller and Schreck (1969)
benzoyltrifluoroacetone	solv. extract.	$\beta = 16.06$ $\mu = 0.1$	Keller and Schreck (1969)
naphthoyltrifluoroacetone	solv. extract.	$\beta = 18.83$ $\mu = 0.1$	Keller and Schreck (1969)
nitrilodiaceto-monopropionic acid	ion exchange	$\beta_1 = 10.94$ $\beta_2 = 18.45$	Eberle and Ali (1968) Eberle and Ali (1968)
nitrilotriacetic acid	ion exchange	$\beta_1 = 11.92$ $\beta_1 = 11.3$ $\beta_2 = 21.0$ $\mu = 0.1$	Stary (1966)
N-2-hydroxyethyl-ethylenediaminetriacetic acid	ion exchange	$\beta_1 = 16.27$ $\beta_2 = 28.5$ $\mu = 0.1$	Eberle and Ali (1968) Eberle and Bayat (1967)
2-hydroxy-1,3diamino-propane tetraacetic acid		$\beta_1 = 13.18$ $\mu = 0.1$	Baybarz (1967)
5,7-dichloro-8-hydroxyquinoline	solv. extract.	$\beta_3 = 22.59$	Feinauser and Keller (1969)
4-benzolyl-3-methyl-1-phenyl-2-pyrozolin-5-one	solv. extract	$\beta_3 = 17.78$ $\mu = 0.1$	Keller (1971)

4-acetyl-3-methyl-1-phenyl-2-pyrozolin-5-one	solv. extract	$\beta_3 = 13.48$ $\mu = 0.1$	Keller (1971)
2-hydroxyethyl-iminodiacetic acid	solv. extract.	$\beta_1 = 9.61$ $\mu = 0.1$	Ermakov *et al*. (1971b)
o-hydroxyphenyl-iminodiacetic acid		$\beta_1 = 7.38$ $\beta_2 = 12.28$ $\mu = 0.1$	Ermakov *et al*. (1971)
2-ethylhexylphenyl-phosphoric acid		$\beta_1 = 6.03$ $\beta_2 = 2.00$ $\mu = 0.1$	Barketov *et al.* (1975)
thenoyltrifluoroacetone		$\beta_1 = 6.90$ $\mu = 0.1$	Khopkar and Mathur (1977)

[a] Overall formation constants:

$$\beta_1 = \frac{[\mathrm{CfA}^{(3-n)+}]}{[\mathrm{Cf}^{3+}][\mathrm{A}^{n-}]}, \quad \beta_2 = \frac{[\mathrm{CfA}_2^{(3-2n)+}]}{[\mathrm{Cf}^{3+}][\mathrm{A}^{n-}]^2} \quad \text{etc.}$$

stepwise constants:

$$K_2 = \frac{[\mathrm{CfA}^{(3-2n)+}]}{[\mathrm{CfA}^{(3-n)+}][\mathrm{A}^{n-}]} \quad \text{etc.}$$

A similar situation exists for the thiocyanate complexes reported for Cf(III). Initially a 1:1 complex, $Cf(SCN)^{2+}$, was reported (Choppin and Ketels, 1965), but subsequent work indicated that three different complexes could form: $Cf(SCN)^{2+}$, $Cf(SCN)_2^+$, and $Cf(SCN)_3$, where the 1:3 complex was of the inner-sphere type (Coleman, 1972).

The hydrolysis behavior of Cf(III) is expected to be similar to that of trivalent lanthanides, and more specifically to that of Eu(III) or Gd(III), which have nearly the same ionic radii. The first hydrolysis reaction (i.e. $Cf^{3+} + H_2O \rightarrow CfOH^2 + H^+$; i.e. the K_1 value) has also been determined for Cf(III); log K_1 values for it were given as –5.62 (Desiré *et al.*, 1969) and –5.05 (Hussonnois *et al.*, 1973).

Several quite stable complexes can be formed with Cf(III) (see Table 11.13). Complexes of diketones and aminopolycarboxylic acids have been found to be considerably more stable than those of tartrate, lactate, oxalate, etc. In some cases, adduct chelates can also form with Cf(III), such as with the californium thenoyltrifluoroacetone (TTA) chelate and methyl isobutyl ketone (MIBK) (i.e. $Cf(TTA)^{3+}$ and Cf(TTA) → MIBK or Cf(TTA)3−2 MIBK; Desiré *et al.*, 1969).

With the monodentate ligands, such as tributyl phosphate (TBP), the extractable californium adduct from nitric acid solutions has been assigned as being a 1:3 species $Cf(NO_3)_3 \cdot 3$ TBP (Healy and McKay, 1956). Quaternary ammonium bases and alkylpyrocatechols (i.e. 4-dioctylethyl pyrocatechol) can form californium complexes in alkaline solutions (Derevyanko *et al.*, 1976), which affords a different medium for complexation. One recent extraction study has examined the influence of the extractant's structure on the extraction behavior of californium (Derevyanko *et al.*, 1976). A large number of materials have been investigated for forming extractable complexes of californium, and the reader is referred to reviews on the subject (Ishimori, 1980; Myasoedov *et al.*, 1980; Shoun and McDowell, 1980). Takeiski *et al.* (2001) have discussed the solvent extraction of californium by deratives of bis(1-phenyl-3-methyl-4-acylpyrazol-5-one) .

Exchange kinetics of Cf(III) with europium ethylenediaminetetraacetate (Eu EDTA) in aqueous solution ($\mu = 0.1$) has also been reported (Williams and Choppin, 1974). The exchange was found to be a first-order reaction having both acid-dependent and acid-independent terms.

From a study of the relationship between distribution coefficients for californium with sodium nitrate in extractions using organic ammonium nitrates, the apparent mean molar activity coefficient of Cf(III) was calculated in terms of a polynomial ($\log k = a + bm + cm^2 + dm^3$, where $a = 0.00397$, $b = -0.154$, $c = 0.0252$, and $d = 0.00119$) (Chudinov and Pirozhkov, 1973).

Some initial studies of californium complexes involving 6-methyl 2-(2-pyridyl)-benzimidazole and derivatives of it have been carried out. The initial studies involved photoluminescence and Raman spectroscopy investigations, where it was concluded that 1:1, 1:2, 1:3, and 1:4 complexes were formed (Assefa *et al.*, 2005).

A general discussion of the hydrolysis of actinide ions is given in a review by Ahrland (1991). Although little is mentioned about californium, several general concept discussed there are useful for the trivalent actinides. In another review, Bhattacharyya and Natarajan (1991) discuss the radiation chemistry of actinide solutions. A rate constant for the oxidation of Cf^{2+} by water ($K = 7 \times 10^4$ м$^{-1}$ s^{-1}) and a rate constant for the reduction of Cf^{3+} ($K = 3 \times 10^9$ м$^{-1}$ s^{-1}) at a pH of 5.3 are quoted.

11.8.4 Thermodynamic data

The thermodynamic behavior of californium has been addressed in Chapter 19. Given there are the recommended values for californium that have been arrived at after considering various reports.

Selected thermodynamic data for the formation of Cf(III) in solution (according to the following reaction):

$$Cf_{(s,a)} + 3H^+_{(aq)} = Cf(III)_{(aq)} + 3/2H_{2(g)}$$

are given in Table 11.14 (also see Section 11.6.2 on californium metal for comments on its enthalpy of solution), which has been used for calculating the enthalpy of formation of aqueous ions. The enthalpy of formation, $\Delta H^\circ_{298,f}(Cf^{3+},aq))$ was derived from the enthalpy of solution (Fuger *et al.*, 1984) as being –577(5) kJ mol^{-1}. The entropy, S° (Cf^{3+}, aq)), has been accepted as –197(17) J K^{-1}·mol^{-1} (see Chapter 19). Using these values and S°(Cf, cr, α phase, 298.15 K) = 81(5) (Ward, 1983; see Chapter 19) one obtains $\Delta_f G(Cf^{3+},aq)$ = –533(7) kJ mol^{-1}. A standard potential for the Cf(III)/Cf(0) couple was calculated to be –(1.92 ± 0.03) V in that work. Earlier estimates for this potential ranged from –1.95 to –2.03 V (Nugent, 1975; David *et al.*, 1976a,b; David *et al.*, 1978; Samhoun and David, 1979).

Other estimates for ΔH_f (Cf^{3+},aq) have appeared in the literature. Nugent *et al.* (1973a,b) proposed a value of –623 kJ mol^{-1}; David *et al.* (1986) suggested –(586 ± 21) kJ mol^{-1}; and Nugent (1975) subsequently arrived at a value of –(602 ± 21) kJ mol^{-1}. A value of –603 kJ mol^{-1} was estimated for californium in a comparison given for thermochemical properties for the lanthanide and actinide elements (Morss, 1983). This latter work also presents other thermochemical values for californium.

Predictions of the standard free energy (ΔG_f) and the enthalpy of hydration (ΔH_{hyd}) for the trivalent californium ion have been made based on an electrostatic hydration model (Goldman and Morss, 1975). Assuming a crystallographic radius of 0.94 Å and a gas-phase radius of 1.516 Å for Cf(III), and using a primary hydration number of 6.1, ΔG°_{298} and ΔH°_{298} were calculated to be –3385 and –3582 kJ mol^{-1}, respectively.

Thermodynamic data for the 1:1 complex, $Cf(SO_4)^+$, have been calculated from the temperature dependence of the stability constant (De Carvalho and

Table 11.14 *Thermodynamic data for californium.*

A. Metal, crystal at 298.15 K and 10^5 Pa

S° (J K^{-1} mol^{-1})	$\Delta_{sub}H^\circ$ (kJ mol^{-1})
81(5)	196 (10)

B. Metal, gas at 298.15 K and 10^5 Pa

S° (J $K^{-1}mol^{-1}$)	Cp (J $K^{-1}mol^{-1}$)
201.3(30)	20.786(20)

C. High temperature heat capacity of the metal [Cp/J K^{-1} $mol^{-1} = a(T/K)^{-2} + b + c(TK) + d(T/K)^2 + e(T/K)^3$]

form	$A\times10^{-6}$	*b*	$C\times10^3$	$D\times10^6$	*e*	*T*/*K*	$\Delta_{trs}H$ (kJ mol^{-1})
dhcp		23.651	9.7865	9.0983		863	2.64
fcc	0.0580	37.6				1173	7.51

D. Aqueous ions at 298.15 K

Cf^{3+}	Cf^{3+}	Cf^{4+}	Cf^{4+}
S° (J K^{-1} mol^{-1})	Δ_fH° (kJ mol^{-1})	S° (J K^{-1} mol^{-1})	Δ_fH° (kJ mol^{-1})
–197(17)	–577(5)	–405(17)	–483(5)

E. Solid CfO_2 at 298.15 K

S_{exs} (J K^{-1} mol^{-1})	S° (J K^{-1} mol^{-1})	Δ_fH° (kJ mol^{-1})
21.3	87(5)	–858

F. Standard entropy and enthalpy of formation of Cf_2O_3 at 298.15 K

S° (J K^{-1} mol^{-1})	Δ_fH° (kJ mol^{-1})
176.0(50)	–1653(10)

G. Properties of californium halides at 298.15 K.

Halide	S° (J K^{-1} mol^{-1})	Δ_fH° (kJ mol^{-1})
CfF_4		–1623
CfF_3		–1553(35)
$CfCl_3$	167.2(6)	–965(20)
$CfBr_3$	202(5)	–752.5
CfI_2	154	–669

Source: Chapter 19.

Choppin, 1967). Values for this complex are: $\Delta G_{298} = -7.9$ kJ mol^{-1}, $\Delta H_{298} =$ 19 kJ mol^{-1}, and $\Delta S_{298} = 88$ kJ mol^{-1}. Similarly, data for the 1:1 CfF^{2+}complex have been calculated (Nugent *et al.*, 1973a,b), and have been given as: $\Delta G_{298} =$ 17.3 kJ mol^{-1}, $\Delta H_{298} = 27.2$ kJ mol^{-1}, and $\Delta S_{298} = 14$ kJ mol^{-1}.

Other thermodynamic data have also been reported for californium (David *et al.*, 1978). The reader is also referred to Chapter 19 for a more complete summary of thermodynamic data for californium.

11.8.5 Solution absorption spectra

The first absorption spectrum for Cf(III) was obtained from the solid state (Green, 1965; see Section 11.7.6). The first solution absorption spectrum was obtained shortly thereafter, using 592 μg of mainly ^{252}Cf isotope, which introduced experimental problems regarding both shielding and radiolytic gassing. Nineteen absorption bands were recorded between 280 and 1600 nm from a 1 M $DClO_4$ solution (see Table 11.15; Fig. 11.6). The absorption spectrum from this work was confirmed using milligram quantities of ^{249}Cf (Carnall and Fried, 1976).

Table 11.15 *Absorption data for Cf(III) in* 1 M $DClO_4$.[a]

Wavelength (nm)	*Wavelength* (cm^{-1})	*Absorption coefficient*, μ (L mol^{-1} cm^{-1})
1560.0	6 410	5.3
1211.0	8 260	1.6
840.3	11 900	2.5
769.8	12 990	6.3
745.2	13 420	6.4
673.8	14 840	2.5
640.2	15 620	1.7
602.0	16 610	4.9
490.0	20 410	1.9
469.9	21 280	8.9
442.1	22 620	10.3
434.8	23 000	9.8
401.9	24 880	0.9
353.4	28 300	1.0
334.0	29 940	1.5
325.0	30 770	3.8
304.9	32 800	1.1
295.0	33 900	2.4
284.0	35 210	1.9

[a] Conway *et al.* (1966).

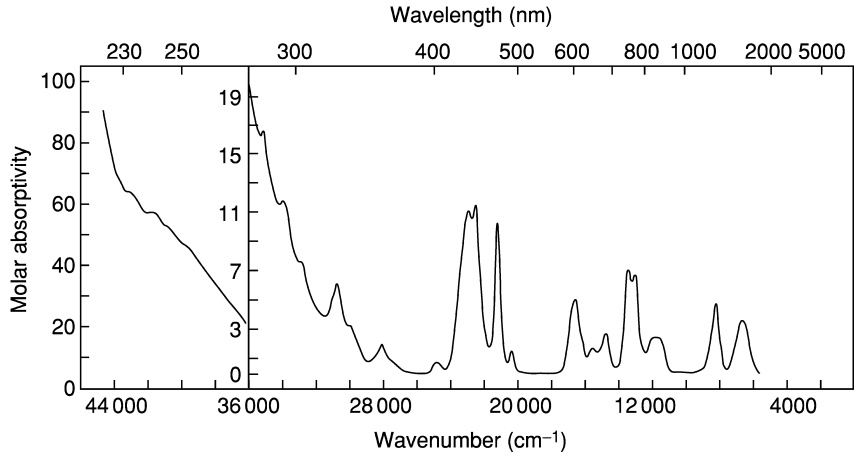

Fig. 11.8 *Solution absorption spectrum of Cf(III) in* 0.1 M $HClO_4$–$DClO_4$.

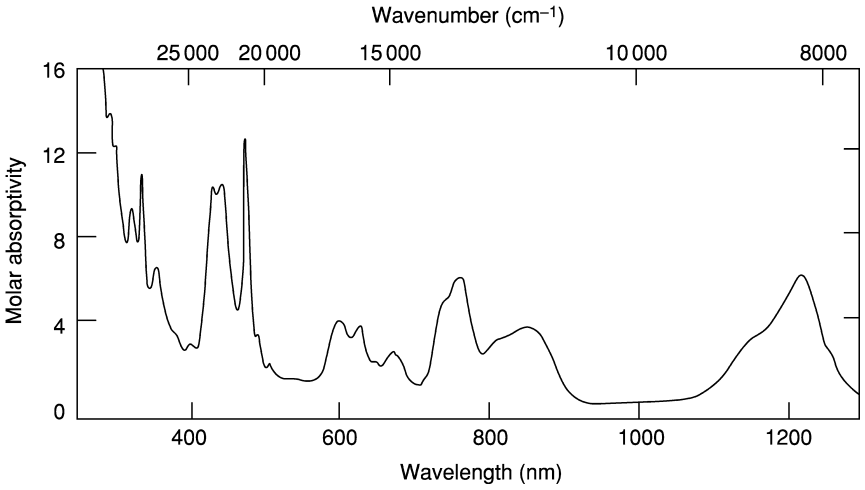

Fig. 11.9 *Solution absorption spectra of Cf(III) in* 0.12 M Na_2CO_3 *at pH* 12.

Fig. 11.8 shows the Cf(III) absorption spectrum obtained from a 0.1 M $HClO_4$–$DClO_4$ solution. The absorption spectrum of Cf(III) in 2 M Na_2CO_3 (Hobart *et al.*, 1982) is shown in Fig. 11.9, and the intensities of the absorptions in the carbonate solution is given in Table 11.16. The spectrum of Cf(III) in the Na_2CO_3 solution is similar to that observed in 1 M $DClO_4$, but shifts in wavelength and enhancement of intensity occur for some peaks. See Chapter 16 for a comprehensive overview of actinide spectroscopy.

Table 11.16 *Absorption data for Cf(III) in* 2 m Na_2CO_3.[a]

Wavelength (nm)	*Wavelength* (cm^{-1})	*Absorption coefficient,* μ (L mol^{-1} cm^{-1})
293	34 100	14
303	33 000	12
322	31 000	9.3
336	29 800	11
355	28 200	6.5
402	24 900	2.9
430	23 200	10
443	22 600	11
474	21 100	13
491	20 400	3.3
506	19 800	2.0
600	16 700	4.0
625	16 000	3.8
674	14 800	2.4
740	13 500	4.9
757	13 200	6.0
850	11 800	3.7
1140	770	2.8
1214	8 240	6.1

[a] Hobart *et al.* (1983).

The absorption spectrum of Cf(IV) and Cf(III) in a potassium phosphotungstate medium has been reported (Kosyakov *et al.*, 1977; Myasoedov, 1982). The phosphotungstate ion stabilizes the Cf(IV) oxidation state sufficiently to permit spectra to be obtained (half-life approximately 70 min at room temperature). This Cf(IV) oxidation state was achieved by using potassium persulfate at elevated temperatures; attempts to oxidize (Cf(III) electrochemically in this medium were not successful. The absorption spectrum of Cf(IV) in this medium is characterized by a broad absorption band beginning at 1030 nm and increasing in intensity down to 390 nm. The maximum absorption appears at about 450 nm, which is similar to the absorption maximum obtained for Cm(IV) and Tb(IV) in this medium (Myasoedov, 1982). The absorption of a comparable Cf(III) phosphotungstate solution did not show a significant absorbance over this spectral region.

11.9 GAS-PHASE STUDIES

In addition to studies in the solid phase and in solution, investigations of reactions in the gas phase provide important insights into the chemistry and electronic make-up of californium. These studies in the gaseous state examine the reactions of Cf ions with other molecules, as opposed to addressing the vaporization of the metal (see Section 11.6), or other solids such as oxides

(see Section 11.7.3), which can provide important thermodynamic parameters for these materials (i.e. their enthalpies of vaporization and formation).

The gas-phase chemistry of californium has been studied by mass spectrometry time-of-flight, and Fourier transform ion resonance mass spectrometry (FTIRMS), and the latter offers an especially powerful technique in this regard. In this technique, metal ions can be isolated and then reacted with other specific materials, which can lead to bond dissociation energies, reaction kinetics, and ionization potentials for the metal ions being studied. Important information about californium's electronic configuration, which can be used for systematic comparisons with other actinides, is also be obtained from these gas-phase reactions.

One area of this californium gas-phase chemistry has involved the dehydrogenation of alkenes, thiols, ethers, and perfluorohydrocarbons by Cf^+ (Gibson and Haire, 2000). The emphasis in that work was on the efficiency of dehydrogenation of alkenes by Cf^+ ions, and direct comparisons with the comparable reactivities of Cm^+, Pr^+, and Tm^+ for similar reactions. It was determined that Cf^+ is inefficient at C–H bond activation, due to its particular electronic structure and energy levels, and evidence was not found for the direct participation of its 5f electrons in the reactions studied.

In related studies, organometallic ions of californium were produced in the gas phase by laser ablation of Cf_2O_3 dispersed in polyimide matrices. This process was followed by mass spectrometric analyses (Gibson and Haire, 2001). Primary products formed were: CfC_2H^+, $CfCN^+$, CfC_4H^+, $Cf(OH)(CN)^+$, $CfOCN^+$, $CfOH^+$, $Cf(OH)_2^+$, and CfO^+. Some of these products represent the first organometallic materials for californium where it is directly bonded to carbon. It was concluded that the composition and abundance of the products are dependent on the ability of californium to have two non–5f valence electrons at the Cf^+ center for participation in the bonding, which involves a single sigma-type bond with the organic material. Thus californium exhibits 'monovalent character' (one direct actinide–carbon bond; as do americium and berkelium) versus 'divalent character' of thorium, uranium, neptunium, plutonium, and curium (two direct actinide-carbon bonds)

This behavior is electronically orientated and associated with the $f \rightarrow d$ promotion energies of the actinides to give a chemically active 6d orbital. As the promotion energy for californium is higher (i.e. $\sim$200 kJ mol^{-1}, see Fig. 11.10) than earlier actinides, this diminishes the generation of reaction products for it. More recent work with Cf^+ and Es^+ (see Chapter 12) has shown that a greater reactivity is observed with pentamethylcyclopentadiene than with most other alkenes. It was found that Cf^+ reacts with this reagent to produce $[MCp^*]^+$ and other products. This behavior of Cf^+ allows estimates for low-lying electronic levels (Gibson and Haire, 2005).

In studies of californium with several alkenes (Gibson and Haire, 2004), it was determined that the relative C–H activation of Cf^+ was $<1\%$ of that for Cm^+. Thus, instead of C–H activation from insertion of the metal center into a

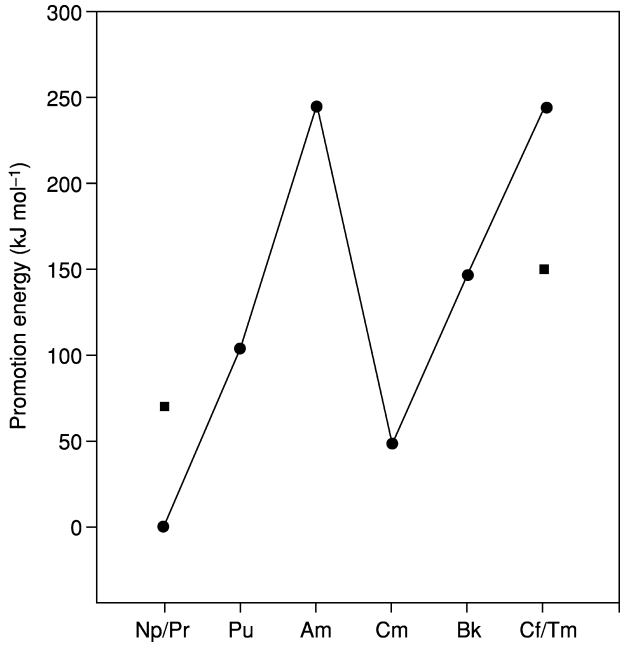

Fig. 11.10 *The f–d promotion energies for selected actinides. Values for Pr and Tm* (*solid blocks*) *are given for comparison*. (*Gibson*, 2003).

C–H bond (i.e. C–Cf^+–H), reactions of Cf^+ with butryonitrile produces an adduct, M^+-butrynitrile. Californium also resisted the formation of CfO^+ ions, consistent with its preference to be 'divalent' rather than 'trivalent' – attempts to oxidize Cf^+ with N_2O to yield CfO^+ in the gas phase were not successful.

In reactions of Cf^+ with perfluorophenanthrene (Gibson and Haire, 2005) only minor yields of CfF_2^+ were observed, again in accord with its propensity to remain divalent. This is also in accord with results noted in the vaporization of Cf_2O_3 at high-temperatures (Haire, 1994). Very little CfO is found in the vapor state as compared to atomic Cf vapor (see Section 11.7.3). This latter behavior is similar to that observed with Eu_2O_3 and Yb_2O_3 and results from the lower dissociation energy of CfO compared to CmO (Haire, 1994). The dissociation energies of the monoxides are also linked to the f–d promotion energies for f-electrons and the formation and availability of active 6d orbital–7s electron orbitals (Haire, 1994; Gibson, 2003).

11.10 CONCLUDING REMARKS

A considerable quantity of chemical and physical data have been acquired for californium over the years. In many instances this information was obtained

using tracer levels or microgram quantities of the element, often using the ^{252}Cf isotope. With the availability of multi-milligram amounts of ^{249}Cf isotope, it became possible to expand studies of californium and prepare pure samples of the metal. This allowed important information to be obtained for californium; acquiring the enthalpy of solution (Fuger *et al.*, 1984) and the sublimation of californium metals (Ward *et al.*, 1980) are two such examples. These data then allowed thermodynamic cycles to be established for the element and many of its compounds.

Given the limited supplies of ^{249}Cf (i.e. perhaps a total of some 50–100 mg exist) as well as other experimental limitations (given its radioactive decay process, the accompanying heat, personnel radiation exposures, etc.) it may not be possible to perform all the desired experiments or to be able to carry them out to the degree of perfection that may be desired. However, californium is the element with the highest atomic number in the periodic table expected to be available in weighable amounts (milligrams) and that has a reasonably long half-life. This allows many studies with it that cannot be done with higher members of the actinide series or periodic table. The next element, einsteinium (see Chapter 12) is available in only multi-microgram amounts, but its very high specific radioactivity and the short half-lives of its isotopes severely limit the experiments can be performed with it. Therefore, data on californium can provide insights/extrapolations into the chemical/physical properties of the higher members of the actinide series, in addition to the importance of its own data in providing a better understanding of the architecture of the periodic table.

Oxidation states of 0, II, III, and IV have been established for Cf, with the III state being the most prevalent and the only state presently known to have a reasonable stability in aqueous solutions. The existence of Cf(V) has been suggested but needs confirmation. In may be more probable to generate this oxidation state in solids or nonaqueous solutions and/or molten salts than in aqueous solutions. Future investigations of californium may place emphasis on stabilizing oxidation states other than Cf(III).

Studies of californium in the gaseous state offer important new thrusts in californium chemistry. Using ion cyclotron resonance mass spectrometry, californium ions can be selected, held, and then reacted with a variety of materials to establish important parameters, thermodynamic properties, bond dissociation energies, reaction kinetics, etc.

Although a considerable amount of information has been acquired for californium metal, there are still unanswered questions about it, for example, concerning a potential divalent form of the metal under certain conditions. Recent high-pressure diffraction studies on the metals have provided important new aspects about the behavior of their 5f electrons under pressure and reduced interatomic distances. Indeed, under these very high pressures (i.e. 100 GPa or higher), the electronic nature of californium metal changes, and it adopts

lower-symmetry structures normally displayed by the lighter actinide metals (Pa–Pu), which have itinerant 5f electrons at atmospheric pressure. These high pressures on californium metal forces the involvement of its 5f electrons into its bonding and changes its physical properties. Thus, pressure can bring about a form of modern alchemy in californium metal with regard to its structure and properties.

There is also a considerable amount of work that can be done on californium compounds, such as the monopnictides and chalcogenides – the mononitride and monosulfide both offer interesting compounds to study in detail. Investigations of its compounds under high pressure should also provide new findings about californium's chemistry. Applying modern tools (synchrotron-based, EXAFS, XANES, photon scattering, etc.) offers the potential to learn new facets about californium materials.

In short, there is a considerable amount of scientific work that needs to be done on californium, perhaps the highest atomic numbered element available for performing the usual actinide studies. The scope of such studies will be limited only by the imagination and skill of the investigators.

ACKNOWLEDGMENTS

The author gratefully acknowledges the assistance of several personnel at the Oak Ridge National Laboratory, as well as other institutions, for helpful discussions, references, comments, and in some cases collaborative studies on californium. The research reported herein was sponsored by the Division of Chemical Sciences, U.S. Department of Energy, under contract DE-AC05-00OR22725 with UT-Battelle, LLC.

REFERENCES

Adar, S., Sjoblom, R. K., Barnes, R. F., Fields, P. R., Hulet, E. K., and Wilson, H. D. (1963) *J. Inorg. Nucl. Chem.*, **25**, 447–52.

Ahmad, I. (1980) *Abstr. Pap. Am. Chem. Soc.*, **179** (Mar) 122-NUCL.

Ahrland, S. (1991) in *Handbook on the Chemistry and Physics of the Actinides,* vol. 6 (eds. A. J. Freeman and C. Keller), North-Holland, New York, pp. 471–510.

Aizenberg, M. I., Fedoseev, E. V., and Travnikov, S. S. (1988) *Sov. Radiochem.*, **30**(3), 299–302.

Aleksandrov, B. M., Malysheva, L. P., Savoskina, G. P., Smirnova, E. A., and Krivokhat-skii, A. S. (1972) *Radiokhimiya*, **19**, 472–7.

Allen, J. W., Johanson, L. I., Bauer, R. S., and Lindau, I. (1978) *Phys. Rev. Lett.*, **41**, 1499–502.

Aly, H. F. and Latimer, R. M. (1970) *Radiochim. Acta*, **14**, 27–31; and (1979) in *Actinide Chemistry and Spectroscopy* (ed. N. M. Edelstein) (ACS Symp. Ser. 131), American Chemical Society, Washington, DC, pp. 199–220.

Aly, H. F. and Abdelras, A. A. (1972) *Z. Anorg. Allg. Chem.*, **387**(2), 252–7.

Asprey, L. B. (1970) unpublished results; cited in Baybarz, Haire and Fahey (1972) *J. Inorg. Nucl. Chem.*, **35**, 1171–7.

Asprey, L. B. and Haire, R. G. (1973) *Inorg. Nucl. Chem. Lett.*, **9**, 1121–8.

Assefa, Z., Yaita, T., Haire, R. G., and Tachimori, S. (2005) *J. Solid State Chem.*, **178**, 505–11.

Bakiev, S. A., Kist, A. A., Rakhmanov, Z., and Flitsiyan, E.S. (1991) *J. Radioanal. Nucl. Chem.*, **147**(1), 59–68.

Baring, A.M. and Smith, J. L. (2000) USDOE Report LA-UR-00-4100, pp. 90–128.

Barketov, E. S., Zaitsev, A. A., and Felermonov, V. T. (1975) *Sov. Radiochem.*, **17**, 383–7.

Barnanov, A. A., Simakin, G. A., Kosyakov, V. N., Rin, E. A., Kopytov, V. V., Timofeev, G. A., and Rykov, A. G. (1981) *Radiokhimiya*, **23**(1), 127–9; (1981) *Sov. Radiochem.*, **23**, 104–6.

Bärnighausen, H. (1976) in *Proc. 12th Rare Earth Research Conf.* (ed. C. E. Lundin), Vail, Colo., July 1976, pp. 404–13.

Baybarz, R. D., Weaver, B. S., and Kinser, H. B. (1963) *Nucl. Sci. Eng.*, **17**, 457–62.

Baybarz, R. D. (1965) *J. Inorg. Nucl. Chem.*, **2**, 1831–9.

Baybarz, R. D. (1966a) *J. Inorg. Nucl. Chem.*, **28**, 23–31.

Baybarz, R. D. (1966b) *J. Inorg. Nucl. Chem.*, **28**, 1055–61.

Baybarz, R. D. (1967) USAEC Report ORNL-4145, p. 225.

Baybarz, R. D., Haire, R. G., and Fahey, J. A. (1972) *J. Inorg. Nucl. Chem.*, **34**, 5576–85.

Baybarz, R. D., Knauer, J. B., and Orr, P. B. (1973) USAEC Report ORNL-4672, Oak Ridge National Laboratory.

Baybarz, R. D. (1973) *J. Inorg. Nucl. Chem.*, **35**, 4149–58.

Baybarz, R. D., Fahey, J. A., and Haire, R. G. (1974) *J. Inorg. Nucl. Chem.*, **36**, 2023–7.

Baybarz, R. D. and Haire, R. G. (1976) *J. Inorg. Nucl. Chem.*, Suppl., 7–12.

Beamer, J. L., Mahony, T. D., and Sullivan, M. F. (1974) *Radiat. Res.*, **36**(6), 1295–302.

Belenkll, B. G., Bondarenko, P. V., Gankina, E. S., *et al.* (1991) *Vysokomol Soedin*, A**33**(9), 2020–6.

Benedict, U., Peterson, J. R., Haire, R. G., and Dufour, C. (1984) *J. Phys. F.: Metal Phys.*, **14**, L43–7.

Benker, D. E., Chattin, F. R., Collins, E. D., Knauer, J. B., Orr, P. B., Ross, R. G., and Wiggins, J. T. (1981) in *Transplutonium Elements – Production and Recovery* (eds. J. D. Navratil and W. W. Schulz) (ACS Symp. Ser. 161), American Chemical Society, Washington, DC, pp. 161–72.

Berger, H. (2004) *Appl. Radiat. Isot.*, **61**(4), 437–42.

Bhattacharyya, P. K. Natarajan, R. and (1991) in *Handbook on the Chemistry and Physics of the Actinides,* vol. 6 (eds. A. J. Freeman and C. Keller), North-Holland, New York, pp. 597–640.

Bigelow, J. E. (1974) in *Gmelin Handbuch der Anorganischen Chemie*, Suppl. Ser., *Transuranium*, Springer-Verlag, New York, vol. 7b, part Al, II, The Elements, pp. 326–36.

Bigelow, J. E., Collins, E. D., and King, L. J. (1980) in *Actinide Separations* (eds. J. D. Navratil, and W. W. Schulz) (ACS Symp. Ser. 117), American Chemical Society, Washington, DC, pp. 147–55.

Bigelow, J. E., Corbett, B. L., King, L. J., McGuire, S. C., and Sims, T. M. (1981) in *Transplutonium Elements – Production and Recovery* (eds. J. D. Navratil and W. W. Schulz) (ACS Symp. Ser. 161), American Chemical Society, Washington, DC, pp. 3–18.

Biggs, F., Mendelsohn, L. B., and Mann, J. B. (1975) *At. Data Nucl. Data Tables*, **16**, 201–309.

Blaise, J. and Wyart, J. F. (1992) Energy levels and atomic spectra of actinides, in *International Tables of Selected Constants*, Curie University, Paris, pp. 401–7; and the WEB, www.lac.u-psud.fr/Database/Tab-energy-californium.

Bouissières, G., Jouniaux, B., Legoux, Y., Merinis, J., David, F., and Samhoun, K. (1980) *Radiochem. Radioanal. Lett.*, **45**(2), 121–8.

Brandau, E. (1971) *Inorg. Nucl. Chem. Lett.*, **7**, 1177–81.

Brewer, L. (1971a) *J. Opt. Soc. Am.*, **61**, 1101–11.

Brewer, L. (1971b) *J. Opt. Soc. Am.*, **61**, 1666–82.

Brooks, M. S. S., Johansson, B., and Skriver, H. L. (1984) in *Handbook on the Physics and Chemistry of the Actinides* (eds. A. J. Freeman and G. H. Lander), North-Holland, New York, pp. 153–271.

Brown, D. (1968) in *Halides of the Lanthanides and Actinides*, John Wiley, London, pp. 48–78.

Burns, J. H., Peterson, J. R., and Baybarz, R. D. (1973) *J. Inorg. Nucl. Chem.*, **35**(4), 1171–7.

Burns, J. H., Peterson, J. R., and Stevenson, S. N. (1975) *J. Inorg. Nucl. Chem.*, **37**, 743–9.

Burns, J. B., Haire, R. G., and Peterson, J. R. (1998) *J. Alloys. Compd.*, **271**, 676–9.

Caird, J. A., Hessler, J. P., Paszek, A. P., Carnall, W. T., Crosswhite, H. M., Crosswhite, H., Diamond, H., and Williams, C. W. (1976) *Bull. Am. Phys. Soc.*, **21**, 1284–7.

Californium (^{252}Cf) Progress Reports and Bibliography are available from: (a) Californium Information Center, Savannah River Laboratory, Aiken, SC 29801, USAEC Report 1969; (b) Oak Ridge User Facility, Oak Ridge, TN 37831.

Campbell, D. O. (1981) in *Transplutonium Elements – Production and Recovery* (eds. J. D. Navratil and W. W. Schulz) (ACS Symp. Ser. 161), American Chemical Society, Washington, DC, pp. 189–202.

Carlson, T. A. and Nestor, C. W. Jr (1977) *At. Data Nucl. Data Tables*, **19**(2), 15373.

Carnall, W. T., Fried, S. M., Wagner, F. Jr, Barnes, R. F., Sjoblom, R. K., and Fields, P. R. (1972) *Inorg. Nucl. Chem. Lett.*, **8**, 773–4.

Carnall, W. T., Fried, S., and Wagner, F. Jr (1973) *J. Chem. Phys.*, **58**, 1938–49.

Carnall, W. T. and Fried, S. (1976) in *Proc. Symp. Commemorating the 25th Anniversary of the Elements 97 and 98*, Lawrence Berkeley Laboratory LBL-Report 4366, pp. 61–9.

Carnall, W. T., Crosswhite, H. M., Crosswhite, H., Hessler, J. P., Aderhold, C., Caird, J. A., Paszek, A., and Wagner, F. W. (1977) in *Proc. 2nd Int. Conf. on Electronic Structure of the Actinides* (eds. J. Mulak, W. Suski, and R. Troc), Wroclaw, Poland, pp. 105–10.

Carter, F. L. (1979) *J. Physique*, Suppl. **C–4**, 228–9.

Carvalho, F. P. and Fowler, S. W. (1985) *Mar. Biol.*, **89**(2), 173–81.
Castro, J. R., Oliver, G. D., and Withers, H. R. (1973) *Am J. Roentgenol.*, **117**(1), 182–94.
Cebulska- Wasilewska, A., Rekas, K., and Kim, J. K. (1999) *Nukleonika* **44**(1), 15–30.
Chakravortty, V., Perevalov, S. A., and Kulyako, Y. M. (1989) *J. Radioanal. Nucl. Chem. Lett.*, **136**(2), 85–94.
Chang, C. T. P, Haire, R. G., and Nave, S. E. (1990) *Phys. Rev.*, **B41**(13-A), 9045–8.
Chen, M. H., Crasemann, B., Huang, K.-N., Aoyagi, M., and Mark, H. (1977) *At. Data Nucl. Data Tables*, **19**(2), 97–151.
Choppin, G. R., Harvey, B. G., and Thompson, S. G. (1956) *J. Inorg. Nucl. Chem.*, **2**, 66–8.
Choppin, G. R. and Ketels, J. (1965) *J. Inorg. Nucl. Chem.*, **27**, 1335–9.
Choppin, G. R. and Schneider, J. K. (1970) *J. Inorg. Nucl. Chem.*, **32**, 3283–8.
Choppin, G. R. and Degischer, G. (1972) *J. Inorg. Nucl. Chem.*, **34**, 3473–7.
Choppin, G. R. and Unrein, P. J. (1976) in *Transplutonium 1975* (eds. W. Müller and R. Lindner), North-Holland, New York, 97–107.
Chudinov, E. G. and Pirozhkov, S. V. (1973) *Sov. Radiochem.*, **15**, 195–9.
Cohen, L. H., Aten, A. H. W. Jr, and Kooi, J. (1968) *Inorg. Nucl. Chem. Lett.*, **4**, 249–52.
Coleman, C. F. (1972) *J. Inorg. Nucl. Chem.*, **34**, 1381–97.
Collins, E. D., Benker, D. E., Chattin, F. R., Orr, P. B., and Ross, R. G. (1981) in *Transplutonium Elements – Production and Recovery* (eds. J. D. Navratil and W. W. Schulz) (ACS Symp. Ser. 161), American Chemical Society, Washington, DC, pp. 147–60.
Conway, J. G., Bruger, J. B., Hulet, E. K., Morrow, R. J., and Gutmacher, R. G. (1962a) *J. Chem. Phys.*, **36**, 189–90.
Conway, J. G., Hulet, E. K., and Morrow, R. J. (1962b) *J. Opt. Soc. Am.*, **52**, 222.
Conway, J. (1976) in *Proc. Symp. Commemorating the 25th Anniversary of the Elements 97 and 98*, Lawrence Berkeley Report LBL 4366, pp. 70–5.
Conway, J. G., Worden, E. F., Blaise, J., and Verges, J. (1977) *Spectrochim. Acta B*, **32**, 97–9.
Conway, J. G., Worden, E. F., and Blaise, J. (1995) *J. Opt. Soc. Am.*, **B12**(7), 1186–202.
Copeland, J. C. and Cunningham, B. B. (1969) *J. Inorg. Nucl. Chem.*, **31**, 733–40.
Crosswhite, H. M. (1977) *Coll. Int. CNRS*, Spectroscopie des Eléments de Transition et des Elements Lourds dans les Solides, Editions du CNRS, Paris, pp. 65–9.
Cunningham, B. B. (1959) *J. Chem. Educ.*, **36**, 32–7.
Cunningham, B. B. and Ehrlich, P. (1970) USAEC Report UCRL-205426, p. 239.
Cunningham, B. B. and Parsons, T. C. (1970) USAEC Report UCRL-205426, pp. 239–40.
Cunningham, B. B., Morss, L. R., and Parsons, T. C. (1970) USAEC Report UCRL-19530, p. 276.
Damien, D. A., Haire, R. G., and Peterson, J. R. (1979) *J. Physique*, Suppl. **C–4**, 95–100.
Damien, D., Haire, R. G., and Peterson, J. R. (1980) *Inorg. Nucl. Chem. Lett.*, **16**, 537–41.
Damien, D., Haire, R. G., and Peterson, J. R., unpublished data.
David, F. and Bouissières, G. (1968) *Inorg. Nucl. Chem. Lett.*, **4**, 153–9.
David, F. (1970a) *C. R. Acad. Sci. Paris C*, **270**, 2112–15.
David, F. (1970b) *Radiochem. Radioanal. Lett.*, **5**, 279–85.
David, F. (1970c) *Rev. Chim. Minér.*, **7**, 1–10.

David, F. (1986) *J. Less-Common Metals*, **121**, 27–42.
David, F., Samhoun, K., and Guillaumont, R. (1976a) in *Transplutonium 1975* (eds. W. Müller and R. Lindner), North-Holland, Amsterdam, pp. 297–304.
David, F., Samhoun, K., Guillaumont, R., and Nugent, L. J. (1976b) in *Heavy Element Properties* (eds. W. Müller and H. Blank), North-Holland, New York, pp. 97–104.
David, F., Samhoun, K., Guillaumont, R., and Edelstein, N. (1978) *J. Inorg. Nucl. Chem.*, **40**, 69–74.
David, F., Maslennikov, A. G., and Peretrukhin, V. P. (1990a) *J. Radioanal. Nucl. Chem.*, **143**(2), 415–26.
David, F., Peretrukin, V. F., and Maslennikov, A. G. (1990b) *Radiochim. Acta.*, **50**(3), 151–4.
De Carvalho, R. H. and Choppin, G. R. (1967) *J. Inorg. Nucl. Chem.*, **29**, 725–36.
Dedov, V. B., Trukhlyaev, P. S., and Kalinichenko, B. S. (1986a) *Sov. Radiochem.*, **28**(5), 579–82.
Dedov, V. B., Trukhlyaev, P. S., and Kalinichenko, B. S. (1986b) *Sov. Radiochem.*, **28**(5), 583–6.
Derevyanko, E. P., Pirozkhov, S. V., and Chudinov, E. G. (1976) *Sov. Radiochem.*, **17**(2), 295–9.
Desiré, B., Hussonnois, M., and Guillaumont, R. (1969) *C. R. Acad. Sci. Paris C*, **269**, 448–51.
Dittner, P. E. and Bemis, C. E. (1972) *Phys. Rev. A*, **5**(2), 481–8.
Dullmann, C. E., Eichler, B., Eichler, R. *et al.* (2003) *Nucl. Instrum. Method A*, **512**(3), 595–605.
Eberle, S. H. and Bayat, I. (1967) *Radiochim. Acta*, **7**, 214–17.
Eberle, S. H. and Ali, S. A. (1968) *Z. Anorg. Allg. Chem.*, **361**, 1–14.
Edelstein, N. and Karraker, D. (1976) in *Proc. Symp. Commemorating the 25th Anniversary of Elements 97 and 98*, Lawrence Berkeley Laboratory Report LBL4366, pp. 75–84; and (1975) *J. Chem. Phys.*, **62**, 3–8.
Eichler, B., Hubener, S., and Erdmann, N. (1997) *Radiochim. Acta*, **79**(4), 221–33.
Elesin, A. A., Nikolaev, V. M., and Shalimov, V. V. (1986) *Sov. Radiochem.*, **28**, 723–6.
Erdmann, N., Nunnemann, M., Eberhardt, K., Herrmann, G., Huber, G., Kohlër, S., Kratz, J. V., Passler, G., Peterson, J. R., Trautmann, N., and Waldek, A. (1998) *J. Alloys Compd.*, **271–273**, 837–40.
Erin, E. A., Vityutnev, V. M., and Kopytov, V. V. (1981) *Sov. Radiochem.*, **23**(3), 277–80.
Ermakov, V. A. and Stary, J. (1967) *Sov. Radiochem.*, **9**, 195–8.
Ermakov, V. A., Vorob'eva, V. V., Zaitsev, A. A., and Yakovlev, G. N. (1971) *Sov. Radiochem.*, **13**, 710–13.
Feinauser, D. and Keller, C. (1969) *Inorg. Nucl. Chem. Lett.*, **5**, 625–30.
Ferris, L. M. and Mailen, J. C. (1970) *J. Inorg. Nucl. Chem.*, **32**, 2019–35.
Ferris, L. M. and Mailen, J. C. (1971) *J. Inorg. Nucl. Chem.*, **33**, 1325–35.
Fields, P. R., Wybourne, B. G., and Carnall, W. T. (1964) Argonne National Laboratory Report ANL-6911.
Filippov, E. M. (1979) *Sov. At. Energy*, **47**(4), 841–3.
Firsova, L. A., Chuveleva, E. A., and Kharitonov, O. V. (1990) *Sov. Radiochem.*, **32**(2), 372–5.

Firsova, L. A., Chuveleva, E. A., and Kharitonov, O. V. (1996) *Radiochemistry*, **38**(5), 407–9.
Firsova, L. A., Chuveleva, E. A., and Kharitonov, O. V. (1998) *Radiochemistry*, **40**(3), 254–6.
Florjan, D., Niedzwiedz, W., and Schneider (1999) *Neoplasma*, **46** (Suppl. S), 88–9.
Frenkel, V. Y., Kulyako, Y. M., and Chistyakov, V. M. (1986) *J. Radioanal. Nucl. Chem.*, **104**(4), 191–200.
Fried, S. and Cohen, A. (1968) *Inorg. Nucl. Chem. Lett.*, **4**, 611–15.
Fried, S., Cohen, D., Siegal, S., and Taire, B. (1968) *Inorg. Nucl. Chem. Lett.*, **4**, 4948.
Fried, S. M., Wagner, F. Jr, and Carnall, W. T. (1973) Argonne National Laboratory Report ANL-7996, p. 5.
Friedman, H. A., Stokely, J. R., and Baybarz, R. D. (1972) *Inorg. Nucl. Chem. Lett.*, **8**, 433–41.
Fu, K. and Phillips, T. L. (1973) *Radiat. Res.*, **55**(3), 605.
Fuger, J. (1958) *J. Inorg. Nucl. Chem.*, **5**, 332–8.
Fuger, J. (1975) in *MTP International Review of Science,* (eds. H. J. Emeleus and K. W. Bagnall), Inorganic Chemistry, ser. II, vol. 7 , Butterworths, London, pp. 151–94.
Fuger, J., Haire, R. G., and Peterson, J. R. (1984) *J. Less Common Metals*, **98**, 315–21.
Fuger, J., Haire, R. G., and Wilmarth, W. R. (1990) *J. Less Common Metals*, **158**(1), 99–104.
Fuger, J. and Matzke, H. J. (1991) in *Handbook on the Chemistry and Physics of the Actinides* vol. 6 (eds. A. J. Freeman and C. Keller), North-Holland, New York, pp. 641–84.
Fujita, D. K. and Cunningham, B. B. (1969) USAEC Report UCRL-19507, p. 136.
Fujita, D. K., Parsons, T. C., Edelstein, N., Noé, M., and Peterson, J. R. (1976) in *Transplutonium Elements 1975* (eds. W. Müller and R. Lindner), North-Holland, Amsterdam, pp. 173–9.
Gavrilov, K. A., Gwozdz, E., Stary, J., and Seng, W. T. (1966) *Talanta*, **13**, 471–6.
Ghiorso, A. (1983) *Int. J. Mass Spectrom.*, **53**, 21–6.
Gibson, J. K. and Haire, R. G. (1985) *Radiochim. Acta*, **38**(4), 193–6.
Gibson, J. K. and Haire, R. G. (1987) *J. Less Common Metals*, **127**, 257–67.
Gibson, J. K. and Haire, R. G. (2000) *Int. J. Mass Spectrom.*, **203**(1–3), 127–42.
Gibson, J. K. and Haire, R. G. (2001) *Radiochim. Acta*, **89**(6), 363–9.
Gibson, J. K. (2003) *J. Phys. Chem.* A **107**, 7891–9.
Gibson, J. K. and Haire, R. G. (2004) *J. Alloys and Compounds*, **363**, 112–16.
Gibson, J. K. and Haire, R. G. (2005) *Organometallics*, **24**, 119–26.
Goldman, S. and Morss, L. R. (1975) *Can. J. Chem.*, **53**, 2685–700.
Green, J. L. (1965) PhD Thesis, UCRL Report 16516, pp. 41–9.
Green, J. L. and Cunningham, B. B. (1966) *Inorg. Nucl. Chem. Lett.*, **2**, 365–71. 157.
Green, J. L. and Cunningham, B. B. (1967) *Inorg. Nucl. Chem. Lett.*, **3**, 43–9.
Gruen, D. M., Koehler, W. C., and Katz, J. J. (1951) *J. Am. Chem. Soc.*, **73**, 1475–9.
Guillaumont, R. and Bourderie, L. (1971) *Bull. Soc. Chim. Fr.*, **8**, 2806–9.
Guminski, C. (1996) *J. Phase Equilib.*, **17**(5), 443–4.
Guseva, L. I., Myasoedov, B. F., and Tikhomir, G. S. (1973) *J. Radioanal. Chem.*, **13**(2), 292–300.
Haire, R. G., Baybarz, R. D., and Fahey, J. A. (1972) *Inorg. Nucl. Chem.*, **34**, 557–62.

Haire, R. G. and Asprey, L. B. (1973) *Inorg. Nucl. Chem. Lett.*, **9**, 869–74.
Haire, R. G. and Baybarz, R. D. (1973a) *J. Inorg. Nucl. Chem.*, **35**, 489–96.
Haire, R. G. and Baybarz, R. D. (1973b) *Inorg. Nucl. Chem. Lett.*, **9**, 1121–4.
Haire, R. G. and Baybarz, R. D. (1974) *J. Inorg. Nucl. Chem.* **36**, 1295–302.
Haire, R. G. and Baybarz, R. D. (1979) Proc. 3rd International Conference on Electronic Structure of the Actinides, *J. de Physique Suppl.* C4 195.
Haire, R. G. (1974) USAEC Report 4966, p. 19.
Haire, R. G. and Asprey, L. B. (1975) *Proc. Berkelium and Californium Symposium*, Berkeley, CA, Jan. 20, 1975.
Haire, R. G. and Asprey, L. B. (1976) *Inorg. Nucl. Chem. Lett.*, **12**, 73–84.
Haire, R. G. (1976) in *Proc. 12th Rare Earth Research Conf.*, vol. II (ed. C. E. Lundin), Vail, Colo., July 1976, Denver Research Institute, pp. 584–93.
Haire, R. G., Young, J. P., Peterson, J. R., and Fellows, R. L. (1978) in *The Rare Earths in Modern Science and Technology* (eds. G. J. McCarthy and J. J. Rhyne), Plenum, New York, pp. 501–6.
Haire, R. G. (1978) USDOE Report ORNL–5485, p. 52; (1980) USDOE Report ORNL-5665, p. 71; and (1981) USDOE Report–5817, p. 65.
Haire, R. G., Young, J. P., Peterson, J. R., Ensor, D. D., and Asprey, L. B. (1980) unpublished data, presented at SE/SW Regional ACS Meeting, December 1980, New Orleans.
Haire, R. G. (1982) in *Actinides in Perspective* (ed. N. Edelstein), Pergamon Press, New York, pp. 309–42.
Haire, R. G., Benedict, U., Peterson, J. R., Dufour, C., and Dabos, S. (1986) *Physica*, **144B**, 19–22.
Haire, R. G. (1988) USDOE Report ORNL-5485, 52.
Haire, R. G. and Gibson, J. K. (1989) *J. Radioanal. Nucl. Chem.*, **143**(1), 35–51.
Haire, R. G. (1990) in *Metals Handbook*, ASM International, Materials Park, OH, pp. 1198–201.
Haire, R. G. (1994) *J. Alloys Compd.*, **213**, 185–90.
Haire, R. G. and Eyring, L. (1994) in *Handbook on the Physics and Chemistry of the Rare Earths* (eds. K. A. Gschneidner, L. Ewing, G. R. Choppin, and G. H. Lander), North-Holland, Amsterdam, pp. 449–505.
Haire, R. G. (1997) *J. Nucl. Mat.*, **247**, 1–6.
Haire, R. G. and Sato, T. (1998) unpublished work.
Haire, R. G., Raison, E. P., and Assefa, Z. (2002) *J. Nucl. Sci. and Technol.*, **3** (Suppl.), 616–19.
Haire, R. G., Heathman, S., Le Bihan, T., Lindbaum, A., and Iridi, M. (2004) *Mat. Res. Symp. Proc.*, **802**, 15–21.
Hannink, N. J., Hoffman, D. C., and Smith, B. F. (1992) *Solvent Extr. Ion Exch.*, **10**(3), 431–8.
Haschke, J. M. (1976) *Inorg. Chem.*, **15**, 298–303.
Haug, H. W. and Baybarz, R. D. (1975) *Inorg. Nucl. Chem. Lett.*, **11**, 847–55.
Haung, K., Aoyagi, M., Chen, M. H., Crasemann, B., and Mark, H. (1976) *At. Data Nucl. Data Tables*, **18**, 243–91.
Healy, T. V. and McKay, H. A. C. (1956) *Rec. Trav. Che. Pay-Bas*, **75**, 730–6.
Heathman, S., Haire, R. G., Le Bihan, T., Lindbaum, A., Litfin, K., Mèresse, Y., and Libotte, H. (2000) *Phys. Rev. B*, **63**, 214101.

Hessler, J. P., Caird, J. A., Carnall, W. T., Crosswhite, H. M., Sjoblom, R. K., and Wagner, F. Jr (1978) in *The Rare Earths in Modern Science and Technology* (eds. G. J. McCarthy and J. J. Rhyne), Plenum, New York, pp. 507–12.

Hessler, J. P. and Carnall, W. T. (1980) in *Lanthanide and Actinide Chemistry and Spectroscopy* (ed. N. M. Edelstein) (ACS Symp. Ser. 131), American Chemical Society, Washington, DC, pp. 349–68.

Hobart, D. E., Samhoun, K., Young, J. P., Norvell, V. E., Mamantov, G., and Peterson, J. R. (1981) *Inorg. Nucl. Chem. Lett.*, **16**, 321–8.

Hobart, D. E., Samhoun, K., and Peterson, J. R. (1982) *Radiochim. Acta*, **31**, 139–45.

Hobart, D. E., Varlashkin, P. G., Samhoun, K., Haire, R. G., and Peterson, J. R. (1983) *Rev. Chim. Minér.*, **20**, 817–27.

Horwitz, E. P., Bloomquist, C. A., Sauro, L. J., and Henderson, D. J. (1966) *Inorg. Nucl. Chem.*, **28**(10), 2313–24.

Horwitz, E. P., Sauro, L. J., Bloomquist, C. A. (1967) *Inorg. Nucl. Chem.*, **29**(8), 2033–46.

Horwitz, E. P., Bloomquist, C. A., Henderson, D. J. (1969a) *Inorg. Nucl. Chem.*, **31**(4), 1149–59.

Horwitz, E. P., Bloomquist, C. A., Henderson, D. J., *et al.* (1969b) *Inorg. Nucl. Chem.*, **31**(10), 3255–64.

Horwitz, E. P., Chiarizia, R., and Dietz, M. L. (1992) *Solvent Extr. Ion Exch.*, **10**, 313–16.

Horwitz, E. P., Chiarizia, R., and Dietz, M. L. (1993) *Anal. Chim. Acta*, **281**, 361–7.

Horwitz, E. P., Dietz, M. L., Chiarizia, R., Diamond, H., Maxwell, S. L. III, and Nelson, M. R. (1995) *Anal. Chim. Acta*, **310**, 63–8.

Hübener, S. and Zvara, I. (1982) *Radiochim. Acta*, **31**, 89–93.

Hübener, S., Eichler, B., and Schadel, M. (1994) *J. Alloys Compd.*, **213**, 429–32.

Hubert, S., Hussonnois, M., Brillard, L., Goby, G., and Guillaumont, R. (1974) *J. Inorg. Nucl. Chem.*, **36**(10), 2361–6.

Huray, P. G. and Nave, S. A. (1987) in *Handbook of the Physics and Chemistry of the Actinides,* vol. 2 (eds. A. J. Freeman and G. L. Lander), North-Holland, Amsterdam, pp. 311–72.

Hussonnois, M., Hubert, S., Brillard, L., and Guillaumont, R. (1973) *Radiochem. Radioanal. Lett.*, **15**, 47–56.

Hyde, E. K., Perlman, I., and Seaborg, G. T. (1971) *The Nuclear Properties of the Heavy Elements,* vol. II, Dover, New York, pp. 923–43.

Ionova, G. V., Spitsyn, V. I., and Pershina, V. G. (1980) in *Proc. 10ème Journées des Actinides* (eds. B. Johansson and A. Rosengren), Stockholm, Sweden, May 27–28, 1980, pp. 126–59.

Ionova, G. V., Pershina, V. G., and Suraeva, N. I. (1989a) *Sov. Radiochem.*, **31**(1), 9–14.

Ionova, G. V., Pershina, V. G., and Suraeva, N. I. (1989b) *Sov. Radiochem.*, **31**(4), 379–86.

Ishimori, T. (1980) in *Actinide Separations* (eds. J. D. Navratil and W. W. Schulz) (ACS Symp. Ser. 117), American Chemical Society, Washington, DC, pp. 333–50.

Johansson, B. and Rosengren, A. (1975a) *Phys. Rev. B*, **11**(4), 1367–73.

Johansson, B. and Rosengren, A. (1975b) *Phys. Rev. B*, **11**(4), 2740–3.

Johnson, E. and Fricke, B. (1991) *J. Phys. Chem.*, **95**, 7082.

Jones, A. D. and Choppin, G. R. (1969) *Actinides Rev.*, **1**, 311–36.

Jouniaux, B. (1979) Thesis, University of Paris, pp. 34–86.
Karalova, Z. K., Lavrinovich, E. A., and Myasoedov, B. F. (1990) *Sov. Radiochem.*, **32**(2), 93–6.
Karraker, D. G., and Dunlap, B. D. (1976) *J. Chem. Phys.* **65**, 2032–3.
Karelin, Y. A., Gordeev, Y. N., and Karasev, V. I. (1997) *Appl. Radiat. Isot.*, **48**(10–12), 1563–6.
Kasimov, F. D. and Skobelev, N. F. (1987) *Sov. Radiochem.*, **29**(5), 591–4.
Katz, J. J. and Seaborg, G. T. (1957) *The Chemistry of the Actinide Elements,* John Wiley, New York, pp. 386–99.
Keller, C. and Schreck, H. (1969) *J. Inorg. Nucl. Chem.*, **31**, 1121–32.
Keller, C. (1971) *The Chemistry of the Transuranium Elements,* Verlag Chemie, Weinheim, pp. 217–49 and 565–80.
Khopkar, P. K. and Mathur, J. N. (1977) *J. Inorg. Nucl. Chem.*, **39**, 2063–7.
Kimura, T. and Akatsu, J. (1991) *J. Radioanal. Nucl. Chem.*, **149**(1), 25–31.
King, L. J., Bigelow, J. E., and Collins, E. D. (1981) in *Transplutonium Elements – Production and Recovery* (eds. J. D. Navratil and W. W. Schulz) (ACS Symp. Ser. 161), American Chemical Society, Washington, DC, pp. 133–46.
Knapp, F. F., Beets, A. L., and Mirzadeh, S. (1999) *Czech. J. Phys.*, **49**, 799–809.
Knighton, J. B. and Steunenberg, R. K. (1966) US Patent 3276 861.
Kosyakov, V. N., Timofeev, G. A., Erin, E. A., Kopytov, V. V., and Andreev, V. J. (1977) *Radiokhimiya*, **19**(1), 82–4; (1977) *Sov. Radiochem*., **19**, 66–7.
Kosyakov, V. N., Erin, E. A., and Vityutnev, V. M. (1982a) *Sov. Radiochem.*, **24**(5), 455–7.
Kosyakov, V. N., Erin, E. A., Vityutnev, V. M., Kopytov, V. V., and Rykov, A. G. (1982b) *Radiokhimiya*, **24**(5), 551–3.
Kovantseva, S. N., Kasimova, V. A., and Filimonov, V. T. (1986) *Sov. Radiochem.*, **28**(2), 174–7.
Krause, M. O., Haire, R. G., Keski-Rahkonen, O., and Peterson, J. R. (1988). *J. Electron Spectrosc. Relat. Phenom.*, **47**, 215–26.
Kulyukhin, S. A., Mikheev, N. B., and Rumer, I. A. (1997) *Radiochemistry*, **39**(2), 130–2.
Laubereau, P. G. and Burns, J. H. (1970a) in *Proc. 8th Rare Earth Research Conf*., vol. I (T. Henrie and R. Lindstrom), Reno, Nev., pp. 258–65.
Laubereau, P. G. and Burns, J. H. (1970b) *Inorg. Chem.*, **9**, 1091–5.
Lazarev, Y. A., Shirokovsky, I. V., Utyonkov, V. K., *et al.* (1995) *Nucl. Phys.*, **A588**(2), 501–9.
Lebedev, I. A. and Mazur, Y. F. (1981) *Sov. Radiochem.*, **23**(3), 291–9.
Leger, J. M., Yacoubi, N., and Loriers, J. (1980) in *The Rare Earths in Modern Science and Technology,* vol. II (eds. G. J. McCarthy, J. J. Rhyne, and H. B. Silber), Plenum Press, New York, pp. 203–8.
Liu, G. K., Huang, J., and Beitz, J. V. (1993) *Phys. Rev. B*, **48**(18), 13351–60.
Lloyd, R. D., Atherton, D. R., and Taylor, G. N. (1972a) *Radiat. Res.*, **51**(2), 542–7.
Lloyd, R. D., Mays, C. W., and Taylor, G. N. (1972b) *Health Phys.*, **22**(6), 667–71.
Lloyd, R. D., May, C. W., and McFarland, S. S. (1976) *Radiat. Res.*, **65**(3), 462–73.
Luke, H. and Eick, H. A. (1976) in *Proc. 12th Rare Earth Research Conf*. (ed. C. E. Lundin), Vail, Colo., July 1976, Denver Research Institute, pp. 424–32.
Mahony, T. D., Beamer, J. L., and Sullivan, M. F. (1973) *Radiat. Res.*, **55**(3), 606.

Mailen, J. C. and Ferris, L. M. (1971) *Inorg. Nucl. Chem. Lett.*, **7**(5), 431–8.
Maly, J. and Cunningham, B. B. (1967) *Inorg. Nucl. Chem. Lett.*, **3**, 445–51.
Maly, J. (1969) *J. Inorg. Nucl. Chem.*, **31**, 1007–18.
Manson, S. T. and Kennedy, D. J. (1974) *At. Data Nucl. Data Tables*, **14**(2), 111–20.
Marcus, Y., Givon, H., and Choppin, G. R. (1963) *J. Inorg. Nucl. Chem.*, **25**, 1457–63.
Martin, W. C., Hagan, L., Reader, J., and Sugar, J. (1974) *J. Phys. Chem. Ref. Data*, **3**(3), 771–5.
Martin, R. C., Laxson, R. R., and Knauer, J. B. (1997) *Appl. Radiat. Isot.*, **48**(10–12), 1691–5.
Martin, R. C., Byrne, T. E., and Miller, L. F. (1998) *J. Radioanal. Nucl. Chem.*, **236**(1–2), 5–10.
Martin, R. C., Knauer, J. B., and Balo, P. A. (2000) *Appl. Radiat. Isot.*, **53**(4–5), 785–92.
Martin, R. C., Glasgow, D. C., and Martin, M. Z. (2004) in *ACS Symp. Ser. 868*, American Chemical Society, Washington, DC, pp. 88–104.
Maruyama, Y., Feola, J. M., Tai, D., Wison, L. C., Van Nagel, J. R., and Yoneda, J. (1978) *Oncology*, **35**(4), 172–8.
Maruyama, Y., Yoneda, J., and Krolikiewicz, H. (1980) *Int. J. Radiat. Oncol.*, **6**(12), 1629–37.
Maruyama, Y., Vannagell, J. R., and Yoneda, J. (1991) *Cancer*, **68**(6), 1189–97.
McDowell, W. J. and Coleman, C. F. (1972) *J. Inorg. Nucl. Chem.*, **3**, 2837–50.
Miglio, J. J. (1978) *Int. J. Appl. Radiat. Isot.*, **29**(9–10), 581–4.
Mignano, J. and Rivard, M. (2004) *Radiothermodyn. Oncol.*, **71** (Suppl. 2), S77–8.
Mikheev, N. B., Spitsyn, V. I., Kamenskaya, A. N., Rozenkevich, N. A., Rumer, I. A., and Auerman, L. N. (1971) *Radiokhimiya*, **14**, 486–7; (1972) *Sov. Radiochem.*, **14**, 494–5.
Mikheev, N. B., Auerman, L. N., Spitsyn, V. I. (1972a) *Inorg. Nucl. Chem. Lett.*, **8**(10), 869–73.
Mikheev, N. B., Kamenskaia, A. N., Rumer, I. A., Spitsyn, V. I., Diatokova, R. A., and Rosenkevitch, N. A. (1972b) *Radiochem. Radioanal. Lett.*, **9**, 247–54.
Mikheev, N. B., Spitsyn, V. I., Dyachkova, R. A., and Auerman, L. N. (1979) *J. Physique*, **C-4**(Suppl.), 230–2.
Miller, W. (1967) *Actinides Rev.*, **1**, 71–119.
Moore, F. L. (1964) *Anal. Chem.*, **36**, 2158–62.
Moore, F. L. (1966) *Anal. Chem.*, **38**, 510–14.
Moore, J. R., Nave, S. E., Haire, R. G., and Huray, P. G. (1986) *J. Less Common Metals*, **121**, 187–92.
Moore, J. R., Nave, S. E., Haire, R. G. and Hurray, P. G. (1998) Unpublished work presented at the Rare Earths Conference (1988), Lake Geneva, WI, Sept. 12-16.
Morss, L. R. (1983) *J. Less Common Metals*, **93**, 301–21.
Morss, L. R., Fuger, J., Goffart, J., and Haire, R. G. (1983) *J. Less Common Metals*, **127**, 79–85.
Morss, L. R., Fuger, J., Goffart, J., Edelstein, N. M., and Shalimoff, G. V. (1987) *J. Less Common Metals*, **127**, 251–7.
Musikas, C., Haire, R. G., and Peterson, J. R. (1981) *J. Inorg. Nucl. Chem.*, **43**, 2935–41.
Myasoedov, B. F., Guseva, L. I., Lebedev, I. A., Milyukova, M. S., and Chmutova, M. K. (1974) in *Analytical Chemistry of Transplutonium Elements* (ed. D. Slutzk), John Wiley, New York, pp. 122–32.

Myasoedov, B. F., Chmutova, M. K., and Karalova, Z. K. (1980) in *Actinide Separations* (eds. J. D. Navratil and W. W. Schulz) (ACS Symp. Ser. 117), American Chemical Society, Washington, DC, pp. 101–15.

Myasoedov, B. F. (1982) in *Actinides in Perspective* (ed. N. M. Edelstein), Pergamon Press, New York, pp. 509–40.

Myasoedov, B. F., Leedev, I. A., Khizhnyak, P. L. Timofeev, G. A., and Frenkel, V. Y. A. (1986) *J. Less Common Metals*, **122**, 189–93.

Myasoedov, B. F. and Lebedev, I. A. (1991) in *Handbook on the Chemistry and Physics of the Actinides,* vol. 6 (eds. A. J. Freeman and C. Keller), North-Holland, Amsterdam, pp. 551–96.

Nave, S. E., Haire, R. G. and Hurray, P. G. (1981) Actinides-81 Conference abstracts, Asilomar, CA., Sept. 10-15, p. 144.

Nave, S. E., Haire, R. G., and Huray, P. G. (1983) in USDOE Report ORNL-5954, pp. 63–5.

Nave, S. E., Haire, R. G., and Huray, P. G (1984) in *Proc. Conf. on Electronic Structure and Properties of Rare Earth and Actinide Intermetallics*, St. Polten, Austria, Sept. 3–6, pp. 220–7.

Nave, S. E., Moore, J. R., Spaar, M. T., Haire, R. G., and Huray, P. G. (1985) *Physica B*, **130B**, 225–7.

Nave, S. E., Moore, J. R., Haire, R. G., Peterson, J. R., Damien, D. A., and Huray, P. G. (1986) *J. Less Common Metals*, **121**, 319–24.

Noé, M. and Peterson, J. R. (1976) in *Transplutonium 1975* (eds. W. Mller and R. Lindner), North-Holland, Amsterdam, pp. 69–77.

Nugent, L. J., Baybarz, R. D., and Burnett, J. L. (1969) *J. Phys. Chem.*, **73**, 1177–8.

Nugent, L. J., Baybarz, R. D., Burnett, J. L., and Ryan, J. L. (1971) *J. Inorg. Nucl. Chem.*, **33**, 2503–30.

Nugent, L. J., Baybarz, R. D., Burnett, J. L., and Ryan, J. L. (1973a) *J. Phys. Chem.*, **77** (12), 1528–39.

Nugent, L. J., Burnett, J. L., and Morss, L. R. (1973b) *J. Chem. Thermodyn.*, **5**, 665–78.

Nugent, L. J. (1975) *J. Inorg. Nucl. Chem.*, **37**, 1767–75.

Osborne-Lee, I. W. and Alexander, C. W. (1995) ORNL/TM–12760, pp. 1–43, and references therein.

Patchell, R. A., Yaes, R. J., Beach, L., Kryscio, R. J., Davis, D. G., Tibbs, P. A., and Young, B. (1997) *Br. J. Radiol.*, **70**(839), 1162–8.

Payne, G. L. and Peterson, J. R. (1987) *Inorg. Chim. Acta*, **139**, 111–12.

Pershina, V., Fricke, B., Inova, G. V., and Johnson, E. (1994) *J. Phys. Chem.*, **98**, 1482.

Peterson, J. R. and Burns, J. H. (1968) *J. Inorg. Nucl. Chem.*, **30**, 2955–8.

Peterson, J. R. and Baybarz, R. D. (1972) *Inorg. Nucl. Chem. Lett.*, **8**, 423–31.

Peterson, J. R., Fellows, R. L., Young, J. P., and Haire, R. G. (1977) *Radiochem. Radional. Lett.*, **31**(4–5), 277–82.

Peterson, J. R., Benedict, U., Dufour, C., Birkel, I., and Haire, R. G. (1983) *J. Less Common Metals*, **93**, 353–6.

Peterson, J. R., Young, J. P., and Haire, R. G. (1985) *Abstr. Am. Chem. Soc. Natl. Meeting* I985 S190:334-INR.

Peterson, J. R. and Xu, W. (1996) *J. Radioanal. Nucl. Chem.*, **203**(2), 301–7.

Poda, G. A. and Hall, R. M. (1975) *Health Phys.*, **29**(3), 407–9.

Popov, Y. S., Efremov, Y. V., and Borisenkov, V. I. *et al.* (1966) *Radiochemistry* **38**(2), 124–6.
Porter, C. E., Riley, F. D., and Vandergriff, R. D. (1997) *Sep. Sci. Technol.*, **32**(1–4), 83–92 and 227–34.
Propst, R. L. and Hyder, M. L. (1969) *Nature*, **221**, 1141–2.
Radchenko, V. M., Seleznev, A. G., and Droznik, R. R. (1986a) *Sov. Radiochem.*, **28**(4), 401–4.
Radchenko, V. M., Shushakov, V. D., and Seleznev, A. G. (1986b) *Sov. Radiochem.*, **28**(4), 405–8.
Raschella, D. L., Haire, R. G., and Peterson, J. R. (1982) *Radiochim. Acta*, **30**, 41–3.
Rivard, M. J. (1999a) *Med. Phys.*, **26**(1), 87–96.
Rivard, M. J. (1999b) *Med. Phys.*, **26**(8), 1503–14.
Rivard, M. J., Wierzbicki, J. G., den Heuvel, Van Chuba, P. J., Fontanesi, J., Martin, R., Mahon, C., and Haire, R. G. (1999) *Med. Phys.*, **26**(1), 87–96.
Rivard, M. J. (2000a) *Med. Phys.*, **27**(8), 1761–9.
Rivard, M. J. (2000b) *Med. Phys.*, **27**(12), 2803–15.
Rivard, M. J. (2000c) *Med. Phys.*, **27**(12), 2816–20.
Rivard, M. J., Sganga, J. K., d'Errico, F., Tsai, J.-S., Ulin, K., and Engler, M. J. (2002) *Nucl. Instrum. Methods A*, **476**(1–2), 119–22.
Rivard, M. J., Evans, K. E., Leal, L. C., and Kirk, B. L. (2004) *Nucl. Instrum. Methods B*, **213**, 621–5.
Rykov, V. A. and Yudin, G. L. (1998) *Dokl. Akad. Nauk.*, **360**(2), 186–9.
Sakanoue, M. and Amano, R. (1976) in *Transplutonium 1975* (eds. W. Müller and R. Lindner), North-Holland, Amsterdam, pp. 123–9.
Samhoun, K. and David, F. (1976) in *Transplutonium 1975* (eds. W. Müller and R. Lindner), North-Holland, Amsterdam, pp. 297–304.
Samhoun, K. and David, F. (1979) *J. Inorg. Nucl. Chem.*, **41**, 357–63.
Scofield, J. H. (1974) *At. Data Nucl. Data Tables*, **14**(2), 121–37.
Seaborg, G. T. and Loveland, W. D. (1990) *The Elements Beyond Uranium,* John Wiley, New York, p. 28.
Seleznev, A. G., Radchenko, V. M., and Shushakov, V. D. (1989) *Sov. Radiochem.*, **(6)**, 637–41.
Seleznev, A. G., Radchenko, V. M., and Shushakov, V. D. (1990) *J. Radioanal. Nucl. Chem.*, **143**(1), 253–9.
Senftle, F. E., Duffey, D., and Wiggins, P. E. (1969) *Mar. Technol. Soc. J.*, **3**(5), 9–11.
Shannon, R. D. (1976) *Acta Crystallogr.*, **A32**, 751–64.
Shleien, B., Slaback, L. A. Jr, and Birky, B. K. (eds) (1998) in *Handbook of the Health Physics and Radiological Health*, 3rd edn, Williams and Wilkins, Baltimore, p. 14.
Shoun, R. R. and McDowell, W. J. (1980) in *Actinide Separations* (eds. J. D. Navratil and W. W. Schulz) (ACS Symp. Ser. 117), American Chemical Society, Washington, DC, pp. 71–87.
Sikkeland, T. and Ghiorso, A. (1967) *Phys. Lett. B*, **24**(7), 333–4.
Skiokawa, Y. and Suzuki, S. (1984) *Bull. Chem. Soc. Jpn.*, **57**(10), 2910–13.
Smith, J. L. and Haire, R. G. (1978) *Science*, **200**, 535–9.
Smith, J. L. (1979) USDOE Report LA-UR-79–1666, pp. 1–13.
Smith, J. L. (1980) USDOE Report LA-UR-80–762, pp. 1–5.

Spitsyn, V. I. (1977) in *Proc. 2nd Int. Conf. on Electronic Structure of the Actinides* (eds. J. Mulak, W. Suski, and R. Troc), Wroclaw, Poland, pp. 25–38.
Stary, J. (1966) *Talanta*, **13**, 421–37.
Stepanov, A. V. (1971) *Russ. J. Inorg. Chem.*, **16**, 1583–6.
Stevenson, J. N. (1973) PhD Thesis University of Tennessee, (Knoxville), U. S. Energy Research and Development Admin. Doc. ORO-4447-004 (TID-26453) p. 49.
Stevenson, J. N. and Peterson, J. R. (1973) *J. Inorg. Nucl. Chem.*, **35**, 3481–6.
Street, K. Jr and Seaborg, G. T. (1950) *J. Am. Chem. Soc.*, **72**, 2790–2.
Sugar, J. (1973) *J. Chem. Phys.*, **59**, 788.
Surls, Jr and J. P. Choppin, G. R. (1957) *J. Inorg. Nucl. Chem.*, **4**, 62–73.
Sykora, R. E., Raison, P. E. and Haire, R. G. (2005) *J. Solid State Chemistry*, **178**(2), 578–83.
Sykora, R. E., Assefa, Z., Haire, R. G., and Albrecht-Schmitt, T. E. (2006) *Inorg. Chem.*, **45**, 475–77.
Tacev, T., Zaloudik, J., Janakova, L., and Vagunda, V. (1998) *Neoplasma*, **45**(2), 96–101.
Tacev, T., Grigorov, G., Papirek, T., and Kolarik, V. (2003a) *Strahlenther. Onkol.*, **179** (6), 113–17.
Tacev, T., Ptackova, B. N., and Strnad, V. (2003b) *Strahlenther. Onkol.*, **179**(6), 377–84.
Tacev, T., Grigorov, G., Papirek, T., and Kolarik, V. (2004a) *Nucl. Instrum. Methods B*, **213**, 626–8.
Tacev, T., Ptackova, B. N., and Strnad, V. (2004b) *Radiothermodyn. Oncol.*, **71**, S8–18.
Taut, S., Hübener, S., and Eichler, B. (1997) *Radiochim. Acta*, **78**, 33–8.
Taylor, G. N., Jee, W. S., Mays, C. W., Dell, R. B., Williams, J. L., and Shabestari, L. (1972) *Health Phys.*, **22**(2), 691–3.
Todd, P., Feola, J. M., and Maruyama, Y. (1984) *Am. J. Clin. Oncol. – Cancer*, **7**(5), 495–8.
Topp, N. E. (1965) in *Chemistry of the Rare Earth Elements*, Elsevier, New York, pp. 71–3.
Turcotte, R. P. and Haire, R. G. (1976) in *Transplutonium Elements 1975* (eds. W. Müller and R. Lindner), North-Holland, Amsterdam, pp. 267–77.
Turcotte, R. P. (1980) *J. Inorg. Nucl. Chem.*, **42**, 1735–7.
Varga, L. P., Baybarz, R. D., Reisfeld, M. J., and Asprey, L. B. (1973a) *J. Inorg. Nucl. Chem.*, **35**, 2775–86.
Varga, L. P., Baybarz, R. D., Reisfeld, M. J., and Volz, W. B. (1973b) *J. Inorg. Nucl. Chem.*, **35**, 2787–94.
Veal, B. W., Lam, D. J., Diamond, H., and Hoekstra, H. R. (1977) *Phys. Rev. B*, **15**(6), 2929–42.
Vobecky, M. (1989) *J. Radioanal. Nucl. Chem.*, **135**(3), 165–9.
Wanwilairat, S., Schmidt, R., and Vilaithong, T. (2000) *Med. Phys.*, **27**(10), 2357–62.
Ward, J. W. and Hill, H. H. (1976) in *Heavy Element Properties* (eds. W. Müller and H. Blank), North-Holland, Amsterdam, pp. 65–79.
Ward, J. W., Kleinschmidt, P. D., and Haire, R. G. (1979) *J. Physique*, **C–4**(Suppl.), 233–5.
Ward, J. W., Kleinschmidt, P. D., Haire, R. G., and Brown, D. (1980) in *Lanthanide and Actinide Chemistry and Spectroscopy* (ed. N. M. Edelstein) (ACS Symp. Ser. 131), American Chemical Society, Washington, DC., pp. 199–221.
Ward, J. W. (1983) *J. Less Common Metals*, **93**, 279–92.

Ward, J. W., Kleinschmidt, P. D. and Peterson, D. E. (1986) in *Handbook of the Physics and Chemistry of the Actinides,* vol. 4 (eds. A. J. Freeman and C. Keller), North-Holland, Amsterdam ch. 7.

Warden, J., Gutmacher, R. G., and Lougheed, R. W. (1970) *J. Opt. Soc. Am.*, **60**, 1555.

Weber, M. J. (1980) in *Lanthanide and Actinide Chemistry and Spectroscopy* (ed. N. Edelstein) (ACS Symp. Ser. 131), American Chemical Society, Washington, DC., pp. 275–311.

Wiggins, P. F., Senftle, F. E., and Duffey, D. (1969) *Trans. Am. Nucl. Soc.*, **12**(2), 492–7

Wild, J. F., Hulet, E. K., Lougheed, R. W., Hayes, W. N., Peterson, J. R., Fellows, R. L., and Young, J. P. (1978) *J. Inorg. Nucl. Chem.*, **40**, 811–17.

Williams, K. R. and Choppin, G. R. (1974) *J. Inorg. Nucl. Chem.*, **36**, 1849–53.

Wilmarth, W. R., Young, J. P., Haire, R. G., and Peterson, J. R. (1988) *J. Less Common Metals*, **143**(1–2), 183–93.

Wilmarth, W. R. and Peterson, J. R. (1991a) in *Handbook on the Chemistry and Physics of the Actinides,* vol. 6 (eds. A. J. Freeman and C. Keller), North-Holland, New York, pp. 61–38.

Wilmarth, W. R. and Peterson, J. R. (1991b) in *Handbook on the Chemistry and Physics of the Actinides,* vol. 6 (eds. A. J. Freeman and C. Keller), North-Holland, New York, pp. 1–38.

Worden, E. F. and Conway, J. G. (1970) *J. Opt. Soc. Am.*, **60**, 1144–5.

Yanch, J. C., Kim, J. K., and Wilson, M. J. (1993) *Phys. Med. Biol.*, **38**(8), 1145–55.

Young, J. P., Vander Sluis, K. L., Werner, G. K., Peterson, J. R., and Noé, M. (1975) *J. Inorg. Nucl. Chem.*, **37**(12), 2497–501.

Young, J. P., Haire, R. G., Fellows, R. L., Noé, M., and Peterson, J. R. (1976) in *Transplutonium 1975* (eds. W. Müller and R. Lindner), North-Holland, Amsterdam, pp. 227–33.

Young, J. P., Haire, R. G., Fellows, R. L., and Peterson, J. R. (1978) *J. Radioanal. Chem.*, **43**, 479–88.

Young, J. P., Haire, R. G., Peterson, J. R., Ensor, D. D., and Fellows, R. L. (1980) *Inorg. Chem.*, **19**, 209–12.

Young, J. P., Haire, R. G., Peterson, J. R., Ensor, D. D., and Fellows, R. L. (1981) *Inorg. Chem.*, **20**, 3979–83.

Young, J. P., Haire, R. G., Peterson, J. R., and Ensor, D. D. (1984) in *Geochemical Behavior of Disposed Radioactive Waste* (eds. G. S. Barney, J. D. Navratil, and W. W. Schulz) (ACS Symp. Ser. 246), American Chemical Society, Washington, DC, pp. 335–46.

Zachariasen, W. H. (1975) *J. Inorg. Nucl. Chem.*, **37**(6), 1441–2.

Zech, P., Guey, A., Leitienne, P., Meary, M. F., Pozet, N., Moskovtchenko, J. F., and Traeger, J. (1976a) *J. Urol. Nephrol.*, **82**(4–5), 315–19.

Zech, P., Guey, A., and Leitienne, P. (1976b) *Kidney Int.*, **9**(6), 524.

CHAPTER TWELVE

EINSTEINIUM

Richard G. Haire

12.1 INTRODUCTION

The discovery of einsteinium, element 99, came about during the analyses of nuclear products produced in and then recovered from test debris following a thermonuclear explosion (weapon test device, 'Mike', November 1952) at Eniwetok Atoll in the Pacific Ocean. The uranium present in this device was subjected to a very intense neutron flux (integrated fluence of about 10^{24} neutrons) in an extremely short time frame (few nanoseconds), which allowed a large number of multiple neutron captures with a minimal degree of decay of the products formed. Nuclei were formed with usually high neutron/proton ratios (very 'heavy' uranium isotopes), which then rapidly beta-decayed into new, transuranium isotopes through element 100. Scientists from several U.S. Government laboratories separated and analyzed extensively the debris samplings in the following weeks. From these investigations came the discovery and identification of einsteinium and fermium. The first element was named in honor of Albert Einstein, and assigned the symbol, E (later changed to the current symbol, Es). Additional details and discussions about the discovery of this element and the scientists involved are given in several references (Thompson *et al.*, 1954; Ghiorso *et al.*, 1955; Fields *et al.*, 1956; Hyde *et al.*, 1964; Seaborg and Loveland, 1990).

Subsequently, einsteinium has been produced in accelerator targets, and in reactors via successive neutron captures, starting with targets of plutonium or higher actinides. The first macroscopic and weighable quantities of einsteinium

(few hundredths of a microgram of ^{253}Es) were obtained in 1961. Today, up to ~2 mg can be present in special high-flux isotope reactor targets at the time of release from a reactor.

The transplutonium elements, where einsteinium is the fifth, have chemistries similar to those of the lanthanide elements, especially in their ionic states and in compounds. In essence, elements in the series sequentially add one f-electron in progressing to higher atomic numbers. Einsteinium is therefore an f-electron element, and its 5f electrons are considered fully localized, as opposed to those in the protactinium through plutonium grouping.

Oxidation states of II, III, and IV have been reported for einsteinium, where the best-established state is III (state normally observed in solution) followed by divalent einsteinium, which can be obtained in solid compounds. The tetravalent state has been postulated from vapor transport studies using tracer levels of einsteinium, but this state has not been established fully. More remote is the potential for a hexavalent state, based on the conception that this state may acquire stability from attaining a half-filled, 5f shell ($5f^{11}$ down to $5f^{7}$), by losing a total of six electrons (Liebman, 1978).

An exception of this similarity of einsteinium to the regular lanthanide elements occurs with the elemental state of einsteinium, where its properties and bonding compare more closely to those for europium and ytterbium metals, rather than to the other lanthanide elements, or more specifically to its apparent lanthanide homolog, holmium. This difference in behavior for einsteinium is readily seen by examining the atomic volumes of the two f-series that are shown in Fig. 12.1. Einsteinium is therefore unique in that it is the first divalent

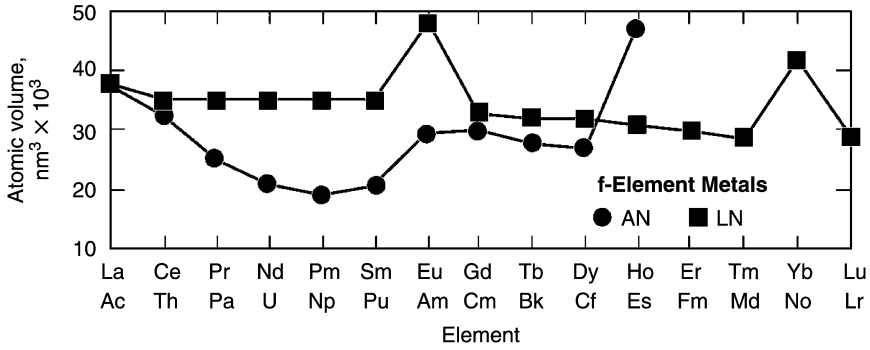

Fig. 12.1 *Atomic volumes of the two f-electron series of elements are shown. The behavior of einsteinium shows it is the first divalent actinide metal, with bonding similar to that for europium and ytterbium metals. This behavior for einsteinium metal is very different than that observed with Es(II) and Es(III) in compounds, which is similar to that for the lanthanides in these states.* (*Haire* et al., 2004).

actinide metal. In the lanthanide elements, europium and ytterbium are also divalent metals (two bonding electrons rather than three). The rationale for their metallic divalency is due to stabilization from a half-filled (Eu) or full (Yb) 4f-orbital arrangement. But this is not an appropriate explanation for the divalency of einsteinium metal. As discussed in Section 12.4, this situation for einsteinium is explained by its high 5f-electron promotion energy (energy to change an f→d).

There are 16 established isotopes of einsteinium (with three isomers), with many having very short half-lives. The longest-lived isotope is ^{252}Es ($t_{1/2} = 471.7$ days), but the ^{253}Es ($t_{1/2} = 20.47$ days) isotope is available in the largest quantity and obtained primarily from nuclear reactors. The quantities of the latter isotope are normally limited to hundreds of micrograms, but frequently only a few micrograms are employed in studies at one time. Up to 2 mg can be discharged from special reactors (i.e. High Flux Isotope Reactor (HFIR) at Oak Ridge National Laboratory, ORNL) once every 6 months to 2 years, depending on the production schedule used. Even so, studies with it are also severely hindered by its half-life (~3% daughter 'impurity' ingrowth per day) and intense self-radiation (6.6 MeV alpha, self-heating of 1000 W g^{-1}), which are often detrimental to the studies being performed. A feeling for the magnitude of the energy released by the decaying einsteinium is obtained by looking at Fig. 12.2. The illumination is associated with the radioactive decay from 300 μg of ^{253}Es solid that is in the bottom of a 9 mm diameter quartz cone.

In essence, there are not many practical applications for einsteinium isotopes. Applications are found as target materials for producing elements with even higher atomic numbers, use of the self-irradiation fields of einsteinium for damage studies, and the use of its radiation for medical treatments. The latter application has been limited, but in principle would employ einsteinium chemically bound to biological agents that could deliver the radiation of einsteinium to biological sites for treatment of different disorders. In this regard, studies have been performed where beagles have been injected einsteinium citrate (Lloyd *et al.*, 1975). Other experiments along this line have been tried with the shorter-lived (~20 h) ^{255}Fm isotope, a daughter product of ^{255}Es; the latter is present in einsteinium products from reactors.

Einsteinium can also be useful in certain chemical studies, where its intense self-irradiation can be used for evaluating radiation damage and radiolysis effects both in solution and in the solid phase. One example of the latter would be to prepare a compound of einsteinium and then follow the chemistry of the daughter and granddaughter (i.e. from ^{253}Es one obtains ^{249}Bk, and ^{249}Cf, respectively) products as they grow into the einsteinium material (Young *et al.*, 1981). The main point is that knowing and understanding the science of einsteinium is important for actinide systematics and understanding the changing role of 5f electrons across the series.

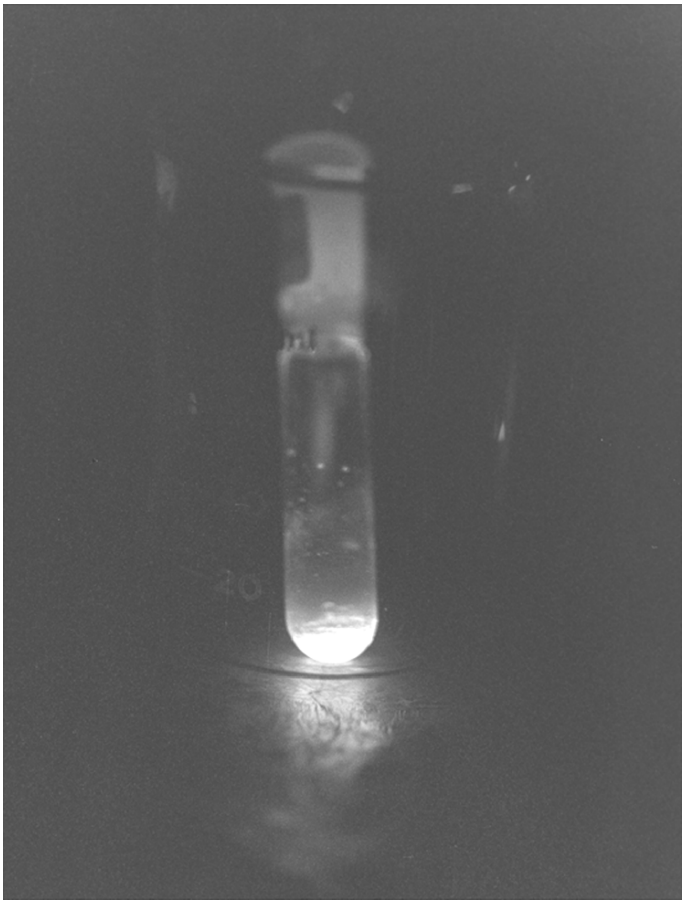

Fig. 12.2 *Self-luminescence arising from the intense radiation from* ~300 μg *of* ^{253}*Es in a quartz cone. The heat and radiation accompanying decay often generate detrimental effects in studies of Es.*

12.2 PRODUCTION AND NUCLEAR PROPERTIES

The primary nuclear properties and production schemes for einsteinium are outlined in Table 12.1 and in Appendix II. The reader is also directed in this regard to references discussing these isotopes (Hyde *et al*., 1964; Seaborg and Loveland, 1990). The nuclear levels of their daughters and the exact atomic mass of each isotope can be established by relating the total decay energies with the masses of the daughter products through studies of the decay processes.

The discovery of einsteinium in nuclear debris involved primarily the ^{253}Es and ^{255}Es isotopes, which have half-lives of 20.47 days and 39.8 h, respectively.

Table 12.1 *Nuclear properties of einsteinium isotopes.*[a]

Mass number	*Half-life*	*Mode of decay*	*Main radiations* (MeV)	*Method of production*
241	8 s	α	α 8.11	^{245}Md daughter
242	13.5 s	α	α 7.92	^{233}U(^{14}N,5n)
243	21 s	α	α 7.89	^{233}U(^{15}N,5n)
244	37 s	EC 96% α ∼ 4%	α 7.57	^{233}U(^{15}N,4n) ^{237}Np(^{12}C,5n)
245	1.1 min	EC 60% α ∼ 40%	α 7.73	^{237}Np(^{12}C,4n)
246	7.7 min	EC 90% α 10%	α 7.35	^{241}Am(^{12}C,α3n)
247	4.55 min	EC ∼ 93% α ∼ 7%	α 7.32	^{241}Am(^{12}C,α2n) ^{238}U(^{14}N,5n)
248	27 min	EC 99.7% α ∼ 0.3%	α 6.87 γ 0.551	^{249}Cf(d,3n)
249	1.70 h	EC 99.4% α 0.57%	α 6.770 γ 0.380	^{249}Cf(d,2n)
250[b]	8.6 h	EC	γ 0.829	^{249}Cf(d,n)
250[b]	2.22 h	EC	γ 0.989	^{249}Cf(d,n)
251	33 h	EC 99.5% α 0.49%	α 6.492 (81%) 6.463 (9%) γ 0.177	^{249}Bk(α,2n)
252	472 d	α 78% EC 22%	α 6.632 (80%) 6.562 (13.6%) γ 0.785	^{249}Bk(α,n)
253	20.47 d 6.3×10^5 yr	α SF β stable	α 6.633 (89.8%) 6.592 (7.3%)	multiple neutron capture
254g	275.7 d $>2.5 \times 10^7$ yr	α SF	α 6.429 (93.2%) 6.359 (2.4%) γ 0.062	multiple neutron capture
254m	39.3 h $>1 \times 10^5$ yr	β^- 99.6 SF α 0.33% EC 0.08%	α 6.382 (75%) 6.357 (8%)	^{253}Es(n,γ)
255	39.8 d	β^- 92.0% α 8.0% SF 4×10^{-3}%	α 6.300 (88%) 6.260 (10%)	multiple neutron capture
256[b]	25.4 min	β^-		^{255}Es(n,γ)
256[b]	∼7.6 h	β^-		^{254}Es(t,p)

[a] Appendix II.
[b] Not known whether ground state nuclide or isomer (Appendix II).
EC = Electron capture
SF = Spontaneous fission

Both elution behavior during ion-exchange purification and the nuclear properties of these isotopes were used to establish the existence of this new element. These two isotopes together with ^{254g}Es ($t_{1/2} = 275.7$ d) are produced by neutron-capture processes. All three isotopes are obtained in high-flux reactors designed to produce synthetic elements, but ^{253}Es and ^{254g}Es are the isotopes normally used for physicochemical studies other than for tracer work given their greater quantities.

The lighter isotopes of einsteinium are prepared in smaller quantities using accelerators and often other actinides as target materials (see Table 12.1). The synthesis of einsteinium isotopes using bombardment of targets with nitrogen isotopes has been discussed (Mikheev *et al*., 1967), as has been the alpha decay properties of some lighter einsteinium isotopes (Ahmad and Wagner, 1977). The half-life of ^{252}Es is also addressed specifically in Ahmad *et al*. (1970). McHarris *et al*. (1966) have addressed the decay scheme of ^{254g}Es. Einsteinium isotopes have also been produced by bombardment of ^{209}Bi with ^{40}Ar ions (Ninov *et al*., 1996). The electron-capture decay fission processes in neutron-deficient einsteinium isotopes have also been discussed (Shaugnessy *et al*., 2000).

At the present time, einsteinium can be produced in the HFIR at the ORNL, Oak Ridge, Tennessee, and at the Research Institute of Atomic Reactors in Dimitrovgrad, Russia. At the HFIR, the targets for neutron irradiation consist mainly of curium isotopes (^{244}Cm through ^{248}Cm), which are irradiated in the reactor to produce the transcurium elements through fermium. The process involves successive neutron captures and beta decays to reach ^{253}Cf, which then β^- decays to ^{253}Es. The latter einsteinium isotope captures neutrons to reach ^{256}Es (possibility even ^{257}Es) but the einsteinium isotopes removed from the reactor targets consist of essentially ^{253}Es, ^{254g}Es, and ^{255}Es. The HFIR can produce einsteinium once every 12–24 months. The SM-2 loop reactor in Russia has similar power and flux levels, also giving it the potential for producing quantities of these transcurium isotopes.

The direct production in the HFIR in the U.S. is less than 2 mg of ^{253}Es, with the ^{254g}Es and ^{255}Es contents being ~0.3 and 0.06%, respectively, at discharge. However, ^{253}Cf is present in the californium isotope fraction that is chemically separated and it β^- decays to ^{253}Es. By subsequent chemical separation of the californium fraction of isotopes, it is possible to obtain chemically the ^{253}Es daughter from the californium fraction at a later time (weeks) and recover isotopically pure ^{253}Es at levels up to 200 μg.

From the mixed einsteinium isotope fraction received from the reactor there are two considerations to be addressed for using this einsteinium fraction. The first concerns the decay of the ^{255}Es present, which is a source of ^{255}Fm at the nanogram level (the longer-lived ^{257}Fm is produced directly in the reactor at only a 1 pg level). Chemical separations of the einsteinium fraction for multiple weeks (i.e. for about a total of four ^{255}Es half-lives) produces a repeated source of a few nanograms of ^{255}Fm. Another aspect is that after decay of —six to ten half-lives of ^{253}Es, the original einsteinium fraction is almost pure ^{254g}Es, and

some 4 μg of it can be obtained essentially free of ^{253}Es. The latter isotope is highly desirable for nuclear syntheses but is of more limited value for physiochemical work, despite its longer half-life. This is due not only to the smaller amounts of it but also to the highly penetrating radiation field generated from its short-lived ^{250}Bk daughter ($t_{1/2}$ = 3.217 h with β^- decay having a 45% branching ratio for a ~1 MeV gamma emission) in equilibrium with it. Thus, decisions must be made regarding the needs and the different choices available for the einsteinium products generated.

More detailed discussions on the nuclear properties, preparation of einsteinium isotopes, and their decay schemes are provided in the references. The K-series X-ray energies of einsteinium isotopes are discussed in Dittner and Bemis (1972). The electron-capture delayed fission processes of neutron-deficient isotopes, ^{242}Es and ^{244}Es, have also been reported, and highly asymmetric mass distributions have been noted (Kosyakov *et al.*, 1974). Average pre-neutron total kinetic energies of (183 ± 18) and (186 ± 9) MeV, respectively, were found. The probability of delayed fission was determined to be (6 ± 2) × 10^{-3} and (1.2 ± 0.4) ×10^{-4}, respectively; smaller probabilities were given for the ^{246}Es and ^{248}Es isotopes.

12.3 PURIFICATION AND ISOLATION

The techniques used for the isolation, recovery, and purification of einsteinium isotopes are very dependent on the method of production. Accelerator production often involves thin foils or targets, where the einsteinium products are either recovered simply (washed off) from the target or from 'catcher' foils located behind a thin target. Recovery from 'catcher' foils can be straightforward, and recovery of products may only involve dissolution or washing of the foil followed by a minor purification of the einsteinium product.

In contrast, recovery of einsteinium following a neutron irradiation process can be rather complex. Larger quantities of very radioactive materials are involved in this process and it requires hot cell operations. The actinide targets are placed in some form of 'container' for the reactor irradiation (normally in aluminum rods), which must then be removed mechanically or chemically to reach the irradiated starting and product materials. At that point, one is faced with the starting material (i.e. curium oxide) and various fission products, in addition to the desired transcurium products (i.e. berkelium, californium, einsteinium, and some fermium). The purification and recovery of einsteinium then involves: (1) separation from lanthanide fission products; and (2) separation from curium, berkelium, and the adjacent actinides, californium and fermium. The major obstacle is the great similarity in the chemical properties of their trivalent actinide ions in solution, given their similar ionic radii.

There is only a small contraction in radii with increasing atomic number in the case of transplutonium elements, which provides a small increase in covalency

and complexing ability, but these are sufficient to allow chromatographic methods to be used for separations. An advantage is acquired in the case of berkelium (which is also a daughter product of einsteinium), as this element can be oxidized to a tetravalent state and separated from the curium through fermium trivalent elements. Separation of einsteinium from its berkelium daughter product can be accomplished by solvent extraction. If solvent extraction is used to remove tetravalent berkelium, the extraction can then leave trivalent californium, einsteinium, and fermium ions together. These elements would have to be separated by subsequent ion exchange or chromatography techniques. A schematic for the separation of einsteinium is given in Fig. 12.3, parts A and B.

The details of various chemical separation processes have been published and presented as reviews. Two earlier reviews cover the approaches in the U.S. (Hulet and Bodé, 1972) and in Russia (Myasoedov *et al.*, 1974). A more general overview for separation of the transuranium elements is also available (Hyde *et al.*, 1964), and individual accounts of procedures used worldwide have been published (Müller, 1967; Bigelow, 1974; Ishimori, 1980; King *et al.*, 1981; Collins *et al.*, 1981). The early scheme used for products from the HFIR at ORNL has also been published in separate reports (Baybarz *et al.*, 1973; Benker *et al.*, 1981). Many of these procedures have not changed significantly over the years.

The removal of lanthanides from the actinides can be accomplished in different ways. An early method, suited for laboratory separations of smaller quantities, was through the use of alcoholic hydrochloric acid as an elutant for the

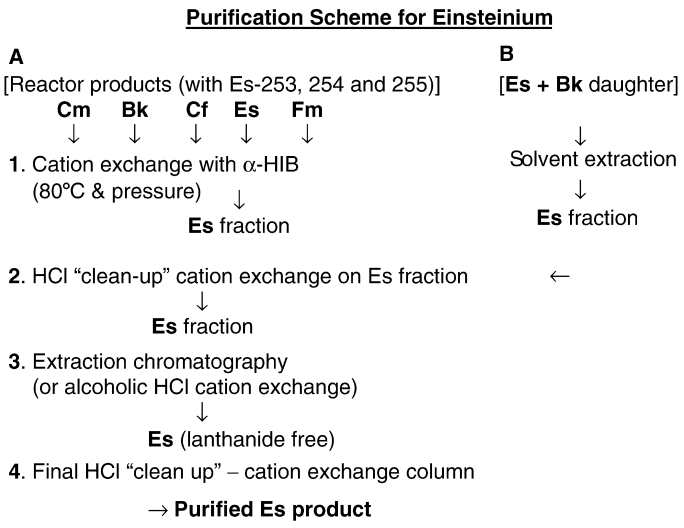

Fig. 12.3 *Einsteinium purification scheme.*

transcurium elements sorbed on cation resin (Street and Seaborg, 1950), where the greater complexing ability of the actinides allowed their desorption as chloride complexes ahead of the lanthanides. A preferred method for larger-scale operations is a lithium chloride anion-exchange process (Shoun and McDowell, 1980), which partitions the actinides from the lanthanides. For small amounts of lanthanides from einsteinium (i.e. the final removal of trace amounts of lanthanides of similar ionic radii) an extraction chromatography column employing ammonium thiocyanate and formic acid can be used (TEVA™ columns; see Horwitz *et al*., 1994; Porter *et al*., 1997). These special columns are also available commercially and give excellent separations between the lanthanide and actinide groups.

When the three elements californium, einsteinium, and fermium are considered, the individual elements can be separated by cation-exchange processes. One method that has been used for several decades is to sorb the three ions on a cation resin from dilute acids (i.e. 0.1 M hydrochloric acid) and selectively elute them with ammonium alpha-hydroxyisobutyrate (α-HIB) solutions at a pH in the range 3.8–4.2 (Choppin and Silva, 1956; Baybarz *et al*., 1973; Bigelow *et al*., 1980; Myasoedov *et al*., 1980; Shoun and McDowell, 1980; Campbell, 1981). The elution order is fermium, einsteinium, and then californium; a high-pressure, ion-exchange column operated at 80°C gives the best results. Separation factors are not great but sufficient, ranging from 1 to 2 for different conditions. Details of using high-pressure columns for separation of f-elements have been given by Campbell (1981). However, even when working with only 10–20 μg of ^{253}Es, care must be exercised, as its radiation level is sufficient to char the resin upon standing and makes it difficult to recovery fully the einsteinium from the resin.

Another approach employs extraction chromatography, where either bis(2-ethylhexyl)phosphoric acid (HDEHP) or 2-ethylhexylphenylphosphonic acid (HEMΦP) are placed on an inert (i.e. fine glass particles) support. The actinides are loaded on this column and eluted with a dilute 0.3 M nitric acid solution (Hulet and Bodé, 1972). Separation factors for these actinide elements are again between 1 and 2. Ion-exchange separations of einsteinium from irradiated californium have also been discussed by Elesin *et al*. (1986).

The extraction chromatography behavior of einsteinium with a quaternary ammonium nitrate has been discussed (Horwitz *et al*., 1966), and extraction of einsteinium with bis(2-ethylhexyl)phosphoric acid was also reported (Horwitz *et al*., 1969). The extraction of einsteinium by bis(2-ethylhexyl)phosphoric acid and the stability constants for hydroxycarboxylic acids is reported by Aly and Latimer (1970a). The extraction of Es by dibutyl *N*,*N*,-diethyl carbamyl phosphate is also discussed (Aly and Latimer, 1970b). The current separation procedure for einsteinium from neutron-irradiated targets at ORNL dates back many years and has been summarized by Campbell (1970). Other separation methods for einsteinium have been provided by Horwitz *et al*. (1994).

12.4 ELECTRONIC PROPERTIES AND STRUCTURE

Chapter 16 is concerned with spectra and electronic structure of free actinide atoms and ions, and these topics are only touched upon here. As einsteinium belongs to the actinide series of elements it can be considered a 5f electron element, which has localized (non-bonding) 5f electrons, and potentially a 'dsp' or an 's^2' type of bonding. In addition, both non-relativistic and relativistic approaches (appropriate because of its high atomic number einsteinium) should be considered with regard to its behavior.

From non-relativistic considerations, the radial probability distributions of the 5f electrons are well within the principal confines of the 6d, 7s, and 7p orbitals, although there is some 'tailing' to the outer regions. This tailing or extension relative to the 7s and 7p orbitals lends itself to a slightly greater degree of covalency than found for the lanthanide's 4f electrons. With the transplutonium elements, the degree of covalency increases slightly when moving to elements with increased atomic number for a given ionic state.

For the relativistic situation, the binding of the electrons becomes greater with higher atomic numbers, which can affect the energies for the different electronic states. Also, potential effects may be found with regard to radii and energies of certain orbitals, spin–orbit splitting, and the expansion of the d- and f-orbitals, all of which can affect chemical behavior. An overview of this electronic picture has been given (Seaborg and Loveland, 1990).

The electronic configurations of einsteinium in neutral and singly ionized gaseous atoms have been analyzed via emission spectra (Gutmacher *et al.*, 1967; Conway, 1979), although full characterization of the ~20000 lines collected is still incomplete. Worden *et al.* (1974) have provided term assignments to a small number of these lines, and Brewer (1971a,b) had estimated energies for the lower spectroscopic terms. Brewer estimated that for a singly ionized atom the $f^{10}s^2$, f^{12}, and $f^{11}d$ levels should be lower in energy than the $f^{11}p$ level reported by Worden *et al.* (1974).

For the gaseous atom of einsteinium, a $5f^{11}7s^2$ ground state is assumed, and the successively ionized neutral gaseous atom loses first one, then two 7s electrons, while the third and even fourth electron lost are 5f electrons, to give a $5f^9$ configuration for the potential ion. It must be remembered that the gaseous atom configurations are different from those encountered in the metals, which are influenced by other factors including crystal energies.

Brewer (1971a,b) has calculated that for einsteinium metal the bonding configuration could be $5f^{10}$dsp, where the 6d and 7p orbitals play important roles. In this case, einsteinium would have three bonding electrons in its conduction band. Alternative configurations would be $5f^{11}$sp or $5f^{11}s^2$, where only two bonding electrons are present, and in this case, einsteinium would be the first divalent actinide metal. The latter configuration appears to be the correct configuration for einsteinium metal. The reason for the divalency of einsteinium metal can be found in the promotion energy for changing an f-electron to a

d-electron, which would then provide three electrons rather than two electrons for the metallic bonding.

A plot of promotion energies for the actinide is shown in Fig. 12.4 (Haire, 1994), which shows einsteinium's promotion energy as being just above the border between divalent and trivalent metal bonding. This 'borderline' energy relates to the crystal energy recovered when the metal atoms crystallize. Thus, when gaseous atomic einsteinium ($5f^{11}7s^2$) condenses to form a crystal, promotion of a 5f electron must occur to provide three rather than two bonding electrons in the solid if a trivalent metal (i.e. with a ds^2 configuration) is to form. For the earlier transplutonium metals, this promotion energy is provided from the greater crystal energy acquired, but with einsteinium, the promotion

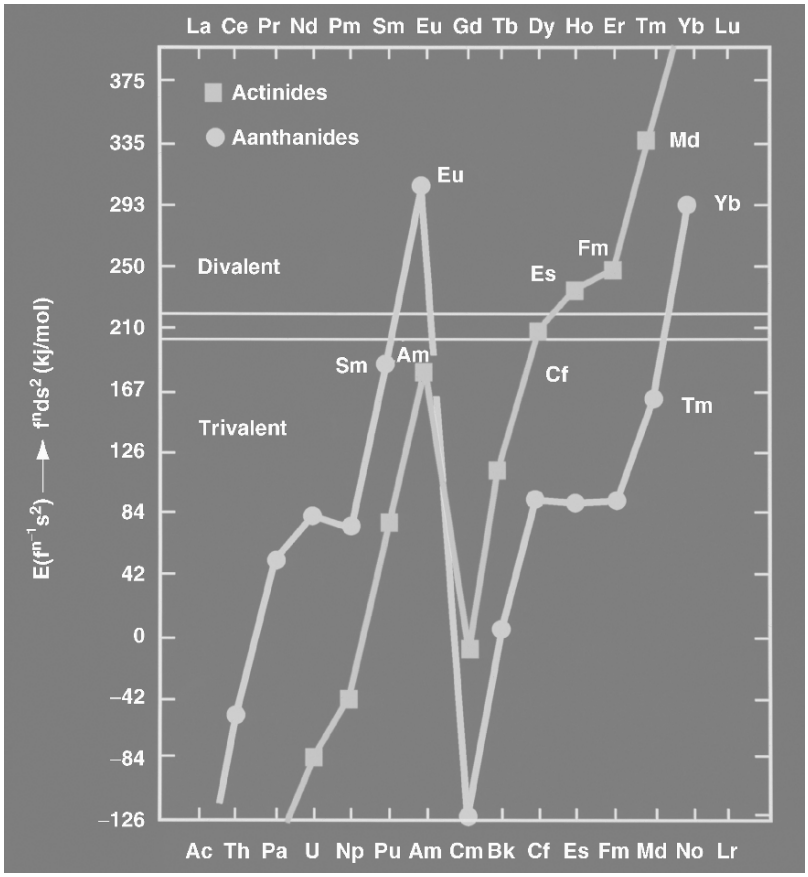

Fig. 12.4 *The f→d promotion energies for the f-elements* (*bar across figure is estimate of crystal energy needed to compensate for promotion of an electron from an f to a d level*).

energy needed exceeds the crystal energy recovered. Thus, einsteinium remains a divalent metal, as do the next three metals in the series.

Recent gas-phase studies of einsteinium have also provided important new insights into its chemistry. The behavior of einsteinium ions in the gas phase is discussed in Section 12.6.6 and the concept of f→d promotion energy again is seen as being important for the different gas species and their reactions.

Blaise and Wyart (1992) have provided tabulated values for einsteinium's energy levels and atomic spectra. Tabulated values for the newer values are given in Table 12.2 for Es(I). The reader is referred to Blaise and Wyart (1992) or Wyart *et al.* (2005) for more extensive data and values for Es(II). Some other atomic values for einsteinium and its ionization potentials are also given in Table 12.3. Estimations of the first ionization potential for einsteinium were earlier given to be 6.42(3) eV (Rajnak and Shore, 1978) but the ionization potential has now been determined accurately by resonance ionization mass spectroscopy using some 10^{12} atoms of ^{254g}Es in an atomic beam (Erdmann *et al.*, 1998; Peterson *et al.*, 1998). The method used is based on measuring photoionization thresholds as a function of an applied electric field, followed by an extrapolation to a zero electric field. The first ionization potential determined experimentally was found to be to be 6.367(5) eV (see Table 12.3). Goodman *et al.* (1975) also examined the nuclear and quadrupole moments of einsteinium. Table 12.3 provides some basic values for Es, but the reader may find more details in the references.

12.5 THE METALLIC STATE

The scarcity and the high specific radioactivity of einsteinium isotopes have in general impeded the investigation of its chemistry, but particularity so for its metallic state. The self-radiation and accompanying heat are imposing factors, and the former rapidly destroys the metal's crystal lattice. The transplutonium elements are all electropositive metals, and react with water and the oxygen in air, but einsteinium metal is even more reactive. Strong reducing agents are needed to convert einsteinium oxide or its halides to the metal. Einsteinium is the most volatile of all the actinides preceding it, which dictates the preparative methods that can be used. It has been concluded that einsteinium is the first divalent actinide metal, in the sense that there are two bonding electrons in its conduction band compared to three or higher for the preceding actinide metals (see Section 12.4). It is followed by divalent fermium metal, and presumably divalent mendelevium and nobelium metals. The last member of the series, lawrencium, is presumably again a trivalent metal. It is likely to have a filled 5f level and a single d-electron; therefore, the promotion of an f-electron is not necessary for it to become trivalent. Thus, einsteinium is divalent like europium and ytterbium metals, but not trivalent like its homolog holmium, the other lanthanide metals, or the americium through californium metals.

Table 12.2 *Atomic properties of einsteinium(I).*[a]

Configuration	*Term*	J	*Energy* (cm^{-1})	w (10^{-3} cm^{-1})	A (10^{-3} cm^{-1})	B (10^{-3} cm^{-1})
$5f^{11}7s^2$	$^4I^0$	15/2	0.00	1543	2 725 729	−1 438 749
$5f^{11}7s^2$	$^4F^0$	9/2	7894.54	>792	25 905	159.1
$5f^{11}7s^2$	$^2H^0$	11/2	8759.27	1216	29 109	36
$5f^{11}7s^2$		137/2	10 244.29	>1391	3113	−1922
$5f^{11}(^4I_{15/2})7s8s$	$(15/2,1)^0$	17/2	33 829.35	6252		
$5f^{11}(^4I_{15/2})7s8s$	$(15/2,1)^0$	15/2	34 068.94	4153		
$5f^{11}7s7p$	^6I	15/2	17 803.09	3838	68 293	−793
$5f^{11}7s7p$	^6I	17/2	19 209.15	5938	93 954	−2173
$5f^{10}6d7s^2$	^6I	17/2	19 367.85	−245	−3777	14
$5f^{11}7s7p$		13/2, 15/2	19 788.32	−2103		
$5f^{10}6d7s^2$		13/2	28 118.65	2170	43 477	−289
$5f^{10}6d7s^2$		13/2, 15/2, 17/2	28 372.78	52		
$5f^{11}7s7p$		13/2	28 447.02	4576	92 872	−1714
$5f^{10}6d7s^2$		15/2, 17/2	28 578.60	−266		
$5f^{10}6d7s^2$		15/2, 17/2	28 689.74	837		
		15/2, 17/2	29 159.28	952		
$5f^{11}7s7p$		13/2	29 204.89	3138	63 762	−763
		11/2	31 829.03	4037	96 233	203
$5f^{10}6d7s^2$		13/2	31 886.3	1590		
		13/2	32 770.06	4437	91 272	573
		9/2	34 192.6			
		13/2	35 507.74			
		11/2	38 634.04			

[a] See Blaise and Wyart (1992) or Wyart *et al.* (2005) for complete set of data including Es(I) and Es(II) and references.

Table 12.3 *Properties of* ^{253}*Es.*

Property	*Value*	*References*
first ionization potential	6.42(3) eV (calc.)	Sugar (1974); Rajnak and Shore (1978)
first ionization potential	6.3676(5) eV (exp.)	Peterson *et al.* (1998); Erdmann *et al.* (1998)
nuclear spin	$I = 7/2$	Appendix I
electronic ground state	$J = 15/2$	
nuclear dipole moment, μ	$4.10(7)\mu_N$	Appendix I
nuclear quadrupole moment, Q_s	6.7(8)	Appendix I
K X-ray energies	$K\alpha_2$ 112.501(10)	Dittner and Bemis (1972)
	$K\alpha_1$ 118.018(10)	Dittner and Bemis (1972)
	$K\beta_3$ 131.848(20)	Dittner and Bemis (1972)
	$K\beta_1$ 133.188(20)	Dittner and Bemis (1972)

Small quantities of transplutonium metals have traditionally been prepared by different methods, two of which are mentioned here (Haire, 1982). The first is reduction of an actinide halide by an active metal (alkali or alkaline earth), and the desired actinide metal is left as a product. This is a suitable technique if the actinide has a lower volatility than the reductant or its halide product (i.e. lithium and lithium fluoride, which are both sufficiently volatile). The second approach is to reduce the actinide oxide with thorium or lanthanum metal and distill away the actinide product. The choice frequently depends on the volatility of the actinide metal. In the case of einsteinium, the latter technique is the most appropriate given its higher volatility. If einsteinium fluoride was reduced with lithium metal, it would be difficult to obtain the metal free of lithium fluoride in the distilled/condensed product.

The first reported attempt to prepare einsteinium metal (Cunningham and Parsons, 1971) used less than 1 μg of einsteinium, and involved distilling lithium metal onto EsF_3. The temperature was raised to 800°C and the sample than quench-cooled to give a material contaminated with lithium fluoride. Thin films of pure einsteinium were prepared subsequently by reducing Es_2O_3 with lanthanum metal followed by collecting the einsteinium metal distillate on electron microscopy grids (Haire and Baybarz, 1979). This reduction approach has become the normal preparative route for einsteinium metal, and has provided the first diffraction data from pure einsteinium metal.

Electron diffraction data for the metal prepared by oxide reduction consisted of over 14 diffraction lines and were obtained from 10–200 ng deposits. The very thin films reduced effects from both self-irradiation damage and self-heating in the metal from the ^{253}Es isotope, and they also allowed diffraction powder patterns to be obtained in a few seconds versus the 30–120 min often needed

for X-ray powder analysis. The diffraction data obtained showed a face-centered cubic (fcc) (*Fm*3*m*) symmetry and generated a lattice parameter of 5.75(1) Å, which corresponds to a metallic radius of 2.03 Å. This radius compares with radii of 2.042 and 1.940 Å (Topp, 1965) for divalent europium and ytterbium metals, respectively, compared to much smaller radii (i.e. 1.734–1.877 Å) for the trivalent lanthanide metals and 1.691–1.725 Å for the trivalent americium through californium metals (Haire, 1990). The radii of Ba, Eu, Es, and Yb form a smooth curve, if radii are plotted versus atomic number (see Fig. 12.1 for the volume behavior of the latter three elements). These findings led to the conclusion that einsteinium is indeed the first divalent actinide metal, and this was subsequently supported by studies of the enthalpy of sublimation of einsteinium (see subsequent discussion) and thermochromatography studies with tracer levels of einsteinium. Selected data for einsteinium and selected f-element metals are given in Tables 12.4 and 12.5.

The elements americium through californium are trivalent metals and exhibit a double hexagonal close-packed (dhcp) room-temperature and an

Table 12.4 *Structural and physical properties of Es versus other f-electron metals.*

		Lattice parameters					
Metal	*Structure type*	a_0 (Å)	b_0 (Å)	c_0 (Å)	*Atomic radius* (Å)	*Atomic volume* (Å)	*References*
Es	fcc (*Fm*3*m*)	5.75(1)			2.03	47.5	Haire and Baybarz (1979)
Eu	bcc	4.578(1)			2.04	48.0	Topp (1965)
Yb	fcc	5.481(1)			1.940	41.2	Topp (1965)
Cf	fcc	4.78(1)			1.69	27.3	Haire (1990)
Cf	dhcp ($P6_3/mmc$)	3.384		11.040	1.691	27.37	Haire (1990)

Table 12.5 *Physical properties of Es versus Cf metals.*[a]

Metal	*Structure type*	*Density* (g cm^{-3})	*Melting point* (K): *boiling point* (K)	*Enthalpy of sublimation at* 298 K (kJ mol^{-1})	*Entropy* (J K^{-1} mol^{-1})	*Bulk modulus* (GPa)	*References*
Es	fcc (*Fm*3*m*)	8.84	1133:1269	134	89.4	15	Haire (1990)
Cf	dhcp ($P6_3/mmc$)	15.10	1173:2018	196	80.3	50	Haire (1990)

[a] Note: Am, Cm, and Bk metal values are similar to those for Cf; all four are 'trivalent' metals, while Es is a 'divalent' metal.

elevated-temperature fcc structure. The densities of the four trivalent transplutonium metals range from 13.6 to 15.1 g cm^{-3}, while einsteinium has a density of 8.84 g cm^{-3} (Haire, 1990). The cubic structure of einsteinium should be considered as reflecting its electronic bonding configuration rather than being a high-temperature form, as are the room temperature structures of europium (body-centered cubic, bcc) and ytterbium (fcc) in the lanthanide series. Europium remains bcc down to 5 K, even with 'cold working' of the material. In contrast, ytterbium transforms from its fcc structure to a hcp form below 270 K, which can be retained at room temperature. Einsteinium metal has been examined at liquid nitrogen temperature (Haire, 1980), where evidence for a hexagonal structure was obtained. However, it was not resolved in that work whether this was a temperature-induced change (comparable to ytterbium metal) or reflected a change from the effects of radiation damage to the einsteinium lattice.

Alloys of einsteinium with europium and with ytterbium (~1 mol%) have also been prepared by co-distilling the metals (Haire, 1982) from mixed oxides (einsteinium–europium and einsteinium–ytterbium) after reacting the oxide mixtures with lanthanum metal. With 100 μg of ^{253}Es, the self-heating/radiation in an Es–Yb alloy was sufficient to give rise to partial sublimation of the einsteinium product when it was isolated in vacuum.

A value for the melting point of einsteinium was obtained by observing the heating of deposits in an electron microscope (Haire and Baybarz, 1979). The melting point was taken as the point where ''micro-puddles'' were formed, in conjunction with calibration studies with other known metals done in a similar fashion. A value of (1133 ± 50) K was reported for the melting point of einsteinium metal. This value can be compared to the melting points of 1099 and 1097 K for europium and ytterbium metals, respectively, while the values for the trivalent lanthanide and americium through californium metals are higher, being (1173–1620) K (Haire, 1990).

At the tracer level, einsteinium–calcium metal mixtures were prepared and studied via thermochromatographic metal columns, where their sorption/condensation behaviors were monitored (Hübener, 1980). Data from this work supported the divalency of einsteinium metal. It was determined that ytterbium, einsteinium, fermium, and mendelevium all condensed at the same column length (~700 K), but deviations were found for europium, samarium, and calcium, where their behaviors were intermediate to the divalent and trivalent metals. One aspect of this thermochromatographic technique has been variation in results when different metals are used for the sorbers or columns.

Volatilities of these metals are correlated with f-electron promotional energies and the number of bonding electrons – the fewer the bonding electrons the higher the volatility. Estimates have been given by Nugent *et al.* (1969a) for the enthalpy of sublimation of these metals via extrapolations. Kleinschmidt *et al.* (1984, 1985) and Haire and Gibson (1989) have also reported experimental data for the enthalpies of sublimation and entropies of einsteinium metal.

The enthalpy for einsteinium also supports that it is a divalent metal. The enthalpy of sublimation of einsteinium is given as 133 kJ $mol^{-1}$and was found to agree closely with that for fermium (143 kJ mol^{-1}) (Haire and Gibson, 1989), the second divalent actinide metal. In the latter work on fermium, the enthalpy for einsteinium was reevaluated, and a value of 134 kJ mol^{-1} was determined for einsteinium, this value being slightly lower than that for fermium. However, this difference is not significant, given that error bars were estimated at $\pm$ 12 kJ mol^{-1}. In essence, the two values for einsteinium and that for fermium can be considered the same.

Subsequent studies of heavy elements (including einsteinium) via thermochromatography have been performed (Hübener *et al.*, 1994; Taut *et al.*, 1997, 1998) and results varied significantly with the metal of the columns used – five different metals were used in the work. With iron columns, californium, einsteinium, and fermium behaved the same; with niobium columns, einsteinium was intermediate to positions for californium and fermium, and in titanium columns, einsteinium and fermium behaved similarly (Hübener *et al.*, 1994). It was concluded that einsteinium and fermium were acting as divalent actinide metals while californium was 'borderline' between divalent and trivalent. Subsequently, similar studies with californium, einsteinium, and fermium tracers estimated einsteinium's enthalpy of sublimation to be 167 kJ mol^{-1} (Taut *et al.*, 1997), a significantly higher value than reported earlier by more direct methods (134 kJ mol^{-1}) but still lower than the enthalpy for californium determined by this technique (close to 200 kJ mol^{-1}). It was stated in Taut *et al.*'s work (1997) that the value for einsteinium is still typical for a divalent metal, although it was higher than that for fermium. Additional discussions on einsteinium thermochromatography are given together with the work on nobelium, where the two models are discussed in conjunction with *ab initio* calculations for actinide adsorption enthalpies (Eichler *et al.*, 2002), and in diffusion studies into tantalum (Legoux and Merinis, 1986).

The crystal entropy of einsteinium has been calculated using a correlation (Ward and Hill, 1976; Ward *et al.*, 1980; Ward, 1986) based on ytterbium metal, and a value of (89.4 $\pm$ 0.8) J K^{-1} mol^{-1} at 298 K was determined. For the 1133 K melting point of einsteinium (Haire and Baybarz, 1979), the enthalpy of melting was calculated to be 9.40 kJ mol^{-1} and the entropy as 8.30 J K^{-1} mol^{-1} by Ward and Hill (1976). The magnetic entropy for a $5f^{11}$ configuration gives a total angular momentum of $J = 15/2$ for the divalent einsteinium. A boiling point of 1269 K was also calculated (Kleinschmidt *et al.*, 1984) for the metal. One additional piece of information has been reported for the metal; its thermal conductivity has been estimated to be 10 W m^{-1} K^{-1} at 300 K (Ho *et al.*, 1972). The bulk modulus of einsteinium was estimated to be similar to those for europium and ytterbium metals. See Tables 12.4 and 12.5 for selected properties and values of einsteinium.

More recent work on the preparation of einsteinium metal provided the first isolated piece of pure einsteinium metal ($\sim$100 μg) and a 60 μg deposit ($\sim$200 μm

in diameter) on platinum. These efforts were in conjunction with attempts to study the high-pressure behavior of the metal (Haire and Heathman, 2000) by energy-dispersive X-ray diffraction using high-intensity tungsten radiation. The pressure behavior of einsteinium metal is very interesting, as it could become a trivalent metal under pressure, where pressure provides the energy necessary to promote an f-electron to a bonding state. In essence, the volume of einsteinium may be reduced under pressure to force additional bonding, similar to that found in the trivalent Am through Cf metals. It was anticipated that applying additional pressure on a potential trivalent einsteinium product could even lead to a further reduction in volume and result in the formation of an einsteinium metal product with itinerant 5f electrons (Haire *et al.*, 2004). This can be understood by examining the volume curves shown in Fig. 12.1, where the volume reduction induces greater bonding. However, the intended study of einsteinium under pressure was not successful, as the intense self-irradiation of einsteinium destroyed both its crystal lattice and the platinum pressure marker present within a few minutes. But the recent preparative effort with einsteinium allowed a new level to be reached in obtaining elemental einsteinium – namely, an einsteinium metal product free of a supporting substrate (i.e. a 100 μg 'bulk form' of pure einsteinium metal).

12.6 COMPOUNDS OF EINSTEINIUM

12.6.1 Crystal data

Once the existence of a new element has been established, scientists strive to determine its chemical and physical properties. The extent to which this is possible depends on the availability and nature of the material, and the techniques that are or can be established to study it. With the availability of multiple micrograms of einsteinium it became feasible to prepare and examine 'bulk forms' of its compounds, although not without perturbations and limitations caused by its short half-life, high self-radiation field, and the heat associated with the decay (^{253}Es alpha decay corresponds to 15312 kJ mol^{-1} min^{-1}). For the preparation of compounds, one normally uses the ^{253}Es isotope (see earlier discussion on isotopes), given its greater availability. Some of the techniques used for microgram-sized samples of einsteinium have been discussed (Haire, 1981, 1982).

Only a few compounds of einsteinium have been prepared and have had their crystal structures identified. In this realm, there are induced changes or destruction of crystal lattices by the isotope's self-irradiation (alpha emission plus nucleus recoil) and the rapid ingrowth of the berkelium daughter (~3% per day, berkelium 'impurity'). For diffraction studies, the accompanying penetrating radiation (L, M and N X-rays, the gamma emissions from ^{254g}Es and its short-lived daughter, ^{250}Bk, also have serious effects on both X-ray

detectors and/or X-ray film in a short time frame (the film is often used for small 1–2 μg sized samples).

Even with rotating anode-type generators with higher X-ray intensities, these difficulties with einsteinium are not overcome. Electron diffraction techniques do afford major advantages, as only small, very thin samples (which can be smaller than the alpha particle's range, where a minimum amount of its energy is transferred) are needed. This technique requires very short exposure times (seconds) and that the detection mode is located approximately 1 m from the sample, which avoids film or detector problems from the einsteinium radiations.

Although synchrotron radiation can supply more intense radiation for diffraction studies with einsteinium samples, two difficulties are encountered: (1) the destruction of the crystal lattice during the time of 'transportation' to the synchrotron beamline; (2) the difficulty of obtaining approvals to use the activity levels from the einsteinium at the synchrotron, or for setting up an apparatus for *in situ* preparation of the compounds on the beamline. Yet, the latter remains an option for dealing with some of the experimental problems with einsteinium's rapid radioactive decay.

As with many of the transuranium compounds, halides and oxides were among the first compounds of einsteinium to be prepared and studied, which is in accord with the fact that these have frequently been among the first to be prepared for new elements. These are also used often as a starting platform for synthesizing other materials. To overcome the experimental difficulties encountered with diffraction analysis of ^{253}Es or ^{254g}Es compounds, three approaches have been successful. One has been constant resynthesis of the compound during X-ray analysis, while another has been the use of very thin films, especially in conjunction with electron diffraction. The third has been to use very short exposures as can be accomplished by electron diffraction. Crystal data have been collected for the following materials: $EsCl_3$, EsOCl, Es_2O_3, $EsBr_3$, and EsI_3 (See Table 12.6). A discussion of X-ray diffraction techniques for einsteinium compounds is also available (Haire and Peterson, 1979).

The first crystal data for einsteinium compounds were obtained for the trichloride and the oxychoride via the constant synthesis technique (Fujita *et al*., 1969a,b). The approach was to resynthesize these materials *in situ* at ~430°C. The trichloride was found to be hexagonal, isostructural with the actinium through californium trichlorides and the lanthanum through gadolinium trichlorides (UCl_3-type, space group $C^2_{6h}-C6_3/m$). The oxychloride was found to crystallize in the tetragonal PbFCl structure (space group $D^7_{4h}-P4/nmm$) and is isostructural with the trivalent lanthanum through erbium oxychlorides and the known actinium through californium oxychlorides. The lattice parameters, corrected to 298 K, are given in Table 12.6.

Einsteinium sesquioxide was the next compound for which diffraction data were acquired, and this involved the use of the electron diffraction technique. The samples were prepared by calcining an einsteinium nitrate salt *in situ* on

Table 12.6 *Compounds of di- and trivalent einsteinium characterized by structural and/or spectroscopic analysis.*

Compound	*Structure type*	*Lattice parameters*				*Major absorption bands* (cm^{-1})	*References*
		a_0 (Å)	b_0 (Å)	c_0 (Å)	β(degree)		
Es_2O_3	Mn_2O_3-bcc	10.766(6)				–	Haire and Baybarz (1973)
Es_2O_3	monoclinic	14.1	3.59	8.80	100	–	Haire and Eyring (1994)
Es_2O_3	La_2O_3-hexagonal	3.7		6.0		–	Haire and Eyring (1994)
$EsCl_3$	UCl_3-hexagonal	7.40(2)		4.07(2)		12 800,20 000, 23 000	Fujita *et al*. (1969a,b)
$EsCl_2$	–					11 100, 18 500, 24 500	Peterson *et al*. (1979); Fellows *et al*. (1977)
EsOCl	PbFCl-tetragonal	3.948(4)		6.702(19)		12 800,16 300	Young *et al*. (1981)
$EsBr_3$	$AlCl_3$-monoclinic	7.27(2)	12.59(3)	6.81(2)	110.8(2)	12 600, 19 800	Fellows *et al*. (1975)
$EsBr_2$	–					11 100,18 300	Young *et al*. (1976)
EsOBr	–					12 700	Peterson *et al*. (1979)
EsI_3	BiI_3-hexagonal	7.53(4)		20.84(5)		12 300	Haire (1978); Peterson (1979)
EsI_2	–					11 100	Young *et al*. (1981)
EsOI	–					12 700,16 100	Young *et al*. (1981)
EsF_3	–					13 200, 20 300, 27 000	Ensor *et al*. (1981)

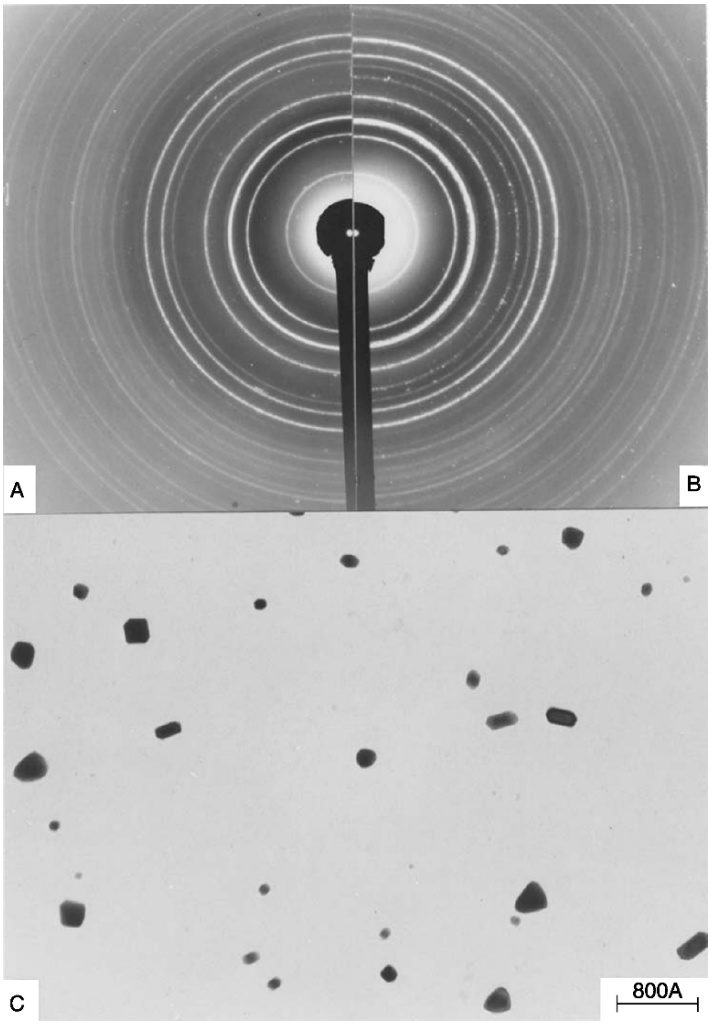

Fig. 12.5 *Electron diffraction patterns of* (*a*) Es_2O_3 *and* (*b*) Gd_2O_3; *particles of* (*c*) Es_2O_3 (*Haire and Baybarz*, 1973).

electron microscope grids in different atmospheres up to 1000°C, and then analyzing the products by electron diffraction (Haire and Baybarz, 1973).

Fig. 12.5 shows an electron diffraction pattern of cubic Es_2O_3 together with isostructural Gd_2O_3 and the small particles from which the einsteinium pattern was obtained. A bcc (α-Mn_2O_3-type, space group *Ia*3) Es_2O_3 was formed, which had a lattice parameter of 10.766(6) Å. Evidence for a higher oxide of einsteinium was not obtained. The parameter and ionic metal radius (calculated to be

Table 12.7 *Ionic radii of einsteinium and selected f-elements.*[a]

Ion	M^{2+} (CN 6)	M^{3+} (CN 6)	M^{3+} (CN 8)	M^{4+} (CN 6)	M^{4+} (CN 8)	*References*
Selected values from calculations						
Cf	1.125	0.945	1.066	0.827	0.925	David (1986)
Es	1.102	0.934	1.053	[0.818]	[0.914]	David (1986)
Fm	1.083	0.922	1.040	[0.811]	[0.906]	David (1986)
Eu	1.166	0.946	1.065	[0.807]	[0.903]	David (1986)
Gd	[1.140]	0.937	1.055	[0.799]	[0.894]	David (1986)
Tb	[1.119]	0.923	1.040	0.792	0.886	David (1986)
Calculated from consistent set of experimental oxide data						
Cf	–	0.949	–	0.859	–	Haire and Eyring (1994)
Es	–	0.928	–	–	–	Haire and Eyring (1994)
Eu	–	0.950	–	–	–	Haire and Eyring (1994)
Gd	–	0.938	–	–	–	Haire and Eyring (1994)
Tb	–	0.920	–	0.817	–	Haire and Eyring (1994)

[a] Radii are given in Å; [–] indicates interpolations.

0.928 Å) for this oxide were intermediate to those for Gd_2O_3 and Tb_2O_3, and just smaller than those for Cf_2O_3 (see Table 12.7).

Lattice parameters and ionic radii for the cubic sesquioxides of the f-elements are shown in Fig. 12.6, where a smooth relationship can be seen. These behaviors differ from the volume behaviors of the metals (see Fig. 12.1). The properties of einsteinium oxide and a comparison of its properties are also discussed in reviews (Baybarz and Haire, 1976; Haire and Eyring, 1994). As opposed to the metal, compounds of einsteinium (i.e. the oxide here) display lattice parameters and ionic radii similar to the comparable transplutonium and lanthanide compounds. All of the first five transplutonium sesquioxides form this cubic crystal form, but some may also exist in a monoclinic structure (Sm_2O_3-type, space group $C2/m$) or a hexagonal form (La_2O_3-type, space group $P3m1$), depending on the thermal history and the particular element in question (see Haire and Eyring, 1994).

Self-irradiation may also convert one structural form of the sesquioxide to another; this radiation effect has been discussed in an earlier review (Fuger, 1975). For einsteinium sesquioxide, both a monoclinic and a hexagonal form have been recorded (Haire *et al*., 1985; Haire and Eyring, 1994). The monoclinic form was observed during oxidation of metal films below 1273 K, and this effect has also been observed with gadolinium metal films. The hexagonal oxide was observed in 'aged' cubic einsteinium sesquioxide. It could not be ascertained whether the monoclinic and/or hexagonal forms of Es_2O_3 resulted from being heated, from self-heating, or from self-irradiation damage. It is probable that the hexagonal form resulted from one of both of the latter two consequences; the hexagonal form of Es_2O_3 would be expected from systematics to be formed

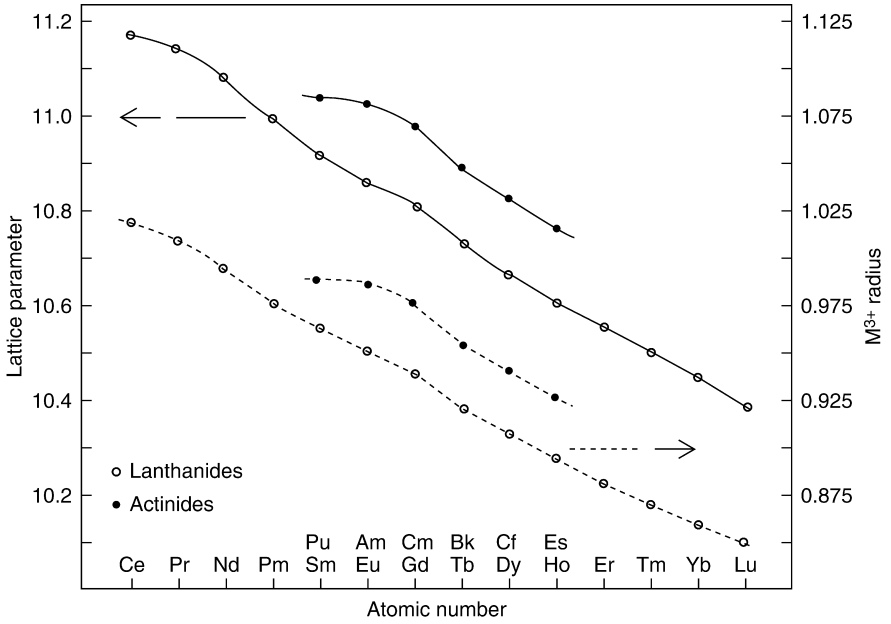

Fig. 12.6 *Lattice parameters and calculated radii for the cubic sesquioxides. A regular trend is observed with Es(III), as opposed to the different behavior observed with Es metal (Haire and Eyring, 1994). Parameters and radii are given in Å.*

only near its melting point (Baybarz and Haire, 1976; Haire and Eyring, 1994). Lattice parameters for the monoclinic and/or hexagonal structural forms of einsteinium sesquioxide must also be considered in this context. The monoclinic form of einsteinium sesquioxide was obtained after heating at temperatures lower than would be expected to bring about the thermal transformation from its cubic form. The values for the lattice parameters of the monoclinic and hexagonal forms of Es_2O_3 are however reasonable, based on ionic systematics for the lanthanide and first four transplutonium sesquioxides (Haire and Eyring, 1994), and allowing for some lattice expansion due to self-irradiation.

X-ray data were also obtained for $EsBr_3$ (Fellows *et al.*, 1975, 1977) and EsI_3 (Peterson, 1979; Haire, 1980). The $EsBr_3$ data were acquired from very small ($\sim$1 μg) pieces immediately after annealing at 400°C. Fifteen diffraction lines were obtained and indexed as a monoclinic $AlCl_3$-type structure, which is isostructural with $BkBr_3$ and $CfBr_3$ (Burns *et al.*, 1975). The information for EsI_3 was obtained from freshly sublimed films formed in a quartz capillary. The diffraction lines were indexed as belonging to a hexagonal BiI_3-type structure, which is also formed by the transneodynium triiodides and the five transplutonium triiodides. The first four lanthanide triiodides form a $PuBr_3$-type structure (Brown, 1968). Important factors in obtaining these diffraction data were the very small samples or thin films and some luck.

12.6.2 Spectrometry – solids

Another important technique for characterizing einsteinium compounds was the use of absorption spectrometry of solids (as well as for actinides in solution, see Section 12.6.3). Divalent compounds of einsteinium were characterized entirely by this technique, given the difficulties in obtaining diffraction data. A great aid in this technique was incorporation of a 'fingerprint' approach, where correlations between spectra and short-range local environment ('crystal environment'; X-ray diffraction requires 'longer-range order') allowed important conclusions to be drawn for the einsteinium compounds. This technique depends partly on the changes in metal ion coordination in the structures. One advantage of this technique is it allows samples to be prepared, annealed, and/or chemically converted in quartz capillaries, while permitting spectral analyses of intermediate products to follow the completeness of the changes being sought (i.e. reduction of a trihalide with hydrogen) in the same system. This approach was particularly suited to halides, as they had modest melting points, and with care, the melts can be solidified to transparent solids or even single crystals. The technique employed a microscope–spectrometer system, which has been described (Young *et al.*, 1976, 1978, 1981). The einsteinium solid-state absorption spectra are characterized normally by sharp electronic f–f transitions. In addition, luminescence spectra have been obtained but the self-radiation of einsteinium also excites trace amounts of impurities and the quartz envelopes containing it, producing an additional source of luminescence that must be considered. Some of the solid-state absorption spectra for einsteinium compounds are shown in Fig. 12.7.

As discussed in Section 12.6.5, potentials ranging from –1.6 to –1.2 V are reported for the Es^{3+}–Es^{2+} couple in aqueous solutions; a value of –1.3V is adopted in Chapter 19. This potential offers an explanation for the ability to reduce einsteinium trihalides with hydrogen at elevated temperatures. This potential for einsteinium contrasts with the more negative $Am^{3+} - Am^{2+}$ through $Bk^{3+} - Bk^{2+}$ potentials, whose trihalides cannot be reduced by hydrogen. This smaller potential is in accord with the greater tendency for obtaining divalency with einsteinium (also see Section 12.6.5).

Several halide materials have been prepared and their solid-state absorption spectra obtained: $EsCl_2$ (Fellows *et al.*, 1975, 1977; Peterson *et al.*, 1977, 1979; Peterson, 1979; Young *et al.*, 1981); $EsBr_2$ and EsI_2 (Young *et al.*, 1976, 1978; Peterson *et al.*, 1979); for EsF_3 (Ensor *et al.*, 1981); and $EsBr_3$ and $EsCl_3$ (Fellows *et al.*, 1975, 1977; Peterson *et al.*, 1979; Young *et al.*, 1981). Efforts to prepare EsF_2 have not been successful and attempts to prepare EsI_3 have encountered difficulties involving the thermal reduction to EsI_2. The spectra obtained for the three divalent halides of einsteinium and that for $EsBr_3$ are shown in Fig. 12.7 (Peterson *et al.*, 1979). The distinct differences between the spectra of $EsBr_2$ and $EsBr_3$ are obvious, while the similarities in the spectra for the three dihalides are also evident. The cutoff in the near UV for the diiodide reflects charge transfer occurring in this sample. The absorption spectrum of

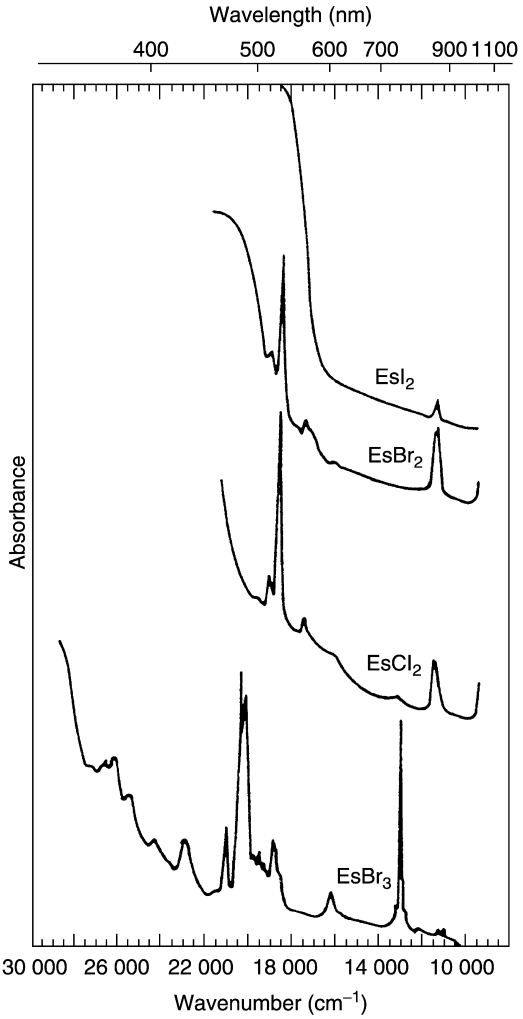

Fig. 12.7 *Solid-state absorption spectra for Es halides* (*Peterson* et al., 1979).

EsOBr is similar to that of $EsBr_3$, but it is sufficiently different to differentiate between the spectra of the two compounds and identify them.

Absorption spectrometry has also been used to study EsF_3 (Ensor *et al.*, 1981) and to then follow the decay products (^{249}Bk and ^{249}Cf, daughter and granddaughter) as they formed in the solid-state sample. From the spectrometric data, it was concluded that EsF_3 initially formed as a LaF_3-type trigonal phase.

Silicate matrices containing ^{253}Es have also been prepared. Results of recent spectroscopic investigations of their properties have been reported (Assefa *et al.*, 1999; Assefa and Haire, 2000, 2001). These studies concentrated on

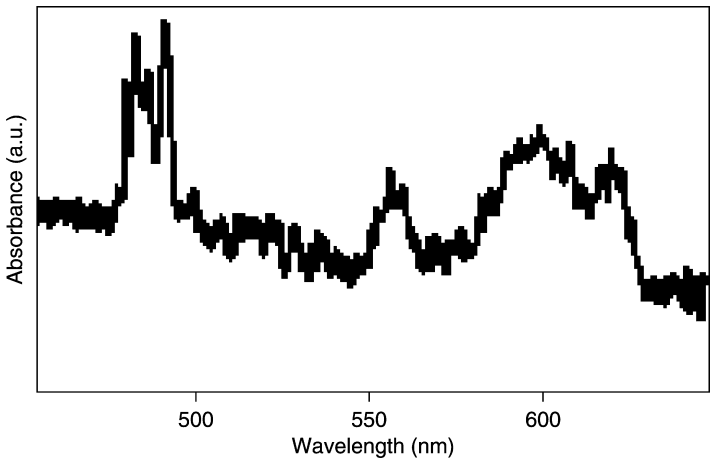

Fig. 12.8 *Absorption spectrum of Es in a borosilicate glass: absorption bands correspond to Es(III)* (*Assefa and Haire*, 2001).

self-luminescence from the materials, and examined the effects of the excitation source used, power of excitation, sample age, and nature of the sample matrix. Also obtained in that work were the absorption spectra of the einsteinium in this host matrix. The self-luminescence arising from einsteinium in these matrices was attributed to defect centers within the Si–O–Si network, nonbonding oxygen holes and Si cluster sites. It was determined that Es(III) was present; evidence for Es(II) was not found. The different spectra obtained for einsteinium in silicate matrices are shown in Figs. 12.8 and 12.9.

12.6.3 Other results – solids

Electron paramagnetic resonance spectra have been obtained for einsteinium placed in single-crystal hosts of CaF_2 (Edelstein *et al.*, 1970; Edelstein, 1971), in BaF_2 and SrF_2 (Bouissières *et al.*, 1980), and in BaF_2 and $SrCl_2$ (Boatner *et al.*, 1976). The spectra of Es^{2+} were similar in CaF_2 and BaF_2. The immediate reduction of Es(III) to Es(II) in the matrix from electron displacement via the alpha radiation field was suggested as the cause of the einsteinium reduction observed in these efforts. A $5f^{11}$ configuration with a ground state close to the $^4I_{15/2}$ (with a small admixture of a $^2K_{15/2}$ state) state was assigned to einsteinium. This indicated that only a minor perturbation of the inner 5f orbitals occurred from the crystal fields in the solids. A value of $\mu_n = 3.62(50)$ nm was reported for einsteinium.

Some information has also been acquired for the magnetism of einsteinium compounds. Preliminary magnetic measurements on einsteinium metal did not show a low temperature transition (Huray *et al.*, 1983). Studies on Es_2O_3 and EsF_3 indicated moments of 10.2(1) and 10.5(1) Bohr magetons, respectively. When corrected for the berkelium ingrowth present in the oxide sample, a value

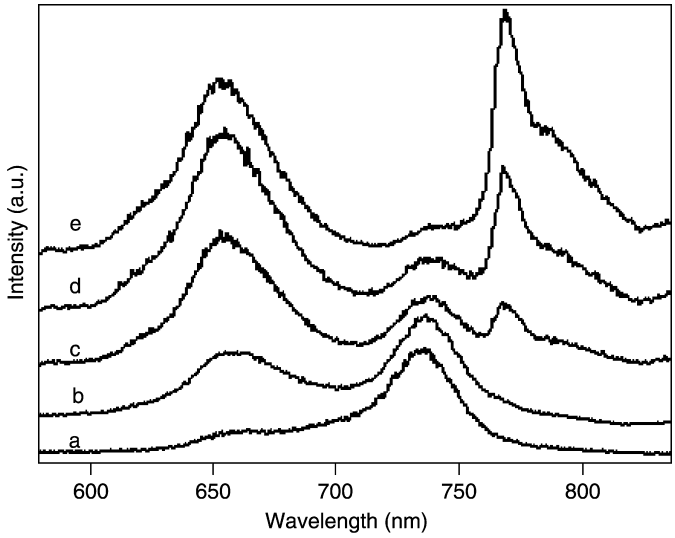

Fig. 12.9 *Photoluminescence spectra from a borosilicate glass doped with Es: excitation was with* 488 nm. *Spectra were recorded at laser powers of* (*a*) 100; (*b*) 310; (*c*) 600; (*d*) 800*; and* (*e*) 1000 mW (*Assefa and Haire*, 2001).

of 10.6(1) is obtained, which is in excellent agreement with a calculated $5f^{10}$ free-ion value (Huray *et al*., 1983; Huray and Nave, 1987).

Preliminary information for the vaporization behavior of Es_2O_3 has been reported (Haire, 1994). The primary mode of vaporization for this oxide is the generation of atomic metal vapor, rather than via a monoxide (Es/EsO in the vapor was greater than 10:1). This situation arises as a result of the lower dissociation energy of EsO, which was estimated to be 460 kJ mol^{-1}. More recent calculations and work (Gibson, 2003; Gibson and Haire, 2003) discuss the electronic states, dissociation energies, and gaseous behavior of einsteinium. A brief discussion on these topics is given in Section 12.6.6.

The thermal behavior of einsteinium sesquioxide and the reduced formation of EsO(g) compares closely to the behaviors of europium and ytterbium oxides. The sesquioxides of europium and ytterbium also decompose mainly to atomic europium and ytterbium rather than form monoxides. A calculated estimate for the standard Gibbs energy of formation of Es_2O_3 at 298 K has been given as –1605 kJ mol^{-1}, and that for EsO_2 as –701 kJ mol^{-1} (Chapter 19). A tentative value for the Gibbs energy of formation for Es_2O_3 based on experimental behavior was given to be between –1650 and –1700 kJ mol^{-1} (Haire, 1994). Attempts to form EsO_2 or other compounds containing Es(IV) (i.e. $BaEsO_3$ or other materials that might help stabilize Es(IV)) have produced negative results (Haire and Bourges, 1980). Several estimated values for thermodynamics of formation of Es_2O_3, EsO_2, EsF_3, EsF_4, $EsCl_2$, and $EsCl_3$ are also given in Chapter 19.

12.6.4 Spectrometry – solutions

Spectrometry of einsteinium in solution has also been pursued, but only its trivalent state has been observed. The solution properties of the trivalent state are similar to those of the previous four transplutonium elements, and coordination number is an important variable. Given that the trivalent ion is present, bonding with ligands is often due to electrostatic effects. But as covalence for a given oxidation state increases across the series, second-order contributions from covalent interactions are possible. The ionic radius of einsteinium in solution should be only slightly smaller than that of californium(III). The free-ion energy levels for trivalent actinides have been given by Blaise and Wyart (1992) and Wyart *et al.* (2005). The ground state of einsteinium (Es(I)) is given as $^5I_8$, with the first excited state appearing at $\sim 10 \times 10^3$ cm^{-1} higher in energy (see Table 12.2).

The first observation of a solution spectrum was for $EsCl_3$ in hydrochloric acid by Cunningham *et al.* (1967), which was obtained by a special technique, where the micro-sized volume of the solution was kept constant by 'pumping' in liquid to overcome evaporation/radiolysis effects. Superior results were obtained subsequently with larger amounts of einsteinium, and 18 peaks between 370 and 1060 nm were obtained in a later work (Fujita *et al.*, 1969b). Electronic energy level and intensity correlations have also been made for Es(III) aquo ion, using data from dilute perchloric acid solutions (Carnall *et al.*, 1973). The absorption spectrum of Es(III) in solution, as demonstrated by Carnall *et al.*, is shown in Fig. 12.10. The band structure and intensities of einsteinium have also been discussed (Nugent *et al.*, 1969b, 1970; Varga *et al.*, 1973a,b).

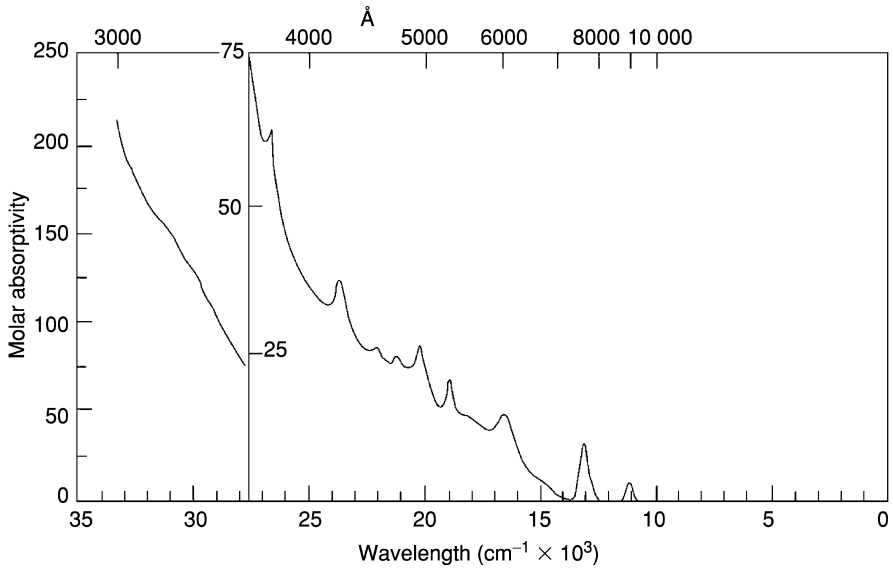

Fig. 12.10 *Solution spectrum of Es(III) in dilute perchloric acid* (*Carnall* et al., 1973).

The spectra fit the behavior expected for an Es(III) free ion, where the f–f transitions were believed to arise from mixed eigenstates, due to coupling that was intermediate between LS and jj.

Photoelectron spectrometry of einsteinium oxide provided spectra of the 4f lines obtained with MgKα excitation (Krause *et al.*, 1988). Binding energies for $4f_{5/2}$ (569.3(4) eV) and $4f_{7/2}$ (550.8(3) eV) of einsteinium were reported and compared to values for other actinides. These values compared well (within –1.0 and –0.1 eV, respectively) with theoretical binding energies The spin–orbit splitting for the 4f level was also measured and compared to the values obtained from theory. Beitz *et al.* (1992, 1998) have reported on the spectrometry and dynamics of the 5f electron states in Es(III) placed in a LaF_3 matrix.

The consequences of self-irradiation from einsteinium on selected clay minerals for waste isolation have also been probed employing ^{253}Es in solution. The einsteinium was sorbed from aqueous solution using two different clay minerals (kaolin and attapugite) and the morphology of the clay was followed with time using electron microscopy (Haire and Beall, 1979). The conclusion reached was that although the clay structure became damaged, einsteinium was still retained by the clay debris and not released to the solution.

12.6.5 Related studies in solution

The complex-ion chemistry of einsteinium has often been studied in conjunction with an examination of the stabilities of other trivalent actinide ions in solution, and often at the tracer level. Although einsteinium exhibits oxidation states of II, III with a potential for IV in the solid state, its solution chemistry is essentially that of a trivalent ion, and is often comparable to the actinide and lanthanide ions having similar radii. A list of the reported stability constants for einsteinium is given in Table 12.8. It has been concluded that chloride and possibly some thiocyanate complexes are the only outer-sphere complexes (water of hydration found between the ligand and the metal ion). The majority of the complexes are instead the inner-sphere type, which has been inferred from an increased stability constant as a function of increased atomic number, and from the enthalpy and entropy values for the formation of the complexes. Several different complexes have been studied, and these are shown in Table 12.8.

The radii and hydration numbers for actinide(III) ions have been derived from the Stokes' law approach using migration rates in electric fields or diffusion coefficients of tracers in electrolytes (Lundqvist *et al.*, 1981; Latrous *et al.*, 1982; Fourest *et al.*, 1983). David (1986) have also discussed the radii of actinides. In line with an expected greater covalent nature when progressing across the series, the Es(III) and Fm(III) hydrated ions are larger than those for earlier members of the series. A value of 0.492 nm (with up to $\sim$16 molecules of water in the hydration sphere) has been estimated for the radius of einsteinium(III).

Several thermodynamic values have also been reported for einsteinium: (1) the molar activity coefficient in sodium nitrate solutions (Chudinov and Pirozhkov,

Table 12.8 *Cumulative stability constants of einsteinium complexes.*

	Log stability constants			
*Complex**	β_1	β_2	β_3	*References*
$EsCl^{2+}$	–0.18			Harmon and Peterson (1972a)
$EsOH^{2+}$	8.86			Hussonnois *et al.* (1973)
$Es(SO_4)_n^{3-2n}$	−2.19	−4.3	−4.93	McDowell and Coleman (1972)
$Es(SCN)_n^{3-n}$	0.559	−1.4	0.468	Harmon and Peterson (1972b)
$EsHCit^{2-}$	10.6			Hubert *et al.* (1974)
$Es(Cit)_2^{3-}$	12.1			Hubert *et al.* (1974)
$Es(\alpha HIB)^{2+}$	4.29			Aly and Latimer (1970a)
$Es(tartrate)^{+}$	5.86			Aly and Latimer (1970a)
$Es(malate)^{+}$	7.06			Aly and Latimer (1970a)
$EsDTPA^{2-}$	22.62			Myasoedov *et al.* (1974)
$EsDCTA^{-}$	19.43			Myasoedov *et al.* (1974)
$EsEDTA^{-}$	19.11			Myasoedov *et al.* (1974)
Es(II) PB (water)	6.2	106.4		Mikheev *et al.* (1988a)
Es(II) PB (acetonitrile)	6.6			Mikheev *et al.* (1988a)
Es(II) 18-6	log $K = 2.64$ water log $K = 4.70$ ethanol–water			Mikheev *et al.* (1986, 1988a,b, 1993a,b); Veleshko *et al.* (1993)

* Cit = citrate ion; αHIB = alphahydroxyisobutyrate; DTPA = diethylenetriaminepentaacetate; DCTA = trans-1,2 diamino cyclohexanetetraacetate ion; EDTA = ethylenediaminetetraacetate ion; PB = tetraphenyl borate; 18-6 = 18-crown-6.

1973); and (2) the Gibbs energy, enthalpy, and entropy of formation (Nugent, 1975; David *et al.*, 1978, 1986; Lebedev, 1978). The following values given were: enthalpy of formation, $\Delta_f H^0 = -603\,\text{kJ mol}^{-1}$; the entropy of formation, $\Delta_f S^0 = -100\,\text{J K}^{-1}\,\text{mol}^{-1}$; and the Gibbs energy, $\Delta_f G^0 = -573\,\text{kJ mol}^{-1}$.

Morss (1986) has provided estimates for several thermodynamic properties of einsteinium, ranging from the formation of aqueous ions, the activity products for the trihydroxide and dioxide, hydration enthalpies and ionization energies, and the enthalpies of formation and solution for the sesquioxide and dioxide. Also given are the calculated enthalpies of formation and solution for the dichlorides and trihalides (fluoride, chloride, bromide, and iodide) and the enthalpy of formation of the four tetrahalides.

Electrode potentials and diffusion coefficients for einsteinium were measured by radiopolarography using solutions and a dropping mercury cathode (Samhoun and David, 1979). A single half-wave for the III to 0 standard potential for reduction/amalgamation was reported as –1.460(5) V and a diffusion coefficient of $6 \times 10^{-6}\,\text{cm}^2\,\text{s}^{-1}$. Nugent (1975) suggested a corrected, more negative value (−1.98(7) V; after correcting for the amalgamation energy) as given in

Chapter 19. David (1986) discussed other values and gave selected ionic radii for several actinides, including einsteinium.

The amalgamation behavior of einsteinium and other actinide elements had been investigated earlier, where it was noted that amalgams of californium, einsteinium, and fermium displayed an anomalous behavior (Maly, 1969). This work suggested that these three elements may display a divalent state, given their preference to form amalgams in comparison to other actinides. Radiopolarography frequently employs mercury as one phase but phase diagrams for mercury alloys or dilute amalgams are not available for many of the transplutonium elements. One report (Guminski, 1996) has tabulated information from pre-1970 publications that contained incorrect data, which makes this publication of limited value.

Although einsteinium is the first element in the series to be divalent, the divalent ionic states of americium and californium have also been reported (see Chapters 8 and 11). The III→II reduction potential for einsteinium was initially estimated to be –1.6V, based on the lowest state for electron transfer (Nugent *et al*., 1969b; Nugent, 1975), but was later suggested to be –1.21 V (from work with chloroaluminate salts (Duyckaerts and Gilbert, 1977)) and –1.18 V from radiopolarographic experiments (David *et al*., 1978). Using a method of co-crystallization of einsteinium tracer with $SmCl_2$, Mikheev *et al*. (1972a,b) and Mikheev and Rumer (1972) had suggested einsteinium's reduction potential should be close to that for samarium (−1.55(6) V). A value of −1.3 V is adopted in Chapter 19 for the standard potential of the $Es^{3+}-Es^{2+}$ couple.

A series of papers over several years have dealt with Es^{2+} in selected solutions. These have been tracer-level studies involving different facets of the co-crystallization technique and of complexation studies. One of these papers (Mikheev *et al*., 1986) investigated the cocrystallization of divalent ions of californium, einsteinium, fermium, samarium, europium, and ytterbium with SrI_2 (18-crown-6) using tetrahydrofuran as a solvent. The Tm^{2+} ion controlled the oxidation potential of the solution. Cocrystallization coefficients relative to strontium were given as close to 1, where the coefficients of the three actinides fell between values of 1.10 for samarium and 0.83 for ytterbium.

The behavior of einsteinium (together with other Am, Cf, and Fm) in $LiCl–NdCl_2–NdCl_3$ and in $LiI–PrI_2$ systems was examined (Kulyukhin *et al*., 1997a,b). In the first molten salt, Nd(II) reduced Cf and Fm to a divalent state. In the second salt system, it was not clear if these actinides were reduced to their divalent or monovalent states. Ratios of the actinide distribution coefficients to those of samarium were reported for both salt systems. Mikheev *et al*. (2004) have reviewed the lower oxidation states of actinides with regard to cocrystallization coefficients in melts, and provided a distribution coefficient for einsteinium versus strontium ($D_{Es/Sm} = 0.94$).

Complexation and cocrystallization of einsteinium with 18-crown-6 in water and water–ethanol mixtures were reported by Mikheev *et al*. (1993a,b). Log K values measured for water and the water–ethanol mixtures were 2.64

and 4.70, respectively. The solvent effects on cocrystallization of Es^{2+} with $SrCl_2$ were reported by Mikheev *et al.* in the 1993b reference. Mikheev *et al.* (1986) had also looked at cocrystallization of Es^{2+} with SrI_2–18-crown-6 complexes, and the effects of water on the cocrystallization and solubility of einsteinium in $Sr(Sm)SO_4$ systems (Mikheev *et al.*, 1987). In the latter work, hydration values could be estimated for Es^{2+} from radii considerations of the different ions. Solubility products for einsteinium complexes with 18-crown-6, boron tetrafluoride, and boron tetraphenyl in tetrahydrofuran were discussed by Kulyukin and Mikheev (1997a,b). The distribution of einsteinium in molten salts containing reductants was described by Kulyukin *et al.* (1997). Veleshko *et al.* (1993) discussed the complexation of Es^{2+} with tetraphenylborate in acetonitrile, and Mikheev *et al.* (1988b) reported the data for the latter with water–ethanol mixtures.

Another study examined the effects of water on the cocrystallization of divalent europium, ytterbium, and einsteinium ions in the $Sr(Sm)SO_4$–ethanol system (Mikheev *et al.*, 1988a,b). Water affected the Es^{2+} coefficients up to 10 M water. The Gibbs energies of hydration were given for Eu^{2+}, Yb^{2+}, and Sr^{2+} ions and were assumed to extend to Es^{2+}. Values ranged from 1361 to 1461 kJ mol^{-1}. The coordination of these three ions was also examined with sodium tetraphenylborate in water–ethanol solutions (Mikheev *et al.*, 1988b). The coordination constants, β_1 and β_2, were determined and the observed trend suggested that the hydrated Es^{2+} ion was smaller than the two divalent lanthanide ions. The β_1 and β_2 values were given as log values: 6.2 and 106.4 for Es^{2+}; 1.7 and 52.7 for Eu^{2+}; and 6.5 and 25.7 for Yb^{2+}.

The effect of the solvent on the cocrystallization of Es^{2+} complexed with tetraphenylborate in acetonitrile and tetrahydrofuran was reported (Mikheev *et al.*, 1993a,b), where the einsteinium was complexed in the acetonitrile but not in the other solvent. The stability constants of the Es^{2+} complexes in acetonitrile were given as $\log \beta_1 = 6.6$ and $\log \beta_2 = 16.0$. Additional work on the complexation of Eu^{2+}, Yb^{2+}, and Es^{2+} with this reagent in different solvents suggested that outer sphere complexes are formed due to electron tunneling from the cation into the unsaturated π-bonds of the anion to form a single-electron bond (Mikheev *et al.*, 1993). The β_1 and β_2 values were given for the three divalent ions in water–ethanol mixtures, acetonitrile, and tetrahydrofuran. From the complexation of Es^{2+} in ethanol–water, acetonitrile, and tetrahydrofuran with the tetraphenylborate ion, it was concluded that complexes are not formed in tetrahydrofuran, as the solvent molecule is too large (Veleshko *et al.*, 1993). In the other two solvents, the smaller solvent molecule is inner sphere and complexes are formed.

The complexation of Es^{2+} with 18-crown-6 in aqueous ethanol and in water was studied, and the stability constants of the complex were determined (Mikheev *et al.*, 1993a,b). The log K values for einsteinium were given as 2.70 in water and 4.70 in ethanol–water (10 M). In both solvents, the log k varied in the order: $Eu^{2+} > Es^{2+} > Yb^{2+}$. The effect of perchlorate, tetrafluoroborate,

and tetraphenylborate ions on the crystallization behavior of Es^{2+} with Sr–10-crown-6)I in tetrahydrofuran was reported (Kulyukhin and Mikheev, 1997a,b). The first two ions affected the cocrystallization constants but the tetraphenylborate ion did not, as it did not form complexes with the metal ion in this solvent. The stability constants were found to increase in going from the tetrafluoroborate to the perchlorate ions.

12.6.6 Compounds in the vapor state

The chemistry of elemental einsteinium in the vapor state was covered in Section 12.5. Elemental einsteinium vapor was generated by direct vaporization of it while ions as Es^+ or EsO^+ were produced by laser ablation of solid matrices or by heating oxides.

Recent gas-phase studies of einsteinium have provided important new insights into its chemistry. The concept of f→d promotion energy is also very important for different gas species and their reactions. The promotion energies for einsteinium's 5f electrons in the elemental state and in different ions are given in Figs. 12.11–12.13, which are taken from Gibson and Haire (2003). One plot is for the promotion energies for An^+ and Ln^+ ions from their ground state electronic configuration to the lowest-lying configurations that have two unpaired non-f valence electrons (i.e. $5f^{n-2}6d7s$), where the value for einsteinium requires some 150 kJ mol^{-1} more energy than its homolog, holmium. The second plot in Fig. 12.12 compares promotion energies for an An^+ ion from the ground state to a configuration having two non-5f valence electrons, a $5f^{n-2}6d7s$ versus a $5f^{n-2}7s^2$ state. The promotion energy for an einsteinium ion having two unpaired 7s electrons is lower. The third comparison in

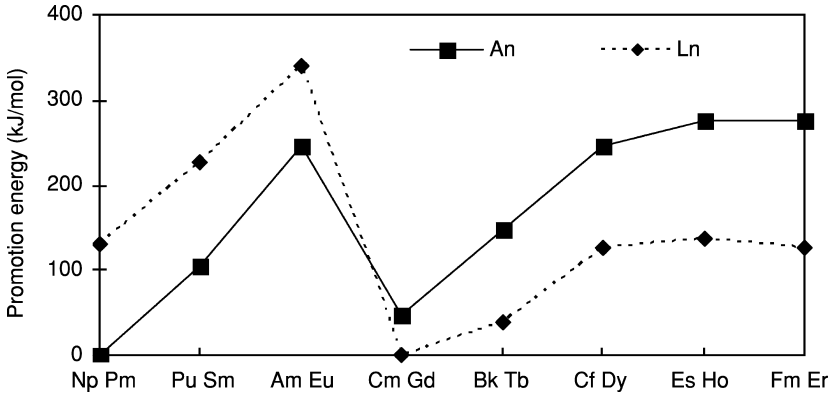

Fig. 12.11 *Promotion energies for An^+ and Ln^+ from ground states to the reactive lowest lying onfiguration having two unpaired, non-f electrons.* (*Gibson and Haire*, 2003). *Note the different trend with the higher members of each series.*

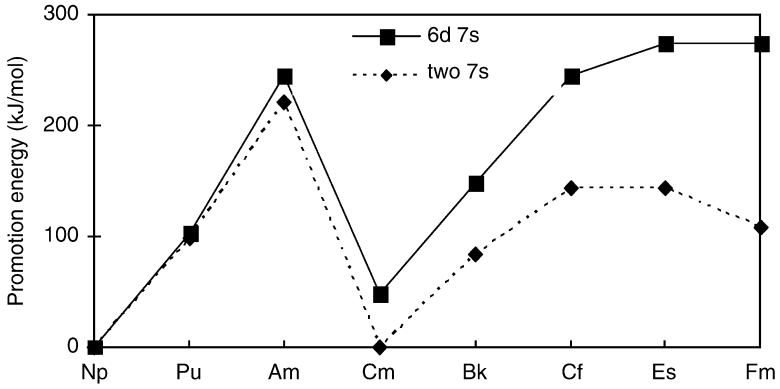

Fig. 12.12 *Promotion energies for An^+ ground state to produce a reactive state with two unpaired f electrons and a 6d7s* state (*solid line*) *versus a paired $7s^2$ state* (*dashed line*). *Additional energy is needed to acquire the 6d7s reactive state.* (*Gibson and Haire*, 2003).

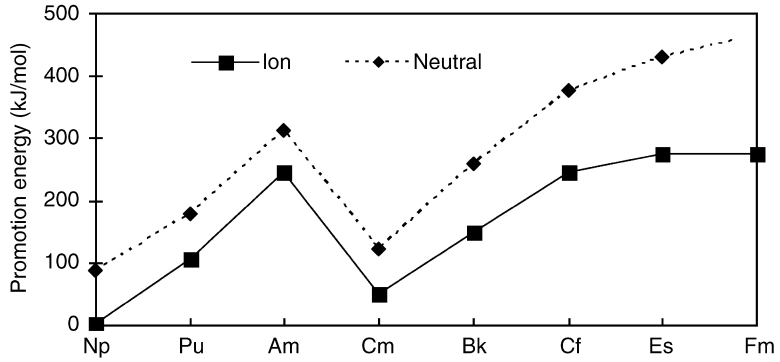

Fig. 12.13 *Promotion energies for An^+ for atomic ions and for An neutral atoms. The energies are for excitation from the ground states to 6d7s "divalent" configurations for An^+ and for 6d7s "trivalent" configurations for the atoms.* (*Gibson and Haire*, 2003).

Fig. 12.13 is made for the promotion energies from the ground state to the neutral atom ('trivalent' configuration, $5f^{n-3}$ $6d^27s$) and the Es^+ ion ('divalent' configuration, $5f^{n-2}6d7s$), where the neutral atom has a promotion energy twice that for forming the An^+ ion.

Important information has been acquired from gas-phase studies of einsteinium, where laser ablations were used in conjunction with mass spectrometry (Gibson and Haire, 2003). The small yields of EsO^+ obtained relative to Es^+ ions indicated that the Es^+–O bond is significantly weaker than that for the earlier actinides.

Fluorination of Es^+ by extraction of fluorine atoms from hexafluoropropene demonstrated the stability of the divalent state of einsteinium. Using this technique, the first organometallic complex of einsteinium was observed ($EsC_4H_8^+$) in the gas phase. From this work the bond dissociation energy for EsO^+ was established and it was found to be smaller than those for EuO^+ and YbO^+, being more similar to that for TmO^+.

Systematic trends of einsteinium's chemistry terms of electronic structure and the energetics of the actinides and lanthanides were developed in this work (Gibson and Haire, 2003). The bond dissociation energy for Es^+–O was estimated to be (470 ± 60) kJ mol^{-1}, higher than the values for Eu^+−O (389 kJ mol^{-1}) and Yb^+−O (372 kJ mol^{-1}), but similar to that for Tm^+–O (478 kJ mol^{-1}) (Gibson and Haire, 2003). The dissociation energy for EsO was earlier reported to be 443 kJ mol^{-1} (Haire, 1994), smaller than dissociation energies for the americium through californium monoxides but similar to those for europium and ytterbium. Thus, einsteinium sesquioxide at high temperatures produces mainly elemental einsteinium rather than a monoxide, where the latter is found when heating curium sesquioxide to very high temperatures.

An important finding was that for einsteinium to become a reactive species, it was necessary to promote the Es^+ ion's ground state electronic configuration to the lowest-lying configuration having two unpaired non-5f valence electrons (i.e. 6d7s rather than $7s^2$). The Es^+ ion was found to be the least efficient of the Th^+ through Cf^+ ions at the dehydrogenation of organic materials, although it was only slightly less efficient than Am^+ and Cf^+ ions (Gibson and Haire, 2003).

In conjunction with the proposal that a hexavalent state of einsteinium could exist based on the added stability acquired from formation of a half-filled 5f orbital (i.e. $[Rn]5f^{11}7s^2 \rightarrow [Rn]5f^7$ for Es(VI)); Liebman, 1978), a potential compound could be the hypothetical EsF_6. As a molecular material, it would be expected to be volatile like UF_6 and PuF_6. From limited attempts to make this material, there is no experimental evidence to support its existence. Attempts to prepare AmF_6 have also proven it to be an elusive material, and far less stable than UF_6 or PuF_6. Therefore, it is unlikely that EsF_6 would be stable.

Studies have also been performed on the formation of volatile molecules using the concepts of thermochromatography (see Section 12.5), and the idea that a molecule in an unusual oxidation state may have a greater potential to form or to exist in the vapor state. From tracer experiments with ^{254}Es, evidence was claimed to support the existence of EsF_4 (Bouissières *et al.*, 1980). The technique consisted of treating EsF_3 with flowing fluorine and determining the temperature where the einsteinium's activity was deposited. This temperature was correlated with deposition temperatures for five other (Pu–Cf) actinide materials, also assumed to be transported as tetrafluorides. The volatility of fluorides should increase with higher oxidation states, so that the order of volatility would be expected to be hexafluoride > tetrafluoride > trifluoride. A point of concern with einsteinium may be the ability to form a tetrafluoride from its trifluoride at temperatures above the expected

decomposition temperature of the tetrafluoride, as estimated from the behaviors of other actinide tetrafluorides.

Thermochromatography of ^{254g}Es in chlorinating carrier gas was used to estimate the adsorption of $EsCl_3$, and was found to be in agreement with a Monte Carlo model for its behavior (Eichler *et al*., 2002). Volatile einsteinium hexafluoroacetylacetonate (HHFA) complexes have also been reported (Fedoseev *et al*., 1987a,b). At the tracer level, these materials can form by passing vapors of the HHFA over einsteinium chloride solids at 200°C. A thermochromatographic study was then used to follow the reaction products. Mixed ligand complexes and lanthanide complexes were also studied. Solvated complexes of HHFA (as well as other organic materials) and the oxychlorides were found to be less volatile in the system. It was concluded that the complexes contained Es(III) rather than Es(II), the latter having a lower volatility.

The gas-phase chemistry of Es^+ and EsO^+ ions has been studied by a laser ablation technique (Gibson and Haire, 2003). The behavior of the Es^+ ion was found to be comparable to that of other actinide ions. The yield of EsO^+ ions suggests that the Es^+–O bond energy is significantly lesser that that of other such actinide ions (i.e. Bk^+–O). By performing chemical reactions in the gas phase between these einsteinium ions and other materials (halogenated organics, alkenes, etc.), it was possible to ascertain important aspects of the chemical behavior of einsteinium in the gas phase, and the ability to form organometallic compounds of einsteinium.

12.7 ATOMIC AND IONIC RADII, AND PROMOTION ENERGIES – THEIR IMPORTANCE IN EINSTEINIUM'S OVERALL SCIENCE

The radii of ions, molecules, and atoms are important in the chemistry and physics of materials as well as for estimation/interpolation of their behaviors. For einsteinium there is a considerable difference in its atomic radius compared to the four previous transplutonium elements, and this is reflected in its properties and science. For divalent and trivalent einsteinium ions, much of their solid and solution behaviors reflect their radii, and in these states einsteinium often behaves similarly to the comparable oxidation states of the other transplutonium and lanthanide ions. In the gas state, bonding energies and potentials (oxidation and promotion) are also of major chemical importance.

The atomic and ionic radii for a given number of bonding electrons or for an oxidation state of the f-elements, in principle, should decrease in a uniform manner across each series (well-established f-element contraction phenomena). This contraction with atomic number has been found to be is in good agreement with multidimensional Dirac–Fock calculations (Desclaux and Freeman, 1984). Ionova *et al*. (1978) have also calculated einsteinium's radius via Hartree–Fock approximations. Thus, these radii are often useful for extrapolations of behavior and properties.

In the case of atomic radii, one observes that einsteinium's radius compares well with radii of europium and ytterbium; as a result of it being a divalent rather than a trivalent metal (see Section 12.5 and Fig. 12.1). The divalent atomic radii of these elements are considerably larger than the trivalent atomic radii of these f-elements, as expected from one less bonding electron. This comes about in part due to the larger promotion energy for changing an f-electron in einsteinium to a 'd' state to enable additional bonding. As a result, einsteinium is the first divalent actinide metal.

With ionic compounds, many are found to form similar, isostructural phases, which is well established in oxide systems (Haire and Eyring, 1994). The ion-exchange behavior of the trivalent ions in solution also shows this correlation (Seaborg and Loveland, 1990). The ionic radius of Es(III), which varies with the coordination number, has been determined from different compounds. From sesquioxide lattice parameters for the actinides and lanthanides (Haire and Eyring, 1994), the ionic radius of Es^{3+} (0.928 Å) is slightly smaller than that of Cf^{3+}, and midway between the radii for Tb^{3+} (0.920 Å) and Gd^{3+} (0.938 Å). Another set of ionic radii has been given by David (1986), which shows a similar relationship. Thus, similar oxide-phase behavior is expected for these ions. The relative behaviors of the sesquioxide lattice parameters and the ionic radii are shown in Fig. 12.6 and Table 12.7, including calculated radii for Es(II) ions. Values are also given for potential Es(IV) ions; these ions would have different coordination numbers and show somewhat different behaviors than the Es(II) and Es(III) ions.

Einsteinium's sesquioxide and trivalent halide-phase behaviors in several solid compounds are found to be comparable to the lanthanides discussed above. In the case of cation-exchange behavior, the elution behavior from ion-exchange columns for a given oxidation state is generally in the order of the radii of the hydrated ions, with the largest or more readily complexed ions eluting first (einsteinium before californium). With elution from a cation column using α-HIB, einsteinium is found at a position between dysprosium and holmium (einsteinium's lanthanide homolog; Seaborg and Loveland, 1990).

Thus, einsteinium's atomic and ionic radii are important factors in the science of einsteinium. They often serve as useful information to understand, predict, and/or extrapolate the behavior of einsteinium. And the f→d electron promotion energy is also very important to understanding elemental einsteinium, as well as several facets of einsteinium's gas-phase chemistry.

ACKNOWLEDGMENTS

Research was sponsored by the Division of Chemical Sciences, Geosciences and Biosciences, Office of Basic Energy Sciences, U.S. Department of Energy, under contract DE-ACO5-00OR22725 with Oak Ridge National Laboratory, managed and operated by UT-Battelle, LLC.

REFERENCES

Ahmad, I., Sjoblom, R. K., and Barnes, R. F. (1970) *Nucl. Phys. A*, **141**, 141–7.

Ahmad, I. and Wagner, F. (1977) *J. Inorg. Nucl. Chem.*, **39**, 1509–11.

Aly, H. F. and Latimer, R. M. (1970a) *Radiochim. Acta*, **14**, 27–31.

Aly, H. F. and Latimer, R. M. (1970b) *J. Inorg. Nucl. Chem.*, **32**, 3081–7.

Aly, H. F., Sjoblom, R. K., and Barnes, R. F. (1970) *Radiochim Acta*, **14**, 27–31.

Assefa, Z., Haire, R. G., and Stump, N. A (1999) Abstract NUCL-164 American Chemical Society, 218th National Meeting, New Orleans, LA.

Assefa, Z. and Haire, R. G. (2000) Abstract NUCL-146, American Chemical Society, 219th National Meeting, San Francisco, CA.

Assefa, Z. and Haire, R. G. (2001) ACS Symp. Ser. 778 (eds. P. G. Elter and W. R. Heineman), American Chemical Society, Washington, DC, ch. 20, pp. 329–66.

Baybarz, R. D., Knauer, J. B., and Orr, P. B. (1973) USAEC Report, ORNL-4672, Oak Ridge National Laboratory.

Baybarz, R. D. and Haire, R. G. (1976) *J. Inorg. Nucl. Chem.*, Suppl., pp. 7–11.

Beitz, J. V., Liu, G. K., Morss, L. R, and Williams, C. W. (1992) Abstract NUCL-105 American Chemical Society, 203th National Meeting, San Francisco, CA.

Beitz, J. V., Williams, C. W., and Liu, G. K. (1998) *J. Alloys Compds*, **271**, 850–3.

Benker, D. E., Chattin, F. R., Collins, E. D., Knauer, J. B., Orr, P. B., Ross, R. G., and Wiggens, J. T. (1981) in *Transplutonium Elements, Production and Recovery,* ACS Symp. Ser. 161 (eds. J. D. Navratil and W. W. Schultz), American Chemical Society, Washington, DC, pp. 161–72.

Bigelow, J. E. (1974) in *Gmelin Handbuch der Anorganischen Chemie, Suppl. Ser., Transuranium*, vol.7b, part A1, II, *The Elements*, Springer-Verlag, Berlin, pp. 326-36.

Bigelow, J. E., Collins, E. D., and King, L. J. (1980) in *Actinide Separations* ACS Symp. Ser. 117 (eds. J. D. Navratil and W. W. Schulz), American Chemical Society, Washington, DC, pp.147–55.

Blaise, J. and Wyart, J.-F. (1992) Energy Levels and Atomic Spectra of Actinides. in *International Tables of Selected Constants*, Curie University, Paris, pp. 401–7; and the WEB, www.lac.u-psud.fr/Database/Tab-energy (einsteinium).

Boatner, L. A., Reynolds, R. W., Finch, C. B., and Abraham, M. M. (1976) *Phys. Rev. B*, **13**, 953–8.

Bouissières, G. Jouniaux, B., Legoux, Y., Mérinis, J., David, F., and Samhoun, K. (1980) *Radiochem. Radioanal. Lett.*, **45**, 121–8.

Brewer, L. (1971a) *J. Opt. Soc. Am.*, **61**, 1101–11.

Brewer, L. (1971b) *J. Opt. Soc. Am.*, **61**, 1666–82.

Brooks, M. S. S., Johansson, B., and Skriver, H. K. (1984) Electronic Structure and Bulk Ground State Properties of the Actinides. in *Handbook on the Physics and Chemistry of the Actinides* vol.1 (eds. A. J. Freeman and G. H. Lander), North-Holland, Amsterdam, pp. 165–76.

Brown, D. (1968) *Halides of the Lanthanides and Actinides,* John Wiley, London, pp. 117–71.

Burns, J. H., Peterson, J. R., and Baybarz, R. D. (1975) *J. Inorg. Nucl. Chem.*, **35**, 1171–7.

Campbell, D. O. (1970) *Ind. Eng. Chem. Process. Des. Dev.*, **9**, 95–9.

Campbell, D. O. (1981) in *Transuranium Elements – Production and Recovery,* ACS Symp. Ser. 161 (eds. J. D. Navratil and W. W. Schulz), American Chemical Society, Washington, DC, pp. 133–46.

Carnall, W. T., Cohen, D., Fields, P. R., Sjoblom, R. K., and Barnes, R. F. (1973) *J. Chem. Phys.*, **59**, 1785–9; and references therein.

Choppin, G. R. and Silva, R. J. (1956) *J. Inorg. Nucl. Chem.*, **3**, 153–4.

Chudinov, E. G. and Pirozhkov, S. V. (1973) *Sov. Radiochem.*, **15**, 195–9.

Collins, E. D., Benker, D. E., Chattin, F. R. Orr, P. B., and Ross, R. G. (1981) in *Transuranium Elements – Production and Recovery,* ACS Symp. Ser. 161 (eds. J. D. Navratil and W. W. Schulz), American Chemical Society, Washington, DC, pp. 147–60.

Conway, J. G. (1979) in *Proc. Symp. Commemorating the 25th Anniversary of Elements 99 and 100*, Report LBL-7701 (ed. G. T. Seaborg), Nat. Tech. Serv., Springfield, VA, p. 9.

Conway, J. G. (1986) in *The Chemistry of the Actinide Elements,* 2nd edn, vol. 2 (eds. J. J. Katz, G. T. Seaborg, and L. R. Morss), Nuclear Spins and Moments of the Actinides, Appendix I, Chapman & Hall, New York, pp. 1647–48; and references therein.

Cunningham, B. B., Peterson, J. R., Baybarz, R. D., and Parsons, T. C. (1967) *Inorg. Nucl. Chem. Lett.*, **3**, 519–21.

Cunningham, B. B. and T. C. Parsons, (1971) USAEC Doc. URCL-20426, p. 239.

David, F., Samhoun, K., Guillaumont, R., and Edelstein, N. (1978) *J. Inorg. Nucl. Chem.*, **40**, 69–74.

David, F. (1986) *J. Less Common Metals*, **121**, 27–42.

Desclaux, J. P. and Freeman, A. J. (1984) Atomic Properties of the Actinides, in The Handbook on the Physcis and Chemistry of the Actinides (eds. A.J. Freeman and G. H. Lander), Elsevier, North-Holland, Amsterdam, pp. 1–78.

Dittner, and P. E. Bemis, C. E. (1972) *Phys. Rev A*, **5**, 481–7.

Duyckaerts, and G. Gilbert, B. (1977) *Inorg. Nucl. Chem. Lett.*, **13**, 537–42.

Edelstein, N., Conway, J. G., and Fujita, D. (1970) *J. Chem. Phys.* **52** (12), 6425–30.

Edelstein, N. (1971) *J. Chem. Phys.*, **54**, 2488–91.

Eichler, B., Adams, J., Eichler, R., Gäggeler, H. W., and Peterson, J. R. (2002) *Radiochim. Acta*, **90**, 895–7.

Elesin, A. A., Nikolaev, V. M., and Shalimov, V. V. (1986) *Sov. Radiochem.*, **28**, 723–6.

Ensor, D. D., Peterson, J. R., Haire, R. G., and Young, J. P. (1981) *J. Inorg. Nucl. Chem.*, **43**, 2425–7.

Erdmann, N., Nunnemann, M., Eberhardt, K., Huber, G., Köhler, S., Kratz, J. V., Passler, G., Peterson, J. R., Trautmann, N., and Waldek, A. (1998) *J. Alloys Compds*, **271/273**, 837–40.

Fedoseev, E. V., Aizenberg, M. I., and Travnikov, S. S. (1987a) *Sov. Radiochem.*, **29**(6), 677–81.

Fedoseev, E. V., Aizenberg, M. I., and Travnikov, S. S. (1987b) *Sov. Radiochem.*, **116**(1), 183–92.

Fellows, R. L., Peterson, J. R., Noé, M., Young, J. P., and Haire, R. G. (1975) *Inorg. Nucl. Chem. Lett.*, **11**, 737–42.

Fellows, R. L., Young, J. P., Haire, R. G., and Peterson, J. R. (1977) in *The Rare Earths in Modern Science and Technology* (eds. G. J. McCarthy and J. J. Rhyne), Plenum Press, New York, pp. 493–9; also cited in Report LBL-7701, p. 55.
Fields, P. R., Studier, M. H., Diamond, H., Mech, J. F., Inghram, M. G., Pyle, G. L., Stevens, C. M., Fried, S., Manning, W. M., Ghiorso, A., Thompson, S. G., Higgins, G. H., and Seaborg, G. T. (1956) *Phys. Rev.*, **102**, 180–2.
Fourest, B., Duplessis, J., and David, F. (1983) *J. Less Common Metals*, **92**, 17–27.
Fuger, J. J. (1975) in*International Review of Science, Inorganic Chemistry,* ser. II, vol.7 *Lanthanides and Actinides* (ed. K. W. Bagnall), Butterworths, London, pp. 151–94.
Fujita, D. K., Cunningham, B. B., Parsons, T. C., and Peterson, J. R. (1969a) *Inorg. Nucl. Chem. Lett.*, **5**, 245–50.
Fujita, D. K., Cunningham, B. B., and Parsons, T. C. (1969b) *Inorg. Nucl. Chem. Lett.*, **5**, 307–13.
Ghiorso, A., Thompson, S. G., Higgins, G. H., Seaborg, G. T., Studier, M. H., Fields, P. R., Fried, S. M., Diamond, H., Mech, J. F., Pyle, G. L., Huizenga, J. R., Hirsch, A., Manning, W. M., Browne, C. I., Smith, H. L., and Spence, R. W. (1955) *Phys. Rev.*, **99**, 1048–9.
Gibson, J. K. (2003) *J. Phys. Chem. A*, **107**, 7891–9.
Gibson, J. K. and Haire, R. G. (2003) *Radiochim. Acta*, **91**, 441–8.
Goodman, L. S., Diamond, H., and Shanton, H. E. (1975) *Phys. Rev. A*, **11**, 499–504.
Guminski, C. (1996) *J. Phase Equilib.*, **17**(5), 443–4.
Gutmacher, R. G., Evans, J. E., and Hulet, E. K. (1967) *J. Opt. Soc. Am.*, **57**, 1389–90.
Haire, R. G. and Baybarz, R. D. (1973) *J. Inorg. Nucl. Chem.*, **35**, 489–96.
Haire, R. G. (1978) unpublished data, ORNL Report 5485.
Haire, R. G. and Baybarz, R. D. (1979) *J. Phys. Colloq.*, **40**(C4), 101–2.
Haire, R. G. and Beall, G. W. (1979) in *Consequences of Radiation from Sorbed Transplutonium Elements on Clays Selected for Waste Isolation,* ACS Symp. Ser. 100 (ed. S. Fried), American Chemical Society, Washington, DC, pp. 291–5.
Haire, and R. G. Peterson, J. R. (1979) *Advances in X-ray Analysis,* vol. 22 (eds. G. J. McCarthy, C. S. Barrett, and C. O. Rund), Plenum Press, New York, pp. 101–9.
Haire, R. G. (1980) in USDOE Report, ORNL-5665, 71.
Haire, R. G. and Bourges, J. (1980) Presented at Journées de Actinides, Stockholm, Sweden, unpublished work.
Haire, R. G. (1981) in USDOE Report, ORNL-5817, p. 60.
Haire, R. G. (1982) Preparation of Transplutonium Metals and Compounds in *Actinides in Perspective* (ed. N. M. Edelstein), Pergamon, Oxford, pp. 309–42.
Haire, R. G., Young, J. P., and Peterson, J. R. (1985) Abstract NUCL-24, American Chemical Society, 189th National Meeting, Miami Beach, FL.
Haire, R. G. and Gibson, J. K. (1989) *J. Chem. Phys.*, **91**, 7085–96.
Haire, R. G. (1990) in *Properties of the Transplutonium Metals*, ASM International, Materials Park, Ohio, pp. 1198–201.
Haire, R. G. (1994) *J. Alloys Compds*, **213/214**, 185–93.
Haire, R. G. and Eyring, L. (1994) in *Handbook on the Physics and Chemistry of Rare Earths,* vol. 18 *Lanthanides and Actinides Chemistry* (eds. K. A. Gschneidner, Jr, L. Eyring, G. R. Choppin, and G. H. Lander), North-Holland, New York, pp. 414–505.
Haire, R. G. and Heathman, S. (2000) unpublished data.

Haire, R. G., Heathman, S., Le Bihan, T., Lindbaum, A., and Iridi, M. (2004) Investigations of Actinide Metals and Compounds Under Pressure Provide Important Insights Into Bonding and Chemistry. in *Materials Research Society Proceedings, Actinides –Basic Science, Applications and Technology,* vol. 802 (eds. L. Soderholm, J. J. Joyce, M. F. Nichols, D. K. Shuh, and J. G. Tobin), MRS, Warrendale, PA, pp. 15–21.

Harbour, R. M. (1972) *J. Inorg. Nucl. Chem.*, **34**, 2680–1.

Harmon, H. D. and Peterson, J. R. (1972a) *Inorg. Nucl. Chem. Lett.*, **8**, 57–63.

Harmon, H. D. and Peterson, J. R. (1972b) *J. Inorg. Nucl. Chem.*, **34**, 1381–97.

Hatsukaway, Y., Ohtsuki, T., and Sueki, K. (1989) *Nucl. Phys. A*, **500**(1), 90–110.

Ho, C. Y., Powell, R. W., and Lilly, P. E. (1972) *J. Phys. Chem. Ref. Data*, **1**, 418

Horwitz, E. P., Sauro, L. J., and Bloomquist, C. A. (1966) *J. Inorg. Nucl. Chem.*, **29**, 2033–7.

Horwitz, E. P., Bloomquist, C. A. A., and Henderson, D. J. (1969) *J. Inorg. Nucl. Chem.*, **31**, 1149–70.

Horwitz, E. P., Chiarizia, R., Dietz, M. L., Diamond, H., and Nelson, D. M. (1993) *Anal. Chim. Acta*, **281**, 361–72.

Horwitz, E. P., Chiarixia, R., and Alexandratos, S. (1994) *Solv. Extr. Ion Exch.*, **12**(4), 831–45.

Hübener, S. (1980) *Radiochem. Radioanal. Lett.*, **44**, 79–86.

Hübener, S., Eichler, S. B., and Schädel, M. (1994) *J. Alloys Compds*, **213**, 429–32.

Hubert, S., Hussonnois, M., Billard, L., Goby, G., and Guillaumont, R. (1974) *J. Inorg. Nucl. Chem.*, **36**, 2361–6.

Hulet, E. K., Gutmacher, R. G., and Coops, M. S. (1961) *J. Inorg. Nucl. Chem.*, **17**, 350–60.

Hulet, E. K. and Bodé, D. D. (1972) in *MTP International Review of Science, Inorganic Chemistry,* Ser. I, vol. 7 *Lanthanide and Actinides* (ed. K. W. Bagnall), Butterworths, London, pp. 1–46.

Huray, P. G., Nave, S. E., and Haire, R. G. (1983) *Magnetism of the Heavy 5f Elements,* in *The Rare Earths in Modern Science and Technology* (eds. J. J. Rhyne, H. B. Silber, and G. J. McCarthy), Elsevier, New York, pp. 293–300.

Huray, P. G. and Nave, S. E. (1987) Magnetic studies of the Transplutonium Actinides, in *Handbook on the Physics and Chemistry of the Actinides* (eds. A. J. Freeman and G. H. Lander), vol. 5, 311–72.

Hussonnois, M., Hubert, S., Billard, L., and Guillaumont, R. (1973) *Radiochem. Radioanal. Lett.*, **15**, 4756

Hyde, E. K., Perlman, I., and Seaborg, G. T. (1964) The Transuranium Elements. in *The Nuclear Properties of the Heavy Elements II,* Prentice-Hall, Englewood Cliffs, NJ, pp. 946–64.

Ionova, G. V., Mikheev, N. B., and Spitsyn, V. I. (1978) *Sov. Radiochem.*, **20**, 89–92.

Ishimori, T. (1980) in *Actinide Separations,* ACS Symp. Ser. 117 (eds. J. D. Navratil and W. W. Schulz), American Chemical Society, Washington, DC, pp. 333–50.

King, L. J., Bigelow, J. E., and Collins, E. D. (1981) in *Transuranium Elements – Production Recovery,* ACS Symp. Ser. 161 (eds. J. D. Navratil and W. W. Schulz), American Chemical Society, Washington, DC, pp. 133–46.

Kleinschmidt, P. D., Ward, J. W., Matlack, G. M., and Haire, R. G. (1984) *J. Chem. Phys.*, **81**, 473–7.

Kleinschmidt, P. D., Ward, J. W., Matlack, G. M., and Haire, R. G. (1985) *High Temp. Sci.*, **19**(3), 267–74.
Kosyakov, V. N., Chudinov, N., and Shvetsov, I. K. (1974) *Sov. Radiochem.*, **16**, 722–8.
Krause, M. N., Haire, R. G., Keski-Rahkonen, O., and Peterson, J.R. (1988) *J. Electron Spectrosc. Related Phenom.*, **47**, 215–26.
Kulyukhin, S. A. and Mikheev, N. B. (1990) *J. Radioanal. Nucl. Chem.*, **143**(2), 415–26.
Kulyukhin, S. A. and Mikheev, N. B. (1997a) *Radiochemistry*, **39**(2), 123–5.
Kulyukhin, S. A. and Mikhee, N. B. (1997b) *Radiochemistry*, **39**(2), 126–7.
Kulyukhin, S. A., Mikheev, N. B., and Rumer, I. A. (1997) *Radiochemistry*, **39**(2), 130–32; and references therein.
Latrous, H., Oliver, J., and Chemla, M. (1982) *Radiochem. Radioanal. Lett.*, **53**, 81–8.
Lebedev, I. A. (1978) *Sov. Radiochem.*, **20**, 556–62.
Legoux, Y. and Merinis, J. (1986) *J. Less Common Metals*, **121**, 49–54.
Liebman, J. F. (1978) *Inorg. Nucl. Chem. Lett.*, **14**, 245–7.
Lloyd, R. D., Dockum, J. G., and Atherton, D. R. (1975) *Health Phys.*, **28**(5), 585–9.
Lundqvist, R. D., Hulet, E. K., and Baisden, P. A. (1981) *Acta Chem. Scand. A*, **35**, 653–61.
Maly, J. (1969) *J. Inorg. Nucl. Chem.*, **31**, 1007–17.
McDowell, W. J. and Coleman, C. F. (1972) *J. Inorg. Nucl. Chem.*, **34**, 2837–50.
McHarris, W., Stephens, F. S., and Asaro, F. (1966) *Phys. Rev.*, **144**, 1031–7.
Mikheev, N. B. and Rumer, I. A. (1972) *Sov. Radiochem.*, **14**, 502–3.
Mikheev, N. B., Spitsyn, V. I., Kamenskaya, A. N., Rozenkevich, N. A., Rumer, I. A., and Auerman, L. N. (1972a) *Sov. Radiochem.*, **14**, 494–5.
Mikheev, N. B., Auerman. and L. N., Spitsyn, V. I. (1972b) *Inorg. Chem. Lett.*, **8**(10), 869–73; *Sov. Radiochem.*, **14,** 494–5.
Mikheev, N. B. (1986) *J. Less Common Metals*, **121**, 652–3.
Mikheev, N. B., Kamenskaya, A. N., and Kulyukhin, S. A. (1986) *Sov. Radiochem.*, **28**(5), 532–34.
Mikheev, N. B., Kamenskaya, A. N., and Kulyukhin, S. A. (1988a) *Sov. Radiochem.*, **30**(2), 196–200.
Mikheev, N. B., Kulyukhin, S., and Rumer, I. A. (1988b) *Sov. Radiochem.*, **30**(2), 200–4.
Mikheev, N. B. and Kamenskaya, A. N. (1992) in *Transuranium Elements: a Half Century*, ACS Symp. (eds. L. Morss and J. Fuger), Americian Chemical Society, Washington, DC, pp. 469–80; and references therein.
Mikheev, N. B., Kulyukhin, S. A., and Veleshko, I. E. (1993a) *Radiochemistry*, **35**(5), 527–30.
Mikheev, N. B., Veleshko, I. E., And Kulyukhin, S. A. (1993b) *Radiochemistry*, **35**(5), 518–20; and references therein.
Mikheev, and N. B. Rumer, I. A. (1999) *Radiochim. Acta*, **85**(1–2), 49–55.
Mikheev, N. B., Kulyukhin, S. A., Kamenskaya, A. N., Rumer, I. A., and Konovalova, N. A. (2004) *Radiochemistry*, **46**(4), 324–39; and references therein.
Mikheev, V. L., Ilyushch, V. I., and Miller, M. B. (1967) *Sov. J. Nucl. Phys.*, **5**, 35–7.
Morss, L. R., (1986) in *The Chemistry of the Actinide Elements*, (eds. Katz, Seaborg and Morss) Chapter 17, Thermodynamics, Chapman and Hall, New York, pp. 1278–360.
Müller, W. (1967) *Actinides Rev.*, **1**, 71–119.

Myasoedov, B. F., Guseva, L. I., Lebedev, I. A., Milyukova, M. S., and Weinheim, M. K. (1974) in *Analytical Chemistry of the Transplutonium Elements* (ed. D. Slutzkin), John Wiley, New York, pp. 122–32.

Myasoedov, B. F., Chmutova, M. K., and Karalova, Z. K. (1980) in *Actinide Separations,* ACS Symp. Ser. 117 (eds. J. D. Navratil and W. W. Schulz), American Chemical Society, Washington, DC, pp. 101–15.

Ninov, V., Hessberger, F. P., and Hofmann, S. (1996) *Z. Phys. A-Hadron Nucl.*, **356**(1), 11–12.

Nugent, L. J., Burnett, J. L., Baybarz, R. D., Werner, G. K., Tanner, S. R., Tarrant, J. R., and Keller, O. L. Jr (1969a) *J. Phys. Chem.*, **73**, 1540–9.

Nugent, L. J., Baybarz, R. D., and Burnett, J. L. (1969b) *J. Phys. Chem.*, **73**, 1177–8.

Nugent, L. J., Baybarz, R. D., Werner, G. K., and Friedman, H. A. (1970) *Chem. Phys. Lett.*, **7**, 179–82.

Nugent, L. J., Baybarz, R. D., Burnett, J. L., and Ryan, J. L. (1971) *J. Inorg. Nucl. Chem.*, **33**, 2503–30.

Nugent, L. J., Burnett, J. L., and Morss, L. R. (1973) *J. Phys. Chem.*, **77**, 1528–39.

Nugent, L. J. (1975) *J. Inorg. Nucl. Chem.*, **37**, 1767–70.

Peterson, J. R., Ensor, D. D., Fellows, R. L., Haire, R. G., and Young, J. P. (1977) *Rev. Chim. Minér.*, **14**, 172–7.

Peterson, J. R. (1979) in *Proc. Symp. Commemorating the 25th Anniversary of Elements 99 and 100* (ed. G. T. Seaborg), Report LBL-7701, p. 55; and references therein.

Peterson, J. R., Ensor, D. D., Fellows, R. L., Haire, R. G., and Young, J. P. (1979) *J. Phys. Colloq.*, **40**(C4), 111–13; and references therein.

Peterson, J. R. (1994) American Chemical Society, Abstract NUCL-14, 207th National Meeting, San Diego, CA.

Peterson, J. R., Erdmann, N., Nunnemann, M., Eberhardt, K., Huber, G., Kratz, J. V., Passler, G., Stetzer, O., Thorle, P., Trautmann, N., and Waldek, A. (1998) *J. Alloys Compds*, **271/273**, 876–78.

Porter, C. E., Riley, F. D., Vandergrift, R. D., and Felker, L. K. (1997) *Sep. Sci. Technol.*, **32**(1–4), 83–92.

Rajnak, and K. Shore, B. W. (1978) *J. Opt. Soc. Am.*, **68**, 360–7.

Samhoun, and K. David, F. (1979) *J. Inorg. Nucl. Chem.*, **41**, 357–63; and references therein.

Seaborg, G. T. and Loveland, W. D. (1990) *The Elements Beyond Uranium,* John Wiley, New York, pp. 28–38.

Shaugnessy, D. A., Gregorich, K. E., Adams, J., Laue, C. A., Lane, M., Lee, D., McGrath, C. A., Patin, J. B., Strellis, D. A., Sylwester, E. R., Wilk, P. A., and Hoffman, D. C. (2000) American Chemical Society, Abstract NUCL-78, 220th National Meeting, Washington, DC.

Shoun, and R. R. McDowell, W. J. (1980) in *Actinide Separations,* ACS Symp. Ser. 117 (eds. J. D. Navratil and W. W. Schulz), American Chemical Society, Washington, DC, pp. 71–87.

Sugar, J. (1974) *J. Chem. Phys.*, **60**, 4103–10.

Street, K. J., and Seaborg, G. T. (1950) *J. Am. Chem. Soc.*, **72**, 2790–2.

Taut, S. S., Hübener, S., Eichler, B., Gäggeler, H. W., Schädel, M., and Zvara, I. (1997) *Radiochim. Acta*, **78**, 33–8.

Taut, S. S., Hübener, S., Eichler, B., Turler, A., Gäggeler, H. W., Timokhin, S. N., and Zvara, I. (1998) *J. Alloys Compds*, **271**, 316–21.

Thompson, S. G., Harvey, B. G., Choppin, G. R., and Seaborg, G. T. (1954) *J. Am. Chem. Soc.*, **76**, 6229–303.

Topp, N. E. (1965) *The Chemistry of the Rare-Earth Elements,* Elsevier, New York, pp. 125–55.

Varga, L. P., Baybarz, R. D., Reisfeld, M. J., and Asprey, L. B. (1973a) *J. Inorg. Nucl. Chem.*, **35**, 2775–85.

Varga, L. P., Baybarz, R. D., Reisfeld, M. J., and Mann, J. B. (1973b) *J. Inorg. Nucl. Chem.*, **35**, 2303–10.

Veleshko, I. E., Mikheev, N. B., and Kulyukhin, S. A. (1993) *Radiochemistry*, **35**(5), 523–26.

Ward, J. W. and Hill, H. H. (1976) in *Heavy Element Properties* (eds. W. Müller and H. Blank), Elsevier, New York, p. 65.

Ward, J. W., Kleinschmidt, P. D., Haire, R. G., and Brown, D. (1980) in *Lanthanides and Actinides Chemistry and Spectroscopy* (ed. N. Edelstein), ACS Symp. Ser. 131, American Chemical Society, Washington, DC, p. 199.

Ward, J. W. (1986) *J. Less Common Metals*, **121**, 1–15.

Worden, E. F., Lougheed, R. W., Gutmacher, R. G., and Conway, J. G. (1974) *J. Opt. Soc. Am.*, **64**, 77–85.

Wyart, J. F., Blaise, J., and Worden, E. F. (2005) *J. Solid State Chem.*, **178**(2), 589–602.

Young, J. P., Haire, R. G., Fellows, R. L., Noé, M., and Peterson, J. R. (1976) Spectroscopic and X-ray Diffraction Studies of the Bromides of Cf-249 and Es-253, in *Transplutonium 1975* (eds. W. Müller and R. Lindner), North-Holland, Amsterdam, pp. 227–34.

Young, J. P., Haire, R. G., Fellows, R. L., and Peterson, J. R. (1978) *J. Radioanal. Chem.*, **43**, 479–88.

Young, J. P., Haire, R. G., Peterson, J. R., Ensor, D. D., and Fellows, R. L. (1981) *Inorg. Chem.*, **20**, 3979–83.

CHAPTER THIRTEEN

FERMIUM, MENDELEVIUM, NOBELIUM, AND LAWRENCIUM

Robert J. Silva

13.1 GENERAL

Because of conflicting claims, the International Union of Pure and Applied Chemistry (IUPAC) recently reviewed the names of all the trans-fermium elements; Münzenberg (1999) has published a detailed discussion of the problems and the resolution. First, a Transfermium Working Group decided the priority of discoveries. Next, the discoverers proposed names to the IUPAC and names were officially accepted by that body. The names for the elements mendelevium, nobelium, and lawrencium were retained as originally proposed at the time of their discoveries.

As of this writing, the number of known isotopes of Fm, Md, No, and Lr is 58, ranging in half-life from as short as 0.25 ms for ^{250}No to as long as 100.5 days for ^{257}Fm. Relativistic effects have been predicted to affect ground state electronic configurations, ionic radii, and oxidation state for the heavier actinides. While the 3+ oxidation state remains a dominant feature of the heavier actinides, a tendency toward the formation of lower oxidation states has emerged. Divalency had been observed in solution for fermium through nobelium, in fact, the elements Fm, Md, and No are divalent in the metallic state. Due to increased 5f electron binding of the filled $5f^{14}$ shell, the 2+ oxidation state is the most stable in aqueous solution for nobelium. However, lawrencium, the last member of the actinide series, returns to the 3+ oxidation state as the most stable in aqueous solution, as predicted (Seaborg, 1949).

Due to the short half-lives and low production yields of Fm–Lr, all available chemical information has been obtained from experiments with tracer quantities. In fact, in many cases, chemical experiments were performed with only a few atoms or even one atom at a time. These experiments have necessarily been rather simple in principle, aimed primarily at making comparative studies with elements of known chemical properties. Nevertheless, all available experimental and theoretical evidence supports the original prediction of an actinide series (Seaborg, 1945) involving filling of the 5f electron shell, analogous to the lanthanide series resulting from the filling of the 4f electron shell, and that element 103 is the last member of this series of elements (Seaborg, 1949). The next element, atomic number 104, would be expected to fall into the next chemical group, i.e. Group IVB, of the periodic table.

13.2 FERMIUM

13.2.1 Introduction

The first isotope of element 100 was discovered in heavy-element samples obtained after the 'Mike' thermonuclear explosion of 1952, during the same set of experiments that resulted in the discovery of element 99. A joint effort by the researchers from the Lawrence Berkeley National Laboratory, the Argonne National Laboratory, and the Los Alamos National Laboratory resulted in the chemical isolation and identification of the 20 h half-life isotope ^{255}Fm (Ghiorso *et al*., 1955a). The production involved rapid, multiple neutron capture by uranium nuclei in the nuclear device to form neutron-rich uranium isotopes of heavy mass followed by beta decay to elements of higher atomic number. The ^{255}Fm in the samples, produced from the beta decay of the longer-lived ^{255}Es, was purified and chemically identified by cation-exchange chromatography and detected through the use of alpha particle energy analysis. The name, fermium, was proposed in 1955 in honor of the leader in nuclear science, Enrico Fermi, and the name was subsequently accepted by the IUPAC.

13.2.2 Isotopes of fermium

As can be seen in Table 13.1, there are 19 known isotopes of element 100, ranging from atomic masses 242 through 260. Isotopes with masses 254 through 257 have been identified in samples of plutonium or elements of higher atomic number following neutron irradiation in nuclear reactors. All the other isotopes can only be produced by charged-particle bombardments of targets of elements of lower atomic number at charged-particle accelerators, e.g. cyclotrons, linear accelerators, etc.

The isotope that can be produced in largest quantities on an atomic basis is ^{257}Fm. This isotope is also the nuclide of highest atomic and mass number ever

Table 13.1 *Nuclear properties of fermium isotopes.*

Mass number	*Half-life*	*Mode of decay*	*Main radiations* (MeV)	*Method of production*
242	0.8 ms	SF		^{204}Pb(^{40}Ar,2n)
243	0.18 s	α	α 8.546	^{206}Pb(^{40}Ar,3n)
244	3.3 ms	SF		^{206}Pb(^{40}Ar,2n)
				^{233}U(^{16}O,5n)
245	4.2 s	α	α 8.15	^{233}U(^{16}O,4n)
246	1.1 s	α 92%	α 8.24	^{235}U(^{16}O,5n)
		SF 8%		^{239}Pu(^{12}C,5n)
247[a]	35 s	α ≥ 50%	α 7.93 (∼ 30%)	^{239}Pu(^{12}C,4n)
		EC ≤ 50%	7.87 (∼70%)	
247[a]	9.2 s	α	α 8.18	^{239}Pu(^{12}C,4n)
248	36 s	α 99.9%	α 7.87 (80%)	^{240}Pu(^{12}C,4n)
		SF 0.1%	7.83 (20%)	
249	2.6 min	α	α 7.53	^{238}U(^{16}O,5n)
				^{249}Cf(α,4n)
250	30 min	α	α 7.43	^{249}Cf(α,3n)
		SF 5.7×10^{-4}%		^{238}U(^{16}O,4n)
250 m	1.8 s	IT		^{249}Cf(α,3n)
251	5.30 h	EC 98.2%	α 6.834 (87%)	^{249}Cf(α,2n)
		α 1.8%	6.783 (4.8%)	
252	25.39 h	α	α 7.039 (84.0%)	^{249}Cf(α,n)
		SF 2.3×10^{-3}%	6.998 (15.0%)	
253	3.0 d	EC 88%	α 6.943 (43%)	^{252}Cf(α,3n)
		α 12%	6.674 (23%)	
			γ 0.272	
254	3.240 h	α > 99%	α 7.192 (85.0)	^{254m}Es daughter
		SF 0.0592%	7.150 (14.2%)	
255	20.07 h	α	α 7.022 (93.4%)	^{255}Es daughter
		SF 2.4×10^{-5}%	6.963 (5.0%)	
256	2.63 h	SF 91.9%	α 6.915	^{256}Md daughter
		α 8.1%		^{256}Es daughter
257	100.5 d	α 99.79%	α 6.695 (3.5%)	multiple n capture
		SF 0.21%	6.520 (93.6%)	
			γ 0.241	
258	0.37 ms	SF		^{257}Fm(d,p)
259	1.5 s	SF		^{257}Fm(t,p)
260	4 ms	SF		^{260}Md daughter

[a] Not known whether ground-state nuclide or isomer.

isolated from either reactor or thermonuclear-produced materials. The neutron capture production chain essentially terminates at mass 257 owing to the very short spontaneous fission half-lives of the heavier isotopes. The current annual reactor production rate is in the picogram range (Porter *et al.*, 1997). However, in the thermonuclear explosion of 1969 called 'Hutch,' about 10^8 higher production was achieved (Hoff and Hulet, 1970), but only one

part in 10 million of the total number of atoms of ^{257}Fm imbedded in tons of geologic debris was recovered, i.e. a 10 kg sample of debris yielded about 10^{10} atoms.

Though ^{257}Fm is produced in larger amounts, ^{255}Fm has been more available on a regular basis from the beta decay of reactor-produced ^{255}Es ($t_{1/2} = 38.3$ days) and is more frequently used for chemical studies at the tracer level. Radioactivity levels in excess of 10^8 alpha disintegrations per minute of ^{255}Fm can be obtained from periodic chemical separations of Fm, 'milkings,' from purified Es samples.

13.2.3 Preparation and purification

Because of their strong chemical similarity, the only satisfactory methods of separation of the trivalent actinides are by cation exchange or solvent extraction chromatography. The procedure most often selected is separation by elution from a cation-exchange resin column, e.g. Dowex 50 × 8 or × 12 resin, using an aqueous solution of the chelating agent ammonium α-hydroxyisobutyrate (α-HIB) as eluant. This combination, developed in 1956 (Choppin *et al.*, 1956) primarily for the isolation and identification of new actinide elements, remains the main process method for the separation of trivalent actinides (Porter *et al.*, 1997). The actinides exhibit increasing complexation strength with the organic ligand with increasing atomic number, attributed to the decreasing ionic radii due to the actinide contraction (Katz *et al.*, 1986) and are eluted from the column in a regular sequence with the higher atomic number elements eluting first. Fig. 13.1 shows a typical separation of trace amounts of trivalent actinides using this method.

Vobecký *et al.* (1991) have obtained similar sequential elution and separation of 3+ actinides from a column of the spheroidal cation exchanger OSTION using a solution of ammonium α-hydroxy-α-methylbutyrate as the eluant.

Porter *et al.* (1997) have described a process method for the isolation and purification of fermium from other actinides and from rare earth fission produce from reactor target material. In addition to the standard series of transcurium actinide separations through the use of ammonium α-HIB eluant and cation-exchange resin, final purification of the fermium from small amounts of rare earth impurities that could contribute to the mass of the sample was accomplished using a solvent extraction chromatographic resin (the quaternary amine, Aliquat-336, impregnated into Amberchrom CG-71 ms support resin) that is marketed under the trade name TEVA.

Mikheev *et al.* (1983) have developed a rapid method for the separation of fermium from californium, einsteinium, and lanthanide elements based on the cocrystallization of reduced ^{254}Fm(II) with sodium chloride in aqueous ethanol solutions containing Yb(II). The coefficient of separation of Fm

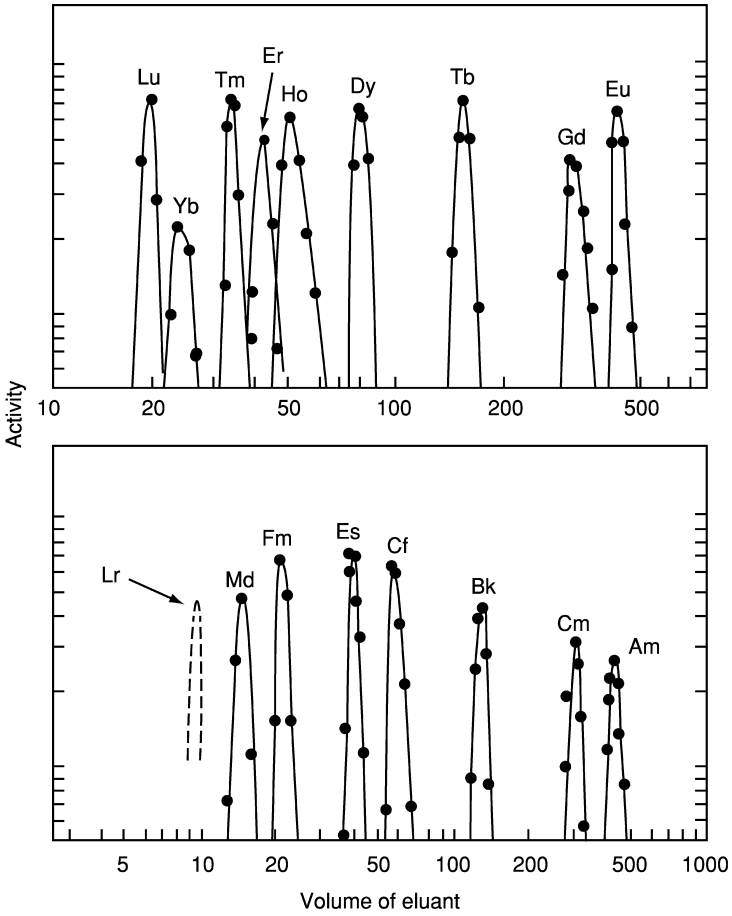

Fig. 13.1 *Elution of homologous trivalent actinides and lanthanides from a Dowex* 50 *cation-exchange resin column at* 87°C *with ammonium α-hydroxyisobutyrate as eluant. The broken curve for element* 103 (*Lr*) *is an estimate based on its predicted radius.*

from its elemental analogs in one cocrystallization step is 10^3 to 10^4 and the separation takes about 10 min.

Fermium has also been separated rapidly from the other transplutonium elements via chromatography using strongly basic anion-exchange resin and mixtures of nitric acid and methyl alcohol at elevated temperatures for the elutions (Usuda *et al.*, 1987).

Volatile hexafluoroacetylacetonates of Md and Fm have been prepared and could be the bases for chemical isolation by thermochromatography (Fedoseev *et al.*, 1990).

13.2.4 Atomic properties

Goodman *et al.* (1971) have used the atomic-beam magnetic resonance technique, adapted to the measurement of radioactive samples, to determine the magnetic moment, g_j, of the atomic ground state of neutral atoms of ^{254}Fm to be 1.16052 ± 0.00014. A comparison of the experimentally measured value with values obtained from intermediate coupling calculations for several likely electron configurations was made. The measured value of g_j was found to be in close agreement only with that calculated for the $^3H_6$ level of the $5f^{12}7s^2$ electronic configuration. This agreement was taken as a conclusive evidence for the assignment of this configuration to the ground state of fermium.

The inner-shell binding energies and X-ray energies for the heavy elements have been estimated from total energies obtained from a Dirac–Fock computer code of Desclaux by Carlson and Nestor (1977). In these calculations, small empirical corrections were added as a result of comparing calculations with experimentally determined binding energies for elements of $Z > 95$. Where comparisons have been made for higher Z elements, the results of the calculations have agreed well with the experimentally measured values. Fricke *et al.* (1972) have also published electron binding energies in fermium obtained from Dirac–Fock calculations and compared them to the values of Porter and Freedman (1971) measured experimentally via spectroscopic measurements of internal conversion electrons emitted following the beta decay of ^{254m}Es to ^{254}Fm. Das (1981) calculated the binding energies in fermium by using a relativistic local density functional theory. Porter and Freedman (1978) have recommended atomic binding energies of the K, L, M, N, O, and P shells for heavy elements from $Z = 84$ to 103. A table of electron binding energies based on the latter is given by Firestone *et al.* (1996). The values for Fm differ slightly from their earlier experimental values (Porter and Freedman, 1971). The results of the three theoretical calculations are compared with the recommended values of Porter and Freedman in Table 13.2. The agreement is quite good and demonstrates that these types of theoretical calculations are consistent and quite useful for predictive purposes.

Dittner *et al.* (1971) have measured the K-series X-rays of ^{251}Fm emitted following the alpha decay of ^{255}No. The K-series X-ray energies derived experimentally from these studies are compared with the values calculated using the binding energies of Porter and Freedman (1978) in Table 13.2.

13.2.5 The metallic state

Fermium metal has not been prepared, however, measurements have been performed on alloys with rare earth metals and a number of predictions about it have been made.

Johansson and Rosengren (1975) have correlated the measured and predicted cohesive energies of the lanthanide and actinide elements in both the divalent and trivalent metallic states. They concluded that the gain in energy of binding

Table 13.2 *Comparison of calculated and measured electron binding and X-ray energies for fermium.*

	Binding energy (−eV)					*X-ray energy* (keV)	
Shell	*Calc.*[a]	*Calc.*[b]	*Calc.*[c]	*Meas.*[d]	*Transition*	*Calc.*[e]	*Meas.*[f]
1s	1 41 943	1 41 953	1 42 573	1 41 962			
2s	27 584	27 581	27 503	27 573			
$2p_{1/2}$	26 643	26 646	26 608	26 644	$K_{\alpha 2}$ ($2p_{1/2} \rightarrow 1s_{1/2}$)	115.285	115.280
$2p_{3/2}$	20 872	20 869	20 783	20 868	$K_{\alpha 1}$ ($2p_{3/2} \rightarrow 1s_{1/2}$)	122.058	121.070
3s	7 206	7 213	7 127	7 200			
$3p_{1/2}$	6 783	6 783	6 710	6 779	$K_{\beta 3}$ ($3p_{1/2} \rightarrow 1s_{1/2}$)	135.150	135.2
$3p_{3/2}$	5 414		5 341	5 408	$K_{\beta 1}$ ($3p_{3/2} \rightarrow 1s_{1/2}$)	136.521	136.6
$3d_{3/2}$	4 757		4 726	4 746			
$3d_{5/2}$	4 497		4 460	4 484			
4s	1 954		1 904	1 940			
$4p_{1/2}$	1 753		1 712	1 743	$K_{\beta 2}$ ($4p_{1/2} \rightarrow 1s_{1/2}$)	140.177	140.1
$4p_{3/2}$	1 383		1 340	1 371			
$4d_{3/2}$	1 071		1 046	1 059			
$4d_{5/2}$	1 005		979	989			
$4f_{5/2}$			591				
$4f_{7/2}$			572				
5s			440				
$5p_{1/2}$			361				
$5p_{3/2}$			264				
$5d_{3/2}$			150				
$5d_{5/2}$			144				

[a] Carlson and Nester (1977).
[b] Fricke *et al.* (1972).
[c] Das (1981).
[d] Porter and Freedman (1971).
[e] Porter and Freedman (1978).
[f] Dittner *et al.* (1971).

of the $5f^n6d^17s^2$ (trivalent) configuration over the $5f^{n+1}7s^2$ (divalent configuration) is less than the energy necessary to promote one 5f electron to the 6d state in the final members of the actinide series. Therefore, Es, Fm, Md, and No prefer a divalent metallic state similar to Eu and Yb rather than a trivalent one. However the energy difference is small for Es and Fm and, at modest compression, the divalent metallic state may convert to the trivalent one.

The sublimation enthalpy, a fundamental metallic property, is connected directly with the valence electronic structure of the metal. The enthalpy of sublimation of fermium has been determined directly by measuring the partial pressure of Fm over Fm–Sm and Fm, Es–Yb alloys for the temperature range 642–905 K (Haire and Gibson, 1989). Based on their combined second law and third law measured values for the enthalpy of sublimation of Fm, they reported a value of (142 ± 13) kJ mol^{-1} for ΔH_{298}. Because the enthalpy of sublimation

of Fm was similar to those of divalent Es, Eu, and Yb, it was concluded that Fm is divalent in the metallic state. Comparisons with radii and melting points of Eu, Yb, and Es metals have yielded estimated values of 0.198 nm and 1125 K for Fm by these authors. David *et al.* (1978) have estimated a divalent metallic radius of 0.194 nm for Fm, in close agreement.

Because the heaviest actinides are available only in trace amounts, innovative experimental approaches must be used in order to characterize their elemental state properties. Zvara and coworkers (Zvara *et al.*, 1976) compared the evaporation rates of trace amounts of Es, Fm, and Md from molten La with those of Ce, Eu, Yb, Am, and Cf to obtain information on their metallic states. Hübener (1980) compared the thermochromatographic behavior of Es, Fm, and Md evaporated from molten La in titanium columns with those of Na, Sc, Sm, Eu, Yb, Bk, and Cf. The conclusion reported in both of these papers supported the idea that Es, Fm, and Md prefer the divalent metallic state. The adsorption behavior of Cf, Es, Fm, and Md on titanium and molybdenum thermochromatographic columns was compared to a number of monovalent, divalent, and trivalent elements and enthalpies of adsorption determined (Hübener and Zvara, 1982). From the data, the authors also concluded that Es, Fm, and Md are divalent in the metallic state and that the position of the f-energy levels relative to the Fermi-energy is lower than in the cases of Cf and Yb. A nearly linear correlation was found between the experimental enthalpies of adsorption of the heavy actinides and their predicted enthalpies of sublimation.

Thermochromatographic studies of the adsorption of Cf, Es, and Fm on several metals were conducted by Taut *et al.* (1997) and enthalpies of sublimation inferred from the measured enthalpies of adsorption. The results support the value of the enthalpy of sublimation of Fm published by Haire and Gibson (1989).

13.2.6 Solution chemistry

The chemical properties of fermium have been studied only with trace quantities. The chemical properties of Fm have been discussed by Thompson *et al.* (1954). Under conditions not strongly reducing, fermium behaves in aqueous solution as expected for a trivalent actinide ion. Fermium coprecipitates with rare earth fluorides and hydroxides. The elution of fermium just before einsteinium from cation-exchange resin columns with hydrogen ion and the complexing ligands citric acid, lactic acid, and α-HIB is consistent with the existence of a trivalent ion (Katz and Seaborg, 1957). In concentrated hydrochloric acid, nitric acid, and ammonium thiocyanate solutions, fermium forms anion complexes with these ligands that can be adsorbed onto and subsequently eluted from anion-exchange columns (Thompson *et al.*, 1954). In this case, fermium follows einsteinium in the elution sequence. Both types of column results indicate that Fm forms a slightly stronger complex with the ligands than Es, which is due to the slightly smaller ionic radius of Fm as a result of the actinide contraction

(Katz *et al.*, 1986). Fermium also exhibits a more acidic behavior than the preceding actinides in aqueous solution, having a first hydrolysis constant of 1.6×10^{-4} (Hussonnois *et al.*, 1972).

David *et al.* (1978) have estimated some thermodynamic properties of the 5f elements obtained from theoretical considerations and empirical correlations drawn from observed trends in the 4f series. They proposed an ionic radius of 0.0922 nm for Fm^{3+}. From the linear correlation of log distribution coefficients with ionic radius obtained from elution positions from α-HIB/cation-exchange column separations, a value of 0.0911 nm was calculated for the ionic radius of Fm^{3+} (Brüchle *et al.*, 1988). Lundqvist *et al.* (1981) have studied the migration rates of Fm^{3+} in an electrical potential gradient using paper electrophoresis and reported a hydrated radius of 0.495 nm and a hydration number of 16.9 in aqueous perchlorate solutions.

Fermium readily forms complexes with a variety of organic ligands, e.g., β-diketones (Hussonnois *et al.*, 1972), hydroxycarboxylic acids (Thompson *et al.*, 1954; Choppin *et al.*, 1956; Baybarz, 1965, 1966; Ermakovl and Stary, 1967; Hubert *et al.*, 1974), organophosphorus esters (Baybarz, 1963; Stary, 1966; Horwitz *et al.*, 1969), and alkylamines (Müller, 1967). α-HIB has long been used as the eluant for inner series separation of trivalent actinides by cation-exchange chromatography as stated above. However, bis(2-ethylhexyl)phosphoric acid (HDEHP) (Horwitz and Bloomquist, 1973) and Alamine 336 (a mixed *n*-octyl and *n*-decyl tertiary amine) (Leuze *et al.*, 1963) have also been used for similar separations of Fm by solvent extraction column chromatography. Gorski *et al.* (1990) have investigated the complex formation of several transplutonium elements, including Fm, with 1,2-diaminocyclohexane tetraacetic acid (DCTA) and shown the correlation of ionic radii with the values of the log of the complex stability constants. A linear dependence is observed for lanthanides while it deviates from linearity for the heavy actinides. The author's postulate that, since the stability of chelate complexes are determined by the positive change of entropy of the reaction, the change in stability constants of the heavy actinides is due to an entropy effect rather than to the change in the ionic radii.

The behavior of Sr, Y, Sm, Eu, Am, Cf, Es, and Fm in the molten salt mixtures LiCl–$NdCl_2$–$NdCl_3$ and LiI–PrI_2 have been studied (Kulyukhin, 1997). In the presence of Nd^{2+}, Cf, Es, and Fm are reduced to the 2+ oxidation state. The results obtained in the LiI–PrI_2 system were ambiguous as to whether the actinides Cf–Fm were reduced to the 1+ or 2+ oxidation states.

The tendency of Fm to form a divalent ion under strong reducing conditions was first suggested by the work of Maly (1967). Mikheev *et al.* (1972) reported the reduction of Fm^{3+} to Fm^{2+} in 1972 from the results of reduction/cocrystallization experiments with $SmCl_2$. The reduction of Fm^{3+} to Fm^{2+} with $SmCl_2$ has also been observed by Hulet *et al.* (1979). Mikheev *et al.* (1977) were able to estimate the reduction potential to be very nearly the same as the $Yb^{3+} \rightarrow Yb^{2+}$ couple or −1.15 V. This value is in reasonably good

agreement with the value of $-(1.1 \pm 0.2)$ V calculated by Nugent (1975) using refined electron-spin-pairing theory.

Using a refined radiopolarographic technique, Samhoun and David (1976) measured the half-wave potential for the $Fm^{2+} \rightarrow Fm(Hg)$ reduction at a dropping mercury electrode as $-(1.47 \pm 0.01)$ V. By applying an estimated amalgamation potential correction of 0.90 V obtained from correlations of other divalent ions, a value for E° ($Fm^{2+} \rightarrow Fm^0$) of $-(2.37 \pm 0.1)$ V was reported. Using this latter value of Samhoun and David, combined with Mikheev's value of -1.15 V for the $Fm^{3+} \rightarrow Fm^{2+}$ couple, a value of $-(1.96 \pm 0.13)$ V can be calculated for E° ($Fm^{3+} \rightarrow Fm^0$). Nugent (1975) has estimated $E^\circ(Fm^{4+} \rightarrow Fm^{3+})$ to be $+4.9$ V. These values (Table 13.8) are consistent within uncertainties with those in Chapter 19 (Fig. 19.9).

Unless otherwise indicated, all electrode potentials in this chapter are with reference to the normal hydrogen electrode (NHE) and the 1969 IUPAC convention, i.e. the more positive the potential the more stable the reduced form (McGlashan, 1970).

13.3 MENDELEVIUM

13.3.1 Introduction

The first isotope of element 101 was produced in 1955 by Ghiorso *et al*. (1955b). It was synthesized in the bombardment of approximately one billion atoms of ^{253}Es with 41 MeV alpha particles and produced at a rate of only about two atoms per 3 h bombardment. A chemical identification was made on the basis of its elution position just before Fm from a cation-exchange resin column using ammonium α-HIB as eluant in a series of repetitive experiments. It was not detected directly but by the observation of spontaneous fission events arising from its electron-capture daughter ^{256}Fm. Additional analysis of the data, coupled with further experimentation, showed the isotope to have mass 256 and to decay by electron capture with a half-life of 1.5 h. The name mendelevium was proposed for the element in honor of Dimitri Mendeleev, in recognition of his contributions to the development of the chemical periodic system, and it was accepted by IUPAC.

13.3.2 Isotopes of mendelevium

Sixteen isotopes of mendelevium from mass 245 to 260 are known (see Table 13.3) . All of its isotopes can only be produced through charged-particle irradiations at accelerators. Although ^{258}Md, with a half-life of 51 days, is the longest-lived isotope, ^{256}Md remains the isotope most often used in chemical experiments because it can be produced in relatively larger quantities. Using microgram amounts of ^{253}Es presently available, more than a million

Table 13.3 *Nuclear properties of mendelevium isotopes.*

Mass number	*Half-life*	*Mode of decay*	*Main radiations* (MeV)	*Method of production*
245	0.4 s	α	α 8.680	^{209}Bi(^{40}Ar,4n)
	0.9 ms	SF		
246	1.0 s	α	α	^{209}Bi(^{40}Ar,3n)
247	1.12 s	α 80%	α 8.424	^{209}Bi(^{40}Ar,2n)
	0.27 s			
248	7 s	EC ~ 80%	α 8.36 (~25%)	^{241}Am(^{12}C,5n)
		α ~ 20%	8.32 (~75%)	^{239}Pu(^{14}N,5n)
249	24 s	EC ≤ 80%	α 8.03	^{241}Am(^{12}C,4n)
		α ≥ 20%		
250	52 s	EC 94%	α 7.830 (~25%)	^{243}Am(^{12}C,5n)
		α 6%	7.750 (~75%)	^{240}Pu(^{15}N,5n)
251	4.0 min	EC ≥ 94%	α 7.55	^{243}Am(^{12}C,4n)
		α ≤ 6%		^{240}Pu(^{15}N,4n)
252	2.3 min	EC > 50%	α 7.73	^{243}Am(^{13}C,4n)
		α < 50%		
253	6 min		^{238}U(^{19}F,5n)	
254[a]	10 min	EC		^{253}Es(α,3n)
254[a]	28 min	EC		^{253}Es(α,3n)
255	27 min	EC 92%	α 7.333	^{253}Es(α,2n)
		α 8%	γ 0.453	^{254}Es(α,3n)
256	1.27 h	EC 90.7%	α 7.205 (63%)	^{253}Es(α,n)
		α 9.9%	7.139 (16%)	
257	5.52 h	EC 90%	α 7.069	^{254}Es(α,n)
		α 10%		
258[a]	51.5 d	α	α 6.790 (28%)	^{255}Es(α,n)
			6.716 (72%)	
258[a]	57 min	EC ?		^{255}Es(α,n)
259	1.60 h	SF		^{259}No daughter
260	31.8 d	SF > 73%		^{254}Es(^{18}O,^{12}C)
		EC < 15%		

[a] Not known whether ground-state nuclide or isomer.

atoms per hour of ^{256}Md can be produced by alpha-particle bombardments (Hulet *et al.*, 1967).

13.3.3 Preparation and purification

The isotope ^{256}Md can best be produced for chemical study by the ^{253}Es(α,n) or ^{254}Es(α,2n) reactions at cyclotrons or linear accelerators. The isotope ^{254}Es would be the target material of choice if available. It has a half-life of 276 days compared to only 20.5 days for ^{253}Es and thus it would have a longer usable target lifetime.

The discovery experiments on mendelevium were the first in which the recoil momentum imparted by the bombarding ion to a product atom during its formation was used to carry out an instantaneous physical separation of the product atom from the target material (Seaborg, 1963). The recoil atoms were collected on a thin metal foil placed behind the target in an evacuated reaction chamber. This eliminated the time needed to separate the product atoms from the target atoms, previously accomplished by chemical means, and made it possible to use the same valuable target in repeated bombardments. A few years later, it was found that the recoil atoms could be slowed down and stopped in a gaseous atmosphere, frequently helium. The gas could be pumped out of the reaction chamber through a small orifice to form a 'gas-jet.' If this jet was impinged onto the surface of a foil, some fraction (frequently 75% or more) of the nonvolatile product atoms carried along with the gas were deposited permanently on the foil surface (Ghiorso, 1959; Macfarlane and Griffioen, 1963). The foil could be removed periodically for processing and a new foil installed. A good description of this system has been giving by Hoffman (1994).

After removal of the Md atoms from the collector foil by acid etching or following total dissolution of the thin metal foil, they can be purified and isolated from other product activities by several other techniques.

Md can be separated from the dissolved 'catcher' foil material, e.g. Be, Al, Pt, or Au, and most fission-product activities by coprecipitation with lanthanum fluoride. Subsequent separation of trivalent actinides from lanthanide fission products and La carrier can be accomplished with a cation-exchange resin column using a 90% water/10% ethanol solution saturated with HCl as eluant (Thompson *et al.*, 1954). When a very thin gold foil is used as the 'catcher' foil, after dissolution with aqua regia, a rapid separation of the Md from the Au can be made by anion-exchange chromatography using 6 M HCl as eluant. The gold remains on the column while the Md and other actinides pass through.

Final isolation of Md^{3+} from other trivalent actinides can be accomplished by selective elution from a cation-exchange resin column using ammonium α-HIB (Choppin *et al.*, 1956). When using the gas-jet system, the first two steps can frequently be eliminated.

In more recent years, it was found that, using the 'gas-jet' method, the recoil product atoms could be transported many meters with the stopping gas through a long capillary tube to the chemistry/counting area (Macfarlane and McHarris, 1974). In this case, effective transport over long distances requires the presence of large clusters, frequently KCl aerosols, in the 'carrier' gas. By this method, it is possible to transport and collect individual product atoms in a fraction of a second some tens of meters away from the target area. This method is quite generally used nowadays in the production and isolation of transeinsteinium elements.

A good separation of Md and Fm has been performed on a spheroidal cation-exchanger OSTIN using ammonium α-hydroxy-α-methylbutyrate (Vobecký *et al.*, 1991). The isotope ^{256}Md is most easily detected through the measurement

of the spontaneous fission activity of its daughter ^{256}Fm; however, in the presence of other fissioning nuclides, the detection of alpha particles of the characteristic energy of ^{256}Md associated with the 10% alpha decay branch can be used for identification.

Intragroup separation of the 3+ actinides has also been achieved by solvent extraction chromatography using HDEHP as the stationary organic phase and HNO_3 as the mobile aqueous phase (Horwitz and Bloomquist, 1969). Here, the actinide elution sequence is reversed from that of the cation-exchange resin column. This method gives a somewhat better final separation of Md from Fm than the cation-exchange resin column. It has the advantage that the final solution containing the Md is free of organic complexing agents compared to the resin column but has the disadvantage that Md elutes after Fm late in the sequence.

Following the discovery that Md can form a divalent state, extraction chromatography using HDEHP was used to show that the elution behavior of Md^{2+} is dissimilar to that of Es^{3+} and Fm^{3+} (Hulet *et al.*, 1967). This became the basis for a rapid separation method for the isolation of Md (Hulet *et al.*, 1979; Lundqvist *et al.*, 1981). After the initial steps of dissolution from the 'catcher' foil and coprecipitation with terbium fluoride, the mendelevium and 50 mg of Cr (added as a holding reductant) in 0.1 M HCl are co-reduced with Zn(Hg). The solution is passed through a solvent extraction column containing HDEHP on an inert support as the stationary organic phase. The actinides in the trivalent and tetravalent states as well as the trivalent lanthanides are extracted by the HDEHP and are retained on the column while the divalent Md is not appreciably extracted and appears in the 0.1 M HCl washes of the column. After reoxidation of the Md and Cr to the trivalent states with H_2O_2, the residual impurities, including the Cr, are separated from the Md by selective elution with 2 M (to remove the impurities) and 6 M HCl (to remove the Md) from a small column of Dowex 50 $\times$ 12 colloidal resin. Guseva *et al.* (1988) have reported a similar method for isolating Md where, using one column with cationite and zinc amalgam and a solution of 1 M HCl as the eluant, Md is reduced and washes through the column with the alkaline earth elements.

Volatile hexafluoroacetylacetonates of Md and Fm have been prepared and could be the bases for chemical isolation by thermochromatography (Fedoseev *et al.*, 1990).

13.3.4 Atomic properties

The electronic structure of the ground state of gaseous mendelevium atoms has been predicted to be the $^2F_{7/2}$ level of the $5f^{13}7s^2$ configuration (Martin *et al.*, 1974). An experimental confirmation has not yet been made. No experimental measurements of inner-shell binding energies or X-ray energies have been reported but estimated values have been reported by Firestone *et al.* (1996)

Table 13.4 *Estimated electron binding and X-ray energies for mendelevium, nobelium, and lawrencium.*

	Binding energy (−eV)				*X-ray energy* (keV)		
Shell	*Md*	*No*	*Lr*	*Transition*	*Md*	*No*	*Lr*
1s	1 46 526	1 49 208	1 52 970	$K_{\alpha1}$ ($2p_{3/2} \rightarrow 1s$)	125.17	127.36	130.61
				$K_{\alpha2}$ ($2p_{1/2} \rightarrow 1s$)	119.09	120.95	123.87
2s	28 387	29 221	30 083	$K_{\alpha3}$ ($2s \rightarrow 1s$)	118.14	119.99	122.89
$2p_{1/2}$	27 438	28 255	29 103				
$2p_{3/2}$	21 356	21 851	22 359	$K_{\beta1}$ ($3p_{3/2} \rightarrow 1s$)	140.97	143.51	147.11
				$K_{\beta2}$ ($4p_{3/2,1/2} \rightarrow 1s$)	144.91	147.53	151.23
3s	7 440	7 678	7 930	$K_{\beta3}$ ($3p_{1/2} \rightarrow 1s$)	139.53	141.98	145.50
$3p_{1/2}$	7 001	7 231	7 474	$K_{\beta4}$ ($4d_{5/2,3/2} \rightarrow 1s$)	145.46	148.10	151.82
$3p_{3/2}$	5 552	5 702	5 860	$K_{\beta5}$ ($3d_{3/2,1/2} \rightarrow 1s$)	141.77	144.32	147.94
$3d_{3/2}$	4 889	5 028	5 176				
$3d_{5/2}$	4 615	4 741	4 876	$L_{\alpha1}$ ($3d_{5/2} \rightarrow 2p_{3/2}$)	16.74	17.10	17.48
				$L_{\alpha2}$ ($3d_{3/2} \rightarrow 2p_{3/2}$)	16.47	16.82	17.18
4s	2 024	2 097	2 180				
$4p_{1/2}$	1 816	1 885	1 963	$L_{\beta1}$ ($3d_{3/2} \rightarrow 2p_{1/2}$)	22.55	23.23	23.93
$4p_{3/2}$	1 424	1 469	1 523	$L_{\beta2}$ ($4d_{5/2,3/2} \rightarrow 2p_{3/2}$)	20.29	20.74	21.21
$4d_{3/2}$	1 105	1 145	1 192	$L_{\beta3}$ ($3p_{3/2} \rightarrow 2s$)	22.84	23.52	24.22
$4d_{5/2}$	1 034	1 070	1 112	$L_{\beta4}$ ($3p_{1/2} \rightarrow 2s$)	21.39	21.99	22.61
$4f_{5/2}$	618	645	680	$L_{\beta5}$ ($5d_{5/2,1/2} \rightarrow 2p_{3/2}$)	21.21	21.70	22.20
$4f_{7/2}$	597	624	658	$L_{\beta6}$ ($4s \rightarrow 2p_{3/2}$)	19.33	19.75	20.18
5s	471	490	516	$L_{\gamma1}$ ($4d_{3/2} \rightarrow 2p_{1/2}$)	26.33	27.11	27.91
$5p_{1/2}$	389	406	429	$L_{\gamma2}$ ($4p_{1/2} \rightarrow 2s$)	26.57	27.34	28.12
$5p_{3/2}$	272	280	296	$L_{\gamma3}$ ($4p_{3/2} \rightarrow 2s$)	26.96	27.75	28.56
$5d_{3/2}$	154	161	174	L_l ($3s \rightarrow 2p_{3/2}$)	13.92	14.17	14.43
$5d_{5/2}$	137	142	154	L_ν ($3s \rightarrow 2p_{1/2}$)	20.00	20.58	21.17
$5f_{5/2}$	12.9	13.6	19.9				
$5f_{7/2}$	10.5	11.1	17.0				

based on the values recommended by Porter and Freedman (1978). The results are given in Table 13.4.

13.3.5 The metallic state

While mendelevium metal has not been prepared, Johansson and Rosengren (1975) predicted that, for the same reasons as discussed above for Fm, Md would prefer a divalent metallic state similar to Eu and Yb rather than a trivalent one.

As was the case with Fm, thermochromatographic studies conducted with trace amounts of Md by Zvara *et al*. (1976), Hübener (1980), and Hübener and Zvara (1982) led to the conclusion that Md forms a divalent metal. If the enthalpies of sublimation determined for Es and Fm from alloys are accepted, then, using the measured enthalpies of adsorption and the established correlation between the sublimation and adsorption enthalpies, Haire and Gibson (1990) estimated that Md has an enthalpy of sublimation in the range of

134–142 kJ mol^{-1}. Using empirical correlation methods, David *et al.* (1978) have estimated a divalent metallic radius of (0.194 ± 0.010) nm.

13.3.6 Solution chemistry

Before mendelevium was discovered, the trivalent state was predicted to be the most stable in aqueous solution and, therefore, it was expected to exhibit a chemical behavior similar to the other 3+ actinides and lanthanides (Seaborg and Katz, 1954). The elution of Md just before Fm in the elution sequence of trivalent actinides from a cation-exchange resin column observed in the discovery experiments appeared to confirm this prediction. Later, Md was indeed found to form insoluble hydroxides and fluorides that are quantitatively coprecipitated with trivalent lanthanides (Hulet *et al.*, 1967). Both the cation-exchange resin column (Choppin *et al.*, 1956) and HDEHP solvent extraction column (Horwitz and Bloomquist, 1969) elution data are consistent with a trivalent state for Md and an ionic radius slightly smaller than Fm.

Using empirical correlations, David *et al.* (1978) have estimated an ionic radius of 0.0912 nm (coordination number (CN) 6) for Md^{3+}. In addition to the ionic radius, a number of enthalpies and entropies of formation and sublimation were also estimated for Md. Hoffman *et al.* (1988) and Brüchle *et al.* (1988) compared the distribution coefficients for Lr, Md, and Fm with those of Tm, Er, and Ho obtained from ammonium α-HIB elutions from cation-exchange resin columns. Using the known ionic radii for the trivalent rare earths and the linear correlation of log distribution coefficient with ionic radius (for the same coordination number), an average ionic radius of 0.0896 nm was estimated for Md^{3+} and a heat of hydration of $-(3654 \pm 12)$ kJ mol^{-1} calculated using empirical models and the Born–Haber cycle.

Gorski *et al.* (1990) have studied the extraction behavior of Md with trioctylphosphine oxide in the presence of complexing agents and compared it to other transplutonium elements. They have also investigated the complex formation of several transplutonium elements, including Md, with DCTA and shown the correlation of ionic radii with the values of the log of the complex stability constants. The observed deviation from linearity by the heavy actinides is discussed in Section 13.2.5.

Hulet *et al.* (1967) first observed an anomalous chemical behavior for Md in certain chemical systems involving reducing conditions. With 10^5 to 10^6 atoms per experiment, coprecipitation with $BaSO_4$ and solvent extraction chromatography experiments using HDEHP were carried out in the presence of a number of different reducing agents. These experiments showed that Md^{3+} could be easily reduced to a stable Md^{2+} in aqueous solution. An estimate was made for the standard potential of the half-reaction $E^\circ(Md^{3+} \rightarrow Md^{2+})$ of approximately −0.2 V. Maly and Cunningham (1967) also produced the divalent state of Md and, from experiments similar to Hulet *et al.*, estimated $E^\circ(Md^{3+} \rightarrow Md^{2+})$ at −0.1 V. David (1986a) estimated $E^\circ(Md^{3+} \rightarrow Md^{0})$ to be −1.74 V. David

et al. (1981, 1990a) measured $-(1.51 \pm 0.01)$ V for the polarographic $E_{1/2}$ of the couple $Md^{2+} \rightarrow Md^{0}$ which (with correction for amalgamation potential of 1.0 V) yields an estimated $E^{\circ}(Md^{2+} \rightarrow Md^{0}) = -2.5$ V (SHE). These values (Table 13.8) are consistent with those in Chapter 19 (Fig. 19.9).

Guseva *et al.* (1988) compared the elution behavior of Md^{2+} with Sr^{2+} and Eu^{2+} from a cationite and zinc amalgam ion-exchange column using 1 M HCl. On the basis of the elution peak position of Md relative to the Sr and Eu and the known ionic radii of the latter two elements, a value for the ionic radius of Md^{2+} was estimated to be 0.115 nm. Using this value for the radius, the enthalpy of hydration of Md^{2+} was calculated to be -1413 kJ mol^{-1}.

In 1973, Mikheev *et al.* reported that a stable monovalent Md ion could be produced in neutral water–ethanol solutions and that it cocrystallized with CsCl (Mikheev *et al.*, 1973). However, studies of the overall reduction of Md^{3+} to Md^{0} (Hg) using controlled potential radiocoulometry (Samhoun *et al.*, 1979) and radiopolarography (David *et al.*, 1981) led to the conclusion that Md could not be considered as a cesium-like element and no evidence was obtained consistent with the formation of a monovalent state. Electrode reduction proceeded in two steps, $3+ \rightarrow 2+$ and $2+ \rightarrow 0$. Hulet *et al.* (1979) repeated some of the cocrystallization experiments of Mikheev and performed a series of new experiments in an attempt to prepare Md^{+} by reduction with Sm^{2+} in ethanol solutions and also in fused KCl. In these experiments, the coprecipitation behavior of Md was compared to tracer quantities of Es, Fm, Eu, Sr, Y, and Cs. Md consistently followed the behavior of Fm^{2+}, Eu^{2+}, and Sr^{2+} rather than Cs^{+}. They concluded that Md could not be reduced to a monovalent state with Sm^{2+} as claimed by Mikheev. However, on the basis of the results of further thermodynamic studies of the cocrystallization process of mendelevium with chlorides of alkali metals, the Russian investigators maintain that Md can be reduced to the monovalent state in water–ethanol solutions and that the cocrystallization of Md^{+} with salts of divalent ions can be explained as being due to the formation of mixed crystals (Mikheev *et al.*, 1980, 1981a; Spitsyn *et al.*, 1982). An ionic radius of 0.117 nm was calculated for Md^{+} from the results of the cocrystallization studies (Mikheev *et al.*, 1981b, 1982).

Unsuccessful attempts have been made to oxidize Md^{3+} to Md^{4+} using the strong oxidant sodium bismuthate (Hulet *et al.*, 1967). Thus, Md^{3+} is not readily oxidized as would be expected from the value of $+5.4$ V predicted by Nugent (1975) for the $E^{\circ}(Md^{4+} \rightarrow Md^{3+})$ couple.

13.4 NOBELIUM

13.4.1 Introduction

The discovery of element 102 was first reported in 1957 by an international research team working at the Nobel Institute in Stockholm, Sweden (Fields *et al.*, 1957). During the bombardment of a ^{244}Cm target with ^{13}C ions from the

Nobel Institute cyclotron, an 8.5 MeV alpha particle activity was produced which decayed with a half-life of approximately 10 min. The alpha activity eluted just before Es and Fm from a cation-exchange resin column using ammonium α-HIB as eluant and also appeared in the trivalent actinide fraction along with Cf and Fm, also produced in the irradiations, from a cation-exchange resin column using 6 M HCl as eluant. This behavior was taken as chemical evidence for the production of an isotope of element 102. From half-life systematics and reaction energetics, an isotope with a mass number of 253 or 255 was thought to have been produced. The name, nobelium, was proposed in honor of Alfred Nobel, in recognition of his support of the natural sciences, and in honor of the Nobel Institute where the experiments were conducted.

During the following 10 years, researchers at both the Lawrence Berkeley National Laboratory and the Dubna Research Center, Russia, attempted to repeat the Nobel Institute experiments, but were unsuccessful. However, the Berkeley group did succeed in identifying an alpha-emitting isotope of element 102 in 1958 using a newly developed method called the 'double recoil technique' (Ghiorso *et al.*, 1958) and assigned a mass of 254. Where the same isotopes have been studied, the Dubna and Berkeley groups are in substantial agreement (Ghiorso and Sikkeland, 1967). The results of the efforts of both groups exclude the likelihood of any isotope of element 102 having a half-life of 10 min with the emission of 8.5 MeV alpha particles. Further, chemical studies by Maly *et al.* (1968) showed that, because of its divalency in aqueous solutions, element 102 could not have exhibited the trivalent cation-exchange column elution behavior attributed to the 10 min activity. On the basis of their 1958 and later work, the Berkeley group claimed discovery of element 102 and, because of the wide use of the name over many years, suggested that nobelium be retained as the name of element 102 (Ghiorso and Sikkeland, 1967).

Because No is normally a divalent ion in aqueous solution and is difficult to oxidize and hold in the trivalent state, it has not been possible to make a chemical identification of the atomic number in the same manner as the preceding 3+ actinides, i.e. identification by their unique positions in the elution sequence from a cation-exchange resin column. However, in 1971, the atomic number of ^{255}No was unequivocally determined through the observance of characteristic K-series X-rays from the daughter isotope ^{251}Fm in coincidence with the alpha particles from the decay of the parent, ^{255}No (Dittner *et al.*, 1971).

13.4.2 Isotopes of nobelium

The known isotopes of nobelium range from mass 250 through 262, with the exception of 261 (Table 13.5) . The isotope ^{259}No is the longest-lived with a half-life of 58 min. However, the isotope ^{255}No has a considerably higher production rate and is most often used for chemical studies.

Table 13.5 *Nuclear properties of nobelium isotopes.*

Mass number	*Half-life*	*Mode of decay*	*Main radiations* (MeV)	*Method of production*
250	0.25 ms	SF		$^{233}U(^{22}Ne,5n)$
251	0.8 s	α	α 8.68 (20%) 8.60 (80%)	$^{244}Cm(^{12}C,5n)$
252	2.27 s	α 73% SF 27%	α 8.415 (∼ 75%) 8.372 (∼ 25%)	$^{244}Cm(^{12}C,4n)$ $^{239}Pu(^{18}O,5n)$
253	1.62 min	α	α 8.01	$^{246}Cm(^{12}C,5n)$ $^{242}Pu(^{16}O,5n)$
254	51 s	α	α 8.086	$^{246}Cm(^{12}C,4n)$ $^{242}Pu(^{16}O,4n)$
254 m	0.28 s	IT		$^{246}Cm(^{12}C,4n)$ $^{249}Cf(^{12}C,\alpha 3n)$
255	3.1 min	α 61.4% EC 38.6%	α 8.121 (46%) 8.077 (12%)	$^{248}Cm(^{12}C,5n)$ $^{249}Cf(^{12}C,\alpha 2n)$
256	2.91 s	α ∼ 99.7% SF ∼ 0.3%	α 8.43	$^{248}Cm(^{12}C,4n)$
257	25 s	α	α 8.27 (26%) 8.22 (55%)	$^{248}Cm(^{12}C,3n)$
258	1.2 ms	SF		$^{248}Cm(^{13}C,3n)$
259	58 min	α ∼ 75% EC ∼ 25%	α 7.551 (22%) 7.520 (25%)	$^{248}Cm(^{18}O,\alpha 3n)$
260	106 ms	SF, α		$^{254}Es(^{18}O,x)$
262	5 ms	SF		^{262}Lr daughter

13.4.3 Preparation and purification

The isotope ^{255}No can be produced for chemical study via the ^{249}Cf ($^{12}C,\alpha 2n$) reaction; about 1200 atoms were produced in a 10 min irradiation of a 350 μg cm^{-2} target of ^{249}Cf with 3×10^{12} particles per second of 73 MeV ^{12}C ions (Dittner *et al.*, 1971).

As with Md, the physical separation of the nobelium atoms from the target material can be made using the recoil-atom catcher foil technique. It is preferable to combine this with the 'gas-jet' technique since the product atoms can be deposited on the 'catcher' foil in a chemistry area separate from the bombardment area. The nearly monolayer of collected atoms can then be easily rinsed off the surface of the foil with dilute acid without dissolution of the foil. Isolation of the No from other actinides produced in the bombardment and from any target material transferred to the foil can be readily made using schemes based on the separation of divalent ions from trivalent ones, e.g. selective elution by solvent extraction chromatography using HDEHP as the stationary organic phase and 0.05 M HCl as the mobile aqueous phase (Silva *et al.*, 1969). Under these conditions, No passes through the column in the first few column volumes while the trivalent actinides are strongly adsorbed on the column. Selective

elution from a cation-exchange resin column, e.g. Dowex 50 × 4, can also be made using 3 M HCl as eluant. Here, No again elutes in a few column volumes and the trivalent actinides remain on the column (Silva *et al.*, 1973). When using a direct 'catcher' foil, e.g. gold, a more elaborate scheme involving separation of the gold by anion-exchange chromatography is necessary (David *et al.*, 1990b). This can be followed by selective isolation of the No from contaminants by elution from a chromatographic extraction column using HDEHP.

13.4.4 Atomic properties

The electronic ground state of gaseous nobelium atoms has been predicted to be the $^1S_0$ level of the $5f^{14}7s^2$ configuration (Martin *et al.*, 1974). No experimental information is available. No experimental measurements of inner-shell binding energies have been reported but estimated values have been published by Firestone *et al.* (1996), along with X-ray energies, based on the values recommended by Porter and Freedman (1978). The results are given in Table 13.4.

The characteristic K-series X-rays of ^{253}No emitted following the alpha decay of ^{257}Rf have been measured in alpha/X-ray coincidence experiments by Bemis *et al.* (1973). Values for $K_{\alpha 2}$ and $K_{\alpha 1}$ were reported as (120.9 ± 0.3) and (127.2 ± 0.3) keV, respectively.

13.4.5 The metallic state

Nobelium metal has not been prepared; however Johansson and Rosengren (1975) predicted that, for the same reasons as discussed above for Fm, No would prefer a divalent metallic state similar to Eu and Yb rather than a trivalent one. An estimate of 126 kJ mol^{-1} for the enthalpy of sublimation of No has been reported (David, 1986a). This value is similar to that of Es, Fm, and Md and supports the suggestion that No would form a divalent metal (Haire and Gibson, 1990). David (1986a) estimated a divalent metallic radius of 0.197 nm.

13.4.6 Solution chemistry

Before discovery, nobelium was expected to be a trivalent ion in aqueous solution and to exhibit a chemical behavior similar to the elements preceding it in the actinides series. However, in 1949, Seaborg (1949) predicted that a relatively stable 2+ state might exist for element 102 due to the special stability of the filled $5f^{14}$ shell in the $5f^{14}7s^2$ electronic configuration. Twenty years later, this prediction was confirmed.

In over 600 experiments, Maly *et al.* (1968) subjected about 50000 atoms of ^{255}No to cation-exchange chromatography and coprecipitation experiments. These tracer experiments showed that nobelium exhibits a chemical behavior substantially different from the trivalent actinides but similar to the divalent alkaline earth elements, Sr, Ba, and Ra. Thus, the divalent ion of nobelium was

shown to be the most stable species in aqueous solution in the absence of strong oxidizing agents.

Chuburkov *et al.* (1967) have compared the behavior of nobelium to those of Tb, Cf, and Fm during experiments where the atoms were first chlorinated and subsequently were carried by gas along a tube with a thermal gradient. From the position of deposition of atoms along the tube, they concluded that the chloride of No undergoes strong adsorption on solid surfaces and therefore is not very volatile; its volatility is close to the chlorides of Tb, Cf, and Fm. The chloride of either divalent or trivalent nobelium would be expected to exhibit a low volatility.

Silva *et al.* (1974) have conducted solvent extraction and cation-exchange chromatography studies of nobelium. Its complexing ability with chloride ions were compared with that of divalent mercury, cadmium, copper, cobalt, and barium in a tri-*n*-octylamine chloride/HCl liquid extraction system, and it was found to be most similar to the relatively weakly complexed alkaline earth element. The elution behavior of nobelium was also compared with that of Be, Mg, Ca, Sr, Ba, and Ra in a cation-exchange resin column/4 M HCl system and found to elute with Ca^{2+}. Further, comparison with these alkaline earth elements in an HDEHP/HCl liquid chromatography system showed nobelium to elute between Ca^{2+} and Sr^{2+}. The ionic radius of No^{2+} was estimated as 0.11 nm from a linear correlation of ionic radius with log distribution coefficient for several divalent ions obtained using an HDEHP/HNO_3 liquid–liquid extraction system. Using a similar correlation, a value of 0.10 nm was obtained from the cation-exchange chromatography data. From the results of relativistic Hartree–Foch–Slater calculations (Lu *et al.*, 1971), a value of 0.11 nm was suggested for the ionic radius of No^{2+}. The single-ion heat of hydration, calculated using an empirical form of the Born equation (Phillips and Williams, 1966) was 1486 kJ mol^{-1}. From correlations of ionic radii of actinides and lanthanides with atomic number, an ionic radius for No^{3+} of 0.90 and 1.02 Å for CNs 6 and 8, respectively, have been estimated. (David *et al.*, 1978; David, 1986b).

The formation of divalent nobelium complexes with citrate, oxalate, and acetate ions in aqueous solution of 0.5 M NH_4NO_3 have been studied by McDowell *et al.* (1976) using solvent extraction techniques. In general, the complexing tendency of nobelium with these ligands is between that of Ca and Sr, being somewhat more like Sr.

Silva *et al.* (1969) have studied the reduction potential of the No(III)–No(II) couple in aqueous solution with 50–100 atoms per experiment using HDEHP extraction column chromatography to distinguish between No^{2+} and No^{3+}. By comparing the extraction of nobelium from dilute acid solutions containing oxidants of differing potentials with the extraction behavior of tracer quantities of Cf, Cm, Ra, Tl, and Ce, the standard potential $E^{\circ}(No^{3+} \rightarrow No^{2+})$ was estimated to be between +1.4 and +1.5 V.

Meyer *et al.* (1976) used a modified radiopolarographic technique and ^{255}No to measure the half-wave potential for the reduction of nobelium at a mercury electrode and reported a value for $E^{\circ}(No^{2+} \rightarrow No^{0}(Hg))$ of −1.6 V. After

applying an estimated amalgamation potential correction, a value of −2.6 V was calculated for the standard potential of the $No^{2+} \rightarrow No^0$ couple. More recently David *et al.* (1990b) have measured amalgamation potentials of nobelium using radiocoulometry with the isotope ^{259}No. From the data, they estimated the $No^{2+} \rightarrow No^0$ couple standard potential as $-(2.49 \pm 0.06)$ V. This couple, combined with the measured $3+ \rightarrow 2+$ potential of 1.45 V (Silva *et al.*, l969) resulted in an estimated value for E° ($No^{3+} \rightarrow No^0$) of −1.18 V by David *et al.* (1990b). David (1986a, 1986b) estimated E° ($No^{3+} \rightarrow No^0$) to be −1.26 V, which leads to a calculated E° ($No^{2+} \rightarrow No^0$) = −2.61 V; these values were selected for Table 13.8 and Fig. 19.9 because of the consistent systematics (David, 1986a, 1986b) among many actinide species. David *et al.* (1990b) also estimated Gibbs energies of formation of −480 and −342 kJ mol^{-1} for No^{2+} (aq) and No^{3+} (aq), respectively. From a semiempirical technique for the linearization of actinide and lanthanide electrode potentials, Nugent (1975) has calculated a value of +6.5 V for $E^\circ(No^{4+} \rightarrow No^{3+})$.

13.5 LAWRENCIUM

13.5.1 Introduction

In 1961, Ghiorso, Sikkeland, Larsh, and Latimer of the Lawrence Berkeley National Laboratory reported the discovery of element 103 (Ghiorso *et al.*, 1961). An alpha particle activity of 8.5 MeV energy with a half-life of 8 s was produced in bombardments of a Cf target with both ^{10}B and ^{11}B ions. Owing to the short half-life, a chemical identification was not possible but the alpha activity was attributed to an isotope of element 103 on the basis of convincing nuclear evidence, i.e. the results of cross-bombardments with other targets and projectiles. However, because the target consisted of a mixture of californium isotopes, masses 249 through 252, an unambiguous mass assignment was not possible. Though isotopes of masses 255–259 could have been produced, based on cross-section considerations, the highest yield was expected for mass 257. The discoverers suggested the name lawrencium, symbol Lw, for the new element in honor of E. O. Lawrence, inventor of the cyclotron and founder of the Lawrence Berkeley National Laboratory. The name was accepted by IUPAC, but the symbol was changed to Lr.

The results of subsequent studies on the production and identification of ^{255}Lr, ^{256}Lr, and ^{257}Lr by researchers at the Joint Institute for Nuclear Research (JINR) at Dubna, Russia, appeared to conflict with the Berkeley mass assignment because none of the above isotopes had the decay properties of the original Berkeley alpha activity (Druin, 1971). However, in 1971, six alpha particle emitting isotopes of lawrencium, masses 255–260, were identified at Berkeley in bombardments of nearly isotopically pure targets of ^{248}Cm with ^{14}N and ^{15}N and ^{249}Cf with ^{10}B and ^{11}B ions, respectively, and an explanation for the discrepancy was suggested (Eskola *et al.*, 1971). From the Berkeley experiments, ^{257}Lr was found to emit

alpha particles of 8.8 MeV with a half-life of only 0.6, but ^{258}Lr was found to have a half-life of 4.2 s with the emission of 8.62 MeV alpha particles. Thus, Ghiorso and associates considered that the mass assignment made in 1961 should have been 258. The difference in the new half-life value compared to the 1961 value was attributed to relatively poor counting statistics resulting from the small number of alpha particle events observed in the earlier work.

13.5.2 Isotopes of lawrencium

Twelve isotopes of lawrencium are known with masses ranging from 252 through 262 (Table 13.6). The longest-lived isotope is ^{262}Lr, with a half-life of 3.6 h. The isotope ^{256}Lr, half-life of 26 s, was used in the early chemical studies; however, the longer-lived isotope ^{260}Lr ($t_{1/2} = 3$ min) has been used in more recent experiments.

13.5.3 Preparation and purification

The production of ^{256}Lr is best accomplished through the ^{249}Cf(^{11}B,4n) reaction using 70 MeV boron ions while ^{260}Lr is produced via the ^{249}Bk(^{18}O, α3n) reaction using 117 MeV oxygen ions.

As with Md and No, the physical separation of the Lr atoms from the target material and subsequent rapid collection is best accomplished using a recoil-atom gas-jet system coupled to a capillary transport system of some type (Hoffman *et al.*, 1988).

Because of their short half-lives, there is insufficient time to obtain a rigorous chemical purification of ^{256}Lr or ^{260}Lr. The isotope, ^{256}Lr was first isolated from

Table 13.6 *Nuclear properties of lawrencium isotopes.*

Mass number	*Half-life*	*Mode of decay*	*Main radiations* (MeV)	*Method of production*
252	0.36 s	α	α 9.018 (75%)	^{256}Db daughter
253 m	1.5 s	α	α 8.722	^{257}Db daughter
253	0.57 s	α	α 8.794	^{257}Db daughter
254	13 s	α	α 8.460 (64%)	^{258}Db daughter
255	21.5 s	α	α 8.43 (40%)	^{243}Am(^{16}O,4n)
			8.37 (60%)	^{249}Cf(^{11}B,5n)
256	25.9 s	α	α 8.52 (19%)	^{243}Am(^{18}O,5n)
			8.43 (37%)	^{249}Cf(^{11}B,4n)
257	0.65 s	α	α 8.86 (85%)	^{249}Cf(^{11}B,3n)
			8.80 (15%)	^{249}Cf(^{14}N,α2n)
258	3.9 s	α	α 8.621 (25%)	^{248}Cm(^{15}N,5n)
			8.595 (46%)	^{249}Cf(^{15}N,α2n)
259	6.2 s	α	α 8.45	^{248}Cm(^{15}N,4n)
260	3.0 min	α	α 8.03	^{248}Cm(^{15}N,3n)
261	39 min	SF		^{254}Es(^{22}Ne,x)
262	3.6 h	SF, EC		^{254}Es(^{22}Ne,x)

reaction products by a rapid solvent extraction technique using the chelating agent thenoyltrifluoroacetone (TTA) dissolved in methyl isobutyl ketone (MIBK) as the organic phase and buffered acetate solutions as the aqueous phase (Silva *et al.*, 1970). This method did not separate individual trivalent actinides so identification of Lr was made on the basis of its unique alpha particle energy of 8.24 MeV.

When the capillary transport system is used, the longer-lived isotope, ^{260}Lr, can be washed from the 'catcher' foil along with the small amount of aerosol carrier particles with 0.05 M HCl. Kept to a few drops of volume, this solution can be placed on the top of a cation-exchange resin column and isolation of Lr^{3+} from other trivalent actinides can be accomplished by selective elution with ammonium α-HIB (Hoffman *et al.*, 1988). An automated system called Automated Rapid Chemistry Apparatus (ARCA) has been developed and used to carry out this separation (Brüchle *et al.*, 1988).

13.5.4 Atomic properties

The electronic structure of the ground state of neutral atoms of Lr was predicted in 1970 as the $^2D_{3/2}$ level of the $5f^{14}6d^17s^2$ configuration (Moeller, 1970) similar to the rare earth homolog Lu, $4f^{14}5d^16s^2$, as one would expect from a simple extrapolation from the chemical periodic table. This prediction was brought into question in 1971 by Brewer who calculated, by a semiempirical method, a configuration of $5f^{14}7s7p^1$ (Brewer, 1971). Later the results of relativistic Dirac–Hartree–Fock calculations by Nugent *et al.* (1974) concluded that the energy difference between these two configurations was quite small and either configuration could be the ground state. On the basis of the results of multiconfiguration Dirac–Fock calculations, Desclaux and Fricke (1980) predicted the $5f^{14}7s^27p^1$ configuration as the ground state. Later, multiconfiguration Dirac–Hartree–Fock calculations by Wijesundera *et al.* (1995) and relativistic Fock-space coupled-cluster method by Eliav *et al.* (1995) led to a similar conclusion, i.e. the s^2p $J = 1/2$ is energetically favored over the s^2d $J = 3/2$ state. This result is due to the relativistic mass increase of the electrons that are strongly accelerated near the highly charged nucleus. This effect is strongest for the spherical s and $p_{1/2}$ orbitals that have high densities near the nucleus.

In 1988, Eichler and coworkers proposed gas adsorption chromatography experiments to distinguish between the two ground state configurations s^2d and s^2p. They calculated that there should be a measurable difference in the enthalpies of adsorption on metal surfaces for the two different configurations (Eichler *et al.*, 1988). The s^2p was predicted to be less volatile, perhaps similar to the p-element Pb, than the s^2d configuration with estimated sublimation energies of about 134 and 400 kJ mol^{-1}, respectively. Online gas chromatography was applied to study the volatility of Lr by Jost *et al.* (1988) and to determine the enthalpy of adsorption. No evidence for Lr as a volatile element was found under reducing conditions at a temperature of about 1000°C. Their

Table 13.7 *Comparison of calculated and measured L-series X-rays for Lr.*

	X-ray energy (keV)	
Transition	*Calculated*[a]	*Measured*[b]
$L_{\gamma 1}$ ($4d_{3/2} \rightarrow 2p_{1/2}$)	27.91	27.97 (15)[c]
$L_{\beta 1}$ ($3d_{3/2} \rightarrow 2p_{1/2}$)	23.93	24.03 (14)
$L_{\beta 4}$ ($3p_{1/2} \rightarrow 2s$)	22.61	22.61 (18)
$L_{\beta 2}$ ($4d_{5/2} \rightarrow 2p_{3/2}$)	21.21	21.35 (20)
$L_{\alpha 1}$ ($3d_{5/2} \rightarrow 2p_{3/2}$)	17.48	17.57 (12)
L_l ($3s \rightarrow 2p_{3/2}$)	14.43	14.43 (20)

[a] Firestone *et al.* (1996).
[b] Bemis *et al.* (1977).
[c] Error in last two digits.

results gave a lower limit for the adsorption enthalpy for Lr on quartz and Pt surfaces at 290 kJ mol^{-1}, significantly higher than the estimated values for Lr (s^2p). The configuration of the ground state of lawrencium is still in doubt.

No experimental measurements of inner-shell binding energies have been reported but estimated values have been published by Firestone *et al.* (1996), along with X-ray energies, based on the values recommended by Porter and Freedman (1978). The results are given in Table 13.4.

The characteristic L-series X-rays of ^{256}Lr have been observed in coincidence with alpha particles of the parent ^{260}Db by Bemis *et al.* (1977). The results are presented in Table 13.7. They agree very well with those given by Firestone *et al.* (1996).

13.5.5 Metallic state

Lawrencium metal has not been prepared. An estimate of 352 kJ mol^{-1} for the enthalpy of sublimation of Lr has been reported (David *et al.*, 1978). This value is similar to that of Lu and supports the suggestion that Lr would prefer the formation of a trivalent metal as expected for the last member of the actinide series. Systematic properties of heats of vaporization, bulk modulus, and atomic volumes suggest that Lr would be a trivalent metal with a volume similar to that of Lu (Haire and Gibson, 1990). David *et al.* (1978) estimated a trivalent metallic radius of 0.171 nm.

13.5.6 Solution chemistry

In 1949, element 103 was predicted by Seaborg (1949) to be the last member of the proposed actinide or 5f series of elements and to be similar to lutetium with respect to the stability of the 3+ oxidation state in aqueous solution. It required nearly 20 years to finally synthesize this element and to conduct chemical experiments to confirm this prediction.

Silva *et al.* (1970) employed a fast solvent extraction procedure using MIBK containing the chelating agent TTA as the organic phase and buffered acetate solutions of differing pH as the aqueous phase to distinguish between the 2+, 3+, and 4+ oxidation states. In over 200 separate experiments, approximately 1500 atoms of ^{256}Lr were produced for study and the extraction behavior of Lr was compared with a number of tetravalent (Th, Pu), trivalent (Fm, Cf, Cm, Am, Ac), and divalent ions (No, Ba, Ra). In these experiments, lawrencium was found to extract into the organic phase over the pH range of 3+ ions along with Fm and Cf. Thus, it was concluded that the 3+ oxidation state is the most stable oxidation state for Lr in aqueous solution. Unfortunately, because of the short half-life, there was insufficient time to perform a cation-exchange resin column separation to confirm its predicted elution position just ahead of Md^{3+}.

From studies comparing the retention times of chlorinated atoms of several different actinides and transactinides as they passed through a heated glass column, Chuburkov *et al.* (1969) concluded that the chloride of element 103 has an adsorbability on solid surfaces, and hence volatility, similar to the chlorides of Cm, Fm, and No and to be much less volatile than the chlorides of element 104, Rf.

Because Lr is a trivalent ion in aqueous solution, it should exhibit a chemical behavior similar to the other 3+ actinides and lanthanides, e.g. insoluble fluoride and hydroxide. One would expect Lr^{3+} to have a slightly smaller ionic radius than Md^{3+}, due to the actinide contraction, and to elute just before Md from a cation-exchange resin column using ammonium α-HIB as eluant (see Fig. 13.1). From correlations of ionic radius with atomic number for actinide and lanthanide elements, David *et al.* (1978) estimated an ionic radius of 0.0893 nm for Lr^{3+}.

By 1987, a longer-lived isotope of lawrencium, ^{260}Lr, with a half-life of 3 months and alpha particle energy of 8.03 MeV, was available for chemical studies. Hoffman *et al.* (1988) repeated the solvent extraction experiments of Silva *et al.* (1970) and confirmed the trivalent nature of Lr in aqueous solution. Further, elutions of Lr from a cation-exchange resin columns using ammonium α-HIB as eluant were conducted and compared with the elution behavior of Md and the rare earths Tm, Er, and Ho (Hoffman *et al.*, 1988). Lr was found to elute between Ho and Tm, and approximately with the Er tracer. Seven alpha events attributable to Lr^{260} were detected. The distribution coefficients were determined from the elution positions and, using the linear correlation of ionic radius with log distribution coefficient, an ionic radius was calculated for each Lr event. The average Lr^{3+} radius was found to be 0.0886 ± 0.0003 nm assuming an ionic radius of 0.0881 nm for Er for CN 6 (Templeton and Dauben, 1954). This result was surprising to the authors because it gave a difference of only 0.0015 nm for the step of 2 in atomic number between Md, with an ionic radius of 0.0896 nm, and Lr. This is substantially smaller than the 2Z difference of 0.0021 for the analogous trivalent rare earth ions Tm and Lu and indicates

an ionic radius for Lr larger than expected. Therefore, Lr elutes later than predicted in Fig. 13.1.

In later experiments, a German–American collaboration (Brüchle *et al.*, 1988) used the ARCA (Automated Rapid Chemistry Apparatus) system to check the earlier results of Hoffman *et al.* (1988) and to increase the number of Lr atoms studies and thus the statistical significance. The earlier work was confirmed and a value of 0.0881 ± 0.0001 nm was obtained from the elution data for Lr. A heat of hydration of $-(3685 \pm 13)$ kJ mol^{-1} was calculated from the radius using empirical models and the Born–Haber cycle. Brüchle *et al.* (1988) pointed out that the difference between the radii of Md^{3+}, Fm^{3+}, and Es^{3+} is 0.0016 nm while this difference is 0.0012 nm for the analogous lanthanide ions. This suggests that the contraction at the end of the actinides series is larger than the analogous lanthanide contraction, perhaps due to relativistic effects (Seth *et al.*, 1994), with the exception of the last member of the actinide series, Lr.

It is possible that relativistic effects could stabilize the $7s^2$ closed shell so that only the $7p_{1/2}$ or 6d electron would be ionized under reducing conditions to give a monovalent Lr. Several attempts have been made to reduce Lr^{3+} to a divalent or monovalent ion in aqueous solution. Hoffman *et al.* (1988) used a solvent extraction column with HDEHP as the stationary organic phase and dilute HCl as the mobile aqueous phase to separate 1+ and 2+ ions from 3+ and 4+ ions, the former passing through the column while the latter remain fixed. Solutions containing $^{260}Lr^{3+}$ were passed through the column where the Lr remained fixed. The reducing agent hydroxylamine hydrochloride was added to the HCl and the resulting solution passed through the column for 20 s at 80°C in an attempt to reduce and elute any Lr. The attempt was unsuccessful, however, as the authors noted, the kinetics of the reduction are slow. In companion experiments, Scherer *et al.* (1988) used the HDEHP solvent extraction column

Table 13.8 *Summary of chemical properties of elements* 100–103.

Element	100	101	102	103
electronic configuration[a]	$5f^{12}7s^2$	$5f^{13}7s^2$	$5f^{14}7s^2$	$5f^{14}6d^1(7p^1)7s^2$
stable oxidation states[b]	3, 2	3, 2	3, 2	3
ionic radius of indicated ion (nm)	0.0911(3+)	0.0896(3+)	0.105(2+)	0.0886(3+)
standard electrode potentials (V)[c]				
$3+ \rightarrow 2+$	−1.15	−0.15	+1.45	<−0.44
$3+ \rightarrow 0$	−1.96	*−1.74*	*−1.26*	*−2.06*
$2+ \rightarrow 0$	−2.37	*−2.5*	*−2.61*	
first ionization potential (V)[d]	6.50	6.58	6.65	

[a] Free neutral atom + Rn core.
[b] Most stable state in aqueous solution underlined.
[c] Values in italics are estimates.
[d] From Martin *et al.* (1974).

method, with the ARCA system, to attempt reductions of Lr to di- or monovalent ions (Scherer *et al.*, 1988). In a series of experiments using the reducing agents V^{2+} and Cr^{2+} in the dilute HCl-eluting solutions, there was no evidence for the reduction of Lr^{3+} to either the 2+ or 1+ oxidation state. From the results, a limit of <-0.44 V was estimated for the $Lr^{3+} \rightarrow Lr^{2+,\ 1+}$ reduction potential. Using the newly discovered Lr^{262} ($t_{1/2} = 3.6$ h), Lougheed *et al.* (1988) attempted to reduce Lr with Sm^{2+}, $E^{\circ}(Sm^{3+} \rightarrow Sm^{2+}) = -1.55$ V, and coprecipitate Lr^{1+} with Rb using sodium tetraphenylborate or chloroplatinic acid but were unsuccessful. The 2+ and 3+ actinide ions do not coprecipitate under these conditions. On the basis of 20 Lr events, they calculated an upper limit of -1.56 V for $E^{\circ}(Lr^{3+} \rightarrow Lr^{1+})$ and concluded that it is unlikely that Lr^{1+} can exist in aqueous solutions. Nugent (1975) has calculated values of -2.06 V for $E^{\circ}(Lr^{3+} \rightarrow Lr^{0})$ and $+7.9$ V for $E^{\circ}(Lr^{4+} \rightarrow Lr^{3+})$.

A summary of some of the chemical properties of fermium, mendelevium, nobelium, and lawrencium is given in Table 13.8.

REFERENCES

Baybarz, R. D. (1963) *Nucl. Sci. Eng.*, **17**, 463–7.

Baybarz, R. D. (1965) *J. Inorg. Nucl. Chem.*, **27**, 1831–9.

Baybarz, R. D. (1966) *J. Inorg. Nucl. Chem.*, **28**, 1055–61.

Bemis, C. E. Jr, Silva, R. J., Hensley, D. C., Keller, O. L. Jr, Tarrant, J. R., Hunt, L. D., Dittner, P. F., Hahn, R. L., and Goodman, C. D. (1973) *Phys. Rev. Lett.*, **31**, 647–50.

Bemis, C. E. Jr, Dittner, P. F., Silva, R. J., Haoh, R. L., Tarrant, J. R., Hunt, L. D., and Hensley, D. C. (1977) *Phys. Rev. C*, **16**, 1146–58.

Brewer, L. (1971) *J. Opt. Soc. Am.*, **61**, 1101–11.

Brüchle, W., Schädel, M., Scherer, U. W., Kratz, J. V., Gregorich, K. E., Lee, D., Nurmia, M., Chasteler, R. M., Hall, H. L., Henderson, R. A., and Hoffman, D. C. (1988) *Inorg. Chim. Acta*, **146**, 267–76.

Carlson, T. A. and Nestor, C. W. Jr (1977) *At. Data Nucl. Data Tables*, **19**, 153–73.

Choppin, G. R., Harvey, B. G., and Thompson, S. G. (1956) *J. Inorg. Nucl. Chem.*, **2**, 66–8.

Chuburkov, Y. T., Caletka, R., Shalaevskii, M. R., and Zvara, I. (1967) *Radiokhimiya*, **9**, 637–42.

Chuburkov, Y. T., Belov, V. Z., Caletka, R., Shalaevsky, M. R., and Zvara, I. (1969) *J. Inorg. Nucl. Chem.*, **31**, 3113–18.

David, F., Samhoun, K., Guillaumont, R., and Edelstein, N. (1978) *J. Inorg. Nucl. Chem.*, **40**, 69–74.

David, F., Samhoun, K., Hulet, E. K., Baisden, P. A., Dougan, R., Landrum, J. H., Lougheed, R. W., Wild, J. F., and O'Kelley, G. D. (1981) *J. Inorg. Nucl. Chem.*, **43** (11), 2941–5.

David, F. (1986a) Oxidation Reduction and Thermodynamic Properties of Curium and Heavier Actinide Elements, in *Handbook on the Physics and Chemistry of the Actinides,* vol. 4 (eds. A. J. Freeman and C. Keller), North-Holland, Amsterdam, pp. 97–128.

David, F. (1986b) *J. Less Common Metals*, **121**, 27–35.

David, F., Maslennikov, A. G., and Peretrukhin, V. P. (1990a) *J. Radioanal. Nucl. Chem. Articles*, **143**(2), 415–26.

David, F., Samhoun, K., Lougheed, R. W., Dougan, R. J., Wild, J. F., Landrum, J. H., Dougan, A. D., and Hulet, E. K. (1990b) *Radiochim. Acta*, **51**, 65–70.

Das, M. P. (1981) *Phys. Rev. A*, **23**(2), 391–4.

Desclaux, J. P. and Fricke, B. (1980) *J. Phys.*, **41**, 943–6.

Dittner, P. F., Bemis, C. E. Jr, Hensley, D. C., Silva, R. J., and Goodman, C. C. (1971) *Phys. Rev. Lett.*, **26**, 1037–40.

Druin, V. A. (1971) *Sov. J. Nucl. Phys.*, **12**, 146–7.

Eichler, B., Hübener, S., Gäggeler, H. W., and Jost, D. T. (1988) *Inorg. Chim. Acta*, **146**, 261–5.

Eliav, E., Kaldor, U., and Ishikawa, Y. (1995) *Phys. Rev. A*, **52**, 291–6.

Ermakovl, V. A. and Stary, I. (1967) *Radiokhimiya*, **9**, 197–201.

Eskola, K., Eskola, P., Nurmia, M., and Ghiorso, A. (1971) *Phys. Rev. C*, **4**, 632–42.

Fedoseev, E. V., Aizenberg, I., Timokhin, S. N., Travnikov, S. S., Zvara, I., Davydov, A. V., and Myasedov, B. F. (1990) *J. Radioanal. Nucl. Chem. Articles*, **142**(2), 459–65.

Fields, P. R., Friedman, Am. M., Milstead, J., Atterling, H., Forsling, W., Holm, L. W., and Aström, B. (1957) *Phys. Rev.*, **107**, 1460–2.

Firestone, R. B., Shirley, V. S., Baglin, C. M., Chu, S. Y., and Zipkin, J. (1996) *Table of Isotopes,* 8th edn, vol. 2, Appendix F, John Wiley, New York, pp. F37–9; F47.

Fricke, B., Desclaux, J. P., and Waber, J. T. (1972) *Phys. Rev. Lett.*, **28**(12), 714–16.

Ghiorso, A., Thompson, S. G., Higgens, G. H., Seaborg, G. T., Studier, M. H., Fields, P. R., Fried, S. M., Diamond, H., Mech, J. F., Pyle, G. L., Huizengo, J. R., Hirsch, A., Manning, W. M., Browne, C. I., Smith, H. L., and Spencer, R. W. (1955a) *Phys. Rev.*, **99**, 1048–9.

Ghiorso, A., Harvey, B. G., Choppin, G. R., Thompson, S. G., and Seaborg, G. T. (1955b) *Phys. Rev.*, **5**, 1518–19.

Ghiorso, A., Sikkeland, T., Walton, J. R., and Seaborg, G. T. (1958) *Phys. Rev. Lett.*, **1**, 18–20.

Ghiorso, A. (1959) LBNL Report UCRL-8714, Berkeley, CA, USA.

Ghiorso, A., Sikkeland, T., Larsh, A. E., and Latimer, R. M. (1961) *Phys. Rev. Lett.*, **6**, 473–5.

Ghiorso, A. and Sikkeland, T. (1967) *Phys. Today*, **20**(9), 25–32.

Goodman, L. S., Diamond, H., Stanton, H. E., and Fred, M. S. (1971) *Phys. Rev. A*, **4**, 473–5.

Gorski, B., Buklanov, G. V., Dok, L. D., Gleisberg, B., Timokhin, S. N., Milek, A., and Salamatin, L. I. (1990) *Radiochim. Acta*, **51**, 59–63.

Guseva, L. I., Tikhomirova, G. S., Buklanov, G. V., Pkhar, Z. Z., Lebedev, I. A., Katargin, N. V., and Myasoedov, B. F. (1988) *Radiokhimiya*, **30**(1), 21–5.

Haire, R. G. and Gibson, J. K. (1989) *J. Chem. Phys.*, **91**(11), 7085–96.

Haire, R. G. and Gibson, J. K. (1990) *J. Radioanal. Nucl. Chem. Articles*, **143**, 35–51.

Hoff, R. W. and Hulet, E. K. (1970) *Proc. Am. Nucl. Soc. Symp.*, in *Engineering with Nuclear Explosives*, vol. 2, pp. 1283–94.

Hoffman, D. C., Henderson, R. A., Gregorich, K. E., Bennett, D. A., Chasteler, R. M., Gannett, C. M., Hall, H. L., Lee, D. M., Nurmia, M. J., Cai, S., Agarwal, R., Charlop, A. W., Chu, Y. Y., Seaborg, G. T., and Silva, R. J. (1988) *J. Radioanal. Nucl. Chem. Articles*, **124**, 135–44.

Hoffman, D. C. (1994) The Heaviest Elements, in *Chem. Eng. News*, **72**(18), 24–34.
Horwitz, E. P. and Bloomquist, C. A. A. (1969) *Chem. Lett.*, **5**, 753–9.
Horwitz, E. P., Bloomquist, C. A. A., and Henderson, D. J. (1969) *J. Inorg. Nucl. Chem.*, **31**, 1149–66.
Horwitz, E. P. and Bloomquist, C. A. A. (1973) *J. Inorg. Nucl. Chem.*, **35**, 271–84.
Hübener, S. (1980) *Radiochem. Radioanal. Lett.*, **44**(2), 79–86.
Hübener, S. and Zvara, I. (1982) *Radiochim. Acta*, **31**, 89–94.
Hubert, S., Hussonnois, M., Brillard, L., Goby, G., and Guillaumont, R. (1974) *J. Inorg. Nucl. Chem.*, **36**, 2361–6.
Hulet, E. K., Lougheed, R. W., Brady, J. D., Stone, R. E., and Coops, M. S. (1967) *Science*, **158**, 486–8.
Hulet, E. K., Lougheed, R. W., Baisden, P. A., Landrum, J. H., Wild, J. F., and Lundqvist, R. F. (1979) *J. Inorg. Nucl. Chem.*, **41**, 1743–7.
Hussonnois, H., Hubert, S., Aubin, L., Guillaumont, R., and Boussieres, G. (1972) *Radiochem. Radioanal. Lett.*, **10**, 231–8.
Johansson, B. and Rosengren, A. (1975) *Phys. Rev. B*, **11**, 1367–73.
Jost, D. T., Gäggeler, H. W., Vogel, Ch., Schädel, M., Jäger, E., Eichler, B., Gregorich, K. E., and Hoffman, D. C. (1988) *Inorg. Chim. Acta*, **146**, 255–9.
Katz, J. J. and Seaborg, G. T. (1957) *Chemistry of the Actinide Elements,* Methuen, London, p. 404.
Katz, J. J., Seaborg, G. T., and Morss, L. R. (1986) *The Chemistry of the Actinide Elements*, Chapman & Hall, London, p. 1165.
Kulyukhin, S. A., Mikheev, N. B., and Rumer, I. A. (1997) *Radiochemistry*, **39**(2), 130–2.
Leuze, R. E., Baybarz, R. D., and Weaver, B. (1963) *Nucl. Sci. Eng.*, **17**, 252–8.
Lougheed, R. W., Moody, K. J., Dougan, R. J., Wild, J. F., and Hulet, E. K. (1988) LLNL report, Nuclear Chemistry Division FY 1988 Annual Report, Livermore.
Lu, C. C., Carlson, T. A., Malik, F. B., Tucker, T. C., and Nester, C. W. Jr (1971) *At. Data*, **3**, 1–131.
Lundqvist, R., Hulet, E. K., and Baisden, T. A. (1981) *Acta. Chem. Scand.*, **A35**, 653–61.
Macfarlane, R. D. and Griffioen, R. D. (1963) *Nucl. Inst. Methods*, **24**, 461–4.
Macfarlane, R. D. and McHarris, W. (1974) in *Nuclear Spectroscopy and Reactions,* vol. A (ed. J. Cerny), Academic Press, New York, p. 24.
Maly, J. (1967) *Inorg. Nucl. Chem. Lett.*, **3**, 373–81.
Maly, J. and Cunningham, B. B. (1967) *Inorg. Nucl. Chem. Lett.*, **2**, 445–51.
Maly, J., Sikkeland, T., Silva, R. J., and Ghiorso, A. (1968) *Science*, **160**, 1114–15.
Martin, W.C., Hagan, L., Reader, J., and Sugar, J. (1974) *J. Phys. Chem. Ref. Data*, **3**, 771–9.
McDowell, W. J., Keller, O. L. Jr, Dittner, P. F., Tarrant, J. R., and Case, G. N. (1976) *J. Inorg. Nucl. Chem.*, **38**, 1207–10.
McGlashan, M. L. (1970) *J. Pure Appl. Chem.*, **21**, 1–44.
Meyer, R. I., McDowell, W. J., Dittner, P. F., Silva, R. J., and Tarrant, J. R. (1976) *J. Inorg. Nucl. Chem.*, **38**, 1171–3.
Mikheev, N. B., Spitsyn, V. I., Kamenskaya, A. N., Gvozdec, B. A., Druin, V. A., Rumer, I. A., Dyachkova, R. A., Rozenkevitch, N. A., and Auerman, L. N. (1972) *Inorg. Nucl. Chem. Lett.*, **8**, 929–36.

Mikheev, N. B., Spitsyn, V. I., Kamenskaya, A. M., Rumer, I. A., Gvozdev, B. A., Rozenkevich, N. A., and Auerman, L. N. (1973) *Dokl. Akad. Nauk SSSR*, **208**, 1146–9.

Mikheev, N. B., Spitsyn, V. I., Kamenskaya, A. N., Konovalova, N. A., Rumer, I. A., Auerman, L. N., and Podorozhnyi, A. M. (1977) *Inorg. Nucl. Chem. Lett.*, **13**, 651–6.

Mikheev, N. B., Spitsyn, V. I., Kamenskaya, A. N., Mikulski, J., and Petryna, T. (1980) *Radiochem. Radioanal. Lett.*, **43**, 85–92.

Mikheev, N. B., Kamenskaya, A. N., Spitsyn, V. I., Mikul'skil, Ya., Petryna, T., and Konovalova, N. A. (1981a) *Radiokhimiya*, **23**(5), 736–42.

Mikheev, N. B., Kamenskaya, A. N., Berdonosov, S. S., and Klimov, S. I. (1981b) *Radiochimiya*, **23**(6), 793–5.

Mikheev, N. B., Spitsyn, V. I., Kamenskaya, A. N., and Berdonosov, S. S. (1982) *Radiochem. Radioanal. Lett.*, **51**(4), 257–64.

Mikheev, N. B., Kamenskaya, A. N., Konovalova, N. A., Rumer, I. A., and Kulyukhin, S. A. (1983) *Radiokhimiya*, **25**(2), 158–61.

Moeller, T. (1970) *J. Chem. Educ.*, **47**, 417–23.

Müller, W. (1967) *Actinides Rev.*, **1**, 71–119.

Münzenberg, G. (1999) *J. Phys G: Nucl. Part. Phys.*, **25**, 717–25.

Nugent, L. J., Vander Sluis, K. L., Fricke, B., and Mann, J. B. (1974) *Phys. Rev. A*, **9**(6), 2270–2.

Nugent, L. J. (1975) in *MTP Review of Inorganic Chemistry*, vol. 7 (ed. K. W. Bagnall), Butterworths, London, pp. 195–219.

Phillips, C. S. G. and Williams, R J. P. (1966) in *Inorganic Chemistry*, vol. 2, Oxford University Press, London, p. 56.

Porter, C. E., Riley, F. D. Jr, Vandergriff, R. D., and Felker, L. K. (1997) *Sep. Sci. Technol.*, **32**, 83–92.

Porter, F. T. and Freedman, M. S. (1971) *Phys. Rev. Lett.*, **27**, 293–7.

Porter, F. T. and Freedman, M. S. (1978) *J. Phys. Chem. Ref. Data*, **7**(4), 1267–84.

Samhoun, K. and David, F. (1976) in *Transplutonium Elements, Proc. 4th Int. Transplutonium Elements Symp.*, 1975 (eds. W. Müller and R. Lindner), North-Holland, Amsterdam, pp. 1297–304.

Samhoun, K., David, F., Hahn, R. L., O'Kelley, G. D., Tarrant, J. R., and Hobart, D. E. (1979) *J. Inorg. Nucl. Chem.*, **41**, 1749–54.

Scherer, U. W., Kratz, J. V., Schädel, M., Brüchle, W., Gregorich, K. E., Henderson, R. A., Lee, D., Nurmia, M., and Hoffman, D. C. (1988) *Inorg. Chim. Acta*, **146**, 249–54.

Seaborg, G. T. (1945) *Chem. Eng. News*, **23**, 2190–3.

Seaborg, G. T. (1949) in *The Transuranium Elements* (eds. G. T. Seaborg, J. J. Katz, and W. M. Manning), Natl. Nucl. Energy Ser., Div. IV, 14B, McGraw-Hill, New York, pp. 1492–524.

Seaborg, G. T. and Katz, J. J. (1954) in *The Transuranium Elements,* Natl. Nucl. Energy Ser., Div. IV, 14A, McGraw-Hill, New York, pp. 733–68.

Seaborg, G. T. (1963) *Man-Made Transuranium Elements,* Prentice-Hall, Englewood Cliffs, NJ, pp. 26–30.

Seth, M., Dolg, M., Fulde, P., and Schwerdtfeger, P. (1994) *J. Am. Chem. Soc.*, **117**, 6597–8.

Silva, R. J., Sikkeland, T., Nurmia, M., and Ghiorso, A. (1969) *J. Inorg. Nucl. Chem.*, **31**, 3405–9.

Silva, R. J., Sikkeland, T., Nurmia, M., and Ghiorso, A. (1970) *Inorg. Nucl. Chem. Lett.*, **6**, 733–9.

Silva, R. J., Dittner, P. F., Keller, O. L. Jr, Eskola, K., Eskola, P., Nurmia, M., and Ghiorso, A. (1973) *Nucl. Phys. A*, **216**, 97–108.

Silva, R. J., McDowell, W. J., Keller, O. L. Jr, and Tarrant, J. R. (1974) *J. Inorg. Nucl. Chem.*, **13**, 2233–7.

Spitsyn, V. I., Mikheev, N. B., Kamenskaya, A. N., Berdonosov, S. S., and Mikul'skii, Ya. (1982) *Radiokhimiya*, **24**(5), 615–17.

Stary, I. (1966) *Talanta*, **13**, 421–37.

Taut, S., Hübener, S., Eichler, B., Gäggeler, M., Schädel, M., and Zvara, I. (1997) *Radiochim. Acta*, **78**, 33–8.

Templeton, D. H. and Dauben, C. H. (1954) *J. Am. Chem. Soc.*, **76**, 5237–9.

Thompson, S. G., Harvey, B. G., Choppin, G. R., and Seaborg, G. T. (1954) *J. Am. Chem. Soc.*, **76**, 6229–36.

Usuda, S.,Shinohara, N., Yoshikawa, S., and Suzuki, T. (1987) *J. Radioanal. Nucl. Chem. Articles*, **116**(1), 125–32.

Vobecký, M., Buklanov, G. V., Maslov, O. D., Salamatin, L. I., Schumann, D., Sen, W. G., and Yakushev, A. B. (1991) *J. Radioanal. Nucl. Chem. Lett.*, **154**(1), 73–8.

Wijesundera, W. P., Vosko, S. H., and Parpia, F. A. (1995) *Phys. Rev. A*, **51**, 278–82.

Zvara, I., Belov, V. Z., Domanov, V. P., Zhuikov, B. L., Huebener, S., and Shalaevskii, M. R. (1976) Joint Inst. Nucl. Res. Report JINR P6-10334, Dubna, Russia.

CHAPTER FOURTEEN

TRANSACTINIDE ELEMENTS AND FUTURE ELEMENTS

Darleane C. Hoffman, Diana M. Lee, and Valeria Pershina

14.1 INTRODUCTION

This chapter gives a brief summary of the reported discoveries, confirmation, and nuclear properties of the claimed and confirmed transactinide elements through the year 2004. However, the primary emphasis is on the chemical properties – experimental, theoretical, and predicted – of the transactinides and a comparison of measured properties with theoretical predictions. The experimental studies of chemical properties are especially challenging because of the low production rates and the short half-lives and the need for very special facilities and the use of atom-at-a-time chemistry. The discovery of a new element must furnish evidence that its atomic number is different from those of all the currently known elements and first claims to discovery often lacked such positive identification. As a result, there were uncertainties and controversies over priority of discovery, nuclear and chemical properties, and assignment of names. The first *positive identification* of the atomic number of all these elements was accomplished using 'physical' rather than chemical techniques.

The authors of this chapter have made a conscientious effort to present a balanced view of research on the properties of the transactinides. The chapter also includes predictions of the nuclear and chemical properties of the

SuperHeavy Elements (SHEs). The term originally referred to an 'island of nuclear stability' around the predicted closed spherical shells at 112 to 114 protons and 184 neutrons. Revisions due to recent experiments and theoretical calculations are discussed.

As of 1997, discoveries of the transactinide elements 104 through 109 had been recognized by the International Union of Pure and Applied Chemistry (IUPAC) and the International Union of Pure and Applied Physics (IUPAP). The names and symbols for these elements as finally approved by IUPAC in 1997 (CNIC, 1997) and the year of discovery are given in Table 14.1.

Claims to the discovery of element 110 were made by researchers at the Lawrence Berkeley National Laboratory (LBNL) (Ghiorso *et al*., 1995a,b), by researchers at the Gesellschaft für Schwerionenforschung (GSI) in Darmstadt, Germany (Hofmann *et al*., 1995a), and by a Dubna/Livermore group working at the Joint Institute for Nuclear Research (JINR) in Dubna, Russia (Lazarev *et al*., 1996).

The published analysis of these claims by a Joint Working Party (JWP) of IUPAC/IUPAP (Karol *et al*., 2001) gave credit for the synthesis of element 110 to the GSI group and invited them to propose a name. They proposed the name 'Darmstadtium' with the symbol Ds after the place in Germany where the element 110 discovery experiments were conducted. The IUPAC Commission on Nomenclature of Inorganic Chemistry (CNIC) considered the proposal and in March 2003 (Corish and Rosenblatt, 2003) recommended to the IUPAC Bureau that it be accepted. It was officially approved by the IUPAC Council at the 42nd General Assembly in Ottawa, Canada, on August 16, 2003.

The discovery of elements 111 and 112 was reported by the GSI group in 1995 (Hofmann *et al*., 1995b, 1996) and confirmatory experiments were reported in 2002 (Hofmann *et al*., 2002). In mid-2003 the JWP assigned credit for discovery of element 111 to the GSI group and asked them to propose a name (Corish and Rosenblatt, 2003; Karol *et al*., 2003), but judged that the evidence for assigning

Table 14.1 *CNIC/IUPAC compromise recommendation for names of transactinide elements. Approved by IUPAC, August* 30, 1997, *Geneva, Switzerland.*

Element	*Name*	*Symbol*	*Discovery year*
104	Rutherfordium	Rf	1969
105	Dubnium (Hahnium)[a]	Db (Ha)[a]	1970
106	Seaborgium	Sg	1974
107	Bohrium	Bh	1981
108	Hassium	Hs	1984
109	Meitnerium	Mt	1982

[a] Many publications of chemical studies before 1997 use hahnium (Ha) for element 105.

credit for the discovery of element 112 was insufficient. The element 111 discovery team proposed the name 'Roentgenium' with symbol Rg after Wilhelm Conrad Roentgen, the discoverer of X-rays. A provisional recommendation for approval of the proposal was sent (Corish and Rosenblatt, 2004) to the IUPAC Bureau and Council and was approved in late 2004. A modern periodic table showing elements through $Z = 154$ is given in Fig. 14.1.

Evidence for elements 112 through 116 has been reported from 1999 to early 2004 by groups working at Dubna (Oganessian, 1999a–c, 2001, 2002; Lougheed *et al.*, 2000; Oganessian *et al.*, 2000a,b, 2002, 2004a–c). However, it should be emphasized that as yet there is no confirmation by other groups of the isotopes of these elements and their decay products. Nuclear properties of the transactinide elements including half-life, mode of decay, main radiations, and method of production based on reports published through early 2004 are given in Table 14.2 and in Appendix II. Nuclides for which only one decay chain has been reported are not listed. Charts of the isotopes of Lr (the last of the actinides) through 109 and for 110 through 116 are shown in Fig. 14.2(a) and (b).

The transactinide elements begin with element 104 (rutherfordium) and include all the elements beyond lawrencium, the element that ends the actinide series with the filling of the 5f electron shell. According to results of atomic relativistic calculations (Fricke, 1975), the filling of the 6d shell takes place in the

1																	18
1 H	2											13	14	15	16	17	2 He
3 Li	4 Be											5 B	6 C	7 N	8 O	9 F	10 Ne
11 Na	12 Mg	3	4	5	6	7	8	9	10	11	12	13 Al	14 Si	15 P	16 S	17 Cl	18 Ar
19 K	20 Ca	21 Sc	22 Ti	23 V	24 Cr	25 Mn	26 Fe	27 Co	28 Ni	29 Cu	30 Zn	31 Ga	32 Ge	33 As	34 Se	35 Br	36 Kr
37 Rb	38 Sr	39 Y	40 Zr	41 Nb	42 Mo	43 Tc	44 Ru	45 Rh	46 Pd	47 Ag	48 Cd	49 In	50 Sn	51 Sb	52 Te	53 I	54 Xe
55 Cs	56 Ba	57 La	72 Hf	73 Ta	74 W	75 Re	76 Os	77 Ir	78 Pt	79 Au	80 Hg	81 Tl	82 Pb	83 Bi	84 Po	85 At	86 Rn
87 Fr	88 Ra	89 Ac	104 Rf	105 Db (Ha)	106 Sg	107 Bh	108 Hs	109 Mt	110 Ds	111 Rg	*112*	*113*	*114*	*115*	*116*	(117)	(118)
(119)	(120)	(121)	(154)														

LANTHANIDES	58 Ce	59 Pr	60 Nd	61 Pm	62 Sm	63 Eu	64 Gd	65 Tb	66 Dy	67 Ho	68 Er	69 Tm	70 Yb	71 Lu
ACTINIDES	90 Th	91 Pa	92 U	93 Np	94 Pu	95 Am	96 Cm	97 Bk	98 Cf	99 Es	100 Fm	101 Md	102 No	103 Lr
SUPERACTINIDES	(122)	(123)	(124)	(125)	(126)									(153)

Fig. 14.1 *Periodic table showing placement of transactinides through element* 154. (*Italics indicate elements reported but not yet confirmed. Undiscovered elements are shown in parentheses.*)

Table 14.2 *Nuclear properties of transactinide elements.*

Mass number	*Half-life*	*Mode of decay*	*Main radiations* (MeV)	*Method of production*
rutherfordium (Rf)				
253	~48 μs	SF		^{206}Pb(^{50}Ti,3n)
254	22.3 μs	SF		^{206}Pb(^{50}Ti,2n)
255	1.64 s	α 48%	α 8.722 (94%)	^{207}Pb(^{50}Ti,2n)
		SF 52%		
256	6 ms	SF, α	α 8.79	^{208}Pb(^{50}Ti,2n)
257	4.7 s	α ~ 80%	α 9.012 (18%)	^{208}Pb(^{50}Ti,n)
		SF ~ 2%	8.977 (29%)	^{249}Cf(^{12}C,4n)
		EC ~ 18%		
258	12 ms	SF		^{246}Cm(^{16}O,4n)
259	3.1 s	α 93%	α 8.87 (~40%)	^{249}Cf(^{13}C,3n)
		SF 7%	8.77 (~60%)	^{248}Cm(^{16}O,5n)
260	20 ms	SF		^{248}Cm(^{16}O,4n)
261	75.5 s	α	α 8.28	^{248}Cm(^{18}O,5n)
	4.2 s	α, SF	8.52	
262	2.1 s	SF		^{248}Cm(^{18}O,4n)
	47 ms	SF		
dubnium (Db)				
256	1.6 s	EC, α	α 9.014 (~67%)	^{209}Bi(^{50}Ti,3n)
257	1.5 s	α, SF	α 8.967, 9.074	^{209}Bi(^{50}Ti,2n)
257 m	0.76 s	α, SF	9.163	^{209}Bi(^{50}Ti,2n)
258	4.4 s	α	α 9.19	^{262}Bh daughter
			9.07	
259	0.51 s	α	α 9.47	^{241}Am(^{22}Ne,4n)
260	1.5 s	α ≥ 90%	α 9.082 (25%)	^{249}Cf(^{15}N,4n)
		SF ≤ 9.6%	9.047 (48%)	^{243}Am(^{22}Ne,5n)
		EC ≤ 2.5%		
261	1.8 s	α ~ 75%	α 8.93	^{243}Am(^{22}Ne,4n)
		SF ~ 25%		^{249}Bk(^{16}O,4n)
262	34 s	α > 67%	α 8.66 (~20%)	^{249}Bk(^{18}O,5n)
		SF + EC < 33%	8.45 (~80%)	
263	27 s	α, SF	α 8.36	^{249}Bk(^{18}O,4n)
268	16 h	SF		115 decay product
seaborgium (Sg)				
258	2.9 ms	SF		^{209}Bi(^{51}V,2n)
259	0.48 s	α	α 9.62 (78%)	^{208}Pb(^{54}Cr,3n)
260	3.6 ms	α	α 9.77 (83%), SF	^{208}Pb(^{54}Cr,2n)
261	0.23 s	α, SF	α 9.56 (60%)	^{208}Pb(^{54}Cr,n)
262	6.9 ms	α ≤ 22%		^{270}110 decay
		SF ≥ 78%		product
263	0.9 s	α	α 9.06 (90%)	^{249}Cf(^{18}O,4n)
	0.3 s	α	α 9.25	
265	7.4 s	α	α 8.84 (46%)	^{248}Cm(^{22}Ne,5n)
266	21 s	α	α 8.77, 8.52	^{248}Cm(^{22}Ne,4n)

Table 14.2 (*Contd.*)

Mass number	*Half-life*	*Mode of decay*	*Main radiations* (MeV)	*Method of production*
bohrium (Bh)				
261	12 ms	α	α 10.10 (40%)	^{209}Bi(^{54}Cr,2n)
262	0.1 s	α	α 10.06, 9.91, 9.74	^{209}Bi(^{54}Cr,n)
	8.0 ms	α	α 10.37, 10.24	^{209}Bi(^{54}Cr,n)
264	1.0 s	α	α 9.48, 9.62	111 decay product
266	∼1 s	α	α 9.3	^{249}Bk(^{22}Ne,5n)
267	17 s	α	α 8.85	^{249}Bk(^{22}Ne,4n)
272	9.8 s	α	α 9.02	115 decay product
hassium (Hs)				
264	0.26 ms	α, SF	α 10.43	^{207}Pb(^{58}Fe,n)
265	1.7 ms	α	α 10.30 (90%)	^{208}Pb(^{58}Fe,n)
	0.8 ms	α	α 10.57 (63%)	^{208}Pb(^{58}Fe,n)
266	2.3 ms	α	α 10.18	^{270}110 daughter
267	59 ms	α	α 9.88, 9.83, 9.75	^{271}110 daughter
269	14 s	α	α 9.23, 9.17	112 decay product
270	∼4 s	α		^{248}cm(^{26}Mg,4n)
meitnerium (Mt)				
266	1.7 ms	α	α 10.46, 11.74	^{209}Bi(^{58}Fe,n)
268	42 ms	α	α 10.10, 10.24	111 daughter
276	0.72 s	α	α 9.71	115 decay product
darmstadtium (Ds)				
267	3.1 μs	α	α 11.6	^{209}Bi(^{59}Co,n)
269	0.17 ms	α	α 11.11	^{208}Pb(^{62}Ni,n)
270	0.10 ms	α	α 11.03	^{207}Pb(^{64}Ni,n)
	6.0 ms	α	α 12.15	^{207}Pb(^{64}Ni,n)
271	56 ms	α	α 10.71	^{208}Pb(^{64}Ni,n)
	1.1 ms	α	α 10.74, 10.68	
273	0.15 ms	α	α 11.08	112 daughter
280	7.6 s	SF		114 decay product
roentgenium (Rg)				
272	1.6 ms	α	α 11.0	^{209}Bi(^{64}Ni,n)
280	3.6 s	α	α 9.75	115 decay product
element 112				
277	0.6 ms	α	α 11.65, 11.45	^{208}Pb(^{70}Zn,n)
283	3 min	α, SF		^{238}U(^{48}Ca,3n); 114 daughter
284	0.75 min	α	α 9.15	114 daughter
element 113				
284	0.48 s	α	α 10.00	115 daughter
element 114				
287	5 s	α	α 10.29	^{242}Pu(^{48}Ca,3n)
288	2.6 s	α	α 9.82	^{244}Pu(^{48}Ca,4n)
element 115				
288	87 ms	α	α 10.46	^{243}Am(^{48}Ca,3n)
element 116				
292	53 ms	α	α 10.53	^{248}Cm(^{48}Ca,4n)

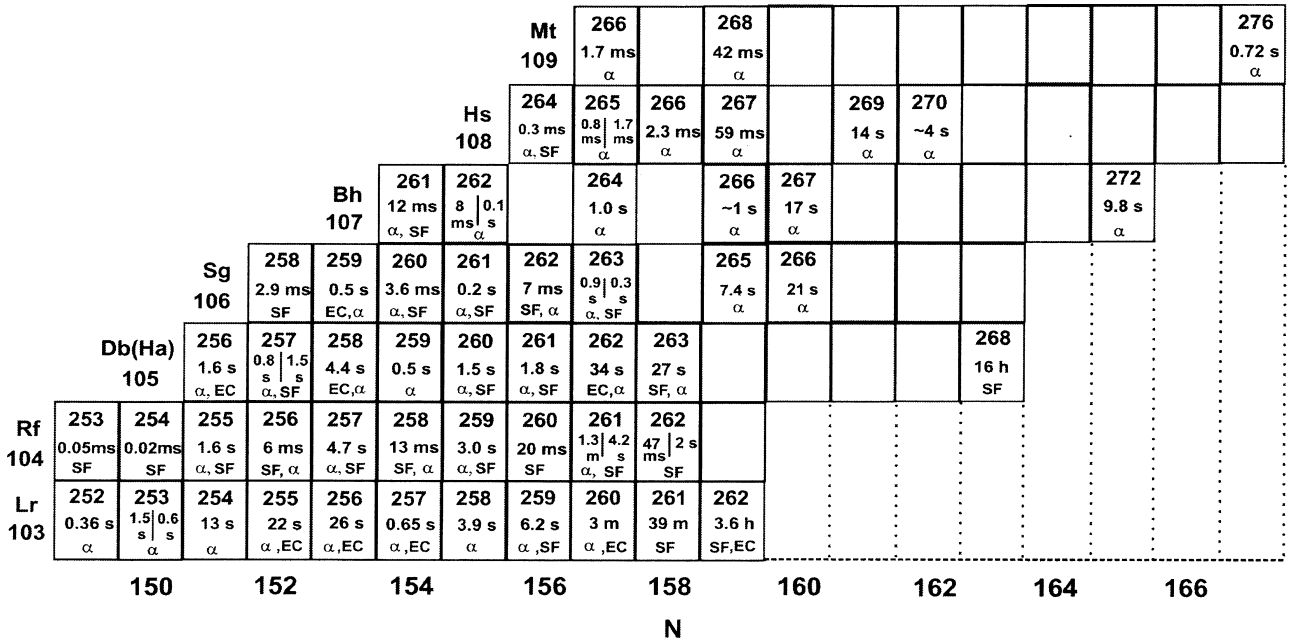

Fig. 14.2 (*a*) *Chart of all isotopes reported for elements* 103 *through* 109.

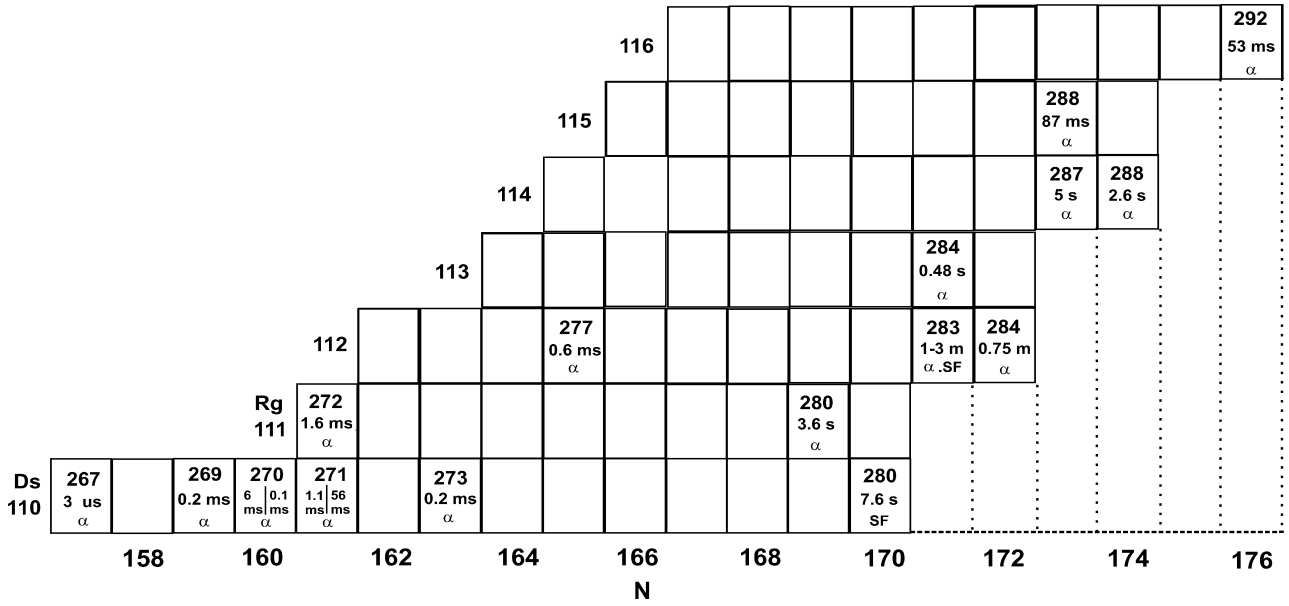

Fig. 14.2 (*b*) *Chart of all isotopes reported for elements* 110 *through* 116.

first nine of the transactinide elements ($Z = 104$ through 112). In elements 113 through 118 the 7p shell is being filled and element 118 is the heaviest member of the noble gas group. Filling of the 8s shell is expected to occur with elements 119 and 120, making them homologs of elements in groups 1 and 2. Accurate relativistic calculations (Eliav *et al.*, 1998a) show that element 121 will have an 8p electron in its ground state configuration in contrast to the 7d electron expected from simple extrapolation of the members of group 3 in the periodic table. A 7d electron will be added in element 122 to give it the [118] $8s^2 7d 8p$ configuration (Eliav *et al.*, 2002), in contrast to thorium, which has the configuration $[Rn]7s^2 6d^2$.

No accurate calculations exist beyond element 122 (Eliav *et al.*, 1992), where the situation becomes more complicated because the energy spacings for the 7d, 6f, and 5g levels and later on for the 9s, $9p_{1/2}$, and $8p_{3/2}$ become so close that in the region of $Z = 160$ the usual classification on the basis of a simple electronic configuration may become invalid. Clear structures on the basis of pure p-, d-, f-, and g-blocks are no longer distinguishable. Chemical properties of the elements influenced by these mixed electronic shells will then be so different from anything currently known that classification on the basis of the known periodic table will be impossible.

In order to positively identify a new element and place it in its proper position in the periodic table, its atomic number (proton number) must be determined or deduced in some way. For transactinide elements it became necessary to develop new methods for positive identification of atomic number. One widely used technique is that of correlation of the unknown element's decay to a known daughter and/or granddaughter, which can be identified either chemically or by its decay characteristics. The method of $\alpha-\alpha$ correlations has been widely used for elements that decay by alpha emission to subsequent known α emitters. Another definitive method is measurement of the characteristic X-rays of the new element. This technique was used by Bemis *et al.* (1973, 1977) to confirm the discovery and reported properties of elements 104 and 105, but it requires considerably larger samples than the α–α correlation method. Although detection of spontaneous fission (SF) is a very sensitive technique, determination of the Z of the parent fissioning nuclide is extremely difficult and depends on some other indirect method such as excitation functions, half-life systematics, production in other reactions, or determination of the atomic number of *both primary fragments* from the same SF event in order to add them together to get the Z of the fissioning new element. Detection of only SF decay has led to many controversies concerning discoveries of the transactinide elements.

In 1974, IUPAC and IUPAP appointed an *ad hoc* committee of neutral experts, consisting of three members from the USA, three from the USSR, and three from other countries (including the chairman), to consider the claims of priority to discovery of elements 104 and 105 and attempt to get agreement between the research groups at Berkeley (USA) and Dubna (USSR). The

committee was finally disbanded without finishing the report, but the American members eventually published their own in-depth report (Hyde *et al*., 1987) that summarized the claims and counterclaims together with a critical assessment of both the physical and the chemical evidence relating to discovery of these elements during the period 1960–77. Reference tables with all the known information for each element, a comprehensive bibliography including internal laboratory reports from Dubna and Berkeley, and all articles published in refereed journals related to the first synthesis and identification of the isotopes of elements 104 and 105, and a summary and conclusions were presented. They concluded that the information published for element 104 (Ghiorso *et al*., 1969) and element 105 (Ghiorso *et al*., 1970, 1971) was correct and fully met the criteria for discovery of new elements stated by Harvey *et al*. (1976) and Flerov and Zvara (1971) and that priority for discovery of elements 104 and 105 clearly belonged to the Berkeley group and endorsed their proposal that they be named rutherfordium (Rf) and hahnium (Ha).

However, the combined IUPAC and IUPAP Transfermium Working Group (TWG) came to different conclusions in their reports (Barber *et al*., 1991, 1992, 1993) on the final assignment of credit for discovery of elements 101 through 109. An immediate rebuttal to the initial assignments of credit for discovery (Barber *et al*., 1991) of element 102 to Dubna, and assignment of shared credit to Berkeley/Dubna for elements 104 and 105, and to GSI/Dubna for element 107 was sent in 1991 in a message from Ghiorso and Seaborg to the chairman of the joint IUPAC/IUPAP TWG. A longer response is found in Ghiorso and Seaborg (1993a), as part of the responses invited from Berkeley, Dubna (Oganessian and Zvara, 1993), and GSI (Armbruster *et al*., 1993). These were published immediately following the TWG report (Barber *et al*., 1993). The response from Ghiorso and Seaborg (1993b) was also published in *Progress in Particle and Nuclear Physics* because IUPAP had given them no opportunity to respond to the companion 'discovery' article published there (Barber *et al*., 1992). A long period of dissent ensued after the CNIC resolved that 'an element could not be named after a living person' and, therefore, the name seaborgium for element 106 already approved by the American Chemical Society could not be accepted. The names for elements 101 through 103 were accepted as mendelevium, nobelium, and lawrencium, but dubnium (Db), joliotium (Jl), rutherfordium (Rf), bohrium (Bh), hahnium (Ha), and meitnerium (Mt) were recommended for elements 104 through 109 by IUPAC/CNIC and approved by the IUPAC Bureau in September 1994. This resulted in protest and criticism from around the world as names that had been in common use were scrambled and the historical right of discoverers of a new element to name it was ignored. A long period of negotiation ensued and resulted in 1995 in the suggestion of still another 'compromise' set of names. This time nobelium (102) was replaced with the name flerovium (Fl), and dubnium, joliotium, seaborgium, nielsbohrium, hahnium, and meitnerium were suggested for elements 104 through 109. This slate did not meet with any more approval than the previous one and in an

unprecedented step the IUPAC Bureau rescinded the previously approved names and solicited comments over a 5-month period. Finally, the CNIC/IUPAC compromise recommendation shown in Table 14.1 was approved by the IUPAC Bureau on August 30, 1997. The long negotiations and final compromise that resulted in the naming of elements 104 through 106 as rutherfordium, dubnium, and seaborgium, and elements 107 through 109 as bohrium, hassium, and meitnerium have been described in detail in the book *The Transuranium People* (Hoffman *et al.*, 2000a).

14.2 NUCLEAR PROPERTIES OF THE TRANSACTINIDE ELEMENTS

All known isotopes of the transactinides are radioactive. The longest known confirmed half-life for these elements ranges from 75 s for ^{261}Rf to only 42.7 ms for ^{268}Mt, the daughter of ^{272}111 (see Fig. 14.2). No transactinide elements have been found in nature although early predictions (Myers and Swiatecki, 1966; Meldner, 1967) that an 'island of SHEs' well beyond uranium might exist around elements with atomic numbers 114 or 126 raised the tantalizing possibility that very long-lived SHEs might still exist on Earth after having been formed during the last nucleosynthesis in our solar system some 5 billion years ago. Later theoretical studies based on new theories of nuclear structure (Strutinsky, 1966; Nilsson *et al.*, 1969a,b; Fiset and Nix, 1972; Randrup *et al.*, 1974) confirmed that an island of nuclear stability stabilized by spherical nuclear shells should be centered around 110 to 114 protons and 184 neutrons. Some calculations even indicated that element 110 with 184 neutrons (^{294}110) should be the longest-lived, with a half-life in the range of hundreds of thousands to a billion years. These predictions sparked a host of experimental investigations to try to detect SHEs in a wide variety of natural sources, but by 1987 no credible evidence for SHEs in nature remained (Hoffman *et al.*, 2000b).

14.3 ONE-ATOM-AT-A-TIME CHEMISTRY

14.3.1 Challenges

Special challenges are involved in studying the chemical properties of the transactinide elements because of their short half-lives, low production rates, the presence of many other unwanted activities, the necessity for producing them in accelerators with high-intensity beams, and the need to build special radiochemistry laboratory and detection facilities nearby. In addition, it is often necessary to prepare and use highly radioactive and rare targets, e.g. ^{248}Cm, ^{249}Bk, ^{249}Cf. Techniques have been developed for detection of a single atom at a time, usually by measuring its radioactive decay. Often the longest-lived known isotope of the element that is used for chemical studies is not the isotope first

discovered. Knowledge of the nuclear decay properties and a measurement technique that positively shows that the detected decay arises from the element in question are required. The technique of α–α correlation to known daughter or granddaughter activities can provide such positive identification and has been widely used because many of the transactinide isotopes decay by alpha emission to known alpha-decaying daughter isotopes. Measurement of characteristic X-rays associated with the decay can also provide positive identification of atomic number, but the technique is difficult to apply when only a few atoms can be detected.

14.3.2 Production methods and facilities required

Chemical studies require use of an isotope with a half-life long enough to permit chemical separation and a reasonable production and detection rate, which for the transactinide elements may range from a few atoms per minute for Rf to only an atom per week in the case of Hs. In addition, the isotope must have unique decay characteristics so that it can be positively identified even on an atom-at-a-time basis in order to prove that it belongs to the element whose chemistry is being studied. The isotopes of elements Rf through Hs that were used in the first definitive chemical studies for each element, their production modes, approximate cross sections, and approximate detection rates for the initial experiments that had different overall efficiencies and transport times are listed in Table 14.3, together with those for Lr, the last of the actinides.

14.3.3 Chemical procedures

The chemical procedures used in atom-at-a-time studies must be fast enough to be accomplished in times comparable to the half-lives of the isotopes used in those studies and must give the same results for a few atoms as for macro

Table 14.3 *Isotopes used in first definitive chemical studies of Lr through Hs.*

Nuclide (half-life)	*Reaction*	*Cross section*	*Estimated rate*	*Year*
^{256}Lr (26 s)	^{249}Cf (^{11}B,4n)	~5 nb	3 min^{-1}	1970[a]
^{261}Rf (75 s)	^{248}Cm(^{18}O,5n)	~5 nb	3 min^{-1}	1970[b]
^{262}Ha (34 s)	^{249}Bk(^{18}O,5n)	~6 nb	1 min^{-1}	1988[c]
^{266,265}Sg (21 s, 7 s)	^{48}Cm(^{22}Ne,4n,5n)	0.03 nb	1-2 d^{-1}	1997[d]
^{267}Bh (17 s)	^{249}Bk(^{22}Ne,4n)	~60 pb	2 week^{-1}	2000[e]
^{270,269}Hs (~4 s, 14 s)	^{248}Cm(^{26}Mg,4,5n)	~5 pb	1 week^{-1}	2001[f]

[a] Silva *et al.* (1970a).
[b] Silva *et al.* (1970b).
[c] Gregorich *et al.* (1988).
[d] Schädel *et al.* (1997b).
[e] Eichler *et al.* (2000).
[f] Düllmann *et al.* (2002a,b); Kirbach *et al.* (2002).

amounts. Chemical methods in which a single atom rapidly participates in many identical chemical interactions in two-phase systems with fast kinetics that reach equilibrium quickly have proven to be valid. Adloff and Guillaumont (1993) have given a thorough discussion of the validity of conclusions about chemical behavior obtained from very small numbers of atoms. An equilibrium constant was defined for such reactions in terms of the probabilities of finding the species in one phase or the other. Adloff and Guillaumont concluded that it is valid to combine the results of many separate one-atom-at-a-time experiments in order to get statistically significant results. Thus the results obtained from many identical experiments, each performed with only a single atom, can be added together to obtain statistically significant information about chemical behavior (Guillaumont *et al*., 1989, 1991).

In early studies, activities recoiling from the target were deposited on a thin 'catcher' foil placed directly behind the target in the production chamber of the accelerator. The foil was then removed manually or remotely shuttled to a detection system without disturbing the accelerator vacuum, and its alpha and SF activity measured with appropriate radiation detectors. Alternatively, the collector foil was removed and chemically processed. In either case, the valuable target is not destroyed, and considerable decontamination from all of the activity remaining in the target itself is achieved. Later, gas transport systems using a variety of gases and aerosols were developed to rapidly and efficiently transport reaction products to collection sites outside the radiation field where chemistry can be carried out within a few seconds, either manually or with computer-controlled automated systems that have been developed for both aqueous- and gas-phase chemistry. Although the automated systems are not necessarily faster, they usually give more reproducible results and are more appropriate for carrying out the many repetitive, around the clock experiments lasting weeks at a time that are required to get statistically significant information. Several detailed reviews (Gäggeler, 1990; Hoffman, 1994; Wierczinski and Hoffman, 1996; Hoffman and Lee, 1999; Kratz, 1999a) of these methods have been given.

(a) Gas-phase chemistry

Both thermochromatographic and isothermal methods have been used to study gas-phase properties of the heaviest elements. These methods are particularly useful for short-lived isotopes because the lengthy process of evaporating liquid samples that is required in most aqueous chemistry experiments is avoided. Gas-phase chromatographic methods permit determination of the adsorption enthalpy, ΔH_{ads}, by using correlations between measured properties such as temperature of adsorption and ΔH_{ads}. The latter were shown to be linearly related to the sublimation enthalpy, ΔH_{sub} (Zvara *et al*., 1970), which is used to compare the volatilities with lighter homologs.

Pioneering studies of the volatilities of the halides of elements 104 and 105 were carried out in the late 1960s and 1970s by Zvara *et al*. (1974, 1976) using thermochromatographic separations. In this method, a longitudinal, negative temperature gradient is established along a chromatographic column through which a gas stream is conducted. It contains the volatile species of interest that deposit on the surface of the column according to their volatilities. Later, the deposition zones are determined from fission tracks registered in detectors positioned along the column. These fissions are associated with specific deposition temperatures, which are then correlated with ΔH_{ads}. The advantage of this method is that production and separation of the detected species takes place very rapidly and species with half-lives as short as a few seconds can be measured. It also has some disadvantages. Positions of the deposition zones are determined only after the experiments are finished. This makes the interpretation of the results very difficult because it is necessary to correct for the half-lives of the various species involved before their volatilities can be compared. Furthermore, real-time observation of the nuclear decay and the determination of the half-lives of the detected species are not possible. Another difficulty is that if only SF activity is measured in the experiments, it is difficult to prove what the atomic number of the detected species actually was because only the fission fragments are detected (see discussion in Section 14.1).

Improved gas thermochromatographic systems have now been developed in which volatile species are transported through a thermochromatographic column (TC) where they are deposited directly on the surface of the pairs of opposing (Si) photodiode detectors that form the column. Both the radiations from the radioactive species and their deposition positions as a function of temperature along the column can be determined simultaneously and recorded. In this way, the isotope (and element) being studied can be positively identified and its deposition temperature at various positions along the TC (Si) (subjected to an appropriate negative temperature gradient) can be determined. Such a cryogenic on-line TC system was used (Düllmann *et al*., 2002b) to perform the first successful chemical studies of element 108 (Hs) using the alpha-emitting isotopes ^{269,270}Hs and compare the behavior of Hs with Os, its lighter group 8 homolog. These investigations are described in detail in Section 14.6.4b.

Recent studies of gas-phase chemistry have utilized isothermal chromatographic systems such as the On-Line Gas Analyzer (OLGA) developed by Gäggeler (1994) and the Heavy Element Volatility Instrument (HEVI) developed by Kadkhodayan *et al*. (1996) and the alpha-emitting isotopes shown in Table 14.3 to compare the behavior of the halides and oxyhalides of elements 104 through 107 with those of their lighter homologs in groups 4 through 7 of the periodic table. In such systems the entire chromatographic column (usually quartz) is kept at a constant temperature. Volatile species pass through the column and undergo numerous sorption/desorption steps. Chromatographic experiments are carried out at a series of temperatures and the chemical yield of

the volatile, short-lived species is studied as a function of temperature. Retention time is indicative of the volatility at each isothermal temperature and can be deduced from the observed changes in the yield from low to high values. The half-life of the nuclide under investigation serves as an 'internal' clock for the process. Just half of the atoms introduced into the isothermal gas chromatographic column will exit from the other end when the time it takes for an atom to pass through the column (the retention time) corresponds to its half-life. That is, the retention time in the chromatographic column at the temperature where the yield is 50% ($T_{50\%}$) of this maximum value is equal to the half-life of the short-lived nuclide (Gäggeler, 1997) and can be used as a relative measure of volatility. If the retention time is very short compared to the known half-life, the yield through the column will approach 100%. A Monte Carlo program taking account of all the experimental conditions is used to deduce the ΔH_{ads} for the measured species. Examples of these studies are discussed in Section 14.6.

(b) Solution chemistry

The Automated Rapid Chemistry Apparatus (ARCA) and the microcentrifuge system SISAK (Special Isotopes Studied by the AKUFE, Swedish acronym for the centrifuge liquid–liquid extraction technique) are examples of automated, computer-controlled systems that have been used in studies of solution chemistry of the heaviest elements.

(*i*) *ARCA*

ARCA can be used to perform rapid, repeated, high-pressure liquid chromatography column experiments on a timescale of seconds. The separations usually are carried out using microscale ion-exchange resin columns. After sorption on the column, the absorbed species are eluted and distribution coefficients are determined from the retention times of the species on the column. The collected liquid samples must then be dried before measurement of alpha emission and/or SF decay with high-resolution solid-state detectors, thus limiting detection to nuclides with half-lives longer than ~30 s. However, longer-lived daughter products can be detected in subsequent steps and used to infer properties of the parent element. The ARCA system has been used successfully for separations of elements 104 through 106, as described in detail in several reviews (Hoffman, 1994; Schädel, 1995; Hoffman and Lee, 1999; Kratz, 1999a,b).

(*ii*) *SISAK*

SISAK is a well-established on-line technique that has been used for studies of gamma-emitting nuclides with half-lives as short as 0.8 s, e.g., ^{109,110}Tc (Alzitzoglou *et al.*, 1990) and was later adapted for use with alpha emitters (Alstad *et al.*, 1995). The SISAK system can be used to perform liquid–liquid

extractions on the timescale of a few seconds and has been coupled to a flowing liquid scintillation system to provide continuous separation and measurement of α–α correlations and SFs for nuclides as short as a few seconds (Omtvedt *et al.*, 1998). This permits chemical studies of shorter-lived nuclides, but the detection energy resolution is not as good. However, a recent experiment by Omtvedt *et al.* (2002) showed that rapid pre-separation by the Berkeley Gas-filled Separator (BGS) furnished sufficient decontamination from the extremely high background of unwanted activities so that the SISAK system could be used to obtain more detailed information about the chemical properties of Rf using 4.7-s ^{257}Rf produced in the ^{208}Pb(^{50}Ti,n) reaction. The same technique can be extended to studies of 4.4-s ^{258}Db produced via ^{208}Pb(^{51}V,n) or ^{209}Bi(^{50}Ti,n) reactions as well as to still heavier elements although the production rates are steadily decreasing as Z increases. Additional developments to increase production rates will be required. Another limitation will be the requirement to choose extraction systems with fast enough kinetics to achieve equilibrium.

14.4 RELATIVISTIC EFFECTS ON CHEMICAL PROPERTIES

14.4.1 Relativistic effects on atomic electronic shells

The relativistic mass increase can be expressed as $m = m_0\sqrt{1-(v/c)^2}$ where m_0 is the rest mass and v is the velocity of an electron. As the Z of the heavy elements increases, the stronger attraction to the core causes the electrons to move faster, and the resultant mass increase leads to a decrease in the Bohr radius of the hydrogen-like s and $p_{1/2}$ electrons: $a_B = \hbar^2/mc^2 = a_B^0\sqrt{1-(v/c)^2}$. The contraction and stabilization of these orbitals is the direct relativistic effect; it was shown to originate from the region of the inner K- and L-shells (Schwarz *et al.*, 1989; Baerends *et al.*, 1990). This effect was originally thought to be large only for the 'fast' electrons in inner core shells of heavy atoms. Later, it was also found to be large for the outer s and $p_{1/2}$ valence electrons. For example, the relativistic contraction for the 7s orbital in Db is $\Delta_R\langle r\rangle_{ns} = (\langle r\rangle^{nr} - \langle r\rangle^{rel}/\langle r\rangle^{nr}) = 25\%$, as shown in Fig. 14.3. As a consequence, the relativistic stabilization of this 7s orbital is 2.6 eV, as shown in Fig. 14.4.

The effect of the *n*s orbital contraction reaches its maximum in the 6th period with Au (17.3%) and in the 7th period with element 112 (31%); the phenomenon has been called the relativistic effect gold maximum and group 12 maximum, respectively (Pyykkö, 1988; Schwerdtfeger and Seth, 1998). The same maximum is, consequently, observed with the relativistic stabilization of the 6s and 7s orbitals (Fig. 14.5). The shift of the maximum to element 112 in the 7th period in contrast to gold in the 6th period is due to the fact that in both elements 111 and 112 the ground state electronic configuration is d^qs^2, while the electronic configuration changes from Au ($d^{10}s^1$) to Hg ($d^{10}s^2$). (See the discussion of relativistic effects in relation to electronic configurations by Autschbach *et al.* (2002).)

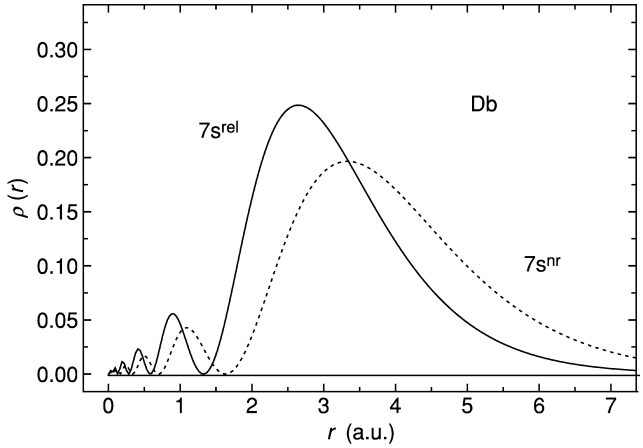

Fig. 14.3 *Relativistic* (*solid line*) *and nonrelativistic* (*dashed line*) *radial distribution of the* 7*s valence electrons in Element* 105, *Db.*

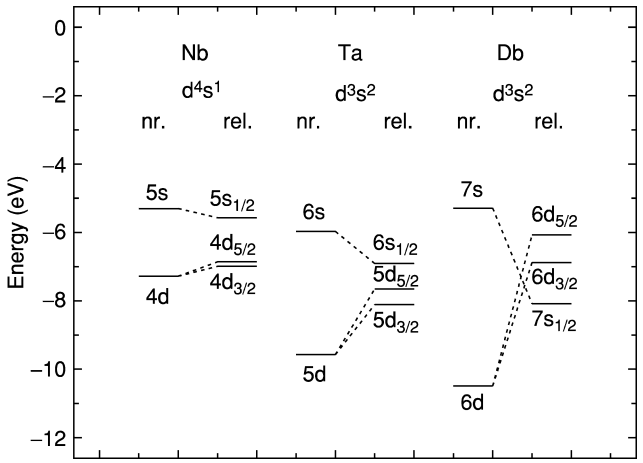

Fig. 14.4 *Relativistic stabilization of the* n*s orbitals, the destabilization of the* (n − 1)*d orbitals and their SO splitting for the group* 5 *elements. Dirac–Fock values are from Desclaux* (1973).

The contraction of the outer s and $p_{1/2}$ orbitals was recently explained as due to the admixture of higher bound and (partially) continuum orbitals due to relativistic perturbations (Schwarz *et al.*, 1989; Baerends *et al.*, 1990).

The relativistic contraction of the s and $p_{1/2}$ shells results in a more efficient screening of the nuclear charge so that orbitals of the outer d- and f-electrons, which never come close to the core, become more expanded and energetically destabilized. This is called the second or indirect relativistic effect. It was

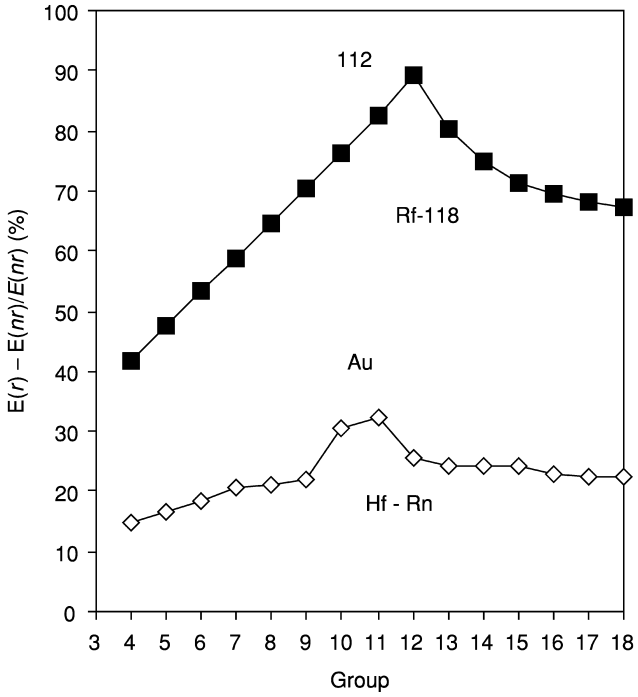

Fig. 14.5 *Relativistic stabilization of the* 6*s and* 7*s orbitals in the* 6*th and* 7*th periods of the periodic table. Redrawn from the data of Schwerdtfeger and Seth* (1998). *Relativistic Dirac–Fock data are from Desclaux* (1973). E(r) *is the relativistic orbital energy and* E(nr) *is the nonrelativistic orbital energy.* (*Figure from Pershina,* 2003).

realized that though contracted s and $p_{1/2}$ core (innermost) orbitals cause indirect destabilization of the outer orbitals, relativistically expanded d- and f-orbitals cause the indirect stabilization of the outer valence s- and p-orbitals. That partially explains the very large relativistic stabilization of the 6s and 7s orbitals in Au and in element 112, respectively (Fig. 14.5). Since both d-shells and f-shells become fully populated at the end of the d- and f-series, respectively, a maximum of indirect stabilization of the valence s- and p-orbitals will occur (Schwarz *et al.*, 1989) there. An example of the relativistic destabilization of the $(n - 1)$d orbitals is shown in Fig. 14.4 for the group 5 elements. This figure shows that trends in the relativistic and nonrelativistic energies of the valence electrons are opposite in going from the 5d to the 6d elements. Their spatial distributions show a similar effect (Fig. 14.3). Thus, only the relativistic description of the wave function can give the appropriate predictions of trends in properties within the chemical groups.

The third relativistic effect is the well-known spin–orbit (SO) splitting of levels with $l > 0$ (p-, d-, f-electrons, etc.) into $j = l \pm 1/2$. It also originates in

the vicinity of the nucleus. The SO splitting decreases with increasing l quantum number: $\mathrm{SO}(n\mathrm{p}_{1/2} - n\mathrm{p}_{3/2}) > \mathrm{SO}(n\mathrm{d}_{3/2} - n\mathrm{d}_{5/2}) > \mathrm{SO}(n\mathrm{f}_{5/2} - n\mathrm{f}_{7/2})$. All three of these effects are of the same order of magnitude and increase roughly as Z^2. The effects can be seen from the energies of one-electron levels of the 7th series of the elements shown in Fig. 14.6.

Breit effects (accounting for magnetostatic interactions) on energies of the valence orbitals and on ionization potentials (IPs) are usually small, e.g. 0.02 eV for element 121 (Eliav *et al.*, 1998a). They can, however, reach a few percent for the fine structure level splitting, e.g. 3.6% of the total amount of the Tl ^{2}P splitting. Quantum electrodynamic (QED) effects are known to be very important for the inner shells, e.g. in accurate calculations of x-ray spectra. The effects were shown to be small, but not negligible for the valence electron shells, and are of the order of 1–2% of the kinetic relativistic effects. That means that existing studies of relativistic effects have uncertainties of no more than 2% (Pyykkö *et al.*, 1998). Recent monographs are recommended for a discussion of relativistic effects on chemical properties (Schwarz, 1990; Wilson *et al.*, 1991).

14.4.2 Current relativistic quantum-chemical methods

Early predictions of chemical properties of the heaviest elements were made in the 1970s on the basis of relativistic atomic electronic structure calculations and extrapolations of properties from the lighter elements (Keller *et al.*, 1970, 1973; Fricke and Waber, 1971; Fricke, 1975; Penneman and Mann, 1976). Influenced by the success of chemical experiments on the heaviest elements and due to the further development of the quantum-mechanical theory, a new wave of predictions of chemical properties based on relativistic molecular calculations

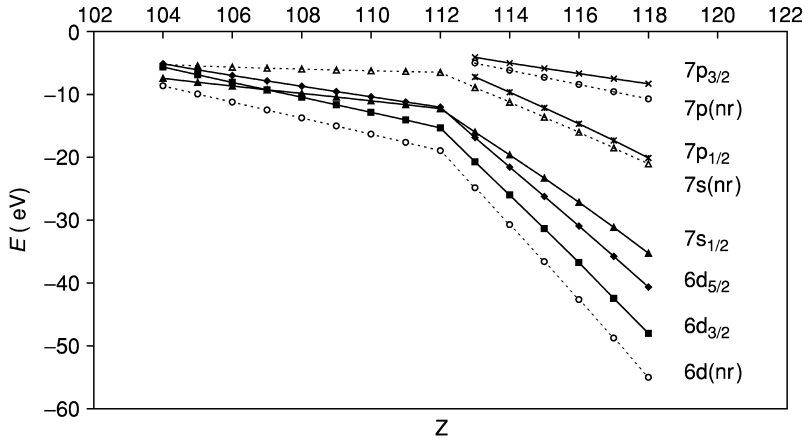

Fig. 14.6 *Relativistic* (*Dirac–Fock, solid lines*) *and nonrelativistic* (*Hartree–Fock, dashed lines*) *orbital energies for elements* 104 *through* 118. *The Dirac–Fock data are from Desclaux* (1973)*; Hartree–Fock data are from Schwerdtfeger and Seth* (1998).

appeared, beginning in the 1990s. These calculations were performed using the most advanced quantum-chemical methods at the time. Overviews of their application to transition elements are given by Pyykkö (1988), to actinides by Pepper and Bursten (1991), and to transactinides by Pershina (1996, 2003), Pershina and Hoffman (2003), and Schwerdtfeger and Seth (1998). All-electron *ab initio* methods based on the Dirac–Coulomb–Breit (DCB) Hamiltonian with some possible corrections such as the radiative correction, the extension of the finite nuclei, and coupling with nuclear spin offer fully relativistic treatment of any atomic system. Since the Dirac equation is written for one electron, the real problem of *ab initio* methods is the treatment of the instantaneous electron–electron interaction, called electron correlation. Correlation effects are taken into account by the configuration interaction (CI) technique, the many-body perturbation theory (MBPT) and currently, most accurately by the Fock-space coupled cluster (CC) procedure, called single double CC excitations (CCSDs) (Ishikawa and Kaldor, 1996; Kaldor and Eliav, 1998, 2000). However, the CCSD method is presently limited to treating electronic configurations with no more than two electrons or holes beyond the closed shell. The DCB CCSD calculations have been performed for elements as heavy as 103, 104, 111–115, 118–122 (Kaldor and Eliav, 2000; Eliav *et al*., 2002).

Atomic calculations using approximations of the DCB equations and some numerical techniques were very successful in the past. Calculations of the electronic structures of the heaviest elements up to very high Z were performed by Desclaux (1973), Mann and Waber (1970), Fricke and Waber (1971), and Fricke *et al*. (1971) using the one-configuration Dirac–Fock (DF) or the Dirac–Slater (DS) methods. (The DS method contains the Slater potential for the exchange-correlation term.) Later, a correlated method, the multi-configuration Dirac–Fock (MCDF) in some slightly different modifications (Desclaux, 1975; Grant, 1986; Parpia *et al*., 1996), was applied in calculations of the electronic structures of many of the heaviest elements up to $Z = 118$ (Desclaux and Fricke, 1980; Pyper and Grant, 1981; Glebov *et al*., 1989; Johnson *et al*., 1990, 1999, 2002; Fricke *et al*., 1993).

Molecular fully relativistic DF linear combination of atomic orbitals (DF-LCAO) codes including correlation effects are still under development (Grant, 1994; Grant and Quiney, 2000). Calculations are restricted to molecules with very few atoms, such as $(113)_2$ (Wood and Pyper, 1981), 111H, 117H, (113), (117), and $114H_4$ (Saue *et al*., 1996; Seth *et al*., 1996; Faegri and Saue, 2001). Algebraic solution of the molecular Dirac equation encounters difficulties due to the fact that the Dirac operator is unbound. Some special techniques like the projection operator technique are used to avoid the variational collapse connected with it. In contrast to nonrelativistic calculations, large basis sets are needed to describe accurately the inner-shell region where relativistic perturbation operators are dominant. The condition of kinetic balance relating the large and small components of the four-component wave function (Grant, 1986) must be observed. Kinetically balanced Gaussian type wave functions

with a Gaussian distribution for the nuclear potential are presently the best suited for these purposes. These methods place heavy demands on computer memory and computational time.

Some pseudopotentials (PPs) (Schwerdtfeger *et al.*, 1989; Schwerdtfeger and Seth, 1998) or relativistic effective core potentials (RECPs) (Ermler *et al.*, 1988; Nash *et al.*, 1997; Han and Lee, 1999) are used to solve the many-electron problem in an efficient way. According to these approximations, frozen inner shells are omitted and replaced in the Hamiltonian by an additional PP term. As a result, the number of basis functions is drastically reduced, and, hence the number of two-electron integrals is reduced. Then, the one-electron integrals are solved for the valence basis functions and this additional term by applying *ab initio* schemes at the self-consistent-field (SCF) level or with electron correlation (CI, MBPT, or CCSD) included. The RECP and the PP have been generated for the transactinides (Nash *et al.*, 1997; Schwerdtfeger and Seth, 1998) and quite a number of calculations have been performed for gas-phase compounds of the heaviest elements.

The next group of methods that can successfully be applied to the calculations of the ground state properties of large, chemically interesting systems are methods based on the density functional theory (DFT). This is a theory of the electronic ground state structure couched in terms of the electronic density distribution $\rho(r)$ (Kohn *et al.*, 1996; Rosen, 1997). It has become increasingly useful in calculations of the ground state density and energy of molecules, clusters, and solids, as well as of solvation and adsorption processes. It is an alternative and complementary approach to the traditional methods of quantum chemistry expressed in terms of the many-electron wave function $\psi(r_1, \ldots, r_N)$. The modern DFT is exact and the methods are accurate upon the introduction of the non-local effects via accurate exchange-correlation potentials, like the relativistic general gradient approximation (RGGA). The electronic structures of a number of the heaviest element compounds have been calculated (Bastug *et al.*, 1993; Varga *et al.*, 1999; Pershina and Bastug, 2000; Pershina *et al.*, 2001, 2002a,b) using the fully relativistic four-component RGGA DFT method. A slightly different Beijing DFT code (Liu *et al.*, 1997; Liu and van Wüllen, 1999) was used for some calculations on the simple heaviest systems. The DS discrete-variational (DS-DV) method, a predecessor of the RGGA DFT method which is intrinsically approximate, was extensively used previously by Pershina *et al.* Reviews of the systems for the heaviest elements are given in Pershina (1996), Pershina and Fricke (1999), Pershina and Hoffman (2003), and Pershina (2003).

There are many other theoretical methods appropriate for calculations of the electronic structures of the heaviest element systems, with some limitations. Their descriptions can be found elsewhere (Pepper and Bursten, 1991; Pershina, 1996; Schwerdtfeger and Seth, 1998). Presently, the combination of the PP (RECP) and DFT methods is the best way to study the electronic structures of the heaviest systems.

14.5 PREDICTIONS OF CHEMICAL PROPERTIES FOR ELEMENTS 104 THROUGH 112

14.5.1 Atomic properties

(a) Electronic configurations

Table 14.4 shows the current best calculations of the electronic configurations of the 6d element atoms and ions in comparison with their 5d homologs. The filling of the 6d shell takes place in the first nine of the transactinide elements, $Z = 104$ through 112. Relativistic changes in the energies of the 7s and 6d electrons (Fig. 14.6) result in the stabilization of the $7s^2$ electronic pair in the ground and first ionized states over the entire 7th period of the periodic table, which is different from the ground states of Pt($5d^9 6s$) and Au($5d^{10} 6s$) or from some of the 1+ and 2+ ionized states, as shown in Table 14.4. For example, the nonrelativistic configuration of element 111 is $6d^{10}7s$ according to Eliav *et al.* (1994). It was thought earlier that the relativistic stabilization of the $7p_{1/2}$ electrons of Rf (the $7s^2 7p6d$ ground state) indicated by MCDF calculations (Glebov *et al.*, 1989; Johnson *et al.*, 1990) would influence the properties of its compounds, but the $7s^2 7p6d$ electronic configuration was not confirmed by the more accurate CCSD calculations of Eliav *et al.* (1995a). Inclusion of dynamic correlation was required to obtain the correct $6d^2 7s^2$ ground state for Rf. However, the CCSD calculations of Eliav *et al.* (1995b) did confirm the $7s^2 7p_{1/2}$ ground state of Lr obtained earlier from the MCDF calculations of

Table 14.4 *Electronic configurations of 5d and 6d elements.*

5d elements[a]				*6d elements*			
Element	Atom	M^+	M^{2+}	Element	Atom	M^+	M^{2+}
Hf	$5d^2 6s^2$	$5d6s^2$	$5d^2$	Rf[b]	$6d^2 7s^2$	$6d7s^2$	$7s^2$
Ta	$5d^3 6s^2$	$5d^3 6s$	$5d^3$	Db[c]	$6d^3 7s^2$	$6d^2 7s^2$	$6d^3$
W	$5d^4 6s^2$	$5d^4 6s$	$5d^4$	Sg[d]	$6d^4 7s^2$	$6d^3 7s^2$	$6d^3 7s$
Re	$5d^5 6s^2$	$5d^4 6s^2$	$5d^5$	Bh[e]	$6d^5 7s^2$	$6d^4 7s^2$	$6d^3 7s^2$
Os	$5d^6 6s^2$	$5d^6 6s$	$5d^5 6s$[e]	Hs[e]	$6d^6 7s^2$	$6d^5 7s^2$	$6d^5 7s$
Ir	$5d^7 6s^2$	$5d^6 6s^2$?	$5d^7$?	109[f]	$6d^7 7s^2$	$6d^6 7s^2$	?
Pt	$5d^9 6s$	$5d^9$	$5d^8$	110[f]	$6d^8 7s^2$	$6d^7 7s^2$	?
Au	$5d^{10} 6s$	$5d^{10}$	$5d^9$	111[g]	$6d^9 7s^2$	$6d^8 7s^2$	?
Hg	$5d^{10} 6s^2$	$5d^{10} 6s$	$5d^{10}$	112[h]	$6d^{10} 7s^2$	$6d^9 7s^2$	$6d^8 7s^2$

[a] Experimental values (Moore, 1958).
[b] CCSD calculations (Eliav *et al.*, 1995a).
[c] MCDF calculations (Fricke *et al.*, 1993).
[d] MCDF calculations (Johnson *et al.*, 1999).
[e] MCDF calculations (Johnson *et al.*, 2002).
[f] DF calculations (Fricke, 1975).
[g] CCSD calculations (Eliav *et al.*, 1994).
[h] CCSD calculations (Eliav *et al.*, 1995b).

Desclaux and Fricke (1980). The relativistic stabilization of the $7p_{1/2}$ electrons manifests itself in some excited states of the transactinides that are different from those of their lighter homologs. For example, the first excited state of Rf is $6d7s^27p(^3D_2)$, only 0.3 eV above its $6d^27s^2(^3F_2)$ ground state (Eliav *et al.*, 1995a), in contrast to Hf, whose first excited state is $5d^26s^2(^3F_3)$, although its ground state is $5d^26s^2(^3F_2)$. Ionized states of elements 104 through 112 show no 7p character, so properties of their compounds in the most typical oxidation states also should not be influenced by this orbital.

(b) Stabilities of oxidation states and ionization potentials

The most accurate IPs calculated for the 6d elements are given in Table 14.5. IPs for elements of the 7th period are shown in Fig. 14.8 in comparison with those of elements of the 6th period. Earlier predictions of stable oxidation states were made on the basis of atomic DF calculations as given in the review of Fricke (1975). They indicated the 4+, 5+, and 6+ states as the most stable for gaseous compounds of Rf, Db, and Sg, respectively, although in solutions the 4+ state was suggested as the most stable for Sg, though not confirmed by later calculations (Pershina *et al.*, 1999). The close proximity of the energy levels of the 7s and 6d electrons (Fig. 14.6) is the reason for the increased stability of the maximum oxidation states of the 6d elements. Indeed, recent MCDF calculations for elements 104 through 108 (Johnson *et al.*, 1990, 1999, 2002; Fricke *et al.*, 1993) have shown a decrease in the multiple IP ($0 \rightarrow Z^+_{max}$) within the transition element groups 4 through 8, as illustrated in Fig. 14.7. This is also the reason that lower oxidation states are not stable at the beginning of the 6d series: the 7s and 6d levels are spatially so close to each other that the stepwise ionization process, for example, for Db or Sg, results in the $6d^2$ and not in the $7s^2$ configuration of Db^{3+} or Sg^{4+} (Pershina *et al.*, 1999). Since the 6d orbitals of the 6d elements are more destabilized than the 4d and 5d orbitals of the 4d and

Table 14.5 *Calculated ionization potentials for the* 6*d elements.*

IP	*Rf*[a]	*Db*[b]	*Sg*[b]	*Bh*[b]	*Hs*[b]	109[c]	110[c]	111	112
IP_1	6.01	6.89	7.85	7.7	7.6	8.3	9.9	10.6[a]	11.97[a]
IP_2	14.4	16.03	17.96	17.5	18.2	(18.9)	(19.6)	(21.5)	22.49[a]
IP_3	23.8	24.65	25.74	26.6	29.3	(30.1)	(31.4)	(31.9)	(32.8)
IP_4	31.9	34.19	35.40	37.3	37.7	(40)	(41)	(42)	(44)
IP_5		44.62	47.28	49.0	51.2	(51)	(53)	(55)	(57)
IP_6			59.24	62.1	64.0				
IP_7				74.9	78.1				
IP_8					91.8				

[a] CCSD calculations: 104 (Eliav *et al.*, 1995a), 111 (Eliav *et al.*, 1994), and 112 (Eliav *et al.*, 1995b).
[b] MCDF calculations; 104 (Johnson *et al.*, 1990), 105 (Fricke *et al.*, 1993), 106 (Johnson *et al.*, 1999), 107, and 108 (Johnson *et al.*, 2002).
[c] DF calculations, best expectation value (Fricke, 1975). Values in parentheses are estimates.

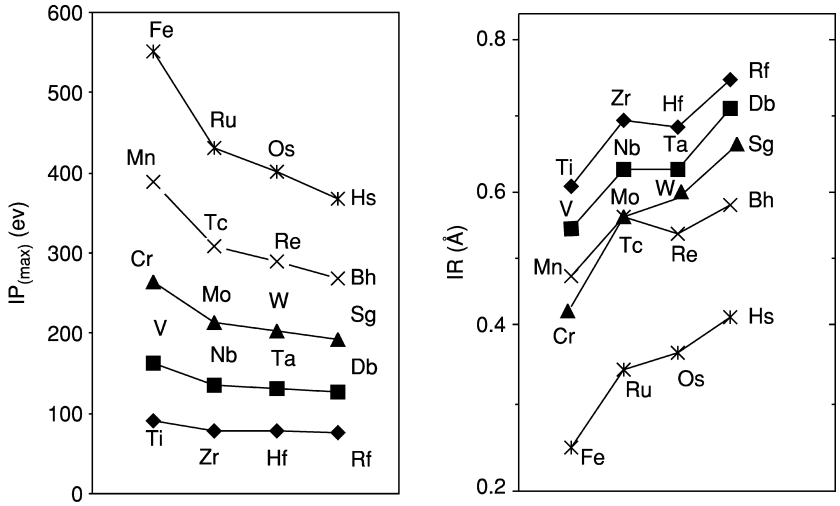

Fig. 14.7 *Ionization potentials (IP_{max}) and ionic radii (IR) for elements* 104 *through* 108 *in their maximum oxidation states obtained as a result of the MCDF calculations* (*Johnson* et al., 1990, 1999, 2002; *Fricke* et al., 1993).

5d elements, respectively, Db^{3+} and Sg^{4+} will be even less stable than Ta^{3+} and W^{4+}. Redox potentials estimated on the basis of these MCDF calculations, as discussed in Section 14.5.3a, indicate that the 6+ state of Sg will also be the most stable in solutions (Pershina *et al.*, 1999).

Predicted stable oxidation states of elements 107 through 110 vary widely. They were discussed in an early paper of Penneman and Mann (1976) that used relativistic Hartree–Fock calculations of the gaseous ion and the hydration parameters of Jorgensen to predict that the most stable oxidation states of elements 107 through 110 in aqueous solutions would be 3+, 2+, 1+, and 0. Earlier, Cunningham (1969) predicted 7+, 8+, 6+, 6+, respectively, for oxidation states of these elements, based on extrapolation by group in the periodic table. Since the Jorgensen hydration parameters did not consider the stabilizing effects of oxyanion formation as observed experimentally for W(VI) and for Re and Os, the higher oxidation states suggested by Cunningham are probably more realistic for solutions where oxyanions can be formed. No predictions based on modern relativistic calculations have been reported for elements 107 through 110.

A most stable oxidation state of 3+ was suggested for element 111, predicted to be a noble metal. It was considered to be as reactive as Au^{3+}, but with more extensive complex formation. Oxidation state 1− was also thought to be possible by analogy to Au^-, while 1+ was predicted to be less stable than for Au. The destabilization of the 6d orbitals at the end of the transactinide series is a reason for the 6d electrons to be chemically active. As a consequence, an enhanced

stability of higher oxidation states can be expected, for example, of the 5+ states of element 111, and of the 4+ state of element 112 (Fricke, 1975; Schwerdtfeger and Seth, 1998).

It was suggested that the 2+ oxidation state of element 112 would be less stable than that of Hg as its IP_2 of 22.49 eV is larger than that for Hg of 18.75 eV (see Table 14.5). The 1+ state of element 112 also will be less stable than that of Hg (see Fig. 14.8) and probably will not be realized in element 112 at all, since compounds of Hg(I) exhibit the diatomic species $(Hg–Hg)^{2+}$. Higher oxidation states such as 4+ will surely be important in aqueous solutions and in compounds. The neutral state of element 112 is also likely to be very stable due to the inertness of the $7s^2$ electrons.

(c) Ionic radii and polarizability

The ionic radii (IR) of elements are defined by the maximum of the radial charge density, r_{max}, or the expectation values $\langle r_{nj} \rangle$ of an outer valence orbital of an ion. The DF $\langle r_{nj} \rangle$ values for elements up to $Z = 120$ were tabulated by Desclaux (1973). The MCDF r_{max} for elements 104 through 108 in various oxidation states were calculated by Johnson *et al.* (1990, 1999, 2002) and by Fricke *et al.* (1993). Using these r_{max}, IR of elements 104 through 108 were estimated by these workers using a linear correlation between r_{max} and the experimentally known IR for the lighter group 4 to 8 elements (Shannon, 1976). The predictions

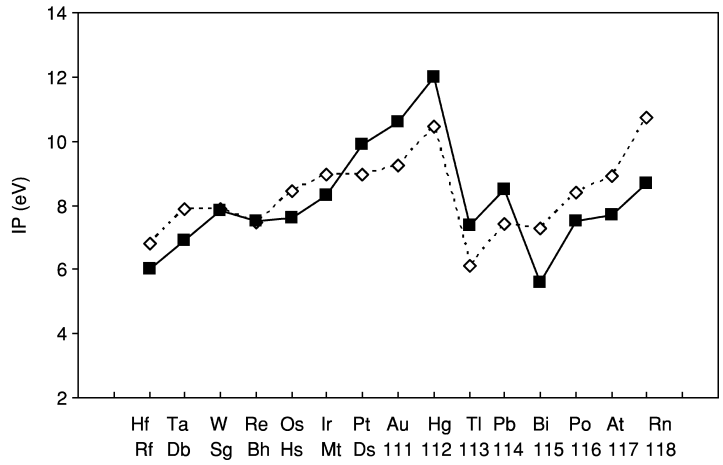

Fig. 14.8 *First ionization potentials for the* 7*th period* (*calculated, solid line*) *and the* 6*th period elements* (*experimental, dashed line*). *CCSD calculations for Rf and elements* 111 *through* 115 (*Eliav* et al., 1994, 1995*b*, 1996*a*, 1998*a*,*b*; *Landau* et al., 2001); *MCDF for elements* 105 *through* 108 (*Fricke* et al., 1993; *Johnson* et al., 1999, 2002; *Pyper and Grant*, 1981).

for the IR of Rf through Hs in their highest oxidation states are summarized in Table 14.6 and Fig. 14.7 together with experimental values for the lighter elements.

The indicated IR of the 4d and 5d elements are almost equal due to the lanthanide contraction, which is 86% a nonrelativistic effect, while the IR of the transactinides are about 0.05 Å larger than the IR of the 5d elements due to an orbital expansion of the $6p_{3/2}$ orbitals, the outer orbitals for the maximum oxidation state. Nevertheless, they are still smaller than the IR of the actinides due to actinide contraction (of 0.030 Å), which is mostly a relativistic effect. Relativistic effects on polarizability (α) change roughly as Z^2 and α should be the smallest in group 12 and in the 7th period for element 112. Its α is relativistically decreased from 74.66 to 25.82 a.u., as shown by PP CCSD(T) calculations (Seth *et al.*, 1997). As a consequence, element 112 is expected to have the weakest van der Waals bond and be extremely volatile.

14.5.2 Gas-phase compounds

(a) Electronic structures of Rf through element 112 and role of relativity

(*i*) *Rf through Hs*

A large series of calculations were performed for halides, oxides, and oxyhalides of Rf through Hs using the DFT and RECP methods: MCl_4 (M = Zr, Hf, and Rf), MCl_5 and MBr_5, $MOCl_3$, and $MOBr_3$ (M = V, Nb, Ta, and Db), MF_6 and MCl_6, $MOCl_4$, MO_2Cl_2, and MO_4^{2-} (M = Mo, W, and Sg) (Pershina, 1996, Pershina and Fricke, 1999), MO (M = Nb, Ta, and Db) (Dolg *et al.*, 1993), $M(CO)_6$ (M = Mo, W, and Sg) (Nash and Bursten, 1995; Nash and Bursten, 1999b), MO_3Cl (M = Tc, Re, and Bh) (Pershina and Bastug, 2000), and MO_4 (M = Ru, Os, and Hs) (Pershina *et al.*, 2001). Various electronic structure

Table 14.6 *MCDF values of IR* (*in* Å) *for the coordination number CN* = 6 *of elements* 104 *through* 108 *in the maximum oxidation states estimated by Johnson* et al. (1990, 1999) *and Fricke* et al. (1993). *Experimental data* (*Shannon,* 1976) *where available are given for the lighter elements*.

Group 4		*Group* 5		*Group* 6		*Group* 7		*Group* 8[a]	
Ti^{4+}	0.61	V^{5+}	0.54	Cr^{6+}	0.44	Mn^{7+}	0.46	Fe^{8+}	0.23
Zr^{4+}	0.72	Nb^{5+}	0.64	Mo^{6+}	0.59	Tc^{7+}	0.57	Ru^{8+}	0.36
Hf^{4+}	0.71	Ta^{5+}	0.64	W^{6+}	0.60	Re^{7+}	0.53	Os^{8+}	0.39
Rf^{4+}	0.79[b]	Db^{5+}	0.74[b]	Sg^{6+}	0.65	Bh^{7+}	0.58	Hs^{8+}	0.45

[a] For CN = 4.
[b] More realistic values obtained from the geometry optimization of molecular compounds are IR = 0.76 Å for Rf^{4+} (Varga *et al.*, 2000) and 0.69 Å for Db^{5+} (Han *et al.*, 1999a).

properties such as IP, electron affinity (EA), electron transition energies, charge density distribution and bonding, as well as their trends in the groups, have been predicted.

Bonding in the compounds of Rf through Hs was shown to be typical of d-element compounds. The bonding is dominated by the large participation of both $6d_{3/2}$ and $6d_{5/2}$ orbitals. The 7s orbital, as well as both $6p_{1/2}$ and $6p_{3/2}$ orbitals, each contribute about 15% to the bonding, and this contribution is increased relative to that of the lighter homologs. The contribution of the $7p_{1/2}$ orbital of 9.4% in $DbCl_5$ is, for example, 50% larger than the contribution of the $5p_{1/2}$ orbital of Nb in $NbCl_5$ (Pershina *et al.*, 1992a). The contribution of the 6d orbitals with respect to that of the 7s and $7p_{1/2}$ orbitals is thus decreased, although it does not change the d-character of the chemical properties.

Molecular orbital (MO) levels for the highest chlorides of Rf, Db, and Sg are shown in Fig. 14.9. They are similar to those of d-element compounds. The group of binding (occupied) levels (with the upper MOs of predominantly 3p character of Cl) is separated from the group of the unoccupied levels of d-character by the energy gap ΔE. A decrease in ΔE from $RfCl_4$ to $SgCl_6$ is indicative of a decrease in the metal–ligand overlap of the atomic wave functions.

The most common feature found in the calculations for all these compounds is an increase in covalence, i.e. a decrease in the effective charge, Q_M, and an increase in the overlap population (OP), as shown in Figs. 14.10 and 14.11. The OP is the amount of the electronic density localized on the bond between atoms in a molecule and is a direct counterpart of the covalent contribution to the

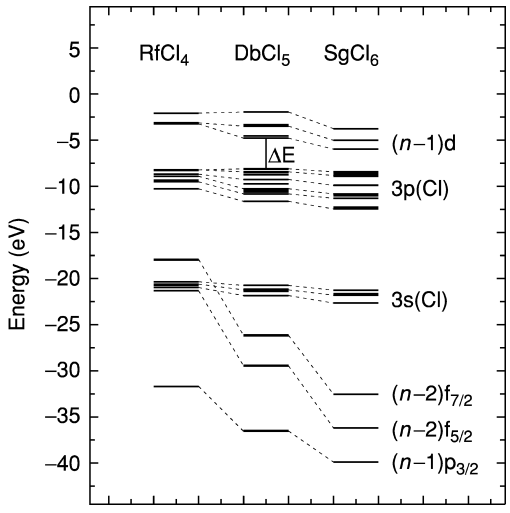

Fig. 14.9 *MO levels for $RfCl_4$, $DbCl_5$, and $SgCl_6$* (*Pershina and Fricke*, 1994).

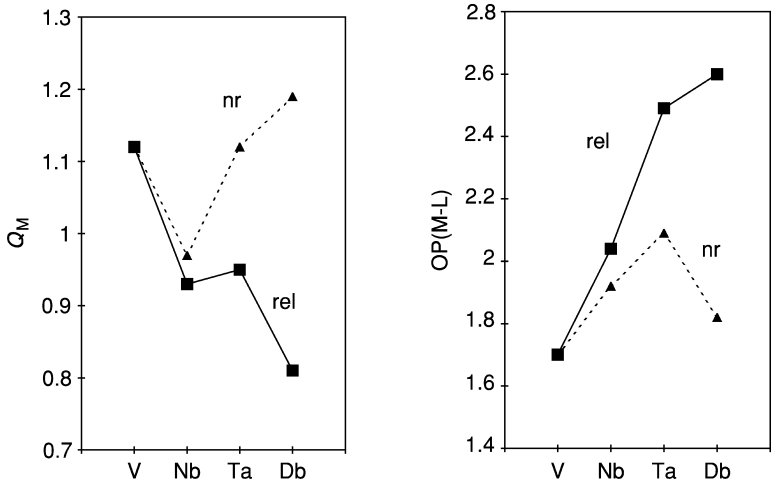

Fig. 14.10 *Relativistic* (*rel*) *and nonrelativistic* (*nr*) *values of the effective charge* (Q_M) *and overlap population* (*OP*) *in* MCl_5, *where* $M = V$, *Nb, Ta, and Db* (*Pershina and Fricke,* 1993).

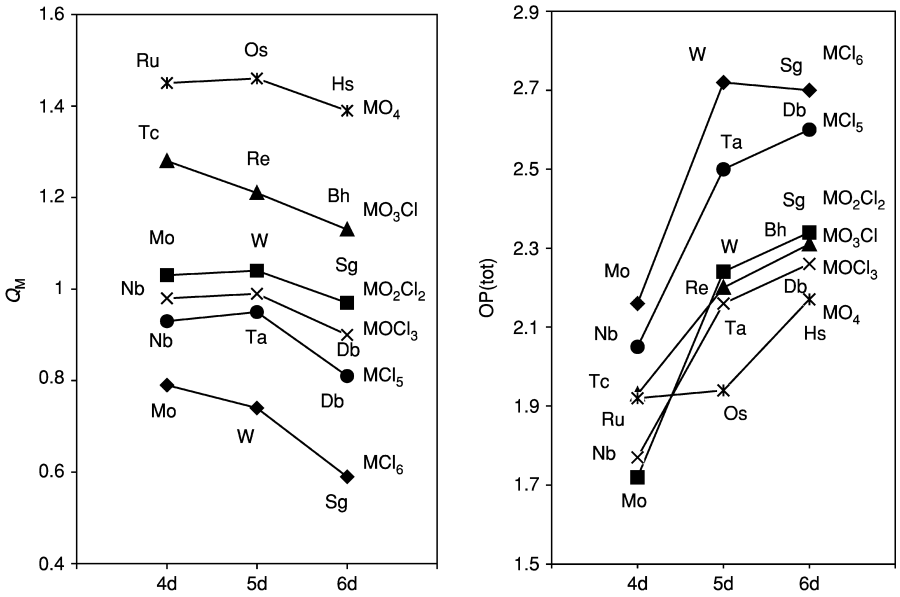

Fig. 14.11 *Effective charges* (Q_M) *and total overlap populations* (*OPs*) *for group* 4 *through* 8 *halides and oxyhalides obtained in various calculations* (*Pershina,* 2003).

binding energy (Mulliken, 1955). Comparison of the relativistic with nonrelativistic calculations (Fig. 14.10) shows this increase to be a purely relativistic effect due to the increasing contribution of the relativistically stabilized and contracted 7s and $7p_{1/2}$ atomic orbitals (AOs), as well as of the expanded 6d AOs in bonding (Pershina and Fricke, 1993).

Calculated molecular properties of gas-phase chlorides, oxychlorides, and oxides of groups 4 through 8 elements and of their homologs studied experimentally are summarized in Table 14.7. Results of molecular calculations (Pershina and Fricke, 1993; Pershina, 1996) have shown that relativistic effects increase IP, decrease EA, and increase the stability of the maximum oxidation state in each compound of the *n*d transition elements, with these effects increasing with increasing Z within the chemical groups. As a consequence, IP, ΔE, and the stabilities of the maximum oxidation states increase from the 4d to the 6d compounds, while the EAs decrease. Nonrelativistically, trends in all these properties would just be reversed from the 5d to the 6d compounds, similarly to the Q_M and OP shown in Fig. 14.10.

Trends in binding energies, D_e, and equilibrium bond distances, R_e, for various types of compounds are depicted in Fig. 14.12. There is a decrease in D_e for almost all of the 6d relative to the 5d element compounds except for MO_4 (M = Ru, Os, and Hs) and MCl_6 (M = Mo, W, and Sg). Within all the groups, relativistic effects enhance bonding of the compounds with increasing Z, though increasing SO splitting of the d-orbitals partially diminishes the binding energy, reaching a decrease of about 1.5 eV for 6d element compounds like SgO_2Cl_2, as shown by RECP calculations (Han *et al.*, 1999a). This is one of the reasons that most of the transactinide compounds have atomization energies lower than those of the homologous 5d elements. The other reason is a decrease in the ionic contribution to bonding, which is also a relativistic effect. The calculated R_e (Fig. 14.12) reflect the experimentally known similarities of bond lengths for the 4d and 5d compounds (due to the lanthanide contraction) and they show an increase in R_e of about 0.05 Å in the transactinide compounds compared to the 5d compounds.

Another important trend is the decrease in the metal–ligand single bond strength in going from the group 4 to the group 6 halides, as well as a decrease in the relative stability of the maximum oxidation state. As a consequence, volatile species such as $SgCl_6$ and $SgOCl_4$ are expected to decompose (a weak Sg–Cl bond) into compounds of Sg(v) at high temperatures by analogy with $MoCl_6$ and $MoOCl_4$. SgO_2Cl_2 was found to be the most stable of all the halides or oxyhalides and was, therefore, recommended (Pershina, 1996) for gas-phase chromatography experiments (Schädel *et al.*, 1997a). An increase in dipole moment, μ, of the low-symmetry molecules within the transition element groups was predicted for all the group 4 to 7 compounds (Table 14.7). The μ and α, as well as the molecular sizes, are decreased by relativistic effects. The PP calculations performed for the gas-phase MO (M = Nb, Ta, and Db) (Dolg *et al.*, 1993) have shown that relativistic effects stabilize the $^2\Delta$ ground state by 2.74 eV

Table 14.7 *Calculated molecular properties of transactinide compounds and of some lighter homologs experimentally studied: ionization potentials (IPs), electron affinities (EAs), energies of the lowest charge-transfer transitions* ($E_{\pi\rightarrow d}$), *equilibrium bond lengths* (R_e), *bond strengths* (D_e), *or dissociation energies* (ΔH_{diss}), *and dipole moments* (μ).

Compound	*IP* (eV)	*EA* (eV)	$E_{\pi\rightarrow d}$ (eV)	R_e (Å)	D_e (eV) (ΔH_{diss})	μ (D)	*Reference*
$ZrCl_4$				2.32[a]	20.32[b]		Girichev *et al.* (1981) (exp.)
$HfCl_4$				2.318[a]	20.53[b]		Girichev *et al.* (1981) (exp.)
$RfCl_4$				2.36	18.97		Han *et al.* (1999a)
				2.38	18.8		Varga *et al.* (2000)
$NbCl_5$	10.77	2.04	2.98	2.34/2.24[c]	19.25[b]		Pershina *et al.* (1992a)
$TaCl_5$	10.73	1.53	3.41	2.37/2.23[c]	19.47[b]		Pershina *et al.* (1992a)
$DbCl_5$	10.83	1.49	3.70	2.42/2.26[c]	17.76		Pershina *et al.* (1992a)
$NbOCl_3$	11.60	0.77	4.57	1.66/2.24[c]		0.91	Pershina *et al.* (1992b)
$TaOCl_3$	11.57	0.29	4.98	1.67/2.25[c]		0.99	Pershina *et al.* (1992b)
$DbOCl_3$	11.64	0.45	4.94	1.72/2.30[c]		1.27	Pershina *et al.* (1992b)
$MoCl_6$	11.06		1.92	2.25	19.29[b]		Pershina and Fricke (1994)
WCl_6	11.13		2.37	2.36[d]	21.65[b]		Pershina and Fricke (1994)
			2.32		19.9		Han *et al.* (1999a)
$SgCl_6$	11.17		2.65	2.38	20.05		Pershina and Fricke (1994)
				2.36	19.9		Han *et al.* (1999a)
$MoOCl_4$				1.658/2.279[e]	20.5[b]	0.14	Pershina and Fricke (1995)
$WOCl_4$				1.685/2.280[e]	22.1[b]	0.49	Pershina and Fricke (1995)
				1.670/2.317	21.5	0.24	Han *et al.* (1999a)

$SgOCl_4$				21.2	1.03	Pershina *et al.* (1995)
			1.720/2.364	21.0	0.77	Han *et al.* (1999a)
MoO_2Cl_2		4.06	1.698/2.259[f]	21.08[b]	1.04	Pershina and Fricke (1996)
WO_2Cl_2		4.48	1.710/2.27[g]	23.5[b]	1.35	Pershina and Fricke (1996)
			1.70/2.28	22.2	1.51	Han *et al.* (1999a)
SgO_2Cl_2		4.33		21.8	1.83	Pershina *et al.* (1996b)
			1.75/2.34	21.0	2.39	Han *et al.* (1999a)
TcO_3Cl	12.25		1.69/2.30[c]	23.12	0.93	Pershina and Bastug (2000)
ReO_3Cl			1.761/2.23			Amble *et al.* (1952) (exp.)
	12.71		1.71/2.28	24.30	1.29	Pershina *et al.* (2000)
BhO_3Cl	13.05		1.77/2.37	22.30	1.95	Pershina *et al.* (2000)
RuO_4	12.19[i]		1.706[h]	27.48		Pershina *et al.* (2001)
OsO_4	12.35[i]		1.711[h]	27.71		Pershina *et al.* (2001)
HsO_4	12.28		1.775	28.44		Pershina *et al.* (2001)

[a] Exp. (Girichev *et al.*, 1981).
[b] From a Born–Haber cycle.
[c] Estimated from IR.
[d] Exp. (Brown, 1973).
[e] Exp. (Lijima and Shibata, 1974, 1975)
[f] Exp. (Zharskii *et al.*, 1975).
[g] Exp. (Jampolskii, 1973).
[h] Exp. (Krebs and Hasse, 1976).
[i] Exp. (Burroughs *et al.*, 1974).

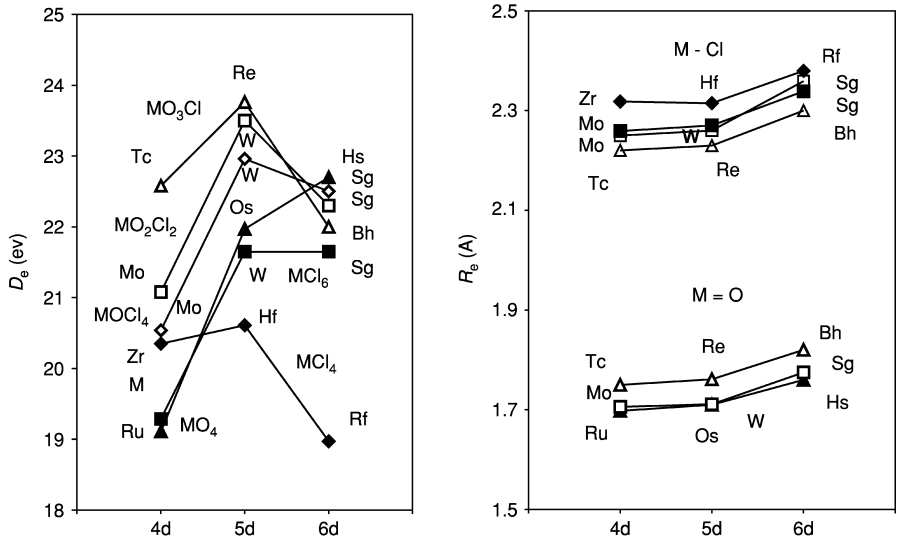

Fig. 14.12 *Binding energies* (D_e, *the dissociation energy of the molecule into its atoms*) *and optimized bond lengths* (R_e) *for various halides, oxides, and oxyhalides of group* 4 *through* 8 *elements* (*Pershina,* 1996*; Han* et al., 1999*a; Pershina and Bastug,* 2000*; Pershina* et al., 2001). *Symbols for both* D_e *and* R_e *are open triangles* = MO_3Cl, *open squares* = MO_2Cl_2, *open rhomboids* = $MOCl_4$, *solid rhomboids* = MCl_4, *solid triangles* = MO_4, *solid squares* = MCl_6.

(the nonrelativistic configuration is $^4\Sigma^-$) in contrast to the $^4\Sigma^-$ state observed for NbO. The relativistic effects also stabilize the binding energy of DbO by 1.93 eV. (Σ and Δ denote molecular spectroscopic states.)

(*ii*) *Mt through element* 112

Elements 109 (Mt) and 110 (Ds) have received little attention in recent years. The position of these elements in the periodic table indicates that they should be noble metals. Volatile hexafluorides and octafluorides might be produced and used for chemical separations. The relativistic DS-DV molecular calculations of Rosen *et al.* (1979) and of Waber and Averill (1974) performed for DsF_6 have shown that its electronic structure is very similar to that of PtF_6, with similar values of IP.

Earlier detailed predictions of chemical properties of element 111 based on atomic calculations were made by Keller *et al.* (1973). Due to the fact that the maximum of relativistic effects in the *n*s shell in group 11 occurs at element 111, there has been widespread interest in the electronic structure of its compounds. The effect of the 7s orbital contraction was investigated for the simplest molecule, 111H, whose electronic structure was calculated by a variety of methods including the fully relativistic DCB *ab initio* method (Seth *et al.*, 1996; Liu and

van Wüllen, 1999). The bonding was shown to be considerably increased by relativistic effects, which doubled the dissociation energy, though the SO splitting diminished it by 0.7 eV. Calculations (Liu and van Wüllen, 1999) were also performed for other dimers, AuX and 111X where X = F, Cl, Br, O, Au, and 111.

The stability of higher oxidation states of element 111 was examined in calculations of energies of the decomposition reactions $MF_6^- \rightarrow MF_4^- + F_2$ and $MF_4^- \rightarrow MF_2^- + F_2$ using the relativistic PP method (Seth *et al.*, 1998a,b). The results support the earlier predictions that the 3+ and 5+ oxidation states will be more stable for this element than they are for Au (due to a larger participation of the 6d orbitals in bonding) and that the 1+ oxidation state of element 111 may be difficult to prepare. The SO coupling was shown to stabilize the molecules in the following order: $MF_6^- > MF_4^- > MF_2$. This order is consistent with the relative involvement of the $(n-1)$d electrons in bonding for each type of molecule.

The most interesting among the heaviest elements from the chemical point of view is element 112, where the maximum of relativistic effects on the 7s shell in the entire 7th period and within group 12 occurs (see Fig. 14.5). Due to the strong relativistic contraction and stabilization of the 7s orbitals (and accordingly its highest IP in group 12) and its closed-shell configuration, it is expected to be rather inert and may be a distinctly noble metal. It was suggested that the interatomic interaction in the metallic state will be small, possibly even leading to high volatility as in the noble gases. Pitzer (1975a) estimated that the very high excitation energy of about 8.6 eV for the $6d^{10}7s^2 \rightarrow 6d^{10}7s7p$ transition into the configuration of the metallic state will not be compensated by the energy gain of the metal–metal bond formation. An extrapolation of the sublimation enthalpy from its homologs, Zn, Cd, and Hg, also suggests that element 112 should be quite volatile (Eichler, 1974). Recently, a similar conclusion was obtained by using a more sophisticated empirical model (Ionova *et al.*, 1996).

Estimates of adsorption enthalpies of element 112 on various metal surfaces using some adsorption models suggest, nevertheless, that element 112 can be deposited on some metals, like Ag, Au, Pd, or Pt (Eichler and Rossbach, 1983). The ability of element 112 to form a metal–metal bond was also predicted by recent relativistic MO calculations for 112M, where M = Cu, Pd, Pt, Ag, and Au (Pershina *et al.*, 2002a). Element 112 was calculated to form a rather strong bond with the above-mentioned transition elements, only about 15–20 kJ mol^{-1} weaker than that of HgM, with the D_e of 112Pd being the largest.

Molecular relativistic PP calculations (Seth *et al.*, 1997) have predicted that the 2+ oxidation state of element 112 will be less stable than that of Hg. They have calculated that $112F_2$ is, indeed, less stable than HgF_2 and that it will decompose readily into 112 and F_2. Seth *et al.* (1997) also came to the conclusion that element 112 should exhibit a typical transition element character in higher oxidation states, because its 6d orbitals are relativistically destabilized and, therefore, should participate more in coordination bonding. Thus, for

example, the 4+ oxidation state of element 112 as in $112F_4$ may be accessible while the 2+ state may not. In combination with an appropriate polar solvent, the species $112F_5^-$ and/or $112F_3^-$ should be formed rather than $112F_4$ or $112F_2$, although these compounds will probably undergo strong hydrolysis in aqueous solutions, and perhaps bromides or even iodides will be more stable and would be better for experimental investigations.

(b) Predictions of volatilities

A more extensive series of the DFT calculations (Pershina, 1996; Pershina and Bastug, 2000; Pershina *et al.*, 2001) permitted establishment of some relationships between molecular properties such as covalence or dipole moment and volatility. Because covalent compounds are typically more volatile than ionic compounds, the higher covalence of high-symmetry halides or oxides of the transactinides is expected to result in their higher volatilities compared with those of their 4d and 5d homologs. For example, $RfCl_4$ is expected to be more volatile than $HfCl_4$ since it is more covalent and is expected to have the T_d symmetry shown by $HfCl_4$ in the vapor phase. Low-symmetry compounds, e.g. oxyhalides of C_n symmetry, have dipole moments and, therefore, are attracted more strongly to the surface of a chromatographic column due to an additional electrostatic (dipole moment–surface charge) interaction than are high-symmetry compounds of the same element such as pure halides. Therefore, one expects that $DbCl_5$ (D_{3h} symmetry) will be more volatile than $DbOCl_3$ (C_{3v} symmetry). For low-symmetry compounds, a trend in volatility in a chemical group will be opposite to the trend in μ, since larger dipole moments cause stronger electrostatic interactions with the surface of a chromatography column. Accordingly, the following decreasing trends in volatility were predicted: $MoO_2Cl_2 > WO_2Cl_2 > SgO_2Cl_2$ and $TcO_3Cl > ReO_3Cl > BhO_3Cl$. These trends are opposite to the increasing dipole moments. Indeed, these trends were confirmed experimentally by the observations (Kadkhodayan, 1993; Kadkhodayan *et al.*,1996; Türler *et al.*, 1998b; Sylwester *et al.*, 2000) that $RfCl_4$ is more volatile than $HfCl_4$, while $DbOCl_3$ (Türler *et al.*, 1996), SgO_2Cl_2 (Schädel *et al.*, 1997a; Türler *et al.*, 1999), and BhO_3Cl (Eichler *et al.*, 2000) are less volatile than the corresponding compounds of their lighter homologs in the respective chemical groups.

In addition, enthalpies of adsorption, $\Delta H_{ads}(BhO_3Cl) = -78.5$ kJ mol^{-1} compared to $\Delta H_{ads}(TcO_3Cl) = -48.2$ kJ mol^{-1} and ΔH_{ads} $(ReO_3Cl) = -61$ kJ mol^{-1}, on the quartz surface of the chromatography column were predicted by Pershina and Bastug (2000) using a model of physisorption and by performing calculations of the electronic structures of those molecules. The obtained adsorption enthalpies indicate that volatility decreases as $TcO_3Cl > ReO_3Cl > BhO_3Cl$, in excellent agreement with the experimental value $\Delta H_{ads}(BhO_3Cl) = -77.8$ kJ mol^{-1} (Eichler *et al.*, 2000). In a similar way, $\Delta H_{ads} = -(36.7 \pm 1.5)$ kJ mol^{-1} on a quartz surface was predicted by Pershina *et al.* (2001) for HsO_4

as compared to $\Delta H_{ads}(RuO_4) = -(40.4 \pm 1.5)$ kJ mol^{-1} and ΔH_{ads} $(OsO_4) = -(38.0 \pm 1.5)$ kJ mol^{-1}. Thus, the volatility of group 8 tetroxides in the specific experiments is expected to change as $RuO_4 < OsO_4 \leq HsO_4$. Such a sequence is also expected from an extrapolation of this property within the group (Düllmann *et al.*, 2002b). This trend is in accord with the idea of increasing volatility with increasing covalence of compounds.

14.5.3 Solution chemistry

(a) Redox potentials

Some earlier estimates of oxidation states of the transactinides made on the basis of empirical modifications of the Born–Haber cycle were reviewed by Fricke (1975). They were mostly related to simple M^{z+} ions, and the results were rather inconsistent. Recently, redox potentials (E°) for complex species of Rf, Db, and Sg in aqueous solutions were estimated (Ionova *et al.*, 1992; Pershina and Fricke, 1994; Pershina *et al.*, 1999) using correlations between the MCDF-calculated IPs (Johnson *et al.*, 1990; 1999; Fricke *et al.*, 1993) and the tabulated redox potentials for group 4, 5, and 6 elements (Bratsch, 1989). Two correlation plots for groups 5 and 6 are shown in Fig. 14.13.

These estimates indicate that the stability of the maximum oxidation state increases with Z within groups 5 and 6, while that of lower oxidation states decreases. Thus, the 5+ and 6+ states of Db and Sg will be more stable than their 3+ and 4+ states, respectively. The 3+ state of Db will be less stable than the 3+ states of Nb or Ta, and the 4+ state of Sg will be less stable than the 4+ states of Mo and W.

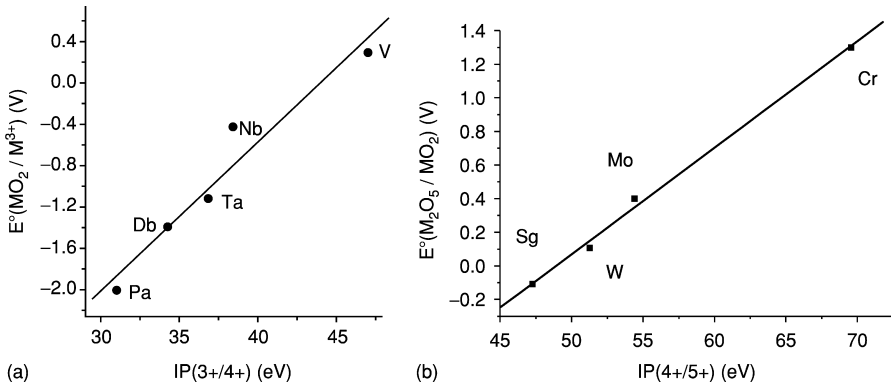

Fig. 14.13 (*a*) *Correlation between IP*(3+/4+) *and the standard potentials* $E^o(MO_2/M^{3+})$ *where M = V, Nb, Ta, Db, Pa. The standard potential for Db is from Ionova* et al. (1992). *The standard potentials for Nb, Ta, and Pa are from Bratsch* (1989). (*b*) *Correlation between IP*(4+/5+) *and the standard potentials* $E^o(M_2O_5/MO_2)$ *where M=Cr, Mo, W, and Sg* (*Pershina* et al., 1999).

The increasing stability of the maximum oxidation state and the decreasing stability of lower oxidation states at the beginning of the 6d series is a relativistic effect caused by destabilization of the 6d orbitals, as discussed earlier. Along the 6d series, the stability of the maximum oxidation state decreases in the order: $Lr^{3+} > Rf^{4+} > Db^{5+} > Sg^{6+}$. For comparison, the results are summarized in Table 14.8, together with those for Lr, the last of the actinides.

(b) Hydrolysis

Aqueous ions of transition elements undergo strong hydrolysis, as do their heaviest homologs. In acidic solutions, hydrolysis involves either the cation $M(H_2O)_n^{Z+} \Leftrightarrow MOH(H_2O)_{n-1}^{(Z-1)+} + H^+$ or the anion, or both. The hydrolysis of cations of a given oxidation state is known to decrease within groups 4, 5, and 6 as one proceeds down the periodic table and it increases from group 4 to group 6 (Baes and Mesmer, 1976). Hydrolysis/protonation of group 4, 5, and 6 cations and of their compounds was considered theoretically on the basis of relativistic DFT calculations (Pershina, 1998a,b; Pershina and Kratz, 2001; Pershina *et al*., 2002b).

For group 4 elements, about 50% of each type of the species indicated in the following equilibrium exists in aqueous solutions at pH = 0: $M(H_2O)_8^{4+} \Leftrightarrow MOH(H_2O)_7^{3+}$. For this reaction, the following trend in hydrolysis of the group 4 elements was predicted from the calculated Gibbs energy changes: Zr > Hf > Rf (Pershina *et al*., 2002b). The first hydrolysis constant

Table 14.8 *Calculated redox potentials of Lr, Rf, Db, and Sg in aqueous acidic solutions.*

Potential	*Lr*[a]	*Rf*	*Db*[b]	*Sg*[c]
$E^\circ(M^{6+}/M^{5+})$	–	–	–	–0.046 (MO_3/M_2O_5) –0.05 (M^{6+}, H^+/M)
$E^\circ(M^{5+}/M^{4+})$	–	–	–1.0 (M_2O_5/MO_2) –1.13 (MO_2^+/MO^{2+})	0.11 (M_2O_5/MO_2) –0.35 (M^{5+}, H^+/M^{4+}, H^+)
$E^\circ(M^{4+}/M^{3+})$	8.1	–1.5 (M^{4+}/M^{3+})[d]	–1.38 (MO_2/M^{3+})	–1.34 (MO_2/M^{3+}) –0.98 ($M(OH)_2^{2+}/M^{3+}$)
$E^\circ(M^{3+}/M^{2+})$	–2.6	–1.7 (M^{3+}/M^{2+})[d]	–1.20	–0.11
$E^\circ(M^{3+}/M)$	–1.96[e]	–1.97 (M^{3+}/M)[f]	–0.56	0.27
$E^\circ(M^{4+}/M)$	–	–1.85 (M^{4+}/M)[g] –1.95 (MO_2/M)[g]	–0.87 (MO_2/M)[f]	–0.134 (MO_2/M) –0.035 ($M(OH)_2^{2+}/M$)
$E^\circ(M^{5+}/M)$	–	–	–0.81 (M_2O_5/M)	–0.13 (M_2O_5/M)[f]
$E^\circ(M^{6+}/M)$	–	–	–	–0.12 (MO_3/M) –0.09 (M^{6+}, H^+/M)

[a] Bratsch and Lagowski (1986).
[b] Ionova *et al*. (1992).
[c] Pershina *et al*. (1999).
[d] Johnson and Fricke (1991).
[e] Bratsch (1989).
[f] Roughly estimated from the other E°.
[g] Pershina *et al*. (1994).

$\log K_{11}(\mathrm{Rf}) \approx -4$ was then calculated and compared to $\log K_{11}(\mathrm{Zr}) = 0.3$ and $\log K_{11}(\mathrm{Hf}) = -0.25$. This hydrolysis sequence is in agreement with the order of extraction of group 4 elements into thenoyltrifluoroacetone (TTA) obtained in the experiments described in Section 14.6.1c(iv).

For group 5 elements and Pa, hydrolysis proceeds very rapidly, with the ultimate formation of products such as $M(OH)_5(aq)$. Hydrolysis of group 5 cations was studied theoretically for the following reaction: $M(H_2O)_6^{5+} \Leftrightarrow M(OH)_6^- + 6H^+$ where M = Nb, Ta, Db, and Pa. Calculations (Pershina, 1998a) of the Gibbs energy changes of this reaction showed that the trend toward decreasing hydrolysis is continued with Db, giving the sequence Nb > Ta > Db >> Pa.

Hydrolysis of group 6 elements proceeds even further than that of the group 5 elements, with the formation of MO_4^{2-} at higher pH according to the following scheme: $M(H_2O)_6^{6+}$ (this species is not observed) $\Leftrightarrow \ldots \Leftrightarrow [M(OH)_4(H_2O)]^{2+}$ $\Leftrightarrow [MO(OH)_3(H_2O)_2]^+ \Leftrightarrow MO_2(OH)_2(H_2O)_2 \Leftrightarrow [MO_3(OH)]^- \Leftrightarrow MO_4^{2-}$. The protonation process, the reverse of the reaction shown above, was considered theoretically (Pershina and Kratz, 2001). The resulting relative values of Gibbs energy changes suggest that for the first two protonation steps (see Table 14.12) the trend in group 6 should be W > Sg ≥ Mo rather than Sg > W > Mo. For the third and subsequent protonation processes, the trend should be Sg > W > Mo. The values of log *K* were defined for Sg, as shown in Table 14.9. The predicted trends in log *K* are in agreement with experiments on Mo and W at various pH values (Baes and Mesmer, 1976) and with Sg for the protonation/hydrolysis of the positively charged complexes (Schädel *et al.*, 1998).

(c) Complexation

If one molecular complex ML_i, among many others, is extracted into an organic phase, the distribution coefficient, K_d (expressed in terms of the complex formation constant β_i), is a good measure of its stability and the sequence in the K_d values for a given series should reflect the sequence in the stability of the complexes (Ahrland *et al.*, 1973). Thus, by predicting $\log\beta_i = \Delta G^r/2.3RT$ one

Table 14.9 *Values of log* K *for the stepwise protonation of* MO_4^{2-} (*M = Mo, W, and Sg*) (*Pershina and Kratz*, 2001).

	log K_n		
Reaction	*Mo*	*W*	*Sg*
$MO_4^{2-} + H^+ \Leftrightarrow MO_3(OH)^-$	3.7	3.8	3.74
$MO_3(OH)^- + H^+ + 2H_2O \Leftrightarrow MO_2(OH)_2(H_2O)_2$	3.8	4.3	4.1 ± 0.2
$MO_4^{2-} + 2H^+ + 2H_2O \Leftrightarrow MO_2(OH)_2(H_2O)_2$	7.50	8.1	8.9 ± 0.1
$MO_2(OH)_2(H_2O)_2 + H^+ \Leftrightarrow MO(OH)_3(H_2O)_2^+$	0.93	0.98	1.02

can predict sequences in the extraction of complexes into an organic phase or their sorption by cation- or anion-exchange resins.

Complex formation is known to increase within the transition element groups with increasing Z. However, in aqueous solutions it competes with hydrolysis as described by the following equilibrium: $x\mathrm{M(H_2O)}_{w^\circ}^{z+} + y\mathrm{OH}^- + i\mathrm{L}^- \Leftrightarrow \mathrm{M}_x\mathrm{O}_u\mathrm{(OH)}_{z-2u}\mathrm{(H_2O)}_w\mathrm{L}_a^{(xz-y-i)} + (xw^\circ + u - w)\mathrm{H_2O}$. This may change trends in the stabilities of the complexes and, consequently, their extraction into an organic phase.

(*i*) *Rf through Sg*

Complexation of group 4 elements in HF solutions is described by the following equilibria:

$$\mathrm{M(H_2O)}_8^{4+} \Leftrightarrow \mathrm{MF(H_2O)}_7^{3+} \Leftrightarrow \mathrm{MF_3(H_2O)}_5^- \Leftrightarrow \tag{14.1}$$

$$\mathrm{MF_4(H_2O)_4} \Leftrightarrow \mathrm{MF_5(H_2O)}^- \Leftrightarrow \mathrm{MF}_6^{2-}. \tag{14.2}$$

Results of DFT calculations of the relative Gibbs energy changes of these equilibria (Pershina *et al.*, 2002b) suggest that the trend in the formation of the positively charged complexes according to equation (14.1) should be Zr $\geq$ Hf $>$ Rf. This means that the K_d values for sorption by a cation resin of the positively charged complexes formed at HF concentrations below $<$0.01 M will have the following trend in group 4: Rf $>$ Hf $\geq$ Zr. (In the case of the formation of positively charged complexes of a lower charge from complexes with a higher charge (equation (14.1)), the sequence in the K_d values is opposite to the sequence in the complex formation, since complexes with a lower positive charge are more poorly sorbed on cation exchange resin than those with a higher charge.) For the formation of anionic complexes (equation (14.2)) sorbed by an anion-exchange resin, the trend becomes more complicated depending on the pH, i.e. depending on whether the fluorination process starts from the hydrated or the hydrolyzed species. Thus, for experiments conducted at HF concentrations above 0.001 M where some hydrolyzed or partially fluorinated species are present, the trend for the formation of MF_6^{2-} (equation (14.2)) and hence of K_d should be reversed in group 4: Rf $\geq$ Zr $>$ Hf.

The predicted sequences are in agreement with experiments on cation- and anion-exchange resin separations of Zr, Hf, and Rf from mixed HF/HCl solutions, where fluorinated complexes were sorbed on the resin and Cl^- ions served as counter-ions competing for its active centers (Trubert *et al.*, 1999). At high HCl concentrations, where no hydrolysis takes place, the complexation reaction is $\mathrm{M(H_2O)}_8^{4+} + 6\mathrm{HCl} \Leftrightarrow \mathrm{MCl}_6^{2-}$. Results of the DFT calculations of Gibbs energy changes for this reaction (Pershina *et al.*, 2002b) suggest that the trend in complex formation and in the K_d values should definitely be continued with Rf to give the sequence Zr $>$ Hf $>$ Rf.

Group 5 elements form a large variety of complexes, such as $M(OH)_2Cl_4^-$, $MOCl_4^-$, $MOCl_5^{2-}$, and MCl_6^- (M = Nb, Ta, Db, and Pa), in HCl solutions with different degrees of hydrolysis. Their formation is described in a general form by the following equilibrium reactions: $M(OH)_6^- + iL^- \Leftrightarrow MO_u(OH)_{z-2u}L_i^{(6-i)-}$. The DFT calculations of Gibbs energy changes for these reactions (Pershina, 1998b) showed the following trend in the complex formation and extraction of group 5 elements: Pa >> Nb $\geq$ Db > Ta. Thus, a reversal of the trend from Ta to Db was predicted for group 5 elements. The following sequence in the formation of various types of complexes as a function of increasing acid concentration was predicted (Pershina and Bastug, 1999): $M(OH)_2Cl_4^- > MOCl_4^- > MCl_6^-$. For the acids of interest, the sequence was predicted as: $MF_6^- > MCl_6^- > MBr_6^-$.

Complex formation of the group 6 elements, Mo, W, and Sg, in HF solutions is described as: MO_4^{2-} (or $MO_3(OH)^-$) + HF $\Leftrightarrow$ $MO_3F^- \Leftrightarrow MO_2F_2(H_2O)_2 \Leftrightarrow MO_2F_3(H_2O)^- \Leftrightarrow MOF_5^-$. The calculated Gibbs energy changes of these reactions show a very complicated dependence of trends in the complex formation on HF concentration and pH. Thus, at low [HF] $< \sim$0.1 M, a reversal of the trend from W to Sg should occur, while at high [HF] > 0.1 M, the trend is continued with Sg: Sg > W > Mo. It should be noted that such complicated trends could not be obtained by any extrapolation of properties within the group, but are the result of considering complex formation in equilibrium with hydrolysis and by calculating relativistically the electronic structure of the complexes.

(*ii*) *Bh through element* 112

The aqueous chemistry of these elements promises to be very interesting and should provide extensive information about complexing ability as well as information about the potential reduction reactions. Some general considerations on the basis of atomic calculations are presented by Fricke and Waber (1971); Fricke (1975). Some aspects of the complex formation of elements 107 through 112 in aqueous solution were discussed by Keller and Seaborg (1977) and Seaborg and Keller (1986). It is expected that element 112 will have extensive complex-ion chemistry, as do other elements of the second half of the 6d transition series. From early relativistic atomic calculations, Pitzer (1975a) postulated some very interesting properties for element 112 caused by relativistic effects on the $7s^2$ shell. He suggested that element 112, eka-Hg, would be more noble than Hg, and even though the oxide, the chloride, and the bromide would be unstable, $112Cl_4^{2-}$ and $112Br_4^{2-}$ would exist in solution, and $112F_2$ would be stable.

Recently, Seth *et al.* (1997) have considered the possibility of formation of $112F_5^-$ and $112F_3^-$, by analogy with Hg where the addition of F^- to HgF_2 or HgF_4 was found to be energetically favorable. However, in aqueous solutions these complexes probably undergo strong hydrolysis. Thus, experiments might only be possible with $112Br_5^-$ or $112I_5^-$.

14.6 MEASURED CHEMICAL PROPERTIES FOR ELEMENTS 104 THROUGH 112

The experimental results for Rf, Db, and Sg, the results of the first experimental investigations for Bh and Hs, and a preliminary report of experiments designed to study element 112 are briefly reviewed. Several more detailed reviews of the experimental techniques, measured chemical properties of Rf, Db (Ha), and Sg, and prospects for studies of still heavier elements are available and should be consulted for additional information (Schädel, 1995, 2002; Gregorich, 1997a; Hoffman and Lee, 1999; Kratz, 1999b).

A summary of some predicted chemical properties of elements 104 through 112 is given in Table 14.10. First experimental investigations of the chemical properties of the transactinides focused on the most fundamental and simplest properties. For example, the determination that the most stable oxidation states of elements 104 and 105 in aqueous solutions were 4+ and 5+, respectively, allowed their placement at the bottom of groups 4 and 5 in the periodic table as members of the 6d transition series. In later experiments, attempts were made to perform more complex studies of transactinide properties for comparison with their lighter homologs in the periodic table. Such studies present even greater challenges because of the need to investigate the transactinides and their lighter homologs under exactly the same chemical conditions – the ideal situation being to measure them all in the same on-line experiments conducted at the accelerators where they are produced.

14.6.1 Chemistry of rutherfordium (104)

(a) Historical

In early gas-phase studies at Dubna, Zvara *et al.* (1969, 1970) reported that the chloride of a 0.3-s SF activity produced in the ^{242}Pu(^{22}Ne,4n) reaction and initially assigned to ^{260}Rf formed a chloride, presumably $RfCl_4$, that was less volatile than $HfCl_4$. However, the existence of such an isotope has never been confirmed (see Fig. 14.2) and these claims were apparently incorrect as discussed in detail by Kratz (1999b). Zvara *et al.* (1972) later proposed that they were actually measuring the SF branch of the known alpha-emitting 3-s ^{259}104, which was produced in the same experiments via the ^{242}Pu(^{22}Ne,5n) reaction. They then reported that the volatility of the Rf tetrachloride was similar to that of $HfCl_4$ and much more volatile than the chlorides of the actinides and Sc. They concluded from their results that Rf properly belonged to group 4 of the periodic table. However, only SF events were measured and there is still some doubt about the magnitude of the SF branch of ^{259}104, which decays predominantly by alpha emission. The results could not be considered definitive because positive identification of the element being studied was not possible since only SF decay was detected.

Table 14.10 *Predicted chemical properties of elements* 104 *through* 112.

	Rf	Db	Sg	Bh	Hs	Mt	110	111	112
chemical group	4	5	6	7	8	9	10	11	12
stable oxidation states[a,b]	**4**,3	**5**,4,(3)	**6**,5,4,(3)	**7**,5,4,3	**8**,6,4,3	6,3,1	6,4,2,0	5,**3**,–1	**4**,2,**0**
first ionization potential (eV)[c]	6.01	6.89	7.85	7.7	7.6	8.7	9.6	10.6	11.97
standard electrode potential in aqueous solution (V)[d]	(4+→0)	(5+→0)	(6+→0)	(5+→0)	(4+→0)	(3+→0)	(2+→0)	(3+→0)	(2+→0)
	–1.85	–0.81	–0.12	+0.1	+0.4	+0.8	+1.7	+1.9	+2.1
ionic radius of indicated ion (Å)[e]	0.76(4+)	0.69(5+)	0.65(6+)	0.83(5+) 0.58(7+)	0.80(4+) 0.45(8+)	0.83(3+)	0.80(2+)	0.76(3+)	0.75(2+)
atomic radius (Å)[f]	1.50	1.39	1.32	1.28	1.26	1.22	1.18	1.14	1.10
density (g cm^{-3})[f]	23	29	35	37	41	37.4	34.8	28.7	23.7
ΔH_{sub} (kJ mol^{-1})[g]	694	795	858	753	628	594	481	335	29
boiling point (K)[g]	5800								
melting point (K)[g]	2400								

[a] Bold type: most stable in gas phase; underlined = most stable in aqueous solutions; non-bold: less stable; ( ) = least stable.
[b] Fricke (1975), Pershina *et al.* (1999), Schwerdtfeger and Seth (1998).
[c] See Table 14.5.
[d] See Table 14.8 for Rf through Sg; see Seaborg and Keller (1986) for elements Bh through 112.
[e] See Table 14.6 for maximum oxidation states of Rf through Hs; see Seaborg and Keller (1986) for Mt through 112.
[f] See Seaborg and Keller (1986) for Rf through Hs and Fricke (1975) for Mt through 112.
[g] Seaborg and Keller (1986).

Studies of the solution chemistry of element 104 were conducted in 1970 by Silva *et al.* (1970b) using 75-s ^{261}Rf (see Table 14.3). Positive identification of ^{261}Rf was made by measuring its known half-life and characteristic alpha-decay sequence. Elutions with α-hydroxyisobutyrate solutions from cation-exchange resin columns were used to compare the behavior of ^{261}Rf with No^{2+}, trivalent actinides, Hf^{4+}, and Zr^{4+}. In several hundred repetitive experiments in which 100 atoms were produced for study, the behavior of element 104 was shown to be similar to that of the group 4 elements Zr and Hf, which did not sorb on the column. Its behavior was entirely different from that of No^{2+} and the trivalent actinides that did sorb on the column at pH 4.0.

Some time later, Hulet *et al.* (1980) used ^{261}Rf to perform further experiments to compare the anionic chloride complexes of Rf with those of Hf, Cm, and Fm. Extraction chromatography with a column containing trioctylmethylammonium chloride on an inert fluorocarbon powder was used rather than an ion-exchange resin column because of the faster kinetics. The products recoiling from the nuclear reaction were transported to a fast computer-controlled apparatus that performed the many repetitive experiments necessary to get statistically significant information. The results showed that in 12 M HCl solutions the anionic chloride complexes of Rf and the Hf tracer were strongly extracted by the quaternary amine while the trivalent actinides were not and ran through the column. The chloride complexation of Rf was clearly similar to Hf and much stronger than that of the trivalent actinides, again confirming its position in group 4 of the periodic table. This experiment is especially noteworthy in that it was the first sophisticated, computer-controlled automated system to be used to perform very rapid solution chemistry experiments on an atom-at-a-time basis.

Following these pioneering studies of Rf, a rather long period of time elapsed before additional experiments were conducted in the late 1980s. MCDF calculations (Desclaux and Fricke, 1980; Glebov *et al.*, 1989) indicated that relativistic effects might cause replacement of the expected 6d orbital in Lr by $7p_{1/2}$ orbitals. Spurred by Keller's (1984) extrapolation that Rf might have the configuration $7s^27p^2$ rather than $6d^27s^2$ as expected by analogy to the $5d^26s^2$ configuration of Hf, experimental investigations of relativistic effects in Rf were undertaken. In 1989, Zhuikov *et al.* (1989) examined the volatility of 3-s ^{259}Rf relative to Au, Tl, and Pb tracers in on-line measurements in a quartz column at 1170°C. Under reducing conditions using Ar/H_2 carrier gas, they found that Hf and Rf did not pass through the column while the other elements did. They deduced a lower limit of 370 kJ mol^{-1} for the sublimation enthalpy of metallic 104, much higher than for Pb and other heavy 'p-elements'. Later MCDF relativistic calculations (Glebov *et al.*, 1989; Johnson *et al.*, 1990) indicated that the ground state of Rf is 80% [$6d7s^27p$] while the $7s^27p^2$ state is 2.9 eV above the ground state. Zhuikov *et al.* (1990) and Ryzhkov *et al.* (1992) further concluded that there was no basis for expecting any distinct 'p-character' in the chemical properties of Rf and evaluated various experimental approaches for investigating relativistic effects, including volatilities in the elemental state,

thermochromatography of tetrahalides, and the stability of lower oxidation states. Zhuikov *et al*. warned that gas chromatography experiments that depend on Rf or Hf in the atomic state are not useful for investigating relativistic effects because of the difficulty in stabilizing the atomic states at the temperatures above 1500°C that are needed for chromatography columns. However, they suggested that thermochromatography of the tetrahalides appeared promising.

(b) Gas-phase chemistry

In the late 1980s an international team of scientists from Switzerland, Germany, and the USA studied the gas-phase properties of the tetrahalides of Rf using the automated isothermal systems OLGA (Türler *et al*., 1996) and HEVI (Kadkhodayan *et al*., 1992). The alpha-emitting isotope 75-s ^{261}Rf (see Table 14.3), produced at the LBNL 88-Inch Cyclotron, was used in the experiments and was positively identified by using surface barrier detectors to measure α–α correlations from its known decay scheme. The Zr and Hf activities were identified via gamma spectroscopy. A schematic diagram of HEVI and the arrangement used in some of the gas-phase studies of element 104 tetrachlorides and tetrabromides at LBNL is shown in Fig. 14.14.

The adsorption enthalpies on the SiO_2 surface of the column were calculated from Monte Carlo fits to the measurements of the relative yields as a function of the isothermal temperature between about 100 and 600°C. The Monte Carlo model was introduced by Zvara (1985) and adapted for use with isothermal gas chromatography by Türler (1996). The calculation takes account of the flow rate, half-life of the isotope, temperature, and other variables to generate yield curves as a function of temperature. A rather complete description of this model has been given by Gäggeler (1997). The adsorption enthalpies resulting from the most recent experiments on the tetrabromides (Sylwester *et al*., 2000) are shown, together with those for the tetrachlorides (Kadkhodayan *et al*., 1996), in Fig. 14.15.

Under these conditions, Rf produced volatile $RfCl_4$ at about the same temperature as $ZrCl_4$, indicating their similar volatilities. $HfCl_4$ was unexpectedly less volatile. The analysis of the data using the Monte Carlo model gave the following ΔH_{ads} for group 4 chlorides on SiO_2: –(74 ± 5) kJ mol^{-1} for Zr, –(96 ± 5) kJ mol^{-1} for Hf, and –(77 ± 6) kJ mol^{-1} for Rf (Fig. 14.14). $RfCl_4$ showed about the same volatility as $ZrCl_4$ within the error bars as expected from relativistic calculations (Pershina and Fricke, 1994). 'Nonrelativistic' extrapolations gave lower volatility for $RfCl_4$ (Türler *et al*., 1996). The observation of the relatively high volatily of $RfCl_4$ was a confirmation of the influence of relativistic effects. Experiments with the bromides showed that they are generally less volatile than the chlorides and that $RfBr_4$ is more volatile than $HfBr_4$ (Fig. 14.14), in agreement with theoretical predictions (Pershina and Fricke, 1999). No attempts to measure the volatilities of the fluorides have yet been reported.

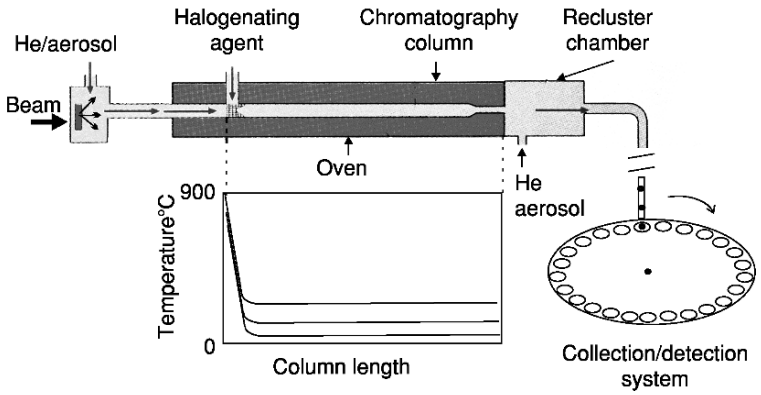

Fig. 14.14 *Schematic diagram of a system used for gas-phase studies is shown. The recoiling products from the reaction are attached to either KCl, KBr, or* MoO_3 *aerosols and transported in He gas to the entrance to HEVI where they were deposited on a quartz wool plug and halogenated at* 900°C. *Volatile products are transported through the quartz column in flowing He gas and are again attached to aerosols and transported in a gas-jet system and deposited on thin polypropylene films placed on the periphery of a horizontal wheel that is rotated so as to position the foils successively between pairs of surface barrier detectors for* alpha *and SF spectroscopy.*

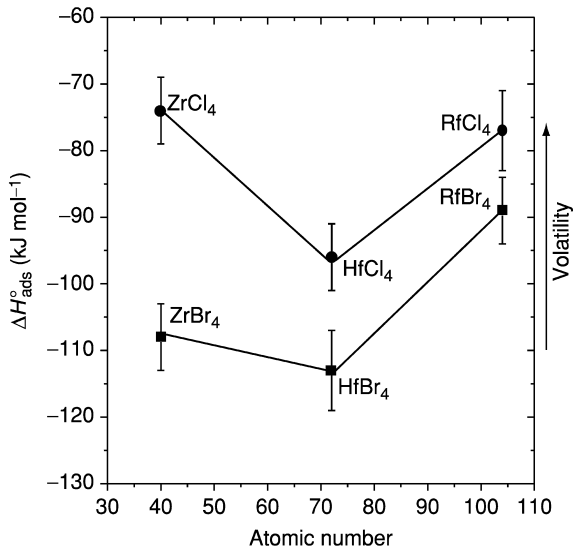

Fig. 14.15 *Adsorption enthalpy values on* SiO_2 *for Zr, Hf, and Rf chlorides and bromides* (*Kadkhodayan,* 1993*; Kadkhodayan* et al., 1996*; Sylwester* et al., 2000).

(c) Solution chemistry

Additional experimental investigations of the solution chemistry of Rf were initiated in the late 1980s. Manual studies to compare the extraction from aqueous solutions into triisooctylamine (TIOA), tri-*n*-butylphosphate (TBP), and TTA of 75-s ^{261}Rf, its lighter homologs Zr and Hf, and the pseudohomologs Th(IV) and Pu(IV) were reported by the Berkeley group (Czerwinski, 1992b; Czerwinski *et al*., 1994a,b; Bilewicz *et al*., 1996; Kacher *et al*., 1996a,b; Hoffman and Lee, 1999). A comprehensive review and summary, as of 1997, of the results from experiments on the extraction behavior of Rf was given by Gregorich (1997a). Later studies used ARCA for repeated chromatographic studies and SISAK for very rapid automated liquid–liquid extractions (Alstad *et al*., 1995; Omtvedt *et al*., 2002).

(*i*) *Extraction of anionic species*

Batch extractions

In repeated manual extractions taking about a min each and using only microliters of each phase, the effect of chloride concentration and pH on extractions into TIOA were investigated. In general, these extractions (Czerwinski *et al*., 1994a,b; Kacher *et al*., 1996a,b) confirmed the earlier results (Hulet *et al*., 1980), showing that Rf generally behaves as a group 4 element, and unlike the trivalent actinides, forms negatively charged complexes in concentrated HCl that are extracted efficiently. Rf is nearly 100% extracted into TIOA from 12 M HCl, as are Zr and Nb, while Th and trivalent actinides and lanthanides are poorly extracted.

Extractions into TIOA/xylene from HF solutions were also performed (Kacher *et al*., 1996b). Although there were some experimental difficulties with the experiments, they clearly showed that Rf was extracted from 0.5 M HF but not from 4 M HF. This was attributed to the extraction of F^- at the higher fluoride concentrations, which complexes all of the TIOA, thus limiting the extraction of the anionic metal fluoride complexes. The extractability of the group 4 elements was found to decrease in the order: Ti > Zr ~ Hf > Rf. This behavior was cited as evidence that the equilibria for the group 4 elements are the same and that Rf is extracted in the chemical form RfF_6^{2-} similarly to Ti, Zr, and Hf, which are extracted as MF_6^{2-} complexes.

Column separations

Pfrepper *et al*. (1998) produced ^{261}Rf and $^{165–169}$Hf isotopes (few-minute half-lives) simultaneously at the Dubna U-400 cyclotron and devised a multi-column technique for continuous on-line processing and detection of ^{253}Es, the long-lived descendant of ^{261}Rf. Using an anion-exchange column with 0.27 M HF/0.1–0.2 M HNO_3 as the eluant, Es was eluted and measured to obtain the K_d values for Rf, which were nearly the same as those for Hf. The ionic charge of

the Rf complex was obtained from measurements of K_d vs. [HNO_3]. The ionic charge was calculated to be –(1.9 ± 0.2), similar to that of Hf, indicating formation of RfF_6^{2-}. This again indicates that Rf is similar to Hf and to other members of group 4. The technique, though extremely complex, ensures that equilibrium has been attained and has the virtue of measuring both Rf and Hf in the same experiment. However, it does not give any additional information about specific differences in the chemical behavior of Rf and of its lighter homologs and pseudohomologs.

Other researchers (Haba *et al.*, 2002) used batch extractions with an anion-exchange resin (CA08Y) to determine K_d values for the Rf homologs Zr and Hf, and the pseudohomologs Th(IV) and Pu(IV) as a function of HCl and HNO_3 concentrations in order to determine appropriate conditions for on-line studies with ^{261}Rf and ^{169}Hf at the same time. They then performed on-line measurements of ^{261}Rf and ^{169}Hf produced in ^{18}O-induced reactions with a ^{248}Cm target containing natural Gd, to study their sorption behavior on this anion-exchange resin in solutions of 1.0–11.5 M HCl and in 8 M HNO_3 using an automated ion-exchange separation apparatus coupled to an alpha-spectroscopy detection system. They found that the adsorption of Rf increased steeply with increasing HCl concentration between 7.0 and 11.5 M, as did the adsorption of Zr and Hf, indicating that like Zr and Hf, anionic complexes such as $Rf(OH)Cl_5^{2-}$ or $RfCl_6^{2-}$ are formed. Their results are consistent with previous experiments with Aliquat 336 (Hulet *et al.*, 1980) and TIOA (Czerwinski *et al.*, 1994a). The adsorption order in the region of 9 M HCl was Rf > Zr > Hf. This behavior is quite different from that of Th(IV), whose distribution coefficients are less than 1 and further decrease in this region. In 8 M HNO_3, more than 80% of Rf, Hf, and Zr were eluted while 99% of the pseudohomolog Th(IV) was retained, indicating that Rf, like Hf and Zr, formed cationic or neutral species, unlike Th(IV) or Pu(IV).

(*ii*) *Extraction of neutral complexes with TBP*

It is well known that TBP extracts neutral complexes by forming adducts with neutral metal salts that are extractable into the TBP organic phase. The adduct is presumed to have the form $ML_4 \cdot xTBP_{(org)}$ where x can be determined by measuring the slope of log K_d as a function of log [TBP]. If the TBP concentration is too high, aggregation of the TBP molecules may give erroneous results. Furthermore, there are very large statistical uncertainties in determination of K_d values when the small number of atoms produced is measured only in the organic phase. The calculation of K_d = (extraction yield)/(1−extraction yield) is probably only accurate for relatively small K_d values because if the K_d values are high the denominator becomes a very small difference between two very similar numbers with large errors. Extractions from HCl into TBP are also unusually dependent on both [H^+] and [A^-], indicating that hydrolysis plays an important role.

Batch extractions

Extractions of ^{261}Rf, Hf, Zr, Th, and Pu into TBP were first studied by Czerwinski *et al*. (1994b) using manual extractions from aqueous solutions of 8, 10, and 12 M HCl, with $[H^+]$ held constant at 8, 10, and 12 M and $[Cl^-]$ adjusted with LiCl to 8, 10, and 12 M. The Zr, Th, and Pu(IV) results were obtained from off-line tracer experiments. In pure HCl solutions, the extraction of Pu, Th, and Zr was nearly 100% at all three molarities, consistent with previously reported (Peppard *et al*., 1956) data for Zr and Th, while extraction of Rf and Hf was low at 8 M and increased to higher values at 10 and 12 M HCl. Extraction of Hf remained lower than that of Rf at all molarities. With $[H^+]$ held at 8 M, an increase in $[Cl^-]$ to 10 and 12 M resulted in significant decreases of both Rf and Pu extraction into TBP/benzene while extraction of Zr, Hf, and Th remained high. This was interpreted as indicating that chloride complexation is stronger for Rf than for Zr, Hf, and Th, and that Rf, similarly to Pu(IV), forms anionic species of the type MCl_6^{2-}, which does not extract into TBP. The trends in extraction yields vs. $[H^+] = 8$, 10, and 12 M for $[Cl^-]$, which are constant at 12 M, show that the Hf yields are independent of $[H^+]$ and remain nearly constant between 75 and 80% while the extraction yields for Rf sharply increase, indicating different extraction mechanisms for Rf and Hf. At the highest $[Cl^-]$ concentrations, the extraction yield for Hf follows that of Th, which does not form anionic chloride complexes, while the trend for Rf follows Pu(IV), which does. Problems with losses of Rf and Hf on Teflon collector foils used in some of the on-line studies resulted in absolute values that were probably too low for the higher K_d values. Nevertheless, much useful information can be obtained from an examination of relative extraction yields.

The extractability decreases in the order Zr > Pu > Rf > Hf > Th for 8 M HCl, in the order Zr > Pu > Rf ~ Th > Hf for 10 M HCl, and in the order Zr ~ Rf ~ Pu > Th > Hf for 12 M HCl. A striking observation that needs to be investigated further is that with $[H^+]$ held constant at 8 M the extraction of Rf increases to ~80% when $[Cl^-]$ is increased to 10 M and then decreases sharply to ~25% when $[Cl^-]$ is increased to 12 M, similar to the extraction of Pu(IV), which decreases to less than 20% while that of Zr remains at ~100% and Hf and Th increase to 80–90%. This would indicate formation of an anionic species of Rf similar to $PuCl_6^{2-}$ and unlike all the other group 4 elements and Th. Extraction as a function of $[H^+]$ between 8 and 12 M with $[Cl^-]$ constant at 12 M indicated little effect on the extraction of Zr and Hf, but the extraction of Rf increased from 25 to ~100%. The extracted complex might be of the type $RfCl_4 \cdot x HCl \cdot y TBP$, where x is 1 or 2, values that have been observed in extraction of other elements into TBP.

Kacher *et al*. (1996a) conducted studies to compare extractions of these elements from HBr solutions into TBP with the results of the previous HCl/TBP experiments. They expected the stability of the bromide complexes to differ from that of the HCl complexes because bromide is a larger and more polarizable anion than chloride. They found that the most likely extracted form of Zr

was $ZrBr_4 \cdot \sim 1TBP$ for the HBr/TBP system and $\sim 2TBP$ for the HCl/TBP system. In general, the extraction of these elements from HBr is much lower than from HCl, and 0.35 M TBP was used to obtain increased extraction. At 9 M HBr, essentially no Rf was extracted but increasing $[Br^-]$ with LiBr to 10, 12, and 13 M resulted in more than 88% extraction of Zr and Rf and ~80% extraction of Th throughout this range while extraction of Pu(IV) increased from about 25 to 70%. In these experiments, Pt collection foils were used to avoid losses of the on-line cyclotron-measured isotopes Rf and Hf. (The Pu tracer was fumed with $NaNO_2$ to make sure it was in the tetravalent state.) Extraction as a function of [HBr] from 7.75 to 9 M HBr solutions was investigated, but without addition of LiBr neither Th nor Rf was extracted. Zr begins to extract at a somewhat lower concentration than Hf, indicating a somewhat stronger tendency to form neutral complexes; Ti extracted only above 9 M HBr. Thus the order of extractability is Zr > Hf >> Ti ~ Rf, a reversal in the trend Zr > Rf > Hf seen in the HCl/TBP extractions. Experiments to examine the extraction at concentrations up to 12 M HBr are necessary to confirm this trend.

Column experiments

In order to check and resolve some of the differences in the previously reported results for the TBP/HCl system, Brüchle *et al*. (1998) and Günther *et al*. (1998) measured K_d values for the TBP/HCl system for the carrier-free radionuclides ^{98}Zr (from fission), and ^{169}Hf and ^{261}Rf produced on-line at the Paul Scherrer Institute (PSI) cyclotron. The recoiling products were transferred via He(KCl) jet to ARCA II whose 40 microchromatographic columns (1.6-mm diameter × 8-mm long) were filled with the inert support Voltalef™ (Lehmann & Voss, Hamburg, Germany) coated with undiluted TBP. The use of undiluted TBP is expected to shift the complete extraction of both Zr and Hf to higher HCl concentrations, as shown earlier (Czerwinski *et al*., 1994b), and prior batch experiments from >10 M HCl confirmed this. From 8 M HCl, 80% Zr and only 20% Hf extraction was found. Chromatographic separations of Zr and Hf were then conducted with ARCA. The radioactive ions were sorbed from 12 M HCl. Most (75%) of the Hf and no Zr were eluted with 8 M HCl and then the remaining Hf and Zr were stripped with 2 M HCl. The K_d for Hf was calculated to be 53 from the relationship, $K_d = [(100)(\%aq)^{-1}–1][vol_{aq}/vol_{org}]$, consistent with batch measurements. Subsequent experiments to determine the K_d for Rf in 8 M HCl were conducted at the PSI cyclotron in the same way. After 90 s collection times, the reaction products were sorbed on the columns in 12 M HCl. Hf and Zr fractions were eluted with 8 and 2 M HCl, respectively, and analyzed for alpha decays from ^{261}Rf and its daughter ^{257}No. Two α–α mother–daughter correlations were observed in the Hf fraction and three in the Zr fraction, indicating that Rf extraction is somewhere between that of Hf and Zr in 8 M HCl. After lengthy and complex considerations of contributions from random and background effects, they (Günther *et al*., 1998) concluded that the K_d for Rf is 150 compared to the K_d of 1180 for Zr and of 60 for Hf obtained

from the batch experiments with 8 M HCl, giving the order of decreasing extraction Zr > Rf > Hf. The percentage extraction in their work, 52% for Rf and 25% for Hf from 8 M HCl, appears to be consistent with that of ~60% for Rf and ~25% for Hf obtained by Czerwinski *et al.* (1994b). In a detailed discussion of corrections for the differences in volumes used in the two studies and the dependence of the equilibrium constant on the differences in the TBP concentrations in the organic phase, they finally concluded that Czerwinski's K_d values for Hf and probably for Rf are significantly too low (probably due to sorption on the Teflon collection foils), but that their K_d values were also lower than expected for undiluted TBP because of aggregation effects.

Thus it appears that measurements of relative extractability can be obtained for experiments carried out under exactly the same conditions, but that determination of absolute K_d values is subject to numerous difficulties. The inconsistencies in the K_d results reported by various researchers are probably due in large part to differences in the exact details of the experimental conditions and can greatly affect the measurements, as pointed out above. In addition, results of on-line experiments for the transactinides often are compared with results of off-line tracer studies of their homologs. Furthermore, in the very rapid separations with ion-exchange resin columns required in the study of short-lived isotopes it is necessary to make sure that equilibrium is attained in order to obtain valid results. Some evidence of non-equilibrium effects was reported by Paulus *et al.* (1999) for most amines other than Aliquat 336 and will require further study. Care must be taken in batch experiments to remove any fluoride ion that may have been present in stored tracer solutions. Kacher *et al.* (1996b) found that fluoride ion concentrations as low as 0.02 M reduced the K_d values for extraction into TBP from HBr by about 2 for Hf and 10 for Zr.

(*iii*) *Extraction of fluoride complexes*

Cationic complexes

The fluoride complexation of Zr, Hf, ^{261}Rf, and Th in mixed HNO_3/HF solutions was investigated (Strub *et al.*, 2000) by studying K_d values for both anion- and cation-exchange resins using ARCA. A detailed study of the complexation as a function of fluoride- and nitrate-ion concentrations was performed. They found all four elements to be strongly sorbed on the cation-exchange resin Aminex A6 at HF concentrations below 0.001 M. The K_d values for Zr and Hf decreased between 0.001 and 0.01 M HF, presumably due to the formation of fluoride complexes. Those for Rf and Th decreased at an order of magnitude higher HF concentrations, and the K_d for Rf remained very high even in 0.01 M HF. The K_d for Rf was found to be >148 in 0.1 M HNO_3/5×10^{-4} M HF while under these conditions ^{265}Sg had been found to elute (Türler *et al.*, 1998a). As discussed in Section 14.5.3c (Eqs. 14.1 and 14.2) at [HF] < 0.01 M, positively charged complexes of higher charge will be formed, which will sorb on the cation resin. The observed order of sorption Rf > Hf ≥ Zr

corresponds to the opposite trend in the complex formation, as discussed in Section 14.5.3c, in agreement with theoretical predictions.

Anionic complexes

Trubert *et al.* (1999) determined distribution coefficients for Zr, Hf, and Rf on the macroporous anion exchanger Bio-Rad (Bio-Rad Laboratory, Hercules, CA, USA) AG® MP-1 from HF/HCl media with concentrations between 0.02 M and concentrated HF and [HCl] $\leq$ 0.8 M. They used batch experiments with Zr and Hf tracers and examined the K_d values as a function of free H^+, Cl^-, and F^- species in solution. They performed on-line column experiments using their automated system at the tandem accelerator at Orsay where ^{261}Rf and ^{167}Hf were produced.

A rather complicated two-column technique (Pfrepper *et al.*, 1998) was used in which the Rf or Hf parents were partially sorbed on a first anion-exchange resin column and the remainder plus the trivalent decay products Fm and Lu are sorbed on a subsequent cation-exchange resin column. One-hour irradiation times were used and the longer-lived ^{253}Fm–^{253}Es granddaughters of ^{261}Rf were finally measured to deduce the K_d for Rf. The one K_d value for Rf obtained for 0.02 M HF/0.4 M HCl was slightly higher than those for Zr and Hf, respectively, in agreement with the theoretically predicted trend Rf $>$ Hf $\geq$ Zr (Section 14.5.3c), but more data are needed before any conclusions can be drawn.

An increase in K_d values for Zr and Hf was observed by Strub *et al.* (2000) with the anion-exchange resin (similar to Bio-Rad AG®1-X8) and solutions between 0.001 and 0.01 M HF, consistent with the observation of decreasing values in the HF range for the cation-exchange resin. Surprisingly, the results of the experiments showed that again Rf and Th behaved differently from Zr and Hf and did not show the high K_d values expected for anionic fluoride complexes even at HF concentrations as high as 1 M. Rf seemed to resemble Th rather than Zr and Hf, which was different from the theoretical predictions (Pershina *et al.*, 2002b). There were indications that the action of the counter-ion was responsible for the unexpected behavior, and by varying the NO_3^- concentration Strub *et al.* (2000) were able to show that Rf did form anionic species, but apparently NO_3^- competed more effectively than F^- for the binding sites on the anion resin. Additional experiments are needed to investigate the effect of varying [NO_3^-] at constant [F^-] and varying [F^-] at much lower [NO_3^-].

(*iv*) *Extraction of cationic complexes*

TTA batch extractions

The chelating agent TTA extracts cationic species from aqueous solutions. Its electron donor groups are oxygen atoms and the tendency for different metals to be extracted is a measure of their affinity for oxygen atoms. This affinity should have a strong correlation with the log of the first hydrolysis constants of the metal ions. Thus TTA can be used to obtain information about hydrolysis of the group 4 ions.

The Berkeley group (Czerwinski, 1992b) performed some preliminary measurements of the extraction of the group 4 elements, Th, and Pu from 0.1 and 0.4 M HCl into 0.5 M TTA/benzene. The initial measurements gave K_d values, decreasing in the order Zr > Hf ~ Pu > Rf > Th, similar to the decreasing values of the logs of the first hydrolysis constants that have been measured for Zr, Hf, Th, and Pu (Baes and Mesmer, 1976). These extraction results are discussed by Gregorich (1997b), who states that on this basis the tendency for Rf to hydrolyze should be between that for Th and Pu and less than that for Zr and Hf. This prediction is in agreement with the theoretical calculation for the hydrolysis of group 4 elements (Pershina *et al.*, 2002b). However, more tracer measurements of the effect on extraction as a function of [HCl] and [TTA] are needed to determine if the equilibria involved in the extraction of Pu and Th are the same as for the group 4 elements. The kinetics of TTA extractions are relatively slow so they may not be the best choice for rapid separations of short-lived species.

HDBP extractions with SISAK

The SISAK microcentrifuge liquid–liquid extraction system described in Section 14.3.3b was used to study extraction of 4.7-s ^{257}Rf [1] from 6 M HNO_3 and 0.25 M dibutylphosphoric acid (HDBP) in toluene. ^{257}Rf was produced at the LBNL 88-Inch Cyclotron in the ^{208}Pb(^{50}Ti,n) reaction, with a cross section of ~10 nb.[1] In preliminary test experiments, ^{257}Rf was pre-separated in the BGS, which reduced unwanted background activities by more than three orders of magnitude, and then transferred to the specially designed Recoil Transfer Chamber (RTC) attached at the BGS focal plane (Kirbach *et al.*, 2002). The Rf ions passed from the BGS detector chamber (held at a pressure of only 1.3 mbar) through a thin Mylar window into the RTC containing He gas whose pressure could be varied from 480 to 2000 mbar, as appropriate, to stop the separated ions. The positive identification of Rf atoms entering the RTC was accomplished by measuring their α decay with an array of Si-strip detectors and six to seven ^{257}Rf–^{253}No α–α correlations per hour were found in these experiments. They were then sorbed on aerosols in a He/KCl gas-jet system and transported without chemical separation directly to the SISAK liquid scintillation detection cells. The transport time was measured with $^{170-x}$Hf isotopes (half-lives > 1 min) produced at the same time in ^{120}Sn(^{50}Ti,xn) reactions. An alpha event in the appropriate preset energy range caused the cell to close and to switch to daughter mode. The cell remained closed for more than five ^{253}No ($t_{1/2}$ = 1.6 min) daughter half-lives. In this way an α–α correlation matrix was successfully obtained and clearly showed that the SISAK liquid scintillation system could detect nuclides at a rate of less than one atom per hour. A number

[1] ^{257}Rf has been reported (Hessberger *et al.*, 1997) to have a metastable state with a half-life of ~4.0 s from which ~60% of the α-decay is estimated to originate and a ground state that α-decays with a half-life of ~3.5 s, but this has not yet been confirmed. Both decay primarily by α-emission so for the purposes of this experiment it makes very little difference.

of other important improvements including pulse-shape discrimination to reduce the beta-background, real-time scintillation yield monitoring by continuous measurement of the Compton edge of ^{137}Cs γ-rays, and improvements in the detection cell efficiencies were also made. Experimental details of the system have been published (Omtvedt *et al.*, 2002). The pre-separation thus permits designing studies of the chemical properties of Rf without the necessity for adding time-consuming and yield-loss steps to remove radioactive isotopes that would interfere with its detection and measurement.

After this successful demonstration, liquid–liquid extraction experiments were performed to compare the extraction behavior of Rf from 6 M HNO_3 into 0.25 M HDBP/toluene with that of its lighter homologs Zr and Hf. A schematic diagram of the setup is shown in Fig. 14.16. The activity-containing aerosols in the He jet are dissolved in the 'de-gasser' centrifuge containing 6 M HNO_3 and the He gas is removed. The main extraction is performed in the next centrifuge. An important step is to wash any dissolved HNO_3 from the organic phase before adding the scintillator ingredients because the acid will cause degradation of the energy resolution, as will any O_2. It is removed by sparging with He, which is removed in the last centrifuge. Flow rates of the order of 0.4–0.8 ml s^{-1} were used and the centrifuges typically operate at 25000–40000 rpm. This was the first time a transactinide, Rf, was extracted and unequivocally identified by the SISAK liquid scintillation system and demonstrates that this method can be used to investigate the chemical properties of the transactinides. The results indicate that Rf behaves similarly to Zr and Hf, as expected. In this demonstration, the conditions were chosen to maximize extraction of Rf and the other group 4 elements rather than to investigate possible differences among them. The next step will be to use the pre-separation technique to conduct experiments with chemical systems designed to distinguish differences in the behavior of individual elements within a periodic table group.

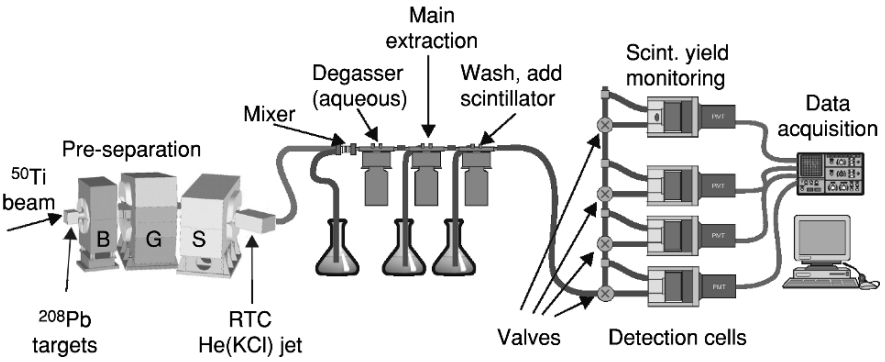

Fig. 14.16 *Schematic diagram of a typical SISAK liquid–liquid extraction configuration with BGS as a pre-separator.*

14.6.2 Chemistry of dubnium/(hahnium) (105)

As discussed in Section 14.5 and shown in Tables 14.4–14.6, the ground state configuration for element 105 is predicted to be $6d^37s^2$ although the relativistic destabilization of the 6d electrons and the close proximity of the 7s and 6d levels should stabilize the higher oxidation states of the 6d elements relative to their 5d homologs. Thus, the most stable oxidation state of Db is expected to be 5+ and the 3+ and 4+ states are even less stable than in its lighter homolog Ta.

(a) Historical

In the only published studies of the early chemistry of element 105, Zvara *et al.* (1974, 1976) reported investigations of the volatilities of the chlorides and bromides of element 105 with 1.8-s ^{261}Db compared to those of Nb and Hf. They used a thermochromatographic system similar to that used in the studies of Rf. Again, they detected SF events from the SF branch in mica track detectors placed along the chromatography column. After corrections for the much shorter half-life of ^{261}Db, the distribution of the fission tracks was compared with the adsorption zones of the tracers (3.3-min ^{169}Hf and 14.6-h ^{90}Nb). From these experiments, Zvara *et al.* concluded that the volatility of Db bromide was less than that of Nb bromide and about the same as that of Hf bromide. Again, only SF events were detected and because the SF branch ($\leq$18%?) is still not well known, it is not certain that the detected fissions belonged to element 105. A complete discussion of these early results was given by Hyde *et al.* (1987), who interpreted these results as indicating that Db behaved more like the group 4 element Hf than like Nb and Ta.

(b) Solution chemistry

No further studies of element 105 chemistry were reported until 1988 when Gregorich *et al.* (1988) reported the very first study of its behavior in aqueous solutions. These experiments were undertaken simply to show whether its most stable oxidation state in aqueous solution was 5+. At that time it had been postulated (Keller, 1984) that Ha might have a $7s^26d7p^2$ rather than a $6d^37s^2$ valence configuration expected by analogy with Ta, whose most stable state in aqueous solution is 5+. The α-emitting, 35-s ^{262}Db (then called Ha), produced in the reaction of ^{18}O with the radioactive target, 320-d ^{249}Bk (see Table 14.3) at the LBL 88-Inch Cyclotron, was used. The recoiling reaction products attached to KCl aerosols were transferred from the target system and outside the cyclotron shielding via a He gas-jet system to a 4-position collection site in a fume hood located outside the radiation area. Here very simple 'manual' chemistry was performed using only a few microliters of solution. The sorption of Ha on glass cover slips after fuming twice with concentrated nitric acid and washing

with 1.5 M HNO_3 was compared with that of tracers of the group 5 elements Nb and Ta and with the group 4 elements Zr and Hf produced on-line under similar conditions. These group 5 elements are known to sorb on glass surfaces while the group 4 elements do not. Measurements of the energy and time distribution of the alpha decay and of time-correlated pairs of alphas from ^{262}Db and its 4-s daughter ^{258}Lr were recorded and analyzed to provide positive identification that element 105 was detected. Some 800 manual extractions taking about 50-s each were performed and a total of 26 alpha and 26 SF events were recorded. Element 105, like its group 5 homologs Nb(V) and Ta(V), was found to sorb on the glass surfaces while Zr and Hf and the trivalent actinides did not. This confirmed the group 5 character of Ha and demonstrated that it properly belonged in the periodic table as the heaviest member of group 5. Its extraction behavior into methylisobuytlketone from mixed HNO_3/HF solutions under conditions in which Ta was extracted but Nb was not was also investigated (Gregorich *et al.*, 1988). Surprisingly, it was found that element 105 did not extract and that its behavior was more like Nb than Ta, indicating that details of complexing behavior cannot be predicted based only on simple extrapolations of trends within a group in the periodic table. This behavior was explained much later (Pershina, 1998b), as discussed in detail in Sections 14.5.3b and 14.5.3c.

This surprising result provided the impetus for further exploration of the complex behavior of element 105. Chromatographic experiments using ARCA II to carry out the thousands of required repetitive experiments were performed jointly by the GSI/Mainz, PSI/Bern, and LBL/Berkeley groups in 1988, 1990, and 1993 at LBL, and in 1992 at GSI. In the first extraction chromatography column separations with the anion exchanger TIOA on inert supports, all the group 5 elements and Pa(V) were extracted from concentrations of HCl > 10 M. At lower concentrations of HCl, small amounts of added HF gave selective back extraction, showing different chemical behavior for these elements (Kratz *et al.*, 1989; Zimmermann *et al.*, 1993). Element 105 showed a marked non-Ta-like behavior at concentrations below 12 M HCl and follows the behavior of Nb and the pseudohomolog Pa(V). Because of this similarity to Nb and Pa, it was concluded that the complex was $DbOX_4^-$ or $[Db(OH)_2X_4]^-$. ARCA was also used to investigate the extraction of Db from HBr into diisobutyl carbinol (DIBC), a specific extractant for Pa, with subsequent elutions with mixed HCl/HF and HCl. The extraction sequence Pa > Nb > Db was obtained and attributed to the increasing tendency to form non-extractable polynegative complexes (Gober *et al.*, 1992). Due to the difficulties encountered in the theoretical interpretation of the results of these experiments because of the small amounts of HF added to the various halide solutions (long recommended for reducing hydrolysis of group 5 elements to prevent them from unwanted sorption on containers, etc.), it was recommended that future experiments be carried out in pure rather than mixed halide solutions (Pershina, 1998b).

Experiments conducted with ARCA also showed that Ha was eluted promptly from cation-exchange columns with α-hydroxyisobutyrate (Kratz *et al.*, 1992;

Schädel *et al.*, 1992) together with Nb, Ta, and Pa, whereas trivalent and tetravalent ions were retained, again confirming that Ha is most stable in aqueous solution as a pentavalent species. The new isotope 27-s ^{263}105 was also identified in these experiments.

Subsequently, Pershina (1998b) and Pershina and Bastug (1999) predicted the sequence Pa >> Nb ≥ Db > Ta for extraction into the anion exchanger TIOA from halide solutions. Paulus *et al.* (1999) remeasured K_d values for Nb, Ta, and Pa in new batch extraction experiments with the quaternary ammonium salt Aliquat-336 and pure HCl, HBr, and HF solutions. New chromatographic column separations with ARCA II were then conducted to study chloride and fluoride complexation separately. The Aliquat-336/HCl experiments confirmed the extraction sequence Pa >> Nb ≥ Db > Ta, as theoretically predicted. In the Aliquat 336/HF system the K_d value for element 105 in 4 M HF was >570, close to those for Nb and Ta of >1000 and different from that of ~10 for Pa.

In his review of transactinide chemistry, Kratz (1999b) discussed all the results for the ARCA experiments on element 105 in detail and concluded that the amine extraction behavior of dubnium halide complexes is always close to Nb, consistent with the predicted inversion of the trend in properties between the 5d and the 6d elements. In pure HF solution, Db differs most from Pa, and in pure HCl solution, it differs from both Pa and Ta. In mixed HCl/HF solutions, it differs markedly from Ta. The experimental results are in agreement with the calculated Gibbs energy changes (see Section 14.5.3c) of 12, 20, and 22 eV for the reactions for complex formation (Pershina *et al.*, 2002b) of the fluorides, chlorides, and bromides, respectively. For example, the equilibrium between hydrolysis and halogenation always favors formation of an extractable fluoride complex rather than the hydrolyzed species even at very low HF concentrations, whereas [HCl] > 3 M is required for formation of extractable chloride complexes, and [HBr] > 6 M is required for the formation of extractable bromide complexes.

(c) Gas-phase chemistry

The first on-line isothermal gas chromatography experiments were performed by an international group (Gäggeler *et al.*, 1992; Türler *et al.*, 1992) using OLGA II with 35-s ^{262}Db. The volatile species were deposited on a moving tape that was subsequently stepped in front of six large-area-passivated implanted planar Si detectors to measure alpha particles and SF events to identify element 105. From the yields as a function of isothermal temperature measured for the bromides of Nb, Ta, and Db, adsorption enthalpies of –88, –94, and –155 kJ mol^{-1}, respectively, were obtained from least-squares fits of Monte Carlo simulations to the isothermal yield curves. Within the error limits, the adsorption enthalpies (volatilities) are nearly the same for Nb and Ta, but Db appears to be significantly less volatile. It was postulated that traces of oxygen in the system might have led to formation of the oxytribromide of Db,

which was predicted to be less volatile than the pentabromide (Pershina *et al*., 1992b), and Db was also predicted to have a much stronger tendency to form oxyhalides than Nb or Ta, as discussed in Section 14.5.2b.

Investigations (Kadkhodayan *et al*., 1996; Türler, 1996) of the volatility of the chlorides of the group 5 elements showed that they were more volatile than their respective bromides, with element 105 being similar to Nb, but for Ta, only a species with much lower volatility, presumably $TaOCl_3$, was observed. In more recent experiments conducted by Türler *et al*. (1996) the volatilities of Db and Nb chlorides were studied as a function of controlled partial pressures of O_2. It was shown that the concentrations of O_2 and oxygen-containing compounds were extremely important in determining whether or not the oxychlorides were formed and in determining the resultant volatilities of the Nb and Db compounds. The results showed that for pO_2 between 1 ppm (vol.) and 80 ppm (vol.) both a volatile species and a less volatile species, presumably MCl_5 and $MOCl_3$, were formed in about equal amounts. The more volatile species, $NbCl_5$, was shown to be the major component at $pO_2 \leq 1$ ppm (vol.). Subsequent experiments with Db were conducted under similar conditions and a two-step yield curve was obtained indicating that both $DbCl_5$ and $DbOCl_3$ were present. Adsorption enthalpies of –80 and –99 kJ mol^{-1} for the Nb species and –98 and –117 kJ mol^{-1} for the Db species were deduced, indicating that the Db species are less volatile than those of Nb. As predicted, the oxychlorides are less volatile than the chlorides, but the experiments need to be extended to lower temperatures for Db with pO_2 kept as low as possible to see if $DbCl_5$ can be measured as a single component, and the measurements need to be extended to Ta.

14.6.3 Chemistry of seaborgium (106)

(a) Historical

Early attempts were made to study the chemistry of Sg using 0.9-s ^{263}Sg produced in the $^{249}Cf(^{18}O,4n)$ reaction at the U-400 cyclotron at Dubna (Timokhin *et al*., 1996; Yakushev *et al*., 1996). Recoiling reaction products were thermalized and carried in Ar gas from the target chamber into a fast on-line TC consisting of a 3.5 mm i.d. by 120 cm long tube of fused SiO_2 where air saturated with $SOCl_2$ was used as a chlorinating agent. The inner surface of the silica column served as a solid-state detector for SF events. In two experiments, Timokhin *et al*. (1996) found a total of 29 fission tracks in zones in the temperature region of 150–250°C, close to the deposition temperature of 16-s ^{166}W. No tracks were found in the start zone or outside the indicated region while alpha activities from actinide products were seen mostly in the start zone. They claimed that this was the first chemical identification of element 106 as SgO_2Cl_2 and that it formed an oxychloride similar to that of W. However, the assignment of the fissions to element 106 based on detection of a small

fission branch of ^{263}Sg is uncertain because it was not shown that the observed fissions did not belong to elements 104 or 105. Kratz (1999b) gave a detailed critique of the Timokhin reports and concluded that their conclusions were not justified.

The discovery by a Dubna–Lawrence Livermore National Laboratory (LLNL) collaboration (Lazarev *et al*., 1994; Lougheed *et al*., 1994) of the longer-lived isotopes ^{266}Sg and ^{265}Sg in ^{248}Cm(^{22}Ne,4n,5n) reactions with cross sections of ~80 and 260 pb for 116 and 121 MeV ^{22}Ne projectiles, respectively, made chemical studies of element 106 much more feasible. These new isotopes were separated and identified using the gas-filled recoil separator at the Dubna U-400 cyclotron. The partial alpha half-lives of 2–30 s for ^{265}Sg and 10–30 s for ^{266}Sg had to be estimated from the measured alpha-decay energies because the time intervals between the Sg isotopes and their Rf daughters were not measured as the signals from the implanted Sg isotopes were below the threshold of their detector system. On-line procedures for studying the chemistry of element 106 with both OLGA and ARCA were developed using W and Mo, the presumed lighter group 6 homologs of element 106.

(b) Gas-phase chemistry

Theoretical predictions (Pershina and Fricke, 1996) based on relativistic MO calculations indicated that SgO_2Cl_2 was the most stable of the Sg oxychlorides. Based on this prediction, the gas-phase chromatography experiments discussed in Section 14.5.2b were conducted under conditions designed to study and identify SgO_2Cl_2. The trend in volatilities of these oxychlorides within group 6, which was predicted using relationships between molecular properties such as covalence or dipole moment and volatility, was $MoO_2Cl_2 > WO_2Cl_2 > SgO_2Cl_2$. Eichler *et al*. (1999) estimated the thermochemical quantities for chlorides, oxychlorides, and oxides of Sg by extrapolation. By the use of empirical correlations, they also found SgO_2Cl_2 to be the most suitable compound for the gas-phase chemistry experiments and expected its standard sublimation enthalpy to be between 125 and 144 kJ mol^{-1}, resulting in an adsorption enthalpy between –97 and –108 kJ mol^{-1} and less volatile than its W homolog.

OLGA III was used in experiments to study the behavior of fission-product Mo isotopes and short-lived W isotopes produced at the PSI Philips cyclotron in preparation for studies of element 106 (Gärtner *et al*., 1997). The reactive gas mixture O_2, Cl_2, and $SOCl_2$ at 900°C was used; adsorption enthalpies of −90 and −100 kJ mol^{-1} were measured for MoO_2Cl_2 and WO_2Cl_2, respectively, in agreement with predictions. The isothermal yield curve was measured for 58-min ^{229}U produced in the ^{232}Th(α,7n) reaction and the resulting adsorption enthalpy of −91 kJ mol^{-1} was interpreted as indicating formation of UCl_6.

The first chemical experiments on Sg were conducted in 1995 and in 1996 at the Universal Linear Accelerator (UNILAC) at GSI using the ^{248}Cm

(^{22}Ne,4n,5n) reactions to produce ^{266,265}Sg. The reaction products recoiling out of the target were thermalized in helium gas containing carbon aerosols ($\sim 0.1 - 1$ μm diameter, generated using a spark discharge generator). In about 3 s, the flowing helium gas continuously transported the reaction products attached to the carbon aerosols through a capillary to a quartz wool plug in the reaction chamber (900–1000°C) at the inlet of OLGA III. There the reactive chlorinating gas consisting of O_2, Cl_2, and $SOCl_2$ was added to form volatile compounds, which were transported through the 1.5-mm i.d. × 1.8 m long isothermal quartz chromatography column to a recluster chamber where the chemically separated volatile Sg compounds were again attached to aerosol particles. They were transported within about 6 s to a rotating wheel system and collected on thin polypropylene foils placed in the 64-collection positions located around the periphery of a wheel that was stepped every 10 s to move the collected activity consecutively between pairs of Passivated Ion-implanted Planar Silicon (PIPS) detectors for measurement of alpha and SF activities. The times, energies, and positions of all events were recorded in list mode by a computer. A mother–daughter stepping mode was used to avoid interference from 45-s ^{212}Po^{m} contamination in the alpha energy region of interest (8.8 MeV). In this mode every other position on the 64-position wheel was left empty. When an alpha particle with the decay energy of ^{265,266}Sg was detected in a bottom detector, the daughter Rf nucleus was assumed to have recoiled out of this aerosol deposit onto the top detector. This initiated the daughter mode, causing a single step that positioned the empty collection sites between the detector pairs. The system waited for 2 min to permit the Rf daughter on the detector to decay in an environment clean of contamination. In the first experiment, two decays of ^{265}Sg were identified in daughter mode, one triple correlation was observed in parent mode, and one $\alpha-\alpha$ correlation from ^{266}Sg–^{262}Rf was recorded (Schädel *et al.*, 1997a).

The isothermal temperature was varied in the second experiment conducted in 1996 (Türler *et al.*, 1999) to obtain the adsorption enthalpy for Sg. The experimental conditions were similar except that a 200 s wait in the daughter mode was used. The yield of short-lived W isotopes produced from ^{22}Ne reactions with ^{152}Gd incorporated in the ^{248}Cm target was measured with a high-purity Ge detector and used to monitor the yield of the chemical separation. An adsorption enthalpy of $-(96 \pm 1)$ kJ mol^{-1} was obtained for $^{168}WO_2Cl_2$, in agreement with the previous measurement. The isothermal yield curves obtained for SgO_2Cl_2 along with those for the Mo and W compounds are shown in Fig. 14.17. Based on detection of 11 events attributable to Sg, an adsorption enthalpy of $-(100 \pm 4)$ kJ mol^{-1} was derived. Adsorption enthalpies of $-(90 \pm 3)$ kJ mol^{-1} and $-(96 \pm 1)$ kJ mol^{-1} were obtained for Mo and W oxychlorides, respectively. Thus the volatility sequence is $MoO_2Cl_2 > WO_2Cl_2 > SgO_2Cl_2$, as theoretically predicted. Türler *et al.* (1998a) analyzed the decay properties of the 13 correlated chains of ^{265}Sg and ^{266}Sg observed in these experiments and recommended the following half-lives and cross sections for

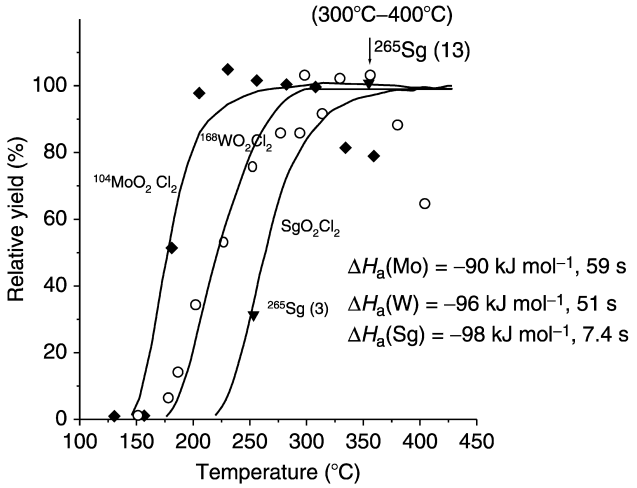

Fig. 14.17 *Relative yields vs. isothermal temperatures for* MoO_2Cl_2 (*solid diamonds*), WO_2Cl_2 (*open circles*), *and* SgO_2Cl_2 (*solid triangles*). (*Data from Türler* et al., 1999).

^{22}Ne energies between 120 and 124 MeV: ^{265}Sg, $t_{1/2} = 7.4^{+3.3}_{-2.7}$ s, cross section ~240 pb; ^{266}Sg, $t_{1/2} = 21^{+20}_{-12}$ s, cross section ~25 pb.

Hübener *et al.* (2001) reported that Sg forms volatile oxide-hydroxides similar to those of U and the group 6 elements Mo and W. They used high-temperature on-line isothermal gas chromatography with quartz columns to study Sg and W in the O_2–H_2O(g)/SiO_2 system. ^{266}Sg, produced as above, was transported in a He/MoO_3 gas-jet system into the chromatography system. Group 6 elements formed oxide-hydroxides that were volatile at a temperature of 1325 K upon addition of O_2. ^{266}Sg was unambiguously identified by measuring its decay chain. They postulated a dissociative adsorption and associative desorption process to explain their results.

(c) Solution chemistry

The first successful studies of the chemical properties of Sg in aqueous solution were reported by Schädel *et al.* (1997a,b) using ^{265,266}Sg produced in the reaction of 121 MeV ^{22}Ne projectiles with ^{248}Cm targets of 0.15 mg cm^{-2} in the first experiment and 0.95 mg cm^{-2} in the second experiment at the UNILAC at GSI. The emphasis in these experiments was on rapid preparation of samples for alpha spectroscopy with decontamination from the high-energy Bi and Po alpha activities and of trivalent actinides, and efficient separation of the Rf and No daughter activities from Sg. If these conditions are met, Rf and No isotopes observed later in the chemically separated Sg fraction can be presumed to be daughters of Sg precursor nuclei. A system with anionic or possibly neutral oxy- and oxyfluoride compounds was chosen because the formation of neutral and

anionic complexes with F^- ions is a characteristic property of group 4, 5, and 6 elements, with distinct differences between the behaviors of the three groups. Based on previous on-line tracer experiments, a solution of 0.1 M HNO_3/5 × 10^{-4} M HF was used to elute the activity from the columns of the cation-exchange resin Bio-Rad AG Aminex A6. The recoiling activities attached to KCl aerosols were swept from the recoil chamber with He gas into a capillary and transported in flowing He some 18 m to ARCA II where they were collected, dissolved, and fed into the 1.8-mm i.d. × 8-mm chromatographic columns filled with the cation-exchange resin Aminex A6. The transport and collection efficiency of about 45% was monitored frequently by checking the production rate of $^{252-255}$Fm isotopes of known cross section. Although the mean separation time of Sg from Rf and No took only 5 s, the evaporation of the eluted samples took about 20 s and on the average, α-particle and SF measurements using a system of eight PIPS detectors were not begun until 38 s after the end of the collection. The energies, times, and detector positions were recorded in list mode on a magnetic disk and tape for later data analysis and identification of the Sg isotopes. Collections times of 45 s were used for most of the 3900 collection and elution cycles. Observation of three correlated α−α events identified as the ^{261}Rf(78 s)→^{257}No(26 s)→decay sequence indicated the decay of ^{265}Sg in the chemically separated Sg fractions. From this observation, it was concluded that Sg behaved as a typical hexavalent group-6 element as did W studied previously in similar on-line experiments. This indicated the formation of SgO_2F_2 by analogy to its Mo and W homologs and showed behavior different from the pseudohomolog U(VI), which remained on the column, presumably as UO_2^{2+}.

An investigation of the fluoride complexation of Zr, Hf, Rf, and Th in mixed HNO_3/HF solutions was undertaken (Strub *et al.*, 2000) to verify experimentally that under the conditions of the first experiments on the solution chemistry of Sg using ARCA, ^{261}Rf would not be eluted from the cation-exchange resin. These detailed studies of sorption on both cation- and anion-exchange resins using ARCA confirmed the validity of the assumption in the Sg experiments that Rf would remain on the Aminex A6 cation-exchange resin column. Therefore, it was concluded that Rf could only have been in the Sg fraction as a result of the alpha decay of 7-s ^{265}Sg.

A new series of 4575 experiments was conducted (Schädel *et al.*, 1998) with ARCA using the same Aminex A6 cation-exchange resin to determine if Sg would form SgO_4^{2-} under the same conditions as before if fluoride ions were not present. The activity was dissolved in 0.1 M HNO_3 without any HF; subsequent analysis of the effluent showed that Sg still remained on the column while W was eluted with 0.1 M HNO_3. This non-tungsten-like behavior of Sg was tentatively attributed to its weaker tendency to hydrolyze in dilute HNO_3 so that its hydrolysis stopped at $M(OH)_4(H_2O)_2^{2+}$ or $MO(OH)_3(H_2O)_2^+$ while hydrolysis of Mo and W proceeded to the neutral species $MO_2(OH)_2$. Thus, in the previous experiments in the presence of fluoride ions, Sg might have been eluted from the

cation-exchange column as neutral or anionic fluoride complexes of the type SgO_2F_2 or $SgO_2F_3^-$ rather than as SgO_4^{2-}.

This hypothesis has been examined theoretically by considering hydrolysis of group 6 elements, as described in Sections 14.5.3b and 14.5.3c. The calculations (Pershina and Kratz, 2001) show that between a pH of 0 and 1, Sg forms complexes with charges of 1+ or 2+ while W forms neutral complexes. Hydrolysis of group-6 elements proceeds even faster at higher pH and a reversal of the trend in group-6 should be observed at pH > 4 (see Section 14.5.3b). Theoretical considerations of complex formation in HF solutions (Pershina *et al.*, 2002b) indicate that it competes with hydrolysis in aqueous solutions, that the dependence on pH and HF concentrations is very complicated, and that reversals of the trends occur. Further experiments can be planned based on the theoretical predictions that cover a wide range of pH values. These reversals of trends among the group 6 elements and U(IV) should be investigated experimentally.

14.6.4 Chemistry of bohrium (107) and hassium (108)

(a) Bohrium

The isotope, 17-s ^{267}Bh (Wilk *et al.*, 2000), produced in the ^{249}Bk(^{22}Ne,4n) reaction, was used in studies to compare the volatility of the oxychloride of Bh with those of its group 7 homologs Re and Tc in on-line isothermal gas chromatographic experiments using the OLGA system (Eichler *et al.*, 2000) conducted at the PSI cyclotron. The recoiling reaction products were sorbed on carbon particles suspended in He gas and continuously transported over a distance of a few meters to the OLGA where they were treated with HCl and oxygen to produce the volatile oxychlorides. These were conducted into the quartz chromatographic column, where their retention time is primarily dependent on the sorption interaction with the chlorinated column surface at a given isothermal temperature and the carrier gas velocity. The molecules passing through the column were attached to aerosols and then deposited stepwise on foils placed in positions on the circumference of a rotating wheel where their decay by alpha emission and SF was measured to identify them positively as ^{267}Bh based on their decay sequences to known daughter activities as reported in Wilk *et al.* (2000). Six such decay chains were observed over nearly 1 month of irradiation time. The relative yields for the trioxychlorides of ^{267}Bh as well as for those for Re and Tc obtained in similar experiments as a function of the isothermal temperatures are shown in Fig. 14.18.

A Monte Carlo program based on a microscopic model of the adsorption process was used to deduce ΔH_{ads} of –75 kJ mol^{-1} with a 68% confidence interval of –66 to –81 kJ mol^{-1} for BhO_3Cl, the most probable oxychloride under these conditions. The ΔH_{ads} values for the Tc and Re oxychlorides studied under the same conditions are –51 and –61 kJ mol^{-1}, respectively. Thus Bh oxychloride shows a stronger adsorption interaction with the chlorinated quartz

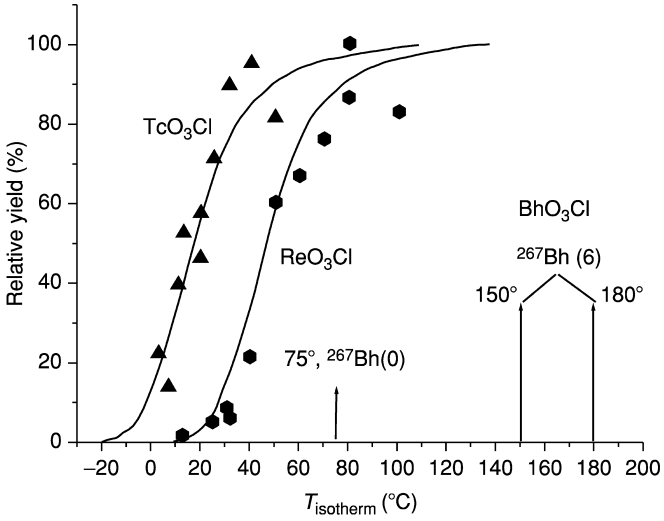

Fig. 14.18 *Relative yields vs. isothermal temperatures for TcO_3Cl (solid triangles) and ReO_3Cl (solid hexagons). A total of six events attributed to ^{267}Bh were detected at the isothermal temperatures of* 150 *and* 180°*C* (*Eichler* et al., 2000). *No events were detected at* 75°*C.*

surface than either Tc or Re compounds and it is less volatile than Re and Tc. This is in very good agreement with the calculations (Pershina and Bastug, 2000) where ΔH_{ads} of –48.2 kJ mol^{-1} for Tc and –78.5 kJ mol^{-1} for Bh were predicted, giving a volatility sequence of $TcO_3Cl > ReO_3Cl > BhO_3Cl$ (see discussion in Section 14.5.2).

(b) Hassium

Systems were developed for separating and detecting Hs as a volatile oxide based on the expectation that it would form a highly volatile tetroxide, as do its group 8-homologs osmium and ruthenium. Fully relativistic density functional calculations have been performed for MO_4 (M = Ru, Os, and Hs), as discussed in Section 14.5.2b. The volatility sequence for the tetroxides was predicted to be $HsO_4 \geq OsO_4 > RuO_4$ based on the calculated adsorption enthalpies of –(36.7 ± 1.5), –(38.0 ± 1.5), and –(40.4 ± 1.5) kJ mol^{-1}, respectively (Pershina *et al.*, 2001).

In preparation for experiments with Hs, Kirbach *et al.* (2002) developed the Cryo-Thermochromatographic Separator (CTS) to perform on-line investigations of the oxides of the α-emitters ^{171,172}Os (8 s,19 s) produced in ^{118,120}Sn (^{56}Fe,3–5*n*) reactions at the LBNL 88-Inch Cyclotron. The CTS consists of a channel formed by two facing rows of 32 PIN (Positive Implanted N-type silicon) diode α-particle detectors upon which a negative temperature gradient

from 247 K at the entrance to 176 K at the exit was maintained. The volatile species deposit on the detector surfaces at a characteristic temperature and are identified from their measured α-decay energies.

After pre-separation with the BGS to remove unwanted transfer reaction products and scattered beam particles, the separated Os ions were stopped in the RTC (described earlier) in a mixture of He gas containing 10 vol% O_2 at 100 kPa. The Os activities were transferred in a continuously flowing He/O_2 mixture through a Teflon capillary to a quartz tube heated to 1200 K where OsO_4 was formed and then transported through another capillary to the CTS. The detector pair in which the activity was deposited and the alpha spectra at each position were recorded to identify these activities. The temperature was determined from thermocouple measurements and also from the measured resistances of the PIN diodes. Monte Carlo fits to the adsorption distributions were obtained by adjusting the model to more closely approximate the slit-like CTS cross section and resulted in an adsorption enthalpy of $-(40.2 \pm 1.5)$ kJ mol^{-1} for quartz surfaces.

Düllmann *et al.* (2002a) devised the *In-situ* Volatilization and On-line detection apparatus (IVO) in which products recoiling from a nuclear reaction are thermalized and stopped in a recoil chamber containing He gas while the high-energy beam particles travel directly through the chamber to a beam stop, thus removing them from the system. The thermalized recoil products are then converted *in situ* to the volatile species to be studied and are swept by the carrier gas to a chromatography column. Volatile species pass through the column to a recluster chamber where they are sorbed on aerosols and transported via gas jet either to an additional quartz column to measure the retention times of the volatile species or directly to an on-line detection system. Short-lived Os isotopes were used to test IVO for future chemical studies with Hs. From the Monte Carlo simulations an adsorption enthalpy of $-(38.0 \pm 1.5)$ kJ mol^{-1} was obtained for $^{173}OsO_4$ on quartz surfaces, in agreement within the uncertainty limits with the value of $-(40.2 \pm 1.5)$ kJ mol^{-1} obtained by Kirbach *et al.* (2002). Subsequent to these prototype experiments, an international team of scientists (Düllmann *et al.*, 2002b) conducted the first studies of the chemistry of hassium, the heaviest element to date whose chemistry has been successfully investigated. The $^{248}Cm(^{26}Mg,5n,4n)$ reactions with estimated production cross sections of only a few picobarns were used to produce $\sim$10 s ^{269}Hs reported previously (Hofmann *et al.*, 1996, 2002) and possibly ^{270}Hs ($\sim$4 s) (Türler *et al.*, 2003) at the UNILAC at GSI. Three ^{248}Cm targets were positioned on a rotating wheel to increase the production rate. The IVO device was used to transport recoiling products to a quartz wool plug where Os and Hs were oxidized to the tetroxides by treatment with oxygen at 600°C. They were transported in helium through a Teflon capillary to the entrance to the Cryo On-Line Detector (COLD) TC formed by 12 pairs of opposing Si PIN-photodiode detectors with an outermost layer of Si_3N_4 positioned so that the gas flow was confined to the active detector surfaces. A schematic diagram of the system is shown in Fig. 14.19.

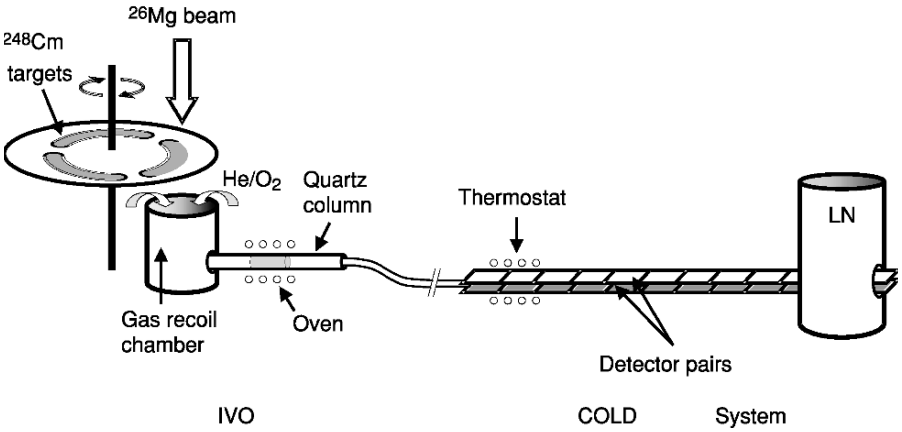

Fig. 14.19 *Schematic of IVO-COLD system for study of gas-phase properties of HsO_4 and lighter homologs* (*adapted from Düllmann* et al., 2002*b*).

Spectra of the alpha particles and SFs of the species deposited within each of the detectors of the array were measured and recorded to provide identification of the ^{269,270}Hs isotopes. The detection efficiency was about 77% for detection of a single alpha particle. A negative temperature gradient from –20 to –170°C was established along the TC formed by the detector array and measured at five positions. The system was checked at the beginning and at the end of the experiment by on-line measurements of the short-lived Os isotopes. In the 64 h experiment performed to produce Hs, three $\alpha-\alpha$-correlated decay chains were detected and assigned to the decay of ^{269}Hs. Two others, possibly due to the new nuclide ^{270}Hs or an isomer of ^{269}Hs, were detected, but a definite assignment could not be made. Based on detection of the three decay chains attributable to ^{269}Hs and two to a new nuclide ^{270}Hs (Türler *et al.*, 2003), HsO_4 was found to condense at a higher temperature than OsO_4 under similar conditions, indicating that the Hs oxide is less volatile than that of Os. The data for Hs and Os are shown in Fig. 14.20.

The Monte Carlo simulations that best fit these data give an adsorption enthalpy of $-(39 \pm 1)$ kJ mol^{-1} for OsO_4 on the silicon nitride surface, in good agreement with the previously measured values for SiO_2. An adsorption enthalpy of $-(46 \pm 2)$ kJ mol^{-1} was deduced for HsO_4 using only the three events assigned to ^{269}Hs and a $t_{1/2}$ value of 11 s in the analysis. This value is considerably more negative than the predicted value of $-(36.7 \pm 1.5)$ kJ mol^{-1} and suggests that HsO_4 is less volatile than OsO_4, in disagreement with calculations (Pershina, 1998a) that indicated that they should be nearly the same. More data and a better half-life measurement for ^{269}Hs are needed to investigate this discrepancy further. The possibility of different behaviors of HsO_4 on the Si_3N_4 detector surface compared to the SiO_2-coated detector surfaces should

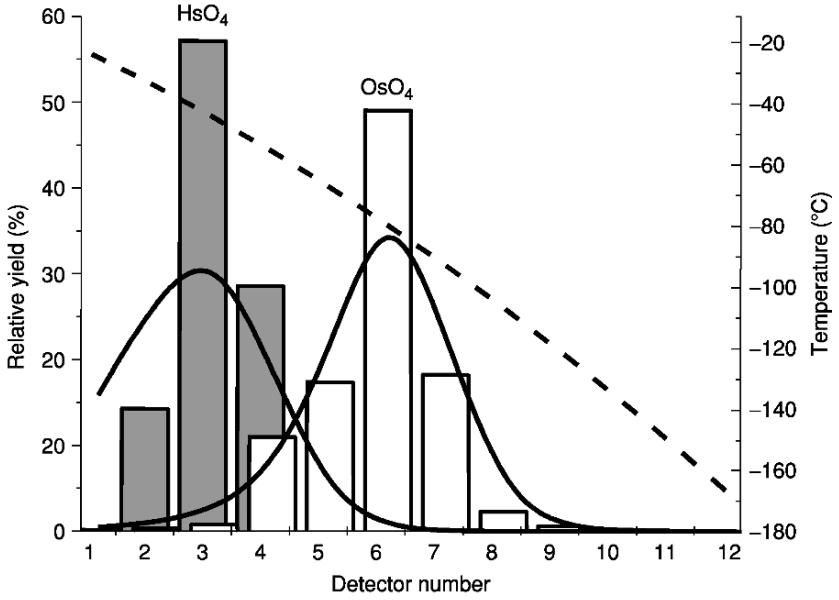

Fig. 14.20 *Combined thermochromatograms for Hs and Os oxides based on deposition positions (temperatures) for each of the* 12 *detector pairs. Dashed line indicates the temperature profile. The bars represent measured values and the curves result from Monte Carlo simulations of the migration process along the column.*

be considered and experiments with the tetroxide of Ru, predicted to be more volatile than those of either Os or Hs, should be conducted on both surfaces to investigate possible differences and the possibility that other oxides may be formed.

14.6.5 Summary of measured compared to predicted chemical properties

(a) Gas-phase studies

Observed trends in the volatility of the compounds of groups 4 through 8 compared to the theoretical predictions are summarized in Table 14.11. It can be seen that the measured and predicted trends in volatilities of the halide and oxyhalide compounds are in excellent agreement. However, in the case of the presumed tetroxides of Os and Hs there appears to be a discrepancy. This discrepancy emphasizes the need for additional investigations because few Hs disintegrations events were measured and their nuclear characteristics have not been unequivocally established.

Table 14.11 *Comparison of measured and predicted trends in volatilities of the compounds of Rf, Db, Sg, Bh, and Hs and their lighter homologs in periodic table groups* 4 *through* 8.

Group	*Compounds*	*Predicted volatility*	*Reference*	*Measured volatility*	*Reference*
4	MCl_4, MBr_4	Rf>Hf	Pershina and Fricke (1999)	Rf >Hf	Kadkhodayan *et al*. (1996); Sylwester *et al*. (2000)
5	ML_5 (L = Cl, Br)	Db >Ta > Nb	Pershina *et al*. (1992b)	(DbO_3Br)	Türler *et al*. (1996)
		$DbCl_5 > DbOCl_3$	Pershina *et al*. (1992b)	$DbCl_5$>$DbOCl_3$	Türler *et al*. (1996)
6	MO_2Cl_2	Mo > W > Sg	Pershina and Fricke (1996)	Mo > W > Sg	Schädel *et al*. (1997a); Türler *et al*. (1999)
7	MO_3Cl	Tc > Re > Bh	Pershina and Bastug (2000)	Tc > Re > Bh	Eichler *et al*. (2000)
8	MO_4	Hs = Os >Ru	Pershina *et al*. (2001)	Os > Hs	Düllmann *et al*. (2002b)

(b) Aqueous-phase studies

The measured trends in hydrolysis, complex formation, and extraction of complexes of Rf, Db, and Sg and their lighter homologs in groups 4 through 6 of the periodic table under a variety of experimental conditions compared to theoretical predictions for the same systems are summarized in Table 14.12. Care must be taken to ensure that the conditions for the experimental studies are the same as for the theoretical predictions since small differences in pH, purity of halide solutions, etc. can affect the equilibria that determine whether hydrolysis or complex formation dominates and whether the resultant complexes are neutral or charged. The order of extraction into organic solvents and sorption in cation- and anion-exchange chromatography differs greatly, depending on the charge on the complex. In general, agreement of the experimental results with the predictions is excellent when these factors are carefully controlled, as discussed in Section 14.5.3c.

There are some prospects for studies of the aqueous chemistry of elements heavier than 106 as well as for more detailed studies of elements 104, 105, and 106 using shorter-lived isotopes that may have higher production rates. The RTC (Kirbach *et al.*, 2002) coupled with the BGS could be used so that the separated isotopes can be transported to different rapid chemical separation systems such as SISAK-III described earlier (Omtvedt *et al.*, 2002) for few-second liquid–liquid extractions or other automated systems such as ARCA. This might permit detailed studies of complex formation of elements Bh and Hs that would be of special interest in acid solutions.

14.6.6 Prospects for experimental studies of chemistry of Mt through element 112

(a) Predictions of half-lives and production modes

Prospects for chemical studies of Mt depend on the confirmation of longer-lived isotopes than ^{268}Mt, currently the longest-lived known isotope of Mt. This isotope decays primarily by alpha emission, with a half-life reported to be about 40 ms; it was detected as the alpha-decay product of ^{272}111 produced with a cross section of 2.5 pb in the ^{209}Bi(^{64}Ni,n) reaction (Hofmann *et al.*, 2002). The half-lives of the ^{264}Bh daughter and the ^{260}Db granddaughter of ^{268}Mt are only about 1 s, so even techniques involving chemical separation of the daughters to infer the parent chemical properties do not appear feasible. Longer-lived isotopes of Mt are expected around the deformed nuclear shell at 162 neutrons and might be produced using the ^{238}U(^{37}Cl,4n) or the ^{249}Bk (^{26}Mg,4n) reaction to make ^{271}Mt. The half-life of this odd-proton, odd-neutron isotope was estimated from interpolation of Smolańczuk's (1997) calculations

Table 14.12 *Comparison of measured with predicted trends in hydrolysis and complex formation of some compounds of Rf, Db, and Sg and their lighter homologs in periodic table groups* 4 *through* 6.

Group	*Complexes*	*Experimental conditions*	*Predictions*	*Reference*	*Measured*	*Reference*
4	hydrolysis of M^{4+}	$pH \leq 2$	Zr > Hf > Rf	Pershina *et al.* (2002b)	Zr > Hf > Rf	Czerwinski (1992a)
	$MF_x(H_2O)_{8-x}^{z-x} (x \leq 4)$	$[HF] < 10^{-1}$ M	Zr > Hf > Rf	Pershina *et al.* (2002b)	Zr > Hf > Rf	Strub *et al.* (2000)
	MF_6^-	$[HF] > 10^{-3}$ M	Rf ≥ Zr > Hf	Pershina *et al.* (2002b)	Rf ≥ Zr > Hf	Trubert *et al.* (1999)
	MCl_6^-	4–8 M [HCl]	Zr > Hf > Rf	Pershina *et al.* (2002b)	Rf > Zr > Hf	Haba *et al.* (2002)
5	hydrolysis of M^{5+}	all pH	Nb > Ta > Db	Pershina (1998a)	Nb > Ta	Baes and Mesmer (1976)
	$M(OH)_2Cl_4^-$	all [HCl]	Pa >> Nb ≥ Db > Ta	Pershina (1998b)	Pa >> Nb ≥ Db >Ta	Paulus *et al.* (1999)
	$MOCl_4^-$, MCl_6^-					
6	hydrolysis of M^{6+}	$0 < pH < 1$	Mo > W > Sg	Pershina and Kratz (2001)	Mo > W > Sg	Schädel *et al.* (1998)
	hydrolysis of $MO_2(OH)_2$	$pH > 1$	Mo > Sg > W	Pershina and Kratz (2001)	Mo > W	Baes and Mesmer (1976)

for even proton–even neutron nuclides to be a few seconds and decay primarily by alpha emission. The cross section for the first reaction is expected to be similar to that of 2.5 pb, measured for the ^{238}U(^{34}S, 5n)$\rightarrow$^{267}Hs reaction (Lazarev *et al.*, 1995) as the enhancement of the cross section due to the extra two neutrons in ^{37}Cl compared to ^{34}S is expected to balance the decrease due to the higher Z of Mt. Based on this cross section, detection of two or three chains a week might be expected using multiple ^{238}U targets in the BGS. The BGS is capable of positively separating and identifying such a new nuclide based on measurement of the known alpha-decay chain of its daughters even if the ^{271}Mt half-life is as short as a few tenths of a second. The overall yield for the reaction with the highly radioactive target ^{249}Bk will be much lower because the cross section is expected to be only a few tenths of 1 pb and it is much more difficult to use multiple targets.

The production of longer-lived isotopes of elements 110, 111, and 112 with half-lives in the range of seconds to minutes have now been reported using 'warm/hot' fusion reactions or as decay products of elements 114 and 115. (See Table 14.2 and Fig. 14.2(b) and discussion in Section 14.1.) It may be possible to produce ^{277}110 directly in the 'warm' fusion reaction ^{232}Th(^{48}Ca,3n), but the cross section may be low and the systematics of these reactions need to be investigated further. The isotope ^{280}110 with a half-life of 7.6 s has been reported as the granddaughter of ^{288}114 produced in a four neutron out reaction in the bombardment of ^{244}Pu targets with ^{48}Ca (Oganessian *et al.*, 2000a; Oganessian, 2001), but this indirect production method is not favorable for chemical studies. Currently, there appear to be no suitable reactions for direct production of the very neutron-rich isotopes of Ds.

Some isotopes of the odd-proton element 111 should have half-lives of seconds or more and hindrances toward fission and alpha decay should exist. An isotope with mass number 280 and with a half-life of 3.6 s has been reported in the alpha-decay chain of ^{288}115 produced in the bombardment of ^{243}Am with ^{48}Ca projectiles (Oganessian *et al.*, 2004a).

SF activity attributed to ^{283}112 produced in the ^{238}U(^{48}Ca,3n) reaction and from the alpha decay of ^{287}112 produced via the ^{242}Pu(^{48}Ca,3n) reaction has been reported by Oganessian *et al.* (1999a,c, 2004b) who obtained a half-life of $\sim$5 min by averaging these results. However, as discussed in Section 14.1, it is difficult to positively identify a new nuclide that decays only by SF and even if this assignment is verified, its positive identification in chemical studies would be equally difficult and likely to be inconclusive. The production of 112 isotopes in ^{238}U(^{48}Ca,xn) reactions should be investigated further to determine the cross sections and if there is an alpha branch in ^{283}112 or ^{284}112. Then more definitive chemical studies could be undertaken. Such experiments would also help to assess the usefulness of 'warm' fusion reactions for production of a broad range of heavy element reactions for chemical studies.

(b) Chemical methods

Even though it appears that isotopes of the elements from Mt through element 112 can exist with half-lives long enough for chemical studies, the most difficult problem will be to increase the production rates and to perform on-line experiments with continuous separation and detection capabilities that can be operated for times long enough to obtain statistically significant results. These times will be of the order of weeks or months and will certainly require computer-controlled automated systems to carry out both gas-phase and solution chemistry. As the production cross sections for the elements of interest become ever smaller, the use of some pre-separation technique – either physical such as BGS or chemical such as IVO – will become mandatory in order to separate out the multitude of unwanted products before use of the more selective systems mentioned below.

The stable oxidation states of these elements both in the gas phase and in solution are predicted to vary widely, as shown in Table 14.10. From element 107 on, the maximum oxidation state is expected to be relatively unstable in aqueous solutions. Experimental studies designed simply to try to determine the most stable oxidation states in aqueous solution should be devised. Thus, for example, the stability of Bh(IV) relative to Bh(VII), or Hs(IV) relative to Hs(VIII) could be investigated by performing anion-exchange separations from HCl solutions in which the 4+ states might form negatively charged complexes that would be retained on the anion column. The relative positions of the peaks of the elution curves associated with reduction would give information about relative stabilities of lower oxidation states. Complex formation can also be studied for elements 109 and heavier. The imaginative gas-separation techniques developed for study of Bh and Hs can be applied to Mt and Ds, which are predicted to form volatile hexafluorides and octafluorides, as discussed in Section 14.5.2b.

Some preliminary chemical experiments on element 112 have been reported by Yakushev *et al.* (2001) and by Yakushev (2002) using the spontaneously fissioning nuclide $^{283}112$ ($\sim$5 min) reported by Oganessian *et al.* (1999a, 2004b) to be formed in the $^{238}U(^{48}Ca,3n)$ reaction with a cross section of 5 pb. The experiment was designed to determine whether element 112 behaved similarly to its periodic table homolog Hg, which had been shown to deposit on Au- or Pd-coated silicon surface barrier detectors (Yakushev *et al.*, 2001), or whether it behaved as a noble gas like Rn and remained in the gas phase. An unambiguous answer about the physical or chemical properties of element 112 was not obtained. The system was improved by introducing a special ionization chamber after the silicon detectors to measure alpha decays and SF events of nuclei remaining in the gas. More than 95% of the simultaneously produced Hg isotopes were deposited on the first Au-coated detector. Again, no events attributable to element 112 were detected on either the Au- or the Pd-coated

silicon detectors, but eight SF events were registered in the ionization chamber (Yakushev, 2002). These SF events were attributed to element 112, which indicates that it is more chemically inert than Hg and remained in the gas phase. The ΔH_{ads} of element 112 was deduced to be more positive than –55 kJ mol^{-1}. Further experiments with a temperature gradient in the chromatography column are now planned to better define ΔH_{ads}. It is also important to confirm that the observed SF events actually belong to element 112. If an alpha-decaying isotope of element 112 with a suitable half-life and production rate can be identified it would be much more suitable for chemical studies because it could be positively identified from its half-life and characteristic alpha-decay chain.

Experiments on element 112, similar to those conducted in Dubna, are planned by researchers at PSI (Soverna *et al.*, 2001) using a chromatographic column with a negative temperature gradient from 35 to –190°C. Silicon detectors coated with Au and Pd will be placed along the chromatographic column to detect element 112 and its deposition temperature will be determined relative to those of Hg at 115°C and Rn at –115°C in order to deduce ΔH_{ads}.

Eichler and Schädel (2002) investigated the adsorption of Rn on polycrystalline surfaces of transition metals and found the strength of adsorption to decrease in the order: Ni > Pd ≈ Cu > Au > Ag. They suggest that low-temperature vacuum thermochromatographic techniques could be used to rapidly separate element 112 from 114 and Rn and to determine whether its behavior is more like its lighter homolog Hg or an inert noble gas.

Isotopes of Hg have been studied by carrying them on Pd aerosols to serve as a model system for possible studies of elements 112 or 114 (Düllmann *et al.*, 2002a). Recoiling Hg isotopes produced in ^{168}Yb(^{22}Ne,xn)$^{190-x}$Hg reactions in the IVO setup at the PSI Philips cyclotron were thermalized in He, swept through an isothermal quartz column at 800°C to the re-cluster chamber, and transported on Pd aerosols to a suitable detection device for measurement of alpha spectra. The short-lived nuclides $^{183-185}$Hg were identified, indicating that volatile metals such as Hg can be transported in gas-flow systems without the presence of aerosol particles and then quickly adsorbed on metal aerosols if the enthalpy of adsorption is sufficiently large. The aerosols can then be transported to a detection system for measurements at low pressure and room temperature. Such a technique may also be applicable to measurements of transactinides with $Z = 112$ to 117.

Plans to separate elements with $Z > 108$ as noble metals by electrochemical deposition from aqueous solutions have been described (Kratz, 1999a). The choice of an appropriate electrode material is very important and estimates of suitable electrodes have been made for lighter homologs of the heaviest elements (Eichler and Kratz, 2000). Pd and Pt were found to be suitable electrode metals for the deposition of Hg, Tl, Pb, Bi, and Po, the homologs of elements 112 through 116.

14.7 FUTURE: ELEMENTS BEYOND 112 (INCLUDING SHEs)

14.7.1 Predictions of electronic structures and chemical properties

(a) Introduction

The ground state configurations of the free neutral atoms of elements 113 through 184 obtained from relativistic DF calculations are summarized in Table 14.13.

Table 14.13 *Dirac–Fock ground state configurations of free neutral atoms of elements* 113 *through* 184.[a]

Rn 'core' + $5f^{14} + 6d^{10} + 7s^2$ +								*Element* 120 *'core'* + $5g^{18} + 8p_{1/2}^2$ +					
	$5g$	$6f$	$7p_{1/2}$	$7p_{3/2}$	$7d$	$8s$	$8p_{1/2}$		$6f$	$7d$	$9s$	$9p_{1/2}$	$8p_{3/2}$
113			1					145	3	2			
114			2					146	4	2			
115			2	1				147	5	2			
116			2	2				148	6	2			
117			2	3				149	6	3			
118			2	4				150	6	4			
119			2	4		1		151	8	3			
120			2	4		2		152	9	3			
121			2	4		2	1	153	11	2			
122			2	4	1	2	1	154	12	2			
123		1	2	4	1	2	1	155	13	2			
124		3	2	4		2	1	156	14	2			
125	1	3	2	4		2	1	157	14	3			
126	2	2	2	4	1	2	1	158	14	4			
127	3	2	2	4		2	2	159	14	4	1		
128	4	2	2	4		2	2	160	14	5	1		
129	5	2	2	4		2	2	161	14	6	1		
130	6	2	2	4		2	2	162	14	8			
131	7	2	2	4		2	2	163	14	9			
132	8	2	2	4		2	2	164	14	10			
133	8	3	2	4		2	2	165	14	10	1		
134	8	4	2	4		2	2	166	14	10	2		
135	9	4	2	4		2	2	167	14	10	2	1	
136	10	4	2	4		2	2	168	14	10	2	2	
137	11	3	2	4	1	2	2	169	14	10	2	2	1
138	12	3	2	4	1	2	2	170	14	10	2	2	2
139	13	2	2	4	2	2	2	171	14	10	2	2	3
140	14	3	2	4	1	2	2	172	14	10	2	2	4
141	15	2	2	4	2	2	2	...					
142	16	2	2	4	2	2	2	...					
143	17	2	2	4	2	2	2	184	172 'core' + $6g^5 7f^4 9d^3$				
144	18	1	2	4	3	2	2						

[a] Fricke (1975).

Chemical properties for elements 113 through 121, as predicted by various researchers, are summarized in Table 14.14. A rather complete discussion and summary of the chemical properties predicted for these elements as of 1986 was given by Seaborg and Keller (1986).

(b) Elements 113 through 115

In elements 113 through 118, the filling of the 7p shell is expected to takes place. Chemistry of these elements will be strongly influenced by relativistic effects: the large relativistic stabilization of the $7s^2$ electron pair (a large 7s–7p gap hindering the hybridization) and a very large SO splitting of the 7p levels into $7p_{1/2}$ and $7p_{3/2}$, reaching 11.8 eV for element 118 (Fig. 14.21). Since the electrons occupying the $7p_{1/2}$ orbital will then form a closed subshell, an enhanced stability of lower oxidation states of these elements is expected. However, destabilization of the 6d levels would contribute to a more transition element character for the earlier 7p elements (Han *et al*., 1999b; Seth *et al*., 1999).

(*i*) *Element* 113

Element 113 has one electron in the $7p_{1/2}$ valence shell. Due to relativistic stabilization of the $7p_{1/2}$ electrons, its first IP of 7.306 eV, as shown in Table 14.15, is the largest in group 13 (Eliav *et al*., 1996a). The 1+ state is thus predicted to be the most stable.

The CCSD calculations (Eliav *et al*., 1996a) revealed a dramatic reduction in the excitation energy of an electron from the d^{10} shell: the $d^{10}s \rightarrow d^9s^2$ energy of 113^{2+} is 0.1 eV as compared to 8 eV for Tl^{2+}. It is, therefore, predicted that divalent or trivalent compounds of element 113 with an open $6d^9$ shell could exist. The calculated EA of Tl and element 113 are 0.4 and 0.68 eV, respectively.

The very large SO splitting of the 7p orbital will influence the chemistry of element 113 compounds by destabilizing the binding energy by almost 1 eV in the monohydride 113H. In this molecule, the 6d and 7s orbitals were shown to participate little in bonding (Han *et al*., 1999a,b, 2000; Seth *et al*., 1999) and all the effects are defined by the large participation of the $7p_{1/2}$ shell. Element 113 was calculated to be more electronegative than Ga, In, Tl, and even Al among all the monohydrides. Involvement of the 6d electrons in bonding in element 113 was confirmed by PP calculations (Han *et al*., 1999b; Seth *et al*., 1999) for $113H_3$, $113F_3$, and $113Cl_3$. As a consequence, a T-shape geometric configuration rather than a trigonal planar was predicted for these molecules. The stability of a high-coordination compound MF_6^- with the metal in the 5+ oxidation state is foreseen. $113F_5$ will probably be unstable since the energy of the reaction $113F_5 \rightarrow 113F_3 + F_2$ is only –53.4 kJ mol^{-1} (Seth *et al*., 1999). The calculated energies of the decomposition reaction $MX_3 \rightarrow MX + X_2$ (M = B, Al, Ga, In, Tl and element 113) confirmed a decrease in the stability of the 3+ oxidation state in group 13.

Table 14.14 *Predicted chemical properties of elements* 113 *through* 121.

	113	114	115	116	117	118	119	120	121
Chemical group	13	14	15	16	17	18	1	2	3
stable oxidation states[a,b,c]	**1**,3	**2**,0,(4)	**1**,3	**2**,4	**1**,**3**,5,(–1)	**4**,2,–1,(6)	**1**,3	2,4	**3**
first ionization potential (eV)[d]	7.306[d]	8.539[d]	5.58[d]	7.5[c]	7.7[c]	8.7[c]	4.53[e]	6.0[c]	4.45[f]
standard electrode potential in aqueous solution (V)	+0.6	+0.9	–1.5	+0.1	–0.25, 0.5		–2.7	–3.0	+2.1
	+0.6	+0.9	–1.5	+0.1	–0.25, 0.5		–2.7	–3.0	+2.1
ionic radius of indicated ion (Å)	1.4(1+)	1.2(2+)	1.5(1+) 1.0(3+)	0.83(4+) 0.58(7+)	0.80(4+) 0.58(7+)		1.8(1+)	1.6(2+)	
atomic radius (Å)[b]	1.7	1.6	2.0				2.4[c]	2.0[c]	
density (g cm^{-3})[b]	18 (16[c])	22 (14[c])	11 (13.5[c])	12.9[c]			3[c]	7[c]	
ΔH_{sub} (kJ mol^{-1})[b]	142(129[c])	42	142	197[c]			42	138	
boiling point (K)[b]	1400	420	~1400		883	263			
melting point (K)[b]	700	340	~700		623–823[c]	258[c]	273–303[c]	953[c]	

[a] Bold type: most stable in gas phase; underlined = most stable in aqueous solutions; non-bold: less stable; ( ) = least stable.
[b] Keller and Seaborg (1977) and Seaborg and Keller (1986).
[c] Fricke (1975).
[d] See Table 14.15.
[e] Lim *et al.* (1999).
[f] Eliav *et al.* (1998a).

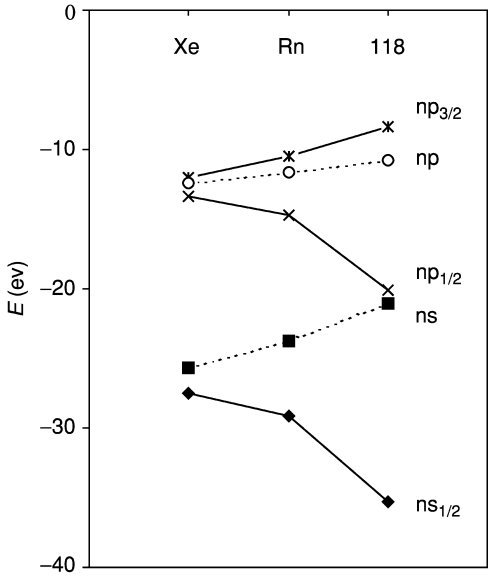

Fig. 14.21 *Relativistic stabilization of the ns and* $np_{1/2}$ *orbitals and the spin–orbit splitting of the np orbitals for the noble gases Xe, Rn, and element* 118. *DF atomic energies* (—) *are from Desclaux* (1973) *and HF values* (---) *are from Schwerdtfeger and Seth* (1998).

The standard electrode potential $E^{\circ}(113^{+}/113)$ was predicted to be +0.6 eV and 113^{+} is expected to be more easily complexed than Tl^{+} and to be similar to Ag^{+} (Keller *et al.*, 1970). For example, the solubility of TlCl in water is not increased much by adding excess HCl (Alekseeva *et al.*, 1972) or NH_3, whereas AgCl dissolves when NH_3 is added. Element 113 is expected to be more like silver in this respect. The smallest sublimation enthalpy in the group was predicted for element 113 by extrapolation (Keller *et al.*, 1970) and can be explained by the relativistic stabilization of the $7p_{1/2}$ orbital.

(*ii*) *Element* 114

The most interesting among the 7p elements is element 114 where a very large SO splitting of the 7p orbital and the relativistically stabilized 7s and $7p_{1/2}$ electrons result in a closed-shell ground state $7s^2 7p_{1/2}{}^2$, suggesting that the element should be rather inert. This is also reflected by the largest IP in group 14 (Table 14.15). One of the most striking features seen in Table 14.14 is the great decrease in boiling point in going from element 113 to element 114. This decrease was predicted by Keller *et al.* (1970) on the basis of extrapolations of the heats of sublimation of the group 13 and 14 elements versus periods of the periodic system. The boiling points were then calculated using Trouton's rule. This effect is a result of adding a second $7p_{1/2}$ electron in element 114 to form a

Table 14.15 *Ionization potentials* (*in* eV) *for the* 7*p elements.*

Calculated	113	114	115	116	117	118	*Reference*
DF	7.4[a]	8.5[a]	5.5[a]	7.5[a]	7.7	8.7	Fricke (1975)
MCDF	7.11	8.04 (8.51[b])	4.65	5.96	6.51	7.74 (7.6[b])	Pyper and Grant (1981)
CCSD	7.306[c]	8.539[d]	5.58[e]	–	–		Eliav *et al*. (1996a),[c] Eliav *et al*. (1998b),[d] Landau *et al*. (2001)[e]

[a] DF values corrected for the difference between theoretical and experimental values for the elements of the 6th period.
[b] Relativistic CI version of RECP (Nash and Bursten, 1999a).
[c] Eliav *et al*. (1996a).
[d] Eliav *et al*. (1998b).
[e] Landau *et al*. (2001).

closed-shell $7p_{1/2}{}^2$ configuration, similar to the s^2 one, making this configuration responsible for much weaker bonding in a metallic state.

The group 14 elements show increasing stability of the 2+ oxidation state relative to the 4+ state as one goes to higher atomic numbers. Lead is known to be most stable of the group 14 elements in the 2+ oxidation state. Due to the very large 7s orbital stabilization, the sp^3 hybridization energy needed for the 4+ valence is very large in element 114, so that the 4+ oxidation state of element 114 is expected to be unstable, while the 2+ state should be the most stable in the group. Recent calculations (Liu *et al*., 2001) have, indeed, shown $114O_2$ to be thermodynamically unstable in contrast to PbO_2. Energies of the decomposition reactions $MX_4 \rightarrow MX_2 + X_2$ and $MX_2 \rightarrow M + X_2$ (M=Ge, Sn, and Pb; X = H, F, and Cl) were calculated at the PP level (Seth *et al*., 1998b; Nash and Bursten, 1999a). The results confirm a trend of decreasing stability of the 4+ oxidation state in the group. The neutral (monatomic) state was calculated to be more stable for element 114 than for Pb. Element 114 should also have a greater tendency to form complexes in solutions than Pb. Because the stability of the 2+ state increases within group 14, element 114 would probably form MX^+, MX_2, MX_3^-, or MX_4^{2-} (X = Cl, Br, and I) by analogy with Pb. $114F_6^{2-}$, suggested by Seth *et al*. (1998b), will probably be unstable in the aqueous phase due to strong hydrolysis of the fluorides in aqueous solutions. Thus, aqueous complexes of element 114 such as $114Br_3^-$ or $114I_3^-$ should be preferentially formed. Pitzer (1975a) predicted stable $(114)X_2$ (X = F, Cl, and Br). The standard electrode potential $E^\circ(114^{2+}/114)$ was estimated as +0.9 V by Keller *et al*. (1970). We thus see that relativistic effects on the $7p_{1/2}$ electrons cause a diagonal relationship to be introduced into the periodic table near element 114, causing 114^{2+} to be somewhere between Hg^{2+} or Cd^{2+} and Pb^{2+} in its chemistry and causing 113^+ to act more like Ag^+ than Tl^+.

(*iii*) *Element* 115

In element 115, one electron is located in the relativistically destabilized $7p_{3/2}$ orbital and, therefore, is loosely bound,while $7p_{1/2}{}^2$ serves as an inert pair. Thus, the 1+ oxidation state of element 115, like that of Tl^+, should be preferred. This is also supported by a drastic decrease in the first IP between 114 and 115 (Fig. 14.8). Furthermore, calculations show that element 115 has the smallest IP in group 15 and in the 7th period, as shown in Table 14.15 and Fig. 14.8. Keller *et al*. (1974) made some detailed predictions of the chemical properties of element 115 based on extrapolations of the properties of group 15 elements and relativistic atomic DS and DF calculations. Their results indicate that the chemical properties of element 115 should be analogous through a diagonal relationship to those of Tl (group 13) as well as to those of Bi. They predicted a standard electrode potential $E^\circ(115^+/115) = -1.5$ V, indicating that element 115 metal should be quite reactive. They also suggested that 115(III) should be relatively stable and have some chemical properties somewhat similar

to Tl(III), but that its chemical properties will be closer to those of Bi(III). The 5+ state seems unlikely. Melting and boiling points of the metal should be close to those of element 113.

(c) Elements 116 through 118

The chemistry of elements 116 through 118 will be defined mostly by the participation of the $7p_{3/2}$ orbital in bonding. Certain predicted volatility characteristics of elements 116, 117, and 118 or their compounds may offer advantages for chemical identification. This will be especially true for element 118. The chemical properties of element 116 can be deduced by extrapolations from Po, though the 2+ state should be more stable than the 4+ state because the $7p_{1/2}^2$ electrons are expected to be rather inert. Estimates of formation enthalpies of MX_2 and MX_4 (X = F, Cl, Br, I, SO_4^{2-}, CO_3^{2-}, NO_3^-, and PO_4^{3-}) for Po and element 116 (Grant and Pyper, 1977) on the basis of the MCDF atomic calculations are consistent with the expected instability of 116^{4+}. The chemistry of element 116 is expected to be mainly cationic, i.e. the relative ease of formation of the divalent compounds should approach that of Be or Mg, and tetravalent compounds such as $116F_4$ should be formed only with the most electronegative atoms.

In element 117, the 1– oxidation state becomes less important than that of the lighter group 17 halide ions due to the destabilization of the $7p_{3/2}$ orbital. The EA of element 117 is the smallest in the group (2.6 eV as predicted by Cunningham, 1969 and 1.8 eV as given by Waber *et al.*, 1969). Therefore, the 3+ state should be at least as important as the 1– state, so that element 117 might resemble Au^{3+} in its ion-exchange behavior in halide media. The trend to decreasing participation of the $np_{1/2}$ orbital bonding in group 17 was found to be continued further with element 117 (Hoffman, 1996; Saue *et al.*, 1996; Nash and Bursten, 1999c; Han *et al.*, 2000). In the group HI, HAt, and H117, an increasing trend in R_e and a decreasing trend in D_e are continued with H117. Analogous to its lighter homologs, Element 117 should form dimers X_2. The DCB CCSD(T) calculations for X_2 (X = F through At) (Visscher *et al.*, 1996) found a considerable antibonding σ-character in the HOMO of At_2 due to the SO coupling while without the SO coupling it is an antibonding π-orbital. The bonding in $(117)_2$ is predicted to continue this trend and have a strong π-character.

The elements in the noble gas group become less inert with increasing Z. Earlier predictions of properties of element 118 were made by extrapolation from lighter homologs within the group (Grosse, 1965; Pitzer, 1975a,b). Early calculations of Penneman and Mann (1976) indicated that ionization energies of element 118 should be less than the experimental values for xenon, and that chemical compounds should be expected for 118. The first IP of element 118 is 8.7 eV (see Table 14.15), about the same as the IP(114) = 8.54 eV and smaller than IP(Rn) = 10.74 eV and IP(112) = 11.97 eV. The outer 8s orbital of element 118 is relativistically stabilized to give the atom a positive EA of 0.056 eV, as

shown by recent CCSD calculations (Eliav *et al.*, 1996b). The polarizability of 118 is expected to be the largest in group 18. Its largest polarizability, together with its smallest IP, implies that it will have the highest reactivity in the group. It should be stable in the 4+ oxidation state, and should form stable tetrafluorides and tetrachlorides as well. Recent RECP calculations (Han and Lee, 1999) of free energies of the reactions $M + F_2 \rightarrow MF_2$ and $MF_2 + F_2 \rightarrow MF_4$, where M = Xe, Rn, and element 118, confirmed an increase in the stabilities of the 2+ and 4+ oxidation states in group 18. The SO effects were shown to stabilize $118F_4$ by a significant amount, about 2 eV, though they elongate R_e by 0.05 Å. The influence of the SO interaction on the geometry of MF_4 was investigated by RECP calculations (Han and Lee, 1999; Nash and Bursten, 1999a,b). It was found that the D_{4h} geometrical configuration for XeF_4 and RnF_4 becomes slightly unstable for $118F_4$. A T_d configuration was shown to be more stable than D_{4h} by about 0.20 eV. The reason was the availability of only stereochemically active $7p_{3/2}$ electrons for bonding. An important observation was made that the fluorides of element 118 will most probably be ionic rather than covalent as is the case of Xe. Therefore, they are predicted to be non-volatile.

(d) Elements 119 through 121

In elements 119 and 120, the filling of the 8s shell will take place, so that these elements should be homologs of the alkali and alkaline earth elements in groups 1 and 2 and will be stable in the 1+ and 2+ oxidation states, respectively. Their first IPs (Fricke, 1975) should be about 0.5 eV higher than those of Fr and Ra, respectively, due to the relativistic stabilization of the 8s electrons, and closer to the values of Rb and Sr. Thus, an upturn in the IPs from Cs to element 119 and from Ba to element 120 (see Fig. 14.22) was predicted (Penneman and Mann, 1976). Recent DK CCSD calculations (Lim *et al.*, 1999) showed the first IP of element 119 to be relativistically increased from 3.31 to 4.53 eV, while polarizability is decreased from 693.94 to 184.83 a.u. Due to the relativistic stabilization of the 8s orbital, the EA for element 119, of 662 meV, is 20 meV higher (being the highest in the group) than that for Fr, according to recent DCB CCSD calculations (Landau *et al.*, 2001).

The atomic radii of elements 119 and 120 are expected to be 2.4 and 2.0 Å, respectively, very similar to the values of Rb and Sr, as shown in Fig. 14.23. They show the same reversal of the trend (a downturn from Cs/Ba to 119/120) as do the IPs in groups 1 and 2 (Fricke, 1975). Thus, the chemical properties of elements 119 and 120 should be close to those of Rb and Sr, respectively, rather than to Fr and Ra in the 1+ and 2+ oxidation states. On the other hand, the ions will have larger radii than Rb^+ and Sr^{2+} because of the larger extension of the filled 7p shell compared to the lower p-shells. Another important point is that due to the relatively small ionization energy of the outer $7p_{3/2}$ electrons and their spatial extension, higher oxidation states like 3+ or 4+, respectively, could be reached in elements 119 and 120.

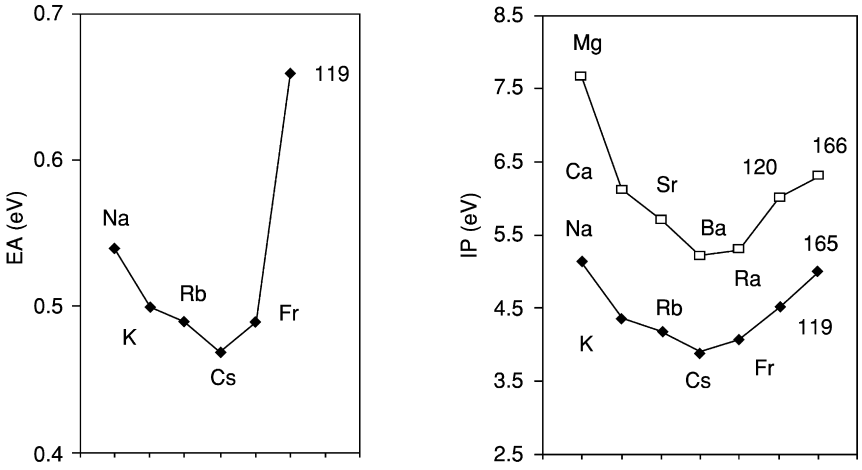

Fig. 14.22 *Electron affinities* (*EAs*) *and ionization potentials* (*IPs*) *for alkali and alkaline-earth elements. The data for Na through Fr and Mg through Ra are experimental. The value for Element* 119 *is from DF CCSD calculations* (*Landau* et al., 2001). *The values for elements* 120, 165 *and* 166 *are from DF calculations* (*Fricke,* 1975).

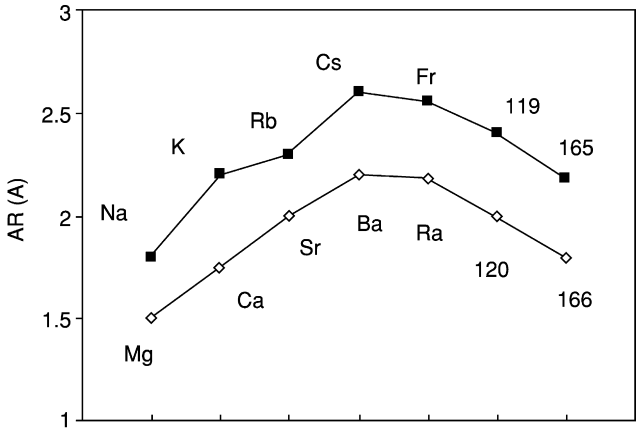

Fig. 14.23 *Atomic radii* (*AR*) *of alkali and alkaline earth elements. The data for Na through Cs and Mg through Ra are experimental. The other data are from DS calculations.* (*Redrawn from Fricke,* 1975).

The next element, 121, will have a relativistically stabilized 8p electron in its ground state electronic configuration $8s^2 8p_{1/2}$ (see Table 14.13) in contrast to that of $8s^2 7d$ predicted by a simple extrapolation within the group. As early as 1969, Griffin *et al.* (1969) showed that the large SO splitting brings an 8p

electron into the stable atomic ground state. Recent CCSD calculations for element 121 (Eliav *et al.*, 1998a) gave $IP_1 = 4.45$ eV and EA = 0.75 eV, the highest EA in group 3. Griffin *et al.* also showed that large changes occur in the spatial distribution of the valence orbitals in going from element 120 to 121. For example, the effective radius of the 5g electrons changes from 25 Bohr units for element 120 in the excited configuration $8s^15g^1$ to 0.8 Bohr units for element 121 in the configuration $8s^17d^15g^1$. This phenomenon, called 'radial collapse', occurs as late as element 125 as a consequence of indirect relativistic effects. Due to the proximity of the valence levels, higher oxidation states are possible.

(e) Superactinide elements and beyond

Element 122 belongs to a very long, unprecedented transition series that is characterized by the filling of not only 6f but also 5g orbitals with partially filled $8p_{1/2}$ orbitals, which is a direct relativistic effect. These elements were dubbed 'superactinides' by Seaborg (1968) as early as 1968. Quite a number of theoretical calculations of the ground state electronic configurations (Griffin *et al.*, 1969; Mann, 1969; Mann and Waber, 1970; Fricke *et al.*, 1971) were performed for this region and the results have been summarized by Fricke (1975). The calculated ground state configurations of the free neutral atoms of elements 113 through 184 are listed in Table 14.13. Here, at the beginning of the superactinides, not only two but four electron shells, namely $8p_{1/2}$, $7d_{3/2}$, $6f_{5/2}$, and $5g_{7/2}$, are expected to compete simultaneously. These open shells, together with the 8s electrons, determine the chemistry.

As shown in Table 14.13, a 7d electron is added to the ground state in element 122 and the 8p electron is relativistically stabilized so that the configuration is $8s^27d8p$, in contrast to the $7s^26d^2$ state of Th. This is the last element where accurate CCSD calculations (Eliav *et al.*, 2002) exist. The first four calculated IPs of element are 5.6, 11.3, 20.4, and 27.14 eV as compared to the first and the fourth IPs, 6.54 and 28.75 eV, of Th. A decrease in the first IP from Th to element 122 is due to the ionized $8p_{1/2}$ electron.

Elements 122 through 152 might have chemical properties somewhat similar to those of the actinides but there will be some differences. The very small binding energies of all the valence electrons will cause the higher oxidation states to be reached in these elements. This will be a continuation of the trend from the lanthanides (where 3+ states are highest) to the superactinides.

For ionic compounds it is important to establish which external orbitals are left after all outer s-, p-, and d-electrons are removed. Will there be some g- and f-electrons left or will they be easily excited to an outer electron shell, so that they can be removed as well? Some investigations showed that for element 126 in the divalent state, one g-electron will move to an f-electronic state, and the 8s electrons will not be the first to be removed. Thus, the divalent ions are expected

to act as soft Lewis acids and possibly form covalent complex ions readily. From some calculations of excited states, it is assumed that very high oxidation states may be possible around element 128 in complex compounds, but that normally these elements will have 4+ as their main oxidation state in ionic compounds. The maximum valence will be reduced to 6+ at element 132 and in the region of 140, it will be 3+ to 4+. At the end of the superactinide series, the normal oxidation states are expected to be only 2+ because the 6f shell will be buried deep inside the electron core and the 8s and $8p_{1/2}$ orbitals will be strongly bound. At element 156, only two 7d relativistically destabilized electrons will be available for bonding. This behavior should be similar to that of the low oxidation states of elements at the end of the actinides. Thus, at the end of the superactinide series, the elements will be more noble.

A contraction of bond lengths, analogous to the actinide contraction, is expected for the superactinide series. The total effect will be very large because of the 32 electrons, with the expected contraction of 0.02 Å per element. The predictions of chemical properties by extrapolation will be very difficult und unreliable in this area, since most of the elements have no homologs. From atomic calculations, one can already say that the behavior will be very different due to the stronger relativistic effects.

The fifth series of transition elements is expected to begin beyond the superactinides. Several early DF calculations in this region were performed. In elements 155 to 164, the filling of the 7d shell will take place so that they will be the d transition elements of the 8th period. The 8s and $8p_{1/2}$ electrons will be bound so strongly in these elements that they will not participate in the chemical bonding in contrast to the 7s electrons of the 7th period. Nevertheless, the 9s and $9p_{1/2}$ states will be easily available in 164 for hybridization so that the chemical behavior is expected to be similar to that of other d-elements. From DF calculations of excited states of element 164, Penneman and Mann (1976) suggested that the 7d orbitals will be chemically very active. Thus, in aqueous solutions, strong ligands can form tetra- and hexavalent bonds in addition to the predominant bivalent bonds. Consequently, tetrahedral $164(CO)_4$, $164(PF_3)_4$, and linear $164(CN)_2^{2-}$ might be prepared, which would be a striking contrast to lead (Fricke, 1975). The softness of element 164 should be similar to that of Hg, so that its location in the same group in the periodic table is justified. The metallic state of element 164 should have a larger cohesive energy than almost any other element because of covalent bonding, so that the melting point should be high (Fricke and Waber, 1971). The same authors indicated that the properties of elements 118 and 164 might also be analogous.

In elements 165 and 166, the 9s shell will be filled, suggesting that they should be homologs of group 1 and 2 elements and that their IPs and IR (Fricke, 1975) will be similar to those of the group 1 and 2 elements, respectively. Nevertheless, because of the underlying 7d shell, elements 165 and 166 might exhibit

properties similar to those of the group 13 and 14 elements. Therefore, higher oxidation states than 1+ and 2+, respectively, might occur.

In elements 167 through 172 the $9p_{1/2}$ shell will fill before the $8p_{3/2}$ shell. The energies of these orbitals are so close to each other that this situation is analogous to the nonrelativistic p-shell in the 3d period. Thus, the common oxidation states of elements 167 to 179 will be 3+ to 6+. Element 171 is expected to have many states from 1– to 7+, as do halogens. H(171) would form due to its high electron affinity of 3.0 eV (Fricke *et al.*, 1971). Compounds with F and O are also expected. Element 172 might be a noble gas similar to Xe due to the similar values of their IPs. The major difference is that element 172 is predicted to be a liquid or a solid at normal temperatures because of its large atomic weight.

Mann reported that his program was unable to go beyond $Z = 176$. Model calculations of Fricke and Waber (1972) took into account a phenomenological formulation of quantum electrodynamic effects and made it possible to extend the DF calculations to even higher elements. They calculated the DF ground state for element 184, as shown in Table 14.13. The 10s and $10p_{1/2}$ electrons do not appear in the ground state configuration and only $8d^3$ and $7f^4$ electrons might be available for chemical bonding. The chemical behavior will be then even simpler than that of the early superactinides. With increasing ionization of the 184 ion, a redistribution of electrons occurs between the 6g and 7f shells so that the number of electrons in the 6g shell increases. Since the 6g electrons are very deep inside the ion, only 7f electrons will be available for bonding. By analogy to U, the 5+ and 6+ states may be easily reached, but in aqueous solution the 4+ oxidation state will be the most stable. Higher oxidation states are not likely because the binding energy of the electrons in the deeply buried 6g shell will increase rapidly with higher ionization. Thus, in the very long SHE transition series, where many outer electron shells are being filled simultaneously in the neutral atom, a large increase in ionization energies will occur so that extremely high or unusual oxidation states are not expected.

In summary, in the area of the SHEs, the relativistic effects are so strong that any classification based on the knowledge of their electronic configurations or extrapolations of properties from the known elements is inappropriate. It is interesting to note that even without relativistic effects, the chemistry of the heaviest SHEs would be different from that of their lighter homologs due to very large shell-structure effects. The nonrelativistic expansion and destabilization of the *n*s valence orbitals and contraction and stabilization of the *n*d, *n*f, and orbitals of higher angular quantum number *l* with very large *n* also would have drastically changed the properties of the SHEs. However, due to the opposite actions of relativistic and shell-structure effects, the relativistic and nonrelativistic changes are predicted to go in opposite directions. A more detailed periodic table up to element 172 was given by Fricke (1975). Some discussions of the chemistry of SHEs can be found in Penneman *et al.* (1971),

Fricke (1975), and Jorgensen (1968), and more recently in a review of the evolution of the periodic table by Seaborg (1996).

14.7.2 Prospects for experimental studies of chemistry of elements beyond element 112, including SHEs

The prerequisites for successful studies of the chemistry of elements beyond 112 will be similar to those discussed previously for Mt through 112. These include the existence of isotopes with long enough half-lives for chemical studies, knowledge of their nuclear decay properties so that they can be positively identified as belonging to the element being studied, synthesis reactions with the highest possible cross sections, techniques for increasing the production rates such as cooled, multiple targets, the highest possible beam currents at accelerators with facilities for conducting these studies, and, ideally, dedicated beamlines for optimal utilization of facilities by international groups of scientists. After the chemistry of a given element is known, the atomic number of new isotopes can be positively assigned based on their established chemical properties and detailed studies of nuclear properties such as SF can be conducted on chemically separated samples.

(a) Chemical methods

A useful technique that should prove invaluable in the study of very low-yield, short-lived elements is pre-separation of the nuclides of interest from the host of unwanted activities using a dedicated on-line separator such as the BGS at the appropriate accelerator. At the focal plane the separated isotopes can be stopped in an RTC containing an appropriate gas and can even be treated chemically to adjust oxidation states and volatility. The resultant volatile species can then be rapidly and continuously transported to a cryo-thermochromatographic separator or any other desired chemical separation/detection system.

The ingenious isothermal gas-phase techniques that have already been applied in the studies of volatile Hs oxides can be used to study other volatile species that can be similarly swept in carrier gas directly to an on-line detection system or to a cryogenic TC composed of the particle detectors. In this way, simultaneous on-line measurements can be performed of the decay properties of the radioactive nuclides in the volatile species and their deposition temperature on the surface of the detectors that form the chromatography column. Vacuum cryo-thermochromatographic techniques in which the relative reactivity of elements 114 through 118 are determined based on their sorption on a variety of transition metal surfaces might be used to assess whether their behavior is more like their lighter homologs or the inert noble gases.

The continuous, computer-controlled automated procedures discussed in the previous sections can be used and other procedures designed specifically to exploit the chemistry predicted for each of these elements. Continuously

operating, rapid systems for liquid–liquid extractions followed by detection in flowing liquid-scintillation detectors such as the SISAK-III/liquid scintillation system (Omtvedt *et al.*, 1998, 2002) can be used for on-line studies of isotopes with half-lives as short as a few seconds provided chemical systems that rapidly come to equilibrium can be devised. Alternatively, they could be used to continuously purify longer-lived SHEs. A variety of computer-controlled, continuous multi-ion-exchange column techniques that include automated transport of samples to the detection equipment have been developed (Haba *et al.*, 2002; Nagame *et al.*, 2002) for performing rapid separations of isotopes with half-lives as short as a few seconds and then inferring their presence based on detection of their longer-lived daughters in subsequent chemical separations. Such continuous systems might also be adapted for processing longer-lived SHEs for subsequent off-line detection.

New methods for studying gas-phase ion chemistry in a Penning trap have been reported by Rieth *et al.* (2002) and it has been shown by the ISOLTRAP group at the Centre Européen pour la Recherche Nucléaire (CERN) (Kugler *et al.*, 1992; Bollen *et al.*, 1996) that nuclides as short as a few tenths of a second can be used with Penning trap mass spectrometers. These techniques have potential application to gas-phase studies of elements beyond 112. Kinetic data on ion–molecule interactions can be obtained with single-ion detection, and mass spectrometry can be used to unambiguously determine the stoichiometry of the reaction products. However, the reaction rates must be increased in order to make the technique viable for the low production rates of less than one atom per week expected for the heaviest elements.

(b) Predicted and reported half-lives and nuclear properties of SHEs

One of the most significant nuclear properties of elements 107 through 112 is that they decay predominantly by alpha emission rather than SF, contrary to earlier predictions. This experimental discovery sparked a renewal of interest in searching for elements beyond 112 and revived hope that the long-predicted island of SHEs might finally be reached. Armbruster and Münzenberg (1989) proposed that even though the neutron-deficient isotopes of elements 107 through 112 are probably not spherical, they should qualify as SHEs because without the stabilization of nuclear shells they would not exist. These elements have not been generally recognized as SHEs.

The discovery of longer-lived isotopes in this region, ^{265,266}Sg, ^{267}Bh, and ^{269,270}Hs, substantiated the theoretical model and calculations (Sobiczewski *et al.*, 1994; Smolańczuk *et al.*, 1995) predicting a doubly magic deformed region of extra stability in the vicinity of proton number 108 and neutron number 162 in addition to the island of spherical stability originally predicted to be around $Z = 114$ and $N = 184$, as shown in Fig. 14.24.

Evidence for three isotopes of element 114, ^{287,288,289}114, has been reported (Oganessian *et al.*, 1999a) although only one event of 21-s ^{289}114 was detected

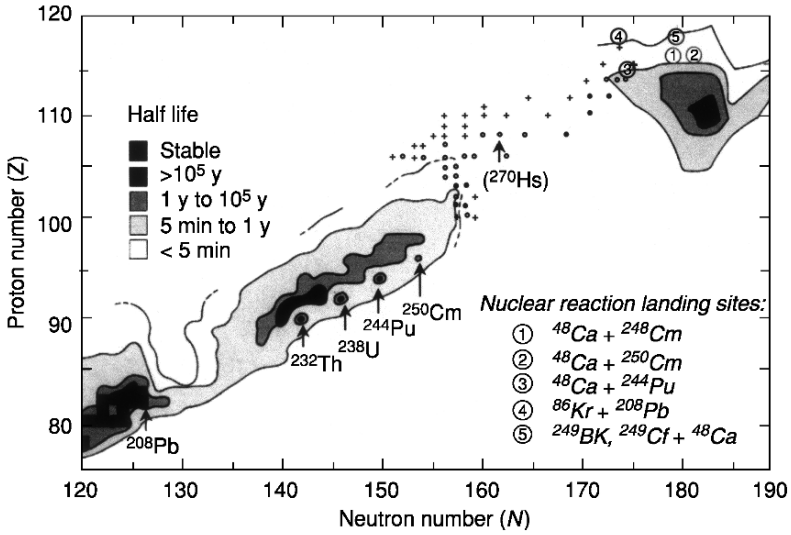

Fig. 14.24 *Updated plot of heavy element topology from* 1978 *showing some landing points for proposed reactions. Heavy element isotopes reported since* 1978 *up to mid-*2002 *are indicated with symbols denoting the following half-life ranges:* 0.1 ms to 0.1 s (+); 0.1 s to 5 min (○); > 5 min (●).

and it was not confirmed in subsequent experiments (Lougheed *et al.*, 2000). The discovery of isotopes of element 116, $^{292}116$, has been discussed by Oganessian (2002) and Oganessian *et al.* (2002, 2004c). Calculations (Smolańczuk, 1997) indicate that these isotopes are nearly spherical with deformation energies ranging from only about 0.1 MeV for $^{292}116$ to 0.3–0.2 MeV for the 114 isotopes, compared to zero deformation energy for the spherical doubly magic $^{298}114$ and 7.8 MeV for the doubly deformed magic nucleus, $^{270}108$. Thus, element 114 and 116 isotopes qualify as spherical SHEs even though they do not have the full complement of 184 neutrons. However, their existence still awaits confirmation by other groups.

Recent theoretical predictions (Chasman and Ahmad, 1997; Smolańczuk, 2001a,b) indicate that isotopes with half-lives of microseconds or longer will exist all along the way to the predicted islands of stability. However, the half-lives predicted for nuclei in the region of the spherical island of stability have decreased dramatically since the 1970s when half-lives of billions of years were predicted. For example, Smolańczuk (2001a,b) predicted that the spherical doubly magic superheavy nucleus $^{298}114$ will decay predominantly by alpha emission with a half-life of only 12 min, but that ^{292}Ds may alpha decay with a half-life of about 50 years.

Some other recent calculations (Kruppa *et al.*, 2000) predict that the strongest spherical shell effects might be at $Z = 124$ or 126 and $N = 184$ while still others

propose the maximum effect might be at $Z = 120$ and $N = 172$. Doughnut-like, toroidal nuclear shapes with lower densities or a hole in the middle to alleviate the effects of Coulomb repulsion have even been postulated. How many more elements can exist is still unclear and it is even more unclear how many of these we can actually produce.

(c) Production reactions

So-called 'cold' fusion reactions in which the compound nucleus is produced with small excitation energy and emits only a single neutron were used to discover the elements from Bh through 112 (Hofmann, 1998). After the discovery of element 112 in 1996 (Hofmann *et al*., 1996), researchers at GSI unsuccessfully attempted to produce element 113 using the cold fusion reaction ^{209}Bi (^{70}Zn,n) ^{278}113 (Hofmann and Münzenberg, 2000). From two experiments lasting about 3 weeks each, they set a limit of 0.6 pb on the cross section at a mean excitation energy of 10.5 MeV. They concluded that the cross section for production of element 116 would be only 1 femtobarn and that their experimental setup would have to be greatly improved in order to investigate this region further. Contrary to these expectations that the production cross sections for the 1n evaporation channel in cold fusion reactions to produce elements above 112 would continue to decrease exponentially with the proton number of the projectile, Smolańczuk (1999a) suggested that the cold fusion reaction ^{208}Pb(^{86}Kr,n) reaction to produce the hypothetical spherical SHE nuclide ^{293}118 with an excitation energy of only 13 MeV would have an unusually large cross section of a few hundred picobarns. The predicted increase in formation cross section was attributed to the fact that ^{86}Kr contains the magic number of 50 neutrons, which leads to a larger Q value with a subsequent increase in the transmission probability through the Coulomb barrier. He also predicted that ^{293}118 would decay by a unique decay sequence of six high-energy alpha particles. However, the results of Gregorich *et al*. (2002) setting upper limits of less than 1 pb for the formation cross section for this reaction based on detection of the predicted high-energy alpha-decay chain make the use of cold fusion reactions appear less attractive for production of SHEs. Estimates of the predicted cross section were later lowered to about 6 pb (Smolańczuk, 2001b), and it was pointed out that the excitation functions are quite narrow and have a rather sharp threshold (Smolańczuk, 1999c) so use of too low a bombarding energy might result in a negative result and the idea should not be totally abandoned.

Similar cold fusion reactions with ^{208}Pb or ^{209}Bi targets with ^{87}Rb or ^{86}Kr projectiles could be used to produce ^{294}119 (Smolańczuk, 1999a,b), whose half-life is estimated to be only microseconds. However, ^{294}119 is predicted to decay to isotopes of the new longer-lived, odd-Z elements 117, 115, and 113 via a succession of alpha emissions, ending with the known isotope 3.6-h ^{262}Lr. Production of ^{295}120 ($\sim$2 μs) via the ^{208}Pb(^{88}Sr,1n) reaction and detection of its high-energy alpha-decay chain have also been proposed (Smolańczuk, 2001a).

The reported elements 114 and 116 were synthesized using reactions of ^{244}Pu and ^{248}Cm with ^{48}Ca projectiles to form the compound nuclei ^{292}114 and ^{296}116, which then emitted four neutrons to produce 2.6-s ^{288}114 and 53-ms ^{292}116 (Oganessian *et al*., 2000a,b; Oganessian, 2001, 2002). They were calculated to have excitation energies of only 33 and 31 MeV, respectively, due to the stability of the doubly magic projectile, compared to >45 MeV for 'hot' fusion reactions. The detection limit of these experiments was about 0.5 pb, several orders of magnitude more sensitive than in the unsuccessful attempt reported in 1984 by an international group of nuclear scientists, both chemists and physicists (Armbruster *et al*., 1985), who conducted an exhaustive 'final' investigation of the reaction of ^{248}Cm with ^{48}Ca projectiles to produce SHEs. Oganessian also proposed that the reaction of ^{48}Ca with ^{249}Cf targets be used to produce element ^{294}118 via the '3n out' reaction. However, the viability of the '3n out' reactions in this region has yet to be confirmed. Loveland *et al*. (2002) set a limit of <2 pb for SF and alpha events for the ^{238}U(^{48}Ca,3n)^{283}Ds reaction. Hot fusion reactions between ^{48}Ca projectiles and ^{249}Bk and ^{249}Cf targets to produce elements ^{293,294}117 and ^{293,294}118, respectively, are under investigation by the Dubna/LLNL group.

The ^{237}Np and ^{249}Bk targets with ^{48}Ca projectiles can probably be used to make the odd-proton element 113 and more neutron-rich isotopes of element 117, respectively. Other highly radioactive targets such as ^{249}Cf or even ^{254}Es with appropriate projectiles might be used to make more neutron-rich isotopes of elements as heavy as 118, but considerable development work will be required.

Reactions that can produce a higher ratio of neutrons to protons will certainly be most advantageous and need to be investigated. Myers and Swiatecki (2000) have suggested that so-called 'unshielded' reactions in which the Coulomb barrier has sunk below the bombarding energy may result in enhanced production yields for some of the higher Z elements. Their hypothesis that the cross section for ^{277}112 produced in the symmetric reaction ^{142}Ce(^{136}Xe,n) might be much larger than that for the 112 discovery reaction ^{208}Pb(^{70}Zn, n)^{277}112 should be tested experimentally. If so, the unshielded reaction ^{170}Er (^{136}Xe,n) reaction to make ^{305}122, which has 183 neutrons, might be a method for getting closer to these regions. It should decay by successive alpha emission to the isotope ^{289}114, reported by the Dubna/LLNL group. Whether additional SHEs can be produced depends very much upon whether the cross sections for the 'cold' fusion reactions in which only a single neutron is emitted and the 'warm'/'hot' fusion reactions with three or four neutrons emitted are large enough to permit detection.

It now appears likely that many more relatively long-lived nuclides can exist than are presently known, but a major research effort to explore new types of production reactions, imaginative techniques for optimizing overall yields by using multiple targets and higher beam currents, innovative chemical separations, and a dedicated on-line installation for chemical studies at an appropriate

accelerator with access to a pre-separator will be required in order to fully explore their chemical properties. If, on the other hand, relatively long-lived new elements are discovered, then methods for 'stockpiling' them for off-line studies or producing them as by-products of other experiments must be devised to facilitate studies of their chemistry. The prospect lies ahead of a whole new landscape for the exploration of the chemical properties of the heaviest elements and their compounds, determining the influence of relativistic effects, assigning their positions in the periodic table, and extending and further defining the architecture of the periodic table.

REFERENCES

Adloff, J. -P. and Guillaumont, R. (1993) *Fundamentals of Radiochemistry*, CRC Press, Boca Raton, pp. 327–52.

Ahrland, S., Liljenzin, J. O., and Rydberg, J. (1973) in *Comprehensive Inorganic Chemistry*, vol. 5 (ed. J. Bailar), Pergamon Press, Oxford, pp. 519–42.

Alekseeva, T. E., Arkhipova, N. F., and Rabinovitch, V. A. (1972) *Russ. J. Inorg. Chem.* **17**, 140–1.

Alstad, J., Skarnemark, G., Haberberger, F., Herrmann, G., Nähler, A., Pense-Maskow, M., and Trautmann, N. (1995) *J. Radioanal. Nucl. Chem. Articles*, **189**, 133.

Alzitzoglou, T., Rogowski, J., Skålberg, M., Alstad, J., Herrmann, G., Kaffrell, N., Skarnemark, G., Talbert, W., and Trautmann, N. (1990) *Radiochim. Acta*, **51**, 145–50.

Amble, E., Miller, S. L., Schawlaw, A. L., and Townes, C. H. (1952) *J. Chem. Phys.,* **20**, 192.

Armbruster, P., Agarwal, Y. K., Brüchle, W., Brügger, M., Dufour, J. P., Gäggeler, H., Hessberger, F. P., Hofmann, S., Lemmertz, P., Münzenberg, G., Poppensieker, K., Reisdorf, W., Schädel, M., Schmidt, K. H., Schneider, J. H. R., Schneider, W. F. W., Sümmerer, K., Vermeulen, D., Wirth, G., Ghiorso, A., Gregorich, K. E., M., D. L., Leino, M., Moody, K. J., Seaborg, G. T., Welch, R. B., Wilmarth, P., Yashita, S., Frink, C., Greulich, N., Herrmann, G., Hickmann, U., Hildebrand, N., Kratz, J. V., Trautmann, N., Fowler, M. M., Hoffman, D. C., Daniels, W. R., Gunten, H. R. V., and Dornhöfer, H. (1985) *Phys. Rev. Lett.,* **54**, 406–9.

Armbruster, P. and Münzenberg, G. (1989) *Sci. Am,* **66**, 66–72.

Armbruster, P., Hessberger, F. P., Hofmann, S., Leino, M., Münzenberg, G., Reisdorf, W., and Schmidt, K.-H. (1993) *Pure Appl. Chem*., **65**, 1822–4.

Autschbach, J., Siekierski, S., Seth, M., Schwerdtfeger, P., and Schwarz, W. H. E. (2002) *J. Comput. Chem*., **23**, 804–13.

Baerends, E. J., Schwarz, W. H. E., Schwerdtfeger, P., and Snijders, J. G. (1990) *J. Phys. B,* **23**, 3225–40.

Baes, C. F. and Mesmer, R. E. (1976) *The Hydroysis of Cations*, Wiley Interscience, New York, pp. 152–91.

Barber, R. C., Greenwood, N. N., Hrynkiewicz, A. Z., Jeannin, Y. P., Lefort, M., Sakai, M., Ulehla, I., Wapstra, A. H., and Wilkinson, D. H. (1991) *Pure Appl. Chem*., **63**, 879–86.

Barber, R. C., Greenwood, N. N., Hrynkiewicz, A. Z., Jeannin, Y. P., Lefort, M., Sakai, M., Ulehla, I., Wapstra, A. H., and Wilkinso, D. H. (1992) *Prog. Part. Nucl. Phys*., **29**, 453–530.

Barber, R. C., Greenwood, N. N., Hrynkiewicz, A. Z., Jeannin, Y. P., Lefort, M., Sakai, M., Ulehla, I., Wapstra, A. H., and Wilkinso, D. H. (1993) *Pure Appl. Chem.,* **65**, 1757–813.

Bastug, T., Heinemann, D., Sepp, W.-D., Kolb, D., and Fricke, B. (1993) *Chem. Phys. Lett*., **211–224**, 119–24.

Bemis, C. E. Jr, Silva, R. J., Hensley, D. C., Keller, O. L. Jr, Tarrant, J. R., Hunt, L. D., Dittner, P. F., Hahn, R. L., and Goodman, C. D. (1973) *Phys. Rev. Lett.,* **31**, 647–50.

Bemis, C. E. Jr, Dittner, P. F., Silva, R. J., Hahn, R. L., Tarrant, J. R., Hunt, L. D., and Hensley, D. C. (1977) *Phys. Rev. C,* **16**, 1146–57.

Bilewicz, A., Kacher, C. D., Gregorich, K. E., Lee, D. M., Stoyer, N. J., Kadkhodayan, B., Kreek, S. A., Lane, M. R., Sylwester, E. R., Neu, M. P., Mohar, M. F., and Hoffman, D. C. (1996) *Radiochim. Acta*, **75**, 121–6.

Bollen, G., Becker, S., Kluge, H.-J., Konig, M., Moore, R. B., Otto, T., Raimbault-Hartmann, H., Savard, G., Schweikhard, L., and Stolzenberg, H. (1996) *Nucl. Instrum. Methods A,* **368**, 675–97.

Bratsch, S. G. and Lagowski, J. J. (1986) *J. Phys. Chem.,* **90**, 307–12.

Bratsch, S. G. (1989) *Phys. Chem. Ref. Data,* **18**, 1–21.

Brown, D. (1973) *Comprehensive Inorganic Chemistry*, vol. 3, Pergamon Press, Oxford, pp. 553–622.

Brüchle, W., Jäger, E., Pershina, V., Schädel, M., Schausten, B., Günther, R., Kratz, J. V., Paulus, W., Seibert, A., Thörle, P., Zauner, S., Schümann, D., Eichler, B., Gäggeler, H., Jost, D., and Türler, A. (1998) *J. Alloy Compds*, **271–273**, 300–2.

Burraghs, P., Evans, S., Hamnett, A., Orchard, A. F., and Richardson, N. V. (1974) *J. Chem. Soc. Faraday Trans.* 2, **70**, 1895.

Chasman, R. R. and Ahmad, I. (1997) *Phys. Lett. B,* **392**, 255–61.

CNIC, Commission on Nomenclature of Inorganic Chemistry of IUPAC (1997) *Pure Appl. Chem.*, **69**, 2471–3.

Corish, J. and Rosenblatt, G. M. (2003) *Pure Appl. Chem*., **75**, 1613–15.

Corish, J. and Rosenblatt, G. M. (2004) *Pure Appl. Chem*. **76**, 2101–3.

Cunningham, B. B. (1969) in *Proc. Robert A. Welch Foundation, XIII, The Transuranium elements – The Mendeleev Centennial*, pp. 307–22, Houston, Texas.

Czerwinski, K. R. (1992a) *Studies of Fundamental Properties of Rutherfordium (element 104) Using Organic Complexing Agents*, Doctoral Thesis, LBL-32233, Berkeley.

Czerwinski, K. R. (1992b) *Studies of Fundamental properties of Rutherfordium (element 104) Using Organic Complexing Agents*, Ph.D. Thesis, Berkeley, LBL-32233, pp. 83–102.

Czerwinski, K. R., Gregorich, K. E., Hannink, N. J., Kacher, C. D., Kadkhodayan, B. A., Kreek, S. A., Lee, D. M., Nurmia, M. J., Türler, A., Seaborg, G. T., and Hoffman, D. C. (1994a) *Radiochim. Acta,* **64**, 23–8.

Czerwinski, K. R., Kacher, C. D., Gregorich, K. E., Hamilton, T. M., Hannink, N. J., Kadkhodayan, B. A., Kreek, S. A., Lee, D. M., Nurmia, M. J., Türler, A., Seaborg, G. T., and Hoffman, D. C. (1994b) *Radiochim. Acta,* **64**, 29–35.

Desclaux, J. P. (1973) *Data Nucl. Data Tables*, **12**, 311–406.

Desclaux, J. P. (1975) *Comp. Phys. Commun*., **9**, 31–45.

Desclaux, J. P. and Fricke, B. (1980) *J. Phys.*, **41**, 943–6.
Dolg, M., Stoll, H., Preuss, H., and Pitzer, R. M. (1993) *J. Phys. Chem.*, **97**, 5852–9.
Düllmann, C. E., Eichler, B., Eichler, R., Gäggeler, H. W., Jost, D. T., Piguet, D., and Türler, A. (2002a) *Nucl. Instrum. Methods A*, **479**, 631–9.
Düllmann, C. E., Brüchle, W., Dressler, R., Eberhardt, K., Eichler, B., Eichler, R., Gäggeler, H. W., Ginter, T. N., Glaus, F., Gregorich, K. E., Hoffman, D. C., Jäger, E., Jost, D. T., Kirbach, U. W., Lee, D. M., Nitsche, H., Patin, J. B., Pershina, V., Piguet, D., Qin, Z., Schädel, M., Schausten, B., Schimpf, E., Schött, H.-J., Soverna, S., Sudowe, R., Thörle, P., Timokhin, S. N., Trautmann, N., Türler, A., Vahle, A., Wirth, G., Yakushev, A. B., and Zielinski, P. M. (2002b) *Nature,* **418**, 859–62.
Eichler, B. (1974) Dubna Report JINR P12–7767.
Eichler, B. and Rossbach, H. (1983) *Radiochim. Acta,* **33**, 121–5.
Eichler, B., Türler, A., and Gäggeler, H. W. (1999) *J. Phys. Chem. A,* **103**, 9296–306.
Eichler, B. and Kratz, J. V. (2000) *Radiochim. Acta,* **88**, 475–82.
Eichler, R., Brüchle, W., Dressler, C. E., Düllman, C. E., Eichler, B., Gäggeler, H. W., Gregorich, K. E., Hoffman, D. C., Hübener, S., Jost, D. T., Kirbach, U. W., Laue, C. A., Lavanchy, V. M., Nitsche, H., Patin, J. B., Piguet, D., Schädel, M., Shaughnessy, D. A., Strellis, D. A., Taut, S., Tobler, L., Tsyganov, Y. S., Türler, A., Vahle, A., Wilk, P. A., and Yakushev, A. B. (2000) *Nature (Lett.),* **407**, 63–5.
Eichler, R. and Schädel, M. (2002) *J. Phys. Chem. B,* **106**, 5413–20.
Eliav, E., Landau, A., Ishikawa, Y., and Kaldor, U. (1992) *J. Phys. B,* **35**, 1693.
Eliav, E., Kaldor, U., Schwerdtfeger, P., Hess, B. A., and Ishikawa, Y. (1994) *Phys. Rev. Lett.,* **73**, 3203–6.
Eliav, E., Kaldor, U., and Ishikawa, Y. (1995a) *Phys. Rev. Lett.,* **74**, 1079–82.
Eliav, E., Kaldor, U., and Ishikawa, Y. (1995b) *Phys. Rev. A,* **52**, 2765–9.
Eliav, E., Kaldor, U., Ishikawa, Y., Seth, M., and Pyykkö, P. (1996a) *Phys. Rev. A,* **53**, 3926–33.
Eliav, E., Kaldor, U., Ishikawa, Y. M., and Pyykkö, P. (1996b) *Phys. Rev. Lett.*, **77**, 5350–2.
Eliav, E., Shmulyian, S., Kaldor, U., and Ishikawa, Y. (1998a) *J. Chem. Phys.*, **109**, 3954–8.
Eliav, E., Kaldor, U., and Ishikawa, Y. (1998b) *Mol. Phys.*, **94**, 181–7.
Eliav, E., Landau, A., Ishikawa, Y., and Kaldor, U. (2002) *J. Phys. B,* **35**, 1693–700.
Ermler, W. C., Ross, R. B., and Christiansen, P. A. (1988) *Adv. Quant. Chem.,* **19**, 139–82.
Faegri, K. and Saue, T. (2001) *J. Chem. Phys.*, **115**, 2456–64.
Fiset, E. O. and Nix, J. R. (1972) *Nucl. Phys.*, **A193**, 647.
Flerov, G. N. and Zvara, I. (1971) Joint Institute of Nuclear Research, Dubna, USSR, Report D7-6031, August 1971.
Fricke, B., Greiner, W., and Waber, J. T. (1971) *Theor. Chim. Acta,* **21**, 235–60.
Fricke, B. and Waber, J. T. (1971) *Actinides Rev.*, **1**, 433–85.
Fricke, B. and Waber, J. T. (1972) *J. Chem. Phys.*, **56**, 3246.
Fricke, B. (1975) in *Structure and Bonding*, vol. 21 (ed. J. D. Dunitz), Springer-Verlag, Berlin, pp. 89–144.
Fricke, B., Johnson, E., and Rivera, G. M. (1993) *Radiochim. Acta,* **62**, 17–25.

Gäggeler, H. W. (1990) Chemistry of the transactinide elements, in *The Robert A. Welch Foundation Conference on Chemical Research XXXIV. Fifty Years with Transuranium Elements*, pp. 255–76, Houston, Texas.

Gäggeler, H. W., Jost, D. T., Kovacs, J., Scherer, U. W., Weber, A., Vermeulen, D., Türler, A., Gregorich, K. E., Henderson, R. A., Czerwinski, K. R., Kadkhodayan, B., Lee, D. M., Nurmia, M., Hoffman, D. C., Kratz, J. V., Gober, M. K., Zimmermann, H. P., Schädel, M., Bruchle, W., Schimpf, E., and Zvara, I. (1992) *Radiochim. Acta,* **57**, 93–100.

Gäggeler, H. W. (1994) *J. Radioanal. Nucl. Chem. Articles,* **183**, 261.

Gäggeler, H. W. (1997) Fast chemical separation procedures for transactinides, in *The Robert A. Welch Foundation 41st Conference on Chemical Research the Transuranium Elements*, pp. 47–51, Houston, Texas.

Gärtner, M., Boettger, M., Eichler, B., Gäggeler, H. W., Grantz, M., Hubener, S., Jost, D. T., Piguet, D., Dressler, R., Türler, A., and Yakushev, A. B. (1997) *Radiochim. Acta,* **78**, 59–68.

Ghiorso, A., Nurmia, M., Harris, J., Eskola, K., and Eskola, P. (1969) *Phys. Rev. Lett.,* **22**, 1317.

Ghiorso, A., Nurmia, M., Eskola, K., Harris, J., and Eskola, P. (1970) *Phys. Rev. Lett.,* **24**, 1498–503.

Ghiorso, A., Nurmia, M., Eskola, K., and Eskola, P. (1971) *Phys. Rev C,* **4**, 1850–5.

Ghiorso, A. and Seaborg, G. T. (1993a) *Pure Appl. Chem*., **65**, 1815–20.

Ghiorso, A. and Seaborg, G. T. (1993b) *Prog. Part. Nucl. Phys*., **31**, 233–7.

Ghiorso, A., Lee, D., Somerville, L. P., Loveland, W., Nitschke, J. M., Ghiorso, W., Seaborg, G. T., Wilmarth, P., Leres, R., Wydler, A., Nurmia, M., Gregorich, K., Czerwinski, K., Gaylord, R., Hamilton, T., Hannink, N. J., Hoffman, D. C., Jarzynski, C., Kacher, C., Kadkhodayan, B., Kreek, S., Lane, M., Lyon, A., McMahan, M. A., Neu, M., Sikkeland, T., Swiatecki, W. J., Türler, A., Walton, J. T., and Yashita, S. (1995a) *Nucl. Phys*., **583**, 861–6.

Ghiorso, A., Lee, D., Somerville, L. P., Loveland, W., Nitschke, J. M., Ghiorso, W., Seaborg, G. T., Wilmarth, P., Leres, R., Wydler, A., Nurmia, M., Gregorich, K., Czerwinski, K., Gaylord, R., Hamilton, T., Hannink, N. J., Hoffman, D. C., Jarzynski, C., Kacher, C., Kadkhodayan, B., Kreek, S., Lane, M., Lyon, A., McMahan, M. A., Neu, M., Sikkeland, T., Swiatecki, W. J., Türler, A., Walton, J. T., and Yashita, S. (1995b) *Phys. Rev. C,* **51**, R2293–7.

Girichev, G. V., Petrov, V. M., Giricheva, N. I., Utkin, A. N., and Petrova, V. N. (1981) *Zh. Strukt. Khim.,* **22**, 6.

Glebov, V. A., Kasztura, L., Nefedov, V. S., and Zhuikov, B. L. (1989) *Radiochim. Acta*, **46**, 117–21.

Gober, M. G., Kratz, J. V., Zimmermann, H. P., Schädel, M., Brüchle, W., Schimpf, E., Gregorich, K. E., Türler, A., Hannink, N. J., Czerwinski, R. K., Kadkhodayan, B., Lee, D. M., Nurmia, M. J., Hoffman, D. C., Gäggeler, H., Jost, D., Kovacs, J., Scherer, U. W., and Weber, A. (1992) *Radiochim. Acta*, **57**, 77–84.

Grant, I. P. and Pyper, N. C. (1977) *Nature (Lett.)*, **265**, 715–17.

Grant, I. P. (1986) *J. Phys. B,* **19**, 3187–205.

Grant, I. P. (1994) *Adv. Mol. Phys.,* **32**, 169–86.

Grant, I. P. and Quiney, H. (2000) *Int. J. Quant. Chem*., **80**, 283–97.

Gregorich, K. E., Henderson, R. A., Lee, D. M., Nurmia, M. J., Chasteler, R. M., Hall, H. L., Bennett, D. A., Gannett, C. M., Chadwick, R. B., Leyba, J. D., Hoffman, D. C., and Herrmann, G. (1988) *Radiochim. Acta*, **43**, 223–31.

Gregorich, K. E. (1997a) Radiochemistry of rutherfordium and hahnium, in *The Robert A. Welch Foundation 41st Conference on Chemical Research the Transuranium Elements*, pp. 95–124, Houston, Texas.

Gregorich, K. E. (1997b) Radiochemistry of rutherfordium and hahnium, in *The Robert A. Welch Foundation 41st Conference on Chemical Research the Transuranium Elements*, pp. 103–8, Houston, Texas.

Gregorich, K. E., Ginter, T., Loveland, W., Peterson, D., Patin, J. B., Folden, C. M. III, Hoffman, D. C., Lee, D. M., Nitsche, H., Omtvedt, J. P., Omtvedt, L. A., Stavsetra, L., Sudowe, R., Wilk, P. A., Zielinski, P., and Aleklett, K. (2002) *Eur. Phys. J. A,* **18**, 633–8.

Griffin, D. C., Andrew, K. L., and Cowan, R. D. (1969) *Phys. Rev.,* **177**, 62–71.

Grosse, A. V. (1965) *J. Inorg. Nucl. Chem.,* **27**, 509–20.

Guillaumont, R., Adloff, J.-P., and Peneloux, A. (1989) *Radiochim. Acta,* **46**, 169–76.

Guillaumont, R., Adloff, J.-P., Peneloux, A., and Delamoye, P. (1991) *Radiochim. Acta,* **54**, 1–15.

Günther, R., Paulus, W., Kratz, J. V., Seibert, A., Thorle, P., Zauner, S., Bruchle, W., Jager, E., Pershina, V., Schädel, M., Schausten, B., Schumann, D., Eichler, B., Gäggeler, H. W., Jost, D. T., and Türler, A. (1998) *Radiochem. Acta,* **80**, 121–8.

Haba, H., Tsukada, K., Asai, M., Goto, S., Toyoshima, A., Nishinaka, I., Akiyama, K., Hirata, M., Ichikawa, S., Nagame, Y., Shoji, Y., Shigekawa, M., Koike, T., Iwasaki, M., Shinohara, A., Kaneko, T., Maruyama, T., Ono, S., Kudo, H., Oura, Y., Sueki, K., Nakahara, H., Sakama, M., Yokoyama, A., Kratz, J. V., Schädel, M., and Brüchle, W. (2002) *J. Nucl. Radiochem. Sci.,* **3**, 143–6.

Han, Y.-K. and Lee, Y. S. (1999) *J. Phys. Chem. A,* **103**, 1104–8.

Han, Y.-K., Son, S.-K., Choi, Y. J., and Lee, Y. S. (1999a) *J. Phys. Chem.,* **103**, 9109–15.

Han, Y.-K., Bae, C., and Lee, Y. S. (1999b) *J. Chem. Phys.,* **110**, 8986–75.

Han, Y.-K., Bae, C., Son, S.-K., and Lee, Y. S. (2000) *J. Chem. Phys.,* **112**, 2684–91.

Harvey, B. G., Gunther, H., Hoff, R., Hoffman, D. C., Hyde, E. K., Katz, J. J., and Seaborg, G. T. (1976) *Science,* **193**, 271–3.

Hessberger, F. P., Hofmann, S., Ninov, V., Armbruster, P., Folger, H., Munzenberg, G., Schott, H. J., Popeko, A. G., Yeremin, A. V., Andreyev, A. N., and Saro, S. (1997) *Z. Phys. A,* **359**, 415–25.

Hoffman, D. C. (1994) *Chem. Eng. News*, 24–34.

Hoffman, D. C. (1996) *Radiochim. Acta,* **72**, 1–6.

Hoffman, D. C. and Lee, D. M. (1999) *J. Chem. Educ.,* **76**, 331–47.

Hoffman, D. C., Ghiorso, A., and Seaborg, G. T. (2000a) *The Transuranium People: The Inside Story*, Imperial College Press, London, pp. 258–98; 379–96.

Hoffman, D. C., Ghiorso, A., and Seaborg, G. T. (2000b) *The Transuranium People: The Inside Story*, Imperial College Press, London, pp. 400–17.

Hofmann, S., Ninov, V., Hessberger, F. P., Armbruster, P., Folger, H., Münzenberg, G., Schott, H. J., Popeko, A. G., Yeremin, A. V., Andreyev, A. N., Saro, S., Janik, R., and Leino, M. (1995a) *Z. Phys.,* **A350**, 277–80.

Hofmann, S., Ninov, V., Hessberger, F. P., Armbruster, P., Folger, H., Münzenberg, G., and Leino, M. (1995b) *Z. Phys.,* **A350**, 281–2.

Hofmann, S., Ninov, V., Hessberger, F. P., Armbruster, P., Folger, H., Münzenberg, G., Schott, H. J., Popeko, A. G., Yeremin, A. V., Saro, S., Janik, R., and Leino, M. (1996) *Z. Phys.,* **A354**, 229–30.

Hofmann, S. (1998) *Rep. Prog. Phys.,* **61**, 639–89.

Hofmann, S. and Munzenberg, G. (2000) *Rev. Modern Phys.,* **72**, 733–67.

Hofmann, S., Hessberger, F. P., Ackermann, D., Münzenberg, G., Antalic, S., Cagarda, P., Kindler, B., Kojouharova, J., Leino, M., Lommel, B., Mann, R., Popeko, A. G., Reshitko, S., Saro, S., Uusitalo, J., and Yeremin, A. V. (2002) *Eur. Phys. J. A,* **14**, 147–57.

Hübener, S., Taut, S., Vahle, A., Dressler, R., Eichler, B., Gäggeler, H. W., Jost, D. T., Piguet, D. T., Türler, A., Brüchle, W., Jäger, E., Schädel, M., Schimpf, E., Kirbach, U., Trautmann, N., and Yakushev, A. B. (2001) *Radiochim. Acta,* **89**, 737–41.

Hulet, E. K., Lougheed, R. W., Wild, J. F., and Landrum, J. H. (1980) *J. Inorg. Nucl. Chem.,* **42**, 79–82.

Hyde, E. K., Hoffman, D. C., and Keller, O. L. Jr (1987) *Radiochim. Acta,* **42**, 57–102.

Ionova, G. V., Pershina, V., Johnson, E., Fricke, B., and Schädel, M. (1992) *J. Phys. Chem.,* **96**, 11096–101.

Ionova, G. V., Pershina, V., Zuraeva, I. T., and Suraeva, N. I. (1996) *Sov. Radiochem.,* **37**, 282–91.

Ishikawa, Y. and Kaldor, U. in *Computational Chemistry, Reviews of Current Trends* (1996) (ed. J. Leszczynski), Worlds Scientific, Singapore, Vol. 1, pp. 1–52.

Jampolskii, V. I. (1973) Doctoral Thesis, Moscow State University.

Johnson, E., Fricke, B., Keller, O. L. Jr, Nestor, C. W. Jr, and Ticker, T. C. (1990) *J. Chem. Phys.,* **93**, 8041–50.

Johnson, E. and Fricke, B. (1991) *J. Phys. Chem.,* **95**, 7082–4.

Johnson, E., Pershina, V., and Fricke, B. (1999) *J. Phys. Chem.,* **103**, 8458–62.

Johnson, E., Fricke, B., Jacob, T., Dong, C. Z., Fritzsche, S., and Pershina, V. (2002) *J. Chem. Phys.,* **116**, 1862–8.

Jorgensen, C. K. (1968) *Chem. Phys. Lett.,* **2**, 549–50.

Kacher, C. D., Gregorich, K. E., Lee, D. M., Watanabe, Y., Kadkhodayan, B., Yang, B. J., Hsu, M., Hoffman, D. C., and Bilewicz, A. (1996a) *Radiochim. Acta,* **75**, 127–33.

Kacher, C. D., Gregorich, K. E., Lee, D. M., Watanabe, Y., Kadkhodayan, B., Wierczinski, B., Lane, M. R., Sylwester, E. R., Keeney, D. A., Hendricks, M., Hoffman, D. C., and Bilewicz, A. (1996b) *Radiochim. Acta,* **75**, 135–9.

Kadkhodayan, B., Türler, A., Gregorich, K. E., Nurmia, M. J., Lee, D. M., and Hoffman, D. C. (1992) *Nucl. Instrum. Methods,* **A317**, 254–61.

Kadkhodayan, B. (1993) *On-Line Gas Chromatographic Studies of Rutherfordium (element 104), Hahnium (element 105), and Homologs*, Doctoral Thesis, LBL-33961, Berkeley.

Kadkhodayan, B., Türler, A., Gregorich, K. E., Baisden, P. A., Czerwinski, K. R., Eichler, E., Gäggeler, H. W., Hamilton, T. M., Stoyer, N. J., Jost, D. T., Kacher, C. D., Kovacs, A., Kreek, S. A., Lane, M. R., Mohar, M. F., Neu, M. P., Sylwester, E. R., Lee, D. M., Nurmia, M. J., Seaborg, G. T., and Hoffman, D. C. (1996) *Radiochim. Acta,* **72**, 169–78.

Kaldor, U. and Eliav, E. (1998) *Adv. Quantum. Chem.,* **31**, 313–36.

Kaldor, U. and Eliav, E. (2000) Energies and other properties of heavy atoms and molecules, in *Quantum Systems in Chemistry and Physics,* vol. II (eds. A. Hernandes-Laguna, J. Maruani, R. McWeeny, S. Wilson), Kluwer, Dordrecht, vol. 1, pp. 161–176.

Karol, P. J., Nakahara, H., Petley, B. W., and Vogt, E. (2001) *Pure Appl. Chem.,* **73**, 959–67.

Karol, P. J., Nakahara, H., Petley, B. W., and Vogt, E. (2003) *Pure Appl. Chem.,* **75**, 1601–11.

Keller, O. L. Jr, Burnett, J. L., Carlson, T. A., and Nestor, C. W. J. (1970) *J. Phys. Chem.,* **74**, 1127–34.

Keller, O. L. Jr, Nestor, C. W., Carlson, T. A., and Fricke, B. (1973) *J. Phys. Chem.,* **77**, 1806–9.

Keller, O. L. Jr, Nestor, C. W., and Fricke, B. (1974) *J. Phys. Chem.,* **78**, 1845–9.

Keller, O. L. Jr and Seaborg, G. T. (1977) *Annu. Rev. Nucl. Sci.,* **27**, 139–66.

Keller, O. L. Jr (1984) *Radiochim. Acta,* **37**, 169–80.

Kirbach, U. W., Folden, C. M. III, Ginter, T. N., Gregorich, K. E., Lee, D. M., Ninov, V., Omtvedt, J. P., Patin, J. B., Seward, N. K., Strellis, D. A., Sudowe, R., Türler, A., Wilk, P. A., Zielinski, P. M., Hoffman, D. C., and Nitsche, H. (2002) *Nucl. Instrum. Methods A,* **484**, 587–94.

Kohn, W., Becke, A. D., and Parr, R. G. (1996) *J. Phys. Chem.,* **100**, 12974–80.

Kratz, J. V., Zimmermann, H. P., Scherer, U. W., Schädel, M., Brüchle, W., Gregorich, K. E., Gannett, C. M., Hall, H. L., Henderson, R. A., Lee, D. M., Leyba, J. D., Nurmia, M. J., Hoffman, D. C., Gäggeler, H. W., Jost, D., Baltensperger, U., Ya, N. Q., Türler, A., and Lienert, C. (1989) *Radiochim. Acta,* **48**, 121–33.

Kratz, J. V., Gober, M. K., Zimmermann, H. P., Schädel, M., Brüchle, W., Schimpf, E., Gregorich, K. E., Türler, A., Hannink, N. J., Czerwinski, K. R., Kadkhodayan, B., Lee, D. M., Nurmia, M. J., Hoffman, D. C., Gäggeler, H. W., Jost, D., Kovacs, J., Scherer, U. W., and Weber, A. (1992) *Phys. Rev. C,* **45**, 1064–9.

Kratz, J. V. (1999a) Fast chemical separation procedures for transactinides, in *Heavy Elements and Related New Phenomena* (eds. W. Greiner and R. K. Gupta), World Scientific, Singapore, pp. 43–63.

Kratz, J. V. (1999b) Chemical properties of the transactinide elements, in *Heavy Elements and Related New Phenomena* (eds. W. Greiner and R. K. Gupta), World Scientific, Singapore, pp. 129–93.

Krebs, B., and Hasse, K. D. (1976) *Acta Crystallogr., B* **32**, 1334

Kruppa, A. T., Bender, M., Nazarewicz, W., Reinhard, P. G., Vertse, T., and Cwiok, S. (2000) *Phys. Rev. C,* **61** 034313-1–13.

Kugler, E., Fiander, D., Jonson, B., Haas, H., Przewloka, A., Ravn, H. L., Simon, D. J., and Zimmer, K. (1992) *Nucl. Instrum. Methods. B,* **70**, 41–9.

Landau, A., Eliav, E., Ishikawa, Y., and Kaldor, U. (2001) *J. Chem. Phys.,* **114**, 2977–80.

Lazarev, Y. A., Lobanov, Y. V., Oganessian, Y. T., Utyonkov, V. K., Abdullin, F. S., Buklanov, G. V., Gikal, B. N., Iliev, S., Mezentsev, A. N., Polyakov, A. N., Sedykh, I. M., Shirokovsky, I. V., Subbotin, V. G., Sukhov, A. M., Tsyganov, Y. S., Zhuchko, V. E., Lougheed, R. W., Moody, K. J., Wild, J. F., Hulet, E. K., and McQuaid, J. H. (1994) *Phys. Rev. Lett.,* **73**, 624–7.

Lazarev, Y. A., Lobanov, Y. V., Oganessian, Y. T., Tsyganov, Y. S., Utyonkov, V. K., Abdullin, F. S., Iliev, S., Polyakov, A. N., Rigol, J., Shirokovsky, I. V., Subbotin, V. G., Sukhov, A. M., Buklanov, G. V., Gikal, B. N., Kutner, V. B., Mezentsev, A. N., Sedykh, I. M., Vakatov, D. V., Lougheed, R. W., Wild, J. F., Moody, K. J., and Hulet, E. K. (1995) *Phys. Rev. Lett.,* **75**, 1903–6.

Lazarev, Y. A., Lobanov, Y. V., Oganessian, Y. T., Utyonkov, V. K., Abdullin, F. S., Polyakov, A. N., Rigol, J., Shirokovsky, I. V., Tsyganov, Y. S., Iliev, S., Subbotin, V. G., Sukhov, A. M., Buklanov, G. V., Gikal, B. N., Kutner, V. B., Mezentsev, A. N., Subotic, K., Wild, J. F., Longheed, R. W., and Moody, K. J. (1996) *Phys. Rev. C,* **54**, 620–5.

Lijima, K. and Shibata, S. (1974) *Bull. Chem. Soc. Jpn.,* **47**, 1393.

Lijima, K. and Shibata, S. (1975) *Bull. Chem. Soc. Jpn.,* **48**, 666.

Lim, I., Pernpointner, M., Seth, M., and Schwerdtfeger, P. (1999) *Phys. Rev. A,* **60**, 2822–8.

Liu, W., Hong, G., Dai, D., Li, L., and Dolg, M. (1997) *Theor. Chem. Acc.,* **96**, 75–83.

Liu, W. and van Wüllen, C. (1999) *J. Chem. Phys.,* **110**, 3730–5.

Liu, W., van Wüllen, C., Han, Y. K., Choi, Y. J., and Lee, Y. S. (2001) *Adv. Quant. Chem.,* **39**, 325–55.

Lougheed, R. W., Moody, K. J., Wild, J. F., Hulet, E. K., McQuaid, J. H., Lazarev, Y. A., Lobanov, Y. V., Oganessian, Y. T., Utyonkov, V. K., Abdullin, F. S., Buklanov, G. V., Gikal, B. N., Iliev, S., Mezentsev, A. N., Polyakov, A. N., Sedykh, I. M., Shirokovsky, I. V., Subbotin, V. G., Sukhov, A. M., Tsyganov, Y. S., and Zhuchko, V. E. (1994) *J. Alloys Compds,* **213**, 61–6.

Lougheed, R. W., Moody, J., Wild, J. F., Stoyer, N. J., Stoyer, M. A., Oganessian, Y. T., Utyonkov, V. K., Lobanov, Y. V., Abdullin, F. S., Polyakov, A. N., Shirokovsky, I. V., Tsyganov, Y. S., Gulbekian, G. G., Gobomolov, S. L., Gikal, B. N., Mezentsev, A. N., Iliev, S., Subbotin, V. G., Sukhov, A. M., Buklanov, G. V., Subotic, K., and Itkis, M. G. K. (2000) NUCL Abstract 19, San Francisco, CA, March 27.

Loveland, W., Gregorich, K. E., Patin, J. B., Peterson, D., Rouski, C., Zielinski, P., and Aleklett, K. (2002) *Phys. Rev. C,* **66** 044617-1–5.

Mann, J. B. (1969) *J. Chem. Phys.,* **51**, 841.

Mann, J. B. and Waber, J. T. (1970) *J Chem. Phys.,* **53**, 2397.

Meldner, H. (1967) *Ark. Fys.,* **36**, 593–8.

Moore, C. E. (1958) Atomic Energy Levels, Natl. Bur. Stand. (U. S.) Circ. No. 467 (U. S. GPO, Washington, DC, 1952), Vol. II; III.

Mulliken, R. S. (1955) *J. Chem. Phys.,* **23**, 1833–46.

Myers, W. D. and Swiatecki, W. J. (1966) *Nucl. Phys.,* **81**, 1.

Myers, W. D. and Swiatecki, W. J. (2000) *Phys. Rev. C,* **6204**, 312–17.

Nagame, Y., Asai, M., Haba, H., Tsukada, K., Goto, S., Sakama, M., Nishinaka, I., Toyoshima, A., Akiyama, K., and Ichikawa, S. (2002) *J. Nucl. Radiochem. Sci.,* **3**, 129–32.

Nash, C. S. and Bursten, B. E. (1995) *New J. Chem.,* **19**, 669–75.

Nash, C. S., Bursten, B. E., and Ermler, W. C. (1997) *J. Chem. Phys.,* **106**, 5133–42.

Nash, C. S. and Bursten, B. E. (1999a) *J. Phys. Chem. A,* **103**, 402–10.

Nash, C. S. and Bursten, B. E. (1999b) *Angew. Chem. Int. Ed. Engl.,* **38**, 151–3.

Nash, C. S. and Bursten, B. E. (1999c) *J. Phys. Chem. A,* **103**, 632–6.

Nilsson, S. G., Tsang, C. F., Sobiczewski, A., Szymanski, Z., Wycech, S., Gustafsson, G., Lam, I. L., Möller, P., and Nilsson, B. (1969a) *Nucl. Phys.,* **A131**, 1.

Nilsson, S. G., Thompson, S. G., and Tsang, C. F. (1969b) *Phys. Lett.,* **28B**, 458.

Oganessian, Y. T. and Zvara, I. (1993) *Pure Appl. Chem.,* **65**, 1820–1.

Oganessian, Y. T., Yeremin, A. V., Popeko, A. G., Bogomolov, S. L., Buklanov, G. V., Chelnokov, M. L., Chepigin, V. I., Gikal, B. N., Gorshkov, V. A., Gulbekian, G. G., Itkis, M. G., Kabachenko, A. P., Lavrentev, A. Y., Malyshev, O. N., Rohac, J., Sagaidak, R. N., Hofmann, S., Saro, S., Giardinas, G., and Morita, K. (1999a) *Nature,* **400**, 242–5.

Oganessian, Y. T., Utyonkov, V. K., Lobanov, Y. V., Abdullin, F. S., Polyakov, A. N., Shirokovsky, I. V., Tsyganov, Y. S., Gulbekian, G. G., Gobomolov, S. L., Gikal, B. N., Mezentsev, A. N., Iliev, S., Subbotin, V. G., Sukhov, A. M., Buklanov, G. V., Subotic, K., Itkis, M. G., Moody, K. J., Wild, J. F., Stoyer, N. J., Stoyer, M. A., and Lougheed, R. W. (1999b) *Phys. Rev. Lett.,* **83**, 3154–7.

Oganessian, Y. T., Yeremin, A. Y., Gulbekian, G. G., Bogomolov, S. L., Chepigin, V. I., Gikal, B. N., Gorshkov, V. A., Itkis, M. G., Kabachenko, A. P., Kutner, V. B., Lavrentev, A. Y., Malyshev, O. N., Popeko, A. G., Rohac, J., Sagaidak, R. N., Hofmann, S., Münzenberg, G., Veselsky, M., Saro, S., Iwasa, N., and Morita, K. (1999c) *Eur. Phys. J. A,* **5**, 63–8.

Oganessian, Y. T., Utyonkov, V. K., Lobanov, Y. V., Abdullin, F. S., Polyakov, A. N., Shirokovsky, I. V., Tsyganov, Y. S., Gulbekian, G. G., Bogomolov, S. L., Gikal, B. N., Mezentsev, A. N., Iliev, S., Subbotin, V. G., Sukhov, A. M., Ivanov, O. V., Buklanov, G. V., Subotic, K., Itkis, M. G., Moody, K. J., Wild, J. F., Stoyer, N. J., Stoyer, M. A., and Lougheed, R. W. (2000a) *Phys. Rev. C,* **62** 041604 (R) 1–4.

Oganessian, Y. T., Utyonkov, V. K., Lobanov, Y. V., Abdulin, F. S., Polyakov, A. N., Shirokovsky, I. V., Tsyganov, Y. S., Gulbekian, G. G., Bogomolov, S. L., Gikal, B. N., Mezentsev, A. N., Iliev, S., Subbotin, V. G., Sukhov, A. M., Ivanov, O. V., Buklanov, G. V., Subotic, K., Itkis, M. G., Moody, K. J., Wild, J. F., Stoyer, N. J., Stoyer, M. A., Lougheed, R. W., Laue, C. A., Karelin, Y. A., and Tatarinov, A. N. (2000b) *Phys. Rev. C,* **63** 011301 (R) 1–2.

Oganessian, Y. T. (2001) *Nucl. Phys. A,* **685**, 17c.

Oganessian, Y. T. (2002) *J. Nucl. Radiochem. Sci.,* **3**, 5–8.

Oganessian, Y. T., Utyonkov, V. K., Lobanov, Y. V., Abdullin, F. S., Polyakov, A. N., Shirokovsky, I. V., Tsyganov, Y. S., Gulbekian, G. G., Bogomolov, S. L., Gikal, B. N., Mezentsev, A. N., Iliev, S., Subbotin, V. G., Sukhov, A. M., Ivanov, O. V., Buklanov, G. V., Subotic, K., Voinov, A. A., Itkis, M. G., Moody, K. J., Wild, J. F., Stoyer, N. J., Stoyer, M. A., Lougheed, R. W., and Laue, C. A. (2002) *Eur. Phys. J. A,* **15**, 201–4.

Oganessian, Y. T., Utyonkoy, V. K., Lobanov, Y. V., Abdullin, F. S., Polyakov, A. N., Shirokovsky, I. V., Tsyganov, Y. S., Gulbekian, G. G., Bogomolov, S. L., Mezentsev, A. N., Iliev, S., Subbotin, V. G., Sukhov, A. M., Voinov, A. A., Buklanov, G. V., Subotic, K., Zagrebaev, V. I., Itkis, M. G., Patin, J. B., Moody, K. J., Wild, J. F., Stoyer, M. A., Stoyer, N. J., Shaughnessy, D. A., Kenneally, J. M., and Lougheed, R. W. (2004a) *Phys. Rev. C,* **69**, 021601(R).

Oganessian, Y. T., Yeremin, A. V., Popeko, A. G., Malyshev, O. N., Belozerov, A. V., Buklanov, G. V., Chelnokov, M. L., Chepigin, V. I., Gorshkov, V. A., Hofmann, S., Itkis, M. G., Kabachenko, A. P., Kindler, B., Munzenberg, G., Sagaidak, R. N., Saro,

S., Schott, H.-J., Streicher, B., Shutov, A. V., Svirikhin, A. I., and Vostokin, G. K. (2004b) *Eur. Phys. J. A,* **19**, 3–6.

Oganessian, Y. T., Utyonkov, V. K., Lobanov, Y. V., Abdullin, F. S., Polyakov, A. N., Shirokovsky, I. V., Tsyganov, Y. S., Gulbekian, G. G., Bogomolov, S. L., Gikal, B. N., Mezentsev, A. N., Iliev, S., Subbotin, V. G., Sukhov, A. M., Voinov, A. A., Buklanov, G. V., Subotic, K., Zagrebaev, V. I., Itkis, M. G., Patin, J. B., Moody, K. J., Wild, J. F., Stoyer, M. A., Stoyer, N. J., Shaughnessy, D. A., Kenneally, J. M., and Lougheed, R. W. (2004c) *Phys. Rev. C,* **69**, 054607.

Omtvedt, J.-P., Alstad, J., Eberhardt, K., Fure, K., Malmbeck, R., Mendel, M., Nähler, A., Skarnemark, G., Trautmann, N., Wiehl, N., and Wierczinski, B. J. (1998) *J. Alloys Compds,* **271**, 303.

Omtvedt, J. P., Alstad, J., Breivik, H., Dyve, J. E., Eberhardt, K., Folden, C. M. III, Ginter, T., Gregorich, K. E., Hult, E. A., Johansson, M., Kirbach, U. W., Lee, D. M., Mendel, M., Nahler, A., Ninov, V., Omtvedt, L. A., Patin, J. B., Skarnemark, G., Stavsetra, L., Sudowe, R., Wiehl, N., Wierczinski, B., Wilk, P. A., Zielinski, P. M., Kratz, J. V., Trautmann, N., Nitsche, H., and Hoffman, D. C. (2002) *J. Nucl. Radiochem. Sci.,* **3**, 121–4.

Parpia, F. A., Froese-Fisher, S., and Grant, I. P. (1996) *CPC,* **94**, 249–71.

Paulus, W., Kratz, J. V., Strub, E., Zauner, S., Brüchle, W., Schädel, M., Schausten, B., Adams, J. L., Gregorich, K. E., Hoffman, D. C., Laue, C., Lee, D. M., McGrath, C. A., Shaughnessy, D. K., Strellis, D. A., and Sylwester, E. R. (1999) *Radiochim. Acta,* **84**, 69–77.

Penneman, R. A., Mann, J. B., and Jorgensen, C. K. (1971) *Chem. Phys. Lett.,* **8**, 321–6.

Penneman, R. A. and Mann, J. B. (1976) Calculational Chemistry of the Superheavy Elements; Comparison with elements of the 7th Period, in *J. Inorg. Chem. Suppl., Proc. Moscow Symp. on Chemistry of the Transuranium Elements,* pp. 257–63.

Peppard, D. F., Mason, G. W., and Maier, J. L. (1956) *J. Inorg. Nucl. Chem.,* **3**, 215.

Pepper, M. and Bursten, B. E. (1991) *Chem. Rev.,* **91**, 719–40.

Pershina, V., Sepp, W.-D., Fricke, B., and Rosen, A. (1992a) *J. Chem. Phys.,* **96**, 8367–78.

Pershina, V., Sepp. W.-D., Bastug, T., Fricke, B., and Ionova, G. V. (1992b) *J. Chem. Phys.,* **97**, 1123–31.

Pershina, V. and Fricke, B. (1993) *J. Chem. Phys.,* **99**, 9720–9.

Pershina, V. and Fricke, B. (1994) *J. Phys. Chem.,* **98**, 6468–73.

Pershina, V. and Fricke, B. (1995) *J. Phys. Chem.,* **99**, 144–7.

Pershina, V. (1996) *Chem. Rev.,* **96**, 1977–2010.

Pershina, V. and Fricke, B. (1996) *J. Phys. Chem.,* **100**, 8748–51.

Pershina, V. (1998a) *Radiochim. Acta,* **80**, 65–73.

Pershina, V. (1998b) *Radiochim. Acta,* **80**, 75–84.

Pershina, V. and Bastug, T. (1999) *Radiochim. Acta,* **84**, 79–84.

Pershina, V. and Fricke, B. (1999) Electronic Structure and Chemistry of the Heaviest Elements, in *Heavy Elements and Related New Phenomena,* vol. 1, (eds. W. Greiner and R. K. Gupta), World Scientific, Singapore, pp. 184–262.

Pershina, V., Johnson, E., and Fricke, B. (1999) *J. Phys. Chem. A,* **103**, 8463–70.

Pershina, V. and Bastug, T. (2000) *J. Chem. Phys.,* **113**, 1441–6.

Pershina, V., Bastug, T., Fricke, B., and Varga, S. (2001) *J. Phys. Chem.,* **115**, 792–9.

Pershina, V. and Kratz, J. V. (2001) *Inorg. Chem.,* **40**, 776–80.

Pershina, V., Bastug, T., Jacob, T., Fricke, B., and Varga, S. (2002a) *Chem. Phys. Lett.,* **365**, 176–83.

Pershina, V., Trubert, D., Le Naour, C., and Kratz, J. V. (2002b) *Radiochim. Acta,* **90**, 869–77.

Pershina, V. (2003) Theoretical chemistry of the heaviest elements, in *The Chemistry of Superheavy Elements* (ed. M. Schädel), Kluwer Academic Publishers, Dordrecht, The Netherland, pp. 31–94.

Pershina, V. and Hoffman, D. C. (2003) The chemistry of the heaviest elements, in *Theoretical Chemistry and Physics of Heavy and Superheavy Elements* in the series Comput. Phys. Commun. *Progress in Theoretical Chemistry and Physics* (eds. U. Kaldor and S. Wilson), Kluwer Academic Publishers, Dordrecht, The Netherlands, ch. 3, pp. 55–114.

Pfrepper, G., Pfrepper, R., Krauss, D., Yakushev, A. B., Timokhin, S. N., and Zvara, I. (1998) *Radiochim. Acta,* **80**, 7–12.

Pitzer, K. S. (1975a) *J. Chem. Phys.,* **63**, 1032–3.

Pitzer, K. S. (1975b) *J. Chem. Soc., Chem. Commun.*, 760–1.

Pyper, N. C. and Grant, I. P. (1981) *Proc. R. Soc. Lond. A,* **376**, 483–92.

Pyykkö, P. (1988) *Chem. Rev.,* **88**, 563–94.

Pyykkö, P., Tokman, M., and Labzowsky, L. N. (1998) *Phys. Rev. A,* **57**, R689–92.

Randrup, J., Larsson, S. E., Moller, P., Sobiczewski, A., and Kukasiak, A. (1974) *Phys. Scr.,* **10A**, 60–4.

Rieth, U., Herlert, A., Kratz, J. V., Schweikhard, L., Vogel, M., and Walther, C. (2002) *Radiochim. Acta,* **90**, 337–43.

Rosen, A., Fricke, B., Morovic, T., and Ellis, D. E. (1979) *J. Phys. C4, Suppl. 4,* **40**, C4/218–19.

Rosen, A. (1997) *Adv. Quant. Chem.,* **29**, 1–30.

Ryzhkov, M. V., Gubanov, V. A., and Zvara, I. (1992) *Radiochim. Acta,* **57**, 11–14.

Saue, T., Faegri, K., and Gropen, O. (1996) *Chem. Phys. Lett.,* **263**, 360–6.

Schädel, M., Brüchle, W., Schimpf, E., Zimmermann, H. P., Gober, M. K., Kratz, J. V., Trautmann, N., Gäggeler, H., Jost, D., Kovacs, J., Scherer, U. W., Weber, A., Gregorich, K. E., Türler, A., Czerwinski, K. R., Hannink, N. J., Kadkhodayan, B., Lee, D. M., Nurmia, M. J., and Hoffman, D. C. (1992) *Radiochim. Acta,* **57**, 85–92.

Schädel, M. (1995) *Radiochimica Acta,* **70/71**, 207–23.

Schädel, M., Brüchle, W., Dressler, R., Eichler, B., Gäggeler, H. W., Günther, R., Gregorich, K. E., Hoffman, D. C., Hübener, S., Jost, D. T., Kratz, J. V., Paulus, W., Schumann, D., Timokhin, S., Trautmann, N., Türler, A., Wirth, G., and Yakuschev, A. (1997a) *Nature* (*Lett.*), **388**, 55–7.

Schädel, M., Brüchle, W., Schausten, B., Schimpf, E., Jäger, E., Wirth, G., Günther, R., Kratz, J. V., Paulus, W., Seibert, A., Thorle, P., Trautmann, N., Zauner, S., Schumann, D., Andrassy, M., Misiak, R., Gregorich, K. E., Hoffman, D. C., Lee, D. M., Sylwester, E. R., Nagame, Y., and Oura, Y. (1997b) *Radiochim. Acta,* **77**, 149–59.

Schädel, M., Brüchle, W., Jäger, E., Schausten, B., Wirth, G., Paulus, W., Günther, R., Eberhardt, K., Kratz, J. V., Seibert, A., Strub, E., Thörle, P., Trautmann, N., Waldek, W., Zauner, S., Schumann, D., Kirbach, U., Kubica, B., Misiak, R., Nagame, Y., and Gregorich, K. E. (1998) *Radiochim. Acta,* **83**, 163–5.

Schädel, M. (2002) *J. Nucl. Radiochem. Sci.,* **3**, 113–20.

Schwarz, W. H. E., Van Wezenbeek, E. M., Baerends, E. J., and Snijders, J. G. (1989) *J. Phys. B,* **22**, 1515–30.

Schwarz, W. H. E. (1990) *Theoretical Models of Chemical Bonding,* Springer, Berlin, pp. 593–643.

Schwerdtfeger, P., Dolg, M., Schwarz, W. H. E., Bowmaker, G. A., and Boyd, P. W. D. (1989) *J. Chem. Phys.,* **91**, 1762–74.

Schwerdtfeger, P. and Seth, M. (1998) Relativistic effects on the superheavy elements, in *Encyclopedia on Computational Chemistry*, vol. 4, John Wiley, New York, pp. 2480–99.

Seaborg, G. T. (1968) *Annu. Rev. Nucl. Sci.,* **18**, 53.

Seaborg, G. T. and Keller, O. L. Jr (1986) Future elements, in *The Chemistry of the Actinide Elements,* 2nd edn, vol. II (eds. J. J. Katz, G. T. Seaborg, and L. R. Morss), Chapman & Hall, London, pp. 1635–43.

Seaborg, G. T. (1996) *J. Chem. Soc., Dalton Trans.*, 3899–907.

Seth, M., Schwerdtfeger, P., Dolg, M., Faegri, K., Hess, B. A., and Kaldor, U. (1996) *Chem. Phys. Lett.,* **250**, 461–5.

Seth, M., Schwerdtfeger, P., and Dolg, M. (1997) *J. Chem. Phys.,* **106**, 3623–32.

Seth, M., Cooke, F., Schwerdtfeger, P., Heully, J.-L., and Pelissier, M. (1998a) *J. Chem. Phys.,* **109**, 3935–43.

Seth, M., Faegri, K., and Schwerdtfeger, P. (1998b) *Angew. Chem. Int. Ed. Engl.,* **37**, 2493–6.

Seth, M., Schwerdtfeger, P., and Faegri, K. (1999) *J. Chem. Phys.,* **111**, 6422–33.

Shannon, R. D. (1976) *Acta Crystallogr. A,* **32**, 751–67.

Silva, R. J., Sikkeland, T., Nurmia, M., and Ghiorso, A. (1970a) *Inorg. Nucl. Chem. Lett.,* **6**, 733–9.

Silva, R., Harris, J., Nurmia, M., Eskola, K., and Ghiorso, A. (1970b) *Inorg. Nucl. Chem. Lett.,* **6**, 871–7.

Smolańczuk, R., Skalski, J., and Sobiczewski, A. (1995) *Phys. Rev. C,* **52**, 1871–80.

Smolańczuk, R. (1997) *Phys. Rev. C,* **56**, 812–24.

Smolańczuk, R. (1999a) *Phys. Rev. C,* **59**, 2634–9.

Smolańczuk, R. (1999b) *Phys. Rev. Lett.,* **83**, 4705–8.

Smolańczuk, R. (1999c) *Phy. Rev. C,* **61** 011601-1–4.

Smolańczuk, R. (2001a) *Phys. Lett. B,* **509**, 227–30.

Smolańczuk, R. (2001b) *Phys. Rev. C,* **63** 044607-1–8.

Sobiczewski, A., Smolańczuk, R., and Skalski, J. (1994) *J. Alloys Compds,* **213**, 38–42.

Soverna, S., Aebersold, H. U., Düllman, C. E., Eichler, B., Gäeggeler, H. W., Tobler, L., Türler, A., and Thi, Q. (2001) The GDCh Conference, Würzburg, Germany, September 2001.

Strub, E., Kratz, J. V., Kronenberg, A., Nähler, A., Thörle, P., Zauner, S., Brüchle, W., Jäger, E., Schädel, M., Schausten, B., Schimpf, E., Zongwei, L., Kirbach, U., Schumann, D., Jost, D., Türler, A., Asai, M., Nagame, Y., Sakara, M., Tsukada, K., Gäggeler, H. W., and Glanz, J. P. (2000) *Radiochim. Acta,* **88**, 265–71.

Strutinsky, V. M. (1966) *Sov. J. Nucl. Phys.,* **3**, 449–57.

Sylwester, E. R., Gregorich, K. E., Lee, D. M., Kadkhodayan, B., Türler, A., Adams, J. L., Kacher, C. D., Lane, M. R., Laue, C. A., McGrath, C. A., Shaughnessy, D. A., Strellis, D. A., Wilk, P. A., and Hoffman, D. C. (2000) *Radiochim Acta,* **88**, 837–43.

Timokhin, S. N., Yakushev, A. B., Xu, H. G., Perelygin, V. P., and Zvara, I. (1996) *J. Radioanal. Nucl. Chem. Lett.,* **212**, 31–4.

Trubert, D., Le Naour, C., Hussonois, M., Brillard, L., Montroy Gutman, F., Le Du, J. F., Constantinescu, O., Barci, V., Weiss, B., Gasparro, J., and Ardisson, G. (1999) in *Abstracts of the 1st Int. Conf. on Chemistry and Physics of the Transactinides*, Seeheim, September 26–30.

Türler, A., Gäggeler, H. W., Gregorich, K. E., Barth, H., Bruchle, W., Czerwinski, K. R., Gober, M. K., Hannink, N. J., Henderson, R. A., Hoffman, D. C., Jost, D. T., Kacher, C. D., Kadkhodayan, B., Kovacs, J., Kratz, J. V., Kreek, S. A., Lee, D. M., Leyba, J. D., Nurmia, M. J., Schädel, M., Scherer, U. W., Schimpf, E., Vermeulen, D., Weber, A., Zimmermann, H. P., and Zvara, I. (1992) *J. Radioanal. Nucl. Chem. Articles,* **160**, 327–39.

Türler, A. (1996) *Radiochim. Acta,* **72**, 7–17.

Türler, A., Eichler, B., Jost, D. T., Piguet, D., Gäggeler, H. W., Gregorich, K. E., Kadkhodayan, B., Kreek, S. A., Lee, D. M., Mohar, M., Sylwester, E., Hoffman, D. C., and Hübener, S. (1996) *Radiochim. Acta,* **73**, 55–66.

Türler, A., Dressler, R., Eichler, B., Gäggeler, H. W., Jost, D. T., Schädel, M., Bruchle, W., Gregorich, K. E., Trautmann, N., and Taut, S. (1998a) *Phys. Rev. C,* **57**, 1648–55.

Türler, A., Buklanov, G. V., Eichler, B., Gäggeler, H. W., Grantz, M., Hübener, S., Jost, D. T., Lubedev, V. Y., Piguet, D., Timokhin, S. N., Yakushev, A. B., and Zvara, I. (1998b) *J. Alloys Compds,* **271**, 287–91.

Türler, A., Brüchle, W., Dressler, R., Eichler, B., Eichler, R., Gäggeler, H. W., Gartner, M., Glatz, J. P., Gregorich, K. E., Hübener, S., Jost, D. T., Lebedev, V. Y., Pershina, V. G., Schädel, M., Taut, S., Timokhin, S. N., Trautmann, N., Vahle, A., and Yakushev, A. B. (1999) *Angew. Chem Int. Ed. Engl.,* **38**, 2212–13.

Türler, A., Düllman, C. E., Gäggeler, H. W., Kirbach, U. W., Yakushev, A. B., Schädel, M., Brüchle, W., Dressler, R., Eberhardt, K., Eichler, B., Eichler, R., Ginter, T. N., Glaus, F., Gregorich, K. E., Hoffman, D. C., Jäger, E., Jost, D. T., Lee, D. M., Nitsche, H., Patin, J. B., Pershina, V., Piguet, D., Qin, Z., Schausten, B., Schimpf, E., Schött, H.-J., Soverna, S., Sudowe, R., Thörle, P., Timokhin, S. N., Trautmann, N., Vahle, A., Wirth, G., and Zielinski, P. (2003) *Eur. Phys. J. A,* **17**, 505–8.

Varga, S., Engel, E., Sepp, W.-D., and Fricke, B. (1999) *Phys. Rev. A,* **59**, 4288–94.

Varga, S., Fricke, B., Hirata, M., Bastug, T., Pershina, V., and Fritzsche, S. (2000) *J. Phys. Chem. A,* **104**, 6495–8.

Visscher, L., Lee, T. J., and Dyall, K. G. (1996) *J. Chem. Phys.,* **105**, 8769–76.

Waber, J. T., Cromer, D. T., and Liberman, D., (1969) *J. Chem. Phys.* **51**, 664.

Waber, J. T. and Averill, F. W. (1974) *J. Chem. Phys.,* **60**, 4460–70.

Wierczinski, B. and Hoffman, D. C. (1996) Instrumentation for atom-at-a-time chemistry of the heavy elements, in *IANCAS Frontiers in Nuclear Chemistry* (eds. D. D. Sood, P. K. Reddy, and A. V. R. Pujari), Perfect Prints, Thane, India, pp. 171–91.

Wilk, P. A., Gregorich, K. E., Türler, A., Laue, C. A., Eichler, R., Ninov, V., Adams, J. L., Kirbach, U. W., Lane, M. R., Lee, D. M., Patin, J. B., Shaughnessy, D. A., Strellis, D. A., Nitsche, H., and Hoffman, D. C. (2000) *Phys. Rev. Lett.,* **85**, 2697–700.

Wilson, S., Grant, I. P., and Gyoffry, B. L. (1991) *The Effects of Relativity in Atoms, Molecules and the Solid State,* Plenum, New York.

Wood, C. P. and Pyper, N. C. (1981) *Chem. Phys. Lett.,* **84**, 614–21.

Yakushev, A. B., Timokhin, S. N., Vedeneev, M. V., Xu, H. G., and Zvara, I. (1996) *J. Radioanal. Nucl. Chem. Articles,* **205**, 63–7.

Yakushev, A. B., Buklanov, G. V., Chelnokov, M. L., Chepigin, V. I., Dmitriev, S. N., Gorshkov, V. A., Hübener, S., Lebedev, V. Y., Malyshev, O. N., Oganessian, Y. T., Popeko, A. G., Sokol, E. A., Timokhin, S. N., Türler, A., Vasko, V. M., Yeremin, A. V., and Zvara, I. (2001) *Radiochim. Acta,* **89**, 743–5.

Yakushev, A. B. (2002) Workshop on Recoil Separator for Superheavy Element Chemistry, March 20–21, 2002, Darmstadt.

Zharskii, I. M., Zasorin, E. Z., Spiridonov, V. P., Novikov, G. I., and Kupreev, V. N. (1975) *Koord. Khim.,* **1**, 574.

Zhuikov, B. L., Chuburkov, Y. T., Timokhin, S. N., Jin, K. U., and Zvara, I. (1989) *Radiochim. Acta,* **46**, 113–17.

Zhuikov, B. L., Glebov, V. A., Nefedov, V. S., and Zvara, I. (1990) *Radioanal. Nucl. Chem. Articles,* **143**, 103–11.

Zimmermann, H. P., Gober, M. K., Kratz, J. V., Schädel, M., Brüchle, W., Schimpf, E., Gregorich, K. E., Türler, A., Czerwinski, K. R., Hannink, N. J., Kadkhodayan, B., Lee, D. M., Nurmia, M. J., Hoffman, D. C., Gäggeler, G., Jost, D., Kovacs, J., Scherer, U. W., and Weber, A. (1993) *Radiochimica Acta,* **60**, 11–16.

Zvara, I., Chuburkov, Y. T., Tsaletka, R., and Shalaevskii, M. R. (1969) *Sov. Radiochem.,* **11**, 161–70.

Zvara, I., Chuburkov, Y. T., Belov, V. Z., Buklanov, G. V., Zakhvataev, B. B., Zvarova, T. S., Maslov, O. D., Caletka, R., and Shalaevsky, M. R. (1970) *J. Inorg. Nucl. Chem.,* **32**, 1885–94.

Zvara, I., Belov, V. Z., Domanov, V. P., Korotkin, Y. S., Chelnokov, L. P., Shalaevsky, M. R., Shchegolev, V. A., and Hussonois, M. (1972) *Sov. Radiochem.,* **14**, 115–18.

Zvara, I., Aikhler, V., Belov, V. Z., Zvarova, T. S., Korotkin, Y. S., Shalaevskii, M. R., Shchegolev, V. A., and Yussonnua, M. (1974) *Sov. Radiochem.,* **16**, 709–15.

Zvara, I., Belov, V. Z., Domanov, V. P., and Shalaevskii, M. R. (1976) *Sov. Radiochem.,* **18**, 328–34.

Zvara, I. (1985) *Radiochim. Acta,* **38**, 95–101.

CHAPTER FIFTEEN

SUMMARY AND COMPARISON OF PROPERTIES OF THE ACTINIDE AND TRANSACTINIDE ELEMENTS

Norman M. Edelstein, Jean Fuger,
Joseph J. Katz, and Lester R. Morss

15.1 INTRODUCTION

15.1.1 Scope

This chapter is intended to provide a unified view of selected aspects of the physical, chemical, and biological properties of the actinide elements, their typical compounds, and their ions in aqueous solutions. The f-block elements have many unique features, and a comparison of similar species of the lanthanide and actinide transition series provides valuable insights into the properties of both. Comparative data are presented on the electronic configurations, oxidation states, oxidation–reduction (redox) potentials, thermochemical data, crystal structures, and ionic radii of the actinide elements, together with

important topics related to their environmental properties and toxicology. Many of the topics in this chapter, and some that are not discussed here, are the subjects of subsequent chapters of this work, which should be consulted for more comprehensive treatments. This chapter provides an opportunity to discuss the biological and environmental aspects of the actinide elements, subjects that were barely mentioned in the first edition of this work and discussed only briefly in the second edition, but have assumed great importance in recent years. This chapter also provides a summary of the chemical properties of the transactinide elements that have been characterized.

15.1.2 The actinide concept

The actinide concept has achieved nearly universal acceptance as a way of integrating the transuranium elements into the periodic table. This concept was first expounded by G. T. Seaborg in 1944 (Seaborg *et al.*, 1949, pp. 1492–524, especially pp. 1517–20) and first enunciated in public on November 16, 1945 (C&E News, 1945). The chemical and electronic evidence that established the actinides as an inner transition series has been recently reviewed (Gruen, 1992). A succinct summary of this important principle will therefore be sufficient here.

The actinide concept considers the elements with atomic numbers 89–103 to be members of a transition series, the first member of which is actinium (atomic number 89). The elements with atomic numbers 89–103 are thus analogs of the lanthanide transition series that starts with lanthanum (atomic number 57) and includes the rare earth elements cerium through lutetium (atomic number 71). It is important, in comparing the lanthanide and actinide transition series, to keep in mind that the electronic configuration of any given element may be significantly different in the gaseous atoms, in ions in solids or solutions, and in the metallic state. In the lanthanide 3+ ions, 14 4f electrons are added in sequence beginning with cerium, atomic number 58 (Table 15.3). In the actinide series, 5f electrons are added successively beginning formally with thorium (atomic number 90) and ending with lawrencium (atomic number 103). Note the qualification 'formally.' No compelling evidence exists to show that thorium metal, or thorium ions in solution or in any of its well-defined compounds, contain 5f electrons. There is convincing evidence that protactinium metal displays 5f electron character, as is expected for the third member of an actinide series (Zachariasen, 1973; Fournier, 1976; Haire *et al.*, 2003).

The subsequent trivalent ions of the actinide series contain their appropriate complements of 5f electrons. Although there are important differences between the actinide and lanthanide elements, there are also striking similarities. The metallic elements and 3+ ions with half-filled f-electron shells, for example, are of special interest because of the enhanced stability of this particular electron configuration. Curium (atomic number 96), with seven 5f electrons in the metal and 3+ species, has magnetic, optical, and chemical properties that are remarkably similar to those of gadolinium (atomic number 64), with seven

4f electrons, as would be expected from the actinide concept. The principal differences between the two transition series arise largely from the lower binding energies and less effective shielding by outer electrons of 5f as compared to 4f electrons. Both the similarities and the differences between the actinide and lanthanide series have had great heuristic value in actinide element research. Further discussion of the electronic structure of the actinide elements is given in Section 15.4. Much more detailed expositions of the actinides as a 5f transition series are given in subsequent chapters.

15.2 SOURCES OF ACTINIDE AND TRANSACTINIDE ELEMENTS

15.2.1 Natural sources

The elements actinium through plutonium occur in nature. Only the elements thorium, protactinium, and uranium are present in amounts sufficient to warrant extraction from natural sources. Thorium and uranium are widely disseminated in the Earth's crust ($\sim$10000 and $\sim$3000 μg kg^{-1} respectively), and, in the case of uranium, in significant concentrations in the oceans (3.3 μg L^{-1}). More importantly, thorium and uranium are found highly enriched in certain mineral formations, and are obtained by conventional mining operations. The richest deposits of uranium are found in northern Saskatchewan, Canada. The annual world production of uranium from uranium ore in the period 1995–2000 was about 35000 metric tons of uranium oxide. Proven uranium reserves were about 3.2 million metric tons, with the richest deposits in Canada, Kazakhstan, USA, and Australia (World Energy Council, 1988). Thorium reserves were estimated at 1.2 million metric tons in 2004 (U.S. Geological Survey, 2002), but this estimate would be much higher if thorium extraction were economically viable; the largest deposits are in India, Australia, and the U.S. Extraction of thorium and uranium from their ores had been practiced for many years before the discovery of the transuranium elements, and an extensive technology exists for the extraction of thorium and uranium from many different types of ores.

Hundreds of thousands of tons of uranium have been processed for isotopic separation. Five grades of isotopically separated uranium are commonly recognized: depleted uranium (less than 0.71% ^{235}U), natural uranium (0.71% ^{235}U), low-enriched uranium (LEU) (0.71–20% ^{235}U), highly enriched uranium (HEU) (20–90% ^{235}U), and weapon-grade uranium (greater than 90% ^{235}U). Of these grades, HEU and weapon-grade uranium are the most important. HEU is produced (almost in equal amounts by gaseous diffusion or centrifuge enrichment) from natural uranium for use in nuclear weapons and for use in commercial nuclear reactors. Worldwide, at the end of 1994, 450 metric tons of HEU (calculated as weapon-grade equivalent) was inside nuclear weapons and 1300 metric tons had been removed from weapons. An additional 20 metric tons exist

in civil inventories. This total (1770 metric tons) is slowly decreased (20 metric tons per year in 1996) by blending down of Russian HEU (Albright *et al.*, 1996).

Neptunium (^{237}Np and ^{239}Np) and plutonium (^{239}Pu) are present in extremely minute amounts in nature as a result of natural nuclear reactions with neutrons in uranium ores. The longer-lived ^{244}Pu has been found in the rare earth mineral bastnasite to the extent of 1 part in 10^{18}, and may possibly be a primordial endowment (see Section 15.8.1).

15.2.2 Neutron irradiation

Actinium and protactinium are decay products of the naturally occurring uranium isotope ^{235}U and are present in uranium minerals in such low concentration that recovery from natural sources is a very difficult task. By comparison, it is relatively straightforward to obtain actinium, protactinium, and most of the remaining transuranium elements by neutron irradiation of elements of lower atomic number in nuclear reactors (Seaborg, 1963, 1978; Hyde *et al.*, 1964). Thus, actinium has been produced in multigram quantities by the transmutation of radium with neutrons produced in a high-flux nuclear reactor:

$$^{226}\mathrm{Ra} + \mathrm{n} \rightarrow {}^{227}\mathrm{Ra} + \gamma$$

$$^{227}\mathrm{Ra} \rightarrow {}^{227}\mathrm{Ac} + \beta^{-}$$

The product actinium can be separated from the precursor radium by solvent extraction or ion exchange, and gram amounts of actinium have been obtained by these procedures. This is not at all an easy task, considering the highly radioactive substances involved and the hazards of radon emission that accompanies these nuclear reactions, but it is preferable by far to extraction from natural sources. Protactinium can be produced by the nuclear reactions:

$$^{230}\mathrm{Th} + \mathrm{n} \rightarrow {}^{231}\mathrm{Th} + \gamma$$

$$^{231}\mathrm{Th} \rightarrow {}^{231}\mathrm{Pa} + \beta^{-}$$

The amount of ^{231}Pa produced in this way, however, is much less than the amounts (more than 100 g) of protactinium obtained from residues accumulated from the very large-scale extraction of uranium from ores. Because of the extreme tendency of protactinium(v) to form colloidal polymers that are easily adsorbed on solid surfaces, and cannot be removed from aqueous media by solvent extraction, the recovery of protactinium from uranium ore processing residues can only be described as a heroic enterprise.

Neptunium-237 is a long-lived isotope of element 93 that is produced in kilogram amounts. It is formed as a by-product in nuclear reactors when neutrons produced in the fission of uranium-235 react with uranium-238:

$$^{238}\mathrm{U} + \mathrm{n} \rightarrow {}^{237}\mathrm{U} + 2\mathrm{n}$$

$$^{237}\mathrm{U} \rightarrow {}^{237}\mathrm{Np} + \beta^{-}$$

Neptunium-237 is also formed by neutron capture in uranium-235:

$$^{235}\mathrm{U} + \mathrm{n} \rightarrow {}^{236}\mathrm{U} + \gamma$$

$$^{236}\mathrm{U} + \mathrm{n} \rightarrow {}^{237}\mathrm{U} + \gamma$$

$$^{237}\mathrm{U} \rightarrow {}^{237}\mathrm{Np} + \beta^{-}$$

The waste solutions from the processing of irradiated uranium fuel usually contain the neptunium, which can be isolated and purified by a combination of solvent extraction, ion exchange, and precipitation techniques.

The strategically important isotope ^{239}Pu is produced by the ton in nuclear reactors. Excess neutrons from the fission of uranium-235 are captured by uranium-238 to yield plutonium-239:

$$^{238}\mathrm{U} + \mathrm{n} \rightarrow {}^{239}\mathrm{U} \rightarrow {}^{239}\mathrm{Np} \rightarrow {}^{239}\mathrm{Pu}$$

Neutrons also cause the uranium nuclei to fission:

$$^{235}\mathrm{U} + \mathrm{n} \rightarrow \text{fission products} + 2.5n + 200\ \mathrm{MeV}$$

After removal from the reactor, the irradiated fuel can be chemically separated to extract the plutonium and also to separate the highly radioactive fission products.

Plutonium produced in nuclear reactors in which the fuel is irradiated for long periods of time contains plutonium isotopes with mass numbers up to 244, formed from ^{239}Pu by successive neutron capture. Industrial-scale processes for the separation and purification of plutonium are described in detail in Chapter 7. Three grades of plutonium are commonly recognized: weapon-grade plutonium (less than 7% ^{240}Pu), fuel-grade plutonium (7–18% ^{240}Pu), and reactor-grade plutonium (more than 18% ^{240}Pu).

Plutonium is an element that was until recently produced in 'production' reactors, i.e. reactors that were dedicated to produce nuclear materials for military purposes. More than 260 metric tons of military plutonium have been produced and separated worldwide (Albright *et al.*, 1996). Plutonium is also formed as a by-product of electricity production in all commercial (civilian) nuclear power reactors. As of 2000 the total 'discharge' of plutonium (plutonium in and separated from civilian spent fuel) from commercial nuclear power reactors was estimated to be 1380 metric tons, and this amount is predicted to increase by 741 metric tons in the decade 2001–10 (Albright *et al.*, 1996).

Although HEU and weapon-grade plutonium are primarily for military purposes and the lower grades are used in commercial nuclear reactors, enriched

uranium and plutonium of all grades are commonly discussed together because ^{235}U and ^{239}Pu are the two primary fissile isotopes and because they have the greatest security risk of potential diversion from peaceful to military or terrorist uses. Therefore, the total inventory must include both military and civilian stocks.

Plutonium has been separated from civilian reactor fuel principally at the B205 reprocessing plant in UK, at three reprocessing plants (UP1, UP2, UP3) in France, at Wiederaufarbeitungsanlage Karlsruhe (WAK) in Germany, and at Tokaimura in Japan. As of 1995, 132 metric tons of civilian plutonium had been removed at these plants. When plutonium separated by other countries is added, the total at the end of 1993 was 145 metric tons, of which 21 metric tons was in use in fast reactors and 17 metric tons in thermal reactors. The world annual separation of civilian plutonium continues at the rate of ca. 16 metric tons per year. By 2010, it is predicted that 437 metric tons will have been separated (Albright *et al.*, 1996).

Worldwide, at the end of 1994, 70 metric tons of plutonium were contained in nuclear weapons and 160 metric tons had been removed from weapons. The world inventory of all types of plutonium was 1160 metric tons at the end of 1994. The majority of this plutonium, 755 metric tons, was unseparated plutonium remaining in spent reactor fuel. This increases at the rate of approximately 70 metric tons per year.

The isotope ^{238}Pu is an important heat source for terrestrial and extraterrestrial applications (Section 15.11.2). The heat is generated by its nuclear alpha-particle decay. This isotope is available in kilogram quantities from the neutron irradiation of neptunium-237:

$$^{237}Np + n \rightarrow {}^{238}Np \rightarrow {}^{238}Pu$$

followed by chemical separation. Its 87.7 year half-life makes it the best isotope for this purpose. High-level waste from the isolation of plutonium-239 contains much larger quantities of plutonium-238, as well as heavier plutonium isotopes, formed by various nuclear reactions in reactor fuel elements, but the isotopic separation would be difficult and prohibitively expensive. The plutonium in a typical pressurized water reactor (PWR) fuel is approximately 1.3% ^{238}Pu after 33000 MWd ton^{-1} burnup (Albright *et al.*, 1996). As of 2000 approximately 10 metric tons of plutonium-238 exists in stored spent fuel elements and process residues accumulated in the U.S. and by the European Community, mixed with heavier plutonium isotopes (Albright *et al.*, 1996).

The elements americium and curium are obtained as by-products of the large-scale production of plutonium-239, or by the irradiation of plutonium-239 or isotopes of transplutonium elements in special high-neutron-flux reactors. The plutonium in a typical PWR fuel is approximately 14% ^{241}Pu after 33000 MWd ton^{-1} burnup (Albright *et al.*, 1996), producing ^{241}Am by beta decay with a half-life of 13.2 years. Kilogram quantities of americium-241 can be separated from

irradiated fuel by a combination of precipitation, ion exchange, and solvent extraction.

Isotopes of curium are also found in waste streams from plutonium-239 production, but in amounts smaller than those of americium. Curium (as ^{242}Cm and ^{244}Cm) is produced in nuclear reactors primarily by the beta decay of ^{242}Am and ^{244}Am, isotopes that were formed by neutron capture in ^{241}Am and ^{243}Am, respectively. The amount of ^{244}Cm accumulated in process wastes and in unprocessed irradiated fuel elements as of 2000 is estimated to be more than 1 metric ton (NEA, 2002). The high specific radioactivity (18.1-year half-life) of ^{244}Cm means that it has to be considered in separation schemes for reprocessing and transmutation, but it decays to low enough levels in a few hundred years that long-term storage is not a concern. Separation and purification of curium and americium is best carried out by the solvent extraction procedures described below because both are present as 3+ ions, which have similar chemical properties (see Section 15.3.6).

The sequence of neutron captures and beta decays that forms transuranium elements by slow neutron capture starting with plutonium-239 is shown in Fig. 15.1. A high neutron flux is essential to expedite the production of transplutonium elements. Fig. 15.2 shows that, even with a neutron flux in excess of 10^{14} cm^{-1} s^{-1}, years of irradiation may be required to attain useful conversions. Starting with 1 kg of ^{239}Pu, about 1 mg of ^{252}Cf would be present after 5–10 years of continuous irradiation at a neutron flux of 3×10^{14} cm$^{-1} \cdot$ s^{-1}. To increase the production rate, large quantities of ^{239}Pu can first be irradiated in production reactors, followed by continued irradiation in higher-neutron-flux reactors. The High Flux Isotope Reactor (HFIR) at Oak Ridge National

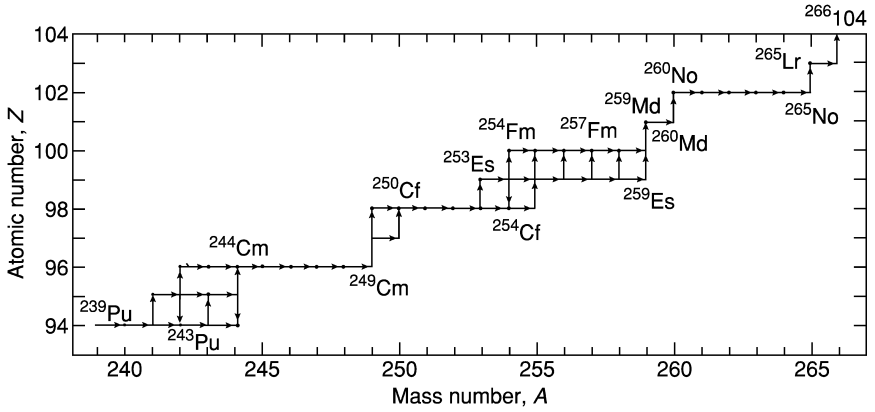

Fig. 15.1 *Nuclear reaction sequence for production of transplutonium elements by intensive slow-neutron irradiation. The principal path is shown by heavy arrows (horizontal, neutron capture; vertical, beta decay). The sequence above ^{258}Fm is a prediction.*

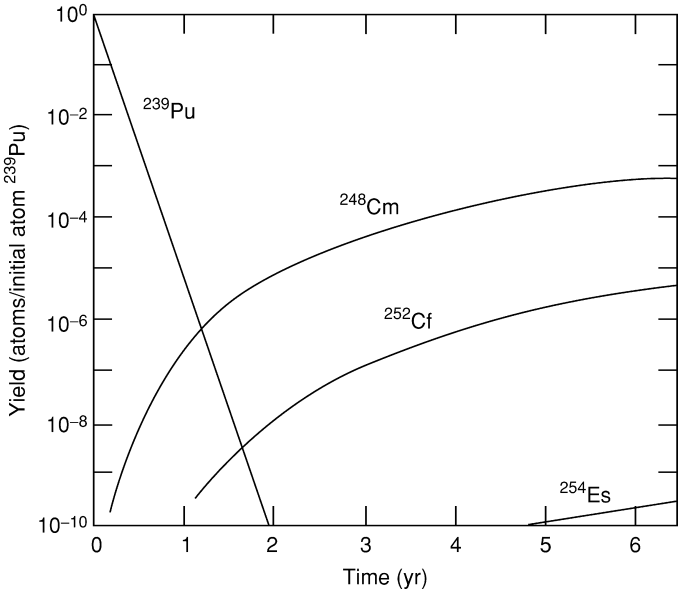

Fig. 15.2 *Production of some transplutonium nuclides by irradiation of* ^{239}*Pu at a neutron flux of* 3×10^{14} cm^{-2} s^{-1}.

Laboratory in Tennessee can provide neutron fluxes of about 2×10^{15} $cm^{-2} \cdot s^{-1}$. This reactor and tritium-production reactors that were in operation from 1953 to 1993 at the Savannah River Site in South Carolina, have made major contributions to the production of transcurium elements. A special facility, presently called the Radioisotope Engineering Development Center (REDC), was established at Oak Ridge in 1966 to fabricate plutonium targets, to extract transplutonium elements from the highly irradiated targets, and to provide pure samples of transplutonium isotopes as heavy as ^{257}Fm for research and industry. Neutron irradiation cannot be used to prepare the elements beyond fermium (^{257}Fm) because some of the intermediate nuclides have such short half-lives that the low equilibrium concentrations present effectively prevent the formation of significant amounts of the desired isotopes. Thus, only milligram amounts of einsteinium and picogram amounts of fermium can be obtained by protracted neutron irradiation even under the most favorable circumstances. Table 15.1 lists the past production rates of isotopes of elements from curium-248 to fermium-257 in the Oak Ridge HFIR/REDC operation (National Research Council, 1983; Keller *et al.*, 1984; Alexander, 2005). The SM-2 loop reactor in Russia has similar power and flux levels, giving it the potential for producing similar quantities of these transcurium isotopes. Isotopes that are sufficiently long-lived for work in weighable amounts are obtainable at least in

Table 15.1 *Production of transcurium isotopes in the U.S.*[a]

Isotope	*Half-life*	*Amount/year* (1983)	*Amount/campaign* (2004)
^{248}Cm	3.48×10^5 yr	150 mg[b]	100 mg[b]
^{249}Bk	330 d	50 mg	45 mg
^{249}Cf	351 yr	50 mg[c]	<45 mg[c]
^{252}Cf	2.645 yr	500 mg	400 mg
^{253}Es	20.47 d	2 mg[d]	1–2 mg[d]
^{254}Es	275.7 d	3 μg	4 μg
^{257}Fm	100.5 d	1 pg	1 pg

[a] One or two separation campaigns per year until about 1995; one campaign every 18–24 months from about 1995 to 2003.
[b] From alpha decay of ^{252}Cf.
[c] From beta decay of ^{249}Bk.
[d] Mixed with 0.06–0.3% ^{254}Es; chemical separation of ^{253}Cf followed by its beta decay can yield ~200 μg of isotopically pure ^{253}Es.

principle for all of the actinide elements through einsteinium. The elements above einsteinium appear likely to remain amenable to chemical study only by tracer techniques because (except for ^{257}Fm) only isotopes with short half-lives are known, and because it is unlikely that isotopes of the elements beyond einsteinium can be formed in weighable quantities by neutron irradiation or any other process.

Very heavy elements have been detected under circumstances where very intense neutron fluxes were produced. Such is the case for a few microseconds after a thermonuclear explosion. Isotopes of einsteinium and fermium were first discovered in the debris of the first thermonuclear explosion detonated at Eniwetok Atoll in November 1952 (Hyde *et al.*, 1964; Choppin *et al.*, 2002, p. 423). The route whereby elements of high atomic number are formed in the detonation of a thermonuclear device is again multiple neutron capture in ^{238}U, which is a component of the thermonuclear device. Thus, the synthesis of ^{255}Fm in the explosion occurred by way of ^{255}U (formed by the capture of 17 neutrons in ^{238}U) followed by a long sequence of short-lived beta decays that take place after the neutron capture reactions are complete:

$$^{238}\mathrm{U} + 17\mathrm{n} \rightarrow {}^{255}\mathrm{U} \xrightarrow{\beta^-} {}^{255}\mathrm{Np} \xrightarrow{\beta^-} {}^{255}\mathrm{Pu} \xrightarrow{\beta^-} {}^{255}\mathrm{Fm}$$

15.2.3 Heavy-ion bombardment

In lieu of the extraordinarily intense neutron fluxes associated with a thermonuclear explosion, synthesis of the transfermium elements in amounts sufficient to study their chemical properties has depended on nuclear reactions of charged particles (i.e. ^{4}He, ^{10}B, ^{12}C, and ^{16}O accelerated to appropriate energies in

heavy-ion accelerators) with targets of an actinide element of a lower atomic number. Such syntheses are made very difficult by the limited availability of target materials of high atomic number, by the low reaction yields, and by the difficulties inherent in the separation, isolation, and characterization of very short-lived radioactive isotopes. A distinctive feature of these procedures is that the product nuclide is produced and collected one atom at a time, necessitating isolation and identification procedures that are highly innovative. However, the obstacles have been successfully surmounted, and numerous isotopes of the heaviest actinide elements mendelevium, nobelium, and lawrencium have been produced, their nuclear properties measured, and salient features of their chemical properties established (Ghiorso, 1982 and Chapter 13, this work).

The currently known transactinide elements 104 through 111 were discovered at Berkeley, Dubna, and Darmstadt (see Table 1.1 and Chapter 14) using physical and nuclear techniques for synthesis, separation, and identification. The longest known confirmed half-lives for these elements range from 75 s for Rf to only ~40 ms for Mt. Discoveries of isotopes of Rf and Db with half-lives of seconds to minutes permitted investigations of their chemical properties after 1970. However, the first isotope discovered for element 106, Sg, had a half-life of just under a second, and the first-discovered isotopes of elements 107 through 111 had half-lives of only milliseconds. Nuclear theorists predicted that half-lives of isotopes of these elements near the deformed nuclear shells they calculated to be at $Z = 108$ and $N = 162$ would be stabilized by orders of magnitude. These predictions motivated experimentalists to design suitable production reactions, and in 1994 isotopes of Sg with alpha decay half-lives estimated to be tens of seconds were produced in reactions of the actinide target ^{248}Cm with ^{22}Ne beams and detected by physical means by a Dubna/Lawrence Livermore National Laboratory (LLNL) collaboration. These results helped to substantiate the theoretical predictions and innovative techniques to perform chemical investigations of Sg, Bh, and Hs were undertaken during the period 1997–2003. Isotopes of these elements with half-lives as long as 15–20 s were successfully identified in these studies by observation of their alpha decay to known daughter isotopes. These studies furnished valuable information about the chemical properties of Sg in both gas and aqueous phases, and of Bh and Hs in the gas phase.

Comparison of the observed chemical properties with the proposed lighter homologs in the periodic table confirms their placement in the periodic table as members of a 6d transition series; nevertheless there is some evidence for deviations that may be attributable to the influence of relativistic effects, expected to be strongest in the heaviest elements. To date, no chemical studies have been conducted beyond Hs because longer-lived isotopes of Mt have not yet been identified. A surprising amount of information has been obtained about the oxidation states of the transfermium and transactinide ions in solution even though in many cases only a few atoms or even a single atom at

a time was available for study. Discoveries of isotopes of elements 110, 111, and 112 were reported in 1995; for element 110 the reports have been confirmed and the name darmstadtium, symbol Ds, was approved by IUPAC in 2003. The name roentgenium, symbol Rg, for element 111 was approved by IUPAC late in 2004. A consortium of scientists from Dubna and LLNL has reported elements 113 through 116 (Table 1.1), but these have not yet been confirmed at another laboratory. The chemistry of transactinide elements and their predicted chemical and nuclear properties is discussed in Chapter 14.

An exciting frontier is the additional exploration of the chemical properties of the heavier transactinides, especially those beyond element 108 where relativistic effects become ever more important. Effects on chemical bonding have not been investigated satisfactorily even for the beginning of the transactinides. The synthesis of longer-lived isotopes of the elements beyond ^{108}Hs will be required to investigate even their rudimentary chemical properties, e.g. whether element 112 is a noble metal or a rare gas.

Some recent theoretical calculations indicate that in addition to the experimentally confirmed island of deformed stability near $Z = 108$, $N = 162$ and the island of spherical stability originally predicted to be around atomic number $Z = 114$ and neutron number $N = 184$, there may be islands of spherical stability around $Z = 120$ and $N = 172$, and $Z = 124$ or 126 and $N = 184$. If the reports by the Dubna/LLNL collaboration of the production in relatively high yield of neutron-rich, long-lived isotopes of elements 112 through 116 in irradiations of ^{244}Pu and other actinide targets with ^{48}Ca projectiles are confirmed, then many isotopes will become available for chemical studies. This would constitute a whole new region of nuclear stability with neutron numbers from $\sim$163 to $\sim$173, which could truly be called a region of 'superheavy elements.' The chemical properties of elements beyond 122 are currently impossible to predict and classify on the basis of the periodic table because the energy spacing for the 7d, 6f, and 5g levels, and later, for the 9s, $9p_{1/2}$, and $8p_{3/2}$ levels become so close and overlapping that clear structures on the basis of pure p, d, f, and g blocks are no longer distinguishable. An international collaborative effort will be required to initiate and implement such a frontier research program.

15.2.4 Atomic weights

The question of atomic weights deserves a brief comment. Many of the radionuclides listed in Table 15.2 can be obtained in high isotopic purity. Compounds of curium, for example, will have different formula weights depending on the particular curium isotope that is present in the compound. Atomic and molecular weights must be calculated from the relative abundances of isotopes present in a given sample.

Table 15.2 *Long-lived actinide nuclides suitable for physical and chemical investigation.*

Element	*Isotope*	*Half-life*
actinium	^{227}Ac	21.772 yr
thorium	^{232}Th	1.405×10^{10} yr
protactinium	^{231}Pa	3.276×10^{4} yr
uranium	^{233}U	1.592×10^{5} yr
	^{238}U[a]	4.468×10^{9} yr
neptunium	^{236}Np	1.54×10^{5} yr
	^{237}Np	2.144×10^{6} yr
plutonium	^{238}Pu	87.7 yr
	^{239}Pu	2.411×10^{4} yr
	^{240}Pu	6564 yr
	^{242}Pu	3.733×10^{5} yr
	^{244}Pu	8.08×10^{7} yr
americium	^{241}Am	432.2 yr
	^{243}Am	7370 yr
curium	^{244}Cm	18.10 yr
	^{245}Cm	8500 yr
	^{246}Cm	4760 yr
	^{247}Cm	1.56×10^{7} yr
	^{248}Cm	3.48×10^{5} yr
	^{250}Cm	$\sim$8300 yr[b]
berkelium	^{247}Bk[c]	1380 yr
	^{249}Bk	330 d
californium	^{249}Cf	351 yr
	^{252}Cf	2.645 yr
einsteinium	^{253}Es	20.47 d
	^{254}Es	275.7 d
	^{255}Es	39.8 d
fermium	^{257}Fm	100.5 d

[a] Natural isotopic composition is 99.275% ^{238}U, 0.720% ^{235}U, and 0.005% ^{234}U. Half-life given is for the major constituent ^{238}U.
[b] Produced only in very small amounts from neutron irradiations in thermonuclear explosions.
[c] Produced so far only in tracer quantities from charged particle irradiations.

15.3 EXPERIMENTAL TECHNIQUES

15.3.1 Hazards

All of the actinide elements, with the exception of uranium and thorium, are radioactive to such a degree that handling requires special equipment and shielded facilities (Gmelin, 1973; Choppin *et al.*, 2002, pp. 498–513; this work, Figs. 1.2–1.4) when samples above the tracer level are handled. The special containment and manipulation techniques for work with the actinide

elements are necessitated by the potential health hazards to the investigator and other occupants of the laboratory. Containment in the form of hoods and gloved boxes is now standard, and these are available through normal commercial channels. Shielded facilities are more specialized, and, for the most part, are found in laboratories devoted to the study or processing of the actinide elements.

The toxicity of the actinide elements, which requires an absolute barrier between the experiment and the experimenter, is dictated to only a small extent by external radiation hazards. Plutonium-239 is intensely radioactive, emitting 1.4×10^8 alpha particles per milligram per minute. However, the alpha radiation from plutonium-239 can easily be shielded by even a thin sheet of paper. It is the consequences of inhalation and ingestion that make plutonium-239 and most isotopes of the other actinide elements such toxic substances. Plutonium-239, inhaled into the lungs as fine particulate matter, is deposited in the lungs or translocated to the bone, and, over a period of time, may give rise to lung or bone neoplasms (see Section 15.10). The biological properties of the actinide elements are discussed in more detail in Sections 15.9 and 15.10 and in Chapter 31.

15.3.2 Long-lived actinide nuclides

Isotopes sufficiently long-lived for work with weighable amounts are in principle available for all the actinide elements through einsteinium (element 99). Long-lived actinide isotopes particularly suitable for physical and chemical investigations by more or less ordinary laboratory procedures are listed in Table 15.2. Not all of these are available in high isotopic purity. The elements above fermium, it appears, will always require tracer techniques for their investigation. This is not as restrictive a prospect as it may seem, for an astonishing amount of chemical information has been acquired from the few atoms of the heaviest actinide and transactinide elements that have already been prepared.

Most of the chemical studies with plutonium have been carried out with ^{239}Pu, but the isotopes ^{242}Pu and ^{244}Pu are more suitable (but available in very limited quantities) because of their longer half-lives and therefore lower specific activities. The solution chemistry of shorter-lived actinide ions in concentrated aqueous solution is complicated by radiolysis products such as hydrogen peroxide rapidly formed by the high-energy alpha particles produced by radioactive decay. In solid compounds, the high-energy heavy recoil particles can seriously damage or even destroy the crystal lattice. Americium chemistry, often studied with ^{241}Am, which emits about 8×10^9 alpha particles per milligram per minute, has fewer ambiguities when the studies are performed with ^{243}Am, which has a specific alpha activity about 20 times less than ^{241}Am. Much of the early research with curium used the isotopes ^{242}Cm and ^{244}Cm. The heavier curium isotopes, especially ^{248}Cm, obtained in relatively

high isotopic purity as the alpha-particle decay daughter of ^{252}Cf, make life much simpler for the investigator, although ^{248}Cm decays in small part by spontaneous fission, which creates a significant neutron hazard. The isotope ^{249}Bk and Cf as a mixture of the isotopes ^{249}Cf, ^{250}Cf, ^{251}Cf, and ^{252}Cf are available from the intense neutron irradiation of lighter elements. The most useful isotope for the study of californium is ^{249}Cf, which can be isolated in pure form from the beta decay of its parent ^{249}Bk. The isotope ^{253}Es (half-life 20.47 days), another product of intense neutron irradiation, is used to study the chemical properties of einsteinium, but the longer-lived ^{254}Es (half-life 275.7 days) would be more useful for work with macroscopic quantities. However, it is not produced initially free of ^{253}Es. There are severe problems in working with weighable amounts of berkelium, californium, and einsteinium because of their intense radioactivity. Spontaneous fission is an important mode of decay for ^{252}Cf (half-life 2.645 years): 1 μg of this isotope emits approximately 1.4×10^8 neutrons min^{-1}. Californium produced in the highest-flux reactors contains sufficient ^{252}Cf to cause very severe handling and shielding problems because of the spontaneous-fission neutron flux. Remote control manipulation is essential when more than a few micrograms of ^{252}Cf are used. While spontaneous fission makes for problems in chemical studies, ^{252}Cf provides very convenient neutron and fission fragment sources, which have important scientific, medical, and industrial uses (see Sections 15.11.3 and 15.11.4).

15.3.3 Tracer techniques

Investigations may be carried out on the tracer level, where solutions are handled in ordinary-sized laboratory equipment, but where the substance studied is present in extremely low concentrations. Concentrations of the radioactive species of the order of 10^{-12} M or much less are not unusual in tracer work with radioactive nuclides. A much larger amount of a suitably chosen nonradioactive host or carrier is subjected to chemical manipulation, and the behavior of the radioactive species (as monitored by its radioactivity) is determined relative to the behavior of the carrier. Thus the solubility of an actinide compound can be judged by whether the radioactive ion is carried by a precipitate formed by the nonradioactive carrier. Interpretation of such studies is made difficult by the adsorption of radioactive ions on vessel walls or colloidal particles in solution. Tracer studies provide information on the oxidation states of ions and complex-ion formation, and are used in the development of liquid–liquid solvent extraction and chromatographic separation procedures. Tracer techniques are not applicable to solid state or to most spectroscopic studies. Despite the difficulties inherent in tracer experiments, these methods continue to be used with the heaviest actinide and transactinide elements, where only a few to a few score atoms may be available (Benes and Majer, 1980).

15.3.4 Ultramicrochemical manipulations

Chemistry under the microscope often provides an alternative to tracer techniques. It is possible to work with microgram or even smaller amounts of material in very small volumes of solution not visible to the naked eye at ordinary concentrations, say 10^{-1} M to 10^{-3} M. Ultramicrochemical investigations yield results of normal validity, but skill, experience, a good microscope, and much patience are necessary to carry out such experiments. X-ray diffraction methods can be applied to microgram or even smaller samples of solid compounds. Many actinide element compounds have been identified and their molecular formulas established on samples of a few micrograms synthesized directly in the capillary that is subsequently used to record the X-ray diffraction pattern. With milligram amounts, operations can be readily carried out in a conventional manner. Most of the chemical results described in this book were obtained on about the milligram scale by semi-micro procedures. With highly radioactive isotopes (e.g. ^{253}Es), the microgram scale may still be preferred even when larger amounts of material are available. In the past, usable X-ray diffraction patterns were difficult to obtain from highly radioactive crystals because of radiation damage. Such problems are considerably ameliorated when smaller samples and modern methods of obtaining X-ray diffraction patterns are used.

15.3.5 Ion-exchange chromatography

Separations based on ion exchange have contributed to the science and technology of actinides in a variety of ways. In particular, the development of ion-exchange materials based on functionalized polymers (with well-characterized and reproducible properties) have enabled important procedures for both analysis and purification of actinides. Both cation-exchange resins containing (in particular) sulfonic and carboxylic acid groups, and anion-exchange resins with quaternary ammonium or methylpyridinium groups have been employed to separate actinides or to separate actinides from fission product lanthanides. Inorganic ion-exchange materials also have been used in actinide separations, particularly for waste management purposes. In this chromatographic technique (see Chapter 24), actinides, either as cations or anionic coordination complexes, are partitioned between a mobile aqueous phase and the solid resin phase. Actinide ions in the III, IV, V, and VI oxidation states are sorbed to different degrees and in different orders on cation and anion-exchange resins. The selectivity of separations is often determined by the complexants present in the mobile phase.

Ion-exchange separations can be rapid and selective and offer the inherent enhanced separation efficiency of being operable in a chromatographic mode. Because the elution order and approximate peak positions can be predicted with considerable confidence, ion exchange has been the key to the discovery of the transcurium elements. The power of the method can be judged from Fig. 15.3,

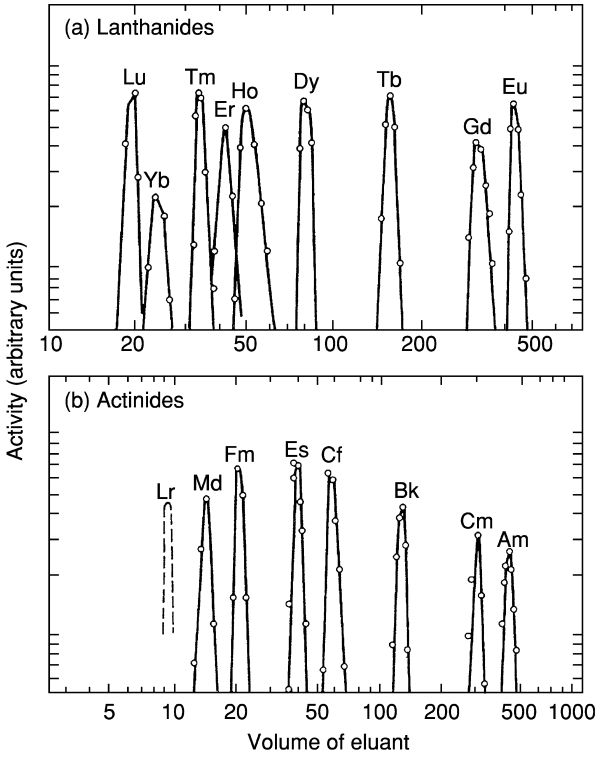

Fig. 15.3 *Elution of tripositive lanthanide and actinide ions on Dowex* 50 *cation-exchange resin and ammonium* α*-hydroxyisobutyrate eluant.* Lr^{3+} *band* (*dashed line*) *was predicted.*

which compares the order of elution of the trivalent lanthanide and actinide ions from the cation-exchange resin Dowex 50 (a copolymer of styrene and divinylbenzene containing sulfonic acid groups). The eluting agent is an aqueous solution of ammonium α-hydroxyisobutyrate. In this system elution occurs in the inverse order of atomic number for both lanthanide and actinide elements. The order of elution is determined by the relative stability of the aqueous complexes formed in the mobile phase. As a result, the differences between these adjacent metal ions are correlated with the variation of ionic radius with atomic number. There are many similarities between the 4f and 5f series of elements, but few parallels are more striking than those observed for the trivalent ions in ion exchange.

15.3.6 Liquid–liquid extraction

Liquid–liquid (or solvent) extraction is a separation technique that depends on the partition of ions between two immiscible liquid phases, one of which is usually an acidic aqueous solution (see Chapter 24). Under most circumstances,

the organic phase contains a strongly lipophilic extracting agent that interacts with a metal cation to form an electroneutral lipophilic complex. Among the most important actinide extractants are tri(*n*-butyl)phosphate (TBP) (basis of the PUREX process), bis(2-ethylhexyl)phosphoric acid, octyl(phenyl)-*N*,*N*-diisobutyl-carbamoylmethylphosphine oxide (basis of the TRUEX process), and *N*,*N*-dimethyl-*N*′,*N*′-dibutyl-2-hexoxyethylmalonamide (basis of the DIAMEX process). Tertiary (e.g. tricaprylamine or trilaurylamine) or quaternary amines (e.g. tricaprylammonium chloride) can also accomplish effective and selective separations of actinide ions through the formation of lipophilic ion pairs of actinide ions associated with enough normally hydrophilic anions (like Cl^- or NO_3^-) to create an anionic coordination complex. As is the case for ion exchange, the most effective separations in solvent extraction are those relying on the differences in actinide oxidation states. Some classes of solvent extraction reagents are capable of the separation of the individual trivalent actinide cations, as in the ion exchange example above. In recent years, solvent extraction reagents capable of efficiently separating trivalent actinides from fission product lanthanides have emerged. Separations are achieved because the partition coefficients of individual actinide ions in a mixture are significantly different. For production purposes, solvent extraction enables rapid and efficient separations when applied in a countercurrent multistage process. Solvent extraction is widely used for actinide element separations both in laboratory investigations and on a large industrial scale.

15.3.7 Column partition chromatography

A technique closely related to liquid–liquid extraction, also discussed in Chapter 24, is column partition chromatography, sometimes referred to as extraction chromatography. Partition chromatography is essentially a solvent extraction system in which one of the liquid phases is made stationary by adsorption on a solid support. The other liquid phase is mobile. Extraction chromatographic materials are usually (but not always) employed for analytical separations using column chromatography, which significantly increases separation efficiency. Either the aqueous or the organic phase can be immobilized. The aqueous phase can be made stationary by adsorption on silica gel, diatomaceous earth, or 5–10 μm diameter microspheres of silica. The same extracting agents that are used in ordinary solvent extraction can be used in partition chromatography. The organic phase can be adsorbed on beads (50–200 μm in diameter) of poly(vinylchloride), poly(tetrafluoroethylene), poly(monochlorotrifluoroethylene), or other solid support. When the stationary phase is organic, the technique is referred to as reversed-phase partition chromatography. This technique is widely used in radioanalytical chemistry, though its application to large-scale separation of actinides from dissolved spent fuel has been considered.

15.4 ELECTRONIC CONFIGURATION

15.4.1 General considerations

Establishing the electronic configuration of the elements and their ions has historically been a primary objective in physical and chemical research. This stems from the conviction that it ought to be possible to deduce *a priori* many of the properties of an element and its compounds from a detailed knowledge of its electronic configuration, a goal that is still approaching full realization. There are other reasons why such information is of particular interest in actinide chemistry. The f-block elements have unusual electronic configurations, and the comparative aspects of lanthanide and actinide electronic structures, as manifested in the chemical and physical properties of homologous elements, is a matter of keen interest. The striking similarities and differences between corresponding elements of the two series provide important insights into the contributions that the valence-electron quantum numbers make to the physical and chemical properties of the f-block elements.

Information relevant to the electronic configuration can be obtained from X-ray absorption spectroscopy, atomic emission spectroscopy (AES), X-ray photoelectron spectroscopy, paramagnetic susceptibility measurements, electron paramagnetic resonance, electronic transition spectroscopy, transmission electron microscopy, X-ray and neutron crystallography, and atomic-beam experiments. Discussions of the theoretical and experimental aspects of atomic spectroscopy, magnetic properties, crystal structures of solids, and electronic absorption spectroscopy are found in the later chapters of this work.

15.4.2 Spectroscopic studies

In AES and inductively coupled plasma mass spectrometry (ICP-MS) the wavelengths of light emitted from a vaporized atom in an excited electronic state are used as a 'signature' of the atomic number of the atom. These techniques are now used routinely for elemental analyses of research, industrial, and environmental materials, but AES was essentially the technique used originally to characterize the electronic properties of actinides. In an electrical discharge most of the species produced are electrically neutral atoms, but among them are small numbers of ionized species that have lost one, two, or three of their valence electrons. Because the spectra result from changes in the quantum numbers of the valence electrons present in the atom or ion, it is possible in principle to make deductions about the electronic energy levels of the emitting species. In practice, however, there are very severe problems in the interpretation of the emission spectra of the actinide elements. In the free atoms in the gas phase, the valence electrons interact strongly with the 5f electrons and also with each other. Each 5f level is split by these interactions to give many energy levels that are more widely split than the 5f levels themselves. The result is an

enormous number of lines in the emission spectra of actinide elements. In the uranium spectrum, 100000 lines have been measured, and between 5000 and 20000 lines have been measured for each of the elements from plutonium to berkelium. The number of assigned lines varies considerably but is much smaller, from about 2500 for uranium to about 100 for curium. The ground electronic configurations of neutral actinium, thorium, uranium, americium, berkelium, californium, and einsteinium were determined by atomic spectroscopy. The ground electronic structures of protactinium, neptunium, plutonium, curium, and fermium were deduced from atomic-beam experiments (Gmelin, 1973; see Chapter 16).

The dominant features of the electronic transition spectra of actinide ions in solution or in solid crystals arise for the most part from transitions within the $5f^N$ subshell. However, in the gas phase the predominant population consists of neutral atoms, which possess all of their valence electrons and therefore experience more interactions between the 5f electrons and the d- and s-shell valence electrons. The 5f electrons in actinide ions, either in crystals or in solution, are perturbed to a lesser extent because valence electrons in the 6d and 7s subshells are missing, and the 5f electrons are shielded from the electric fields of other ions by the remaining 6s and 6p electrons. The electronic transition spectra of actinide ions in solution therefore provide more information about the structure of the 5f levels, but the free-atom spectra provide more information about the interactions between the 5f and the valence electrons.

15.4.3 Electronic structure

Table 15.3 shows the assignments of the configuration (beyond the radon structure) of the ground-state gas-phase neutral atom of each of the elements from actinium to lawrencium, as well as the configurations of the singly charged, doubly charged, and triply charged gaseous atoms. Included for comparison are the ground-state neutral-atom and triply charged electronic configurations (beyond the xenon structure) of the 4f lanthanide elements and the configurations of the 3+ ions of both series. The similarities between the lanthanide and actinide elements were recognized from very early work on the actinides. It can be seen from Table 15.3 that the incorporation of the 14 5f electrons into the elements of the actinide series is not as regular as in the 4f series, especially in the actinide elements preceding curium.

The atomic spectra indicate quite clearly that the 6d levels of thorium in the gas-phase neutral atom are lower in energy than the 5f levels. As in other transition series, the relative energy levels of the electron shell being filled become lower as successive electrons are added, and, in the elements following thorium, the 5f shell appears clearly to be of lower energy than the 6d shell. Triply ionized Th^{3+} has one 5f electron in the gas phase as the ground configuration with the 6d configuration ~1.25 eV higher. But in the very few molecular Th^{3+} compounds synthesized to date, the 6d configuration is stabilized by the

Table 15.3 *Electronic configurations of f-block and transactinide atoms and ions.*[a]

		Lanthanide series				*Actinide series*				
Element	*Gaseous atom*	M^{3+}(g)	M^{3+}(aq)	*Element*	*Gaseous atom*	M^{+}(g)	M^{2+}(g)	M^{3+}(g)	M^{3+}(aq)	M^{4+}(g)
La	$5d6s^2$			Ac	$6d7s^2$	$7s^2$	7s			
Ce	$4f5d6s^2$	4f	4f	Th	$6d^27s^2$	$6d7s^2$	5f6d	5f		
Pr	$4f^36s^2$	$4f^2$	$4f^2$	Pa	$5f^26d7s^2$	$5f^27s^2$	$5f^26d$	$5f^2$		(5f)
Nd	$4f^46s^2$	$4f^3$	$4f^3$	U	$5f^36d7s^2$	$5f^37s^2$		$5f^3$	$5f^3$	$5f^2$
Pm	$4f^56s^2$	$4f^4$	$4f^4$	Np	$5f^46d7s^2$			$5f^4$	$5f^4$	($5f^3$)
Sm	$4f^66s^2$	$4f^5$	$4f^5$	Pu	$5f^67s^2$	$5f^67s$	$5f^6$	$5f^5$	$5f^5$	($5f^4$)
Eu	$4f^76s^2$	$4f^6$	$4f^6$	Am	$5f^77s^2$	$5f^77s$	$5f^7$	$5f^6$	$5f^6$	($5f^5$)
Gd	$4f^75d6s^2$	$4f^7$	$4f^7$	Cm	$5f^76d7s^2$	$5f^77s^2$	$5f^8$	$5f^7$	$5f^7$	($5f^6$)
Tb	$4f^96s^2$	$4f^8$	$4f^8$	Bk	$5f^97s^2$	$5f^97s$	$5f^9$	$5f^8$	$5f^8$	($5f^7$)
Dy	$4f^{10}6s^2$	$4f^9$	$4f^9$	Cf	$5f^{10}7s^2$	$5f^{10}7s$	$5f^{10}$	$5f^9$	$5f^9$	($5f^8$)
Ho	$4f^{11}6s^2$	$4f^{10}$	$4f^{10}$	Es	$5f^{11}7s^2$	$5f^{11}7s$	$5f^{11}$	$5f^{10}$	$5f^{10}$	($5f^9$)
Er	$4f^{12}6s^2$	$4f^{11}$	$4f^{11}$	Fm	$5f^{12}7s^2$			$5f^{11}$	$5f^{11}$	($5f^{10}$)
Tm	$4f^{13}6s^2$	$4f^{12}$	$4f^{12}$	Md	$5f^{13}7s^2$			$5f^{12}$	$5f^{12}$	($5f^{11}$)
Yb	$4f^{14}6s^2$	$4f^{13}$	$4f^{13}$	No	$5f^{14}7s^2$		($5f^{14}$)	$5f^{13}$	$5f^{13}$	($5f^{12}$)
Lu	$4f^{14}5d6s^2$	$4f^{14}$	$4f^{14}$	Lr	($5f^{14}6d7s^2$ or $5f^{14}7s^27p$)			$5f^{14}$	$5f^{14}$	($5f^{13}$)
				Rf	($5f^{14}6d^27s^2$)					($5f^{14}$)
				Db	($6d^37s^2$)	($6d7s^2$)	($7s^2$)			
				Sg	($6d^47s^2$)	($6d^27s^2$)	($6d^3$)			
				Bh[e]	($6d^57s^2$)	($6d^37s^2$)	($6d^37s$)			
				Hs	($6d^67s^2$)	($6d^47s^2$)	($6d^37s^2$)			
				109	($6d^77s^2$)	($6d^57s^2$)	($6d^57s$)			
				110	($6d^87s^2$)	($6d^67s^2$)	?			
				111	($6d^97s^2$)	($6d^77s^2$)	?			
				112	($6d^{10}7s^2$)	($6d^87s^2$)	?			

[a] Configurations from Chapters 14 and 16. Predicted configurations are given in parentheses.

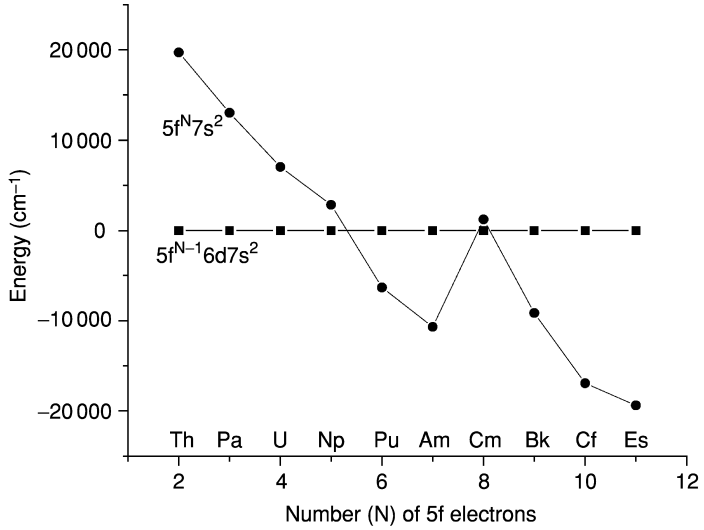

Fig. 15.4 *Relative energies of the $5f^N7s^2$ and $5f^{N-1}6d7s^2$ electron configurations in the gaseous actinide atoms showing the stabilization of the $5f^N7s^2$ as the atomic number Z ($Z = 88 + N$) increases.*

ligand field relative to the 5f configuration, and is found to be the ground configuration. For the elements beyond neptunium, the electronic configurations of the 4f and 5f elements strongly resemble each other. That the relative energy levels of the outer d- and s-shell electrons relative to the 5f electrons are not identical to those observed in the 4f block elements is not unexpected. Fig. 15.4 represents the relative energies of electron configurations that interchange 5f and 6d electrons for most of the actinide elements; as the curves intersect, inversion of behavior is inevitable.

15.4.4 Position in the periodic table

Before 1944, the elements thorium, protactinium, and uranium were assigned positions in the periodic table immediately below the elements hafnium, tantalum, and tungsten. It became evident that to accommodate the transuranium elements in the periodic table would require a radically new arrangement. The arguments for positioning them as a new 'actinide' transition series, similar to the rare earths, became strong by 1944 but experimental data to support this view were still scanty. With the passage of time the evidence in favor of a new transition series has become very convincing. Fig. 15.5 shows a modern periodic table, which not only includes the actinide elements as a transition series, but also indicates the location of the transactinides and a new superactinide transition series that may never be discovered.

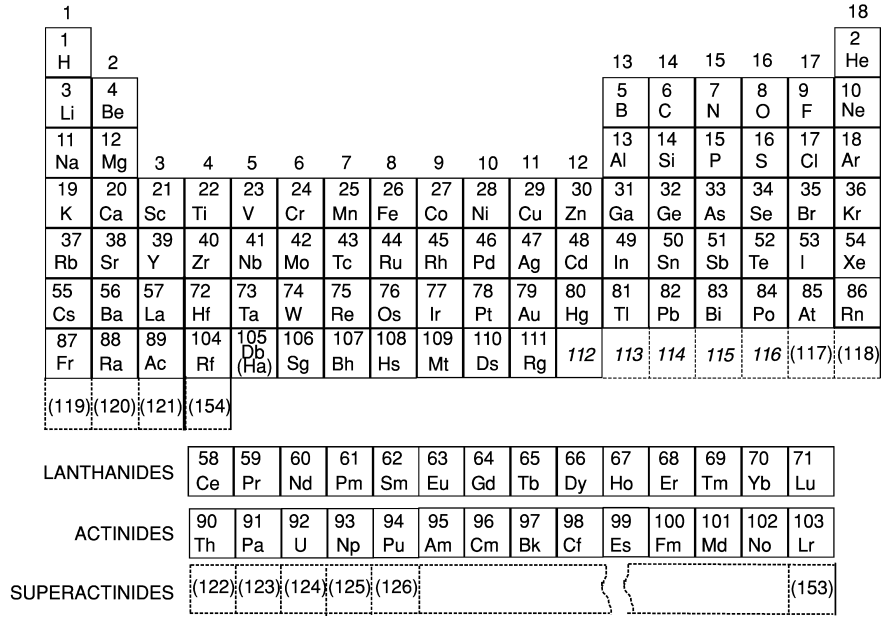

Fig. 15.5 *Modern periodic table showing predicted locations of many undiscovered transuranium elements (atomic numbers in parentheses). For element* 105 *two symbols are shown. The official IUPAC name is dubnium (Db), adopted in* 1997. *Hahnium (Ha) is also shown; this name also was used for a number of years after the discovery of this element.*

15.5 OXIDATION STATES

15.5.1 Ions in aqueous solution

Tables 15.4 and 15.6 list the oxidation states of the actinide elements and the color of the actinide ions, respectively. It is clear that the actinide oxidation states are far more variable than those of the lanthanides. The close proximity of the energy levels of the 7s, 6d, and 5f electrons almost guarantees multiple oxidation states for the actinide ions, at least in the first half of the actinide series. The multiplicity of oxidation states, coupled with the hydrolytic behavior of the ions, make the chemical behavior of the elements from protactinium to americium among the most complex of the elements in the periodic table.

In Table 15.4, the most stable states are shown in bold type and the more unstable states are indicated by parentheses. Oxidation states that have been claimed to exist, but not independently substantiated, are indicated with question marks. The most unstable oxidation states have only been observed in solid compounds, or produced as transient species in solution by pulse radiolysis (Sullivan *et al.*, 1976a,b, 1982; Gordon *et al.*, 1978). In this very interesting technique, a beam of energetic electrons is injected into an aqueous

Table 15.4 *The oxidation states of the actinide elements.*

Atomic No. *Element*	89 *Ac*	90 *Th*	91 *Pa*	92 *U*	93 *Np*	94 *Pu*	95 *Am*	96 *Cm*	97 *Bk*	98 *Cf*	99 *Es*	100 *Fm*	101 *Md*	102 *No*	103 *Lr*
Oxidation states													1?		
		(2)					(2)			(2)	(2)	2	2	**2**	
	3	(3)	(3)	3	3	3	**3**	**3**	**3**	**3**	**3**	**3**	**3**	3	**3**
		4	4	4	4	**4**	4	4	4	4	4?				
			5	5	**5**	5	5	5?		5?					
				6	6	6	6	6?							
					7	7	7?								
						8?									

Bold type, most stable; ( ), unstable; ?, claimed but not substantiated.

Table 15.5 *The oxidation states of the transactinide elements.*

Atomic No. *Element*	104 *Rf*	105 *Db*	106 *Sg*	107 *Bh*	108 *Hs*	109 *Mt*	110 *Rg*	111	112
Oxidation states								–1 ?	
							0 ?		**0 ?**
						1 ?		**3 ?**	
							2 ?		2 ?
	3	(3)	(3)	**3**	**3**	**3 ?**		**5** ?	
	4	4	4	4	**4**		4 ?		**4 ?**
		5	5	5					
			6		6	**6 ?**	6 ?		
				7					
					8				

Bold type, most stable; ( ), unstable; ?, predicted but not experimentally substantiated.

solution of the ion (for actinides, mainly the 3+ ions) under investigation. When N_2O is present in the reaction mixture, the hydrated electrons formed by the injection of the electrons into water are converted into OH radicals, which are strong oxidants. If *t*-butanol is present in place of nitrous oxide, the OH radicals are scavenged, and only the hydrated electron, e^-(aq), a powerful reducing agent, is formed. The reactions of these reagents with actinide ions are followed spectrophotometrically. Reaction of the 3+ ions in 0.1 M perchloric acid with e^-(aq) forms Am(II), Cm(II), and Cf(II). When OH radicals react, Am(IV) and Cm(IV), but no Cf(IV), are produced. All of the 2+ and 4+ species are transient. The 2+ species disappear with rate constants of about 10^5 s^{-1} by what appears to be a first-order process. Am(II), Cm(II), and Cf(II) have half-lives of the order of 5–20 μs. Am(IV) appears to be

appreciably more stable and has a half-life of about 1 ms. Pulse radiolysis has been shown to be a widely applicable method for producing ionic species in oxidation states that are difficult or impossible to access by conventional chemical procedures.

With the exception of thorium and protactinium, all of the actinide elements show a 3+ state in aqueous solution, although the 3+ state does not become the preferred or stable oxidation state under ordinary conditions until americium is reached. Stable organometallic compounds of Th(III) have been characterized and have a $6d^1$ configuration as the ground state (Blake *et al.*, 2001). A stable 4+ state is observed in the elements thorium through plutonium and in berkelium. Am(IV) can be stabilized in aqueous media by very strong complexing agents such as carbonate, tungstophosphate and tungstosilicate heteropolyanions. The 5+ oxidation state is well established for the elements protactinium through americium, and the 6+ state in the elements uranium through americium. The 4+ state in curium is confined to a few solid compounds, particularly CmO_2 and CmF_4, and appears to be present in a stable complex ion that exists in concentrated cesium fluoride solution. The Cf(IV) state is limited to the solid compounds CfO_2, CfF_4, a complex oxide $BaCfO_3$, and in tungstophosphate solutions; the oxidation of Cf(III) to Cf(IV) in strong carbonate solutions is a disputed topic.

The 2+ oxidation state first appears at americium in a few solid compounds and then at californium in the second half of the series. The II oxidation state becomes increasingly more stable in proceeding to nobelium. Md(II) and No(II) have been observed in aqueous solution and this appears to be the most stable oxidation state for nobelium. Am(II) has not only been encountered in solid compounds, but also in electrochemical and pulse radiolysis experiments in acetonitrile solution. The formation of Bk(IV) is associated with enhanced stability of the half-filled 5f configuration ($5f^7$), and the No(II) state reflects the stability of the full 5f shell ($5f^{14}$). The increase in the stability of the lower oxidation states of the heavier actinide elements relative to the lanthanides may be the result of stronger binding of the 5f (and 6d) electrons in the elements near the heavy end of the actinide series. Claims have been advanced that all the elements from plutonium to nobelium can be prepared in the 2+ state, and that this is a stable oxidation state for the elements fermium to nobelium (Mikheev, 1984). There has been no confirmation of these claims. The findings from pulse radiolysis show that even the 2+ state of the actinides preceding einsteinium are transient species, and have very short lifetimes (Gordon *et al.*, 1978; Sullivan *et al.*, 1982). Mendelevium has been reported to possess a stable 1+ oxidation state (Mikheev, 1984), but the evidence for monovalent ions of the actinide elements is doubtful. (See chapter 13.)

The transactinide elements rutherfordium through hassium have been studied by innovative chemical techniques, in particular thermochromatography (by which the relative volatilities of halides of elements 104–108 have been determined). The resulting oxidation states are shown in Table 15.5.

15.5.2 Ion types

Actinide ions in the same oxidation state have essentially the same coordination environments. In aqueous solutions at a pH < 3, four structural types of actinide cations exist. Formulas and colors of these ions are listed in Table 15.6. Only simple (uncomplexed) ions are listed. The ions of the type M^{3+} or M^{4+}, as is the case for cations with a high charge, show a strong inclination to solvation, hydrolysis, and polymerization (see Section 15.5.3). For the actinide elements in higher oxidation states (U through Am), the effective charge on the simple ion is decreased by the formation of oxygenated species of the general type MO_2^+ and MO_2^{2+}. The actinyl ions MO_2^+ and MO_2^{2+} are remarkably stable, having strong covalently bonded O=M=O ions, and persisting as a unit through a great variety of chemical transformations. Infrared spectroscopy shows conclusively that the ion MO_2^{2+} exists as a symmetrical, linear or very nearly linear, group. Crystallographic studies have shown that in solids UO_2^{2+} have four, five, or six ligands, typically in an equatorial plane perpendicular to the O=U=O axis; X-ray scattering in dilute perchloric acid solution shows UO_2^{2+} coordinated to five water molecules (Neuefeind *et al.*, 2004). The stability and linearity of the MO_2^{2+} ions are understood from theoretical bonding arguments (Zhang and Pitzer, 1999; Hay *et al.*, 2000). The corresponding 5+ state actinyl ions, AnO_2^+ (An = U, Np, Pu, Am), have the same symmetrical linear structure but with weaker metal–oxygen bonds. There is a regular decrease in the strength of the metal–oxygen bond with increasing atomic number in the actinyl ions from uranium to americium. The 7+ oxidation state, found in some

Table 15.6 *Ion types and colors for actinide ions in aqueous solution.*

Element	M^{3+}	M^{4+}	MO_2^+	MO_2^{2+}	$MO_4(OH)_2^{3-}$ (*alkaline soln.*)
actinium	colorless				
thorium		colorless			
protactinium		colorless	colorless		
uranium	red	green	color unknown	yellow	
neptunium	blue to purple	yellow-green	green	pink to red	dark green
plutonium	blue to violet	tan to orange	reddish-purple	yellow to pink-orange	dark green
americium	pink or yellow	color unknown	yellow	rum-colored	
curium	pale green	color unknown			
berkelium	green	yellow			
californium	green				

compounds of neptunium and plutonium in alkaline aqueous solution, contains in some cases tetroxo species $MO_4(OH)_2^{3-}$ (Williams *et al.*, 2001). The existence of Am(VII), even in alkaline media, is still a matter of debate (see Chapter 8). In acid solution, actinide ions in the 7+ oxidation state oxidize water rapidly.

Reduction potentials for the actinide elements are shown in Fig. 15.6. These show standard potentials in volts in aqueous acidic solution relative to the standard hydrogen electrode. The measured potentials were determined by electrochemical cells at or near equilibrium, and enthalpy of reaction measurements coupled with entropy measurements or estimates. Species not found in aqueous solution, but whose thermodynamic properties have been estimated, are indicated in parentheses.

The M^{4+}/M^{3+} and the MO_2^{2+}/MO_2^{+} couples are reversible, and, as expected, rapid reactions occur with one-electron oxidizing and reducing agents when no bond breaking or making takes place. The MO_2^{+}/M^{3+}, MO_2^{+}/M^{4+}, and MO_2^{2+}/M^{4+} couples are not reversible, presumably because of the barrier introduced by formation and rupture of covalent 'yl' bonds and the subsequent reorganization of the solvent shell, and also because some of these are two-electron reductions.

A summary of qualitative information about the oxidation–reduction characteristics of the actinide ions is presented in Table 15.7. The disproportionation and redox reactions of UO_2^{+}, Pu^{4+}, PuO_2^{+}, and AmO_2^{+} are especially complex, and, despite extensive study, many aspects of these reactions still remain to be explored. In the case of plutonium, the situation is especially complicated, because ions in all four oxidation states 3+, 4+, 5+, and 6+ can exist simultaneously in aqueous solution in comparable concentrations. The kinetics of the redox reactions of the actinide elements were reviewed by Newton (1975) and are presented in Chapter 23. Mechanisms of redox reactions involving uranium species are discussed in Chapter 5.

15.5.3 Hydrolysis and polymerization

All metal cations in aqueous solution interact extensively with the solvent water, and to a lesser or greater extent exist as hydrated cations (Baes and Mesmer, 1976; Burgess, 1978). The more highly charged the naked cation, the greater the extent of interaction with the solvent. Aquo cations, especially those of 4+, 3+, and small 2+ ions, act as acids in solution:

$$M(OH_2)_x^{n+} \rightarrow M(OH_2)_{x-1}(OH)^{(n-1)+} + H^+$$

This reaction illustrates the increase in acidity caused by hydrolysis of water as a protic ligand coordinated to metal cations. Because the acidity of water coordinated to 3+ and 4+ species is the more strongly enhanced the higher the charge on the metal cation, actinide elements in their most frequently encountered oxidation states undergo extensive hydrolytic reactions. Th^{4+}(aq) begins to hydrolyze to $Th(OH)^{3+}$ below pH 2. At higher pH, more hydrolyzed and

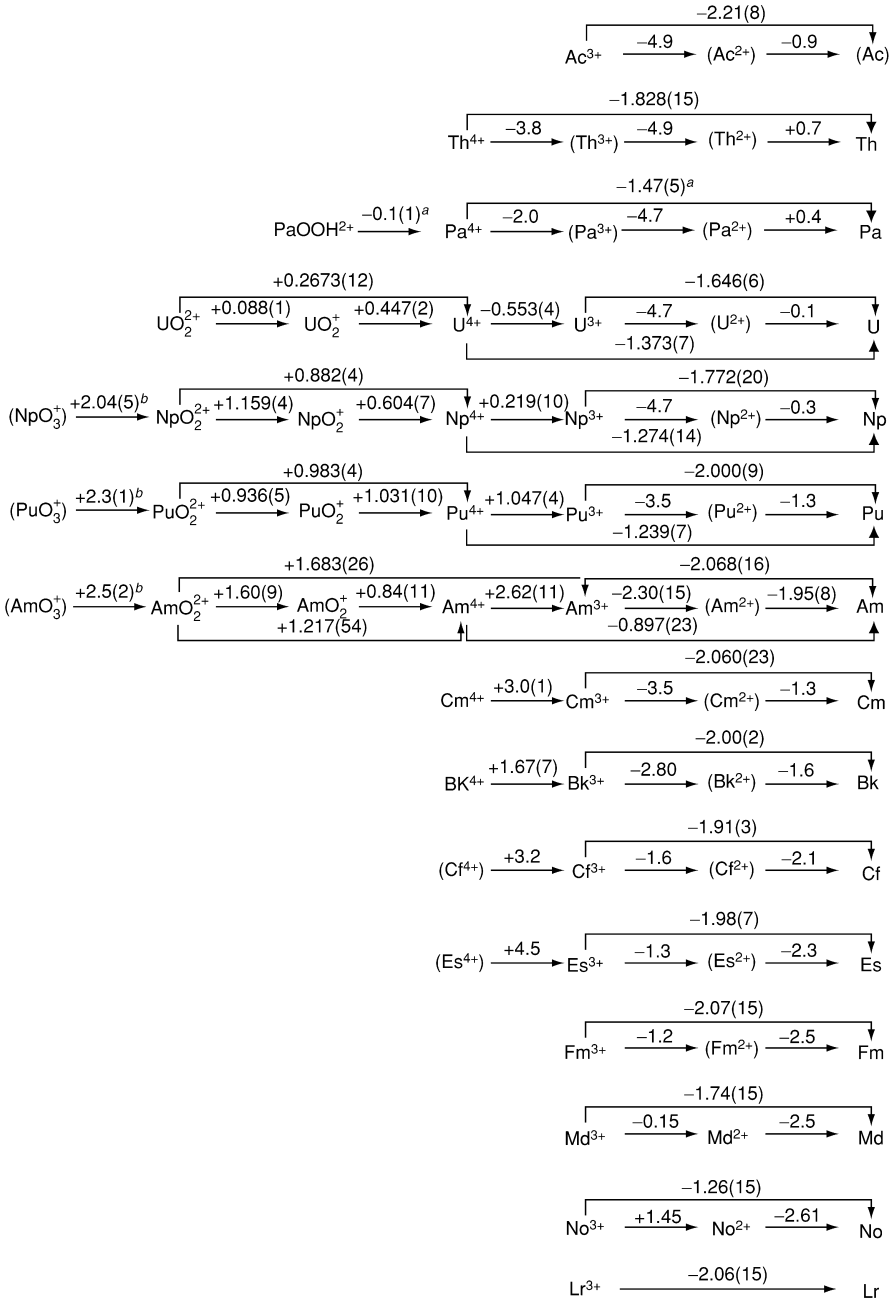

Fig. 15.6 *Standard reduction potentials diagrams for the actinide ions. Values in volts versus standard hydrogen electrode; footnote a indicates that the solvent is* 1 M *HCl, footnote b refer to the potentials in* 1 M $HClO_4$.

Table 15.7 *Stability of actinide ions in aqueous solution* (*usually acidic*).

Ion	*Stability*
Md^{2+}	stable to water, but readily oxidized
No^{2+}	stable
Ac^{3+}	stable
U^{3+}	oxidizes to U^{4+} and reduces water; aqueous solutions evolve H_2 on standing
Np^{3+}	stable to water, but easily oxidized by air to
Pu^{3+}	stable to water and air, but easily oxidized to Pu^{4+}
Am^{3+}	stable; can be oxidized with difficulty
Cm^{3+}	stable
Bk^{3+}	stable; can be oxidized to Bk^{4+}
Cf^{3+}	stable
Es^{3+}	stable
Fm^{3+}	stable
Md^{3+}	stable, but rather easily reduced to Md^{2+}
No^{3+}	easily reduced to No^{2+}
Lr^{3+}	stable
Th^{4+}	stable
Pa^{4+}	stable to water, but readily oxidized
U^{4+}	stable to water, but slowly oxidized by air to UO_2^{2+}
Np^{4+}	stable to water, but slowly oxidized by air to NpO_2^+
Pu^{4+}	stable in concentrated acid, e.g. 6 M HNO_3, but disproportionates to Pu^{3+} and PuO_2^{2+} at lower acidities
Am^{4+}	known in solution only in presence of strong complexants
Cm^{4+}	known in solution only in presence of strong complexants
Bk^{4+}	marginally stable; easily reduced to Bk^{3+}
Pa^{5+}	stable, hydrolyses readily
UO_2^+	disproportionates to U^{4+} and UO_2^{2+}; most nearly stable at pH 2–4
NpO_2^+	stable; disproportionates only at high acidities
PuO_2^+	tends to disproportionate to Pu^{4+} and PuO_2^{2+} (ultimate products); most nearly stable at very low acidities
AmO_2^+	disproportionates in strong acid to Am^{3+} and AmO_2^{2+}; reduces fairly rapidly under the action of its own a radiation at lower acidities (as ^{241}Am isotope)
UO_2^{2+}	stable; difficult to reduce
NpO_2^{2+}	stable; easy to reduce
PuO_2^{2+}	stable; easy to reduce; reduces slowly under the action of its own alpha radiation (as ^{239}Pu isotope)
AmO_2^{2+}	easy to reduce; reduces fairly rapidly under the action of its own alpha radiation (as ^{241}Am isotope)
$NpO_4(OH)_2^{3-}$	observed only in alkaline solution
$PuO_4(OH)_2^{3-}$	observed only in alkaline solution; oxidizes water

polymerized Th(IV) species begin to predominate. The mononuclear Pa(IV) species $PaO^{2+}(aq)$ or $Pa(OH)_2^{2+}(aq)$ have been claimed to exist at low concentrations; however, polymers are already evident at protactinium concentrations well below micromolar and in tracer experiments. U(IV) begins to undergo

hydrolysis in aqueous solution above pH 2.9, and, at somewhat higher pH, is largely present as hydrolyzed and polymerized species. $U(OH)^{3+}$ has been identified as the predominant U(IV) species in solution at low uranium concentrations and moderate acidities. Pu(IV) requires strongly acid conditions to exist as a simple Pu^{4+}(aq) ion. Even in moderately acid solutions, Pu(IV) hydrolyzes extensively, and may form polymers of high molecular weight. The actinyl ions typical of the 5+ and 6+ states presumably are formed with great speed whenever oxidation to the 5+ and 6+ states occurs in water. Once the uranyl, neptunyl, plutonyl, and americyl ions are formed, the only practical way to remove the coordinated oxygen atoms is by reduction to the 4+ or 3+ state. Although uranyl nitrate can be obtained as an anhydrous compound, in this form it is coordinatively unsaturated, and it is usually encountered as the hexahydrate or coordinated to equivalent ligands.

It is well known that aquo cations of heavy elements in the 3+ oxidation state or higher readily lose protons to form hydroxo complexes. Subsequent condensation reactions between the hydroxo complexes can then form polynuclear species in which the metal ions are linked through hydroxo (M–OH–M) or oxo (M–O–M) bridges. For the formation of polynuclear species, the pH range is critical; at too low a pH the ion will exist as the simple aquo cation, and at too high a pH the hydrous oxide or hydroxide precipitates. The actinide ions with oxidation number 4+ are particularly prone to hydrolysis and polymerization, but the MO_2^{2+} oxo cations also have considerable tendencies toward polynuclear ion formation. Among the 4+ cations, Th(IV), U(IV), and especially Pu(IV) form polymeric species. Th(IV) has a very complicated solution chemistry and, except in strong acid solutions, polynuclear species are easily generated in which Th(IV) ions are cross-linked by hydroxo bridges. Similarly, U(IV) forms polynuclear aggregates that may contain both hydroxo and oxo bridges. The $U(OH)^{3+}$ ion, which predominates in acidic solutions and low uranium concentrations, rapidly undergoes polymerization in solutions of moderate or low acidity. The formation of very large polymers occurs with U(IV) at much lower ligand numbers than is the case for Th(IV). The hydrolytic behavior of the Np(IV) ion is similar to that of Pu(IV), although Np^{4+} is an appreciably weaker acid.

The hydrated Pu(IV) ion is a stronger acid than the U(IV) ion, and it is exceptionally prone to polymer formation. As hydrolysis proceeds and before actual precipitation occurs, positively charged polymers of colloidal dimensions with molecular weights as high as 10^{10} have been observed. Although all of the polynuclear species of the actinide ions are of scientific interest, the polymers of Pu(IV) have attracted the most attention because of practical considerations. The effect of concentration, acidity, temperature, and ionic strength on polymer formation are ill-defined, and, as the Pu(IV) polymers are very stable and depolymerization is not at all easily affected, unpredictable behavior of Pu(IV) solutions can pose major problems and create potentially serious hazards, such as criticality, in nuclear fuel processing.

The actinyl ions MO_2^+ and MO_2^{2+} are considerably less acidic than are the 4+ state monomeric ions, and therefore have a smaller tendency to undergo hydrolysis. Hydrolysis decreases in the order $M^{4+} > MO_2^{2+} > M^{3+} > MO_2^+$. This trend follows the expected decreasing ratio of charge to ion size as the determining factor in hydrolysis.

The order of acidity for the 4+ species is $Pu^{4+} \approx Np^{4+} > U^{4+} \gg Th^{4+}$ (Neck and Kim, 2001). The similar hydrolytic behavior of Np^{4+} and Pu^{4+} cannot be understood simply in terms of charge-to-size considerations. On the basis of increasing charge and decreasing ionic size, it is expected that the degree of hydrolysis for a series of ions of any charge in the actinide series would increase with atomic number. This hydrolytic behavior of Np(IV) implies that additional, and as yet unidentified, factors make important contributions to the interaction of the actinide ions with water.

The actinyl(V) ions, which carry the low charge of 1+, are weak acids, with the singular exception of Pa(V). The protactinyl(V) ion is a much stronger acid than its successors in the actinide series and, in fact, the least hydrolyzed species of Pa(V) appears to be $PaO(OH)^{2+}$. In both its 4+ and 5+ oxidation states, protactinium shows a very unusual tendency to hydrolyze. Experience with protactinium chemistry in extremely dilute acidic solutions indicates that Pa(V) is already extensively hydrolyzed. The chemical investigation of protactinium at any level is rendered extremely difficult by the formation of intractable polymers. The use of strong complexing agents such as fluoride circumvents some of these difficulties.

The actinyl(VI) ions all undergo hydrolysis to an appreciable extent. Hydrolysis of UO_2^{2+} even in dilute solution results in almost total conversion to polynuclear species. These are small polymers, containing fewer than five uranium atoms. The tendency to form polymers of colloidal dimensions thus appears to be much diminished in the actinyl(VI) ions relative to the actinide(IV) ions. Precipitation occurs gradually or rapidly, depending on the kinetics of colloidal aggregation. The strong inclination to form insoluble precipitates after only a small amount of hydrolysis makes characterization of the water-soluble polymers of the actinyl ions a difficult challenge.

15.5.4 Complex-ion formation

The tendency to form complex ions in solution is to a considerable extent an expression of the same forces that lead to hydrolysis. The high positive charge on a bare 3+ or 4+ ion provides a strong driving force for interaction with nucleophiles. Water is only one example of such a nucleophilic ligand. Other nucleophiles that may be present in a solution can compete for coordination to the electrophilic cation to form complex ions. In most cases of complex formation, water molecules directly bound to the metal cation are displaced by the entering ligand to form an inner-sphere complex that may or may not contain water still bound to the metal ion. Alternatively, ligands may form hydrogen

bonds to water molecules of the outer hydrate shell to form outer-sphere complexes. Strong complexes are for the most part of the inner-sphere type. For inorganic anions, the complexing power of the actinide cations is in the order fluoride > nitrate > chloride > perchlorate for the singly charged anions, and carbonate > oxalate > sulfate for doubly charged anions. The stability of the complexes for a given ligand follows the order $M^{4+} > MO_2^{2+} \approx M^{3+} > MO_2^{+}$. For ions of the same charge, the stability of the complex increases with decreasing ionic radius in the first half of the actinide series. Many irregularities are encountered in the series of ions of uranium through americium, just as in the hydrolytic behavior of the tetravalent actinides. Overall, however, the stability of the actinide complexes increases as the ratio of effective charge to ionic radius increases. As a general rule, the actinide ions form somewhat more stable complexes than do the homologous lanthanide ions.

The phosphate anion PO_4^{3-} and organic phosphates are powerful complexing agents for actinide ions. The phosphate anion acts as a bridge between metal ions to form aggregates that are insoluble in water. The M^{4+} and MO_2^{2+} ions form complexes with many organic phosphates, either neutral or anionic, that are preferentially soluble in nonpolar aliphatic hydrocarbons. Typical of such ligands are TBP and dibutyl phosphate (DBP). Phosphine oxides are also potent coordinating ligands. Oxygen-containing donor compounds such as the ketones, diisopropyl ketone or methyl isobutyl ketone, and the ethers, diethyl ether, ethyleneglycol diethyl ether, or diethyleneglycol dibutyl ether, act likewise and are good complexing agents for actinide ions. All of these ligands have oxygen atoms with lone electron pairs not otherwise engaged in chemical bonding that can act as electron donors in coordination interactions. Complexes with such reagents have been used on a very large scale in the extraction and separation of the actinide elements by liquid–liquid extraction. In recent years, extractants containing soft donor atoms (nitrogen, sulfur) have received much attention, especially as they offer great potential for the separation of trivalent actinides from the chemically similar lanthanides. Among other compounds, polyaza and dithiophosphinic acid derivatives are investigated extensively. The reader is referred to Chapter 24 for a discussion of the comparative merits of various extractant systems.

Chelating ligands form strong complexes with actinide ions. Examples of such are the β-diketones, the tropolones, 8-hydroxyquinoline and its derivatives, and ethylenediaminetetraacetic acid (EDTA), among many others. In its enol form, acetylacetone, a typical diketone, forms very strong complexes with M^{4+} ions. Even though these complexes have significant water solubility, they are easily and completely extracted by benzene, carbon tetrachloride, or similar nonpolar solvents. The acetylacetone complexes of the MO_2^{2+} actinyl ions form weaker complexes that show little preference for a nonpolar organic phase. The structure of the diketone can be modified to enhance the preferential solubility of the metal complex for the organic phase. The most important of such modified diketone chelating agents is 2-thenoyltrifluoroacetone ($C_4H_3COCH_2COCF_3$),

which has been widely used to extract plutonium from aqueous solutions into nonpolar solvents. Tropolone ($C_7H_6O_2$, 2-hydroxy-2,4,6-cycloheptatrien-1-one) is a seven-membered cyclic carbon compound containing a keto carbonyl function and a weakly acid hydroxyl group, both of which are able to form strong complexes with highly charged metal cations. EDTA is an effective sequestering agent for the actinide ions in aqueous solutions. The strongest EDTA complexes are formed by M^{4+}. The strength of the EDTA complexes with M^{3+} ions increases steadily from Pu^{3+} to Cf^{3+}. Possibly for steric reasons, EDTA interacts in a different way with actinyl(VI) ions; in these systems EDTA is a bridging ligand, and gives rise to linear polynuclear complexes.

There is a great deal more to be said about the actinide ions in solution, about hydrolytic phenomena, and about complex-ion formation. For a comprehensive and authoritative treatment of these important subjects, the reader is referred to Chapters 23 and 24.

15.6 THE METALLIC STATE

The actinide metals pose some of the most interesting problems in actinide research and, in fact, in all of materials science. Many actinide compounds behave in a perfectly conventional way (except for radioactivity), and have properties that can be safely inferred from lanthanide chemistry or the chemistry of similar compounds of well-studied elements. For no category of materials is this less true than for the actinide metals and intermetallics. Many of the actinides in their elemental state and in intermetallic compounds are unique. They have metallurgical properties that are unprecedented in conventional metals, and their properties cannot be described by conventional theories of the metallic state. The theoretical framework of the metallic state has been broadened to accommodate this group of unusual metals, and this led to a better understanding of complex phenomena not only in the actinide series but also in such complex materials as high-temperature superconductors (Santini *et al.*, 1999; Sarrao *et al.*, 2002).

15.6.1 Preparation

The actinide metals are highly electropositive and may react, especially on surfaces and in finely divided form, with water vapor, oxygen, nitrogen, and hydrogen. The chemical reactivity and radioactivity of most of the actinides makes confinement in atmosphere-controlled gloved boxes compulsorily. For some of the heavier actinide metals, shielding is required because of gamma rays or because of neutrons released by spontaneous fission. The actinide elements form very stable oxides and fluorides, so that vigorous reducing agents and high temperatures are necessary for their reduction to the metals. The earliest preparations of the actinide metals were carried out by reduction of the anhydrous

actinide tri- or tetrafluoride with the appropriate alkali or alkaline earth metal at high temperature. For submilligram amounts this is still the method of choice, especially with lithium or barium as reductants. Alternatively, especially at the industrial scale, the actinide oxide is reduced at high temperature with lanthanum or thorium metal. All of the starting materials must be as pure as possible to yield a pure product. Reduction of the oxide is the preferred route to milligram-to-gram amounts of Ac, Am, Cm, Bk, Cf, and submilligram amounts of Es (Heathman and Haire, 1998). Uranium, thorium, and plutonium metals are obtained from appropriate industrial-scale operations.

Much modern research on the metallic state requires very pure metals. Depending on the nature of the impurities, the actinide metals can be purified by volatilization of the impurities in a very high vacuum, by volatilization of the metal itself to form films of very pure metal, or by electrodeposition from molten salt baths. Very pure protactinium and thorium metals can be obtained by the van Arkel process, which consists of converting the crude metal to the volatile iodide by reaction with elemental iodine at an elevated temperature, and decomposing the gaseous metal iodide on a hot filament (Müller and Spirlet, 1985). This process produces exceptionally pure metals, which have been used for such demanding purposes as superconductivity measurements that require metals of the highest purity.

15.6.2 Crystal structures

The crystal structures, phase transformations, and metallic radii of the actinide metals are listed in Table 15.8, together with melting points, densities, and enthalpies of sublimation. The crystal structures of metallic protactinium, uranium, neptunium, and plutonium are complex, have no counterparts among the lanthanide metals, and resemble the 3d transition metals more closely than the lanthanides. The lanthanide metals show a generally uniform hexagonal close-packed (hcp) or face-centered cubic (fcc) crystal structure pattern at low temperatures, and body-centered cubic (bcc) at high temperatures. The lighter actinide elements have a bcc structure at the melting point, which changes to fcc in the elements after plutonium. For the actinide elements americium through einsteinium, the characteristic crystal structures at all temperatures below the melting point are the fcc and double hexagonal close-packed (dhcp) structures. In uranium, neptunium, and plutonium, complex crystal structures are observed at low temperatures.

The differences between the actinide and lanthanide metals can be rationalized by a consideration of the differences between the 4f and 5f electron shells (Santini *et al*., 1999). In the 4f series, all the 4f electrons (added after cerium) are buried in the interior of the electron cloud. The 4f electrons thus experience relatively little interaction with valence electrons in the outer shells. The maxima in the 4f radial charge density occur well inside the usual interatomic distances in solids, and consequently the 4f electron properties of the free atoms are

Table 15.8 *Selected properties of actinide metals.*[a]

Element	*Melting point* (K)	*Enthalpy of sublimation at* 298.15 K (kJ mol^{-1})	*Lattice symmetry*	*Temperature range* (K)	*Lattice constants*[b] a_0 (Å)	b_0 (Å)	c_0 (Å)	β (deg)	*X-ray density* (g cm^{-3})	*Z (atoms per unit cell)*	*Metallic radius CN* 12 (Å)[d]
actinium	1323 ± 50	418 ± 20	fcc		5.315				10.01	4	1.878
thorium		602 ± 6	α, fcc	below 1633	5.0842				11.724	4	1.798
	2023 ± 10		β, bcc	1633–2023	4.11 (1723 K)					2	~1.80
protactinium		570 ± 10	α, bcc tetrag.	below 1443	3.929		3.241		15.37	2	1.642
	1845 ± 20		β, bcc or fcc	1443–1845							
uranium		533 ± 8	α, orthorh.	below 941	2.854	5.870	4.955		19.04	4	1.542
			β, tetrag.	941–1049	5.656 (5) (995 K)	10.759 (5)	10.759 (5)		18.11	30	1.548
	1408 ± 2		γ, bcc	1049–1408	3.524 (2) (1078 K)				18.06	2	1.548
neptunium		465.1 ± 3.0	α, orthorh.	below 553	6.663 (293 K)	4.723	4.887		20.48	8	1.503
			β, tetrag.	553–849	4.897 (586 K)		3.388		19.38	4	1.511
	912 ± 3		γ, bcc	849–912	3.518 (873 K)				18.08	2	1.53
plutonium		349.0 ± 3.0	α, monocl.	below 397.6	6.183 (294 K)	4.822	10.963	101.79	19.85	16	1.523
			β, monocl.	397.6–487.9	9.284 (463 K)	10.463	7.859	93.13	17.71	34	1.571
			γ, orthorh.	487.9–593.1	3.159 (508 K)	5.768	10.162		17.15	8	1.588
			δ, fcc	593.1–736.0	4.637 (593 K)				15.92	4	1.640
			δ′, bcc tetrag.	736.0–755.7	3.34 (738 K)		4.44		16.03	2	1.640
	913.0 ± 2.0		ε, bcc	755.7–913.0	3.6361 (763 K)				16.51	2	1.592
americium		283.8 ± 1.5	α, dhcp	below 1042	3.47		11.25		13.67	4	1.730
			β, fcc	1042–1350	4.89				13.69	4	1.730
	1449 ± 5		γ, bcc?	1350–1449	unknown						
curium		384 ± 10	α, dhcp	below 1568	3.500(3)[c]		11.34(1)[c]		13.5	4	1.743
	1619 ± 50		β, fcc	1568–1619	5.065				12.7	4	1.782
berkelium		310 ± 10	α, dhcp	below 1250	3.416 (3)		11.069 (7)		14.79	4	1.704
	1323 ± 50		β, fcc	1250–1323	4.997(4)				13.24		1.767
californium		196 ± 10	α, dhcp	below ~973	3.384		11.040		15.1	4	1.691
	1173 ± 30		β, fcc	~973–1173	4.78				15.1	4	1.69
einsteinium	1133	130 ± 10	fcc	ambient	5.75				8.84	4	2.03

[a] Chapter 21, Table 21.1, which contains additional data.
[b] At 298.15 K, unless otherwise stated.
[c] Stevenson, J. N. and Peterson, J. R. (1979) *J. Less Common Metals*, **66**, 201–10.
[d] Zachariasen, W. H. (1973) *J. Inorg. Nucl. Chem.* 35, 3487–97. Zachariasen adjusted high-temperature radii to room temperature. For Ac, Cf, and Es see Chapter 2, 11, 12 respectively.

retained in the metallic as well as ionic lanthanide solids. Cerium is the only 4f metal that does not conform to this generalization, presumably because its 4f electron shell is not yet fully stabilized. The actinide 5f electrons behave quite differently. For the early members of the actinide series, the 5f electrons have a greater radial distribution than do their 4f homologs. The first few 5f electrons are not confined to the core of the atom, and they can therefore interact or mix with the other valence electrons to affect interatomic interactions in the solid state. Beyond plutonium, all the 5f electrons are localized within the atomic core, and the resemblance between the f-block elements becomes closer. Americium is the first actinide metal whose crystal structure resembles that of the lanthanide metals. In the transcurium metals, the resemblance to the lanthanide metals becomes increasingly strong. The room temperature crystal structure for the elements for Am to Cf is dhcp, just as it is in the light lanthanides (see Table 15.8).

A natural consequence of the increase in nuclear charge along the actinide series for a given oxidation state is an increasing tendency for the 6d and 7s electrons to experience less shielding from the nuclear charge. This leads to a contraction of the atomic radius. Shielding of the valence electrons from the nucleus is also diminished by delocalization of the 5f electrons in the early part of the actinide series. In metals, the atomic radius expands significantly when the 5f electrons are localized in the core, which occurs at americium and curium. The transition from delocalized to localized f-electron behavior at americium is clearly reflected in the complex chemical and physical properties of uranium, neptunium, and especially plutonium metals in the crossover region of the actinide series. Recent experiments have shown that americium metal exhibits delocalized 5f electron behavior and a structure similar to alpha uranium under high pressure (Lindbaum *et al*., 2003).

15.6.3 Polymorphic transformations

Protactinium, uranium, neptunium, and plutonium metal have complex structures unlike anything encountered in the lanthanide metals (see Table 15.8). For example, plutonium metal is unique among metals, having no fewer than six allotropic modifications between room temperature and its melting point at 913.0 K. A remarkable phenomenon occurs as plutonium metal is heated. Plutonium metal undergoes a 26% volume increase going from room temperature through the α, β, γ, and δ phases with increasing temperature. However as the temperature continues to increase the δ and δ' phases undergo a contraction with a concomitant increase in density. An immense effort has been expended to map the phase transformations in uranium and plutonium metals and their alloys because of their great importance in nuclear technology. Details of the electronic properties of the actinide metals can be found in Chapter 21 and in Lam *et al*. (1974) and Spirlet (1982). The metallurgy of Pu and its phase transitions are discussed in Chapter 7.

15.6.4 Electronic structures

We have noted in Section 15.6.2 the effects of localized and delocalized 5f electrons on the crystal structures and phase transformations of the actinide metals. These effects are observed in many materials, but perhaps most clearly in the actinide metals. The basis for the differences observed for localized and delocalized 5f electrons has been discussed briefly in Section 15.4, but because of their importance in the metallic state some additional discussion of the electronic state in the actinide metals is appropriate. The classical d-electron or d-block transition series and the f-block elements have as a principal feature of their electronic architecture the filling of the 3d, 4d, and 5d electron shells for the d-block series, and the 4f and 5f energy levels in the lanthanide and actinide series. The f electrons occupy energy levels or orbitals closer to the nucleus of the atom than do the outer s and p valence electrons. In the lanthanide elements beyond cerium, the 4f levels are highly localized and, because overlap between the levels is minimal, these energy levels are not broadened to any appreciable extent by 4f–4f interactions. Nor do the 4f electrons mix significantly with the d, s, or p valence electrons. In the d-block metals, the d-electron levels have significant overlap with other d-electrons; the d-electrons also mix or hybridize with s and p levels. The extensive mixing of the d, s, and p orbitals in d-block elements generates broad energy bands whose existence is reflected in the magnetic and electrical properties of the d-block transition metals.

The electronic properties of the 5f elements are intermediate between those of the d-block elements and the 4f elements. At the beginning of the actinide series, the 5f electrons interact strongly with each other, and the band character of the delocalized (itinerant) 5f electrons inhibits the development of magnetism. As the 5f shell is filled, the 5f electrons become increasingly localized and the energy levels fall so that they are well below the Fermi band level. The transition from delocalized to localized 5f electrons takes place in the vicinity of plutonium, as shown in schematic fashion in Fig. 15.7. In the crossover region, which extends from uranium to americium, the electronic behavior is especially complicated because the energy differences between localized and delocalized 5f electrons is small. Comparatively small perturbations can convert the localized 5f electrons into mobile electrons with a band structure, or the reverse. This delicate balance near the middle of the actinide series gives rise to unusual crystal structures, unusual thermodynamic and mechanical properties, multiple valence states, and collective phenomena such as magnetism, superconductivity, and valence fluctuations. So complex are the phenomena near the middle of the actinide series that modern theories of the metallic state have serious difficulties in dealing with them, a situation that is under active study and may well turn out to be not the least valuable contribution that the study of the actinide elements will have made to the understanding of the solid state (Albers, 2001).

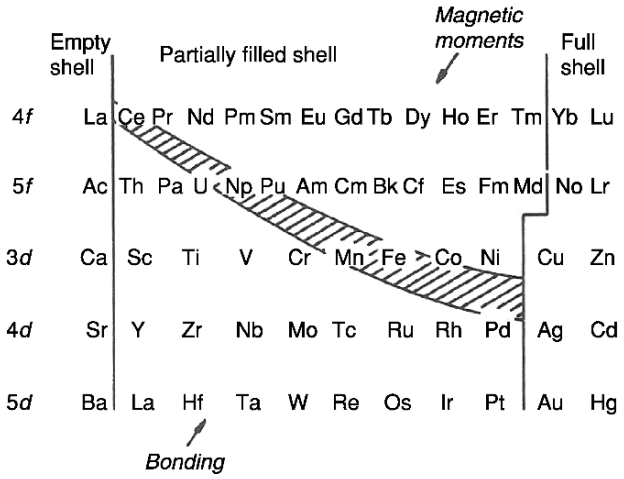

Fig. 15.7 *Transition metals* (*f- and d-series*) *showing the crossover from delocalized* (*bonding*) *to localized* (*magnetic moments*) *f- and d-electron behavior. From Smith and Kmetko* (1983), *with permission.*

One of the most powerful techniques for the elucidation of the electronic states of the actinide elements is the application of high pressure (Benedict, 1984; Haire *et al.*, 2004). The early actinides at 1 atm exhibit complex phase structures due to the behavior of the itinerant (nonlocalized) 5f electrons. The transplutonium elements do not have 5f itineracy contributing to the bonding and show complex phase behavior under high pressures. For americium metal, these 5f electrons become delocalized at high pressures, and the same crystal structures found for the light actinides are obtained (Lindbaum *et al.*, 2003). Pressure also affects the superconducting transition temperature and the magnetic properties of the actinide metals. Similarly, large pressure effects have been observed in actinide alloys and compounds (Heathman and Haire, 1998; Haire *et al.*, 2004).

15.6.5 Superconductivity

Superconductivity in the actinide metals is closely related to the degree of delocalization of the 5f electrons. Highly localized 5f electrons, which are characteristic of the latter portion of the actinide series, are associated with temperature-dependent paramagnetism and the absence of superconductivity. Delocalized 5f electrons participate in chemical bonding, show small temperature-independent magnetic moments, and are conducive to superconductivity. Protactinium metal becomes superconducting at 1.4 K, thorium metal at 1.368 K, and uranium metal at 0.68 K. These three elements have delocalized (itinerant) 5f electrons. Neptunium and plutonium, especially the latter, are

anomalous. The 5f electrons in americium are localized, but americium metal is superconducting at 0.625 K, because its spin and orbital angular momenta cancel one another and its magnetic moment at low temperature is almost zero. The transamericium actinide metals all contain strongly localized 5f electrons, are not superconductors, and have large magnetic moments at low temperatures. Plutonium is not superconducting, but the intermetallic compound $PuCoGa_5$ shows a superconducting transition at $T_c = 18.5$ K. This surprising result is attributed to the presence of a local magnetic moment in the normal state. The superconductivity in this compound is of an unconventional type and could be due to magnetically mediated superconductivity. Thus the transuranics appear to represent a promising area of superconductor research, intermediate between known heavy fermion materials and the high-temperature superconductors derived from copper oxides (Sarrao *et al*., 2002).

15.7 SOLID COMPOUNDS

15.7.1 Introductory remarks

Thousands of compounds of the actinide elements have been prepared (Gmelin, 1972; Müller and Blank, 1975; Müller and Lindner, 1975; Shannon, 1976). Compounds that have special scientific or technological importance are described in the preceding chapters on the chemistry of the individual actinide elements, and in a systematic way in Chapter 22. In the past few years there have been important additions to the roster of actinide compounds and new chemical phenomena that are particularly characteristic of, although perhaps not entirely confined to, the chemical behavior of the actinide compounds, and these are commented on here.

15.7.2 Binary compounds

Table 15.9 lists the binary hydrides, oxides, and halides of the actinide elements along with their melting points, color, and crystallographic parameters. The properties of the hydrides and oxides in Table 15.9 are for compounds that are stoichiometric or come close to the indicated stoichiometric composition. The methods of preparation of the compounds in Table 15.9 are essentially classical procedures adapted to a micro- or semi-microscale and to the radioactivity of the actinide elements (Müller, 1983). There are claims in the literature for the synthesis of actinide halides in which the actinide element is in an unusually high or low oxidation state. Reports of the synthesis of the higher-valent actinide fluorides PuF_5, EsF_4, AmF_6, and CmF_6 have not been confirmed. Following the discovery of the lanthanide dihalides $NdCl_2$ and $TmCl_2$, the dichlorides, dibromides, and diiodides of americium and californium have been prepared. These studies were reviewed by Morss and Edelstein (1984).

Table 15.9 *Properties and crystal structure data for some important actinide binary compounds. References are in Chapters* 2–12.

Compound	*Color*	*Melting point* (°C)	*Symmetry*	*Space group or structure type*	*Lattice parameters*				*Density* (g cm^{-3})
					a_0 (Å)	b_0 (Å)	c_0 (Å)	β (deg)	
ThH_2	black		tetragonal	I4/*mmm*	4.055		4.965		9.50
Th_4H_{15}	black		cubic	$I\bar{4}3d$	9.116				8.25
α-PaH_3	gray		cubic	P*m*3*n*	4.150				10.87
β-PaH_3	black		cubic	β-W (P*m*3*n*)	6.648				10.58
α-UH_3	?		cubic	β-W	4.160				11.12
β-UH_3	black		cubic	β-W	6.6444				10.92
NpH_2	black		fcc	fluorite (F*m*3*m*)	5.343				10.41
NpH_3	black		trigonal	NpF_3 $(P\bar{3}c1)$	6.51		6.72		9.64
PuH_2	black		fcc	fluorite	5.359				10.40
PuH_3	black		trigonal	NpF_3	6.55		6.76		9.61
AmH_2	black		fcc	fluorite	5.348				10.64
AmH_3	black		trigonal	NpF_3	6.53		6.75		9.76
CmH_2	black		fcc	fluorite	5.322				10.84
CmH_3	black		trigonal	NpF_3	6.528		6.732		10.06
BkH_2	black		fcc	fluorite	5.248				11.57
BkH_3	black		trigonal	NpF_3	6.454		6.663		10.44
Ac_2O_3	white		hexagonal	La_2O_3 $(P\bar{3}m1)$	4.07		6.29		9.19
Pu_2O_3	?		cubic	I*a*3	11.03				10.44
Pu_2O_3	black	2085	hexagonal	La_2O_3 $(P\bar{3}m1)$	3.841		5.958		11.47
Am_2O_3	tan		hexagonal	La_2O_3 $(P\bar{3}m1)$	3.817		5.971		11.77
Am_2O_3	reddish brown		cubic	I*a*3	11.03				10.57
Cm_2O_3	white to faint tan	2260	hexagonal	La_2O_3 $(P\bar{3}m1)$	3.792		5.985		12.17
Cm_2O_3	light green		monoclinic	Sm_2O_3(C2/*m*)	14.282	3.641	8.883	$\beta = 100.29$	11.90
Cm_2O_3	white		cubic	I*a*3	11.002				10.80
Bk_2O_3	light green		hexagonal	La_2O_3 $(P\bar{3}m1)$	3.754		5.958		12.47
Bk_2O_3	yellow-green		monoclinic	C2/*m*	14.197	3.606	8.846	$\beta = 100.23$	12.20
Bk_2O_3	yellowish brown		cubic	I*a*3	10.998				11.66
Cf_2O_3	pale green		hexagonal	La_2O_3 $(P\bar{3}m1)$	3.72		5.96		12.69
Cf_2O_3	lime green		monoclinic	C2/*m*	14.12	3.591	8.809	$\beta = 100.34$	12.37

Table 15.9 (*Contd.*)

Compound	*Color*	*Melting point* (°C)	*Symmetry*	*Space group or structure type*	*Lattice parameters*				*Density* (g cm^{-3})
					a_0 (Å)	b_0 (Å)	c_0 (Å)	β (deg)	
Cf_2O_3	pale green		cubic	I*a*3	10.839				11.39
Es_2O_3	white		hexagonal	La_2O_3 $(P\bar{3}m1)$	3.7		6.0		12.7
Es_2O_3	white		monoclinic	C2/*m*	14.1	3.59	8.80	$\beta = 100$	12.4
Es_2O_3	white		cubic	I*a*3	10.766				11.79
ThO_2	white		f. c. cubic	fluorite	5.592				10.00
PaO_2	black		f. c. cubic	fluorite	5.509				10.45
UO_2	black or brown		f. c. cubic	fluorite	5.4704				10.95
NpO_2	apple green		f. c. cubic	fluorite	5.4334				11.14
PuO_2	yellow-green		f. c. cubic	fluorite	5.3960				11.46
AmO_2	black		f. c. cubic	fluorite	5.374				11.68
CmO_{2-x}	black		f. c. cubic	fluorite	5.358				11.92
BkO_2	yellowish-brown		f. c. cubic	fluorite	5.3315				12.31
CfO_{2-x}	black		f. c. cubic	fluorite	5.310				12.46
Pa_2O_5	white		cubic	fluorite-related	5.446				11.14
Np_2O_5	dark brown		monoclinic	$P2_1/c$	4.183	6.584	4.086	$\beta = 90.32$	8.18
α-U_3O_8	black-green	1150 (dec)	orthorhombic	C2*mm*	6.716	11.960	4.147		8.39
β-U_3O_8	black-green		orthorhombic	C*mcm*	7.069	11.445	8.303		8.32
γ-UO_3	orange	650 (dec)	orthorhombic	F*ddd*	9.813	19.93	9.711		7.80
$AmCl_2$	black		orthorhombic	$PbCl_2$ (P*bnm*)	8.963	7.573	4.532		6.78
$CfCl_2$	red-amber		?						
$AmBr_2$	black		tetragonal	$SrBr_2$ (P4/*n*)	11.592		7.121		7.00
$CfBr_2$	amber		tetragonal	$SrBr_2$	11.500		7.109		7.22
β-ThI_2	gold		hexagonal	$P6_3/mmc$	3.97		31.75		7.45
AmI_2	black	~700	monoclinic	EuI_2 ($P2_1/c$)	7.677	8.311	7.925	$\beta = 98.46$	6.60
CfI_2	violet		hexagonal	$CdI_2(P\bar{3}m1)$	4.557		6.992		6.63
CfI_2	violet		rhombohedral	$CdCl_2$ $(R\bar{3}/m)$	7.434			$\alpha = 35.83$	6.58

AcF_3	white		trigonal	LaF_3 $(P\bar{3}c1)$	7.41		7.53	7.88
UF_3	black	disproportionates above 1000	trigonal	LaF_3	7.173		7.341	8.95
NpF_3	purple		trigonal	LaF_3	7.129		7.288	9.12
PuF_3	purple	1425	trigonal	LaF_3	7.092		7.254	9.33
AmF_3	pink	1393	trigonal	LaF_3	7.044		7.225	9.53
CmF_3	white	1406	trigonal	LaF_3	7.014		7.194	9.85
BkF_3	yellow-green		orthorhombic	YF_3 (P*nma*)	6.70	7.09	4.41	9.70
BkF_3	yellow-green		trigonal	LaF_3	6.97		7.14	10.15
CfF_3	light green		orthorhombic	YF_3	6.653	7.039	4.393	9.88
CfF_3	light green		trigonal	LaF_3	6.945		7.101	10.28
$AcCl_3$	white		hexagonal	UCl_3	7.62		4.55	4.81
UCl_3	green	835	hexagonal	$P6_3/m$	7.452		4.328	5.51
$NpCl_3$	green	~800	hexagonal	UCl_3	7.413		4.282	5.60
$PuCl_3$	emerald green	760	hexagonal	UCl_3	7.394		4.243	5.71
$AmCl_3$	pink or yellow	715	hexagonal	UCl_3	7.382		4.214	5.87
$CmCl_3$	white to pale green	695	hexagonal	UCl_3	7.374		4.185	5.95
$BkCl_3$	green	603	hexagonal	UCl_3	7.382		4.127	6.02
α-$CfCl_3$	green	545	orthorhombic	$TbCl_3$ (C*mcm*)	3.859	11.748	8.561	6.07
β-$CfCl_3$	green		hexagonal	UCl_3	7.379		4.090	6.12
$EsCl_3$	white to orange		hexagonal	UCl_3	7.40		4.07	6.20
$AcBr_3$	white		hexagonal	UBr_3	8.06		4.68	5.85
UBr_3	red	730	hexagonal	$P6_3/m$	7.942		4.441	6.54
$NpBr_3$	green		hexagonal	UBr_3	7.919		4.392	6.65
$NpBr_3$	green		orthorhombic	$TbCl_3$ (C*mcm*)	4.109	12.618	9.153	6.67
$PuBr_3$	green	681	orthorhombic	$TbCl_3$	4.097	12.617	9.147	6.72
$AmBr_3$	white to pale yellow		orthorhombic	$TbCl_3$	4.064	12.661	9.144	6.85
$CmBr_3$	pale yellow-green	625 ± 5	orthorhombic	$TbCl_3$	4.041	12.700	9.135	6.85

Table 15.9 (*Contd.*)

Compound	*Color*	*Melting point* (°C)	*Symmetry*	*Space group or structure type*	*Lattice parameters*				*Density* (g cm^{-3})
					a_0 (Å)	b_0 (Å)	c_0 (Å)	β (deg)	
$BkBr_3$	light green		monoclinic	$AlCl_3$ (C2/*m*)	7.23	12.53	6.83	$\beta = 110.6$	5.604
$BkBr_3$	light green		orthorhombic	$TbCl_3$	4.03	12.71	9.12		6.95
$BkBr_3$	yellow green		rhombohedral	$FeCl_3$ $(R\bar{3})$	7.66			$\alpha = 56.6$	5.54
$CfBr_3$	green		monoclinic	$AlCl_3$	7.215	12.423	6.825	$\beta = 110.7$	5.673
$CfBr_3$	green		rhombohedral	$FeCl_3$	7.58			$\alpha = 56.2$	5.77
$EsBr_3$	straw		monoclinic	$AlCl_3$	7.27	12.59	6.81	$\beta = 110.8$	5.62
β-ThI_3			orthorhombic	C*ccm*	8.735	20.297	14.661		
UI_3	black		orthorhombic	$TbCl_3$ (C*mcm*)	4.334	14.024	10.013		6.78
NpI_3	brown		orthorhombic	$TbCl_3$	4.30	14.03	9.95		6.82
PuI_3	green		orthorhombic	$TbCl_3$	4.33	13.95	9.96		6.92
AmI_3	pale yellow		hexagonal	BiI_3 $(R\bar{3})$	7.42		20.55		6.35
AmI_3	yellow		orthorhombic	$TbCl_3$	4.28	13.94	9.974		6.95
CmI_3	white		hexagonal	BiI_3	7.44		20.40		6.40
BkI_3	yellow		hexagonal	BiI_3	7.584		20.87		6.02
CfI_3	red-orange		hexagonal	BiI_3	7.587		20.81		6.05
EsI_3	amber to light yellow		hexagonal	BiI_3	7.53		20.84		6.18
ThF_4	white	1068	monoclinic	UF_4 (C2/*c*)	13.049	11.120	8.538	$\beta = 126.31$	6.20
PaF_4	reddish-brown		monoclinic	UF_4	12.88	10.88	8.49	$\beta = 126.4$	6.38
UF_4	green	1036	monoclinic	C2/*c*	12.7941	10.7901	8.3687	$\beta = 126.25$	6.71
NpF_4	green		monoclinic	UF_4	12.68	10.66	8.34	$\beta = 126.3$	6.86
PuF_4	brown or pink		monoclinic	UF_4	12.59	10.69	8.29	$\beta = 126.0$	7.05
AmF_4	tan		monoclinic	UF_4	12.56	10.58	8.25	$\beta = 125.9$	7.23
CmF_4	light gray-green		monoclinic	UF_4	12.50	10.49	8.18	$\beta = 126.1$	7.36
BkF_4	pale yellow-green		monoclinic	UF_4	12.396	10.466	8.118	$\beta = 126.33$	7.55
CfF_4	light green		monoclinic	UF_4	12.38	10.44	8.12	$\beta = 126.2$	7.57

α-$ThCl_4$	white		tetragonal	$I4_1/a$	6.408		12.924		
β-$ThCl_4$	white	770	tetragonal	UCl_4 ($I4_1/amd$)	8.491		7.483		
$PaCl_4$	greenish-yellow		tetragonal	UCl_4	8.377		7.481		4.72
UCl_4	green	590	tetragonal	$I4_1/amd$	8.3018		7.4813		4.87
$NpCl_4$	red-brown	518	tetragonal	UCl_4	8.266		7.475		4.96
α-$ThBr_4$	white		tetragonal	$I4_1/a$	6.737		13.601		5.94
β-$ThBr_4$	white		tetragonal	UCl_4	8.971		7.912		
$PaBr_4$	orange-red		tetragonal	UCl_4	8.824		7.957		5.90
UBr_4	brown	519	monoclinic	$C2/m$	10.92	8.69	7.05	$\beta = 93.9$	5.55
$NpBr_4$	dark red	464	monoclinic	$C2/m$	10.89	8.74	7.05	$\beta = 94.19$	
ThI_4	yellow	556	monoclinic	$P2_1/n$	13.216	8.068	7.766	$\beta = 98.68$	6.00
PaI_4	black								
UI_4	black		monoclinic	$C2/c$	13.967	8.472	7.510	$\beta = 90.54$	
PaF_5	white		tetragonal	$I\bar{4}2d$	11.53		5.19		
α-UF_5	grayish white		tetragonal	$I4/m$	6.5259		4.4717		5.81
β-UF_5	pale yellow		tetragonal	$I\bar{4}2d$	11.469		5.215		6.45
NpF_5			tetragonal	$I4/m$	6.53		4.45		
$PaCl_5$	yellow	306	monoclinic	$C2/c$	8.00	11.42	8.43	$\beta = 106.4$	
α-UCl_5	brown		monoclinic	$P2_1/n$	7.99	10.69	8.48	$\beta = 91.5$	3.81
β-UCl_5	red-brown		triclinic	$P\bar{1}$	7.07	9.65	6.35	$\alpha = 89.10$; $\beta = 117.36$; $\gamma = 108.54$	
α-$PaBr_5$			monoclinic	$P2_1/c$	12.64	12.82	9.92	$\beta = 108$	
β-$PaBr_5$	orange-brown		monoclinic	$P2_1/n$	9.385	12.205	8.95	$\beta = 91.1$	
UBr_5	brown		triclinic	$P\bar{1}$	7.449	10.127	6.686	$\alpha = 89.25$; $\beta = 117.56$; $\gamma = 108.87$	5.07
PaI_5	black		orthorhombic	unknown	7.22	21.2	6.85		
UF_6	white	64.02 at 151.6 kPa	orthorhombic	$Pnma$	9.924	8.954	5.198		5.06
NpF_6	orange	55	orthorhombic	$Pnma$	9.909	8.997	5.202		5.00
PuF_6	reddish-brown	52	orthorhombic	$Pnma$	9.888	8.961	5.202		5.085
UCl_6	dark green	178	hexagonal	$P\bar{3}m1$	10.95		6.016		3.594

15.7.3 Other compounds

The actinide M^{3+} ions in aqueous solution resemble the tripositive lanthanide ions in their precipitation reactions, allowing for differences in the redox properties of early members of the actinide series. The chloride, bromide, nitrate, bromate, and perchlorate anions form water-soluble salts, which can be isolated as hydrated solids by evaporation. The acetates, iodates, and iodides are somewhat less soluble in water. The sulfates are sparingly soluble in hot solutions, and somewhat more soluble in the cold. Insoluble precipitates are formed with hydroxide, fluoride, carbonate, oxalate, and phosphate anions. Precipitates formed from aqueous solution are usually hydrated, and the preparation of anhydrous salts from the hydrates without formation of hydrolyzed species can only be accomplished with difficulty. The actinide(IV) ions resemble Ce(IV) in forming fluorides and oxalates that are insoluble even in acid solution. The nitrates, sulfates, perchlorates, and sulfides are all water-soluble. The 4+ state actinide ions form insoluble iodates and arsenates even in rather strong acid solution. The actinyl(V) ions can be precipitated as the insoluble potassium salts from concentrated carbonate solutions. Actinyl(VI) ions in solutions containing high concentrations of acetate ions form an insoluble crystalline double salt, $NaAnO_2(O_2CCH_3)_3$ (An = actinide). The hydroxides or hydrous oxides of any of the actinide ions in all oxidation states are insoluble in water. Some complex oxides such as $M^{I}_2U_2O_7$ or $M^{II}U_2O_7$(with $M^{I} = Na, NH_4 \ldots$; $M^{II} = Mg \ldots$) can be precipitated from moderately alkaline solutions. The actinyl(VII) ions NpO_5^{3-} and PuO_5^{3-} exist as $MO_4(OH)_2^{3-}$ in alkaline solution, from which they can be precipitated by several di- and tripositive cations.

Actinide(IV) ions form insoluble peroxy compounds with hydrogen peroxide in moderately acid solution. The solid peroxy compounds incorporate inorganic anions such as sulfate, nitrate, or chloride that may be present in the solution. Phosphates, arsenates, cyanides, cyanates, thiocyanates, selenocyanates, sulfites, selenates, selenites, tellurates, and tellurites of some actinides have all been prepared, but our knowledge of these compounds is far from thorough.

15.7.4 Oxides and nonstoichiometric systems

There are many inorganic compounds whose composition is not necessarily expressible as the ratio of small whole numbers. Instead, they exist over a range of compositions. Compounds of variable composition often have electrical, magnetic, and thermal properties that are exceedingly sensitive to the exact composition. Nonstoichiometry is purely a solid-state phenomenon, which is associated with vacancies and/or interstitial ions in or near cation or anion sites in a crystal lattice (Anderson, 1970). Electrical neutrality in the crystal must of course be maintained, and deviations from exact stoichiometry can only exist if compensated by a change in the oxidation state of another constituent of the

crystal. Nonstoichiometry is therefore encountered in binary and ternary compounds of transition elements with hydrogen, oxygen, chalcogens, pnictogens, carbon, silicon, and boron. The presence of a metallic ion in more than one oxidation state in a crystal endows nonstoichiometric compounds with a variety of interesting properties: they may be highly colored; they may show metallic electrical conductivity, or they may be semiconductors; they frequently show marked catalytic activity; and they may differ significantly in chemical reactivity from the stoichiometric compounds of the same elements. Nonstoichiometric compounds are important as transistors, thermistors, rectifiers, ionic electrical conductors, thermoelectric generators, photodetectors, and other electronic and optical devices. The actinide elements, because of the multiplicity of oxidation states that they can assume, are particularly prone to the formation of nonstoichiometric systems. This is especially true for the elements uranium through curium. The oxide systems illustrate many of the salient features of nonstoichiometry in actinide element chemistry.

The first actinide element to form nonstoichiometric oxides is protactinium. It is also the first of the actinide elements to have two readily accessible oxidation states. The black dioxide PaO_2 is obtained by reduction of Pa_2O_5 with hydrogen or carbon. Intermediate phases with the composition $PaO_{2.18–2.20}$, $PaO_{2.33}$, $PaO_{2.40–2.42}$, and $PaO_{2.42–2.44}$ have been identified by X-ray crystallography. Pa_2O_5 itself occurs in several crystal modifications determined by the method and temperature of preparation. The black color of PaO_2 indicates that it is probably nonstoichiometric and the white color of Pa_2O_5 indicates that it is stoichiometric.

The complexity of the uranium–oxygen system is awesome. In the composition range UO_2 to UO_3 there are close to a dozen phases, many of which exist in several crystal modifications. UO_3 itself occurs in six polymorphs. The complex phase relationships result from the easy change in oxidation state of the uranium as additional oxygen is introduced into the UO_2 lattice. The additional oxygen incorporated in hyperstoichiometric UO_{2+x} is distributed at random into vacant lattice sites. The original fluorite structure is distorted, but remains recognizably the same phase over a range of compositions. The stoichiometric range of a phase is a measure, at a particular temperature and oxygen pressure, of its ability to accommodate randomly distributed oxygen without change in the long-range order of a crystal. When random incorporation is no longer possible, additional oxygen is ordered in a superlattice structure, and a new phase appears, possibly because of variable composition. In the uranium–oxygen system such an abrupt transformation occurs at the composition $UO_{2.4}$. Six more phases occur between $UO_{2.4}$ and UO_3.

Only two neptunium oxide phases, with compositions of NpO_2 to $NpO_{2.5}$, are known. The composition of the latter oxide is consistent with the well-known stability of the Np(v) state. Plutonium has two oxides corresponding to the oxidation states 3+ and 4+, and an oxide of intermediate composition, $PuO_{1.61}$. Despite the existence of stable 6+ states for both neptunium and plutonium, no

binary oxide corresponding to the 6+ oxidation state is known for neptunium but hyperstoichiometric PuO_{2+x} does appear to exist (Haschke *et al.*, 2000). Recent spectroscopic evidence indicates that it contains Pu(v) rather than Pu(vi) (Conradson *et al.*, 2004).

For the transplutonium elements through fermium, the 3+ oxidation state is the stable one, and the actinide elements following plutonium have (or should have, for Fm–Lr) oxides of the composition An_2O_3. All of the transplutonium elements to californium also form oxides in which the actinide elements have the formal oxidation state 4+, which is consistent with the known ability of these elements to assume oxidation states higher than 3+. The relative ease of formation of the transplutonium dioxides from $MO_{1.5}$ is in the order $BkO_2 > AmO_2 > CmO_2 > CfO_2$. Curium and californium are also reported to form intermediate oxides of the composition $CmO_{1.714}$ and $CfO_{1.714}$. In the case of $CfO_{1.714}$, this is the highest oxide that can be prepared in air or in oxygen at 1 atm pressure. The oxide systems of the transcalifornium elements still remain to be explored. By comparison, the nonstoichiometric compounds of the actinides elements with the chalcogenides and pnictides have only received a modest amount of study.

15.7.5 Crystal structures and ionic radii

The vast accumulation of crystallographic structural data, especially structures of ionic compounds solved by single-crystal diffractometry, has provided the basis for the determination of the ionic radii of monatomic ions in several coordination numbers. Actinide ionic radii for coordination number 6 are presented in Table 15.10. Ionic radii for the lanthanide series are listed for comparison. For both the 3+ and 4+ ions of the actinide series, the ionic radii decrease with increasing atomic number, a phenomenon that is caused by decreased shielding by f-electrons of the outer valence electrons from the increasing nuclear charge. This behavior, termed 'actinide contraction,' is very similar to the corresponding 'lanthanide contraction.' As a consequence of the ionic character of most actinide compounds, and the similarity of the ionic radii for a given oxidation state, analogous compounds of lanthanide and actinide ions with similar ionic radii are generally isostructural. In the series UBr_3, $NpBr_3$, $PuBr_3$, and $AmBr_3$, for example, the structural type changes with increasing atomic number, which is consistent with the contraction in ionic radius and with lanthanide tribromides that have similar Ln^{3+} ionic radii (Brown, 1968; Eick, 1994). The extraordinary stability of the fluorite-type MO_2 structure is responsible for the existence of such compounds as PaO_2, AmO_2, CmO_2, and CfO_2, despite the relative instability of the 4+ oxidation state of these elements in solution and in many solids. The actinide contraction and the isostructural relationships among the compounds of 4f and 5f elements are particularly convincing examples of evidence for the actinide elements as a 5f transition series.

Table 15.10 *Ionic radii of lanthanides and actinides* (*coordination number* 6) (*Shannon*, 1976, *except as noted*).

No. of 4f or 5f electrons	*Lanthanide series*						*Actinide series*					
	2+ *ion*	*Radius* (Å)	3+ *ion*	*Radius* (Å)	4+ *ion*	*Radius* (Å)	2+ *ion*	*Radius* (Å)	3+ *ion*	*Radius* (Å)	4+ *ion*	*Radius* (Å)
0			La^{3+}	1.032	Ce^{4+}	0.87			Ac^{3+}	1.12	Th^{4+}	0.94
1			Ce^{3+}	1.01	Pr^{4+}	0.85			Th^{3+}		Pa^{4+}	0.90
2			Pr^{3+}	0.99					Pa^{3+}	1.04	U^{4+}	0.89
3			Nd^{3+}	0.983					U^{3+}	1.025	Np^{4+}	0.87
4	Nd^{2+}	1.20[a]	Pm^{3+}	0.97					Np^{3+}	1.01	Pu^{4+}	0.86
5			Sm^{3+}	0.958					Pu^{3+}	1.00	Am^{4+}	0.85
6	Sm^{2+}	1.18[a]	Eu^{3+}	0.947					Am^{3+}	0.975	Cm^{4+}	0.84[b]
7	Eu^{2+}	1.17	Gd^{3+}	0.938	Tb^{4+}	0.76	Am^{2+}	1.16[a]	Cm^{3+}	0.97	Bk^{4+}	0.83
8			Tb^{3+}	0.923					Bk^{3+}	0.96	Cf^{4+}	0.821
9			Dy^{3+}	0.912					Cf^{3+}	0.95	Es^{4+}	0.81[c]
10	Dy^{2+}	1.07	Ho^{3+}	0.901			Cf^{2+}	1.14[d]	Es^{3+}	0.93[b]		
11			Er^{3+}	0.890					Fm^{3+}			
12			Tm^{3+}	0.880					Md^{3+}			
13	Tm^{2+}	1.03	Yb^{3+}	0.868					No^{3+}			
14	Yb^{2+}	1.02	Lu^{3+}	0.861			No^{2+}	1.05[e]	Lr^{3+}			

[a] Corrected to coordination number 6 using Fig. 2 of Shannon (1976).
[b] Shannon (1976) gives 0.85 Å, which is not consistent with lattice parameters of dioxides (Table 15.9).
[c] Chapter 12.
[d] Mean of values of Chapter 11 (0.01 smaller than IR(Eu^{2+}) and David (1984) (1.125 Å), both for coordination number 6.
[e] Estimated by David (1984).

15.7.6 Organoactinide compounds

When the first edition of this book was in preparation (1956), the prospects of an organoactinide chemistry, i.e. compounds containing an actinide–carbon bond, were judged to be very dim. At this time of writing, the situation is very different. A rich organometallic chemistry of the actinide elements has come into existence in the last four decades, so luxuriant in fact that presenting a concise summary that does justice to the subject is not possible. This field of inquiry is one of the most active and important in current actinide element research (see Chapters 25 and 26). Not only are new organoactinide compounds with remarkable properties appearing, but studies of their structure and physical properties by the use of nuclear magnetic resonance (NMR), optical and vibrational spectroscopy, photoelectron spectroscopy, crystallography, and many other physical and chemical techniques are contributing valuable information on the electronic structure and the nature of chemical bonding in the 5f elements, subjects that are of great importance in every aspect of actinide element chemistry.

The large size and the generally ionic bonding for the 5f ions result in different reactivities and coordination with the same ligands as compared to the d-transition series. In addition, the early actinides, uranium, neptunium, and plutonium in particular, have stable oxidation states ranging from trivalent to hexavalent, which introduces a range of possible organometallic compounds with varying formal charge on the metal ion. Due to the relatively easy availability of thorium and uranium starting materials and the low specific activity of the naturally occurring isotopes of these elements, most of the work to date has been done with thorium and uranium. Only a few organometallic compounds of the transuranium elements have been characterized.

The best known covalent organometallic compound of a transition metal, $Fe(C_5H_5)_2$ (ferrocene), was synthesized in 1951 (Keally and Pauson, 1951). The main group elements were well known to form compounds in which covalent metal–carbon bonds were formed, but transition metals were widely regarded as incapable of forming stable bonds of this kind. The first stable transition-metal organometallic compounds were derivatives of cyclopentadiene, C_5H_6. Its anion, cyclopentadienide ion (Cp^-), is aromatic and possesses 6 π electrons capable of coordination to vacant d-orbitals on a transition metal. In 1956, uranium, newly recognized as a member of a 5f transition element series, became the first of the actinide elements to yield a stable cyclopentadienyl (Cp) compound, tris(cyclopentadienyl)uranium chloride, Cp_3UCl (Reynolds and Wilkinson, 1956). A decade was to pass before the first transuranium organometallic derivative, tris(cyclopentadienyl)neptunium chloride, was prepared (Baumgartner *et al.*, 1965). Since then, hundreds of organometallic derivatives of the actinide metals have been prepared. Among these are compounds containing other π-donor ligands, such as indenyl and cyclooctatetraenyl groups. The introduction of bulky alkyl- and silyl-substituted derivatives of

these π-donor ligands has extended the scope of these reactions and allowed the isolation of discrete molecular entities because the large ionic radii of the actinide ions require sterically demanding ligands so that only one or a few coordinatively unsaturated sites are available for reaction. These compounds provide an excellent environment for the study of chemical bonding in the f-block elements.

Cyclopentadienyl organoactinide compounds can be prepared by a variety of reactions (Marks and Fischer, 1979). One method for actinides in the 3+ and 4+ oxidation states is by reaction of potassium or sodium cyclopentadienide with the anhydrous actinide halide (AnX_n) in an organic solvent such as tetrahydrofuran (THF), toluene, or diethyl ether:

$$AnX_4 + 4KCp \rightarrow AnCp_4 + 4KX$$

$$AnX_4 + 3KCp \rightarrow Cp_3AnX + 3KX$$

$$AnX_3 + 3KCp \rightarrow AnCp_3 + 3KX$$

The actinide compounds are recovered from the reaction mixture by extraction with an appropriate organic solvent, and can be further purified by sublimation in a good vacuum when the volatility of the compound permits. The actinide cyclopentadienylides can also be prepared by metathesis in the molten phase by heating the actinide halide with beryllium or magnesium cyclopentadienides. The tris(cyclopentadienyl) compounds are strong Lewis acids and form adducts with many Lewis bases. They are ionic substances, although the bonding has more covalent character than in the corresponding lanthanide compounds. All of the actinide(III) compounds, with the exception of the uranium compound, are soluble in organic solvents, are reasonably stable, and are appreciably volatile, but all are sensitive to air. The tetrakiscyclopentadienyl complexes are soluble in organic solvents and moderately stable to air; they are not, however, appreciably volatile.

Compounds of the type Cp_3AnX, where the actinide element is in the 4+ oxidation state and X is an anion, have been prepared in large numbers and with a great variety of anions. Evidence has been adduced that the uranium tris (cyclopentadienyl) chloride ionizes in oxygen-free water to form the UCp_3^+ and Cl^- ions. The halide ion (X^-) in compounds of the type Cp_3AnX can be exchanged in solution by reaction with KX'. Anions (X'^-) that can be introduced include not only other halides, but also sulfate, perchlorate, nitrate, thiocyanate, etc., and also more exotic anions such as BH_4^-, BPh_3CN^-, $Co_3(CO)_{10}^-$, and OR^- (where R is an alkyl or other organic entity). These compounds have been subjected to structural analysis as well as examination by modern spectroscopic techniques. NMR spectroscopy has shown that the hydrogen atoms in the borohydride derivatives are all equivalent. The crystal structure indicates that in the BH_4^- anion there are two structurally distinct hydrogen atoms, bridging and terminal atoms. The equivalence of the hydrogen

atoms on the NMR timescale demonstrates the existence of a rapid internal dynamic exchange process. The NMR studies have not only revealed unusual features of the structure of the organometallic compounds but have also contributed to the theory of NMR paramagnetic chemical shifts by virtue of the magnetic properties of the 5f electrons in the compounds.

The discovery in 1968 by Streitwieser and coworkers (Streitwieser and Muller-Westerhof, 1968; Seyferth, 2004) that the dianion of cyclooctatetraene (COT), $C_8H_8^{2-}$, can act as a ligand to the actinide elements signaled an important new development in organoactinide chemistry. The first compound of this class was uranocene, prepared by reaction of UCl_4 with potassium salt of COT:

$$UCl_4 + 2K_2(COT) \rightarrow U(COT)_2 + 4KCl$$

Subsequently, the corresponding compounds of Th, Pa, Np, and Pu have been prepared. All have a sandwich structure in which two planar COT dianion rings enclose a metal atom. Uranocene is the most intensively studied of these compounds. It is exceedingly reactive toward oxygen, but it reacts only slowly with water or acetic acid. Unlike the cyclopentadienyl compounds of the actinides, all reactions with strong electrophiles completely decompose uranocene. The nature of the bonding in the actinide bis-cyclooctatetraene compounds has naturally attracted much interest. From crystal structure data, ionic bonding seems plausible, but photoelectron, NMR, and Mössbauer spectroscopy all suggest substantial covalency. This conclusion is reinforced by *ab initio* calculations on this series of molecules. NMR has been especially useful in studying ligand-exchange reactions, in mapping the electron spin distribution, and in exploring the dynamic processes in these compounds.

Attempts to prepare organometallic compounds that contain a direct metal–carbon bond were made in the very early days of the Manhattan Project, with the objective of producing compounds sufficiently volatile to be useful in isotope separation by diffusion or electromagnetic separation methods. All products prepared by the reactions then available for the synthesis of σ metal–carbon bonds gave products that were unstable at room temperature. The first cyclopentadienyl compound containing a true σ metal–carbon bond was obtained by alkylation of tris(cyclopentadienyl) uranium(IV) chloride (Brandi *et al.*, 1973; Gebala and Tsutsui, 1973; Marks *et al.*, 1973):

$$UCp_3Cl + RLi \rightarrow UCp_3R + LiCl$$

where R = methyl, and many other straight- and branched-chain alkyl groups, unsaturated alkenes such as allyl and vinyl, aromatic radicals such as phenyl, tolyl, or benzyl, or many other functional groups. Analogous compounds of thorium, but not of the other actinide elements, have also been reported. The structure of the UCp_3R compounds is basically a distorted tetrahedron with the three cyclopentadienyl rings at three of the corners, and the sigma bonded alkyl

group at the fourth corner on the three-fold axis of rotation of the molecule. The NMR spectra are very informative about the structure, the spin delocalization of U(IV), and the structural dynamics of the molecule. At room temperature the three cyclopentadienyl rings are magnetically equivalent, but at low temperature the equivalence vanishes because of restricted rotation about the uranium–carbon σ bond.

The chemistry of the actinide–carbon σ bond has been studied intensively. The Cp_3AnR (and alkyl- or silyl-substituted Cp) compounds are extremely sensitive to air, have high thermal stability, and completely lack any tendency for β-hydride elimination by the alkyl moiety. Hydrogen elimination is a common process in d-block organometallic compounds, and its complete suppression in the actinide hydrocarbyl derivatives is noteworthy. Uranium(IV) and thorium(IV) bis(pentamethylcyclopentadienyl) dichlorides can be readily alkylated with lithium reagents in diethyl ether solutions to yield the air-sensitive but thermally stable bis(pentamethylcyclopentadienyl) actinide dialkyls. These actinide hydrocarbyls are highly reactive. Hydrogenolysis yields organoactinide hydrides; this constituted the first preparation of a member of this class of compounds. The dialkyls also show remarkable reactivity with carbon monoxide at low temperatures to form metal–oxygen and carbon–carbon double bonds, reactions that are of interest in catalysis.

A complete review of the present state of organometallic chemistry of the actinides (including the details and references to the work described here) is presented in Chapter 25 and the use of organoactinide compounds in catalysis is given in Chapter 26. Chapter 17 covers the bonding in organometallic compounds of the actinides as described by *ab initio* calculations.

15.8 ENVIRONMENTAL ASPECTS OF THE ACTINIDE ELEMENTS

The development of a large-scale nuclear power industry and the detonation of nuclear weapons in the atmosphere have created worldwide anxiety about the long-term consequences arising from the introduction of transuranium elements into the atmosphere, the hydrosphere, and the biosphere. The radioactive nature of the transuranium elements, and the relatively long half-lives of many of these radionuclides, provide ample reasons for concern. In this section, a summary of the distribution and migration of the actinide elements in the environment is presented. In the preparation of this section we have made extensive use of a number of reviews (Walters *et al.*, 1983; Allard *et al.*, 1984; Bidoglio *et al.*, 1984; Scoppa, 1984; Silva and Nitsche, 1995; Runde, 2000; Choppin *et al.*, 2002, 2003; this work, Chapter 22). A summary of the environmental research on the transuranium elements conducted under the auspices of the U.S. Department of Energy to 1980 provides a comprehensive and authoritative guide to the voluminous literature on the subject (Hanson, 1980).

15.8.1 Actinide elements of natural origin

Several of the actinide elements are natural constituents of the Earth's crust. Of these, thorium and uranium are relatively common and, in the aggregate, occur in enormous quantities in the lithosphere. Uranium and thorium, in fact, are present in the Earth's crust to a larger extent than such familiar elements as mercury, bismuth, tin, cadmium, and silver, and in about the same concentration as lead. The uranium concentration is estimated at 1–10 $\mu g\ g^{-1}$ (1–10 ppm) in the igneous rocks of the Earth's crust; some sedimentary rocks contain much more, as also do some granites. The concentration of thorium in igneous rock is somewhat higher than that of uranium, in the range 5–20 $\mu g\ g^{-1}$ (Hedrick, 1999). The uranium content of seawater is 3.3 $\mu g\ L^{-1}$; thorium concentrations in water are much lower (6×10^{-4} $\mu g\ L^{-1}$) (Allard *et al.*, 1984). Estimates of about 10^{14} tons for the uranium content of the Earth's crust (to a depth of 20 km) have been made, and about 10^{10} tons of uranium may be contained in the Earth's oceans. Other naturally occurring radioactive elements, which are all decay progeny of long-lived thorium or uranium isotopes, are present in the lithosphere and oceans to much smaller extents: protactinium and radium have an abundance of about 10^{-12} mass percent, and the remaining radioactive isotopes as little as several orders of magnitude less. The concentration of radioactive nuclides in secular equilibrium with the progenitors of the natural uranium and thorium decay series is determined by the half-lives of the daughter radionuclides, and, unless concentrated by some geochemical process, they will be present in very small concentrations. Radioactivity is a primeval endowment of the world we inhabit.

Neptunium and plutonium are found in nature in minute amounts, formed by nuclear reactions with fission neutrons in uranium. The ratio of $^{239}Pu/^{238}U$ is on the order of 10^{-12} (see Chapter 7, Table 7.3). Longer-lived ^{244}Pu, which may be primordial in origin, is present in the rare earth mineral bastnasite to the extent of 1 part in 10^{18} (Hoffman *et al.*, 1971). The amount of the naturally occurring plutonium isotopes are so small that for all practical purposes any of the transuranium elements encountered in the environment must be taken as man-made.

There is convincing evidence that some uranium ores have in past geological epochs sustained natural chain reactions. Some samples of pitchblende, U_3O_8, from the Oklo Mine in Gabon, Africa, have a ^{235}U content distinctly lower than the natural average of 0.72%. Some samples contained less than 0.5% ^{235}U, and other elements in these samples had isotopic compositions that varied considerably from the norm. For example, some of the pitchblende from the Oklo Mine had an unusually high content of ^{143}Nd, and an equally unusually low content of ^{142}Nd. Fission-product neodymium contains a high percentage of ^{143}Nd, whereas ^{142}Nd is not formed in the fission of ^{235}U. A high ^{143}Nd content is found in ore that has a low ^{235}U content. These observations strongly suggest that in some remote bygone age, ^{235}U had undergone fission, a conclusion

supported by the unusual isotopic compositions of elements in the ore, indicating they were produced by fission. It is not likely that similar natural 'reactors' are in operation today. Fissile ^{235}U has a much shorter half-life than ^{238}U. In the early days of the Earth, the ^{235}U content of uranium minerals relative to ^{238}U was therefore higher. The age of the Oklo deposit has been established at 1.74×10^9 years. Calculation indicates that the ^{235}U content of the Oklo pitchblende 1.74×10^9 years ago was about 3%. At this concentration of fissile material, water suffusing the ore deposit could have brought regions of the deposit to criticality, and a slow or intermittent chain reaction could have ensued. It is believed that other concentrated uranium ore deposits could have achieved supercriticality in the presence of water as a neutron moderator $(2–3) \times 10^9$ years ago. Such chain reactions conceivably played an important part in early geological events. It is interesting to note that the fission products produced at Oklo over an estimated period of 10^6 years are still retained in the rock in which they were formed more than a billion years ago (Maurette, 1976; Casas *et al.*, 2004).

15.8.2 Man-made actinides

In terms of amount, by far the most significant of the synthetic actinide elements is plutonium. Commercial nuclear power reactors produce approximately 70 metric tons per year worldwide of a mixture of plutonium isotopes as a by-product. About 1380 metric tons of plutonium was estimated to be in the world plutonium inventory in 2000, mostly still in unprocessed spent fuel assemblies from nuclear reactors (Albright *et al.*, 1996). Plutonium produced for nuclear weapons is mainly ^{239}Pu, but plutonium produced as a by-product of energy production contains substantial amounts of ^{240}Pu, ^{241}Pu, and ^{242}Pu and small amounts of ^{238}Pu (Albright *et al.*, 1996, p. 20).

The plutonium in the terrestrial environment (at or near the Earth's surface and in ocean sediment) is due, in decreasing order of importance, to the testing of nuclear weapons in the atmosphere, the reentry into the atmosphere and disintegration of satellites equipped with ^{238}Pu power sources, and the processing of irradiated nuclear reactor fuel.

(a) Nuclear weapons testing

A total of approximately 7700 kg of plutonium has been released in atmospheric and underground nuclear explosions. During the period 1950–63, when testing nuclear weapons in the atmosphere was regarded as acceptable practice by the USSR and the U.S., 4400 kg of plutonium, primarily ^{239}Pu and ^{240}Pu, were injected into the atmosphere in 543 acknowledged atmospheric detonations, mostly as plutonium oxide (Kim, 1986; Hobart, 1990). More than 99% of this has by now been redeposited on Earth; 10.87 PBq of ^{239,240}Pu has been deposited on the ocean (UNSCEAR, 2000); the concentration varies greatly as a

function of latitude, longitude, and depth (Nakano and Povinec, 2003). The highest Pu concentrations in the ocean near the end of the 20th century were $\sim$0.1 Bq m^{-3} in the vicinity of Eniwetok and Bikini atolls at a depth of about 800 m. Of the original 12.8 PBq (1.28×10^{16} Bq, 3.5×10^{5} Ci) of plutonium originally present in the atmosphere of the Northern Hemisphere, about 37 TBq (1000 Ci) remain, a decrease by a factor of 1000 or more (Olivier *et al.*, 2004). Another 1.4 metric tons of plutonium have been deposited in the ground in the course of surface and subsurface testing of nuclear devices (Allard *et al.*, 1984). When more recent weapons tests are included, approximately 6 metric tons of plutonium have been deposited in the Earth's environment from weapons tests that peaked in 1963 (Allard *et al.*, 1984; Olivier *et al.*, 2004).

(b) Disintegration of satellites

Plutonium that is highly enriched in ^{238}Pu has been released into the atmosphere, largely the result of the disintegration over the Indian Ocean in 1964 of a Transit satellite (Table 15.12) carrying a nuclear power source (Nenot and Metivier, 1984).

(c) Nuclear fuel processing and storage

The amount of plutonium in the environment resulting from nuclear reactors and fuel reprocessing operations is small. Measurements in the waters of the Seine Bay (taken near the La Hague fuel reprocessing plant) indicated a plutonium concentration of about 10000 times less than the concentration of natural uranium (Nenot and Metivier, 1984). Since that time the amounts of plutonium released from all these sources has been much smaller. However, there is a potential for future release from stored spent nuclear fuel: Examination of accelerated commercial spent fuel corrosion products by electron microscopy showed that U–Pu enriched layers exist in the corroded fuel and that some of the plutonium may be present as soluble and mobile Pu(v) (Buck *et al.*, 2004).

What complicates the environmental situation is that plutonium is not the only transuranium element produced in nuclear reactors. Americium and curium are also formed by multiple neutron capture (see Fig. 15.1). The amounts of long-lived actinides in spent fuel as a function of time after removal from a reactor are shown in Table 15.11. The elements americium and curium formed in the reactor undergo radioactive decay to produce radioactive daughter species (Allard *et al.*, 1984):

$$^{245}\mathrm{Cm} \rightarrow {}^{241}\mathrm{Pu} \rightarrow {}^{241}\mathrm{Am} \rightarrow {}^{237}\mathrm{Np} \rightarrow {}^{233}\mathrm{U} \rightarrow {}^{229}\mathrm{Th}$$

$$^{242}\mathrm{Am} \rightarrow {}^{242}\mathrm{Cm} \rightarrow {}^{238}\mathrm{Pu} \rightarrow {}^{234}\mathrm{U} \rightarrow {}^{230}\mathrm{Th} \rightarrow {}^{226}\mathrm{Ra}$$

$$^{243}\mathrm{Am} \rightarrow {}^{239}\mathrm{Pu} \rightarrow {}^{235}\mathrm{U} \rightarrow {}^{231}\mathrm{Pa} \rightarrow {}^{227}\mathrm{Ac}$$

Table 15.11 *Long-lived actinides in spent fuels*[a] (*Allard* et al., 1984).

Nuclide	*Half-life*[b] (yr)	*Activity* (GBq/ton U) *after*		
		40 yr	100 yr	1000 yr
^{229}Th	7.340×10^3	–	–	0.006
^{230}Th	7.538×10^4	0.018	0.048	0.74
^{231}Pa	3.276×10^4	0.001	0.002	0.011
^{232}U	68.9	0.78	0.44	–
^{233}U	1.592×10^5	0.003	0.007	0.15
^{234}U	2.455×10^5	52	67	89
^{235}U	7.038×10^8	0.52	0.52	0.52
^{236}U	2.3415×10^7	10	10	10
^{238}U	4.468×10^9	12	12	12
^{237}Np	2.144×10^6	16	19	48
^{239}Pu	2.411×10^4	1.1×10^4	1.1×10^4	1.1×10^4
^{240}Pu	6.564×10^3	1.4×10^4	1.4×10^4	1.3×10^4
^{241}Pu	14.35	9.3×10^5	5.2×10^4	12
^{242}Pu	3.733×10^5	110	110	110
^{241}Am	432.2	1.8×10^5	1.9×10^5	4.4×10^4
^{243}Am	7.37×10^3	0.0012	0.0012	0.0011

[a] PWR, 38 000 MW d ton^{-1} U.
[b] Appendix II, this work.

The effect of radioactive decay of the americium and curium is an increase in the intensity of radioactivity with time after removal from the reactor. For a period from 10 to 10^3–10^4 years after discharge from the reactor, the environmental hazards will be preponderantly due to ^{241}Am; from 10^4 to 10^5 years the nuclides ^{239}Pu and ^{240}Pu will be the principal actinides present; and for the period after 10^6 years, ^{237}Np will be the principal actinide present. The chemical properties of uranium, neptunium, plutonium, and americium thus determine the mode and extent of dispersion of alpha-emitting radionuclides introduced into the environment from nuclear operations. Table 15.12 indicates the amounts of transuranium elements released into the atmosphere as of 1980. The disposal of low-level waste streams from nuclear fuel reprocessing in the sea is estimated to add considerably less than 0.1 kg (0.3 TBq) per year of plutonium to the environmental inventory (Allard *et al.*, 1984).

15.8.3 Actinides in the hydrosphere

From the discussion of ions in solution and their redox and hydrolytic properties in Section 15.5, it can be inferred that the transuranium elements in a marine (ocean) environment will tend to form insoluble compounds. Under the redox conditions that obtain in the ocean, the stable oxidation states of plutonium,

Table 15.12 *Transuranium elements released to the atmosphere* (*Allard* et al., 1984; *LANL*, 2000, *pp.* 36–47).

Nuclide	*Amount* (TBq)
^{238}Pu[a]	890[b]
^{239}Pu	5.7×10^3
^{240}Pu	7.7×10^3
^{241}Pu	3.6×10^5[c]
^{241}Am	1.2×10^4[d]

[a] Half-life 87.7 years.
[b] Including 590 TBq from a SNAP 9A radionuclide battery in a Transit satellite that vaporized upon reentering the atmosphere in April 1964.
[c] Largely decayed to ^{241}Am.
[d] Largely from ^{241}Pu.

americium, and curium are expected to be Pu(IV), Pu(V), Am(III), and Cm(III). Under reducing conditions, neptunium is expected to be in the Np(IV) state and to behave much as does Pu(IV). Under oxidizing conditions, however, the neptunyl(V) ion, NpO_2^+, will be the stable species, and the similar Pu(V) ion PuO_2^+ predominates; these ionic species have smaller tendency to undergo hydrolysis or to form strong complexes than do the 4+ state ions or other actinyl ions in the 6+ oxidation state (Orlandini *et al.*, 1986). Plutonium and the other transplutonium elements in the 3+ and 4+ oxidation states readily undergo hydrolysis at the normal pH of marine waters to form hydroxides and oxides that are essentially insoluble in water. However, these ions form strong complexes with oxygen-containing ligands, which may change their redox potentials significantly, and this may render them oxidizable. The overall effect of the formation of higher oxidation states and complex ions is to produce actinide ions that are more soluble in water. The carbonate ion in particular is important because it is present in natural waters; it forms soluble complexes that stabilize the higher oxidation states of neptunium and plutonium. Allard *et al.* (1984) made a detailed analysis of the interaction of the transuranium elements with natural complexing agents as a function of concentration and pH, and calculated solubilities in water that may be expected for these elements under various conditions. Because natural conditions vary a great deal, it is difficult to make precise generalizations, but general trends can be discerned without too much difficulty. The transuranium actinides under most conditions form insoluble species that result in actinide enrichment in bottom sediments. The tendency to form strong complexes with water-insoluble oxygen-containing ligands (e.g. the exoskeletons of marine organisms) is another route for the removal of the transuranium actinides from the water column to the bottom sediments. The nature of the chemical forms in which the actinide elements occur in marine sediments, and the chemical processes that occur between

seawater and sediments, are topics of active research (Morse and Choppin, 1986; McCubbin *et al*., 2002).

The availability of ocean transuranium elements to marine organisms has received attention. Plutonium is accumulated quite efficiently by benthic (sea-bottom) algae and invertebrates and by plankton. While it is a fairly straightforward matter to determine the plutonium content of harvested organisms, it is not so simple to decide the route by which the plutonium entered or just where in the organism the plutonium is retained. Transfer of plutonium in the water to starfish can take place via ingested food, but it can also occur by adsorption on the surface of the organism. The high concentration of plutonium in starfish appears to be due largely to the strong affinity of polymeric plutonium hydrosols or simple plutonium ions for the mucus sheath that coats the organism. Neptunium, as the NpO_2^+ ion, is rapidly accumulated and excreted by marine zooplankton, but appears, on the basis of limited observations, to be less available than either plutonium or americium.

The transfer rate of americium from sediments containing it in insoluble form is low, and it appears for the most part to be adsorbed on the exterior of bivalve molluscs, *Polychaeta* (marine worms), and isopods (crustaceans). In the presence of higher concentrations of carbonate (Atlantic sediments containing 83% carbonate as compared to Pacific sediments containing only 8% carbonate), the transfer of americium to living organisms increased several fold (Scoppa, 1984). Experiments in which the marine environment was simulated show that the accumulation of ^{241}Am by tiny crustaceans (krill) occurred mainly by adsorption on the exoskeleton, and that only a small amount of americium was retained by the krill after molting. Americium sorbed on diatoms ingested by krill was not assimilated and was excreted in a short time.

Based on a limited amount of data acquired in the Irish Sea near the reprocessing plant at Sellafield, UK, invertebrates and algae accumulate higher concentrations of curium than do the edible parts of fish. The behavior of californium has been studied in a preliminary way in seawater, sediments, and plankton (Scoppa, 1984). Cf(III) is rapidly adsorbed by particulate matter and sediments with distribution coefficients of 10^4 to 10^5. It is also taken up rapidly by marine zooplankton. The relative order of uptake by krill is Cf(III) > Am(III) > Pu(V+VI) > Np(V). Assimilation and incorporation of Cf(III) by the zooplankton in the internal tissues is extremely low in these organisms, and take-up is most likely due to adsorption on the surface of the organisms.

Actinide elements have been released into freshwater (rivers and lakes) as a result of subsurface plumes from leaking waste tanks or other storage of nuclear wastes at former military reactor processing sites. At the Hanford site (Washington state, USA) several tons of uranium, accompanied by other radionuclides, has contaminated the vadose zone. Synchrotron X-ray spectroscopy and diffraction studies of borehole samples showed uranium to be present in the U(VI) solids that are known forms. These solids make it unlikely that uranium is

migrating in the vadose zone but will make it difficult to remove the uranium as a remediation option (Catalano *et al.*, 2004).

15.8.4 Actinide sorption and mobility

Polymeric actinide ions carry a positive charge, and are easily scavenged by negatively charged surfaces. As depolymerization is a very slow process even in strong acid solution, the Pu(IV) polymer is an attractive candidate for an explanation of the ease with which it is removed and the tenacity with which it is retained by clays or soils. Many minerals, especially clays with zeolitic channels and cages, have ion-exchange properties. Ion-exchange sites firmly bind the simple actinide ions in the III and IV oxidation states, and binding of the actinyl ions in the 5+ and 6+ states is considerably weaker. Plutonium is strongly sorbed on many minerals in the pH range normally encountered in the environment under both oxidizing and reducing conditions.

The overall effect of ion exchange and other sorption processes by solid phases is to remove actinides at tracer concentrations from an aqueous phase. The uptake on solids is in the same sequence as the order of hydrolysis: Pu(IV) > U(VI) > Am(III) > Np(V).

Assimilation in plants commonly declines in the order: Np(V) > U(VI) > Am (III) > Pu(IV), Np(IV). Both phenomena are evidently contingent on the species formed by hydrolysis: the easily immobilized species are also assimilated with difficulty by plants. The uptake of actinides by living organisms from solid phase is minor, and this is also the case for actinide elements immobilized on food. Of the 4400–7700 kg of plutonium that came to Earth after atmospheric testing of nuclear weapons, the total amount fixed in the world population is estimated to be less than 1 g (Allard *et al.*, 1984). Allard *et al.* (1984) conclude from the available evidence that plutonium in the environment is not concentrated in the food chain. Surface-adsorbed actinides appear to be the major mechanism for the introduction of transuranium elements into the terrestrial food chain even though the actinides are not actually incorporated into the internal tissues of the organisms (Teale and Brown, 2003). The enrichment of actinides in the food chain to humans is minimized by discrimination against the absorption of actinides by organisms at higher levels in the food chain. Thus, it is unlikely that the concentration of plutonium in a human being will significantly exceed the concentration in natural waters, regardless of the mode of ingestion.

Organic and inorganic particles or colloids to which actinide elements are attached constitute a major mode of dissemination of the actinide elements in the environment. Natural waters contain particulate silt and organic matter, which may or may not be living. Transport of actinide elements adsorbed on particulate matter will then depend on particle size, water flow, and factors other than the chemical properties of the actinide species themselves.

Living organisms can also act as carriers even if the actinide elements are not actually incorporated into the tissues of the organism.

15.8.5 Nuclear waste disposal

The fate of actinide elements introduced into the environment is not merely a scientific issue. The disposal of the by-products of the nuclear power industry has become a matter of industrial and public concern. For each 1000 kg of uranium fuel irradiated in a typical nuclear reactor for a 3 year period, about 50 kg of uranium are consumed. In addition to a large amount of energy evolved as heat, 35 kg of radioactive fission products and 15 kg of plutonium and transplutonium elements are produced. Many of the fission-product nuclides are stable or are short-lived radionuclides that decay to stable isotopes, but others are highly radioactive for decades or longer. All of the fission products are isotopes of elements whose chemical properties are well understood. The transuranium elements produced in the reactor by neutron capture, however, have unique chemical properties, which are reasonably well understood but are not easily inferred by extrapolation from the chemistry of the classical elements. Plutonium is fissile and can be recycled as a nuclear fuel in conventional or breeder reactors, but the transplutonium elements are not fissile to the extent of supporting a nuclear chain reaction, and in any event they are produced in amounts too small to be of interest for large-scale uses. The transplutonium elements must therefore be secured and stored.

The exact form in which fission products and heavy elements are extracted from spent fuel elements is determined by the chemical process used to treat the spent fuel. In the past, most fuel reprocessing has been by solvent extraction, and it is probable that solvent extraction will continue to be the most widely used processing procedure, at least until new reactor types are introduced. Solvent extraction is efficient in separating uranium, fission products, and transuranium elements, but large volumes of liquid waste streams with rather low but not negligible levels of radioactivity are generated in the process. The plutonium is generally separated from the transplutonium elements, leaving a complex mixture of fission products and americium, curium, and transcurium elements, which as they decay form isotopes of neptunium, uranium, and natural radioactive elements. These must be immobilized and stored in a way and in places where no geological or man-made catastrophe will release the radioactive material into the environment, even over an enormously long timespan.

Many schemes have been considered for disposal of both fission products and actinide elements. These proposals has been discussed by Choppin *et al*., 2002, pp. 599–640), National Academy of Sciences (1995), and Van Tuyle *et al*. (2002) among others. Nuclear 'incineration,' the transmutation of excess plutonium and the 'minor actinides' neptunium, americium, and curium (which are the predominant source of radioactivity from spent fuel after about 600 years)

in nuclear reactors after their separation from other components of spent fuel, is a realistic option pursued in several countries. Prolonged neutron irradiation in a conventional fission nuclear reactor, or possibly in a fast breeder reactor, will transmute long-lived actinide isotopes, especially excess weapons plutonium, to short-lived radioactive or stable isotopes faster than they will be formed from the uranium or uranium–plutonium mixed oxide (MOX) fuel in the reactor, especially if the nuclear fuel is an 'inert matrix' ceramic oxide that has no uranium. The actinide elements subjected to nuclear incineration in a reactor must be free of lanthanide fission products, as some of these have very large cross sections for neutron capture and thus could adversely affect the neutron economy of a nuclear reactor. A drawback of reactor incineration is that some plutonium is bred; this drawback can be mitigated by the use of uranium-free 'inert matrix fuels' that are ceramic oxides such as yttria stabilized zirconia or zirconates. These fuels are inert in the sense that the fuel cannot breed plutonium (Degueldre and Yamashita, 2003).

Another transmutation scheme is accelerator transmutation of long-lived nuclear wastes. An accelerator generates high neutron fluxes by spallation. These neutrons drive a subcritical reactor to fission the long-lived actinide isotopes without breeding additional plutonium. This technology can transmute fissile ^{235}U and ^{239}Pu, as well as the isotopes ^{237}Np, ^{241}Pu, and ^{241}Am that dominate both the long-term heat load and radiotoxicity of the waste.

Immobilization and disposal in appropriate geological formations has received the most attention. The first step in immobilization is to convert the liquid waste streams from fuel processing into dry solids by evaporation or some other drying process. The dry residue is calcined to convert the radioactive mix to metal oxides. In this form the calcined oxides are leachable and can easily become airborne. Their thermal conductivity is low, and good heat conductivity is essential to dissipate the heat liberated by radioactive decay. A great variety of glassy and crystalline matrices have been explored. Prime requirements are stability to radiation and to chemical attack by or to solubility in water, since exposure to groundwater is a possibility that must be guarded against in any subterranean repository. Borosilicate glasses are preferred matrices in most countries, and in fact France (La Hague) and the U.S. (Savannah River plant) have glass melters that have been in operation for one or more decades (CEA, 2002). Additional encapsulation of the solidified waste is generally considered mandatory, and for this purpose corrosion-resistant metals such as copper or C-22 alloy (UNS 06022, a nickel–chromium–molybdenum–tungsten alloy) have been selected for waste canisters.

The requirements for a geological repository are quite stringent. The repository must be sited in a region of high geological stability, free of earthquakes and volcanic activity. The chosen stratum must be free of vents to the surface, and it must have little or no groundwater circulation. It is important that the geological formation have good heat conduction properties to enable heat evolved by radioactive decay, which is very substantial, to be conducted away

rapidly enough to prevent destruction of the containment by high temperature. Rock salt, granite, and clay all have their proponents. Disposal in the Arctic ice caps and burial in deep seabeds also have been considered. Rock salt formations, at least in the U.S., appear to be the geological stratum of choice for transuranic wastes. Unaltered rock salt formations of great age and of unquestionable seismic stability are known. Rock salt has exceptionally good heat transfer properties. Extremely dry salt domes that have existed for more than 100 million years without appreciable alteration exist in many places. Salt is plastic, and holes and fractures in the salt bed will self-seal. As long as the surface layers are not breached by drilling, and that provision is made in repository design for the corrosive properties of brine, rock salt domes appear to have most of the features required for a secure repository.

Clays likewise have desirable properties. The migration rate of fission products and actinides through clay is very slow and, once adsorbed in such a matrix, the transuranium elements are effectively immobilized. However, clay deposits frequently are percolated by water, and it is difficult to guarantee that even a bed dry for geological epochs will remain that way. Still, even radionuclides that enter underground water are readily removed and immobilized by ion exchange on clays and other minerals. A very good example of efficient and extraordinarily effective immobilization of radioactive fission products by natural processes is found in the Oklo mineral formation, where the products of a natural chain reaction have remained in close proximity to their point of origin although the rock formation has been suffused repeatedly by water in the past billion years (see Section 15.8.1). Although there are unanswered questions about nuclear repositories, there are many reasons to expect that the technical problems in nuclear waste disposal can be solved satisfactorily. Indeed, most of the necessary technology has been in existence for some time, and a high level of technical sophistication has been available for many years (Topp, 1982). It seems likely that interim or monitored retrieval storage will be the method of choice for the storage of nuclear waste. Storage of this kind is easier to prove safe and could be useful for a century or more.

15.9 BIOLOGICAL BEHAVIOR OF THE ACTINIDE ELEMENTS

15.9.1 General considerations

In this section we have made extensive use of several authoritative reviews (Bulman, 1980; Raymond and Smith, 1981; Nenot and Metivier, 1984; Banaszak *et al.*, 1999; Gorden *et al.*, 2003) that emphasize aspects of importance in the biological behavior of the actinide elements, both in the ecosphere and in humans. None of the elements heavier than iodine (atomic number 53) is, so far as is known, essential to life, and an intrusion by any of them into living organisms is generally regarded as a noxious event best avoided. Studies on

the heavier elements tend to be sparse or fragmentary except where special circumstances apply, e.g. mercury or lead. Were it not for the long-lived radioactivity of the actinide elements, it is likely that they too would attract little interest. Uranium, neptunium, plutonium, and americium are regarded as the major health hazards among the actinide elements, and thus have been the focus of research activity (Thompson, 1982). Recently, interest in the oxidation–reduction and coordination of neptunium with microorganisms and their organic by-products (e.g. humic and fulvic acids) has reawakened and is now a theme in bioremediation research because Np(V) appears to be the most mobile of the actinide ionic species (Songkasiri *et al.*, 2002). This, coupled with the realization that long-lived ^{237}Np formed by the radioactive decay of ^{241}Pu (via the decay sequence

$$^{241}\mathrm{Pu} \xrightarrow{\beta^-} {}^{241}\mathrm{Am} \xrightarrow{\alpha} {}^{237}\mathrm{Np}$$

in nuclear waste) makes ^{237}Np the major contributor to the radioactivity of nuclear waste at times greater than 10^5 years, has stimulated new interest in the biological properties of neptunium. A comprehensive treatment of the behavior of actinides in animals and man is found in chapter 31.

15.9.2 State of actinide elements in body fluids

The forms in which plutonium, americium, and curium occur in blood and urine are continuing topics of major concern, for they are intimately involved in transport in the body after ingestion and in subsequent excretion. Boocock and Popplewell (1965) found that plutonium injected intravenously into the rat was bound in the blood serum to transferrin, a protein produced in the liver that transports iron between tissues and bone marrow. Pu(IV) in the blood is rapidly and firmly bound to transferrin. By far the greater part of the plutonium is captured by transferrin, but small amounts are believed to be complexed by citrate ion or low-molecular-weight carbohydrates or peptides. This may reflect a complex equilibrium situation, or may be an indication that more than one ionic species of plutonium in more than one oxidation state is present. The binding of plutonium to transferrin is strong, but Fe(III) can displace it, and plutonium is not bound by iron-saturated transferrin. Bicarbonate ion is required to bind iron to transferrin, and this is also the case for plutonium. The half-life for the removal of transferrin-bound iron and plutonium from the circulation is the same. The exact nature of the binding sites remains unknown, and whether the same site is used for binding iron and plutonium is unsettled. Transferrin contains a sialic acid component (an oligo- or polysaccharide containing an acidic sugar, *N*-acetylneuraminic acid), which is an excellent complexing agent for metal ions. However, destruction of the polysaccharide moiety inhibits the binding of Pu(IV) but not of Fe(III), suggesting a more complicated binding site situation than at first anticipated. Pu(IV) shows

remarkable similarity to Fe(III) in its coordination behavior, attributed by Raymond *et al.* (1984) to similar ratios of charge to ionic radius for Pu(IV) ($4.6e$ Å^{-1}) and Fe(III) ($4.2e$ Å^{-1}). The 3+ ions of americium, curium, and the transcurium elements bind very weakly, if at all, to transferrin. Instead, the actinide(III) ions present in biological fluids are weakly associated with various plasma proteins. Uranium, present as the uranyl ion UO_2^{2+}, which has a much diminished tendency to form complex ions as compared to uranium in lower oxidation states, is found in the blood in roughly equal amounts associated with protein and as uranyl carbonate complex ions. U(IV), however, binds strongly to protein and is excreted very slowly.

Such studies as are available indicate that plutonium, americium, and curium are cleared through the kidneys and excreted in the urine as citrate complexes, whereas uranyl ion is excreted as a bicarbonate complex. Although there is by now a considerable body of information on the rate of excretion of plutonium in the urine as influenced by a variety of additives and presumptive therapeutic agents, much remains to be learned about the chemistry of the elimination of the actinide elements through the kidney.

Plutonium, americium, and curium are cleared from the liver through bile, which is the principal source of these elements in feces. The clearance of the actinide elements through the feces, however, constitutes only a very small fraction of the radioactivity transported in mammals. Transport of the actinide elements also appears to take place in lymph fluid. This is presumed to be the mode of transport of plutonium introduced in a wound. Plutonium as a simple ion in the lymphatic system moves with the fluid flow, but plutonium as a colloid or as particulate matter is transported in lymphocytes whose function is to scavenge ingested particulate matter. Plutonium in the fluid phase of the lymph migrates as a transferrin complex (Bulman, 1980). The behavior of plutonium and the transplutonium elements in the lymphatic system may well have an important bearing on the decorporation of ingested actinide elements, but too little information is available to make any definitive declarations on this point.

15.9.3 Uptake of actinide elements in the liver

Actinide elements are rapidly cleared from the body fluids. As is usual in the removal of xenobiotics, the first repository is the liver. According to Bulman (1980), the mechanism by which plutonium, americium, and curium are removed from the blood and trapped in the liver is not well understood. The actinide elements bound by transferrin are transferred in the liver to ferritin, an iron storage protein, but nothing is known about the transfer process. It might be expected that actinide element colloids would be taken up by endocytosis, the process of cellular uptake or internalization by which particles, macromolecules, and fluid droplets are removed from the bloodstream and incorporated

into living cells. However, the literature does not support this view. Endocytosis (or pinocytosis as the process is also known) is not considered to play an important part in the incorporation of actinide elements into liver cells (Taylor, 1972). What seems well established is the critical role of phospholipids in the uptake of the actinide elements by the liver. Actinide(III) and (IV) ions are complexed strongly by phosphates in simple aqueous systems. Th(IV) likewise interacts strongly with phospholipids (Boocock and Popplewell, 1965; Barton, 1968). Such behavior for other actinides ions in the 3+ and 4+ oxidation states would not be unexpected. Phospholipids could thus act as ionophores in the concentration of the actinide elements in the liver. The evidence in support of this hypothesis is mostly indirect. Based on the behavior of Fe(III) and the uptake of plutonium in animals treated so as to have a much higher than normal concentration of phospholipids in the liver, there is reason to suppose that phospholipids cause concentration of plutonium by the liver. Thioacetamide characteristically increases the accumulation of acidic phospholipids in the liver, and this compound is found to cause a 2.5-fold increase in the uptake of Pu(IV) by the liver. The effect of various phospholipids on the liquid–liquid partition of Pu(IV), Am(III), and Cm(III) between water and water-immiscible organic solvents provides additional evidence of the ionophore capabilities of phospholipids. Nevertheless, the exact nature of the receptors involved in actinide uptake (if indeed there are specific receptors) remains to be established.

Several research groups have provided evidence that plutonium, americium, and curium are taken up by lysosomes in the liver. Lysosomes are specialized parts of cells or organelles in which an important part of the cellular metabolism is carried out. The lysosome is surrounded by a single membrane and contains a complex mixture of hydrolytic enzymes; together these enzymes are able to dismantle proteins, nucleic acids, polysaccharides, and lipids to their component parts. The actinide elements not translocated from the liver remain associated with the lysosomes, possibly bound to the iron storage proteins ferritin and hemosiderin. Lysosomes are associated with endocytosis and at least a fraction of the lysosomes are formed by endocytosis. If the main part of the actinide uptake is really associated with liver lysosomes, then it may be premature to exclude endocytosis as a primary event in liver uptake of actinide ions. A substantial association of the cellular actinide content with mitochondria is also probable.

A body of evidence indicates that, within 3 days of administration, considerable amounts of plutonium are bound to lysosomal ferritin, and similar findings have been reported for americium and curium administered as monomeric citrates (Boocock *et al.*, 1976). Americium has been reported to associate with lysosomal ferritin and lipofuscin, a yellow-brown pigment that accumulates in aging cells. Lipofuscin contains phospholipids and is known to bind metal ions.

15.9.4 Uptake of actinides by bone

The ultimate fate of plutonium that is not excreted promptly after administration or ingestion is deposition in the bone and other mineralized tissues. Whether the mineralization is phosphate- or carbonate-based appears to be immaterial. In cartilaginous fish, plutonium is concentrated in the skeleton to a significant extent, and in fish with a bony skeleton, the plutonium concentration in the soft tissues may be less than 1% of that in the skeleton. The uptake of actinide elements from the body fluids by bone is a slow process, because of the strong binding of plutonium by transferrin. Autoradiography of bone shows quite different patterns of deposition for plutonium and americium compared to the deposition of radioactive calcium. Calcium deposition is uniform, whereas actinide deposition is irregular. The lack of uniformity in the distribution of the actinides deposited in bone may be related to variations in the pH of the bone surface, or to different concentrations of citrate ion at different locations on the bone surface.

Glycoprotein has been suggested as the important agent in the fixation of plutonium, but glycoprotein is less important for americium or curium (Mahlum, 1967). Glycoproteins that have a high acidic amino acid content bind plutonium *in vitro*. Calcium ion is required for plutonium fixation, which suggests that calcium nucleation sites are necessary for plutonium uptake. Phospholipids have also been implicated in the process, and a lysosome–inositol triphosphatide complex that plays an important part in a model of bone calcification is known to complex Pu(IV), Am(III), and Cm(III) from citrate solutions or plasma (Bulman and Griffin, 1980). Eventually the plutonium in bone accumulates in immobilized deposits of hemosiderin, which, unlike the iron storage protein ferritin, is insoluble in aqueous media. Hemosiderin contains a large core of iron hydroxides and phosphates, and is the repository of the iron content of heme liberated by the catabolism of hemoglobin. Hemosiderin deposits are located close to the surfaces of the bone in the reticuloendothelial cells of the bone marrow (Durbin, 1975). Once plutonium is incorporated into bone, it is not totally immobilized, but the rate at which it leaves the bone is slow and the process by which it is released is unknown. The half-time for the spontaneous removal of plutonium from bone has been estimated as 65–130 years (Bulman, 1980). Release of plutonium from hemosiderin should not be taken to imply that the mobile plutonium will be excreted through the kidney. More probably, it will be bound to transferrin and recycled into the liver and bone.

15.9.5 Bioremediation of actinides from the environment

Biological treatments of organic, agricultural, and domestic wastes have been in use for centuries and are used very widely. Bioremediation of such wastes is usually ecologically and economically preferable to chemical treatment. These

wastes can be converted to harmless and sometimes beneficial products. Although the biotreatment of metals, especially radioactive metals, cannot decrease the elemental composition of the metal or the specific activity of radionuclides in waste, it can increase the concentration of metallic species to facilitate their removal from the environment or cause the metal to precipitate to prevent its migration. Therefore the bioremediation of actinides requires microbial interactions that changes the actinide's complexation behavior or oxidation state.

Thomas and McCaskie (1996) demonstrated that microorganisms (especially *Pseudomonas*) can hydrolyze the widely used extractant TBP into phosphate and also precipitate U(VI) as a uranyl phosphate, thereby breaking down an organophosphorus pollutant and immobilizing a dissolved actinide. Microbes can serve as reducing agents to convert mobile actinides, e.g. U(VI), Np(V), and Pu(VI) to readily precipitated tetravalent ions. Banaszak *et al.* (1999) presented the redox couples of many important electron transport coenzymes and showed how these coenzymes can catalyze the reduction of actinide ions via sulfate reduction, Fe(III)/Fe(II) reduction, or other electron transfer processes at pH 7. Reductants that can reduce Fe(III) to Fe(II), or are more reducing, can reduce U(VI) to U(IV), Np(V) to Np(IV), and Pu(V) to Pu(IV) or Pu(III). The more reduced actinide ions can be precipitated, a process referred to as biomineralization. Bioremediation research utilizes the disciplines of microbiology, enzymology, actinide chemistry, and environmental science (NABIR, 2003).

15.10 TOXICOLOGY OF THE ACTINIDE ELEMENTS

Although plutonium has been known since 1940 and has been manufactured and handled on a large scale, there have been few cases of injury to workers and the average intakes by most workers have been consistently low. In recent years, information has become available from Russia where there have been instances of high-level exposure to plutonium with a reported increase in lung cancer deaths compared to other workers whose exposure was within occupational limits (see Section 15.10.3). Most of the information about the toxicity of plutonium has been learned from animal experimentation. The application of information acquired in this way to human toxicology can only be estimated by extrapolation (Clarke *et al.*, 1996). The information available about the other actinide elements is much less abundant, and some generalizations must be accepted with reservations.

15.10.1 Ingestion and inhalation

Any of the actinide elements in the environment can enter the human body by ingestion, by inhalation of particulate matter, by passage through the skin, or by accidents accompanied by forcible introduction of the actinide into the body. Absorption through the intestinal tract appears to be one of the least important

routes for the incorporation of plutonium and the transplutonium elements. Plutonium has not been found to concentrate in the food chain (see Section 15.8.4); however, solubilizing ligands have been found to increase the uptake of plutonium and americium into plants, presenting a possible means of their introduction into the food chain (Francis, 1973; Bulman, 1978; Vyas and Mistry, 1983). Plutonium itself is not very bioavailable as it does not readily pass through the intestinal wall when ingested. Unbroken skin presents an essentially impermeable barrier to the passage of actinide ions. Likewise, the fate of plutonium deposited in an open wound is largely dependent on the chemical state of the plutonium. If the plutonium is in a soluble form such as a citrate complex, it will rapidly reach the circulatory system and form a transferrin complex. If it is deposited in a wound as an insoluble compound, translocation is slower (Clarke *et al.*, 1996). The toxic effects and ability of Pu (IV) to form strong complexes with bone and tissue is similar to the behavior of Fe(III). The currently available treatments for chelation therapy to extract actinides that have been introduced into the body are most effective if administered within hours of exposure. After this point, the actinides can be incorporated into bone and tissues, rendering them fixed (Durbin *et al.*, 1998).

By far the most likely (and serious) mode of entry for plutonium into the body is inhalation of insoluble particulate matter into the lungs. Factors that influence the translocation of plutonium oxides from the lung to other parts of the body include particle size, chemical composition, lung burden, calcination temperature, and isotopic composition (Lataillade *et al.*, 1995). Extremely small particles (1 nm in diameter) of PuO_2 are quickly absorbed from the lung and enter the circulation as low-molecular-weight complexes. Large particles (0.025–0.22 μm) clear very slowly. AmO_2 made by calcination of americium oxalate at 650°C was observed to be removed so rapidly from the lung as to raise questions whether the compound should continue to be considered insoluble. It is possible that the americium dioxide preparation was actually americium hydroxide polymer, and it may be that small deviations from stoichiometry could have a considerable effect on the rate of dissolution and removal from the lung. Variations in stoichiometry are expected to be much more prominent in plutonium than in americium, which may be responsible for the surprising differences in the behavior of the oxides of these actinide elements. Curium dioxide behaves quite similarly to americium dioxide, but there is at least one important and puzzling difference between the two. While americium dioxide does not bind to protein, curium dioxide does (Bulman, 1980). In the absence of information about the stoichiometry of the actinide oxide, or the preparations used in the experiments, it is difficult to ascertain whether it is particle size or deviations from stoichiometry that are responsible for the biological behavior of the actinide oxides. Many questions about the behavior of actinide particulates in the lung remain, and the answers could have implications for other lung pathologies. It has been found that $^{238}PuO_2$ clears the lung much faster than does $^{239}PuO_2$ (NCRP, 2001). The magnitude of the difference is clearly beyond

the range of ordinary isotope effects, and must be attributed to the increased radiation damage incurred by the oxide particles from the more energetic alpha particles emitted by the shorter-lived radionuclide ^{238}Pu (Bulman, 1980).

15.10.2 Acute toxicity of plutonium

There is general agreement that the chemical toxicity of plutonium is inconsequential compared to the radiotoxicity, or the effects caused by its alpha radiation (Bulman, 1980; Nenot and Metivier, 1984; Clarke *et al*., 1996; Voelz, 2000; Guilmette, 2001). By far, the greatest risk from plutonium is the long-term possibility to develop cancer. One way to compare risks between two materials is by a comparison of relative limits on concentration in air of the two substances. These limits are extrapolated from experimental observations with animals. The limit in air for plutonium is referred to as the derived air concentration (C_{DAC}). This is the concentration in air which, if breathed alone for one work year, would irradiate 'reference man' to the limits for occupational exposure, and is 0.006 μCi cm^{-3} for ^{239}Pu (4×10^{-4} μg m^{-3}). Comparing plutonium-239 to most materials handled on the small industrial scale shows plutonium-239 to be a very toxic material. Its toxicity per unit mass is similar to that of long-lived fission products such as strontium-90 and cesium-137 but less than that of short-lived fission products such as iodine-121 (Clarke *et al*., 1996).

All data on the chemical toxicity of plutonium are derived from animal experiments. On the assumption that ions of similar size and charge will have similar toxicological properties, which is reasonable in this situation, to produce a similar change in an adult human liver would require the intravenous injection of about 200 mg of plutonium (Bulman, 1980). Further evidence supports this conclusion. The amount of material that causes death in 50% of animals after n days is known as the $LD_{50}(n)$ value. The $LD_{50}(30)$ value obtained from studies on dogs after intravenous injection of plutonium is about 0.32 mg per kg of tissue. When extrapolated to a human of 70 kg, the $LD_{50}(30)$ value is about 22 mg (Voelz, 2000). Neptunium-237 injected into rats intravenously at 3 mg kg^{-1} induces short-term subacute changes in the liver, but is nowhere near as toxic as strychnine. There is substantial evidence that the chemical toxicity of plutonium is comparable to that of neptunium, and that plutonium is not an extraordinarily virulent chemical poison. The toxic manifestations of plutonium are due to long-term effects of radiation damage from its radioactive decay.

The acute toxicity of uranium in the form of the uranyl ion varies considerably with the experimental animal; the acute dose in the rabbit and guinea-pig is in the range 0.1–0.3 mg kg^{-1}, and in mice it may be as much as 20–25 mg kg^{-1} (Bulman, 1980). Differences in toxicity in different species have been attributed to differences in diet that result in the excretion of urine of widely differing pH. Herbivores excrete very acidic urine, which interferes with the formation of carbonate and citrate complexes of uranyl ion. These are the forms in which

uranium is cleared through the kidneys. Under conditions that lower the carbonate and citrate concentrations, uranium clears the organism more slowly, and a given dose of uranium in a herbivore appears to have a higher toxicity than in an organism that can eliminate uranium more rapidly. Acute toxic symptoms produced in yeast by uranyl salts appear to be a result of the suppression of glucose metabolism by interaction of the uranyl ion with the cell surface. Reagents such as phosphate that complex uranyl ion strongly reverse the inhibition of respiratory activity (Bulman, 1980). The small amount of data gathered from human studies indicates that the renal injury is consistent to what is seen in animal models (Diamond, 1989).

15.10.3 Long-term effects of ingested plutonium

The maximum allowed dose of ^{239}Pu in humans was referred to as maximum permissible body burden and was set at 0.65 μg for radiation workers from 1953 to 1977. The International Commission on Radiation Protection published a series of reports between 1977 and 1988 that effectively decreased the lifetime body burden of ^{239}Pu to 0.5 μg (0.05 Sv) for U.S. radiation workers; these values are approximate because dose calculations must be made for internal deposition of each isotope to specific organs (Voelz, 2000). A population of 26 white male workers at Los Alamos National Laboratory who acquired plutonium body burdens between 260 and 8510 Bq (0.1–3.7 μg if pure ^{239}Pu) during World War II was followed for 50 years. As of 1994, seven persons were dead compared with the expected 16 deaths based on mortality rates for white males in the U.S. in the general population and age group. Comparing the mortality rate of the exposed workers with that of 876 unexposed Los Alamos workers of the same period, the mortality rate of the exposed workers is not elevated. As of 1995, the 16 living white males had diseases and physical changes expected of a male population with a median age of 72 years. Out of 26 white male workers, eight had been diagnosed as having one or more cancers, within the expected range for a similar, unexposed population. The cause of death in three of the seven deceased men was cancer of the prostate, lung, and bone; however mortality from all cancers was not statistically elevated (Voelz *et al*., 1997).

Long-term chromosomal analyses of British plutonium workers who had more than 20% of the maximum permissible body burden of ^{239}Pu (doses greater than 0.25 Sv) showed no evidence for induction of persistent transmissible genomic instability (Whitehouse and Tawn, 2001). However, some Russian workers have been exposed to much higher levels of plutonium at the Mayak nuclear facility (among 2283 plutonium workers from 1948 to 1958, the mean accumulated dose was 8 Sv for males and 14 Sv for females). An increased risk of lung, liver, and bone cancers was associated with these higher exposures (Tokarskaya *et al*., 1997; Koshurnikova *et al*., 1998; Gilbert *et al*., 2000; Voelz, 2000; Grogan *et al*., 2001). In many cases, the ingrowth of ^{241}Am from decay of ^{241}Pu that is present in most plutonium samples is actually the largest

contributor to the dose from inhaled or ingested plutonium (Hisamatsu and Takizawa, 2003).

Most of the available information on the effects of plutonium in mammals has come from animal experiments. Low doses of radiation in the lungs of rats produce three types of cancer: sarcomas (10%), bronchoalveolar cancers (40%), and bronchogenic cancers (50%). The lowest dose at which a significant increase in lung cancers occurs is 37 Bq g^{-1} of lung tissue for inhaled insoluble plutonium compounds. The mode of distribution of plutonium in the lung has a large effect, and whether the plutonium was acquired in a single exposure or by multiple exposures is also a factor that is important in subsequent pathology. In the dose range 0.06–37 kBq kg^{-1} of bone, an osteosarcoma incidence from 31% to 100% has been observed in dogs. Organisms experiencing rapid bone growth are more sensitive to osteosarcomas from plutonium than are adults. Liver appears to be less sensitive to alpha radiation than either lung or bone. The effects of ingested plutonium on the blood are largely due to irradiation of the hematopoietic tissues where blood cells are formed. No leukemia has ever been detected in dogs. In humans exposed to plutonium, stable chromosomal aberrations in the blood have been seen. Finally, no hereditary diseases have been observed in the progeny of animals whose bodies contained plutonium (Nenot and Metivier, 1984; ICRP, 1986).

15.10.4 Removal of actinide elements from the body

Once plutonium has gained access to the bloodstream, there is no normal physiological process that will eliminate it rapidly from the body. Foreign chemicals or organic poisons that are introduced into the body are converted in the liver by oxidation and conjugation into compounds that can be excreted. Heavy metals are either deposited in insoluble form or else they become complexed to body constituents, and no such metabolic elimination pathway exists. Plutonium retention is not absolute, but the excretion rate is so slow that in a normal lifespan only a fraction of the deposited actinide will be removed from the body. Early attempts to increase the rate of plutonium excretion were based on competitive displacement by innocuous metal ions of a size and charge that would enable them to compete successfully with Pu(IV) for binding sites or crystal lattice sites. Zirconyl(IV) citrate was found to accelerate considerably the excretion of injected plutonium, but only if the zirconium was administered within a very short time after the plutonium. Zirconyl citrate appears to be reasonably effective in displacing Pu(IV) from the bloodstream but not from body tissues. Other hydrous metal oxides such as those of thorium or aluminum minimize deposition of plutonium in bone, but increase the amount of plutonium deposited in the liver. Therapeutic approaches along these lines have therefore fallen into disuse.

The only practical strategy for increasing the excretion of plutonium is based on the use of chelating agents to form water-soluble complexes of plutonium

(ICRP, 1990). Citrate and ascorbate are effective complexing agents to a degree, but are metabolized too rapidly to be of practical utility. Useful therapeutic agents have been sought among the numerous chelating agents that have been synthesized for ion sequestration purposes, particularly derivatives and analogs of EDTA. EDTA itself is quite effective in accelerating the excretion of plutonium, provided it is administered within a short time after plutonium ingestion, but it is much less effective when the interval between ingestion and therapy is of the order of weeks (Schubert, 1955; Durbin, 1973; Vaughn *et al*., 1973). Of the considerable number of derivatives and analogs of EDTA that have received attention, the most successful is diethylenetriaminepentaacetic acid (DTPA). This compound has one carboxyl group more available for chelation than EDTA, making it an octadentate ligand system capable of fully complexing Pu(IV) in its preferred coordination geometry, thus significantly enhancing the stability of the complex. DTPA administered promptly in a single dose after plutonium ingestion causes the excretion of about 90% of the plutonium in the following 6 days as compared to less than 5% excretion in controls; when pigs were used as the experimental animal (Taylor, 1978). To achieve such good results, DTPA must be administered within 30 min after plutonium injection in beagles. A delay in the administration of DTPA for as little as 2 h results in only 15% of the injected plutonium being excreted during the first day. Delayed treatment with multiple doses of DTPA is effective in removing moderate amounts of plutonium from the pig. In these experiments, it was observed that the principal source of the excreted plutonium was the soft tissues, and that removal of plutonium from the bone did not proceed to the point where the number of bone tumors formed was significantly reduced (James and Taylor, 1971). DTPA is also limited in that it must be administered as the calcium or zinc salt to prevent toxicity from the depletion of these essential divalent metals. Additional details on the use of DTPA can be found elsewhere (Rosenthal and Lindenbaum, 1967; Smith, 1972; Durbin, 1973; Vaughn *et al*., 1973; Bruenger *et al*., 1991; Durbin *et al*., 1998). Many other chelating agents related in structure to EDTA and DTPA (for example, citrate and nitrilotriacetic acid, NTA) have been studied, but none of these are significantly better performers. Increasing the number of carboxyl groups does not improve decorporation, and the replacement of oxygen functions by sulfur or phosphorus analogs degrades their performance.

The *in vivo* situation of chelating agents is much more complicated than sequestration of alkaline earth ions in a detergent solution, or in laboratory systems arranged for the measurements of complexation constants. It has been recognized for some time (Schubert, 1955) that, because the calcium-ion concentration in serum is much greater than that of other metal ions, unless a chelating agent has a much lower affinity for calcium ion than for another metal ion, the chelating agent will exist predominantly as the calcium complex in the circulatory system. The apparent efficacy of a chelating agent is thus increased by a low affinity for calcium ion as well as by an enhanced affinity

for plutonium. A foreign metal ion will be partitioned between natural chelators engaged in the transport or metabolic activities of metal ions and any chelating agents that may be introduced for therapeutic purposes. The naturally occurring iron sequestering agent desferrioxamine (DFO) is a very much weaker complexing agent for calcium ion than is DTPA, and even though it does not bind much more strongly to Fe(III) than does DTPA, it is much more effective in removing iron from the body, presumably because of its lower affinity for calcium ion. Whereas DFO is more efficient in plutonium removal than DTPA, provided it is administered within an hour after injection of plutonium, its efficacy decreases more rapidly than that of DTPA as the time interval between plutonium incorporation and therapy increases. Combined use of DTPA and DFO appears to remove the greatest amount of plutonium. The presumption is that plutonium ion liberated from the Pu(IV)–DFO complex is recomplexed and excreted as the DTPA complex before irreversible deposition of the plutonium can occur. Once plutonium has been deposited in insoluble form or incorporated into bone, no known therapeutic approach is efficacious. Inhalation of insoluble plutonium can only be countered by repeated pulmonary lavage with isotonic saline solution (Nenot and Metivier, 1984).

While conventional chelating agents have received by far the most attention in search for effective decorporation of plutonium, other work has aimed at the development of new more selective ligand systems. Raymond *et al.* (1982) have undertaken a search for new chelating agents that would bind strongly to and be specific for actinide ions. They have adopted a biomimetic approach in which compounds are modeled after the powerful and highly specific siderophores, natural iron sequestering agents used by microorganisms to acquire Fe(III) from the environment. Ligands have been generated which incorporate hydroxamic acid, hydroxypyridonate (HOPO), catecholamide (CAM), and terephthalamide (TAM) chelating subunits analogous to those found in the siderophores into a variety of backbones (Gorden *et al.*, 2003). The rationale behind their design method was that by introducing several coordinating functional groups, enough binding sites on the ligand are provided to occupy all of the coordination sites on the metal ion. Enterobactin, a hexadentate siderophore containing three CAM subunits, has the largest formation constant and complexation ability for Fe(III). An octadentate system should be more selective for the larger Pu(IV) ion. The metal ion is then encapsulated, so to speak, by the chelating agent, preventing deposition, increasing solubility and hence, excretion. Siderophore-like systems have also been explored by other researchers to see if they have the potential to introduce Pu or the actinides into the food chain (Ruggiero *et al.*, 2002).

The Raymond–Durbin collaboration has developed a large number of new ligands. Many of these have been tested in mice as actinide decorporation agents. Of these, the best chelating systems for Pu(IV) were, as expected, octadentate ligand systems, e.g. the Pu(IV)–HOPO molecule in Fig. 15.8 , but many

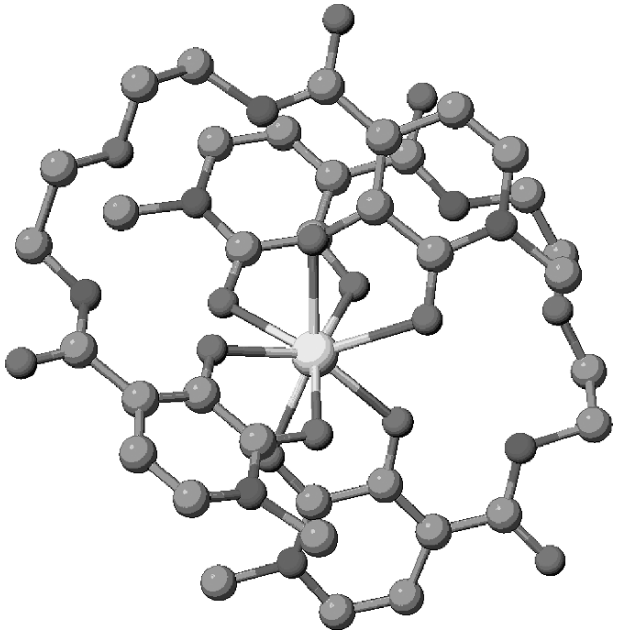

Fig. 15.8 *Molecular structure of Pu(IV)-(5-LIO-Me-3,2-HOPO)$_2$ generated from crystallographic data showing octadentate coordination about the Pu(IV) ion. The geometric arrangement of the ligands about the Pu ion is best described as a distorted bicapped trigonal prism* (*Gorden* et al., 2005).

questions remain about the importance of denticity, binding group acidity, backbone flexibility, and solubility in the development of a highly effective, orally bioavailable chelator of low toxicity. Octadentate HOPO systems have been shown to be as much as 40% more effective in mice than an equimolar amount of $CaNa_3$–DTPA, the current clinical drug of choice, as well as to be orally active. Other systems have also been demonstrated to be effective for the chelation of Am(III) as well as U(VI), Th(IV), and Np(IV/V), for which DTPA is not effective (Gorden *et al*., 2003). Preliminary *in vitro* studies suggest that these complexes are also capable of redissolving Pu(IV) or Am(III) after it has deposited in bone mineral (Guilmette *et al*., 2003).

15.11 PRACTICAL APPLICATIONS OF THE ACTINIDE ELEMENTS

The principal application of the actinide elements is in the production of nuclear energy. Although this is by far the most important use for any of the actinide elements, a surprising number of other uses have been found. These include the

use of short-lived (tens of years) actinide isotopes as portable power supplies for satellites; in ionization smoke detectors; in the therapy of cancer; in neutron radiography; in mineral prospecting and oil-well logging; as neutron sources in nuclear reactor start-up; and as neutron sources in a variety of analytical procedures, the most important of which are neutron activation analysis and heavy-ion desorption mass spectroscopy.

15.11.1 Nuclear power

The practical importance of the actinide elements derives from the discovery of nuclear fission by Hahn and Strassmann in 1939. Atoms of one naturally occurring isotope (0.72% abundance) of uranium, ^{235}U, split into two approximately equal fragments by the capture of a neutron, an event that releases an enormous amount of energy. Approximately 2.5 neutrons are released per fission event, making it possible to initiate an explosive chain reaction in the pure fissile isotope; alternatively, controlled fission in a nuclear reactor can be used to provide heat to generate electricity. The plutonium isotope ^{239}Pu is produced in chain-reacting nuclear reactors by capture of excess neutrons in nonfissionable ^{238}U. Plutonium-239 itself is also fissionable with slow (essentially zero-energy) neutrons. The naturally occurring thorium isotope ^{232}Th, which does not undergo fission, can be converted by neutron capture to ^{233}U, which is a fissionable nuclide. The complete utilization of nonfissionable ^{238}U (through conversion to fissionable ^{239}Pu) and nonfissionable ^{232}Th (through conversion to fissionable ^{233}U) can be accomplished by breeder reactors. The fissile isotopes ^{233}U, ^{235}U, and ^{239}Pu constitute an enormous, effectively inexhaustible, energy resource. The future of nuclear power, however, is clouded by technological and social problems. The technical problems relate to the safety of nuclear reactors, to the ability to prevent access of radioactive substances to the environment, and to the prevention of the diversion of plutonium for the clandestine manufacture of nuclear weapons. We adhere to the school of thought that believes the technological problems of safe nuclear energy and environmental contamination are soluble problems. Indeed, many of these problems have already been solved, and those that remain do not require the discovery of new or unheard of scientific principles for their solution. The social, economic, and political problems are another matter. The fully justified fear of nuclear war is projected onto nuclear power, as if nuclear power and nuclear war were synonymous, and as if the fear of nuclear war could be exorcised by abolishing nuclear power. Prevention of nuclear war and the proliferation of nuclear weapons can only be accomplished by international statesmanship, not by a refusal to make use of the limitless energy that can be supplied by fission.

Some countries (France and Japan are notable examples) have embraced nuclear power, with the probable result that they will have a future economic advantage in world trade from the cheaper electric power that nuclear energy can provide. Nuclear power promises a more prosperous future, but whether the

promise becomes a reality in many additional countries will depend on the solution of the social, economic, and international problems that enmesh the issue of nuclear energy.

15.11.2 Portable power sources

Radioactive decay is accompanied by the evolution of heat, and radioactive nuclides can therefore be used as portable heat sources. One gram of ^{238}Pu produces about 0.56 W of thermal power, primarily from its 87.7 year alpha decay, and this isotope of plutonium has found use in space vehicles to drive thermoelectric power units. Several satellites with ^{238}Pu generators that produce 25 W have been deployed in space. Several of the Apollo spacecrafts carried a ^{238}Pu generator that produced 73 W of electrical power, fueled with 2.6 kg of ^{238}Pu in the form of PuO_2, to run the scientific experiments of some Apollo lunar expeditions. The satellite that sent the amazing photographs of Jupiter and the outer planets back to Earth used a 50 W ^{238}Pu power supply for this purpose. Space Nuclear Auxiliary Power (SNAP) thermoelectric power units containing 54 kg of plutonium-238 provide the nuclear-powered energy in the Cassini–Huygens 1966–2005 mission to Saturn and its moon Titan (see Chapter 7, section 7.2, of this book). This space probe is expected to accompany Saturn for 4 years. Much smaller ^{238}Pu generators were implanted as human cardiac pacemakers beginning in 1970; although chemical battery and electronics technologies have rendered nuclear pacemakers obsolete, several nuclear pacemakers have been in operation for over 30 years (see Chapter 7, section 7.2, of this book and section 15.11.4).

15.11.3 Neutron sources

The radionuclide americium-241 emits alpha particles, which produce neutrons by an (α,n) nuclear reaction with light elements. A mixture of americium-241 with beryllium produces 1.0×10^7 neutrons per second per gram of ^{241}Am. A large number of ^{241}Am–Be sources are in daily use worldwide in oil-well logging operations to measure the amount of oil produced in a given period of time. These sources have also been used to measure the water content of soils, and to monitor process streams in industrial plants. ^{241}Am itself has extensive uses in dissipating static electrical charges and in smoke detectors, where it functions to ionize air.

The radioactive decay of the nuclide californium-252 is largely by alpha emission, but part of the decay is by spontaneous fission. ^{252}Cf thus provides an intense neutron source: 1 g emits 2.4×10^{12} neutrons per second. ^{252}Cf is the only commercially available nuclide that can be fabricated into small neutron sources that produce an intense neutron flux over a useful period of time. The physical size of these sources is considerably smaller than alpha neutron sources, and less space must be provided in the ^{252}Cf sources to accommodate gaseous products. Since ^{252}Cf neutron sources became available in 1975, a

surprising variety of industrial and scientific uses have been developed for them (Martin *et al.*, 2000).

One of the largest uses of these sources is in reactor start-up operations. Before achieving criticality, a neutron source is inserted into the reactor to allow instrument calibration and observation of the approach to criticality. ^{252}Cf sources are used in reactor start-up all over the world because of the high neutron flux that can be obtained and their small size (<1 cm^3), which is very advantageous in the start-up procedure. ^{252}Cf neutron sources are used in the nuclear power industry as fuel-rod scanners, a procedure in which the amount and uniformity of the fissile material in the fuel rod is measured. This is the second largest industrial application of californium neutron sources.

Applications to neutron activation analysis constitute another important use of ^{252}Cf neutron sources. Neutron capture in many elements forms radioactive species that then decay with highly characteristic γ-ray emissions. This analytical procedure is very sensitive and specific, and is widely used for the analysis of trace elements. Neutron activation finds use in uranium borehole logging to make accurate determinations of the uranium concentrations in boreholes, and as little as 100 ppm of U_3O_8 can be detected by this procedure. Other industrial uses for ^{252}Cf sources are in the continuous monitoring of the sulfur and ash content of coal on a moving conveyor belt at the rate of 50 metric tons h^{-1}. Batch analysis of the vanadium content of crude oil is still another application of neutron activation analysis.

15.11.4 Medical and other applications

Americium-241 has found use in the diagnosis of thyroid disorders, because the 59.6 keV γ-rays allow determination of iodine in the thyroid by X-ray fluorescence (Reiners *et al.*, 1998). Americium-241 is used worldwide in ionization smoke detectors because it emits alpha particles, has a relatively long half-life, and decays to ^{237}Np, which has a much longer half-life. Household smoke detectors contain a small quantity (<35 kBq, approximately 200 μg) of ^{241}Am as AmO_2. Ionization smoke detectors in public or commercial buildings contain up to 2 MBq of ^{241}Am. The nearly monoenergetic alpha particles and 59.6 keV γ-rays of ^{241}Am have made it useful in thickness gauges and radiography (see Chapter 8, section 8.3, of this book).

Miniature power generators using ^{238}Pu have been developed for use in heart pacemakers. The pacemaker itself is a device planted in the chest and connected to the heart muscles; a programmed electrical pulse is periodically administered, which assures regularity in the heartbeat. A typical nuclear-powered heart pacemaker contains about 160 mg of ^{238}Pu encased in a tantalum–iridium–platinum alloy. Several thousand such devices were in use worldwide by 1980 and some remain in use in 2005, having been functioning for over 30 years (see Section 7.2). Heart pacemakers that operate from chemical batteries have a limited life, and must be replaced periodically by a surgical procedure, but they

have replaced nuclear pacemakers since about 1980 because of their efficiency and safety (Parsonnet, 2005).

Actinium-225 is used in alpha-particle generators for tumor radiotherapy (see Chapter 2, section 2.9.3, of this book). Californium-252 attracted early attention as a possible therapeutic agent in cancer treatment. The general impression formed from early work was that neutron therapy was inferior to X-ray therapy. More recent studies, however, indicate that neutron irradiation may have advantages over X-rays or γ-rays in certain situations. In the period 1976–82, several hundred cancer cases were treated by neutron irradiation supplied by ^{252}Cf (Murayama, 1991). Although not a cure, ^{252}Cf neutron therapy appears to have promise in the treatment of pelvic cancer and in brachytherapy (short exposure therapy). Sources containing ≤ 30 μg of ^{252}Cf as a Cf_2O_3 wire in a Pd matrix have been prepared by the Radiochemical Engineering Development Center of Oak Ridge National Laboratory (Martin *et al.*, 1997). Neutron sources have also been prepared by the Research Institute of Atomic Reactors (RIAR), Dimitrovgrad, Russia (Karelin *et al.*, 1997). Neutrons appear to have particular utility in tumors whose oxygen supply is impaired, and which, as a consequence, are relatively insensitive to X-rays or γ-rays. While the applications of neutrons in the treatment of cancer are still experimental, there is a possibility that further clinical studies may well find a use for the neutron-emitting californium isotopes in therapy.

ABBREVIATIONS

AES	atomic emission spectroscopy
Bq	SI derived unit of radioactivity, 1 disintegration per second
CAM	catecholamide
Ci	Curie $= 3.7 \times 10^{10}$ disintegrations per second $= 3.7 \times 10^{10}$ Bq.
Cp	cyclopentadienyl, C_5H_5
CEA	Commission de l'Energie Atomique
COT	cyclooctatetrene, C_8H_8
DFO	desferrioxamine
DIAMEX	DIAMide EXtraction process used to separate the lanthanides and the "minor actinides" Np, Am, Cm from fission products
DTPA	diethylenetriaminepentaacetic acid
EDTA	ethylenediaminetetraacetic acid
HEU	highly enriched uranium (20–90% ^{235}U)
HFIR	High Flux Isotope Reactor
HOPO	hydroxypyridonate
ICP-MS	inductively-coupled plasma mass spectroscopy
IUPAC	International Union of Pure and Applied Chemistry
LEU	low enriched uranium (0.7–20% ^{235}U)

LLNL	Lawrence Livermore National Laboratory
MOX	Mixed oxide fuel (usually UO_2-PuO_2 solid solution)
MWd	Megawatt-days
NMR	nuclear magnetic resonance
NTA	nitrilotriacetic acid
PBq	petabequerel (1×10^{15} Bq)
PUREX	Plutonium uranium reduction extraction
PWR	pressurized water reactor
RIAR	Research Institute of Atomic Reactors
REDC	Radioisotope Engineering Development Center
SNAP	Space Nuclear Auxiliary Power
Sv	Sievert (derived SI unit of equivalent dose used for radiation protection purposes); 1 Sv = 1 J kg^{-1} = 100 rem
TAM	terephthalamide
TBP	tri(*n*-butyl)phosphate
TBq	terabecquerel (1×10^{12} Bq)
THF	tetrahydrofuran

ACKNOWLEDGMENT

Part of the work reported herein was performed under the auspices of the Office of Basic Energy Sciences, U.S. Department of Energy under Contract W-31–109-ENG-38.

REFERENCES

Albers, R. C. (2001) *Nature*, **410**, 759–61.

Albright, D., Berkhout, F., and Walker, W. (1996) *Plutonium and Highly Enriched Uranium, 1996: World Inventories, Capabilities and Policies*, Oxford University Press, Oxford.

Alexander, C. (2005) Oak Ridge National Laboratory, personal communication to L. Morss.

Allard, B., Olofsson, V., and Torstenfelt, B. (1984) *Inorg. Chim. Acta*, **94**, 205–21.

Anderson, J. S. (1970) in *Modern Aspects of Solid State Chemistry* (ed. C. N. R. Rao), Plenum Press, New York, pp. 29–105.

Baes, C. F. and Mesmer, R. E. (1976) *The Hydrolysis of Cations*, John Wiley, New York.

Banaszak, J. E., Rittmann, B. E., and Reed, D. T. (1999) *J. Radioanal. Nucl. Chem.*, **241**, 385–435.

Barton, P. G. (1968) *J. Biol. Chem.*, **243**, 3884–90.

Baumgartner, F., Fischer, E. O., and Laubereau, P. (1965) *Naturwissenschaften*, **52**, 560.

Benedict, U. (1984) *J. Less Common Metals*, **100**, 153–70.

Benes, P. and Majer, V. (1980) *Tracer Chemistry of Aqueous Solutions*, Elsevier, Amsterdam.
Bidoglio, G., De Plano, A., Avogadro, A., and Murray, C. N. (1984) *Inorg. Chim. Acta*, **95**, 1–3.
Blake, P. C., Edelstein, N. M., Hitchcock, P. B., Kot, W. K., Lappert, M. F., Shalimoff, G. V., and Tian, S. (2001) *J. Organomet. Chem.* **636**, 124–9.
Boocock, G. and Popplewell, D. S. (1965) *Nature*, **208**, 282–3.
Boocock, G., Danpure, C. J., Popplewell, D. S., and Taylor, D. M. (1976) *Radiat. Res.*, **42**, 381–96.
Brandi, G., Brunelli, M., Lugli, G., and Mazzei, A. (1973) *Inorg. Chim. Acta*, **7**, 319–22.
Brown, D (1968) *Halides of the Lanthanides and Actinides*, Wiley-Interscience, London.
Bruenger, F. W., Taylor, D. M., Taylor, G. N., and Lloyd, R. D. (1991) *Int. J. Radiat. Biol.*, **60**, 803–18.
Buck, E. C., Finn, P. A., and Bates, J. K. (2004) *Micron*, **35**, 235–43.
Bulman, R. A. (1978) *Struct. Bond.*, **34**, 39–77.
Bulman, R. A. (1980) *Coord. Chem. Rev.*, **31**, 221–50.
Bulman, R. A. and Griffin, R. G. (1980) *Metab. Bone Dis. Relat. Res.*, **2**, 281–3.
Burgess, J. (1978) *Metal Ions in Solution*, John Wiley, New York.
Casas, I., de Pablo, J., Perez, I, Gimenez, J., Duro, L., and Bruno, J. (2004) *Environ. Sci. Technol.*, **38**, 3310–15.
Catalano, J. G., Heald, S. M., Zachara, J. M., and Brown, G. E., Jr (2004) *Environ. Sci. Technol.*, **38**, 2822–8.
C&E News (1945) Chem. Eng. News, 23, 21903. (Speech given by G. T. Seaborg at Chicago Section of American Chemical Society, Nov. 16, 1945.)
CEA (2002) *Radioactive Waste Management Research*, Clefs CEA No. 46, http://www.cea.fr/gb/publications/Clefs46/pagesg/clefs46_43.html
Choppin, G. R., Liljenzin, J.-O., and Rydberg, J. (2002) *Radiochemistry and Nuclear Chemistry*, 3rd edn, Butterworth-Heinemann, Woburn, MA.
Choppin, G. R. (2003) *Radiochim. Acta*, **91**, 645–9.
Clarke, R. H., Dunster, J., Nenot, J.-C., Smith, H., and Voelz, G. (1996) *J. Radiol. Prot.*, **16**, 91–105.
Conradson, S. D., Begg, B. D., Clark, D. L., *et al.* (2004) *J. Am. Chem. Soc.*, **126**, 13443–58.
David, F. (1984) in *Handbook on the Physics and Chemistry of the Actinides*, vol. 4 (eds. A. J. Freeman and C. Keller), North-Holland, Amsterdam, pp. 97–128.
Degueldre, C. and Yamashita, T. (2003) *J. Nucl. Mater.*, **319**, 1–5.
Diamond, G. L. (1989) *Rad. Prot. Dosim.*, **26**, 33–6.
Durbin, P. W. (1973) *Handb. Exp. Pharmacol.*, **36**, 739–896.
Durbin, P. W. (1975) *Health Phys.*, **29**, 495–510.
Durbin, P. W., Kullgren, B., Xu, J., and Raymond, K. N. (1998) *Radiat. Prot. Dosim.*, **79**, 433–43.
Eick, H. A. (1994) in *Handbook on the Physics and Chemistry of the Rare Earths*, vol. 18 (eds. K. A. Gschneidner, L. Eyring, G. R. Choppin, and G. L. Lander), Elsevier, New York, pp. 365–411.
Fournier, J.-M. (1976) *J. Phys. Chem. Solids*, **37**, 235–44.
Francis, C. W. (1973) *J. Environ. Qual.*, **2**, 67–70.
Gebala, A. E. and Tsutsui, M. (1973) *J. Am. Chem. Soc.*, **95**, 91–3.

Ghiorso, A. (1982) in *Actinides in Perspective* (ed. N. M. Edelstein), Pergamon Press, Oxford, pp. 23–56.

Gilbert, E. S., Koshurnikova, N. A., Sokolnikov, M., Khokhryakov, V. F., Miller, S., Preston, D. L. S., Romanov, A., Shilnikova, N. S., Suslova, K. G., and Vostrotin, V. V. (2000) *Radiat. Res.*, **154**, 246–52.

Gmelin Handbuch der Anorganischen Chemie, Suppl. Ser., *Transurane*, Verlag Chemie, Weinheim, Springer-Verlag, Berlin, Heidelberg & New York, parts Dl and D2, *Chemistry in Solution* (1974, 1975).

Gmelin Handbuch der Anorganischen Chemie, Suppl. Ser., *Transurane*, Springer Verlag, Berlin, part C, *The Compounds* (1972).

Gmelin, Handbuch der Anorganischen Chemie, Suppl. Ser., *Transurane*, Verlag Chemie, Weinheim, part A2, *The Elements* (1973).

Gorden, A. E. V., Xu, J., Raymond, K. N., and Durbin, P. W. (2003) *Chem. Rev.*, **103**, 4207–82.

Gorden, A. E. V., Shuh, D. K., Tiedemann, B. E. F., Wilson, R. E., Xu, J., and Raymond, K. N. (2005) *Chem. Eur. J.*, **11**, 2842–8.

Gordon, S., Mulac, W., Schmidt, K. H., Sjoblom, R. K. and Sullivan, J. C. (1978) *Inorg. Chem.*, **17**, 294–6.

Grogan, H. A., Sinclair, W. K., and Volleque, P. G. (2001) *Health Phys.*, **80**, 447–61.

Gruen, D. M. (1992) in *Transuranium Elements – A Half Century* (eds. L. R. Morss and J. Fuger), American Chemical Society, Washington, DC, pp. 63–77.

Guilmette, R. A. (2001) *Scientific Basis for Evaluating the Risks to Populations from Space Applications of Plutonium: Recommendations of the National Council on Radiation Protection and Measurements*, National Council on Radiation Protection and Measurements (NCRP) Report. No. 131, Bethesda, MD.

Guilmette, R. A., Hakimi, R., Durbin, P. W., Xu, J., and Raymond, K. N. (2003) *Rad. Prot. Dosim.*, **105**, 527–34.

Haire, R. G., Heathman, S., Idiri, M., Le Behan, T., Lindbaum, A., and Rebizant, J. (2003) *Phys. Rev. B*, **67**, 134101.

Haire, R. G., Heathman, S., Le Bihan, T., Lindbaum, A., and Iridi, M. (2004) *Mat. Res. Soc. Symp. Proc*. Vol. 802, paper DD.1.5.1.

Hanson, W. C. (ed.) (1980) *Transuranic Elements in the Environment*, DOE/TIC-22800.

Haschke, J. M., Allen, T. H., and Morales, L. A. (2000) *Science*, **287**, 285–7.

Hay, P. J., Martin, R. L., and Schreckenbach, G. (2000) *J. Phys. Chem. A* **104**, 6259–70.

Heathman, S. and Haire, R. G. (1998) *J. Alloys Compd.*, **271**, 342–6.

Hedrick, J. B. (1999) *Thorium – 1999*, http://minerals.usgs.gov/minerals/pubs/commodity/thorium/690499.pdf

Hisamatsu, S. and Takizawa, Y. (2003) *Health Phys.*, **85**, 701–8.

Hobart, D. E. (1990) in *Actinides in the Environment*, Proc. Robert A Welch Foundation Conference, pp. 379–436.

Hoffman, D. C., Lawrence, F. D., Mcwherter, J. L., and Rourke, F. M. (1971) *Nature*, **234**, 132–4.

Hyde, E. K., Perlman, I., and Seaborg, G. T. (1964) *Nuclear Properties of the Heavy Elements*, vol. II, *Detailed Radioactivity Properties*, Prentice-Hall, Englewood Cliffs, NJ.

ICRP (1986) *ICRP Publication 48*, *Radiation Protection – The Metabolism of Plutonium and Related Elements*, *Annals of the ICRP*, **16**(2–3).

ICRP (1990) *ICRP Publication 60. Recommendations of the International Commission on Radiological Protection. Annals of the ICRP 21.*

James, A. C. and Taylor, D. M. (1971) *Health Phys.*, **21**, 31–9.

Karelin, Y. A., Gordeev, Y. N., Karasev, V. I., Radchenko, V. M., Schimbarev, Y. V., and Kuznetsov., R. A. (1997) *Appl. Radiat. Isot.,* **48**, 1563–6.

Keally, T. J. and Pauson, P. L. (1951) *Nature*, **168**, 1039–40.

Keller, O. L. Jr, Hoffman, D. C., Penneman, R. A., and Choppin, G. R. (1984) *Phys. Today*, March, 35–41.

Kim, J. I. (1986) in *Handbook on the Physics and Chemistry of the Actinides*, vol. 4 (eds. A. J. Freeman and C. Keller), pp. 413–55.

Koshurnikova, N. A., Bolotnikova, M. G., Ilyin, L. A., Keirim-Markus, I. B., Menshikh, Z. S., Okatenko, P. V., Romanov, S. A., Tsvetkov, V. I., and Shiknikova, N. S. (1998) *Radiat. Res.*, **149**, 366.

Lam, D. J., Darby, J. B. Jr, and Nevitt, M. V. (1974) in *The Actinides: Electronic Structure and Related Properties* (eds. A. J. Freeman and J. B. Darby Jr), vols I and II, Academic Press, New York, pp. 119–84.

LANL (2000) Los Alamos Science, **26**, Los Alamos National Laboratory, New Mexico.

Lataillade, G., Verry, M., Rateau, G., Métivier, H., and Masse, R. (1995) *Int. J. Radiat. Biol.*, **67**, 373–80.

Lindbaum, A., Heathman, S., Le Bihan, T., Haire, R. G., Idiri, M., and Lander, G. H. (2003) *J. Phys.:Conden. Matter*, **15**, S297–303.

Mahlum, D. D. (1967) *Toxicol. Appl. Pharmacol.*, **11**, 264–71.

Marks, T. J., Seyam, A. M., and Kolb, J. R. (1973) *J. Am. Chem. Soc.*, **95**, 5529–39.

Marks, T. J. and Fischer, R. D. (eds) (1979) *Organometallics of the f-Elements*, Reidel, Dordrecht.

Martin, R. C., Laxson, R. R., Miller, J. H., Wierzbicki, J. G., Rivard, M. J., and Marsh, D. L. (1997) *Appl. Radiat. Isot.*, **48**, 1567–70.

Martin, R. C., Knauer, J. B., and Balo, P. A. (2000) *Appl. Radiat. Isot.*, **53**, 785–92.

Maurette, M. (1976) *Annu. Rev. Nucl. Sci.*, **26**, 319–50.

McCubbin, D., Leonard, K. S., and Emerson, H. S. (2002) *Mar. Chem.*, **80**, 61–77.

Mikheev, N. B. (1984) *Inorg. Chim. Acta*, **94**, 241–8.

Morse, J. W. and Choppin, G. R. (1986) *Mar. Chem.*, **20**, 73–89.

Morss, L. R. and Edelstein, N. (1984) *J. Less Common Metals*, **100**, 15–28.

Müller, W. and Blank, H. (eds) (1975) *Heavy Element Properties, Proc. Joint Session Transplutonium Element Symp. and 5th Int. Conf. on Plutonium and Other Actinides*, Baden-Baden, North-Holland, Amsterdam and Oxford, Sept. 13, 1975; Elsevier, New York.

Müller, W. and Lindner, R. (eds) (1975) *Transplutonium 1975*, *Proc. 4th Int. Transplutonium Symp*., Baden-Baden, Sept. 13–17, 1975, North-Holland, Amsterdam.

Müller, W. (1983) *Chem. Z.*, **106**, 105–12.

Müller, W. and Spirlet, J. C. (1985) *Struct. Bond.*, **59/60**, 57–73.

Murayama, Y. (1991) *Cancer*, **68**, 1189–97.

NABIR (2003) *Bioremediation of Metals and Radionuclides*, 2nd edn, LBNL-42595, Lawrence Berkeley National Laboratory, http://www.lbl.gov/NABIR/generalinfo/03_NABIR_primer.pdf

Nakano, M. and Povinec, P. P. (2003) *J. Environ. Radioact.*, **69**, 85–106.

National Academy of Sciences (1995) *Management and Disposition of Excess Weapons Plutonium*, 2 vols, National Academy Press, Washington, DC.
National Research Council (1983) *Opportunities and Challenges in Research with Transplutonium Elements*, National Research Council, Washington, DC.
NCRP (2001) *Scientific Basis for Evaluating the Risks to Populations from Space Applications of Plutonium*, National Council on Radiation Protection Report 131.
NEA (2002) ORIGEN-ARP 2.00, Isotope Generation and Depletion Code System.
Neck, V. and Kim, J. I. (2001) *Radiochim. Acta*, **89**, 1–16.
Nenot, J. C. and Metivier, H. (1984) *Inorg. Chim. Acta*, **94**, 165–70.
Neuefeind, J., Soderholm, L., and Skanthakumar, S. (2004) *J. Phys. Chem. A*, **108**, 2733–9.
Newton, T. W. (1975) *The Kinetics of Oxidation–Reduction Reactions of Uranium, Neptunium, Plutonium and Americium in Aqueous Solution*, TID-26506.
Olivier, S., Bajo, S., Fifield, L. K., Gaggeler, H. W., Papina, T., Santschi, P. H., Schotterer, U., Schwikowski, M., and Wacker, L. (2004) *Environ. Sci. Technol.*, **38**, 6507–12.
Orlandini, K. A., Penrose, W. R., and Nelson, D. M. (1986) *Mar. Chem.*, **18**, 49–57.
Parsonnet, V. (2005) personal communication to L. R. Morss.
Raymond, K. N. and Smith, W. L. (1981) *Struct. Bond.,* (Berlin), **43**, 159–86.
Raymond, K. N., Koppel, M. J., Pecoraro, V. L., Harris, W. R., Carrano, C. J., Weill, F. L., and Durbin, P. W. (1982) in *Actinides in Perspective* (ed. N. M. Edelstein), Pergamon Press, Oxford, pp. 491–507.
Raymond, K. N., Freeman, G. E., and Kappel, M. J. (1984) *Inorg. Chim. Acta*, **94**, 193–204.
Reiners, C., Hanscheid, H., Lassmann, M., Tiemann, M., Kreissl, M., Rendl, J., and Bier, D. (1998) *Exp. Clin. Endocrinol. Diabetes*, **106**, S31–3.
Reynolds, L. T. and Wilkinson, G. (1956) *J. Inorg. Nucl. Chem.*, **2**, 246–53.
Rosenthal, M. W. and Lindenbaum, A. (1967) *Radiat. Res.*, **31**, 506–21.
Ruggiero, C. E., Matonic, J. H., Reilly, S. D., and Neu, M. P. (2002) *Inorg. Chem.*, **41**, 3593–5.
Runde, W. (2000) in *Los Alamos Science*, **26**, pp. 392–411.
Santini, P., Lémanski, R., and Erdös, P. (1999) *Adv. Phys.*, **48**, 537–653.
Sarrao, J. L., Morales, L. A., Thompson, J. D., Scott, B. L., Stewart, G. R., Wastin, F., Rebizant, J., Boulet, P., Colineau, E., and Lander, G. H. (2002) *Nature*, **420**, 297–9.
Schubert, J. (1955) *Annu. Rev. Nucl. Sci.*, **5**, 369–412.
Scoppa, P. (1984) *Inorg. Chim. Acta*, **95**, 23–7.
Seaborg, G. T., Katz, J. J., and Manning, W. M. (eds) (1949) *The Transuranium Elements: Research Papers*, Natl. Nucl. En. Ser., Div. IV, 14B, McGraw-Hill, New York.
Seaborg, G. T. (1963) *Man-Made Transuranium Elements*, Prentice-Hall, Englewood Cliffs, NJ.
Seaborg, G. T. (ed.) (1978) *Transuranium Elements. Benchmark Papers in Physical Chemistry and Chemical Physics*, vol. 1, Dowden, Hutchinson & Ross, Stroudsburg, PA.
Seyferth, D. (2004) *Organometallics*, **23**, 3562–83.
Shannon, R. D. (1976) *Acta Crystallogr. A*, **32**, 751–67.
Silva, R. J. and Nitsche, H. (1995) *Radiochim. Acta*, **70/71**, 377–96.
Smith, V. H. (1972) *Health Phys.*, **22**, 765–78.

Smith, J. L. and Kmetko, E. A. (1983) *J. Less Common Metals*, **90**, 83–8.
Songkasiri, W., Reed, D. T., and Rittmann, B. E. (2002) *Radiochim. Acta*, **90**, 785–9.
Spirlet, J. C. (1982) in *Actinides in Perspective* (ed. N. M. Edelstein), Pergamon Press, Oxford, pp. 361–80.
Streitwieser, A. Jr and Muller-Westerhof, U. (1968) *J. Am. Chem. Soc.*, **90**, 7364.
Sullivan, J. C., Gordon, S., Mulac, W. A., Schmidt, K. H., Cohen, D., and Sjoblom, R. (1976a) *Inorg. Nucl. Chem. Lett.*, **12**, 599–601.
Sullivan, J. C., Gordon, S., Cohen, D., Mulac, W, and Schmidt, K. H. (1976b) *J. Phys. Chem.*, **80**, 1684–6.
Sullivan, J. C., Morss, L. R., Schmidt, K. H., Mulac, W. A., and Gordon, S. (1982) *Inorg. Chem.*, **22**, 2338–9.
Taylor, D. M. (1972) *Health Phys.*, **22**, 575–81.
Taylor, G. N. (1978) *Health Phys.*, **35**, 201–10.
Teale, P. and Brown, J. (2003) *Modelling Approach for the Transfer of Actinides to Fruit Species of Importance in the UK*, NRPB-W46, National Radiological Protection Board, Chilton, Didcot, Oxon OX11 0RQ, UK, http://www.nrpb.org/publications/w_series_reports/2003/nrpb_w46.pdf.
Thomas, R. A. P. and McCaskie, L. E. (1996) *Environ. Sci. Technol.*, **30**, 2371–5.
Thompson, R. C. (1982) *Radiat. Res.*, **90**, 1–32.
Tokarskaya, Z. B., Okladnikova, N. D., Belyaeva, Z. D., and Drozhko, E. G. (1997) *Health Phys.*, **73**, 899–905.
Topp, S. V. (ed.) (1982) *Scientific Basis for Nuclear Waste Management*, vol. 6, Materials Research Society Symp. Proc., Elsevier, Amsterdam.
UNSCEAR (2000) *United nations scientific committee on the effects of atomic radiation exposures to the public from man-made sources of radiation, in Sources and Effects of Ionizing Radiation*, United Nations, New York.
U.S. Geological, Survey (2002) *Mineral Resources Program* http://minerals.usgs.gov/index.html
Van Tuyle, G. J., Bennett, D. R., Herczeg, J. W., Arthur, E. D., Hill, D. J., and Finch, P. J. (2002) *Prog. Nucl. Energy*, **40**, 357–64.
Vaughn, J., Bleany, B., and Taylor, D. M. (1973) *Handb. Exp. Pharmacol.*, **36**, 349–502.
Voelz, G. L., Lawrence, J. N.P., and Johnson, E. R. (1997) *Health Phys.*, **73**, 611–19.
Voelz, G. L. (2000) in *Los Alamos Science*, **26**, pp. 75–89.
Vyas, B. N. and Mistry, K. B. (1983) *Plant Soil*, **73**, 345–53.
Walters, R. L., Hakonson, T. E., and Lane, L. J. (1983) *Radiochim. Acta*, **32**, 89–103.
Whitehouse, C. A. and Tawn, E. J. (2001) *Radiat. Res.*, **156**, 467–75.
Williams, C. W., Blaudeau, J.-P., Sullivan, J. C., Antonio, M. R., Bursten, B. E., and Soderholm, L. (2001) *J. Am. Chem. Soc.*, **123**, 4346–7.
World Energy Council (1988) *Survey of Energy Resources*.
Zachariasen, W. H. (1973) *J. Inorg. Nucl. Chem.*, **35**, 3487–97.
Zhang, Z. and Pitzer, R. M. (1999) *J. Phys. Chem. A*, **103**, 6880–6.

CHAPTER SIXTEEN

SPECTRA AND ELECTRONIC STRUCTURES OF FREE ACTINIDE ATOMS AND IONS

Earl F. Worden, Jean Blaise, Mark Fred*,
Norbert Trautmann, and Jean-François Wyart

Dedicated to Mark Fred (1912–1994), John G. Conway (1922–1995), and Frank Tomkins (1915–1999).

* Deceased.

16.1 INTRODUCTION

This chapter reviews the spectra and the deduced electronic properties of isolated actinide atoms and ions observed in the vapor phase at low density. The free atoms or ions have all or most of the valence electrons present, and the observed spectra can be assigned to transitions due essentially to changes in the quantum numbers of the valence electrons. This is in contrast to the spectra of actinides in crystals or in solution (dealt with in depth in Chapter 18), where the observed spectra are largely due to transitions within the 5f shell. In crystals, the actinide ions are exposed to the electric field of the surrounding ions, which produces a Stark effect on the levels. The magnitude of the effect is relatively small because the 5f electrons are shielded from the crystal field by the 6s and 6p electrons. The result is a small perturbation in which each 5f level is split into a number of close components. In free atoms, the valence electrons interact strongly with the 5f electrons and also with each other. Hence each 5f level gives rise to many daughter levels that are more widely split than the parent separations and have large angular momentum contributions from the parent. The result in this case is a great number of levels whose structure is not simply related to the structure of the 5f levels or to the structure of the valence-electron levels by themselves. It is evident that the 5f level structure can be obtained more directly from crystal spectra but the properties of the valence electrons (in particular, implications for the chemical properties) must be deduced from the free-atom spectra.

Historically, the correlation between actinide chemistry and spectroscopy was anticipated before much experimental information was available in either field. Therefore interest in actinide spectroscopy was as an aid to predicting actinide chemistry, in the expectation that smaller quantities of these elements would be required. In practice, the chemistry developed first as soon as sufficient amounts of material were produced, while the spectroscopy encountered difficulties because the complexities were underestimated. The difficulty was not so much as the enormous total number of levels, which could be counted readily, but the extent to which the levels interacted so as to preclude simplification.

The interaction implies that each level is a mixture of various pure states labeled by quantum numbers for the 5f shell and also by quantum numbers for each valence-electron shell. Different levels have different mixtures, and the composition of each level cannot be deduced by inspection because of the large number of quantum numbers, with a different energy dependence for each. Thus the compositions must be derived by comparison with theoretical calculations. The calculations are difficult to perform even with a large computer, and because of the mixing, the results do not give a simple picture of the way in which the energy of an actinide atom depends on the valence-electron configuration. This complexity is inherent in atoms with 5f electrons, and the chemistry is correspondingly more difficult to predict. Nevertheless, it is clearly desirable to attempt it.

We begin with a discussion of some experimental techniques, then present an introduction to the theory, and finally relate the electronic structure obtained from the spectroscopic data to the chemistry of the actinide elements. Laser spectroscopic techniques are discussed, which have improved the quality of isotope shift (IS) and hyperfine structure (hfs) data. These methods have increased the accuracy of the ionization potentials (IPs) of the actinide elements where sufficient (and in some cases only very small) quantities of atoms can be produced. A few new energy levels have been found for Fm and Es by the resonance ionization mass spectroscopy (RIMS) technique, but no new information has been obtained to date on the electronic structure of the heavier actinides (beyond Fm). A discussion of the spectroscopy of deformed isomers of Am is included.

16.2 EXPERIMENTAL SPECTROSCOPY OF FREE ACTINIDE ATOMS AND IONS

The main interest in actinide spectra, besides finding lines useful for chemical analyses of the elements, is in energy level analysis. This methodology determines the relative energies of various electron configurations for each actinide and the way the interactions between different kinds of electrons vary along the actinide series. The first step in this process is to obtain the complete (as possible) spectra for each element. For conventional actinide spectroscopy, the limit is Es, the element with atomic number 99. Thus four elements, Fm to Lw, have little experimental spectroscopic results. Limited beam and laser spectroscopy, plus extrapolation and theory, are all that is available for determining the optical spectra and electronic structure of these four elements.

In each actinide spectrum, tens of thousands of spectral lines are observed and many more are possible but weak. No order is apparent. The determination of the energy levels from the lines is based chiefly on the search for recurrent differences (or sums) between the energies (wavenumbers) of various pairs of lines, indicating pairs of transitions to a given pair of levels from levels of opposite parity. The level structure can be derived in principle by establishing a number of such level pairs. For actinide spectra, a purely numerical approach is not possible for the following reasons:

(1) The large line density usually yields many more fortuitous recurrences than real ones, but improvement in the accuracy of the line list can significantly reduce the number.
(2) The real recurrences due to transitions involving a given pair of levels are limited by selection rules.
(3) The strong lines can often be paired with weak lines that may be too weak to be observed and thus be missed.

Hence one needs to observe the energies of as many lines as possible, measured with the highest accuracy and resolution, as contrasted with spectrochemical analysis, where only a relatively small number of strong lines are required. Corroborative information, such as Zeeman data, ISs, hfs, vapor absorption or self-absorption in an electrodeless discharge lamp (EDL), spectral assignment, is essential.

Experimental techniques have been adequate for the production of neutral (atomic, An I where An represents any actinide element) and first-ion spectra (singly ionized, An II), in spite of the limitations of available sample size and the associated radioactivity for all the actinides up to and including Es. The usual light source is an EDL made from quartz tubing with about 2–3 mm i.d., 5–6 mm o.d., and about 22–25 mm long, into which the sample ($\sim$0.1 mg as anhydrous An iodides) is sublimed. The lamp is then sealed off under vacuum, as described in Tomkins and Fred (1957) and in Worden *et al.* (1963). A microwave discharge supplies the heat to volatilize the sample, and the electron energy to dissociate the molecules and excite the atomic spectrum. This source is sensitive, confines the radioactivity, gives sharp lines, and can be run in a magnetic field. It can also be used to differentiate lines of the neutral spectrum from those of the first ion by observation of the spectrum at high and low microwave powers (or high and low atom density). At very high power or high atom density, self-reversal of lines from the low-lying levels of the neutral atoms, and in some cases the first ion of the element, were observed. The lamps allow complete recovery of the element after use. This is a very important consideration for rare isotopes where the cost of production is high and only limited quantities are available. Unfortunately a comparable source for the higher ions (much higher electron temperature required) is not yet available. A few lines of the third spectrum of some actinides have been observed in special hollow cathode lamps but not from EDLs.

The design and construction of EDLs of Es, when amounts of $\sim$100 mg or more became available, had to be changed because of the poor yields ($<$15%) obtained with no carrier element present (Worden *et al.*, 1968, 1970 and especially Worden *et al.*, 1974). These changes are described in detail in Appendix 16.1.

Initial analyses of all actinide spectra are based on measurements of photographic plates taken on the Argonne National Laboratory (ANL) 9.15 m Paschen-Runge and 3.4 m Ebert spectrographs with high-angle gratings (now decommissioned). These instruments covered a large wavelength range at high resolving power with a single exposure (providing wavenumber (energy) accuracy of 0.02 cm^{-1} or higher (Tomkins and Fred, 1963; Worden and Conway, 1970; Worden *et al.*, 1970, 1974, 1987). Because photographic plates were used, several exposures were required. The plates were measured using semiautomatic comparators with 1 μm accuracy (Tomkins and Fred, 1951). The thorium spectrum was used in order to provide standards to establish the unknown

wavelengths. In the case of the highly radioactive elements, it was essential to remove the lines of the decay products as well as other impurity lines from the line list before beginning the analyses of the spectra. The near-infrared and infrared spectra of the actinide elements were observed with Fourier transform spectrometers (FTSs) (see for example Conway *et al*., 1976). The assembly of an accurate line list and other supporting data suitable for level analysis required 3–6 years. The hfs and IS can be obtained with FTSs, but calibration of the IS data is needed when using separated isotopes in EDLs where there are no internal standard lines for production of a calibrated energy scale (Pulliam *et al*., 2003).

An FTS with comparable resolving power but better energy accuracy (0.005 cm^{-1} or higher) than the ANL spectrograph has been operational at the Laboratoire Aimé Cotton (LAC), Orsay, France, since 1970. Built initially for the infrared region, it covers the region 4000–400 nm (Connes *et al.*, 1970). A second FTS covered the visible and ultraviolet regions down to 345 nm. By 1976, another high-resolution FTS had been built at the National Solar Observatory, Kitt Peak, Arizona (Brault, 1976). All the actinide spectra from Th to Cf have now been recorded with one or more of these instruments. Observation of the infrared spectrum with high resolution and accuracy is especially important for the term analyses of the lanthanide and actinide spectra because of the large number of low-lying energy levels that give transitions in this spectral region. The spectra of a number of actinides have been recorded over the full range ($\sim$1800 to 50 000 cm^{-1}, or because of quartz lamp limitations, 3500–45 000 cm^{-1}) on the 1 m FTS at Kitt Peak.

The advent of atomic vapor laser isotope separation (AVLIS) in the early 1970s stimulated considerable interest in the laser spectroscopy of actinides, primarily on U and other light actinide elements that continues to the present. These efforts involve many countries besides the USA, including Canada, France, England, Germany, Italy, Japan, India, and China. More conventional actinide spectroscopy, in addition to laser spectroscopy, has continued in France and Germany. Blaise and Wyart at LAC are compiling actinide energy levels and extending current analyses and theory for some heavier actinides. German work is based on the low-level detection of actinides, and has resulted in the very accurate determination of actinide IPs, the study of isomer shifts, and recently the finding of a limited number of levels in Es (Peterson *et al*., 1998) and Fm (Sewtz *et al*., 2003) by laser techniques. Complete line lists with level assignments of some of the actinides are now available from the National Institute of Standards and Technology (NIST). Atlases that include scans, line frequencies, and level assignments for FTS observations are available from Los Alamos National Laboratory (LANL) on Th (Palmer and Engleman, 1983) and U (Palmer *et al*., 1980).

The present status of the term analyses of actinide spectra varies from essentially complete for the elements with even atomic number (Th, U, Pu, Cm, and Cf) to partial analyses for some of the odd isotopes. In the first category, nearly

all the strong and moderate-intensity lines have been classified and only weak lines remain to be assigned. However, these are a considerable fraction of the total number. Conventional publication of so much data is impracticable; thus this information is in some cases available only in the laboratory doing the work. Nevertheless, wavelengths of the strongest emission lines of all the actinides from Ac through Cf have been tabulated according to the stage of ionization (Reader and Corliss, 1980). Blaise and Wyart (1992) have published all known energy levels of the actinides analyzed up to that time and list ionization stage, energies, intensities, *J*-values, and level assignments of selected lines of all actinides through Es. The contents of this volume are being transferred and updated on a database at LACs website www.lac.u-psud.fr. Table 16.1 summarizes the lowest determined level for each known configuration of the actinide elements. In some cases, the references in Table 16.1 include extensive line lists of the classified lines and known energy levels.

After a major campaign in 1975–76 to observe the ^{253}Es and ^{250}Cf atomic spectra, the number of workers doing energy-level analyses has steadily decreased worldwide. At the present time only a very few laboratories are pursuing studies of this type.

16.3 EMPIRICAL ANALYSIS OF ACTINIDE SPECTRA

A neutral actinide has typically less than a 1000 known experimental levels, the first ion somewhat fewer, primarily due to the low excitation energy of the EDL source. The levels are organized by half-dozen into terms, some dozens of terms form a configuration, and there are often ten or more configurations identified for a given stage of ionization. The order in this hierarchy, however, is not evident. There is considerable overlapping of different terms and of different configurations. The terms are not pure in any coupling scheme but must be described as mixtures to account for their properties, and there is more often than not mixing of configurations. The only way most levels can be identified with a given configuration is by the use of the observed IS, the intensities of its transitions to levels of known configurations, and by comparison with theoretical calculations with appropriate parameters.

There are several fortunate circumstances that make it possible to identify the lowest level of each configuration and thereby the relative energies of the configurations (for interpretation of the structure). In *SL* coupling the lowest level of a configuration is usually found to be fairly pure and follows Hund's rules, i.e. this term has maximum multiplicity and maximum orbital angular momentum. Fig. 16.1 shows, as an example of Hund's rules, the lowest term of a number of configurations in neutral plutonium. Although Hund's rules apply only in configurations of equivalent electrons, they are followed, with few exceptions, in configurations with several open subshells.

Table 16.1 *Lowest levels found for identified configurations, with parity, terms, IS values, and hfs widths* (*Widths are negative for inverted hfs splitting*). *Under configuration all have the radon core as part of the configuration. Under references, the first initial of all authors plus the date gives the reference. A question mark means the data are missing or in question.*

Spectrum measured isotopes	*Configuration*	*Parity/term*		*Level* (cm^{-1})	g_{obs}	*IS* (10^{-3} cm^{-1})	*hfs* (10^{-3} cm^{-1})	*References*[a]
Ac III	7s	E	$^2S_{1/2}$	0.0				Meggers *et al.* (1957)
	6d	E	$^2D_{3/2}$	801.0				
	5f	O	$^2F_{5/2}$	23 454.5				
	7p	O	$^2P_{1/2}$	29 465.9				
Ac II	$7s^2$	E	$^1S_0$	0.00				Meggers *et al.* (1957)
	6d7s	E	$^3D_1$	4739.63				Klinkenberg and Lang (1949)
	$6d^2$	E	$^3F_2$	13 236.46				
	7s7p	O	$^3P_0$	20 956.40				
	6d7p	O	$^3P_2$	26 446.96				
	5f7s	O	$^3F_2$	31 878.87				
	5f6d	O	$^3H_4$	39 807.14				
	7s8s	E	$^3S_1$	51 680.55				
	5f7p	E	$^3F_2$	54 633.05				
Ac I	$6d7s^2$	E	$^2D_{3/2}$	0.00				Meggers *et al.* (1957)
	$6d^27s$	E	$^4F_{3/2}$	92 17.28				
	$7s^27p$	O	$^2P_{1/2}$	?				
	6d7s7p	O	$^4F_{3/2}$	13 712.90				
	$6d^27p$	O	$^4G_{5/2}$	31 494.68				
Th IV	5f	O	$^2F_{5/2}$	0.00				Klinkenberg and Lang (1949)
232	6d	E	$^2D_{3/2}$	9193.245				Klinkenberg (1988)
	7s	E	$^2S_{1/2}$	23 130.75				
	7p	O	$^2P_{1/2}$	60 239.10				
	8s	E	$^2S_{1/2}$	119 621.60				
	7d	E	$^2D_{3/2}$	119 684.60				
	6f	O	$^2F_{5/2}$	127 269.2				

	8p	O	$^2P_{1/2}$	134 516.50				
	5g	E	$^2G_{9/2}$	159 371.				
	9s	E	$^2S_{1/2}$	160 728.1				
	8d	E	$^2D_{3/2}$	161 954.				
	7f	O	$^2F_{5/2}$	164 554.7				
	6g	E	$^2G_{9/2}$	181 674.				
	10s	E	$^2S_{1/2}$	182 441.				
Th III	5f6d	O	$^3H_4$	0.000	0.89			Klinkenberg (1950)
232	$6d^2$	E	$^3F_2$	63.267	0.744			Litzen (1974)
	5f7s	O	$^3F_3$	2527.095	1.071			Wyart and Kaufman (1981)
	6d7s	E	$^3D_1$	5523.881	0.50			Klinkenberg and Uylings (1986)
	$7s^2$	E	$^1S_0$	15 148.519	0.81			
	5f7p	E	$^3G_3$	33 562.349	0.849			
	6d7p	O	$^3F_2$	37 280.229	0.793			
	7s7p	O	$^3P_0$	42 259.714				
	5f8s	O	$J = 2$	74 644.27				
	5f7d	O	$J = 3$	78 327.71				
	6d8s	E	$^3D_1$	81 706.37				
	6d7d	E	$J = 1$	83 358.66				
	5f8p	E	$J = 3$	86 086.37				
	5f6f	E	$J = 5$	86 933.97				
	6d6f	O	$J = 4$	94 657.94				
Th II	$6d^27s$	E	$^4F_{3/2}$	0.000	0.639	0	–141	Zalubas and Corliss (1974)
232	$6d7s^2$	E	$^2D_{3/2}$	1859.938	0.586	34	–102	Giacchetti *et al.* (1974)
IS	$5f7s^2$	O	$^2F_{5/2}$	4490.256	0.856	–554	17	Engleman and Palmer (1984)
232–230	5f6d7s	O	$^4H_{7/2}$	6168.351	0.718	–371		
hfs	$6d^3$	E	$^4F_{3/2}$	7001.425	0.800	–422		
229	$5f6d^2$	O	$^4H_{7/2}$	12 485.688	0.855	–680		
	6d7s7p	O	$^4F_{3/2}$	23 372.582	1.067	–554		
	$5f^27s$	E	$^4H_{7/2}$	24 381.802	0.70	–590		
	5f7s7p	E	$^4G_{5/2}$	26 488.644	0.776	–305		
	$6d^27p$	O	$^4G_{5/2}$	28 243.812	0.922	–421		
	5f6d7p	E	$^4I_{9/2}$	30 452.723	1.035	–640		

Table 16.1 (*Contd.*)

Spectrum measured isotopes	*Configuration*	*Parity/term*	*Level* (cm^{-1})	g_{obs}	*IS* (10^{-3} cm^{-1})	*hfs* (10^{-3} cm^{-1})	*References*[a]
	$7s^2 7p$	O $^2P_{1/2}$	31 625.680	0.344	–139		
	$5f^2 6d$	E $^4K_{11/2}$	32 620.859	0.826	–948		
Th I	$6d^2 7s^2$	E $^3F_2$	0.000	0.736	0		Zalubas (1975)
232	$6d^3 7s$	E $^5F_1$	5563.143	0.065	–328		Palmer and Engleman (1983)
IS	$5f6d7s^2$	O $^3H_4$	7795.270	0.863	–244		Engleman and Palmer (1983)
232–230	$6d7s^2 7p$	O $^3F_2$	10 783.153	0.732	–33		Blaise *et al.* (1988a)
	$6d^2 7s7p$	O $^5G_2$	14 465.220	0.810	–209		
	$5f6d^2 7s$	O $^5H_3$	15 618.985	0.600	–535		
	$5f7s^2 7p$	E $^3G_3$	18 431.685		–162		
	$6d^4$	E $^5D_0$	21 176.012		–655		
	5f6d7s7p	E $^5I_4$	22 098.187	0.742	–484		
	$5f^2 7s^2$	E $^3H_4$	27 495.589	1.005	–396		
	$5f6d^3$	O $^5I_4$	31 194.705	0.735	–789		
	$6d^3 7p$	O $^5G_2$	32 575.421	0.720	–672		
	$5f6d^2 7p$	E $^5K_5$	35 300.914	0.875	–671		
Pa II	$5f^2 7s^2$	E $^3H_4$	0.00	0.8212		0	Giacchetti (1967)
231	$5f^2 6d7s$	E $^5K_5$	823.265			–1410	Giacchetti and Blaise (1970)
hfs	$5f6d^2 7s$	O $^5I_4$	4751.660			–1065	
231	$5f6d7s^2$	O $^3H_4$	7312.695			–130	
	$5f^2 6d^2$	E $^5L_6$	7454.030	0.77		205	
	$5f^3 6d$	O $^5L_6$?	19 162.305			315	
	$5f^2 7s7p$	O $^5I_4$	22 549.535?			–680	
Pa I	$5f^2 6d7s^2$	E $^4K_{11/2}$	0.000	0.820		0	Giacchetti (1966)
231	$5f6d^2 7s^2$	O $^4H_{7/2}$	1978.220	0.790		–130	Blaise and Giacchetti (1970)
hfs	$5f^2 6d^2 7s$	E $^6L_{11/2}$	7000.290			–1030	Blaise *et al.* (1985)
231	$5f6d^3 7s$	O $^6I_{7/2}$	7585.025			–585	
	$5f^2 7s^2 7p$	O $^4I_{9/2}$	11 444.705	0.88		145	

	$5f^3 7s^2$	O	$^4I_{9/2}$	13 018.610	0.81		–100	
	$5f6d7s^2 7p$	E	$^4I_{9/2}$	14 227.130?	0.980		–155	
	$5f^2 6d7s7p$	O	$^6L_{11/2}$	14 393.410	0.675		–745	
	$5f6d^2 7s7p$	E	$^6I_{7/2}$	15 061.150			–705	
	$5f^2 6d^2 7p$	O	$^6M_{13/2}$	25 106.985	0.980		–310	
U VI	5f	O	$^2F_{5/2}$	0.0				Kaufman and Radziemski (1976)
238	6d	E	$^2D_{3/2}$	90 999.6				
	7s	E	$^2S_{1/2}$	141 447.5				
	7p	O	$^2P_{1/2}$	193 340.2				
U V	$6p^6 5f^2$	E	$^3H_4$	0.00				Wyart *et al.* (1980)
238	$6p^6 5f6d$	O	$^3H_4$	59 183.36				Van Deurzen *et al.* (1984)
	$6p^6 5f7s$	O	$^3F_2$	94 069.53				
	$6p^6 6d^2$	E	$^3F_2$	137 608.14				
	$6p^6 5f7p$	E	$^3G_3$	139 140.96				
	$6p^5 5f^3$	E	$J = 4$	145 870.70				
U III	$6p^6 5f^4$	E	$^5I_4$	0.000		0		Blaise *et al.* (1984)
238	$6p^6 5f^3 6d$	O	$^5L_6$	210.265		291		Blaise *et al.* (1987)
IS	$6p^6 5f^3 7s$	O	$^5I_4$	3743.963		1340		
238–235	$5f^2 6d^2$	E	$^5L_6$	19 416.772		719		
	$5f^3 7p$	E	$^5K_5$	36 651.404		824		
U II	$5f^3 7s^2$	O	$^4I_{9/2}$	0.000	0.765	0		Steinhaus *et al.* (1971)
238	$5f^3 6d7s$	O	$^6L_{11/2}$	289.040	0.655	–788		Blaise *et al.* (1980)
IS	$5f^3 6d^2$	O	$^6M_{13/2}$	4585.434	0.785	–1286		Palmer *et al.* (1980)
238–235	$5f^4 7s$	E	$^6I_{7/2}$	4663.803	0.480			Conway *et al.* (1984)
	$5f^4 6d$	E	$^6L_{11/2}$	12 513.885	0.680			Blaise *et al.* (1994)
	$5f^2 6d^2 7s$	E	$^6L_{11/2}$	13 783.030	0.685			
	$5f^2 6d7s^2$	E	$^4K_{11/2}$	17 434.364?	0.795			
	$5f^3 7s7p$	E	$^6K_{9/2}$	23 315.090	0.880			
	$5f^3 6d7p$	E	$^6M_{13/2}$	26 191.309	0.890			
	$5f^4 7p$	O	$^6K_{9/2}$	30 599.179	0.900			
U I	$5f^3 6d7s^2$	O	$^5L_6$	0.000	0.750	0	–112	Steinhaus *et al.* (1971)
238	$5f^3 6d^2 7s$	O	$^7M_6$	6249.029	0.625	–565		Blaise and Radziemski (1976)
IS	$5f^4 7s^2$	E	$^5I_4$	7020.710	0.660	–310		Rajnak (1979)

Table 16.1 (*Contd.*)

Spectrum measured isotopes	*Configuration*	*Parity/term*	*Level* (cm^{-1})	g_{obs}	*IS* (10^{-3} cm^{-1})	*hfs* (10^{-3} cm^{-1})	*References*[a]
238–235	$5f^26d^27s^2$	E $^5L_6$	11 502.624	0.775	450		Childs *et al.* (1979a,b)
hfs 235	$5f^37s^27p$	E $^5K_5$	11 613.975	0.740	175		Engleman and Palmer (1980)
	$5f^36d7s7p$	E $^7M_6$	14 643.867	0.675	–380		Palmer *et al.* (1980)
	$5f^46d7s$	E $^7L_5$	14 839.736	0.565	–380		Conway (1984)
	$5f^47s7p$	O $^7K_4$	22 792.372	0.645	–665		
	$5f^36d^3$	O $^7M_6$	23 084.307?	0.825	–699?		
	$5f^26d^27s7p$	O $7M_7$?	27 576.161	0.99	–170		
	$5f^36d^27p$	E $7N_7$	27 886.992	0.850	–580		
	$5f^37d7s^2$	O $^5L_6$	27 920.942	0.835	40		
	$5f^36d7s8s$	O $^7L_5$	32 857.449	0.760	–360		
	$5f^36d7s8p$	E $^7M_6$	33 639.562	0.820	–420		
	$5f^46d7p$	O $^7M_6$	34 160.569	0.890	–770		
Np II	$5f^46d7s$	E $^7L_5$	0.000			–1722	Fred *et al.* (1976)
237	$5f^47s^2$	E $^5H_4$	24.270	0.650		776	Blaise *et al.* (1977)
hfs 237	$5f^57s$	O $^7H_2$	83.490			–1585	Blaise *et al.* (1980)
	$5f^56d$	O $^7K_4$	9446.880	0.485		936	
	$5f^47s7p$	O $J = 4$	21 922.530			–528	
	$5f^57p$	E $J = 4$	22 720.500			670	
Np I	$5f^46d7s^2$	E $^6L_{11/2}$	0.000	0.655		777	Fred *et al.* (1977)
237	$5f^57s^2$	O $^6H_{5/2}$	2831.140	0.43		534	Blaise *et al.* (1980)
hfs 237	$5f^46d^27s$	E $^8M_{11/2}$	7112.430	0.48		–924	
	$5f^47s^27p$	O $^6K_{9/2}$	11 940.075	0.625		976	
	$5f^56d7s$	O $^8K_{7/2}$	13 384.205			–1008	
	$5f^46d7s7p$	O $^8M_{11/2}$	14 338.880			–661	
	$5f^57s7p$	E $^8I_{5/2}$	18 654.895	0.71		75	
	$5f^36d^27s^2$	O $^6M_{13/2}$	20 050.905	0.780		842	
	$5f^46d^27p$	O $^8N_{13/2}$	28 551.035	0.940		1183	

	$5f^4 7s7p^2$	E	$^8K_{7/2}$	32 896.360	0.86		467	
Pu II	$5f^6 7s$	E	$^8F_{1/2}$	0.000	3.150	381		McNally and Griffin (1959)
240	$5f^5 7s^2$	O	$^6H_{5/2}$	8198.665	0.414	896		Bauche *et al.* (1963a,b)
IS	$5f^5 6d7s$	O	$^8K_{7/2}$	8709.640	0.308	555		Bauche-Arnoult *et al.* (1973)
240–239	$5f^6 6d$	E	$^8H_{3/2}$	12 007.503	–0.019	77		Blaise *et al.* (1980)
hfs 239	$5f^5 6d^2$	O	$^8L_{9/2}$	17 296.880	0.494	242		Blaise *et al.* (1983)
	$5f^6 7p$	O	$^8G_{1/2}$	22 038.950	0.345	287		
	$5f^5 7s7p$	E	$^8I_{5/2}$	30 956.355	0.646	424		
	$5f^5 6d7p$	E	$^8L_{9/2}$	33 793.295	0.800	208		
	$5f^4 6d^2 7s$	E	$^8M_{11/2}$	37 640.775	0.70	813		
Pu I	$5f^6 7s^2$	E	$^7F_0$	0.000		465		Blaise *et al.* (1962)
240	$5f^5 6d7s^2$	O	$^7K_4$	6313.866	0.487	653		Bauche *et al.* (1963a,b)
IS	$5f^6 6d7s$	E	$^9H_1$	13 528.246	–0.59	253		Blaise *et al.* (1980)
240–239	$5f^5 6d^2 7s$	O	$^9L_4$	14 912.011	0.496	488		Striganov (1983
	$5f^6 7s7p$	O	$^9G_0$	15 449.475		336		Blaise *et al.* (1984b)
	$5f^5 7s^2 7p$	E	$^7I_3$	17 897.917	0.450	691		Blaise *et al.* (1986)
	$5f^5 6d7s7p$	E	$^9L_4$	20 828.475	0.352	467		
	$5f^7 7s$	O	$^9S_4$	25 192.231	1.768	273		
	$5f^6 7s8s$	E	$^9F_1$	31 572.610	2.403	446		
	$5f^6 6d^2$	E	$^9I_2$	31 710.912	0.200	115		
	$5f^6 6d7p$	O	$^9I_2$	33 070.577	0.673	293		
	$5f^4 6d^2 7s^2$	E	$^7M_6$	36 050.520	0.850	535		
	$5f^5 6d^2 7p$	E	$^9M_5$	37 415.495	0.980	403		
	$5f^5 6d7s8s$	O	$^9K_3$	39 618.178	0.27	503		
Am II	$5f^7 7s$	O	$^9S_4$	0.00		400	1726	Fred and Tomkins (1957)
241	$5f^7 6d$	O	$^9D_3$	14 222.21		–17	–260	
IS 243–241	$5f^6 6d7s$	E	$J = 2$	20 501.00		547	–929	
hfs 241	$5f^7 7p$	E	$^9P_3$	23 117.18		507	1084	
Am I	$5f^7 7s^2$	O	$^8S_{7/2}$	0.000	1.937	0	–11	Fred and Tomkins (1957)
241	$5f^6 6d7s^2$	E	$^8H_{3/2}$	10 683.568		268	83	Marrus *et al.* (1960)
IS 243–241	$5f^7 6d7s$	O	$^{10}D_{5/2}$	14 506.922		–269	1021	Blaise *et al.* (1980)
hfs 241	$5f^7 7s7p$	E	$^{10}P_{7/2}$	15 608.260	1.382	–210	933	Pulliam (1985)
	$5f^6 6d^2 7s$	E	$^{10}I_{3/2}$	20 522.51				Pulliam *et al.* (2003)

Table 16.1 (*Contd.*)

Spectrum measured isotopes	*Configuration*	*Parity/term*	*Level* (cm^{-1})	g_{obs}	*IS* (10^{-3} cm^{-1})	*hfs* (10^{-3} cm^{-1})	*References*[a]
	$5f^6 7s^2 7p$	O $^8G_{1/2}$	22 860.445				
	$5f^6 6d7s7p$	O $^{10}I_{3/2}$	25 876.47		–17		
	$5f^7 7s8s$	O $^{10}S_{9/2}$	30 884.995		–130	1859	
	$5f^7 6d^2$	O $^{10}F_{3/2}$	33 972.03		–520		
Cm II	$5f^7 7s^2$	O $^8S_{7/2}$	0.00	1.935	0		Worden and Conway (1967)
244	$5f^8 7s$	E $^8F_{13/2}$	2093.870	1.500	–738		Conway *et al.* (1976)
IS	$5f^7 6d7s$	O $^{10}D_{5/2}$	4010.645	2.492	–496		Worden *et al.* (1976a)
246–244	$5f^7 6d^2$	O $^{10}F_{3/2}$	14 830.150	3.009	–962		Blaise *et al.* (1980)
	$5f^8 6d$	E $^8G_{13/2}$	17 150.790	1.415	–1177		Blaise *et al.* (1981)
	$5f^7 7s7p$	E $^{10}P_{7/2}$	24 046.385	2.098	–403		Worden *et al.* (1986)
	$5f^8 7p$	O $^8F_{11/2}$	27 065.085	1.51	–972		
	$5f^7 6d7p$	E $^{10}F_{3/2}$	32 034.430	2.933	–923		
Cm I	$5f^7 6d7s^2$	O $^9D_2$	0.000	2.563	0		Conway *et al.* (1976)
244	$5f^8 7s^2$	E $^7F_6$	1214.203	1.452	–275		Worden *et al.* (1976a)
IS 246–244	$5f^7 7s^2 7p$	E $^9P_3$	9263.374	2.112	118		Lobikov *et al.* (1979)
	$5f^7 6d^2 7s$	O $^{11}F_2$	10 144.927	2.873	–339		Worden and Conway (1976b)
	$5f^7 6d7s7p$	E $^{11}F_2$	15 252.710	2.835	–269		Blaise *et al.* (1980)
	$5f^8 6d7s$	E $^9G_7$	16 932.750	1.466	–586		Worden *et al.* (1985)
	$5f^8 7s7p$	O $^9D_6$	17 656.657	1.621	–463		Blaise *et al.* (1988b)
	$5f^7 7s^2 8s$	O $^9S_4$	28 635.020	1.731	–126		
	$5f^7 6d^3$	O $^{11}F_2$	30 443.915	2.53	–619		
	$5f^7 7s7p^2$	O $^{11}P_4$	31 167.969	1.759	–180		
	$5f^8 6d7p$	O $^9H_8$	32 876.853		–720		
	$5f^8 7s8s$	E $^9F_7$	33 013.035	1.54	–450		
	$5f^7 6d7s8s$	O $^{11}D_3$	34 255.170	2.064	–220		
	$5f^7 6d^2 7p$	E $J = 5$	34 290.497	1.466	–526		
	$5f^7 7s^2 8p$	E $^9P_3$	35 540.695	2.00	135		

	$5f^8 6d7p$	O	$J = 7$	35 694.690	1.358	–677		
	$5f^7 7d7s^2$	O	$^9D_2$	36 481.435	2.373	105		
	$5f^8 7p^2$	E	$^9F_6$	37 631.966	1.48	–813		
	$5f^8 7s8p$	O	$J = 6$	38 092.623	1.47	–435		
Bk II	$5f^9 7s$	O	$^7H_8$	0.00			6195	Worden *et al.* (1967)
249	$5f^8 7s^2$	E	$^7F_6$	7040.98			820	Conway *et al.* (1977a)
hfs 249	$5f^8 6d7s$	E	$J = 8$	12 340.96			8678	Worden and Conway (1978)
	$5f^9 6d$	O	$J = 8$	16 360.00			670	Blaise *et al.* (1980)
	$5f^9 7p$	E	$J = 7$	26 938.26			2050	Worden *et al.* (1987)
	$5f^8 7s7p$	O	$J = 6$	32 025.72			3445	
Bk I	$5f^9 7s^2$	O	$^6H_{15/2}$	0.00	1.28		1150	Worden *et al.* (1967)
249	$5f^8 6d7s^2$	E	$^8G_{13/2}$	9141.115	1.415		836	Conway *et al.* (1977a)
hfs 249	$5f^9 7s7p$	E	$J = 15/2$	16 913.770			3168	Worden and Conway (1978)
	$5f^9 6d7s$	O	$J = 17/2$	17 182.482			4472	Blaise *et al.* (1980)
	$5f^8 7s^2 7p$	O	$J = 11/2$	17 777.808			157	Worden *et al.* (1987)
	$5f^8 6d^2 7s$	E	$^{10}G_{13/2}$	21 506.406	1.550		3596	
	$5f^8 6d7s7p$	O	$J = 13/2$	24 652.405	1.38		1157	
	$5f^9 7s8s$	O	$^8H_{17/2}$	32 488.850			6306	
	$5f^9 6d7p$	E	$J = 17/2$	36 952.610			1800	
Cf II	$5f^{10} 6s$	E	$^6I_{17/2}$	0.00	1.28			Worden and Conway (1970)
249	$5f^{10} 6d$	E	$J = 15/2$	19 359.06				Conway *et al.* (1977a)
hfs 249	$5f^9 6d7s$	O	$J = 19/2$	24 213.34	1.27			Blaise *et al.* (1980)
	$5f^{10} 7p$	O	$J = 15/2$	26 858.90	1.26			Conway *et al.* (1995)
Cf I	$5f^{10} 7s^2$	E	$^5I_8$	0.000	1.213		0	Worden and Conway (1970)
249	$5f^9 6d7s^2$	O	$J = 8$	16 909.355	1.301		–40	Conway *et al.* (1977a)
hfs 249	$5f^{10} 7s7p$	O	$J = 8$	17 459.210	1.277		–140	Blaise *et al.* (1980)
	$5f^{10} 6d7s$	E	$J = 8$	20 043.930			–210	Conway *et al.* (1995)
	$5f^9 7s^2 7p$	E	$J = 7$	24 727.600			60	
	$5f^{10} 7s8s$	E	$^7I_9$	32 983.180	1.300		–490	
	$5f^9 6d7s7p$	E	$J = 8$	33 952.135			–200	
	$5f^{10} 7s8p$	O	$J = 8$	38 225.945			–410	
	$5f^{10} 7s7d$	E	$J = 8$	39 081.175	1.245			
	$5f^9 7s^2 8s$	O	$J = 8$	45 183.155			–150	

Table 16.1 (*Contd.*)

Spectrum measured isotopes	*Configuration*	*Parity/term*		*Level* (cm^{-1})	g_{obs}	*IS* (10^{-3} cm^{-1})	*hfs* (10^{-3} cm^{-1})	*References*[a]
Es II	$5f^{11}7s$	O	$^5I_8$	0.00			7086	Gutmacher *et al.* (1967)
253	$5f^{11}6d$	O	$J = 7?$	21 639.58			1250	Worden *et al.* (1970)
hfs 253	$5f^{11}7p$	E	$J = 7$	27 751.12			442	Worden *et al.* (1974)
								Blaise *et al.* (1980)
								Blaise *et al.* (2003)
Es I	$5f^{11}7s^2$	O	$^4I_{15/2}$	0.00	1.185		1543	Worden *et al.* (1968)
253	$5f^{11}7s7p$	E	$J = 15/2$	17 802.87			3838	Worden *et al.* (1974)
hfs 253	$5f^{10}6d7s^2$	E	$J = 15/2$	20 162.56			1550	Blaise *et al.* (1980)
	$5f^{11}7s8s$	O	$^6I_{17/2}$	33 829.35			6280	Blaise *et al.* (2003)
	$5f^{10}6d7s7p$	O	$J = 15/2$	37485.58			3870	Wyart *et al.* (2005)
	$5f^{11}7s7d$	O	$J = 13/2$	40478.25			6557	Wyart *et al.* (2005)

[a] Complete energy levels etc. of all the atoms and ions in this table are given in BW92.

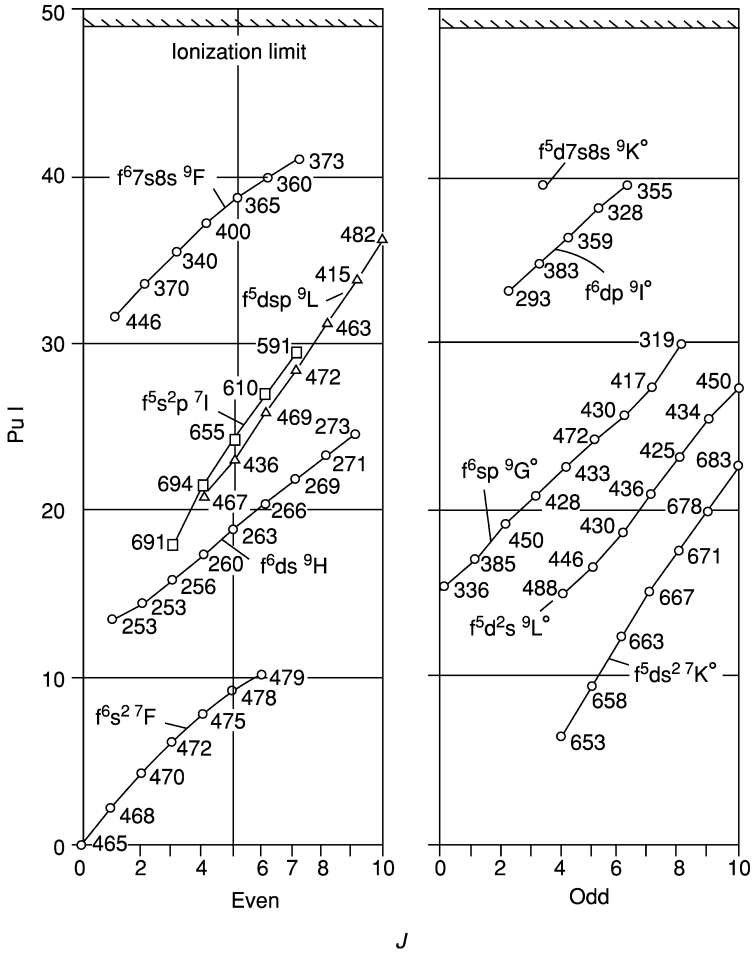

Fig. 16.1 *Hund's rule multiplet of various electron configurations of neutral plutonium,* Pu(*I*). *The number opposite each fine-structure level is the observed isotope shifts* (^{240}Pu–^{239}Pu) *in* 10^{-3} cm^{-1}.

One of the most useful types of experimental corroboration can be obtained from IS values. In the heavy elements the difference in energy of an atomic level from one isotope to another is due to the difference in nuclear volume between the isotopes. For an electron very near the center of the atom, the Coulomb attraction is decreased from that for a point nucleus. The effect is greater for heavier (larger) isotopes. The IS is also greater for electron configurations with more s-electrons since s-electrons have (nonrelativistically) a finite electron

density at the nucleus. The IS is therefore larger for the $5f^n7s^2$ configuration than for the $5f^n7s7p$ configuration. The size of the shift is not directly proportional to the number of 7s electrons because the total s-electron density at the nucleus is modified by the mutual shielding among the electrons. If two 7s electrons are present, the inner electron density of one to some extent shields the outer density of the other from the nuclear attraction, and consequently the $7s^2$ central density is less than twice that for $7s^1$. The presence of an inner electron (5f or, somewhat less so, 6d) also shields a 7s electron. So converting a 5f to a 6d electron reduces the shielding of the 7s electron and increases the IS. Nonrelativistic Hartree–Fock (HF) calculations (Wilson, 1968) gave the result that in converting from one type of valence electron to another, the 5s and 6s electron densities also changed appreciably and had to be considered since it is the total density of all the s-electrons that is responsible for the IS. Relativistic HF calculations (Rajnak and Fred, 1977), on the other hand, ascribe the shift to changes in the shielding of just the 7s electron. Fig. 16.2 shows the experimental shifts and calculated densities at the nucleus for a number of Pu I configurations, illustrating the linear relationship. The experimental shifts are also given for the fine-structure levels of the terms plotted in Fig. 16.1, showing that there is a sensibly constant shift within each set of levels. They are, in fact, fairly constant not only within the lowest term, but also for all the levels of a configuration. The fluctuation is evidently due to varying amounts of configuration interaction (CI), which mixes different configurations and hence mixes the shifts in proportion. The IS values thus make it possible to assign many experimental levels to a definite configuration, which is a very valuable property even though it says nothing about the assignment of term quantum numbers to individual levels within a configuration.

16.4 ELECTRONIC CONFIGURATIONS OF ACTINIDES, SYSTEMATICS OF ACTINIDE CONFIGURATIONS, AND RELATION TO CHEMISTRY

Electron configurations, analogous to the Pu configurations shown in Fig. 16.1, occur in the other actinide elements, i.e. configurations with the same combination of valence electrons but with the number of 5f electrons increasing as Z, the atomic number, increases. These can be generalized into various series, such as $5f^n7s^2$, $5f^{n-1}6d7s^2$, etc., where for the neutral atom $n = Z-88$. Within a series, the S and L of the Hund's rules term change from series member to member because of the changing contribution from the 5f shell. There are also corresponding series for the ions, e.g. $5f^n7s$, $5f^{n-1}6d7s$.

The usefulness of the series concept comes from the regularity in energy of the lowest term. The relative energies of different series change with Z but the change is systematic. This is illustrated in Fig. 16.3(a) and (b) for the neutral

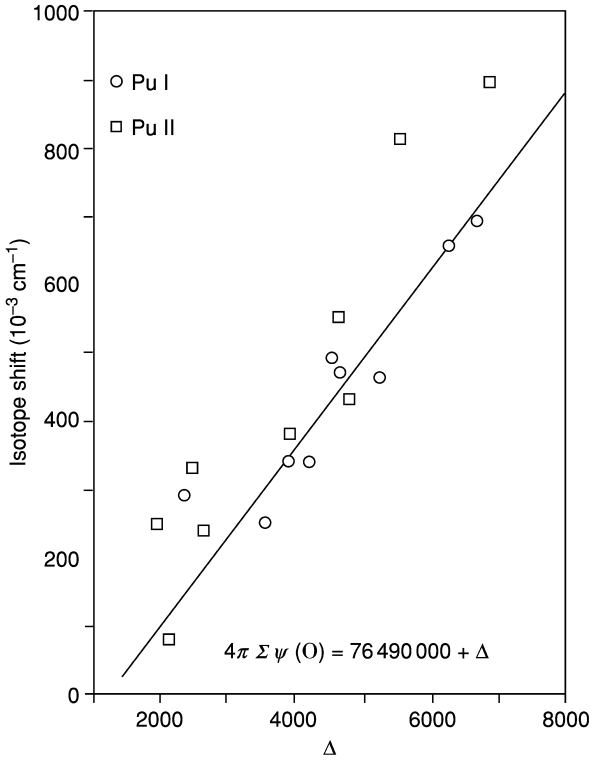

Fig. 16.2 *Isotope shifts of configurations of Pu I and Pu II as a function of electron density at the nucleus.*

atoms; the data are given in Tables 16.1 and 16.2. The absolute binding energies increase with Z (become more negative), but the quantity of interest is usually the relative energy between series. In Fig. 16.3(a) the zero energy for each element has been taken arbitrarily as the configuration $5f^{n-1}6d7s^2$ (the lowest with three valence electrons, trivalent) and in Fig. 16.3(b) the lowest configuration is taken as $5f^n7s^2$ (divalent). The regularity provides independent evidence of the correct assignment of levels to the various series for the individual actinide elements, except for the irregular behavior near the middle of the 5f shell.

This irregularity is due mainly to the fact that the overall spread in energy of the f^n configurations is greatest for the half-filled shell, $n = 7$. (Each f^n configuration consists of a number of SL terms due to the 5f–5f repulsion, and these terms have quite different energies.) Fig. 16.4 shows the approximate position of the lowest term of each f^n configuration with respect to the weighted average of the configuration, and also with respect to the lowest term of f^{n-1}. When f^n is

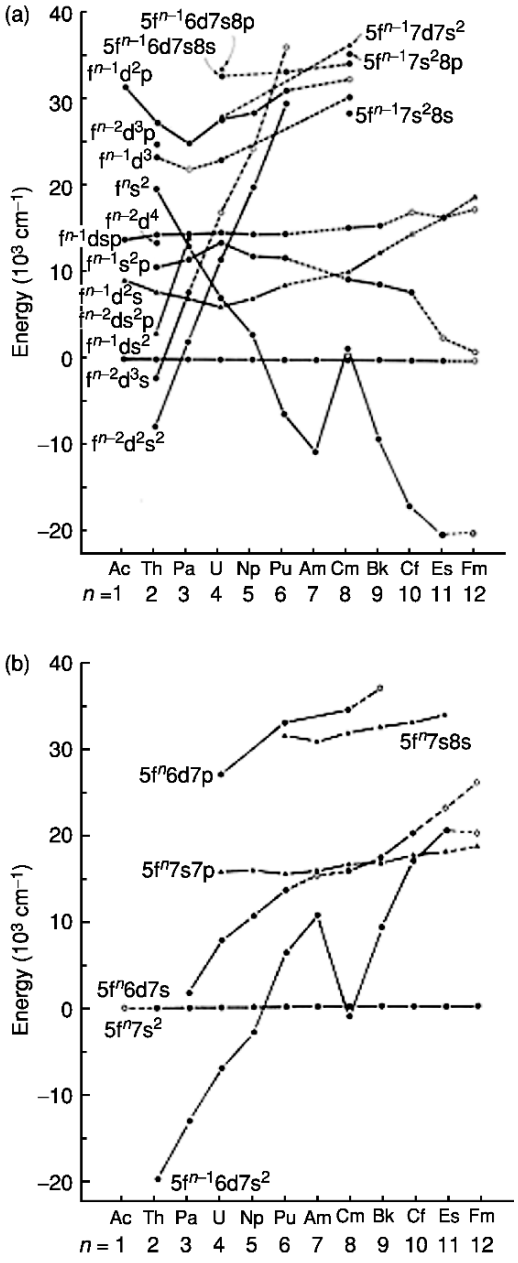

Fig. 16.3 *Energies of various series of configurations in the neutral actinides compared to* $5f^{n-1}6d7s^2$ (*a*) *and* $5f^n7s^2$ (*b*). *The open circles indicate estimates from Brewer* (1971a,b, 1984).

Table 16.2 *Lowest levels of some common configurations of the neutral actinide elements.*

	Ac (*Z* = 89, *N* = 1)	*Th* (90, 2)	*Pa* (91, 3)	*U* (92, 4)	*Np* (93, 5)	*Pu* (94, 6)	*Am* (95, 7)	*Cm* (96, 8)	*Bk* (97, 9)	*Cf* (98, 10)	*Es* (99, 11)	*Fm* (100, 12)	*Md* (101, 13)
$5f^{n-1}6d7s^2$	0	7795	0	0	0	6314	10 684	0	9141	16 909	20 163	(20 000)	(30 000)
$5f^{n-1}6d^27s$	9217	15 619	7000	6249	7112	14 912	20 523	10 145	21 506	(31 500)	(36 000)	(39 000)	(51 000)
$5f^{n-1}7s^27p$	(9500)	18 432	11 445	11 614	11 940	17 898	22 860	9263	17 778	24 728	(22 000)	(21 000)	(28 000)
$5f^{n-1}6d7s7p$	13 713	22 098	14 393	14 644	14 339	20 828	25 876	15 253	24 652	33 952	(36 000)	(37 500)	(48 000)
$5f^n7s^2$	(30 000)	27 496	13 019	7021	2831	0	0	1214	0	0	0	0	0
$5f^n6d7s$	(42 000)	(39 000)	14 693	14 840	13 384	13 528	14 507	16 933	17 182	20 044	(23 000)	(26 000)	(28 000)
$5f^n6d^2$	(59 000)	(57 000)	(39 000)	(34 000)	(27 000)	31 711	33 972	(41 000)	(45 000)	(50 000)	(54 000)	(58 000)	(62 000)
$5f^n7s7p$	(43 000)	(42 000)	(25 600)	22 792	18 655	15 449	15 608	17 657	16 914	17 459	17 803	(18 500)	(19 000)
$5f^{n-2}6d^27s^2$		0	1978	11 503	20 050	36 050	(51 000)	(50 000)					
$5f^{n-2}6d^37s$		5563	7585	(16 930)	(24 500)	(42 500)							

Values in parenthesis are estimates taken from Brewer (1984).

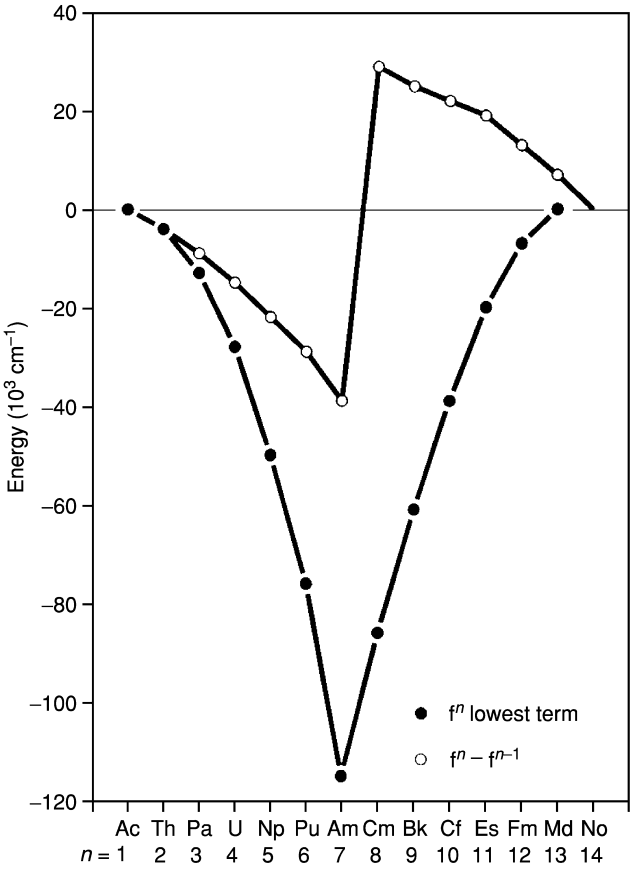

Fig. 16.4. *Approximate energy of the lowest term of f^n relative to the weighted average of f^n and of f^{n-1}.*

compared with $f^{n-1}d$ (the $7s^2$ electrons do not contribute to the structure), the irregularity is reduced because the f–d electrostatic interaction changes sign at $n = 8$, and also slope.

Inspection of Fig. 16.3(a) shows three families of series based on f^n, f^{n-1}, and f^{n-2} having respectively negative, zero, and positive slope. The relative positions of different series characterized by various configurations of outer electrons tend to repeat for each family, and consequently the existence of families is clearly due to the properties of the 5f electrons. For simplicity, Fig. 16.4 presents the lowest series of each family, those configurations with $7s^2$. Now HF calculations show that most of the energy in actinide configurations comes from the electrostatic attraction between the individual 5f electrons and the nucleus. This

attraction increases with Z (the actinide contraction) and the total of the 5f attraction energy is proportional to the number of 5f electrons. The $7s^2$ energy is nearly constant with Z and so does not affect the trend of the series. The 6d energy is also nearly constant but gives an additional (almost constant) contribution to $5f^{n-1}6d7s^2$ and twice as much to $5f^{n-2}6d^27s^2$; it affects the absolute positions of the three series but not the slopes (see Fig. 16.3a). The three series have roughly equal energies for atomic numbers around that of uranium ($Z = 92$). For smaller Z, the 6d binding energy is more important than the 5f binding energy, but for larger Z the 5f becomes increasingly more stable due to an increase with both Z and n.

The electron–nucleus attraction energy is related by the virial theorem to the mean value of r (the electron–nucleus separation) for the different kinds of electrons. Fig. 16.5 shows (nonrelativistic) HF solutions for the radial distribution $P(r)$ for plutonium as a typical actinide. The abscissa is chosen as $r^{1/2}$ (in atomic units) in order to show more detail at small r and less at large r. The figure also shows the total electron density due to the first 86 electrons in the radon core, plotted to a reduced ordinate scale. At the bottom of the figure is Z^*, the effective Z, which describes how the nuclear charge seen by an electron at separation r is reduced by the shielding due to the electron density between zero and r. The 5f electrons clearly see a larger Z^* than do 6d or 7p. The 5f Coulomb energy $-Z^*e^2/\langle r\rangle$ is more negative ($\langle r\rangle$ is the expectation value of r,

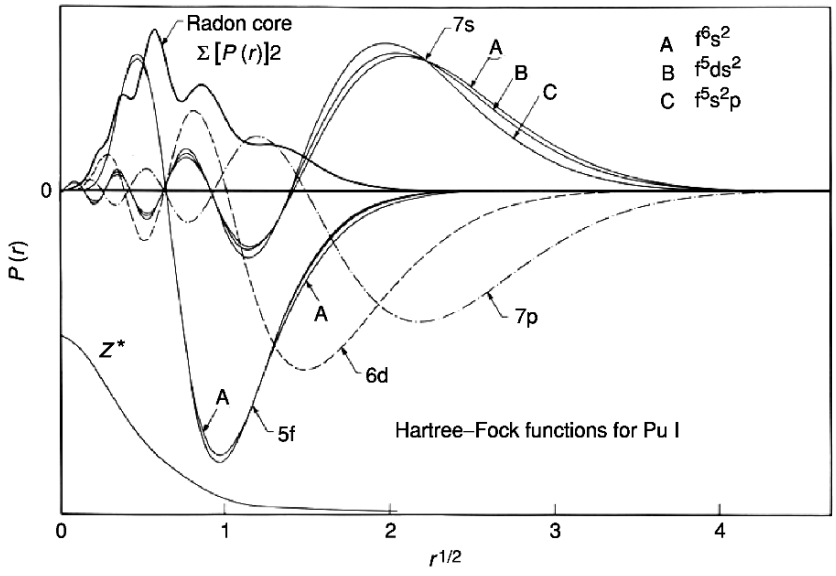

Fig. 16.5 *Radial distribution functions of valence electrons in neutral plutonium.*

i.e. r averaged over the radial density distribution). The total energy also includes a centrifugal term $+l(l+1)/r^2$ (l is the azimuthal quantum number), which tends to equalize the 5f, 6d, and 7p Coulomb energies, and the details vary along the actinide series as first shown by Goeppert Mayer (1941). It can be seen that the 7s radial function has its main contribution well outside the radon core, the 6d not quite so much, while the 5f electron is completely inside the core. The 5f electron is an inner electron and not much affected by the environment outside the core.

The determination of the electronic structure of the actinide elements through spectroscopy was expected to lend considerable knowledge to the chemistry of the elements. In fact the opposite is true because of complications in the observation and the analyses of the spectra, the chemistry was well known before elucidation of the spectra was possible. There are clear implications for actinide chemistry in the relative energies and radial distributions of the last ($Z-86$) electrons of a neutral actinide atom (see Fig. 16.5). For a typical actinide, the 6d and $7s^2$ electrons extend beyond the radon core and are available for forming chemical bonds, i.e. a typical actinide should be trivalent. At the beginning of the series, however, the 5f electron is not so firmly bound and has a larger $\langle r \rangle$, which reduces the amount of shielding of the nuclear charge as seen by the 6d electron. Hence for thorium, 6d is favored over 5f because of its larger Z^* and smaller centrifugal loss, and the ground state is $6d^27s^2$, resulting in a neutral atom with four external electrons (quadrivalent).

The tendency of the actinides to be multivalent in the first part of the actinide series because of the presence of 7s, 7p and 6d and 5f electrons of about equivalent energy is well known. The tendency to become more lanthanide-like in behavior toward the middle of the series and then have more divalent character near and beyond Es is related to the known electronic structure of these actinides. The increased stability of the 5f electrons as the atomic number is increased can be determined from the systematics of the electronic structure. At the heavy end of the actinide series, the 5f electrons become increasingly bound compared with 6d and it is more favorable to convert an added electron to another 5f, producing $5f^n7s^2$ as the ground state (divalent). This change in valence along the series is reduced in the lanthanides, as is shown in Fig. 16.6, where the relative energy of configurations $4f^n6s^2$, $4f^{n-1}5d6s^2$, and $4f^{n-1}5d6s6p$ are compared with the corresponding actinide configurations. The increased stability of 5f vs 4f in the second half of the series is evident and explains the tendency toward divalent character in the actinides beyond Es. The first actinide to show a stable divalent ion in solution was Md (Hulet *et al.*, 1967).

Brewer (1971a,b, 1984) developed methods based on the thermodynamic data of actinide metals and the regularities of the lowest energy levels of known actinide configurations (described above) to estimate the lowest energy levels of missing configurations of free atoms and ions in the 4f and 5f series.

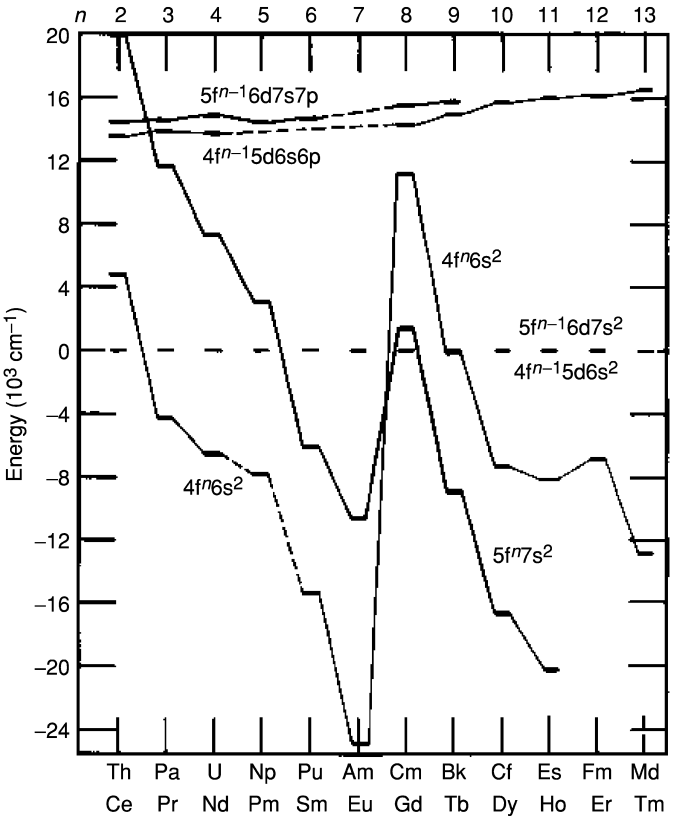

Fig. 16.6 *The energies of the lowest levels of the configurations, $f^n s^2$, $f^{n-1}ds^2$, and $f^{n-1}dsp$ for the actinides (5f) and lanthanides (4f) plotted vs n with the lowest level of the $f^{n-1}ds^2$ configuration at zero. Level energies with dashed level and connector lines are predicted values from Brewer* (1971a). *The lower energy for $5f^n7s^2$ for Cm and beyond is evident as the actinide series is ascended. This explains the tendency for the actinides to be more lanthanide-like at the center then become more divalent in character for the heavier actinides of Es and beyond.*

His estimates have proven to be very useful in assigning unknown configurations during spectral analyses.

These qualitative considerations are compared with some solution chemistry results in Fig. 16.7(a) and (b). The standard oxidation–reduction potentials $E^{\circ}(M^{(n+1)+}/M^{n+})$, converted from volts to cm^{-1}, are plotted for comparison with the energies of f–d transitions in free atoms. The full symbols are experimental values, the open symbols the calculated ones (Nugent, 1975). The similarity in shape of the two sets of curves is evident. There are approximate shifts of about 30000 cm^{-1} for the (III)/(II) potentials (Fig. 16.7(a)) and

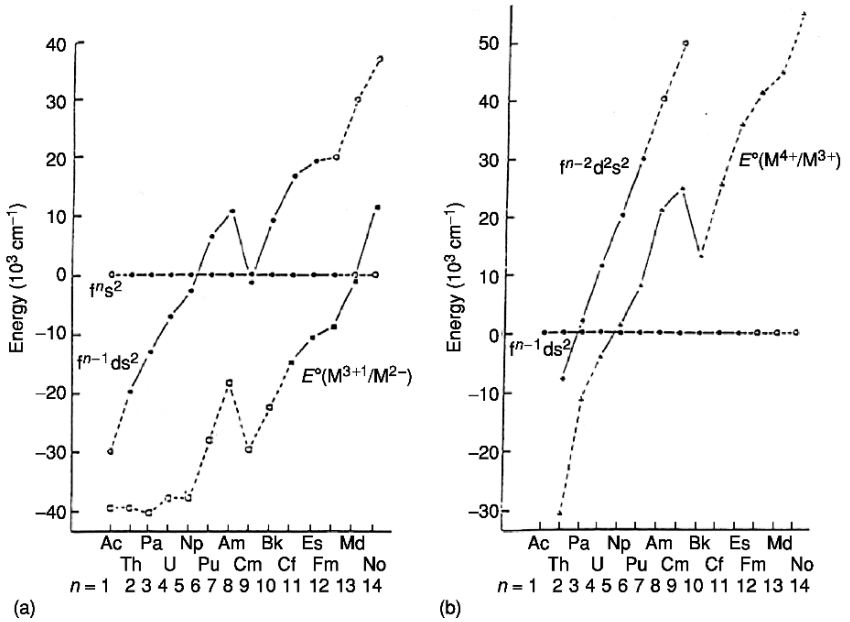

Fig. 16.7 *Comparison of actinide standard oxidation–reduction potentials and the relative energies of the series on converting a 5f electron to a 6d electron across the series.*

about 20000 cm^{-1} for (IV)/(III) (Fig. 16.7(b)) in the same direction, i.e. less energy is required for f→d conversion in solution than in the free neutral atom.

16.5 THEORETICAL TERM STRUCTURE OF THE FREE ACTINIDES

The energy of an atomic level results from various interactions and is an eigenvalue of the Hamiltonian operator describing the N-electron atom. If relativistic effects are first neglected, the Schrödinger equation $H\Psi = E\Psi$ is to be solved with

$$H = \sum_{i=1}^{N} \left(\frac{p_i^2}{2m} - \frac{Ze^2}{r_i} \right) + \sum_{i>j=1}^{N} \left(\frac{e^2}{r_{ij}} \right)$$

where $p_i^2/2m$ represents the kinetic energy and r_i the distance to the nucleus for electron i of mass m and electron charge e. The last term in H (named Q hereafter) accounts for the repulsions between all pairs of electrons separated by the distance r_{ij} and is too large to be treated as a perturbation. The central field approximation of Slater (1929), i.e. electrons being assumed to move in

a spherically symmetric potential $-U(r_i)/e$, gives the following equation H' considered as zeroth-order perturbation theory

$$H' = \sum_i \left(\frac{p_i^2}{2m} + U(r_i) \right).$$

The difference, H–H', is the perturbation potential,

$$H - H' = \sum_{i=1}^{N} \left(-U(r_i) - \frac{Ze^2}{r_i} \right) + \sum_{i)j=1}^{N} \left(\frac{e^2}{r_{ij}} \right)$$

The eigenvalues of H' depend on the n and l quantum numbers only, defining the configurations $\ldots n_a l_a^p n_b l_b^q \ldots$ and the first summation in the $H-H'$ equation contributes as a global shift for each configuration. The *active* two-electron part Q splits the highly degenerate states of the configurations into terms of definite total spin S and total orbital angular momenta L. Spin-dependent interactions have a leading term that couples the spin angular momentum s_i and the orbital angular momentum l_i of each of the electrons e_i. The spin–orbit operator

$$\Lambda = \sum_i \xi(r_i) s_i l_i$$

is then added to $H-H'$. The matrix elements of Λ have radial parts, the spin–orbit radial integrals ζ_{nl}, which increase rapidly with atomic number. Consequently, Λ can be considered a perturbation on SL terms for low Z elements only, where all levels with total angular momentum J ($\mathbf{J} = \mathbf{L} + \mathbf{S}$) allowed in a term ($| L - S | \leq J \leq L + S$) are close in energy. In actinides, the spin–orbit splitting (fine structure) of the terms is larger than their separations. LS coupling selection rules for transitions are violated and prevent total spin and orbital momenta S and L, respectively, from being quantum numbers of interest. The complexity of the actinide spectra is correlated with the relative magnitude of various parts in Q and in Λ. All the individual s and l angular momenta sum as $\mathbf{J} = \Sigma_i(\mathbf{s}_i + \mathbf{l}_i)$ with intermediate steps and the angular momenta associated with these steps define a coupling scheme. It is chosen so that the off-diagonal elements of the matrix of the $Q + \Lambda$ operator are as small as possible. In odd-Z elements, due to the nuclear magnetic moment $\mathbf{I}$ and its coupling with $\mathbf{J}$, the total angular momentum $\mathbf{J}$ should be replaced by $\mathbf{F} = \mathbf{I} + \mathbf{J}$. Then the hyperfine Hamiltonian $\mathbf{A} \cdot \mathbf{I} \cdot \mathbf{J}$ has to be added to $Q + \Lambda$. Actinides display the largest hfs patterns of all spectra; however, the hyperfine splitting is small compared with level separations and may be interpreted as a perturbation of the fine-structure levels with wave functions $|\alpha J M_J>$, α being a symbol for all couplings ending on J.

The angular and radial parts in the monoelectronic eigenfunctions and in the Hamiltonian operators lead to separate radial and angular integrals. All radial integrals needed in any configuration (electrostatic Slater integrals and spin–orbit integrals), and how they can be determined from experimental energy

levels in two-electron configurations, are fully described (Condon and Shortley, 1935). The application of this parametric approach to larger atomic systems needed Racah methods to be achieved. Racah derived the symmetry properties in configurations of l^N and the double tensor $\mathbf{w}^{(\kappa k)}$ properties of the operators involved in the Hamiltonian and showed how their ranks κ and k in the spin and orbital spaces explain selection rules and some singularities in matrix elements (Racah, 1942, 1943, 1949; Judd, 1963).

Although globally satisfactory, the first-order parametric theory faces certain problems. The electrostatic operator Q has matrix elements between configurations of the same parity $p = (-1)^{\Sigma l}$ and this would lead to the calculation of the H_1 operator with a basis set of many configurations. This was done with success by Racah (1950) for the two-electron configurations of Th III, but even with present-day computers the size of matrices that can be diagonalized is limited. Perturbation theory allows CI to be calculated as second-order effects, as long as they are distant (Rajnak and Wybourne, 1964). In case of f^n, two-particle operators lead to the correction terms $\alpha L(L+1) + \beta G(G2) + \gamma G(R7)$, where α, β and γ are effective parameters and $G(G2)$ and $G(R7)$ are Casimir operators of symmetry groups needed to classify f^n states. Three-particle operators involved in f^n to $f^{n\pm1}n'l'^{\mu l}$ excitations also lead to six additional parameters (Judd, 1966). In the case of several open shells, two-electron electrostatic operators lead to Slater-type effective parameters (Feneuille and Pelletier-Allard, 1968; Crosswhite, 1971). Although λ is an effective operator valid in a given configuration, second-order operators acting on spin and orbital spaces (cross products $Q \times \Lambda$) have been investigated (Goldschmidt, 1983). Further details are not given here as they can be found in several textbooks (Slater, 1960; Wybourne, 1965; Cowan, 1981; Rudzikas, 1997).

Judd (1985) has made a survey of atomic structure theory for complex spectra. He included a new way of parameterization. Radial integrals and the usual effective parameters are correlated in the sense that the introduction of a neglected parameter changes the values of those already used in the analysis. This can be overcome by replacing the usual operators by linear combinations associated with 'orthogonal' parameters. An application to Pr III $4f^3$ was made (Judd and Crosswhite, 1984) and the angular coefficients of relevant operators were further studied (Hansen *et al.*, 1996; Judd and Lo, 1996) but the actinides have not yet been investigated in this way.

16.6 DETERMINATION OF RADIAL PARAMETERS

A description of the level structure of an actinide configuration as given by the eigenvalues and eigenvectors of the energy matrix H has been outlined above. To obtain quantitative information, it is necessary to provide numerical values for the matrix elements and then to diagonalize the matrix. The problem thus divides naturally into several stages: evaluating the angular coefficients f_k, g_k of

the electrostatic integrals $R^k(n^a l^a\, n^b l^b, n^c l^c\, n^d l^d)$ with ($a = c$, $b = d$) for the direct Slater integrals, F^k, and ($a = d$, $b = c$) for the Slater exchange integrals, G^k. The same procedure may be applied for the spin–orbit integrals, for the electrostatic CI integrals R^k, and for effective CI parameters. Then initial values are provided for the radial integrals and the effective parameters, followed by diagonalization and optimization of the effective parameters by comparison of the calculated energy levels with the assigned experimental levels.

The angular coefficients are calculated exactly by application of the Wigner–Eckart theorem and by means of Racah algebra techniques as described by Judd (1963). They are products of phase factors, n–j symbols, and contain sums over the states of the parent configuration f^{n-1} as the decoupling of one (or more) f electrons out of f^n is needed. For that purpose, fractional parentage coefficients can be found in Nielson and Koster (1964). The analytic expression of angular coefficients was used as input in the first computer programs to determine numerical values of the angular coefficients (Racah, 1951; Bordarier, 1970). As an intricate function of all spin and orbital momenta involved in the selected coupling scheme, it was subject to errors although an implicit check of the Racah algebra consistency was provided by the integer form $a(b)^{1/2}/c$ of the whole numerical process. A nearly automatic code was developed at LANL (Cowan, 1968, 1981), requiring only the number of electrons in each open shell, input of the fractional parentage coefficients, and a list of terms for each shell. This code is widely distributed and was adapted at other sites, such as ANL (Crosswhite, 1975) and for PC users (Kramida, 1997). It runs faster than the earlier codes as all calculations are performed in the decimal form.

After an initial set of radial integrals is chosen, the Slater–Condon method of treating them as adjustable parameters may be applied. Upon diagonalization, the eigenfunctions lead to coefficients of the parameters in intermediate coupling and to a linear expansion for the energy of each level. In the subsequent least-squares minimization of $\Delta_i = E_i(\text{exp})$–$E_i(\text{th})$ (where $E_i(\text{exp})$ and $E_i(\text{th})$ are the experimental and calculated levels), and the mean error $\sigma = (\Sigma \Delta_i^2/(N_{\text{lev}}$–$N_{\text{par}}))^{1/2}$ measures the quality of the fit and is critically dependant on the number of known levels N_{lev} relative to the number N_{par} of unknown parameters. Some iterations of the diagonalization/least-squares fits lead after convergence to a set of fitted parameters with standard errors. In the complex first and second spectra, inappropriate initial parameters may lead to term inversions in the comparisons of $E_i(\text{exp})$ vs $E_i(\text{th})$ and it sometimes happens that iterations diverge when processed in an automatic way.

Besides obtaining a low mean error on energies, validity checks of the parametric study may be obtained by using the eigenfunctions for the calculations of hfs constants. This was done for U I (Avril *et al.*, 1994). In addition, theoretical studies of the IS may be used, e.g. in Th(I,II) (Blaise *et al.*, 1988a). For even-Z elements, all investigated with the support of Zeeman effect, first checks are provided by comparisons between large sets of Landé factors $g_i(\text{exp})$ and easily derived $g_i(\text{calc})$ values.

16.7 ACTINIDE PARAMETERS

16.7.1 Least-squares fitted values

Actinide parameter values cannot be derived in a straightforward way because of the difficulties discussed above. In almost no case can the parameters be determined precisely; the values obtained depend on the assumptions made in defining the energy matrix and these vary from case to case and cannot be compared reliably. The early actinides (Th to Np) are more completely known but have more close configurations, and so the parameter values derived are sensitive to how much CI is included. The middle actinides (Pu to Cf) have larger configuration separations but more terms in each, leaving the choice between complete configurations with CI neglected or truncated subconfigurations with CI considered. The late actinides (Es and beyond), which get some simplicity being closer to $5f^{14}$, may provide values that are still unavailable from lower-Z elements. A rare example taken from einsteinium (Worden *et al.*, 1974; Blaise *et al.*, 2003) is shown in Fig. 16.8. In the first excited configuration of Es I $5f^{11}7s7p$, the lowest level $^4I_{15/2}$ of the core $5f^{11}$ is relatively well isolated from others and the relationships $Q(7s,7p) > \Lambda(7p) > Q(5f,7s)$, $Q(5f,7p)$ lead to a case

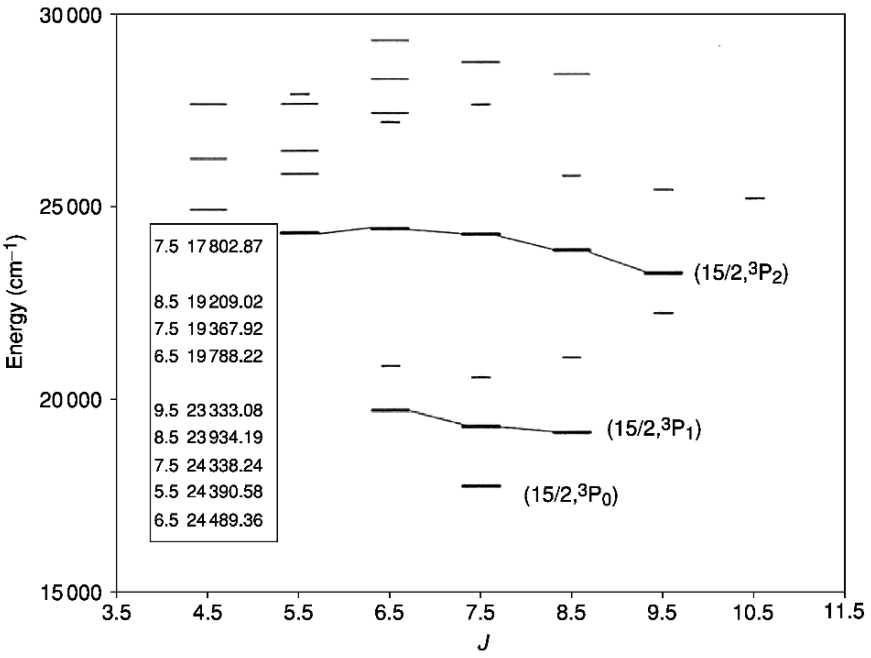

Fig. 16.8 *The low-lying levels for various configurations of Es I. The experimental values for the $5f^{11}7s7p$ of Es (heavy bars) are grouped in J_c–J_2 multiplets. Some predicted levels of $5f^{10}6d7s^2$ (light short bars) and of $5f^{11}7s7p$ (light long bars) are also given.*

of ($5f^{11}$ J_c–($7s7p)^3P$ J_2) J coupling with a clear separation of (15/2, $^3P_0$) and multiplets (15/2, $^3P_1$) and (15/2,$^3P_2$). As the theoretical splitting of any sp^3P term is approximately equal to $1.5\zeta_p$, an approximate value of 4100 cm^{-1} is readily derived for the ζ_{7p} spin–orbit parameter. Conversely, a case of complexity characterizing most of the lanthanides is found in the study of $5f^36d7s^2$ + $5f^36d^27s$ configurations of U I (Petit, 1999) using an extended version of RCG/RCE codes (Cowan, 1981). The complete basis sets of both configurations lead to 3642 theoretical levels, of which 155 are identified and 29 parameters are fitted with an excellent mean error. The eigenfunctions of the lower levels describe Landé g-values properly. On the other hand, the lack of experimental evidence for the expected perturbing configuration $5f^36d^3$ and the large number of levels without g-values or IS set the limit for additional theoretical assignments.

The small value of the ratio $N_{known}/N_{predict}$ mentioned for U I is usual in the I (free atom) and II (singly ionized ion) spectra of f-elements. Not all parameters involved in the description of a configuration can be derived reliably from the least-squares fitting on its very low energy part. If SL coupling is obeyed, all levels of a term have the same dependence on Slater integrals and the determination of the F^k(ff) ($k = 0,2,4,6$) parameters would require at least four terms of f^n to be known, which is not fulfilled in many free atoms and ions of actinides. The lowest terms of highest multiplicity have separations that are a function of only one parameter, the Racah parameter $E^3 = (1/135)F^2 + (2/1089)F^4 - (175/42471)F^6$. Owing to the strength of the 5f spin–orbit interaction, its off-diagonal matrix elements lead to term mixings and those intermediate coupling conditions lead to the differentiation of the coefficients of the electrostatic parameters for all the levels. Hence the least-squares fit does yield values of all the F^k(ff) but with rather large statistical errors.

In order to reduce those statistical errors and to improve the predictive character of the parametric calculations, the techniques of generalized least-squares (GLS) first used by Racah and coworkers in 3d-elements have been applied to actinides (Blaise *et al.*, 1980). It is known that for long periodic trends, the parameters determined as described above have a slow empirical dependence on Z. The simple expansions of the parameters as $P = A(P) + (n–7)B(P) + (n–7)^2C(P)$ lead to the determination from all the known levels of $5f^n7s^2$ and $5f^n7s$, of the A, B, and C GLS-constants for the parameters F^k(ff), α, β and γ. In the singly ionized free ion spectra, 112 levels of seven elements from U II $5f^47s$ through Es II $5f^{11}7s$ were interpreted by this GLS method with 22 free parameters and a small error of $\sigma = 84$ cm^{-1}.

16.7.2. Comparisons with *ab initio* radial integrals

Various *ab initio* studies of atomic systems have confirmed Racah's empirical statement that in $3d^n$ atoms and ions the radial integrals are smoothly Z-dependent. The same trends are found in the 4d, 4f, 5d, and 5f elements. Consider the theoretical values from relativistic HF (HFR) calculations

(Crosswhite, 1975). Fig. 16.9(a) shows various cases with certain regularities. The integrals F^k(ff) all increase with atomic number, the increase approaching linearity for the second half of the series. The ratios of the limiting slopes of F^2:F^4:F^6 are 1:0.643:0.464. The numerical values of the integrals for $5f^n7s^2$ are for Th I 49704:31366:22660 = 1.0:0.631:0.456 and for Fm I 90499:58914:43210 = 1:0.651:0.477. For hydrogenic-shaped 5f radial functions, the ratios are 1:0.688:0.527. The similarity to hydrogen can be taken to mean that over the range in r which includes most of the HF 5f radial function, the potential does not change greatly from that for a fairly constant effective nuclear charge Z^*. The increase of the F^k integrals with Z corresponds to the actinide contraction.

Fig 16.9(a) shows that the HF values of F^k(ff) are only mildly affected by changes in the outer electrons and for each k, converge toward the same limit with increasing Z, independent also of ionic charge. The change in the integral for constant Z but varying number of 5f electrons is much greater and amounts to a constant shift. All these effects are in the direction expected for changes in the shielding of the 5f electrons. The HFR overlap integrals F^k(5f6d) and G^k(5f6d) in Fig. 16.9(b) and (c) show the opposite effect: they decrease with Z because the 5f functions contract while the 6d functions remain constant, and they are more sensitive to the number of 7s electrons, that affects their relative shielding. The one-electron integrals ζ_f, which are proportional to $<1/r^3>$, increase with Z and their dependence on outer electrons is consistent with shielding effects. The effect of increasing Z on ζ_d and ζ_f is shown in Fig. 16.9(d).

Now consider the experimental parameters and how they compare with theory. Table 16.3 presents some experimental values of F^k(ff) parameters, the corresponding HFR integrals and several ways of comparing them. The experimental parameters P_{exp} are all smaller than the calculated integrals P_{HFR}, which is an almost universal characteristic throughout the periodic table. The ratio (P_{exp}/P_{HFR}) is roughly 2/3 with irregular variations. Another ratio is F^k/F^2 that can be formed independently for P_{exp} and P_{HFR}. A third possibility is the difference (P_{exp}–P_{HFR}) that was found to be nearly constant for each F^k for tripositive lanthanide ions (Carnall *et al.*, 1978). It should be stressed that parameter comparisons are meaningful only if they have been derived with similar approximations, i.e. the same terms in the Hamiltonian operator were calculated on similar sets of configurations, only the number n of core electrons being varied. Parametric studies still continue to make general trends better known.

16.8 SUMMARY OF ACTINIDE CONFIGURATIONS

Table 16.1 lists the lowest level of all known actinide configurations of the species studied and Table 16.2 shows the lowest level of some common configurations of the neutral actinide spectra. Thousands of higher levels are known, but for this survey we are more interested in generalities than in details. The

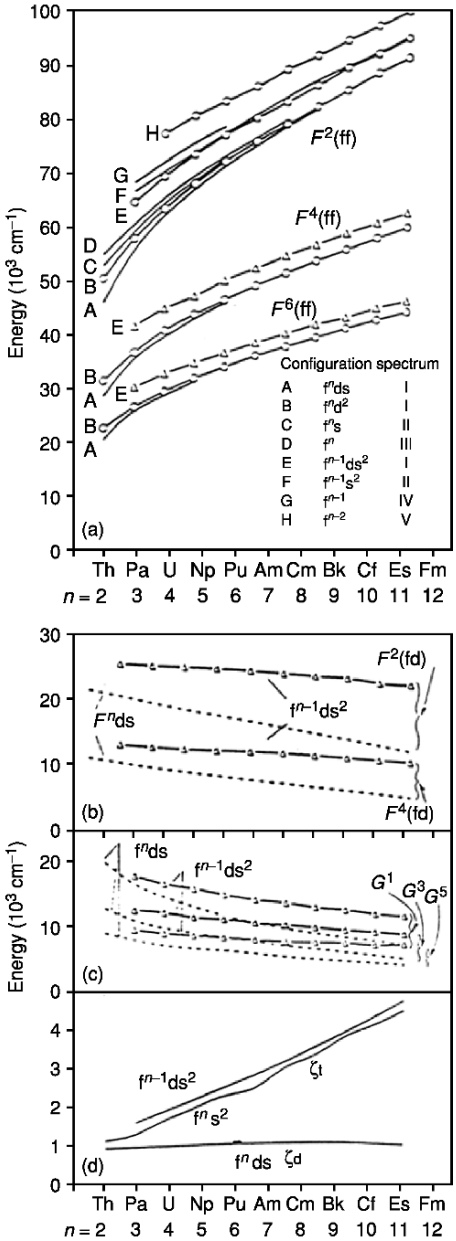

Fig. 16.9 *Relativistic Hartree–Fock calculations of some actinide radial integrals:* (*a*) $F^k(ff)$; (*b*) $F^k(fd)$; (*c*) $G^k(fd)$, *and* (*d*) ζ_f *and* ζ_d.

Table 16.3 *Some experimental values of F^k(ff) parameters, Hartree–Fock values, and ratios F^k/F^2 for a number of actinide elements.*

					F^k/F^2				
Configuration	*Element*	*Parameter*	*Experiment*	*Hartree–Fock*	*Expt*	*HF*	F^k_{Expt}/F^k_{HF}	$F^k_{HF} - F^k_{Expt}$	*References*
$5f^4 7s^2$	U(I)	F^2	36 505	62 891	1.000	1.000	0.580	26 386	Rajnak (1979)
		F^4	28 474	40 290	0.780	0.641	0.707	11 816	
		F^6	20 808	29 304	0.570	0.466	0.710	8496	
$5f^5 7s^2$	Np(I)	F^2	39 797	67 452	1.000	1.000	0.590	27 655	Crosswhite (1986)
		F^4	31 017	43 381	0.779	0.643	0.715	12 364	
		F^6	23 044	31 611	0.579	0.469	0.729	8567	
$5f^6 7s^2$	Pu(I)	F^2	42 935	71 461	1.000	1.000	0.601	28 526	Crosswhite (1986)
		F^4	33 472	46 094	0.780	0.645	0.726	12 622	
		F^6	24 959	33 638	0.580	0.471	0.742	8679	
$5f^8 7s^2$	Cm(I)	F^2	51 025	78 531	1.000	1.000	0.650	27 506	Crosswhite (1986)
		F^4	39 133	50 868	0.767	0.648	0.769	13 883	
		F^6	30 579	37 204	0.599	0.474	0.822	8229	
$5f^{10} 7s^2$	Cf(I)	F^2	57 870	84 799	1.000	1.000	0.682	26 929	Wyart (1998)
		F^4	45 052	55 085	0.779	0.650	0.818	10 033	
		F^6	31 873	40 345	0.551	0.476	0.790	8472	
$5f^3 6d7s^2$	U(I)	F^2	43 891	68 684	1.000	1.000	0.639	24 793	Petit (1999)
		F^4	32 431	44 396	0.739	0.646	0.730	11 965	
		F^6	23 128	32 417	0.527	0.472	0.713	9289	
$5f^4 6d7s^2$	Np(I)	F^2	43 317	72 662	1.000	1.000	0.596	29 345	Crosswhite (1986)
		F^4	37 170	47 094	0.858	0.648	0.789	9924	
		F^6	23 286	34 436	0.538	0.474	0.676	11 150	
$5f^5 6d7s^2$	Pu(I)	F^2	47 975	76 279	1.000	1.000	0.629	28 304	Wyart (1998)
		F^4	37 590	49 543	0.783	0.649	0.758	11 953	
		F^6	33 441	36 268	0.697	0.475	0.921	2827	

trend of analogous configurations as a function of atomic number in the neutral atoms has been shown in Figs. 16.3(a), (b), and 16.6. The relative configuration energies as a function of ionization stage are given in Table 16.4 for Th I–IV 5f, 6d, 7s, and 7p, showing that the 5f configuration becomes increasingly more stable as outer electrons are removed (5f gains 17000 cm^{-1} over 6d in going from Th I to Th IV). The change in 5f energy with increase in atomic number corresponds to the actinide contraction, which increases the effective nuclear charge Z^*. Increasing ionization also increases Z^* by reducing the shielding of 5f electrons from the nucleus as outer electrons are removed. The effect on the 5f energy is thus in the same direction as with increasing Z. The outer electrons 7s and 7p are more nearly hydrogenic and have energies that become more negative as approximately the square of the ionic charge (about the same for all Z). Hence the 7s–7p difference increases with ionic charge.

Racah (1950) treated the term structure of Th III in a classic paper on least-squares parameter fitting in intermediate coupling with CI. With these off-diagonal matrix elements included, the calculated energies were in much better agreement with observation, and in addition, the calculated g-values were also in better agreement than the pure SL Landé g-factors. This has been the general experience in fitting spectra with more than two electrons: the better the energy fit, the better the g-value fit; it also applies to other properties such as IS, hfs, and relative intensities of transitions, and thus lends confidence to the calculation. Attempts to make the g-value fit more exact by trying to fit the energies and g-values simultaneously have not been successful because these are not independent quantities. If the calculated g-values are not more or less in agreement with observation, it is an indication that some interactions are missing from the energy matrix. Since parameter fits in the general case are not exact and are in a state of flux, no attempt has been made in Table 16.1 or 16.2 to try to include calculated g-values or other calculated properties. Comparison of g (exp) with calculated SL g-values serves as an indication of how much intermediate coupling and CI are present and not that the assignment is in doubt. Tables 16.1 and 16.2 show that, in moving toward the middle of the actinide series, the multiplicity increases in accord with Hund's rules.

Thus in Pa I (the first true actinide with a 5f electron in the ground state), there are quartets and sextets (and also doublets in the higher states), whereas in Am I there are octets and decets (and also sextets, quartets, and doublets). This has a profound effect on the intensity distribution of the observed spectral lines. In pure SL coupling, there is a selection rule $\Delta S = 0$ (octet terms have transitions only to octets, etc.). In intermediate coupling, as obtains in the actinides, there are off-diagonal spin–orbit matrix elements between terms of adjacent multiplicity ($\Delta S = 0, \pm 1$), which means that octet terms, for example, will also have some decet and sextet eigenvector components, and therefore have transitions to decet and sextet terms. There will be, however, no transitions to quartet and doublet terms. The strong lines (those involving the low terms) will therefore consist of transitions between terms of high multiplicity that are

Table 16.4 *Comparison of thorium configurations in four stages of ionization.*

Th IV (Th^{3+})		*Th* III (Th^{2+})		*Th* II (Th^{+})		*Th* I (Th^{0})	
Configuration	*Level* (cm^{-1})	*Configuration*	*Level* (cm^{-1})	*Configuration*	*Level* (cm^{-1})	*Configuration*	*Level* (cm^{-1})
5f	0	5f 7s	2527	$5f\,7s^2$	4490	$5f\,7s^27p$	18 432
6d	9193	6d7s	5524	$6d7s^2$	1860	$6d7s^27p$	10 783
Δ(5f–6d)	–9193		–2997		2630		7649
7s	23 130	$7s^2$	11 961	$6d7s^2$	4113	$6d^27s^2$	0
7p	60 239	7s7p	42 260	6d7s7p	23 373	$6d^27s7p$	14 465
Δ(7s–7p)	–37 109		–30 299		–19 260		–14 465

comparatively few in number. There will also be transitions among the terms of low multiplicity but these will be very numerous and weak. The observed Am I spectrum thus consists of a relatively small number of strong lines superimposed on a weak complex background. The strong lines are easy to classify into a transition array; the weak lines are not. The determination of the G^k parameters requires knowledge of terms of all multiplicities, not obtainable from just the strong lines. At the beginning of the actinide series, by contrast, the multiplicities are all low and the ΔS selection rule is not so restrictive, hence the range in intensity is not so great. In fact Pa I appears at first sight to have the most complex spectrum of all the actinides because of the comparatively uniform intensities, despite fewer expected terms. The Pa spectrum is further complicated by the presence of hfs. Many transitions have four hfs components that have a large degradation in intensity because of the low nuclear spin (^{231}Pa, $I = 3/2$) and low J values, so they often cannot be distinguished from neighboring weak lines. In Am (for the relatively long half-life isotopes ^{241}Am and ^{243}Am, $I = 5/2$), each level has six hfs components when $J \geq 5/2$, in Bk and Es (for ^{249}Bk and ^{253}Es, $I = 7/2$) each level has eight hfs components when $J \geq 7/2$, with less degradation so they usually stand out from the background. Hence the analysis and interpretation of a spectrum like Pa is no easier than for later elements with larger multiplicities.

Another characteristic of the actinide series is the fact that the L values for f^n go through a maximum not at the half-filled shell, as in the case of the S values, but at the one-fourth and three-fourths-filled shells. Thus the ground state of Np I f^4ds^2 is $^6L_{11/2-21/2}$ and for Np(I) f^4d^2s it is $^8M_{11/2-25/2}$. These high J values are poorly excited by electron collision in the light source, so transitions to the highest J levels are weak and hard to find, in contrast to multiplets at the beginning of the actinides. For the three-fourths-filled f^n shell, the multiplets are inverted and not so much of a problem. The high L values for Np have a considerable effect on the hfs because the large orbital angular momentum produces a high magnetic field at the nucleus that increases the orbital contribution. The Np I ground level has a total width of 0.776 cm^{-1} in spite of having no unpaired s-electron, the usual source of large hfs (Fred *et al.*, 1977). Bk I and Es I have even larger widths, 1.150 and 1.532 cm^{-1}, due to larger nuclear spin, larger J value, and larger Z (Worden *et al.*, 1974, 1987). The ability to measure the intervals of the hfs patterns to better than 1 part in 1000 is a great help in the empirical analysis of these spectra. Moreover, the quantum numbers of the various levels can be obtained by comparing the relative widths with those calculated by standard hfs theory.

To summarize, the spectroscopic properties of all the actinide elements that can be studied by conventional emission spectroscopy, Ac to Es, have now been investigated experimentally and theoretically. The present status is satisfactory in that most of the electronic structure information of interest for actinide chemistry is available. The experimental completion of the determination of the electronic structure of the last four elements in the actinide series will

take considerable effort and new techniques due to the limited availability of the elements and their short half-lives. Theoretical estimates together with extrapolations (e.g. Vander Sluis and Nugent, 1972; Brewer, 1984) from the known structure of the lower actinide elements are needed. In addition, further efforts are required to provide the complete details for some of the lighter actinide elements.

16.9 NEW PROPERTIES OF ACTINIDES DETERMINED BY CONVENTIONAL SPECTROSCOPY AND MATERIAL LEFT FOR DATA REDUCTION

The signs of the nuclear magnetic moments in both ^{249}Cf and ^{251}Cf have been determined to be negative (Conway *et al.*, 1995). From the examination of the direction of degradation of the hfs of the ground and first excited levels in the second spectrum of ^{249}Cf, the $^{6}I_{17/2}$ and the $^{4}I_{15/2}$ of $5f^{10}7s$ were found to be inverted and regular, respectively. Since the hfs of both isotopes degraded in the same direction, it was concluded from this data that the sign of the nuclear magnetic dipole moment of both isotopes is negative. The nuclear spins of both isotopes were confirmed as 9/2 for ^{249}Cf and 1/2 for ^{251}Cf. A large number of ^{251}Cf lines with two components were observed indicating the nuclear spin of this isotope is 1/2. With the high J values involved in most Cf transitions, the off-diagonal components for ^{251}Cf are very weak (3% or less of the total intensity when $J > 3$) (White, 1934) and so they were not observed in the spectra resulting in many lines with two components.

There is considerable actinide spectroscopic data awaiting analyses. One complete set of photographic plates for Bk taken on the ANL spectrograph is in storage at LLNL. The Bk structure was determined from measurements of photographic plates taken on a 3.4 m Ebert spectrometer with a special high-angle grating and order sorter (the resolution and dispersion were about equal to that of the ANL spectrograph). Worden, using a Grant comparator at LLNL, measured the plates and then the data were analyzed (Worden *et al.*, 1987). Some of the Zeeman spectra taken on the ANL spectrograph were measured (again by Worden) to determine Landé g-values used in the level analyses. A complete set of plates was taken in 1976 on the ANL spectrograph using EDLs with the major isotope ^{250}Cf and known ^{249}Cf, ^{251}Cf, and ^{252}Cf content, including some with an additional spike of ^{252}Cf. The IS values for ^{250}Cf vs ^{249}Cf, ^{251}Cf, and ^{252}Cf should result from measurements of these plates as well as a better set of wavelengths (there are no hfs and subsequent broadening with ^{250}Cf as there is with the current ^{249}Cf-line list). Improved analyses of the neutral and especially the first ion spectra (where the hfs is larger) should be possible.

The complete Es spectrum was measured on the ANL spectrograph in 1975. Earlier measurements were done at LLNL (Worden *et al.*, 1974). The ANL

photographic plates should produce a much more complete list and many more levels should be obtained. Blaise and Wyart are currently working on these data to improve the analyses of the Es I and II spectra (Blaise *et al.*, 2003; Wyart *et al.*, 2005).

16.10 LASER SPECTROSCOPY OF ACTINIDES

A large number of hfs A and B factors for ^{235}U have been determined by laser spectroscopy. The data list included 35 odd (28 low-lying odd levels of the configuration $5f^36d7s^2$) and 34 even levels from 15500 to 31000 cm^{-1}, many with very high precision (Childs *et al.*, 1979a,b; Hackel *et al.*, 1979; Greenland *et al.*, 1981; Avril *et al.*, 1986, 1994; Demers *et al.*, 1986). A very large number of high-lying upper levels of both parities have been found by multi-step laser spectroscopy of U by researchers in the USA, France, England, India, Japan, and China. However, these level determinations are inaccurate (uncertainties ranging from 0.5 to 2 cm^{-1}) as compared with typical emission spectra levels derived from grating spectrographs or FTS instruments (with 0.02 to 0.001 cm^{-1} uncertainty) so no references are given.

The signs of the ground state A and B factors of neutral ^{241}Am (Le Garrec and Petit, 1986) and ^{243}Am (Meisel *et al.*, 1987) have been determined by high-resolution laser spectroscopy of the Am isotopes to be $A < 0$ and $B > 0$. The ^{242m}Am isotope has the same sign because the hfs has the same degradation. Considerable laser spectroscopy of Pu has been accomplished, but little except the IP has been published in the open literature (Worden *et al.*, 1993). The same is true of Np where the energy separation of 24.27 cm^{-1} between the two lowest levels of Np II (Fred and Blaise, 1978) was used to help confirm the observation of Rydberg series in Np I (Worden and Conway, 1979). A review of multi-step laser excitation of lanthanides and actinides has been published (Worden and Conway, 1980) with a discussion of properties that can be determined by the use of laser spectroscopy.

16.11 IONIZATION POTENTIALS OF ACTINIDES BY LASER SPECTROSCOPY

The precise determination of the first IP of the actinide elements is important for the identification of systematic trends in binding energies of the elements. It is also important for drawing conclusions about the electronic structure of the atoms, since the first IP is directly connected to the atomic spectra. Information about the electronic structure of the actinides is required to predict deviations from the regularities of the periodic table (Pyykkö and Desclaux, 1979) caused by relativistic effects which are expected in this region as a result of the relativistic mass increase of the inner electrons (Pyykkö, 1988). The IPs are useful

quantities in the Born–Haber cycle (Morss, 1971) and also allow comparison with predictions of multi-configuration Dirac–Fock calculations (Fricke *et al.*, 1993), a successful theoretical treatment for heavy multi-electron atoms.

Ionization energies of the neutral atoms were derived by Sugar using interpolation of the series properties of the $5f^n7s8s$ configurations. They are given in Table 16.5 (Sugar, 1974). The first accurate experimental value of an IP of an actinide element was by multi-step laser spectroscopic observation of reasonably long high-energy Rydberg series in uranium by Solarz *et al.* (1976) who obtained the value 49958.1(4.0) cm^{-1}. In the Solarz technique, delayed ionization by use of a CO_2 laser was employed to separate the short-lived valence levels from the long-lived Rydberg levels enabling their detection in the very complex spectrum. The photoionization limit was often determined first to limit the scan range needed for measuring Rydberg levels to less than 50 to 100 cm^{-1}. Such a limit is usually easy to detect by the sharp rise in ions as the photoionization laser is scanned in a multi-step excitation scheme. These were normally determined with the apparatus used in the configuration without delayed field ionization (Worden *et al.*, 1978). In an experiment similar to that of Solarz *et al.*, Coste *et al.* (1982) used delayed field ionization to measure an

Table 16.5 *First IPs (IP_{exp}) of the actinide elements determined by RIMS. Tabulated are also IPs (IP) from laser spectroscopy measurements. The method and reference is given in column* 5 *(RA = comparison of lifetimes of Rydberg and autoionizing states, RC = Rydberg convergence limits). The predictions by extrapolation of spectroscopic data* (*Sugar*, 1974) *are given in column* 6.

Actinide element	$IP_{exp.}$ (cm^{-1}) (*RIMS*)	$IP_{exp.}$ (eV) (*RIMS*)	*IP* (cm^{-1}) (*others*)	*Method and references*	*Extrapolated* (*Sugar*, 1974)
Ac	43 398(3)	5.3807(3)			41 700(1000)
Th	50 867(2)	6.3067(2)	50 890 (20)	RA (Johnson *et al.*, 1992)	49 000(1000)
Pa	—	—			47 500(1000)
U	49 957(2)	6.1939(2)	49 958(4)	RC (Solarz *et al.*, 1976)	48 800(600)
			49 958.4 (5)	(Coste *et al.*, 1982)	
Np	50 535(2)	6.2655(2)	50 536(4)	RC (Worden and Conway, 1979)	49 900(1000)
Pu	48 601(2)	6.0258(2)	48 604(1)	RC (Worden *et al.*, 1993)	48 890(200)
Am	48 180(3)	5.9736(3)			48 340(80)
Cm	48 324(2)	5.9914(2)			48 560(200)
Bk	49 989(2)	6.1978(2)			50 240(200)
Cf	50 665(2)	6.2817(2)			50 800(200)
Es	51 358(3)	6.3676(3)			51 800(200)

RA, Rydberg autoionization; RC, Rydberg convergence of relative long series.

IP of 49958.4(5) cm^{-1} for the U atom. The IP of neutral Np was measured at 50 536(4) cm^{-1} using similar laser techniques (Worden and Conway, 1979). These values are, respectively, 2 and 1% larger than Sugar's estimates (see Table 16.5). Rydberg levels have been measured by delayed field ionization and were created by a number of different processes (Worden *et al.*, 1978; Worden and Conway, 1980) including collisional ioniziation converging to the ground state and auto-ionization levels converging to excited levels in the ion. The IP of ^{239}Pu was measured using a number of laser methods by Worden *et al.* (1993) to obtain the value 48 604(1) cm^{-1}. The experiments included the observation and measurement of hfs of ^{239}Pu and the IS of ^{240}Pu–^{239}Pu in auto-ionization levels, the first such measurement for an actinide.

16.12 FIRST IONIZATION POTENTIALS OF THE ACTINIDES BY RESONANCE IONIZATION MASS SPECTROMETRY

The first IPs of the common lighter actinide elements Th, U, Np, and Pu have been determined by laser spectroscopy (Solarz *et al.*, 1976; Worden and Conway, 1979; Coste *et al.*, 1982, Johnson *et al.*, 1992; Worden *et al.*, 1993). The most precise measurements were performed by the study of long-lived Rydberg series converging to one or more limits in the ion. For these elements, gram amounts of the metal were readily available for use in experiments. About 1 g of material was used to determine the IP of Np by these techniques (Worden and Conway, 1979). As much as 2 g of ^{239}Pu was used for the determination of the IP of ^{239}Pu by the observation of the threshold of ionization and of a large number of Rydberg series that converged to five separate limits in the ion (Worden *et al.*, 1993). A large amount of other types of spectroscopy was done with these samples that was not part of the IP determination and has not been published.

RIMS, first developed for ultra-trace analysis of actinide nuclides (Ruster *et al.*, 1989), has been introduced as a method that allows the accurate determination of the first IP of the actinides with samples of only 10^{12} atoms ($\sim$400 pg) or less. This makes possible the measurement of IPs of the heavier actinides and some light actinides that can be conveniently handled only in small quantities because of the strong radioactivity or that may be available only in very limited amounts.

The method is based on the determination of the photoionization thresholds in the presence of an external electric field and is explained in detail in a number of papers (Riegel *et al.*, 1993; Trautmann, 1994; Köhler *et al.*, 1997; Erdmann *et al.*, 1998). There it is shown that the observed ionization threshold is proportional to the square root of the electric field strength E. For the determination of the first IP, the wavelength of the laser for the ionizing step in a multi-step process is scanned across the threshold in the presence of E. The ionization threshold $W_{th}(E)$, the total energy of the exciting lasers, is indicated by a sudden increase of the ion count rate. This procedure is repeated for various electric

field strengths and the extrapolation of $W_{th}(E)$ to zero field strength leads to the energy of the first IP.

The experimental set-up (Ruster *et al.*, 1989) for resonance ionization mass spectrometry generally consists of three tunable dye lasers pumped by two pulsed copper vapor lasers (6.5 kHz pulse repetition rate, with 30 and 50 W average output power, 30 ns pulse duration) and a time-of-flight (TOF) mass spectrometer. The dye laser beams are focused into the TOF region where they interact perpendicularly with the atomic beam of the element under investigation. Ionization by two- or three-step resonant laser excitation takes places in the presence of an electric field. The importance of 6.5 kHz excitation is for efficient excitation of the atoms in the atomic beam of this set-up. Special care is taken to make the electric field homogenous and to keep it free of stray electric fields by use of corrective electrodes.

For the determination of the first IP of actinium (Waldek *et al.*, 2001), a frequency doubled titanium–sapphire laser pumped by a NdYAG laser (Grüning *et al.*, 2004) was used for one-step resonant excitation and a dye laser for the ionization step. In all experiments, the wavelengths of the laser beams were measured by pulsed wavemeters with a precision of $\Delta\lambda/\lambda = 10^{-6}$.

One crucial part for the application of resonance ionization mass spectrometry to determine the first IP is the creation of an atomic actinide beam. This is achieved by resistive heating of a sandwich filament consisting of a thin tantalum foil on which the element under investigation is electrochemically deposited in the form of the hydroxide (3 mm spot) and covered with a thin layer ($\sim$1 μm) of titanium or zirconium produced by sputtering. By heating such a sandwich filament, the hydroxide is converted to the oxide, which is reduced to the metallic state during diffusion through the covering layer. For the elements of uranium up to fermium, a titanium layer was used whereas for actinium the reduction by titanium was not efficient and therefore zirconium was used. Efficient release from these filaments occurs at temperatures between 800 and 1200°C, depending on the element. For protactinium, it was not possible to produce an atomic beam in this way, not even with thorium as reducing agent. As a result, an experimental value of the first IP of protactinium with RIMS is still missing.

For all the measurements of the photoionization thresholds either two-step (Ac, Np) or three-step (Th, U, Pu, Am, Cm Bk, Cf, Es) excitation schemes were used, each starting from the atomic ground state (Table 16.6). The wavelengths for the excitation steps were selected by use of energy levels published by Blaise and Wyart (1992) or by finding levels with scans of the appropriate laser. The photo-ionization thresholds were determined with various electric field strengths of 1.6–340 V cm^{-1}. The precision of the photo-ionization threshold method was checked by the re-determination of the first IP of Th, U, Np, and Pu. There is excellent agreement as can be seen from Table 16.5. With quantities of only $\sim 10^{12}$ atoms each, the first IPs of Ac, Am, Cm, Bk, Cf, and Es were determined for the first time by RIMS. Plots of the obtained ionization

Table 16.6 *Excitation schemes of the actinide elements used for the determination of the first IP by RIMS. The last step laser wavelength is approximate because the laser is scanned in the presence of an electric field of various voltages.*

Actinide element	λ_1 (nm) *air*	*First excited state* (cm^{-1})	λ_2 (nm) *air*	*Second excited state* (cm^{-1})	*Ionizing* λ (nm)
Ac	388.56	25 729.0	—	—	≈568
Th	580.42	17 224.3	622.90	33 273.8	≈568
U	639.54	15 631.9	591.47	32 534.1	≈577
			585.85	32 696.3	≈582
Np	311.81	32 061.3	—	—	≈541
Pu	648.89	15 406.6	629.57	31 285.9	≈579
Am	640.52	15 608.5	654.41	30 885.1	≈578
Cm	655.46	15 252.2	640.56	30 859.1	≈573
Bk	565.90	17 666.0	720.50	31 541.3	≈544
			664.52	32 710.3	≈581
Cf	572.61	17 459.2	625.04	33 453.7	≈583
Es	561.53	17 803.5	661.13	32 924.9	≈544

thresholds of these elements versus the square root of the applied electric field strength E are shown in Fig. 16.10. The values fit perfectly the linear extrapolation to zero field strength by least-squares fits. The first IP of all the actinide elements from Ac to Es with the exception of Pa have been determined with RIMS (Riegel *et al*., 1993; Trautmann, 1994; Deissenberger *et al*., 1995; Köhler *et al*., 1996, 1997; Erdmann *et al*., 1998; Peterson *et al*., 1998; Waldek *et al*., 2001). The results are summarized in Table 16.5 together with experimental data obtained by other methods and published in the literature (Solarz *et al*., 1976; Worden and Conway, 1979; Johnson *et al*., 1992; Worden *et al*., 1993) as well as with predictions from extrapolation of spectroscopic data (Sugar, 1974). The uncertainties of the RIMS values are statistical errors given as two standard deviations (2σ) derived from the least-squares fits including weighted errors for each data point.

An attempt to determine the first IP of Fm with 2 to 5×10^{10} atoms of ^{255}Fm ($t_{1/2} = 20.1$ h) with RIMS failed due to the short half-life of ^{255}Fm and the fact that no spectroscopic data for Fm were available. However, with a sandwich filament, where 2.7×10^{10} atoms of ^{257}Fm were electrodeposited on a Ta backing and covered with ~1 μm Ti, an atomic beam of Fm was produced at ~1000°C. The atoms were stored for ~40 ms in argon gas buffer-optical cell. They were resonantly excited and ionized with two beams of an excimer-dye consisting of a 200 Hz excimer pump laser that runs on XeF at wavelengths of 351/353 nm, and a one-step tunable dye laser. The resulting ions were identified after extraction from the optical cell with a quadrupole mass filter and a channeltron detector. Two atomic resonances of Fm were observed for the first time in this experiment at wavenumbers of 25099.80(4) cm^{-1} and 25111.80(4) cm^{-1}, and their lifetimes were estimated (Sewtz *et al*., 2003).

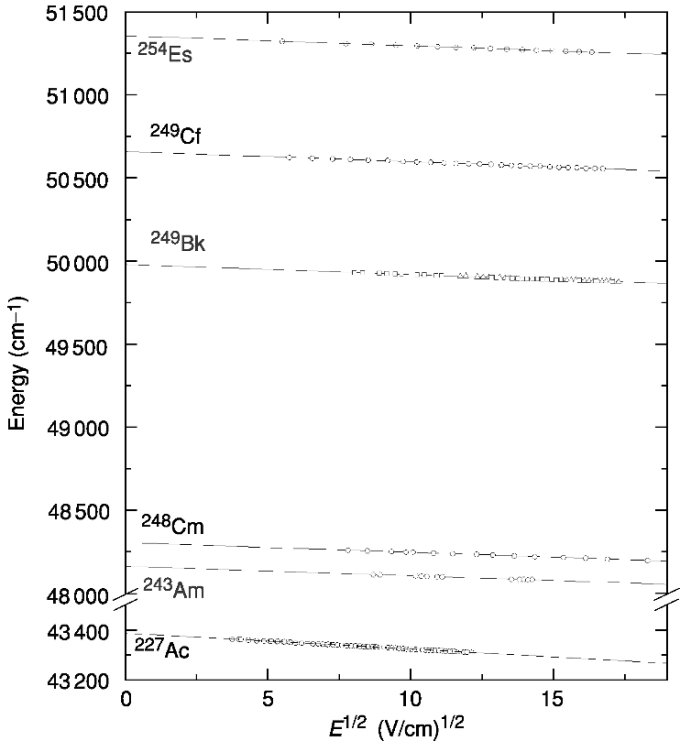

Fig. 16.10 *Plot of the measured ionization thresholds vs the square root of the electric field strength* E *for Ac, Am, Cm, Bk, Cf, and Es. Extrapolation to zero field strength yields the first IP. With this method, the first IPs of the six actinide elements shown here were determined experimentally for the first time.*

The ionization energies of the process $f^n s^2 \rightarrow f^n s$ were calculated by means of semiempirical Slater–Condon and *ab initio* HF calculations (Rajnak and Shore, 1978). For the lanthanides as well as for the actinides, the removal of an s-electron from the lowest $f^n s^2$ level producing an ion in the lowest $f^n s$ level is the most frequent mode of ionization in the f-series, and these ionization energies are called 'normalized IP–IP_n'. In all cases where the ground states differ from the configurations $f^n s^2$ and $f^n s$, corrections must be made by use of the known level energies of the lowest levels of the $f^n s^2$ and $f^n s$ configurations in the neutral and singly ionized atoms. In the lanthanide series (Worden *et al.*, 1978), it was observed that in a plot of IP_n versus n, the plot forms two straight lines connected at the half-filled shell ($n = 7$). The change in slope is interpreted as an effective exchange integral. A similar behavior is expected for the first IPs of the actinide elements.

In order to compare the experimental results with theoretical predictions (Sugar, 1974; Rajnak and Shore, 1978), the first IPs, normalized to

$5f^n7s^2 \rightarrow 5f^n7s$, are plotted versus the number of 5f electrons in Fig. 16.11. The experimental values of the heavier actinide elements are a little bit lower than the extrapolated data (Sugar, 1974) and slightly above the HF calculations (Rajnak and Shore, 1978). For the lighter actinides, the experimental IPs show strong deviations from the linear dependence, which might be connected to the fact that the ground states differ from f^ns^2 and most likely are due to CI. As pointed out (Rajnak and Shore, 1978), the actinide IPs should follow the trend for binding energies of the s-electrons by forming two straight lines, with a change of slope at Am, the half-filled f-shell. While the early actinides show considerable scatter, the higher actinides do follow the predicted behavior very well.

The high precision of RIMS in measuring the first IP of the actinides may also enable a determination of the isotope dependence of the IP, especially for elements which differ significantly in their neutron number, like ^{232}U and ^{238}U or ^{236}Pu and ^{244}Pu. The extension of the method to elements beyond Fm is difficult due to the limited amounts of material available and the short half-lives of the transfermium isotopes. For such investigations with online produced isotopes, an apparatus for RIMS in a buffer gas cell has been developed and might be suitable (Backe *et al.*, 1997). This method is based on resonance ionization in an argon buffer gas cell followed by ion-guide extraction and mass-selective direct detection of the resonantly ionized atoms.

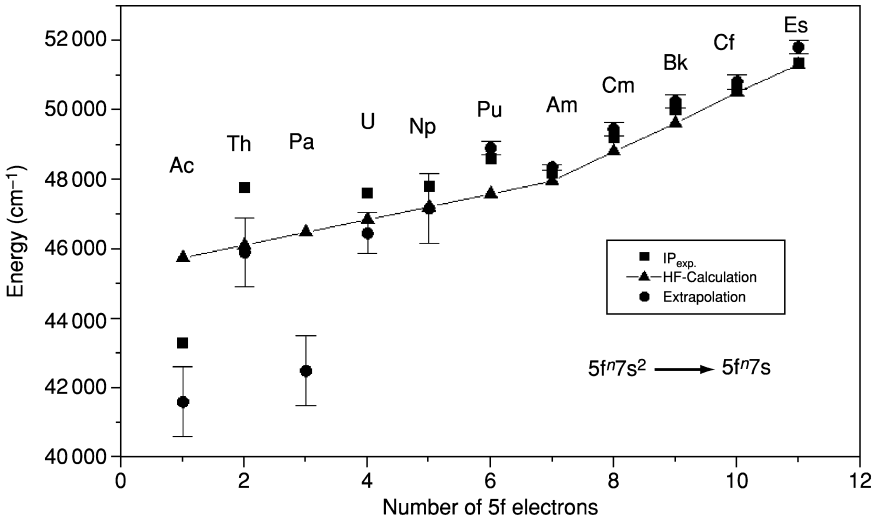

Fig. 16.11 *Comparison of the experimentally determined IPs of the actinides with two predictions* (*Sugar*, 1974; *Rajnak and Shore*, 1978). *The normalized first IPs* (IP_n) *are plotted for the ionization process* $5f^n7s^2 \rightarrow 5f^n7s$ *as a function of n, the number of 5f electrons. A straight line is drawn through the data from Hartree–Fock* (*HF*) *calculations* (*Rajnak and Shore*, 1978) (— ▲ —); *the values from extrapolated spectral properties* (*Sugar*, 1974) (●) *and the experimental data* $IP_{exp.}$ (▪) *are given with their errors.*

16.13 LASER SPECTROSCOPY OF SUPER-DEFORMED FISSION ISOMERS OF AMERICIUM

Fission isomers are interpreted as shape isomers (Bjornholm and Lynn, 1980; Metag *et al.*, 1980) corresponding to a second minimum in the potential energy surface (Strutinsky, 1967, 1968). The structure of the fission barrier with a double hump results from the superposition of shell corrections to the nuclear binding energy onto the rather flat maximum of the macroscopic part of the deformation energy as described by the liquid drop model. The double-humped fission barrier explains the basic features of fission isomers; e.g. their excitation energy of 2–3 MeV, their stability against γ-decay due to the inner barrier, and their short half-lives for spontaneous fission determined by the penetration of the outer barrier that is much smaller than the barrier for the spontaneous fission decay from the ground state. The fission isomers are mainly located in the actinide region and their half-lives are in the ps- to ms-range and thus 24–30 orders of magnitude shorter than those for spontaneous fission from the respective nuclear ground states.

The deformation parameter, the magnetic moment, and the nuclear spin can best be obtained by optical IS and hfs spectroscopy (Otten, 1989). These are valuable data for testing nuclear matter in the state of extreme deformation as is the case for fission isomers. A measurement of the IS allows the determination of the nuclear deformation parameter β_2. If the IS can be measured in chains of fission isomers, information on the stability of nuclear deformation as a function of the neutron number can be obtained. Furthermore, by resolved optical hyperfine spectroscopy, the intrinsic quadrupole moment, the nuclear spin, and the g-factor can be deduced. However, such experiments are not easy to perform due to the low production rate of fission isomers, on the order of a few per second and their very short half-lives ($t_{1/2} \leq 14$ ms).

Bemis and coworkers (Bemis *et al.*, 1979) provided the first direct experimental proof for the large deformation in ^{240f}Am ($t_{1/2} = 0.9$ ms) by laser spectroscopy. With the laser-induced nuclear polarization (LINUP) technique, they determined the relative IS ratio $IS^{240f/241}/IS^{243/241} = 26.8\ (20)$ by measuring the 640.5 nm optical transition ($^{10}P_{7/2} \rightarrow {}^{8}S_{7/2}$) for the isotopes ^{240f}Am, ^{241}Am, and ^{243}Am.

In order to extend the optical measurements on fission isomers, an ultrasensitive technique, radioactive-detected resonance ionization spectroscopy (RADRIS) in a buffer gas cell, has been developed (Backe *et al.*, 1992b, 1998) to perform hyperfine spectroscopy of fission isomers produced in heavy-ion-induced reactions. The method is based on resonance ionization in a buffer gas cell combined with radioactive decay detection and its feasibility was demonstrated with the β-active isotope ^{208}Tl (Lauth *et al.*, 1992). The first experiment on ^{242f}Am with the RADRIS technique was done at the Max-Planck-Institut für Kernphysik in Heidelberg (Backe *et al.*, 1992b). The experimental set-up is shown in Fig. 16.12. The ^{242f}Am fission isomers were produced via the reaction

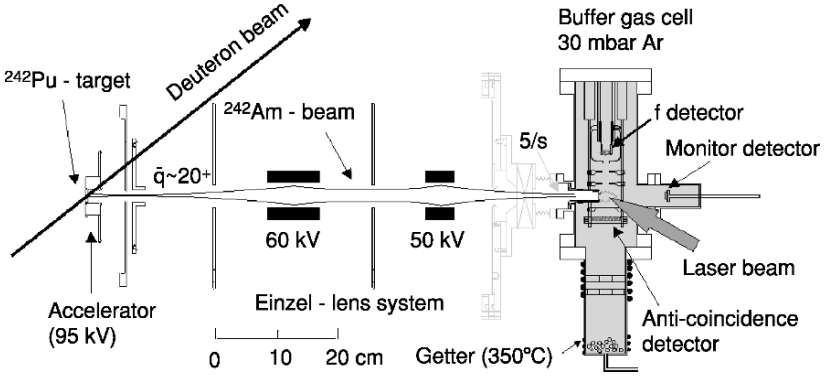

Fig. 16.12 *Experimental set-up for fission-detected resonance ionization spectroscopy in a buffer gas cell* (*Backe* et al., 1998). *For the production of* ^{242f}*Am a deuteron beam hits a* ^{242}*Pu-target and the fission isomers recoiling out of the target are accelerated and focused with an Einzel-lens system onto the entrance window of the optical buffer gas cell. The anti-coincidence fission detector is a PIN PD chip and the fission detector a windowless PIN photodiode. A dye laser and an excimer laser are used for resonance excitation and ionization. Getter techniques are applied to purify the gases.*

^{242}Pu (d,2n) ^{242f}Am by using a pulsed (5 ms on, 5 ms off) 12 MeV deuteron beam on a 50 μg/cm^2 $^{242}PuF_3$-target with a thin carbon backing. The fission isomers leaving the target have a recoil energy <100 keV and non-equilibrium ionic charge states between 10^+ and 35^+ (Metag *et al.*, 1980) as a result of conversion electron transitions followed by Auger cascades. After post-acceleration at a potential of 95 kV, the energy of the fission isomers was high enough to penetrate a 50 μg/cm^2 thick entrance window of the optical cell. On their way to the buffer gas cell, the fission isomers were focused with an Einzel-lens system. The ^{242f}Am beam at the entrance of the cell amounted typically to 5/s at a deuteron beam current of 5 μA. The optical cell, filled with 30 mbar argon and as quenching gas 0.3 mbar nitrogen, was loaded with the fission isomers during the beam-on periods. A fraction of ~15% of the recoiling ions was neutralized in the gas (Backe *et al.*, 1992a). The ions, not neutralized in the collision with the buffer gas, were fixed onto a thin electrode foil (250 μg/cm^2) in front of the anti-coincidence fission detector by applying an electric field. The gas acted as a storage medium for the neutral fission isomers. The diffusion time to the cell walls has been estimated to be ~30 ms. Resonance ionization was performed in the beam-off periods by two-color excitation/ionization. For this, an excimer laser (EMG 104 MSC, Lambda Physik) lasing with XeF at 351 and 353 nm for the second step and a dye laser (FL 2001, Lambda Physik) for the first excitation step were used. The resonantly ionized fission isomers were transported within 1.40(8) ms in an electric field of the ion electrode system to the fission detector. Fission events originating from isomers sticking on the foil

in front of the anti-coincidence detector or from neutrals in the gas phase were completely rejected by the signal, which the simultaneously emitted second fission fragment generated in the anti-coincidence detection. The bandwidth of the dye laser could be improved from 6 to 1.5 GHz by means of an intercavity etalon. Wavelength calibrations and the optimization of the laser system were performed in an off-line buffer gas cell with the long-lived α-active isotopes ^{243}Am and ^{241}Am (Backe *et al.*, 1993). During the online experiments, the wavelength of the dye laser was continuously monitored with absorption in Te_2 vapor (Cariou and Luc, 1980).

In addition to the fission isomer ^{242f}Am, the ^{240f}Am and ^{244f}Am fission isomers were produced. The reaction ^{242}Pu(p,3n) ^{240f}Am (σ = 10 μb) with a pulsed (2 ms on, 2 ms off) proton beam of 23 MeV energy (Backe *et al.*, 1998) produced the ^{240f}Am fission isomer. A 14 MeV deuteron beam on a ^{244}Pu target of 30 μg/cm^2 thickness (2 ms on, 2 ms off) was used to create the ^{244f}Am fission isomer with $t_{1/2}$ = 1.0 ms via the reaction ^{244}Pu (d,2n) ^{244f}Am (Backe *et al.*, 2000). The target consisted of $^{244}PuO_2$ (97.88% ^{244}Pu) on a thin carbon backing (34 μg/cm^2).

Most of the measurements were done with ^{242f}Am. The IS of ^{242f}Am has been measured for three optical transitions for which the IS values IS$^{243/241}$ between the ^{243}Am and ^{241}Am isotopes are known (Worden, 1991–1993; Blaise and Wyart, 1992). The initial IS measurement was performed at λ_1 = 468.17 nm (Backe *et al.*, 1992b, 1993). An IS$^{242f/241}$ (468 nm) = –1.18(9) cm^{-1} was determined, corresponding to an IS ratio IS$^{242f/241}$/IS$^{243/241}$ = 24.6(24) using IS$^{243/241}$ = 0.048(3) cm^{-1} for this wavelength. A second measurement (Backe *et al.*, 1998) with λ_1 = 499.08 nm yielded an IS$^{242f/241}$ (499 nm) = +2.83(9) cm^{-1} and an isotope ratio IS$^{242f/241}$/IS$^{243/241}$ = 44.9(26) with IS$^{243/241}$ (499 nm) = 0.063(3) cm^{-1}. The disagreement of the two isotope ratio values originates from an anomaly in the 468.17 nm transition caused by configuration mixing. The same explanation can be given for the disagreement with the ~41 value and the value of 26.8 obtained by Bemis *et al.* at the 640.5 nm transition. The configuration mixing is between the 15608 cm^{-1} level and a level at 15273 cm^{-1} of the same parity and J with a large IS of opposite sign. A third measurement (Backe *et al.*, 1996, 1998) at λ_1 = 500.02 nm resulted in an IS$^{242f/241}$ (500 nm) = +10.358(14) cm^{-1}. The isotope ratio of IS$^{242f/241}$/IS$^{243/241}$ = 41.4(8) was obtained with IS$^{243/241}$ = 0.250(5) cm^{-1} in good agreement with the value at λ_1 = 499.08 um.

The IS measurements of ^{240f}Am at the 500 nm transition (Backe *et al.*, 1998) delivered a resonance signal just 0.56 cm^{-1} away from the one of ^{242f}Am. The IS$^{240f/241}$ = 9.80(3) cm^{-1} corresponds to an IS ratio IS$^{240f/241}$/IS$^{243/241}$ = 39.2(8). The IS of ^{244f}Am relative to ^{241}Am at a wavelength of 500 nm was determined to be IS$^{244f/241}$ = 10.49(4) cm^{-1}, with a signal very close to ^{240f}Am and ^{242f}Am, which gives an IS ratio IS$^{244f/241}$/IS$^{241/243}$ = 42.0(9) (Backe *et al.*, 2000, 2001). Fig. 16.13 summarizes the resonance ionization signals at the 500.02 nm transition of the fission isomers ^{244f}Am, ^{242f}Am and ^{240f}Am relative to ^{241}Am.

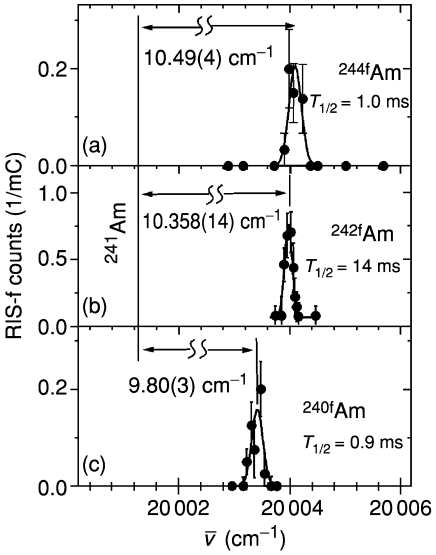

Fig. 16.13 *Resonance ionization signals of the fission isomers* ^{244f}*Am* (*a*), ^{242f}*Am* (*b*), *and* ^{240f}*Am* (*c*) *at the* 500.02 nm *transition* (*Backe* et al., 2001). *The IS values to the reference isotope* ^{241}*Am are indicated.*

Table 16.7 *Isotope shifts* $IS^{24xf/241}$, *IS ratios* $IS^{24xf/241}/IS^{243/241}$, *and nuclear parameters* $\lambda^{24xf/241}$ *for the fission isomers* ^{240f}*Am,* ^{242f}Am, and ^{244f}*Am. The measurements were performed at the* 500 nm *transition. The deformation parameters* β_2 *and the quadrupole moments* Q_{20} *have been calculated with the deformed droplet model* (*Backe* et al., 2001).

Isomer	$IS^{24xf/241}$ (cm^{-1})	$IS^{24xf/241}/IS^{243/241}$	$\lambda^{24xf/241}$ (fm^2)	β_2	Q_{20} (eb)
^{240f}Am	9.80(3)	39.2(8)	5.06(30)	0.690	33.9
^{242f}Am	10.358(14)	41.4(8)	5.34(28)	0.699	34.5
^{244f}Am	10.49(4)	42.0(9)	5.41(31)	0.694	34.4

In the determination of the deformation of the fission isomeric states, the mass shift contributions were neglected because the normal mass shift is only 0.004% of the measured IS of the fission isomers. The deformation parameters β_2 and the intrinsic quadrupole moments Q_{20} of the fission isomeric states have been evaluated (Backe *et al.*, 1998) on the basis of the droplet model (Meyers and Schmidt, 1983) and from the nuclear parameters employing a charge distribution of the deformed Fermi model (Brack *et al.*, 1974) with the assumption that the IS between ^{243}Am and ^{241}Am comes from a pure nuclear volume change. The results obtained with the deformed droplet model are presented in Table 16.7 for the three fission isomers of Am. In the analysis, a hexadecapole parameter $\beta_4^{II} = 0.08$ has been assumed, which is a theoretical prediction value

(Howard and Möller, 1980). The small differences of the nuclear charge parameters of the three fission isomers (e.g. $\Lambda^{244f/242f} = 0.069(21)$ fm^2) result in small changes of the deformation parameters β_2 and the quadrupole moments Q_{20}, as can be seen from Table 16.7.

Precise IS measurements are now available for the fission isomers ^{240f}Am, ^{242f}Am, and ^{244f}Am obtained with the fission RADRIS method in a buffer gas cell at very low production rates of ~5/s. The results demonstrate the stability of the deformation in the second potential minimum if neutron pairs are added in accordance with earlier calculations (Howard and Möller, 1980). The experimentally determined deformation parameters are a little bit larger than the theoretically calculated value $\beta_2 = 0.61$ (Howard and Möller, 1980). The laser spectroscopic method corroborates independently the charge plunger measurements (Metag *et al.*, 1980) and confirms the extreme deformation of fission isomers. To illustrate this, Fig. 16.14 shows the quadrupole moments of fission isomers and nuclear ground states for the lighter actinides. First hyperfine spectroscopic measurements, required for the determination of the nuclear spin and the *g*-factor, have been performed at the 466.28 nm transition of ^{242f}Am (Backe *et al.*, 1996). From the obtained data, a negative *g*-factor and a spin of $I = 2$–3 were derived (Lauth *et al.*, 1998). However, more detailed deformed shell-model calculations are required for the interpretation of the measured *g*-factor of ^{242f}Am. In addition to the results obtained with resonance ionization spectroscopy in a buffer gas cell, this method should also be applicable for studies of the atomic and nuclear properties of transeinsteinium elements (Backe *et al.*, 1997; Sewtz *et al.*, 2003).

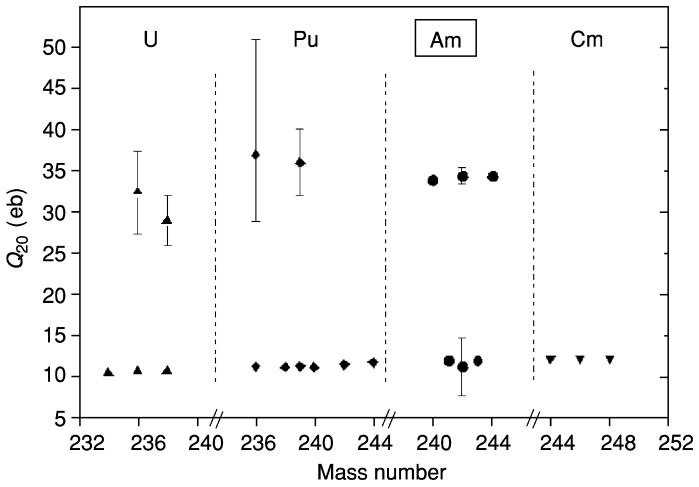

Fig. 16.14 *Quadrupole moments* Q_{20} *in the actinide region for the nuclear ground state and for the fission isomeric state.*

APPENDIX 16.1 THE CONSTRUCTION OF Es ELECTODELESS LAMPS

The design and construction of the EDL was modified when amounts of ~100 μg or more of Es became available because of the poor yields (<15%) obtained with no carrier element present (Worden *et al.*, 1968, 1970, and especially Worden *et al.*, 1974). The vacuum system used to prepare the pure Es lamps is shown in Fig. A16.1. A 6 mm outer diameter (o.d.) quartz frit was used to collect and wash ~100 μg of Es oxalate precipitated from a recently purified Es solution taken from a resin column. The high specific activity (5.6×10^{10} alpha activity per min per microgram) of ~100 μg of Es prevented collecting and washing of the precipitate in the usual 6 mm o.d. cone (because the intense alpha activity stirred up the solid) as done in normal lamp preparation. The quartz frit was inserted into reaction tube (at this point not sealed to the vacuum system as shown in Fig. A16.1) and the Es oxalate converted to Es_2O_3 by heating with a torch to red heat in the quartz frit with air present. The constriction at B was then made with a torch while holding the reaction tube vertical. The reaction tube was then turned horizontal and sealed to the Pyrex system at A in Fig. A16.1.

The assembly was pumped down to high vacuum ($<10^{-3}$ Pa) and the entire quartz part of the assembly was out-gassed with a tube furnace at ~1000°C. The thin capillary containing the AlI_3 was moved so that the iron slugs could break the tip using external magnets. Then the capillary assembly was moved so that the tip of the capillary was inside the reaction tube at constriction B. The AlI_3 was then sublimed into the reaction tube with a torch. The Es material and sublimed AlI_3 reactant and the final lamp were sealed off together at point B under high vacuum. The reaction at 560°C was carried out in a tube furnace with the reaction tube and lamp blank contained in a stainless steel tube with a

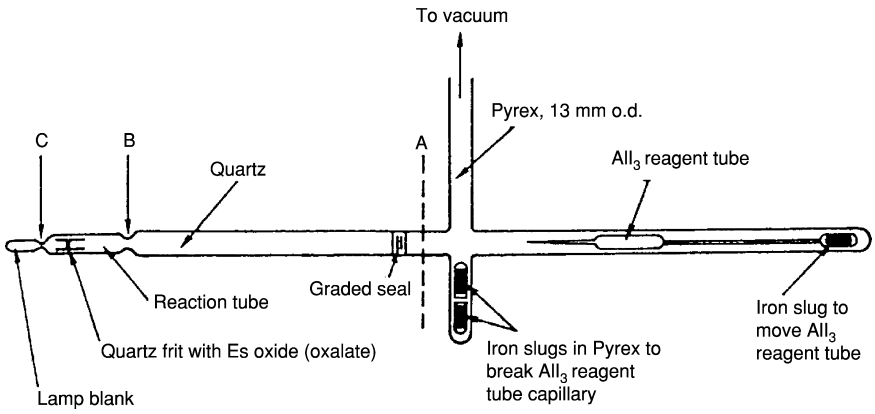

Fig. A16.1 *Vacuum apparatus for the preparation of einsteinium electrodeless lamps.*

sealed screw top for about 3 h. The stainless steel tube was cooled and the reaction tube and lamp blank removed. The product EsI_3 plus the excess AlI_3 was sublimed at ~750–800°C into the lamp blank cooled with wet asbestos cloth on the end of the lamp. The oven temperature was then reduced to ~500°C and the AlI_3 and other high vapor pressure impurities were sublimed into the reaction tube cooled with wet asbestos cloth. The lamp was then separated from the reaction tube at point C using a torch with wet asbestos cloth covering the lamp and reaction tube. This produced a lamp with up to 90% of the Es in the lamp, but also many impurities. The lamp life was about the same as lamps of other actinides prepared by the standard technique.

These procedures for the pure Es lamps were carried out at ANL so the time from purification of the 20.5 day half-life ^{253}Es to observation of the spectrum on the ANL spectrograph was reduced. The minimum time for the process was reduced to about 12 h vs the previous times of 2–3 days.

ACKNOWLEDGMENTS

This work was performed in part under the auspices of the U.S. Department of Energy by University of California, Lawrence Livermore National Laboratory under Contract W-7405-Eng-48. This document was prepared as an account of work sponsored by an agency of the United States Government. Neither the United States Government nor the University of California nor any of their employees, makes any warranty, express or implied, or assumes any legal liability or responsibility for the accuracy, completeness, or usefulness of any information, apparatus, product, or process disclosed, or represents that its use would not infringe privately owned rights. Reference herein to any specific commercial product, process, or service by trade name, trademark, manufacturer, or otherwise, does not necessarily constitute or imply its endorsement, recommendation, or favoring by the United States Government or the University of California. The views and opinions of authors expressed herein do not necessarily state or reflect those of the United States Government or the University of California, and shall not be used for advertising or product endorsement purposes.

LIST OF ABBREVIATIONS

ANL	Argonne National Laboratory
AVLIS	Atomic Vapor Laser Isotope Separation
EDL	electrodeless discharge lamp
FTS	Fourier Transform Spectrometers
GLS	generalized-least-squares
hfs	hyperfine structure
IP	ionization potential
IS	isotope shifts

LAC	Laboratoire Aimé Cotton
LINUP	laser-induced nuclear polarization
LLNL	Lawrence Livermore National Laboratory
NIST	National Institute of Standards and Technology
RADRIS	radioactive-detected resonance ionization spectroscopy
RIMS	resonance ionization mass spectroscopy
TOF	time of flight

REFERENCES

Avril, R., deLabachellerie, M., Viala, F., and Petit, A. (1986) *J. Less Common Metals,* **122**, 47–53.

Avril, R., Ginibre, A., and Petit, A. (1994) *Z. Phys. D,* **29**, 91–102.

Backe, H., Lauth, W., Achenbach, W., Hain, M., Hies, M., Scherrer, A., Steinhof, A., Tölg, S., and Ziegler, S. (1992a) *Nucl. Instrum. Methods Phys. Res.,* **B70**, 521–31.

Backe, H., Blönningen, Th., Dahlinger, M., Doppler, U., Graffé, P., Habs, D., Hies, M., Illgner, Ch., Kunz, H., Lauth, W., Schöpe, H., Schwamb, P., Theobald, W., and Zahn, R. (1992b) *Hyperfine Interact.,* **74**, 47–57.

Backe, H., Graffé, P., Habs, D., Hies, M., Illgner, Ch., Kunz, H., Lauth, W., Schöpe, H., Schwamb, P., Theobald, W., Thörle, P., Trautmann, N., and Zahn, R. (1993) *Hyperfine Interact.,* **78**, 35–45.

Backe, H., Baum, R.-R., Fricke, B., Habs, D., Hellmann, K., Hies, M., Illgner, Ch., Krameyer, Ch., Kunz, H., Lauth, W., Martin, R., Schwamb, P., Theobald, W., Thörle, P., and Trautmann, N. (1996) *Hyperfine Interact.,* **97/98**, 535–41.

Backe, H., Eberhardt, K., Feldmann, R., Hies, M., Kunz, H., Lauth, W., Martin, R., Schöpe, H., Schwamb, P., Sewtz, M., Thörle, P., Trautmann, N., and Zauner, S. (1997) *Nucl. Instrum. Methods Phys. Res.,* **B126**, 406–10.

Backe, H., Hies, M., Kunz.,H., Lauth, W., Curtze, O., Schwamb, P., Sewtz, M., Theobald, W., Zahn, R., Eberhardt, K., Trautmann, N., Habs, D., Repnow, R., and Fricke, B. (1998) *Phys. Rev. Lett.,* **80**, 920–3.

Backe, H., Dretzke, A., Hies, M., Kube, G., Kunz, H., Lauth, W., Sewtz, M., Trautmann, N., Repnow, R., and Maier, H. J. (2000) *Hyperfine Interact.,* **127**, 35–9.

Backe, H., Dretzke, A., Habs, D., Hies, M., Kube, G., Kunz, H., Lauth, W., Maier, H. J., Repnow, R., Sewtz, M., and Trautmann, N. (2001) *Nucl. Phys.,* **A690**, 215c–18c.

Bauche-Arnoult, C., Gerstenkorn, S., Verges, J., and Tomkins, F. S. (1973) *J. Opt. Soc. Am.,* **63**, 1199–203.

Bauche, J., Blaise, J., and Fred, M. (1963a) *C. R. Acad. Sci. Paris*, **256**, 5091–3.

Bauche, J., Blaise, J., and Fred, M. (1963b) *C. R. Acad. Sci. Paris*, **257**, 2260–3.

Bemis, C. E. Jr, Beene, J. R., Young, J. P., and Kramer, S. D. (1979) *Phys. Rev. Lett.,* **43**, 1854–8.

Bjornholm, S. and Lynn, J. E. (1980) *Rev. Mod. Phys.,* **52**, 725–931.

Blaise, J., Fred, M., Gerstenkorn, S., and Judd, B. R. (1962) *C. R. Acad. Sci. Paris*, **255**, 2403–5.

Blaise, J. and Radziemski, L. J. Jr (1976) *J. Opt. Soc. Am.,* **66**, 644–59.

Blaise, J., Luc, P., and Verges, J. (1977) *9th EGAS Conf*., Cracow.

Blaise, J., Wyart, J.-F., Conway, J. G., and Worden, E. F. (1980) *Phys. Scr.,* **22**, 224–30.
Blaise, J., Verges, J., Wyart, J.-F., Conway, J. G., and Worden, E. F. (1981) *Eur. Conf At. Phys.*, Heidelberg, vol. 5A, part I, pp. 102–3.
Blaise, J., Fred, M., Carnall, W. T., Crosswhite, H. M., and Crosswhite, H. (1983) *Plutonium Chemistry* (ACS Symp. Ser. no. 216), American Chemical Society, Washington DC, pp. 173–98.
Blaise, J., Wyart, J.-F., Palmer, B. A., and Engleman, R. Jr (1984a) *16th EGAS Conf.*, London.
Blaise, J., Fred, M., and Gutmacher, R. G. (1984b) Argonne National Laboratory Report ANL-83–95.
Blaise, J., Ginibre, A., and Wyart, J.-F. (1985) *Z. Phys. A. Atoms and Nuclei***, 321**, 61–3.
Blaise, J., Fred, M., and Gutmacher, R G. (1986) *J. Opt. Soc. Am. B*, 3, 403–18.
Blaise, J., Wyart, J.-F., Palmer, B. A., Engleman, R. Jr, and Launay, F. (1987) *19th EGAS Conf.*, Dublin, Europhys. Conf. Abstracts **11E**, A3–08.
Blaise, J., Wyart, J.-F., Engleman, R. J., and Palmer, B. A. (1988a) *J. Opt. Soc. Am. B,* **5**, 2087–92.
Blaise, J., Worden, E. F., and Conway, J. G. (1988b) *J. Opt. Soc. Am. B***, 5**, 2093–106.
Blaise, J. and Wyart, J.-F. (1992) *Energy Levels and Atomic Spectra of Actinides*. Tables Internationales de Constantes Sélectionées, Université Pierre et Marie Curie, Paris, vol. 20.
Blaise, J., Wyart, J.-F., Verges, J., Engleman, R. Jr, Palmer, B. A., and Radziemski, L. J. Jr (1994) *J. Opt. Soc. Am. B***, 11**, 1897–929.
Blaise, J., Worden, E. F., and Wyart, J.-F. (2003) analysis in progress.
Bordarier, Y. (1970) Thesis, University of Paris; Bordarier, Y., Bachelier, A., Sinzelle, J., computer codes (unpublished).
Brack, M., Ledergerber, T., Pauli, H. C., and Jensen, A. S. (1974) *Nucl. Phys. A,* **234**, 185–215.
Brault, J. W. (1976) *J. Opt. Soc. Am.,* **66**, 1081A.
Brewer, L. (1984) *High Temp. Sci.,* **17**, 1–30; (1971) *J. Opt. Soc. Am.*, **61**, 1101–11; 1666–82.
Cariou, J. and Luc, P. (1980) *Atlas du Spectre d'Absorption de la Molecule Tellure*, Laboratoire Aimé Cotton, CNRS II, Orsay, France.
Carnall, W. T., Crosswhite, H., and Crosswhite, H. M. (1978) *Energy Level Structure and Transition Probabilities of the Trivalent Lanthanides in* LaF_3, Argonne National Laboratory Report ANL-78-77.
Childs, W. J., Poulsen, O., and Goodman, L. S. (1979a) *Opt. Lett.,* **4**, 35–7.
Childs, W. J., Poulsen, O., and Goodman, L. S. (1979b) *Opt. Lett.,* **4**, 63–5.
Condon, E. U. and Shortley, G. H. (1935) *The Theory of Atomic Spectra*, Cambridge University Press, Cambridge, ch. VI.
Connes, J., Delouis, H., Connes, P., Guelachvili, G., Maillard, J.-P., and Michel, G. (1970) *Nouv. Rev. Opt. Appl. Fr.,* **1**, 3–22.
Conway, J. G., Blaise, J., and Verges, J. (1976) *Spectrochim. Acta B,* **31**, 31–47.
Conway, J. G., Worden, E. F., Blaise, J., and Verges, J. (1977a) *Spectrochim. B. Acta***, 32**, 97–9.
Conway, J. G., Worden, E. F., Blaise, J., Camus, P., and Verges, J. (1977b) *Spectrochim. Acta B***, 32**, 101–6.

Conway, J. G., Worden, E. F., Brault, J. W., Hubbard, R. P., and Wagner, J. J. (1984) *At. Data Nud. Data Tables*, **31**, 299–358

Conway, J. G., Worden, E. F., and Blaise, J. (1995) *J. Opt. Soc. Am. B,* **12**, 1186–202.

Coste, A., Avril, R., Blancard, P., Chatelet, J., Lambert, D., Legre, J., Liberman, S., and Pinard, J. (1982) *J. Opt. Soc. Am.,* **72**, 103–9.

Cowan, R. D. (1968) *J. Opt. Soc. Am.,* **58**, 808–18.

Cowan, R. D. (1981) *The Theory of Atomic Structure and Spectra*, University of California Press, Berkeley, CA.

Crosswhite, H. M. (1971) *Phys. Rev. A,* **4**, 485–9.

Crosswhite, H. M. (1975) Private communication to M. Fred.

Crosswhite, H. M. (1986) Private communication.

Deissenberger, R., Köhler, S., Ames, F., Eberhardt, K., Erdmann, N., Funk, H., Herrmann, G., Kluge, H.-J., Nunnemann, M., Passler, G., Riegel, J., Scheerer, F., Trautmann, N., and Urban, F.-J. (1995) *Angew. Chem. Int. Ed. Engl.,* **34**, 814–15.

Demers, Y., Gagne, J. M., Dreze, C., and Pianarosa, P. (1986) *J. Opt. Soc. Am. B,* **3**, 1678–80.

Engleman, R. Jr and Palmer, B. A. (1980) *J. Opt. Soc. Am.,* **70**, 308–17.

Engleman, R. Jr and Palmer, B. A. (1983) *J. Opt. Soc. Am.,* **73**, 694–701

Engleman, R. Jr and Palmer, B. A. (1984) *J. Opt. Soc. Am. B*, **1**, 782–7.

Erdmann, N., Nunnemann, M., Eberhardt, K., Herrmann, G., Huber, G., Köhler, S., Kratz, J. V., Passler, G., Peterson, J. R., Trautmann, N., and Waldek, A. (1998) *J. Alloys Compds,* **271–273**, 837–40.

Feneuille, S. and Pelletier-Allard, N. (1968) *Physica,* **40**, 347–56.

Fred, M. and Tomkins, F. S. (1957) *J. Opt. Soc. Am.,* **47**, 1076–87.

Fred, M., Tomkins, F. S., Blaise, J., Camus, P., and Verges, J. (1976) Argonne National Laboratory Report ANL-76-68.

Fred, M., Tomkins, F. S., Blaise, J., Camus, P., and Verges, J. (1977) *J. Opt. Soc. Am.,* **67**, 7–23.

Fred, M. and Blaise, J. (1978) private communication of the 0.00 to 24.27 cm^{-1} low level separation in Np(II).

Fricke, B., Johnson, E., and Rivera, G. M. (1993) *Radiochimica Acta,* **62**, 17–25.

Giacchetti, A. (1966) *J. Opt. Soc. Am.,* **56**, 653–7.

Giacchetti, A. (1967) *J. Opt. Soc. Am.,* **57**, 728–33.

Giacchetti, A. and Blaise, J. (1970) *2nd EGAS Conf.*, Hanover.

Giacchetti, A., Blaise, J., Corliss, C. H., and Zalubas, R. J. (1974) *J. Res. NBS,* **78A**, 247–81.

Goeppert Mayer, M. (1941) *Phys. Rev.,* **60**, 184–7.

Goldschmidt, Z. B. (1983) *Phys. Rev. A,* **27**, 740–53.

Greenland, P. T., Pritchard, S. E., and Wort, D. J. H. (1981) Poster AERE Harwell OX11 ORA.

Grüning, C., Huber, G., Klopp, P., Kratz, J. V., Kunz, P., Passler, G., Trautmann, N., Waldek, A., and Wendt, K. (2004) *Int. J. Mass Spectrometry*, **235**, 171–8.

Gutmacher, R. G., Evans, J. E., and Hulet, E. K. (1967) *J. Opt. Soc. Am.,* **57**, 1389–90.

Hackel, L. A., Bender, C. A., Johnson, M. A., and Rushford, M. A. (1979) *J. Opt. Soc. Am.,* **69**, 230–2.

Hansen, J. E., Judd, B. R., and Crosswhite, H. (1996) *At. Data Nuc. Data Tables,* **62**, 1–49.

Howard, W. M. and Möller, P. (1980) *At. Data Nucl. Data Tables,* **25**, 219–85.
Hulet, E. K., Lougheed, R. W., Brady, J. D., Stone, R. E., and Coops, M. S. (1967) *Science,* **158**, 486–8.
Johnson, S. G., Fearey, B. L., Miller, C. M., and Nogar, N. S. (1992) *Spectrochim. Acta B,* **47**, 633–43.
Judd, B. R. (1963) *Operator Techniques in Atomic Spectroscopy*, Wiley Interscience, New York.
Judd, B. R. (1966) *Phys. Rev.,* **141**, 4–14.
Judd, B. R. and Crosswhite, H. M. (1984) *J. Opt. Soc. Am. B,* **1**, 255–60.
Judd, B. R. (1985) *Rep. Prog. Phys.,* **48**, 907–54.
Judd, B. R. and Lo, E. (1996) *At. Data Nucl. Data Tables,* **62**, 51–75.
Kaufman, V. and Radziemski, L. J. Jr (1976) *J. Opt. Soc. Am.,* **66**, 599–600.
Klinkenberg, P. F. A. and Lang, R. G. (1949) *Physica,* **15**, 774–88.
Klinkenberg, P. F. A. (1950) *Physica,* **16**, 618–50.
Klinkenberg, P. F. A. and Uylings, P. H. M. (1986) *Phys. Scr.,* **34**, 413–22.
Klinkenberg, P. F. A. (1988) *Physica***, 151**, 552–67.
Köhler, S., Erdmann, N., Nunnemann, M., Herrmann, G., Huber, G., Kratz, J. V., Passler, G., and Trautmann, N. (1996) *Angew. Chem. Int. Ed. Engl.,* **35**, 2856–8.
Köhler, S., Deißenberger, R., Eberhardt, K., Erdmann, N., Herrmann, G., Huber, G., Kratz, J. V., Nunnemann, M., Passler, G., Rao, P. M., Riegel, J., Trautmann, N., and Wendt, K. (1997) *Spectrochim. Acta B,* **52**, 717–26.
Kramida, A. E. (1997) PC version of the RCN/RCG/RCE Cowan codes available on the web site plasma-gate@weizmann.ac.il
Lauth, W., Backe, H., Dahlinger, M., Klaft, I., Schwamb, P., Schwickert, G., Trautmann, N., and Othmer, U. (1992) *Phys. Rev. Lett.,* **68**, 1675–8.
Lauth, W., Backe, H., Hies, M., Kolb, T., Kunz, H., Schütze, Th., Sewtz, M., Steinhof, A., Eberhardt, K., Trautmann, N., and Repnow, R. (1998) in *Heavy Ion Physics* (eds. Yu. Ts. Oganessian and R. Kalpakchieva) World Scientific Publishing, Singapore, pp. 588–97.
Le Garrec, B. and Petit, A. (1986) *J. Less Common Metals,* **122**, 55–8.
Litzen, U. (1974) *Phys. Scr.,* **10**, 103–4.
Lobikov, E. A., Striganov, A. R., Labozin, V. P., Odintsova, N. K., and Pomytkin, V. F. (1979) *Opt. Spekctrosk.,* **46**, 1054–60; *Opt. Spectrosc.*, **46**, 596–9.
Marrus, R., Nierenberg, W. A., and Winocur, J. (1960) *Phys. Rev.,* **120**, 1429–35.
McNally, J. R. Jr and Griffin, P. M. (1959) *J. Opt. Soc. Am.,* **49**, 162–6.
Meggers, W. F., Fred, M., and Tomkins, F. S. (1957) *J. Res. NBS,* **58**, 297–315.
Meisel, G., Bekk, K., Rebel, H., and Schatz, G. (1987) *Hyperfine. Interact.,* **38**, 723–40.
Metag, V., Habs, D., and Specht, H. J. (1980) *Phys. Rep.,* **65**, 1–41.
Meyers, W. D. and Schmidt, K. H. (1983) *Nucl. Phys. A,* **410**, 61–73.
Morss, L. R. (1971) *J. Phys. Chem.,* **75**, 392–9.
Nielson, C. W. and Koster, G. F. (1964) *Spectroscopic Coefficients for p^n, d^n, and f^n Configurations*, MIT Press, Cambridge, MA.
Nugent, L. J. (1975) *MTP International Review of Science, Inorganic Chemistry*, sec. 2, vol. 7, Butterworths, London, pp. 195–219.
Otten, E. W. (1989) *Treatise on Heavy-Ion Science*, Plenum, vol. 8.
Palmer, B. A., Keller, R. A., and Engleman, R. Jr (1980) *An Atlas of Uranium Emission Intensities in a Hollow Cathode Discharge*, Los Alamos Scientific Laboratory Report LA-8251-MS.

Palmer, B. A. and Engleman, R. Jr (1983) *Atlas of the Thorium Spectrum*, Los Alamos National Laboratory Report LA-9615.
Palmer, B. A. and Engleman, R. Jr (1984) *J. Opt. Soc. Am. B*, **1**, 782–7.
Peterson, J. R., Erdmann, N., Nunnemann, M., Eberhardt, K., Huber, G., Kratz, J. V., Passler, G., Stetzer, O., Thörle, P., Trautmann, N., and Waldek, A. (1998) *J. Alloys Compds,* **271–273**, 876–8.
Petit, A. (1999) *Eur. Phys. J. D,* **6**, 157–70.
Pulliam, B. V. (1985) private communication to J. Blaise.
Pulliam, B. V., Conway, J. G., and Worden, E. F. (2003) unpublished results.
Pyykkö, P. and Desclaux, J. P. (1979) *Acc. Chem. Res.,* **12**, 276–81.
Pyykkö, P. (1988) *Chem. Rev.,* **88**, 563–94.
Racah, G. (1942) *Phys. Rev.,* **62**, 438–62.
Racah, G. (1943) *Phys. Rev.,* **63**, 367–82.
Racah, G. (1949) *Phys. Rev.,* **76**, 1352–65.
Racah, G. (1950) *Physica,* **16**, 651–66.
Racah, G. (1951) *Bull. Res. Counc. Isr.,* **8F**, 1–14.
Rajnak, K. and Wybourne, B. G. (1964) *Phys. Rev. A,* **134**, 596–600.
Rajnak, K. and Fred, M. (1977) *J. Opt. Soc. Am.,* **67**, 1314–23.
Rajnak, K. and Shore, B. W. (1978) *J. Opt. Soc. Am.,* **68**, 360–7.
Rajnak, K. (1979) private communication to M. Fred.
Reader, J. and Corliss, C. H. (1980) *Wavelengths and Transition Probabilities for Atoms and Atomic Ions, Part I, Wavelengths,* NSRDS-NBS 68, Washington DC.
Riegel, J., Deissenberger, R., Herrmann, G., Köhler, S., Sattelberger, P., Trautmann, N., Wendeler, H., Ames, F., Kluge, H.-J., Scheerer, F., and Urban, F.-J. (1993) *Appl. Phys.,* **B56**, 275–80.
Rudzikas, Z. (1997) *Theoretical Atomic Spectroscopy*, Cambridge University Press, Cambridge, England.
Ruster, W., Ames, F., Kluge, H.-J., Otten, E.-W., Rehklau, D., Scheerer, F., Herrmann, G., Mühleck, C., Riegel, J., Rimke, H., Sattelberger, P., and. Trautmann, N. (1989) *Nucl. Instrum. Methods Phys. Res. A,* **281**, 547–58.
Sewtz, M. H., Backe, A., Dretzke, G., Kube, W., Lauth, P., Schwamb, K., Eberhardt, C., Grüning, P., Thörle, P., Trautmann, N., Kunz, P. J., Lassen, G., Passler, G., Dong, C. Z., Fritsche, S., and Haire, R. G. (2003) *Phys. Rev. Lett.,* **90**, 163002–1-4.
Slater, J. C. (1929) *Phys. Rev.*, **34**, 1293–322.
Slater, J. C. (1960) *Quantum Theory of Atomic Structure*, vol. I, McGraw-Hill, New York.
Solarz, R. W., May, C. A., Carlson, L. R., Worden, E. F., Johnson, S. A., Paisner, J. A., and Radziemski, L. J. Jr (1976) *Phys. Rev. A,* **14**, 1129–36.
Steinhaus, D. W., Radziemski, L. J. Jr, Cowan, R. D., Blaise, J., Guelachvili, G., Ben Osman, Z., and Verges, J. (1971) Los Alamos Scientific Laboratory Report LA-4501.
Striganov, A. R. (1983) *Atomic Spectrum and Energy Levels of the Neutral Atom of Plutonium*, Energoatomisdat, Moscow (in Russian).
Strutinsky, V. M. (1967) *Nucl. Phys.,* **A95**, 420–42.
Strutinsky, V. M. (1968) *Nucl. Phys.,* **A122**, 1–33.
Sugar, J. (1974) *J. Chem. Phys.,* **60**, 4103.
Tomkins, F. S. and Fred, M. (1951) *J. Opt. Soc. Am.,* **41**, 641–3.
Tomkins, F. S. and Fred, M. (1957) *J. Opt. Soc. Am.,* **47**, 1087–91.
Tomkins, F. S. and Fred, M. (1963) *Appl. Opt.,* **2**, 715–25.

Trautmann, N. (1994) *J. Alloys Compds,* **213–214**, 28–32.
Van Deurzen, C. H. H., Rajnak, K., and Conway, J. G. (1984) *J. Opt. Soc. Am. B,* **1**, 45–7.
Vander Sluis, K. L. and Nugent, L. J. (1972) *Phys. Rev. A,* **6**, 86–94.
Waldek, A., Erdmann, N., Grüning, C., Huber, G., Kunz, P., Kratz, J. V., Lassen, J., Passler, G., and Trautmann, N. (2001) *Resonance Ionization Spectroscopy 2000* (eds. J. E. Parks and J. P. Young), AIP Conf. Proc., 584, American Institute of Physics, Melville, NY, 219–24.
White, H. E. (1934) *Introduction to Atomic Spectra*, McGraw-Hill, New York, p. 441
Wilson, M. (1968) *Phys. Rev.,* **176**, 58–63.
Worden, E. F., Gutmacher, R. G., and Conway, J. G. (1963) *Appl. Opt.,* **2**, 707–13.
Worden, E. F. and Conway, J. G. (1967) *Physica*, **33**, 274.
Worden, E. F., Hulet, E. K., Lougheed, R. M., and Conway, J. G. (1967) *J. Opt. Soc. Am.,* **57**, 550.
Worden, E. F., Gutmacher, R. G., Lougheed, R. W., Evans, J. E., and Conway, J. G. (1968) *J. Opt. Soc. Am.,* **58**, 998–9.
Worden, E. F. and Conway, J. G. (1970) *J. Opt. Soc. Am.,* **60**, 1144–5.
Worden, E. F., Gutmacher, R. G., Lougheed, R. W., Conway, J. G., and Mehlhorn, R. J. (1970) *J. Opt. Soc. Am.,* **60**, 1297–302.
Worden, E. F., Lougheed, R. W., Gutmacher, R. G., and Conway, J. G. (1974) *J. Opt. Soc. Am.,* **64**, 77–85.
Worden, E. F., Hulet, E. K., Gutmacher, R. G., and Conway, J. G. (1976) *At. Data Nucl. Data Tables***, 18**, 459–95.
Worden, E. F. and Conway, J. G. (1976) *J. Opt. Soc. Am.,* **66**, 109–21.
Worden, E. F. and Conway, J. G. (1978) *At. Data Nucl. Data Tables***, 22**, 329–66.
Worden, E. F., Solarz, R. W., Paisner, J. A., and Conway, J. G. (1978) *J. Opt. Soc. Am.,* **68**, 52–61.
Worden, E. F. and Conway, J. G. (1979) *J. Opt. Soc. Am.,* **69**, 733–8.
Worden, E. F. and Conway, J. G. (1980) *Lanthanide and Actinide Chemistry and Spectroscopy* (ed. N. M. Edelstein), American Chemical Society, Washington DC, 381–425.
Worden, E. F., Conway, J. G., and Blaise, J. (1985) *Americium and Curium Chemistry and Technology* (eds. N. M. Edelstein, J. D. Navratil, and W. W. Schultz), D. Reidel Publishing Co, 123–34.
Worden, E. F., Conway, J. G., and Blaise, J. (1986) *J. Opt. Soc. Am. B***, 3**, 1092–101.
Worden, E. F., Conway, J. G., and Blaise, J. (1987) *J. Opt. Soc. Am. B,* **4**, 1358–68.
Worden, E. F. (1991–1993) private communications to W. Lauth.
Worden, E. F., Carlson, L. R., Johnson, S. A., Paisner, J. A., and Solarz, R. W. (1993) *J. Opt. Soc. Am. B***, 10**, 1998–2006.
Wyart, J.-F., Kaufman, V., and Sugar, J. (1980) *Phys. Scr.,* **22**, 389–96.
Wyart, J.-F. and Kaufman, V. (1981) *Phys. Scr.,* **24**, 941–52.
Wyart, J.-F. (1998) unpublished calculations.
Wyart, J.-F., Blaise, J. and Worden, E. F. (2005) *J. Sol. State. Chem*., **178**, 589–602.
Wybourne, B. G. (1965) *Spectroscopic Properties of Rare Earths*, John Wiley, New York.
Zalubas, R. and Corliss, C. H. (1974) *J. Res. NBS,* **78A**, 163–246.
Zalubas, R. (1975) *J. Res. NBS,* **80A**, 221–358.

CHAPTER SEVENTEEN

THEORETICAL STUDIES OF THE ELECTRONIC STRUCTURE OF COMPOUNDS OF THE ACTINIDE ELEMENTS

Nikolas Kaltsoyannis, P. Jeffrey Hay, Jun Li,
Jean-Philippe Blaudeau, and Bruce E. Bursten

17.1 INTRODUCTION

In this chapter, we will present an overview of the theoretical and computational developments that have increased our understanding of the electronic structure of actinide-containing molecules and ions. The application of modern electronic structure methodologies to actinide systems remains one of the great challenges in quantum chemistry; indeed, as will be discussed below, there is no other portion of the periodic table that leads to the confluence of complexity with respect to the calculation of ground- and excited-state energies, bonding descriptions, and molecular properties. But there is also no place in the periodic table in which effective computational modeling of electronic structure can be more useful. The difficulties in creating, isolating, and handling many of the

actinide elements provide an opportunity for computational chemistry to be an unusually important partner in developing the chemistry of these elements.

The importance of actinide electronic structure begins with the earliest studies of uranium chemistry and predates the discovery of quantum mechanics. The fluorescence of uranyl compounds was observed as early as 1833 (Jørgensen and Reisfeld, 1983), a presage of the development of actinometry as a tool for measuring photochemical quantum yields. Interest in nuclear fuels has stimulated tremendous interest in understanding the properties, including electronic properties, of small actinide-containing molecules and ions, especially the oxides and halides of uranium and plutonium. The synthesis of uranocene in 1968 (Streitwieser and Müller-Westerhoff, 1968) led to the flurry of activity in the organometallic chemistry of the actinides that continues today. Actinide organometallics (or organoactinides) are nearly always molecular systems and are often volatile, which makes them amenable to an arsenal of experimental probes of molecular and electronic structure (Marks and Fischer, 1979). Theoretical and computational studies of the electronic structure of actinide systems have developed in concert with the experimental studies, and have been greatly facilitated by the extraordinary recent advances in high-performance computational technology.

We will focus on computational studies of the electronic structure of discrete (molecular or ionic) actinide-containing systems. We begin by discussing some of the general tenets of bonding that are relevant to the actinide elements and some of the challenges that are unique to this field. We then present the results of computational electronic structure studies on a variety of molecular actinide systems. The literature of molecular electronic structure of actinide systems has been compiled by Pyykkö (1986, 1993, 2000b), as well as being available as a database on the web (http://www.csc.fi/rtam). Pepper and Bursten (1991) reviewed the methodology and applications in the field in 1991. The reader is referred to those reviews for some of the details on earlier studies in this field. We restrict our discussion in this chapter to molecular actinide systems and do not discuss the extensive body of research in the use of theoretical electronic structure methods to model solid-state actinide chemistry. The reader is referred to Chapter 21 and some recent review articles (Lander *et al.*, 1994; Soderlind, 1998; Wills and Eriksson, 2000) for discussions of theoretical electronic structure methods applied to the metallic actinide elements and solid-state actinide compounds. We will also have minimal discussion of compounds of the transactinide elements in this chapter. The electronic structure of compounds of the transactinides is discussed in Chapter 14 and in the excellent review by Pershina (1996).

17.1.1 Electronic structure of actinide atoms

The challenge in undertaking theoretical studies of actinide complexes begins, of course, with the complex electronic structure of the actinide atoms. The lanthanide and actinide elements are distinct from the p- and d-block elements

in having f-orbitals as part of the active valence orbitals of the atom. The methodologies that can be successful in describing the electronic structure of such systems must obviously be able to accommodate valence f-orbitals. The historical development of methods that could handle f-electrons has been discussed by Pepper and Bursten (1991) and will be briefly recounted later in this chapter.

The most common representation of the angular functions of the seven real f-orbitals is presented in Table 17.1 and Fig. 17.1. Real orbitals are constructed by forming linear combinations of the spherical harmonics $Y_{l,m_l}(\theta,\phi)$ with common $|m_l|$ values, such as $Y_{3,1} \pm Y_{3,-1}$. The resulting real orbitals can be described with Cartesian labels in the same way we do for p- and d-orbitals. They are characterized by a distinct $|m_l|$ value, giving axially quantized orbitals of σ ($m_l = 0$), π ($|m_l| = 1$), δ ($|m_l| = 2$), and ϕ ($|m_l| = 3$) symmetry with respect to the z-axis. In addition, a set of f-orbitals convenient for systems with cubic symmetry can be formed via linear combinations of these real f-orbitals (see, for example, Cotton, 1990).

Both the lanthanide and actinide elements have valence f-orbitals, but they have distinct differences that originate in electronic structure. The 5f orbitals of the actinide elements are in close energetic proximity to other valence orbitals, which leads to complex and fluctuating electron distributions for the early actinide elements. Table 17.2 compares the ground electron configurations of isovalent lanthanide and actinide atoms. It is evident that, when comparing the early members of each series, the 6d orbitals of the actinide elements are more energetically accessible than are the 5d orbitals of the lanthanide elements. The radial functions for the outer orbitals of actinide atoms also indicate that the characterization of these elements as ones for which the chemistry is dominated by the behavior of the 5f electrons might be considered somewhat of a misnomer. Fig. 17.2 shows the radial functions obtained for the Pu atom from recent relativistic Cowan–Griffin *ab initio* atomic calculations of Seijo *et al.* (2001). As expected, the 7s and 6d radial functions are significantly more diffuse than the 5f radial function. Somewhat more surprising, the 6s and 6p orbitals, which are typically considered to be core orbitals, have radial functions of comparable or greater extension than the 5f radial function. These results underscore the fact that the electronic structure of actinide atoms can involve complex electron occupancies that span several different n and l values, even in the absence of spin–orbit effects.

The fact that there are so many atomic orbitals (AOs) in spatial and energetic proximity near the highest valence level of the actinide atoms leads to another complicating factor in describing the electronic structure of actinide systems, namely the presence of a large number of electronic states close to the ground state. Particularly for the early actinides and their simple ions, the presence of multiple $5f^n6d^m7s^k$ configurations of comparable energy, and the energetically close multiplets that can arise from each of these configurations, leads to the enormously complex state energetics and optical spectra observed for these

Table 17.1 *The angular functions of the seven real f-orbitals in the axially quantized representation.*

Axial symmetry	*Spherical harmonics*	*Cartesian representation*	*Usual label*
σ	$Y_{3,0}$	$z(5z^2–3r^2)$	f_{z^3}
π	$Y_{3,1} \pm Y_{3,-1}$	$x(5z^2–r^2)$, $y(5z^2–r^2)$	f_{xz^2}, f_{yz^2}
δ	$Y_{3,2} \pm Y_{3,-2}$	$z(x^2–y^2)$, zxy	$f_{z(x^2–y^2)}$, f_{zxy}
ϕ	$Y_{3,3} \pm Y_{3,-3}$	$x(x^2–3y^2)$, $y(3x^2–y^2)$	$f_{x(x^2–3y^2)}$, $f_{y(3x^2–y^2)}$

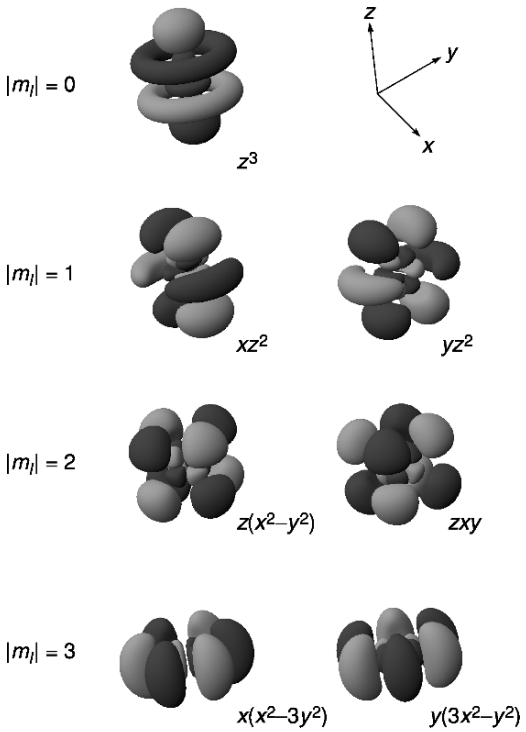

Fig. 17.1 *Representation of the angular functions for the seven real 5f-orbitals in the axially quantized representation.*

systems (Wybourne, 1965; Dieke, 1968; Carnall and Crosswhite, 1986). With the exception of $5f^1$ complexes (Kaltsoyannis and Bursten, 1995; Seijo and Barandiarán, 2001), the various multiplets of actinide systems in general cannot be described within a single-configuration framework, which has greatly hindered the use of first-principles calculations of the electronic state energies. As a result, until recently most efforts to understand the optical spectra of actinide ions involved crystal-field models that incorporated empirically obtained parameters (Crosswhite and Crosswhite, 1984; Carnall, 1992). In

Table 17.2 *Ground state electron configurations of the lanthanide and actinide atoms.*[a]

La	$[Xe]5d^16s^2$	Ac	$[Rn]6d^17s^2$	Gd	$[Xe]4f^75d^16s^2$	Cm	$[Rn]5f^76d^17s^2$
Ce	$[Xe]4f^15d^16s^2$	Th	$[Rn]6d^27s^2$	Tb	$[Xe]4f^96s^2$	Bk	$[Rn]5f^97s^2$
Pr	$[Xe]4f^36s^2$	Pa	$[Rn]5f^26d^17s^2$	Dy	$[Xe]4f^{10}6s^2$	Cf	$[Rn]5f^{10}7s^2$
Nd	$[Xe]4f^46s^2$	U	$[Rn]5f^36d^17s^2$	Ho	$[Xe]4f^{11}6s^2$	Es	$[Rn]5f^{11}7s^2$
Pm	$[Xe]4f^56s^2$	Np	$[Rn]5f^46d^17s^2$	Er	$[Xe]4f^{12}6s^2$	Fm	$[Rn]5f^{12}7s^2$
Sm	$[Xe]4f^66s^2$	Pu	$[Rn]5f^67s^2$	Tm	$[Xe]4f^{13}6s^2$	Md	$[Rn]5f^{13}7s^2$
Eu	$[Xe]4f^76s^2$	Am	$[Rn]5f^77s^2$	Yb	$[Xe]4f^{14}6s^2$	No	$[Rn]5f^{14}7s^2$

[a] There have been discussions about whether the lanthanide and actinide series should begin with La and Ac, respectively, as has been done here, or with Ce and Th, respectively. See Jensen (1982).

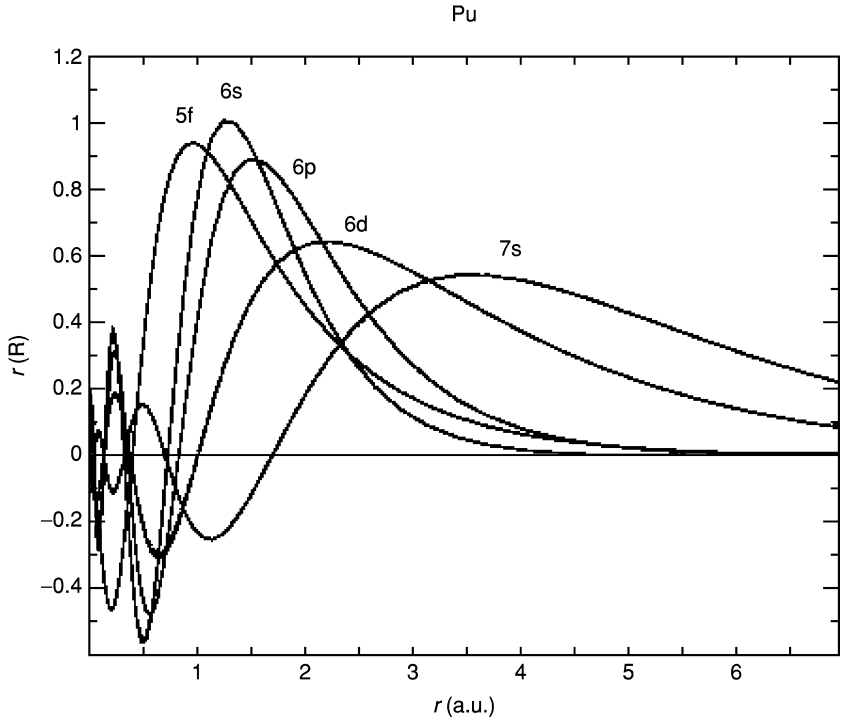

Fig. 17.2 *Radial functions for the outer orbitals of a Pu atom from relativistic atomic calculations* (*reproduced from Seijo* et al., 2001).

recent years, correlated electronic structure methods with spin–orbit operators have been used to address optical excitations in f^n ($n > 1$) actinide-containing systems (Matsika and Pitzer, 2000; Gagliardi *et al.*, 2001b; Matsika *et al.*, 2001; Mochizuki and Tatewaki, 2002), but this still remains as one of the biggest challenges in computational actinide chemistry.

17.1.2 Relativistic effects

Another challenge in describing the electronic structure of the actinide and transactinide elements is the necessity to include the effects of relativity on the behavior of the electrons. Although Dirac (1929) merged special relativity and quantum mechanics in 1929, and Breit (1932) extended Dirac's ideas to many-electron systems shortly thereafter, the importance of relativistic corrections in molecular quantum chemistry was not fully appreciated until the 1970s. Dirac himself was not convinced of the importance of relativistic effects, which he said would be "of no importance in the consideration of atomic and molecular structure and ordinary chemical reactions" (1929). Dirac clearly understated the chemical consequences of his discovery! Beginning with the third-row transition metal atoms, and even more so for the actinide and transactinide atoms, the high kinetic energy of the core electrons, which correspond to classical speeds close to the speed of light, leads to large relativistic effects. Powell (1968) presented an early and readily understood introduction to the derivation of Dirac's relativistic quantum mechanics and its impact on chemistry, and a number of more detailed reviews (Pyykkö, 1978, 1988; Pitzer, 1979; Pyykkö and Desclaux, 1979; Christiansen *et al.*, 1985; Balasubramanian and Pitzer, 1987; Ermler *et al.*, 1988; Balasubramanian, 1989; Schwarz, 1990; Kaltsoyannis, 1997; Bond, 2000) and monographs (Malli, 1983; Balasubramanian, 1989, 1994, 1997; Dolg and Stoll, 1996; Schwerdtfeger, 2002, 2004; Hess, 2003; Hirao and Ishikawa, 2004) over the last 25 years discuss the chemical consequences of relativistic effects in greater detail. We provide a brief recap here of the major relativistic effects that influence the electronic structure of actinide complexes.

Because most of the chemical distinctiveness of the actinide elements results from the presence of valence f-electrons, much of our focus will be on the effects of relativity on the 5f orbitals. The magnitude of many of the relativistic effects increases as Z^n (Z = atomic number; $n > 1$). Hence, relativistic effects are more pronounced for the actinide elements than for the lanthanide elements. This trend is apparent in Fig. 17.3, in which the nonrelativistic and Dirac–Fock relativistic atomic orbital energies obtained by Desclaux (1973) for lanthanide and corresponding actinide atoms are compared. This figure illustrates the two general classes of relativistic effects on the electronic structure, both of which are greater for the actinides than for the lanthanides. The first effect is the increase in the energies of the nf and $(n + 1)$d orbitals relative to the $(n + 1)$p and $(n + 2)$s orbitals ($n = 4$ and 5). These overall changes in the orbital energies are primarily due to 'classical' relativistic effects, such as the relativistic mass correction for core electrons, that lead to greater shielding of the higher l-value orbitals. The 5f orbitals in actinides are more destabilized by relativistic effects than are the 4f orbitals of the lanthanides. As a result, the valence 5f electrons in the actinide elements are more weakly bound, and hence more chemically active, than the 4f electrons in the lanthanide elements.

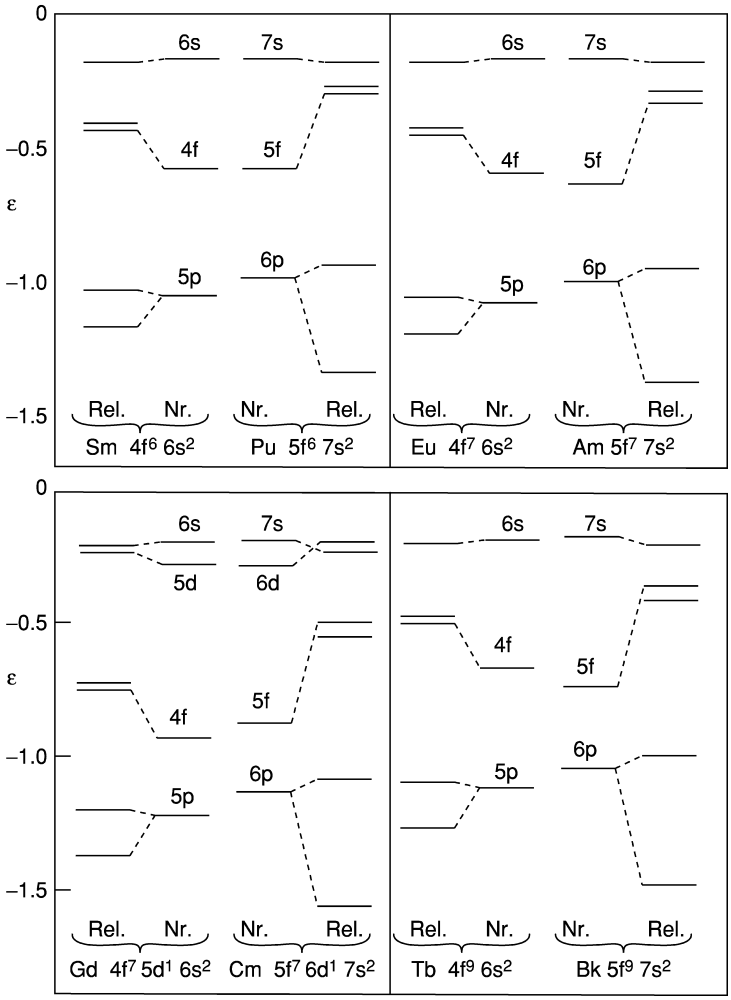

Fig. 17.3 *The Dirac–Fock average of configuration orbital energies* (a.u.) *obtained by Desclaux* (1973) *for the lanthanides Sm, Eu, Gd, and Tb and for the corresponding actinides Pu, Am, Cm, and Bk. The inner columns for each lanthanide–actinide pair denote nonrelativistic orbital energies. The shifts in energy due to the relativistic effects are evident in the relativistic orbital energies, displayed in the outer columns for each lanthanide–actinide pair* (*adapted from Pyykkö,* 1978).

The second relativistic effect is the splitting of subshells with $l \geq 1$ because of spin–orbit coupling, which can be considered a 'quantum' relativistic effect. The spin–orbit splitting generally decreases with the increase of l and with increasing orbital energy. In Fig. 17.3, for example, the $(n + 1)$p orbitals are split more

than the *n*f orbitals. These two classes of relativistic effects are lucidly discussed in a review by Pitzer (1979) and spin–orbit effects in molecules have recently been reviewed by Marian (2001).

The various methods for the inclusion of relativistic effects in electronic structure calculations have been discussed briefly by Pepper and Bursten (1991) and in greater detail by Balasubramanian (1997). They will also be developed more fully in Section 17.2. In general, the methods can be separated into two broad classes depending on how the relativistic effects are incorporated into the molecular Hamiltonian. In the so-called *scalar* relativistic methods, the relativistic mass–velocity and Darwin terms are incorporated into the Hamiltonian in such a way that preserves the separation of the spatial and spin components of the resultant wavefunction. Scalar relativistic methods thus generate wavefunctions that are bases for the representations of the familiar single point groups used in nonrelativistic calculations. Spin–orbit effects are not explicitly included in scalar-relativistic calculations, although they can be included via perturbative methods.

In the second general approach to relativistic molecular electronic structure calculations, the full Dirac equation is solved using a variety of simplifying formalisms, such as the Dirac–Fock approach that is the relativistic analog to nonrelativistic Hartree–Fock (HF) methods. Spin–orbit coupling is explicitly included in these methods, which yield four-component wavefunctions. The two small components, which are usually needed only for calculations involving electromagnetic field interactions, are often omitted from the molecular wavefunction. Because the spatial and spin components of the electronic wavefunction are coupled in these approaches, the calculated orbitals are bases for the less-familiar double point groups, which sometimes complicates the interpretation of the results.

As this chapter develops, we will see that scalar-relativistic methods, which use *LS* labels for the molecular states, are generally adequate for the calculation of many of the ground state properties of actinide systems, including molecular geometries and vibrational frequencies, although the reader is referred to the discussion concerning the plutonyl (PuO_2^{2+}) ion below. The calculation of excited state properties, especially optical excitation energies, almost always demands an approach that includes spin–orbit effects explicitly. When these effects are included, double-group labels are required. For example, for linear molecules, the states are labeled based on Ω values rather than on Λ values.

17.1.3 Actinide–ligand bonding: General considerations

In this chapter, we will address a number of different molecular and ionic systems that contain a variety of ancillary atoms and ligands bonded to an actinide center. Although these systems might appear at first glance to be very different, there are some general observations that can be made about the nature of the ligand-to-actinide bonding.

The actinide elements are classified as hard Lewis acids, especially in their more positive oxidation states (Katz *et al.*, 1986; Kaltsoyannis and Scott, 1999). The interactions of ligands with an actinide center are conventional Lewis acid–base interactions in which the ligand serves as an electron donor to a vacant acceptor orbital on the metal. In this sense, the formation of actinide–ligand complexes is entirely analogous to the formation of metal–ligand bonds in transition-metal coordination chemistry. There are several general factors that distinguish actinide coordination chemistry from that of the transition metals and the lanthanide elements:

(1) As hard Lewis acids, both the actinide and lanthanide ions generally prefer to coordinate hard Lewis bases such as F^-, O^{2-}, and other O-containing ligands, including OH^- and H_2O. Indeed, the chemistry of the actinides tends to be dominated by aqua complexes, fluorides, oxides, and oxyfluorides, although much of our subsequent discussion will involve different types of ligands, such as hydrocarbyls.
(2) The 4f orbitals of the lanthanides are too contracted in their radial distributions to be involved to any significant extent in covalent interactions with ligands, particularly in the +3 oxidation state that dominates lanthanide chemistry. The 5f orbitals of the early actinide elements are less contracted and can therefore have significant overlap with ligand orbitals. The 5f orbitals contract as one moves across the actinide series, which is consistent with the observation that the chemistry of the later actinides is similar to that of the lanthanides. As a consequence, the bonding in the lanthanides and the later actinides tends to be largely ionic, whereas significant covalent character can be found in the early actinides (Burns and Bursten, 1989).
(3) For most of the actinide (An) systems, we will see that the An 6d orbitals serve as more effective acceptor orbitals than the An 5f orbitals because the former are more diffuse than the latter. Thus, if a choice is allowed by symmetry, the ligands tend to interact more strongly with the 6d orbitals than the 5f orbitals. In centrosymmetric systems, such as the actinyl ions(AnO_2^{q+}), the actinide hexafluorides (AnF_6) and the actinocenes (An (η^8-$C_8H_8)_2$), interactions of the ligands with the An 6d and 5f orbitals will be partitioned based on the inversion symmetry of the ligand group orbitals.
(4) In most cases, any metal-based electrons will reside primarily in the 5f orbitals of the An center. For example, in U(IV) complexes the two electrons formally remaining on the U atom will be localized within the U 5f orbitals.

As noted earlier, the large number of An atomic orbitals generally leads to a large number of electronic states close to the ground state. Strong interactions of the An center with ligands serve to destabilize some of the An orbitals and greatly increase the energy of configurations that involve those orbitals. Thus, the distribution of states near the ground state can be somewhat simpler than that for free ions or atoms of the elements.

17.2 RELATIVISTIC APPROACHES FOR ELECTRONIC STRUCTURE OF ACTINIDES

A variety of methods are used in electronic structure calculations on actinide molecules. Some of these methods and their historical development were outlined in the 1991 review by Pepper and Bursten (1991). In this section, we will touch upon some of the salient features covered in that review as well as address recent developments and applications over the past decade. In discussing these theoretical approaches, it is useful to categorize them according to three aspects: (a) whether the electronic structure calculation is based on wavefunction-based *ab initio* approaches, such as Hartree–Fock and CI, or by density functional theory (DFT) approaches, such as local density and generalized-gradient methods; (b) the manner in which relativistic effects are included; and (c) whether the approach explicitly involves all-electron or only valence-electron character.

17.2.1 Hartree–Fock and density functional approaches

While electronic structure approaches for molecules differ in their methodologies, they share many common features. The starting point is the molecular energy expressed in terms of the total wavefunction for the molecule and a Hamiltonian describing the interactions. The total wavefunction, in turn, is comprised of an antisymmetrized product of one-electron molecular orbitals (ϕ_i). By applying the variational principle to the expression for the molecular energy, one obtains a set of self-consistent field (SCF) equations that are solved iteratively to obtain the molecular orbitals (MOs). The MOs are typically represented as linear combinations of atomic orbitals (LCAO), which may be expanded in terms of Gaussian- or Slater-type functions. From the molecular orbitals, one can then calculate the energy of the molecule, the total charge density, and other molecular properties.

In Hartree–Fock calculations, the exchange interaction is treated explicitly in the expression for the molecular energy:

$$E_{\mathrm{HF}} = E_{\mathrm{kin}} + E_{\mathrm{coul}} + E_{\mathrm{exch}}$$

where E_{HF}, E_{kin}, E_{coul}, and E_{exch} are the Hartree–Fock total energy, the electron kinetic energy, the Coulomb repulsion energy, and the exchange energy, respectively. The nonlocal Hartree–Fock exchange operator is associated with interchanging electrons of the same spin. Electron correlation effects are treated by including excitations from occupied to virtual levels by perturbation theory (e.g. second-order Møller–Plesset perturbation theory (MP2) to fourth-order Møller–Plesset perturbation theory (MP4)) (Møller and Plesset, 1934; Pople *et al.*, 1977), coupled-cluster theory (Bartlett, 1981, 1989), including coupled cluster with single and double excitations (CCSD; Purvis and Bartlett, 1982) and coupled cluster singles, doubles and perturbative triples (CCSD(T); Raghavachari *et al.*, 1989; Watts *et al.*, 1993), and configuration interaction

(CI, e.g. configuration interaction with single and double excitations [CISD]) (Shavitt, 1977; Szabo and Ostlund, 1989; Jensen, 1999).

DFT is based on the famous Hohenberg–Kohn theorem (Hohenberg and Kohn, 1964), which states that the electronic ground state of a molecule can be obtained uniquely from knowledge of the electron density $\rho(r)$ at all points in the molecule. Exchange and correlation effects are treated by the use of exchange and correlation functionals, which depend on the density, and lead to an expression for the energy similar to that for Hartree–Fock except for the 'exchange-correlation' energy, E_{xc}:

$$E_{DFT} = E_{kin} + E_{coul} + E_{xc}(\rho)$$

By expanding the electron density via a set of Kohn–Sham (KS) orbitals, one can derive the one-electron KS equation, similar to the Hartree–Fock equation (Kohn and Sham, 1965; Koch and Holthausen, 2001).

At the time of the 1991 review by Pepper and Bursten, DFT methods were very much in their infancy. At that time the majority of DFT methods used the local density approximation (LDA), in which the functional depends only on the density. Among the early LDA approaches that were widely applied to inorganic systems including actinides were the Xα-scattered wave (Xα-SW) and Dirac–Slater (DS) discrete variational (DV) methods, including early versions of the quasi-relativistic Hartree–Fock–Slater (HFS) approach (see relativistic methods in next section). At that time, the Xα variant of the LDA methods had questionable reliability with respect to the calculation of total energy and could not be used generally to determine geometries and vibrational properties. Pepper and Bursten (1991) made the following statement about DFT in the conclusion of their review:

> "Recent developments in density functional theory, including improved functionals and methods for the accurate calculation of binding energies, also bode well for computational actinide chemistry. These methods have the advantage of providing easily interpreted information about bonding interactions in actinide systems, and have proved useful for many years in organotransition metal and organoactinide chemistry. Again, the improved approaches are just beginning to be applied to actinide systems, with promising results."

Indeed, as will be evident in this chapter, DFT methods have become a major contributor to our understanding of actinide electronic structure. We will briefly discuss some of the major developments in DFT since the 1991 review, including the improved accuracies of molecular energies and other quantities using DFT methods as well as the development of improved functionals for DFT calculations.

Among numerous efforts in developing 'good' exchange-correlation functionals beyond the LDA, Becke (1988) developed a gradient-corrected exchange functional in 1988. This exchange functional depends both on the density, ρ, and on its gradient, $\nabla\rho$, at any point in space. In the past decade, developments by many individuals, including Lee *et al.* (1988), Perdew and Wang (1992),

Perdew *et al*. (1992), Becke (1993a), and others have led to new functionals [often known as generalized-gradient approximations (GGA)] for both exchange and correlation that have received wide usage by the community because of the improvements in orbital energies, bond energies, structures, and other properties.

In 1993 Becke launched another revolution in the density functional world by developing a 'hybrid' functional (Becke, 1993b). The hybrid approach differs in the treatment of exchange by adding a certain amount of the nonlocal exact exchange calculated in Hartree–Fock formalism to the local and gradient-corrected terms of the exchange functional of traditional DFT. Overall the form of the functional had three linear parameters that determined the amount of exact exchange as well as the relative amounts of local and gradient-corrected terms in the exchange and correlation functionals. The parameters were determined for a set of small organic molecules by the best fit to a set of experimental energies. When combining with appropriate correlation functionals (e.g. LYP and PW91), these functionals, denoted as B3LYP and B3PW91, have achieved great success in the computational chemistry of organic and inorganic molecules. The performance of these hybrid functionals in the prediction of thermochemical properties and molecular structures has led numerous investigators to apply these functionals to actinide chemistry as well.

Finally, another crucial development in the past decade for both Hartree–Fock and DFT methods has been the implementation of techniques for calculating the gradient and second derivative of the molecular energy as a function of nuclear coordinates. The information on the gradient gives directly the forces on the nuclei for a particular molecular configuration and this, in turn, enables the optimization of molecular geometries to be carried out routinely for various functionals, Hartree–Fock methods, and the hybrid approaches. Similarly the second derivatives provide the vibrational frequencies at the equilibrium structure and the Hessian matrix to characterize stationary points (e.g. minima and saddle points) and to move along molecular potential energy surfaces.

17.2.2 Relativistic effects

Relativistic effects are incorporated into electronic structure calculations by a variety of techniques that are partially summarized in Table 17.3. They are categorized on the basis of whether they are Hartree–Fock- or DFT-based, on how many components of the wavefunction are treated (see below), and on other characteristics.

The formal starting point for most relativistic methods is the Dirac equation (Dirac, 1929). In the previous section, each molecular orbital ϕ_i was a scalar function associated with either up or down spin. In relativistic theory ϕ_i is represented as a four-component spinor comprised of 'large' (or *electronic*) and 'small' (or *positronic*) components with each component having spin up (α) and spin down (β). For a one-electron system the Dirac equation is

Table 17.3 *Summary of theoretical methods for treating molecules including heavy atoms divided according to wave-function-based (Hartree-Fock) or density-functional-based approaches.*

Wave-function-based approaches	*Density functional approaches*
nonrelativistic	
HF	LDA, GGA, hybrid functional, meta-GGA
MP2–MP4	(all-electron, frozen-core, and ECP)
CCSD(T)	
scalar relativistic	
HF with RECP	quasi-relativistic Pauli formalism
MP*n*, CCSD(T) with RECP	ZORA
CASPT2, MRCI with RECP	LDA, GGA, hybrid, meta-GGA with RECP
two-component relativistic	
SO multi-configuration SCF	SO DFT
SO-CASPT2, SO-MRCI	two-component ZORA
	two-component DKH
four-component relativistic	
Dirac–Hartree–Fock	Dirac–Kohn–Sham

$$H\Psi = \left[\vec{\alpha} \cdot \vec{p} + (\beta - 1)mc^2 + V\right]\Psi = \mathrm{i}\hbar\frac{\partial\Psi}{\partial t}$$

The $\vec{\alpha}$ and β are the Dirac matrices and are 4 $\times$ 4 dimensional (the $\vec{\sigma}$ are the familiar 2 $\times$ 2 Pauli matrices and I is the 2 $\times$ 2 identity matrix):

$$\vec{\alpha} = \begin{pmatrix} 0 & \vec{\sigma} \\ \vec{\sigma} & 0 \end{pmatrix} \qquad \beta = \begin{pmatrix} I & 0 \\ 0 & -I \end{pmatrix}$$

For many-electron systems, in analogy to the nonrelativistic many-electron Schrödinger equation, the relativistic equation is termed the Dirac–Coulomb equation (here h_{D} is the one-electron Dirac equation):

$$H_{\mathrm{Dirac}} = \sum_i h_{\mathrm{D}}(i) + \sum_{i>j}\frac{1}{r_{ij}}$$

Analogous to the nonrelativistic Hartree–Fock (for wavefunction methods) and Kohn–Sham (for DFT methods) equations, these equations are the bases for the Dirac–HF and Dirac–Kohn–Sham methods, respectively. Dirac-based codes are thus four-component methods that are computationally extremely demanding and, for this reason, such methods have been applied to relatively few actinide molecules. There are several well-known codes [e.g. MOLFDIR (MOLFDIR), DIRAC (DIRAC; Saue *et al*., 1997)], Beijing density functional code (BDF; Liu *et al*., 2004), BERTHA (BERTHA; Grant and Quiney, 2000), and PORPHET4R (Matsuoka and Watanabe, 2004) that have been developed for these methods (Hirao and Ishikawa, 2004).

Several techniques exist to separate the large and small components, thus enabling a formal treatment of only the electronic (i.e. large) components and resulting in two-component methods (one for spin up and one for spin down). One such method is the Foldy–Wouthuysen transformation (Foldy and Wouthuysen, 1950; Foldy, 1956), which results in a two-component Hamiltonian (to order α^2, where α is the fine structure constant) called the Pauli Hamiltonian:

$$H = H_{\mathrm{NR}} + H_{\mathrm{mv}} + H_{\mathrm{D}} + H_{\mathrm{so}}$$

In the Pauli Hamiltonian, H_{NR}, H_{mv}, H_{D}, and H_{so} are the nonrelativistic Hamiltonian, the mass–velocity term, the Darwin term, and the spin–orbit coupling term, respectively:

$$H_{\mathrm{mv}} = \frac{-p^4}{8m^3c^2}$$

$$H_{\mathrm{D}} = \frac{1}{8m^2c^2}\left(p^2 V_{\mathrm{ext}}\right)$$

$$H_{\mathrm{so}} = \frac{1}{4c^2}\left(\nabla(V_{\mathrm{N}} + V_{\mathrm{el}}) \times \vec{p}\right) \bullet \vec{s}$$

Baerends and coworkers have developed a zeroth-order regular approximation (ZORA) that overcomes some of the problems of the Pauli formalism (*vide infra*). Rösch and coworkers (Knappe and Rösch, 1990; Rösch *et al*., 1996) have developed a linear combination of Gaussians DFT method in the PARAGAUSS program (PARAGAUSS) that implements the all-electron second-order Douglas–Kroll–Hess (DKH) scheme (Douglas and Kroll, 1974; Jansen and Hess, 1989) for transforming the Dirac equation. The DKH method has also been implemented by de Jong and coworkers and Hirata *et al.* (de Jong *et al*., 2001a; Hirata *et al*., 2004) in the software package NWChem (NWChem) in scalar form and by Peralta and Scuseria (2004) in Gaussian in both scalar and spin–orbit forms. Dyall (1997, 2001) proposed an alternative series of transformations via so-called normalized elimination of the small components (NESC) from the four-component wavefunctions. Nakajima and Hirao (1999) suggested a formalism named relativistic scheme by eliminating small components (RESC).

As noted in Section 17.1.2, when spin–orbit coupling effects are ignored or averaged out, the relativistic methods reduce to scalar relativistic (one-component) methods. The vast majority of electronic structure calculations on actinide species use these simpler 'scalar relativistic' methods in which the wavefunction has the same form as in nonrelativistic quantum chemistry and each orbital has either α or β spin. In these scalar relativistic methods, only the mass–velocity and Darwin terms are included in addition to the usual nonrelativistic Hamiltonian. Scalar relativistic methods include calculations

with effective core potentials (ECPs; see next section), where the relativistic terms are implicitly incorporated into the potential.

Among density functional approaches the quasi-relativistic (QR) and ZORA are popular relativistic methods that are included in the Amsterdam Density Functional (ADF) software. The quasi-relativistic method of Ziegler *et al.* (1989) is based on the Pauli formalism, where only the first-order terms are retained. These methods treat the relativistic terms self-consistently and are typically employed with frozen relativistic core orbitals to reduce variational instabilities. The ZORA method (van Lenthe *et al.*, 1993, 1994), which is equivalent to the earlier CPD (Chang, Pelissier, and Durand) method (Chang *et al.*, 1986), includes higher order effects in a slightly different manner. ZORA is also implemented by van Wullen (1999), by the Li group in BDF (Wang *et al.*, 2000; Hong *et al.*, 2001), and Gagliardi *et al.* (1998, 2001c) in three other DFT codes. These QR, ZORA, and DKH approaches can utilize either the LDA or GGA DFT functionals. Such approaches are beginning to be applied to the chemistry of heavy atoms, including the two-component ZORA method, implemented in ADF (ADF) and MAGIC (MAGIC), and spin–orbit DFT, which is now part of NWChem (NWChem).

17.2.3 Relativistic effective core potentials

An alternative approach to including relativistic effects is to replace the inner core electrons using relativistic effective core potentials (RECPs) derived from all-electron relativistic atomic calculations. RECPs have been recently reviewed by Dolg (2002). With these methods, the quantum chemical calculations are carried out in nonrelativistic fashion without any explicit relativistic terms in the calculation. In addition to including the effects of the core electrons, the RECPs implicitly treat the relativistic effects on the valence orbitals, since relativistic orbitals were used to construct the RECPs. A major question, especially for actinides, concerns which electrons should be included in the core. For an atom such as U, the 'large core' would treat the outer $6s^2 6p^6 7s^2 5f^3 6d^1$ electrons as valence electrons and treat the remaining 78 electrons as core electrons. Note that the 'large core' approach actually includes a smaller number of electrons than are in the noble gas configuration of [Xe], which includes the so-called semi-core 6s and 6p electrons. As noted elsewhere, the 6s and 6p electrons are energetically and spatially in the same region as the other valence electrons and play an important role in the valence electronic structure. The other common choices for core size are a 68-electron core (with the 5d shell in the valence space) and a 60-electron core (with the 5s and 5p shells in the valence).

RECPs have been developed starting with numerical Dirac–Fock orbitals by Pitzer, Christiansen, Ermler and colleagues (Lee *et al.*, 1977; Christiansen *et al.*, 1979). After transforming to a two-component 'spinor' equation, they obtain two spin–orbit-coupled RECPs for each orbital (such as $6p_{1/2}$ and $6p_{3/2}$), except for the case of s orbitals. The two RECPs can be combined in a weighted

average to obtain an average RECP (AREP) to facilitate calculations in scalar relativistic mode. The other combination of RECPs yields a rigorous spin–orbit potential that can be used in two-component SCF or spin–orbit CI calculations. Atomic RECPs for the entire periodic chart have been derived according to this procedure. Of interest for 5f elements are potentials for Fr–Pu by Ermler *et al.* (1991) and for Am through element 118 by Nash *et al.* (1997, 1999).

Starting from a scalar relativistic Cowan–Griffin numerical atomic wavefunction (Cowan and Griffin, 1976), Hay, Wadt, Kahn and coworkers developed the first RECPs for uranium and applied it to UF_6 (Hay *et al.*, 1979). They have subsequently developed RECPs for much of the periodic table (Hay and Wadt, 1985). In their approach, an 'average' RECP is directly obtained because there is only one radial function for, for example, the 6p shell of U atom. Spin–orbit effects have been treated by an approximate operator. The most recent versions of these potentials have been reported for U, Np, and Pu (Hay and Martin, 1998).

Alternative approaches developed by Preuss, Stoll, Dolg and coworkers fit the RECP parameters to calculated levels from all-electron relativistic methods (Küchle *et al.*, 1994). The atomic results can be obtained either from Dirac-based methods or an alternative scalar-relativistic method developed by Wood and Boring (1978), which is analogous to the Cowan–Griffin method. In addition to 'large core' actinide RECPs, 'small-core' RECPs have been developed in which the 5s, 5p, and 5d shells are also treated as valence electrons, because they are in the same principal quantum shell as the 5f electrons, even though these electrons are 'deep' in terms of energy. Among the codes that have capabilities for relativistic ECPs are GAUSSIAN (GAUSSIAN), GAMESS (GAMESS), TURBOMOLE (TURBOMOLE), NWChem (NWChem), and COLUMBUS (Pitzer and Winter, 1988; Shepard *et al.*, 1988).

An alternative to RECPs are those based on the Huzinaga–Cantu equation (Huzinaga and Cantu, 1971) and are known as model potentials. For these potentials, the valence-space orbitals, unlike those previously discussed, preserve the nodal (radial) structure of the all-electron orbitals. The most commonly used form is the so-called *ab initio* model potentials (AIMP) of Seijo, Barandiarán, and coworkers (Huzinaga *et al.*, 1987; Seijo and Barandiarán, 1999), who have recently published a set of AIMPs, with appropriate basis sets, for lanthanides and actinides (Seijo *et al.*, 2001). These potentials are based on a spin-dependent relativistic Wood–Boring AIMP Hamiltonian, which can be divided into a Cowan–Griffin spin-free relativistic Hamiltonian and a pure spin–orbit Hamiltonian.

The model potentials are formed by replacement of the core operators in two ways: for local, long-range operators, such as the Coulomb operator, a simple local operator is used. For local, short-range, or non-local operators, such as the exchange or the mass–velocity and Darwin Cowan–Griffin operators, a spectral representation is used (Seijo *et al.*, 2003). Recently, alternate formulations of incorporating relativistic effects, namely the aforementioned relativistic

elimination of small components (RESC) (Motegi *et al.*, 2001) and the DKH approaches (Paulovic *et al.*, 2002, 2003) have been incorporated into AIMP methods.

In the latter of these studies, spin–orbit relativistic (i.e. two-component) calculations are performed in a two-step procedure: a large scalar relativistic (one-component) calculation is used to incorporate electron correlation followed by a smaller spin–orbit (two-component) calculation. There are some important assumptions made in this approach. Its underlying principle is that the correlation calculation converges more slowly than the spin–orbit one, and that the two results are additive. The CIPSO code of Teichteil and coworkers (Teichteil and Spiegelmann, 1983; Teichteil *et al.*, 1983) is a well-known example of this method and has been applied to actinides in several studies (Maron *et al.*, 1999; Vallet *et al.*, 1999a,b). Recently, this method has been extended to the EPCISO code, which accounts for spin–orbit polarization effects (Vallet *et al.*, 2000). Another implementation of the two-step method has been developed by the Roos group; the first step being a complete active space plus second-order perturbation theory (CASPT2) correlation calculation (Andersson *et al.*, 1992), followed by a restricted active space self-consistent field (RASSCF) state interaction (RASSI) method to perform the spin–orbit calculation (Malmqvist *et al.*, 2002).

The COLUMBUS codes of Pitzer *et al.* (Pitzer and Winter, 1988; Shepard *et al.*, 1988) have incorporated RECPs within a two-component approach. Initially their methodology was developed by using the observation that when the calculations are carried out under C_{2v}^*, D_2^*, or D_{2h}^* double-group symmetry (see Section 17.2.5), the spin–orbit integrals are either pure real or pure imaginary, thus allowing the program to use real arithmetic. Recently, Yabushita *et al.* (1999) developed a spin–orbit formalism for the COLUMBUS graphical-unitary group approach (GUGA) CI program. Their method uses configuration state functions (CSFs) based on spatial orbitals (e.g. from a one-component SCF or multi-configuration self-consistent field [MCSCF] calculation) in a CI expansion that uses a spin–orbit Hamiltonian. Thus, the correlation and the spin–orbit effects are treated simultaneously and variationally via the spin–orbit CI approach. This method has been used with CI expansions of the order of a million CSFs on actinide systems, including several of the actinyl ions (Zhang and Pitzer, 1999; Matsika and Pitzer, 2000; Matsika *et al.*, 2001).

17.2.4 Excited electronic states

The preceding discussion has focused primarily on methodologies for calculating properties of the electronic ground state of actinide molecules. There has been considerably less activity involving excited states, in part because of the unique challenges actinides present with respect to the importance of spin–orbit and other relativistic effects, and in part because of the inherent challenge of

many electronic states involving unpaired 5f electrons in multiple electron configurations (Section 17.1.1). For Hartree–Fock-based methods, CI techniques have been the most popular approach to determining excited-state energies. For a ground state with no unpaired electrons, single excitations from occupied MOs to virtual MOs provide a zero-order description of the electronic states. Inclusion of higher order excitations explicitly treats the electron correlation effects needed for more quantitative results. Spin–orbit CI calculations (Pitzer and Winter, 1988; Yabushita *et al.*, 1999) have evolved to the point where fairly accurate calculations can be carried out on complexes of modest size. Illustrations of spin–orbit configuration interaction (SOCI) results will be presented in the section on the spectroscopy of actinyl species. There is also a recent review on the development and application of the multi-configuration-based relativistic quantum chemistry in exploring excited states of heavy elements, including actinides (Roos and Malmqvist, 2004).

While DFT is based on the ground electronic state of a system (or the lowest state of a given spin and symmetry), there have been various developments for treating excited electronic states within a DFT approach. Among the earliest LDA approaches was the transition state theory of Slater (1974), in which the prescription of exciting one-half electron from occupied to virtual level corresponded to the proper excitation energy in DFT. Within the QR and ZORA techniques in the ADF program and others, one can solve self-consistently for the excited states by progressively removing an electron from various occupied orbitals and promoting it into the virtual levels.

More recently, time-dependent DFT (TD-DFT) techniques have been developed (van Gisbergen *et al.*, 1995; Jamorski *et al.*, 1996; Petersilka *et al.*, 1996; Casida *et al.*, 1998) in terms of 'response functions' to provide an alternative description of the excited states in molecules. In TD-DFT, an excited state is made up of all possible particle–hole excitations (as well as counter-intuitive hole–particle 'de-excitations') between occupied and virtual MOs. This approach is applicable to closed-shell ground states to compute excited singlet and triplet excited states, and to open-shell ground states as well. Numerous TD-DFT results with a variety of functionals (LDA, GGA, and hybrid) have been reported for organic molecules and transition metal complexes. To date, very little work has been done on actinide species, mainly because the calculated excitation energies would hardly be useful without including spin–orbit coupling effects. Notably, recent developments by Liu and coworkers that allow calculations of TD-DFT excitation energies with spin–orbit coupling is a highly promising approach for tackling excited states of actinides (Gao *et al.*, 2004).

17.2.5 Double groups

As previously mentioned, the incorporation of a spin–orbit operator in the Hamiltonian requires the use of two-component wavefunctions and double groups, because the operator allows the mixing of functions with different

spins. Thus, one needs to incorporate a framework where spin functions are allowed to transform under symmetry operations of a point group. Originally suggested by Bethe (1929), double groups incorporate such transformations (Wigner, 1959; Herzberg, 1991). Before describing double groups, it is instructive to review some of the tenets of angular momentum coupling and term symbols in atoms and molecules. The following discussion is based on the development in Levine's textbook on quantum chemistry (Levine, 2000); readers are also referred to the classic series of texts by Herzberg (1944, 1989, 1991).

For atoms, the two most common methods for coupling spin and angular momenta are the *LS* and the *j–j* coupling schemes. *LS*, or Russell–Saunders, coupling is used when the electronic repulsion splitting is greater than the spin–orbit splitting, whereas *j–j* coupling is used if the latter is greater than the former. When coupling two angular momenta $\overrightarrow{j_1}$ (characterized by quantum number j_1) and $\overrightarrow{j_2}$ (characterized by j_2), one uses vector sums to obtain the possible quantum numbers characterizing the total angular momentum, which are defined by the following relation:

$$j = j_1 + j_2, j_1 + j_2 - 1, j_1 + j_2 - 2, ..., |j_1 - j_2|$$

To couple any number of angular momenta, one first couples two angular momenta according to the formula above, then couples the resulting values with the third angular momentum, and repeats the procedure as needed.

In *LS* coupling, there is a defined total electronic orbital angular momentum, labeled by $\overrightarrow{L}$, characterized by the quantum number L, formed by the vector sum of the individual electron orbital angular momenta, $\overrightarrow{l}_i$. Analogously, there is a defined total spin angular momentum, labeled by $\overrightarrow{S}$, characterized by S, formed by the vector sum of the individual electron spin angular momenta, $\overrightarrow{s_i}$. The total electronic angular momentum, $\overrightarrow{J}$, characterized by J, is the vector sum of $\overrightarrow{L}$ and $\overrightarrow{S}$. The possible J values for a given L and S are:

$$J = L + S, L + S - 1, ..., |L - S|$$

In *j–j* coupling, the orbital angular momentum, $\overrightarrow{l_i}$, characterized by l_i and the spin angular momentum, $\overrightarrow{s_i}$, characterized by s_i, for each electron is coupled to form the total angular momentum for the particular electron, $\overrightarrow{j_i}$, characterized by j_i. The total angular momentum is the vector sum of these individual angular momenta, the J values are obtained using:

$$\overrightarrow{J} = \sum_i \overrightarrow{j_i}$$

For a non-spin–orbit Hamiltonian, the total orbital and total spin angular momentum operators, which correspond to the quantum numbers L and S, commute with the Hamiltonian, and are good quantum numbers – enabling their use in the labeling of wavefunctions (i.e. the electronic states). The labels for atomic states, called term symbols, use the multiplicity, defined as

the quantity $2S + 1$, as a left superscript and using a capital letter to represent the total orbital angular momentum: S for $L = 0$, P for 1, D for 2, F for 3, G for 4, and then alphabetically (omitting J). Thus one obtains ${}^{2S+1}L$ for the term symbol, and ^{1}P, ^{2}D, and ^{3}S as examples. When one includes the J values, which are subscripts, one would obtain ${}^{2S+1}L_J$ and for the previous examples: ${}^1\mathrm{P}_1$; ${}^2\mathrm{D}_{3/2}$, ${}^2\mathrm{D}_{5/2}$; and ${}^3\mathrm{S}_1$.

For linear molecules, including diatomics, the total angular momenta are no longer good quantum numbers, but their z-components are. Thus, when coupling angular momenta for linear molecules, algebraic sums are used rather than vector sums. Greek letters are used for the z-component of orbital angular momenta, the total z-component angular momentum is now characterized by the quantum number Λ, and the analogous coupling to LS coupling is referred to as ΛS coupling. To couple two individual electron z-components, one obtains (note that each λ quantum number corresponds to a z-component of $\pm M_\lambda$ where $\lambda = M_\lambda$):

$$\lambda = \lambda_1 + \lambda_2 \quad \text{and} \quad \lambda = \lambda_1 - \lambda_2$$

Again, to couple more than two angular momenta z-components, one uses the above relation repeatedly. The total orbital momentum is now labeled Σ for $\Lambda = 0$, Π for 1, Δ for 2, Φ for 3, Γ for 4, and so on. Since (for a non-spin–orbit Hamiltonian) the total spin is still a good quantum number, the molecular term symbols are ${}^{2S+1}\Lambda$. For Σ ($\Lambda = 0$) states, there is an additional label, corresponding to reflection symmetry in a mirror plane containing the internuclear axis. Σ states, symmetric with respect to this symmetry operation, have a plus sign as a right superscript and Σ states antisymmetric with respect to this operation have a minus sign. The total component angular momentum is labeled Ω and is obtained by coupling Λ with the z-component of spin (called Σ). The values of $\Lambda + \Sigma$ are thus, note that this value may be negative:

$$\Lambda + S, \Lambda + S - 1, ..., \Lambda - S$$

The possible values of Ω, the total z-component angular momentum are:

$$\Omega = \Lambda + S, \Lambda + S - 1, ..., |\Lambda - S|$$

The molecular term symbol is ${}^{2S+1}\Lambda_{\Lambda+\Sigma}$, thus a ${}^4\Pi$ state will split into ${}^4\Pi_{5/2}$, ${}^4\Pi_{3/2}$, ${}^4\Pi_{1/2}$, and ${}^4\Pi_{-1/2}$ states.

The coupling for linear molecules analogous to j–j coupling for atoms is called ω–ω coupling. The z-component angular momentum for each electron is coupled to the spin z-component to form the individual electron total z-component angular momenta, ω_i. The individual ω_i are then coupled to form the Ω values.

For nonlinear polyatomics, electronic states are labeled by the irreducible representations of the point group of the molecule and the multiplicity of the state, referred to as ΓS coupling. The term symbols are ${}^{2S+1}\Gamma$. In analogy to j–j and ω–ω coupling, one can incorporate spin into a total symmetry label, but

that involves determining how spin functions transform, invoking double groups.

When spin functions are allowed to transform under symmetry operations, the fact that they are antisymmetric with respect to a rotation of 2π leads to the necessary modification of the identity operator, which now corresponds to a rotation of 4π. The operator corresponding to a rotation of 2π is labeled R, and the number of symmetry operators is now doubled (hence the name *double* group). An alternative perspective for atoms, more mathematical, is use of the nomenclature of Lie groups, for which a 2-to-1 homomorphism can be shown to exist between the two-dimensional special unitary group, SU(2), and the full special three-dimensional rotation group, SO(3) or O_3^+ (Arfken, 1985; Hamermesh, 1989). The resulting double point groups have double the number of operators than the simple groups, although the number of classes is not necessarily doubled. Character tables for these double groups are available in various references (Koster *et al.*, 1963; Pyykkö and Toivonen, 1983; Herzberg, 1991). Due to the additional classes, there are additional irreducible representations in these groups, referred to as double-valued representations, corresponding to states that change sign upon rotation by 2π. It can be shown that odd-electron functions necessarily transform as one of these double-valued representations, while even-electron functions transform as one of the irreducible representations of the simple group, now referred to as single-valued representations. Of particular importance for Hartree–Fock or DFT calculations that include a spin–orbit operator is that, because orbitals are one-electron functions, they now carry labels from the double-valued irreducible representations. Calculations that include only the spin–orbit operator in the subsequent correlation step and perform the Hartree–Fock calculations with a spin-free Hamiltonian retain the single-valued irreducible representation labels for the orbitals.

Of importance for chemical purposes is how functions transform. For example, for two electrons, the singlet spin function transforms as the totally symmetric irreducible representation and the triplet functions transforms in the same fashion as the angular momentum vector operators – e.g. functions with a z-axis projection of zero, such as S_z, transform under the same irreducible representation as L_z does. To obtain the double-group label of a function, the direct product of the irreducible representation for the spatial function and the irreducible representations for the spin function are determined. For atoms, this procedure is analogous to obtaining J values. S^2 and L^2 no longer commute with the Hamiltonian and their magnitudes are no longer good quantum numbers, but the magnitude of the total angular momentum, J, is still good. For example, for a ^{3}P function, one obtains J values of 2, 1, and 0 and the states are labeled $^3P_2$, $^3P_1$, and $^3P_0$. The spin–orbit operator allows mixing of the $^3P_1$ with a $^1P_1$ function. Where the spin–orbit interaction is much larger than electron–electron repulsion, the states are more properly labeled by J values alone, which leads to the progression from Russell–Saunders (or LS) coupling

to *j–j* coupling. For linear molecules, the double-group irreducible representations correspond to Ω values, where Ω is the *z*-component of the total angular momentum. The *z*-component of the orbital angular momentum, Λ, is no longer a good quantum number, Ω is still a valid quantum number. For a $^3\Pi$ state, one obtains Ω values of 2, 1, 0^+, and 0^- and the states are labeled $^3\Pi_2$, $^3\Pi_1$, $^3\Pi_{0+}$, and $^3\Pi_{0-}$. The $^3\Pi_1$ can mix with $^1\Pi_1$. For linear molecules, the analog to *j–j* coupling is *ω–ω* coupling. For nonlinear polyatomics, the double-group label is obtained by first determining the representation of the spin functions. For example, in C_{2v}^*, the triplet functions transform as $A_2 + B_1 + B_2$, while the singlet function transforms as the A_1 irreducible representation. Thus, a $^3B_1$ function in *ΓS* coupling transforms, after the direct product is taken, as the B_2, A_1, and A_2 irreducible representations of the double group. A $^1A_2$ function would transform as the A_2 irreducible representation of the double group and would be able to mix with the A_2 portion of the triplet function. Note that the double-group label does not have an explicit spin label as a superscript; the spin symmetry is incorporated in the label itself.

A final point is that different authors use different labels for the additional irreducible representations of the double group. For example, for the O_h^* group, Herzberg (1991) uses two sets of labels $E_{1/2g}$, $E_{5/2g}$, $G_{3/2g}$, $E_{1/2u}$, $E_{5/2u}$, and $G_{3/2u}$, while other authors use the labels Γ_{6g}, Γ_{7g}, Γ_{8g}, Γ_{6u}, Γ_{7u}, and Γ_{8u}.

17.3 THEORETICAL STUDIES OF THE ACTINYL IONS AND ACTINIDE OXO COMPLEXES

Because the actinide elements, and especially the most studied early actinides, tend to be very electropositive, much of their chemistry is dominated by high positive oxidation states. The electropositive nature of the actinides leads to high oxophilicity, as exemplified by the high-valent (typically +5 and +6 oxidation states) actinide elements in actinyl ions, AnO_2^{q+}. The U(VI) uranyl ion, UO_2^{2+}, is by far the most studied of the actinyl ions, and the electronic structure of this isolated species has been the subject of numerous theoretical studies. In the next section, the bonding in UO_2^{2+} is discussed briefly, followed by discussion of actinyl complexes of the general form $[AnO_2(L)_n]^q$. This is followed by sections on the spectroscopy of 'bare' actinyl species and actinyls in ionic solids. The section ends with discussion of other high-valent actinide oxo compounds and of actinide oxyfluorides.

17.3.1 The uranyl ion and related species

The most common oxidation state for uranium is +6, which corresponds to an f^0 center with a radon-like electron configuration. In the presence of oxygen, the most common discrete ionic and molecular uranium species formed contain the

uranyl ion, UO_2^{2+}, which nearly always has a linear O–U–O linkage. Similarly, neptunium and plutonium commonly form NpO_2^{q+} and PuO_2^{q+} species in which the actinide center is in the +5 or +6 oxidation state. The 'bare' uranyl species has not been isolated in the gaseous state, and can only be approached in matrix isolation studies or in ionic lattices, as will be discussed in later sections.

Electronic structure calculations on UO_2^{2+} have served as benchmarks for theoretical methods as well as a means for understanding the bonding in this relatively simple system and in the complexes it forms with other ligands. As has been detailed by Pepper and Bursten (1991), the electronic structure of UO_2^{2+} has been surprisingly controversial, especially given the apparent simplicity of this symmetric, linear, triatomic system. Among the significant questions addressed by these calculations are the following: (a) how important are relativistic effects on the electronic structure of the uranyl and related ions? (b) how covalent are the U–O bonds? (c) what are the relative contributions of the U 5f and 6d orbitals in the U–O interactions? and (d) what are the bonding principles that cause UO_2^{2+} to favor a linear geometry? Many of these questions are general ones that serve as proxies for the challenges in all electronic structure calculations on molecular actinide systems. Inasmuch as the uranyl ion is the smallest commonly found molecular actinide ion, it is not surprising that it has received intense scrutiny by theoretical methods. To provide an historical framework, the contributions of electronic structure theory in addressing the above questions about the uranyl ion will be briefly discussed here, followed by discussion of some of the recent advances in applications of theoretical methods to the chemistry of the actinyl ions.

The high symmetry and small size of the UO_2^{2+} ion has made it an attractive early candidate for electronic structure calculations of actinide complexes. McGlynn and Smith (1961) presented a nonrelativistic semiempirical MO description of the electronic structure of the uranyl ion in 1961. The importance of relativistic effects in the bonding of the uranyl ion was recognized as early as 1965, and all of the theoretical methods used to study UO_2^{2+} over the last 40 years have included explicit or implicit relativistic corrections. Many of the early and more recent studies of the bonding in uranyl have addressed the debate over 5f contributions to the U–O bonds, a seemingly straightforward question that has led to lively debates among theoretical and experimental actinide chemists.

The question of 5f covalency in actinide systems is not a new one. Chemical evidence for f-orbital covalency in actinyl nitrates was provided in 1950 by Glueckauf and McKay (1950), but was disputed shortly thereafter by Katzin (Glueckauf and McKay, 1950; Katzin, 1950). In 1952, Connick and Hugus used experimental data for UO_2^{2+} to propose U 5f orbital participation in the U–O bonds (Connick and Hugus, 1952). In 1953, Elliott used a model involving 5f interactions to explain the temperature dependence of paramagnetism in NpO_2^{2+} and PuO_2^{2+} (Elliott, 1953). Eisenstein proposed group theoretical arguments in favor of 5f and 6d covalency in uranyl and other actinide compounds (Eisenstein and Pryce, 1955; Eisenstein, 1956). Coulson and Lester (1956) soon

after proposed that f-orbital interactions must contribute to the bonding in hexavalent actinyl complexes, but that ionic interactions are probably dominant. They surprisingly proposed that the 6f orbitals of the actinides would dominate any f-orbital interactions because of the contracted nature of the 5f orbitals. At roughly the same time, Seaborg and coworkers attributed the difference in the ion-exchange behavior of analogous lanthanide and actinide complexes to significant 5f orbital contributions in the actinide systems (Diamond *et al*., 1954).

Although relativistic quantum chemical methodology continued to grow in sophistication from the 1960s through the 1980s, there was still surprisingly little agreement among quantum chemists concerning the 5f contributions to and the energetic ordering of the highest occupied orbitals in UO_2^{2+}. Because it is an f^0 ion, the highest-energy orbitals of UO_2^{2+} are predominantly O 2p in character. For the linear ion, the formally filled O 2pσ orbitals lead to group orbitals of σ_g and σ_u symmetry. Likewise, the formally filled doubly-degenerate O 2pπ orbitals generate filled doubly-degenerate π_g and π_u orbitals of UO_2^{2+}. Because of the centrosymmetric symmetry of the linear ion, the allowed interactions of the U 6d and 5f orbitals are mutually exclusive; the gerade 6dσ and 6dπ orbitals can interact with the O 2p σ_g and π_g combinations, whereas the ungerade 5fσ and 5fπ orbitals can interact with the σ_u and π_u ligand group orbitals. A qualitative MO diagram for UO_2^{2+} is presented in Fig. 17.4. All of the orbital methods agree that the four highest occupied MOs are the O 2p-based σ_g, σ_u, π_g, and π_u MOs, followed by low-lying U 5f virtual orbitals. There has been marked disagreement over the actual ordering of the highest filled orbitals, however. The disagreements about the orbital orderings in UO_2^{2+} were especially marked in the late 1970s and early 1980s when a number of relativistic methods were applied to the ion, including the relativistic extended Hückel (REX) calculations of Pyykkö and Lohr (1981), the quasi-relativistic multiple-scattering (QR-MS) Xα calculations of Wood and Boring (Boring *et al*., 1975; Boring and Wood, 1979; Wood *et al*., 1981), the Dirac–Slater multiple-scattering (DS-MS) Xα calculations of Yang *et al*. (1978), the Dirac–Slater discrete-variational (DS-DV) Xα calculations of Ellis *et al.* (1975), the Hartree–Fock calculations with RECPs by Wadt (1981), and the relativistic HFS calculations of DeKock *et al.* (1984). Jørgensen and Reisfeld (1983) compared the lack of quantitative agreement among these various methods for the orbital ordering in UO_2^{2+} to the 'effect of throwing dice'. Most of these early calculations predict a σ_u highest occupied molecular orbital (HOMO), as shown in Fig. 17.4. A detailed discussion of the lively debate over the ordering of the O 2p-based orbitals in linear UO_2^{2+} is given in the review by Pepper and Bursten (1991). As an illustrative example of a very recent calculation, the following ordering was obtained in a hybrid DFT calculation (Sonnenberg *et al*., 2005) for the highest occupied orbitals for the bare uranyl ion: π_g (–24.91 eV) < π_u (–24.56) < σ_g (–24.27) < σ_u (–23.63). The 5f-based virtual orbitals had the ordering ϕ_u (–18.38) < δ_u (–17.95) < π_u (–15.49).

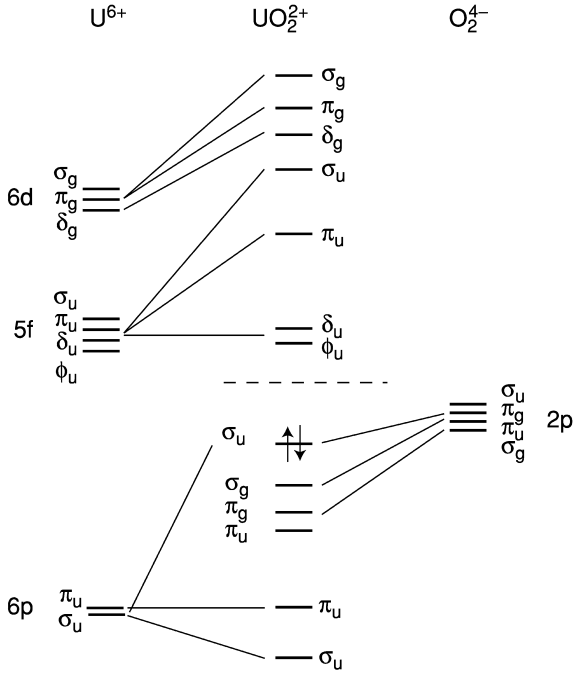

Fig. 17.4 *Schematic diagram of the MO interactions in* UO_2^{2+}, *showing the interaction of the U* 6*d and* 5*f atomic orbitals with the oxygen* 2*s and* 2*p orbitals* (*adapted from Pepper and Bursten*, 1991).

It is now clear that accurate accounting of both electron correlation and relativistic effects are essential for the prediction of the ordering of these frontier orbitals.

The electronic structural origins of the nearly invariably linear geometry of the UO_2^{2+} ion have been the focus of many theoretical studies, especially given that isoelectronic ThO_2 and the analogous transition metal ion MoO_2^{2+} typically exhibit bent geometries. The issue was first addressed on the basis of extended Hückel calculations by Tatsumi and Hoffmann (1980) and later using REX by Pyykkö *et al.* (1989) The factors include the relative admixture of 5f(σ_u) vs 6d as the ion bends, the role of the filled 'outer core' U 6p shell, and the relative contributions of covalent and ionic bonding. RECP calculations at the Hartree–Fock level by Wadt correctly predicted bent ThO_2 and linear UO_2^{2+} but disagreed in the interpretation of the role of U 6p orbitals (Wadt, 1981).

Dyall (1999) has carried out Dirac–Hartree–Fock calculations on ThO_2, PaO_2^+, and UO_2^{2+} and has analyzed in detail the role of the actinide 6p, 6d, and 5f orbitals across the series on the basis of the more sophisticated results.

He observes that the energy of the U 6d orbitals remain roughly unchanged across this region of the actinide series whereas the 5f orbitals drop in energy and becoming more radially contracted. For Th, the 5f orbitals lie above the 6d and it is favorable to bend and use f–d hybrids in the bonding, while for U the lower energy of the 5f orbitals favors linearity. In Fig. 17.5, the energy of the orbitals (actually spinors from the Dirac–Hartree–Fock [DHF] results) as a function of bending is shown. The highest-energy spinor, which corresponds to the σ_u orbital, increases in energy with bending for UO_2^{2+} but decreases for ThO_2.

A summary of the results of recent theoretical calculations on UO_2^{2+} using a variety of methods (Wahlgren *et al.*, 1998; Dyall, 1999; Ismail *et al.*, 1999; Vallet *et al.*, 1999b; Han and Hirao, 2000; Zhou *et al.*, 2000; de Jong *et al.*, 2001b; Garcia-Hernandez *et al.*, 2002), is given in Table 17.4. The methods are grouped into Hartree–Fock-based and density functional theory categories. Both of these include all-electron (AE) calculations along with calculations employing RECPs. The latter include two types denoted 'large core' with 78 electrons replaced by the RECP (Ermler *et al.*, 1991; Hay and Martin, 1998) and 'small core' with 60 electrons replaced (Küchle *et al.*, 1994). Among all-electron calculations, the U=O bond length is calculated to be about 1.65 Å from the various Hartree–Fock-based methods (DHF and DK-HF). With the small-core

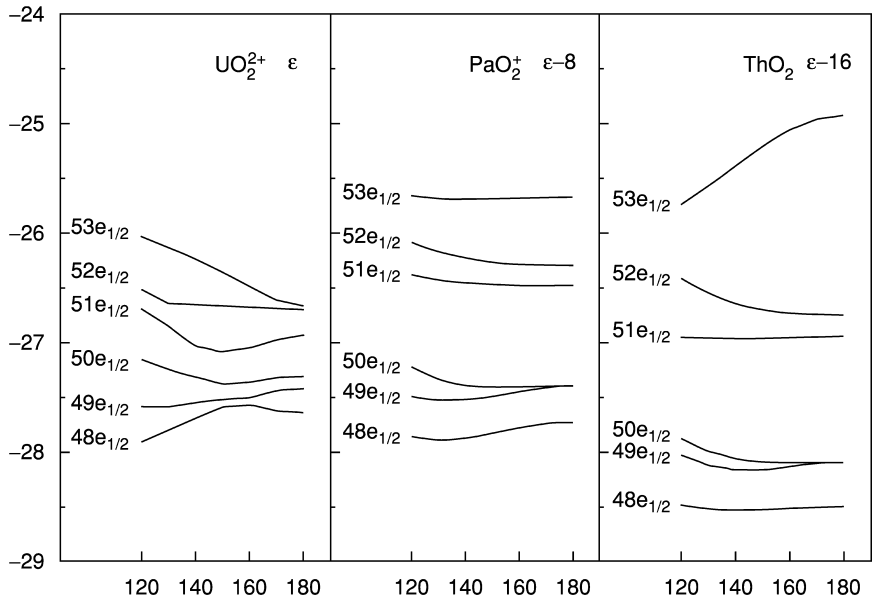

Fig. 17.5 *Valence spinor energies* (eV) *energies as a function of bending angle* (*degrees*) *for* ThO_2, PaO_2^+, *and* $[UO_2]^{2+}$ *from relativistic calculations at* $M–O = 1.9$ Å (*adapted from Dyall*, 1999).

Table 17.4 *Comparison of the calculated properties of UO_2^{2+} from various theoretical methods using all-electron (AE) approaches or employing using either small core (SC) or large core (LC) relativistic effective core potentials (RECP).*

Method	*AE or ECP*	$R_{U=O}$ (Å)	ν_1 (cm^{-1})	ν_2 (cm^{-1})	ν_3 (cm^{-1})	*References*
HF-based						
DK-HF	AE	1.651				Wahlgren *et al.* (1998)
	AE	1.647				Vallet *et al.* (1999b)
DHF	AE	1.651	1240	241	1326	de Jong *et al.* (2001b)
	AE	1.650	1234	246	1294	Dyall (1999)
HF	SC KDSP[a]	1.643				Vallet *et al.* (1999b)
	SC KDSP[a]	1.642	1243	268	1394	Han and Hirao (2000)
	SC KDSP[a]	1.654	1221	260	1301	Ismail *et al.* (1999)
	LC K[b]	1.613	1275	287	1321	Zhou *et al.* (2000)
	LC K[b]	1.631	1250	271	1301	de Jong *et al.* (2001b)
	LC HM[c]	1.646	1228	270	1280	de Jong *et al.* (2001b)
correlated						
DK CCSD(T)	AE	1.706				Vallet *et al.* (1999b)
DHF CCSD(T)	AE	1.715	974	164	1121	de Jong *et al.* (2001b)
CCSD(T)	SC KDSP	1.702	1025	192	1113	Han and Hirao (2000)
DFT scalar						
DK SVWN	AE	1.705	1034	263	1142	Garcia-Hernandez *et al.* (2002)
SVWN	SC KDSP	1.697	1029	134	1124	Zhou *et al.* (2000)
		1.709	1059	65	1165	Ismail *et al.* (1999)
		1.698	1031	221	1133	Garcia-Hernandez *et al.* (2002)
	LC K	1.670	1056	87	1138	Zhou *et al.* (2000)
	LC HM	1.728	931	84	961	Garcia-Hernandez *et al.* (2002)
	LC ERC[d]	1.691	1005	34	1096	de Jong *et al.* (2001b)
DFT hybrid						
B3LYP	SC KDSP	1.694	1051	174	1142	Ismail *et al.* (1999)
	SC KDSP	1.705	1041	161	1140	Zhou *et al.* (2000)
	SC KDSP	1.696	1049	163	1142	de Jong *et al.* (2001b)

Table 17.4 (*Contd.*)

Method	*AE or ECP*	$R_{U=O}$ (Å)	ν_1 (cm^{-1})	ν_2 (cm^{-1})	ν_3 (cm^{-1})	*References*
	LC K	1.661	1090	181	1166	Han and Hirao (2000)
	LC HM	1.704	1011	139	1101	de Jong *et al.* (2001b)
	LC ERC	1.679	1047	166	1135	de Jong *et al.* (2001b)

[a] Küchle *et al.* (1994).
[b] RECP for U:http://www.theochem.uni-stuttgart.de/pseudopotentials/index.en.html
[c] Hay and Martin (1998).
[d] Ermler *et al.* (1991).

relativistic effective core potentials (RECPs), Hartree–Fock calculations lead to similar bond lengths to those found using the all-electron DHF method, while there are slightly greater differences noted with the large-core RECPs. When correlation effects are explicitly included, as in CCSD(T) approaches, the bond length increases to 1.71 Å. The density functional results (for the LDA and B3LYP functionals summarized in the table) that incorporate correlation effects through the exchange-correlation functional reasonably reflect this with predicted U=O bond lengths ranging from 1.69 to 1.71 Å. Again larger discrepancies arise with the large core RECP.

The calculated vibrational stretching frequencies generally follow the trend that higher frequencies are associated with shorter U=O bond lengths. DHF calculations, with shorter bond lengths, predict symmetric and asymmetric stretching frequencies of 1240 and 1300 cm^{-1}, while the correlated methods and DFT approaches give 1020–1050 and 1110–1140 cm^{-1} for the same values. Comparison with experiment is problematic in the absence of isolated gas-phase spectroscopic studies, but comparisons with observed frequencies will be given below for uranyl complexes.

Garcia-Hernandez *et al.* (2002) examined the Np(VI) analog $[NpO_2]^{2+}$ with a $5f^1$ configuration using all-electron Douglas–Kroll–Hess approaches. For the Np–O bond length they obtained 1.698, 1.716, and 1.718 Å using the VWN, BP, and PBEN functionals, respectively. Results with spin–orbit DKH showed practically no change in the computed bond lengths. For symmetric stretch frequencies, the same calculations predicted 1009 cm^{-1} (VWN), 972 cm^{-1} (BP), and 969 cm^{-1} (PBEN).

17.3.2 Actinyl complexes

In solution and the solid state, additional ligands bind to the actinyl ions in the equatorial plane of the O=An=O unit. Among the most common characterized species are the aqua complexes $[UO_2(H_2O)_5]^{2+}$ found at low pH, the hydroxo

complexes $[UO_2(OH)_4]^{2-}$, $[UO_2(OH)_5]^{3-}$, and $[UO_2(OH)_4(H_2O)]^{2-}$ found at high pH, and the halide species $[UO_2X_4]^{2-}$ found in crystals (Fig. 17.6). In this class of $[UO_2L_n]$ complexes, the equatorial ligands are weak σ-donors. In this case, the U atom can use acceptor orbitals oriented in the equatorial plane that are not utilized in the bonds with the actinyl oxo atoms. The orbitals that in principle can act as acceptors in the equatorial plane include the 6d(x^2–y^2), 6d(xy), 5f(x^3–$3xy^2$) and 5f(y^3–$3x^2y$), and, to a lesser extent, the 7s and 7p orbitals. In the case of hydroxo complexes, the OH^- ligands can be π-donors and can compete with the metal orbitals involved in the U=O π_u and π_g bonds.

Clavaguéra-Sarrio *et al.* (2003b) have recently reported a DFT study of the binding energies and geometries of $UO_2L_2^{q+}(q = 0, 2)$ complexes with 33 different ligands L with the goal of predicting preferred coordination geometries. They determined that ligand polarization and charge transfer to the uranyl ion are likely to be necessary in any force-field model for uranyl–ligand bonding.

(a) Aqua complexes

Aqua complexes of actinyls have been studied in solution and the solid state using extended X-ray absorption fine structure (EXAFS) spectroscopy (Allen *et al.*, 1997), X-ray crystallography (Alcock and Esperas, 1977; Aaberg *et al.*, 1983), and X-ray scattering (Neuefeind *et al.*, 2004). The experimental studies show a preferred coordination number of five water molecules. The $[UO_2(H_2O)_5]^{2+}$ ion is the commonly observed U(VI) species in aqueous solution at low pH (Fig. 17.6) and consequently this complex has been the subject of several recent theoretical studies (Gropen, 1999; Spencer *et al.*, 1999; Tsushima and Suzuki, 1999; Wahlgren *et al.*, 1999; Hay *et al.*, 2000; Fuchs *et al.*, 2002; Clavaguéra-Sarrio *et al.*, 2003a) including DFT-based approaches and model potentials with Douglas–Kroll corrections. The oxygen atoms of the five water molecules are coordinated in nearly perfect five-fold symmetry about the uranyl ion, with the water molecules nearly perpendicular to the equatorial plane. Subtle differences in the structure of this complex are obtained among the calculations (Table 17.5). The AIMP-DK and DFT calculations with LDA and B3LYP functionals all predict U=O bond lengths in the range 1.75–1.78 Å. These theoretical results are in good agreement with the EXAFS solution bond length of 1.76 Å, which is slightly longer than the solid state value of 1.71 Å. The U-OH_2 bond lengths are predicted to be 2.42–2.52 Å in the DFT calculations, which compare favorably with the experimental bond lengths of 2.41–2.45 Å (Hay *et al.*, 2000). In the DKH studies (Fuchs *et al.*, 2002), the effects of solvation were included where the U=O bond length decreased from 1.771 to 1.662 Å while the U–OH_2 bond length increased from 2.530 to 2.639 Å.

Several studies have addressed the issue of why five is the preferred coordination number for H_2O with UO_2^{2+} (Spencer *et al.*, 1999; Tsushima and Suzuki, 1999; Hay *et al.*, 2000). In particular, several groups have explored the relative

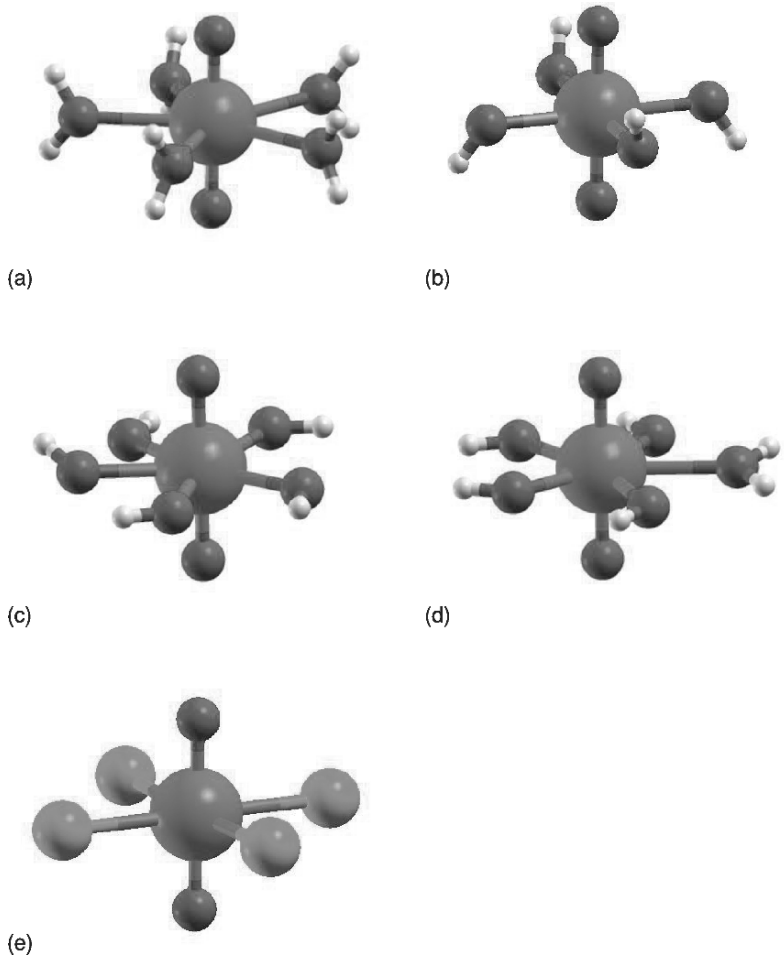

Fig. 17.6 *Structures of* (*a*) $[UO_2(H_2O)_5]^{2+}$, (*b*) $[UO_2(OH)_4]^{2-}$, (*c*) $[UO_2(OH)_5]^{3-}$, (*d*) $[UO_2(OH)_4(H_2O)]^{2-}$, *and* (*e*) $[UO_2Cl_4]^{2-}$ *as determined by DFT calculations* (*rendered from results reported in Schreckenbach* et al.*,* 1998, 1999*; Wahlgren* et al.*,* 1999*; Clavaguéra-Sarrio* et al., 2003*a; Sonnenberg* et al.*,* 2005).

energetics of binding four, five, or six water molecules to various actinyl ions. These approaches used a combination of energies from density functional calculations, thermodynamic quantities derived from calculated vibrational frequencies, and solvation energies from dielectric continuum models. Spencer *et al.* (1999) used DFT (Becke–Lee–Yang–Parr functional [BLYP]) calculations to obtain the relative ordering 5 < 4 (+7.2 kcal mol^{-1}) < 6 (+18.5) for $[UO_2(H_2O)_n]^{2+}$ species. They obtained a similar ordering pattern for $[PuO_2(H_2O)_n]^{2+}$ ions. Calculations using DFT (B3LYP) and different solvent

Table 17.5 *Calculated properties of* $[UO_2(H_2O)_5]^{2+}$ *from various theoretical methods, compared to experimental values for the uranyl aqua complex.*

Method	$R_{U=O}$ (Å)	$R_{U-O(H)}$ (Å)	ν_{sym} (cm^{-1})	ν_{asym} (cm^{-1})	*References*
BLYP	[1.746]	2.550			Spencer *et al.* (1999)
AIMP-DK	1.750	2.421			Wahlgren *et al.* (1999)
HF RECP	1.694	2.545	1091	1149	Hay *et al.* (2000)
LDA RECP	1.778	2.423	854	945	Hay *et al.* (2000)
BLYP RECP	1.803	2.516	787	893	Hay *et al.* (2000)
B3LYP RECP	1.756	2.516	910	1003	Hay *et al.* (2000)
PBEN (AE)	1.771	2.530			Fuchs *et al.* (2002)
PBEN (AE+solv)	1.662	2.639			Fuchs *et al.* 2002
Expt.	1.76	2.41	869	965	Allen *et al.* (1997)

models gave a slightly different ordering of $5 < 6 < 4$ water molecules in the first coordination shell (Tsushima and Suzuki, 1999; Hay *et al.*, 2000). Additional structures are found with at least one water molecule displaced from the first shell into the second shell, where the molecule is hydrogen bonded to the uranyl oxygen atoms rather than directly coordinated to the uranium center.

As one proceeds across the actinide series, there is only a slight change in the experimental An–O bond length as measured in solution by EXAFS: 1.76 Å in $[UO_2(H_2O)_5]^{2+}$ (Allen *et al.*, 1997), 1.75 Å in $[NpO_2(H_2O)_5]^{2+}$ (Reich *et al.*, 2000; Den Auwer *et al.*, 2003), and 1.74 Å in $[PuO_2(H_2O)_5]^{2+}$ (Conradson, 1998). DFT (B3LYP) calculations using LC-RECPs predict a slight shortening of bond length of 1.756–1.742 Å across U(VI) to Pu(VI) (Hay *et al.*, 2000) (Fig. 17.7). In addition the calculations reasonably well describe the decrease in symmetric and antisymmetric O=An=O stretch frequencies across the series (Jones and Penneman, 1953; Basile *et al.*, 1974). It is somewhat curious that as the bond lengths are getting slightly shorter, the frequencies are actually decreasing – the reverse of the usual correlation. This trend is attributed to the decrease in An(5f)–O(2p) overlap going across the series as the 5f orbitals become more radially contracted.

The mechanisms for exchange of water (H_2O^*) with the aqua complex $[UO_2(H_2O)_5]^{2+}$ were investigated by Vallet *et al.* (2001). The possibilities of associative (via a six-coordinate intermediate), dissociative (via four-coordinate intermediate), and interchange (via a concerted symmetric transition state) pathways were probed using a combination of Hartree–Fock, MP2, and CPCM (conductor-like polarizable comtinuum model) solvent model (Fig. 17.8). The calculated activation energies were 74, 19, and 21 kJ mol^{-1}, respectively, for the D-, A- and I-mechanisms in the solvent. Comparison with the experimental value of 26 ± 1 kJ mol^{-1} eliminates the D mechanism, leaving it difficult to distinguish between the A- and I-mechanisms. A later study extended

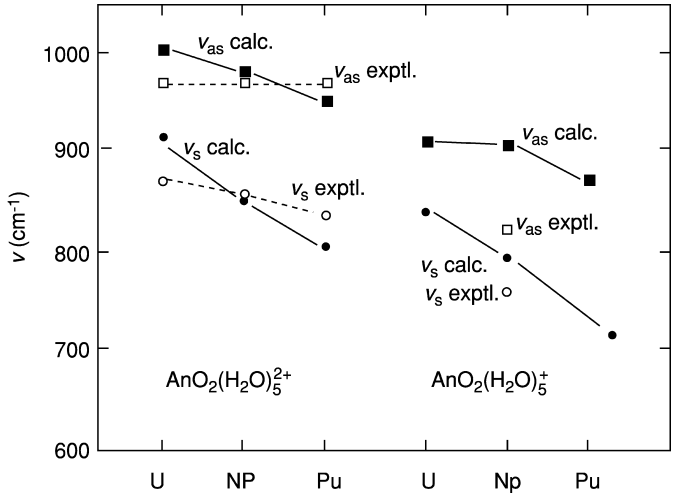

Fig. 17.7 *Plots of calculated and experimental vibrational frequencies for* $[AnO_2(H_2O)_5]^{2+}$ *and* $[AnO_2(H_2O)_5]^{+}$ *species* (*reproduced from Hay* et al., 2000).

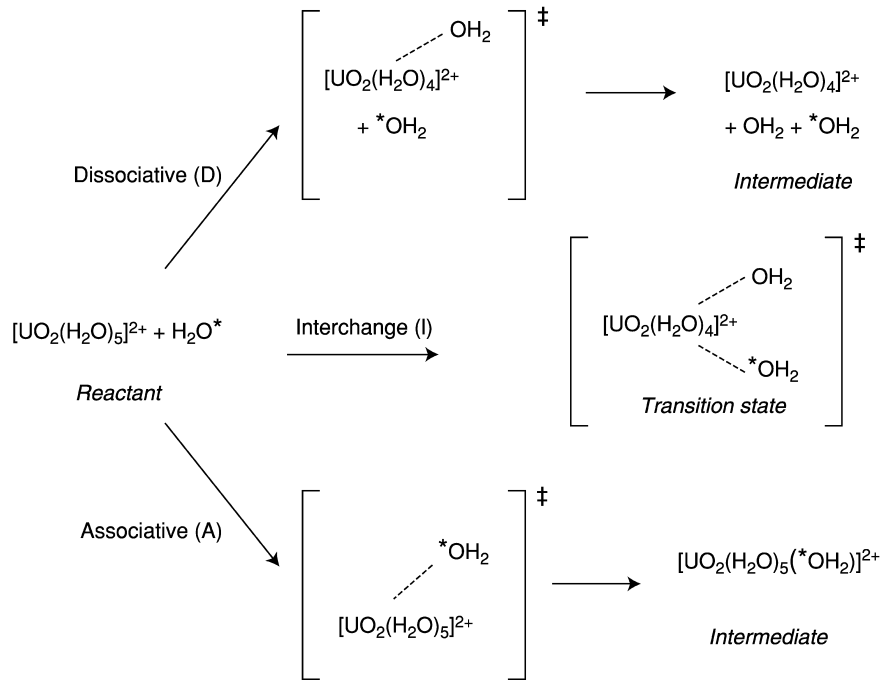

Fig. 17.8 *Intermediates for exchange of water molecules in* $[UO_2(H_2O)_5]^{2+}$ *by associative* (*A*), *dissociative* (*D*), *and interchange* (*I*) *mechanisms* (*adapted from Vallet* et al., 2001).

these studies to exchange in aqua complexes of UO_2^+, NpO_2^{2+}, and AmO_2^{2+} with similar findings (Vallet *et al.*, 2004). This same group has modeled electron exchange between UO_2^+ and UO_2^{2+} in solution, examining potential intermediates in both outer-sphere and inner-sphere electron-exchange mechanisms (Privalov *et al.*, 2004). Other than this contribution, relatively little work has been done on dimeric and polymeric species that can be the dominant species in solution depending on the conditions. Schlosser *et al.* (2003) compared all-electron DFT results on one of the few dimeric complexes for which there is a crystal structure, $[(UO_2)_2(\mu^2\text{-}OH)_2Cl_2(H_2O)_4]$. In addition, the role of hydrogen bonding in the crystal was studied by adding a layer of water molecules.

(b) Hydroxide complexes

At higher pH, one finds uranyl species with hydroxide ligands displacing water molecules coordinated to the metal. The first hydrolysis product formed is $[UO_2(H_2O)_4(OH)]^+$, which can also exist in dimeric form (Clark *et al.*, 1995). At much higher pH, the $[UO_2(OH)_4]^{2-}$ species has been observed and characterized in the solid state (Clark *et al.*, 1999). The structures of the tetrahydroxide species have been investigated using DFT techniques with RECPs (Schreckenbach *et al.*, 1998) and with model potentials with Douglas–Kroll corrections (AIMP-DK) (Wahlgren *et al.*, 1999). As shown in Table 17.6, the calculated U=O distances agree rather well with experiment while the U–OH bond lengths are overestimated somewhat by ~0.1 Å compared to the crystal structure.

The U=O bonds in the hydroxide complexes are longer than those in the aqua complexes. This observation indicates weaker U=O interactions because of the competition with the equatorial OH^- ligands, which are acting as strong π-donors. The lone pair orbitals on the OH^- ligands have the proper symmetry to interact with the π_u and π_g U–O bonding orbitals of the UO_2^{2+} moiety (Schreckenbach *et al.*, 1998).

Solution EXAFS studies of uranyl hydroxide complexes in two different alkaline environments found relatively similar U–OH bond lengths (2.22–2.24 Å) that differ only slightly from the X-ray structure of $[UO_2(OH)_4]^{2-}$ (Clark *et al.*, 1999; Wahlgren *et al.*, 1999). The number of oxygen atoms in the equatorial plane was found to be 5 ± 0.5. Clark *et al.* interpret this result in terms of a $[UO_2(OH)_5]^{3-}$ structure. Calculations on the pentahydroxide structure by Wahlgren *et al.* gave U–OH bond lengths 0.3 Å longer, and hence they ruled out this form in favor of the tetrahydroxide. They also examined a third species with one water and four hydroxide ligands bound to the uranyl. More recently, Sonnenberg *et al.* (2005) found a stable pentahydroxide species with C_{5v} symmetry with no imaginary frequencies having U–OH bond lengths of 2.45 Å without incorporating solvent effects, which would be 0.2 Å longer than the derived value from the EXAFS analysis.

Table 17.6 *Theoretical and experimental geometries of hydroxyl complexes including* $[UO_2(OH)_4]^{2-}$ *and related complexes.*

Method	$R_{U=O}$ (Å)	$R_{U-O(H)}$ (Å)		*References*
$[UO_2(OH)_4]^{2-}$				
AIMD-DK	1.80	2.36–2.38		Wahlgren *et al.* (1999)
B3LYP LC-RECP	1.842	2.33		Schreckenbach *et al.* (1998)
	1.87	2.27–2.35	*cis*-O=U=O form	
B3LYP SC-RECP	1.84	2.31		Sonnenberg *et al.* (2005)
Expt (solid)	1.80–1.83	2.23–2.36		Clark *et al.* (1999)
$[UO_2(OH)_5]^{3-}$ and related species				
AIMD-DK	1.80	2.50	$[UO_2(OH)_4]^{2-}$	Wahlgren *et al.* (1999)
	1.80	2.36–2.38	$[UO_2(OH)_4(H_2O)]^{2-}$	
B3LYP SC-RECP	1.83	2.455	$[UO_2(OH)_5]^{3-}$	Sonnenberg *et al.* (2005)
EXAFS soln	1.79	2.22	$N_{eq} = 5.3 \pm 0.5$[a]	Clark *et al.* (1999)
EXAFS soln	1.82	2.24	$N_{eq} = 5.0 \pm 0.5$[a]	Wahlgren *et al.* (1999)

[a] Values for the coordination number from the EXAFS experiments.

Schreckenbach *et al.* (1998) investigated the possible isomerization of the tetrahydroxide in which protons are transferred from the equatorial hydroxides to the uranyl oxygen atoms to reconstitute the tetrahydroxide. Such a mechanism was suggested to account for the scrambling of ^{18}O in the complex in basic solution (Fig. 17.9). They found an unusual *cis*-oxo form with a bent O=U=O bond angle of 128° (Table 17.6) to be a local minimum with a calculated energy 18 kcal mol^{-1} above the more stable 'usual' *trans*-oxo form. The barrier between the two forms was calculated to be 38 kcal mol^{-1}, too high to account for rapid isomerization via a unimolecular mechanism.

(c) Complexes with bidentate ligands

Actinyl species can be found complexed to other inorganic ligands in a variety of conditions. Because waste treatments of actinides in solution use nitrates, actinyl complexes with coordinated nitrate ligands are common (Castellato *et al.*, 1981; Allen *et al.*, 1996). Actinyl complexes with carbonate ligands are also common and are especially relevant to studies of actinides in the environment with naturally occurring minerals, carbonate species are another important actinide complex (Clark *et al.*, 1995). Craw *et al.* examined prototypical nitrate complexes $UO_2(NO_3)_2(H_2O)_2$ at the Hartree–Fock level (Table 17.7) as well as a sulfate complex and their Pu(VI) analogs (Craw *et al.*, 1995). As shown

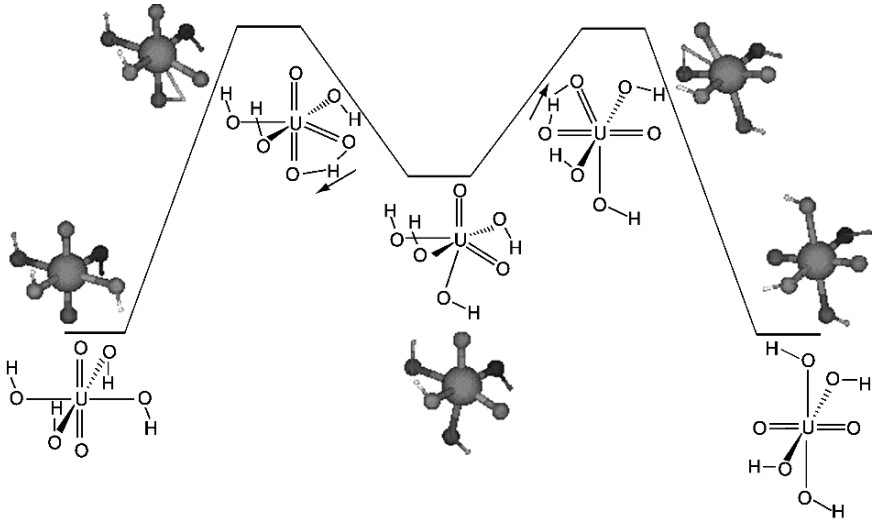

Fig. 17.9 *Isomers of* $[UO_2(OH)_4]^{2-}$ *involving conventional trans and unusual cis-O=U=O linkages* (*reproduced from Schreckenbach* et al., 1998).

in Fig. 17.10, the nitrato complexes are coordinated in a bidentate mode. An analysis of the bonding in these complexes showed primarily ionic bonding dominated by electrostatic forces.

Gagliardi and Roos (Gagliardi *et al.*, 2001a; Gagliardi and Roos, 2002) have used complete active space self-consistent field (CASSCF)/CASPT2 calculations to examine carbonato complexes of the uranyl and neptunyl ions that have been the focus of several experimental studies (Clark *et al.*, 1995, 1996; Docrat *et al.*, 1999). Solid-state structures with both $[UO_2(CO_3)_3]^{4-}$ and $[UO_2(CO_3)_3]^{5-}$ are known. In both cases, three carbonates bind in the equatorial plane in a bidentate mode. Experimentally the U=O bond length increases from 1.80 to 1.90 Å when the extra electron is added in going from the U(VI) to the U(V) complex. The calculations also give an increase in the U=O bond length of 1.845 to 1.929 Å between the U(VI) and U(V) complexes. Similar increases in the $U–O_{eq}$ bond length are also noted. For the Np(V) species $[NpO_2(CO_3)_2(H_2O)_2]^{3-}$, the calculated Np=O bond length, 1.854 Å, is between the U(VI)=O and U(V)=O values and is in excellent agreement with the experimental value of 1.85 Å.

Vázquez *et al.* (2003) studied tris-carbonato, tris-acetato, and related uranyl complexes using gradient-corrected DFT using the ADF code also employing a solvent continuum model. They also explored dimeric complexes with bridging hydroxide groups and examined the role of Ca^{2+} counter-ions and explicit water molecules. Coupez and Wipff (2003) reported Hartree–Fock and DFT calculations with diamide ligands (malonamide and succinamide) comparing the

Table 17.7 *Theoretical and experimental bond lengths* (Å) *of actinyl complexes with multidentate ligands.*

Complex	*Method*	*R(U=O)*	*R(U–O)*	*R(U–O_H)*	*References*
$UO_2(NO_3)_2(H_2O)_2$	HF	1.72	2.56	2.40	Craw *et al.* (1995)
	expt	1.76		2.40	
$PuO_2(NO_3)_2(H_2O)_2$	HF	1.68		2.45	Craw *et al.* (1995)
$UO_2(SO_4)(H_2O)_3$	HF	1.74	2.57	2.64	Craw *et al.* (1995)
	expt	1.75		2.40	
$PuO_2(SO_4)(H_2O)_3$	HF	1.70		2.47	Craw *et al.* (1995)
$[UO_2(CO_3)_3]^{4-}$	MBPT2	1.88	2.407		Gagliardi *et al.* (2001a)
	solv. PW91	1.86	2.44		Vazques *et al.* (2003)
	expt	1.80	2.43		Clark *et al.* (1996)
$[UO_2(CO_3)_3]^{5-}$	MBPT2	1.933	2.529		Gagliardi *et al.* (2001a)
	expt	1.90	2.50		Docrat *et al.* (1999)
$[NpO_2(CO_3)_2(H_2O)_2]^{3-}$	CASPT2	1.854	2.548	2.585	Gagliardi *et al.* (2001a)
	expt	1.85	2.48		Clark *et al.* (1996)
$[UO_2(acetate)_3]^{1-}$	solv. PW91	1.81	2.50		Vazques *et al.* (2003)
	expt	1.76	2.48		Navaza *et al.* (1991)

relative stabilities of six- and seven-membered chelate rings in their bidentate coordination to the uranyl.

17.3.3 'Bare' actinyl species and actinyl ions in solids

While uranyl is the prototypical actinyl ion, with an oxidation state of +6, high-valent dioxo species are also well known for Np, Pu, and Am. For these actinides, the -yl name has also been applied to the +5 and +6 oxidation states (Katz *et al.*, 1986). In an overview of the electronic structure and spectra of these ions, Matsika *et al.* (2001) were able to characterize the strengths of different interactions found in actinyls. The strongest interaction is the antibonding one between the $5f\sigma_u$ and the $5f\pi_u$ and the ligand orbitals, resulting in high orbital energies for the molecular orbitals mostly derived from these 5f orbitals. Comparisons between the actinide electron repulsion parameters and the actinide spin–orbit parameter (ζ_{5f}) indicate that the electron repulsion is more

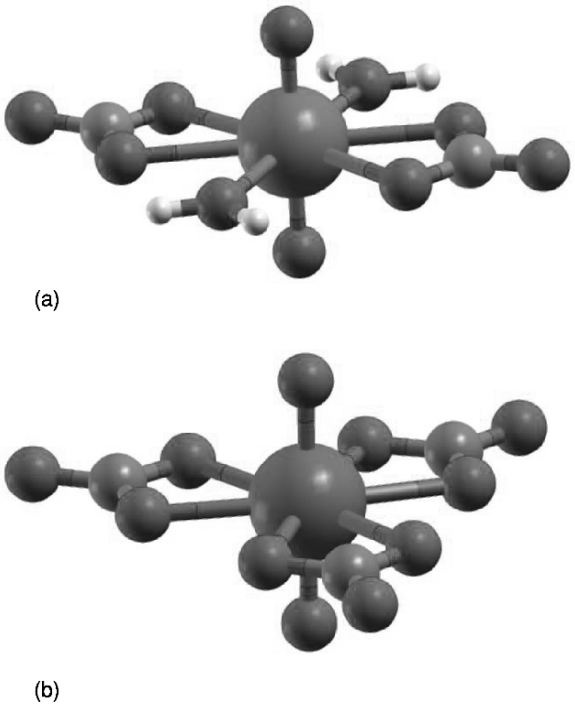

Fig. 17.10 *Calculated structures of bidentate complexes with* (*a*) *nitrate and* (*b*) *carbonate ligands* (*see Craw* et al.*,* 1995*; Gagliardi and Roos,* 2002).

significant, but that the spin–orbit splitting needs to be included. Lastly, the $5f\delta_u$ and the $5f\phi_u$ orbitals display weak-field coupling, i.e. the two-electron open-shell state is $\delta_u^1\phi_u^1$ rather than δ_u^2 or ϕ_u^2. The electron configurations for these ions can thus be characterized as $\sigma_u^2(\delta_u\phi_u)^n$,$\sigma_u^2(\delta_u\phi_u)^{n-1}\pi_u^1$,$\sigma_u^1(\delta_u\phi_u)^{n+1}$, with n ranging from zero to four, the ground states for these configurations for the various actinyl species are listed in Table 17.8. For example, for f^2 systems, the two actinyl ions studied were NpO_2^+ and PuO_2^{2+}. The lowest state for a given electron configuration is listed – for example, for the $\sigma_u{}^1(\delta_u\phi_u)$ ^3H configuration, that state would be $^5\Phi_{1g}$ for each of the two actinyl ions. Note that the occupation number for the δ_u and the ϕ_u orbitals are given together due to the strength of the electronic interactions listed above.

As mentioned previously, the COLUMBUS codes have recently enabled two-component multi-reference configuration interaction singles and doubles (SO-MRCISD) using CSF expansions on the order of millions. The great advantage of these calculations for linear molecules is that since the spin–orbit effects are incorporated in the variational calculation, the resultant states are eigenfunctions of the total z-component angular momentum, Ω. A survey of the computational uranyl literature referred to above reveals little information concerning

Table 17.8 *Lowest energy electronic states for various f^n actinyl electron configurations* (*see Matsika* et al., 2001).

Electronic configuration[a]	$n = 0$ UO_2^{2+} NpO_2^{3+}	$n = 1$ UO_2^{+} NpO_2^{2+} PuO_2^{3+}	$n = 2$ NpO_2^{+} PuO_2^{2+}	$n = 3$ PuO_2^{+} AmO_2^{2+}	$n = 4$ AmO_2^{+}
$\sigma_u^2(\delta_u\phi_u)^n$	$^1\Sigma^+_{0^+g}$	$^2\Phi_{5/2u}$	$^3H_{4g}$	$^4\Phi_{3/2u}$	$^5\Sigma^+_{0^+g}$
$\sigma_u^2(\delta_u\phi_u)^{n-1}\pi_u^1$		$^2\Pi_{1/2u}$	$^3\Gamma_{3g}$	$^4I_{9/2u}$	$^5\Gamma_{2g}$
$\sigma_u^1(\delta_u\phi_u)^{n+1}$	$^3\Delta_{1g}$	$^4H_{7/2u}$	$^5\Phi_{1g}$	$^6\Sigma^+_{1/2u}$	$^5\Delta_{4g}$

[a] Note that the σ_u orbital refers to the highest ligand-based occupied orbital.

excited states. Experimentally, much of the spectroscopic work is based on actinyl ions in crystalline environments or in solutions. Computational modeling of the latter is discussed elsewhere in this review; as for the former, there are two well-known approaches: embedded potentials using AIMP, developed by Seijo and Barandiarán (1999), recently applied to Pa^{4+} and U^{4+} defects in chloride hosts (Barandiarn *et al.*, 2003) and to a study of Pa^{4+} defects in Cs_2ZrCl_6 (Seijo and Barandiarán, 2001), and a layered-cluster computational model developed by Winter and Pitzer (1985) and applied to actinyl systems by Matsika and Pitzer (2001). These authors have also examined the spectral intensities of actinyl ions (Matsika *et al.*, 2000).

The low-lying transitions of non-f^0 actinyl species are known to be f→f transitions, which are formally electric-dipole forbidden if the molecule has a center of symmetry based on group theory (Matsika *et al.*, 2001). By adding equatorial ligands to the actinyl complexes, the center of inversion can be removed. A study of intensities for $NpO_2^+ + nCl^-$ complexes reveals that, for the odd n cases (odd being required to remove the inversion point), the $n = 5$ case reproduces the experimental spectrum (Matsika *et al.*, 2000). Analysis of the crystal field shows that five-coordination allows for mixing between the 5fϕ and 6dδ orbitals, resulting in calculated oscillator strengths that can reproduce the experimental spectrum.

The excited states of the uranyl ion have been calculated for both gas-phase and crystalline environments by SO-MRCISD (Zhang and Pitzer, 1999; Matsika and Pitzer, 2001) and by CASPT2 [using Douglas–Kroll for scalar relativistic effects and RASSI (restricted active space state interaction) with atomic mean field integrals for spin–orbit effects] (Pierloot, 2003) methods. Both methods agree with the experimental results (Denning, 1992) as to the progression of the Ω values of the low-lying excited states: 1_g, 2_g, 3_g, 2_g, 3_g, and 4_g. The first three spin–orbit states are derived from the ΛS term $^3\Delta_g$ and the next three from $^3\Phi_g$–note that there is mixing between the two ΛS states in the $\Omega = 2_g$ and $\Omega = 3_g$ states. The latter method appears to have better quantitative agreement for transition energies (T_e) for the fluorescent transition, which is the $1_g \rightarrow 0_g^+$ transition: 20 363 cm^{-1} (for $Cs_2UO_2Cl_4^{2-}$) using

SO-MRCISD, 20 028 cm^{-1} (for the isolated $UO_2Cl_4^{2-}$ complex) using CASPT2, and 20096 cm^{-1} from experiment.

There are far fewer experimental and computational studies for the neptunyl ions as compared to uranyl. For the NpO_2^{2+} ion, which is an f^1 system, the SO-MRCISD method gives a bond length of 1.66 Å and a symmetric stretching frequency of 1059 cm^{-1} for the gas phase (Matsika and Pitzer, 2000). All-electron scalar-relativistic DFT studies give values from 1.701 to 1.721 Å for the former and 1011 to 970 cm^{-1} for the latter, depending on the functional used (Garcia-Hernandez *et al*., 2002). The experimental values (in solution and in the solid state) range from 1.75 (Clark, 1999; Tait, 1999) to 1.80 Å (Volkoy and Kapshuhof, 1976) and from 863 to 914 cm^{-1} (Basile *et al*., 1974; Budantseva *et al*., 2000). Matsika and Pitzer (2001) calculated a bond length of 1.70 Å and 950 cm^{-1} for NpO_2^{2+} doped into $Cs_2UO_2Cl_4$, values that are much closer to experiment and which emphasizes the need for comparing theory and experiment for the same phase of matter. The excited states show an interesting pattern: the ground state is an $\Omega = 5/2u$ state that is 86% $^2\Phi_{5/2u}$ and 14% $^2\Delta_{5/2u}$, the first excited state is an $\Omega = 3/2u$ that is predominantly $^2\Delta_{3/2u}$, followed by a 5/2u state (86% $^2\Delta_{5/2u}$ and 14% $^2\phi_{5/2u}$) and a 7/2u state ($^2\Phi_{7/2u}$). Although the 5fδ orbital is lower in energy than the 5fϕ orbital, the latter participates more in the ground state due to the greater spin–orbit splitting of the fϕ orbital. For NpO_2^{2+} doped into $Cs_2NpO_2Cl_4$, the calculated T_e values for the analogs of these states are 0, 1663, 5775, and 8463 cm^{-1} compared to the experimental 0, 1000, 6880, and 7990 cm^{-1} (Denning *et al*., 1982a,b), which is good agreement for this level of theory (Matsika and Pitzer, 2001). Calculations on the energy of the first charge transfer state, a $^4H_{7/2u}$ state from a $\sigma_u^1\delta_u^1\phi_u^1$ configuration, are very dependent on the level of correlation. The experimental value is 13264.9 cm^{-1} above the ground state, and the calculated values differ between 12622 cm^{-1} (for 15 electrons correlated, in the isolated ion) and 18236 cm^{-1} (for seven electrons correlated, in the crystal).

The Pu(VI) plutonyl ion, PuO_2^{2+}, is an f^2 system for which there are very little experimental data. The ground state has been determined by electron spin resonance (Bleaney, 1955) and spectroscopic methods (Denning, 1992) to be $^3H_{4g}$. Initial calculations on PuO_2^{2+} led to the proposal of a $^3\Sigma_g^-$ ground state derived from a δ_u^2 configuration (Craw *et al*., 1995). However, as mentioned above, the δ_u and ϕ_u orbitals are weak-field-coupled and the ground state is proposed by several authors to be a ^3H_g state from a $\delta_u^1\phi_u^1$ configuration (Ismail *et al*., 1999; Maron *et al*., 1999; Hay *et al*., 2000). The bond lengths for this ground state vary from 1.6770 Å using averaged quadratic coupled cluster (AQCC; Maron *et al*., 1999) to 1.6883 Å using B3LYP (Ismail *et al*., 1999). Examination of vertical excitations show the importance of spin–orbit splitting, as the ground state is more properly labeled as an $\Omega = 4_g$ state. The progression of states shows the interposition of states derived from different ΛS states, the total spin–orbit splitting between the $\Omega = 4_g$ and $\Omega = 6_g$ states is 7849 cm^{-1} from two-step quasi-degenerate perturbation theory calculations by Maron *et al.* (1999)

and 9613 cm^{-1} from a SO-MRCISD calculation (Blaudeau *et al.*, unpublished). Hay *et al.* (2000) also performed spin–orbit studies on plutonyl, as well as on the aqua complexes. Recently, an EPCISO calculation has been performed by Clavaguéra-Sarrio *et al.* (2004), which predicts the splitting between the $\Omega = 4_g$ and $\Omega = 6_g$ states to be 14329 cm^{-1} (see Table 17.9 for the splittings of the ^3H_g and $^3\Sigma_g^-$ states; note that there are other states in the spectra that are not listed in the table). Their explanation of the discrepancy between this calculation and the previous ones are due to the inclusion of spin–orbit polarization effects in the EPCISO method. All of the calculations show the interspersing of the Ω states derived from different ΛS states, and thus the importance of incorporating spin–orbit methods in the calculations. A charge-transfer state, $^5\Phi_{1g}$ state from a $\sigma_u^1\delta_u^2\phi_u^1$ configuration, is found in the latter set of calculations at an adiabatic T_e of 20279 cm^{-1}; the experimental value is 19000 cm^{-1} (Jørgensen, 1970). Comparing the calculated excited states for the isoelectronic species NpO_2^+ and PuO_2^{2+}, the transition energies are lower for the monocation, e.g. the first excited state, with $\Omega = 0_g^+$, lies at 3366 cm^{-1}, compared to 3951 cm^{-1} for the plutonium species (Matsika and Pitzer, 2000; Blaudeau *et al.*, unpublished).

What is most significant for these results is that they illustrate the absolute need to include spin–orbit effects for open-shell actinide systems. Interestingly, the study by Clavaguéra-Sarrio *et al.* (2004) show that the geometries and frequencies of these states are very similar due to the atomic nature of the 5fδ and the 5fϕ orbitals. Thus, single-reference methods, such as DFT, can still predict the structural properties of these molecules, although wavefunction techniques that include spin–orbit effects are required to predict the electronic spectra.

17.3.4 Other high oxidation state oxygen species

There has been much recent experimental and theoretical interest in actinide oxide species with formal metal oxidation states greater than +6. Domanov *et al.* report the formation of a volatile species they tentatively identify as a Pu(VIII) oxide, PuO_4 (Domanov *et al.*, 2002). They refer to previous work by

Table 17.9 *Vertical excitations* (cm^{-1}) *for the Ω states derived from the* ^3H_g *and* $^3\Sigma_g^-$ *states of* PuO_2^{2+}*, showing interspersing of the Ω states.*

Ω	*Major ΛS state*	*CIPSO*[a]	*EPCISO*[b]	*Variational spin–orbit MRCISD*[c]
6_g	^3H_g	7849	14329	9613
1_g	$^3\Sigma_g^-$	7044	6068	5816
5_g	^3H_g	6593	8037	5158
0_g^+	$^3\Sigma_g^-$	4295	4194	3951
4_g	^3H_g	0	0	0

[a] Maron *et al.* (1999).
[b] Clavaguéra-Sarrio *et al.* (2004).
[c] Blaudeau *et al.* (unpublished).

Pershina and coworkers that had concluded that such a species in solution would be thermodynamically unstable (Ionova *et al.*, 1981; Pershina *et al.*, 1982). Pyykkö *et al.* speculated on the existence of neutral UO_6, with a formal oxidation state of +12 for the uranium atom (Pyykkö *et al.*, 2000). The octahedral structure of this hexaoxide is a minimum for several computational methods, including DFT and MRCI. However, it is found to have an imaginary frequency at the Dirac–Fock level. Some earlier studies included calculations on anionic U(VI) oxides, including UO_4^{2-} and UO_4^{6-}, with good agreement to experimental geometries (Ellis *et al.*, 1982; Pyykkö and Zhao, 1991).

Np(VII) species in solution have been studied by two groups. Williams *et al.* (2001) found a NpO_4^- complex, which, in agreement with DFT calculations, has D_{2d} symmetry. The deviation from planar geometry is slight (the *trans*-O–Np–O angle is 169.8°) but significant, as the planar form has an imaginary frequency. On the other hand, Bolvin *et al.* undertook calculations on the isoelectronic ions NpO_4^- and UO_4^{2-} and found the former to be square planar and the latter to be tetrahedral (Bolvin *et al.*, 2001a,b). Both studies agree that the increased contribution of the 5f orbitals destabilize the tetrahedral forms, and the different geometries for the Np and the U complexes are due to the lower energy of the 5f orbitals for Np(VII) compared to U(VI).

17.4 ACTINIDE HALIDE COMPLEXES

The actinide halides, particularly UF_6, have occupied a central role in actinide chemistry since the Manhattan Project. The high vapor pressure of UF_6 at room temperature made it the compound of choice to use in the gaseous diffusion cascade process for the separation of uranium isotopes. In addition, UF_6 is the most promising candidate for laser-induced isotope enrichment, in which the isotopic shifts of optical excitations are used to achieve isotope separation. The irradiation of UF_6 also generates the unsaturated photoproducts UF_5 and UF_4, which formally are f^1 U(V) and f^2 U(IV) complexes, respectively. Because of the dominant role these compounds play in actinide technology, the electronic structure of the ground and excited states of these highly symmetric (in the gas phase) uranium fluorides and related actinide halides has intrigued experimental and theoretical actinide chemists. In this section, some of the more recent theoretical calculations on the electronic structure of molecular actinide halides will be presented.

17.4.1 UF_6 and related complexes

The properties of actinide halides have been extensively studied both experimentally and theoretically. Much as the uranyl ion has been for oxo chemistry, the hexafluoride UF_6 has been the benchmark for theoretical studies of actinide halides over the past 25 years. Early electronic structure studies of UF_6 have

been extensively reviewed by Pepper and Bursten (1991) and included REX, nonrelativistic and relativistic MS-Xα calculations, and relativistic ECP calculations. The principal focus of these studies was on the energies of the occupied orbitals, the participation of the 5f orbitals in the bonding, and the nature of the excited states. The highest occupied valence orbitals, shown schematically in Fig. 17.11, arise naturally from the symmetry-adapted combination of six sets of fluorine 2p orbitals with admixture of 6d and 5f character on U. The two lowest

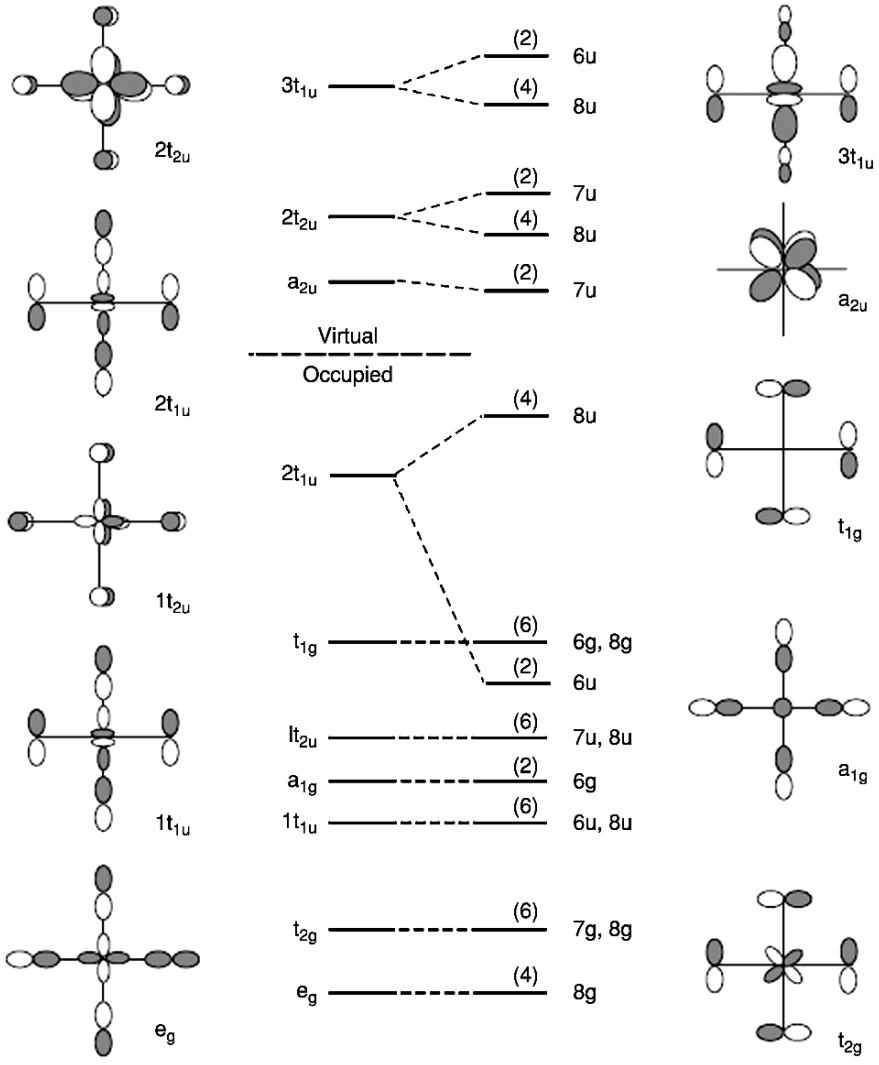

Fig. 17.11 *Schematic energy-level diagram for* UF_6 *without* (*left*) *and with* (*right*) *spin–orbit coupling* (*adapted from Hay*, 1983).

orbitals in this set, of e_g and t_{2g} symmetry, are of the proper symmetry for 6d mixing from the U, while the higher energy occupied orbitals of t_{1u} and t_{2u} symmetry can have 5f admixture. The lowest virtual orbitals having a_{2u}, t_{2u}, and t_{1u} symmetry essentially comprise the 5f set of orbitals. As one goes down the actinide series from UF_6, a formally $5f^0$ system, to NpF_6 ($5f^1$) and PuF_6 ($5f^2$), the additional electrons populate this manifold of orbitals that are unoccupied in UF_6. When spin–orbit effects are included, only modest splittings are observed with the exception of the highest occupied orbital ($2t_{1u}$), which, in addition to some 5f character, also has significant mixing with the occupied 6p orbital of U. This mixing leads to a large splitting ($\sim$1.2 eV) between the two spinor components γ_{8u} and γ_{6u}, where γ_{8u} and γ_{6u} are the double-group symmetries arising from the $2t_{1u}$ level when spin–orbit effects are included.

Several studies in recent years of UF_6 have been carried out using the modern approaches described in the earlier section. Hartree–Fock-based approaches include all-electron Hartree–Fock and Dirac HF calculations by de Jong and Nieuwpoort (1996) and RECP studies (Hay and Martin, 1998). Density functional approaches include DS-DV by Onoe *et al.* (1993), all-electron Douglas–Kroll local density (SVWN), and valence-electron SVWN by Garcia-Hernandez *et al.* (2002), and quasi-relativistic BLYP using ADF by Schreckenbach (2000). In Table 17.10, the energies of the occupied orbitals are shown from selected theoretical Hartree–Fock and DFT approaches. In general, we note that the predicted ionization potentials from Hartree–Fock-based methods using the orbital energies according Koopmans' theorem begin around 17 eV, which is considerably higher than the first observed peak at 14.1 eV in the photoelectron spectra. DFT methods give somewhat correspondingly lower predicted IPs ranging from 8 eV for a scalar (DV-DS), 11 eV for gradient-corrected (QR-PW91), and 12 eV for hybrid (B3LYP). Analysis of the bonding for the DHF wavefunctions showed a charge of +2.22 on U and populations 5f (1.82), 6d (1.31), 7s (0.06), while the DV-DS results showed a charge of 1.39 on U and populations 5f (2.51), 6d (1.83).

As mentioned in the earlier section on methods, one of the major developments over the past decade has been the capability to calculate geometries and frequencies using analytic derivative techniques. The geometries and frequencies of the AnF_6 hexafluorides have been determined using these capabilities, quasi-relativistic DFT by Schreckenbach *et al.* with ADF, and all-electron Douglas–Kroll DFT by Garcia-Hernandez *et al.* (Hay and Martin, 1998; Schreckenbach *et al.*, 1999; Garcia-Hernandez *et al.*, 2002) and with RECPs using Hartree–Fock and DFT approaches. The results are summarized in Table 17.11 and compared with experiment (Seip, 1965; Kimura *et al.*, 1968; McDowell *et al.*, 1974). Generally the experiences from these investigations have shown that methods that predict bond lengths accurately also typically calculate vibrational frequencies in good agreement with experiment. In this regard the LDA approaches (SWVN) either with RECPs or in all-electron DKH calculations are a good compromise in computational effort and

Table 17.10 *Calculated energy levels in UF_6 from various relativistic methods* (*in* eV). *Symmetries of MOs are labeled according to the O_h group for the calculations without spin–orbit coupling, while the double-group labels of the O_h^* group are used to label the MOs when spin–orbit effects are included.*

		Hartree–Fock methods			*DFT methods*	
O_h symmetry	*O_h^* double-group symmetry*	*Dirac HF de Jong and Nieuwpoort* (1996)	*HF-SO*[a] *Hay* (1983)	*DV-DS Onoe* et al. (1993)	*QRPW91 Schreckenbach* (2000)	*B3LYP*[b] *Batista* et al. (2004b)
$2t_{1u}$	γ_{8u}	17.31	17.69	8.16	10.75	12.06
	γ_{6u}	18.47	18.58	9.29		
t_{1g}	γ_{6g}	18.45	18.59	9.14	11.16	12.47
	γ_{8g}	18.51	18.49	9.12		
a_{1g}	γ_{6g}	19.27	18.84	10.06	12.23	13.48
t_{2u}	γ_{8u}	19.50	20.14	10.09	11.97	13.33
	γ_{7u}	19.53	20.13	10.09		
$1t_{1u}$	γ_{8u}	19.91	20.14	10.52	12.38	13.78
	γ_{6u}	19.99	20.13	10.52		
t_{2g}	γ_{7g}	20.65	20.67	10.99	12.71	14.17
	γ_{8g}	20.67	20.70	10.99		
e_g	γ_{8g}	21.18	20.84	11.10	13.30	14.76

[a] LC-RECP.
[b] SC-RECP.

Table 17.11 *Experimental and calculated bond lengths* (Å) *and vibrational frequencies* (cm^{-1}) *for* UF_6.

		VWN				
	Expt	*RECP* (60e)	*RECP* (78e)	*DK-VWN*	*QR-BLYP*	*B3LYP RECP* (78e)
R(U–F)	1.996, 1.999	2.000	1.992	1.998	2.010	2.014
ν_1 (a_{1g})	667	652	658	655	654	653
ν_2 (e_g)	534	565	552	547	541	552
ν_3 (t_{1u})	626	657	630	626	618	647
ν_4 (t_{1u})	186	174	175	167	185	191
ν_5 (t_{2g})	200	169	147	142	183	178
ν_6 (t_{2u})	143	141	110	104	141	150
|avg. error|	–	20	21	24	8	15
References	Seip (1965); Kimura *et al.* (1968)	Garcia-Hernandez *et al.* (2002)	Hay and Martin (1998)	Garcia-Hernandez *et al.* (2002)	Schreckenbach *et al.* (1999)	Hay and Martin (1998)

accuracy. Hartree–Fock approaches underestimate U–F bond lengths (and overestimate vibrational frequencies) whereas the opposite is true for gradient-corrected DFT methods. Hybrid approaches give predictions of bond lengths and frequencies similar to local density approaches.

The calculation of bond energies is a more difficult challenge for theoretical methods. Coupled with this is the relatively sparse database of thermochemical properties for actinide-containing molecules. For the uranium fluorides and chlorides, however, there is thermochemical data for most of these species, and the bond energy in UF_6 to form $UF_5 + F$ is especially well known: 70 ± 2 kcal mol^{-1}, as measured by Hildenbrand and Lau (1991). Recently Batista *et al.* (2004b) carried out a systematic study of DFT approaches in their predictions of this bond energy. In addition the results of all-electron Douglas–Kroll–Hess results were compared using the same functionals. These results are summarized in Table 17.12. Among the main conclusions is that the SC-RECP (60-electron) potential of Küchle *et al.* is required to give agreement with the all-electron DKH results with a given functional. By contrast the results with the 78-electron LCRECP (not shown in the table) overestimates the bond energy for a particular method by 40–50 kcal mol^{-1} compared to the SC-RECP and DKH result. When corrected for zero-point and spin–orbit effects, the agreement between the hybrid DFT (B3LYP, PBE0), all-electron DKH and experiment is within the experimental uncertainties. These authors also presented an analysis of the effects on vibrational frequencies with variation of functionals and types of core potentials.

Table 17.12 *Comparison of calculated and experimental values of the bond dissociation energy of* UF_6 (kcal mol^{-1}) (*see Batista* et al., 2004*b*).

	Scalar-relativistic		*SO and ZPE corrections*	
Method	*SC-RECP*	*DKH*	*SC-RECP*	*DKH*
HF	–5.7	7.7		
LSDA (scal)	124.4	123.7		
PBE (grad corr)	98.6	99.1		
PBE0 (hybrid)	73.8	74.4	68.3	68.9
B3LYP (hybrid)	75.0	75.8	69.6	70.4
Expt [a]			70 ± 2	

[a] Hildenbrand and Lau (1991).

The spectroscopy of the excited electronic states of UF_6 shows broad relatively unstructured bands in the ultraviolet region with the first strong peak occurring at 5.4–5.8 eV (C-band) and weaker peaks at lower energies 3.2–3.4 eV (A-band) and 3.8–4.6 eV (B-band) (Hay, 1983). Excited states were probed using earlier QR-MS (Boring and Wood, 1979), DS-DV (Koelling *et al.*, 1976), and RECP-SO (Hay, 1983) methods; there have been surprisingly few recent studies using newer techniques. Qualitatively the methods assign the weaker bands to 'u-to-u' dipole-forbidden excitations such as t_{1u} (8u) to the virtual 5f manifold while the strong C band is variously assigned to allowed 'g-to-u' excitations such as t_{1g}–t_{1u}, a_{1g}–t_{1u}, and t_{1g}–t_{2u}.

The structures and vibrational properties of UF_6, NpF_6, and PuF_6 were studied using DFT approaches with LC-RECPs (Hay and Martin, 1998) where the best agreement with available experimental data was obtained at the local density (SVWN) and hybrid (B3LYP) functionals. All-electron DKH calculations on NpF_6 had similar conclusions (Garcia-Hernandez *et al.*, 2002). The predicted Np–F bond lengths were 1.978 Å (VWN), 2.008 Å (BP), and 2.019 Å (PBEN) of which the local density VWN value agrees most closely with experiment (1.981 Å). By comparison the LC-RECP calculations with B3LYP hybrid functional and VWN functionals predicted a bond length of 2.013 and 1.998 Å, respectively.

Schreckenbach (2000) compared QR-PW91 and ECP-B3LYP calculations on the chlorine-substituted fluoride series $UF_{6-n}Cl_n$ and the related methoxide series $UF_{6-n}(OCH3)_n$. Batista *et al.* (2004a) computed the equilibrium structures of the UF_n and UCl_n series of halide species for $n = 1$–6 using ECP-B3LYP calculations. They found structures and corresponding symmetries as follows: UF_5 (C_{4v}), UF_4 (T_d), UF_3 (C_{3v}), and UF_2 (C_{2v}), as shown in Fig. 17.12, and similarly for the chloride analogs. Gagliardi *et al.* (2002) optimized the equilibrium geometries of ThX_4 (X = F, Cl, Br, and I) and computed the vibrational frequencies, of which only ν_3 and ν_4 had been measured for gas-phase ThF_4 and only ν_3 had been measured for gas-phase $ThCl_4$. Mochizuki and Tatewaki (2003)

have reported DHF studies on CmF_n ($n = 1$–4). The bonding was found to be largely ionic in character, with some donation from the F 2p to the Cm 6d orbitals.

The electronic structure of the $5f^1$ actinide hexahalide complexes PaX_6^{2-} (X = F, Cl, Br, I), UX_6^- (X = F, Cl, Br), and NpF_6 were studied using relativistic DV-Xα approach (Kaltsoyannis and Bursten, 1995). Increased 5f participation was found in going from Pa to U to Np while the metal character remained relatively unchanged as one proceeds from F down to I. Electronic transition energies were calculated using the Slater's transition state method (Slater, 1974).

17.4.2 Actinide oxyhalides

Complexes containing halides and the actinyl AnO_2^{2+} unit represent another interesting class of species. The properties of uranyl halide species $[UO_2X_4]^{2-}$ are known in solid state structures for the chlorides but there are no known structures for the fluorides. While $[UO_2F_n]^{2-n}$ species exist in solution for $n = 0$–5, the solid state fluoride structures include dimers, neutral UO_2F_2 with six equatorial fluorine ligands around each U, and uranyl complexes with five or six equatorial F or H_2O ligands. In Table 17.13, the results of calculations on $[UO_2F_4]^{2-}$ and $[UO_2Cl_4]^{2-}$ are shown along with experimental values for various crystal structures of the chloride complexes. The bonding is analogous to the tetrahydroxide species discussed above except that the halides are much poorer π-donors than hydroxide ligands. The computational studies to date have focused primarily on the structures, vibrational frequencies, and to some extent on the thermodynamics with regard to overall stability with less emphasis on the nature of the bonding.

Recently, Straka *et al.* (2001) have examined all possible $[UO_2F_n]^{q+}$ species with f^0 configuration using DFT approaches. These include the known UO_2F_2 species and other reactive forms, some of which have been detected in mass spectra and matrix isolation studies. Some of these predictions are also given in Table 17.13. In addition, they examined other actinides from Pa through Am with f^0 configurations where the trends in bond lengths as a function of the actinide and the coordination number were examined (Fig. 17.13). Most recently, Straka (2005) has used DHF calculations to explore the bonding in later actinide AnO_2F_4 (An = Pu, Cm, Cf, Fm) complexes. These calculations suggest that the Pu and Cm species have D_{4h} symmetry and are stable with respect to decomposition to the elements. Infante and Visscher (2004a) investigated solvated forms of $[UO_2F_4]^{2-}$ complexes and especially on the relative stability of one vs two aqua equatorial groups in the first coordination shell in a study that combined quantum and classical (QM/MM) methods. In a related study, Wang and Pitzer (2001) studied the various structures arising from $UO_2F_2(H_2O)_n$, for $n = 2$–4 and the results for $n = 2$ are shown in Table 17.13. The possibilities of bonding in the series UF_4X_2 for a variety of pseudohalide ligands

Table 17.13 *Calculated structures of* $[UO_2X_n]^q$ *species.*

Species/Method	*R*(*U–O*), Å	*R*(*U–X*), Å	∠*O–U–O* (°)	∠*X–U–X* (°)	*References*
$[UO_2F_4]^{2-}$					
QR-BLYP	1.847	2.205	180	180	Schreckenbach *et al.* (1999)
RECP-B3LYP	1.823	2.259			Schreckenbach *et al.* (1999)
RECP B3LYP	1.819	2.233			Straka *et al.* (2001)
RECP MP2	1.839	2.223			Straka *et al.* (2001)
$[UO_2Cl_4]^{2-}$					
QR-BLYP	1.780	2.784	180	180	Schreckenbach *et al.* (1999)
RECP-B3LYP	1.799	2.730			Schreckenbach *et al.* (1999)
Expt (var.cryst.)	1.72–1.81	2.64–2.71			Schreckenbach *et al.* (1999)
$UO_2F_3^-$					
B3LYP RECP	1.790	2.161	180	120	Straka *et al.* (2001)
MP2 RECP	1.811	2.156			Straka *et al.* (2001)
UO_2F_2					
B3LYP RECP	1.768	2.075	168	114	Straka *et al.* (2001)
MP2 RECP	1.794	2.070	169	112	Straka *et al.* (2001)
UO_2F^+					
B3LYP RECP	1.731	2.000	120		Straka *et al.* (2001)
MP2 RECP	1.760	1.996	124		Straka *et al.* (2001)
$UO_2F_2(H_2O)_2$					
Cis LDA RECP	1.795	2.082	167	108	Wang and Pitzer (2001)
Trans LDA RECP	1.791	2.066	177	180	Wang and Pitzer (2001)

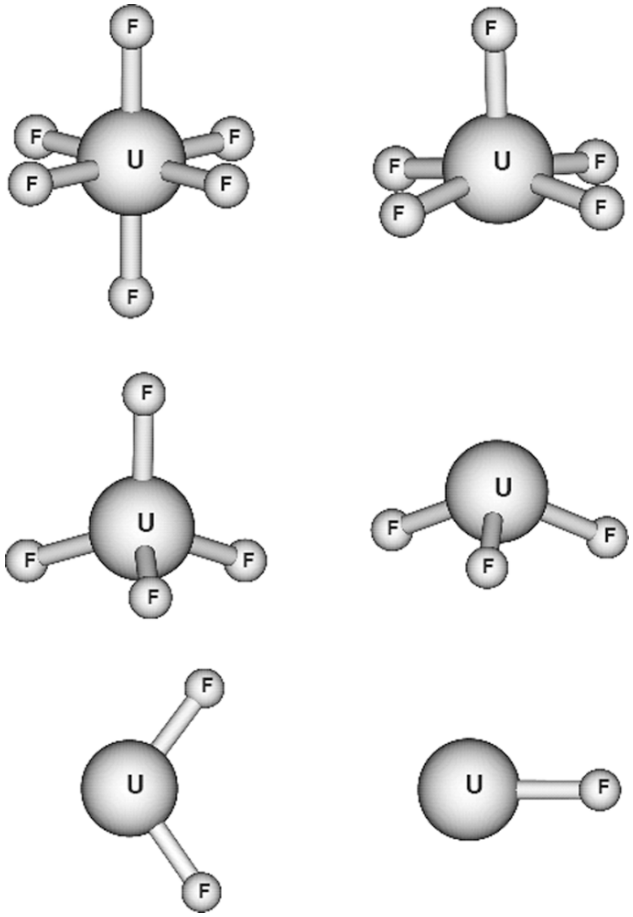

Fig. 17.12 *Calculated structures of* UF_n ($n = 1$–6) *species* (*adapted from Batista* et al., 2004*a*).

X (H,Cl, CN, etc.) were probed by Straka *et al.* (2003) by computing the structures, frequencies, and thermochemistry with SC RECP calculations with the B3LYP functional. By examining substitution energies of 2X for 2F in UF_6, they were able to gauge relative stabilities. While none of the complexes was more stable than UF_6, they found relative stabilities NCO < Cl < NC < NCS < CN < OCN < SCN and related these trends to the poorer π-accepting ability of CN, for example, relative to NC and other ligands.

Kovács *et al.* (2004) used the ZORA approach to determine the structures, vibrational analyses, and bonding of UX_6 and UO_2X_2 (X = F, Cl, Br, I) molecules. The UX_6 complexes maintained O_h symmetry, while the UO_2X_2 complexes, which have C_{2v} symmetry, showed structural variations with the heavier halides, with the O=U=O and X–U–X bond angles decreasing as the

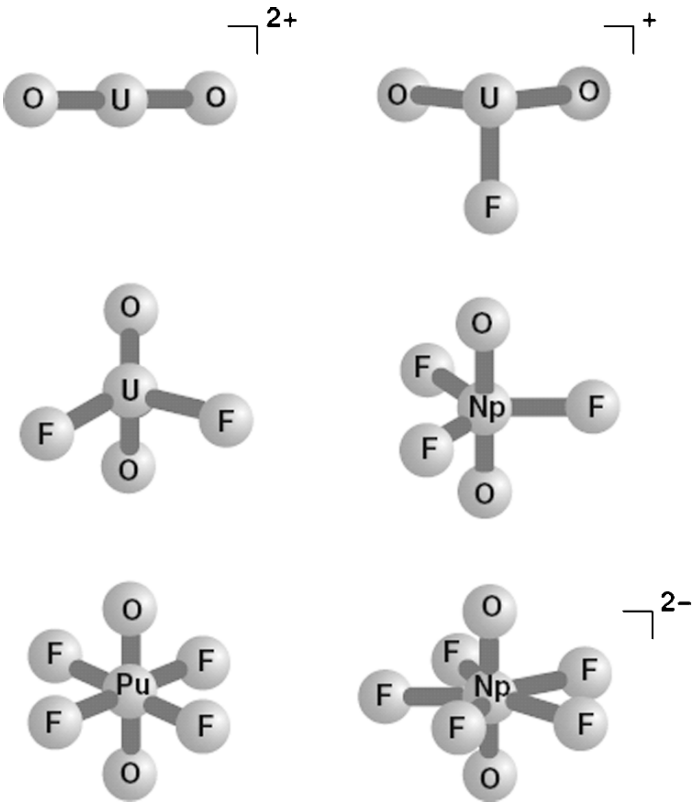

Fig. 17.13 *Calculated structures of* AnO_2F_n ($n = 1$–5) *species* (*adapted from Straka* et al., 2001).

halide ligands get heavier. For example, the X–U–X angle decreases from 110.6° for UO_2F_2 to 97.5° for UO_2I_2. They report the uranium 5f plays a predominant role in the orbital interactions, with increased contribution from the 6d in the heavier halide complexes.

17.5 ACTINIDE ORGANOMETALLICS

The growth in actinide chemistry following the Manhattan Project coincided with the birth of modern organometallic chemistry that followed the discovery of ferrocene in the early 1950s. It is therefore not surprising that actinide organometallic chemistry has developed into a thriving field. The growth in the chemistry and spectroscopy of actinide organometallics has been nicely reviewed in a series of articles by Marks (1976, 1979, 1982) and in Chapters 25 and 26. The study of organoactinide compounds benefits from some of the typical advantages of organometallic chemistry, including the use

of weakly coordinating nonaqueous solvents, the intrinsically molecular nature of organometallic compounds, and the well-developed arsenal of spectroscopic probes developed for organometallic systems. In this section, we will discuss theoretical aspects of the electronic structure of the major classes of organoactinide complexes, with an emphasis on systems in which an actinide atom is bonded to two or more cyclic hydrocarbyl ligands.

17.5.1 Actinocenes

The history of the actinocenes, $An(COT)_2$ ($COT = \eta^8\text{-}C_8H_8$), dates back to 1963, when R.D. Fischer first predicted that uranocene would be a stable compound, i.e. the actinide analog of the prototypical d-element sandwich molecule ferrocene (Fischer, 1963). Five years later, Streitwieser and Müller-Westerhoff (1968) reported the synthesis and characterization of $U(COT)_2$, thereby opening up a whole new area of organometallic chemistry. Subsequently several other actinocenes and actinocene anions were reported (Streitwieser, 1984; Streitwieser and Kinsley, 1985; Parry *et al.*, 1999), with An = Th, Pa, Np, Pu, and Am. Much of the chemistry of actinocenes has been the subject of recent reviews (see, for example, Roesky, 2001; Seyferth, 2004) and is detailed in Chapter 25.

The actinocenes have proved an irresistible challenge for many theoretical groups, due partly to the high molecular symmetry (which allows the relative roles of the 6d and 5f orbitals of the metal to be differentiated) and to the fact that $M(COT)_2$ compounds occur only in the f-block. These researchers have employed many different computational techniques, ranging from relativistic EHMO theory (Pyykkö and Lohr, 1981), to intermediate neglect of differential overlap (INDO; Cory *et al.*, 1994), to more sophisticated *ab initio* methods (Chang and Pitzer, 1989; Chang *et al.*, 1994; Dolg *et al.*, 1995; Liu *et al.*, 1997), as well as density functional approaches (Rösch and Streitweiser, 1983; Boerrigter *et al.*, 1988; Kaltsoyannis and Bursten, 1997; Li and Bursten, 1998). In this section, we shall review the issues that have been addressed by these studies, and summarize the key conclusions.

(a) Geometric structures of the actinocenes

The crystal structures of $Th(COT)_2$ and $U(COT)_2$ were reported in 1972 by Avdeef *et al.* (1972). Both molecules were found to have planar and parallel carbocyclic rings, sandwiching the metal center in an eclipsed (D_{8h}) orientation. It has been common practice for theoretical studies to assume the crystallographic geometry (e.g. Pyykkö and Lohr, 1981; Chang and Pitzer, 1989; Kaltsoyannis and Bursten, 1997), and there have been very few attempts to calculate the geometry of actinocenes. Most of these have focussed on optimizing the metal–ring distance while retaining both D_{8h} symmetry and planar rings. The results are summarized in Table 17.14, from which it can be seen that the metal–ring distance is generally overestimated.

Table 17.14 *Optimized metal–ring centroid distances* (Å) *in* $An(COT)_2$ ($M = Th$ *to* Pu).

	Method				
Metal	*HFS*[a]	*MP2*[b]	*MCSCF*[c]	*PW91*[d]	*Expt.*[e]
Th	2.08	1.998			2.004
Pa	2.02			1.975	
U	1.98		2.047		1.923
Np	1.97				
Pu	1.96				

[a] Boerrigter *et al*. (1988).
[b] Dolg *et al*. (1995).
[c] Liu *et al*. (1997).
[d] Li and Bursten (1998).
[e] Avdeef *et al*. (1972).

In 1998, Li and Bursten reported fully optimized geometries for $Pa(COT)_2$ using relativistic DFT with a variety of different functionals (Li and Bursten, 1998). They found that the D_{8h} and D_{8d} (staggered) structures were essentially isoenergetic (providing some late-in-the-day computational justification of the ubiquitous assumption of D_{8h} symmetry in previous theoretical studies), and that the PW91 functional best reproduced the average of the experimental metal–ring distances in $Th(COT)_2$ and $U(COT)_2$. They also found that the hydrogen atoms are tilted toward the metal atom by as much 9°, suggesting that the previous universal assumption of ring planarity in $Pa(COT)_2$ in particular and actinocenes in general may be a source of error and a possible reason for discrepancies between theoretical and experimental data. A ball-and-stick representation of the optimized PW91 geometry of $Pa(COT)_2$ under the constraint of D_{8h} symmetry is shown in Fig. 17.14.

(b) Orbital interactions in the actinocenes

In 1998, Dolg and Fulde wrote: "any discussion of atomic or molecular electronic structure in terms of orbitals and single configurations....is a simplification, which works in many but not in all cases" (Dolg and Fulde, 1998). They were writing with reference to the lanthanocenes and actinocenes, and in particular to their finding that the ground state of the 4f systems are not well represented by a single configuration, a result which they predicted to also hold for the later actinocenes. Notwithstanding these observations, we will set out the basic electronic structure of the actinocenes within the usual orbital approach. This brings with it the conceptual advantages of the independent-particle description, and serves as a good starting point for discussion of the effects of relativity, the calculation of excited-state properties, and the introduction of multi-configurational character to the molecular wavefunctions.

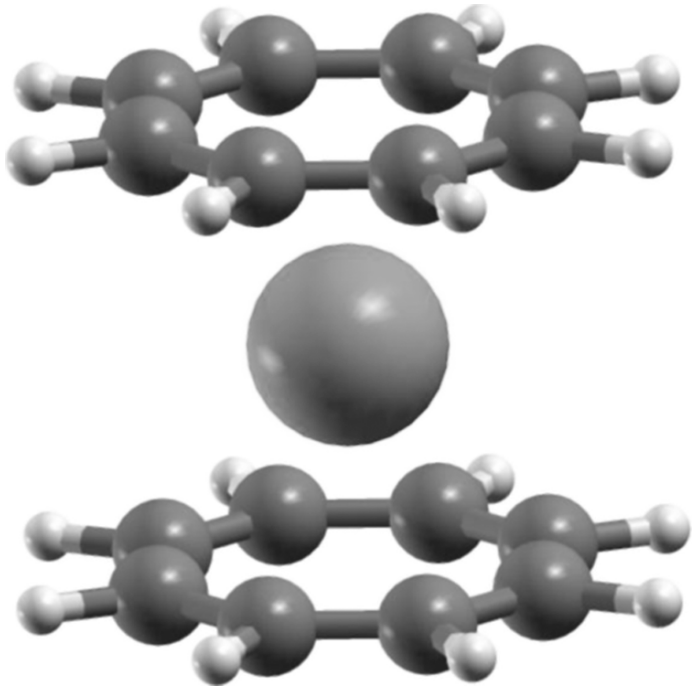

Fig. 17.14 *Representation of the optimized structure of protactinocene, Pa(η^8-C_8H_8)$_2$, from scalar-relativistic DFT (PW91) calculations (apdated from Li and Bursten, 1998).*

The generally accepted orbital interaction diagram for the actinocenes is given in Fig. 17.15. The eight-carbon 2pπ atomic orbitals of a D_{8h} C_8H_8 ring give rise to eight molecular orbitals (MOs) transforming as a_{2u}, e_{1g}, e_{2u}, e_{3g}, and b_{1u} in order of increasing energy. These orbitals are commonly denoted π_n ($n = 0$–4), where n is the number of vertical nodes (i.e. nodes perpendicular to the plane of the ring). In a ligand field of two COT rings, these π MOs give rise to the combinations shown in the second column from the right in Fig. 17.15. The valence atomic orbitals (AOs) of the actinide elements that interact with the $(COT)_2$ ligands are primarily the 5f and the 6d. It is common practice to take advantage of the pseudoaxial nature of the D_{8h} $(COT)_2$ ligand-field and label the metal orbitals as σ, π, δ, and ϕ, corresponding to $m_l = 0$, ±1, ±2, or ±3 respectively. In the absence of spin–orbit coupling, the 5f orbitals split in the $(COT)_2$ ligand field as e_{3u} (fϕ) $\approx$ a_{2u} (fσ) $<$ e_{1u} (fπ) $\ll$ e_{2u} (fδ), the strong destabilization of the latter resulting from their significant interaction with the highest occupied e_{2u} ring pπ levels. The 6d orbitals split as a_{1g} (dσ) $\ll$ e_{2g} (dδ) $<$ e_{1g} (dπ), and the total d-orbital splitting is larger than for the 5f on account of their greater radial extension and hence greater interaction with the ligand field.

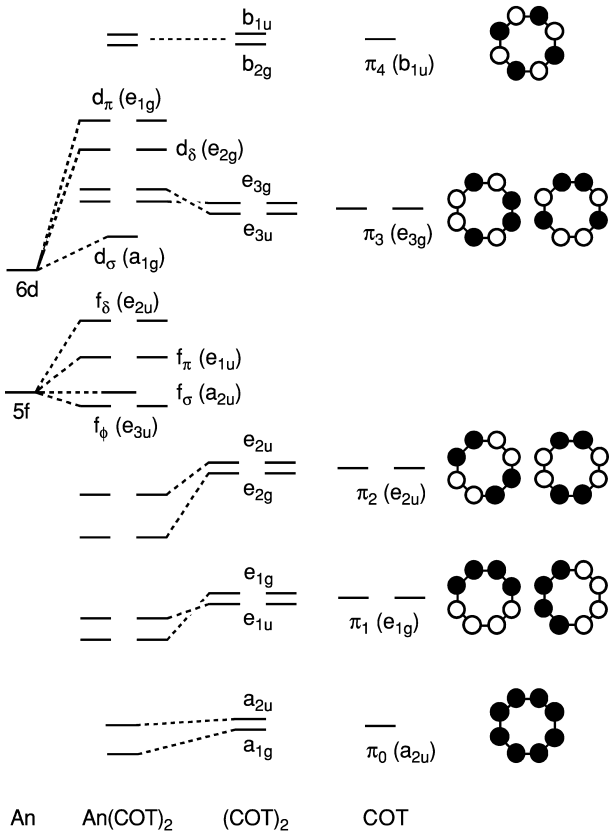

Fig. 17.15 *Principal interactions between the orbitals of two COT rings and the valence orbitals of an actinide atom in forming the frontier MOs of the actinocenes under D_{8h} single-group symmetry* (*reproduced from Li and Bursten*, 1998).

(c) Electronic configurations, ground states, and oxidation states in the actinocenes

In their 1994 INDO study, Cory *et al.* found that the highest occupied MO (HOMO) of $Th(COT)_2$ was the ring e_{2u} orbital, and that the metal-based levels were empty (Cory *et al.*, 1994). Moving across the actinides increased the number of metal electrons from 1 for $Pa(COT)_2$ to 4 for plutonocene, and it was found that all of these electrons occupy the e_{3u} ($f\phi$) orbitals. These findings are consistent with the experimental observations that $Th(COT)_2$ and $Pu(COT)_2$ are diamagnetic (although the magnetic moment of $Pu(COT)_2$ exhibits unusual temperature dependence), that $Pa(COT)_2$ and $Np(COT)_2$ have doublet ground states, and that uranocene has a triplet ground state (Karraker *et al.*, 1970; Hayes and Edelstein, 1972; Karraker, 1973). Chang *et al.* (1994) also

concluded that $An(COT)_2$ (An = Pa to Pu) have the $5f^n$ ($n = 1$–4) ground state configuration.

Earlier *ab initio* (SOCI) work by Chang and Pitzer (1989) on $U(COT)_2$ also concluded that it has an f^2 ground state configuration. These authors reported that the best simple description of the ground state was weak-field L–S $^3H_4$, with $|M_j| = 3$, where M_j is the magnetic quantum number. In the notation of the D_{8h}^* double point group, the spin–orbit-coupled ground state is E_{3g} (see below for more on spin–orbit coupling). Several configurations were found to contribute to this state, the leading one being $\pi(e_{2u})^4 e_{3u}^1 e_{1u}^1$, i.e. $f\phi^1 f\pi^1$. Several years later, Liu *et al.* (1997) also found that the ground configuration of uranocene is $5f^2$, although they calculated that the leading configuration to the ground state is $f\phi^1 f\sigma^1$.

In 1995 Dolg *et al.* used the MRCI and averaged coupled-pair functional (ACPF) *ab initio* methods to study $Th(COT)_2$ and its lanthanide analog $Ce(COT)_2$. They concluded that the ground state of $Th(COT)_2$ is $^1A_{1g}$, and that the dominant configuration to this state is $\pi(e_{2u})^4 f^0 d^0$, i.e. that there are no metal-based valence electrons (Dolg *et al.*, 1995). $Ce(COT)_2$ was also found to have a $^1A_{1g}$ ground state, but the $\pi(e_{2u})^4$ configuration was in this case found to contribute only $\approx 20\%$ to the ground state. The dominant contribution ($\approx 80\%$) comes from the $\pi(e_{2u})^3 f\delta^1$ configuration, in which the electrons are antiferromagnetically coupled in two MOs, and the direct product of their spatial symmetries is A_{1g}. Thus $Ce(COT)_2$ is best described as having a single metal-localized valence f-electron, i.e. as a Ce(III) compound containing two formally $COT^{1.5-}$ rings. This view, which was soon verified experimentally by Edelstein *et al.* (1996), is by contrast to that held historically, which saw both $Ce(COT)_2$ and $Th(COT)_2$ as M(IV) species.

Dolg and Fulde (1998) subsequently concluded that all of the lanthanocenes are Ln(III) compounds, and predicted that the later actinocenes should also be viewed in this way. By contrast, the early actinocenes are best described in the traditional manner, i.e. as An(IV) compounds with two COT^{2-} rings and a single dominant $\pi(e_{2u})^4 f^n$ configuration. It is perhaps rather fortunate then that the only actinocenes to have been studied by single-reference density functional methods are $Th(COT)_2$–$Pu(COT)_2$, precisely those that *ab initio* calculations suggest should be amenable to study by single-reference techniques.

Of those density functional studies, the most comprehensive remains the 1988 contribution from Boerrigter *et al.* (1988), which surveyed the first five actinocenes from $Th(COT)_2$ to $Pu(COT)_2$ using both nonrelativistic and relativistic HFS techniques. Their nonrelativistic calculations concluded that $Th(COT)_2$–$Pu(COT)_2$ have between 0 and 4 5f electrons, respectively, and that these electrons occupy the $f\phi$, $f\sigma$, and $f\pi$ levels equally. The relativistic spin–orbit-coupled calculations also find 0–4 5f electrons, occupying closely spaced $e_{5/2u}$ and $e_{1/2u}$ levels (D_{8h}^*). They concluded that both of these spin–orbit-coupled levels are composed primarily of atomic $5f_{5/2}$ character, and may be traced mainly to the $f\phi$ nonrelativistic molecular orbital. Two subsequent DFT studies of $Pa(COT)_2$

(Kaltsoyannis and Bursten, 1997; Li and Bursten, 1998) concur with the findings of Boerrigter *et al.*

(d) Metal–ring covalency

One of the most appealing features of actinocene electronic structure is the way in which the D_{8h} point group separates the metal's d- and f-orbitals into irreducible representations of g and u parity, thus preventing them from mixing with the same $(COT)_2^{4-}$ levels. There have been many estimates of covalency in the actinocenes, and in particular much has been made of its separation into d and f contributions. The metal content of the ring-based e_{2g} and e_{2u} levels has been a popular method for estimating the extent of covalency, and Table 17.15 collects the data from a range of studies. Uranocene is clearly the molecule for which most data are available, and it is notable that, while the exact numbers differ from study to study, all of the calculations show significant metal character to the e_{2g} and e_{2u} levels (or their spin–orbit-coupled equivalents). Boerrigter *et al.* (1988) find that the relative roles of the 6d and 5f orbitals alter from Th $(COT)_2$ to Pu$(COT)_2$, with the extent of 5f covalency significantly increasing with increasing actinide atomic number.

Other estimates of covalency have been made that do not explicitly involve the e_{2u}/e_{2g} composition. Chang and Pitzer (1989) calculated a metal charge of +0.98 in U$(COT)_2$, much reduced from the formal value of +4. They concluded

Table 17.15 *Metal 5f* (e_{2u}) *and 6d* (e_{2g}) *content (%) of the* $(COT)_2$*-based* e_{2u} *and* e_{2g} *molecular orbitals of An*$(COT)_2$ (*M = Th to Pu*).

		Method				
Metal	*Orbital*	*REX*[a]	*QR-SW-Xα*[b]	*HFS*[c,f]	*DV-Xα*[d,f]	*MRCI*[e]
Th	e_{2u}			12		
	e_{2g}			19		
Pa	e_{2u}			16	17	
	e_{2g}			18	20	
U	e_{2u}	12	33	22		15
	e_{2g}	11	20	16		17
Np	e_{2u}			27		
	e_{2g}			15		
Pu	e_{2u}			33		
	e_{2g}			15		

[a] Pyykkö and Lohr (1981).
[b] Rösch and Streitweiser (1983).
[c] Boerrigter *et al.* (1988).
[d] Kaltsoyannis and Bursten (1997).
[e] Liu *et al.* (1997).
[f] Average of $f_{7/2}/f_{5/2}$ and $d_{5/2}/d_{3/2}$ contributions to spin–orbit-coupled components of e_{2u} and e_{2g}.

that there is extensive metal–ring covalency, and that this is mainly through the uranium 6d AOs as the total $(COT)_2^{4-} \rightarrow U^{4+}$6d donation is 1.98 electrons, significantly larger than the 0.5 electrons donated into the metal 5f orbitals. Dolg *et al.* (1995) found that the bonding in thoracene is also significantly covalent and is mainly 6d-based, using analysis methods similar to those employed by Chang and Pitzer. Cory *et al.* (1994) used the metal fδ and dδ populations to also conclude that 6d covalency is larger than 5f, although the fδ population increases from $Th(COT)_2$ to $Pu(COT)_2$ while the dδ remains approximately constant.

The consensus from all of these studies is that there is significant mixing of the metal AOs with the highest occupied pπ MOs of the COT rings and that, for the early actinocenes at least, 6d covalency is larger than that involving the 5f orbitals. Experimental estimates of covalency are not easy to obtain, and hence it can be difficult to assess the reliability of the computational results. However, a very important experimental contribution in this area came in 1989 from Brennan *et al.* (1989), who studied $U(COT)_2$ by variable photon energy photoelectron spectroscopy. They concluded that (a) the second and third ionization bands are due unequivocally to the ring e_{2u}^{-1} and e_{2g}^{-1} ionizations, respectively (providing good evidence for the MO ordering shown in Fig. 17.15), (b) there is direct evidence for significant U 5f orbital character to the ring e_{2u}-based MOs, and (c) that the position of the e_{2g} ionization band at higher energy than the e_{2u} band is strong indirect evidence for an even larger U 6d contribution to these MOs.

(e) Electronic transitions in the actinocenes

Thus far we have not considered in detail the effects of relativity on actinocene electronic structure. However, almost all of the data discussed to this point are taken from calculations in which some or all of the so-called scalar-relativistic corrections – e.g. the Darwin and mass–velocity terms – have been incorporated in one way or another. Such an approach is in many cases adequate, but is not really satisfactory when attempting to understand the electronic transitions of actinocenes, especially where comparisons with experiment are sought. This type of investigation requires that spin–orbit coupling effects are also taken into account. Indeed, non-spin–orbit-coupled calculations typically give poor agreement with experiment when excited states are involved.

(*i*) *Pa*(*COT*)$_2$

Barring f^0 thoracene, $Pa(COT)_2$, is in principle the simplest actinocene in terms of its electronic transitions, as it has only one metal-localized valence f-electron. It has proved a fertile testing ground for both *ab initio* (Chang *et al.*, 1994) and density functional studies (Kaltsoyannis and Bursten, 1997; Li and Bursten, 1998). The effect of spin–orbit coupling on a free f^1 atom or ion is to split the

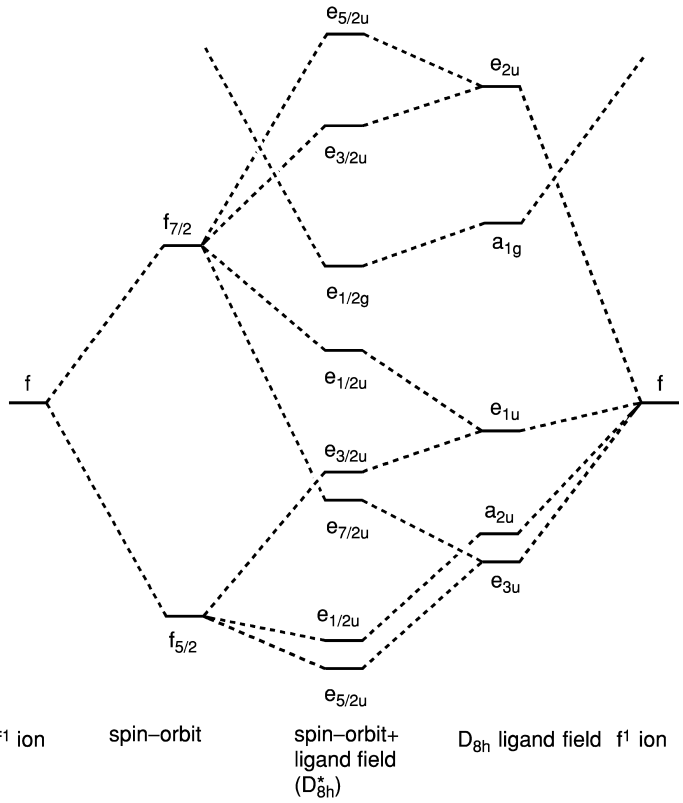

Fig. 17.16 *Correlation of the orbitals of an f1 Pa^{4+} ion split by spin–orbit coupling with the spin–orbit-coupled orbitals of $Pa(COT)_2$ under the D^*_{8h} double group (adapted from Li and Bursten*, 1998).

f-orbitals into a lower energy $f_{5/2}$ level and a higher energy $f_{7/2}$ level, which are respectively six- and eight-fold spin–orbit degenerate. This splitting is indicated on the left-hand side of Fig. 17.16, which is a correlation diagram showing the effects of spin–orbit coupling and the D_{8h} ligand field on an f^1 ion in a $(COT)_2^{4-}$ environment. In the absence of spin–orbit coupling but in the D_{8h} field, the f-orbitals are split as shown on the right-hand side of the figure. This f-orbital ordering is as presented in Fig. 17.15.

One of the main reasons for the complexity of actinide molecular electronic spectra is that both the effects of the ligand field and spin–orbit coupling must be taken into account. This is in contrast to the situation in the d-block, where ligand-field effects dominate, and to the lanthanides where spin–orbit coupling is the principal perturbation. The central column of Fig. 17.16 shows the combined effects of spin–orbit coupling and the D_{8h} ligand field on the f^1 ion.

All of the spin–orbitals now carry one of the labels of the D^*_{8h} double group, reflecting the fact that they are now properly characterized by non-integral total angular momentum, (i.e. spin + orbital). These arguments have been developed in greater detail (Kaltsoyannis and Bursten, 1997; Li and Bursten, 1998).

In Fig. 17.15, the metal d-based MOs are shown as being less stable than those arising from the 5f orbitals. While this is certainly the case for uranium/neptunium onwards, for the very early actinides the 6dσ level is comparable in energy with the 5f manifold. Indeed, the DFT calculations of Boerrigter *et al.* (1988) predict the lowest unoccupied molecular orbital (LUMO) of $Th(COT)_2$ to be the 6dσ orbital, while for $Pa(COT)_2$ this level lies in amongst the f-manifold. This result has been confirmed by other studies (Chang *et al.*, 1994; Kaltsoyannis and Bursten, 1997; Li and Bursten, 1998) and is taken into account on Fig. 17.16 by the presence of the $e_{1/2g}$ (a_{1g}) orbital. It might be expected that the presence of a low-lying d-based orbital would have a significant effect on calculations of the electronic transitions of $Pa(COT)_2$, and this has indeed been found to be the case.

Although the optical spectrum of $Pa(COT)_2$ has not been reported, limited data are available for the octamethyl derivative $Pa(TMCOT)_2$ (Solar *et al.*, 1980). The latter has an absorption maximum at 380 nm, with a low-energy shoulder at 490 nm. Based on comparison with the bathochromic shifts induced by the replacement of COT by TMCOT in other actinocenes, Solar *et al.* estimated that the absorption maximum in $Pa(COT)_2$ would occur at ca. 365 nm. There have been three attempts to calculate the electronic transitions of $Pa(COT)_2$, and three different assignments of the proposed 365 nm band. All of the f → f and many of the f → d transitions are formally forbidden, and Chang *et al.* (1994) concluded that the 365 nm peak arises from a ligand-to-metal charge transfer (LMCT) transition from the highest occupied ring π_2 levels into the $e_{1/2g}$ (dσ) orbital, calculated at 341 nm. Later, Kaltsoyannis and Bursten (1997) suggested that the band arises from both f → π_3 metal-to-ligand charge transfer (MLCT) and π_2 → f LMCT transitions at 351 and 360 nm, respectively. Most recently, Li and Bursten (1998) concluded that the band is due to a 368 nm ligand-field transition from the (predominantly fϕ) $e_{5/2u}$ HOMO to one of the spin–orbit-coupled components of the dδ levels. This latter study, which is the most complete and convincing, also concluded that the experimental low-energy shoulder is due to the π_2 → dσ transition.

(*ii*) *Th*(*COT*)$_2$ *and U*(*COT*)$_2$

As noted above, $Th(COT)_2$ has no metal-localized valence electrons. Experimentally it has a strong absorption at ca. 450 nm (Streitwieser, 1979), which Rösch and Streitwieser assigned to an LMCT π_2 → fϕ transition (Rösch and Streitweiser, 1983). Subsequent calculations by Dolg *et al.* (1995) placed this transition at 230 nm, and assigned the experimental peak to an LMCT π_2 → dσ transition. This ties in well with the DFT calculations of Boerrigter *et al.* (1988)

which, as we saw previously, predict the LUMO of $Th(COT)_2$ to be the $6d\sigma$ level.

The actinocene for which the most extensive experimental transition energy data are available is $U(COT)_2$ (Dallinger *et al.*, 1978; Amberger, 1983). These electronic transitions have been studied computationally by two groups using SOCI *ab initio* techniques (Chang and Pitzer, 1989; Chang *et al.*, 1994; Liu *et al.*, 1997). The experimental and theoretical (allowed transitions only) data are collected in Table 17.16, from which it may be seen that the two studies concur as to the assignment of the lowest energy transition, but differ over the nature of the experimental transition at 0.290 eV. It should be noted that $U(COT)_2$ is computationally significantly more difficult to handle than either $Th(COT)_2$ or $Pa(COT)_2$, owing to the presence of two 5f-based electrons and their significant mutual repulsion. Such difficulties manifest themselves in the discrepancies between experimental and theoretical data.

17.5.2 Actinide–cyclopentadienyl complexes

It is now 50 years since the discovery of the first organometallic sandwich molecule, ferrocene $[FeCp_2]$ ($Cp = \eta^5\text{-}C_5H_5$) (Wilkinson *et al.*, 1952; Wilkinson, 1975), and in the intervening period, the cyclopentadienyl ligand has become almost synonymous with organometallic chemistry. Indeed, the first organoactinide compound to be reported was the Cp derivative $[UCp_3Cl]$ (Reynolds and Wilkinson, 1956), and there have been hundreds more subsequently. As with the actinocenes, Cp–actinide systems have been a target of many theoretical studies, and those up to 1990 have been reviewed by Bursten and Strittmatter (1991). In this section, we will summarize these efforts and set out their key conclusions.

Several structural motifs are commonly observed for Cp–actinide complexes. $[AnCp_4]$ systems feature four η^5-bonded Cp rings, and are without parallel in transition metal chemistry. 'Base-free' tris-Cp complexes and their pseudotetrahedral derivatives $[AnCp_3X]$ (X = wide variety of ligands) are common and

Table 17.16 *Experimental and calculated transition energies* (eV) *in* $U(COT)_2$.

Experimental energy[a]	*Calculated energy*[b]	*Assignment*[b]	*Calculated energy*[c]	*Assignment*[c]
0.058	0.109	$E_{3g} \rightarrow E_{2g}\ f^2 \rightarrow f^2$	0.062	$E_{3g} \rightarrow E_{2g}\ f^2 \rightarrow f^2$
0.290	0.360, 0.364	$E_{3g} \rightarrow B_{2g}, B_{1g}\ f^2 \rightarrow f^2$	0.411	$E_{3g} \rightarrow E_{1g}\ f^2 \rightarrow f^2$
1.881	2.728	$E_{2g} \rightarrow E_{2u}\ f^2 \rightarrow f^1d^1$		
1.939	2.837	$E_{3g} \rightarrow E_{2u}\ f^2 \rightarrow f^1d^1$		
2.017	2.905	$E_{3g} \rightarrow E_{3u}\ f^2 \rightarrow f^1d^1$		
	3.322	$\pi_2 \rightarrow f^2d^1$ LMCT		

[a] Dallinger *et al.* (1978) and Streitwieser (1979).
[b] Chang and Pitzer (1989).
[c] Liu *et al.* (1997).

have been widely studied, as have the bis-Cp systems [$AnCp_2$] and [$AnCp_2X_2$]. The present review makes the somewhat arbitrary division of Cp–actinide chemistry into these three motifs, i.e. we group the compounds according to the number of carbocyclic rings bonded to the metal. The motifs are collected in Fig. 17.17.

(a) [$AnCp_4$] complexes

These compounds are known for Th, Pa, U, and Np, and the crystal structure of [UCp_4] shows it to contain four η^5-Cp ligands in a pseudotetrahedral arrangement (Burns, 1973). These systems were the subject of semiempirical and early DFT studies in the 1970s and 1980s, though they have not been subsequently probed by more modern methods. Quasi-relativistic Xα-SW (QR-Xα-SW) calculations on [$ThCp_4$] and [UCp_4] showed that, with the exception of a small An 7s contribution, the metal does not interact with the π_0 MOs of the Cp rings (i.e. those C 2pπ orbitals with no vertical nodes) (Bursten *et al.*, 1985). By contrast, the Cp π_1 levels interact significantly with the An, with donation into the 6d and, to a lesser extent, 5f orbitals. The 6d–Cp interaction was found to be more stabilizing than donation to the 5f levels (Bursten and Fang, 1985). The two metal-based electrons in the formally U(IV) [UCp_4] were found to

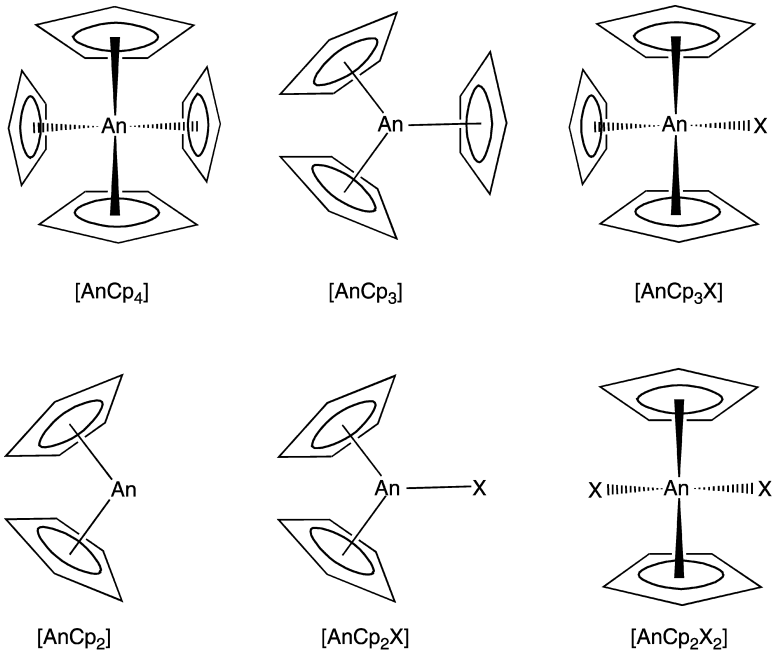

Fig. 17.17 *Structural motifs exhibited in complexes with actinide atoms and pentahapto-cyclopentadienyl ligands.*

occupy an essentially pure U 5f orbital of t_2 symmetry (T_d single-point group notation) with parallel spins.

Extended Hückel calculations on $[U(\eta^5\text{-}Cp)_4]$ and $[U(\eta^5\text{-}Cp)_3(\eta^1\text{-}Cp)]$ probed the actinide preference for η^5 coordination (Tatsumi and Nakamura, 1984). The conclusion from these studies was that the all-η^5 system is indeed more stable than the $(\eta^5)_3/\eta^1$ arrangement, in agreement with experiment.

(b) 'Base-free' $[AnCp_3]$ complexes

The $[AnCp_3]$ complexes without an additional axial ligand are perhaps the most widely studied Cp–actinide system. The metal and the Cp centroids are coplanar, giving rise to a virtually D_{3h} molecular symmetry. The interactions of a Cp_3 ligand field with a central metal are now well established, based on the results of extended Hückel, QR-Xα-SW, and DV-Xα studies (Lauher and Hoffmann, 1976; Bursten *et al.*, 1989a; Strittmatter and Bursten, 1991; Kaltsoyannis and Bursten, 1997), and we now set out the key features. The principal metal–ring bonding occurs between the valence AOs of the central atom and the highest occupied π_1 MOs of the Cp rings (e_1'' in the D_{5h} symmetry of a Cp ring), with a lesser interaction between the metal AOs and the Cp $\pi_0(a_2'')$ level (as was found for the $[AnCp_4]$ systems). In a C_{3v} ligand field, the Cp π_0 orbitals give rise to $a_1 + e$ symmetry combinations, while the π_1 orbitals result in $a_1 + a_2 + 2e$ levels. Ligand–ligand interactions result in the a_2 π_1 combination being destabilized above the others. This a_2 combination is important in that its interaction (or lack thereof) with the central metal elegantly rationalizes the paucity of the $[MCp_3]$ unit when M is a transition metal and the abundance of this unit for the actinides. There is no d AO that transforms as a_2 symmetry in C_{3v}. By contrast, the $f_{y(3x^2-y^2)}$ orbital can stabilize the ligand a_2 combination and provide significant metal–ligand bonding in the process.

A qualitative energy level diagram for the interaction of an actinide atom with the Cp π_1 MOs in a C_{3v} $[AnCp_3]$ complex is shown in Fig. 17.18. The 5f/π_1 a_2 interaction is shown as being the most important involving the 5f orbitals; the other six 5f-based levels span a very narrow energy range, reflecting their largely actinide nature. The relative position of the 5f manifold and the $6d_{z^2}$ level has been extensively studied, due in part to the experimental observation that $[ThCp_3''](Cp_3'' = \eta^5 - C_5H_3(SiMe_3)_2)$ possesses a $6d^1$ ground configuration (Kot *et al.*, 1988). The evidence from both Xα-SW (Bursten *et al.*, 1989a) and DV-Xα (Kaltsoyannis and Bursten, 1997) calculations is that at the start of the actinide series, the $6d_{z^2}$ orbital lies below the 5f manifold in $[AnCp_3]$ complexes. Furthermore, the d-below-f ordering is found to be a relativistic effect, as nonrelativistic DV-Xα calculations predict a $5f^1$ ground configuration for $[ThCp_3]$ (Kaltsoyannis and Bursten, 1997). Xα-SW studies predict that as the actinide series is crossed the 5f manifold is stabilized with respect to the $6d_{z^2}$ level, and hence that the later $[AnCp_3]$ compounds have a $5f^n >$ ground state configuration (Bursten *et al.*, 1989a).

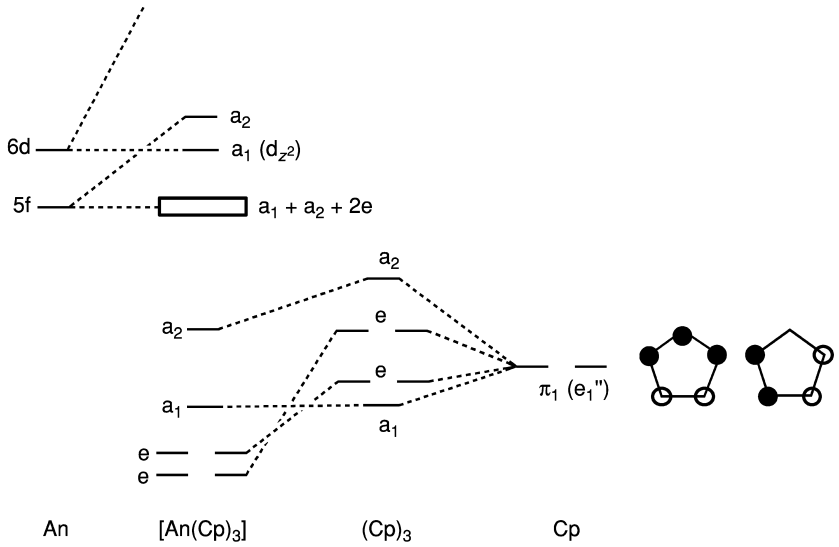

Fig. 17.18 *Qualitative energy-level diagram for the interaction of an actinide atom with the Cp π_1 MOs in a C_{3v} [$AnCp_3$] complex.*

The discrepancy between the nonrelativistic and relativistic results for the ground state configuration of [$ThCp_3$] is an excellent example of the need to incorporate relativity when calculating actinide electronic structure. More specifically, the calculated electronic absorption spectrum of $6d^1$ [$ThCp_3$] is very different from that from a $5f^1$ ground state configuration, with intense d $\rightarrow$ f transitions as opposed to weak Laporte-forbidden f $\rightarrow$ f transitions. The experimental spectrum of [$ThCp_3''$] indeed displays intense peaks, consistent with the $6d^1$ ground state configuration (Kot *et al.*, 1988).

As ever, the nature and extent of metal–ligand covalency has been the subject of extensive research and discussion (Burns and Bursten, 1989; Jensen and Bond, 2002). In particular, the relative contributions of the An 6d and 5f AOs to the two Cp π_1-based e symmetry MOs has come under scrutiny, as these are the two π_1-based MOs to which both An 6d and 5f AOs can contribute (the a_2 level can only have metal 5f character by symmetry, and the a_1 orbital is found to contain almost no metal contribution). Xα-SW calculations find that the 6dδ and 6dπ contributions to these orbitals are much larger than those of the 5f for the early An, with increasing 5f character to one of the levels (6dπ) with increasing An atomic number (Strittmatter and Bursten, 1991). The total metal involvement is in the 15–25% range, depending upon the orbital and compound in question. These results were later corroborated for [$ThCp_3$] by DV-Xα calculations (Kaltsoyannis and Bursten, 1997). The An 5f content of the a_2 level was found by Xα-SW to increase very significantly across the actinides,

to as high as 55% in [$CfCp_3$]. By contrast, the DV-Xα studies of [$ThCp_3$] find only 10% metal 5f content in this level.

(c) [$AnCp_3X$] complexes

When a fourth ligand X binds to a [$AnCp_3$] fragment, the Cp ligands pyramidalize to open up a coordination site for the X moiety. Several groups have investigated the nature of the An–X interaction, with much attention being paid to the An orbitals involved in the An–X bond. Early extended Hückel work on $[UCp_3]^+$ indicated that pyramidalization causes a stabilization and hybridization of the metal $6d_{z^2}$ and $7p_z$ AOs, resulting in a low-lying σ orbital that can accept charge from the X ligand (Tatsumi and Nakamura, 1984). A similar conclusion was drawn from Xα-SW calculations on [UCp_3] and [$ThCp_3$] (Bursten *et al.*, 1989a), although these studies suggested that the vacant hybrid is approximately isoenergetic with the 5f levels, in contrast to the extended Hückel calculations, which place the σ acceptor level well above the 5f manifold.

Xα-SW studies of the U–H bonding in [UCp_3H] support the results of the pyramidal base-free calculations in concluding that the U–H bond is indeed dominated by the U $6d_{z^2}$ AO (Bursten *et al.*, 1989b). Subsequent nonrelativistic DV-Xα calculations on [UCp_3X] (X = Me, NH_2, BH_4, NCS) suggest that the situation may be more complex, however, in that the U AO involved in the U–X σ bond depends upon the energies of the X orbitals (Gulino *et al.*, 1992). Thus, when X = NH_2 or NCS, the σ-bond is dominated by U $6d_{z^2}$, while for X = Me the U $5f_{z^3}$ plays a much larger role in σ-bonding. By contrast, RECP *ab initio* studies by the same workers on [$AnCp_3Me$] (An = Th, U) concluded that the An–Me σ bond is dominated by the metal $6d_{z^2}$ AO (Di Bella *et al.*, 1993).

The bonding of X to the An center is not necessarily restricted to purely σ interactions; π-donor and even π-acceptor ligands can also bind to the [$AnCp_3$] moiety as well. Quasi-relativistic Xα-SW calculations on [UCp_3CO], a model for the experimentally characterized $[UC_3^{\dagger}CO]$($Cp^{\dagger} = \eta^5$-$C_5H_4SiMe_3$) (Brennan *et al.*, 1986), found a U–C σ-bond similar in nature to those discussed above (i.e. a CO $5\sigma \rightarrow$ U $6d_{z^2}$ donation) (Bursten and Strittmatter, 1987). However, in addition, there is significant π-backbonding from the U 5fπ AOs into the vacant CO π^* orbitals. Thus, the overall U–CO interaction is an excellent example of the classic Dewar–Chatt–Duncanson model of synergic bonding, more usually associated with transition metal carbonyl complexes. Furthermore, the computational evidence for U $\rightarrow$ CO π-backbonding provides solid rationalization of the experimental observation that the CO stretching vibration in $[UCp_3^{\dagger}CO]$ is about 170 cm^{-1} lower than in free CO. Since that initial synthesis, a number of other UCp_3CO complexes with different substituents on the Cp rings have been synthesized and characterized (Parry *et al.*, 1995; Del Mar Conejo *et al.*, 1999; Evans *et al.*, 2003). The observed C–O stretching frequencies of these complexes show some surprising trends that will stimulate further theoretical studies (Kaltsoyannis, 2003). Recent experimental and theoretical studies

by Andersen, Eisenstein and coworkers have addressed the bonding of CO to organolanthanide complexes of the type Cp^*_2Ln, and propose significant differences between the binding of CO to 4f metals relative to 5f metals (Maron *et al.*, 2002).

Compounds in which there is π donation from ligand to metal have also been investigated computationally. Cramer *et al.* (1988) conducted extended Hückel calculations on N-based π-donor [UCp_3X] complexes where X = NH_2, NPH_3, $NHCHCHPH_3$, and NPh. They concluded that, for the latter three complexes, there is significant N 2pπ → U π donation, mainly into the U 6dπ levels. Subsequent DV-Xα calculations on similar complexes where X = NH_2 and NCS also found π character to the U–N bond, although they indicated that the donation is from N 2pπ → U 5fπ (Gulino *et al.*, 1992). Interestingly, this study found that alterations in X produced almost no change in the metal's charge (+1.8 ± 0.06) or configuration ($5f^{3.4}6d^{0.7}$). The conclusion was that this electronic 'buffering' of the U is facilitated by changes in the U–Cp bonding; as the donation from X, and hence U–X covalency, increases, the U–Cp bonding becomes more ionic.

In addition to N-donor ligands, complexes containing alkoxide groups have also been studied, using extended Hückel (Gulino *et al.*, 1992), Xα-SW (Bursten *et al.*, 1989b), DV-Xα and fully relativistic local density Dirac–Slater (Gulino *et al.*, 1993) approaches. The conclusions from all studies are broadly similar; the An–O bond has both σ and π character, with significant O 2pπ → An 6d and (lesser) 5f π donation. A comparison of [$ThCp_3OMe$] with the U analog found that 1.895 e^- are transferred to the Th center (along the Me→O→$AnCp_3$ direction), increasing to 2.185 e^- in [UCp_3OMe], i.e. the U compound was found to be more covalent (Gulino *et al.*, 1993). These workers noted, as have others (Bursten and Strittmatter, 1991), that the partial π character of the An–O bond may account for the prevalence of linear (or nearly linear) An–O–R vectors in actinide alkoxide systems.

(d) [$AnCp_2X_2$], [$AnCp_2X$], and [$AnCp_2$] complexes

The metallocene structures MCp_2X_2 are common structures for the transition metal, lanthanide, and actinide elements, and thus provide an opportunity to compare and contrast the electronic structure of d- and f-block metals. Many of the f-element complexes of formulation MCp_2X_2 contain the sterically bulky and electron-rich pentamethylcyclopentadienyl (η^5-C_5Me_5, denoted Cp^*) ligand; the steric bulk of the Cp^* ligand is often needed to avoid the coordination of more than two Cp ligands about the large f-element centers (Janiak and Schumann, 1991).

The 1980s saw a number of extended Hückel calculations on compounds of the general formula [$AnCp_2X_2$], in which unsubstituted Cp rings were used to model the much bulkier Cp^* groups used in synthetic investigations (Tatsumi *et al.*, 1985; Smith *et al.*, 1986; Tatsumi and Nakamura, 1987). These extended

Hückel calculations are well summarized in the 1991 review by Bursten and Strittmatter (1991), and space does not allow us to go into detail here. Topics covered include (a) rationalization of the existence of both 'O inside' and 'O outside' structures in $[UCp_2Cl(\eta^2\text{-COR})]$, by contrast to the transition metal preference for O inside (Tatsumi *et al.*, 1985), (b) rationalization of the preference for the butadiene *s-cis* geometry in $[AnCp_2(C_4H_6)]$ (An = Th, U) (Smith *et al.*, 1986), (c) determination that the actinacyclopentadiene complex is ca. 250 kJ mol^{-1} more stable than the corresponding cyclobutadiene structure in $[UCp_2(C_4H_4)]$ (Tatsumi and Nakamura, 1987), and (d) studies of CO insertion pathways in $[UCp_2Me_2]^{2+}$ (Tatsumi *et al.*, 1985). Slightly earlier, quasi-relativistic Xα-SW calculations on $[UCp_2X_2]$ (X = Cl, Me) were used to show that Me^- is a stronger σ donor than Cl^- to the actinide center, and concluded that there no significant $Cl^- \rightarrow U$ π donation (Bursten and Fang, 1983). Hay has recently reported DFT calculations on models of the formally U(VI) bis-imido complexes $Cp^*_2U(=NR)_2$ and related N-ligand systems (Hay, 2003). These systems demonstrate some of the complex chemical transformations that can occur at a uranium center (Arney *et al.*, 1992; Warner *et al.*, 1998; Kiplinger *et al.*, 2002), and an understanding of their behavior challenges the ability of calculations to determine reaction pathways for large actinide-containing systems.

In 1996, Di Bella *et al.* used configuration interaction *ab initio* methods to study the formally U(III) $[UCp_2CH(SiH_3)_2]$ (Di Bella *et al.*, 1996). The U center was found to have a $5f^3$ ground state configuration, and it was argued that the stability of this configuration vs $5f^26d^1$ correlates well with the inherent chemical stability of U(III) organometallics in comparison with $6d^1$ Th(III) analogs. In agreement with previous studies, the U–Cp bonding was found to be primarily U 6d/Cp π_1, with the metal 5f electrons being only marginally involved in bonding. The U–$CH(SiH_3)_2$ bond is σ only.

More recently, Kaltsoyannis and Russo (2002) have used ZORA relativistic gradient-corrected DFT to show that the equilibrium geometry of $[NoCp^*_2]$ is bent by 26° (i.e. the angle subtended by the centroids of the Cp^* rings and the No atom is 154°), this structure being ca. 9 kJ mol^{-1} more stable than the linear arrangement. This study also examined the lanthanide analog, $[YbCp^*_2]$, and also found it to be bent, in excellent agreement with gas-phase electron diffraction data (Andersen *et al.*, 1986). The bent structure of $[NoCp^*_2]$ was traced to a combination of valence orbital and electrostatic factors. The involvement of the No 5f AOs in bonding to the Cp^* rings is minimal, although ca. 10% metal d content is found in the Cp^* ring pπ e_{1g} levels.

(e) Bis(cyclopentadienyl) actinide complexes with metal–metal bonds

Despite extensive efforts, no organometallic (or nonorganometallic!) compound has been synthesized containing a direct An–An bond. Nevertheless, organometallic systems do exist that contain a bond between an actinide metal and a

transition metal (both direct and bridged), and some have been investigated computationally. Xα-SW calculations have been performed on [MCp_2(I)–$RuCp(CO)_2$] (M = Zr, Th) (Bursten and Novo-Gradac, 1987), a model for the first ever compound with a direct actinide–transition metal bond (Sternal *et al.*, 1985). The M–Ru bonding was found to be very similar in the transition metal and actinide systems, consisting of donation from the filled $4d_{z^2}$ orbital of Ru to the empty d_{z^2} valence function of Zr or Th. The bond is highly polarized toward the Ru, and is best described as a dative donor–acceptor bond from [$RuCp(CO)_2$]$^-$ to the d^0 Zr(IV) or d^0f^0 Th(IV) center.

Extended Hückel (Ortiz, 1986), Xα-SW (Makhyoun *et al.*, 1987), and *ab initio* (HF + generalized valence bond [GVB]) calculations (Hay *et al.*, 1986) have been performed on bis-Cp systems containing bridged bonds between Th and a late transition metal (Ni or Pt). The latter study took [$Th(Cl)_2(\mu\text{-}PH_2)_2Pt(PH_3)$] as a model for the experimental Cp^*_2 system (the replacement of Cp by Cl is a computational simplification often made in early calculations on large systems, justified on the grounds that both ligands possess one filled σ and two filled π orbitals with respect to the ligand–metal axis), and concluded that there is direct M–M bonding between the $5d_{x^2-y^2}$ orbital of Pt and the $6d_{x^2-y^2}$ orbital of Th, with the larger fraction of the electron density on the Pt. The bond is best described as dative, from the formally filled $5d^{10}$ shell of the Pt into the formally empty 6d shell of Th.

17.5.3 Sandwich complexes with six- and seven-membered rings: $An(\eta^6\text{-}C_6H_6)_2$ and $An(\eta^7\text{-}C_7H_7)_2$

In 1999, Hong *et al.* published the results of an in-depth *ab initio* study of the energetics and bonding in [MBz_2] (M = Th, U, variety of lanthanide elements; Bz = η^6-C_6H_6) (Hong *et al.*, 1999). These calculations employed extensive electron correlation techniques (e.g. state-averaged CASSCF, MRCI, and CCSD(T)) in conjunction with large pseudopotential basis sets, and assumed D_{6h} molecular symmetry (i.e. the Bz rings were fixed to be parallel to one another). It was found that both [$ThBz_2$] and [UBz_2] are stable with respect to dissociation into two benzene rings plus the metal, but that the An–ring bonding is weaker than in analogous bis-COT systems due to the lack of ionic contributions to the bonding (Bz is, of course, formally neutral and closed shell).

In a conclusion reminiscent of their earlier work on the lanthanocenes and actinocenes (Dolg *et al.*, 1995; Dolg and Fulde, 1998), these workers found that the ground state of both [$ThBz_2$] and [UBz_2] is not completely described by a single configuration. Thus, while the leading configuration to the ground state of the Th and U compounds is $e^4_{2g}5f^0$ and $e^4_{2g}5f^2$, respectively (the e_{2g} level being a mixture of An $6d_{\pm2}$ and ring π_2), the ground state wavefunctions have a contribution from the $e^2_{2g}a^2_{1g}5f^0$ (Th) and $e^2_{2g}a^2_{1g}5f^2$ (U) configurations (the a_{1g} orbital is a mixture of An 7s and $6d_0$). The principal source of metal–ring

covalency is a backbonding interaction from the An $6d_{\pm 2}$ levels to the ring π_2 orbitals, although there is some evidence for weak $5f_{\pm 2}$ involvement in this process.

Hong *et al.*'s assumption of D_{6h} symmetry for $[MBz_2]$ was called into question by the work of Li and Bursten (1999), published in the same year. These workers used gradient-corrected DFT to probe the geometric structures of $[AnBz_2]$ (An = Th to Am) and $[An(\eta^6\text{-}C_6H_3R_3)_2]$ (An = Th, U, Pu; R = Me, ^{t}Bu). They found that the equilibrium geometry of $[AnBz_2]$ is significantly bent, with the angle subtended by vectors connecting the ring centroids and the metal ranging from 135 to 142°, depending on the metal. This bending is electronically driven, with greater covalency in the bent geometry arising from greater Bz → An 6d and 5f donation. Fig. 17.19 shows the calculated energy curves for the $TiBz_2$ and $ThBz_2$ as a function of the centroid–metal–centroid angle, showing that the former is 'linear' whereas the latter is predicted to prefer a 'bent' geometry.

Replacement of three H atoms on each ring by Me groups also results in bent equilibrium geometries. However, when the Me groups are replaced by the much bulkier ^{t}Bu units the equilibrium geometry reverts to linear, i.e. for very bulky R substituents, the steric repulsion between the rings overcomes the electronic preference for bending. These conclusions are summarized in Fig. 17.20, which shows the calculated structures of $U(\eta^6\text{-}C_6H_3Me_3)_2$ and $U(\eta^6\text{-}C_6H_3{}^tBu_3)_2$. The former is found to have a bent geometry with a centroid–U–centroid angle of 139.8° whereas the latter is found to be linear. It is notable that the experimental crystal structure of $Gd(\eta^6\text{-}C_6H_3{}^tBu_3)_2$ is indeed linear (Brennan *et al.*, 1987).

Shortly after Li and Bursten's work was published, Hong *et al.* (2000) revisited $[ThBz_2]$ and $[UBz_2]$ using both *ab initio* and ZORA DFT methods. They found that neither molecule is bent at the *ab initio* SCF level. Inclusion of electron correlation, however, using MP2 and CCSD(T) methods, results in significantly bent structures (ca. 140–145°), although the energy differences between the linear and bent geometries is so small that the equilibrium geometry cannot be unequivocally established using these *ab initio* techniques, probably because of the use of an unrelaxed structure for the rings. Hong *et al.* then went on to conduct ZORA DFT studies which also indicated that the bent structures are the most stable, and hence they concluded that "qualitatively...we confirm their [Li and Bursten] result that the bis benzene complexes of Th and U have bent structures", and that bending enhances the metal–ring bonding. Dolg (2001) has also reported additional calculations on these systems at the scalar-relativistic level using a combination of energy-consistent *ab initio* pseudopotentials and gradient-corrected density functionals.

A number of recent investigations have focused on actinide sandwich molecules involving the cycloheptatrienyl ligand (Cht = η^7-C_7H_7). In 1995, Ephritikhine and coworkers isolated a salt of the $[U(Cht)_2]^-$ anion, which is the first and, to date, only experimental example of a sandwich complex involving two Cht ligands (Arliguie *et al.*, 1995). The $[U(Cht)_2]^-$ anion was characterized

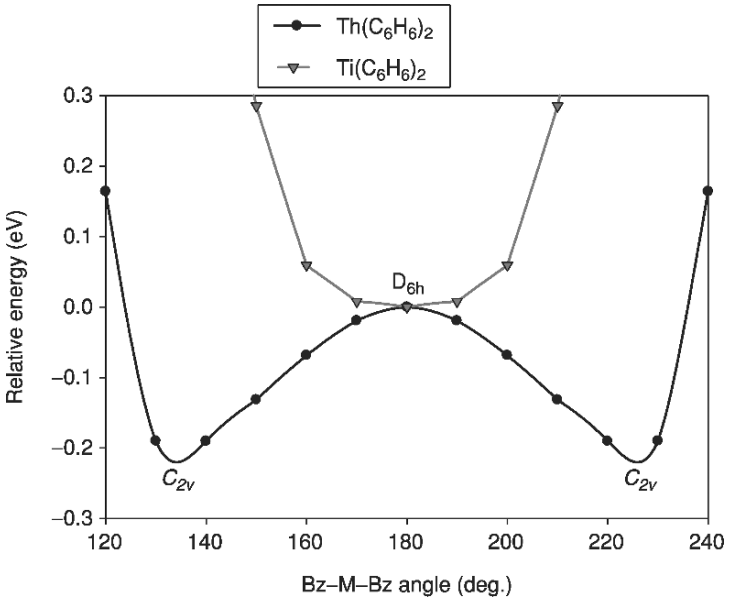

Fig. 17.19 *DFT-calculated potential energy curves for* $Ti(\eta^6\text{-}C_6H_6)_2$ *and* $Th(\eta^6\text{-}C_6H_6)_2$ *as a function of centroid–metal–centroid angle* (*reproduced from Li and Bursten*, 1999).

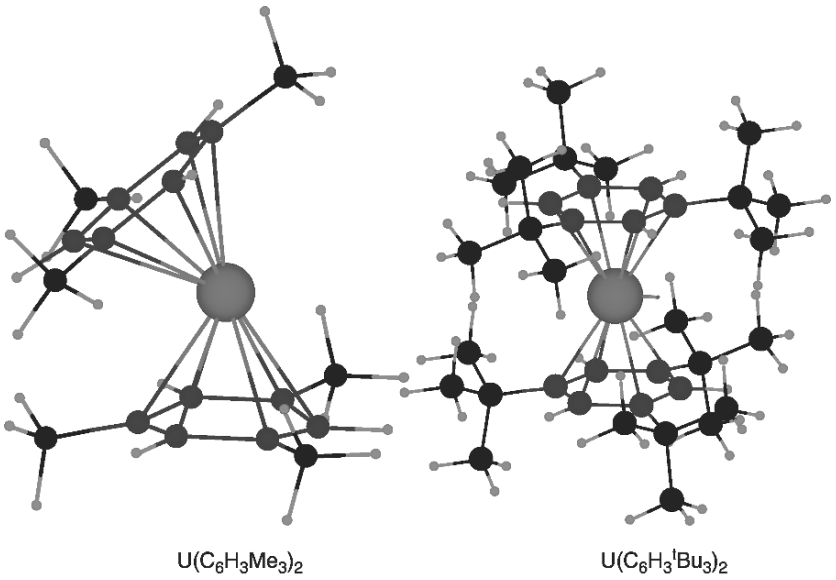

Fig. 17.20 *DFT-calculated structures of* $U(\eta^6\text{-}C_6H_3Me_3)_2$ *and* $U(\eta^6\text{-}C_6H_3{}^tBu_3)_2$ *as a function of centroid–metal–centroid angle* (*reproduced from Li and Bursten*, 1999).

crystallographically and was found to be a 'parallel' sandwich complex, i.e. the two Cht ligands are parallel to one another with a centroid–U–centroid angle of 180°.

Li and Bursten (1997) reported relativistic DFT calculations at both the LDA and Becke–Perdew86 (BP86) levels on $[An(Cht)_2]^q$ (An = Th to Am; $q = 2-$, $1-$, 0, $1+$) complexes. The geometries were optimized in both D_{7h} and D_{7d} symmetries, with the latter (staggered rings) arrangement being found to be 2–4 kJ mol^{-1} more stable. The H atoms were found to be canted in toward the metal atom (e.g. by 4° in $[UCht_2]^-$), reminiscent of the results of similar calculations by the same researchers on protactinocene (Section 17.5.1) (Li and Bursten, 1998).

The metal–ring bonding was found to involve both the An 5fδ and 6dδ levels. The former interact with the e_2'' π_2 levels of the Cht ligands, and are as important as the 6dδ in stabilizing the frontier pπ orbitals of the rings. As the actinide atomic number increases, the An 5f and ring frontier pπ orbitals come into closer energetic proximity, resulting in an increase in the 5f contribution to the ring e_2'' levels and a decrease in the 6d content.

One of the most interesting aspects of this study concerns the formal oxidation states of the Cht rings and hence the metal centers. Formal charges of $1+$ and $3-$ for a Cht ring satisfy the Hückel $4n+2$ rule for aromaticity. When reporting the experimental characterization of $[U(Cht)_2]^-$, Ephritikhine *et al.* suggested that the complex is a U(v) f^1 system with two $3-$ rings (Arliguie *et al.*, 1995). Li and Bursten, however, suggest that this is not the best description on the grounds that the $3e_2''$ level of $[U(Cht)_2]$ (HOMO) and $[U(Cht)_2]^-$ (HOMO–1) is an approximately equal mixture of U 5f and Cht π_2. They argued that two of the four electrons in this level should be associated with the metal and two with the rings, resulting in an f^2 U(IV)/2 × Cht^{2-} description for $[U(Cht)_2]$, with $[U(Cht)_2]^-$ being a U(III) f^3 system. That the formal description of the oxidation state of the Cht ligand is intermediate between the +1 and –3 limits is in agreement with previous experimental and theoretical studies of mixed ring transition metal Cht/Cp complexes (Green *et al.*, 1992, 1994; Kaltsoyannis, 1995). Gourier *et al.* (1998) performed an EPR and angle-selected ENDOR study of the $[U(Cht)_2]^-$ anion to determine the ordering of the electronic energy levels and the metal–ligand interaction. They indeed find that the single electron is localized in the U 5f-orbital, a spin–orbit-coupled mixture of fσ and fπ orbitals, and there exists strong participation of the fδ orbitals in the covalent bonding.

17.5.4 π-Backbonding in U(III) complexes containing N-based ligands

In our discussion of $[AnCp_3X]$ complexes, we came across Xα-SW calculations on $[UCp_3CO]$ (Bursten and Strittmatter, 1987), which found a significant π-backbonding interaction between the 5f AOs of the U(III) center and the CO π^* levels. Slightly over a decade after these calculations were published, Roussel and Scott (1998) reported the synthesis and

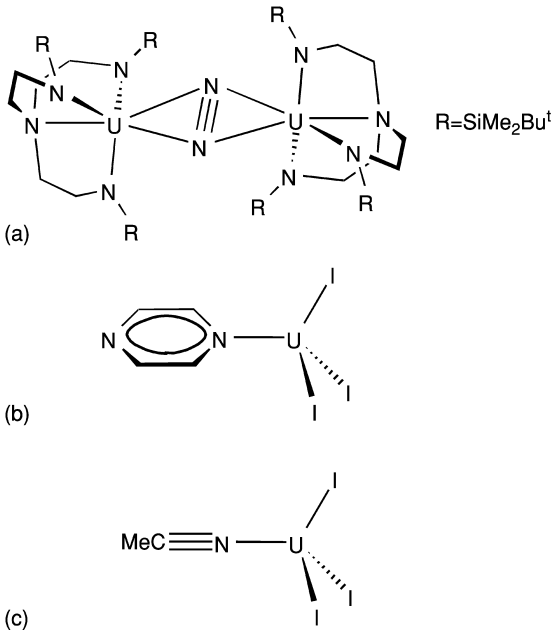

Fig. 17.21 *Molecular structures of three uranium compounds featuring metal→ligand π-backbonding* (*see Roussel and Scott*, 1998; *Mazzanti* et al., 2002).

characterization of the first dinitrogen compound of an actinide element, $[\{(NN_3)U\}_2(\mu^2 + \eta^2 : \eta^2 + N_2)]$ $[NN_3 = N(CH_2CH_2NSiBu^tMe_2)_3]$ (Fig. 17.21a). The fact that the N–N distance in this compound is essentially the same as in free dinitrogen prompted these workers to conclude that the interaction between the N_2 and U centers is σ-donation from ligand to metal. Subsequent quasi-relativistic gradient-corrected DFT calculations on the model complex $[\{(NH_2)_3(NH_3)U\}_2(\mu^2\text{-}\eta^2\text{:}\eta^2\text{-}N_2)]$ (Kaltsoyannis and Scott, 1998), however, found that the only significant metal–N_2 interaction is π-backbonding from the 5f AOs of the formally U(III) centers into the N_2 π_g N–N antibonding MOs, very reminiscent of the earlier Xα-SW calculations on $[UCp_3CO]$. A three-dimensional representation of one of the two such π-backbonding MOs is shown in Fig. 17.22.

One of the more curious aspects of the work on $[\{(NH_2)_3(NH_3)U\}_2(\mu^2\text{-}\eta^2\text{:}\eta^2\text{-}N_2)]$ is the N–N bond length. Significant population of the N_2 π_g level should result in an increase in the N–N distance, and geometry optimizations of $[\{(NH_2)_3(NH_3)U\}_2(\mu^2\text{-}\eta^2\text{:}\eta^2\text{-}N_2)]$ indeed lead to a shortening of the U–N (N_2) distance and a lengthening of the N–N distance in comparison with experiment. These conclusions were reinforced by analogous DFT studies of UN_2 (Brown and Kaltsoyannis, 1999) and U_2N_2 (Roussel *et al.*, 2001).

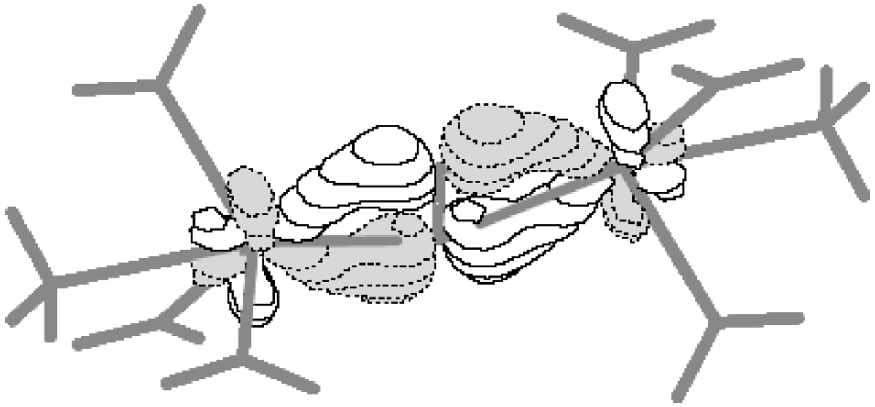

Fig. 17.22 *Three-dimensional representation of one of the two* $U_2 \rightarrow N_2$ *π-backbonding MOs in* $[\{(NH_2)_3(NH_3)U\}_2(\mu^2\text{-}\mu^2\text{:}\eta^2\text{-}N_2)]$, *a computational model for* $[\{(NH_2)_3(NH_3)U\}_2(\mu^2\text{-}\eta^2\text{:}\eta^2\text{-}N_2)]$ (*see Fig.* 17.21(*a*) *and Kaltsoyannis and Scott*, 1998).

A possible explanation for the discrepancy between theory and experiment is that the NN_3 ligands are so bulky that they prevent the two ends of the molecule from coming any closer together, as would accompany a reduction in the U–N (N_2) distance. The conclusion was therefore that there is an electronic driving force toward U–N(N_2) shortening and N–N lengthening, but that this is opposed (and overcome) by the highly sterically demanding NN_3 ligands.

Recent experimental work by Cloke and Hitchcock (2002) has, however, called this conclusion into question. These workers have synthesized and characterized a bimetallic dinitrogen uranium complex with $CpCp^*$ and pentalene ancillary ligands, $[(U(\eta^5\text{-}C_5Me_5)(\eta^8\text{-}C_8H_4\{Si^iPr_3\text{-}1,4\}_2))_2(\mu\text{-}\eta^2\text{:}\eta^2\text{-}N_2)]$. By contrast to triamidoamine system of Roussel and Scott, the N–N distance in the Cloke complex is significantly longer than in free N_2, consistent with the presence of an N=N double bond. Intriguingly, however, the U–N distances are essentially the same as in $[\{(NN_3)U\}_2\ (\mu^2\eta^2\text{:}\eta^2\text{-}N_2)]$, and Cloke has suggested that the difference between $[\{(NN_3)U\}_2\ (\mu^2\text{-}\eta^2\text{:}\eta^2\text{-}N_2)]$ and $[(U(\eta^5\text{-}C_5Me_5)(\eta^8\text{-}C_8H_4\{Si^iPr_3\text{-}1,4\}_2))_2(\mu\text{-}\eta^2\text{:}\eta^2\text{-}N_2)]$ may be a consequence of different frontier orbital geometries in the two ligand environments.

A model for the Cloke pentalene system has been studied computationally by Cloke *et al*. (2004). These relativistic, gradient-corrected DFT studies reinforce the conclusions from the previous work on $[\{(NH_2)_3(NH_3)U\}_2(\mu^2\text{-}\eta^2\text{:}\eta^2\text{-}N_2)]$, i.e. both complexes contain two $5f^2$ U(IV) centers, with substantial covalent interaction between the U 5f atomic orbitals and one component of the N_2 π_g orbitals. The interaction may be characterized as reduction of the N_2 to N_2^{2-}, and geometry optimizations of the Cloke model concur with experiment in finding an N–N distance appreciably longer than in free N_2. However, this agreement between theory and experiment is only achieved at the expense of a

non-Aufbau electronic occupation. The origin of the short N–N distance in $[(N_3N']U)_2(\mu\text{-}\eta^2\text{:}\eta^2\text{-}N_2)]$ is therefore still not unambiguously resolved.

Mazzanti *et al.* (2002) have recently reinforced previous conclusions that U(III) can function as a π basic center. These workers have conducted quasi-relativistic gradient-corrected DFT calculations on [M(pyrazine)I_3] (Fig. 17.21b), [M(acetonitrile)I_3] (Fig. 17.21c), and [M(pyrazine)$_3I_3$] (M = La, Nd, U), models for experimentally characterized tris[(2-pyrazinyl)methyl]amine systems. Geometry optimizations of these compounds reproduce experimental trends, i.e. there is a reduction in M–N from La to U even though the ionic radii of La^{3+} and U^{3+} are very similar. The calculations reveal that there is essentially no orbital interaction between Ln^{3+} and the N-donor ligands, in contrast to the actinide system in which there is π-backdonation from the 5f AOs of U^{3+} into the π^* levels of both acetonitrile and pyrazine. This interaction leads to a larger total bonding energy for the U(III) species compared with the Ln systems (even though the shorter U–N distances produce larger Pauli repulsion energies).

Meyer *et al.* have also encountered π effects in uranium–nitrogen chemistry (Castro-Rodrigues *et al.*, 2003b). These researchers have conducted DFT calculations on uranium tris-aryloxide derivatives supported by triazacyclononane, in which the metal center is also bonded to $NCCH_3$, $NSi(CH_3)_3$, or N_3. In the $NCCH_3$ and $NSi(CH_3)_3$ systems, the acetonitrile– and imido–uranium bonds display strong covalent π interactions; interestingly, the azide derivative features an essentially electrostatic U–N_3 interaction. The uranium tris-aryloxide moiety has also been employed by the same researchers in the synthesis of an alkane-coordinated system (Castro-Rodrigues *et al.*, 2003a). Preliminary DFT calculations of this complex indicate a weak σ-type orbital interaction between the (η^2-H,C)-coordinated alkane and U-based fragments.

17.5.5 Miscellaneous organometallic systems

In 1989, Van der Sluys *et al.* reported the synthesis and structure of U[CH$(SiMe_3)_2]_3$, a U(III) complex that was the first homoleptic alkyl complex of an actinide element (Van der Sluys *et al.*, 1989). The molecule exhibits a somewhat nonintuitive pyramidal structure that could have been motivated for electronic or steric reasons. Ortiz *et al.* (1992) used *ab initio* CASSCF methods to study the electronic and geometric structures of [$AnMe_3$] (An = U, Np, Pu) as models of the isolated complex. They found that the pyramidal structure was more stable than the planar for the ground state of each molecule. The driving force toward pyramidalization is increased An 6d orbital participation in the An–C bonding orbitals. For example, the U $6d_{xz}$ and $6d_{yz}$ atomic populations increase from 0.04 to 0.34 electrons as [UMe_3] pyramidalizes from 0 to 23° out of plane. Further evidence for the key role of the 6d AOs come from the observation that if these functions are removed from the basis set, the planar geometry is the most stable for each molecule. Later scalar-relativistic DFT calculations by

Joubert and Maldivi (2001) lead to similar conclusions. Schneider *et al.* (1991) used Dirac–Fock–Slater calculations based on the discrete-variational Xα method to investigate the effects of spin–orbit and ligand-field effects on UH_3 and $U(NH_2)_3$. They found that the metal–ligand σ-bonding predominantly involves the U 6d orbitals and that the trigonal ligand field effectively quenches the spin–orbit coupling in the 6d manifold.

Nash and Bursten (1995) used relativistic DV-Xα calculations to study the electronic structure of octahedral $[M(CO)_6]$ (M = Cr, W, U, Sg). Population analyses and electron density plots indicate that there is more extensive π-backbonding in the actinide system than in the transition metal molecules. However, while $[Cr(CO)_6]$ and $[W(CO)_6]$ are stable species, $[U(CO)_6]$ cannot be isolated outside of a cold matrix, perhaps at odds with the electronic structure results. The rationalization of theory and experiment is that for the U species only there is a high density of 5f-based dissociative states close in energy to the ground state. Indeed, the calculations on $[U(CO)_6]$ required a thermal spreading factor (a Boltzmann weighting of orbital populations around the HOMO) to achieve SCF convergence. The authors conclude that "the 'clean' MO description of the transition metal systems is lost in $[U(CO)_6]$ owing to the energetic closeness of the U 5f and 6d AOs". The same authors also performed higher-level (MP2, CCSD(T)) calculations on $Sg(CO)_6$ (Nash and Bursten, 1999). These calculations affirm that $Sg(CO)_6$ is predicted to be a d^6 transition-metal carbonyl complex analogous to $Mo(CO)_6$ and $W(CO)_6$.

Recently, Korobkov *et al.* (2001) reported the results of hybrid DFT (B3LYP) studies on a model binuclear tetrapyrrole system $[(TP)U_2I_4]^{2-}$, in which the bridging $C(CH_2)_5$ units of the experimentally characterized molecule are replaced by CH_2 groups. Both high- and low-spin calculations were performed, essentially corresponding to ferromagnetic and antiferromagnetic coupling of the two U(III) $5f^3$ centers. The results, in agreement with experimental magnetic measurements, indicate that the ground state is low spin, but only by a very small energy (ca. 1 kJ mol^{-1}). The unpaired electrons are found in all spin cases to be nearly pure U 5f in character.

As we have seen, there has been a great deal of interest in organoactinide sandwich molecules and, more recently, in bimetallic uranium complexes involving π-backbonding from the U centers. Cummins *et al.* have synthesized and studied computationally inverted sandwich molecules of the form $[\{L_nU\}_2(\mu\text{-}R)]$, where L is a nitrogen-based ligand and R is toluene, naphthalene, or COT (Diaconescu *et al.*, 2000; Diaconescu and Cummins, 2002). The ORTEP of $[\{(N[Ad]Ar)_2U\}_2(\mu\text{-}C_7H_8)]$ is shown in Fig. 17.23, and it can clearly be seen how the carbocyclic toluene ligand bridges the two U centers. DFT calculations reveal that the primary bonding interaction between the metals and the bridging ligand in $[\{(NH_2)_2U\}_2(\mu\text{-}C_6H_6)]$, a model for $[\{(N[Ad]Ar)_2U\}_2(\mu\text{-}C_7H_8)]$, is δ-backbonding from the U 5f atomic orbitals into the free arene LUMO. Fig. 17.24 presents three-dimensional representations of the two near-degenerate δ-backbonding levels. It is noticeable that the computed arene ring

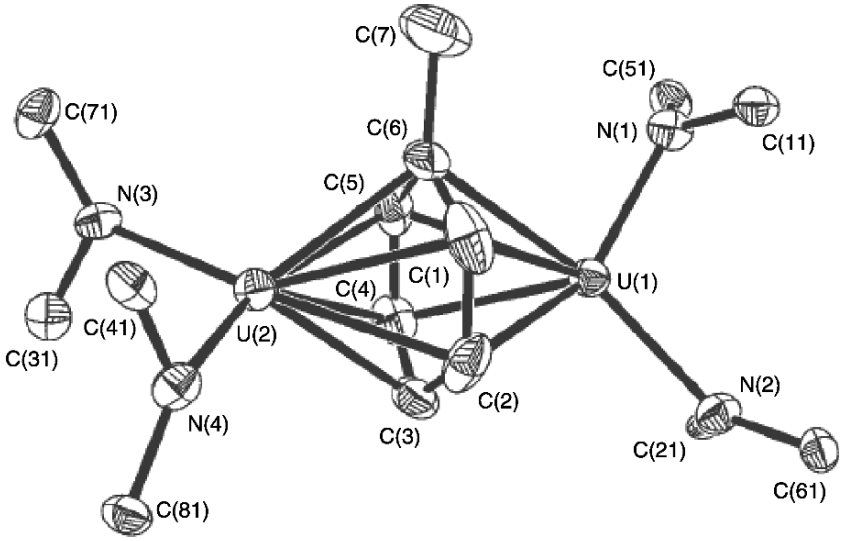

Fig. 17.23 *Structural drawing of* [{(N[*Ad*]*Ar*)$_2$*U*}$_2$(μ-C_7H_8)] (*reproduced from Diaconescu* et al., 2000).

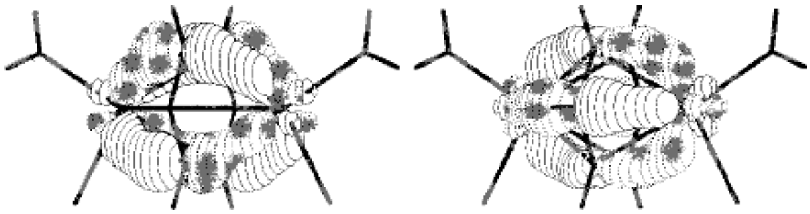

Fig. 17.24 *Two near-degenerate δsymmetry U→Bz backbonding orbitals in* [{(NH_2)$_2$*U*}$_2$ (μ-C_6H_6)], *a model for* [{(N[*Ad*]*Ar*)$_2$*U*}$_2$(μ-C_7H_8)] (*reproduced from Diaconescu* et al., 2000).

C–C distance is 1.461 Å, significantly longer than in free benzene (1.39 Å), as expected for partial population of the e_2 symmetry-free benzene LUMO. Similar conclusions concerning the nature of the bonding between the U centers and the arene bridge in $[(C_5Me_5)_2U]_2(\eta\text{-}\mu^6\text{:}\mu^6\text{-}C_6H_6)$ were drawn by Evans *et al.* (2004).

17.6 MATRIX-ISOLATED ACTINIDE MOLECULES

In previous sections of this chapter, we have examined the electronic structure of some very small and some very large actinide-containing molecules and ions. Part of the appeal of the actinyl ions discussed in Section 17.3 is their small size

and their high symmetry, both of which facilitate high-level electronic structural studies. In contrast, the large organometallic complexes discussed in Section 17.5 present a much larger challenge to computational methods. One difficulty in comparing calculated electronic structural properties of the AnO_2^{q+} actinyl ions with experimental data is the fact that actinyl ions are generally found experimentally with equatorial ligands. Indeed, the experimental properties of isolated AnO_2^{q+} ions are largely unknown.

In this section, we will discuss another class of small actinide-containing species, namely those that can be isolated and detected in low-temperature matrices. Matrix isolation has been proven to be an effective way to stabilize reactive or transient species so that spectroscopic characterizations can be performed on otherwise thermodynamically unstable molecules (Bondybey *et al.*, 1996; Himmel *et al.*, 2002). Inert gas (e.g. noble-gas, N_2, H_2) matrices are frequently used because they usually protect (or prevent) the newly formed gas-phase products from undertaking further reactions. For several decades, matrix isolation techniques have helped scientists to identify and characterize thousands of new compounds, including many species that are unexpected from the traditional point of view of chemistry (Jacox, 2003). The first studies of matrix-isolated transient actinide molecules occurred in the early 1970s. These early studies reported the first data on matrix-isolated UO, UO_2, and UO_3 (Abramowitz *et al.*, 1971; Leary *et al.*, 1971; Abramowitz and Acquista, 1972; Carstens *et al.*, 1972), as well as the first uranium carbonyl complexes (Slater *et al.*, 1971), and the generation of UF_5 in matrices (Paine *et al.*, 1976; Jones and Ekberg, 1977). Reedy and coworkers performed a series of matrix-isolation experiments in the 1970s that led to a number of new species that will be discussed below. In the last decade, Andrews and coworkers have extensively explored the chemistry of Th and U in noble-gas (Ng) matrices, and these more recent studies will be much of the focus of the remainder of this section.

The generation of isolated small actinide transients is a very fertile area for electronic structure calculations, especially given some of the potential difficulties in characterizing transient molecules using only experimental methods (Beattie, 1999). Many of the new actinide molecules that have been detected in solid matrices are formed from the reaction of electronically excited actinide atoms, typically generated via laser ablation, with small substrate molecules, such as O_2, CO, NO, N_2, H_2O, and CO_2. Vibrational spectroscopy has been the most common and sensitive experimental probe of the products trapped within the low-temperature matrices. In addition, the use of isotopomers of the substrate molecules has allowed the vibrational studies to determine the stoichiometries of the reactions as well as the isotope shifts in the vibrational frequencies. Thus, the experimental studies typically can determine the reaction stoichiometries between the actinide atoms and the substrate molecules, and provide the vibrational frequencies of multiple isotopomers of the actinide-containing products. Theoretical studies of the matrix-isolated species can provide predictions of the geometric structures, relative isomer energies, and

electronic structures of the proposed products. In recent years, the ability to determine vibrational frequencies and normal modes directly from the electronic structure calculations has provided an important benchmark for the quality of the theoretical methods. Indeed, the understanding of matrix-isolated actinide molecules has greatly benefited from the synergy between experimental and theoretical studies, and the combination of experiments and theory has led to much more progress than either would in isolation.

Here we will provide a brief summary of recent developments in this fruitful field of actinide chemistry, with particular focus on the actinide oxides, nitrides, nitride–oxides, and carbide–oxides. The analogous transition-metal species characterized using the same technique have been reviewed recently (Zhou *et al.*, 2001; Andrews and Citra, 2002). The geometries, electronic structures, and vibrational frequencies of UO_2^{2+}, UO_2, UN_2, PuO_2^{2+}, and PuN_2 were recently investigated (Clavaguéra-Sarrio *et al.*, 2004). We will proceed by discussing the molecular and electronic structures of the actinide molecules formed upon the reactions of laser-ablated actinide atoms with various small molecules. Typically, the reaction of laser-ablated actinide atoms with small molecules leads to the formation of many products because of the excess energy of the laser-ablated atoms and the existence of multiple reaction channels. We will focus on some selected matrix-isolated actinide molecules that have been definitively characterized via experiment and are of fundamental importance in actinide chemistry. Also, we will limit our discussion primarily to molecules with three atoms or more that result from the addition of actinide atoms to diatomic or larger substrate molecules.

Many of the species that we will discuss in this section are triatomic molecules of the type XAnY involving a variety of actinide atoms in different oxidation states. This chemistry becomes closely linked to that of the actinyl ions, AnO_2^{q+}, that were discussed in Section 17.3. Not surprisingly, the majority of actinide matrix-isolation experiments have involved uranium because of the availability of the element and the relative ease with which it can be handled. Thus, many of the matrix-isolated species will be closely related to the uranyl ion, UO_2^{2+}, which, as we have pointed out, is probably the most prevalent species in uranium chemistry. In order to give a sense of the electronic structural diversity even among formally U(VI) species isoelectronic to UO_2^{2+}, we will present first a comparison of the energy-level diagrams for the isoelectronic series UO_2^{2+}, NUO^+, and CUO. The electronic structure of this series was first considered by Pyykkö *et al.* (1994) via Hartree–Fock calculations with quasi-relativistic pseudopotentials. The relative MO energies of UO_2^{2+}, NUO^+, and CUO from recent scalar-relativistic DFT calculations (Bursten *et al.*, 2003) are presented in Fig. 17.25. The electronic structures of these U(VI) f^0 species are qualitatively similar inasmuch as the highest occupied MOs form the familiar $(\sigma)^2(\pi)^4(\pi)^4(\sigma)^2$ manifold that is derived from the formally filled 2p orbitals of the $(O\cdots O)^{4-}$, $(N\cdots O)^{5-}$, and $(C\cdots O)^{6-}$ ligand sets. Quantitatively, however, the relative positions of the MOs vary substantially across the series because of

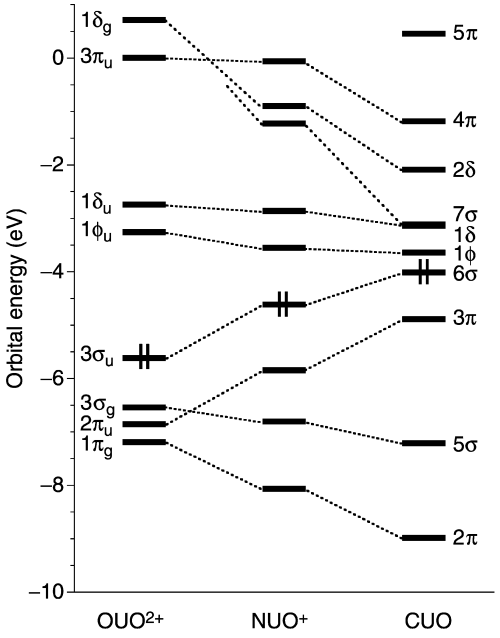

Fig. 17.25 *MO energies of the isoelectronic series* UO_2^{2+}, *NUO*$^+$, *and CUO from scalar-relativistic DFT calculations. The orbitals are labeled under* $D_{\infty h}$ *symmetry for* UO_2^{2+} *and* $C_{\infty v}$ *symmetry for NUO*$^+$ *and CUO* (*reproduced from Bursten* et al., 2003).

the changes in the relative energies of the 2p orbitals for O, N, and C atoms. In particular, the rise of the HOMO across the series places it closer to the LUMO, which is a U-localized 5fφ orbital in each case. We will find the energetic ordering of the MOs in this figure and the trends in orbital energies to be useful in this section.

17.6.1 Matrix-isolated actinide dioxides

The oxides occupy a central place in the natural, environmental, and technological aspects of actinide chemistry (Matthews, 1987). A variety of actinide oxides exist as solids or aqueous solutions in nature and in human-made reservoirs, such as nuclear fuel rods, nuclear waste repositories, and actinide storage tanks. We will focus our discussion here on the electronic structure of molecular actinide oxides, and particularly some of the actinide dioxides, that have been isolated in low-temperature matrices. As noted above, the largest body of research in this area has involved uranium chemistry. In addition to the ubiquitous chemistry of the uranyl ion, gas-phase reactions of uranium and other actinide atoms with atmospheric components are of great interest because

actinide metals experience oxidation when exposed to the atmosphere. Reactions of actinide atoms with oxygen, and the products thereof, thus represent one of the most important aspects of actinide chemistry.

Matrix-isolated uranium oxides were first explored in the early 1970s and the infrared (IR) spectra of UO, UO_2, and UO_3 were observed and assigned in several laboratories (Abramowitz *et al.*, 1971; Leary *et al.*, 1971; Abramowitz and Acquista, 1972; Carstens *et al.*, 1972). The IR spectra and assignments reported by Reedy and coworkers for UO, UO_2, and UO_3 (Gabelnick *et al.*, 1973a,b,c) and for ThO and ThO_2 (Green *et al.*, 1980) are generally accepted and has led to the interesting observation that UO_2 is linear (like UO_2^{2+}) whereas molecular ThO_2 has a bent structure (Pepper and Bursten, 1991). Green and Reedy (1978a) also reported the IR spectra of PuO and PuO_2 in Ar and Kr matrices. Because of the difficulty in handling the radioactive Pu systems, there are comparatively few experimental data available for them, although Green (1980) has also reported the gas-phase enthalpies of formation of PuO and PuO_2, and Capone *et al.* (1999) have reported an ionization energy for gaseous PuO_2.

In 1993, Andrews and coworkers generated UO_n species in an argon matrix via the reaction of laser-ablated U atoms with O_2 molecules in an argon carrier followed by condensation of a solid matrix at low temperature, and were able to obtain more accurate IR frequencies for UO, UO_2, and UO_3 (Hunt and Andrews, 1993). These species are also formed upon the reaction of laser-ablated U atoms with other substrates that can provide O atoms (e.g. NO, CO, CO_2) as will be discussed later. Interestingly, despite its stability and ubiquitous presence in solution and coordination chemistry, the UO_2^{2+} dication has not yet been observed in noble-gas matrices. The 'bare' UO_2^{2+} ion was first observed in the gas phase in 1996 (Cornehl *et al.*, 1996), although the vibrational properties of the bare ion are still unknown experimentally. Because the uranyl ion is highly charged, it is expected to have strong electrostatic or even covalent interactions with the matrix atoms or other residue counter-anions in the reactions. To date, the best known matrix-isolated species containing the UO_2^{2+} ion are those with various counter-ions, such as $UO_2^{2+}(NO^-)$, $UO_2^{2+}(NO_2^-)$, and $UO_2^{2+}(O_2^-)$ (Green *et al.*, 1976; Hunt and Andrews, 1993).

As shown in Section 17.3, there have been a great number of theoretical calculations on the free uranyl dication and other actinyl cations, and those results will not be repeated here. In order to relate the neutral uranium oxides detected via matrix isolation to the UO_2^{2+} ion, however, it is relevant to discuss briefly here the electronic structures of the UO_2^q $(q = +2,\ +1,\ 0,\ -1)$ series. With reference to Fig. 17.25, the UO_2^{2+} ion has a closed-shell $^1\Sigma_g^+$ ground state with a $(3\sigma_u)^2(f\phi_u)^0(f\delta_u)^0$ electron configuration, consistent with the notion that uranyl is a U(VI) complex with an f^0 configuration. The UO_2^+ cation, which has one more electron than UO_2^{2+}, has a $^2\Phi_u$ ground state corresponding to the $(3\sigma_u)^2(f\phi_u)^1(f\delta_u)^0$ configuration. Although the $^2\Delta_u$ state, from the $(3\sigma_u)^2(f\phi_u)^0(f\delta_u)^1$ configuration, is only slightly higher in energy, the first-order

spin–orbit splitting of $^2\Phi_u$ is much larger than that of $^2\Delta_u$, which renders the $^2\Phi_u$ as the ground state. Upon adding two electrons to UO_2^{2+} to form neutral UO_2, we see the effect that changing the oxidation state of U has upon the relevant atomic orbital energies and, hence, the ground state of the molecule. At first glance one might expect that UO_2 would have a ^3H_g state derived from the $(3\sigma_u)^2(f\phi_u)^1(f\delta_u)^1$ configuration, which is the case for the isoelectronic PuO_2^{2+} ion. However, because of the increase in the U–O bond lengths and the decrease in the formal oxidation state to U(IV), the U 7s orbital is energetically very close to the $(f\phi_u f\delta_u)$ manifold in UO_2. As we will discuss in detail below, the free UO_2 molecule has a 'nonintuitive' $^3\Phi_u$ state derived from the $(3\sigma_u)^2(f\phi_u)^1(f\delta_u)^0(7s)^1$ configuration. Similarly, the UO_2^- anion has a $^2\Phi_u$ ground state from the $(3\sigma_u)^2(f\phi_u)^1(f\delta_u)^0(7s)^2$ configuration.

The nonintuitive ground state of UO_2 is a problem of great current interest and serves as a paradigm of the challenges in determining the electronic structures of even small actinide molecules. Part of the current interest in the electronic structure of matrix-isolated UO_2 is due to some current experimental anomalies that, at the time of this writing, are not resolved. UO_2 has very different IR-active U–O stretching frequencies in solid argon than in solid neon. In 1993, Hunt and Andrews reported that UO_2 in solid argon has an antisymmetric stretching mode at 776.0 cm^{-1} (Hunt and Andrews, 1993), a value that is in close agreement with earlier Knudsen effusion studies (Gabelnick *et al.*, 1973a). In 2000, Zhou *et al.* reported that UO_2 in solid neon exhibits a stretch at 914.8 cm^{-1}, ca. 139 cm^{-1} higher than in solid argon (Zhou *et al.*, 2000). The large shift in frequency from an argon to a neon matrix is unlikely to be due to typical polarizability-based matrix effects, which tend to cause shifts on the order of 5–20 cm^{-1} in vibrational frequencies (Jacox, 1994). As will be discussed in detail below, similar large frequency shifts were seen for matrix-isolated CUO and were ultimately shown to be the result of a noble-gas induced change in the electronic state of that molecule due to direct U–Ng bonds.

Calculations on the isolated UO_2 molecule have been carried out at several different levels of theory over the past few years, starting with some early Hartree–Fock–Slater work by Baerends *et al.* (Allen *et al.*, 1988; van Wezenbeek *et al.*, 1991). Zhou *et al.* (2000) reported DFT calculations on UO, UO_2^q ($q = 1+, 0, 1-$), and UO_3, including the calculation of vibrational frequencies and were the first to propose that neutral UO_2 has a $^3\Phi_u$ ground state arising from a $5f^17s^1$ configuration for the U(IV) center. Their calculated antisymmetric stretching frequency for UO_2 was 931 cm^{-1}, which is in good agreement with the experimental value observed in solid neon. Gagliardi and Roos with coworkers carried out CASSCF/CASPT2 and CASPT2/SO calculations on the geometries, electronic states, and vibrational frequencies of UO_2^{2+}, UO_2^+, and UO_2 (Gagliardi and Roos, 2000; Gagliardi *et al.*, 2001b). They also concluded that UO_2 has a $^3\Phi_u$ ($\Omega = 2$) ground state and found that the lowest state

derived from the $5f^2$ configuration was the ^3H_g ($\Omega = 4$) state, which was 0.52 eV above the ground state. Chang and Pitzer performed SOCI calculations on neutral UO_2 (Chang, 2002). They also found a $^3\Phi_u$ ($\Omega = 2$) ground state, with the ^3H_g ($\Omega = 4$) state only 0.20 eV above the ground state. Majumdar *et al.* (2002) also calculated the geometries and frequencies of the UO_2^q ($q = 2+,\ 1+,\ 0,\ 1-$) series using CASSCF and MRCI methods. A summary of the calculated geometric parameters and vibrational frequencies of the various uranium oxide species is presented in Table 17.17.

The theoretical results on isolated UO_2 could not be used to reconcile the difference in the experimentally observed IR stretching frequencies of UO_2 in argon and neon. Li *et al.* (2004) have performed scalar-relativistic DFT and CCSD(T) calculations on a series of UO_2 and $UO_2(Ar)_n$ complexes to explore the possibility that the electronic state of UO_2 is different in Ar than in Ne. Their calculated geometries and vibrational frequencies for UO_2, $UO_2(Ar)$, and $UO_2(Ar)_5$ are listed in Table 17.18, and Fig. 17.26 shows their linear transit potential energy curves for the interaction between five Ar atoms and UO_2 in two different electronic states of the model complex $UO_2(Ar)_5$. On the basis of these calculations, Li *et al.* proposed that UO_2 forms direct U–Ar bonds in the argon matrix, and that these bonds lead to stabilization of the $5f^2$-derived ^3H_g state below the $5f^17s^1$-derived $^3\Phi_u$ state that is the apparent ground state for UO_2 in solid neon. The significantly lower U–O antisymmetric stretching frequency for the ^3H_g state of UO_2 relative to the $^3\Phi_u$ state was proposed to explain the different IR frequencies of UO_2 in argon and neon matrices.

Recent experiments by Heaven *et al.* suggest that UO_2 is in the same electronic state in the gas phase and in an argon matrix (Han *et al.*, 2003). By using resonance-enhanced multiphoton ionization (REMPI) spectroscopy, they obtained a new value of 6.13 eV for the first ionization energy of UO_2, which was in good agreement with the calculated values of Zhou *et al.* (2000) and Gagliardi *et al.* (2001b). Their results were consistent with a $^3\Phi_u$ ground state for UO_2. They have also obtained dispersed fluorescence spectra for molecular UO_2 in solid argon, which suggest that UO_2 has the same ground state in the matrix as in the gas phase (Lue *et al.*, 2004), although these results cannot reconcile the different stretching frequencies of UO_2 in solid neon relative to solid argon. There are clearly still some unanswered questions with regard to the electronic state of UO_2 in noble-gas matrices. The recent calculation of the electronic spectra of isolated UO_2 by Gagliardi *et al.* (2005) represents one of such efforts. Nevertheless, the mystery of the different results from the two experiments will likely persist until it is possible to perform accurate theoretical calculations on the electronic spectra of UO_2 with the Ar matrix environment included.

The proposal of direct U–Ar bonds when UO_2 is in an argon matrix followed shortly after the proposal of the first uranium-to-noble-gas bonds, which involved the CUO molecule that will be discussed in the next section. Other recent discoveries in the interactions of noble-gas atoms with metal

Table 17.17 *Selected calculated bond lengths, bond angles, and vibrational frequencies of UO,* UO_2^q ($q = +2,\ +1,\ 0,\ -1$), *and* UO_3.[a]

Species	*Method*	*State*	*U–O*	*∠O–U–O*	ν_b[b]	$\nu_s(U–O)$[b]	$\nu_{as}(U–O)$[b]	*References*
UO	B3LYP	$^5\Gamma$	1.850	–			846	[c]
UO_2^{2+}	B3LYP	$^1\Sigma_{g}^{+}$	1.705	180°	161×2	1041	1140	[c]
	CASPT2	$^1\Sigma_{g}^{+}$	1.705	180°	–	959	1066	[d]
	MP2	$^1\Sigma_{g}^{+}$	1.728	180°	126×2	923	1024	[e]
	CCD	$^1\Sigma_{g}^{+}$	1.678	180°	194×2	1100	1179	[e]
UO_2^{+}	B3LYP	$^2\Phi_u$	1.764	180°	148×2	936	1010	[c]
	CASPT2	$^2\Phi_u$	1.773	180°	–	858	942	[d]
	MP2	$^2\Phi_u$	1.780	180°	101×2	901	955	[e]
	CCD	$^2\Phi_u$	1.744	180°	146×2	971	1031	[e]
UO_2	B3LYP	$^3\Phi_u$	1.800	180°	138×2	874	931	[c]
	CASPT2	$^3\Phi_u$	1.806	180°	–	809	932	[f]
	CASPT2/SO	$^3\Phi_u(\Omega = 2)$	1.766	180°	–	948	923	[f]
	MP2	$^3\Phi_u$	1.795	180°	149×2	896	913	[e]
	CCD	$^3\Phi_u$	1.766	180°	168×2	927	958	[e]
UO_2^{-}	B3LYP	$^2\Phi_u$	1.828	180°	136×2	825	874	[c]
	MP2	$^2\Phi_u$	1.825	180°	150×2	869	856	[e]
	CCD	$^2\Phi_u$	1.797	180°	160×2	872	895	[e]
UO_3	B3LYP	$^1A_1$	1.810, 1.853	100.6°, 158.8°	887 (a_1)	885 (b_2)	782 (a_1)	[c]

[a] Bond lengths in Å, bond angles in degrees, and frequencies in cm^{-1}.
[b] ν_b, ν_s(U–O), and ν_{as}(U–O) are the bending, symmetric stretching, and antisymmetric stretching frequencies of the UO_2^q species. For UO and UO_3, these categories do not apply.
[c] Zhou *et al.* (2000).
[d] Gagliardi and Roos (2000).
[e] Majumdar *et al.* (2002).
[f] Gagliardi *et al.* (2001b).

Table 17.18 *Calculated DFT and CCSD(T)*[a] *bond lengths* (Å) *and U–O stretching frequencies* (cm^{-1}) *for the* $^3\Phi_u$- *and* ^3H_g-*derived states of* UO_2 ($D_{\infty h}$), $UO_2(Ar)$ (C_{2v}), *and* $UO_2(Ar)_5$ (D_{5h}) (*see Li* et al., 2004).

Molecule	*State*	*U–O*	*U–Ar*	$\nu_s(U–O)$	$\nu_{as}(U–O)$[b]
UO_2	$^3\Phi_u$	1.807 (1.835)	–	856	919
	^3H_g	1.851 (1.893)	–	779	824
$UO_2(Ar)$	"$^3\Phi_u$"	1.808 (1.834)	4.30 (4.006)	855	918
	"^3H_g"	1.851 (1.895)	3.28 (3.192)	765	806
$UO_2(Ar)_5$	"$^3\Phi_u$"	1.808 (1.833)	4.31 (4.097)	851	917
	"^3H_g"	1.856 (1.901)	3.37 (3.216)	755	805

[a] CCSD(T) values are listed in parenthesis when available.
[b] Only the antisymmetric stretches (ν_{as}) are infrared active.

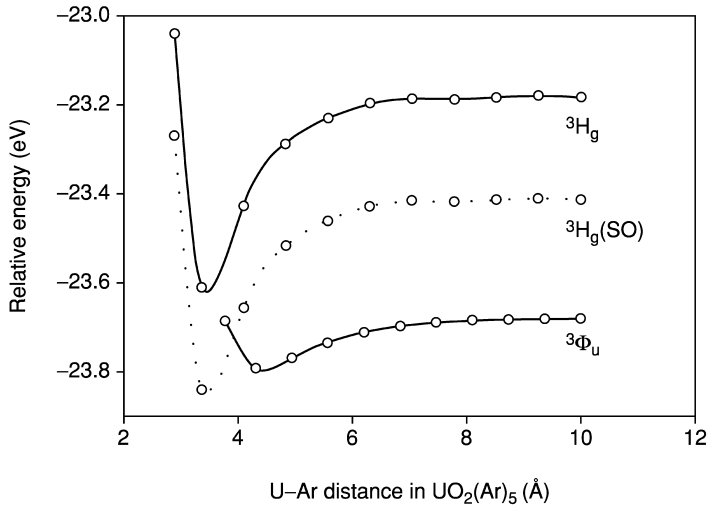

Fig. 17.26 *Calculated linear-transit potential energy curves for* D_{5h} $(UO_2)(Ar)_5$ *for the* $^3\Phi_u$ *and* ^3H_g *electronic states of* UO_2. *The dotted line represents a lowering of the curve for the* ^3H_g *state by* 0.23 eV, *the differential stabilization due to spin–orbit effects found by Gagliardi* et al. (2001*b*) (*reproduced from Li* et al., 2004).

centers, notably the remarkable stability of the $[AuXe_4]^{2+}$ complex (Seidel and Seppelt, 2000), suggest that the interaction of Ng atoms will be stronger with cationic centers because of electrostatic stabilization. Consistent with this notion, recent experimental and theoretical results suggest U–Ng interactions in a series of $UO_2^+(Ng)_n(Ng = Ne, Ar, Kr, Xe)$ complexes in low-temperature matrices that are stronger than those for neutral UO_2 (Wang *et al.*, 2004).

A recent combined experimental and computational study also provides evidence for the formation of Ar atom binding to the simplest neutral uranyl complex, i.e. $H_2UO_2(Ar)_n$ (Liang *et al.*, 2005).

There have been other neutral actinide oxide molecules that have been studied by matrix-isolation techniques. As noted earlier, the bent structure of ThO_2 was indicated by the IR spectra of the matrix-isolated molecule. The interesting observation that ThO_2 is bent whereas the isoelectronic UO_2^{2+} ion is linear has stimulated a number of theoretical investigations. Much of the early work in this area was covered in detail by Pepper and Bursten (1991). Since that review was written, there have been applications of higher-level methods by Dyall (1999) and by Straka *et al.* (2001). The bent structure of ThO_2 is attributed to the favorable mixing of the Th 5f and 6d orbitals that can occur upon bending. Liang and Andrews (2002) recently generated ThS and ThS_2 in an argon matrix and investigated these molecules using scalar-relativistic DFT calculations. The IR spectrum of matrix-isolated ThS_2 indicates that it is also a bent molecule, and the DFT calculations predict a S–Th–S bond angle of 112°.

As noted earlier, Green and Reedy (1978a) reported the matrix isolation of PuO_2 in 1978, formed from the sputtering of a plutonium cathode with Ar/O or Kr/O mixtures. Isotopic labeling of the O atoms allowed them to conclude that PuO_2 was a linear molecule. PuO_2 is formally a Pu(IV) complex with four metal-based electrons, and based on our discussion this far it is anticipated to have a complex electronic structure. To date, the only detailed electronic structure calculations on PuO_2 have been carried out by Archibong and Ray (2000), who used coupled-cluster and CAS calculations with RECPs. They found that the two lowest-energy states of PuO_2 are nearly degenerate, namely a $^5\Sigma_g^+$ state derived from the $(f\delta_u)^2(f\phi_u)^2$ electron configuration and a $^5\Phi_u$ state from the $(f\delta_u)^2(f\phi_u)^1(7s\sigma)^1$ configuration. Because these states are derived from different configurations (f^4 vs f^3s^1), they have significantly different calculated properties, as has been proposed for UO_2 and CUO. The calculated Pu–O bond lengths in the $^5\Sigma_g^+$ state range from 1.85 to 1.88 Å, depending on the method, and from 1.78 to 1.80 Å in the $^5\Phi_u$ state. The shorter An–O bonds in the states derived from the $f^{n-1}s^1$ configuration relative to those from the f^n configuration is consistent with what was observed for UO_2 (Table 17.18). Based on a comparison of the calculated antisymmetric stretching frequencies and $^{16}O/^{18}O$ isotopic ratios, Archibong and Ray propose that the $^5\Sigma_g^+$ state is the likely ground state of PuO_2.

17.6.2 Matrix-isolated actinide carbide oxides

One of the most interesting aspects of the chemistry of matrix-isolated actinide atoms has involved their reactions with CO and CO_2 as matrix substrates. The activation and sequestration of these two important molecules are and will continue to be fundamental areas of research. As we will see in this section,

actinide atoms, and particularly laser-ablated actinide atoms, have a remarkable ability to react with CO and CO_2. We will also see that some atypical species have been formed as well as some unusual types of bonds, providing many challenges to electronic structure calculations. To date, the experimental studies have been limited to reactions of Th and U with CO and CO_2, and we will limit our discussion here to some of the carbide–oxide products that form from these reactions. A discussion of some of the carbonyl species formed in these reactions will be presented later in this section.

The reaction of laser-ablated U atoms with CO produces a number of interesting products corresponding to the addition of one or more CO molecules to a U atom (Tague *et al.*, 1993; Zhou *et al.*, 1999a; Andrews *et al.*, 2000b). The 1:1 stoichiometry products are UCO and CUO, and the 2:1 products are $U(CO)_2$, OUCCO, and $(\eta^2\text{-}C_2)UO_2$. Evidence has also been found for the higher binary carbonyl complexes $U(CO)_n$ (n = 3–6). Table 17.19 presents the calculated scalar-relativistic DFT relative energies, geometric parameters, and some of the calculated vibrational frequencies of the 1:1 and 2:1 adducts of CO to U (Zhou *et al.*, 1999a). In both the isomers of UCO and $U(CO)_2$, the calculated lowest energy isomer is the one that involves the maximum number of U–O bonds, consistent with the high oxophilicity of uranium.

Table 17.19 *Relative energies, geometric parameters, and vibrational frequencies for the isomers of UCO and $U(CO)_2$ from scalar-relativistic DFT calculations, along with the experimental frequencies of the matrix-isolated species in solid neon* (*see Zhou* et al., 1999*a*).

Species	*Structure*	*Relative energy* (eV)	*Geometry*	*Frequencies* (cm^{-1}) *Calculated*	*Ne matrix*
UCO	linear, $C_{\infty v}$	+2.29	U–C = 2.236 Å C–O = 1.178 Å	1818	1918[a]
CUO ($^1\Sigma^+$)	linear, $C_{\infty v}$	0	U–C = 1.764 Å U–O = 1.808 Å	874 1049	872 1047
$U(CO)_2$	bent, C_{2v}	+4.44	U–C = 2.236 Å ∠U–C–O = 179.4° ∠C–U–C = 76.2°	1810 1861	1791 1840
OUCCO	linear, $C_{\infty v}$	+1.42	U–O = 1.795 Å U–C = 2.026 Å C–C = 1.298 Å C–O = 1.176 Å	897 1393 2125	841 1362 2052
$(\eta^2\text{-}C_2)UO_2$	C_2	0	U–C = 2.289 Å U–O = 1.796 Å C–C = 1.271 Å ∠O–U–O = 155.8° CUC/OUO dihedral = 55°	849 910	843 922

[a] This value is uncertain.

Of the species formed in these reactions, the CUO molecule is especially interesting from an electronic structural viewpoint for several reasons. CUO is isoelectronic with UO_2^{2+} and can be considered as an f^0 U(VI) complex like the uranyl ion. Fig. 17.27 shows a qualitative interaction diagram that compares the valence MOs of CUO to those of UO_2^{2+}. This diagram is constructed by allowing the MOs of the f^0 fragment UO^{4+} to interact with the AOs of either O^{2-} or C^{4-}. As expected for isoelectronic systems, there is a one-to-one correspondence of the filled MOs of UO_2^{2+} (labeled under $D_{\infty h}$ symmetry) and CUO ($C_{\infty v}$ symmetry). The energies of the MOs in CUO differ from those of UO_2^{2+} because of the higher energy of the C 2s and 2p orbitals relative to the O 2s and 2p orbitals. In particular, the C 2p-based 4σ HOMO of CUO is much closer in energy to the empty 5f-based MOs than is the corresponding $2\sigma_u$ HOMO of UO_2^{2+}. As shown, the CUO molecule has a closed-shell $^1\Sigma^+$ ground state analogous to the $^1\Sigma_g^+$ ground state of UO_2^{2+}.

The CUO molecule was first isolated in 1993 by Andrews and coworkers (Tague *et al.*, 1993) in solid argon, where it exhibits stretching modes at 804.4 and 852.6 cm^{-1}. Later studies of CUO in solid neon led to very different frequencies, 1047.3 and 872.2 cm^{-1}, which isotopic substitution showed predominantly U–C and U–O stretching modes, respectively (Zhou *et al.*, 1999a). These large frequency shifts upon changing the matrix are greater than would be expected for normal polarizability-based matrix effects. As shown in Fig. 17.27, CUO is expected to have a $^1\Sigma^+$ ground state with a $(4\sigma)^2(5f\phi)^0$ configuration. However, the U–C-based 4σ orbital is so close in energy to the U $5f\phi$ orbital that the open-shell $^3\Phi$ excited state corresponding to the $(4\sigma)^1(5f\phi)^1$ configuration is very close in energy to the $^1\Sigma^+$ ground state. Initial scalar-relativistic DFT calculations predicted that the $^3\Phi$ excited state is only about 1 kcal mol^{-1} higher in energy than the singlet 'ground state' of free CUO and that the two states would have very different vibrational frequencies because they arise from different electronic configurations. The experimentally observed large vibrational frequency shifts were thus preliminarily explained in terms of a matrix-induced ground state reversal (Andrews *et al.*, 2000a).

To understand the ground-state reversal of CUO in the Ne and Ar matrices, further detailed theoretical calculations were performed to model the interaction between CUO and the noble-gas matrix. It was discovered that the CUO molecule tends to form direct albeit weak bonds to the Ar atoms in the matrix, leading to the proposal of a $CUO(Ar)_n$ complex that has a U–Ar bond (Li *et al.*, 2002). The formation of the U–Ar bond stabilizes the $^3\Phi$ ($^3A''$ under C_s symmetry) state of the molecule to such an extent that it drops below the $^1\Sigma^+$ ($^1A'$ under C_s) ground state of the isolated CUO molecule, as shown by the DFT energy curves shown in Fig. 17.28. This proposal of the first U–Ar bonding was affirmed by matrix experiments that showed that the U–Ar interactions occur even in a matrix of 1% Ar in neon (Fig. 17.29). The discovery of direct actinide-to-noble-gas bonding adds to the recent renaissance in noble-gas chemistry (Pyykkö, 2000a; Christe, 2001).

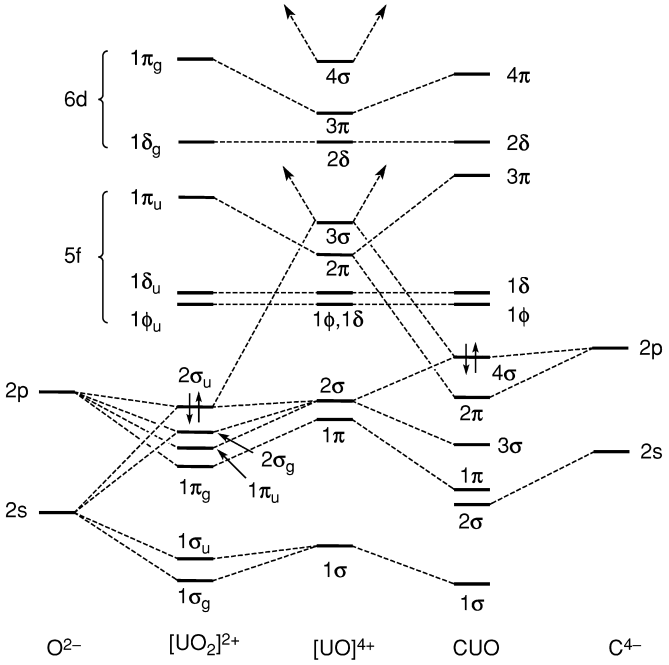

Fig. 17.27 *Qualitative interaction diagram showing the formation of the molecular orbitals of* UO_2^{2+} *and CUO by the interaction of* O^{2-} *and* C^{4-} *with* UO^{4+}. *Only the 5f and 6d orbitals of U are shown, although the U 7s and 7p AOs contribute non-negligibly to the bonding* (*reproduced from Zhou* et al., 1999*a*).

As noted above, the very small energetic separation (1 kcal mol^{-1}) between the $^1\Sigma^+$ ground state and the $^3\Phi$ excited state of CUO was first found using scalar-relativistic DFT calculations. The validity of this small gap was questioned because of concerns about the ability of DFT to calculate excited-state energies reliably and the lack of inclusion of spin–orbit effects, which are expected to affect the two states to a different extent. Recent CCSD(T) calculations with geometry optimizations on CUO and CUO(Ng) (Ng = Ne, Ar, Kr, Xe) confirm that the previous DFT triplet–singlet energy difference is underestimated and that the coordination of one (or more) heavier Ng atom indeed stabilizes the $^3\Phi$ excited state more than the $^1\Sigma^+$ ground state of CUO (Bursten *et al.*, 2003). This energy difference is found to be around 16 kcal mol^{-1} from CCSD(T) calculations without including spin–orbit effects. Roos *et al.* (2003) performed CASPT2/SO calculations with spin–orbit effects included and found that the $^3\Phi$ state is stabilized by spin–orbit coupling by about 8–10 kcal mol^{-1} relative to the $^1\Sigma^+$ state. The additional differential stabilization of the $^3\Phi$ state upon multiple coordination of heavier Ng atoms would therefore seem to make the proposed ground-state reversal of CUO quite feasible. A recent study by

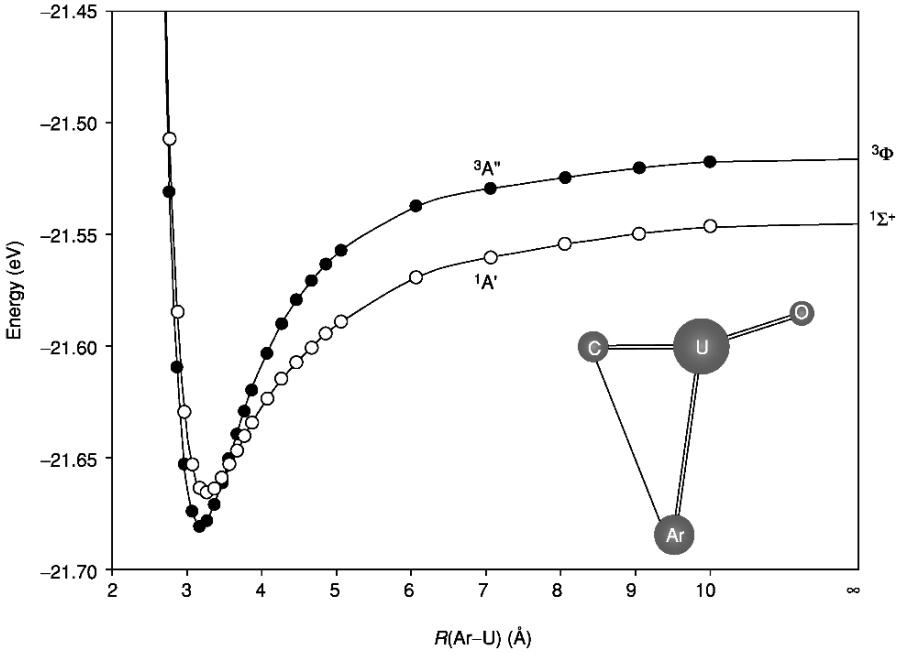

Fig. 17.28 *Potential energy curves for the* $^1A'$ *and* $^3A''$ *states of CUO(Ar) as a function of the U–Ar distance. The U–Ar bond length in this complex is* 3.16 Å (*reproduced from Li* et al., 2002).

Infante and Visscher (2004b) at the fully relativistic CCSD(T) level has confirmed that with inclusion of the high-level electron correlation and spin–orbit effects the $^3\Phi$ triplet state lies ~14 kcal mol^{-1} above the $^1\Sigma^+$ ground state for isolated CUO. They concluded that "our result gives further justification to the interpretation of the measured frequency shifts of this species (CUO) in various noble gas matrices as being caused by significant interaction between the uranium and the heavier noble gas atoms."

Binding energy calculations on $CUO(Ng)_n$ (Ng = Ar, Kr, Xe; n = 1–6) predicted that CUO prefers five-coordination for Ar and Kr, and four-coordination for Xe. Experimental efforts indeed uncovered the coordination of CUO by multiple noble-gas atoms (Liang *et al.*, 2002; Andrews *et al.*, 2003). Recent experiments further confirm that the multiple coordination of CUO is necessary for the ground state reversal, with the experimentally determined singlet-to-triplet crossover points as $CUO(Ar)_3$, $CUO(Kr)_3$, and $CUO(Xe)_4$ (Liang *et al.*, 2003, 2004; Andrews *et al.*, 2004).

The only other CAnO species that has been detected thus far experimentally is the CThO molecule, which is formed upon the reaction of laser-ablated Th atoms with CO in excess neon (Zhou *et al.*, 1999b; Li *et al.*, 2001). The properties of the CThO molecule differ markedly from those of CUO because of the

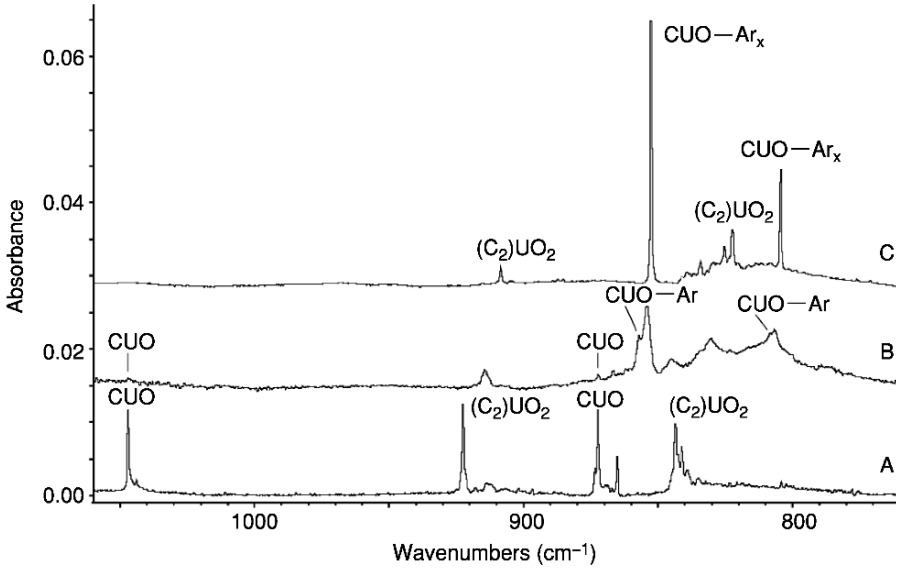

Fig. 17.29 *Infrared spectra in the* 1060–760 cm^{-1} *region for laser-ablated U atoms co-deposited with CO in excess noble gas.* (*A*) *Spectrum obtained when U atoms and* 0.1% *CO in Ne are deposited for* 30 min, *followed by full-arc photolysis and annealing at* 10 K. (*B*) *Spectrum obtained when U atoms*, 0.1% *CO*, *and* 1% *Ar in Ne are deposited for* 30 min, *followed by full-arc photolysis and annealing at* 10 K. (*C*) *Spectrum obtained when U atoms and* 0.3% *CO in Ar are deposited for* 15 min, *followed by full-arc photolysis and annealing at* 35 K (*reproduced from Li* et al., 2002).

difference in the number of valence electrons for Th and U. As discussed earlier, the $^1\Sigma^+$ state of CUO is isoelectronic with UO_2^{2+} and is best considered as a U(VI) complex. Because Th has only four valence electrons, the maximum oxidation state of Th is +4. The most obvious Lewis structure of CThO is the carbene :C=Th=Ö:, which is the actinide analog of the organic carbene ketenylidene, (:C=C=Ö:). Ketenylidene, which has been detected in interstellar space (Ohishi *et al.*, 1991), is a linear radical with a triplet ground state (Devillers and Ramsay, 1971). It was not apparent *a priori* whether CThO is linear or bent, and whether its ground state is a singlet or a triplet. Fig. 17.30 shows linear-transit potential energy curves from scalar-relativistic DFT calculations for the lowest singlet and triplet states of CThO (Li *et al.*, 2001). These studies predict that CThO prefers a highly bent structure ($\angle$CThO = 108.9°) with a triplet ground state. The bending of CThO is caused by factors similar to those used to explain the bent structure of ThO_2. From the CUO energy level in Fig. 17.25, linear CThO is expected to be a closed-shell molecule with a $(3\pi)^4(6\sigma)^0$ configuration. Because the 6dσ orbital participates strongly in the 6σ orbital, the unoccupied 6σ and occupied 3π MOs are very close in energy in linear structure; thus, a bending distortion via a second-order Jahn–Teller

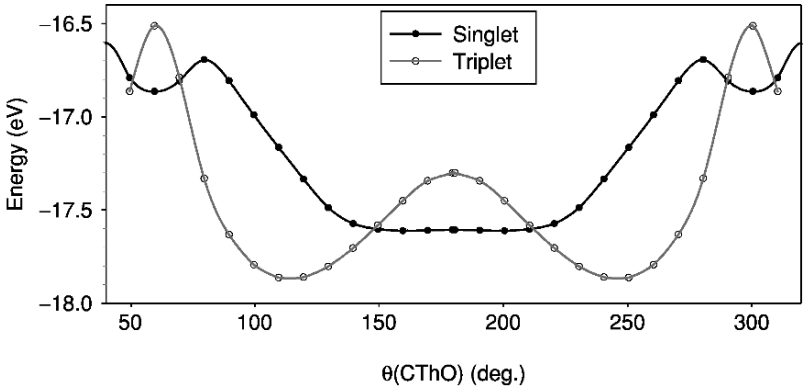

Fig. 17.30 *Linear-transit energy curves for the lowest singlet and triplet states of CThO* (*reproduced from Li* et al., 2001).

interaction is energetically favorable. The degenerate 3π orbital splits into $a' + a''$ upon bending, and the ground state of bent CThO corresponds to an $(a'')^2(a')^1(a')^1$ configuration that correlates with the $(3\pi)^3(6\sigma)^1$ configuration of the linear molecule.

The difference in the valence electronic structures of CUO and CThO has a remarkable effect on the observed stretching frequencies of the molecules. CThO in solid neon exhibits stretches at 617.7 and 812.2 cm^{-1}, and isotopic substitution demonstrates that these are predominantly Th–C and Th–O modes, respectively. The scalar-relativistic DFT calculations on isolated CThO model these vibrations extremely well, with calculated frequencies of 621 and 811 cm^{-1} and excellent calculated values for the isotopic ratios. Some of the properties of $^1\Sigma^+$ CUO and $^3A'$ CThO are compared in Table 17.20. Particularly notable are the changes in the calculated An–C bond lengths and the calculated and experimental An–C stretching frequencies. The Th–C bond length in CThO is more than 0.35 Å longer than the U–C bond length in CUO, and the predominantly Th–C stretching frequency is more than 400 cm^{-1} lower than the predominantly U–C stretching frequency. Both of these changes are consistent with a significantly lower bond order for the Th–C bond in CThO relative to the U–C bond in CUO, which is consistent with the simple Lewis structures of the molecules. The Th–O bond in CThO is slightly longer and weaker than the U–O bond in CUO, although the difference of the An–O bonding is not nearly as great as for the An–C bonds.

We will briefly discuss here the electronic structural aspects of some of the other products of the reactions of laser-ablated U and Th atoms with CO (Zhou *et al.*, 1999a; Li *et al.*, 2001). The most stable product from the addition of two CO molecules to a U atom is the unusual molecule $(\eta^2\text{-}C_2)UO_2$. This molecule results from the insertion of a U atom into two CO molecules, and its stability

Table 17.20 *Comparison of the properties of* $^1\Sigma^+$ *CUO and* $^3A'$ *CThO calculated from scalar-relativistic DFT calculations, along with the experimental frequencies of the matrix-isolated species in solid neon* (*see Zhou* et al., 1999*a*; *Li* et al., 2001).

	CUO	*CThO*
ground state	$^1\Sigma^+$	$^3A'$
An–C (Å)	1.764	2.124
An–O (Å)	1.808	1.889
∠C–An–O (°)	180	108.9
ν(An–C)[a] (cm^{-1}), calc	1049	621
ν(An–C) (cm^{-1}), expt	1047.3	617.7
ν(An–O) (cm^{-1}), calc	874	811
ν(An–O) (cm^{-1}), expt	872.2	812.2

[a] The vibrations are labeled 'An–C' and 'An–O' based on the predominant component of the normal mode.

relative to the other isomers [$U(CO)_2$ and OUCCO] is a consequence of the high oxophilicity of uranium and its preference for the +6 oxidation state. (η^2-C_2)UO_2 can be viewed as a closed-shell organometallic complex of the uranyl ion with a C_2^{2-} ligand that is obtained by deprotonating acetylene. Experimentally, (η^2-C_2)UO_2 shows two vibrational frequencies in the U–O stretching region at 843.2 and 922.1 cm^{-1}. Scalar-relativistic DFT calculations found a minimum structure with calculated symmetric and antisymmetric U–O stretching frequencies at 849 and 910 cm^{-1}, respectively, in good agreement with the experimental values. The calculated structure of (η^2-C_2)UO_2 is unusual in two respects. First, the UO_2 moiety is bent (∠O–U–O = 155.8°), which is highly unusual for uranyl complexes. Second, the dihedral angle between the C–U–C and O–U–O planes is 55°, nearly halfway between a pseudotetrahedral (C_{2v}) structure with a dihedral angle of 90° and a completely planar structure. It is proposed that the 'twisted' C_2 structure allows for the maximum donation from the filled π orbitals of the C_2^{2-} ligand to the f^0d^0 UO_2^{2+} fragment (Zhou *et al.*, 1999a). There is no experimental evidence for the formation of the analogous (η^2-C_2)ThO_2 molecule. Because Th cannot achieve a +6 oxidation state, this isomer is calculated to be considerably higher in energy than OTh(η^3-CCO), which is a lower oxidation state complex of Th (Li *et al.*, 2001). The OUCCO and OTh (η^3-CCO) molecules are highly unusual inasmuch as they are the first examples of mononuclear ketenylidene complexes (Geoffrey and Bassner, 1988).

The major products of the reaction of laser-ablated Th or U atoms with CO_2 are the OThCO and OUCO molecules (Tague *et al.*, 1993; Andrews *et al.*, 2000b). These oxocarbonyl complexes were the first reported complexes of Th(II) and U(II). They provide an interesting contrast in structure and bonding because of the presence of a π-basic oxo ligand, which typically favors high oxidation states, and a π-acidic CO ligand, which generally favors lower oxidation states. Scalar-relativistic DFT calculations on these products lead to the prediction that they are high-spin complexes with linear CO ligands and

severely bent O–U–C linkages. The calculated electronic states, geometries, and vibrational frequencies, along with the experimental frequencies in solid neon, are presented in Table 17.21.

The OUCO molecule is predicted to be a planar, bent molecule with four unpaired electrons that correspond to a $(7s)^1(5f)^3$ configuration at the U(II) center. The bending of the molecule is a consequence of a Renner–Teller distortion that splits the 5fϕ orbitals, which are degenerate in the linear geometry. The bent geometry allows the U atom to serve as an efficient conduit of electron density from the strongly donating oxo ligand to the CO ligand, thus helping to explain the ca. 300 cm^{-1} reduction of the C–O stretching frequency in OUCO relative to free CO.

The bonding in OThCO differs substantially from that in OUCO because Th(II) has only two metal-localized valence electrons. Further, because the 6d orbitals of Th are lower in energy than the 5f orbitals, the two metal-based electrons are predicted to adopt a $(7s)^1(6d)^1$ electron configuration. Linear OThCO is predicted to have a Renner–Teller-active $^3\Pi$ state. Distortion causes OThCO to bend even more severely than OUCO, and it has a quite remarkable 90° O–Th–C angle. The greater radial extension of the 6d orbitals relative to the 5f orbitals allows the former to interact more strongly with the 2π orbitals of the CO ligand. As a result, the calculated and observed C–O stretching frequencies in OThCO are lower than those for OUCO even though the Th–C bond is predicted to be longer than the U–C bond.

17.6.3 Matrix-isolated actinide binary carbonyls

Binary zero-valent carbonyl complexes of the actinides have been a long-sought goal of actinide chemists because of their potential attractiveness in isotope-separation processes. In 1971, Slater *et al.* reported the isolation of

Table 17.21 *Predicted properties of OThCO and OUCO from scalar-relativistic DFT calculations, along with the experimental frequencies of the matrix-isolated species in solid neon* (*see Andrews* et al., 2000*b*).

	OThCO	*OUCO*
ground state	$^3A''$	$^5A''$
An–O (Å)	1.871	1.828
An–C (Å)	2.488	2.259
C–O (Å)	1.161	1.174
∠O–An–C (°)	90.8	113.8
∠An–C–O (°)	176.8	179.1
ν (C–O) (cm^{-1}), calc.	1789	1842
ν (C–O) (cm^{-1}), expt.	1778.4	1806.9
ν (An–O) (cm^{-1}), calc.	850	859
ν (An–O) (cm^{-1}), expt.	[a]	823.2

[a] Not observed.

$U(CO)_n$ ($n = 1$–6) in solid argon (Slater *et al.*, 1971). Since then there have been some reports of isolable carbonyl complexes of uranium, most notably the U(III) cyclopentadienyl carbonyl complexes discussed in Section 17.5.2. To date, however, the only reports of binary actinide carbonyls have involved matrix-isolated species. In this section, we will discuss the electronic structures of some actinide mono- and dicarbonyls. The higher carbonyls tend to be harder to characterize experimentally and there has been only one theoretical study of one of these species (Nash and Bursten, 1995).

The binary uranium carbonyls $U(CO)_n$ ($n = 1$–6) were reinvestigated by Zhou *et al.* (1999a) in a neon matrix. The monocarbonyl UCO was difficult to identify experimentally and a vibrational band at 1917.8 cm^{-1} was tentatively assigned to this species. The dicarbonyl $U(CO)_2$ exhibited absorptions at 1840.2 and 1790.8 cm^{-1}, which were assigned to the symmetric and antisymmetric C–O stretching modes, respectively, of a bent (C_{2v}) molecule. It is to be noted that the stretches assigned to $U(CO)_2$ are both at significantly lower frequencies than that for UCO, which is counter-intuitive. ThCO and $Th(CO)_2$ have both been identified in a neon matrix, along with the first report of the higher binary carbonyls of Th (Li *et al.*, 2001). The C–O stretch for ThCO is observed at 1817.5 cm^{-1} and the symmetric and antisymmetric stretches of $Th(CO)_2$ are assigned at 1827.7 and 1775.6 cm^{-1}, respectively. The reduction of the C–O stretching frequencies in these complexes by more than 300 cm^{-1} below that of free CO is quite striking given that Th is considered an early metal with only four electrons for potential backbonding.

Theoretical studies of even these simple mono- and dicarbonyl complexes are extremely challenging because of the presence of four (Th) or six (U) metal-based valence electrons at the An(0) center. The coordinative unsaturation of these complexes combined with the energetic closeness of the An 7s, 5f, and 6d orbitals leads to a large number of low-lying states that will almost certainly demand multiconfigurational approaches to discern. To date, the only computational studies of these molecules have used scalar-relativistic DFT, which is intrinsically a single-configuration approach. Nevertheless, the results reported do provide useful information about the bonding in these complexes and we will discuss them briefly here. We will focus on ThCO and $Th(CO)_2$, which are somewhat cleaner systems than the uranium complexes because of the smaller number of metal-based electrons.

Scalar-relativistic DFT calculations on ThCO predict that it is a linear molecule with Th–C = 2.261 Å and C–O = 1.181 Å, and a $^3\Sigma^-$ ground state that corresponds to a $(7s)^2(6d\pi)^2$ electron configuration at Th. Two other states, namely a $^5\Delta$ $[(7s)^1(6d\pi)^2(5f\delta)^1]$ and a $^3\Pi$ $[(7s)^1(6d\pi)^3]$ are found at 3.2 and 11.1 kcal mol^{-1} above the ground state, respectively. The calculated C–O stretching frequency of ThCO is 1790 cm^{-1}, in good agreement with the experimental neon-matrix value, and the calculated $^{12}C/^{13}C$ and $^{16}O/^{18}O$ isotopic vibrational ratios are also in excellent agreement with the experimental values.

An energy level diagram for ThCO is presented in Fig. 17.31 (Li *et al*., 2001). This diagram illustrates some of the important features of the bonding within actinide carbonyl complexes. The relativistic destabilization of the Th 5f orbitals and stabilization of the Th 7s orbital are shown in the first two columns, which compare atomic results on Th at the nonrelativistic and scalar-relativistic levels. The dominant interactions involve the Th 6d orbitals. The Th 6dσ orbital is strongly destabilized by interaction with the filled 5σ orbital of CO whereas the 6dπ orbitals are stabilized by a backbonding interaction with the CO 2π orbitals. In contrast, the Th 7s and 5f orbitals are minimally affected by the CO ligand. The $^3\Sigma^-$ ground state of ThCO corresponds to the $(3\pi)^2(6\sigma)^2$ MO configuration in which only two of the four Th-based electrons are involved in Th-to-CO π-backbonding. The large reduction in the C–O stretching frequency with only two π-electrons involved is attributed to the highly electropositive nature of Th, which leads to very effective charge transfer from Th to CO. The authors also reported a calculation on the hypothetical $^1\Sigma^+$ excited state that arises from the $(3\pi)^4(6\sigma)^0$ configuration in which all four of the Th-based electrons are involved in π-backbonding. This excited state is found ca. 36 kcal mol^{-1} above the $^3\Sigma^-$ ground state, and leads to a predicted C–O stretching frequency of 1630 cm^{-1}, a value considerably lower than the lowest known CO-stretching frequency of any terminal metal carbonyl.

Scalar-relativistic DFT calculations on $Th(CO)_2$ also led to some interesting and unusual results. Three relatively low-lying states were found, each with different spin multiplicities. The ground state is predicted to be a closed-shell $^1A_1$ state in which two MOs that each involve strong Th 6d → CO 2π-backbonding are doubly occupied. The two occupied MOs are sketched in Fig. 17.32. By doubly occupying these MOs, all four of the metal-based electrons are involved in metal-to-ligand backbonding. The calculated geometry of ground state $Th(CO)_2$ is highly unusual inasmuch as it has two terminal CO ligands with ∠C–Th–C = 49.6°. This very acute angle is a consequence of the strong desire of electropositive Th to transfer its electrons to the ligands. At this small angle, the CO ligands are brought into close enough proximity (1.89 Å) to produce a significant C–C bonding interaction, which lowers the energies of the 2π orbitals and facilitates even better Th-to-CO donation. In essence, the strong Th 6d → CO 2π-backbonding has led to partial reductive coupling of the two carbon atoms. The low-lying triplet and quintet excited states depopulate the MOs in Fig. 17.32, leading to longer C–C interactions and correspondingly larger C–Th–C angles.

The calculated symmetric and antisymmetric C–O stretching frequencies for $^1A_1$ $Th(CO)_2$ are 1766 and 1734 cm^{-1}, respectively, which are slightly lower than the neon-matrix experimental values. Both the experimental and calculated mean C–O stretching frequencies of $Th(CO)_2$ are lower than the corresponding values for ThCO, which seems consistent with (i) the fact that two electrons are involved in backbonding in ThCO whereas four electrons are involved in $Th(CO)_2$ and (ii) the acute C–Th–C angle in $Th(CO)_2$ allows for

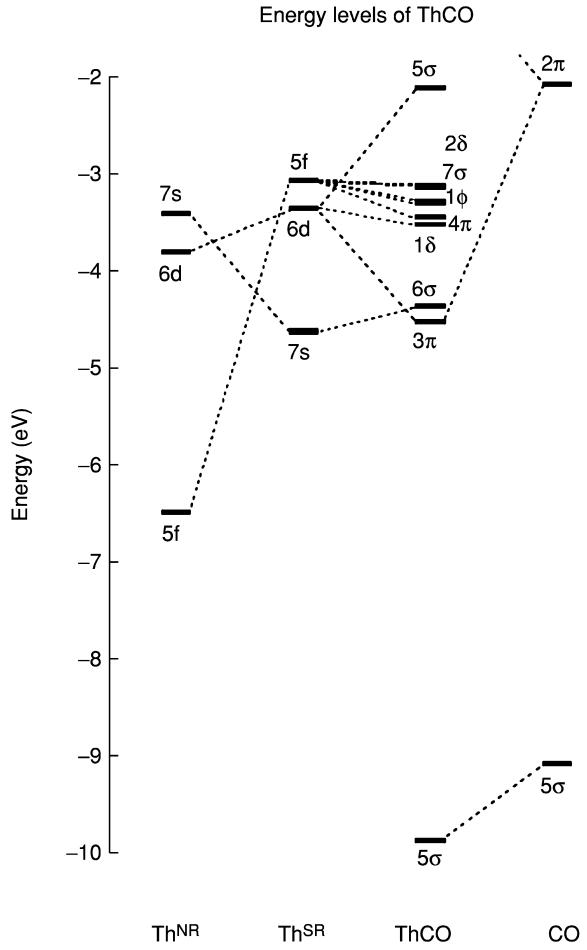

Fig. 17.31 *Energy-level diagram showing the interaction of a CO ligand with a Th atom to form ThCO. The atomic energy levels of Th^{NR} and Th^{SR} are for nonrelativistic and scalar-relativistic calculations on Th, respectively* (*reproduced from Li* et al., 2001).

better backbonding than can occur for a single CO ligand. The extreme ability of Th(0) to transfer electron density to CO is remarkable and is unprecedented among the transition metals.

17.6.4 Matrix-isolated actinide nitrides

The dinitrogen molecule is one of the most stable molecules with the N≡N bond energy of 225 kcal mol^{-1} (9.76 eV) (Gingerich, 1967). As a result, significant activation energy is needed to activate the N_2 molecule, as is the case for

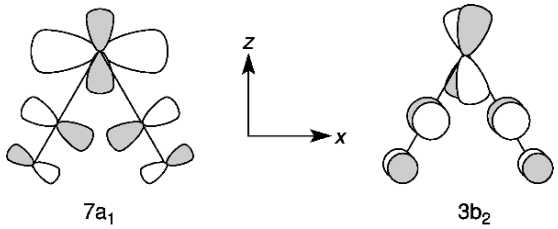

Fig. 17.32 *Sketches of the two highest occupied MOs of the calculated ground state of* $Th(CO)_2$. *Both MOs are doubly occupied in the ground state* (*reproduced from Li* et al., 2001).

activating the CO molecule. In the preceding sections we have seen that laser-ablated actinide atoms have sufficient activity to insert into the CO molecule, and the dinitrogen molecule can analogously be activated by energetic actinide atoms. Green and Reedy first generated the mono- and dinitrides of Th, U, and Pu via reactions of cathode-sputtered actinides with N_2 in a solid argon matrix (Green and Reedy, 1976, 1978b, 1979). By reacting laser-ablated Th and U atoms with N_2, N_2/O_2 mixtures, NO, NO_2, and N_2O, the Andrews group isolated the actinide mononitrides (AnN), dinitrides (NAnN), and some dinuclear actinide species in noble-gas matrices (Hunt *et al.*, 1993; Kushto *et al.*, 1997, 1998). Sankaran *et al.* (2001) also reported the matrix IR spectra of the UN and NUN molecules.

DFT calculations have been carried out on the matrix-isolated AnN and NAnN molecules using the ADF program with the PW91 and BP86 functional (Kushto *et al.*, 1997, 1998). It is predicted that without spin–orbit coupling the ThN, UN, and PuN are in $^2\Sigma$, $^4\Sigma$, and $^6\Pi$ electronic states, respectively, and the optimized bond lengths are consistent with triple bonds for these diatomic actinide molecules. All the NAnN (An = Th, U, Pu) molecules are predicted to be linear, consistent with the experimental IR spectra. Because the NUN molecule is isoelectronic to the uranyl ion, the electronic structures of these NAnN molecules can be qualitatively deduced from Fig. 17.27. Specifically, NUN is expected to have a $^1\Sigma_g^+$ ground state corresponding to the $(3\sigma_u)^2(f\phi_u)^0(f\delta_u)^0$ configuration, and NThN and NPuN should have the $(3\sigma_u)^0(f\phi_u)^0(f\delta_u)^0$ and $(3\sigma_u)^2(f\phi_u)^1(f\delta_u)^1$ configuration, respectively. The DFT calculations on the Th, U, and Pu dinitrides confirm these expectations: the Th and U dinitrides are found to have singlet states, while the NPuN molecule is in triplet state. Note instead of the $^3\Pi_g$ state assigned originally, the ground state of NPuN should be a ^3H_g state with a $(5f\phi)^1(5f\delta)^1$ configuration, as is confirmed in later calculations (Clavaguéra-Sarrio *et al.*, 2004).

The DFT-optimized An–N bond lengths and calculated vibrational frequencies of AnN and NAnN complexes are listed in Table 17.22, together with the experimentally measured data in Ar and N_2 matrixes. In agreement with the predicted linear structure of the NAnN molecules, only one IR absorption,

Table 17.22 *Predicted bond lengths* (Å) *and vibrational frequencies* (cm^{-1}) *of the AnN and NAnN molecules from scalar-relativistic DFT calculations, along with the experimental frequencies of the matrix-isolated species in solid argon and dinitrogen matrices* (*see Kushto* et al., 1997, 1998).

			ν_{sym} (*An–N*)	$\nu_{antisym}$(*An–N*)	
	An–N	ν_{bend}	*Calculated*	*Calculated*	*Experimental*
ThN	1.795			999	934.3 (Ar), 835.6 (N_2)
UN	1.746			1045	1000.9 (Ar), 890.5 (N_2)
PuN	1.756			863	855.73 (Ar)
NThN	1.864	64 × 2	828	830	756.6 (Ar), 716.4 (N_2)
NUN	1.717	53 × 2	1087	1123	1050.8 (Ar), 1010.3 (N_2)
NpuN	1.703	143 × 2	1012	1091	1029.74 (Ar)

corresponding to the antisymmetric stretching mode, was observed for each NAnN species in the matrices. By using the Ar matrix frequencies for different isotopomers, the NUN symmetric stretching frequency is estimated to be 1008.3 cm^{-1} via an F–G matrix approach (Hunt *et al.*, 1993). The large differences of the calculated 'gas-phase' antisymmetric frequencies and those measured in the Ar and N_2 matrices imply that, like the CUO and UO_2 molecules, these highly unsaturated species have significant chemical and physical interactions with the micro-solvating atoms in the Ar matrix, and even stronger interactions with those in the N_2 matrix. A recent CCSD(T) calculation on the $(f\phi_u)^1(f\delta_u)^1$ electron configuration of NPuN by Archibong and Ray (2000) leads to an optimized Pu–N bond length of 1.719 Å and the antisymmetric stretching frequency at 1117 cm^{-1}, in good agreement with the predictions from the DFT calculations. Gagliardi *et al.* (2003) also performed a CASPT2/SO calculation to explore the reaction energetics of U inserting to N_2 molecule.

The NThN molecule offers some interesting questions with respect to bonding. Terminal nitride ligands are generally formulated as N^{3-} and thus NUN and NPuN are considered complexes of U(VI) and Pu(VI) that have An≡N triple bonds. Because the maximum oxidation state of Th is +4, the bonds in NThN must be considered double bonds and the nitride ligands in this complex are formally N^{2-}. The calculated bond length for NThN is considerably longer than that in NUN and NPuN, consistent with these expected differences in the bonding.

17.6.5 Matrix-isolated actinide nitride–oxides

The NO^+ ion is another member of the isoelectronic series that includes N_2 and CO. Andrews and coworkers have examined the reactions of laser-ablated U and Th atoms with N_2/O_2 mixtures or NO. They have determined the

vibrational spectra and molecular structures of a series of actinide molecules of formula NAnO and $NAnO^+$ (An = Th, U) and have also performed DFT calculations on some of these species (Kushto *et al*., 1997; Kushto and Andrews, 1999; Zhou and Andrews, 1999). The NUO^+ ion was also observed by Heinemann and Schwarz (1995) in gas-phase ion–molecule reactions. Inasmuch as the NUO^+ molecule is isoelectronic with UO_2^{2+} and CUO, and the NUO molecule is isoelectronic with the UO_2^+ ion, it is not unexpected that both NUO and NUO^+ are predicted to be linear. In contrast, the NThO molecule is bent, with an optimized N–Th–O angle of 127.5°, similar to the OThO and CThO molecules. From Fig. 17.27, the NUO^+ ion is expected to have an electron configuration of $(6\sigma)^2(f\phi)^0(f\delta)^0$. However, because the N 2p orbitals are lower in energy than the C 2p orbitals, the HOMO–LUMO gap of NUO^+ is larger than that of CUO. As a result, a ground-state reversal such as that observed for CUO is unlikely to occur. The NUO molecule has a $^2\Phi$ ground state with the $(6\sigma)^2(f\phi)^1(f\delta)^0$ configuration. The geometric parameters and vibrational frequencies of the actinide nitride–oxides from the DFT calculations reported by Zhou and Andrews (1999) are summarized in Table 17.23. Gagliardi and Roos (2000) also have reported CASPT2 calculations on the geometric structures and vibrational frequencies of NUO and the NUO^+ ion.

In this section, we have summarized the geometric structures, electronic structures, and vibrational frequencies of some of the small molecules and ions that have been detected experimentally via matrix isolation. The combined efforts of low-temperature matrix-isolation experiments with state-of-the-art computational chemistry methods have greatly helped to rationalize and understand the chemistry of these unique actinide species. Further experimental and theoretical studies on these and other actinide species will greatly advance our

Table 17.23 *Predicted bond lengths* (Å) *and vibrational frequencies* (cm^{-1}) *of NUO, NUO^+, and NThO from B3LYP DFT calculations, along with the experimental frequencies of the matrix-isolated species in solid neon and argon matrices* (*see Zhou and Andrews*, 1999).

		N–An	*An–O*	*∠NAnO*	ν_{bend}	ν(*An–O*)	ν(*N–An*)
NUO	calc.	1.735	1.811	180°	125, 139	856	1063
	expt. (Ne)					833.5	1004.9
	expt. (Ar)					818.9	983.6
NUO^+	calc.	1.685	1.746	180°	129 × 2	1005	1191
	expt. (Ne)					969.8	1118.6
	expt. (Ar)					(882.5)	(1035.8)
NThO	calc.	1.957	1.901	127.5°	117 × 2	785	708
	expt. (Ne)					784.2	709.8
	expt. (Ar)					760.3	697.3

understanding of the structure and bonding of actinide complexes. In particular, the presumably innocent noble-gas matrices have been shown to play sometimes significant roles in the geometries, electronic structures, and spectroscopy of actinide compounds. The existence of the noble-gas actinide bonding indicates that the long overlooked role of noble gas atoms will have to be considered in future matrix-isolation experiments and in reinterpreting previous experimental results.

17.7 SPECIATED ACTINIDE IONS

In contrast to the high-valent actinyl series, An(III) and An(IV) ions exist in solution as bare ions (surrounded, of course, with solvent molecules and counter-ions). As with the actinyl ions, the characterization of their behavior in aqueous solution, i.e. their speciation, is of great interest in order to obtain a better understanding of their structures, stabilities, reactivities, and solution chemistry and of their environmental implications.

Recently, a hydration (electrostatic) model to describe monoatomic ions has been developed by David and Vokhmin (2001). They predict experimental An–O distances of 2.56, 2.52, 2.51, 2.51, and 2.44 Å for U^{3+}, Np^{3+}, Pu^{3+}, Am^{3+}, and Cf^{3+}, respectively. Their coordination numbers for the first solvation shell are between 9 and 10 for the first four ions and 8.5 for Cf^{3+}. Blaudeau and coworkers performed DFT (PW91) calculations on the hydrated Pu^{3+} ion and predicted a coordination number of eight or nine in the complex (Blaudeau *et al.*, 1999). Their calculated bond lengths were 2.508 Å for the eight-coordinate complex in which the water molecules form a nearly cubic cage around the plutonium ion with a total symmetry of D_{2d}, and 2.585 Å (axial) and 2.491 Å (equatorial) for a D_{3h} nine-coordinate tricapped trigonal prismatic complex. These values were in good agreement with a subsequent crystal structure determination of $[Pu(H_2O)_9][CF_3SO_3]_3$ (Fig. 17.33), which contains an isolated $Pu(H_2O)_9^{3+}$ ion with Pu–O distances of 2.574 Å (axial) and 2.476 Å (equatorial) (Matonic *et al.*, 2001). Earlier solution EXAFS studies, which are not as definitive concerning coordination number as the X-ray crystallography, had concluded that Pu–O = 2.51 Å and the coordination number was 9 or 10 for Pu^{3+} (Ankudinov *et al.*, 1998; Gropen, 1999).

Yang *et al.* (2001) performed quantum mechanical and molecular dynamics (MD) calculations on the Th^{4+} ion using DFT (B3LYP) methodology and AMBER force fields. In the aqueous phase, calculated using a polarized continuum model (PCM), they found a C_{4v} nine-water capped-square-antiprism complex to be the most stable. Their calculated Th–O bond distance was 2.54 Å. These results compare reasonably well with experimental EXAFS measurements, for which a coordination number of 9–11 and a bond length of 2.45 Å were found (Moll *et al.*, 1999). The MD simulations lead to a well-defined

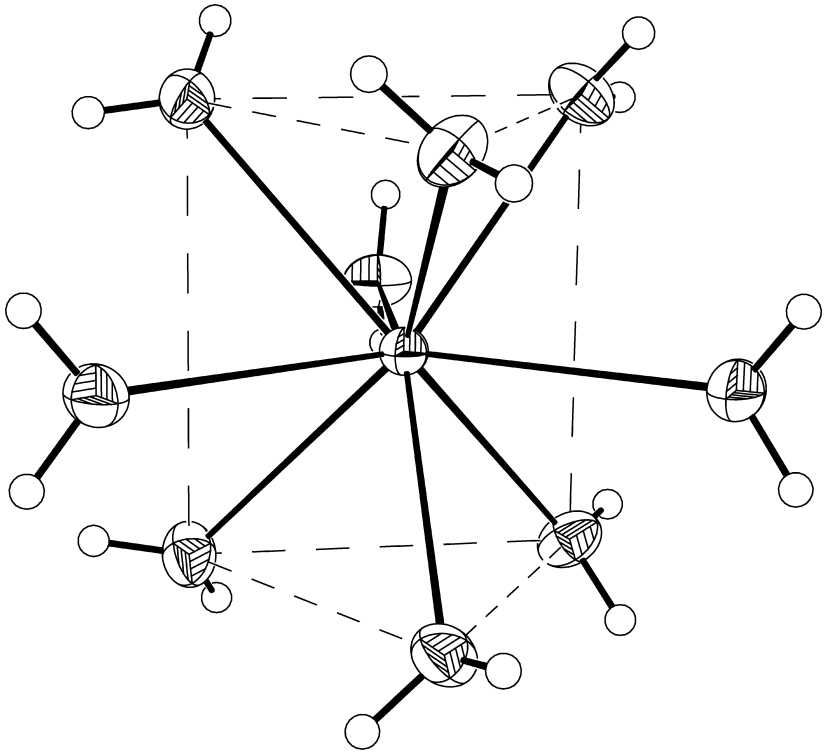

Fig. 17.33 *The structure of the* $[Pu(H_2O)_9]^{3+}$ *ion from the X-ray crystal structure of* $[Pu(H_2O)_9][CF_3SO_3]_3$ (*reproduced from Matonic* et al., 2001).

second shell consisting of 18.9 water molecules at a distance of 4.75 Å from the metal ion. In a further study, Tsushima *et al.* (2003) concluded that incorporation of the second shell in the geometry optimizations improves the Th–O bond distance to 2.50 Å. Mochizuki and Tsushima (2003) performed RECP-based B3LYP calculations with a conductive PCM and found a reduction in the calculated bond length to 2.47 and 2.48 Å. They also performed DIRAC four-component all-electron calculations of the $Ac(H_2O)_n^{3+}$ ($n = 1$, 2, 4, and 6) complexes and the analogous Th^{4+} complexes. They found that the thorium complexes have a shorter metal–oxygen distance, larger stabilization energies, and larger amounts of ligand-to-metal electron donation. Mochizuki and Tatewaki (2002) performed similar calculations on the analogous Cm^{3+} complexes. They found the curium–oxygen bond distance to increase with the number of water molecules in the complex and the stabilization energy per water molecule was reduced. These studies provide important information about the solvation properties of actinides ions. Further theoretical calculations are needed to address the important chemical properties (e.g. charge-transfer or redox chemistry) of actinide ions in solutions.

17.8 UNSUPPORTED METAL–METAL BONDS CONTAINING ACTINIDE ATOMS

The rich manifold of s, p, d, and f orbitals on actinide atoms has led to numerous theoretical explorations on the possibility of forming discrete complexes that contain direct metal–metal bonds involving one or more actinide atoms. As noted earlier, one bonding motif that contains an unsupported (and therefore unambiguous) metal–metal bond involving an actinide atom is the $Cp^*_2(X)Th - RuCp(CO)_2(X = Cl, I)$ system reported by Marks and coworkers in 1985 (Sternal *et al.*, 1985). This system was studied theoretically using quasi-relativistic Xα-SW calculations (Bursten and Novo-Gradac, 1987), which indicated that the $CpRu(CO)_2$ fragment in the molecule is best considered as an 'organometallic pseudohalide' that leads to a very polarized Ru–Th bond characteristic of 'early–late' heterodimetallic complexes (Gade, 2000). The conclusions of this theoretical study were applied in the synthesis of other organometallic complexes that contain unsupported actinide–transition metal bonds, such as the $Cp_3An–MCp(CO)_2$ (An = Th, U; M = Fe, Ru) complexes (Sternal and Marks, 1987). Mass spectrometric evidence has been presented for the formation of cationic complexes that contain direct An–M bonds from the reaction of Th^+ and U^+ with $Fe(CO)_5$ (da Conceicao Vieira *et al.*, 2001). The proposed complexes, $[AnFe(CO)_n]^+$ (An = Th, U) have the potential to lead to more covalent An–Fe bonding because of the lower oxidation state of the actinide centers, but theoretical studies are yet to be done for this structurally uncharacterized system.

Gagliardi (2003) recently exploited the pseudohalide characteristics of Au atoms as ligands to explore the structure and bonding in UAu_4 at the DFT and CASPT2 levels of theory. It is predicted that UAu_4 has a geometry slightly distorted from tetrahedral with U–Au bond lengths of 2.72 Å. The molecule is predicted to have a triplet ground state, analogous to the uranium tetrahalides. The U–Au bond is predicted to be ionic, although a comparison of the atomic populations of UAu_4 with those of other MAu_4 (M = Ti, Zr, Hf, Th) complexes indicates that the U–Au bond should have greater covalency than the other systems. Gagliardi and Pyykkö (2004) extended the analogy between An–main group and An–transition metal bonding to explore the possibility of strong U–M bonding in species such as NUIr, which is electronically similar to NUN. NUIr is predicted to be a closed-shell molecule with a very short U–Ir bond of 2.15 Å at the CASPT2 level with an extended basis. The bond is predicted to be polar, with a partial positive charge on U and partial negative charges on N and Ir, although less so than the other systems mentioned in this section. Similar results were obtained for the neutral isoelectronic molecules FURe, OUOs, and CUPt.

Truly covalent metal–metal bonds involving actinide atoms could be made in principle via direct actinide–actinide bonding in a symmetric discrete complex. To date, there are no well-characterized complexes that contain direct

actinide–actinide bonds; indeed, such systems remain as an experimental 'holy grail' in actinide chemistry. Most of the attention to the bonding and electronic structure of actinide–actinide bonded systems has focused on homonuclear diatomic molecules. March *et al.* have used simple models to predict that homonuclear diatomics of the heavy elements are unlikely to exist (Mucci and March, 1985; Pucci and March, 1986). Contrary to this prediction, the diatomic molecule U_2 has been detected in the gas phase via mass spectrometry (Gorokhov *et al.*, 1974; Gingerich, 1980), and was proposed to have a dissociation enthalpy of 52 ± 5 kcal mol^{-1}. This molecule has been the subject of several theoretical studies. Bursten and Ozin (1984) first examined the electronic structure of U_2 and Np_2 at an assumed bond distance of 2.2 Å using the quasi-relativistic Xα-SW method. They proposed that these molecules could form ϕ bonds via the 'face-to-face' interaction of the An 5fϕ AOs. Pepper and Bursten (1990) later used CASSCF and single-reference CI calculations to explore the bonding in U_2. They found a complex electronic structure for this molecule, including a relatively low-spin short-bond-length (SBL) state, and completely spin-uncoupled long-bond-length (LBL) state. Interestingly, they found the LBL minimum (at ca. 3.0 Å) to be lower in energy than the SBL minimum (at ca. 2.2 Å), although they expressed concerns about the lack of inclusion of spin–orbit effects in their calculations. Archibong and Ray (1999) have used DFT, CISD, and CCSD(T) calculations with RECPs to explore the possible existence of the Pu_2 diatomic molecule. They find that the molecule is bound, but that the Pu 5f electrons are localized, which leads to a rather weak interaction. The predicted Pu–Pu bond length, 4.4–4.5 Å depending on the method, is quite long and the predicted ground state is $^{13}\Sigma_g$ in the absence of spin–orbit effects.

Most recently, Gagliardi and Roos (2005) have reexamined the bonding in the U_2 molecule using CASSCF/CASPT2 methodology that includes spin–orbit effects. They find that the molecule has a very complex electronic structure: six of the 12 valence electrons fully occupy 7sσ and 6dπ bonding orbitals, one electron each occupy the 6dσ and 6dδ orbitals, one electron each occupy the weakly bonding 5fπ and 5fδ orbitals, and the last two electrons are essentially localized in the 5fϕ atomic orbitals on the two U atoms. They therefore describe the bonding in the molecule as having "three strong 'normal' electron-pair bonds, two fully developed one-electron bonds, two weak one-electron bonds, and two localized electrons," leading to the prediction of a net quintuple bond in the molecule. Fig. 17.34 depicts the active MOs of U_2 used to construct this unusual bond, and the occupation number of each from the CASPT2 calculations. With the inclusion of spin–orbit coupling, they predict a U–U bond length of 2.43 Å and a bond dissociation energy of 30.5 kcal mol^{-1}. It is highly unusual that a molecule with a quintuple bond possesses a dissociation energy lower than that of most systems with single bonds, which emphasize the weakness and complexity of the actinide–actinide bonds.

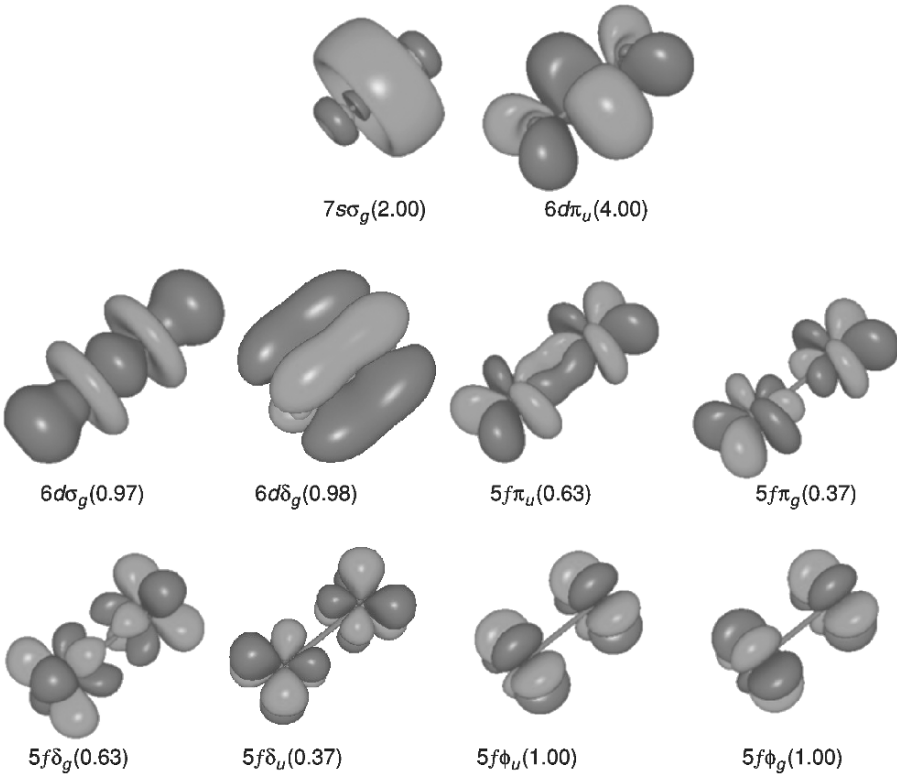

Fig. 17.34 *The active MOs that form the bond in U_2 from CASPT2 calculations. The number in parentheses is the electron occupation of the orbital in the ground state* (*reproduced from Gagliardi and Roos*, 2005).

17.9 CONCLUDING COMMENTS

We hope that this chapter has given the reader a sense of the challenges and complexity of obtaining and describing the electronic structure of discrete actinide-containing systems. As was stated at the outset, the large number of active atomic orbitals on actinide atoms and ions, the necessarily large number of electrons, the need to include relativistic effects, and the generally large coordination numbers all serve to make the electronic structure of molecular actinide complexes appreciably more complicated than that of transition-metal systems (and, perforce, purely organic systems). We have attempted to show the reader how recent advances in computational resources coupled with new theoretical methodologies have led to great progress in the quantitative description of actinide electronic structure. In particular, the growth of density functional methods and new electron correlation techniques during the last

10–15 years has greatly facilitated advances in this field, particularly with respect to the calculation of geometries, vibrational frequencies, and ground state metal–ligand interactions.

In spite of the progress that has been made, there are areas of actinide electronic structure that still require a great deal of development so as to allow computational actinide chemistry to be an even stronger partner to the experimental studies of actinide science. Very recent developments have led to better descriptions of the electronic structure of excited states of actinide systems, to improved treatment of dynamic correlation effects with the inclusion of scalar and spin–orbit relativistic effects, and to more effective combining of quantum mechanics and molecular mechanics methods (QM/MM methods) for the theoretical analysis of very large actinide molecular systems, such as those that are relevant to the interaction of actinide atoms and ions with biomolecules. These new capabilities portend an even greater role that theoretical studies will play in the understanding of experimental observations and the prediction of new properties of actinide systems.

Improved methods and enhanced computational capabilities will enable higher quality calculations of the types of actinide systems discussed in this chapter. They will also allow computational actinide chemists to address the 'next generation' of actinide electronic structure problems, including the interaction of actinide-containing molecules with realistically modeled solvents and surfaces and the complex equilibria exhibited in actinide chemistry (particularly aqueous actinide chemistry). We anticipate that the next decade will be one of continued growth in the scope and utility of theoretical actinide chemistry. Continuing efforts to improve relativistic electronic structural methodologies within DFT and electron correlation techniques, coupled with ever-increasing computational capabilities, will provide new, more powerful electronic structure codes for addressing actinide electronic structure. We expect that more reliable methods will be developed for exploring excited states of actinide systems, including the complex multiplets that are characteristic of the optical spectroscopy of actinide complexes. Improved methods for the calculation of the molecular energetics of actinide complexes could lead to predictive capabilities with thermodynamic accuracy. We are also hopeful that relativistic molecular electronic structure approaches will be improved to the point of allowing for the facile calculation of potential energy surfaces for actinide-containing molecules, including reaction transition states. It will be an exciting time for our field.

LIST OF ABBREVIATIONS

ADF	Amsterdam density functional code
AIMP	*ab initio* model potential
An	Actinide

AO	atomic orbital
ACPF	averaged coupled-pair functional
AQCC	averaged quadratic coupled cluster
B3LYP	Becke's three parameter exchange functional plus the correlation functional of Lee, Yang and Parr
BDF	Beijing density functional code
BLYP	Becke–Lee–Yang–Parr functional
BP86	Becke–Perdew 86 functional
Bz	Benzene
CASPT2	complete active space plus second-order perturbation theory
CASSCF	complete active space self-consistent field
CCSD	coupled cluster with single and double excitations
CCSD(T)	coupled cluster singles, doubles and perturbative triples
Cht	cycloheptatrienyl
CISD	configuration interaction with single and double excitations
COT	cyclooctatetraene
Cp	cyclopentadienyl
Cp*	pentamethylcyclopentadienyl
DFT	density functional theory
DHF	Dirac–Hartree–Fock method
DKH	Douglas–Kroll–Hess hamiltonian
DV-Xα	discrete variational Xα method
ECP	effective core potential
EHMO	extended Hückel molecular orbital
Gaussian	Gaussian computational chemistry code
GGA	generalized gradient approximation
GVB	generalized valence bond
HF	Hartree–Fock
HFS	Hartree–Fock–Slater
HOMO	highest occupied molecular orbital
INDO	intermediate neglect of differential overlap
IR	infrared
LCAO	linear combination of atomic orbitals
LDA	local density approximation
LMCT	ligand-to-metal charge transfer
LUMO	lowest unoccupied molecular orbital
MCSCF	multi-configuration self-consistent field
MLCT	metal-to-ligand charge transfer
MO	molecular orbital
MP2	second-order Møller–Plesset perturbation theory
MRCI	multi-reference configuration interaction
MRCISD	multi-reference configuration interaction with single and double excitations
NESC	normalized elimination of the small components

Ng	noble gas
NWChem	Northwest computational chemistry code
PCM	polarized continuum model
PW91	Perdew–Wang 1991 functional
QR-SW-Xα	quasi-relativistic scattered wave Xα
RASSCF	restrictive active space self-consistent field
RESC	relativistic scheme by eliminating small components
RECP	relativistic effective core potential
REX	relativistic extended Hückel
SCF	self-consistent field
SO	spin–orbit
SOCI	spin–orbit configuration interaction
SO-MRCISD	spin-orbit multi-reference configuration interaction singles and doubles
SW-Xα	scattered-wave Xα method
TD-DFT	time-dependent density functional theory
TMCOT	tetramethylcyclooctatetraene
Tp	tetrapyrrole
ZORA	zeroth-order regular approximation (to the Dirac equation)

ACKNOWLDEGMENTS

NK acknowledges the EPSRC for support of actinide chemistry in the UK. PJH and BEB acknowledge support by the Division of Chemical Sciences, Geosciences, and Biosciences, Office of Basic Energy Sciences, U.S. Department of Energy. PJH also acknowledges support for actinide research by Laboratory Directed Research and Development at Los Alamos National Laboratory under the auspices of the U.S. DOE, and BEB also acknowledges computational support from the Ohio Supercomputer Center. JL acknowledges the computational resources from the Molecular Science Computing Facility and the support from EMSL, a national scientific user facility sponsored by the U.S. DOE, OBER and located at PNNL. The authors thank Dr. Constance Brett for assistance in preparing the manuscript.

REFERENCES

Aaberg, M., Ferri, D., Glaser, J., and Grenthe, I. (1983) *Inorg. Chem.,* **22**, 3986–9.

Abramowitz, S., Acquista, N., and Thompson, K. R. (1971) *J. Phys. Chem.,* **75**, 2283–5.

Abramowitz, S. and Acquista, N. (1972) *J. Phys. Chem.,* **76**, 648–9.

ADF: Scientific Computing and Modeling (SCM) NV, *Theoretical Chemistry*, Vrije Universiteit, Amsterdam, The Netherlands. http://www.scm.com

Alcock, N. W. and Esperas, S. (1977) *J. Chem. Soc., Dalton Trans.*, 893–6.
Allen, G. C., Baerends, E. J., Vernooijs, P., Dyke, J. M., Ellis, A. M., Feher, M., and Morris, A. (1988) *J. Chem. Phys.,* **89**, 5363–72.
Allen, P. G., Veirs, D. K., Conradson, S. D., Smith, C. A., and Marsh, S. F. (1996) *Inorg. Chem.,* **35**, 2841–5.
Allen, P. G., Bucher, J. J., Shuh, D. K., Edelstein, N. M., and Reich, T. (1997) *Inorg. Chem.,* **36**, 4676–83.
Amberger, H. D. (1983) *J. Less Common Metals,* **93**, 233–41.
Andersen, R. A., Boncella, J. M., Burns, C. J., Blom, R., Haaland, A., and Volden, H. V. (1986) *J. Organomet. Chem.,* **312**, C49–52.
Andersson, K., Malmgyist, P.-A., and Roos, B. O. (1992) *J. Chem. Phys.,* **96**, 1218–26.
Andrews, L., Liang, B. Y., Li, J., and Bursten, B. E. (2000a) *Angew. Chem. Int. Edn.,* **39**, 4565–7; *Angew. Chem.*, **112**, 739–41.
Andrews, L., Zhou, M. F., Liang, B. Y., Li, J., and Bursten, B. E. (2000b) *J. Am. Chem. Soc.,* **122**, 11440–9.
Andrews, L. and Citra, A. (2002) *Chem. Rev.,* **102**, 885–912.
Andrews, L., Liang, B. Y., Li, J., and Bursten, B. E. (2003) *J. Am. Chem. Soc.,* **125**, 3126–39.
Andrews, L., Liang, B. Y., Li, J., and Bursten, B. E. (2004) *New J. Chem.,* **28**, 289–94.
Ankudinov, A. L., Conradson, S. D., de Leon, J. M., and Rehr, J. J. (1998) *Phys. Rev. B,* **57**, 7518–25.
Archibong, E. F. and Ray, A. K. (1999) *Phys. Rev. A,* **60**, 5105–7.
Archibong, E. F. and Ray, A. K. (2000) *J. Mol. Struct.* (*Theochem*), **530**, 165–70.
Arfken, G. (1985) *Mathematical Methods for Physicists,* Academic Press, New York.
Arliguie, T., Lance, M., Neirlich, M., Vigner, J., and Ephritikhine, M. (1995) *J. Chem. Soc., Chem. Commun.*, 183–4.
Arney, D. S. J., Burns, C. J., and Smith, D. C. (1992) *J. Am. Chem. Soc.,* **114**, 10068–9.
Avdeef, A., Raymond, K. N., Hodgson, K. O., and Zalkin, A. (1972) *Inorg. Chem.,* **11**, 1083–8.
Balasubramanian, K. and Pitzer, K. S. (1987) *Adv. Chem. Phys.,* **67**, 287–319.
Balasubramanian, K. (1989) *J. Phys. Chem.,* **93**, 6585–96.
Balasubramanian, K. (1994) in *Handbook on the Physics and Chemistry of Rare Earths,* vol. 18 (eds. K. A. Gschneidner and L. Eyring), North-Holland, Amsterdam, p. 29–158.
Balasubramanian, K. (1997) *Relativistic Effects in Chemistry, Part A: Theory and Techniques,* John Wiley, New York.
Barandiarán, Z. and Seijo, L. (2003) *J. Chem. Phys.,* **119**, 3785–90.
Bartlett, R. J. (1981) *Ann. Rev. Phys. Chem.,* **32**, 359–401.
Bartlett, R. J. (1989) *J. Phys. Chem.,* **93**, 1697–708.
Basile, L. J., Sullivan, J. C., Ferraro, J. R., and LaBonville, P. (1974) *Appl. Spectrosc.,* **28**, 142–5.
Batista, E. R., Martin, R. L., and Hay, P. J. (2004a) *J. Chem. Phys.,* **121**, 11104–11.
Batista, E. R., Martin, R. L., Hay, P. J., Peralta, J. E., and Scuseria, G. E. (2004b) *J. Chem. Phys.,* **121**, 2144–50.
Beattie, I. R. (1999) *Angew. Chem. Int. Edn.,* **38**, 3294–306.
Becke, A. D. (1988) *Phys. Rev. A,* **38**, 3098–100.
Becke, A. D. (1993a) *J. Chem. Phys.,* **98**, 1372–7.

Becke, A. D. (1993b) *J. Chem. Phys.,* **98**, 5648–52.
BERTHA: Grant, I. P. (1999) in *Supercomputers, Collision Processes and Applications* (eds. K. L. Bell, K. A. Berrington, D. S. F. Crothers, and K. T. Taylor), Plenum, New York, pp. 213–24.
Bethe, H. (1929) *Ann. Physik,* **3**, 133–208.
Blaudeau, J.-P., Zygmunt, S. A., Curtiss, L. A., Reed, D. T., and Bursten, B. E. (1999) *Chem. Phys. Lett.,* **310**, 347–54.
Blaudeau, J.-P., Bursten, B. E., and Pitzer, R. M. unpublished results.
Bleaney, B. (1955) *Discuss. Faraday Soc.,* **19**, 112–18.
Boerrigter, P. M., Baerends, E. J., and Snijders, J. G. (1988) *Chem. Phys.,* **122**, 357–74.
Bolvin, H., Wahlgren, U., Gropon, O., and Marsden, C. (2001a) *J. Phys. Chem. A,* **105**, 10570–6.
Bolvin, H., Wahlgren, U., Moll, H., Reich, T., Geipel, G., Fanghänel, T., and Grenthe, I. (2001b) *J. Phys. Chem. A,* **105**, 11441–5.
Bond, G. C. (2000) *J. Mol. Catal. A,* **156**, 1–20.
Bondybey, V. E., Smith, A. M., and Agreiter, J. (1996) *Chem. Rev.,* **96**, 2113–34.
Boring, M., Wood, J. H., and Moskowitz, J. W. (1975) *J. Chem. Phys.,* **63**, 638–42.
Boring, M. and Wood, J. H. (1979) *J. Chem. Phys.,* **71**, 392–9.
Breit, G. (1932) *Phys. Rev.,* **39**, 616–24.
Brennan, J. G., Andersen, R. A., and Robbins, J. L. (1986) *J. Am. Chem. Soc.,* **108**, 335–6.
Brennan, J. G., Cloke, F. G. N., Sameh, A. A., and Zalkin, A. (1987) *J. Chem. Soc., Chem. Commun.*, 1668–9.
Brennan, J. G., Green, J. C., and Redfern, C. M. (1989) *J. Am. Chem. Soc.,* **111**, 2373–7.
Brown, K. L. and Kaltsoyannis, N. (1999) *J. Chem. Soc., Dalton Trans.*, 4425–30.
Budantseva, N. A., Fedosseey, A. M., Bessonov, A. A., and Grigoriev, M. S. (2000) *Radiochim. Acta,* **88**, 291–5.
Burns, J. H. (1973) *J. Am. Chem. Soc.,* **95**, 3815–17.
Burns, C. J. and Bursten, B. E. (1989) *Comments Inorg. Chem.,* **9**, 61–93.
Bursten, B. E. and Fang, A. (1983) *J. Am. Chem. Soc.,* **105**, 6495–6.
Bursten, B. E. and Ozin, G. A. (1984) *Inorg. Chem.,* **23**, 2910–11.
Bursten, B. E., Casarin, M., Di Bella, S., Fang, A., and Fragalà, I. L. (1985) *Inorg. Chem.,* **24**, 2169–73.
Bursten, B. E. and Fang, A. (1985) *Inorg. Chim. Acta,* **110**, 153–60.
Bursten, B. E. and Novo-Gradac, K. J. (1987) *J. Am. Chem. Soc.,* **109**, 904–5.
Bursten, B. E. and Strittmatter, R. J. (1987) *J. Am. Chem. Soc.,* **109**, 6606–8.
Bursten, B. E., Rhodes, L. F., and Strittmatter, R. J. (1989a) *J. Am. Chem. Soc.,* **111**, 2756–8.
Bursten, B. E., Rhodes, L. F., and Strittmatter, R. J. (1989b) *J. Am. Chem. Soc.,* **111**, 2758–66.
Bursten, B. E. and Strittmatter, R. J. (1991) *Angew. Chem. Int. Edn. Engl.,* **30**, 1069–85.
Bursten, B. E., Drummond, M. L., and Li, J. (2003) *Faraday Discuss.,* **124**, 1–24, 457–8.
Capone, F., Colle, Y., Hiernaut, J. P., and Ronchi, C. (1999) *J. Phys. Chem. A,* **103**, 10899–906.
Carnall, W. T. and Crosswhite, H. M. (1986) in *Chemistry of the Actinide Elements*, vol. 2 (eds. J. J. Katz, G. T. Seaborg, and L. R. Morss), Chapman & Hall, London, ch 16.
Carnall, W. T. (1992) *J. Chem. Phys.,* **96**, 8713–26.

Carstens, D. H. W., Gruen, D. M., and Kozlowski, J. F. (1972) *High Temp. Sci.,* **4**, 436–44.
Casida, M. E., Jamorski, C., Casida, K. C., and Salahub, D. R. (1998) *J. Chem. Phys.,* **108**, 4439–49.
Castellato, U., Vigato, A., and Vidali, M. (1981) *Coord. Chem. Rev.,* **36**, 183–265.
Castro-Rodrigues, I., Nakai, H., Gantzel, P., Zakharov, L. N., Rheingold, A. L., and Meyer, K. (2003a) *J. Am. Chem. Soc.,* **125**, 15734–5.
Castro-Rodrigues, I., Olsen, K., Gantzel, P., and Meyer, K. (2003b) *J. Am. Chem. Soc.,* **125**, 4565–71.
Chang, C., Pelissier, M., and Durand, P. (1986) *Phys. Scr.,* **34**, 394–404.
Chang, A. H. H. and Pitzer, R. M. (1989) *J. Am. Chem. Soc.,* **111**, 2500–7.
Chang, A. H. H., Zhao, K., Ermler, W. C., and Pitzer, R. M. (1994) *J. Alloys Compd.,* **213–214**, 191–5.
Chang, Q. (2002) MS Thesis, The Ohio State University.
Christe, K. O. (2001) *Angew. Chem. Int. Edn.,* **40**, 1419–21.
Christiansen, P. A., Lee, Y. S., and Pitzer, K. S. (1979) *J. Chem. Phys.,* **71**, 4445–50.
Christiansen, P. A., Ermler, W. C., and Pitzer, K. S. (1985) *Ann. Rev. Phys. Chem.,* **36**, 407–32.
Clark, D. L., Hobart, D. E., and Neu, M. P. (1995) *Chem. Rev.,* **95**, 25–48.
Clark, D. L., Conradson, S. D., Ekberg, S. A., Hess, N. J., Neu, M. P., Palmer, P. D., Runde, W., and Tait, C. D. (1996) *J. Am. Chem. Soc.,* **113**, 2089–90.
Clark, D. L. (1999) Presented at the Symposium of Heavy Element Complexes: The Convergence of Theory and Experiment, 217th ACS National Meeting, Anaheim, CA.
Clark, D. L., Conradson, S. D., Donohoe, R. J., Keogh, D. W., Morris, D. E., Palmer, P. D., Rogers, R. D., and Tait, C. D. (1999) *Inorg. Chem.,* **38**, 1456–66.
Clavaguéra-Sarrio, C., Brenner, V., Hoyau, S., Marsden, C. J., Millié, P., and Dognon, J.-P. (2003a) *J. Phys. Chem. B,* **107**, 3051–60.
Clavaguéra-Sarrio, C., Hoyau, S., Ismail, N., and Marsden, C. J. (2003b) *J. Phys. Chem. A,* **107**, 4515–25.
Clavaguéra-Sarrio, C., Vallet, V., Maynau, D., and Marsden, C. J. (2004) *J. Chem. Phys.,* **121**, 5312–21.
Cloke, F. G. N. and Hitchcock, P. B. (2002) *J. Am. Chem. Soc.,* **124**, 9352–3.
Cloke, .F. G. N., Green, J. C., and Kaltsoyannis, N. (2004) *Organometallics,* **23**, 832–5.
Connick, R. E. and Hugus, Z. Z. Jr (1952) *J. Am. Chem. Soc.,* **74**, 6012–15.
Conradson, S. D. (1998) *Appl. Spectrosc.,* **52**, 252A–79A.
Cornehl, H. H., Heinemann, C., Marcalo, J. Pires de Matos, P., and Schwarz, H. (1996) *Angew. Chem. Int. Edn. Engl.,* **35**, 891–4.
Cory, M. G., Köstimeier, S., Kotzian, M., Rösch, N., and Zerner, M. (1994) *J. Chem. Phys.,* **100**, 1353–65.
Cotton, F. A. (1990) *Chemical Applications of Group Theory,* John Wiley, New York.
Coulson, C. A. and Lester, G. R. (1956) *J. Chem. Soc.*, 3650–9.
Coupez, B. and Wipff, G. (2003) *Inorg. Chem.,* **42**, 3693–703.
Cowan, R. A. and Griffin, G. C. (1976) *J. Opt. Soc. Am. B.,* **66**, 1010–14.
Cramer, R. E., Edelmann, F., Mori, A. L., Roth, S., Gilje, J. W., Tatsumi, K., and Nakamura, A. (1988) *Organometallics,* **7**, 841–9.
Craw, J. S., Vincent, M. A., Hillier, I. H., and Wallwork, A. L. (1995) *J. Phys. Chem.,* **99**, 10181–5.

Crosswhite, H. M. and Crosswhite, H. (1984) *J. Opt. Soc. Am. B,* **1**, 246–54.
da Conceicao Vieira, M., Marcalo, J., and Pires de Matos, A. (2001) *J. Organomet. Chem.,* **632**, 126–32.
Dallinger, R. F., Stein, P., and Spiro, T. G. (1978) *J. Am. Chem. Soc.,* **100**, 7865–70.
David, F. H. and Vokhmin, V. (2001) *J. Phys. Chem. A,* **105**, 9704–9.
de Jong, W. A. and Nieuwpoort, W. C. (1996) *Int. J. Quantum Chem.,* **58**, 203–16.
de Jong, W. A., Harrison, R. J., and Dixon, D. A. (2001a) *J. Chem. Phys.,* **114**, 48–53.
de Jong, W. A., Harrison, R. J., Nichols, J. A., and Dixon, D. A. (2001b) *Theo. Chem. Acta*, **107**, 22–6. (Erratum: *Theo. Chem. Acta*, **107**, 318)
De Kock, R. L., Baerends, E. J., Boerrigter, P. M., and Snijders, J. G. (1984) *Chem. Phys. Lett.,* **105**, 308–16.
Del Mar, Conejo, M., Parry, J. S., Carmona, E., Schultz, M., Brennan, J. G., Beshouri, S. M., Andersen, R. A., Rogers, R. D., Coles, S., and Hursthouse, M. (1999) *Chem. Eur. J.,* **5**, 3000–9.
Den Auwer, C., Simoni, E., Conradson, S., and Madic, S. (2003) *Eur. J. Inorg. Chem.*, **21**, 3843–59.
Denning, R. G., Norris, J. O. W., and Brown, D. (1982a) *Mol. Phys.,* **46**, 287–323.
Denning, R. G., Norris, J. O. W., and Brown, D. (1982b) *Mol. Phys.,* **46**, 325–64.
Denning, R. G. (1992) *Struct. Bond.* (*Berlin*), **79**, 215–76.
Desclaux, J.-P. (1973) *At. Data Nucl. Data Tables,* **12**, 311–406.
Devillers, C. and Ramsay, D. A. (1971) *Can. J. Phys.,* **49**, 2839–58.
Di Bella, S., Gulino, A., Lanza, G., Fragalà, I. L., and Marks, T. J. (1993) *J. Phys. Chem.,* **97**, 11673–6.
Di Bella, S., Lanza, G., Fragalà, I. L., and Marks, T. J. (1996) *Organometallics,* **15**, 205–8.
Diaconescu, P. L., Arnold, P. L., Baker, T. A., Mindiola, D. J., and Cummins, C. C. (2000) *J. Am. Chem. Soc.,* **122**, 6108–9.
Diaconescu, P. L. and Cummins, C. C. (2002) *J. Am. Chem. Soc.,* **124**, 7660–1.
Diamond, R. M., Street, K. Jr, and Seaborg, G. T. (1954) *J. Am. Chem. Soc.,* **76**, 1461–9.
Dieke, G. H. (1968) in *Spectra and Energy Levels of Rare Earth Ions in Crystals* (eds. H. M. Crosswhite and H. Crosswhite), Interscience, New York.
DIRAC: Department of Chemistry, University of Southern Denmark, Odense M., Denmark. http://dirac.chem.sdu.dk
Dirac, P. A. M. (1929) *Proc. R. Soc. London, Ser. A,* **123**, 714–33.
Docrat, T. I., Mosselmans, J. F. W., Charnock, J. M., Whiteley, M. W., Collison, D., Livens, F. R., Jones, C., and Edmiston, M. J. (1999) *Inorg. Chem.,* **38**, 1879–82.
Dolg, M., Fulde, P., Stoll, H., Preuss, H., Chang, A., and Pitzer, R. M. (1995) *Chem. Phys.,* **195**, 71–82.
Dolg, M. and Stoll, H. (1996) in *Handbook on the Physics and Chemistry of Rare Earths,* vol. 22 (eds. K. A. Gschneidner and L. Eyring), Elsevier Science B.V., Amsterdam, pp. 607–729.
Dolg, M. and Fulde, P. (1998) *Chem. Eur. J.,* **4**, 200–4.
Dolg, M. (2001) *J. Chem. Inf. Comput. Sci.,* **41**, 18–21.
Dolg, M. (2002) *Theor. Comput. Chem.* **11**, 793–862.
Domanov, V. P., Buklanov, G. V., and Lebanov, Y. V. (2002) *Radiochemistry,* **44**, 114–20.
Douglas, M. and Kroll, N. M. (1974) *Ann. Phys.* (*N. Y.*), **82**, 89–155.

Dyall, K. G. (1997) *J. Chem. Phys.,* **106**, 9618–26.
Dyall, K. G. (1999) *Mol. Phys.,* **96**, 511–18.
Dyall, K. G. (2001) *J. Chem. Phys.,* **115**, 9136–43.
Dyall, K. G. (2005) *Chem. Phys.,* **311**, 19–24.
Edelstein, N. M., Allen, P. G., Bucher, J. J., Shuh, D. K., Sofield, C. D., Sella, A., Russo, M., Kaltsoyannis, N., and Maunder, G. (1996) *J. Am. Chem. Soc.,* **118**, 13115–16.
Eisenstein, J. C. and Pryce, M. H. L. (1955) *Proc. R. Soc. London,* **A229**, 20–38.
Eisenstein, J. C. (1956) *J. Chem. Phys.,* **25**, 142–6.
Elliott, R. J. (1953) *Phys. Rev.,* **89**, 659–60.
Ellis, D. E., Rosén, A., and Walch, P. F. (1975) *Int. J. Quantum Chem. Symp.,* **9**, 351–8.
Ellis, D. E., Rosen, A., and Gubanov, V. A. (1982) *J. Chem. Phys.,* **77**, 4051–60.
Ermler, W. C., Ross, R. B., and Christiansen, P. A. (1988) *Adv. Quantum Chem.,* **19**, 139–82.
Ermler, W. C., Ross, R. B., and Christiansen, P. A. (1991) *Int. J. Quantum Chem.,* **40**, 829–46.
Evans, W. J., Kozimor, S. A., Nyce, G. W., and Ziller, J. W. (2003) *J. Am. Chem. Soc.,* **125**, 13831–5.
Evans, W. J., Kozimor, S. A., Ziller, J. W., and Kaltsoyannis, N. (2004) *J. Am. Chem. Soc.,* **126**, 14533–47.
Fischer, R. D. (1963) *Theor. Chim. Acta* (*Berlin*), **1**, 418–31.
Foldy, L. L. and Wouthuysen, S. A. (1950) *Phys. Rev.,* **78**, 29–36.
Foldy, L. L. (1956) *Phys. Rev.,* **102**, 568–81.
Fuchs, M. S. K., Shor, A. M., and Rosch, N. (2002) *Int. J. Quantum. Chem.,* **86**, 485–501.
Gabelnick, S. D., Reedy, G. T., and Chasanov, M. G. (1973a) *J. Chem. Phys.,* **58**, 4468–75.
Gabelnick, S. D., Reedy, G. T., and Chasanov, M. G. (1973b) *Chem. Phys. Lett.,* **19**, 90–3.
Gabelnick, S. D., Reedy, G. T., and Chasanov, M. G. (1973c) *J. Chem. Phys.,* **59**, 6397–404.
Gade, L. H. (2000) *Angew. Chem. Int. Edn.,* **39**, 2658–78.
Gagliardi, L., Handy, N. C., Ioannou, A. G., Skylaris, C.-K., Spencer, S., Willetts, A., and Simper, A. M. (1998) *Chem. Phys. Lett.,* **283**, 187–93.
Gagliardi, L. and Roos, B. O. (2000) *Chem. Phys. Lett.,* **331**, 229–34.
Gagliardi, L., Grenthe, I., and Roos, B. O. (2001a) *Inorg. Chem.,* **40**, 2976–8.
Gagliardi, L., Roos, B. O., Malmqvist, P., and Dyke, J. M. (2001b) *J. Phys. Chem. A,* **105**, 10602–6.
Gagliardi, L., Schimmelpfennig, B., Maron, L., Wahlgren, U., and Willetts, A. (2001c) *Chem. Phys. Lett.,* **344**, 207–12.
Gagliardi, L. and Roos, B. O. (2002) *Inorg. Chem.,* **41**, 1315–19.
Gagliardi, L., Skylaris, C.-K., Willets, A., Dyke, J. M., and Barone, V. (2002) *Chem. Phys.,* **2**, 3111–14.
Gagliardi, L. (2003) *J. Am. Chem. Soc.,* **125**, 7504–5.
Gagliardi, L., La Manna, G., and Roos, B. O. (2003) *Faraday Discuss.,* **124**, 63–8.
Gagliardi, L. and Pyykkö, P. (2004) *Angew. Chem. Int. Edn.,* **43**, 1573–6.
Gagliardi, L., Heaven, M. C., Krogh, J. W., and Roos, B. O. (2005) *J. Am. Chem. Soc.,* **127**, 86–91.
Gagliardi, L. and Roos, B. (2005) *Nature,* **433**, 848–51.

GAMESS: "General Atomic and Molecular Electronic Structure System," Schmidt, M. W., Baldridge, K. K., Boatz, J. A., Elbert, S. T., Gordon, M. S., Jensen, J. H., Koseki, S., Matsunaga, N., Nguyen, K. A., Su, S. J., Windus, T. L., Dupuis, M., and Montgomery, J. A. (1993) *J. Comput. Chem.,* **14**, 1347–63.
Gao, J., Liu, W., Song, B., and Liu, C. (2004) *J. Chem. Phys.,* **121**, 6658–66.
Garcia-Hernandez, M., Lauterbach, C., Kruger, S., Matveev, A., and Rösch, N. (2002) *J. Comput. Chem.,* **23**, 834–46.
GAUSSIAN: GAUSSIAN03, Frisch, M. J. *et al.*, Gaussian, Inc., Wallingford, CT. http://www.gaussian.com
Geoffrey, G. L. and Bassner, S. L. (1988) *Adv. Organomet. Chem.,* **28**, 1–83.
Gingerich, K. A. (1967) *J. Chem. Phys.,* **47**, 2192–3.
Gingerich, K. A. (1980) *Symp. Faraday Soc.,* **14**, 109–25.
Glueckauf, E. and McKay, H. A. C. (1950) *Nature,* **165**, 594–5.
Gorokhov, L. N., Emel'yanov, A. M., and Khodeev, Y. S. (1974) *Teplofiz. Vys. Temp.,* **12**, 1307–9.
Gourier, D., Caurant, D., Arliguie, T., and Ephritikhine, M. (1998) *J. Am. Chem. Soc.,* **120**, 6084–92.
Grant, I. P. and Quiney, H. M. (2000) *Int. J. Quantum. Chem.,* **80**, 283–97.
Green, D. W., Gabelnick, S. D., and Reedy, G. T. (1976) *J. Chem. Phys.,* **64**, 1697–705.
Green, D. W. and Reedy, G. T. (1976) *J. Chem. Phys.,* **65**, 2921–2.
Green, D. W. and Reedy, G. T. (1978a) *J. Chem. Phys.,* **69**, 544–51.
Green, D. W. and Reedy, G. T. (1978b) *J. Chem. Phys.,* **69**, 552–5.
Green, D. W. and Reedy, G. T. (1979) *J. Mol. Spectrosc.,* **74**, 423–34.
Green, D. W. (1980) *Int. J. Thermophys.,* **1**, 61–71.
Green, D. W., Reedy, G. T., and Gabelnick, S. D. (1980) *J. Chem. Phys.,* **73**, 4207–16.
Green, J. C., Green, M. L. H., Kaltsoyannis, N., Mountford, P., Scott, P., and Simpson, S. J. (1992) *Organometallics,* **11**, 3353–61.
Green, J. C., Kaltsoyannis, N., Mac Donald, M. A., and Sze, K. H. (1994) *J. Am. Chem. Soc.,* **116**, 1994–2004.
Gropen, O. (1999) *J. Phys. Chem. A,* **103**, 8257–64.
Gulino, A., Ciliberto, E., Di Bella, S., Fragalà, I., Seyam, A. M., and Marks, T. J. (1992) *Organometallics,* **11**, 3248–57.
Gulino, A., Di Bella, S., Fragalà, I. L., Casarin, M., Seyam, A. M., and Marks, T. J. (1993) *Inorg. Chem.,* **32**, 3873–9.
Hamermesh, M. (1989) *Group Theory and its Application to Physical Problems,* Dover, Mineola, New York.
Han, Y. and -K. Hirao, K. (2000) *J. Chem. Phys.,* **113**, 7345–50.
Han, J., Kaledin, L. A., Goncharov, V., Komissarov, A. V., and Heaven, M. C. (2003) *J. Am. Chem. Soc.,* **125**, 7176–7.
Hay, P. J., Wadt, W. R., Kahn, L. R., Raffenetti, R. C., and Phillips, D. H. (1979) *J. Chem. Phys.,* **71**, 1767–79.
Hay, P. J. (1983) *J. Chem. Phys.,* **49**, 5468–82.
Hay, P. J. and Wadt, W. R. (1985) *J. Chem. Phys.,* **82**, 270–83.
Hay, P. J., Ryan, R. R., Salazar, K. V., Wrobleski, D. A., and Sattelberger, A. P. (1986) *J. Am. Chem. Soc.,* **108**, 313–15.
Hay, P. J. and Martin, R. L. (1998) *J. Chem. Phys.,* **109**, 3875–81.
Hay, P. J., Martin, R. L., and Schreckenbach, G. (2000) *J. Phys. Chem. A,* **104**, 6259–70.

Hay, P. J. (2003) *Faraday Discuss.,* **124**, 69–83.
Hayes, R. G. and Edelstein, N. M. (1972) *J. Am. Chem. Soc.,* **94**, 8688–91.
Heinemann, C. and Schwarz, H. (1995) *Chem. Eur. J.,* **1**, 7–11.
Herzberg, G. (1944) *Atomic Spectra and Atomic Structure,* Dover, New York.
Herzberg, G. (1989) *Molecular Spectra and Molecular Structure Volume I – Spectra of Diatomic Molecules,* Krieger, Malaber, FL.
Herzberg, G. (1991) *Molecular Spectra and Molecular Structure Volume III – Electronic Spectra and Electronic Structure of Polyatomic Molecules,* Krieger, Malaber, FL.
Hess, B. A. (2003) *Relativistic Effects in Heavy-Element Chemistry and Physics,* JohnWiley, Chichester.
Hildenbrand, D. and Lau, K. H. (1991) *J. Chem. Phys.,* **94**, 1420–5.
Himmel, H.-J., Downs, A. J., and Greene, T. M. (2002) *Chem. Rev.,* **102**, 4191–241.
Hirao, K., and Ishikawa, S., (eds.) (2004) *Recent Advances in Relativistic Molecular Theory, Recent Advances in Computational Chemistry*, vol 5, World Scientific, Singapore.
Hirata, S., Yanai, T., de Jong, W. A., Nakajima, T., and Hirao, K. (2004) *J. Chem. Phys.,* **120**, 3297–310.
Hohenberg, and P. Kohn, W. (1964) *Phys. Rev. B,* **136**, 864–71.
Hong, G., Schautz, F., and Dolg, M. (1999) *J. Am. Chem. Soc.,* **121**, 1502–12.
Hong, G., Dolg, M., and Li, L. (2000) *Int. J. Quantum. Chem.,* **80**, 201–9.
Hong, G., Dolg, M., and Li, L. (2001) *Chem. Phys. Lett.,* **334**, 396–402.
Hunt, and R. D. Andrews, L. (1993) *J. Phys. Chem.,* **98**, 3690–6.
Hunt, R. D., Yustein, J. T., and Andrews, L. (1993) *J. Chem. Phys.,* **98**, 6070–4.
Huzinaga, and S. Cantu, A. A. (1971) *J. Chem. Phys.,* **55**, 5543–9.
Huzinaga, S., Seijo, L., Barandiarán, Z., and Klobukowski, M. (1987) *J. Chem. Phys.,* **86**, 2132–45.
Infante, and I. Visscher, L. (2004a) *J. Comput. Chem.,* **25**, 386–92.
Infante, and I. Visscher, L. (2004b) *J. Chem. Phys.,* **121**, 5783–8.
Ionova, G. V., Mironov, V. S., Spitsyn, V. I., and Pershina, V. G. (1981) *Radiokhimiya,* **23**, 6–11.
Ismail, N., Heully, J.-L., Saue, T., Daudey, J.-P., and Marsden, C. J. (1999) *Chem. Phys. Lett.,* **300**, 296–302.
Jacox, M. E. (1994) *Chem. Phys.,* **189**, 149–70.
Jacox, M. E. (2003) *J. Phys. Chem. Ref. Data,* **32**, 1–441.
Jamorski, C., Casida, M. E., and Salahub, D. R. (1996) *J. Chem. Phys.,* **104**, 5134–47.
Jensen, W. B. (1982) *J. Chem. Educ.,* **59**, 634.
Jansen, G. and Hess, B. A. (1989) *Phys. Rev. A,* **39**, 6016–17.
Janiak, C. and Schumann, H. (1991) *Adv. Organomet. Chem.,* **33**, 291–393.
Jensen, F. (1999) *Introduction to Computational Chemistry,* John Wiley, New York.
Jensen, M. P. and Bond, A. H. (2002) *J. Am. Chem. Soc.,* **124**, 9870–7.
Jones, L. H. and Penneman, R. A. (1953) *J. Chem. Phys.,* **21**, 542–4.
Jones, L. H. and Ekberg, S. (1977) *J. Chem. Phys.,* **67**, 2591–5.
Jørgensen, C. K. (1970) *Prog. Inorg. Chem.,* **12**, 101–58.
Jørgensen, C. K. and Reisfeld, R. (1983) *J. Electrochem. Soc.,* **130**, 681–4.
Joubert, L. and Maldivi, P. (2001) *J. Phys. Chem. A,* **105**, 9068–76.
Kaltsoyannis, N. (1995) *J. Chem. Soc., Dalton Trans.*, 3727–30.
Kaltsoyannis, N. and Bursten, B. E. (1995) *Inorg. Chem.,* **34**, 2735–44.

Kaltsoyannis, N. (1997) *J. Chem. Soc., Dalton Trans.*, 1–11.
Kaltsoyannis, N. and Bursten, B. E. (1997) *J. Organomet. Chem.,* **528**, 19–33.
Kaltsoyannis, N. and Scott, P. (1998) *Chem. Commun.*, 1665–6.
Kaltsoyannis, N. and Scott, P. (1999) *The f-Elements,* Oxford University Press, Oxford.
Kaltsoyannis, N. and Russo, M. R. (2002) *J. Nucl. Sci. Technol.,* Suppl. 3, 393–9.
Kaltsoyannis, N. (2003) *Chem. Soc. Rev.,* **32**, 9–16.
Karraker, D. G., Stone, J. A., Jones, E. R. Jr, and Edelstein, N. M. (1970) *J. Am. Chem. Soc.,* **92**, 4841–5.
Karraker, D. G. (1973) *Inorg. Chem.,* **12**, 1105–8.
Katz, J. J., Seaborg, G. T., and Morss, L. R. (eds.) (1986) *Chemistry of the Actinide Elements,* vol. 2, Chapman & Hall, London.
Katzin, L. I. (1950) *Nature,* **166**, 605.
Kimura, M., Schomaker, V., Smith, D. W., and Weinstock, B. (1968) *J. Chem. Phys.,* **48**, 4001–12.
Kiplinger, J. L., John, K. D., Morris, D. E., Scott, B. L., and Burns, C. J. (2002) *Organometallics,* **21**, 4306–8.
Knappe, P. and Rösch, N. (1990) *J. Chem. Phys.,* **92**, 1153–62.
Koch, W. and Holthausen, M. C. (2001) *A Chemist's Guide to Density Functional Theory,* Wiley-VCH, Weinheim.
Koelling, D. D., Ellis, D. E., and Artlett, R. J. (1976) *J. Chem. Phys.,* **65**, 3931–40.
Kohn, W. and Sham, L. J. (1965) *Phys. Rev.,* **140**, A1133.
Korobkov, I., Gambarotta, S., Yap, G. P. A., Thompson, L., and Hay, P. J. (2001) *Organometallics,* **20**, 5440–5.
Koster, G. F., Dimmock, J. O., Wheeler, R. G., and Staz, H. (1963) *Properties of the Thirty-Two Point Groups,* MIT Press, Cambridge, MA.
Kot, W. K., Shalimoff, G. V., Edelstein, N. M., Edelman, M. A., and Lappert, M. F. (1988) *J. Am. Chem. Soc.,* **110**, 986–7.
Kovács, A. and Konings, R. J. M. (2004) *J. Mol. Struct.* (*Theochem*), **684**, 35–42.
Küchle, W., Dolg, M., Stoll, H., and Preuss, H. (1994) *J. Chem. Phys.,* **100**, 7535–42.
Kushto, G. P., Souter, P. F., Andrews, L., and Neurock, M. (1997) *J. Chem. Phys.,* **106**, 5894–903.
Kushto, G. P., Souter, P. F., and Andrews, L. (1998) *J. Chem. Phys.,* **108**, 7121–30.
Kushto, G. P. and Andrews, L. (1999) *J. Phys. Chem. A,* **103**, 4836–44.
Lander, G. H., Fisher, E. S., and Bader, S. D. (1994) *Adv. Phys.,* **43**, 1–111.
Lauher, J. W. and Hoffmann, R. (1976) *J. Am. Chem. Soc.,* **98**, 1729–42.
Leary, H. J., Rooney, T. A., Cater, E. D., and Friedrich, H. B. (1971) *High Temp. Sci.,* **3**, 433–43.
Lee, Y. S., Ermler, W. C., and Pitzer, K. S. (1977) *J. Chem. Phys.,* **67**, 5861–76.
Lee, C., Yang, W., and Parr, R. G. (1988) *Phys. Rev. B,* **37**, 785–9.
Levine, I. N. (2000) *Quantum Chemistry,* Prentice-Hall, Upper Saddle River, NJ.
Li, J. and Bursten, B. E. (1997) *J. Am. Chem. Soc.,* **119**, 9021–32.
Li, J. and Bursten, B. E. (1998) *J. Am. Chem. Soc.,* **120**, 11456–66.
Li, J. and Bursten, B. E. (1999) *J. Am. Chem. Soc.,* **121**, 10243–4.
Li, J., Bursten, B. E., Zhou, M., and Andrews, L. (2001) *Inorg. Chem.,* **40**, 5448–60.
Li, J., Bursten, B. E., Liang, B. Y., and Andrews, L. (2002) *Science,* **295**, 2242–5.
Li, J., Bursten, B. E., Andrews, L., and Marsden, C. J. (2004) *J. Am. Chem. Soc.,* **126**, 3424–5.

Liang, B. and Andrews, L. (2002) *J. Phys. Chem. A,* **106**, 4038–41.
Liang, B. Y., Andrews, L., Li, J., and Bursten, B. E. (2002) *J. Am. Chem. Soc.,* **124**, 9016–17.
Liang, B. Y., Andrews, L., Li, J., and Bursten, B. E. (2003) *Chem. Eur. J.,* **9**, 4781–8.
Liang, B. Y., Andrews, L., Li, J., and Bursten, B. E. (2004) *Inorg. Chem.,* **43**, 882–94.
Liang, B., Hunt, R. D., Kushto, G. P., Andrews, L., Li, J., and Bursten, B. E. (2005) *Inorg. Chem.,* **44**, 2159–68.
Liu, W., Dolg, M., and Fulde, P. (1997) *J. Chem. Phys.,* **107**, 3584–91.
Liu, W., Wang, F., and Li, L. (2004) Recent advances in molecular theory, in *Recent Advances in Computational Chemistry,* vol. 5 (eds. K. Hirao and S. Ishikawa), World Scientific, Singapore, pp. 257–82.
Lue, C. J., Jin, J., Ortiz, M. J., Rienstra-Kiracofe, J. C., and Heaven, M. C. (2004) *J. Am. Chem. Soc.,* **126**, 1812–15.
MAGIC: Willetts, A., Gagliardi, L., Ioannou, A. G., Simper, A. M., Skylaris, C.-K., Spencer, S., and Handy, N. C. (2000) *Int. Rev. Phys. Chem.,* **19**, 327–62.
Majumdar, D., Balasubramanian, K., and Nitsche, H. (2002) *Chem. Phys. Lett.,* **361**, 143–51.
Makhyoun, M. A., El-Issa, B. D., and Salsa, B. A. (1987) *J. Mol. Struct.* (*Theochem*), **38**, 241–8.
Malli, G. L. (ed.) (1983) *Relativistic Effects in Atoms, Molecules and Solids,* NATO ASI Ser. B, 87, Plenum, New York.
Malmqvist, P.-A., Roos, B. O., and Schimmelpfennig, B. (2002) *Chem. Phys. Lett.,* **357**, 230–40.
Marian, C. M. (2001) *Rev. Comput. Chem.,* **17**, 99–204.
Marks, T. J. (1976) *Acc. Chem. Res.,* **9**, 223–30.
Marks, T. J. (1979) *Prog. Inorg. Chem.,* **25**, 223–333.
Marks, T. J. and Fischer, R. D. (eds.) (1979) *Organometallics of the f-Elements,* NATO Advanced Study Institutes, Series C, *Mathematical and Physical Sciences*, 44, Reidel, Dordrecht.
Marks, T. J. (1982) *Science,* **217**, 989–97.
Maron, L., Leininger, T., Schimmelpfennig, B., Vallet, V., Heully, J.-L., Teichteil, C., Gropen, O., and Wahlgren, U. (1999) *Chem. Phys.,* **244**, 195–201.
Maron, L., Perrin, L., Eisenstein, O., and Andersen, R. A. (2002) *J. Am. Chem. Soc.,* **124**, 5614–15.
Matonic, J. H., Scott, B. L., and Neu, M. P. (2001) *Inorg. Chem.,* **40**, 2638–9.
Matsika, S. and Pitzer, R. M. (2000) *J. Phys. Chem. A,* **104**, 4064–8.
Matsika, S., Pitzer, R. M., and Reed, D. T. (2000) *J. Phys. Chem. A,* **104**, 11983–92.
Matsika, S. and Pitzer, R. M. (2001) *J. Phys. Chem. A,* **105**, 637–45.
Matsika, S., Zhang, Z., Brozell, S. R., Blaudeau, -P., J.Wang, Q., and Pitzer, R. M. (2001) *J. Phys. Chem. A,* **105**, 3825–8.
Matsuoka, O. and Watanabe, Y. (2004) Recent advances in relativistic molecular theory, in *Recent Advances in Computational Chemistry,* vol. 5 (eds. K. Hirao and Y. Ishikawa), World Scientific, Singapore, pp. 247—55.
Matthews, J. R. (1987) *J. Chem. Soc., Faraday Trans. 2,* **83**, 1273–85.
Mazzanti, M., Wietzke, R., Pécaut, J., Latour, J.-M., Maldivi, P., and Remy, M. (2002) *Inorg. Chem.,* **41**, 2389–99.
McDowell, R. S., Asprey, L. B., and Paine, R. T. (1974) *J. Chem. Phys.,* **61**, 3571–80.

McGlynn, S. P. and Smith, J. K. (1961) *J. Mol. Spectrosc.,* **6**, 164–87.
Mochizuki, Y. and Tatewaki, H. (2002) *J. Chem. Phys.,* **116**, 8838–42.
Mochizuki, Y. and Tatewaki, H. (2003) *J. Chem. Phys.,* **118**, 9201–7.
Mochizuki, Y. and Tsushima, S. (2003) *Chem. Phys. Lett.,* **372**, 114–20.
MOLFDIR: Visscher, L., Visser, O., Aerts, P. J. C., Merenga, H., and Nieuwpoort, W. C. (1994) *Comput. Phys. Commun.,* **81**, 120–44. http://theochem.chem.rug.nl/~broer/Molfdir/Molfdir.html
Moll, H., Denecke, M. A., Jalilehvand, F., Sandström, M., and Grenthe, I. (1999) *Inorg. Chem.,* **38**, 1795–9.
Møller, C. and Plesset, M. S. (1934) *Phys. Rev.,* **46**, 618–22.
Motegi, K., Nakajima, T., Hirao, K., and Seijo, L. (2001) *J. Chem. Phys.,* **114**, 6000–6.
Mucci, J. F. and March, N. H. (1985) *J. Chem. Phys.,* **82**, 5099–101.
Nakajima, T. and Hirao, K. (1999) *Chem. Phys. Lett.,* **302**, 383–91.
Nash, C. S. and Bursten, B. E. (1995) *New J. Chem.,* **19**, 669–75.
Nash, C. S., Bursten, B. E., and Ermler, W. C. (1997) *J. Chem. Phys.,* **106**, 5133–42.
Nash, C. S. and Bursten, B. E. (1999) *J. Am. Chem. Soc.,* **121**, 10830–1.
Nash, C. S., Bursten, B. E., and Ermler, W. C. (1999) *J. Chem. Phys.,* **111**, 2347 (erratum).
Navaza, A., Charpin, P., Vigner, D., and Heger, G. (1991) *Acta Crystallogr.,* **C47**, 1842–5.
Neuefeind, J., Soderholm, L., and Skanthakumar, S. (2004) *J. Phys. Chem. A,* **108**, 2733–9.
NWChem: William R. Wiley Environmental Molecular Sciences Laboratory, Pacific Northwest National Laboratory, Richland, Washington.http://www.emsl.pnl.gov/docs/nwchem/nwchem.html
Ohishi, M., Suzuki, H., Ishikawa, S., Yamada, C., Kanamori, H., Irvine, W. M., Brown, R. D., Godfrey, P. D., and Kaifu, N. (1991) *Astrophys. J.,* **380**, L39–42.
Onoe, J., Takeuchi, K., Nakamatsu, H., Mykoyama, T., Sekine, R., Kim, B. I., and Adachi, H. (1993) *J. Chem. Phys.,* **99**, 6810–17.
Ortiz, J. V. (1986) *J. Am. Chem. Soc.,* **108**, 550–1.
Ortiz, J. V., Hay, P. J., and Martin, R. L. (1992) *J. Am. Chem. Soc.,* **114**, 2736–7.
Paine, R. T., McDowell, R. S., Asprey, L. B., and Jones, L. H. (1976) *J. Chem. Phys.,* **64**, 3081–3.
PARAGAUSS: Belling, T., Grauschopf, T., Krüger, S., Nörtemann, F., Staufer, M., Mayer, M., Nasluzov, V. A., Birkenheuer, U., Hu, A., Matveev, A. V., Shor, A. M., Fuchs-Rohr, M. S. K., Neyman, K. M., Ganyushin, D. I., Kerdcharoen, T., Woiterski, A., Gordienko, A. B., Majumder, S., and Rösch, N., Technische Universi•tät München, München, Germany, 2004.
Parry, J., Carmona, E., Coles, S., and Hursthouse, M. (1995) *J. Am. Chem. Soc.,* **117**, 2649–50.
Parry, J. S., Cloke, F. G. N., Coles, S. J., and Hursthouse, M. B. (1999) *J. Am. Chem. Soc.,* **121**, 6867–71.
Paulovic, J., Nakajima, T., Hirao, K., and Seijo, L. (2002) *J. Chem. Phys.,* **117**, 3597–604.
Paulovic, J., Nakajima, T., Hirao, K., Lindh, R., and Malmqvist, P. A. (2003) *J. Chem. Phys.,* **119**, 798–805.
Pepper, M. and Bursten, B. E. (1990) *J. Am. Chem. Soc.,* **112**, 7803–4.

Pepper, M. and Bursten, B. E. (1991) *Chem. Rev.,* **91**, 719–41.
Peralta, J. E. and Scuseria, G. E. (2004) *J. Chem. Phys.,* **120**, 5875–81.
Perdew, J. P., Chevary, J. A., Vosko, S. H., Jackson, K. A., Pederson, M. R., Singh, D. J., and Fiolhais, C. (1992) *Phys. Rev. B,* **46**, 6671–87.
Perdew, J. P. and Wang, Y. (1992) *Phys. Rev. B,* **45**, 13244–9.
Pershina, V. G., Ionova, G. V., and Spitsyn, V. I. (1982) *Radiokhimiya,* **24**, 154–63.
Pershina, V. G. (1996) *Chem. Rev.,* **96**, 1977–2010.
Petersilka, M., Grossmann, U. J., and Gross, E. K. U. (1996) *Phys. Rev. Lett.,* **76**, 1212–15.
Pierloot, K. (2003) *Mol. Phys.,* **101**, 2083–94.
Pitzer, K. S. (1979) *Acc. Chem. Res.,* **12**, 271–5.
Pitzer, R. M. and Winter, N. W. (1988) *J. Phys. Chem.,* **92**, 3061–3.
Pople, J. A., Seeger, R., and Krishna, R. (1977) *Int. J. Quantum. Chem. Symp.,* **11**, 149–63.
Powell, R. E. (1968) *J. Chem. Educ.,* **45**, 558–63.
Privalov, T., Macak, P., Schimmelpfennig, B., Fromager, E., Grenthe, I., and Wahlgren, U. (2004) *J. Am. Chem. Soc.,* **126**, 9801–8.
Pucci, R. and March, N. H. (1986) *Phys. Rev. A,* **33**, 3511–14.
Purvis, G. D. and Bartlett, R. J. (1982) *J. Chem. Phys.,* **76**, 1910–18.
Pyykkö, P. (1978) *Adv. Quantum Chem.,* **11**, 353–409.
Pyykkö, P. and Desclaux, J.-P. (1979) *Acc. Chem. Res.,* **12**, 276–81.
Pyykkö, P. and Lohr, L. L. Jr (1981) *Inorg. Chem.,* **20**, 1950–9.
Pyykkö, P. and Toivonen, H. (1983) *Tables of Representation and Rotation Matrices for the Relativistic Irreducible Representations of 38 Point Groups, Acta Acad. Aboensis,* Ser. B, No. 2, Åbo Akademi, Åbo, Finland.
Pyykkö, P. (1986) Relativistic theory of atoms and molecules. A bibliography 1916–1985, in *Lecture Notes in Chemistry*, vol. 41, Springer-Verlag, Berlin.
Pyykkö, P. (1988) *Chem. Rev.,* **88**, 563–94.
Pyykkö, P., Laakkonen, L. J., and Tatsumi, K. (1989) *Inorg. Chem.,* **28**, 1801–5.
Pyykkö, P. and Zhao, Y. (1991) *Inorg. Chem.,* **30**, 3787–8.
Pyykkö, P. (1993) Relativistic theory of atoms and molecules II. A bibliography 1986–1992, in *Lecture Notes in Chemistry*, vol. 60, Springer-Verlag, Berlin.
Pyykkö, P., Li, J., and Runeberg, N. (1994) *J. Phys. Chem.,* **98**, 4809–13.
Pyykkö, P. (2000a) *Science,* **290**, 117–18.
Pyykkö, P. (2000b) Relativistic theory of atoms and molecules III. A bibliography 1993–1999, in *Lesture Notes in Chemistry*, vol. 76, Springer-Verlag, Berlin.
Pyykkö, P., Runeberg, N., Straka, M., and Dyall, K. G. (2000) *Chem. Phys. Lett.,* **328**, 415–19.
Raghavachari, K., Trucks, G. W., Pople, J. A., and Head-Gordon, M. (1989) *Chem. Phys. Lett.,* **157**, 479–83.
Reich, T., Bernhard, G., Geipel, G., Funke, H., Heining, C., Rosber, A., Matz, W., Schnell, N., and Nitsche, H. (2000) *Radiochim. Acta,* **88**, 633–7.
Reynolds, L. T. and Wilkinson, G. (1956) *J. Inorg. Nucl. Chem.,* **2**, 246–53.
Roesky, P. W. (2001) *Eur. J. Inorg. Chem.*, 1653–60.
Roos, B. O., Widmark, P.-O., and Gagliardi, L. (2003) *Faraday Discuss.,* **124**, 57–62.
Roos, B. O. and Malmqvist, P.-A. (2004) *Phys. Chem. Chem. Phys.,* **6**, 2919–27.
Rösch, N. and Streitweiser, A. J. (1983) *J. Am. Chem. Soc.,* **105**, 7237–40.

Rösch, N., Kruger, S., Mayer, M., and Nasluzov, V. A. (1996) *Theor. Comput. Chem.,* **4**, 497–566.

Roussel, P. and Scott, P. (1998) *J. Am. Chem. Soc.,* **120**, 1070–1.

Roussel, P., Errington, W. B., Kaltsoyannis, N., and Scott, P. (2001) *J. Organomet. Chem.,* **635**, 69–74.

Sankaran, K., Sundararajan, K., and Viswanathan, K. S. (2001) *J. Phys. Chem. A,* **105**, 3995–4001.

Saue, T., Fægri, K., Helgaker, T., and Gropen, O. (1997) *Mol. Phys.,* **91**, 937–50.

Schlosser, F., Kruger, S., and Rösch, N. (2003) *Eur. J. Inorg. Chem.*, **17**, 3144–51.

Schneider, W. F., Strittmatter, R. J., Bursten, B. E., and Ellis, D. E. (1991) in *Density Functional Methods in Chemistry* (eds. J. K. Labanowski and J. W. Andzelm), Springer-Verlag, New York, pp. 247–60.

Schreckenbach, G., Hay, P. J., and Martin, R. L. (1998) *Inorg. Chem.,* **37**, 4442–51.

Schreckenbach, G., Hay, P. J., and Martin, R. L. (1999) *J. Comput. Chem.,* **20**, 70–90.

Schreckenbach, G. (2000) *Inorg. Chem.,* **39**, 1265–74.

Schwarz, W. H. E. (1990) in *Theoretical Models of Chemical Bonding* (ed. Z. B. Maksic), Springer-Verlag, Berlin p. 595.

Schwerdtfeger, P. (ed.) (2002) *Relativistic Electronic Structure Theory: Part I, Fundamentals Theoretical and Computational Chemistry,* vol. 11, , Elsevier Science B. V., Amsterdam.

Schwerdtfeger, P. (ed.) (2004) *Relativistic Electronic Structure Theory, Part II: Applications Theoretical and Computational Chemistry,* vol. 14, Elsevier Science B. V., Amsterdam.

Seidel, S. and Seppelt, K. (2000) *Science,* **290**, 117–18.

Seijo, L. and Barandiarán, Z. (1999) in *Computational Chemistry: Reviews of Current Trends*, vol. 4, (ed. J. Leszczynski), World Scientific, Singapore, pp. 55–152.

Seijo, L. and Barandiarán, Z. (2001) *J. Chem. Phys.,* **115**, 5554–60.

Seijo, L., Barandiarán, Z., and Harguindey, E. (2001) *J. Chem. Phys.,* **114**, 118–29.

Seijo, L., Barandiarán, Z., and Ordejon, B. (2003) *Mol. Phys.,* **101**, 73–80.

Seip, H. M. (1965) *Acta Chem. Scand.,* **19**, 1955–68.

Seyferth, D. (2004) *Organometallics,* **23**, 3562–83.

Shavitt, I. (1977) in *Methods of Electronic Structure Theory* (ed. H. F. Schaefer III), Plenum, New York, pp. 189–276.

Shepard, R., Shavitt, I., Pitzer, R. M., Comeau, D. C., Pepper, M., Lischka, H., Szalay, P. G., Ahlrichs, R., Brown, F. B., and Zhao, J. G. (1988) *Int. J. Quantum Chem., Quantum Chem. Symp.,* **22**, 149–65.

Slater, J. L., Sheline, R. K., Lin, K. C., and Weltner, J. W. (1971) *J. Chem. Phys.,* **55**, 5129–30.

Slater, J. C. (1974) *The Self-Consistent Field for Molecules and Solids,* McGraw-Hill, New York.

Smith, G. M., Suzuki, H., Sonnenberger, D. C., Day, V. W., and Marks, T. J. (1986) *Organometallics,* **5**, 549–61.

Soderlind, P. (1998) *Adv. Phys.,* **47**, 959–98.

Solar, J. P., Burghard, H. P. G., Banks, R. H., Streitwieser, A. Jr., and Brown, D. (1980) *Inorg. Chem.,* **19**, 2186–8.

Sonnenberg, J. L., Hay, P. J., Martin, R. L., and Bursten, B. E. (2005) *Inorg. Chem.,* **44**, 2255–62.

Spencer, S., Gagliardi, L., Handy, N. C., Ioannou, A. G., Skylaris, C.-K., Willets, A., and Simper, A. M. (1999) *J. Phys. Chem. A,* **103**, 1831–7.
Sternal, R. S., Brock, C. P., and Marks, T. J. (1985) *J. Am. Chem. Soc.,* **107**, 8270–2.
Sternal, R. S. and Marks, T. J. (1987) *Organometallics,* **6**, 2621–3.
Straka, M., Dyall, K. G., and Pyykko, P. (2001) *Theor. Chem. Acc.,* **106**, 393–403.
Straka, M., Patzschke, M., and Pyykko, P. (2003) *Theor. Chem. Acc.,* **109**, 232–40.
Streitwieser, A. J. and Müller-Westerhoff, U. (1968) *J. Am. Chem. Soc.,* **90**, 7364.
Streitwieser, A. Jr. (1979) in *Organometallics of the f-Elements* (eds. T. J. Marks and R. D. Fischer), Reidel, Dortrecht, pp. 149–77.
Streitwieser, A. Jr. (1984) *Inorg. Chim. Acta,* **94**, 171–7.
Streitwieser, A. Jr. and Kinsley, S. A. (1985) *NATO ASI Ser. C,* **155**, 77–114 and references therein.
Strittmatter, R. J. and Bursten, B. E. (1991) *J. Am. Chem. Soc.,* **113**, 552–9.
Szabo, A. and Ostlund, N. S. (1989) *Modern Quantum Chemistry: Introduction to Advanced Electronic Structure Theory,* McGraw-Hill, New York.
Tague, T. J., Andrews, L., and Hunt, R. D. (1993) *J. Phys. Chem.,* **97**, 10920–4.
Tait, C. D. (1999) The Convergence of Theory and Experiment, Presented at the Symposium of Heavy Element Complexes, 217th ACS National Meeting, Anaheim, CA.
Tatsumi, K. and Hoffmann, R. (1980) *Inorg. Chem.,* **19**, 2656–8.
Tatsumi, K. and Nakamura, A. (1984) *J. Organomet. Chem.,* **272**, 141–53.
Tatsumi, K., Nakamura, A., Hofmann, P., Stauffert, P., and Hoffmann, R. (1985) *J. Am. Chem. Soc.,* **107**, 4440–51.
Tatsumi, K. and Nakamura, A. (1987) *J. Am. Chem. Soc.,* **109**, 3195–206.
Teichteil, C., Pelissier, M., and Spiegelmann, F. (1983) *Chem. Phys.,* **81**, 273–82.
Teichteil, C. and Spiegelmann, F. (1983) *Chem. Phys.,* **81**, 283–96.
Tsushima, S. and Suzuki, A. (1999) *J. Mol. Struct*. (*Theochem*), **487**, 33–8.
Tsushima, S., Yang, T., Mochizuki, Y., and Okamoto, Y. (2003) *Chem. Phys. Lett.,* **375**, 204–12.
TURBOMOLE: Quantum Chemistry Group, University of Karlsruhe, Karlsruhe, Germany. http://www.turbomole.com
Vallet, V., Maron, L., Schimmelpfennig, B., Leininger, T., Teichteil, C., Gropen, O., Grenthe, I., and Wahlgren, U. (1999a) *J. Phys. Chem. A,* **103**, 9285–9.
Vallet, V., Schimmelpfennig, B., Maron, L., Teichteil, C., Leininger, T., Gropen, O., Grenthe, I., and Wahlgren, U. (1999b) *Chem. Phys.,* **244**, 185–93.
Vallet, V., Maron, L., Teichteil, C., and Flament, J.-P. (2000) *J. Chem. Phys.,* **113**, 1391–402.
Vallet, V., Wahlgren, U., Schimmerlpfenning, B., Szabo, Z., and Grenthe, I. (2001) *J. Am. Chem. Soc.,* **123**, 11999–2008.
Vallet, V., Privalov, T., Wahlgren, U., and Grenthe, I. (2004) *J. Am. Chem. Soc.,* **126**, 7766–7.
Van der Sluys, W. G., Burns, C. J., and Sattelberger, A. P. (1989) *Organometallics,* **8**, 855–7.
van Gisbergen, S. J. A., Snijders, J. G., and Baerends, E. J. (1995) *J. Chem. Phys.,* **103**, 9347.
van Lenthe, E., Baerends, E. J., and Snijders, J. G. (1993) *J. Chem. Phys.,* **99**, 4597–610.
van Lenthe, E., Baerends, E. J., and Snijders, J. G. (1994) *J. Chem. Phys.,* **101**, 9783–92.

van Wezenbeek, E. M., Baerends, E. J., and Snijders, J. G. (1991) *Theor. Chem. Acc.,* **81**, 139–55.
van Wullen, C. (1999) *J. Comput. Chem.,* **20**, 51–62.
Vázquez, J., Bo, C., Poblet, M. M., de Pablo, J., and Bruno, J. (2003) *Inorg. Chem.,* **42**, 6136–41.
Volkoy, Y. F. and Kapshuhof, I. I. (1976) *Radiokhimiya,* **18**, 284.
Wadt, W. R. (1981) *J. Am. Chem. Soc.,* **103**, 6053–7.
Wahlgren, U., Schimmelpfennig, B., Jusuf, S., Stromsnes, H., Gropen, O., and Maron, L. (1998) *Chem. Phys. Lett.,* **287**, 525–30.
Wahlgren, U., Moll, H., Grenthe, I., Schimmelpfennig, B., Maron, L., Vallet, V., and Gropen, O. (1999) *J. Phys. Chem. A,* **103**, 8257–64.
Wang, F., Hong, G. Y., and Li, L. M. (2000) *Chem. Phys. Lett.,* **316**, 318–23.
Wang, Q. and Pitzer, R. M. (2001) *J. Phys. Chem. A,* **105**, 8370–5.
Wang, X., Andrews, L., Li, J., and Bursten, B. E. (2004) *Angew. Chem. Int. Edn.,* **43**, 2554–7.
Warner, B. P., Scott, B. L., and Burns, C. J. (1998) *Angew. Chem. Int. Edn. Engl.,* **37**, 959–60.
Watts, J. D., Gauss, J., and Bartlett, R. J. (1993) *J. Chem. Phys.,* **98**, 8718–33.
Wigner (1959) *Group Theory and its Application to the Quantum Mechanics of Atomic Spectra,* Academic Press, New York.
Wilkinson, G., Rosenblum, M., Whiting, M. C., and Woodward, R. B. (1952) *J. Am. Chem. Soc.,* **74**, 2125–6.
Wilkinson, G. (1975) *J. Organomet. Chem.,* **100**, 273–8.
Williams, C. W., Blaudeau, J.-P., Sullivan, J. C., Antonio, M. R., Bursten, B. E., and Soderholm, L. (2001) *J. Am. Chem. Soc.,* **123**, 4346–7.
Wills, J. M. and Eriksson, O. (2000) *Los Alamos Sci.,* **26**, 129–51.
Winter, N. W. and Pitzer, R. M. (1985) *Springer Ser. Opt. Sci.* (*Tunable Solid State Lasers*), **47**, 164–71.
Wood, J. H. and Boring, A. M. (1978) *Phys. Rev. B,* **18**, 2701–11.
Wood, J. H., Boring, M., and Woodruff, S. B. (1981) *J. Chem. Phys.,* **74**, 5225–33.
Wybourne, B. G. (1965) *Spectroscopic Properties of the Rare Earths,* Interscience, New York.
Yabushita, S., Zhang, Z., and Pitzer, R. M. (1999) *J. Phys. Chem. A,* **103**, 5791–800.
Yang, C. Y., Johnson, K. H., and Horsley, J. A. (1978) *J. Chem. Phys.,* **68**, 1001–5.
Yang, T., Tsushima, S., and Suzuki, A. (2001) *J. Phys. Chem. A,* **105**, 10439–45.
Zhang, Z. and Pitzer, R. M. (1999) *J. Phys. Chem. A,* **103**, 6880–6.
Zhou, M. F. and Andrews, L. (1999) *J. Chem. Phys.,* **111**, 11044–9.
Zhou, M. F., Andrews, L., Li, J., and Bursten, B. E. (1999a) *J. Am. Chem. Soc.,* **121**, 9712–21.
Zhou, M. F., Andrews, L., Li, J., and Bursten, B. E. (1999b) *J. Am. Chem. Soc.,* **121**, 12188–9.
Zhou, M., Andrews, L., Ismail, N., and Marsden, C. (2000) *J. Phys. Chem. A,* **104**, 5495–502.
Zhou, M., Andrews, L., and Bauschlicher, C. W. Jr (2001) *Chem. Rev.,* **101**, 1931–62.
Ziegler, T., Tschinke, V., Baerends, E. J., Snijders, J. G., and Ravenek, W. (1989) *J. Phys. Chem.,* **93**, 3050–6.

CHAPTER EIGHTEEN

OPTICAL SPECTRA AND ELECTRONIC STRUCTURE

Guokui Liu and James V. Beitz

18.1 INTRODUCTION

Much of our knowledge of the electronic properties of actinides in solutions and solids is obtained from optical spectroscopy. One of the features that sets actinide spectra apart from those of other elements in the periodic table, aside from the lanthanide series, is that their f-orbitals can be considered both as containing optically active electrons and as belonging to the core of inner shells. As a result of this dominant characteristic, the spectra of these elements, particularly of the lower valence states, are moderately insensitive to changes in the ionic environment. Although ion–ligand interactions shift and split the energy levels of the f-orbitals, the scale of this crystal-field splitting is generally smaller than the intra-ionic Coulomb interaction and spin–orbit coupling. The relative insensitivity of these f-electrons to external forces also means that for these elements there is a close connection between energy levels in compounds and those in gaseous free atoms and ions. Table 18.1 lists the scales of various mechanisms of electronic interactions that will be discussed in this chapter through analysis and modeling of the optical spectra of the various valence states of actinide ions in solutions and compounds.

Table 18.1 *Energy level scales of actinide ions in crystals.*

Interaction mechanism	*Energy* (cm^{-1})[a]	*Optical probe*
configuration splitting ($5f^N$–$5f^{N-1}6d$)	10^5	visible and UV spectroscopy
splitting within a $5f^N$ configuration		
noncentral electrostatic field	10^4	absorption, fluorescence, and laser excitation spectroscopy
spin–orbit interaction	10^3	
crystal-field interaction	10–10^2	
hyperfine splitting	10^{-3}–10^{-1}	selective and nonlinear laser spectroscopy

[a] 1 eV = 8065.7 cm^{-1}.

For the actinide valence states of most interest to chemists, 1+ through 7+, very few gaseous free-ion spectra have been sufficiently analyzed to provide a basis for guiding theoretical interpretations. From an experimental point of view, optical spectroscopy usually probes energy levels with photon sources in the infrared, visible, and ultraviolet (UV) region with energies below 45 000 cm^{-1}. This situation is responsible for the fact that most of our structural information for the f^N states comes from observation of forced electric dipole absorption and luminescence transitions in optically clear crystals. The latter analysis is much simplified by the fact that only transitions between nominal f^N levels are involved. Electric dipole transitions normally are forbidden by the parity selection rule, but in crystals such as $LaCl_3$ that have no center of symmetry, enough of the character of opposite-parity configurations can be mixed in to induce such transitions. At the same time, the admixture (of the order 0.1%) is small enough for the actinide ions in low-lying states of a $5f^N$ configuration that the f-character of the levels is preserved and level calculations can be made on the assumption of a pure $5f^N$ configuration.

The stability of f-orbitals against changes in the ionic environment results in energy levels of various compounds being closely correlated among themselves as well as with those of the free ion, where known. In consequence, *ab initio* free-ion calculations have proven to be very useful for interpreting spectra of the same ion in a solid, and a parametric model based on these calculations has been developed for systematic analyses of the $4f^N$ (lanthanides) (Crosswhite, 1977; Carnall *et al.*, 1989) and $5f^N$ (actinides) (Carnall, 1992; Liu *et al.*, 1994b) optical spectra. This model can be applied in a consistent way to ions of both the actinide and lanthanide series (Crosswhite and Crosswhite, 1984; Görller-Walrand and Binnemans, 1996; Liu, 2000). The free-ion energy levels for trivalent actinide ions in $5f^N$ ($N = 2$ through 13) configurations may be calculated using the parametric model as shown in Fig. 18.1 by the horizontal lines.

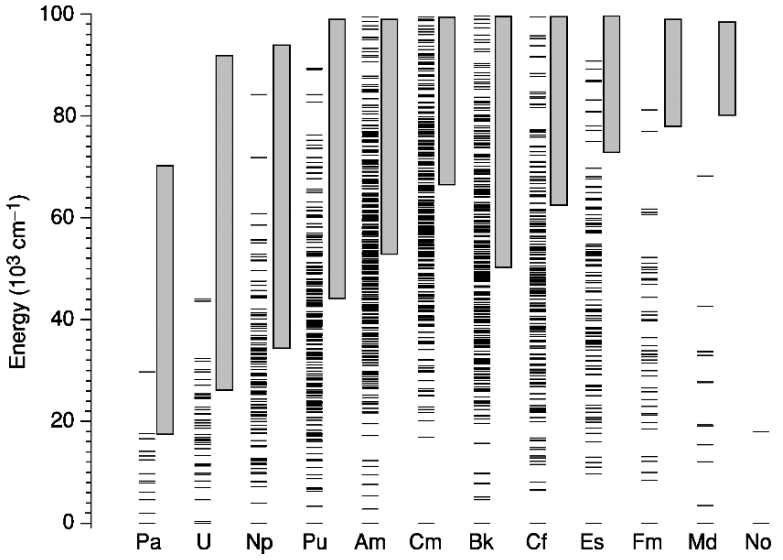

Fig. 18.1 *Calculated free-ion energy levels* (*horizontal lines*) *for the trivalent ions in the* $5f^N$*configurations and the energy range* (*shaded vertical bars*) *for the excited configurations.*

The method of parametric modeling is discussed here to help systematize the overall view of actinide spectra. This chapter is based primarily on Chapter 16 by Carnall and Crosswhite in the second edition of this series. In this review advances in actinide spectroscopy are updated, and in particular, recent progress in the optical spectroscopy of trivalent and tetravalent actinide ions in crystals are included. Our emphasis is on the fundamental understanding of actinide spectra that are interpreted by a parametric model in terms of free-ion and crystal-field interactions (Wybourne, 1965a; Hüfner, 1978; Judd, 1988).

With the experimental techniques used, highly excited states belonging to many different configurations may be produced simultaneously, making interpretation difficult. The estimated energy ranges of the $5f^{N-1}6d$, $5f^{N-1}7s$, and $5f^{N-1}7p$ configurations are plotted in Fig. 18.1 as gray bars for comparison with the calculated energy levels of the free-ion states of the $5f^N$ configurations of trivalent actinide ions (Brewer, 1971a). It is obvious that large portions of the upper states of $5f^N$ configurations overlap with the low-lying states of $5f^{N-1}6d$, $5f^{N-1}7s$, and $5f^{N-1}7p$ configurations. Therefore, a major complicating factor in the theoretical interpretation of $5f^N$ spectra is the extensive inter-configurational mixing, often termed as configurational interaction (Wybourne, 1965a; Dieke, 1968; Goldschmidt, 1978; Hüfner, 1978; Crosswhite and Crosswhite, 1984).

These effects of mixing other configurations into the $5f^N$ states involve not only competing configurations with large overlaps but also cumulative interactions with infinitely many distant electronic configurations. That this is a serious problem is demonstrated by analysis of isotope shifts and hyperfine structure in actinide free-ion spectra (Fred, 1967). The parameters that describe the energy level structure for a configuration would show less variation if the independent-particle model provided a fully accurate description of actinide free-ion spectra. In the parametric model for f-element spectral analysis, the effects of configuration interaction are partially compensated by the use of effective operators in the atomic Hamiltonian for f^N shells (Wybourne, 1965a; Judd, 1966, 1968a,b; Crosswhite *et al.*, 1968; Goldschmidt, 1978; Poon and Newman, 1983; Judd and Crosswhite, 1984; Judd and Suskin, 1984).

Qualitatively, the spectroscopic properties of lanthanides and actinides are very similar because both f-shell electron densities are primarily within already filled s- and p-shells of one higher principal quantum number, which partially shield the f-shells from external influences. A comparison of the Nd^{3+} and U^{3+} analogs is shown in Fig. 18.2, where the squares of the f-electron radial functions are multiplied by an arbitrary factor for emphasis. The same theoretical framework has been used successfully in modeling solid-state spectra of trivalent (Edelstein *et al.*, 1967; Carnall, 1989) and tetravalent actinides (Edelstein, 1987; Krupa, 1987; Liu *et al.*, 1994b; Liu, 2000), as well as for the lanthanide series (Crosswhite, 1977; Carnall *et al.*, 1989; Görller-Walrand and Binnemans, 1996).

Notice that in Fig. 18.2 for U^{3+} (relative to Nd^{3+} $4f^3$) the $5f^3$ peak is considerably displaced toward greater r values with respect to the shielding of s- and p-shells, and the relative magnitude of the 5f electron tail at large r with respect to the rest of the core function is larger and more exposed. Because of the greater extension of the 5f orbitals with respect to those of the shielding 6s and 6p shells, they are more sensitive to changes in the valence electron situation than is the case for the corresponding lanthanide ions. As a result, actinides in solution and in solids, particularly in the first half of the $5f^N$ series, appear in different valence states from 3+ to 6+, making 5f spectroscopy extremely rich and complicated.

18.2 RELATIVE ENERGIES OF ACTINIDE ELECTRONIC CONFIGURATIONS

In order to emphasize the systematic correlations found in the energy level structure of actinide ions both as a function of atomic number Z and for configurations with the same number of f-electrons but different charge states, we begin by considering the types of interactions that have been used successfully to account for observed energy level structures. In the discussion of atomic spectra, attention is focused on identification of the ground (lowest-energy) and

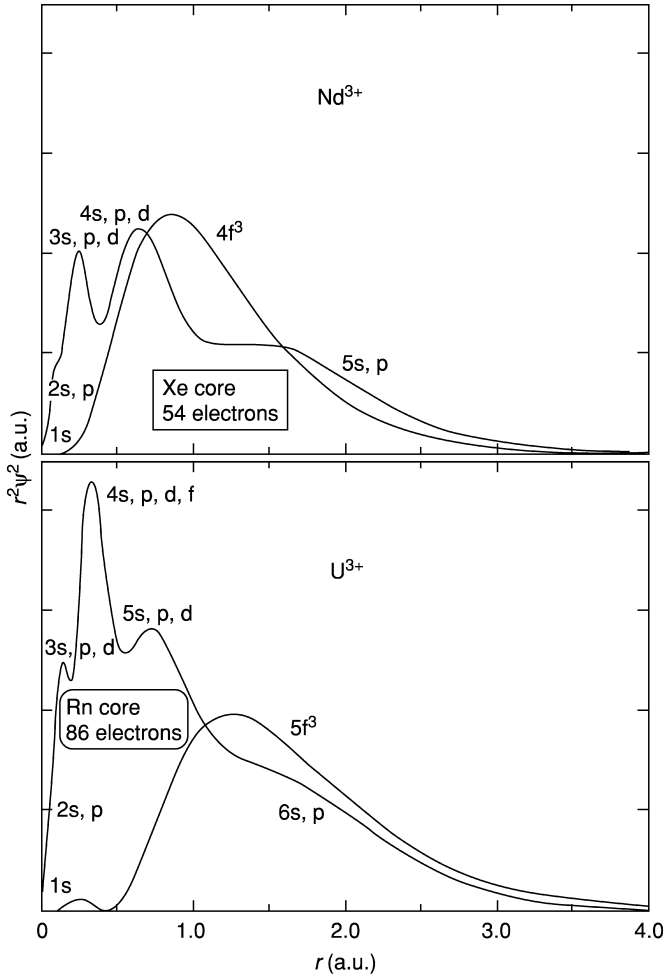

Fig. 18.2 *Comparison of the overlap of* $4f^3$–$5s,p$ *configurations and those of* $5f^3$–$6s,p$ *configurations for* Nd^{3+} *and* U^{3+}, *respectively.*

excited electronic configurations of neutral as well as ionized species. The relative energies of the various electronic configurations thus established provide the basis for extending the interpretation of spectra (and thus electronic structure) to condensed media. In gaseous atomic or ionic species, the energy level structure is attributed primarily to the interactions between electrons in unfilled shells. In condensed media, the additional effect of the ligand field is superimposed. Several summaries of the atomic spectra of the actinides have been published (Kanellakopulos and Fischer, 1973; Peterson, 1976;

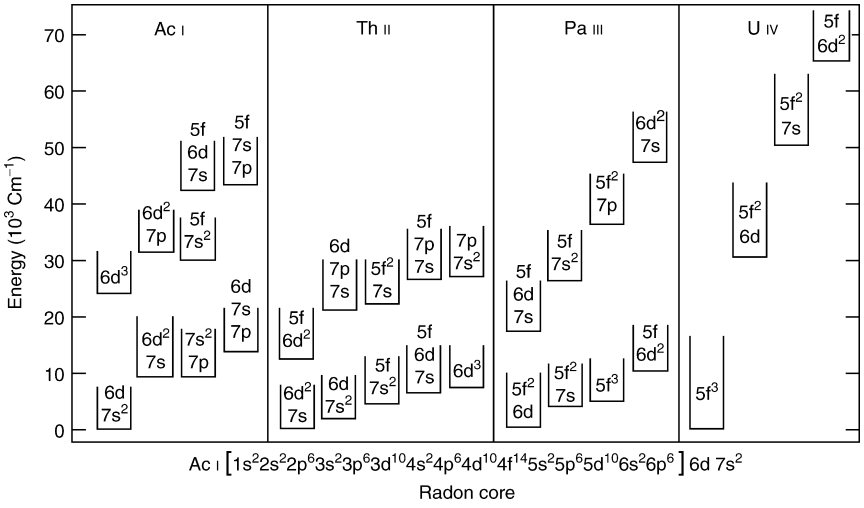

Fig. 18.3 *Three-electron configurations beyond the radon core.*

Crosswhite, 1982; Blaise *et al.*, 1983; Crosswhite and Crosswhite, 1984; Worden *et al.*, 2005).

The progenitor of the actinide (5f) series is actinium. The electronic structure of zero-valent actinium Ac I[1] is represented as three electrons ($6d7s^2$) outside the radon core. This can be written [Rn] ($6d7s^2$), but in the subsequent discussion the core symbol [Rn] will be omitted from the notation. All of the actinide atomic and ionic species are built on the radon core, but the properties of the electronic structure beyond the core depend on the energy with respect to the ground state, atomic number Z, and the state of ionization (Brewer, 1971a,b, 1983). Thus, within the energy range indicated in Fig. 18.3, in addition to configurations involving 6d and 7s electrons, there are those containing 7p and 5f electrons.

Fig. 18.3 is to be interpreted in the following manner. In Ac I the lowest-energy electron states result from the coupling of two 7s electrons and one 6d electron. Further, an energy equivalent to about 9000 cm^{-1} is sufficient to promote a ground-state 7s electron to the 6d shell, thus forming the lowest level of the excited configuration ($6d^27s$). Essentially the same energy is required to promote a ground-state 6d electron to the 7p shell, giving the excited configuration ($7s^27p$). Only the lowest-energy state (relative to the ground state) for each configuration is indicated in the figure. In most cases large numbers of excited states exist within each of the configurations, so that the density of levels from overlapping configurations increases appreciably with

[1] In atomic spectroscopy, Roman letters I, II, III, IV,...refer to ionic oxidation states 0, 1+, 2+, 3+,... respectively, while in some chemistry literature, notations such as An(I) refers to An^+.

excitation energy. However, since the coupling of two 7s electrons result in a filled subshell, the ground configuration in Ac I ($6d7s^2$) is simple in structure, involving only the states of a single 6d electron, $^2D_{3/2}$ and $^2D_{5/2}$. Such states, written in terms of the quantum numbers S, L, and J, are subsequently referred to as free-ion states.

In Th II, the ground state belongs to $6d^27s$, but as Fig. 18.3 indicates, the spectrum at lower energies is very complex due to a number of electronic configurations with nearly the same energy relative to the ground state. In Pa III, the three electrons beyond the Rn core in the ground state belong to the $5f^26d$ configuration. In U IV, further stabilization of the 5f orbital has taken place and excited configurations occur at much higher energies relative to the ground state than was the case in Pa III, Th II, and Ac I. Thus in U IV, the only electronic transitions observed in absorption in the range up to ~30 000 cm^{-1} are those *within* the $5f^3$ configuration.

Experimentally, free-ion spectra (for both neutral and ionic species) usually have been observed in emission, and the underlying energy level structures are deduced from coincidences of energy differences of pairs of spectral lines, subject to verification by isotope shift, hyperfine structure, and magnetic g-factor tests. In condensed phases, spectra are more commonly measured in absorption. Since the application of tunable lasers, laser-induced fluorescence spectra and excitation spectra also have been used in condensed phases to probe energy levels of actinide ions that possess a metastable emitting state. Relative intensities associated with 'parity-allowed' and 'forbidden' transitions are reflected in the nature of two processes: transitions in which the initial and final states belong to electronic configurations of different parity (parity-allowed transitions, e.g. $5f^3 \rightarrow 5f^26d$) and those in which both states belong to the same configuration (parity-forbidden transitions, e.g. $5f^3 \rightarrow 5f^3$). The latter are weak and sharp. The former are much more intense and are associated with broader absorption bands.

The primary purpose of this chapter is to elucidate the electronic energy level structure of the $5f^N$ configurations of actinide ions in condensed phases. The energy levels of trivalent and tetravalent actinide ions in $5f^N$ configurations spread up to ~100 000 cm^{-1} for $4 \leq N \geq 10$, and even extend higher than 150 000 cm^{-1} for $N = 6, 7, 8$. However, as shown in Fig. 18.3, the energy levels of the excited state configurations, specifically, $5f^{N-1}6d$, $5f^{N-1}7s$, and $5f^{N-1}7p$ are present below 100 000 cm^{-1} and thus overlap the energy levels of the $5f^N$ states. This overlap induces complexity in modeling the energy level structures, since the commonly used theory treats the inter-configurational coupling as a perturbation, an approximation that is valid only when the respective configurations are well separated. In this section, a systematic comparison of the energies between the ground states of $5f^N$ configurations and the higher-lying energy configurations that are accessible via optical excitation is given. The energy required to promote an electron from a 5f to a 6d orbital varies rapidly in an irregular manner as the nuclear charge is increased, but a large portion of the

variation and most of the irregularity can be attributed to the pairing energy within the $5f^N$ configuration (Jørgensen, 1975, 1980). A method of using thermodynamic and spectroscopic data for calculating energies of various electronic configurations of lanthanide and actinide ions was developed by Brewer (1971a,b).

For the case of electrons in a 6d orbital, ion–lattice coupling is much stronger than for a 5f orbital. As a result, the energy levels of the $5f^{N-1}6d$ configuration exhibits much stronger host dependence than that of the $5f^N$ configurations. Systematic variation of the $5f^{N-1}6d$ energy level structures for trivalent lanthanide ions in CaF_2 was measured in ultraviolet absorption spectra (Loh, 1966). (van Peterson *et al.*, 2002) conducted further experimental measurements and theoretical modeling of the inter-configuration $4f^N$ to $4f^{N-1}5d$ transitions of rare earth (RE) ions in $LiYF_4$ and YPO_4. For actinide ions, extensive studies of $5f^N$ to $5f^{N-1}6d$ transitions are limited to the $5f^1$ and $5f^2$ configurations. The 6d states of Pa^{4+} in several crystalline hosts were measured based on observed 5f−6d electronic transitions (Piehler *et al.*, 1991; Edelstein *et al.*, 1992). The lowest-energy level of the 6d state is only $\sim$20 000 cm^{-1} above the ground state of Pa^{4+}. In the series of $5f^1$ ions, the differences between the lowest 6d energy level and the ground $5f^1$ level for U^{5+} and Np^{6+} increase as do the total splittings of the 5f energy levels with atomic number (Carnall and Crosswhite, 1985).

18.3 MODELING OF FREE-ION INTERACTIONS

The well-developed theoretical framework for modeling the electronic interactions and analyzing the optical spectra of lanthanide ions has been adopted to modeling the actinides because of the similarities in the electronic properties of actinides in the $5f^N$ configurations and the lanthanides in the $4f^N$ configurations (Crosswhite, 1977; Edelstein, 1979, 1995; Carnall and Crosswhite, 1985; Carnall *et al.*, 1991; Liu *et al.*, 1994b; Liu, 2000). In this section a brief review of the free-ion part of the model theory and its applications to actinide spectroscopy is given.

18.3.1 Central field approximation

Interpretation of optical spectra of actinides in condensed phases follows the general approach in atomic spectroscopy that utilizes the central field approximation and Hartree–Fock method (Hartree, 1957; Slater, 1960; Weissbluth, 1978). In the central field approximation, each electron is assumed to move independently in the field of the nucleus and a central field made up of the spherically averaged potential fields of each of the other electrons. The non-spherical part of the electronic interactions is treated as a perturbation to a spherically symmetric potential, so that the basis of the hydrogen atom wave functions can be used to construct the eigenstates of an N-electron atom (ion). The same method has been used to classify electronic states and evaluate energy levels of lanthanide and actinide ions (Judd, 1963b; Wybourne, 1965a).

The primary terms of the Hamiltonian for an N-electron ion in the absence of external fields are commonly expressed as

$$\mathscr{H} = \mathscr{H}_0 + \mathscr{H}_{\mathrm{C}} + \mathscr{H}_{\mathrm{S-O}}, \tag{18.1}$$

where

$$\mathscr{H}_0 = -\sum_{i=1}^{N} \frac{\hbar^2}{2m} \boldsymbol{\nabla}_i^2 - \sum_{i=1}^{N} \frac{Ze^2}{r_i}, \tag{18.2}$$

$$\mathscr{H}_{\mathrm{C}} = \sum_{i<j}^{N} \frac{e^2}{r_{ij}}, \tag{18.3}$$

$$\mathscr{H}_{\mathrm{S-O}} = \sum_{i}^{N} \xi(r_i) \boldsymbol{l}_i \cdot \boldsymbol{s}_i. \tag{18.4}$$

In equation (18.2), the first term is the kinetic energy and the second term is the potential energy of the electrons in the field of the nucleus. All levels that belong to a particular configuration are shifted equally by this term, which is purely radial, without affecting the energy level structure of the configuration. The term $\mathscr{H}_{\mathrm{C}}$ in equation (18.3) represents the inter-electron Coulombic repulsion between a pair of electrons at a distance of r_{ij}, which varies for different states of the same configuration. The term $\mathscr{H}_{\mathrm{S-O}}$ describes the spin–orbit interactions, which can be understood as magnetic dipole–dipole interactions between the spin and angular momenta of the electrons. In equation (18.4), the spin–orbit coupling constant $\xi(r_i)$ is defined as solely a function of r_i.

Exact solutions of Schrödinger's equation are not possible for systems with more than one electron. In the framework of the central field approximation, one assumes that it is possible to construct a potential energy function $U(r_i)$, which is a spherically symmetric, one-electron operator, and is a good approximation to the actual potential energy of the electron i in the field of the nucleus and the other $N-1$ electrons. Therefore, $\mathscr{H}_0$ can be replaced by (Weissbluth, 1978)

$$\mathscr{H}_0' = \sum_{i=1}^{N} \left[-\frac{\hbar^2}{2m} f \boldsymbol{\nabla}_i^2 + U(r_i) \right], \tag{18.5}$$

with

$$\sum_{i=1}^{N} U(r_i) = -\sum_{i=1}^{N} \frac{Ze^2}{r_i} + \left\langle \sum_{i<j}^{N} \frac{e^2}{r_{ij}} \right\rangle. \tag{18.6}$$

The second term in equation (18.6) is an average over a sphere of the electron repulsion. This term is therefore independent of the angular coordinates. Since $\mathscr{H}_0'$ contains the kinetic energy, the potential energy of N-electrons, and most of the inter-electron repulsion, it is called the Hamiltonian of the central

field. Since most of the inter-electron repulsion is included in the central field Hamiltonian equation (18.5), the second term in equation (18.1) can be rewritten as

$$\mathscr{H}'_{\mathrm{c}} = \sum_{i<j}^{N} \frac{e^2}{r_{ij}} - \left\langle \sum_{i<j}^{N} \frac{e^2}{r_{ij}} \right\rangle, \tag{18.7}$$

which is small enough to be treated, along with the spin–orbit Hamiltonian (equation (18.4)), as a perturbation to the central field potential.

The eigenfunctions of $\mathscr{H}'_0$ for a N-electron ion are obtained as a linear combination of one-electron wave functions that satisfy the Pauli exclusion principle and are subject to the orthonormality condition. This method, known as the Hartree–Fock approach, is generally used for seeking an approximate solution to the N-electron Schrödinger equation (Hartree, 1957; Weissbluth, 1978). All effects of noncentral field interactions including spin–orbit coupling and many-body collective electronic interactions are considered by introducing additional effective operators and diagonalizing the Hamiltonian with parameters determined in comparison with experiments.

In the Hartree–Fock method, the wave function of each electron is expressed as a product of radial functions and angular functions of the spherical harmonics multiplied by a spin function

$$\Psi_{nlm_{\mathrm{l}}m_{\mathrm{s}}}(\mathbf{r}, m_s) = \frac{1}{r} R_{n\mathrm{l}}(r)\, Y_{lm_{\mathrm{l}}}(\theta, \varphi)\sigma(m_{\mathrm{s}}), \tag{18.8}$$

where the radial function $R_{nl}(r)$ depends on the central field potential, which determines the radial charge distribution functions such as that plotted in Fig. 18.2 for U^{3+}. The spherical harmonic function $Y_{lm_{\mathrm{l}}}(\theta, \varphi)$ in equation (18.8) is characterized by the four conventional quantum numbers n, l, m_{l}, and m_{s}, which define a unique state of an electron in an atom. For electrons in a $5f^N$ configuration,

$$\begin{aligned} &n = 5, \\ &l = 3, m_{\mathrm{l}} = -l, -l, +1, ..., l, \\ &m_{\mathrm{s}} = \frac{1}{2} \end{aligned} \tag{18.9}$$

The central field wave function for N-electrons thus may be written in the form of a determinant as

$$\Psi(\lambda_1, \lambda_2, ..., \lambda_N) = \frac{1}{\sqrt{N!}} \begin{vmatrix} \Psi_1(\lambda_1) & \Psi_2(\lambda_1) & \cdots & \Psi_N(\lambda_1) \\ \Psi_1(\lambda_2) & \Psi_2(\lambda_2) & \cdots & \Psi_N(\lambda_2) \\ \vdots & & & \\ \Psi_1(\lambda_N) & \Psi_2(\lambda_N) & \cdots & \Psi_N(\lambda_N) \end{vmatrix}, \tag{18.10}$$

in which $\Psi_i(\lambda_j)$ are spin orbital wave functions in the form of equation (18.8). The subscript i identifies a particular choice of the four quantum numbers n, l,

m_l, and m_s, where λ_j represents the space and spin coordinates of the jth electron. The primary purpose of the central field approximation is to use the N-electron wave functions defined by equation (18.10) as the basis functions for the perturbation terms of a Hamiltonian that includes inter-electron Coulomb (18.3) and spin–orbit interactions (18.4).

18.3.2 *LS* coupling and intermediate coupling

To construct wave functions for a multielectron atom on the basis of the central field approximation, one needs to choose a coupling scheme for angular momentum summation to determine the wave functions of the N-independent electrons defined by equation (18.10). There are two coupling schemes that are commonly used for two extreme cases in atomic spectroscopy (Judd, 1963b; Cowan, 1981). In lighter atoms, where spin–orbit interactions (equation (18.4)) tend to be small compared with the electrostatic interactions between electrons (equation (18.3)), the so-called Russell–Saunders coupling scheme, or LS coupling scheme is a good choice, since L and S are approximately good quantum numbers. With increasing Z, electrostatic interactions decrease and spin–orbit interactions become more important, and in the heavier atoms, spin–orbit interactions become much stronger than the Coulomb interactions. Thus, one should consider the j–j coupling scheme. For f-elements, the Coulomb electrostatic interactions and spin–orbit interactions have the same order of magnitude. Therefore, neither coupling scheme is really appropriate. Calculations of energy levels of actinide ions involve a mathematically more complicated scheme that is called intermediate coupling, which is usually developed from the LS scheme.

In the LS coupling scheme, orbital momentum (l) and spin momentum (s) of individual electrons are summed separately (Weissbluth, 1978; Cowan, 1981). Thus

$$\boldsymbol{L} = \sum_{i=1}^{N} \boldsymbol{l}_i, \quad \boldsymbol{S} = \sum_{i=1}^{N} \boldsymbol{s}_i, \tag{18.11}$$

where $\boldsymbol{L}$ and $\boldsymbol{S}$ are the total orbital and total spin momentum operators, respectively. $\boldsymbol{J}$ defined as

$$\boldsymbol{J} = \boldsymbol{L} + \boldsymbol{S}, \tag{18.12}$$

is the total angular momentum operator which has $2J+1$ eigenstates represented by the magnetic quantum number $M = -J, -J+1, \ldots, J$.

In the LS coupling scheme, the electronic states of an actinide ion may be specified completely by writing the basis states as

$$\Psi = |nl\tau LSJM\rangle, \tag{18.13}$$

where nl, which is 5f or 6d for actinide ions, represents the radial part of the basis states. Usually, the symbol ${}^{2S+1}L_J$ is used to label a free-ion state that is

Table 18.2 *Electronic configurations and ground states of divalent (An^{2+}), trivalent (An^{3+}), and tetravalent (An^{4+}) actinide ions.*

Atomic number	*Element*	An^{2+}	An^{3+}	An^{4+}
89	Ac actinium	$5f^1$, $^2S_{1/2}$	$5f^0$, $^1S_0$	
90	Th thorium	$6d^2$, $^3F_2$	$6d^1$, $^2D_{3/2}$	$5f^0$, $^1S_0$
91	Pa protactinium	$5f^26d^1$, $^4I_{11/2}$	$5f^2$, $^3H_4$	$5f^1$, $^2F_{5/2}$
92	U uranium	$5f^36d^1$, $^5L_6$	$5f^3$, $^4I_{9/2}$	$5f^2$, $^3H_4$
93	Np neptunium	$5f^5$, $^6H_{5/2}$	$5f^4$, $^5I_4$	$5f^3$, $^4I_{9/2}$
94	Pu plutonium	$5f^6$, $^7F_0$	$5f^5$, $^6H_{5/2}$	$5f^4$, $^5I_4$
95	Am americium	$5f^7$, $^8S_{7/2}$	$5f^6$, $^7F_0$	$5f^5$, $^6H_{5/2}$
96	Cm curium	$5f^8$, $^7F_6$	$5f^7$, $^8S_{7/2}$	$5f^6$, $^7F_0$
97	Bk berkelium	$5f^9$, $^6H_{15/2}$	$5f^8$, $^7F_6$	$5f^7$, $^8S_{7/2}$
98	Cf californium	$5f^{10}$, $^5I_8$	$5f^9$, $^6H_{15/2}$	$5f^8$, $^7F_6$
99	Es einsteinium	$5f^{11}$, $^4I_{15/2}$	$5f^{11}$, $^5I_8$	$5f^9$, $^6H_{15/2}$
100	Fm fermium	$5f^{12}$, $^3H_6$	$5f^{11}$, $^4I_{15/2}$	$5f^{11}$, $^5I_8$
101	Md mendelevium	$5f^{13}$, $^2F_{7/2}$	$5f^{12}$, $^3H_6$	$5f^{11}$, $^4I_{15/2}$
102	No nobelium	$5f^{14}$, $^1S_0$	$5f^{13}$, $^2F_{7/2}$	$5f^{12}$, $^3H_6$

called a multiplet. Whereas S and J are specified with numbers $(0, \frac{1}{2}, 1, ...)$, L is traditionally specified with letters S, P, D, F, G, H, ... respectively, for $L = 0$, 1, 2, 3, 4, 5, ... Table 18.2 lists the electronic configurations and ground states identified by $^{2S+1}L_J$ for divalent, trivalent, and tetravalent ions in the actinide series. All tetravalent ions (An^{4+}) have the lowest spectroscopic energies in $5f^N$ configurations, however, this is not true for the lighter divalent ions. For Th^{3+}, the ground state in known compounds is $6d^1$, $^2D_{3/2}$ instead of the calculated $5f^1$, $^2F_{5/2}$ (Brewer, 1971a,b).

An additional quantum number τ, the seniority number, is needed for distinguishing the states that have the same L and S quantum numbers. In fact, two more quantum numbers are needed to completely define the states of an f^N configuration. One such classification number is $W = (w_1w_2w_3)$, with three integers for characterizing the irreducible representations of the seven-dimensional rotational group R_7. The other classification number is $U = (u_1u_2)$ for characterizing the irreducible representations of the group G_2. Details as to classification of the f^N states are given by Judd (1963b) and Wybourne (1965a). Table 18.3 lists the classification of the states for the f^N configurations with $N \leq 7$. Columns 5 and 11 list the LS terms with the same S, and columns 6 and 12 list the number of $^{2S+1}L_J$ multiplets in the classification. The LS terms of the $5f^{14-N}$ configuration are identical for those of the $5f^N$ configuration ($N \leq 7$), although the seniority of the states is different.

Inclusion of spin–orbit coupling breaks the symmetry of the LS coupling scheme. In this case,

$$\begin{aligned} \left[\mathscr{H}_{\text{S–O}}, \boldsymbol{L}\right] \neq 0, \left[\mathscr{H}_{\text{S–O}}, \boldsymbol{S}\right] \neq 0, \\ \left[\mathscr{H}_{\text{S–O}}, J^2\right] = \left[\mathscr{H}_{\text{S–O}}, J_Z\right] = 0, \end{aligned} \tag{18.14}$$

Table 18.3 *Classification of the free-ion states of the f^N configurations* (*Wybourne,* 1965a).

N	τ	W	U	^{2S+1}L	N_J	N	τ	W	U	^{2S+1}L	N_J
1	1	(100)	(10)	^{2}F	2				(20)	^{5}DGI	15
2	2	(110)	(10)	^{3}F	3		6	(221)	(10)	^{3}F	3
			(11)	^{3}PH	6				(11)	^{3}PH	6
	2	(200)	(20)	^{1}DGI	3				(20)	^{3}DGI	9
	0	(000)	(00)	^{1}S	1				(21)	^{3}DFGHKL	18
3	3	(111)	(00)	^{4}S	1				(30)	^{3}PFGHIKM	21
			(10)	^{4}F	4				(31)	^{3}PDFFGHHIIK-KLMNO	45
			(20)	^{4}DGI	12		4	(211)	(10)	^{3}F	3
	3	(210)	(11)	^{2}PH	4				(11)	^{3}PH	6
			(20)	^{2}DGI	6				(20)	^{3}DGI	9
			(21)	^{2}DFGHKL	12				(21)	^{3}DFGHKL	18
	1	(100)	(10)	^{2}F	2				(30)	^{3}PFGHIKM	21
4	4	(111)	(00)	^{5}S	1		2	(110)	(10)	^{3}F	3
			(10)	^{5}F	5				(11)	^{3}PH	6
			(20)	^{5}DGI	15		6	(222)	(00)	^{1}S	1
	4	(211)	(10)	^{3}F	3				(20)	^{1}DGL	3
			(11)	^{3}PH	6				(30)	^{1}PFGHIKM	7
			(20)	^{3}DGI	9				(40)	^{1}SDFGGHIIK-LLMNQ	14
			(21)	^{3}DFGHKL	18		4	(220)	(20)	^{1}DGI	3
			(30)	^{3}PFGHIKM	21				(21)	^{1}DFGHKL	6
	2	(110)	(10)	^{3}F	3				(22)	^{1}SDGHILN	7
			(11)	^{3}PH	6		2	(200)	(20)	^{1}DGI	3
	4	(220)	(20)	^{1}DGI	3		0	(000)	(00)	^{1}S	1
			(21)	^{1}DFGHKL	6	7	7	(000)	(00)	^{8}S	1
			(22)	^{1}SDGHILN	7		7	(200)	(20)	^{6}DGI	17
	2	(200)	(20)	^{1}DGI	3		5	(110)	(10)	^{6}F	6
	0	(000)	(00)	^{1}S	1				(11)	^{6}PH	9
5	5	(110)	(10)	^{6}F	6		7	(220)	(20)	^{4}DGI	12
			(11)	^{6}PH	9				(21)	^{4}DFGHKL	24
	5	(211)	(10)	^{4}F	4				(22)	^{4}SDGHILN	25
			(11)	^{4}PH	7		5	(211)	(10)	^{4}F	4
			(20)	^{4}DGI	12				(11)	^{4}PH	7
			(21)	^{4}DFGHKL	24				(20)	^{4}DGI	12
			(30)	^{4}PFGHIKM	27				(21)	^{4}DFGHKI	24
	3	(111)	(00)	^{4}S	1				(30)	^{4}PFGHIKM	27
			(10)	^{4}F	4		3	(111)	(00)	^{4}S	1
			(20)	^{4}DGI	12				(10)	^{4}F	4
	5	(221)	(10)	^{2}F	2				(20)	^{4}DGI	12
			(11)	^{2}PH	4		7	(222)	(00)	^{2}S	1
			(20)	^{2}DGI	6				(10)	^{2}F	2
			(21)	^{2}DFGHKL	12				(20)	^{2}DGI	6
			(30)	^{2}PFGHIKM	14				(30)	^{2}PFGHIKM	14
			(31)	^{2}PDFFGHH-IIKKLMNO	30				(40)	^{2}SDFGGHII-KLLMNQ	27
	3	(210)	(11)	^{2}PH	4		5	(221)	(10)	^{2}F	2
			(20)	^{2}DGI	6				(11)	^{2}PH	4

Table 18.3 (*Contd.*)

N	τ	W	U	^{2S+1}L	N_J	N	τ	W	U	^{2S+1}L	N_J
			(21)	^{2}DFGHKL	12				(20)	^{2}DGI	6
	1	(100)	(10)	^{2}F	2				(21)	^{2}DFGHKL	12
6	6	(100)	(10)	^{7}F	7				(30)	^{2}PFGHIKM	14
	6	(210)	(11)	^{5}PH	8				(31)	^{2}PDFFGHHII-KKLMNO	30
			(20)	^{5}DGI	15		3	(210)	(11)	^{2}PH	4
			(21)	^{5}DFGHKL	30				(20)	^{2}DGI	6
	4	(111)	(00)	^{5}S	1				(21)	^{2}DFGHKL	12
			(10)	^{5}F	5		1	(100)	(10)	^{2}F	2

namely, J^2 and M still commute, but $\boldsymbol{L}$ and $\boldsymbol{S}$ do not. Thus L and S are no longer good quantum numbers, but J and M are still good; therefore, the wave functions $|nl\tau LSJM\rangle$ are not eigenfunctions of the Hamiltonian shown in equation (18.1). One may obtain a new set of eigenfunctions by diagonalizing the primary terms of the Hamiltonian defined by equations (18.4) and (18.7) with the basis set in terms of $|nl\tau LSJM\rangle$ based on perturbation theory and the concept of the central field approximation. As a result, the new eigenfunctions are linear combinations of the LS basis sets, and are known as the free-ion wave functions in the intermediate coupling scheme. If we do not include inter-configurational coupling, the eigenfunctions in the intermediate coupling scheme are expressed as

$$\Psi(nlJ) = \sum_{\tau LS} a_{\tau LSJ} |nl\tau LSJ\rangle, \tag{18.15}$$

where the coefficients $a_{\tau LSJ}$ are determined by the matrix elements

$$a_{\tau LSJ} = \sum_{\tau' L' S'} \langle nl\tau LSJ| \mathscr{H}_{\mathrm{C}} + \mathscr{H}_{\mathrm{S-O}} |nl\tau' L' S' J'\rangle \delta_{JJ'}. \tag{18.16}$$

The energy levels of the free-ion states are independent of M, so they are $(2J+1)$-fold degenerate. The new basis set (equation (18.15)) in the intermediate coupling scheme describes the energy states of a Hamiltonian that includes Coulomb and spin–orbit interactions and is obtained from the mixing of all LS terms with the same J in a given $5f^N$ configuration. The transformation coefficients of $a_{\tau SLJ}$ are the components of the eigenvector pertaining to the basis state in the LS coupling (Judd, 1963b).

18.3.3 Effective-operator Hamiltonian

In spectroscopy, a powerful method for evaluating atomic energy level structure is to define and diagonalize an effective-operator Hamiltonian with the wave functions of the central field Hamiltonian. Racah (1949) used this method for

calculating the matrix elements of tensor operators of the electronic angular momentum (Racah, 1949). Since then, many developments have been made, particularly for applications of the effective-operator method to rare earth spectroscopy (Judd, 1963b; Wybourne, 1965a). An essential part of the effective-operator method is to determine the matrix elements of irreducible tensor operators using the Wigner–Eckart theorem. According to the Wigner–Eckart theorem, for a tensor operator $\mathbf{T}^{(k)}$ of rank k with $2k+1$ components $T_q^{(k)}(q = -k, -k+1, \ldots, k)$ that acts on a set of basis functions $|\tau LSJM\rangle$, each of which is an eigenfunction of the operators J^2 and J_z, the matrix elements of $T_q^{(k)}$ can be reduced as

$$\left\langle \tau LSJM \middle| T_q^{(k)} \middle| \tau' L' S' J' M' \right\rangle = (-1)^{J-M} \begin{bmatrix} J & k & J' \\ -M & q & M' \end{bmatrix} \left\langle \tau LSJ \middle\| \mathbf{T}^{(k)} \middle\| \tau' L' S' J' \right\rangle, \tag{18.17}$$

where the $3-j$ symbols involve only geometrical properties of the tensor operator (Rotenberg *et al.*, 1959). The physical nature of the operator is contained entirely in the reduced matrix elements $\left\langle \tau LSJ \middle\| T^{(k)} \middle\| \tau' L' S' J' \right\rangle$. Information on the use of tensor operators in atomic spectroscopy is provided in several textbooks (Judd, 1963b, 1975; Weissbluth, 1978).

In central field approximation, the orbital electronic wave functions of an actinide ion are represented by products of radial and angular parts as shown in equation (18.8). The effective operator for Coulomb electrostatic intra-ion interaction may be expressed by expanding $1/r_{ij}$ into scalar products of tensor operators of spherical harmonics. Therefore, for N-equivalent electrons in orbital nl, the matrix elements of the effective-operator Hamiltonian for the Coulomb electrostatic interaction may be expressed as:

$$\left\langle l^N \tau LS \middle| \sum_{i>j}^{N} \frac{e^2}{r_{ij}} \middle| l^N \tau' \; L' S' \right\rangle = \sum_k f_k(l,l) F^{(k)}(nl, nl), \tag{18.18}$$

where $F^k(nl, nl)$, with $k = 0, 2, 4, 6$, are the Slater radial integrals for the radial part of the electrostatic interaction, which is defined as:

$$F^k(nl, nl) = e^2 \int_0^\infty \int_0^\infty \frac{r_<^k}{r_>^{k+1}} [R_{nl}(r_i)]^2 \left[R_{nl}\left(r_j\right)\right]^2 \mathrm{d}r_i \mathrm{d}r_j \tag{18.19}$$

The value of F^k may be calculated using the Hartree–Fock method, but in analyses of actinide-ion spectra, F^k is considered as an experimentally determined parameter.

The angular part of the matrix element in equation (18.18) is defined as

$$f_k(l,l) = \left\langle l^N \tau LS \middle| \sum_{i>j} \mathbf{C}^{(k)}(i) \cdot \mathbf{C}^{(k)}(j) \middle| l^N \tau' L' S' \right\rangle. \tag{18.20}$$

Using the Wigner–Eckart theorem, the matrix elements in equation (18.20) are best handled by introducing the tensor operator $\mathbf{U}^{(k)}$. In combination with the symmetry properties of angular momentum, f_k can be expressed in terms of the reduced matrix elements of $\mathbf{U}^{(k)}$ as:

$$f_k(l,l) = \frac{1}{2}(2l+1)^2 \begin{pmatrix} l & k & l \\ 0 & 0 & 0 \end{pmatrix}^2 \left\{ \frac{1}{2L+1} \sum_{\tau' L'} \left| \left\langle l^N \tau L S \middle\| \mathbf{U}^{(k)} \middle\| l^N \tau' L' S \right\rangle \right|^2 - \frac{N}{2l+1} \right\}. \tag{18.21}$$

In the particular case of $k = 0$, it is easy to find that

$$f_0(l,l) = N(N-1)/2. \tag{18.22}$$

For the d^N and f^N configurations, the values for the reduced matrix elements of tensor operator $\mathbf{U}^{(k)}$ have been tabulated (Nielson and Koster, 1963). Because of the symmetry properties of the $3-j$ symbol, $f_k(l,l)$ has nonzero values only if $l+l \geq k \geq |l-l|$; and k is even. For f-electrons, $l = 3$, thus f_k vanishes except for $k = 0, 2, 4, 6$.

As defined in equation (18.4), the Hamiltonian for spin–orbit coupling for N-electrons in an actinide ion is a linear summation of the independent spin–orbit interaction for a single electron. In LS coupling, the N-equivalent electronic matrix element of the spin–orbit interaction is expressible in terms of the tensor operator $\mathbf{V}^{(11)}$. Hence the matrix element of spin–orbit interaction for N-equivalent electrons can be expressed as

$$\left\langle nl^N \tau L S J \middle| \sum_{i=1}^{N} \xi(r_i) \boldsymbol{l}_i \cdot \boldsymbol{s}_i \middle| nl^N \tau' L' S' J' \right\rangle = \zeta_{nl} A_{nl}(ls), \tag{18.23}$$

where ζ_{nl} is the spin–orbit interaction parameter defined as a radial integral

$$\zeta_{nl} = \int_0^\infty [R_{nl}(r)]^2 \xi(r) \mathrm{d}r. \tag{18.24}$$

where $R_{nl}(r)$ is the radial wave function.

The spin–orbit parameter can be evaluated numerically using the Hartree–Fock central field potential, but it is usually adjusted to obtain the experimentally observed energies. The matrix element in equation (18.23) can be expressed as (Sobelman, 1972)

$$A_{nl}(ls) = (-1)^{L+S'+J} \sqrt{(2l+1)(l+1)l} \delta_{JJ'} \delta_{MM'} \begin{Bmatrix} L & S & J \\ S' & L' & 1 \end{Bmatrix} \left\langle \tau L S \middle\| \mathbf{V}^{(11)} \middle\| \tau' L' S' \right\rangle, \tag{18.25}$$

where $\{\ldots\}$ is a $6-j$ symbol, and the values for the reduced matrix elements of the tensor operators $\mathbf{V}^{(11)}$ have been tabulated by Slater (1960), Sobelman (1972), and Nielson and Koster (1963).

The electrostatic and spin–orbit interactions usually give the right order for the energy level splitting of the f^N configurations. However, these primary terms of the free-ion Hamiltonian do not accurately reproduce the experimentally measured energy level structures. The reason is the parameters F^k and ζ_{nf}, which are associated with interactions within a f^N configuration, cannot absorb all the effects of additional mechanisms such as relativistic effects and configuration interactions. Introduction of new terms in the effective-operator Hamiltonian is required to better interpret the experimental data. It was demonstrated (Judd and Crosswhite, 1984) that, in fitting the experimental free-ion energy levels of Pr^{3+} (f^2 configuration), the standard deviation between observed and calculated f-state energies could be reduced from 733 to 24 cm^{-1} by adding nine more parameterized effective operators into the Hamiltonian.

Among several corrective terms included in the effective-operator Hamiltonian, a significant contribution to the f^N energy level structure is from configuration interactions between configurations of the same parity. This contribution can be taken into account by a set of three two-electron operators (Wybourne, 1965a):

$$\mathscr{H}_{c1} = \alpha L(L+1) + \beta G(G_2) + \gamma G(R_7) \tag{18.26}$$

where α, β, and γ are the parameters associated with the continuous groups $G(G_2)$ and $G(R_7)$ (Rajnak and Wybourne, 1963, 1964) the latter being eigenvalues of Casimir operators for the groups G_2 and R_7 (Judd, 1963a).

For f^N configurations of $N \geq 3$, three-body interaction terms were introduced by Judd (1966) and Crosswhite *et al.* (1968) as

$$\mathscr{H}_{c2} = \sum_{i=2,3,4,6,7,8} T^i t_i \tag{18.27}$$

where T^i are parameters associated with three-particle operators t^i. This set of effective operators scaled with respect to the total spin $\boldsymbol{S}$ and total orbital angular momentum $\boldsymbol{L}$ are needed in the Hamiltonian to represent the coupling of the f^N states to those in the higher energy configurations (d, p, s) via inter-electron Coulombic interactions. It is common to include six three-electron operators $t^i (i = 2, 3, 4, 6, 7, 8)$. When perturbation theory is carried beyond the second order, an additional eight three-electron operators t^i ($11 \leq i \leq 19$, with $i = 13$ excluded) are required (Judd and Lo, 1996). A complete table of matrix elements of the 14 three-electron operators for the f-shell have been published (Hansen *et al.*, 1996).

In addition to the magnetic spin–orbit interaction parameterized by ζ_{nf}, relativistic effects including spin–spin and spin–other–orbit, both being

parameterized by the Marvin integrals M^0, M^2, and M^4 (Marvin, 1947), are included as the third corrective term of the effective-operator Hamiltonian (Judd *et al.*, 1968).

$$\mathscr{H}_{c3} = \sum_{i=0,2,4} M^i m_i, \tag{18.28}$$

where m_i is the effective operator and M^i is the radial parameter associated with m_i.

As demonstrated (Judd *et al.*, 1968; Carnall *et al.*, 1983), for improving the parametric fitting of the f-element spectra, two-body effective operators can be introduced to account for configuration interaction through electrostatically correlated magnetic interactions. This effect can be characterized by introducing three more effective operators as

$$\mathscr{H}_{c4} = \sum_{i=2,4,6} P^i p_i, \tag{18.29}$$

where p_i is the operator and P^i is the radial parameter.

In summary, 20 effective operators are utilized for fitting spectra, including those for two- and three-electron interactions. The total effective-operator Hamiltonian for free-ion interactions is

$$\begin{aligned}\mathscr{H}_{FI} = &\sum_{k=0,2,4,6} F^k f_k + \zeta_{nl} A_{nl} + \alpha L(L+1) + \beta G(G_2) + \gamma G(R_7) \\ &+ \sum_{i=2,3,4,6,7,8} T^i t_i + \sum_{i=0,2,4} M^i m_i + \sum_{i=2,4,6} p_i P^i.\end{aligned} \tag{18.30}$$

This effective-operator Hamiltonian has been used as the most comprehensive free-ion Hamiltonian in previous spectroscopic analyses of f-element ions in solids (Crosswhite, 1977; Crosswhite and Crosswhite, 1984; Carnall *et al.*, 1989; Liu, 2000). The 20 parameters associated with the free-ion operators are adjusted in the fitting of experimental energy levels.

18.3.4 Reduced matrices and free-ion state representation

In equation (18.30), all effective operators for the free-ion interactions have well-defined group-theoretical properties (Judd, 1963b; Wybourne, 1965a). Within the intermediate coupling scheme, all matrix elements can be reduced, using the Wigner–Eckart theorem, to new forms that are independent of J, viz.

$$\langle \tau SLJ | \mathscr{H}_i | \tau' S' L' J' \rangle = P_i \delta_{JJ'} c(SLS'L'J) \langle \tau SL \| O_i \| \tau' S' L' \rangle, \tag{18.31}$$

where P_i is the parameter, $c(SLS'L'J)$ is a numerical coefficient, and $\langle \tau SL \| O_i \| \tau' S' L' \rangle$ is the reduced matrix element of the effective-operator O_i. Once the reduced matrix elements are calculated, it is not difficult to diagonalize the entire free-ion Hamiltonian with the wave functions in the LS basis set. The free-ion eigenfunctions are thus obtained in the form of the intermediate

coupling representation. All matrix elements of the effective-operator Hamiltonian are evaluated in terms of the parameters of the effective operators.

Because the reduced matrix elements are independent of J, the matrix of the free-ion Hamiltonian thus can be reduced into a maximum of 13 independent submatrices for $J = 0, 1, 2, \ldots, 12$ for even N and $J = \frac{1}{2}, \frac{3}{2}, \frac{5}{2}, \ldots, \frac{25}{2}$ *for odd N* in an f^N configuration. The number of submatrices and their size can be determined from the values of N_J (the number of J levels for a given SL multiplet) given in Table 18.3. Separation of the free-ion matrix into submatrices greatly facilitates the evaluation of free-ion energy levels. However, evaluation of matrix elements is still a considerable effort, particularly with inclusion of the corrective terms in the Hamiltonian. For an f^N configuration with $3 < N < 11$, there are more than 10^4 free-ion matrix elements and each of them may have as many as 20 terms to be evaluated on the basis of angular momentum operations. Fortunately, several groups have calculated the matrix elements that are available on web sites (http://chemistry.anl.gov) from which one may download a MS-Windows based computer program named SPECTRA to calculate the eigenvalues and eigenfunctions of the free-ion Hamiltonian defined in equation (18.30). As discussed in the following sections, SPECTRA can also be used for nonlinear least-squares fitting of observed levels to determine values of the Hamiltonian parameters.

Due to the SL–$S'L'$ mixing in the intermediate coupling scheme, labeling a multiplet as $^{2S+1}L_J$ is incomplete. In most cases, the nominal labeling of a free-ion state as $^{2S+1}L_J$ only indicates that this multiplet has a leading component from the pure LS basis $|LSJ\rangle$. Diagonalization of each of the submatrices produces free-ion eigenfunctions in the form of equation (18.15). As an example, the leading LS terms for the free-ion wave functions of the nominal $^4I_{9/2}$ ground state of the $4f^3$ ion Nd^{3+} and the $5f^3$ ion $U^{3+}$are:

$$\Psi(4f^3, {}^4I_{9/2}) = 0.984\,{}^4I - 0.174\,{}^2H - 0.017\,{}^2G + \text{etc.}$$

$$\Psi(5f^3, {}^2I_{9/2}) = 0.912\,{}^4I - 0.391\,{}^2H - 0.081\,{}^2G + 0.048\,{}^4G + 0.032\,{}^4F + \text{etc.}$$

In general, SL–$S'L'$ mixing becomes more significant in the excited multiplets.

18.3.5 Parameterization of the free-ion Hamiltonian

In an empirical approach to interpretation of the experimentally observed energy level structure of an f-element ion in solids, establishing accurate parameters for the model Hamiltonian essentially relies on systematic analyses that encompass theoretical calculations for incorporating trends of parameter variation across the f-element series. In the previous work that led to the establishment of the free-ion parameters for the trivalent actinide ions (Carnall, 1992) and the tetravalent actinide ions (Carnall *et al.*, 1991; Liu *et al.*, 1994b), the results of analyses of simpler spectra were carried over to more complex ones through consideration of their systematic trends and symmetry properties.

Table 18.4 lists values of the free-ion interaction parameters obtained from analyses of the spectra of An^{3+}:$LaCl_3$.

In early attempts to develop a systematic interpretation of trivalent actinide and lanthanide spectra, initial sets of F^k and ζ_{nf} for some members of the series had to be estimated. This was done by a linear extrapolation based on the fitted parameters that were available from the analyses of other individual spectra. As more extensive data and improved modeling yielded better determined and more consistent F^k and ζ_{nf} values for the 3+ actinides (and lanthanides), it became apparent that the variation in the parameters was nonlinear, as indicated for F^2(5f,5f) in Fig. 18.4. This nonlinearity could also be observed in the values of parameters of the *ab initio* calculations. The difference between the *ab initio* and fitted values of parameters (ΔF) appears to exhibit a much more linear variation with Z than do the parameter values. Consequently, ΔF has been adopted as the basis for a useful predictive model.

For the trivalent actinides, the values of ΔF are not constant over the series, but use of a single average value over a group of four or five elements is not an unreasonable approximation. Thus, in developing a predictive model for the F^k and ζ_{nf} parameters, an attempt is made to establish average values of ΔF for a particular valence state and type of crystal-field interaction. The energy level structure computation based on the predicted parameters can be compared to that observed, and then appropriate modifications sought by a fitting procedure where necessary.

Detailed results of Hartree–Fock calculations on f-electrons were previously analyzed (Carnall *et al.*, 1983; Crosswhite and Crosswhite, 1984). The most important trends are those of the electrostatic-interaction parameters F^k and spin–orbit parameters ζ_{nf} which increase with the number of f-electrons, N. The experimentally determined values of F^k and ζ_{nf} for trivalent actinides in $LaCl_3$ are shown as a function of N in Figs. 18.4 and 18.5, respectively. These values were obtained from the systematic analyses of experimental spectra (Carnall, 1992). Fig. 18.5 also shows the systematic trends for ζ_{nf} for the trivalent actinide ions that were obtained from Hartree–Fock calculations. Although the Hartree–Fock calculations predict the same trends across the series, the Hartree–Fock values for F^k and ζ_{nf} are always larger than the empirical parameters obtained by allowing them to vary in fitting experimental data. The relativistic Hartree–Fock (HFR) values of ζ_{nf} agree remarkably well with empirical values, whereas the F^k values remain considerably larger than the empirical values. Presumably, this is because, in addition to relativistic effects, f-electron coupling with orbitals of higher-lying energies reduces the radial integrals assumed in the HFR approximation. Moreover, the experimental results are obtained for ions in condensed phases, not in a gaseous phase, which leads on average to an ~5% change (Crosswhite, 1977). Because of the absence of mechanisms that absorb these effects in the HFR model, HFR values of F^ks cannot be used directly as initial parameters for the least-squares fitting process. Scaling of HFR values to the experimentally determined ones is

Table 18.4 *Energy-level parameters for trivalent actinide ions in* $LaCl_3$ (*in* cm^{-1}), *from Carnall* (1992).[a]

	U^{3+}	Np^{3+}	Pu^{3+}	Am^{3+}	Cm^{3+}	Bk^{3+}	Cf^{3+}	Es^{3+}	Fm^{3+}	Md^{3+}
F^2	39 611(222)	45 382(80)	48 679(89)	[51 900]	[55 055]	[57 697]	[60 464]	63 174(142)	65 850	68 454
F^4	32 960(418)	37 242(215)	[39 333 R]	[41 600]	43 938(148)	[45 969]	[48 026]	[50 034 R]	52 044	54 048
F^6	23 084(352)	25 644(196)	27 647(89)	[29 400]	32 876(154)	[32 876]	[34 592]	[36 199 R]	37 756	39 283
ζ	1626(3)	1937(2)	2242(2)	2564(3)	2889(4)	3210(4)	3572(2)	3944(3)	4326	4715
α	29.26(0.44)	31.78(0.30)	30.00(0.16)	26.71(0.31)	29.42(0.32)	29.56(0.42)	27.36(0.26)	30.21(1.1)	30	30
β	–824.6(29)	–728.0(18)	–678.3(12)	–426.6(42)	–362.9(51)	–564.9(47)	–587.5(21)	–761.0(55)	–600	–600
γ	1093(105)	840.2(61)	1022(31)	977.9(28)	[500]	839.8(28)	753.5(14)	488.2(39)	450	450
T^2	306(64)	[200]	190(8)	150(20)	[275]	127(15)	105(11)	[110]	100	100
T^3	42(14)	45(7)	54(10)	[45]	[45]	24(59)	48(11)	[45]	45	
T^4	188(20)	50(6)	[45]	[45]	[60]	70(54)	59(21)	[50]	50	
T^6	–242(40)	–361(18)	–368(19)	–487(31)	–289(22)	–388(44)	–529(31)	–256(43)	–300	
T^7	447(61)	427(23)	363(14)	489(28)	546(95)	525(29)	630(34)	648(66)	640	
T^8	[300]	340(17)	322(10)	228(32)	528(52)	378(34)	270(14)	408(44)	400	
M^0	[0.672]	[0.773]	[0.877]	[0.985]	[1.097]	[1.213]	[1.334]	[1.458]	1.587	1.720
M^2	[0.372]	[0.428]	[0.486]	[0.546]	[0.608]	[0.672]	[0.738]	[0.807]	0.878	0.951
M^4	[0.258]	[0.297]	[0.388]	[0.379]	[0.423]	[0.468]	[0.514]	[0.562]	0.612	0.662
P^{2b}	1 216(77)	1009(30)	949(24)	613(42)	1054(36)	667(83)	820(42)	506(102)	600	600
B_0^2	287(32)	164(26)	197(22)	242(34)	[280]	280(40)	306(29)	[306]	306	306
B_0^4	–662(93)	–559(44)	–586(38)	–582(80)	[–884]	–884(62)	–1062(56)	[–1062]	–1062	–1062
B_0^6	–1 340(89)	–1 673(49)	–1723(39)	–1 887(83)	[–1 293]	–1293(68)	–1441(48)	[–1441]	–1441	–1441
B_6^6	1070(63)	1033(34)	1011(34)	1122(49)	[990]	990(40)	941(36)	[941]	941	941
σ^c	29	22	18	21	23	22	19	22		
η^c	82	167	193	79	84	83	110	47		

[a] The values in parentheses are errors in the indicated parameters. The values in brackets were either not allowed to vary in the parameter fitting, or if followed by an *R*, were constrained: For Pu^{3+}, $F^4/F^2 = 0.808$; for Es^{3+}, $F^4/F^2 = 0.792$, $F^6/F^2 = 0.573$. All parameters for Fm^{3+} and Md^{3+} are extrapolated values.
[b] P^2 was varied freely, P^4 and P^6 were constrained by ratios $P^4 = 0.5P^2$, $P^6 = 0.1P^2$.

[c] Deviation $\sigma = \sqrt{\sum_i \Delta_i^2/(n-p)}$, where i is an index that runs over the assigned levels, Δ_i is the difference between observed and calculated energies for the ith assigned level, n is the number of levels fit, and p is the number of parameters freely varied.

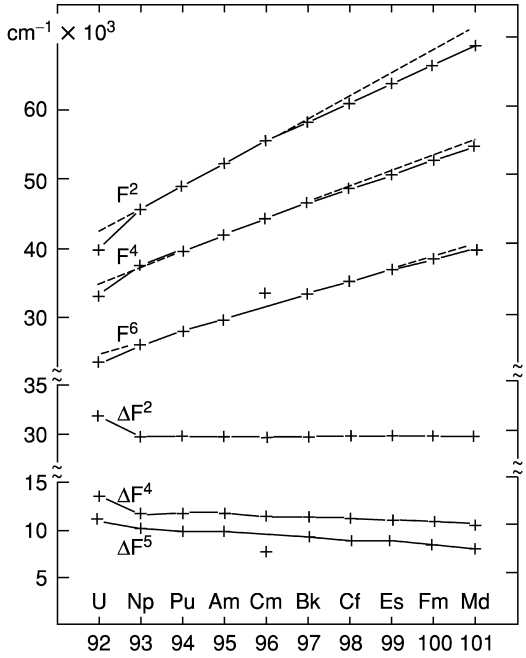

Fig. 18.4 *Variation of the parameters* F^2, F^4, F^6, ΔF^2, ΔF^4, ΔF^6 *where* $\Delta F^N = F^N$ (*HFR*) $-F^4$ (*expt*) *in* cm^{-1} *for* An^{3+}:$LaCl_3$ *as a function of atomic number.* (*Reprinted with permission from Carnall,* 1992. *Copyright* 1992, *American Institute of Physics.*)

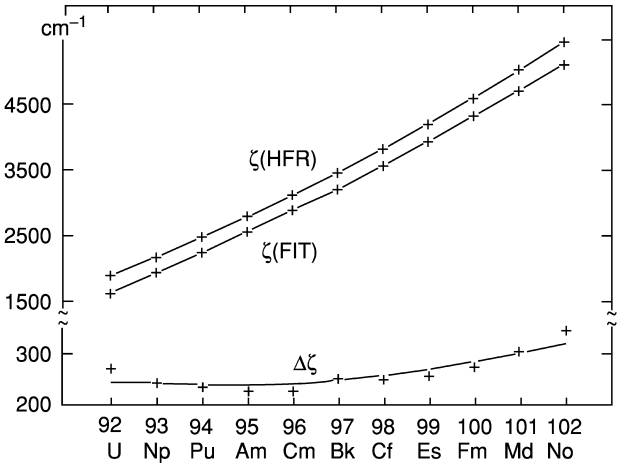

Fig. 18.5 *Variation of the parameter* ζ(*expt*), ζ(*expt*), *and* $\Delta\zeta$(*expt*) *in* cm^{-1} *for* An^{3+}: $LaCl_3$ *as a function of atomic number.* (*Reprinted with permission from Carnall,* 1992. *Copyright* 1992, *American Institute of Physics.*)

necessary to establish a systematic trend for a specific parameter. With this procedure, linear extrapolations of model parameters from one ion to another lead to values consistent with those obtained in the actual fitting process.

In addition to HFR calculations of F^ks and ζ_{nf}, estimated values for $M^k (k = 0, 2, 4)$ can also be computed using the HFR method (Judd *et al.*, 1968). These parameters do not vary dramatically across the f-series. In practice, experience has shown that they can be taken as given or varied as a single parameter while maintaining the HFR ratios $M^2/M^0 = 0.56$ and $M^4/M^0 = 0.31$ (Carnall, 1989). For actinide ions, the ratio M^4/M^0 may be maintained at 0.38−0.4 (see Table 18.4).

For the rest of the free-ion effective operators introduced above, no direct Hartree–Fock calculated values can be derived. Only a term-by-term HFR calculation is possible to give additional guidance for parameter estimates. For example, the HFR values of P^ks for Pr^{2+} and Pr^{3+} have been determined by Copland *et al.* (1971). In establishing systematic trends of parameters for An^{3+}:$LaCl_3$, Carnall (1989) constrained the P^k parameters by the ratios $P^4 = 0.5P^2$ and $P^6 = 0.1P^2$ whereas P^2 was varied freely along with other parameters. These ratios are consistent with the HFR estimation. The variation of these parameters across the series is not significant, and no obvious systematic trends have been established.

Once the systematic trends of free-ion parameters are established, constraints can be imposed on other parameters that are relatively insensitive to the available experimental data. Some parameters such as T^i, M^k, and P^k do not vary significantly across the series and as a good approximation can be fixed at the same values for neighboring ions in the same series. In fact, most of the free-ion parameters are not host sensitive. Typically, there are changes of ~1% in the values of the free-ion parameters between different lattice environments. The free-ion parameters given in Table 18.4 can be used as initial inputs for least-squares fitting of the energy level structure of a trivalent f-element ion in any crystalline lattice. If there is a limited number of experimentally determined levels, one may allow only the F^k and ζ_{nf} parameters to vary freely along with the crystal field parameters and keep the other free-ion parameters fixed. For further improvement of the fits, α, β, and γ can be released. For a final refinement, M^0 and P^2 may be varied freely with $M^{2,4}$ and $P^{4,6}$ varied following M^0 and P^2, respectively, at fixed ratios.

Multiconfiguration calculations have shown that similar values of these effective-operator parameters are to be expected at both ends of the lanthanide sequence (Morrison, 1972), and empirical evaluations are in agreement with this for both the lanthanides and actinides. For three (or 11) electrons, similar arguments show the need for additional (three-body) operators to parameterize the electrostatic interactions completely. If consideration is limited to the interactions arising from second-order perturbation theory, only six new operators are needed (Judd *et al.*, 1968; Judd and Suskin, 1984), and their experimental

evaluation is consistent with results expected from first-principles calculations (Poon and Newman, 1983).

Similar arguments hold for corrections to the spin–orbit interaction, as well as additional terms of relativistic origin such as the spin–other–orbit and spin–spin interactions. Hartree–Fock calculations give good estimates of the Marvin radial integrals $M^k(k = 0, 2, 4)$ associated with spin–other-orbit and spin–spin interactions (Judd *et al.*, 1968). Experimental investigations are needed for evaluation of the magnetic corrections associated with configuration interactions, but experience has shown that a single set of parameters $P^k\left(k = 2, 4, 6 \text{ with } P^4 = 0.75P^2 \text{ and } P^6 = 0.50P^2\right)$ accounts for a large part of this class of corrections (Judd *et al.*, 1968). Use of sets of all of the foregoing parameters has been explored in detail for all of the trivalent ions from U^{3+} through Es^{3+}, and values are shown in Table 18.4 for An^{3+}: $LaCl_3$.

18.4 MODELING OF CRYSTAL-FIELD INTERACTION

When an actinide or lanthanide ion occurs in a condensed-phase medium, the spherical symmetry of its electronic structure is destroyed, and ionic energy levels shift and split under the influence of the electric field produced by the crystalline environment. The energy level shifts and splittings depend on the nature and strength of the interaction with the environment. Some of this interaction can be absorbed by the nominal 'free-ion' parameters themselves and a measure of this contribution would give clues as to the nature of the interactions. Unfortunately, mainly because of the different methods by which the free-ion and condensed-phase levels are determined, there are very few cases in which both sets of parameters are known well enough for meaningful comparisons to be drawn.

In addition to modifications of the atomic parameters, there are medium-related effects that must be taken into account explicitly. The broken spherical symmetry that normally results when an isolated free gaseous ion is placed in a ligand field gives rise to a splitting of the free-ion level into a maximum of $(2J+1)$ components. A single-particle crystal field model has had remarkable success for lanthanide ions and a somewhat qualified, but nevertheless satisfactory, success for the trivalent actinide ions in providing an interpretation of experimental data (Dieke, 1968; Hüfner, 1978; Carnall, 1992; Liu, 2000). The degree to which the $2J+1$ fold degeneracy of a free-ion state is removed depends only on the point symmetry about the ion. The magnitude of crystal-field splittings is determined primarily by the crystal field strength that is expressed in terms of the crystal field parameters of the effective-operator Hamiltonian. The 5f electrons of actinide ions, which participate primarily in ionic bonding with surrounding ligands, have localized states that are conventionally described in the framework of crystal field theory (Stevens, 1952; Wybourne, 1965a). Using effective-operator techniques and the parameterization method,

the framework of crystal field theory has been developed with the same basis set of eigenfunctions of the effective-operator Hamiltonian for the free-ion interactions discussed in Section 18.3.5.

Because electronic interactions in solids are complex, various interaction mechanisms that influence the electronic states of an actinide ion in a solid environment may not be accurately calculated in the framework of current crystal field theory. Evaluation of the crystal field parameters, however, is theoretically much more difficult than predicting the number of energy levels for each free-ion state. To date, an empirical approach has been the most effective method for evaluation of the crystal field parameters of f-states of actinide ions (Krupa, 1987; Carnall, 1992; Liu *et al*., 1994b). Phenomenological modeling and *ab initio* calculations of ion–ligand interactions are able to provide theoretical guidance for the analysis of crystal field spectra. From theoretical approaches, analytical expressions of crystal field parameters using phenomenological models are available for calculating the crystal field parameters of actinide and lanthanide ions in a specific crystalline lattice. The exchange charge model (Malkin *et al*., 1970; Malkin, 1987) and the superposition model (Newman, 1971; Newman and Ng, 1989a) are two crystal field models that have achieved significant success and are useful for guiding spectral analyses. In addition, *ab initio* calculations of the solid-state electronic energy level structure have advanced significantly along with the rapid development of computer technology and are likely to be increasingly important in future studies (Matsika *et al*., 2001; Seijo and Barandiaran, 2001).

18.4.1 Correlation of free-ion and condensed-phase energy level structures

It was pointed out earlier that, because of the different techniques used in studying condensed-phase and free-ion spectra, the configurations available for direct comparison in the two cases have very little overlap. When crystals or solutions are cooled to near 4 K so that only the lowest (ground) electronic state is populated, the resultant absorption spectrum is directly interpretable in terms of energy levels, and, except for complications of superimposed vibronic bands and the added perturbations of crystal field effects themselves, the analysis can proceed to energy level assignments and parametric fitting. In free-ion emission studies, on the other hand, many overlapping transition arrays between the multiple configurations displayed in Fig. 18.1 are obtained simultaneously, and one must first analyze this complex structure. This can only be done with the aid of additional tags on the energy levels such as isotope shift, hyperfine structure, or Landé *g*-factor information, which requires that multiple experiments be performed. Of the many configurations that finally result, most are too heavily involved with s-, p-, and d-orbitals for easy comparison with the f-shell cases discussed here. See Chapter 16 for a detailed discussion of free-atom and free-ion spectra. Nevertheless, with some assistance from theory,

cases are available from which to begin constructing a useful interpretative and predictive model.

Considering the analogous lanthanide situation, nearly all the $4f^2$ atomic levels are known for Pr^{3+} as a free-ion (Pr IV; Crosswhite *et al.*, 1965) and as an ion in $LaCl_3$ (Crosswhite *et al.*, 1965; Rana *et al.*, 1984) and LaF_3 (Carnall *et al.*, 1969, 1989) hosts. The corresponding parametric results are given in Table 18.5. This is the only example now available in either the lanthanide or actinide series for which this direct comparison can be made. For this reason, this case will be examined more closely. Columns 2 (free-ion) and 3 ($LaCl_3$ crystal) in the upper part of Table 18.5 give the results found for the parametric model. Comparing the two cases line-by-line, significant differences can be seen for the major parameters F^k and ζ_{4f}, and lesser ones for α and β. Any possible differences in the M^k and P^k values are masked by the statistical uncertainties. The parameter shifts attributed to the Pr^{3+} environment are given in column 4 and the relative change of the crystal values, compared to those of the free ion, in column 5. Note that the most important change, nearly 5%, occurs for F^2, and about half of this for F^4, F^6, and ζ_{4f}. Also α is in the same range, but with a large uncertainty. The most striking change seems to be for β, which shows an increase in magnitude of some 10–15%.

The $5f^2$ free-ion configurations are completely known for both Th III (deBruin *et al.*, 1941) and U V (Wyart *et al.*, 1980; Van Deurzen *et al.*, 1984), but the Th^{2+} condensed-phase analog is not known, and analyzed data for U^{4+} are limited in scope. The $4f^3$ Pr III configuration is nearly completely known (Suger, 1963), but

Table 18.5 *Medium shift of free-ion parameters for selected f-element ions.*

	Pr IV (cm^{-1})	Pr^{3+}:$LaCl_3$ (cm^{-1})	*Medium shift* (cm^{-1})	*Relative change* (%)
F^2	71 822(41)	68 498(20)	–3324	–4.63 ± 0.08
F^4	51 829(112)	50 317(50)	–1512	–2.92 ± 0.33
F^6	33 889(72)	33 127(38)	–762	–2.25 ± 0.32
α	23 939(322)	22 866(173)	–1073	–4.5 ± 2.1
β	–599(19)	–678(9)	–79	+13 ± 5
ζ	766(3)	749(1)	–17	–2.0 ± 0.5
M^0	2.0(0.4)	1.7(0.2)	0	
P^2	168(58)	248(32)	0	

	Pu II $5f^5 7s^2$ (exp.) (cm^{-1})	*Pu IV* $5f^5$ (est.) (cm^{-1})	Pu^{3+}:$LaCl_3$ (exp.) (cm^{-1})	*Medium shift* (cm^{-1})	*Relative change* (%)
F^2	49 066(770)	50 015	48 670(154)	–1345(924)	–2.7 ± 1.8
F^4	39 640(719)	40 322	39 188(294)	–1134(1 013)	–2.8 ± 2.5
F^6	26 946(785)	27 466	27 493(153)	+27(938)	+0.1 ± 3.4
ζ	2275(27)	2305	2241(2)	–64(29)	–2.8 ± 1.3

there is no corresponding divalent crystal case for comparison. On the other hand, both the Nd^{3+}:$LaCl_3$ (Crosswhite *et al.*, 1976) and U^{3+}:$LaCl_3$ (Crosswhite *et al.*, 1980) spectra are very well documented, but experimental work for both Nd IV and U IV are incomplete. In fact, except for thorium, no doubly or triply ionized actinide free-ion analyses are known.

Although the parametric analyses are incomplete, enough free-ion data are available in a few cases to permit a determination of one or both of the major parameters F^k and ζ_{nf}. For the actinides, these are all neutral atomic and singly ionized cases, for which, again, no condensed-phase analogs are available. These are U I $5f^47s^2$, U II $5f^37s^2$, Pu I $5f^67s^2$, Pu II $5f^57s^2$, and Cf I $5f^{10}7s^2$, all of which contain the closed shell $7s^2$. Using Hartree–Fock (Cowan and Griffin, 1976) results to make corrections for the removal of the $7s^2$ shells, parametric values for the divalent U III, Pu III, and Cf III, and trivalent U IV and Pu IV cases can be inferred. The best example is for Pu IV. A comparison of estimated free-ion parameters with the Pu^{3+}:$LaCl_3$ results is given in Table 18.5. Although the statistical uncertainties are large, the relative changes are consistent with those for Pr^{3+} in the same host.

Because the shifts due to the crystalline environment and those due to the addition of the $7s^2$ shell are nearly the same, it has turned out that, for initial identification, the crystal absorption lines can be related directly to the free-ion spectral lines, at least in those cases for which the crystal field can be treated in the weak-field approximation.

18.4.2 Crystal-field Hamiltonian and matrix element evaluation

Based on the concept that the crystal-field interaction can be treated approximately as a point-charge perturbation on the free-ion energy states, which have their eigenfunctions constructed with the basis of spherical harmonic functions, the effective operators of crystal-field interaction may be defined with the tensor operators of the spherical harmonics $\mathbf{C}^{(k)}$. Following Wybourne's formalism (Wybourne, 1965a,b), the crystal field potential may be defined by:

$$\mathscr{H}_{\mathrm{CF}} = \sum_{k,q,i} B_q^k C_q^{(k)}(i), \tag{18.32}$$

where the summation involving i is over all the equivalent electrons of the open shell of the ion of interest; where the B_q^k are crystal field parameters and the $C_q^{(k)}$ are components of the tensor operators $\mathbf{C}^{(k)}$ that transform like spherical harmonics.

In addition to Wybourne's formalism for crystal field parameters, the Stevens' notation of crystal field parameters $A_k^q\langle r^k\rangle$ are often found in the literature. The crystal-field interaction is often characterized by quantitative comparison of the crystal field strength defined as (Wybourne, 1965a; Auzel and Malta, 1983):

$$N_v = \left[\frac{1}{4\pi}\sum_{q,k}\frac{\left(B_q^k\right)^2}{2k+1}\right]^{1/2}, \tag{18.33}$$

With tensor operators, evaluation of the crystal field matrix elements can be performed with the same methods used for the free-ion matrix elements. Upon application of the Wigner–Eckart theorem, the matrix elements of the crystal-field interaction can be expressed with the reduced matrix elements of a unit tensor $\mathbf{U}^{(k)}$ (Wybourne, 1965a; Weissbluth, 1978):

$$\left\langle l\tau SLJM\left|\sum_i C_q^k(i)\right|l\tau' L'J'M'\right\rangle = (-1)^{J-M}\begin{pmatrix} J & k & J' \\ -M & q & M'\end{pmatrix} \left\langle l\tau SLJ\|\boldsymbol{U}^{(k)}\|l'\tau' S'L'J'\right\rangle\left\langle l\left\|\boldsymbol{C}^{(k)}\right\|l\right\rangle. \tag{18.34}$$

In *LS* coupling, the matrix elements of the unit tensor can be further reduced to

$$\left\langle l\tau LSJ\|\mathbf{U}^{(k)}\|l\tau' L'S'J'\right\rangle = (-1)^{S+L'+J+k}[(2J+1)(2J'+1)]^{1/2} \begin{Bmatrix} J & J' & k \\ L' & L & S\end{Bmatrix}\left\langle l\tau LS\|\boldsymbol{U}^{(k)}\|l\tau' L'S'\right\rangle \tag{18.35}$$

With equations (18.34) and (18.35), the reduced matrix elements of the crystal-field Hamiltonian can be written as:

$$\langle l\tau SLJM\,|\,\mathscr{H}_{\mathrm{CF}}|l\tau' S'L'J'M'\rangle = \sum_{k,q} B_q^k(-1)^{J-M}\begin{pmatrix} J & k & J' \\ -M & q & M'\end{pmatrix} D_J^k, \tag{18.36}$$

where

$$D_J^k = (-1)^{S+L'+J+k}[(2J+1)(2J'+1)]^{1/2}\begin{Bmatrix} J & J' & k \\ L' & L & S\end{Bmatrix} \left\langle l\tau SL\|\mathbf{U}^{(k)}\|l\tau' S'L'\right\rangle(-1)^l(2l+1)\begin{pmatrix} l & k & l \\ 0 & 0 & 0\end{pmatrix} \tag{18.37}$$

where $l = 3$ for f^N configurations. Since all the coefficients, including the values of the $3{-}j$ and $6{-}j$ symbols and the doubly reduced matrix elements of the unit tensor, are known for a given free-ion multiplet, it is obvious that evaluation of crystal-field splittings can be performed by fitting the crystal field parameters B_q^k.

The doubly reduced matrix elements of $\mathbf{U}^{(k)}$ may be obtained directly from Nielson and Koster (1963) or from the SPECTRA program. The values of the $3{-}j$ ( ) and $6{-}j$ { } symbols can be obtained from the compilation of Rotenberg *et al*. (1959) or by direct computer evaluation. The values of k and q for which the matrix elements are nonzero are determined by the symmetry of the crystal

field and the f-electron angular momentum. For f^N configurations ($l = 3$), the $3-j$ symbols in equation (18.37) require that $k = 0, 2, 4, 6$, and $|q| \leq k$. The values of q are also restricted by the point group of the f-ion site, because the crystal-field Hamiltonian has to be invariant under all symmetry operations of the point group. Restrictions due to point group symmetry properties on the nonzero matrix elements of the crystal-field Hamiltonian are discussed later in this section.

For the matrix element of $k = q = 0$, the zero-order of crystal-field interaction is spherically symmetric and does not split the free-ion energy levels, but induces a shift to all energy levels in the same f^N configuration. In general, B_0^0 is not included in evaluation of the crystal-field splitting. Therefore, its contribution to energy level shift is combined with the spherically symmetric component of the free-ion electrostatic interactions. One parameter, namely F^0, absorbs contributions from spherically symmetric components of free-ion and crystal-field interactions.

Once the matrix elements in equation (18.36) are evaluated, the Hamiltonian of the crystal-field interaction may be diagonalized together with the free-ion Hamiltonian to obtain the crystal-field splittings as a function of crystal field parameters. For spectral analysis, the free-ion parameters may also be considered as variables for fitting an experimental spectrum. As a result of the crystal-field interactions, each of the $^{2S+1}L_J$ multiplets splits into crystal field levels. Because the off-diagonal matrix elements of the crystal field between different J-multiplets may not be zero, crystal field operators induce J-mixing. In consequence, for actinide ions in crystals, both J and M are no longer good quantum numbers.

As a result of J-mixing, the eigenfunction of a crystal field level is expressed as

$$|\mu\rangle = \sum_{J,M} a_{JM} |JM\rangle, \tag{18.38}$$

where, in principle, the summation is over all JM terms of a given f^N configuration. However, inclusion of all J-multiplets results in extremely large matrices, particularly, for the configurations with $4 \leq N \leq 10$. Diagonalization of the effective-operator Hamiltonian on the entire $LSJM$ basis could be very time-consuming in an analysis of an experimental spectrum from optical spectroscopy. Such spectra usually cover energy levels that are less than 40 000 cm^{-1} above the ground state (Carnall, 1992; Liu *et al.*, 1994b). Off-diagonal matrix elements between free-ion states separated by a large energy gap are small. As an approximation, crystal field calculations without including J-mixing is appropriate only for the isolated multiplets, such as the first $^5D_1$ excited state of Am^{3+} or the $^8S_{7/2}$ ground state of Cm^{3+}. In practice, the crystal field energy level structure of a $5f^N$ configuration is usually calculated over the restricted energy region in which experimental data are available. Free-ion multiplets with energy

levels far from this region usually are not be included in the calculation. Namely, the free-ion eigenfunction basis may be truncated before diagonalizing the matrix of crystal-field Hamiltonian. Theoretically, this truncation of free-ion states is justified because crystal-field coupling diminishes between two free-ion multiplets as their energy gap increases. From the perturbation point of view, the leading contribution of J-mixing to the energy level splitting of the J-multiplets is proportional to $1/\Delta E_{JJ'}$. Given that the crystal-field splitting of a free-ion multiplet is about 100−1000 cm^{-1}, multiplets that are separated by 10^4 cm^{-1} should have no significant influence on each other.

In computational analyses of experimental spectra, one may truncate the free-ion states whose energy levels are far from the region of interest. This is readily accomplished after diagonalization of the free-ion matrix to produce a calculated free-ion energy level structure. These levels are considered to be the centers of gravity for the crystal-field splitting (Carnall *et al.*, 1983; Carnall, 1992). One chooses the numbers of J-multiplets to be included in the crystal-field matrices for each J-value. Therefore, the chosen J-multiplets are still complete sets of free-ion eigenfunctions that contain all SL components of the given J. This way of free-ion state truncation ensures that no contribution from the free-ion interactions is lost when constructing the free-ion wave functions for each J-multiplet.

One example is the $^8S_{7/2}$ ground state of ions in a $5f^7$ configuration for Am^{2+}, Cm^{3+}, or Bk^{4+} in which both diagonal and off-diagonal matrix elements of the crystal field operators vanish (Wybourne, 1966; Newman, 1970; Liu *et al.*, 1993; Newman and Ng, 2000). The observed crystal-field splittings must be attributed to the contributions of the mixture of other LS terms in the ground state free-ion wave function and nonzero off-diagonal matrix elements between different J values (Liu *et al.*, 1993, 1998; Murdoch *et al.*, 1996, 1998). Because of large energy gaps from the ground state to the excited multiplets ($\sim$16 000 cm^{-1}), J-mixing is negligible in this case. It has been shown that for the $^8S_{7/2}$ ground state splitting, the leading contributions are from the fourth and higher orders of the coupled matrix elements between the spin–orbit ($\mathbf{V}^{(11)}$) and crystal field ($\mathbf{U}^{(k)}$) operators (Liu *et al.*, 1993; Brito and Liu, 2000). Without inclusion of J-mixing, the leading contributions to the crystal-field splitting of the $^8S_{7/2}$ multiplet of an f_7 configuration are from the mixed matrix elements such as

$$\begin{aligned}&\left\langle {}^8S\middle|\mathbf{V}^{(11)}\middle|{}^6P\right\rangle\left\langle {}^6P\middle|\mathbf{U}^{(2)}\middle|{}^6D\right\rangle\left\langle {}^6D\middle|\mathbf{U}^{(2)}\middle|{}^6P\right\rangle\left\langle {}^6P\middle|\mathbf{V}^{(11)}\middle|{}^8S\right\rangle\\&\left\langle {}^8S\middle|\mathbf{V}^{(11)}\middle|{}^6P\right\rangle\left\langle {}^6P\middle|\mathbf{U}^{(11)}\middle|{}^6I\right\rangle\left\langle {}^6I\middle|\mathbf{U}^{(6)}\middle|{}^6P\right\rangle\left\langle {}^6P\middle|\mathbf{V}^{(11)}\middle|{}^8S\right\rangle.\end{aligned} \tag{18.39}$$

It is obvious that truncation of LS terms in the $J = 7/2$ multiplets should affect the scale of the coupled matrix elements, and thus affect the calculated crystal-field splitting. The same situation occurs for the off-diagonal matrix elements between different J-levels, but is less important because of the large energy gap between the ground state and the first excited state.

18.4.3 Symmetry rules

The geometric properties of the crystal field operators will now be discussed in more detail. In addition to the angular momentum of the f-ions that restricts k and q for a set of nonvanishing crystal field operators, the site symmetry in a crystalline lattice also imposes limits on crystal field operators. The tensor operators for the crystal-field interaction must be invariant under the point group symmetry operations imposed by the site symmetry of the ion in question. Here the interest is to identify the nonvanishing components of crystal field operators and their matrix elements. First, for states of the same parity, namely $l = l'$, k must be even. It is also required that B_q^k must be real in any symmetry group that contains a rotation operation about the y-axis by π or a reflection through the $x-z$ plane; otherwise B_q^k ($q \neq 0$) is complex. In the latter case, one of the B_q^k can be made real by a rotation of the coordinate system about the z-axis. The B_q^k for $q < 0$ are related to those of $q > 0$ by

$$B_{-q}^k = (-1)^q B_q^{k*}. \tag{18.40}$$

Also under the invariant conditions of the point group theory, the crystallographic axis of the lowest symmetry determines the values of q for the nonvanishing crystal field operators. For example, at a site of C_{3v} symmetry, there is a three-fold axis of rotational symmetry with a reflection plane that contains the C_3 axis (Tinkham, 1964; Hüfner, 1978). The ligand field must exhibit this symmetry. Hence, if a $2\pi/3$ rotation is performed on the crystal field potential followed by a reflection with regard to the plane, the potential is invariant only if $q = 0$, ± 3, and ± 6. Thus, within an f^N configuration, the crystal-field Hamiltonian may be written as

$$\begin{aligned}\mathscr{H}(C_{3v}) = \sum_i [&B_0^2 C_0^{(2)}(i) + B_0^4 C_0^{(4)}(i) + B_3^4 (C_{-3}^{(4)}(i) - C_3^{(4)}(i)) \\ &+ B_0^6 C_0^{(6)}(i) + B_3^6 (C_{-3}^{(6)}(i) - C_3^{(6)}(i)) + B_6^6 (C_{-6}^{(6)}(i) + C_6^{(6)}(i))].\end{aligned} \tag{18.41}$$

If the reflection plane is perpendicular to the C_3 axis, the site symmetry becomes C_{3h}, which occurs for doped f^N impurity ions in lanthanum ethylsulfate, $LaCl_3$, and $LaBr_3$ (Morosin, 1968). This potential invariant property requires $q = 0$, ± 6 only, but, since there is no rotation symmetry about the y-axis by π or a reflection through the x–z plane for the C_{3h} site, there is an imaginary noncylindrical term in the Hamiltonian:

$$\begin{aligned}\mathscr{H}(C_{3h}) = \sum_j [&B_0^2 C_0^{(2)}(j) + B_0^4 C_0^{(4)}(j) + B_0^6 C_0^{(6)}(j) + B_6^6 (C_{-6}^{(6)}(j) \\ &+ C_6^{(6)}(j)) + iB_6'^6 (C_6^{(6)}(j) - C_{-6}^{(6)}(j))].\end{aligned} \tag{18.42}$$

D_{3h} is a symmetry group that includes all rotation and reflection operations of C_{3h} (Tinkham, 1964; Hüfner, 1978). The crystal field operators for ions at a

D_{3h} site are the real terms for C_{3h} without the imaginary term $iB_6'^6(C_6^{(6)} - C_{-6}^{(6)})$. The nonvanishing terms of crystal field operators for various lattice sites of f-ions in crystals are listed in Table 18.6.

The free-ion degeneracy in M may be partially or completely removed by the crystal-field interaction. In the crystal-field energy matrix using the JM basis set, the terms for which $M-M' = q$ for the operator $C_q^{(k)}$ are nonzero. Otherwise the crystal-field matrix elements are zero. Based on this property, the crystal-field matrix may be reduced into several independent submatrices, each of which is characterized by a crystal quantum number μ (or γ). Each μ represents a group of M, such that $M-M' = q(0, 2, 3, 4, 6)$ belongs to the same submatrix (Hüfner, 1978). All matrix elements between the submatrices are zero. The crystal field quantum number may be used to classify the crystal field energy levels even when J and M are not good quantum numbers. Considering C_{3h} (and D_{3h}) as an example, the JM and $J'M'$ (J may be equal to J') with $M-M' = 6$ belong to the same crystal field submatrix. For an even number of f-electrons, there are four independent submatrices, and for an odd number of f-electrons, there are three independent submatrices. The parameters of nonvanishing crystal field terms for symmetries of common crystal hosts of f-element ions are given in Table 18.6 along with the numbers of reduced crystal-field matrices.

Without a magnetic field, the electrostatic crystal field alone does not completely remove the free-ion degeneracy for the odd-numbered electronic configurations. Known as Kramers' degeneracy (Kramers, 1930; Hüfner, 1978), all crystal field levels are at least doubly degenerate. The crystal quantum number and JM classification schemes are given for D_{3h} symmetry in Table 18.7. In calculation of energy level structure for degenerate doublets, one may cut off half of the submatrix elements. In many cases, calculations of crystal field energy levels have been carried out usefully by assuming a higher site symmetry than the real one so that fewer parameters are required. In some cases, this approach was used because actinide ions in many solids occupy a low-symmetry site and the limited number of observed energy levels could not accurately determine a large number of crystal field parameters (Carnall *et al.*, 1991). In other cases, a crystal lattice that does not have mirror symmetries in its coordinates requires complex crystal field parameters for the $q \neq 0$ terms (Table 18.6). If one uses as an approximation only the real part of the crystal field operators, energy level calculation becomes much easier. Because the use of high symmetry as an approximation is equivalent to upgrading a lower-symmetry site to a higher one within the same crystal symmetry group, this approach has been called the descent-of-symmetry method (Görller-Walrand and Binnemans, 1996). This method may be applied to the groups of monoclinic, trigonal, and tetragonal structures listed in Table 18.6. For example, the C_{3h} symmetry of $LaCl_3$ was replaced by D_{3h} (Morrison and Leavitt, 1982); the S_4 site symmetry of trivalent lanthanide ions in $LiYF_4$ is often treated as D_{2d} (Esterowitz *et al.*, 1979; Görller-Walrand *et al.*, 1985; Liu *et al.*, 1994a). Similarly, the actual C_2 symmetry of LaF_3 was replaced by C_{2v} (Carnall *et al.*, 1989).

Table 18.6 *Nonvanishing terms of crystal field (CF) parameters B_q^k, numbers of reduced matrices and crystal field quantum number μ for f^N configurations in crystals of various symmetries.*[a,b]

Crystal structure	*Site symmetry*	*Example*	B_q^{kc}	μ *for even* N[d]	*μ for odd* N[d]
monoclinic	C_s, C_2,C_{2h}	LaF_3	$B_0^2, B_0^4, B_0^6, \mathrm{Re}(B_2^2), B_2^4, B_2^6, B_4^4, B_4^6, B_6^6$	±0, ±1 (S)	1/2 (D)
rhombic	C_{2v}, D_2, D_{2h}	$Y_3Al_5O_{12}$	$B_0^2, B_0^4, B_0^6, \mathrm{Re}\left(B_2^2, B_2^4, B_2^6, B_4^4, B_4^6, B_6^6\right)$		
trigonal	C_3, $S_6(C_{3i})$	$LiNbO_3$	$B_0^2, B_0^4, B_0^6, \mathrm{Re}(B_3^4), B_3^6, B_6^6$	±0 (S), 1 (D)	1/2, 3/2 (D)
	C_{3v}, D_3, D_{3d}	Y_2O_2S	$B_0^2, B_0^4, B_0^6, \mathrm{Re}\left(B_3^4, B_3^6, B_6^6\right)$		
tetragonal	C_4, S_4, C_{4h}	$LiYF_4$	$B_0^2, B_0^4, B_0^6, \mathrm{Re}\left(B_4^4\right), B_4^6$	±0, ±2 (S), 1 (D)	1/2, 3/2 (D)
	D_4,C_{4v}, D_{2d}, D_{4h}	YPO_4	$B_0^2, B_0^4, B_0^6, \mathrm{Re}\left(B_4^4, B_4^6\right)$		
hexagonal	C_6,C_{3h}, C_{6h},D_6, C_{6v}, D_{3h}, D_{6h}	$LaCl_3$	$B_0^2, B_0^4, B_0^6, \mathrm{Re}\left(B_6^6\right)$	±0, ±3 (S), 1, 2 (D)	1/2, 3/2, 5/2 (D)
cubic	T, T_d, T_h, O, O_h	CeO_2	$B_0^4, B_0^6, \mathrm{Re}\left(B_4^4, B_4^6\right)$[e]	±0, ±4 (S), 2, 6 (D), 1 (T)	1/2, 7/2 (D), 3/2 (Q)

[a] Morrison and Leavitt (1982).
[b] Hüfner (1978).
[c] For $q \neq 0$, $B_q^k$are complex except for the real terms $\mathrm{Re}\left(B_q^k\right)$.
[d] S, singlet; D, doublet; T, triplet; Q, quartet.
[e] $B_4^4 = \frac{5}{\sqrt{70}} B_0^4, \quad B_4^6 = -\sqrt{\frac{7}{2}} B_0^6$

Table 18.7 *Classification of crystal field energy levels for D_{3h} symmetry.*

(*a*) *Even number of electrons*

	$\mu = 0\ (^1\Gamma_{1,\,2})$	$\mu = \pm 1\ (^2\Gamma_5)$	$\mu = \pm 2\ (^2\Gamma_6)$	$\mu = 3\ (^1\Gamma_{3,\,4})$	*No. levels*
J	*M*	*M*	*M*	*M*	
0	0				1
1	0	± 1			2
2	0	± 1	± 2		3
3	0	± 1	± 2	$3, -3$	5
4	0	± 1	$\pm 2, \mp 4$	$3, -3$	6
5	0	$\pm 1, \mp 5$	$\pm 2, \mp 4$	$3, -3$	7
6	$-6, 0, 6$	$\pm 1, \mp 5$	$\pm 2, \mp 4$	$3, -3$	9
7	$-6, 0, 6$	$\pm 7, \pm 1, \mp 5$	$\pm 2, \mp 4$	$3, -3$	10
8	$-6, 0, 6$	$\pm 7, \pm 1, \mp 5$	$\pm 8, \pm 2, \mp 4$	$3, -3$	11

(*b*) *Odd number of electrons*

	$\mu = \pm 1/2\ (^2\Gamma_7)$	$\mu = \pm 3/2\ (^2\Gamma_8)$	$\mu = \pm 5/2\ (^2\Gamma_9)$	*No. levels*
J	*M*	*M*	*M*	
1/2	$\pm 1/2$			1
3/2	$\pm 1/2$	$\pm 3/2$		2
5/2	$\pm 1/2$	$\pm 3/2$	$\pm 5/2$	3
7/2	$\pm 1/2$	$\pm 3/2$	$\pm 5/2, \mp 7/2$	4
9/2	$\pm 1/2$	$\pm 3/2, \mp 9/2$	$\pm 5/2, \mp 7/2$	5
11/2	$\pm 1/2, \mp 11/2$	$\pm 3/2, \mp 9/2$	$\pm 5/2, \mp 7/2$	6
13/2	$\pm 13/2, \pm 1/2, \mp 11/2$	$\pm 3/2, \mp 9/2$	$\pm 5/2, \mp 7/2$	7
15/2	$\pm 13/2, \pm 1/2, \mp 11/2$	$\pm 15/2, \pm 3/2, \mp 9/2$	$\pm 5/2, \mp 7/2$	8

In general, use of the descent-of-symmetry method may have more complicated consequences than that of the above examples. For a specific symmetry modification, one may estimate the changes in crystal field parameters based on the rotational symmetry of point charges in polar coordinates (θ,ϕ) and assuming that the ligand ions in each coordination shell are at the same distance from the f-element ion. For an arbitrary rotation, the B_0^k parameters should only depend on the θ-coordinates, whereas the B_q^k parameters ($q \neq 0$) depend on both θ- and ϕ-coordinates. Changes in the ϕ-coordinates have no influence on B_0^k and $|B_q^k| = [(\mathrm{Re}B_q^k)^2 + (\mathrm{Im}B_q^k)^2]^{1/2}$. Descent-of-symmetry operations that have this property are $C_{n\mathrm{h}} \rightarrow D_{n\mathrm{h}}$, $S_4 \rightarrow D_{2\mathrm{d}}$, and $C_n \rightarrow C_{n\mathrm{v}}$. The symmetry changes that incorporate a change in θ-coordinates will change all parameters, such as $D_{n\mathrm{h}} \rightarrow C_{n\mathrm{v}}$ and $D_{n\mathrm{h}} \rightarrow C_n$. If the symmetry of the f-element site is lowered, not only are additional parameters required, but there are also changes in the crystal field parameters found in the higher symmetry. In consequence, there is far less rationale for using D_n has an approximation for C_n and $C_{n\mathrm{v}}$.

Site distortion is a common phenomenon when f-element ions are doped into crystals. A dopant ion may have site symmetry lower than that of the host ion it replaces. This is especially true if the charge on the dopant ion and/or its ionic radius is different from that of the host ion. Accordingly, both the sign and magnitude of crystal field parameters are subject to change. As discussed above, different crystal structures may undergo different types of distortion that reflect the properties of the specific coordination polyhedron in a given crystal. Görller-Walrand and Binnemans (1996) give a detailed description of the effects of structural distortion in terms of changes in the θ- and ϕ-coordinates. However, changes in radial distances may occur as well. For ions at a distorted site that further reduces the degeneracy of electronic states, analyses of crystal field spectra must be conducted using a lower symmetry.

18.4.4 Empirical evaluation of crystal field parameters

Extensive mixing of *SL*-basis states, brought about by the spin–orbit and crystal-field interactions for each *J*-multiplet, can result in the least-squares method for empirical evaluation of crystal field parameters converging to a false solution. A false solution can be recognized if there is sufficient characterization of the states from supplementary data, such as Zeeman splitting factors or polarized spectra. However, this in itself may not produce the true solution. The latter can only be found if sufficiently accurate initial parameters are available for the least-squares fitting process to be effective. Therefore, establishing accurate parameters for the model Hamiltonian essentially relies on systematic analyses that encompass theoretical calculations for incorporating trends of parameter variation across the f-element series (Carnall, 1989; Liu *et al.*, 1994b; Liu, 2000). The results of analyses of simpler spectra are carried over to more complex ones through consideration of their symmetry properties.

For f-element ions in crystals of well-defined site symmetry, crystal field theory is widely used along with group theory for predicting the number of energy levels and determining selection rules for electronic transitions between crystal field levels. Whereas the number of nonvanishing crystal field parameters can be determined by the symmetry arguments, their values are usually determined by analyzing the experimentally observed crystal-field splittings. Experimental data that carry supplementary spectroscopic information, such as polarized transitions allowed by electric or magnetic dipolar selection rules, ensure the accuracy of the experimentally fitted crystal field parameters (Liu *et al.*, 1992, 1994a, 1998). In addition, the temperature dependence of observed crystal-field splittings may be analyzed to distinguish pure electronic lines from vibronic features. Properties such as magnetic susceptibility as a function of temperature may be calculated from the empirical wave functions as a further check on the accuracy of the crystal field parameters. If multiple sites exist, site-resolved spectra are required to distinguish energy levels of ions at different sites (Tissue and Wright, 1987; Liu *et al.*, 1994b; Murdoch *et al.*, 1996). Accordingly, as a procedure of

parametric modeling, correct assignment of observed energy levels is crucial to avoid a false solution. For spectra that lack sufficient experimental information to achieve unambiguous assignment, this procedure may involve several iterations of trial calculations and analyses that require a firm understanding of the basics of crystal-field splitting of free-ion states (Carnall, 1989, 1992).

For setting initial parameters of the crystal-field Hamiltonian to be fit by observed energy levels, one may simply use the previously established parameters for different f-element ions in the same or similar host materials. For the series of trivalent actinide ions in $LaCl_3$, one of the most extensively studied host crystals, the parameters of free-ion and crystal-field interactions are listed in Table 18.4. Comprehensive summaries of previously studied lanthanide systems are given (Morrison and Leavitt, 1982; Görller-Walrand and Binnemans, 1996). Alternatively, the signs and magnitudes of crystal field parameters can be predicted according to the coordination of the f-element ion using the point charge model of the electrostatic crystal field potential. For this purpose, only the nearest ligand (NL) atoms need to be considered. As a function of the radial and angular coordinates, the expressions for the B_q^k parameters are given in the following section. The signs of the crystal field parameters are determined by the angular part of the electrostatic potential and may be obtained by symmetry analysis. The predicted signs are important for checking the signs of the parameters obtained by the fitting procedure. Some sign combinations may correspond to a coordination that is physically impossible. Generally, determination of the magnitudes requires more quantitative calculations of the overlap integrals between the f-electrons and the electrons of the ligands. The electrostatic interactions beyond the nearest ligands may bring about significant contributions to the parameters with $k = 2$. For these parameters, the total contribution from the long-range interactions may exceed that of the NL so that a change in the sign of B_q^2 determined by the NL atoms is possible (Zhorin and Liu, 1998). Moreover, the electrostatic point charge model is not realistic in describing the short-range interactions between the f-element ion and its nearest ligands. Charge exchange interactions including covalency may dominate the crystal field parameters with $k = 4$ and 6. For these reasons, an empirical approach with theoretical guidance is necessary to ensure that the parameterization is within the limitations of physical interactions.

In a nonlinear least-squares fitting process, the magnitudes and signs of crystal field parameters are varied to best reproduce the observed energy level structure. This is actually a process of optimizing crystalline structure within a given restriction through variation of the crystal field parameters. The parameters that have higher weight are better determined than the parameters that have less influence on the observed energy levels. Adding an imaginary parameter may only change the real part of the term that has the same q and k but does not have much influence on other parameters. If the values of the crystal field parameters for a system of higher symmetry are used as initial values of the parameters for a different system of lower symmetry, the fitting may either

fall into a false solution or leave the added parameters less accurately determined. In this case, one should assign the unambiguously observed energy levels, most likely the isolated multiplets, and only allow the most significant crystal field parameters to vary freely. Once these weighted parameters converge, further fitting should be performed on the entire set of crystal field parameters, along with the variation of the free-ion parameters.

18.4.5 Theoretical evaluation of crystal field parameters

Quantum mechanical calculations of crystal field energies and corresponding crystal field parameters for f-element ions in compounds with different chemical characteristics were carried out by several groups in the framework of the cluster approximation. For an f-ion and its nearest ligands (chlorine, fluorine, or oxygen ions), the fully antisymmetric and orthonormalized wave functions of zero-order are constructed as linear combinations of products of individual ion wave functions, and the energy matrix is built with the complete Hamiltonian that contains one- and two-electron operators including the interaction with the electrostatic field created by the rest of the crystal. The first-order contributions to the energy matrix include integrals over one-electron wave functions of the occupied states of the cluster. Higher-order contributions correspond to configuration mixing. The procedure and details of calculations have been described in several original and review papers (Newman, 1971; Eremin, 1989; Garcia and Faucher, 1995; Shen and Bray, 1998; Zhorin and Liu, 1998; Newman and Ng, 2000). Here we present only a brief description of the results of *ab initio* simulations that are important for modeling of the main physical mechanisms responsible for crystal-field splittings.

The first-order terms in the energy matrix include Coulombic, exchange, and overlap integrals over 5f orbitals of the actinide ion and outer orbitals of ligand ions. From these terms, the 5f-electron energy in the electrostatic field of the ligand point multipole moments and the charge penetration contribution may be singled out. The second-order terms may be classified according to intermediate (virtual) excited states of the cluster. In this regard, the following electronic excitations should be considered:

(1) Intra-ion excitations from the filled electronic shell of the actinide ion to the empty excited shell (in particular, $6p^6 \rightarrow 6p^5 6d^1$). These processes shield the inner valence $5f^N$ shell and may be accounted for, at least partly, by introducing shielding (or antishielding) factors into the multipole moments of the valence electron $\left(\langle 5f|r^k|5f\rangle \rightarrow (1-\sigma_k)\langle 5f|r^k|5f\rangle\right)$ (Rajnak and Wybourne, 1964).
(2) Intra-ion excitations from the valence shell into empty shells and from the filled shells into the valence shell (in particular, $5f^N \rightarrow 5f^{N-1}6d^1$ or $6p^6 \rightarrow 6p^5 5f^{N+1}$). These processes contribute to the linear shielding and cause additional corrections to parameters of the effective Hamiltonian bilinear in parameters of the electrostatic field.

(3) Inter-ion excitations, mainly into the charge-transfer states of the actinide ion with the extra electron in the valence shell promoted from the outer-filled shell of the ligand. Actually, mixing of the ground configuration with the charge-transfer states corresponds to a partially covalent character in the chemical bonding between an actinide ion and its ligands.

It should be noted that the effective-operator Hamiltonian (equation (18.32)) with a single set of crystal field parameters, operating within the total space of wave functions of $5f^N$ configuration, can be introduced if all excited configurations of the cluster under consideration are separated from the ground configuration by an energy gap that is much larger than the width of the energy spectrum of the ground configuration. Otherwise the crystal field parameters become term (*LSJ*) dependent. In particular, a crystal field analysis carried out on an extended basis containing the ground $4f^2$ and excited 4f5d, 4f6p configurations of Pr^{3+} in YPO_4 (Moune *et al*., 2002) greatly improved the agreement between the experimental data and the calculated energy levels. For the $5f^N$ configurations, the inter-configuration coupling is anticipated to be much stronger because of smaller gaps between the ground and excited state configurations, particularly, for the lighter actinides in the first half of the $5f^N$ series.

A general conclusion about the dominant role of overlap and covalent contributions to the crystal field parameters B_q^4 and B_q^6 follows from all *ab initio* calculations carried out up to the present time. When Hartree–Fock one-electron wave functions of free ions are used in simulations, relative differences between the theoretical and experimental values of these parameters do not exceed 50%. However, for the quadrupole component of the crystal field parameters B_q^2, contributions from the long-range interactions of valence electrons with point charges, dipole, and quadrupole moments of ions in the crystal lattice are comparable to contributions from the interactions with the nearest ligand ions, and the theoretical estimations differ substantially from the experimental data.

Whereas the free-ion parameters vary smoothly across the 5f series, trends in crystal field parameters, particularly B_q^4 and B_q^6, usually break at the f^7 configuration. Experimental evidence for this effect is evident in the systematic analysis of the spectra of trivalent actinides doped into single-crystal $LaCl_3$ (Carnall, 1992) and trivalent lanthanides in LaF_3 (Carnall *et al*., 1989). An abrupt change in the magnitude of parameters with $k = 4$ and 6 occurs at the center of the series. Judd (1979) has interpreted this effect as a problem of the one-electron operators of the crystal-field Hamiltonian. One-electron operators, $\mathbf{U}^k$, change sign at the center of the series. Inclusion of two-electron operators in the crystal-field Hamiltonian would likely remove this discontinuity.

Although extensive Hartree–Fock calculations have been utilized for establishing systematic trends of free-ion interactions that lead to the determination of the parameters of the effective-operator Hamiltonian, most analyses of crystal-field interactions are carried out with the crystal field parameters determined by the fitting of experimental data. Attempts to calculate the crystal field

parameters from first principles may not be realistic. Given the complexity of electronic interactions in solids, *ab initio* calculations of electronic structure of heavy element ions in solids currently are not capable of achieving accuracy that is comparable to experimental results. Therefore, theoretical models, more or less phenomenological on the basis of the point-charge approximation, are essential in providing a clear theoretical understanding of electronic interactions of the f-element ions in solids. Model calculations do not only generate the phenomenological crystal field parameters that provide guidance to parametric modeling of the crystal field spectra of f-element ions in solids, but also reveal more fundamental aspects of the ion–ligand interactions that are poorly characterized by the point-charge approximation itself. Among the crystal field models introduced in the literature, the angular overlap model (Jørgensen *et al.*, 1963), the exchange charge model (Malkin *et al.*, 1970; Malkin, 1987), and the superposition model (Newman, 1971; Newman and Ng, 1989b, 2000) have been used for calculations of crystal field parameters for both 4f elements and 5f elements in various crystals.

Detailed discussions of the superposition model of the crystal field and its application to analysis of experimental spectra were provided by Newman and Ng (1989b, 2000). The superposition model neglects the ligand–ligand overlap effects and reflects the total crystal-field interaction as a linear 'superposition' of local ion–ligand pair-wise electrostatic interactions. The crystal field parameters are expressed as a sum of individual contributions from ions in the host crystal lattice,

$$B_q^k = \sum_L \bar{B}_k(R_L) g_{k,q}(\theta_L, \varphi_L), \tag{18.43}$$

where $g_{k,q}$ are normalized spherical harmonic functions, and R_L, θ_L, φ_L locate the position of ligand L in the lattice coordination environment. The distance-dependent parameters $\bar{B}_k(R_L)$ are referred to as intrinsic crystal field parameters, which by definition are dependent only on the radial distance between the f-ion and the ligand L. Based on the assumption of the point charge model that the ion–ligand electrostatic interaction has a specific power law dependence, the intrinsic parameters can be defined as

$$\bar{B}_k(R) = \bar{B}_k(R_0)(R_0/R)^{t_k}, \tag{18.44}$$

where R_0 is the distance between the f-ion and a reference ligand located on the z-axis of the crystalline lattice, and τ_k are power law exponents that reflect the distance dependence of the ion–ligand interaction (Newman and Ng, 2000). $\bar{B}_k(R_0)$and τ_k can be empirically determined as phenomenological parameters. It should be noted that the parameters τ_k are not generally in agreement with the electrostatic power law components $\tau_2 = 3$, $\tau_4 = 5$, $\tau_6 = 7$. For chloride ligands, in particular, $\tau_4 = 12 - 16$, $\tau_6 = 5 - 7$ for different RE ions (Reid and Richardson, 1985). Values of the rank 4 and 6 parameters quickly decrease with R, and the corresponding sums (equation (18.43)) are limited to the nearest neighbors of the f-ion. Because of their long-range effect, values of the rank 2

parameters are often difficult to determine. One may break the rank 2 operator into two terms, labeled as p and s (Levin and Cherpanov, 1983):

$$\bar{B}_2(R_L) = \bar{B}_2^p(R_0)(R_0/R_L)^3 + \bar{B}_2^s(R_0)(R_0/R_L)^{10} \tag{18.45}$$

to represent, respectively, the ligand point charge contribution and the short-range contribution.

Apparently, model calculations of crystal field parameters result in less discrepancies for some systems than for others. This is mainly due to uncertainties in structure information to which crystal field calculations, particularly of the rank 4 and 6 parameters, are extremely sensitive. Crystal lattice constants determined from X-ray diffraction or neutron scattering may be of very high resolution only for intrinsic sites. For impurity f-element ions doped into host materials, an unknown structural distortion is induced in most cases. The doping-induced site distortion depends in part on the ionic radius difference between the host ion and the doped f-element ion. If a model calculation is conducted based on the structure of the host, the calculated crystal field parameters are expected to be more or less different from those determined by fitting experimental data for the system.

The exchange charge model (ECM) (Malkin *et al.*, 1970; Larionov and Malkin, 1975; Malkin, 1987) is an extension of the angular overlap model (Jørgensen, 1962). It considers both long-range and short-range interactions between the actinide or lanthanide ion and lattice ions. The effective crystal-field Hamiltonian is assumed to be a sum

$$\mathscr{H}_{\mathrm{CF}} = \mathscr{H}^{\mathrm{pm}} + \mathscr{H}^{\mathrm{ec}} \tag{18.46}$$

where the first term corresponds to the electrostatic interaction of valence electrons localized on the f-element ion with point multipole moments of the lattice ions. The second term approximates all contributions due to the spatial distribution of electron density. Both terms have the form of equation (18.44) with parameters $B_q^{(\mathrm{pm})k}$ and $B_q^{(\mathrm{ec})k}$. Matrix elements of the effective-operator Hamiltonian $\mathscr{H}^{\mathrm{ec}}$ in the basis of one-electron wave functions of the metal ion interacting with spherical ligand ions may be calculated (Malkin *et al.*, 1970; Malkin, 1987).

To gain a greater insight into the energy level calculations, it is instructive to compare contributions to the electrostatic crystal field parameters with those from overlap and covalency effects. The ECM introduces the renormalization of the parameters of the electrostatic crystal field only and does not change the structure of the Hamiltonian $\mathscr{H}^{\mathrm{pm}}$. This renormalization may be considered to be a result of the 'nonlocal' interaction of the valence electron with the exchange charges localized at the bonds connecting the metal ion with its nearest neighbor ions. The concept of exchange charge, for which the crystal field model under consideration was named, and was first introduced by Dick and Overhauser (1958) in the theory of dielectric properties of solids. Values of exchange charges are proportional to the linear combinations of the overlap integrals and depend on the rank k of the corresponding tensor $\boldsymbol{B}^{(k)}$ of crystal field parameters. It is

Table 18.8 *Crystal field parameters from ECM calculation and experimental fit* (cm^{-1}).[a]

	Nd^{3+}:$LaCl_3$	(C_{3h} *symmetry*)	Cm^{3+}:$LuPO_4$	(D_{2d} *symmetry*)
	Calculated[b]	*Experimental*[b] (*fit to* D_{3h})	*Calculated*[c]	*Experimental*[c]
B_0^2	−78(39)	81	450(180)	399
B_0^4	−78(−57)	−42	370(230)	363
B_0^6	−44(−41)	−44	−2500(−2050)	−2470
ReB_4^4			2400(1200)	2261
ReB_4^6			200(185)	167
ReB_6^6	299(279)	439		
ImB_6^6	−239(−226)			

[a] The values in parentheses are the contribution from exchange-charge interactions.
[b] Zhorin and Liu (1998).
[c] Liu *et al.* (1998).

important that the ECM allows for consideration of both even and odd components of the crystal field. In particular, integral intensities of spectral lines in the intra-configurational $5f^N-5f^N$ spectra and their frequencies may be fitted in the framework of a single model.

As an example of ECM calculation, Table 18.8 lists the values of crystal field parameters calculated by using the ECM in comparison with the experimentally determined ones. It is evident that the dominant contributions to B_q^2 are from electrostatic interactions, whereas those to B_q^4 and B_q^6 are from short-range interactions. It is generally realized that the second-order parameters B_q^k with $k = 2$ are less accurately determined by the model calculation, particularly for a disordered lattice. This is because the second-order parameters characterize the long-range electrostatic interactions that are difficult to calculate accurately. It should be noted that the contradiction between the calculated and experimental values of the B_0^2 parameter in Nd^{3+}:$LaCl_3$ (in particular, different signs) may be removed when taking into account large contributions due to point dipole and quadrupole moments of chlorine ions (Eremin, 1989).

18.4.6 Corrections to the crystal-field Hamiltonian

As described in earlier sections, the parameterization approach is able to reproduce the crystal field energy level structures of actinide or lanthanide ions in satisfactory agreement with high-resolution absorption and luminescence spectra. The standard deviation in a nonlinear least-squares fit to experimental spectra in the low-lying energy levels (40 000 cm^{-1}) can be less than 10 cm^{-1} for lanthanide ions (Liu *et al.*, 1994a). However, crystal field modeling of energy levels for some particular states in the 4f configurations is invariably poor as, for instance, in the cases of the $^2H_{11/2}$ multiplet of Nd^{3+} and $^3K_8$ of Ho^{3+}. The discrepancies are much larger for the actinides in $5f^N$ configurations

(Edelstein, 1979; Carnall, 1992; Liu *et al*., 1994b; Murdoch *et al*., 1997; Liu, 2000). Faucher *et al*. (1996) reported in energy level analysis of U^{4+} in the octahedral sites of Cs_2UBr_6 and Cs_2ZrBr_6 evidence of strong interaction between the $5f^2$ and $5f^17p^1$ configurations. Adjustment of the parameters in the free-ion Hamiltonian does not result in much improvement. This problem is primarily due to the exclusion of the electron correlation effect in the one-electron crystal field model. The effects of electron–electron interaction cannot be completely absorbed into the effective-operator Hamiltonian of the one-electron crystal field model. Reid and coworkers (Reid, 2000) have reviewed progress in the modification of the one-electron crystal field theory with inclusion of correlation crystal field operators in the Hamiltonian.

There are various physical mechanisms that contribute to multiplet-dependent crystal-field splittings that can be described generally as correlation effects. The two obvious mechanisms, namely, the spin-correlated crystal field potential (Newman, 1971; Judd, 1977b) and the anisotropic ligand polarization effect, also known as nephelauxetic effect (Jørgensen, 1962; Gerloch and Slade, 1973), have been identified as large contributors, although, it is not clear what physical mechanisms produce the dominant contribution to shift the f-electron energy levels. To correct the discrepancy that appears in analyses of optical spectra with the one-electron crystal field model, it becomes necessary to introduce a full parameterization of the anisotropic two-electron interaction. To facilitate calculations of the matrix elements with the same basis for the one-electron operator Hamiltonian, Judd's $\mathbf{g}_{iq}^{(k)}$ operators (Judd, 1977a), which are orthogonal over the complete f^N basis sets, are used to define the correlation crystal field (CCF) Hamiltonian (Reid, 1987):

$$\mathscr{H}_{\mathrm{CCF}} = \sum_{ikq} G_{iq}^{k} \mathbf{g}_{iq}^{(k)}, \tag{18.47}$$

where G_{iq}^{k} are parameters of CCF. The index k runs through the even integers from 0 to 12 ($4l$, for f^N configurations). The parameter q is restricted by symmetry, and the number of operators varies with k. The operators $\mathbf{g}_{i}^{(k)}$with $k = 0$ correspond to Coulomb interactions and those with $i = 1$ to one-electron operators, in fact $\mathbf{g}_{1}^{(k)} \equiv \mathbf{U}^{(k)}$.

The main problem in the application of the CCF Hamiltonian is the very large number of parameters that are necessary to account for electron–electron correlation. However, the successful parameterization of f-ion crystal field energy level structure is largely dependent on the accuracy and the number of observed and properly assigned energy levels. In general, nonlinear least-square fitting requires that the number of assigned energy levels should be much larger than the total number of freely varied parameters. Expansion of the effective-operator Hamiltonian by including the operators for the correlation crystal-field interaction is effective only if there are sufficient experimental data and correctly determined parameters for the free-ion and one-electron crystal-field Hamiltonian for initial input. Otherwise, fits may fall into false minima and

produce inconsistent parameters. To correct the one-electron crystal field discrepancy by adding more terms to the crystal-field interaction, one should always consider restrictions on operators and introduce constraints based on physical relationships to reduce the number of freely varied parameters.

As discussed in Section 18.3, the effective-operator Hamiltonian for the free-ion interaction includes a corrective term (equation (18.26)) due to configuration interaction. In crystal field theory, the effect of configuration interaction was also considered (Rajnak and Wybourne, 1964). For a configuration of equivalent electrons l^N, most mechanisms of configuration interaction lead to a simple scaling of the crystal field parameters B_q^k. However, a one-electron excitation, either from the l^N shell to unfilled orbitals or from closed shells into the l^N shell, also results in effects that cannot be accommodated by a scaling of the B_q^k parameters alone. As a result, the crystal field parameters are expected to vary from one multiplet to another.

For the weak crystal-field interaction of the f-element ions in crystals, the usual method of a second-order perturbation theory can be used to characterize the configuration interaction (Judd, 1963a; Rajnak and Wybourne, 1963, 1964). The single particle operator $C_q^{(k)}$ in equation (18.32) can only couple configurations that differ by the excitation of a single electron. Thus, for an nl^N-type configuration, only three types of configurations are coupled:

(1) $nl^N n'l'^{4l'+1}$ with $nl^N n'l'^{4l'+1}n'l''$;
(2) nl^N with $nl^{N-1}n'l'$;
(3) $nl^N n'l'^{4l'+2}$ with $nl^{N+1}n'l'^{4l'+2}$.

As a result of the interaction between these configurations, each matrix element of equation (18.32) must be replaced by

$$(1+\Delta)\left\langle l^N\tau SLJM\left|B_q^k C_q^{(k)}\right|l^N\tau' S'L'J,M'\right\rangle \tag{18.48}$$

where Δ is known as the configuration interaction correction factor. This factor is the sum of two terms Δ_1 and Δ_2, where

$$\Delta_1 = \frac{-1}{E}\sum_m \frac{\langle nl^N\psi|\mathscr{H}_{\mathrm{CF}}|m\rangle\langle m|\mathscr{H}_{\mathrm{CF}}|nl^N\psi'\rangle}{\langle nl^N\psi|\mathscr{H}_{\mathrm{CF}}|nl^N\psi'\rangle}, \tag{18.49}$$

and

$$\Delta_2 = \frac{-2}{E}\sum_m \frac{\langle nl^N\psi|\mathscr{H}_{\mathrm{CF}}|m\rangle\langle m|\mathscr{H}_{C}|nl^N\psi'\rangle}{\langle nl^N\psi|\mathscr{H}_{\mathrm{CF}}|nl^N\psi'\rangle} \tag{18.50}$$

and E is the mean excitation energy of the excited electron, m is a state of the perturbing configuration, $\mathscr{H}_{\mathrm{CF}}$ is the crystal-field Hamiltonian, and $\mathscr{H}_{\mathrm{C}}$ is the Coulomb interaction in the free-ion Hamiltonian.

The first correction factor Δ_1 corresponds to configuration mixing purely by the crystal field, whereas the second factor Δ_2 represents an electrostatically correlated crystal-field interaction between the configurations. Methods for

evaluating the matrix elements have been discussed in detail in previous work (Judd, 1963a; Rajnak and Wybourne, 1964). It has been shown that the primary effect of configuration interaction is simply to scale the crystal field parameters B_q^k. The individual parameters are shielded (or antishielded) by different amounts depending on the perturbing configuration. This overall scaling effect is absorbed into the crystal field parameters determined from the experimental data. However, it has been shown that the second factor Δ_2 may be different for different *SL* states. This means that the crystal field parameters are no longer independent of free-ion states. If this mechanism is important, the crystal field parameters determined in fitting observed states in the narrow energy range of the low-lying multiplets give an inadequate description of the crystal-field splittings of the multiplets at higher energies.

18.5 INTERPRETATION OF THE OBSERVED SPECTRA OF TRIVALENT ACTINIDE IONS

Most of the actinide elements may be easily stabilized as trivalent ions in solids. Accordingly, a majority of the spectroscopic studies of actinides has been performed on the trivalent ions in $5f^N$ configurations. Whereas higher oxidation states can be stabilized for the lighter members in the first half of the actinide series, the 3+ oxidation state is most stable for the spectroscopically studied heavier actinides in condensed phases. Spectroscopic analyses and empirical modeling of the free-ion and crystal-field Hamiltonian were successfully conducted first on the trivalent ions using the model Hamiltonian reviewed in Section 18.4.6. Similarities are found between the series of trivalent actinide and lanthanide ions in terms of free-ion interactions and crystal-field splittings of the energy levels of the f-electrons.

When the results of a Hartree–Fock calculation are compared to those of a parametric analysis of experimentally identified levels for a given element, the magnitude of the computed energies, particularly those for F^k, are generally found to be too high. For a more realistic Hamiltonian, using parametric approach, one can apply subtractive corrections to the estimates derived from *ab initio* calculations. These corrections turn out to be essentially constant over the series and almost identical for both $4f^N$ and $5f^N$ shells (Crosswhite, 1977; Liu, 2000). The significance of this is that mixing with high configurations can be taken as essentially a fixed contribution to a global parametric model (Crosswhite and Crosswhite, 1984; Carnall, 1992; Liu *et al*., 1994b).

Many of the early spectroscopic studies of actinides in solids were conducted on actinide chlorides or trivalent actinide ions doped into crystals of $LaCl_3$ (Carnall, 1992), which can incorporate the actinide series from U^{3+} through Es^{3+} as impurities that substitute at the La^{3+} lattice site (C_{3h} symmetry). These studies, supplemented by Zeeman-effect studies of the influence of applied magnetic fields on the energy levels, provided the basis for experimental

characterization of the observed transitions in terms of the free-ion *SLJ* and crystal field quantum numbers. The available data for the $5f^N$ energy levels of trivalent actinide ions in $LaCl_3$ and actinide chlorides have enabled a systematic analysis and modeling of the $5f^N$ energy level structure (Carnall, 1992). The significance of such a systematic analysis and theoretical modeling, like that for the lanthanide series in $LaCl_3$ and LaF_3, is to provide a fundamental understanding of the electronic properties of actinides in solids along with values of free-ion interaction parameters that can be used for analyzing the spectra of the actinide ions in other compounds and solutions.

The relative energies of some of the low-lying states in U^{3+}:$LaCl_3$ are shown in Fig. 18.6 (Crosswhite *et al.*, 1980). As indicated, each free-ion state is split by the crystal field. When measured at the temperature of liquid He (~4 K), only transitions from the lowest state (taken as the zero of energy and having a

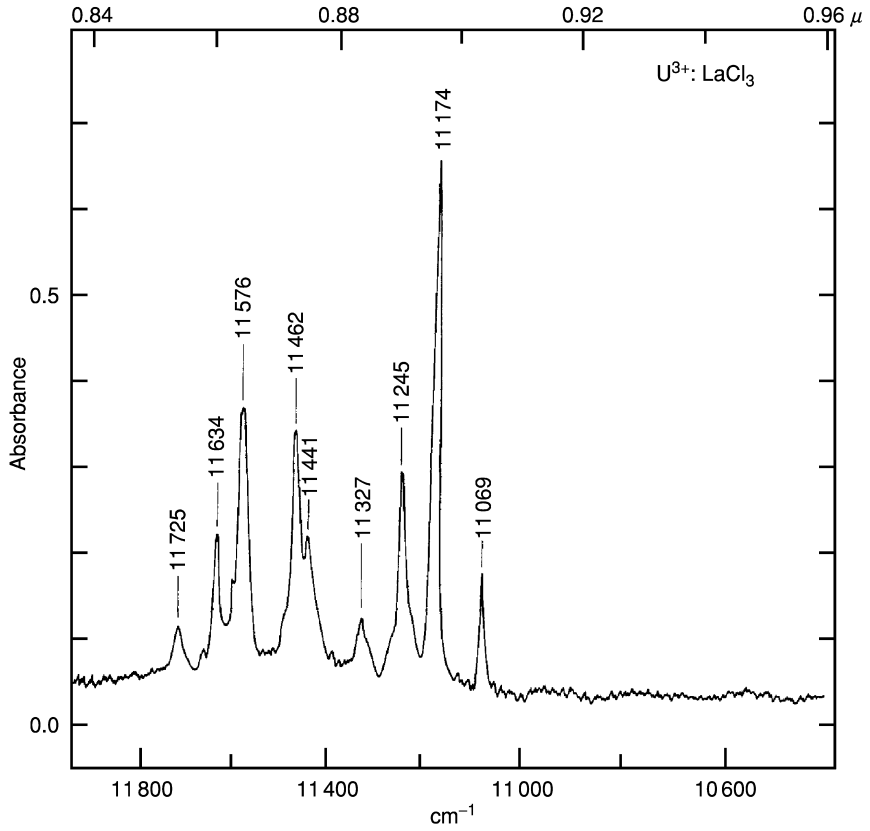

Fig. 18.6 *Absorption spectrum of the crystal-field splittings of* U^{3+}*:*$LaCl_3$ *in the range* 11 000–11 800 cm^{-1} *at* 4 K. (*Reprinted with permission from Crosswhite* et al., 1980. *Copyright* 1980, *American Institute of Physics.*)

crystal field quantum number $\mu = 5/2$ in this case) are observed. Most of the experimental results that have been reported were photographed using high-resolution grating spectrographs. Transitions to only three levels $^4I_{11/2}$ were readily observed in absorption; that to a $\mu = 1/2$ state (found by other techniques near 4580 cm^{-1}) were too weak to be apparent. Fig. 18.6 shows the absorption spectrum of U^{3+}:$LaCl_3$ in the range of 11 000 cm^{-1}. Lines in this spectrum are attributed the multiplets of $^4G_{5/2}$, $^4I_{15/2}$, $^4S_{3/2}$, and $^4F_{7/2}$ (Carnall, 1992). Electric dipole selection rules between the ground (μ=5/2) and excited (μ=5/2) states show that absorption transitions are forbidden, so the levels that would have corresponded to absorption transitions at 4556 and 4608 cm^{-1} had to be established by fluorescence methods. Assigning energies corresponding to the centers of these components, thus defining the 'free-ion' levels for the ion in a particular medium yields the energy level scheme indicated at the left in Fig. 18.7. Although the levels are shifted to somewhat lower energies than those of the true gaseous free-ion states, the basic structure appears to be preserved and is usually only moderately changed from medium to medium for trivalent lanthanides and actinides. For example, the center of gravity of the $^4I_{11/2}$ state in U^{3+}:$LaCl_3$ in Fig. 18.7 is 4544 cm^{-1}.

As the energies of the components of various groups are established experimentally, the model free-ion and crystal field parameters that reproduce the splittings can be computed by a suitable (nonlinear least-squares) fitting procedure. The computed values are then used to predict the splitting patterns in other groups where not all of the allowed components can be observed. Thus in the analysis of such spectral data there is a continual interplay between theory and experiment. When large numbers of levels have been experimentally confirmed, most (in some cases, all) of the parameters of the model can be varied simultaneously to establish the final values (Table 18.4). Fig. 18.8 shows the calculated energy levels that result from crystal-field splitting for An^{3+} in $LaCl_3$ (Carnall, 1992).

In typical analyses of actinide and lanthanide spectra in condensed phases, the range of observation may extend well into the near-ultraviolet region. The number of assignments made to different multiplets and states is usually sufficient to determine most of the energy level parameters. However, in Fig. 18.8 some of the observations on which this diagram is based were limited to less than 50% of the total extent of the f^N configurations. The accuracy of predicted energy level in the ultraviolet range clearly remains to be thoroughly tested. The Slater parameters in An^{3+} are typically only two-thirds as large as those for the Ln^{3+}, but ζ_{5f} is a factor of 2 larger than ζ_{4f}; so while the total energy range of the $5f^N$ configuration is reduced, the states are significantly more mixed in character because of the increased spin–orbit interaction.

The lanthanide orthophosphates, such as $LuPO_4$ and YPO_4, are good hosts for the incorporation of dilute f^N impurities. A wide variety of lanthanide and actinide ions, diluted in these materials, have been produced to carry out fundamental spectroscopic investigations (Morrison and Leavitt, 1982; Görller-Walrand and Binnemans, 1996). For the actinide series, Cm^{3+} doped

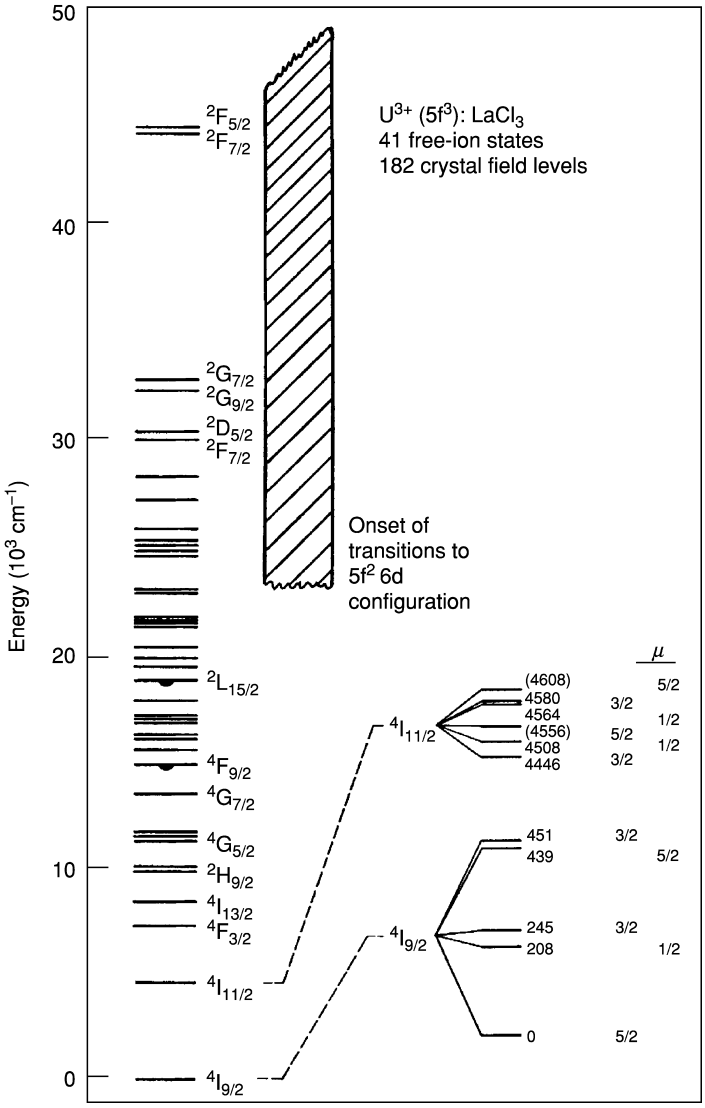

Fig. 18.7 *Energy level structure for* U^{3+}*:*$LaCl_3$.

into $LuPO_4$ and YPO_4, has been the most extensively studied system (Murdoch *et al.*, 1996, 1997; Liu *et al.*, 1998). The greater spatial extent of the 5f electron shell results in a smaller electrostatic interaction between equivalent electrons in the 5f shell than in the 4f shell. Thus for Cm^{3+}, the energy level of the first excited multiplet ($J = 7/2$) is at $\sim$16 000 cm^{-1}. Utilizing this metastable emitting state, excited state absorption studies allowed the collection of data to

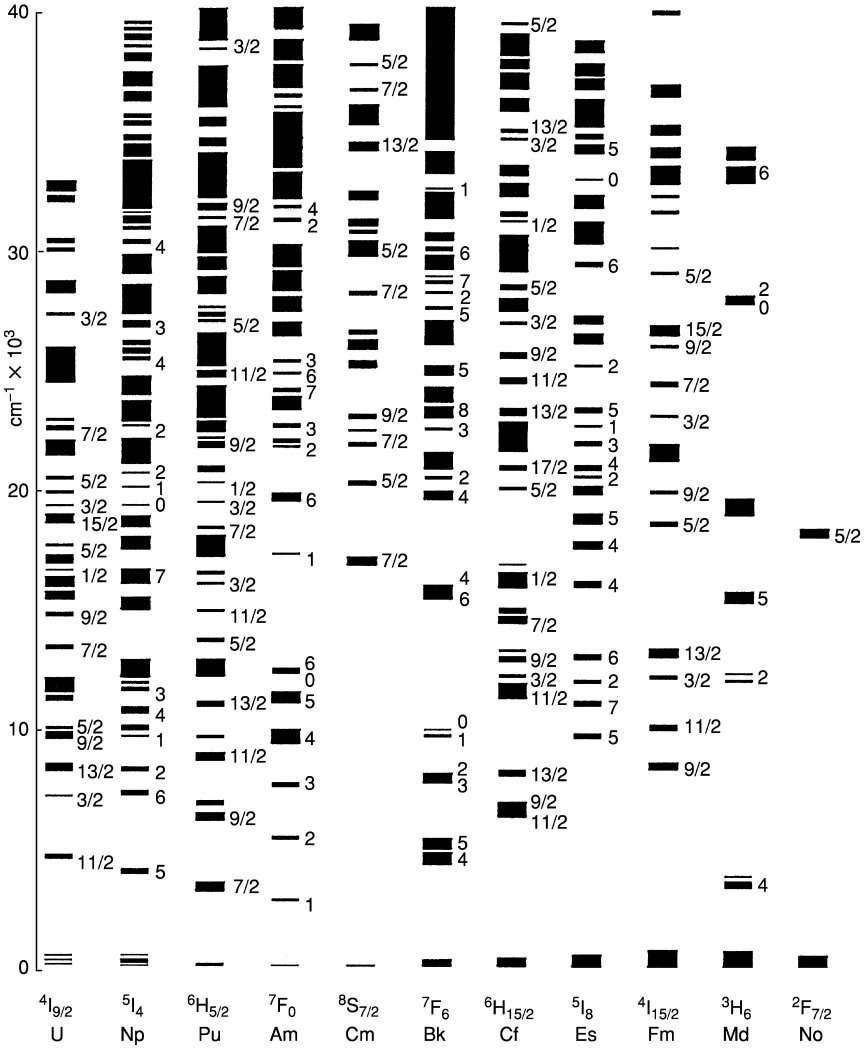

Fig. 18.8 *Energy level structure of An^{3+}:$LaCl_3$ based on computed crystal field energies in the range* 0–40 000 cm^{-1}. (*Reprinted with permission from Carnall,* 1992. *Copyright* 1992, *American Institute of Physics.*)

40 000 cm^{-1} using two visible lasers (Murdoch *et al.*, 1997). The ground term multiplet splitting is small, because the largest component of the ground multiplet has zero angular momentum. Early detailed studies of the Cm^{3+} optical spectra were performed with the ^{244}Cm isotope. During the past decade or so, multimilligram quantities of ^{248}Cm have become available. Several single crystals were doped with the ^{248}Cm isotope and optical studies of these samples

were performed using laser-selective excitation and fluorescence techniques. Edelstein (2002) has recently published a review of the spectroscopic studies of Cm^{3+} in various hosts.

The free-ion model based on studies of the 3+ actinide ions in $LaCl_3$ has been used in analysis of the optical spectra of Cm^{3+} in $LuPO_4$. For the crystal-field splitting, because the metal ion site is D_{2d} in the phosphates instead of C_{3h} in $LaCl_3$, a different set of crystal field parameters must be established. Fig. 18.9 shows the excitation spectra of Cm^{3+} in $LuPO_4$ (Fig. 18.9a) and YPO_4

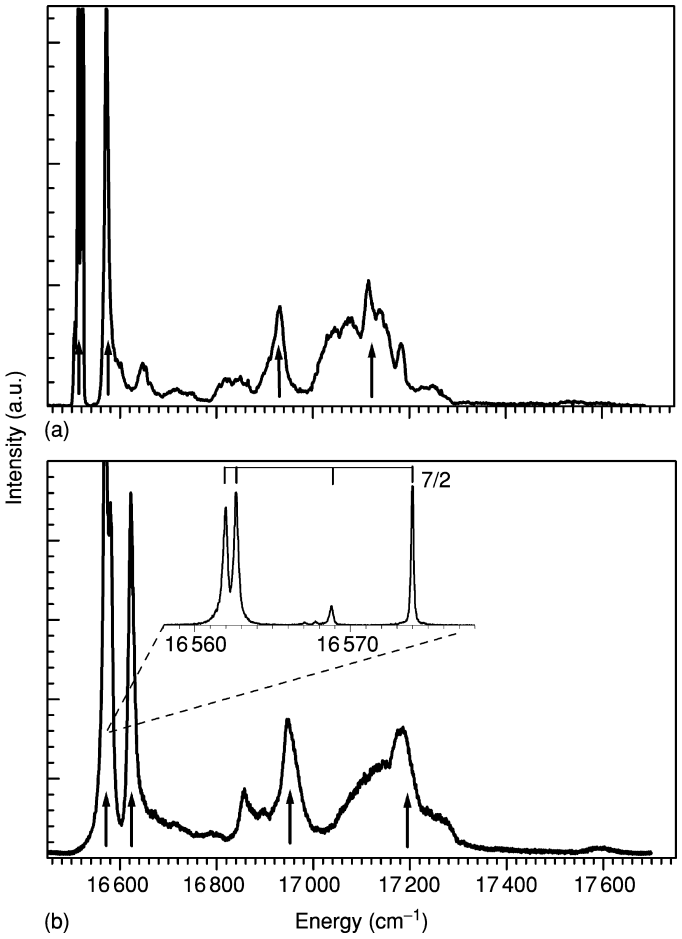

Fig. 18.9 *Excitation spectra of transitions from the* $^8S_{7/2}$ *ground state multiplets to the* $^6D_{7/2}$ *excited state of the* Cm^{3+} *ion in* (*a*) $LuPO_4$ *and* (*b*) YPO_4 *at* 4 K. (*Reprinted with permission from Liu* et al., 1998. *Copyright* 1998, *American Institute of Physics.*) *The emission was monitored at* 16 563.0 cm^{-1} *for* Cm^{3+}:YPO_4 *and* 16 519.5 cm^{-1} *for* Cm^{3+}:$LuPO_4$. *The insert shows the crystal-field splitting of the ground state of* Cm^{3+} *in* YPO_4.

(Fig. 18.9b) in which the crystal field energy levels for the first excited multiplet (nominal $^6D_{7/2}$) were observed to extend from 16 560 to 17 200 cm^{-1}. In addition to the zero-phonon lines (ZPL) indicated by the vertical arrows, vibronic sidebands have intensities comparable to those of the upper ZPLs. The insert in Fig. 18.9b shows the crystal-field splitting in the ground state which also is a $J = 7/2$ (nominal $^8S_{7/2}$). Whereas the excited state crystal-field splitting is more than 800 cm^{-1}, the ground state splitting is only 12 cm^{-1}. As pointed out in Section 18.4.2, the crystal-field interaction vanishes in the ground state of an f^7 configuration unless a fourth-order coupling to the excited states is considered (Liu *et al.*, 1993). Although the excited $^6D_{7/2}$ also has no first-order crystal-field splitting, the more significant mixture of *LS* terms in its wave functions results in much larger crystal-field splitting. Many experimental results of the ground state splitting of actinide ions in the $5f^7$ configuration, which include Am^{2+}, Cm^{3+}, and Bk^{4+} in different crystalline hosts, have been reported (Edelstein and Easley, 1968; Liu *et al.*, 1996; Murdoch *et al.*, 1996; Brito and Liu, 2000).

In different hosts, the values for the An^{3+} free-ion parameters listed in Table 18.4 may vary 1% or less. In fitting the Cm^{3+}:$LuPO_4$ (or YPO_4) data, the parameters of three-body coupling operators, T^k, were kept fixed at the values for Cm^{3+} in $LaCl_3$ (Murdoch *et al.*, 1996, 1997). The energy levels of Cm^{3+} in $LuPO_4$ up to 35 000 cm^{-1} were probed by high-resolution techniques using two-step excited state absorption and one color two-phonon absorption methods (Murdoch *et al.*, 1997). The modeling of the Cm^{3+}:$LuPO_4$ energy level structure with the experimental data up to 35 000 cm^{-1} did not result in significant changes in the free-ion parameters determined in the systematic analysis of the $5f^N$ ions in $LaCl_3$. This consistency leads to two important conclusions as regards the applications of the free-ion and crystal field model: (a) the free-ion interaction parameters are relatively insensitive to host lattice; and (b) the parameters determined by analysis of the low-lying energy states can reproduce energy levels of high-lying states with satisfactory accuracy.

In appropriate hosts, the $^5D_1$ state of Am^{3+} ($5f^6$ configuration) is a metastable emitting state as is the $^6D_{7/2}$ state of Cm^{3+} ($5f^7$ configuration) (Carnall, 1992). In such cases, both ions emit visible luminescence so they are very suitable for laser-induced fluorescence excitation studies. In addition to $LaCl_3$ and $LuPO_4$, these two ions in other crystalline hosts such as Cs_2NaYCl_6 (Murdoch *et al.*, 1998), ThO_2 (Hubert *et al.*, 1993; Thouvenot *et al.*, 1993a, 1994), and $CaWO_4$ (Liu *et al.*, 1997a,b) have been investigated using laser spectroscopic methods. These studies showed that Am^{3+} and Cm^{3+} exhibit spectroscopic properties that are similar to those found in studies in $LaCl_3$, although the strength of the crystal-field interaction may be significantly different. Table 18.9 provides a comparison between the free-ion and crystal-field interactions of Eu^{3+} and Am^{3+} both of which have the f^6 configuration.

The ratios of free-ion interactions and crystal field strength for the 4f and 5f ions listed in Table 18.9 indicate that the electrostatic interaction is reduced approximately to 60% and the spin–orbit coupling is increased by 190%

Table 18.9 *Comparison of interaction parameters of* Am^{3+} $(5f^6)$ *and* $Eu^{3+}(4f^6)$ (cm^{-1}).

	$LaCl_3$[a]	ThO_2[b]
$F^2(Eu^{3+})$	84 400	80 335
$F^2(Am^{3+})$	51 900	48 038
$\boldsymbol{F^2(Am^{3+})/F^2(Eu^{3+})}$	**0.62**	**0.60**
$\zeta_{4f}(Eu^{3+})$	1 328	1 337
$\zeta_{5f}(Am^{3+})$	2 564	2 511
$\boldsymbol{\zeta_{5f}(Am^{3+})/\zeta_{4f}(Eu^{3+})}$	**1.93**	**1.88**
$N\nu(Eu^{3+})$	329	1 231
$N\nu(Am^{3+})$	628	2 953
$\boldsymbol{N\nu(Am^{3+})/N\nu(Eu^{3+})}$	**1.9**	**2.4**

[a] Carnall (1992) and Crosswhite (1977).
[b] Hubert *et al.* (1993).

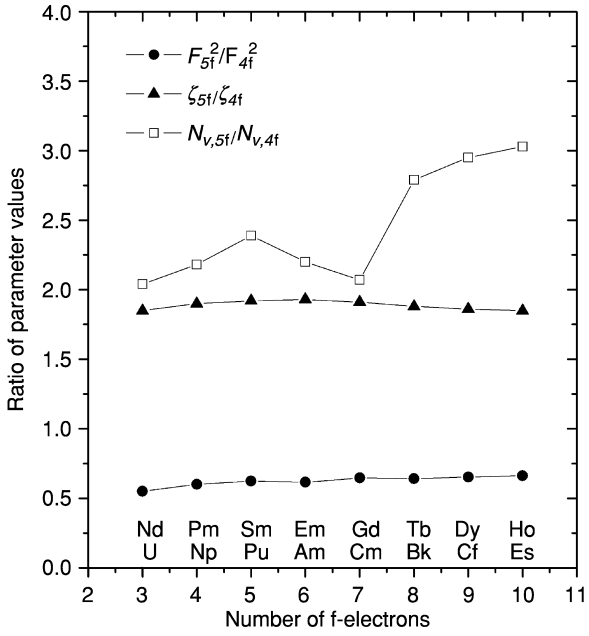

Fig. 18.10 *Comparison of the parameter ratios for trivalent lanthanide and actinide ions in* $LaCl_3$ (*Data from Crosswhite*, 1977 *and Carnall, 1992*).

(Edelstein and Easley, 1968) for the values of the lanthanide analogs in the same f^N configuration. These changes are attributed to the more extended 5f orbitals of Am^{3+} in comparison with the 4f orbitals of Eu^{3+}. In addition, the strength of the crystal-field interaction is doubled for the actinide ion. This trend of

variations is shown systematically in Fig. 18.10 for the two series of ions in the $LaCl_3$ crystal lattice (Liu, 2000).

Edelstein and Easley (1968) observed the trivalent state for ^{243}Am and ^{244}Cm doped into CaF_2 when the crystals were initially grown. However, due to the high level of radioactivity caused mainly by the alpha decay of ^{244}Cm ($t_{1/2}$ = 18.1 years) part of the Am^{3+} was reduced to Am^{2+} and part of the Cm^{3+} was oxidized to Cm^{4+}. It was observed that the ratio of Am^{2+} to Am^{3+} in the cubic sites of CaF_2 was approximately 10:1. The energy level structures of Am^{2+} and Cm^{3+} in CaF_2 were probed and analyzed based on the crystal field model for $5f^7$ configuration (Edelstein *et al.*, 1966; Edelstein and Easley, 1968). A recent study (Beitz *et al.*, 1998) reported that Es^{3+} ($5f^{10}$) can be stabilized in LaF_3 and its spectroscopic properties in terms of free-ion interactions are very similar to Es^{3+} in $LaCl_3$, although a crystal field strength approximately twice of that for Ho^{3+} ($4f^{10}$) in LaF_3 is expected. Although the spectra of several organometallic 3+ actinides, such as plutonium tricyclopentadienide, have been measured, the analysis of data is still quite incomplete (Carnall, 1979b). Nevertheless, it seems apparent that now the energy level parameters for such systems can be approximated by those characteristics of the trivalent actinide in the $LaCl_3$ host.

There have been several recent laser spectroscopic studies on U^{3+} ions in various ternary chloride and bromide crystalline systems. Because of relatively low-phonon energies of lattice vibration, strong luminescence from U^{3+} can be observed in these crystals. Using effective-operator Hamiltonian and parameterization method, Karbowiak and colleagues have analyzed the absorption and emission spectra of U^{3+} in Ba_2YCl_7, $CsCdBr_3$, and Cs_2NaYBr_6, respectively. Both U^{3+} and U^{4+} were observed in the Ba_2YCl_7 system, which possesses monoclinic symmetry. For uranium ions at a C_1 site, a total of 27 crystal field parameters are required to calculate the energy levels (Karbowiak *et al.*, 1997, 2003). Using time-resolved and site-selected laser excitation methods, this group has investigated the spectroscopic and excited state dynamics of U^{3+} in RbY_2Cl_7. The strength of the free-ion and crystal-field interaction in these systems is generally consistent with that for the U^{3+}:$LaCl_3$ systems. A general correlation between the magnitudes of crystal field parameters and the U^{3+} luminescence decay rate has been realized in the analyses of the site-selected spectra and luminescence dynamics.

18.6 INTERPRETATION OF THE OBSERVED SPECTRA OF TETRAVALENT ACTINIDE IONS

It is well known that a major difference between the lanthanide and actinide series is the greater stability of 4+ and higher valance states of the actinides, particularly in the first half of the respective series. There have been numerous analyses of the spectra of tetravalent uranium compounds, whereas the number

of published spectroscopic analyses rapidly decreases as heavier members of the actinide series in the 4+ valence states are considered. The reasons are, first of all, differences in stability of the tetravalent state for actinide compounds are such that reducing and then oxidizing conditions become necessary as the actinide atomic number increases. Secondly, the low specific radioactivity of uranium of natural isotopic abundance makes the doped crystalline materials easy to handle and limits radiolytic degradation. Moreover, the f^2 configuration of U^{4+} provides experimental features that are suitable for theoretical analyses and constitute a useful basis for extending the interpretation of spectra of other An^{4+} ions in condensed media. There is a series of crystalline hosts, notably ThX_4 and Cs_2MX_6 (M = Zr, Th; X = Cl, Br), $ThSiO_4$, and $ZrSiO_4$, in which $Pa^{4+}(5f)$ and $U^{4+}(5f^2)$ can be doped for spectroscopic studies (Krupa, 1987). In addition, Np^{4+}, Pu^{4+}, and Am^{4+} have been successfully doped into $ThSiO_4$ (Krupa *et al.*, 1983; Krupa and Carnall, 1993). However, in contrast to most other binary compounds, the tetravalent actinides as fluorides are sufficiently stable and PaF_4 through CfF_4 can be prepared and are isostructural to UF_4 and CeF_4 (Brown, 1968; Morss, 2005).

Since 1986, significant progress in analyses of the crystal field spectra of tetravalent actinide ions in solids has been reported. The structural characteristic of f→f transitions has been observed and analyzed using the theoretical model of free-ion and crystal-field interactions that was discussed in Sections 18.3 and 18.4. The observations are consistent with trends indicated in Fig. 18.1, which suggest that transitions to the $f^{N-1}d$ configurations in An v will lie even higher in energy relative to the lowest-energy f^N state than in the corresponding transitions for An iv. The lowest f→d transition in the atomic spectrum of U v was assigned at 59 183 cm^{-1} (Van Deurzen *et al.*, 1984). Consequently, broad and intense band structure in the spectra of An^{4+} compounds beginning near 40 000–45 000 cm^{-1} would be consistent with the onset of f→d transitions. The energy level structure of the free-ion U^{4+} ($5f^2$) configuration has provided a valuable basis for comparison in developing the analysis of An^{4+} spectra in solids.

Krupa (1987) reviewed spectroscopic properties of $Pa^{4+}(5f^1)$, $U^{4+}(5f^2)$, and $Np^{4+}(5f^3)$ in crystalline host $ThBr_4$, $ThCl_4$, and $ThSiO_4$. For Pa^{4+} in Cs_2ZrCl_6, electron paramagnetic resonance and near-infrared absorption spectra were measured and the data analyzed by Axe *et al.* (1961) in terms of the crystal-field and spin–orbit interactions for a $5f^1$ electron. Additional optical studies have been reported for pure Pa^{4+} hexahalo compounds and Pa^{4+} diluted into Cs_2ZrCl_6 (Brown *et al.*, 1974, 1976; Edelstein *et al.*, 1974, 1992; Piehler *et al.*, 1991). For this one-electron system, there are no electrostatic terms for the free-ion interactions, thus the splitting of the free-ion energy states, which consist of the $^2F_{5/2}$ ground state and the $^2F_{7/2}$ excited state, is solely due to spin–orbit coupling. Crystal-field splittings in the tetravalent ions are much larger than those of the trivalent ions. Table 18.10 lists the spectroscopic parameters of Pa^{4+} in $ThCl_4$ and $ThBr_4$ in D_{2d} symmetry (Malek and Krupa, 1986; Krupa,

Table 18.10 *Energy parameters of Pa^{4+} and U^{4+} in $ThCl_4$, $ThBr_4$, and $ThSiO_4$ in D_{2d} symmetry* (cm^{-1}).[a]

	Pa^{4+}		U^{4+}		
	$ThCl_4$	$ThBr_4$	$ThCl_4$	$ThBr_4$	$ThSiO_4$
F^2			42 752(162)	42 253(127)	43 110(245)
F^4			39 925(502)	40 458(489)	40 929(199)
F^6			24 519(479)	25 881(383)	23 834(639)
ζ	1524.4(5)	1532.8(5)	1808(8)	1783(7)	1840(2)
α			30.4(2)	31(1)	32.3(0.4)
β			−492(84)	−644(75)	−663(144)
γ			[1200]	[1200]	[1200]
B_0^2	−1405(50)	−1047(52)	−1054(117)	−1096(80)	−1003(127)
B_0^4	1749(94)	1366(138)	1146(200)	1316(146)	1147(281)
B_4^4	−2440(98)	−1990(102)	−2767(147)	−2230(85)	−2698(251)
B_0^6	−2404(607)	−1162(541)	−2315(404)	−3170(379)	−2889(557)
B_4^6	−195(267)	623(174)	−312(227)	686(246)	−208(333)
n[b]	7	7	25	26	25
σ[b]	23.6	19.4	46	36	71

[a] Krupa (1987).
[b] Number of assigned levels (n) and deviation (σ), see Table 18.4, footnote c.

1987). The data for Pa^{4+} in Cs_2ZrCl_6 are considerably better than for the ThX_4 systems. Also some data are given for the excited 6d system.

Analysis of the spectra of U^{4+} in both high-symmetry (O_h) and relatively low-symmetry (D_{2d} and D_2) sites have been published. Somewhat in contrast to observations made with trivalent ions, the magnitude of the crystal-field splitting in the two cases differs significantly. An example of the high-symmetry case is that of U^{4+} in Cs_2UCl_6 (Johnston *et al.*, 1966a,b). The low-symmetry (D_{2d}) case is illustrated in the analysis of U^{4+}:$ThBr_4$ (Delamoye *et al.*, 1983). Recently, spectroscopic analyses were reported by Karbowiak *et al.* (2003) for U^{4+} in Ba_2YCl_7. In this work, values of the 27 crystal field parameters of the Hamiltonian were determined in fitting a total of 60 observed crystal field energy levels to the model Hamiltonian. The crystal-field splitting in the Cs_2UCl_6 is over twice as large as that in U^{4+}:$ThBr_4$. As a result, much more complex structure caused by the mixing of states of different J in close proximity occurs within a given energy range in Cs_2UCl_6 compared to the U^{4+}:$ThBr_4$ case. In the analyses of the crystal field spectrum of U^{4+} on the octahedral sites of Cs_2UBr_6 and Cs_2ZrBr_6, Faucher *et al.* (1996) reported that there is a strong coupling between the $5f^2$ and $5f^17p^1$ configurations. Therefore, additional effective operators for the configuration interaction are necessary to better interpret the observed energy level structure.

The extensive analysis of the data for U^{4+}:$ThBr_4$ and the similar crystal field parameters deduced for Pa^{4+}:$ThCl_4$ (Krupa *et al.*, 1983) have provided a new

basis for examining other An^{4+} spectra. As Auzel and coworkers have shown (Auzel *et al.*, 1982), band intensities in the spectrum of aquated U^{4+} can be assigned in terms of crystal-field split *SLJ* levels similar to those deduced for U^{4+}:$ThBr_4$. Using the method of extrapolation discussed in Sections 18.3 and 18.4, energy level parameters that are consistent with those for Pa^{4+}:$ThCl_4$ and U^{4+}:$ThBr_4$ can be extrapolated to obtain a set for Np^{4+}, and a good correlation is found between this energy level structure and the band structure observed for aquated Np^{4+}. That the apparent correlation between band structure observed for the iso-f-electron configurations of aquated An^{4+} and aquated An^{3+} ions continues along the series is evident when comparing the spectra of aquated Pu^{4+} and aquated Np^{3+}. Jørgensen called attention to this apparent correlation in the band structure observed for the iso-f-electron configurations An^{3+} and An^{4+} spectra at a time when little was known about the extent of the ligand fields involved (Jørgensen, 1959). Concern that the data for aquated An^{4+} should be interpreted in terms of large ligand-field splitting characteristic of Cs_2UCl_6, instead of a weaker-field case may have been partially responsible for the slow pace in exploration of Jørgensen's insight. Of course, development of this An^{3+}/An^{4+} spectral correlation also required an understanding of the energy level structures in An^{3+}, which was not well understood in 1959. Adopting the electrostatic and spin–orbit parameters for U^{4+}:$ThBr_4$ as a basis for estimating parameters for the An^{4+} ions, the general character of the spectra of the An^{4+} ions can be interpreted (Conway, 1964).

In solid compounds such as Cs_2UCl_6, where the 4+ ions occupy sites of inversion symmetry, the observed structure is almost exclusively vibronic in character, as contrasted with the electronic transitions characteristic of 3+ compounds. The electronic origins were deduced from progressions in the vibronic structure, because the electronic transitions themselves were symmetry-forbidden. An analysis of the intensities of vibronic bands has been reported (Satten *et al.*, 1983; Reid and Richardson, 1984). Other extensive analyses of the spectra of U^{4+} in crystalline hosts include those for U^{4+}:$ZrSiO_4$ (Richman *et al.*, 1967; Mackey *et al.*, 1975).

Because of much stronger ion–lattice coupling for the 6d orbitals, in contrast to the 5f−5f transitions in which vibronic coupling is relatively weak, the spectra of 5f↔6d transitions, however, are often dominated by the vibronic bands associated with the f−d electronic transitions in both absorption and emission spectra even when there is no inversion symmetry. The assignment and analyses of the crystal field spectra become difficult, because the pure electronic transitions (ZPL) may be obscured by the broad and intense vibronic sidebands. Fig. 18.11 shows the emission spectrum of the $6d^2D_{3/2}$ (Γ_{8g}) $\rightarrow 5f^2F_{5/2}$ (Γ_{8u}) electronic transition of Pa^{4+}:Cs_2ZrCl_6, with the zero-phonon line at 17 847 cm^{-1} accompanied by various vibronic sidebands (Piehler *et al.*, 1991). From the optical spectra, the vibrational frequencies of different modes can be measured and assigned to the local and lattice modes that couple to the electronic transitions. In the 5f−6d spectra (see Fig. 18.11), and also in charge-transfer spectra

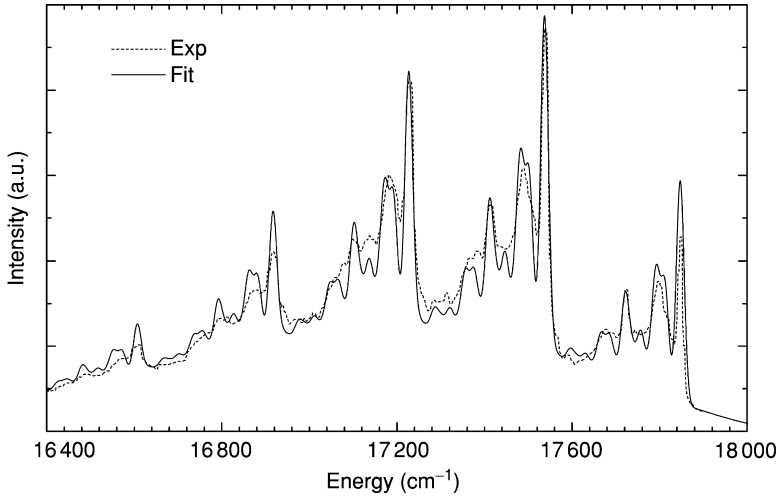

Fig. 18.11 *The emission spectrum of the* $6d^2D_{3/2}(\Gamma_{8g}) \rightarrow 5f^2F_{5/2}(\Gamma_{8u})$*electronic vibronic transitions for* Pa^{4+} *in* Cs_2ZrCl_6 *at* 4.2 K (*experimental data from Piehler* et al., 1991). *The energy of the zero-phonon line of the electronic transition is* 17 847 cm^{-1}. *The vibrational frequencies obtained from fitting the spectrum are* $\nu_1(A_{1g}) = 310$ cm^{-1}, ν_5 $(T_{2g}) = 123$ cm^{-1}, ν_{L1} $(T_{1g}) = 35$ cm^{-1}, *and* ν_{L2} $(T_{2g}) = 55$ cm^{-1}.

(discussed later), certain vibrational progression frequencies have harmonics up to fifth order, whereas others appears only to first order. Liu *et al*. (2002) demonstrated recently that the progressions of multiple vibrational frequencies can be simulated using a modified model of the Huang–Rhys theory of electron–phonon interaction (Huang and Rhys, 1950). The dashed line in Fig. 18.11 is a model fit to the experimental spectrum.

A systematic analysis of crystal field spectra has been reported for tetravalent actinide ions from U^{4+} through Bk^{4+} in AnF_4 and An^{4+}:CeF_4 (Carnall *et al*., 1991; Liu *et al*., 1994b). The tetravalent fluorides were chosen because An^{4+} (An = U to Cf) can be stabilized and they all, including CeF_4, which has no f-electron in the lowest-energy configuration, are isostructural. The absorption spectrum of UF_4 is plotted in Fig. 18.12 in comparison with that of U^{4+} ion in aqueous solution, and the liquid helium temperature absorption spectra of NpF_4 and PuF_4 are shown in Fig. 18.13 (Carnall *et al*., 1991). Crystal structure data for UF_4 established that there are two different low-symmetry sites, C_1 and C_2, for the An^{4+} ion. Both sites have eight nearest neighbor fluorine ions arranged in a slightly distorted antiprismatic configuration; however, there are twice as many C_1 as C_2 sites in the unit cell which aids in identifying sites in the site-resolved spectra. The site-selective excitation spectra of the $^7F_0 - ^5L_6$ transitions are shown in Fig. 18.14 for a 0.1% Cm^{4+}:CeF_4 sample at 4.3 K. Crystal field modeling was conducted based on an approximate C_2 site symmetry. The spectra have similar characteristics as those of An^{3+} ions in crystals

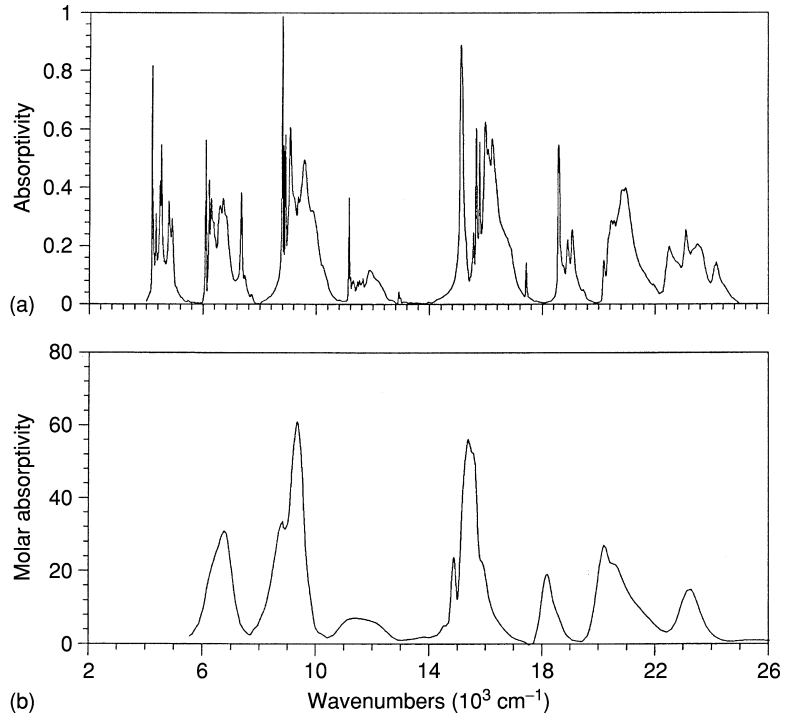

Fig. 18.12 *Absorption spectra of* (*a*) UF_4 *in a KBr pellet at* ~4 K*;* (*b*) *aquated* U^{4+} *at* 298 K *both in the near-infrared to visible range.* (*Reprinted with permission from Carnall* et al., 1991. *Copyright* 1991*, American Institute of Physics.*)

(see Fig. 18.9 for Cm^{3+}:$LuPO_4$). Sharp ZPL are resolved in the low-energy region and broad vibronic transitions that span ~800 cm^{-1} with the strongest features ~400 cm^{-1} above the first ZPL are also found. The vibronic lines in the An^{4+} spectra are relatively stronger than those in An^{3+} spectra. This suggests a stronger ion–ligand coupling for tetravalent ions, which is consistent with the larger crystal-field splittings in the An^{4+} systems.

Optical spectroscopic data, including low-temperature absorption (see Figs. 18.12 and 18.13) and laser excitation and luminescence spectra of tetravalent actinides in fluoride compounds, have provided adequate experimental information for a systematic analysis and parameterization of the free-ion and crystal-field interactions. The Hamiltonian of the free-ion and crystal-field interactions has been established through the same parameterization method used for the trivalent ions that was discussed in Section 18.5. The Hamiltonian parameters for An^{4+} in CeF_4 are listed in Table 18.11. The parameterization method ensures a consistent set of free-ion and crystal field parameters from one ion to the next. Given the limited number of energy levels that could be assigned

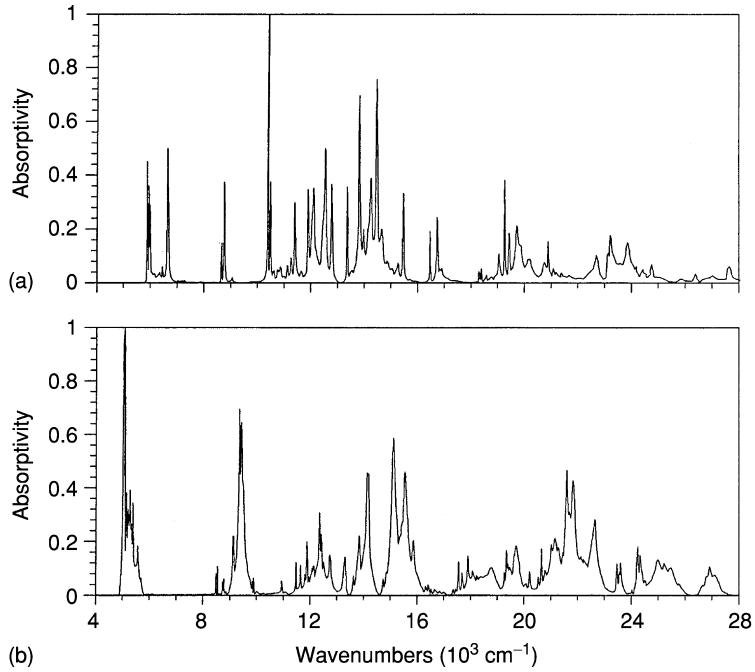

Fig. 18.13 *Absorption spectra of* (*a*) NpF_4 *in a KBr pellet at* ~4 K*;* (*b*) PuF_4 *in KBr pellet at* ~4 K *in the range* 4000–30 000 cm^{-1}. (*Reprinted with permission from Carnall* et al., 1991. *Copyright* 1991, *American Institute of Physics.*)

without ambiguity, the observed spectra of AnF_4 were modeled based on the standard model crystal field with constrained parameters. For instance, the three-body parameters T^i were fixed at average values determined in the analysis of An^{3+}:$LaCl_3$ spectra (Carnall, 1992). The M^h values were assigned in each case based on *ab initio* calculations and were not varied. Although P^2 was varied, in all cases P^4 and P^6 were constrained by the ratios $P^4 = 0.5P^2$ and $P^6 = 0.1P^2$. In fitting experimental data, the modeling, therefore, relied on the systematic variations of F^k and ζ_{5f}. In UF_4, it was pointed out that the magnitude of the crystal-field interaction was relatively large, and *J*-mixing was very significant in higher energy states, the ground crystal field state remained more than 95% pure in terms of *J*-character. Although the excited states above 50 000 cm^{-1} were truncated in the construction of the free-ion wave functions for Pu^{4+}, Am^{4+}, Cm^{4+}, and Bk^{4+}, the ground state eigenfunctions had relatively pure *J*-character, fully consistent with the results for U^{4+} and Np^{4+}. The nominal $^6H_{5/2}$ ground state in Am^{4+} is more than 96% $J = 5/2$, whereas the $^7F_0$ ground state in Cm^{4+} is more than 98% $J = 0$ character. Thus the experimental problem of interpreting magnetic susceptibility measurements in CmF_4 where temperature-dependent results are not consistent with a $J = 0$ ground state (Nave

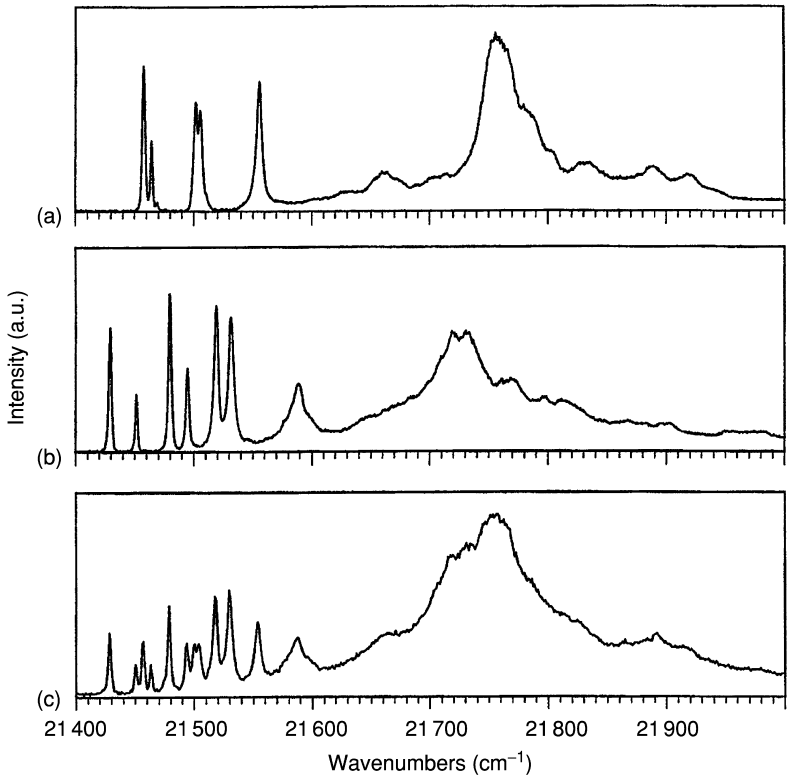

Fig. 18.14 *Site-elective excitation spectra of the* $^7F_0$–$^5L_0$ *transitions in* 0.1% Cm^{4+}:CeF_4 *at* 4.3 K. (*a*) *The spectrum of* Cm^{4+} *ions on site* A *recorded with emission at* 16 603 cm^{-1}; (*b*) *the spectrum of* Cm^{4+} *on site B recorded with emission at* 16 584 cm^{-1}; *and* (*c*) *the excitation spectrum without emission selection. The broad features in the high-energy range are due to vibronic transitions.* (*Reprinted with permission from Liu et al.,* 1994*b*. *Copyright* 1994, *American Institute of Physics.*)

et al., 1983) seems unlikely to be rationalized by assuming appreciable *J*-mixing. For Bk^{4+}, the $J = 0$ character is more than 99.5%, but the contribution from the pure $^8S_{7/2}$ is reduced to 75.5% (Brito and Liu, 2000).

Systematic analysis of the free-ion and crystal-field interactions in AnF_4 (An = U–Bk) provides a useful comparison of the trends in free-ion parameter values between those that would have been expected based on parameters computed using *ab initio* methods and those obtained from fitting the experimental data. As shown in Fig. 18.15, when plotted as a function of atomic number, the model free-ion parameters for An^{4+} exhibit similar increasing trends as those predicted by Hartree–Fock calculations. However, the normalized Hartree–Fock-based values of F^k were typically found to show a steeper slope than those obtained in fitting the experimental data.

Table 18.11 *Energy-level parameters for tetravalent actinide ions in actinide tetrafluorides* (*in* cm^{-1}) (*Liu* et al., 1994*a*,*b*).[a]

	U^{4+}	Np^{4+}	Pu^{4+}	Am^{4+}	Cm^{4+}	Bk^{4+}
F^2	44 784	47 630	50 000	51 824(47)	53 051(38)	55 300
F^4	43 107	42 702 ($0.896F^2$)	44 500 ($0.89F^2$)	$0.89F^2$	$0.893F^2$	$0.88F^2$
F^6	25 654	29 623 ($0.622F^2$)	30 500 ($0.61F^2$)	$0.61F^2$	$0.619F^2$	$0.60F^2$
ζ	1761(3)	2021(4)	2315(7)	2604(6)	3017(5)	3244
α	34.74	34.89	35	35	35	34
β	−767.3	−743.2	−740	−740	−740	−740
γ	913.9	890.7	900	900	900	1000
T^2		200	200	200	200	200
T^3		50	50	50	50	50
T^4		50	50	50	50	50
T^6		−360	−360	−360	−360	−360
T^7		425	425	425	425	425
T^8		340	340	340	340	340
$M^{0,b}$	0.775	0.877	0.984	1.094	1.204	1.314
M^2	0.434	0.489	0.546	0.608	0.671	0.733
M^4	0.294	0.340	0.381	0.424	0.468	0.512
$P^{2,c}$	2715(94)	2700	2200	1623(71)	633(96)	1064
B_0^2	1183(28)	1127(92)	1127	1302(59)	1209(75)	1150
B_2^2	29(27)	45	45	45	45	45
B_0^4	−2714(99)	−2818 (193)	−2818	−2822	−2820	−2720
B_2^4	3024(71)	3090 (171)	3090	3219(135)	3304(99)	3000
B_4^4	−3791(53)	−3584 (170)	−3584	−3337(101)	−3243(90)	−3275
B_0^6	−1433(148)	−1427 (382)	−1427	−1500	−1500	−1700
B_2^6	1267(101)	1267	1267	1400	1400	1500
B_4^6	−1391(93)	−1147 (181)	−1147	−1147	−1142	−1200
B_6^6	1755(82)	1819 (129)	1819	1819	1820	1800
σ^d	31	41	30	31	28	27
n^d	69	57	23	61	38	25

[a] The values in parentheses are errors in the indicated parameters.
[b] The M^k values were assigned in each case based on *ab initio* calculation and were not varied.
[c] P^2 was varied freely, P^4 and P^6 were constrained by ratios $P^4 = 0.5P^2$, $P^6 = 0.1P^2$.
[d] Deviation (σ) and number of assigned levels (n), see Table 18.4, footnote c.

It has been shown that a significant change in the ratios of F^4/F^2 and F^6/F^2 from U^{4+} to Np^{4+} is required to fit the experimental data (Carnall *et al.*, 1991; Liu *et al.*, 1994b). However, in the analysis of the transneptunium ions, the ratios of F^4/F^2 and F^6/F^2 could be held constant. In this context, values of F^2

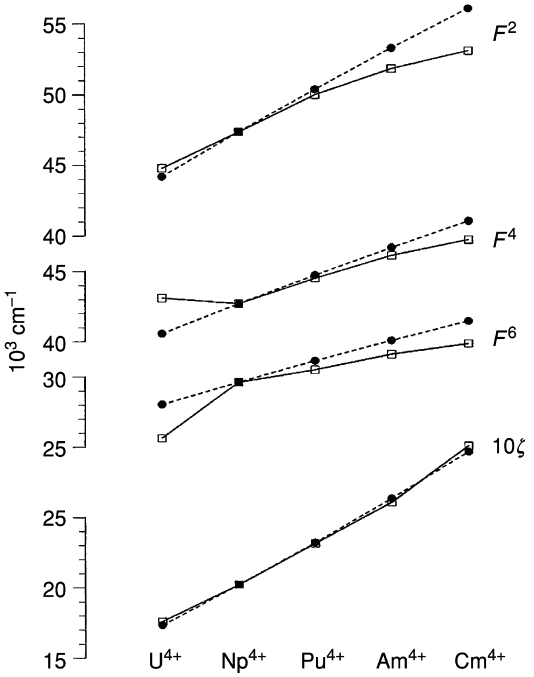

Fig. 18.15 *Systematic trends in free-ion parameters of the effective-operator Hamiltonian for AnF_4 ($An = U$ through Bk). The dots (•) connected by the dashed lines are calculated using Hartree–Fork methods, and the squares (□) connected by solid lines are from fitting experimental data. All values are normalized to those for NpF_4.* (*Reprinted with permission from Liu* et al., 1994a,b. *Copyright* 1994, *American Institute of Physics.*)

for all the ions studied exhibited a functional (but not linear) increase with atomic number. It is important to note that the values of F^2 for all transneptunium members of the AnF_4 series would be poorly estimated based solely on linear projections from U^{4+} or Np^{4+}. Similar to the An^{3+} series, a regular behavior appears to be characteristic of the transneptunium actinide tetrafluorides. The computed values of ζ_{5f} from fitting the experimental data are generally quite consistent with *ab initio* values normalized to agree with the empirical value for NpF_4. In comparison to the An^{3+} series, the slope found for the variation of F^k for An^{4+} as a function of atomic number is reduced. This is particularly evident for F^2 in Fig. 18.15 and provides the rationale for increasingly similar energies found in the lower energy free-ion states of iso-f-electron An^{3+} and An^{4+} spectra as a function of increasing atomic number.

The parametric free-ion electrostatic interaction parameters F^k for UF_4 and NpF_4 are a few percent larger than those that have been determined by fitting spectroscopic data for the tetravalent chlorides and bromides listed in Table 18.10, and those for UF_4 are smaller than the gaseous free-ion values for UV

(Van Deurzen *et al.*, 1984), as expected. Indeed all the free-ion parameter values used in the analysis of AnF_4 spectra are fully consistent with those available from other analysis of An^{4+} spectra in a variety of crystal environments (Krupa, 1987).

For tetravalent actinide ions, it is useful to emphasize that the crystal field is no longer a small interaction relative to that of the free ion, but is capable of radically transforming the energy level scheme without any change in magnitude in the free-ion interaction parameters. This is readily evident in comparing the parameters and energy level schemes for UCl_4 and Cs_2UCl_6. One of the consequences of this change in the hierarchy of interactions that comprise the theoretical model is that there is a decreased sensitivity in energy level structure calculations to the values of the F^k integrals in the analysis of An^{4+} compared to An^{3+} and Ln^{3+} spectra. This is a direct result of the stronger crystal-field and spin–orbit interactions. Recognition of this fact is important because it explains the relatively uncertain F^k values obtained from fitting experimental data. In most cases, very few free-ion states are actually included in the calculation. Indeed, those states that are included tend to be the lowest-energy states in the configuration and to exhibit the smallest J-mixing that would aid in defining the parameters.

Most of the experimental data from absorption spectra include contributions from An^{4+} ions on two crystallographic sites. One of the basic aspects of modeling the AnF_4 crystal field spectra is the reliance, not only on the results of a model calculation of the crystal field parameters in the actual C_2 symmetry, but also the assumption that for purposes of interpreting the observed energy level structure, it is possible to use an approximate C_{2v} symmetry. It was shown that the predictions that were made as a result of this approximation could be directly related to the observed structure and were consistent with the few available measurements that had been obtained independently. In fact, as shown in Table 18.11, very little change in crystal field parameter values over the series was required. This again confirms the arguments in Section 18.4.3 on using the descent-of-symmetry method to simplify the analysis of crystal field spectra of lanthanide and actinide ions in crystals of low symmetry.

In the history of f-element spectroscopy, theoretical interpretations of the crystal-field splitting of the $^8S_{7/2}$ ground state in a half-filled shell of the f^7 configuration have been contradictory. The lanthanides in such a configuration are Eu^{2+}, Gd^{3+}, and Tb^{4+}; and the actinide ions include Am^{2+}, Cm^{3+}, and Bk^{4+}. Early arguments were focused on the Gd^{3+} ion because the ground state crystal-field splitting observed in EPR experiments was less than 0.5 cm^{-1} (Hubert *et al.*, 1985) and could not be interpreted by the crystal field theory. A series of mechanisms were considered but failed to provide a consistent interpretation (Wybourne, 1966; Newman, 1970, 1975). However, the $^8S_{7/2}$ ground-state splittings in the actinide ions is much larger than that of the Gd^{3+}. For Am^{2+} and Cm^{3+}, the observed splitting varies from 2 to 20 cm^{-1}

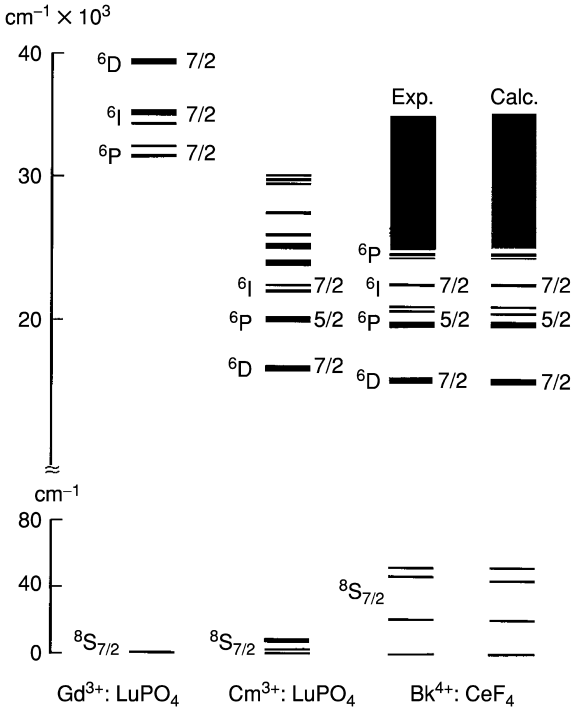

Fig. 18.16 *Partial energy level diagrams of Gd^{3+}, Cm^{3+}, and Bk^{4+} based on computed and experimental crystal field energies.* (*Reprinted with permission from Brito and Liu,* 2000. *Copyright* 2000, *American Institute of Physics.*)

(Edelstein and Easley, 1968; Liu *et al.*, 1993; Murdoch *et al.*, 1996; Edelstein, 2002), while for Bk^{4+} it is on the order of 60 cm^{-1} (Liu *et al.*, 1994b; Brito and Liu, 2000).

As a summary of previous work on the $5f^7$ ion, a comparison of the crystal-field splittings of Gd^{3+}, Cm^{3+}, and Bk^{4+} ions including the ground-state splitting is shown in Fig. 18.16. For the $5f^7$ systems, no additional mechanisms other than the crystal-field interaction are needed to provide a satisfactory interpretation to the observed splitting in the $^8S_{7/2}$ ground state of actinide ions (Liu *et al.*, 1993; Brito and Liu, 2000). As indicated in Section 18.4.2, the observed crystal-field splittings must be attributed to the contributions of the mixture of other *LS* terms into the ground state free-ion wave function (see equation (18.39)) and nonzero off-diagonal matrix elements between different *J*-multiplets. Because of the large energy gaps from the ground state to the excited multiplets of Gd^{3+}, the excited state *LS* components in the ground state is small, and *J*-mixing is also negligible in this case. However, for the actinide ions in $5f^N$ configurations, as discussed in Section 18.3, the ground-state wave

functions contains considerable *LS* components of the excited states, and thus lead to much larger splittings that should not occur for a pure *S*-state.

18.7 SPECTRA AND ELECTRONIC STRUCTURE OF DIVALENT ACTINIDE IONS AND ACTINIDES IN VALENCE STATES HIGHER THAN 4+

Although spectra of actinide compounds and solutions exhibiting other than the 3+ and 4+ valence states are well known, systematic analyses of the electronic structure in other valence states are very tentative now. Extensive analysis is limited to a few isolated cases. However, tabulations of electrostatic (Varga *et al.*, 1970) and spin–orbit integrals (Lewis *et al.*, 1970), computed using *ab initio* methods, have been published, and the relative energies of electronic configurations occurring within the usual spectral range of interest to chemists have been estimated from free-ion spectra (Brewer, 1971a,b).

The electrostatic and spin–orbit interactions in any given valence state are expected to vary systematically across the series. However, in the trivalent and tetravalent series it was necessary to introduce effective operators to explicitly screen the effects of configuration interaction to obtain good correlation with the experiment. In the absence of these correction terms, the values of the Slater integrals obtained in fitting the data exhibited a much more erratic behavior when plotted as a function of Z. In the discussion of 2+ and high valent actinides, it should be noted that the role of second-order correction terms has not been studied in detail for these oxidation states. What is clear is that the importance of both spin–orbit coupling and crystal-field interactions relative to the electrostatic interaction increases with increasing valence.

One of the reasons for introducing the theoretical interpretation of trivalent and tetravalent spectra in some detail was to provide the basis for discussing models appropriate to other valence states. Although detailed models have yet to be constructed, and may lead to revision of some of the values given here, it is advantageous to introduce a generalizing element into the discussion and relate available spectra to this central theme rather than approach each different actinide ion as a unique entity.

It has been realized for An^{2+} that the interactions appear to be of the same relative magnitude as for An^{3+}; however for An^{4+} and An^{5+} the crystal-field interaction becomes, relatively, much more important, and extraction of well-defined parameters for the free-ion and crystal-field interactions becomes more difficult. In An^{3+} spectra, the correction terms H_{corr} act mainly on the electrostatic part of the free-ion Hamiltonian, although some provision for second-order magnetic effects are included. In this discussion it is assumed that it is not necessary to modify the magnitudes of the terms associated with H_{corr} in treating other valence states. Since the crystal-field splitting is computed using a single-particle model, corrections to E_{cf} may be required as the relative magnitude of the crystal field increases.

In early attempts to develop a systematic interpretation of trivalent actinide and lanthanide spectra, initial sets of F^k and ζ_{nf} for some members of the series had to be estimated. This was done by linear extrapolation based on the fitted parameters that were available from the analyses of other individual spectra. As more extensive data and improved modeling yielded better determined and more consistent F^k and ζ_{nf} values for the 3+ actinides (and lanthanides), it became apparent that the variation in the parameters was nonlinear, as indicated for F^2 (5f,5f) in Fig. 18.4. This nonlinearity could also be observed in the values of parameters obtained from the *ab initio* calculations. The difference between the *ab initio* and fitted values of parameters (ΔP) appears to exhibit a much more linear variation with Z than do the parameter values. Consequently, ΔP has been adopted as the basis for a useful predictive model (Carnall *et al.*, 1966; Crosswhite, 1977; Crosswhite and Crosswhite, 1984).

For the trivalent actinides the values of ΔP are not constant over the series, but use of a single average value over a group of four or five elements is not an unreasonable approximation. Thus, in developing a predictive model for the F^k and ζ_{nf} parameters, an attempt is made to establish average values of ΔP for a particular valence state and type of crystal-field interaction. The energy level structure computation based on the predicted parameters can be compared to that observed, and then appropriate modifications sought by a fitting procedure where necessary.

18.7.1 Divalent actinide-ion spectra

Efforts to prepare divalent actinide compounds and analyze their spectra have been less successful than was the case for lanthanides, where the divalent ion for each member of the series could be stabilized in CaF_2 (McClure and Kiss, 1963). In both Am^{2+}:CaF_2 and Es^{2+}:CaF_2 (Edelstein *et al.*, 1966, 1967, 1970; Baybarz *et al.*, 1972), intense absorption bands were observed. These bands could be attributed to either f→d or charge-transfer transitions. The presence of divalent actinide ions in these cases was established by measurements of the electron paramagnetic resonance spectra, not on the basis of the observed optical spectra. In contrast to the more intense absorption bands reported for Es^{2+}:CaF_2, weak absorption bands consistent with the intensities expected for f→f transitions were identified in the 10 000–20 000 cm^{-1} region in both $EsCl_2$ and Es^{2+}:$LaCl_3$ (Fellows *et al.*, 1978). The relatively narrow band structure exhibited by the Es^{2+} halides was also found to be characteristic of the Cf^{2+} halides (Peterson *et al.*, 1977; Wild *et al.*, 1978).

Although it was not possible to stabilize Cm^{2+} in CaF_2 under the same conditions that yielded for Am^{2+}:CaF_2, evidence for the formation of both Am^{2+} and Cm^{2+} has been obtained in solution in pulse radiolysis studies; however, as in the spectrum of Am^{2+}:CaF_2, the absorption bands were broad and intense. The nature of the absorption process is therefore not clear. A charge-transfer process cannot be excluded (Sullivan *et al.*, 1976).

Because the available spectroscopic results for divalent actinides are fragmentary, a consistent interpretation that accounts for all observations and predicts the energies of other bands that might be accessible to observation will be adopted. The basic aspects of this tentative model can be deduced in part from available data for divalent lanthanide spectra.

The free-ion spectra of Ce III and Pr IV are known. Initial estimates of F^k and ζ_{4f} values appropriate to Ln^{2+} in condensed phases can be made by assuming that the change observed in these parameters for iso-f-electron couples such as Ce III/Pr IV (both $4f^2$) will also be characteristic of the couple Ce^{2+}/Pr^{3+} in condensed phases. This suggests a reduction of 20–30% in comparing values of F^k and ζ_{4f} for divalent compared to isoelectronic trivalent-ion cases. Comparing the results for Eu^{2+}:CaF_2 (Downer *et al.*, 1983) with those for Gd^{3+}:LaF_3 (Carnall *et al.*, 1971), the parameters for Eu^{2+} ($4f^7$) are 82–86% of those for Gd^{3+} ($4f^7$). The little information available on divalent lanthanide ion crystal-field splitting (Dieke, 1968) suggests that the crystal-field interaction is even smaller than for the trivalent case. This also was suggested in an analysis of Eu^{2+} in strontium fluoride (Downer *et al.*, 1983).

Based on the small crystal-field splitting indicated for the divalent lanthanides, it is reasonable to assume as a first-order approximation that the corresponding actinide crystal-field splitting will be small. Although fragmentary, available spectroscopic data for An^{2+} appear to be consistent with this estimate. The initial model can consequently be limited to free-ion considerations. The initial F^k and ζ_{5f} parameters for An^{2+} may be estimated to be 85–90% of those for the iso-f-electronic An^{3+}:$LaCl_3$ ion. The effects of configuration interaction for An^{2+} can be taken to approximate those for An^{3+}. The resulting model energy level schemes for An^{2+} are plotted in Fig. 18.17 where the overlap of the $5f^{N-1}6d$ and $5f^N$ configurations is also indicated (Brewer, 1971a,b).

Examining the range of energies in which f→f transitions might be observed, it is seen from the figure that the largest 'optical windows' are expected in Am^{2+}, Cf^{2+}, and Es^{2+}. In Np^{2+}, Pu^{2+}, Cm^{2+}, and Bk^{2+}, it is probable that f→f transitions will only be observed in the infrared range. This of course assumes that the $5f^N$ is consistently the ground state configuration. Transitions resulting from the promotion of f→d would be expected to result in intense (allowed) absorption bands such as those observed in Ln^{2+} spectra (McClure and Kiss, 1963). The much weaker f→f transitions occurring in the same energy range as the allowed transitions would be masked, so the optical window corresponding to the pure f→f energy spectrum will be somewhat smaller than that for the gaseous free-ion f→d transition energies indicated in Fig. 18.17 (Brewer, 1971a,b). The computed level structure for Cf^{2+} and Es^{2+} agree with the experimental results, but indicate the existence of bands not yet reported.

Systematic energy level calculations are of considerable importance in predicting the energies at which luminescence might be observed. In general, the longest-lived luminescence will originate from the state with the largest energy gap between it and the next lower-energy state. Based on the computed large

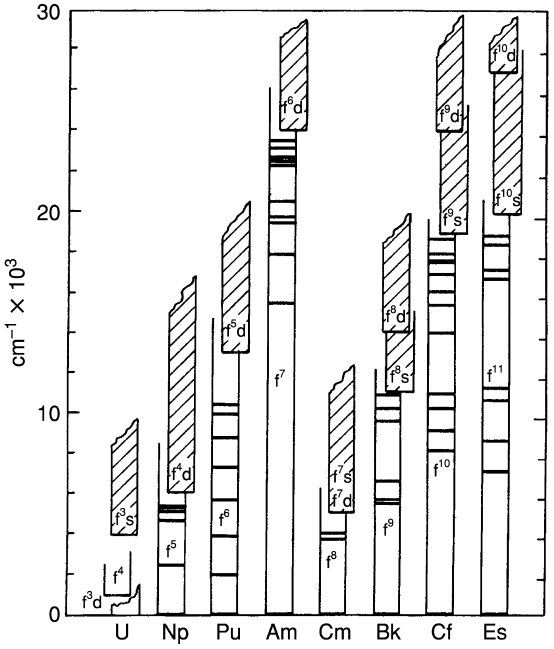

Fig. 18.17 *Estimated ranges of energies in which 5f–5f transitions in An^{2+} may be experimentally observed.*

energy gap between the ground ($^8S_{7/2}$) and first excited ($^6P_{7/2}$) states in Am^{2+} ($5f^7$), isolated Am^{2+} sites would be expected to exhibit luminescence near 14 000 cm^{-1} (Edelstein *et al.*, 1966; Edelstein and Easley, 1968; Edelstein, 1991).

18.7.2 Spectra of actinide ions in the pentavalent and hexavalent states

The actinide ions with well-defined valence states greater than VI are confined to the light half of the 5f series. A large number of stable compounds are known, and spectra have been recorded in solution, in solids, and in gas phase. However, there have been relatively few attempts to develop detailed energy level analyses. Although Hartree–Fock type calculations of F^k and ζ_{nf} can be carried out for any arbitrary state of ionization of an actinide ion, the relative importance of the ligand (or crystal) field must also be established to develop a correlation for experimentally observed transition energies. *Ab initio* models of the ligand field are characteristically very crude. The spectra of penta- and higher-valent actinides are strong crystal field cases and the development of correction terms for first-order crystal field model may well be essential to any detailed analysis.

Two types of ionic structure are normally encountered in the higher-valent species: the actinyl ions AnO_2^+ and AnO_2^{2+} (Denning, 1992; Matsika and Pitzer,

2001; Denning *et al.*, 2002), and halides such as UCl_5, $CsUF_6$, and PuF_6. Mixed oxohalide complexes are also known. In the actinyl ions (An = U, Np, Pu, Am) the axial field imposed by the two nearest-neighbor (−y1) oxygen atoms plays a dominant role in determining the observed energy level structure (Eisenstein and Pryce, 1966; Bell, 1969). The analysis of spectra of higher-valent actinide halides is also based on a strong ligand-field interaction, but the symmetry is frequently found to be octahedral or distorted octahedral (Goodman and Fred, 1959; Eisenstein and Pryce, 1960; Kugel *et al.*, 1976; Eichberger and Lux, 1980). Typical iso-f-electronic penta- and higher-valent actinide species are shown in Table 18.12, where X is a halide ion.

Aqueous solution spectra characteristic of the NpO_2^+ and PuO_2^{2+} ions, both having the $5f^2$ electronic structure, are shown in Fig. 18.18. Some qualitative similarities in band patterns for these iso-f-electronic ions appear to exist, but detailed analysis of the observed structure in terms of a predictive model is tentative. Charge-transfer bands for NpO_2^{2+} (20 800 cm^{-1}), PuO_2^{2+} (19 000 cm^{-1}), and AmO_2^{2+} (∼18 000 cm^{-1}) have been identified (Jørgensen, 1970). Spectra of the actinyl ions and the molar absorptivities of the more intense bands in aqueous solution have been tabulated (Carnall, 1973, 1982). The charge-transfer transitions in crystalline $CsNpO_2Cl_4$ and $CsNpO_2(NO_3)$ as reported by Denning *et al.* (1982) are apparently much lower than that predicted for NpO_2^{2+} (20 800 cm^{-1}). In their analysis, Denning *et al.* (1982) assigned five charge-transfer bands of $CsNpO_2Cl_4$ and $CsNpO_2(NO_3)$ between 13 000 and 20 000 cm^{-1}.

Attempts to interpret the spectra of the penta- and hexahalides of the actinides have used the effective-operator Hamiltonian discussed in Sections 18.3 and 18.4. However, the results are limited primarily to U^{5+} and Np^{6+}, both having the $5f^1$ configuration and Np^{5+} and Pu^{6+} with the $5f^2$ configuration. The magnitude of the spin–orbit interaction is known for U v. Its free-ion spectrum has been interpreted in terms of a coupling constant, $\zeta_{5f} = 2173.9$ cm^{-1}, based on a $^2F_{5/2} \rightarrow {}^2F_{7/2}$ energy difference of 7608.6 cm^{-1} (Kaufman and Radziemski, 1976). The optical properties of Np and Pu ions and compounds were analyzed by Edelstein (1992). The spectra of several complex pentavalent uranium halide

Table 18.12 *Some iso-f-electron penta- and higher-valent actinide species.*[a]

Number of 5f electrons =	0	1	2	3	4
	UO_2^{2+} Np VIII UF_6 UCl_6	UO_2^{+} NpO_2^{2+} Pu VIII NpF_6 UX_6^{-} UF_5	PuO_2^{2+} NpO_2^{+} PuF_6 NpX_6^{-}	AmO_2^{2+} PuO_2^{+} PuX_6^{-}	AmO_2^{+}

[a] X, halide ion.

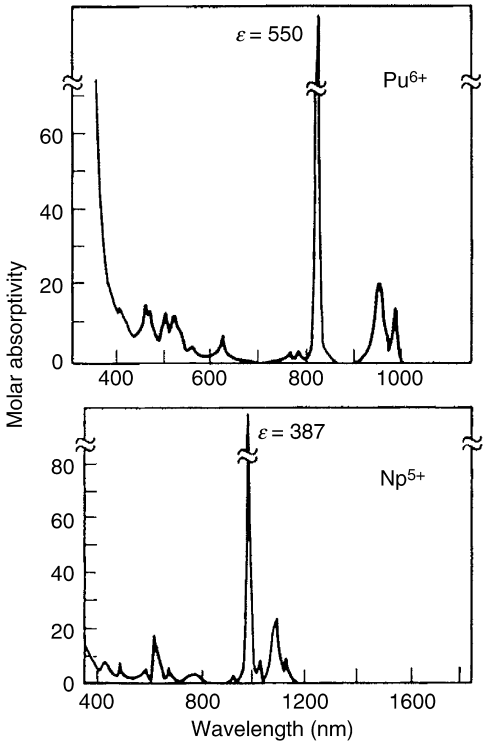

Fig. 18.18 *Aqueous solution absorption spectra of* PuO_2^{2+} (Pu^{6+}) *and* NpO_2^{+} (Np^{5+}).

compounds appear in the literature and, based on representative crystallographic determinations, the site symmetry usually is close to octahedral. The combined effect of the spin–orbit and octahedral ligand-field interactions is to split the parent ^2F state into five components whose irreducible double group labels are indicated in Fig. 18.19.

The energy level structures of several actinide 4+, 5+, and 6+ compounds with the $5f^1$ ion at a site of octahedral (or approximated as octahedral) symmetry are compared in Table 18.13. As indicated in Table 18.13, there has been considerable variation in the ligand field parameters deduced by different investigators from absorption spectra in which the energies of observed features are surprisingly consistent. The case of UCl_5, which has a dimeric structure that gives rise to approximately octahedral U^{5+} sites, is particularly interesting because the spectra of solutions (UCl_5 in $SOCl_2$) (Karraker, 1964), of a single crystal (Leung and Poon, 1977), and of the vapor phase, $(UCl_5)_2$ or $UCl_5 \cdot AlCl_3$ (Gruen and McBeth, 1969), all give absorption features that are similar to both the relative intensities of the transitions and their energies. The importance of the nearest-neighbor coordination sphere in determining the spectra, essential

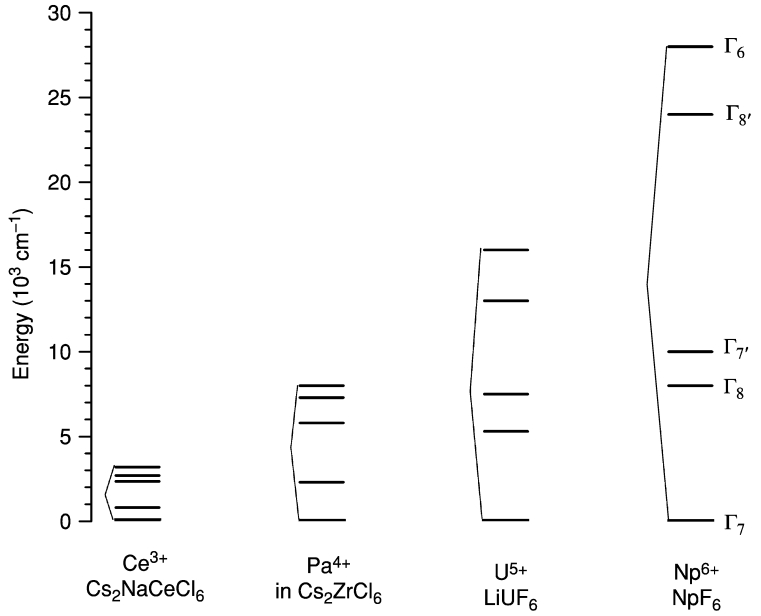

Fig. 18.19 *Comparison of crystal-field splittings of the $5f^1$ states of actinide ions in various hosts.*

to the exclusion of the effects of long-range order, is consistent with the behavior expected for strong octahedral bonding. However, more evidence is needed to justify the assignments and to establish uniquely the limits over which the ligand field parameters may vary.

The spectra of $CsUF_6$ (Reisfeld and Crosby, 1965) and $CsNpF_6$ (Hecht *et al.*, 1979) have been reported and analyzed, and that of $CsPuF_6$ has been measured (Morss *et al.*, 1983). However, the treatment of $CsUF_6$, which has been considered to be a model for other cases of distorted octahedral symmetry, has been questioned both experimentally (Ryan, 1971) and on theoretical grounds. Both Leung (1977) and Soulie (1978) have pointed out that there is actually a very significant distortion of the O_h symmetry originally assumed for $CsUF_6$ (Reisfeld and Crosby, 1965), with D_{3d} symmetry providing the basis for a much improved interpretation. If electrostatic interaction parameters of the same order of magnitude as those suggested by Poon and Newman (1982) are utilized for $CsNpF_6$, together with the D_{3d} ligand field parameters for $CsUF_6$, and further extrapolation of these results is carried out to provide values for the $CsPuF_6$ case, the resulting energy level structure is that indicated in Fig. 18.20. The general aspects of this predicted structure appear to be consistent with available experimental data. Aside from the structure of the ground state, a relatively isolated $^3F_2$ state in $CsNpF_6$ should be observed. However, with the

Table 18.13 *Energy parameters for* $An^{4+,\ 5+,\ 6+}$ *compounds* (in cm^{-1}).[a]

	$(5f^1)$ Pa^{4+}: Cs_2ZrCl_6[b]	$(5f^1)$ UCl_5[c]	$(5f^1)$ $CsUF_6$[d]	$(5f^1)$ NpF_6[e]	$(5f^2)$ $CsNpF_6$[f]	$(5f^2)$ PuF_6[g]	$(5f^3)$ $CsPuF_6$[f]
F^2					48 920	36 026 (2 472)	51 760
F^4					42 300	72 458 (3 054)	44 200
F^6					27 700	40 535 (3 877)	29 120
ζ	1539.6	1559 (115)	1910.2 (13)	2448.4 (33)	2200	2551 (46)	2510
α					30 000	[35 500]	30 000
β					−660	[−664]	−660
γ					700	[744]	700
B_0^2			534.2 (139)		534.2		543.2
B_0^4	6945.3	13 479 (1 125)	−14 866 (66)	44 553 (211)	−14 866	48 377(803)	−14 866
B_0^6	–162.7	–158.6 (745)	3305 (78)	7992 (105)	3305	8690(180)	3305
σ[h]		370	33	73		54.2	

[a] Values in parentheses are errors in the indicated parameters. Values in brackets were not allowed to vary in the parameter fitting.
[b] Piehler *et al.* (1991).
[c] Leung and Poon (1977).
[d] Ryan (1971).
[e] Goodman and Fred (1959).
[f] Estimated parameter values shown. In addition to those parameters tabulated, the following were included: $P^2 = 500$, $P^4 = P^6 = 0$ (for both $CsNpF_6$ and $CsPuF_6$); $T^2 = 200$, $T^3 = 50$, $T^4 = 100$, $T^6 = -300$, $T^7 = 400$, $T^8 = 350$ (for $CsPuF_6$ only).
[g] Edelstein (1992). $M^0 = 0.987$, $M^2 = 0.55$, $M^4 = 0.384$, $P^2 = 573$, $P^4 = 524$, $P^6 = 1173$.
[h] Deviation as defined in footnote c of Table 18.4.

exception of this $^3F_2$ state, neither the spectrum of $CsNpF_6$ nor that of $CsPuF_6$ is expected to exhibit any extensive, easily recognizable band structure. A relatively high density of excited states is predicted and detailed analysis will be difficult.

The actinide hexafluorides, UF_6, NpF_6, and PuF_6, form a unique group of volatile actinide molecular species. They are not regarded as strongly bonded since the metal–fluorine distances tend to be rather large (~1.98 Å) (Claassen, 1959). The combination of well-characterized spectroscopic and magnetic (Goodman and Fred, 1959; Hutchison and Weinstock, 1960; Edelstein, 1992) results for NpF_6 and PuF_6 has served to establish a reasonable basis for the energy level analysis in octahedral symmetry summarized in Table 18.13. A consistent set of F^k and ζ_{5f} parameters can be combined with the crystal field for NpF_6 to yield an estimate of the parameters set for PuF_6 and AmF_6. However, in terms of the free-ion interaction parameters, no consistent results have been

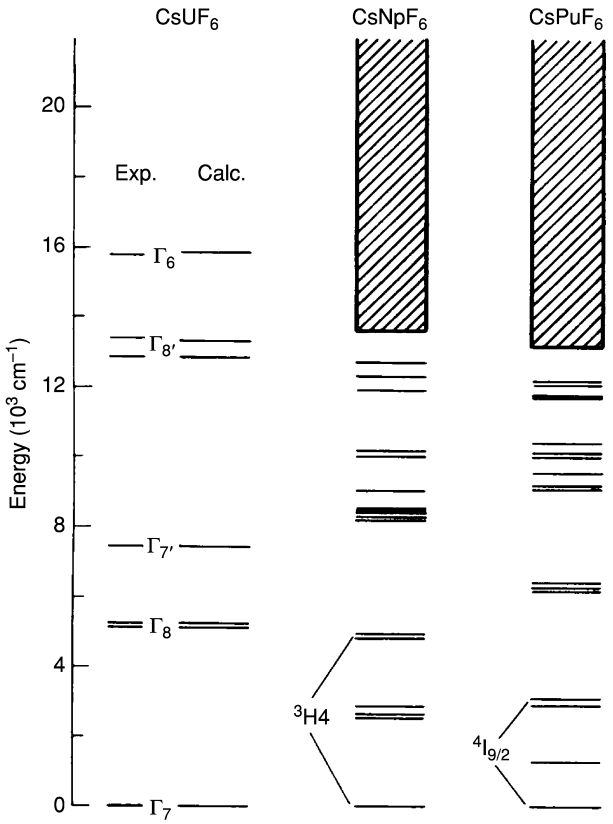

Fig. 18.20 *Computed energy levels schemes for $CsUF_6$, $CsNpF_6$, and $CsPuF_6$. The cross-hatched areas indicate that a relative dense energy structure is predicted.*

achieved when the parameters are varied in fitting of the observed energy levels of PuF_6 (Edelstein, 1992). As listed in Table 18.13, the value of F^2 for PuF_6 is reduced by greater than 50% from its Hartree–Fock value and F^4 is greater than the calculated Hartree–Fock value (Wadt, 1987). In comparison with Hartree–Fock values and the parameters for NpF_6, the empirical values for F^6 and ζ seem to be of reasonable magnitude. The energies of some of the lower-lying states in NpF_6 and PuF_6 are shown in Fig. 18.21. The two upper levels of NpF_6 at 23 500 and 28 000 cm^{-1} were not well resolved in absorption spectra (Steindler and Gerding, 1966) and the uncertainty in assigning these two levels could result in uncertainties in the spin–orbit and crystal field parameters. The indicated structure is consistent with the principal features in the absorption spectrum of PuF_6 (Kugel *et al.*, 1976) as shown in Fig. 18.22. Detection of luminescence in the selective excitation of NpF_6 and PuF_6 and at energies in

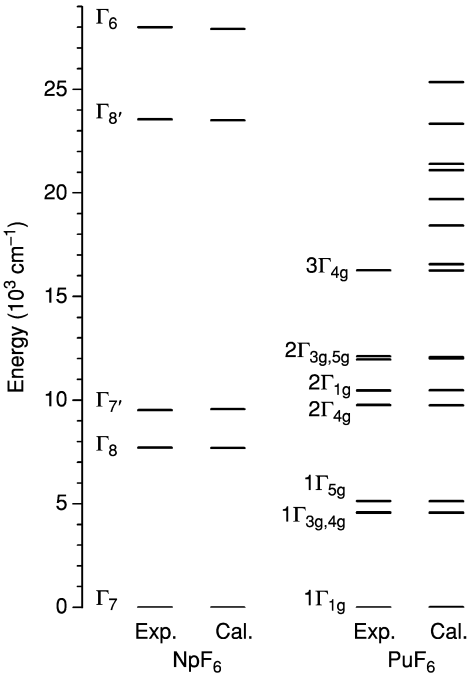

Fig. 18.21 *Comparison of observed and computed energy level schemes for NpF_6 (data from Goodman and Fred,* 1959) *and PuF_6 (data from Edelstein,* 1992). *Analysis of near-infrared spectra of matrix-isolated NpF_6 was also reported* (*Mulford* et al., 1991)

agreement with the energy gaps between the predicted ground and first excited states in both spectra has been reported (Beitz *et al.*, 1982).

18.7.3 Charge-transfer transitions and structure of actinyl ions

In addition to electronic transitions from $5f^N$ to excited configurations, an electron may be excited from a ligand to a 5f orbital, creating a charge-transfer state, with a configuration consisting of $5f^{N+1}$ plus a ligand 'hole'. The spectra of UO_2^{2+}, UF_6, and Np^{7+} shows typical charge-transfer transitions for the actinide series since, in contrast to the transitions between states within the $5f^N$ configuration which characterize most of the actinide spectra discussed in previous sections; the above species contain no f-electrons in open shells. The energies of these states are highly ligand-dependent and, especially in organic systems, they can be at a lower energy than the $5f^{N-1}6d$ states. For lighter actinide ions in oxygen environments, actinyl ions are formed through charge-transfer bonding (Jørgensen, 1957). The most extensive studies of ion-to-ligand charge transfer have been conducted on uranyl (UO_2^{2+}) ion in various solutions and compounds (Denning *et al.*, 1982, 2002; Denning, 1992). Fig. 18.23 shows

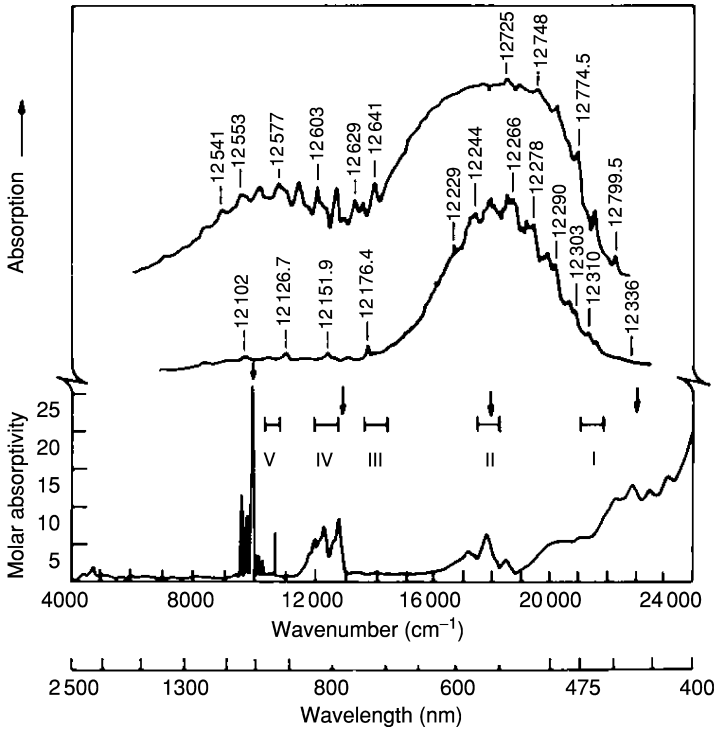

Fig. 18.22 *The absorption spectrum of PuF_6. Arrows indicate regions reported to show vibrational structure. Bars indicate regions examined by intra-cavity laser absorption:* I, 455–470; II, 550–574; III, 697–729; IV, 786–845; V, 918–971 nm. *At the top is a densitometer trace of the high-resolution absorption spectrum of PuF_6 in the* 781–830 nm *region obtained in multipass experiments. Data from Kugel* et al. (1976).

the energy level structure of UO_2^{2+} charge-transfer states in comparison with that of the U^{6+} and O^{2-} ions. The lowest-energy level of the excited charge-transfer states starts at (20 000 cm^{-1} for uranyl ion and at (14 000 cm^{-1} for neptunyl ion (NpO_2^{2+}), which is below the energy levels of several 5f states of the Np^{6+} core (Denning *et al.*, 1982, 2002). In the neptunyl case, energy levels of different origins, namely $5f^N$, $5f^{N-1}6d$, and ion–ligand charge transfer, may overlap in the same energy region, and thus make spectrum analysis difficult. Emission from charge-transfer states of actinide ions in condensed phase is relatively rare except for the case of uranyl (UO_2^{2+}) ions, which often exhibit a strong luminescence in solution. This is because of the large energy gap between its ground and excited charge-transfer states that suppresses quenching due to nonradiative phonon relaxation (Riseberg and Moos, 1968).

The spectra of UO_2^{2+} compounds with a characteristic structure in the visible–ultraviolet range below 400 nm are commonly observed charge-transfer

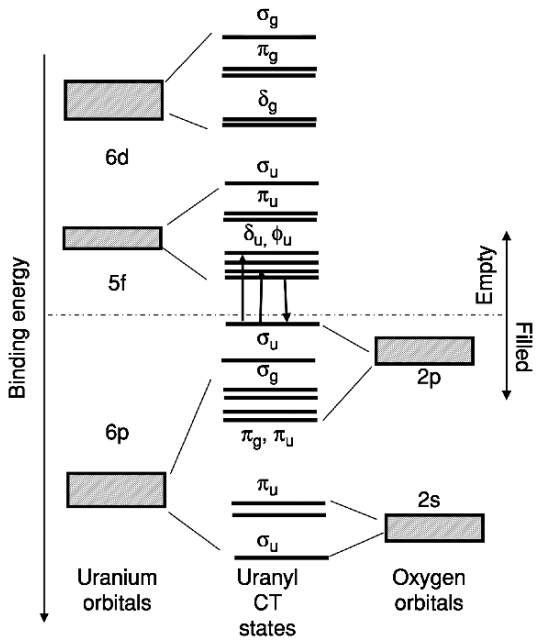

Fig. 18.23 *Illustration of electronic energy level scheme of uranyl ion* UO_2^{2+}.

transitions in the actinide series. Analyses of crystal spectra such as that for $Cs_2UO_2Cl_4$ are now available (Denning *et al.*, 1980, 1982; Denning, 1992). Because of the energy gap between the emitting and ground states as shown in Fig. 18.23 is much larger than the vibration energies, in many cases including uranyl species in solutions, fluorescence emission is often the dominant channel of relaxation from the lowest level of the excited charge-transfer states. Fig. 18.24(a) shows the fluorescence spectrum of $UO_2Cl_4^{2-}$:Cs_2ZrCl_6 single crystal at 20 K (Metcalf *et al.*, 1995). The ZPL is accompanied by a progression of vibronic lines due to the O–U–O stretching and bending modes, which characterize the uranyl structure and are relatively insensitive to the environment of the uranyl ion in the equatorial plane. Usually, the linear dioxo cation O–U–O is coordinated by an additional four to six ligand ions in its equatorial plane. The vibrational frequencies of different modes of the complexed ion can be determined directly from the spectrum. They are typically 820, 900, and 240 cm^{-1} for the symmetric, asymmetric, and bending modes of the UO_2^{2+} ion, respectively. As to the nature of the uranyl bonding, variation of the vibrational frequencies is correlated with the energy levels of the charge-transfer states (Denning, 1992). The spectrum of the uranyl ion in single crystals of $UO_2Cl_4^{2-}$:Cs_2ZrCl_6 exhibits extremely sharp line widths, indicating that the uranyl ions in the crystal have highly identical local structure so that

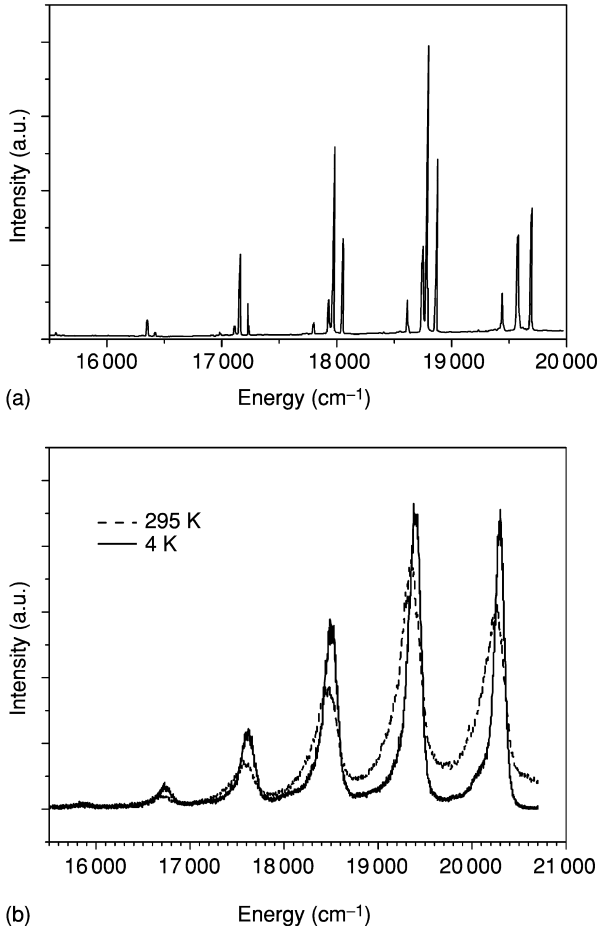

Fig. 18.24 *Spectra of uranyl charge-transfer vibronic transitions:* (*a*) *fluorescence spectrum of* UO_2^{2+} in Cs_2ZrCl_6 *at* 20 K (*data from Metcalf* et al., 1995) *and* (*b*) *fluorescence spectra of* UO_2^{2+} *in* B_2O_3 *glass at* 4 *and* 295 K.

inhomogeneous line broadening induced by structure defects is not significant. If structure variation and impurity phases exist, inhomogeneous line broadening would obscure the features due to different vibrational modes. Fig. 18.24(b) shows the emission spectra of uranyl in B_2O_3 glass matrix at 4 and 295 K. In comparison with Fig. 18.24(a), the lines become much broader, whereas the changes in the overall spectral profile and line locations are insignificant. Given the nature of charge-transfer states, it is apparent that the energy levels of charge-transfer states are more sensitive to local structure disordering than that of the 5f−5f transitions. Therefore, in structurally disordered environments such as glasses and solutions, inhomogeneous line broadening obscures

observation of separated lines of the asymmetric and bending modes. Only the progression of the symmetric mode, up to five quanta of phonon sidebands, is often observed. Based on the theory of ion–phonon interaction (Huang and Rhys, 1950), the spectra of charge-transfer vibronic transitions of uranyl species may be theoretically simulated using a model proposed by Liu *et al*. (2002). The Huang–Rhys parameter of the uranyl vibronic coupling is typically in the range of 1.0–1.5.

For the closely related case of NpO_2^{2+} ion doped into single-crystal $Cs_2UO_2Cl_4$, detailed spectroscopic studies have identified a single electronic transition belonging to the $5f^1$ configuration, but the other structure observed is similar in origin to that reported for UO_2^{2+}, i.e. transitions to molecular-orbital states (Stafsudd *et al*., 1969; Jørgensen, 1982; DeKock *et al*., 1985). Extensive analyses of the absorption and fluorescence spectra of UF_6 have been published, and are covered in a review (Carnall, 1982). In the visible to near-ultraviolet range, the character of the spectrum is similar to that of UO_2^{2+}.

18.8 RADIATIVE AND NONRADIATIVE ELECTRONIC TRANSITIONS

18.8.1 Intensity of 5f–5f transitions

A systematic understanding of the energy level structure for An^{3+} serves as a foundation upon which to base the interpretation of other physical measurements. Considerable success has now been achieved in developing a parameterized model of f → f transition intensities.

The intensity of an absorption band can be defined in terms of the area under the band envelope normalized for the concentration of the absorbing ion and the path length of light in the absorbing medium. A proportional quantity, the oscillator strength P, has been tabulated for trivalent actinide-ion absorption bands in aqueous solution. The experimentally determined oscillator strengths of transitions can in turn be related to the mechanisms by which light is absorbed (Condon and Shortley, 1963; Reid, 2000):

$$P = \frac{8\pi^2 mc\sigma}{3he^2(2J+1)}\left(\chi\overline{F}^2 + n\overline{M}^2\right) \tag{18.51}$$

where $\overline{F}$and $\overline{M}$ are, respectively, the matrix elements of the electric dipole and magnetic dipole operators joining the initial state J to a final state J', $\chi = (n^2+2)^2/9n$ and n is the refractive index of the medium, σ is the energy of the transition (cm^{-1}), and the other symbols have their usual meanings.

Only a few transitions observed for the 3+ actinide ions have any significant magnetic dipole character; however, the matrix elements of $\bar{M}^2$ can be evaluated directly from the knowledge of the eigenvectors of the initial (ΨJ) and final ($\Psi' J'$) states. Following the results of Condon and Shortley (1963), the magnetic dipole operator is given as

$$M = -\frac{e}{2mc}\sum_i (l_i + 2s_i). \tag{18.52}$$

The matrix elements of the operator in equation (18.51) can then be written as

$$\overline{M}^2 = \frac{e^2}{4m^2c^2}\langle \Psi J \| L + 2S \| \Psi' J' \rangle^2. \tag{18.53}$$

The nonzero matrix elements, which should be calculated in the intermediate coupling scheme, will be those diagonal in the quantum numbers τ, S, and L. The selection rule on J is $\Delta J = 0, \pm 1$.

The Judd–Ofelt theory (Judd, 1962; Ofelt, 1962) has successfully addressed the problem of computing the matrix elements of $\overline{F}^2$, and can be written in the form:

$$\overline{F}^2 = e^2 \sum_{k=2,4,6} \Omega_k \left\langle \Psi J \left\| \mathbf{U}^{(k)} \right\| \Psi' J' \right\rangle^2 \tag{18.54}$$

where Ω_k are three parameters which in practice are evaluated from measured band intensities. These parameters involve the radial parts of the f^N wave functions, the wave functions of perturbing configurations such as $5f^{N-1}6d$, and the interaction between the central ion and the immediate environment. Since the Ω_k parameters contain many contributions, model calculations are not possible. Nevertheless, the relative simplicity of the intensity calculations using equation (18.51) have resulted in extremely useful analyses of experimental data. The matrix elements in equation (18.54) may be calculated using the SPECTRA program. For the trivalent actinide ions, the matrix elements of $\mathbf{U}^{(k)}$ have been tabulated (Carnall, 1989) for states of $5f^3$ to $5f^{12}$ configurations with energies up to 40 000 cm^{-1}. It should be noted that the intensity theory presented here is applied only to the free-ion multiplets, and the empirical values for the intensities of these multiplets are obtained by integrating over the band intensities in solution.

Judd (1962) showed that the theory could successfully reproduce the observed intensities of bands of Nd^{3+} and Er^{3+} in aqueous solution ($RE(H_2O)_x$ where x is 8 or 9) throughout the optical range, and that the intensity parameters Ω_k computed from first principles were consistent with those derived from fitting experimental data. Later systematic treatments of the intensities observed in the spectra of all aquated Ln^{3+} ions have confirmed and extended the original correlation (Carnall *et al.*, 1968; Carnall, 1979a) and, more recently, it was found that a similar systematic treatment of band intensities for aquated An^{3+}-ion spectra could be successfully carried out with only Ω_4 and Ω_6 treated as variables (Carnall *et al.*, 1984). The emphasis on aquated f^N-ion spectra comes from the ability to identify many relatively isolated bands with single or very limited numbers of *SLJ* states, the corresponding unambiguous quantitative nature of the oscillator-strength calculation, and the wide range of data

available, i.e. most members of the 4f and 5f series can be readily obtained as trivalent aquated ions in dilute acid solution. Intensity correlations for Ln^{3+} ion in many different host crystals, as well as in vapor complexes, have been developed (Beitz, 1994b; Reid, 2000). For the actinides, systematic and quantitative examination of transition intensities is presently restricted to aquated An^{3+}.

Examination of Fig. 18.8 shows that, particularly for U^{3+}, Np^{3+}, and Pu^{3+}, the density of states is high and few of the observed bands can be uniquely identified. Both the relative intensities of observed transitions and the density of states decrease in magnitude with increasing atomic number. Starting with aquated Cm^{3+}, the heavy-actinide aquated-ion spectra are all amenable to intensity analyses with excellent correlation found between observed oscillator strengths and intensities computed using the Judd parameterization (Carnall *et al.*, 1983). The oscillator strengths of aquated An^{3+} bands tend to be a factor of 10−100 greater than those observed for the lanthanides, Starting with aquated Bk^{3+}, there is an apparent transition to a heavy-lanthanide-like character in the spectra, with no bands being disproportionately intense. Analysis reveals that the trends in the intensity parameter values over the series can be correlated with the extent to which higher-lying opposite-parity configurations like $f^{N-1}d$ are mixed into the f^N configuration. There is much less mixing of $f^{N-1}d$ states into $5f^8(Bk^{3+})$ than in $5f^3(U^{3+})$ which it is consistent with the energy level structures of the $f^{N-1}d$ and f^N configurations of the two ions. An example of the type of correlation obtained between experiment and theory for aquated An^{3+} was previously discussed for aquated Cm^{3+} (Carnall and Rajnak, 1975). Figs. 18.25 and 18.26 compare the observed absorption spectra of U^{3+} and Cf^{3+} in dilute perchloric acid, respectively. These spectra are from the work of Carnall (1992) and have been published, along with those of other An^{3+} ions, with split abscissa scales to highlight weakly absorbing transitions (Beitz, 1994b). Also shown in Figs. 18.25 and 18.26 as vertical bars are the centers of gravity expected for the actinide ion's 5f electron states based on the free-ion parameters established for trivalent actinide ions in single crystals of lanthanum trichloride. It is evident in Fig. 18.26 that the free-ion states provide an excellent basis for interpretation and assignment of the parity-forbidden f–f absorption bands of Cf^{3+}. The very strong absorption bands that occur in the blue and ultraviolet spectral ranges of the U^{3+} spectrum can be assigned as arising from parity-allowed transitions. In addition, it is evident that the f–f absorption bands of U^{3+} at longer wavelengths are significantly more intense than those of the comparatively heavy actinide ion Cf^{3+}. Qualitatively, the high intensity of U^{3+} f–f transitions can be attributed to interaction with the low-lying opposite-parity states of U^{3+}. Put another way, the f-electron states of light actinide ions contain a larger contribution from opposite-parity states than is the case for heavier actinide ions.

Band intensities of spectra such as those shown in Figs. 18.25 and 18.26 have been analyzed systematically (Carnall and Crosswhite, 1985; Carnall *et al.*, 1985;

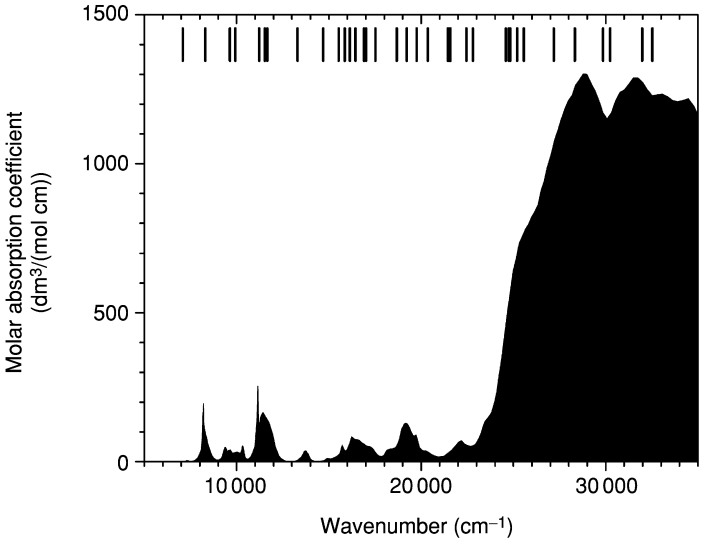

Fig. 18.25 *Optical absorption spectrum of* U^{3+} *in dilute acid solution* (*shaded curve*) *compared to the* 5*f electron free-ion state energies from studies on* U^{3+} *in* $LaCl_3$ (*vertical bars*). *Data from Carnall* (1992).

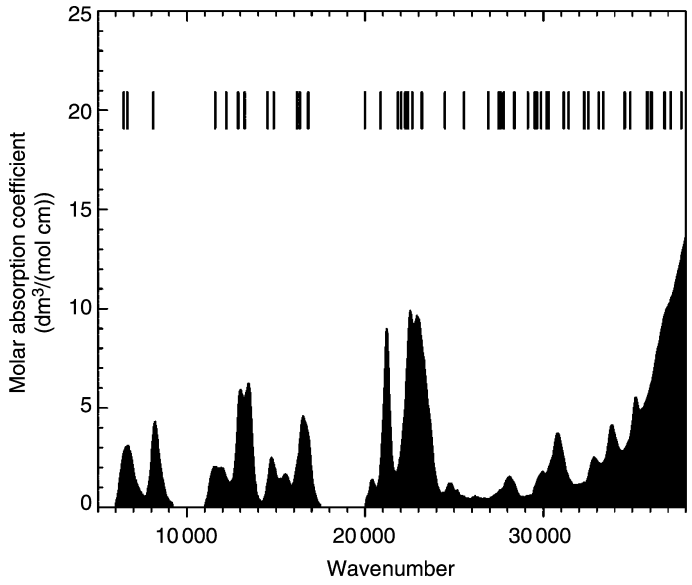

Fig. 18.26 *Optical absorption spectrum of* Cf^{3+} *in dilute acid solution* (*shaded curve*) *compared to the* 5*f electron free-ion state energies from studies on* Cf^{3+} *in* $LaCl_3$ (*vertical bars*). *Data from Carnall* (1992).

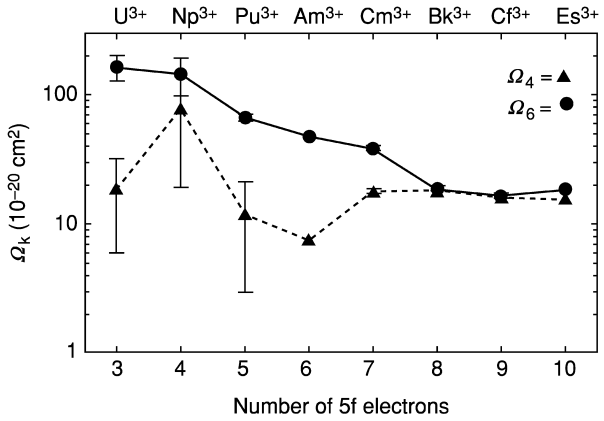

Fig. 18.27 *Trends in the values of the Judd–Ofelt theory Ω_4 and Ω_6 parameters across the trivalent actinide ion series.* (*Data from Carnall and Crosswhite,* 1985*; Carnall* et al., 1985*; Beitz,* 1994b).

Beitz, 1994b) from the f–f transition intensities using the Judd–Ofelt formalism (see equation (18.54)). The results of these analyses for aquated U^{3+} through aquated Es^{3+}, based on a fixed value of the Judd–Ofelt parameter Ω_2 at 1×10^{-20} cm^2, are shown in Fig. 18.27. The difficulty in uniquely determining band areas for the strongly overlapping bands of light actinide ions results in large error estimates for these ions. The Judd–Ofelt parameters for aquated trivalent lanthanide ions become nearly constant in value beginning at neodymium and continuing across the series of lanthanide elements (Carnall, 1979a). A similar trend is evident in Fig, 18.27 beginning at Bk^{3+} for aquated trivalent actinide ions. Few opportunities exist for experimentally establishing Ω_2 values for trivalent actinide ions. One such case is found in the branching ratios for emission from the $^5D_1$ state of aquated Am^{3+}. Partial measurement of those ratios led Beitz (1994a) to conclude that an Ω_2 value of 7×10^{-20} cm^2 was consistent with the Ω_4 and Ω_6 values shown in Fig. 18.27 (Beitz, 1994a). Görller-Walrand and Binnemans (1998) have reviewed the application of Judd–Ofelt theory to lanthanide and actinide f–f transitions.

18.8.2 Florescence lifetimes

One reason of interest for determining absorption intensity correlations is that, once the parameters of the Judd–Ofelt theory are evaluated, they can be used to compute the radiative lifetime of any excited state of interest via the Einstein expression

$$A(\Psi J, \Psi' J') = \frac{64\pi^2\sigma^3}{3h(2J+1)}\left(\chi'\overline{F}^2 + n^3\overline{M}^2\right) \tag{18.55}$$

where $|\Psi J\rangle$ and $|\Psi' J'\rangle$ are the initial and final states, A is the rate of relaxation of ΨJ by radiative processes, and $\overline{F}^2$ and $\overline{M}^2$ are the terms defined in equations (18.52) and (18.54). The observed fluorescent lifetime of a particular excited state, τ_T, is determined by the sum of the inverse of the radiative and nonradiative lifetimes. Usually the nonradiative relaxation mechanisms are dominant. Thus

$$(\tau_T)^{-1} = A_T(\Psi J) + W(\Psi J) \tag{18.56}$$

where A_T (ΨJ) is the total radiative relaxation rate from state $|\Psi J\rangle$, that is, the sum of the rates of radiative decay to all states with energy less than that of $|\Psi J\rangle$. If τ_R (calc) is the (computed) total radiative lifetime of $|\Psi J\rangle$, then τ_R (calc) $= [A\ (\Psi J)]^{-1}$. Similarly, $W_T(\Psi J)$ is a total rate summed over all nonradiative relaxation processes. The magnitude of the energy gap between a fluorescing state and the next lower-energy state appears to play a major role in determining the nonradiative lifetime of that state; shorter empirical fluorescent lifetimes are correlated with narrower gaps for the same fluorescing level in different systems.

On the basis of the existence of relatively large energy gaps in the spectra of some of the heavier actinides (Fig. 18.8), experiments were initiated and luminescence lifetimes were successfully measured in solution for some of the excited states of aquated Bk^{3+} and Es^{3+} (Beitz *et al.*, 1981), as well as aquated Cm^{3+} (Beitz and Hessler, 1980) and aquated Am^{3+} (Beitz *et al.*, 1987). As indicated in Fig. 18.28, which shows the lower energy level structure for the heavier aquated

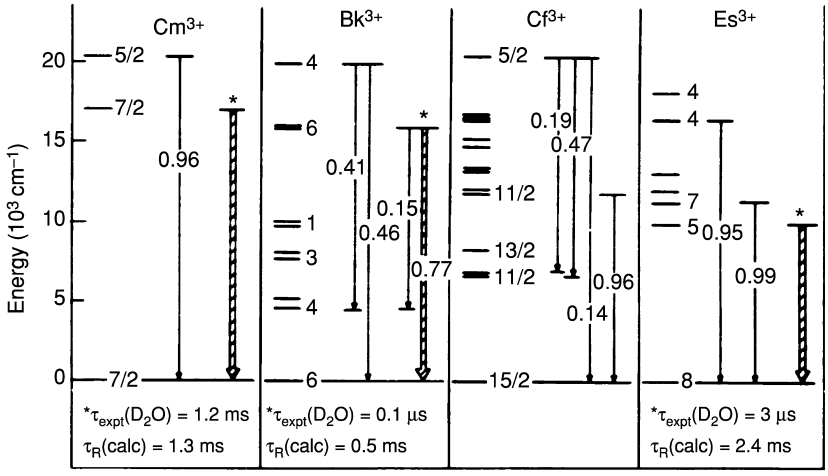

Fig. 18.28 *Energy level schemes and selected branching ratios for radiative relaxation for Cm^{3+} through Es^{3+}.*

An^{3+} ions, only in aquated Cm^{3+} does the observed lifetime of 1.2 ms in D_2O (Kimura *et al.*, 2001) compare well with the computed radiative lifetime, $\tau_R = 1.3$ ms. With smaller energy gaps, the nonradiative relaxation rate clearly becomes rate-determining. Inability to observe a luminescing state for aquated Cf^{3+} in preliminary experiments suggests that lifetimes may be in the nanosecond time range (Beitz *et al.*, 1981; Carnall *et al.*, 1983).

In addition to computing radiative lifetimes, it is instructive to establish the most probable pathway for fluorescence from a given state. Thus the branching ration, β_R, from a given relaxing state to a particular final state is

$$\beta_R(\Psi J, \Psi' J') = \frac{A(\Psi J, \Psi' J')}{A_T(\Psi J)}. \tag{18.57}$$

As indicated in Fig. 18.28 for Cf^{3+}, $\beta_R = 0.47$ for emission from an excited ($J = 5/2$) state to a lower-lying ($J = 11/2$) state, whereas $\beta_R = 0.14$ for emission to the ground state. In the case of $J = 5/2$ state, it would be appropriate to monitor for luminescence near 13 000 cm^{-1} as well as near 20 000 cm^{-1}.

18.8.3 Nonradiative phonon relaxation

The identification of the mechanisms of nonradiative relaxation of actinide ions in solution as well as in solids remains an important area for research (Hessler *et al.*, 1980; Liu and Beitz, 1990a,b). The nonradiative relaxation rate between crystal field energy levels belonging to different multiplets is predominantly determined by temperature, the energy gap, and the lattice phonon modes of the particular host crystal (Riseberg and Moos, 1968; Miyakawa and Dexter, 1970). With the assumption that the phonons involved are of equal energy, a commonly used expression for the temperature-dependent multiphonon relaxation rate is (Riseberg and Moos, 1968)

$$W(T) = W(0)\left[\frac{\exp(\hbar\omega_m/kT)}{\exp(\hbar\omega_m/kT) - 1}\right]^{\Delta E/\hbar\omega_m}, \tag{18.58}$$

where $\hbar\omega_m$ is the maximum phonon energy the lattice vibrations that couples to the electronic transition of the metal ion, ΔE is the energy gap between the populated state and the next low-lying state, and $W(0)$ is the spontaneous transition rate at $T = 0$ when the phonon modes are all initially in their ground state. At low temperatures where $\hbar\omega_m \gg kT$, nonradiative relaxation rate is dominated by $W(0)$, which can be expressed as a simple exponential function depending on the energy gap, ΔE

$$W(0) = C\exp(-\alpha\Delta E/\hbar\omega_m), \tag{18.59}$$

where C and α are empirical parameters which are characteristic of the particular crystal. Known as the energy gap law, this exponential dependence of the transition rate on the energy gap has been used to describe quite generally the

energy gap dependence of multiphonon transitions rates for the 4f and 5f states (Riseberg and Moos, 1967, 1968).

Extensive experimental results for lanthanide systems are available for comparison with those obtained for actinide ions. It should be possible to explore bonding differences between selected actinides and lanthanides by examining their excited state relaxation behavior. Because of smaller electrostatic interaction and larger spin–orbit coupling and crystal-field splittings, the energy gaps between different *J*-multiplets of actinide ions are much smaller than that of the isoelectronic lanthanide ions. Therefore, phonon-induced nonradiative relaxation in actinide systems is more efficient than in the lanthanide systems. Except for a few cases, such as the $^6D_{7/2}$ state of Cm^{3+} and Bk^{4+}, that have a large energy gap to the low-lying states, the lifetime of most 5f–5f electronic transitions of actinide ions in solids and solutions are predominantly determined by nonradiative relaxation. A direct comparison of the use of the energy gap law for Cm^{3+} in $LaCl_3$ and the trivalent rare earth ions in $LaCl_3$ has been reported (Illemassene *et al.*, 1997). A comparison of the emitting state lifetimes of Cm^{3+} in various crystals is given in Fig. 18.16. A summary of spectroscopic studies of Cm^{3+} in crystals $LaCl_3$, $LuPO_4$, ThO_2, Cs_2NaYCl_6, and $CsCdBr_3$ was given in a review paper (Edelstein, 2002). The lifetimes of the actinide ions with the $5f^7$ configuration (Cm^{3+}, Bk^{4+}) are roughly consistent with the energy gap law in that for the hosts $LuPO_4$, ThO_2, and in CeF_4, only one or at most two levels luminesce. For the heavier halide hosts, the vibrational spread is small and the crystal field strength is relatively small so many more levels luminesce.

Early studies on multiphonon relaxation of 5f states of aquated trivalent actinide ions have been reviewed (Yusov, 1993; Beitz, 1994a) and compared to similar work on 4f states of aquated trivalent lanthanide ions (Beitz, 1994b). Aquated ions are those whose inner coordination sphere consists only of water molecules. Systematic studies of the 5f state luminescence lifetimes of aquated trivalent actinide ions began in 1980 with the work of Beitz and Hessler (1980) who reported the luminescence emission spectra of $^{248}Cm^{3+}$ in dilute perchloric or hydrochloric acid as well as luminescence lifetimes in H_2O and D_2O solutions. They assigned the emission as arising from the electronically excited $^6D_{7/2}$ state of Cm^{3+} based on a study of the solution absorption spectrum of Cm^{3+} in perchloric acid (Carnall and Rajnak, 1975). A subsequent study by Beitz and coworkers on the luminescence of $^{244}Cm^{3+}$ in dilute acid solution showed that speciation studies on ultratrace levels of Cm^{3+} could be carried out using elementary laser-induced fluorescence techniques (Beitz *et al.*, 1988). Laser-induced luminescence studies also have been reported on Am^{3+} (Beitz *et al.*, 1987; Yusov, 1990; Thouvenot *et al.*, 1993b; Kimura and Kato, 1998), Bk^{3+} (Carnall *et al.*, 1984) and Es^{3+} (Beitz *et al.*, 1983) in dilute acid solutions and as well as additional studies on aquated Cm^{3+} (Yusov, 1987; Kimura and Choppin, 1994; Kimura *et al.*, 1996, 1997). In all cases, the observed luminescence bands were assigned as arising from a 5f state lying at or below the energy

of the exciting photons and that, among all such states, in addition possessed the largest ΔE value. The reported 5f state emission spectra of aquated trivalent actinide ions are in good agreement with the calculated free-ion states of trivalent actinide ions doped into lanthanum trichloride (Carnall, 1992).

Aquated actinide ions are prototypical species for the investigation of coordination complexes that form as ligands other than water become associated with an actinide ion. It should be appreciated that the coordination sphere of trivalent actinide ions is dynamic unless there is an exceptionally strong ligand bonding. For example, using nanosecond laser excitation, there are no reports of emission from aquated actinide ions that differ as to the number of coordinated water molecules, which suggests that the coordination environment of aquated actinide ions reaches equilibrium on the submicrosecond timescale. In the case of aquated actinide ions, interest naturally exists as to the number of inner-sphere coordinated water molecules, and luminescence studies have been reported that provide a measure of that number.

Kimura and Choppin (1994) doped Cm^{3+} into a series of solid-hydrated lanthanum compounds and determined the influence of the number of inner-sphere coordinated water molecules on the observed Cm^{3+} luminescence lifetimes. Their data are plotted in Fig. 18.29 where the solid line expresses the resulting correlation as

$$n_{H_2O} = 0.65k_{obs} - 0.88 \tag{18.60}$$

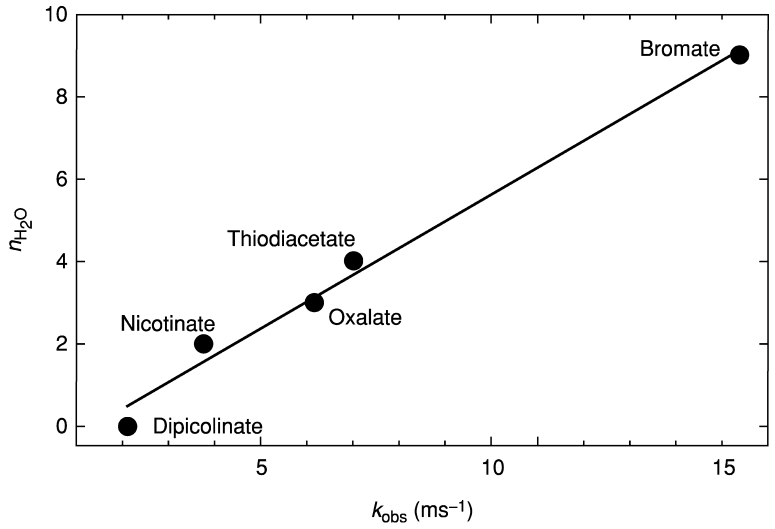

Fig. 18.29 *Observed $^{248}Cm^{3+}$ luminescence decay rate, $k_{obs,}$ from Cm^{3+} doped into a series of solid-hydrated lanthanum compounds at Cm:La = 1:6.9 × 10^3 as a function of the number of inner-sphere coordinated water molecules, n_{H_2O}. Data from Kimura and Choppin* (1994).

where n_{H_2O} is the number of inner-sphere coordinated water molecules and k_{obs} is the measured luminescence lifetime in units of ms^{-1}. Analysis of the data in Fig. 18.29 using equation (18.60) results in a calculated 95% confidence limit of $\pm$ 0.74 for n_{H_2O} values, if one assumes that there is no error as to the number of inner-sphere coordinated water molecules in a given compound. The correlation embodied in equation (18.60) should be valid as long as there is no contribution from ligands other than H_2O or HDO to de-excitation of the emitting state and the purely radiative decay rate of the emitting state remains essentially unchanged across the series of compounds. The value of n_{H_2O} for aquated Cm^{3+} reported by Kimura and Choppin was 9.2 $\pm$ 0.5 water molecules.

Subsequently, Kimura and Kato (1998) studied aquated and complexed $^{241}Am^{3+}$ luminescence via its $^5D_1 \rightarrow {}^7F_1$ transition. They reported $k_{obs} = 24.6 \pm 0.6$ ns for aquated Am^{3+} in H_2O and 162 $\pm$ 4 ns for Am^{3+} in 99.9% D_2O. They adopted a different analysis procedure based on the assumption that the number of inner-sphere water molecules is 9 for aquated Am^{3+} and aquated Cm^{3+}. With that assumption and from the linear correlation they observed between the observed luminescence decay rate, k_{obs}, and the deuterium mole fraction in H_2O–D_2O mixtures, they determined

$$n_{H_2O} = 2.56 \times 10^{-4} k_{obs} - 1.43 \tag{18.61}$$

for the case of aquated Am^{3+} and

$$n_{H_2O} = 0.612\, k_{obs} - 0.48 \tag{18.62}$$

for the case of aquated Cm^{3+}. Subsequently, Kimura and coworkers studied the luminescence lifetimes of Am^{3+} and Cm^{3+} of unstated actinide isotopic composition at 25°C (Kimura *et al.*, 2001). They reported lifetime values for aquated Am^{3+} in H_2O of 25 $\pm$ 0.75 and 160 $\pm$ 5 ns for aquated Am^{3+} in 99.95% D_2O along with the values of 65 $\pm$ 2 μs for aquated Cm^{3+} in H_2O and 1200 $\pm$ 36 μs for aquated Cm^{3+} in 99.95% D_2O. These values together with equations (18.61) and (18.62) give $n_{H_2O} = 8.9$ for aquated Cm^{3+} and $n_{H_2O} = 8.8$ for aquated Am^{3+}. On the basis of preferential solvation in the nonaqueous solutions, an estimate of the Gibbs free energy of transfer of Am^{3+} and Cm^{3+} ions from aqueous to nonaqueous solutions also was obtained using the observed luminescence lifetimes in mixtures of water and organic solvents.

Due to its spectroscopy and photophysics, Cm^{3+} is the trivalent actinide ion most commonly studied in solution using luminescence techniques. As noted earlier, luminescence from three other aquated trivalent actinide ions has been reported. Selected lifetime values from these studies are shown in Table 18.14. In nearly all cases where the stated measurement errors were 5% or less of the observed value and the lifetime was at least a factor of 10 longer than the excitation pulse width, the reported lifetime values are concordant at the 95% confidence level. The seeming exception occurs for Cm^{3+} in D_2O solution. Beitz and Hessler (1980) reported that the luminescence lifetime of Cm^{3+} in 1 M $DClO_4$ solution was 940 $\pm$ 40 μs, whereas Kimura and coworkers reported

Table 18.14 *Selected 5f state luminescence lifetimes, τ, for actinide ions in dilute acid solution at ambient temperature.*[a]

Actinide ion	*Emitting state*[b]	*τ in H_2O*	*τ in D_2O*
U^{4+}	$^1S_0$	<20 ns	
Am^{3+}	$^5D_1$	22 ± 3 ns	160 ± 5 ns
Cm^{3+}	$^6D_{7/2}$	65 ± 3 μs	1200 ± 36 μs
Bk^{3+}	$^7F_6$		100 ± 20 ns
Es^{3+}	$^5F_5$	1.05 ± 0.05 μs	2.87 ± 0.09 μs

[a] See text for selection basis and literature references.
[b] Term symbols for emitting states from the work of Carnall and coworkers (Carnall *et al.*, 1991; Carnall, 1992).

that the lifetime of aquated Cm^{3+} in 0.01 M $DClO_4$ was 1200 ± 36 μs (Kimura *et al.*, 2001). Both studies reported that the lifetime of Cm^{3+} in H_2O was 65 μs. Beitz and Hessler used triply distilled D_2O that was 99% D_2O by near-infrared absorption spectroscopy to make up their solutions whereas Kimura and coworkers used as-received 99.95% D_2O. The work of Kimura and coworkers provides evidence that the observed luminescence lifetime of Cm^{3+} in a mixture of H_2O and D_2O is given by the expression

$$k_{obs} = (1 - \chi)\, k_{H_2O} + \chi\, k_{D_2O} + C, \tag{18.63}$$

where k_{obs} is the observed Cm^{3+} luminescence lifetime in a mixture of H_2O and D_2O in which χ is the deuterium mole fraction of the solution, C is a constant, and k_{H_2O} and k_{D_2O} are the luminescence decay rates of Cm^{3+} in 100% H_2O and 100% D_2O solutions, respectively. Taking into account the stated errors in the measured luminescence lifetimes and equation (18.63), the reported 940 ± 40 and 1200 ± 36 μs Cm^{3+} lifetime values in heavy water solutions agree with each other at the 95% confidence level given the differing degree of solvent deuteration in the two studies.

Reported lifetimes for the $^5D_1$ state of aquated Am^{3+} in H_2O are more discordant which can be attributed primarily to the use of excitation pulses whose width was not insignificant compared to the luminescence decay time of aquated Am^{3+}. The value reported by Beitz (1994a) is selected for inclusion in Table 18.14 because a deconvolution procedure was used to correct for the finite excitation pulse width. The lifetimes reported by Kimura and coworkers for Cm^{3+} and Am^{3+} (Kimura *et al.*, 2001) in D_2O were selected for inclusion in Table 18.14 because of the higher level of solution deuteration in their studies in comparison with earlier studies by others.

A limit for the luminescence lifetime of the $^1S_0$ state of U^{4+} in 1 M perchloric acid has been reported (Kiarshima *et al.*, 2003) and is included in Table 18.14. Based on their excitation and emission spectra, the energy gap between the U^{4+} emitting state and its next lower 5f state is comparable to the Cm^{3+} energy gap. In consequence, one might have expected that nonradiative decay would

only moderately diminish the observed lifetime of the $^1S_0$ state. However, Kiarshima and coworkers report that the luminescence lifetime of the $^1S_0$ state of aquated U^{4+} is <20 ns. Evidently the $^1S_0$ state is primarily quenched by processes other than those that are responsible for the nonradiative decay of the observed 5f emitting states of aquated trivalent actinide ions. Candidate processes for U^{4+} include intersystem crossing to a lower-lying opposite-parity state of U^{4+} and electron transfer to or from neighboring ligands.

Insight into the factors influencing the nonradiative decay of emitting 5f states of aquated trivalent actinide ions can be obtained by plotting the data of Table 18.14 for such ions semilogarithmically as shown in Fig. 18.30. The solid and dashed lines are fits of the data for ions in H_2O and D_2O, respectively, to equation (18.59). Use of this equation is justified ($\hbar\omega_m \gg kT$) if energy is transferred to a stretching or bending vibrational modes of water at ambient temperature. The resulting fit values for $(\alpha/\hbar\omega_m)$ are 6.23×10^{-4} cm for H_2O solutions and 7.52×10^{-4} cm for D_2O solutions. Based on equation (18.59), nonradiative decay occurs primarily to stretching vibrational modes of water for Es^{3+} and Cm^{3+}. However, the currently available data for aquated trivalent actinide ions in H_2O are too less to determine if energy transfer to bending vibrational modes of water makes a significant contribution to the overall nonradiative decay rate at low values of ΔE as might be expected from recent studies on multiphonon-induced nonradiative decay in single crystals (Ermeneux *et al.*, 2000).

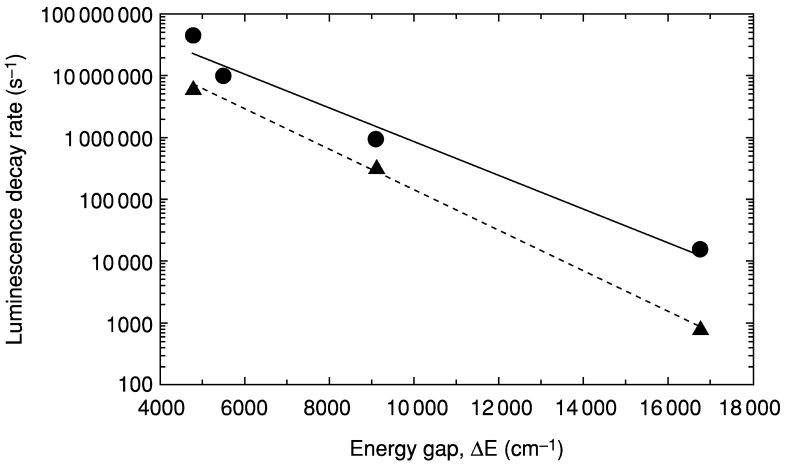

Fig. 18.30 *Energy gap law plot of the luminescence decay rates from Table* 18.14 *of aquated trivalent actinide ions in H_2O* (•) *and D_2O* (▲) *solutions. The solid and dashed lines are fits of equation* (18.59) *to the observed data for H_2O and D_2O solutions, respectively.*

18.8.4 Ion–ion interaction and energy transfer

The success of the single-particle model for interpretation of the solid-state actinide spectra is largely due to the localized nature of the 5f electrons. In the modeling of $5f^N$ electronic energy level structure, the coupling between neighboring f-element ions is neglected even for actinides in stoichiometric compounds, although ion–ion interaction induced band structure and cooperative pair transitions have been observed in lanthanide compounds (Cone and Meltzer, 1987) and are expected to be more significant in the actinide compounds because of more extended 5f orbitals (Fig. 18.3). However, the effects of ion–ion interactions on the excited state dynamics such as luminescence decay are very significant even in dilute crystals with actinide doping level below 1% (Liu and Beitz, 1990a). As a result of ion–ion interactions, luminescence emission from a $5f^N$ state is usually observed only in dilute crystals. The excited state lifetime and the luminescence decay dynamics are strongly dependent on the actinide ion concentration as well as on sample temperature. Fig. 18.31 shows the $^5D_1$ luminescence decay of 0.1 at% Cm^{4+} (a) and 5 at% Cm^{4+} (b) in crystalline CeF_4 at 4 K. There is an obvious deviation from a single exponential decay for the 0.1 at% Cm^{4+}:CeF_4 sample and the decay rate in the long time range is approximately $5 \times 10^3\ s^{-1}$. In the 5 at% Cm^{4+}:CeF_4 sample, most Cm^{4+} ions relaxed from the excited state within 15 μs. At long times, behavior similar

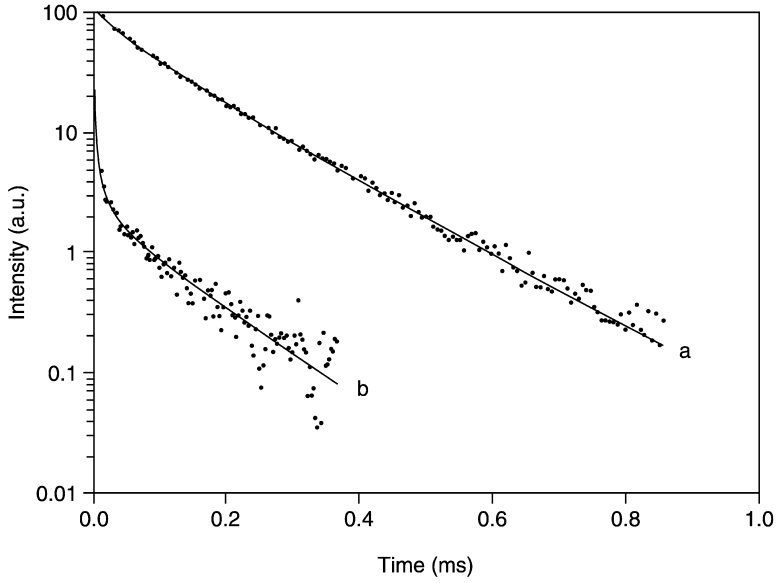

Fig. 18.31 *Nonexponential fluorescence decays of Cm^{3+} ions in CeF_4 induced by interionic excitation energy transfer.* (*a*) *the $^5D_1$ fluorescence decay of* 0.1% (*atom*) *Cm^{4+}:CeF_4 at* 4 K*; and* (*b*) *the $^5D_1$ fluorescence decay of* 5% (*atom*) *Cm^{4+}:CeF_4 at* 4 K. (*Reprinted with permission from Liu and Beitz,* 1990b. *Copyright* 1990, *Elsevier.*)

to that of the 0.1 at% Cm^{4+}:CeF_4 sample is due to the contribution from Cm^{4+} ions at isolated sites where energy transfer is improbable.

The theory of energy transfer of luminescent ions in solids has been developed for interpretation of sensitized luminescence (Förster, 1948; Dexter, 1953). This theory is based on the assumption that the rate of excitation energy transfer (W_{da}) from a donor, d, to an acceptor, a, depends on the distance between d and a, R_{da}, as

$$W_{da} = \alpha\left(\frac{R_0}{R_{da}}\right)^s, \tag{18.64}$$

where the parameter α contains the matrix elements of the interaction between d and a, and R_0 is the distance between the nearest neighbors. These matrix elements depend on the transition probabilities as well as the energy mismatches if d and a do not have identical excitation energy levels. In equation (18.64), s takes an integer value of 6, 8, or 10 for electric dipole–dipole, dipole–quadrupole, or quadrupole–quadrupole interactions, respectively. For the simple case where energy-transfer processes are irreversible, the luminescence decay rate may be evaluated using

$$\frac{dP_d}{dt} = -\kappa P_d - \sum_a W_{da} P_d, \tag{18.65}$$

where P_d is the probability of excitation of the donor, κ is for the intrinsic decay rate, and the summation is over all possible acceptors. In f-element ions in dielectric crystals, the donors and acceptors are the same. It is often difficult, especially for the doped crystals or structurally disordered solids, to perform the lattice summation over the occupied acceptor sites in equation (18.65). Inokuti and Hirayama (1965) first obtained a general approximate solution for ion concentration $c \ll 1$:

$$\ln\frac{P(0)}{P(t)} = \kappa t + c\Gamma(1 - 3/s)(\alpha t)^{3/s}, \tag{18.66}$$

where $\Gamma(1 - 3/s)$ is the gamma function and other quantities are the same as defined in equations (18.64) and (18.65). The solid line in Fig. 18.31 are fitted results using the Inokuti and Hirayama model.

Although nonexponential luminescence decay is the direct consequence of ion–ion interactions that are easy to measure by experiment, there are different microscopic mechanisms that may not be revealed in detail in the analysis of the decay dynamics alone. Analysis of energy level structure is often critical in understanding the energy-transfer processes. For actinide and lanthanide ions in insulating crystals, resonant migration excitation of excitation among the identical ions is common, and if there is inhomogeneous line broadening, phonon-assisted (phonon absorption from or emission to the lattice) energy-transfer results in temperature-dependent spectral diffusion as well as nonexponential luminescence decay (Yen, 1987). In many cases, energy transfer occurs in such a way that the donor gives the acceptor a part of its excitation energy and

nonradiatively relaxes to an intermediate state, whereas with this amount of energy the acceptor is excited into the same or a different intermediate state. This type of energy transfer is called cross-relaxation. As shown in Fig. 18.31, the nonexponential decay of Cm^{4+} in the $^5D_1$ level is dependent on the Cm^{4+} doping level. The mechanism for the nonexponential decay is mainly due to the cross-relaxation into the low-lying excited states of $^7F_{3,4}$ states (Liu and Beitz, 1990a). A special type of cross-relaxation is up-conversion energy transfer. In this process, the donor and acceptor are both in metastable states while the donor relaxes into a low-lying state and the acceptor is further excited into a high-lying state. This energy-transfer process enables emission of a photon with energy higher than the initial excitation energy. Instead of emission of a higher energy photon, this type of energy transfer may end up with energy lost to the lattice or lead to ionization, a process called annihilation.

Extensive studies of the microscopic mechanisms of ion–ion interactions and various consequences of energy-transfer processes have been done for lanthanide ions and detailed reviews of the previous work have been published (Cone and Meltzer, 1987; Yen, 1987). Much less work has been conducted on actinide systems. Many experimental results from the actinide systems may be interpreted using the same framework developed from modeling the lanthanide systems, such as those of Cm^{4+}:CeF_4 (Liu and Beitz, 1990a,b). The excited state dynamics of both U^{3+} and U^{4+} ion in a host crystal of Ba_2YCl_7 was recently reported. It is shown that energy transfer induced up-conversion of U^{4+} excitation leads to strong luminescence from the $^1I_6$ state at 19 600 cm^{-1} (Karbowiak *et al.*, 2003). Consistent with the observations in analyses of crystal-field splittings and ion–phonon coupling, ion–ion interactions in the actinide systems with the same level of ion concentration are much stronger than that in the lanthanide systems. This explains in general the more significant nonexponential decay and quenching of actinide luminescence emission.

ACKNOWLEDGMENTS

We dedicate this chapter to the memory of William T. Carnall who was our actinide spectroscopy mentor, colleague, and friend. We also thank him for permission to base our present work on the chapter that he coauthored in the second edition of this work. This work was performed under the auspices of the Office of Basic Energy Sciences, Office of Science, U.S. Department of Energy under contract W-31-109-ENG-38.

REFERENCES

Auzel, F., Hubert, S., Delamoye, P., and Hussonnois, M. (1982) *J. Lumin.*, **26**, 251–62.
Auzel, F. and Malta, O. L. (1983) *J. Phys.*, **44**, 201–6.
Axe, J. D., Stapleton, H. J., and Jeffiries, C. D. (1961) *Phys. Rev.*, **121**, 1630–7.

Baybarz, R. D., Asprey, L. B., Strouse, C. E., and Fukushima, E. (1972) *J. Inorg. Nucl. Chem.*, **34**, 3427–31.
Beitz, J. V. and Hessler, J. P.(1980) *Nucl. Technol.*, **51**, 169–77.
Beitz, J. V., Carnall, W. T., and Wester, D. W. (1981) in *Lawrence Berkeley Laboratory Report LBL-12441*, Lawrence Berkeley Laboratory, Berkeley, CA, pp. 108–10.
Beitz, J. V., Williams, C. W., and Carnall, W. T. (1982) *J. Chem. Phys.*, **76**, 2756–7.
Beitz, J. V., Wester, D. W., and Williams, C. W. (1983) *J. Less Common Metals*, **93**, 331–8.
Beitz, J. V., Jursich, G., and Sullivan, J. C. (1987) in *Rare Earths 1986, Proc. of the 17th Rare Earth Research Conference*, vol. 1 (eds. H. B. Silber, L. R. Morss, and L. E. DeLong), Elsevier Sequoia, Lausanne, p. 301.
Beitz, J. V., Bowers, D. L., Doxtader, M. M., Maroni, V. A., and Reed, D. T. (1988) *Radiochim. Acta*, **44/45**, 87–93.
Beitz, J. V. (1994a) *J. Alloys Compds*, **207/208**, 41–50.
Beitz, J. V. (1994b) in *Handbook on the Physics and Chemistry of Rare Earths,* vol. 18 (eds. K. A. Gschneidner Jr, L. Eyring, G. R. Choppin, and G. H. Lander), North-Holland, Amsterdam, pp. 159–95.
Beitz, J. V., Williams, C. W., and Liu, G. K. (1998) *J. Alloys Compds*, **271**, 850–3.
Bell, J. T. (1969) *J. Inorg. Nucl. Chem.*, **31**, 703–10.
Blaise, J., Fred, M. S., Carnall, W. T., Crosswhite, H. M., and Crosswhite, H. (1983) *ACS Symp. Ser.*, **216**, 173–98.
Brewer, L. (1971a) *J. Opt. Soc. Am.*, **61**, 1101–11.
Brewer, L. (1971b) *J. Opt. Soc. Am.*, **61**, 1666–82.
Brewer, L. (1983) in *Systematics and the Properties of the Lanthanides,* Reidel, Boston, pp. 17–63.
Brito, H. F. and Liu, G. K. (2000) *J. Chem. Phys.*, **112**, 4334–41.
Brown, D. (1968) *Halides of the Lanthanides and Actinides,* John Wiley, New York.
Brown, D., Whittaker, B., and Edelstein, N. (1974) *Inorg. Chem.*, **13**, 1805–8.
Brown, D., Lidster, P., Whittaker, B., and Edelstein, N. (1976) *Inorg. Chem.*, **15**, 511–14.
Carnall, W. T., Walker, A., and Neufeldt, S. J. (1966) *Inorg. Chem.*, **5**, 2135–40.
Carnall, W. T., Fields, P. R., and Rajnak, K. (1968) *J. Chem. Phys.*, **49**, 4412–23.
Carnall, W. T., Fields, P. R., and Sarup, R. (1969) *J. Chem. Phys.*, **51**, 2587–91.
Carnall, W. T., Fields, P. R., and Sarup, R. (1971) *J. Chem. Phys.*, **54**, 1476–9.
Carnall, W. T. (1973) in *Gmelin Handbuch der Anorganishce Chemie,* Vol. *Transurane A2*, Verlag Chemie, Weinheim, pp. 49–80.
Carnall, W. T. Rajnak, and K. (1975) *J. Chem. Phys.*, **63**, 3510–14.
Carnall, W. T. (1979a) in *Handbook on the Physics and Chemistry of the Rare Earths,* vol. 3 (eds. K. A. Gschneidner Jr, and L. Eyring) North-Holland, Amsterdam, pp. 171–208.
Carnall, W. T. (1979b) *NATO Adv. Study Inst. Ser., Ser. C: Math. Phys. Sci.*, **44**, 281–307.
Carnall, W. T. (1982) in *Gmelin Handhuch der Anorganischen Chemie,* 8th edn., Uranium Suppl. A5, Springer-Verlag, Berlin, pp. 69–161.
Carnall, W. T., Beitz, J. V., Crosswhite, H., Rajnak, K., and Mann, J. B. (1983) in *Systematics and the Properties of the Lanthanides* (ed. S. P. Sinha), Reidel, Dordrecht, pp. 389–450.
Carnall, W. T., Beitz, J. V., and Crosswhite, H. (1984) *J. Chem. Phys.*, **80**, 2301–8.

Carnall, W. T. and Crosswhite, H. M. (1985) *Argonne National Laboratory Report ANL-84-90,* Argonne National Laboratory, Argonne, IL, 154 pp.
Carnall, W. T., Crosswhite, H., and Rajnak, K. (1985) in *Rare Earths Spectroscopy* (eds. B. Jezowska-Trzebiatowska, J. Legendziewicz, and W. Strek), World Scientific Publishing, Singapore, pp. 267–97.
Carnall, W. T. (1989) *Argonne National Laboratory Report ANL-89/39,* Argonne National Laboratory, Argonne, IL, p. 285.
Carnall, W. T., Goodman, G. L., Rajnak, K., and Rana, R. S. (1989) *J. Chem. Phys.*, **90**, 3443–57.
Carnall, W. T., Liu, G. K., Williams, C. W., and Reid, M. F. (1991) *J. Chem. Phys.*, **95**, 7194–203.
Carnall, W. T. (1992) *J. Chem. Phys.*, **96**, 8713–26.
Claassen, H. H. (1959) *J. Chem. Phys.*, **30**, 968–9.
Condon, E. U. and Shortley, G. H. (1963) *The Theory of Atomic Spectra,* Cambridge University Press, Cambridge.
Cone, R. L. and Meltzer, R. S. (1987) in *Spectroscopy of Solids Containing Rare Earth Ions* (eds. A. A. Kaplyanskii and R. M. Macfarlane), North-Holland, Amsterdam, pp. 481–556.
Conway, J. G. (1964) *J. Chem. Phys.*, **41**, 904–5.
Copland, G. M., Newman, D. J., and Taylor, C. D. (1971) *Journal of Physics B: Atomic and Molecular Physics*, **4**, 1605–10.
Cowan, R. D. and Griffin, C. D. (1976) *J. Opt. Soc. Am.*, **66**, 1010–14.
Cowan, R. D. (1981) *The Theory of Atomic Structure and Spectra,* University of California Press, Berkeley.
Crosswhite, H. M., Dieke, G. H., and Carter, W. J. (1965) *J. Chem. Phys.*, **43**, 2047–54.
Crosswhite, H., Crosswhite, H. M., and Judd, B. R. (1968) *Phys. Rev.*, **174**, 89–94.
Crosswhite, H. M., Crosswhite, H., Kaseta, F. W., and Sarup, R. (1976) *J. Chem. Phys.*, **64**, 1981–5.
Crosswhite, H. M. (1977) *Colloq. Int. CNRS*, **255**, 65–9.
Crosswhite, H. M., Crosswhite, H., Carnall, W. T., and Paszek, A. P. (1980) *J. Chem. Phys.*, **72**, 5103–7.
Crosswhite, H. M. (1982) in *Gmelin Handbuch der Anorganischen Chemie,* 8th edn, Uranium Suppl. A5, Springer-Verlag, Berlin, pp. 1–68.
Crosswhite, H. M. and Crosswhite, H. (1984) *J. Opt. Soc. Am. B*, **1**, 246–54.
de Bruin, T. L., Klinkenberg, P. F. A., and Schuutmans, P. (1941) *Z. Phys.*, **118**, 58–87.
DeKock, R. L., Baerends, E. J., Boerrigter, P. M., and Snijders, J. G. (1985) *Chem. Phys. Lett.*, **105**, 308–16.
Delamoye, P., Rajnak, K., Genet, M., and Edelstein, N. (1983) *Phys. Rev. B*, **28**, 4923–30.
Denning, R. G., Norris, J. O. W., Short, I. G., Snellgrove, T. R., and Woodwark, D. R. (1980) in *ACS Symposium Series: Lanthanide and Actinide Chemistry and Spectroscopy,* vol. 131 (ed. N. Edelstein), American Chemical Society, Washington, DC, pp. 313–30.
Denning, R. G., Norris, J. O. W., and Brown, D. (1982) *Mol. Phys.*, **46**, 287–364.
Denning, R. G. (1992) in *Structure and Bonding,* vol. 79 (ed. M. J, Clarke), Springer-Verlag, Berlin, pp. 215–76.

Denning, R. G., Green, J. C., Hutchings, T. E., Dallera, C., Tagliaferri, A., Giarda, K., Brookes, N. B., and Braicovich, L. (2002) *J. Chem. Phys.*, **117**, 8008–20.
Dexter, D. L. (1953) *J. Chem. Phys.*, **21**, 836–50.
Dick, B. G. and Overhauser, A. (1958) *Phys. Rev.*, **112**, 90–103.
Dieke, G. H. (1968) *Spectra and Energy Levels of Rare Earth Ions in Crystals,* John Wiley, New York.
Downer, M. C., Cordero- Montalvo, C. D., and Crosswhite, H. (1983) *Phys. Rev. B*, **28**, 4931–43.
Edelstein, N., Easley, W., and McLaughlin, R. (1966) *J. Chem. Phys.*, **44**, 3130–1.
Edelstein, N., Easley, W., and McLaughlin, R. (1967) *Adv. Chem. Ser.*, **71**, 203–10.
Edelstein, N. and Easley, W. (1968) *J. Chem. Phys.*, **48**, 2110–15.
Edelstein, N., Conway, J. G., Fujita, D. K., Kolbe, W., and McLaughlin, R. (1970) *J. Chem. Phys.*, **52**, 6425–6.
Edelstein, N., Brown, D., and Whittaker, B. (1974) *Inorg. Chem.*, **13**, 563–7.
Edelstein, N. M. (1979) in *Organometallics of the f-elements* (eds. T. J. Marks and R. D. Fischer), Reidel, Dordrecht, pp. 37–79.
Edelstein, N. (1987) *J. Less Common Metals*, **133**, 39–51.
Edelstein, N. M. (1991) *Eur. J. Solid State Inorg. Chem.*, **28**, 47–55.
Edelstein, N. (1992) in *Transuranium Elements: A Half Century* (eds. L. R. Morss and J. Fuger), American Chemical Society, Washington, DC, pp. 145–58.
Edelstein, N., Kot, W. K., and Krupa, J. C. (1992) *J. Chem. Phys.*, **96**, 1–4.
Edelstein, N. M. (1995) *J. Alloys Compds*, **223**, 197–203.
Edelstein, N. (2002) *Proc. SPIE-Int. Soc. Opt. Eng.*, **4766**, 8–21.
Eichberger, K. and Lux, F. (1980) *Ber. Bunsenges. Phys. Chem.*, **84**, 800–7.
Eisenstein, J. C. and Pryce, M. H. L. (1960) *Proc. Roy. Soc. A*, **255**, 181–98.
Eisenstein, J. C. and Pryce, M. H. L. (1966) *J. Res. NBS*, **70A**, 165–7.
Eremin, M. V. (1989) in *Spectroscopy of Crystals* (ed. A. A. Kaplyanskii), Nauka, Leningrad, p. 30.
Ermeneux, F. S., Goutaudier, C., Moncorge, R., Sun, Y., Cone, R. L., Zannoni, E., Cavalli, E., and Bettinelli, M. (2000) *Phys. Rev. B*, **61**, 3915–21.
Esterowitz, L., Bartoli, F. J., Allen, R. E., Wortman, D. E., Morrison, C. A., and Leavitt, R. P. (1979) *Phys. Rev. B*, **19**, 6442–55.
Faucher, M. D., Moune, O. K., Garcia, D., and Tanner, P. (1996) *Phys. Rev. B*, **53**, 9501–4.
Fellows, R. L., Peterson, J. R., Young, J. P., and Haire, R. G. (1978) in *The Rare Earths in Modern Science and Technology* (eds. G. J. McCarthy and J. J. Ryne), Plenum, New York, pp. 493–9.
Förster, T. (1948) Ann. Phys.(Germany), **2**, 55-75.
Fred, M. (1967) in *Lanthanide/Actinide Chemistry,* vol. 71 (eds. P. R. Fields and T. Moeller) ACS Adv. Chem. Ser. American Chemical Society, Washington, DC, pp. 180–202.
Garcia, D. and Faucher, M. (1995) in *Handbook on the Physics and Chemistry of Rare Earths,* vol. 21 (eds. K. A. Gschneidner Jr and L. Eyring), Elsevier, Amsterdam, p. 263.
Gerloch, M. and Slade, R. C. (1973) *Ligand-Field Parameters,* Cambridge University Press, Cambridge.
Goldschmidt, Z. B. (1978) in *Handbook on the Physics and Chemistry of Rare Earths,* vol. 1 (eds. K. A. Gschneidner Jr and L. Eyring), North-Holland, New York, pp. 1–172.

Goodman, G. L. and Fred, M. (1959) *J. Chem. Phys.*, **30**, 849–50.
Görller-Walrand, C., Behets, M., Porcher, P., Moune-Minn, O. K., and Laursen, I. (1985) *Inorg. Chim. Acta*, **109**, 83–90.
Görller-Walrand, C. and Binnemans, K. (1996) in *Handbook on the Physics and Chemistry of Rare Earth,* vol. 23 (eds. K. A. Gschneidner Jr and L. Eyring), Elsevier, Amsterdam.
Görller-Walrand, C. and Binnemans, K. (1998) in *Handbook on the Physics and Chemistry of Rare Earths,* vol. 25 (eds. K. A. Gschneidner Jr and L. Eyring), Elsevier, Amsterdam, pp. 101–264.
Gruen, D. M. and McBeth, R. L. (1969) *Inorg. Chem.*, **8**, 2625–33.
Hansen, J. E., Judd, B. R., and Crosswhite, H. (1996) *At. Data and Nucl. Data Tables*, **62**, 1–49.
Hartree, D. R. (1957) *The Calculation of Atomic Structures,* John Wiley, New York.
Hecht, H. G., Varga, L. P., Lewis, W. B., and Boring, A. M. (1979) *J. Chem. Phys.*, **70**, 101–8.
Hessler, J. P., Brundage, R. T., Hegarty, J., and Yen, W. M. (1980) *Opt. Lett.*, **5**, 348–50.
Huang, K. and Rhys, A. (1950) *Proc. Roy. Soc. A*, **204**, 406–23.
Hubert, S., Emery, J., Edelstein, N., and Fayet, J. C. (1985) *Solid State Commun.*, **54**, 1085–90.
Hubert, S., Thouvenot, P., and Edelstein, N. (1993) *Phys. Rev. B*, **48**, 5751–60.
Hüfner, S. (1978) *Optical Spectra of Transparent Rare Earth Compounds,* Academic Press, New York.
Hutchison, C. A. and Weinstock, B. (1960) *J. Chem. Phys.*, **32**, 56–61.
Illemassene, M., Murdoch, K. M., Edelstein, N. M., and Krupa, J. C. (1997) *J. Lumin.*, **75**, 77–87.
Inokuti, M. and Hirayama, F. (1965) *J. Chem. Phys.*, **43**, 1978–89.
Johnston, D. R., Satten, R. A., Schreiber, C. L., and Wong, E. Y. (1966a) *J. Chem. Phys.*, **44**, 3141–3.
Johnston, D. R., Satten, R. A., and Wong, E. Y. (1966b) *J. Chem. Phys.*, **44**, 687–91.
Jørgensen, C. K. (1957) *Acta Chem. Scand.*, **11**, 166–78.
Jørgensen, C. K. (1959) *Mol. Phys.*, **2**, 96–108.
Jørgensen, C. K. (1962) *Orbits in Atoms and Molecules,* Academic Press, London.
Jørgensen, C. K., Pappalardo, R., and Schmidtke, H. H. (1963) *J. Chem. Phys.*, **39**, 1422–30.
Jørgensen, C. K. (1970) *Prog. Inorg. Chem.*, **12**, 101–52.
Jørgensen, C. K. (1975) in *Structure and Bonding,* vol. 22, Springer-Verlag, New York, pp. 49–81.
Jørgensen, C. K. (1980) *Isr J. Chem.*, **19**, 174–92.
Jørgensen, C. K. (1982) *Chem. Phys. Lett.*, **89**, 455–8.
Judd, B. R. (1962) *Phys. Rev.*, **127**, 750–61.
Judd, B. R. (1963a) *Proc. Phys. Soc.*, (*London*) **82**, 874–81.
Judd, B. R. (1963b) *Operator Techniques in Atomic Spectroscopy,* McGraw-Hill, New York.
Judd, B. R. (1966) *Phys. Rev.*, **141**, 4–14.
Judd, B. R. (1968a) *Phys. Rev.*, **173**, 40–3.
Judd, B. R. (1968b) *Phys. Rev.*, **173**, 39–40.
Judd, B. R., Crosswhite, H. M., and Crosswhite, H. (1968) *Phys. Rev.*, **169**, 130–8.

Judd, B. R. (1975) *Angular Momentum Theory for Diatomic Molecules,* Academic Press, New York.
Judd, B. R. (1977a) *Phys. Rev. Lett.*, **39**, 242–4.
Judd, B. R. (1977b) *J. Chem. Phys.*, **66**, 3163–70.
Judd, B. R. (1979) *J. Lumin.*, **18–19**, 604–8.
Judd, B. R. and Crosswhite, H. (1984) *J. Opt. Soc. Am. B*, **1**, 255–60.
Judd, B. R. and Suskin, M. A. (1984) *J. Opt. Soc. Am. B*, **1**, 261–5.
Judd, B. R. (1988) in *Handbook on the Physics and Chemistry of Rare Earths,* vol. 11 (eds. K. A. Gschneidner Jr and L. Eyring), North-Holland, Amsterdam, pp. 81–195.
Judd, B. R. and Lo, E. (1996) *At. Data Nucl. Data Tables*, **62**, 51–75.
Kanellakopulos, B. and Fischer, R. D. (1973) in *Gmelin Handhuch der Anorganischen Chemie, Transurane A2,* Verlag Chemie, Weinheim, pp. 1–48.
Karbowiak, M., Drozdzynski, J., Murdoch, K. M., Edelstein, N. M., and Hubert, S. (1997) *J. Chem. Phys.*, **106**, 3067–77.
Karbowiak, M., Mech, A., and Drozdzynski, J. (2003) *Phys. Rev. B*, **67**, 195108–17.
Karraker, D. G. (1964) *Inorg. Chem.*, **3**, 1618–22.
Kaufman, V. and Radziemski, L. J. (1976) *J. Opt. Soc. Am.*, **66**, 599–601.
Kiarshima, A., Kimura, T., Tochiyama, O., and Yoshida, Z. (2003) *Chem. Commun.*, **2003**, 910–11.
Kimura, T. and Choppin, G. R. (1994) *J. Alloys Compds*, **213/214**, 313–17.
Kimura, T., Choppin, G. R., Kato, Y., and Yoshida, Z. (1996) *Radiochim. Acta*, **72**, 61–4.
Kimura, T., Kato, Y., and Choppin, G. R. (1997) in *Recent Progress in Actinides Separation Chemistry, Proc. Workshop on Actinides Solution Chemistry*, WASC '94, Tokai, Japan, September 1–2, 1994, pp. 149–64.
Kimura, T. and Kato, Y. (1998) *J. Alloys Compds*, **271–273**, 867–71.
Kimura, T., Nagaishi, R., Kato, Y., and Yoshida, Z. (2001) *Radiochim. Acta*, **89**, 125–30.
Kramers, H. A. (1930) *Proc. Amsterdam Acad.*, **33**, 959.
Krupa, J. C., Hubert, S., Foyentin, M., Gamp, E., and Edelstein, N. (1983) *J. Chem. Phys.*, **78**, 2175–9.
Krupa, J. C. (1987) *Inorg. Chim. Acta*, **139**, 223–41.
Krupa, J. C. and Carnall, W. T. (1993) *J. Chem. Phys.*, **99**, 8577–84.
Kugel, R., Williams, C., Fred, M., Malm, J. G., Carnall, W. T., Hindman, J. C., Childs, W. J., and Goodman, L. S. (1976) *J. Chem. Phys.*, **65**, 3486–92.
Larionov, A. L. and Malkin, B. Z. (1975) *Opt. Spektrosk.*, **39**, 1109–13.
Leung, A. F. (1977) *J. Phys. Chem. Solids*, **38**, 529–32.
Leung, A. F. and Poon, Y. M. (1977) *Can. J. Phys.*, **55**, 937–42.
Levin, L. I. and Cherpanov, V. I. (1983) *Sov. Phys.: Solid State*, **25**, 394–9.
Lewis, W. B., Mann, J. B., Liberman, D. A., and Cromer, D. T. (1970) *J. Chem. Phys.*, **53**, 809–20.
Liu, G. K. and Beitz, J. V. (1990a) *Phys. Rev. B*, **41**, 6201–12.
Liu, G. K. and Beitz, J. V. (1990b) *J. Lumin.*, **45**, 254–6.
Liu, G. K., Beitz, J. V., and Carnall, W. T. (1992) in *Transuranium Elements: A Half Century* (eds. L. R. Morss and J. Fuger), American Chemical Society, Washington, DC, pp. 181–6.
Liu, G. K., Beitz, J. V., and Huang, J. (1993) *J. Chem. Phys.*, **99**, 3304–11.

Liu, G. K., Carnall, W. T., Jones, R. P., Cone, R. L., and Huang, J. (1994a) *J. Alloys Compds*, **207–208**, 69–73.
Liu, G. K., Carnall, W. T., Jursich, G., and Williams, C. W. (1994b) *J. Chem. Phys.*, **101**, 8277–89.
Liu, G. K., Cao, R., Beitz, J. V., and Huang, J. (1996) *Phys. Rev. B*, **54**, 483–7.
Liu, G. K., Beitz, J. V., Huang, J., Abraham, M. M., and Boatner, L. A. (1997a) *J. Alloys Compds*, **250**, 347–51.
Liu, G. K., Huang, J., and Abraham, M. M. (1997b) *Phys. Rev. B*, **55**, 8967–72.
Liu, G. K., Li, S. T., Zhorin, V. V., Loong, C.-K., Abraham, M. M., and Boatner, L. A. (1998) *J. Chem. Phys.*, **109**, 6800–8.
Liu, G. K. (2000) in *Crystal Field Handbook* (eds. D. J. Newman and B. K. C. Ng), Cambridge University Press, Cambridge, pp. 65–82.
Liu, G. K., Chen, X. Y., and Huang, J. (2002) *Mol. Phys.*, **101**, 1029–36.
Loh, E. (1966) *Phys. Rev.*, **147**, 332.
Mackey, D. J., Runciman, W. A., and Vance, E. R. (1975) *Phys. Rev. B*, **11**, 211–18.
Malek, C. K. and Krupa, J. C. (1986) *J. Chem. Phys.*, **84**, 6584.
Malkin, B. Z., Ivanenko, Z. I., and Aizenberg, I. B. (1970) *Fiz. Tverd. Tela (USSR)*, **12**, 1873–80.
Malkin, B. Z. (1987) in *Spectroscopy of Solids Containing Rare Earth Ions* (eds. A. A. Kaplyanskii and R. M. Macfarlane), North-Holland, Amsterdam, pp. 13–50.
Marvin, H. H. (1947) *Phys. Rev.*, **71**, 102–10.
Matsika, S. and Pitzer, R. M. (2001) *J. Chem. Phys.*, **105**, 637–45.
Matsika, S., Zhang, Z., Brozell, S. R., Blaudeau, J.-P., Wang, Q., and Pitzer, R. M. (2001) *J. Phys. Chem. A*, **105**, 3825–8.
McClure, D. S. and Kiss, Z. (1963) *J. Chem. Phys.*, **39**, 3251–7.
Metcalf, D. H., Dai, S., Del Cul, G. D., and Toth, L. M. (1995) *Inorg. Chem.*, **34**, 5573–7.
Miyakawa, T. and Dexter, D. L. (1970) *Phys. Rev. B*, **1**, 2961–9.
Morosin, B. (1968) *J. Chem. Phys.*, **49**, 3007–12.
Morrison, J. C. (1972) *Phys. Rev. A*, **6**, 643–50.
Morrison, C. A. and Leavitt, R. P. (1982) in *Handbook on the Physics and Chemistry of Rare Earths,* vol. 5 (eds. K. A. Gschneidner Jr and L. Eyring), North-Holland, Amsterdam, pp. 461–692.
Morss, L. R., Williams, C. W., and Carnall, W. T. (1983) *ACS Symp. Ser.*, **216**, 199–210.
Morss, L. R. (2005) in this volume, see Chapter 19.
Moune, O. K., Faucher, M. D., and Edelstein, N. (2002) *J. Lumin.*, **96**, 51–68.
Mulford, R. N., Dewey, H. J., and Barefield II, J. E. (1991) *J. Chem. Phys.*, **94**, 4790–6.
Murdoch, K. M., Edelstein, N. M., Boatner, L. A., and Abraham, M. M. (1996) *J. Chem. Phys.*, **105**, 2539–46.
Murdoch, K. M., Nguyen, A. D., Edelstein, N. M., Hubert, S., and Gacon, J. C. (1997) *Phys. Rev. B*, **56**, 3038–45.
Murdoch, K. M., Cavellec, R., Simoni, E., Karbowiak, M., Hubert, S., Illemassene, M., and Edelstein, N. M. (1998) *J. Chem. Phys.*, **108**, 6353–61.
Nave, S., Haire, R. G., and Huary, P. G. (1983) *Phys. Rev. B*, **28**, 2317–27.
Newman, D. J. (1970) *Chem. Phys. Lett.*, **6**, 288–90.
Newman, D. J. (1971) *Adv. Phys.*, **20**, 197–256.
Newman, D. J. (1975) *J. Phys. C: Solid State Phys.*, **8**, 1862–8.
Newman, D. J. and Ng, B. (1989a) *J. Phys.: Condensed Matter*, **1**, 1613–19.

Newman, D. J. and Ng, B. (1989b) *Rep. Prog. Phys.*, **52**, 699–763.
Newman, D. J. and Ng, B. (2000) in *Crystal Field Handbook* (eds. D. J. Newman and B. Ng), Cambridge University Press, Cambridge, pp. 140–59.
Nielson, C. W. and Koster, G. F. (1963) *Spectroscopic Coefficients for the pn, dn, and fn Configurations,* MIT Press, Cambridge.
Ofelt, G. S. (1962) *J. Chem. Phys.*, **37**, 511–20.
Peterson, J. R. (1976) in *Gmelin Handhuch der Anorganischen Chemie,* 8th edn, Uranium Suppl. A5, Springer-Verlag, Berlin, pp. 57–84.
Peterson, J. R., Fellows, R. L., Young, J. P., and Haire, R. G. (1977) *Radiochem. Radioanal. Lett.*, **31**, 277–82.
Piehler, D., Kot, W. K., and Edelstein, N. (1991) *J. Chem. Phys.*, **94**, 942–8.
Poon, Y. M. and Newman, D. J. (1982) *J. Chem. Phys.*, **77**, 1077–9.
Poon, Y. M. and Newman, D. J. (1983) *J. Phys. B: At. Mol. Phys.*, **16**, 2093–101.
Racah, G. (1949) *Phys. Rev.*, **76**, 1352–65.
Rajnak, K. and Wybourne, B. G. (1963) *Phys. Rev.*, **132**, 280–90.
Rajnak, K. and Wybourne, B. G. (1964) *J. Chem. Phys.*, **41**, 565–9.
Rana, R. S., Cordero- Montalvo, C. D., and Bloembergen, N. (1984) *J. Chem. Phys.*, **81**, 2951–2.
Reid, M. F. and Richardson, F. S. (1984) *Mol. Phys.*, **51**, 1077–94.
Reid, M. F. and Richardson, F. S. (1985) *J. Chem. Phys.*, **63**, 95.
Reid, M. F. (1987) *J. Chem. Phys.*, **87**, 2875–84.
Reid, M. F. (2000) in *Crystal Field Handbook* (eds. D. J. Newman and B. Ng), Cambridge University Press, Cambridge, pp. 190–226.
Reisfeld, M. J. and Crosby, G. A. (1965) *Inorg. Chem.*, **4**, 65–70.
Richman, I., Kisliuk, P., and Wong, E. Y. (1967) *Phys. Rev.*, **155**, 262–7.
Riseberg, L. A. and Moos, H. W. (1967) *Phys. Rev. Lett.*, **25**, 1423–6.
Riseberg, L. A. and Moos, H. W. (1968) *Phys. Rev.*, **174**, 429–38.
Rotenberg, M., Bivins, R., Metropolis, R. B. N., and Wooten, J. K. Jr (1959) *The 3-j and 6-j Symbols,* MIT Press, Cambridge.
Ryan, J. L. (1971) *J. Inorg. Nucl. Chem.*, **33**, 153–77.
Satten, R. A., Schreiber, C. L., and Wong, E. Y. (1983) *J. Chem. Phys.*, **78**, 79–87.
Seijo, L. and Barandiaran, Z. (2001) *J. Chem. Phys.*, **115**, 55554–60.
Shen, Y. and Bray, K. L. (1998) *Phys. Rev. B*, **58**, 5305–13.
Slater, J. C. (1960) *Quantum Theory of Atomic Structure,* McGraw-Hill, New York.
Sobelman, I. I. (1972) *Theory of Atomic Spectra,* Pergamon, Oxford.
Soulie, E. (1978) *J. Phys. Chem. Solids*, **39**, 695–8.
Stafsudd, O. M., Leung, A. F., and Wong, E. Y. (1969) *Phys. Rev.*, **180**, 339–43.
Steindler, M. J. and Gerding, T. J. (1966) *Spectrochim. Acta*, **22**, 1197–200.
Stevens, K. W. H. (1952) *Proc. Phys. Soc.*, (*London*) **A65**, 209–15.
Suger, J. (1963) *J. Opt. Soc. Am.*, **53**, 831–5.
Sullivan, J. C., Gordon, S., Mulac, W. A., Schmidt, K. H., Cohen, D., and Sjoblom, R. (1976) *Inorg. Nucl. Chem. Lett.*, **12**, 599–601.
Thouvenot, P., Hubert, S., and Edelstein, N. (1993a) *Phys. Rev. B*, **48**, 5751–60.
Thouvenot, P., Hubert, S., Moulin, C., Decambox, P., and Mauchien, P. (1993b) *Radiochim. Acta*, **61**, 15–21.
Thouvenot, P., Hubert, S., and Edelstein, N. (1994) *Phys. Rev. B*, **50**, 9715–20.
Tinkham, M. (1964) *Group Theory and Quantum Mechanics,* McGraw-Hill, New York.

Tissue, B. M. and Wright, J. C. (1987) *Phys. Rev. B*, **36**, 9781–9.
Van Deurzen, C. H. H., Rajnak, K., and Conway, J. G. (1984) *J. Opt. Soc. Am. B*, **1**, 45–7.
van Pieterson, L., Reid, M. F., Burdick, G. W. and Meijerink, A. (2002a) *Phys. Rev. B*, **65**, 045114.
van Pieterson, L., Reid, M. F., Burdick, G. W. and Meijerink, A. (2002b) *Phys. Rev. B*, **65**, 045113.
Varga, L. P., Brown, J. D., Reisfeld, M. J., and Cowan, R. D. (1970) *J. Chem. Phys.*, **52**, 4233–41.
Wadt, W. R. (1987) *J. Chem. Phys.*, **86**, 339–46.
Weissbluth, M. (1978) *Atoms and Molecules,* Academic Press, New York.
Wild, J. F., Hult, E. K., Lougheed, R. W., Hayes, W. N., Peterson, J. R., Fellows, R. L., and Young, J. P. (1978) *J. Inorg. Nucl. Chem.*, **40**, 811–16.
Worden, E. F. J., Blaise, J., Trautmann, N., and Wyart, J. F. (2005) in this volume, see Chapter 16.
Wyart, J. F., Kaufman, V., and Suger, J. (1980) *Phys. Scr.*, **22**, 389–96.
Wybourne, B. G. (1965a) *Spectroscopic Properties of Rare Earths,* Wiley Interscience, New York.
Wybourne, B. G. (1965b) *J. Opt. Soc. Am.*, **55**, 928–35.
Wybourne, B. G. (1966) *Phys. Rev.*, **148**, 317–27.
Yen, W. M. (1987) in *Spectroscopy of Solids Containing Rare Earth Ions* (eds. A. A. Kaplyanskii and R. M. Macfarlane), North-Holland, Amsterdam, pp. 185–249.
Yusov, A. B. (1987) *Radiokhimiya*, **29**, 118–21.
Yusov, A. B. (1990) *J. Radioanal. Nucl. Chem.*, **143**, 287–94.
Yusov, A. B. (1993) *Radiokhimiya*, **35**, 3–25.
Zhorin, V. V. and Liu, G. K. (1998) *J. Alloys Compds*, **275–277**, 137–41.

SUBJECT INDEX

Vol. 1: 1–698, Vol. 2: 699–1395, Vol. 3: 1397–2111, Vol. 4: 2113–2798, Vol. 5: 2799–3440.

Page numbers suffixed by t and f refer to Tables and Figures respectively.

AUTHOR INDEX

Vol. 1: 1–698, Vol. 2: 699–1395, Vol. 3: 1397–2111, Vol. 4: 2113–2798, Vol. 5: 2799–3440.

Page numbers suffixed by t and f refer to Tables and Figures respectively.

CHAPTER NINETEEN

THERMODYNAMIC PROPERTIES OF ACTINIDES AND ACTINIDE COMPOUNDS

Rudy J. M. Konings, Lester R. Morss, and Jean Fuger

19.1 INTRODUCTION

The necessity of obtaining accurate thermodynamic quantities for the actinide elements and their compounds was recognized at the outset of the Manhattan Project, when a dedicated team of scientists and engineers initiated the program to exploit nuclear energy for military purposes. Since the end of World War II, both fundamental and applied objectives have motivated a great deal of further study of actinide thermodynamics. This chapter brings together many research papers and critical reviews on this subject. It also seeks to assess, to systematize, and to predict important properties of the actinide elements, ions, and compounds, especially for species in which there is significant interest and for which there is an experimental basis for the prediction.

Many experimental and theoretical studies of thermochemical and thermophysical properties of thorium, uranium, and plutonium species were undertaken by Manhattan Project investigators. Some of these reports appeared in

the National Nuclear Energy Series (Seaborg *et al*., 1949). These papers, and others in the literature through 1956, formed the basis for Table 11.11 *Summary of thermodynamic data for the actinide elements* of the first edition of this work. This table, compiled by J. D. Axe and E. F. Westrum Jr., listed 126 species, of which the properties of 40 were estimates. A fair measure of the progress in actinide thermodynamics is the number of subsequent research papers and reviews.

Two other monumental works, which appeared in 1952, must be mentioned here: the U.S. National Bureau of Standards Circular no. 500 (Rossini *et al*., 1952) included all known data through uranium, and Latimer's oxidation potentials (Latimer, 1952) included oxidation–reduction data on all actinides through americium. Following the publication of the first edition of this work, with its thermodynamic summary in Table 11.11, the only major reviews of actinide thermodynamics during the decade 1960–69 were the monograph of Rand and Kubaschewski (1963) on uranium, the IAEA panel reports on oxides (IAEA, 1965, 1967) and carbides (Rand, 1968), and long reviews by Rand (1966) and Oetting (1967). However, until the 1970s, the reviews of actinide thermodynamics lagged behind the reports of these measurements themselves.

Critical efforts to compile and to assess actinide thermodynamic properties improved during the 1970s and 1980s. Krestov (1972) prepared an extensive compilation of rare earth and actinide thermochemical properties. Rand (1975) comprehensively and critically reviewed thorium thermodynamics, and the thermodynamics group of the U.S. National Bureau of Standards (Wagman *et al*., 1981) published the final volume of the Technical Note 270 series, which included the elements actinium through uranium. At nearly the same time the parallel compendium of Glushko *et al*. (1978) was published in the USSR. The most contemporary and thoroughly annotated compilation is the 14-part series issued under the auspices of the International Atomic Energy Agency, *The Chemical Thermodynamics of Actinide Elements and Compounds*, of which ten volumes have been published (Fuger and Oetting, 1976; Oetting *et al*., 1976; Cordfunke and O'Hare, 1978; Chiotti *et al*., 1981; Fuger *et al*., 1983; Flotow *et al*., 1984; Grønvold *et al*., 1984; Holley *et al*., 1984; Hildenbrand *et al*., 1985; Fuger *et al*., 1992). The nine volumes of this compilation published before 1986 formed the basis for most of the data in the second edition of this work.

After this 'golden age' of thermodynamics of the actinides a significant decrease in the number of experimental studies occurred during the last two decades, when the programs in many laboratories in the U.S. and Europe faced significant budget reductions. Also the review activities at the IAEA stopped before the series was completed. Fortunately many new review activities in this field started in the 1990s. The Nuclear Energy Agency (NEA) of the OECD initiated a project, the Thermodynamic Database Project (NEA-TDB), with the goal to assess and publish the thermochemical data of those actinides that are highly relevant to waste disposal studies: uranium, neptunium, plutonium, and americium (Grenthe *et al*., 1992; Silva *et al*., 1995; Lemire *et al*., 2001;

Guillaumont *et al.*, 2003). The volumes for these elements, which strongly rely upon the work done in the frame of the IAEA activities, have all been published and a supplement with extensions and corrections has been issued recently (Guillaumont *et al.*, 2003). At the Institute for Transuranium Elements (ITU), a systematic review of lanthanide and actinide elements and compounds was undertaken, with the goal of establishing a web-based information center (Konings, 2004b) focused on high-temperature properties. The results of these two projects form, together with the IAEA series, the basis for the present chapter. The thermodynamic studies on the transactinide elements are restricted to a few experimentally determined adsorption enthalpies of halides of elements 104, 105, and 106 on metal surfaces and quantum chemical calculations. For that reason these elements will not be dealt with in this chapter. The reader is referred to Chapter 14.

19.2 ELEMENTS

19.2.1 Actinides in the condensed phase

A systematic and critical review of the available thermodynamic quantities for the actinide elements was made by Ward *et al.* (1986), which is much more complete than the earlier reviews by Hultgren *et al.* (1973) and Oetting *et al.* (1976). Since then the thermodynamic quantities of some actinide elements were reviewed individually in other compilations. Thorium and uranium were carefully reviewed by the CODATA Workgroup for Key Values for Thermodynamics (Cox *et al.*, 1989) and recommended values for the standard entropy, heat capacity, and enthalpy of sublimation at room temperature were given. Reviews for plutonium and americium were reported by Cordfunke and Konings (1990), for uranium, neptunium, plutonium, and americium by the NEA-TDB Project teams (Grenthe *et al.*, 1992; Silva *et al.*, 1995; Lemire *et al.*, 2001; Guillaumont *et al.*, 2003), and for americium and curium by Konings (2001b, 2002). These reviews are essentially based on the same information as the work of Ward *et al.* Because few new measurements have been reported since 1986, the differences in values between these reviews mainly arise from the estimation methods, as explained below.

(a) Entropy

The low-temperature heat capacities have been measured for the actinides Th through Am. The experimental measurements were reviewed by Ward *et al.* (1986). The values given by Ward *et al.* (1986) for the heat capacity and entropy of Pa are based on the estimates of Oetting *et al.* (1976), but thereafter heat capacity measurements were reported by Hall *et al.* (1990) from 10 to 300 K.

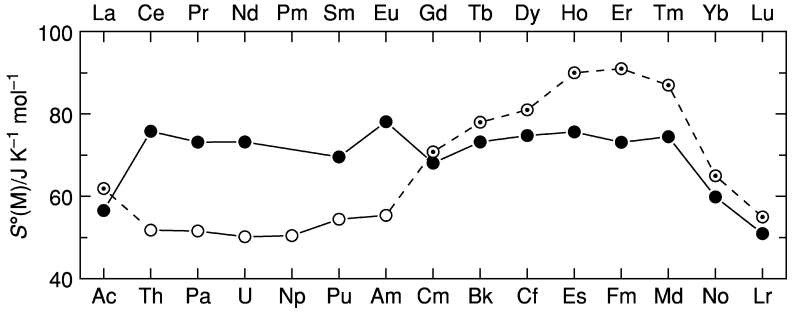

Fig. 19.1 *The standard entropies of lanthanide* (•) *and actinide* (○) *metals at* $T = 298.15$ K; *estimated values are indicated by* (⊙).

These authors reported preliminary results on several occasions but because the numbers given vary somewhat, the results cited here are from their final report.

The variation of the standard entropies along the actinide metal series is shown in Fig. 19.1. The entropies of the elements Th to Am are below the lattice entropies of the corresponding lanthanides, showing the absence of magnetic contributions. At Cm a distinct increase of the entropy occurs, showing the magnetic character of this element. Konings (2001b) suggested that the entropy of this element can be estimated by adding the excess entropy of Gd to that of Am. Ward and his colleagues (Kleinschmidt *et al.*, 1983; Ward *et al.*, 1986) suggested a more general formula to estimate the entropies of the metals heavier than americium from those of lanthanide and lighter actinide metals by correlation with metallic radius (r), atomic weight (M), and magnetic entropy (S_μ):

$$S_u(298.15\ \text{K}) = S_k(298.15\ \text{K})(r_u/r_k) + \frac{3}{2}R\ \ln(M_u/M_k) + S_\mu \qquad (19.1)$$

where u refers to the unknown element and k to the known element. S_μ is taken equal to $S_{\text{spin}} = (2J + 1)$, where J is the total angular momentum quantum number. The selected values for the entropies of the actinide elements are listed in Table 19.1.

(b) High-temperature properties

High-temperature heat capacity data have only been measured for Th, U, and Pu and the results allow an adequate description of the thermal functions of these elements into the liquid phase. Measurements for Np have only been made up to 480 K (Evans and Mardon, 1959). Oetting *et al.* (1976) and Ward *et al.* (1986) presented estimates for most other actinide metals based on a simple empirical correlation with the lanthanide metals, often adjusted to fit the second- and third-law analysis of the vapor pressure studies. Very similar data for Np and Am were presented in the OECD-NEA project. A semi-empirical

Table 19.1 *Thermodynamic properties of the actinide metals and gaseous elements at* 298.15 K *and* 10^5 Pa*; estimated values are in italics.*

	Crystal		*Gas*			
	C_p(298.15 K) (J K^{-1} mol^{-1})	$S°$(298.15 K) (J K^{-1} mol^{-1})	C_p(298.15 K) (J K^{-1} mol^{-1})	$S°$(298.15 K) (J K^{-1} mol^{-1})	$\Delta_{sub}H°$(298.15 K) (kJ mol^{-1})	*References*
Ac	*26 ± 2*	*61.9 ± 0.8*	20.817 ± 0.040	188.045 ± 0.10	*418 ± 20*	[a]
Th	26.23 ± 0.20	51.8 ± 0.5	20.790 ± 0.020	190.17 ± 0.05	602 ± 6	[b]
Pa	28.2 ± 0.4	51.6 ± 0.8	22.91 ± 0.05	198.11 ± 0.10	570 ± 10	[c]
U	27.66 ± 0.05	50.20 ± 0.20	23.690 ± 0.020	199.79 ± 0.10	533 ± 8	[b]
Np	29.62 ± 0.80	50.46 ± 0.80	20.824 ± 0.020	197.719 ± 0.005	465.1 ± 3.0	[d]
Pu	31.49 ± 0.40	54.46 ± 0.80	20.854 ± 0.010	177.167 ± 0.005	349.0 ± 3.0	[d]
Am	25.5 ± 1.5	55.4 ± 2.0	20.786 ± 0.010	194.55 ± 0.05	283.8 ± 1.5	[d]
Cm	*28.8 ± 1.5*	*70.8 ± 3.0*	28.106 ± 0.020	197.5 ± 5.0	384 ± 10	[e]
Bk		*78 ± 5*	20.786 ± 0.020	200.6 ± 3.0	310 ± 10	[f]
Cf		*81 ± 5*	20.786 ± 0.020	201.3 ± 3.0	196 ± 10	[f]
Es		*89 ± 5*	20.786 ± 0.020	201.0 ± 5.0	130 ± 10	[f]
Fm		*91 ± 5*	20.786 ± 0.020	199.4 ± 5.0	141 ± 13	[f]
Md		*87 ± 5*	20.786 ± 0.020	195.4 ± 5.0	*141 ± 13*	[f]
No		*65 ± 5*	20.786 ± 0.020	178.2 ± 5.0	*141 ± 13*	[f]
Lr		*55 ± 5*	20.786 ± 0.020	184.0 ± 5.0	*341 ± 13*	[f]

[a] Estimated in this work.
[b] Cox *et al.* (1989).
[c] Ward *et al.* (1986).
[d] NEA-TDB (Silva *et al.*, 1995; Lemire *et al.*, 2001; Guillaumont *et al.*, 2003).
[e] Konings (2001a).
[f] See text.

approach was used by Konings (2003) who presented the heat capacity of α- and β-Am as the sum of the harmonic, anharmonic, dilatation, electronic, and magnetic contributions:

$$C_p = C_{har} + C_{anh} + C_{dil} + C_{ele} + C_{mag} \quad (19.2)$$

This approach gives a good agreement with the low-temperature values; at elevated temperatures the results are somewhat higher than the earlier estimated heat capacity data. Larger differences were found for γ-Am and liquid Am, for which simplified versions of equation (19.2) were used.

Table 19.2 summarizes the transition temperatures and enthalpies for which, again, the data from the above-mentioned reviews have been adopted in most cases. The melting points are plotted in Fig. 19.2 together with those of the lanthanide metals. The melting points in the lanthanide series increase regularly, indicating an increasing cohesive energy in the condensed phase. Eu and Yb form exceptions to this trend as they have a divalent state, whereas the other lanthanides have a predominantly trivalent state. In the actinide series, tetravalent (Th–Pu), trivalent (Ac, Am–Cf, Lr), and divalent (Es–No) states are present, explaining why the melting points of the actinide metals are significantly different from those of the lanthanides. In this context, it is interesting to examine the variation in the sum of the transition entropies of the actinides, shown in Fig. 19.3. Clearly the elements U–Am have a considerably higher value of $\Sigma(\Delta_{trs}S)$ compared to the other actinide metals, for which the values are almost identical to the lanthanide elements. The value for Am is to be discussed in somewhat greater detail (Konings, 2003). The selected values for this element in the NEA-TDB review are based on the work of Wade and Wolf (1967) that was made on massive samples of Am. These values disagree seriously with those of the recent work of Gibson and Haire (1992). However, the values of $\Sigma(\Delta_{trs}S)$ derived from both these studies do not fit the trend suggested by Fig. 19.3. The results of Seleznev *et al.* (1977, 1978) are intermediate between these two studies and $\Sigma(\Delta_{trs}S)$ of Am derived from this work (8.7 J K^{-1} mol^{-1}) fits well in the trend for the trivalent lanthanide metals. Therefore Seleznev's values have been recommended (Konings, 2003). Clearly more work is required for this element.

The trend of the heat capacity of the actinides in the liquid phase is shown in Fig. 19.4 together with that for the liquid lanthanides. The actinides Th–Pu, for which experimental data are available, are tetravalent in the liquid, which explains why the two patterns are different. Am and Cm have a trivalent state, like the lanthanides (except Eu and Yb which are divalent).

The recommended heat capacity functions are summarized in Table 19.2.

19.2.2 Actinides in the gas phase

Heat capacity and entropy of the gaseous actinide elements have been calculated from atomic parameters and electronic energy levels. As discussed by Brewer (1984) the levels for the actinides are complete (through experiments and

Table 19.2 *High-temperature heat capacity of the crystalline and liquid actinide metals;* $C_p/(\mathrm{J\ K^{-1}\ mol^{-1}}) = a(\mathrm{T/K})^{-2} + b + c(\mathrm{T/K}) + d(\mathrm{T/K})^2 + e(\mathrm{T/K})^3$ (*estimated values are in italics*).

		a ($\times 10^{-6}$)	b	c ($\times 10^{3}$)	d ($\times 10^{6}$)	e ($\times 10^{9}$)	T (K)	$\Delta_{trs}H$ (kJ mol^{-1})	*References*
Ac	α		*25.45*	*−0.584*	*8.095*		*1323 ± 50*	*10.8 ± 2.0*	[a]
	liq		*35*						[a]
Th	α		23.435	8.945			1633 ± 20	3.50	[b]
	β	0.0114	15.70	11.951			2023 ± 10	13.8	[b]
	liq		46.00						[b]
Pa	α		21.6522	12.426			1443 ± 20	6.6	[c]
	β		39.7				1845 ± 20	12.3	[c]
	liq		47.3						[c]
U	α		26.9200	−2.5020	26.5558		941 ± 2	2.791	[b,d]
	β	−0.07699	42.9278				1049 ± 2	4.757	[b,d]
	γ		38.2836				1408 ± 2	9.142	[b,d]
	liq		48.660						[b,d]
Np	α	0.805714	−4.0543	82.555			553 ± 3	5.607 ± 0.500	[d]
	β		39.33				849 ± 3	5.272 ± 0.500	[d]
	γ		36.40				912 ± 3	5.188 ± 0.500	[d]
	liq		45.396						[d]
Pu	α		18.1258	44.820			397.6 ± 1.0	3.706 ± 0.100	[e]
	β		27.4160	13.060			487.9 ± 1.0	0.478 ± 0.020	[d]
	γ		22.0233	22.959			593.1 ± 1.0	0.713 ± 0.040	[d]
	δ		28.4781	10.807			736.0 ± 2.0	0.084 ± 0.020	[d]
	δ′		35.560				755.7 ± 2.0	1.841 ± 0.100	[d]
	ε		33.720				913 ± 2	2.824 ± 0.100	[d]
	liq		42.248						[d]
Am	α		30.0399	−29.053	52.026	−18.961	1042 ± 30	0.34 ± 0.08	[e]
	β		8.4572	33.167	−7.587		1350 ± 5	3.8 ± 0.4	[e]
	γ		43.0				1449 ± 5	8.0 ± 1.3	[e]
	liq		52.0						[e]

Table 19.2 (*Contd.*)

		a ($\times 10^{-6}$)	b	c ($\times 10^{3}$)	d ($\times 10^{6}$)	e ($\times 10^{9}$)	T (K)	$\Delta_{trs}H$ (kJ mol^{-1})	*References*
Cm	α		28.409	−0.8284	4.920		*1568 ± 30*	*4.5 ± 0.5*	[e]
	β		28.3				1619 ± 50	11.7 ± 1.0	[e]
	liq		37.2						[e]
Bk	α		27.437	−14.882	21.586		1250 ± 50	3.66	[f]
	β	0.1059	36.9				1323 ± 50	7.916	[f]
	liq		42.6						
Cf	α		23.651	9.7865	9.0983		863	2.64	[f]
	β	0.0580	37.6				1173	7.51	[f]
	liq		42.5						
Es	α		27.919	4.1825			1133	9.40	[f]
	liq	−0.2157	37.0						

[a] Estimated in this work.
[b] Cox *et al.* (1989).
[c] Oetting *et al.* (1976).
[d] NEA-TDB (Grenthe *et al.*, 1992; Silva *et al.*, 1995; Lemire *et al.*, 2001; Guillaumont *et al.*, 2003).
[e] Konings (2001b, 2003).
[f] Ward *et al.* (1986).

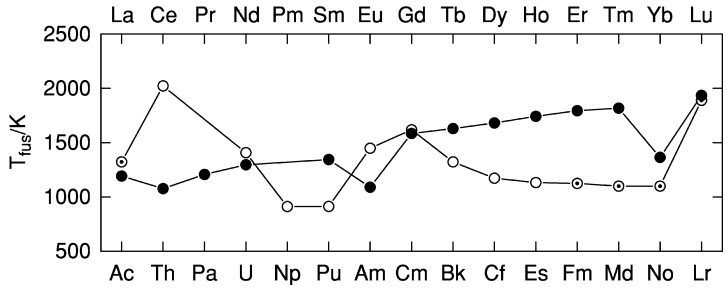

Fig. 19.2 *The melting points of lanthanide* (●) *and actinide* (○) *metals; estimated values are indicated by* (⊙).

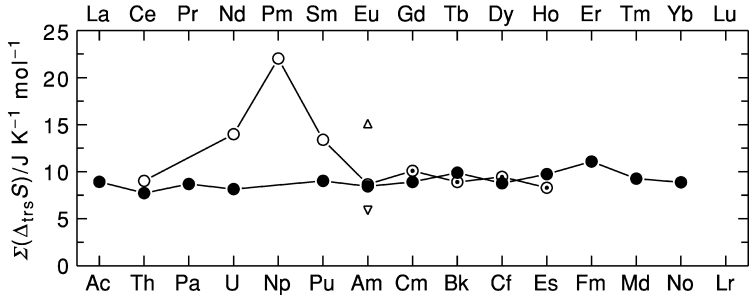

Fig. 19.3 *The sum of the transition entropies of lanthanide* (●) *and actinide* (○) *metals;* ▽, *results for Am from Wade and Wolf* (1967); Δ, *results for Am from Gibson and Haire* (1992)*; estimated values are indicated by* (⊙).

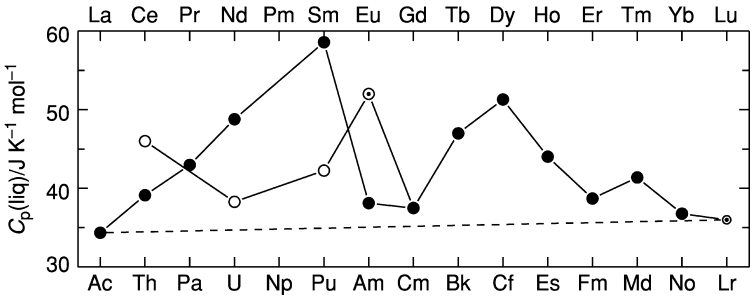

Fig. 19.4 *The heat capacity of the lanthanide* (●) *and actinide* (○) *metals in the liquid state; estimated values are indicated by* (⊙).

estimations) to about 15000 cm^{-1}, which permits the calculation of the values up to about 2000 K with reasonable accuracy. The room temperature values are shown in Table 19.1. The gaseous ions, for which thermodynamic data are also available, are dealt with extensively in Chapter 16 and are excluded from this chapter.

With these data and the thermal functions for the solid, sublimation enthalpies can be derived from the vapor pressure measurements for the actinide elements. Such measurements have been performed for all actinide metals except Md, No, and Lr, though the measurements for Ac (Foster, 1953) are of a very approximate nature. The work performed at Los Alamos and Oak Ridge National Laboratories is noteworthy because these researchers extended the measurements of the transplutonium elements to Cf and finally measured the vapor pressure of Es (Kleinschmidt *et al.*, 1984) and Fm (Haire and Gibson, 1989) using samples containing 10^{-5} to 10^{-7} at% of the actinides in rare earth alloys by applying Henry's law for dilute solutions. The enthalpies of sublimation derived from these studies are listed in Table 19.1. They are plotted in Fig. 19.5 together with the sublimation enthalpies of the lanthanide metals. The trend in the latter series shows a typical pattern, with La, Gd, and Lu forming an approximate linear baseline from which the others systematically deviate. This trend can be understood from the electronic states of the condensed and gaseous atoms, as discussed by Nugent *et al.* (1973), who showed that the difference between the value linearly interpolated in the La–Gd–Lu series and the experimental value corresponds to the energy difference between the lowest electronic energy level of the $f^n s^2 d^1$ configuration and the lowest level of the $f^{n+1} s^2$ configuration. An exception is Eu, which is divalent in the condensed state.

The trend in the actinide series decreases more as a function of Z compared to that for the lanthanides. The explanation for this is found in the complexity of the valence states, as discussed in Section 19.2.2. Several predictions of $\Delta_{sub}H$ for Ac, Md, No, and Lr were made. Nugent *et al.* (1973) correlated energetics of divalent and trivalent lanthanides and actinides. Fournier (1976) correlated

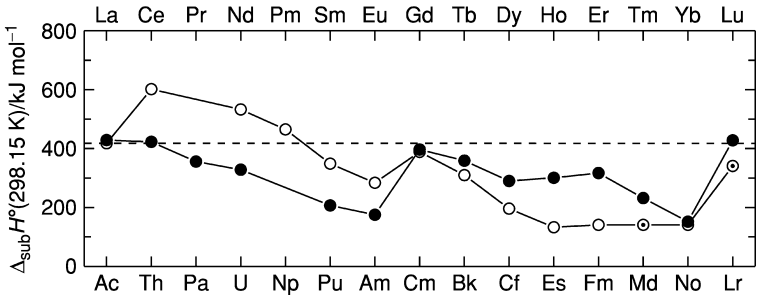

Fig. 19.5 *Enthalpies of sublimation of lanthanide* (•) *and actinide* (○) *metals at* $T =$ 298.15 K*; estimated values are indicated by* (⊙).

electronic configuration with metallic radius, melting temperature, and enthalpy of sublimation. A more reliable series of sublimation properties was generated by David *et al.* (1978) and David (1986), who included experimental radioelectrochemical measurements in the correlation. An independent method of estimation of sublimation properties is that of thermochromatography, which has been utilized effectively for the actinides (Hubener and Zvara, 1982). There is general agreement that the enthalpy of sublimation of Lr is in the range 320–350 kJ mol^{-1}, and we select the value estimated by David (1986). His values for Md and No must, however, be considered to be somewhat too high as the estimate for Fm is 32 kJ mol^{-1} higher than the experimental value by Kleinschmidt *et al.* (1984). Fournier estimated the sublimation enthalpies of Fm–No to be approximately the same, as was approximately the case for the results of David. We therefore suggest the same enthalpy of sublimation for Md and No as for Fm. The results are summarized in Table 19.1.

19.3 IONS IN AQUEOUS SOLUTIONS

19.3.1 Enthalpy of formation

For most of the transuranium elements, the enthalpy of formation of aqueous ions were the first thermochemical property to be determined. One reason was that the measurement of the 'heat of solution' of metals or, later, of enthalpies of redox reactions between actinide ions was an appropriate step in the determination of enthalpies of formation of compounds. A more fundamental reason is that the enthalpy of formation of an aqueous ion establishes a fundamental property of that ion and is a reference for all stability studies of compounds of that ion. Because solution microcalorimetry is more readily done than combustion microcalorimetry, milligram-scale enthalpy-of-formation studies of aqueous ions have been possible whereas such studies of oxides and halides by combustion calorimetry have not. In fact, microcalorimetry studies of transuranium elements have been carried out for more than 50 years, with barely an order of magnitude improvement in sensitivity in all that time!

The existing values of actinide aqueous-ion enthalpies of formation of actinium through berkelium were assessed by Fuger and Oetting (1976) in the frame of a series of publications under the auspices of the IAEA (Vienna). More recently, reassessments of the values for the ions of U, Np, Pu, and Am were presented in the NEA-TDB reviews, and for Cm ions by Konings (2001a). For these ions, the new values are preferred to those of Fuger and Oetting. Only in a few instances the differences are significant. For the quadrivalent (and pentavalent) Pa aqueous species, the values accepted here are very marginally different from those recommended by Fuger and Oetting, because of the later measurements with metal samples in the standard body-centered tetragonal form (Fuger *et al.*, 1978) instead of a quenched face-centered cubic form. For berkelium and californium,

newer measurements (Fuger *et al.*, 1981, 1984) have provided the tabulated enthalpies of formation. All An^{3+} values are plotted in Fig. 19.6, together with the Ln^{3+} values. The latter vary smoothly within a small band, with exception of Eu^{3+} and Yb^{3+}. These two metals are divalent in the crystal state, whereas the other lanthanide metals are trivalent. In the actinide series the electronic structure is more complex, as discussed in the previous sections, leading to a much more irregular pattern.

An important correlation between trivalent f-block ions and their 'trivalent' atoms ($f^n ds^2$) is the promotion energy function $P(M)$ proposed by Nugent *et al.* (1973), who utilized it for predicting enthalpies of formation of aqueous ions systematically (Fig. 19.7). David (1986) used the heavy actinide thermodynamic properties to establish a $P(M)$ function relating all of the actinide metals and their 3+ aqueous ions. Morss and Sonnenberger (1985) used newer data to

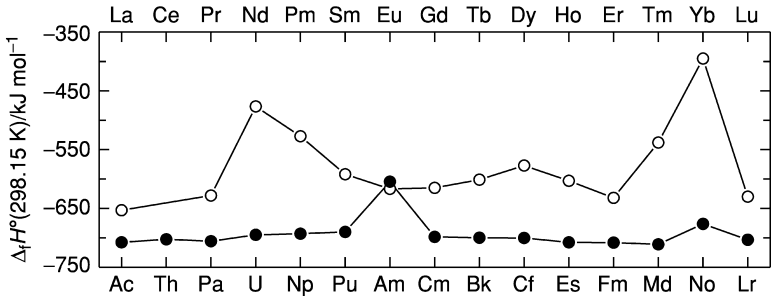

Fig. 19.6 *The enthalpy of formation of the lanthanide* (•) *and actinide* (○) *trivalent aqueous ions at* $T = 298.15$ K.

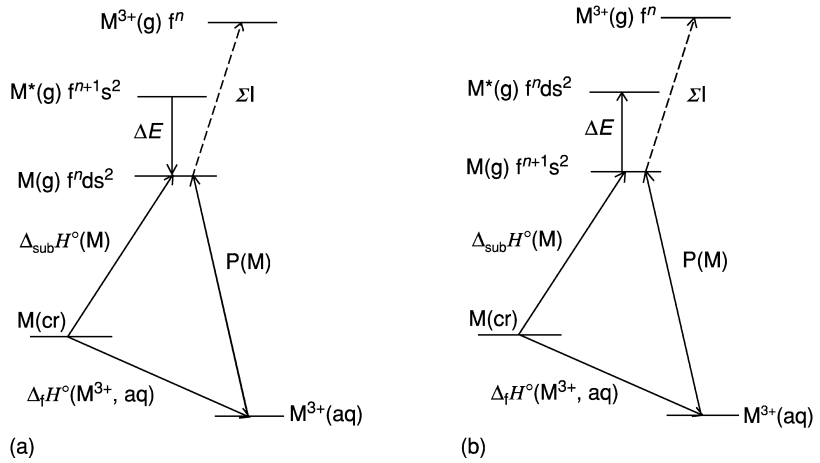

Fig. 19.7 P(M) (*energy level*) *diagrams for trivalent species:* (*a*) *for M = La, Ce, Gd, Lu, Ac–Np, and Cm;* (*b*) *for other lanthanides, and Pu, Am, and Bk–No.*

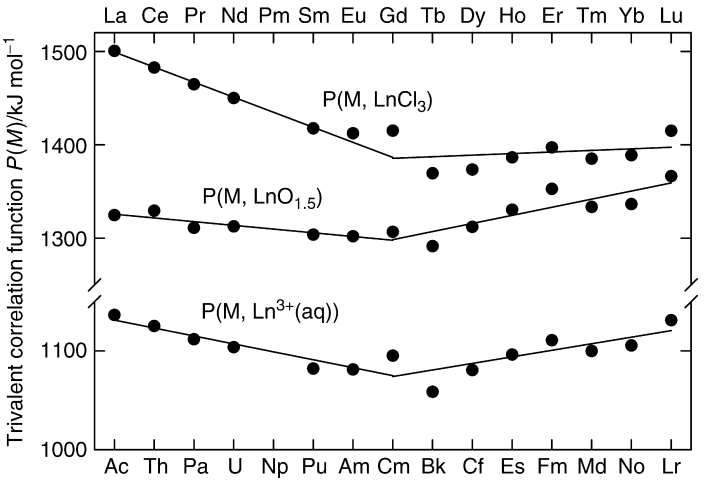

Fig. 19.8 P(M) *function for f-element trichlorides, sesquioxides, and aquo ions.*

refine this $P(M)$ function and to develop similar $P(M)$ plots relating f-block metals and their sesquioxides and trichlorides (Fig. 19.8). David's predictions for $\Delta_f H^\circ(Bk^{3+})$ and $\Delta_f H^\circ(Cf^{3+})$ have been borne out by experiments and consequently, their estimates for the heaviest trivalent actinides are used here. Some enthalpies of formation of tetravalent and higher ions have been calculated from Gibbs energies (electromotive force (EMF) measurements) and entropies (estimates) (Fuger and Oetting, 1976).

Enthalpies of formation of the tetravalent ions Am^{4+} and Cm^{4+} have been estimated from enthalpies of formation and solution of the dioxides (Morss and Fuger, 1981; Morss, 1983, 1985). The enthalpy of formation of Cf^{4+} was obtained from that of Cf^{3+}, the semiempirically deduced standard potential for the Cf^{4+}/Cf^{3+} couple, 3.2 V (see below), and the assumption that the difference in entropies between the Cf^{4+} and the Cf^{3+} ions is the same as for the corresponding Bk system.

19.3.2 Entropies

Entropies of aqueous ions can be determined directly by measuring the enthalpy and Gibbs energy of solution of a salt that contains the ions, and also by measuring the heat capacity of the solid salt and calculating its entropy.

$$\Delta_f S^\circ = (\Delta_f H^\circ - \Delta_f G^\circ)/T \tag{19.3}$$

The absolute entropy of the ion is then calculated from the equation representing $\Delta_f S^\circ$:

$$MX_n(cr) = M^{n+}(aq) + nX^-(aq) \tag{19.4}$$

Standard-state entropies of aqueous ions are by convention referenced to $S^\circ(H^+(aq)) = 0$. Four actinide aqueous-ion entropies (Th^{4+}, Pu^{3+}, UO_2^{2+}, and NpO_2^{2+}) have been determined by the former method.

The temperature coefficient of the EMF of an equilibrium reaction involving the ion can be used to calculate the entropy of the reaction, from which, using auxiliary data, the entropy of formation of the ion can be calculated. This is, for instance, the case of the entropy of the $Pu^{4+}(aq)$ ion. When, for a given reaction, the standard enthalpies of formation of the intervening ions, as well as the standard potential, are known, then the entropy change for this reaction is, of course, fixed. Alternatively, the experimental knowledge of the standard potential and of the entropy change fixes the standard enthalpy of formation.

Fuger and Oetting (1976) summarized all experimental data and selected or estimated entropies of the aqueous ions of Th through Bk. We have adopted their values for the ions of Th, Pa, and Cm. For Bk, we have used the temperature dependence of the Bk^{4+}/Bk^{3+} potential by Simakin *et al.* (1977). For the ions of U, Np, Pu, and Am, the values recommended by the NEA-TDB assessment (Grenthe *et al.*, 1992; Silva *et al.*, 1995; Lemire *et al.*, 2001; Guillaumont *et al.*, 2003) have been taken. For the aqueous ions beyond Bk, only estimated entropies are available. These estimates are fairly trustworthy because they depend only upon the ionic charges, the ionic radii, and the magnetic degeneracy of the ground states.

Several semiempirical equations have been proposed to fit entropies of aqueous ions to the above parameters, for example (Morss, 1976; Morss and McCue, 1976):

$$S(M^{z+}) = \frac{3}{2}R\ \ln(\text{at.wt.}) + R\ \ln(2J+1) + 256.8 - 32.84(|z|+3)^2/(r+c) \tag{19.5}$$

where $R = 8.314\ \text{J K}^{-1}\ \text{mol}^{-1}$, J is the total angular momentum quantum number of the ion, z is the ionic charge, r is the ionic radius (in nm) for coordination number 6 taken from Shannon (1976) (except that coordination number 8 is used for $z = 4$), and c is a term added to the radius to represent the inner-sphere hydration: $c = 0.120$ nm for cations and $c = 0.040$ nm for anions. David (1986) has proposed the following equation:

$$S(M^{z+}) = \frac{3}{2}R\ \ln(\text{at. wt.}) + R\ \ln(2J+1) + S_c(r) \tag{19.6}$$

where $S_c(r)$ is a structural entropy term, dependent for a given z only on the hydrated-ion structure. Equation (19.6) was devised by David to take into account the change in inner-sphere hydration number from 9 to 8 between Sm and Tb in the Ln^{3+} ions and between Cm and Es in the An^{3+} ions. Very recently, David and coworkers (David and Vokhmin, 2001, 2002; David *et al.*, 2001) developed a hydration and entropy model for covalent and ionic ions, leading to estimates very close to those obtained earlier. We thus accept David's estimates

of the heavy An^{3+} ion entropies. Equation (19.5) has been used for divalent and tetravalent ions (Table 19.3). The necessary ionic radii for equation (19.5) were estimated by comparison of isoelectronic 4f and 5f ions as well as by Shannon-type plots of unit-cell volumes of dihalides and dioxides against r^3. Other predictive equations give fairly consistent entropy estimates (Lebedev, 1981; David, 1986) even though ionic radii as small as 100 pm for No^{2+} have been estimated (Silva *et al.*, 1974; David, 1986).

For the An^{4+} ions the situation is less clear. Entropy values have been derived for Th^{4+}, U^{4+}, Np^{4+}, and Pu^{4+} from experiments. However, the trend in the values for these compounds, even when corrected for the $R\ln(2J+1)$ contribution, is not smooth as one could expect from equation (19.6), as shown by Konings (2001a), who suggested that the Np^{4+} value may be in error. He suggested $S°(Np^{4+}, aq, 298.15\ K) = -414\ J\ K^{-1}\ mol^{-1}$, which is the lower limit of the experimental value, $-(426.4 \pm 12.4)\ J\ K^{-1}\ mol^{-1}$ as given by NEA (Lemire *et al.*, 2001). Also his estimate for Am^{4+} ($-422\ J\ K^{-1}\ mol^{-1}$) is different from the NEA value $-(406 \pm 21)\ J\ K^{-1}\ mol^{-1}$ (Silva *et al.*, 1995). Clearly further experiments are needed to resolve these discrepancies.

19.3.3 Electrode potentials

Fuger and Oetting (1976) assessed the reversible cell EMF and polarographic data that allowed them to calculate Gibbs energy differences between many aqueous-ion pairs. By this way they were able to connect all aqueous ions and to tabulate Gibbs energies of formation of all actinide aqueous ions in acid solution. Comprehensive summaries of reduction potential literature values have been assembled by Martinot (1978) and Martinot and Fuger (1985). The latter authors have presented reduction potentials in acid solution for all of these elements including estimates of the reduction potentials for the Bk^{3+}/Bk and Cf^{3+}/Cf couples, based on calorimetric measurements on $Bk^{3+}(aq)$ and $Cf^{3+}(aq)$ (Fuger *et al.*, 1981, 1984). The reduction potentials of the U, Np, Pu, and Am ions were discussed extensively and assessed in the NEA-TDB series (Grenthe *et al.*, 1992; Silva *et al.*, 1995; Lemire *et al.*, 2001; Guillaumont *et al.*, 2003).

No selection was made by Fuger and Oetting (1976) and by Lemire *et al.* (2001) for the heptavalent/hexavalent neptunium and plutonium couples, although the literature values were discussed. We adopt here, for the formal potentials in 1 mol dm^{-3} NaOH the values (0.59 ± 0.05) V and (0.85 ± 0.05) V for the Np(VII/VI) and Pu(VII/VI) couples, respectively, from the review of Perethrukhin *et al.* (1995). Conventionally, we write the heptavalent species as MO_3^+, noting that, in neptunium, strong arguments have been brought recently in support of the existence of the tetroxo species $NpO_4(OH)_2^{3-}$ in 1 mol dm^{-3} NaOH (Williams *et al.*, 2001). Reduction of Np(VII) to NpO_2^{2+} in acid media occurs rapidly: we will take for the 1 mol dm^{-3} $HClO_4$ medium,

Table 19.3 *Thermodynamic properties of the actinide aqueous ions, see text for references; estimated values in italics.*

	An^{3+}		An^{4+}		AnO_2^+		AnO_2^{2+}		
	S°(298.15 K) (J K^{-1} mol^{-1})	$\Delta_f H^\circ$(298.15 K) (kJ mol^{-1})	S° (298.15 K) (J K^{-1} mol^{-1})	$\Delta_f H^\circ$(298.15 K) (kJ mol^{-1})	S°(298.15 K) (J K^{-1} mol^{-1})	$\Delta_f H^\circ$(298.15 K) (kJ mol^{-1})	S°(298.15 K) (J K^{-1} mol^{-1})	$\Delta_f H^\circ$(298.15 K) (kJ mol^{-1})	*References*
Ac	*–180 ± 17*	*–653 ± 25*							[a]
Th			–422.6 ± 16.7	–769.0 ± 2.5					[a]
Pa			*–397 ± 40*	–621.4 ±14.3[b,c]	*–21 ± 21*	–1115 ± 21[c,d]			[b]
U	–188.2 ± 13.9	–489.1 ± 3.7	–416.9 ± 12.6	–591.2 ±3.3	–25 ± 8	–1025.1 ± 3.0	–98.2 ± 3.0	–1019.0 ± 1.5	[e]
Np	–193.6 ± 20.3	–527.2 ± 2.1	–426.4 ± 12.4	–556.0 ± 4.2	–45.9 ± 10.7	–978.2 ± 4.6	–92.4 ± 10.5	–860.7 ± 4.7	[e]
Pu	–184.5 ± 6.2	–591.8 ± 2.0	–414.5 ± 10.2	–539.9 ± 3.1	1 ± 30	–910.1 ± 8.9	–71.2 ± 22.1	–822.0 ± 6.6	[e]
Am[i]	–201 ± 15	–616.7 ± 1.5	–406 ± 6	–406 ± 21	–21 ± 10	–804.3 ± 5.4	–88 ± 10	–650.8 ± 4.8	[e]
Cm	–191 ± 10	–615.0 ± 6.0	–439 ± 15	–380 ± 10					[f]
Bk	*–194 ± 17*	–601 ± 5	–402 ± 17	–483 ± 5					[g]
Cf	*–197 ± 17*	–577 ± 5	*–405 ± 17*	*311 ± 13*					[h]
Es	*–206 ± 17*	*–603 ± 21*							[h]
Fm	*–215 ± 25*	*–632 ± 42*							[h]
Md	*–224 ± 25*	*–538 ± 42*							[h]
No	*–231 ± 25*	*–395 ± 42*							[h]
Lr	*–255 ± 25*	*–630 ± 42*							[h]

[a] Fuger and Oetting (1976).
[b] Recalculated by the present authors from Fuger *et al.* (1983).
[c] In 1 mol dm^{-3} HCl.
[d] For the species $PaOOH^{2+}$.
[e] NEA-TDB (Grenthe *et al.*, 1992; Silva *et al.*, 1995; Lemire *et al.*, 2001; Guillaumont *et al.*, 2003).
[f] Konings (2001a).
[g] See text.
[h] Estimated.
[i] S° (Am^{2+}, aq, 298.15 K) = −(1 ± 15) J K^{-1} mol^{-1} and $\Delta_f H^\circ$ (Am^{2+}, aq, 298.15 K) = −(355 ± 16) kJ mol^{-1}.

the value (2.04 ± 0.05) V from the determination of Musikas *et al.* (1974). For the corresponding Pu and Am couples in the same medium, Perethrukhin suggested the values (2.3 ± 0.1) V and (2.5 ± 0.1) V, respectively. The uncertainties have been increased, compared to those given in the references cited. No value exists for the corresponding Pu couple in acid media, which is even more oxidizing. The question of the existence of any Am(VII), even in basic media, has been briefly discussed by Silva *et al.* (1995), and no selection was made.

The heavier actinide ions present especially challenging problems. These elements have short-lived isotopes with available amounts ranging between micrograms and single atoms. They also have accessible divalent states. To achieve meaningful experimental measurements on these ions, Maly (1967) and Maly and coworkers (Maly and Cunningham, 1967; Maly *et al.*, 1968), as well as Samhoun and David (1976) and David (1986) developed radioelectrochemical tracer methods, and Mikheev (1983) and his coworkers developed co-crystallization systematics. Judicious application of radiopolarography, radiocoulometry, amalgamation energies, and co-crystallization has yielded E° for An^{3+}/An^{2+}, An^{2+}/An, and An^{3+}/An couples (David, 1986) and has provided Gibbs energies of formation for Es^{3+}, Md^{3+}, and No^{3+}. The best Gibbs energies of formation of Fm^{3+} and Lr^{3+} have actually been calculated from estimates of enthalpies of sublimation, promotion energies $P(M)$, and entropies (David, 1986). Fig. 19.9 summarizes standard reduction potentials that are consistent with the Gibbs energies of formation calculated from enthalpies of formation and standard entropies. Because of the necessity of making EMF measurements in strongly acidic solution, and the impossibility of making measurements approaching standard state (nearly neutral solution), both the Gibbs energies of formation and reduction potentials refer to formal potentials rather than standard potentials (unit concentration rather than unit activity of hydrogen ion). When no thermochemical data were available, notably for the divalent ions, the potentials have been estimated.

The reduction potentials in Fig. 19.9 are 'Latimer' diagrams showing the potentials of half-reactions in which the left-hand species is reduced to the right-hand species with the appropriate number of electrons, H^+, and H_2O to balance the half-reaction. (Species not found in aqueous solution, but whose thermodynamic properties have been estimated, are indicated in parentheses.)

The potentials are summarized in Fig. 19.10 as nE°, a property proportional to $\Delta_f G^\circ$, versus n, the oxidation state, so that the lowest-lying species for each element is the one most stable in equilibrium with the H^+/H_2 couple.

A substantial number of studies have dealt with the electrochemical behavior of complexed actinides in aqueous solution. Complexation of f-block ions by ligands such as carbonate and polyphosphotungstate has allowed otherwise unstable species such as Am(IV) and U(V) to be studied electrochemically (Kosyakov *et al.*, 1977; Volkov *et al.*, 1981; Hobart *et al.*, 1982, 1983). Carbonate and bicarbonate stabilize acidic cations at relatively high pH (typical

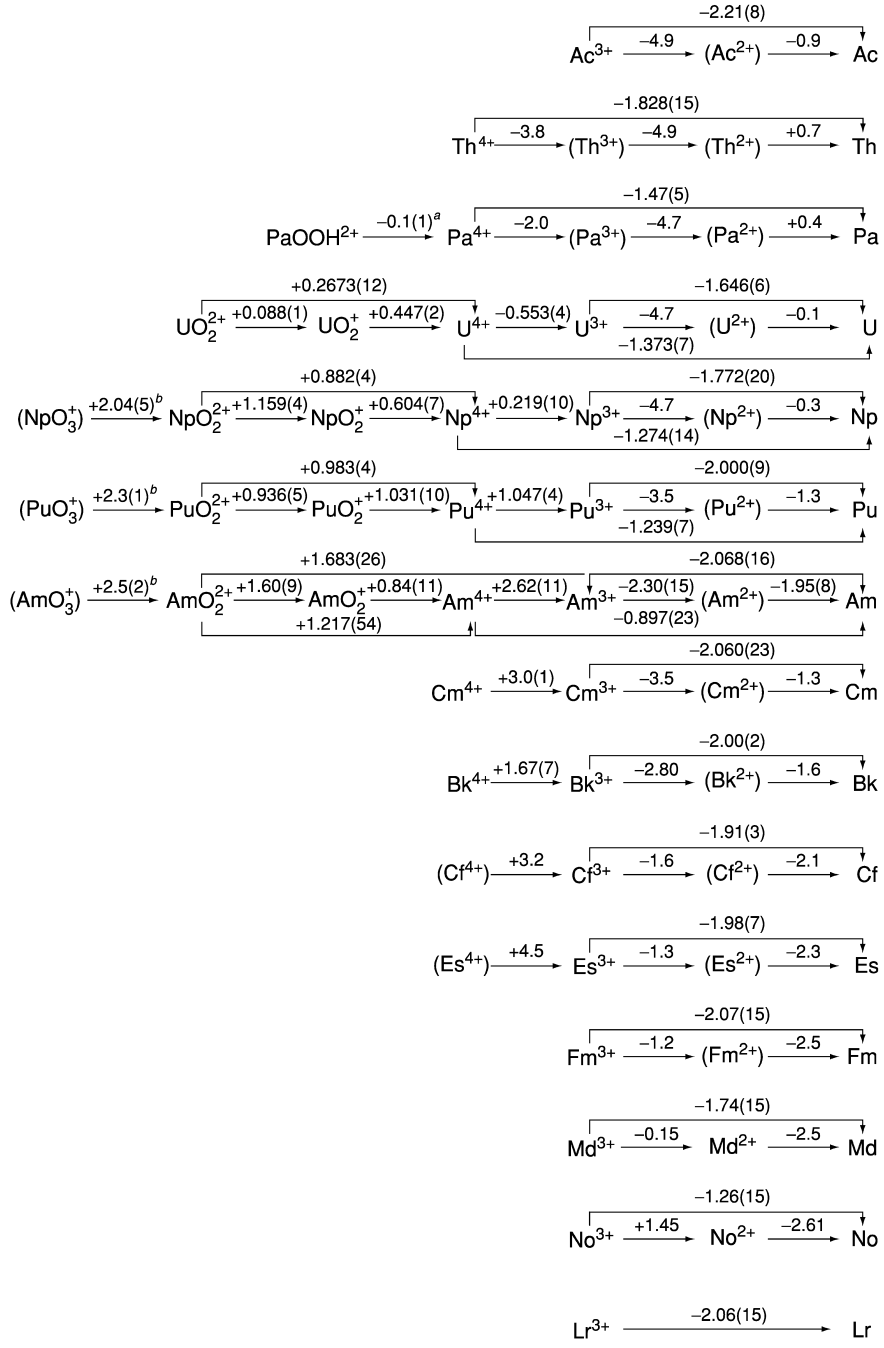

Fig. 19.9 *Standard reduction potentials diagrams for the actinide ions* (*values in volts versus standard hydrogen electrode*); [a] *indicates that the solvent is* 1 mol dm^3 *HCl,* [b] *refers to the potentials in* 1 mol dm^3 $HClO_4$.

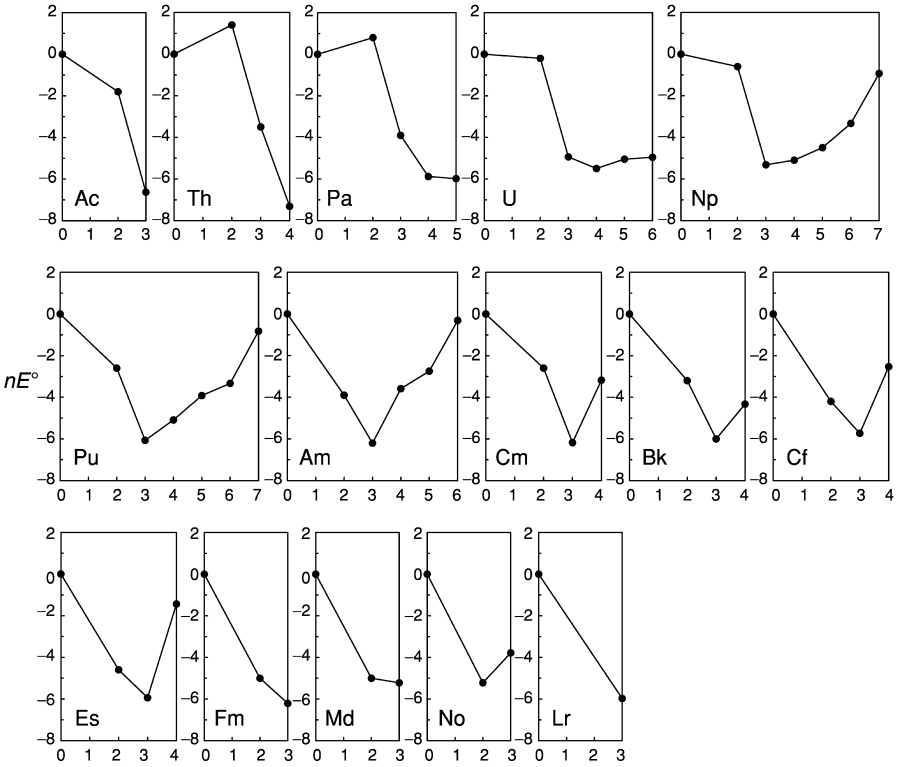

Fig. 19.10 *Comparative stability of actinide aqueous ions* (*relative to the* $H^+(aq)/H_2(g)$ *couple*).

of environmental and biological systems), and many actinide–carbonate studies have been reviewed (Cleveland, 1979; Newton and Sullivan, 1985).

Ions that are stabilized as complexes can be utilized to determine standard redox potentials. The $E°(Am^{4+}/Am^{3+})$ measured by cyclic voltammetry in 2 M $Na_2CO_3/NaHCO_3$ at pH 9.7, namely (0.92 ± 0.01) V, could be corrected for the preferred complexation of Am(IV) in this medium by 1.7 V to yield $E°(Am^{4+}/Am^{3+}) = (2.6 \pm 0.1)$ V (Hobart *et al.*, 1982), in good agreement with the accepted (Fig. 19.2) thermochemical value of (2.62 ± 0.09) V.

Polyphosphotungstate appears to be able to complex Cm(IV) and Cf(IV) sufficiently well to stabilize these ions in aqueous solution (Kosyakov *et al.*, 1977). Because the An^{4+}/An^{3+} potential shift of 1.7 V in carbonate is more favorable for stabilization of An^{4+} than is the shift of 1.0 V in polyphosphotungstate (Volkov *et al.*, 1981), it was expected that Cm(IV) and Cf(IV) would be readily produced in carbonate. Such was not found to be the case, however (Hobart *et al.*, 1983).

19.3.4 Heat capacities

Heat capacities, as well as entropies, of aqueous ions are the fundamental thermodynamic properties that reflect their structure and hydration. Heat capacities are also necessary for the calculation of other thermodynamic properties at temperatures other than 298.15 K. For the actinides, high-temperature properties (at least to 473 K) are essential for calculation of redox, complexation, and heterogeneous equilibria, which are useful in separation and waste management technologies.

The most thorough treatment of uranium and plutonium aqueous-ion equilibria over extended temperatures is that of Lemire and Tremaine (1980). This paper uses the systematic relationships developed by Criss and Cobble (1964), which relate aqueous-ion entropies, heat capacities, and their high-temperature behavior. Lemire and Tremaine had to rely on estimated heat capacities for almost all of their calculations, and most of their equilibrium constants are uncertain by two or more orders of magnitude. Lemire (1984) has also written a report on neptunium aqueous-ion equilibria over extended temperatures. However, in more recent years, the limitations of the Criss–Cobble relationships, when applied to tri- and quadrivalent aqueous species became more apparent. For instance, Shock *et al*. (1997), using the revised Helgerson–Kirkham–Flowers equation of state for aqueous ions, estimated $C^{o}_{p,m}(U^{3+}, aq, 298.15\ K) = -125.3\ J\ K^{-1}\ mol^{-1}$, distinctly more negative than the value $-(64 \pm 22)\ J\ K^{-1}\ mol^{-1}$ (mean value over the temperature range 298–473 K) accepted by Grenthe *et al*. (1992) from the estimate reported by Lemire and Tremaine. For another trivalent ion, Al^{3+}, Hovey and Tremaine (1986) have determined $C^{o}_{p,m}(Al^{3+}, aq, 298.15\ K) = -119\ J\ K^{-1}\ mol^{-1}$, whereas the Criss–Cobble relationship leads to $16\ J\ K^{-1}\ mol^{-1}$.

For quadrivalent actinide ions, the Criss–Cobble relation leads to −28, −48, and $-63\ J\ K^{-1}\ mol^{-1}$ for Th^{4+} (Morss and McCue, 1976), U^{4+}, and Pu^{4+} (Lemire and Tremaine, 1980), respectively. However, Hovey (1997) has determined recently $C^{o}_{p,m}(Th^{4+}, aq, 298.15\ K) = -(224 \pm 5)\ J\ K^{-1}\ mol^{-1}$. The flow microcalorimetric technique used by this author, under conditions minimizing hydrolysis and complexation, is far superior to measurements of integral heats of dilution or solution used in two previous studies (Apelblatt and Sahar, 1975; Morss and McCue, 1976). From the above, it appears that the Criss–Cobble relationships underestimate the heat capacities of tri- and quadrivalent ions by 100–160 $J\ K^{-1}\ mol^{-1}$. The values adopted recently by the NEA-TDB assessment (Guillaumont *et al*., 2003) $C^{o}_{p,m}(U^{3+}, aq, 298.15\ K) = -(150 \pm 50)\ J\ K^{-1}\ mol^{-1}$ and $C^{0}_{p,m}(U^{4+}, aq, 298.15K) = -(220 \pm 50) J\ K^{-1}\ mol^{-1}$ are in line with $C^{o}_{p,m}(Th^{4+}, aq, 298.15\ K) = -(224 \pm 5)\ J\ K^{-1}\ mol^{-1}$ (Hovey, 1997).

The value $C^{o}_{p,m}(UO_2^{2+}, aq, 298.15\,K) = (42.4 \pm 3.0)\ J\ K^{-1} mol^{-1}$, and the function $C^{o}_{p,m}(UO_2^{2+}, aq, T) = \{350.5 - 0.8722(T/K) - 5308((T/K) - 190)^{-1})\}$

$J\,K^{-1}mol^{-1}$, for the temperature range 283–328 K, adopted in the NEA assessment (Grenthe *et al.*, 1992) is also based on sound experiments (Hovey *et al.*, 1989).

For actinide ions, with 1+ charge, the only experimental results $C^{o}_{p,m}(NpO_2^+, aq, 298.15\ K) = -(4 \pm 25)\,J\,K^{-1}\,mol^{-1}$, and $C^{o}_{p,m}(NpO_2ClO_4, aq, T) = \{3.56779 \times 10^3 - 4.95931(T/K) - 6.32244 \times 10^5 (T/K)^{-1}\}\,J\,K^{-1}\,mol^{-1}$ in the temperature range 291–373 K, adopted in the NEA assessment (Lemire *et al.*, 2001) depend on measurements by Lemire and coworkers (Lemire *et al.*, 1993; Lemire and Campbell, 1996a) on NpO_2ClO_4 solutions. Use of $C^{o}_{p,m}(HClO_4, aq, T) = \{3.25118 \times 10^3 - 4.86333(T/K) - 5.45295 \times 10^5 (T/K)^{-1}\}\,J\,K^{-1}\,mol^{-1}$, in the same temperature range, from Lemire and Campbell (1996b) leads to $C^{o}_{p,m}(NpO_2^+, aq, T) = \{0.31661 \times 10^3 - 0.09598(T/K) - 0.87049 \times 10^5 (T/K)^{-1}\}\,J\,K^{-1}\,mol^{-1}$, with $C^{o}_{p,m}(H^+, aq, T) = 0\,J\,K^{-1}\,mol^{-1}$ in the reported temperature range.

Obviously, in recent years, progress has been made in our knowledge of the behavior of the electrolytes at high temperature. Nevertheless, more heat capacity data are needed for the multicharged ions.

19.4 IONS IN MOLTEN SALTS

Electrochemistry of actinides in molten salts has been pursued by many authors. The main incentives have been the molten salt reactor development and the pyrochemical reprocessing of spent fuel. The early work (up to 1980) has been summarized through reviews (Gruen, 1976; Plambeck, 1976; Martinot, 1978, 1982). In some cases, such as hydroxide and carbonate melts, high oxidation states of the actinides are stabilized, whereas in halide melts the use of strong Lewis acid molten salts stabilizes lower oxidation states (4+, 3+, and 2+). Coprecipitation of lanthanide tri- and dichlorides and oxychlorides with trace amounts of some actinides has yielded some An^{3+}/An^{2+} E° values and has produced evidence (unconfirmed by other methods) of divalent Pu, Cm, and Bk (Mikheev, 1983).

We will briefly summarize the data for the fluoride ($LiF–BeF_2$) and chloride (LiCl–KCl) systems as these are of interest to the renewed studies of the molten salt reactor and the pyrochemical reprocessing of spent fuel, in the framework of the partitioning and transmutation (P&T) and advanced nuclear reactor development programs worldwide. The apparent standard potentials are summarized in Tables 19.4 and 19.5.

The data for the actinide fluorides in $LiF–BeF_2$ (0.67:0.33 molar ratio) are taken from the review of Martinot (1982) who selected the data assessed by Baes (1966, 1969) for the Molten Salt Reactor Experiment (MSRE). These data are not based on electrochemical measurements but are derived from chemical

Table 19.4 *Apparent standard potentials in molten LiF–BeF_2* (0.67:0.33 molar ratio) *calculated versus the* $HF(g) + e^- = F^- + H_2(g)$ *reference system* [*after Baes* (1966, 1969)].

	E^0 (V)	T (K)	$\Delta_f S°$ (J K^{-1} mol^{-1})	$\Delta_f H°$ (kJ mol^{-1})
Th^{4+}/Th^0	$-2.498 + 0.720\ 10^{-3}(T/K)$	700–1000	–277.9	–964.1
U^{3+}/U^0	$-2.059 + 0.626\ 10^{-3}(T/K)$	700–1000	–181.2	–596.0
U^{4+}/U^0	$-2.007 + 0.671\ 10^{-3}(T/K)$	700–1000	–259.0	–774.6
Pu^{3+}/Pu^0	$-2.313 + 0.788\ 10^{-3}(T/K)$	700–1000	–228.1	–669.5

Table 19.5 *Apparent standard potentials in molten LiCl–KCl* (*eutectic*) *calculated versus the* Cl_2/Cl^- *reference system; estimated values are in italics.*

	E^0 (V)	T (K)	$\Delta_f S°$ (J K^{-1} mol^{-1})	$\Delta_f H°$ (kJ mol^{-1})	*References*
Th^{4+}/Th^0	$-2.86 + 0.50 \times 10^{-3}(T/K)$	673–773			[a,b]
Pa^{4+}/Pa^0	$-2.754 + 0.60 \times 10^{-3}(T/K)$	673–773	–231.6	–1062.9	[b]
U^{3+}/U^0	$-2.962 + 0.6115 \times 10^{-3}(T/K)$	673–773	–177.0	–857.4	[b]
U^{4+}/U^0	$-2.677 + 0.5726 \times 10^{-3}(T/K)$	673–773	–221.0	–1033.2	[b]
Np^{3+}/Np^0	$-3.119 + 7.45 \times 10^{-4}(T/K)$	673–773	–231.6	–902.9	[c]
Pu^{3+}/Pu^0	$-3.319 + 7.45 \times 10^{-4}(T/K)$	673–773	–203.9	–960.6	[c]
Am^{2+}/Am^0	$-3.259 + 5.50 \times 10^{-4}(T/K)$	673–773	–106.1	–628.8	[d]
Am^{3+}/Am^0	$-3.55 + 1.0 \times 10^{-3}(T/K)$	723–773	–289.5	–1028.4	[d]
Cm^{3+}/Cm^0	*–2.83*	723	–	–	[e]

[a] Plambeck (1976).
[b] Martinot (1982).
[c] Roy *et al.* (1996).
[d] Fusselman *et al.* (1999).
[e] Estimated in this work.

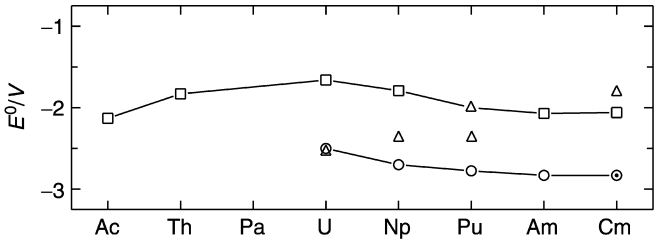

Fig. 19.11 *The electrode potentials of* An^{3+}/An^0 *couples in aqueous solution* (□) *and in LiCl–KCl eutectic at* 773 K (○)*; the results of Martinot* (1982) *are also shown* (Δ) *for information* (*see text*)*; estimated values are indicated by* (⊙).

equilibria in LiF–BeF_2 (0.67:0.33). For example, the uranium potentials were derived from the equilibria:

$$UO_2(s) = U^{4+}(sln) + 2\,O^{2-}(sln) \tag{19.7}$$

$$\frac{1}{2}\,H_2(g) + UF_4(sln) = UF_3(sln) + HF(g) \tag{19.8}$$

via the Gibbs energies of formation, scaling the results to the HF/F^- and the Be^{2+}/Be^0 couples.

Martinot (1982) summarized the data for the actinides in molten chloride salts, primarily based on his own electrochemical measurements. But recently many new studies have been reported on plutonium and americium in LiCl–KCl (Roy *et al*., 1996; Fusselman *et al*., 1999; Lambertin *et al*., 2000; Serp *et al*., 2004). Here a contradictory observation is made: the results of Martinot indicate an increase of the apparent potential of the An^{3+}/An^0 couple from U to Cm, whereas the more recent results indicate the opposite trend (Fig. 19.11), which is in agreement with the trend in potentials of the aqueous ions. Baes (1966) indeed noted that the potentials in molten salts correlate very well with those in solutions, and for that reason we reject the results of Martinot. Recently, data on Am^{2+}/Am^0 couple have been obtained (Fusselman *et al*., 1999). Yamana and Moriyama (2002) measured the Ln^{2+}/Ln^{3+} couples of Nd, Eu, Dy, and Yb and showed an excellent correlation with the aqueous Ln^{2+}/Ln^{3+} potentials.

19.5 OXIDES AND COMPLEX OXIDES

19.5.1 Binary oxides with O/An > 2.00

Many binary uranium oxides with O/U > 2.00 are known, and the thermodynamic properties of most of them are well established (see Table 19.6). The room temperature values for γ-UO_3 and U_3O_8 are CODATA Key Values (Cox *et al*., 1989); those of the other binary uranium compounds have been reviewed

Table 19.6 *Thermodynamic properties of the crystalline binary actinide oxides with O/An >2.00; estimated values in italics.*

	C_p(298.15 K) (J K^{-1} mol^{-1})	$S°$(298.15 K) (J K^{-1} mol^{-1})	$\Delta_f H°$(298.15 K) (kJ mol^{-1})	*References*
γ-UO_3	81.67 ± 0.16	96.11 ± 0.40	–1223.8 ± 1.2	a,b
β-UO_3	81.34 ± 0.16	96.32 ± 0.40	–1220.3 ± 1.3	a
α-UO_3	81.84 ± 0.30	99.4 ± 1.0	–1212.41 ± 1.45	a
δ-UO_3			–1213.73 ± 1.44	a
ε-UO_3			–1217.2 ± 1.3	a
am-UO_3			–1207.9 ± 1.4	a
α-$UO_{2.95}$			–1211.28 ± 1.28	a
U_3O_8	237.93 ± 0.48	282.55 ± 0.50	–3574.8 ± 2.5	a
α-U_3O_7	214.26 ± 0.90	246.51 ± 1.50		a
β-U_3O_7	215.52 ± 0.42	250.53 ± 0.60	–3423.0 ± 6.0	a
U_4O_9	293.36 ± 0.45	334.12 ± 0.68	–4512.0 ± 6.8	a
NpO_3	–	*100 ± 10*	*–1070 ± 6*	c
Np_2O_5	–	*174 ± 20*	–2162.7 ± 9.5	a,c

[a] NEA-TDB (Grenthe *et al*., 1992; Lemire *et al*., 2001; Guillaumont *et al*., 2003).
[b] Cox *et al*. (1989).
[c] Morss and Fuger (1981).

by Grenthe *et al*. (1992). Pa_2O_5 and Np_2O_5 are the only other well-known binary oxide with O/An > 2.00. None of the thermodynamic properties of Pa_2O_5 have been measured. Those of Np_2O_5 are fairly well established through enthalpy of formation measurements (Belyaev *et al*., 1979; Merli and Fuger, 1994) and high-temperature enthalpy increment measurements (Belyaev *et al*., 1979) that have been reviewed by Lemire *et al*. (2001). Because of the better stoichiometry and better thermochemical cycle used by Merli and Fuger, the $\Delta_f H°(Np_2O_5,cr)$ derived from that work has been accepted. No lanthanide comparison for these compounds can be made because there are no lanthanide oxides with O/Ln > 2.00. Recently the existence of PuO_{2+x} with x up to 0.5 has been claimed (Haschke *et al*., 2001) and its thermodynamic properties have been estimated (Haschke and Allen, 2002).

19.5.2 Dioxides

(a) Enthalpy of formation

The dioxides from ThO_2 through CfO_2 are all known, but many of these have not been studied thermodynamically (see Table 19.7). Because the enthalpy of formation values of ThO_2, UO_2 (CODATA Key Values, see Cox *et al*., 1989) and NpO_2 to CmO_2 are based on a sound experimental basis, the values for the other actinide dioxides can be estimated with reasonable accuracy.

Table 19.7 *Thermodynamic properties of the crystalline actinide dioxides at* 298.15 K*; estimated values are in italics.*

	S_{exs} (J K^{-1} mol^{-1})	$S°$(298.15 K) (J K^{-1} mol^{-1})	$\Delta_f H°$(298.15 K) (kJ mol^{-1})	*References*
ThO_2	0	65.23 ± 0.20	–1226.4 ± 3.5	[a]
PaO_2	*14.90*	*80 ± 5*	*–1107 ± 15*	[b]
UO_2	9.34	77.03 ± 0.20	–1085.0 ± 1.0	[a]
NpO_2	14.15	80.30 ± 0.40	–1074.0 ± 2.5	[c]
PuO_2	1.55	66.13 ± 0.26	–1055.8 ± 1.0	[c]
AmO_2	12.46	*78 ± 5*	–932.3 ± 2.5	[c,d]
CmO_2	0.00	*65 ± 5*	–912.1 ± 6.8	[d]
BkO_2	*17.29*	*83 ± 5*	*–1023 ± 9*	[b]
CfO_2	*21.3*	*87 ± 5*	*–857 ± 14*	[b]

[a] Cox *et al.* (1989).
[b] Estimated in the present work.
[c] NEA-TDB (Silva *et al.*, 1995; Lemire *et al.*, 2001; Guillaumont *et al.*, 2003).
[d] Konings (2001b).

Morss and Fuger (1981) established that the reaction enthalpy of the idealized dissolution reaction

$$AnO_2(c) + 4H^+(aq) \rightarrow An^{4+}(aq) + 2H_2O(l) \qquad (19.9)$$

varies regularly in the actinide series. The enthalpy of this reaction represents in part the difference between the lattice enthalpy of the crystalline dioxide and the enthalpy of hydration of its ionic components. Both these properties are difficult to calculate and change substantially as a function of ionic properties, whereas their difference (the enthalpy of solution) should change slowly and smoothly as a function of ionic size. Because the enthalpies of formation of $H^+(aq)$ and $H_2O(l)$ are constant in this equation, the quantity $\{\Delta_f H°(MO_2, cr) - \Delta_f H°(M^{4+}, aq)\}$ can be used for establishing relationships. Fig. 19.12 shows the relation with the molar volume of the unit cell. Ionic radii could have been used, because these are tabulated as a function of coordination number, but often they are reliable to only two significant figures. The values for PaO_2, BkO_2, and CfO_2 can be derived by interpolation or extrapolation of the linear relationship. These values are included in Table 19.7.

(b) Entropy

The low-temperature heat capacities have been measured for the solid dioxides from ThO_2 to PuO_2 and standard entropies for these compounds are known (see Table 19.7). The values for ThO_2 and UO_2 are CODATA Key Values (Cox *et al.*, 1989), those for NpO_2 and PuO_2 have been evaluated by the NEA-TDB (Lemire *et al.*, 2001). Konings (2001a) estimated the entropies of AmO_2 and CmO_2, proposing that the $S°$(298.15 K) of these compounds can be adequately

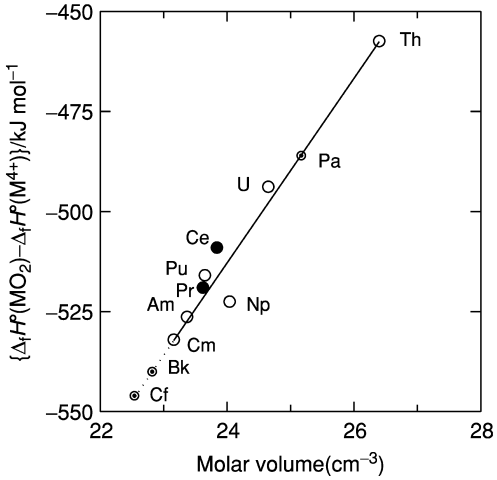

Fig. 19.12 *The difference between the enthalpies of formation of f-element dioxides and the corresponding* M^{4+} *aqueous ions; lanthanides* (•), *actinides* (○), *and estimated values* (⊙).

described as the sum of a lattice component and an excess component arising from f-electron excitation:

$$S = S_{\text{lat}} + S_{\text{exs}} \tag{19.10}$$

S_{lat} was assumed to be the value for ThO_2 and S_{exs} was calculated from the crystal field energies of these compounds (Krupa and Gajek, 1991; Krupa, 2001). Good agreement with the experimental values for UO_2, NpO_2, and PuO_2 was found and the description explains the significantly lower entropy value of PuO_2 among these compounds. This estimation procedure was adopted in the recent evaluation of the entropies of Am compounds by the NEA-TDB project (Guillaumont *et al.*, 2003). In a subsequent study, Konings (2004a) argued that the experimental data give evidence that S_{exs} is composed of two terms, the f-electron excitation and a residual term:

$$S_{\text{exs}} = S_{\text{f}} + S_{\text{res}} \tag{19.11}$$

We have used a similar method to estimate the entropies of PaO_2, BkO_2, CfO_2, and EsO_2, where in absence of crystal field data, the excess contribution was calculated from the degeneracy of the unsplit ground state, which probably overestimates the entropy somewhat.

(c) High-temperature properties

The high-temperature properties of the major actinide dioxides (UO_2, ThO_2, PuO_2) have been reviewed by many authors. The data are mostly restricted to the solid phase, except for UO_2, which has been studied in detail in the crystal,

liquid, and gas phases (up to 8000 K) for obvious reasons. Fink (2000) reviewed the thermophysical properties of UO_2 recently and presented recommended values for a large number of thermodynamic and thermophysical properties. Numerous equations of state for UO_2 have been published, the most recent and complete one by Ronchi *et al.* (2002). Also the high-temperature properties of thorium oxide in the crystal phase are reasonably well established (Bakker *et al.*, 1997). The melting points of the actinide dioxides are shown in Fig. 19.13 along with those for the lanthanide and actinide sesquioxides.

The high-temperature heat capacities of ThO_2, UO_2, and PuO_2 are shown in Fig. 19.14. The heat capacity approaches the Dulong–Petit value ($9R = 74.8$ J K^{-1} mol^{-1}) between 500 and 1500 K. In this temperature range the lattice contributions dominate the heat capacity with a minor but significant

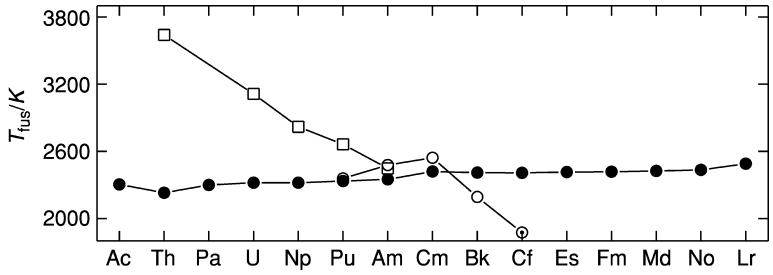

Fig. 19.13 *The melting points of the lanthanide sesquioxides* (•), *the actinide sesquioxides* (○) *and actinide dioxides* (□)*; estimated values are indicated by* (⊙).

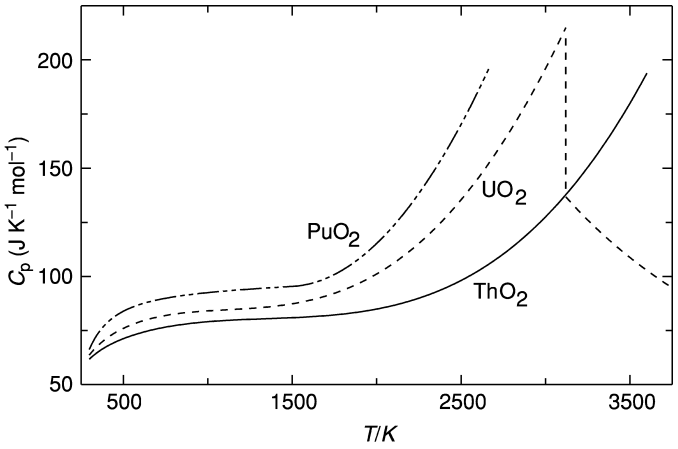

Fig. 19.14 *The high-temperature heat capacity of the actinide dioxides* (*see Table* 19.9).

contribution of 5f electron excitations. Peng and Grimvall (1994) showed that for ThO_2 and UO_2 the harmonic lattice contributions dominate up to about 500 K; above that temperature, the anharmonic contributions should be included.

As discussed in Section 19.5.2(b), the difference between the heat capacity of ThO_2 and the other actinide dioxides in the temperature range up to 1500 K is mainly due to the excess contribution arising from the population of excited f-electron levels of the An^{4+} ions:

$$C_p = C_{lat} + C_{exs} \tag{19.12}$$

Thus the heat capacity of the other actinide dioxides can be approximated by adding C_{exs}, which can be calculated from electronic energy levels.

Above 1500 K, the heat capacity strongly increases towards the melting point. In this temperature range, λ-type phase transitions have been observed for UO_2 (Hiernaut *et al.*, 1993) as well as ThO_2 (Ronchi and Hiernaut, 1996) at about $0.85T_{fus}$, which are related to order–disorder anion displacements in the oxygen sublattice. Below the phase transition, the formation of Frenkel lattice defects is the main cause of the rapid increase of the heat capacity; above the phase transition, Schottky defects become more important. The experimental data for PuO_2 by Ogard (1970) suggest a similar effect above 2400 K, but it has been attributed to partial melting of PuO_2 through interaction with the tungsten container (Fink, 1982; Oetting and Bixby, 1982). Because no clear evidence exists for this interaction, it has been included in the recommended equations given in this work (unlike in Cordfunke and Konings, 1990; Lemire *et al.*, 2001).

The experimental heat capacity data for NpO_2 (Arkhipov *et al.*, 1974) are in poor agreement with the low-temperature data and with the values estimated by Yamashita *et al.* (1997) and Serizawa *et al.* (2001). These authors calculated the lattice heat capacity from the phonon and dilatation contributions using Debye temperature, thermal expansion, and Grüneisen constants, and the electronic contributions from crystal field energies. No experimental data are known for PaO_2 and AmO_2. CmO_2 is unstable above 653 K.

As shown in Fig. 19.13 the melting points of the dioxides steadily decrease from ThO_2 to PuO_2, the change being more than 1200 K. This strong variation is accompanied by a strong increase in the oxygen pressure as the dioxides start to lose oxygen according to the reaction

$$MO_2(c) = MO_{2-x}(s) + \frac{x}{2}O_2(g) \tag{19.13}$$

which for PuO_2 and AmO_2 is already significant below the melting point, which means that the melting points are only defined in an oxygen atmosphere. The decrease of stability is related to the strong changes in stability of the 4+ oxidation states. Only the melting enthalpy of UO_2 is known with some accuracy. The values for the other dioxides have been estimated assuming that the entropy of melting is constant along the AnO_2 series.

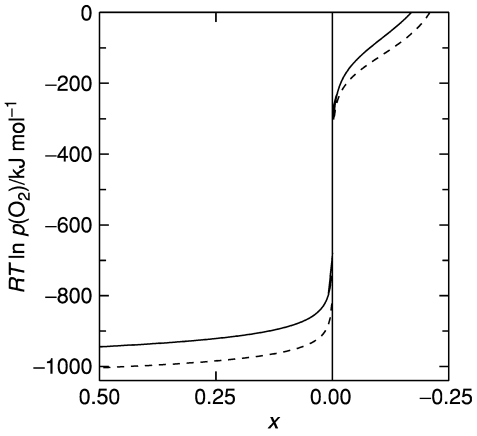

Fig. 19.15 *The oxygen potential of* UO_{2-x} *at* 1500 K (*solid line*) *and* 1250 K (*broken line*) *as a function of x calculated from the Lindemer and Besmann* (1985) *model; note that the hyperstoichiometric range is given with negative values.*

Recommended equations for the high-temperature heat capacity are given in Table 19.8.

(d) Nonstoichiometry

The actinide dioxides are well known for their wide ranges of nonstoichiometry. Hypostoichiometry has been reported for all actinide dioxides. Hyperstoichiometry is only known for UO_2 although recent studies have presented evidence that it could also occur in PuO_2 (Haschke *et al.*, 2001).

Lindemer and Besmann (1985) presented a thermochemical model to represent the oxygen potential–temperature–composition data for $AnO_{2\pm x}$ assuming a solution of two fluorite structures with different O/An ratios. The reaction can be represented by

$$\left(\frac{2a}{b-2a}\right)\mathrm{AnO_2} + \mathrm{O_2} = \left(\frac{2}{b-2a}\right)\mathrm{An}_a\mathrm{O}_b \tag{19.14a}$$

for the hyperstoichiometric range and

$$\left(\frac{2}{2a-b}\right)\mathrm{An}_a\mathrm{O}_b + \mathrm{O_2} = \left(\frac{2a}{2a-b}\right)\mathrm{AnO_2} \tag{19.14b}$$

for the hypostoichiometric range. In these equations, An_aO_b is a hypothetical end-member of the fluorite solid solution $AnO_{2\pm x}$. The oxygen potential can then be represented by:

$$RT\ln(p\mathrm{O_2}) = \Delta_r H - T\Delta_r S + RTf(x) + Ef'(x) \tag{19.15}$$

Table 19.8 *High-temperature heat capacity of the binary actinide oxides;* $C_p/(\mathrm{J\ K^{-1}\ mol^{-1}}) = a(\mathrm{T/K})^{-2} + b + c(\mathrm{T/K}) + d(T/K)^2 + e(\mathrm{T/K})^3 + f(\mathrm{T/K})^4$ (*estimated values are in italics*); *temperature T indicates the transition or melting temperatures except marked with m, when it indicates the maximum valid temperature of the polynomial equation.*

		a ($\times 10^{-6}$)	b	c ($\times 10^{3}$)	d ($\times 10^{6}$)	e ($\times 10^{9}$)	f ($\times 10^{12}$)	T (K)	$\Delta_{trs}H$ (kJ mol^{-1})	*References*
ThO_2	(cr)	–0.574031	55.9620	51.2579	–36.8022	9.2245		3651 ± 17	*82 ± 10*	[a]
	(liq)		61.76							[a]
UO_2	(cr)	–0.71391	52.1743	87.951	–84.2411	31.542	–2.6334	3110 ± 10	70 ± 4	[b]
	(l)	1328.8	0.25136							[b]
U_4O_9	(α)	–3.9602	319.163	49.691				348	2.594	[c]
	(β)	–3.9602	319.163	49.691				1400^{m}	11.9	[c]
U_3O_8	(cr)	–4.3116	279.267	27.480				2000^{m}		[c]
UO_3	(γ)	–1.00903	88.701	14.4896				1200^{m}		[c]
NpO_2	(cr)	–0.8969	73.662	8.8125				2820 ± 60	*63 ± 6*	[d]
PuO_2	(cr)	0.34759	36.2952	152.25	−127.255	36.289		2633 ± 40	*60 ± 10*	[e]
Pu_2O_3	(cr)	*–1.75053*	*130.6670*	*18.4357*				2358 ± 25	*113 ± 20*	[e]
AmO_2	(cr)	−1.9285	84.739	10.72	−0.8159			2000^{m}		[c]
Am_2O_3	(cr)	−1.071	113.93	59.37	−0.2301			1000^{m}		[c]
		−9.8742	153.13	3.573	2.372			2000^{m}		[c]
Cm_2O_3	(cr)	*–1.3489*	*123.532*	*14.550*				2543 ± 25		[e]
Bk_2O_3	(cr)							2196 ± 25		
Cf_2O_3	(cr)							*1875 ± 30*		

[a] Bakker *et al.* (1997).
[b] Fink (2000).
[c] NEA-TDB (Grenthe *et al.*, 1992; Lemire *et al.*, 2001; Guillaumont *et al.*, 2003).
[d] Fit of the estimated data by Serizawa *et al.* (2001).
[e] Konings (2004b).

where $f(x)$ and $f'(x)$ are functions of x that follow from the mass balance, and E is a temperature-dependent interaction energy term that was used in modeling the experimental data:

$$E = \Delta H_e - T\Delta S_e \tag{19.16}$$

Lindemer and Besmann (1985) analyzed the vast amount of experimental data and showed that hyperstoichiometric UO_{2+x} can be represented as a mixture of UO_2 and U_3O_7 for oxygen potentials above $RT\ln(p) = -26\,6700 + 16.5(T/K)$, or $U_2O_{4.5}$ below this limit; hypostoichiometric UO_{2-x} as a mixture of UO_2 and the hypothetical end-member compound $U_{1/3}$. Besmann and Lindemer (1985, 1986) showed that PuO_{2-x} can be represented as a mixture of PuO_2 and $Pu_{4/3}O_2$.

Also for the Np–O, Am–O, Cm–O, Bk–O, and Cf–O systems, the $T-p(O_2)-x$ relations have been measured. The Np–O system was studied by Bartscher and Sari (1986) using the gas equilibrium technique, the other systems by Eyring and coworkers (Chikalla and Eyring, 1967; Turcotte *et al.*, 1971, 1973, 1980; Haire and Eyring, 1994) using oxygen decomposition measurements, and the Am–O system by Casalta (1996) using a galvanic cell. The data of most of these systems, however, do not allow a detailed description of the $T-p(O_2)-x$ relations due to insufficient knowledge of the composition of the solid phase. An exception is the Am–O system and Thiriet and Konings (2003) applied the Lindemer–Besmann approach to the results of Chikalla and Eyring (1967), showing that AmO_{2-x} can be represented as a mixture of $Am_{5/4}O_2$ and AmO_2.

19.5.3 Sesquioxides

(a) Enthalpy of formation

Unlike the 4f elements, for which sesquioxides are ubiquitous, only the sesquioxides of Ac and Pu through Es have been prepared (Haire and Eyring, 1994). Experimental data from solution calorimetry are available for Am_2O_3, Cm_2O_3, and Cf_2O_3 and the enthalpies of formation of these three compounds are well established (although by only one set of measurements). Their values, the former taken from the most recent assessments (Silva *et al.*, 1995; Konings, 2001b) and Cf_2O_3 from the original paper (Morss *et al.*, 1987), are given in Table 19.9.

As discussed for the dioxides, a systematic approach to the prediction of the enthalpies of formation of other sesquioxides can be made on the basis of the reaction enthalpy of the idealized dissolution reaction

$$An_2O_3(cr) + 6H^+(aq) \rightarrow 2An^{3+}(aq) + 3H_2O(l) \tag{19.17}$$

The enthalpy of this reaction can be used for establishing a relationship with molar volume, which was chosen as a parameter because there are three different sesquioxide structures with different coordination numbers and numbers of molecules per unit cell, as shown in Fig. 19.16. It is evident that, for all the three structure types, the enthalpies of solution of actinide sesquioxides are

Table 19.9 *Standard entropies and enthalpies of formation of the crystalline actinide and lanthanide sesquioxides; estimated values are in italics.*

An	$S°$(298.15 K) (J K^{-1} mol^{-1})	$\Delta_f H°$(298.15 K) (kJ mol^{-1})	*References*	*Ln*	$S°$(298.15 K) (J K^{-1} mol^{-1})	$\Delta_f H°$(298.15 K) (kJ mol^{-1})	*References*
Ac	*141.1 ± 5.0*	*–1756*	[a]	La	127.32	–1791.6 ± 2.0	[c,f]
Th				Ce	148.8	–1813.0 ± 2.0	[c,f]
Pa				Pr	*160.5*	–1809.9 ± 3.0	[c,f]
U	*176 ± 5.0*	*–1456*	[a]	Nd	158.45	–1806.9 ± 3.0	[c,f]
Np	*173 ± 5.0*	*–1522*	[a]	Pm	*158.0*	*–1811 ± 21*	[c,f]
Pu	163.02 ± 0.65	–1656 ± 10	[b]	Sm	150.62	–1823.0 ± 4.0	[c,f]
Am	*133.6 ± 5.0*	–1690.4 ± 8.0	[b,c]	Eu	*137.4*	–1650.4 ± 4.0	[c,f]
Cm	*167.0 ± 5.0*	–1684 ± 14	[d]	Gd	152.73	–1819.7 ± 3.6	[c,f]
Bk	*173.8 ± 5.0*	*–1694*	[a]	Tb	*159.2*	–1865.2 ± 6.0	[c,f]
Cf	*176.0 ± 5.0*	–1653 ± 10	[a,e]	Dy	149.78 ± 0.42	–1863.4 ± 5.0	[c,f]
Es	*180.0 ± 5.0*	*–1696*	[a]	Ho	158.16	–1883.3 ± 8.2	[c,f]
Fm		*–1694*	[a]	Er	153.13 ± 0.42	–1900.1 ± 6.5	[c,f]
Md		*–1535*	[a]	Tm	139.75	–1889.3 ± 5.7	[c,f]
No		*–1260*	[a]	Yb	133.05 ± 0.42	–1814.5 ± 6.0	[c,f]
Lr		*–1766*	[a]	Lu	109.96	–1877.0 ± 7.7	[c,f]

[a] Estimated in the present work.
[b] NEA-TDB (Silva *et al.*, 1995; Lemire *et al.*, 2001; Guillaumont *et al.*, 2003).
[c] Konings (2001b, 2002).
[d] Konings (2001a).
[e] Morss *et al.* (1987).
[f] Cordfunke and Konings (2001c).

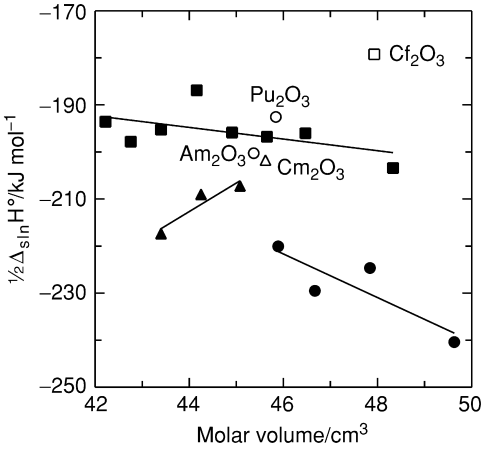

Fig. 19.16 *The enthalpy of solution* (*reaction* 19.17) *of the f-element sesquioxides; closed symbols, lanthanides; open symbols, actinides;* (●, ○), *hexagonal,* (▲, △), *monoclinic,* (■, □), *cubic.*

significantly less exothermic than for structurally similar lanthanide sesquioxides. With the exception of the enthalpy of formation of Pu_2O_3 (see below), the enthalpies of formation of the other sesquioxides were estimated from Fig. 19.16, taking in account their known or expected structural type.

Using the calculated enthalpies of formation of the sesquioxides of U and Np, it can be shown that these sesquioxides are thermodynamically unstable with respect to disproportionation to the metals and the much more stable dioxides, e.g. using enthalpies of formation and estimated entropies:

$$2Np_2O_3(c) = 3NpO_2(c) + Np(c), \quad \Delta G^\circ = -162 \text{ kJ mol}^{-1} \qquad (19.18)$$

The corresponding U reaction has $\Delta G = -322$ kJ mol^{-1}. The case of Pu_2O_3 deserves special mention. Its enthalpy of formation has been estimated as $-(1710 \pm 13)$ kJ mol^{-1} (IAEA, 1967) from high-temperature EMF measurements, as $-(1685 \pm 21)$ kJ mol^{-1} (Chereau *et al.*, 1977) from high-temperature calorimetry, and as -1656 kJ mol^{-1} (Besmann and Lindemer, 1983) from earlier measurements and more recent heat capacity values. The last value is adopted in Lemire *et al.* (2001). Because there is an experimentally derived standard entropy of Pu_2O_3, we can calculate its Gibbs energy of reaction (19.17), -289 kJ mol^{-1}, for comparison with that of the structurally similar Nd_2O_3, -332 kJ mol^{-1}. Actinide sesquioxides appear to be more stable than structurally similar lanthanide sesquioxides in comparison with the corresponding aqueous solutions, so that nuclear waste oxide matrices that accept lanthanide ions should bind corresponding trivalent actinides (Pu^{3+}, Am^{3+}) even more strongly. The reason for this behavior is not clear; a rationalization is that the 5f covalence is stronger to oxygen in solid oxides than in hydrated ions.

Recommended values for the standard enthalpies of formation and entropies of the actinide and lanthanide sesquioxides are assembled in Table 19.9.

(b) Entropy

Low-temperature heat capacity measurements have been reported for Pu_2O_3 only (Flotow and Tetenbaum, 1981). This value was used to derive the entropies of Am_2O_3 and Cm_2O_3 (Konings, 2001a; Konings *et al.*, 2005) using equation (19.10), calculating the excess entropy from known crystal field energies. Because information on the lattice component in the actinide sesquioxide series is missing, and the lattice component was obtained by scaling the values derived from the isostructural lanthanide series (Fig. 19.17). In this series the lattice entropy can be described by a simple linear relation between La_2O_3 and Gd_2O_3, for which the lattice values are well known due to the f^0 and f^7 configurations.

(c) High-temperature properties

High-temperature properties of the actinide sesquioxides have hardly been studied. The phase transitions in the sesquioxides have been determined and it has been shown that the sesquioxides exhibit a polymorphism: bcc → monoclinic → hexagonal. The cubic to monoclinic transition is, however, irreversible, and the monoclinic form is thought to be the thermodynamically stable phase. The measured melting points of Pu_2O_3, Am_2O_3, Cm_2O_3, and Bk_2O_3 are plotted in Fig. 19.13 and show a maximum at Cm_2O_3.

The only measurements of high-temperature properties are for Pu_2O_3, Am_2O_3, Cm_2O_3, and Bk_2O_3. The most extensive are the studies made for $^{244}Cm_2O_3$,

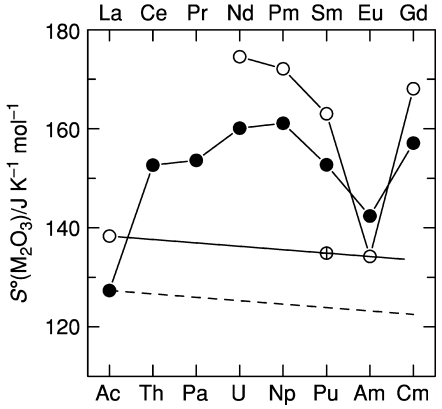

Fig. 19.17 *The entropy of the hexagonal/monoclinic lanthanide sesquioxides* (•), *showing the linear lattice component derived for the* f^0 *and* f^7 *configuration as a dotted line. The entropies of the actinide sesquioxides* (○) *are calculated for a parallel lattice component based on the* Pu_2O_3 *value* (⊕).

which was considered as an isotopic heat source in the 1970s. Vapor pressure studies (see Section 19.5.5) and thermal conductivity and thermal diffusivity measurements were reported. To convert the latter measurements to thermal conductivity, Gibby *et al.* (1970) estimated the heat capacity of Cm_2O_3. As discussed by Konings (2001a), these values are very high when compared to the lanthanide sesquioxide data. Since reliable high-temperature heat capacity data for the lanthanide sesquioxides are available, the functions of the actinide sesquioxides can be estimated from those by simple correlation (equation (19.13)).

19.5.4 Monoxides

Solid monoxides of Th and of U through Am have been reported as surface layers on the metals, as the reduction product of PuO_2 with Pu or C, or as the product of reaction of Am with HgO. However, these solid 'monoxides' may be oxycarbides (Larson and Haschke, 1981). Usami *et al.* (2002) claim the formation of AmO by lithium reduction of AmO_2. The product was, however, not characterized but its formation was deduced from a mass balance. The authors estimated its Gibbs energy of formation as -481.1 kJ mol^{-1} at 923 K.

Among the reported lanthanide monoxides, only EuO is well characterized, impure YbO can be prepared with difficulty, and 'metallic' (trivalent) monoxides of La, Ce, Pr, Nd, and Sm can be synthesized at high temperature and pressure. Earlier reports of lanthanide monoxides as surface phases are believed to be oxynitrides, oxycarbides, or hydrides (Morss, 1983). Thermodynamic calculations have shown how marginally stable the few lanthanide monoxides are, even under the exotic conditions of their preparation, and that classical (divalent) CfO should be unstable with respect to disproportionation (Morss, 1983). Thus the only hope of synthesis of actinide monoxides would appear to be the high-pressure route for AmO and CfO, an extremely demanding synthetic procedure.

19.5.5 Oxides in the gas phase

Gaseous actinide oxide molecules of the types AnO, AnO_2, and AnO_3 have all been identified in Knudsen cell effusion or matrix isolation experiments of vapors above the solid oxides. The experimental work is restricted to the oxides of Th to Cm.

Thorium dioxide principally vaporizes to give ThO_2 molecules. Numerous vapor pressure studies have been performed for the solid–gas equilibrium, none of them, however, with techniques to confirm the vapor composition. Ackermann and Rauh (1973a) as well as Belov and Semenov (1980) reported the existence of the monoxide ThO in the vapor phase using mass spectrometry. Ackermann and Rauh (1973b) derived enthalpies of formation of the two molecules from the existing studies by correcting the vapor pressure studies for the ThO contribution. The thermal functions of the gaseous molecules have

been calculated from molecular parameters (Rand, 1975). The properties of the ThO molecule are based on experimental results as summarized by Rand (1975) and have been confirmed by quantum chemical calculations (Küchle *et al*., 1994). ThO_2 is a bent molecule, as was derived from matrix-isolation and molecular beam deflection studies (Linevsky, 1963; Kaufman *et al*., 1967; Gabelnick *et al*., 1974).

In the Pa–O system the monoxide and dioxide species have been identified in the vapor above PaO_{2-x} (Kleinschmidt and Ward, 1986) and above Pa metal in the presence of small amounts of oxygen (Bradbury, 1981).

The situation for uranium is more complex. The binary molecules UO, UO_2, and UO_3 coexist above solid and liquid UO_2, and at very high temperatures even dimeric molecules of these species and ionic species contribute to the vapor pressure. The UO_2 molecule does not have a bent structure, like ThO_2, but is linear; UO_3 is planar with a T-shaped geometry (Green, 1980). The relative fractions of these species are highly dependent on the temperature and O/U ratio of the condensed phase. Ronchi *et al*. (2002) have presented a detailed analysis of these complex equilibria, for which a large number of studies has been made up to very high temperatures, and their recommended values for the enthalpies of formation and entropies are listed in Table 19.10.

Ackermann *et al*. (1966a) measured the vapor pressure of NpO_2 by the Knudsen effusion technique. Mass spectrometric measurements confirmed that NpO_2 is the dominant vapor species but that NpO(g) also has a significant contribution to the vapor. Ackermann and Rauh (1975) studied the isomolecular

Table 19.10 *Thermodynamic properties of the gaseous polyatomic actinide oxides; estimated values are in italics.*

	$S°$(298.15 K) (J K^{-1} mol^{-1})	$\Delta_f H°$(298.15 K) (kJ mol^{-1})	*References*
UO_3	309.5 ± 2.0	–795.0 ± 10.0	[a]
ThO_2	281.7 ± 4.0	–455.2 ± 10.0	[b]
UO_2	266.4 ± 4.0	–476.2 ± 10.0	[a]
NpO_2	276.5 ± 5.0	–444 ± 20	[e]
PuO_2	278.0 ± 5.0	–410 ± 20	[c]
ThO	240.1 ± 2.0	–20.9 ± 10.0	[b]
UO	248.8 ± 2.0	24.7 ± 10.0	[a]
NpO	257.9 ± 5.0	−9 ± 5	[e]
PuO	248.1 ± 3.0	–60.0 ± 10.0	[c]
CmO	261.9 ± 10.0	–175 ± 15	[d]

[a] Ronchi *et al*. (2002).
[b] IVTAN-THERMO Database of the Institute for High Temperatures of the Russian Academy of Sciences.
[c] Glushko *et al*. (1978).
[d] Konings (2002).
[e] Ackermann *et al*. (1966a).

exchange reactions with La and Y by mass spectrometry. In addition, Ackermann and Rauh (1975) studied the NpO vapor pressure over the univariant system (NpO_2(cr)+Np(l)+vapor) by Knudsen effusion technique. This approach yields results that are within the limits of uncertainty of the analysis of the isomolecular exchange reactions. The selected enthalpies of formation are derived from these studies.

In the Pu–O system, it has been thought for a long time that only PuO_2 and PuO exist as binary molecular species, but recently the existence of the PuO_3 molecule has been reported (Ronchi *et al.*, 2000). Matrix-isolation spectroscopy (Green and Reedy, 1978a,b) has established the linear molecular structure of PuO_2 and yielded values for the vibrational stretching frequencies. Archibong and Ray (2000) calculated the molecular properties of PuO_2 using quantum chemical techniques. They found that the $^5\Sigma_g^+$ and the $^5\Phi_u$ states are both candidates for the ground state, being almost equal in energy, the former preferred because of somewhat better agreement with the experiments for the two stretching frequencies. However, the data for the internuclear distance and the bending frequency for the $^5\Sigma_g^+$ state differ considerably from the estimates by Green (1980) on basis of the UO_2 data, whereas the data for the $^5\Phi_u$ state agree reasonably. The enthalpies of formation of PuO and PuO_2 are taken from Glushko *et al.* (1978).

The vapor pressure of americium oxides has been deduced from measurements of plutonium oxides containing small amounts of ^{241}Am as decay product using Raoult's law (Ackermann *et al.* 1966b; Ohse, 1968). Although no direct measurement of the vapor species was made in either study, it was assumed that the AmO and AmO_2 molecules are present. These data do not, however, allow the derivation of formation properties.

For the Cm–O system, Knudsen cell effusion measurements have been performed (Smith and Peterson, 1970) from which it was concluded that Cm_2O_3 vaporizes according to the reaction:

$$Cm_2O_3(cr,l) = 2\,CmO(g) + O(g) \tag{19.19}$$

which is analogous to the lanthanide sesquioxides. Hiernaut and Ronchi (2004) recently measured the vapor pressure of $(Cm,Pu)_2O_3$ by Knudsen effusion mass spectrometry, confirming the results and conclusions of Smith and Peterson (1970).

The dissociation energy of the actinide monoxides are plotted in Fig. 19.18 together with those of the lanthanide monoxides (Pedley and Marshall, 1983). The pattern that emerges for the actinide monoxides is parallel to that of the lanthanide monoxides and the dissociation energies of AmO can be estimated. Haire (1994) discussed this pattern in more detail, and extended the estimates to the heaviest actinides. He described the dissociation energy by a base energy $D_{0,\mathrm{base}}$ and a ΔE value (as proposed by Murad and Hildenbrand (1980)):

$$D_0 = D_{0,\mathrm{base}} + \Delta E \tag{19.20}$$

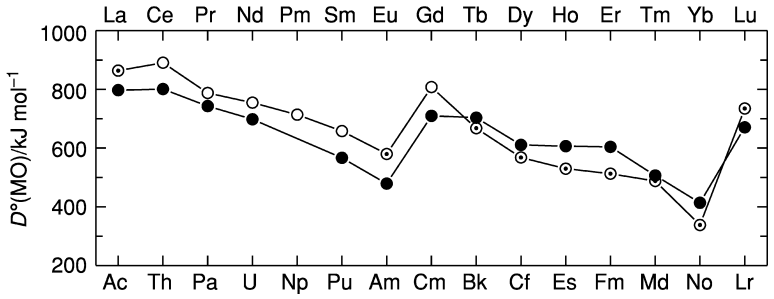

Fig. 19.18 *Dissociation energy of lanthanide* (•) *and actinide* (○) *monoxides; estimated values* (*see text*) *are indicated by* (⊙).

A ds-state was assumed for these molecules, which means that a promotion energy of a f-electron to a d-state is required. This is the origin of the ΔE value, which can be derived from theoretical calculation (Brooks *et al.*, 1984). The $D_{0\ \mathrm{base}}$ value was represented by interpolation of the LaO–GdO–LuO line, i.e. those lanthanides that already have one d-electron. In transposing this relationship to the actinides, Haire assumed that the base relation is the same in the 4f and 5f series but the value for CmO adopted here (the actinide analog of GdO) suggests that there is a systematic difference of about 70 kJ mol^{-1} (Fig. 19.18). We have corrected Haire's values for this difference and the data for the monoxides beyond CmO thus obtained are shown in Fig. 19.18.

Recently Santos *et al.* (2002a,b) suggested that the excited 'bonding' state is obtained by promotion of an s-electron to a d-level to create the double bond. The lowest-lying excited states to be considered are $4f^{n-3}5d^26s$ and $4f^{n-2}5d6s$. Gibson (2003) showed how the energy required to promote gaseous lanthanide atoms to the excited 'bonding' state is responsible for the trends in the LnO dissociation energies. He defined the intrinsic Ln=O bond energy as "the bonding interaction between an oxygen atom and a lanthanide atom, Ln*, that has an electron configuration suitable for formation of the covalent formally double bond in the Ln=O molecule." He identified the $4f^{n-3}5d^26s$ configuration as the appropriate one for bonding and the two 5d electrons as the electrons that provide bonding with the oxygen. Thus the trend was explained as:

$$D^0(\mathrm{LnO}) = D^{0*}(\mathrm{LnO}) = \Delta E\ [\mathrm{ground} \rightarrow \mathrm{bonding\ configuration}] \qquad (19.21)$$

19.5.6 Complex oxides

(a) Ternary and quaternary oxides with alkali metal ions

An extensive number of thermodynamic studies of the alkali uranates have been reported and the existing thermochemical data have been assessed by Cordfunke and O'Hare (1978) and Grenthe *et al.* (1992), the latter study

updated by Guillaumont *et al.* (2003). These thermochemical data are, however, much fewer than the large number of phases existing in the A_2O–UO_3–UO_2 phase diagrams (Lindemer *et al.*, 1981). And no thermodynamic studies exist for ternary compounds with the alkali ions containing tetravalent actinide ions. Thermochemical measurements have also been reported for a few ternary oxides of alkali metals and Np(VI). No thermochemical measurements have been reported for compounds of the alkali metal with other actinide oxides, surprisingly not even for the sodium plutonates.

(*i*) *Enthalpy of formation*

The enthalpies of formation of the alkali uranates are generally derived from enthalpy of solution measurements in hydrochloric or nitric acid, often involving very complex reaction cycles to compensate the oxidation of uranium. The measurements have been made for mixed compounds of the general formulas $nA_2O \cdot mUO_3$ (hexavalent U) and $nA_2O \cdot mUO_{2.5}$ (pentavalent U). All existing literature have been reviewed by Grenthe *et al.* (1992) and Guillaumont *et al.* (2003) using currently accepted auxiliary data. Johnson (1975) as well as Lindemer *et al.* (1981) discussed correlations and methods to estimate unknown enthalpies of formation for the complex alkali uranates up to high n/m ratios (e.g. $Cs_2O \cdot 15UO_3$), but their procedures are quite arbitrary.

For the alkali metal neptunates(VI) with the general formulas A_2NpO_4, $A_2Np_2O_7$, and A_4NpO_5, the enthalpies of formation were derived from the enthalpies of solution of the compounds in hydrochloric acid. These results were recently assessed by Lemire *et al.* (2001). The values of the enthalpies of formation of all these compounds are given in Table 19.11.

(*ii*) *Entropy*

Only a few low-temperature heat capacity measurements have been made for the alkali uranates, and they are restricted to sodium and cesium compounds (see Table 19.11). Lindemer *et al.* (1981) estimated the entropy values for the other alkali uranates assuming that $\Delta_r S$ for the formation reaction from the oxides is zero. The experimental results show that this is not the case and that the values for $\Delta_r S$ strongly depend on the crystallographic modification and tend to be slightly positive. For these reasons, the values by Lindemer *et al.* (1981) have not been included in the present tabulations.

(*iii*) *High-temperature properties*

High-temperature enthalpy increment measurements have been made for a few alkali uranates. These are essentially the same compounds for which low-temperature measurements have been performed. Most of the early data have been reviewed by Cordfunke and O'Hare (1978) and Cordfunke and Konings (1990) and they are summarized in Table 19.13. In the 1990s, the

Table 19.11 *Entropies and enthalpies of formation of crystalline complex alkali actinide oxides, from NEA-TDB* (*Grenthe* et al., 1992; *Lemire* et al., 2001; *Guillaumont* et al., 2003); *see text for explanation.*

	Li		*Na*		*K*		*Rb*		*Cs*	
	$S°$ (298.15 K) ($J K^{-1} mol^{-1}$)	$\Delta_f H°$ (298.15 K) ($kJ mol^{-1}$)	$S°$ (298.15 K) ($J K^{-1} mol^{-1}$)	$\Delta_f H°$ (298.15 K) ($kJ mol^{-1}$)	$S°$ (298.15 K) ($J K^{-1} mol^{-1}$)	$\Delta_f H°$ (298.15 K) ($kJ mol^{-1}$)	$S°$ (298.15 K) ($J K^{-1} mol^{-1}$)	$\Delta_f H°$ (298.15 K) ($kJ mol^{-1}$)	$S°$ (298.15 K) ($J K^{-1} mol^{-1}$)	$\Delta_f H°$ (298.15 K) ($kJ mol^{-1}$)
M_4UO_5	133.0 ± 6.0	–2639.4 ± 1.7		–2457.0 ± 2.2[a]						
M_2UO_4		–1968.2 ± 1.3	166.0 ± 0.5[b]	–1897.7 ± 3.5[b] –1884.6 ± 3.6[a]	*180 ± 8*	–1920.7 ± 2.2	*203 ± 8*	–1922.7 ± 2.2	219.66 ± 0.44	–1928.0 ± 1.2
MUO_3		–1522.3 ± 1.8	132.84 ± 0.40	–1494.9 ± 10.0		–1522.9 ± 1.7		–1520.9 ± 1.8		
$M_2U_2O_7$		–3213.6 ± 5.3	275.9 ± 1.0	–3203.8 ± 4.0		–3250.5 ± 4.5		–3232.0 ± 4.3	327.75 ± 0.66	–3220 ± 10
$M_2U_3O_{10}$		–4437.4 ± 4.1								
$M_2U_4O_{12}$									526.4 ± 3.5	–5571.8 ± 3.6
M_3UO_4			198.2 ± 0.4	–2024 ± 8						
$M_6U_7O_{24}$				–10841.7 ± 10.0						
M_2NpO_4		–1828.2 ± 5.8		–1763.8 ± 5.7[b] –1748.5 ± 6.1[a]		–1784.3 ± 6.4				–1788.1 ± 5.7
$M_2Np_2O_7$				–2894 ± 11		–2932 ± 11		–2914 ± 12		
M_4NpO_5				–2315.4 ± 5.7[a]						

[a] Beta form.
[b] Alpha form.

Indian group led by Venugopal and coworkers measured the enthalpy increments of a number uranates of potassium, rubidium, and cesium. They were reviewed by Guillaumont *et al.* (2003), and some of their recommendations have been included in Table 19.13.

(b) Ternary and quaternary oxides with alkaline-earth ions

(*i*) *Enthalpy of formation*

The following perovskites with alkaline-earth ions containing tetravalent actinide ions have been studied thermodynamically: $BaUO_3$ (Williams *et al.*, 1984; Cordfunke *et al.*, 1997), $BaPuO_3$ (Morss and Eller, 1989), $BaAmO_3$ and $SrAmO_3$ (Goudiakas *et al.*, 1990), $BaCmO_3$, and $BaCfO_3$ (Fuger *et al.*, 1993). Efforts to obtain the strontium analog of $BaUO_3$, $SrUO_3$, resulted in a perovskite phase with the empirical formula $Sr_2UO_{4.5}$ (crystallographic formula $Sr_2(Sr_{2/3}U_{1/3})UO_6$) (Cordfunke and IJdo, 1994). Also $BaUO_3$ cannot be prepared with a Ba/U ratio of exactly 1, as was found independently by Barrett *et al.* (1982), Williams *et al.* (1984), and Cordfunke *et al.* (1997). The latter two groups determined the enthalpy of the ideal composition by extrapolating the data for different Ba/U ratios and found excellent agreement [$-(1690 \pm 10)$ kJ mol^{-1} and $-(1680 \pm 10)$ kJ mol^{-1}]. However, there are several reports of studies on materials claimed to be $SrUO_3$ and $BaUO_3$. Huang *et al.* (1997a) derived the enthalpy of formation of $SrUO_{3.1}$ from Knudsen effusion mass spectrometric measurements. Ali *et al.* (2001) used a comparable method (but a complex reaction) for $SrThO_3$.

Using the Goldschmidt tolerance factor t, expressed as $t = (R_{Ba} + R_O)/(2^{1/2})(R_{An} + R_O)$, where R_{Ba}, R_O, and R_{An} represent the ionic radii of Ba^{2+}, O^{2-}, and the actinide 4+ ion, respectively, Morss and Eller (1989) showed that the enthalpy of formation of the complex oxides from BaO and AnO_2 becomes less favorable as t decreases. This correlation was extended by Fuger *et al.* (1993) to a large number of complex oxides of the general formula $MM'O_3$ (M = Ba, and M′ = Ti, Hf, Zr, Ce, Tb, U, Pu, Am, Cm, and M = Sr, and M′ = Ti, Mo, Zr, Ce, Tb, Am) and allowed the prediction of the enthalpy of formation of yet unprepared actinide(IV) complex oxides with BaO and SrO. This correlation was in accordance with the inability to obtain stoichiometric $BaUO_3$.

Cordfunke *et al.* (1997) suggested that a continuous series exists between $BaUO_3$–$Ba_{1+y}UO_{3+x}$–Ba_3UO_6. The oxidation of U^{4+} ions is accompanied by the formation of metal vacancies on the Ba and U sites, and Ba substitution on the U-vacancies, finally resulting in $Ba_2(Ba,U)O_6$. $Ba_2U_2O_7$ does not belong to this series, which is explained by the fact that $Ba_2U_2O_7$ is a complex oxide containing pentavalent uranium. For the system Sr–U–O it was shown by Cordfunke *et al.* (1999) that the enthalpies of formation of the U(VI) compounds linearly depend on the Sr/U ratio (Fig. 19.19). The data fall into two groups, the

pseudo-hexagonal types ($Sr_3U_{11}O_{36}$, $Sr_2U_3O_{11}$, $SrUO_4$, and UO_3) and the perovskite types ($Sr_5U_3O_{14}$, Sr_2UO_5, Sr_3UO_6). Takahashi *et al.* (1993) studied the enthalpies of formation of $SrUO_{4-y}$ ($0 \leq y \leq 0.5$) also finding an almost linear relationship.

Complex oxides of the formula $nAO \cdot mAnO_3$ with alkaline-earth ions containing hexavalent actinides are well known. AUO_4 compounds have been identified and thermochemically characterized for magnesium, calcium, strontium, and barium. Also the enthalpies of formation of many A_3AnO_6 (An = U, Np, Pu) and quaternary $Ba_2A'AnO_6$ (A′ = Mg, Ca, Sr and An = U, Np, Pu) compounds have been determined (see Table 19.12). All the values listed have been taken from the NEA assessments (Grenthe *et al.*, 1992; Silva *et al.*, 1995; Lemire *et al.*, 2001; Guillaumont *et al.*, 2003) except for those on curium and californium compounds (Fuger *et al.*, 1993).

The enthalpy of formation from the binary oxides, here called the enthalpy of complexation $\Delta_{cplx}H$, is an excellent measure for the stability of these compounds. It can be calculated easily for the uranates, but not for complex Np(VI) oxides or for complex Pu(VI) oxides, because NpO_3(c) and PuO_3(c) are unknown. For the construction of Fig. 19.20, we have therefore utilized the value estimated in Section 19.5.1. The exothermic enthalpy effect of the reactions indicated in Fig. 19.20 implies that the compounds are thermodynamically stable at room temperature, assuming a negligible entropy change upon the formation of the complex oxides from the binary oxides. Extrapolation of the trends indicated that the beryllium compounds are not stable under these conditions.

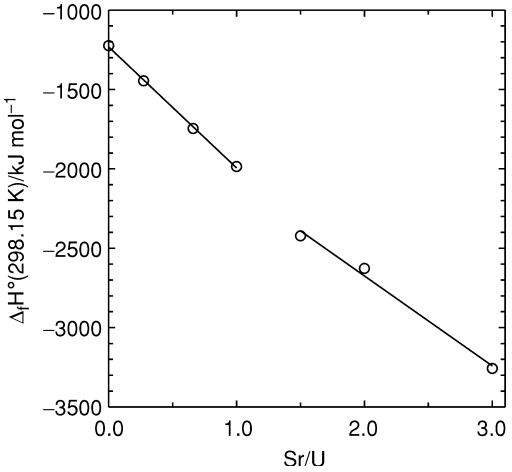

Fig. 19.19 *The enthalpy of formation in the strontium uranates in the Sr–U*^{VI}*–O system* (*after Cordfunke* et al., 1999).

Table 19.12 *Entropies and enthalpies of formation of crystalline complex alkaline-earth actinide oxides, from NEA-TDB* (*Grenthe* et al., 1992; *Silva* et al., 1995; *Lemire* et al., 2001; *Guillaumont* et al., 2003) *except for those on curium and californium compounds* (*Fuger* et al., 1993).

	Mg		*Ca*		*Sr*		*Ba*	
	$S°$(298.15 K) (J K^{-1} mol^{-1})	$\Delta_f H°$(298.15 K) (kJ mol^{-1})	$S°$(298.15 K) (J K^{-1} mol^{-1})	$\Delta_f H°$(298.15 K) (kJ mol^{-1})	$S°$(298.15 K) (J K^{-1} mol^{-1})	$\Delta_f H°$(298.15 K) (kJ mol^{-1})	$S°$(298.15 K) (J K^{-1} mol^{-1})	$\Delta_f H°$(298.15 K) (kJ mol^{-1})
MUO_3						–1672.6 ± 8.6		–1690 ± 10
MUO_4	131.95 ± 0.17	–1857.3 ± 1.5	121.1 ± 0.17	–2002.3 ± 2.3	153.15 ± 0.17[a]	–1989.6 ± 2.8[a] –1988.4 ± 5.4[b]	153.97 ± 0.31	–1993.8 ± 3.3
MU_2O_7							*260 ± 15*	–3237.2 ± 5.0
MU_3O_{10}	338.6 ± 1.0							
$M_2UO_{4.5}$						–2494.0 ± 2.3		
MU_4O_{13}						–5920 ± 20		
M_2UO_5						–2632.9 ± 1.9		
$M_2U_2O_7$							*296 ± 15*	–3740.0 ± 6.3
$M_2U_3O_{11}$						–5243.7 ± 5.0		
M_3UO_6				–3305.4 ± 4.1		–3263.4 ± 3.0	*298 ± 15*	–3210.4 ± 8.0
Ba_2MUO_6		–3245.9 ± 6.5		–3295.8 ± 5.9		–3257.3 ± 5.7		
$M_3U_2O_9$						–4620.0 ± 8.0		
$M_3U_{11}O_{36}$						–15903.8 ± 16.5		
$M_5U_3O_{14}$						–7248.6 ± 7.5		
M_3NpO_6						–3125.8 ± 5.9		–3085.6 ± 9.6
Ba_2MNpO_6		–3096.9 ± 8.2		–3159.3 ± 7.9		–3122.5 ± 7.8		
$MPuO_3$								–1654.2 ± 8.3
M_3PuO_6						–3042.1 ± 7.9		–2997 ± 10
Ba_2MPuO_6		–2995.8 ± 8.8		–3067.5 ± 8.9		–3023.3 ± 9.0		
$MAmO_3$						–1539.0 ± 7.9		–1544.6 ± 3.4
$MCmO_3$								–1517.8 ± 7.1
$MCfO_3$								–1477.9 ± 5.6

[a] Alpha form (rhombohedral).
[b] Beta form (orthorhombic).

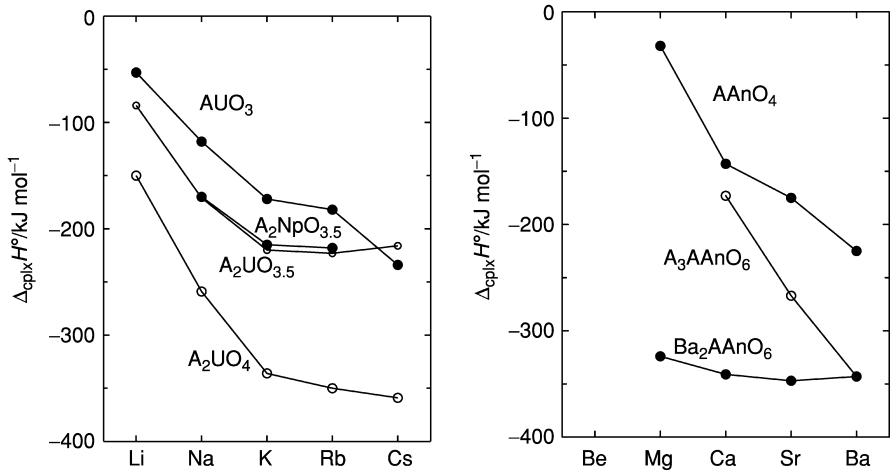

Fig. 19.20 *Enthalpies of complexation of complex actinide(VI) oxides where A represents a alkali or alkaline earth and An an actinide ion.*

There are, as of the time of writing, no thermochemical data on complex oxides containing trivalent actinides (e.g. $AmAlO_3$ or $SrAm_2O_4$). Indeed, such measurements are still lacking for the lanthanides.

(*ii*) *Entropy*

Low-temperature heat capacity measurements have been reported for a few alkaline-earth uranates. The data for the AUO_4 monouranates of the series A = Mg to Ba (Table 19.12) need some further discussion. The two measurements for $BaUO_4$ are discordant, though made by well-known research groups. The results of Westrum *et al.* (1980) give $S°(298.15\ K) = 177.84\ J\ K^{-1}\ mol^{-1}$ whereas the results of O'Hare *et al.* (1980) gave $153.97\ J\ K^{-1}\ mol^{-1}$. In most assessments the latter value is selected because the sample was better characterized. However, the values for the other alkaline-earth monouranates are from the same set of measurements by Westrum *et al.* (1980) and the reported data indicate a regular trend with molar volume for the orthorhombic compounds (A = Mg, Sr, Ba). The value of O'Hare *et al.* (1980) does not fit in the series, which would imply that the values for the other compounds measured by Westrum *et al.* (1980) are in error, which is not considered in the NEA-TDB selections (Grenthe *et al.*, 1992). Another way of looking at this problem is to consider the entropy of complexation from the oxides. The values for the orthorhombic monouranates derived from the measurements of Westrum *et al.* (1980) all suggest that the quantity $\Delta_{cplx}S°(298.15\ K)$ is positive which is

the case for most orthorhombic complex oxides. The result for $BaUO_4$ from O'Hare *et al.* (1980) in contrast, suggests a negative value. Clearly further measurements are required to solve this problem.

(*iii*) *High-temperature properties*

High-temperature heat capacity data have been measured for the AUO_4 compounds of the series A = Mg to Ba and have been evaluated by Cordfunke and O'Hare (1978); the resulting recommended equations are summarized in Table 19.13. They agree with the less exhaustive selections of the NEA assessment (Grenthe *et al.*, 1992). Melting points of these compounds are not known. The high-temperature properties of the other alkaline-earth compounds are poorly known. Recently, Japanese researchers have extensively studied materials claimed to be stoichiometric $BaUO_3$ and $SrUO_3$. The heat capacity (Matsuda *et al.*, 2001), thermal expansion, thermal conductivity and melting point (Yamanaka *et al.*, 2001), and the vaporization behavior (Huang *et al.*, 1997a) were measured. Vaporization measurements have also been made for $SrUO_3$ (Huang *et al.*, 1997b) and $BaPuO_3$ (Nakajima *et al.*, 1999b). Dash *et al.* (2000) reported enthalpy increments of $Sr_3U_{11}O_{36}$ and $Sr_3U_2O_9$. The relevant thermodynamic data extracted from these studies are listed in Table 19.12.

(c) Other ternary and quaternary oxides/oxysalts

Enthalpies of formation data for uranium carbonates, nitrates, phosphates, arsenates, and silicates have been measured and the available data were reviewed and summarized in the NEA-TDB assessments (Grenthe *et al.*, 1992; Guillaumont *et al.*, 2003). Heat capacity and entropy data have hardly been measured for these compounds and only estimates are available. The data are summarized in Table 19.14. Also included are the enthalpies of formation of several actinide (Th,U) bearing mineral phases reported by Helean *et al.* (2002, 2003) and by Mazeina *et al.* (2005) using high temperature solution calorimetry. Data for complex oxides or oxyacids of other actinides are not known with sufficient accuracy for inclusion in this chapter.

19.6 HALIDES

Because of the fundamental and applied interest in the many actinide halides, their thermodynamic properties have received much attention. The authoritative assessment by Fuger *et al.* (1983), which formed the basis for the data in the second edition of this work, is still the major source of information though parts of it have been updated in the NEA-TDB series on *Chemical Thermodynamics* (U through Am).

Table 19.13 *High-temperature heat capacity of selected crystalline complex actinide oxides;* $C_p/(\mathrm{J\ K^{-1}\ mol^{-1}}) = a(\mathrm{T/K})^{-2} + b + c(\mathrm{T/K}) + d(\mathrm{T/K})^2$ (*estimated values are in italics, maximum temperatures in brackets*).

		a ($\times 10^{-6}$)	b	c ($\times 10^{3}$)	d ($\times 10^{6}$)	T (K)	ΔH (kJ mol^{-1})	*References*
$NaUO_3$		–1.0966	115.491	19.1672		[1000]		[a]
Na_2UO_4	(α)	–2.09664	162.5384	25.8857		1193	20.92	[b]
	(β)		224.6743					[b]
Na_3UO_4		–2.08007	188.901	25.1788				[c]
$Na_2U_2O_7$	(α)	–3.54904	262.831	14.6532				[a]
	(β)		280.571					[a]
KUO_3			133.258	12.558		[800]		[d]
$K_2U_2O_7$			149.084	269.5		[800]		[d]
Cs_2UO_4		–1.52851	164.8814	17.0232				[c]
$Cs_2U_2O_7$		–1.13403	221.532	75.3158				[c]
$Cs_2U_4O_{12}$		–5.4375	423.7262	71.9406				[c]
$MgUO_4$			110.2681	66.7959	23.4381			[b]
$CaUO_4$	(α)		115.6039	46.819		1025	0.920	[b]
	(β)		113.0100	52.6347				[b]
$SrUO_4$	(α)	0.64475	102.7703	69.0394				[c]
$Sr_3U_2O_9$		–4.6201	319.18	116.02				[e]
$Sr_3U_{11}O_{36}$		–0.3954	962.72	355.26		[1000]		[e]
$BaUO_4$		–2.7776	153.7812	9.1788				[c]
$BaUO_3$		–0.142	126.6	16.1		2450		[f]

[a] Cordfunke *et al.* (1982).
[b] Cordfunke and O'Hare (1978).
[c] Cordfunke and Konings (1990).
[d] Guillaumont *et al.* (2004).
[e] Dash *et al.* (2000).
[f] Matsuda *et al.* (2001); Yamanaka *et al.* (2001).

Table 19.14 *Thermodynamic properties of selected crystalline miscellaneous actinide oxyacids and oxysalts.*

	$S°$(298.15 K) (J K^{-1} mol^{-1})	$\Delta_f H°$(298.15 K) (kJ mol^{-1})	*References*
$Th(NO_3)_4$		–1445.6 ± 12.6	a
$Th(NO_3)_4 \cdot 4H_2O$		–2707.0 ± 12.6	a
$Th(NO_3)_4 \cdot 5H_2O$	543.1 ± 0.4	–3007.9 ± 4.2	a
$ThTi_2O_6$		–3096.5 ± 4.3	b
$ThSiO_4$ (thorite)		–2117.6 ± 4.2	b
$ThSiO_4$ (huttonite)		–2110.9 ± 4.7	b
UO_2CO_3	144.2 ± 0.3	–1691.3 ± 1.8	c
$UO_2(NO_3)_2$	*241 ± 9*	–1351.0 ± 5.0	c
$UO_2(NO_3)_2 \cdot 2H_2O$	*327.5 ± 8.8*	–1978.7 ± 1.7	c
$UO_2(NO_3)_2 \cdot 3H_2O$	*367.9 ± 3.3*	–2280.4 ± 1.7	c
$UO_2(NO_3)_2 \cdot 6H_2O$	505.6 ± 2.0	–3167.5 ± 1.5	c
$UO_3 \cdot 1/2NH_3 \cdot 1⅓H_2O$		–1770.3 ± 0.8	a
$UO_3 \cdot ½NH_3 \cdot 1½H_2O$		–1741.3 ± 0.8	a
$UO_3 \cdot ⅔NH_3 \cdot 1⅓H_2O$		–1705.8 ± 0.8	a
$USiO_4$	*118 ± 12*	–1991.3 ± 5.4	c
$U_{0.97}Ti_{2.03}O_6$		–2977.9 ± 3.5	b
$Ca_{1.46}U_{0.69}Ti_{1.85}O_7$		–3610.6 ± 4.1	b
$(UO_2)_3(PO_4)_2$	*410 ± 14*	–5491.3 ± 3.5	c
$(UO_2)_2P_2O_7$	*296 ± 21*	–4232.6 ± 2.8	c
UPO_5	*137 ± 10*	–2064 ± 4	c
UP_2O_7	*204 ± 12*	–2852 ± 4	c
UO_2SO_4	*163.2 ± 8.4*	–1845.1 ± 0.84	c
$UO_2SO_4 \cdot 2.5H_2O$	*246.1 ± 6.8*	–2607.0 ± 0.9	c
$UO_2SO_4 \cdot 3H_2O$	*274.1 ± 16.6*	–2751.5 ± 4.6	c
$UO_2SO_4 \cdot 3.5H_2O$	*286.5 ± 6.6*	–2901.6 ± 0.8	c
$U(SO_4)_2$	*180 ± 21*	–2309.6 ± 12.6	c
$U(SO_4)_2 \cdot 4H_2O$	*359 ± 32*	–3483.2 ± 6.3	c
$U(SO_4)_2 \cdot 8H_2O$	*538 ± 52*	–4662.6 ± 6.3	c
$(UO_2)_3(AsO_4)_2$	*387 ± 30*	–4689.4 ± 8.0	c
$(UO_2)_2As_2O_7$	*307 ± 30*	–3426.0 ± 8.0	c
$UO_2(AsO_3)_2$	*231 ± 30*	–2156.6 ± 8.0	c
$NpO_2(NO_3)_2 \cdot 6H_2O$	*516.3 ± 8.0*	–3008.2 ± 5.0	c
$PuTi_2O_6$		*–2909 ± 8*	b

[a] Cordfunke and O'Hare (1978).
[b] Helean *et al.* (2002, 2003); Mazeina *et al.* (2005).
[c] NEA-TDB (Grenthe *et al.*, 1992; Silva *et al.*, 1995; Lemire *et al.*, 2001; Guillaumont *et al.*, 2003).

19.6.1 Hexahalides

(a) Solid hexahalides

The enthalpy of formation of UF_6 is a key value for the U–F thermochemistry. This value is well established by fluorine combustion calorimetry (Johnson, 1979). The heat capacity of UF_6 has been measured accurately up to the melting point and beyond (Brickwedde *et al.*, 1948), from which the entropy can be

Table 19.15 *Thermodynamic properties of the crystalline hexa- and pentahalides at* 298.15 K*; estimated vales are given in italics.*

	C_p(298.15 K) (J K^{-1} mol^{-1})	$S°$(298.15 K) (J K^{-1} mol^{-1})	$\Delta_f H°$(298.15 K) (kJ mol^{-1})	*References*
UF_6	166.8 ± 0.2	227.6 ± 1.3	–2197.7 ± 1.8	[a]
UCl_6	175.7 ± 4.2	285.5 ± 1.7	–1066.5 ± 3.0	[a]
NpF_6	167.44 ± 0.40	229.09 ± 0.50	*–1970 ± 20*	[a]
PuF_6	*168.1 ± 2.0*	221.8 ± 1.1	*–1861 ± 20*	[a]
$PaCl_5$	–	*238 ± 8*	–1147.8 ± 14.4	[b]
$PaBr_5$	–	*289 ± 17*	–866.8 ± 14.9	[b]
$UF_5(\alpha)$	132.2 ± 4.2	199.6 ± 3.0	–2075.3 ± 5.9	[a]
$UF_5(\beta)$	*132.2 ± 12.0*	*179.5 ± 12.6*	–2083.2 ± 4.2	[a]
UCl_5	*150.6 ± 8.4*	*242.7 ± 8.4*	–1039.0 ± 3.0	[a]
UBr_5	*160.7 ± 8.0*	*292.9 ± 12.6*	–810.4 ± 8.4	[a]
NpF_5	*132.8 ± 8.0*	*200 ± 3*	*–1941 ± 25*	[a]

[a] NEA-TDB (Grenthe *et al*., 1992; Lemire *et al*., 2001; Guillaumont *et al*., 2003).
[b] Fuger *et al*. (1983) taking in account the enthalpy of dissolution of the standard state of the metal (Fuger *et al*., 1978) and more recent auxiliary values.

derived. The resulting values are summarized in Table 19.15. Unfortunately the situation is different for NpF_6 and PuF_6. Low-temperature heat capacity measurements have been made for NpF_6, also into the liquid range, but a determination of its enthalpy of formation is lacking. Lemire *et al*. (2001) derived this quantity from the estimated difference $\{\Delta_f H°(MF_6, cr) - \Delta_f H°(MO_2^{2+}, aq)\}$ obtained by interpolation in the AnF_6 series. For PuF_6, no thermodynamic measurements of the solid phase have been made except for the vapor pressure. But since the properties of the gas phase are well established (see below), the enthalpy of formation and the standard entropy can be derived with reasonable accuracy.

UCl_6 is the only known solid actinide hexachloride. Its thermochemical properties were intensely studied in the World War II period. Thereafter Gross *et al*. (1971) and Cordfunke *et al*. (1982) performed enthalpy-of-solution studies on this compound and derived the enthalpy of formation. As discussed by Grenthe *et al*. (1992) the values for UCl_6 from these two studies disagree (unlike similar work for UCl_5) and the results of Cordfunke *et al*. (1982) were selected. The heat capacity and entropy for UCl_6 at low temperature were measured by Ferguson and Rand in the early 1940s, as reported in Katz and Rabinowitch (1951); the high-temperature heat capacity of UCl_6 is an estimate by Barin and Knacke (1973).

The high-temperature heat capacity equations plus the melting data of the hexahalides are summarized in Table 19.16.

(b) Gaseous hexahalides

The gaseous hexafluorides of U, Np, and Pu were studied extensively in the 1950s and 1960s. Gas-phase electron diffraction, Raman, and infrared studies

have established the octahedral structure (O_h symmetry) and the molecular and vibrational parameters. From these data the entropies can be calculated accurately; the major uncertainty coming from neglect of excited electronic states for incompletely filled f-shells. The enthalpies of formation of these species can then be obtained from analyses of the vapor pressure measurements that have been performed and such data have been derived in the NEA-TDB series (Grenthe *et al.*, 1992; Lemire *et al.*, 2001; Guillaumont *et al.*, 2003). The molecular properties of AmF_6, and thus the entropy, can be extrapolated from those of the other actinide hexahalides (Kim and Mulford, 1990). Its enthalpy of formation is derived from the extrapolation of the mean bond enthalpy of the other actinide hexahalides, which linearly varies along the actinide series.

Except for UCl_6, no other gaseous hexachlorides are known. The molecular properties of UCl_6 have not been determined experimentally. Estimates (Hildenbrand *et al.*, 1985) have been used in the NEA assessments (Grenthe *et al.*, 1992; Guillaumont *et al.*, 2003) but more recently reliable results from quantum chemical calculations have become available (Han, 2001). An approximate value for the enthalpy of formation of UCl_6 is derived from vapor pressure measurements performed in the 1940s (see Grenthe *et al.* (1992)).

19.6.2 Pentahalides

(a) Solid pentahalides

Fuger *et al.* (1983) accepted the enthalpies of formation of $PaCl_5$, $PaBr_5$, and α-UF_5 and β-UF_5 (as well as some intermediate uranium fluorides) to be well established based upon single reliable thermochemical studies by Fuger and Brown (1975) for the Pa compounds, and by O'Hare *et al.* (1982) for the UF_5 modifications. For UCl_5, Fuger *et al.* (1983) discussed the results of three different studies, but these gave an unclear picture. The discrepancy seems to be resolved by the measurements of Cordfunke *et al.* (1982). Properties of UBr_5 are based on high-temperature heterogeneous equilibria and have large uncertainties when extrapolated to 298.15 K. The other pentahalides (PaF_5, NpF_5) have not been studied thermochemically. The properties of PaF_5 cannot yet be estimated because of insufficient experimental data. Those of NpF_5 have been approximated by Lemire *et al.* (2001) on the basis of the experimental observation that NpF_5 does not disproportionate to NpF_6(g) and NpF_4(cr) below 591 K (Malm *et al.*, 1993).

The experimental basis for the entropies of the actinide pentahalides is very poor. Low-temperature heat capacity measurements have only been reported for UF_5 (Brickwedde *et al.*, 1951), but the sample contained 17% UF_4 and UO_2F_2. Fuger *et al.* (1983) adjusted the result for S°(298.15 K) by $+11.3\ J\ K^{-1}\ mol^{-1}$, to be consistent with dissociation pressure measurements in the U–F system. Fuger *et al.* also gave (rough) estimates of the entropies of $PaCl_5$, $PaBr_5$, and UCl_5, based on a systematic difference between MX_4 and MX_5 compounds.

Table 19.16 *High-temperature heat capacity of the actinide halides;* $C_p/(\mathrm{J\ K^{-1}\ mol^{-1}}) = a(\mathrm{T/K})^{-2} + b + c(\mathrm{T/K}) + c(\mathrm{T/K})^2$ (*estimated values in italics*); $T_{min} = 298.15$ K*;* T_{trs} *and* $\Delta_{trs}H$ *refer to transition or fusion, as can be deduced from the phase indicators.*

		a ($\times 10^6$)	b	c ($\times 10^3$)	T_{trs} (K)	$\Delta_{trs}H$ (kJ mol^{-1})	*References*
UF_6	cr		52.318	383.798	337.20	19.196	a
	l	–2.87646	215.338	1.9962			a
NpF_6	cr		62.333	352.547	327.91	17.520	a
	l		150.344	110.076			a
PuF_6	cr		168.1		*317*	*17.0*	a
UCl_6	cr	–0.7406	173.427	35.0619	*452*	*20.9*	b
	l		214				b
UF_5	β	–0.1926	125.478	30.2085	398		a
UF_5	α	–0.1926	125.478	30.2085	621		a
$PaCl_5$	cr				579	31.5	b
UCl_5	cr		140.164	35.564	*600*	*35.6*	a
$PaBr_5$	cr				556	35.4	b
ThF_4	cr	–1.255	122.173	8.37	1383	*41.8*	b
	l		*133.9*				b
UF_4	cr	–0.41316	114.5194	20.5549	1309	44.79	c
	l		174.0				c
NpF_4	cr	–0.83646	122.635	9.684	*1305*	*47*	a
PuF_4	cr	–1.091	127.53	3.114	*1300*	*47*	a
$ThCl_4$	cr	*–0.615*	*120.290*	*23.267*	1043	61.5	b
	l		*167.4*				b
$PaCl_4$	cr				*950*		b
UCl_4	cr	–0.0900	106.859	48.6448	863	49.8	a
	l		162.34				a
$NpCl_4$	cr	*–0.11*	*112.5*	*36*	*811*	*59.6*	a

$ThBr_4$	β	*–0.62*	*127.6*	*15.1*	952	*54.4*	c
	l		171.5				c
UBr_4	cr		119.244	29.7064	791	36 ± 5	a
	l		*172*				b
$NpBr_4$	cr		119	30	*800*	*50*	a
ThI_4	cr	*–0.6067*	*129.7*	*12.97*	843	*48*	b
	l		176				b
UI_4	cr	–1.97485	145.603	9.9579	*779*	*38*	a,b
	l		165.7				b
UF_3	cr	–1.0355	106.541	0.70542	1768	36.8	a
NpF_3	cr	–1.0	105.2	0.812	*1735*	*36.1*	a
PuF_3	cr	–1.0355	104.078	0.707	1700	*35.4*	a
AmF_3	cr				1666 ± 20		e
CmF_3	cr				1679 ± 20		e
UCl_3	cr	0.4583	87.78	31.120	1115	49.0	a
$NpCl_3$	cr	0.36	89.6	27.5	*1075*	*50*	a
$PuCl_3$	cr	0.24	91.35	24	1041	55	a
$AmCl_3$	cr				990 ± 5	48.1 ± 0.4	d,e,f
$CmCl_3$	cr				997 ± 5	47.9 ± 0.4	d,e
UBr_3	cr		97.971	26.360	1003	43.9	a
$NpBr_3$	cr	–0.32	101.23	20.68	*975*	*48*	a
$PuBr_3$	cr	–0.638	104.5	15.0	935	47.1	a
UI_3	cr		105.018	24.2672	*800*		a

[a] NEA-TBD (Grenthe *et al.*, 1992; Lemire *et al.*, 2001; Guillaumont *et al.*, 2003).
[b] Fuger *et al.* (1983).
[c] Rand (1975).
[d] Burnett (1966).
[e] Weigel and Kohl (1985).
[f] Peterson and Burns (1973).

Their value for $PaCl_5$ is, however, significantly lower than that derived by Kovács *et al.* (2003) by combining the entropy of sublimation from the work of Weigel *et al.* (1969) with the entropy of the gas obtained from quantum chemical data. A comparison to other MCl_5 compounds showed that this value for solid $PaCl_5$ is unexpectedly high compared to UCl_5 and the transition metal pentahalides, which Kovács *et al.* attributed to the distinctly different crystal structure of $PaCl_5$ (pentagonal bipyramidal). However, no calorimetric measurements have been performed for any of the pentachloride compounds, and all entropies have been derived from (other complex) solid–gas equilibria.

The selected solid pentahalide data are listed in Table 19.15.

(b) Gaseous pentahalides

$PaCl_5$, $PaBr_5$, UF_5, UCl_5, UBr_5, and PuF_5 are the only gaseous pentahalides that have been studied experimentally. Vapor pressure measurements for the protactinium pentahalides were reported by Weigel *et al.* (1969, 1974) from which the enthalpy of formation of $PaCl_5$ has been derived (see Table 19.17). The interpretation of the UF_5 vapor pressure measurements is complicated due to the existence of dimeric molecules and dissociation reactions. The enthalpy of formation of UF_5 can also be derived from molecular equilibrium measurements by mass spectrometry. At least six such studies have been performed. They were reviewed in the NEA-TDB (Grenthe *et al.*, 1992; Guillaumont *et al.*, 2003) and the recommended values from that work are included in Table 19.17. Also for UCl_5(g) and UBr_5(g), molecular equilibrium studies have been performed. The derived enthalpies of formation are included in Table 19.17. An approximate value for the enthalpy of formation of PuF_5 was calculated indirectly from ionization potential measurements by Kleinschmidt (1988), but since this value is rather uncertain, it is not included.

Table 19.17 *Thermodynamic properties of the gaseous hexa- and pentahalides; estimated values are given in italics.*

	$S°$(298.15 K) (J K^{-1} mol^{-1})	$\Delta_f H°$(298.15 K) (kJ mol^{-1})	*References*
UF_6	376.3 ± 1.0	–2148.6 ± 1.9	[a]
UCl_6	438.0 ± 5.0	–985.5 ± 5	[a]
NpF_6	376.643 ± 0.500	–1921.66 ± 20.00	[a]
PuF_6	368.90 ± 1.00	–1812.7 ± 20.1	[a]
AmF_6	399.0 ± 5.0	*–1606 ± 30*	[a]
PaF_5	385.6	–2130 ± 50	[b]
$PaCl_5$	440.8	–1042 ± 15	[b]
UF_5	386.4 ± 10.0	–1913 ± 15	[a]
UCl_5	438.7 ± 5.0	– 900 ± 15	[a]
UBr_5	498.7 ± 5.0	–648 ± 15	[a]

[a] NEA-TDB (Grenthe *et al.*, 1992; Lemire *et al.*, 2001; Guillaumont *et al.*, 2003).
[b] Kovács *et al.* (2003).

Little experimental information exists on the molecular properties of the actinide pentahalides. Spectroscopic experiments of matrix-isolated UF_5 molecules (Kunze *et al.*, 1976; Paine *et al.*, 1976; Jones and Ekberg, 1977) indicate a tetragonal pyramidal structure (C_{4v}). Quantum chemical calculations (Wadt and Hay, 1979; Onoe *et al.*, 1997) showed that energy barrier between the C_{4v} and the trigonal bipyramidal structure (D_{3h}) is small (<4 kJ mol^{-1}) and it was suggested that the structure of UF_5 may be fluxional between C_{4v} and D_{3h} at high temperatures. Quantum chemical calculations of PaF_5 and $PaCl_5$ gave similar results (Kovács *et al.*, 2003). The derived entropy values are included in Table 19.17. It is likely that the Pa compounds follow the trend in the d-transition metal halides and have a D_{3h} equilibrium structure, whereas the U pentahalides have a C_{4v} equilibrium structure as a result of stronger participation of the 5f electrons in the An–F bonding.

19.6.3 Tetrahalides

(a) Solid tetrahalides

(*i*) *Enthalpy of formation*

Knowledge of actinide tetrafluoride enthalpies of formation is relatively poor. UF_4 has been studied extensively but the review by Grenthe *et al.* (1992) lists 14 experimental studies that show considerable scatter. Their selected value is based on reliable thermochemical cycles with UF_6(cr) using fluorine combustion calorimetry (Johnson, 1985) and UO_3(cr) using solution calorimetry (Cordfunke and Ouweltjes, 1981), which yielded values that differ by 10.7 kJ mol^{-1}. For ThF_4 the values derived from combustion calorimetry and high-temperature equilibria are discordant, as was discussed in detail by Wagman *et al.* (1977). We adopt here the value recommended by these authors, with increased uncertainty limits. For PuF_4, there are only estimates from the high-temperature equilibria, as discussed in detail by Lemire *et al.* (2001). Estimates of the enthalpies of formation of AmF_4 and CmF_4 can be derived from decomposition measurements by Gibson and Haire (1988a,b). We have accepted the assessed values for UF_4, NpF_4, and PuF_4 of the NEA-TDB (Grenthe *et al.*, 1992; Silva *et al.*, 1995; Lemire *et al.*, 2001) and made estimates of tetrafluoride thermochemistry with those of other tetravalent compounds.

The situation for the other tetrahalides is globally better. The most reliable values for UCl_4 of the ten studies performed cluster around −1019 kJ mol^{-1} (Grenthe *et al.*, 1992). Also the enthalpies of formation of thorium, protactinium, uranium, and neptunium tetrahalides appear to be well established. For the thorium and protactinium compounds, we have accepted the recommended values by Fuger *et al.* (1983) for the uranium, neptunium, plutonium, and americium compounds as the recommended values of NEA-TDB (Grenthe *et al.*, 1992; Lemire *et al.*, 2001; Guillaumont *et al.*, 2003). Table 19.18

Table 19.18 *Thermodynamic properties of crystalline actinide(IV) halides at* 298.15 K (*estimated values in italics*); *see text for references.*

	AnF_4(cr)		$AnCl_4$(cr)		$AnBr_4$(cr)		AnI_4(cr)	
An	$S°$(298.15 K) (J K^{-1} mol^{-1})	$\Delta_f H°$(298.15 K) (kJ mol^{-1})	$S°$(298.15 K) (J K^{-1} mol^{-1})	$\Delta_f H°$(298.15 K) (kJ mol^{-1})	$S°$(298.15 K) (J K^{-1} mol^{-1})	$\Delta_f H°$(298.15 K) (kJ mol^{-1})	$S°$(298.15 K) (J K^{-1} mol^{-1})	$\Delta_f H°$(298.15 K) (kJ mol^{-1})
Th	142.05 ± 0.21	–2097.9 ± 8.4	*183.5 ± 5*	–1186.2 ± 1.7	*227 ± 5*	–964.4 ± 2.1[a]	*251 ± 5*	–670.7 ± 2.1
Pa	*153 ± 3*	*–1946*	*196 ± 5*	–1046.3 ± 14.3	*238 ± 5*	–828.4 ± 14.3	*262 ± 5*	–525.2 ± 16.6
U	151.7 ± 0.2	–1914.2 ± 4.2	197.2 ± 0.8	–1018.8 ± 2.5	*240 ± 5*	–802.1 ± 2.5	*264 ± 5*	–518.3 ± 2.8
Np	*148 ± 3*	*–1874 ± 16*	*196 ± 5*	–984.0 ± 1.8	*233 ± 5*	–771.2 ± 1.8		
Pu	147.25 ± 0.37	*–1850 ± 20*	*195 ± 5*[b]	*–968.7 ± 5.0*[b]				
Am	*149 ± 5*	*–1724 ± 17*						
Cm	*135 ± 5*	*–1689*						
Bk		*–1793*						
Cf		*–1623*						
Es		*–1521*[b]						

[a] Beta modification.
[b] Believed to be unstable.

lists and Fig. 19.21 plots the enthalpies of formation of all known tetravalent actinide compounds and the aqueous ions as a function of Z. The enthalpy scale has been compressed to facilitate comparison. Interpolations can be made, using the best-fit curves shown, because each set of tetravalent compounds is isostructural, and other enthalpies of formation have thereby been estimated. The differences between the values thus calculated and those predicted by Fuger *et al.* (1983) are relatively small.

An interesting but unstable compound is $PuCl_4$. It has been detected in the gas phase by Gruen and DeKock (1967). Abraham *et al.* (1949) observed an increased volatility of $PuCl_3$ in a stream of chlorine gas. This was explained by the formation of gaseous $PuCl_4$, which decomposed to form solid $PuCl_3$ and Cl_2 upon condensation. Nevertheless, by comparison with other tetrahalides and complex chlorides, the enthalpy of formation of $PuCl_4$(s) is predictable within narrow error limits and has been included in Table 19.18 and Fig. 19.21.

(*ii*) *Heat capacity and entropy*

The low-temperature heat capacities of ThF_4, UF_4, PuF_4, and UCl_4 have been measured experimentally. The results for the fluorides are reliable. The measurements for UF_4 have been made down to 1.3 K and include careful analysis of the excess entropy contribution arising from the Schottky anomaly that corresponds to a crystal field level of 10.7 cm^{-1} for the U^{4+} ions at the C_2 symmetry site (one-third of the ions). The heat capacity measurements for UCl_4 (15–355 K) date from the World War II period and have only been reported in summary in the *Chemistry of Uranium* by Katz and Rabinowitch (1951). The recommended entropies of these actinide tetrahalides are listed in Table 19.18. We have estimated the entropies of the other tetrafluorides and tetrachlorides from these values using equations (19.10) and (19.11), and the procedure described for the dioxides.

The values for the tetrabromides and tetraiodides are estimates based on extrapolation of the trend F to I. It is known from transition metal and lanthanide halides that the entropies regularly increase as a function of the logarithm of the halide mass. Fig. 19.22 shows the relationship between the entropy divided by the number of halide ligands (n) for the uranium and europium halides. We have extrapolated the almost parallel relations as indicated, and used the estimated values for the UBr_4 and UI_4 as a basis for the estimation.

(*iii*) *High-temperature properties*

High-temperature data for the actinide tetrahalides are even more problematic. Experimental enthalpy increment data have been measured for UF_4 and ThF_4 crystal, but the results of ThF_4 are unpublished (see Fuger *et al.* (1983) and references therein). No high-temperature data for the tetrabromides have been

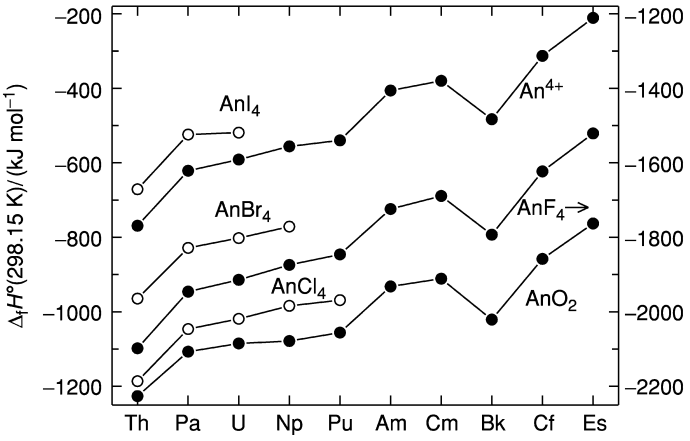

Fig. 19.21 *Comparison of enthalpies of formation of actinide(IV) species.*

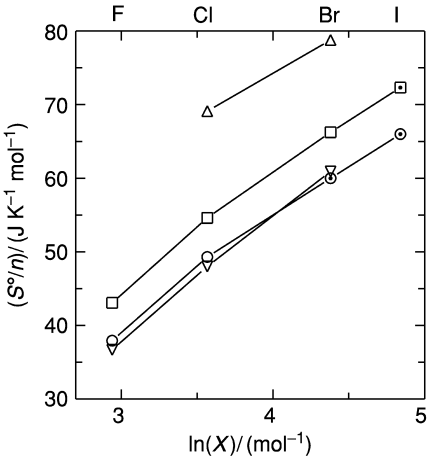

Fig. 19.22 *The relation between the entropy divided by the number of halide ligands n and the logarithm of the halide mass (X), for the uranium and europium halides;* □, UX_3, ○, UX_4, Δ, UOX_2, ▽, EuX_3. *Estimated values are indicated by dotted symbols.*

reported, but a heat capacity study of UI_4 was made by Popov *et al.* (1959). This study indicated a phase transition close to the melting point. From these data the heat capacity of the other actinide tetrahalides were estimated with reasonable accuracy by Fuger *et al.* (1983) and later by the NEA-TDB (Grenthe *et al.*, 1992; Lemire *et al.*, 2001; Guillaumont *et al.*, 2003). The values thus obtained are listed in Table 19.16.

(b) Gaseous tetrahalides

The gaseous tetrahalides of uranium have been the subject of studies for many years. Early electron diffraction studies were interpreted as a tetrahedral (T_d) structure whereas later measurements on UX_4 molecules seem to indicate a distorted tetrahedron. The latter seemed to be confirmed by analyses of vapor pressure data (Hildenbrand, 1988), which gave good second/third law agreement in case a C_{2v} molecular structure was assumed. Only in the 1990s it was established with certainty by a combination of gas-phase electron diffraction, high-temperature gas-phase infrared spectroscopy, and quantum chemical calculations that UF_4 and UCl_4 have a tetrahedral structure (Haaland *et al.*, 1995; Konings *et al.*, 1996). The entropies of UF_4 and UCl_4 calculated from the molecular and vibrational parameters derived from these studies are consistent with the entropies obtained from vapor pressure measurements, which have been reported for most of these compounds. Konings and Hildenbrand (1998) discussed in detail that this is essentially true for all known gaseous actinide tetrahalides, for which they estimated the molecular and vibrational parameters in a systematic manner. Since then further electron diffraction results and also results from quantum chemical calculations have become available, which have led to further refinement of the recommended values.

The calculated entropies and the enthalpies of formation derived from vapor pressure measurements for these species are listed in Table 19.19. The numbers principally come from the NEA-TDB reviews, in which the most recent refinements have not been included and a simplified approach to the estimation of the vibrational frequencies was used. However, since this will have a moderate effect, we have accepted these numbers.

19.6.4 Trihalides

(a) Solid trihalides

(*i*) *Enthalpy of formation*

Trigonal trifluorides are known for all the actinides Ac and U–Cf. Surprisingly, thermodynamic measurements have been performed only for UF_3 and PuF_3; even more surprising is the unsatisfactory situation regarding even these two trifluorides. Fuger *et al.* (1983) and later Grenthe *et al.* (1992) have evaluated all of the experimental results and listed their unresolved questions. For UF_3 several independent thermochemical pathways have been used, yielding unresolvable inconsistencies with a variety of uranium species; sample impurities plagued the fluorine combustion measurements and complex thermochemical cycles, involving many species, obfuscate the solution calorimetry measurements. For PuF_3 the one measurement (Westrum and Eyring, 1949) is uncertain primarily because it was a reaction to an unanalyzed trifluoride precipitate assumed to be anhydrous but probably $PuF_3 \cdot 0.4H_2O$. Nevertheless,

Table 19.19 *Thermodynamic properties of the gaseous tetra- and trihalides; estimated values are in italics.*

Molecule	$S°$(298.15 K) (J K^{-1} mol^{-1})	$\Delta_f H°$(298.15 K) (kJ mol^{-1})	*References*
ThF_4	351.6 ± 3.0	–1748.2 ± 8.4	[a]
$ThCl_4$	398.5 ± 3.0	–953.4 ± 1.8	[a]
$ThBr_4$	443.6 ± 3.0	–746.3 ± 2.3	[a]
ThI_4	503.8 ± 5.0	–436.9 ± 2.3	[a]
UF_4	360.7 ± 5.0	–1605.2 ± 6.5	[b]
UCl_4	409.3 ± 5.0	–815.4 ± 4.7	[b]
UBr_4	451.9 ± 5.0	–605.6 ± 4.7	[b]
UI_4	499.1 ± 8.0	–305.0 ± 5.7	[b]
NpF_4	369.8 ± 10.0	–1561 ± 22	[b]
$NpCl_4$	423.0 ± 10.0	–787.0 ± 4.6	[b]
PuF_4	359.0 ± 10.0	–1548 ± 22	[b]
$PuCl_4$	409.0 ± 10.0	–792.0 ± 10.0	[b]
UF_3	347.5 ± 10.0	–1065 ± 20	[b]
UCl_3	380.3 ± 10.0	–523 ± 20	[b]
UBr_3	403 ± 15	–371 ± 20	[b]
UI_3	431.2 ± 10.0	–137 ± 25	[b]
PuI_3	*435 ± 15*	*– 305 ± 15*	[b]
NpF_3	330.5 ± 5.0	–1115 ± 25	[b]
$NpCl_3$	362.8 ± 10.0	–589.0 ± 10.4	[b]
PuF_3	336.1 ± 10.0	–1167.8 ± 6.2	[b]
$PuCl_3$	368.6 ± 10.0	–647.4 ± 4.0	[b]
$PuBr_3$	423 ± 15	–488 ± 15	[b]
AmF_3	330.4 ± 8.0	–1156.5 ± 16.6	[b]

[a] Recalculated in this study.
[b] NEA-TDB (Grenthe *et al.*, 1992; Lemire *et al.*, 2001; Guillaumont *et al.*, 2003).

these two data points must be used to compare and to predict the properties of all f-element trifluorides.

Fortunately, there are enthalpy-of-formation data on almost all lanthanide trifluorides, though not all of them are reliable (Konings and Kovács, 2003). Table 19.20 and Fig. 19.23 present these data along with structural data that permit a correlation of the quantity $\{\Delta_f H°(MF_3,cr) - \Delta_f H°(M^{3+},aq)\}$ with the ionic radii. It can be seen that the most reliable data for the lanthanide trifluorides fall into two groups of different crystal structures (trigonal/hexagonal and orthorhombic), and that the two actinide trifluorides (trigonal) do not clearly fit to this trend. Clearly, the correlation is less evident than for the lanthanide chlorides, bromides, and iodides so that the correlation will have limited value until better lanthanide and actinide trifluoride enthalpy measurements are made.

Trichlorides, tribromides, and triiodides of all elements from uranium through einsteinium are known. Solution calorimetry enthalpies of formation

Table 19.20 *Enthalpies of formation and entropies of the crystalline lanthanide and actinide trifluorides; estimated values are in italics.*

	$S°$(298.15 K) (J K^{-1} mol^{-1})	$\Delta_f H°$(298.15 K) (kJ mol^{-1})	*References*		$S°$(298.15 K) (J K^{-1} mol^{-1})	$\Delta_f H°$(298.15 K) (kJ mol^{-1})	*References*
AcF_3	*115.8 ± 4.0*	*–1670 ± 40*		LaF_3	106.98 ± 0.11	–1699 ± 2	[d]
				CeF_3	*119.7*	–1703	[d]
				PrF_3	121.22 ± 0.12	–1689 ± 3	[d]
UF_3	129.22 ± 0.5	–1501.4 ± 4.7	[a,b]	NdF_3	120.79 ± 0.12	–1679 ± 2	[d]
NpF_3	*130.6 ± 3.0*	*–1529 ± 8*	[a,b]	PmF_3	*120.6*	*–1668*	[d]
PuF_3	126.11 ± 0.36	–1586.7 ± 3.7	[a,b]	SmF_3	*116.5*	–1669 ± 5	[d]
AmF_3	*110.6 ± 3.0*	*–1594 ± 14*	[a,b]	EuF_3	*110.1*	–1571	[d]
CmF_3	*127.0 ± 3.0*	*–1599 ± 35*	[a]	GdF_3	114.77 ± 0.22	–1699 ± 2	[d]
BkF_3	*130.0 ± 5.0*	*–1581 ± 35*	[c]	TbF_3	*119.9*	–1707	[d]
CfF_3	*131.0 ± 5.0*	*–1553 ± 35*	[c]	DyF_3	119.07 ± 0.12	–1692 ± 2	[d]
EsF_3		*–1575 ± 40*	[c]	HoF_3	*120.3*	–1698 ± 2	[d]
				ErF_3	116.86 ± 0.12	–1694 ± 2	[d]
				TmF_3	*115.0*	–1656	[d]
				YbF_3	*111.8*	–1570	[d]
				LuF_3	116.86 ± 0.12	–1701	[d]

[a] Konings (2001a).
[b] NEA-TDB (Grenthe *et al.*, 1992; Silva *et al.*, 1995; Lemire *et al.*, 2001; Guillaumont *et al.*, 2003).
[c] Estimated in present work.
[d] Konings and Kovács (2003).

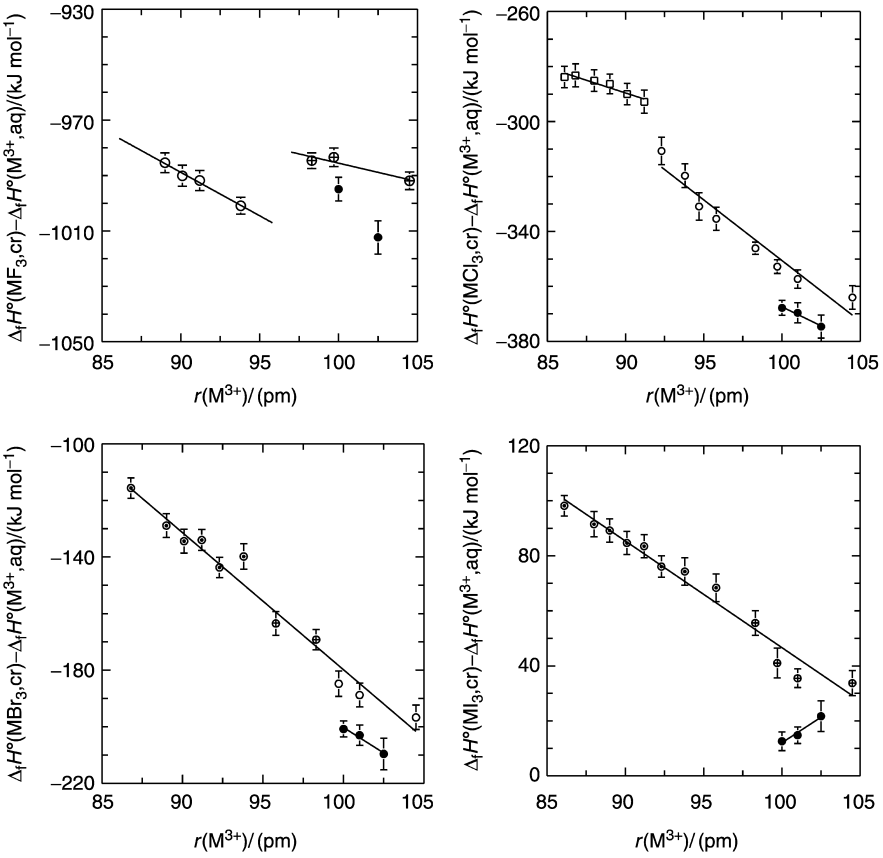

Fig. 19.23 *The difference between the enthalpies of formation of f-element trihalides* (*at* 298.15 K) *and the corresponding* M^{3+} *aqueous ions; the lanthanides are shown by open symbols that indicate the different crystallographic structures; the actinides are shown by closed symbols.*

are known for these trihalides of uranium through plutonium, although that of $NpCl_3$ requires an estimate of its heat of solution (Fuger *et al.*, 1983). In addition, the enthalpies of formation of $AmCl_3$ and $CfBr_3$ are known from solution calorimetry; that of other actinide trihalides as well as heavier trihalides must be estimated. This can be done by a correlation of the quantity $\{\Delta_f H°(MX_3,cr) - \Delta_f H°(M^{3+},aq)\}$ with ionic radius for isostructural compounds (Fig. 19.23). It can be seen that the trend in the actinide chloride and bromides series is parallel to that in the lanthanide series and thus permits extrapolation beyond Pu. In the actinide iodides, the trend is opposite. Such data sets are shown in Tables 19.21–19.23. The resultant enthalpies of formation are consistent with the data reported in the NEA-TDB project.

Table 19.21 *Enthalpies of formation and entropies of the crystalline lanthanide and actinide trichlorides; estimated values are in italics.*

	$S°$(298.15 K) (J K^{-1} mol^{-1})	$\Delta_f H°$(298.15 K) (kJ mol^{-1})	*References*		$S°$(298.15 K) (J K^{-1} mol^{-1})	$\Delta_f H°$(298.15 K) (kJ mol^{-1})	*References*
$AcCl_3$	*148.7 ± 6.0*	*–1053*	[a]	$LaCl_3$	137.57	–1071.6 ± 1.5	[d]
				$CeCl_3$	*151.0*	–1059.7 ± 1.5	[d]
				$PrCl_3$	153.30	–1058.6 ± 1.5	[d]
UCl_3	163.90 ± 0.50	–863.7 ± 2.0	[b,c]	$NdCl_3$	153.43	–1040.9 ± 1.0	[d]
$NpCl_3$	*165.2 ± 6.0*	–896.8 ± 3.0	[b,c]	$PmCl_3$	*153.3*	*–1030 ± 10*	[d]
$PuCl_3$	*161.4 ± 6.0*	–959.6 ± 1.8	[b,c]	$SmCl_3$	150.12	–1025.3 ± 2.0	[d]
$AmCl_3$	*146.2 ± 6.0*	–977.8 ± 1.3	[b,c]	$EuCl_3$	144.06	–935.4 ± 3.0	[d]
$CmCl_3$	*163.1 ± 6.0*	–969.6 ± 6.7	[a]	$GdCl_3$	151.42	–1019.2 ± 1.5	[d]
$BkCl_3$	*164.6 ± 6.0*	*–952 ± 15*	[a]	$TbCl_3$	*176.7*	–1010.6 ± 3.0	[d]
$CfCl_3$	*167.2 ± 6.0*	*–965 ± 20*	[a]	$DyCl_3$	175.4	–993.1 ± 3.0	[d]
$EsCl_3$		*–950 ± 24*	[a]	$HoCl_3$	177.1	–997.7 ± 2.5	[d]
$FmCl_3$		*–963 ± 44*	[a]	$ErCl_3$	175.1	–994.4 ± 2.0	[d]
$MdCl_3$		*–864 ± 50*	[a]	$TmCl_3$	173.5	–996.3 ± 2.5	[d]
$NoCl_3$		*–716 ± 50*	[a]	$YbCl_3$	169.3	–959.5 ± 3.0	[d]
				$LuCl_3$	153.0	–987.1 ± 2.5	[d]
$PuCl_3 \cdot 6H_2O$	*420 ± 5*	–2773.4 ± 2.1	[b]				

[a] Estimated in the present work.
[b] NEA-TDB (Grenthe *et al.*, 1992; Silva *et al.*, 1995; Lemire *et al.*, 2001).
[c] Konings (2001a).
[d] Konings and Kovács (2003).

Table 19.22 *Enthalpies of formation and entropies of the crystalline lanthanide and actinide tribromides; estimated values are in italics.*

	$S°$(298.15 K) (J K^{-1} mol^{-1})	$\Delta_f H°$(298.15 K) (kJ mol^{-1})	*References*		$S°$(298.15 K) (J K^{-1} mol^{-1})	$\Delta_f H°$(298.15 K) (kJ mol^{-1})	*References*
$AcBr_3$	*164 ± 6*	*–896 ± 30*	[a]	$LaBr_3$	*177.1*	–904.4 ± 1.5	[d]
				$CeBr_3$	*191.2*	–891.2 ± 1.5	[d]
				$PrBr_3$	*193.8*	–890.5 ± 4.0	[d]
UBr_3	198.74 ± 0.40	–698.7 ± 4.2	[b]	$NdBr_3$	*193.6*	–864.0 ± 3.0	[d]
$NpBr_3$	*200 ± 6*	–730.2 ± 2.9	[b]	$PmBr_3$	*192.6*	*–858 ± 10*	[d]
$PuBr_3$	*196 ± 6*	–792.6 ± 2.0	[b]	$SmBr_3$	*189.4*	–853.4 ± 3.0	[d]
$AmBr_3$	*181 ± 6*	*–804.0 ± 6.0*	[b]	$EuBr_3$	182.8	*–759 ± 10*	[d]
$CmBr_3$	*198 ± 6*	*–800.3 ± 7.0*	[c]	$GdBr_3$	*209.0*	–838.2 ± 2.0	[d]
$BkBr_3$	*199 ± 6*	*–781.5 ± 6.5*	[c]	$TbBr_3$	*212.3*	–843.5 ± 3.0	[d]
$CfBr_3$	*202 ± 6*	–752.5 ± 3.2	[c]	$DyBr_3$	*213.4*	–834.3 ± 2.5	[d]
				$HoBr_3$	*213.1*	–842.1 ± 3.0	[d]
				$ErBr_3$	*212.2*	–837.1 ± 3.0	[d]
				$TmBr_3$	*210.2*	*–832 ± 10*	[d]
				$YbBr_3$	*204.8*	–791.9 ± 2.0	[d]
				$LuBr_3$	*188.7*	–814 ± 10	[d]

[a] Estimated in present work.
[b] NEA-TDB (Grenthe *et al.*, 1992; Silva *et al.*, 1995; Lemire *et al.*, 2001; Guillaumont *et al.*, 2003).
[c] Fuger *et al.* (1990).
[d] Konings and Kovács (2003).

Table 19.23 *Enthalpies of formation and entropies of the crystalline lanthanide and actinide triiodides; estimated values are in parentheses.*

	$S°$(298.15 K) (J K^{-1} mol^{-1})	$\Delta_f H°$(298.15 K) (kJ mol^{-1})	*References*		$S°$(298.15 K) (J K^{-1} mol^{-1})	$\Delta_f H°$(298.15 K) (kJ mol^{-1})	*References*
				LaI_3	*196.3*	–673.9 ± 2.0	[c]
				CeI_3	*210.4*	–666.8 ± 3.0	[c]
				PrI_3	*213.0*	–664.7 ± 5.0	[c]
UI_3	*217 ± 5*	–466.9 ± 4.2	[a]	NdI_3	*212.8*	–639.2 ± 4.0	[c]
NpI_3	*218 ± 5*	–512.4 ± 2.2	[b]	PmI_3	*230.6*	*–634 ± 10*	[c]
PuI_3	*214 ± 5*	–579.2 ± 2.8	[b]	SmI_3	*227.4*	–621.5 ± 4.0	[c]
AmI_3	*199 ± 3*	*–615 ± 9*	[b]	EuI_3	*220.8*	*–538 ± 10*	[c]
				GdI_3	*220.8*	–624.1 ± 3.0	[c]
				TbI_3	*228.2*	–623.8 ± 3.0	[c]
				DyI_3	*231.5*	–616.7 ± 3.0	[c]
				HoI_3	*232.5*	–622.9 ± 3.0	[c]
				ErI_3	*232.3*	–619.0 ± 3.0	[c]
				TmI_3	*228.7*	–619.7 ± 3.5	[c]
				YbI_3	*223.1*	*–578 ± 10*	[c]
				LuI_3	206.7	–605.1 ± 2.2	[c]

[a] NEA-TDB (Grenthe *et al.*, 1992; Silva *et al.*, 1995; Lemire *et al.*, 2001; Guillaumont *et al.*, 2003).
[b] Estimated in the present work.
[c] Konings and Kovács (2003).

(*ii*) *Heat capacity and entropy*

Low-temperature heat capacities of UF_3 and PuF_3 have been measured, and high-temperature data are only available for UF_3. Recently, an inconsistency between the low-temperature data for these compounds was pointed out by Konings (2001a). The entropy value of PuF_3, derived from measurements by Osborne *et al*. (1974), yields a lattice entropy that is significantly higher than that of UF_3 derived from data by Cordfunke and Westrum, which are only published as a summary (Cordfunke *et al*., 1989). This lattice entropy is not consistent with those of the lanthanide trifluorides and it was suggested that the extrapolation to 0 K of the UF_3 value did not include the magnetic contribution, which is equal to R ln(2) and completely removes the inconsistency. From the results for PuF_3 and those for the lanthanide trifluorides, Konings (2001a) estimated the lattice entropies of NpF_3, AmF_3, and CmF_3 which were combined with an excess entropy calculated from crystal field levels to give the standard entropy. These values are given in Table 19.20.

Heat capacity and thus entropy data for the other actinide trihalides have only been reported for UCl_3 and UBr_3. As discussed above the entropy values for UCl_3 and UBr_3 derived from the results of Cordfunke *et al*. (1989) must be R ln(2) higher to account for the magnetic contribution at low temperatures (Konings, 2001a). Estimates for the standard entropies of the transuranium trichlorides up to $CmCl_3$ were presented by Konings (2001a) and are included in Table 19.21. Estimates for the standard entropy for the uranium triiodide and the bromides and iodides of neptunium, plutonium, and americium were presented in the NEA-TDB project, but the method used is less accurate than that proposed by Konings (2001a). In the case of the americium compounds, where the differences between the two sets of data largely exceeds the uncertainty limits, the values proposed by Konings (2001a) have been adopted by the NEA-TDB project (Guillaumont *et al*., 2003). The value for $PuCl_3 \cdot 6H_2O$ is included in Table 19.21 as it is a key value for the estimation of the entropies of the aqueous ion of this element.

(*iii*) *High-temperature properties*

The high-temperature heat capacity of solid UF_3, UCl_3, and UBr_3 has been derived from enthalpy increment measurements (Cordfunke *et al*., 1989). Measurements for other actinide trihalides have not been made. As discussed by Konings and Kovács (2003) the heat capacity of the lanthanide trihalides can be described very well as the sum of the lattice and excess components, the latter arising from the electronic states of the lanthanide ions. A similar approach can be used for the estimation of the heat capacity of the actinide trihalides. The recommended functions are listed in Table 19.16.

The melting point and melting enthalpy of many trihalides have been reported. They are summarized in Table 19.16. The data for the trichlorides

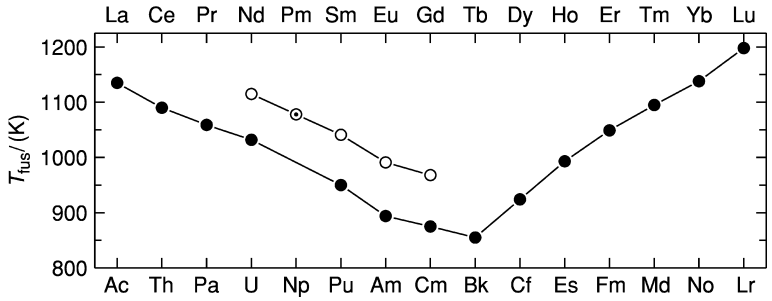

Fig. 19.24 *Melting temperature of the lanthanide* (•) *and actinide* (○) *trichlorides; estimated values are indicated by* (⊙).

are the most extensive; they are known from UCl_3 to $CmCl_3$. These values are of the same order as those of the lanthanide trichlorides and the trend in the actinide trichlorides series is parallel, as shown in Fig. 19.24.

(b) Gaseous trihalides

The situation for the gaseous actinide trihalides is complicated: the measured condensed gas-phase equilibria are not always clearly defined, the condensed phase data are often uncertain (see above) and the molecular geometry of these species has not been measured except for UCl_3 and UI_3. For these two compounds, gas-phase electron diffraction (ED) measurements have been reported (Bazhanov *et al.*, 1990a,b), which indicated a pyramidal structure with a X–M–X bond angle close to 90°. Quantum chemical calculations for the uranium(III) halides also indicate a pyramidal structure (Joubert and Maldivi, 2001) but with a bond angle much closer to the planar 120°. Fortunately, the molecular properties of the lanthanide trihalides are much better known and can be used for comparison. Experimental and theoretical studies have indicated a gradual increase of the X–Ln–X bond angle to the planar 120° from F to I and La to Lu (Molnar and Hargittai, 1995; Konings and Kovács, 2003), which is consistent with simple steric considerations. The lanthanide trifluorides are most probably pyramidal, the trichlorides, tribromides, and triiodides are quasi-planar (light lanthanides) or planar (heavy lanthanides). Quantum chemical calculations for UCl_3 and UI_3 agree with this trend but the experimental bond angles for UCl_3 $(95 \pm 3)°$ and UI_3 $(89 \pm 3)°$ disagree. The situation for the vibrational frequencies is equally complicated. The asymmetric stretching frequency of UCl_3 was determined experimentally by high-temperature infrared spectroscopic measurements (Kovács *et al.*, 1996), but the value (275 cm^{-1}) is considerably lower than those estimated from the electron diffraction data (310 ± 30 cm^{-1}) and derived from the quantum chemical calculations (300 cm^{-1} to 341 cm^{-1}, depending on the theoretical level). Clearly further research is needed to establish the molecular and thus the thermodynamic properties

of the gaseous actinide trihalides more precisely. For the present chapter we accept the estimated values given in the NEA-TDB reviews, but increased the uncertainties assigned in that work. The values are given in Table 19.19.

Enthalpies of formation of gaseous UF_3, UCl_3, and UBr_3 have been evaluated from experimental studies by Grenthe *et al.* (1990) and the enthalpies of formation derived in this work are listed in Table 19.19. For UF_3, vapor pressure and molecular equilibria studies were used, and are in fair agreement. For UCl_3 and UBr_3, only the molecular equilibria studies were used. Such data are also available for the lower thorium fluorides, chlorides, and bromides. Vapor pressure measurements have been reported also for the trifluorides AmF_3, PuF_3, and CfF_3 and the trichlorides $PuCl_3$ and $AmCl_3$, and the tribromide $PuBr_3$.

Fig. 19.25 shows the mean bond enthalpy of the actinide trifluorides as well as of the lanthanide trifluorides. The figure shows approximately the same trend for the two groups, the actinide series being somewhat shifted compared to the lanthanide series. From this trend, the enthalpies of formation of the other gaseous trihalides can be estimated with confidence.

19.6.5 Di- and monohalides

(a) Solid dihalides

The existence of the dichlorides, dibromides, and diiodides of Am and Cf has been reported. However, no experimental thermochemical data are available. Because these dihalides parallel lanthanide dihalides of similar M^{2+} ionic radii, it is possible to estimate their enthalpies of formation by a method similar to that used by Morss and Fahey (1976), based on the difference $\{\Delta_f H^\circ(MX_2,cr) - \Delta_f H^\circ(M^{2+},aq)\}$. Konings (2002a) estimated the standard entropy of $AmCl_2$ as $S^\circ(298.15\ K) = (148.1 \pm 5.0)\ J\ K^{-1}\ mol^{-1}$. This value is the sum of a lattice contribution estimated from the experimental data for some lanthanide

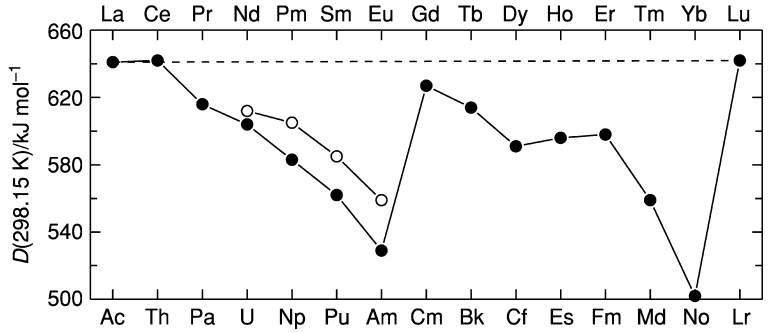

Fig. 19.25 *The mean bond enthalpy at* 298.15 K *of the gaseous lanthanide* (•) *and actinide trifluorides* (○).

dichlorides and the excess contribution $R \ln(8)$. Using a similar approach, we estimate the entropies of some other actinide dichlorides.

The data for these estimations, and the resulting predicted enthalpies of formation, are shown in Table 19.24. The Gibbs energies of these reactions are given in the following equations:

$$\mathrm{Am(cr)} + 2\mathrm{AmCl_3(cr)} = 3\mathrm{AmCl_2(cr)}, \quad \Delta_r G = -35 \text{ kJ mol}^{-1} \tag{19.22}$$

and

$$\mathrm{Cf(cr)} + 2\mathrm{CfCl_3(cr)} = 3\mathrm{CfCl_2(cr)}, \quad \Delta_r G = -91 \text{ kJ mol}^{-1} \tag{19.23}$$

illustrate the relative difficulty and ease of preparing the dihalides of americium compared to californium.

(b) Gaseous di- and monohalides

The di- and monohalides of thorium and uranium have been identified in mass spectrometric measurements by different authors. Lau and coworkers (Lau and Hildenbrand, 1982; Lau *et al*., 1989) studied the exchange reactions of the lower thorium and uranium fluorides with BaF; Gorokhov *et al*. (1984) and Hildenbrand and Lau (1991) studied the molecular equilibria between the uranium fluorides among themselves. The results for the uranium compounds have been analyzed in detail by Grenthe *et al*. (1990) and updated by Guillaumont *et al*. (2003), who demonstrated that the results are in reasonable agreement, considering the large number of approximations made in the analysis. Similar studies have been made for the lower chlorides and bromides (Lau and Hildenbrand, 1984, 1987, 1990; Hildenbrand and Lau, 1990). Almost no experimental data on the molecular properties of these species are available and thus all thermal functions are based on rather qualitative estimates (using alkaline-earth dihalide data), introducing large uncertainties. For this reason, the recommended values for the lower uranium halide species given in Table 19.25 should be used with caution, especially when used well outside the temperature range of the experimental studies.

As discussed by Lau and Hildenbrand (1982), the mean bond energy decreases gradually in the uranium halide series (Fig. 19.26). This trend can be used to approximate the enthalpies of formation of the lower halides of other actinides, when needed.

19.7 COMPLEX HALIDES, OXYHALIDES, AND NITROHALIDES

19.7.1 Solid complex halides

Many complex halides of thorium and uranium have been prepared for crystallographic, magnetic, and spectroscopic studies. Preparative conditions suggested that these compounds are more stable than the parent (binary)

Table 19.24 *Enthalpies of formation and entropies of the crystalline lanthanide and actinide dichlorides; estimated values are in italics.*

	$S°$(298.15 K) (J K^{-1} mol^{-1})	$\Delta_f H°$(298.15 K) (kJ mol^{-1})	*References*		$S°$(298.15 K) (J K^{-1} mol^{-1})	$\Delta_f H°$(298.15 K) (kJ mol^{-1})	*References*
				$NdCl_2$	141.5	–707	[a,b]
				$PmCl_2$	*139.4*	–691	[a,b]
$PuCl_2$		*–528*	[a]	$SmCl_2$	132.2	–802	[a,b]
$AmCl_2$	*148.1*	*–654*	[a,b]	$EuCl_2$	138.5	–824	[a,b]
$CmCl_2$		*–516*	[a]				
$BkCl_2$		*–584*	[a]				
$CfCl_2$	*154*	*–669*	[a]	$DyCl_2$	141.7	–693	[a,b]
$EsCl_2$		*–694*	[a]				
$FmCl_2$		*–748*	[a]				
$MdCl_2$		*–752*	[a]	$TmCl_2$	137.4	–709	[a,b]
$NoCl_2$		*–763*	[a]	$YbCl_2$	120.0	–800	[a,b]

[a] Morss and Fahey (1976).
[b] Konings (2002a) and references therein.

Table 19.25 *Thermodynamic properties of the gaseous actinide di- and monohalides; estimated values are in italics from NEA-TDB* (*Grenthe* et al., 1992; *Guillaumont* et al., 2003).

	$S°$(298.15 K) (J K^{-1} mol^{-1})	$\Delta_f H°$(298.15 K) (kJ mol^{-1})
UF_2	315.7 ± 10.0	–540 ± 25
UCl_2	339.1 ± 10.0	–155 ± 20
UBr_2	359.7 ± 10.0	–40 ± 15
UI_2	376.5 ± 10.0	103 ± 25
UF	251.8 ± 3.0	–47 ± 20
UCl	265.6 ± 3.0	187 ± 20
UBr	278.5 ± 3.0	245 ± 20
UI	286.5 ± 5.0	342 ± 20

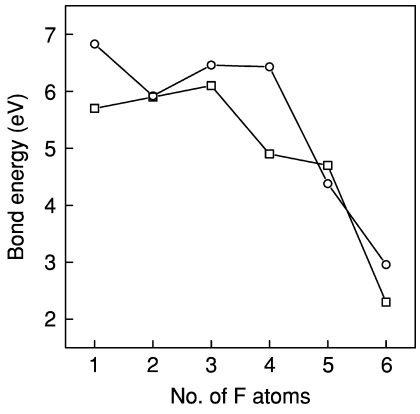

Fig. 19.26 *The bond dissociation energy of the $F_{n-1}AnF$ molecules as a function of n, the number of fluorine atoms in the molecule;* ○, *uranium fluorides;* □, *plutonium fluorides.*

halides. For example, UF_5 is difficult to prepare but complex halides such as $CsUF_6$ are relatively stable. Among the transuranium elements, fewer high-valent binary halides are known, but complex halides (e.g. Cs_2PuCl_6 and $CsPuF_6$) are known whereas the binary actinide halides ($PuCl_4$ and PuF_5) have been sought without success. Some of these complex halides have been exploited in separation schemes for the actinides. As discussed by Fuger *et al.* (1983), their thermodynamic properties have been of interest since the beginning of the 20th century.

Fuger *et al.* (1983) also assessed all of their thermodynamic properties. More recently the compounds of Np, Pu, and Am were also reviewed by the NEA-TDB teams (Silva *et al.*, 1995; Lemire *et al.*, 2001; Guillaumont *et al.*, 2003). In Table 19.26 the values selected by the NEA teams are given for compounds of Np, Pu, and Am and the values selected by Fuger *et al.* (1983) for compounds of Th, Pa, and U. All these data have been recalculated using the latest NEA-selected values. In the framework of a general study on several $Cs_2NaAnCl_6$ compounds, Schoebrechts *et al.* (1989) also reported the enthalpy of formation of $Cs_2NaCfCl_6$ and estimates for the corresponding compounds of Cm and Bk. These values are also given in Table 19.26.

Fig. 19.27 displays the enthalpies of complexation, e.g.

$$2CsCl(cr) + UCl_4(cr) = Cs_2UCl_6(cr), \quad \Delta H = \Delta_{cplx}H \tag{19.24}$$

of some of these compounds. Interpolation and extrapolation of $\Delta_{cplx}H$ along with enthalpies of formation of the binary compounds provide the values necessary to predict the enthalpies of formation of several of these complex halides. Note that $\Delta_{cplx}H$ becomes more favorable (exothermic) as the alkali-metal ion A^+ becomes larger and, to a lesser extent, as the actinide ion An^{4+} becomes smaller. As with complex oxides, these are both structural-packing (ionic) and acid–base (covalent) effects.

19.7.2 Solid oxyhalides and nitrohalides

There are many oxyhalides of actinide oxidation states +3 through +6. In general these are more stable than a mixture of oxide and halide, e.g.

$$UF_6(cr) + 2UO_3(c,\gamma) = 3UO_2F_2(cr), \quad \Delta_rG^\circ = -318 \text{ kJ mol}^{-1} \tag{19.25}$$

reflecting the acid–base nature of the reactions. In some cases, however, e.g.

$$UCl_4(cr) + UO_2(cr) = 2UOCl_2(cr), \quad \Delta_rG^\circ = +12 \text{ kJ mol}^{-1} \tag{19.26}$$

$$NpCl_4(cr) + NpO_2(cr) = 2NpOCl_2(cr), \quad \Delta_rG^\circ = +59 \text{ kJ mol}^{-1} \tag{19.27}$$

the Gibbs energy of the reactions is positive, reflecting the limited stability of such oxyhalides with respect to the stoichiometric mixture of the oxide and chloride in the same oxidation state.

We have accepted the assessed enthalpies of formation from calorimetric and vapor–solid hydrolysis equilibria by Fuger *et al.* (1983) for Th, Pa, and Cm compounds, and the more recently assessed values by the NEA teams for compounds of U to Am (Table 19.27). Also included are the recent results of Burns *et al.* (1998) for CfOCl and BkOCl, the former based on experiments, the latter based on an interpolation in the AnOCl series (An = U, Pu, Am, Cm, and Cf).

Heat capacity data have been reported for uranium oxyhalides UO_2F_2, UO_2Cl_2, $UOCl_2$, and $UOBr_2$. The entropy values derived in these studies have been accepted in the NEA-TDB review (Grenthe *et al.*, 1992). High-temperature

Table 19.26 *Thermodynamic properties of crystalline actinide complex halides and oxyhalides with alkali metals; estimated values are in italics; see text for references.*

	S° (298.15 K) (J K^{-1} mol^{-1})	$\Delta_f H^\circ$ (298.15 K) (kJ mol^{-1})		S° (298.15 K) (J K^{-1} mol^{-1})	$\Delta_f H^\circ$ (298.15 K) (kJ mol^{-1})		S° (298.15 K) (J K^{-1} mol^{-1})	$\Delta_f H^\circ$ (298.15 K) (kJ mol^{-1})		S° (298.15 K) (J K^{-1} mol^{-1})	$\Delta_f H^\circ$ (298.15 K) (kJ mol^{-1})
			Na_3UF_7		-3672.0 ± 4.6	$NaUF_6$		-2694 ± 13[a]	$NaUF_7$	*272 ± 12*	-2804.9 ± 10.5
									Na_2UF_8	*330 ± 13*	-3391.8 ± 12.6
									$Na_3UO_2F_5$		-3115.0 ± 2.5
									$Na(UO_2)_2F_5$		-3917.7 ± 2.9
						KUF_6		-2731.0 ± 5.0	$K_3UO_2F_5$		-3484.0 ± 2.5
									$K(UO_2)_2F_5$		-3954.9 ± 2.9
									$K_5(UO_2)_2F_9$		-6377.3 ± 6.6
			Rb_3UF_7		-3734.6 ± 3.3	$RbUF_6$		-2740.5 ± 5.9	$Rb_3UO_2F_5$		-3472.3 ± 3.3
									$Rb(UO_2)_2F_5$		-3964.8 ± 3.8
									$Rb_5(UO_2)_2F_9$		-6373.9 ± 7.5
			Cs_2UF_6		-3156.4 ± 4.2	$CsUF_6$		-2756.0 ± 5.4	$Cs_3UO_2F_5$		-3468.8 ± 6.3
									$Cs(UO_2)_2F_5$		-3977.8 ± 4.0
									$Cs_5(UO_2)_2F_9$		-6374.6 ± 10.3
			$LiThCl_5$		-1619.6 ± 4.2						
			Li_2ThCl_6		-2038.9 ± 6.3						
			Li_2UCl_6		-1831.3 ± 3.8						
			Na_2ThCl_6		-2041.4 ± 6.3						
			Na_2UCl_6		-1848.1 ± 2.1	$NaUCl_6$		-1472.3 ± 3.3[b]			
			K_2ThCl_6		-2110.8 ± 6.3						
			$KUCl_5$		-1481.1 ± 3.3						
			K_2UCl_6		-1931.8 ± 2.1	$KUCl_6$		-1525.5 ± 2.9			
			Rb_2ThCl_6		-2157.3 ± 6.3						
			Rb_4ThCl_8		-3063.5 ± 8.0						
			$RbUCl_5$		-1497.9 ± 4.2						
			Rb_2UCl_6		-1956.6 ± 3.6	$RbUCl_6$		-1553.5 ± 2.5			
			Rb_4UCl_8		-2828.7 ± 4.2						
			Cs_4ThCl_8		-3053.1 ± 8.0				$Cs_2UO_2Cl_4$		-2204.5 ± 2.5
			Cs_2ThCl_6		-2147.6 ± 2.1				$Cs_2NpO_2Cl_4$		-2056.1 ± 5.4
			Cs_2PaCl_6		-2030.8 ± 14.4[c]				$Cs_3NpO_2Cl_4$		-2449.1 ± 4.8

Table 19.26 (*Contd.*)

	S° (298.15 K) (J K^{-1} mol^{-1})	$\Delta_f H^\circ$ (298.15 K) (kJ mol^{-1})		S° (298.15 K) (J K^{-1} mol^{-1})	$\Delta_f H^\circ$ (298.15 K) (kJ mol^{-1})		S° (298.15 K) (J K^{-1} mol^{-1})	$\Delta_f H^\circ$ (298.15 K) (kJ mol^{-1})		S° (298.15 K) (J K^{-1} mol^{-1})	$\Delta_f H^\circ$ (298.15 K) (kJ mol^{-1})
Cs_2NaUCl_6		–2173.8 ± 4.1	CsU_2Cl_9		–2534.7 ± 7.7						
			$CsUCl_5$		–1518.4 ± 4.2	$CsUCl_6$		–1574.4 ± 2.5			
			Cs_2UCl_6		–2010.5 ± 4.2						
$Cs_2NaNpCl_6$		–2217.2 ± 3.1	Cs_2NpCl_6	*410 ± 15*	–1976.2 ± 1.9						
$Cs_2NaPuCl_6$	*440 ± 15*	–2294.2 ± 2.6	Cs_2PuCl_6	*412 ± 15*	–1982.0 ± 5.0						
Cs_3PuCl_6	*455 ± 11*	–2364.4 ± 9.0									
$CsPu_2Cl_7$	*424 ± 7*	–2399.4 ± 5.7									
$Cs_2NaAmCl_6$	*421* ± 15	–2315.8 ± 1.8									
$Cs_2NaCmCl_6$		*–2325 ± 7*									
$Cs_2NaBkCl_6$		*–2315* ± 7									
$Cs_2NaCfCl_6$		–2292.4 ± 5.8									
			Na_2UBr_6		–1529.7 ± 2.7						
K_2UBr_5		–1513.3 ± 4.5	K_2UBr_6		–1632.3 ± 2.7						
Rb_2UBr_5		–1528.8 ± 4.4	Rb_2UBr_6		–1653.7 ± 2.6						
Cs_2UBr_5		–1552.4 ± 4.9	Cs_2UBr_6		–1709.4 ± 2.6	$Cs_2UO_2Br_4$		–2008.7 ± 1.5			
			Cs_2NpBr_6	*469 ± 10*	–1682.3 ± 2.0						
			Cs_2PuBr_6	*470 ± 15*	–1697.4 ± 4.2						

[a] For the alpha form; $\Delta_f H^\circ(NaUF_6, \beta, 298.15\ K) = -(2708.3 \pm 5.4)$ kJ mol^{-1}.
[b] For the alpha form; $\Delta_f H^\circ(NaUCl_6, \beta, 298.15\ K) = -(1472.1 \pm 29)$ kJ mol^{-1}.
[c] Recalculated using $\Delta_f H^\circ(PaCl_4, cr, 298.15\ K)$ from Table 19.18.

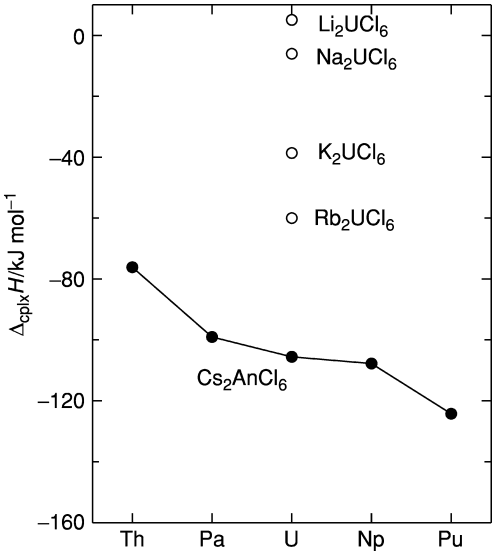

Fig. 19.27 *Enthalpies of complexation of complex actinide(IV) halides.*

enthalpy increments of UO_2X_2 (for X = F, Cl, and Br) have been measured by Cordfunke *et al.* (1979). Their data are in reasonable to good agreement with the low-temperature data. Cordfunke and Kubaschewski (1984) also cite unpublished experimental data for $UOCl_2$ and $U_2O_2Cl_5$ by Cordfunke, and estimated the heat capacity functions of other oxyhalides. They are listed in Table 19.28.

In contrast, data for mixed nitride halides are scarce. Recently Akabori *et al.* (2002) and Huntelaar *et al.* (2002) have presented data for the enthalpy of formation, the entropy, and high-temperature heat capacity of UNCl, which are included in Tables 19.27 and 19.28.

19.7.3 Gaseous oxyhalides

Several oxyhalides are stable in the gaseous phase and experimental vapor pressure data have been reported for UO_2F_2, UOF_4, and UO_2Cl_2 from which the enthalpies of formation of the gaseous molecules can be derived. In the NEA-TDB review, these studies were analyzed by third-law method using estimated molecular parameters from Glushko *et al.* (1978). The estimates for structure parameters and vibrational frequencies of UO_2F_2 differ considerably from those obtained by Privalov *et al.* (2002) using quantum chemical calculations at different theoretical levels (SCF, B3LYP). Souter and Andrews (1997) identified the molecules UO_2F_2, UOF_4, and UO_2F by infrared matrix-isolation spectroscopy. The asymmetric O–U–O stretching frequency found is in reasonable

Table 19.27 *Thermodynamic properties of crystalline actinide oxyhalides and complex actinide oxyhalides; estimated values are in italics.*

	S° (298.15 K) (J K^{-1} mol^{-1})	$\Delta_f H^\circ$ (298.15 K) (kJ mol^{-1})		S° (298.15 K) (J K^{-1} mol^{-1})	$\Delta_f H^\circ$ (298.15 K) (kJ mol^{-1})		S° (298.15 K) (J K^{-1} mol^{-1})	$\Delta_f H^\circ$ (298.15 K) (kJ mol^{-1})		S° (298.15 K) (J K^{-1} mol^{-1})	$\Delta_f H^\circ$ (298.15 K) (kJ mol^{-1})	*References*
			$ThOF_2$	*101.3 ± 8.4*	–1669.4 ± 10.5							a
			UOF_2	119.2 ± 4.2	–1504.6 ± 6.3				UO_2F_2	135.56 ± 0.42	–1653.5 ± 1.3	b
									UOF_4	*195 ± 5*	–1924.6 ± 4.0	b
PuOF	*96 ± 10*	*–1140 ± 20*										b
			$ThOCl_2$	114.6 ± 4.2	–1232.6 ± 8.4							a
			$PaOCl_2$	*125.5 ± 8.4*	*–1096 ± 9*							a
UOCl	*102.5 ± 8.4*	–833.9 ± 4.2	$UOCl_2$	138.32 ± 0.21	–1069.3 ± 2.7	$UOCl_3$	*170.7 ± 8.4*	–1140.0 ± 8.0	UO_2Cl_2	150.54 ± 0.31	–1243.6 ± 1.3	b
			$U_2O_2Cl_5$	*326.3* ± 8.4	–2197.4 ± 4.2	UO_2Cl	*112.5* ± 8.4	–1171.1 ± 8.0				b
						$U_5O_{12}Cl$	*465* ± 30	–5854.4 ± 8.6				b
			$NpOCl_2$	*143.5 ± 5.0*	–1030.0 ± 8.0							b
PuOCl	105.6 ± 3.0	–931.0 ± 1.7										b
AmOCl	*92.6 ± 10*	–949.8 ± 6.0										b
CmOCl	*105 ± 21*	–963.2 ± 6.7										a
BkOCl		*–944 ± 10*										c
CfOCl		–920 ± 7										c
			$ThOBr_2$	*129.7 ± 12.6*	–1129.7 ± 12.6							a
			$PaOBr_2$	*142.3 ± 16.7*	–1002.9 ± 15.5							a,d
			$UOBr_2$	157.57 ± 0.29	–973.6 ± 8.4	$UOBr_3$	*205.0 ± 12.6*	–954 ± 21	UO_2Br_2	169.5 ± 4.2	–1137.4 ± 1.3	b
PuOBr	*127 ± 10*	–870.0 ± 8.0										b
AmOBr	*104.9 ± 12.8*	–887.0 ± 9.0										
			$ThOI_2$	*144.8 ± 4.2*	–996.6 ± 2.5							a
PuOI	*130 ± 15*	*–802 ± 20*										b
			UNCl	96.54 ± 0.10	–559 ± 4							e

[a] Fuger *et al.* (1983).
[b] NEA-TDB (Grenthe *et al.*, 1992; Silva *et al.*, 1995; Lemire *et al.*, 2001; Guillaumont *et al.*, 2003).
[c] Burns *et al.* (1998).
[d] Recalculated with the accepted value for $\Delta_f H^\circ(Pa^{4+}, aq, 298.15\ K)$.
[e] Huntelaar *et al.* (2002) and Akabori *et al.* (2002).

Table 19.28 *High-temperature heat capacity of the crystalline uranium oxyhalides and oxynitrides;* $C_p/(\mathrm{J\ K^{-1}\ mol^{-1}}) = a(T/\mathrm{K})^{-2} + b + c(T/\mathrm{K})$ (*estimated values are in italics*).

	a ($\times 10^{-6}$)	b	c ($\times 10^{3}$)	T_{max} (K)	*References*
UO_2F_2	–1.0208	106.238	28.326		[a]
UO_2Cl_2	–1.1418	115.275	18.2232		[a,b]
UO_2Br_2		104.270	37.938		[a,b]
UNCl	–0.97344	79.7373	2.3703	1000	[c]

[a] NEA-TDB (Grenthe *et al*., 1992; Silva *et al*., 1995; Lemire *et al*., 2001; Guillaumont *et al*., 2003).
[b] Cordfunke and Ouweltjes (1981).
[c] Huntelaar *et al*. (2002).

Table 19.29 *Thermodynamic properties of some gaseous oxyhalides; estimated vales are given in italics.*

	$S°$(298.15 K) (J K^{-1} mol^{-1})	$\Delta_f H°$(298.15 K) (kJ mol^{-1})	*References*
UO_2F_2	342.7 ± 6.0	–1352.5 ± 10.1	[a]
UOF_4	363.2 ± 8.0	–1763 ± 20	[a]
UO_2Cl_2	373.4 ± 6.0	–970.3 ± 15.0	[a]

[a] NEA-TDB (Grenthe *et al*., 1992; Silva *et al*., 1995; Lemire *et al*., 2001; Guillaumont *et al*., 2003).

agreement with the B3LYP results of Privalov *et al*. (2002), which also give the best agreement with the estimates used in the NEA-TDB review. The recommended values of the NEA-TDB review for the species UO_2F_2, UOF_4, and UO_2Cl_2 are given in Table 19.29.

19.8 HYDRIDES

19.8.1 Enthalpy of formation

The enthalpies of formation of the actinide hydrides have been principally derived from hydrogen pressure measurements in which the pressure–temperature–composition relation was studied. The equilibrium reaction in these metal–hydrogen systems can be described as:

$$\left(\frac{2}{2-s-x}\right)\mathrm{AnH}_s + \mathrm{H}_2 = \left(\frac{2}{2-s-x}\right)\mathrm{AnH}_{2-x} \qquad (19.28)$$

where s and $(2-x)$ both generally have the values 1.3, 2, 3, and 3.75. The AnH_2 compounds occur in all systems from Th to Cm, except U. In the U–H system, only the trihydride occurs, which is also found in the systems with Np, Pu, and

Am, though almost no data exist for the latter. The composition H/An = 1.3 is typical for the Pa–H system, and H/An = 3.75 for the Th–H system.

Flotow *et al.* (1984) systematically analyzed the equilibrium data for Th, Pa, U, Np, Pu, and Am, and their recommended enthalpies of formation for the hydrides of Th, Pa, U, and Pu are summarized in Table 19.30. Ward *et al.* (1987) measured the hydrogen dissociation pressure in the Np–H and derived thermodynamic data for NpH_2, $NpH_{2.6}$, and NpH_3. Gibson and Haire (1990) measured the hydrogen dissociation pressures of milligram-sized samples of the americium and curium hydrides, and made comparison to the lanthanide hydrides (Dy, Ho). Their results for AmH_2 are in good agreement with the recommended values by Flotow *et al.* (1984), who selected the average results of two discordant studies; their results for CmH_2 are the first ones to be reported. They have been included in Table 19.30. The variation of the enthalpy of formation of the actinide dihydrides is shown in Fig. 19.28, together with the data for the lanthanide dihydrides (Libowitz and Maeland, 1979). As observed for the elements and many compounds, the trend in light actinides dihydrides is significantly different from that of the lanthanides and the two curves approach each other near Am and Cm.

19.8.2 Entropy

Low-temperature heat capacity measurements (up to 300 K) have been reported for ThH_2, $ThH_{3.75}$, UH_3, and $PuH_{1.9}$ and the entropy values at 298.15 K recommended by Flotow *et al.* (1984) are listed in Table 19.30. The entropies of the other compounds have been derived by Flotow *et al.* (1984) from the high-temperature hydrogen equilibrium measurements, using estimated heat capacity data. Flotow *et al.* (1984) also estimated the entropy of CmH_2 by linear extrapolation of the data of the dihydrides of Np, Pu, and Am, but it is doubtful whether this is correct in view of the trend shown for the enthalpies of formation, which indicates that CmH_2 resembles more the lanthanide dihydrides than the light actinide dihydrides.

19.8.3 High-temperature properties

High-temperature heat capacity data have been reported only for PuH_2 (Oetting *et al.*, 1984). The high-temperature heat capacity of ThH_2, $ThH_{3.75}$, and UH_3 were calculated by Flotow *et al.* (1984). They described the total heat capacity as the sum of the electronic, optical mode, and residual contributions:

$$C_p = C_{ele} + C_{\mu H} + C_{residual} \tag{19.29}$$

where the electronic heat capacity coefficient and the residual term were obtained from the low-temperature measurements, which extent to 350 K, and

Table 19.30 *Enthalpies of formation and entropies of the crystalline actinide hydrides, estimated values are given in italics.*

	AnH_2		AnH_3		$AnH_{3.75}$		
	$S°$(298.15 K) (J K^{-1} mol^{-1})	$\Delta_f H°$ (298.15 K) (kJ mol^{-1})	$S°$(298.15 K) (J K^{-1} mol^{-1})	$\Delta_f H°$(298.15 K) (kJ mol^{-1})	$S°$ (298.15 K) (J K^{-1} mol^{-1})	$\Delta_f H°$(298.15 K) (kJ mol^{-1})	*References*
Th	50.73 ± 0.10	–145.1 ± 1.0			54.43 ± 0.13	–215.8 ± 4.3	[a]
Pa							
U			63.68 ± 0.13	–127.0 ± 0.13			[a]
Np	*66.1*	–119		–230.9 ± 3.3			[b]
Pu	72.84 ± 0.38	–164.4		*–236.4*			[a]
Am	*48.1*	–177 ± 12					[a,c]
Cm		–187 ± 14					[c]

[a] Flotow *et al.* (1984).
[b] Ward *et al.* (1987).
[c] Gibson and Haire (1990).

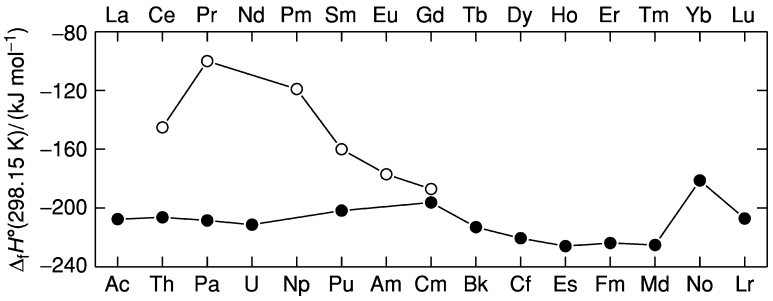

Fig. 19.28 *Enthalpies of formation of lanthanide* (•) *and actinide* (○) *dihydrides.*

Table 19.31 *High-temperature heat capacity of selected crystalline actinide hydrides;* $C_p/(J\ K^{-1}\ mol^{-1}) = a(T/K)^{-2} + b + c(T/K) + d(T/K)^2$ (*estimated values are given in italics*), *from Flotow* et al. (1984).

	a ($\times 10^{-6}$)	b	c ($\times 10^{3}$)	d ($\times 10^{6}$)	T_{max} (K)
ThH_2	–0.17364	166.566	149.725	–69.113	800
$ThH_{3.75}$		–192.918	272.726	–120.387	800
UH_3	–0.48392	6.05878	189.349	–87.514	800
NpH_2		32.4395	50.1072	–1.1138	900
PuH_2	2.1711	–78.1827	405.219	–264.995	600

the optical modes were obtained from spectroscopic measurements. Polynomial fits of the heat capacity function thus obtained by Flotow *et al*. for temperatures up to maximum 800 K are listed in Table 19.31.

19.9 HYDROXIDES AND OXYHYDRATES

19.9.1 Trihydroxides

(a) Enthalpy of formation

The only experimental determinations of the enthalpy of formation of a trivalent actinide hydroxide are two solution-calorimetry studies for $Am(OH)_3$, but the two results differ considerably (Morss and Williams, 1994; Merli *et al.*, 1997) due to a difference of enthalpies of solution of the trihydroxide of (23 ± 8) kJ mol^{-1}. The value selected in Table 19.32 is that calculated by Guillaumont *et al.* (2003), based primarily on the measured solubility product of $Am(OH)_3$ measured by Silva (1982) corrected for hydrolysis and ionic strength, and an estimated entropy of $Am(OH)_3$ (Guillaumont *et al.*, 2003). The selected value

Table 19.32 *Enthalpies of formation and entropies of the crystalline lanthanide and actinide trihydroxides; estimated values are given in italics.*

An(OH)$_3$	$S°$(298.15 K) (J K^{-1} mol^{-1})	$\Delta_f H°$(298.15 K) (kJ mol^{-1})	*Ln(OH)*$_3$	$S°$(298.15 K) (J K^{-1} mol^{-1})[a]	$\Delta_f H°$(298.15 K) (kJ mol^{-1})
			$La(OH)_3$	117.81	–1415.6 ± 2.0[b]
			$Ce(OH)_3$	*130.2*	
			$Pr(OH)_3$	*132.6*	–1409.7 ± 4.9[c]
			$Nd(OH)_3$	129.87	–1415.6 ± 2.3[b]
			$Pm(OH)_3$	*131.2*	*–1419 ± 10*[d]
$Pu(OH)_3$	*134 ± 8*[e]		$Sm(OH)_3$	*126.7*	–1406.6 ± 2.2[b]
$Am(OH)_3$	*116 ± 8*[f]	–1353.2 ± 6.4[f]	$Eu(OH)_3$	119.88	*–1319 ± 10*[d]
$Cm(OH)_3$	*134 ± 8*[e]		$Gd(OH)_3$	126.63	*–1409 ± 10*[d]
$Bk(OH)_3$			$Tb(OH)_3$	128.37	*–1415 ± 10*[d]
$Cf(OH)_3$			$Dy(OH)_3$	*130.0*	*–1428 ± 10*[d]
$Es(OH)_3$			$Ho(OH)_3$	130.04	*–1431 ± 10*[d]

[a] As compiled by Konings (2001a).
[b] Merli *et al.* (1997).
[c] Morss and Hall (1994); Diakonov *et al.* (1998b) recommend –(1414 ± 10) kJ mol^{-1}.
[d] Diakonov *et al.* (1998a,b).
[e] Following the procedure of Guillaumont *et al.* (2003), p. 350, for $S°(Am(OH)_3,cr) = S_{lat} + S_{exc}$ using data from Konings (2001a) and estimating S_{exc} from that of sesquioxides Pu_2O_3 and Cm_2O_3.
[f] Guillaumont *et al.*(2003).

is nearly consistent with the experimental value of Merli *et al.* (1997), $\Delta_f H°(M(OH)_3,cr) = -(1343.6 \pm 1.8)$ kJ mol^{-1}. Their sample was well characterized and their calorimetric results are supported by similar measurements that they carried out for lanthanide hydroxides, which are consistent with solubility data.

(b) Entropy

The entropies of the solid trihydroxides $An(OH)_3$ have been estimated using the approach outlined earlier (equation (19.10)) (Konings, 2001a). The lattice component was estimated from the lanthanide trihydroxides, assuming the displacement of the trend to be the same as for the sesquioxides. The excess entropy was calculated from the degeneracy of the ground state. The values thus obtained are listed in Table 19.32 together with data for the lanthanide trihydroxides.

(c) Solubility products

Solubility products, often denoted 'solubility constants,' refer to equilibria such as:

$$M(OH)_3(cr) = M^{3+}(aq) + 3\,OH^-(aq), \quad K = K^0_{s,0} \tag{19.30}$$

Because americium has important long-lived isotopes and because it exists in solution as Am(III), its hydrolysis and solubility in aqueous solutions have been

the most carefully studied of the An(III) ions. The NEA review (Guillaumont *et al.*, 2003) selected the value of (15.6 ± 0.6) for the equilibrium

$$Am(OH)_3(cr) + 3\ H^+(aq) = Am^{3+}(aq) + 3\,H_2O(l), \quad K = {}^*K^0_{s,0} \qquad (19.31)$$

from the study of Silva (1982) because the solid phase in equilibrium with the solution was crystalline $Am(OH)_3$. The asterisk (*) in this notation refers to the protonation that is part of the equilibrium. For this equilibrium at 298.15 K, $\log_{10} K^0_{s,0} = \log_{10} {}^*K^0_{s,0} - 3\log_{10} K_w = 15.6 - 3 \times 14 = -26.4$. Guillaumont *et al.* (2003) also selected the value $\log_{10} {}^*K^0_{s,0} = (16.9 \pm 0.8)$ for the equilibrium (equation (19.31)) with $Am(OH)_3$(am), where 'am' refers to the precipitate that was amorphous to X-rays after aging for 4 months.

Latimer (1952) estimated the solubility products of actinide(III) hydroxides, $An(OH)_3$, from corresponding values for freshly precipitated hydroxides of the lanthanides. It is well known that, as these gelatinous precipitates age, their crystallinity increases and their solubility product decreases, so that the aged precipitates more nearly reflect equilibrium conditions. Baes and Mesmer (1976) exhaustively surveyed the literature and evaluated heterogeneous equilibria for lanthanide and actinide hydroxides and hydrated oxides. Additional thermochemical and extensive solubility data are available for the lanthanide trihydroxides. Diakonov *et al.* (1998a,b) carried out an extensive critical review of the thermochemical and solubility literature on rare earth hydroxides. These authors showed that there is a systematic trend of $\log_{10} K^0_{s,0}$ data for all rare earth hydroxides as a function of M^{3+} ionic radii. Specifically, the values of solubility product $\log_{10} K^0_{s,0}$ and $\log_{10} {}^*K_{s,0}$ become more positive as Z increases, because the ionic radii decrease and the Ln^{3+} ions become more acidic.

This trend could be extended to estimate solubility products for actinide trihydroxides. After the review of Diakonov *et al.* was published, Cordfunke and Konings (2001c) critically reviewed all the literature on enthalpy of formation of rare earth aqueous ions and recommended a set of values that are more comprehensive than the enthalpies of formation of rare earth aqueous ions used by Diakonov *et al.* One could use the recommended values of Diakonov *et al.*, with corrections for Cordfunke and Konings enthalpies of formation of rare earth aqueous ions, to extrapolate the relation between $\{\Delta_f H^\circ(M(OH)_3,cr) - \Delta_f H^\circ(M^{3+}, aq)\}$ and the M^{3+} ionic radii to derive estimates of $\log_{10} {}^*K_{s,0}$ for $An(OH)_3$. However, the one 'anchor,' $Am(OH)_3$, has such a significant uncertainty that such an extrapolation is considered too speculative for this chapter. Because the calorimetric data of Merli *et al.* for $Am(OH)_3$ are not quite in agreement with solubility data, enthalpy and entropy estimates for other actinide trihydroxides were not used to estimate solubility product measurements for other actinide trihydroxides in this chapter. We do cite the value of $\log_{10} {}^*K_{s,0} = (15.8 \pm 1.5)$ calculated for $Pu(OH)_3$ (Felmy *et al.*, 1989). This value is slightly smaller than the estimate for $Am(OH)_3$ cited above, consistent with the systematic trend for rare earth hydroxides as a function of ionic radius.

19.9.2 Oxides, hydrated oxides, and oxyhydroxides of An(IV), An(V), and An(VI)

The thermodynamics of crystalline anhydrous oxides was discussed in Section 19.5. Therefore, for these compounds, only solubility product values of interest are mentioned here for comparison with those of the amorphous corresponding compounds.

Under basic conditions, all actinide ions precipitate as hydroxides or hydrated oxides. Very few of these precipitates have been thoroughly characterized; interpolations, extrapolations, and approximations are usually necessary. Lemire *et al.* (2001) and Guillaumont *et al.* (2003) evaluated the literature results on the solubilities of some amorphous and crystalline actinide oxides, hydrated oxides, and oxyhydroxides. Their recommended values are given in Table 19.33. In this table the solubility product refers to the equilibrium constant for reactions such as

$$MO_2(\text{am or cr}) + 2\ H_2O\,(l) = M^{4+}(aq) + 4\ OH^-(aq), \quad K = K^0_{s,0} \quad (19.30a)$$

$$NpO_2OH(am) + H^+(aq) = NpO_2^+(aq) + H_2O(1), \quad K = {}^*K^0_{s,0} \quad (19.31a)$$

As mentioned in equation (19.31), the asterisk (*) in this notation refers to the protonation that is part of the equilibrium.

Selections were also made (Grenthe *et al.*, 1992; Guillaumont *et al.*, 2003) for other hydrates of UO_3. We cite here two properties of $UO_3 \cdot 2H_2O$(cr) ('schoepite'): $S°(298.15) = (188.54 \pm 0.38)$ J K^{-1} mol^{-1} and $\Delta_f H°(298.15) = -(1826.1 \pm 1.7)$ kJ mol^{-1}, as given by NEA-TDB (Grenthe *et al.*, 1992) based on measurements by Tasker *et al.* (1988). The solubility product of this compound is given in Table 19.33. We note that $UO_3 \cdot 2H_2O$(cr), which is often called schoepite, should be referred to as metaschoepite (Finch *et al.*, 1998).

The enthalpy of formation of the uranium(VI) peroxide studtite, $(UO_2)O_2(H_2O)$(cr), has been determined to be $-(2344.7 \pm 4.0)$ kJ mol^{-1} (Hughes-Kubatko *et al.*, 2003). The authors calculated the solubility at 298.15 K,

$$UO_2^{2+}(aq) + H_2O_2(aq) + 4\,H_2O(l) = (UO_2)O_2(H_2O)(cr) + 2\,H^+(aq) \quad (19.33)$$

and concluded that this peroxide is stable under the conditions where aqueous peroxide is formed from radiolysis of water by alpha particles.

The enthalpy of formation of NpO_2OH(am) was selected as $-(1222.9 \pm 5.5)$ kJ mol^{-1} by Lemire *et al.* (2001) from enthalpy of solution measurements by two different groups (Campbell and Lemire, 1994; Merli and Fuger, 1994) who used material containing different amounts of water.

The enthalpy of formation of $UO_3 \cdot H_2O(\beta)$ was selected as $-(1533.8 \pm 1.3)$ kJ mol^{-1} by Grenthe *et al.* (1992) from the difference in the enthalpy of solution of this compound (Cordfunke, 1964) and that of γ-UO_3. The enthalpy of formation of $NpO_3 \cdot H_2O$(cr) (= $NpO_2(OH)_2$(cr)) was selected as $-(1377 \pm 5)$ kJ mol^{-1}

Table 19.33 *Solubility products of the actinide crystalline and amorphous oxides at* 298.15 K, *from NEA-TDB* (*Grenthe* et al., 1992; *Silva* et al., 1995; *Lemire* et al., 2001; *Guillaumont* et al., 2003).

Solid phase	*Equilibrium*	*Th*	*U*	*Np*	*Pu*	*Am*
$An(OH)_3$(am)	$\log_{10}K^0_{s,0}$					–(25.1 ± 0.8)
$An(OH)_3$(cr)	$\log_{10}K^0_{s,0}$				–(26.2 ± 1.5)	–(26.4 ± 0.6)
AnO_2(am)	$\log_{10}K^0_{s,0}$	–(47.0 ± 0.8)	–(54.5 ± 1.0)	–(56.7 ± 0.5)	–(58.33 ± 0.52)	
AnO_2(cr)	$\log_{10}K^0_{s,0}$	–(54.3 ± 1.1)	–(60.86 ± 0.36)	–(65.75 ± 1.07)	–(64.04 ± 0.51)	–(65.4 ± 1.7)
An_2O_5(cr)	$\log_{10}{}^*K_{s,0}$			+(1.8 ± 0.8)		
AnO_2OH(am) 'fresh'	$\log_{10}{}^*K_{s,0}$			+(5.3 ± 0.2)		+(5.3 ± 0.5)
AnO_2OH(am) 'aged'	$\log_{10}{}^*K_{s,0}$			+(4.7 ± 0.5)	+(5.0 ± 0.5)	
$AnO_3 \cdot H_2O(\beta)$	$\log_{10}{}^*K_{s,0}$		+(4.90 ± 0.50)	+(5.47 ± 0.40)	+(5.80 ± 1.00)	
$AnO_3 \cdot 2H_2O$(cr)	$\log_{10}{}^*K_{s,0}$		+(4.81 ± 0.43)		+(5.5 ± 1.0)	

by Lemire *et al.* (2001), primarily from the enthalpy of solution measurements by Fuger *et al.* (1969).

No other hydroxides of tetravalent or higher-valent actinides have been adequately characterized for thermodynamic property determinations and calculations of solubility at equilibrium conditions.

19.9.3 Gaseous oxyhydroxides

It has been shown by several authors that the volatility of the uranium oxides is significantly enhanced in the presence of water vapor, as a result of the formation of the gaseous species $UO_2(OH)_2$ (Dharwadkar *et al.*, 1975; Krikorian *et al.*, 1993a). The equilibrium data of these studies were analyzed in the NEA-TDB review (Guillaumont *et al.*, 2003) using second- and third-law methods to derive the enthalpy of formation. The agreement between the studies is very poor. Moreover, the thermal functions for the third-law analysis, obtained from two sets of estimated molecular parameters (Ebbinghaus, 1995; Gorokhov and Sidorova, 1998), result in appreciably different entropy values. For that reason no selected values were presented by NEA-TDB. Recently, Privalov *et al.* (2002) calculated the geometry and vibrational frequencies of $UO_2(OH)_2$ using quantum chemical techniques. The thermodynamic functions calculated from their results are close to those of Gorokhov and Sidorova (1998). Also an increased volatility was reported in the presence of steam for the oxides of Pu and Am (Krikorian *et al.*, 1993b).

19.10 CARBIDES

The thermodynamic properties of the binary actinide carbides in the Th–C, U–C, Np–C, Pu–C, and Am–C systems were reviewed by Holley *et al.* (1984) as part of the IAEA series on the chemical thermodynamics of the actinide elements and compounds. In the NEA-TDB series that covers the compounds from U to Am (Grenthe *et al.*, 1992; Lemire *et al.*, 2001), most of the data by Holley *et al.* (1984) were accepted unchanged. Solid dicarbides, sesquicarbides, and monocarbides of the actinides have all been reported to exist, all generally showing wide ranges of nonstoichiometry, which makes the comparison of the different experimental results difficult. For the Pu–C system also, the compound Pu_3C_2 has been found.

19.10.1 Solid carbides

(a) Enthalpy of formation

The dicarbide exists in the Th–C and U–C systems with certainty, and in the Pu–C system only at high temperatures. The situation for the Pa–C and Np–C

systems is not yet fully clear, but claims for the synthesis of the dicarbides have been made. The measurements for thorium and uranium dicarbide have all been made on samples that are slightly substoichiometric ($C/M \approx 1.90$–1.97), and contain variable amount of oxygen impurities. Holley *et al.* (1984) gave recommended values for the composition $C/M = 1.94$ for both Th and U, probably the most stable composition, based on an analysis of the high-temperature equilibria and combustion calorimetry, which are given in Table 19.34.

The sesquicarbide is known for the U–C, Np–C, Pu–C, and Am–C systems, and measurements of the enthalpies of formation are only known for the first three compounds. Of these compounds, U_2C_3 is probably not thermodynamically stable at room temperature (its lower stability limit is estimated to be 1200 K) but samples have been cooled down without difficulty. High-temperature equilibria and combustion calorimetry have been reported, data which were analyzed by Holley *et al.* (1984). The value for Np_2C_3 is based on a preliminary measurement by combustion calorimetry; for U_2C_3 and Pu_2C_3 the combustion values at 298.15 K were slightly adjusted by Holley *et al.* (1984) to get a reasonable agreement with the high-temperature Gibbs energy values. From these values, Holley *et al.* (1984) estimated the enthalpy of formation of Am_2C_3 as $\Delta_f H^\circ(298.15\ \text{K}) = -(151 \pm 42)\ \text{kJ mol}^{-1}$.

The monocarbides are best described by the formula MC_{1-x}; they are known for all actinide–carbon systems from Th to Pu. The boundary compositions are $ThC_{0.98}$, UC, $NpC_{0.94}$, and $PuC_{0.84}$ and the enthalpies of formation of compositions, close to those recommended by Holley *et al.* (1984), are included in Table 19.34.

The enthalpy of formation of Pu_3C_2 was calculated by Holley *et al.* (1984) from phase considerations: (i) Pu_3C_2 is stable with respect to Pu and $PuC_{0.88}$ from 300 to 800 K and (ii) Pu_3C_2 decomposes to Pu and $PuC_{0.78}$ at 848 K.

(b) Entropy

A relatively large number of low-temperature heat capacity measurements have been made for the actinide carbides. For the Pu–C system measurements for 16 compositions have been reported, with reasonable though not complete consistency (see Holley *et al.*, 1984). Thus most of the entropy values listed in Table 19.34 are based on experimental studies; exceptions are Np_2C_3 and Pu_3C_2. Most of the experimental values have been corrected for the randomization entropy:

$$S_{\text{ran}} = x\ \ln\ x - (1-x)\ln(1-x) \tag{19.32}$$

which arises from the random ordering of the carbon and vacancies in the monocarbide, and of C and C_2 groups in the dicarbides.

Table 19.34 *Enthalpies of formation and entropies of the crystalline actinide carbides, pnictides and chalcogenides; see text for reference* (*estimated values are given in italics*). *The values for the compounds thorium are from the IAEA reviews* (*Chiotti* et al., 1981; *Holley* et al., 1984), *those for the compounds uranium, neptunium, and plutonium are from NEA-TDB* (*Grenthe* et al., 1990*; Lemire* et al., 2001*; Guillaumont* et al., 2003), *the values for* Am_2C_3 *are from Holley* et al. (1984).

	Th		*U*		*Np*		*Pu*		*Am*	
	$S°$ (298.15 K) ($J\ K^{-1}\ mol^{-1}$)	$\Delta_f H°$ (298.15 K) ($kJ\ mol^{-1}$)	$S°$ (298.15 K) ($J\ K^{-1}\ mol^{-1}$)	$\Delta_f H°$ (298.15 K) ($kJ\ mol^{-1}$)	$S°$ (298.15 K) ($J\ K^{-1}\ mol^{-1}$)	$\Delta_f H°$ (298.15 K) ($kJ\ mol^{-1}$)	$S°$ (298.15 K) ($J\ K^{-1}\ mol^{-1}$)	$\Delta_f H°$ (298.15 K) ($kJ\ mol^{-1}$)	$S°$ (298.15 K) ($J\ K^{-1}\ mol^{-1}$)	$\Delta_f H°$ (298.15 K) ($kJ\ mol^{-1}$)
An_3C_2							*210 ± 5*	*–113.0*		
AnC_{1-x}	59.0 ± 2.0	–125.5 ± 6.3	59.3 ± 0.2	–97.9 ± 4.0	72.2 ± 2.4	–71.1 ± 10.0	74.8 ± 2.1	–45.2 ± 8.0		
An_2C_3			137.8 ± 0.3	–183.3 ± 10.0	*135 ± 10*	–187.4 ± 19.2	*150 ± 2.9*	–149.4 ± 16.7	145 ± 20	–151 ± 42
$AnC_{1.94}$	70.4 ± 6.7	–125.5 ± 6.7	68.3 ± 2.0	–87.2 ± 2.1						
AnN	56.1 ± 0.8	–378 ± 10	62.43 ± 0.22	–290.0 ± 3.0	*63.9 ± 3.0*	*–305 ± 10*	64.81 ± 1.50	–299.2 ± 2.5		
$AnN_{1.466}$			*64.5 ± 1.0*	–362.2 ± 2.3						
An_3N_4	182.8 ± 2.1	–1305 ± 25								
AnP			78.28 ± 0.42	–269.8 ± 11.1			81.32 ± 6.00	–318 ± 21		
An_3P_4			259.4 ± 2.6	–843 ± 26						
AnP_2			100.7 ± 3.2	–304 ± 15						
AnAs			97.4 ± 2.0	–234.3 ± 8.0			94.3 ± 7.0	–240 ± 20		
An_3As_4			309.07 ± 0.60	–720 ± 18						
$AnAs_2$			123.05 ± 0.20	–252 ± 13						
AnSb					101.4 ± 6.1		106.9 ± 7.5	–150 ± 20		
$AnSb_2$			141.46 ± 0.13	–173.6 ± 10.9						
An_3Sb_4			349.8 ± 0.4	–451.9 ± 22.6						

(c) High-temperature properties

Enthalpy increment measurements have been reported for the three uranium carbides as well as PuC and Pu_2C_3. All data show a steep rise in the derived heat capacity above 1200 K, as is also observed in the oxides and nitrides and which have been attributed to the contribution of lattice vacancies. Fig. 19.29 shows the heat capacity of the three uranium carbides indicating rather similar behavior. Holley *et al*. (1984) estimated the heat capacity of ThC and ThC_2 from these data assuming a similar shape of the C_p curve. The heat capacity equations are summarized in Table 19.35.

19.10.2 Gaseous carbides

Gupta and Gingerich (1979, 1980) have detected gaseous AnC_n molecules with $n = 1$ to 6 in the Th–C and U–C systems by mass spectrometry. In the Th–C system, the molecules ThC_2 and ThC_4 contribute significantly to the vapor pressure, and in the ThC_2–C region the contribution of the former is about equal to that of Th(g). In the U–C system, only UC_2 has significant contribution for thermodynamic measurements. Holley *et al*. (1984) give estimated molecular properties for the thorium compounds ThC_2 and ThC_4 from which the thermal functions have been calculated. They assume a linear Th–C–C structure for ThC_2 and a linear C_2–Th–C_2 structure for ThC_4. With these functions they derived the enthalpies of formation of these molecules using third-law analysis. The resulting values are given in Table 19.36. Such treatment was not followed for UC_2 because of insufficient and inconsistent information.

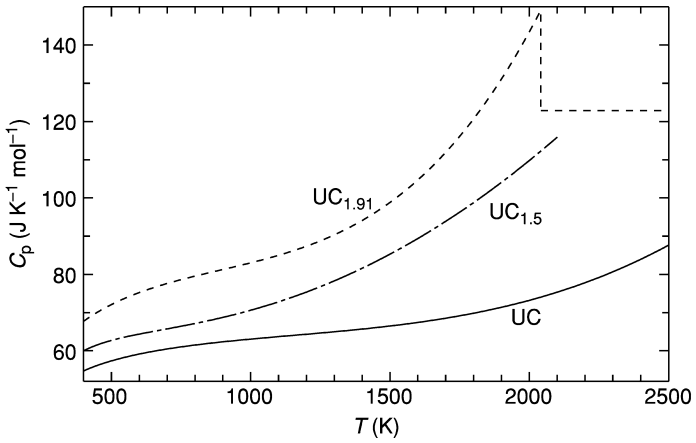

Fig. 19.29 *The high-temperature heat capacity of the uranium carbides.*

Table 19.35 *High-temperature heat capacity of the crystalline actinide nitrides and carbides;* $C_p/(\mathrm{J\ K^{-1}\ mol^{-1}}) = a(T/\mathrm{K})^{-2} + b + c(T/\mathrm{K}) + d(T/\mathrm{K})^2 + e(T/\mathrm{K})^3$ *(estimated values in italics); temperature* T_{max} *indicates the transition or melting temperature except values in brackets, which indicate the maximum valid temperature of the polynomial equation.*

	a ($\times 10^{-6}$)	b	c ($\times 10^{3}$)	d ($\times 10^{6}$)	e ($\times 10^{9}$)	T_{max} (K)	$\Delta_{trs}H$ (kJ mol^{-1})	*References*
ThC	*–0.6276*	*46.024*	*25.522*	*–18.828*	*5.439*	[2270]		[a]
$ThC_{1.94}$	*–0.5858*	*44.769*	*83.68*	*–79.496*	*30.426*	[1700]		[a]
UC	–0.618395	50.9235	25.7065	–18.6711	5.71334	2780		[a]
U_2C_3	–2.90503	150.6366	–47.8717	41.3588		[2100]		[a]
$UC_{1.91}$	–0.59258	48.9654	82.4867	–78.1086	30.2671	2041	10.083	[a]
		122.88						[a]
$PuC_{0.84}$	–0.15659	57.848	–14.4904	7.7048	8.6115	[1875]		[a]
Pu_2C_3	–0.5200	156.0004	–79.8726	70.4167		2285		[a]
ThN	*–0.4787*	*47.447*	*9.523*			[2000]		[b]
Th_3N_4	*–2.230*	*164.557*	*26.108*			[2000]		[b]
UN	–0.23304	40.4263	41.1928	–31.3066	10.0570	3123		[c]
$UN_{1.54}$	*–1.6788*	*65.040*	*19.288*			[1700]		[d]
PuN		45.002	15.420			[2000]		[e]
NpN	–0.0908	43.3	23.1	–7.62		[2000]		[f]

[a] Holley *et al.* (1984).
[b] Rand (1975).
[c] Refit of the equation by Hayes *et al.* (1990).
[d] Tagawa (1974).
[e] Lemire *et al.* (2001).
[f] Nakajima and Arai (2003).

Table 19.36 *Thermodynamic properties of the gaseous actinide carbides; estimated values are given in italics, from Holley* et al. (1984).

	$S°$(298.15 K) (J K^{-1} mol^{-1})	$\Delta_f H°$(298.15 K) (kJ mol^{-1})
ThC_2	256.7	720.5 ± 33.5
ThC_4	294.0	855.6 ± 41.8

19.11 PNICTIDES

The planned volume on the actinide pnictides in the IAEA series on the chemical thermodynamics of the actinide elements and compounds has not been completed and as a result a systematic review of the actinide nitride series is not available. However, in the NEA-TDB series, the data for the nitride compounds of uranium, neptunium, and plutonium have been reviewed, but with emphasis on the room temperature data.

19.11.1 Solid nitrides

(a) Enthalpy of formation

The enthalpies of formation of the mononitrides for ThN, UN, and PuN are based on calorimetric studies, as are those of the sesquinitrides $UN_{1.5+x}$ (α-U_2N_3) and $UN_{1.466}$ (β-U_2N_3) and Th_3N_4. The selected data for the compounds of U and Pu, which are summarized in Table 19.34, are from the NEA-TDB reports (Grenthe *et al.*, 1992; Lemire, *et al.*, 2001; Guillaumont *et al.*, 2003), the value of ThN and Th_3N_4 are taken from the assessment by Rand (1975).

The measurements for the uranium nitrides have not been made for the stoichiometric compositions as these are often difficult to prepare or do not exist: in α-U_2N_3, the N/U ratio varies from 1.54 to 1.75, in β-U_2N_3 from 1.45 to 1.49. The enthalpies of formation of the various uranium nitrides vary linearly as a function of the N/U ratio, as shown in Fig. 19.30. Thus the enthalpy of formation of α-U_2N_3 is represented by the following equation:

$$\Delta_f H°(UN_{1.5+x},\ \text{cr},\ 298.15\ \text{K})/\text{kJ mol}^{-1} = -366.7 - 138.2x$$

which is a simple linear representation of the two compositions with N/U 1.606 and 1.674 for which experimental measurements have been made (see Grenthe *et al.*, 1992).

The enthalpy of formation of ThN is significantly more negative than that of UN and PuN. This can be explained by the fact that the chemical bonding in ThN is less ionic and more covalent than in UN and PuN. Kuznietz (1968)

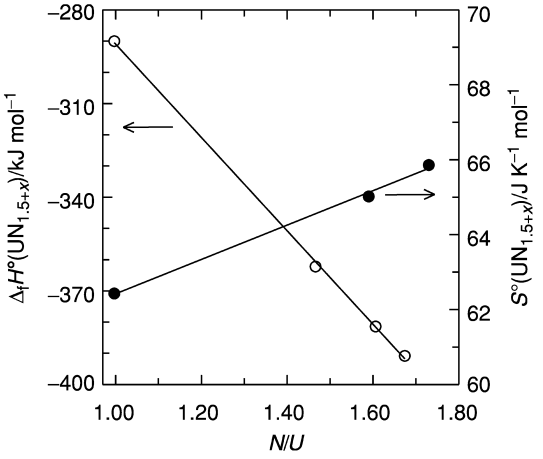

Fig. 19.30 *The enthalpy of formation* (○) *and the standard entropy* (●) *of the uranium nitrides as a function of the N/U ratio.*

proposed that the ThN lattice consists of Th^{4+} and N^{3-} ions with one conduction electron for each Th atom. Recently some indirect information on the enthalpies of formation of the mononitrides NpN and AmN was obtained from high-temperature Knudsen cell studies. Nakajima *et al.* (1997, 1999a) studied the vaporization of NpN and (Np,Pu)N. From their results, they found that the Gibbs energy of formation of NpN is between the values for UN and PuN. This is a justification for the approach of Lemire *et al.* (2002) who estimated the enthalpy of NpN by interpolation of the values for UN and PuN. Ogawa *et al.* (1995) studied the vaporization of PuN containing small amount of ^{241}Am as decay product. From these results, they estimated the enthalpy of formation of AmN as -294 kJ mol^{-1} at 1600 K.

(b) Entropy

Low-temperature heat capacity measurements of three mononitrides have been reported: ThN, UN, and PuN. As is the case for the enthalpies of formation, the value for ThN is distinctly different (lower) from that of UN and PuN. Lemire *et al.* (2001) assumed the entropy of NpN to be between the values for UN and PuN. Low-temperature heat capacity measurements have also been reported for Th_3N_4 and α-U_2N_3 (two compositions with N/U 1.59 and 1.73). The recommended values are summarized in Table 19.34. Like the enthalpy of formation, the standard entropy varies linearly with the N/U ratio, as shown in Fig. 19.30, and the value for $UN_{1.466}$ is obtained by interpolation. Based on

this observation, the standard entropy of α-U_2N_3 is represented by the following equation:

$$S^\circ(UN_{1.5+x},\ \text{cr},\ 298.15\ \text{K})/\text{J K}^{-1}\ \text{mol}^{-1} = 64.48 + 6.00x$$

(c) High-temperature properties

The high-temperature properties of UN and PuN were reviewed by Matsui and Ohse (1987), those of UN by Hayes *et al.* (1990), and more recently by Chevalier *et al.* (2000). These are the only two mononitrides for which calorimetric enthalpy increment measurements are available. Below 1700 K, the UN data recommended by Matsui and Ohse (1987) and Hayes *et al.* (1990) are in good agreement, as they are based on the same set of experimental data. But Hayes *et al.* (1990) indicate that UN shows a nonlinear increase in the heat capacity at high temperatures, likely due to the contribution of lattice defects, based on measurements by Conway and Flagella (1969), which were not considered by Matsui and Ohse (1987). This effect has not been observed in PuN, but the experimental data for this compound are limited to 1560 K. This situation is similar to the dioxides. Kurosaki *et al.* (2000) performed molecular dynamics calculations of the heat capacity of UN, and obtained a good agreement with the experimental results up to 1500 K, where the effects of lattice defects are marginal. Experimental high-temperature heat capacity data for the higher nitrides are scarce. The heat capacity of NpN has been measured by Nakajima and Arai (2003) by differential scanning calorimetry. The recommended high-temperature heat capacity functions are given in Table 19.35.

The actinide mononitrides vaporize to give An(g) and N_2(g) molecules, as has been demonstrated experimentally for ThN, UN, PuN, and NpN. The detailed mass spectrometric studies for UN have demonstrated also that the UN molecule occurs in the vapor phase, though its pressure is about three orders of magnitude lower than that of U(g). The decomposition temperatures under 1 bar nitrogen are 3053 K for UN, 2948 K for NpN, and 2843 K for PuN. Under nitrogen pressure, the mononitrides melt congruently: 3080 K at 2–3 bar N_2 for ThN (Rand, 1975), 3123 K at 2.5 bar N_2 for UN (Matsui and Ohse, 1987), 3103 K at 9.9 bar N_2 for NpN, and 3103 K at 5 bar N_2 for PuN (Lemire *et al.*, 2001). Th_3N_4 decomposes to ThN before melting.

19.11.2 Gaseous nitrides

The actinide mononitrides principally vaporize to give the gaseous elements, but molecular UN has been identified in the vapor as a minor species by mass spectrometry (Gingerich, 1969; Venugopal *et al.*, 1992). Molecular ThN, UN, and PuN species were also identified by infrared absorption spectroscopy in

low-temperature inert-gas matrices (Ar) as reported by Green and Reedy (1976, 1978b, 1979). From these measurements the harmonic frequency ω_e and the first anharmonic correction coefficient were derived. Unlike the actinide monoxides, the experimental data for mononitrides do not show a regular decrease from ThN to PuN. The value for UN ($\omega_e = 1007.7$ cm^{-1}) is significantly higher than the values for ThN ($\omega_e = 941.9$ cm^{-1}) and PuN ($\omega_e = 861.8$ cm^{-1}). The reason for this is not clear. Overall the experimental data are insufficient to derive reliable thermodynamic properties.

19.11.3 Phosphides, arsenides, and antimonides

The thermodynamic data on phosphides, arsenides, and antimonides are restricted to the uranium compounds, some plutonium compounds and a single neptunium compound. They are summarized in Table 19.37, and have been

Table 19.37 *Thermodynamic properties of selected crystalline actinide chalcogenides; estimated values are given in italics.*

	C_p(298.15 K) (J K^{-1} mol^{-1})	$S°$(298.15 K) (J K^{-1} mol^{-1})	$\Delta_f H°$(298.15 K) (kJ mol^{-1})	*References*
ThS		69.79 ± 0.33	–399.6 ± 4.2	[a]
Th_2S_3		*180 ± 17*	–1083.7 ± 12.6	[a]
Th_7S_{12}		*641 ± 59*	–4130 ± 146	[a]
ThS_2		96.2 ± 8.4	–628 ± 42	[a]
Th_2S_5		215 ± 17	–1272 ± 84	[a]
US	50.54 ± 0.08	77.99 ± 0.21	–320.9 ± 12.6	[a,b]
U_2S_3	133.7 ± 0.8	199.2 ± 1.7	–880 ± 67	[a,b]
U_3S_5		*291 ± 25*	–1431 ± 100	[a,b]
US_2	74.64 ± 0.13	110.42 ± 0.21	–520.4 ± 8.0	[a,b]
U_2S_5		*243 ± 25*		[a,b]
US_3	95.60 ± 0.25	138.49 ± 0.21	–539.6 ± 10.6	[a,b]
USe	54.81 ± 0.17	96.52 ± 0.21	–275.7 ± 14.6	[a,b]
USe_2 (α)	79.16 ± 0.17	134.98 ± 0.25	–427 ± 42	[a,b]
USe_3		*177 ± 17*	–452 ± 42	[a,b]
U_2Se_3		261.4 ± 1.7	*–711 ± 75*	[a,b]
U_3Se_4		*339 ± 38*	–983 ± 85	[a,b]
UTe		*112 ± 5*	–182 ± 11	[a]
UTe_3	117.2 ± 1.0	214.2 ± 1.7	*–284 ± 63*	[a]
U_3Te_4			–684 ± 142	[a,b]
PuS		*74 ± 5*	*–364 ± 38*	[a]
PuS_2		*107 ± 13*	*–529 ± 54*	[a]
Pu_2S_3		*188 ± 17*	*–987 ± 100*	[a]
PuSe	59.7 ± 1.2	92.1 ± 1.8		[b]
PuTe	73.1 ± 2.9	107.9 ± 4.3		[b]

[a] Grønvold *et al.* (1984).
[b] NEA-TDB (Grenthe *et al.*, 1990; Guillaumont *et al.*, 2003).

taken from the assessments by the NEA teams (Grenthe *et al.*, 1992; Lemire *et al.*, 2001; Guillaumont *et al.*, 2003).

19.12 CHALCOGENIDES

19.12.1 Sulfides

The experimental thermodynamic data on the actinide sulfides are restricted to the compounds of thorium and uranium. Data for the other actinides, essentially neptunium and plutonium, are based on estimates. A thorough review of the thermodynamic properties of the actinide sulfides (and the selenides and tellurides) was made by Grønvold *et al.* (1984), after which little new information has become available. For these systems, compounds with a wide variety of S/An ratios have been reported: the solids AnS, An_3S_4, An_2S_3, An_7S_{12}, AnS_2, An_2S_5, and AnS_3, and the gases AnX and AnX_2. The thermodynamic data for the solid compounds are summarized in Table 19.37, which is essentially based on the analyses by Grønvold *et al.* (1984). The values in the NEA-TDB report on uranium are essentially revisions of this work and are adopted here. The entropies of the uranium sulfides are a linear function of the S/U ratio, as shown in Fig. 19.31, confirming the estimates for U_3S_5 and U_2S_5.

19.12.2 Selenides and tellurides

Very few data also exist for the selenides and tellurides, again mainly for uranium compounds. However, for this compound group some plutonium compounds have been reported. Low-temperature heat capacities of PuSe and

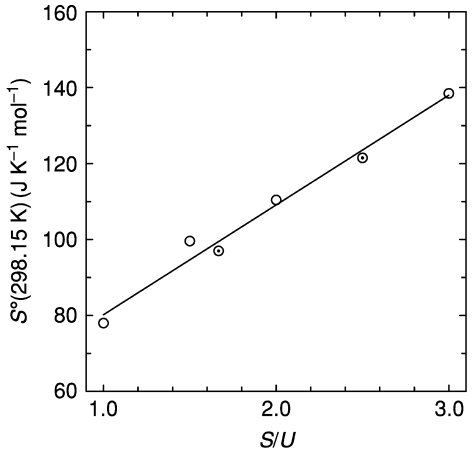

Fig. 19.31 *The entropies of the uranium sulfides* (*per mole of U*) *as a function of the S/U ratio; estimated values are indicated by* (⊙).

PuTe were measured by Hall *et al.* (1990, 1992) (see Table 19.37). No experimental determinations of the enthalpies of formation of these compounds exist.

19.13 OTHER BINARY COMPOUNDS

19.13.1 Compounds with group IIA elements

Thermodynamic data for binary compounds with group IIA elements are restricted to the actinide–beryllium systems. The compounds $ThBe_{13}$, UBe_{13}, and $PuBe_{13}$ have been characterized. A relatively complete data set is only available for UBe_{13} (see Tables 19.38 and 19.39) and have been assessed by the NEA team (Grenthe *et al.*, 1992). They include low-temperature heat capacity, enthalpy of formation and high-temperature heat capacity, and enthalpy increment measurements, the latter, however, in a limited temperature range (273–379 K). Unfortunately the high-temperature data are not consistent, and for this reason they give no recommendation. The value for the enthalpy of formation of $PuBe_{13}$ is taken from the assessment by Chiotti *et al.* (1981), and is based on an assessment of enthalpy of solution measurements.

19.13.2 Compounds with group IIIA elements

The systems of the actinides with group IIIA elements have significant technological relevance: the U–Al system for (materials testing) reactor fuel and the Pu–Ga for nuclear weapons. Also uranium borides have been considered for nuclear fuel materials. It is not surprising that these systems have been studied in more detail. Thermodynamic data for UB_2 are well established, and the high-temperature enthalpy increment measurement extend up to 2300 K. An anomalous increase of the heat capacity is observed (Fig. 19.32), as for many uranium compounds. The data have been assessed by Chiotti *et al.* (1981) and their selected values are included in Tables 19.38 and 19.39. For the U–Al compounds, only enthalpy of solution and EMF measurements have been made. However, Chiotti *et al.* (1981) do not give recommended values for the enthalpies of formation of the U–Al compounds. In Table 19.38 we have listed the values derived by Chiotti and Kately (1969), which are in good agreement with the other measurements. For the U–Ga system, Chiotti *et al.* (1981) cite only EMF and vapor pressure measurements and do not give thermodynamic values at 298.15 K. However, Palenzona and Cirafici (1975) measured the enthalpy of formation of UGa_3 and Prabhahara *et al.* (1998) measured the enthalpy of formation of UGa_3 and UGa_2 by solution calorimetry. Their results for UGa_3 are in poor agreement, but the results of Prabhahara *et al.* (1998) agree nicely with the EMF and vapor pressure studies. Their values are given in Table 19.38. In contrast, enthalpy of solution measurements are known for a number

Table 19.38 *Thermodynamic properties of other selected crystalline binary actinide compounds; estimated values are given in italics.*

	C_p(298.15 K) (J K^{-1} mol^{-1})	$S°$(298.15 K) (J K^{-1} mol^{-1})	$\Delta_f H°$(298.15 K) (kJ mol^{-1})	*References*
$ThSi_2$			–174.4	[a]
UBe_{13}	242.3 ± 4.2	180.1 ± 3.3	–163.6 ± 17.5	[b]
UB_2	55.35 ± 0.13	55.10 ± 0.13	–144.8 ± 12.6	[a]
UAl_2			–92.5 ± 8.4	[a]
UAl_3			–108.4 ± 8.4	[a]
UAl_4			–124.7 ± 8.4	[a]
UGa_3			–153.2 ± 17.6	[c]
UGa_2			–121.2 ± 18.0	[c]
USi_3			–132.2 ± 0.4	[a]
USi_2			–130.1 ± 1.3	[a]
USi			–80.3 ± 1.3	[a]
U_3Si_2			–170.3 ± 2.1	[a]
UGe_3		170.7	–106.7	[a]
UGe_2		130.5	–87.4	[a]
U_3Ge_5		351.9	–239.7	[a]
UGe		90.4	–61.5	[a]
U_5Ge_3		374.9	–23.1	[a]
UPd_3	102.10 ± 0.20	176.35 ± 0.30	–286 ± 22	[d]
URh_3	103.01 ± 0.20	152.24 ± 0.30	–302.0 ± 0.2	[d,e]
URu_3	101.42 ± 0.20	144.50 ± 0.29	–153.2 ± 0.2	[d]
$PuBe_{13}$			–149.4 ± 23.4	[a]
$PuAl_2$			–142.3 ± 10.0	[a]
$PuAl_3$ (hex)			–180.7 ± 10.0	[a]
$PuAl_4$ (α)			–180.7 ± 10.0	[a]
Pu_6Fe		425.6 ± 4.4	*–13.8 ± 4.6*	[a]
Pu_3Ga (β)			–158.2 ± 20.9	[a]
$PuGa_2$			–190.4 ± 31.4	[a]
$PuGa_6$			–238.1 ± 37.7	[a]
$PuSn_3$			–219.7 ± 11.3	[a]

[a] Chiotti *et al.* (1981).
[b] NEA-TDB (Grenthe *et al.*, 1992; Lemire *et al.*, 2001; Guillaumont *et al.*, 2003).
[c] Prabhahara *et al.* (1998).
[d] Cordfunke and Konings (1990).
[e] See text.

of compounds in the Pu–Ga system, and the assessed values by Chiotti *et al.* (1981) are included in Table 19.38.

19.13.3 Compounds with group IVA elements

The phase diagrams of the systems of the actinides with Si, Ge, Sn, and Pb have been studied in detail but thermodynamic data are scarce. Chiotti *et al.* (1981) did not give recommended values for the enthalpies of formation of any of the

Table 19.39 *High-temperature heat capacity of other crystalline actinide binary compounds;* $C_p/(\mathrm{J\ K^{-1}\ mol^{-1}}) = a(T/\mathrm{K})^{-2} + b + c(T/\mathrm{K}) + d(T/\mathrm{K})^2 + e(T/\mathrm{K})^3$ (*estimated values are given in italics*).

	a ($\times 10^{-6}$)	b	c ($\times 10^{3}$)	d ($\times 10^{6}$)	e ($\times 10^{9}$)	T (K)	*References*
UB_2		16.0498	167.8	–131.52	36.553	2658	[a]
UPd_3	–0.28221	110.8964	–28.865	33.5733		1973	[b,c]
URu_3	–0.47184	101.224	18.46028			2123	[c]
URh_3	–0.61003	104.445	18.20548			2013	[c]

[a] Chiotti *et al.* (1981).
[b] See Fig. 19.32.
[c] Cordfunke and Konings (1990).

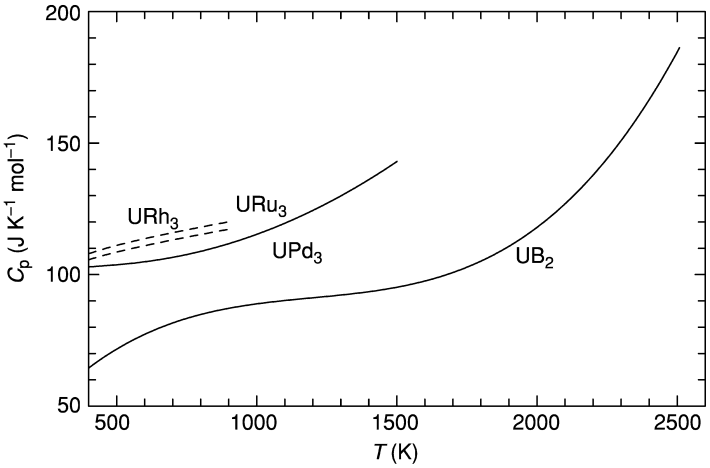

Fig. 19.32 *High-temperature heat capacity of some uranium intermetallic compounds. The UPd_3 curve is composed from the results of Burriel* et al. (1988) *and Arita* et al. (1997) *by scaling of the latter.*

compounds of these systems, except the U–Ge system. This is because there is often a distinct difference between the results from calorimetric (solution) measurements and EMF or vapor pressure measurement. However, measurement of the enthalpy of formation has been made that can be considered reliable. Robbins and Jenkins (1955) measured the enthalpy of formation of $ThSi_2$, Gross *et al.* (1962) measured the enthalpy of formation of USi_3, USi_2, USi, and U_3Si_2. For the U–Ge system, Chiotti *et al.* (1981) selected the values derived by Rand and Kubaschewski (1963) from vapor pressure measurements. These data are included Table 19.38.

19.13.4 Compounds with the transition elements (IB–VIIIB)

Chiotti *et al.* (1981) and Colinet and Pasturel (1994) discussed the thermodynamic data of the actinide intermetallic compounds with the transition metals in detail, Ward *et al.* (1986) the actinide–noble metal intermetallic compounds. The experimental basis for these compounds is limited and most of the work is done for the compounds of Th, U, and Pu.

(a) Enthalpies of formation

Extensive data exist for the systems An–Cd, An–Zn, and An–Bi that are of relevance to pyrochemical reprocessing, although the thermodynamic characterization of the compounds in these systems is limited. In most cases, only ΔG

functions at elevated temperatures have been reported, derived from EMF or vapor pressure measurements (see Chiotti *et al.*, 1981).

A large number of thermodynamic studies have been performed on the intermetallic compounds of uranium and the noble metals Ru, Rh, and Pd. The data were reviewed by Cordfunke and Konings (1990) and the recommended values are included in Table 19.38. The experimental EMF data on URu_3 and URh_3 reasonably agree, but a big discrepancy exists for UPd_3 for which a fluorine combustion study gave a much more negative value (-524 kJ mol^{-1}) than the value derived from vapor pressure measurements (-260 kJ mol^{-1}). Jung and Kleppa (1991) performed direct reaction calorimetry on these three compounds, and their result for UPd_3 $-(286 \pm 22)$ kJ mol^{-1} suggests that the fluorine combustion values are found to be in error. On the other hand, Prasad *et al.* (2000) reported a value close to the combustion value, derived from gas-equilibrium measurements. This example shows the difficulties determining accurate thermochemical data for these compounds.

Two semiempirical models are generally used to explain the trends and to estimate the unknown thermodynamic quantities of the actinide intermetallic compounds: the Engel–Brewer model and the Miedema model, as discussed extensively by Chiotti *et al.* (1981) and Ward *et al.* (1986). The Engel–Brewer model correlates thermodynamic properties with electronic structure. Brewer postulated that the s- and p-electrons involved in the bonding determine the crystal structure, whereas the d-electrons affect the chemical bonding and thermodynamic properties. The Engel–Brewer model is based on the promotion of atoms to valence states involving unpaired electrons suitable for bond formation with covalent character. The promotional energy to unpair the electrons was found to be 67 kJ mol^{-1} for the d^3s state in Th, 75 kJ mol^{-1} for the f^3d^2s state in U, and 180 kJ mol^{-1} for the f^5d^2s state in Pu (Brewer, 1970).

The Miedema model (de Boer *et al.*, 1988) correlates the enthalpy of formation of an intermetallic compound with the electronegativity and the electron density at the atomic cell boundary:

$$\Delta H = f(c)\left[-P(\Delta\phi^*)^2 + Q_0\left(\Delta n_{\mathrm{ws}}^{1/3}\right)^2\right] \tag{19.33}$$

where $f(c)$ is a function of the concentration of the metals, ϕ^* and Δn_{ws} the electronic work function of a pure metal and the electronic potential at the cell boundary, and P and Q_0 are constants. Fig. 19.33 shows the enthalpies of formation of actinide AnM_2 compounds with the 3d, 4d, and 5d transition elements predicted by this model (Ward *et al.*, 1986), indicating the limited stability of actinide compounds with the early d-transition elements (IVB, VB, and VIB) and a high stability of the compound with late d-transition elements. The Miedema model predicts $\Delta_f H^\circ(298.15\ \mathrm{K}) = -244$ kJ mol^{-1} for UPd_3 (de Boer *et al.*, 1988), which is close to the experimental values obtained by reaction calorimetry and vapor pressure measurements (see above). As concluded by Chiotti *et al.* (1981) after a systematic analysis of the thermodynamic

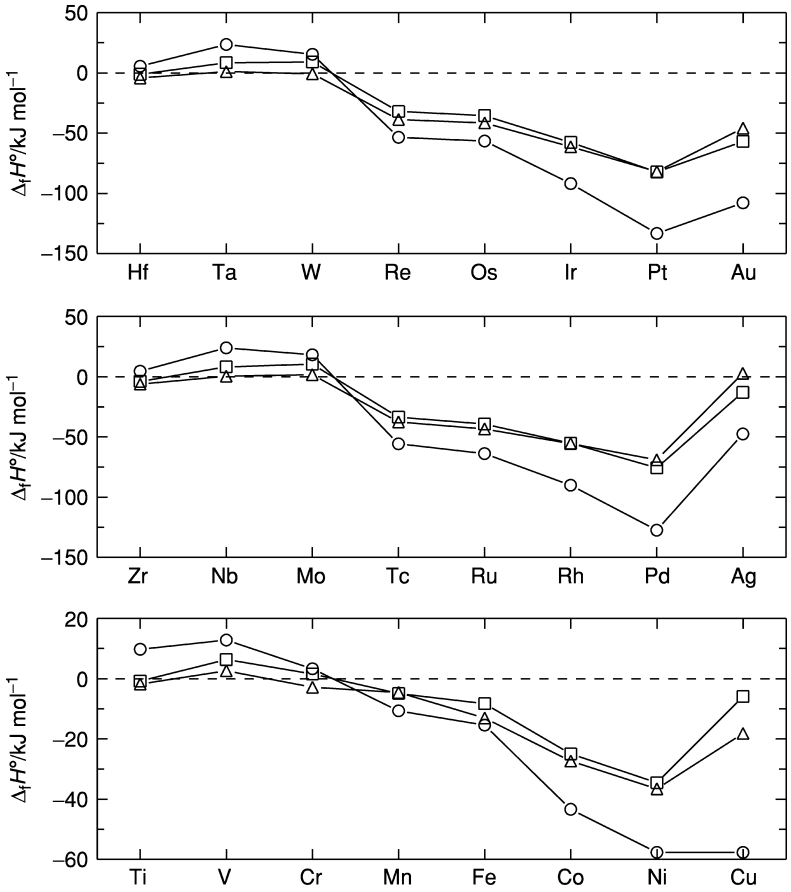

Fig. 19.33 *The enthalpies of formation predicted for actinide intermetallic phases* AnM_2 *from the Miedema correlation, as a function of the transition metal component,* (○) *Th,* (□) *U and* (Δ) *Pu* (*after Ward* et al., 1986).

data for intermetallic actinide compounds, estimates with Miedema's model are seldom in error by more than 20%, though it does not take into account the role of 5f electrons.

(b) Heat capacity and entropy

Accurate low-temperature (up to 300 K) heat capacity measurements have only been made for a limited number of uranium intermetallic compounds (URu_3, URh_3, and UPd_3). The derived entropy values at 298.15 K are given in Table 19.38. Also heat capacity measurements for some plutonium intermetallic compounds (Pu_6Fe) have been made, but of significantly less accuracy due to the small sample masses used. It should be noted, however, that low-temperature

heat capacity measurements below 50 K have been made for many actinide intermetallic compounds, due to their interesting magnetic and superconducting properties. It can be noted here that the heat capacity data for UPd_3 confirm that the f-electrons in this compound are localized, leading to discrete energy levels, in contrast to URu_3 and URh_3, in which the f-electrons are itinerant.

Moriyama *et al.* (1990) proposed a correlation to estimate the entropies of intermetallic compounds based on the assumption that the (vibrational) entropy is proportional to the logarithm of the bond energy. The entropies of the MA_n compound and the elements M and A are described by:

$$S(MA_n) = a \ln[\{E(M) + nE(A) - \Delta_f H^\circ\}/(1+n)] + b_1 \tag{19.34}$$

$$S(M) = a \ln E(M) + b_2$$

$$S(A) = a \ln E(A) + b_3$$

where E is the bond energy of the metal, which was approximated by the sublimation enthalpy. The entropy of formation of the MA_n compound was then calculated from the equation:

$$\Delta_f S(MA_n) - a \ln H' + b' \tag{19.35}$$

with $H' = [\{E(M) + nE(A) - \Delta_f H^\circ(MA_n)\}/(1+n)]^{(1+n)} E(M)^{-1} E(A)^{-n}$. Indeed a linear relation was found for the actinide intermetallics considered. The coefficient a was determined empirically to be –61.9 J K^{-1} mol^{-1} and b was found to be zero, using known entropy values for actinide intermetallics.

(c) High-temperature properties

High-temperature heat capacities of only a limited number of intermetallic actinide compounds have been measured. Systematic studies have been made on the intermetallic compounds of uranium with the noble metals Rh, Ru, and Pd. Cordfunke *et al.* (1985) and Burriel *et al.* (1988) have reported enthalpy increment measurements for URh_3, URu_3, and UPd_3 and found excellent agreement with the low-temperature data. Arita *et al.* (1997) measured the heat capacity of UPd_3 but their results poorly agree with the enthalpy data of Burriel *et al.* (1988). However, their results indicate a rapid increase above 900 K (Fig. 19.32) that was attributed to lattice defect formation. The recommended heat capacity functions are summarized in Table 19.39. No data are known for the liquid phase of any of these compounds.

19.14 CONCLUDING REMARKS

The present chapter shows that a steady progress has been made in the determination and understanding of the thermodynamic properties of the actinide elements and compounds since the first edition of this work. Not only

the number of compounds has been extended considerably, but also the quality of the data and the quality of the methods for estimation has improved considerably. In general it can be concluded that the systematics in the thermodynamic properties reflect the well-known change from itinerant f-electrons at the beginning of the actinide series to localized f-electrons from Am and beyond.

However, the overall quality of the thermodynamic data differs considerably between the various groups of compounds:

- The thermodynamic properties of the main actinide elements are fairly well established. Improvement is still needed for Ac, Pa, and the elements from Am onwards, but due to the high radioactivity of these elements and their limited availability, many additional measurements are not to be expected in the coming decades. But since the trends in the thermodynamic properties are reasonably well understood, the estimates presented here must be considered reliable.
- The thermodynamic data for actinide ions in aqueous solutions are still not satisfactory, even for the main actinides. Especially the values for the standard entropies of the aqueous species are based on few experiments and need improvement. The thermodynamic data of ions in molten salts have improved considerably for the LiCl–KCl (eutectic) but are still of poor quality for LiF–BeF_2. Other molten salt solvents have hardly been studied.
- The solid oxides (binary, ternary, quaternary) have been studied extensively and many systematics have been established. For this group there is a considerable mismatch between the large number of enthalpy of formation data and the limited number of entropy data. Also the high-temperature heat capacity data are limited. This is very apparent for the complex solid oxides. The data for the gaseous binary oxides are incomplete and require further studies: experimental studies to identify the molecular species and quantum chemical studies to estimate their properties.
- The actinide halides show the largest number of different oxidation states in both solid and gaseous state. Except for some technologically important halides (UF_6) the thermodynamic properties of this group are still surprisingly poorly characterized in spite of many studies, and for the solid dihalides, for example, no measurements exist at all. Trends and systematics in the AnX_n series and comparison to the LnX_3 and LnX_2 series, however, allow reasonable estimates, but there is still a need for experimental studies, especially heat capacity data at low and high temperatures.
- Relatively many studies of the dissociation pressures of the An–H_2 systems have been performed. However, the thermodynamic properties of only limited number of compounds can be derived from these data.
- The properties of the actinide hydroxides have hardly been studied, and the few experimental results (e.g. $Am(OH)_3$) are not consistent.

- The thermodynamic data for the carbides, pnictides, and chalcogenides are restricted to compounds of Th, U, and Pu. Because of their potential technological interest as nuclear fuels, the data are quite complete generally and extend up to high temperatures, though the available data on the gaseous molecules is scanty. The carbides, pnictides, and chalcogenides of other actinide have hardly been studied.
- Although the binary phase diagrams of actinides and other elements are generally well established, the basic thermodynamic data for alloys and intermetallic compounds are poorly known, even for technologically relevant systems. Predictive models have been developed, but the lack of reliable data makes it difficult to judge them. Moreover, the chemical bonding in actinide compounds is much more complex than in lanthanide or transition metal compounds, and possibly beyond the applicability of these models.

The need for further thermodynamic studies is thus as relevant as in the past decades. This is especially true because the trends in nuclear technology are moving in the direction of advanced nuclear systems for energy production with fuel cycles that include the proper treatment of plutonium and the minor actinides: fast reactors with innovative fuels, molten salt reactors, and advanced reprocessing (hydrochemical or pyrochemical). The development of these technologies demands better data for many actinide compounds, not only the pure substances but also their multicomponent mixtures, which have not been addressed in this chapter. To assure that such data will become available, the expertise in the field of actinide thermodynamics (both experimental and theoretical) must thus be maintained at a level that is needed for engineering, safety, and environmental applications, which is not evident now.

The data presented in this chapter are included in the f-MPD web-based material property information center of the Institute for Transuranium Elements (www.f-elements.net), from which complete thermodynamic tables can be retrieved. Corrections and updates will also be available from this site.

REFERENCES

Abraham, B. M., Brody, B. B., Davidson, N. R., Hagemann, F., Karle, I., Katz, J. J., and Wolf, M (1949) in *The Transuranium Element-Collected Papers* (eds. G. T. Seaborg, J. J. Katz, and W. M. Manning), McGraw-Hill, New York, pp. 740–58.

Ackermann, R. J., Faircloth, R. L., Rauh, E. G., and Thorn, R. J. (1966a) *J. Inorg. Nucl. Chem.*, **28**, 111–18.

Ackermann, R. J., Faircloth, R. L., and Rand, M. H. (1966b) *J. Phys. Chem.*, **70**, 3698–706.

Ackermann, R. J. and Rauh, E. G. (1973a) *Rev. Hautes Temp. Refract. Fr.*, **15**, 259–80.

Ackermann, R. J. and Rauh, E. G. (1973b) *High Temp. Sci.*, **5**, 462–73.

Ackermann, R. J. and Rauh, E. G. (1975) *J. Chem. Phys.*, **62**, 108–12.

Akabori, M., Kobayashi, F., Hayashi, H., Ogawa, T., Huntelaar, M. E., Booij, A. S., and Van Vlaanderen, P. (2002) *J. Chem. Thermodyn.*. **34**, 1461–6.

Ali, M., Mishra, R., Bharadwaj, S. R., Kerkar, A. S., Dharwadkar, S. R., and Das, D. (2001) *J. Nucl. Mater.*, **299**, 165–70.

Apelblatt, A. and Sahar, A. (1975) *JCS Faraday Trans. I*, **71**, 1667–70.

Archibong, E. F. and Ray, A. K. (2000) *J. Mol. Struct. (THEOCHEM)*, **530**, 165–70.

Arita, Y., Sasajima, N., and Matsui, T. (1997) *J. Nucl. Mater.*, **247**, 232–4.

Arkhipov, V. A., Gutina, E. A., Dobretsov, V. N., and Ustinov, V. A. (1974) *Sov. Radiochem.*, **16**, 122–4.

Bakker, K., Cordfunke, E. H. P., Konings, R. J. M., and Schram, R. P. C. (1997) *J. Nucl. Mater.*, **250**, 1–12.

Barin, I. and Knacke, O. (1973) *Thermochemical Properties of Inorganic Substances*, Springer Verlag, Berlin.

Barrett, S. A., Jacobson, A. J., Tofield, B. C., and Fender, B. E. F. (1982) *Acta Crystallogr.*, **B38**, 2775–8.

Bartscher, W. and Sari, C. (1986) *J. Nucl. Mater.*, **140**, 91–3.

Baes, C. F. Jr (1966) in *Thermodynamics*, vol. 1, IAEA, Vienna, pp. 409–33.

Baes, C. F. Jr (1969) in *Reprocessing of Nuclear Fuel*, Conf. 690–801; USAEC, p. 617.

Baes, C. F. Jr and Mesmer, R. E. (1976) *The Hydrolysis of Cations*, Wiley Interscience, New York.

Bazhanov, V. I., Ezhov, Yu. S., and Komarov, S. A. (1990a) *Zh. Strukt. Khim.*, **31**, 152–3.

Bazhanov, V. I., Komarov, S. A., Sevast'yanov, V. G., Popik, M., Kuznetsov, N. T., and Ezhov, Yu. S. (1990b) *Vysochist. Veshchestva*, **1**, 109–10.

Belov, A. N. and Semenov, G. A. (1980) *Zh. Fiz. Khim.*, **54**, 1537–41.

Belyaev, Yu. I., Smirnov, N. L., and Taranov, A. P. (1979) *Radiokhimiya*, **21**, 682–6.

Besmann, T. M. and Lindemer, T. B. (1983) *J. Am. Ceram. Soc.*, **66**, 782–5.

Besmann, T. M. and Lindemer, T. B. (1985) *J. Nucl. Mater.*, **130**, 489–504.

Besmann, T. M. and Lindemer, T. B. (1986) *J. Nucl. Mater.*, **137**, 292–3.

Bradbury, M. H. (1981) *J. Less Common Metals*, **78**, 207–18.

Brewer, L. (1970) *Plutonium 1970 and Other Actinides*, Nucl. Met. Ser. (AIME), **17**, 650.

Brewer, L. (1984) *High Temp. Sci.*, **17**, 1–30.

Brickwedde, F. G., Hodge, H. J., and Scott, R. B. (1948) *J. Chem. Phys.*, **16**, 429–36.

Brickwedde, F. G., Hodge, H. J., and Scott, R. B. (1951) in *The Chemistry of Uranium* (eds. J. J. Katz and E. Rabinowitch), Dover Publications, New York.

Brooks, M. S. S., Johnson, B., and Skriver, H. L. (1984) in *Handbook on the Chemistry and Physics of the Actinides* (eds. A. J. Freeman and G. L. Lander), North-Holland, Amsterdam, pp. 153–270.

Burnett, J. L. (1966) *J. Inorg. Nucl. Chem.*, **28**, 2454–6.

Burns, J. B., Haire, R. G., and Peterson, J. R. (1998) *J. Alloys Compds*, **271–273**, 676–9.

Burriel, R., To, M., Zaniel, H., Westrum, E. F. Jr, Cordfunke, E. H. P., Muis, R. P., and Wijbenga, G. (1988) *J. Chem. Thermodyn.*, **20**, 815–23.

Campbell, A. B. and Lemire, R. J. (1994) Atomic Energy of Canada Limited Report RC-1278, COG-I-94–399.

Casalta, S. (1996) Etude des proprietes du systeme Am-O en vue de la transmutation de l'americium 241 en reacteur a neutrons rapides, Ph.D. Thesis, University Aix-Marseille I.

Chereau, P., Dean, G., De Franco, M., and Gerdanian, P. (1977) *J. Chem. Thermodyn.*, **9**, 211–19.
Chevalier, P.-Y., Fischer, E., and Cheynet, B. (2000) *J. Nucl. Mater.*, **280**, 136–50.
Chikalla, T. D. and Eyring, L. (1967) *J. Inorg. Nucl. Chem.*, **29**, 2281–93.
Chiotti, P. and Kately, J. A. (1969) *J. Nucl. Mater.*, **32**, 135–42.
Chiotti, P., Akhachinskij, V. V., Ansara, I., and Rand, M. H. (1981) The chemical thermodynamics of actinide elements and compounds, part 5, *The Actinide Binary Alloys*, STI/PUB/424/5, International Atomic Energy Agency, Vienna.
Cleveland, J. M. (1979) in *Chemical Modeling in Aqueous Systems* (ed. E. A. Jenne), (Am. Chem. Soc. Symp. Ser. 93), Washington, DC, pp. 321–38.
Colinet, C. and Pasturel, A. (1994) in *Handbook on the Chemistry of Rare Earths* (eds. K. A. Gschneidner Jr, L. Eyring, G. H. Lander and G. R. Choppin), vol. 19, ch. 134.
Conway, J. B. and Flagella, P. N. (1969) Report GEMP-1012, p. 61.
Cordfunke, E. H. P. (1964) *J. Phys. Chem.*, **68**, 3353–6.
Cordfunke, E. H. P. and O'Hare, P. A. G. (1978) The chemical thermodynamics of actinide elements and compounds, part 3, *Miscellaneous Actinide Compounds*, STI/PUB/424/3, International Atomic Energy Agency, Vienna.
Cordfunke, E. H. P., Muis, R. P., and Prins, G. (1979) *J. Chem. Thermodyn.*, **11**, 819–23.
Cordfunke, E. H. P. and Ouweltjes, W. (1981) *J. Chem. Thermodyn.*, **13**, 193–7.
Cordfunke, E. H. P., Ouweltjes, W., and Prins, G. (1982) *J. Chem. Thermodyn.*, **14**, 495–502.
Cordfunke, E. H. P., Muis, R. P., Ouweltjes, W., Flotow, H. E., and O'Hare, P. A.G. (1982) *J. Chem. Thermodyn.*, **14**, 313–22.
Cordfunke, E. H. P. and Kubaschewski, O. (1984) *Thermochim. Acta*, **74**, 235–45.
Cordfunke, E. H. P., Muis, R. P., Wijbenga, G., Burriel, R., To, M., Zaniel, H., and Westrum, E. F. Jr (1985) *J. Chem. Thermodyn.*, **17**, 1035–44.
Cordfunke, E. H. P., Konings, R. J. M., and Westrum, E. F. Jr (1989) *J. Nucl. Mater.*, **167**, 205–12.
Cordfunke, E. H. P. and Konings, R. J. M. (1990) *Thermochemical Data for Reactor Materials and Fission Products*, Elsevier, Amsterdam.
Cordfunke, E. H. P. and IJdo, D. J. W. (1994) *J. Solid State Chem.*, **109**, 272–6.
Cordfunke, E. H. P., Booij, A. S., Smit-Groen, V. S., van Vlaanderen, P., and Ijdo, D. J. W. (1997) *J. Solid State Chem.*, **131**, 341–9.
Cordfunke, E. H. P., Booij, A. S., and Huntelaar, M. E. (1999) *J. Chem. Thermodyn.*, **31**, 1337–45.
Cordfunke, E. H. P. and Konings, R. J. M. (2001a) *Thermochim. Acta*, **375**, 17–50.
Cordfunke, E. H. P. and Konings, R. J. M. (2001b) *Thermochim. Acta*, **375**, 51–64.
Cordfunke, E. H. P. and Konings, R. J. M. (2001c) *Thermochim. Acta*, **375**, 65–79.
Cox, J. D., Wagman, D. D., and Medvedev, V. A. (1989) *CODATA Key Values for Thermodynamics*, Hemisphere, New York.
Criss, C. M. and Cobble, R. W. (1964) *J. Am. Chem. Soc.*, **86**, 5385–9.
Dash, S., Singh, Z., Prasad, R., and Venugopal, V. (2000) *J. Nucl. Mater.*, **279**, 84–90.
David, F., Samhoun, K., Guillaumont, R., and Edelstein, N. (1978) *J. Inorg. Nucl. Chem.*, **40**, 69–74.
David, F. (1986) in *Handbook on the Chemistry of the Actinides* (eds. A. J. Freeman and C. Keller), vol. 4, ch. 3.

David, F. H. and Vokhmin, V. (2001) *J. Phys. Chem. A*, **105**, 9704–9.
David, F. H., Vokhmin, V., and Ionova, G. (2001) *J. Mol. Liquids*, **90**, 45–62.
David, F. H. and Vokhmin, V. (2002) *J. Nucl. Sci. Technol.*, Suppl. 3, 286–9.
De Boer, F. R., Boom, R., Matthens, W. C. M., and Miedema, A. R. (1988) *Cohesion in Metals*, Elsevier, Amsterdam.
Dharwadkar, S. R., Tripathi, S. N., Karkhana, M. D., and Chandrasekharaiah, M. S. (1975) in *Proc. Symp. on Thermodynamics of Nuclear Materials 1974*, IAEA, Vienna, vol. II, pp. 455–65.
Diakonov, I. I., Tagirov, B. R., and Ragnarsdottir, K. V. (1998a) *Radiochim. Acta*, **81**, 107–16.
Diakonov, I. I., Tagirov, B. R., and Ragnarsdottir, K. V. (1998b) *Chem. Geol.*, **151**, 327–47.
Ebbinghaus, B. B. (1995) Report UCRL-JC-122278, Lawrence Livermore National Laboratory.
Evans, J. H. and Mardon, P. G. (1959) *J. Phys. Chem. Solids*, **10**, 311–18.
Felmy, A. R., Rai, D., Schramke, J. A., and Ryan, J. L. (1989) *Radiochim. Acta*, **48**, 29–35.
Finch, R. J., Hawthorne, F. C., and Ewing, R. C. (1998) *Can. Miner.*, **36**, 831–45.
Fink, J. K. (1982) *Int. J. Thermophys.*, **3**, 165–200.
Fink, J. K. (2000) *J. Nucl. Mater.*, **279**, 1–18.
Flotow, H. E. and Tetenbaum, M. (1981) *J. Chem. Phys.*, **74**, 5269–77.
Flotow, H. E., Haschke, J. M., and Yamauchi, S. (1984) The chemical thermodynamics of actinide elements and compounds, Part 9, *The Actinide Hydrides*, STI/PUB/424/9, International Atomic Energy Agency, Vienna.
Foster, K. W. (1953) Report MLM-901.
Fournier, J. M. (1976) *J. Phys. Chem. Solids*, **37**, 235–44.
Fuger, J., Brown, D., and Easey, J. F. (1969) *J. Chem. Soc. A*, 2995–8.
Fuger, J. and Brown, D. (1975) *J. Chem. Soc., Dalton Trans.*, 225–31.
Fuger, J. and Oetting, F. L. (1976) The chemical thermodynamics of actinide elements and compounds, part 2, *The Actinide Aqueous Ions*, STI/PUB/424/2, International Atomic Energy Agency, Vienna.
Fuger, J., Bohet, J., Müller, W., Whittacker, B., and Brown, D. (1978) *Inorg. Nucl. Chem. Lett.*, **14**, 11–18.
Fuger, J., Haire, R. G., and Peterson, J. R. (1981) *J. Inorg. Nucl. Chem.*, **43**, 3209–15.
Fuger, J., Parker, V. B., Hubbard, W. N., and Oetting, F. L. (1983) The chemical thermodynamics of actinide elements and compounds, part 8, *The Actinide Halides*, STI/PUB/424/8, International Atomic Energy Agency, Vienna.
Fuger, J., Haire, R. G., and Peterson, J. R. (1984) *J. Less Common Metals*, **98**, 315–21.
Fuger, J., Haire, R. G., Wilmarth, W. R., and Peterson, J. R. (1990) *J. Less Common Metals*, **158**, 99–104.
Fuger, J., Khodakovsky, I. L., Sergeyeva, E. I., Medvedev, V. A., and Navratil, J. D. (1992) The chemical thermodynamics of actinide elements and compounds, part 12, *The Actinide Aqueous Inorganic Complexes*, STI/PUB/424/12, International Atomic Energy Agency, Vienna.
Fuger, J., Haire, R. G., and Peterson, J. R. (1993) *J. Alloys Compds*, **200**, 181–5.
Fusselman, S. P., Roy, J. J., Grimmet, D. L., Grantham, L. F., Krueger, C. L., Nabalek, C. R., Storvick, T. S., Inoue, T., Hijikata, T., Kinoshita, K., Sakamura, Y., Uozumi, K., Kawai, T., and Takahashi, N. (1999) *J. Electrochem. Soc.*, **146**, 2573–80.

Gabelnick, S. D., Reedy, G. T., and Chasanov, M. G. (1974) *J. Chem. Phys.*, **60**, 1167.
Gibby, R. L., McNeilly, C. E., and Chikalla, T. D. (1970) *J. Nucl. Mater.*, **34**, 299–306.
Gibson, J. K. and Haire, R. G. (1988a) *Thermochim. Acta.*, **133**, 241–7.
Gibson, J. K. and Haire, R. G. (1988b) *J. Solid State Chem.*, **73**, 524.
Gibson, J. K. and Haire, R. G. (1990) *J. Phys. Chem.*, **94**, 935.
Gibson, J. K. and Haire, R. G. (1992) *J. Nucl. Mater.*, **195**, 156–65.
Gibson, J. K. (2003) *J. Phys. Chem. A*, **107**, 7891–9.
Gingerich, K. A. (1969) *J. Chem. Phys.*, **67**, 4433.
Glushko, V. P., Medvedev, V. A., Bergman, G. A., Gurvich, L. V., Vorob'ev, A. F., Vasil'ev, V. P., Kolesov, V. P., Yungman, V. S., Reznutskij, L. R., Baibuz, V. F., Gal'chenko, G. L., and Yatzimirskij, K. B. (1978) *Thermodynamic Constants Of Substances*, Academy of Science Publishing House, Moscow.
Gorokhov, L. N., Smirnov, V. K., and Khodeev, Yu. S. (1984) *Russ. J. Phys. Chem.*, **58**, 980–7.
Gorokhov, L. N. and Sidorova, I. V. (1998) *Russ. J. Phys. Chem.*, **72**, 1038–42.
Goudiakas, J., Haire, R. G., and Fuger, J. (1990) *J. Chem. Thermodyn.*, **22**, 577–87.
Green, D. W. and Reedy, G. T. (1976) *J. Chem. Phys.*, **65**, 2921–7.
Green, D. W. and Reedy, G. T. (1978a) *J. Chem. Phys.*, **69**, 544–51.
Green, D. W. and Reedy, G. T. (1978b) *J. Chem. Phys.*, **69**, 552–5.
Green, D. W. and Reedy, G. T. (1979) *J. Mol. Spectrosc.*, **74**, 423–34.
Green, D. W. (1980) *Int. J. Thermophys.*, **1**, 61.
Grenthe, I., Fuger, J., Konings, R. J. M., Lemire, R. J., Muller, A. B., Nguyen-Trung, Cregu, C., and Wanner, H. (1992) *Chemical Thermodynamics of Uranium* (eds. H. Wanner and I. Forest), North Holland, Amsterdam.
Grønvold, F., Drowart, J., and Westrum, E. F. Jr (1984) The chemical thermodynamics of actinide elements and compounds, part 4, *The Actinide Chalcogenides (Excluding Oxides)*, STI/PUB/424/4, International Atomic Energy Agency, Vienna.
Gross, P., Hayman, C., and Clayton, H. (1962) in *Proc. Thermodyn. Nucl. Mater.*, IAEA, Vienna, pp. 653–65.
Gross, P., Hayman, C., and Wilson, G. L. (1971) *Monathsh. Chem.*, **102**, 924–8.
Gruen, D. M. and DeKock, C. W. (1967) *J. Inorg. Nucl. Chem.*, **29**, 2569.
Gruen, D. M. (1976) *Proc. Int. Symp. Molten Salts*, Washington, DC, p. 204.
Guillaumont, R., Fanghänel, T., Fuger, J., Grenthe, I., Neck, V., Palmer, D., and Rand, M. H. (2003) *Update on the Chemical Thermodynamics of Uranium, Neptunium, Plutonium, Americium and Technetium*, Elsevier, Amsterdam.
Gupta, S. K. and Gingerich, K. A. (1979) *J. Chem. Phys.*, **71**, 3072.
Gupta, S. K. and Gingerich, K. A. (1980) *J. Chem. Phys.*, **72**, 2795.
Haaland, A., Martinsen, K.-G., Swang, O., Volden, H., Booij, A. S., and Konings, R. J. M. (1995) *J. Chem. Soc., Dalton Trans.*, 185–90.
Haire, R. G. and Gibson, J. K. (1989) *J. Chem. Phys.*, **91**, 7085–96.
Haire, R. G. (1994) *J. Alloys Compds*, **213/214**, 185–91.
Haire, R. G. and Eyring, L. (1994) Comparisons of the binary oxides, in *Handbook of the Rare Earths,* vol. 18 (eds. K. A. Gschneidner, L. Eyring, G. H. Lander, and G. R. Choppin), North-Holland, Amsterdam, 18: 413.
Hall, R. O. A., Jeffery, A. J., Mortimer, M., and Spirlet, J. C. (1990) Report AERE-R-13490.
Hall, R. O. A., Mortimer, M., Harding, S. R., and Spirlet, J. C. (1992) Report AEA-FS-0048H.

Hall, R. O. A., Mortimer, M., and Spirlet, J. C. (1990) Report AERE-R-13768.
Han, Y.-K. (2001) *J. Comp. Chem.*, **22**, 2010–221.
Haschke, J. M., Allen, T. H., and Morales, L. A. (2001) *J. Alloys Compds*, **314**, 78–84.
Haschke, J. M. and Allen, T. H. (2002) *J. Alloys Compds*, **336**, 124–30.
Hayes, S. L., Thomas, J. K., and Pedicord, K. L. (1990) *J. Nucl. Mater.*, **171**, 300–18.
Helean, K. B., Navrotsky, A., Vance, E. R., Carter, M. L., Ebbinghaus, B., Krikorian, O., Lian, J., Wang, L. M., and Catalano, J. G. (2002) *J. Nucl. Mater.*, **303**, 226–39.
Helean, K. B., Navrotsky, A., Lumpkin, G. R., Colella, M., Lian, J., Ewing, R. C., Ebbinghaus, B., and Catalano, J. G. (2003) *J. Nucl. Mater.*, **320**, 231–44.
Hiernaut, J. P., Hyland, G. J., and Ronchi, C. (1993) *Int. J. Thermophys.*, **14**, 609–18.
Hiernaut, J. P. and Ronchi, R. (2004) *J. Nucl. Mater.*, **334**, 133–8.
Hildenbrand, D. L., Gurvich, L. V., and Yungman, V. S. (1985) The chemical thermodynamics of actinide elements and compounds, part 13, *The Gaseous Actinide Ions*, STI/PUB/424/13, International Atomic Energy Agency, Vienna.
Hildenbrand, D. L. (1988) *Pure Appl. Chem.*, **60**, 303–10.
Hildenbrand, D. L. and Lau, K. H. (1990) *J. Chem. Phys.*, **90**, 5983.
Hildenbrand, D. L. and Lau, K. H. (1991) *J. Chem. Phys.*, **94**, 1420.
Hobart, D. E., Samhoun, K., and Peterson, J. R. (1982) *Radiochim. Acta*, **31**, 139.
Hobart, D. E., Varlashkin, P. G., Samhoun, K., Haire, R. G., and Peterson, J. R. (1983) *Rev. Chim. Miner.*, **20**, 817–27.
Holley, C. E., Rand, M. H., and Storms, E. K. (1984) The chemical thermodynamics of actinide elements and compounds, part 6, *The Actinide Carbides*, STI/PUB/424/6, International Atomic Energy Agency, Vienna.
Hovey, J. K. and Tremaine, P. R. (1986) *Geochim. Cosmochim. Acta*, **50**, 453.
Hovey, J. K., Nguyen-Trung, C., and Tremaine, P. R. (1989) *Geochim. Cosmochim. Acta*, **53**, 1503–9.
Hovey, J. K. (1997) *J. Phys. Chem. B*, **101**, 4321.
Huang, J., Yamawaki, M., Yamaguchi, K., Yasumoto, M., Sakurai, H., and Suzuki, Y. (1997a) *J. Nucl. Mater.*, **247**, 17–20.
Huang, J., Yamawaki, M., Yamaguchi, K., Yasumoto, M, Sakurai, H., and Suzuki, Y. (1997b) *J. Nucl. Mater.*, **248**, 257–61.
Hubener, S. and Zvara, I. (1982) *Radiochim. Acta*, **31**, 89–94.
Hughes-Kubatko, K.-A., Helean, K. B., Navrotsky, A., and Burns, P. C. (2003) *Science*, **302**, 1191–3.
Hultgren, R., Desai, P. D., Hawkins, D. T., Gleiser, M., Kelley, K. K., and Wagman, D. D. (1973) *Selected Values of the Thermodynamic Properties of the Elements*, American Society for Metals, Metals Park, Ohio.
Huntelaar, M. E., Booij, A. S., Ijdo, D., van Genderen, A., Akabori, M., Gaune- Escard, M., and Rycerz, L. (2002) *J. Nucl. Sci. Technol.*, Suppl. 3, 599–602.
IAEA (1965) *Thermodynamic and Transport Properties of Uranium Dioxide and Related Phases*, Technical Reports Series no. 39, International Atomic Energy Agency, Vienna.
IAEA (1967) *The Plutonium-Oxygen and Uranium-Plutonium-Oxygen Systems: A Thermochemical Assessment*, Technical Reports Series no. 79, International Atomic Energy Agency, Vienna.
Johnson, G. K. (1979) *J. Chem. Thermodyn.*, **11**, 483–9.
Johnson, G. K. (1985) *J. Nucl. Mater.*, **130**, 102–8.

Johnson, I. (1975) Report ANL-RDP-26.
Jones, L. H. and Ekberg, S. (1977) *J. Chem. Phys.*, **67**, 2591–8.
Joubert, L. and Maldivi, P. (2001) *J. Phys. Chem. A*, **105**, 9068–76.
Jung, W.-G. and Kleppa, O. J. (1991) *J. Chem. Thermodyn.*, **23**, 147.
Katz, J. J. and Rabinowitch, E. (1951) *The Chemistry of Uranium*, McGraw-Hill, New York.
Kaufman, M. J., Muenter, J., and Klemperer, W. (1967) *J. Chem. Phys.*, **47**, 3365–70.
Kim, K. C. and Mulford, R. N. (1990) *J. Mol. Struct. (THEOCHEM)*, **207**, 293.
Kleinschmidt, P. D., Ward, J. W., and Haire, R. G. (1983) *Proc. II Symp. on High Temperature Materials Chemistry* (eds. Z. Munir and D. Cubiciotti), Electrochemical Society, Pennington, NJ, pp. 23–31.
Kleinschmidt, P. D., Ward, J. W., and Haire, R. G. (1984) *J. Phys. Chem.*, **81**, 473.
Kleinschmidt, P. D., and Ward, J. W. (1986) *J. Less Common Metals*, **121**, 61.
Kleinschmidt, P. D. (1988) *J. Chem. Phys.*, **89**, 6897.
Konings, R. J. M., Booij, A. S., Kovács, A., Girichev, G. V., Giricheva, N. I., and Krasnova, O. G. (1996) *J. Mol. Struct.*, **378**, 121–31.
Konings, R. J. M. and Hildenbrand, D. L. (1998) *J. Alloys Compds*, **271–273**, 583–6.
Konings, R. J. M. (2001a) *J. Nucl. Mater.*, **295**, 57–63.
Konings, R. J. M. (2001b) *J. Nucl. Mater.*, **298**, 255–68.
Konings, R. J. M. (2002) *J. Nucl. Mater.*, **301**, 223–6.
Konings, R. J. M. (2003) *J. Alloys Compds*, **348**, 38–42.
Konings, R. J. M. and Kovács, A. (2003) in *Handbook on the Physics and Chemistry of Rare Earths*, vol. 33, ch. 213 (eds. K. A. Gschneidner Jr and J.-C. G. Bünzli, and V. K. Pecharsky) Elsevier, pp. 147–247.
Konings, R. J. M. (2004a) *J. Chem. Thermodyn.*, **36**, 121–6.
Konings, R. J. M. (2004b) www.f-elements.net.
Konings, R. J. M., van Miltenburg, J. C., and van Genderen, A. G. C. (2005) *J. Chem. Thermodyn.*, **37** (2005), 1219–25.
Kosyakov, V. N., Timofeev, G. A., Erin, I. A., Kopytov, V. V., and Andreev, V. J. (1977) *Radiokhimiya*, **19**, 82.
Kovács, A., Booij, A. S., Cordfunke, E. H. P., Kok-Scheele, A., and Konings, R. J. M. (1996) *J. Alloys Compds*, **241**, 95–7.
Kovács, A., Konings, R. J. M., and Nemcsok, D. S. (2003) *J. Alloys Compds*, **353**, 128–32.
Krestov, G. A. (1972) *Thermochemistry of Compounds of Rare-Earth and Actinide Elements*, Atomizdat, Moscow (English translation, AEC-tr-7505, National Technical Information Service, Springfield, VA 22151).
Krikorian, O. H., Ebbinghaus, B. B., Adamson, M. G., Fontes, A. S. Jr, and Fleming, D. L. (1993a) Report UCRL-ID-112994.
Krikorian, O. H., Condit, R. H., Fontes, A. S. Jr, Fleming, D. L., Magana, J. W., Morris, W. F., and Adamason, M. G. (1993b) Report UCRL-ID-114774.
Krupa, J. C. and Gajek, Z. (1991) *Eur. J. Solid State Chem.*, **28**, 143.
Krupa, J. C. (2001) personal communication to R. J. M. Konings.
Küchle, W., Dolg, M., Stoll, H., and Preus, H. (1994) *J. Chem. Phys.*, **100**, 7535.
Kunze, K. R., Hauge, R. H., Hamill, D., and Margrave, J. L. (1976) *J. Chem. Phys.* **65**, 2026.

Kurosaki, K., Yano, K., Yamada, K., Uno, M., and Yamanaka, S. (2000) *J. Alloys Compds*, **297**, 1.
Kuznietz, M. (1968) *J. Chem. Phys.*, **49**, 3731.
Lambertin, D., Lacquement, J., Sanchez, S., and Picard, G. S. (2000) *Plasmas and Ions*, **3**, 65.
Larson, D. T. and Haschke, J. M. (1981) *Inorg. Chem.*, **20**, 1945–50.
Latimer, W. M. (1952) *Oxidation Potentials*, 2nd edn, Prentice-Hall, New York.
Lau, K. H. and Hildenbrand, D. L. (1982) *J. Chem. Phys.*, **76**, 2646.
Lau, K. H. and Hildenbrand, D. L. (1984) *J. Chem. Phys.*, **80**, 1312.
Lau, K. H. and Hildenbrand, D. L. (1987) *J. Chem. Phys.*, **86**: 2949.
Lau, K. H. and Hildenbrand, D. L. (1990) *J. Chem. Phys.*, **92**: 6124–6130.
Lau, K. H., Brittain, R. D., and Hildenbrand, D. L. (1989) *J. Chem. Phys.*, **90**, 1158.
Lau, K. H., and Hildenbrand, D. L., (1989) *J. Chem. Phys.*, **90**, 1158.
Lebedev, L. A. (1981) *Radiokhimiya*, **23**, 12.
Lemire, R. J. and Tremaine, P. R. (1980) *J. Chem. Eng. Data*, **25**, 361–70.
Lemire, R. J. (1984) Atomic Energy of Canada Ltd Report AECL-7817, Whiteshell Nuclear Research Establishment.
Lemire, R. J., Campbell, A. B., Saluja, P. P. S., and Le Blanc, J. C. (1993) *J. Nucl. Mater.*, **201**, 165–75.
Lemire, R. J. and Campbell, A. B. (1996a) *Radiochim. Acta*, **73**, 131–7.
Lemire, R. J. and Campbell, A. B. (1996b) *Thermochim. Acta*, **286**, 225–31.
Lemire, R. J., Fuger, J., Nitsche, H., Potter, P., Rand, M. H., Rydberg, J., Spahiu, K., Sullivan, J. C., Ullman, W. J., Vitorge, P., and Wanner, H. (2001) *Chemical Thermodynamics of Neptunium and Plutonium*, Elsevier, Amsterdam.
Libowitz, G. G. and Maeland, A. J. (1979) in *Handbook on Physics and Chemistry of Rare Earths* (eds. L. R. Eyring and K. A. Gschneidner Jr), vol. 3, pp. 299–336.
Lindemer, T. B., Besmann, T. M., and Johnson, C. E. (1981) *J. Nucl. Mater.*, **100**, 178–226.
Lindemer, T. B. and Besmann, T. M. (1985) *J. Nucl. Mater.*, **130**, 473–88.
Linevsky (1963) General Electric Report WADD-TR-60-646.
Malm, J. G., Williams, C. W., Soderholm, L., and Morss, L. R. (1993) *J. Alloys Compds*, **194**, 133.
Maly, J. (1967) *Inorg. Nucl. Chem. Lett.*, **3**, 373.
Maly, J. and Cunningham, B. B. (1967) *Inorg. Nucl. Chem. Lett.*, **3**, 445.
Maly, J., Sikkeland, T., Silva, R., and Ghiorso, A. (1968) *Science*, **160**, 1114–15.
Martinot, L. (1978) *Encyclopedia of Electrochemistry of the Elements*, vol. VIII (ed. A. J. Bard), Marcel Dekker, New York, pp. 149–206.
Martinot, L. (1982) in *Handbook on the Physics and Chemistry of the Actinides* (eds. A. J. Freeman and C. Keller), vol. 6, ch. 4, North-Holland, Amsterdam, p. 241.
Martinot, L., and Fuger, J. (1985) *Standard Potentials in Aqueous Solutions* (eds. A. J. Bard, R. Parsons, and J. Jordan), Marcel Dekker, New York. ch. 21.
Matsuda, T., Yamanaka, S., Kurosaki, K., Uno, M., and Kobayashi, S. (2001) *J. Alloys Compds*, **322**, 77.
Matsui, T., and Ohse, R. W. (1987) *High Temp.–High Press.*, **19**, 1–17 (see also Report EUR 10858 EN).
Mazeina, L., Ushakov, S. V., Navrotsky, A., and Boatner, L. A. (2005) *Geochim. Cosmochim. Acta*, **69**, 4675–83.

Merli, L. and Fuger, J. (1994) *Radiochim. Acta*, **66/67**, 109–13.
Merli, L., Lambert, B., and Fuger, J. (1997) *J. Nucl. Mater.*, **247**, 172–6.
Mikheev, N. B. (1983) *Radiochim. Acta*, **32**, 69.
Molnar, J. and Hargittai, M. (1995) *J. Phys. Chem.*, **99**, 10780.
Moriyama, H., Konoshita, K., and Ito, Y. (1990) *J. Nucl. Sci. Technol.*, **27**, 827–34.
Morss, L. R. (1976) *Chem. Rev.*, **76**, 827–41.
Morss, L. R. and Fahey, J. A. (1976) *Proc. 12th Rare Earth Res. Conf.*, vol. 1, Denver Research Institute, Denver, CO, pp. 443–50.
Morss, L. R. and McCue, M. C. (1976) *J. Chem. Eng. Data*, **21**, 337–41.
Morss, L. R. and Fuger, J. (1981) *J. Inorg. Nucl. Chem.*, **43**, 2059–64.
Morss, L. R. (1983) *J. Less Common Metals*, **93**, 301–21.
Morss, L. R. (1985) in *Americium and Curium Chemistry and Technology* (ed. N. Edelstein), D. Reidel, Dordrecht, The Netherlands, pp. 147–58.
Morss, L. R. and Sonnenberger, D. C. (1985) *J. Nucl. Mater.*, **130**, 266–72.
Morss, L. R., Fuger, J., Goffart, J., Edelstein, N., Shalimoff, G. V. (1987) *J. Less Common Metals*, **127**, 251.
Morss, L. R. and Eller, P. G. (1989) *Radiochim. Acta*, **47**, 51–4.
Morss, L. R. and Hall, J. P. (1994) *49th Annual Calorimetry Conference*, Santa Fe, NM, July 31–Aug 5, paper No. 63.
Morss, L. R. and Williams, C. W. (1994) *Radiochim. Acta*, **66/67**, 89–93.
Murad, E. and Hildenbrand, D. L. (1980) *J. Chem. Phys.*, **73**, 4005–11.
Musikas, C., Couffin, F., and Marteau, M. (1974) *J. Chim. Phys. Phys.-Chim. Biol.*, **5**, 641–8.
Nakajima, K., Arai, Y., and Suzuki, Y. (1997) *J. Nucl. Mater.*, **247**, 33–6.
Nakajima, K., Arai, Y., and Suzuki, Y. (1999a) *J. Nucl. Mater.*, **275**, 332–5.
Nakajima, K., Arai, Y., Suzuki, Y., and Yamawaki, M. (1999b) *J. Mass Spectrom. Soc. Jpn*, **47**, 46–8.
Nakajima, K. and Arai, Y. (2003) *J. Nucl. Sci. Technol.*, Suppl. 3, 620–623.
Newton, T. W. and Sullivan, J. C. (1985) in *Handbook on the Chemistry of the Actinides*, vol. 3 (eds. A. J. Freeman, G. L. Lander, and C. Keller), pp. 387–406.
Nugent, L. J., Burnett, J. L., and Morss, L. R. (1973) *J. Chem. Thermodyn.*, **5**, 665–72.
Oetting, F. L. (1967) *Chem. Rev.*, **67**, 261–97.
Oetting, F. L., Rand, M. H., and Ackermann, R. J. (1976) The chemical thermodynamics of actinide elements and compounds, part 1, *The Actinide Elements*, STI/PUB/424/1, International Atomic Energy Agency, Vienna.
Oetting, F. L. and Bixby, G. E. (1982) *J. Nucl. Mater.*, **105**, 257–61.
Oetting, F. L., Hodges, A. E., Haschke, J. M., and Flotow, H. E. (1984) *J. Chem. Thermodyn.*, **16**, 1089–102.
Ogard, A. E. (1970) in *Plutonium 1970 and Other Actinides*, vol. I, p. 78.
O'Hare, P. A. G., Flotow, H. E., and Hoekstra, H. R. (1980) *J. Chem. Thermodyn.*, **12**, 1003–8.
O'Hare, P. A. G., Malm, J. G., and Eller, P. G. (1982) *J. Chem. Thermodyn.*, **14**, 323–30.
Ohse, R. W. (1968) Institute for Transuranium Elements, Progress Report no. 5, p. 26.
Ogawa, T., Ohmichi, T., Maeda, A., Arai, Y., and Suzuki, Y. (1995) *J. Alloys Compds*, **224**, 55.

Onoe, J., Nakamatsu, H., Mukoyama, T., Sekine, R., Adachi, H., and Takeuchi, K. (1997) *Inorg. Chem.*, **36**, 1934.

Osborne, D. W., Flotow, H. E., Fried, S. M., and Malm, J. G. (1974) *J. Chem. Phys.*, **61**, 1463.

Palenzona, A. and Cirafici, S. (1975) *Thermochim. Acta*, **13**, 357–61.

Paine, R. T., McDowell, R. S., Asprey, L. B., and Jones, L. H. (1976) *J. Chem. Phys.*, **64**, 3081.

Pedley, J. B. and Marshall, E. M. (1983) *J. Phys. Chem. Ref. Data*, **12**, 967–1031.

Peng, S. and Grimvall, G. (1994) *J. Nucl. Mater.*, **210**, 115–22.

Perethrukhin, V. F., Shilov, V. P., and Pikaev, A. K. (1995) Technical Report-0817, Westinghouse Hanford Company, Richland, WA, USA.

Peterson, J. R. and Burns, J. H. (1973) *J. Inorg. Nucl. Chem.*, **35**, 1525.

Plambeck, J. A. (1976) Encyclopedia of electrochemistry of the elements, vol. X, *Fused Salt Systems* (ed. A. J. Bard), Marcel Dekker, New York.

Popov, M. M., Gal'chenko, G. L., and Senin, M. D. (1959) *Russ. J. Inorg. Chem.*, **4**, 560.

Prabhahara, R. B., Babu, R, Nagarajan, K., and Vasudeva- Rao, P. R. (1998) *J. Alloys Compds*, **271–273**, 395–8.

Prasad, R., Dash, S., Parida, S. C., Singh, Z., and Venugopal, V. (2000) *J. Nucl. Mater.*, **277**, 45–8.

Privalov, T., Schimmelpfennig, B., Wahlgren, U., and Grenthe, I. (2002) *J. Phys. Chem.*, **106**, 11277.

Rand, M. H. and Kubaschewski, O. (1963) *The Thermochemical Properties of Uranium Compounds*, Interscience, New York.

Rand, M. H. (1966) *At. Energy Rev.*, **4**, Spec. Issue no. 1, 7–51.

Rand, M. H. (1968) *Technical Panel on Uranium and Plutonium Carbides*, International Atomic Energy Agency, Vienna.

Rand, M. H. (1975) *At. Energy Rev.*, Spec. Issue no. 5, 7–85.

Robbins, D. A. and Jenkins, J. (1955) *Acta Metall.*, **3**, 598–605.

Ronchi, C. and Hiernaut, J. P. (1996) *J. Alloys Compds*, **240**, 179–85.

Ronchi, C., Capone, F., Colle, J. Y., and Hiernaut, J. P. (2000) *J. Nucl. Mater.*, **280**, 111–15.

Ronchi, C., Iosilevsji, I. L., and Yakub, E. (2002) *Equation of State of Uranium Dioxide*, Springer, Berlin, 2004.

Rossini, F. D., Wagman, D. D., Evans, W. H., Levine, S., and Jaffe, L. (1952) *Selected Values of Chemical Thermodynamic Properties*, U.S. Natl. Bur. Stand. Circ. 500, U.S. Govt. Printing Office, Washington, DC.

Roy, J. J., Grantham, L. F., Grimmett, D. L., Fusselman, S. P., Krueger, C. L., Strovick, T. S., Inoue, T., Sakamura, Y., and Takahashi, N. (1996) *J. Electrochem. Soc.*, **143**, 2487–93.

Samhoun, K. and David, F. (1976) in *Transplutonium Elements, Proc. 4th Int. Transplutonium Elements Symp.*(eds. W. Müller and R. Linder), North Holland, Amsterdam, pp. 297–319.

Santos, M., Marçalo, J., Pires de Matos, A., Gibson, J. K., and Haire, R.G. (2002a) *J. Phys. Chem. A*, **106**, 7190–4.

Santos, M., Marçalo, J., Leal, P., Pires de Matos, A., Gibson, J. K., and Haire, R. G. (2002b) *Int. J. Mass Spectrom.*, **228**, 457–65.

Schoebrechts, J.-P., Fuger, J., and Morss, L. R. (1989) *Thermochim. Acta*, **139**, 49–55.
Seaborg, G. T., Katz, J. J., and Manning, W. M. (eds.) (1949) *The Transuranium Elements: Research Papers*, Natl. Nucl. En. Ser., Div. IV, 14B, McGraw-Hill, New York.
Seleznev, A. G., Kosulin, N. S., Kosenkov, V. M., Shushakov, V. D., Stupin, V. A., Demeshkin, V. A. (1977) *Fiz. Met. Metall.*, **44**, 654–7.
Seleznev, A. G., Shushakov, V. D., and Kosulin, N. S. (1978) *Fiz. Met. Metall.*, **46**, 1109–12.
Serizawa, H., Arai, Y., and Nakajima, K. (2001) *J. Chem. Thermodyn.*, **33**, 615–28.
Serp, J., Konings, R. J. M., Malmbeck, R., Rebizant, J., Scheppler, C., and Glatz, J.-P. (2004) *J. Electroanal. Chem.*, **561**, 143–8.
Shannon, R. D. (1976) *Acta Crystallogr. A*, **32**, 751–67.
Shock, E. L., Sassani, D. C., Willis, M., and Svergensky, D. A. (1997) *Geochim. Cosmochim. Acta*, **61**, 907–50.
Silva, R. J., McDowell, W. J., Keller, Jr, and O. L. Tarrant, J. R. (1974) *Inorg. Chem.*, **13**, 2233–8.
Silva, R. J. (1982) Lawrence Berkeley Laboratory Report LBL-15055, 57 pp.
Silva, R. J., Bidoglio, G. R., Rand, M. H., Robouch, P. B., Wanner, H., and Puigdomenech, I. (1995) *Chemical Thermodynamics of Americium*, Elsevier, Amsterdam.
Simakin, G. A., Baranov, A. A., Kosyakov, V. N., Timofeev, G. A., Erin, E. A., and Lebedev, I. A. (1977) *Sov. Radiochem.*, **19**, 307–9.
Smith, P. K. and Peterson, D. E. (1970) *J. Chem. Phys.*, **52**, 4963–70.
Souter, P. F. and Andrews, L. (1997) *J. Mol. Struct.*, **412**, 161–5.
Tagawa, H. (1974) *J. Nucl. Mater.*, **51**, 78–89.
Takahashi, K., Fujino, T., and Morss, L. R. (1993) *J. Solid State Chem.*, **105**, 234–42.
Tasker, I., O'Hare, P. A. G., Lewis, B. M., Johnson, G. K., and Cordfiunke, E. H. P. (1988) *Can. J. Chem.*, **66**, 620–5.
Thiriet, C. and Konings, R. J. M. (2003) *J. Nucl. Mater.*, **320**, 292–8.
Turcotte, R. P., Chikalla, T. D., and Eyring, L. (1971) *J. Inorg. Nucl. Chem.*, **33**, 3749–60.
Turcotte, R. P., Chikalla, T. D., and Eyring, L. (1973) *J. Inorg. Nucl. Chem.*, **35**, 809–17.
Turcotte, R. P., Chikalla, T. D., and Haire, R. G. (1980) *J. Inorg. Nucl. Chem.*, **42**, 1729–35.
Usami, T., Kato, T., Kurata, M., Inoue, T., Sims, H. E., Beetham, S. A., and Jenkins, J. A. (2002) *J. Nucl. Mater.*, **304**, 50–5.
Venugopal, V., Kulkarni, S. G., Subbanna, C. S., and Sood, D. D. (1992) *J. Nucl. Mater.*, **186**, 259–68.
Volkov, Yu. F., Visyashcheva, G. I., Tomilin, S. V., Kapshukov, I. I., and Rykov, A. G. (1981) *Radiokhimiya*, **23**, 243–7.
Wade, W. Z. and Wolf, T. (1967) *J. Inorg. Nucl. Chem.*, **29**, 2577–82.
Wadt, W. R. and Hay, P. J. (1979) *J. Am. Chem. Soc.*, **101**, 5198–205.
Wagman, D. D., Schumm, R. H., and Parker, V. B. (1977) Report NBSIR 77–1300.
Wagman, D. D., Evans, W. H., Parker, V. B., Schumm, R. H., and Nuttall, R. L. (1981) U.S.. Natl. Bur. Stand. Tech. Note 270–8, U.S. Govt. Printing Office, Washington, DC; (1982) *J. Phys. Chem. Ref. Data*, **11**, Suppl. 2.
Ward, J. W., Kleinschmidt, P. D., and Peterson, D. E. (1986) in *Handbook on the Physics and Chemistry of the Actinides* (eds. A. J. Freeman and C. Keller), vol. 4, ch. 7.
Ward, J. W., Batscher, W., and Rebizant, J. (1987) *J. Less Common Metals*, **130**, 431–6.

Weigel, F., Hoffmann, G., and Ter Meer, N. (1969) *Radiochim. Acta*, **11**, 210–16.
Weigel, F., Hoffmann, G., Wishnevsky, V., and Brown, D. (1974) *J. Chem. Soc. Dalton Trans.*, 1473–7.
Weigel, F. and Kohl, R. (1985) in *Americium and Curium Chemistry and Technology* (eds. N. M. Edelstein, J. D. Navratil, and W. W. Schultz), D. Reidel, Dordrecht, The Netherlands, p. 159.
Westrum, Jr and E. F. Eyring, L. (1949) in *The Transuranium Elements* (eds. G. T. Seaborg, J. J. Katz, and W. M. Manning), Natl. Nucl. En. Ser., Div. IV, 14B, McGraw-Hill, New York, paper 6.52.
Westrum, E. F. Jr, Zainel, H. A., and Jakes, D. (1980) in *Proc. Symp. Thermodyn. Nucl. Mater. 1979*, IAEA, Vienna, vol. II, pp. 143–54.
Williams, C. W., Morss, L. R., and Choi, I.-K. (1984) in *Geochemical Behavior of Disposed Radioactive Waste* (eds. G. S. Barney, J. D. Navratil, and W. W. Schulz), Am. Chem. Soc. Symp. Ser. 246, American Chemical Society, Washington, DC, pp. 323–34.
Williams, C. W., Blaudeau, J.-P., Sullivan, J. C., Antonio, M. R., Bursten, B. E., and Soderholm, L. (2001) *J. Am. Chem. Soc.*, **123**, 4346–7.
Yamashita, T., Nitani, N., Tsuji, T., and Kato, T. (1997) *J. Nucl. Mater.*, **247**, 90–3.
Yamana, H. and Moriyama, H. (2002) Personal communication.
Yamanaka, S., Kurosaki, K., Matsuda, T., and Uno, M. (2001) *J. Nucl. Mater.*, **294**, 99–103.

CHAPTER TWENTY

MAGNETIC PROPERTIES

Norman M. Edelstein and Gerard H. Lander

20.1 INTRODUCTION

20.1.1 Magnetic measurements

The magnetic properties of actinide ions and compounds arise from the spin and orbital angular momenta of the unpaired electrons. The theoretical basis for understanding these properties was provided by Van Vleck in 1932 in his classic work *The Theory of Electric and Magnetic Susceptibilities* (Van Vleck, 1932). The Van Vleck equation is expressed as follows:

$$\chi_M = \frac{N \sum_i [(E_i^{(1)})^2/kT - 2E_i^{(2)}] \exp(-E_i^0/kT)}{\sum_i \exp(-E_i^0/kT)} \tag{20.1}$$

where χ_M is the molar susceptibility and E_i the energy of the ith energy level, which can be expanded as a power series in the magnetic field H:

$$E_i = E_i^0 + E_i^{(1)}H + E_i^{(2)}H^2 + \cdots \tag{20.2}$$

The material can possess no residual moment in the absence of a magnetic field, so that:

$$\sum_i E_i^{(1)} \exp(-E_i^0/kT) = 0 \tag{20.3}$$

The term in equation (20.1) involving $E^{(1)}$ is the first-order Zeeman interaction and the term involving $E^{(2)}$ is the second-order Zeeman interaction. If the ground crystal field (CF) state is a singlet and the next state is greater than kT away in a particular temperature range, the first-order term will be zero and only the second-order term will contribute to the paramagnetic susceptibility, which will be independent of temperature (temperature-independent paramagnetism, TIP).

If enough information is available about an ion or molecule (i.e. from optical spectroscopy) such that the properties of the energy levels in a magnetic field can be calculated, magnetic susceptibility measurements provide a good test for the eigenfunctions. Conversely, magnetic data can be used to determine information about energy levels and their eigenfunctions. Magnetic measurements usually are performed in the temperature range 2–300 K (energy range $\sim$1.5–200 cm^{-1}). From optical data, the crystal or ligand-field splittings of the ground state of some $5f^1$ hexahalo compounds are shown in the second column of Table 20.1 and vary from 1730 cm^{-1} in Pa^{4+} to about 7500 cm^{-1} for Np^{6+}. For $5f^2$ U^{4+} compounds, the total crystal-field splitting of the ground $^3H_4$ term is about 2240 cm^{-1} in Cs_2UCl_6 (Johnston *et al.*, 1966), about 2000 cm^{-1} in Cs_2UBr_6 (Johnston *et al.*, 1966), about 2400 cm^{-1} in $U(C_5H_5)_4$ (Amberger, 1976b), and about 1800 cm^{-1} for $U(BH_4)_4$ diluted in $Zr(BH_4)_4$ (Bernstein and Keiderling, 1973). For the $5f^3$ and $5f^4$ ions, U^{3+} and Np^{3+} diluted in $LaCl_3$, the total crystal-field splitting of the ground terms are 451 and 465 cm^{-1}, respectively (Carnall, 1992). From the above data, it is clear that temperature-dependent magnetic susceptibility measurements provide information only about the ground crystal field state and possibly a few lower-lying states. Most susceptibility measurements are performed on polycrystalline samples that give only the average susceptibility. Magnetic susceptibility values can also be performed on liquid solutions of pure compounds by use of the Evans nuclear magnetic resonance (NMR) method (Evans, 1959).

Electron paramagnetic resonance (EPR) measurements for actinide ions are usually made at liquid-helium temperatures in order to lengthen the spin–lattice relaxation time (T_1) so that the resonance can be observed (Abragam and Bleaney, 1970; Boatner and Abraham, 1978). Consequently information is obtained only about the ground crystal field state and possibly the first excited state. The spectra are interpreted in terms of an effective spin Hamiltonian:

$$H = \mu_B(g_x H_x S_x + g_y H_y S_y + g_z H_z S_z) \tag{20.4}$$

where μ_B is the Bohr magneton, and g_i, H_i, and S_i ($i = x, y, z$) are the components of the g-tensor, the magnetic field, and the spin operator along the principal axes of the crystal field. For a crystal or molecule with the highest-symmetry rotation axis (the z-axis by definition) of three-fold symmetry or greater, $g_x = g_y = g_\perp$ and $g_z = g_{||}$. For T_d or O_h symmetry, the g-value is isotropic (except when a Γ_8 state is lowest). For this review, hyperfine and quadrupole effects usually are not considered.

Table 20.1 *Optical transitions, g-values, and the best-fit parameters to the Eisenstein–Pryce theory for some* $5f^1$ *hexahalo compounds* (*Eichberger and Lux,* 1980).

	Electronic transitions and ground state g-value					*Best-fit parameters*				
Compound	Γ_7–Γ_8 (cm^{-1})	Γ_7–$\Gamma_{7'}$ (cm^{-1})	Γ_7–$\Gamma_{8'}$ (cm^{-1})	Γ_7–Γ_6 (cm^{-1})	$\lvert g\rvert$	ζ (cm^{-1})	θ (cm^{-1})	φ (cm^{-1})	k	k'
$((C_2H_5)_4N)_2PaCl_6$[a]	1730	5330	7140	8011	1.141	1689	600	3525	0.83	0.46
$CsUF_6$	5363	7400	13 800	15 900	0.708	2206	3335	8050	0.84	0.61
$RbUCl_6$	3800	6794	10 137	11 520	1.12	2219	826	5794	0.78	0.45
$CsUBr_6$	3700	6830	9761	10 706	1.21	2190	99	5746	0.79	0.32
NpF_6	7543	9348	24 000	27 000	0.605	2697	4775	16 921	0.85	0.60

[a] See Piehler *et al.* (1991) for more accurate optical data on Pa^{4+} diluted in Cs_2ZrCl_6.

An electron configuration with an odd number of electrons ($f^1, f^3, \ldots$., etc.) has a Kramers degeneracy that can be lifted by a magnetic field but not by a crystal field. However, it is possible that the pair of states that lies lowest will not have an EPR signal because the selection rule $\Delta J_z = \pm 1$ will be violated. For example, consider a $J = 5/2$ term in a purely axial crystal field. This term will be split into three doublets: $J_z = \pm 1/2$, $\pm 3/2$, and $\pm 5/2$. If the crystal field is such that the $J_z = \pm 3/2$ or $J_z = \pm 5/2$ state is lowest, there will be no EPR transitions allowed.

An ion with an electron configuration with an even number of electrons($f^2, f^4, \ldots$., etc.) is called a non-Kramers ion. If the highest-symmetry axis is a C_2 axis, the crystal field will split an integer J term into $2J + 1$ singlets, and EPR will not be observed. If the highest-symmetry axis is C_3 or higher, a doubly or triply degenerate crystal field state could be lowest, and EPR might be observed. However, EPR has been reported only for the non-Kramers ions U^{4+} and PuO_2^{2+}, both $5f^2$, in the actinide series. Non-Kramers ions are discussed in detail by Abragam and Bleaney (1970).

For an f^n configuration, where n is the number of equivalent electrons, the electrostatic interaction between two f electrons results in a series of terms that can be classified by the total orbital and spin angular momenta, L and S, defined as:

$$L = \sum_i^n l_i \qquad S = \sum_i^n s_i \tag{20.5}$$

where l_i and s_i are the orbital and spin angular momenta of the ith electron. The eigenstates are then labeled by the quantum numbers (or symbols) ^{2S+1}L. This classification is called Russell–Saunders coupling. Inclusion of the spin–orbit interaction will cause mixing of the spin and orbital angular momenta and requires the use of J, the total angular momentum, defined as:

$$\boldsymbol{J} = \boldsymbol{L} + \boldsymbol{S} \tag{20.6}$$

The ^{2S+1}L multiplet is split into levels labeled by their J eigenvalues, $J = L + S, L + S - 1, \ldots., L - S + 1, L - S$, where each J level has a $2J + 1$ degeneracy. It is this J degeneracy which is split by the crystal field (Judd, 1963; Wybourne, 1965). Usually, the lowest J level is relatively isolated, the ligand-field splittings are approximately 100–1000 cm^{-1}, and only the lowest few crystal field states as indicated above provide the main contribution to the measured magnetic susceptibility. The effects of the various interactions are shown in Fig. 20.1 for the f^2 configuration.

A large number of magnetic susceptibility and EPR measurements have been made on actinide ions in crystal fields of O_h or T_d symmetry. In these symmetries, the ordering of the energy levels of a J-term depends only on the ratio of two crystal field parameters, the fourth-order term and the sixth-order term. From magnetic data, the ground crystal field state may be determined, which in

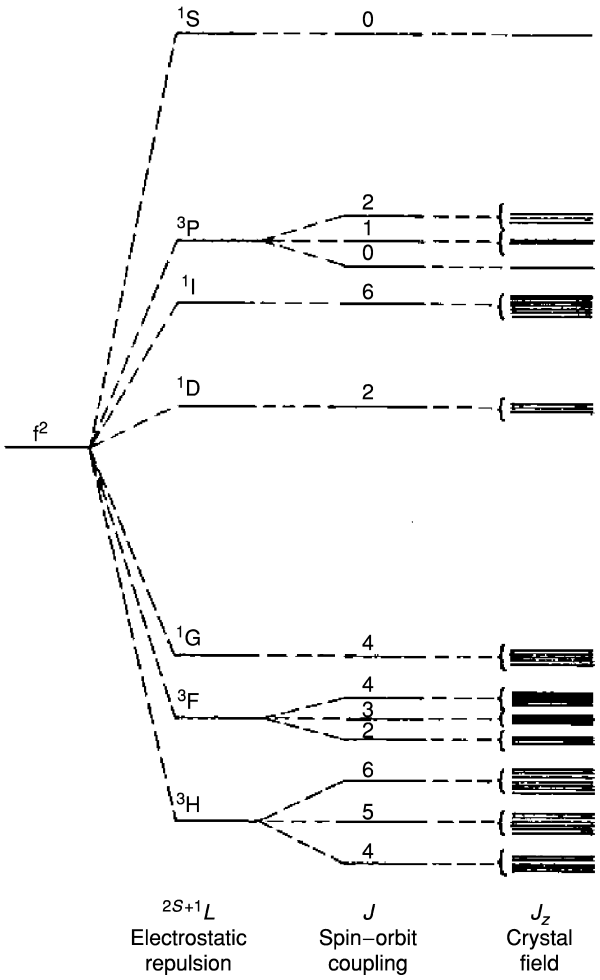

Fig. 20.1 *Schematic of the effects of the electrostatic, spin–orbit, and crystal field interactions on the f^2 configuration.*

turn can set a limit on the ratio of the fourth- to the sixth-order term. Lea *et al.* (1962) tabulated the results in reduced coordinates for all J levels of interest and their nomenclature is widely used. An illustration of the application of the Lea, Leask, and Wolf method (plus the effects of mixing other J states by the crystal field) is given in the study of Hendricks *et al.* (1974) on the temperature dependence of the magnetic susceptibility of the isostructural series, Cs_2NaMCl_6, M = U^{3+}, Np^{3+}, Pu^{3+}, Am^{3+}, Cm^{3+}, and Bk^{3+}. The data are shown in Table 20.2. From a consideration of these data, limits were placed on the possible values of the fourth- and sixth-order crystal field parameters B_0^4

Table 20.2 *Magnetic data for octahedral actinide(III) chlorides. Taken from Hendricks* et al. (1974) *unless otherwise noted.*

Compound	*T range* (K)	μ_{eff} (μ_B)	θ (K)	χ_{TIP} (10^{-6} emu mol^{-1})
Cs_2NaUCl_6	4–20	2.49 (6)	–0.53	
Cs_2NaUCl_6	25–50	2.92 (6)	–9.6	
$Cs_2NaNpCl_6$	3–50	1.92 (5)	–0.47	
$Cs_2NaPuCl_6$	3–21	0.97 (5)	–1.3	
$Cs_2NaPuCl_6$	25–50	1.16 (8)	–12.4	
$Cs_2NaAmCl_6$	15–70			5400 (400)
$Cs_2NaAmCl_6$[a]	40–300			660 (40)
$Cs_2NaCmCl_6$[b]	7.5–25	7.90 (10)	–3.87	
$Cs_2NaCmCl_6$[b]	25–45	7.48 (50)	–1.15	
$Cs_2NaBkCl_6$[b]	10–40			192 000 (30 000)
$Cs_2NaCfCl_6$[c,d]	2.2–14	7.36 (2)	–2.8	
$Cs_2NaCfCl_6$[c,d]	20–100	10.0 (1)	13.5 (4)	

[a] Soderholm *et al.* (1986).
[b] Diluted into $Cs_2NaLuCl_6$.
[c] Karraker and Dunlap (1976).
[d] Diluted into Cs_2NaYCl_6.

and B_0^6 (defined as described by Wybourne (1965)). However, recent optical results on U^{3+} ion diluted into the elpasolite host Cs_2NaYCl_6 yielded much different crystal field parameters than those obtained by Hendricks *et al.* (Karbowiak *et al.*, 1998).

Magnetic susceptibility data are usually represented by a plot of $1/\chi_M$ vs T. This plot is linear over a particular range of temperatures, and the data are fitted to the Curie–Weiss law:

$$\chi_M = C/(T - \theta) \tag{20.7}$$

where χ_M is the molar magnetic susceptibility (expressed in cgs units in cm^3 mol^{-1} or emu mol^{-1}), T and θ (the Weiss constant) are expressed in K (kelvin), and C is the Curie constant. Note that equation (20.7) uses (T–θ) in the denominator. Some authors use (T+θ) and this is a point of great confusion. All data quoted in this chapter using the Curie–Weiss law will use the form in equation (20.7).

Sometimes, in order to analyze magnetic susceptibility data that shows temperature-dependent behavior, a modified Curie law of the form

$$\chi = \chi_0 + C/T \tag{20.8}$$

has been utilized where χ_0 is the temperature-independent susceptibility and μ_{eff} may be obtained from the value of C, the Curie constant.

Another common way of representing data is to use the effective moment, μ_{eff} (in units of the Bohr magneton μ_B):

$$\mu_{\text{eff}} = 2.828\ C^{1/2} = 2.828\,[\chi_{\text{M}}(T-\theta)]^{1/2} \tag{20.9}$$

or

$$\mu_{\text{eff}}^2 = 8.0\,\chi_{\text{M}}(T-\theta) \tag{20.10}$$

If the data do not follow the Curie–Weiss law, μ_{eff} is commonly defined as:

$$\mu_{\text{eff}} = 2.828\,(\chi_{\text{M}}T)^{1/2} \tag{20.11}$$

Considering the temperature range where only the ground crystal field state is populated and there is no second-order Zeeman effect, the molar susceptibility in the z-direction may be written as:

$$\chi_z = N\mu_{\text{B}}^2 g_z^2/4kT \tag{20.12}$$

with similar equations for the x- and y-directions. In eq. 20.12 N is Avogadro's number and k is the Boltzmann factor. Because $\chi_{\text{ave}} = 1/3(\chi_x + \chi_y + \chi_z)$, therefore:

$$\chi_{\text{ave}} = \frac{N\mu_{\text{B}}^2(g_x^2 + g_y^2 + g_z^2)}{12kT} \tag{20.13}$$

The g_x, g_y, and g_z in equation (20.13) are the same g-values obtained from EPR measurements on the ground crystal field state. Magnetic susceptibility measurements and units are discussed in detail by Myers (1973) and Boudreaux and Mulay (1976). All data quoted in this chapter will be in cgs units (see equation (20.7)).

For the lanthanide series, it is common to assume the ground term crystal-field splitting is much less than kT where k is the Boltzmann constant and $T \sim$300 K (at 300 K, $kT = 208.34\ \text{cm}^{-1} = 25.85$ meV). In this case

$$\mu_{\text{eff}} = g_J[J(J+1)]^{1/2} \tag{20.14}$$

where g_J is the free-ion g-value of the particular ground J multiplet. This equation is usually *not* valid for actinide compounds at room temperature as in most cases (see above) the crystal-field splittings of the ground term are larger than kT. Exceptions are found in the case of the $5f^7$ ions, Am^{2+}, Cm^{3+}, and Bk^{4+}. For the Am^{2+} and Cm^{3+} ions, the total crystal-field splitting of the ground terms are much less than 100 cm^{-1}. Thus for Cm^{3+} compounds, $\mu_{\text{eff}} = 7.62\mu_{\text{B}}$ with $g_J = 1.925$ (Edelstein and Easley, 1968).

20.1.2 Introduction to neutron and synchrotron X-ray scattering

The techniques discussed so far, magnetic susceptibility and EPR, are useful in the sense that they can determine many details about the magnetic state of an actinide ion. On the other hand, what they cannot determine is the interaction *between* actinide ions. For example, at low temperature the actinide ions,

especially those with a Kramers ground state, frequently order magnetically. The *exchange interaction* between the actinide ions energetically prefers a certain configuration of neighboring dipoles. Naturally, it is important to know the exact form of this magnetic structure. In certain cases EPR and Mössbauer spectroscopies (which are both single-site sensitive) are able to determine the magnetic structure. For example, if all the moments are aligned along the unique axis in a uniaxial crystal structure, then this symmetry will be reflected in the spectra. In general, however, one needs a technique that is sensitive to the long-range ordering of the moments and one naturally turns to methods involving the scattering of radiation.

The technique of choice for studies of this type is the scattering of thermal neutrons. Pioneered for magnetic structures in the period 1949–60 at Oak Ridge National Laboratory by Shull and his collaborators, this technique is in very wide use and there are a number of good books introducing the technique (Bacon, 1962; Squires, 1978; Kostorz, 1979; Skold and Price, 1987). In very early work (Shull and Wilkinson, 1955; Wilkinson *et al*., 1955) the famous ferromagnet UH_3 was examined (although to reduce the incoherent scattering from H they made a sample of isostructural UD_3). The key to magnetic structure determination is that for most antiferromagnetic (AF) structures, the repeat distances of the magnetic structure is more complex than the chemical structure. The result is new neutron diffraction peaks when the magnetic moments order. From the position and intensity of these diffraction peaks, the periodicity and the arrangements of the ordered moments, as well as their magnitude, may be deduced. Neutrons can, of course, be used also for chemical structure determinations, and the fact that the scattering from an actinide atom and an oxygen atom are roughly comparable means that the contrast is completely different from that of studies using X-rays. Much work in this respect is done on oxides and nitrides, and a summary of some of this work has been given (Lander, 1993) with particular reference to actinides. A good example of a study of this sort will be described later in connection with UO_2 at low temperature.

The *magnetic* scattering of neutrons is by the magnetic dipole moments in the material. For the actinides this arises from the 5f electrons around the nucleus. If the magnetic structure is well known, then the intensities may be measured as a function of momentum transfer Q ($= 4\pi \sin\theta/\lambda$, where θ is the Bragg angle and λ is the wavelength of the incident radiation) to give a so-called magnetic form factor $f(Q)$. By analogy with the scattering factor in X-ray studies, $f(Q)$ is proportional to the Fourier transform of the distribution of the outer 5f electrons. Again this is discussed (Lander, 1993), and there have been many studies of this type in actinides, including some Pu compounds.

Finally, thermal neutrons at 300 K have an energy corresponding to kT ($= 25.85$ meV, $= 208.34$ cm^{-1}) so that it is possible for them to lose energy to (or gain from) the sample and this energy change may be measured by inelastic neutron scattering. As with EPR and optical spectroscopies, the crystal field levels may be determined. Most importantly, and unlike spectroscopic methods

based on photons, the neutrons (which are electrically neutral) can penetrate deep into the solid so this technique is good also for opaque materials. This means that complex experimental environments can readily be used, for example, at low temperatures down to 100 mK, high temperatures up to 2500°C, and high magnetic fields. Furthermore, if single crystals are available, then the neutrons can map out the dispersion curves of both the phonons and the magnons. UO_2 is a famous example of this, where both types of excitations were published more than 30 years ago (Cowley and Dolling, 1968).

Unfortunately, there are two major disadvantages for neutron studies. The first one is caused by the presence of resonant terms in the neutron-nuclear cross sections for actinides (Lander, 1993). This interaction is a complex one, not easy to calculate from first principles. However, generally speaking, the heavier nuclides are less stable than the lighter ones, and part of this trend toward instability results in resonant terms in the cross section. Thus, when a neutron impinges upon the nucleus there are probabilities for scattering and absorption. The latter results in the formation of a compound nucleus, which usually rapidly decays and gives rise to other types of radiation. If a neutron is captured then it is no longer available for scattering; the beam penetration is restricted. Materials like Cd and Gd have enormous absorption cross sections for thermal neutrons, and are frequently used to stop neutron beams. In the actinides there is an appreciable absorption cross section for ^{237}Np, but, of course, the most famous absorption cross sections are those due to the fission process in both ^{235}U and ^{239}Pu. In the case of ^{235}U, the fission cross section is actually for low-energy neutrons, which can penetrate the nuclear barrier, forming an unstable compound nucleus that then breaks up with the emission of fast neutrons and γ-rays. This, of course, was the famous discovery of Hahn and Strassman in 1938. Fortunately, ^{235}U is only a small fraction of normal uranium. However, the most common isotope of Pu is ^{239}Pu with a very large cross section, so for most neutron experiments using Pu, the heavier isotope ^{242}Pu should be used.

The second disadvantage for neutrons is the available intensities. Neutron sources are weak, much weaker (in terms of flux per $cm^2\ s^{-1}$) than synchrotron or laser sources, mainly because they are impossible to focus. Large samples are therefore needed. For neutron powder diffraction, samples of up to several grams are frequently used, although studies of much smaller samples are possible. Examples are the work on CmO_2 (Morss *et al.*, 1989) and Cm_2CuO_4 (Soderholm *et al.*, 1999), discussed below, in which amounts of $\sim$50 mg were studied. For single-crystal studies, the samples can be at the few milligram level, but this still contrasts with samples of $\sim$50 μg that can be examined by conventional laboratory X-ray sources. For inelastic neutron scattering and the study of phonons, samples sizes of grams are again required. This is a serious handicap for neutron diffraction on *any* element in the periodic table. For many studies, this is not a problem, but the acquisition of large single crystals for phonon or magnon measurements can be a serious limitation. For example,

despite the huge effort on high T_c superconducting materials after their discovery in 1986, it took approximately 5 years until the first details of the phonon and magnetic excitation spectra were published. This did not represent a lack of interest on the part of neutron specialists, but rather an absence of suitable crystals. Moreover, this technique can, of course, only be done at a central user facility, either a spallation source or reactor. The difficulty for actinides as compared to most other elements is that their quantity in user facilities is frequently restricted. The large quantities required in neutron scattering studies are not a problem with uranium, but have severely limited the possible range of experiments on transuranium materials. The restrictions continue to become more severe in 'open' facilities, and experiments that were readily performed (for example at Argonne in the 1970s) are no longer possible at most facilities.

Synchrotron radiation (another activity performed at large user facilities) is making a sizeable impact in actinide science, especially in the field of environmental studies using methods based on absorption spectroscopy. Can such beams be of any use in magnetic studies, the subject of this chapter? Initially, when the synchrotrons were built, their impact on magnetism was predicted to be small. It was known, for example, that photons do indeed have a 'magnetic' cross section, but it was very small. For example, for iron the magnetic photon cross section is some six orders of magnitude smaller than the Thompson (charge) cross section (Blume, 1985; Blume and Gibbs, 1988; Lovesey and Collins, 1996). Indeed, this cross section has been of only limited use, although as the synchrotron fluxes continually increase in intensity, this may change. One example is the work on UAs (Langridge *et al*., 1997) in which the spin and orbital contributions to the magnetism were separated. The weak intensities resulted in large uncertainties, but this technique may well become more popular as synchrotron fluxes increase.

Synchrotron radiation is, of course, tunable in the sense that any wavelength (energy) may be chosen, unlike laboratory-based sources. This naturally led to the idea that the energy should be tuned to a resonant absorption edge – something incidentally also useful in protein crystallography as the cross section for charge scattering also changes appreciably near an absorption edge (James, 1962). The result in magnetic studies was the discovery of large *enhancements* in the (weak) non-resonant magnetic scattering. Although there had been some attempts to see these previously, the first really large effects were observed in holmium metal by Gibbs and his collaborators (Gibbs *et al*., 1988) and were immediately interpreted in terms of atomic resonance theory (Hannon *et al*., 1988). This general technique is called resonant X-ray scattering (RXS).

Turning to the actinides, enhancements at the M_4 and M_5 edges are shown in Fig. 20.2 taken from McWhan *et al*. (1990) on the antiferromagnetic material UAs. M-edges correspond to the initial states having a principal quantum number n of 3. The M_4 and M_5 edges have the azimuthal quantum number $l = 2$ and correspond to transitions from $3d_{3/2}$ and $3d_{5/2}$ core states, respectively.

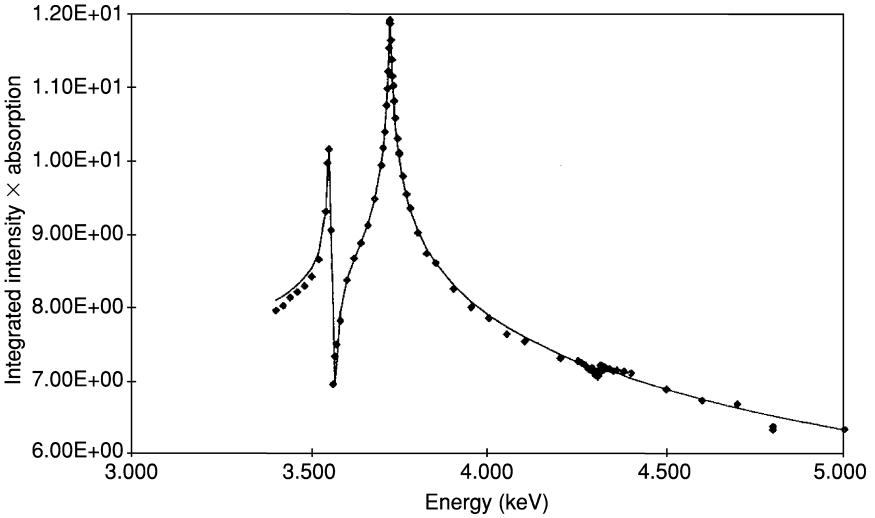

Fig. 20.2 *Intensity of the* (003/2) *reflection from a single crystal of UAs at* $T = 10$ K *as a function of photon energy. UAs* (*simple fcc NaCl crystal structure*) *has a magnetic structure that repeats in two unit cells. This results in magnetic reflections occurring at half integer Miller indexes. Notice that the intensity is plotted on a log scale so that the enhancement approaches* 10^6 *as compared to the intensity off resonance. The positions of the M resonances are* $M_5 = 3.550$, $M_4 = 3.726$, *and* $M_3 = 4.304$ keV. *The solid line is the result of a calculation involving three dipole oscillators, and fits the data very well. Reprinted from McWhan* (1998), *Copyright* 1998 *with permission from Elsevier.*

Electric dipole (E1) transitions change the azimuthal quantum number by ± 1 so that the final states involve the $5f_{5/2}$ and $5f_{7/2}$ states, the valence band states. However, in the actinides, there may be already electrons in the 5f states. In UAs, for example, one would expect most of the three 5f electrons to be in the lower energy $5f_{5/2}$ orbitals. At low temperature, these states become polarized, leading to a magnetic moment on the atom. The promotion of an electron into the valence band 5f states causes a resonance between the states already there, resulting in a reemission of radiation when the excited state decays to annihilate the core hole. In the case of the valence states being polarized, as when UAs becomes antiferromagnetically ordered below T_N, the emitted radiation is also polarized, and it is this that leads to the large enhancement of magnetic scattering at the resonant energy. One can see immediately from this that for the light actinides the signal at the M_4 edge should be greater than that at the M_5, because the 5f polarized states are mostly in $5f_{5/2}$ levels corresponding to the M_4 transition. (Transitions at the M_5 edge involve mainly $5f_{7/2}$ states but also $5f_{5/2}$ with smaller matrix elements, hence the intensities are smaller. For a half-filled shell the intensities at the two edges should be similar.)

The process involving resonance effects also occurs in absorption spectroscopy. The development of the two techniques, so-called X-ray magnetic circular dichroism (XMCD) has been remarkably parallel (Thole *et al.*, 1985; Schütz *et al.*, 1987). The amplitude of the effects in either technique depends on a number of factors, in particular the overlap of the wavefunctions of the core and valence states and matrix elements summed over all possible excited states. The advantage of XMCD is that (provided a model of the magnetism is available) the signal may be related directly to the orbital moment of the valence states, and it is also possible with reasonable assumptions to deduce the spin moment. These so-called 'sum rules' (Carra and Altarelli, 1990) can be derived primarily because absorption involves only the imaginary part of the cross section. In the case of scattering one must deduce *both* the real and imaginary parts, and that has proved intractable so far for resonance scattering experiments. XMCD also has the advantage (see below) that any edge can be accessed without the necessity to fulfill Bragg's law as is necessary for scattering. However, XMCD has the major *disadvantage* that it cannot give any information about the spatial extent of the scattering centers as it is restricted to $Q = 0$, where Q is the momentum transfer. Moreover, it cannot examine antiferromagnets since (by definition) they have no net magnetization so no magnetic signal at $Q = 0$. (X-ray linear dichroism is a possible technique to overcome this, but the matrix elements are very small.) From this discussion, it is clear that RMS and XMCD are indeed complementary. There have been a number of experiments reported on U compounds (none yet on transuranium compounds), especially on UFe_2 (Finazzi *et al.*, 1997) and on the heavy-fermion intermetallic materials (Dalmas de Rotier *et al.*, 1999; Bombardi *et al.*, 2001).

Scattering experiments have played an important role in studies of one of the oxides, NpO_2. Before discussing particular experiments, a general overview (Fig. 20.3) of the energies of the resonances will be given. The boxes in Fig. 20.3 give the ranges of the electron binding energies across a series that are of interest for magnetism. For example in the 3d series the K-edges correspond to transitions from the 1s to the 4p states. Since the 4p states are not expected to be polarized strongly, the matrix elements are small. On the other hand, transitions at $L_{2,3}$ edges are to the strongly polarized 3d states, so it is these edges that need to be used to observe an appreciable signal. Similarly (as explained above) it is the $M_{4,5}$ edges that will be useful for f magnetism as found in the rare earths and actinides. No modification of these electron-binding energies is possible except perhaps at enormous pressures. For scattering processes Bragg's law, $2d \sin \theta/\lambda$, is utilized where d is the interplanar spacing, θ is Bragg's angle, and λ is the wavelength of the radiation. Using the relationship for photons that $E = 12.4/\lambda$, where E is in keV, and λ in Å, Bragg's law demands d spacings *larger* than 3.1 Å for radiation less than 2 keV in energy. Now 3.1 Å has been chosen as it represents a large d-spacing from a simple solid. Larger d-spacings require either more complex solids or the examinations of d-spacings in multilayers or domains. The latter can reach up to $\sim$1000 Å and represent science on the

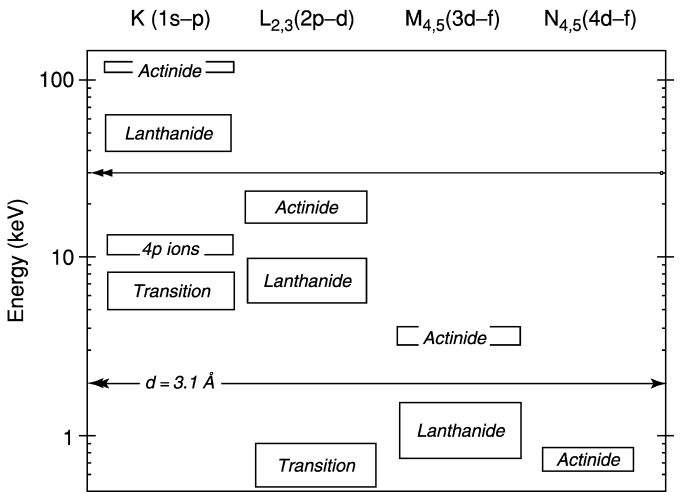

Fig. 20.3 *Each box shows the energy spread of the electron binding energies across the series for the transitions marked at the top of the figure. The upper horizontal line gives the approximate maximum energy* (∼30 keV) *of most magnetic scattering beamlines. The lower horizontal line gives the d-space corresponding to the maximum that will fulfill Bragg's law for an incident photon energy of* 2 keV. *For lower energies, such as the transition metal* $L_{2,3}$ *edges, greater d-spaces are required. For a normal crystal structure with a small unit cell this implies these edges are beyond the Bragg cut-off and no scattering can be observed. For dichroism there are no such restrictions, and, in principle, all edges are accessible. Reprinted from Lander* (2002). *Copyright* 2002 *with permission from Elsevier.*

nanoscale. Now it can be understand why this technique has not been enormously useful for Å-level magnetism in the transition-element series, the important edge is simply too low in energy (Lander, 2002). Similarly, even in the rare earths most of the work is done at the L-edges, which represent transitions to the (sparsely polarized) 5d states. It is only recently with the building of dedicated magnetic scattering beamlines in vacuum that work on the rare-earth M-edges is being reported (Schüssler-Langeheine *et al.*, 2001). The M-edges of the actinides are then unique, magnetism on the atomic scale with the largest resonance effects can be examined. Accordingly a large amount of work, starting with the first study of UAs as shown in Fig. 20.2, has been done with U, Np, and even Pu compounds (Langridge *et al.*, 1994a,b; Lander, 2002; Normile *et al.*, 2002).

Compared to neutrons RXS can use minute amounts of material. Samples of about 1 mg are regularly used, and intensity corresponding to a doping of ∼40 μg of Np was seen in one crystal. On the other hand, no method (yet) is available to relate the observed signal to the magnetic moment. In addition, it has not proved possible to observe signals from polycrystalline samples (except with

very poor *q*-space resolution (Collins *et al*., 1995)). In principle, this could be remedied by building a special apparatus to collect more of the solid angle from the Debye–Scherrer cone, but the strong absorption means that the beam only would penetrate a few micrometers at most (and only ~0.2 μm at the U M-edges) so the sampling through the powder would always be poor. Since neutrons are so good at sampling a large volume of material, very little effort has been made at synchrotron sources with RXS, but it might be justified for actinides because of the small sample quantities that could be used.

As is so often the case, the techniques are really complementary and scientists in this field should choose the technique for the problem, and not vice versa!

20.1.3 Scope, other reviews, and units

Although in this chapter the coverage has been primarily restricted to *ionic* actinide compounds, in actinide condensed matter physics a major interest is actually in studies of intermetallic and semiconductor compounds. Chapter 21 reviews the physical properties of actinide metals and alloys, including their magnetic properties. The two volumes edited by Freeman and Darby (1974) contain information about the magnetic properties of many actinide materials, including a review by Lam and coworkers (Lam and Chan, 1974; Lam and Aldred, 1974) on actinide salts, carbides, chalcogenides, pnictides (group V), and various intermetallic compounds, plus another review by Nellis and Brodsky (1974) on the pure metals and alloys. A later review article by Brodsky (1978) covered the magnetic properties of the actinide elements and their magnetic compounds. An earlier review covers the $5f^0$, $5f^1$, and some selected data for $5f^2$ and higher configurations (Sidall, 1976). Some magnetic data are given in the review by Keller (1972) on lanthanide and actinide mixed oxides and by Dell and Bridger (1972) in their review of actinide chalcogenides and pnictides. The review article by Boatner and Abraham (1978) summarizes all the EPR data on actinide ions published through 1976. Kanellakopulos (1979) reviewed the magnetic properties of cyclopentadienyl compounds of the trivalent and tetravalent actinides. Fournier (1985) reviewed the magnetic properties of actinide solid compounds and Huray and Nave (1987) have surveyed magnetic measurements on transplutonium actinides. A comprehensive survey of actinide metals and their compounds is given in Landolt-Börnstein (Troc *et al*., 1991; Troc and Suski, 1993). Santini *et al*. (1999) reviewed the magnetism of actinide compounds that can be categorized as actinide intermetallics and strongly correlated systems.

The discovery of heavy-fermion materials in the early 1980s and the accompanying interplay between magnetism and superconductivity has been of great interest both in the neutron and synchrotron communities, as well as in the larger solid state physics community. Much of the corresponding neutron work has been reviewed (Lander and Aeppli, 1991; Lander, 1993; Holland-Moritz

and Lander, 1994). The general neutron trends were illustrated in the following papers (Bernhoeft *et al.*, 1998; Metoki *et al.*, 1998). For the high-intensity X-ray case, a good background and useful references are given in the reviews by McWhan (1998) and Lander (2002). Further excitement in the condensed matter physics community has been caused by the discovery of the *ferromagnetic* superconductor UGe_2 with $T_c \sim 0.5$ K (Saxena *et al.*, 2000), and the recent discovery of a Pu-based compound ($PuCoGa_5$) that becomes a superconductor at the astonishingly high temperature of 18 K (Sarrao *et al.*, 2002).

The remainder of this chapter is divided into two major sections. In the first section, the actinide ions are classified according to their electron configuration, and magnetic measurements are reviewed for each electron configuration. The actinide dioxides (AnO_2) are not included in this section but are reviewed separately in the second major section. The actinide dioxides are isostructural with a face-centered cubic (fcc) fluorite structure. Thus the crystal field parameters (which determine the ground state electronic and magnetic properties) for each of the dioxides should be correlated. Therefore, in principle, the results of the analyses for one of the dioxides should be relevant to the series. In fact the actinide dioxide story is complicated and considerable efforts, both experimental and theoretical, have been expended to try to understand their properties. For these reasons this subject is best treated separately.

Two different energy units are used in this review depending on the discussion. The units are meV and cm^{-1}. The conversions between these units are as follows: (1 eV = 8065.479 cm^{-1}); (1 meV = 0.001 eV = 8.065 cm^{-1}); (1 cm^{-1} = 1.2399×10^{-4} eV or 0.12399 meV). It is useful to note that kT (where k is the Boltzmann constant) at 300 K = 25.85 meV = 208.34 cm^{-1}.

20.2 $5f^0\ ^1S_0$; Th^{4+}, Pa^{5+}, U^{6+}, UO_2^{2+}

For a closed-shell configuration, compounds formed with these ions should be diamagnetic. This is found to be true for Th^{4+} and Pa^{5+}, but uranyl compounds and UF_6 exhibit TIP. The weak paramagnetism for UF_6 was attributed by Eisenstein and Pryce (1960) to the coupling of higher-energy states into the ground configuration by the magnetic field. From an analysis of the observed susceptibility they concluded that the bonding in the actinide hexafluorides is at least partially covalent. A similar model was proposed earlier by Eisenstein and Pryce (1955) and later by McGlynn and Smith (1962) to explain the weak paramagnetism of uranyl salts. Studies by Denning and coworkers (Denning, 1992) on the high-resolution spectral characteristics, including Zeeman effect measurements of the uranyl ion in tetragonal and trigonal equatorial fields (perpendicular to O–U–O bond axis), has resulted in the determination of paramagnetic magnetic moments for some excited states and a consistent description of the bonding within the uranyl group. The magnetism of a number of ternary U(VI) oxides have been measured and their TIP were

Table 20.3 *Magnetic susceptibilities for some $5f^0$ uranates and neptunates. These data are from Bickel and Kanellakopulos* (1993). *The original references are given in this paper.*

Compound	χ_{TIP} (10^{-6} emu mol^{-1})
α-Na_2UO_4	152
β-Na_2UO_4	114
Li_2UO_4	240[a]
β-Na_4UO_5	142
$Li_2U_2O_7$	135
$Na_2U_2O_7$	133
Sr_3UO_6	158
Ca_3UO_6	156
$BaUO_4$	134
$SrUO_4$	143
Na_4UO_5	162
Li_5NpO_6	225
Li_5NpO_6	217[b]

[a] High value attributed to a ferromagnetic impurity.
[b] Second reported measurement.

attributed to a nonnegligible degree of covalency in the An–O bonds (Bickel and Kanellakopulos, 1993). These data are listed in Table 20.3.

20.3 $5f^1\ {}^2F_{5/2}$; Th^{3+} ($6d^1$), Pa^{4+}, U^{5+}, Np^{6+}, NpO_2^{2+}, Pu^{7+}

The $5f^1$ ions are good examples for the interpretation of magnetic data because electron repulsion is absent and at most six transitions are allowed in the optical spectrum.

An interesting change in the ground configuration occurs for the known Th^{3+} compounds. Initially a purple trivalent thorium complex, formulated as $Th(C_5H_5)_3$, was reported by Kanellakopulos *et al.* (1974), with a room-temperature magnetic moment of $0.331\mu_B$. A second compound, also formulated as $Th(C_5H_5)_3$ but green in color, was prepared by Kalina *et al.* (1977), who reported a magnetic moment of $0.404\mu_B$. Trisindenylthorium(III) has been prepared by Goffart and also has a very low magnetic moment (Kanellakopulos, 1979). Blake *et al.* (1986) prepared the first crystallographically characterized Th^{3+} compound, $[Th\{\eta^5\text{-}C_5H_3(SiMe_3)_2\}_3]$. Kot *et al.* (1988) showed that this compound has a room-temperature EPR spectrum that is consistent only with a $6d^1$ ground state. Subsequently two other Th^{3+} compounds (Parry *et al.*, 1999; Blake *et al.*, 2001) have been synthesized and shown to have EPR spectra consistent with the $6d^1$ ground configuration rather than a $5f^1$ configuration. Because the relative energies of these two configurations are so close in energy (for the Th^{3+} free ion, the ground configuration is $5f^1$ with the start of the $6d^1$

configuration at 9192.84 cm^{-1}, see Chapter 16, Table 16.1) it is possible that other new Th^{3+} compounds may indeed have a $5f^1$ ground configuration.

The magnetic susceptibility of protactinium tetrachloride was measured between 3.2 and 296 K (Hendricks *et al.*, 1971), follows the Curie–Weiss law from 182 to 210 K with $\mu_{\text{eff}} = 1.04(6)\mu_B$ and $\theta = +158$ K, and exhibits a ferromagnetic transition at 182 ± 2 K. A high degree of covalency has been suggested to explain this relatively high transition temperature. The magnetic susceptibility of protactinium tetraformate (Schenk *et al.*, 1975) was measured from 80 to 300 K and follows the Curie–Weiss law with $\mu_{\text{eff}} = 1.23\mu_B$ and $\theta = -3$ K. The crystal structure of this compound and its Np analog were reported to have the M^{4+} ion at the center of a nearly undistorted cube of eight oxygen atoms. However, the U analog was stated to have lower symmetry, which appears inconsistent (Hauck, 1976). By assuming that the $J = 5/2$, Γ_7 state was lowest and is the only one that contributes to the measured susceptibility, a value of $\mu_{\text{eff}} = 1.24\mu_B$ (with $g_J = 6/7$) was calculated from the wave functions given by Lea *et al.* (1962), in good agreement with the experimental value.

The susceptibility of tetrakis(cyclopentadienyl)protactinium was measured between 4.2 and 300 K (Kanellakopulos, 1979). Above 90 K, the magnetic susceptibility followed the Curie–Weiss law with θ = –8.6 K, and the magnetic moment at room temperature is $0.725\mu_B$. A $J = 5/2$ state will split into at most three Kramers doublet levels, and in this compound it is reported that the first two levels are separated by approximately 15–30 cm^{-1} and that the third level is at about 600 cm^{-1}. J mixing cannot explain the low magnitude of the magnetic moment.

A large number of magnetic measurements have been reported for $5f^1$ ions in compounds with octahedral or pseudo-octahedral nearest neighbor coordination. These studies include EPR measurements of the $5f^1$ ion (Pa^{4+}, U^{5+}, Np^{6+}, and in one case Pu^{7+}) diluted in nonmagnetic hosts or magnetic susceptibility measurements of the $5f^1$ compounds, either pure or again diluted in a host matrix. For a $5f^1$ ion only the crystal (or ligand) field and the spin–orbit coupling are the important interactions. The necessary theory to interpret the magnetic and optical measurements may be easily formulated starting from the one-electron f-orbitals in a crystal field as the basis set (S, S_z representation) or from the spin–orbit coupled (J, J_z representation) basis set (Axe, 1960; Eisenstein and Pryce, 1960; Hutchison and Weinstock, 1960; Axe *et al.*, 1961; Judd, 1963; Reisfeld and Crosby, 1965; Hecht *et al.*, 1971). For O_h symmetry, the energy levels and magnetic properties are dependent upon two crystal field parameters and the spin–orbit parameter as shown schematically in Fig. 20.4.

For one $5f^1$ electron in a free ion (no crystal field), the ^2F Russell–Saunders state splits into two J states, $J = 5/2$ and $J = 7/2$, when the effect of spin–orbit interaction ζ is included with an energy splitting between the two states of $7\zeta/2$ (far right side of Fig. 20.4). Now assuming an octahedral array of ligands about the metal ion, the $J = 5/2$ state breaks up into a doubly degenerate

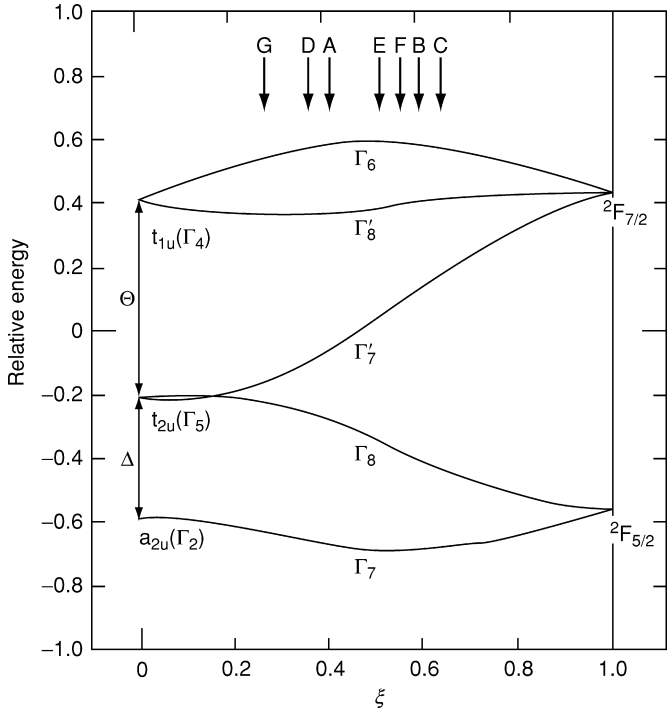

Fig. 20.4 *Relative energy splittings of an f^1 ion (O_h symmetry) as a function of the relative magnitudes of the crystal field and spin–orbit coupling interactions. The ordinate is defined as relative energy* $= E/[(\Delta + \Theta)^2 + (7\zeta/2)^2]^{1/2}$ *and the abscissa* ξ *can be determined from the equation* $\xi = [(7\zeta/2)/(\Delta + \Theta)]/[1+(7\zeta/2)/(\Delta + \Theta)]$. *The figure is drawn for the ratio* $\Theta/\Delta = 13/8$. *The arrows at the top represent the approximate parameter values for A,* $(NEt_4)_2PaF_6$*; B,* $(NEt_4)_2PaCl_6$*; C,* $(NEt_4)_2PaBr_6$*; D,* $(NEt_4)UF_6$*; E,* $(NEt_4)UCl_6$*; F,* $(NEt_4)UBr_6$*; G,* NpF_6. *The data are from Brown* et al. (1976).

Γ_7 state and a four-fold degenerate Γ_8 state. The higher-lying $J = 7/2$ state breaks up into two doubly degenerate states, Γ_6 and Γ'_7, and one four-fold degenerate Γ'_8 state. The ground state in this symmetry is the $J = 5/2$, Γ_7 state. The parameters Θ and Δ represent the splittings of the f-orbitals for O_h symmetry when the spin–orbit interaction is zero. This is represented at the far left side of Fig. 20.4. As the relative strengths of the crystal field and spin–orbit interactions become comparable, the relative energy splittings change as shown in the center of Fig. 20.4. The ground Γ_7 state g-value depends only on the spin–orbit coupling constant and the difference in energy between the two lowest f-orbitals (Δ) in the limit of zero spin–orbit coupling.

If the ground Γ_7 state were a pure $J = 5/2$ state, the measured g-value could easily be calculated. However, the crystal field interaction is not small as compared to the spin–orbit coupling interaction so the excited $J = 7/2$,

Γ_7' state is mixed into the ground $J = 5/2$, Γ_7 state via this interaction. The resulting expression for the ground state g-value in $5f^1$ octahedrally coordinated complexes is given by Axe (1960):

$$g = -2\left(\frac{5}{7}\cos^2\phi - \frac{4\sqrt{3}}{21}\sin 2\phi - \frac{12}{7}\sin^2\phi\right)$$

where

$$\Gamma_7^{(1)} = |^2F_{5/2}\Gamma_7 > \cos\phi - |^2F_{7/2}\Gamma_7' > \sin\phi$$

and ϕ is determined by the relative magnitudes of the crystal field parameters. There are four electronic transitions (O_h symmetry) that should be observed in these systems. Three optical and/or near-infrared transitions between the $J = 5/2$ and $J = 7/2$ states have been reported for most of these octahedral complexes. In some cases the $\Gamma_7 \rightarrow \Gamma_8$ transition of the $J = 5/2$ state that occurs in the infrared or near-infrared region has also been observed. These electronic absorption data plus the EPR data on the ground state allow the parameters (including orbital reduction factors) of the Eisenstein–Pryce model (Eisenstein and Pryce, 1960; Hecht *et al.*, 1971; Edelstein, 1977; Eichberger and Lux, 1980) for an octahedral f^1 system to be evaluated as shown in Table 20.1. Note the much different ground state g-values for various compounds.

A careful study of the magnetic susceptibility of NpF_6 and NpF_6 diluted in UF_6 (very slightly distorted O_h symmetry) in the temperature range 4.2–336.9 K has been reported by Hutchison *et al.* (1962). The g-value extrapolated to infinite dilution was found to be 0.605 ± 0.004. The g-value was found to vary as a function of the mole fraction of NpF_6 (six different samples of varying mole fractions were measured), with a maximum value of 0.694 ± 0.011 at a mole fraction of 0.34. No explanation has been given for these observations. The magnetic measurements agree with EPR measurements of NpF_6 diluted in UF_6 (Hutchison and Weinstock, 1960) and with the calculations of Eisenstein and Pryce (1960). Analysis of the fluorine superhyperfine structure measured by electron-nuclear double resonance (ENDOR) in single crystals of NpF_6 diluted in UF_6 (Butler and Hutchison, 1981) indicates that 5f orbital covalency effects are approximately an order of magnitude larger in NpF_6 than in 4f complexes. This is consistent with the larger radial extension of 5f orbitals as compared to 4f orbitals. Similarly, a series of papers on the EPR of U^{5+} in complexes of the type MUF_6 (M = Li, Na, Cs, NO) measured at 77 K have been reported (Rigny and Plurien, 1967; Drifford *et al.*, 1968; Rigny *et al.*, 1971a). These octahedral complexes showed a small g-value anisotropy due to axial distortions. The data have been analyzed on this basis. Other, similar complexes with M = K, NH_4, Rb, Ag, and Tl showed no EPR spectra at 77 K, which has been attributed to larger distortions of theUF_6^- octahedra. Selbin and coworkers (Selbin *et al.*, 1972; Selbin and Sherrill, 1974) have measured and analyzed the room-temperature EPR spectra of a number of polycrystalline salts of the type

UX_6^- and UOX_5^{2-} (X = F^-, Cl^-, Br^-, no signal observed for UF_6^-). Their analysis was based on an extension of the standard octahedral theory to include a tetragonal distortion. Although observations of the room temperature signals for the UOX_5^{2-} species have been questioned (Lewis *et al.*, 1973), the magnitude of the *g*-value obtained is consistent with that of other $5f^1$ hexahalide or distorted hexahalide complexes. Some EPR and optical measurements have been reported or reanalyzed for NpF_6, UX_6^- (X = F, Cl, Br) (Eichberger and Lux, 1980), and PaX_6^{2-} (X = F, Cl, Br, I) (Brown *et al.*, 1976) (see Table 20.1).

Early studies on the optical and magnetic properties have been reported for $5f^1$ ions in uranates, neptunates, and one plutonate (Keller, 1972; Miyake *et al.*, 1977a, 1979, 1982, 1984; Kanellakopulos *et al.*, 1980a). For these compounds, the magnetic ions (U^{5+}, Np^{6+}, Pu^{7+}) are surrounded by an octahedral or distorted octahedral array of oxygen atoms. Hinatsu, in a series of recent papers, has reanalyzed earlier data and provided new measurements on some compounds plus other distorted actinide perovskites. He has given a consistent analysis of this body of data (Hinatsu and Edelstein, 1991; Hinatsu *et al.*, 1992a,b; Hinatsu, 1994a,b). Hinatsu's results are consistent with the *g*-values of about 0.7 reported by Lewis *et al.* (1973) from EPR measurements for U^{5+} diluted in $LiNbO_3$, $LiTaO_3$, and $BiNbO_4$. The latter study could not find any verifiable EPR spectra due to U^{5+} in a number of magnetically concentrated crystals including $NaUO_3$ and $LiUO_3$.

In an interesting paper, Bickel and Kanellakopulos (1993) compiled magnetic data on a number of $5f^1$ ternary actinide oxides that they analyzed in terms of a temperature-dependent term and a temperature-independent term (see equation 20.8). Table 20.4 lists the results of the magnetic measurements and some crystallographic data for a number of compounds. The compounds studied have the $5f^1$ ion at the center of a more or less distorted AnO_6 anionic array. For U^{5+} and Np^{6+} compounds in this symmetry, the first excited level is more than $\sim$4000 cm^{-1} higher in energy. Therefore the room-temperature moment should reflect the value of $1.24\mu_B$ obtained from a Γ_7 ground state. Table 20.4 shows the experimental values, all of which are lower than the theoretical value. Bickel and Kanellakopulos (1993) argue that this can be interpreted, along with the observed TIP for these compounds, as due to the degree of covalency. They also point out that the observation of low-temperature magnetic transitions in these compounds, due to exchange interactions, depends on the shortest An–An distance. This behavior is reminiscent of that found in actinide metals and alloys. In that case, when the actinide ion–actinide ion distance is less than a certain critical distance (the Hill parameter), approximately 3.5 Å, the material exhibits itinerant behavior (TIP). At a distance greater than the critical distance, localized magnetism is found. For the ionic compounds discussed by Bickel and Kanellakopulos, the equivalent behavior is exchange interactions at shorter distances vs no magnetic ordering at larger distances. See Chapter 21 for further discussion.

Table 20.4 *Magnetic and crystallographic data for $5f^1$ ternary actinide oxides. All data are taken from Bickel and Kanellakopulos* (1993).

Compound	*Crystal symmetry*	*Shortest An–An distance* (pm)	χ_{TIP} (10^{-6} emu mol^{-1})	μ_{eff} (~300 K) (μ_B)	T_0 (K)*
$LiUO_3$	rhombohedral	400	364	1.117	16.9
$NaUO_3$	orthorhombic	413	395	1.125	31.1
KUO_3	cubic	429	440	1.216	16.0
$RbUO_3$	cubic	432		1.216	32.0
Li_3UO_4	tetragonal	449	280	0.922	6
Li_7UO_6	hexagonal	615	238	0.873	[a]
Na_2NpO_4	orthorhombic	444	372	1.053	7
K_2NpO_4	tetragonal	423			19.5
Li_4NpO_5	tetragonal	443	331	0.994	20
Na_4NpO_5	tetragonal	459	342	1.018	[a]
Li_6NpO_6	hexagonal	520	389	1.083	[a]
Na_6NpO_6	hexagonal	567	376	1.005	[a]
Ba_3NpO_6	orthorhombic	627	340	1.012	[a]
Sr_3NpO_6	orthorhombic	598	283	0.933	[a]
Ca_3NpO_6	orthorhombic	574	347	1.089	[a]
$BaNpO_4$	orthorhombic	404	335	1.089	18.3
Li_5PuO_6			300	0.955	

* Ordering temperature.
[a] No ordering observed above 4.2 K.

A recent report of a newly synthesized U^{5+} hexakisamido complex (Meyer *et al.*, 2000) reported $g = 1.12$ as measured by EPR at 20 K with a $\mu_{\text{eff}} = 1.16$ BM from 5 to 35 K. This complex has six N atoms arranged in octahedral coordination around the U^{5+} ion from each of six dbabh groups (dbabh = 2,3:5,6-dibenzo-7-azabicyclo[2.2.1]hepta-2,5-diene) and its g-value is in accord with those measured for hexahalogenated U^{5+} complexes.

The magnetic susceptibility of UCl_5 (a dimeric compound with a pseudo-octahedral array of chlorine atoms, two of which are bridging) as a function of temperature was first reported by Handler and Hutchison (1956) and later by Fuji *et al.* (1979). The latter authors have also reported the g-value as measured by EPR (Miyake *et al.*, 1977b). They have combined the magnetic data with optical measurements by Leung and Poon (1977) and fitted all the data with a crystal field model based on a weak C_{2v} distortion of the predominantly octahedral (O_h) crystal field. However, they calculated an isotropic g-value on the basis of octahedral symmetry when in fact their model predicts an anisotropic g-tensor. Soulie and Edelstein (1980) have adopted a different point of view by noting the large difference in distances between the two bridging chlorines (U–Cl ~2.68 Å) and the four nonbridging chlorines (U–Cl ~2.43 Å) in the crystal structure. They used the Newman superposition model (Newman, 1971) and fitted the optical and magnetic data. Their best fit gave $g_x = 0.226$ and $g_y \approx g_z \approx 1.186$, as observed. This g_x-value could not be experimentally observed because

of the large magnetic field necessary to do so. However the derived spin–orbit coupling constant of 1196 cm^{-1} is much smaller than that observed in any U^{5+} compound and the calculated $\mu_{eff} \sim 0.85\mu_B$ is lower than the measured value of $1.08\mu_B$.

In the eight-fold cubic coordination of Na_3UF_8, Lewis *et al.* (1973) measured a *g*-value of 1.2 at 7 K. The magnetic susceptibilities of M_3UF_8 (M = Na, Cs, Rb, and NH_4) have been measured from 8 to 300 K (Rigny *et al.*, 1971b). The experimental data were fitted very satisfactorily with a model that assumed a trigonal (D_{3d}) distortion to the eight-fold cubic coordination of the fluorine atoms.

An interesting EPR study of six organouranium(v) complexes (five organouranium amides and one organouranium alkoxide) in dilute frozen solutions at 15 K has been published (Gourier *et al.*, 1997). From an interpretation of the anisotropic *g*-values obtained from the EPR spectra, a picture of the bonding was established for these compounds. The major assumption made was that all ligands, with the exception of the alkoxide ligands, were bound only weakly with the 5f orbitals of the U(v) ion so that only the ground $J = 5/2$ crystal field state has to be considered. With this assumption the experimental *g*-values of the organouranium(v) amide complexes could be quantitatively fit. This model did not work with the organouranium(v) alkoxide compound. This was attributed to a strong U(v) 5f-OR (where R is the alkyl group on the alkoxide) interaction so that the above weak field approximation is not valid.

The magnetic uranium bis-cycloheptatrienyl sandwich compound $[K(C_{12}H_{24}O_6)][U(\eta^7\text{-}C_7H_7)_2]$ has been synthesized (Arliguie *et al.*, 1995). The ionic configuration of the U ion should be $5f^3$ since the formal charge on each of the cycloheptatrienyl rings is -3. However, theoretical calculations by Li and Bursten (1997) have shown that the U ion has a localized $5f^1$ configuration. Thus this molecule can be considered as the $5f^1$ analog of uranocene because the molecular orbitals of the C_7H_7 rings have the same group theoretical symmetries as the cyclooctatetraenyl rings of uranocene. The EPR spectrum of a frozen solution of this compound in methyl-tetrahydrofuran (THF) was measured below 15 K and the ENDOR spectrum was measured at selected fields at 4 K (Gourier *et al.*, 1998). From an analysis of the measured *g*-tensor they concluded that the strong participation of the $5f_\delta$ orbitals in bonding and spin–orbit effects were responsible for the f-orbital composition of the singly occupied molecular orbital. The proton ENDOR measurements allowed a lower limit of $\rho_\pi \geq 4 \times 10^{-2}$ to be set for the positive spin density on the $2p\pi$ carbon orbitals of the cycloheptatrienyl ligands in this compound.

Two bimetallic, pentavalent uranium derivatives $[(MeC_5H_4)_3U]_2[\mu\text{-}1,4\text{-}N_2C_6H_4]$ and $[(MeC_5H_4)_3U]_2[\mu\text{-}1,3\text{-}N_2C_6H_4]$ have been synthesized and magnetic measurements have been performed from room temperature to 5 K (Rosen *et al.*, 1990). In each of these dimers, the two U atoms are coupled to the imido N atoms on the substituted benzene rings. The U-dimer coupled by the $[\mu\text{-}1,4\text{-}N_2C_6H_4]$ moiety can form a conjugated ring while the other U-compound

Table 20.5 *Magnetic data for some U(v) compounds. The values given below are for the range of temperatures where the Curie–Weiss formula approximately holds. The references should be checked for details.*

Compound	*T range* (K)	θ (K)	μ_{eff}[a] (μ_B)	*References and notes*
$[(Me_3Si)_2N]_3UN(p\text{-}C_6H_4CH_3)$	5–40 140–240	–1.3 –98	1.49 2.26	Stewart and Andersen (1998)
$[(Me_3Si)_2N]_3UNSiMe_3$	5–40 140–280	–3.6 –54	1.61 2.04	Stewart and Andersen (1998)
$(C_5H_5)_3UNSiMe_3$	5–40 140–280	–0.7 –82	1.19 1.83	Rosen *et al.* (1990)
$(MeC_5H_4)_3UNPh$	5–40 140–280	1.03 –110	1.25 1.96	Rosen *et al.* (1990)
$[(MeC_5H_4)_3U]_2[\mu\text{-}1,3\text{-}N_2C_6H_4]$	5–40 140–280	–3.95 –134	1.30 2.12	Rosen *et al.* (1990)
$[(MeC_5H_4)_3U]_2[\mu\text{-}1,4\text{-}N_2C_6H_4]$	5–40 140–280	 –147	 2.08	Rosen *et al.* (1990). This compound becomes antiferromagnetic at ~20 K. See discussion in text

[a] All magnetic data are given per U atom. To obtain the value per formula unit for dimeric compounds multiply by the sqrt(2).

cannot. From room temperature down to ~40 K the magnetic susceptibility measurements of these two compounds were similar. Below ~40 K an antiferromagnetic coupling was observed for the $[2\mu\text{-}1,4\text{-}N_2C_6H_4]$ coupled dimer but no such coupling was observed from the $[\mu\text{-}1,3\text{-}N_2C_6H_4]$ coupled dimer. A value of the exchange constant J, of ~–19 cm^{-1}, was obtained for the magnitude of the exchange interaction by a fit of the observed magnetism to that calculated for an isolated one-dimensional dimer as a model for the $[\mu\text{-}1,4\text{-}N_2C_6H_4]$ coupled dimer. Table 20.5 lists the magnetic properties of some U(v) imide compounds.

20.4 $5f^2\ ^3H_4$; U^{4+}, Np^{5+}, Pu^{6+}

U(IV) compounds have been widely studied. The total crystal-field splitting for the $^3H_4$ ground term of the $5f^2$ configuration is usually of the same order as or greater than 200 cm^{-1} (kT at room temperature). Thus only the ground crystal field state or perhaps the two or three lowest-lying states will provide first-order contributions to the observed magnetic susceptibility. Measurements over

as wide a temperature range as possible are clearly desirable. For most U^{4+} compounds, few optical data are available so magnetic data are usually interpreted by considering only the ground $^3H_4$ term, determining the crystal-field splittings for a particular point symmetry group (usually from crystallographic data), choosing a ground state either empirically or by calculation (e.g. point-charge or angular-overlap model), and then calculating the susceptibility. A $J = 4$ state in a point group symmetry lower than tetragonal will split into nine singlet states. In higher symmetries, there will be some singlet states and some doubly and/or triply degenerate states. If a singlet state lies lowest there will be a range of temperatures for which the compound will exhibit only TIP. Some examples from the voluminous literature follow.

One of the few cases for which anisotropic magnetic susceptibility measurements of a single crystal have been reported is UCl_4 (Gamp *et al.*, 1983). In this compound, the anisotropy of the susceptibility is very large ($\chi_\perp > \chi_\parallel$) which makes powder measurements difficult because the crystallites tend to reorient in a static homogeneous magnetic field with the axis of greatest susceptibility parallel to the field. This effect is stronger at low temperatures and depends on the magnitude of the applied field. Gamp *et al.* (1983) found it impossible to obtain reliable powder susceptibility data for UCl_4 at temperatures below 20 K, even with a field as small as 0.05 T. The powder reoriented slowly and the measured susceptibility data increased with time until it reached the value of $\chi_\perp$ measured in the single crystal. This is illustrated in Fig. 20.5. Using the available optical data, Gamp *et al.* (1983) obtained a reasonable fit between the calculated single crystal susceptibilities and the experimental values. The fit could easily have been improved with only minor changes in the crystal field parameter set or the introduction of orbital reduction factors.

The UCl_4 crystal field scheme was examined directly by neutron inelastic scattering by Delamoye *et al.* (1986). The first excited state ($\Gamma_4 \rightarrow \Gamma_5$) was found at 92(1) cm^{-1}, which is in disagreement with the 109 cm^{-1} deduced from susceptibility (Gamp *et al.*, 1983). The neutron study also observed the next higher level (Γ_5') at 1125(3) cm^{-1}. This last level is in good agreement with the predictions of the susceptibility. Here is an example where the susceptibility predicts a value of the crystal field energy splitting too large compared to that measured by neutrons. As in PuO_2 (see below), one could invoke the exchange interaction (Colarieti-Tosti *et al.*, 2002), but there appears a more direct explanation in terms of coupling between the magnetic and lattice modes (phonons). This is illustrated by the most unusual behavior of the temperature dependence of the $\Gamma_4 \rightarrow \Gamma_5$ excitation as shown in Fig. 20.6. From simple Boltzmann statistics, the peak should decrease by only 20% of its strength between 10 and 50 K. Instead it has lost 70% of its intensity, broadened considerably, and shifted to lower energy. At 160 K (where the peak should still be ~40% of its 10 K value), it has lost about 90% of its intensity and shifted to ~75 cm^{-1}, a decrease in frequency of almost 20%. The only explanation for these effects is that there is strong coupling to the lattice vibrations (phonons). It is not

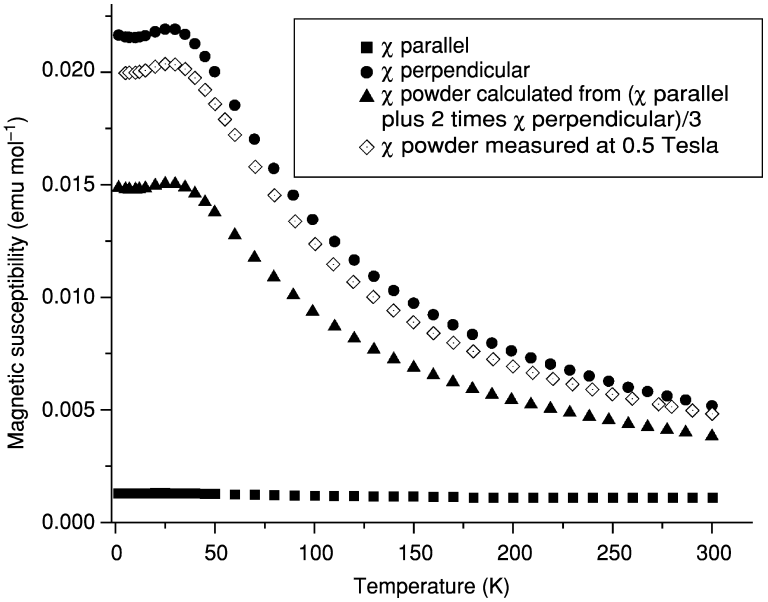

Fig. 20.5 *The values of $\chi_{\|}$ and $\chi_{\perp}$ obtained from measurements on a single crystal of UCl_4 and the calculated average magnetic susceptibility of polycrystalline UCl_4 derived from these measurements. The calculated average susceptibility is compared with susceptibility measurements on a polycrystalline sample of UCl_4 at* 0.5 T. *For the polycrystalline sample in a magnetic field, a strong force is applied along the strong magnetic axis of the crystallites and tends to reorient the crystallites. Thus the measured value of a powdered sample has a susceptibility greater than that calculated from the values of $\chi_{\|}$ and $\chi_{\perp}$ obtained from the single crystal measurements. See Gamp* et al. (1983) *for details.*

surprising, therefore, that simple predictions of the crystal-field splittings from the susceptibility should not agree with the neutron measurements, as interactions with the phonons are not considered. Efforts to include configuration interaction to explain the discrepancy between simple models and the experiments may also have to be taken into account (Zolnierek *et al.*, 1984), but before these large interactions with the lattice modes are understood, such an effort would appear premature.

Another interesting experiment was performed on UCl_4 to look for covalency effects between the U and Cl atoms (Lander *et al.*, 1985). In these experiments a single crystal is placed in a high magnetic field (4.6 T in this case) and then from the scattering of polarized neutrons the magnetization in the unit cell is deduced. If, for example, there would be strong mixing of the U 5f and Cl p-states then one might expect to observe a reduced spin density at the Cl site. Naively, it would be expected that covalency is small in compounds such as UCl_4, and such mixing of the 5f states unlikely. This indeed was the case, and no spin density was found at the Cl site. However, a small spin density midway between the

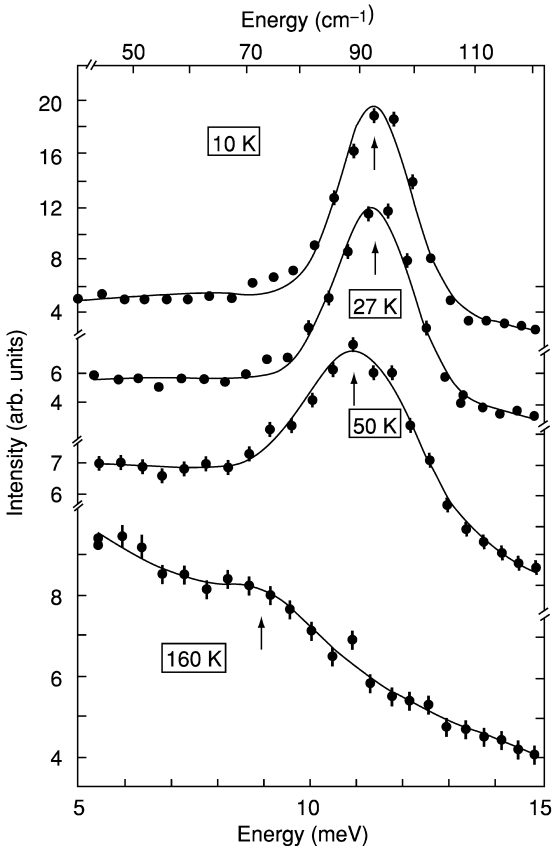

Fig. 20.6 *The temperature dependence of the intensities of the neutron inelastic scattering of the* $\Gamma_4 \rightarrow \Gamma_5$ *excitation in* UCl_4. *The shift in energy and the loss of intensity provide evidence for strong electronic–phonon coupling. Reprinted from Delamoye* et al. (1986). *Copyright* 1986 *with permission from Elsevier.*

U and Cl ions was modeled as an electron transfer from the 5f to the 6d antibonding orbital, and then a covalent bond formed between the U 6d and Cl p-states. Given the interesting possibilities for covalency in 5f compounds, it is perhaps surprising that experiments such as these have not been more common in the actinides. The difficulty is that single crystals are required (and they must be at least 10 mm^3) and their low-temperature properties must be well-known. For example, an experiment was reported on UCp_3Cl, where the covalency effects would be expected to be much larger than in the tetrachloride. Unfortunately, although good crystals were available, on cooling to low temperature many phase transitions occurred (Raison *et al.*, 1994a,b). Such complexities made it impossible to examine the spin densities and learn the details of the covalency. New efforts along these lines would seem worthwhile, especially

as neutron intensities have increased (which means that smaller crystals can be used), available magnetic fields have increased (now up to 10 T and in special cases to 15 T), and local-spin-density-approximation methods can be used to calculate the expected covalency effects.

Blaise *et al.* (1986) have measured the temperature-dependent magnetic susceptibility of a single crystal of tetrakis(1,1,1-trifluoro-4-phenylbutane-2,4-dionato) U(IV). The data were fit with a crystal field model based on distorted cubic symmetry. Optical and magnetic studies on $U(NCS)_8(NEt_4)_4$ ($Et = C_2H_5$) have been published by several groups (Folcher *et al.*, 1976; Soulie and Goodman, 1976, 1979; Carnall *et al.*, 1980; Kanellakopulos *et al.*, 1980c). In this compound the uranium ion is at a site of cubic symmetry (in cubic symmetry no magnetic anisotropy is possible) in the first coordination sphere surrounded by eight nitrogen atoms from the thiocyanate groups. By fitting the measured magnetic susceptibility in the temperature range 4.2–290 K, Soulie and Goodman (1976, 1979) evaluated the appropriate free-ion and crystal field parameters. They found good agreement above 30 K with the measured susceptibility but with significant deviations below this temperature. These deviations were attributed to a slight D_{4h} distortion of the cubic symmetry (confirmed by Raman spectra), which was not taken into account in their calculations. Subsequently Kanellakopulos and coworkers (Carnall *et al.*, 1980; Kanellakopulos *et al.*, 1980c) determined another set of empirical parameters using cubic crystal field parameters obtained from the assignment of the optical spectrum. They then took into account the lower symmetry by using perturbation theory to split the ground triplet state in cubic symmetry into a singlet state and a higher-lying doublet state. The use of this model and the introduction of an orbital reduction factor resulted in satisfactory agreement between the calculated and experimental susceptibility data.

The optical spectra of $U(BD_4)_4$ diluted in $Zr(BD_4)_4$ were measured by Bernstein and Keiderling (1973) and reinterpreted by Rajnak *et al.* (1984b). The U^{4+} ion in the $U(BD_4)_4$ molecule in this host crystal has tetrahedral symmetry (T_d) but the pure compound is polymeric with a lower site symmetry at the metal ion. Shinomoto *et al.* (1983) synthesized the $U(BH_3CH_3)_4$ compound which is monomeric and has the same (T_d) symmetry found for $U(BD_4)_4$ diluted in $Zr(BD_4)_4$. The magnetic susceptibility of $U(BH_3CH_3)_4$ has been measured from 2 to 330 K. Using the eigenvectors obtained from the reanalysis of the Keiderling data, the magnetic data could be fit. However in order to get the best fit, Rajnak *et al.* (1984b) empirically adjusted the energy splitting between the ground E-state and the first excited T_1 state (T_d) and included an orbital reduction factor of $k = 0.85$. In addition to the magnetic susceptibility, the temperature dependence of the solution shifts of the ^1H, ^{11}B, and ^{13}C NMR have been obtained for the $M(BH_3CH_3)_4$ (M = Pa, Th, U, Np) (Gamp *et al.*, 1987; Kot and Edelstein, 1995). Because of the high symmetry at the paramagnetic actinide metal ion, there is no contribution due to the metal ion dipolar term. Thus the measured NMR shifts should arise from the unpaired spin

density transferred from the metal ion to the ligand orbitals. The traditional equation used to determine the unpaired spin density is:

$$\frac{\Delta H}{H_0} = \frac{\beta}{3kT}\langle S_z\rangle \frac{A}{\gamma(h/2\pi)} \tag{20.15}$$

where $\Delta H/H_0$ is the NMR shift, β is the Bohr magneton, k is the Boltzmann constant, A is the hyperfine constant in energy units, γ is the nuclear gyromagnetic ratio, and h is Planck's constant. $\langle S_z\rangle$ is the thermal average of the spin operator and can be calculated from the eigenvectors obtained from the optical analyses. The usual assumptions made in these types of analyses is that the above equation is valid for all crystal field states using the same value of A, and that each of the f-orbitals is equally effective in transferring spin into ligand orbitals. Difficulties were encountered in analyzing the NMR shifts in the actinide methylborohydrides. McGarvey (1998) has shown that the data can be explained if it is assumed that each of the f-orbitals contributes a different amount of spin into the ligand orbitals.

The temperature dependence of the magnetic susceptibility of three U^{4+} sulfates, $U(SO_4)_2 \cdot 4H_2O$, $U_6O_4(OH)_4(SO_4)_6$, and $U(OH)_2SO_4$, in the temperature range 4.2–300 K has been reported by Mulak (1978). These three compounds have a similar antiprismatic coordination about the U^{4+} ion by oxygen anions with almost the same U–O distances. Using a simplified model of the U^{4+} ion with a $^3H_4$ ground term, $J = 4$ as a good quantum number in a D_{4d} crystal field, and only the energy splittings between the two lowest crystal field states as empirical parameters, the temperature dependence of the magnetic susceptibility was fitted. A further low-symmetry distortion has to be introduced (which split the energy levels that were doubly degenerate in D_{4d} symmetry) in order to obtain satisfactory agreement. Despite the very similar coordination environment about the U^{4+} ion in the three compounds, there are significant differences in the low-temperature magnetic behavior. In particular, the magnetic susceptibility for $U(OH)_2SO_4$ from 4.2 to 21 K is approximately constant while above 21 K the susceptibility decreases with a temperature dependence typical of a paramagnetic compound with a degenerate ground state. This low-temperature behavior was attributed to a crystallographic transition induced by the cooperative Jahn–Teller effect. Hinatsu *et al.* (1981) reported the temperature dependence from 1.8 to 300 K of a crystalline uranium(IV) sulfate that showed a broad maximum in the susceptibility at 21.5 K. They assumed a one-dimensional chain structure with U atoms linked by hydroxyl groups (or possibly oxygen atoms) and fitted their data to an exchange interaction between uranium atoms along this one-dimensional chain.

The synthesis of the organometallic 'sandwich' compound uranocene, $U(C_8H_8)_2$, by Müller-Westerhoff and Streitwieser (1968) led to a renaissance in the organometallic chemistry of the actinide series (Seyferth, 2004). Magnetic susceptibility measurements have played an important role in the discussions

of the electronic structure of these types of compounds. Karraker *et al.* (1970) initially reported the temperature-dependent susceptibility of $U(C_8H_8)_2$ and interpreted the data on the basis of a crystal field of C_{8h} symmetry acting on the $^3H_4$ ground term. The data were fitted with a $J_z = \pm 4$ ground state and the inclusion of an orbital reduction factor to account for covalency. This model also fitted the experimental results for $Np(C_8H_8)_2$ and $Pu(C_8H_8)_2$. Hayes and Edelstein (1972) then proceeded to calculate the necessary crystal field parameters using molecular orbital theory and the Wolfsberg–Helmholz approximation. From the calculated crystal field parameters and published free-ion parameters they found the ground crystal field state to be the $J_z = \pm 3$ level. More careful measurements by Karraker (1973) have shown that the susceptibility of $U(C_8H_8)_2$ at low temperature became temperature independent and was attributed by Hayes and Edelstein as being due to a possible low-temperature crystal structure phase transition causing the U^{4+} ion to be at a symmetry site lower than C_{8h}. This model was disputed by Amberger *et al.* (1975). They recalculated the crystal field parameters for uranocene in three ways: using the purely electrostatic approach, the angular overlap model, and a molecular orbital model. Assuming rigorous D_{8h} symmetry, they found that a crystal-field splitting with a singlet ground state ($J_z = 0$) and an excited doublet state at 17 cm^{-1} ($J_z = \pm 1$) gave the best agreement with their molecular orbital calculation and the experimental data. Subsequently, Edelstein *et al.* (1976) showed that some uranocene-type molecules with alkyl or phenyl groups attached to the cyclooctatetraene rings showed the temperature-dependent behavior expected for a degenerate ground state down to 4.2 K. This behavior is inconsistent with the Amberger *et al.* model. Warren (1977) has discussed the magnetic properties of uranocene-type compounds in his extensive review on ligand field theory of f-orbital sandwich complexes. Later experimental and theoretical papers have utilized the magnetic data as tests of the validity of their data and/or calculations (Dallinger *et al.*, 1978; Boerrigter *et al.*, 1988; Chang and Pitzer, 1989).

Another class of organometallic U(IV) compounds that have been thoroughly studied is tetrakis(cyclopentadienyl)uranium(IV), UCp_4, and its tris(cyclopentadienyl) derivatives, Cp_3UR, where R = BH_4, BF_4, OR, F, Cl, Br, I, etc (Kanellakopulos, 1979). These compounds have been divided into two categories: those showing a small dipole moment and a small range of temperature-independent susceptibilities; and a second category exhibiting larger dipole moments and a more extended range of temperature-independent susceptibilities. These differences have been attributed to an increasing trigonal distortion in the second category of compounds. Amberger *et al.* (1976) have used three different semiempirical calculations to estimate the two crystal field parameters needed for the assumed T_d symmetry of UCp_4. The temperature-dependent magnetic susceptibility of UCp_4 was then fitted assuming a weak crystal field of lower symmetry that split the tetrahedral energy levels. The tetrahedral wave functions were used for the calculations and the energy differences of four levels

plus one scaling parameter were varied. Satisfactory agreement with the experimental data was obtained. Amberger (1976a,b) also analyzed optical spectra of UCp_4 and Cp_3UCl assuming T_d symmetry. He further analyzed the fine structure of the spectrum and determined the crystal-field splitting of the ground $^3H_4$ term. Using tetrahedral wave functions and the crystal-field splitting of the ground term he was able to satisfactorily fit the observed susceptibility using only one scaling parameter. Magnetic data for a number of Cp_3UR compounds have been given by Aderhold *et al.* (1978).

A number of other structurally characterized U(IV) compounds were synthesized and magnetic measurements are reported. Some results are listed in Table 20.6. Most of these compounds are monomeric, but a number of dimers and even some higher oligomers have been found. Compounds with amido, amidoamine, alkoxide, and other ligands were characterized and are given in Table 20.6.

In general for U(IV) compounds Curie–Weiss behavior is found at higher temperatures with the susceptibility tending toward temperature-independent behavior at the lowest temperatures. The U^{4+} ion is a non-Kramers' ion with two 5f electrons and will usually have an orbital singlet ground state at low temperatures (this depends on the point symmetry at the U^{4+} ion and will generally be true for lower-symmetry groups) which is the reason for the temperature-independent behavior. For dimeric U^{4+} compounds and higher oligomers, if the U–U distances are short (less than 3.6 Å) or if the bridging ligand(s) facilitate electron exchange, deviations from this type of behavior suggest magnetic interactions between the two U centers.

Le Borgne *et al.* (2002) reported the syntheses, crystal structures, and magnetic properties of heteronuclear trimetallic compounds of the type $[\{ML(py)\}_2U]$ (M = Co, Ni, Zn) and $[\{CuL(py)\}M'\{CuL\}]$ (M′ = U, Th, Zr) where L = *N*,*N*′-bis(3-hydroxysalicylidene)-2,2-dimethyl-1,3-propanediamine and py is pyridine. The crystal structures show that the two ML fragments are orthogonal and linked to the central U ion by two pairs of oxygen atoms from each of the Schiff base ligands. In each of the compounds the three metal ions are linear and the eight oxygen atoms exhibit similar dodecahedral geometry around the U ion. The magnetic susceptibilities of the Co_2U, Ni_2U, and Cu_2U compounds were measured and compared with that of the appropriate Zn_2U derivative, where the paramagnetic 3d ion was replaced by the diamagnetic Zn^{2+} ion. By subtracting the magnetic data of the U–3d diamagnetic ion complexes from similar data for the U–paramagnetic 3d ion complexes (in the temperature range from 300 to 2 K), a weak antiferromagnetic coupling was observed between the Ni^{2+} and the U^{4+} ions, and a ferromagnetic interaction was found between the Cu^{2+} and U^{4+} ions. In a later paper (Salmon *et al.*, 2003), this same group synthesized and magnetically and structurally characterized $[ML^2(py)U(acac)_2]$ and $[(ML^2)_2U]$, where M = Cu and Zn and L^2 = *N*, *N*′-bis(3-hydroxysalicylidene)-2-dimethyl-1,3-propanediamine, and acac is acetylacetonate ($C_5H_7O_2$). Again the Cu, U compounds and the Cu, Zn analogs

Table 20.6 *Magnetic data for some U(IV) and neptunyl(V) compounds. The values given below are for the range of temperatures where the Curie–Weiss formula approximately holds. At lower temperatures more complex magnetic behavior is observed. The references should be checked for details.*

Compound	*T range* (K)	θ (K)	μ_{eff}* (μ_B)	*References and notes*
Cp_3UOH	110–300	–125	2.45 ± 0.01	a
$[Cp_3U]_2O$	140–300	–108	2.17 ± 0.01	a
Cp_3USH	110–300	–83	2.65 ± 0.01	a
$[Cp_3U]_2S$	120–300	–62.5	2.64 ± 0.01	a
$Cp^+_2UCl_2$	100–300	–7.6	3.32	b
$Cp^+_2UF_2$	100–300	–137	3.11	b
$FU[N(Me_3Si)_2]_3$	5–280	–7	2.91	c
$MeU[(Me_3Si)_2N]_3$	25–100	–14	2.99	c
	120–280	–32	3.18	
$Te\{U[N(Me_3Si)_2]_3\}_2$	5–140	–19	3.10	c
	140–280	–40	3.28	
$\{U[N(Me_3Si)_2]_2\}_2[\mu-N(p\text{-tolyl})]_2$	5–40		4.37	c
	160–280		3.34	
$MeU[OC(CMe_3)_3]_3$	80–280	–54	3.15	c
$U[OC(CMe_3)_2H]_4$	5–120	–17	2.59	c
	140–280	–33	2.71	
$U[OSi(CMe_3)_3]_4$	5–90	–11	2.69	c
	100–200	–22	2.82	
$[(MeC_5H_4)_3U]_2[\mu\text{-}CS_2]$	120–300	–12.5	3.01	d
$[(MeC_5H_4)_3U]_2[\mu\text{-S}]$	100–300	–84.5	2.93	d
$[(MeC_5H_4)_3U]_2[\mu\text{-Se}]$	110–300	–72.2	2.85	d
$[(MeC_5H_4)_3U]_2[\mu\text{-Te}]$	120–300	–11.8	3.02	d
$[(MeC_5H_4)_3U]_2[\mu\text{-PhNCO}]$	110–300	–89.5	2.87	d
$U[N(CH_2CH_3)_2]_4$	20–100	–4.8	2.74	e
$U[N(CH_2CH_2CH_3)_2]_4$	30–102	7.2	2.69	e
$U[N(CH_2CH_2CH_2CH_3)_2]_4$	27–84	2.2	2.44	e
$U[N(C_6H_5)_2]_4$	40–90	24.8	2.84	e
$[U(CH_3NCH_2CH_2NCH_3)_2]_3$	4.6–100	–30.5	2.5	f
$(H_3N(CH_2)_3NH_3)U_2F_{10}\cdot 2H_2O$	20–300	–24.7 ± 1.3	4.00	g
$(H_3N(CH_2)_4NH_3)U_2F_{10}\cdot 3H_2O$	20–300	–30.9 ± 0.4	3.47	g
$(H_3N(CH_2)_6NH_3)U_2F_{10}\cdot 2H_2O$	20–300	–41.7 ± 1.1	3.94	g
$(C_5H_{14}N_2)_2U_2F_{12}\cdot 2H_2O$	150–300	–1.3	3.09	h
$(C_2H_{10}N_2)U_2F_{10}$	150–300	+21	3.24	h
$[(C_5N_2H_{14})_2(U_2F_{12})\cdot 2H_2O]$	40–350	14.7	3.59	i
$[(C_5N_2H_{14})_2(H_3O)(U_2F_{11})]$	40–350	78.8	3.72	i
$[(C_4N_2H_{12})_2(U_2F_{12})\cdot H_2O]$	40–350	15.7	3.35	i
$[(C_6N_2H_{14})_2(U_3O_4F_{12})]$	40–350	153.6	4.01	j
$(NpO_2)_2C_2O_4\cdot 4H_2O$	15–40	12.5	2.71	k
$[NpO_2(O_2CH)(H_2O]$	50–300	12.7	2.81	l
$(NpO_2)_2(O_2C)_2C_6H_4\cdot 6H_2O$	10–70	7.75	2.54	m
	150–300	29.8	2.29	

* All magnetic data are given per U atom. To obtain the value per formula unit for dimeric compounds multiply by the sqrt(2).

[a] Spirlet *et al.* (1996). $Cp = C_5H_5$.

were shown to be very similar structurally so that the magnetism of the appropriate Zn, U compound could be subtracted from the magnetism of the Cu, U compound to obtain the influence of the Cu^{2+} ion on the exchange interactions between the Cu and U ions. For the dimeric compound the difference in χT vs T was approximately constant from 300 to 100 K with a value of 040 ± 0.05 cm^3 mol^{-1} K, similar to that of an isolated Cu^{2+} ion. Below 100 K the difference in magnetic behavior is indicative of antiferromagnetic exchange between the U^{4+} – Cu^{2+} ions. Similar experiments were performed with the trimetallic $[(ML^2)_2U]$ complexes and it was found that the low-temperature magnetic behavior of the $[(CuL^2)_2U]$ compound was also antiferromagnetic. The low-temperature magnetism in the latter compound is different from ferromagnetic interaction found in the somewhat structurally similar [{CuL(py)}U{CuL}] described earlier.

A similar type of experiment has been reported for an oxalate-bridged U(IV)–Mn(II) compound, $K_2MnU(C_2O_4)_4 \cdot 9H_2O$ (Mortl *et al.*, 2000). In this compound the U(IV) ion is linked to four Mn(II) ions by each of the oxalate ligands and each of the Mn(II) ions are also linked by the oxalate ligands to four U(IV) ions. The magnetic susceptibility of this compound has been measured from 2 to 300 K. For this compound, the experimental magnetic measurements have been interpreted as the sum of the individual U(IV) and Mn(II) contributions. No indication of magnetic coupling has been found between the U(IV) ion and the Mn(II) ion down to 2 K.

A number of complex U^{4+} fluoride compounds have been synthesized and structurally characterized. As part of the determination of their physical properties, the temperature-dependent magnetic susceptibilities have been measured and analyzed (over the appropriate temperature range using the Curie–Weiss equation). Table 20.6 lists magnetic data for some structurally diverse U(IV) complex fluoride compounds.

---

[b] Lukens *et al.* (1999). $Cp^{\ddagger} = 1,3\text{-}(Me_3C)_2C_5H_3$.
[c] Stewart (1988). If no θ values are given, the data are not very linear ($1/\chi$ vs T) in the given range and the μ_{eff} values are approximate.
[d] Brennan *et al.* (1986).
[e] Reynolds and Edelstein (1977).
[f] Reynolds *et al.* (1977). Three uranium atoms form a linear chain with the central U atom linked to the two terminal U atoms by a triple nitrogen bridge.
[g] Francis *et al.* (1998).
[h] Almond *et al.* (2000).
[i] Allen *et al.* (2000). The data ($1/\chi$ vs T) are not very linear in the 40–350 K range, the μ_{eff} values are approximate.
[j] Allen *et al.* (2000). This compound is formulated as a ($U_2^{VI}U^{IV}O_4F_{12}$) complex, the μ_{eff} given is for the formula unit or per the U(IV) atom, and is an approximate value due to the nonlinearity of the $1/\chi$ vs T data.
[k] Jones and Stone (1972).
[l] Nakamoto *et al.* (1999).
[m] Nakamoto *et al.* (2001).

There have been a few measurements performed on NpO_2^+ compounds. The compounds that are formulated as having dimeric neptunyl $(NpO_2^+)_2$ units exhibit complex magnetic behavior at low temperatures. Metamagnetism, that is the field-induced transformation of a compound from an antiferromagnetic state to a ferromagnetic state, was originally reported by Jones and Stone (1972) for the neptunyl(v) oxalate complex, $(NpO_2)_2C_2O_4 \cdot 4H_2O$. This compound exhibited Curie–Weiss behavior above 15 K (see Table 20.6). The susceptibility displayed a peak characteristic of an antiferromagnetic transition with $T_N = 11.6 \pm 0.1$ K. However the susceptibility maximum shifted to lower temperatures as the external magnetic field was increased, and above 0.075 T the susceptibility peak disappeared and ferromagnetic saturation was observed. From these observations, it was concluded that this compound was metamagnetic. Recent magnetic studies have been reported for neptunyl(v) formate and phthalate compounds $[NpO_2(O_2CH)(H_2O)]$ and $(NpO_2)_2(O_2C)_2C_6H_4 \cdot 6H_2O$ (Nakamoto *et al.*, 1999, 2001). The formate complex, which forms infinite two-dimensional sheets linked by NpO_2^+ bonding, follows the Curie–Weiss law from 50 K to room temperature (see Table 20.6). Below 50 K, this neptunyl compound exhibits complex magnetic behavior that is attributed to ferromagnetic ordering with $T_c = 12$ K. The authors note the situation in the neptunyl(v) formate complex is similar to that found earlier in the neptunyl(v) oxalate complex and attributed in the earlier work to metamagnetism. The neptunyl phthalate magnetic data can be fit in two regions with the Curie–Weiss law as shown in Table 20.6. Below 4.5 K, complex magnetic ordering is found that is attributed to the existence of two kinds of Np sublattices, one is ferromagnetic and the other is antiferromagnetic.

20.5 $5f^3\ ^4I_{9/2}$; U^{3+}, Np^{4+}, Pu^{5+}

UH_3 has a ferromagnetic transition at approximately 172 K and a saturation magnetic moment in the temperature range 63–196 K of approximately $1\mu_B$ (Gruen, 1955). The magnetic susceptibilities of the uranium(III) halides are listed in Table 20.7 (Berger and Sienko, 1967; Jones *et al.*, 1974). UF_3 followed the Curie–Weiss law down to about 125 K, below which temperature the susceptibility increased more rapidly than expected from the higher-temperature data (Berger and Sienko, 1967). Jones *et al.* (1974) reported the magnetic susceptibilities of U trihalides (Cl, Br, and I). For the most part, the properties could be understood on the basis of crystal field calculations. Of special interest was the report of antiferromagnetic magnetic ordering (as judged by a maximum in the susceptibility) at 22.0, 15.0, and 3.4 K in the U-trihalides Cl, Br, and I. Extensive neutron studies have also been performed on these compounds (Murasik and Furrer, 1980; Murasik *et al.*, 1981, 1985, 1986; Schmid *et al.*, 1990). Neutron diffraction confirmed the hexagonal crystal structure for UCl_3 and UBr_3, but then surprisingly found that the assumed T_N values of Jones *et al.* were not

Table 20.7 *Magnetic data for some M(III) actinide halides, M = U^{3+}, Np^{3+}, and Pu^{3+}.*

Compound	*T range* (K)	θ (K)	μ_{eff} (μ_B)	T_N (K)	χ_{TIP} (10^{-6} emu mol^{-1})	*References*
UF_3	125–293	–110 ± 5	3.67 ± 0.06			[a]
UCl_3	25–117	–89	3.70 ± 0.08	22.0 ± 1.0		[b,c]
UBr_3	25–76	–54	3.57 ± 0.08	15.0 ± 0.5		[b,c]
UI_3	5–14	–9.1	2.67 ± 0.10	3.4 ± 0.2		[b,c]
UI_3	25–200	–34	3.65 ± 0.05			[b]
$NpCl_3$	3.5–50				6400 ± 100	[b]
$NpCl_3$	75–240	–83.5	2.81 ± 0.09			[b]
α-$NpBr_3$	10–30				10 850 ± 320	[b,d]
α-$NpBr_3$	50–125	–86	3.26 ± 0.40			[b]
NpI_3	3–15				17 000 ± 7 000	[b]
NpI_3	25–60	–42	3.17 ± 0.40			[b]
$PuCl_3$	5–100	–7.9	1.11 ± 0.04	4.5 ± 0.5		[b]
$PuBr_3$	2.2–20	–0.55	0.81 ± 0.08			[b]
$PuBr_3$	25–60	–10.5	1.01 ± 0.10			[b]
PuI_3	5–50	+4.15	0.88 ± 0.08	4.75 ± 0.10		[b,e]

[a] Berger and Sienko (1967).
[b] Jones *et al.* (1974).
[c] Further magnetic ordering in these compounds have been observed from neutron scattering experiments (Murasik *et al.*, 1986; Schmid *et al.*, 1990).
[d] Sample is estimated to contain 5% $NpOI_2$ impurity.
[e] Low-temperature phase is ferromagnetic.

correct. The actual ordering temperatures in UCl_3 and UBr_3 are 6.5 and 5.4 K, respectively. The ordered moments are $\sim 2\mu_B$ for both systems. However, at lower temperatures there is a second transition (3.8 K for UCl_3 and 3.0 K for UBr_3) to a more complex magnetic structure. On cooling, the moments are initially parallel to the crystallographic *c*-axis, but then rotate to perpendicular to *c*-axis at low temperature, and with a magnetic moment of only about $0.8\mu_B$. These lower-temperature transitions were not apparently observed by Jones *et al.* (1974). The neutron work also determined the crystal field transitions that range from about 20 to 400 cm^{-1}. From the crystal field level scheme they showed that many of the properties could be understood on the basis of the extreme magnetic anisotropy. There is antiferromagnetic exchange *only* along the chains of U atoms along the *c*-axis. The peak in the susceptibility in this case is actually *not* an indication of the antiferromagnetic order, but rather the competition between the exchange and anisotropic contributions to the susceptibility. All these measurements, both the original magnetic and more recent neutron studies, were performed on polycrystalline samples, which makes the amount of information extracted in the neutron study quite remarkable.

Furthermore, a relatively sharp mode was observed at 32 cm^{-1} in both UCl_3 and UBr_3 at low temperature and was assigned to one-dimensional spin–wave excitations along the *c*-axis.

These studies would be most interesting to continue with single crystals. The whole question of one-dimensional magnetism is now much in fashion; the exchange interactions in actinides are usually stronger than in the lanthanides, thus making the examples more interesting. It is furthermore a salutary lesson in making a simple interpretation of the susceptibility curves.

EPR measurements have been reported for surprisingly few U^{3+} compounds and the data up to 1977 were discussed by Boatner and Abraham (1978). Crosswhite *et al.* (1980), from their analysis of the optical spectrum of U^{3+} diluted in $LaCl_3$, have calculated $g_{\|} = -4.17$, which agrees well with the magnetic resonance value of $|g_{\|}| = 4.153$ (Hutchison *et al.*, 1956). Magnetic susceptibility data for Cs_2NaUCl_6 (Hendricks *et al.*, 1974) (Table 20.2) as a function of temperature have been given. A recent optical study of U^{3+} diluted in Cs_2NaYCl_6 has given the energy levels for this system and shown that a Γ_8 (O_h) state is lowest in energy (Karbowiak *et al.*, 1998) consistent with the magnetic data.

The temperature-dependent magnetic susceptibility of a number of substituted tris-cyclopentadienyl U and Nd compounds and their Lewis base adducts has been measured and are listed in Table 20.8. The EPR spectra of these compounds also have been measured as powders or frozen glasses and compared with the corresponding Nd^{3+} compounds ($4f^3$ configuration) (Lukens, 1995).

Table 20.8 *Magnetic data for some* Cp''_3 *M and* Cp''_3 *M L complexes* (*M = Nd, U*).[a,b]

	μ_{eff}[c] (5 K) (μ_B)	μ_{eff}[d] (200–300 K) (μ_B)	g_1[e]	g_2[e]	g_3[e]	μ_{eff}[f] (5 K) (μ_B)
Cp''_3Nd	1.65	3.70	2.48 (48)	2.08 (1.29)	0.18 (0.69)	1.62
$Cp''_3Nd \cdot (C_6H_{11}NC)$	1.75	3.60	2.51 (21)	1.76 (29)	0.88 (7)	1.60
$Cp''_3Nd \cdot (^t BuNC)$	1.69	3.91	2.25 (19)	2.08 (11)	0.86 (9)	1.59
Cp''_3U	2.03	3.32	3.41 (50)	1.65 (2.08)	0.85 (75)	1.94
$Cp''_3U \cdot (C_6H_{11}NC)$	1.76	3.25	2.51 (96)	1.59 (1.17)	0.72 (1.76)	1.53
$Cp''_3U \cdot (^t BuNC)$	1.78	3.14	2.41 (12)	1.75 (9)	0.29 (65)	1.49
$Cp^{\ddagger}_3U$	2.13	3.37	3.60 (16)	2.36 (34)	0.70 (0.98)	2.21

[a] From Lukens (1995).
[b] $Cp'' = 1,3\text{-}(Me_3Si)_2C_5H_3$, $Cp^{\ddagger} = 1,3\text{-}(Me_3C)_2C_5H_3$.
[c] Calculated directly from measured magnetic susceptibility value at 5 K, $\chi = C/T$, $\mu_{eff} = (8C)^{1/2}$.
[d] $\chi = C/(T-\theta)$, $\mu_{eff} = (8C)^{1/2}$, θ values are not given.
[e] Values obtained by fitting EPR spectra obtained from powders at ~5 K. The g_3 component has been obtained for some complexes solely from the least squares fit. In cases where the error is greater than the value, g_3 is considered unreliable.
[f] Calculated from the EPR *g*-values.

Table 20.9 *Magnetic data for some U(III) compounds. The values given below are for the range of temperatures where the Curie–Weiss formula approximately holds. At lower temperatures more complex magnetic behavior is observed. The references should be checked for details.*

Compound	*T range* (K)	θ (K)	μ_{eff}[a] (μ_B)	*References and notes*
$SrUCl_5$	90–300	–127	3.65	Karbowiak and Drozdzynski (1998a)
Ba_2UCl_7	105–300	–95	3.25	Karbowiak and Drozdzynski (1998a)
$CsUCl_4$	60–300	–36	3.16	Karbowiak and Drozdzynski (1998b)
Cs_2LiUCl_6	85–300	–103	3.56	Karbowiak and Drozdzynski (1998b)
RbU_2Cl_7	210–300	–80	3.74	Karbowiak *et al.* (1996)
$[(Me_3Si)_2N]_3U$	35–280	-12 ± 1	3.37 ± 0.02	Stewart and Andersen (1998)
$\{U[N(Me_3Si)_2]_2\}_2$	80–280	–71	3.53	Stewart (1988)
$[\mu-N(H)(2,4,6\text{-}Me_3C_6H_2)]_2$	9–60	–22.5	2.87	

[a] All magnetic data are given per U atom. To obtain the value per formula unit for dimeric compounds multiply by the sqrt(2).

Magnetic susceptibility results for some other U(III) compounds are given in Table 20.9.

Two interesting dimeric molecules were reported by Korobkov *et al.* (2001). One of these two dimeric molecules, $[Li(THF)_4]_2\{U_2[(-CH_2-)_5]_4$-calix[4]tetrapyrrole$\}[\mu\text{-}I]_4$ had two U(III) ions held together by the $[(-CH_2-)_5]_4$-calix[4]tetrapyrrole ligand with a short U–U distance of 3.4560(8) Å. The second compound $[Li(THF)_2]_2(\mu\text{-}Cl)_2\{U_2[(\text{-}CH_2\text{-})_5]_4$-calix[4]tetrapyrrole$\}Cl_2 \cdot THF$, formally a mixed valence U(III)–U(IV) dimer with a similar geometry as the first dimer, also had a short U–U distance of 3.365(6) Å. The magnetic moment of the U(III)–U(III) dimer was $1.99\mu_B$ (per U) at 300 K falling to $0.55\mu_B$ (per U) at 2 K. For the U(III)–U(IV) dimer the magnetic moment at 300 K was $3.04\mu_B$ (per mole) and $1.03\mu_B$ (per mole) at 2 K. The authors suggest that the low moment for the U(III)–U(III) dimer could be due to antiferromagnetic behavior at low temperatures while the U(III)–U(IV) dimer could be explained by the sum of the magnetic moments of two isolated U(III) and U(IV) compounds (no magnetic exchange). Clearly much further work has to be done to determine whether magnetic exchange takes place in these dimers.

$NpCl_4$ (Table 20.7) was reported to have a ferromagnetic transition at 6.7 K (Stone and Jones, 1971). Kanellakopulos *et al.* (1980c) reported the temperature dependence of the magnetic susceptibility data for $NpCl_4$ and $((C_2H_5)_2N)_4Np(NCS)_8$ and presented an analysis of these data. This group (Stollenwerk *et al.*, 1979; Dornberger *et al.*, 1980; Stollenwerk, 1980) also measured and discussed

the optical spectra and magnetic susceptibilities of Cp_4Np ($Cp = C_5H_5$) and Cp_3NpX where X = Cl, Br, and I. Low-temperature magnetic susceptibility data for $NpBr_4$ are given in Table 20.7.

From magnetic susceptibility measurements (Karraker and Stone, 1980) and EPR measurements (Bernstein and Dennis, 1979; Edelstein *et al.*, 1980) of hexachloro complexes of Np^{4+}, the ground state of the $^4I_{9/2}$ term was shown to be Γ_8 (O_h). Limits on the ratios of the fourth- to the sixth-order crystal field parameters have been determined, and these limits are consistent in the isostructural series MCl_6^{2-}, $M = Pa^{4+}, U^{4+}, Np^{4+}$. Depending on the cation involved, the Γ_8 state may be split by 5–10 cm^{-1} due to small deviations from O_h symmetry. The free-ion *g*-value ($\sim$0.6) for Np^{4+} deduced from the data are much reduced from the value of 0.77 obtained from optical data. Warren (1983) has suggested that the rather large value of the orbital reduction factor needed to fit the EPR data could be due to the occurrence of the Ham effect (which would change the value of the ratios of the crystal field parameters needed to fit the data). However EPR data obtained at liquid-helium temperatures for Np $(BH_4)_4$ and $Np(BD_4)_4$ diluted in the corresponding $Zr(BH_4)_4$ and $Zr(BD_4)_4$ hosts show that the doublet Γ_6 state (T_d) of the $^4I_{9/2}$ term is lowest (Rajnak *et al.*, 1984a). Again the free-ion *g*-value (0.515) is much lower than expected. Richardson and Gruber (1972) claimed that they observed the EPR spectrum of Np^{4+} diluted in ThO_2. EPR and optical spectra of Np^{4+} diluted in $ZrSiO_4$ at 4.2 K were obtained by Poirot *et al.* (1988) with measured ground Γ_6 state (D_{2d} symmetry) *g*-values of $|g_{\|}| = 0.8$ (6) and $|g_{\perp}| = 2.59$ (2), consistent with the optical analysis.

$SrNpO_3$ and $BaNpO_3$ show magnetic transitions at 31 and 48 K, respectively (Kanellakopulos *et al.*, 1980b; Bickel and Kanellakopulos, 1993). A sharp increase in magnetization was observed below the transition temperature, which suggests a complicated magnetic structure.

20.6 $5f^4\ ^5I_4$; Np^{3+}, Pu^{4+}

The magnetic susceptibility and magnetization of NpH_x ($x = 2.04$, 2.67, and 3) have been measured in the temperature range 4–700 K (Aldred *et al.*, 1979). The dihydride data could be fitted with a crystal field model based on cubic symmetry (O_h) for the Np^{3+}, $5f^4$ configuration, with a nominal $^5I_4$ ground state split into a ground Γ_3 doublet and a Γ_4 and a Γ_5 triplet at 512 and 549 cm^{-1}, respectively. The Γ_1 singlet is calculated to be at 1851 cm^{-1} above the Γ_5 state. Magnetic data for $Cs_2NaNpCl_6$ (Hendricks *et al.*, 1974) are shown in Table 20.2 and were assigned as due to the magnetic properties of the Γ_5 (O_h) ground state. The magnetic properties of NpX_3 (X = Cl, Br, and I) are given in Table 20.7 (Jones *et al.*, 1974).

Magnetic susceptibilities from 2.5 to 50 K for Pu^{4+} in three hexachloro complexes were reported by Karraker (1971). Surprisingly, one of the compounds,

Cs_2PuCl_6, had a temperature-dependent paramagnetism at low temperatures, which means a non-Kramers doublet is the lowest state. The other two $PuCl_6^{2-}$ complexes had temperature-independent susceptibilities at the lowest temperatures, which arises from a singlet state being the ground state. These data have been interpreted on the basis of a model based on the distorted O_h symmetry of the $PuCl_6^{2-}$ octahedron.

Magnetic susceptibility measurements have been reported for $Pu(C_8H_8)_2$ and $Pu(C_8H_7R)_2$, where R is an alkyl group (Karraker *et al.*, 1970; Karraker, 1973). These compounds were reported to be diamagnetic. However, the susceptibility is expected to exhibit TIP for the $^5I_4$ state in C_{8h} symmetry if the $J_z = 0$ state is lowest.

20.7 $5f^5\ ^6H_{5/2}$; Pu^{3+}, Am^{4+}

The magnetic properties of PuH_x ($2.0 \leq x \leq 3$) have been measured between 4 and 700 K (Aldred *et al.*, 1979). The cubic PuH_2 appears to order antiferromagnetically at 30 K. Cubic Pu compounds with higher hydrogen concentrations order ferromagnetically with higher transition temperatures as x increases. A maximum is reached at $T = 66$ K and $x = 2.7$. Hexagonal PuH_3 becomes ferromagnetic at 101 K. The temperature dependence of the magnetic susceptibility indicates that the ground state configuration is Pu^{3+}, $5f^5$. The magnetic properties of PuX_3 (X = Cl, Br, and I) (Jones *et al.*, 1974) are given in Table 20.7. $PuCl_3$ shows an antiferromagnetic transition at 4.5 K while PuI_3 has a ferromagnetic transition at 4.75 K. For $PuCl_3$, magnetic susceptibility calculations using wave functions obtained from optical data on Pu^{3+} diluted in $LaCl_3$ reproduce the observed susceptibility. Magnetic data for the octahedral complex $Cs_2NaPuCl_6$ (Hendricks *et al.*, 1974) are given in Table 20.2.

EPR measurements of $|g_{\|}| = 0.585$ (2) and $|g_{\perp}| = 0.875$ (1) were reported for $^{239}Pu^{3+}$ diluted in $LaCl_3$ at 4.2 K by Lämmermann and Stapleton (1961). These values agreed well with the results obtained from a subsequent optical analysis of this system (Lämmermann and Conway, 1963). Kot *et al.* (1993b) measured the EPR spectra of Pu^{3+} in $LuPO_4$ at 4.2 K and found $|g_{\|}| = 0.772(2)$ and $|g_{\perp}| = 0.658(2)$. Pu_2O_3 becomes antiferromagnetic at $T_N = 19$ K, as judged by the specific heat (Flotow and Tetenbaum, 1981). Magnetic susceptibility and neutron diffraction measurements ($T = 4$–300 K) also indicate that hexagonal β-Pu_2O_3 becomes antiferromagnetic at $T \sim 19$ K (McCart *et al.*, 1981) with a second transition at 4 K. Neutron diffraction was not initially able to determine the magnetic configurations, but in subsequent neutron work by Wulff and Lander (1988) the configuration with a moment of $0.60\mu_B$/Pu and the moments aligned parallel to the unique c-axis of the hexagonal structure were determined. The ground state moment is consistent with that from the Kramers doublet $|J = 5/2, J_z = \pm 3/2\rangle$ and the valence state is (as expected) trivalent Pu.

Table 20.10 *Measured g-values for $5f^5$ ions at cubic sites in crystals with the fluorite structure. For each type of host or ion, the matrices are listed in order of increasing lattice constant, or decreasing CF. Data taken at ~5 K (Kolbe* et al., 1974).

Matrix	*Ion*	$\|g\|$
CeO_2	Pu^{3+}	1.333 (1)
ThO_2	Pu^{3+}	1.3124 (5)
CaF_2	Pu^{3+}	1.297 (2)
SrF_2	Pu^{3+}	1.250 (2)
BaF_2	Pu^{3+}	1.187 (4)
$SrCl_2$	Pu^{3+}	1.1208 (5)
CeO_2	Am^{4+}	1.3120 (5)
ThO_2	Am^{4+}	1.2862 (5)

EPR measurements on Pu^{3+} and Am^{4+} at liquid-helium temperatures in various cubic hosts have been summarized by Boatner and Abraham (1978). For both Pu^{3+} and Am^{4+} with a nominally $^6H_{5/2}$ ground state, strong intermediate-coupling effects cause the Γ_7 state (O_h) to be the ground crystal field state, rather than the Γ_7 (O_h) state as expected for pure Russell–Saunders coupling (Edelstein *et al.*, 1969). Crystal field mixing between the ground state and the excited *J*-states makes the measured *g*-value a very sensitive indicator of the magnitude of the crystal field (Lam and Chan, 1974). Table 20.10 illustrates the effect of the decreasing crystal field strength on the measured ground state *g*-values. For each type of crystal or ion, the crystal field decreases (the lattice constant of the host matrix increases) as one scans down Table 20.10, and the magnitude of *g* decreases also. In the limit of zero crystal field mixing of excited multiplets, the ground state *g*-value should be $|g| = 0.700$. ENDOR measurements on Pu^{3+} in CaF_2 have shown the interaction with the nearest neighbor fluorine ions is much stronger than found for the 4f series (Kolbe and Edelstein, 1971). The magnetic data for Am^{4+} given above have been utilized in conjunction with optical data for Am^{3+} in ThO_2 to estimate the crystal field parameters for AnO_2 series (Hubert *et al.*, 1993).

The magnetic susceptibility of the high-T_c superconductor-related compound $Pb_2Sr_2AmCu_3O_8$ has been measured from ~4 to 300 K. The data can be fit with an effective moment for the Am^{4+} ion of $0.94\mu_B$ after subtracting off the contribution from the Cu sublattice. This compound shows no superconductivity (Soderholm *et al.*, 1996).

20.8 $5f^6\ ^7F_0$; Am^{3+}, Cm^{4+}

A $^7F_0$ ground term has a singlet ground state that is expected to show TIP. The magnitude of the TIP depends on the energy differences to the excited states. Measurements on some Am^{3+} and Cm^{4+} compounds sometimes show a

Table 20.11 *Magnetic susceptibility of Am metal, and some Am^{3+} and Cm^{4+} compounds. If more than one set of data are given, the results are from different samples.*

Compound	*Temp. range* (K)	*TIP* (10^{-6} emu mole^{-1})	μ_{eff} (μ_B)	*References and comments*
^{241}Am metal	102–848	881 (62)		Cunningham (1962)
^{241}Am metal	~50–300	675		Nellis and Brodsky (1974)
^{241}Am metal	100–300	780 (10), 880 (40)		Kanellakopulos *et al.* (1975)
$^{241}Am^{3+}$ in solution	room temperature	720		Howland and Calvin (1950)
$^{243}Am(C_5H_5)_3$	30–300	715 (14)		Kanellakopulos *et al.* (1978)
$Cs_2Na^{243}AmCl_6$	15–70	5400 (400)		Hendricks *et al.* (1974)
$Cs_2Na^{243}AmCl_6$	40–300	660 (40)		Soderholm *et al.* (1986)
$^{243}Am_2O_3$	5–300	640 (20)		Soderholm *et al.* (1986)
$^{243}AmF_3$	~4.2–280	714	0.63	Nave *et al.* (1983)
$^{248}CmF_4$	~4.2–280	328 (144), 1700 (527), 2800 (224)	3.24 (4), 3.49 (7), 3.04 (3)	Nave *et al.* (1983)
$Ba^{248}CmO_3$	~4.2–300	2130 (213), 988 (20)	1.63 (6), 1.71 (1)	Nave *et al.* (1983)
$^{248}CmO_2$	~4.2–300	1900 (171), 4100 (164), 2464 (1232)	1.63 (4), 1.96 (3), 2.27 (20)	Nave *et al.* (1983)
$^{248}CmO_2$	5–125		3.36 (6)	Morss *et al.* (1989)

temperature dependence that is not understood. In order to analyze these data, a modified Curie law has been utilized and is given in equation (20.8).

The few available data for these ions are given in Table 20.11. Karraker *et al.* measured the magnetic susceptibility of $Cs_2NaAmCl_6$ (Hendricks *et al.*, 1974) and found the susceptibility was temperature independent, as expected for a $J = 0$ ground state, but the magnitude found was much larger than that calculated considering only the second-order Zeeman effect to the optically determined $J = 1$ state at 2720 cm^{-1}. Subsequent measurements on $Cs_2NaAmCl_6$ and Am_2O_3 agreed much better with the calculated value (Soderholm *et al.*, 1986). Am metal was found to exhibit TIP, suggesting a localized $5f^6$ configuration plus conduction electrons (Cunningham, 1962; Nellis and Brodsky, 1974; Kanellakopulos *et al.*, 1975). The susceptibility of $^{248}CmO_2$ should also be temperature-independent but exhibits Curie–Weiss behavior (Nave *et al.*, 1983; Morss *et al.*, 1989). Nave *et al.* (1983) also have measured two other $^{248}Cm^{4+}$ compounds and have found complex magnetic behavior that they have analyzed using equation (20.8). Their measurements were performed on samples of mass ~50–1000 μg and it should be noted that measurements of different samples of nominally the same material were not very reproducible. A recent

calculation of the Cm magnetic moment in CmO_2 gave $3.39\mu_B$/atom. The authors suggested that an itinerant magnetism model based on delocalized electrons might be more appropriate for this system rather than the usual crystal field theory (Milman *et al.*, 2003). See Section 20.14.5 for a more detailed discussion of CmO_2.

20.9 $5f^7\ ^8S_{7/2}$; Am^{2+}, Cm^{3+}, Bk^{4+}

In the limit of pure Russell–Saunders coupling an f^7-configuration has an $^8S_{7/2}$ ground term. A crystal field interaction will not split the orbitally non-degenerate S state. For the $4f^7$ ion, Gd^{3+}, it is indeed found that crystal-field splittings of the ground $J = 7/2$ term are of the order of about 0.2 cm^{-1}. However, the ground term for Cm^{3+} is only 87% $^8S_{7/2}$ because spin–orbit coupling mixes in substantial amounts of the $^6P_{7/2}$, $^6D_{7/2}$, and higher terms that result in crystal-field splittings of about 5–100 cm^{-1}. Early EPR studies have been reviewed by Boatner and Abraham (1978). The first authentic identification of the EPR spectra of the Cm^{3+} ion was by Abraham *et al.* (1963) in single crystals of lanthanum ethylsulfate and lanthanum trichloride. The strongest observed EPR resonance for Cm^{3+} in $LaCl_3$ was assigned as the ground state with $J_z = \pm 1/2$. Later calculations based on optical data conflicted with this assignment (Carnall, 1992). High-resolution laser spectroscopy measurements (Liu *et al.*, 1993) have shown the total ground term $J = 7/2$ splitting is $\sim$2 cm^{-1} and that the $J_z = \pm 1/2$ level is not the ground state but the first excited state, in agreement with the Carnall's assignments. Am^{2+} ions have approximately the same magnetic properties as Cm^{3+}, and it was this fact that was used for the first identification of Am^{2+} as a chemically stable oxidation state (Edelstein *et al.*, 1966). A considerable amount of EPR studies have been performed on the Cm^{3+} and Am^{2+} ions at cubic symmetry sites in single crystals with the fluorite structure MX_2 (M = Ca, Sr, Ba; X = F), $SrCl_2$, ThO_2, and CeO_2. For a $5f^7$ ion in this symmetry, the ground state is an isotropic Γ_6 state and the first excited state is a Γ_8 state. If the splitting between these two states is of the order of magnitude of the magnetic splittings, these states can be mixed by the magnetic field in the EPR experiment and will result in the ground Γ_6 state showing anisotropy as the crystal orientation is changed with respect to the magnetic field. From the magnitude of the anisotropy, the Γ_6–Γ_8 splitting can be deduced. Later optical measurements on Cm^{3+} in ThO_2 confirmed the Γ_6–Γ_8 splitting of 15.5 (3) cm^{-1} found for this system (Thouvenot *et al.*, 1994). The measured ground state *g*-values and splittings are shown in Table 20.12. Detailed EPR measurements have been reported for Cm^{3+} in YPO_4 and $LuPO_4$ (Abraham *et al.*, 1987; Kot *et al.*, 1993a). Interestingly, for the Cm^{3+} diluted into $LuPO_4$ system, EPR measurements at $\sim$300 K were observed for the Cm^{3+} ion. Subsequent high-resolution optical measurements showed the zero-field splittings deduced from the EPR spectra were not accurately determined

Table 20.12 *EPR g-values and zero-field splittings for Cm^{3+} and Am^{2+} ions in cubic sites in fluorite-type crystals. Under O_h symmetry, a $J = 7/2$ state will split into a ground Γ_6 state, a Γ_8 state, and the highest energy Γ_7 state.*

Crystal	*Ion*	ΔE (Γ_6–Γ_8)	g_J[a]	$g(\Gamma_6)$[b]	*References*
$SrCl_2$	Cm^{3+}	5.13 (5)[c]	1.928 (2)	$g_{100} = 4.501$ (2) $g_{111} = 4.473$ (2) $g_{110} = 4.482$ (2)	Kolbe *et al.* (1972)
SrF_2	Cm^{3+}	11.2 (4)	1.9257 (10)	4.493	Kolbe *et al.* (1972)
CaF_2	Cm^{3+}	13.4 (5)	1.926 (1)	4.492 (2)	Edelstein and Easley (1968)
ThO_2	Cm^{3+}	15.5 (3)	1.9235 (20)	4.484 (2)	Kolbe *et al.*, (1972); Abraham *et al.* (1968)
CeO_2	Cm^{3+}	17.8 (3)	1.918	4.475 (2)	Abraham *et al.* (1968); Kolbe *et al.* (1973)
$SrCl_2$	Am^{2+}	5.77 (5)	1.9283 (8)	$g_{100} = 4.504$ (3) $g_{111} = 4.481$ (3) $g_{110} = 4.489$ (3)	Abraham *et al.* (1970)
SrF_2	Am^{2+}	15.2 (4)	1.9254 (10)	4.493	Kolbe *et al.* (1972)
CaF_2	Am^{2+}	18.6 (5)	1.926 (1)	4.490 (2)	Edelstein and Easley (1968)
ThO_2	Bk^{4+}	>50	1.923	4.488	Boatner *et al.* (1972)

[a] Derived free-ion *g*-value.
[b] Measurements at ~9.2 GHz and 4.2 K.
[c] For Cm^{3+} in $SrCl_2$ $\Delta E(\Gamma_8$–$\Gamma_7) = 15.3$ (4) cm^{-1}.

(Murdoch *et al.*, 1996). In the Cm^{3+}:$LuPO_4$ system, the energy levels occur in pairs with two lowest levels separated by 3.49 cm^{-1} and the two highest levels separated by 1.39 cm^{-1}. The splitting between these pairs of levels is 4.64 cm^{-1}. This splitting was not determined accurately in the EPR measurements because the data were not sensitive to small perturbations of the first-order Zeeman splitting of each of the Kramers' doublets that occurs between Kramers' doublets separated by such a large energy gap.

There has been one early study of the magnetic properties of AmI_2, a divalent Am compound. The results are given in Table 20.13 along with values for Cm metal and some trivalent Cm compounds.

As discussed earlier, Cm^{3+} compounds are expected to have ground term crystal-field splittings of less than 50 cm^{-1}. Thus at temperatures where all the ground term levels are populated, μ_{eff} should equal the free-ion value of $7.64\mu_B$. Early work on the preparation of Cm compounds and the metal were performed with ^{244}Cm, $\tau_{1/2} = 18.1$ years. Later studies have been conducted with ^{248}Cm, $\tau_{1/2} = 340000$ years. Studies with ^{248}Cm should, in principle, be more reliable as problems from radiation damage and the growth of daughter isotopes are minimized. Magnetic susceptibility measurements of Cm^{3+} diluted in $Cs_2NaLuCl_6$ (Table 20.2) suggested a crystal-field splitting of 5–10 cm^{-1}. Recent optical studies on the related system, Cm^{3+} diluted in Cs_2NaYCl_6, have

Table 20.13 *Summary of magnetic susceptibility data for $5f^7$ compounds and Cm metal.*

Compound	*T range* (K)	μ_{eff} (BM)	Θ (K)	T_o (K)	*References and comments*
$^{243}AmI_2$	37–180	6.7 (7)			a
^{244}Cm metal	145–550	7.99 (15)			b
^{244}Cm metal	100–300	8.07, 8.8	–386, –560	52 (1)	c
^{248}Cm metal	270–307	5.5	176	$T_N = 65$ K, $T_o = \sim 200$ K	d
^{248}Cm metal	200–300	6.2	202		e
^{248}Cm metal	300–340	7.7	138		e
^{244}Cm metal	140–300	6.0	72.2		f
$^{244}CmF_3 \cdot 1/2H_2O$	77–298	7.7	–5		g
$^{244}CmF_3$ in LaF_3	77–298	7.7	–6		g
$^{248}CmF_3$	~30–280	7.67	3.6		h
$^{244}CmOCl$	77–298	7.6	–22		g
$^{244}Cm^{3+}$:$Cs_2NaLuCl_6$	7.5–25	7.90 (10)	–4		i
$^{244}Cm^{3+}$:$Cs_2NaLuCl_6$	25–45	7.48 (50)	–1		i
$^{248}Cm_2O_3$	20–80	8.20	–149		j
$^{248}Cm_2O_3$	100–300	7.89	–130		j
$^{248}Cm_2O_3$	50–300	7.74	–130	$T_N \sim 15$ K	h
$^{248}Cm_2O_3$	4.2–300	7.51	–110		h
$^{248}CmBa_2Cu_3O_7$	~50–300	8.9 (3)		$T_N = 22$	k
$^{248}CmCuO_4$	50–300	7.89 (5)		$T_N = 25$	l
$Pb_2Sr_2{}^{248}CmCu_3O_8$	120–320	8.7 (2)	–96.8		m
$Pb_2Sr_2{}^{248}CmCu_3O_8$	30–90	7.8 (2)		$T_N = 18$	m

[a] Baybarz *et al.* (1972).
[b] Marei and Cunningham (1972). The Cm metal sample measurement was repeated four times with widely varying Θ values.
[c] Kanellakopulos *et al.* (1975) and Fournier *et al.* (1977). The first value of Θ is associated with the first value of μ_{eff}, etc.
[d] Huray *et al.* (1980) dhcp phase.
[e] Huray *et al.* (1980). fcc phase, another more complex analysis is also given.
[f] Fujita *et al.* (1976).
[g] Marei and Cunningham (1972).
[h] Nave *et al.* (1983).
[i] Hendricks *et al.* (1974).
[j] Morss *et al.* (1983).
[k] Soderholm *et al.* (1989) and Soderholm (1992). Includes a contribution from the Cu^{2+} ions to μ_{eff}.
[l] Soderholm *et al.* (1999). No value of Θ is given, low-temperature neutron diffraction indicates the spins order ferromagnetically within the *a–b* plane and are antiferromagnetically ordered along the *c*-axis.
[m] Skanthakumar *et al.* (2001). The large value of μ_{eff} above 100 K is attributed to a local paramagnetic moment on Cu^{2+} plus that of the Cm^{3+} ion. It is suggested that Cu^{2+} moment ordering occurs below 100 K resulting in the expected Cm^{3+} free-ion moment.

reported a 4.8 cm^{-1} splitting between the ground state and the first excited state. Because the ionic radius of the Lu^{3+} ion is less than that of the Y^{3+} ion, the crystal-field splitting in the Lu system should be larger, in accord with the susceptibility measurement. Above 7.5 K, there is reasonably good agreement

with the calculated free-ion moment. The temperature-dependent magnetic susceptibility of BkO_2 diluted in ThO_2 showed the ground state to be a Γ_6 (O_h) and the excited Γ_8 (O_h) state to be at about 80 cm^{-1} (Karraker, 1975b). The *g*-value of the ground state was 5.04, about 10% higher than the more accurate value of 4.488 ± 0.004 measured by EPR (Boatner *et al.*, 1972). The total overall splitting of the ground $J = 7/2$ state was estimated to be about 300 cm^{-1}. A possible antiferromagnetic transition at 3 K has been suggested to account for the anomalous magnetic behavior of these samples below 10 K. This transition would require segregation of the BkO_2 in the host ThO_2 matrix. Nave *et al.* (1983) measured the magnetic susceptibility of a 56.6 μg sample of BkO_2 (containing a 3% Cf impurity at the time of the measurement) and find Curie–Weiss behavior from 4.2 to 300 K with $\mu_{eff} = 7.92\mu_B$ and $\theta = -250$ K. Their value agrees with the calculated value for an $^8S_{7/2}$ state. However, it does conflict with the EPR results and Karraker's results which indicate a considerable splitting of the ground $J = 7/2$ term.

Interactions involving Cm^{3+} may be judged from a very complete work on Cm_2CuO_4 by Soderholm *et al.* (1999), where $\mu_{eff} = 7.89\ (5)\mu_B$, $T_N = 25$ K, and the ordered moment is $4.8\ (2)\mu_B$ at 15 K. This is a lower moment than expected, which might be due to measurements being made at an elevated temperature compared to T_N, but also may be caused also by covalency effects. The sample used for the neutron experiments was 42 mg (^{248}Cm), and the magnetic structure is the same as found for Gd_2CuO_4, which orders at 6.4 K. As far as known this is the only observation of magnetism in a Cm compound with neutrons. Cm_2CuO_4 is isostructural with the famous high-T_c-related La_2CuO_4 and it would be interesting to know what is the value of the moment on the Cu atom in the Cm compound. Unfortunately, this was below their experimental cut-off.

Another similar study (but without neutrons) was done by Skanthakumar *et al.* (2001) on the compound $Pb_2Sr_2Cm_{1-x}Ca_xCu_3O_8$ with $x = 0$ and 0.5. Again, these materials are related to high-T_c analogs with rare earths, although none of the Cm-doped compounds becomes superconducting.

A number of magnetic susceptibility measurements have been reported for Cm metal (Table 20.13), but reports by various investigators disagree (Marei and Cunningham, 1972; Kanellakopulos *et al.*, 1975; Fournier *et al.*, 1977; Huray *et al.*, 1980). The Soderholm group has been using the Cm^{3+} ion as a probe to study the influence of magnetic electrons on the superconductivity of some high-T_c-related oxides (Soderholm, 1992). In the course of this work, some new Cm compounds have been synthesized and their susceptibilities determined as shown in Table 20.13.

20.10 $5f^8$ $^7F_6$; Bk^{3+}, Cf^{4+}

The magnetic data for $^{249}Bk^{3+}$ diluted in $Cs_2NaLuCl_6$ are given in Table 20.2 (Hendricks *et al.*, 1974). The magnetic susceptibility is temperature independent, which shows that a singlet state is the ground state. From the systematics

of the crystal field parameters for the host crystal, the ground state is assigned as a Γ_1 (O_h) state, and from the magnitude of the susceptibility, the first excited state is calculated to be a triplet Γ_4 (O_h) state at about 85 cm^{-1}. Magnetic measurements for other ^{249}Bk compounds and the metal are listed in Table 20.14. The theoretical value for the $5f^8$ ground term free-ion g-value in intermediate coupling is 1.446 (1.50 for the pure $^7F_6$ ground term). From the magnetic susceptibility of Bk^{3+} adsorbed on ion-exchange beads, Fujita (1969) measured from 9.3 to 298 K (Table 20.14) a $\mu_{eff} = 9.40(6)\mu_B$, which corresponds to a free ion $g = 1.452$ (8) in excellent agreement with the expected value. The magnetic susceptibility of $^{249}BkF_3$ has also been reported and is in agreement with the free-ion value. The results of measurements of the magnetic susceptibility of Bk metal (Fujita, 1969; Nave *et al.*, 1980) are also given in Table 20.14. These measurements were performed on very small amounts (μg) of ^{249}Bk metal. Since $\tau_{1/2}$ of ^{249}Bk is only 320 days, there were varying amounts of ^{249}Cf metal (although corrections were applied for the amount of Cf) in the samples. Thus it is not surprising that different ^{249}Bk samples showed different magnetic behavior, especially at lower temperatures. Clearly these very difficult measurements need to be repeated. Measurements have been reported for $^{249}CfO_2$ and for $^{249}Cf_7O_{12}$. The latter compound can be thought of as comprising 40% Cf^{3+} and 60% Cf^{4+} and, assuming that susceptibilities can be simply added, the free-ion moment should be $9.7\mu_B$. As can be seen from Table 20.14, the measured higher temperature values are slightly lower than the expected free-ion values.

20.11 $5f^9\ ^6H_{15/2};\ Cf^{3+}$

The EPR spectrum of $^{249}Cf^{3+}$ in $Cs_2NaLuCl_6$ powder has been observed at 4.2 K (Edelstein and Karraker, 1975). From the measured isotropic g-value of 6.273 (10), the ground crystal field was identified as the Γ_6 (O_h) state and a free-ion g-value of 1.255 was deduced as compared with a calculated intermediate-coupling g-value of 1.279 for the nominally $^6H_{15/2}$ term. For the $4f^9$ analog, Dy^{3+}, the free-ion g-value is 1.333. The magnetic susceptibility of $^{249}Cf^{3+}$ (~2.4 mg) diluted into octahedral Cs_2NaYCl_6 (Table 20.2) was reported in the temperature range from 2.2 to 100 K (Karraker and Dunlap, 1976). From an analysis of the data, the Γ_6 state was determined to be the ground state, in agreement with EPR measurements, with a Γ_8^1 level as the first excited level at about 50 cm^{-1}. The total crystal-field splitting was calculated to be about 860 cm^{-1}. Limits were set for the ratio of B_0^4/B_0^6, which were consistent with those determined previously for the trivalent actinide compounds Cs_2NaMCl_6 $(M = U^{3+}, \ldots, Bk^{3+})$. EPR measurements of $|g_\parallel| = 3.56(2)$ and $|g_\perp| = 7.79(3)$ were reported for Cf^{3+} diluted in $LuPO_4$ at 4.2 K by Kot *et al.* (1993b).

Table 20.14 also lists magnetic susceptibility data for $^{249}Cf^{3+}$ compounds and for ^{249}Cf metal. From the magnetic susceptibility of Cf^{3+} adsorbed on ion-exchange beads (Fujita, 1969) measured from 77 to 297 K (Table 20.14),

Table 20.14 *Magnetic data for $5f^8$ and $5f^9$ metals, ions, and compounds.*

Compound	*T range* (K)	θ (K)	μ_{eff} (μ_B)	T_N (K)	*References and notes*
^{249}Bk metal	170–350	64.4	8.23	$T_o = 140$ (15)	[a]
^{249}Bk metal	50–298	–72.7	8.52	35 (3)	[b]
^{249}Bk metal	100–298	–33.0	8.83		[c]
^{249}Bk metal	70–300	–101.6	9.69	~34	[d]
^{249}Bk metal	70–300	–84.4	8.82	~34	[e]
$^{249}Bk^{3+}$	~10–300	–11.0 (1.9)	9.40 (6)		[f]
$^{249}BkF_3$	4.2–300	–77.9	9.38		[g]
$^{249}CfO_2$	~80–320	–70 (10)	9.1 (2)	7 (2)	[h]
$^{249}Cf_7O_{12}$	~80–320	95 (15)	9.5 (2)	8 (2)	[i]
$^{249}CfF_4$	150–340	–51 (3)	9.4 (1)		[j]
$^{249}CfF_4$	150–340	–33 (3)	9.1 (1)	9–12	[k]
^{249}Cf metal	28–298	3.24	9.84		[l]
^{249}Cf metal	22–298	–3.00	9.67		[l]
^{249}Cf metal	100–340	40 (3)	9.7 (2)	$T_o = 51$ (2)	[m]
$^{249}Cf^{3+}$	77–298	–5.6 (3.2)	9.14 (6)		[n]
$Ba^{249}CfO_3$	~80–320	–210 (20)	9.2 (2)	7 (2)	[o]
$^{249}Cf_2O_3$	~80–320	–80 (15)	10.1 (2)	8 (2)	[p]
$^{249}Cf_2O_3$	~80–320	–115 (15)	9.8 (2)	19 (2)	[q]
$^{249}Cf_2O_3$	90–300	–80 (10)	9.7 (2)		[r]
$^{249}CfF_3$	150–340	–20 (3)	10.2 (1)	6–7	[s]
$^{249}CfCl_3$	100–340	37 (10)	10.3 (2)	13	[t]
$^{249}CfCl_3$	60–340	13 (5)	10.1 (2)	7	[u]
$Cs_2Na^{249}CfCl_6$	2.2–14	–2.8 (1)	7.36 (20)		[v]
$Cs_2Na^{249}CfCl_6$	20–100	–13.5 (4)	10.0 (1)		[v]

[a] Fujita (1969) predominantly fcc, mass 1.669 μg, ~20% ^{249}Cf, possible ferromagnetic impurities.
[b] Fujita (1969) predominantly dhcp, mass 5.629 μg, ~16% ^{249}Cf.
[c] Fujita (1969) approximately equal amounts of the dhcp and fcc phases, mass 1.725 μg, ~1.7% ^{249}Cf.
[d] Nave *et al.* (1980) dhcp, ~12% ^{249}Cf, 21.0 (3) μg.
[e] Nave *et al.* (1980) mainly dhcp, some fcc, ~16% ^{249}Cf, 19.0 (3) μg, indication of a second transition (small amplitude) at ~42 K.
[f] Bk^{3+} absorbed on ion-exchange beads, two samples of 0.546 and 1.012 μg, less than 0.8 and 0.4 at % ^{249}Cf respectively in the two samples. Average value is given.
[g] Nave *et al.* (1981) 143 μg sample.
[h] Moore *et al.* (1986) fcc, two samples of 6 and 53 μg.
[i] Moore *et al.* (1986) rhombohedral, three samples of 25, 42, and 100 μg.
[j] Chang *et al.* (1990) monoclinic, results for two of three freshly prepared samples of mass ranging from 30 to 90 μg.
[k] Chang *et al.* (1990) monoclinic, results for two aged and one of three freshly prepared samples of mass ranging from 30 to 90 μg. The aged samples showed antiferromagnetic behavior.
[l] Fujita *et al.* (1976) fcc, two samples of 8.85 (top) and 5.64 μg (next).
[m] Nave *et al.* (1985) dhcp, two samples of 73.0 and 98.0 μg, average value is given.
[n] Fujita (1969) Cf^{3+} absorbed on ion-exchange beads, three samples of 0.342, 0.806, and 1.190 μg, average value is given.
[o] Moore *et al.* (1986) perovskite type, 24 μg sample.
[p] Moore *et al.* (1986) monoclinic, two samples of 11 and 22 μg.
[q] Moore *et al.* (1986) bcc, 31 μg sample.
[r] Morss *et al.* (1987) bcc, two samples of 3.097 and 1.23 μg, the numbers given in the table are the recommended average of measurements on the two samples, no indication of magnetic ordering was observed down to ~2 K.
[s] Chang *et al.* (1990) one hexagonal and three orthorhombic samples, masses ranging from 30 to 90 μg, high temperature results did not depend on the age of the samples.

a $\mu_{eff} = 9.14(6)\mu_B$ was obtained. This value is significantly lower than the expected free-ion value of $10.21\mu_B$ for the $^6H_{15/2}$ ground term. The magnetic susceptibilities of a number of compounds of Cf^{3+} have been measured. For the most part, the high-temperature data that could be fit by the Curie–Weiss law gave effective moments that were close to the free-ion value. However, as found before for small samples of highly radioactive isotopes, the low-temperature data were quite complex and sample dependent. Magnetic susceptibility measurements of ^{249}Cf metal samples were reported by two groups and are listed in Table 20.14. The high-temperature results are in fair agreement although one group reported complex low-temperature data for the metal.

20.12 $5f^{10}$; $^5I_8$; Es^{3+}

Very few measurements have been reported for trivalent Es compounds because of the difficulties associated with measurements on materials with short-lived isotopes. The most abundant isotope of Es is ^{253}Es with $\tau_{1/2} = 20.4$ days. A magnetic susceptibility measurement was reported for Es_2O_3 in the temperature range 4.2–180 K on an amorphous sample. The data fit the Curie–Weiss law with $\mu_{eff} = -10.5\mu_B$ and $\Theta = -53$ K. Correcting for the growth of ^{249}Bk (the sample was 4 days old and contained 13% Bk) gave a value of $10.5\mu_B$, consistent with the free-ion value. Measurements were reported for a 3.25 μg sample of EsF_3 in the temperature range 4.2–200 K 10 days after separation and preparation, which meant there was 31% ^{249}Bk in the sample. The data were fit with the Curie–Weiss law with $\mu_{eff} = -10.9\mu_B$ and $\Theta = -37$ K. After correction for the Bk content, the effective moment was $11.4\mu_B$. These measurements on Es samples should be treated conservatively as the true sample temperatures, the container corrections, and ^{249}Bk corrections lead to large uncertainties (Huray and Nave, 1987).

Elements beyond Es have half-lives that are too short to permit magnetic measurements of metals or compounds by conventional methods discussed here.

20.13 $5f^{11}$; $^4I_{15/2}$; Es^{2+}

The only reported Es metal (a divalent metal) magnetic measurement was made on a 0.25 μg sample. The purity of this sample is questionable since the preparative method may have resulted in an Au–Es alloy. Data were taken for

---

[t] Nave *et al.* (1987) and Moore *et al.* (1988) orthorhombic form obtained after melting the hexagonal samples, two polycrystalline samples of mass of 12.3 and 19.3 μg, exhibits metamagnetic behavior at low temperatures.

[u] Nave *et al.* (1987) and Moore *et al.* (1988) hexagonal, two microcrystalline samples of mass of 12.3 and 19.3 μg, exhibits metamagnetic behavior at low temperatures.

[v] Karraker and Dunlap (1976) 2.37 mg of $^{249}Cf^{3+}$ diluted in ~0.2 g of polycrystalline Cs_2NaYCl_6.

this sample with apparent temperature readings from 4.2 to 90 K. In this interval, a local moment of $11.3\mu_B$ was obtained, higher than the $10.2\mu_B$ free-ion value. The authors note the small sample size, large corrections for the sample holder, and uncertainty in the sample temperature due to self-heating as well as corrections for ^{249}Bk growth lead to a large uncertainty in the measured value (Huray and Nave, 1987).

The EPR spectrum at 4.2 K of $^{253}Es^{2+}$ diluted in CaF_2 was reported by Edelstein and coworkers (Edelstein *et al.*, 1970; Edelstein, 1971) and used to identify the stabilization of this oxidation state by the CaF_2 host. The measured *g*-value of 5.809 ± 0.005 identified the ground state as a Γ_6 (O_h) state. Subsequently, Boatner *et al.* (1976) found that the ground state of $^{253}Es^{2+}$ diluted in $SrCl_2$ had a *g*-value of 6.658 ± 0.003, which was assigned to the Γ_7 (O_h) state. Boatner *et al.* (1976) also reported the EPR spectrum of $^{253}Es^{2+}$ diluted in BaF_2, which was similar to that of Es^{2+} in CaF_2. Thus, the ratio of the crystal field parameters changed on going from CaF_2 or BaF_2 to $SrCl_2$, causing the ground state to switch. Analogous behavior had been found for the $4f^{11}$ ion, Ho^{2+}, in the same host crystals. The magnitude of the measured *g*-values is smaller than expected, and has been attributed primarily to covalency effects (Edelstein, 1971; Boatner *et al.*, 1976).

20.14 THE ACTINIDE DIOXIDES

Starting with the actinide oxides, AnO_2, one would intuitively expect that the situation might be relatively simple. If one takes oxygen as divalent, then an ionic compound can be made with An^{4+} and $2O^{2-}$. Indeed, from many considerations this appears a good approximation. All compounds have the well-known fcc CaF_2 fluorite structure. (See Chapter 15, Table 15.9, for a list of lattice constants.) This apparently simple cubic structure belies the complications that occur for the different oxides. As in so many cases, the devil is in the details. Despite half a century of effort, there remain many puzzles in the actinide dioxides, and they will be discussed at some length in this article. The magnetic properties should reflect this ionic nature, i.e. for UO_2 a $5f^2$ configuration is anticipated with a crystal-field splitting that gives a well-defined ground state.

20.14.1 Uranium dioxide

Early work on the magnetic susceptibilities of solid solutions of UO_2 in ThO_2 (cubic symmetry) was interpreted as showing 'spin only' behavior for the d^2 configuration on extrapolation to infinite dilution. Subsequently Hutchison and Candela (1957) showed that a model based on the $5f^2$ configuration with a strong spin–orbit interaction and the ratio of the crystal field parameters such that the Γ_5 (O_h) triplet state is lowest would also fit the observed magnetism. Ordered magnetism of UO_2 was first suggested by Jones *et al.* (1952) from their

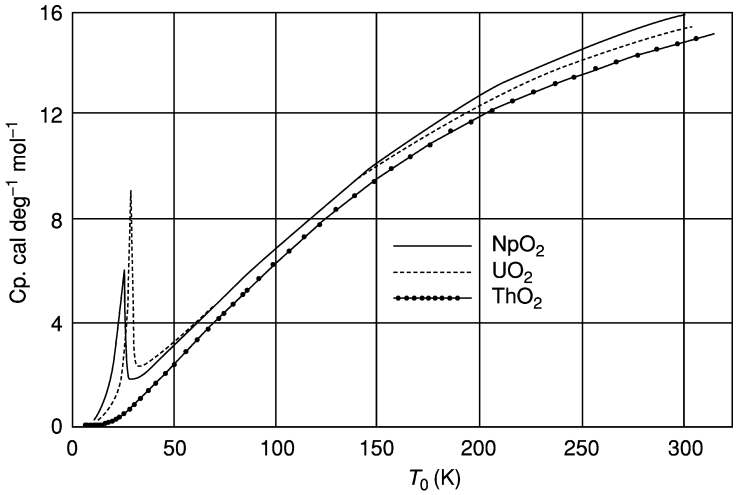

Fig. 20.7 *Heat capacities of ThO_2, UO_2, and NpO_2. Figure reprinted with permission from Osborne and Westrum* (1953). *Copyright* 1953 *by the American Institute of Physics.*

heat capacity measurements. Within a year, the heat capacities of ThO_2, UO_2, and NpO_2 were measured (Osborne and Westrum, 1953) and are reproduced in Fig. 20.7. These showed important anomalies for UO_2 and NpO_2, at 30 and 25 K, respectively. The assumption, of course, was that both materials exhibited a phase transition to a magnetically ordered state. Although magnetic susceptibility measurements were made on UO_2 in 1950, the best data were presented by Arrott and Goldman (1957). They showed that the magnetic phase transition disappeared when additional oxygen entered the lattice to the level of $UO_{2.07}$. Almost a decade then passed before the microscopic proof of antiferromagnetism was given by neutron diffraction. Two papers were published essentially simultaneously, Willis and Taylor (1965) and Frazer *et al.* (1965). Both reported work on single crystals and showed that UO_2 has a first-order transition to an antiferromagnetic state at 30.8 K. The uranium moments (of $1.75\mu_B$ at 5 K) are aligned in alternating ferromagnetic (100) sheets in a sequence $+ - + -$. The magnetic repeat may be characterized by a wave vector of $\mathbf{k} = 1$, i.e. the magnetic and chemical unit cells are the same. The magnetic moments are perpendicular to the propagation direction, i.e. $\boldsymbol{\mu} \perp \mathbf{k}$, in what may be described as a transverse structure (Fig. 20.8). These experiments, the availability of single crystals, and the increasing interest in f-electron magnetism ushered in the 'golden era' of experiments on UO_2, essentially the period from 1965 to 1980. Blume (1966), assuming a model where the electronic structure of U^{4+} consisted of a nonmagnetic singlet ground state with a low-lying magnetic triplet state and including bilinear isotropic exchange interactions, was able to account semiquantitatively for the first-order magnetic phase transition (see also

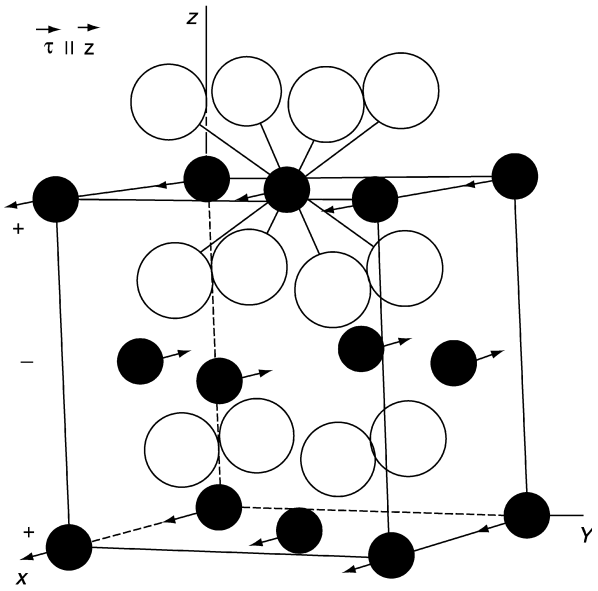

Fig. 20.8 *Magnetic structure of UO_2. The open circles are oxygen and the closed circles are uranium. In the arrangement shown the propagation direction* $\mathbf{k} = [001]$, (**k** *and* $\boldsymbol{\tau}$ *are equivalent*) *and the moments are transverse to this direction. There are two domains, one with* $\mu \parallel [100]$, *and the other with* $\mu \parallel [010]$. *Figure reprinted with permission from Faber and Lander* (1976). *Copyright* 1976 *by the American Physical Society.*

Alessandrini *et al.*, 1976). Rahman and Runciman (1966) showed that this was unlikely, their full manifold calculation showed that the crystal field ground state was most probably the triplet Γ_5. This could also explain the moment (which should be $2.0\mu_B$ for a pure $^3H_4$ ground state) as the mixing of higher L and S components would tend to reduce the ordered moment. They obtained crystal field parameters $V_4 = -409$ meV and $V_6/V_4 \sim -0.06$. They could not easily explain the first-order phase transition, but did predict a splitting of $\sim$171 meV between the ground state and the doublet Γ_4 and $\sim$630 meV to the next excited crystal field state. Neutron inelastic scattering was incapable of verifying these energy splittings in the 1960s and the opaque character of UO_2 make the optical technique of limited value. However, on a lower energy scale, neutrons had already been used to measure the complete phonon dispersion spectra at room temperature (Dolling *et al.*, 1965). At lower temperature, the neutron inelastic experiments by Cowley and Dolling (1968) showed a possible strong interaction between the magnons and the lattice, and this was reinforced by the elastic constant measurements as measured by Brandt and Walker (1967, 1968). Interestingly, they showed that the c_{44} elastic mode actually started to soften just below room temperature, and showed a strong minimum at the phase

transition. Within a year, in two remarkable papers, Allen (1968a,b) proposed a theory for the spin–lattice interaction in UO_2 that was based on a Jahn–Teller (JT) interaction and first introduced the idea of *quadrupole* interactions in the actinides. Allen proposed that the quadrupoles ordered and would thus give rise to an internal strain that would lead to a change in the position of the oxygen atoms without giving rise to an external change in the symmetry of UO_2. No measurements had found evidence for a large *external* (i.e. a lowering of the overall cubic symmetry) crystallographic distortion at the phase transition. Pirie and Smith (1970), using X-rays, searched for possible shifts of the U-atoms, but in such a measurement any oxygen shift would have been impossible to observe.

Following the work of Allen, an important paper was published by Sasaki and Obata (1970) giving new insights into the Jahn–Teller effects that might occur in the oxides. Their essential contribution was to realize that there could also be a *dynamic* JT effect that could occur at temperatures above the phase transition, and by coupling to the lattice this would explain the anomalies found in both the elastic constant work of Brandt and Walker (1967, 1968), and the susceptibility measurements of Arrott and Goldman (1957).

There is no evidence that the neutron experts understood the theory of Allen, which was advanced for its time, or Sasaki and Obata's work. It was not until 1975 that the internal distortion of the oxygen cage was discovered with neutron diffraction in the course of precise measurement of the intensities from a single crystal (Faber *et al.*, 1975; Faber and Lander, 1976). The experiment was designed to study something completely different, the magnetic form factor of U^{4+} at high values of Q, and the observation of the oxygen internal distortion was accidental! The full theory of this distortion was published by Siemann and Cooper (1979). The exact internal modes proposed by Allen are incorrect, but other modes are found. This does not distract from the originality of Allen's ideas. The coupling of magnetism and internal modes is illustrated in Fig. 20.9. The oxygen displacement from the equilibrium position is 0.014 Å. That such a small movement of the oxygen atoms could be measured is an example of how the neutrons are sensitive to light atoms in the presence of heavy ones.

The next step in the UO_2 saga came with the experiments on many actinide compounds at the Commissariat à l'Energie Atomique (CEA) in Grenoble, France during the period 1977–87 under the leadership of J. Rossat-Mignod. This group determined that many of the NaCl-type actinide compounds had a more complicated form of magnetic structure than originally proposed (Rossat-Mignod *et al.*, 1984). Instead of having a single **k** propagation vector in a certain volume of the crystal, a number of symmetry equivalent **k** vectors coexist in the same volume of the crystal. UO_2 was determined to have a triple **k** magnetic structure both by cooling the material in a magnetic field, as well as by applying uniaxial stress to the sample. This does not change the understanding of the magnetic structure or internal distortion, as long as one realizes that only one component of the moment and distortion are shown in Figs. 20.8 and 20.9. It did, however, lead to a reinterpretation of the magnon dispersion curves of

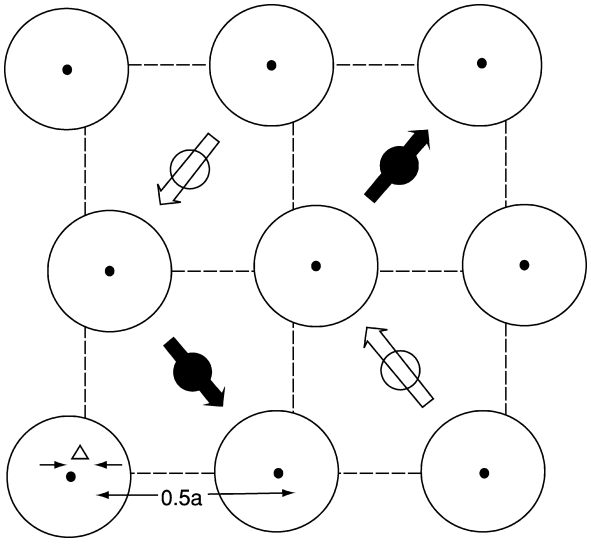

Fig. 20.9 *The* (001) *projection of the fluorite structure. The large circles represent oxygen atoms at* $z = 1/4$ *and* 3/4 *displaced from the ideal fluorite structure* (*indicated by the dashed lines*). *The shift of the oxygen atoms is not drawn to scale,* $\Delta = 0.014$ Å. *The smaller closed and open circles represent the uranium atoms at* $z = 0$ *and* 1/2, *respectively. The arrows indicate the directions of moments for the four sublattice antiferromagnetic structure. Figure reprinted with permission from Faber and Lander* (1976). *Copyright* 1976 *by the American Physical Society.*

Cowley and Dolling (1968) and Giannozzi and Erdos (1987). However, efforts to reproduce the dispersion of the magnons (discussed later), despite the 3**k**-structures were not successful. Apparently some element was still missing in the understanding of these curves.

During this period many other experiments were, of course, conducted on UO_2. It is a semiconductor with a band gap of $\sim$2 eV, and much of the electronic structure aspects were reviewed by Schoenes (1980) and by Brooks *et al.* (1984). There is little doubt from photoemission that the 5f states are considerably removed from the Fermi level E_F in UO_2. They are measured at 1.4 eV below E_F, a strong indication of the localization of the $5f^2$ state. Kelly and Brooks (1987) have shown that the local density approximation can account for the lattice parameter and estimate the width of the valence band. However, these electronic structure calculations show also that the simple concept of an ionic solid is not a good approximation in any of the light actinide oxides. There is appreciable mixing of the actinide 6p states with the 2p states of oxygen resulting in a measure of covalency for all actinide oxides.

In examining the optical properties (Schoenes, 1980) the localized nature of the 5f electrons in UO_2 also became apparent, and many features of the

electronic structure were observed as interband transitions. One extraordinary effect, shown in Fig. 20.10a was the presence below T_N of intense and sharp peaks at 151 and 154 meV. Schoenes identified these as two-phonon excitations as they are at exactly double the highest energy longitudinal optic (LO) modes involving principally oxygen atoms as measured by Dolling *et al.* (1965). The question is why they should be so strong and temperature dependent

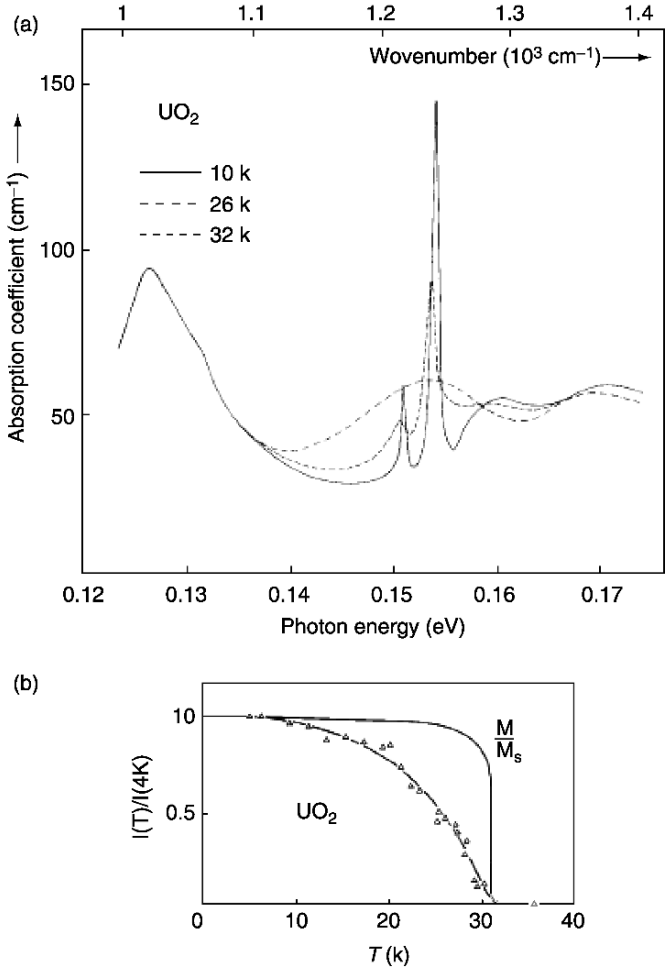

Fig. 20.10 (*a*) *The absorption coefficient of* UO_2 *measured in optical spectroscopy for various temperatures above and below* $T_N = 30.8$ K. *The sharp peaks at* 151 *and* 154 meV *are thought to be multiphonon excitations.* (*b*) *The temperature dependence of the area of the* 154 meV *peak compared to the normalized sublattice magnetization as measured by neutrons. Reprinted from Schoenes* (1980), *Copyright* 1980 *with permission from Elsevier.*

(see Fig. 20.10b)? As found from the experiments that will be described for NpO_2 (see below), it now appears that these excitations are a consequence of the LO phonon coupling to the quadrupolar distortion induced by the 5f quadrupole moment around the uranium nucleus. The fact that the T-dependence is continuous rather than discontinuous, as seen in the sublattice magnetization, suggests that the quadrupole coupling is a higher-order effect, and the dipole ordering is the primary-order parameter. It would seem worthwhile to measure this LO phonon as a function of temperature with neutron inelastic scattering.

Rahman and Runciman (1966) utilized the crystal field model to predict that there was a large splitting of the $^3H_4$ ground state manifold, with the first excited state being at least 150 meV above the ground state. With the advent of spallation neutron sources in the early 1980s, these types of crystal field energies became accessible, and the first indication for crystal field excitations in UO_2 was published in 1985 (Kern *et al.*, 1985). *Two* excitations were observed at 155 and 172 meV, whereas only *one* was expected according to the Rahman and Runciman calculation. These authors suggested that the R&R calculations might still be correct but that the V_6/V_4 ratio might be rather different from the –0.06 suggested by Rahman and Runciman. Three years later, using the more powerful spallation source ISIS near Oxford in UK, Osborn *et al.* (1988) showed that the crystal field spectra of UO_2 consisted of *four* excitations spread over the range 152–183 meV; these are shown for various temperatures in Fig. 20.11. They also searched up to energy transfers of 800 meV, but found no evidence of further transitions. The first point to note is that in the crystal field model for the $^3H_4$ multiplet there should be only two transitions in the ground state multiplet. (Transitions from Γ_5 to Γ_3 and Γ_4 are allowed, but not to Γ_1.) Since the overall multiplet is now within 180 meV, rather than the $\sim$700 meV proposed by Rahman and Runciman, the crystal field interaction is much weaker than in the Rahman and Runciman model. In a detailed paper, Amoretti *et al.* (1989) showed that $V_4 \sim -123$ meV, less than 1/3 that was proposed by Rahman and Runciman, and $V_6/V_4 = -0.21$. The extra lines (above the two expected) arise from the lowering of the symmetry due to the internal distortion of the oxygen cage (Fig. 20.9). Amoretti *et al.* (1989) were able to show that the spectra are better explained with a 3**k** magnetic structure (physical displacements along $\langle 111 \rangle$) rather than a 2**k** model (physical displacements along $\langle 110 \rangle$). Interestingly, one can see that the four lines are still present *above* T_N, whereas there is no longer a static distortion of the oxygen cage. However, dynamic effects are still present, as pointed out by Sasaki and Obata (1970), and these will give rise to a splitting of the crystal field levels, although it is noticeable that the transitions are starting to broaden in width by 35 K.

Following this direct measurement of the crystal-field splitting, the theorists returned to the fray and showed that the smaller value of V_4 (as compared to the original calculations of Rahman and Runciman) could be understood (Gajek *et al.*, 1988; Rahman, 1998). The latter paper shows that the ground state is $\sim$90% $^3H_4$, justifying the approximations made in interpreting the neutron

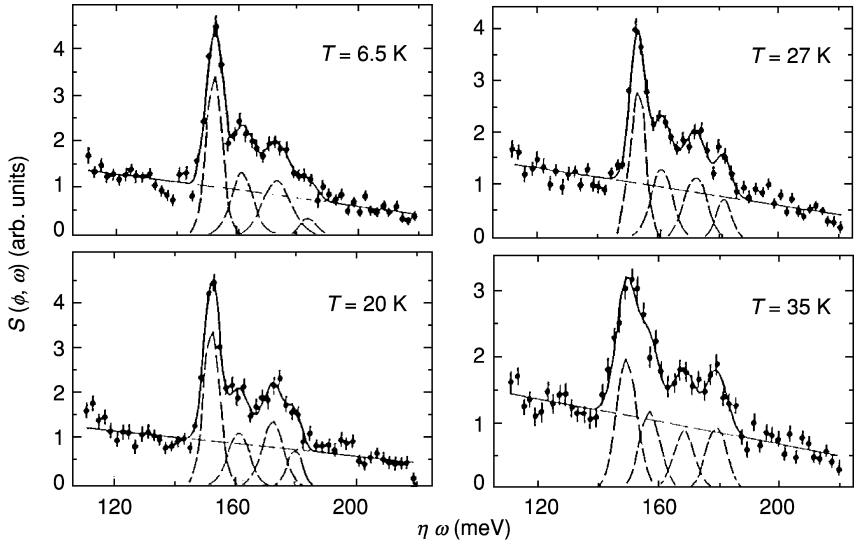

Fig. 20.11 *Neutron spectra measured with an incident energy of* 290 meV *for different temperatures between* 6.5 *and* 35 K, *where* $T_N = 30.8$ K. *The smooth line is the fit to four Gaussian line shapes and a sloping background. These five components are shown by the dashed lines. Figure reprinted with permission from Amoretti* et al. (1989). *Copyright* 1989 *by the American Physical Society.*

spectra. The moment calculated is $1.94\mu_B$, only a small reduction from the $2.00\mu_B$ in the simple Russell–Saunders coupling for the Γ_5 ground state. The reduction from 1.94 to $1.75\mu_B$ is thus due to the JT effect, as discussed above. All of this established beyond doubt that the ground state was the triplet Γ_5.

For the ground states of the heavier actinides, more mixing of excited states into the ground state is expected, but this work on UO_2 shows that although taking into account intermediate coupling (mixing of excited L and S values) is necessary, J-mixing is probably not so important for *any* ground state properties of the actinides. This result suggests many of the earlier calculations, e.g. Chan and Lam (1974) were not relevant. Furthermore, this has important implications for studies of intermetallics compounds, which are not covered in this review (but see Chapter 21 and Vol. 17, 19, and 32 of *Handbook of Physics and Chemistry of the Rare-Earths*). Because the conduction-electron states in intermetallic compounds are known to shield the crystal field interactions, the crystal field parameters are expected to be *lower* than in the actinide oxides. Thus it is expected that crystal-field splittings in intermetallics should be in the range 20–50 meV, as compared to 150 meV in UO_2. The range for intermetallics is thus excellently matched to neutron spectroscopy, and in practice this has been found (Holland-Moritz and Lander, 1994). However, when the crystal field transitions in intermetallics are *not* observed with neutron spectroscopy, it

cannot be argued that the crystal field transitions are outside the range of neutron spectroscopy. More subtle interactions, due to the hybridization of the 5f electrons with the conduction-electron states, are involved.

An elegant NMR study has been performed at low temperature on both the ^{235}U and ^{17}O NMR nuclei in UO_2 (Ikushima *et al.*, 2001). The results lend support to the idea of a 3**k** magnetic structure in UO_2 below T_N. Furthermore, Ikushima *et al.* (2001) give strong evidence for a local distortion driven by the U quadrupoles, and an excitation spectrum that shows the presence of magnon–phonon coupling.

The understanding of UO_2 is almost complete, but there are still the magnon dispersion curves, first measured in 1968, that still defy a complete theoretical interpretation, despite the realization of the 3**k** state. Again, new neutron technology has come into play, in this case in the ability to have enough neutron intensity to analyze the polarization of the scattered neutrons. Briefly, when a neutron is scattered from a magnetic moment the spin state of the neutron is *changed*; on the other hand, when the neutron is scattered from a nucleus, the spin state is *unchanged*. With a sufficiently large single crystal of UO_2, it proved possible to examine the magnon dispersion curves with polarization analysis, and the results are shown in Fig. 20.12 (Caciuffo *et al.*, 1999). The hope in these

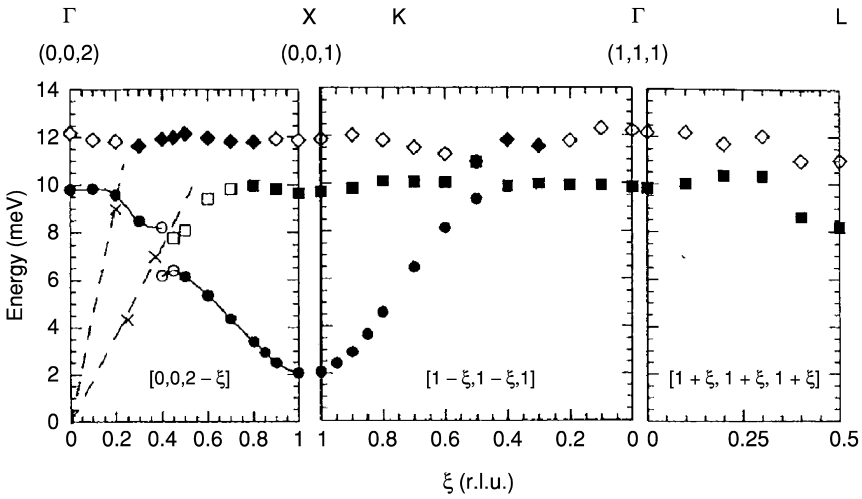

Fig. 20.12 *Magnon dispersion curves of UO_2 measured at* 16.5 K *along the principal crystallographic directions. The broken lines and crosses correspond to acoustic phonon branches measured at* 270 K. *Open symbols indicate a qualitatively smaller magnon intensity than the filled points. In all measurements the neutron spin state was spin flip, i.e. changed, and the nonspin-flip cross section was found negligible. Figure reprinted with permission from Caciuffo* et al. (1999). *Copyright* 1999 *by the American Physical Society.*

experiments was that a 'mixed' mode would be found to identify the famous magnon–phonon coupling first proposed by Cowley and Dolling (1968). No sign of this interaction was found. However, if it occurs in the region $\xi \sim 0.5$ in the $[00\bar{2}\xi]$ zone, then it is difficult to observe as the intensity drops to almost zero, for reasons that are not immediately clear. Theory is still unable to reproduce the magnon dispersion curves. This is certainly the most important question to resolve before a complete understanding of the magnetism of UO_2 is achieved.

In this long story of the magnetism of UO_2 not a word has been said about the new technique of RXS. In a sense this technique came too late! One discovery still needing confirmation in UO_2 is the presence of the quadrupole moments. Rather than treat this here, it is more appropriate to raise it after the discussion of NpO_2 (below). However, one interesting story using synchrotrons is worth recounting. The signal from uranium in resonant magnetic scattering is so strong (see Fig. 20.2 and discussion) that it opens the possibility for doing different kinds of experiments. One of these is the possibility of observing the scattering from *surface magnetism* in UO_2. Experiments of this sort to study the surface *charge* arrangements are common with synchrotrons, but are extremely rare for *magnetism* because they require scattering from a very small magnetic volume near the surface of the material. After many efforts involving surface preparation and different experiments, *surface magnetic scattering* was observed from UO_2 (Watson *et al.*, 1996). Strictly speaking, the parameters investigated have little specific to UO_2; they concern what happens near the surface of an antiferromagnet that undergoes a discontinuous phase transition in which the magnetism melts. One of the more interesting aspects is that as emphasis is put more and more on the surface layers it is found that the phase transition is in fact continuous. The crucial data are shown in Fig. 20.13. Although it is not strictly correct to interpret the different values of the L index in Fig. 20.13 as representing different depths into the antiferromagnet, as a first approximation it is acceptable. The bulk magnetism signal (similar to that observed with neutrons) is shown at (001). The model of magnetism near the surface in UO_2 is that near the phase transition, the top few surface layers lose their magnetism, and below them is an interfacial layer of reduced moments that grows in spatial extent as the temperature approaches T_N. These results are in agreement with some of the theories, based on symmetry arguments, but in disagreement with a simple melting transition, which is observed for ferromagnets. That there is a difference is perhaps not surprising as a ferromagnet has a net magnetization, which couples to the lattice, whereas such an interaction is absent in an antiferromagnet. More recent experiments have gone on to study the roughening of the magnetic order just before the phase transition. Interestingly, such studies are relevant to a current problem in magnetic multilayers, viz. the interplay of charge and magnetic roughness in defining the interfacial structure of the multilayers.

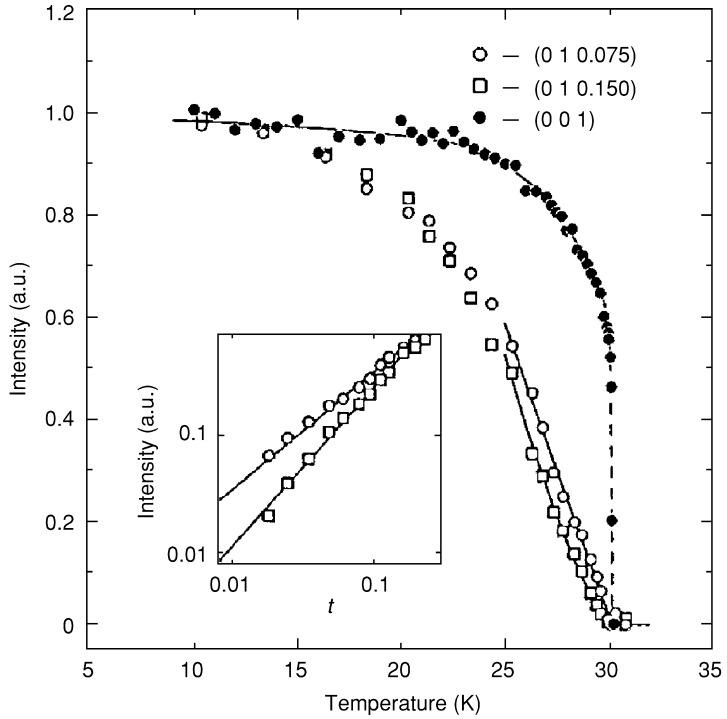

Fig. 20.13 *Temperature dependence of the magnetic scattering at the* (001) *bulk Bragg reflection* (*solid circles, which agrees with neutrons*) *and at various positions along the* (01*L*) *magnetic truncation rod* (*open symbols*). *Essentially one can think of these data having a greater component of the surface as L increases. Data are normalized to unity at low temperature. Inset: log–log plot of the scattering intensity at two different positions along the* (01*L*) *rod as a function of reduced temperature. Figure reprinted with permission from Watson* et al. (2000). *Copyright* 2000 *by the American Physical Society.*

20.14.2 Neptunium dioxide

Progress in understanding was slow and steady over the last 50 years in the study of UO_2. Not so with NpO_2. The problem turned out to be considerably more complicated. The story starts with the same paper on the heat capacity from Osborne and Westrum (1953) (Fig. 20.7). Since NpO_2 has a $5f^3$:Np^{4+} configuration, the ground state is $^4I_{9/2}$, a Kramers' ion in which the lowest ground state must be a magnetic doublet. This means given even the smallest amount of magnetic exchange the compound should order magnetically as no crystal field interaction can induce a singlet (nonmagnetic) state. The transition at $T_o = 25$ K in the heat capacity was thus assumed to be due to magnetic ordering. Note that the entropy at the transition (area under the curve) is very similar for both UO_2 and NpO_2, reinforcing the supposition of

ordered magnetism in both. Magnetic susceptibility measurements by Ross and Lam (1967) showed a strong peak at T_o, again suggesting antiferromagnetic order, as in UO_2. The first surprise came when neutron diffraction (on polycrystalline samples) by Cox and Frazer (1967) and Heaton *et al.* (1967) failed to find any change in the diffraction pattern on cooling below 25 K. They put an upper limit of $\sim 0.4\mu_B$ on any possible moment, much less than expected from the $5f^3$ ground state quartet. This limit was drastically reduced by the Mössbauer experiments of Dunlap *et al.* (1968) that showed that there was a very small amount of line broadening developing below T_o. When interpreted in terms of magnetic dipole ordering, this line broadening suggested a moment of $\sim 0.01\mu_B$. At that time, in the 1960s, a moment so small was unheard of, so the problem remained unsolved. The discovery of the internal distortions in UO_2 in the mid-1970s led those involved, especially theorists, to return to the unsolved mystery of NpO_2. Erdos and coworkers published a number of papers trying to explain the low-temperature magnetic properties of NpO_2 (Erdos *et al.*, 1980; Solt and Erdos, 1980). The essential point was to introduce a *quadrupole* interaction and allow this to cause an internal distortion. The magnetism was then 'removed' by postulating an unusual ground state or other assumptions about the presence of Np^{3+} ions. Since the UO_2 studies had shown that small extra diffraction peaks were present at low temperature as a consequence of the rearrangement of the oxygen atoms, an effort was made to see whether similar peaks could be found from NpO_2. Boeuf *et al.* (1983) reported a null effect, but the crystals of NpO_2 were small (no crystals larger than ~ 2 mm^3 have ever been produced), so these experiments could not be as sensitive as in the case of UO_2. Given the sensitivity of the Mössbauer signal from the ^{237}Np ion, it was not surprising that Friedt *et al.* (1985) returned to this technique and made a series of precise measurements down to 1.5 K, including applying a magnetic field. They suggested that there was *no* dipole magnetism at all, and that all the effects could be explained by a JT distortion of the oxygen cage. However, since this had not been observed in the experiments of Boeuf *et al.* (1983), they suggested that the distortion should be dynamic in nature. If it were, then this should give rise to a change in the phonon spectra, which might be reflected in the thermal parameters at low temperatures. Caciuffo *et al.* (1987) searched for any such changes, but without success.

By this time experimentalists were unenthusiastic about working on NpO_2, but it seemed at least important to establish the crystal field parameters, as there had been the suggestion that NpO_2 was not even Np^{4+} (Zolnierek *et al.*, 1981). The first attempts by Kern *et al.* (1988) showed that any crystal field peaks were broad, much broader than the experimental resolution. The problem needed the higher intensity of the ISIS (UK) source and this experiment was performed by Amoretti *et al.* (1992). The data and fits are shown in Fig. 20.14. Clearly these are less convincing than those found for UO_2 (Fig. 20.11). Any crystal field scheme with Np^{4+} predicts the highest Γ_6 state at well over 200 meV and the matrix element is small. The transition(s) observed, therefore, must be between

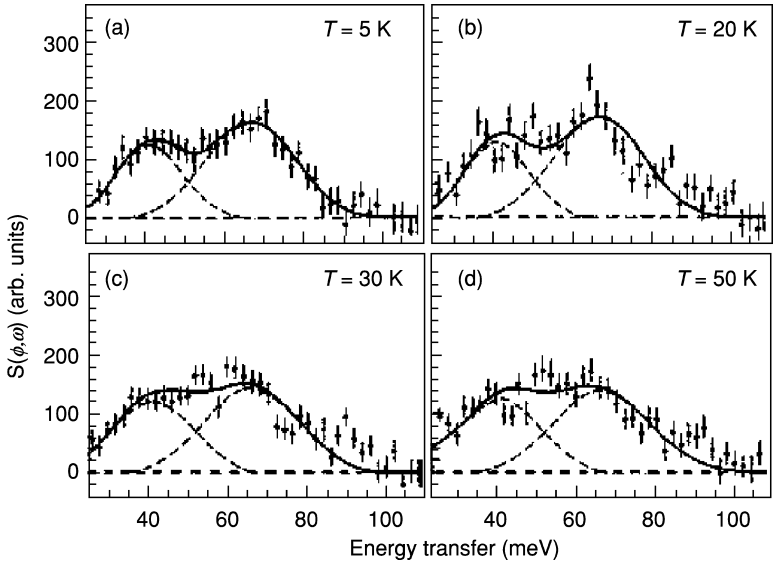

Fig. 20.14 *Neutron inelastic magnetic scattering cross section for NpO_2 as a function of temperature. The incident neutron energy was* 180 meV *and the average scattering angle* 5°. *The phonon contribution, which is small at these angles, has been subtracted. The full curve is a fit to the data of two Gaussians* (*shown as broken curves*) *plus a background. Reprinted from Amoretti* et al. (1992). *Copyright* 1992 *with permission from Elsevier.*

the two Γ_8 states. The extent of this splitting, around 55 meV, with evidence for a splitting of the peak as observed in UO_2, is completely consistent with the V_4 parameter deduced for UO_2, after taking into account the change in the cation. Amoretti *et al.* (1992) also made measurements at lower energy and saw an interesting effect as the temperature was lowered through T_o, which is shown in Fig. 20.15. The transition must correspond to the splitting of the ground state Γ_8 quartet below T_o. It thus appeared after these measurements that the crystal field parameters were as expected (based on UO_2) for NpO_2 and one really had a Np^{4+} ion (as the chemists and the Mössbauer spectroscopists insisted all the time!) and there was a need for a new idea.

Muon spectroscopy (Kalvius *et al.*, 2001) is also sensitive to the presence of dipole moments. The difficulty with this method is that there is always some uncertainty about at which point the muon annihilates, giving rise to the measured signal. However, Kopmann *et al.* (1998) showed that the signal from magnetic ordering was readily observed in UO_2 and went on to observe a small effect in NpO_2. Again, as with the neutron signal shown in Fig. 20.15, there is an 'effect' at T_o, but if it was dipole moment ordering, then the Mössbauer spectroscopy would have observed it.

Given the huge sensitivity to magnetism in 5f shells that was discussed in connection with RXS (see Fig. 20.2), one of the first samples to try with this

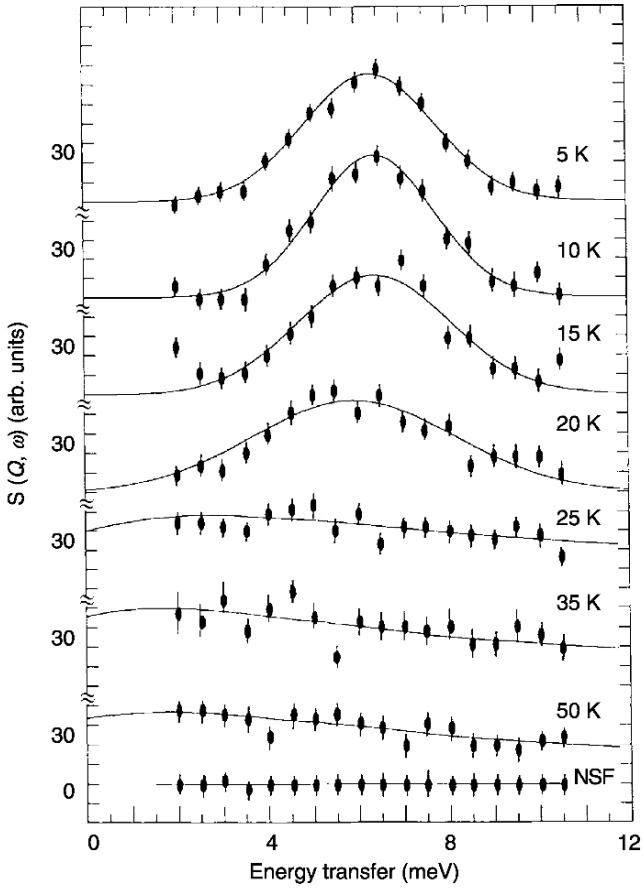

Fig. 20.15 *Evolution of the spin-flip scattering* (*i.e. the neutron spin state is changed on scattering indicating a magnetic cross section*) *as the temperature is lowered through the* 25 K *transition in* NpO_2. *The momentum transfer is* $Q = 1.3$ Å^{-1} *and the sample is polycrystalline. The solid lines are fits to the data with a Gaussian function. The transition energy is* 6.3 meV. *Reprinted from Amoretti* et al. (1992). *Copyright* 1992 *with permission from Elsevier.*

technique was NpO_2, once the problem of looking at transuranium samples at the ESRF in Grenoble was solved. A large signal was indeed observed below T_o by Mannix *et al.* (1999). Because Mannix *et al.* (1999) did not have all the necessary tools to analyze the polarization of the scattered photons, they were cautious in ascribing this signal to dipole ordering, and, of course, the RXS technique cannot relate the intensity of the scattering to the magnitude of the dipole moment. They did, however, measure the dependence of the scattered intensity on the photon energy, and this is shown for UO_2 and NpO_2 in

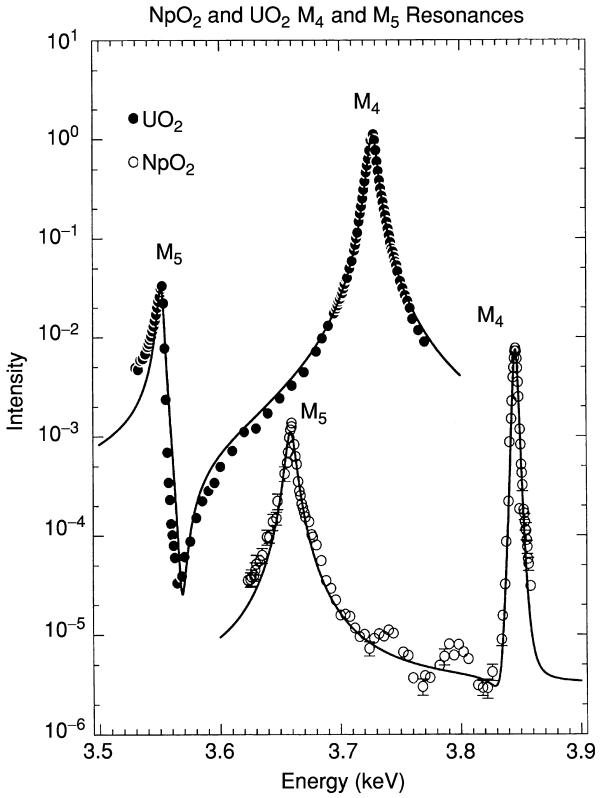

Fig. 20.16 *The energy dependence of the integrated intensity from UO_2 and NpO_2 as a function of incident photon energy. Note that the signal for UO_2 is fit to simple Lorentzian curves, as was the case for UAs, shown in Fig.* 20.2. *On the other hand, the NpO_2 spectra, especially that at the strong M_4 cannot be fit to a Lorentzian and requires a Lorentzian-squared function to fit the observed variation. Notice also the different energies for the $M_{4,5}$ edges for U and Np. This allows the RXS technique to be element selective, and one can look at mixed $(U,Np)O_2$ oxides and probe independently the magnetism on the two types of cations. For a study like this see Normile* et al. (2002). *Reprinted from Lander* (2002). *Copyright* 2002 *with permission from Elsevier.*

Fig. 20.16. The energy dependence, which was not published by Mannix *et al.* (1999), as it was not understood, suggested that perhaps the scattering was not simple dipole.

At the same time that these experiments were in progress, Santini and Amoretti (2000) proposed that the ordering in NpO_2 was not dipole $\langle M \rangle$ but rather of an octupole $\langle M^3 \rangle$ nature. These can be best understood in terms of the shapes of the resulting charge distributions. For dipole ordering the magnetic moment is a vector quantity but it does not require a distortion of the charge density, which can then remain spherical around the atom. For *quadrupole*

ordering $\langle M^2 \rangle$ there is *no* net magnetic moment as the (even) operator does not destroy time reversal symmetry, however, it does change the shape of the charge density of the electrons around the nucleus. Shapes such as prolate or oblate are typical symmetries of quadrupoles. For octupole moments $\langle M3 \rangle$ time reversal symmetry is broken as the operator is odd; in addition, the charge distributions become even more aspherical. Santini and Amoretti (2000, 2002) proposed this model for NpO_2 to explain the essentially 'zero' of Mössbauer spectroscopy, and yet to have a magnetic operator that would break time-reversal symmetry to explain the results of the muon experiments.

As the capabilities increased at the ESRF synchrotron, it became important to return to these experiments on NpO_2. The new capabilities allowed the polarization of the scattered photons to be analyzed and, at the same time, the crystal to be rotated about the scattering vector while the intensity was monitored. This proved crucial. The scattering at the (001) and (003) reflections, first reported by Mannix *et al.* (1999), were found to originate totally from *quadrupole* charge distributions. This can be understood by both the azimuthal and polarization dependence, see Paixão *et al.* (2002). Furthermore, the absence of either internal or external lattice distortions in NpO_2 implies that the configuration involves 3**k** quadrupole ordering. A schematic picture of this is shown in Fig. 20.17. It is important to realize that the scattering observed here is *not* magnetic in origin. It arises from the aspherical nature of the charge distribution

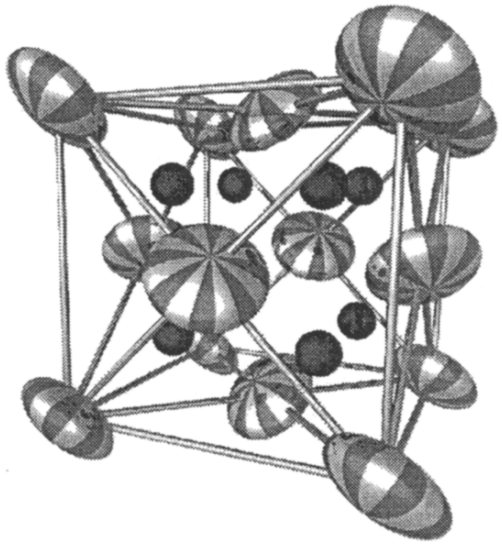

Fig. 20.17 *Crystal structure of NpO_2 in the antiferromagnetic-quadrupole state. The ellipsoids represent the orientation of the local symmetry axis at the Np position, not the actual charge distributions. The oxygen atoms are shown as spheres. Figure reprinted with permission from Paixão* et al. (2002). *Copyright* 2002 *by the American Physical Society.*

of the 5f states. The local symmetry around the Np atoms is broken by the quadrupole distribution of the 5f states, and this gives rise to new reflections that are not allowed by the original space group. RXS is a particularly powerful tool as it tells us the nature of the electrons that make up the quadrupole distribution. In this case the strong energy dependence (Fig. 20.16) is related to the particular matrix elements that give rise to the scattering. This particular feature of RXS is becoming more important, and has also been used in the 3d series, see for example, Zimmerman *et al.* (2001). In general this is called Templeton scattering, after the pioneering crystallography of Templeton and Templeton (1985) even before tunable synchrotron beams were available.

This section on NpO_2 will finish by returning to UO_2 and asking whether it would not also be possible to demonstrate directly the presence of the quadrupoles. Indeed, it would be, but in the case of UO_2 there is also strong *dipole* scattering. If both of these occur at the same place in the reciprocal lattice then distinguishing the much weaker quadrupole effects becomes difficult. As far as known, NpO_2 is the only material that exhibits quadrupolar ordering without an ordering of dipoles at the same or a lower temperature. On the other hand, the observation of a temperature-independent susceptibility (Erdos *et al.*, 1980) and the asymmetry in the muon experiments suggests that there exists an operator that lifts time reversal. (This cannot be done by the quadrupole operator as it is even in M.) The only possibility is that there is simultaneous ordering of an octupole moment, but a symmetry analysis has shown that it must be a different type from that proposed by Santini and Amoretti (2000). Observing this is almost impossible with the RXS technique and 5f electrons because the matrix elements will be small. Thus, the saga of NpO_2 is not over completely, but at least the field now is illuminated, as opposed to the darkness surrounding research on NpO_2 for almost 50 years!

20.14.3 Plutonium dioxide

The electronic state of Pu^{4+} is $5f^4$:$^5I_4$ and relatively simple considerations lead to the suggestion that the crystal field ground state might be a singlet Γ_1. (In a simple picture, the crystal field states for Pu^{4+} are simply the inverse of those for U^{4+}.) This idea was strongly reinforced by the first reported measurement of the susceptibility of stoichiometric PuO_2 by Raphael and Lallement (1968). Remarkably they showed that the susceptibility was completely independent of temperature up to 1000 K, with a value 0.54×10^{-3} emu mol^{-1} (after correcting for the small diamagnetism of the radon core). In order to calculate the above value of the TIP from the simple crystal field model, the necessary crystal-field splitting between the ground state (singlet) Γ_1 and first excited (triplet) Γ_4 was found to be $\sim$280 meV. (If χ is temperature independent up to 1000 K, then the magnetically active triplet state must be at least $\sim$2000–3000 K away in energy). The resulting V_4 is approximately –320 meV, and this is not far from the value first proposed for UO_2 (Rahman and Runciman, 1966) of $V_4 \sim$ –400 meV.

Yet, as discussed above, this value was found to be much smaller from experiments on UO_2.

Performing crystal field measurements on PuO_2 with neutrons proved *much* harder than on UO_2. For these measurements, samples of 30–80 g of materials are needed; moreover, it is quite impossible to use the ^{239}Pu isotope for inelastic scattering, so one has to use samples with the rare isotope ^{242}Pu. Still, these measurements were clearly of great importance, and finally a suitable sample (79 g, triply encapsulated) was transported to Intense Pulsed Neutron Source (IPNS) at Argonne and the experiment performed. At least *two* peaks were seen, spread over ~85–125 meV. In the crystal field scheme only *one* transition is expected as the matrix elements for transitions from the Γ_1 singlet state are zero except for the one transition $\Gamma_1 \rightarrow \Gamma_4$. However, by examining the Q-dependence of the scattering it became clear that most of the observed peaks increased in intensity with Q, whereas electronic transitions should decrease with Q. In fact only the transition at ~120 meV appeared electronic and the others were assigned to H-modes from an impurity, probably from water in the PuO_2 (Kern *et al.*, 1990). (Neutron scattering is extremely sensitive to hydrogen and, although these impurities were later detected by infrared spectroscopy, neutrons are still a wonderful analytical tool – if rather expensive – for free or bound H.) This was rather an unfortunate situation, and it took almost a decade to get the sample purified at Los Alamos, and then actually run on the Los Alamos spallation source. However, the result (Kern *et al.*, 1999) merited the wait. A single peak at 123 (4) meV was observed, but with a width significantly greater than the experimental resolution (Fig. 20.18). By calibrating the spectrometer with the known scattering from vanadium, Kern *et al.* (1999) were able to put the scattering on an absolute scale. They then took the crystal field parameters (V_4 and V_6) from UO_2 and extrapolated them to PuO_2 where they predicted a single transition at 115 meV. Moreover, the absolute calculated intensity of the transition also agreed perfectly with the experiment, so this gives considerable confidence to the crystal field parameters.

However, there is now a *major* discrepancy between χ as determined by Raphael and Lallement (1968) and χ calculated from the crystal field scheme. Using the observed V_4 and V_6 parameters, the calculated $\chi = 0.90 \times 10^{-3}$ emu mol^{-1}, a value almost twice as great as measured! Many thought that the 1968 measurement must be wrong, but any impurities in the Pu would normally lead to a *larger* value, and the amount of diamagnetic impurities (e.g. ThO_2) to make the difference exceeded 10% and appeared unreasonable. Recently, this value of the experimental χ has been remeasured (Kolberg *et al.*, 2002) and found to be correct.

Earlier attempts by Goodman (Kern *et al.*, 1990) to question the crystal field scheme and develop a so-called strong coupling approach are still a possibility to explain these results (and those for CmO_2 as discussed below), but they have not yet been fully developed. More recently, Colarieti-Tosti *et al.* (2002) have reported on a first principles calculation of the crystal field scheme, and they

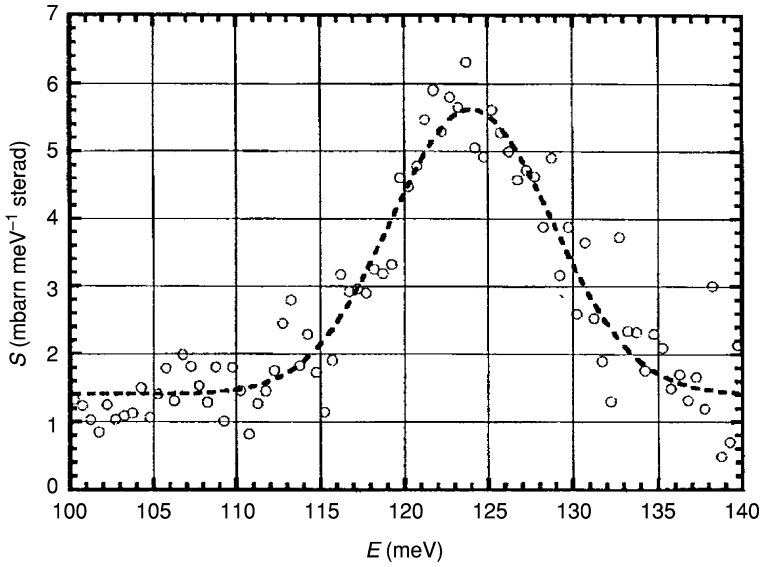

Fig. 20.18 *Neutron inelastic spectra from PHAROS of* 29 g *of* $^{242}PuO_2$ *at* $T = 30$ K. *The incident neutron energy was* 184 meV. *The resolution of the instrument is* ~4 meV *at these energy transfers, but the Gaussian fit gives a width of* 11 meV. *No other electronic signal was found between* 10 *and* 100 meV. *Figure reprinted with permission from Kern* et al. (1999). *Copyright* 1999 *by the American Physical Society.*

arrive at an energy separation $\Gamma_1 \rightarrow \Gamma_4 \sim 99$ meV, which is relatively close to the observed value of 123 meV. These authors went on to consider the discrepancy between the measured and calculated susceptibility, and they introduced the idea that there is an *antiferromagnetic* exchange interaction between the Pu^{4+} ions, mediated by the admixture of the actinide 6d states into valence band. Knowing that UO_2 orders antiferromagnetically, a rough value of the exchange parameter may be deduced, and then scaled to the case of Pu. The resulting calculations (demonstrated with other data in Fig. 20.19) are in good agreement with experiment, except that they show some curvature for $T > \sim 400$ K. It is still difficult to understand what appeared to be the amazingly uninteresting susceptibility of PuO_2 first measured in 1968.

Recently Kolberg *et al.* (2002) have suggested that the dynamical JT effect may play a role also in $(U,Pu)O_2$ materials, as discussed earlier for pure UO_2. Indeed, with this additional interaction agreement between theory and experiment might be possible. All this work shows that the complications in PuO_2 have, like those in the other oxides, now stretched over almost half a century. The broadening of the crystal field transition remains so far unexplained. However, a slight broadening of the excited Γ_4 state could either come from antiferromagnetic exchange or the dynamic JT effect.

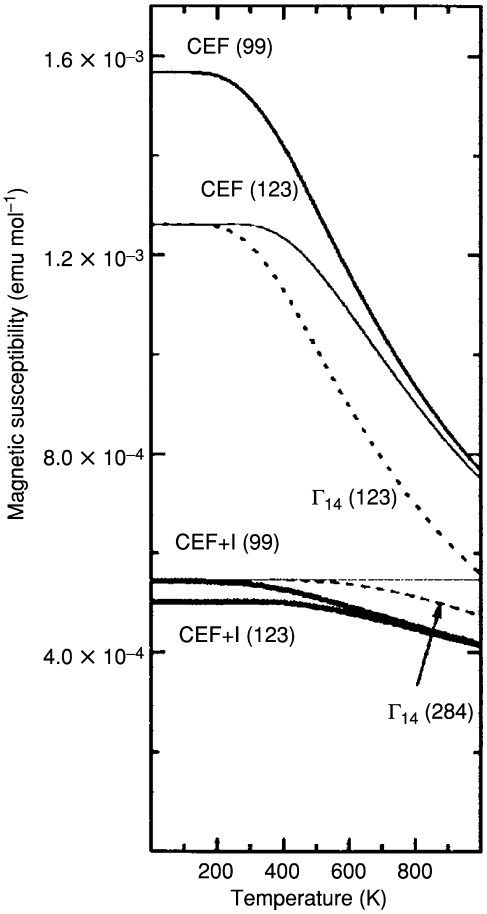

Fig. 20.19 *The magnetic susceptibility of PuO_2. The measurements are the T-independent straight dotted line. The calculated bare susceptibility with a single $\Gamma_1 \rightarrow \Gamma_4$ excitation energy of* 284 meV *fits the data at $T = 0$ and is shown as the dashed line labeled Γ_{14}* (284). *The corresponding bare susceptibility with $\Gamma_1 \rightarrow \Gamma_4 =$* 123 meV, *which fits the neutron experiment, is the dotted line labeled Γ_{14}* (123). *Adding additional CF transitions to the* 123 meV *model produces the improvement shown by the solid line labeled CEF* (123). *Similarly the CEF* (99) *line uses all the CF transitions with $\Gamma_1 \rightarrow \Gamma_4 =$* 99 meV. *The effect of using the antiferromagnetic molecular field deduced from that of UO_2 to enhance the bare susceptibility is given by the curves labeled CEF+I. Figure reprinted with permission from Colarieti-Tosti* et al. (2002). *Copyright* 2002 *by the American Physical Society.*

20.14.4 Americium dioxide

For the heavier elements starting with Am, experiments become really sparse. Am^{4+} in AmO_2 should have a ground $5f^5$:$^6H_{5/2}$ state, i.e. a Kramers' ion so that the degeneracy cannot be lifted by a crystal field interaction (the same as Np in

NpO_2). EPR studies of Am^{4+} doped into ThO_2 and CeO_2 establish the Γ_7 doublet as the ground state (Abraham *et al.*, 1971; Kolbe *et al.*, 1974) with a $g_{\text{eff}} = 1.27$. Karraker (1975a) has made susceptibility measurements (on a sample with 224 mg of ^{243}Am and a radiation field of $\sim$150 roentgen h^{-1} at the sample!) and found an effective moment of $1.31\mu_B$ at low temperature. Since $S = 5/2$, this gives $g = 0.44$ which is in excellent accord with the value for a $5f^5$ state when intermediate coupling is taken into account (Lander, 1993). With an effective spin of $S_{\text{eff}} = 1/2$, corresponding to the Γ_7 doublet, one obtains $g_{\text{eff}} = 1.51$, in reasonable agreement with the EPR work.

Karraker (1975a) also found clear evidence for a phase transition at $T_o = 8.5$ K. The susceptibility shows a peak and then decreases as the temperature decreases. This was puzzling at the time, as a Mössbauer experiment (Kalvius *et al.*, 1969) had found *no* evidence for any phase transition. Later, Boeuf *et al.* (1979) prepared another sample of $^{243}AmO_2$ and performed neutron scattering experiments at the Institute Laue Langevin in Grenoble. They observed no magnetic diffraction peaks below T_o in agreement with the Mössbauer results. No further experiments have been reported on the low-temperature properties of AmO_2 since 1979.

Of course, given what happens in the case of NpO_2 (the ordering of the quadrupoles) in a Kramers ion with an odd number of 5f electrons (Paixão *et al.*, 2002), it is easy to suggest that the same thing happens in AmO_2. This would make a really beautiful experiment with RXS, but one would need a single crystal, even if only of $\sim$20 μg.

20.14.5 Curium dioxide

With Cm^{4+} the ground state should be a $5f^6\ ^7F_0$ state. Since $L = |S| = 3$, there should be *no* sign whatsoever of magnetism, particularly in the susceptibility. The splitting to the first excited state is at $\sim$400 meV, so the susceptibility should be temperature-independent and small. The difficulty is that Cm^{3+} is more stable thermodynamically than Cm^{4+} so it is not difficult to imagine small amounts of Cm^{3+} in the CmO_2 matrix. Cm^{3+} has the $5f^7\ ^8S_{7/2}$ configuration and so it could contribute $\sim 7\mu_B$ of magnetism. Many early efforts on CmO_2 reported a sloping susceptibility, but in all cases it was expected that was a consequence of contamination with Cm^{3+}.

In 1986 Morss at Argonne set out to make stoichiometric CmO_2 from the rare isotope ^{248}Cm. This had the advantage that the radiation from ^{248}Cm is relatively small compared to the more abundant ^{244}Cm so that radiation damage and production of defects, which could convert Cm^{4+} into Cm^{3+}, were reduced. The sample ($\sim$55 mg) was then studied with neutron diffraction at the IPNS spallation source at Argonne. The small sample and the relatively modest flux at IPNS meant that the strongest powder diffraction peak in CmO_2 gave $\sim$1 ct min^{-1}, with a peak/background ratio of 0.6. (Part of the background came from the neutrons emitted from the ^{248}Cm sample itself.) Despite these difficulties,

Rietveld analysis was successful and gave a Cm:O stoichiometry of 1.97 (3), which is statistically insignificant from the stoichiometric composition (Morss *et al.*, 1989). The X-ray pattern from CmO_2 is, of course, totally dominated by the scattering from the Cm, so this is a good illustration of the power of neutrons, where the scattering from curium and oxygen have almost equal scattering lengths. In agreement with X-rays, no evidence of additional phases was found.

Susceptibility measurements were then made and showed, once again, a slope, which corresponded to $\mu_{\text{eff}} = 3.36\ (6)\mu_{\text{B}}$. More than 10 years have gone by since this work and no suggestion has been made to resolve the difficulty between simple crystal field theory (with a $^7F_0$ ground state) and the finite effective moment. However, taking the theory, developed for another *even* 5f electron material (Pu with four 5f electrons), can be utilized by assuming that the susceptibility is affected by the exchange and possibly also JT interactions as found in another even-f system, UO_2. Although $J = 0$, there is an S quantum number of 3 (6f electrons) and the spin state of Cm will give rise to antiferromagnetic exchange via coupling to the excited (magnetic) $J = 1$ state. Detailed calculations for this have not been made, but should be. Furthermore, this effect is not expected to give a constant μ_{eff} for all Cm^{4+} ions. The antiferromagnetic exchange passes through the actinide 6d states and their mixing with the oxygen p-states. This will change depending on the anions involved, for example it will be different for CmO_2 than CmF_4. More experiments on these materials would be interesting and should further increase our understanding of the interactions in the ionic actinide systems. As discussed in Section 20.8, Milman *et al.* (2003) performed density functional theory (DFT) calculations for Cm compounds and suggested that an itinerant magnetism model might be appropriate for CmO_2.

20.14.6 Summary of the magnetic properties of the actinide dioxides

Many physicists have been kept busy for the last half a century studying the properties of the actinide dioxides. Initially it was expected that the data would be relatively straightforward to analyze because of the very simple fcc structure. As happens frequently in actinide research, the trail has been tortuous, and in all cases there are still experiments to be done, although a general understanding of the ground state magnetic properties now appears reasonably sound. Neutron inelastic scattering has played an important role in establishing the crystal field interactions and showing that the earlier theoretical models were incorrect. The crystal field ground states are then perturbed by higher-order interactions, notably the quadrupolar ones, and this is a consequence of the aspherical nature of the 5f electron states. The effect is particularly apparent in NpO_2 ($5f^3$), in which the quadrupoles order at 25 K, presumably because of their interactions with the lattice, and there is *no* accompanying dipole ordering (at least down to 1.5 K). For the moment NpO_2 appears unique in this respect, but no doubt

other materials will be found; AmO_2 appears a good candidate. The interactions with the lattice are very strong for all the oxides, and give rise to a number of effects. Most notably, the Jahn–Teller interactions cause an internal *static* distortion in UO_2, but can be dynamic in nature as well (Sasaki and Obata, 1970). If the susceptibility of PuO_2 ($5f^4$) is reasonably well explained by the indirect exchange through the oxygen p-states (thus implying a measure of covalency in these materials), the situation in CmO_2 ($5f^6$) is more complicated. Perhaps some of the same arguments can be used, together with the JT effect, but it is still not possible to exclude the presence of Cm^{3+} ions in the compound, and these would give a large susceptibility term, as they are $5f^7$. The detailed exchange interactions (measured by neutron inelastic scattering on single crystals, Caciuffo *et al.*, 1999) in UO_2 still are not understood from first principles, illustrating the complexity of the interactions that occur in these oxides.

ABBREVIATIONS

AF	antiferromagnetic
bcc	body-centered cubic
BM (β)	Bohr magneton
^{t}Bu	^{t}butyl – tertiary butyl – $(CH_3)_3C$
CEA	Commissariat à l'Energie Atomique
CF	crystal field
cm^{-1}	wave numbers
Cp	cyclopentadienyl – C_5H_5
dhcp	double hexagonal close-packed
DFT	density functional theory
ENDOR	electron-nuclear double resonance
EPR or epr	electron paramagnetic resonance
Et	ethyl – C_2H_5 – CH_3CH_2
fcc	face-centered cubic
IPNS	Intense Pulsed Neutron Source
JT	Jahn–Teller
LO	longitudinal optic
Me	methyl – CH_3
meV	millielectron volts
mK	milli-Kelvin
NMR or nmr	nuclear magnetic resonance
RXS	resonant X-ray scattering
T_c	temperature below which superconductivity occurs
TIP	temperature-independent paramagnetism
T_N	Neel temperature

T_o	Temperature at and below which a magnetically ordered phase appears
XMCD	X-ray magnetic circular dichroism

UNITS

Two different energy units are used in this review depending on the discussion. The units are meV and cm^{-1}. The conversion between these units is as follows: (1 eV = 8065.479 cm^{-1}); (1 meV = 0.001 eV = 8.065 cm^{-1}); (1 cm^{-1} = 1.2399 × 10^{-4} eV or 0.12399 meV). It is useful to note that kT (where k is the Boltzmann constant) at 300 K = 25.85 meV = 208.34 cm^{-1}.

REFERENCES

Abragam, A. and Bleaney, B. (1970) *Electron Paramagnetic Resonance of Transition Ions,* Clarendon Press, Oxford.

Abraham, M. M., Judd, B. R., and Wickman, H. H. (1963) *Phys. Rev.*, **130**, 611–12.

Abraham, M. M., Finch, C. B., and Clark, G. W. (1968) *Phys. Rev.*, **168**, 933.

Abraham, M. M., Boatner, L. A., Finch, C. B., Reynolds, R. W., and Zeldes, H. (1970) *Phys. Rev. B*, **1**, 3555–60.

Abraham, M. M., Boatner, L. A., Finch, C. B., and Reynolds, R. W. (1971) *Phys. Rev. B*, **3**, 2864

Abraham, M. M., Boatner, L. A., Finch, C. B., Kot, W. K., Conway, J. G., Shalimoff, G. V., and Edelstein, N. M. (1987) *Phys. Rev. B*, **35**, 3057–61.

Aderhold, C., Baumgartner, F., Dornberger, E., and Kanellakopulos, B. (1978) *Z. Naturforsch.*, **33a**, 1268–80.

Aldred, A. T., Cinader, G., Lam, D. J., and Weber, L. W. (1979) *Phys. Rev. B*, **19**, 300–5.

Alessandrini, V. A., Cracknell, A. P., and Przystawa, J. A. (1976) *Commun. Phys.*, **1**, 51–5.

Allen, S. J. (1968a) *Phys. Rev.*, **167**, 492–6.

Allen, S. J. (1968b) *Phys. Rev.*, **166**, 530–9.

Allen, S., Barlow, S., Halasyamani, P. S., Mosselmans, J. F. W., O'Hare, D., Walker, S. M., and Walton, R. I. (2000) *Inorg. Chem.*, **39**, 3791–8.

Almond, P. M., Deakin, L., Porter, M. J., Mar, A., and Albrecht- Schmitt, T. E. (2000) *Chem. Mater.*, **12**, 3208–13.

Amberger, H. -D., Fischer, R. D., and Kanellakopulos, B. (1975) *Theor. Chim. Acta*, **37**, 105–27.

Amberger, H.-D. (1976a) *J. Organomet. Chem.*, **116**, 219–29.

Amberger, H.-D. (1976b) *J. Organomet. Chem.*, **110**, 59–66.

Amberger, H.-D., Fischer, R. D., and Kanellakopulos, B. (1976) *Z. Naturforsch.*, **B31**, 12–21.

Amoretti, G., Blaise, A., Caciuffo, R., Fournier, J. M., Hutchings, M. T., Osborn, R., and Taylor, A. D. (1989) *Phys. Rev. B*, **40**, 1856–70.

Amoretti, G., Blaise, A., Caciuffo, R. C., Di Cola, D., Fournier, J. M., Hutchings, M. T., Lander, G. H., Osborn, R., Severing, A., and Taylor, A. D. (1992) *J. Phys. Condensed Matter*, **4**, 3459–78.

Arliguie, T., Lance, M., Nierlich, M., Vigner, J., and Ephritikhine, M. (1995) *J. Chem. Soc. Chem. Commun.*, 183–4.
Arrott, A. and Goldman, J. E. (1957) *Phys. Rev.*, **108**, 948.
Axe, J. D. (1960) University of California, Radiation Laboratory Report, UCRL-9293.
Axe, J. D., Stapleton, H. J., and Jeffries, C. D. (1961) *Phys. Rev.*, **121**, 1630.
Bacon, G. E. (1962) *Neutron Diffraction,* Oxford University Press, Oxford.
Baybarz, R. D., Asprey, L. B., Strouse, C. E., and Fukushima, E. (1972) *J. Inorg. Nucl. Chem.*, **34**, 3427–31.
Berger, M. and Sienko, M. J. (1967) *Inorg. Chem.*, **6**, 324–6.
Bernhoeft, N., Sato, N., Roessli, B., Aso, N., Hiess, A., Lander, G. H., Endoh, Y., and Komatsubara, T. (1998) *Phys. Rev. Lett.*, **81**, 4244.
Bernstein, E. R. and Keiderling, T. A. (1973) *J. Chem. Phys.*, **59**, 2105–22.
Bernstein, E. R. and Dennis, L. W. (1979) *Phys. Rev. B*, **20**, 870.
Bickel, M. and Kanellakopulos, B. (1993) *J. Solid State Chem.*, **107**, 273–84.
Blaise, A., Genet, M., Chong- Li, S., and Soulie, E. (1986) *J. Less Common Metals*, **121**, 209–15.
Blake, P. C., Lappert, M. F., Atwood, J. L., and Zhang, H. (1986) *J. Chem. Soc., Chem. Commun.*, 1148.
Blake, P. C., Edelstein, N. M., Hitchcock, P. B., Kot, W. K., Lappert, M. F., Shalimoff, G. V., and Tian, S. (2001) *J. Organomet. Chem.*, **636**, 124–9.
Blume, M. (1966) *Phys. Rev.*, **141**, 517–24.
Blume, M. (1985) *J. Appl. Phys.*, **57**, 3615.
Blume, M. and Gibbs, D. (1988) *Phys. Rev. B*, **37**, 1779.
Boatner, L. A., Reynolds, R. W., Finch, C. B., and Abraham, M. M. (1972) *Phys. Lett. A*, **42**, 93–4.
Boatner, L. A., Reynolds, R. W., Finch, C. B., and Abraham, M. M. (1976) *Phys. Rev. B,* **13**, 953–8.
Boatner, L. A. and Abraham, M. M. (1978) *Rep. Prog. Phys.*, **41**, 87–155.
Boerrigter, P. M., Baerends, E. J., and Snijders, J. G. (1988) *Chem. Phys.*, **122**, 357–74.
Boeuf, A., Rustichelli, F., Fournier, J. M., Gueugnon, J. F., Manes, L., and Rebizant, J. (1979) *J. Phys.* (*Paris*), *Lett.*, **40**, L335–8.
Boeuf, A., Caciuffo, R. C., Fournier, J. M., Manes, L., Rebizant, J., Rustichelli, F., Spirlet, J. C., and Wright, A. (1983) *Phys. Status Solidi A*, **79**, K1–3.
Bombardi, A., Kernavanois, N., Dalmas de Réotier, P., Lander, G. H., Sanchez, J. P., Yaouanc, A., Burlet, P., Lelievre-Berna, E., Rogalev, A., Vogt, O., and Mattenberger, K. (2001) *Eur. Phys. J. B*, **21**, 547
Boudreaux, E. A. and Mulay, L. N. (1976) *Theory and Applications of Molecular Paramagnetism,* Wiley, New York.
Brandt, O. G. and Walker, C. T. (1967) *Phys. Rev. Lett.*, **18**, 11.
Brandt, O. G. and Walker, C. T. (1968) *Phys. Rev.*, **170**, 528–41.
Brennan, J. G., Andersen, R. A., and Zalkin, A. (1986) *Inorg. Chem*, **25**, 1761–5.
Brodsky, M. B. (1978) *Rep. Prog. Phys.*, **41**, 1547–608.
Brooks, M. S. S., Johansson, B., and Skriver, H. L. (1984) *in Handbook of the Physics and Chemistry of the Actinides* (ed. A. J. Freeman and G. H. Lander), North-Holland, Amsterdam, pp. 153–269.
Brown, D., Lidster, P., Whittaker, B., and Edelstein, N. (1976) *Inorg. Chem.*, **15**, 511–14.
Butler, J. E. and Hutchison, C. A. Jr (1981) *J. Chem. Phys.*, **74**, 3102–19.

Caciuffo, R. C., Lander, G. H., Spirlet, J. C., Fournier, J. M., and Kuhs, W. F. (1987) *Solid State Commun.*, **64**, 149.

Caciuffo, R. C., Amoretti, G., Santini, P., Lander, G. H., Kulda, J., and Du Plessis, P. D. V. (1999) *Phys. Rev. B*, **59**, 13892.

Carnall, W. T., Kanellakopulos, B., Klenze, R., and Stollenwerk, A. (1980) in *Proc. 10eme Journees des Actinides* (eds. B. Johansson and A. Rosengren), pp. 201–16.

Carnall, W. T. (1992) *J. Chem. Phys.*, **96**, 8713–26.

Carra, P. and Altarelli, M. (1990) *Phys. Rev. Lett.*, **64**, 1286.

Chan, S. K. and Lam, D. J. (1974) *in The Actinide Electronic Structure and Related Properties,* vol. 1 (ed. A. J. Freeman and J. B. Darby), Academic Press, New York.

Chang, A. H. H. and Pitzer, R. M. (1989) *J. Am. Chem. Soc.*, **111**, 2500

Chang, C. T., Haire, R. G., and Nave, S. E. (1990) *Phys. Rev. B Condensed Matter*, **41**, 9045–8.

Colarieti-Tosti, M., Eriksson, O., Nordström, L., Wills, J., and Brooks, M. S. S. (2002) *Phys. Rev. B*, **65**, 195102

Collins, S. P., Laundy, D., Tang, C. C., and Cernik, R. J. (1995) *J. Phys. Condensed Matter*, **7**, L223.

Cowley, R. A. and Dolling, G. (1968) *Phys. Rev.*, **167**, 464.

Cox, D. E. and Frazer, B. C. (1967) *J. Phys. Chem. Solids*, **28**, 1649.

Crosswhite, H. M., Crosswhite, H., Carnall, W. T., and Paszek, A. P. (1980) *J. Chem. Phys.*, **72**, 5103–17.

Cunningham, B. B. (1962) Thermodynamics of the Actinides. *Thermodynamics of Nuclear Materials. International Atomic Energy Agency Symposium held in Vienna, Austria, May 21–25, 1962. Proc. Ser. STI/PUB/58*, 61–70.

Dallinger, R. F., Stein, P., and Spiro, T. G. (1978) *J. Am. Chem. Soc.*, **100**, 7865

Dalmas de Réotier, P., Yaouanc, A., Van Der Laan, G., Kernavanois, N., Sanchez, J. P., Smith, J. L., Hiess, A., Huxley, A., and Rogalev, A. (1999) *Phys. Rev. B*, **60**, 10606.

Delamoye, P., Krupa, J. C., Kern, S., Loong, C. -K., and Lander, G. H. (1986) *J. Less Common Metals*, **122**, 59–63.

Dell, R. M. and Bridger, N. J. (1972) in *MTP International Review of Science, Inorganic Chemistry, ser. I, Lanthanides and Actinides,* vol. 7 (ed. K. W. Bagnall), Butterworths, London, pp. 211–74.

Denning, R. G. (1992) *Struc. Bonding* (*Berlin*), **79**, 215–71.

Dolling, G., Woods, A. B. D., and Cowley, R. A. (1965) *Can. J. Phys.*, **43**, 1397.

Dornberger, E., Kanellakopulos, B., Klenze, R., and Stollenwerk, A. H. (1980) Crystal field spectra and magnetic properties of neptuniumtetracyclopentadienide, $(C_5H_5)_4Np$, and triscyclopentadienylneptuniumchloride, $(C_5H_5)_3NpCl$, in *Proc. 10eme Journees des Actinides* (ed. B. Johansson and A. Rosengren), pp. 58–73.

Drifford, M., Rigny, P., and Plurien, P. (1968) *Phys. Lett.*, **27A**, 620.

Dunlap, B. D., Kalvius, G. M., Lam, D. J., and Brodsky, M. B. (1968) *J. Phys. Chem. Solids*, **29**, 1365.

Edelstein, N., Easley, W., and Mclaughlin, R. (1966) *J. Chem. Phys.*, **44**, 3130–1.

Edelstein, N. and Easley, W. (1968) *J. Chem. Phys.*, **48**, 2110.

Edelstein, N., Mollet, H. F., Easley, W. C., and Mehlhorn, R. J. (1969) *J. Chem. Phys.*, **51**, 3281–5.

Edelstein, N., Conway, J. G., Fujita, D., Kolbe, W., and Mclaughlin, R. (1970) *J. Chem. Phys.*, **52**, 6425–6.

Edelstein, N. (1971) *J. Chem. Phys.*, **54**, 2488–91.
Edelstein, N. and Karraker, D. G. (1975) *J. Chem. Phys.*, **62**, 938–40.
Edelstein, N., Streitwieser, A. J., Morrell, D. G., and Walker, R. (1976) *Inorg. Chem.*, **15**, 1397–8.
Edelstein, N. (1977) *Rev. Chim. Miner.*, **14**, 149.
Edelstein, N., Kolbe, W., and Bray, J. E. (1980) *Phys. Rev. B*, **21**, 338–42.
Eichberger, K. and Lux, F. (1980) *Ber. Bunsenges. Phys. Chem.*, **84**, 800–7.
Eisenstein, J. C. and Pryce, M. H. L. (1955) *Proc. R. Soc. A*, **A229**, 20–38.
Eisenstein, J. C. and Pryce, M. H. L. (1960) *Proc. R. Soc. Lond. A*, **A255**, 181–98.
Erdos, P., Solt, G., Zolnierek, Z., Blaise, A., and Fournier, J. M. (1980) *Physica*, **102B**, 164–70.
Evans, D. F. (1959) *J. Chem. Soc.*, 2003–5.
Faber, J., Lander, G. H., and Cooper, B. R. (1975) *Phys. Rev. Lett.*, **35**, 1770–3.
Faber, J. Jr and Lander, G. H. (1976) *Phys. Rev. B*, **14**, 1151–64.
Finazzi, M., Sainctavit, P., Dias, A. M., Kappler, J. P., Krill, G., Sanchez, J. P., Dalmas De Rotier, P., Yaouanc, A., Rogalev, A., and Goulon, J. (1997) *Phys. Rev. B*, **55**, 3010.
Flotow, H. E. and Tetenbaum, M. (1981) *J. Chem. Phys.*, **74**, 5269.
Folcher, G., Marquet- Ellis, H., Rigny, P., Soulie, E., and Goodman, G. (1976) *J. Inorg. Nucl. Chem.*, **38**, 747–53.
Fournier, J. M., Blaise, A., Muller, W., and Spirlet, J. C. (1977) *Physica B*, **86–88**, 30–1.
Fournier, J. M. (1985) Magnetic properties of actinide solids, in *Structure and Bonding 59/60: Actinides-Chemistry and Physical Properties* (ed. L. Manes), Springer-Verlag, Berlin, pp. 127–96.
Francis, R. J., Halasyamani, P. S., and O'Hare, D. (1998) *Chem. Mater.*, **10**, 3131–39.
Frazer, B. C., Shirane, G., Cox, D. E., and Olsen, C. E. (1965) *Phys. Rev A*, **140**, 1448–52.
Freeman, A. J. and Darby, J. B. J. (1974) *The Actinides: Electronic Structure and Related Properties,* vols. 1 and 2, Academic Press, New York.
Friedt, J. M., Litterst, F. J., and Rebizant, J. (1985) *Phys. Rev. B*, **32**, 257
Fuji, K., Miyake, C., and Imoto, S. (1979) *J. Nucl. Sci. Technol.*, **16**, 207–13.
Fujita, D. K. (1969) University of California Radiation Laboratory Report, UCRL-19507.
Fujita, D. K., Parsons, T. C., Edelstein, N., Noe, M., and Peterson, J. R. (1976) The magnetic susceptibility of ^{244}Cm metal and ^{249}Cf metal, in *Transplutonium Elements* (eds. W. Muller and R. Lindner), North-Holland, Amsterdam, pp. 173–8.
Gajek, Z., Lahalle, M. P., Krupa, J. C., and Mulak, J. (1988) *J. Less Common Metals*, **139**, 351.
Gamp, E., Edelstein, N., Khan Malek, C., Hubert, S., and Genet, M. (1983) *J. Chem. Phys.*, **79**, 2023–6.
Gamp, E., Shinomoto, R., Edelstein, N., and McGarvey, B. R. (1987) *Inorg. Chem.*, **26**, 2177.
Giannozzi, P. and Erdos, P. (1987) *J. Magn. Magn. Mater.*, **67**, 75.
Gibbs, D., Hrashman, D. R., Isaacs, E. D., Mcwhan, D. B., Mills, D., and Vettier, C. (1988) *Phys. Rev. Lett.*, **61**, 1241.
Gourier, D., Caurant, D., Berthet, J. C., Boisson, C., and Ephritikhine, M. (1997) *Inorg. Chem.*, **36**, 5931–36.
Gourier, D., Caurant, D., Arliguie, T., and Ephritikhine, M. (1998) *J. Am. Chem. Soc.*, **120**, 6084–92.

Gruen, D. M. (1955) *J. Chem. Phys.*, **23**, 1708–10.
Handler, P. and Hutchison, C. A. Jr (1956) *J. Chem. Phys.*, **25**, 1210–13.
Hannon, J. P., Trammell, G. T., Blume, M., and Gibbs, D. (1988) *Phys. Rev. Lett.*, **62**, 2644.
Hauck, J. (1976) *Inorg. Nucl. Chem. Lett.*, **12**, 617–22.
Hayes, R. G. and Edelstein, N. (1972) *J. Am. Chem. Soc.*, **94**, 8688.
Heaton, L., Mueller, M. H., and Williams, J. M. (1967) *J. Phys. Chem. Solids*, **28**, 1651.
Hecht, H. G., Lewis, W. B., and Eastman, M. P. (1971) *Adv. Chem. Phys.*, **21**, 351.
Hendricks, M. E., Jones, E. R. Jr, Stone, J. A., and Karraker, D. G. (1971) *J. Chem. Phys.*, **55**, 2993–7.
Hendricks, M. E., Jones, E. R. Jr, Stone, J. A., and Karraker, D. G. (1974) *J. Chem. Phys.* **60**, 2095–103.
Hinatsu, Y., Miyake, C., and Imoto, S. (1981) *J. Nucl. Sci. Technol.*, **18**, 349–54.
Hinatsu, Y. and Edelstein, N. (1991) *J. Solid State Chem.*, **93**, 173.
Hinatsu, Y., Fujino, T., and Edelstein, N. (1992a) *J. Solid State Chem.*, **99**, 182–8.
Hinatsu, Y., Fujino, T., and Edelstein, N. (1992b) *J. Solid State Chem.*, **99**, 95–102.
Hinatsu, Y. (1994a) *J. Alloys Compd*, **203**, 251–7.
Hinatsu, Y. (1994b) *J. Solid State Chem.*, **109**, 1–6.
Holland-Moritz, E. and Lander, G. H. (1994) in *Handbook on the Physics and Chemistry of Rare Earths,* vol. 19 (eds. K. A. Gschneidner Jr, L. Eyring, G. H. Lander, and G. R. Choppin), North-Holland Physics, Amsterdam, pp. 1–121.
Howland, J. J. Jr and Calvin, M. (1950) *J. Chem. Phys.*, **18**, 239.
Hubert, S., Thouvenot, P., and Edelstein, N. (1993) *Phys. Rev. B*, **48**, 5751–60.
Huray, P. G., Nave, S. E., Peterson, J. R., and Haire, R. G. (1980) *Physica*, **102B+C**, 217–20.
Huray, P. G. and Nave, S. E. (1987) Magnetic studies of transplutonium actinides, in *Handbook on the Physics and Chemistry of the Actinides,* vol. 5 (eds. A. J. Freeman and G. H. Lander), North-Holland, Amsterdam, pp. 311–72.
Hutchison, C. A. Jr, Llewellyn, P. M., Wong, E., and Dorain, P. B. (1956) *Phys. Rev.*, **102**, 292.
Hutchison, C. A. Jr and Candela, G. A. (1957) *J. Chem. Phys.*, **27**, 707–10.
Hutchison, C. A. Jr and Weinstock, B. (1960) *J. Chem. Phys.*, **32**, 56–61.
Hutchison, C. A. Jr, Tsang, T., and Weinstock, B. (1962) *J. Chem. Phys.*, **37**, 555–62.
Ikushima, K., Tsutsui, S., Haga, Y., Ysauoka, H., Walstedt, R. E., Masaki, N. M., Nakamura, A., Nasu, S., and Onuki, Y. (2001) *Phys. Rev. B*, **63**, 104404.
James, R. W. (1958) *The Optical Principles of the Diffraction of X Rays*, G. Bell & Sons, London.
Johnston, D. A., Satten, R. A., Schreiber, C. L., and Wong, E. Y. (1966) *J. Chem. Phys.*, **44**, 3141.
Jones, E. R. Jr and Stone, J. A. (1972) *J. Chem. Phys.*, **56**, 1343.
Jones, E. R. Jr, Hendricks, M. E., Stone, J. A., and Karraker, D. G. (1974) *J. Chem. Phys.*, **60**, 2088–94.
Jones, W. M., Gordon, J., and Long, E. A. (1952) *J. Chem. Phys.*, **20**, 695.
Judd, B. R. (1963) *Operator Techniques in Atomic Spectroscopy,* McGraw-Hill, New York.
Kalina, D. G., Marks, T. J., and Wachter, W. A. (1977) *J. Am. Chem. Soc.*, **99**, 3877–9.

Kalvius, G. M., Ruby, S. L., Dunlap, B. D., Shenoy, G. K., Cohen, D., and Brodsky, M. B. (1969) *Phys. Lett. B*, **29**, 489.

Kalvius, G. M., Noakes, D. R., and Hartmann, O. (2001) (μ)SR studies of rare earth and actinide magnetic materials, in *Handbook on the Physics and Chemistry of Rare Earths,* vol. 32 (eds. K. A. Gschneidner Jr, L. Eyring, and G. H. Lander), North-Holland, Amsterdam.

Kanellakopulos, B., Dornberger, E., and Baumgartner, F. (1974) *Inorg. Nucl. Chem. Lett.*, **10**, 155–60.

Kanellakopulos, B., Blaise, A., Fournier, J. M., and Muller, W. (1975) *Solid State Commun.*, **17**, 713–15.

Kanellakopulos, B., Aderhold, C., Dornberger, E., Müller, W., and Baybarz, R. D. (1978) *Radiochim. Acta*, **25**, 85–92.

Kanellakopulos, B. (1979) Cyclopentadienyl compounds of the actinide elements, in *Organometallics of the f-Elements* (eds. T. J. Marks and R. D. Fischer), Reidel, Boston, pp. 1–35.

Kanellakopulos, B., Henrich, E., Keller, C., Baumgartner, F., Konig, E., and Desai, V. P. (1980a) *Chem. Phys.*, **53**, 197–213.

Kanellakopulos, B., Keller, C., Klenze, R., and Stollenwerk, A. H. (1980b) *Physica*, **102B**, 221–5.

Kanellakopulos, B., Klenze, R., and Stollenwerk, A. (1980c) Magnetic properties of the cubic octa-thiocyanato complexes, $(Et_4N)_4An(NCS)_8$, and of the tetra-chlorides, $AnCl_4$, of uranium and neptunium, in *Proc. 10eme Journees des Actinides* (eds. B. Johansson and A. Rosengren), pp. 217–31.

Karbowiak, M. and Drozdzynski, J. (1998a) *J. Alloys Compds*, **271–273**, 863–6.

Karbowiak, M. and Drozdzynski, J. (1998b) *J. Alloys Compds*, **275–277**, 848–51.

Karbowiak, M., Hanuza, J., Drozdzynski, J., and Hermanowicz, K. (1996) *J. Solid State Chem.*, **121**, 312–18.

Karbowiak, M., Drozdzynski, J., Hubert, S., Simoni, E., and Strek, W. (1998) *J. Chem. Phys.*, **108**, 10181–6.

Karraker, D. G., Stone, J. A., Jones, E. R. Jr, and Edelstein, N. (1970) *J. Am. Chem. Soc.*, **92**, 4841.

Karraker, D. G. (1971) *Inorg. Chem.*, **10**, 1564–6.

Karraker, D. G. (1973) *Inorg. Chem.*, **12**, 1105–8.

Karraker, D. G. (1975a) *J. Chem. Phys.*, **63**, 3174–5.

Karraker, D. G. (1975b) *J. Chem. Phys.*, **62**, 1444–6.

Karraker, D. G. and Dunlap, B. D. (1976) *J. Chem. Phys.*, **65**, 2032–3.

Karraker, D. G., and Stone, J. A. (1980) *Phys. Rev. B*, **22**, 111–14.

Keller, C. (1972) in *MTP International Review of Science, Inorganic Chemistry, ser. I, Lanthanides and Actinides,* vol. 7 (ed. K. W. Bagnall), Butterworths, London, pp. 47–85.

Kelly, P. J. and Brooks, M. S. S. (1987) *J. Chem. Soc., Faraday Trans. 2*, **83**, 1189–203.

Kern, S., Loong, C.-K., and Lander, G. H. (1985) *Phys. Rev. B*, **32**, 3051–7.

Kern, S., Morris, J., Loong, C. K., Goodman, G. L., Lander, G. H., and Cort, B. (1988) *J. Appl. Phys.*, **63**, 3598–600.

Kern, S., Loong, C.-K., Goodman, G. L., Cort, B., and Lander, G. H. (1990) *J. Phys. Condensed Matter*, **2**, 1933–40.

Kern, S., Robinson, R. A., Nakotte, H., Lander, G. H., Cort, B., Watson, P., and Vigil, F. A. (1999) *Phys. Rev. B*, **59**, 104–6.
Kolbe, W. and Edelstein, N. (1971) *Phys. Rev. B*, **4**, 2869–75.
Kolbe, W., Edelstein, N., Finch, C. B., and Abraham, M. M. (1972) *J. Chem. Phys.*, **56**, 5432–3.
Kolbe, W., Edelstein, N., Finch, C. B., and Abraham, M. M. (1973) *J. Chem. Phys.*, **58**, 820–1.
Kolbe, W., Edelstein, N., Finch, C. B., and Abraham, M. M. (1974) *J. Chem. Phys.*, **60**, 607–9.
Kolberg, D., Wastin, F., Rebizant, J., Boulet, P., Lander, G. H., and Schoenes, J. (2002) *Phys. Rev. B*, **66**, 214418.
Kopmann, W., Litterst, F. J., Klauss, H. H., Hillberg, M., Wagener, W., Kalvius, G. M., Schreier, E., Burghart, F. J., Rebizant, J., and Lander, G. H. (1998) *J. Alloys Compds*, **271**, 463–6.
Korobkov, I., Gambarotta, S., Yap, G. P. A., Thompson, L., and Hay, P. J. (2001) *Organometallics*, **20**, 5440–5.
Kostorz, G. E. (1979) Neutron scattering, in *Treatise on Materials Science and Technology*, vol. 15, Academic Press, New York.
Kot, W., Shalimoff, G., Edelstein, N., Edelman, M. A., and Lappert, M. F. (1988) *J. Am. Chem. Soc.*, **110**, 986.
Kot, W. K., Edelstein, N. M., Abraham, M. M., and Boatner, L. A. (1993a) *Phys. Rev. B*, **48**, 12704–12.
Kot, W. K., Edelstein, N. M., Abraham, M. M., and Boatner, L. A. (1993b) *Phys. Rev. B*, **47**, 3412–14.
Kot, W. K. and Edelstein, N. M. (1995) *New J. Chem.*, **19**, 641–54.
Lam, D. J. and Aldred, A. T. (1974) in *The Actinides: Electronic Structure and Related Properties*, vol. I, Academic Press, New York, pp. 109–79.
Lam, D. J. and Chan, S. K. (1974) *Phys. Rev. B*, **9**, 808–14.
Lämmermann, H. and Conway, J. G. (1963) *J. Chem. Phys.*, **38**, 259–69.
Lämmermann, H. and Stapleton, H. J. (1961) *J. Chem. Phys.*, **35**, 1514–16.
Lander, G. H., Brown, P. J., Spirlet, J. C., Rebizant, J., Kanellakopulos, B., and Klenze, R. (1985) *J. Chem. Phys.*, **83**, 5988–97.
Lander, G. H. and Aeppli, G. (1991) *J. Magn. Magn. Mater.*, **100**, 151–72.
Lander, G. H. (1993) in *Handbook on the Physics and Chemistry of Rare Earths,* vol. 17 (eds. K. A. Gschneidner Jr, L. Eyring, G. H. Lander, and G. R. Choppin), North-Holland Physics, Amsterdam, pp. 635–709.
Lander, G. H. (2002) *J. Magn. Magn. Mater.*, **242–245**, 3–8.
Langridge, S., Stirling, W. G., Lander, G. H., and Rebizant, J. (1994a) *Phys. Rev. B*, **49**, 12010–21.
Langridge, S., Stirling, W. G., Lander, G. H., and Rebizant, J. (1994b) *Phys. Rev. B*, **49**, 12022.
Langridge, S., Lander, G. H., Bernhoeft, N., Stunault, A., Vettier, C., Grübel, G., Sutter, C., Nuttall, W. J., Stirling, W. G., Mattenberger, K., and Vogt, O. (1997) *Phys. Rev. B*, **55**, 6392.
Lea, K., Leask, M., and Wolf, W. (1962) *J. Phys. Chem. Solids*, **23**, 1381–405.
Le Borgne, T., Riviere, E., Marrot, J., Thuery, P., Girerd, J. J., and Ephritikhine, M. (2002) *Chem. Eur. J.*, **8**, 774–83.

Leung, A. F. and Poon, Y. M. (1977) *Can. J. Phys.*, **55**, 937–42.
Lewis, W. B., Hecht, H. G., and Eastman, M. P. (1973) *Inorg. Chem.*, **12**, 1634–9.
Li, J. and Bursten, B. E. (1997) *J. Am. Chem. Soc.*, **119**, 9021–32.
Liu, G. K., Beitz, J. V., and Huang, J. (1993) *J. Chem. Phys.*, **99**, 3304–11.
Lovesey, S. W. and Collins, S. P. (1996) *X-ray Scattering and Absorption by Magnetic Materials,* Oxford Science Publications, New York.
Lukens, W. W. (1995) *Trivalent Metallocene Chemistry of Some Uranium, Titanium, and Zirconium Complexes*, Ph.D. Thesis, LBL-37646, University of California, Berkeley.
Lukens, W. W., Beshouri, S. M., Blosch, L. L., Stuart, A. L., and Andersen, R. A. (1999) *Organometallics*, **18**, 1235–46.
Mannix, D., Lander, G. H., Rebizant, J., Caciuffo, R., Bernhoeft, N., Lidstrom, E., and Vettier, C. (1999) *Phys. Rev. B*, **60**, 15187–93.
Marei, S. A. and Cunningham, B. B. (1972) *J. Inorg. Nucl. Chem.*, **34**, 1203–6.
McCart, B., Lander, G. H., and Aldred, A. T. (1981) *J. Chem. Phys.*, **74**, 5263–8.
McGarvey, B. R. (1998) *Inorg. Chim. Acta*, **272**, 43–54.
McGlynn, S. P. and Smith, J. K. (1962) *J. Mol. Spectrosc.*, **6**, 164.
McWhan, D. B., Vettier, C., Isaacs, E. D., Ice, G. E., Siddons, D. P., Hastings, J. B., Peters, C., and Vogt, O. (1990) *Phys. Rev. B*, **42**, 6007.
McWhan, D. B. (1998) *J. Alloys Compds*, **271–273**, 408.
Metoki, N., Haga, Y., Koike, Y., and Onuki, Y. (1998) *Phys. Rev. Lett.*, **80**, 5417.
Meyer, K., Mindiola, D. J., Baker, T. A., Davis, W. M., and Cummins, C. C. (2000) *Angew. Chem. Int. Ed. Engl.*, **39**, 3063–66.
Milman, V., Winkler, B., and Pickard, C. J. (2003) *J. Nucl. Mater.*, **322**, 165–79.
Miyake, C., Fuji, K., and Imoto, S. (1977a) *Chem. Phys. Lett.*, **46**, 349.
Miyake, C., Fuji, K., and Imoto, S. (1977b) *Inorg. Nucl. Chem. Lett.*, **13**, 53–5.
Miyake, C., Fuji, K., and Imoto, S. (1979) *Chem. Phys. Lett.*, **61**, 124–6.
Miyake, C., Takeuchi, H., Ohya-Nishiguchi, H., and Imoto, S. (1982) *Phys. Status Solidi* (*a*), **74**, 173.
Miyake, C., Takeuchi, H., Fuji, K., and Imoto, S. (1984) *Phys. Status Solidi* (*a*), **83**, 567.
Moore, J. R., Nave, S. E., Haire, R. G., and Huray, P. G. (1986) *J. Less Common Metals*, **121**, 187–92.
Moore, J. R., Nave, S. E., Hart, R. C., Wilmarth, W. R., Haire, R. G., and Peterson, J. R. (1988) *Phys. Rev. B Condensed Matter*, **38**, 2695–702.
Morss, L. R., Fuger, J., Goffart, J., and Haire, R. G. (1983) *Inorg. Chem.*, **22**, 1993–6.
Morss, L. R., Fuger, J., Goffart, J., Edelstein, N., and Shalimoff, G. (1987) *J. Less Common Metals*, **127**, 251.
Morss, L. R., Richardson, J. W. Jr, Williams, C. W., Lander, G. H., Lawson, A. C., Edelstein, N., and Shalimoff, G. (1989) *J. Less Common Metals*, **156**, 273–89.
Mortl, K. P., Sutter, J. P., Golhen, S., Ouahab, L., and Kahn, O. (2000) *Inorg. Chem.*, **39**, 1626–7.
Müller-Westerhoff, U. and Streitwieser, A. J. (1968) *J. Am. Chem. Soc.*, **90**, 7364–5.
Mulak, J. (1978) *J. Solid State Chem.*, **25**, 355–66.
Murasik, A. and Furrer, A. (1980) *Physica*, **102B+C**, 185–7.
Murasik, A., Fischer, P., and Szczepaniak, W. (1981) *J. Phys. C*, **14**, 1847–54.
Murasik, A., Fischer, P., Furrer, A., and Szczepaniak, W. (1985) *J. Phys. C: Solid State Phys.*, **18**, 2909–21.

Murasik, A., Fischer, P., Furrer, A., Schmid, B., and Szczepaniak, W. (1986) *J. Less Common Metals*, **121**, 151–5.

Murdoch, K. M., Edelstein, N. M., Boatner, L. A., and Abraham, M. M. (1996) *J. Chem. Phys.*, **105**, 2539–46.

Myers, R. J. (1973) *Molecular Magnetism and Magnetic Resonance Spectroscopy,* Prentice-Hall, New York.

Nakamoto, T., Nakada, M., Nakamura, A., Haga, Y., and Onuki, Y. (1999) *Solid State Commun.*, **109**, 77–81.

Nakamoto, T., Nakada, M., and Nakamura, A (2001) *Solid State Commun.*, **119**, 523–6.

Nave, S. E., Huray, P. G., and Haire, R. G. (1980) The magnetic susceptibility of sup 249/Bk metal. *Proc. Int. Conf. Crystalline Electric Field and Structural Effects in f-Electron Systems,* Plenum, 1980, pp. 269–74, New York.

Nave, S. E., Haire, R. G., and Huray, P. G. (1981) in *Actinides-1981, Abstracts,* Lawrence Berkeley Laboratory Report LBL-12441, pp. 144–6.

Nave, S. E., Haire, R. G., and Huray, P. G. (1983) *Phys. Rev. B*, **28**, 2317–27.

Nave, S. E., Moore, J. R., Spaar, M. T., Haire, R. G., and Huray, P. G. (1985) *Physica*, **130B+C**, 225–7.

Nave, S. E., Moore, J. R., Peterson, J. R., and Haire, R. G. (1987) *J. Less Common Metals*, **127**, 79–85.

Nellis, W. J. and Brodsky, M. B. (1974) *in The Actinides: Electronic Structure and Related Properties,* vol. II (eds. A. J. Freeman and J. B. J. Darby), Academic Press, New York, pp. 265–88.

Newman, D. J. (1971) *Adv. Phys.*, **20**, 197–256.

Normile, P. S., Stirling, W. G., Mannix, D., Lander, G. H., Wastin, F. J., Rebizant, J., Boudarot, F., Burlet, P., Lebech, B., and Coburn, S. (2002) *Phys. Rev. B*, **66**, 014405.

Osborn, R., Taylor, A. D., Bowden, Z. A., Hackett, M. A., Hayes, W., Hutchings, M. T., Amoretti, G., Caciuffo, R., Blaise, A., and Fournier, J. M. (1988) *J. Phys. C*, **21**, L931–7.

Osborne, D. W. and Westrum, E. F. (1953) *J. Chem. Phys.*, **21**, 1884.

Paixão, J. A., Detlefs, C., Longfield, M. J., Caciuffo, R., Santini, P., Bernhoeft, N., Rebizant, J., and Lander, G. H. (2002) *Phys. Rev. Lett.*, **89**, 187202–1–4.

Parry, J. S., Cloke, F. G. N., Coles, S. J., and Hursthouse, M. B. (1999) *J. Am. Chem. Soc.*, **121**, 6867–71.

Piehler, D., Kot, W. K., and Edelstein, N. (1991) *J. Chem. Phys.*, **94**, 942–8.

Pirie, J. D. and Smith, T. (1970) *Phys. Status Solidi*, **41**, 221.

Poirot, I., Kot, W., Shalimoff, G., Edelstein, N., Abraham, M. M., Finch, C. B., and Boatner, L. A. (1988) *Phys. Rev. B*, **37**, 3255–64.

Rahman, H. U. and Runciman, W. A. (1966) *J. Phys. Chem. Solids*, **27**, 1833–5.

Rahman, H. U. (1998) *Physica B*, **252**, 160.

Raison, P., Delapalme, A., Kiat, J. M., Schweiss, P., Kanellakopulos, B., Rebizant, J., Apostolides, C., Gonthier-Vassal, A., Lander, G. H., and Brown, P. J. (1994a) *Z. Kristallogr.*, **209**, 720.

Raison, P., Lander, G. H., Delapalme, A., Williams, J. H., Kahn, R., Carlile, C. J., and Kanellakopulis, B. (1994b) *Mol. Phys.*, **81**, 369.

Rajnak, K., Banks, R. H., Gamp, E., and Edelstein, N. (1984a) *J. Chem. Phys.*, **80**, 5951–62.

Rajnak, K., Gamp, E., Shinomoto, R., and Edelstein, N. (1984b) *J. Chem. Phys.*, **80**, 5942–50.
Raphael, G. and Lallement, R. (1968) *Solid State Commun.*, **6**, 383–5.
Reisfeld, M. J. and Crosby, G. A. (1965) *Inorg. Chem.*, **4**, 65.
Reynolds, J. G. and Edelstein, N. (1977) *Inorg. Chem.*, **16**, 2822–25.
Reynolds, J. G., Zalkin, A., Templeton, D. H., and Edelstein, N. (1977) *Inorg. Chem.*, **6**, 599–603.
Richardson, R. P. and Gruber, J. B. (1972) *J. Chem. Phys.*, **56**, 256–60.
Rigny, P. and Plurien, P. (1967) *J. Phys. Chem. Solids*, **28**, 2589.
Rigny, P., Dianoux, A. J., and Plurien, P. (1971a) *J. Phys. Chem. Solids*, **32**, 1175.
Rigny, P., Dianoux, A. J., and Plurien, P. (1971b) *J. Phys. Chem. Solids*, **32**, 1901–8.
Rosen, R. K., Andersen, R. A., and Edelstein, N. (1990) *J. Am. Chem. Soc.*, **112**, 4588–90.
Ross, J. W. and Lam, D. J. (1967) *J. Appl. Phys.*, **38**, 1451–3.
Rossat-Mignod, J., Lander, G. H., and Burlet, P. (1984) in *Handbook of the Physics and Chemistry of the Actinides* (eds. A. J. Freeman and G. H. Lander), North-Holland, Amsterdam, pp. 415–515.
Salmon, L., Thuery, P., Riviere, E., Girerd, J. J., and Ephritikhine, M. (2003) *Chem. Commun*, **21**, 762–3.
Santini, P., Lémanski, R., and Erdös, P. (1999) *Adv. Phys.*, **48**, 537–653.
Santini, P. and Amoretti, G. (2000) *Phys. Rev. Lett.*, **85**, 2188–91.
Santini, P. and Amoretti, G. (2002) *J. Phys. Soc. Jpn.*, **71**, 11.
Sarrao, J. L., Morales, L. A., Thompson, J. D., Scott, B. L., Stewart, G. R., Wastin, F., Rebizant, J., Boulet, P., Colineau, E., and Lander, G. H. (2002) *Nature*, **420**, 297–9.
Sasaki, K. and Obata, T. (1970) *J. Phys. Soc. Jpn.*, **28**, 1157.
Saxena, S. S., Agarwal, P., Ahilan, K., Grosche, F. M., Haselwimmer, R. K. W., Steiner, M. J., Pugh, E., Walker, I. R., Julian, S. R., Monthoux, P., Lonzarich, G. G., Huxley, A., Sheikin, I., Braithwaite, D., and Floquet, J. (2000) *Nature*, **406**, 587.
Schenk, H. J., Bohres, E. W., and Schwochau, K. (1975) *Inorg. Nucl. Chem. Lett.*, **11**, 201–6.
Schmid, B., Murasik, A., Fischer, P., Furrer, A., and Kanellakopulos, B. (1990) *J. Phys. Condensed Matter*, **2**, 3369–80.
Schoenes, J. (1980) *Phys. Rep.*, **63**, 301–36.
Schüssler-Langeheine, C., Weschke, E., Grigoriev, A. Y., Ott, H., Meier, R., Vyalikh, D. V., Mazumdar, C., Sutter, C., Abernathy, D., Grübel, G., and Kaindl, G. (2001) *J. Electron Spectrom. Related Phenom.*, **114–116**, 953.
Schütz, G., Wagner, W., Wilhelm, W., Zeller, R., Frahm, R., and Materlik, G. (1987) *Phys. Rev. Lett.*, **58**, 737.
Selbin, J., Ballhausen, C. J., and Durrett, D. G. (1972) *Inorg. Chem.*, **11**, 510.
Selbin, J. and Sherrill, H. J. (1974) *Inorg. Chem.*, **13**, 1235.
Seyferth, D. (2004) *Organometallics*, **23**, 3562–83.
Shinomoto, R., Gamp, E., Edelstein, N., Templeton, D. H., and Zalkin, A. (1983) *Inorg. Chem.*, **22**, 2351.
Shull, C. G. and Wilkinson, M. K. (1955) Oak Ridge National Laboratory, ORNL-1879, pp. 24–7.
Sidall, T. H., III. (1976) in *Theory and Applications of Molecular Paramagnetism* (eds. E. A. Boudreaux and L. N. Mulay), Wiley-Interscience, New York, pp. 317–48.

Siemann, R. and Cooper, B. R. (1979) *Phys. Rev. B*, **20**, 2869–85.
Skanthakumar, S., Williams, C. W., and Soderholm, L. (2001) *Phys. Rev. B Condensed Matter*, **64**, 144521/1–8.
Skold, K. and Price, D. L. (1987) *Neutron Scattering, Parts A, B, and C,* Academic Press, New York.
Soderholm, L., Edelstein, N., Morss, L. R., and Shalimoff, G. V. (1986) *J. Magn. Magn. Mater.*, **54–57**, 597–8.
Soderholm, L., Goodman, G. L., Welp, U., Williams, C. W., and Bolender, J. (1989) *Physica C*, **161**, 252–6.
Soderholm, L. (1992) *J. Alloys Compds*, **181**, 13–22.
Soderholm, L., Williams, C., Skanthakumar, S., Antonio, M. R., and Conradson, S. (1996) *Z. Phys. B*, **101**, 539–45.
Soderholm, L., Skanthakumar, S., and Williams, C. W. (1999) *Phys. Rev. B Condensed Matter*, **60**, 4302–8.
Solt, G. and Erdos, P. (1980) *J. Magn. Magn. Mater.*, **15–18**, 57.
Soulie, E. and Goodman, G. (1976) *Theor. Chim. Acta*, **41**, 17–36.
Soulie, E. and Goodman, G. (1979) *Erratum: Theor. Chim. Acta*, **51**, 259–60.
Soulie, E. and Edelstein, N. (1980) *Physica*, **102B**, 93–9.
Spirlet, M. R., Rebizant, J., Apostolidis, C., Dornberger, E., Kanellakopulos, B., and Powietzka, B. (1996) *Polyhedron*, **15**, 1503–8.
Squires, G. L. (1978) *Thermal Neutron Scattering,* Cambridge University Press, New York.
Stewart, J. L. (1988) *Tris[bis(trimethylsilyl)amido]uranium: Compounds with Tri-, Tetra-, and Pentavalent Uranium*. Ph.D. Thesis, LBL-25240, University of California, Berkeley.
Stewart, J. L. and Andersen, R. A. (1998) *Polyhedron*, **17**, 953–8.
Stollenwerk, A. H., Klenze, R., and Kanellakopulos, B. (1979) *J. Phys. (Paris), Colloq.*, **40** (C4), 179–80.
Stollenwerk, A. H. (1980) Institut für Heisse Chemie, Kernforschungszentrum Karlsruhe, pp. 1–202.
Stone, J. A. and Jones, E. R. Jr (1971) *J. Chem. Phys.*, **54**, 1713–18.
Templeton, D. H. and Templeton, L. K. (1985) *Acta Crystallogr.*, **A41**, 133–42.
Thole, B. T., Van Der Laan, G., and Sawatzky, G. (1985) *Phys. Rev. Lett.*, **55**, 2086.
Thouvenot, P., Hubert, S., and Edelstein, N. (1994) *Phys. Rev. B*, **50**, 9715–20.
Troc, R., Suski, W., Franse, J. J. M., and Gersdorf, R. (1991) Actinide elements and their compounds with other elements, part 1, in *Landolt-Börnstein Group III: Condensed Matter Volume 19 Magnetic Properties of Metals Subvolume F1* (ed. H. P. J. Wijn), Springer-Verlag, Berlin.
Troc, R. and Suski, W. (1993) Actinide elements and their compounds with other elements, part 2, in *Landolt-Börnstein Group III: Condensed Matter Volume 19 Magnetic Properties of Metals Subvolume F2* (ed. H. P. J. Wijn), Springer-Verlag, Berlin.
Van Vleck, J. H. (1932) *The Theory of Electric and Magnetic Susceptibilities,* Oxford University Press, Oxford.
Warren, K. D. (1977) *Struct. Bonding*, **33**, 97–138.
Warren, K. D. (1983) *Chem. Phys. Lett.*, **99**, 427–31.
Watson, G. M., Gibbs, D., Lander, G. H., Gaulin, B. D., Berman, L. E., Matzke, H., and Ellis, W. (1996) *Phys. Rev. Lett.*, **77**, 751.

Watson, G. M., Gibbs, D., Lander, G. H., Gaulin, B. D., Berman, L. E., Matzke, H., and Ellis, W. (2000) *Phys. Rev. B*, **61**, 8966.
Wilkinson, M. K., Shull, C. G., and Rundle, R. E. (1955) *Phys. Rev.*, **99**, 627.
Willis, B. T. M. and Taylor, R. I. (1965) *Phys. Lett.*, **17**, 188.
Wulff, M. and Lander, G. H. (1988) *J. Chem. Phys.*, **89**, 3295.
Wybourne, B. G. (1965) *Spectroscopic Properties of Rare Earths,* Interscience Publishers, New York.
Zimmermann, M. V., Nelson, C. S., Hill, J. P., Gibbs, D., Blume, M., Casa, D., Keimer, B., Murakami, Y., Kao, C. C., Venkataraman, C., Gog, T., Tomioka, Y., and Tokura, Y. (2001) *Phys. Rev. B*, **64**, 195133.
Zolnierek, A., Solt, G., and Erdos, P. (1981) *J. Phys. Chem. Solids*, **42**, 773–6.
Zolnierek, Z., Gajek, Z., and Khan Malek, C. (1984) *Physica*, **125B**, 199–214.

CHAPTER TWENTY ONE

5f-ELECTRON PHENOMENA IN THE METALLIC STATE

A. J. Arko, John J. Joyce, and Ladia Havela

21.1 INTRODUCTION

In this chapter, the properties of actinides in the metallic state will be reviewed with an emphasis on those properties which are unique or predominantly found in the metallic solid state. Such properties include magnetism, superconductivity, enhanced mass, spin and charge-density waves, as well as quantum critical points. An introduction to fundamental condensed matter principles is included to focus the discussion on the properties in the metallic state. Systematics of the actinide 5f electronic structure will be presented for elements, alloys, metallic, and semi-metallic compounds so as to elucidate the unique characteristics that arise from the properties of actinides and 5f electrons in a periodic potential.

There are two defining characteristics to materials in the metallic state: first, the material exhibits a periodic potential which controls much of the electronic structure, and second, there is a finite density of electronic states at the chemical potential which influences, among other properties, the thermodynamic and

transport characteristics. For the early actinide metals, these two characteristics are often manifested as narrow bands containing a substantial 5f electron component. Complexity in material properties often arises when competing or overlapping energy scales are available. In the metallic state, with a continuum of electron energy levels available, there is the possibility for interaction of charge with spin and lattice degrees of freedom. Because the actinides have an open 5f electron shell which, in the metallic state, often straddles the boundary between localized and itinerant character, the interplay between spin, charge, and lattice degrees of freedom leads to varied and interesting properties. In order to better understand the controlling role of the 5f electrons in the metallic state, one should look beyond the elements and beyond standard temperature and pressure. To elucidate the fundamental properties of 5f electrons in the metallic state, we consider the actinide elements at low temperature and high pressure. An additional dimension to the understanding of the 5f metals can be attained by considering the actinide elements in a metallic host matrix, e.g. alloys and compounds.

Atoms in a closely spaced periodic environment (crystalline condensed matter) experience an overlapping of outer electron shells with neighboring atoms. If the outer shells are open, then these electrons are shared between neighboring atoms and can travel from atom to atom through the periodic array. This sharing of electrons, a form of bonding, becomes the glue that holds the atoms together. In the crudest sense, this is the metallic state. Here attention is given to those atoms (materials) whose outer shell comprises an unfilled 5f shell, namely, actinide materials. A thorough treatment of the subject covers volumes (Kittel, 1963, 1971; Ziman, 1972; Ashcroft and Mermin, 1976; Harrison, 1980, 1999), so the overview presented here is cursory. The intent is primarily to cover those aspects of the metallic state that differentiate 5f electron systems from simpler metals containing only s, p, or d electrons, since many properties of 5f systems appear anomalous by comparison.

In the atomic and molecular configurations of f-electron materials, the highly directional nature of the f-orbitals plays a central role in the unique properties of the lanthanides and actinides. In the metallic state, however, it is widely accepted that it is the very limited radial extent of the 5f wave functions relative to the s, p, or d wave functions of the valence band that is at the heart of the exotic phenomena (consequently the 5f electrons are nearly localized), though the understanding of the actinides and their compounds is still incomplete. These metals and their compounds are among the most complex in the periodic table, displaying some of the most unusual behaviors relative to non-f systems, such as very low melting temperatures, large anisotropic thermal expansion coefficients, very low-symmetry crystal structures, many solid-to-solid phase transitions, exotic magnetic states, incommensurate charge-density waves, etc. Some insights can be gained by using the 4f series as a guide, but the comparison is limited since the radial extent of the 4f electrons is even smaller than that of the 5f electrons.

A comprehensive picture of actinides in the metallic state is slowly emerging. Many of the very unusual properties appear to be a direct consequence of the formation of extremely narrow 5f bands in which the electrons are not completely free. Rather, their motion is affected by the presence of neighboring 5f electrons. This differs from the lanthanide metals whose 4f electrons tend to be localized in atomic states except perhaps for Ce and Yb (Gschneidner and Eyring, 1993).

In recent years, there have been many advances in the theoretical capability to calculate the electronic structure of materials that form narrow bands. In particular, extensions to density functional theory (DFT) now allow the inclusion of some of the electron–electron interactions that previously were the exclusive domain of many-body physics. Yet even this approach often proves insufficient.

The problem of narrow bands or localization of electrons in an unfilled shell is strongly related to magnetic properties as well. However, there is a fundamental difference between band magnetism and localized magnetism. Although the electronic and magnetic properties of a material are related, the pervasiveness and sheer volume of unusual magnetic behavior observed in the 5f series suggest that they be treated separately.

21.2. OVERVIEW OF ACTINIDE METALS

The anomalous nature of the electronic properties of the 5f series of metals is apparent when considering the electrical resistivity, atomic volume (or equivalently the Wigner–Seitz radius), and a composite crystallographic phase diagram of the actinide metals through Cm. These physical properties are shown in Figs. 21.1–21.3. While these data have been presented on numerous occasions, they remain most illuminating, clearly showing a transition from itinerant (participating in bonding) behavior of the 5f electrons in the light actinides to localized (limited to an atomic site) behavior beyond Pu. It is the transition region that is least understood and where much of the anomalous behavior is centered.

Fig. 21.1 shows the electrical resistivity, ρ, as a function of temperature for the actinides through Cm (the last element obtained in sufficient bulk to allow such measurements). One immediately sees that the overall resistivity increases dramatically up to α-Pu (the low-temperature stable phase of Pu) and then begins to drop for Am. The α-Pu value of 150 $\mu\Omega$ cm ($\mu\Omega$ cm) is much higher than that of Cu (as a material with conventional metallic properties) where the room temperature value is of the order of 1 $\mu\Omega$ cm. The resistivity is intimately tied to the electronic structure of the material and several models ranging in complexity detail the relationship between resistivity and electronic structure. Within the free-electron model, ρ is related to the relaxation time τ of electrons

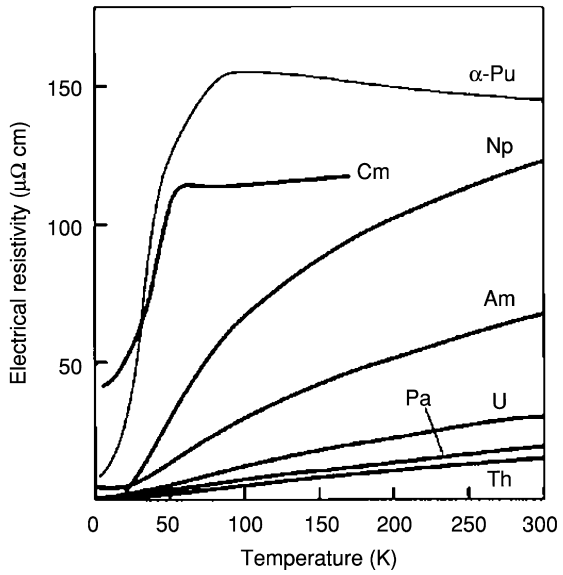

Fig. 21.1 *Electrical resistivity as a function of temperature between* 0 *and* 300 K *for the actinides metals Th through Cm* (*after Hecker,* 2001).

and mean free path defined as $\lambda = v_F\tau$, where v_F is the velocity of electrons at the Fermi surface, called Fermi velocity, by the relationship

$$\rho = m^*/Ne^2\tau \tag{21.1}$$

where m^* is the effective mass of electrons of charge e whose density is N. Clearly the mean free path of conduction electrons in 5f metals is very short and τ is the time between two scattering events compared to normal metals. It is shortest for α-Pu and begins to increase again with Am. Indeed, for α-Pu the mean free path of the conduction electrons is no more than the interatomic spacing. One can hardly call these free electrons.

Additionally, the α-Pu resistivity increases with decreasing temperature, an effect contrary to normal metals like Cu, while it appears relatively normal for Th through U. Such a negative temperature dependence is often associated with magnetic scattering of electrons (thus decreasing their mean free path) although experimental evidence indicates a lack of magnetism in Pu metal.

The Wigner–Seitz radius (Wigner and Seitz, 1933), or the equilibrium atomic volume of an atom in a metallic lattice, is likewise instructive, especially when compared to the volumes occupied by atoms in metals with an open 5d or 4f shell. Fig. 21.2 compares the Wigner–Seitz radius of the lanthanides and actinides with those of the 5d transition metals. It was shown by Friedel (1969) that the atomic volume should display a parabolic dependence with increasing atomic number Z as one fills an open shell of electrons involved in bonding

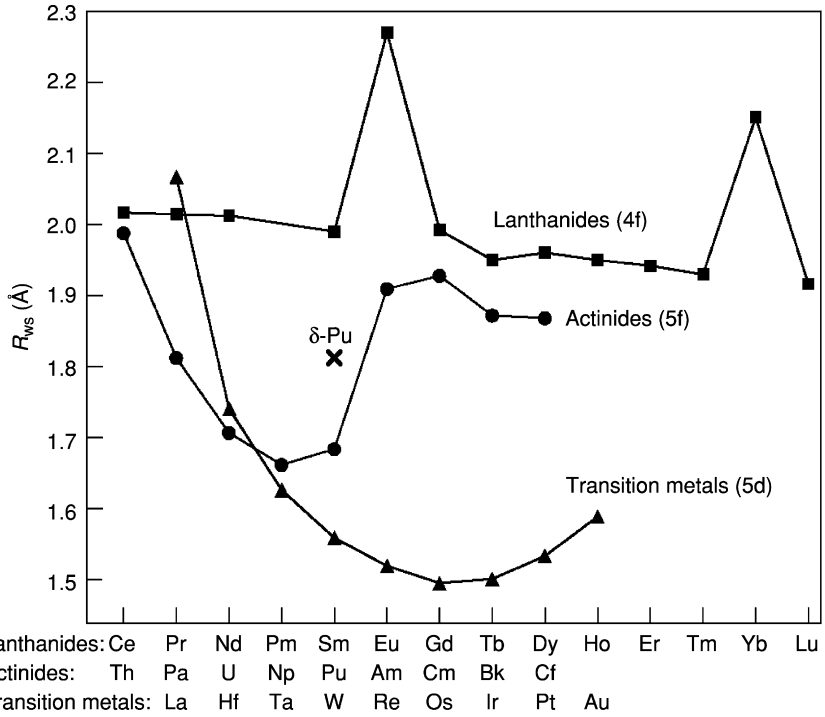

Fig. 21.2 *The Wigner–Seitz radius* (R_{WS}) *for the lanthanides, actinides and the* 5*d transition metal series. The transition metals show a parabolic dependence with bonding d-orbitals in accordance with the predictions of Friedel. The lanthanides display a nominally constant volume with non-bonding 4f states. The actinides show mixed character with Th through* α*-Pu on the bonding Friedel curve while Am–Cf look lanthanide-like with a non-bonding f-character* (*courtesy of Los Alamos Science*).

and conduction (i.e. the 5d electrons in Fig. 21.2). This is attributed to an increasing nuclear charge with its increasing Coulomb attraction, which is not completely screened by outer electrons shared by their neighbors, thus resulting in a volume contraction. But then, as the shell fills, the screening is again effective and the atom relaxes.

If, on the other hand, the outer electrons are instead localized as is the case of the 4f electrons in lanthanides, then the nuclear charge for each value of Z is effectively screened by the localized electrons, and the atomic volume remains unaffected as Z increases. This is clearly evident for the lanthanides in Fig. 21.2, except for Eu and Yb, exhibiting valency irregularities (the metals are divalent, not trivalent as the other lanthanides). The atomic volumes of early actinides appear to follow a parabolic curve up to the metal Np, suggesting 5f participation in bonding, but then begin to strongly deviate, behaving more like the

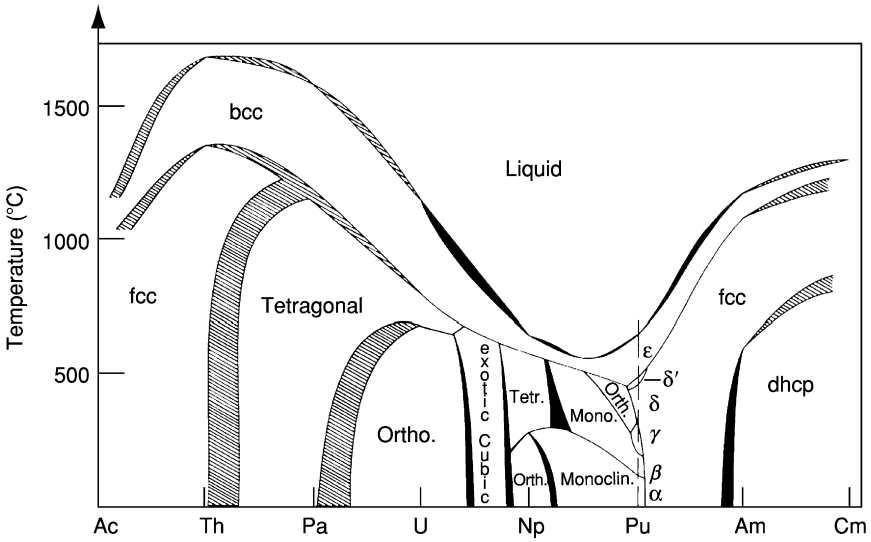

Fig. 21.3 *The binary phase diagram for the actinides Am through Cm showing the reduction in melting point and increase in complexity of the crystal structure and phases as the series moves from bonding (Ac–U) through localized (Am, Cm) with Pu having the lowest symmetry α-phase as well as the lowest melting point and six solid state allotropes (after Smith and Kmetko,* 1983).

localized 4f electrons beyond Pu (i.e. the atomic volumes remain relatively constant with increasing Z). It is as if there were two distinct 5f series: the first ending with Np and the second beginning with Am. In the intermediate region, the various phases of Pu are found, and also much of the correlated electron behavior of interest in this chapter.

The abrupt ending of the parabolic dependence of the equilibrium volumes of the actinides between plutonium and americium differentiates them from the lanthanides and the transition metals. But in addition, the transition metals and actinides also differ in their low-temperature crystal structures. The transition metals form close-packed, high-symmetry structures, such as hexagonal close-packed (hcp), face-centered cubic (fcc), and body-centered cubic (bcc), whereas the light actinides form at low temperatures low-symmetry, open-packed structures. For instance, protactinium forms a body-centered tetragonal (bct) structure, and uranium and neptunium form orthorhombic structures with two and eight atoms per cell, respectively. These data suggest that anomalous behavior already starts in the light actinides where many compounds of the light actinides display strongly correlated electron behavior (Ott and Fisk, 1987; Stewart, 2001).

The crystal structures, along with alloying information, are summed up in the composite phase diagram of Fig. 21.3 (Smith and Kmetko, 1983).

This phase diagram is composed of a series of binary phase diagrams of adjacent actinide metals from Ac to Cm plotted side by side (the x-axis between any two adjacent metals varies from 0 to 100% of the content of the heavier metal). The shaded areas having no crystal structure label represent areas of uncertainty.

In the early part of the series (between Ac and Th) structures are obtained somewhat similar to transition metals while beyond Am, typical structures of the rare earth metals are found. Indeed, it appears that beyond Am the anticipated 'second rare earth series' is obtained. In the region of Np and Pu, however, striking deviations from normal behavior are observed. The most obvious is the large drop in the melting temperature, reaching a value as low as 600°C near Np and Pu. Equally anomalous in this region, however, are the large number of allotropes, or solid-state crystalline phases. In fact, the actinides have the largest number of allotropes of any series in the periodic table. Also in this region one obtains the highest number of bonding f-electrons.

Many of these relevant parameters to actinide metals are captured in Table 21.1. Note the appearance of magnetism in the second rare earth series above Am, as well as the absence of many-body ordering phenomena in Pu and Np and the superconductivity in the light actinides (Am would nominally be magnetic if not for a fortuitous $J = 0$ ground state allowing for superconductivity). The occurrence of interesting electronic properties increases enormously as one changes from the pure actinide elements to actinide alloys and compounds.

Figs. 21.1–21.3 are entirely consistent with each other. The metallic radii are smallest at the crossover to localization, and as shown in Fig. 21.2, the low-temperature phases of the heavier actinides (beginning with americium) form dhcp structures. As in most metals, it is the bcc phase that forms prior to melting. However, the temperature range over which this phase is formed in the actinides is very small compared to transition metals and appears to be another signature of narrow bands, as described below (Wills and Eriksson, 2000).

A detailed description of the properties for Pu metal is presented in Chapter 7. Here the emphasis is on overall 5f electronic properties and their differences from simpler metals. To recognize these differences, a short discussion of free electron and condensed-matter behavior is presented. The papers by Boring and Smith (2000), and Wills and Eriksson (2000) serve as more detailed references and the main sources for this material.

21.3 BASIC PROPERTIES OF METALS (FREE-ELECTRON MODEL)

21.3.1 Formation of energy bands in simple metals

In general, most materials (metal or non-metal), when condensed in the solid state, form a crystalline array of repeating unit cells. Indeed, it is this repetition in space that allows for the mathematical determination of the electron wave

Table 21.1 *Properties of actinide metals.*

Element	*Melting point*[a,b] (K)	*Enthalpy of sublimation*[a,b] *at* 298.15 K (kJ mol^{-1})	*Lattice symmetry*[a–c]	*Temperature range* (K)[a–c]	*Lattice constants*[a,c] a_o (Å)	b_o (Å)	c_o (Å)	β (deg)	*X-ray density* (g cm^{-3}) (calc)	*Z (atoms per unit cell)*[a,c]	*Metallic radius CN* 12 (Å)[a,c,e]	*Bulk modulus* (GPa)[f]	*Low T specific heat coeff.* γ (mJ/mol K^2)[g]	χ_0 (10^{-4}emu/mol)[h,i]	μ_{eff} (μ_B)[j]	*Ordering temp.* (K)[l]
actinium	1323 ± 50	418 ± 20	fcc		5.315(5)				10.01	4	1.878					
thorium		602 ± 6	α, fcc	below 1633	5.0842				11.724	4	1.798	59.0(9)	4	.93		1.37 SC
	2023 ± 10		β, bcc	1633–2023	4.11 (1450K)					2	1.80					
protactinium		570 ± 10	α, bc tetrag.	below 1443	3.929		3.241		15.37	2	1.643	118(2)	6.6	2.7		1.4 SC
	1845 ± 20		β, bcc or fcc	1443–1845												
uranium		533 ± 8	α, orthorh.	below 941	2.854	5.87	4.955		19.04	4	1.542	104(2)	10	3.8		0.68 SC
			β, tetrag.	941–1049	5.656(5) (995K)	10.759(5)	10.759(5)		18.11	30	1.548					
	1408 ± 2		γ, bcc	1049–1408	3.524(2) (1078K)				18.06	2	1.548					
neptunium		465.1 ± 3.0	α, orthorh.	below 553	6.663 (293K)	4.723	4.887		20.48	8	1.503	118	14	5.5		
			β, tetrag.	553–849	4.897 (586K)		3.388		19.38	4	1.511					
	912 ± 3		γ, bcc	849–912	3.518 (873K)				18.08	2	1.53					
plutonium		349.0 ± 3.0	α, monocl.	below 397.6	6.183 (294 K)	4.822	10.963	101.79	19.85	16	1.523	43(2)	17(1)	5.3		
			β, monocl.	397.6–487.9	9.284 (463K)	10.463	7.859	93.13	17.71	34	1.571			5.5		

			γ, orthorh.	487.9–593.1	3.159 (508K)	5.768	10.162	17.15	8	1.588			5.2		
			δ, fcc	593.1–736.0	4.637 (593K)			15.92	4	1.640	29.9	64(3)	5.1		
			δ′, bc tetrag.	736.0–755.7	3.34 (738K)		4.44	16.03	2	1.640			5.1		
	913 ± 2		ε, bcc	755.7–913.0	3.6361 (763K)			16.51	2	1.592			5.2		
americium		283.8 ± 1.5	α, dhcp	below 1042	3.47		11.25	13.67	4	1.730	30	2	6.8		0.79 SC
			β, fcc	1042–1350	4.89			13.69	4	1.730					
	1449 ± 5		γ, bcc?	1350–1449	unknown										
curium		384 ± 10	α, dhcp	below 1568	3.500(3)[d]		11.34(1)[d]	13.5	4	1.743	33			8.07[k]	52 AF[k]
	1619 ± 50		β, fcc	1568–1619	5.065			12.7	4	1.782					
berkelium		310 ± 10	α, dhcp	below 1250	3.416(3)		11.069(7)	14.79	4	1.704	25			8.5	34 AF
	1323 ± 50		β, fcc	1250–1323	4.997(4)			13.24	4	1.767					
californium		196 ± 10	α, dhcp	below ∼973	3.384(3)		11.040	15.1	4	1.691	50			9.7	51 FM
	1173 ± 30		β, fcc	∼973–1173	4.78(1)			15.1	4	1.69					
einsteinium	1133	130 ± 10	fcc		5.75(1)			8.84	4	2.03				11.3?	

[a] Values from Chapters 2–12.
[b] Values taken from Chapter 19.
[c] Values taken from Chapter 22, at 298.15 K, except as noted.
[d] From Stevenson and Peterson (1979).
[e] See also Zachariasen (1973).
[f] Th (Benedict and Holzapfel, 1993); Pa, U, and Am (Lindbaum *et al.*, 2003); Np (Dabos *et al.*, 1987); α-Pu (Dabos-Seignon *et al.*, 1993); δ-Pu, from measurements on a single crystal of Pu with 3.3 atomic% Al (Ledbetter and Moment, 1976); Cm, Bk, and Cf (Benedict, 1987).
[g] Th (Gordon *et al.*, 1966); Pa (Spirlet *et al.*, 1987); U (Bader *et al.*, 1975); Np (Mortimer, 1979); α-Pu and δ-$Pu_{0.95}5Al_{0.05}$ (Lashley *et al.*, 2003); Am (Smith *et al.*, 1979).
[h] Temperature-independent susceptibility χ_0.
[i] Most of these elements show a slight temperature dependence, possibly due to impurities. Data taken from Nellis and Brodsky (1974) except Th (Greiner and Smith, 1971); Pu (Olsen *et al.*, 1992).
[j] Effective magnetic moment in units of Bohr magnetons (μ_B). Different samples show rather different values. Representative values given. Data taken from Chapter 20 except as noted.
[k] This Cm value is from Kanellakopulos *et al.* (1975).
[l] Superconducting (SC), antiferromagnetic (AF), ferromagnetic(FM). Data for ordering temperatures of the transamericium actinides are from Chapter 20 except as noted.

functions to within a phase factor. These cyclic wave functions are called Bloch states after Felix Bloch, who first introduced them (Bloch, 1928). The simplest elements, with a single outer electron, such as lithium or sodium, typically form cubic crystal structures at room temperature. The outer electrons from their atomic valence shells become conduction electrons traveling almost freely through the lattice. That is, these valence electrons occupy one-electron Bloch states, and they are therefore responsible for bonding in the solid.

A logical progression can be followed for band formation starting from the isolated atom, to molecules and finally, band formation and the formation of Bloch states in a metal. In the isolated atom, the electrons exist in a potential well with well-defined energy levels or states. The levels representing the outermost, or valence states, are responsible for bonding. Considering first the case of only two isolated atoms (i.e. molecular case), when two atoms are brought together, their outer electron wave functions (orbitals) overlap, and the valence electrons feel a strong electrostatic pull from both nuclei (typically depicted as a double-well electrostatic potential). The atomic orbitals combine to form molecular orbitals that may bind the two atoms into a diatomic molecule. The single atomic energy level splits into two allowed states: one lower in energy, or bonding, and the other higher in energy, or antibonding. The energy difference between these two levels is proportional to the amount of overlap of the two-electron atomic orbitals, and the molecular orbitals (wave functions) corresponding to the bonding and antibonding energy levels are the sum and difference, respectively, of the atomic orbitals.

If one generalizes to the case of N atoms brought close together to form a perfect crystal, the single valence electron now sees the periodic electrostatic potential due to all N atoms (where N is a number of order 10^{23}). The wave function (Bloch state) is now a combination of overlapping wave functions from all the atoms and extends over the entire volume occupied by those atoms. As in the molecular case, that wave function can be a bonding state or an antibonding state. The original atomic valence levels generalize to a band of very closely spaced energy levels, half of them bonding and half of them antibonding, and the width of the energy band is approximately equal to the energy splitting between the bonding and antibonding energy levels in the diatomic molecule. This broad band forms whether the crystal is an insulator, a metal, or a semiconductor, the metal being the case where the uppermost band is not completely occupied by the available electrons.

Because in a macroscopic sample the number of energy levels in the energy band is large (approximately 10^{23}, corresponding to the number of valence electrons in the crystal) and the spacing between these energy levels is small, the electron energies may be considered to be a continuous variable. The number of electron energy levels per unit energy is then described in terms of a density of states (DOS) that varies with energy. Because each electron must have a slightly different energy (the Pauli exclusion principle), electrons fill up

the energy levels one by one, in the order of increasing energy (in accordance with the Fermi–Dirac statistics). This concept will be detailed below.

21.3.2 Brillouin zones

A Bloch state, or the three-dimensional extended wave function of a valence electron in a solid, may be represented in one dimension by the valence electron wave function appearing at every atomic site along a line of atoms, but its amplitude is modulated by the plane wave $e^{i\boldsymbol{k}\cdot\boldsymbol{r}}$ where $\boldsymbol{k}$ is the momentum of the allowed state and $\boldsymbol{r}$ is the position vector. As mentioned before, this general form for a Bloch state in a solid emerges from the requirement of translational invariance. That is, the electron wave function in a given unit cell must obey the Bloch condition

$$u_k(r + \boldsymbol{T}_n) = u_k(r), \tag{21.2}$$

where $\boldsymbol{T}_n$ is a set of vectors connecting equivalent points of the repeating unit cells of the solid and u_k is the one-electron potential. The wave function must therefore be of the form

$$\Psi_k(r) = e^{i\boldsymbol{k}\cdot\boldsymbol{r}} u_k(r), \tag{21.3}$$

where a plane wave with wave vector $\boldsymbol{k}$ modulates the atomic wave function in a solid. The wave vector $\boldsymbol{k}$, or the corresponding crystal momentum $\boldsymbol{p} = h\boldsymbol{k}$, is the quantum number characterizing that Bloch state, and the allowed magnitudes and directions of $\boldsymbol{k}$ reflect the periodic structure of the lattice. Indeed, the momentum vectors $\boldsymbol{k}$ are related to the vectors of the unit cell in an inverse fashion. For example, if $\boldsymbol{T}_n$ is the vector in a unit cell in real space (e.g. along the [100] direction) which connects equivalent points, then the corresponding crystal momentum vector is $2\pi/\boldsymbol{T}_n$ which connects equivalent points in momentum space (i.e. a reciprocal lattice vector). The most basic periodic crystal unit is not necessarily the unit cell. Often a unit cell can be further reduced to a primitive cell, or a Bravais lattice, which defines the most basic repetitive unit. One can then derive a set of real space vectors that define a Bravais lattice. The inverse of these vectors defines the most basic repetitive unit in momentum space – the Brillouin zone. Energy bands are defined within this three-dimensional reciprocal, or momentum space having axes of k_x, k_y, and k_z. For a simple cubic unit cell, both the primitive cell in real space and its associated Brillouin zone are likewise simple cubic. Allowed energy band states, of course, can have a continuously varying set of momentum states, with the reciprocal lattice vectors being only a special set of crystal momenta defining the Brillouin zone boundaries along various high-symmetry directions. Within a solid, the periodic, crystalline symmetries replace the more common localized potentials of atoms and molecules. Also, the crystal momentum quantum numbers replace the usual orbital angular-momentum components. Within this framework, the metallic,

condensed matter properties of magnetism, superconductivity, enhanced mass, spin, and charge-density waves are quantified.

21.3.3 Complex and hybridized bands

The electronic structure gets more complicated in metals containing more than one type of valence electrons. A typical band structure for uranium metal (Wills and Eriksson, 2000) is shown in Fig. 21.4. Here the multiple overlapping bands are created when the conduction electrons in a solid originate from various s, p, d, and f valence orbitals of an atom. In general, the width of each band increases as the interatomic distance decreases and the overlap of the wave functions increases. Also, the s and p bands are always wider (span a wider energy range) than the d band, which in turn is always wider than the f band, reflecting the larger radial extent of the non-f wave functions. The overlapping bands in Fig. 21.4 portray a case where at a given value of $\boldsymbol{k}$ (a position vector in momentum space) one has wave functions of more than one orbital symmetry (angular momentum) but having nearly the same energy. This implies that the Bloch functions with a given quantum number (wave vector) $\boldsymbol{k}$ could be represented as a linear combinations of states originating from the s, p, d, and f atomic orbitals. In other words, the Bloch states could be 'hybridized' states containing many angular-momentum components, in contrast to atomic

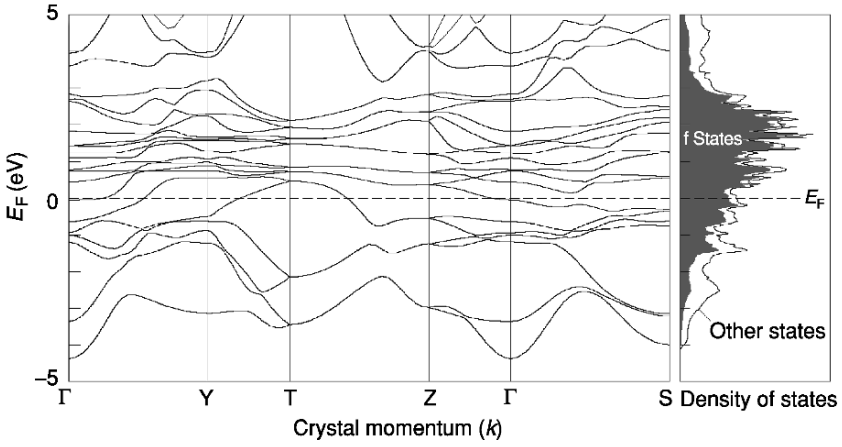

Fig. 21.4 *An electronic structure calculation for α-U metal including energy bands and the density of states. The DFT predictions for the energy bands* E(**k**) *are plotted along several different directions in the unit cell of the reciprocal lattice. The labels on the* **k***-axis denote different high-symmetry points in reciprocal space:* $\Gamma = (000)$, $Y = (100)$, $T = (111)$. *The narrow bands close to the Fermi level are dominated by the 5f levels. Some of the bands cross the Fermi level making α-uranium a metal. The shaded area for the density of states curve represents the 5f orbital contribution* (*courtesy of Los Alamos Science*).

orbitals that contain only one angular-momentum component. The angular-momentum mixture for a given band can vary from point to point in momentum space. Near $\boldsymbol{k}$-values where several bands are nearly degenerate one obtains a strong admixture, while for regions in $\boldsymbol{k}$-space where bands do not cross each other, the orbital symmetry of a band may contain only a single component. The dashed line in Fig. 21.4 is the Fermi energy (E_F) and separates the occupied from unoccupied energy levels.

The 5f states dominate the bonding primarily because there are three 5f electrons per atom and only one d-electron per atom occupying the Bloch states and participating in bonding. The narrow 5f band is referred to as the dominant band. Because narrow bands correspond to small overlaps of wave functions, these 5f band electrons may be easily pushed toward localization by various effects, in which case they do not contribute to bonding. Compared with the band widths of non-f metals, the actinide 5f bands are narrow and reflect the limited wave function overlap between f-orbitals on adjacent sites. The narrowness of the 5f bands and the proximity to the Fermi energy make the 5f bands central to understanding the actinide metallic state.

21.3.4 Density of states

A very useful concept to consider is the concept of the density of allowed energy states per unit energy interval. Recall that the allowed states in a band are not actually continuous, but are very closely spaced. Since each band of allowed states may contain two electrons from each atom (spin up and spin down), one can see that bands that disperse rapidly with energy will have fewer allowed states per unit energy interval than slowly dispersing or 'flat' bands. The right frame of Fig. 21.4 shows the DOSs resulting from the multiband structure on the left panel of Fig. 21.4. Note that the 5f states outnumber all the others at the Fermi energy E_F (see below for description). If an energy sub-band is filled (two electrons of opposite spin occupy all its energy levels), there will be no electron density at E_F and the solid is an insulator. If a band is only partially filled, the solid is a metal.

21.3.5 The Fermi energy and effective mass

Electrons, being spin-½ particles, obey Fermi statistics with the occupation of states occurring in order of increasing energy. The mathematical expression for Fermi–Dirac statistics is

$$f = 1/[\exp\{(E - E_F)/k_B T\} + 1]. \tag{21.4}$$

where k_B is the Boltzmann factor. The probability, f, for occupation of states at $T = 0$ is unity up to the Fermi energy, E_F, and zero above this energy. E_F is defined as the highest occupied energy state in a metal after all the electrons in a crystal (or in a box in the case of true free electrons) have been accounted for at

$T = 0$. As the atomic levels are filled up and the band states (i.e. the valence states involved in bonding) become occupied, the energy or momentum of a band electron from a particular atom is not precisely known. One only knows that it occupies one of the near continuum of allowed energies in a band and that the lowest states in a band must be occupied first.

In many elements (e.g. the alkali metals), the atom has only one electron to contribute to the uppermost or valence band. In that case, the uppermost band is unfilled (half filled for the alkali metals). More importantly, in the case of complex systems as shown in Fig. 21.4, the complexities introduced by the crystal structure and the subsequent hybridization result in an overlapping of valence bands, such that some states from a higher band actually lie below a lower one. This is clearly shown in Fig. 21.4 where the s–d bands cross the f-bands. In this case, the upper band begins to be filled before the lower one is fully occupied, so that, when all the electrons are exhausted, neither band is filled, and empty states exist just above E_F. The highest occupied energy (at $T = 0$ K) is E_F and the material is a metal because the electrons occupying the highest energy state have many empty allowed states in their vicinity into which they can scatter in order to travel throughout the crystal. By contrast, in the case of insulators where the uppermost band is fully occupied and there is an energy gap before the next band that is unoccupied, the Pauli exclusion principle prevents the occupation of states that already contain two electrons. Thus the electrons are not free to change states and move throughout the crystal unless they obtain sufficient energy to access an empty state beyond the energy gap between filled and empty states.

At finite temperature T, some electrons within k_BT below E_F can occupy empty states within k_BT above E_F. This is shown in Fig. 21.5 where the Fermi–Dirac distribution function has been convoluted with a model DOS. The probability of occupation of states below E_F is unity except within a few k_BT of E_F where some electrons can scatter into empty states within a few k_BT above E_F. Fig. 21.5 shows that electrons with binding energies higher than $(E_F - k_BT)$ contribute to the bonding, and only the narrow stripe just above E_F is responsible for the metallic behavior. Most of the properties of a metal (excluding magnetism) are determined by the band states within a few k_BT of E_F. The sudden drop in occupation is referred to as the Fermi edge. One immediately begins to see that densities of states whose width is of the order of k_BT will be dramatically affected by temperature. Of course, in complex systems electrons from more than one band and angular momentum are allowed to scatter into empty states. The substantive effects of the Fermi function are generally considered to occur within $\pm 2.2k_BT$ of the Fermi level. These values represent the 90% (below E_F) and 10% (above E_F) occupancy values for electron states at a finite temperature T.

Within the free-electron model (i.e. free-electron gas in a box) the energy is measured from the bottom of the free-electron band parabola. The electron energy dispersion is

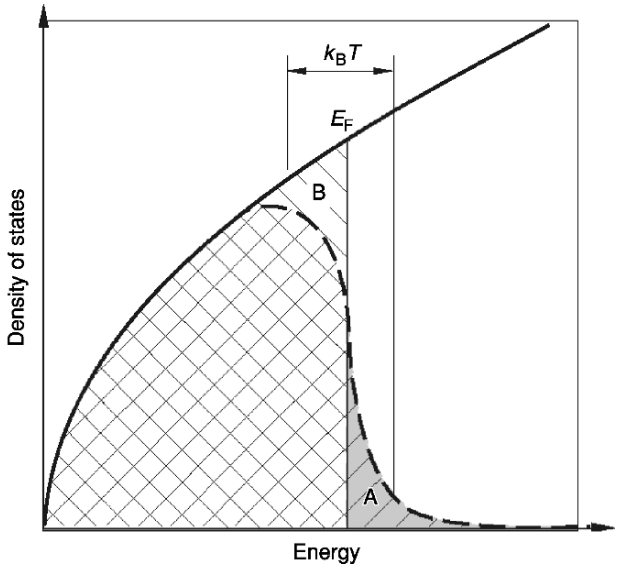

Fig. 21.5 *The solid line is the density of states for a free-electron gas plotted as a function of one-electron energy. At* T = 0, *electrons occupy all the states up to the Fermi energy* E_F. *The dashed curve shows the density of filled states at a finite temperature* T. *Only electrons within* k_BT *of the Fermi level can be thermally excited from states below the Fermi energy* (*region B*) *to states above that level* (*region A*) (*courtesy of Los Alamos Science*).

$$E = (\boldsymbol{p})^2/2m^*, \tag{21.5}$$

where $\boldsymbol{p}$ is the momentum and m^* is effective mass of the electron. The uppermost filled level is at the Fermi energy and is given by $E_F = (\boldsymbol{p}_F)^2/2m^*$, where $\boldsymbol{p}_F$ is the momentum of this uppermost level. Here E_F essentially corresponds to the bandwidth of the occupied states. If one then takes a repetitive box (i.e. a crystal lattice) one fulfills the requirement of periodicity, so that a free-electron parabola exists in each box – or Brillouin zone. The parabola from each Brillouin zone may extend through many other adjacent zones so that the resulting band (reduced or folded back into the first zone by virtue of periodicity) can be very complex. Nonetheless, in the case of alkali metals and other simple metals the bandwidth definition of the Fermi energy is still often used. The crystal momentum is zero at the center of the reciprocal lattice where $k = 0$. In a complex band system such as shown in Fig. 21.4, this definition loses some of its meaning. Nonetheless, if one adheres to this definition, one may define the Fermi temperature, $T_F = E_F/k_B$, as well as the Fermi velocity, $v_F = [2E_F/m^*]^{1/2}$. The use of m^* rather than m_o is appropriate in the formula because even the periodic crystal potential has some effect on the effective mass. Indeed many of

the properties of the free-electron model can be transferred to real material systems by substituting m^* for m_o.

The effective mass is essentially a measure of the interactions (correlations) that slow down (sometimes even speed up) the electron motion. Because of electron–electron interactions $\boldsymbol{v}_F$ can be smaller for a given $\boldsymbol{p}$, sometimes much smaller, than predicted by free-electron theory. It is as if the electron were much heavier than a free electron. Formally,

$$m^* = \hbar/(\mathrm{d}^2E(k)/\mathrm{d}k^2), \tag{21.6}$$

where $E(k)$ is a band that crosses the Fermi level and the derivative is evaluated at the Fermi level. It is easy to see that a very slowly dispersing or nearly flat band (this is obviously no longer a free-electron parabola) will have a much larger m^* than a rapidly varying band such as is found for s- and p-electrons where the wave function overlap is large. Correlations can be viewed as effectively resulting in a flattening of the bands at the Fermi edge.

21.3.6 Fermi surface

If one draws the energy band states in three dimensions defined by the crystal momentum $\hbar\boldsymbol{k}$ (in Fig. 21.4 they are shown in one dimension along a major symmetry axis) and connects all the points where each band crosses E_F, then these points trace out a surface in momentum space (or $\boldsymbol{k}$-space) known as the Fermi surface. In the free-electron model, each state on the Fermi surface corresponds to an electron having a constant absolute value of Fermi momentum $|\boldsymbol{p}_F|$ with kinetic energy given by the free particle formula above. In the case of a free-electron parabolic band, the Fermi surface is essentially a sphere, provided that the Fermi momentum $\boldsymbol{p}_F$ exists within the first Brillouin zone. If it extends into the next zone, one may still simply reconstruct the Fermi surface from a lattice of overlapping spheres. Again, in complex systems where several bands of differing angular momentum and bandwidth cross the Fermi energy, the topology of the Fermi surface can become extremely complex, one cannot use the simple bandwith definition of the Fermi energy, and $\boldsymbol{p}_F$ must be defined for each band.

The topology of the Fermi surface can be experimentally determined by means of de Haas–van Alphen (dHvA) oscillations. While a complete description of this effect is far beyond the scope of this chapter, qualitatively this is a measurement of the oscillatory diamagnetic susceptibility. For metal single crystals at low temperatures in the presence of a changing magnetic field, B, the diamagnetic susceptibility is influenced by B because the presence of B imposes an additional quantum condition on the free-electron orbits. The energy states of the electrons in the allowed orbits are called Landau levels, and these change with changing B. Without going into detail, the changing Landau levels (as B is varied) induce oscillations in the susceptibility, the frequency of

which (proportional to $1/B$) is directly related to the cross-sectional area of the Fermi surface in momentum space. By measuring the oscillations for differing directions of B, one can reconstruct the topology of the Fermi surface. Furthermore, by measuring the amplitude of the oscillations as a function of temperature, it is possible to determine the m^* of the orbiting electrons.

21.3.7 Electronic heat capacity

For a gas of free particles heated from absolute zero to a temperature T, classical statistical mechanics would predict that, on the average, the kinetic energy of each particle would increase by an amount $k_B T$. But because of the Pauli exclusion principle, the electrons obey Fermi–Dirac statistics and only those conduction electrons occupying states within $k_B T$ of the Fermi level E_F can be heated (by phonon scattering) because only they can access states not occupied by other electrons (see Fig. 21.5). The number of electrons that participate in properties such as electrical conduction and electronic heat capacity decreases to a fraction T/T_F of the total number of conduction electrons in the metal. At room temperature, T/T_F is about 1/200 in most metals. Thus, replacing the classical Maxwell–Boltzmann statistics with the Fermi–Dirac quantum statistics implied by the exclusion principle has a profound impact on the electronic properties of metals.

The factor T/T_F shows up explicitly in the low-temperature specific heat of a metal. In general, the specific heat is the sum of a lattice-vibration term (proportional to T^3) and an electronic term γT, which is due to the thermal excitation of the electrons. The classical coefficient of the electronic term is $\gamma = Nk_B$ (where N is the number of conduction electrons) but because of the exclusion principle, it becomes

$$\gamma = 2Nk_B T/T_F, \tag{21.7}$$

and only electrons near the Fermi energy can be excited. Thus, in simple metals obeying the free-electron model, γ is inversely proportional to T_F, or equivalently, E_F, and therefore proportional to m^* (see above), or to the density of electronic states at the Fermi level, $N(E_F)$. The prefactor 2 represents two possible spin directions.

A common unit of γ is (mJ mol^{-1} K^{-2}) and the value is about 1 for a typical free-electron metal like Cu. In strongly correlated actinide materials, values as large as 1000 have been observed. Here electrons behave more like strongly interacting particles of a liquid, e.g. more like a Fermi liquid. Because of interactions, m^* increases and shows an increase in the value of γ over that predicted by the free-electron model. Thus, low-temperature specific heat measurements reveal the strength of the electron–electron correlations in a metal and therefore provide a major tool for identifying unusual metals.

21.3.8 Electrical resistivity

For free electrons the resistivity ρ is given by equation (21.1). In a perfect crystal, electrical resistance would be zero near the classical $T = 0$ limit because the non-interacting conduction electrons, acting as waves, would move through the perfect lattice unimpeded. Above $T = 0$, the thermal excitations of lattice vibrations (phonons) affect the lattice periodicity and thus scatter the Bloch waves which depend on periodicity. Near $T = 0$, in the absence of strong electron–electron (e–e) interactions and impurities, $\rho(T)$ increases as T^5, while at higher temperatures $\rho(T) = AT$, where A is a constant. In general, anything that destroys the perfect translational invariance of the crystal lattice will scatter electrons. This is reflected in the mean free path of electrons, λ, the distance traveled by electrons between scattering events (see equation (21.1)). Foreign atoms, lattice vacancies, more complicated defects such as stacking faults, and finally, magnetic moments in an array without the full symmetry of the lattice can scatter electrons since they destroy the periodicity. Many of these imperfections are temperature-independent and lead to a finite limiting resistance as $T = 0$ is approached, called the residual resistance or ρ_0. Hence, this limit is used as a measure of the quality of metal samples, for which the lowest ρ_0 signifies the most perfect sample. It has been shown that correlated electron materials (and actinide metals in particular, see Fig. 21.1) often have anomalously high $\rho(T)$ and ρ_0 despite very small or zero magnetic moments at low temperatures. For systems with a high $N(E_F)$, strong electron–electron scattering gives rise to a term aT^2, where the prefactor a reflects the e–e correlations so that a/γ^2 is approximately constant for various materials.

21.3.9 One-electron band model

It has been shown that even a free-electron model for a periodic system yields a relatively complex band structure. The periodic potential actually introduces gaps at the Brillouin zone boundaries, and, depending on $\boldsymbol{p}_F$ relative to the zone boundaries, the Fermi surface can be very complicated. To obtain the band structure in materials with several valence electrons having more than one type of angular momentum requires substantial calculations. However, the problem of dealing with 10^{23} electrons can be reduced to a one-electron problem by assuming that an electron sees only an averaged potential between the ions and the remaining electrons, and that this periodic electrostatic potential can be modeled in a self-consistent fashion.

Slater first proposed calculating the electronic states, the energy bands in Fig. 21.4, of solids by the same self-consistent method that had been applied so successfully to describe the electronic states of atoms and molecules (Slater, 1937). In this method, one treats electrons as independent particles and calculates the average Coulomb forces on a single electron. The equation for the one-electron states is essentially the time-independent Schrödinger equation,

$$(T + V_{\text{eff}})\psi_{\text{i}}(\boldsymbol{r}) = E_i\psi_i(\boldsymbol{r}) \tag{21.8}$$

where T is a kinetic energy operator (e.g. $-\hbar^2\nabla^2/2m$ in a non-relativistic approximation and ∇ is the derivative with respect to position, V_{eff} is the average effective potential, and E_i are the eigenstates. The other electrons and all the ions in the solid are the source of these Coulomb forces on one electron and give rise to the V_{eff}. This calculation, repeated for all the electrons in the unit cell, leads to a charge distribution

$$n(r) = \Sigma|\psi_i(\boldsymbol{r})|^2 \tag{21.9}$$

from which a new electrostatic potential seen by the electrons can be obtained as a solution of the Poisson equation. Using the new electrostatic potential, one then repeats the calculations for each electron until the charge density (distribution of electrons) and the crystal potential (forces on the electrons) have converged to self-consistent values. Slater's approach led to all the modern electronic band structure calculations commonly labeled one-electron methods. These one-electron band-structure methods are adaptations of the familiar Hartree–Fock methods that work so well for atoms and molecules. They were put on a more rigorous footing through Kohn's development of DFT. Unlike the genuine Hartree–Fock method, the non-local part of electron–electron interaction is treated less formally, but it includes the long-range screening, unimportant for simple molecules but prominent in the electron gas.

Once a metal is formed, its conduction electrons (approximately 10^{23} per cubic centimeter) can act collectively, in a correlated manner, giving rise to what is called quasiparticle behavior (not determined by averaged electrostatic forces) and to collective phenomena such as superconductivity and magnetism. These phenomena are outside the scope of the independent electron model, which cannot accommodate all the electron–electron interactions found in the actinide series. Many-body interactions do not readily lend themselves to reduction to an average potential. Nevertheless, great strides have been made toward including correlations into the one-electron picture. In particular, DFT described below can incorporate the concept of exchange as well as Coulomb correlation. These electron correlations are described in the next section.

21.3.10 Electron–electron correlations

Electrons in a crystal are simultaneously attracted to the ions and repelled from each other via Coulomb repulsion. To minimize the total energy of the system, the electrons must minimize the electron–electron repulsion while maximizing the electron–ion attraction, and the way to minimize the Coulomb repulsion is for them to stay as far from each other as possible. In calculations on the helium atom it was found that: first, the two He electrons are indistinguishable – that is, electron 1 can be in orbital A or B, and so can electron 2; second, the electrons have to obey the Pauli exclusion principle, which means

that the total wave function for the two electrons has to be antisymmetric, and that antisymmetry implies that the Hamiltonian must contain an exchange term. This exchange term determines the probability that two electrons of the same spin can exist near each other. It is what separates the Hartree–Fock calculations of many-electron atoms from the original Hartree calculations of those atoms.

When the exchange term was included in the calculation of an electron gas, it was found that around each electron, there is a 'hole', or depression in the probability of finding another electron close by. Indeed, this probability was found to be one-half the value it would have without the exchange term. This exchange hole demonstrates that the electron motion of the two electrons is correlated with each other, in the sense that electrons with the same spin cannot get close to each other.

In the 1930's, Wigner performed similar calculations for electrons of opposite spins, which led to a 'correlation' hole (very similar to the exchange hole) for the probability of finding an electron of opposite spin near a given electron (Wigner, 1934). The picture of an exchange hole and a correlation hole around each electron is a great visual image of electron correlations in solids. Modern one-electron calculations include these correlations in an average way because these terms can be calculated from the average electron density around a given electron. The cost in energy of putting two electrons on the same site is referred to as the Coulomb correlation energy.

Several theories will be considered in this chapter that include interactions beyond the one-electron method, these approaches are termed correlated-electron theory. Likewise, any solid (metal, insulator, and so on) that exhibits behavior not explained by either the free-electron model or the one-electron band model is considered a correlated-electron system. If the properties of a solid deviate strongly from the predictions of free-electron or band models (e.g. heavy fermions), that solid is called a strongly correlated system. While many actinide metals and compounds fall within this group, still many others can be described as weakly correlated systems that are quite tractable within the one-electron approach.

21.3.11 Density functional theory

This section concludes with a brief description of DFT, a one-electron band structure approach which includes both exchange and correlation, and which has been very successful in describing weakly correlated systems. Two common variants are used: the local density approximation (LDA), which expresses the exchange and correlation potential, $E_{xc}(n(\boldsymbol{r}))$, as a function of local electron density, while the generalized gradient approximation (GGA) includes, in addition to these terms, the gradient of $n(\boldsymbol{r})$ as well. Formally, as in the Slater approach, the starting point for DFT calculations is the time-independent Schrödinger equation (similar to equation (21.8) above).

One would, in principle, calculate the ground-state (lowest-energy configuration) total electronic energy from

$$H\psi(\boldsymbol{r}_1, \boldsymbol{r}_2, \ldots \boldsymbol{r}_n) = E\psi(\boldsymbol{r}_1, \boldsymbol{r}_2, \ldots \boldsymbol{r}_n)\,, \tag{21.10}$$

where H is the Hamiltonian containing the kinetic energy and all the interactions of the system (i.e. electron–electron correlation and exchange and electron–nuclei interactions) and $\boldsymbol{r}_1$,$\boldsymbol{r}_2$,... $\boldsymbol{r}_n$ are the n position vectors. However, in the most generalized form $\psi(\boldsymbol{r}_1$,$\boldsymbol{r}_2$,... $\boldsymbol{r}_n)$ is now a many-electron wave function of the n-electron system, and E is the total electron energy of the entire system in the ground state. The input parameters in equation (21.10) are the atomic numbers of the atoms and the geometry of the crystal (the lattice constant, the crystal structure, and the atomic positions). From the solution of this equation, one should, in principle, be able to calculate the equilibrium crystal structure, the cohesive energy, as well as the band structure. Unfortunately, there is no practical way to solve equation (21.10) for a solid.

To get around this problem, Hohenberg and Kohn (1964), Kohn and Sham (1965), and Dreitzler and Gross (1990) pointed out that the total energy of a solid (or atom) may be expressed uniquely as a functional of the electron density (equation (21.9) (i.e. $E = E[n(\boldsymbol{r})]$ just as E_{xc} above). This function can be minimized in order to determine the ground-state energy. Therefore, instead of working with a many-electron wave function, $\psi(\boldsymbol{r}_1$,$\boldsymbol{r}_2$,... $\boldsymbol{r}_n)$, one can express the ground-state energy in terms of the electron density at a single point (as in equation (21.9)), where that density is due to all the electrons in the solid.

In addition, Hohenberg and Kohn (1964), Kohn and Sham (1965), and Dreitzler and Gross (1990) demonstrated that, instead of calculating the electron density from the many-electron wave function, one may work with the solutions to an effective one-electron problem (equation (21.8)). The method uses the form of the total-energy functional to identify an effective potential $V_{\mathrm{eff}}(r)$ as described above for one-electron states, and then to solve for the one-electron states to produce a density equal to the many-electron density. To account for the relativistic effects in actinides, it is necessary to replace the non-relativistic Schrödinger-like one-electron equation (equation (21.8)) by the relativistic Dirac equation. By finding the correct form for the effective potential, the electron density in equation (21.9) will be the same as that required by DFT.

The one-electron problem defined by equation (21.8) has the same form as the equations solved by band theorists before DFT was invented, and the eigenvalues of those equations as a function of crystal momentum are precisely the energy bands. The contribution of DFT is to provide a rigorous prescription for determining the new effective potential and for calculating the total ground-state energy, $E[n(\boldsymbol{r})]$.

The total energy functional within DFT is given by

$$E[n(\boldsymbol{r})] = T[n(\boldsymbol{r})] + E_{\mathrm{H}}[n(\boldsymbol{r})] + E_{\mathrm{xc}}[n(\boldsymbol{r})] + E_{\mathrm{eN}}[n(\boldsymbol{r})] + E_{\mathrm{NN}}, \tag{21.11}$$

where T is the effective kinetic energy of the one-electron states obtained from equation (21.9), E_{H} is the usual classical Hartree interaction between an electron and a charge cloud, E_{eN} is the interaction between an electron and nuclei, and E_{NN} is the inter-nuclear Coulomb interaction. The important term is E_{xc}, which is the one part of equation (21.11) that goes beyond the classical Hartree term obtained from the expression

$$E_{\mathrm{xc}}[n(\boldsymbol{r})] = \int n(\boldsymbol{r})\varepsilon_{\mathrm{xc}}(n(\boldsymbol{r}))\mathrm{d}\boldsymbol{r}. \tag{21.12}$$

This term represents the difference between the true energy of the eigenstates and the one-electron eigenstates. The operator of exchange-correlation $\varepsilon_{\mathrm{xc}}[n(\boldsymbol{r})]$ represents the sum of the exchange term $\varepsilon_{\mathrm{x}}(\boldsymbol{r})$ plus the correlation term $\varepsilon_{\mathrm{c}}(\boldsymbol{r})$.

The new (and presumably more correct) effective potential can now be obtained from the relationship

$$V_{\mathrm{eff}}(\boldsymbol{r}) = \delta/\delta n(\boldsymbol{r})[E_{\mathrm{H}}(n(\boldsymbol{r})) + E_{\mathrm{xc}}(n(\boldsymbol{r})) + E_{\mathrm{eN}}(n(\boldsymbol{r}))]. \tag{21.13}$$

With this new potential, the problem again reduces to a one-electron problem by substituting this potential into equation (21.8). From these definitions, it is clear that the effective potential in which the electron moves has contributions from the electron's interaction with the nuclei and the other electrons in the solid both by the classical Hartree term and by the quantum mechanical exchange and correlation terms.

Because all electron–electron interactions that go beyond the classical Hartree term are found in $E_{\mathrm{xc}}[n(\boldsymbol{r})]$, it is crucial to have a good approximation for this term. Unfortunately, there is no exact form of this term for a real solid. However, if one assumes the functional to be local, a numerical form may be obtained from many-body calculations (quantum Monte Carlo or perturbation series expansion), and very good values may be obtained for the ground-state energy for different values of the electron density. If the electron density of a real system varies smoothly in space, one expects that a form of E_{xc} taken from a uniform electron gas should be applicable to the real system as well. This approximation is none other than the LDA. The good agreement, for many solids, on cohesive energy, equilibrium volume, and structural properties between this approximate theoretical approach and experimental values suggests that the LDA form of E_{xc} works even if the electron density varies rapidly in space.

Thus, the total ground-state energy can be obtained by solving an effective one-electron equation. This tremendous simplification of replacing interacting electrons with effective one-electron states will work only if one can find the correct, effective one-electron potential. Good approximations can be obtained for $\varepsilon_{\mathrm{x}}(\boldsymbol{r})$ and $\varepsilon_{\mathrm{c}}(\boldsymbol{r})$ as determined by comparisons between the thus calculated band structures and experimental band structures measured by optical properties and photoelectron spectroscopy (PES).

21.4 GENERAL OBSERVATIONS OF 5f BANDS IN ACTINIDES

21.4.1 Narrow 5f bands

It is correct to say that the short radial extent of the 5f wave function yields only a small overlap between electrons from neighboring atoms and that this in turn results in very narrow 5f bands. Nevertheless, if the atomic spacing were sufficiently small, the overlap would be significant, as it is for 5f metals up to α-Pu. Why then does one not get a continuation of the actinide contraction (see Fig. 21.2) if the 5f electrons are involved in bonding?

Boring and Smith (2000) in their review argue that it is the presence of non-f bands at E_F (i.e. the 6p, 7s and to some extent the 6d bands), which contributes a repulsive force to the interatomic bonding forces (i.e. the s, p, d electrons with their larger radial extent, begin to repel each other at much larger distances). This is shown in Fig. 21.6 where the atomic-sphere approximation is used to calculate the contributions to bonding from individual bands for Pu (for

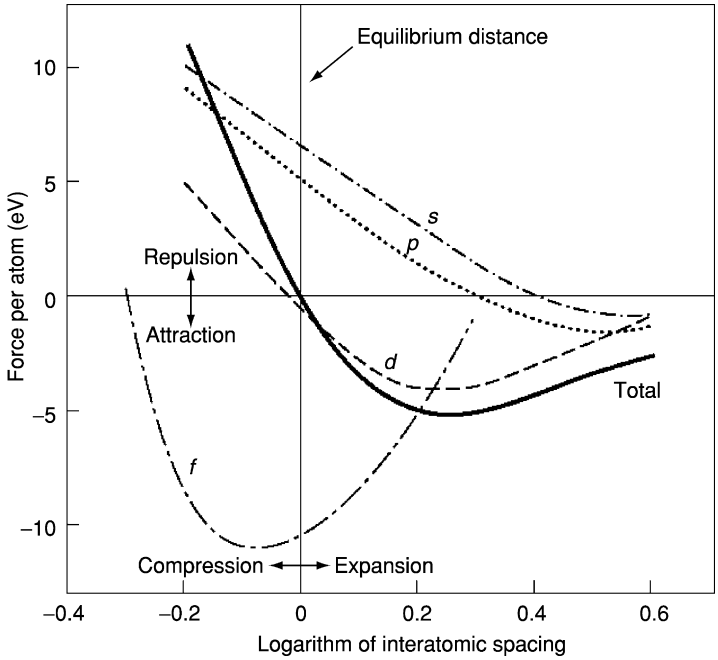

Fig. 21.6 *The force per atom as a function of interatomic spacing. DFT predictions for the bonding curves of δ-Pu in the fcc structure are plotted vs the interatomic spacing* $x = \ln(a/a_0)$. *Included are the curve for the total cohesive energy per atom, and the individual contributions from the s, p, d, and f states. The f band is narrow at this larger volume* (*courtesy of Los Alamos Science*).

simplicity, in the fcc phase) as a function of interatomic spacing. For any single band, the calculated equilibrium spacing is that at which the interatomic forces on the atom are zero – i.e. where the calculated curve crosses the horizontal zero line.

From Fig. 21.6, one can see that if plutonium had only an f-band contribution, its equilibrium lattice constant would be smaller than that found. The f-band would be wider, and Pu would stabilize in a high-symmetry crystal structure. In reality, the contribution from the s–p band (a repulsive term at true equilibrium) helps to stabilize plutonium at a larger volume; the f-band is narrow at that larger volume, and the narrowness leads to the low-symmetry crystal structure. This argument is universal for multiband metals. In the transition metals, the s–p band is repulsive at equilibrium and leads to slightly larger volumes than would be the case if these metals had only d bands. For metals above Pu the repulsive force of the s–p bands is sufficient to prevent additional lattice contraction. The additional f-electron is no longer involved in bonding and it becomes energetically favorable for the entire f-subshell to localize. Another factor to the total energy balance is the correlation energy of electrons localized in atomic 5f states. The system gains the 5f bonding energy by the 5f delocalization, but as the electrons in atomic states can be better correlated than in band states, part of the correlation energy is lost.

In actinide compounds the whole range of narrow band behavior is observed, from transition-metal-like to localized. The existence of non-actinide atoms in compounds immediately yields a larger An–An separation so that a greater tendency toward localization is expected even in uranium compounds. This is in fact the case.

21.4.2 Low-symmetry structures from 5f bands

Fig. 21.3 shows a large number of low-symmetry crystal structures among the actinide metals. Actinide compounds, especially the more strongly correlated materials, show the same tendencies. It has long been assumed (at least for the pure metals) that it is the directional nature of the 5f bonds which leads to the low-symmetry structures. In recent years, the charge density for several actinides using the full-potential DFT method has been calculated. For elemental actinides up to Pu, no dominant directional 5f bonds have been found and, most importantly, no charge buildup between atoms (Söderlind *et al.*, 1995). What, then, is the driving force for the numerous transitions and low-symmetry allotropic phases? A general reason can be seen in the narrow 5f bands themselves. There exists a high density of 5f states at or near E_F so that a lowering of the electronic energy can occur through a Peierls-like distortion (Merrifield, 1966). The original Peierls distortion model was demonstrated in a one-dimensional lattice. It was shown that a row of perfectly spaced atoms can lower the total energy by forming pairs (or dimers). The lower symmetry causes the otherwise degenerate electronic energy levels to split, some becoming lower

Table 21.2 *Typical energies of the various interactions characterizing the localized picture of magnetism for ions with 3d, 5f or 4f unfilled shells.*

Interaction	3*d* (meV)	5*f* (meV)	4*f* (meV)
coulomb (U)	1000–10000	1000–10000	1000–10000
spin–orbit (Δ_{S-O})	10–100	300	100
crystal field (CF)	1000	100	10
exchange	100	10	1
bandwidth (W)	4000–10000	700–5000	<500–2000

and others becoming higher in energy. The lowered levels are occupied by electrons, and therefore the distortion increases the bonding and lowers the total energy of the system. In the one-dimensional system, the distortion opens an energy gap at the Fermi level and makes the system an insulator. However, in the higher dimensional systems, the material can remain a metal in spite of the distortion because there are Bloch states from other bands that fill this gap.

In real three-dimensional lattices, the energy levels are degenerate along high-symmetry directions. If those levels lie close to E_F, a Peierls-like distortion of the crystal (i.e. a lowering of the symmetry) would increase the one-electron contribution to bonding, just as in the one-dimensional case described above. The Peierls mechanism is particularly effective if there are many degenerate levels near E_F, that is, if the energy bands are narrow, the DOS is large, and a large energy gain results from the distortion and filling of the lowered bands. Materials with broad bands (wider than 4 eV), gain less energy from level splitting because there are fewer levels near E_F. Indeed, symmetry-lowering distortions are rare in these materials. This is the dominant mechanism in cases where the energy is not lowered by other mechanisms removing part of the high-density states from the vicinity of E_F (magnetic ordering, superconductivity). In Table 21.2, a list of interaction energy ranges is given which highlights the types of interactions that are relevant in the actinides as well as the lanthanides and transition metals. The table shows Coulomb, spin–orbit, crystal field, exchange and bandwidth parameters. In the actinides, the large values and overlapping energy ranges for the interactions make the electronic structure calculations (and understanding) challenging.

21.4.3 The Hill plot

A very informative look at the effect of An–An spacing, and hence the effect of bandwidth, is provided in Fig. 21.7. This figure shows the transition temperatures for various uranium compounds, both magnetic and superconducting, plotted as a function of An–An spacing. Superconducting or magnetic-transition temperatures are plotted vertically, and the spacing between the f-electron elements is plotted horizontally. Hill first presented these results in the early

1970s (Hill, 1970) and found similar results for many different actinides and lanthanides. However, the presentation of data for uranium compounds yields much of the necessary information. Although some of this discussion pertains to magnetism, it is nevertheless presented here owing to its association with narrow 5f bands.

Fig. 21.7 shows that the crossover from itinerant to localized electrons can clearly be achieved if the actinide atoms are spread out. The most important aspect of Fig. 21.7 is the observation that a very limited number of magnetic uranium compounds are found with actinide spacing (in this case U–U) of less than about 3.4 Å. Inasmuch as magnetism is generally associated with more localized electrons, one may surmise that the 5f bandwidths for An–An separations smaller than 3.4 Å become too broad to support magnetism. Indeed, at these separations one may obtain direct f–f overlap. In Hill's initial plot, the known behaviors fell into only two of the four quadrants – large spacing correlated with magnetism and short spacing with superconductivity. Hill originally conjectured that the f-electrons could hybridize only with f-electrons at

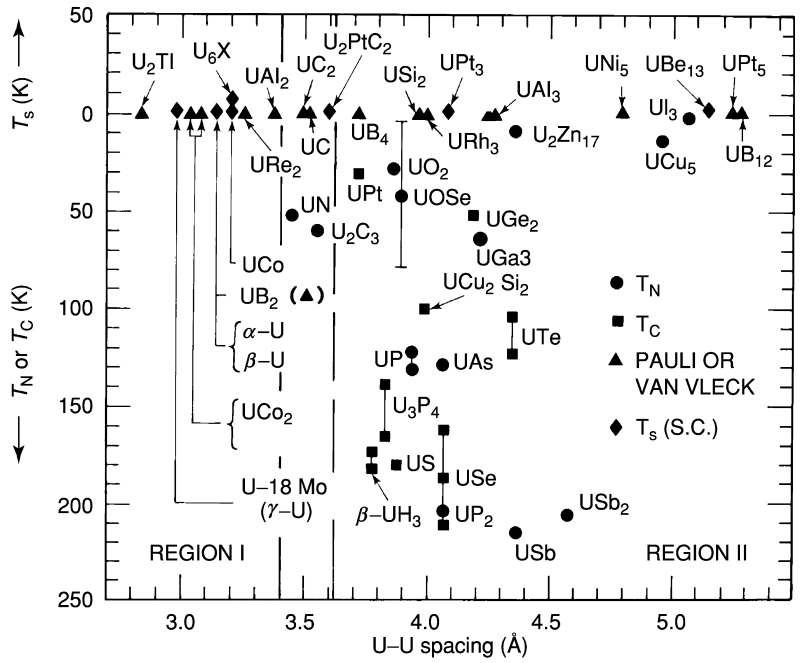

Fig. 21.7 *The 'Hill' plot for uranium compounds shows the interactinide spacing against a transition temperature* (*magnetic or superconducting*). *It is a general observation that magnetism is favored with the U–U spacing greater than 3.4Å while non-magnetic ground states are common below the separation. For uranium compounds, this distance roughly defines the localized/itinerant boundary for 5f states* (*after Hill*, 1970).

other sites and that the intervening non-f-electron atoms were just spacers to change the degree of overlap between the f-electron wave functions. Hill's plot became a major step toward understanding the light actinides, but it is now clear that the situation is more complex.

Fig. 21.7 depicts many more materials than were plotted in Hill's initial version. A large number of materials with large separations are now known to be non-magnetic. The existence of superconducting compounds is also found which, based on the relatively large distance between two f-electron atoms, should be magnetic. Two such compounds, namely, UPt_3 and UBe_{13}, are plotted in Fig. 21.7. They belong to a class of materials known as heavy-fermion superconductors first discovered in $CeCu_2Si_2$ (Steglich *et al.*, 1979) and later discovered in UBe_{13} (Ott *et al.*, 1983) and UPt_3 (Stewart *et al.*, 1984) setting off a period of intense research in heavy fermion and unconventional superconductivity research.

To understand the existence of non-magnetic compounds despite the large An–An separation, the concept of hybridization described in Section 21.3.3 above is utilized. It is not necessary to have direct f–f overlap of wave functions to produce relatively broad f-bands. Hybridization produces relatively wide f-bands that are broadened by the admixture of other symmetry components (the spd bands). It was shown by Koelling *et al.* (1985) that the lobes of the f-wave function allow the $AuCu_3$ simple cubic structure to be particularly amenable to hybridization with p- or d-bands along certain high-symmetry directions. Most materials having this structure are non-magnetic. Another observation is that for compounds in which the ligand atom contributes a high d-density at E_F, one generally obtains a strong f–d hybridization and a suppression of magnetism.

However, it is not true that the 5f-electrons are necessarily localized in compounds that are magnetic. Only one binary intermetallic compound (UPd_3) has been shown to exhibit true localized behavior of the 5f electrons. In nearly all other compounds, the hybridization with ligand sp bands is weak and leads to narrow band magnetism. In the case of extremely weak hybridization, one obtains the heavy-fermion compounds, among which those that have a superconducting transition (e.g. UPt_3 and UBe_{13} in Fig. 21.7) are very likely unconventional superconductors (Ott and Fisk, 1987).

21.5 STRONGLY HYBRIDIZED 5f BANDS

From the above Hill plot (Fig. 21.7), it is evident that many uranium compounds (and other actinide compounds also, particularly with Th and Pa, that are not shown in Fig. 21.7) have the characteristics of simple transition metals. This is true for the pure metals Th, Pa, and U as well (Np and α-Pu are questionable owing to a dearth of microscopic measurements). This class of materials is considered first. Because the pure metals are difficult to obtain in

single-crystal form, the compound UIr_3 will be considered as representative for this class of materials.

21.5.1 Fermi surface measurements in UIr_3

The $AuCu_3$-type compounds were perhaps the most extensively studied within the actinide group in the early years. They form readily (the phase often forms congruently from the melt and thus allows for very pure single crystals) which is just one more indication of strong bonding. UIr_3, like many of its isostructural materials, displays a large but temperature-independent paramagnetic susceptibility (of the order of 10^{-8} m^3/mol), thus indicating no localized magnetic moments. Its resistivity (linear with T at high temperatures) is of the order 20 $\mu\Omega$ cm at 300 K, which is again large but not when compared to Pu. It does, however, indicate that even in these relatively simple metals, one obtains some correlated electron behavior, not explained by the free-electron model.

In the 1970s, Koelling and coworkers calculated the electronic structure of UIr_3 as well as other U compounds using DFT, and found excellent agreement with experiment (see Arko *et al.*, 1985). Fig. 21.8 shows the measured de Haas–van Alphen frequencies (proportional to the extremal cross-sectional areas of the various pockets of the Fermi surface) for various directions of the magnetic field along symmetry lines. These are superimposed on dHvA frequencies calculated from the DFT band structure (solid lines) along the same symmetry directions. The agreement is phenomenal, especially when one considers that many of the refinements of DFT were not yet available in the early 1970s. Both the calculated Fermi surface volume and the topology are experimentally reproduced (Arko *et al.*, 1985).

It has been assumed that the Fermi surface remains unaltered in the presence of electron–electron correlations from what it would be in the absence of such interactions (Luttinger theorem; Luttinger, 1960). Thus, under this supposition, calculating the Fermi surface correctly is no proof of the validity of DFT. However, the Luttinger theorem states that only the Fermi surface volume is preserved, since the number of quasiparticle (defined below) states corresponds to the number of free-electron states. The topology, on the other hand, might be allowed to change if bands at the Fermi energy are altered by the interactions. Calculating the correct topology from DFT would suggest that the correlations are relatively weak and their effects have been included. In the case of UIr_3, this appears to be the case. This conclusion is reinforced by the observation that the measured m^* values do not exceed five times m_0. Recall that m^* is a rough measure of the electron–electron correlation strength.

21.5.2 Background on photoemission measurements

Since the dHvA effect only probes the states near E_F it is useful to consider other measurements that probe the electronic structure at higher binding energies. Perhaps the most direct such measurement is PES. In its simplest form this

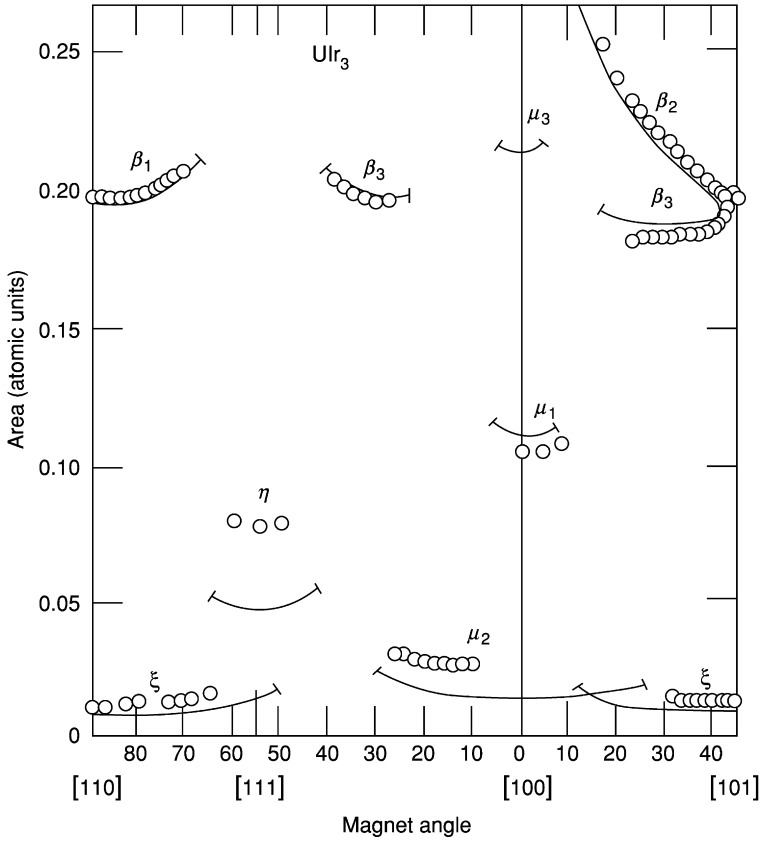

Fig. 21.8 *de Haas–van Alphen results indicating extremal areas for the Fermi surface of* UIr_3. *The open circles are the experimental data and the solid line is the DFT calculation. The agreement between experiment and theory is quite good over a large portion of the crystal structure* (*after Arko* et al., 1985).

measurement assumes that when an electron in quantum state $\boldsymbol{k}$ and energy eigenvalue E_k absorbs a photon and is ejected from the solid, the measured binding energy, E_B, is

$$E_B = E_{B,k} = -E_k \tag{21.14}$$

and the spectral function is a delta function at $E = -E_{kv}$ (i.e. absorption occurs at E_B and not elsewhere). This is referred to as Koopmans' theorem or the sudden approximation. For a non-interacting free-electron gas, this approximation seems reasonable. Even in the presence of small interactions, the above rule holds to a good approximation. However, in an interacting system, there occurs

a relaxation in the (N–1) electron solid and the relationship no longer holds. It becomes necessary to renormalize E_k by adding a correcting self-energy term $\Sigma(k,E)$ (Louie, 1992).

Assuming small corrections by measuring both the kinetic energy in vacuum, E_{Kin}, and angle θ of the outgoing electron (θ is measured relative to the surface normal), it is possible to determine both the energy and the momentum of the electron prior to the absorption of the photon; i.e. its energy state in the metal. The relationship is given by $E_{\mathrm{Kin}} = h\nu - E_{\mathrm{B}} - \phi$, where E_{Kin} is as above, $h\nu$ is the photon energy, E_{B} is the binding energy (or E_k) of the electron, and ϕ is the work function, or the energy lost in exiting the surface of the sample. The momentum components parallel and perpendicular to the sample surface are given by:

$$k_{||} = (\sqrt{2mE_{\mathrm{Kin}}})\sin(\theta), \quad \text{and} \quad k_{\perp} = (\sqrt{2mE_{\mathrm{Kin}}})\cos(\theta). \tag{21.15}$$

Since a photon does not change the direction of electron motion, the momentum information is preserved on photon absorption (so-called direct transitions). Indeed, as the electron exits through the sample surface, $k_{||}$ is preserved. An excellent reference for photoemission is the volume edited by Kevan (1992).

It is possible to determine electron momentum, $\boldsymbol{k}$, and map out the $E(\boldsymbol{k})$ vs $\boldsymbol{k}$ dispersion – i.e. the band structure by selectively sampling only electrons emitted in a narrow range of angles θ and measuring their energy. This is the so-called angle-resolved photoemission spectroscopy (ARPES). On the other hand, if the measurement accepts all electrons with a wide range of θ into the spectrometer, this will integrate over all momenta and yield, to a first approximation, the DOS. This is referred to as angle-integrated photoemission, or PES.

An important variation of PES is the so-called resonant photoemission. In simplified form, the data are taken at two photon energies: at the Fano resonance and at the Fano anti-resonance (Fano, 1961). The resonant energy roughly corresponds to a core level binding energy (in the case of U, $h\nu = 98$ eV, which is nearly the binding energy of the $5d_{5/2}$ core level). At this photon energy, the 5f photoemission cross section is greatly enhanced, while at the anti-resonance ($h\nu = 92$ eV for U), the 5f emission is strongly suppressed. By subtracting a PES spectrum taken at $h\nu = 92$ eV from one taken at $h\nu = 98$ eV one obtains the PES emission due to 5f electrons only. To a first approximation, this allows the measurement of the 5f DOS. Clearly this is a powerful tool. A fine reference for actinide photoemission is the chapter by Naegele *et al.*, (1985).

21.5.3 Photoemission in UIr_3

The ARPES measurements on UIr_3 is shown in Fig. 21.9 (Arko *et al.*, 1983). Most of the experimental data points ($E_{\mathrm{B},k}$) fall on top of the calculated bands, the notable exception being the experimental band labeled 'e' (see below). Since this data was obtained on a first generation synchrotron at 300 K with

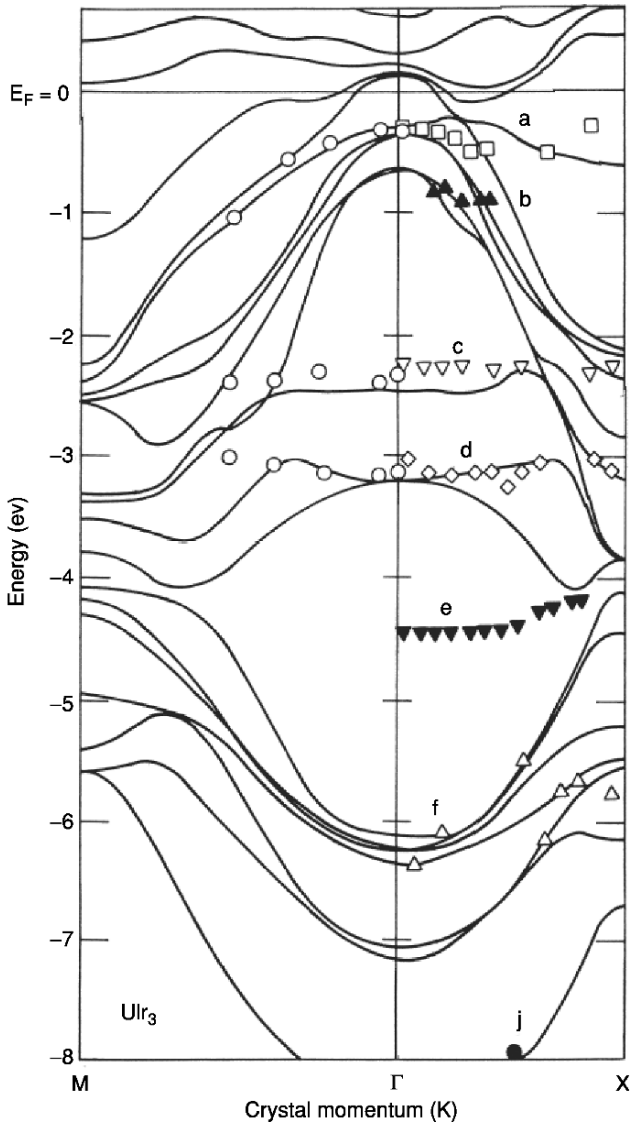

Fig. 21.9 *ARPES measurements and comparison to DFT calculations for* Uir_3. *The experimental data are the symbols and the calculation is represented by the solid lines. The agreement between experiment and theory is again quite good. The synergy between ARPES and DFT calculations is obvious in this comparison between the experimental and computational* E(**k**) *diagrams* (*after Arko* et al., 1983).

resolution no better than 200 meV, the agreement between experiment and theory is quite good. High-resolution low-temperature data would clear up the details at E_F, but from the data above the calculated bands at E_F are correct.

The 5f DOS is obtained by the resonance photoemission measurement described above (Arko *et al.*, 1983). Fig. 21.10 shows the calculated 5f DOS in UIr_3 as well as the measured result labeled 5f PES (dashed line). Although there appears to be a problem with intensity, it is necessary to consider that the 5f photoemission cross section varies with binding energy. If the 5f photoemission cross section is convoluted with the calculated 5f DOS, nearly perfect agreement with experiment is obtained. Thus UIr_3 (and the analogous compound URh_3) are simple band-like materials.

A vexing problem is band 'e' in Fig. 21.9, which has all the characteristics of a satellite. It is situated in a large gap in the calculated bands so that it is unlikely to be reproduced by DFT even with today's refinements. It was initially

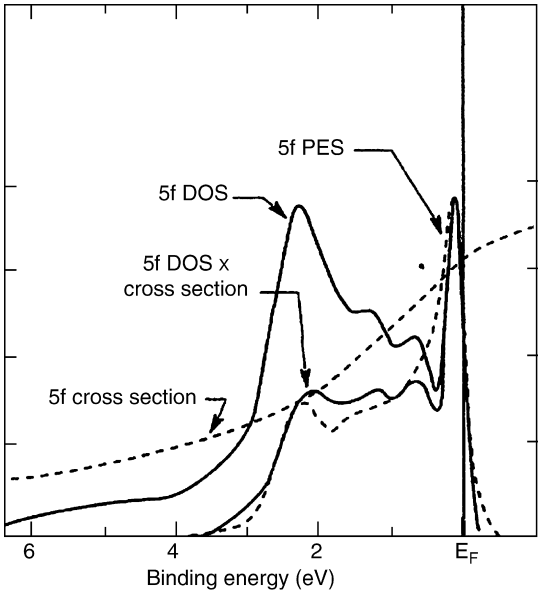

Fig. 21.10 *The calculated density of electronic states for UIr_3 compared against resonance photoemission. The resonance PES strongly enhances the 5f character in the spectrum. By separating the 5f component of the density of states in the DFT calculation, a direct comparison is made between experiment and theory. When the theoretical 5f DOS is modulated by the 5f cross section as a function of binding energy before comparison to the resonance photoemission, the results again show very good agreement between experiment and theory.*

attributed to Umklapp processes (translations by a reciprocal lattice vector, Arko *et al*., 1985). While this may yet prove to be the case there is a possibility that it is due to correlations that are not contained within the DFT calculation. Band 'e' suggests that despite the general agreement with DFT, there is more to the story. It suggests electron correlation effects that are not strong enough to result in a renormalization of the band structure. While satellites are common in core level and atomic spectra, DFT is unable to account for such essentially final-state effects. By contrast, Fermi liquid theory, because of its different approach to weak correlations, yields a satellite as a natural consequence of the incoherent part of quasiparticle (see below) spectral weight (Kevan, 1992). Although band 'e' is not assigned to the incoherent part of the 5f spectral weight (it appears to be at a very high binding energy), this point is considered because of its applicability to more strongly correlated systems considered later.

21.6 WEAK CORRELATIONS – LANDAU FERMI LIQUID

Prior to the development of DFT, Landau (1957) argued that electrons in the conduction band act as if they were nearly free even though the individual electrons are subject to strong Coulomb forces. Landau's idea was based on the effect of the electrons' correlated motions from mutual interactions in the solid. The electrons tend to 'clothe' themselves, so as to screen their charge (the details are complex and involve the entire system). These 'clothed' electrons were called 'quasiparticles'. Based on properties of strongly interacting electrons at the Fermi level, Landau showed that the system of strongly interacting electrons can be remapped onto a system of weakly interacting quasiparticles, which preserve some characteristics of electrons such as spin, momentum, and charge, while other quantities like the mass are renormalized. The consequence is that expressions known from weakly interacting electrons and describing temperature dependences of magnetic susceptibility, electrical resistivity, and specific heat preserve the same analytical form, while only prefactors are renormalized by the interactions. In mathematical terms, E_k is renormalized, as above, so that $E_k^1 = E_k^0 + \Sigma(k, E)$, where E_k^0 is the free particle eigenvalue, and $\Sigma(k,E)$ is the self-energy term with real and imaginary components. For the weakly interacting Fermi liquid, $\Sigma(k,E)$ can be parameterized in the form

$$\Sigma(k, E) = \alpha E + \mathrm{i}\beta E^2 \tag{21.16}$$

The general effect of $\Sigma(k,E)$ on photoemission (see Kevan, 1992 for a complete derivation) is to yield a spectral function (for E_k^1) consisting of a coherent part called the quasiparticle peak, and an incoherent part which can, in a loose fashion, be associated with a satellite resulting from a relaxation of the (N–1) particle system. A schematic of such a spectral function is shown in

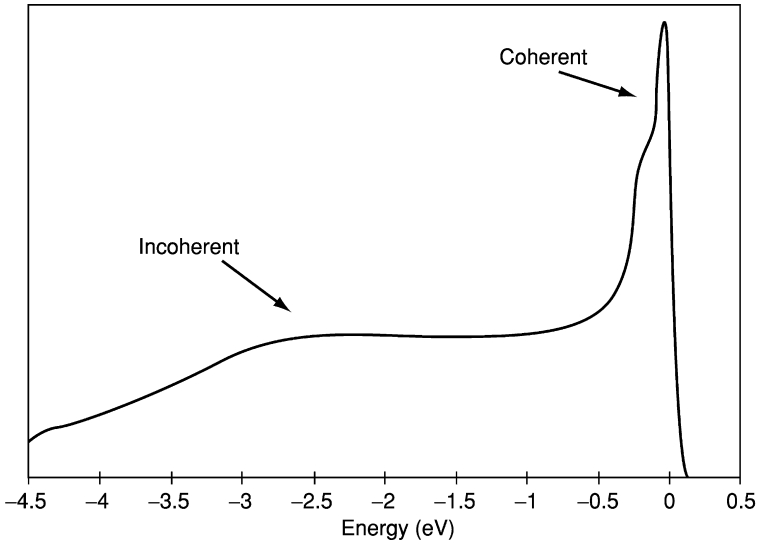

Fig. 21.11 *A schematic representation of a photoemission spectrum within a correlated electron description of the system. The coherent portion of the spectrum would represent the well-defined quasiparticle character described by Landau's Fermi liquid theory, and the incoherent portion would represent emission not consistent with such well-defined quasiparticles. The self-energy which contains all of the interactions beyond the one-electron picture may represent both a shift in energy and a broadening from the one-electron states.*

Fig. 21.11. In atomic spectra such satellites are referred to a shake-up satellites. The strength of the incoherent peak increases with increasing interaction strength. For the weakly interacting Fermi liquid it can be shown that the coherent part of E_{k}^{1} (the position of the quasiparticle peak) is given by

$$E_k^1 = E_k^0(1-\alpha)^{-1}. \tag{21.17}$$

The resolution at E_{F} in Fig. 21.9 is insufficient to draw conclusions regarding E_{k}^{1}, but it is possible that the very weak band "e" can be associated with the incoherent part of E_{k}^{1}.

It is useful to look at the signature that a Fermi liquid has on electrical resistivity. The net effect of the correlations is to contribute a quadratic temperature term to the resistivity at low temperatures; i.e., $\rho(T) = aT^2$ where a is a constant. If the interaction is sufficiently strong, this term, due to electron–electron interactions, will dominate over the weak T^5 term at very low temperatures. At higher temperatures, of course, the usual linear term may be expected. Fig. 21.12 shows plots of resistivity vs temperature for several actinide

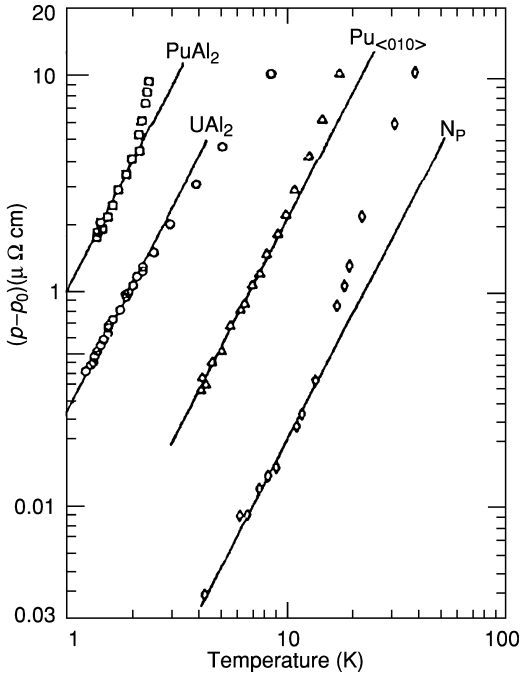

Fig. 21.12 *Resistivity for Np, Pu, $PuAl_2$, and UAl_2 as a function of temperature. The T^2 dependence of the resistivity clearly places these materials in the Fermi liquid category of metals. At higher temperatures, additional effects beyond the electronic contributions begin to have a substantial role in the resistivity* (*after Arko* et al., 1972).

systems where clearly the T^2 term is dominant. The T^2 term persists in strongly correlated systems so that all compounds are considered Fermi liquids if they display a T^2 rise in resistivity at low temperatures.

21.7 STRONG CORRELATIONS

21.7.1 Heavy fermions

Perhaps the most interesting compounds in the actinide series are the so-called heavy-fermion compounds. In general, these are very narrow band materials on the verge of localization whose conduction 5f electrons behave as if they had an extremely heavy effective mass. Indeed they blur the distinction between itinerant and localized states, making it seem as if there was a continuous transition. Fully localized electrons, with their definite energy levels, can be thought of as belonging to an infinitely narrow band and having an infinite effective mass

since they are unable to travel beyond the bounds of their atomic site. The effective masses of heavy-fermion materials, by contrast, range from tens to hundreds of times the mass of a typical itinerant electron in normal metals, indicating a very low but finite velocity through the crystal.

The unusual collective ground states of heavy fermions arise from very strong electron correlations involving the electrons in their narrow bands, and their low-energy excitations are associated with the spin and charge fluctuations in that narrow band. Of the light-actinide metals, only δ-Pu might be associated with heavy-fermion behavior, and even here there is room for debate. It is the large An–An separation in compounds that results in the narrow bands, particularly when hybridization is weak. Recent experiments on the phonon dispersions by inelastic X-ray scattering for delta phase Pu (Wong *et al.*, 2003) demonstrate the unique nature of Pu and the complex interactions involving electron-phonon coupling in this material.

Heavy-fermion behavior was first discovered in Ce compounds having one 4f electron; in particular, $CeCu_2Si_2$. Despite their magnetic susceptibility that at high temperatures suggested magnetic behavior, the susceptibility became temperature-independent at the low-T end and the material exhibited a superconducting transition with an extremely large specific heat anomaly. Subsequently similar behavior was observed in materials having 5f electrons, initially UPt_3 and UBe_{13}. This was most unusual since it was assumed that nearly localized electrons cannot even conduct electricity, much less support superconductivity. It slowly became clear that a new ground state of matter existed, one in which electron interactions were so highly correlated that only an extreme quasiparticle picture could cause that behavior. More specialized information on heavy fermion (both actinide and anomalous lanthanide) systems can be found in reviews of Grewe and Steglich (1991) and Nieuwenhuys (1995).

The unusual bulk properties of UBe_{13} are displayed in Fig. 21.13. The behavior of specific heat C_P at low temperatures, particularly the extremely large C_P/T ratio (in normal metals it is of the order 1 mJ mol^{-1} K^{-2}) points to an m^* perhaps on the order of 1000 and is also reflected in the large superconducting anomaly. Note that the low-temperature state of heavy fermions can be superconducting, antiferromagnetic, or simply paramagnetic. In all cases, however, as shown for UBe_{13} in Fig. 21.13, the magnetic susceptibility (plotted as $1/\chi$ in Fig. 21.13) exhibits Curie–Weiss behavior at high temperatures, but then levels off or even decreases at low temperatures. The upper critical field is extremely high, reaching a value of 6 T at 0.4 K. A most unusual property is the electrical resistivity, ρ, which has a negative temperature dependence down to about 10 K, and then drops precipitously.

Although there remains disagreement as to the nature of this ground state, the most widely accepted model is the so-called single impurity model (SIM). The origins of the SIM stem from the theory used for transition metal impurities in a noble metal matrix, a true impurity scenario. The model was extended to f-electron systems and later to situations where the 'impurity' nature of the

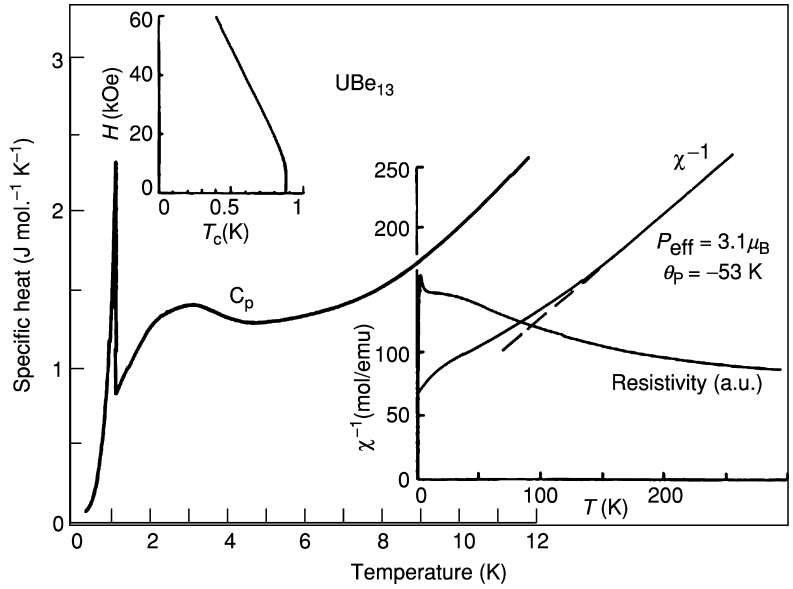

Fig. 21.13 *The thermodynamic properties (magnetic susceptibility, specific heat, and magnetic field dependence of* T_C*) of the heavy-fermion–superconductor* UBe_{13} *are plotted against temperature. The superconducting transition just below* 1 K *is clear from the specific heat while the anomalous resistivity and susceptibility for a metal are plotted on a much larger temperature scale showing the heavy-fermion nature of* UBe_{13} *(after Fisk* et al.*,* 1985).

problem was far exceeded. This model presumably strictly applies to Ce compounds having only one f-electron, but the similarities of properties in all heavy fermions suggest that one model might qualitatively apply to all. Attempts to compensate for the SIM shortcomings in the area of periodicity have given rise to extensions of the original idea in a periodic array with the Kondo lattice and Anderson lattice being two such models. A more detailed description of these models and predictions may be found in Arko *et al.* (1999). The description given here is for completeness and due to the lack of a more comprehensive model.

Within the SIM picture, the 4f or 5f electrons behave at high temperatures as if they were localized magnetic impurities at binding energy ε_f (sometimes called the bare f-level), having no interaction with each other or non-f electrons. As the temperature is lowered, however, they do hybridize slightly with the remaining non-f conduction electrons via a Kondo-like interaction whereby the conduction electrons align antiparallel to the f spin in order to screen the magnetic moment. The hybridization strength Δ is generally small. When the moment is fully screened, the susceptibility becomes independent of T. At still lower temperatures, this cloud of conduction electrons, which through hybridization has acquired a small amount of f-character, forms a coherent

ordered array (Kondo and Anderson lattice models) and a very narrow f-band at the Fermi energy. The amount of f-character at the Fermi energy is $(1-n_f)$ where n_f is nearly unity and represents the f-character remaining in the localized f-state at ε_f – the bare f-level. Essentially, $\Delta(1-n_f)$ is the probability that a conduction electron will occupy an already occupied f-level. A very loosely defined characteristic temperature, the Kondo temperature or $T_K = \Delta(1-n_f)/k_B$, approximates the onset of coherence. Indeed, most properties of heavy fermions in principle scale with T_K.

The SIM more or less successfully explains the bulk properties shown in Fig. 21.13. The heavy mass arises from the screening cloud and associated spin fluctuations, the negative $\rho(T)$ from the scattering from localized impurity moments, and the precipitous drop in ρ is due to coherence. However, there are numerous unresolved problems even for Ce compounds, among which is the fact that the approximations of SIM are only valid for n_f near unity (Arko *et al.*, 1999), whereas n_f values as low as 0.5 have been erroneously ascribed to heavy fermions.

Since the bare 5f-level, essential to SIM, has never been clearly observed in actinide compounds, Fig. 21.14 portrays instead photoelectron spectra of $CeBe_{13}$, having a T_K of 400 K in order to elucidate some of the problems. The near-E_F peak in the figure has been associated with the f-density acquired by the conduction electrons (the Kondo resonance), while the feature near -2.5 eV has been associated with the bare f peak. Despite its crucial importance to the validity of SIM, an unconventional temperature dependence has never been established for the near-E_F peak. The problem remains unresolved in large part due to the difficulty of the measurement and is outside the scope of this chapter. Instead the focus is on only one of the many discrepancies with SIM, namely the $\boldsymbol{k}$-dependence of the bare f-peak evident in the figure between the (100) and the (110) directions. This is totally inconsistent with the concept of a localized state.

While the SIM appears to capture some of the physics associated with bulk properties, its failure to incorporate periodicity causes it to fail the test of microscopic measurements. Newer models such as the periodic Anderson model (PAM) or the dynamical mean-field theory (DMFT) (Savrasov *et al.*, 2001) do incorporate the f-electron periodicity and show some promise, though the calculations are extremely difficult. It is useful to also point out that in the mid-1990s, Bedell and his coworkers developed very simplified one- and two-band Fermi liquid models of heavy-fermion compounds such as UPt_3 (Sanchez-Castro and Bedell, 1993). The surprise was that these simplified models yielded quantitative results in agreement with the low-energy and low-temperature physics of these materials. This is presented here because the dispersing bare-f level of Fig. 21.14, while totally inconsistent with SIM, is consistent with Landau's incoherent state. It would appear that Landau's principle of one-to-one correspondence between electron and quasiparticle states continues to have validity and yields profound insights into systems of strongly interacting particles.

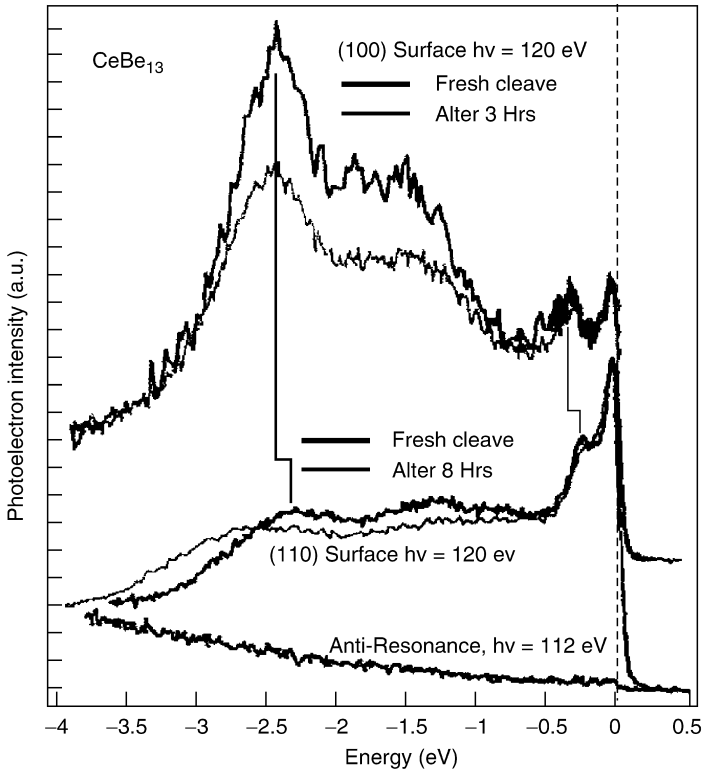

Fig. 21.14 *Resonance photoemission data for the enhanced mass compound $CeBe_{13}$ with a characteristic temperature of 400* K. *The PES data show two crystallographic orientations which demonstrate major variations in the electronic structure of the material, particularly the 5f levels, as a function of position in reciprocal space. The dotted vertical line at the zero of binding energy is the Fermi level. The peaks centered between* 2 *and* 2.5 eV *below the Fermi energy are attributed to the 'bare' f^0 peak in Kondo-type description of the system. The data are presented for freshly cleaned samples and three hour old samples in order to assess the role of surface features in the electronic structure* (*after Arko* et al., 1999).

21.7.2 Special case of plutonium systems

Plutonium and its compounds appear to present ground states different from heavy fermions or predictions from DFT-derived band structure calculations. Even α-Pu, which has been considered a relatively ordinary transition-metal-like system based on the ability to correctly calculate its atomic volume, does not yield PES results consistent with DFT calculations. All phases in the ordered state, however, conform to the requirements of a Fermi liquid as shown in Fig. 21.12. While the resistivities of both α-Pu and δ-Pu closely resemble resistivities of heavy fermions (see Fig. 21.15), the magnetic susceptibilities are

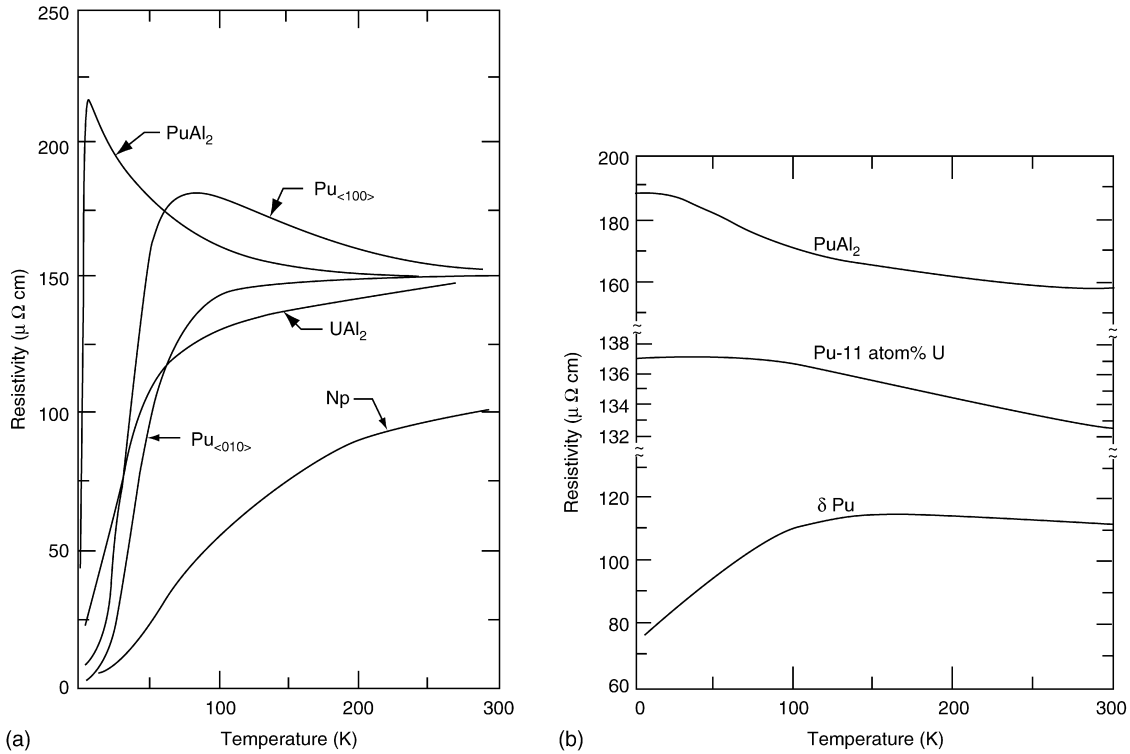

Fig. 21.15 *Electrical resistivity as a function of temperature for $PuAl_2$ and other actinides. The role of disorder and radiation are manifest in the resistivity. The difference in the low-temperature resistivity for $PuAl_2$ in* (*a*) *and* (*b*) *is a result of radiation damage. A similar effect may be generated by alloying where the impurities disrupt the integrity of the lattice as seen in* (*b*). *Separating intrinsic many-body phenomena such as quantum criticality from radiation and impurity effects is an ongoing challenge in actinide metals, alloys, and compounds* (*after Arko* et al., 1972).

temperature-independent, albeit large (of the order of 10^{-9} m^3 mol^{-1}). The specific heat γ-values are 17 and $\approx$ 64 mJ/mol. K^2 for α- and δ-Pu, respectively, which places them near the bottom of the range for heavy fermions (Lashley *et al.*, 2003). Eriksson *et al.* (1999) took a novel approach to the Pu problem and explored the localization of an integral fraction of the 5f electrons in δ-Pu in their DFT calculation (actually, the generalized gradient approximation or GGA, which extends LDA), while allowing other 5f electrons to be itinerant and involved in bonding. This is the mixed-level model (Eriksson *et al.*, 1999; Wills *et al.*, 2004). Using this technique, they were able to correctly calculate the atomic volume of δ-Pu, as well as obtain agreement with PES spectra (Joyce *et al.*, 2004). Indeed, the same approach appears to work for several other Pu compounds as well (Joyce *et al.*, 2003). This computational scheme provides an understanding of the 5f electronic structure as consisting of 5f electrons both in a localized as well as in an itinerant configuration for Pu, which is the cross-over point in the actinide series between localized and itinerant f-electron characteristics. The concept of the 5f electrons having a dual nature is not unique to Pu metal or its intermetallic compounds. This approach of separating the 5f character into localized and itinerant can also be found in insulating Pu oxides and other actinide systems (Petit *et al.*, 2003), the magnetically mediated, heavy-fermion superconductor UPd_2Al_3 (Sato *et al.*, 2001) and for the original actinide heavy-fermion superconductor UPt_3 (Zwicknagl and Fulde, 2003). For the δ-phase of Pu metal, the dual nature of the 5f electrons was initially proposed by Joyce *et al.* (1998). In Fig. 21.16 the energies are calculated for localized and itinerant 5f electrons for U, Pu, and Am. Clearly, an itinerant 5f framework is appropriate for U and just as clearly, a localized model is the choice for Am. In the boundary region of Pu, the energy level for localized and itinerant 5f character are nearly degenerate, and thus this mixed level character in Pu and Pu-based compounds would not be surprising.

An alternative interpretation for Pu PES results was considered (Gouder *et al.*, 2000; Havela *et al.*, 2002, 2003). The fact that a number of Pu-based systems show similar characteristic narrow features in the range 0–1 eV below E_F led to a conjecture that details of particular band structure are not dominant in this energy range. Instead final-state effects, either a fingerprint of atomic-state multiplet (whose high-energy lying states can be seen due to the excitation at the photoemission process) in analogy to 4f systems, or a general structure originating from many-electron process, are responsible for the observed structures (Fig. 21.17). It is interesting that the 5f states tend to localize in ultra-thin layers, as the reduced mean number of nearest neighbors leads to a preference for nonbonding 5f states. Calculations based on a DMFT may yield better agreement in the future, but these calculations at this point are in the early stages (see Savrasov *et al.*, 2001).

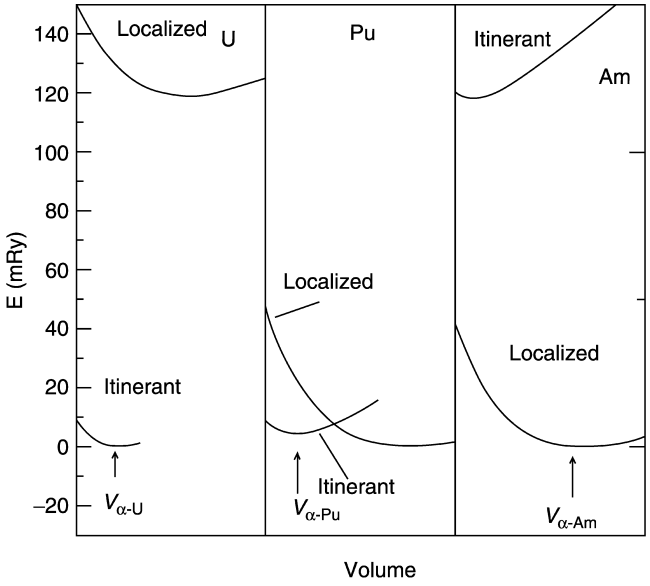

Fig. 21.16 *Total energy vs metallic radius (volume) for uranium, plutonium, and americium treating the 5f electrons as either localized or itinerant. For uranium, the calculation strongly favors an itinerant character to the 5f levels while for americium the localized 5f character is favored. Plutonium sits at the boundary between localized and itinerant. The boundary position of Pu supports the mixed-level approach to treating Pu 5f electrons (after Wills and Eriksson,* 2000).

21.7.3 Non-Fermi liquid effects and the quantum critical point

Actinide metals and most of their associated compounds typically follow the Fermi liquid scaling of electrical resistivity and electronic specific heat. Their respective coefficients reach the strongly renormalized (enhanced) values for narrow 5f-band systems. This contrasts with the systems with broad 5f-bands on one side and magnetic materials with sizeable moments on the other side, where the respective coefficients reach smaller values. The latter case deals with correlations of non-f electrons only. But some compounds persistently fail to meet the Fermi liquid rules at all. While the Fermi liquid concept requires resistivity to increase from zero temperature with a T^2 dependence, in such anomalous cases the value of the exponent can be lower. Instead of the normal constant value for C/T, logarithmically increasing C/T values with decreasing T are found. Such behavior can be encountered in the vicinity of the onset of magnetic ordering, in particular, if the parameters of the system are tuned so that its critical temperature for magnetic ordering reaches the $T = 0$ K limit. In such a situation, thermal fluctuations are suppressed and quantum fluctuations start to dominate.

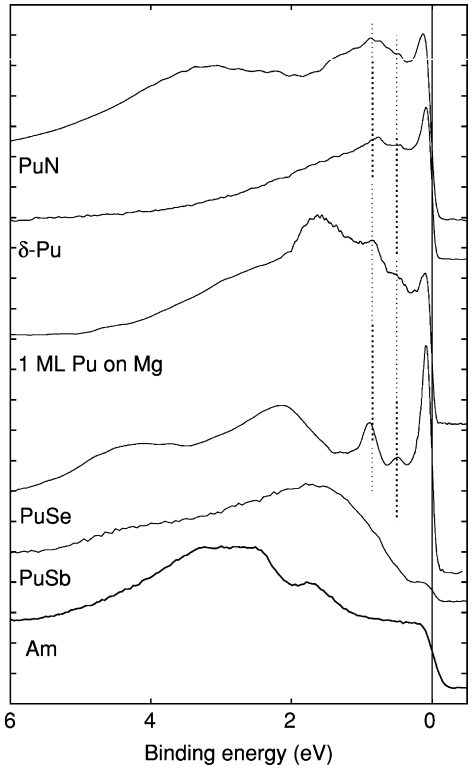

Fig. 21.17 *Examples of UPS valence-band spectra* ($h\nu = 40.8$ eV) *of selected Pu systems and Am demonstrate the effect of the* 5*f localization* (*in Am and PuSb*), *which reduces the spectral intensity at the Fermi level* (E = 0). *More itinerant Pu systems* (*PuN, δ-Pu, PuSe*) *exhibit a high spectral intensity at* E_F, *while a variable fraction of the localized* 5*f states is observed* 1–3 eV *below* E_F. *The latter dominates also for one monolayer of Pu on Mg. The dotted lines indicate positions of rather generally occurring features, which do not belong to particular DFT electronic states.* (*Reprinted with permission from Havela* et al., 2003.)

Unfortunately, efforts to bring a system to this so-called quantum critical point by the proper doping of impurities into the system also results in a randomness in the structure due to the statistical occupation of atomic positions. In most instances of non-Fermi liquid (NFL) behavior, the explanation has been one of disorder. Fig. 21.15a shows the resistivities of $PuAl_2$ and other materials whose low-temperature resistivity has been shown to vary as T^2 in Fig. 21.12. Upon disorder (via self-damage by α-particles), the resistivity of $PuAl_2$ in Fig. 21.15b no longer drops at low temperatures, but rather seems to level off. Only about 1% of the sample is estimated to sustain disorder caused by damage from α-particle bombardment during 1 month of shelf time, assuming that no room temperature annealing occurred. This shows how little disorder it takes

to destroy coherence in very narrow bands. The resistivity of Fig. 21.15a can be entirely reproduced by annealing the specimen at 1000°C for 12 h (Arko *et al.*, 1973).

One of the microscopic models accounting for the NFL behavior in such inhomogeneous systems is based on a distribution of Kondo temperatures T_K due to the atomic disorder. Numerous such systems include $(U,Y)Pd_3$, $U(Cu,Pd)_5$, or $(U,Th)Ru_2Si_2$. A summary of NFL features in actinides and lanthanides can be found in Stewart (2001). Sometimes NFL scaling is observed even in undoped systems. Undoubtedly in such a case the sample has the real characteristics of strongly correlated systems. Approximate theories indicate several fundamental classes of NFL behavior (instead of one class of FL scaling) which depend on the character of magnetic interactions (ferro- or antiferromagnetic) and on dimensionality (for example f-sites may form weakly interacting sheets or chains, thus reducing the effective dimensionality). These parameters determine the degrees of freedom of the quantum fluctuations, which affect the type of analytical behavior describing basic quantities. For example, in the proximity of three-dimensional ferromagnetism, the characteristics $\rho \sim T^n$, $n = 5/3$ and $C/T \sim -\ln(T/T_0)$ are expected. For antiferromagnetic coupling, the n value is reduced to 3/2 and further reduction takes place for lower dimensionality. In the two-dimensional case, $n = 4/3$ and 1 for the ferromagnetic and antiferromagnetic coupling, respectively. Although the majority of undoped NFL systems are found among Ce or Yb intermetallics, there are also a few U-based intermetallics. For example, at ambient pressure, NFL features are observed in UCoAl, U_2Co_2Sn, or U_2Pt_2In. The review article by Stewart (2001) describes these and other examples.

21.8 CONVENTIONAL AND UNCONVENTIONAL SUPERCONDUCTIVITY

Superconductivity, with its basic characteristic of the complete disappearance of electrical resistivity at low temperatures, has been traditionally considered as a contradiction to magnetic ordering. The reason is related to the Cooper pairs, consisting of two electrons with opposite momentum and spin, which are the basic ingredient of the superconducting state (Bardeen *et al.*, 1957). Indeed, a very small admixture of magnetic ions into a normal superconductor rapidly suppresses the superconductivity, and this phenomenon has to be attributed to the breaking of such electron pairs by exchange interactions, which prefer a parallel orientation of electron spins.

This conventional superconductivity is commonly found in actinides that are only weakly magnetic, although the critical temperatures T_c are very low. For example, $T_c = 1.37$ K for Th (Gordon *et al.*, 1966), 1.4 K for Pa (Fowler *et al.*, 1965), and 0.68 K for α-U (Hein *et al.*, 1957). For heavier actinides, superconductivity was found for Am ($T_c = 0.79$ K) (Smith and Haire, 1978). Similarly, intermetallic compounds with high actinide content also tend toward

superconductivity. The highest T_c values are found in compounds of the form U_6T, where T = Mn, Fe, Co, Ni, reaching the highest $T_c = 3.7$ K for U_6Fe, and U_3Ir ($T_c = 1.24$). Several others, U_3Si, U_3Os, U_2Ti, all have T_c below 1 K (see Sechovsky and Havela, 1988 and references therein). The same is true for amorphous U-rich systems (metallic glasses) (Poon *et al.*, 1985), while similar Th-based systems (e.g. $Th_{80}Co_{20}$) reach T_c at nearly 4 K. For lower U content, a tendency to magnetic ordering appears and superconductivity ceases. But this is not universally the case. A strange island of superconductivity was discovered for some compounds with a high inter-uranium spacing, which have characteristics close to a normal magnetic ordering (UBe_{13}, UPt_3, see above). (Ott and Fisk, 1987). Some variations of these compounds even order antiferromagnetically and the magnetic order and superconductivity coexist. In this case of so-called unconventional superconductivity, the pairing mechanism of the Cooper pairs is related to magnetic interactions instead of the electron–phonon coupling of normal Cooper pairs (Bardeen *et al.*, 1957) in the BCS mechanism. Here the superconducting state may be based on electrons with parallel spins (as opposed to antiparallel) with the total wave function therefore having a different symmetry. This phenomenon is called d-wave or p-wave symmetry in contrast to the s-wave symmetry in conventional BCS superconductivity. Such superconductors can be strongly anisotropic, including the anisotropy of the superconducting gap, and the superconducting state also can be much more resistant against a magnetic field (Ott and Fisk, 1987). The intimate connection of the superconductivity and the heavy-fermion character of the electronic structure is manifest in the huge jump of the specific heat C, scaling with γT_c. This scaling strongly suggests that the heavy-fermion character and the superconductivity are related to the same set of 5f electrons.

The most prominent materials among unconventional superconductors were already mentioned in the Heavy Fermion section. In the first of these, UBe_{13}, T_c can reach 0.85–0.90 K, and is very dependent on the actual purity of the sample (Ott and Fisk, 1987). This compound is of particular interest by virtue of its enormous γ ($\gamma = 1100$ mJ mol^{-1}K^{-2} and it is one of the U compounds with the most 'heavy' electrons) and its strongly anomalous resistivity in the normal state, increasing with decreasing T towards a sharp maximum at $T = 2.5$ K. It was first assumed to be non-magnetic, but very small static magnetic moments of $0.001\mu_B$ were deduced from muon spin-relaxation studies (Heffner *et al.*, 1990). The very high upper critical field $B_{c2} = 9$ T (considering the low T_c value) is consistent with the unconventional nature of the superconductivity.

UPt_3 with $\gamma = 420$ mJ mol^{-1} K^{-2} can be also classified as a heavy-fermion superconductor. The superconducting transition temperature again depends strongly on the sample quality. A T_c of 0.53 K can be obtained in well-annealed samples (Franse *et al.*, 1984). Unlike UBe_{13}, UPt_3 displays well-documented antiferromagnetic correlations, shown by neutron scattering experiments. An unusual static magnetic order with very low magnetic moments develops below about 5 K (Aeppli *et al.*, 1988).

Superconductivity ($T_c = 0.8$ K) and antiferromagnetism ($T_N = 17.5$ K) coexist also in URu_2Si_2, which has only a moderate γ value (75 mJ mol^{-1} K^{-2}) (Maple *et al.*, 1986). Although ordered magnetic moments do not exceed $0.04\mu_B$/U where μ_B is the Bohr magneton, the specific heat anomaly at T_N and the total entropy related to magnetic ordering is so large that there appeared numerous speculations about other type of ordering (e.g. quadrupolar), invisible to the neutron diffraction, which could induce a secondary weak magnetic ordering. The search for this so-called hidden order is still in progress (see for example Chandra *et al.*, 2002). An alternative approach, based on dynamic long-range correlations carrying a large magnetic entropy, has been proposed (Bernhoeft *et al.*, 2003).

Even larger ordered moments and higher superconducting transition temperatures are found in the superconducting antiferromagnets UPd_2Al_3 and UNi_2Al_3. UPd_2Al_3 has a higher ordered moment $(0.85 \pm 0.03)\mu_B$/U and ordering temperature of 14.4 K (Krimmel *et al.*, 1993). Unlike the Néel temperature, the superconducting critical temperature is strongly sample dependent, varying with a slight off-stoichiometry and/or heat treatment of single crystalline samples between 1.5 and 2.0 K. An interplay of superconductivity and magnetic fluctuations revealed by inelastic neutron scattering (Bernhoeft *et al.*, 1998) indicates importance of magnetic interactions in the unconventional superconductivity mechanism. UNi_2Al_3 orders antiferromagnetically below $T_N = 4.5$ K and the magnetic order coexists with superconductivity below $T_c \approx 1$ K (Geibel *et al.*, 1991), γ reaches 140 and 120 mJ mol^{-1} K^{-2} for the Pd and Ni compounds, respectively.

All these compounds are very exotic, but even more surprising was the recent discovery of the ferromagnetic superconductors UGe_2 and URhGe. The superconductivity in UGe_2 appears only in a state induced by high pressure. Although high pressure finally led to the suppression of magnetism, at pressures around 12 GPa, where the superconducting temperature reaches its maximum (about 0.7 K), the magnetization still corresponded to about $0.8\mu_B$/U with the Curie temperature at about 30 K. The superconductivity disappeared in fields of several tesla, where a high-magnetization state was induced in a first-order magnetic phase transition. An overview of the data on this compound as well as on URhGe is given in Flouquet *et al.* (2003). On the other hand, URhGe is already superconducting at ambient pressure. Its critical temperature reaches only 0.3 K ($T_c = 9.5$ K), with U moments around $0.4\mu_B$/U.

The most recent breakthrough in the superconductivity of actinides was the discovery of Pu-based nearly magnetic systems with superconductivity in the temperature range exceeding 18 K (Sarrao *et al.*, 2002). The fact is surprising because $PuCoGa_5$ is the first known Pu superconductor. The Ce-based isostructural compounds $CeCoIn_5$, and $CeIrIn_5$ are superconducting also, but only in the 1 K range, and for $CeRhIn_5$ only under pressure. The high γ value of $PuCoGa_5$, 77 mJ mol^{-1} K^{-2} points to strong electron–electron correlations. This value, and the high estimated upper critical field 74 T, is indicative of

an unconventional superconductivity. The T_c of $PuCoGa_5$ can be further enhanced to about 22 K by applying pressure (Griveau *et al.*, 2004). $PuRhGa_5$ is superconducting, as well, with $T_c = 8.6$ K (Bauer *et al.*, 2004).

21.9 MAGNETISM IN ACTINIDES

The peculiar character of the electronic structure of actinides, with the 5f states ranging between localized and itinerant, implies an extreme variability of magnetic features of elemental actinides as well as actinide-based alloys and intermetallic compounds. The gradual filling of the 5f shell in the sequence of actinide elements does not dominate the development of the magnetic properties of the pure elements in the way expected on the basis of parallel lanthanide series. This is especially true for the early actinides, in which a 5f band is formed, as described in Sections 21.3 and 21.4. Therefore more similarity is found with the d transition metals, exhibiting broad s and p bands and narrow d bands. As a consequence, the density of electronic states at the Fermi level, $N(E_F)$, is a more important parameter than the filling of the 5f band itself. The interactinide spacing has a crucial role. For pure elements, it is too small, and substantial 5f–5f overlap leads to a rather broad 5f band and weak magnetic behavior.

For heavier actinides (from Am onwards) the 5f localization was documented for the pure elements, and atomic correlations in analogy to rare earths leads to the formation of local moments and their ordering. At closer inspection, specific features of band magnetism appear in systems based on elements up to Pu. The main characteristics of the 5f band magnetism comprise strong spin–orbit interaction, leading to large orbital moments formed even in the case of band-like states, exchange interactions mediated or assisted by the hybridization of the 5f states with the ligand states, and enormous magnetic anisotropy arising from the anisotropy of the hybridization (bonding anisotropy). Another characteristic is a high sensitivity of magnetic properties to external variables, like pressure, magnetic field, and to fine details of composition. More detailed information can be found in review chapters (Sechovský and Havela, 1988, 1998). Electronic structure calculations based on the density functional approach are discussed by Johansson and Brooks (1993) and by Norman and Koelling (1993). The impact of magnetism on transport properties for actinides and lanthanides are compared by Fournier and Gratz (1993).

21.9.1 General features of magnetism of light-actinide systems

The fundamental difference between the character of the 4f electron states in lanthanides and the 5f states in light actinides can be attributed to a much larger spatial extent of the 5f wave functions, and thus a much stronger interaction with their metallic environment, compared to the 4f case. The 5f electrons are, as

a rule, delocalized due to their participation in bonding, which leads to a considerable hybridization of the 5f states with the valence states of neighboring atoms (5f-ligand hybridization). The delocalization of the 5f electrons has serious consequences, such as the formation of a more or less narrow 5f band intersected by the Fermi energy E_F (the bandwidth W_{5f} is of the order of several eV) rather than discrete energy levels. Consequently, the magnetic moments due to the itinerant 5f electrons are much smaller than expected for a free ion (irrespective whether the L–S or j–j coupling schemes are used – ground state magnetic moments are similar), and magnetic moments can disappear in a broadband limit leading to weak temperature-independent (Pauli) paramagnetism. This situation resembles to a certain extent the 3d transition metals. The strength of magnetic coupling in cases of existing 5f moments is typically much larger than for the 4f moments interacting via the Ruderman–Kittel–Kasuya–Yosida (RKKY) interaction, which is reflected by higher ordering temperatures compared to isostructural rare earth systems. The impact on magnetic excitations is even more dramatic, no crystal-field excitations can be observed by inelastic neutron scattering in the vast majority of systems studied so far, but a rather broad quasielastic response reflecting the 5f-moments instability in analogy to, for example, cerium mixed valence materials is observed (Holland-Moritz and Lander, 1994).

21.9.2 Magnetism in pure An elements

A small separation between the ions of the pure elements leads to large overlap of the 5f wave functions of nearest neighbors, amounting to the formation of a broad 5f band and weakly paramagnetic behavior. With increasing 5f occupation, the value of the Pauli-type susceptibility increases due to the increase of $N(E_F)$, the DOSs at the Fermi level, which is corroborated by a similar increase in the low-temperature electronic specific heat coefficient γ (see Table 21.1). This tendency is interrupted between Pu and Am, where the 5f states localize, and do not contribute to bonding for heavier actinides. The reason for the localization (and loss of the 5f bonding energy) can be found qualitatively in the gain of electron correlation energy for atomic-like 5f states (which is partly lost in the 5f band case). For details, see Johansson and Brooks (1993).

Quantitatively, the lack of magnetic ordering can be deduced from the Stoner criterion, which specifies conditions for magnetic ordering in band systems. If the Stoner product $U^*N(E_F)$, which contains besides the DOS at the Fermi level the intra-atomic Coulomb interaction parameter U, is larger than 1, the spin-up and spin-down sub-bands are not occupied equally and net magnetization arises. For light-actinide metals, this criterion is not fulfilled and the sub-bands are not split. Light-actinide metals can lower their electron energies by forming different open crystal structures, sometimes of a very low symmetry (in analogy to Jahn–Teller effect). The best example of this phenomenon is Pu having six allotropes, with the ground-state allotrope, α-Pu, showing a

complicated monoclinic structure. A similar situation is found in α-U, the structure of which is orthorhombic, but an incommensurate charge-density wave is formed below $T = 43$ K (Lander *et al.*, 1994). Due to the weakly magnetic character, superconductivity can appear at the beginning of the actinide series, as mentioned earlier.

Plutonium, the element on the verge of localization, exhibits the most complex behavior. Its room temperature phase, α-Pu, is monoclinic with 16 atoms per unit cell. At $T = 388$ K, it undergoes a phase transition to an even more complicated monoclinic β-phase with 34 atoms per unit cell. For remaining phases, most of data exists on the fcc δ-phase with four atoms per unit cell, which has atomic volume expanded by 26% compared to the α-phase, and which can be stabilized by several percent doping with Al, Ce, Ga, or other trivalent elements. Comparing the fcc δ-phase to the data for α-Pu given in Table 21.1, γ is strongly enhanced to (64 ± 3) mJ mol^{-1} K^{-2} (Lashley *et al.*, 2003). It is an interesting fact that all the Pu phases have only a small difference in magnetic susceptibility (see Table 21.1). The highest value was recorded for the β-phase, which also exhibits a noticeable temperature dependence in the narrow temperature range of its existence (Olsen *et al.*, 1992). The most surprising is the lack of magnetic order in the δ-phase with the largest atomic volume. LDA or GGA calculations invariably lead to a magnetic state, with spin and orbital moments only partially canceling each other (Söderlind and Sadigh, 2004). Méot-Reymond and Fournier (1996) discussed the properties of δ-Pu in terms of a Kondo effect (i.e. many-electron effect based on dynamical screening of a local atomic spin by spins of conduction electrons) with the characteristic Kondo temperature T_K higher than room temperature. Also Savrasov *et al.* (2001) suspect dynamic phenomena, described by a DMFT, to wash out magnetism. Another conjecture trying to solve the δ-Pu puzzle is the idea that there are magnetic moments in δ-Pu, but they are disordered, not leading to a long-range order (Niklasson *et al.*, 2003). But as the low δ-Pu susceptibility is quite robust with respect to various dopings or even lattice expansion (Hecker *et al.*, 2004 and references therein), it seems that it is fundamentally non-magnetic. Such non-magnetic character ($S = 0$, $L = 0$) could be obtained using an LDA+U method, where U denotes an explicit involvement of intra-atomic coulomb correlations going beyond LDA (Shick *et al.*, 2005) but this approach needs to be reconciled with the photoemission and the enhanced mass results. Such calculations suggest that the 5f count in δ-Pu is about 5.5, and is not only much higher than typically 5.0 in α-Pu, but relatively close to the non-magnetic $5f^6$ configuration.

The elements beyond Pu behave rather similarly to the lanthanide series. The analogy starts with the crystal structures. Am, Cm, Bk, and Cf all have dhcp structures, but the structures change and the 5f states delocalize under external pressure, yielding low-symmetry structures of the light-actinides type (Lindbaum *et al.*, 2003). The non-magnetic ground state of Am (exhibiting a low value of γ and quite high Van Vleck susceptibility) can be understood in the

framework of either L–S or j–j coupling for the $5f^6$ configuration. Most of information on curium (Cm) was obtained on the ^{244}Cm isotope (half-life 18 years), which is available in large amounts (milligrams) but displays high self-heating and radiation damage. A maximum in the magnetic susceptibility indicating antiferromagnetic (AF) ordering was observed at $T = 52$ K for this isotope, and a simple antiferromagnetic order was indeed confirmed by neutron diffraction. For ^{248}Cm, which has a longer half-life of 340,000 years, but is available only in small amounts, the antiferromagnetic ordering occurred at $T = 64$ K. Values of effective moment are compatible with $\mu_{\text{eff}} = 7.55\mu_{\text{B}}$ expected for the intermediate coupling model. Besides the ground-state dhcp crystal structure, a high-temperature fcc phase can occur in a low-temperature metastable state. Its magnetic ordering temperature is enhanced to $T = 205$ K. Berkelium (Bk) and californium (Cf) can be studied only in sub-milligram quantities. For Bk, antiferromagnetic ordering was deduced below $T = 34$ K. Cf is probably ferromagnetic below approximately 51 K. Both materials display μ_{eff} values compatible with free-ion theoretical values in the paramagnetic state. Einsteinium, which can be studied in sub-microgram quantities only, yields a moment of $11.3\mu_{\text{B}}$, which is even somewhat higher than the theoretical value. For more detailed information on magnetism of transplutonium actinides, see the review of Huray and Nave (1987) and references therein.

21.9.3 Magnetic properties of actinide intermetallic compounds

Similar to pure actinide elements, the magnetic properties of intermetallic compounds reflect the gradual filling of the incomplete 5f-shell. In Th compounds, the very small filling of the 5f states cannot give rise to the 5f magnetic moments, and compounds are typically Pauli paramagnets with susceptibility χ_0 of the order of 10^{-9} to 10^{-8} m^3 mol^{-1} for intermetallic compounds, indicating a low DOS at E_{F}. The ground state is frequently superconducting (Sechovsky and Havela, 1988). Exceptions are compounds such as Th_2Fe_{17} ($T_{\text{C}} = 295$ K) and Th_2Co_{17} ($T_{\text{C}} = 1035$ K), in which the magnetism is dominated by transition-metal components (Buschow, 1971).

In the compounds of U, Np, and Pu magnetic ordering can appear when the actinide–actinide spacing is enhanced to such an extent that the 5f-band narrowing and consequent increase of the DOS at E_{F} leads to the fulfillment of the Stoner criterion. The proximity of these elements to the boundary between the localized and itinerant character of the 5f-electronic states makes them very sensitive to variations of the environment. In the first approximation, the width of the 5f band can be taken as a function of the overlap of the 5f atomic wave functions centered on nearest neighbors, and the increase of the overlap can be taken as the principal delocalizing mechanism of the 5f electrons. The prominence of the Hill limit, introduced earlier (see Fig. 21.7), is evident. The situation is best documented for U compounds, where the Hill distance $d_{\text{U–U}} = 3.4$–3.6 Å is an approximate boundary value of the spacing, corresponding to the critical

5f–5f overlap. For smaller spacing values, most of the compounds are non-magnetic (often superconducting), for d_{U-U} larger than the Hill limit, the compounds usually show a magnetically ordered ground state. The value of the Hill limit should be taken as very approximative, the width of the 5f band is naturally affected also by the coordination number.

For compounds with d_{U-U} larger than the Hill limit, the principal control parameter is not the U–U spacing, but the hybridization of the 5f states with electronic states of other components. In particular, in compounds with transition metals, it is mainly the overlap of the 5f states with the d-states of the transition metal that affects the strength of the hybridization. The 5f states remain pinned at the Fermi level in most cases, whereas the late transition metals (as well as noble metals) being much more electronegative have their particular d states shifted towards higher binding energies thus leaving the 5f–d overlap small on the energy scale. The reduced 5f–d hybridization leads to the onset of the 5f magnetism, whereas the d-states are occupied more than in the pure d-element. Even if the d-element itself is magnetically ordered (Co, Ni, Fe), in the compound with U, it behaves as essentially non-magnetic (a similar effect appears in Th compounds). Exceptions are compounds with very high content of the transition metal component, in which case the d-magnetism can prevail. In compounds with the earlier d-metals like Fe or Ru, the d-states appear closer to the Fermi energy and the 5f–d overlap increases, leading typically to a non-magnetic ground state (as in UFeAl). But in some cases, magnetic moments appear both on the U and transition-metal ions. Prominent examples are Laves phases with Fe, all ordering ferromagnetically. Relatively high T_C values (UFe_2, 162 K; $NpFe_2$, 492 K; $PuFe_2$, 564 K;, $AmFe_2$, 613 K) point to the dominance of Fe–sublattice exchange interactions, but actinide magnetic moments are non-negligible, reaching $1.1\mu_B$/Np or $0.45\mu_B$/Pu. The tiny total moment in the case of U is caused by the orbital ($0.23\mu_B$) and spin ($0.22\mu_B$) components nearly canceling each other (Sechovsky and Havela, 1988 and references therein).

In compounds with non-transition metals, it is mainly the size of ligand atoms that affects the hybridization. Compounds with larger ligands are typically magnetic (e.g. UIn_3), whereas those with smaller ligands and greater hybridization form broad bands with low $N(E_F)$ and are weakly paramagnetic (USi_3). Several characteristic groups of U compounds can be thus distinguished.

(a) Compounds with very high U content

The stoichiometry leads to a small U spacing, d_{U-U}. The consequence is a broad 5f band similar to U metal. These compounds are weakly paramagnetic and superconducting. The examples, U_6Fe, U_6Co, U_6Ni, U_3Ir, U_3Si, U_3Os, and U_2Ti were mentioned in the section on superconductivity. The lower U concentration compound, which can be classified as a regular superconductor with moderate $d_{U-U} = 3.2$ Å, UCo has $T_C = 1.22$ K (Chen *et al.*, 1985).

(b) Lower U content, small $d_{U—U}$ much below the Hill limit

This stoichiometry leads to a weakly paramagnetic behavior, possibly with an influence of spin fluctuations, and the ground state is not superconducting. As examples, one may give U_3Si_2, UAl_2, or UCo_2. The last two compounds belong to an extended group of so-called Laves phases, which combine atoms of two different sizes into a very closely packed cubic or hexagonal structure. Therefore although the U content is relatively low, the packing leads to $d_{U–U}$ much below the Hill limit. Some of these compounds do not undergo magnetic ordering, also partly due to the strong hybridization of the 5f states with the d-state of transition metal constituents (UMn_2, UCo_2, URe_2). But the Laves phases with Fe and Ni are ferromagnets, and belong therefore to the next group (Sechovsky and Havela, 1988 and references therein).

(c) Itinerant ferromagnets with $d_{U—U}$ around or below the Hill limit, 3.4 Å

When proceeding from the most U-rich compounds and decreasing the U concentration, one observes magnetic order (ferromagnetism) at the 1:1 stoichiometry. Typical examples have very small ordered moments and relatively high ordering temperatures (UIr: $T_C = 46$ K, spontaneous magnetic moment $\mu_s = 0.45\mu_B$). For UNi_2, the very small spontaneous moment $0.08\mu_B$/U led to the conjecture that the magnetism was due to a small fraction of Ni atoms occupying wrong crystallographic positions (Franse *et al.*, 1981). But neutron diffraction proved finally that magnetism was not carried by Ni, but by U, and what is observed in the magnetization is a small difference between the orbital and spin moments with antiparallel orientation (Fournier *et al.*, 1986). UFe_2, the first U compound for which magnetic ordering was reported (Gordon, 1949), is a somewhat different case. Fe atoms carry magnetic moments (although much reduced by the hybridization compared to Fe metal) and lead to a high Curie temperature $T_C = 162$ K. The nearly complete mutual cancellation of spin and orbital moments reduces the contribution of U to the total magnetization to practically zero, but polarized neutron diffraction can accurately detect both components (for details, see Sechovsky and Havela, 1988).

Focusing thus on the sequence of the U-3d Laves phases, an interesting non-monotonic development of magnetism is observed. UMn_2 is non-magnetic and strongly hybridized, as the 5f and 3d bands have a strong energy overlap, and this situation does not allow the formation of Mn or U moments. In UFe_2, the 3d states shift towards somewhat higher binding energies, but the hybridization with the 5f states, given by the energy overlap, remains strong. The Fe sublattice orders ferromagnetically, allowing for the formation of the U moments. In UCo_2, the 3d band shifts even deeper and is close to filling. The Fermi level is in a minimum between the 3d and 5f states, therefore magnetism is lost again. For UNi_2, the 3d band is filled, the Fermi level is on the ascending

edge of the 5f band, and the Stoner criterion leads to magnetism of purely 5f origin (Eriksson *et al.*, 1989).

(d) Low U concentration, large $d_{U—U}$, ferromagnetic ground state

Ferromagnetism appears typically for uranium compounds with a moderate U–U spacing. For higher spacing, ferromagnetism changes to antiferromagnetism due to a more indirect exchange interaction. The ferromagnet with the highest $d_{U–U}$ (among known binaries) is UGa_2 (shortest $d_{U–U}$ in UGa_2 is 4.01 Å). It exhibits a sizeable spontaneous moment of $2.7\mu_B$/U and a rather high $T_C = 126$ K (Andreev *et al.*, 1979). As γ is only about 5 mJ mol^{-1} K^{-2} (Ballou, 1983), it was often assumed to form 5f localized states, but both the decreasing magnetization under pressure and microscopic (PES) data point to the itinerant character (Reihl *et al.*, 1985; Gouder *et al.*, 2001). Another prominent representative of this group is UGe_2 ($T_C = 52$ K, $\mu_s = 1.43\mu_B$/U), mentioned in the context of unconventional superconductivity, which was observed under pressure (Saxena *et al.*, 2000).

(e) Compounds with a very low U concentration

Within this group, the U—U spacing is significantly over the Hill limit, and consequently the direct 5f–5f overlap becomes insignificant. The strength of the 5f–ligand hybridization determines whether the ground state is magnetic or non-magnetic. This can be well demonstrated for the series UT_3 where T is a transition metal and UX_3 with X a p-metal, all sharing the $AuCu_3$ cubic structure type. For UX_3, the relation of the hybridization and the radius of the p metal can be found. For large X-radii, the falloff of the wave functions of the X-ligand at the U atom is generally small, and the hybridization is weak. For small X ligands, the spatial variations of their wave functions are larger and the hybridization is stronger (Koelling *et al.*, 1985). The crossover from weak Pauli paramagnetism to magnetic ordering occurs as X gets heavier, where X represents elements from the columns of the periodic table with p^1 and p^2 states. Thus USi_3, UGe_3, and UAl_3 are weak paramagnets, USn_3 still shows non-magnetic spin fluctuations, whereas UGa_3, UPb_3, UIn_3 and UTl_3 are antiferromagnets. The highest ordering temperature $T_N = 95$ K was found in UIn_3. In the group of UT_3 compounds, magnetic ordering depends mainly on the strength of the 5f–d hybridization, modulated by the overlap of the two types of states determined by the energy scale (Koelling *et al.*, 1985). It is generally reduced for T at the end of transition-metal series, as the d band shifts below the Fermi level, whereas the 5f states stay pinned at E_F. The development is similar to that in the Laves phases, but no d-originating magnetism is found in this group. UCo_3, URu_3, URh_3, and UIr_3 are weak paramagnets, nearly magnetic UPt_3 (heavy-fermion superconductor) and UPd_3 with localized $5f^2$ states and a quadrupolar ordering have a different structure type. UPd_3 is thus an interesting reference case; no

other binary compound exhibits the f-states shifted from the Fermi level (shown by PES; see Baer, 1984). Also neutron scattering experiments reveal well-defined crystal-field (CF) excitations (Buyers and Holden, 1985; McEwen *et al.*, 1993), normally absent in the spectra of uranium intermetallics, and γ reaches only 5 mJ mol^{-1} K^{-2} (Andres *et al.*, 1978). Compounds with high concentrations of a transition element can exhibit also high-temperature magnetic ordering. For example, ferromagnetic order with a high Curie temperature (360 K) in $UCo_{5.3}$, studied by Deryagin and Andreev (1978), is undoubtedly related to Co.

(f) Heavy-fermion materials

The last group comprises those having a substantially enhanced γ-coefficient of the specific heat and show a coexistence of magnetic ordering and superconductivity of an unconventional type. If these materials undergo a magnetic ordering, the critical temperatures are very low. Typical examples are UCu_5 ($T_N = 15$ K), U_2Zn_{17} ($T_N = 9.7$ K), UCd_{11} ($T_N = 5$ K), and the heavy-fermion superconductor UBe_{13}. For details, see Ott and Fisk (1987) and references therein.

(g) Other compounds

Besides binary compounds, there exist large groups of ternary compounds, often including a transition metal T and a non-transition metal X (UTX, U_2T_2X, UT_2X_2), which follow the tendencies of the 5f-ligand hybridization mentioned above. The advantage of studies of the *5*f magnetism in such compounds is that both the transition and non-transition metal components can be varied, while the structure type, i.e. the symmetry of environment of actinide atoms, is preserved. Thus the crossover from a non-magnetic to a magnetic ground state can be studied in more detail.

Materials, which are in the boundary region (i.e. nearly or weakly magnetic), show a variety of so-called spin-fluctuation features. Those with a non-magnetic ground state exhibit Curie–Weiss behavior of the magnetic susceptibility at high temperatures, but at low temperatures, a broad maximum in $\chi(T)$ appears (e.g. URuAl, UCoAl), other types of spin fluctuations are characterized by a plateau in $\chi(T)$ below a characteristic temperature, and then a low-temperature upturn as found in URuGa (Sechovsky and Havela, 1998). High ordering temperatures can be achieved with ternary compounds, for example, in compounds of the $UT_{10}Si_2$-type ($ThMn_{12}$ structure type), in which both the U and transition metal T (Fe, Co) carry magnetic moments. The highest $T_C = 750$ K was recorded for $U(Fe_{0.5}Co_{0.5})_{10}Si_2$ (Berlureau *et al.*, 1991).

The occurrence of magnetic ordering in Np-based compounds is dominated by mechanisms analogous to their U-counterparts. Important information is obtained using the ^{237}Np Mössbauer spectroscopy, which can determine microscopic parameters of the Np magnetism such as the magnetic hyperfine field B_{hf} on the Np nucleus. Values were found approximately proportional to the local

Np magnetic moment μ_{Np} (Dunlap and Kalvius, 1985; Potzel *et al.*, 1993): $B_{hf}/\mu_{Np} = 215$ (T/μ_B). The boundary between the magnetic and non-magnetic behavior for different Np materials is not much different than for their U-isotypes and demonstrates that for Np compounds, the mechanisms of the 5f-delocalization play a comparable role. Thus the non-magnetic behavior of Np in $NpGe_3$ and $NpRh_3$ has to be attributed to the 5f–p and 5f–d hybridization in analogy to UGe_3 and URh_3 (Sechovsky and Havela, 1988 and references therein). On the other hand, differences also exist. For example, $NpSn_3$ is an itinerant antiferromagnet, whereas USn_3 shows spin-fluctuations not undergoing magnetic ordering. Such a difference can be generally attributed to a higher 5f count or weaker 5f delocalization. On the other hand, Np_2Rh_2Sn is a non-magnetic spin fluctuator, whereas U_2Rh_2Sn undergoes antiferromagnetic order ($T_N = 24$ K) (Sechovsky and Havela, 1998). Moreover, ^{237}Np Mössbauer spectroscopy under high pressure has been a convenient tool to distinguish different types of magnetically ordered compounds. For those with more stable 5f moments, the Np moment does not decrease with pressure in the GPa range while the ordering temperature increases (e.g. $NpCo_2Si_2$), whereas a pronounced decrease of both parameters points to a stronger 5f-moment instability, e.g. as in Np Laves phases $NpOs_2$ or $NpAl_2$ (Potzel *et al.*, 1993 and references therein).

For intermetallic compounds of Pu, two tendencies cross each other. One is a stronger tendency to 5f localization due to the proximity of the Pu–Am borderline. On the other hand, the tendency to magnetism is diminished by small free-ion magnetic moments of the $5f^5$ state in both *L–S* and *j–j* coupling schemes. For $5f^6$, the moment is zero. For example, $PuMn_2$ is a weak paramagnet (although $NpMn_2$ is a ferromagnet), and a similar situation is found for the couples $NpCo_2$–$PuCo_2$ and $NpNi_2$–$PuNi_2$, and $NpRe_2$–$PuRe_2$. The Pu compounds that order magnetically include $PuRh_2$ ($T_N = 10$ K), $PuFe_2$ ($T_C = 564$ K, due to the ferromagnetism of the iron sublattice), $PuPt_3$ ($T_N = 40$ K), $PuPd_3$ ($T_N = 24$ K), $PuRh_3$ ($T_N = 6.6$ K). The knowledge of magnetism of Am intermetallics is fragmentary. The ferromagnetism of $AmFe_2$ ($T_C = 613$ K) is explained by the properties of the Fe sublattice. $AmRh_2$ is a paramagnet. For details, see Sechovsky and Havela (1988).

21.9.4 Magnetic properties of other actinide compounds

A large majority of actinide compounds even with non-metallic elements have metallic character. The magnetic behavior is dominated by the f–p hybridization, which has a dual role. It leads both to a delocalization of the 5f states and mediates the exchange interaction. The metallic character appears in most of the rocksalt-type of compounds, monopnictides AnX (An = U, Np, Pu, X = P, As, Sb, Bi) and monochalcogenides AnY (An = U, Np, Y = S, Se, Te), which are magnetically ordered and reach appreciable temperatures for the magnetic phase transition, as, for example, $T_N = 213$ K in USb or 285 K in UBi. On the other hand, Pu monochalcogenides are semimetallic and

non-magnetic (for details, see Vogt and Mattenberger, 1993). Carbides, which are of slightly under-stoichiometric ratios (AnC_{1-x}) are weakly magnetic for An = Th, Pa, U. NpC_{1-x} is ferromagnetic below $T = 225$ K, whereas antiferromagnetic ordering is found up to about 300 K, depending on the x values. PuC_{1-x} undergoes antiferromagnetic ordering with T_N ranging between 100 and 30 K, depending on the stoichiometry (Fournier and Troc, 1985). A large data set exists for nitrides AnN. Whereas ThN and AmN are weakly magnetic, magnetic ordering appears for UN ($T_N = 53$ K), NpN ($T_C \approx 90$ K), presumably also in PuN ($T_N = 13$ K), in CmN ($T_C = 109$ K), and data exist even for BkN ($T_C = 88$ K). For other compounds, high-temperature magnetic ordering can be found, for example, in U_3As_4 ($T_C = 196$ K), U_3Sb_4 ($T_C = 146$ K), or even 400 K for antiferromagnetic ordering in U_2N_2As. USb_2 and UAs_2 are antiferromagnets with $T_N = 205$ and 273 K, respectively (Fournier and Troc, 1985). The magnetism of actinide dioxides is covered in Chapter 18.

U forms a trihydride with hydrogen known to be a ferromagnet ($T_C = 180$ K). antiferromagnetic order was found in PuH_2 ($T_N = 30$ K), whereas PuH_3 is ferromagnetic ($T_C = 101$ K) (Aldred *et al.*, 1979) Np hydrides are weakly paramagnetic, which can be understood as due to crystal field effects for the $5f^4$ ionic state (Aldred *et al.*, 1979). For a review covering hydrides, see Wiesinger and Hilscher (1991). Hydrogen can be absorbed also by a number of binary and ternary intermetallic compounds. Similar to elemental light actinides, it strongly supports the tendency to form local 5f magnetic moments and order magnetically, which can be at least be partly attributed to the 5f-band narrowing due to enhanced inter-actinide spacing. Actinide compounds with non-metallic components are, together with discussions of general aspects of actinide compounds, covered in the review of Fournier and Troc (1985). Properties of systems containing boron are covered by Rogl (1991).

21.9.5 Orbital moments in light actinides

Although the majority of light actinides and their intermetallic compounds are characterized by itinerant 5f-states, an important difference with 3d magnetics is in the energy of the spin–orbit coupling Δ_{S-O} and the width of the 3d (5f) band W_{3d} (W_{5f}). Whereas $\Delta_{S-O} << W_{3d}$, their respective values in light actinides become comparable because Δ_{S-O}(5f) is of the order of eV. The relevant energy scales are indicated in Table 21.2. Due to the strong spin–orbit interaction, typically a large orbital magnetic moment μ_L is induced. It is antiparallel to the spin moment for U, in analogy with light lanthanides and the third Hund's rule stating that the total angular momentum is given by $J = L–S$ for the first half of the series. The existence of such orbital moments for the 5f-band systems was revealed first from band structure calculations involving a spin–orbit interaction term coupling the spin and orbital moment densities. Experimentally it was confirmed by the studies of the neutron form-factor, which adopts a very specific shape with a maximum, especially if the spin and orbital moments are

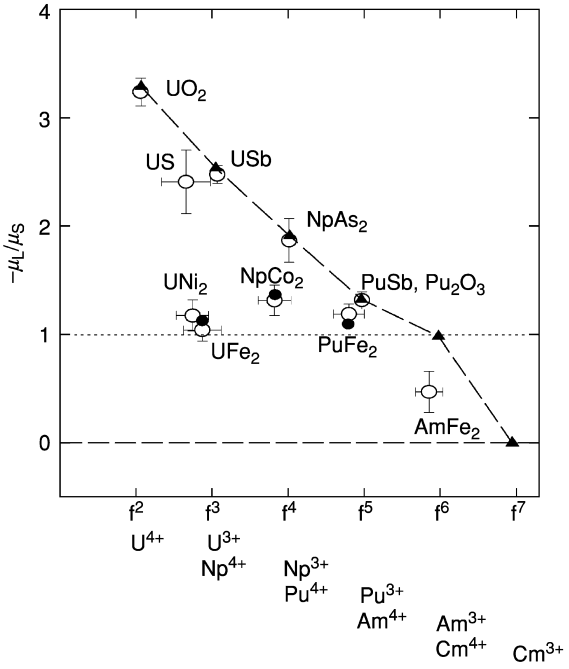

Fig. 21.18 *Ratio of the orbital μ_L and spin μ_S moments in a number of magnetically ordered materials plotted as a function of the number of the 5f-electrons. The triangles, which are connected by a dashed line, are the values derived from single-ion theory including intermediate coupling. Experimental results are shown by open circles. Results of band structure calculations are shown by solid circles.* (*Reprinted from Sechovsky and Havela,* 1998, *with permission from Elsevier.*)

of the same size. Such a case, where the total moment is close to zero, but the spatial extent of spin and orbital moment densities is different, was observed for example in UNi_2 or UFe_2. In the latter case, the U-moment consists of the orbital part $\mu_L = 0.23\mu_B$ and $\mu_S = -0.22\mu_B$. Recently, orbital moments became accessible also in X-ray scattering studies using synchrotron radiation. The strong spin–orbit interaction leads to a characteristic shape for the 5f band consisting of two features, the lower states classified as $j = 5/2$ (containing six states per atom), and the upper states classified as $j = 7/2$ (with eight states per atom). The magnitude of the splitting (up to 3 eV) leads to the formation of a minimum between these features. The weaker tendency to magnetic ordering in Pu systems comparing to Np can be understood as due to the lower sub-band being nearly filled.

A different sensitivity of the spin or orbital moments to external variables led to the assumption that the ratio of orbital and spin moments should reflect the degree of the 5f-delocalization. Indeed, as seen from Fig. 21.18, the compounds showing the least delocalized nature of the 5f states (UO_2, USb, $NpAs_2$, PuSb)

are located on the line representing values of $-\mu_L/\mu_S$ of a free $5f^n$ ion. On the other hand, magnetically ordered materials with presumably the most itinerant 5f states (UFe_2, UNi_2, $NpCo_2$, $PuFe_2$) have this ratio close to 1 (Lander *et al.*, 1991).

Relatively large orbital moments induced by the magnetic field exist probably even in weakly paramagnetic materials like U metal. Surprisingly, in an external magnetic field, the spin and orbital magnetic moments orient parallel to each other, as shown by a simple balance of the Zeeman and spin–orbit energy in the case of weak susceptibility (Hjelm *et al.*, 1993).

21.9.6 Exchange interactions and magnetic anisotropy

Exchange interactions in materials with localized 5f states can be seen as analogous to the lanthanides, for which the indirect exchange of the RKKY-type (oscillatory) is a good approximation. The other limit, systems with strongly itinerant 5f states can be understood in terms of the Stoner–Edwards–Wohlfarth theory for itinerant magnets (one band model), in which the ordering temperature is proportional to the ordered moment. For intermediate delocalization, when the direct 5f–5f overlap is negligible, two types of states have to be considered. 5f states are dominant for the moment formation, but their interaction is mediated by the hybridization with broadband states. Thus a dual role of the 5f–ligand hybridization has to be considered. It destabilizes the 5f magnetic moments, but because the spin information is conserved in the hybridization process, it leads to an indirect exchange coupling. The maximum ordering temperatures consequently can be expected for a moderate strength of hybridization, because a strong hybridization completely suppresses magnetic moments, whereas a weak one leaves moments intact, but their coupling is weak. Cooper and coworkers, on the basis of the Coqblin–Schrieffer approach, have given a model leading to realistic results (Cooper *et al.*, 1985). The mixing term in the Hamiltonian of the Anderson-type is treated as a perturbation, and the hybridization interaction is replaced by an effective f-electron–band-electron resonant exchange scattering. If the ion–ion interaction is considered to be mediated by different covalent-bonding channels, each for a particular magnetic quantum number m_l, then the strongest interaction is for those orbitals, which point along the ion–ion bonding axis, and which represents the quantization axis of the system. The two 5f ions maximize their interaction by compression of the 5f charge towards the direction of the nearest 5f ion. This has serious impacts on magnetic anisotropy, because it means a population of the 5f states with orbital moments perpendicular to the bonding axis. This interaction results in a strong ferromagnetic coupling of actinide atoms along the bonding direction. There is no special general tendency to ferro- or antiferromagnetism in the perpendicular direction, where the interaction is much weaker, and can be comparable to the 'background' isotropic exchange interaction of the standard RKKY-type. Unlike such two-ion hybridization-mediated anisotropy, crystal field (single-ion) effects control the type

and strength of magnetic anisotropy for materials with the localized 5f states, in analogy to lanthanide systems.

The two-ion anisotropy, for which orbital moments are a necessary prerequisite, has been observed in numerous U compounds especially when single-crystal magnetization data exist. The tendency for moments to orient perpendicular to the U—U bonding links leads to a uniaxial anisotropy in crystal structures with U atoms organized in planes with a short in-plane U–U spacing and larger inter-plane spacing, whereas the case of U linear chains leads to a planar type of anisotropy (see Fig. 21.19). The strength of anisotropy, which is observable both in magnetically ordered and paramagnetic phases, can be estimated in some cases from the difference between paramagnetic Curie temperatures when the susceptibility is measured with the magnetic field along different crystallographic directions. Other estimates can be obtained from the extrapolated magnetic field at which magnetization curves along different directions would intersect each other. Typically values of 10^2–10^3 K or 10^2–10^3 Tesla (assuming the anisotropy is energy expressed in $k_B T$ and $\mu_B H$, respectively, where k_B is the Boltzmann constant and μ_B the Bohr magneton) are obtained in this way; see Figs. 21.20 and 21.21).

For large groups of isostructural compounds, the same type of anisotropy is, as a rule, found irrespective of the non-actinide components. The strong generally uniaxial anisotropy of compounds UTX (with the hexagonal structure of the ZrNiAl-type) or tetragonal UT_2X_2, both with strong U bonding within

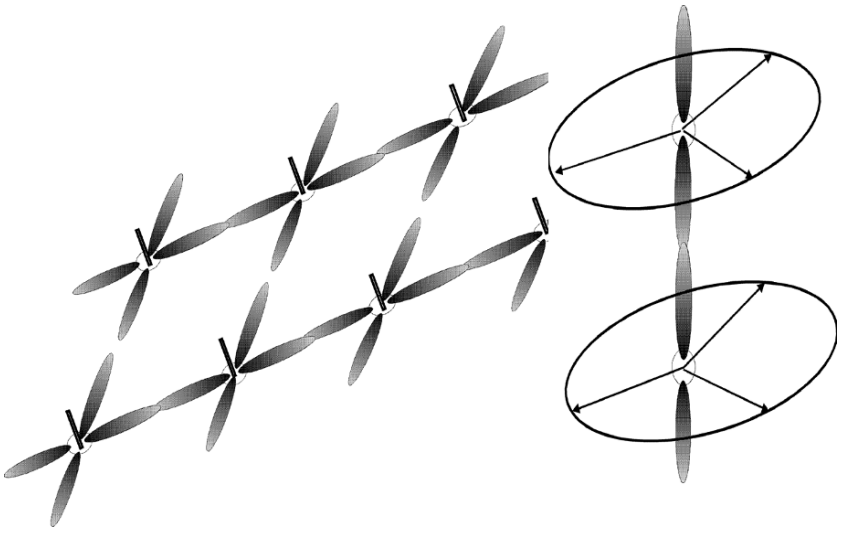

Fig. 21.19 *Schematic view illustrating how the bonding and easy-magnetization directions are related in light actinides. Left part shows the easy-axis anisotropy for planar bonding, right part the easy-plane anisotropy for columnar bonding.* (*Reprinted from Sechovsky and Havela,* 1998, *with permission from Elsevier.*)

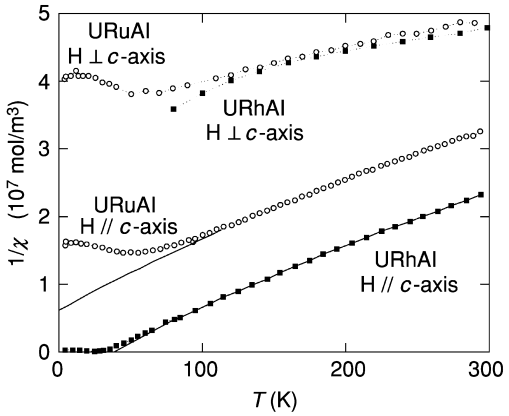

Fig. 21.20 *Temperature dependence of inverse magnetic susceptibility for URuAl and URhAl.* (*Reprinted from Sechovsky and Havela,* 1998, *with permission from Elsevier.*)

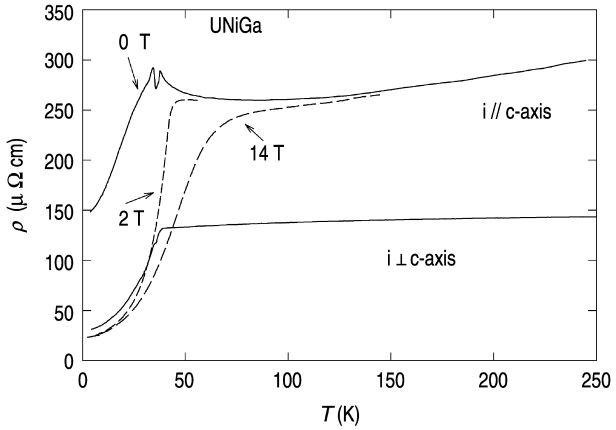

Fig. 21.21 *Temperature dependence of electrical resistivity measured on a single-crystal UNiGa for two current directions and several magnetic field applied along the* c*-axis.* (*Reprinted from Sechovsky and Havela,* 1998, *with permission from Elsevier.*)

planes perpendicular to the hexagonal (tetragonal) axis, and U-moments (or higher susceptibility) along this axis are examples (Sechovsky and Havela, 1998).

21.9.7 Magnetic structures

The specific mechanisms of magnetic anisotropy and exchange interactions both affect the types of magnetic structures in light-actinide materials. Strong anisotropy leads frequently to collinear modulated structures (spin-density

waves), which are preferred over non-collinear equal-moment structures. The reason is that the anisotropy energy is typically stronger than the exchange coupling energies. Non-collinear magnetic structures are stable if the easy-magnetization directions on different sites are non-collinear, as in U_2Pd_2Sn, where they are orthogonal. Also for those cases in which the lattice symmetry imposes no special requirements on the directions of the moments (see Sandratskii, 1998) do non-collinear equal-moment structures appear (e.g. UPtGe). The types of magnetic structures are also affected by the strong ferromagnetic coupling along strong bonding directions (see the hybridization-induced exchange model in Section 21.9.6). For example, the UTX compounds with the hexagonal structure of the ZrNiAl-type tend to magnetic structures consisting of ferromagnetic basal-plane sheets, whereas the inter-sheet exchange interaction is weaker and can be of the ferromagnetic or antiferromagnetic type, leading to a variety of stacking sequences along the hexagonal axis. In this case, ferromagnetic-like alignment can be obtained in moderate magnetic fields applied along the antiferromagnetic stacking direction.

21.9.8 Relation of electronic transport and magnetism – giant magnetoresistance phenomena

The situation in which magnetic moments are strongly coupled to the crystal lattice due to the strong spin–orbit coupling and large orbital moments, and the 5f states are strongly hybridized with other conduction-electron states, is especially favorable to observe any variations of magnetism projected onto electrical resistivity and other transport properties.

The frequently observed anisotropy of exchange coupling (see subsection 21.9.7) often leads to a striking anisotropy in the resistivity. In single crystals of tetragonal, hexagonal, or orthorhombic materials not only the magnitude of resistivity is dependent on the direction of electrical current, but often different directions yield different types of temperature-dependent behavior. In certain directions, antiferromagnetic correlations can be broken by an external magnetic field and a giant magnetoresistance effect can be observed at the critical field. The residual resistivity ρ_0 typically reaches smaller values in ferromagnets. The much larger ρ_0 values observed in antiferromagnets can be understood as due to a gapping of part of the Fermi surface due to an additional periodicity. If, for example, the magnetic structure consists of two sublattices with antiparallel sublattice magnetization, the magnetic unit cell is doubled compared to the crystallographic unit cell (assuming a simple case with one actinide atom in the unit cell). The size of the Brillouin zone is therefore reduced by a factor of 2. As quantum states of electrons must have a gap at every Brillouin zone boundary, a gapping of the Fermi surface will occur if it is cut by the new, inserted, Brillouin zone boundary. This does not bring an extra scattering mechanism, but the effective number of electrons available for the charge transport is reduced, and resistivity therefore increases. This effect is parametrized by the expression:

$$\rho = (\rho_0 + \rho_{e-ph} + \rho_{e-e} \ldots)/[1 - g\ m(T)], \tag{21.18}$$

where $m(T)$ is the temperature dependence of sublattice magnetization and g is a truncation factor modifying the Fermi surface. ρ_0, $\rho_{e-ph,}$ ρ_{e-e} represent individual resistivity terms due to impurity, electron–phonon, and electron–electron scattering, respectively.

The situation can be illustrated by the example of UNiGa (see Fig.21.21), which has an antiferromagnetic ground state. It crystallizes in a layered hexagonal structure (ZrNiAl-type), in which U–Ni and Ni–Al layers alternate along the *c*-axis. Strong ferromagnetic exchange is found within the U–Ni basal planes, where the U-atoms are close together. Magnetic moments are locked along the *c*-axis. The exchange along *c* is weak and antiferromagnetic, and ferromagnetic alignment can be achieved by a magnetic field below 1 T if applied along *c*. The resistivity for current along the *ab*-plane has the character of a ferromagnet, as mostly electrons with the wave vector along *ab* contribute to the conduction. Residual resistivity is low. For current along *c* electrons respond to the antiferromagnetic coupling, and the resistivity is very high. The magnetic unit cell is six times larger than the crystallographic cell along *c*, because the stacking of layers can be described as (++—+–). Fig. 21.21 shows how the high resistivity is suppressed in the metamagnetic state in UNiGa. ρ_0 drops by about 90%. The minimum in $\rho(T)$ for *i*//*c* is due to antiferromagnetic correlations above T_N, which can be suppressed by the magnetic field (Sechovsky and Havela, 1998).

21.10 COHESION PROPERTIES – INFLUENCE OF HIGH PRESSURE

The variable nature of the 5f electronic states in actinide metals is reflected in cohesion properties. Crystal structures of elemental actinide metals are complex and of low symmetry for the earlier actinides (up to Pu), and they show also relatively higher bulk moduli and few (if any) phase transitions under pressure. In contrast, the transplutonium metals do not have the 5f electrons involved in bonding, their atomic volumes are much higher, and they are softer, i.e. with lower bulk moduli. Application of pressure induces a sequence of structural phase transitions, eventually reaching states with itinerant 5f states with corresponding low atomic volumes and low-symmetry structures. In Fig. 21.22, the phase diagram for Ac through Cf as a function of pressure is shown from a more detailed discussion by Lindbaum *et al*. (2003). The reason why the 5f bonding leads to smaller atomic volumes can be seen from two points of view. One is the smaller spatial extent of the 5f states even in bonding situations, when compared to the other bonding states (6d, 7s), as described in section 21.4.1. The bonding energy minimum evaluated for the separate 5f states appears at much smaller inter-atomic spacing than for the 6d–7s states. The real equilibrium volume, obtained by summing both contributions, corresponds

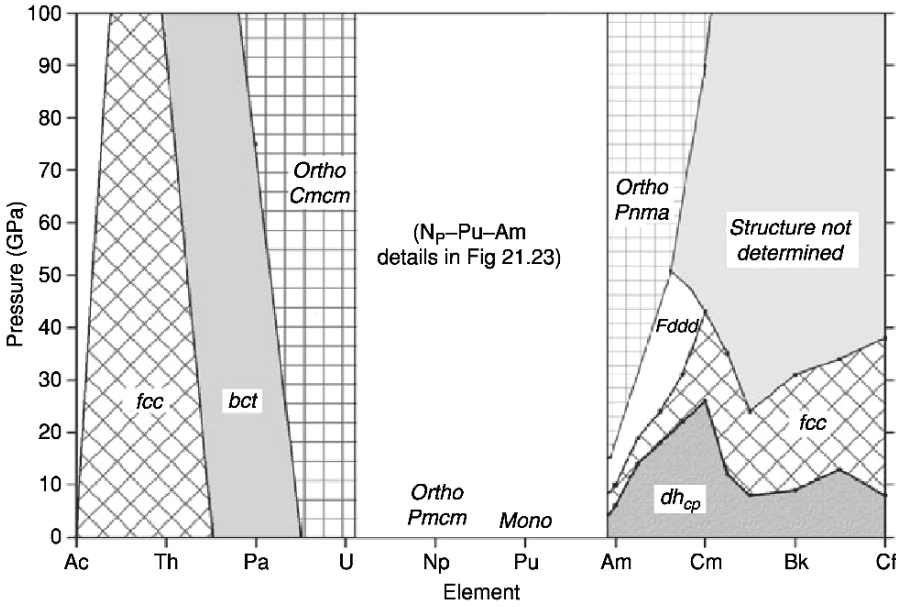

Fig. 21.22 *Phase diagram of the actinides* (*Ac through Cf*) *vs pressure. The complexity of the pressure phase diagram depends in large part on the role of the 5f electrons in bonding and variations in bonding as the interatomic distances are decreased under pressure* (*after Lindbaum* et al., 2003).

then to a compromise between the smaller 5f and larger 6d–7s bonding distance. Releasing the 5f states from bonding leads to the 6d–7s bonding only, with its larger bonding length. The second reason for the volume expansion is the different screening of the ionic potential, attracting the outer (6d–7s) electrons to the ion core. When withdrawn from bonding, the 5f charge density redistributes more towards the ion core, which screens more effectively the attractive potential, and the less attracted 6d and 7s states expand.

The existence of the low-symmetry structures for itinerant 5f electronic states can be caused by an electronic Jahn–Teller effect. In this situation, when the density of electronic states in the vicinity of the Fermi level reaches appreciable values, the total energy can be minimized by redistributing some of the 5f band states towards lower energies, using the degrees of freedom offered by all possible exotic crystal structures. For these high densities of states, such distortions can compensate the loss of the Madelung energy, which favors high-symmetry structures. One can compare this situation with e.g. the late 3d transition metals, similarly characterized by high $N(E_F)$ values. In such a case, the Stoner criterion $U.N(E_F) > 1$ is fulfilled, which leads to magnetic order. Thus the ground state for high $N(E_F)$ values can be either magnetic (in case of sufficient high U) or a low-symmetry crystal structure, if U is not large enough.

The latter case holds in the early actinide metals and in the late actinides in the high-pressure phases. An interesting insight is provided by *ab initio* electronic structure calculations in different structure types (see for example, Wills and Eriksson, 1992 or 2000).

Although specialized review chapters exist covering the structural aspects of actinides at high pressures (Benedict, 1987; Benedict and Holzapfel, 1993), the enormous progress in the last decade has brought numerous new data (extended pressure ranges led to discovery of new phases, improved hydrostatic conditions yield much more precise values of bulk moduli), so that it is worthwhile to provide a more detailed overview for the individual metals. Thorium crystallizes in the fcc structure, but at very high pressure (between 75 and 100 GPa), it undergoes a transition to a body-centered tetragonal structure (Vohra and Akella, 1991). Calculations show that the high-pressure structure can be associated with a population of the 5f band of about 0.6 electrons (Rao *et al*., 1992). This structure is the same as adopted by protactinium at ambient pressure. Pa bulk modulus value, 118(2) GPa obtained from a recent experiment (Le Bihan *et al*., 2003), is much closer to the value of 100 GPa predicted by calculations (Söderlind and Eriksson, 1997) than previous data (Benedict *et al*., 1982). The new experiment also revealed a structural phase transition at 77(5) GPa identified as the α-U structure (Haire *et al*., 2003). The reason for this structure change can be seen in somewhat varying (increasing) 5f occupancy at lower volume.

The same argument, i.e. higher 5f occupancy, is why the orthorhombic α-U structure (*Cmcm* space group) stabilizes in uranium. Its bulk modulus 104(2) GPa (Le Bihan *et al*., 2003) is similar to the value for Pa. Some authors, though, give higher values. For a review of older data, see Benedict (1987) and Benedict and Holzapfel (1993). The α-U structure is stable to at least 100 GPa, in agreement with theory (Le Bihan *et al*., 2003). The ground state structure of neptunium (orthorhombic, space group *Pmcn*) was found to be similarly stable to at least 52 GPa (Dabos *et al*., 1987). The bulk modulus of 118(2) GPa is comparable with the value of 110 GPa obtained from calculations (Johansson and Skriver, 1982).

The qualitative difference of cohesion properties in transplutonium materials is well illustrated by the case of americium (Heathman *et al*., 2000; Lindbaum *et al*., 2001). The initial bulk modulus of 30 GPa leads to a rapid decrease of the volume with applied pressure. A sequence of structural phase transitions starts at 6.1 GPa, at which pressure the dhcp ground-state structure (the same as for Cm, Bf, and Cf) transforms into a fcc structure. The next transition at 11 GPa, accompanied by a volume collapse of 2%, leads to an orthorhombic structure, which is identical with the γ-Pu structure. It has been proposed that this structure already shows 5f bonding. An even larger volume collapse of 7% appears at 16 GPa, and brings Am into an orthorhombic structure with a low compressibility, similar to the α-U-type, and thus confirming the itinerant nature of the 5f states. The volume collapse and 5f bonding was predicted also by theory, although one type of calculation preferred the α-Pu structure as the high-pressure phase (Söderlind *et al*., 2000). On the other hand, calculations of

Pénicaud (2002) are not only consistent with the real orthorhombic structure, but suggest that this so-called Am(IV) structure is also one of the high-pressure structures of Pu. Although Pu has been studied thoroughly, information is lacking in the open literature for the high-pressure range, clearly due to nuclear non-proliferation concerns. But the data available confirm the stability of the α-Pu phase up to 40 GPa (Benedict and Holzapfel, 1993 and Dabos-Seignon *et al.*, 1993). On the other hand, the expanded-volume δ-phase collapses again under a pressure of several few kbar (1 kbar = 0.1 GPa). The opposite experiment, i.e. imposing a negative pressure by doping larger Am atoms, shows that the δ-Pu phase is stabilized over a large concentration range and corresponds actually to the Am(II) fcc structure. Recent results for Cm indicate a lattice structure stabilized by magnetism (Heathman *et al.*, 2005). The interplay between pressure and alloy substitution is shown very nicely in Fig. 21.23 for the Np, Pu, Am solid solution series. The inset in the upper left corner of Fig. 21.23 shows elemental Pu as a function of pressure. There is a strong resemblance to the phases obtained from alloys of Pu with Np, which effectively increases the pressure in the Pu lattice (Hecker, 2000).

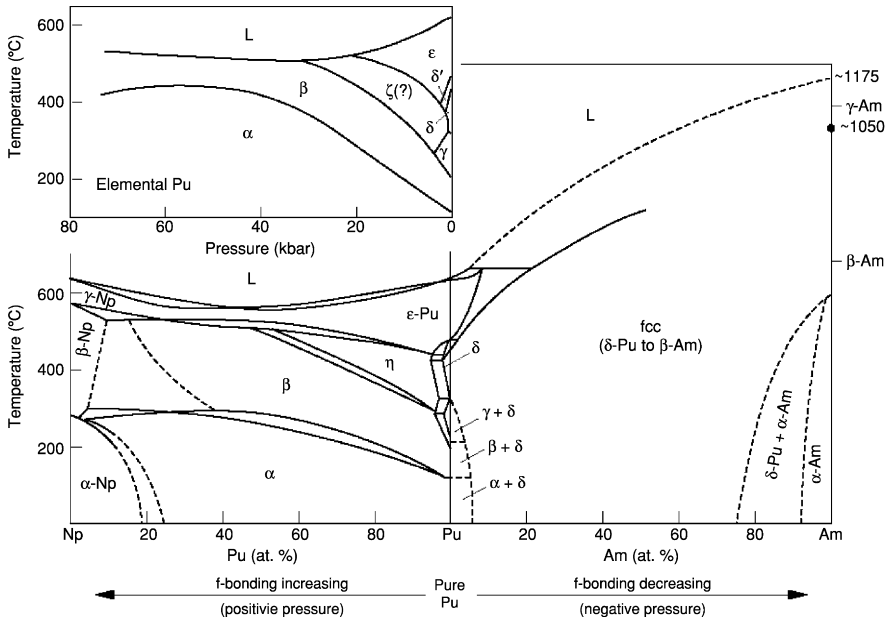

Fig. 21.23 *The binary phase diagram for Np through Am as a function of temperature. The inset in the upper left shows the temperature vs pressure phase diagram for Pu metal. The similarity between the Pu pressure diagram and the Np–Pu binary gives clear indication of how atomic substitution may create effective pressure in metallic solids* (*after Hecker,* 2000).

21.11 CONCLUDING REMARKS

There remains a great deal of uncertainty regarding the understanding of the actinides in the metallic state. For the late actinide metals, much of the uncertainty arises from sample size and purity limitations. For the early actinides (through Pu), the uncertainty is centered on the understanding of the 5f electrons and the nature of the narrow bands in actinide metals. The literature presents many models for treating the 5f electrons from Th through Pu with no clear consensus model for the electronic structure, which is universally applicable. In many cases, it appears that the 5f electrons form narrow bands, which hybridize with the conduction electrons to some extent and give rise to many of the interesting properties of actinides in the metallic state. By expanding the phase space of investigation to include alloys, compounds, and pressure one finds some systematics in the properties of actinide metals. Indeed, Fig. 21.23 demonstrates how pressure and alloying may be considered equivalent knobs to adjust in tuning the properties of metallic actinides. The propensity for rich electronic structure in the metallic actinides is highlighted by the frequent occurrence of correlated electron ground states including magnetism (both local moment and band magnetism), enhanced mass, superconductivity, and charge-density waves. The rich electronic structure is indicative of nearly degenerate energy scales and competing processes to lower the free energy. In the most complex systems, one finds competing ordered ground states such as enhanced mass and superconductivity in UPt_3 and UBe_{13} with truly exceptional characteristics in materials like UPd_2Al_3, which exhibits enhanced mass, magnetism, and superconductivity. The discovery of superconductivity at 18 K in $PuCoGa_5$ in 2002 (Sarrao *et al.*, 2002) ushers in a new era for actinide superconductivity spanning the gap between low-temperature spin-fluctuators and the high temperature oxides exhibiting charge fluctuations. While an uncontested explanation for the electronic properties of metallic actinides is still in the future, the broader understanding of actinide alloys and compounds, along with increased range in pressure and temperature phase space, gives us a better understanding of the intricacies of the elemental actinides in the metallic state such as the charge-density waves in uranium metal as well as the multiple phases, crystal structures, and volumes of plutonium metal.

ABBREVIATIONS

Å	Angström
AF	anti-ferromagnetic
An	actinide
ARPES	angle resolved photoemission
bcc	body-centered cubic
bct	body-centered-tetragonal

T_c	critical temperature
T_C	Curie temperature
DFT	density functional theory
dhcp	double hexagonal close-packed
dHvA	de Haas–van Alpen
DOS	density of states
DMFT	Dynamical Mean Field Theory
m^*	Effective mass
fcc	face-centered cubic
E_F	Fermi Energy
FL	Fermi Liquid
FM	Ferromagnetic
γ	low temperature specific heat coefficient
GGA	generalized gradient approximation
hcp	hexagonal close-packed
LDA	local density approximation
χ	magnetic susceptibility
mono	monoclinic
T_N	Néel temperature
NFL	Non-Fermi-Liquid
orth	Orthorhombic
PAM	Periodic Anderson Model
PES	photoelectron spectroscopy
RKKY	Ruderman-Kittel-Kasuya-Yosida
SC	Superconducting
SIM	single impurity model

ACKNOWLEDGMENTS

Thanks to James L. Smith for a great deal of assistance in figures and scientific input, and in general to John Wills, Jim Smith, Olle Eriksson, and Mike Boring for discussions and previous work which J.J. and A.A. relied heavily upon in writing this review. This work was supported by the U.S. Department of Energy, Office of Science. The work of L.H. at the Charles University was part of the research program MSM 002160834 financed by the Ministry of Education of the Czech Republic.

REFERENCES

Aeppli, G., Bucher, E., Broholm, C., Kjems, J. K., Baumann, J., and Hufnagl, J. (1988) *Phys. Rev. Lett*., **60**, 615.

Aldred, A. T., Cinader, G., Lam, D. J., and Weber, L. W. (1979) *Phys. Rev. B,* **19**, 300–5.

Andreev, A. V., Belov, K. P., Deriagin, A. V., Levitin, R. Z., and Menovsky, A. (1979) *J. Phys. (Paris),* **40**, C4, 82–3.

Andres, K., Davidov, D., Dernier, P., Hsu, F., and Reed, W. A. (1978) *Solid State Commun.,* **28**, 405–8.

Arko, A. J., Brodsky, M. B., and Nellis, W. J. (1972) *Phys. Rev. B,* **5**, 4564.

Arko, A. J., Fradin, F. Y., and Brodsky, M. B. (1973) *Phys. Rev. B,* **8**, 4104.

Arko, A. J., Koelling, D. D., and Reihl, B. (1983) *Phys. Rev. B,* **27**, 3955.

Arko, A. J., Koelling, D. D., and Schirber, J. E. (1985) Energy band structure and fermi surface of actinide materials, in *Handbook on the Physics and Chemistry of the Actinides,* vol. 1 (eds. A. J. Freeman and G. H. Lander), Elsevier, Amsterdam, pp. 175–238.

Arko, A. J., Andrews, A. B., Riseborough, P. S., Joyce, J. J., Tahvildar-Zadeh, A., and Jarrell, M. A. (1999) Photoelectron spectroscopy in heavy fermion systems: emphasis on single crystals, in *Handbook on the Physics and Chemistry of Rare Earths*, vol. 26, Elsevier Science, Amsterdam, p. 265, ch. 172.

Ashcroft, N. E. and Mermin, N. D. (1976) *Solid State Physics,* Holt, Rinhart and Winston, Philadelphia.

Bader, S. D., Phillips, N. E., and Fisher, E. S. (1975) *Phys. Rev. B,* **12**, 4929–40.

Baer, Y. (1984) Electron spectroscopy studies, in *Handbook on the Physics and Chemistry of the Actinides,* vol. 1 (eds. A. J. Freeman and G. H. Lander), Elsevier, Amsterdam, p. 271.

Ballou, R. (1983) Thesis, University of Grenoble.

Bardeen, J., Cooper, L. N., and Schrieffer, J. R. (1957) *Phys. Rev.,* **108**, 1175.

Bauer, E. D., Thompson, J. D., Sarrao, J. L., Morales, L. A., Wastin, F., Rebizant, J., Griveau, J. C., Javorsky, P., Boulet, P., Colineu, E., Lander, G. H., and Stewart, G. R. (2004) *Phys. Rev. Lett.,* **93**, 147005.

Benedict, U., Spirlet, J. C., Dufour, C., Birkel, I., Holzapfel, W. B., and Peterson, J. R. (1982) *J. Magn. Magn. Mater.,* **29**, 287–90.

Benedict, U. (1987) The effect of high pressures on actinide metals, in *Handbook on the Physics and Chemistry of the Actinides,* vol. 5 (eds. A. J. Freeman and G. H. Lander), Elsevier, Amsterdam, pp. 227–69.

Benedict, U. and Holzapfel, W. B. (1993) High-pressure studies – structural aspects, in *Handbook on the Physics and Chemistry of Rare Earths,* vol. 17 (eds. K. A. Gschneidner Jr, L. Eyring, G. H. Lander, and G. Choppin), Elsevier, Amsterdam, pp. 245–300, ch. 113.

Berlureau, T., Chevalier, B., Gravereau, P., Fournès, L., and Etourneau, J. (1991) *J. Magn. Magn. Mater.,* **102**, 166–74.

Bernhoeft, N., Sato, N., Roessli, B., Aso, N., Hiess, A., Lander, G. H., Endoh, Y., and Komatsubara, T. (1998) *Phys. Rev. Lett.,* **81**, 4244.

Bernhoeft, N., Lander, G. H., Longfield, M. J., Langridge, S., Mannix, D., Lidström, E., Colineau, E., Hiess, A., Vettier, C., Wastin, F., Rebizant, J., and Lejay, P. (2003) *Acta Phys. Pol. B,* **23**, 1367.

Bloch, F. (1928) *Z. Phys.,* **52**, 555.

Boring, A. M. and Smith, J. L. (2000) *Los Alamos Science*, vol. 26 (ed. N.G. Cooper), Los Alamos National Laboratory.

Buschow, K. H. J. (1971) *J. Appl. Phys.,* **42**, 3433.

Buyers, W. J. L. and Holden, T. (1985) Neutron scattering from spins and phonons in actinide systems, in *Handbook on the Physics and Chemistry of the Actinides,* vol. 2, (eds. A. J. Freeman and G. H. Lander), Elsevier, Amsterdam, pp. 239–327.

Chandra, P., Coleman, P., Mydosh, J. A., and Tripathi, V. (2002) *Nature,* **417**, 831.

Chen, J. W., Hake, R. R., Lambert, S. E., Maple, M. B., Rossel, C., Torikachvili, M. S., and Yang, K. N. (1985) *J. Appl. Phys.,* **57**, 3090.

Cooper, B. R., Siemann, R., Yang, D., Thayamballi, P., and Banerjea, A. (1985) Hybridization induced anisotropy in cerium and actinide systems, in *Handbook on the Physics and Chemistry of the Actinides,* vol. 2 (eds. A. J. Freeman and G. H. Lander), Elsevier, Amsterdam, pp. 435–98.

Dabos, S., Dufour, C., Benedict, U., and Pages, M. (1987) *J. Magn. Magn. Mater.,* **63 & 64**, 661–3.

Dabos-Seignon, S., Dancausse, J. P., Gering, E., Heathman, S., and Benedict, U. (1993) *J. Alloys and Compd.,* **190**, 237–42.

Deryagin, A. V. and Andreev, A. V. (1978) *Sov. Phys. JETP,* **44**, 610–13.

Dreitzler, R. M. and Gross, E. K. U. (1990) *Density Functional Theory,* Springer-Verlag, Berlin.

Dunlap, B. D. and Kalvius, G. M. (1985) Mössbauer spectroscopy on actinides and their compounds, in *Handbook on the Physics and Chemistry of the Actinides,* vol. 2 (eds. A. J. Freeman and G. H. Lander), Elsevier, Amsterdam, pp. 329–434.

Eriksson, O., Johansson, B., Brooks, M. S. S., and Skriver, H. L. (1989) *Phys. Rev. B,* **40**, 9519.

Eriksson, O., Becker, J. D., Balatsky, A. V., and Wills, J. M. (1999) *J. Alloys compd.,* **287**, 1–5.

Fano, U. (1961) *Phys. Rev.,* **124**, 1866.

Fisk, Z., Ott, H. R., and Smith, J. L. (1985) *Physica,* **130B**, 159–62.

Flouquet, J., Huxley, A., Braithwaite, D., Hardy, F., Knebel, G., Mineev, V., Ressouche, E., Aoki, D., and Brison, J. P. (2003) *Acta Phys. Pol. B,* **34**, 275.

Fournier, J. M. and Troc, R. (1985) Bulk properties of the actinides, in *Handbook on the Physics and Chemistry of the Actinides,* vol. 2 (eds. A. J. Freeman and G. H. Lander), North-Holland, Amsterdam, pp. 29–179.

Fournier, J. M., Boeuf, A., Frings, P., Bonnet, M., Boucherle, J. X., Delapalme, A., and Menovsky, A. (1986) *J. Less Common Metals,* **121**, 249–52.

Fournier, J. M. and Gratz, E. (1993) in *Handbook on the Physics and Chemistry of Rare Earths,* vol. 17 (eds. K. A. Gschneidner Jr, L. Eyring, G. H. Lander, G. R. Choppin), North-Holland, Amsterdam, pp. 409–537.

Fowler, R. D., Matthias, B. T., Asprey, L. B., Hill, H. H., Lindsay, J. D. G., Olsen, C. E., and White, R. W. (1965) *Phys. Rev. Lett.,* **15**, 860.

Franse, J. J. M., Frings, P. H., de Boer, F. R., and Menovsky, A. (1981) in *Physics of Solids under High Pressure* (eds. J. S. Schilling and R. N. Shelton), North-Holland, Amsterdam, p.181.

Franse, J. J. M., Frings, P. H., de Visser, A., Menovsky, A., Palstra, T. T. M., and Mydosh, J. A. (1984) *Physica B,* **126**, 116.

Friedel, J. (1969) *The Physics of Metals* (ed. J. M. Ziman), Cambridge University Press, New York.

Geibel, C., Thies, S., Kaczorowski, D., Mehner, A., Garuel, A., Seidel, B., Ahlheim, U., Helfrich, R., Petersen, K., Bredl, C. D., and Steglich, F. (1991) *Z. Phys. B,* **83**, 305.

Gordon, P. (1949) Thesis, Massachusetts Institute of Technology.

Gordon, J. E., Montgomery, H., Noer, R. J., Pickett, G. R., and Tobón, R. (1966) *Phys. Rev.,* **152**, 432.

Gouder, T., Wastin, F., Rebizant, J., and Havela, L. (2000) *Phys. Rev. Lett.,* **84**, 3378.

Gouder, T., Havela, L., Divis, M., Rebizant, J., Oppeneer, P. M., and Richter, M. (2001) *J. Alloys Compd.,* **314**, 7–14.

Greiner, J. D. and Smith, J. F. (1971) *Phys. Rev. B,* **4**, 3275.

Grewe, N. and Steglich, F. (1991) in *Handbook on the Physics and Chemistry of Rare Earths,* vol. 14 (eds. K. A. Gschneidner Jr and L. Eyring), North-Holland, Amsterdam, p. 343.

Griveau, J.-C., Pfleiderer, C., Boulet, P., Rebizant, J., and Wastin, F. (2004) *J. Magn. Magn. Mater.,* **272–276**, 154.

Gschneidner, K. A. Jr and Eyring, L. (eds.) (1993) *Handbook on the Physics and Chemistry of Rare Earths,* vol. 17, , North-Holland, Amsterdam.

Haire, R. G., Heathman, S., Iridi, M., Le Bihan, T., Lindbaum, A., and Rebizant, J. (2003) *Phys. Rev. B,* **67**, 134101.

Harrison, W. A. (1980) *Solid State Theory,* Dover, New York.

Harrison, W. A. (1999) *Elementary Electronic Structure,* World Scientific, Singapore.

Havela, L., Gouder, T., Wastin, F., and Rebizant, J. (2002) *Phys. Rev. B,* **65**, 235118.

Havela, L., Wastin, F., Rebizant, J., and Gouder, T. (2003) *Phys. Rev. B,* **68**, 085101.

Heathman, S., Haire, R. G., Le Bihan, T., Lindbaum, A., Litfin, K., Mèresse, Y., and Libotte, H. (2000) *Phys. Rev. Lett*. **85**, 2961.

Heathman, S., Haire, R. G., Le Bihan, T., Lindbaum, A., Idira, M., Normile, P., Li, S., Ahuja, R., Johansson, B., and Lander, G. H., (2005) *Science* **309**, 110.

Hecker, S. S. (2000) *Los Alamos Science*, vol. 26 (ed. N.G. Cooper).

Hecker, S. S. (2001) *MRS Bull.,* **26** (9), 672.

Hecker, S. S., Harbur, D. R., and Zocco, T. G. (2004) *Prog. Mater. Sci.,* **49**, 429.

Heffner, R. J., Smith, J. L., Willis, J. O., Birrer, P., Baines, C., Gygax, F. N., Hitti, B., Lippelt, E., Ott, H. R., Schenk, A., Knetsch, E. A., Mydosh, J. A., and McLaughlin, D. E. (1990) *Phys. Rev. Lett.,* **65**, 2816.

Hein, R. A., Henry, W. E., and Wolcott, N. M. (1957) *Phys. Rev.,* **107**, 1517.

Hill, H. H. (1970) in: *Plutonium and Other Actinides,* ed. W. N. Miner (AIME, New York) p.2.

Hjelm, A., Eriksson, O., and Johansson, B. (1993) *Phys. Rev. Lett.,* **71**, 1459–61.

Hohenberg, P. and Kohn, W. (1964) *Phys. Rev. B,* **136**, 864.

Holland-Moritz, E. and Lander, G. H. (1994) in *Handbook on the Physics and Chemistry of Rare Earths,* vol. 19. (eds. K. A. Gschneidner Jr, L. Eyring, G. H. Lander, and G. R. Choppin), North-Holland, Amsterdam, pp. 1–120.

Huray, P. G. and Nave, S. E. (1987) in *Handbook on the Physics and Chemistry of the Actinides,* vol. 5. (eds. A. J. Freeman and S. E. Nave), Elsevier, Amsterdam.

Johansson, B. and Skriver, H. L. (1982) *J. Magn. Magn. Mater.,* **29**, 217.

Johansson, B. and Brooks, M. S. S. (1993) in *Handbook on the Physics and Chemistry of Rare Earths,* vol. 17 (eds. K. A. Gschneidner Jr, L. Eyring, G. H. Lander, and G. R. Choppin), North-Holland, Amsterdam, pp. 149–244.

Joyce, J. J., Arko, A. J., Cox, L., and Czuchlewski, S. (1998) *Surf. Interface Anal.,* **26**, 121.

Joyce, J. J., Wills, J. M., Durakiewicz, T., Butterfield, M. T., Guziewicz, E., Sarrao, J. L., Morales, L. A., Arko, A. J., and Eriksson, O. (2003) *Phys. Rev. Lett.,* **91**, 176401.

Joyce, J. J., Wills, J. M., Durakiewicz, T., Guziewicz, E., Butterfield, M. T., Arko, A. J., Moore, D. P., Sarrao, J. L., Morales, L. A., and Eriksson, O. (2004) *Mat. Res. Soc. Symp. Proc.,* **802**, 239–44.

Kanellakopulos, B., Blaise, A., Fournier, J. M., and Muller, W. (1975) *Solid State Commun.,* **17**, 713–15.
Kevan, S. D. (ed.) (1992) *Angle-Resolved Photoemission Theory and Current Applications,* Elsevier, Amsterdam.
Kittel, C. (1963) *Quantum Theory of Solids,* John Wiley, New York.
Kittel, C. (1971) *Introduction to Solid State Physics,* John Wiley, New York.
Koelling, D. D., Dunlap, B. D., and Crabtree, G. W. (1985) *Phys. Rev. B,* **31**, 4966–71.
Kohn, W. and Sham, L. J. (1965) *Phys. Rev. A,* **140**, 1133.
Krimmel, A., Fischer, P., Roessli, B., Maletta, H., Geibel, C., Schank, C., Grauel, A., Loidl, A., and Steglich, F. (1993) *Z. Phys. B,* **86**, 161.
Landau, L. (1957) *Sov. Phys. JETP,* **3**, 920.
Lander, G. H., Brooks, M. S. S., and Johansson, B. (1991) *Phys. Rev. B,* **43**, 13672–5.
Lander, G. H., Fisher, E. S., and Bader, S. D. (1994) *Adv. Phys.,* **43**, 1–110.
Lashley, J. C., Singleton, J., Migliori, A., Betts, J. B., Fisher, R. A., Smith, J. L., and McQueeney, R. J. (2003) *Phys. Rev. Lett.,* **91**, 205901.
Le Bihan, T., Heathman, S., Idiri, M., Wills, J. M., Lawson, A. C., and Lindaum, A. (2003) *Phys. Rev. B,* **67**, 134102.
Ledbetter, H. M. and Moment, R. L. (1976) *Acta Metall.,* **24**, 891–9.
Lindbaum, A., Heathman, S., Litfin, K., Méresse, Y., Haire, R.G., Le Bihan, T., and Libotte, H. (2001) *Phys. Rev. B,* **63**, 214101.
Lindbaum, A., Heathman, S., Le Bihan, T., Haire, R. G., Diri, M. I., and Lander, G. H. (2003) *J. Phys.: Condens. Matter,* **15**, S2297.
Louie, S. G. (1992) Quasiparticle excitation and photoemission, in *Angle-Resolved Photoemission Theory and Current Applications* (ed. S. D. Kevan), Elsevier, Amsterdam.
Luttinger, J. M. (1960) *Phys. Rev.,* **119**, 1153.
Maple, M. B., Chen, J. W., Dalichaouch, Y., Kohara, T., Rossel, C., Torikachvili, M. S., McElfresh, M. W., and Thompson, J. D. (1986) *Phys. Rev. Lett.,* **56**, 185.
McEwen, K. A., Steinberger, U., and Martinez, J. L. (1993) *Physica B,* **186–188**, 670–4.
Méot-Reymond, S. and Fournier, J. M. (1996) *J. Alloys Compd.,* **232**, 119–25.
Merrifield, R. E. (1966) *J. Chem. Phys.,* **44**, 4005.
Mortimer, M. J. (1979) *J. Phys.* (*Paris*) (*C-4*), **40**, 124.
Naegele, J. R., Ghijen, J., and Manes, L. (1985) Localization and hybridization of 5f states in the metallic and ionic bond as investigated by photoelectron spectroscopy, in *Actinides – Chemical and Physical Properties* (ed. L. Manes), Structure and Bonding 59/60, Springer-Verlag, Berlin, p. 198.
Nellis, W. J. and Brodsky, M. B. (1974) in *The Actinides: Electronic Structure and Related Properties,* vol. 2. (eds. A. J. Freeman and J. B. J. Darby), Academic Press, New York, pp. 265–88.
Nieuwenhuys, G. J. (1995) in *Handbook of Magnetic Materials,* vol. 9 (ed. K. H. J. Buschow), North-Holland, Amsterdam, pp. 1–55.
Niklasson, A. M. N., Wills, J. M., Katsnelson, M. I., Abrikosov, I. A., Eriksson, O., and Johansson, B. (2003) *Phys. Rev. B,* **67**, 235105.
Norman, M. R. and Koelling, D. D. (1993) in *Handbook on the Physics and Chemistry of Rare Earths,* vol. 17 (eds. K. A. Gschneidner Jr, L. Eyring, G. H. Lander, and G. R. Choppin), North-Holland, Amsterdam, pp. 1–86.
Olsen, C. E., Comstock, A. L., and Sandenaw, T. A. (1992) *J. Nucl. Mater.,* **195**, 312–16.

Ott, H. R., Rudigier, H., Fisk, Z., and Smith, J. L. (1983) *Phys. Rev. Lett.,* **50**, 1595.
Ott, H. R. and Fisk, Z. (1987) Heavy-electron actinide materials, in *Handbook on the Physics and Chemistry of Rare Earths,* vol. 17 (eds. A. J. Freeman and G. H. Lander), North-Holland, Amsterdam, pp. 85–225.
Pénicaud, M. (2002) *J. Phys.: Condens. Matter,* **14**, 3575.
Petit, L., Svane, A., Szotek, Z., and Temmerman, W. M. (2003) *Science,* **301**, 498–501.
Poon, S. J., Drehman, A. J., Wong, K. M., and Clegg, A. W. (1985) *Phys. Rev. B,* **31**, 3100.
Potzel, W., Kalvius, G. M., and Gal, J. (1993) in *Handbook on the Physics and Chemistry of Rare Earths,* vol. 17 (eds. K. A. Gschneidner Jr, L. Eyring, G. H. Lander, and G. R. Choppin), North-Holland, Amsterdam, pp. 539–634.
Rao, R. S., Godwal, B. K., and Sikka, S. K. (1992) *Phys. Rev. B,* **46**, 5780.
Reihl, B., Domke, M., Kaindl, G., Kalkowski, G., Laubschat, C., Hulliger, F., and Schneider, W. D. (1985) *Phys. Rev. B,* **32**, 3530–3.
Rogl, P. (1991) The ternary and higher order systems with actinide elements and boron, in *Handbook on the Physics and Chemistry of the Actinides* (eds. A. J. Freeman and G. Keller), North-Holland, Amsterdam, pp. 75–154.
Sanchez-Castro, C. and Bedell, K. S. (1993) *Phys. Rev. B,* **47**, 1203.
Sandratskii, L. M. (1998) *Adv. Phys.,* **47**, 91–160.
Sarrao, J. L., Morales, L. A., Thompson, J. D., Scott, B. L., Stewart, G. R., Wastin, F., Rebizant, J., Boulet, P., Colineau, E., and Lander, G. H. (2002) *Nature,* **420**, 297.
Sato, N. K., Aso, N., Miyake, K., Shiina, R., Thalmeier, P., Varelogiannis, G., Geibel, C., Steglich, F., Fulde, P., and Komatsubara, T. (2001) *Nature,* **410**, 340–3.
Savrasov, S. Y., Kotliar, G., and Abrahams, E. (2001) *Nature,* **410**, 793.
Saxena, S. S., Agarwal, P., Ahilan, K., Grosche, F. M., Haselwimmer, R. K. W., Steiner, M. J., Pugh, E., Walker, I. R., Julian, S. R., Monthoux, P., Lonzarich, G. G., Huxley, A., Sheikin, I., Brathwaite, D., and Flouquet, J. (2000) *Nature,* **406**, 587.
Sechovský, V. and Havela, L. (1988) in *Ferromagnetic Materials – A Handbook on the Properties of Magnetically ordered Substances,* vol. 4 (eds. E. P. Wohlfarth and K. H. J. Buschow), North-Holland, Amsterdam, pp. 309–491.
Sechovský, V. and Havela, L. (1998) in *Handbook of Magnetic Materials,* vol. 11 (ed. K. H. J. Buschow), North-Holland, Amsterdam, pp. 1–289.
Shick, A. B., Drchal, V., and Havela, L. (2005) *Europhys. Lett.,* **69**, 588–94.
Slater, J. C. (1937) *Phys. Rev.,* **51**, 846.
Smith, J. L. and Haire, R. G. (1978) *Science,* **200**, 535.
Smith, J. L., Stewart, G. R., Huang, C. Y., and Haire, R. G. (1979) *J. Phys.* (*Paris*) (*C-4*), **40**, 138.
Smith, J. L. and Kmetko, E. A. (1983) *J. Less Common Metals,* **90**, 83.
Spirlet, J. C., Hall, R. A. O., Jeffrey, A. J., and Mortimer, M. J. (1987) *Proc 17emes Journees des Actinides* (*Signal des Chexbres*), ed. P. Erdös, p. 15.
Steglich, F., Aarts, J., Bredl, C. D., Lieke, W., Meschede, D., Franz, W., and Schafer, H. (1979) *Phys. Rev. Lett.,* **43**, 1892–6.
Stevenson, J. N. and Peterson, J. R. (1979) *J. Less Common Metals,* **66**, 201–10.
Stewart, G. R., Fisk, Z., Willis, J. O., and Smith, J. L. (1984) *Phys. Rev. Lett.,* **52**, 679.
Stewart, G. R. (2001) *Rev. Mod. Phys.,* **73**, 797.
Söderlind, P., Eriksson, O., Johansson, B., Wills, J. M., and Boring, A. M., (1995) *Nature,* **374**, 524.

Söderlind, P. and Eriksson, O. (1997) *Phys. Rev. B,* **56**, 10719.
Söderlind, P., Ahuja, R., Eriksson, O., Johansson, B., and Wills, J. M. (2000) *Phys. Rev. B,* **61**, 8119.
Söderlind, P. and Sadigh, B. (2004) *Phys. Rev. Lett.,* **92**, 185702.
Vogt, O. and Mattenberger, K. (1993) in *Handbook on the Physics and Chemistry of Rare Earths,* vol. 17 (eds. K. A. Gschneidner Jr, L. Eyring, G. H. Lander, and G. R. Choppin), North-Holland, Amsterdam, pp. 301–407.
Vohra, Y. K. and Akella, J. (1991) *Phys. Rev. Lett.,* **67**, 3563.
Wiesinger, G. and Hilscher, G. (1991) in *Handbook of Magnetic Materials,* vol. 6 (ed. K. H. J. Buschow), Elsevier, Amsterdam.
Wigner, E. P. and Seitz, F. (1933) *Phys. Rev.,* **43**, 804.
Wigner, E. (1934) *Phys. Rev.,* **46**, 1002.
Wills, J. M. and Eriksson, O. (1992) *Phys. Rev. B,* **45**, 13879.
Wills, J. M. and Eriksson, O. (2000) *Los Alamos Science*, vol. 26 (ed. N.G. Cooper), Los Alamos National Laboratory.
Wills, J. M., Eriksson, O., Delin, A., Andersson, P. H., Joyce, J. J., Durakiewicz, T., Butterfield, M. T., Arko, A. J., Moore, D. P., and Morales, L. A. (2004) *J. Electron. Spectrosc. Relat. Phenom.,* **135**, 163–66.
Wong, J., Krisch, M., Farber, D. L., Occelli, F., Schwartz, A. J., Chiang, T. C., Wall, M., Boro, C., and Xu, R. Q. (2003) *Science* **301**, 1078–80.
Zachariasen, W. H. (1973) *J. Inorg. Nucl. Chem.,* **35**, 3487–97.
Ziman, J. M. (1972) *Principles of the Theory of Solids,* Cambridge University Press, New York.
Zwicknagl, G. and Fulde, P. (2003) *J. Phys.: Condens. Matter,* **15**, S1911.

CHAPTER TWENTY TWO

ACTINIDE STRUCTURAL CHEMISTRY

Keith E. Gutowski, Nicholas J. Bridges, and Robin D. Rogers

22.1 INTRODUCTION

This chapter focuses on the solid state structural chemistry of actinide materials as determined by single-crystal X-ray diffraction, single-crystal neutron diffraction, powder X-ray diffraction, and powder neutron diffraction techniques. Since Burns' chapter, Structural Chemistry, was published in the 1986 edition of this work, significant improvements in crystallographic technology and instrumentation have advanced the field of solid state chemistry. Some of the most dramatic changes have been in computer technology and software, making the data collection, reduction, and refinement processes highly automated and simplified. As a consequence, X-ray diffractometers have become nearly ubiquitous in research departments globally and neutron-scattering resources have become more advanced and accessible, resulting in the elucidation and publication of a greater number of additional actinide structures since the last edition; these structures are the focus for this chapter.

In the past, the structural study of actinide compounds using diffraction techniques had often entailed complications, many of which were inherent difficulties attributable to the composition (very heavy and very light elements) and radioactivity of the samples themselves. However, modern advances and insights have made the study of actinide-containing compounds almost a routine process. For example, X-ray diffraction of actinide–organic complexes can be complicated by the scattering due to the heavy atoms, which often dominates

that of light atoms; however, the complementary use of neutron diffraction techniques allows for the accurate placement of lighter atoms, particularly hydrogen, along with the heavy atoms (Suortti, 2002). In instances where the growth of sufficiently large single crystals for analysis has been an obstacle, powder diffraction, particularly when coupled with sophisticated refinement techniques, has allowed for the determination of positional and thermal parameters of samples containing randomly oriented crystallites with nearly the same degree of precision as single-crystal techniques (Rietveld, 1967). In addition, advances in the growth of single crystals from melts, solutions, and vapors have enabled many difficulties in this area to be overcome (Spirlet *et al.*, 1991). For many actinide isotopes, radioactive decay can cause defects and dislocations in single-crystal samples. However, substitution of less radioactive isotopes alleviates the rate at which lattice deterioration occurs, creating more stable samples for study. For short-lived isotopes available in larger quantities, self-heating or irradiation problems are encountered; for example, ^{242}Cm ($t_{1/2} = 162.8$ days) produces 122 W/g although substituting ^{244}Cm ($t_{1/2} = 8.1$ years) or ^{248}Cm ($t_{1/2} = 3.4 \times 10^5$ years) reduces that aspect of the problem (Haire and Eyring, 1994).

While our treatment is by no means exhaustive (in the sense that we do not include every actinide structure published in the literature), it is intended to represent a large number of important structures, to illustrate how advances in solid state techniques have led to the generation of larger numbers of structures, and to offer an appreciation for solid state actinide structures in general. In addition, this overview of actinide structural and coordination chemistry has the aim to establish an understanding of how the unique electronic properties of the actinide elements influence chemical bonding in their inorganic, coordination, and organometallic compounds.

22.2 SOLID STATE STRUCTURAL TECHNIQUES

Recent advances in crystallography and structure determination focus on improvements in instrumentation because the theory and preparatory steps (i.e., crystal growing, unit cell/orientation matrix determination) remain the same. Although many actinide inorganic structures were solved several decades ago, the use of state-of-the-art instrumentation for the determination of new structures or the refinement of old ones will be highlighted whenever possible throughout this chapter.

22.2.1 X-ray diffraction techniques

X-ray crystallography as a technique is based on the diffraction of X-rays by electron density that resides in defined planes within the crystalline lattice; the nature of the diffraction is governed by Bragg's law ($n\lambda = 2d\sin\theta$). Thus, X-ray diffraction yields information regarding the distribution of electrons in a crystalline solid. The application of X-ray crystallography to actinide science is

met with a unique challenge; because X-rays are diffracted by electron density, the large, dense actinides can easily overshadow smaller atoms with less electron density. The study of heavy elements in this manner has become routine, however, through use of techniques to circumvent this problem (Deschamps and Flippen-Anderson, 2002).

In most small-scale X-ray diffractometers (i.e., non-synchrotron), X-ray tubes are used to accelerate electrons toward a target material (Mo or Cu), resulting in the generation of X-rays which are then filtered, collimated, and focused through an aligned single crystal that is subsequently rotated through space by a goniometer; the diffracted X-rays are then registered by an area detector, such as a charge coupled device (CCD), resulting in a diffraction pattern that is then interpreted. Current X-ray diffractometers are controlled by computers and software that assist in refining the data and aid in solving the crystal structure, making the method so attractive that it is regarded as an essential analytical instrument in many research departments. In fact, tasks that used to require several months of effort are now easily accomplished in minutes with modern day computational and graphical resources (Suortti, 2002).

The advent of the synchrotron has revolutionized the ways in which X-rays are generated and used for research purposes. Synchrotron radiation is emitted when light, charged particles (e.g., electrons or positrons) moving at relativistic speeds undergo radial acceleration. Unlike laboratory diffractometers, synchrotrons are large-scale facilities that are designated for the production of synchrotron radiation. Small synchrotrons of the past have paved the way for the development of third-generation synchrotron facilities; in the latter, electrons emitted by an electron gun are first accelerated in a linear accelerator (linac) and then transmitted to a circular accelerator (booster synchrotron) where they are accelerated to energy levels of several gigaelectron volts (GeV). These high-energy electrons are then injected into a large storage ring where they circulate in a vacuum environment, at a constant energy, for many hours. Magnets are used to deflect the particles, causing them to change direction and emit synchrotron radiation, which is then directed toward a beamline for use in experiments (Suortti, 2002).

The radiation produced is extremely bright over a broad spectral range; in fact, it is several orders of magnitude brighter than that produced by a conventional X-ray tube. The X-rays produced in this manner are collimated to a narrow beam, polarized, and pulsed (subnanosecond). Synchrotron radiation offers the advantage of being able to analyze very small crystals because 10^{10}–10^{11} photons sec^{-1} can be focused on a sample 10 μm in diameter (Suortti, 2002).

Powder X-ray diffraction refers to the use of a collimated monochromatic beam of X-rays to analyze a sample containing a large number of crystals with random orientations. Diffraction intensity is measured as a function of 2θ, thus allowing a simple application of Bragg's law to determine d-spacings within the lattice. The resulting set of d-spacings is a 'fingerprint' that can uniquely determine crystal symmetry and can identify a crystalline material or a mixture of crystalline materials, typically by comparisons with standards. Powder X-ray

diffraction has become an important tool in the study of actinide compounds because it is often impossible to obtain sufficiently large single crystals for some classes of compounds (Suortti, 2002).

22.2.2 Neutron diffraction techniques

In X-ray diffraction, the scattering power of a given atom for a given reflection, or the 'scattering factor', is strongly dependent on the type of atom, the scattering angle, and thermal motion, thus drastically affecting the resolution and the determination of the position of lighter atoms in the presence of heavy ones. However, scattering in neutron diffraction occurs primarily from the nucleus; since the diameter of the nucleus is small relative to the wavelength of the neutrons, the 'scattering factor' is characteristic of the particular nucleus and independent of scattering angle. As a result, neutron diffraction offers the ability to distinguish among near neighbors in the periodic table, or determine the position of light atoms with the same degree of accuracy as the heavy elements. For example, the scattering amplitudes for ^{2}D and ^{238}U with X-rays are 0.28 and 25.92, respectively, while with neutrons, these values are 0.67 and 0.84, respectively. In this regard, X-ray diffraction and neutron diffraction are often thought of as complementary techniques (Deschamps and Flippen-Anderson, 2002).

Currently, monochromatic neutrons for scattering experiments are produced at large facilities because there is no laboratory-size instrument comparable to the X-ray diffractometer. Nuclear reactors offer a source of steady (i.e., not pulsed) neutrons; high-energy neutrons (1 MeV) from continuous self-sustained fission reactions in ^{235}U are moderated to thermal energies near 40 meV and extracted through holes that penetrate the moderator. Alternatively, pulsed (spallation) sources use short bursts of 1 GeV protons to generate a large number of neutrons by being spalled ('chipped') from target nuclei (e.g., 25 neutrons per incident photon for ^{238}U). The resulting neutrons are moderated (using hydrogenous materials) to a pulse of neutrons with energies less than 10 eV (Suortti, 2002).

Spallation-based neutron scattering has emerged as comparable and complementary to reactor-based neutron scattering, although there are fundamental differences between the experiments. Neutrons from a reactor are separated with a monochromator to provide a small energy band for use in diffraction experiments in a manner similar to the beam from an X-ray tube. Spallation neutrons have a wide energy distribution and diffraction patterns are analyzed as a function of the neutron wavelength by employing time-of-flight diffraction (Suortti, 2002).

Powder neutron diffraction, like its X-ray analog, is an important tool for analyzing samples containing randomly oriented crystallites. However, in recent years, powder X-ray and neutron diffraction have become more widely used due to the advantages offered by the Rietveld refinement technique, originally developed for analyzing neutron diffraction data; here, positional and thermal

parameters can be determined from powder data. In fact, precision comparable to single-crystal X-ray diffraction data is achievable for positional parameters, but thermal parameters are less reliable (by a factor of 2 or 3) (Deschamps and Flippen-Anderson, 2002).

22.3 METALS AND INORGANIC COMPOUNDS

22.3.1 Actinide metals

The temperature-dependent phase diagrams of actinide metals are usually complicated by a variety of allotropic forms as illustrated in Fig. 22.1. As the temperature is increased, the metallic forms of the light actinides, in many cases, go through a series of allotropic changes, the most complicated of which is observed in plutonium metal (Smith and Kmetko, 1983). In general, as the metals approach melting, they take on the body-centered cubic (bcc) form, almost universally observed for high-temperature forms of lanthanide metals; however, this bcc form is predicted to be unstable for the later actinides (Sari *et al*., 1972/73). This change in crystal structure is caused by intricate differences in the electronic nature of the early actinides, while these differences in the later actinides become less clear due to lack of research. In a paper by Wills and Eriksson (1992), predictions of the crystal structure properties of thorium, protactinium, and uranium metal were made based on electronic considerations which successfully reproduced the experimentally observed crystal structures.

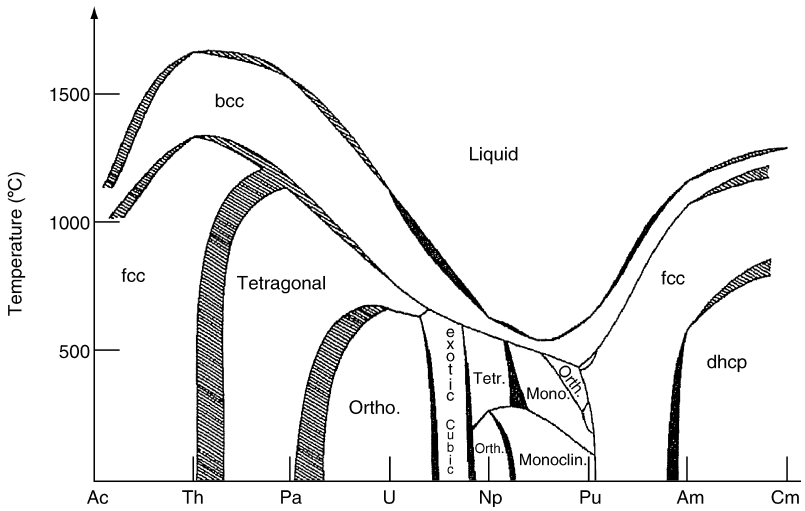

Fig. 22.1 *Binary phase diagram of the light actinides* (*bcc: body-centered cubic; fcc: face-centered cubic; ortho.: orthorhombic; mono.: monoclinic; dhcp: double hexagonal close packed*) (*Smith and Kmetko,* 1983. *Reproduced with permission from Elsevier*).

Described below are the different structural forms of the actinide metals from actinium through einsteinium. The transition temperatures listed reflect the widely agreed upon values from Chapters 2–12, 15, 19, and 21, although may not be reflective of the primary references listed, which have been included for completeness.

(a) Actinium

Actinium metal has a crystal structure identical to that of β-La, the high-temperature form of lanthanum. Actinium metal is a face-centered cubic (fcc) system with unit cell dimensions of 5.31(1) Å as determined by X-ray powder diffraction. Despite the existence of low-temperature α-La, a corresponding α-Ac has not been detected (Farr *et al.*, 1961).

(b) Thorium

Thorium metal exhibits two allotropic forms; at temperatures below 1360°C, the fcc form is present, after which it transforms into a bcc form. The bcc phase is present until the melting point of thorium is reached at 1750°C (Chiotti, 1954).

(c) Protactinium

Low-temperature protactinium metal (less then 1170°C) is a body-centered tetragonal crystal system. Upon heating, the axial ratio (c/a) increases exponentially from 0.8260(7) to 1.00, causing the structure to tend toward bcc at high temperature (up to 1572°C) (Marples, 1965).

(d) Uranium

Uranium metal has three temperature-induced allotropic forms. The room temperature allotropic form, α-phase (below 668°C), was the first to be discovered. This phase was originally reported by Wilson as having a monoclinic structure (Wilson, 1933). Within 4 years, it had been reindexed as an orthorhombic structure (Jacob and Warren, 1937). The last phase to be discovered was the β-phase which belongs to the tetragonal crystal system (Thewlis, 1951). This phase is present over the smallest temperature range, 668–776°C. X-ray single-crystal results are found in an article by Tucker (1951). The high-temperature γ-phase has a bcc crystal structure and is present until the melting point of uranium is reached (1135°C). Tucker (1950) also summarizes structural aspects of the allotropic forms of uranium in detail.

(e) Neptunium

Room-temperature neptunium metal belongs to the orthorhombic crystal system, known as the α-phase, and is different from that of uranium. In the α-phase, two different neptunium environments are present, only one of which

resembles the environment of the atoms observed in α-uranium (Zachariasen, 1952a). The α-phase is stable up to about 280°C, after which it transforms into the β-phase, a tetragonal crystal system. The final phase, present above 576°C, is known as the γ-phase (bcc crystal system) and exists until the metal melts at 639°C (Zachariasen, 1952b).

(f) Plutonium

Plutonium metal, by far the most complex of the actinide metals, has six different temperature-dependent allotropic forms with a wide range of physical properties and crystal structures. The α-phase, present at room temperature, is monoclinic and exists up to 124.4°C, after which it transforms into the β-phase (Zachariasen and Ellinger, 1963a). The α-phase is the densest and has the largest positive thermal expansion coefficient of all the plutonium allotropes (Zachariasen and Ellinger, 1957). A comprehensive list of densities and thermal expansion coefficients for plutonium metal is available from Choppin and Stout (1991). The β-phase is body-centered monoclinic and is stable up to about 214.8°C. The α–β phase transition has no simple geometry transformation, thus making the change sluggish (Zachariasen and Ellinger, 1959, 1963b). Between 214.8 and 320.0°C, the orthorhombic γ-phase is present and is unlike any other metal, having ten close plutonium neighbors at an average distance of 3.157 Å. The mean linear thermal expansion coefficients of the metal are positive along the [010] and [001] crystallographic direction and negative along the [100] direction (Zachariasen and Ellinger, 1955). The δ and the δ′ allotropic forms of plutonium are the only two that exhibit negative thermal expansion, thus introducing special concerns during casting of plutonium metal. The δ-phase is present between 320.0 and 462.9°C and belongs to the fcc crystal system. The δ′-phase is only present in the small range of 462.9–482.6°C and possesses, in magnitude, the largest thermal expansion coefficient of all the plutonium allotropic forms. At temperatures higher then 482.6°C (up to the melting point of plutonium metal at 640°C), the bcc ε-phase is present (Ellinger, 1956). The changes in the thermal expansion coefficients with respect to the allotropic forms of plutonium are shown graphically in Fig. 22.2. A summary of all the physical and crystallographic properties of plutonium metal is presented in greater detail elsewhere (Jette, 1955).

(g) Americium

At room temperature, americium metal, like α-La, belongs to the double hexagonal closed-packed (dhcp) crystal system (Graf *et al*., 1956; McWhan *et al*., 1962). At temperatures between 600 and 700°C, it was originally reported that a dhcp to fcc change occurs; however, a later report by Sari *et al*. refuted the existence of this change and suggested evidence for a solid-solid transition around 1075°C (before melting at 1173°C), although the exact nature of the

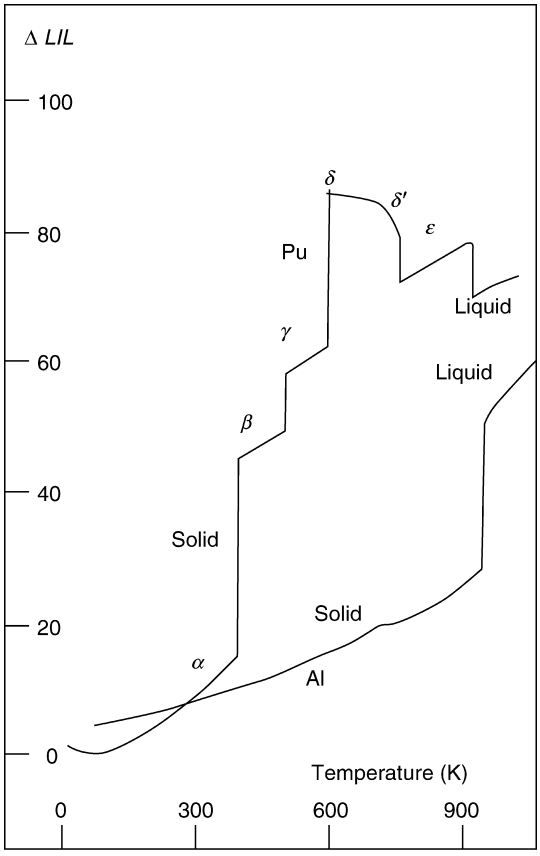

Fig. 22.2 *Dilation of aluminium and plutonium metals as a function of temperature. The allotropes are designated by their symbols* (*Choppin and Stout*, 1991. *Reproduced with permission from The Royal Society of Chemistry*).

modification could not be determined (Sari *et al*., 1972/73). Further evidence supports the α to β-phase at 769°C, β to γ-phase 1077°C with melting occurring at 1176°C, (see chapter 8).

(h) Curium

The crystal structure of curium metal as reported by Cunningham and Wallmann indicates a dhcp form at low temperatures (below 1295°C) that is isostructual with α-La and dhcp americium (1964). A later report by Smith *et al*. saw no evidence for the dhcp form, but rather a cubic close-packed structure. In their study, however, they reported broadened lines indicative of damaged curium structures, as well as weak curium lines compared to the tungsten lines. Also reported was a high-temperature phase (1295–1346°C) with fcc

symmetry where the metallic radius of curium (1.54 Å) is consistent with the 4+ oxidation state (Smith *et al.*, 1969).

(i) Berkelium

X-ray powder diffraction of berkelium metal revealed the existence of two stable room-temperature crystallographic modifications: dhcp and fcc . In preparation of the metal, annealing at 800°C with slow cooling tended to favor the dhcp structure, while annealing at 900°C resulted primarily in the fcc structure (Peterson *et al.*, 1971). Current studies place the α-phase below 977°C while the β-phase exists until melting at 1050°C (see Chapter 10).

(j) Californium

Californium metal was also observed to exist in two allotropic forms at room temperature: fcc and hexagonal close-packed (hcp). Upon heating in a vacuum, the fcc structure usually changed to the hcp structure, but would not revert back to the fcc, even at liquid nitrogen temperatures (Haire and Baybarz, 1974). A subsequent study by Zachariasen (1975) called into question these results, and concluded that the hcp and fcc structures were attributable to Cf_2O_2S and CfS, respectively. Further studies by Haire and Asprey (1976) later showed the existence of two dhcp structures present as a mixture. Analysis of the data and comparisons with previous results suggest that californium metal is one of the most complex transplutonium metals, existing in both a divalent and higher valent form with dhcp, and fcc structures. Current evidence supports the dchp phase below 700°C and the fcc phase between 700 and 900°C (see Chapter 11).

(k) Einsteinium

Einsteinium metal has been investigated through the reduction of a thin film of Es_2O_3 by lanthanum. The metallic einsteinium has a fcc structure and at the present time is the only known allotropic form (Haire and Baybarz, 1979).

22.3.2 Oxides

Actinide oxides (An_xO_y) are refractory materials, indicating their collective resistance to decomposition at high temperatures. For example, ThO_2 has the highest melting point of any oxide (3378°C) (Ronchi and Hiernaut 1996). Research has focused on the use of appropriate actinide oxides as nuclear fuels, although the chemistry associated with the actinide elements tends to be complex and includes polymorphism, non-stoichiometric compounds, and intermediate phases. The oxides are basic in character (they are weak Lewis bases, able to donate electron pairs). Their chemical reactivity is usually influenced by their thermal history; actinide oxides are significantly more inert after they have been ignited (Greenwood and Earnshaw, 2001).

Several early studies of actinide monoxides reported structural data for Th through Am, although definitive evidence is lacking. A later study with plutonium oxides, however, contested their existence and presented data supporting the existence of plutonium oxycarbide rather than monoxide as a phase on plutonium metal surfaces (Larson and Haschke, 1981). Studies of lanthanides (La–Nd, Sm) under high-temperature and high-pressure conditions supported the formation of NaCl-type monoxides, but noted their instability in condensed form under standard conditions. This suggests that PuO may be attainable by similar high-pressure techniques (Leger *et al.*, 1981). Despite this evidence against plutonium monoxide under standard conditions, structural data for the remaining actinide monoxides will be presented herein for completeness.

Structural studies of other actinide oxides have largely been by means of powder diffraction techniques due to the refractory nature of the materials and the difficulty in obtaining single crystals. Actinide dioxides are known for the elements thorium through californium. All are isostructural and adopt the common face-centered cubic (fcc) fluorite structure (CaF_2). The unit cell constants for the dioxides from thorium to Californium are shown in Table 22.1. In the CaF_2 structure, the cations occupy the cubic closest packing sites and the anions fill the remaining tetrahedral holes, resulting in a coordination number (CN) of eight for each cation. Thus, the overall structure is three-dimensional with a strong covalent component due to the high formal charge on the cation, resulting in compounds with unusually high melting points. The dioxides, with the exception of PaO_2, tend to lose oxygen at high temperature and form substoichiometric compounds with oxygen vacancies in the anion part of the lattice; the protactinium and uranium dioxides can form superstoichiometric compounds at room temperature (Keller, 1973).

Actinide sesquioxides (An_2O_3) become increasingly stable progressing from the lighter to the heavier actinide elements. Their structures are analogous to those formed for rare earths and adopt three structures commonly classified according to the following types:

Table 22.1 *Unit cell constants for actinide dioxides.*

Compound	*Cell constant, a* (Å)	*Reference*
ThO_2	5.597	Sellers *et al.* (1954); Leigh and McCartney (1974)
PaO_2	5.505	Sellers *et al.* (1954)
UO_2	5.4704	Grønvold (1955); Hutchings (1987)
NpO_2	5.4334	Fahey *et al.* (1976)
PuO_2	5.396	Gardner *et al.* (1965)
AmO_2	5.373	Hurtgen and Fuger (1977)
CmO_2	5.359	Peterson and Fuger (1971)
BkO_2	5.3315	Fahey *et al.* (1974)
CfO_2	5.310	Baybarz *et al.* (1972a)

A-type: hexagonal structure, with AnO_7 units in capped octahedral arrangement (CN = 7);

B-type: monoclinic structure, with two AnO_7 units in capped trigonal prism arrangement and third in capped octahedral arrangement (CN = 7, possibly 6);

C-type: cubic structure (related to fluorite), where one-quarter of anions have been removed to reduce coordination number to 6, but not octahedral (CN = 6).

As with the lanthanides, the smaller actinides favor the C-type structure (Greenwood and Earnshaw, 2001). However, none of the actinide sesquioxides have been studied using single-crystal X-ray diffraction techniques, thus making precise structural characterization (i.e., atomic positions, bond lengths) impossible. The chemistry of this class of compounds may be further complicated by temperature or pressure dependence on the structures, as detailed by Haire and Eyring (1994).

More complex and less common actinide oxides, including AnO_3, An_3O_8, and An_2O_5, will be discussed on a case by case basis, where appropriate. For example, AnO_3 compounds are known, but typically exist in a hydrated state; the only known anhydrous trioxide is UO_3. Anhydrous uranium trioxide has been isolated in seven polymorphic forms, reflecting the ability of uranium(VI) to exist in a variety of low symmetry, high coordination environments with similar energies (Weller *et al.*, 1988).

(a) Actinium

Only one actinium oxide has been reported. Fried *et al.* (1950) reported that actinium sesquioxide, Ac_2O_3, can be obtained through decomposition of actinium oxalate at 1100°C. The compound has hexagonal symmetry and is isomorphous with certain lanthanide sesquioxides, including those of lanthanum, cerium, and praseodymium (A-type). It is interesting to note that the sample was prepared from less than 10 μg of actinium to minimize fogging of the X-ray film due to high gamma radiation encountered during structural data collection.

(b) Thorium

Two binary oxides have been reported for thorium. Metastable thorium monoxide has been reported to form on the surface of thorium metal exposed to air and subsequent crystallographic analysis revealed an fcc structure with a lattice parameter of 5.302 Å (Ackermann and Rauh, 1973). ThO_2, also with fcc symmetry (CaF_2 structure), is stable up to its melting point of 3390°C, although extensive heating to 1800–2000°C in a vacuum results in a blackened material due to loss of oxygen (Haire and Eyring, 1994).

(c) Protactinium

The oxides of protactinium are more complex than those of the two earlier actinide elements, ascribable to its more complex electronic structure. Three binary oxides are known: PaO, PaO_2, and Pa_2O_5. Several intermediate oxides of variable stoichiometry also exist between PaO_2 and Pa_2O_5, in addition to seven crystal modifications of Pa_2O_5 (Haire and Eyring, 1994).

Crystallographic analysis of the monoxide, PaO, showed the NaCl structure with a lattice cell length of 4.961 Å. This material, like ThO, has been reported to exist as a coating on metal. Its existence is further ascribed as PaO because the substance is slowly oxidized by air to form PaO_2 (Sellers *et al.*, 1954).

The white binary oxide Pa_2O_5 is formed by heating the hydrated oxide ($Pa_2O_5 \cdot nH_2O$), as well as several other protactinium compounds (hydroxide, nitrate, etc.), in air or oxygen above 650°C. The crystalline modification that is obtained (there are seven total, including fcc, tetragonal, hexagonal, orthorhombic, and rhombohedral forms) depends on the temperature to which the starting material is heated. The black dioxide, PaO_2, can be prepared by the reduction of Pa_2O_5 with H_2 at 1550°C and has a fluorite fcc structure (Sellers *et al.*, 1954).

Intermediate compounds with O/Pa ratios between 2.0 and 2.5 are obtained by selective oxidation of PaO_2 or reduction of Pa_2O_5. These compounds have been identified as $PaO_{2.18}$–$PaO_{2.21}$, $PaO_{2.33}$, $PaO_{2.40}$–$PaO_{2.42}$, and $PaO_{2.42}$–$PaO_{2.44}$, having fcc, tetragonal, tetragonal, and rhombohedral symmetries, respectively (Roberts and Walter, 1966).

(d) Uranium

The complexity of uranium oxides is due to the ability of uranium to exist in several valence states, both exclusively and simultaneously. Many uranium oxides are known, including UO_2, U_2O_5, U_3O_8, U_4O_9, and UO_3, each showing a range of content. Diffraction data for the monoxide have been reported and, like the analogous thorium compound, UO is unstable with respect to disproportionation (Ackermann and Rauh, 1973). The compound U_3O_8 is the most stable oxide of uranium under ambient conditions.

Uranium dioxide is the most widely studied of the dioxides due to its use in the nuclear industry. The room-temperature fcc fluorite crystal structure of stoichiometric UO_2 was first determined by Goldschmidt and Thomassen (1923) and they showed that the uranium atoms occupy the face-centered sites, while the oxygen atoms occupy the corners of a cube centered within the unit cell. Earlier, however, Hillebrand established the isomorphism of UO_2 with ThO_2 (Hillebrand, 1893). The fluorite structure possesses two types of lattice holes per unit cell: three positioned in the middle of the unit cell edges at (½, 0, 0), (0, ½, 0), and (0, 0, ½), and one large hole in the cube center at (½, ½, ½). The openness of the structure allows the anions to move toward the holes and causes anharmonic motion of the oxygen atoms (Rouse *et al.*, 1968).

In addition, the holes allow for the addition of oxygen atoms up to a composition of $UO_{2.25}$ without changing the cubic structure of the cell. Several studies have been performed to determine the exact positions of oxygen atoms in UO_{2+x} using X-ray (Belbeoch *et al.*, 1961; Willis, 1978) and neutron diffraction (Willis, 1964). Neutron diffraction on polycrystalline UO_2 has also been reported (Knowles *et al.*, 1981).

Hyperstoichiometric UO_{2+x}, resulting from the addition of oxygen to the dioxide lattice, has been thoroughly investigated using neutron diffraction (Willis, 1963, 1964). Willis showed that the additional oxygen atoms are not exactly on the (½, ½, ½) positions, but are slightly displaced around these holes. Vacancies are also still present in the oxygen sublattice. Electron diffraction of $UO_{2.19}$ revealed a superstructure composed of $4 \times 4 \times 1$ basic cells of UO_2 (fluorite); the oxygen atoms were displaced slightly from ideal locations with local accumulations of three oxygen atoms (Steeb and Mitsch, 1965). The structure of $UO_{2.25}$ (or U_4O_9) has also been thoroughly investigated using X-ray (Belbeoch *et al.*, 1961), neutron (Masaki and Doi, 1972), and electron diffraction (Blank and Ronchi, 1968). The superlattice is cubic with a cell dimension that is four times that of UO_2. The structures, dislocations, and defects in anion-excess uranium oxides are described in detail elsewhere (Vollath, 1984; Willis, 1987).

The three crystalline forms of U_2O_5 exist only at elevated temperature and pressure. The powder pattern of the α-form was not successfully indexed at first, but was observed as the predominant form below 800°C and between 10 and 60 kbar of pressure (Hoekstra *et al.*, 1970). It was later indexed as a monoclinic cell (Haire and Eyring, 1994). The β- and γ-forms exist mainly above 800°C and between 30 and 60 kbar of pressure; they are hexagonal and monoclinic, respectively. Samples prepared at the highest pressure (60 kbar) and above 800°C sometimes appeared as the β-form, and other times as the γ-form (Hoekstra *et al.*, 1970).

The most stable uranium oxide, U_3O_8, has two common polymorphs (α and β) that exist independently. Using neutron diffraction, Loopstra (1964) was able to model the two phases, both of which are orthorhombic. The most stable polymorph is α-U_3O_8 in which the oxygen atoms are all located at the corners of a pentagonal bipyramid around the central uranium. Generation of the β-U_3O_8 polymorph is accomplished by extended heating of α-U_3O_8 to 1350°C in air or oxygen, followed by slow cooling over about 2 weeks. The β-U_3O_8 polymorph exhibits two uranium coordination environments forming two distinct uranium polymeric chains along the *c*-axis. The first set of chains has uranium surrounded by oxygen atoms at the corners of a pentagonal bipyramid, while the remaining chains have the uranium surrounded by both pentagonal bipyramidal and octahedral oxygen atoms in an alternating fashion. Here, all neighbors of octahedrally coordinated uranium are pentagonal bipyramids (Loopstra, 1970). Other uncommon polymorphs include the γ-U_3O_8 which is formed from α-U_3O_8 at pressures and temperatures greater then 16,000 atm and

400°C (Herak and Jovanovic, 1969). If the α-U_3O_8 polymorph is exposed to an oxygen atmosphere for a prolonged time at 1350°C, the lattice converts to δ-U_3O_8 (Amirthalingam, 1966). Another form, p-U_3O_8, was discovered when α-U_3O_8 was held at room temperature and pressures greater than 50 kPa. This polymorph is not stable at temperatures greater then 1100°C in air or an argon atmosphere, and converts back to α-U_3O_8 (Steeb and Brucklacher, 1966).

Seven forms of UO_3, both crystalline and amorphous, have been characterized. Their methods of preparation are illustrated in Fig. 22.3. The amorphous form of the oxide is referred to as A-UO_3 (Hoekstra and Siegel, 1961). The structure of α-UO_3 has gone through many refinements, the latest of which corrects several discrepancies in previous studies. Here, Greaves and Fender (1972)

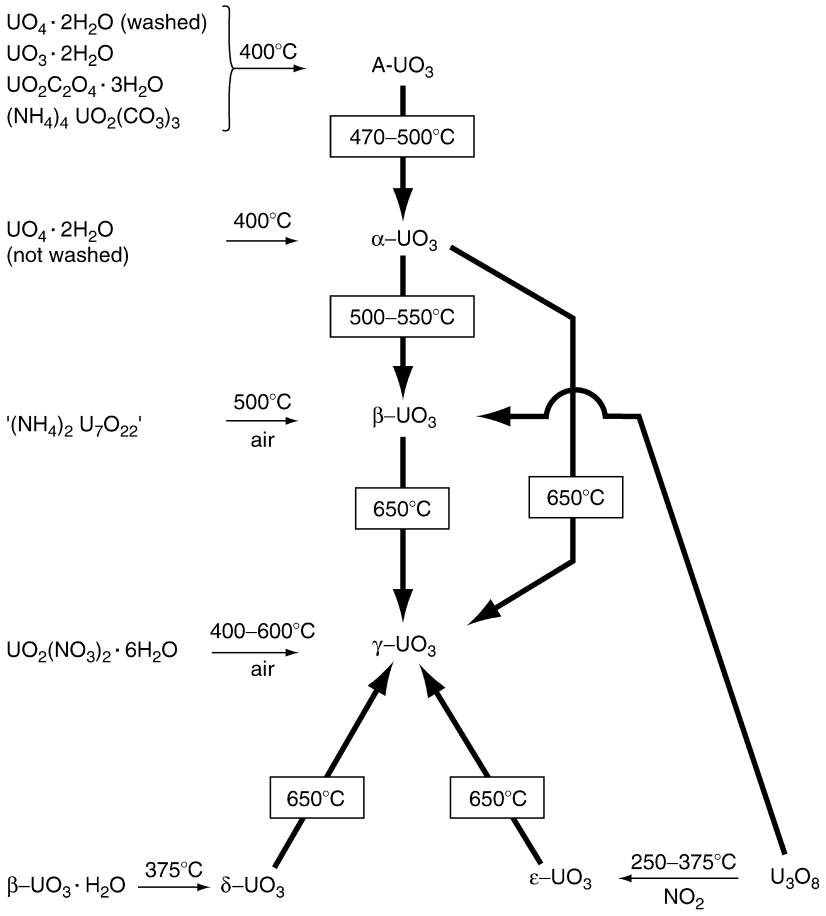

Fig. 22.3 *Uranium trioxide polymorphs and means of preparation* (*Weigel,* 1986. *Reproduced with permission from Chapman and Hall*).

based the structure on uranium-deficient α-U_3O_8; the loss of uranium atoms is countered by the shortening of some U–O distances from 2.1 to 1.6 Å, thus explaining the existence of some uranyl-like bonds. The diffraction pattern of β-UO_3 revealed three different environments for uranium with coordination numbers of 6, 6, and 7. The overall structure may be visualized as layers interconnected by distorted uranyl groups (Debets, 1966). The most recent neutron powder profile of γ-UO_3 shows the existence of three closely related phases between 373 and 77 K. At 373, 323, and 77 K, tetragonal, orthorhombic, and orthorhombic structures are observed, respectively. Of all the UO_3 crystalline phase, γ-UO_3 is the most thermodynamically stable (Loopstra *et al.*, 1977). Cubic δ-UO_3 has an unusual regular octahedral uranium environment and is isostructural with ReO_3. The structure has been confirmed with both powder X-ray diffraction (Wait, 1955), and powder neutron diffraction techniques (Weller *et al.*, 1988). Structural data for ε-UO_3 shows a triclinic cell (Hoekstra and Siegel, 1961). The last form isolated at high pressure, η-UO_3, is seven-coordinate with two *trans* oxygen atoms at 1.80 and 1.85 Å forming the uranyl group, and the remaining five oxygen atoms distributed equatorially in a puckered pentagon (Siegel *et al.*, 1966).

(e) Neptunium

Neptunium monoxide has been reported as having the NaCl structure type with a lattice parameter of 5.00(1) Å (Zachariasen, 1949a). However, like the other actinide monoxides, its existence is a point of debate except as a vapor phase species at high temperature and pressure.

The first neptunium compound to be identified by X-ray powder diffraction was NpO_2 and is isostructural with other actinide dioxides (Zachariasen, 1949a). NpO_2 can be prepared by calcining nitrates, hydroxides, or oxalates of the metal in air or oxygen at 700–1000°C.

Neptunium(v) oxide, Np_2O_5, is prepared by bubbling ozone through a solution of Np(v) in molten $LiClO_4$ at 260°C and displays a very narrow compositional range with limited stability (Cohen, 1963). Anhydrous neptunium oxides above Np_2O_5 are not known. The pentoxide is monoclinic; however, the β angle is nearly 90°, allowing poor crystalline samples to be mistakenly indexed as orthorhombic (Cohen, 1963).

A hydrated oxide, $NpO_3 \cdot 2H_2O$, has been prepared by ozone oxidation of Np(v) in a $LiNO_3$–KNO_3 eutectic at 150°C (Cohen, 1963).

(f) Plutonium

The monoxide of plutonium, previously reported as belonging to the NaCl structure type, is actually a plutonium oxide carbide of the form PuO_xC_y. It is very similar to the samarium oxide carbide analog, thus aiding in its characterization. Due to these similarities, it is suggested that PuO likely exists in

the vapor phase under high temperature and pressure (Larson and Haschke, 1981).

Two sesquioxides of plutonium have been identified. Interestingly, two forms of α-Pu_2O_3 have been observed, both of which are sub-stoichiometric compounds due to loss of oxygen from the dioxide. The first, α-form, is prepared by heating PuO_2 in a vacuum at 1650–1800°C in a tantalum crucible. This compound has a C-type bcc structure and exists at an O/Pu ratio of 1.515. An alternate form of α-Pu_2O_3, referred to as α'-Pu_2O_3, has also been observed at a O/Pu ratio of 1.61, although its classification as fcc is ambiguous. The only purely stoichiometric form, β-Pu_2O_3, is prepared by reducing PuO_2 with 20% excess of Pu metal at 1500°C and adopts an A-type, hexagonal structure. A more comprehensive analysis of plutonium oxide sub-stoichiometric behavior as a function of temperature is available (Gardner *et al.*, 1965).

Crystals of PuO_2, the most stable plutonium oxide, can be obtained by careful temperature control during decomposition in a molten salt (Schlechter, 1970), reaction of Pu with O_2 (Akimoto, 1960), or other methods, including the calcination of plutonium oxalate (or other salts) in air or oxygen to 800–1000°C for several hours. The dioxide is isostructural with other actinide dioxides and adopts the fluorite-type structure (Phipps and Sullenger, 1964).

(g) Americium

Although its existence is questionable, the monoxide of americium (NaCl type) has been reported by Zachariasen (1949b) and Akimoto (1967). Furthermore, the presence of certain X-ray powder diffraction lines from americium metal are possibly attributable to fcc AmO with a lattice parameter of 5.05 Å (McWhan *et al.*, 1960).

Two modifications of americium sesquioxide have been reported. The bcc (C-type) structure is the low-temperature form, prepared by heating the dioxide in H_2 at 600°C. The high-temperature hexagonal (A-type) structure was prepared by ignition of the metal oxalate at 850°C, followed by reduction in H_2 at 800°C (Templeton and Dauben, 1953). Chikalla and Eyring (1968) reported that samples with O/Am ratios between 1.54 and 1.51, when quenched from 800°C or above, gave several weak diffraction lines of neither C-type nor A-type origin. These lines compared reasonably well with those for monoclinic B-type Sm_2O_3 and were assigned as B-type Am_2O_3. The B-type sesquioxide was only found in quenched samples and it exists only at elevated temperatures; its upper temperature limit of stability lies between 950 and 1000°C. It is likely not stable as a dominant phase. The lattice constants for the americium sesquioxides are listed in Table 22.2.

Phase relations of americium oxides in the O/Am range of 1.5–2.0 have also been investigated. The cubic sesquioxide was observed to dissolve excess oxygen at room temperature up to a stoichiometry of $AmO_{1.67}$. In this range, there was either a single phase of continually variable composition or there were several

Table 22.2 *Lattice constants for Am_2O_3* (*Templeton and Dauben,* 1953*; Chikalla and Eyring,* 1968).

Formula	*Symmetry*	*a* (Å)	*b* (Å)	*c* (Å)	*β* (°)
A – Am_2O_3	hexagonal	3.817	–	5.971	–
B – Am_2O_3	monoclinic	14.38	3.52	8.92	100.4
C – Am_2O_3	cubic	11.03	–	–	–

Table 22.3 *Lattice constants for Cm_2O_3* (*Wallmann,* 1964*; Haug,* 1967*; Noé* et al*.,* 1970*; Mosley,* 1972*; Morss* et al*.,* 1983).

Formula	*Symmetry*	*a* (Å)	*b* (Å)	*c* (Å)	*β* (°)
A – Cm_2O_3	hexagonal	3.792	–	5.985	–
B – Cm_2O_3	monoclinic	14.282	3.641	8.883	100.29
C – Cm_2O_3	cubic	11.002	–	–	–

narrow regions separated by miscibility gaps. For stoichiometries between $AmO_{1.67}$ and AmO_2, an intermediate phase is thought to exist, likely from O/Am ratios between 1.67 and 1.80 (Chikalla and Eyring, 1968).

AmO_2 was the first reported americium compound (Zachariasen, 1948a, 1949b) and was shown to crystallize in the fluorite structure. It can be prepared in a variety of ways, including ignition of the nitrate or oxalate in air or oxygen up to 900°C (Templeton and Dauben, 1953). Self-irradiation effects in americium oxides are quite significant. Crystalline AmO_2 expands due to these effects, resulting in an enlargement of the lattice constant, an effect that was unaccounted for in early reports of the structure. Interestingly, lattice expansion varied between those samples stored under vacuum and those stored under O_2, with the latter occurring at a slightly slower rate. Likewise, self-irradiation of the low-temperature cubic form of the sesquioxide caused a transformation to the hexagonal form over the time span of about 3 years (Hurtgen and Fuger, 1977).

(h) Curium

The monoxide of curium has been reported during the study of curium metal, where three extra lines in the diffraction pattern were indexed as fcc CmO with a lattice constant of 5.09 Å (Cunningham and Wallmann, 1964).

Three crystalline forms of Cm_2O_3 have been characterized and the lattice constants are summarized in Table 22.3. The low-temperature bcc (C-type) structure is formed from the hydrogen reduction of a higher curium oxide (Wallmann, 1964). Heating the C-type structure between 800 and 1300°C irreversibly generates the monoclinic (B-type) structure (Mosley, 1972) and is

remarkably stable with respect to self-irradiation (Haug, 1967). The reversible hexagonal (A-type) structure can be prepared in two ways: heating the B-type sesquioxide above 1600°C (Mosley, 1972) or from gradual self-irradiation of the C-type form at room temperature (Wallmann, 1964). In addition, it has been discovered that heating the A-type form to 500°C results in the B-type structure (Noé *et al.*, 1970).

The dioxide of curium can be prepared in several ways, including calcining of salts (i.e., oxalates, hydroxides) in oxygen followed by slow cooling (Asprey *et al.*, 1955) or by oxidation of the cubic sesquioxide at 400°C in air or oxygen for several days (Haug, 1967). Alternatively, CmO_2 can be prepared by thermally decomposing a resin loaded with Cm^{3+} (Hale and Mosley, 1973). The dioxide has the fluorite structure with a lattice parameter of 5.357(1) Å at room temperature, but in the case of ^{244}Cm, can undergo significant lattice damage due to self-irradiation, resulting in a swelling of the lattice parameter to 5.373 Å within 3 days (Mosley, 1972). A powder neutron diffraction study of the dioxide with Rietveld refinement yielded a stoichiometry of $CmO_{1.970 \pm 0.034}$; thus the material is probably hypostoichiometric. In fact, magnetic susceptibility measurements gave an effective moment of 3.36 μ_B, indicative of substantial Cm^{3+} impurity, thus favoring a nominal composition of $CmO_{1.91}$. The discrepancy between neutron diffraction data and thermogravimetric analysis (TGA) data (indicating CmO_2), and magnetic susceptibility data that favor the non-stoichiometric material, is yet to be resolved (Morss *et al.*, 1989).

Thermal decomposition of the dioxide has revealed two intermediate systems, $CmO_{1.81}$, with fluorite symmetry, and Cm_7O_{12}, with rhombohedral symmetry, finally ending with the C-type sesquioxide (Mosley, 1972). The complex nature of the curium–oxygen system bears some resemblance to the analogous plutonium system, and its intricacies are outlined elsewhere (Chikalla and Eyring, 1969).

(i) Transcurium elements

The monoxide of berkelium has been reported as having the NaCl structure type, although its existence is debatable (Fahey *et al.*, 1972).

Three berkelium sesquioxides have been identified as having A-, B-, and C-type structures and their lattice parameters are listed in Table 22.4. The low-temperature cubic C-form is produced by hydrogen reduction of the higher oxide, BkO_2 (Peterson and Cunningham, 1967a; Baybarz, 1968). Irreversible conversion of the C-type sesquioxide to the monoclinic, B-type structure occurs upon heating in the range 1200–1700°C. Further heating of the B-type sesquioxide to temperatures above 1750°C results in the hexagonal, A-type sesquioxide. The melting point occurs at 1920°C (Baybarz, 1973a).

The oxygen dissociation pressure of non-stoichiometric oxides of the form BkO_x, where $1.5 < x < 2.0$, have been investigated, resulting in the identification of three phases, $BkO_{1.5–1.77}$, $BkO_{1.81–1.91}$, and $BkO_{1.93–2.00}$

Table 22.4 *Lattice constants for Bk_2O_3* (*Peterson and Cunningham,* 1967a*; Baybarz,* 1968, 1973*a*).

Formula	*Symmetry*	*a* (Å)	*b* (Å)	*c* (Å)	*β* (°)
A – Bk_2O_3	hexagonal	3.754	–	5.958	–
B – Bk_2O_3	monoclinic	14.197	3.606	8.846	100.23
C – Bk_2O_3	cubic	10.887	–	–	–

Table 22.5 *Lattice constants for Cf_2O_3* (*Copeland and Cunningham,* 1969*; Baybarz,* 1973*a*).

Formula	*Symmetry*	*a* (Å)	*b* (Å)	*c* (Å)	*β* (°)
A – Cf_2O_3	hexagonal	3.72	–	5.96	–
B – Cf_2O_3	monoclinic	14.124	3.591	8.809	100.31
C – Cf_2O_3	cubic	10.839	–	–	–

(Turcotte *et al.*, 1971). A follow-up investigation of the phase behavior was consistent with previous studies, resulting in a phase diagram of the non-stoichiometric area at high temperatures. Two regions were indexed for BkO_x compounds in the non-stoichiometric range: a bcc region for $1.5 < x \leq 1.70$ and a fcc region for $1.78 < x < 2.0$ (Turcotte *et al.*, 1980). A more comprehensive investigation of the phase diagram in the temperature range from 200 to 900°C and from 59 to 67 atomic % oxygen is available from Okamoto (1999).

The stoichiometric dioxide of berkelium is obtained by calcination of berkelium salts (nitrate, oxalate, hydroxide, etc.) in air or oxygen, resulting in a fcc structure. The first structural determination of the dioxide was performed in 1962 using only 4 ng of sample; the diffraction pattern showed four lines that were indexed on the basis of a fcc cell (Peterson and Cunningham, 1967a). Subsequent studies used larger samples (μg) of ^{249}Bk that had been loaded onto an ion exchange resin, calcined, and indexed (Peterson and Cunningham, 1967a; Baybarz, 1968). BkO_2 also undergoes thermal expansion in 1 atm of oxygen, although the phenomenon is reversible with a decrease in temperature (Fahey *et al.*, 1974).

The three known sesquioxides of californium are the A-, B-, and C-type structures and their lattice constants are provided in Table 22.5. The first discovered was the monoclinic, B-type sesquioxide (Green and Cunningham, 1967) followed by the discovery of the cubic, C-type sesquioxide (Copeland and Cunningham, 1969). The hexagonal, A-type sesquioxide was the most difficult to obtain due to its small range of existence between the monoclinic form and the melting point. The low-temperature B-type sesquioxide is transformed to the C-type upon heating between 1200 and 1700°C, followed by a transformation to the A-type sesquioxide above 1700°C and melting at 1750°C (Baybarz, 1973a).

Table 22.6 *Lattice constants for Es_2O_3* (*Haire and Baybarz,* 1973*; Haire and Eyring,* 1994).

Formula	*Symmetry*	*a* (Å)	*b* (Å)	*c* (Å)	*β* (°)
A – Es_2O_3	hexagonal	3.7	–	–	–
B – Es_2O_3	monoclinic	14.1	3.59	8.80	100
C – Es_2O_3	cubic	10.766	–	–	–

An intermediate between the sesquioxide and the dioxide was identified as Cf_7O_{12}. This rhombohedral structure can be prepared by heating the cubic sesquioxide in air or oxygen, at which time the sesquioxide takes up oxygen to an O/Cf ratio of 1.7; its existence is limited to a very narrow range of O/Cf values. It can also be prepared by heating the nitrate, oxalate, or nitrate salts in air or oxygen to 750°C, after which oxygen is lost to form the sesquioxide (Baybarz *et al.*, 1972a).

Californium dioxide has been prepared by the oxidation of the cubic sesquioxide with high-pressure molecular oxygen and by atomic oxygen. The dioxide has the fluorite structure with a lattice parameter of 5.310(2) Å, which has been corrected for expansion due to swelling. Preparation of CfO_2 can also be achieved through self-irradiation of lower californium oxides via the generation of active oxygen species from alpha decay (Baybarz *et al.*, 1972a).

The only characterized oxides of einsteinium have been the sesquioxides, the lattice parameters for which are provided in Table 22.6. The cubic C-type sesquioxide was prepared from the calcination of submicrogram amounts of the metal nitrate and analyzed by electron diffraction (Haire and Baybarz, 1973). The monoclinic B-type sesquioxide was produced from the oxidation of einsteinium metal under oxygen at elevated temperatures (800–1000°C). The hexagonal A-type sesquioxide is produced as a result of the self-irradiation of the monoclinic form. Both the B- and A-types were characterized by electron diffraction (Haire and Eyring, 1994). The rapid appearance of the highly radioactive daughter ^{249}Bk from the parent ^{253}Es (3% per day) has made the study of these compounds quite challenging.

Crystal structures for the oxides of transeinsteinium elements are not available due to limitations in abundance and their short half-lives.

22.3.3 Actinyl compounds

Actinide elements in the hexavalent oxidation state commonly exist as the actinyl (AnO_2^{2+}) ion in both aqueous solutions and solid state. The linear geometry of the uranyl ion with its *trans* oxo ligands (O=U=O) was first elucidated by Fankuchen (1935) from the space group symmetry of sodium uranyl acetate. The stability of the uranyl ion is evident in the hundreds of structural characterizations that have since been published, many of which were

included by Burns in Chapter 20 of the previous edition (pre-1986) as well as Chapter 5 of the current edition. The ubiquity of the hexavalent uranyl moiety in both solution and the solid state has led to numerous studies in a variety of environments, including inclusion into the cavity of macrocyclic ligands (see Section 22.4.2) for separations applications, the interaction with ligands such as carbonate (Morse *et al.*, 1984), and citrate (Pasilis and Pemberton, 2003) to understand environmental mobility and/or immobilization, elucidation of the Lewis base properties of the oxo ligands with respect to ligand exchange, substitution, and cation–cation interactions (Sarsfield and Helliwell, 2004), and computational studies of the role of 5f electrons in bonding, electronic, and structural properties to understand the origin of its linearity (Zhang and Pitzer, 1999).

Hexavalent actinyl ions are also known for transuranic actinides Np (neptunyl), Pu (plutonyl), and Am (americyl). The entire series is isostructural although structural details are limited compared to uranyl. The An–O bond strength, as well as the resistance to reduction, decreases in the order U > Np > Pu > Am. Whereas uranyl salts are highly common, formation of AmO_2^{2+} requires the use of strong oxidizing agents such as peroxodisulfate. The An=O bond length in hexavalent actinyl compounds generally ranges between 1.7 and 2.0 Å. In all cases, the bond is very strong, while in uranyl, it appears that the bond order may be even greater than two as evidenced by the short bond length (Greenwood and Earnshaw, 2001).

The linearity of the uranyl and other hexavalent actinyl ions (Np, Pu, Am) has been the subject of many theoretical inquiries that sought to elucidate the relative contributions of orbitals from the actinide and oxygen atoms. Wadt (1981) noted that the difference in the gas-phase geometries of isoelectronic UO_2^{2+} and ThO_2 is due to the relative ordering of the 5f and 6d levels. In uranium, the 5f orbitals are lower in energy, thus favoring a linear geometry upon interaction with oxygen 2p orbitals. In thorium, however, the 6d orbitals are lower, resulting in a bent geometry. Furthermore, Tatsumi and Hoffmann (1980) and Pyykkö *et al.* (1989) have added that 6p interactions with oxygen are significant in uranium; this repulsive interaction activates the 5f orbitals of uranium in a coorperative manner through a 'pushing from below' mechanism, leading to short, linear oxo bonds. A review of the electronic structure of several actinide-containing molecules is available from Pepper and Bursten (1991).

It is estimated that 98% of all crystal structures have O=U=O angles in the range 174–180° (Sarsfield *et al.*, 2004). Despite the prevalence of the linear dioxo cation, nonlinear uranyl species have been observed. For example, the structure of $UO_2[(SiMe_3N)CPh(NSiMe_3)]_2THF$ contains a uranyl unit with a O=U=O angle of 169.7(2)° (Sarsfield and Helliwell, 2004). While this bend is a dramatic example of nonlinearity, more common deviations are observed in the structures of $UO_2(O\text{-}2,6\text{-}{}^{i}Pr_2C_6H_3)_2(pyr)_2$ (Barnhart *et al.*, 1995a) and $[UO_2(OCH({}^{i}Pr)_2)_2]_4$ (Wilkerson *et al.*, 2000); the O=U=O angles in these examples are 173.4(2)° and 172.6(2)°, respectively.

Accurate determination of the uranium–oxygen bond length of uranyl in its compounds by X-ray diffraction have traditionally been difficult due to the large difference in scattering power (proportional to the number of electrons) between the two atoms. However, advances in neutron diffraction techniques and their wider availability have eliminated this problem. The nuclear cross sections of uranium and oxygen are comparable, thus allowing accurate atomic placement using neutrons.

In general for hexavalent actinyl ions, several factors have been identified that can lead to variations in the U=O bond length. The most significant is the bonding of ligands in the equatorial plane, perpendicular to the O=An=O axis. Actinyls readily form complexes with halides, such as F^- and Cl^-, oxygen donors such as OH^-, SO_4^{2-}, NO_3^-, PO_4^{3-}, and carboxylates, as well as neutral donors, such as H_2O or pyridine. Coordination numbers between four and six from monodentate and bidentate ligands are common in the equatorial plane and generate octahedral, pentagonal bipyramidal, and hexagonal bipyramidal geometries. In uranyl, the formal charge on uranium is 2+, although other evidence suggests that it may be closer to 3+ (the formal charge is different from oxidation state); thus, depending on the extent of orbital overlap from equatorial ligands, the electron density withdrawn from the axial oxygen atoms greatly affects the M=O bond lengths (Sarsfield and Helliwell, 2004). Another factor is the local environment provided by the rest of structure, sometimes resulting in U=O bond lengths that vary within the same compound. For example, in the compound $UO\{OB(C_6F_5)_3\}[(SiMe_3N)CPh(NSiMe_3)]$, the interaction of one oxo ligand (Lewis base) with the borane (Lewis acid) results in an elongated U=O bond (1.898(3) Å) compared to the uncoordinated one (1.770(3) Å) (Sarsfield and Helliwell, 2004). Finally, reduction of the actinide oxidation state from 6+ to 5+ results in a lengthening, and hence weakening, of the oxo bond. Additional information on actinyl structures and structural changes with correlations to vibrational spectra has been compiled by Hoeskstra (1982).

Actinide elements in the pentavalent oxidation state form a less common type of actinyl represented by the formula AnO_2^+. This species is known for U, Np, Pu, and Am. Like AnO_2^{2+}, the AnO_2^+ ion is linear and symmetric, although the low charge on AnO_2^+ prevents the formation of very stable complexes. These compounds are very susceptible to disproportionation into An(IV) and An(VI). The most notable pentavalent actinyl is NpO_2^+; it has recently been observed to form an inclusion complex with the porphyrin, hexaphyrin(1.0.1.0.0.0). Here, the environment around the linear cation results in two different Np=O bond lengths: 1.762(1) and 1.826(1) Å. These distances are unusually short for the neptunyl ion where 1.85 Å is common in simple inorganic salts (Sessler *et al.*, 2001b).

Differences in the An=O bond length are also significantly influenced by the oxidation state of the metal; changing from a hexavalent to a pentavalent actinyl results in a bond length increase of about 0.14 Å (Burns and Musikas, 1977). This change in the bond length implies a weakening of the bond and is

attributed to the additional non-bonding electrons in each AnO_2^+ ion compared to the corresponding AnO_2^{2+} ion. Both AnO_2^+ and AnO_2^{2+} exhibit the actinide contraction where incremental increases in the atomic number result in a lengthening of the An=O bond by about 0.01 Å (Zachariasen, 1954; Musikas and Burns, 1976). Self-assembled uranyl peroxide nanosphere clusters of 24, 28, and 32 polyhedra (some containing neptunyl) that crystallize from alkaline solution have been characterized (Burns *et al*., 2005).

22.3.4 Hydrides, borohydrides, borides, carbides, and silicides

(a) Hydrides

A majority of the actinide hydrides attain either the $AnH_{2\pm x}$ or AnH_3 composition through direct reaction of the metal in a H_2 atmosphere. Structural information is available for hydrides of thorium through californium. The resulting actinide hydrides react readily with oxygen and all are pyrophoric.

(*i*) *Thorium*

Thorium dihydride was originally studied by Rundle *et al*. (1952) using neutron diffraction and was indexed as a body-centered tetragonal (bct) lattice; it is also isomorphous with ZnH_2. However, several weak maxima were observed in the X-ray diffraction pattern that were presumably due to unidentified impurities. An X-ray diffraction study by Korst (1962) examined sub-stoichiometric samples of thorium hydride in the overall composition range $ThH_{1.93}$ to $ThH_{1.73}$. Samples richest in hydrogen ($ThH_{1.93}$ and $ThH_{1.88}$) gave diffraction patterns corresponding to the bct lattice of Rundle *et al*., while the other samples ($ThH_{1.84}$, $ThH_{1.79}$, and $ThH_{1.73}$) contained bct lines as well as face-centered cubic lines in their diffraction patterns. As a result, Korst reindexed all samples as face-centered tetragonal, for which the preferred setting is body-centered tetragonal.

The higher thorium hydride, Th_4H_{15}, was studied by X-ray diffraction and assigned a bcc lattice based on a H/Th ratio of 3.62 (representing the lower limit due to impurities) (Zachariasen, 1953). The structure of Th_4H_{15} was also confirmed by Korst (1962) with a H/Th ratio as high as 3.73.

(*ii*) *Protactinium*

X-ray diffraction studies of the complicated Pa–H system revealed the existence of four protactinium hydride phases during the hydriding process as a function of temperature and pressure. Phase I is present in mixtures with Phase II (>500 K) or Phase IV (<500 K) at H/Pa ratios less than 1.3 and has a body-centered tetragonal structure. Phase II exists solely at temperatures above 500 K in the range corresponding to Pa_3H_4–Pa_3H_5 and has a fcc structure. After a narrow two-phase region above 500 K, Phase III becomes dominant with a wide

composition range corresponding to $2.0 \leq H/Pa \leq 3.0$. This phase has a cubic structure that is isostructural with β-UH_3, which will be described later. Phase IV forms rapidly below 500 K and exhibits an extremely wide composition range corresponding to $1.3 \leq H/Pa \leq 3.0$. This phase also has a cubic structure and is isostructural with α-UH_3 (Ward *et al.*, 1984).

(*iii*) *Uranium*

Two crystalline modifications of uranium trihydride have been characterized and are denoted α-UH_3 and β-UH_3. The first to be discovered was the β-form of the trihydride and was studied using both X-ray (Rundle, 1947) and neutron diffraction (Rundle, 1951). Neutron diffraction of UD_3 shows that each hydrogen atom lies in a distorted tetrahedron, surrounded by four uranium atoms at a distance of 2.32 Å. There are two types of uranium atoms in the lattice; each is surrounded by 12 hydrogens at this distance. Uranium atoms of the first type are surrounded by hydrogen atoms at the corners of an icosahedron (of T_d symmetry), while the uranium atoms of the second type are surrounded by sets of three hydrogen atoms, each forming the face of a different icosahedron. The absence of metallic U–U bonds indicates that the structure is held together solely by U–H interactions.

The less stable α-UH_3 was structurally characterized in 1954 and was found to be a metastable form of UH_3.The crystal structure of α-UH_3 is simple cubic with a lattice parameter of 4.160(5) Å and has U–H distances identical to the β-form. Interestingly, the reaction of hydrogen with uranium powder at the lowest temperatures (–80°C) produced mixtures of the α- and β-forms with the greatest percentage of α-UH_3. Heating of mixtures of known composition at 250°C resulted in total conversion to the β-form, but heating of the same mixture at 100°C resulted in no change in the diffraction pattern. Thus, the appearance of the α-form is only by virtue of it being formed more rapidly than it decomposes at low reaction temperatures (Mulford *et al.*, 1954).

(*iv*) *Transuranium*

The Np–H and Pu–H systems are the most thoroughly studied of the transuranium hydride systems. Two studies of the Np–H system have been performed, the latter of which used ultra-pure metal to confirm the existence of two structural forms, a cubic form and a hexagonal form as well as a two-phase region. An unusually sharp phase boundary is observed at a H/Np ratio of 2.13 marking the disappearance of neptunium metal. At temperatures below 400°C and a H/Np ratio above about 2.3, a cubic region is observed where the dihydride lattice expands upon addition of hydrogen, a phenomenon which has not been observed in any other systems. The transition to a hexagonal/cubic two-phase system occurs at a H/Np ratio of about 2.6, followed by a very narrow hexagonal NpH_{3-x} region, both of which were only observed upon dehydriding. Increasing the H/Np ratio to 3.0 resulted in a hexagonal trihydride

structure with very weak indications of cubic artifacts due to decomposition (Mulford and Wiewandt, 1965; Ward *et al.*, 1987).

The Pu–H system is very complex. A recent study by Haschke *et al.* (1987) indicated the existence of five phases in the range $1.9 \leq \text{H/Pu} \leq 3.0$ during the dehydriding process as a function of temperature. At lower temperatures (75–100°C), only the cubic (fcc) dihydride exists for H/Pu values less than 2.7. In the range of $2.7 < \text{H/Pu} < 2.9$, a two-phase region exists that has both cubic and hexagonal (hcp) structural features. In the small region of H/Pu values between 2.9 and 2.95, only the hexagonal trihydride is present, but the region from 2.95 to 3.0 has not been structurally characterized. A neutron diffraction study describing the occupancy of hydrogen atoms in tetrahedral versus octahedral sites is also described. See Chapter 7, especially section 7.8.1 of this work, for further discussion of Pu hydrides.

X-ray diffraction studies of the americium–hydrogen system revealed both fcc AmH_{2+x} and a hexagonal AmH_3 phases, thus resembling the Np–H and Pu–H systems. The cubic dihydride was observed until a composition of $AmH_{2.7}$ was reached, after which a transition to the hexagonal AmH_3 occurred. As in the Pu–H system, the lattice constant decreases in the cubic region as hydrogen content increases (Olson and Mulford, 1966; Roddy, 1973).

Curium and berkelium hydrides, like their transuranium predecessors, also exhibit both fcc MH_{2+x} (dihydride) and hexagonal MH_3 phases (Gibson and Haire, 1985a,b). Structural data on the cubic californium dihydride has also been collected, but a trihydride has not yet been observed (Gibson and Haire, 1987).

(b) Borohydrides

The limitations of single-crystal X-ray diffraction techniques were evident in the study of $U(BH_4)_4$ as evidenced by an inherent inability to locate hydrogen atoms against the extreme electron density of the actinide (Bernstein *et al.*, 1972a). This problem was easily overcome with neutron diffraction (Bernstein *et al.*, 1972b). Whereas X-ray diffraction only revealed the interaction of uranium with boron atoms of the four bridging and two terminal groups, neutron diffraction data showed that, in actuality, the four bridging BH_4^- groups each donate two hydrogen atoms to the uranium polyhedron (resulting in a helical polymer), and the terminal groups donate three hydrogen atoms, resulting in a uranium coordination number of 14.

Similar borohydride compounds with dimethyl ether, $U(BH_4)_4 \cdot O(CH_3)_2$, and diethyl ether $U(BH_4)_4 \cdot O(C_2H_5)_2$ (Fig. 22.4), show slight variations in the structural trends due to metal–ether bonding. In both cases, the coordination number of 14 is maintained due to 13 hydrogen atoms (4 bridging, 9 terminal) and one ether oxygen atom contributing to the coordination polyhedron (Rietz *et al.*, 1978a). A coordination number of 14 was also observed in the borohydride/tetrahydofuran (THF) compound, $U(BH_4)_4 \cdot (OC_4H_8)_2$ due to 12 hydrogen atoms from borohydride and two oxygen atoms from THF. This is a unique

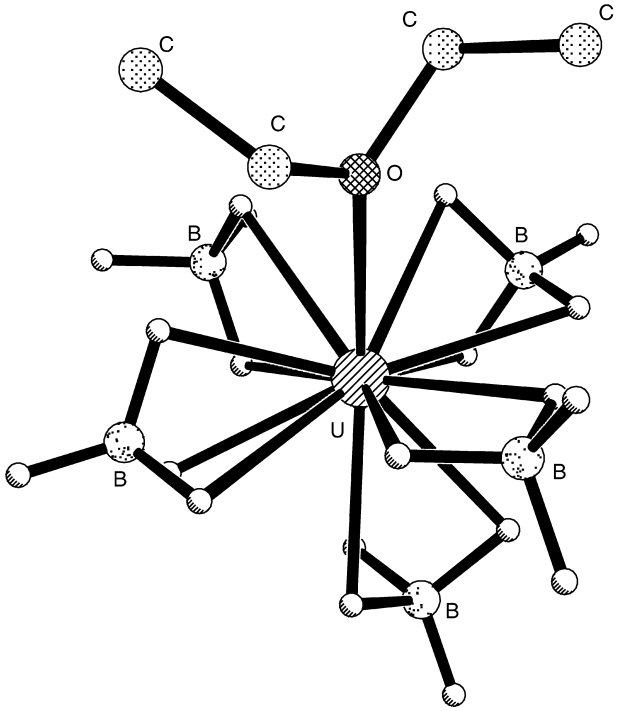

Fig. 22.4 *Crystal structure of* $U(BH_4)_4 \cdot O(C_2H_5)_2$ *with ether hydrogen atoms omitted* (*Rietz* et al., 1978*a*).

example in which all the borohydride groups are terminal, resulting in a monomeric solid state complex (Rietz *et al.*, 1978b). Interestingly, coordination numbers of 13 and 14 are observed for two different uranium atoms in the solid state structure of $U(BH_4)_4 \cdot (n\text{-}C_3H_7)_2$, resulting in an unsymmetrical dimer (Zalkin *et al.*, 1978a).

The stability of the $An(BH_4)_4$ (where An = Th, Pa, U, Np and Pu) compounds of the actinides decreases going from thorium to plutonium; the latter two decompose readily. Structural analyses using X-ray powder diffraction indicate that the Th, Pa, and U compounds are isomorphous tetragonal polymers. The Np and Pu compounds are also isomorphous, but have a different tetragonal structure and are monomeric in the solid state (Banks *et al.*, 1978).

(c) Borides, carbides, and silicides

The structures for actinide borides, carbides, and silicides are summarized in Table 22.7. In general, borides, carbides, and silicides are less chemically reactive relative to the hydrides and are refractory materials, enabling their consideration as nuclear fuels (Naito and Kamegashira, 1976). In general,

Table 22.7 *Actinide borides, carbides, and silicides and their crystal symmetries.*

Boride	*Symmetry*	*References*	*Carbide*	*Symmetry*	*References*	*Silicide*	*Symmetry*	*References*
ThB_4	tetragonal	a	ThC	fcc	g	Th_3Si_2	tetragonal	w
ThB_6	cubic	a	Th_2C_3	bcc	h	ThSi	orthorhombic	w
ThB_{12}	fcc	b	α-ThC_2	monoclinic	i, j	Th_3Si_5	hexagonal	x
–	–	–	β-ThC_2	tetragonal	j	α-$ThSi_2$	tetragonal	y
–	–	–	γ-ThC_2	fcc	j	β-$ThSi_2$	hexagonal	w, y
–	–	–	PaC	fcc	k	–	–	–
–	–	–	PaC_2	bcc	k	–	–	–
UB_2	hexagonal	c, d	UC	fcc	l	U_3Si	tetragonal	z
UB_4	tetragonal	c, d	U_2C_3	bcc	m	U_3Si_2	tetragonal	aa
UB_{12}	fcc	c, d	α-UC_2	tetragonal	n	USi	tetragonal	bb
–	–	–	β-UC_2	fcc	n	U_3Si_5	hexagonal	x
–	–	–	–	–	–	α-USi_2	tetragonal	aa
–	–	–	–	–	–	β-USi_2	hexagonal	aa
–	–	–	–	–	–	USi_3	cubic	cc
NpB_2	hexagonal	e	NpC	fcc	o	Np_3Si_2	tetragonal	dd
NpB_4	tetragonal	e	Np_2C_3	bcc	p	$NpSi_2$	tetragonal	q, aa
NpB_6	cubic	e	NpC_2	tetragonal	q	–	–	–
NpB_{12}	fcc	e	–	–	–	–	–	–
PuB_2	hexagonal	f	PuC	fcc	r	PuSi	orthorhombic	ee
PuB_4	tetragonal	f	Pu_2C_3	bcc	s	Pu_3Si_5	hexagonal	ff
PuB_6	cubic	f	α-PuC_2	tetragonal	t	α-$PuSi_2$	tetragonal	aa, ee
PuB_{12}	fcc	f	β-PuC_2	fcc	u	β-$PuSi_2$	hexagonal	gg, ee
–	–	–	–	–	–	Pu_5Si_3	tetragonal	hh, ee
–	–	–	–	–	–	Pu_3Si_2	tetragonal	ff, ee
AmB_4	tetragonal	e	Am_2C_3	bcc	v	Am_5Si_3	tetragonal	ii
AmB_6	cubic	e	–	–	–	AmSi	orthorhombic	ii, jj
–	–	–	–	–	–	α-$AmSi_2$	tetragonal	ii
–	–	–	–	–	–	"β"-$AmSi_2$	hexagonal	ii
–	–	–	–	–	–	CmSi	orthorhombic	kk
–	–	–	–	–	–	$CmSi_2$	tetragonal	kk
–	–	–	–	–	–	Cm_2Si_3	hexagonal	kk

their stoichiometries are highly varied. The monocarbides, AnC, are semi-metallic and primarily ionic, but with supernumerary electrons in a delocalized conduction band.

Actinide borides (in actuality, metal borides in general) are interstitial compounds through inclusion of the small boron atoms into the lattice holes of the metallic structure which becomes expanded, but maintain their simple structure. Metal borides are characterized by the fact that boron atoms can form direct B–B bonds in the lattice (Vegas *et al.*, 1995). This catenation increases with the concentration of boron atoms in the lattice, where the boron atoms rest at the centers of trigonal prisms of metal atoms (Greenwood and Earnshaw, 2001). Structural details of metal diborides, tetraborides, and hexaborides where the structure of the parent metal is retained are described elsewhere (Vegas *et al.*, 1995).

Actinide borides all contain either two- or three-dimensional lattices of covalent B–B bonds with lengths from 1.72 to 1.83 Å and these bond lengths are typically invariant with respect to changes in the metal atom type. The actinide–boron bonds show a range of distances depending on the crystal structure. They appear to adjust to the more rigid framework of the boron atoms and can be found in several compositions. The hexagonal UB_2 has been characterized by X-ray diffraction (Brewer *et al.*, 1951; Dancausse *et al.*, 1992). The structure contains triangular nets of boron atoms that alternate with similar layers of uranium to form a hexagonal stacking sequence. Alternatively, the structure can be described in terms of boron atoms at the center of trigonal prisms of uranium atoms. Thus, each uranium atom has 12 boron neighbors (Post *et al.*, 1954). The formation of AnB_4 is common and, as detailed for UB_4, the synthesis can be achieved through several methods, including floating zone melting, the tri-arc Czochralski method, and from a molten metal flux (Menovsky *et al.*, 1984). Like ThB_4, the structure of UB_4 consists of B_6 octahedra linked along the *z*-axis and joined in the *xy* plane by pairs of B_2 atoms. The resulting three-dimensional structure has tunnels along the *z*-axis that are filled by metal atoms; thus the B_6 and B_2 units are surrounded by metal cubes and metal trigonal prisms, respectively. Each metal has 18 nearest boron neighbors (Vegas *et al.*, 1995).

The structure of ThB_6 is a three-dimensional array of interconnected B_6 octahedra with An atoms in the lattice holes, forming a primitive cubic structure

---

[a] Konrad *et al.* (1996); [b] Cannon and Farnsworth (1983); [c] Brewer *et al.* (1951); [d] Dancausse *et al.* (1992); [e] Eick and Mulford (1969); [f] Eick (1965); [g] Kempter and Krikorian (1962); [h] Krupka (1970); [i] Gantzeland Baldwin (1964); [j] Bowman *et al.* (1968); [k] Lorenz *et al.* (1969); [l] Olsen *et al.* (1986); [m] Mallett *et al.* (1951); [n] Bowman *et al.* (1966); [o] Lander *et al.* (1969); [p] Lorenzelli (1968); [q] Sheft and Fried (1953); [r] Zachariasen (1949c); [s] Zachariasen (1952c); [t] Chackraburtty and Jayadevan (1965); [u] Harper *et al.* (1968); [v] Mitchell and Lam (1970a); [w] Jacobson *et al.* (1956); [x] Brown and Norreys (1959); [y] Brown (1961); [z] Kimmel (1978); [aa] Zachariasen (1949d); [bb] Le Bihan *et al.* (1996); [cc] Brixner (1963); [dd] Mitchell and Lam (1974); [ee] Boulet *et al.* (2003); [ff] Land *et al.* (1965); [gg] Runnalls and Boucher (1955); [hh] Cromer *et al.* (1964); [ii] Weigel *et al.* (1984); [jj] Weigel *et al.* (1977); [kk] Weigel and Marquart (1983).

expanded by the B_6 clusters; this gives Th a coordination number of 24. The An–An distances in AnB_6 usually are similar to the An–An bond distances in the parent metal. Dodecaborides, AnB_{12}, can be described as a cubic closest packed structure of B_{12} units with actinide cations located in the octahedral lattice holes. The metal is coordinated with 24 boron atoms (Vegas *et al*., 1995).

Heating AnO_2 with excess carbon usually leads to the formation of AnC_2, which may also be prepared by direct reaction of the metal with carbon (Troost, 1893). Three polymorphs of ThC_2 have been detected using both X-ray and neutron diffraction: monoclinic α-ThC_2 at room temperature (Hunt and Rundle, 1951; Bowman *et al*., 1968), tetragonal β-ThC_2 at temperatures between 1430 and 1480°C, and cubic γ-ThC_2 at temperatures above 1480°C (Bowman *et al*., 1968). The dicarbide of uranium has two polymorphs. The α-form is tetragonal (CaC_2-type) at 1700°C and differs from the tetragonal β-form of thorium dicarbide. The β-form of uranium dicarbide is cubic at 1900°C and is analogous to γ-ThC_2 (Bowman *et al*., 1966). The α- and β-forms of PuC_2 are tetragonal (Chakraburtty and Jayadevan, 1965) and fcc (Harper *et al*., 1968), respectively. The tetragonal form adopts the CaC_2 structure type. PaC_2 (Lorenz *et al*., 1969) and NpC_2 (Sheft and Fried, 1953) have been observed with cubic and tetragonal structures, respectively. Careful control of the conditions for preparing AnC_2 can also be used to produce AnC. Structural information on AnC and An_2C_3 structures can be located in Table 22.7.

Of the actinide silicides, the uranium and thorium compounds are the most thoroughly characterized. The α-form of $ThSi_2$ was first identified in 1942 (Brauer and Mitius, 1942); the β-form readily transforms to α-$ThSi_2$ above 1350°C, and is reversible below 1250°C. A defect structure of the non-stoichiometric composition $ThSi_{1.67}$ is also known (Brown, 1961). The structure of USi was the most recent to be determined. Le Bihan *et al*. (1996) describe the synthesis of USi and assign a tetragonal symmetry to this compound despite previous reports of an orthorhombic cell. The unit cell has 68 uranium atoms. The plutonium–silicon binary system contains at least five different compounds, with Pu_5Si_3 being one of the few actinide silicide structures determined from single crystal X-ray diffraction (Cromer *et al*., 1964). The structural determination of AmSi and $AmSi_2$ was first reported by Weigel *et al*. (1984) using X-ray powder diffraction. Further work produced a range of americium silicides between room temperatures and 900°C. Curium silicides were first prepared by Weigel and Marquart (1983) through the reduction of CmF_3 with stoichiometric amounts of elemental Si at 1260°C. The X-ray diffraction data was compared to X-ray data from known analogous compounds of uranium, neptunium, plutonium, and americium. However, the authors caution that, because of the use of ^{244}Cm in the structures, the large amount of self-irradiation that occurs can destroy the lattice and cause inaccuracies due to broadening of and intensity changes in the X-ray lines, although the destruction could be reduced by a factor of 20000 if ^{248}Cm were used in its place (Weigel and Marquart, 1983).

22.3.5 Pnictides and chalcogenides

Actinide pnictides (compounds with N, P, As, Sb, and Bi) and chalcogenides (compounds with S, Se, and Te) are of interest to solid state chemists because these compounds display interesting electronic properties based upon the degree of localization or delocalization of the 5f electrons, resulting in compounds that are not purely ionic. In most cases, the delocalized nature of the 5f electrons in thorium through plutonium (although the transuranium elements become weakly delocalized) allows them to participate in bonding, while the localized nature of these electrons in americium and beyond makes them non-bonding (Damien *et al.*, 1986). In general, the nature of the bonding in these compounds is considered to be semimetallic.

For example, the monopnictides are face-centered cubic (fcc) compounds with lattice parameters decreasing from Th to U, increasing through Cm, and then decreasing again (Damien and de Novion, 1981). This behavior reflects metallic character in ThN, delocalized 5f electrons in UN, less delocalization in NpN, PuN, and AmN, and localized lanthanide-like behavior in CmN and BkN (due to the prevalence of the trivalent oxidation state in the later actinides). Similar behavior is observed in other pnictides; when there is a direct comparison with lanthanide compounds, transamericium compounds show slightly larger lattice parameters than do isoelectronic lanthanides. The delocalized nature of UN, NpN, and PuN 5f electrons is indicative of band formation and metallic conduction. The variation in lattice parameters of monochalcogenides follows a similar trend, but transcurium elements are unknown.

Several structural lattice types are common within these compounds. A list of known actinide–pnictide and actinide–chalcogenide compounds are provided in Tables 22.8 and 22.9, respectively.

The majority of the structures listed in these tables were determined by X-ray powder diffraction (lattice parameters and structural type) because the compounds are sensitive to oxidation in air, are unstable at high temperature due to the considerable partial pressures of the nonmetal elements over the crystalline phases, and have high chemical reactivity at elevated temperatures. Common methods used for growing single crystals of the monopnictides involve considerable difficulties, including selecting sufficiently inert materials for the high-temperature sample container. While some single crystals have been grown for certain compounds in both classes, little has been done in terms of structure determination. Efforts to facilitate the synthesis have been detailed by Horyn *et al.* (1983).

The structural types adopted by actinide pnictides and chalcogenides are quite diverse. All monopnictides and monochalcogenides are NaCl fcc structures except for ThTe which has a CsCl structure. A thorough summary of the structural types of higher pnictides and chalcogenides is available (Damien *et al.*, 1986). Some interesting examples include the body-centered cubic (bcc) form of Th_3P_4

Table 22.8 *Actinide pnictides and their crystal symmetries.*

	N		*P*		*As*		*Sb*		*Bi*	
Composition	*Symmetry*	*References*	*Symmetry*	*References*	*Symmetry*	*References*	*Symmetry*	*References*	*Symmetry*	*References*
ThX	fcc	[a]	fcc	[p]	fcc	[x]	fcc	[ee]	–	–
Th_2X_3	hexagonal	[b]	–	–	–	–	–	–	–	–
Th_3X_4	hexagonal (α)	[c]	bcc	[p, q]	bcc	[x]	bcc	[ee]	bcc	[kk]
	rhombohedral (β)	[d]	–	–	–	–	–	–	–	–
ThX_2	–	–	–	–	orthorhombic (α)	[q]	tetragonal	[ee]	tetragonal	[kk]
	–	–	–	–	tetragonal (β)	[x]	–	–	–	–
PaX	fcc	[e]	–	–	fcc	[y]	–	–	–	–
Pa_3X_4	–	–	bcc	[r]	bcc	[y]	bcc	[ff]	–	–
PaX_2	–	–	tetragonal	[r]	tetragonal	[y]	tetragonal	[ff]	–	–
UX	fcc	[a, f]	fcc	[s]	fcc	[s]	fcc	[s]	fcc	[ll]
U_2X_3	cubic (α)	[g]	–	–	–	–	–	–	–	–
	hexagonal (β)	[h]	–	–	–	–	–	–	–	–

U_3X_4	–	–	bcc	t	bcc	z	bcc	gg	bcc	ll, mm
UX_2	fcc	a	tetragonal (α)	u	tetragonal	v	tetragonal	hh	tetragonal	nn
	–	–	tetragonal (β)	v	–	–	–	–	–	–
NpX	fcc	i	fcc	i	fcc	i	fcc	ii	fcc	i
Np_3X_4	–	–	bcc	w	bcc	aa	–	–	–	–
NpX_2	–	–	–	–	tetragonal	aa	orthorhombic	jj	–	–
PuX	fcc	j, k	fcc	s	fcc	s, bb	fcc	s	fcc	i
PuX_2	–	–	–	–	–	–	orthorhombic	jj	–	–
Pu_4X_3	–	–	–	–	–	–	bcc	i	–	–
AmX	fcc	l, m	fcc	m	fcc	m, bb, cc	fcc	m, cc	fcc	cc
AmX_2	–	–	–	–	–	–	orthorhombic	jj	–	–
Am_4X_3	–	–	–	–	–	–	bcc	m	–	–
CmX	fcc	n	fcc	m, n	fcc	m, n	fcc	m, n	–	–
BkX	fcc	o	fcc	o	fcc	o	fcc	o	–	–
CfX	–	–	–	–	fcc	dd	fcc	dd	–	–

[a] Rundle (1948); [b] Zachariasen (1949b); [c] Benz and Zachariasen (1966); [d] Bowman and Arnold (1971); [e] Bohet and Müller (1978); [f] Marples (1970); [g] Serizawa *et al.* (1994); [h] Masaki and Tagawa (1975); [i] Charvillat (1978); [j] Zachariasen (1949c); [k] Olson and Mulford (1964); [l] Akimoto (1967); [m] Charvillat *et al.* (1975); [n] Damien *et al.* (1979a); [o] Damien *et al.* (1980a); [p] Gingerich and Wilson (1965); [q] Hulliger (1966); [r] Wojakowski *et al.* (1982); [s] Kruger and Moser (1967); [t] Zumbusch (1941); [u] Pietraszko and Lukaszewicz (1971); [v] Iandelli (1952a); [w] Sheft and Fried (1953); [x] Ferro (1955); [y] Calestani *et al.* (1979); [z] Iandelli (1952b); [aa] Wojakowski and Damien (1982); [bb] Charvillat and Damien (1973); [cc] Roddy (1974); [dd] Damien *et al.* (1980b); [ee] Ferro (1956); [ff] Hery *et al.* (1979); [gg] Smetana *et al.* (1975); [hh] Ferro (1952a); [ii] Mitchell and Lam (1971); [jj] Charvillat *et al.* (1977); [kk] Borzone *et al.* (1982); [ll] Ferro (1952b); [mm] Henkie *et al.* (1997); [nn] Ferro (1953).

Table 22.9 *Actinide chalcogenides and their crystal symmetries.*

	S		*Se*		*Te*	
Composition	*Symmetry*	*References*	*Symmetry*	*References*	*Symmetry*	*References*
Ac_2X_3	cubic	a	–	–	–	–
ThX	fcc	b	fcc	x	bcc	ll
Th_2X_3	orthorhombic	b	orthorhombic	x	hexagonal	d
Th_7X_{12}	hexagonal	c	hexagonal	x, y	hexagonal	mm
ThX_2	orthorhombic	b, d	orthorhombic	d, x, y	hexagonal	d
Th_2X_5	orthorhombic	e	orthorhombic	l, x	–	–
ThX_3	–	–	oonoclinic	l	monoclinic	d
PaX_2	orthorhombic	f	hexagonal	f	–	–
UX	fcc	b, g, h	fcc	h	fcc	h
U_3X_4	–	–	bcc	aa	bcc	nn
U_2X_3	orthorhombic	b, g	orthorhombic	bb	bcc	oo
	–	–	–	–	orthorhombic	pp
U_3X_5	orthorhombic	i, g	orthorhombic	cc	orthorhombic	qq
U_7X_{12}	–	–	hexagonal	dd	hexagonal	mm
UX_2	tetragonal (α)	g	tetragonal (α)	ee	orthorhombic	rr
	orthorhombic (β)	g, j	orthorhombic (β)	ff	–	–
	hexagonal (γ)	g, k	hexagonal (γ)	k	–	–
U_2X_5	orthorhombic	l	–	–	monoclinic	ss
UX_3	monoclinic	g	monoclinic	dd	monoclinic (α)	rr
	–	–	–	–	orthorhombic (β)	tt
NpX	fcc	m	fcc	gg	fcc	gg
Np_3X_4	–	–	bcc	hh	bcc	hh
Np_2X_3	orthorhombic (α)	m	cubic (γ)	ii	orthorhombic (η)	uu
	orthorhombic (β)	m	–	–	bcc (γ)	uu
	bcc (γ)	m	–	–	–	–
Np_3X_5	orthorhombic	m	orthorhombic	ii	–	–
NpX_2	orthorhombic	n	–	–	tetragonal	uu
Np_2X_5	orthorhombic	m	orthorhombic	jj	–	–

NpX_3	monoclinic	m	monoclinic	ii	orthorhombic	uu
PuX	fcc	b, h	fcc	h	fcc	u
Pu_2X_3	orthorhombic (α)	o	orthorhombic (η)	o	orthorhombic (η)	vv
	orthorhombic (β)	o	bcc (γ)	o	bcc (γ)	vv
	bcc (γ)	o	–	–	–	–
PuX_2	tetragonal	o	tetragonal	o	tetragonal	vv
PuX_3	–	–	–	–	orthorhombic	vv
AmX	fcc	p	fcc	gg	fcc	gg
Am_3X_4	–	–	bcc	kk	bcc	ww
Am_2X_3	orthorhombic (α)	p	bcc (γ)	w	orthorhombic (η)	ww
	tetragonal (β)	q	–	–	bcc (γ)	ww
	bcc (γ)	b	–	–	–	–
AmX_2	tetragonal	r	tetragonal	r	tetragonal	xx
AmX_3	–	–	–	–	orthorhombic	xx
CmX	fcc	s, t	fcc	s	fcc	s, t
Cm_2X_3	orthorhombic (α)	u	bcc (γ)	v	orthorhombic (η)	yy
	tetragonal (β)	u	–	–	bcc (γ)	t
	bcc (γ)	v	–	–	–	–
CmX_2	tetragonal	v	tetragonal	v	tetragonal	yy
CmX_3	–	–	–	–	orthorhombic	yy
Bk_2X_3	bcc (γ)	w	bcc (γ)	w	orthorhombic (ξ)	w
BkX_2	tetragonal	w	tetragonal	w	tetragonal	w
BkX_3	–	–	–	–	orthorhombic	w
Cf_2X_3	bcc (γ)	w	bcc (γ)	w	–	–
CfX_2	tetragonal	w	tetragonal	w	tetragonal	w

[a] Fried *et al.* (1950); [b] Zachariasen (1949e); [c] Zachariasen (1949f); [d] Graham and McTaggart (1960); [e] Noël and Potel (1982); [f] Hery (1979); [g] Picon and Flahaut (1958); [h] Kruger and Moser (1967); [i] Potel *et al.* (1972); [j] Suski *et al.* (1972); [k] Kohlmann and Beck (1997); [l] Noël (1980); [m] Marcon (1969); [n] Thévenin *et al.* (1984); [o] Marcon and Pascard (1966); [p] Damien (1971); [q] Damien *et al.* (1972); [r] Damien and Jové (1971); [s] Damien *et al.* (1979a); [t] Damien *et al.* (1979b); [u] Damien *et al.* (1976a); [v] Damien *et al.* (1975); [w] Damien *et al.* (1986); [x] D'Eye *et al.* (1952); [y] D'Eye (1953); [z] Kohlmann and Beck (1999); [aa] Noël (1985); [bb] Khodadad (1959); [cc] Moseley *et al.* (1972); [dd] Breeze and Brett (1972); [ee] Noël and Le Marouille (1984); [ff] Noël *et al.* (1996); [gg] Damien and Wojakowski (1975); [hh] Mitchell and Lam (1970b); [ii] Damien *et al.* (1973); [jj] Thévenin *et al.* (1982); [kk] Roddy (1974); [ll] D'Eye and Sellman (1954); [mm] Tougait *et al.* (1998a); [nn] Ferro (1954); [oo] Matson *et al.* (1963); [pp] Tougait *et al.* (1998b); [qq] Tougait *et al.* (1998c); [rr] Stöwe (1997); [ss] Stöwe (1996); [tt] Noël and Levet (1989); [uu] Damien (1974); [vv] Damien (1973); [ww] Damien and Charvillat (1972); [xx] Damien (1972); [yy] Damien *et al.* (1976b).

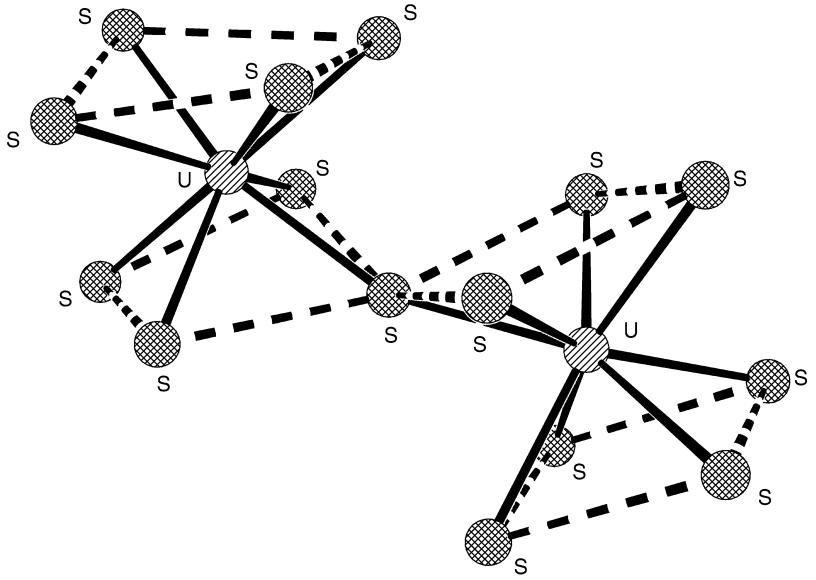

Fig. 22.5 *The two crystallographically independent uranium centers in the crystal structure of α-US_2. Dashed lines are used to delineate square antiprisms* (*Noël and Le Marouille,* 1984).

and the reverse structure, anti-Th_3P_4, adopted by pnictides such as Pu_4Sb_3 and Am_4Sb_3, which are different from hexagonal U_4Sb_3. The dichalcogenides are characterized by a variety of sub-stoichiometric phases that can either crystallize in different forms (i.e., tetragonal $PuS_{1.9}$ vs monoclinic PuS_2) or retain their structures (i.e., transuranium ditellurides). Fig. 22.5 shows the crystal structure of the α-form of the dichalcogenide, US_2. Finally, the sesquichalcogenides (An_2X_3) can take on up to five polymorphic forms, including α (orthorhombic), β (orthorhombic), γ (body-centered cubic), η (orthorhombic), and ξ (orthorhombic). Interestingly, berkelium is the first transuranic element to exhibit the ξ-type modification and an identical $\eta \rightarrow \xi$ transition occurs in the lanthanides at terbium, the homolog of berkelium (Damien *et al.*, 1979b). The existence of the β-modification in the actinides, although widely reported, may in fact be an oxychalcogenide (Damien *et al.*, 1986).

22.3.6 Halides and oxyhalides

The halides are the most widely examined of the actinide compounds from the point of view of structural determination. A review by Taylor (1976) noted that over 70 binary actinide halides, 60 actinide oxyhalides, and 70 binary

transition metal fluorides were known as of 1976. Despite the large number of compounds, their structural study is simplified by the isostructural nature of the series due to common structural types. Thus, powder diffraction data are often sufficient for obtaining adequate structural information about these compounds.

The bonding in actinide halides is largely ionic in nature. In general, the structures of these compounds may be approximated as consisting of positive actinide cations surrounded by negative anions. The shape of the anionic polyhedron around the actinide cation is controlled by many factors, including significant size effects. For a given oxidation state of the metal, coordination number usually decreases in the order F > Cl > Br > I due to increasing size of the anion. In addition, coordination number for a given ligand (i.e., F) typically increases as the oxidation state of the metal decreases due to size effects as in UF_6 (CN = 6) and UF_3 (CN = 11). This variability in size results in a large number of potential polyhedral types, significantly more diverse than those observed in transition metal halides. Further comprehensive structural reviews on actinide and lanthanide halides (Brown, 1968) as well as actinide fluorides (Penneman *et al.*, 1973) are available elsewhere. Important structural types and tables of known structures will be described herein.

In addition to size effects based on ligand type and metal oxidation state, clear trends are often also observed due to the actinide contraction. As one moves from left to right across the actinide series, the cation becomes smaller, resulting in an increasing occurrence of actinide halide polyhedra of lower coordination number. When polymorphism is observed for a given element, the high-temperature polymorph is typically the one of lower coordination number due to the generation of a more open lattice structure. Polymorphism is more common in the lower oxidation states due to larger size of the cation and enhanced ionic bonding (Taylor, 1976).

Dihalides are known for only a few of the actinides due to the instability of the An^{2+} oxidation state. Thorium diiodide was first prepared by the reaction of ThI_4 with Th metal at elevated temperatures and characterized in an X-ray powder pattern by Clark and Corbett (1963). A subsequent single-crystal X-ray diffraction study by Guggenberger and Jacobson (1968) confirmed the prediction by Clark and Corbett that the compound is not a true Th(II) salt, but rather contains Th(IV) with two supernumerary electrons. Thus, ThI_2 should be formulated as $Th^{4+}(I^-)_2(e^-)_2$. The structure contains four two-dimensionally infinite layers that alternate between trigonal prismatic and trigonal antiprismatic layers.

Americium dichloride, dibromide, and diiodide, each of which was prepared by reacting americium metal with the appropriate mercuric halide, have also been indexed using X-ray diffraction. The chloride and bromide belong to orthorhombic and tetragonal crystal systems, respectively (Baybarz, 1973b). The diiodide, AmI_2, has a monoclinic structure (Baybarz *et al.*, 1972b). Some

dihalides of californium(II) have also been characterized; $CfBr_2$ (Peterson and Baybarz, 1972) and CfI_2 (Hulet *et al.*, 1976) are tetragonal and hexagonal, respectively.

The actinide trihalides are the most structurally complete series of all the actinide halides and they form a series of compounds showing strong similarities to the lanthanide trihalides. The trifluorides (through curium) exhibit a nine-coordinate LaF_3-type structure; however, berkelium trifluoride is dimorphic with its low-temperature modification being the eight-coordinate YF_3-type (Brown, 1973). The same type of change occurs in californium trifluoride above 600°C (Stevenson and Peterson, 1973). An analogous structural change occurs in the lanthanide trifluorides between promethium and samarium (Thoma and Brunton, 1966). These structural observations have been related to the actinide contraction in a paper by Brown *et al.* (1968a).

The actinide trichlorides follow a similar trend. At californium, there is a structural change as a consequence of the actinide contraction. The earlier actinides possess the nine-coordinate UCl_3 structure type. Californium trichloride is dimorphic and exhibits both a nine-coordinate UCl_3 modification, and an eight-coordinate $PuBr_3$-type modification. The structural change observed in the trichlorides occurs earlier in the tribromides; Ac through α-$NpBr_3$ are nine-coordinate UCl_3 types, while β-$NpBr_3$ through $BkBr_3$ are eight-coordinate $PuBr_3$ types. The triiodides are quite different altogether. The triiodides from protactinium through americium (α-modification) are $PuBr_3$-type structures, while the compounds from americium (β-modification) through californium are six-coordinate BiI_3-type structures (Brown, 1973). The trichlorides, tribromides, and triiodides are also moisture-sensitive materials and easily form hydrated compounds. The trihalides of the actinides are listed in Table 22.10.

The actinide tetrafluorides (Th–Cf) have been the most extensively characterized class of tetrahalides due to their isostructural nature (all are monoclinic); each eight-coordinate actinide is surrounded by a square antiprism of fluorine ligands (Keenan and Asprey, 1969). Structural details of the remaining tetrahalides are far less available (Table 22.11). The tetrachlorides (Th through Np) are also isostructural and have tetragonal crystal lattices. In $ThCl_4$, thorium is eight-coordinate and the ligands are arranged in a dodecahedron around the actinide. Both β-$ThBr_4$ and $PaBr_4$ are isostructural with the tetrachlorides. Few structural details are available for α-$ThBr_4$, UBr_4, and $NpBr_4$ other than them being orthorhombic, monoclinic, and monoclinic, respectively. Of the tetraiodides, structural data are only available for ThI_4 and UI_4. The former has an eight-coordinate distorted square antiprismatic geometry, while the latter is six-coordinate octahedral (Brown, 1973).

The pentahalides are quite uncommon; the only actinide for which all four pentahalides are known is protactinium, and none are known past neptunium (only NpF_5 is known). These compounds are extremely moisture sensitive and the hydrolysis of some is further complicated by disproportionation. PaF_5 and

Table 22.10 *Actinide trihalides (AnX_3) and their crystal symmetries.*

	Flouride		*Chloride*		*Bromide*		*Iodide*	
	Symmetry	*References*	*Symmetry*	*References*	*Symmetry*	*References*	*Symmetry*	*References*
Ac	hexagonal	[a, b]	hexagonal	[b, g]	hexagonal	[b, g]	–	–
Th	–	–	–	–	–	–	–	–
Pa	–	–	–	–	–	–	orthorhombic	[p]
U	hexagonal	[a]	hexagonal	[g, h]	hexagonal	[g]	orthorhombic	[g, q]
Np	hexagonal	[a]	hexagonal	[g]	hexagonal (α)	[g]	orthorhombic	[g]
	–	–	–	–	orthorhombic (β)	[g]	–	–
Pu	hexagonal	[a]	hexagonal	[g, i]	orthorhombic	[g]	orthorhombic	[g]
Am	hexagonal	[c]	hexagonal	[d, g]	orthorhombic	[d, g]	orthorhombic	[g, r]
	–	–	–	–	–	–	hexagonal	[d]
Cm	hexagonal	[d]	hexagonal	[d, j]	orthorhombic	[d, i]	hexagonal	[d, r]
Bk	orthorhombic	[e]	hexagonal	[k]	monoclinic	[i]	hexagonal	[n]
	trigonal	[e]	–	–	rhombohedral	[i]	–	–
	–	–	–	–	orthorhombic	[i, n]	–	–
Cf	orthorhombic	[f]	hexagonal	[l]	monoclinic	[i]	hexagonal	[s]
	trigonal	[f]	orthorhombic	[l]	rhombohedral	[i]	–	–
Es	–	–	tetragonal	[m]	monoclinic	[o]	–	–
	–	–	hexagonal	[m]	–	–	–	–

[a] Zachariasen (1949b); [b] Fried *et al.* (1950); [c] Templeton and Dauben (1953); [d] Asprey *et al.* (1965); [e] Peterson and Cunningham (1968a); [f] Stevenson and Peterson (1973); [g] Zachariasen (1948b); [h] Taylor and Wilson (1974a); [i] Burns *et al.* (1975); [j] Peterson and Burns (1973); [k] Peterson and Cunningham (1968b); [l] Burns *et al.* (1973); [m] Fujita *et al.* (1969); [n] Cohen *et al.* (1968); [o] Fellows *et al.* (1975); [p] Scherer *et al.* (1967); [q] Levy *et al.* (1975); [r] Haire *et al.* (1983); [s] Fried *et al.* (1968).

Table 22.11 *Actinide tetrahalides (AnX_4) and their crystal symmetries.*

	Fluoride		*Chloride*		*Bromide*		*Iodide*	
	Symmetry	*References*	*Symmetry*	*References*	*Symmetry*	*References*	*Symmetry*	*References*
Th	monoclinic	a, b	tetragonal	h	orthorhombic (α)	m	monoclinic	q
	–	–	–	–	tetragonal (β)	m	–	–
Pa	monoclinic	a, b, c	tetragonal	i, j	tetragonal	i, n	–	–
U	monoclinic	a, b, d, e	tetragonal	h, k	monoclinic	o	monoclinic	r
Np	monoclinic	a, b	tetragonal	l	monoclinic	p	–	–
Pu	monoclinic	a, b	–	–	–		–	–
Am	monoclinic	a, b	–	–	–	–	–	–
Cm	monoclinic	a, b, f	–	–	–	–	–	–
Bk	monoclinic	a, b, g	–	–	–	–	–	–
Cf	monoclinic	a, e	–	–	–	–	–	–

[a] Asprey and Haire (1973); [b] Keenan and Asprey (1969); [c] Stein (1964); [d] Kunitomi *et al.* (1964); [e] Haug and Baybarz (1975); [f] Asprey *et al.* (1957); [g] Haug and Baybarz (1975); [h] Mooney (1949); [i] Brown and Jones (1967); [j] Brown *et al.* (1973); [k] Taylor and Wilson (1973a); [l] Spirlet *et al.* (1994); [m] Scaife (1966); [n] Brown and Jones (1966); [o] Taylor and Wilson (1974b); [p] Brown *et al.* (1970); [q] Zalkin *et al.* (1964); [r] Levy *et al.* (1980).

β-UF_5 are isostructural (Brown, 1973), while the powder data from NpF_5 appears to be similar to that of α-UF_5 (Malm *et al.*, 1993); each has tetragonal crystal symmetry. PaF_5 and β-UF_5 are both seven-coordinate with pentagonal bipyramidal geometry. The structure of α-UF_5, however, is six-coordinate and octahedral. $PaCl_5$ is also seven-coordinate with infinite chains of edge-fused pentagonal bipyramids (Fig. 22.6). Of the remaining pentahalides, α-$PaBr_5$ and UBr_5 are isostructural, β-$PaBr_5$ and α-UCl_5 (cubic close-packed) both form edge-sharing dimers, β-UCl_5 dimers are based on hexagonal close-packing of anions, and PaI_5 is believed to be structurally similar to TaI_5 (Brown *et al.* 1976; Müller, 1979). The pentahalides are listed in Table 22.12.

Some intermediate compounds of the stoichiometries An_2X_9 and An_4X_{17} have also been discovered, including Pa_2F_9, U_2F_9, U_4F_{17}, and Pu_4F_{17}. The former two compounds are isostructural with bcc symmetry. In the nine-coordinate U_2F_9, it is believed that its black color results from resonance between oxidation states four and five. The latter two compounds are structurally uncharacterized (Brown, 1973).

Structural information for only four actinide hexahalides is available (Table 22.13). The hexafluorides of U, Np, and Pu are volatile solids obtained

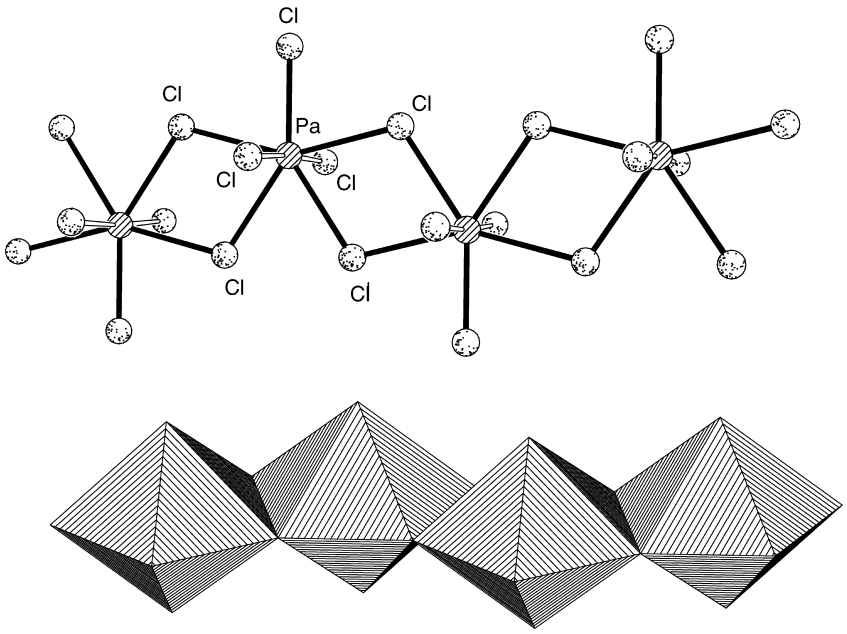

Fig. 22.6 *Crystal structure of $PaCl_5$ (top) with an illustration of the infinite chains of edge-sharing pentagonal bipyramids (bottom)* (*Dodge* et al., 1967).

Table 22.12 *Actinide pentahalides (AnX_5) and their crystal symmetries.*

	Fluoride		*Chloride*		*Bromide*		*Iodide*	
	Symmetry	*References*	*Symmetry*	*References*	*Symmetry*	*References*	*Symmetry*	*References*
Pa	tetragonal	[a]	monoclinic	[h]	monoclinic (α)	[k]	orthorhombic	[o]
	–	–	–	–	monoclinic (β)	[k, l]	–	–
	–	–	–	–	triclinic (γ)	[k]	–	–
U	tetragonal (α)	[b, c, d]	monoclinic (α)	[i]	triclinic	[n]	–	–
	tetragonal (β)	[d, e]	triclinic (β)	[j]	–	–	–	–
Np	tetragonal	[f, g]	–	–	–	–	–	–

[a] Stein (1964); [b] Zachariasen (1948b); [c] Eller *et al.* (1979); [d] Zachariasen (1949g); [e] Ryan *et al.* (1976); [f] Malm *et al.* (1993); [g] Baluka *et al.* (1980); [h] Dodge *et al.* (1967); [i] Smith *et al.* (1967); [j] Mueller and Kolitsch (1974); [k] Brown *et al.* (1969); [l] Brown *et al.* (1968b); [m] Brown (1979); [n] Levy *et al.* (1978); [o] Brown *et al.* (1976).

Table 22.13 *Actinide hexahalides (AnX_6) and their crystal symmetries.*

	Fluoride		*Chloride*	
	Symmetry	*References*	*Symmerty*	*References*
U	orthorhombic	[a, b]	hexagonal	[e, f, g]
Np	orthorhombic	[c]	–	–
Pu	orthorhombic	[d]	–	–

[a] Levy *et al.* (1976); [b] Hoard and Stroupe (1958); [c] Malm *et al.* (1958); [d] Florin *et al.* (1956); [e] Zachariasen (1948b); [f] Zachariasen (1948c); [g] Taylor and Wilson (1974c).

from AnF_4 fluorination, and UCl_6 is obtained from the reaction of $AlCl_3$ with UF_6. AmF_6 has been claimed as the result of oxidation of AmF_3 by KrF_2 in anhydrous HF at 40–60°C, although no structural data is available (Drobyshevskii *et al.*, 1980). All are powerful oxidizing agents and extremely sensitive to moisture; contact with water results in the formation of AnO_2X_2 and HX compounds. The hexafluoride of uranium is important in gaseous diffusion processes for the enrichment of uranium. The hexafluorides are isostructural compounds that form discrete octahedra, although in the case of UF_6, neutron diffraction data suggests that there are significant deviations from the ideal parameters of Hoard and Stroupe due to strong U–U repulsions (Taylor *et al.*, 1973). The hexachloride of uranium (the only other actinide hexahalide) contains a hexagonal crystal lattice with perfect octahedral geometry around uranium. It is isostructural with β-WCl_6 (Taylor, 1976).

Actinide oxyhalides of the type An(VI)O_2X_2, An(V)O_2X, An(IV)OX_2, and An(III)OX are known although less thoroughly characterized than the halides themselves. In general, the higher oxidation state compounds are favored by the early actinides, while the lower oxidation states are favored by the later actinides. The trivalent actinide oxyfluorides are limited to AcOF, ThOF, PuOF, and CfOF. With the exception of PuOF, these oxyhalides have CaF_2 fluorite-type structures with the oxygen and fluorine atoms randomly distributed in the anion sites. The PuOF lattice is a tetragonal modification of the fluorite structure, probably stabilized by excess fluoride (Brown, 1973).

The remaining trivalent actinide oxychlorides, oxybromides, and oxyiodides (where structural data are available) are strictly of the tetragonal PbFCl structure type, thus making their characterization rather straightforward. In this arrangement, the metal atom has four oxygen neighbors and five halide neighbors. It is rather remarkable that compounds formed from both large and small cations ranging in size from Ac^{3+} to Es^{3+} and anions from Cl^- to I^- can all adopt this structure type. The known compounds are listed in Table 22.14.

Tetravalent actinide oxyhalides are very limited in number; none are known beyond neptunium (Table 22.15). With the exception of $ThOF_2$, all adopt the $PaOCl_2$ structure type. This rather unusual structure consists of infinite

Table 22.14 *Trivalent actinide oxyhalides (AnOX) and their crystal symmetries.*

	Fluoride		*Chloride*		*Bromide*		*Iodide*	
	Symmetry	*References*	*Symmetry*	*References*	*Symmetry*	*References*	*Symmetry*	*References*
Ac	fcc	[a]	tetragonal	[a]	tetragonal	[a]	–	–
Th	fcc	[b]	–	–	–	–	–	–
Pa	–	–	–	–	–	–	–	–
U	–	–	tetragonal	[e]	tetragonal	[e]	tetragonal	[e]
Np	–	–	tetragonal	[f]	tetragonal	[f]	tetragonal	[f]
Pu	tetragonal	[a,p]	tetragonal	[a]	tetragonal	[a]	tetragonal	[a]
Am	–	–	tetragonal	[g]	tetragonal	[l]	tetragonal	[o]
Cm	fcc	[c]	tetragonal	[h]	tetragonal	[c]	–	–
Bk	–	–	tetragonal	[i]	tetragonal	[m]	tetragonal	[m]
Cf	fcc	[d]	tetragonal	[j]	tetragonal	[n]	tetragonal	[n]
Es	–	–	tetragonal	[k]	–	–	–	–

[a] Zachariasen (1949b); [b] Rannou and Lucas (1969); [c] Weigel and Kohl (1985); [d] Peterson and Burns (1968); [e] Levet and Noël (1981); [f] Brown and Edwards (1972); [g] Templeton and Dauben (1953); [h] Peterson (1972); [i] Peterson and Cunningham (1967b); [j] Copeland and Cunningham (1969); [k] Fujita *et al.* (1969); [l] Weigel *et al.* (1979); [m] Cohen *et al.* (1968); [n] Fried *et al.* (1968); [o] Haire *et al.* (1983); [p] Zachariasen (1951).

polymeric chains along the *c*-direction with cross-linking in the *ab* plane. The protactinium environments are diverse and can be either seven-, eight-, or nine-coordinate with three- or four-coordinate oxygen atoms. The LaF_3 structure type of $ThOF_2$ is orthorhombic but is largely structurally uncharacterized (Taylor, 1976).

The pentavalent actinide oxyhalides can be of An(v)OX_3, An(v)O_2X, or An(v)$_2OX_8$ composition. In general, structural data are few, if available at all (Table 22.16). The most thoroughly characterized of these oxyhalides are the isostructural $PaOBr_3$ and $UOBr_3$ systems. The structure of the former compound is composed of endless double chains (with random terminations) with pentagonal bipyramidal polyhedra around the Pa atoms. Four out of every five pentagonal edges of the polyhedra are shared (Brown *et al.*, 1975).

Hexavalent actinide oxyhalides are typically of the form An(VI)O_2X_2 (actinyl) or An(VI)OX_4. The actinyl fluorides, UO_2F_2, NpO_2F_2, PuO_2F_2, and AmO_2F_2, are isostructural and have the rhombohedral UO_2F_2 structure type. Here, the linear uranyl cation is surrounded equatorially by six fluorides, generating a coordination number of 8 for uranium. The U–O bond distance of 1.74(2) Å is common for the uranyl cation. Neutron diffraction of UO_2Cl_2 reveals a linear uranyl cation surrounded equatorially by five atoms, four of which are chlorides and the fifth is an oxygen atom from a neighboring uranyl group. Uranyl bromide, UO_2Br_2, is also known structurally, but the last in the series, UO_2I_2, is as of yet unknown. Known compounds are listed in Table 22.17 (Taylor, 1976).

Actinide halo-complexes containing alkali, ammonium, or other cations will not be discussed here. The reader is referred elsewhere for comprehensive reviews of structural characterizations (Brown, 1973).

22.3.6 Carbonates, nitrates, phosphates, arsenates, and sulfates

In general, a limited number of anhydrous binary compounds of actinides and these ligands are reported in the literature. This is due to the greater stability of the hydrated compounds and higher order complexes. In most examples, the common structural feature is that the anions all provide oxygen atoms that surround the actinide cation. Coordination numbers for the metal atom in these compounds can be as high as eight to 12 for tetravalent thorium, but typically decrease across the series to between six and nine due to the actinide contraction. A coordination number of six is observed in a few uranyl structures. The high coordination numbers are predominantly due to the ability of these ligands to act in both monodentate and bidentate (symmetric and asymmetric) coordination modes. Bidentate coordination is most common because of the small 'bite' distance (O $\cdots$ O distance) of the ligand.

Table 22.15 *Tetravalent actinide oxyhalides ($AnOX_2$) and their crystal symmetries.*

	Fluoride		*Chloride*		*Bromide*		*Iodide*	
	Symmetry	*References*	*Symmetry*	*References*	*Symmetry*	*References*	*Symmetry*	*References*
Th	orthorhombic	[a]	orthorhombic	[b]	–	–	orthorhombic	[g]
Pa	–	–	orthorhombic	[b, c, d]	orthorhombic	[c]	orthorhombic	[c]
U	–	–	orthorhombic	[b, e, f]	orthorhombic	[f]	orthorhombic	[f]
Np	–	–	orthorhombic	[b]	–	–	–	–

[a] D'Eye (1958); [b] Bagnall *et al*. (1968a); [c] Brown and Jones (1967); [d] Dodge *et al*. (1968); [e] Taylor and Wilson (1974d); [f] Levet and Noël (1979); [g] Scaife *et al*. (1965).

Table 22.16 *Pentavalent actinide oxyhalides and their crystal symmetries.*

Fluoride			*Bromide*			*Iodide*		
Compound	*Symmetry*	*References*	*Compound*	*Symmetry*	*References*	*Compound*	*Symmetry*	*References*
PaO_2F	orthorhombic	[a]	$PaOBr_3$	monoclinic	[e]	PaO_2I	hexagonal	[h]
Pa_2OF_8	bcc	[b]	–	–	–	–	–	–
Pa_3O_7F	orthorhombic	[a]	–	–	–	–	–	–
UO_2F	monoclinic	[c]	UO_2Br	orthorhombic	[f]	–	–	–
–	–	–	$UOBr_3$	monoclinic	[g]	–	–	–
NpO_2F	tetragonal	[d]	–	–	–	–	–	–
$NpOF_3$	rhombohedral	[d]	–	–	–	–	–	–

[a] Brown and Easey (1970); [b] Stein (1964); [c] Kemmler-Sack (1969); [d] Bagnall *et al.* (1968b); [e] Brown *et al.* (1975); [f] Levet *et al.* (1977); [g] Brown (1973); [h] Brown *et al.* (1967).

Table 22.17 *Hexavalent actinide oxyhalides and their crystal symmetries.*

Fluoride			*Chloride*		
Compound	*Symmetry*	*References*	*Compound*	*Symmetry*	*References*
UO_2F_2	rhombohedral	[a, b]	UO_2Cl_2	orthorhombic	[l, m]
UOF_4 (α)	trigonal	[c, d]	–	–	–
UOF_4 (β)	tetragonal	[e]	–	–	–
NpO_2F_2	rhombohedral	[a, f]	–	–	–
$NpOF_4$	trigonal	[g]	–	–	–
PuO_2F_2	rhombohedral	[h, i]	–	–	–
$PuOF_4$	trigonal	[j]	–	–	–
AmO_2F_2	rhombohedral	[k]	–	–	–

[a] Zachariasen (1949b); [b] Atoji and McDermott (1970); [c] Paine *et al.* (1975); [d] Levy *et al.* (1977); [e] Taylor and Wilson (1974e); [f] Bagnall *et al.* (1968b); [g] Peacock and Edelstein (1976); [h] Florin *et al.* (1956); [i] Alenchikova *et al.* (1958); [j] Burns and O'Donnell (1977); [k] Keenan (1968); [l] Debets (1968); [m] Taylor and Wilson (1973b).

(a) Carbonates

Structures of actinide carbonates number very few in the literature and mostly contain the actinyl cation, thus restricting ligand bonding to the equatorial region. Carbonates typically bond in a bidentate fashion, but instances of monodentate bridging carbonate are also known. Actinide carbonates are sometimes geologically occurring minerals such as rutherfordine. Rutherfordine is the naturally occurring form of the mineral UO_2CO_3 and its structure has been investigated both as the natural mineral (Christ *et al.*, 1955) and a synthetic compound (Cromer and Harper, 1955). The crystal structure of the natural mineral has reccently been refined (Finch *et al.*, 1999). In both cases, UO_2CO_3 crystallizes as an orthorhombic lattice and there are six oxygen atoms bound in the equatorial plane. Two carbonate groups act in a symmetrical bidentate fashion, while the remaining two oxygens are from monodentate carbonate groups, resulting in hexagonal bipyramidal geometry. Other instances of uranyl carbonate compounds are listed in Table 22.18. While the hexagonal bipyramidal geometry is common in several uranyl carbonates, slight differences in the U=O actinyl bond length are still observed; for example, 1.67(9), 1.79(1), and 1.80(1) Å distances are observed in UO_2CO_3, $(NH_4)_4UO_2(CO_3)_3$ (Graziani *et al.*, 1972), and $Tl_4UO_2(CO_3)_3$ (Mereiter, 1986b), respectively.

Simple carbonates of the transuranium actinyls (AnO_2^{2+}) are known for both neptunium and plutonium. NpO_2CO_3 (Thévenin *et al.*, 1986; Kato *et al.*, 1998) and PuO_2CO_3 (Navratil and Bramlet, 1973) are both isostructural with the uranium analog and have orthorhombic lattices. The tetraammonium tricarbonate compounds of neptunyl and plutonyl, $(NH_4)_4NpO_2(CO_3)_3$ and

Table 22.18 *Some actinide carbonates and their crystal symmetries.*

Carbonates	*Symmetry*	*References*
$[C(NH_2)_3]_6[Th(CO_3)_5] \cdot 4H_2O$	monoclinic	Voliotis and Rimsky (1975a)
$Na_6[Th(CO_3)_5] \cdot 12H_2O$	triclinic	Voliotis and Rimsky (1975b)
UO_2CO_3	orthorhombic	Cromer and Harper (1955)
$Sr_2UO_2(CO_3)_3 \cdot 8H_2O$	monoclinic	Mereiter (1986a)
$Na_4UO_2(CO_3)_3$	hexagonal	Císařová *et al.* (2001)
$K_4UO_2(CO_3)_3$	monoclinic	Malcic (1958a)
$Tl_4UO_2(CO_3)_3$	monoclinic	Mereiter (1986b)
$(NH_4)_4UO_2(CO_3)_3$	monoclinic	Graziani *et al.* (1972); Malcic (1958b)
NpO_2CO_3	orthorhombic	Thévenin *et al.* (1986)
$KNpO_2CO_3$	hexagonal	Keenan and Kruse (1964)
$Na_3NpO_2(CO_3)_2 \cdot nH_2O$	monoclinic	Volkov *et al.* (1981)
$Rb_3NpO_2(CO_3)_2 \cdot nH_2O$	orthorhombic	Volkov *et al.* (1981)
$K_4NpO_2(CO_3)_3$	monoclinic	Musikas and Burns (1976)
$(NH_4)_4NpO_2(CO_3)_3$	monoclinic	Marquart *et al.* (1983)
$[Na_6Pu(CO_3)_5]_2 \cdot Na_2CO_3 \cdot 33H_2O$	monoclinic	Clark *et al.* (1998a)
PuO_2CO_3	orthorhombic	Navratil and Bramlet (1973)
$(K,NH_4)PuO_2CO_3$	hexagonal	Ellinger and Zachariasen (1954)
$(NH_4)_4PuO_2(CO_3)_3$	monoclinic	Marquart *et al.* (1983)
$Am_2(CO_3)_3 \cdot 2H_2O$	cubic	Weigel and ter Meer (1967)
$KAmO_2CO_3$	hexagonal	Keenan and Kruse (1964)
$CsAmO_2CO_3$	hexagonal	Keenan (1965)
$RbAmO_2CO_3$	hexagonal	Ellinger and Zachariasen (1954)
$NH_4AmO_2CO_3$	hexagonal	Nigon *et al.* (1954)
$(NH_4,Cs)_4AmO_2(CO_3)_3$	monoclinic	Fedoseev and Perminov (1983)

$(NH_4)_4PuO_2(CO_3)_3$, are also isostructural with the corresponding uranium compound and crystallize in monoclinic crystal systems. Only bidentate coordination of the carbonate ion is observed. Pentavalent actinyl (AnO_2^+) carbonate compounds containing americium have also been studied; the compounds $KNpO_2CO_3$, $KPuO_2CO_3$, and $KAmO_2CO_3$ (Ellinger and Zachariasen, 1954; Keenan and Kruse, 1964) are isostructural with hexagonal symmetry.

Tetravalent thorium and plutonium carbonate compounds include $Na_6Th(CO_3)_5 \cdot 12H_2O$ (Voliotis and Rimsky, 1975b) and $Na_6[Pu(CO_3)_5]_2 \cdot Na_2CO_3 \cdot 33H_2O$ (Clark *et al.*, 1998a); the crystal structure of the latter is shown in Fig. 22.7. In both structures, the actinides are ten coordinate and all the carbonate groups are bidentate. The geometry of each has been described as a modified hexagonal bipyramid; two *trans* carbonate ligands occupy axial positions analogous to the *trans* oxo ligands in an actinyl ion, while the remaining carbonates occupy the equatorial sites, thus forming the hexagon. An example of a trivalent actinide carbonate can be seen in the structure of $Am_2(CO_3)_3 \cdot 2H_2O$ (Weigel and ter Meer, 1967).

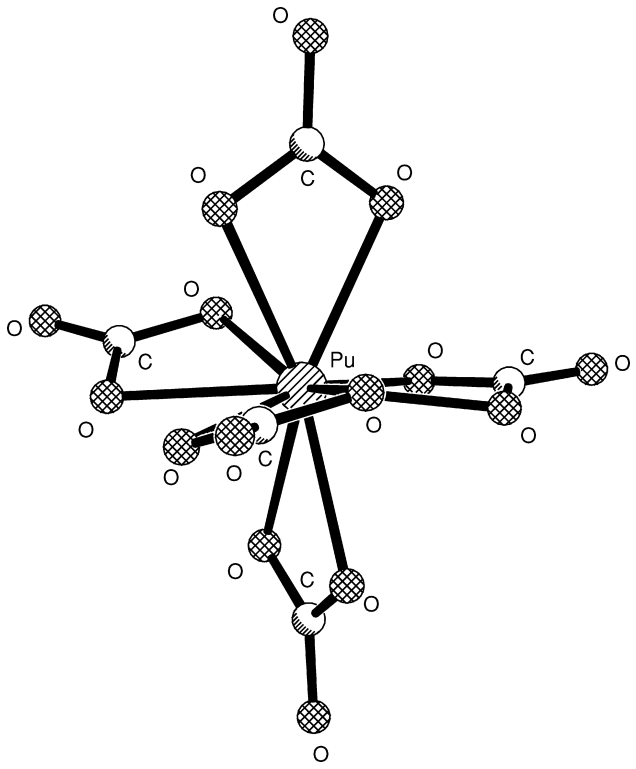

Fig. 22.7 *Coordination geometry of* $[Pu(CO_3)_5]^{6-}$ *anion* (*showing axial and equatorial carbonate ligands*) *in the crystal structure of* $[Na_6Pu(CO_3)_5]_2 \cdot Na_2CO_3 \cdot 33H_2O$ (*Clark* et al., 1998*a*).

(b) Nitrates

Structures of simple actinide nitrates containing only actinide/actinyl cations and nitrate anions are unknown. All known structures are hydrated, contain additional non-actinide monovalent or divalent cations, or contain various donor ligands. Actinide nitrate compounds are limited mainly to Th(VI) and uranyl cations, although a few neptunium and plutonium structures exist. In the tetravalent thorium and plutonium compounds, the nitrate anions are typically bidentate, thus allowing for extraordinarily high coordination numbers ranging from eight to as high as 12. In actinyl compounds, the *trans* oxo ligands enforce equatorial nitrate coordination, thus causing both bidentate as well as monodentate coordination in the case of four equatorial nitrate ligands. Hexagonal bipyramidal geometry is common in this case. Examples of actinide nitrate compounds are available from the previous edition of this work or Brown (1973).

Thorium(IV) nitrate pentahydrate has been investigated using both X-ray and neutron diffraction (Taylor *et al.*, 1966; Ueki *et al.*, 1966). The structure as determined by neutron diffraction is shown in Fig. 22.8. Four bidentate nitrate groups and three of the five water molecules are coordinated to the metal center, resulting in a coordination number of 11. Water–water and water–nitrate hydrogen bonds are significant in terms of stabilizing the overall structure, with the latter being slightly longer than the former by about 0.2 Å. The plutonium analog, $Pu(CO_3)_4 \cdot 5H_2O$, is isostructural with the thorium compound, both of which have orthorhombic symmetry (Staritzky, 1956).

The dihydrate (Dalley *et al.*, 1971), trihydrate (Hughes and Burns, 2003), and hexahydrate (Hall *et al.*, 1965) of uranyl nitrate each exhibit eight-coordinate uranium centers of hexagonal bipyramidal geometry. In each compound, both nitrates are bidentate and two waters are coordinated through oxygen. Once again, extensive hydrogen bonding is present between hydrogen atoms of water molecules and unbound oxygen atoms of the nitrate groups (Hall *et al.*, 1965; Dalley *et al.*, 1971). The U=O bond lengths are shorter in the dihydrate (1.754(4) and 1.763(5) Å) than in the hexahydrate (1.85 and 1.87 Å), presumably due to the greater effects of hydrogen bonding in the latter.

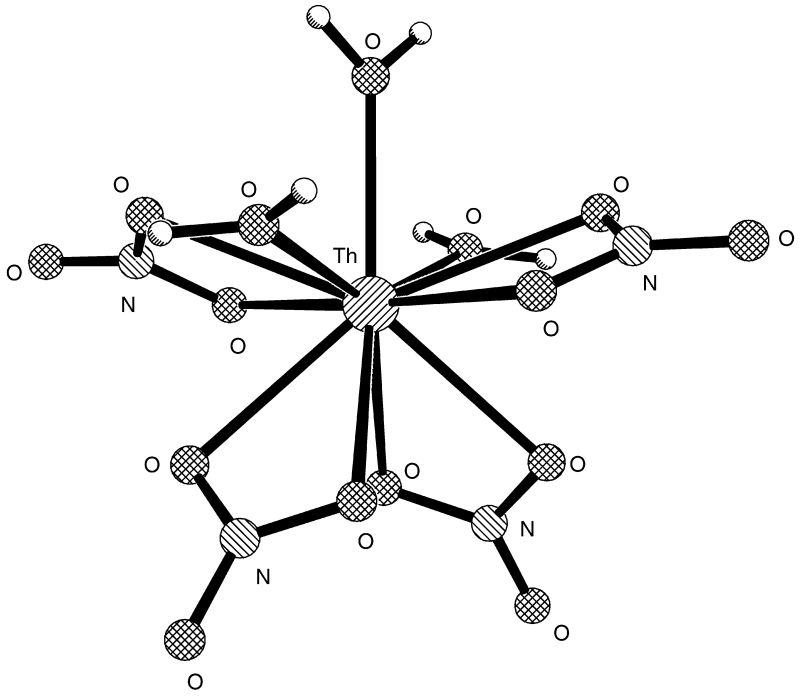

Fig. 22.8 *Coordination environment of thorium in the neutron diffraction crystal structure of* $Th(NO_3)_4 \cdot 5H_2O$ (*Taylor* et al., 1966).

Neptunyl nitrate hexahydrate, $NpO_2(NO_3)_2 \cdot 6H_2O$, has orthorhombic symmetry and appears to be isostructural with the uranium analog. X-ray powder data are also available for the compounds $NpO_2NO_3 \cdot H_2O$ and $Np(NO_3)_4 \cdot N_2O_5$, but structural details are inconclusive (Laidler, 1966).

The series of tetravalent thorium nitrates having the formula M(II)Th$(NO_3)_6 \cdot 8H_2O$ [M(II) = Mg, Mn, Co, Ni, Zn] are isomorphically related. Further studies of the Mg compound have shown that the coordination is best described by the formula $[Mg(H_2O)_6] \cdot [Th(NO_3)_6] \cdot 2H_2O$. All the nitrates bond in a bidentate fashion, leading to a coordination number of 12 for thorium (Šćavničar and Prodić, 1965). In some cases, anhydrous nitrate compounds can be obtained such as $RbUO_2(NO_3)_3$. All the nitrate groups are bidentate to the metal, thus resulting in hexagonal bipyramidal geometry around the uranium atom (Barclay *et al.*, 1965). Also included in the anhydrous uranyl compounds are $KUO_2(NO_3)_3$ (Krivovichev and Burns, 2004) and $CsUO_2(NO_3)_3$ (Zivadinovic, 1967), as well as the tetranitrate $Rb_2[UO_2(NO_3)_4]$ (Irish *et al.*, 1985).

(c) Phosphates and arsenates

Phosphate and arsenate compounds containing the following actinides have been the subject of a series of extensive articles: uranium(VI) (Weigel and Hoffmann, 1976a), neptunium(VI) (Weigel and Hoffmann, 1976b), ammonium–americyl(VI)–phosphate (Weigel and Hoffmann, 1976c), plutonium(VI) (Fischer *et al.*, 1981), americium(VI) (Lawaldt *et al.*, 1982), thorium(IV), uranium(IV), and neptunium(IV) (Bamberger *et al.*, 1984a), and plutonium(III) and plutonium(IV) (Bamberger *et al.*, 1984b). Representative examples of actinide phosphates will be presented herein (Table 22.19).

The structural chemistry of actinide phosphates and arsenates is important on a number of levels. Uranyl phosphates and arsenates in particular are found geologically in large numbers as naturally occurring minerals, which include autenite, tobernite, metazeunerite, and uranocircite. Additionally, the long-term stability of the rare-earth phosphate mineral monazite has led to studies involving the immobilization of actinides in synthetic monazites for long-term storage. Phosphate chemistry is also critically important for understanding the behavior of actinides in the environment as well as in separations schemes.

Actinide phosphate compounds typically contain the orthophosphate (PO_4^{3-}), metaphosphate (PO_3^-), or pyrophosphate ($P_2O_7^{4-}$) anions; arsenate structures are typically limited to the former type. The tetrahedral PO_4^{3-}ion lends itself to both monodentate and bidentate metal bonding, as illustrated in Fig. 22.9. The pyrophosphate anion contains two tetrahedral centers, each of which can be monodentate or bidentate. The various types of phosphate coordination modes in the solid state are exemplified in the structure of $Th_4(PO_4)_4P_2O_7$. Each heavy thorium atom is bound to eight oxygen atoms from five PO_4^{3-} groups and one $P_2O_7^{4-}$ group. One of the former groups is bidentate and the remaining four are monodentate; the pyrophosphate

Table 22.19 *Some actinide phosphates, by type, and their crystal symmetries.*

Phosphate	*Symmetry*	*References*
orthophosphates (*including double phosphates*)		
$AcPO_4 \cdot 0.5H_2O$	hexagonal	Fried *et al.* (1950)
$Th_3(PO_4)_4$	monoclinic	Shankar and Khubchandani (1957)
$U(UO_2)(PO_4)_2$	triclinic	Bénard *et al.* (1994)
$U_3(PO_4)_4$	monoclinic	Burdese and Borlera (1963)
$(U_2O)(PO_4)_2$	orthorhombic	Albering and Jeitschko (1995)
$(UO_2)_3(PO_4)_2(H_2O)_4$	orthorhombic	Locock and Burns (2002)
$PuPO_4$	monoclinic	Bjorklund (1957)
$PuPO_4 \cdot 0.5H_2O$	hexagonal	Bjorklund (1957)
$Pu(PO_4)_3$	orthorhombic	Bamberger *et al.* (1984b)
$AmPO_4$	monoclinic	Keller and Walter (1965)
$AmPO_4 \cdot 0.5\ H_2O$	hexagonal	Keller and Walter (1965)
$CmPO_4$	monoclinic	Weigel and Haug (1965)
$(Li,Na,K,Rb,Cs)Th_2(PO_4)_3$	monoclinic	Matković *et al.* (1968a)
$KTh_2(PO_4)_3$	monoclinic	Matković *et al.* (1968b)
$NaTh_2(PO_4)_3$	monoclinic	Matković and Šljukić (1965)
$Na_2Th(PO_4)_2$	monoclinic	Galešić *et al.* (1984)
$(Ca,Sr,Cd,Ba,Pb)_{0.5}Th_2(PO_4)_3$	monoclinic	Guesdon *et al.* (1999)
$CuTh_2(PO_4)_3$	monoclinic	Louër *et al.* (1995)
$TlTh_2(PO_4)_3$	monoclinic	Laugt (1973)
$PbTh(PO_4)_3$	monoclinic	Quarton *et al.* (1984)
$Pb_3Th_6(PO_4)_{10}$	monoclinic	Quarton *et al.* (1984)
$Pb_7Th(PO_4)_6$	cubic	Quarton *et al.* (1984)
$(H,Li,Na)UO_2PO_4 \cdot 4H_2O$	tetragonal	Weigel and Hoffmann (1976a)
$H_{11}(UO_2)_2(PO_4)_5$	monoclinic	Staritzky and Cromer (1956)
$(Li,Na)U_2(PO_4)_3$	monoclinic	Matković *et al.* (1968a)
$(Na,K,NH_4)UO_2PO_4 \cdot 3H_2O$	tetragonal	Weigel and Hoffmann (1976a)
$(Mg,Ca,Sr,Ba)(UO_2PO_4)_2 \cdot nH_2O$ ($n = 2$–6.5, 8–12)	tetragonal	Weigel and Hoffmann (1976a)
α-$KU_2(PO_4)_3$	monoclinic	Guesdon *et al.* (1999)
β-$(K,Rb)U_2(PO_4)_3$	rhombohedral	Volkov *et al.* (2003)
α-$CaU(PO_4)_2$	orthorhombic	Dusausoy *et al.* (1996)
β-$CaU(PO_4)_2$	monoclinic	La Ginestra *et al.* (1965)
$Ca(UO_2PO_4)_2 \cdot nH_2O$ ($n = 0$–2)	orthorhombic	Weigel and Hoffmann (1976a)
$Cu_2UO_2(PO_4)_2$	monoclinic	Guesdon *et al.* (2002)
$(H,Li)NpO_2PO_4 \cdot 4H_2O$	tetragonal	Weigel and Hoffmann (1976b)
α-$NaNp_2(PO_4)_3$	monoclinic	Nectoux and Tabuteau (1981)
β-$(Na,K,Rb)Np_2(PO_4)_3$	rhombohedral	Volkov *et al.* (2003)
$(Na,K,NH_4)NpO_2PO_4 \cdot 3H_2O$	tetragonal	Weigel and Hoffmann (1976b)
$Mg(NpO_2PO_4)_2 \cdot 9H_2O$	tetragonal	Weigel and Hoffmann (1976b)
$(Ca,Sr,Ba)(NpO_2PO_4)_2 \cdot 6H_2O$	tetragonal	Weigel and Hoffmann (1976b)
$(H,K,NH_4)PuO_2PO_4 \cdot nH_2O$	tetragonal	Fischer *et al.* (1981)
α-$NaPu_2(PO_4)_3$	monoclinic	Burnaeva *et al.* (1992)
β-$(Na,K,Rb)Pu_2(PO_4)_3$	rhombohedral	Burnaeva *et al.* (1992); Volkov *et al.* (2003)
$(K,Rb,Cs,NH_4,)AmO_2PO_4 \cdot nH_2O$	tetragonal	Lawaldt *et al.* (1982)
$NH_4AmO_2PO_4 \cdot 3H_2O$	tetragonal	Weigel and Hoffmann (1976c)

Table 22.19 (*Contd.*)

Phosphate	*Symmetry*	*References*
metaphosphates		
$Th(PO_3)_4$	orthorhombic	Douglass (1962)
$Pa(PO_3)_4$	orthorhombic	Le Cloarec and Cazaussus (1978)
α-$U(PO_3)_4$	monoclinic	Baskin (1967)
β-$U(PO_3)_4$	orthorhombic	Douglass (1962)
α-$Np(PO_3)_4$	tetragonal	Nectoux and Tabuteau (1981)
β-$Np(PO_3)_4$	triclinic	Nectoux and Tabuteau (1981)
γ-$Np(PO_3)_4$	orthorhombic	Nectoux and Tabuteau (1981)
$Pu(PO_3)_4$	orthorhombic	Douglass (1962)
pyrophosphates		
α-ThP_2O_7	cubic	Bamberger *et al*. (1984a); Burdese and Borlera (1963)
β-ThP_2O_7	orthorhombic	Bamberger *et al*. (1984a); Burdese and Borlera (1963)
PaP_2O_7	cubic	Le Cloarec and Cazaussus (1978)
$(PaO)_4(P_2O_7)_3$	monoclinic	Le Cloarec *et al*. (1976)
α-UP_2O_7	cubic	Kirchner *et al*. (1963)
β-UP_2O_7	orthorhombic	Douglass and Staritzky (1956)
NpP_2O_7	cubic	Keller and Walter (1965)
PuP_2O_7	cubic	Bjorklund (1957)
other		
$Th_4(PO_4)_4P_2O_7$	orthorhombic	Bénard *et al*. (1996)
$KThU(PO_4)_3$	monoclinic	Guesdon *et al*. (1999)
$Pa_2O_5 \cdot P_2O_5$	orthorhombic	Le Cloarec *et al*. (1976)
$UXPO_4 \cdot 2H_2O$ (X = Cl, Br)	tetragonal	Bénard-Rocherullé *et al*. (1997)
$U_2(PO_4)(P_3O_{10})$	orthorhombic	Podor *et al*. (2003)
$[(UO_2)_3(PO_4)O(OH)(H_2O)_2](H_2O)$	tetragonal	Burns *et al*. (2004)
$U(HPO_4)_2 \cdot 4H_2O$	N/A	Voinova (1998)

group donates two oxygen atoms, one from each tetrahedral center (Bénard *et al*., 1996).

Actinide pyrophosphates can adopt two different structural modifications: the orthorhombic β-form and the cubic α-form. Structural details of the former type are scarce, but the latter modification is known for structures including the actinides Th, Pa, U, Np, and Pu. These pyrophosphates are all isostructural and lattice parameters decrease with increasing atomic number. Six oxygen atoms are coordinated to the metal center in each instance (Le Cloarec and Cazaussus, 1978). The β-UP_2O_7 modification has orthorhombic symmetry (Douglass and Staritzky, 1956). Simple metaphosphates of tetravalent Th, Pa, U, and Pu of the composition $An(PO_3)_4$ are all isostructural and have orthorhombic symmetry

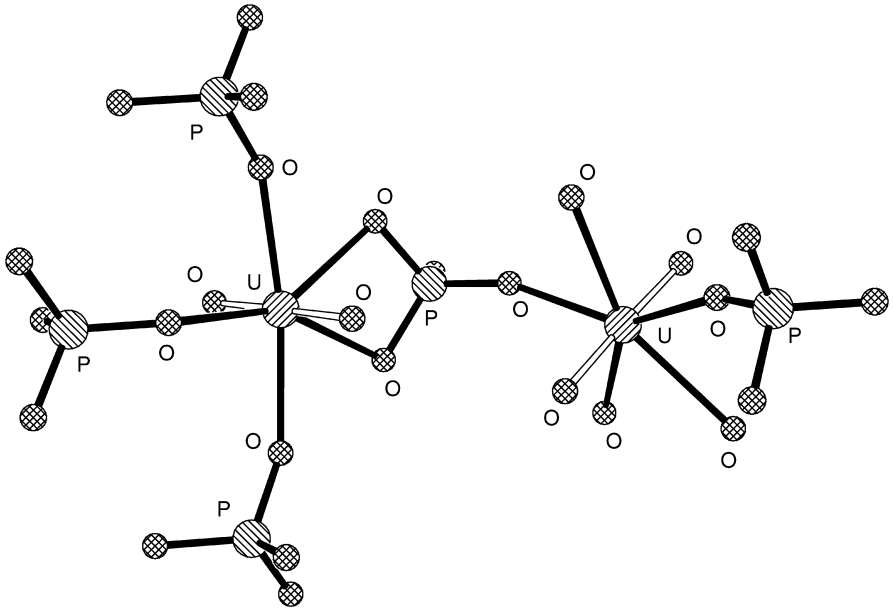

Fig. 22.9 *The two crystallographically independent uranyl centers in the crystal structure of* $(UO_2)_3(PO_4)_2(H_2O)_4$. *Hydrogen atoms have been omitted from the three water molecules bound to the uranium on the right* (*Locock and Burns,* 2002).

(Douglass, 1962; Le Cloarec and Cazaussus, 1978). Structural details for the simple arsenates of $AmAsO_4$ and $PuAsO_4$ (monoclinic symmetry) are available elsewhere (Keller and Walter, 1965).

(d) Sulfates

Actinide sulfates enjoy a unique place in the history of nuclear chemistry; it was A. H. Becquerel who, in 1896, discovered radioactivity in the uranyl double sulfate $K_2UO_2(SO_4)_2 \cdot 2H_2O$. He simply noticed that in the absence of sunlight (actually, in the total darkness of laboratory drawer), the salt will darken a photographic plate and so must spontaneously emit its own type of radiation (Becquerel, 1896).

Additionally, sulfates have traditionally played an important role in the mining of uranium ores. Uranium is leached from crushed ores using sulfuric acid, resulting in soluble ionic species such as $UO_2(SO_4)_3^{4-}$. Despite its prevalence in actinide chemistry, structural characterizations of actinide sulfates are relatively few (Table 22.20).

Actinide sulfate compounds are usually found in hydrated form where as few as one to as many as ten water molecules are present in the structural formula.

Table 22.20 *Some actinide sulfates and their crystal symmetries.*

Sulfate	*Symmetry*	*References*
$Th(SO_4)_2$	hexagonal	Mudher *et al.* (1999)
$Th(SO_4)_2 \cdot 8H_2O$	monoclinic	Habash and Smith (1983)
$Th(OH)_2SO_4$	orthorhombic	Lundgren (1950)
$(NH_4)_2Th(SO_4)_3$	monoclinic	Mudher *et al.* (1999)
$K_4Th(SO_4)_4 \cdot 2H_2O$	triclinic	Arutyunyan *et al.* (1966a)
$H_3PaO(SO_4)_3$	hexagonal	Bagnall *et al.* (1965)
$U(OH)_2SO_4$	orthorhombic	Lundgren (1952)
$U_6O_4(OH)_4(SO_4)_6$	tetragonal	Lundgren (1953)
α-UO_2SO_4	monoclinic	Kovba *et al.* (1965)
β-UO_2SO_4	monoclinic	Brandenburg and Loopstra (1978)
$Cs_2(UO_2)_2(SO_4)_3$	tetragonal	Ross and Evans (1960)
$K_2UO_2(SO_4)F_2 \cdot 2H_2O$	monoclinic	Alcock *et al.* (1980a)
$(NH_4)_2UO_2SO_4 \cdot 2H_2O$	monoclinic	Niinisto *et al.* (1978)
$(K,Rb)_4U(SO_4)_4 \cdot 2H_2O$	monoclinic	Mudher *et al.* (1988)
$(NH_4, K)_2UO_2(SO_4)_2 \cdot 2H_2O$	monoclinic	Weigel and Hellmann (1986)
$UO_2SO_4 \cdot 2.5H_2O$	monoclinic	Weigel and Hellmann (1986)
$UO_2SO_4 \cdot 3H_2O$	orthorhombic	Traill (1952)
$Na_{10}[(UO_2)(SO_4)_4](SO_4)_2 \cdot 3H_2O$	monoclinic	Burns and Hayden (2002)
$U(SO_4)_2 \cdot 4H_2O$	orthorhombic	Kierkegaard (1956)
$(NH_4, Rb)U(SO_4)_2 \cdot 4H_2O$	monoclinic	Chadha *et al.* (1980)
$H_2(UO_2)_2(SO_4)_2 \cdot 5H_2O$	orthorhombic	Traill (1952)
$(NH_4)_2(UO_2)_2(SO_4)_3 \cdot 5H_2O$	orthorhombic	Staritzky *et al.* (1956)
$CsU(SO_4)_2 \cdot 5.5H_2O$	orthorhombic	Chadha *et al.* (1980)
α-$2UO_2SO_4 \cdot 7H_2O$	orthorhombic	Zalkin *et al.* (1978b)
β-$2UO_2SO_4 \cdot 7H_2O$	monoclinic	Brandenburg and Loopstra (1973)
$U_2(SO_4)_3 \cdot 8H_2O$	orthorhombic	Chadha *et al.* (1980)
$(Cs, Rb)_2UO_2(SO_4)_2 \cdot 10H_2O$	orthorhombic	Weigel and Hellmann (1986)
$Cs_2NpO_2(SO_4)_2$	monoclinic	Fedosseev *et al.* (1999)
$Cs_2(NpO_2)_2(SO_4)_3$	tetragonal	Fedosseev *et al.* (1999)
$(Cs, Rb)_2NpO_2(SO_4)_2 \cdot nH_2O$ ($n = 0.5, 4, 10$)	orthorhombic	Weigel and Hellmann (1986)
$(NpO_2)_2SO_4 \cdot H_2O$	orthorhombic	Grigor'ev *et al.* (1993a)
$(NpO_2)_2SO_4 \cdot 2H_2O$	monoclinic	Budantseva *et al.* (1988)
$K_2NpO_2(SO_4)_2 \cdot 2H_2O$	monoclinic	Weigel and Hellmann (1986)
$Cs_2Np(SO_4)_3 \cdot 2H_2O$	monoclinic	Charushnikova *et al.* (2000a)
$Cs_3NpO_2(SO_4)_2 \cdot 2H_2O$	triclinic	Grigor'ev *et al.* (1991a)
$(NH_4)_2NpO_2SO_4 \cdot 2H_2O$	monoclinic	Fedosseev *et al.* (1999)
$NpO_2SO_4 \cdot 2.5H_2O$	monoclinic	Weigel and Hellmann (1986)
$Na_{10}Np_2(SO_4)_9 \cdot 4H_2O$	orthorhombic	Charushnikova *et al.* (2000b)
$Pu(SO_4)_2$	hexagonal	Mudher *et al.* (1999)
$(NH_4)_2Pu(SO_4)_3$	monoclinic	Mudher *et al.* (1999)
$NaPu(SO_4)_2 \cdot H_2O$	hexagonal	Iyer and Natarajan (1989)
$(K, Cs)_2PuO_2(SO_4)_2 \cdot 2H_2O$	monoclinic	Weigel and Hellmann (1986)
$(K, Rb)_4Pu(SO_4)_4 \cdot 2H_2O$	monoclinic	Mudher *et al.* (1988); Mudher and Krishnan (2000)
$PuO_2SO_4 \cdot 2.5H_2O$	monoclinic	Weigel and Hellmann (1986)
α-$Pu(SO_4)_2 \cdot 4H_2O$	orthorhombic	Jayadevan *et al.* (1982)
β-$Pu(SO_4)_2 \cdot 4H_2O$	orthorhombic	Jayadevan *et al.* (1982)
$NH_4Pu(SO_4)_2 \cdot 4H_2O$	monoclinic	Iyer and Natarajan (1990)
$Am_2(SO_4)_3 \cdot 8H_2O$	monoclinic	Burns and Baybarz (1972)

Water molecules can be directly bonded to the metal or take on a non-bonding role in the lattice. In the case of thorium(IV) sulfates, the number of water molecules in the lattice is variable by controlling the temperature of crystallization. The octahydrate is crystallized from neutral aqueous solution at 20–25°C, lower hydrates are obtained by drying at 100–110°C, and the anhydrous form is formed at 400°C. In the octahydrate, the coordination sphere around thorium is occupied by four oxygen atoms from two chelating sulfate groups and the oxygen atoms of six water molecules, resulting in bicapped square antiprismatic geometry. These polyhedra are linked by hydrogen bonding (Habash and Smith, 1983).

Protactinium sulfates are rare, probably due to the difficulties in handling this element. One example is $H_3PaO(SO_4)_3$ which has hexagonal symmetry, but decomposes to amorphous $H_3PaO(SO_4)_3$ at 375°C (Bagnall *et al.*, 1965). Uranyl sulfate structures, however, are more common because they constitute a widespread class of minerals. For example, in the cluster compound $Na_{10}[(UO_2)(SO_4)_4](SO_4)_2 \cdot 3H_2O$, the $[(UO_2)(SO_4)_4]^{6-}$ anion (Fig. 22.10) is composed of a uranyl pentagonal bipyramid that shares an edge with one sulfate tetrahedron and vertices of three tetrahedra (Burns and Hayden, 2002). Polymorphism is displayed in $2UO_2SO_4 \cdot 7H_2O$; the α and β forms are similar, but differ in the

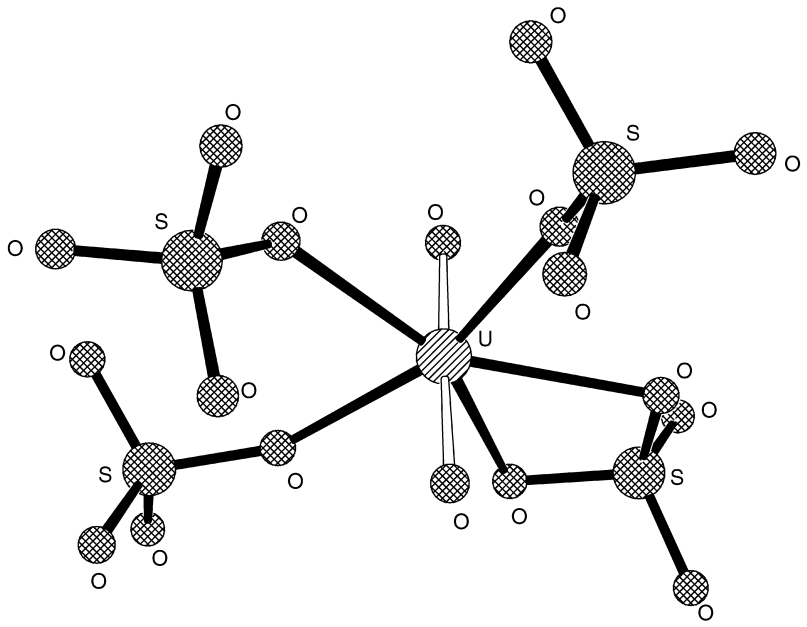

Fig. 22.10 *The uranyl sulfate cluster in the crystal structure of* $Na_{10}[(UO_2)(SO_4)_4](SO_4)_2 \cdot 3H_2O$ (*Burns and Hayden,* 2002).

way in which their chains are repeated and the orientation of their polyhedra (Zalkin *et al.*, 1978b).

Examples of neptunium and plutonium sulfate structures are also available. The compound $(NpO_2)_2SO_4 \cdot H_2O$ is a rare example of cation–cation interactions. Each linear NpO_2^+ unit is coordinated equatorially by three oxygen atoms from three sulfate groups as well as two oxygen atoms from two neighboring neptunyl groups, resulting in pentagonal bipyramidal polyhedra (Grigor'ev *et al.*, 1993a). Higher hydrated forms are also known, depending on the conditions of preparation (Budantseva *et al.*, 1988). The hexavalent actinide compounds of the composition $AnO_2SO_4 \cdot 2.5H_2O$ (An = U, Np, Pu) are isostructural with monoclinic symmetry. Two structural modifications are known for $Pu(SO_4)_2 \cdot 4H_2O$ (α and β), both of which are monoclinic; the latter modification has a lattice constant (*a*-axis) nearly twice as large as the former (Weigel and Hellmann, 1986).

The compound $Am_2(SO_4)_3 \cdot 8H_2O$, a rare americium sulfate, was studied using single-crystal X-ray diffraction. Each trivalent americium atom is coordinated by four oxygen atoms from four sulfate groups and by four water molecules; the resulting polyhedron is intermediate between an antiprism and a dodecahedron. Extensive hydrogen bonding links the polyhedra and the structure is isomorphous with the neodymium analog (Burns and Baybarz, 1972).

22.4 COORDINATION COMPOUNDS

Structural studies of coordination compounds of actinides in the solid state are quite numerous and diverse. Crystallographic information generated from X-ray and neutron diffraction techniques regarding the structural details of such compounds is too extensive to be comprehensively discussed herein. Thus, the following section comprising actinide coordination compounds will focus on two major areas: (1) structures containing carboxylic acid-derived acyclic ligands and (2) structures containing macrocyclic ligands including crown ethers, calixarenes, and porphyrins/phthalocyanines. Organoactinide compounds will be treated separately.

Actinide complexes with acyclic ligands are by no means limited to those involving carboxylic acids; a large number of crystal structures are available for those containing amides, phosphine oxides, and carbonyls, just to name a few. Due to the great diversity in this area, carboxylic acids were chosen owing to their extensive employment as actinide extraction ligands, ion-exchange media, and as agents in other practical applications. Their ability to act in both monodentate and bidentate modes and yield complexes of high coordination number has resulted in a plethora of structural characterizations, which will be illustrated in Section 22.4.1.

Macrocyclic ligands, including crown ethers, calixarenes, and porphyrins/phthalocyanines, have received a lot of attention due to their cyclic arrangement of donor atoms (including oxygen, nitrogen, and sulfur) for coordination to both lanthanide and actinide cations. The ability to vary the ring size of the macrocycle, as well as to alter the identity of the donor atoms (to tune hard/soft properties), has resulted in the generation of a large number of crystal structures that exhibit tremendous diversity, particularly with regard to the role of counter-ions for the generation of inclusion versus exclusion complexes. Examples of structurally characterized actinide/macrocycle complexes will be presented in Section 22.4.2.

Organoactinide structures involving cyclopentadienyl ligands, their derivatives, and related ligands, on account of their distinction from both acyclic and macrocyclic actinide complexes, will be the focus of Section 22.5. In addition, the chemistry of organoactinide complexes, including both synthesis and characterization, is the focus of Chapter 25.

22.4.1 Complexes with carboxylic acids

Carboxylic acids typically form stable coordination complexes with the large actinide ions via monodentate or bidentate donation through the carboxylate oxygen atoms, yielding complexes of high coordination number. Representative carboxylate ligands include monocarboxylate species such as formates, acetates, glycolates, and salicylates, dicarboxylate species such as oxalates and malonates, and pyridine or benzene derivatives containing three or more carboxylate functionalities. Several coordination modes are possible in carboxylic acid complexes with actinides, the major types of which are represented in Fig. 22.11 (for monocarboxylic acids). Carboxylic acid ligands can engage in both monodentate and bidentate coordination modes, as well as provide more than one bonding site per molecule. These features make carboxylic acids highly versatile ligands as evidenced in the high number of structural characterizations that have been made (Tables 22.21–22.23). Structural characteristics of representative examples will be described.

While a large number of carboxylic acid ligands exhibit the potential to chelate actinide cations, crystal structures have been most commonly determined of formates, acetates, oxalates, and malonates. This is due to the small O···O 'bite' distances and the overall relative compactness of the molecules, resulting in easy packing in the crystal lattice. Large or bulky chains attached to the (mono- or di-) carboxylate functionality tend to make crystallization and subsequent structural characterization difficult (Casellato *et al.*, 1978).

Formates are the simplest type of carboxylic acid, where the the R_1 group is a hydrogen atom. Actinide formates are typically prepared in solution using formic acid or a formate salt. Uranium(VI) diformate monohydrate crystallizes in the orthorhombic space group with the uranyl ion coordinated equatorially by five oxygen atoms, resulting in pentagonal bipyramidal geometry around the

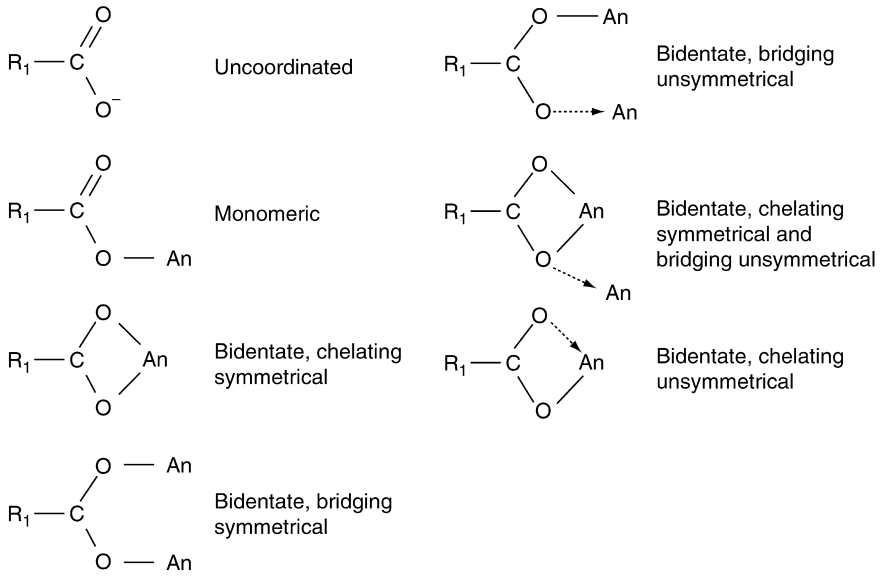

Fig. 22.11 *Summary of possible monocarboxylic acid bonding modes. R_1 can be a hydrocarbon radical or a proton* (*Casellato* et al., 1978).

uranium atom. The equatorial coordination is assigned to one oxygen atom from bound water and four oxygen atoms from the formate ligands, with these nodes forming infinite formate–uranium–formate chains, further stabilized by hydrogen bonding through bound water (Mentzen *et al.*, 1977).

The monoclinic $NaUO_2(HCOO)_3 \cdot H_2O$ lattice contains an interesting combination of structural motifs with two distinct types of formate bonding (Fig. 22.12). First, the uranyl motif contains equatorial pentagonal coordination through five formate oxygen atoms. The two uranyl oxygen atoms reside axially, resulting in a pentagonal bipyramid about uranium. The second motif has hexa-coordination around Na^+ using two oxygen atoms from water and four from formate ligands. Each uranium polyhedron is formed from three types of formate ligands. First, one type of formate bridges adjacent uranium centers, resulting in infinite formate–uranium–formate chains. Second, two infinite chains are bridged by a second type of formate, resulting in a uranium polyhedra 'layer'. Third, layers of sodium polyhedra and uranium polyhedra are bridged by a third type of formate ligand, resulting in an ..ABABA.. layering scheme (Claudel *et al.*, 1976, Mentzen, 1977).

Formate complexes with Th(IV) have also have been structurally investigated. For example, $Th(HCOO)_4 \cdot 3H_2O$ contains a central thorium atom with coordination number of ten, formally described as $[Th(HCOO)_4 \cdot 2H_2O]H_2O$. Each thorium is coordinated to eight oxygen atoms of eight separate bridging formate

Table 22.21 *Monocarboxylic acid compounds with actinides, by type.*

Structure	*References*
formate	
$Am(HCOO)_3$	Weigel and ter Meer (1967)
$Th(HCOO)_4$	Chevreton *et al.* (1968)
$An(HCOO)_4$, [An = Th(IV), Pa(IV), U(IV), Np(IV)]	Hauck (1976)
$Th(HCOO)_4 \cdot 2/3H_2O$	Chevreton *et al.* (1968)
$Th(HCOO)_4 \cdot 3H_2O$	Chevreton *et al.* (1968); Arutyunyan *et al.* (1966b)
$UO_2(HCOO)(OH) \cdot H_2O$	Le Roux *et al.* (1979)
$UO_2(HCOO)_2 \cdot H_2O$	Mentzen *et al.* (1977)
$NaUO_2(HCOO)_3 \cdot H_2O$	Claudel *et al.* (1976); Mentzen (1977)
$(NH_4)_2UO_2(HCOO)_4$	Mentzen *et al.* (1978a)
$SrUO_2(HCOO)_4 \cdot (1 + x)H_2O$	Mentzen *et al.* (1978b)
$(NH_4)NpO_2(CHOO)_2$	Grigor'ev *et al.* (1994)
acetate	
$Th(CH_3COO)_4$	Eliseev *et al.* (1967)
$(CN_3H_6)_2[Th(CH_3COO)_6]$	Arutyunyan *et al.* (1966c)
$[UO_2(CH_3COO)_2Ph_3PO]_2$	Panattoni *et al.* (1969)
$UO_2(CH_3COO)_2(Ph_3PO)_2$	Graziani *et al.* (1967)
$UO_2(CH_3COO)_2Ph_3PO$	Graziani *et al.* (1967)
$[UO_2(CH_3COO)_2Ph_3AsO]_2$	Bandoli *et al.* (1968)
$UO_2(CH_3COO)_2(Ph_3AsO)_2$	Bandoli *et al.* (1968)
$Na[(UO_2)_2(\mu\text{-}OH)_2(CH_3COO)_2(OH)]$	Avisimova *et al.* (2001)
$UO_2(CH_3COO)_2 \cdot 2H_2O$	Howatson *et al.* (1975)
$NaUO_2(CH_3COO)_3$	Zachariasen and Plettinger (1959); Navaza *et al.* (1991)
$(C_6H_{15}N_4O_2)[UO_2(CH_3COO)_3] \cdot CH_3COOH \cdot H_2O$	Silva *et al.* (1999)
$U(CH_3COO)_4$	Jelenić *et al.* (1964)
$(NpO_2)_2(CH_3COO)_2(H_2O) \cdot C_2H_3N$	Charushnikova *et al.* (1995)
$NaNpO_2(CH_3COO)_3$	Zachariasen (1954)
$BaNpO_2(CH_3COO)_3 \cdot 2H_2O$	Burns and Musikas (1977)
$NaPuO_2(CH_3COO)_3$	Zachariasen (1954)
$NaAmO_2(CH_3COO)_3$	Zachariasen (1954)
propionate	
$MUO_2(CH_3CH_2COO)_3$, (M = Cs, Rb, Tl, NH_4)	Burkov *et al.* (1997)
$Ca[UO_2(C_2H_5COO)_3]_2 \cdot 6H_2O$	Benetollo *et al.* (1995)
glycolate	
$UO_2(CH_2OHCOO)_2$	Mentzen and Sautereau (1980)
$U(CH_2OHCOO)_4 \cdot 2H_2O$	Alcock *et al.* (1980b)
$NpO_2(CH_2OHCOO) \cdot H_2O$	Grigor'ev *et al.* (1995)
salicylate	
$[UO_2(NO_3)(C_7H_4O_3)(DMAP)]_2$	Nassimbeni *et al.* (1976)
$[H_3O][UO_2(C_7H_5O_3)_3] \cdot 5H_2O$	Alcock *et al.* (1989)
$Am(C_7H_5O_3)_3 \cdot H_2O$	Burns and Baldwin (1977)

Table 22.21 (*Contd.*)

Structure	*References*
benzoate	
$Na[UO_2(C_6H_5COO)_3] \cdot (C_6H_5COOH) \cdot H_2O$	Benetollo *et al.* (1995)
pyridine-2-carboxylate (*monopicolinate*)	
$[(UO_2)_3(C_5H_4NCOO)_2(NO_3)_2(H_2O)_2] \cdot 2H_2O$	Silverwood *et al.* (1998)
pyridine-3-carboxylate	
$UO_2(C_5H_4NCOO)_2(H_2O)_2$	Alcock *et al.* (1996a)
2,6-dihydroxybenzoate	
$[UO_2(C_6H_3(OH)_2COO)_2(H_2O)_2] \cdot 8H_2O$	Cariati *et al.* (1983)
amino acid	
$UO_2(CO_2CH_2NH_3)_4 \cdot (NO_3)_2$ (glycine)	Alcock *et al.* (1985)
$UO_2(\gamma$-aminobutanoic acid$)_3(NO_3)_2 \cdot H2O$	Bismondo *et al.* (1985)
anthranilate (*1*), *pyrazinate* (*2*)	
$(H_3O)[UO_2(C_6H_4NH_2COO)_3]H_2O$ (1)	Alcock *et al.* (1996b)
$[UO_2(C_4H_3N_2COO)_2(H_2O)] \cdot 2H_2O$ (2)	Alcock *et al.* (1996b)

ligands, resulting in a distorted Archimedic antiprism. The remaining two coordination sites are occupied by oxygen atoms from two water molecules located in the square faces of the antiprism (Chevreton *et al.*, 1968).

Acetate ligands are carboxylates where R_1 is a methyl group, making them compact for packing in a crystal. The uranyl acetate dihydrate lattice contains a uranyl cation equatorially coordinated to an oxygen from a water molecule, two oxygen atoms from a chelating acetate ligand, and two oxygen atoms from two bridging acetate ligands, resulting in a distorted pentagonal bipyramidal geometry around the uranium center. The bridging acetates link the uranium centers together to form propagating chains, and adjacent chains are associated with one another through a lattice water molecule; this water participates in hydrogen bonding to the bound water of one chain and two acetate ligands of the neighboring chain (Howatson *et al.*, 1975).

Acetate complexes with uranyl incorporating phosphine oxides have also been structurally characterized and are significant with regards to separations processes. Certain types of phosphine oxides exhibit functional extractive abilities for actinides such as uranium and plutonium, making them invaluable for remediating acidic media and waste streams. The compound $UO_2(CH_3COO)_2(Ph_3PO)_2$ and the related arsine oxide analog $UO_2(CH_3COO)_2(Ph_3AsO)_2$ were found to be isomorphous by single-crystal X-ray diffraction (Graziani *et al.*, 1967; Bandoli *et al.*, 1968). The related compounds $[UO_2(CH_3COO)_2(Ph_3PO)]_2$ (Panattoni *et al.*, 1969) and $[UO_2(CH_3COO)_2(Ph_3AsO)]_2$ (Bandoli *et al.*, 1968) have also been isolated. The former structure consists of two seven-coordinate uranium centers. Each uranium has two axial uranyl

Table 22.22 *Dicarboxylic acid compounds with actinides, by type.*

Structure	*References*
oxydiacetate	
$[Th(SO_4)(CO_2CH_2OCH_2CO_2)(H_2O)_2] \cdot H_2O$	Graziani *et al.* (1983)
$Th(CO_2CH_2OCH_2CO_2)_2(H_2O)_4 \cdot 6H_2O$	Benetollo *et al.* (1984)
$Na_2[Th(CO_2CH_2OCH_2CO_2)_3] \cdot 2NaNO_3$	Benetollo *et al.* (1984)
$[UO_2(CO_2CH_2OCH_2CO_2)]_n$	Bombieri *et al.* (1972, 1974a)
$[C_2H_5NH_2(CH_2)_2NH_2C_2H_5]$ $[UO_2(CO_2CH_2OCH_2CO_2)_2]$	Jiang *et al.* (2002)
$[(CH_3)_2NH(CH_2)_2NH(CH_3)_2]$ $[UO_2(CO_2CH_2OCH_2CO_2)_2]$	Jiang *et al.* (2002)
$(C_6H_{13}N_4)_2[(UO_2)_2(CO_2CH_2OCH_2CO_2)_2$ $(\mu\text{-}OH)_2] \cdot 2H_2O$	Jiang *et al.* (2002)
$Na_2[UO_2(CO_2CH_2OCH_2CO_2)_2] \cdot 2H_2O$	Bombieri *et al.* (1973)
iminodiacetate	
$[UO_2(CO_2CH_2NH_2CH_2CO_2)]_n$	Battiston *et al.* (1979)
$UO_2(CO_2CH_2NH_2CH_2CO_2)_2$	Bombieri *et al.* (1974b)
$(C_4H_{12}N_2)[(UO_2)_2(CO_2CH_2NHCH_2CO_2)_2$ $(\mu\text{-}OH)_2] \cdot 8H_2O$	Jiang *et al.* (2002)
glutarate	
$UO_2(CO_2(CH_2)_3CO_2)Li(CO_2(CH_2)_3COOH) \cdot 4H_2O$	Benetollo *et al.* (1979)
succinate	
$UO_2(CO_2(CH_2)_2CO_2) \cdot DMSO$	Shchelokov *et al.* (1985)
$UO_2(CO_2(CH_2)_2CO_2) \cdot H_2O$	Bombieri *et al.* (1979)
oxalate	
$Ac_2(C_2O_4)_3 \cdot 10H_2O$	Weigel and Hauske (1977)
$K_4Th(C_2O_4)_4 \cdot 4H_2O$	Akhtar and Smith (1969)
$UO_2(C_2O_4) \cdot 3H_2O$	Jayadevan and Chackraburtty (1972)
$Na_3UO_2(C_2O_4)F_3 \cdot 6H_2O$	Dao *et al.* (1984)
$M_3[UO_2(C_2O_4)_2]F \cdot 2H_2O$ (M = Na, Rb, Cs)	Dao *et al.* (1984)
$M_3UO_2(C_2O_4)F_3 \cdot 2H_2O$ (M = K, Rb, Cs)	Dao *et al.* (1984)
$K_2UO_2(C_2O_4)F_2$	Chakravorti *et al.* (1978)
$K_2(UO_2)_2(C_2O_4)F_4$	Chakravorti *et al.* (1978)
$K_4UO_2(C_2O_4)_2F_2$	Chakravorti *et al.* (1978)
$K_3[UO_2(C_2O_4)_2]F \cdot 3H_2O$	Dao *et al.* (1984)
$K_2(UO_2)_2(C_2O_4)_3 \cdot 4H_2O$	Jayadevan *et al.* (1975)
$K_4U(C_2O_4)_4 \cdot 4H_2O$	Favas *et al.* (1983)
$K_6[(UO_2)_2(C_2O_4)_5] \cdot 10H_2O$	Legros and Jeannin (1976)
$Cs_2UO_2(C_2O_4)(SeO_4)$	Mikhailov *et al.* (2000a)
$Cs_4[UO_2(C_2O_4)_2(SO_4)] \cdot 2.7H_2O$	Mikhailov *et al.* (2000b)
$Ba_2[U(C_2O_4)_4(H_2O)] \cdot 7H_2O$	Spirlet *et al.* (1986, 1987a)
$(NH_4)_2[UO_2(C_2O_4)(SeO_4)] \cdot 1.5H_2O$	Mikhailov *et al.* (1996)
$(NH_4)_2[UO_2(O_2)(C_2O_4)(H_2O)] \cdot 2H_2O$	Baskin and Prasad (1964)
$(NH_4)_3[UO_2(NH_2O)(C_2O_4)_2] \cdot H_2O$	Shchelokov *et al.* (1984)
$(NH_4)_3[UO_2(C_2O_4)_2]F \cdot H_2O$	Dao *et al.* (1984)
$(NH_4)_2UO_2(C_2O_4)_2$	Alcock (1973a)
$(NH_4)_4UO_2(C_2O_4)_3$	Alcock (1973b)
$(NH_4)_2(UO_2)_2(C_2O_4)_3$	Alcock (1973c)

Table 22.22 (*Contd.*)

Structure	*References*
$(NH_4)_2(CH_6N_3)_4[(UO_2)_2(C_2O_4)_5]\cdot 2H_2O$	Chumaevskii *et al.* (1998)
$(N_2H_5)_2UO_2(C_2O_4)_2(H_2O)$	Poojary and Patil (1987)
$(N_2H_5)_6[(UO_2)_2(C_2O_4)_5]\cdot 2H_2O$	Govindarajan *et al.* (1986)
$Tl_2UO_2(C_2O_4)_2\cdot 2H_2O$	Jayadevan *et al.* (1973)
$(NpO_2)_2C_2O_4\cdot 6H_2O$	Grigor'ev *et al.* (1996)
$NpO_2(C_2O_4)\cdot 3H_2O$	Mefod'eva *et al.* (1981)
$Np(C_2O_4)_2\cdot 6H_2O$	Grigor'ev *et al.* (1997)
$H_2Np_2(C_2O_4)_3(C_2O_4)_2\cdot 9H_2O$	Charushnikova *et al.* (1998)
$NaNpO_2(C_2O_4)\cdot 3H_2O$	Tomilin *et al.* (1984)
$K_6(NpO_2)_2(C_2O_4)_5\cdot nH_2O$ ($n = 2$–4)	Mefod'eva *et al.* (1981)
$Cs_2NpO_2(C_2O_4)_2\cdot 2H_2O$	Mefod'eva *et al.* (1981)
$Cs_2(NpO_2)_2(C_2O_4)_3$	Mefod'eva *et al.* (1981)
$(NH_4)NpO_2(C_2O_4)\cdot 8/3H_2O$	Grigor'ev *et al.* (1991b)
$[Co(NH_3)_6][NpO_2(C_2O_4)_2]\cdot nH_2O$ ($n = 3$, 4)	Grigor'ev *et al.* (1991c)
$PuO_2(C_2O_4)\cdot 3H_2O$	Mefod'eva *et al.* (1981)
$Pu_2(C_2O_4)_3\cdot 10H_2O$	Chackraburtty (1963)
$Am_2(C_2O_4)_3\cdot 10H_2O$	Weigel and ter Meer (1967)
malonate	
$(C_2H_{10}N_2)_2[Th(CO_2CH_2CO_2)_4(H_2O)]$	Zhang *et al.* (2000)
$(C_4H_{12}N_2)_2[Th(CO_2CH_2CO_2)_4]\cdot H_2O$	Zhang *et al.* (2000)
$Li_2UO_2(CO_2CH_2CO_2)_2\cdot nH_2O$ ($n = 1$, 3)	Herrero *et al.* (1977)
$Na_2UO_2(CO_2CH_2CO_2)_2\cdot nH_2O$ ($n = 0$, 2)	Herrero *et al.* (1977)
$K_2UO_2(CO_2CH_2CO_2)_2\cdot H_2O$	Herrero *et al.* (1977)
$(NH_4)_2UO_2(CO_2CH_2CO_2)_2\cdot H_2O$	Rojas *et al.* (1979)
$[U(CO_2CH_2CO_2)_2(H_2O)_3]_n$	Zhang *et al.* (2000)
$MUO_2(CO_2CH_2CO_2)_2\cdot 3H_2O$ (M = Ba, Sr)	Bombieri *et al.* (1980)
$(NpO_2)_2(CO_2CH_2CO_2)\cdot nH_2O$ ($n = 3$, 4)	Grigor'ev *et al.* (1993b,c)
methylmalonate	
$(C_4H_{12}N_2)_2[Th(CO_2CH(CH_3)CO_2)_4]\cdot 2H_2O$	Zhang *et al.* (2000)
$[\{Co(NH_3)_6\}\{UO_2(CO_2CH(CH_3)CO_2)(CO_2C(CH_3)_2CO_2)\}]_2Cl_2\cdot 6H_2O$	Zhang *et al.* (2002a)
$(C_4H_{12}N_2)[UO_2(CO_2CH(CH_3)CO_2)_2(H_2O)]\cdot 1.5H_2O$	Zhang *et al.* (2002a)
$(C_4H_{14}N_2)[UO_2(CO_2CH(CH_3)CO_2)_2(H_2O)]\cdot 2H_2O$	Zhang *et al.* (2002a)
dimethylmalonate	
$(C_2H_{10}N_2)_2[Th(CO_2C(CH_3)_2CO_2)_4]\cdot 5H_2O$	Zhang *et al.* (2000)
$(C_{10}H_{26}N_2)[(UO_2)_2(CO_2C(CH_3)_2CO_2)_3]$	Zhang *et al.* (2002b)
$(C_2H_{10}N_2)[UO_2(CO_2C(CH_3)_2CO_2)_2(H_2O)]\cdot H_2O$	Zhang *et al.* (2002b)
$(C_6H_{16}N_2)[(UO_2)_3(CO_2C(CH_3)_2CO_2)_4(H_2O)_2]\cdot 3H_2O$	Zhang *et al.* (2002b)
$(C_7H_{20}N_2)[UO_2(CO_2C(CH_3)_2CO_2)_2]\cdot 3H_2O$	Zhang *et al.* (1998)
$[\{Co(NH_3)_6\}\{UO_2(CO_2C(CH_3)_2CO_2)_2\}Cl]_2\cdot 7H_2O$	Zhang *et al.* (1998)
diethylmalonate	
$(C_4H_{12}N_2)[UO_2(CO_2C(C_2H_5)_2CO_2)_2(H_2O)]\cdot H_2O$	Zhang *et al.* (2002a)
$(C_{10}H_{26}N_2)[UO_2(CO_2C(C_2H_5)_2CO_2)_2(H_2O)]\cdot 2H_2O$	Zhang *et al.* (2002a)
$(C_{10}H_{26}N_2)[(UO_2)_3(CO_2C(C_2H_5)_2CO_2)_5]\cdot 2H_2O$	Zhang *et al.* (2002a)

Table 22.22 (*Contd.*)

Structure	*References*
pyridine-2,6-dicarboxylate (*dipicolinate*)	
$Th[C_5H_3N(COO)_2]_2(H_2O)_4$	Degetto *et al.* (1978)
$\{UO_2[C_5H_3N(COO)_2] \cdot H_2O\}_n$	Immirzi *et al.* (1975)
$U[C_5H_3N(COO)_2]_2(H_2O)_3 \cdot 3.5H_2O$	Haddad *et al.* (1987)
$(Ph_4As)_2UO_2[C_5H_3N(COO)_2]_2 \cdot 6H_2O$	Marangoni *et al.* (1974)
$(Ph_4As)_2U[C_5H_3N(COO)_2]_3 \cdot 3H_2O$	Baracco *et al.* (1974)
$(UO_2)_3[C_5H_3N(COO)(COOH)]_2$ $[C_5H_3N(COO)_2]_2 \cdot 2H_2O$	Cousson *et al.* (1993)
$UO_2(C_7H_3NO_5) \cdot 3H_2O$	Bombieri *et al.* (1977)
$UO_2[C_5H_3N(COO)_2]_2 \cdot (C_5H_4NCOOH) \cdot 6H_2O$	Cousson *et al.* (1991)
fumarate (*1*), *maleate* (*2*)	
$UO_2(C_4H_4O_4)(H_2O)_2$ (1)	Bombieri *et al.* (1982)
$[UO_2(C_4H_2O_4)K(C_4H_3O_4)]$ (2)	Bombieri *et al.* (1981)

Table 22.23 *Tetracarboxylic and hexacarboxylic acid compounds with actinides, by type.*

Structure	*References*
1,2,4,5-benzenetetracarboxylate	
$(NH_4)_3[(NpO_2)_5(C_{10}O_8H_2)_2] \cdot 7H_2O$	Cousson (1985)
$[Na_3NpO_2(C_{10}O_8H_2)]_2 \cdot 11H_2O$	Nectoux *et al.* (1984)
$UO_2(C_{10}O_8H_4) \cdot 2H_2O$	Cousson *et al.* (1986)
benzene hexacarboxylate	
$Na_4(NpO_2)_2(C_{12}O_{12}) \cdot 8H_2O$	Nectoux *et al.* (1984); Cousson *et al.* (1984)

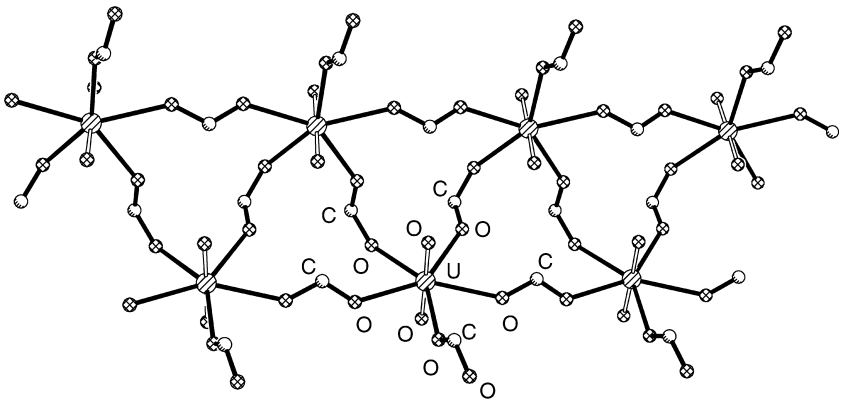

Fig. 22.12 *Crystal structure of anionic portion of* $NaUO_2(HCOO)_3 \cdot H_2O$*, with* Na^+*,* H_2O*, and hydrogen atoms omitted* (*Claudel* et al., 1976). *The coordinates were obtained from the Cambridge Structural Database* (*refcode SURFOR*).

oxygen atoms and pentagonal equatorial coordination provided by a chelating acetate group, two oxygen atoms from bridging acetate groups, and an oxygen atom from a triphenyl phosphine oxide moiety. It is isomorphous with the arsenic-containing analog.

An example of a pentavalent actinide complex is illustrated (Fig. 22.13) in the single-crystal X-ray diffraction structure of $BaNpO_2(CH_3COO)_3 \cdot 2H_2O$. The anion contains a linear NpO_2^+ unit surrounded equitorially by three bidentate acetate groups, resulting in a hexagonal bipyramidal geometry around the neptunium center. The Ba^{2+} cation acts a crosslinker with shared coordination between six acetate oxygen atoms of three different neptunium polyhedra and the oxygen atoms of two lattice water molecules, resulting in a dodecahderal/square antiprism polyhedron. Neptunyl Np–O bond distances are 1.85(2) Å, while $Np–O_{acetate}$ distances range from 2.52(2) to 2.56(2) Å (Burns and Musikas, 1977).

Tetravalent thorium forms an anhydrous complex with four acetate ligands, $Th(CH_3COO)_4$, that is structurally isomorphous (Eliseev *et al.*, 1967) with the uranium(IV) analog (Jelenić *et al.*, 1964). Each thorium center is ten-coordinate;

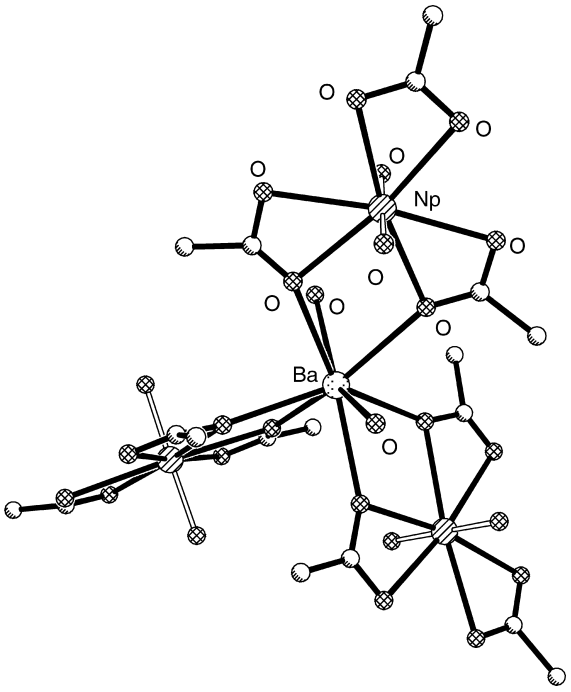

Fig. 22.13 *Crystal strucuture of $BaNpO_2(CH_3COO)_3 \cdot 2H_2O$ with hydrogen atoms omitted* (*Burns and Musikas,* 1977). *The coordinates were obtained from the Cambridge Structural Database* (*refcode BNPTAC*) (*Allen*, 2002).

eight oxygen atoms are provided by eight acetate ligands that bridge between adjacent thorium centers and the remaining two coordination sites are occupied by two of these acetate ligands acting in a tridentate manner (i.e., both oxygen atoms close to the metal center).

Dicarboxylate complexes with actinides are well studied, as evidenced by the large number of crystal structures present in the literature (Table 22.22). Crystallographic information for complexes with the simplest dicarboxylate, the oxalate ligand, is abundant, primarily due to its high affinity for actinides, the ability to form both four- and five-membered rings, and its potential to chelate in a tetradentate manner. An example of the tetradentate ability of oxalate is illustrated in $UO_2(C_2O_4) \cdot 3H_2O$. Each oxalate ligand, through its four oxygen donors, bridges two uranyl ions yielding five-membered rings; additional coordination is provided by the oxygen of a water molecule, making each uranium center hepta-coordinate and pentagonal bipyramidal. The remaining two water molecules, while not participants in direct uranium bonding, engage in hydrogen bonding to further stabilize the complex (Jayadevan and Chackraburtty, 1972).

The crystal structure of monoclinic $K_2(UO_2)_2(C_2O_4)_3 \cdot 4H_2O$ shows the association of three separate oxalate ligands with a single uranyl cation (Fig. 22.14). Each linear uranyl fragment has six oxygen atoms bound equatorially from three oxalate ligands, forming three five-membered rings, with an average

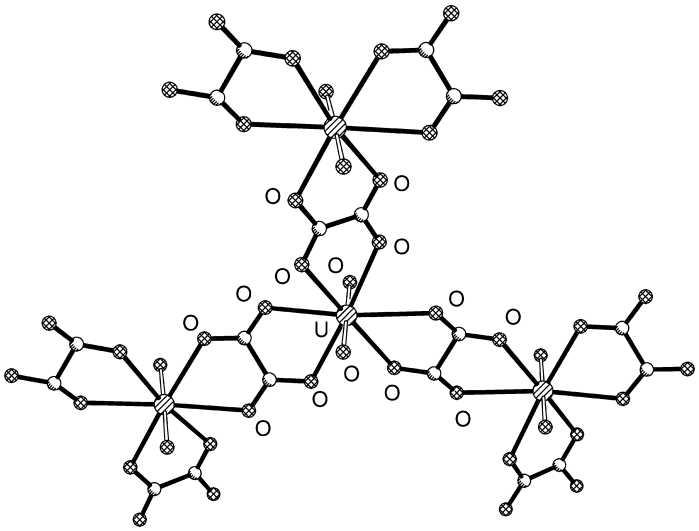

Fig. 22.14 *Crystal strucuture of anionic portion of* $K_2(UO_2)_2(C_2O_4)_3 \cdot 4H_2O$ *with* K^+, H_2O, *and hydrogen atoms omitted* (*Jayadevan* et al., 1975). *The coordinates were obtained from the Cambridge Structural Database* (*refcode KUROXT*).

U–O bond distance of 2.45(4) Å. The geometry around each uranium atom is hexagonal bipyramidal, with the equatorial hexagon being slightly puckered. Each oxalate group takes on a tetradentate role while associated with two uranyl cations, yielding infinite polymeric anions in the crystal lattice; the K^+ cations are associated with eight oxygen atoms from the oxalate ligands and the lattice water molecules within a sphere of about 3.2 Å (Jayadevan *et al.*, 1975).

Bridging oxalate coordination and the absence of uranium-bound water is observed in $K_6[(UO_2)_2(C_2O_4)_5] \cdot 10H_2O$; each uranyl cation in the dinuclear hexavalent anion is five-coordinate equatorially. Two oxalate ligands coordinate in a bidentate manner, forming two five-membered rings, and one oxalate bridges symmetrically, donating one oxygen atom to each uranium center. The pentagonal bipyramidal polyhedron around uranium has an average equatorial U–O bond distance of 2.38 Å (Legros and Jeannin, 1976).

Pyridine-2,6-dicarboxylic acid (pdca) can be multidentate through oxygen only or heteronuclear oxygen/nitrogen donation, and can form monomeric or polymeric metal-templated complexes. A repeating helical pattern is found in the single-crystal X-ray diffraction structure of $[UO_2\{C_5H_3N(COO)_2\} \cdot H_2O]_n$ where pseudo-planar pentagonal equatorial coordination around the linear uranyl ion is provided by two oxygens and one nitrogen from the pdca ligand, oxygen from a water molecule, and oxygen from a neighboring pdca ligand (Fig. 22.15). The bridging provided by the neighboring pdca ligand results in a polymeric structure that takes on a helical shape. In the crystal, all helices are of the same sense and possess a diameter of about 21 Å. Each helix is surrounded

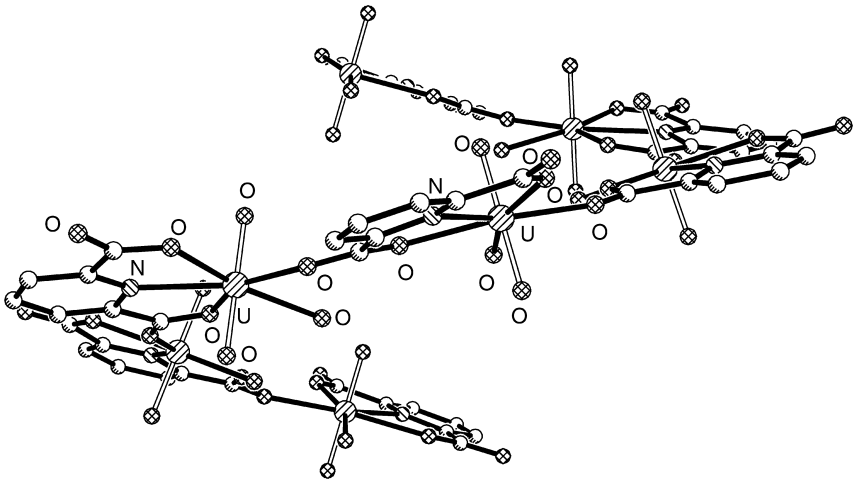

Fig. 22.15 *Crystal strucuture of* $[UO_2\{C_5H_3N(COO)_2\} \cdot H_2O]_n$ *with hydrogen atoms omitted* (*Immirzi* et al., 1975). *The coordinates were obtained from the Cambridge Structural Database* (*refcode PYDCUO*).

by six other helices that are associated with one another via hydrogen bonding between bound water and dangling C–O groups (Immirzi *et al.*, 1975).

Malonate ligands are dicarboxylates, structurally related to oxalates, where the caboxylate functionalities are joined by a methylene group. Several Th(IV) and U(VI) malonato complexes have been structurally characterized, once again taking advantage of the relatively compact nature of the malonate ligand for crystal packing. Malonate ligands have the ability to coordinate with actinides in bidentate, tridentate, and tetradentate modes, examples of which will be shown when available.

The structure of the bispiperazinium complex, $(C_4H_{12}N_2)_2[Th(CO_2CH_2CO_2)_4] \cdot H_2O$, contains an eight-coordinate thorium atom with four 1,5-bidentate malonate ligands, resulting in a monomeric anionic complex (Fig. 22.16). The geometry around the thorium is distorted square antiprismatic, with the Th–O bond distances ranging from 2.337(2) to 2.450(2) Å. The lattice water molecule is uncoordinated. The compounds $(C_2H_{10}N_2)_2[Th(CO_2CH_2CO_2)_4(H_2O)]$, $(C_4H_{12}N_2)_2[Th(CO_2CH(CH_3)CO_2)_4] \cdot 2H_2O$, and $(C_2H_{10}N_2)_2[Th(CO_2C(CH_3)_2\ CO_2)_4] \cdot 5H_2O$ have similar coordination around the thorium center with the exception that the former compound has a bound water, giving

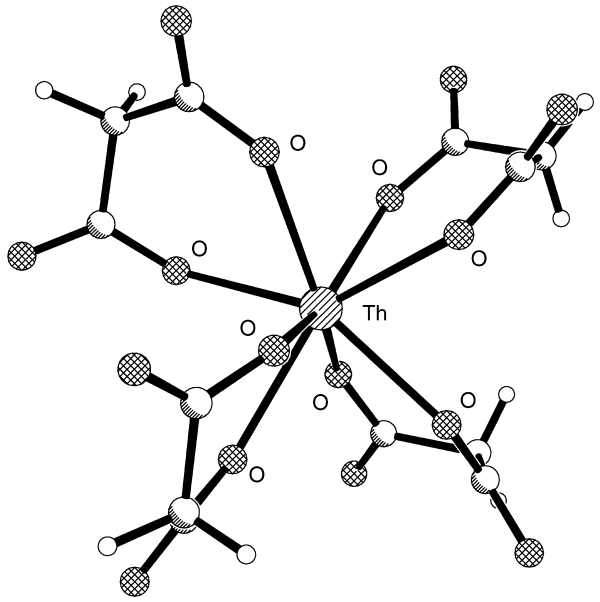

Fig. 22.16 *Crystal strucuture of anioic portion of* $(C_4H_{12}N_2)_2[Th(CO_2CH_2CO_2)_4] \cdot H_2O$ *with* $(C_4H_{12}N_2)^{2+}$ *and* H_2O *omitted* (*Zhang* et al., 2000). *The coordinates were obtained from the Cambridge Structural Database* (*refcode WONKUF*).

the thorium a coordination number of nine and a mono-capped distorted square antiprismatic geometry. The latter two structures contain methylmalonate and dimethylmalonate ligands, respectively (Zhang *et al.*, 2000).

The structure of $[U(CO_2CH_2CO_2)_2(H_2O)_3]_n$, however, contains uranium with a coordination number of nine in a mono-capped square antiprismatic geometry. The coordination sphere is achieved through two 1,5-bidentate malonate ligands, each also bridging to an adjacent uranium through a carbonyl oxygen (thus the malonate ligands are tridentate) and oxygen atoms from three water molecules. The bridging character of the malonate ligands results in the formation of infinite chains. Chelating U–O bond distances are 2.315(4) and 2.434(4) Å, while the bridging U–O distance is 2.420(4) Å (Zhang *et al.*, 2000).

Two other types of malonate binding have also been observed using single-crystal X-ray diffraction. The structure of $(C_6H_{16}N_2)[(UO_2)_3(CO_2C(CH_3)_2CO_2)_4(H_2O)_2]\cdot 3H_2O$ (involving dimethylmalonate), has two distinct uranium sites. The first site shows hexagonal bipyramidal geometry around a single uranium center from two axial uranyl oxygen atoms, two *trans* equatorial water molecules, and two equatorial 1,3-bidentate malonate ligands. The second site shows two crystallographically equivalent uranium atoms, each also with hexagonal bipyramidal geometry. This geometry results from two axial uranyl oxygen atoms, a 1,3-bidenate malonate ligand that bridges the uranium atom at the first site, and two malonate ligands in a μ_2-1,3- and 1,5-bidentate arrangement. The malonate that bridges the two uranium sites is coordinated in a bis(1,3-bidentate) manner, making the ligand tetradenate and the overall structure infinite (Zhang *et al.*, 2002b).

Higher order carboxylate ligands (tetracarboxylate and hexacarboxylate) are shown in Table 22.23, the details of which will not be discussed here.

22.4.2 Complexes with macrocyclic ligands

(a) Crown ethers

Traditional crown ethers are cyclic polyether molecules that interact with the actinide cations in one of two fashions: either through an inner-sphere coordination mode, resulting in direct metal ion inclusion into the crown ether cavity, or through an outer-sphere coordination mode involving hydrogen bonds with the uranyl cation where the metal–crown interaction results in sandwich or polymeric structures. Crown ether derivatives where oxygen has been replaced with nitrogen (azacrowns) or sulfur (thiacrowns) have also been studied, thus taking advantage of the softer character of these elements. The complexation characteristics of crown ethers depend on a variety of factors, including size of cavity (size-fitting effect), nature of the heteroatoms present, as well as the type of counter ions, all of which are critical in obtaining inclusion versus exclusion complexes.

For inclusion complexes, the diameter of the crown ether molecule, and thus the ability for an actinide cation to fit within the cavity, increases from 12-crown-4, to 15-crown-5, to 18-crown-6. Crown ethers are neutral molecules; crystal structures showing metal ion complexation that results in inclusion usually have one or more poorly coordinating anions present to balance the charge on the cation. The formation of crown ether inclusion complexes, as indicated by the few structures available in the literature, takes careful matching of solvent and counter-ions to suitable macrocyclic cavity sizes (Bradshaw *et al.*, 1996). Representative structures of actinide inclusion complexes are shown in Table 22.24.

In UO_2(18-crown-6)$(CF_3SO_3)_2$, an inclusion complex between UO_2^{2+} and 18-crown-6, the trifluoromethanesulfonate anion is not directly bound to the complex, but rather effectively balances the overall charge (Deshayes *et al.*, 1994a). The linear uranyl fragment is perpendicular with respect to the crown plane and the six crown ether oxygen atoms coordinate the uranium atom equatorially, resulting in an overall hexagonal bipyramidal geometry. The average equatorial U–O bond distance is 2.50(5) Å. In the related structure (Fig. 22.17), UO_2(dicyclohexyl-18-crown-6)$(CF_3SO_3)_2$, uranyl insertion into dicyclohexano-18-crown-6 results in a similar 1:1 UO_2:crown inclusion complex where the geometry about the uranium atom is a hexagonal bipyramid (Deshayes *et al.*, 1994a). Here, the average equatorial U–O bond distance is slightly longer at 2.58(7) Å, indicating that the dicyclohexane rings of the crown ether result in a less flexible coordination environment.

The uranyl cation in the related inclusion complex UO_2(18-azacrown-6)$(CF_3SO_3)_2$ is bonded to all six nitrogen atoms of the crown in a hexagonal bipyramidal manner. The six nitrogen atoms in the azacrown ring are in a puckered plane with the uranium atom lying 0.066(1) Å out of this plane. The average U–N bond distance is 2.66(6) Å, indicating the relative weakness of

Table 22.24 *Inclusion compounds of actinides and crown ethers.*

Structure	*References*
UO_2(18-crown-6)$(CF_3SO_3)_2$	Deshayes *et al.* (1994a)
UO_2(18-crown-6)$(ClO_4)_2$	Dejean *et al.* (1987); Folcher *et al.* (1979)
$[UCl_3$(18-crown-6)$]_2[UO_2Cl_3(OH)(H_2O)] \cdot MeNO_2$	Bombieri *et al.* (1978a)
$U(BH_4)_3$(18-crown-6)$_{3/4}$	Moody *et al.* (1979)
UO_2(dicyclohexyl-18-crown-6)$(CF_3SO_3)_2$	Deshayes *et al.* (1994a)
UO_2(dicyclohexyl-18-crown-6)$(ClO_4)_2$	Navaza *et al.* (1984)
$[U(BH_4)_2$(dicyclohexyl-18-crown-6)$]_2[UCl_5(BH_4)]$	Dejean *et al.* (1987)
$[UCl_3$(dicyclohexyl-18-crown-6)$]_2[UCl_6]$	de Villardi *et al.* (1978)
UO_2(18-azacrown-6)$(CF_3SO_3)_2$	Nierlich *et al.* (1994)
UO_2(diaza-18-crown-6)(CF_3SO_3)	Thuéry *et al.* (1995a)
$[NpO_2$(18-crown-6)$](ClO_4)$	Clark *et al.* (1998b)

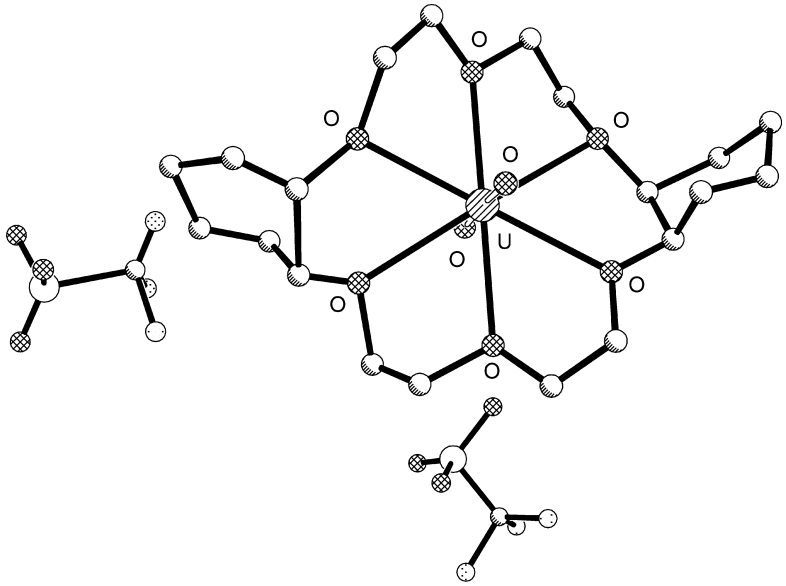

Fig. 22.17 *Crystal strucuture of* UO_2(*dicyclohexyl*-18-*crown*-6)$(CF_3SO_3)_2$ *with hydrogen atoms omitted* (*Deshayes* et al., 1994*a*). *The coordinates were obtained from the Cambridge Structural Database* (*refcode WIFTUA*).

the U–N bond compared to the U–O bond in the above complexes (Nierlich *et al*., 1994).

The compound $[U(BH_4)_2$dicyclohexyl-18-crown-6$]_2[UCl_5(BH_4)]$ contains U(III) macrocyclic coordination along with the coexistence of U(IV) in the same crystal. In the cationic portion, the $U(III)(BH_4)_2^+$ moiety resides in the crown ether cavity and the two BH_4 groups assume axial positions (B–U–B = 173(5)°). All six equatorial oxygen atoms participate in bonding, resulting in hexagonal bipyramidal geometry around uranium. The anion, $(UCl_5BH_4)^{2-}$ contains uranium in the 4+ oxidation state in a pseudo-octahedral environment (Dejean *et al*., 1987). Other crown ether inclusion complexes of uranium include $U(BH_4)_3$(18-crown-$6)_{3/4}$, for which only marginal crystallographic data exist due to crystal disorder, making further structural characterization necessary (Moody *et al*., 1979).

A rare example of a transuranium inclusion compound is $[NpO_2$(18-crown-6)$](ClO_4)$. The NpO_2^+ cation resides within the crown ether cavity and the Np center is equatorially coordinated by the six coplanar oxygen atoms at an average distance of 2.594(10) Å, yielding a hexagonal bipyramidal coordination polyhedron (Fig. 22.18). The average Np–O distances of the *trans* oxo ligands are 1.800(5) Å, unusually short for the NpO_2^+ cation (Clark *et al*., 1998b).

Despite the potential to favorably match crown ether cavities containing five and six donors to the UO_2^{2+} ion that prefers such equatorial coordination

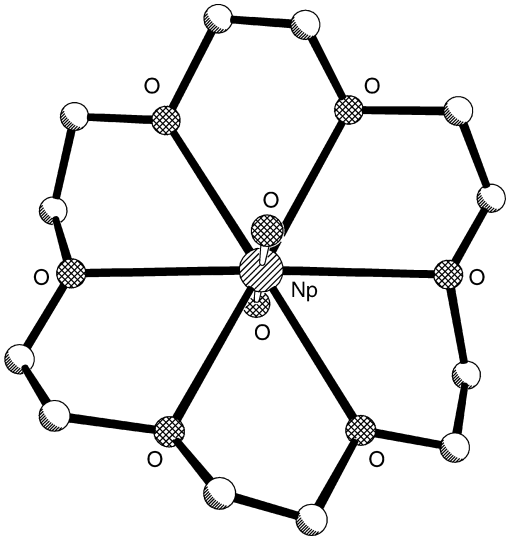

Fig. 22.18 *Crystal strucuture of* [NpO_2(18-*crown*-6)](ClO_4) *with* ClO_4^- *and hydrogen atoms omitted* (*Clark* et al., 1998*b*). *The coordinates were obtained from the Cambridge Structural Database* (*refcode NICFUA*).

environments, the majority of actinide structures in the literature exhibit second sphere/outer sphere exclusion motifs (Thuéry *et al.*, 1995d). The result is the formation of 'supermolecules' usually involving complex hydrogen-bonded networks. Hydrogen bonding between the crown ether oxygen atoms and water molecules coordinated to the metal is commonly observed (but not always) (Rogers *et al.*, 1988). Table 22.25 summarizes representative second sphere/outer sphere actinide-crown ether exclusion complexes.

An interesting example of mistaken identity was observed in the case of $UO_2(NO_3)_2(H_2O)_2 \cdot$(12-crown-4). An initial study by Armağan (1977) contended, based on crystallographic data, that the compound was of the inclusion type. However, all previous and subsequent attempts to place uranyl in the relatively small cavity of 12-crown-4 were unsuccessful. Due to anomalies within the reported results, a follow-up study was done that established the structure as an exclusion complex; $UO_2(NO_3)_2$ nodes are connected to 12-crown-4 molecules through a hydrogen-bonded network enabled by the lattice water molecules (Ritger *et al.*, 1983).

One of the first examples of a hydrogen bonding-stabilized exclusion complex is that of $UO_2(NO_3)_2(H_2O)_2 \cdot 2H_2O \cdot$(18-crown-6). Discrete $UO_2(NO_3)_2(H_2O)_2$ units are separated by crown ether molecules and linked together by hydrogen bonding through intermediary water molecules. Each uranium atom is coordinated to the *trans* uranyl oxygen atoms, two water molecules, and two bidentate nitrate groups (Eller and Penneman, 1976).

Table 22.25 *Exclusion* (*second sphere/outer sphere*) *compounds of actinides and crown ethers.*

Structure	*References*
9-crown-3, 12-crown-4	
UI_3(trithia-9-crown-3)$(MeCN)_2$	Karmazin *et al.* (2002)
$UO_2(SO_4)(H_2O)_2 \cdot$(12-crown-4)$_{0.5} \cdot H_2O$	Rogers *et al.* (1991)
$UO_2(NO_3)_2(H_2O)_2 \cdot$(12-crown-4)	Ritger *et al.* (1983)
$[UO_2Cl_2(H_2O)_2$(12-crown-4)$] \cdot$(12-crown-4)	Rogers *et al.* (1989)
[Li(12-crown-4)]$_2[UO_2Cl_4]$	Danis *et al.* (2001)
[Li(12-crown-4)]$_2[UO_2Br_4]$	Danis *et al.* (2001)
[Na(12-crown-4)$_2$]$_2[UO_2Cl_4] \cdot 2MeOH$	Rogers (1988)
15-crown-5	
$ThCl_4(MeOH)_2(OH_2)_2 \cdot$(15-crown-5) $\cdot$ MeCN	Rogers and Benning (1988a)
$UO_2(NO_3)_2(H_2O)_2$(15-crown-5)	Gutberlet *et al.* (1989)
$UO_2Cl_2(H_2O)_3$(15-crown-5)	Hassaballa *et al.* (1988, 1998)
$(H_5O_2)[UO_2(H_2O)_2Cl_3] \cdot$(15-crown-5)$_2$	Hassaballa *et al.* (1998)
[Na(15-crown-5)]$_2[UO_2Cl_4]$	Danis *et al.* (2001)
[Na(15-crown-5)]$_2[UO_2Br_4]$	Danis *et al.* (2001)
$[(NH_4)$(15-crown-5)$_2]_2(UO_2Cl_4) \cdot 2MeCN$	Rogers *et al.* (1987a)
$[UO_2(H_2O)_5][ClO_4]_2 \cdot$(15-crown-5)$_3 \cdot$ MeCN	Rogers *et al.* (1987b)
$UO_2(SO_4)(H_2O)_2 \cdot$(benzo-15-crown-5)$_{0.5} \cdot 1.5H_2O$	Rogers *et al.* (1991)
$UO_2(NO_3)_2(H_2O)_2$(benzo-15-crown-5)	Deshayes *et al.* (1993)
$[UO_2(TTA)_2H_2O]_2$(benzo-15-crown-5)	Kannan *et al.* (2001)
[Na(benzo-15-crown-5)]$_2(UO_2Cl_4)$	Moody and Ryan (1979)
$UO_2(NO_3)_2(H_2O)_2$(benzo-15-crown-5)$_2$	Deshayes *et al.* (1993)
$UO_2(H_2O)_3(CF_3SO_3)_2 \cdot$(benzo-15-crown-5)$_2$	Thuéry *et al.* (1995b)
$[(H_5O_2)(H_9O_4)$(benzo-15-crown-5)$_2][UO_2Cl_4]$	Rogers *et al.* (1991)
$[(H_5O_2)\{(NO_2)_2$benzo-15-crown-5$\}_2]_2$ $[\{UO_2(NO_3)_2\}_2C_2O_4]$	Rogers *et al.* (1991)
$[(NH_4)$(benzo-15-crown-5)$_2]_2[UCl_6] \cdot 4MeCN$	Rogers *et al.* (1987a)
$[UO_2(NO_3)_2]_2(\mu\text{-}H_2O)_2$(monoaza-15-crown-5)$_2$	Cragg *et al.* (1988)
18-crown-6	
$[ThCl(OH)(H_2O)_6]Cl_4 \cdot$(18-crown-6) $\cdot 2H_2O$	Rogers and Bond (1992)
$[ThCl_2(H_2O)_7]Cl_2 \cdot$(18-crown-6) $\cdot 2H_2O$	Rogers (1989)
$ThCl_4(EtOH)_3(H_2O) \cdot$(18-crown-6) $\cdot H_2O$	Rogers *et al.* (1988)
$Th(NCS)_4(H_2O)(HOCH_2CH_2OH)_2 \cdot$(18-crown-6)	Rogers *et al.* (1998)
$Th(H_2O)_3(NO_3)_4 \cdot$(18-crown-6)	Rogers *et al.* (1987c)
$[(H_3O)$(dicyclohexyl-18-crown-6)$]_2[Th(NO_3)_6]$	Ming *et al.* (1988)
$UO_2(SO_4)(H_2O)_3 \cdot$(18-crown-6)$_{0.5}$	Rogers *et al.* (1991)
$[(H_5O_2)_2$(18-crown-6)$][UO_2Cl_4]$	Rogers *et al.* (1991)
$[UO_2(CH_3COO)(OH)(H_2O)]_2 \cdot$(18-crown-6)	Mikhailov *et al.* (1997)
$UO_2(CH_3COO)_2(H_2O)_2 \cdot (H_2O)_2 \cdot$(18-crown-6)	Mikhailov *et al.* (1997)
$UO_2(NO_3)_2(H_2O)_2$(18-crown-6)	Bombieri *et al.* (1978b)
$UO_2(NO_3)_2(H_2O)_2 \cdot 2H_2O \cdot$(18-crown-6)	Eller and Penneman (1976)
$UO_2(H_2O)_5(CF_3SO_3)_2 \cdot$(18-crown-6)	Deshayes *et al.* (1994b)
$[UO_2(H_2PO_4)_2(H_2O)]_2 \cdot$(18-crown-6) $\cdot 5H_2O$	Danis *et al.* (2000)
$UO_2(H_2PO_4)_2(H_2O) \cdot$(18-crown-6) $\cdot 3H_2O$	Danis *et al.* (2000)
$[U(SCN)_4(H_2O)_4]$[18-crown-6]$_{1.5} \cdot 3H_2O \cdot (C_6H_{12}O)$	Charpin *et al.* (1977)
$UO_2(NCS)_2(H_2O)_3 \cdot$(18-crown-6)$_{1.5} \cdot$ MeCN	Rogers *et al.* (1998)

Table 22.25 (*Contd.*)

Structure	*References*
$[(H_3O)(18\text{-crown-}6)]_2[\{UO_2(NO_3)_2\}_2C_2O_4]$	Rogers *et al.* (1991)
$[UO_2(H_2O)_5][ClO_4]_2 \cdot (18\text{-crown-}6)_2 \cdot 2MeCN \cdot H_2O$	Rogers *et al.* (1987b)
$[NH_4(18\text{-crown-}6)]_2[UCl_6] \cdot 2MeCN$	Rogers and Benning (1988b)
$[NH_4(18\text{-crown-}6)]_2[UO_2(NCS)_4(H_2O)]$	Ming *et al.* (1987a)
$[K(18\text{-crown-}6)]_2[UO_2(NCS)_4(H_2O)]$	Ming *et al.* (1987b)
$[K(18\text{-crown-}6)]_2[UO_2Cl_4]$	Danis *et al.* (2001)
$[K(18\text{-crown-}6)]_2[UO_2Br_4]$	Danis *et al.* (2001)
$[(UO_2)_2(OH)_2(H_2O)_6](ClO_4)_2$ [dicyclohexyl-18-crown-6]$_3 \cdot$ MeCN	Navaza *et al.* (1984)
UO_2Cl_4(dicyclohexyl-18-crown-6 $\cdot H_3O)_2$	Guang-Di *et al.* (1990)
$[UO_2(TTA)_2(\mu\text{-}H_2O)]_2(H_2O)_2$(dibenzo-18-crown-6)	Kannan *et al.* (2001)
$[(NH_4)$(dibenzo-18-crown-6)$]_2[(UO_2Cl_4) \cdot 2MeCN$	Rogers *et al.* (1987a)
24-crown-8	
$[(H_5O_2)$(dicyclohexyl-24-crown-8)$]_2(UO_2Cl_4) \cdot$ MeOH	Rogers and Benning (1991)
$[(H_5O_2)$(dicyclohexyl-24-crown-8)$]_2(UCl_6) \cdot$ MeOH	Rogers and Benning (1991)

The crystal lattice of the compound $[(H_5O_2)\{(NO_2)_2$benzo-15-crown-5$\}_2]_2[\{UO_2(NO_3)_2\}_2C_2O_4]$ contains discrete cation and anion pairs. The anion consists of two $UO_2(NO_3)_2$ groups (each nitrate is bidentate) bridged by a tetradentate oxalate group (forming two five-membered rings); each uranium center is surrounded by a hexagonal bipyramidal polyhedron of ligands. A single $H_5O_2^+$ ion resides between two 15-crown-5 molecules and is stabilized by hydrogen bonding to the ethereal oxygen atoms of the crown ether (Rogers *et al.*, 1991).

Inclusion of H_3O^+ is observed in the structure of $[(H_3O)(18\text{-crown-}6)]_2[\{UO_2(NO_3)_2\}_2C_2O_4]$; the H_3O^+ species resides in the cavity of the crown ether molecule, stabilized by hydrogen bonding (Fig. 22.19). This hydrogen bonding likely occurs with three crown ether oxygen atoms, giving the hydronium a pseudo-pyramidal geometry, residing 0.4 Å out of the plane. The discrete uranyl-containing anion adopts the same conformation as the former molecule, with alternate cation–anion–cation stacking (Rogers *et al.*, 1991).

In $UO_2(SO_4)(H_2O)_2 \cdot (12\text{-crown-}4)_{0.5} \cdot H_2O$, two *trans* uranyl oxygen atoms, two water molecules, and one oxygen each from three sulfate atoms coordinate each uranium atom, generating a pentagonal bipyramid. The sulfate anions bridge each uranium atom to two neighbors, thus forming polymeric double chains. Furthermore, the 18-crown-6 molecule and the uncoordinated water molecule form an organic layer that separates the layers of the uranium polymeric double chains; the layers are stabilized by a hydrogen-bonding network (Rogers *et al.*, 1991).

A series of five alkali metal/crown ether/uranyl halide sandwich exclusion complexes have been structurally characterized and each displays square

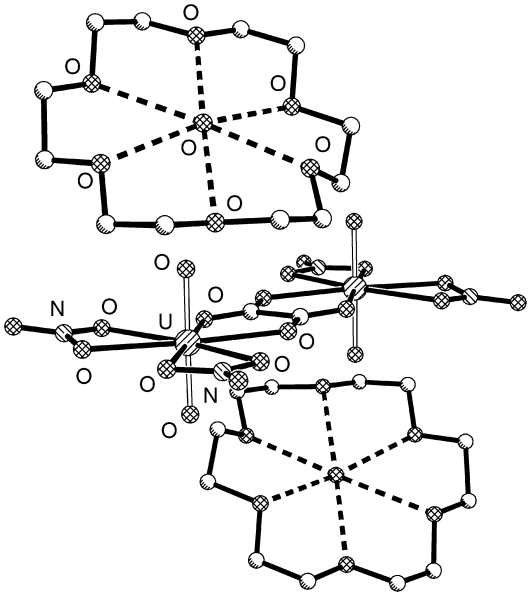

Fig. 22.19 *Crystal strucuture of* $[(H_3O)(18\text{-}crown\text{-}6)]_2[\{UO_2(NO_3)_2\}_2C_2O_4]$ *with hydrogen atoms omitted* (*Rogers* et al., 1991). *The coordinates were obtained from the Cambridge Structural Database* (*refcode SODFUM*).

bipyramidal $[UO_2X_4]^{2-}$ anions sandwiched between two $[A(\text{crown ether})]^+$ cations (X = Cl, Br and A = Li, Na, K). Crown ethers of varying cavity size were investigated, including 18-crown-6, 15-crown-5, and 12-crown-4. The $[K(18\text{-crown-}6)]_2[UO_2Cl_4]$ and $[K(18\text{-crown-}6)]_2[UO_2Br_4]$ complexes display Type I bonding behavior where the K^+ cations form inclusion complexes with the crown ethers. Two uranium-bound halides coordinate in a bridging manner to each K^+ ion and the anionic unit is tilted with respect to the plane of the crown ether toward the K^+ ions to varying degrees (56° for Cl and 63° for Br) (Danis *et al.*, 2001).

The $[Na(15\text{-crown-}5)]_2[UO_2Cl_4]$ has two crystallographically unique anionic units, one of which is Type I bonding, as described above, and the other Type II where only one uranium-bound chloride interacts with each Na^+ ion. Significant tilt of the anionic unit (31°) also occurs. In the Type I bonding, the linear uranyl unit of the anion is aligned parallel to the crown ether plane. If the halide in the aforementioned complex is changed from Cl to Br, a structural shift occurs to Type III bonding. Here, each crown-encapsulated Na^+ ion is bridged by one uranyl bromide and one uranyl oxygen. The linear unbound Br–U–Br unit is aligned parallel to the crown ether plane. Finally, $[Li(12\text{-crown-}4)]_2[UO_2Cl_4]$ and $[Li(12\text{-crown-}4)]_2[UO_2Br_4]$ both exhibit Type IV bonding and are both nearly isostructural. In both complexes, the bonding to each crown-

encapsulated Li^+ is solely through the two uranyl oxygen atoms, resulting in a plane defined by uranium and its four halide atoms that separates the cationic units. The type of bonding exemplified in these structures can be described in terms of hard–soft acid–base theory; in the latter two complexes, the 'hard' Li^+ ion prefers exclusive interaction with the 'hard' uranyl oxygen atoms (Danis *et al.*, 2001).

Exclusion crown ether complexes of uranyl incorporating ligands that are important in uranium chemistry are also known. For example, thenoyl (trifluoroacetone) (HTTA), a β-diketone extractant that acts synergistically with crown ethers in extraction schemes, interacts directly with uranium in $[UO_2\ (TTA)_2H_2O]_2$(benzo-15-crown-5) and $[UO_2(TTA)_2(\mu\text{-}H_2O)]_2(H_2O)_2$(dibenzo-18-crown-6), where the crown ethers are second-sphere and third-sphere ligands, respectively (Fig. 22.20). In both complexes, each uranium attains pentagonal bipyramidal geometry, with equatorial coordination provided by two bidentate HTTA groups and a water molecule. In the former, the bound water hydrogen bonds to the crown ether, making it second sphere. In the latter, intermediate water molecules generate a hydrogen-bonding network (Kannan *et al.*, 2001).

Various forms of phosphate also play significant roles in both processing and environmental aspects of uranium chemistry. The structure of $[UO_2(H_2PO_4)_2(H_2O)]_2 \cdot (18\text{-crown-6}) \cdot 5H_2O$ once again shows pentagonal bipyramidal geometry around uranium, as well as infinite, one-dimensional $[UO_2(H_2PO_4)_2(H_2O)]$ chains that are hydrogen-bonded to uncomplexed crown ether molecules

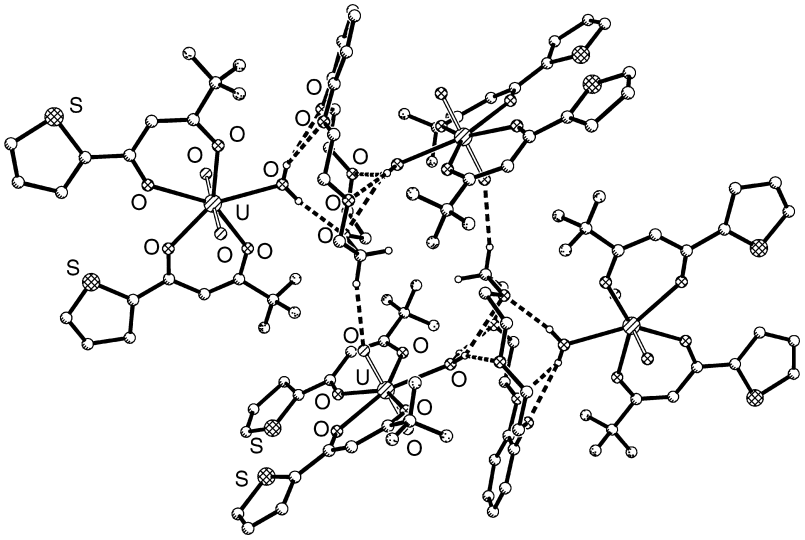

Fig. 22.20 *Crystal strucuture of* $[UO_2(TTA)_2H_2O]_2$(*benzo*-15-*crown*-5) *with hydrogen atoms omitted* (*Kannan* et al., 2001). *The coordinates were obtained from the Cambridge Structural Database* (*refcode RORXIF*).

through solvate lattice water molecules. Each of four $H_2PO_4^-$ units is bound $\mu-\eta^1$ to uranium. A similar situation is observed in the crystal structure of $UO_2(H_2PO_4)_2(H_2O) \cdot (18\text{-crown-6}) \cdot 3H_2O$ (Danis *et al*., 2000).

Although fewer in number, thorium exclusion-type crown ether structures are also known. For example, the crystal structure of $[(H_3O)(\text{dicyclohexano-18-crown-6})]_2[Th(NO_3)_6]$ reveals the thorium atom resting at a center of symmetry and unbound to the crown ether donor atoms. The thorium is 12-coordinate due to bidentate coordination of the six nitrate anions, thus giving it a nearly perfect icosahedral geometry. The Th–O bond distances in this anionic unit range from 2.551 to 2.587 Å. Each H_3O^+ cation rests in the cavity of the crown ether molecules, stabilized by three hydrogen bonds, as well as ion–dipole interactions (Ming *et al*., 1988).

(b) Calixarenes

The class of macrocyclic ligands known as calixarenes is structurally recognized by phenolic subunits joined in a cyclic fashion via methylene linkages; derivatives based on CH_2–X–CH_2 linkages are also commonly used, where X is O, NH, or S. Substitutions at the pendant phenol oxygen site are also possible. The latter types are of interest due to their less rigid character and larger number of potential donor sites. Calixarenes are highly diverse in terms of available ring sizes, making them excellent candidates for systematic analyses concerning their donor properties in binding to groups of metal ions, including lanthanides and actinides. Traditional calixarene chemistry allows for substitutions at either the lower or upper rim of the calixarene and the tuning of their physical properties. The lower rim of a calixarene comprises the cyclic arrangement of alcohol functionalities of the phenol unit. Typically, substitution is directed to the upper rim, leaving the lower rim unsubstituted, thus comprising the class of 'phenolic calixarenes'. Due to the variety of ring sizes available, actinide complexes with calixarenes can be either inclusion or exclusion complexes with the coordination based on considerations such as ligand type, ring diameter, and metal ion radius. For a general overview of phenolic calixarene f-element coordination chemistry, the reader is referred to a review from Thuéry *et al*. (2001d); representative single-crystal X-ray diffraction structures from the literature will be reviewed herein, the likes of which are summarized in Table 22.26.

The complexes formed between $UO_2^{2+}$and triply deprotonated *p-tert*-butylhexahomotrioxacalix[3]arene, studied by Thuéry *et al*. (1999a) show the lowest coordination number (five) observed for a uranyl complex (Fig. 22.21). In the presence of the deprotonating agents triethylamine and DABCO, two isomorphous inclusion-type complexes are formed where the uranyl is located in the center of the lower rim of the calixarene. The uranyl cation is bound in the equatorial plane to the three deprotonated phenolic oxygen atoms with an average $U–O_{eq}$ bond distance of 2.20(3) Å, yielding pseudo-trigonal

Table 22.26 *Representative actinide-calix[n]arene compounds, by type.*

Structure	*References*
calix[3]*arenes*	
$[HNEt_3][UO_2$(*p*-methylhexahomotrioxacalix[3]arene–3H)]	Masci *et al.* (2002a)
$[HN^nPr_3][UO_2$(*p-tert*-butylhexahomotrioxacalix[3]arene–3H)] · MeOH	Masci *et al.* (2002a)
$[H_3N^nBu][UO_2$(*p-tert*-butylhexahomotrioxacalix[3]arene–3H)]	Masci *et al.* (2002a)
$[H_2N^nBu_2][UO_2$(*p-tert*-butylhexahomotrioxacalix[3]arene–3H)] · MeOH	Masci *et al.* (2002a)
$(C_6H_{14}N)[UO_2$(*p-tert*-butylhexahomotrioxacalix[3]arene–3H)] · 2MeOH · H_2O	Masci *et al.* (2002a)
$[UO_2$(*p-tert*-butylhexahomotrioxacalix[3]arene–3H)$(HNEt_3)] \cdot 3H_2O$	Thuéry *et al.* (1999a)
$[UO_2$(*p-tert*-butylhexahomotrioxacalix[3]arene–3H)(HDABCO)] · 3MeOH	Thuéry *et al.* (1999a)
$[UO_2(NO_3)_2$(*p*-chloro-*N*-benzylhexahomotriazacalix[3]arene)] · pyr · $CHCl_3$	Thuéry *et al.* (2001a)
calix[4]*arenes*	
$[UO_2(NO_3)_2$(*p*-methyl-*N*-benzyltetrahomodiazacalix[4]arene)] · 0.5MeOH · H_2O	Thuéry *et al.* (2001a)
$[HNEt_3]_2[UO_2$(*p-tert*-butyltetrahomodioxacalix[4]arene–4H)] · $CHCl_3$ · MeCN	Thuéry *et al.* (2001a)
$[\{UCl$(*tert*-butylcalix[4]arene–4H)$\}_3(\mu_3$-oxo)] · 11.5pyr	Leverd and Nierlich (2000)
$[HNEt_3]_2[UO_2\{$bis(homo-oxa)-*p-tert*-butylcalix[4]arene–4H$\}] \cdot 2H_2O$	Harrowfield *et al.* (1991a)
$[Hpyr][(UO_2)_2$(*p*-methyloctahomotetraoxacalix[4]arene–4H)(OH)$(H_2O)] \cdot 2.5$pyr	Thuéry *et al.* (2001b)
$[(UO_2)_2$(1-acid-3-diethylamide substituted calix[4]arene–2H$)_2] \cdot 10$MeCN · 2MeOH	Beer *et al.* (1998)
$[UO_2$(calix[4]arene–1H$)_2(DMF)_{3.7}(DMSO)_{0.3}] \cdot$ [calix[4]arene(DMF)] · 1.5DMF	Asfari *et al.* (2001)
$[HNEt_3]_2[UO_2$(*p-tert*-butyltetrathiacalix[4]arene–4H)(DMF)] · 2DMF	Asfari *et al.* (2001)
$[HNEt_3]_2[UO_2$(*p-tert*-butyltetrathiacalix[4]arene–4H)(MeCN)] · $\sim$ 1.7DMSO	Asfari *et al.* (2001)
$[Hpyr]_2[UO_2$(*p*-methyl-tetrahomodioxacalix[4]arene–4H)$] \cdot 3H_2O$	Masci *et al.* (2002b)
$[HNEt_3]_2[UO_2$(*p*-phenyl-tetrahomodioxacalix[4]arene–4H)$] \cdot 2CHCl_3$	Masci *et al.* (2002b)
$[H_3N^nBu]_2[UO_2$(*p*-phenyl-tetrahomodioxacalix[4]arene–4H)] · $(H_3N^nBu) \cdot (CH_3COO) \cdot 2H_2O$	Masci *et al.* (2002b)
$[UO_2$(*p*-methyl-*N*-benzyl-tetrahomodiazacalix[4]arene–2H)] · $2CHCl_3$ · MeCN	Thuéry *et al.* (2001c)
calix[5]*arenes*	
$[Hpyr]_2[\{U$(*tert*-butylcalix[5]arene–5H$\}_2(\mu_2$-oxo)] · 4pyr	Leverd and Nierlich (2000)
$[\{U$(*tert*-butylcalix[5]arene–5H$\}_2(\mu_2$-oxo)$]_2 \cdot 5$pyr	Leverd and Nierlich (2000)

Table 22.26 (*Contd.*)

Structure	*References*
$[HNEt_3]_2[UO_2(p\text{-}tert\text{-butylcalix[5]arene–4H})] \cdot 2MeOH$	Thuéry and Nierlich (1997)
calix[6]*arenes*	
$[U(tert\text{-butylcalix[6]arene–3H})_2] \cdot (Hpyr)_2Cl_2 \cdot 10pyr$	Leverd and Nierlich (2000)
$[U\{(tert\text{-butylcalix[6]arene–4H})LaCl_2(pyr)_4\}_2]$	Leverd *et al.* (2002)
$[UO_2(p\text{-}tert\text{-butylcalix[6]arene–4H})]_2 \cdot 2(HNEt_3) \cdot 2(H_3O) \cdot 6MeCN$	Thuéry *et al.* (1996)
$[HNEt_3]_2[UO_2(p\text{-}tert\text{-butyltetrahomodioxacalix[6]arene–4H})] \cdot 3MeCN$	Thuéry *et al.* (2001b)
$[Hpyr]_3[Cs][(UO_2Cl_2)_2(tert\text{-butylcalix[6]arene–4H})] \cdot 7pyr$	Leverd *et al.* (1998)
$[(UO_2)_2Li(OH)(p\text{-}tert\text{-butylhexahomotrioxacalix[6]arene–6H)(pyr)][Li(H_2O)_3(pyr)] \cdot (Hpyr) \cdot H_2O \cdot 4.5pyr$	Thuéry and Masci (2004)
$[UO_2K(p\text{-}tert\text{-butylhexahomotrioxacalix[6]arene–3H)(H_2O)_2]_2 \cdot 14pyr$	Thuéry and Masci (2004)
calix[7]*arenes*	
$[(UO_2)_6(p\text{-benzylcalix[7]arene–7H})_2(O)_2(HDABCO)_6] \cdot 3MeCN \cdot CH_3Cl \cdot 5MeOH \cdot 3H_2O$	Thuéry *et al.* (1999b)
$[HNEt_3]_2[UO_2(p\text{-}tert\text{-butylcalix[7]arene–4H})] \cdot MeNO_2 \cdot MeOH$	Thuéry *et al.* (1998)
$[HNEt_3]_2[UO_2(p\text{-}tert\text{-butylcalix[7]arene–4H})] \cdot MeCN \cdot 2H_2O$	Thuéry *et al.* (1998)
calix[8]*arenes*	
$[Th_4(p\text{-}tert\text{-butylcalix[8]arene–7H})(p\text{-}tert\text{-butylcalix[8]arene–6H)(DMSO)}_4(OH)_3(H_2O)] \cdot (DMSO) \cdot 2H_2O$	Harrowfield *et al.* (1991b)
$[HNEt_3]_2[(UO_2)_4(p\text{-}tert\text{-butyloctahomotetraoxacalix[8]arene–8H)(OH)}_2(H_2O)_4] \cdot 1.5NEt_3 \cdot 2.5H_2O \cdot MeOH$	Thuéry *et al.* (2001b)
$[(HNEt_3)_2(OH)][(UO_2)_2(p\text{-}tert\text{-butylcalix[8]arene–4H)(OH)}] \cdot 2NEt_3 \cdot 3H_2O \cdot 4MeCN$	Thuéry *et al.* (1995c)
$[HNEt_3]_5[(UO_2)_2(p\text{-}tert\text{-butylcalix[8]arene–4H)(OH)}]_2 \cdot 3OH \cdot 3MeCN$	Thuéry *et al.* (1995d)
$[NMe_4][(UO_2)_3(OH)(p\text{-}tert\text{-butylcalix[8]arene–6H)(DMSO)}_2]$	Thuéry *et al.* (2001d)
$[(UO_2)_4O_4(p\text{-}tert\text{-butyloctahomotetraoxacalix[8]arene)}] \cdot 10MeOH$	Thuéry and Masci (2003)
$[(UO_2)_2(pyr)_4(p\text{-}tert\text{-butyloctahomotetraoxacalix[8]arene–4H)}] \cdot pyr$	Thuéry and Masci (2003)
calix[9, 12]*arenes*	
$[HNEt_3]_3[(UO_2)_2(p\text{-}tert\text{-butylcalix[9]arene–5H)}(CO_3)]$	Thuéry *et al.* (2001d)
$[HNEt_3]_2[\{(UO_2)_2(NO_3)(pyr)\}_2(tert\text{-butylcalix[12]arene–8H})] \cdot 9pyr$	Leverd *et al.* (2000)

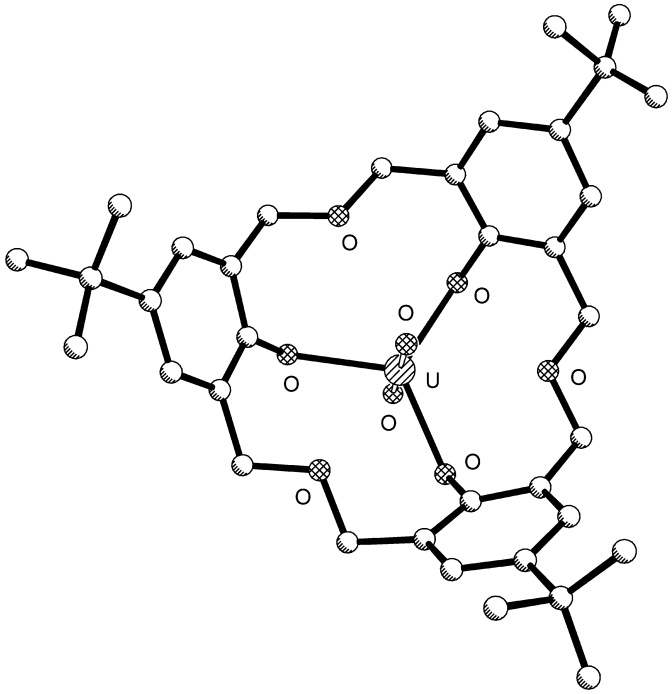

Fig. 22.21 *Crystal strucuture of* [UO_2(p-tert-*butylhexahomotrioxacalix*[3]*arene*–3*H*)(*HDABCO*)]·3*MeOH with MeOH, HDABCO, and hydrogen atoms omitted* (*Thuéry* et al., 1999*a*). *The coordinates were obtained from the Cambridge Structural Database* (*refcode BINKOY*).

bipyramidal geometry around the uranium atom. The oxa-linkages that connect the phenolic units do not take part in the bonding; thus, the five-coordinate environment around uranium is the lowest ever observed. The overall conformation of the calixarene ligand is cone-shaped, and the uranyl is slightly displaced from the plane formed by the three bonding phenolic oxygen atoms. This displacement is counter-ion-dependent, with triethylamine and DABCO resulting in 0.186(4) and 0.248(3) Å displacements, respectively (Thuéry *et al.*, 1999a).

The trigonal equatorial coordination environment around uranium in the two aforementioned complexes changes with alterations to the upper rim as well as the deprotonating agent. Maintaining the *tert*-butyl substitution at the upper rim and changing the deprotonation agent to H_2NBu preserves the trigonal equatorial coordination around uranium; however, in the presence of NPr_3, a distorted tetragonal coordination is observed, with an ether oxygen also taking part in the bonding. Distorted tetragonal coordination is also observed with a methyl substitution and triethylamine. Higher degrees of equatorial coordination are also possible. A *tert*-butyl substitution with 4-methylpiperidine as

the deprotonating agent results in distorted pentagonal coordination aided by the participation of two ether oxygen atoms; an intermediate coordination environment (between tetragonal and pentagonal) occurs with $HNBu_2$ (Masci *et al.*, 2002a).

Calix[4]arene-based actinide complexes are plentiful in the literature, owing to the larger cavity size of the ligand and larger number of potential donor sites. Tetrahomodioxa- and tetrahomodiazacalix[4]arene uranyl structures typically show 1:1 complexes with different complexation modes. The complexation of UO_2^{2+} with *p-tert*-butyltetrahomodioxacalix[4]arene in the presence of triethylamine yields an inclusion complex where the uranyl is bound equatorially in the plane of four deprotonated phenolic oxygen atoms, with the two calixarene ether oxygen atoms taking on a non-bonding role (3.832(4) and 3.820(4) Å from uranium). The geometry around uranium is square bipyramidal with an average $U–O_{eq}$ bond distance of 2.28(3) Å (Thuéry *et al.*, 2001a).

The uranyl/*p*-methyl-*N*-benzyltetrahomodiazacalix[4]arene complex, on the other hand, is of the exclusion type. Interestingly, the complex forms in the absence of base, resulting in a neutral 1:1 complex, where the uranyl is bound to two phenolic oxygens (zwitterionic form) of the calixarene and to two nitrate counter-ions. The uranyl cation rests above the plane of the four phenolic oxygen atoms at a distance of 1.543(8) Å, with the two bound $U–O_{phenol}$ distances at 2.234(9) and 2.269(8) Å. The nitrate anions have different coordination modes, one being mondentate and the other bidentate. The differences observed between the dioxa- and diaza-complexes are presumably due to electrostatic repulsion between the uranyl and the ammonium groups of the diazacalixarene (Thuéry *et al.*, 2001a).

A unique inclusion complex between *p*-methyloctahomotetraoxacalix[4]arene and two uranyl cations has also been structurally characterized (Fig. 22.22). The doubly bridged dinuclear cation rests in the calixarene cavity with the bridging provided by a hydroxide and one oxygen atom from a water molecule. Pentagonal bipyramidal geometry around each uranium results from the two axial uranyl oxygen atoms, the two bridging oxygen atoms, two deprotonated phenolic oxygen atoms, and a single ether oxygen atom. The mean $U–O_{phenoxide}$ bond distances are 2.25(2) Å, while the mean $U–O_{ether}$ distances are significantly longer at 2.67(2) Å (Thuéry *et al.*, 2001b).

The reaction of UO_2^{2+} with *p-tert*-butycalix[5]arene in the presence of triethylamine generates an inclusion complex. The uranyl is bound equatorially to the five phenolic oxygen atoms of the lower rim of the calixarene, generating an overall pentagonal bipyramidal geometry around the uranium atom. Interestingly, only four of the five phenolic sites are deprotonated, suggesting that uranyl ion has an acid-enhancing effect. The $U–O_{eq}$ bond distances vary greatly; three in the range 2.25–2.30 Å, a fourth at 2.571(7) Å, and the longest at 2.836(8) Å. The large variation in the range of $U–O_{eq}$ bond lengths may be due to the calixarene cavity being too large for ideal coordination of the uranyl ion. Finally, the calixarene itself takes on the common cone conformation and

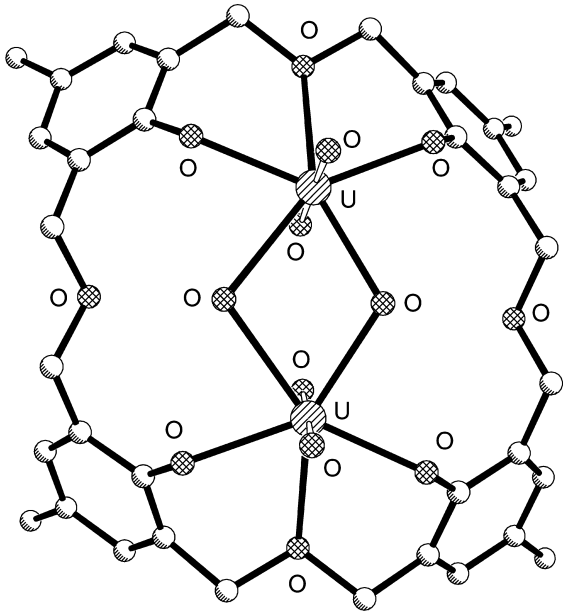

Fig. 22.22 *Crystal strucuture of* [*Hpyr*][$(UO_2)_2$(p-*methyloctahomotetraoxacalix*[4]*arene*–4*H*)(*OH*)(H_2O)] · 2.5*pyr with Hpyr, pyr, and hydrogen atoms omitted* (*Thuéry* et al., 2001*b*). *The coordinates were obtained from the Cambridge Structural Database* (*refcode QOPMIR*).

one of the protonated triethylamine molecules sits in the cavity of the cone, coordinated with an axial uranyl oxygen atom (Thuéry and Nierlich, 1997).

Single crystals of larger calix[*n*]arenes, where $n = 6$, 7, 8, 9, or 12, complexed with actinides have also been isolated and their structures determined. While uranium–calixarene complexes are the most common in the literature, a novel Th(IV) structure with *p-tert*-butylcalix[8]arene has also been solved (DMSO solvate). The structure contains two different calixarene ligands, each with varying degrees of deprotonation (both seven and six protons), bound to four thorium atoms. While the structure itself is very complicated, it is obvious that the two calixarenes attain two different conformations, with one being in a 'propeller' conformation and the other a 'crown'. The two calixarenes form four cone-shaped cavities, the apices of which are defined by a plane of four phenolic oxygen atoms; each cavity is subsequently associated with a single thorium atom. Each thorium center is associated with five phenolic oxygen atoms, three of which are mondentate while the remaining two take on bridging interactions. DMSO and hydroxide molecules also contribute to the bonding (Harrowfield *et al.*, 1991b).

A related uranyl complex incorporating *p-tert*-butylcalix[8]arene is bimetallic and contains only a single calixarene ligand (Fig. 22.23). Here, each uranyl ion

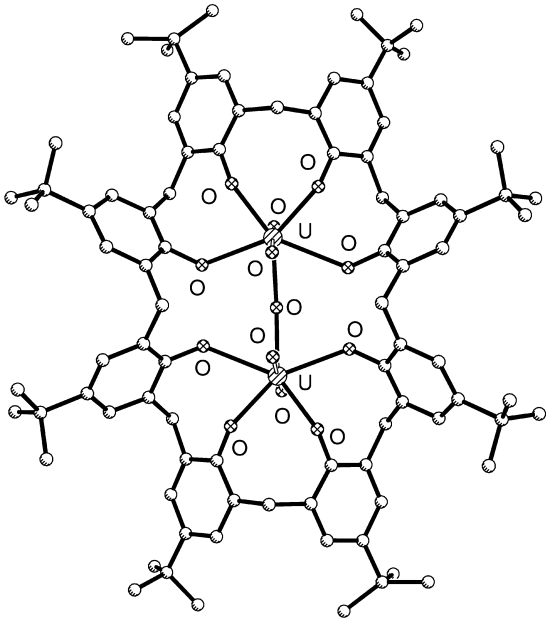

Fig. 22.23 *Crystal strucuture of* $[(HNEt_3)_2(OH)][(UO_2)_2$(p-tert-*butylcalix*[8]*arene*–4*H*)$(OH)] \cdot 2NEt_3 \cdot 3H_2O \cdot 4MeCN$ *with* $[(HNEt_3)_2(OH)]^+$, NEt_3, H_2O, *MeCN, and hydrogen atoms omitted* (*Thuéry* et al., 1995*c*). *The coordinates were obtained from the Cambridge Structural Database* (*refcode ZAMJIG*).

resides in the cavity of the calixarene, making it an inclusion complex, and each is bound equatorially to four phenolic oxygen atoms, two of which are deprotonated. The uranyl ions are also linked via a bridging hydroxide, thus making the overall geometry around each heptacoordinate uranium atom distorted pentagonal bipyramidal. The equatorial U–O bond lengths at the protonated sites are 2.619(9) and 2.476(9) Å, while the corresponding lengths at the deprotonated sites are 2.218(9) and 2.20(1) Å. Two protonated triethylamine molecules are also associated with the complex, each being hydrogen-bonded to a separate axial uranyl oxygen atom. The overall conformation of the bound calixarene has been described as a 'pleated loop' (Thuéry *et al*., 1995c).

The largest calixarene complex of an actinide to date for which a single-crystal X-ray diffraction structure is known is that between *tert*-butylcalix[12]arene and UO_2^{2+} (Fig. 22.24). The resulting inclusion complex contains two uranyl bimetallic units; the uranyl ions in each unit are bridged by a tridentate nitrate ligand. Each bimetallic unit is bound to five phenolic oxygen sites, four of which are deprotonated. One uranyl in each unit is bound to three of the oxygen atoms, while the second is bound to the remaining two and a pyridine molecule (through nitrogen). The resulting geometry around each uranium atom is pentagonal bipyramidal. The four shorter $U–O_{eq}$ bond lengths at each bimetallic

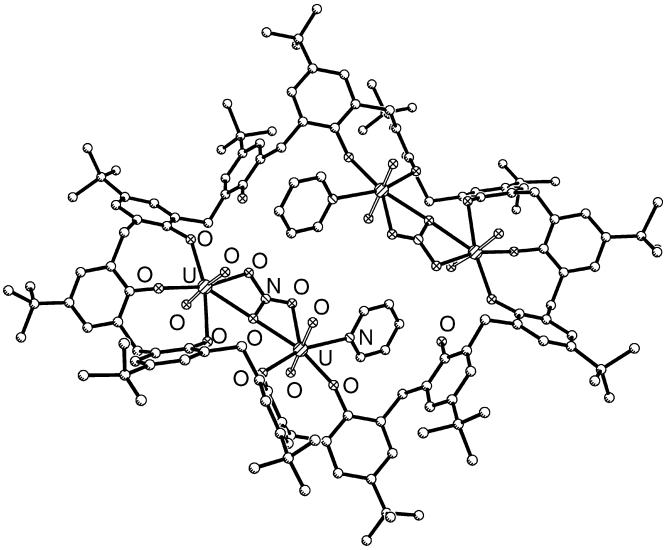

Fig. 22.24 *Crystal strucuture of* $[HNEt_3]_2[\{(UO_2)_2(NO_3)(pyr)\}_2$(tert-*butylcalix*[12]*arene*–8H)$]\cdot 9pyr$ *with* $[HNEt_3]^+$, *pyr*(*unbound*), *and hydrogen atoms omitted* (*Leverd* et al., 2000). *The coordinates were obtained from the Cambridge Structural Database* (*refcode MALGEL*).

unit are about 2.2 Å and correspond to the four deprotonated phenolic sites; the fifth longer bond length at the protonated site is 2.62(3) Å (Leverd *et al*., 2000).

(c) Porphyrins/phthalocyanines

The macrocyclic ligands commonly referred to as porphyrins are ubiquitous in nature. They are structurally described as an arrangement of four pyrrole units linked together in a cyclic manner at the 2- and 5-positions by methine bridges, forming an aromatic, 22-π electron system. The iron-containing porphyrin, commonly known as heme, comprises the primary binding site in hemoglobin that is responsible for dioxygen transport throughout the body. While traditional porphyrins contain only nitrogen-donor atoms, pyrrole-derived macrocycles have also been synthesized that contain pyrrole, furan, and thiophene subunits solely, or combinations thereof. In addition, extensive chemistries have been developed in the synthesis of expanded, contracted, and isomeric porphyrins, the details of which have been described elsewhere. Expanded porphyrins will hereafter be defined as containing at least 17 atoms in a conjugated manner and three pyrrole or pyrrole-like subunits (Sessler and Weghorn, 1997). Porphyrins have been extensively studied as templates for metal ion coordination; the addition of base, such as triethylamine, for the deprotonation of nitrogen sites allows for tetradentate or higher coordination to the metal

centers, often times facilitating electronic transitions in the visible portion of the electromagnetic spectrum that give rise to a wide range of observable color changes. In addition, traditional nitrogen-containing porphyrins give rise to unique coordination complexes with metals that prefer oxygen or sulfur atom donation (Girolami *et al.*, 1994).

Traditionally, oxygen and sulfur atoms, when incorporated into ligand support molecules, have been the atoms of choice for coordination to metal centers; thus, the use of pyrrole-derived porphyrins provides a unique opportunity to study the binding to actinide ions in a non-traditional manner (i.e. all nitrogen atoms) and the subsequent effect on electronic and structural (using X-ray crystallography) motifs. Only a small number of porphyrin–actinide crystal structures have been reported in the literature, indicative of the inherent difficulty in synthesizing these kinds of complexes (as well as the precursors). These structures contain the expanded porphryins, characterized by a bigger core size to accommodate the actinide cations that are considerably larger in diameter than the more commonly used transition metals (Sessler *et al.*, 2001a).

Crystallographic studies of porphyrin- and polypyrrolic-derived ligands with actinides have been limited to tetravalent, pentavalent, and hexavalent cations, including Th(IV), U(IV), Np(V), and U(VI). Table 22.27 lists representative structurally characterized actinide phthalocyanine/porphyrin complexes. The claimed 'first' structural determination of an actinide porphyrin complex was

Table 22.27 *Phthalocyanine and porphyrin compounds of the actinides.*

Structure	*References*
phthalocyanines	
Th(phthalocyanine)$_2$	Kobayashi (1978)
U(phthalocyanine)$_2$	Gieren and Hoppe (1971)
U(diphthalocyanine)$_2$I$_{5/3}$	Janczak and Kubiak (1999)
U(diphthalocyanine)$_2$I$_2$	Anczak *et al.* (2000)
UO$_2$(superphthalocyanine)	Day *et al.* (1975)
porphyrins	
Th(tetraphenylporphyrin)$_2 \cdot C_7H_8$	Girolami *et al.* (1988)
[Th(tetraphenylporphyrin)$_2$][SbCl$_6$] $\cdot$ 2C$_7$H$_8$ $\cdot$ CH$_2$Cl$_2$	Girolami *et al.* (1988)
[Th(tetraphenylporphyrin)(OH)$_2$]$_3 \cdot 2H_2O \cdot 3C_7H_{16}$	Kadish *et al.* (1988)
Th(octaethylporphyrin)$_2$	Girolami *et al.* (1994)
Th(octaethylporphyrin)(acetylacetonate)$_2$	Dormond *et al.* (1986)
U(tetraphenylporphyrin)Cl$_2$(THF)	Girolami *et al.* (1987)
UO$_2$(pentaphyrin)	Burrell *et al.* (1991a)
UO$_2$[hexaphyrin(1.0.1.0.0.0)]	Sessler *et al.* (2001b)
UO$_2$(monooxasapphyrin)	Sessler *et al.* (1998)
UO$_2$(β-methoxysapphyrin)	Burrell *et al.* (1991b)
UO$_2$(grandephyrin)	Sessler *et al.* (2002)
UO$_2$(alaskaphyrin)(CHCl$_3$)$_4$	Sessler *et al.* (1992)
[HNEt$_3$]NpO$_2$[hexaphyrin(1.0.1.0.0.0)]	Sessler *et al.* (2001b)

for U(tpp)Cl_2(THF) with U(IV) and doubly deprotonated tetraphenylporphyrin (tpp). X-ray analysis indicates an exclusion complex, where the U(IV) rests above the plane of the porphyrin (defined by four nitrogen atoms) by 1.29 Å; the two chloride ions and a THF molecule are bound to the metal. The porphyrin itself is not rigorously planar, but rather 'saucer-shaped' to promote bonding of the four nitrogens to uranium. Overall, the coordination geometry about uranium consists of what may be described as a 4:3 piano-stool configuration, with the porphyrin comprising the base of the stool. The U–N bond lengths are 2.41(1) Å, while the U–Cl and U–O bond distances are 2.63(1) and 2.50(1) Å, respectively (Girolami *et al.*, 1987). The structure of Th(octaethylporphyrin)(acetylacetonate)$_2$, incidentally, was reported by Dormond *et al.* in 1986.

The structure of UO_2(pentaphyrin) contains an expanded pentadentate porphyrin that takes on a characteristic saddle-shaped geometry with a uranyl ion located at the center. The uranyl ion is bound symmetrically through uranium to all five nitrogen atoms of the ligand, resulting in a nearly ideal, centrally coordinated pentagonal bipyramid, with U–N and U–O bond distances averaging 2.541(3) and 1.756(5) Å, respectively. Distortions from planarity are due to the oversized diameter of the ligand cavity, thus yielding to the bonding requirements of the uranyl ion (Burrell *et al.*, 1991a).

The complexes of both UO_2^{2+} and NpO_2^+ with hexaphyrin(1.0.1.0.0.0) contain the ligand in its oxidized, aromatic form; the crystal structure of the latter is provided in Fig. 22.25. The linear uranyl ion is completely encapsulated within the porphyrin and is oriented perpendicularly to the plane of the six nitrogen atoms; each nitrogen participates in bonding to the uranium, resulting in a distorted hexagonal bipyramid due to non-centered placement of uranium within the macrocycle cavity. The average U–N bond distance is 2.63(1) Å (considerably longer than U–N distances observed in the former pentaphyrin structure) and U–O distances are 1.760(2) Å (typical for the uranyl cation) (Sessler *et al.*, 2001b).

The analogous NpO_2^+ structure reveals less distortion in the ligand geometry as compared to the uranyl complex, presumably due to a better intrinsic 'fit' between the larger NpO_2^+ cation and the hexaaza ligand core. The geometry around the neptunium center, as in the uranium complex, is roughly a hexagonal bipyramid. The two Np–O bond distances [1.762(1) and 1.826(1) Å] are short for the NpO_2^+ cation (1.85 Å in simple metal salts); the difference in length of these bonds is presumably due to a short-contact interaction between a triethylammonium cation nitrogen atom and a neptunyl oxygen atom. In addition, Np–N bond distances average 2.77(2) Å, nearly 0.14 Å longer than in the corresponding uranyl complex (Sessler *et al.*, 2001b).

Thorium–porphyrin compounds are also relatively common in the literature; for example, Th(IV) and octaethylporphyrin (oep) in the presence of acetylacetonate yield Th(oep)(acac)$_2$. The geometry about the Th(IV) center in the crystal structure is described as a nearly ideal octa-coordinated Archimedean antiprism

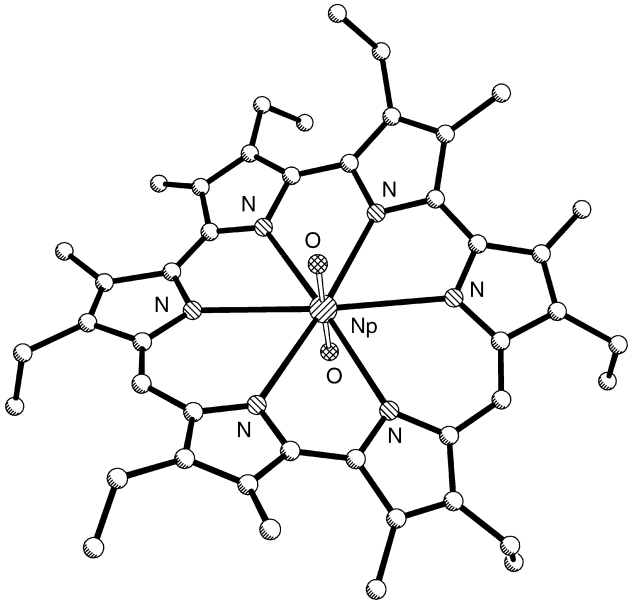

Fig. 22.25 *Crystal strucuture of* $[HNEt_3]NpO_2$[*hexaphyrin*(1.0.1.0.0.0)] *with* $[HNEt_3]^+$ *and hydrogen atoms omitted* (*Sessler* et al., 2001*b*). *The coordinates were obtained from the Cambridge Structural Database* (*refcode QIVCON*).

provided by the four pyrrolic nitrogen atoms and the four oxygen atoms of the two acetylacetonato ligands. The Th(IV) ion is observed to rest closer to the acteylacetonato oxygen atoms than the nitrogen atoms of the porphyrin, making it an exclusion complex. The Th–N and Th–O bond distances average 2.50 and 2.40 Å, respectively, and the geometry of the acetylacetonate ligand is consistent with known carboxylic acid complexes of related type (Dormond *et al*., 1986).

The neutral Th(tetraphenylporphyrin)$_2 \cdot C_7H_8$ and its oxidized π-radical cation in the form of $[Th(tpp)_2][SbCl_6]$ are quite similar and have average Th–N bond distances of 2.55(1) and 2.52(2) Å, respectively. Both metal centers are displaced from the mean plane formed by the pyrrolic nitrogen atoms with an average displacement distance of 1.47 Å for the neutral and 1.45 Å for the cation. The overall geometry around thorium in both the neutral and cationic species may be described as distorted square antiprismatic. Slight differences in the interplanar spacings and twists angles further distinguish the two (Girolami *et al*., 1988).

Phthalocyanines are porphyrin-like macrocycles (aza rather than methine bridge) and may be described as tetrabenzo-tetraazaporphyrins that, unlike porphyrins, are typically prepared via a metal-templated condensation using phthalonitrile and its derivatives (Sessler and Weghorn, 1997). The

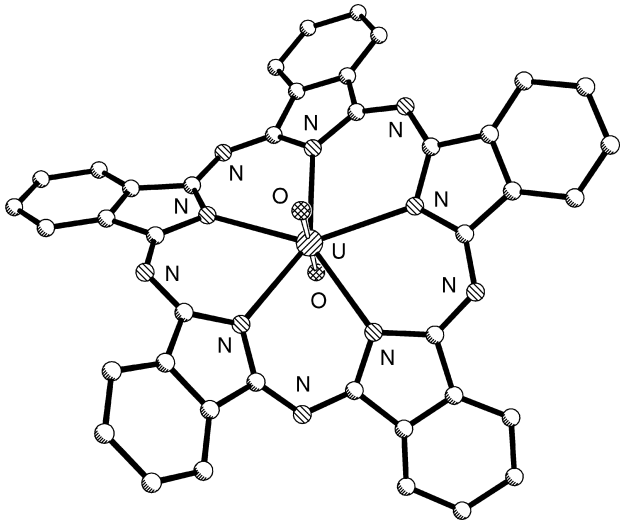

Fig. 22.26 *Crystal strucuture of UO_2(superphthalocyanine) with hydrogen atoms omitted* (*Day* et al., 1975). *The coordinates were obtained from the Cambridge Structural Database* (*refcode CIMINU10*).

uranyl-templated condensation reaction with *o*-dicyanobenzene has yielded an expanded, cyclic five-subunit complex with uranyl known as a 'uranyl superphthalocyanine' (Fig. 22.26). The crystal structure of the UO_2(superphthalocyanine) complex reveals a linear uranyl ion pentacoordinated to the five nitrogen donors of the ligand, creating a near ideal compressed pentagonal bipyramid. The linear [179(1)°] uranyl fragment has an average U–O bond distance of 1.744(8) Å, consistent with other uranyl structures. The average U–N bond distance is 2.524(9) Å and is consistent with other seven-coordinate uranyl/nitrogen complexes. A side-profile of the complex reveals severe distortions from planarity, inherently due to steric strain within the ligand upon metal binding (Day *et al.*, 1975).

22.5 ORGANOACTINIDE COMPOUNDS

Historically, organoactinide chemistry had its origins in the era of the Manhattan Project with unsuccessful attempts to synthesize volatile compounds such as tetraethyl uranium for isotopic enrichment in the gaseous diffusion operations. The synthesis of the unique sandwich compound, uranocene, in 1968, more than previous strides in actinide chemistry with cyclopentadienyl ligands, truly marked the beginning of the organoactinide era, evidenced by the exponential growth thereafter. The subsequent exploration

of organoactinide complexes has mainly focused on π-electron interactions with the cyclopentadienyl and cyclooctatetraenyl ligands and their derivatives, resulting in complexes that take advantage of the potential for high coordination numbers as compared to d-block elements. In addition to the π-bonding ability of these ligands, coordinative saturation of the actinide center can be approached with a variety of other σ- or π-donating ligands (including halides, alkyls, and others), thus introducing a seemingly endless number of possibilities for studying coordination, ligand activation, or reactivity (Marks, 1982a).

Organometallic complexes of lanthanide ions are largely ionic in nature, due to poor overlap between the 4f orbitals and ligand molecular orbitals. As a result, all the lanthanides favor the trivalent oxidation state and display similar chemical reactivity, with differences being primarily due to differences in ionic radii. The 5f electrons of the early actinides, however, are not completely shielded by the 6s and 6p electrons, resulting in a significant radial extension of the 5f orbitals that allows for overlap with ligand orbitals and a covalent bonding contribution. Despite this small covalent contribution, ionic character predominates; in fact, in the later actinides, contraction of the 5f orbitals due to increased nuclear charge results in less metal–ligand orbital overlap and in the predominance of the trivalent oxidation state (Bombieri *et al*., 1998).

The interest surrounding organoactinide chemistry is based on the unique properties of actinide ions (e.g., larger size) that cause them to interact with ligands to produce chemistry that is wholly different from that observed with the d-elements. The larger size of the actinide ions permits coordination numbers (as high as 12) and polyhedra that are unknown or highly unusual for d-elements. This implies a greater control over coordinative unsaturation and a greater number of reactive species can be coordinated and maintained in spatially unusual orientations (Marks, 1982a).

The tremendous growth of organoactinide chemistry since 1968 has resulted in the structural characterization of a wide range of complexes, far too many to be comprehensively presented in this section. The following sections present representative examples, primarily organized in a tabular form, that give the reader an idea of the classes of bonding, as well as the diversity and complexity of organoactinide structural chemistry with brief synopses of select complexes where appropriate. For a more comprehensive treatment of the chemistry and characterization of these compounds, the reader is referred to Chapter 25 of this work, or the annual lanthanide/actinide surveys that are listed in Table 22.28.

22.5.1 Cyclopentadienyl–actinide compounds

Organoactinide complexes of the cyclopentadienyl ligand (η^5-C_5H_5 or Cp) commonly occur as An(η^5-C_5H_5)$_4$, An(η^5-C_5H_5)$_3$X, An(η^5-C_5H_5)$_2$X$_2$, and An(η^5-C_5H_5)X$_3$ where X is a halogen atom, an alkyl, hydride, or alkoxy group, NCS, BH_4, or other ligands with oxygen, nitrogen, or phosphorus donor sites of varying denticity. Typically, the aromatic nature of the Cp ring

Table 22.28 *Annual lanthanide and actinide organometallic surveys* (1964–1998).

Year	*Reference*	*Year*	*References*
1964–1970	Hayes and Thomas (1971)	1983	Rogers and Rogers (1990)
1971	Calderazzo (1973)	1984–1986	Rogers and Rogers (1991)
1972	Calderazzo (1974)	1987–1990	Rogers and Rogers (1992a)
1973	Marks (1974)	1990	Rogers and Rogers (1992b)
1974	Marks (1975)	1991	Rogers and Rogers (1993)
1975	Marks (1976)	1992	Kilimann and Edelmann (1995)
1976	Marks (1977)	1993	Richter and Edelmann (1996)
1977	Marks (1978)	1994	Gun'ko and Edelmann (1996)
1978	Marks (1979a)	1995	Edelmann and Gun'ko (1997)
1979	Marks (1980)	1996	Edelmann and Lorenz (2000)
1980	Marks (1982b)	1997	Hyeon and Edelmann (2003a)
1981	Ernst and Marks (1987)	1998	Hyeon and Edelmann (2003b)
1982	Ernst (1990)	1999	Gottfriedsen and Edelmann (2005)
		2000	Hyeon *et al*., (2005)

Table 22.29 *Representative tetrakis–cyclopentadienyl organoactinide complexes*.

Structure	*References*
Cp_4An (An = Th, U, Np)	Kanellakopulos and Bagnall (1972)
Cp_4Th	Maier *et al*. (1993)
Cp_4U	Burns (1974)

lends itself to a η^5 (pentahapto) bonding mode to the actinide metal via its π-electrons. The following discussion will focus on structural motifs present in representative compounds of mono-, bis-, tris-, and tetrakis-cyclopentadienyl organoactinide complexes (Marks, 1979b).

(a) Tetrakis–cyclopentadienyl complexes

The Cp_4An complexes, shown in Table 22.29, are very few in number and are prepared by heating $AnCl_4$ with KCp. A single-crystal X-ray diffraction study of Cp_4U revealed four identical Cp rings arranged in a tetrahedral fashion around the uranium atom with an average U–C distance of 2.538 Å (Burns, 1974). The single-crystal structure of Cp_4Th is isostructural with the uranium analog with a slightly longer average Th–C distance of 2.606 Å (Maier *et al*., 1993). The arrangement of Cp ligands around the thorium center is illustrated in Fig. 22.27. Furthermore, powder X-ray diffraction techniques have confirmed the isostructural nature of the Th, U, and Np complexes (Kanellakopulos and Bagnall, 1972).

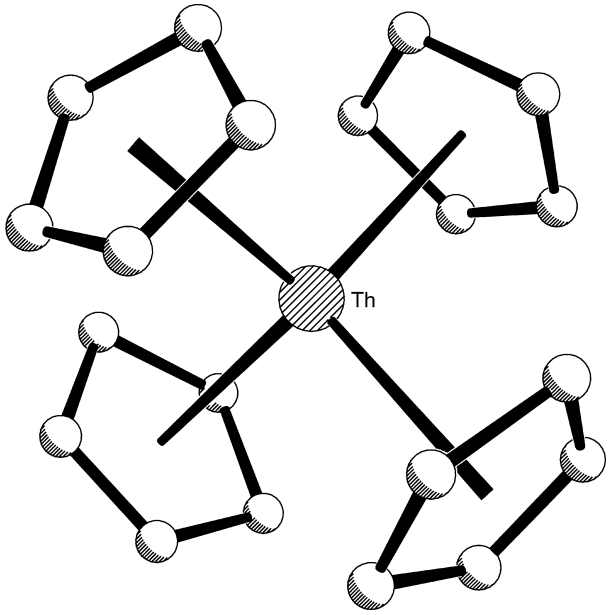

Fig. 22.27 *Crystal strucuture of Cp_4Th with hydrogen atoms omitted* (*Maier* et al., 1993). *The coordinates were obtained from the Cambridge Structural Database* (*refcode LANTEZ*).

(b) Tris-cyclopentadienyl complexes

The tris-cyclopentadienyl complexes of the actinides are known for Th, U, Pu, Am, Cm, Bk, and Cf, but not all have been structurally characterized. The uranium and thorium compounds can be prepared by different methods, including reduction of the tetravalent derivatives or photo-induced β-hydride elimination reactions of Cp_3An–alkyl compounds (Bruno *et al.*, 1982a). The thorium version is a unique example of thorium in the rare trivalent oxidation state and some structural data are available (Kanellakopulos *et al.*, 1974). The uranium complex is a strong Lewis acid and readily favors the formation of adducts with a variety of Lewis bases (Marks, 1982a). Powder diffraction data are available for the Cm, Bk, and Cf compounds, evidence that the trivalent oxidation state is preferred for the heavier actinide elements (Cm, Bk, Cf) (Laubereau and Burns, 1970a,b).

The predominance of Cp_3AnX compounds over Cp_3An (where An is U or Th and X is an anion, Lewis base, or another Cp ring) in organoactinide chemistry depicts the degree to which the tetravalent oxidation state of the metal is preferred over the trivalent state in these complexes, or in cases where the trivalent oxidation state is maintained, the high Lewis acid character of the

precursor (Bombieri *et al.*, 1998). In all the Cp_3AnX compounds, the Cp rings are bound in the traditional η^5 (pentahapto) mode to the actinide cation(s) and the complexes have irregular tetrahedral structure (although there are exceptions). Structural analysis has confirmed that this molecular arrangement exists for other complexes in which the X is varied, revealing not only the retention of the irregular tetrahedral structure, but also the aromatic nature of the Cp rings and the regularity of the An–C bond length.

A series of tris-cyclopentadienyl actinide complexes are tabularized in Table 22.30. The series of Cp_3UX complexes, where X is a halide (F, Cl, Br, I), have been structurally characterized (Wong *et al.*, 1965; Ryan *et al.*, 1975; Spirlet *et al.*, 1989; Rebizant *et al.*, 1991). While each has the same distorted tetrahedral environment around the uranium center, none are isostructural, despite the chloride and bromide being geometrically equivalent (both monoclinic, $P2_1/n$). A neutron diffraction structure of the chloride is also available which shows disorder of the Cp rings as well as a crystallographic phase transition between 80 and 100 K (Delapalme *et al.*, 1988). A structure of the iodide derivative is shown in Fig. 22.28.

A large number of compounds exhibit σ-bonding at the fourth site, such as $Cp_3U(n\text{-}C_4H_9)$, $Cp_3U(p\text{-}CH_2C_6H_4Me)$ (Perego *et al.*, 1976), or $Cp_3U[MeC(CH_2)_2]$ (Halstead *et al.*, 1975), with U—C_σ bond distances of 2.426(23), 2.541(15), and 2.48(3) Å, respectively. In the latter complex, while π-bonding of the methylallyl group is possible, the structure clearly indicates σ-type interactions with the metal center. The result is a distorted tetrahedral geometry with approximate C_{3v} symmetry. An interesting case exists with $[Cp_2Th(\eta^5{:}\eta^1\text{-}C_5H_4)]_2$, where the two Cp_2Th centers are bridged by two $\eta^5{:}\eta^1\text{-}C_5H_4$ ligands, each pentahapto to one thorium and monohapto (σ-bonded) to its neighbor (Baker *et al.*, 1974).

Another interesting situation arises in the pyrazolate complex, $Cp_3U(N_2C_3H_3)$, where endo-bidentate η^2-coordination through both nitrogen atoms to the uranium center is observed; the U–N distances are 2.40 and 2.36 Å (Fig. 22.29). In this compound, the ionic nature of the U–N bond suggests that the N–N bond is involved in a non-directional association with the uranium atom; the resulting geometry may be described as a flattened tetrahedron with bonds joining the uranum atom with the center of the three Cp ligands and the midpoint of the N–N pyrazolate bond (Eigenbrot and Raymond, 1981).

The reaction of $Cp_3U \cdot THF$ with the potentially bidentate phosphine ligand, $Me_2P(CH_2)_2PMe_2$, yields the complex $(Cp_3U)_2[Me_2P(CH_2)_2PMe_2]$ where the phosphine ligand adopts an unusual role (Zalkin *et al.*, 1987a). Here, the phosphine acts as a bridging ligand between each Cp_3U fragment rather that chelating in a bidentate mode through each phosphorus atom. In doing so, the steric repulsions are minimized and the coordination number of the uranium is reduced by one, resulting in an 'economical arrangement'. The U–P bond distance is 3.022(2) Å and the U–$Cp_{centroid}$ distance is 2.52(1) Å, both of which

Table 22.30 *Representative tris-cyclopentadienyl organoactinide complexes and derivatives.*

Structure	*Non-Cp Donors (# per center)*	*References*
Cp		
Cp_3Th	–	Kanellakopulos *et al.* (1974)
Cp_3An (An = Cm, Bk, Cf)	–	Laubereau and Burns (1970a,b)
$[(Cp_3U)_2(\mu\text{-}H)][Na(THF)_2]$	H	Le Maréchal *et al.* (1989a)
$Cp_3U(HBBN)$	H(2)	Zanella *et al.* (1987b)
$Cp_3U(BH_4)$	H(3)	Zanella *et al.* (1988)
Cp_3UF	F	Ryan *et al.* (1975)
Cp_3UCl	Cl	Wong *et al.* (1965); Delapalme *et al.* (1988)
$(Cp_3UClCp_3)[Na(18\text{-crown-}6)(THF)_2]$	Cl	Le Maréchal *et al.* (1989b)
Cp_3UBr	Br	Spirlet *et al.* (1989)
Cp_3UI	I	Rebizant *et al.* (1991)
$[Cp_2Th(\eta^5{:}\eta^1\text{-}C_5H_4)]_2$	C	Baker *et al.* (1974)
$Cp_3U(C{\equiv}CH)$	C	Atwood *et al.* (1976)
$Cp_3U[C{\equiv}CPh]$	C	Atwood *et al.* (1973)
$Cp_3U(n\text{-}C_4H_9)$	C	Perego *et al.* (1976)
$[Cp_3U\text{-}n\text{-}C_4H_9][LiC_{14}H_{28}N_2O_4]$	C	Arnaudet *et al.* (1986)
$Cp_3U(p\text{-}CH_2C_6H_4Me)$	C	Perego *et al.* (1976)
$Cp_3U[MeC(CH_2)_2]$	C	Halstead *et al.* (1975)
$Cp_3U(CHPMe_2Ph)$	C	Cramer *et al.* (1981, 1983)
$Cp_3U(CHPMe_3)$	C	Cramer *et al.* (1988a)
$Cp_3U(CNC_6H_{11})$	C	Kanellakopulos and Aderhold (1973)
$Cp_2Cp^*U(CH_2Ph)$	C	Kiplinger *et al.* (2002a)
$Cp_3U(NCR)$ (R = ^{n}Pr, ^{i}Pr)	N	Adam *et al.* (1993)
Cp_3UNPh_2	N	Cramer *et al.* (1987a)
$Cp_3U(NCS)$	N	Spirlet *et al.* (1993a)
$Cp_3UNC(Me)CHP(Me)(Ph)_2$	N	Cramer *et al.* (1984a)
$Cp_3U(NPPh_3)$	N	Cramer *et al.* (1988b)
$Cp_3U(NCBH_3)(NCMe)$	N(2)	Adam *et al.* (1990)
$[Cp_3U(NCMe)_2]_2[UO_2Cl_4]\cdot(C_4H_6)_2$	N(2)	Bombieri *et al.* (1983a)
$[Cp_3U(NCMe)_2][CpThCl_4(NCMe)]$	N(2); Cl(4), N	Rebizant *et al.* (1987)
$[Cp_3U(NCMe)_2][BPh_4]$	N(2)	Aslan *et al.* (1988)
$Cp_3U(NCS)(NCMe)$	N(2)	Aslan *et al.* (1988); Fischer *et al.* (1978)
$Cp_3U(N_2C_3H_3)$	N(2)	Eigenbrot and Raymond (1981)
$[Ph_4As][Cp_3U(NCS)_2]$	N(2)	Bombieri *et al.* (1983b)
$Cp_3U(OR)$ (R = $C(CF_3)_2CCl_3$, Ph)	O	Knösel *et al.* (1987); Spirlet *et al.* (1990a)
$Cp_3U(THF)$	O	Wasserman *et al.* (1983)
$Cp_3U(OSiPh_3)$	O	Porchia *et al.* (1989)
$Cp_3Np(OPh)$	O	De Ridder *et al.* (1996a)
$(Cp_3U)_2(Me_2P(CH_2)_2PMe_2)$	P	Zalkin *et al.* (1987a)
$Cp_3U(SMe)$	S	Leverd *et al.* (1996)

Table 22.30 (*Contd.*)

Structure	*Non-Cp Donors* (*# per center*)	*References*
Cp		
$Cp_3U[\eta^2\text{-}MeC{=}N(C_6H_{11})]$	C, N	Zanella *et al.* (1985)
$Cp_3U[(NEt_2)C{=}N(C_6H_3Me_2\text{–}2,6)]$	C, N	Zanella *et al.* (1987a)
$Cp_3U(NPh)(O)CCHPMe_2Ph$	O, N	Cramer *et al.* (1987b)
$Cp_3U(\eta^2\text{-}OCCH)P(Me)(Ph)_2$	C, O	Cramer *et al.* (1982)
*Cp**		
$(Cp^*)_3ThH$	H	Evans *et al.* (2001)
$(Cp^*)_3UX$ (X = F, Cl)	F; Cl	Evans *et al.* (2000)
$(Cp^*)_3U(CO)$	C	Evans *et al.* (2003a)
$(Cp^*)_3U(\eta^1\text{-}N_2)$	N	Evans *et al.* (2003b)
MeCp, Me_4Cp, $PhCH_2Cp$		
$(Me_4Cp)_3UCl$	Cl	Cloke *et al.* (1994)
$(PhCH_2Cp)_3UCl$	Cl	Leong *et al.* (1973)
$(Me_4Cp)_3U(CO)$	C	Parry *et al.* (1995)
$(MeCp)_3U(NH_3)$	N	Rosen and Zalkin (1989)
$(MeCp)_3U(NPh)$	N	Brennan and Andersen (1985)
$(MeCp)_3U[N(CH_2CH_2)_3CH]$	N	Brennan *et al.* (1988a)
$(MeCp)_3U(C_7H_{10}N_2)$	N	Zalkin and Brennan (1987)
$(MeCp)_3U(OPPh_3)$	O	Brennan *et al.* (1986b)
$[(MeCp)_3U]_2[\mu\text{-}\eta^1,\eta^2\text{-}PhNCO]$	O; C, N	Brennan and Andersen (1985)
$(MeCp)_3U(PMe_3)$	P	Brennan and Zalkin (1985)
$(MeCp)_3U[P(OCH_2)_3CEt]$	P	Brennan *et al.* (1988a)
$(MeCp)_3U(C_4H_8S)$	S	Zalkin and Brennan (1985)
$[(MeCp)_3U]_2[\mu\text{-}S]$	S	Brennan *et al.* (1986b)
$[(MeCp)_3U]_2[\mu\text{-}\eta^1,\eta^2\text{-}CS_2]$	S; C, S	Brennan *et al.* (1986a)
Cp′, Cp″, Cp^{tt}, $(SiMe_3)_2CHCp$		
$(Cp'')_3Th$	–	Blake *et al.* (1986a, 2001)
$(Cp^{tt})_3Th$	–	Blake *et al.* (2001)
$(Cp')_3U$	–	Zalkin *et al.* (1988a)
$(Cp'')_3ThCl$	Cl	Blake *et al.* (1998)
$(Cp^{tt})_3ThCl$	Cl	Blake *et al.* (1998)
$(Cp'')_2(Cp^*)ThCl$	Cl	Blake *et al.* (1998)
$[(SiMe_3)_2CHCp]_3ThCl$	Cl	Blake *et al.* (1998)
$(Cp'')_3UCl$	Cl	Blake *et al.* (1998)
$(Cp')_3UCH{=}CH_2$	C	Schock *et al.* (1988)
$[Na(18\text{-crown-}6)][(Cp')_3U\text{-}N_3\text{-}U(Cp')_3]$	N	Berthet *et al.* (1991a)
$[(Cp')_3U]_2[\mu\text{-}O]$	O	Berthet *et al.* (1991b)

* Semicolons used to differentiate coordination to different metal centers or different structures.

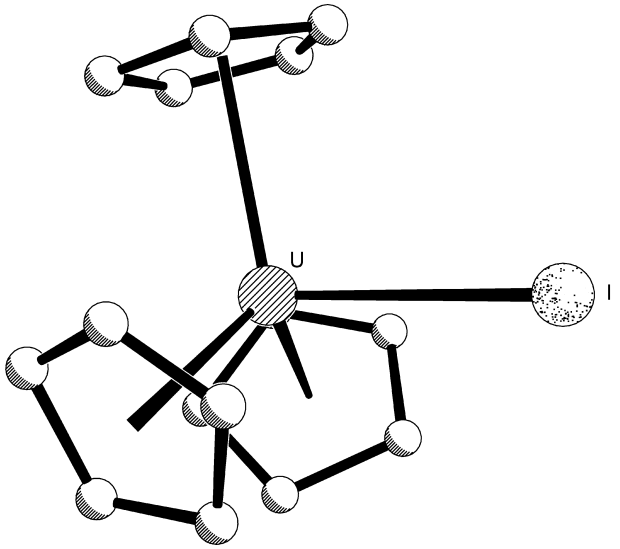

Fig. 22.28 *Crystal strucuture of Cp_3UI with hydrogen atoms omitted* (Rebizant et al., 1991). *The coordinates were obtained from the Cambridge Structural Database* (*refcode JIKGOZ*).

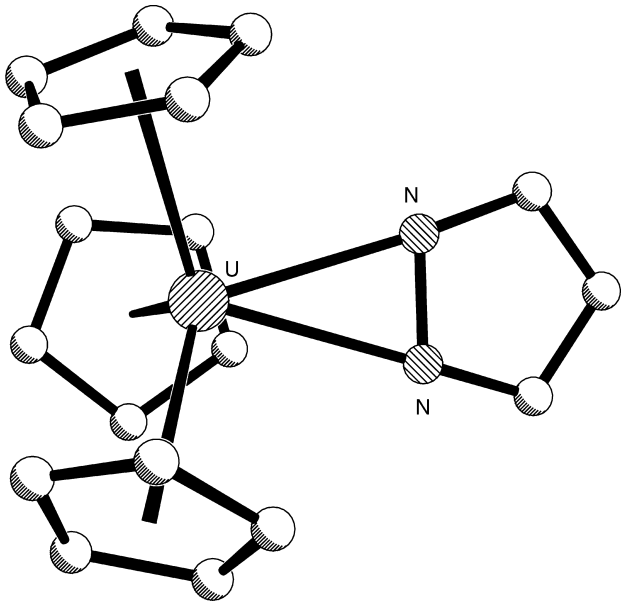

Fig. 22.29 *Crystal strucuture of $Cp_3U(N_2C_3H_3)$ with hydrogen atoms omitted* (*Eigenbrot and Raymond,* 1981). *The coordinates were obtained from the Cambridge Structural Database* (*refcode CPYRZU*).

are comparable to the distances observed in the $(MeCp)_3U(PMe_3)$ complex of 2.972(6) and 2.52(1) Å, respectively (Brennan and Zalkin, 1985).

Several novel tris-cyclopentadienyl complexes have also been studied structurally. In the anionic portion of $[Ph_4As][Cp_3U(NCS)_2]$, the uranium center is surrounded by a trigonal planar arrangement of Cp ligands in the equatorial plane, and the thiocyanate ligands occupy axial positions with U–N bond distances of 2.46 and 2.50 Å (Bombieri *et al.*, 1983a). The first example of the opposite situation, a cationic organoactinide species, was observed in $[Cp_3U(NCMe)_2]_2[UO_2Cl_4]\cdot(C_4H_6)_2$, formed from the reaction of Cp_3UCl in MeCN with gaseous butadiene and traces of O_2 (Fig. 22.30). The cation contains uranium in the tetravalent oxidation state with trigonal bipyramidal geometry (D_{3h}), while the anion has hexavalent uranium with approximate D_{2h} symmetry (Bombieri *et al.*, 1983b). Another cationic organoactinide species is evident in $[Cp_3U(NCMe)_2][CpThCl_4(NCMe)]$ with the familiar trigonal bipyramidal geometry. An interesting aspect of this structure is the simultaneous presence of tetravalent thorium in the anion with octahedral coordination (Rebizant *et al.*, 1987).

In the compound $Cp_3U(NPh)(O)CCHPMe_2Ph$, η^2 coordination of the oxygen and nitrogen atoms of the neutral ligand creates a four-membered ring. The U–N and U–O bond lengths are 2.45(1) and 2.34(1) Å, respectively, indicating the presence of single bonds which are typical for donor atoms carrying a partial negative charge. Due to the sterically crowded nature of the uranium center, the formation of this *cis*-Cp_3UXY-type compound is quite rare; its highly crowded nature is evident in the small ligand bite distance (2.22(2) Å), elongated $U–C_{Cp}$ bonds (average 2.84(2) Å vs 2.72 Å for Cp_3UBr), and compressed $Cp_{centroid}–U–Cp_{centroid}$ angles (Cramer *et al.*, 1987b).

A rare instance of a neptunium-containing organometallic complex (with tetravalent neptunium) is $Cp_3Np(OPh)$. Considering the oxygen atom and the centers of the three Cp ligands as vertices, the structure has flattened tetrahedral geometry and near C_{3v} symmetry (De Ridder *et al.*, 1996a). The Np–O bond

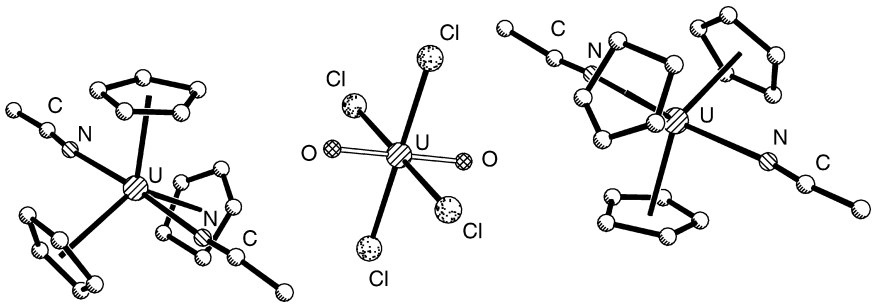

Fig. 22.30 *Crystal strucuture* $[Cp_3U(NCMe)_2]_2[UO_2Cl_4]\cdot(C_4H_6)_2$ *with* (C_4H_6) *and hydrogen atoms omitted* (*Bombieri* et al., 1983*b*). *The coordinates were obtained from the Cambridge Structural Database* (*refcode BUJPOL*).

distance is 2.136(7) Å, considerably shorter than that in $CpNpCl_3(OPMePh_2)_2$ of 2.277(6) Å (Bagnall *et al.*, 1986). $Cp_3Np(OPh)$ is isostructural with its uranium analog $Cp_3U(OPh)$; the U–O bond distance is slightly shorter, however, at 2.119(7) Å, and the flattened tetrahedral geometry is maintained (Spirlet *et al.*, 1990a).

The structure of $[(MeCp)_3U]_2[\mu\text{-}S]$ shows sulfur occupying a bridging role between two $(MeCp)_3U$ moieties, with an average U–S distance of 2.60(1) Å, one of the shortest ever observed. The most interesting aspect of this structure is the bent U–S–U angle of 164.9(4)°. These observed structural features are consistent with a class of bridging sulfur transition metal complexes with nearly linear M–S–M angles (159–180°) and M–S bond lengths shorter than expected for a M–S single bond. This trend suggests that the bridging sulfur may act as a π-donor or π-acceptor towards the metal center; an alternative explanation, however, is an electrostatic one, where steric repulsion due to the bulky $(MeCp)_3U$ groups accounts for the observed structural features (Brennan *et al.*, 1986b).

The first example of end-on binding of N_2 has been observed in the structure of $(Cp^*)_3U(\eta^1\text{–}N_2)$. A solution of $(Cp^*)_3U$ under N_2 at 80 psi darkens with the precipitation of hexagonal crystals of the desired compound. Binding is reversible, with quantitative regeneration of $(Cp^*)_3U$ upon lowering the pressure to 1 atm. The three Cp* ligands are bound pentahapto to the uranium center, with the remaining coordination site filled by N_2, resulting in a trigonal pyramidal geometry (Evans *et al.*, 2003b). The U–N bond distance of 2.492(10) Å is comparable to the 2.485(9) Å $U\text{–}C_{CO}$ distance observed in $(Cp^*)_3U(CO)$. Here, the C≡O ligand is isoelectronic with N_2 and also binds end-on to the uranium center through carbon (Evans *et al.*, 2003a). The isostructural nature of the two compounds is illustrated in Fig. 22.31.

(c) Bis-cyclopentadienyl complexes

Like the tris-compounds, the prevalance of $Cp_2(Th,U)X_2$ compounds over $Cp_2(Th,U)X$ compounds reveals the large preference for the tetravalent oxidation state in these complexes. However, the $Cp_2(Th,U)X_2$ are considerably unstable compared to transition metal and lanthanide analogs towards intermolecular ligand redistribution (Bombieri *et al.*, 1998). For example, Cp_2UCl_2, produced by the reaction of TlCp and UCl_4 in the presence of 1,2-dimethoxyethane (DME), is actually a mixture of Cp_3UCl and $CpUCl_3(DME)$ (Ernst *et al.*, 1979).

The pentamethylcyclopentadienyl ligand (Cp*) has been utilized in organoactinide chemistry to circumvent many of the problems encountered with the unstable $Cp_2(Th,U)X_2$ compounds. As compared to the unsubstituted analog (Cp), Cp* provides increased covalent character of the Cp–M bond, stronger π-donor ability, kinetic stabilization due to steric shielding of the metal, and increased thermal stability. In addition to inhibiting the formation of polymeric structures, the Cp* improves many solution chemistry properties, including

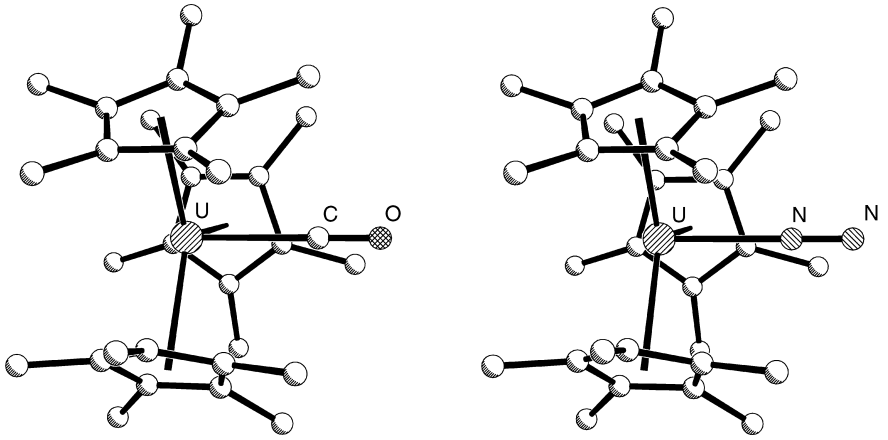

Fig. 22.31 *Crystal strucutures of* $(Cp^*)_3U(CO)$ (*Evans* et al., 2003*a*) *and* $(Cp^*)_3U(\eta^1\text{-}N_2)$ (*Evans* et al., 2003*b*) *with hydrogen atoms omitted. The coordinates were obtained from the Cambridge Structural Database* (*refcodes IMUVAN and ENABUQ*).

crystallizability, thus promoting its widespread use in organoactinide chemistry (Bombieri *et al*., 1998).

The addition of methyl groups to the Cp rings promotes coordinative unsaturation of the actinide metal by preventing the binding of other sterically demanding ligands. In addition, the methyl groups stabilize the organoactinide complexes with respect to ligand redistribution reactions, a feature that dominates the solution chemistry of unsubstituted f-element metallocenes. Ligand rearrangement prevents the cystallization of the Cp_2UCl_2 and $(Cp^*)(Cp)UCl_2$, as well as $[(^t\text{Bu})Cp]_2UCl_2$ and $(Cp')_2UCl_2$ (Lukens *et al*., 1999). In contrast, the $(Cp^*)_2UCl_2$ complex (Fig. 22.32) has normal, monomeric pseudotetrahedral 'bent-sandwich' configuration and has no tendency to undergo ligand redistribution to form the unknown $(Cp^*)_3UCl$ (Spirlet *et al*., 1992a).

A large number of representative bis-cyclopentadienyl actinide complexes are listed in Table 22.31, again illustrating the magnitude and diversity of organoactinide structural chemistry. The list is dominated by Cp* ligands (and other Cp derivative with bulky substituents), a tribute to its prevalence in organometallic chemistry and its usefulness in preventing ligand redistribution.

The series of compounds $Cp_2ThX_2(Me_2P(CH_2)_2PMe_2)$, where X = Cl, Me, or $CH_2C_6H_5$, have been synthesized and structurally characterized. The chloro derivative (Fig. 22.33) was synthesized from the reaction of sodium cyclopentadienide with $ThCl_4 \cdot (CH_3)_2PCH_2CH_2P(CH_3)_2$ in THF at 203 K. The latter two derivatives were synthesized from the reaction of the chloro derivative with methyllithium and benzyllithium, respectively, at 228 K. In accordance with Keppert's rules, the monodentate ligand with the shortest bond distance in each

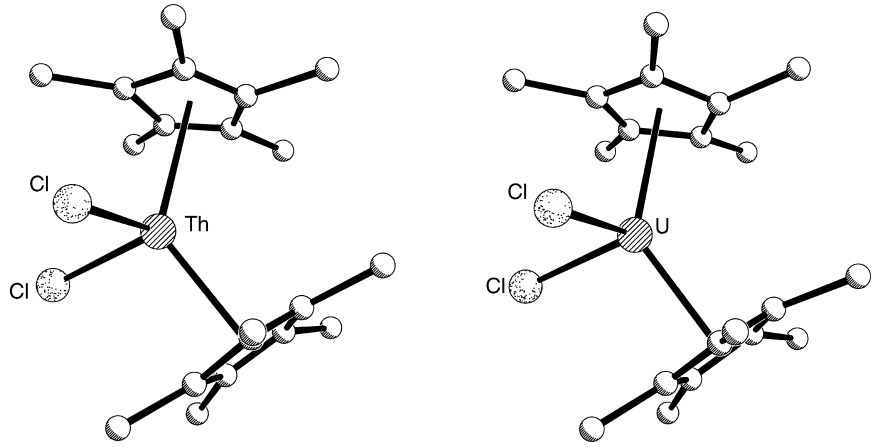

Fig. 22.32 *Crystal strucutures of* $(Cp^*)_2ThCl_2$ *and* $(Cp^*)_2UCl_2$ *with hydrogen atoms omitted* (*Spirlet* et al., 1992*a*). *The coordinates were obtained from the Cambridge Structural Database* (*refcodes VUJRAT and VUJPUL*).

structure (the Th–$Cp_{centroid}$ bond) occupies the site *trans* to the bidentate $Me_2P(CH_2)_2PMe_2$ ligand, thus making the bulky Cp ligands *cis* to one another. This is, in many ways, counter-intuitive in that the bulky Cp ligands should prefer a *trans* configuration to each other to lessen steric hindrance. The average Th–P bond lengths in the above three compounds are 3.147(1), 3.121(1), and 3.19(3) Å, respectively (Zalkin *et al*., 1987b,c).

The compounds $(Cp^*)_2UCl_2(C_3H_4N_2)$, $(Cp^*)_2UCl(C_3H_3N_2)$, and $(Cp^*)_2U(C_3H_3N_2)_2$ exhibit two bonding modes for the pyrazole/pyrazolate ligand. In the first compound, the pyrazole ligand acts as a neutral donor, with donation to the uranium center occurring through only a single nitrogen atom. In the latter two complexes, the pyrazole ligand is in the form of the pyrazolate anion and donates two nitrogen atoms per ligand to the uranium center. In the mono-chloro complex, the geometry can be approximated as tetrahedral by considering the two Cp* centroids, the chloride, and the midpoint of the N–N bond as corners. The U–N nitrogen bond length trend is supported by the nature of the ligand: the longest U–N bonds (2.607(8) Å average) occur for the neutral pyrazole ligand, while the anionic ligand yields the shortest U–N bonds. In the monopyrazolate complex, the two U–N bond lengths are 2.351(5) and 2.349(5) Å, while the dipyrazolate distances are 2.403(4), 2.360(5), 2.363(9), and 2.405(5) Å. Interestingly, in the latter case, the two 'internal' U–N bonds are shorter (greater crowding) than the two 'external' bonds. The pyrazolate U–N bond lengths are consistent with the $Cp_3U(N_2C_3H_3)$ structure (1.36, 1.40 Å) (Eigenbrot and Raymond, 1982).

Table 22.31 *Representative bis-cyclopentadienyl organoactinide complexes and derivatives.*

Structure	*Non-Cp donors (# per center)*	*References*
Cp		
$Cp_2U(BH_4)_2$	H(6)	Zanella *et al.* (1977)
$[\{Cp_2U(\mu\text{-}Cl)\}_3(\mu_3\text{-}Cl)_2][\{CpUCl_2\}_2(\mu\text{-}Cl)_3]\cdot 2(CH_2Cl_2)$	Cl(4); Cl(5)	Arliguie *et al.* (1994a)
$Cp_2ThX_2(Me_2P(CH_2)_2PMe_2)$ (X = Me, Cl, $CH_2C_6H_5$)	C(2), P(2); Cl(2), P(2)	Zalkin *et al.* (1987b,c)
$[Cp_2U(\mu\text{-}CH)(CH_2)P(Ph)_2]_2\cdot(C_2H_5)_2O$	C(3)	Cramer *et al.* (1978, 1980)
M-$[Cp_2U(\mu\text{-}S\text{-}CH)(CH_2)P(Ph)_2]_2\cdot C_5H_{12}$	C(3)	Cramer *et al.* (1980)
$Cp_2Th[(CH_2)(CH_2)PPh_2]_2$	C(4)	Cramer *et al.* (1995a)
*Cp**		
$[(Cp^*)_2Th(H)(\mu\text{-}H)]_2$	H(3)	Broach *et al.* (1979)
$[K(18\text{-crown-}6)][(Cp^*)_2U(Cl)H_6Re(PPh_3)_2]\cdot 0.5(C_6H_6)$	H(3), Cl	Cendrowski-Guillaume *et al.* (1994)
$(Cp^*)_2U(H)(Me_2P(CH_2)_2PMe_2)$	H, P(2)	Duttera *et al.* (1982)
$(Cp^*)_2MCl_2$ (M = Th, U)	Cl(2)	Spirlet *et al.* (1992a)
$[(Cp^*)_2U(\mu\text{-}Cl)]_3$	Cl(2)	Manriquez *et al.* (1979)
$[Li(TMED)][(Cp^*)_2UCl(NC_6H_5)]$	Cl, N	Arney and Burns (1995)
$(Cp^*)_2Th(Cl)(HNC(Me)NC(Me)CHCN)$	Cl, N(2)	Sternal *et al.* (1987)
$(Cp^*)_2UCl(\eta^2\text{-}(N,N')\text{-}MeNN{=}CPh_2)$	Cl, N(2)	Kiplinger *et al.* (2002b)
$(Cp^*)_2UCl_2(C_3H_3N_2)$	Cl, N(2)	Eigenbrot and Raymond (1982)
$(Cp^*)_2UCl_2(C_3H_4N_2)$	Cl(2), N	Eigenbrot and Raymond (1982)
$(Cp^*)_2UCl_2(HNPPh_3)$	Cl(2), N	Cramer *et al.* (1989)
$(Cp^*)_2UCl_2(HNSPh_2)$	Cl(2), N	Cramer *et al.* (1995b)
$(Cp^*)_2ThCl[O_2C_2(CH_2CMe_3)(PMe_3)]$	Cl, O(2)	Moloy *et al.* (1983)
$[(Cp^*)_2ThCl\{\mu\text{-}CO(CH_2CMe_3)CO\}]_2$	Cl, O(2)	Fagan *et al.* (1980)
$(Cp^*)_2ThCl[\eta^2\text{-}COCH_2CMe_3]$	Cl, C, O	Fagan *et al.* (1980)
$(Cp^*)_2ThBr_2(THF)$	Br(2), O	Edelman *et al.* (1995)
$[(Cp^*)_2Th(Me)][B(C_6F_5)_4]$	C	Yang *et al.* (1991)
$(Cp^*)_2Th[(CH_2)_2SiMe_2]$	C(2)	Bruno *et al.* (1982b)
$(Cp^*)_2Th(CH_2SiMe_3)_2$	C(2)	Bruno *et al.* (1983)
$(Cp^*)_2Th(CH_2CMe_3)_2$	C(2)	Bruno *et al.* (1986)
$(Cp^*)_2Th(\eta^4\text{-}C_4H_6)$	C(4)	Smith *et al.* (1986)
$[(Cp^*)_2Th(Me)(THF)_2][BPh_4]$	C, O(2)	Lin *et al.* (1987)
$[(Cp^*)_2U(Me)(OTf)]_2$	C, O(2)	Kiplinger *et al.* (2002b)
$(Cp^*)_2U(N\text{-}2,4,6\text{-}{}^t\!Bu_3C_6H_2)$	N	Arney and Burns (1995)
$(Cp^*)_2U(NC_6H_5)_2$	N(2)	Arney *et al.* (1992)
$(Cp^*)_2U[NH(C_6H_3Me_2\text{–}2,6)]_2$	N(2)	Straub *et al.* (1996)
$(Cp^*)_2U(NCPh_2)_2$	N(2)	Kiplinger *et al.* (2002c)
$(Cp^*)_2U(NSPh_2)_2$	N(2)	Ariyaratne *et al.* (2002)
$(Cp^*)_2U(C_3H_3N_2)_2$	N(4)	Eigenbrot and Raymond (1982)
$[(Cp^*)_2Th(\mu\text{-}O_2C_2Me_2)]_2$	O(2)	Manriquez *et al.* (1978)

Table 22.31 (*Contd.*)

Structure	*Non-Cp donors (# per center)*	*References*
*Cp**		
$(Cp^*)_2U(\eta^2\text{-}(N,N')\text{-}MeNN{=}CPh_2)(OTf)$	O, N(2)	Kiplinger *et al.* (2002b)
$[(Cp^*)_2U(OMe)]_2(\mu\text{-}PH)$	O, P	Duttera *et al.* (1984)
$(Cp^*)_2Th(PPh_2)_2$	P(2)	Wrobleski *et al.* (1986a)
$(Cp^*)_2U(SMe)_2$	S(2)	Lescop *et al.* (1999)
$(Cp^*)_2Th[S(CH_2)_2Me]_2$	S(2)	Lin *et al.* (1988)
$[Na(18\text{-crown-}6)][(Cp^*)_2U(S^tBu)(S)]$	S(2)	Ventelon *et al.* (1999)
$(Cp^*)_2U(S^tBu)(S_2CS^tBu)$	S(3)	Lescop *et al.* (1999)
$(Cp^*)_2ThS_5$	S(4)	Wrobleski *et al.* (1986b)
MeCp		
$[(MeCp)_2U]_2(\mu\text{-}NR)_2$ (R = Ph, $SiMe_3$)	N(2)	Brennan *et al.* (1988b)
Cp′, *Cp″*, Cp^{tt}, $(^tBu)_2Cp$		
$(Cp'')_2UX_2$ (X = BH_4, Cl, OAr)	H(6); Cl(2); O(2)	Hunter and Atwood (1984)
$(Cp'')_2UX_2$ (X = BH_4, Br, I)	H(6); Br(2); I(2)	Blake *et al.* (1995)
$[(^tBu)_2Cp]_2UX_2$ (X = F, Cl)	F(2); Cl(2)	Lukens *et al.* (1999)
$[(Cp'')_2UF(\mu\text{-}F)]_2$	F(3)	Lukens *et al.* (1999)
$[(Cp'')_2U(\mu\text{-}BF_4)(\mu\text{-}F)]_2$	F(4)	Hitchcock *et al.* (1984)
$(Cp'')_2MCl_2$ (M = Th, U)	Cl(2)	Blake *et al.* (1995)
$(Cp'')_2U(\mu\text{-}Cl)_2Li(PMDETA)$	Cl(2)	Blake *et al.* (1988a)
$(Cp'')_2U(\mu\text{-}Cl)_2Li(THF)_2$	Cl(2)	Blake *et al.* (1988b)
$[PPh_4][(Cp'')_2UCl_2]$	Cl(2)	Blake *et al.* (1988a)
$[\{(^tBu)_2Cp\}_2U]_2(\mu\text{-}Cl)_2$	Cl(2)	Zalkin *et al.* (1988b)
$[(Cp'')_2U(\mu\text{-}X)]_2$ (X = Cl, Br)	Cl(2); Br(2)	Blake *et al.* (1986b)
$(Cp'')_2UX_2$ (X = Cl, Me)	Cl(2); C(2)	Lukens *et al.* (1999)
$[(Cp^{tt})_2Th(Cl)\{CH(SiMe_3)_2\}]$	Cl, C	Edelman *et al.* (1995)
$(Cp'')_2UCl[CN(C_6H_3Me_2)]_2$	Cl, C(2)	Zalkin and Beshouri (1989a)
$(Cp'')_2UCl(NCSiMe_3)_2$	Cl, N(2)	Zalkin and Beshouri (1989b)
$[(^tBu)_2Cp]_2Th(\mu,\eta^3\text{-}P_3)Th(Cl)[(^tBu)_2Cp]_2$	Cl, P(3)	Scherer *et al.* (1991)
$(Cp'')_2UBr(CN^tBu)_2$	Br, C(2)	Beshouri and Zalkin (1989)
$[(Cp')_2U(\mu\text{-}O)]_3$	O(2)	Berthet *et al.* (1993)
$[(Cp'')_2U(\mu\text{-}O)]_2$	O(2)	Zalkin and Beshouri (1988)
$[(^tBu)_2Cp]_2Th(\mu,\eta^3,\eta^3\text{-}P_6)Th[(^tBu)_2Cp]_2$	P(3)	Scherer *et al.* (1991)
$[(^tBu)_2Cp]_2Th(\mu,\eta^{2:1:2:1}\text{-}As_6)Th[(^tBu)_2Cp]_2$	As(3)	Scherer *et al.* (1994)

* Semicolons used to differentiate coordination to different metal centers or different structures.

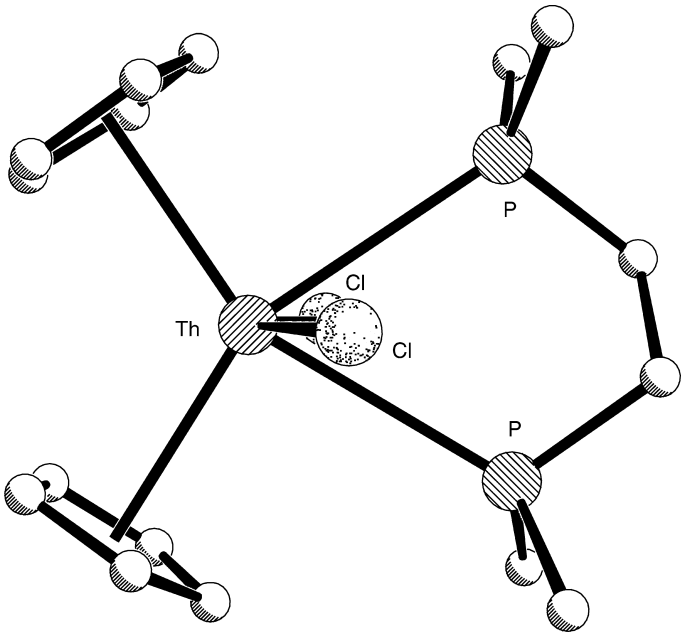

Fig. 22.33 *Crystal strucuture of* $Cp_2ThCl_2(Me_2P(CH_2)_2PMe_2)$ *with hydrogen atoms omitted* (*Zalkin* et al., 1987*b*). *The coordinates were obtained from the Cambridge Structural Database* (*refcode BIXVOT10*).

The first example of an organoactinide polysulfide reveals the unique twist-boat conformation of a ThS_5 ring, generated by the reaction of $(Cp^*)_2ThCl_2$ with Li_2S_5. The crystal structure of $(Cp^*)_2ThS_5$ (Fig. 22.34) is unique compared to transition metal analogs, such as Cp_2TiS_5, Cp_2ZrS_5, and Cp_2HfS_5, which strictly exhibit a MS_5 chair conformation. This anomaly in conformation is likely due to the coordination of four ring sulfur atoms to the uranium center, rather than two. Two types of bonding are thought to occur: two Th–S bonds at 2.768(4) Å are ionic in nature and two at 3.036(3) Å are dative in nature (Wrobleski *et al*., 1986b).

Many polynuclear bis-organoactinide complexes with bridging hydride, halide, and oxo groups are known. For example, the single-crystal neutron diffraction structure of the dimeric compound $[(Cp^*)_2Th(H)(\mu\text{-}H)]_2$, one of the first examples of an actinide hydride complex, contains both bridging and terminal hydrides. Two $(Cp^*)_2Th(H)$ moieties, each containing a terminal hydride, are connected by two bridging hydrides; the terminal and bridging Th–H distances are 2.03(1) and 2.29(3) Å, respectively, with a Th–Th separation of 4.007(8) Å (Broach *et al*., 1979).

The trimeric bridging halide complex, $[(Cp^*)_2U(\mu\text{-}Cl)]_3$, contains three $(Cp^*)_2U$ units, each connected by a bridging chloride and pseudotetrahedral

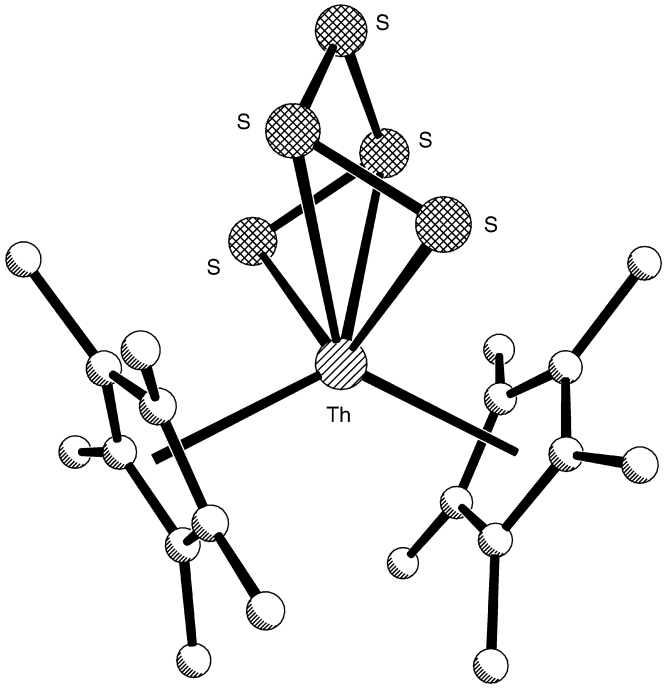

Fig. 22.34 *Crystal strucuture of* $(Cp^*)_2ThS_5$ *with hydrogen atoms omitted* (*Wrobleski* et al., 1986*b*). *The coordinates were obtained from the Cambridge Structural Database* (*refcode DIJRET*).

geometry around each uranium. The cyclic –U–Cl–U–Cl–U–Cl– moiety comprises a nearly planar six-membered ring, with average U–Cl, U–C, and U–U distances of 2.901(5), 2.76(3), and 5.669(2) Å, respectively (Manriquez *et al*., 1979). Finally, the bridging oxo complex, $[(Cp'')_2U(\mu\text{-}O)]_2$, contains two $(Cp'')_2U$ units connected by two bridging oxo ligands and a geometry similar to the chloro complex (Fig. 22.35). The average U–O and U–C distances are 2.213(8) and 2.77(4) Å, respectively. The average $U\text{–}Cp_{centroid}$ distance is 2.496 Å (Zalkin and Beshouri, 1988). For further examples of bridging complexes, the reader is referred to Table 22.31.

(d) Mono-cyclopentadienyl complexes

Mono-cyclopentadienyl organoactinide complexes, while less common, are typically Lewis-base adducts of the type $CpAnX_3L_n$. These complexes are usually sterically and electronically unsaturated, making their synthesis and subsequent crystallization quite challenging. Representative complexes for which structural data are available are listed in Table 22.32. The structures of

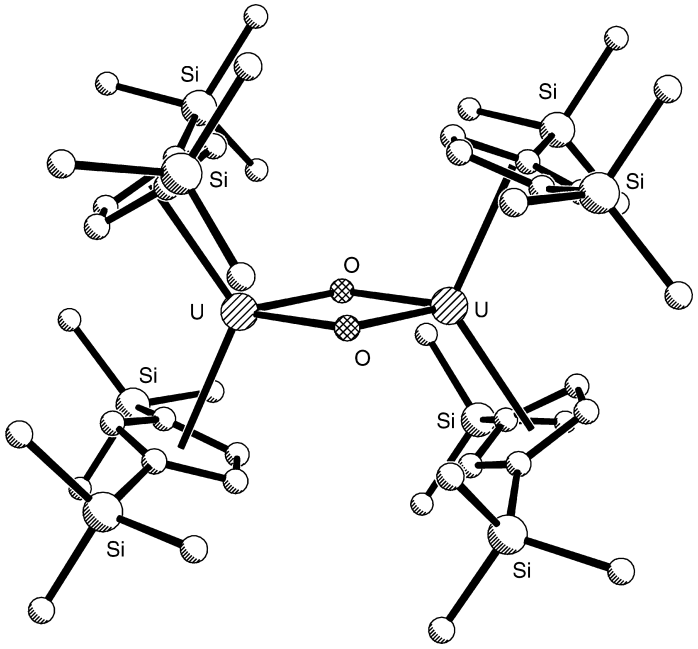

Fig. 22.35 *Crystal strucuture of* $[(Cp'')_2U(\mu\text{-}O)]_2$ *with hydrogen atoms omitted* (*Zalkin and Beshouri,* 1988). *The coordinates were obtained from the Cambridge Structural Database* (*refcode GIFNIS*).

$CpUCl_3(OPPh_3)_2 \cdot THF$ (Bombieri *et al.*, 1978c; Bagnall *et al.*, 1984) and $CpUCl_3[OP(NMe_2)_3]_2$ (Bagnall *et al.*, 1984) show an octahedral environment around the uranium centers with the neutral ligands occupying the *cis* coordination sites. In addition, the chlorine ligands are arranged in a *mer* fashion (as opposed to a *fac* arrangement) and the Cp ligands are *trans* to one of the neutral ligands. One of the few neptunium-containing organoactinide complexes, $CpNpCl_3(OPMePh_2)_2$, is analogous to the uranium structures described above (Fig. 22.36) (Bagnall *et al.*, 1986).

The compound $[CpU(CH_3COO)_2]_4O_2$ has four seven-coordinate uranium centers, each with distorted pentagonal bipyramidal geometry. The pentagonal arrangement around a given uranium center is defined by five oxygen atoms from four different acetate ligands. Two bridging acetates are monodentate simultaneously with respect to two neighboring uranium atoms. The remaining two bridging acetate groups take on a more complex role, each joining two neighboring uranium centers, with one oxygen being mondentate toward one uranium and the other oxygen being bidentate toward both uranium atoms. The remaining coordination sites are occupied by bridging oxo ligands (joining two pairs of uranium atoms), providing the apex of each pentagonal bipyramid,

Table 22.32 *Representative mono-cyclopentadienyl organoactinide complexes.*

Structure	*Non-Cp donors (# per center)*	*References*
Cp		
$CpU(BH_4)_3$	H(9)	Baudry *et al.* (1989a)
$[CpTh_2(O\text{-}^iPr)_7]_3$	O(5)	Barnhart *et al.* (1995b)
$CpUCl(acac)_2(OPPh_3)$	Cl, O(5)	Baudin *et al.* (1988)
$CpUCl_3(OPPh_3)_2 \cdot THF$	Cl(3), O(2)	Bombieri *et al.* (1978c); Bagnall *et al.* (1984)
$CpUCl_3[OP(NMe_2)_3]_2$	Cl(3), O(2)	Bagnall *et al.* (1984)
$CpNpCl_3(OPMePh_2)_2$	Cl(3), O(2)	Bagnall *et al.* (1986)
$CpU[(CH_2)(CH_2)PPh_2]_3$	C(6)	Cramer *et al.* (1984b)
$[Cp(CH_3COO)_5U_2O]_2$	O(6)	Brianese *et al.* (1989)
$[CpU(CH_3COO)_2]_4O_2$	O(6)	Rebizant *et al.* (1992)
*Cp**		
$[Na(THF)_6][Cp^*U(BH_4)_3]_2$	H(9)	Ryan *et al.* (1989)
$[Cp^*(Cl)(HNSPh_2)U(\mu^3\text{-}O)(\mu^2\text{-}O)U(Cl)(HNSPh_2)]_2$	Cl, N, O(3)	Cramer *et al.* (1995b)
$Cp^*UI_2(THF)_3$	I(2), O(3)	Avens *et al.* (2000)
$Cp^*UI_2(pyr)_3$	I(2), N(3)	Avens *et al.* (2000)
$Cp^*U(CH_2Ph)_3$	C(6)	Kiplinger *et al.* (2002a)
$Cp^*U(\eta^3\text{-}2\text{-}MeC_3H_4)_3$	C(9)	Cymbaluk *et al.* (1983)
$Cp^*[(Me_3Si)_2N]Th(\mu_2\text{-}OSO_2CF_3)_3Th[N(SiMe_3)(SiMe_2CH_2)]Cp^*$	C, N, O(3); N, O(3)	Butcher *et al.* (1995)
$Cp^*U[N(SiMe_3)_2]_2$	N(2)	Avens *et al.* (2000)
$[Cp^*U(NEt_2)_2(THF)_2]BPh_4$	N(2), O(2)	Berthet *et al.* (1995)
Cp‴, MeCp		
$[(Cp'''ThCl_3)_2NaCl(OEt_2)]_2$	Cl(5)	Edelman *et al.* (1995)
$Cp'''UCl_2(THF)(\mu\text{-}Cl)_2[Li(THF)_2]$	Cl(4), O(1)	Edelman *et al.* (1987)
$(MeCp)UCl_3(THF)_2$	Cl(3), O(2)	Ernst *et al.* (1979)

* Semicolons used to differentiate coordination to different metal centers or different structures.

and each pentahapto Cp ligand occupies the remaining apex (Rebizant *et al.*, 1992).

A cyclic hexameric thorium organoactinide complex (Fig. 22.37) is evident in the structure of $[CpTh_2(O\text{–}^iPr)_7]_3$. Interestingly, the Cp ligands in this structure take on a bridging role between three $[Th_2(O\text{–}^iPr)_7]$ units, each pentahapto to its neighboring thorium atoms. Each thorium center has distorted octahedral geometry provided by a Cp ligand and five $O\text{–}^iPr$ groups, two of which are bound to a thorium atom and the remaining three bridge between two thorium atoms (Barnhart *et al.*, 1995b).

The two thorium atoms in the triflate-bridged compound isolated by Butcher *et al.* (1995) have different coordination numbers (Fig. 22.38). Each thorium atom has one Cp* ligand bound in a pentahapto fashion and the two centers are

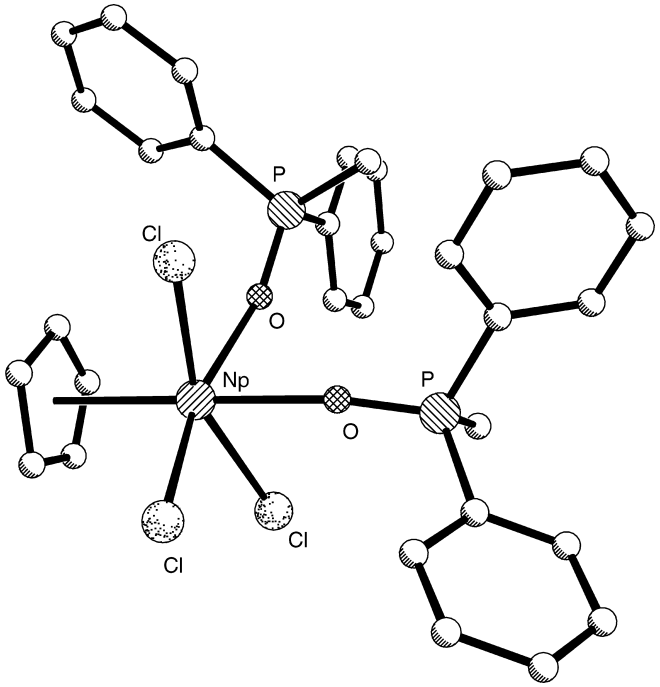

Fig. 22.36 *Crystal strucuture of* $CpNpCl_3(PMePh_2O)_2$ *with hydrogen atoms omitted* (*Bagnall* et al., 1986). *The coordinates were obtained from the Cambridge Structural Database* (*refcode DIXCOC*).

joined by three bridging triflate ligands. One thorium center is coordinated to a cyclometalated amide ligand in a bidenate manner through both nitrogen, and interestingly, carbon, resulting in a hexacoordinate thorium atom (Th–N= 2.26(4) Å, Th–C=2.43(5) Å). The remaining thorium center has a bis-(trimethylsilyl)amide ligand bound in a monodentate fashion only through the nitrogen atom (Th–N=2.24(3) Å), resulting in pentacoordinate thorium.

22.5.2 Cyclooctatetraene–actinide compounds

A milestone in the field of organometallics that effectively marked the beginning of organoactinide chemistry was the synthesis (Streitweiser and Müller-Westerhoff, 1968) and subsequent structural characterization of uranocene. The pursuit of uranocene was a direct result of the idea that it would be analogous to ferrocene with the additional benefit of studying the contribution of f-orbitals to the bonding. Like ferrocene, uranocene is a sandwich complex of D_{8h} symmetry in which the uranium(IV) ion is positioned between two octahapto (η^8-C_8H_8) cyclooctatetraene (COT) dianions. Although eclipsed in

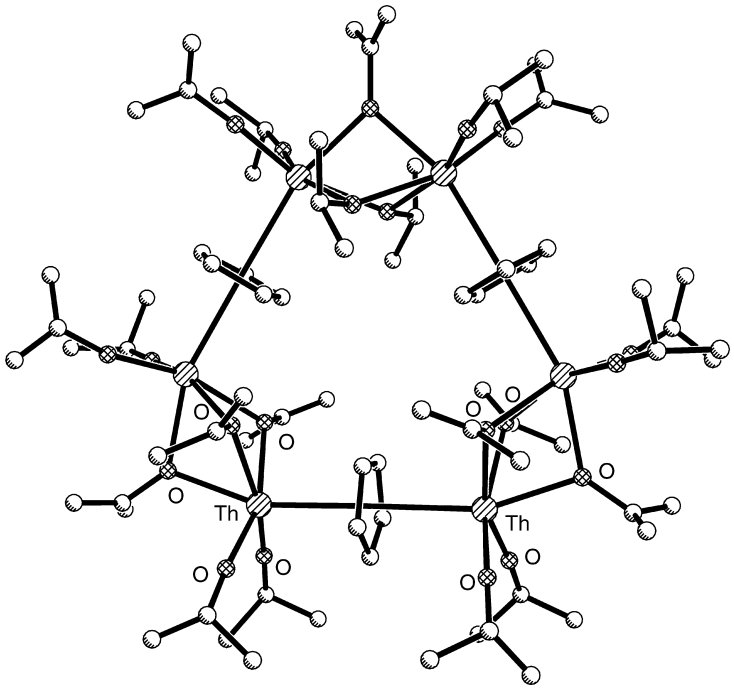

Fig. 22.37 *Crystal strucuture of* $[CpTh_2(O\text{-}^iPr)_7]_3$ *with hydrogen atoms omitted* (*Barnhart* et al., 1995*b*). *The coordinates were obtained from the Cambridge Structural Database* (*refcode ZEJYES*).

uranocene, the COT rings have the potential of being either eclipsed or staggered (Zalkin and Raymond, 1969; Avdeef *et al*., 1972). The thorium analog of uranocene, commonly referred to as thorocene, is isostructural, and both are extremely air-sensitive (Avdeef *et al*., 1972). Both structures consist of the central metal atom participating in symmetrical π-bonding to the COT ligands, related by a crystallographic inversion center. The average Th–C and U–C bond distances are 2.701(4) and 2.647(4) Å, respectively; the corresponding metal-to-centroid distances are 2.004 and 1.924 Å. Spectroscopic studies with uranocene seem to indicate at least some π-interactions between the molecular orbitals of the COT ligands and the 5f orbitals of the metal.

Neptunocene, a transuranic metallocene, is isostructural with both thorocene and uranocene, with an average Np–C bond distance of 3.630(3) Å (De Ridder *et al*., 1996b). Powder diffraction data are available for both $(COT)_2Pa$ and $(COT)_2Pu$ that indicate protactinocene is isostructural with the lower actinide analogs and plutonocene is isomorphous with the series (Karraker *et al*., 1970; Starks *et al*., 1974). Incorporation of the COT ligand is not limited to metallocenes. In fact, a host of other examples containing COT are listed in Table 22.33.

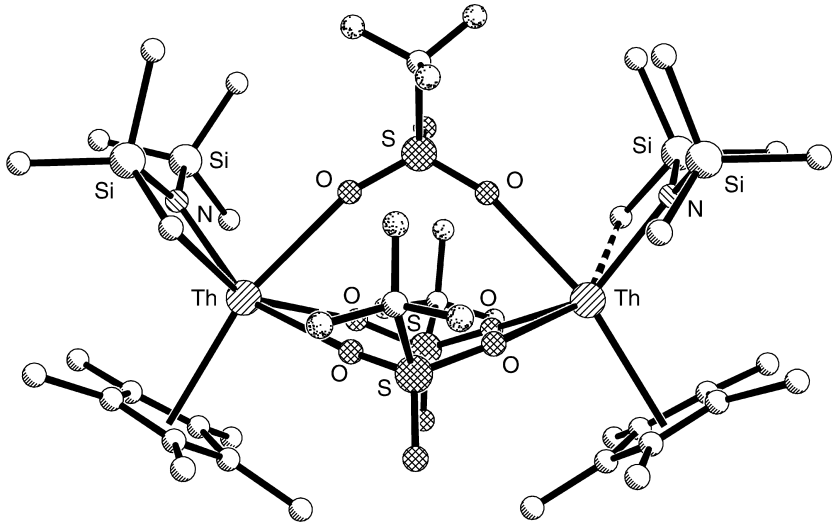

Fig. 22.38 *Crystal strucuture of* $Cp^*[(Me_3Si)_2N]Th(\mu_2\text{-}OSO_2CF_3)_3Th[N(SiMe_3)(SiMe_2CH_2)]Cp^*$ *with hydrogen atoms omitted* (*Butcher* et al., 1995). *The coordinates were obtained from the Cambridge Structural Database* (*refcode ZANJIH*).

A mixed cyclopentadiene/cyclooctatetraene complex is observed in the crystal structure of (COT)(Cp*)U(Me_2bpy) (Schake *et al.*, 1993). The binding of the COT and Cp* rings are η^8 and η^5, respectively, and the bipyridine adduct is bidentate through both nitrogen atoms. The resulting geometry around the uranium is a distorted tetrahedron with a Cp*–U–COT bond angle (from centroids of ligands) of 138.2°, comparable to what is observed in the thorium complexes, (COT)Cp*Th[$CH(SiMe_3)_2$] and (COT)Th(Cp*)(μ-Cl)$_2$Mg($CH_2{}^t$Bu)(THF) · 0.5PhMe (Gilbert *et al.*, 1989).

Butenouranocene, $[C_8H_6(CH_2)_2]_2U$, contains a cyclooctatetraene derivative appended with a cyclobuteno ring (Fig. 22.39). The uranium ion is sandwiched between the two eclipsed rings, but centered on the cyclooctatetraene rings, with an overall C_{2h} symmetry. The average U–C distance of 2.64(2) Å (Zalkin *et al.*, 1979) is comparable to uranocene (2.65 Å) and similar structures.

22.5.3 Other (indenyl, arene, etc.) compounds

Representative organoactinide complexes containing ligands not covered in previous sections are listed in Table 22.34 and include various indenyl, arene, and miscellaneous structures, including bridged Cp ligands. The indenyl ligand, $C_9H_7^-$, is formally analogous to $C_5H_5^-$, yet is more sterically demanding (both substituted and unsubstituted) and can coordinate in pentahapto, trihapto, and monohapto modes (Bombieri *et al.*, 1998).

Table 22.33 *Representative cyclooctatetraenyl organoactinide complexes.*

Structure	*Non-Cp donors (# per center)*	*References*
$(COT)_2Th$	–	Avdeef *et al.* (1972)
$(COT)_2U$	–	Zalkin and Raymond (1969); Avdeef *et al.* (1972)
$(Me_4COT)_2U$	–	Hodgson and Raymond (1973)
$(Ph_4COT)_2U$	–	Templeton *et al.* (1977)
$[C_8H_6(CH_2)_2]_2U$	–	Zalkin *et al.* (1979)
$[C_8H_6(CH_2)_3]_2U$	–	Zalkin *et al.* (1982)
$[C_8H_6(CH)_4]U$	–	Zalkin *et al.* (1985)
$(COT)_2An$ (An = Pa, Np, Pu)	–	Karraker *et al.* (1970); Starks *et al.* (1974)
$(COT)_2Np$	–	De Ridder *et al.* (1996b)
$K(COT)_2An \cdot (THF)_2$ (An = Np, Pu)	–	Karraker and Stone (1974)
$K(COT)_2Pu \cdot [CH_3O(CH_2)_2]_2O$	–	Karraker and Stone (1974)
$(COT)U(\eta^5\text{-}C_4Me_4P)(BH_4)(THF)$	H(3), O	Cendrowski-Guillaume *et al.* (2002)
$[(COT)U(BH_4)(\mu\text{-}OEt)]_2$	H(3), O(2)	Arliguie *et al.* (1992)
$(COT)U(BH_4)_2(OPPh_3)$	H(6), O	Baudry *et al.* (1990a)
$(COT)(Cp^*)Th(\mu\text{-}Cl)_2Mg(CH_2{}^tBu)(THF) \cdot 0.5PhMe$	Cl(2)	Gilbert *et al.* (1989)
$(COT)UCl_2(pyr)_2$	Cl(2), N(2)	Boussie *et al.* (1990)
$(COT)ThCl_2(THF)_2$	Cl(2), O(2)	Zalkin *et al.* (1980)
$(COT)(Cp^*)Th[CH(SiMe_3)_2]$	C	Gilbert *et al.* (1989)
$[(COT)U(mdt)]_2$	C(2), S(4)	Arliguie *et al.* (2003)
$(COT)U(mdt)(pyr)_2$	C(2), N(2), S(2)	Arliguie *et al.* (2003)
$(COT)Th[N(SiMe_3)_2]_2$	N(2)	Gilbert *et al.* (1988)
$(COT)(Cp^*)U(Me_2bpy)$	N(2)	Schake *et al.* (1993)
$(\mu\text{-}\eta^8,\eta^8\text{-}COT)U_2(NC[{}^tBu]Mes)_6$	N(3)	Diaconescu and Cummins (2002)
$[(COT)U]_2[\mu\text{-}\eta^4,\eta^4\text{-}HN(CH_2)_3N(CH_2)_2N(CH_2)_3NH]$	N(4)	Le Borgne *et al.* (2000)
$[(COT)Cp^*U(THF)_2]BPh_4$	O(2)	Berthet *et al.* (1995)
$[(COT)U(O^iPr)(\mu\text{-}O^iPr)]_2$	O(3)	Arliguie *et al.* (1992)
$(COT)U(MeCOCHCOMe)_2$	O(4)	Boussie *et al.* (1990)
$[Na(18\text{-crown-}6)(THF)_2][(COT)U(S^tBu)_3]$	S(3)	Leverd *et al.* (1994)
$[(COT)U(\mu\text{-}S^iPr)_2]_2$	S(4)	Leverd *et al.* (1994)
$[Na(18\text{-crown-}6)(THF)][(COT)U(C_4H_4S_4)_2]$	S(4)	Arliguie *et al.* (2000)

The π-bonding of indenyl ligands to the Th(IV) center in $(C_9H_7)_4Th$ occurs in an η^3 manner, where the five-membered rings of each indenyl ligand form the apices of a distorted tetrahedron. The indenyl bonding occurs through the three non-bridging carbons of each five-membered ring, giving thorium a

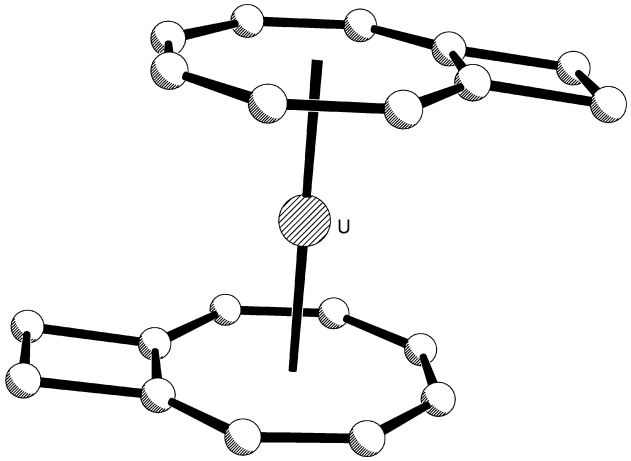

Fig. 22.39 *Crystal strucuture of* $[C_8H_6(CH_2)_2]_2U$ *with hydrogen atoms omitted* (*Zalkin* et al., 1979). *The coordinates were obtained from the Cambridge Structural Database* (*refcode CBOCTU*).

coordination number of 12. The lengthening of the distance between thorium and the remaining two bridging carbons of the five-membered ring is likely a consequence of localization of charge at these sites (Rebizant *et al*., 1986a,b). This is similar to what is observed in $(C_{12}H_{13})_3ThCl$ (containing a trimethyl indenyl ligand) (Spirlet *et al*., 1982) and $(C_9H_7)_3UCl$. In the latter case, the three shorter U–C bond distances range from 2.67(1) to 2.77(1) Å, while the two longer bonds are in the range of 2.79(1)–2.89(1) Å, suggesting trihapto bonding. However, the authors suggest the possibility of pentahapto bonding if one considers steric interferences from chloride and the six-membered ring (Burns and Laubereau, 1971). The trihapto indenyl coordination mode is also reported in the bromide and iodide analogs of the uranium complex (Spirlet *et al*., 1987b; Rebizant *et al*., 1988).

Pentahapto coordination of the indenyl ligand is apparent in the structures of several complexes, including $(C_9H_7)_3U$ (Meunier-Piret *et al*., 1980a), $(C_9H_7)_2U(BH_4)_2$ (Rebizant *et al*., 1989), and $(C_9H_7)UBr_3(THF)(OPPh_3)$ (Meunier-Piret *et al*., 1980b). In the tri-indenyl uranium complex (Fig. 22.40), the $U–C_{indenyl}$ bond distances to the five-membered ring are very similar; for instance, these distances for one of the indenyl rings are 2.846, 2.802, 2.845, 2.833, and 2.804 Å, with no bridging/non-bridging correlation. The first example of monhapto indenyl coordination is in the structure of $(C_{15}H_{19})_3ThCl$, where the hexamethyl indenyl ligand is σ-bonded through one carbon of each five-membered ring to thorium (Spirlet *et al*., 1992b).

Arene complexes of the actinides are very few (and limited to uranium); those for which structures are available show η^6 π-bonding of the aromatic ring

Table 22.34 *Representative other organoactinide complexes.*

Structure	*Other donors (# per center)*	*References*
indenyl		
pentahapto (η^5)		
$(C_9H_7)_3U$	–	Meunier-Piret *et al.* (1980a)
$(C_9H_7)_2U(BH_4)_2$	H(6)	Rebizant *et al.* (1989)
$(C_9H_7)UX_3(THF)_2$ (X = Cl, Br)	Cl(3), O(2); Br(3), O(2)	Rebizant *et al.* (1983, 1985)
$(C_9H_7)UBr_3(THF)(OPPh_3)$	Br(3), O(2)	Meunier-Piret *et al.* (1980b)
trihapto (η^3)		
$(C_9H_7)_4Th$	–	Rebizant *et al.* (1986a,b)
$(C_{11}H_{11})_3ThCl$	Cl	Spirlet *et al.* (1990b)
$(C_{12}H_{13})_3ThCl$	Cl	Spirlet *et al.* (1982)
$(C_9H_7)_3UCl$	Cl	Burns and Laubereau (1971)
$(C_{12}H_{13})_3UCl$	Cl	Meunier-Piret and Van Meerssche (1984)
$(C_9H_7)_3UBr$	Br	Spirlet *et al.* (1987b)
$[(C_9H_7)UBr_2(NCMe)_4]_2[UBr_6]$	Br(2), N(4)	Beeckman *et al.* (1986)
$[\{(C_9H_7)UBr(NCMe)_4\}_2(\mu\text{-}O)][UBr_6]$	Br, N(4), O	Beeckman *et al.* (1986)
$(C_9H_7)_3UI$	I	Rebizant *et al.* 1988)
$(C_{11}H_{11})_3ThCH_3$	C	Spirlet *et al.* (1993b)
$(C_9H_7)_3U(OCH_2CF_3)$	O	Spirlet *et al.* (1993c)
monohapto (σ-*bonded*)		
$(C_{15}H_{19})_3ThCl$	Cl	Spirlet *et al.* (1992b)
arenes		
$(C_6Me_6)U(BH_4)_3$	H(9)	Baudry *et al.* (1989b)
$[(C_6Me_6)UCl_2]_2(\mu\text{-}Cl)_3(AlCl_4)$	Cl(5)	Cotton and Schwotzer (1985)
$[(C_6Me_6)UCl_2(\mu\text{-}Cl)_3Cl_2U(C_6Me_6)][AlCl_4]$	Cl(5)	Campbell *et al.* (1986)
$(C_6Me_6)UCl_2(\mu\text{-}Cl)_3UCl_2(\mu\text{-}Cl)_3Cl_2U(C_6Me_6)$	Cl(5); Cl(8)	Campbell *et al.* (1986)
$(C_6H_6)U(AlCl_4)_3$	Cl(6)	Cesari *et al.* (1971)
$(C_6Me_6)U(AlCl_4)_3$	Cl(6)	Cotton and Schwotzer (1987)
$[U_3(\mu^3\text{-}Cl)_2(\mu^2\text{-}Cl)_3(\mu^1,\eta^2\text{-}AlCl_4)_3(\eta^6\text{-}C_6Me_6)_3][AlCl_4]$	Cl(6)	Cotton *et al.* (1986)
$[U(O\text{-}2,6\text{-}{}^iPr_2C_6H_3)_3]_2$	O(3)	Van Der Sluys *et al.* (1988)

Table 22.34 (*Contd.*)

Structure	*Other donors (# per center)*	*References*
ring-bridged		
$LiU_2Cl_5[CH_2(C_5H_4)_2]_2(THF)_2$	Cl(4)	Secaur *et al.* (1976)
$[Me_2Si(C_5Me_4)_2]U(\mu\text{-}Cl_4)$ $[Li(TMEDA)]_2$	Cl(4)	Schnabel *et al.* (1999)
$[CH_2(C_5H_4)_2]UCl_2(bipy)$	Cl(2), N(2)	Marks (1977)
$\mu\text{-}[2,6\text{-}CH_2C_5H_3NCH_2](\eta^5\text{-}C_5H_4)_2UCl_2$	Cl(2), N	Paolucci *et al.* (1991)
$(Cp^*)(C_5H_4CH_2)U(NAd)(NHAd)$	N(2)	Peters *et al.* (1999)
$[\{Me_2Si(C_5Me_4)(C_5H_4)\}U(\mu\text{-}NPh)]_2$	N(2)	Schnabel *et al.* (1999)
other	*type*	
$[U(C_3H_5)_2(O^iPr)_2]_2$	allyl	Brunelli *et al.* (1979)
$[Li(THF)_4]_2[(C_2B_9H_{11})_2UCl_2]$	dibarbollide	Fronczek *et al.* (1977)
$[U(BH_4)(THF)_5][U(BH_4)_3$ $(\mu\text{-}\eta^7,\eta^7\text{-}C_7H_7)U(BH_4)_3]$	cycloheptatrienyl	Arliguie *et al.* (1994b)
$[K(18\text{-crown-6})][U(\eta\text{-}C_7H_7)_2]$	cycloheptatrienyl	Arliguie *et al.* (1995)
$K_2(\mu\text{-}\eta^6,\eta^6\text{-}C_{10}H_8)[U(NC[^tBu]Mes)_3]_2$	napthalene	Diaconescu and Cummins (2002)
$(Me_4Fv)_2FeThCl_2$	fulvalene	Scott and Hitchcock (1995)
$[(\eta^5\text{-}C_4Me_4P)(\mu\text{-}\eta^5\text{-}C_4Me_4P)U(BH_4)]_2$	phospholyl	Gradoz *et al.* (1994)
$(\eta^5\text{-}C_4Me_4P)_2U(BH_4)_2$	phospholyl	Baudry *et al.* (1990b)
$(\eta\text{-}2,4\text{-}Me_2C_5H_5)U(BH_4)_3$	dimethylpentadienyl	Baudry *et al.* (1989a)

* Semicolons used to differentiate coordination to different metal centers or different structures.

(C_6H_6) to the metal center. For example, in the complexes $(C_6H_6)U(AlCl_4)_3$ (Cesari *et al.*, 1971) and $(C_6Me_6)U(AlCl_4)_3$ (Cotton and Schwotzer, 1987), the hexahapto arene ligands are bound to the uranium centers along with three bidentate $AlCl_4$ ligands (through chlorine), resulting in pentagonal bipyramidal structures (Fig. 22.41). In the case of $[(C_6Me_6)UCl_2]_2(\mu\text{-}Cl)_3(AlCl_4)$, as well as other U(III)–benzene complexes, the U–benzene (centroid) distances are considerably longer than in traditional anionic π-ligands. This is a strong indication of the relatively weak bonds that form in these types of complexes with the neutral arene ligand (Cotton and Schwotzer, 1985).

22.6 SUMMARY

The actinide structures that have been presented herein represent a fraction of known f-element compounds that have been studied by neutron and X-ray diffraction techniques. However, this treatment is by no means exhaustive as it

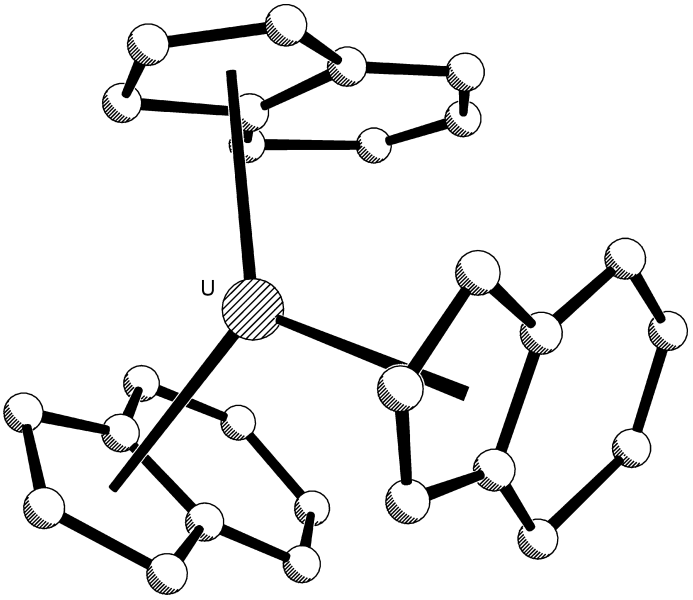

Fig. 22.40 *Crystal strucuture of* $(C_9H_7)_3U$ *with hydrogen atoms omitted* (*Meunier-Piret* et al., 1980*a*). *The coordinates were obtained from the Cambridge Structural Database* (*refcode TRINUR*).

would require several more chapters of comparable length. It should be apparent that the study and structural characterization of actinide compounds continues to play an important role in understanding the nature of this fascinating row of elements. While it is true that most simple and fundamental actinide compounds have been structurally characterized over the past 50 years, these studies are only the 'tip of the iceberg' in terms of what can and has yet to be discovered.

Due to the complex nuclear wastes that exist at many sites, the intricacies of environmental actinide migration and interaction phenomena, the task-specific nature of fuel processing schemes for the recovery of heavy elements, and a continued fundamental academic interest in these elements, advances in actinide chemistry will continue to be increasingly important into the foreseeable future. These advances must necessarily be accompanied by more complex structural analyses that will achieve a more thorough understanding of the chemical behavior of the actinides.

The development of more advanced X-ray and neutron diffraction instrumentation, along with the use of more exotic techniques such as extended X-ray absorption fine-structure (EXAFS) spectroscopy and even highly advanced *ab initio* quantum mechanics tools based on relativistic theory, will be

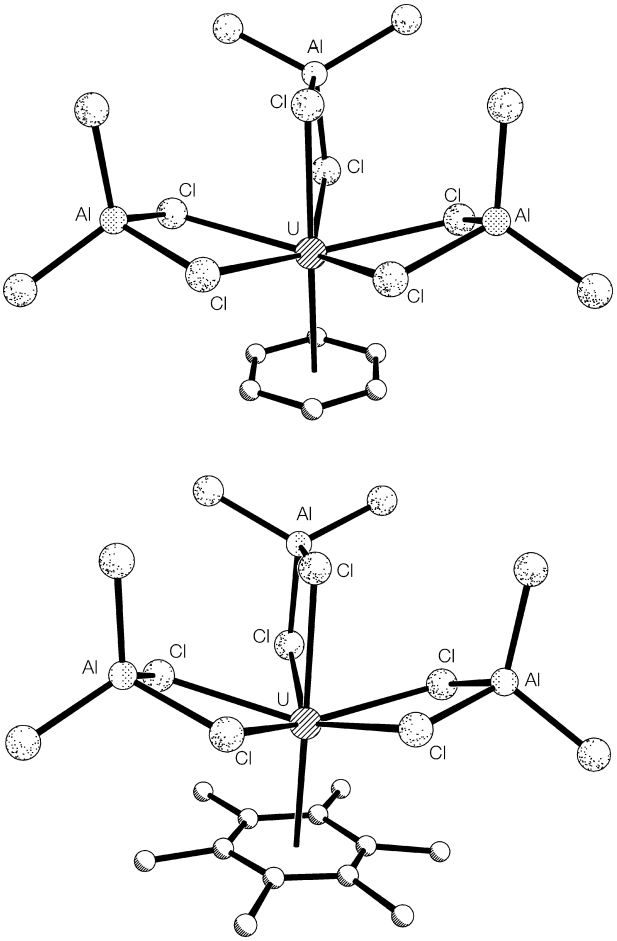

Fig. 22.41 *Crystal strucutures of* $(C_6H_6)U(AlCl_4)_3$ (*Cesari* et al., 1971) *and* $(C_6Me_6)U(AlCl_4)_3$ (*Cotton and Schwotzer,* 1987) *with hydrogen atoms omitted. The coordinates were obtained from the Cambridge Structural Database* (*refcodes BNZUAL and FODRUL*).

paramount in moving forward. These techniques will continue to assist in the elucidation of the critical aspects of actinide electronic structure and bonding, such as the role of 5f electrons in covalent interactions, that are still widely studied and debated. Nonetheless, the actinides are a series of elements unlike any other that will continue to provide ample challenges for chemists worldwide and push the limits of existing technology, particularly in the area of structural determination.

ABBREVIATIONS

Acac	acetylacetonato = 2,4-pentanedionato
BBN	9-borabicyclo(3.3.1)nonane
bipy	2,2′-bipyridyl
^{n}Bu	butyl = C_4H_9–
^{t}Bu	*tert*-butyl = $(CH_3)_3C$–
(^{t}Bu)Cp	η^5-$C_5H_4(^{t}Bu)$
(^{t}Bu)$_2$Cp	η^5-$C_5H_3(^{t}Bu)_2$–1,3
COT	η^8-C_8H_8
Cp	η^5-C_5H_5
Cp*	η^5-$C_5(CH_3)_5$
Cp′	η^5-$C_5H_4[Si(CH_3)_3]$
Cp″	η^5-$C_5H_3[Si(CH_3)_3]_2$–1,3
Cp‴	η^5-$C_5H_2[Si(CH_3)_3]_3$–1,2,4
Cp^{tt}	η^5-$C_5H_3[Si^{t}Bu(CH_3)_2]_2$–1,3
$CpCH_2Ph$	η^5-$C_5H_4(CH_2C_6H_5)$
DABCO	1,4-diazabicyclo[2.2.2]octane
DMAP	dimethylaminopyridine
DMF	dimethylformamide
DMPE	$(Me)_2P(CH_2)_2P(Me)_2$
DMSO	dimethylsulfoxide
Et	ethyl = C_2H_5–
HTTA	thenoyl trifluoroacetone
mdt	1,3-dithiole-4,5-dithiolate
Me	methyl = CH_3–
Me_2bpy	4,4′-dimethyl-2,2′-bipyridine
Me_4COT	η^8-$C_8H_4(CH_3)_4$
MeCp	η^5-$C_5H_4(CH_3)$
Me_4Cp	η^5-$C_5H(CH_3)_4$
Me_4Fv	1,2,3,4-tetramethylfulvalene
Mes	2,4,6-$C_6H_2(CH_3)_3$
NAd	1-adamantyl
OAr	2,5-dimethylphenoxide
OTf	OSO_2CF_3
Ph	phenyl = C_6H_5–
Ph_4COT	η^8-$C_8H_4(C_6H_5)_4$
PMDETA	pentamethyldiethylenediamine = $(Me_2NCH_2CH_2)_2NMe$
^{i}Pr	*iso*-propyl = $(CH_3)_2CH$–
^{n}Pr	*n*-propyl = C_3H_7–
pyr	pyridine = C_5H_5N; Hpyr = C_5H_5NH

$(SiMe_3)_2CHCp$	η^5-$C_5H_4[CH(SiMe_3)_2]$
THF	tetrahydrofuran = OC_4H_8
TMED	tetramethylethylenediamine

ACKNOWLEDGMENT

The authors thank Dr. Ann E. Visser for her early contributions to this chapter.

REFERENCES

Ackermann, R. J. and Rauh, E. G. (1973) *J. Inorg. Nucl. Chem.*, **35**, 3787–94.
Adam, M., Yünlü, K., and Fischer, R. D. (1990) *J. Organomet. Chem.*, **387**, C13–16.
Adam, R., Villiers, C., Ephritikhine, M., Lance, M., Nierlich, M., and Vigner, J.-D. (1993) *J. Organomet. Chem.*, **445**, 99–106.
Akhtar, M. N. and Smith, A. J. (1969) *J. Chem. Soc., Chem. Commun.*, 705–6.
Akimoto, Y. (1960) Chemistry Division Semiannual Report, November 1959, UCRL-9093, p. 73.
Akimoto, Y. (1967) *J. Inorg. Nucl. Chem.*, **29**, 2650–2.
Allen, F. H. (2002) *Acta Crystallogr*. B, **58**, 380–8.
Albering, J. H. and Jeitschko, W. (1995) *Z. Kristallogr.*, **210**, 878.
Alcock, N. W. (1973a) *J. Chem. Soc., Dalton Trans.*, 1614–16.
Alcock, N. W. (1973b) *J. Chem. Soc., Dalton Trans.*, 1610–13.
Alcock, N. W. (1973c) *J. Chem. Soc., Dalton Trans.*, 1616–20.
Alcock, N. W., Roberts, M. M., and Chakravorti, M. C. (1980a) *Acta Crystallogr. B*, **36**, 687–90.
Alcock, N. W., Kemp, T. J., Sostero, S., and Traverso, O. (1980b) *J. Chem. Soc., Dalton Trans.*, 1182–5.
Alcock, N. W., Flanders, D. J., Kemp, T. J., and Shand, M. A. (1985) *J. Chem. Soc., Dalton Trans.*, 517–21.
Alcock, N. W., Kemp, T. J., Leciejewicz, J., and Pennington, M. (1989) *Acta Crystallogr. C*, **45**, 719–21.
Alcock, N. W., Errington, W., Kemp, T. J., and Leciejewicz, J. (1996a) *Acta Crystallogr. C*, **52**, 615–17.
Alcock, N. W., Kemp, T. J., Roe, S. M., and Leciejewicz, J. (1996b) *Inorg. Chim. Acta*, **248**, 241–6.
Alenchikova, I. F., Zaitseva, L. L., Lipis, L. V., Nikolaev, N. S., Fomin, V. V., and Chebotarev, K. (1958) *Zh. Neorg. Khim.*, **3**, 951–5.
Amirthalingam, V. (1966) *J. Nucl. Mater.*, **20**, 193–4.
Ariyaratne, K. A. N. S., Cramer, R. E., and Gilje, J. W. (2002) *Organometallics*, **21**, 5799–802.
Arliguie, T., Baudry, D., Ephritikhine, M., Nierlich, M., Lance, M., and Vigner, J.-D. (1992) *J. Chem. Soc., Dalton Trans.*, 1019–24.
Arliguie, T., Ephritikhine, M., Lance, M., Vigner, J.-D., and Nierlich, M. (1994a) *J. Organomet. Chem.*, **484**, 195–201.

Arliguie, T., Lance, M., Nierlich, M., Vigner, J.-D., and Ephritikhine, M. (1994b) *J. Chem. Soc., Chem. Commun.*, 847–8.
Arliguie, T., Lance, M., Nierlich, M., Vigner, J.-D., and Ephritikhine, M. (1995) *J. Chem. Soc., Chem. Commun.*, 183–4.
Arliguie, T., Fourmigué, M., and Ephritikhine, M. (2000) *Organometallics*, **19**, 109–11.
Arliguie, T., Thuéry, P., Fourmigué, M., and Ephritikhine, M. (2003) *Organometallics*, **22**, 3000–3.
Armağan, N. (1977) *Acta Crystallogr. B*, **33**, 2281–4.
Arnaudet, L., Charpin, P., Folcher, G., Lance, M., Nierlich, M., and Vigner, J.-D. (1986) *Organometallics*, **5**, 270–4.
Arney, D. S. J., Burns, C. J., and Smith, D. C. (1992) *J. Am. Chem. Soc.*, **114**, 10068–9.
Arney, D. S. J. and Burns, C. J. (1995) *J. Am. Chem. Soc.*, **117**, 9448–60.
Arutyunyan, E. G., Porai-Koshits, M. A., and Molodkin, A. K. (1966a) *Zh. Strukt. Khim.*, **7**, 733–7.
Arutyunyan, E. G., Antsyshkina, A. S., and Balta, E. Ya. (1966b) *Zh. Strukt. Khim.*, **7**, 471–2.
Arutyunyan, E. G., Porai-Koshits, M. A., Molodkin, A. K., and Ivanova, O. M. (1966c) *Zh. Prikl. Khim.*, **7**, 813–14.
Asfari, Z., Bilyk, A., Dunlop, J. W. C., Hall, A. K., Harrowfield, J. M., Hosseini, M. W., Skelton, B. W., and White, A. H. (2001) *Angew. Chem. Int. Ed.Engl.*, **40**, 721–3.
Aslan, H., Yünlü, K., Fischer, R. D., Bombieri, G., and Benetollo, F. (1988) *J. Organomet. Chem.*, **354**, 63–76.
Asprey, L. B., Ellinger, F. H., Fried, S., and Zachariasen, W. H. (1955) *J. Am. Chem. Soc.*, **77**, 1707–8.
Asprey, L. B., Ellinger, F. H., Fried, S., and Zachariasen, W. H. (1957) *J. Am. Chem. Soc.*, **79**, 5825.
Asprey, L. B., Keenan, T. K., and Kruse, F. H. (1965) *Inorg. Chem.*, **4**, 985–6.
Asprey, L. B. and Haire, R. G. (1973) *Inorg. Nucl. Chem. Lett.*, **9**, 1121–8.
Atoji, M. and McDermott, M. J. (1970) *Acta Crystallogr. B*, **26**, 1540–4.
Atwood, J. L., Hains, C. F. Jr, Tsutsui, M., and Gebala, A. E. (1973) *J. Chem. Soc., Chem. Commun.*, 452–3.
Atwood, J. L., Tsutsui, M., Ely, N., and Gebala, A. E. (1976) *J. Coord. Chem.*, **5**, 209–15.
Avdeef, A., Raymond, K. N., Hodgson, K. O., and Zalkin, A. (1972) *Inorg. Chem.*, **11**, 1083–8.
Avens, L. R., Burns, C. J., Butcher, R. J., Clark, D. L., Gordon, J. C., Schake, A. R., Scott, B. L., Watkin, J. G., and Zwick, B. D. (2000) *Organometallics*, **19**, 451–7.
Avisimova, N. Yu., Gorbunova, Yu. E., Mikhailov, Yu. N., and Chumaevskii, N. A. (2001) *Zh. Neorg. Khim.*, **46**, 629–32.
Bagnall, K. W., Brown, D., and Jones, P. J. (1965) *J. Chem. Soc.*, 176–81.
Bagnall, K. W., Brown, D., and Easey, J. F. (1968a) *J. Chem. Soc. A*, 288–91.
Bagnall, K. W., Brown, D., and Easey, J. F. (1968b) *J. Chem. Soc. A*, 2223–7.
Bagnall, K. W., Benetollo, F., Bombieri, G., and De Paoli, G. (1984) *J. Chem. Soc., Dalton Trans.*, 67–73.
Bagnall, K. W., Payne, G. F., Alcock, N. W., Flanders, D. J., and Brown, D. (1986) *J. Chem. Soc., Dalton Trans.*, 783–7.
Baker, E. C., Raymond, K. N., Marks, T. J., and Wachter, W. A. (1974) *J. Am. Chem. Soc.*, **96**, 7586–8.

Baluka, M., Yeh, S., Banks, R., and Edelstein, N. (1980) *Inorg. Nucl. Chem. Lett.*, **16**, 75–7.

Bamberger, C. E., Haire, R. G., Begun, G. M., and Hellwege, H. E. (1984a) *J. Less Common Metals*, **102**, 179–86.

Bamberger, C. E., Haire, R. G., Hellwege, H. E., and Begun, G. M. (1984b) *J. Less Common Metals*, **97**, 349–56.

Bandoli, G., Graziani, R., and Zarli, B. (1968) *Acta Crystallogr. B*, **24**, 1129–30.

Banks, R. H., Edelstein, N. M., Rietz, R. R., Templeton, D. H., and Zalkin, A. (1978) *J. Am. Chem. Soc.*, **100**, 1957–8.

Baracco, L., Bombieri, G., Degetto, S., Forsellini, E., Graziani, R., and Marangoni, G. (1974) *Inorg. Nucl. Chem. Lett.*, **10**, 1045–50.

Barclay, G. A., Sabine, T. M., and Taylor, J. C. (1965) *Acta Crystallogr.*, **19**, 205–9.

Barnhart, D. M., Burns, C. J., Sauer, N. N., and Watkin, J. G. (1995a) *Inorg. Chem.*, **34**, 4079–84.

Barnhart, D. M., Butcher, R. J., Clark, D. L., Gordon, J. C., Watkin, J. G., and Zwick, B. D. (1995b) *New J. Chem.*, **19**, 503–8.

Baskin, Y. and Prasad, N. S. K. (1964) *J. Inorg. Nucl. Chem.*, **26**, 1385–90.

Baskin, Y. (1967) *J. Inorg. Nucl. Chem.*, **29**, 383–91.

Battiston, G. A., Sbrignadello, G., Bandoli, G., Clemente, D. A., and Tomat, G. (1979) *J. Chem. Soc., Dalton Trans.*, 1965–71.

Baudin, C., Charpin, P., Ephritikhine, M., Lance, M., Nierlich, M., and Vigner, J.-D. (1988) *J. Organomet. Chem.*, **345**, 263–74.

Baudry, D., Bulot, E., Charpin, P., Ephritikhine, M., Lance, M., Nierlich, M., and Vigner, J.-D. (1989a) *J. Organomet. Chem.*, **371**, 163–74.

Baudry, D., Bulot, E., Charpin, P., Ephritikhine, M., Lance, M., Nierlich, M., and Vigner, J.-D. (1989b) *J. Organomet. Chem.*, **371**, 155–62.

Baudry, D., Bulot, E., Ephritikhine, M., Nierlich, M., Lance, M., and Vigner, J.-D. (1990a) *J. Organomet. Chem.*, **388**, 279–87.

Baudry, D., Ephritikhine, M., Nief, F., Ricard, L., and Mathey, F. (1990b) *Angew. Chem.*, **102**, 1501–2.

Baybarz, R. D. (1968) *J. Inorg. Nucl. Chem.*, **30**, 1769–73.

Baybarz, R. D., Haire, R. G., and Fahey, J. A. (1972a) *J. Inorg. Nucl. Chem.*, **34**, 557–65.

Baybarz, R. D., Asprey, L. B., Strouse, C. E., and Fukushima, E. (1972b) *J. Inorg. Nucl. Chem.*, **34**, 3427–31.

Baybarz, R. D. (1973a) *J. Inorg. Nucl. Chem.*, **35**, 4149–58.

Baybarz, R. D. (1973b) *J. Inorg. Nucl. Chem.*, **35**, 483–7.

Becquerel, A. H. (1896) *Compt. Rend.*, **122**, 501–3.

Beeckman, W., Goffart, J., Rebizant, J., and Spirlet, M. R. (1986) *J. Organomet. Chem.*, **307**, 23–37.

Beer, P. D., Drew, M. G. B., Hesek, D., Kan, M., Nicholson, G., Schmitt, P., Sheen, P.D., and Williams, G. (1998) *J. Chem. Soc., Dalton Trans.*, 2783–5.

Belbeoch, P. B., Piekarski, C., and Pério, P. (1961) *Acta Crystallogr.*, **14**, 837–43.

Bénard, P., Louër, D., Dacheux, N., Brandel, V., and Genet, M. (1994) *Chem. Mater.*, **6**, 1049–58.

Bénard, P., Brandel, V., Dacheux, N., Jaulmes, S., Launay, S., Lindecker, C., Genet, M., Louër, D., and Quarton, M. (1996) *Chem. Mater.*, **8**, 181–8.

Bénard-Rocherullé, P., Louër, M., Louër, D., Dacheux, N., Brandel, V., and Genet, M. (1997) *J. Solid State Chem.*, **132**, 315–22.

Benetollo, F., Bombieri, G., Herrero, J. A., and Rojas, R. M. (1979) *J. Inorg. Nucl. Chem.*, **41**, 195–9.

Benetollo, F., Bombieri, G., Tomat, G., Castellani, C. B., Cassol, A., and Di Bernardo, P. (1984) *Inorg. Chim. Acta*, **95**, 251–61.

Benetollo, F., Bombieri, G., Herrero, P., and Rojas, R. M. (1995) *J. Alloys Compds*, **225**, 400–5.

Benz, R. and Zachariasen, W. H. (1966) *Acta Crystallogr.*, **21**, 838–40.

Bernstein, E. R., Keiderling, T. A., Lippard, S. J., and Mayerle, J. J. (1972a) *J. Am. Chem. Soc.*, **94**, 2552–3.

Bernstein, E. R., Hamilton, W. C., Keiderling, T. A., La Placa, S. J., Lippard, S. J., and Mayerle, J. J. (1972b) *Inorg. Chem.*, **11**, 3009–16.

Berthet, J.-C., Lance, M., Nierlich, M., Vigner, J.-D., and Ephritikhine, M. (1991a) *J. Organomet. Chem.*, **420**, C9–11.

Berthet, J.-C., Le Maréchal, J.-F., Nierlich, M., Lance, M., Vigner, J.-D., and Ephritikhine, M. (1991b) *J. Organomet. Chem.*, **408**, 335–41.

Berthet, J.-C., Ephritikhine, M., Nierlich, M., Lance, M., and Vigner, J.-D. (1993) *J. Organomet. Chem.*, **460**, 47–53.

Berthet, J.-C., Boisson, C., Lance, M., Vigner, J.-D., Nierlich, M., and Ephritikhine, M. (1995) *J. Chem. Soc., Dalton Trans.*, 3027–33.

Beshouri, S. M. and Zalkin, A. (1989) *Acta Crystallogr. C*, **45**, 1221–2.

Bismondo, A., Casellato, U., Sitran, S. and Graziani, R. (1985) *Inorg. Chim. Acta*, **110**, 205–10.

Bjorklund, C. W. (1957) *J. Am. Chem. Soc.*, **79**, 6347–50.

Blake, P. C., Lappert, M. F., Atwood, J. L., and Zhang, H. (1986a) *J. Chem. Soc., Chem. Commun.*, 1148–9.

Blake, P. C., Lappert, M. F., Taylor, R. G., Atwood, J. L., Hunter, W. E., and Zhang, H. (1986b) *J. Chem. Soc., Chem. Commun.*, 1394–5.

Blake, P. C., Lappert, M. F., Atwood, J. L., and Zhang, H. (1988a) *J. Chem. Soc., Chem. Commum.*, 1436–8.

Blake, P. C., Hey, E., Lappert, M. F., Atwood, J. L., and Zhang, H. (1988b) *J. Organomet. Chem.*, **353**, 307–14.

Blake, P. C., Lappert, M. F., Taylor, R. G., Atwood, J. L., Hunter, W. E., and Zhang, H. (1995) *J. Chem. Soc., Dalton Trans.*, 3335–41.

Blake, P. C., Edelman, M. A., Hitchcock, P. B., Hu, J., Lappert, M. F., Tian, S., Müller, G., Atwood, J. L., and Zhang, H. (1998) *J. Organomet. Chem.*, **551**, 261–70.

Blake, P. C., Edelstein, N. M., Hitchcock, P. B., Kot, W. K., Lappert, M. F., Shalimoff, G. V., and Tian, S. (2001) *J. Organomet. Chem.*, **636**, 124–9.

Blank, H. and Ronchi, C. (1968) *Acta Crystallogr. A*, **24**, 657–66.

Bohet, J. and Müller, W. (1978) *J. Less Common Metals*, **57**, 185–99.

Bombieri, G., Forsellini, E., Graziani, R., Tomat, G., and Magon, L. (1972) *Inorg. Nucl. Chem. Lett.*, **8**, 1003–7.

Bombieri, G., Graziani, R., and Forsellini, E. (1973) *Inorg. Nucl. Chem. Lett.*, **9**, 551–7.

Bombieri, G., Croatto, U., Graziani, R., Forsellini, E., and Magon, L. (1974a) *Acta Crystallogr. B*, **30**, 407–11.

Bombieri, G., Forsellini, E., Tomat, G., and Magon, L. (1974b) *Acta Crystallogr. B*, **30**, 2659–63.
Bombieri, G., Degetto, S., Forsellini, E., Marangoni, G., and Immirzi, A. (1977) *Cryst. Struct. Commun.*, **6**, 115–18.
Bombieri, G., De Paoli, G., and Immirzi, A. (1978a) *J. Inorg. Nucl. Chem.*, **40**, 1889–94.
Bombieri, G., De Paoli, G., and Immirzi, A. (1978b) *J. Inorg. Nucl. Chem.*, **40**, 799–802.
Bombieri, G., De Paoli, G., Del Pra, A., and Bagnall, K. W. (1978c) *Inorg. Nucl. Chem. Lett.*, **14**, 359–61.
Bombieri, G., Benetollo, F., Del Pra, A., and Rojas, R. (1979) *J. Inorg. Nucl. Chem.*, **41**, 201–3.
Bombieri, G., Benetollo, F., Forsellini, E., and Del Pra, A. (1980) *J. Inorg. Nucl. Chem.*, **42**, 1423–30.
Bombieri, G., Benetollo, F., Rojas, R. M., and De Paz, M. L. (1981) *J. Inorg. Nucl. Chem.*, **43**, 3203–7.
Bombieri, G., Benetollo, F., Rojas, R. M., De Paz, M. L., and Del Pra, A. (1982) *Inorg. Chim. Acta*, **61**, 149–54.
Bombieri, G., Benetollo, F., Klähne, E., and Fischer, R. D. (1983a) *J. Chem. Soc., Dalton Trans.*, 1115–21.
Bombieri, G., Benetollo, F., Bagnall, K. W., Plews, M. J., and Brown, D. (1983b) *J. Chem. Soc., Dalton Trans.*, 45–9.
Bombieri, G. and Paolucci, G. (1998) in *Handbook on the Physics and Chemistry of Rare Earths*, vol. 25 (eds. K. A. Gschneidner Jr and L. Eyring), Elsevier, Amsterdam, pp. 265–413.
Borzone, G., Borsese, A., and Ferro, R. (1982) *J. Less Common Metals*, **84**, 165–72.
Boulet, P., Wastin, F., Colineau, E., Griveau, J. C., and Rebizant, J. (2003) *J. Phys., Condensed Matter*, **15**, S2305–8.
Boussie, T. R., Moore, R. M. Jr, Streitwieser, A., Zalkin, A., Brennan, J., and Smith, K. A. (1990) *Organometallics*, **9**, 2010–16.
Bowman, A. L., Arnold, G. P., Witteman, W. G., Wallace, T. C., and Nereson, N. G. (1966) *Acta Crystallogr.*, **21**, 670–1.
Bowman, A. L., Krikorian, N. H., Arnold, G. P., Wallace, T. C., and Nereson, N. G. (1968) *Acta Crystallogr. B*, **24**, 1121–3.
Bowman, A. L. and Arnold, G. P. (1971) *Acta Crystallogr. B*, **27**, 243–4.
Bradshaw, J. S., Izatt, R. M., Bordunov, A. V., Chu, C. Y., and Hathway, J. L. (1996) in *Comprehensive Supramolecular Chemistry: Molecular Recognition: Receptors for Cationic Guests,* vol. 1 (ed. G. W. Gokel), Pergamon, Oxford, pp. 35–95.
Brandenburg, N. P. and Loopstra, B. O. (1973) *Cryst. Struct. Commun.*, **2**, 243–6.
Brandenburg, N. P. and Loopstra, B. O. (1978) *Acta Crystallogr. B*, **34**, 3734–6.
Brauer, G. and Mitius, A. (1942) *Z. Anorg. Allg. Chem.*, **249**, 325–39.
Breeze, E. W. and Brett, N. H. (1972) *J. Nucl. Mater.*, **45**, 131–8.
Brennan, J. G. and Andersen, R. A. (1985) *J. Am. Chem. Soc.*, **107**, 514–16.
Brennan, J. G. and Zalkin, A. (1985) *Acta Crystallogr. C*, **41**, 1038–40.
Brennan, J. G., Andersen, R. A., and Zalkin, A. (1986a) *Inorg. Chem.*, **25**, 1756–60.
Brennan, J. G., Andersen, R. A., and Zalkin, A. (1986b) *Inorg. Chem.*, **25**, 1761–5.
Brennan, J. G., Stults, S. D., Andersen, R. A., and Zalkin, A. (1988a) *Organometallics*, **7**, 1329–34.
Brennan, J. G., Andersen, R. A., and Zalkin, A. (1988b) *J. Am. Chem. Soc.*, **110**, 4554–8.

Brewer, L., Sawyer, D. L., Templeton, D. H., and Dauben, C. H. (1951) *J. Am. Ceram. Soc.*, **34**, 173–9.
Brianese, N., Casellato, U., Ossola, F., Porchia, M., Rossetto, G., Zanella, P., and Graziani, R. (1989) *J. Organomet. Chem.*, **365**, 223–32.
Brixner, L. H. (1963) *J. Inorg. Nucl. Chem.*, **25**, 783–7.
Broach, R. W., Schultz, A. J., Williams, J. M., Brown, G. M., Manriquez, J. M., Fagan, P. J., and Marks, T. J. (1979) *Science*, **203**, 172–4.
Brown, A. and Norreys, J. J. (1959) Nature (*UK*), **183**, 673.
Brown, A. (1961) *Acta Crystallogr.*, **14**, 860–5.
Brown, D. and Jones, P. J. (1966) *J. Chem. Soc., Chem. Commun.*, 279–80.
Brown, D., Easey, J. F., and Jones, P. J. (1967) *J. Chem. Soc. A*, 1698–1702.
Brown, D. and Jones, P. J. (1967) *J. Chem. Soc. A*, 719–23.
Brown, D. (1968) *Halides of the Lanthanides and Actinides*, John Wiley, London.
Brown, D., Fletcher, S., and Holah, D. G. (1968a) *J. Chem. Soc. A*, 1889–94.
Brown, D., Petcher, T. J., and Smith, A. J. (1968b) *Nature* (*UK*), **217**, 737–8.
Brown, D., Petcher, T. J., and Smith, A. J. (1969) *Acta Crystallogr. B*, **25**, 178–82.
Brown, D. and Easey, J. F. (1970) *J. Chem. Soc. A*, 3378–81.
Brown, D., Hill, J., and Rickard, C. E. F. (1970) *J. Chem. Soc. A*, 476–80.
Brown, D. and Edwards, J. (1972) *J. Chem. Soc., Dalton Trans.*, 1757–62.
Brown, D. (1973) in *Comprehensive Inorganic Chemistry*, vol. 5 (eds. J. C. Bailar Jr, H. J. Emeléus, S. R. Nyholm, and A. F. Trotman-Dickenson), Pergamon, Oxford., pp. 151–217; 277–318.
Brown, D., Hall, T. L., and Moseley, P. T. (1973) *J. Chem. Soc., Dalton Trans.*, 686–91.
Brown, D., Petcher, D. J., and Smith, A. J. (1975) *Acta Crystallogr. B*, **31**, 1382–5.
Brown, D., Whittaker, B., and De Paoli, G. (1976) *The Thermal Stability and Other Physical Properties of Protactinium Penta- and Tetraiodide*, Report AERE-R 8367, Chem. Div., AERE, Harwell, UK.
Brown, D. (1979) *Inorg. Nucl. Chem. Lett.*, **15**, 219–23.
Brunelli, M., Perego, G., Lugli, G., and Mazzei, A. (1979) *J. Chem. Soc., Dalton Trans.*, 861–8.
Bruno, J. W., Kalina, D. G., Mintz, E. A., and Marks, T. J. (1982a) *J. Am. Chem. Soc.*, **104**, 1860–9.
Bruno, J. W., Marks, T. J., and Day, V. W. (1982b) *J. Am. Chem. Soc.*, **104**, 7357–60.
Bruno, J. W., Marks, T. J., and Day, V. W. (1983) *J. Organomet. Chem.*, **250**, 237–46.
Bruno, J. W., Smith, G. M., Marks, T. J., Fair, C. K., Schultz, A. J., and Williams, J. M. (1986) *J. Am. Chem. Soc.*, **108**, 40–56.
Budantseva, N. A., Fedoseev, A. M., Grigor'ev, M. S., Potemkina, T. I., Afonas'eva, T. V., and Krot, N. N. (1988) *Radiokhimiya*, **30**, 607–10.
Burdese, A. and Borlera, M. L. (1963) *Ann. Chim.*, **53**, 344–55.
Burkov, V. I., Mistryukov, V. E., Mikhailov, Yu. N., and Chuklanova, E. B. (1997) *Zh. Neorg. Khim.*, **42**, 391–5.
Burnaeva, A. A., Volkov, Yu. F., Kryukova, A. I., Korshunov, I. A., and Skiba, O. V. (1992) *Radiokhimiya*, **34**, 13–21.
Burns, J. H. and Laubereau, P. G. (1971) *Inorg. Chem.*, **10**, 2789–92.
Burns, J. H. and Peterson, J. R. (1971) *Inorg. Chem.*, **10**, 147–51.
Burns, J. H. and Baybarz, R. D. (1972) *Inorg. Chem.*, **11**, 2233–7.
Burns, J. H., Peterson, J. R., and Baybarz, R. D. (1973) *J. Inorg. Nucl. Chem.*, **35**, 1171–7.

Burns, J. H. (1974) *J. Organomet. Chem.*, **69**, 225–33.
Burns, J. H., Peterson, J. R., and Stevenson, J. N. (1975) *J. Inorg. Nucl. Chem.*, **37**, 743–9.
Burns, J. H. and Baldwin, W. H. (1977) *Inorg. Chem.*, **16**, 289–94.
Burns, J. H. and Musikas, C. (1977) *Inorg. Chem.*, **16**, 1619–22.
Burns, P. C. and Hayden, L. A. (2002) *Acta Crystallogr. C*, **58**, i121–3.
Burns, P. C., Alexopoulos, C. M., Hotchkiss, P. J., and Locock, A. J. (2004) *Inorg. Chem.*, **43**, 1816–18.
Burns, P. C., Kubatko, K.-A., Sigmon, G., Fryer, B. J., Gagnon, J. E., Antonio, M. R., and Soderholm, L. (2005) *Angew. Chem. Int. Ed.*, **44**, 2135.
Burns, R. C. and O'Donnell, T. A. (1977) *Inorg. Nucl. Chem. Lett.*, **13**, 657–60.
Burrell, A. K., Hemmi, G., Lynch, V., and Sessler, J. L. (1991a) *J. Am. Chem. Soc.*, **113**, 4690–2.
Burrell, A. K., Cyr, M. J., Lynch, V., and Sessler, J. L. (1991b) *J. Chem. Soc., Chem. Commun.*, 1710–13.
Butcher, R. J., Clark, D. L., Grumbine, S. K., and Watkin, J. G. (1995) *Organometallics*, **14**, 2799–805.
Calderazzo, F. (1973) *J. Organomet. Chem.*, **53**, 173–8.
Calderazzo, F. (1974) *J. Organomet. Chem.*, **79**, 175–80.
Calestani, G., Spirlet, J. C., Rebizant, J., and Müller, W. (1979) *J. Less Common Metals*, **68**, 207–12.
Campbell, G. C., Cotton, F. A., Haw, J. F., and Schwotzer, W. (1986) *Organometallics*, **5**, 274–9.
Cannon, J. F. and Farnsworth, P. B. (1983) *J. Less Common Metals*, **92**, 359–68.
Cariati, F., Erre, L., Micera, G., Clemente, D. A., and Cingi, M. B. (1983) *Inorg. Chim. Acta*, **79**, 205.
Casellato, U., Vigato, P. A., and Vidali, M. (1978) *Coord. Chem. Rev.*, **26**, 85–159.
Cendrowski-Guillaume, S. M., Lance, M., Nierlich, M., Vigner, J.-D., and Ephritikhine, M. (1994) *J. Chem. Soc., Chem. Commum.*, 1655–6.
Cendrowski-Guillaume, S. M., Nierlich, M., and Ephritikhine, M. (2002) *J. Organomet. Chem.*, **643–644**, 209–13.
Cesari, M., Pedretti, U., Zazzetta, A., Lugli, G., and Marconi, W. (1971) *Inorg. Chim. Acta*, **5**, 439–44.
Chackraburtty, D. M. (1963) *Acta Crystallogr.*, **16**, 834.
Chackraburtty, D. M. and Jayadevan, N. C. (1965) *Acta Crystallogr.*, **18**, 811–12.
Chadha, A., Sampath, S., and Chackraburtty, D. M. (1980) *Inorg. Chim. Acta*, **42**, 163–7.
Chakravorti, M. C., Bharadwaj, P. K., Pandit, S. C., and Mathur, B. K. (1978) *J. Inorg. Nucl. Chem.*, **40**, 1365–7.
Charpin, P., Costes, R. M., Folcher, G., Plurien, P., Navaza, A., and de Rango, C. (1977) *Inorg. Nucl. Chem. Lett.*, **13**, 341–7.
Charushnikova, I. A., Perminov, V. P., and Katser, S. B. (1995) *Radiokhimiya*, **37**, 493–8.
Charushnikova, I. A., Krot, N. N., and Katser, S. B. (1998) *Radiochemistry (Translation of Radiokhimiya)*, **40**, 558–64.
Charushnikova, I. A., Krot, N. N., and Starikova, Z. A. (2000a) *Radiochemistry (Translation of Radiokhimiya)*, **42**, 42–7.
Charushnikova, I. A., Krot, N. N., and Starikova, Z. A. (2000b) *Radiochemistry (Translation of Radiokhimiya)*, **42**, 37–41.
Charvillat, J. P. and Damien, D. (1973) *Inorg. Nucl. Chem. Lett.*, **9**, 559–63.

Charvillat, J. P., Benedict, U., Damien, D., and Muller, W. (1975) *Radiochem. Radioanal. Lett.*, **20**, 371–81.
Charvillat, J. P., Damien, D., and Wojakowski, A. (1977) *Rev. Chim. Miner.*, **14**, 178–88.
Charvillat, J. P. (1978) *Crystal Chemistry of Tranuranium Pnictides*, Report CEA-R-4933, CEA, Fontenay-aux-Roses, France.
Chevreton, M., Claudel, B., and Mentzen, B. (1968) *J. Chim. Phys. PCB*, **65**, 890–4.
Chikalla, T. D. and Eyring, L. (1968) *J. Inorg. Nucl. Chem.*, **30**, 133–45.
Chikalla, T. D. and Eyring, L. (1969) *J. Inorg. Nucl. Chem.*, **31**, 85–93.
Chiotti, P. (1954) *J. Electrochem. Soc.*, **101**, 567–70.
Choppin, G. R. and Stout, B. E. (1991) *Chemistry in Britain*, **27**, 1126–9.
Christ, C. L., Clark, J. R., and Evans, H. T. Jr (1955) *Science*, **121**, 472–3.
Chumaevskii, N. A., Minaeva, N. A., Mikhailov, Yu. N., Gorbunova, Yu. E., Beirakhov, A. G., and Shchelokov, R. N. (1998) *Zh. Neorg. Khim.*, **43**, 789–95.
Císařová, I., Skála, R., Ondruš, P., and Drábek, M. (2001) *Acta Crystallogr. E*, **57**, i32–4.
Clark, D. L., Conradson, S. D., Keogh, D. W., Palmer, P. D., Scott, B. L., and Tait, C. D. (1998a) *Inorg. Chem.* **37**, 2893–9.
Clark, D. L., Keogh, D. W., Palmer, P. D., Scott, B. L., and Tait, C. D. (1998b) *Angew. Chem. Int. Ed. Engl.*, **37**, 164–5.
Clark, R. J. and Corbett, J. D. (1963) *Inorg. Chem.*, **2**, 460–3.
Claudel, B., Mentzen, B., Navarro, A., and Sautereau, H. (1976) *J. Inorg. Nucl. Chem.*, **38**, 759–62.
Cloke, F. G. N., Hawkes, S. A., Hitchcock, P. B., and Scott, P. (1994) *Organometallics*, **13**, 2895–7.
Cohen, D. M. (1963) *Inorg. Chem.*, **2**, 866–7.
Cohen, D., Fried, S., Siegel, S., and Tani, B. (1968) *Inorg. Nucl. Chem. Lett.*, **4**, 257–60.
Copeland, J. C. and Cunningham, B. B. (1969) *J. Inorg. Nucl. Chem.*, **31**, 733–40.
Cotton, F. A. and Schwotzer, W. (1985) *Organometallics*, **4**, 942–3.
Cotton, F. A., Schwotzer, W., and Simpson, C. Q. (1986) *Angew. Chem.*, **98**, 652–4.
Cotton, F. A. and Schwotzer, W. (1987) *Organometallics*, **6**, 1275–80.
Cousson, A., Dabos, S., Abazli, H., Nectoux, F., Pages, M., and Choppin, G. (1984) *J. Less Common Metals*, **99**, 233–40.
Cousson, A. (1985) *Acta Crystallogr. C*, **41**, 1758–61.
Cousson, A., Stout, B., Nectoux, P., Pages, M., and Gasperin, M. (1986) *J. Less Common Metals*, **125**, 111–15.
Cousson, A., Proust, J., and Rizkalla, E. N. (1991) *Acta Crystallogr. C*, **47**, 2065–9.
Cousson, A., Nectoux, F., Pages, M., and Rizkalla, E. N. (1993) *Radiochim. Acta*, **61**, 177–80.
Cragg, P. J., Bott, S. G., and Atwood, J. L. (1988) *Lanthanide Actinide Res.*, **2**, 265–77.
Cramer, R. E., Maynard, R. B., and Gilje, J. W. (1978) *J. Am. Chem. Soc.*, **100**, 5562–4.
Cramer, R. E., Maynard, R. B., and Gilje, J. W. (1980) *Inorg. Chem.*, **19**, 2564–9.
Cramer, R. E., Maynard, R. B., Paw, J. C., and Gilje, J. W. (1981) *J. Am. Chem. Soc.*, **103**, 3589–90.
Cramer, R. E., Maynard, R. B., Paw, J. C., and Gilje, J. W. (1982) *Organometallics*, **1**, 869–71.
Cramer, R. E., Maynard, R. B., Paw, J. C., and Gilje, J. W. (1983) *Organometallics*, **2**, 1336–40.

Cramer, R. E., Panchanatheswaran, K., and Gilje, J. W. (1984a) *J. Am. Chem. Soc.*, **106**, 1853–4.
Cramer, R. E., Mori, A. L., Maynard, R. B., Gilje, J. W., Tatsumi, K., and Nakamura, A. (1984b) *J. Am. Chem. Soc.*, **106**, 5920–6.
Cramer, R. E., Engelhardt, U., Higa, K. T., and Gilje, J. W. (1987a) *Organometallics*, **6**, 41–5.
Cramer, R. E., Jeong, J. H., and Gilje, J. W. (1987b) *Organometallics*, **6**, 2010–12.
Cramer, R. E., Bruck, M. A., Edelmann, F., Afzal, D., Gilje, J. W., and Schmidbaur, H. (1988a) *Chem. Berichte*, **121**, 417–20.
Cramer, R. E., Edelmann, F., Mori, A. L., Roth, S., Gilje, J. W., Tatsumi, K., and Nakamura, A. (1988b) *Organometallics*, **7**, 841–9.
Cramer, R. E., Roth, S., and Gilje, J. W. (1989) *Organometallics*, **8**, 2327–30.
Cramer, R. E., Hitt, J., Chung, T., and Gilje, J. W. (1995a) *New J. Chem.*, **19**, 509–14.
Cramer, R. E., Ariyaratne, K. A. N. S., and Gilje, J. W. (1995b) *Z. Anorg. Allg. Chem.*, **621**, 1856–64.
Cromer, D. T. and Harper, P. E. (1955) *Acta Crystallogr.*, **8**, 847–8.
Cromer, D. T., Larson, A. C., and Roof, R. B. (1964) *Acta Crystallogr.*, **17**, 947–50.
Cunningham, B. B. and Wallmann, J. C. (1964) *J. Inorg. Nucl. Chem.*, **26**, 271–5.
Cymbaluk, T. H., Ernst, R. D., and Day, V. W. (1983) *Organometallics*, **2**, 963–9.
D'Eye, R. W. M., Sellman, P. G., and Murray, J. R. (1952) *J. Chem. Soc.*, 2555–62.
D'Eye, R. W. M. (1953) *J. Chem. Soc.*, 1670–2.
D'Eye, R. W. M. and Sellman, P. G. (1954) *J. Chem. Soc.*, 3760–6.
D'Eye, R. W. M. (1958) *J. Chem. Soc., Abstr.*, 196–9.
Dalley, N. K., Mueller, M. H., and Simonsen, S. H. (1971) *Inorg. Chem.*, **10**, 323–8.
Damien, D. (1971) *Inorg. Nucl. Chem. Lett.*, **7**, 291–7.
Damien, D. and Jové, J. (1971) *Inorg. Nucl. Chem. Lett.*, **7**, 685–8.
Damien, D. (1972) *Inorg. Nucl. Chem. Lett.*, **8**, 501–4.
Damien, D. and Charvillat, J. P. (1972) *Inorg. Nucl. Chem. Lett.*, **8**, 705–8.
Damien, D., Marcon, J. P., and Jové, J. (1972) *Inorg. Nucl. Chem. Lett.*, **8**, 317–20.
Damien, D. (1973) *Inorg. Nucl. Chem. Lett.*, **9**, 453–6.
Damien, D., Damien, N., Jové, J., and Charvillat, J. P. (1973) *Inorg. Nucl. Chem. Lett.*, **9**, 649–55.
Damien, D. (1974) *J. Inorg. Nucl. Chem.*, **36**, 307–8.
Damien, D. and Wojakowski, A. (1975) *Radiochem. Radioanal. Lett.*, **23**, 145–54.
Damien, D., Charvillat, J. P., and Müller, W. (1975) *Inorg. Nucl. Chem. Lett.*, **11**, 451–7.
Damien, D., Wojakowski, A., and Müller, W. (1976a) *Inorg. Nucl. Chem. Lett.*, **12**, 533–8.
Damien, D., Wojakowski, A., and Müller, W. (1976b) *Inorg. Nucl. Chem. Lett.*, **12**, 441–9.
Damien, D., Haire, R. G., and Peterson, J. R. (1979a) *J. Less Common Metals*, **68**, 159–65.
Damien, D. A., Haire, R. G., and Peterson, J. R. (1979b) *J. Phys., Colloq.*, **40** (C4), 95–100.
Damien, D., Haire, R. G., and Peterson, J. R. (1980a) *J. Inorg. Nucl. Chem.*, **42**, 995–8.
Damien, D., Haire, R. G., and Peterson, J. R. (1980b) *Inorg. Nucl. Chem. Lett.*, **16**, 537–41.

Damien, D. and de Novion, C. H. (1981) *J. Nucl. Mater.*, **100**, 167–77.
Damien, D., de Novion, C. H., and Thévenin, T. (1986) in *Handbook on the Physics and Chemistry of the Actinides,* vol. 4 (eds. A. J. Freeman and C. Keller), North-Holland, Amsterdam, pp. 39–96.
Dancausse, J.-P., Gering, E., Heathman, S., Benedict, U., Gerward, L., Olsen, S. S., and Hulliger, F. (1992) *J. Alloys Compds*, **189**, 205–8.
Danis, J. A., Hawkins, H. T., Scott, B. L., Runde, W. H., Scheetz, B. E., and Eichhorn, B. W. (2000) *Polyhedron*, **19**, 1551–7.
Danis, J. A., Lin, M. R., Scott, B. L., Eichhorn, B. W., and Runde, W. H. (2001) *Inorg. Chem.*, **40**, 3389–94.
Dao, N. Q., Bkouche-Waksman, I., Walewski, M., and Caceres, D. (1984) *Bull. Soc. Chim. Fr.*, 129–32.
Day, V. W., Marks, T. J., and Wachter, W. A. (1975) *J. Am. Chem. Soc.*, **97**, 4519–27.
De Ridder, D. J. A., Apostolidis, C., Rebizant, J., Kanellakopulos, B., and Maier, R. (1996a) *Acta Crystallogr. C*, **52**, 1436–8.
De Ridder, D. J. A., Rebizant, J., Apostolidis, C., Kanellakopulos, B., and Dornberger, E. (1996b) *Acta Crystallogr. C*, **52**, 597–600.
de Villardi, G. C., Charpin, P., Costes, R.-M., Folcher, G., Plurien, P., Rigny, P., and De Rango, C. (1978) *J. Chem. Soc., Chem. Commun.*, 90–2.
Debets, P. C. (1966) *Acta Crystallogr.*, **21**, 589–93.
Debets, P. C. (1968) *Acta Crystallogr. B*, **24**, 400–2.
Degetto, S., Baracco, L., Graziani, R., and Celon, E. (1978) *Transit. Met. Chem.*, **3**, 351–4.
Dejean, A., Charpin, P., Folcher, G., Rigny, P., Navaza, A., and Tsoucaris, G. (1987) *Polyhedron*, **6**, 189–95.
Delapalme, A., Schweiss, P., Spirlet, M. R., Rebizant, J., and Kanellakopulos, B. (1988) *MS Forum*, **27/28**, 211–16.
Deschamps, J. R. and Flippen-Anderson, J. L. (2002) in *Encyclopedia of Physical Science and Technology,* 3rd edn, vol. 4 (ed. R. A. Meyers), Academic Press, San Diego, CA, pp. 121–53.
Deshayes, L., Keller, N., Lance, M., Nierlich, M., and Vigner, J.-D. (1993) *Acta Crystallogr. C*, **49**, 16–19.
Deshayes, L., Keller, N., Lance, M., Navaza, A., Nierlich, M., and Vigner, J.-D. (1994a) *Polyhedron*, **13**, 1725–33.
Deshayes, L., Keller, N., Lance, M., Nierlich, M., Vigner, J.-D. (1994b) *Acta Crystallogr. C*, **50**, 1541–4.
Diaconescu, P. L. and Cummins, C. C. (2002) *J. Am. Chem. Soc.*, **124**, 7660–1.
Dodge, R. P., Smith, G. S., Johnson, Q., and Elson, R. E. (1967) *Acta Crystallogr.*, **22**, 85–9.
Dodge, R. P., Smith, G. S., Johnson, Q., and Elson, R. E. (1968) *Acta Crystallogr. B*, **24**, 304–11.
Dormond, A., Belkalem, B., Charpin, P., Lance, M., Vigner, J.-D., Folcher, G., and Guilard, R. (1986) *Inorg. Chem.*, **25**, 4785–90.
Douglass, R. M. and Staritzky, E. (1956) *Anal. Chem.*, **28**, 1211.
Douglass, R. M. (1962) *Acta Crystallogr.*, **15**, 505–6.
Drobyshevskii, I. V., Prusakov, V. N., Serik, V. F., and Sokolov, V. B. (1980) *Radiokhimiya*, **22**, 591–4.

Dusausoy, Y., Ghermani, N. E., Podor, R., and Cuney, M. (1996) *Eur. J. Miner.*, **8**, 667–73.
Duttera, M. R., Fagan, P. J., Marks, T. J., and Day, V. W. (1982) *J. Am. Chem. Soc.*, **104**, 865–7.
Duttera, M. R., Day, V. W., and Marks, T. J. (1984) *J. Am. Chem. Soc.*, **106**, 2907–12.
Edelman, M. A., Lappert, M. F., Atwood, J. L., and Zhang, H. (1987) *Inorg. Chim. Acta*, **139**, 185–6.
Edelman, M. A., Hitchcock, P. B., Hu, J., and Lappert, M. F. (1995) *New J. Chem.*, **19**, 481–9.
Edelmann, F. T. and Gun'ko, Y. K. (1997) *Coord. Chem. Rev.*, **165**, 163–237.
Edelmann, F. T. and Lorenz, V. (2000) *Coord. Chem. Rev.*, **209**, 99–160.
Eick, H. A. (1965) *Inorg. Chem.*, **4**, 1237–9.
Eick, H. A. and Mulford, R. N. R. (1969) *J. Inorg. Nucl. Chem.*, **31**, 371–5.
Eigenbrot, C. W. Jr and Raymond, K. N. (1981) *Inorg. Chem.*, **20**, 1553–6.
Eigenbrot, C. W. Jr and Raymond, K. N. (1982) *Inorg. Chem.*, **21**, 2653–60.
Eliseev, A. A., Molodkin, A. K., and Ivanova, O. M. (1967) *Zh. Neorg. Khim.*, **12**, 2854–5.
Eller, P. G. and Penneman, R. A. (1976) *Inorg. Chem.*, **15**, 2439–42.
Eller, P. G., Larson, A. C., Peterson, J. R., Ensor, D. D., and Young, J. P. (1979) *Inorg. Chim. Acta*, **37**, 129–33.
Ellinger, F. H. and Zachariasen, W. H. (1954) *J. Phys Chem.*, **58**, 405–8.
Ellinger, F. H. (1956) *J. Met.*, **8**, 1256–9.
Ernst, R. D., Kennelly, W. J., Day, C. S., Day, V. W., and Marks, T. J. (1979) *J. Am. Chem. Soc.*, **101**, 2656–64.
Ernst, R. D. and Marks, T. J. (1987) *J. Organomet. Chem.*, **318**, 29–82.
Ernst, R. D. (1990) *J. Organomet. Chem.*, **392**, 51–92.
Evans, W. J., Nyce, G. W., Johnston, M. A., and Ziller, J. W. (2000) *J. Am. Chem. Soc.*, **122**, 12019–20.
Evans, W. J., Nyce, G. W., and Ziller, J. W. (2001) *Organometallics*, **20**, 5489–91.
Evans, W. J., Kozimor, S. A., Nyce, G. W., and Ziller, J. W. (2003a) *J. Am. Chem. Soc.*, **125**, 13831–5.
Evans, W. J., Kozimor, S. A., and Ziller, J. W. (2003b) *J. Am. Chem. Soc.*, **125**, 14264–5.
Fagan, P. J., Manriquez, J. M., Marks, T. J., Day, V. W., Vollmer, S. H., and Day, C. S. (1980) *J. Am. Chem. Soc.*, **102**, 5393–6.
Fahey, J. A., Peterson, J. R., and Baybarz, R. D. (1972) *Inorg. Nucl. Chem. Lett.*, **8**, 101–7.
Fahey, J. A., Turcotte, R. P., and Chikalla, T. D. (1974) *Inorg. Nucl. Chem. Lett.*, **10**, 459–65.
Fahey, J. A., Turcotte, R. P., and Chikalla, T. D. (1976) *J. Inorg. Nucl. Chem.*, **38**, 495–500.
Fankuchen, I. (1935) *Z. Kristallogr.*, **91**, 473–9.
Farr, J. D., Giorgi, A. L., Bowman, M. G., and Money, R. K. (1961) *J. Inorg. Nucl. Chem.*, **18**, 42–7.
Favas, M. C., Kepert, D. L., Patrick, J. M., and White, A. H. (1983) *J. Chem. Soc., Dalton Trans.*, 571–81.
Fedoseev, A. M. and Perminov, V. P. (1983) *Radiokhimiya*, **25**, 555–7.
Fedosseev, A. M., Budantseva, N. A., Grigoriev, M. S., Bessonov, A. A., Astafurova, L. N., Lapitskaya, T. S., and Krupa, J.-C. (1999) *Radiochim. Acta*, **86**, 17–22.

Fellows, R. L., Peterson, J. R., Noé, M., Young, J. P., and Haire, R. G. (1975) *Inorg. Nucl. Chem. Lett.*, **11**, 737–42.
Ferro, R. (1952a) *Atti. Accad. Nazl. Lincei, Rend., Classe Sci. Fis., Mat. e Nat.*, **13**, 151–7.
Ferro, R. (1952b) *Atti. Accad. Nazl. Lincei, Rend., Classe Sci. Fis., Mat. e Nat.*, **13**, 401–5.
Ferro, R. (1953) *Atti. Accad. Nazl. Lincei, Rend., Classe Sci. Fis., Mat. e Nat.*, **14**, 89–94.
Ferro, R. (1954) *Z. Anorg. Allg. Chem.*, **275**, 320–6.
Ferro, R. (1955) *Acta Crystallogr.*, **8**, 360.
Ferro, R. (1956) *Acta Crystallogr.*, **9**, 817–18.
Finch, R. J., Cooper, M. A., Hawthorne, F. C., Ewing, R. C. (1999) *Can. Miner.*, **37**, 929–38.
Fischer, R. D., Klähne, E., and Kopf, J. (1978) *Z. Naturforsch. B*, **33**, 1393–7.
Fischer, R. D., Werner, G.-D., Lehmann, T., Hoffmann, G., and Weigel, F. (1981) *J. Less Common Metals*, **80**, 121–32.
Florin, A. E., Tannenbaum, I. R., and Lemons, J. F. (1956) *J. Inorg. Nucl. Chem.*, **2**, 368–79.
Folcher, G., Charpin, P., Costes, R. M., Keller, N., and de Villardi, G. C. (1979) *Inorg. Chim. Acta.*, **34**, 87–90.
Fried, S., Hagemann, F., and Zachariasen, W. H. (1950) *J. Am. Chem. Soc.*, **72**, 771–5.
Fried, S., Cohen, D., Siegel, S., and Tani, B. (1968) *Inorg. Nucl. Chem. Lett.*, **4**, 495–8.
Fronczek, F. R., Halstead, G. W., and Raymond, K. N. (1977) *J. Am. Chem. Soc.*, **99**, 1769–75.
Fujita, D. K., Cunningham, B. B., and Parsons, T. C. (1969) *Inorg. Nucl. Chem. Lett.*, **5**, 307–13.
Galešić, N., Matković, B., Topić, M., Coffou, E., and Šljukić, M. (1984) *Croat. Chem. Acta*, **57**, 597–608.
Gantzel, P. K. and Baldwin, N. L. (1964) *Acta Crystallogr.*, **17**, 772–3.
Gardner, E. R., Markin, T. L., and Street, R. S. (1965) *J. Inorg. Nucl. Chem.*, **27**, 541–51.
Gibson, J. K. and Haire, R. G. (1985a) *J. Solid State Chem.*, **59**, 317–23.
Gibson, J. K. and Haire, R. G. (1985b) *J. Less Common Metals*, **109**, 251–9.
Gibson, J. K. and Haire, R. G. (1987) *J. Less Common Metals*, **127**, 267.
Gieren, A. and Hoppe, W. (1971) *J. Chem. Soc., Chem. Commun.*, 413–14.
Gilbert, T. M., Ryan, R. R., and Sattelberger, A. P. (1988) *Organometallics*, **7**, 2514–18.
Gilbert, T. M., Ryan, R. R., and Sattelberger, A. P. (1989) *Organometallics*, **8**, 857–9.
Gingerich, K. A. and Wilson, D. W. (1965) *Inorg. Chem.*, **4**, 987–93.
Girolami, G. S., Milam, S. N., and Suslick, K. S. (1987) *Inorg. Chem.*, **26**, 343–4.
Girolami, G. S., Milam, S. N., and Suslick, K. S. (1988) *J. Am. Chem. Soc.*, **110**, 2011–12.
Girolami, G. S., Gorlin, P. A., Milam, S. N., Suslick, K. S., and Wilson, S. R. (1994) *J. Coord. Chem.*, **32**, 173–212.
Goldschmidt, V. M. and Thomassen, L. (1923) Videnskapsselskapets Skrifter I, *Mat.-Naturv. Klasse*, 48 pp.
Gottfriedsen, J. and Edelmann, F. T. (2005) *Coord. Chem. Rev.*, **249**, 919–69.
Govindarajan, S., Patil, K. C., Poojary, M. D., and Manohar, H. (1986) *Inorg. Chim. Acta*, **120**, 103–7.
Gradoz, P., Ephritikhine, M., Lance, M., Vigner, J.-D., and Nierlich, M. (1994) *J. Organomet. Chem.*, **481**, 69–73.
Graf, P., Cunningham, B. B., Dauben, C. H., Wallmann, J. C., Templeton, D. H., and Ruben, H. (1956) *J. Am. Chem. Soc.*, **78**, 2340.

Graham, J. and McTaggart, F. K. (1960) *Aust. J. Chem.*, **13**, 67–73.
Graziani, R., Zarli, B., and Bandoli, G. (1967) *Ric. Sci.*, **37**, 984–5.
Graziani, R., Bombieri, G., and Forsellini, E. (1972) *J. Chem. Soc., Dalton Trans.*, 2059–61.
Graziani, R., Battiston, G. A., Casellato, U., and Sbrignadello, G. (1983) *J. Chem. Soc., Dalton Trans.*, 1–7.
Greaves, C. and Fender, B. E. F. (1972) *Acta Crystallogr. B*, **28**, 3609–14.
Green, J. L. and Cunningham, B. B. (1967) *Inorg. Nucl. Chem. Lett.*, **3**, 343–9.
Greenwood, N. N. and Earnshaw, A. (2001) *Chemistry of the Elements*, 2nd edn, Butterworth-Heinemann, Oxford., pp. 1227–84.
Grigor'ev, M. S., Yanovskii, A. I., Fedoseev, A. M., Budantseva, N. A., Struchkov, Y. T., and Krot, N. N. (1991a) *Radiokhimiya*, **33**, 17–19.
Grigor'ev, M. S., Bessonov, A. A., Yanovskii, A. I., Struchkov, Yu. T., and Krot, N. N. (1991b) *Radiokhimiya*, **33**, 46–53.
Grigor'ev, M. S., Baturin, N. A., Regel, L. L., and Krot, N. N. (1991c) *Radiokhimiya*, **33**, 19–25.
Grigor'ev, M. S., Baturin, N. A., Budantseva, N. A., and Fedoseev, A. M. (1993a) *Radiokhimiya*, **35**, 29–38.
Grigor'ev, M. S., Charushnikova, I. A., Krot, N. N., Yanovskii, A. I., and Struchkov, Yu. T. (1993b) *Radiokhimiya*, **35**, 24–30.
Grigor'ev, M. S., Charushnikova, I. A., Krot, N. N., Yanovskii, A. I., and Struchkov, Yu. T. (1993c) *Radiokhimiya*, **35**, 31–7.
Grigor'ev, M. S., Charushnikova, I. A., Krot, N. N., Yanovskii, A. I., and Struchkov, Yu. T. (1994) *Zh. Neorg. Khim.*, **39**, 1328–31.
Grigor'ev, M. S., Charushnikova, I. A., Baturin, N. A., and Krot, N. N. (1995) *Zh. Neorg. Khim.*, **40**, 732–5.
Grigor'ev, M. S., Charushnikova, I. A., Krot, N. N., Yanovskii, A. I., and Struchkov, Yu. T. (1996) *Zh. Neorg. Khim.*, **41**, 539–42.
Grigor'ev, M. S., Charushnikova, I. A., Krot, N. N., Yanovskii, A. I., and Struchkov, Yu. T. (1997) *Radiochemistry* (*Translation of Radiokhimiya*), **39**, 420–3.
Grønvold, F. (1955) *J. Inorg. Nucl. Chem.*, **1**, 357–70.
Guang-Di, Y., Yu-Guo, F., and Yan-De, H. (1990) *Science in China* (*Series B*), **33**, 1418–24.
Guesdon, A., Provost, J., and Raveau, B. (1999) *J. Mater. Chem.*, **9**, 2583–7.
Guesdon, A., Chardon, J., Provost, J., and Raveau, B. (2002) *J. Solid State Chem.*, **165**, 89–93.
Guggenberger, L. J. and Jacobson, R. A. (1968) *Inorg. Chem.*, **7**, 2257–60.
Gun'ko, Y. K. and Edelmann, F. T. (1996) *Coord. Chem. Rev.*, **156**, 1–89.
Gutberlet, T., Dreissig, W., Luger, P., Bechthold, H.-C., Maung, R., and Knöchel, A. (1989) *Acta Crystallogr. C*, **45**, 1146–9.
Habash, J. and Smith, A. J. (1983) *Acta Crystallogr. C*, **39**, 413–15.
Haddad, S. F., Al-Far, R. H., and Ahmed, F. R. (1987) *Acta Crystallogr. C*, **43**, 453–6.
Haire, R. G. and Baybarz, R. D. (1973) *J. Inorg. Nucl. Chem.*, **35**, 489–96.
Haire, R. G. and Baybarz, R. D. (1974) *J. Inorg. Nucl. Chem.*, **36**, 1295–302.
Haire, R. G. and Asprey, L. B. (1976) *Inorg. Nucl. Chem. Lett.*, **12**, 73–84.
Haire, R. G. and Baybarz, R. D. (1979) *J. Phys., Colloq.*, 101–2.
Haire, R. G., Young, J. P., and Peterson, J. R. (1983) *J. Less Common Metals*, **93**, 339–45.

Haire, R. G. and Eyring, L. (1994) in *Handbook on the Physics and Chemistry of Rare Earths,* vol. 18 (eds. K. A. Gschneidner Jr, L. Eyring, G. R. Choppin, and G. H. Lander), Elsevier, Amsterdam, pp. 413–505.
Hale, W. H. Jr and Mosley, W. C. (1973) *J. Inorg. Nucl. Chem.*, **35**, 165–71.
Hall, D., Rae, A. D., and Waters, T. N. (1965) *Acta Crystallogr.*, **19**, 389–95.
Halstead, G. W., Baker, E. C., and Raymond, K. N. (1975) *J. Am. Chem. Soc.*, **97**, 3049–52.
Harper, E. A., Hedger, H. J., and Dalton, J. T. (1968) *Nature* (*UK*), **219**, 151.
Harrowfield, J. M., Ogden, M. I., and White, A. H. (1991a) *J. Chem. Soc., Dalton Trans.*, 979–85.
Harrowfield, J. M., Ogden, M. I., and White, A. H. (1991b) *J. Chem. Soc., Dalton Trans.*, 2625–32.
Haschke, J. M., Hodges, A. E. III, and Lucas, R. L. (1987) *J. Less Common Metals*, **133**, 155–66.
Hassaballa, H., Steed, J. W., and Junk, P. C. (1988) *J. Chem. Soc., Chem. Commun.*, 577–8.
Hassaballa, H., Steed, J. W., Junk, P. C., and Elsegood, M. R. J. (1998) *Inorg. Chem.*, **37**, 4666–71.
Hauck, J. (1976) *Inorg. Nucl. Chem. Lett.*, **12**, 617–22.
Haug, H. O. (1967) *J. Inorg. Nucl. Chem.*, **29**, 2753–8.
Haug, H. O. and Baybarz, R. D. (1975) *Inorg. Nucl. Chem. Lett.*, **11**, 847–55.
Hayes, R. G. and Thomas, J. L. (1971) *Organomet. Chem. Rev. A*, **7**, 1–50.
Henkie, Z., Wiśniewski, P., and Gukasov, A. (1997) *J. Crystal Growth*, **172**, 459–65.
Herak, R. and Jovanovic, B. (1969) *Inorg. Nucl. Chem. Lett.*, **5**, 693–7.
Herrero, J. A., Bermudez, J., and Rios, E. G. (1977) *An. Quim.*, **73**, 1271–9.
Hery, Y. (1979) *Synthesis, Crystallographic, and Magnetic Properties of Protactinium Pnictides*, Report CEA-R-4971, CEA, Fontenay-aux-Roses, France.
Hery, Y., Damien, D., and Charvillat, J. P. (1979) *Radiochem. Radioanal. Lett.*, **37**, 17–26.
Hillebrand, W. F. (1893) *Z. Anorg. Allg. Chem.*, **3**, 249–51.
Hitchcock, P. B., Lappert, M. F., and Taylor, R. G. (1984) *J. Chem. Soc., Chem. Commun.*, 1082–4.
Hoard, J. L. and Stroupe, J. D. (1958) *Structure of Crystalline Uranium Hexafluoride*, TID-5290 (Book 1), U.S. Atomic Energy Commun., pp. 325–49.
Hodgson, K. O. and Raymond, K. N. (1973) *Inorg. Chem.*, **12**, 458–66.
Hoekstra, H. R. and Siegel, S. (1961) *J. Inorg. Nucl. Chem.*, **18**, 154–65.
Hoekstra, H. R., Siegel, S., and Galloy, J. J. (1970) *J. Inorg. Nucl. Chem.*, **32**, 3237–48.
Hoekstra, H. R. (1982) in *Gmelin Handbook of Inorganic Chemistry, Uranium*, 8th edn, Suppl. vol. A5 (eds. K.-C. Buschbeck and C. Keller), Springer-Verlag, Berlin., pp. 211–40.
Horyn, R., Henry, J. Y., and Rossat-Mignod, J. (1983) *J. Crystal Growth*, **63**, 407–9.
Howatson, J., Grev, D. M., and Morosin, B. (1975) *J. Inorg. Nucl. Chem.*, **37**, 1933–5.
Hughes, K.-A. and Burns, P. C. (2003) *Acta. Crystallogr.* C, **59**, i7–8.
Hulet, E. K., Wild, J. F., Lougheed, R. W., and Hayes, W. N. (1976) in *Proc. Moscow Symp. Chem. Transuranium Elements*, 1972 (eds. V. I. Spitsyn and J. J. Katz), Pergamon, Oxford, pp. 33–5.
Hulliger, F. (1966) Nature (*UK*), **209**, 499–500.
Hunt, E. B. and Rundle, R. E. (1951) *J. Am. Chem. Soc.*, **73**, 4777–81.

Hunter, W. E. and Atwood, J. L. (1984) *Inorg. Chim. Acta*, **94**, 80.
Hurtgen, C. and Fuger, J. (1977) *Inorg. Nucl. Chem. Lett.*, **13**, 179–88.
Hutchings, M. T. (1987) *J. Chem. Soc., Faraday Trans. 2*, **83**, 1083–103.
Hyeon, J.-Y. and Edelmann, F. T. (2003a) *Coord. Chem. Rev.*, **241**, 249–72.
Hyeon, J.-Y. and Edelmann, F. T. (2003b) *Coord. Chem. Rev.*, **247**, 21–78.
Hyeon, J.-Y., Gottgriedsen, J., and Edelmann, F. T. (2005) *Coord. Chem. Rev.*, **249**, 2787–844.
Iandelli, A. (1952a) *Atti. Accad. Nazl. Lincei, Rend., Classe Sci. Fis., Mat. e Nat.*, **13**, 144–51.
Iandelli, A. (1952b) *Atti. Accad. Nazl. Lincei, Rend., Classe Sci. Fis., Mat. e Nat.*, **13**, 138–43.
Immirzi, A., Bombieri, G., Degetto, S., and Marangoni, G. (1975) *Acta Crystallogr. B*, **31**, 1023–8.
Irish, D. E., Pursel, R., Taylor, N. J., and Toogood, G. E. (1985) *Acta Crystallogr. C*, **41**, 1012–3.
Iyer, P. N. and Natarajan, P. R. (1989) *J. Less Common Metals*, **146**, 161–6.
Iyer, P. N. and Natarajan, P. R. (1990) *J. Less Common Metals*, **159**, 1–11.
Jacob, C. W. and Warren, B. E. (1937) *J. Am. Chem. Soc.*, **59**, 2588–91.
Jacobson, E. L., Freeman, R. D., Tharp, A. G., and Searcy, A. W. (1956) *J. Am. Chem. Soc.*, **78**, 4850–2.
Janczak, J. and Kubiak, R. (1999) *Polyhedron*, **18**, 1621–7.
Janczak, J., Kubiak, R., Svoboda, I., Jezierski, A., and Fuess, H. (2000) *Inorg. Chim. Acta*, **304**, 150–5.
Jayadevan, N. C. and Chackraburtty, D. M. (1972) *Acta Crystallogr. B*, **28**, 3178–82.
Jayadevan, N. C., Dias, R. M. A., and Chakraburtty, D. M. (1973) *J. Inorg. Nucl. Chem.*, **35**, 1037–40.
Jayadevan, N. C., Mudher, K. D. S., and Chackraburtty, D. M. (1975) *Acta Crystallogr. B*, **31**, 2277–80.
Jayadevan, N. C., Mudher, K. D. S., and Chackraburtty, D. M. (1982) *Z. Kristallogr.*, **161**, 7–13.
Jelenić, I., Grdenić, D., and Bezjak, A. (1964) *Acta Crystallogr.*, **17**, 758–9.
Jette, E. R. (1955) *J. Chem. Phys.*, **23**, 365–8.
Jiang, J., Sarsfield, M. J., Renshaw, J. C., Livens, F. R., Collison, D., Charnock, J. M., Helliwell, M., and Eccles, H. (2002) *Inorg. Chem.*, **41**, 2799–806.
Kadish, K. M., Liu, Y. H., Anderson, J. E., Charpin, P., Chevrier, G., Lance, M., Nierlich, M., Vigner, J.-D., Dormond, A., Belkalem, B., and Guilard, R. (1988) *J. Am. Chem. Soc.*, **110**, 6455–62.
Kanellakopulos, B. and Bagnall, K. W. (1972) in *MTP International Review of Science, Inorganic Chemistry,* vol. 7 (ed. K. W. Bagnall), Butterworths, London., pp. 299–322.
Kanellakopulos, B. and Aderhold, C. (1973) *XXIVth IUPAC Congress*, Hamburg, Abstracts, p. 632.
Kanellakopulos, B., Dornberger, E., and Baumgärtner, F. (1974) *Inorg. Nucl. Chem. Lett.*, **10**, 155–60.
Kannan, S., Raj, S. S., and Fun, H.-K. (2001) *Polyhedron*, **20**, 2145–50.
Karmazin, L., Mazzanti, M., and Pécaut, J. (2002) *J. Chem. Soc., Chem. Commun.,* 654–5.

Karraker, D. G., Stone, J. A., Jones, E. R. Jr, and Edelstein, N. (1970) *J. Am. Chem. Soc.*, **92**, 4841–5.
Karraker, D. G. and Stone, J. A. (1974) *J. Am. Chem. Soc.*, **96**, 6885–8.
Kato, Y., Kimura, T., Yoshida, Z., and Nitani, N. (1998) *Radiochim. Acta*, **82**, 63–8.
Keenan, T. K. and Kruse, F. H. (1964) *Inorg. Chem.*, **3**, 1231–2.
Keenan, T. K. (1965) *Inorg. Chem.*, **4**, 1500–1.
Keenan, T. K. (1968) *Inorg. Nucl. Chem. Lett.*, **4**, 381–4.
Keenan, T. K. and Asprey, L. B. (1969) *Inorg. Chem.*, **8**, 235–8.
Keller, C. and Walter, K. H. (1965) *J. Inorg. Nucl. Chem.*, **27**, 1253–60.
Keller, C. (1973) in *Comprehensive Inorganic Chemistry,* vol. 5, (eds. J. C. Bailar Jr, H. J. Emeléus, S. R. Nyholm, and A. F. Trotman-Dickenson), Pergamon, Oxford, pp. 219–76.
Kemmler-Sack, S. (1969) *Z. Anorg. Allg. Chem.*, **364**, 88–99.
Kempter, C. P. and Krikorian, N. H. (1962) *J. Less Common Metals*, **4**, 244–51.
Khodadad, P. (1959) *Compt. Rend.*, **249**, 694–6.
Kierkegaard, P. (1956) *Acta Chem. Scand.*, **10**, 599–616.
Kilimann, U. and Edelmann, F. T. (1995) *Coord. Chem. Rev.*, **141**, 1–61.
Kimmel, G. (1978) *J. Less Common Metals*, **59**, P83–6.
Kiplinger, J. L., Morris, D. E., Scott, B. L., and Burns, C. J. (2002a) *Organometallics*, **21**, 5978–82.
Kiplinger, J. L., John, K. D., Morris, D. E., Scott, B. L., and Burns, C. J. (2002b) *Organometallics*, **21**, 4306–8.
Kiplinger, J. L., Morris, D. E., Scott, B. L., and Burns, C. J. (2002c) *Organometallics*, **21**, 3073–5.
Kirchner, H. P., Merz, K. M., and Brown, W. R. (1963) *J. Am. Ceram. Soc.*, **46**, 137–41.
Knösel, F., Roesky, H. W., and Edelmann, F. (1987) *Inorg. Chim. Acta*, **139**, 187–8.
Knowles, K. J., Rahakrishna, P., and Willis, B. T. M. (1981) *Room-Temperature Study of Uranium Dioxides by Pulse Neutron Powder Diffraction*, AERE-MPD/NBS-169, Sci. Res. Counc., Rutherford Laboratory, Chilton, UK.
Kobayashi, T. (1978) *Bull. Inst. Chem. Res. Kyoto. Univ.*, **56**, 204–212.
Kohlmann, H. and Beck, H. P. (1997) *Z. Anorg. Allg. Chem.*, **623**, 785–90.
Kohlmann, H. and Beck, H. P. (1999) *Z. Kristallogr.*, **214**, 341–5.
Konrad, T., Jeitschko, W., Danebrock, M. E., and Evers, C. B. H. (1996) *J. Alloys Compds*, **234**, 56–61.
Korst, W. L. (1962) *Acta Crystallogr.* **15**, 287–8.
Kovba, L. M., Trunov, V. K., and Grigor'ev, A. I. (1965) *Zh. Strukt. Khim.*, **6**, 919–21.
Krivovichev, S. V. and Burns, P. C. (2004) *Radoichemistry*, **46**, 16–9.
Kruger, O. L. and Moser, J. B. (1967) *J. Phys. Chem. Solids*, **28**, 2321–5.
Krupka, M. C. (1970) *J. Less Common Metals*, **20**, 135–40.
Kunitomi, N., Hamaguchi, Y., Sakamoto, M., Doi, K., and Komura, S. (1964) *J. Phys.* (*Paris*), **25**, 462–8.
La Ginestra, A., Variali, G., and Valigi, M. (1965) *Gazz. Chim. Ital.*, **95**, 1096–9.
Laidler, J. B. (1966) *J. Chem. Soc. A*, 780–4.
Land, C. C., Johnson, K. A., and Ellinger, F. H. (1965) *J. Nucl. Mater.*, **15**, 23–32.
Lander, G. H., Heaton, L., Mueller, M. H., and Anderson, K. D. (1969) *J. Phys. Chem. Solids*, **30**, 733–7.
Larson, D. T. and Haschke, J. M. (1981) *Inorg. Chem.*, **20**, 1945–50.

Laubereau, P. G. and Burns, J. H. (1970a) *Inorg. Chem.*, **9**, 1091–5.
Laubereau, P. G. and Burns, J. H. (1970b) *Inorg. Nucl. Chem. Lett.*, **6**, 59–63.
Laugt, M. (1973) *J. Appl. Crystallogr.*, **6**, 299–301.
Lawaldt, D., Marquart, R., Werner, G.-D., and Weigel, F. (1982) *J. Less Common Metals*, **85**, 37–41.
Le Bihan, T., Noël, H., and Rogl, P. (1996) *J. Alloys Compds*, **240**, 128–33.
Le Borgne, T., Lance, M., Nierlich, M., and Ephritikhine, M. (2000) *J. Organomet. Chem.*, **598**, 313–17.
Le Cloarec, M. F., Dartyge, J. M., Kovacevic, S., and Muxart, R. (1976) *J. Inorg. Nucl. Chem.*, **38**, 737–9.
Le Cloarec, M. F. and Cazaussus, A. (1978) *J. Inorg. Nucl. Chem.*, **40**, 1680–1.
Le Maréchal, J. F., Villiers, C., Charpin, P., Lance, M., Nierlich, M., Vigner, J.-D., and Ephritikhine, M. (1989a) *J. Chem. Soc., Chem. Commun.*, 308–10.
Le Maréchal, J. F., Villiers, C., Charpin, P., Nierlich, M., Lance, M., Vigner, J.-D., and Ephritikhine, M. (1989b) *J. Organomet. Chem.*, **379**, 259–69.
Le Roux, S. D., Van Tets, A., and Adrian, H. W. W. (1979) *Acta Crystallogr. B*, **35**, 3056–7.
Leger, J. M., Yacoubi, N., and Loriers, J. (1981) *J. Solid State Chem.*, **36**, 261–70.
Legros, J.-P. and Jeannin, Y. (1976) *Acta Crystallogr. B*, **32**, 2497–503.
Leigh, H. D. and McCartney, E. R. (1974) *J. Am. Ceram. Soc.*, **57**, 192.
Leong, J., Hodgson, K. O., and Raymond, K. N. (1973) *Inorg. Chem.*, **12**, 1329–35.
Lescop, C., Arliguie, T., Lance, M., Nierlich, M. and Ephritikhine, M. (1999) *J. Organomet. Chem.*, **580**, 137–44.
Leverd, P. C., Arliguie, T., Lance, M., Nierlich, M., Vigner, J.-D., and Ephritikhine, M. (1994) *J. Chem. Soc., Dalton Trans.*, 501–4.
Leverd, P. C., Ephritikhine, M., Lance, M., Vigner, J.-D., and Nierlich, M. (1996) *J. Organomet. Chem.*, **507**, 229–37.
Leverd, P. C., Berthault, P., Lance, M., and Nierlich, M. (1998) *Eur. J. Inorg. Chem.*, 1859–62.
Leverd, P. C., Dumazet-Bonnamour, I., Lamartine, R., and Nierlich, M. (2000) *J. Chem. Soc., Chem. Commun.*, 493–4.
Leverd, P. C. and Nierlich, M. (2000) *Eur. J. Inorg. Chem.*, 1733–8.
Leverd, P. C., Rinaldo, D., and Nierlich, M. (2002) *J. Chem. Soc., Dalton Trans.*, 829–31.
Levet, J. C., Potel, M., and Le Marouille, J.-Y. (1977) *Acta Crystallogr. B*, **33**, 2542–6.
Levet, J. C. and Noël, H. (1979) *J. Solid State Chem.*, **28**, 67–73.
Levet, J. C. and Noël, H. (1981) *J. Inorg. Nucl. Chem.*, **43**, 1841–3.
Levy, J. H., Taylor, J. C., and Wilson, P. W. (1975) *Acta Crystallogr. B*, **31**, 880–2.
Levy, J. H., Taylor, J. C., and Wilson, P. W. (1976) *J. Chem. Soc., Dalton Trans.*, 219–24.
Levy, J. H., Taylor, J. C., and Wilson, P. W. (1977) *J. Inorg. Nucl. Chem.*, **39**, 1989–91.
Levy, J. H., Taylor, J. C., and Wilson, P. W. (1978) *J. Inorg. Nucl. Chem.*, **40**, 1055–7.
Levy, J. H., Taylor, J. C., and Waugh, A. B. (1980) *Inorg. Chem.*, **19**, 672–4.
Lin, Z., Le Maréchal, J.-F., Sabat, M., and Marks, T. J. (1987) *J. Am. Chem. Soc.*, **109**, 4127–9.
Lin, Z., Brock, C. P., and Marks, T. J. (1988) *Inorg. Chim. Acta*, **141**, 145–9.
Locock, A. J. and Burns, P. C. (2002) *J. Solid State Chem.*, **163**, 275–80.
Loopstra, B. O. (1964) *Acta Crystallogr.*, **17**, 651–4.
Loopstra, B. O. (1970) *Acta Crystallogr. B*, **26**, 656–7.

Loopstra, B. O., Taylor, J. C., and Waugh, A. B. (1977) *J. Solid State Chem.*, **20**, 9–19.
Lorenz, R., Scherff, H. L., and Toussaint, N. (1969) *J. Inorg. Nucl. Chem.*, **31**, 2381–90.
Lorenzelli, R. (1968) *Compt. Rend. Acad. Sci. C*, **226**, 900–2.
Louër, M., Brochu, R., Louër, D., Arsalane, S., and Ziyad, M. (1995) *Acta Crystallogr. B*, **51**, 908–13.
Lukens, W. W. Jr, Beshouri, S. M., Blosch, L. L., Stuart, A. L., and Andersen, R. A. (1999) *Organometallics*, **18**, 1235–46.
Lundgren, G. (1950) *Arkiv. Kemi*, **2**, 535–49.
Lundgren, G. (1952) *Arkiv. Kemi*, **2**, 421–8.
Lundgren, G. (1953) *Arkiv. Kemi*, **5**, 349–63.
Maier, R., Kanellakopulos, B., Apostolidis, C., Meyer, D., and Rebizant, J. (1993) *J. Alloys Compds*, **190**, 269–71.
Malcic, S. S. (1958a) *Bull. Inst. Nucl. Sci. Boris Kidrich*, **8**, 99–104.
Malcic, S. S. (1958b) *Bull. Inst. Nucl. Sci. Boris Kidrich*, **8**, 95–7.
Mallett, M. W., Gerds, A. F., and Vaughan, D. A. (1951) *J. Electrochem. Soc.*, **98**, 505–9.
Malm, J. G., Weinstock, B., and Weaver, E. E. (1958) *J. Phys. Chem.*, **62**, 1506–8.
Malm, J. G., Williams, C. W., Soderholm, L., and Morss, L. R. (1993) *J. Alloys Compds*, **194**, 133–7.
Manriquez, J. M., Fagan, P. J., Marks, T. J., Day, C. S., and Day, V. W. (1978) *J. Am. Chem. Soc.*, **100**, 7112–14.
Manriquez, J. M., Fagan, P. J., Marks, T. J., Vollmer, S. H., Day, C. S., and Day, V. W. (1979) *J. Am. Chem. Soc.*, **101**, 5075–8.
Marangoni, G., Degetto, S., Graziani, R., Bombieri, G., and Forsellini, E. (1974) *J. Inorg. Nucl. Chem.*, **36**, 1787–94.
Marcon, J. P. and Pascard, R. (1966) *J. Inorg. Nucl. Chem.*, **28**, 2551–60.
Marcon, J. P. (1969) *Contribution à l'Etude des Sulfures Actinides*, CEA-R-3919, Sous. Dir. Met., CEA, Fontenay-aux-Roses, France.
Marks, T. J. (1974) *J. Organomet. Chem.*, **79**, 181–99.
Marks, T. J. (1975) *J. Organomet. Chem.*, **95**, 301–15.
Marks, T. J. (1976) *J. Organomet. Chem.*, **119**, 229–41.
Marks, T. J. (1977) *J. Organomet. Chem.*, **138**, 157–83.
Marks, T. J. (1978) *J. Organomet. Chem.*, **158**, 325–43.
Marks, T. J. (1979a) *J. Organomet. Chem.*, **180**, 153–75.
Marks, T. J. (1979b) *Prog. Inorg. Chem.*, **25**, 223–333.
Marks, T. J. (1980) *J. Organomet. Chem.*, **203**, 415–48.
Marks, T. J. (1982a) *Science*, **217**, 989–97.
Marks, T. J. (1982b) *J. Organomet. Chem.*, **227**, 317–40.
Marples, J. A. C. (1965) *Acta Crystallogr.*, **18**, 815–17.
Marples, J. A. C. (1970) *J. Phys. Chem. Solids*, **31**, 2431–9.
Marquart, R., Hoffmann, G., and Weigel, F. (1983) *J. Less Common Metals*, **91**, 119–27.
Masaki, N. and Doi, K. (1972) *Acta Crystallogr. B*, **28**, 785–91.
Masaki, N. and Tagawa, H. (1975) *J. Nucl. Mater.*, **58**, 241–3.
Masci, B., Nierlich, M., and Thuéry, P. (2002a) *New J. Chem.*, **26**, 120–8.
Masci, B., Gabrielli, M., Mortera, S. L., Nierlich, M., and Thuéry, P. (2002b) *Polyhedron*, **21**, 1125–31.
Matson, L. K., Moody, J. W., and Himes, R. C. (1963) *J. Inorg. Nucl. Chem.*, **25**, 795–800.

Matković, B. and Šljukić, M. (1965) *Croat. Chem. Acta*, **37**, 115–16.
Matković, B., Prodić, B., and Šljukić, M. (1968a) *Bull. Soc. Chim. Fr.*, **4**, 1777–9.
Matković, B., Prodić, B., Šljukić, M., and Peterson, S. W. (1968b) *Croat. Chem. Acta*, **40**, 147–61.
McWhan, D. B., Wallmann, J. C., Cunningham, B. B., Asprey, L. B., Ellinger, F. H., and Zachariasen, W. H. (1960) *J. Inorg. Nucl. Chem.*, **15**, 185–7.
McWhan, D. B., Cunningham, B. B., and Wallmann, J. C. (1962) *J. Inorg. Nucl. Chem.*, **24**, 1025–38.
Mefod'eva, M. P., Grigor'ev, M. S., Afonos'eva, T. V., and Kryukov, E. B. (1981) *Radiokhimiya*, **23**, 697–703.
Menovsky, A., Franse, J. J. M., and Klaasse, J. C. P. (1984) *J. Crystal Growth*, **70**, 519–22.
Mentzen, B. F. (1977) *Acta Crystallogr. B*, **33**, 2546–9.
Mentzen, B. F., Puaux, J.-P., and Loiseleur, H. (1977) *Acta Crystallogr. B*, **33**, 1848–51.
Mentzen, B. F., Puaux, J.-P., and Sautereau, H. (1978a) *Acta Crystallogr. B*, **34**, 1846–9.
Mentzen, B. F., Puaux, J.-P., and Sautereau, H. (1978b) *Acta Crystallogr. B*, **34**, 2707–11.
Mentzen, B. F. and Sautereau, H. (1980) *Acta Crystallogr. B*, **36**, 2051–3.
Mereiter, K. (1986a) *Acta Crystallogr. C*, **42**, 1678–81.
Mereiter, K. (1986b) *Acta Crystallogr. C*, **42**, 1682–4.
Meunier-Piret, J., Declercq, G., Germain, G., and Van Meerssche, M. (1980a) *Bull. Soc. Chim. Belg.*, **89**, 121–4.
Meunier-Piret, J., Germain, G., Declercq, J. P., and Van Meerssche, M. (1980b) *Bull. Soc. Chim. Belg.*, **89**, 241–5.
Meunier-Piret, J. and Van Meerssche, M. (1984) *Bull. Soc. Chim. Belg.*, **93**, 299–305.
Mikhailov, Yu. N., Gorbunova, Yu. E., Serezhkina, L. B., Losev, V. Yu., and Serezhkin, V. N. (1996) *Zh. Neorg. Khim.*, **41**, 2058–62.
Mikhailov, Yu. N., Kanishcheva, A. S., Gorbunova, Yu. E., Belomestnykh, V. I., and Sveshnikova, L. B. (1997) *Zh. Neorg. Khim.*, **42**, 1980–5.
Mikhailov, Yu. N., Gorbunova, Yu. E., Shishkina, O. V., Serezhkina, L. B., and Serezhkin, V. N. (2000a) *Zh. Neorg. Khim.*, **45**, 1999–2002.
Mikhailov, Yu. N., Gorbunova, Yu. E., Shishkina, O. V., Serezhkina, L. B., and Serezhkin, V. N. (2000b) *Zh. Neorg. Khim.*, **45**, 1825–9.
Ming, W., Pei-Ju, Z., Jing-Zhi, Z., Zhong, C., Jin-Ming, S., and Yong-Hui, Y. (1987a) *Acta Crystallogr. C*, **43**, 873–5.
Ming, W., Pei-Ju, Z., Jing-Zhi, Z., Zhong, C., Jin-Ming, S., and Yong-Hui, Y. (1987b) *Acta Crystallogr. C*, **43**, 1544–6.
Ming, W., Boyi, W., Pei-Ju, Z., Wenji, W., and Jie, L. (1988) *Acta Crystallogr. C*, **44**, 1913–16.
Mitchell, A. W. and Lam., D. J. (1970a) *J. Nucl. Mater.*, **36**, 110–12.
Mitchell, A. W. and Lam, D. J. (1970b) *J. Nucl. Mater.*, **37**, 349–52.
Mitchell, A. W. and Lam, D. J. (1971) *J. Nucl. Mater.*, **39**, 219–23.
Mitchell, A. W. and Lam, D. J. (1974) *J. Nucl. Mater.*, **52**, 125–7.
Moloy, K. G., Marks, T. J., and Day, V. W. (1983) *J. Am. Chem. Soc.*, **105**, 5696–8.
Moody, D. C. and Ryan, R. R. (1979) *Crystal Struct. Commun.*, **8**, 933–6.
Moody, D. C., Penneman, R. A., and Salazar, K. V. (1979) *Inorg. Chem.*, **18**, 208–9.
Mooney, R. C. L. (1949) *Acta Crystallogr.*, **2**, 189–91.

Morse, J. W., Shanbhag, P. M., Saito, A., and Choppin, G. R. (1984) *Chem. Geol.*, **42**, 85–99.
Morss, L. R., Fuger, J., Goffart, J., and Haire, G. (1983) *Inorg. Chem.*, **22**, 1993–6.
Morss, L. R., Richardson, J. W., Williams, C. W., Lander, G. H., Lawson, A. C., Edelstein, N. M., and Shalimoff, G. V. (1989) *J. Less Common Metals*, **156**, 273–89.
Moseley, P. T., Brown, D., and Whittaker, B. (1972) *Acta Crystallogr. B*, **28**, 1816–21.
Mosley, W C. (1972) *J. Inorg. Nucl. Chem.*, **34**, 539–55.
Mudher, K. D. S., Krishnan, K., Chackraburtty, D. M., and Jayadevan, N. C. (1988) *J. Less Common Metals*, **143**, 173–82.
Mudher, K. D. S., Keskar, M., and Venugopal, V. (1999) *J. Nucl. Mater.*, **265**, 146–53.
Mudher, K. D. S. and Krishnan, K. (2000) *J. Alloys Compds*, **313**, 65–8.
Mueller, U. and Kolitsch, W. (1974) *Z. Anorg. Allg. Chem.*, **410**, 32–8.
Müller, U. (1979) *Acta Crystallogr. B*, **35**, 2502–9.
Mulford, R. N. R., Ellinger, F. H., and Zachariasen, W. H. (1954) *J. Am. Chem. Soc.*, **76**, 297–8.
Mulford, R. N. R. and Wiewandt, T. A. (1965) *J. Phys. Chem.*, **69**, 1641–4.
Musikas, C. and Burns, J. H. (1976) in *Transplutonium Elements, Proc. 4th Int. Transplutonium Elements Symp., 1975* (eds. W. Muller and R. Lindner), North-Holland, Amsterdam, pp. 237–45.
Naito, K. and Kamegashira, N. (1976) *Adv. Nucl. Sci. Technol.*, **9**, 99–180.
Nassimbeni, L. R., Rodgers, A. L., and Haigh, J. M. (1976) *Inorg. Chim. Acta*, **20**, 149–53.
Navaza, A., Villain, F., and Charpin, P. (1984) *Polyhedron*, **3**, 143–9.
Navaza, A., Charpin, P., and Vigner, J.-D. (1991) *Acta Crystallogr. C*, **47**, 1842–5.
Navratil, J. D. and Bramlet, H. L. (1973) *J. Inorg. Nucl. Chem.*, **35**, 157–63.
Nectoux, F. and Tabuteau, A. (1981) *Radiochem. Radioanal. Lett.*, **49**, 43–8.
Nectoux, F., Abazli, H., Jové, J., Cousson, A., Pages, M., Gasperin, M., and Choppin, G. (1984) *J. Less Common Metals*, **97**, 1–10.
Nierlich, M., Sabattie, J.-M., Keller, N., Lance, M., and Vigner, J.-D. (1994) *Acta Crystallogr. C*, **50**, 52–4.
Nigon, J. P., Penneman, R. A., Staritzky, E., Keenan, T. K., and Asprey, L. B. (1954) *J. Phys. Chem.*, **58**, 403–4.
Niinisto, L., Toivonen, J., and Valkonen, J. (1978) *Acta Chem. Scand. A*, **32**, 647–51.
Noé, M., Fuger, J., and Duyckaerts, G. (1970) *Inorg. Nucl. Chem. Lett.*, **6**, 111–19.
Noël, H. (1980) *J. Inorg. Nucl. Chem.*, **42**, 1715–17.
Noël, H. and Potel, M. (1982) *Acta Crystallogr. B*, **38**, 2444–5.
Noël, H. and Le Marouille, J. Y. (1984) *J. Solid State Chem.*, **52**, 197–202.
Noël, H. (1985) *Physica B+C*, **130**, 499–500.
Noël, H. and Levet, J. C. (1989) *J. Solid State Chem.*, **79**, 28–33.
Noël, H., Potel, M., Troc, R., and Shlyk, L. (1996) *J. Solid State Chem.*, **126**, 22–6.
Okamoto, H. (1999) *J. Phase Equil.*, **20**, 351.
Olsen, J. S., Gerward, L., Benedict, U., Itié, J.-P., and Richter, K. (1986) *J. Less Common Metals*, **121**, 445–53.
Olson, W. M. and Mulford, R. N. R. (1964) *J. Phys. Chem.*, **68**, 1048–51.
Olson, W. M. and Mulford, R. N. R. (1966) *J. Phys. Chem.*, **70**, 2934–7.
Paine, R. T., Ryan, R. R., and Asprey, L. B. (1975) *Inorg. Chem.*, **14**, 1113–17.

Panattoni, C., Graziani, R., Bandoli, G., Zarli, B., and Bombieri, G. (1969) *Inorg. Chem.*, **8**, 320–5.
Paolucci, G., Fischer, R. D., Benetollo, F., Seraglia, R., and Bombieri, G. (1991) *J. Organomet. Chem.*, **412**, 327–42.
Parry, J., Carmona, E., Coles, S., and Hursthouse, M. (1995) *J. Am. Chem. Soc.*, **117**, 2649–50.
Pasilis, S. P. and Pemberton, J. E. (2003) *Inorg. Chem.*, **42**, 6793–800.
Peacock, R. D. and Edelstein, N. (1976) *J. Inorg. Nucl. Chem.*, **38**, 771–3.
Penneman, R. A., Ryan, R. R., and Rosenzweig, A. (1973) *Struct. Bonding*, **13**, 1–52.
Pepper, M. and Bursten, B. E. (1991) *Chem. Rev.*, **91**, 719–41.
Perego, G., Cesari, M., Farina, F., and Lugli, G. (1976) *Acta Crystallogr. B*, **32**, 3034–9.
Peters, R. G., Warner, B. P., Scott, B. L., and Burns, C. J. (1999) *Organometallics*, **18**, 2587–9.
Peterson, J. R. and Cunningham, B. B. (1967a) *Inorg. Nucl. Chem. Lett.*, **3**, 327–36.
Peterson, J. R. and Cunningham, B. B. (1967b) *Inorg. Nucl. Chem. Lett.*, **3**, 579–83.
Peterson, J. R. and Burns, J. H. (1968) *J. Inorg. Nucl. Chem.*, **30**, 2955–8.
Peterson, J. R. and Cunningham, B. B. (1968a) *J. Inorg. Nucl. Chem.*, **30**, 1775–84.
Peterson, J. R. and Cunningham, B. B. (1968b) *J. Inorg. Nucl. Chem.*, **30**, 823–8.
Peterson, J. R., Fahey, J. A., and Baybarz, R. D. (1971) *J. Inorg. Nucl. Chem.*, **33**, 3345–51.
Peterson, J. R., and Fuger, J. (1971) *J. Inorg. Nucl. Chem.*, **33**, 4111–17.
Peterson, J. R. (1972) *J. Inorg. Nucl. Chem.*, **34**, 1603–7.
Peterson, J. R. and Baybarz, R. D. (1972) *Inorg. Nucl. Chem. Lett.*, **8**, 423–31.
Peterson, J. R. and Burns, J. H. (1973) *J. Inorg. Nucl. Chem.*, **35**, 1525–30.
Phipps, K. D. and Sullenger, D. B. (1964) *Science*, **145**, 1048–9.
Pietraszko, D. and Lukaszewicz, K. (1971) *Roczniki Chemii*, **46**, 1105–17.
Picon, M. and Flahaut, J. (1958) *Bull. Soc. Chim. Fr.*, **25**, 772–80.
Podor, R., Francois, M., and Dacheux, N. (2003) *J. Solid State Chem.*, **172**, 66–72.
Poojary, M. D. and Patil, K. C. (1987) *Proc. Indian. Acad. Sci., Chem. Sci.*, **99**, 311–15.
Porchia, M., Brianese, N., Casellato, U., Ossola, F., Rossetto, G., Zanella, P., and Graziani, R. (1989) *J. Chem. Soc., Dalton Trans.*, 677–81.
Post, B., Glaser, F. W., and Moskowitz, D. (1954) *Acta Met.*, **2**, 20–5.
Potel, M., Brochu, R., Padiou, J., and Grandjean, D. (1972) *Compt. Rend. Acad. Sci. C*, **275**, 1421.
Pyykkö, P., Laakkonen, L. J., and Tatsumi, K. (1989) *Inorg. Chem.*, **28**, 1801–5.
Quarton, M., Zouiri, M., and Freundlich, W. (1984) *Compt. Rend. Acad. Sci. II*, **299**, 785–8.
Rannou, J. P. and Lucas, J. (1969) *Mat. Res. Bull.*, **4**, 443–50.
Rebizant, J., Spirlet, M. R., and Goffart, J. (1983) *Acta Crystallogr. C*, **39**, 1041–3.
Rebizant, J., Spirlet, M. R., and Goffart, J. (1985) *Acta Crystallogr. C*, **41**, 334–6.
Rebizant, J., Spirlet, M. R., Kanellakopulos, B., and Dornberger, E. (1986a) *Acta Crystallogr. C*, **42**, 1497–500.
Rebizant, J., Spirlet, M. R., Kanellakopulos, B., and Dornberger, E. (1986b) *J. Less Common Metals*, **122**, 211–14.
Rebizant, J., Apostolidis, C., Spirlet, M. R., and Kanellakopulos, B. (1987) *Inorg. Chim. Acta*, **139**, 209–10.

Rebizant, J., Spirlet, M. R., Van den Bossche, G., and Goffart, J. (1988) *Acta Crystallogr. C*, **44**, 1710–12.
Rebizant, J., Spirlet, M. R., Bettonville, S., and Goffart, J. (1989) *Acta Crystallogr. C*, **45**, 1509–11.
Rebizant, J., Spirlet, M. R., Apostolidis, C., and Kanellakopulos, B. (1991) *Acta Crystallogr. C*, **47**, 854–6.
Rebizant, J., Spirlet, M. R., Apostolidis, C., and Kanellakopulos, B. (1992) *Acta Crystallogr. C*, **48**, 452–4.
Richter, J. and Edelmann, F. T. (1996) *Coord. Chem. Rev.*, **147**, 373–442.
Rietveld, H. M. (1967) *Acta Crystallogr.*, **22**, 151–2.
Rietz, R. R., Zalkin, A., Templeton, D. H., Edelstein, N. M., and Templeton, L. K. (1978a) *Inorg. Chem.*, **17**, 653–8.
Rietz, R. R., Edelstein, N. M., Ruben, H. W., Templeton, D. H., and Zalkin, A. (1978b) *Inorg. Chem.*, **17**, 658–60.
Ritger, P. L., Burns, J. H., and Bombieri, G. (1983) *Inorg. Chim. Acta*, **77**, L217–19.
Roberts, L. E. J. and Walter, A. J. (1966) in *Physico-Chimie du Protactinium* (eds. G. Bouissières and R. Muxart), Orsay, 2–8 July 1965, Centre National de la Recherche Scientifique, Paris, pp. 51–9.
Roddy, J. W. (1973) *J. Inorg. Nucl. Chem.*, **35**, 4141–8.
Roddy, J. W. (1974) *J. Inorg. Nucl. Chem.*, **36**, 2531–3.
Rogers, R. D., Kurihara, L. K., and Benning, M. M. (1987a) *Inorg. Chem.*, **26**, 4346–52.
Rogers, R. D., Kurihara, L. K., and Benning, M. M. (1987b) *J. Inclusion Phenom.*, **5**, 645–58.
Rogers, R. D., Kurihara, L. K., and Benning, M. M. (1987c) *Acta Crystallogr. C*, **43**, 1056–8.
Rogers, R. D. (1988) *Acta Crystallogr. C*, **44**, 638–41.
Rogers, R. D. and Benning, M. M. (1988a) *Acta Crystallogr. C*, **44**, 641–4.
Rogers, R. D. and Benning, M. M. (1988b) *Acta Crystallogr. C*, **44**, 1397–9.
Rogers, R. D., Kurihara, L. K., and Benning, M. M. (1988) *J. Chem. Soc., Dalton Trans.*, 13–16.
Rogers, R. D. (1989) *Lanthanide Actinide Res.*, **3**, 71–81.
Rogers, R. D., Benning, M. M., Etzenhouser, R. D., and Rollins, A. N. (1989) *J. Chem. Soc., Chem. Commun.*, 1586–8.
Rogers, R. D. and Rogers, L. M. (1990) *J. Organomet. Chem.*, **380**, 51–76.
Rogers, R. D. and Benning, M. M. (1991) *J. Inclusion Phenom. Mol. Recog. Chem.*, **11**, 121–35.
Rogers, R. D., Bond, A. H., Hipple, W. G., Rollins, A. N., and Henry, R. F. (1991) *Inorg. Chem.*, **30**, 2671–9.
Rogers, R. D. and Rogers, L. M. (1991) *J. Organomet. Chem.*, **416**, 201–90.
Rogers, R. D. and Bond, A. H. (1992) *Acta Crystallogr. C*, **48**, 1199–201.
Rogers, R. D. and Rogers, L. M. (1992a) *J. Organomet. Chem.*, **442**, 83–224.
Rogers, R. D. and Rogers, L. M. (1992b) *J. Organomet. Chem.*, **442**, 225–69.
Rogers, R. D. and Rogers, L. M. (1993) *J. Organomet. Chem.*, **457**, 41–62.
Rogers, R. D., Zhang, J., and Campbell, D. T. (1998) *J. Alloys Compds*, **271–273**, 133–8.
Rojas, R., Del Pra, A., Bombieri, G., and Benetollo, F. (1979) *J. Inorg. Nucl. Chem.*, **41**, 541–5.
Ronchi, C. and Heirnaut, J. P. (1996) *J. Alloys Compds*, **240**, 179–85.

Rosen, R. K. and Zalkin, A. (1989) *Acta Crystallogr. C*, **45**, 1139–41.
Ross, M. and Evans, H. T. Jr (1960) *J. Inorg. Nucl. Chem.*, **15**, 338–51.
Rouse. K. D., Wills, B. T. M., and Pryor, A. W. (1968) *Acta Crystallogr. B,* **24**, 117–22.
Rundle, R. E. (1947) *J. Am. Chem. Soc.*, **69**, 1719–23.
Rundle, R. E. (1948) *Acta Crystallogr.*, **1**, 180–7.
Rundle, R. E. (1951) *J. Am. Chem. Soc.*, **73**, 4172–4.
Rundle, R. E., Shull, C. G., and Wollan, E. O. (1952) *Acta Crystallogr.*, **5**, 22–6.
Runnalls, O. J. C. and Boucher, R. R. (1955) *Acta Crystallogr.*, **8**, 592.
Ryan, R. R., Penneman, R. A., and Kanellakopulos, B. (1975) *J. Am. Chem. Soc.*, **97**, 4258–60.
Ryan, R. R., Penneman, R. A., Asprey, L. B., and Paine, R. T. (1976) *Acta Crystallogr. B*, **32**, 3311–13.
Ryan, R. R., Salazar, K. V., Sauer, N. N., and Ritchey, J. M. (1989) *Inorg. Chim. Acta*, **162**, 221–5.
Sari, C., Müller, W., and Benedict, U. (1972/73) *J. Nucl. Mater.*, **45**, 73–5.
Sarsfield, M. J. and Helliwell, M. (2004) *J. Am. Chem. Soc.*, **126**, 1036–7.
Sarsfield, M. J., Helliwell, M., and Raftery, J. (2004) *Inorg. Chem.*, **43**, 3170–9.
Scaife, D. E., Turnbull, A. G., and Wylie, A. W. (1965) *J. Chem. Soc., Abstr.*, 1432–7.
Scaife, D. E. (1966) *Inorg. Chem.*, **5**, 162–4.
Šćavničar, S. and Prodić, B. (1965) *Acta Crystallogr.*, **18**, 698–702.
Schake, A. R., Avens, L. R., Burns, C. J., Clark, D. L., Sattelberger, A. P., and Smith, W. H. (1993) *Organometallics*, **12**, 1497–8.
Scherer, O. J., Werner, B., Heckmann, G., and Wolmershäuser, G. (1991) *Angew. Chem. Int. Ed. Engl.*, **30**, 553–5.
Scherer, O. J., Schulze, J., and Wolmershäuser, G. (1994) *J. Organomet. Chem.*, **484**, C5–7.
Scherer, V., Weigel, F., and Van Ghemen, M. E. (1967) *Inorg. Nucl. Chem. Lett.*, **3**, 589–95.
Schlechter, M. (1970) *J. Nucl. Mater.*, **37**, 82–8.
Schnabel, R. C., Scott, B. L., Smith, W. H., and Burns, C. J. (1999) *J. Organomet. Chem.*, **591**, 14–23.
Schock, L. E., Seyam, A. M., Sabat, M., and Marks, T. J. (1988) *Polyhedron*, **7**, 1517–29.
Scott, P. and Hitchcock, P. B. (1995) *J. Organomet. Chem.*, **497**, C1–3.
Secaur, C. A., Day, V. W., Ernst, R. D., Kennelly, W. J., and Marks, T. J. (1976) *J. Am. Chem. Soc.*, **98**, 3713–15.
Sellers, P. A., Fried, S., Elson, R. E., and Zachariasen, W. H. (1954) *J. Am. Chem. Soc.*, **76**, 5935–8.
Serizawa, H., Fukuda, K., Ishii, Y., Morii, Y., and Katsura, M. (1994) *J. Nucl. Mater.*, **208**, 128–34.
Sessler, J. L., Mody, T. D., and Lynch, V. (1992) *Inorg. Chem.*, **31**, 529–31.
Sessler, J. L. and Weghorn, S. J. (1997) *Tetrahedron Organic Chemistry Series: Expanded, Contracted, and Isomeric Porphyrins,* vol. 15, Pergamon, Oxford.
Sessler, J. L., Gebauer, A., Hoehner, M. C., and Lynch, V. (1998) *J. Chem. Soc., Chem. Commun.*, 1835–6.
Sessler, J. L., Vivian, A. E., Seidel, D., Burrell, A. K., Hoehner, M., Mody, T. D., Gebauer, A., Weghorn, S. J., and Lynch, V. (2001a) *Coord. Chem. Rev.*, **216–217**, 411–34.

Sessler, J. L., Seidel, D., Vivian, A. E., Lynch, V., Scott, B. L., and Keogh, D. W. (2001b) *Angew. Chem. Int. Ed. Engl.*, **40**, 591–4.
Sessler, J. L., Gorden, A. E. V., Seidel, D., Hannah, S., Lynch, V., Gordon, P. L., Donohoe, R. J., Tait, C. D., and Keogh, D. W. (2002) *Inorg. Chim. Acta*, **341**, 54–70.
Shankar, J. and Khubchandani, P. G. (1957) *Anal. Chem.*, **29**, 1375.
Shchelokov, R. N., Orlova, I. M., Beirakhov, A. G., Mikhailov, Yu. N., and Kanishcheva, A. S. (1984) *Koord. Khim.*, **10**, 1644–50.
Shchelokov, R. N., Mikhailov, Yu. N., Orlova, I. M., Sergeev, A. V., Ashurov, Z. K., Tashev, M. T., and Parpiev, N. A. (1985) *Koord. Khim.*, **11**, 1010–14.
Sheft, I. and Fried, S. (1953) *J. Am. Chem. Soc.*, **75**, 1236–7.
Siegel, S., Hoekstra, H. R., and Sherry, E. (1966) *Acta Crystallogr.*, **20**, 292–5.
Silva, M. R., Beja, A. M., Paixão, J. A., da Veiga, L. A., and Martin-Gil, J. (1999) *Acta Crystallogr. C*, **55**, 2039–41.
Silverwood, P. R., Collison, D., Livens, F. R., Beddoes, R. L., and Taylor, R. J. (1998) *J. Alloys Compds*, **271–273**, 180–3.
Smetana, Z., Sechovský, V., and Meňovský, A. (1975) *Phys. Status Solidi A*, **27**, K73–5.
Smith, G. M., Suzuki, H., Sonnenberger, D. C., Day, V. W., and Marks, T. J. (1986) *Organometallics*, **5**, 549–61.
Smith, G. S., Johnson, Q., and Elson, R. E. (1967) *Acta Crystallogr.*, **22**, 300–3.
Smith, J. L. and Kmetko, E. A. (1983) *J. Less Common Metals*, **90**, 83–8.
Smith, P. K., Hale, W. H., and Thompson, M. C. (1969) *J. Chem. Phys.*, **50**, 5066–76.
Spirlet, J. C., Kalbusch, J., Moens, A., Rijkeboer, C., and Rebizant, J. (1991) *Lanthanide Actinide Res.*, **3**, 277–83.
Spirlet, M. R., Rebizant, J., and Goffart, J. (1982) *Acta Crystallogr. B*, **38**, 2400–4.
Spirlet, M. R., Rebizant, J., Kanellakopulos, B., and Dornberger, E. (1986) *J. Less Common Metals*, **122**, 205–10.
Spirlet, M. R., Rebizant, J., Kanellakopulos, B., and Dornberger, E. (1987a) *Acta Crystallogr. C*, **43**, 19–21.
Spirlet, M. R., Rebizant, J., and Goffart, J. (1987b) *Acta Crystallogr. C*, **43**, 354–5.
Spirlet, M. R., Rebizant, J., Apostolidis, C., Andreetti, G. D., and Kanellakopulos, B. (1989) *Acta Crystallogr. C*, **45**, 739–41.
Spirlet, M. R., Rebizant, J., Apostolidis, C., Van den Bossche, G., and Kanellakopulos, B. (1990a) *Acta Crystallogr. C*, **46**, 2318–20.
Spirlet, M. R., Rebizant, J., Bettonville, S., and Goffart, J. (1990b) *Acta Crystallogr. C*, **46**, 1234–6.
Spirlet, M. R., Rebizant, J., Apostolidis, C., and Kanellakopulos, B. (1992a) *Acta Crystallogr. C*, **48**, 2135–7.
Spirlet, M. R., Rebizant, J., Bettonville, S., and Goffart, J. (1992b) *Acta Crystallogr. C*, **48**, 1221–3.
Spirlet, M. R., Rebizant, J., Apostolidis, C., and Kanellakopulos, B. (1993a) *Acta Crystallogr. C*, **49**, 929–31.
Spirlet, M. R., Rebizant, J., Bettonville, S., and Goffart, J. (1993b) *Acta Crystallogr. C*, **49**, 1138–40.
Spirlet, M. R., Rebizant, J., Bettonville, S., and Goffart, J. (1993c) *J. Organomet. Chem.*, **460**, 177–80.
Spirlet, M. R., Jemine, X., and Goffart, J. (1994) *J. Alloys Compds*, **216**, 269–71.
Staritzky, E. (1956) *Anal. Chem.*, **28**, 2021–2.

Staritzky, E. and Cromer, D. T. (1956) *Anal. Chem.*, **28**, 1354–5.
Staritzky, E., Cromer, D. T., and Walker, D. I. (1956) *Anal. Chem.*, **28**, 1634–5.
Starks, D. F., Parsons, T. C., Streitweiser, A. Jr, and Edelstein, N. (1974) *Inorg. Chem.*, **13**, 1307–8.
Steeb, S. and Mitsch, P. (1965) *J. Nucl. Mater.*, **15**, 81–7.
Steeb, S. and Brucklacher, D. (1966) *J. Less Common Metals*, **11**, 263–72.
Stein, L. (1964) *Inorg. Chem.*, **3**, 995–8.
Sternal, R. S., Sabat, M., and Marks, T. J. (1987) *J. Am. Chem. Soc.*, **109**, 7920–1.
Stevenson, J. N. and Peterson, J. R. (1973) *J. Inorg. Nucl. Chem.*, **35**, 3481–6.
Stöwe, K. (1996) *Z. Anorg. Allg. Chem.*, **622**, 1423–7.
Stöwe, K. (1997) *J. Alloys Compds*, **246**, 111–23.
Straub, T., Frank, W., Reiss, G. J., and Eisen, M. S. (1996) *J. Chem. Soc., Dalton Trans.*, 2541–6.
Streitweiser, A. Jr and Müller-Westerhoff, U. (1968) *J. Am. Chem. Soc.*, **90**, 7364.
Suortti, P. (2002) in *Encyclopedia of Physical Science and Technology*, 3rd edn, vol. 17 (ed. R. A. Meyers), Academic Press, San Diego, CA, pp. 989–1023.
Suski, W., Gibinski, T., Wojakowski, A., and Czopnik, A. (1972) *Phys. Status Solidi A*, **9**, 653–8.
Tatsumi, K. and Hoffmann, R. (1980) *Inorg. Chem.*, **19**, 2656–8.
Taylor, J. C., Mueller, M. H., and Hitterman, R. L. (1966) *Acta Crystallogr.*, **20**, 842–51.
Taylor, J. C. and Wilson, P. W. (1973a) *Acta Crystallogr. B*, **29**, 1942–4.
Taylor, J. C. and Wilson, P. W. (1973b) *Acta Crystallogr. B*, **29**, 1073–6.
Taylor, J. C., Wilson, P. W., and Kelly, J. W. (1973) *Acta Crystallogr. B*, **29**, 7–12.
Taylor, J. C. and Wilson, P. W. (1974a) *Acta Crystallogr. B*, **30**, 2803–5.
Taylor, J. C. and Wilson, P. W. (1974b) *Acta Crystallogr. B*, **30**, 2664–7.
Taylor, J. C. and Wilson, P. W. (1974c) *Acta Crystallogr. B*, **30**, 1481–4.
Taylor, J. C. and Wilson, P. W. (1974d) *Acta Crystallogr. B*, **30**, 175–7.
Taylor, J. C. and Wilson, P. W. (1974e) *J. Chem. Soc., Chem. Commun.*, 232–3.
Taylor, J. C. (1976) *Coord. Chem. Rev.*, **20**, 197–273.
Templeton, D. H. and Dauben, C. H. (1953) *J. Am. Chem. Soc.*, **75**, 4560–2.
Templeton, L. K., Templeton, D. H., and Walker, R. (1977) *Inorg. Chem.*, **15**, 3000–3.
Thévenin, T., Pages, M., and Wojakowski, A. (1982) *J. Less Common Metals*, **84**, 133–7.
Thévenin, T., Jové, J., and Pages, M. (1984) *Hyperfine Interact.*, **20**, 173–86.
Thévenin, T., Jové, J., and Madic, C. (1986) *J. Less Common Metals*, **121**, 477–81.
Thewlis, J. (1951) *Nature* (*UK*), **168**, 198–9.
Thoma, R. E. and Brunton, G. D. (1966) *Inorg. Chem.*, **5**, 1937–9.
Thuéry, P., Keller, N., Lance, M., Sabattié, J.-M., Vigner, J.-D., and Nierlich, M. (1995a) *Acta Crystallogr. C*, **51**, 801–5.
Thuéry, P., Nierlich, M., Keller, N., Lance, M., and Vigner, J.-D. (1995b) *Acta Crystallogr. C*, **51**, 1300–2.
Thuéry, P., Keller, N., Lance, M., Vigner, J.-D., and Nierlich, M. (1995c) *Acta Crystallogr. C*, **51**, 1570–4.
Thuéry, P., Keller, N., Lance, M., Vigner, J.-D., and Nierlich, M. (1995d) *New J. Chem.*, **19**, 619–25.
Thuéry, P., Lance, M., and Nierlich, M. (1996) *Supramol. Chem.*, **7**, 183–5.
Thuéry, P. and Nierlich, M. (1997) *J. Inclusion Phenom. Mol. Recog. Chem.*, **27**, 13–20.

Thuéry, P., Nierlich, M., Ogden, M. I., and Harrowfield, J. M. (1998) *Supramol. Chem.*, **9**, 297–303.
Thuéry, P., Nierlich, M., Masci, B., Asfari, Z., and Vicens, J. (1999a) *J. Chem. Soc., Dalton Trans.*, 3151–2.
Thuéry, P., Nierlich, M., Souley, B., Asfari, Z., and Vicens, J. (1999b) *J. Chem. Soc., Dalton Trans.*, 2589–94.
Thuéry, P., Nierlich, M., Vicens, J., Masci, B., and Takemura, H. (2001a) *Eur. J. Inorg. Chem.*, 637–43.
Thuéry, P., Nierlich, M., Vicens, J., and Masci, B. (2001b) *J. Chem. Soc., Dalton Trans.*, 867–74.
Thuéry, P., Nierlich, M., Vicens, J., and Takemura, H. (2001c) *Polyhedron*, **20**, 3183–7.
Thuéry, P., Nierlich, M., Harrowfield, J. M., and Ogden, M. I. (2001d) in *Calixarenes 2001* (eds. Z. Asfari, V. Böhmer, J. Harrowfield, J. Vicens), Kluwer Academic, Dordrecht, pp. 561–82.
Thuéry, P. and Masci, B. (2003) *Polyhedron*, **22**, 3499–505.
Thuéry, P. and Masci, B. (2004) *Polyhedron*, **23**, 649–54.
Tomilin, S. V., Volkov, Yu. F., Visyashcheva, G. I., and Kapshukov, I. I. (1984) *Radiokhimiya*, **26**, 734–9.
Tougait, O., Potel, M., and Noël, H. (1998a) *Inorg. Chem.*, **37**, 5088–91.
Tougait, O., Potel, M., Jevet, J. C., and Noël, H. (1998b) *Eur. J. Solid State Inorg. Chem.*, **35**, 67–76.
Tougait, O., Potel, M., and Noël, H. (1998c) *J. Solid State Chem.*, **139**, 356–61.
Traill, R. J. (1952) *Am. Mineral.*, **37**, 394–406.
Troost, L. (1893) *Compt. Rend. Acad. Sci. Paris*, **116**, 1229.
Tucker, C. W. Jr (1950) *Trans. Am. Soc. Met.*, **42**, 762–70.
Tucker, C. W. Jr (1951) *Acta Crystallogr.*, **4**, 425–31.
Turcotte, R. P., Chikalla, T. D., and Eyring, L. (1971) *J. Inorg. Nucl. Chem.*, **33**, 3749–63.
Turcotte, R. P., Chikalla, T. D., Haire, R. G., and Fahey, J. A. (1980) *J. Inorg. Nucl. Chem.*, **42**, 1729–33.
Ueki, T., Zalkin, A., and Templeton, D. H. (1966) *Acta Crystallogr.*, **20**, 836–41.
Van Der Sluys, W. G., Burns, C. J., Huffman, J. C., and Sattelberger, A. P. (1988) *J. Am. Chem. Soc.*, **110**, 5924–5.
Vegas, A., Martinez-Cruz, L. A., Ramos-Gallardo, A., and Romero, A. (1995) *Z. Kristallogr.*, **210**, 574–80.
Ventelon, L., Lescop, C., Arliguie, T., Leverd, P. C., Lance, M., Nierlich, M., and Ephritikhine, M. (1999) *J. Chem. Soc., Chem. Comm.*, 659–60.
Voinova, L. M. (1998) *Radiokhimiya*, **40**, 299–301.
Voliotis, S. and Rimsky, A. (1975a) *Acta Crystallogr. B*, **31**, 2612–15.
Voliotis, S. and Rimsky, A. (1975b) *Acta Crystallogr. B*, **31**, 2615–20.
Volkov, Yu. F., Visyashcheva, G. I., Tomilin, S. V., Kapshukov, I. I., and Rykov, A. G. (1981) *Radiokhimiya*, **23**, 237–42.
Volkov, Yu. F., Tomilin, S. V., Orlova, A. I., Lizin, A. A., Spiryakov, V. I., and Lukinykh, A. N. (2003) *Radiokhimiya*, **45**, 289–97.
Vollath, D. (1984) in *Gmelin Handbook of Inorganic Chemistry, Uranium*, 8th edn, Suppl. vol. C4 (eds. R. Keim and C. Keller), Springer-Verlag, Berlin, pp. 97–138.
Wadt, W. R. (1981) *J. Am. Chem. Soc.*, **103**, 6053–7.
Wait, E. (1955) *J. Inorg. Nucl. Chem.*, **1**, 309–12.

Wallmann, J. C. (1964) *J. Inorg. Nucl. Chem.*, **26**, 2053–7.
Ward, J. W., Haschke, J. M., Rebizant, J., and Bartscher, W. (1984) *J. Less Common Metals*, **100**, 195–214.
Ward, J. W., Bartscher, W., and Rebizant, J. (1987) *J. Less Common Metals*, **130**, 431–9.
Wasserman, H. J., Zozulin, A. J., Moody, D. C., Ryan, R. R., and Salazar, K. V. (1983) *J. Organomet. Chem.*, **254**, 305–11.
Weigel, F. and Haug, H. (1965) *Radiochim. Acta*, **4**, 227–8.
Weigel, F. and ter Meer, N. (1967) *Inorg. Nucl. Chem. Lett.*, **3**, 403–8.
Weigel, F. and Hoffmann, G. (1976a) *J. Less Common Metals*, **44**, 99–123.
Weigel, F. and Hoffmann, G. (1976b) *J. Less Common Metals*, **44**, 125–32.
Weigel, F. and Hoffmann, G. (1976c) *J. Less Common Metals*, **44**, 133–6.
Weigel, F. and Hauske, H. (1977) *J. Less Common Metals*, **55**, 243–7.
Weigel, F., Wittmann, F. D., and Marquart, R. (1977) *J. Less Common Metals*, **56**, 47–53.
Weigel, F., Wishnevsky, V., and Wolf, M. (1979) *J. Less Common Metals*, **63**, 81–6.
Weigel, F. and Marquart, R. (1983) *J. Less Common Metals*, **90**, 283–90.
Weigel, F., Wittmann, F. D., Schuster, W., and Marquart, R. (1984) *J. Less Common Metals*, **102**, 227–38.
Weigel, F. and Kohl, R. (1985) in *Americium Curium Chem. Technol., Pap. Symp.*, 1984 (eds. N. M. Edelstein, J. D. Navratil, and W. W. Schulz), Reidel, Dordrecht, Netherlands, pp. 159–91.
Weigel, F. (1986) in *Chemistry of the Actinide Elements*, 2nd edn, vol. 1 (eds. J. J. Katz, G. T. Seaborg, and L. R. Morss), Chapman and Hall, New York., p. 267.
Weigel, F. and Hellmann, H. (1986) *J. Less Common Metals*, **121**, 415–23.
Weller, M. T., Dickens, P. G., and Penny, D. J. (1988) *Polyhedron*, **7**, 243–4.
Wilkerson, M. P., Burns, C. J., Dewey, H. J., Martin, J. M., Morris, D. E., Paine, R. T., and Scott, B. L. (2000) *Inorg. Chem.*, **39**, 5277–85.
Willis, B. T. M. (1963) *Nature* (*UK*), **197**, 755–6.
Willis, B. T. M. (1964) *J. Phys.* (*Paris*), **25**, 431–9.
Willis, B. T. M. (1978) *Acta Crystallogr. A,* **34**, 88–90.
Willis, B. T. M. (1987) *J. Chem. Soc., Faraday Trans. 2*, **83**, 1073–81.
Wills, J. M. and Eriksson, O. (1992) *Phys. Rev. B*, **45**, 13879–90.
Wilson, T. A. (1933) *Physica*, **4**, 148–52.
Wojakowski, A. and Damien, D. (1982) *J. Less Common Metals*, **83**, 263–7.
Wojakowski, A., Damien, D., and Hery, Y. (1982) *J. Less Common Metals*, **83**, 169–74.
Wong, C.-H., Yen, T.-M., and Lee, T.-Y. (1965) *Acta Crystallogr.*, **18**, 340–5.
Wrobleski, D. A., Ryan, R. R., Wasserman, H. J., Salazar, K. V., Paine, R. T., and Moody, D. C. (1986a) *Organometallics*, **5**, 90–4.
Wrobleski, D. A., Cromer, D. T., Ortiz, J. V., Rauschfuss, T. B., Ryan, R. R., and Sattelberger, A. P. (1986b) *J. Am. Chem. Soc.*, **108**, 174–5.
Yang, X., Stern, C. L., and Marks, T. J. (1991) *Organometallics*, **10**, 840–2.
Zachariasen, W. H. (1948a) *Phys. Rev.*, **73**, 1104–5.
Zachariasen, W. H. (1948b) *Acta Crystallogr.*, **1**, 265–8.
Zachariasen, W. H. (1948c) *Acta Crystallogr.*, **1**, 285–7.
Zachariasen, W. H. (1949a) *Nat. Nucl. Ener. Ser.*, Manhattan Proj. Tech. Sect., Div. 4, Plutonium Proj. 14B, 1489–91.
Zachariasen, W. H. (1949b) *Acta Crystallogr.*, **2**, 388–90.

Zachariasen, W. H. (1949c) *Nat. Nucl. Ener. Ser.*, Manhattan Proj. Tech. Sect., Div. 4, Plutonium Proj. 14B, 1448–50.
Zachariasen, W. H. (1949d) *Acta Crystallogr.*, **2**, 94–9.
Zachariasen, W. H. (1949e) *Acta Crystallogr.*, **2**, 291–6.
Zachariasen, W. H. (1949f) *Acta Crystallogr.*, **2**, 288–91.
Zachariasen, W. H. (1949g) *Acta Crystallogr.*, **2**, 296–8.
Zachariasen, W. H. (1951) *Acta Crystallogr.*, **4**, 231–6.
Zachariasen, W. H. (1952a) *Acta Crystallogr.*, **5**, 660–4.
Zachariasen, W. H. (1952b) *Acta Crystallogr.*, **5**, 664–7.
Zachariasen, W. H. (1952c) *Acta Crystallogr.*, **5**, 17–19.
Zachariasen, W. H. (1953) *Acta Crystallogr.*, **6**, 393–5.
Zachariasen, W. H. (1954) *Acta Crystallogr.*, **7**, 795–9.
Zachariasen, W. H. and Ellinger, F. H. (1955) *Acta Crystallogr.*, **8**, 431–3.
Zachariasen, W. H. and Ellinger, F. H. (1957) *J. Chem. Phys.,* **27**, 811–12.
Zachariasen, W. H. and Ellinger, F. H. (1959) *Acta Crystallogr.*, **12**, 175–6.
Zachariasen, W. H. and Plettinger, H. A. (1959) *Acta Crystallogr.*, **12**, 526–30.
Zachariasen, W. H. and Ellinger, F. H. (1963a) *Acta Crystallogr.*, **16**, 777–83.
Zachariasen, W. H. and Ellinger, F. H. (1963b) *Acta Crystallogr.*, **16**, 369–75.
Zachariasen, W. H. (1975) *J. Inorg. Nucl. Chem.*, **37**, 1441–2.
Zalkin, A., Forrester, J. D., and Templeton, D. H. (1964) *Inorg. Chem.*, **3**, 639–44.
Zalkin, A. and Raymond, K. N. (1969) *J. Am. Chem. Soc.*, **91**, 5667–8.
Zalkin, A., Rietz, R. R., Templeton, D. H., and Edelstein, N. M. (1978a) *Inorg. Chem.*, **17**, 661–3.
Zalkin, A., Ruben, H., and Templeton, D. H. (1978b) *Inorg. Chem.*, **17**, 3701–2.
Zalkin, A., Templeton, D. H., Berryhill, S. R., and Luke, W. D. (1979) *Inorg. Chem.*, **18**, 2287–9.
Zalkin, A., Templeton, D. H., Le Vanda, C., and Streitweiser, A. Jr (1980) *Inorg. Chem.*, **19**, 2560–3.
Zalkin, A., Templeton, D. H., Luke, W. D., and Streitwieser, A. Jr (1982) *Organometallics*, **1**, 618–22.
Zalkin, A. and Brennan, J. G. (1985) *Acta Crystallogr. C*, **41**, 1295–7.
Zalkin, A., Templeton, D. H., Kluttz, R., and Streitwieser, A. Jr (1985) *Acta Crystallogr. C*, **41**, 327–9.
Zalkin, A. and Brennan, J. G. (1987) *Acta Crystallogr. C*, **43**, 1919–22.
Zalkin, A., Brennan, J. G., and Andersen, R. A. (1987a) *Acta Crystallogr. C*, **43**, 1706–8.
Zalkin, A., Brennan, J. G., and Andersen, R. A. (1987b) *Acta Crystallogr. C*, **43**, 418–20.
Zalkin, A., Brennan, J. G., and Andersen, R. A. (1987c) *Acta Crystallogr. C*, **43**, 421–3.
Zalkin, A. and Beshouri, S. M. (1988) *Acta Crystallogr. C*, **44**, 1826–7.
Zalkin, A., Brennan, J. G., and Andersen, R. A. (1988a) *Acta Crystallogr. C*, **44**, 2104–6.
Zalkin, A., Stuart, A. L., and Andersen, R. A. (1988b) *Acta Crystallogr. C*, **44**, 2106–8.
Zalkin, A. and Beshouri, S. M. (1989a) *Acta Crystallogr. C*, **45**, 1080–2.
Zalkin, A. and Beshouri, S. M. (1989b) *Acta Crystallogr. C*, **45**, 1219–21.
Zanella, P., De Paoli, G., Bombieri, G., Zanotti, G., and Rossi, R. (1977) *J. Organomet. Chem.*, **142**, C21–4.
Zanella, P., Paolucci, G., Rossetto, G., Benetollo, F., Polo, A., Fischer, R. D., and Bombieri, G. (1985) *J. Chem. Soc., Chem. Commun.*, 96–8.

Zanella, P., Brianese, N., Casellato, U., Ossola, F., Porchia, M., Rossetto, G., and Graziani, R. (1987a) *J. Chem. Soc., Dalton Trans.*, 2039–43.

Zanella, P., Ossola, F., Porchia, M., Rossetto, G., Villa, A. C., and Guastini, C. (1987b) *J. Organomet. Chem.*, **323**, 295–303.

Zanella, P., Brianese, N., Casellato, U., Ossola, F., Porchia, M., and Rossetto, G. (1988) *Inorg. Chim. Acta*, **144**, 129–34.

Zhang, Y.-J., Collison, D., Livens, F. R., Helliwell, M., Eccles, H., and Tinker, N. (1998) *J. Alloys Compds*, **271–273**, 139–43.

Zhang, Y.-J., Collison, D., Livens, F. R., Powell, A. K., Wocadlo, S., and Eccles, H. (2000) *Polyhedron*, **19**, 1757–67.

Zhang, Y.-J., Collison, D., Livens, F. R., Helliwell, M., Heatley, F., Powell, A. K., Wocadlo, S., and Eccles, H. (2002a) *Polyhedron*, **21**, 81–96.

Zhang, Y.-J., Livens, F. R., Collison, D., Helliwell, M., Heatley, F., Powell, A. K., Wocadlo, S., and Eccles, H. (2002b) *Polyhedron*, **21**, 69–79.

Zhang, Z. and Pitzer, R. M. (1999) *J. Phys. Chem. A*, **103**, 6880–6.

Zivadinovich, M. S. (1967) *Bull. Boris Kidric Inst. Nucl. Sci.*, **18**, 1–8.

Zumbusch, M. (1941) *Z. Anorg. Allg. Chem.*, **245**, 402–8.

CHAPTER TWENTY THREE

ACTINIDES IN SOLUTION: COMPLEXATION AND KINETICS

Gregory R. Choppin and Mark P. Jensen

23.1 INTRODUCTION

The solution chemistry of the actinide elements has been explored in aqueous and organic solutions. While the relative stabilities of the actinide oxidation states and the types of complexes formed with the actinide cations in these states vary between solvents, the fundamental principles governing their redox reactions and their complexation strengths are the same regardless of the solvent. This chapter focuses on aqueous actinide chemistry, reflecting the wide variety of studies on actinide reactions in aqueous solutions. However, three factors that are important for actinides in non-aqueous solvents should be noted. First, in non-aqueous solvents, the formation of neutral cation–anion ion pairs is often dominant due to the lower (as compared to water) dielectric constants of the solvents. Second, non-aqueous conditions also allow the formation of complexes between actinide cations and ligands containing soft Lewis base groups, such as sulfur. Third, non-aqueous solvents are often useful for

stabilizing redox-sensitive actinide complexes, as oxidation states that are unstable in aqueous solution may be stable in non-aqueous solutions (Mikheev *et al.*, 1977; Hulet *et al.*, 1979).

Actinide cations can exist in a variety of oxidation states (2+ to 7+) in aqueous solution, with trivalent, tetravalent, pentavalent, and hexavalent actinides being the most common. However, there is wide variability in the stability of a particular oxidation state across the actinide series and for some actinides several oxidation states can coexist in the same solution. This is most evident for plutonium as there are small differences in the redox potentials of Pu(III), Pu(IV), Pu(V), and Pu(VI) over a range of pH values (Fig. 23.1).

The divalent oxidation state is the most stable form of nobelium in acidic aqueous solution. It is strongly stabilized, relative to the trivalent state, by the formation of a closed, $5f^{14}$ shell, as reflected in the large reduction potential of the No^{3+} aquo ion [E°(No(III)/No(II)) = +1.45 V vs NHE] (see Chapter 19).

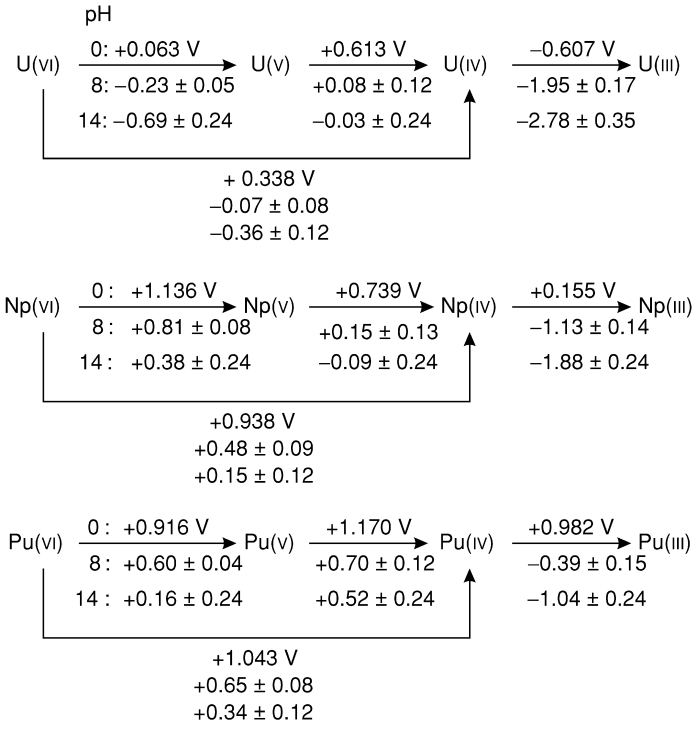

Fig. 23.1 *Reduction potential diagrams for uranium, neptunium, and plutonium for* 1 M $HClO_4$, *pH* 8, *and* 1 M *NaOH* (*Choppin* et al., 2002). *Values for* 1 M $HClO_4$ *are formal potentials for that medium.*

This is in direct contrast to nobelium's lanthanide homolog, ytterbium, which is significantly more stable as E°(Yb(III)/Yb(II)) = –1.05 V vs NHE (Morss, 1985). The stability of No(II) suggests that isoelectronic Md(I) might be expected in aqueous solution. However, while Md(I) has been reported (Mikheev *et al.*, 1980), its existence has not been confirmed (Hulet *et al.*, 1979; Samhoun *et al.*, 1979). Md(II) is moderately stable in acidic solution [E°(Md(III)/Md(II)) = −0.15 V vs NHE], and can be produced through the reduction of Md(III) by Cr(II), Eu(II), or metallic zinc. Nobelium and mendelevium are the only actinides stable as divalent cations in aqueous solution but Am(II), Cm(II), and Cf(II) can be produced transiently in aqueous acidic solutions by pulse radiolysis (Gordon *et al.*, 1978). Trivalent californium, einsteinium, and fermium also can be reduced to the divalent oxidation state by Sm(II) or Yb(II) in 85% ethanol/water.

The trivalent oxidation state is the most stable form of actinium and the transplutonium actinide ions, americium to mendelevium and lawrencium, in aqueous solution. Pu(III) is readily produced by reduction, but it is slowly oxidized to Pu(IV) by the radiolysis products from the α-decay if more than tracer amounts of ^{238}Pu or ^{239}Pu are present. Solutions of the long-lived plutonium isotopes ^{242}Pu and ^{244}Pu in 1 M perchloric acid show little oxidation of Pu(III) after storage for weeks. Np(III) is less stable than Pu(III) but its oxidation to Np(IV) is very slow in the absence of oxygen. U(III) is a strong reducing agent, oxidizing in water. Trivalent thorium and protactinium are not stable in solution.

All the actinides from thorium to californium form tetravalent species in aqueous solution. Th(IV) is the only oxidation state of thorium that is stable in solution. Pa(IV), U(IV), and Np(IV) are stable in the absence of oxygen. Low concentrations of Pu(IV) are stable in acidic aqueous solutions even in the presence of oxygen, but the similarity of the potentials of the Pu(IV)/Pu(V), Pu(V)/Pu(IV), and Pu(IV)/Pu(III) redox couples can make it difficult to prepare and maintain high concentrations of plutonium in a single oxidation state because of the resulting tendency of plutonium to undergo disproportionation reactions (see Section 23.10). Tetravalent americium, curium, berkelium, and californium are much less stable than the other An(IV) species, but they can be prepared in aqueous solution with strong oxidants in the presence of fluoride, phosphate, or polyoxometallate ligands, which form strong complexes with the tetravalent actinides. Bk(IV) is the most stable of the tetravalent transplutonium species with a Bk(IV)/Bk(III) reduction potential similar to that of Ce(IV) [E°(Ce(IV)/Ce(III)) = +1.6 V vs NHE] (Antonio *et al.*, 2002).

The actinides from protactinium to americium can be prepared in the pentavalent oxidation state. Pa(V) and Np(V) are the most stable oxidation states of these elements in aqueous solution, though NpO_2^+ disproportionates to Np(IV) and Np(VI) at high neptunium concentrations and acidities (>8 M HNO_3). UO_2^+ and PuO_2^+ are very susceptible to disproportionation, but become more stable as the uranium or plutonium concentration is decreased or the pH is increased.

PuO_2^+ becomes the predominant dissolved form of plutonium in natural waters (Nelson and Lovett, 1978). AmO_2^+ is a strong oxidant and is reduced to Am(III) by alpha radiolysis.

The hexavalent oxidation state of the actinides, which is present as AnO_2^{2+} ions in aqueous solution, is known for the actinides from uranium to americium. UO_2^{2+} is the most stable form of uranium in solution and is the most stable of the actinyl(VI) cations. The stability of the actinyl(VI) cations decreases in the order $UO_2^{2+} >> PuO_2^{2+} > NpO_2^{2+} > AmO_2^{2+}$. Np(VI) can be reduced by cation exchange resin to Np(V) (Sullivan *et al*., 1955).

The heptavalent actinides, Np(VII) and Pu(VII), are unstable in acidic solution. The reduction of Np(VII) and Pu(VII) to the hexavalent oxidation state is very slow in alkaline solutions (Spitsyn *et al*., 1968; Sullivan and Zielen, 1969), and is reversible in 1 M NaOH (Zielen and Cohen, 1970). The structure of the Np(VII) anion, $NpO_4(OH)_2^{3-}$, is the same in the solid state (Burns *et al*., 1973; Tomilin *et al*., 1981; Grigor'ev *et al*., 1986) and in solution (Appelman *et al*., 1988; Williams *et al*., 2001). The existence of Am(VII) (Krot *et al*., 1974; Shilov, 1976) is still a matter of controversy.

Given the stabilities of the various oxidation states, as well as the limited availability and high specific activity of many of the actinide nuclides, there are comparatively few solution studies of the complexes of actinium, protactinium, and the transplutonium elements from berkelium to lawrencium. Quantitative information about the complexation of actinide ions in the less common oxidation states, An(II) and An(VII), also is very scarce. The lack of data on these species can often be filled by extrapolation from the behavior of other, better studied actinide cations.

Stability constants provide a measure of the resistance of a metal–ligand complex to dissociation in solution, and are directly related to the Gibbs energy of complexation. It is often difficult to measure the chemical activities of actinide ions, ligands, and complexes, so concentrations are used commonly in place of activities for calculations of stability constants. Such concentration stability constants are valid for only a limited range of conditions due to their dependence on the ionic strength of the solution. The concentration stability constant, β_{nq}, for the reaction of an actinide cation, An, with a ligand, L, according to the equation,

$$n\mathrm{An} + q\mathrm{L} \rightleftarrows \mathrm{An}_n\mathrm{L}_q$$

is

$$\beta_{nq} = [\mathrm{An}_n\mathrm{L}_q]/[\mathrm{An}]^n[\mathrm{L}]^q \tag{23.1}$$

This notation is used throughout this chapter to identify stability constants, Gibbs energies (ΔG_{nq}), enthalpies (ΔH_{nq}), and entropies (ΔS_{nq}) of complexation of n actinide cations by q ligands.

23.2 HYDRATION OF ACTINIDE CATIONS

The hydration of an actinide cation is a critical factor in the structural and chemical behavior of the complexes. Although f-element salts generally have large lattice energies, many are fairly soluble in water, reflecting the strength of the interactions between the metal cations and water molecules. Once an actinide cation is dissolved in an aqueous solution, the formation of inner sphere complexes involves displacement of one or more water molecules by each ligand. In the reaction with simple ligands to form inner sphere complexes, the release of water molecules from the hydration spheres of the ligand and actinide ion to the bulk solvent contributes to the thermodynamic strength of the complexes formed by increasing the entropy, but some of this gain is offset by a positive enthalpy contribution.

The size and structure of the hydration sphere of a metal ion have been probed by direct and indirect methods. Direct methods include X-ray and neutron diffraction, X-ray absorption fine structure (XAFS) measurements, luminescence decay, and nuclear magnetic resonance (NMR) relaxation measurements, while the indirect methods involve compressibility, NMR exchange, and optical absorption spectroscopy. Theoretical and computational studies are also becoming important in understanding the coordination geometry and coordination number (CN) of actinide ion hydrates (e.g. Spencer *et al*., 1999; Hay *et al*., 2000; Tsushima and Suzuki, 2000; Antonio *et al*., 2001).

23.2.1 Trivalent actinides

Much of the initial hydration data reported for trivalent actinide cations were derived by analogy to the experimental data for the trivalent lanthanide ions. In the lanthanide studies, the data is consistent with formation of an isostructural series with nine water molecules coordinated to the early members of the lanthanide series that transitions to an isostructural series containing eight water molecules over the middle members of the lanthanide series. This reflects the decrease in radius with increasing atomic number; i.e. the lanthanide (and actinide) contraction. The transition between CN = 9 and 8 occurs between Pm(III) and Dy(III) for the Ln(III) series. The trivalent cations of both the An(III) and Ln(III) series have similar cationic radii, and a similar decrease in hydration number from nine to eight is observed for the trivalent actinide elements between Am(III) and Es(III) (Table 23.1), which span the same range of cationic radii as Pm(III)–Dy(III).

Initial measurements of the hydration of the trivalent actinides involved electrophoretic and diffusion methods in which it is difficult to differentiate between the total hydration (all of the water molecules that feel the effect of a cation over several concentric hydration spheres) and first sphere or primary hydration (i.e. the water molecules directly coordinated to the cation).

Table 23.1 *Hydration radii, R_b, hydration numbers, h, and primary sphere hydration, N_{H_2O}, of trivalent actinide ions obtained by electrophoresis and diffusion measurements* (*Lundqvist* et al., 1981; *Fourest* et al., 1984; *David*, 1986).

An^{3+}	R_b (Å)	h	N_{H_2O}
Am	4.60	13.6	9.0
Cm	4.69	14.4	8.9
	4.55	13.0	–
Cf	4.9	16.4	8.2
	4.64	13.8[a]	–
Es	4.92	16.6	8.0
Fm	4.95	16.9	–
Md	4.88	16.2	–

[a] Data obtained from diffusion measurements.

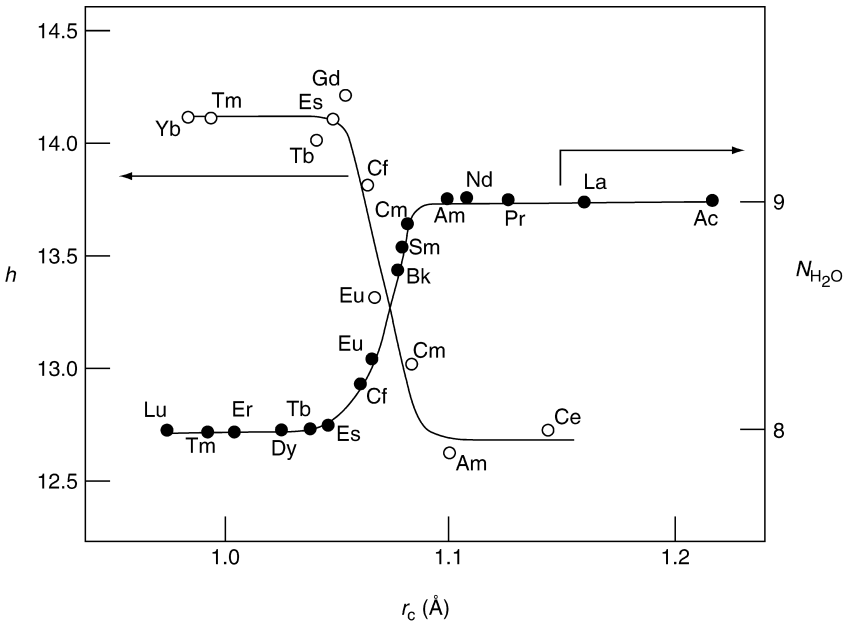

Fig. 23.2 *Total hydration (h) and number of water molecules in the primary coordination sphere(N_{H_2O}) of Ln^{3+} and An^{3+} cations* (*Rizkalla and Choppin,* 1994).

Fourest *et al.* (1984) estimated the primary, inner sphere coordination numbers, N_{H_2O} of the trivalent actinides by interpolation using the values of the lanthanide elements (Habenschuss and Spedding, 1979a, 1979b, 1980). The two sets of hydration numbers for Ln(III) and An(III) cations are presented in Fig. 23.2.

These values show that the primary hydration number, N_{H_2O}, of the trivalent metal ions as a function of cationic radius for coordination number 8 is, in both cases, sigmoidal with smaller primary hydration for the smaller, heavier cations. By contrast the opposite trend is seen for the total hydration number, h, which is smaller for the lighter cations. This was attributed by Fourest's group to the increase in the cationic charge density as the atomic number increases. It should be noted that the break in the properties of the two series also is observed in other physical data such as apparent molal volume, relative viscosity, heat of dilution, and electrical conductivity.

The coordination geometry in the first hydration sphere has been obtained primarily from neutron diffraction measurements and is consistent with formation of nona-coordinate lanthanides with a tricapped trigonal prismatic (TCTP) structure. X-ray crystal structures of nona-coordinate Ln(III) and Pu(III) triflates also show this geometry in the solid state (Chatterjee *et al.*, 1988; Matonic *et al.*, 2001). Similarly, the data for the heavier members of the series, with coordination number 8, are consistent with a square prismatic structure. The ions that are intermediate between these two extremes (Pm–Dy or Am–Es) show an equilibrium mixture of the structures for $N_{H_2O} = 8$ and $N_{H_2O} = 9$. Optical spectroscopy indirectly confirms that the solid state structures of the hydrated An(III) ions persist in solution as well (Carnall, 1989; Matonic *et al.*, 2001), and fluorescence lifetime measurements of Cm(III) solutions give a direct primary hydration number of (9.2 ± 0.5) (Kimura and Choppin, 1994).

While it cannot give the coordination geometry, XAFS measurements are useful for determining the average actinide–oxygen bond distances of the first hydration sphere and N_{H_2O} in liquid samples at concentrations much lower than those accessible by X-ray or neutron diffraction. An–OH_2 bond distances and coordination numbers have been determined by XAFS for all of the An(III) from U(III) to Cf(III) at concentrations of $0.5-20 \times 10^{-3}$ M. The An–O bond distances are all consistent with octa- or nona-coordination, and the average coordination number reported across the actinide series is (9 ± 1). As is the case with the other oxidation states, some investigators report hydration numbers 10–20% higher than this, but this is within the generally accepted absolute uncertainty of XAFS-based coordination number determinations and there are a number of factors that could explain systematic deviations from the true coordination number, as discussed by Allen *et al.* (2000).

23.2.2 Tetravalent actinides

Information relating to the hydration numbers of tetravalent actinide ions is somewhat limited. From NMR peak areas, an estimate of the primary hydration number of Th(IV) in an aqueous acetone solution of $Th(ClO_4)_4$ at $-100°C$ indicated a hydration number of 9 (Butler and Symons, 1969; Fratiello *et al.*, 1970a) whereas an indirect, NMR line width method gave $N_{H_2O} = 10$ (Swift and Sayre, 1966). However, the direct and accurate method of solution X-ray

diffraction gave $N_{H_2O} = (8.0 \pm 0.5)$ for acidic, 1–2 M $Th(ClO_4)_4$ and $ThCl_4$ solutions (Johansson *et al.*, 1991). Other reported values are: Th(IV) (10.8 ± 0.5) and U(IV) (10 ± 1) (Moll *et al.*, 1999), Np(IV) (11.2 ± 0.4) (Allen *et al.*, 1997), Th(IV) 11.0, U(IV) 10.65, Np(IV) 10.2, and Pu(IV) 10.0 (David and Vokhmin, 2003).

An entirely different method for the estimation of total hydration numbers from conductivity measurements has been proposed and developed by Gusev (1971, 1972, 1973). This method gave a value of $h = 20$ for the total hydration number of Th(IV), which can be compared to the values of 22 obtained from compressibility measurements (Bockris and Saluja, 1972a,b) that are based on the lower compressibility of a solvate's solvent molecules as a result of electroconstriction (Passynskii, 1938).

Reviews of the available evidence pertaining to hydration numbers of U(IV) and Np(IV) have suggested that two forms of each of these aquo ions may exist, differing in geometry and possibly coordination number (Rykov *et al.*, 1971; Sullivan *et al.*, 1976). Radial distribution functions from X-ray measurements on 2 M uranium(IV) perchlorate solutions indicate a primary hydration number of $N_{H_2O} = (7.8 \pm 0.3)$ with no perchlorate in the primary coordination sphere (Pocev and Johansson, 1973). XAFS measurements of Np(IV) and Bk(IV) aquo cations gave $N_{H_2O} = (9 \pm 1)$ and (7.9 ± 0.5), respectively (Antonio *et al.*, 2001, 2002). The An–O bond distances derived from XAFS for the An(IV) hydrates, which are more accurate than the coordination numbers, also are most consistent with a primary hydration number of 8. Changes in the optical absorption spectra of U(IV), Np(IV), and Pu(IV) also have been interpreted as consistent with $N_{H_2O} = 8$ (Rykov *et al.*, 1973).

23.2.3 Pentavalent and hexavalent actinides

The hydration of pentavalent actinyl cations has been studied less than any of the other common oxidation states, but the findings are quite consistent from study to study. In the solid state, neptunyl(V) perchlorate has a total equatorial coordination number of 5. Four oxygens come from inner sphere water molecules and a fifth oxygen comes from the '-yl' oxygen of a neighboring NpO_2^+ ion (Grigor'ev *et al.*, 1995), as discussed in Section 23.9. In solutions, where the AnO_2^+ concentration is usually quite small, cation–cation complexes (Section 23.9) of AnO_2^+ are not important, and fully hydrated AnO_2^+ cations are expected. Optical absorption spectra of AnO_2^+ in solution are consistent with a primary hydration number of 5, based on symmetry considerations and comparison with the spectra of solid state complexes of known structures (Garnov *et al.*, 1996). XAFS measurements on solutions containing 1×10^{-3} to 2×10^{-2} M NpO_2^+ agree well with this, consistently giving a hydration number of 5 and Np–O equatorial bond distances that suggest the coordination of 5 water molecules (Combes *et al.*, 1992; Allen *et al.*, 1997; Antonio *et al.*, 2001).

Hydration numbers of the hexavalent actinyl cations have received more attention, particularly for UO_2^{2+}. The Raman spectra of aqueous uranyl

solutions were interpreted to show the presence of six inner sphere water molecules in the plane perpendicular to the O=U=O axis (Sutton, 1952). However, similar hydration numbers have been obtained by methods that are influenced by the second hydration shell. For example, activity coefficient measurements suggest a hydration number of 7.4 relative to an assumed hydration number of zero for Cs(I) (Hinton and Amis, 1971). Similarly, a hydration number of 7 has been derived from conductivity measurements (Gusev, 1971, 1972, 1973).

In the solid state, $UO_2(ClO_4)_2 \cdot 7H_2O$ contains discrete pentagonal bipyramidal $UO_2(H_2O)_5^{2+}$ cations and ClO_4^- anions (Alcock and Esperås, 1977), an indication that, like the actinyl(V) cations, penta hydration may be preferred by actinyl(VI) cations in solution. Garnov *et al.* (1996) also deduced a hydration number of 5 for AnO_2^{2+} from absorption spectra of PuO_2^{2+}. It seems likely that this is correct since XAFS measurements of AnO_2^{2+} solutions also give average hydration numbers of ranging from 4.5 to 5.3 and An–O equatorial bond distances that are close matches for those of pentacoordinate $UO_2(H_2O)_5^{2+}$ in $UO_2(ClO_4)_2 \cdot 7H_2O$ (Allen *et al.*, 1997; Wahlgren *et al.*, 1999; Antonio *et al.*, 2001). In agreement with this, a study of uranyl(VI) perchlorate solutions by X-ray diffraction concluded that the hydration number of UO_2^{2+} could be either 4 or 5 (Åberg *et al.*, 1983a).

23.2.4 Solvation and hydration in non-aqueous media

Solvation numbers of actinide cations in non-aqueous media have been measured for only a few systems. FTIR investigations of the homologous lanthanide solvates $[Ln(NO_3)_3(DMSO)_n]$ in anhydrous acetonitrile (Bünzli *et al.*, 1990) indicated a change in coordination number in the middle of the series near Eu(III) from nine to eight with increasing atomic number. NMR spectroscopy, stoichiometric, and XAFS measurements gave a solvation number of 2 for uranyl nitrate salts in tri(*n*-butyl)phosphate (TBP) solutions. The total coordination number would include two for TBP coordination and four for the bidentate nitrate coordination (Siddall and Stewart, 1967; Den Auwer *et al.*, 1997).

A commonly used extractant ligand in actinide separation science is thenoyltrifluoroacetone, TTA. The luminescent lifetimes of the Cm(III) complex with TTA in various organic solvents was 130–140 μs which gives $N_{H_2O} = (3.8 \pm 0.5)$. This indicates the formation of a Cm–TTA complex with a total CN = 10 (Dem'yanova *et al.*, 1986).

Solvation of UO_2^{2+} ions in water–acetone and water–dioxane mixtures were studied by ultrasound (Ernst and Jezowska-Trzebiatowska, 1975a,b). The resulting hydration numbers are listed in Table 23.2. The data show a decrease in the hydration numbers with increasing dioxane concentration. This can be attributed to a partial replacement of waters of hydration by the organic

Table 23.2 *Hydration numbers of AnO_2^{2+} ions in aqueous and mixed solvents.*

Salt	*Medium*	*Method*	*h*	*References*
UO_2SO_4	water	ultrasound	10.3	Ernst and Jezowska-Trzebiatowska (1975a,b)
$UO_2(NO_3)_2$	water	ultrasound	11.9	Ernst and Jezowska-Trzebiatowska (1975a,b)
UO_2SO_4	dioxane–water (20%)	ultrasound	6.3	Ernst and Jezowska-Trzebiatowska (1975a,b)
$UO_2(NO_3)_2$	dioxane–water (20%)	ultrasound	6.3	Ernst and Jezowska-Trzebiatowska (1975a,b)
UO_2SO_4	dioxane–water (45%)	ultrasound	4.8	Ernst and Jezowska-Trzebiatowska (1975a,b)
$UO_2(NO_3)_2$	dioxane–water (45%)	ultrasound	5.8	Ernst and Jezowska-Trzebiatowska (1975a,b)
$UO_2(ClO_4)_2$	acetone–water	PMR	4.0	Fratiello *et al.* (1970b)
$UO_2(NO_3)_2$	acetone–water	PMR	2.0	Fratiello *et al.* (1970b)
$UO_2(ClO_4)_2$	acetone–water	PMR	6.0	Shcherbakov and Shcherbakova (1976)
$UO_2(NO_3)_2$	acetone–water	PMR	6.0	Shcherbakov and Shcherbakova (1976)
UO_2Cl_2	acetone–water	PMR	6.0	Shcherbakov and Shcherbakova (1976)
$UO_2(ClO_4)_2$	acetone–water	PMR	4.7–4.9	Bardin *et al.* (1998)
$UO_2(ClO_4)_2$	acetone–water	PMR	4.5–4.9	Åberg *et al.* (1983a)
$NpO_2(ClO_4)_2$	acetone–water	PMR	6.0	Shcherbakov *et al.* (1974)
$NpO_2(ClO_4)_2$	acetone–water	PMR	4.8	Bardin *et al.* (1998)

solvent although inner sphere complexation by the anion would also reduce the hydration number.

This result is in agreement with low-temperature ^{1}H-NMR measurements for both UO_2X_2 (X is ClO_4^-, Cl^-, or NO_3^-) (Fratiello *et al.*, 1970b; Shcherbakov and Shcherbakova, 1976) and NpO_2^{2+} (Shcherbakov *et al.*, 1974) compounds (Table 23.2). For uranyl, the average number of bound waters was shown to increase with increasing molar ratio, $[H_2O]/[UO_2^{2+}]$, to a limiting value of six for ratios from 40 to 70 depending on the anion (Shcherbakov and Shcherbakova, 1976). The stronger the complexing ability of the anion, the higher the ratio required to reach maximum hydration. More recent high-field NMR measurements of UO_2^{2+} and NpO_2^{2+} hydration report $N_{H_2O} = 4.7–4.9$ for a range of $[H_2O]/[AnO_2^{2+}]$ ratios (Åberg *et al.*, 1983a; Bardin *et al.*, 1998).

23.2.5 Measurements of N_{H_2O} by TRLF technique

Beitz and Hessler (1980) reported the first study of aqueous Cm(III) photophysics, including measurement of the emission spectrum and lifetimes of aqueous of Cm^{3+} in H_2O and D_2O. Beitz (1994) reported a value of $N_{H_2O} = 9$ for the hydrated Cm^{3+} cation and smaller residual inner sphere hydration numbers for a number of Cm(III) complexes in a review of the theoretical and experimental aspects of such studies to 1994. Studies by time-resolved laser fluorescence (TRLF) with Cm(III) have proven very valuable for understanding the hydration of trivalent actinides. Measurement of the Cm fluorescence decay constant, k(Cm), as a function of residual hydration in crystals of lanthanide complexes of known structure and hydration doped with Cm(III) resulted in equation (23.2) for calculation of the residual hydration numbers (Kimura and Choppin, 1994):

$$N_{H_2O} = 0.65k(\mathrm{Cm}) - 0.88 \tag{23.2}$$

where k(Cm) is expressed in ms^{-1}. This equation assumes no contribution from the ligand to the deexcitation of the luminescence excited state and that quenching of the excitation results only from interaction with the OH vibrators of the water in the first coordination sphere. The absolute uncertainty in the hydration numbers calculated from equation (23.2) is ± 0.5. Use of equation (23.2) gives a value for N_{H_2O} of Cm^{3+} in water of (9.2 ± 0.5).

The residual hydration in the primary coordination sphere of Cm(III) in a number of aminopolycarboxylate complexes (Kimura and Choppin, 1994) is plotted in Fig. 23.3 and shows the variation of the measured hydration number, N_{H_2O}, as a function of pH. These data indicate that the complexation is initiated around pH 2–4 and the hydration number remains constant until pH values of 10 and higher are reached. This constancy over the medium pH range is consistent with the formation of very strong 1:1 complexes. The two plateaus in the data for the NTA complex reflects the successive formation of 1:1 and 1:2 complexes for this smaller ligand. In Table 23.3, the calculated hydration numbers reported for the different complexes are listed for Am(III) and Nd(III) (Kimura and Kato, 1998) and Cm(III) and Eu(III) (Kimura *et al.*, 1996). In these systems, the total coordination number (i.e. the sum of the average number of ligand donor groups and primary water molecules) was (9.3 ± 0.4) for Cm(III), (10.7 ± 0.5) for Am(III), (8.8 ± 0.5) for Eu(III) and (9.9 ± 0.5) for Nd(III) complexation.

The TRLF technique has been used to characterize Cm(III) complexation in natural waters by ligands such as OH^-, CO_3^{2-}, NO_3^- and humic acids (Table 23.4). While the aqueous Cm^{3+} ion has nine water molecules in the primary coordination sphere, $N_{H_2O} = 8.5$, 8.0, 7.0, 5.0, and 3.0 are expected for monohydroxide, dihydroxide, monocarbonate, dicarbonate, and tricarbonate complexes, respectively, from the assumptions that OH vibrators of coordinated water molecules act independently in the de-excitation process and a carbonate ion coordinates with Cm(III) as a bidentate ligand. The N_{H_2O} for each

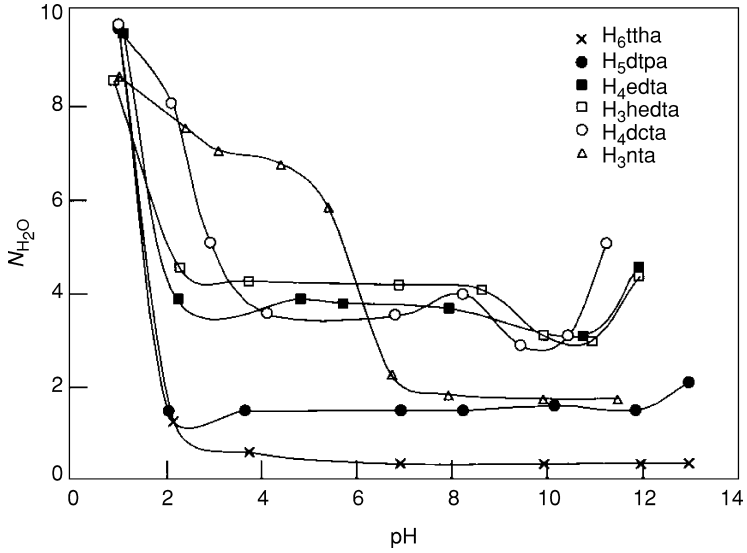

Fig. 23.3 *Dependence of the hydration number of Cm(III) complexes with polyaminopolycarboxylate ligands on pH.* $I = 0.1$ M $NaClO_4$, $[Cm] = 7.3 \times 10^{-6}$ M, $[ligand] = 8 \times 10^{-6}$ M. *H_6ttha = triethylenetetraaminehexaacetic acid, H_5dtpa = diethylenetriaminepentaacetic acid, H_4edta = ethylenediaminetetraacetic acid, H_3hedta = N-(2-hydroxyethyl) ethylenediaminetriacetic acid, H_4dcta = trans-1,2-diaminocyclohexane-tetraacetic acid, H_3nta = nitriliotriacetic acid.*

Table 23.3 *Inner sphere hydration numbers of Am(III), Cm(III), Nd(III) and Eu(III) complexes with aminopolycarboxylate ligands.*

	$N^a_{H_2O}$			
Ligand	*Am(III)*	*Cm(III)*	*Nd(III)*	*Eu(III)*
nta^{3-} (1:1)	6.5	6.3	5.6	4.5
nta^{3-} (1:2)	–	1.7	–	–
$hedta^{3-}$	5.1	4.2	4.5	3.2
$edta^{4-}$	4.8	3.7	4.0	2.7
$dcta^{4-}$	–	3.8	4.5	2.5
$dtpa^{5-}$	3.1	1.7	2.6	1.0
$ttha^{6-}$	1.6	0.6	0.7	1.2

[a] Uncertainties are ±0.5.

species calculated from the lifetime in Table 23.4 agrees with each expected value within the experimental uncertainty. The lifetimes measured for Cm(III) humate and fulvate complexes involves two components, which indicates the presence of two types of complexes. The first component gives an N_{H_2O} of 8.2–8.4 and the second, 3.6–3.7.

Table 23.4 *Inner sphere hydration number of Cm(III) complexes from fluorescence lifetimes.*

Medium	*Excitation* (nm)	*Emission* (nm)	*Lifetime* (μs)	N_{H_2O} (±0.5)	*References*
0.1 M $HClO_4$	396.7	593	68	8.7	Beitz *et al.* (1988)
1.0 M $HClO_4$	375.4	593.8	63	9.4	Klenze *et al.* (1991)
	381.3	–	–	–	
	396.5	–	–	–	
16 M HNO_3	383	603–607	107 ± 3	5.2	Beitz (1991)
0.1 M $HClO_4$	375.4	593.8	72.5 ± 1.3	8.1	Kim *et al.* (1991)
3 M K_2CO_3	337	608	240	1.8	Decambox *et al.* (1989)
1 M $NaCO_3$	383	590(sh)	160 ± 5	3.2	Beitz (1991)
	–	599(sh)	–	–	
0.1 M Na_2CO_3	377.5–399.4	607.4	141	3.7	Klenze *et al.* (1991)
$Cm(OH)^{2+}$	397.2	598.8	72 ± 2	8.2	Wimmer *et al.* (1992)
$Cm(OH)_2^{+}$	399.2	603.5	80 ± 10	7.3	Wimmer *et al.* (1992)
$Cm(CO_3)^{+}$	397.5	598.0	85 ± 4	6.8	Wimmer *et al.* (1992)
$Cm(CO_3)_2^{-}$	398.9	605.9	105 ± 5	5.3	Wimmer *et al.* (1992)
$Cm(CO_3)_3^{3-}$	399.9	607.6	215 ± 6	2.1	Wimmer *et al.* (1992)
Cm humate	398	601.0	72 ± 5 (80%)	8.2	Wimmer *et al.* (1992)
	–	–	145 (20%)	–	
Cm fulvate	374–398.5	600.3	70 ± 5 (80%)	3.6	Wimmer *et al.* (1992)
	–	–	142 (20%)	–	

All of the N_{H_2O} values calculated using equation (23.2) from the fluorescence lifetimes in the literature are chemically reasonable. The determination of the hydration number from fluorescence lifetimes makes it possible to characterize Cm(III) species in aqueous solution at high sensitivity, providing valuable insight into the primary structure of ions in solution.

23.2.6 Hydration in concentrated solutions

Data from luminescence studies in more concentrated media must be evaluated carefully. An example of this is shown in Fig. 23.4 in which the measured hydration number for the trivalent europium ion increases as the perchloric acid concentration increases. This presumably reflects the fact that as the electrolyte concentration increases, the number of water molecules in the

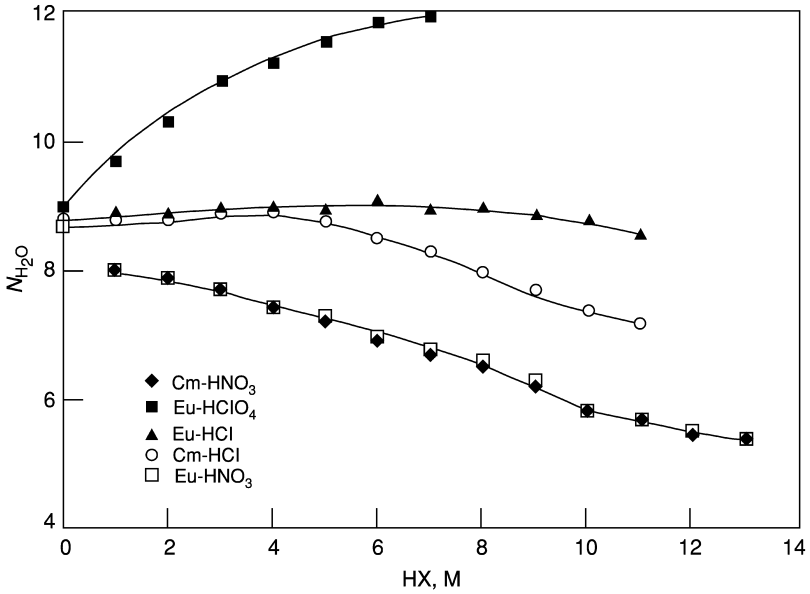

Fig. 23.4 *Variation of the number of water molecules in the primary hydration sphere of trivalent europium and curium ions as determined by TRLF.*

secondary hydration sphere decreases and, consequently, there is a tightening of the bond between the trivalent europium and the hydrate waters in the inner sphere. This tightening allows for more efficient quenching of the fluorescence by the hydroxyl groups of the H_2O. NMR studies (Choppin, 1997) have shown that inner sphere complexation by perchlorate ions does not occur below approximately 8–10 M. Obviously, this calculated increase in hydration number does not represent greater hydration nor does it represent an effect of complexation by perchlorate; rather, it is due to the tighter bonding.

The data in Fig. 23.4 show that the hydration number of the Eu(III) remains relatively constant in hydrochloric acid up to approximately 6–8 M, after which it decreases. The same is true for the Cm(III) hydration number in HCl, which begins a decline at about 5 M HCl. This difference presumably reflects greater complexation of the actinide trivalent ion by the relatively soft anion Cl^-. In fact, this difference in complexation has been used for over 40 years to provide efficient separation of trivalent actinides from trivalent actinides in concentrated HCl solutions by passage through columns of cation exchange resin. Independent studies (Rizkalla and Choppin, 1994) have shown that complexation does occur with the chloride anions for both trivalent actinides and lanthanides in 1.0 M HCl. The constancy of the hydration number in Fig. 23.4 for both

cations to concentrations of ca. 4 M HCl indicates that up to this concentration, only outer sphere complexes are formed and, therefore, the primary hydration sphere is not affected. At higher concentrations, however, there is greater complexation by the soft donor Cl^- with the actinide, which has been interpreted as reflecting an enhanced covalent interaction of trivalent actinide ions relative to that of lanthanide ions of the same ionic radius (Diamond *et al.*, 1954, see Section 23.4). By contrast, in Fig. 23.4 it is seen that the Cm(III) and Eu(III) behavior as a function of nitric acid concentration is very similar from dilute acid to $\geq$12 M. Nitrate ions begin to form inner sphere complexes at lower concentrations than chloride anions do, as reflected in the decreased hydration number even at relatively lower concentrations. However, the oxygens of the nitrate are hard donors and, therefore, there is no evidence of any covalent enhancement in its bonding as is seen with the chloride anions for the trivalent actinide cations relative to the lanthanide cations.

23.2.7 Thermodynamic properties

As Chapter 19 of this work is devoted to the thermodynamic properties of the actinides, their ions and compounds, this section focuses only on the hydration behavior of the actinides to minimize overlap. The values used for the calculations of the thermodynamic properties in this section are taken from literature references, which are sometimes different from those accepted in recent critical assessments of the thermodynamic properties of the actinides (Grenthe *et al.*, 1992; Silva *et al.*, 1995; Lemire *et al.*, 2001; Guillaumont *et al.*, 2003) or those in Chapter 19.

The thermodynamic properties of the actinide ions in the oxidation states III–VI have been reviewed by Morss (1976), Fuger and Oetting (1976), Fuger (1982), and David (1986). Calorimetric measurements of the heats of formation of the trivalent cations are limited to the actinides up to californium that are available in macroscopic quantities and with isotopes of sufficiently low specific radioactivity. Entropies of Pu(III) (Hinchey and Cobble, 1970; Fuger and Oetting, 1976), Th(IV) (Morss and McCue, 1976), and the actinyl ions UO_2^{2+} (Coulter *et al.*, 1940), NpO_2^+ and NpO_2^{2+} (Brand and Cobble, 1970) also have been reported. Data on other actinide species have been estimated across the entire actinide series using various models.

David *et al.* (1985) proposed a general expression for the calculation of the absolute enthalpy of hydration, ΔH°_{hyd}, based on the semiempirical model of Bockris and Reddy (1970). The hydration enthalpy of a cation can be related to the crystallographic radius, R, the hydration number, N_{H_2O}, and the ionic charge, $+Z$, by the equation:

$$\begin{aligned} \Delta H^{\circ}_{hyd} = {} & \alpha Z^2 (R + 2R_W)^{-1} + \beta Z N_{H_2O} (R + R_W)^{-2} \gamma Z N_{H_2O} (R + R_W)^{-3} \\ & + \sigma Z^2 N_{H_2O} (R + R_W)^{-4} + N_{H_2O} W + P(-1)^Z \end{aligned} \tag{23.3}$$

where W is the hydration energy of one water molecule and R_w is the radius of a water molecule, 1.38 Å. The numerical values of the coefficients (α, β, etc.) of equation (23.3) were computed using hydration enthalpies (which included contributions from the hydration of halide anions) of 35 monovalent, divalent, trivalent, and tetravalent ions (David *et al.*, 1985) assuming $N_{H_2O} = 4$ for monovalent, 6 for divalent, and 8 for trivalent and tetravalent cations. The estimated uncertainty between the experimental and calculated enthalpies is 0.4–0.5%.

Bratsch and Lagowski (1985a,b, 1986) proposed an ionic model to calculate the thermodynamics of hydration ΔG°_{hyd}, ΔH°_{hyd}, and ΔS°_{hyd} using standard thermochemical cycles. The model uses the values of the enthalpy of formation of the monoatomic gas $[\Delta H^{\circ}_f(M_g)]$, the ionization potential for the oxidation state under consideration, and the crystal ionic radius of the metal ion. Since the ionization potentials for the actinide ions are not all available, the authors 'back-calculated' an internally consistent set of ionization potentials from selected thermodynamic data (Bratsch and Lagowski, 1986). The general set of equations used are:

$$\Delta H^{\circ}_{hyd}(M^{Z+}) = \Delta H^{\circ}_f(M^{Z+}_{aq}) - \Delta H^{\circ}_f(M^{z+}_g) + Z[\Delta H^{\circ}_f(H^+_g) + \Delta H^{\circ}_{hyd}(H^+_{aq})] \tag{23.4a}$$

$$\Delta S^{\circ}_{hyd}(M^{Z+}) = S^{\circ}(M^{Z+}_{aq}) - S^{\circ}(M^{Z+}_g) + Z[S^{\circ}(H^+_g) + \Delta S^{\circ}_{hyd}(H^+_{aq})] \tag{23.4b}$$

$$\Delta G^{\circ}_{hyd}(M^{Z+}) = \Delta G^{\circ}_f(M^{Z+}_{aq}) - \Delta G^{\circ}_f(M^{Z+}_g) + Z[\Delta G^{\circ}_f(H^+_g) + \Delta G^{\circ}_{hyd}(H^+_{aq})] \tag{23.4c}$$

The calculated Gibbs energies and enthalpies of hydration for the actinide ions are listed in Tables 23.5 and 23.6.

The absolute entropies for the gaseous ions are calculated with the equation (Johnson, 1982):

$$S^{\circ}(M^{Z+}_g) = 1.5R \ln(\text{at wt.}) + R \ln(2J + 1) + 108.75 \tag{23.5}$$

The values of the entropies of the trivalent aquo actinide ions were obtained by interpolation from the dependence of the corrected (structural) entropy term, S°_c (see Chapter 19, equation (19.6)), of the lanthanides on ionic radii (Fig. 23.5) These corrected entropy values are only dependent on the structure of the aquo ion (David *et al.*, 1985). Justification of this approach is provided by the agreement of the calculated value of S°_c of Pu(III) with that from experimental data (Fuger and Oetting, 1976). The entropies are listed in Table 23.7. Similarly, the entropies of the tetravalent actinides were obtained from pertinent data on Th(IV) (Morss and McCue, 1976) and Ce(IV) (Morss, 1976).

Table 23.5 *Gibbs energies of formation and hydration of the gaseous and hydrated actinide ions. Data from Bratsch and Lagowski* (1986) *and Marcus and Loewenschuss* (1986).

	Gas phase ΔG_f° (kJ mol^{-1})			*Aquo ion* ΔG_f° (kJ mol^{-1})				ΔG_{hyd}° (kJmol^{-1})		
Element	+3	+4	+6	+3	+4	+5	+6	+3	+4	+6
Ac	3832	–	–	−614	–	–	–	−3093	–	–
Th	4182	6960	–	−314	−704	–	–	−3143	−5860	–
Pa	4136	7128	–	−411	−606	−1050	–	−3194	−5930	–
U	4114	7259	1177	−477	−539	−969	−953	−3238	−5994	−1228
Np	4115	7357	–	−516	−497	−915	−796	−3278	−6050	–
Pu	4095	7432	–	−571	−475	−850	−757	−3313	−6105	–
Am	4110	7598	–	−590	−356	−741	−587	−3347	−6150	–
Cm	4144	7700	–	−586	−298	–	–	−3377	−6194	–
Bk	4186	7622	–	−574	−416	–	–	−3407	−6234	–
Cf	4222	7822	–	−563	−250	–	–	−3432	−6268	–
Es	4256	7990	–	−554	−116	–	–	−3457	−6302	–
Fm	4285	8076	–	−547	−61	–	–	−3479	−6333	–
Md	4379	8219	–	−476	51	–	–	−3502	−6364	–
No	4523	8477	–	−351	282	–	–	−3521	−6391	–
Lr	4347	8452	–	−546	233	–	–	−3540	−6415	–

Table 23.6 *Standard enthalpies of formation of the gaseous and hydrated actinide ions. Data from Bratsch and Lagowski* (1986) *and Marcus and Loewenschuss* (1986). *Number in brackets denote experimental data.*

	Gas phase ΔH_f° (kJmol^{-1})			*Aquo ion* ΔH_f° (kJmol^{-1})				ΔH_{hyd}° (kJmol^{-1})		
Element	+3	+4	+6	+3	+4	+5	+6	+3	+4	+6
Ac	3885	–	–	−633	–	–	–	−3224	–	–
Th	4242	7022	–	−327	−766	–	–	−3275	−6063	–
Pa	4197	7194	–	−411	−664	−677	–	−3326	−6133	–
U	4176	7327	1210	−423	−595	−1032	(−1019)	−3371	−6197	−1345
Np	4177	7425	–	−528	−553	−978	−861	−3411	−6253	–
Pu	4154	7498	–	−587	−534	−915	−822	−3447	−6307	–
	–	–	–	(−592)	–	–	–	–	–	–
Am	4165	7664	–	−608	−414	−805	−652	−3479	−6353	–
	–	–	–	(−617)	–	–	–	–	–	–
Cm	4199	7756	–	−608	−364	–	–	−3513	−6395	–
	–	–	–	(−615)	–	–	–	–	–	–
Bk	4241	7682	–	−597	−480	–	–	−3544	−6437	–
	–	–	–	(−601)	–	–	–	–	–	–
Cf	4277	7882	–	−587	−314	–	–	−3570	−6471	–
	–	–	–	(−577)	–	–	–	–	–	–
Es	4308	8048	–	−584	−182	–	–	−3598	−6505	–
Fm	4337	8135	–	−580	−127	–	–	−3623	−6437	–
Md	4432	8279	–	−510	−13	–	–	−3648	−6567	–
No	4580	8542	–	−382	223	–	–	−3668	−6594	–
Lr	4402	8518	–	−581	175	–	–	−3689	−6618	–

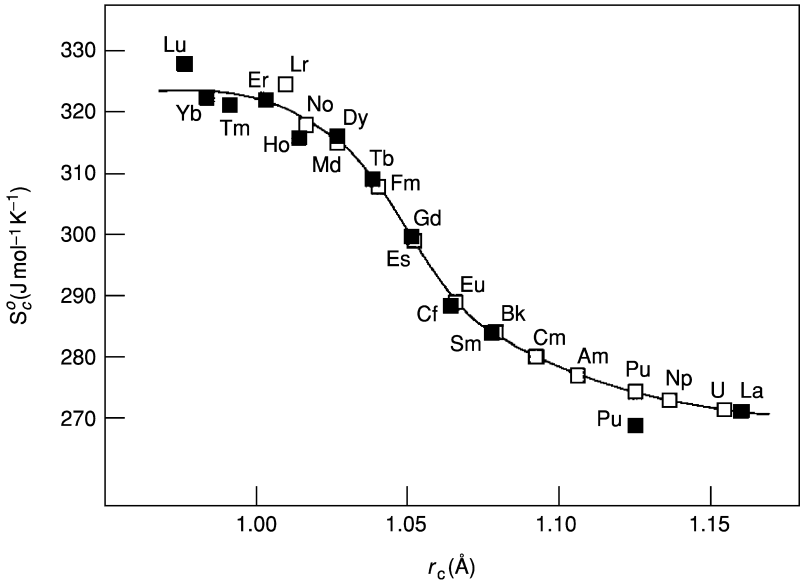

Fig. 23.5 *Variation of the corrected entropy,* S_c^o, *with the crystallographic radius of the trivalent lanthanides and actinides with CN* = 8. (■) *experimental data* (□) *extrapolated data.*

Differences in lanthanide and actinide hydration thermodynamics have been attributed by Bratsch and Lagowski (1986) to relativistic effects in the actinides which perturb the energies of the s, p, d, and f orbitals. The first and second ionization potentials of the 7s electrons of the actinides are higher than those of the 6s electrons of the lanthanides whereas the third ionization potentials are similar for both groups and the fourth ionization potential is lower for the actinides than the lanthanides. A small decrease in IP_3 and IP_4 for the f^7 configuration in the actinides results in smoother variations in the relative stabilities of the adjacent oxidation states across the actinide series while the greater spatial extension of the 5f orbitals increases the actinides' susceptibility to environmental effects (Johnson, 1982).

Nugent *et al*. (1973a,b) proposed equation (23.6) as a basis for comparison of the actinide and lanthanide thermodynamics:

$$P(\mathrm{M}) = \Delta H_\mathrm{f}^\mathrm{o}(\mathrm{M_g}) + \Delta E(\mathrm{M}) - \Delta H_\mathrm{f}^\mathrm{o}(\mathrm{M_{aq}^{3+}}) \qquad (23.6)$$

where ΔE(M) is the promotion energy from the ground state electron configuration to the $f^q d^1 s^2$ configuration where q varies from 0 (La and Ac) to 14 (Lu and Lr). ΔE(M) is approximately zero or near zero for La, Ce, Gd,

Table 23.7 *Standard entropies of the gaseous and hydrated actinide ions and standard entropies of hydration. Data from Bratsch and Lagowski* (1986), *Marcus and Loewenschuss* (1986), *David* (1986). *Number in brackets denote experimental data.*

	Gas phase S° ($JK^{-1}mol^{-1}$)				*Aquo ion* S° ($JK^{-1}mol^{-1}$)				ΔS°_{hyd} ($JK^{-1}mol^{-1}$)			
Element	+3	+4	+5	+6	+3	+4	+5	+6	+3	+4	+5	+6
Ac	176	–	–	–	−199	–	–	–	−441	–	–	–
Th	192	177	–	–	−186	−417	–	–	−444	−682	–	–
Pa	195	192	–	–	−183	−402	−21	–	−444	−682	–	–
U	196	195	296	280	−183	−399	−26	−98	−445	−682	−323	−400
Np	195	196	280	273	−185	−398	−21	−94	−446	−682	−323	−411
Pu	192	196	281	277	−190	−399	−21	−92	−448	−683	−324	−413
Am	177	192	>271	278	−199	−402	−21	−88	−442	−682	<−314	−410
Cm	195	178	–	–	−194	−408	−25	−88	−455	−674	–	–
Bk	199	195	–	–	−194	−399	−30	–	−459	−682	–	–
Cf	201	199	–	–	−197	−395	−22	–	−464	−682	–	–
Es	201	201	–	–	−206	−393	–	–	−473	−682	–	–
Fm	201	202	–	–	−215	−393	–	–	−482	−683	–	–
Md	199	201	–	–	−224	−393	–	–	−489	−682	–	–
No	195	199	–	–	−231	−395	–	–	−492	−682	–	–
Lr	178	195	–	–	−255	−399	–	–	−499	−682	–	–

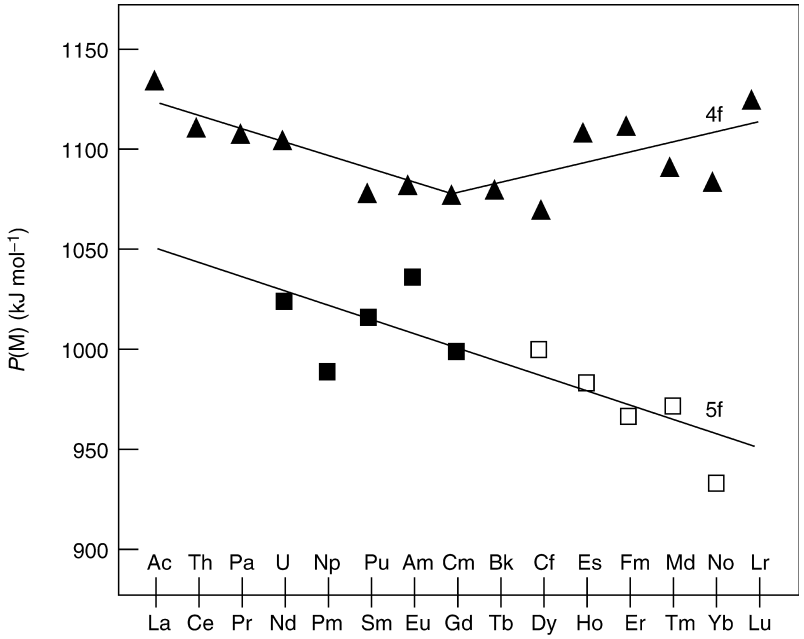

Fig. 23.6 *Plot of* P(*M*) *against atomic number for the lanthanide and actinide series.* (▲) *lanthanide experimental data,* (■) *actinide experimental data, and* (□) *extrapolated actinide data.*

and Lu, and for Ac, Pa, U, Np, Cm, and Lr. For the other f-elements, ΔE(M) is positive with accurately known values from spectroscopic measurements (Bratsch, 1983). Fig. 23.6 shows a graph of P(M) for lanthanide (4f) and actinide (5f) ions.

Only for UO_2^{2+} is there extensive data for the actinyl cations. Comparison of ΔH^o_{hyd} and ΔS^o_{hyd} with other 2+ and 3+ cations indicate that the enthalpy of hydration of actinyl(VI) cations is comparable to those of dipositive ions whereas the entropy of hydration is somewhat between that of dipositive and tripositive ions (Marcus and Loewenschuss, 1986). These authors assigned the increase in entropy to the large effective charge on the uranium center, +3.3. The non-spherical symmetry of the uranium atom caused by the shielding effect of the axial uranyl oxygens results in a lower hydration entropy than those of the typical trivalent cations. However, the strong primary sphere interactions from the charge–dipole effects causes more extensive but weaker secondary hydration. As a result, the net enthalpy of hydration is more similar to that of divalent than to trivalent cations.

23.3 HYDROLYSIS OF ACTINIDE CATIONS

Hydrolysis reactions occur for the f-elements in weakly acidic to alkaline solutions in the 3+, 4+, and 6+ oxidation states and often predominate over other complexation reactions in neutral and basic solutions. Hydrolysis of the pentavalent actinides occurs for pH $\geq$ 8. The hydrolysis reactions can be expressed by the general reaction

$$n\mathrm{An}^{z+} + q\mathrm{H_2O} \rightleftarrows \mathrm{An}_n(\mathrm{OH})_q^{nz-q} + q\mathrm{H}^+ \quad (\mathrm{An} = \mathrm{An(III)},\ \mathrm{An(IV)},\ \mathrm{AnO_2^+},\ \mathrm{AnO_2^{2+}}) \tag{23.7}$$

$$^*\beta_{nq} = [\mathrm{An}_n(\mathrm{OH})_q^{nz-q}][\mathrm{H}^+]^q/[\mathrm{An}^{z+}]^n$$

where $^*\beta_{nq}$ increases with increasing cationic charge density. Such hydrolysis reactions can be described as due to the positive charge of the metal ion polarizing the water molecule(s) sufficiently to release the proton(s). They are related to hydroxide complexation reactions:

$$n\ \mathrm{An}^{z+} + q\ \mathrm{OH}^- \rightleftarrows \mathrm{An}_n(\mathrm{OH})_q^{nz-q} \tag{23.8}$$

$$\beta_{nq} = [\mathrm{An}_n(\mathrm{OH})_q^{nz-q}]/[\mathrm{An}^{z+}]^n[\mathrm{OH}^-]^q$$

by $K_\mathrm{W} = [\mathrm{H}^+][\mathrm{OH}^-]$, making $\beta_{nq} = {}^*\beta_{nq}/K_w^q$. The strength of hydrolysis follows the order:

$$\mathrm{An}^{4+} > \mathrm{AnO_2^{2+}} > \mathrm{An}^{3+} > \mathrm{AnO_2^+}$$

This is consistent with most thermodynamic data and reflects the effective charges on the actinide atoms in the actinyl(V) and actinyl(VI) ions (Section 23.4). Hydroxide-bridged polynuclear complexes have been observed for actinide cations and the tendency toward polymer formation (Fig. 23.7) is a function of the charge density of the actinide cation. In the case of Th^{4+} and U^{4+}, X-ray measurements indicate the formation of clusters built of units with an An–An distance in range 3.95–4.00 Å. The kinetics of polymerization–depolymerization becomes more complicated for Pu^{4+}. The slower rate of

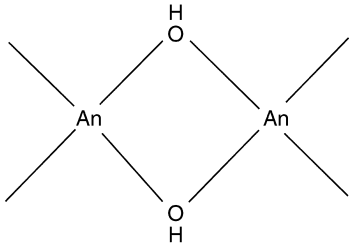

Fig. 23.7 *Structure of hydroxyl bridged actinide hydroxide polymers.*

depolymerization compared with the rate of polymer formation is due to an equilibrium between hydroxo and oxo bridge formation with aging.

23.3.1 Trivalent actinides

With a few exceptions, quantitative hydrolysis measurements of the actinide ions are complicated since the actinide hydroxides are quite insoluble and sorb to surfaces. The increasing pH required for hydrolysis also can result in significant changes in the oxidation state equilibria (e.g. for plutonium). Of the common oxidation states, the trivalent actinides have been the most intensively studied species. Solubility experiments (Rai *et al.*, 1983), solvent extraction (Caceci and Choppin, 1983a), spectroscopy (Stadler and Kim, 1988), and other techniques (Shalinets and Stepanov, 1972) have been used. The low solubility of $An(OH)_3$ in neutral/basic solutions prevents use of conventional absorption spectroscopy. However, time-resolved laser fluorescence spectroscopy allows measurements at the very low concentrations present in neutral/alkaline solutions (Stadler and Kim, 1988).

This laser spectroscopy technique was used to study the hydrolysis of Cm(III) at concentrations as low as 3×10^{-9} M. Values obtained for formation of the 1:1 and 1:2 species at 25°C in 0.10 M ($NaClO_4$) solutions are:

$$\log \beta_{11} = (6.67 \pm 0.18)$$

$$\log \beta_{12} = (12.6 \pm 0.28)$$

The laser fluorescence method has been used by Fanghänel and Kim (1994) to measure the values of $\log \beta_{11}$ and $\log \beta_{12}$ for Cm(III) over a range of ionic strengths from 0.011 to 6.15 M in NaCl solution at pH 8.6.

An evaluation of An(III) hydrolysis has been made by Rai *et al.* (1983). Table 23.8 lists the $\log {}^*\beta_{nq}$ and $\log K_{sp}$ values for the hydrolytic reactions of Am(III) from this reference. In carbonate-free environments, $Am(OH)^{2+}$ and $Am(OH)_2^+$ are the major species at pH 8.2, while, in carbonate-rich waters, $Am(CO_3)^+$ and $Am(CO_3)_2^-$ may also be significant components (Fig. 23.8). Because of the strong sorption characteristics of the hydroxide species, Am(III) is frequently removed from solution onto colloids, sediments, and humic substances. Stadler and Kim (1988) and the OECD-NEA (Silva *et al.*, 1995, Guillaumont *et al.*, 2003) have reviewed americium hydrolysis, while the hydrolysis of trivalent actinides has been reviewed by Fuger *et al.* (1992) and Rizkalla and Choppin (1994).

Polynuclear hydroxides of the formula $An_2(OH)_2^{4+}$ have been reported for Np(III) (Allard *et al.*, 1980) and Pu(III) (Allard and Rydberg, 1983) with values for $\log {}^*\beta_{22}$ of ca. −15 (Np) and −16 (Pu). Values for the $AnOH^{2+}$ hydrolysis formation constants for the trivalent actinide ions are listed in Table 23.9.

Table 23.8 *Hydrolysis constants for Am(III), $I = 0$ M; $T = 22°C$ (Rai* et al., 1983; *Felmy* et al., 1990).

I. $\log {}^{*}\beta_{nq}$ values for formation of $Am(OH)_q^{3-q}$	
$Am^{3+} + H_2O \rightleftarrows Am(OH)^{2+} + H^+$	$\log {}^{*}\beta_{11} \leq -8.2$
$Am^{3+} + 2\ H_2O \rightleftarrows Am(OH)_2^{+} + 2H^+$	$\log {}^{*}\beta_{12} = -17.1$
$Am^{3+} + 3\ H_2O \rightleftarrows Am(OH)_3 + 3H^+$	$\log {}^{*}\beta_{13} = -28.6$
II. $\log K_{sp}$ values for solid $Am(OH)_3$	
$Am(OH)_{3(am)} \rightleftarrows Am^{3+} + 3OH^-$	$\log K_{sp} = -24.5$
$Am(OH)_{3(cr)} \rightleftarrows Am^{3+} + 3OH^-$	$\log K_{sp} = -27.0$

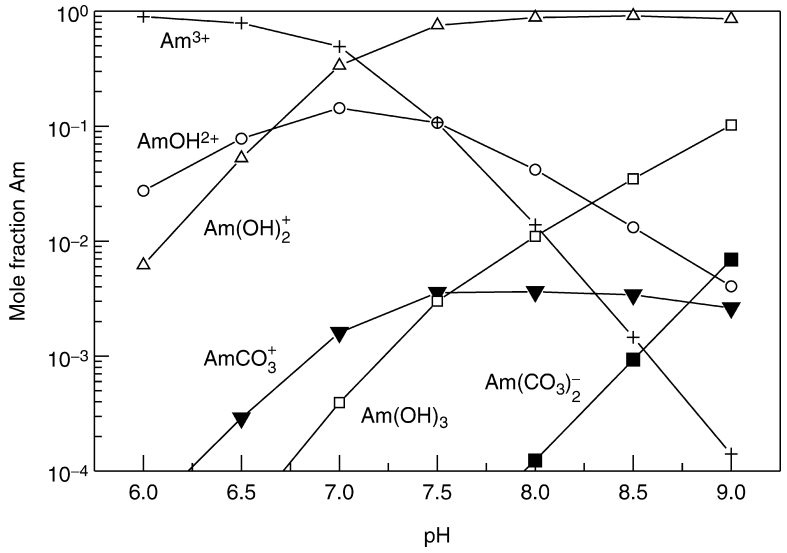

Fig. 23.8 *Fraction of Am(III) species in water in equilibrium with atmospheric carbon dioxide as a function of pH* (*Choppin* et al., 2002).

23.3.2 Tetravalent actinides

Study of the aqueous chemistry of tetravalent actinides can be difficult due to the very strong tendency of the cations to hydrolyze even in acidic solutions (pH $\leq$ ca. 2). Moreover, An(IV) cations of elements from protactinium through americium can undergo redox reactions relatively easily if the pH is not very low or in the absence of a strong complexant, making it difficult to ensure that only the tetravalent oxidation state is present.

Thorium is found in aqueous solution only in the 4+ oxidation state and is often used as a model for Np(IV) and Pu(IV) behavior. However, it has a smaller ionic charge density than these cations, due to its larger ionic radius, that results

Table 23.9 *Hydrolysis constants of trivalent actinide ions; $T = 25°C$ (Rizkalla and Choppin,* 1994).

Species	*Medium*	*Method*[a]	$log\ {}^{*}\beta_{nq}$
$Np(OH)^{2+}$	0.3 M $NaClO_4$	pH	-7.43 ± 0.12
$Pu(OH)^{2+}$	1.0 M $NaClO_4$	pH	-5.53
	0.2 M $LiClO_4$, 23°C	ex	-3.80 ± 0.2
$Am(OH)^{2+}$	1.0 M $NaClO_4$	sol	-7.03 ± 0.05
	1.0 M $NaClO_4$	ex	-7.50 ± 0.3
	0.7 M NaCl, 21°C	ex	-7.54 ± 0.2
	0.5 M$(H,NH_4)ClO_4$	ex	-6.80 ± 0.3
	0.1 M $LiClO_4$, 23°C	ex	-5.92
	0.1 M $LiClO_4$, 23°C	ex	-5.30 ± 0.1
	0.1 M $NaClO_4$	sol	-7.68
	0.1 M $NaClO_4$	sol	-7.93
	0.1 M $NaClO_4$	sol	-6.34 ± 0.83
$Am(OH)_2^+$	0.2 M $NaClO_4$	ex	-14.76
	0.1 M $NaClO_4$	sol	-16.56
	0.1 M $NaClO_4$	sol	-14.77
	0.1 M $NaClO_4$	sol	-13.64 ± 0.63
$Am(OH)_3$	0.1 M $NaClO_4$	sol	-24.84
	0.1 M $NaClO_4$	sol	-24.71
$Cm(OH)^{2+}$	0.1 M $LiClO_4$, 23°C	ex	-5.92 ± 0.13
	0.1 M $LiClO_4$, 23°C	ex	-5.40 ± 0.1
	0.1 M $LiClO_4$	ex	-5.93
$Bk(OH)^{2+}$	0.1 M $LiClO_4$, 23°C	ex	-5.66
$Cf(OH)^{2+}$	0.1 M $LiClO_4$, 23°C	ex	-5.62
	0.1 M $LiClO_4$, 23°C	ex	-5.05
$Es(OH)^{2+}$	0.1 M $LiClO_4$, 23°C	ex	-5.14
$Fm(OH)^{2+}$	0.1 M $LiClO_4$, 23°C	ex	-3.8 ± 0.2

[a] pH, potentiometric titration; sol, solubility; ex, solvent extraction.

in significant differences in the extent of the hydrolytic reactions. The hydrolysis of Th^{4+} involves extensive formation of polynuclear complexes. In the earlier stages of the hydrolysis in perchlorate media, when the number of hydroxide ions per thorium atom in the complexes is ≤ 2, the hydrolytic reactions are fully reversible and equilibrium is quickly reached (Hietanen, 1954; Kraus and Holmberg, 1954; Baes *et al.*, 1965). The first extensive measurements of the hydrolysis behavior were interpreted (Hietanen, 1954) as indicating the formation of an infinite series of 'core + links' complexes, $Th((OH)_3Th)_n^{4+n}$. However, other measurements over large pH and Th(IV) concentration ranges could be satisfactorily fitted with three polymers, $Th_2(OH)_2^{6+}$, $Th_4(OH)_8^{8+}$, and $Th_6(OH)_{15}^{9+}$, and two monomers, $ThOH^{3+}$ and $Th(OH)_2^+$ (Kraus and Holmberg, 1954; Baes *et al.*, 1965). In Table 23.10, the constants ${}^{*}\beta_{nq}$ are listed for the reactions:

$$n\mathrm{Th}^{4+} + q\mathrm{H_2O} \rightleftarrows \mathrm{Th}_n(\mathrm{OH})_q^{4n-q} + q\mathrm{H}^+$$

Of the complexes mentioned, $\mathrm{Th_2(OH)_2^{6+}}$ is significant in chloride media (Hietanen and Sillen, 1968; Baes and Mesmer, 1976; Milic, 1981) as well as $\mathrm{Th_2(OH)_3^{5+}}$ and $\mathrm{Th_6(OH)_{14}^{10+}}$. In nitrate media, the complexes $\mathrm{Th_2(OH)_2^{6+}}$, $\mathrm{Th_6(OH)_{15}^{9+}}$ and $\mathrm{Th_3(OH)_5^{7+}}$ predominate (Milic and Suranji, 1982). Constants for the hydroxo complexes are somewhat smaller in chloride and nitrate than in perchlorate media (Table 23.10).

For values $n \geq 2$ (equation (23.7)), equilibrium is more slowly attained than for mononuclear complex formation, resulting in formation of larger polymers before precipitation takes place. Direct structural determinations by X-ray diffraction on hydrolyzed thorium nitrate solutions confirmed the existence of the dimer $\mathrm{Th_2(OH)_2^{6+}}$ (Johansson, 1968). The Th–Th distance is 3.99 Å, i.e. exactly the same as in the solid $\mathrm{Th_2(OH)_2(NO_3)_6(H_2O)_8}$ that contains dimers joined by double hydroxo bridges. As the hydrolysis reaction proceeds, complexes of higher nuclearity become prominent although the Th–Th distance stays almost the same, approximately 3.94 Å. The hydrolytic complexes formed in concentrated nitrate solutions also contain nitrate ions coordinated as bidentate ligands. As expected, the number of nitrate ions coordinated per thorium decreases as hydrolysis becomes more extensive. Diffraction measurements by Johansson (1968) on hydrolyzed solutions of thorium perchlorate and chloride give the same Th–Th distance 3.94 Å, implying that the same type of hydroxo-bridged complexes are formed in these media.

Rai *et al.* (1997) have reported a value of $\log K_{sp}^0 = -45.5$ for amorphous $\mathrm{Th(OH)_4}$ while Neck and Kim (2001) have proposed for a value of $\log K_{sp}^0$ of $-(47.0 \pm 0.8)$ (Table 23.11). The values of $\log K_{sp}^0$ of Th(IV) are larger than for

Table 23.10 *Hydrolysis constants, log* $^*\beta_{nq}$, *for Th(IV) in different media.*

	T				
n, *q*	0°C 1 M $NaClO_4$[a]	25°C 1 M $NaClO_4$[b]	95°C 1 M $NaClO_4$[a]	25°C 3 M $NaCl$[c]	25°C 3 M $NaNO_3$[d]
1, 1	−4.31	−4.23	−2.25	–	–
1, 2	−8.46	−7.69	−4.51	–	–
2, 2	−5.59	−4.61	−2.59	−4.69	−5.19
2, 3	–	–	–	−8.73	–
4, 8	−22.80	−19.16	−10.44	–	–
6, 14	–	–	–	−36.37	–
6, 15	−43.81	−37.02	−20.61	–	−42.3

[a] Molality scale, Baes *et al.* (1965).
[b] Kraus and Holmberg (1954).
[c] Data recalculated from Hietanen and Silen (1968).
[d] $\mathrm{Th_3(OH)_5^{7+}}$ also suggested with $\log {}^*\beta_{35} = -14.23$, by Milic and Suranji (1982).

Table 23.11 *Hydroxide complexation constants for An(IV) cations, $I = 0$ M (Neck and Kim, 2001).*

	Th(IV)	*U(IV)*	*Np(IV)*	*Pu(IV)*
$\log K^{o}_{sp(cr)}$	-54.2 ± 1.3	-60.86 ± 0.36	-63.7 ± 1.8	-64.0 ± 1.2
$\log K^{o}_{sp(am)}$	-47.0 ± 0.8	-54.5 ± 1.0	-56.7 ± 0.4	-58.5 ± 0.7
$\log \beta^{o}_{11}$	11.8 ± 0.2	13.6 ± 0.2	14.5 ± 0.2	14.6 ± 0.2
$\log \beta^{o}_{12}$	22.0 ± 0.6	26.9 ± 1	28.3 ± 0.3	28.6 ± 0.3
$\log \beta^{o}_{13}$	31.0 ± 1.0	37.3 ± 1	39.2 ± 1	39.7 ± 0.4
$\log \beta^{o}_{14}$	38.5 ± 1.0	46.0 ± 1.4	47.7 ± 1.1	48.1 ± 0.9
$\log \beta^{o}_{24}$	59.1[a]	–	–	–
$\log \beta^{o}_{4,12}$	141.3	–	–	–
$\log \beta^{o}_{6,15}$	176.0	196[b]	–	–

[a] Calculated for $I = 0$ from data in Moon (1989).
[b] $\log \beta_{6,15}$ for $I = 3$ M $NaClO_4$ (Baes and Mesmer, 1976).

the other An(IV) ions, presumably due to inclusion of polynuclear species of Th(IV) in the concentration of the soluble fraction (Neck and Kim, 2001).

Evidence is scarce and conflicting on the hydrolysis of Pa^{4+}. Values of $\log {}^{*}\beta_{11} = -0.14$ and $\log {}^{*}\beta_{12} = -0.52$ have been measured for the first two mononuclear complexes in a 3 M $(Li,H)ClO_4$ medium, by means of a solvent extraction method (Guillaumont, 1968). This would lead to about 50% of the protactinium present as unhydrolyzed Pa^{4+} in 1 M perchloric acid; however, other extraction measurements indicate that $Pa(OH)_2^{2+}$ is the predominant species in 1 M acid (Lundqvist, 1974). The mononuclear complexes are predominant only in extremely dilute solutions. Polymers become significant at protactinium concentrations as low as 10^{-5} M.

Hydrolysis of U(IV) is of concern only in reducing solutions as UO_2^{2+} is the form present in oxic waters. The hydrolysis of U(IV) increases with increasing ionic strength and increasing temperature. Polynuclear hydrolytic species form readily and are likely to be present except in strongly acidic solutions or at very low concentrations of U(IV). Hydrolysis constant values were reported for a series of polynuclear $U_{(n+1)}(OH)_{3n}^{(4+n)+}$complexes in 3 M $(H,Na)ClO_4$ by Hietanen (1956) using a 'core+links' model of thread-like chains of $U(OH)_2U$ links. However, this model has fallen out of favor and reevaluation of these experiments showed that only $U(OH)^{3+}$ and one polynuclear species, $U_6(OH)_{15}^{9+}$, were required to reproduce the data with $\log {}^{*}\beta_{11} = -2.1$ and $\log {}^{*}\beta_{6,15} = -16.9$ (Baes and Mesmer, 1976) except at the highest $q{:}n$ ratios. This suggests that dinuclear or tetranuclear hydroxide complexes are less important for U(IV) than for Th(IV), but that hexanuclear $U_6(OH)_{15}^{9+}$ and higher oligomers of U(IV) with $n > 6$ and $q/n > 2.5$ do form in millimolar solutions of U(IV) when the pH exceeds 1.5.

As can be seen in the data in Table 23.11, the hydrolysis of Np(IV) is quite similar to that of Pu(IV) but greater than that of Th(IV) and U(IV). The ease of oxidation of Np(IV) to NpO_2^+ in non-reducing solutions results in Np(V) being the dominant neptunium species in oxic waters. Although there has been little research on hydrolytic polymers of Np(IV), it is very probable that the same polymers observed for Th(IV), U(IV), and Pu(IV) are formed by Np(IV).

Similar to the situation for Np(IV), the hydrolysis of Pu(IV) is difficult to investigate. At pH $\geq$ 1.0, tetravalent plutonium experiences hydrolysis and also oxidizes to PuO_2^+. Disproportionation reactions also occur in these acid solutions to form Pu(III) and PuO_2^{2+}. Preparation and maintenance of a solution with only Pu(IV) present is a challenge in any investigation of Pu(IV) behavior. This is reflected in the inconsistent data in a number of publications on Pu(IV) hydrolysis. The tendency of hydrolyzed plutonium(IV) to form intrinsic colloids or to sorb on other colloids is also a complicating factor. It has been demonstrated that colloidal Pu(IV) can be present at pH = 0 to 1 and total Pu(IV) concentrations smaller than 10^{-3} M (Kim and Kanellakopulos, 1989). Ultrafiltration removes such colloids if a sufficiently small filter size is used. However, without filtration, the solubility data used to calculate solubility product constants may be more than an order of magnitude too large due to the presence of colloids. Hydrolyzed plutonium species also have a strong tendency to sorb to surfaces. The surfaces of equipment used for plutonium experimentation must be treated to minimize sorption in solubility and extraction measurements (Caceci and Choppin, 1983b).

Freshly precipitated $Pu(OH)_4 \cdot xH_2O$, dehydrates over time with the hydroxo bridges between neighboring plutonium ions converting to an oxo bridged structure (Fig. 23.9). The resulting crystalline PuO_2 has a value of $\log K^{o}_{sp(cr)} = -64$ (Table 23.11), compared to the value of the amorphous hydrate of $\log K^{o}_{sp(am)} = -58.5$. The measured value of $\log K^{o}_{sp(cr)}$ (−64.0) reflects the reduced solubility of the aged precipitate; but measured solubilities in solutions of pH $\geq$ 7 are those of the amorphous solid, independent of whether $An(OH)_{4(am)}$ or $AnO_{2(cr)}$ were used for the initial solid phase. This can be attributed to the bulk crystalline solid being covered by a surface layer of the amorphous species. The amorphous form dissolves readily in strong acid but dissolution of the aged PuO_2 precipitate is very difficult due to the strength of

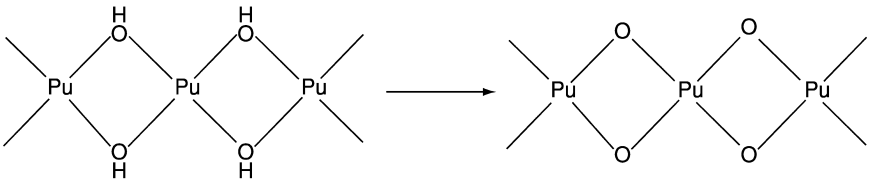

Fig. 23.9 *Conversion of amorphous $Pu(OH)_4$ into crystalline PuO_2 by loss of H_2O.*

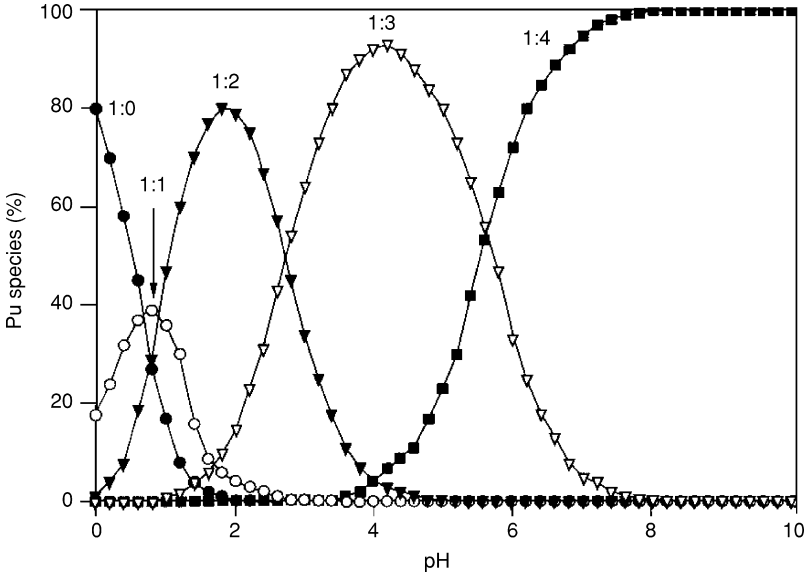

Fig. 23.10 *Fraction of mononuclear plutonium(IV) hydrolysis products as a function of pH in* 1 M $NaClO_4$ *solution* (*Choppin,* 2003).

the Pu–O bonding. Generally, aged $PuO_{2(cr)}$ must be contacted with an acidic oxidizing solution which converts the Pu(IV) to the much more soluble PuO_2^{2+} species.

The variation of mononuclear Pu(IV) hydrolytic species with pH is shown in Fig. 23.10. At pH 1.0, there are almost equal concentrations of Pu^{4+}, $Pu(OH)^{3+}$, and $Pu(OH)_2^{2+}$, demonstrating strong hydrolysis of Pu(IV). The fraction of polynuclear species present increases as the plutonium and/or the pH concentration increases. The hydrolysis constants of Pu(IV) indicate an extremely low value for soluble plutonium in neutral solutions. However, the net plutonium solubility is much larger than predicted ($\leq 10^{-6}$ M) by the constants in Table 23.11, as it is due to the relatively high concentration of PuO_2^+ ($\sim 10^{-6}$ to 10^{-7} M) in redox equilibrium with the ultratrace concentrations of soluble Pu(IV).

23.3.3 Pentavalent actinides

The protactinium(V) ion is a much stronger acid than other pentavalent actinides with $\log {}^*\beta_{11} = -4.5$ in 3.5 M (Li, H)ClO_4 (Guillaumont, 1968). In both the tetravalent and pentavalent states, protactinium hydrolyzes much more readily than do the other actinides. A structure different from the other actinyl(V) ions, e.g. $PaO(OH)_2^+$, with a strongly covalent protactinium–oxo bond has been proposed (Guillaumont *et al.*, 1968).

The tendency of UO_2^+ and PuO_2^+ to disproportionate and the strong oxidation properties of AmO_2^+ have led to few hydrolytic studies of these cations. NpO_2^+ is relatively stable, however, and is the most studied actinyl(V) species. Pentavalent neptunium does not hydrolyze in solutions with pH less than 8. Sullivan *et al.* (1991), Itagaki *et al.* (1992), and Neck *et al.* (1992) have discussed neptunium hydrolysis in some detail. A value of $\log {}^*\beta_{11}$ for NpO_2^+ (ca. -8.85 at $I = 0$) was reported by Baes and Mesmer (1976) and Schmidt *et al.* (1980). The stability of NpO_2^+ has led to its use as a chemical analog for pentavalent plutonium since PuO_2^+ is environmentally important at low concentrations of plutonium (Nelson and Lovett, 1978).

A study of the thermodynamics of NpO_2^+ hydrolysis (Sullivan *et al.*, 1991) in a solution of $I = 1.0$ M $(CH_3)_4NCl$ at $T = 25°C$ gave the following values for the reaction $NpO_2^+ + OH^- \rightleftarrows NpO_2OH$:

$$\log {}^*\beta_{11} = -(9.26 \pm 0.06)$$

$$\Delta H_{11} = -(22.10 \pm 0.04)\,\text{kJ mol}^{-1}$$

$$\Delta S_{11} = (16 \pm 5)\,\text{J K}^{-1}\,\text{mol}^{-1}$$

This value for ${}^*\beta_{11}$ indicates that at pH 9.26, NpO_2^+ is 50% hydrolyzed.

Sullivan *et al.* (1991) estimated that $\log \beta_{11}$ for PuO_2^+ would be ca. 4.5, which indicates that PuO_2^+ does not form a significant fraction of hydroxide species until pH 9. Of all the plutonium oxidation states, the pentavalent state has the least tendency to hydrolyze (Choppin, 1991) and is most stable in basic solution (Peretrukhin *et al.*, 1994). Unlike the case of NpO_2^+, the redox potential of Pu(V)/Pu(IV) and the strong hydrolysis of Pu(IV) limit the concentration of $PuO_2{}^+$ in marine waters. Plutonium redox and sorption have been reviewed by Morse and Choppin (1991) and plutonium hydrolysis by Clark *et al.* (1995).

23.3.4 Hexavalent actinides

The hydrolysis of the uranyl cation, UO_2^{2+}, has been studied more intensely than that of any other actinide cation, partially because the lower level of radioactivity of natural uranium allows use of a wider variety of techniques than for shorter lived actinides. Also, the hydrolysis of U(VI) forms a wide variety of polynuclear hydrolytic species, resulting in a quite complex chemistry (Table 23.12 and Fig. 23.11).

The hydrolysis of the cations of the actinyl(VI) species decreases in the order $UO_2^{2+} > NpO_2^{2+} > PuO_2^{2+}$, with a larger difference between NpO_2^{2+} and PuO_2^{2+} (Table 23.13). The actinide radial contraction with atomic number would lead to the opposite trend. The pattern is different also from that for the actinide(IV) ions where the order of acidities is $U^{4+} > Np^{4+} < Pu^{4+}$. For these ions, the unexpected decrease between U^{4+} and Np^{4+} is followed by a marked reversal at Pu^{4+}.

In very dilute solutions, $\leq 10^{-6}$ M U(VI), the hydrolysis of UO_2^{2+} first forms mononuclear $UO_2(OH)_q^{2-q}$ species, but above this concentration UO_2^{2+} exists mainly in polynuclear species. Within wide ranges of pH and C_M (metal concentration), the predominant complex is the dimer ($(UO_2)_2(OH)_2^{2+}$). As the pH increases, the trimer $(UO_2)_3(OH)_5^+$ becomes prominent (Fig. 23.12). In chloride solutions $(UO_2)_3(OH)_4^{2+}$ is also formed. In concentrated solutions of low pH, $(UO_2)_2OH^{3+}$ may be present. Other complexes which have been proposed to form are $(UO_2)_3(OH)_7^-$, $(UO_2)_3(OH)_{10}^{4-}$, $(UO_2)_4(OH)_6^{2+}$, $(UO_2)_4(OH)_7^+$,

Table 23.12 *Hydrolysis constants at* I = 0 *and* 25°C *for formation of* $(UO_2)_n(OH)_q$ *species.*

n, *q*	$log^*\beta^\circ_{nq}$ (*Palmer and Nguyen-Trung*, 1995)	$log^*\beta^\circ_{nq}$ (*Guillaumont* et al., 2003)
1, 1	-5.42 ± 0.04[a]	-5.25 ± 0.24
2, 2	-5.51 ± 0.04	-5.62 ± 0.04
3, 5	-15.33 ± 0.12	-15.55 ± 0.12
3, 7	-27.77 ± 0.09	-32.2 ± 0.8
3, 8	-37.65 ± 0.14	–
3, 10	-62.4 ± 0.3	–

[a] For $I = 0.10$ M (KNO_3).

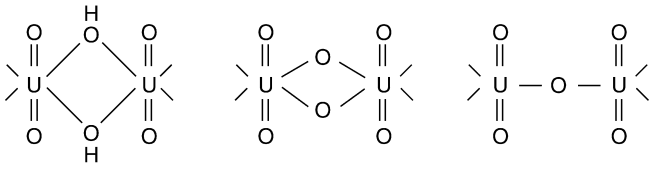

(I) (II) (III)

Fig. 23.11 *Structures of dinuclear uranyl hydroxide and oxide complexes.*

Table 23.13 *Hydrolysis constants,* $log^*\beta_{nq}$, *of hexavalent actinides,* NpO_2^{2+} *and* PuO_2^{2+}, *in* $NaClO_4$ *solution;* $T = 25°C$.

	NpO_2^{2+}	PuO_2^{2+}		
n, *q*	I = 1 M (*Cassol* et al., 1972*a*)	I = 1 M (*Kraus and Dam*, 1949)	I = 1 M (*Cassol* et al., 1972*b*)	I = 3 M (*Schedin*, 1975)
1, 1	−5.17	−5.71	−5.97	–
2, 2	−6.68	–	−8.51	−8.23
3, 5	−18.25	–	−22.16	–
4, 7	–	–	–	−29.13

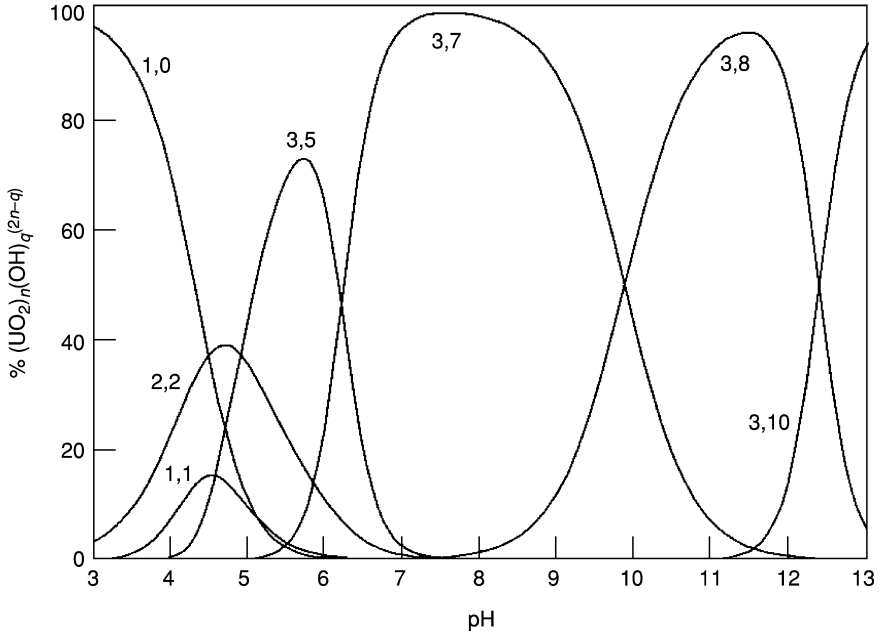

Fig 23.12 *Speciation diagram (n,q) for the formation of* $(UO_2)_n(OH)_q^{(2n-q)}$. $[UO_2^{2+}]_{total} = 4.75 \times 10^{-4} M$, $T = 25\,^{\circ}C$, *from the data of Palmer and Nguyen-Trung* (1995) *extrapolated to* $I = 1.0$ M.

Table 23.14 *Hydrolysis constants for* UO_2^{2+} *at different ionic strengths;* $T = 25^{\circ}C$.

I (M)	$log\ ^{*}\beta_{11}$	$log\,\beta_{11}$
0[a]	−5.88	8.12
0.05	−6.02	7.00
0.1	−6.09	7.70
0.4	−6.20	7.56
0.7	−6.07	7.71
1.0	−6.20	7.82

[a] Extrapolated values.

and $(UO_2)_5(OH)_8^{2+}$. The variation of the hydrolysis constant of $UO_2(OH)^+$ as a function of ionic strength is shown in Table 23.14.

The existence of the dimer $(UO_2)_2(OH)_2^{2+}$ has been confirmed by direct determination of the species present in hydrolyzed uranyl(VI) chloride solutions (Åberg, 1970). Even in the concentrated solutions ($C_M = 3$ M) used in these diffraction studies, the dimer is an important species at the lower ligand numbers investigated.

The average U–U distance in this concentrated solution is 3.88 Å, which is close to the distance of 3.94 Å found in the solids $[(UO_2)_2(OH)_2Cl_2(H_2O)_4]$ and $[(UO_2)_2(OH)_2(NO_3)_2(H_2O)_3]H_2O$ (Åberg, 1969; Perrin, 1976).

23.4 BONDING IN ACTINIDE COMPLEXES

Actinide ions in all common solution oxidation states (2+ to 6+) are hard Lewis acids, and actinide–ligand bonds are predominantly ionic, as expected from the electropositive nature of the actinides. This is manifested in kinetically labile, non-directional bonds, and a marked preference for binding to ligands via hard Lewis base donor atoms like fluorine or oxygen. The thermodynamic bond strengths of actinide–ligand complexes are determined primarily by electrostatic attraction and steric constraints. The electrostatic attraction between an actinide cation and a ligand is proportional to the product of the effective charges of the metal and ligand divided by the actinide–ligand distance. The steric constraints may arise from the properties of the actinide cation (ion size and presence or absence of actinyl oxygen atoms) or of the ligand (number and spatial relationship of donor atoms, size of the chelate rings, and flexibility of ligand conformations).

23.4.1 Ionicity of f-element bonding

As a consequence of the predominantly ionic nature of the metal–ligand bonding in actinide complexes, the strength of the complexes and the associated chemistry are determined primarily by the effective charge of the actinide cation and of the coordinating ligands. Similar to the lanthanide 4f orbitals, the actinide 5f orbitals are well shielded from environmental influences and have little influence on bonding energies of the outer 6d orbitals, which dominate the radii values. The orbital energies and the radii of actinide ions in a given oxidation state vary slowly and smoothly across the actinide series. As a result, the types of actinide complexes formed and the strength of those complexes, as reflected by the stability constants, are relatively uniform within an oxidation state in comparison to transition metal complexes where covalence and ligand field stabilization energies can cause significant variations (Fig. 23.13). An important exception to the regularities of complex formation within an actinide oxidation state is Pa(v), which is the only pentavalent actinide that does not form the linear transdioxo actinyl(v) moiety, and whose chemistry is closer to that of pentavalent niobium and tantalum (Kirby, 1959) than that of AnO_2^+ cations.

23.4.2 Thermodynamics of bonding

The predominantly ionic nature of actinide–ligand bonding also accounts for the enthalpies and entropies of actinide complexation. The formation of inner sphere 1:1 actinide–ligand complexes in aqueous solution is characterized

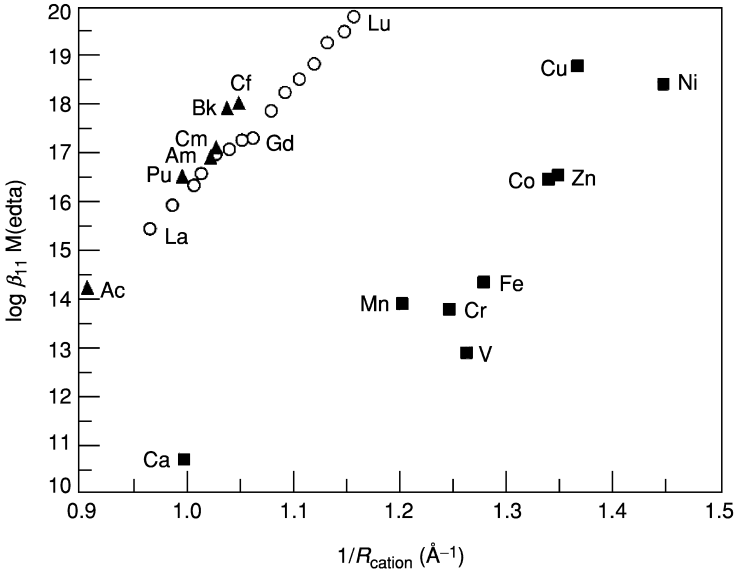

Fig. 23.13 *Variation of the stability constants of metal complexes with ethylenediaminetetraacetate* ($edta^{4-}$) *with ion size for the trivalent actinide* (▲), *trivalent lanthanide* (○), *and divalent fourth row metal cations* (■). *Stability constant data from Martell* et al. (1998) *and Makarova* et al. (1972) *for* I = 0.1 M, *and* $T = 25°C$. R_{cation} *from Shannon* (1976) *for* $CN = 6$.

by positive values of the formation entropies, ΔS_{11}, and of the values of the formation enthalpies, ΔH_{11}, that vary from moderately endothermic (positive and unfavorable) to moderately exothermic (negative and favorable) depending on the charge and coordination number of the ligand. For simple ligands, the entropic component of the Gibbs energy tends to be the more important in determining the magnitude of the Gibbs energy change (ΔG) upon complexation and, hence, of the equilibrium constant. In aqueous media, the entropy changes (ΔS) for formation of 1:1 lanthanide and actinide complexes arise primarily from the partial dehydration of the metal and ligand that is associated with the formation of an inner sphere complex. For a given ligand, the ΔS values tend to increase as the effective charge of the actinide ion increases, as expected for electrostatic bonding (Laidler, 1956). Also, since the complexation entropies are linked to dehydration of the metal and ligand, characteristic values of $\Delta S/n$ exist for a given actinide oxidation state and a particular class of ligands, as shown for actinide carboxylate complexation in Table 23.15 (n can be either the number of donor groups bound to the cation or the number water molecules displaced from the inner coordination sphere of the cation).

Table 23.15 *Average entropy change per coordinated carboxylate group, n, for carboxylate, polycarboxylate, and aminopolycarboxylate ligands* (*standard deviation* ±10%).

Cation	*Average* $\Delta S/n$ ($JK^{-1}mol^{-1}$)	*References*
Th^{4+}	96	Martell *et al.* (1998)
UO_2^{2+}	73	Martell *et al.* (1998)
Am^{3+}	62	Rizkalla *et al.* (1989)
Sm^{3+}	59	Choppin (1993)
NpO_2^+	27	Jensen and Nash (2001)
Ca^{2+}	25	Choppin *et al.* (1992a)

23.4.3 Coordination numbers

Typical coordination numbers of transition metal ions, where d-orbitals participate in the formation of directional covalent bonds, range from four to six, with well-defined stereochemistry (tetrahedral, square planar, octahedral, etc.). In contrast, most actinide–ligand bonds are characterized by a very small degree of covalence, if any, and the coordination geometry of the complexes is not determined by the directionality of the bonding overlap of the actinide and ligand orbitals. Combined with the somewhat larger size of actinide cations relative to the 3d and 4d transition metal cations, this results, for actinide cations, in larger and variable coordination numbers, which are determined by the maximum number of ligands (including Lewis base solvent molecules) that can fit around the actinide. Increasing oxidation state decreases the ionic radii of the actinide ions (Shannon, 1976), thus favoring lower coordination numbers than are observed for actinides in the lower oxidation states. In water, or in other oxygenated solvents with similar steric demands, typical inner sphere coordination numbers of actinide ions range between seven and nine (including the -yl oxygen atoms of the actinyl cations) with coordinated solvent molecules filling space not occupied by other ligands.

The size and shape of the ligands are very important in determining the exact coordination number of actinide cations. Coordination numbers as low as four or five, for example in $U(NPh_2)_4$ (Reynolds *et al.*, 1977) or UO_2(*p-tert*-butylhexahomotrioxacalix[3]arene)$^-$ (Masci *et al.*, 2002), are observed for bulky ligands in low polarity media. In contrast, coordination numbers of 10 or 12 are not uncommon in solid state and solution-phase complexes containing small, bidentate ligands, such as CO_3^{2-} and NO_3^- [e.g. ten-coordinate $An(CO_3)_5^{6-}$ (Clark *et al.*, 1995) and 12-coordinate $An(NO_3)_6^{2-}$ (Ryan, 1960; Ščavnicar and Prodic, 1965)].

The constraints imposed by the presence of the two oxo groups in the linear, pentavalent AnO_2^+ and hexavalent AnO_2^{2+} cations provide an inherent, steric limitation on the number of ligand donor groups that can form bonds to the actinyl cations. The stability constants of the complexes of actinide cations in

each of the common oxidation states with a series of carboxylate and amino-carboxylate ligands are presented as a function of the number of potential donor groups present in each ligand in Fig. 23.14. For the spherical An(III) and An(IV) cations, which lack the -yl oxygen atoms of the higher actinide oxidation states, the stability constants of the metal–ligand complexes increase regularly with the increased number of donor groups in the ligand. The size, spherical symmetry, and lack of strong, directional covalent bonding in these complexes allow An(III) and An(IV) cations to accommodate polydentate ligands that form multiple chelate rings. In contrast, the linear dioxo structure of AnO_2^+ and AnO_2^{2+} cations constrains the interactions with ligands to the

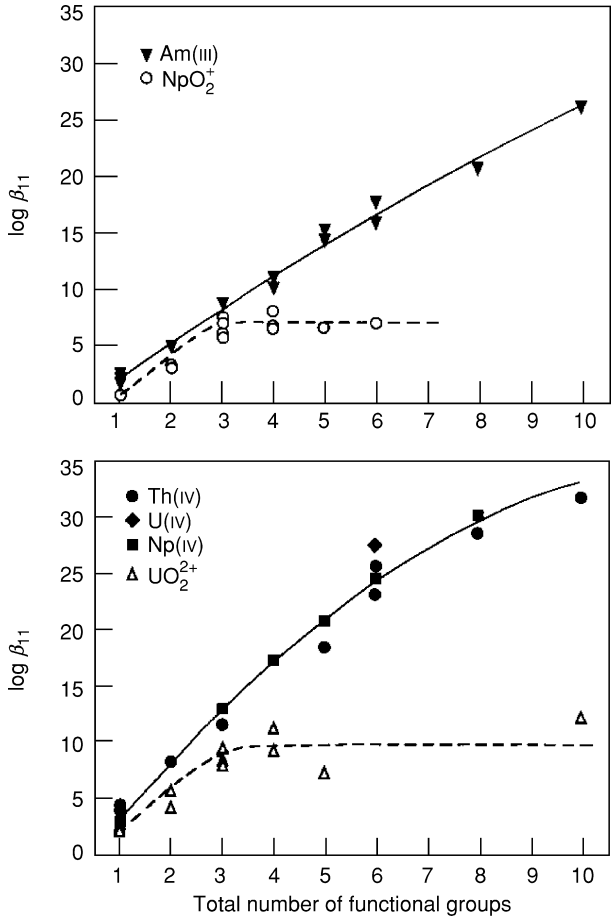

Fig. 23.14 *Effect of the steric constraints imposed by actinyl oxygen atoms of neptunyl(V) and uranyl(VI) on the stability constants of the carboxylate and aminocarboxylate ligands as compared to trivalent and tetravalent actinides. Data from Martell* et al. (1998), *Rizkalla* et al. (1990*a*), *and Tochiyama* et al. (1994).

plane perpendicular to the actinyl oxygens (referred to as the equatorial plane hereafter). Generally, this limits the number of bound donor groups in a single ligand to three or four for the actinyl ions. As shown in Fig. 23.14, the thermodynamic stability of the complexes of AnO_2^+ and AnO_2^{2+} cations increases regularly until three donor groups are present in a given ligand. The presence of additional (more than three) donor groups causes no significant increase in the stability constants of the actinyl complexes because the additional donors do not form bonds with the actinyl cation. Interesting exceptions to this general observation are the pentacoordinate calixarene-based ligands (Shinkai *et al.*, 1987; Guilbaud and Wipff, 1993a), which have the proper geometry to be strong and highly selective complexants for the actinyl(VI) ions.

23.4.4 Steric effects in actinyl bonding

The '-yl' oxygen atoms can interfere with the complexation of rigid ligands, even if the ligand contains three or fewer donor atoms, by restricting ligand donor atoms to bonding only in the equatorial plane of the actinyl ion. In rigid ligands this restriction can cause torsional strain within a bound ligand, or, if the ligand is too large to be contained in the equatorial plane, portions of the ligand and the actinyl oxygens may come into steric conflict. This was reported for the uranyl(VI) complexes of the relatively rigid ligand tetrahydrofuran-2,3,4,5-tetracarboxylic acid, for which the stability constant of the uranyl complex is two orders of magnitude smaller than expected from the stability constants of the complexes of the ligand with the sterically undemanding trivalent lanthanide cations or the uranyl complexes of similar, but more flexible, ligands (Morss *et al.*, 2000).

When steric constraints are not important, the strength of actinide–ligand interactions are primarily governed by electrostatic attraction. Increasing effective charge and decreasing ion size (i.e. increasing charge density) of either the actinide cation or the ligand favor stronger bonds, as discussed in Section 23.6. For a given oxidation state, the radii of actinide ions become progressively smaller with increasing atomic number, imparting a larger charge density to the actinide cation and, generally, making the complexes of the heavier actinides progressively more stable. Unfortunately, little data is available for elements heavier than curium, but the measured stability constants support such correlations.

23.4.5 Relative strength of complexation

For a given ligand, the strength of the actinide complexes usually increases in the order

$$AnO_2^+ < An^{3+} \lesssim AnO_2^{2+} < An^{4+}$$

when steric effects are not important. Obviously the order tracks neither the oxidation state nor the formal charge of the actinide cations. While the overall, formal charges of the actinyl(V) and actinyl(VI) cations are +1 and +2,

respectively, the order of the stability constants implies that the effective charge (Z_{eff}) felt by a ligand bound to the actinyl cations in the equatorial plane is considerably larger. This suggests that the -yl oxygen atoms of the actinyl(v) and actinyl(vi) cations retain a partial negative charge. Assuming completely electrostatic bonding (except for the actinyl oxygens) and that the effective charges of Ca^{2+}, Nd^{3+}, Am^{3+}, and Th^{4+} are equal to their formal charges, the effective charge felt by ligands bound to pentavalent and hexavalent actinyl cations were estimated empirically. For NpO_2^+, Z_{eff} was estimated as $+(2.2 \pm 0.1)$ (Choppin and Rao, 1984). For AnO_2^{2+} (An = U, Np, Pu), cations this approach estimated Z_{eff} between +3.0 and +3.3, depending on the cation and the estimation procedure (Choppin and Unrein, 1976; Choppin, 1983; Choppin and Rao, 1984). In the series of AnO_2^{2+}–fluoride complexes, the derived value of Z_{eff} decreases with increasing atomic number. These experimental Z_{eff} values agree with those from theoretical calculations (Walch and Ellis, 1976; Matsika and Pitzer, 2000), providing theoretical foundations for the observed order of actinide complex stabilities.

The stability constants of a few carboxylate complexes of No^{2+} have been reported (McDowell *et al.*, 1976). They are smaller than those of the actinyl(v) cations, and are similar to those observed for Ca^{2+} or Sr^{2+}. This suggests that the divalent actinides have the lowest effective charge and form the weakest complexes of any actinide oxidation state.

23.4.6 Covalent contribution to bonding

Although an ionic model adequately describes most actinide complexes in solution, measurable covalent bonding is present in the actinide–ligand bonds of some compounds. The most prevalent example of covalence in actinide bonding comes from actinide–ligand multiple bonds (Kaltsoyannis, 2000; Denning *et al.*, 2002), particularly the short (ca. 1.7–1.8 Å) O=An=O bonds in the linear dioxo actinyl ions of the pentavalent and hexavalent light actinides, AnO_2^+ and AnO_2^{2+} (An = U, Np, Pu, Am). Other well-characterized examples of actinide–ligand bonds with some degree of covalence are found in actinide–organometallic complexes (Cramer *et al.*, 1983; Brennan *et al.*, 1987, 1989). More surprising examples come from computation (Pepper and Bursten, 1991) and experiments that suggest that a measurable covalent contribution is present even in An–F bonds, the actinide–ligand bonds expected to be the most strongly ionic. Bleaney *et al.* (1956) and Kolbe and Edelstein (1971) observed superhyperfine splitting, attributable to covalence, in the EPR of trivalent uranium and plutonium fluorides, which are present as cubic AnF_8^{5-} in a fluorite host. In contrast, superhyperfine splitting was not observed for the equivalent compounds of the trivalent lanthanides doped in fluorite, implying that the An–F bonds have measurably greater covalent character than Ln–F bonds. However, the presence of some covalence in the actinide–ligand bonds does not diminish the overarching importance of ionic interactions in the formation of these bonds.

In solution, the best evidence for some degree of covalence in actinide–ligand bonds comes from the thermodynamic differences in the complexes of the trivalent lanthanides and the trivalent actinides with soft donor ligands (i.e. ligands containing N, S, or halide donors other than F^-). The complexes formed by An^{3+} cations and Ln^{3+} cations with hard donor, oxygen-based, ligands (carboxylates, organophosphates) are nearly indistinguishable for Ln^{3+} and An^{3+} ions with similar ionic radii (e.g. Am^{3+} and Pm^{3+}). However, as first observed by Diamond *et al*. (1954), An^{3+} cations form thermodynamically more stable complexes with soft donor ligands than the equivalent Ln^{3+} cations do. This deviation from predictions based solely on electrostatic bonding has been interpreted as indicating slightly greater covalence in the actinide–soft donor ligand bond. The stability constants of aqueous complexes of trivalent lanthanide and actinide cations with some representative hard and soft donor ligands, as well as ligands containing both hard and soft donor groups, are summarized in Table 23.16.

23.4.7 Soft ligand bonding

A greater degree of covalence in the bonds between an actinide ion and soft donor ligand should also be reflected in more exothermic complexation enthalpies, relative to the equivalent lanthanide complexes. Significant differences in the enthalpies of metal–nitrogen bonds were not observed in the aminocarboxylate complexes of americium, curium, and europium (Rizkalla *et al*., 1989). However, large differences in the complexation enthalpies of trivalent lanthanide and actinide cations consistent with enhanced covalence in actinide–soft donor bonds have been reported for ligands containing only soft donor atoms in both aqueous and organic solutions (Zhu *et al*., 1996; Jensen *et al*., 2000a; Miguirditchian, 2003).

The preference of actinide ions for softer donor ligands is the common basis for successful chemical separations of the trivalent actinides from the trivalent lanthanides (Nash, 1993a). Although actinide–soft donor bonds are thermodynamically stronger than the corresponding lanthanide–soft donor bonds, neither series of f-element cations forms particularly strong complexes with ligands containing only soft donors, as illustrated by the stability constants in Table 23.16. The likelihood of observing complexes between actinide ions and soft donor ligands is further reduced in aqueous solution by the high background concentration of the hard Lewis base H_2O, 55 mol L^{-1}. Thus, forming actinide complexes with soft donor ligands in aqueous solution requires either high concentrations of the soft ligand, multiple soft donor sites within a single ligand, or the presence of both hard and soft donors within the same ligand. Soft donor binding in aqueous solution is also encouraged when the soft donor groups are relatively acidic, which allows the soft donor ligand to compete with hydrolysis reactions. As a result, actinide soft donor reactions are most easily observed in non-aqueous solvents.

Table 23.16 *Stability constants of trivalent lanthanide and actinide cations of similar ionic radius with oxygen donor and nitrogen donor ligands in aqueous $NaClO_4$, $T = 25°C$. (Crystal radii according to Shannon (1976) $Nd^{3+} = 1.249$ Å, $Pm^{3+} = 1.233$ Å, $Sm^{3+} = 1.219$ Å, $Am^{3+} = 1.230$ Å for $CN = 8$.)*

Complex formed[a]	$log\,\beta_{1q}$ *Nd*	*Sm*	*Am*	*Ligand donor atoms*	I (M)	*References*
Hard donors						
$M(ac)^{2+}$	1.92	2.03	1.96	1 or 2 O	2	Grenthe (1964); Choppin and Schneider (1970)
$M(ox)^{+}$	5.18 (Pm)	–	5.25	2 O	0.1	Stepanov (1971)
$M(ox)_2^{-}$	8.78 (Pm)	–	8.85	4 O	0.1	Stepanov (1971)
Both hard and soft donors						
$M(edta)^{-}$	15.75	16.20	16.77	4 O, 2 N	0.5	Gritmon *et al.* (1977); Rizkalla *et al.* (1989)
$M(dtpa)^{2-}$	20.09	20.72	21.12	5 O, 3 N	0.5	Gritmon *et al.* (1977); Rizkalla *et al.* (1989)
Soft donors						
MN_3^{2+}	0.4	–	1.3	1 N	–[b]	Musikas *et al.* (1983)
$M(N_3)_2^{+}$	0.6	–	1.6	2 N	–[b]	Musikas *et al.* (1983)
$M(N_3)_3$	0.7	–	1.4	3 N	–[b]	Musikas *et al.* (1983)
$M(tpen)^{3+}$		4.70	6.73	6 N	0.1	Jensen *et al.* (2000a)
$M(tptz)^{3+}$	2.8	3.4	4.2	3 N	1[c]	Musikas (1984)

[a] ac^{-}, acetate; ox^{2-}, oxalate; $edta^{4-}$, ethylenediaminetetraacetate; $dtpa^{5-}$, diethylenetriaminepentaacetate; tpen, *N*,*N*,*N*′,*N*′-tetrakis(2-pyridylmethyl)ethylenediamine; tptz, 2,4,6-tri(2-pyridyl)-1,3,5-triazine.
[b] Ionic strength not given.
[c] 1 M KCl.

In summary, actinide–ligand bonding, though primarily ionic, should be considered as intermediate between the strongly ionic bonding observed in lanthanide complexes and the more covalent bonding found in transition metal complexes. The exact behavior of an actinide ion is determined by its oxidation state, the hard or soft characteristics of the ligand, and the position of an actinide element within the actinide series, with the actinides becoming more lanthanide-like with increasing atomic number.

23.5 INNER VERSUS OUTER SPHERE COMPLEXATION

Although the concept of outer sphere complexation was introduced by Werner (1913) and the theory first given a mathematical base by Bjerrum (1926) progress in understanding the factors involved in the competition between inner and outer sphere complexation was slow.

The term 'outer sphere complex' refers to species in which the ligand does not enter the primary coordination sphere of the cation but remains separated by at least one solvent molecule. Such species are known also as 'solvent separated' ion pairs to distinguish them from inner sphere complexes in which the bonding involves direct contact between the cation and the ligand. Some ligands cannot displace the water and complexation terminates with the formation of the outer sphere species. Actinide cations have been found to form both inner and outer sphere complexes and for some ligands, both types of complexes may be present simultaneously.

For labile complexes, it is often quite difficult to distinguish between inner and outer sphere complexes. Adding to this confusion is the fact that stability constants for such labile complexes determined by optical spectrometry are often lower than those of the same system determined by other means such as potentiometry, solvent extraction, etc. This has led some authors to identify the former as 'inner sphere' stability constants and the latter as 'total' stability constants. However, others have shown that this cannot be correct even if the optical spectra of the solvated cation and the outer sphere complex are the same (Beck, 1968; Johansson, 1971). Nevertheless, the characterization and knowledge of the formation constants of outer sphere complexes are important as such complexes play a significant role in the Eigen–Tamm mechanism for the formation of labile complexes (Eigen and Wilkins, 1965). The Eigen–Tamm mechanism assumes rapid formation of an outer sphere association complex (i.e. an ion pair) and the subsequent rate-determining step in which the ligand displaces one or more water molecules,

$$M(H_2O)_q^{z+} + L^{x-} \rightarrow M(H_2O)_q^{z+}\text{- - -}L^{x-} \rightarrow M(H_2O)_{q-1}L^{z-x} + H_2O$$

The conversion of the outer sphere complex to the inner sphere complex is the rate-determining step and is dependent on the equilibrium concentration of the outer sphere complex. Consequently, calculations of rate constants by the Eigen model involve estimation of the stability constants of the outer sphere species. Actinide cations form labile, ionic complexes of both inner and outer sphere character and serve as useful probes to study the competition between inner and outer sphere complexation due to ligand properties.

It has been proposed (Choppin and Strazik, 1965; Choppin and Ensor, 1977; Khalili *et al*., 1988) that the thermodynamic parameters of complexation can be used as a criterion for evaluation of inner versus outer sphere complexation. For outer sphere complexes, the primary hydration sphere is minimally perturbed. As a result, an exothermic enthalpy results from the cation–ligand interaction while the entropy change can be expected to be negative since the ordering of ionic charges is not accompanied by a compensatory disordering of the hydration sphere. By contrast, when inner sphere complexes are formed, the primary hydration sphere is sufficiently disrupted that this contribution to the entropy and enthalpy of complexation frequently exceeds that of the cation–ligand

interaction and the result is an endothermic enthalpy and a positive entropy change. These considerations have led, for trivalent lanthanides and actinides in their 1:1 complexes (i.e., ML), to assignment of predominately outer sphere character to the Cl^-, Br^-, I^-, ClO_3^-, NO_3^- and sulfonate complexes and of inner sphere character to the F^-, IO_3^- and SO_4^{2-} complexes (Choppin, 1971).

The experimental, total, stability constant, β^{exp} is related to β_{os} and β_{is} by

$$\beta^{exp} = \beta_{is} + \beta_{os}$$

where β_{is} and β_{os} are the stability constants for inner and outer sphere formation, respectively. The effect of cationic charge on the equilibrium between inner and outer sphere complexation by the halate and chloroacetate anions has been investigated (Rizkalla *et al.*, 1990b; Choppin *et al.*, 1992b). In the case of halate systems, the entropy change for the complexation with monochlorate ($pK_a(HClO_3) = -2.7$) was considered to indicate 100% outer sphere character while that of the monoiodate ($pK_a(HIO_3) = 0.7$) led to the assignment of a predominately inner sphere character. The data for the 1:1 europium bromate ($pK_a(HBrO_3) = -2.3$) complex was interpreted to show a mixed nature with the outer sphere character more dominant. For thiocyanate complexes, stepwise stability constant patterns are reported for An(III) (Harmon *et al.*, 1972a) and AnO_2^{2+} (Ahrland and Kullberg, 1971a) to be $K_1 > K_2 < K_3$, indicating predominant outer sphere nature of the 1:1 and 1:2 complexes which changes to inner sphere for the 1:3 system. For An(IV), the pattern (Laubscher and Fouché, 1971) is $K_1 > K_2 > K_3 < K_4$, indicating that inner sphere complexation occurs only in the 1:4 species.

A series of related ligands, acetate and chloroacetates (Ensor and Choppin, 1980), was studied by solvent extraction and calorimetry to ascertain the relationship of ligand pK_a and inner versus outer sphere character. The relationship of experimental values of $\log \beta_{11}$ with the ligand pK_a as well as the relationships of the calculated values of $\log \beta_{is}$ and $\log \beta_{os}$ is shown in Fig. 23.15. Acetate (ac^-, $pK_a = 4.8$) formed inner sphere complexes and trichloroacetate (Cl_3ac^-, $pK_a = -0.5$), outer sphere complexes. The inner sphere nature increased with pK_a (Rinaldi *et al.*, 1979) with estimates for inner character of 100% $La(ac)^{2+}$, 50% $La(Clac)^{2+}$, 22% $La(Cl_2ac)^{2+}$, and 0% $La(Cl_3ac)^{2+}$. These values agreed satisfactorily with calculations using a modified Born equation (Choppin and Strazik, 1965). For the uranyl(VI) system, similar calculations (Khalili *et al.*, 1988) provided the following values for the percent inner sphere character: $UO_2(ac)^+$, 100%; $UO_2(Clac)^+$, 42%; $UO_2(Cl_2ac)^+$, 9%; $UO_2(Cl_3ac)^+$, 4%.

The data are consistent with an increased tendency to outer sphere complexation for the same cation as the ligand pK_a values decrease since the more acidic ligand is less competitive with hydration. Conversely, there is a stronger tendency to outer sphere complexation with increased charge on the metal cation, reflecting the increased hydration strength for higher cation charge. From acetate/haloacetate 1:1 complexation data with An^{3+} and AnO_2^{2+}, it

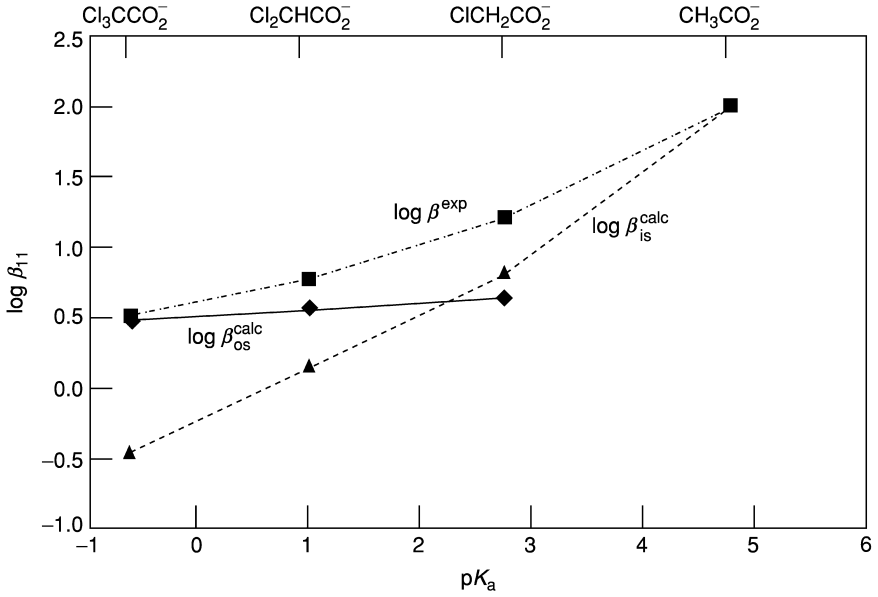

Fig 23.15 *Dependence of the experimentally measured total stability constant,* β^{exp}, *and the calculated inner* (β_{is}) *and outer* (β_{os}) *sphere stability constants for Am*(III) *complexes on the acidity of* $Cl_{3-n}H_nCCO_2H$ *ligands.*

was estimated that equal amounts of inner and outer sphere complexation would be observed for carboxylate ligands of p$K_a \sim 2.8-3.0$ (Khalili *et al.*, 1988). For NpO_2^+ and Th^{4+} cations, equal amounts of inner and outer sphere complexes would be present in 1:1 complexes with carboxylate ligands of p$K_a \sim$ 1.1 and 4.2, respectively (Choppin and Rizkalla, 1994).

The thermodynamic data of Eu(halate)$^{2+}$ and Th(halate)$^{3+}$ complexation are listed in Table 23.17. The entropy for the monochlorate (pK_a $HClO_3 = -2.7$) was interpreted as indicating 100% outer sphere character with Eu(III) and a predominance of it with Th(IV). The values for the monoiodate (pK_a $HIO_3 = 0.7$) complexes led to assignment of a predominately inner sphere character for both Eu(III) and Th(IV) (Choppin and Ensor, 1977). The data for the 1:1 europium complex with bromate (pK_a $HBrO_3 = -2.3$) were interpreted as showing a mixed nature with more outer sphere character. Values of 70, 80, and 85% ($\pm$10%) were estimated as the percent of outer sphere nature in the $EuBrO_3^{2+}$, $UO_2BrO_3^+$, and $ThBrO_3^{3+}$ complexes (Rinaldi *et al.*, 1979; Ensor and Choppin, 1980; Khalili *et al.*, 1988). This is consistent with increased outer sphere nature with larger effective charge of U in UO_2^{2+}. This pattern is likely due to the increase in hydration strength as the cationic charge increases.

Table 23.17 *Thermodynamic parameters for halate complexation.*

Complex	*log* β_{11}	ΔG (kJ mol^{-1})	ΔH (kJmol^{-1})	ΔS (JK^{-1}mol^{-1})	% *inner sphere*
$EuClO_3^{2+}$	0.04	−0.25	−6.3	−20	0
$EuBrO_3^{2+}$	0.59	−3.39	−2.5	3	ca. 30
$EuIO_3^{2+}$	1.14	−6.53	11.0	59	100
$ThClO_3^{3+}$	0.14	−0.78	2.4	11	≥0
$ThBrO_3^{3+}$	0.63	−3.61	2.5	20	ca. 15
$ThIO_3^{3+}$	2.49	−14.24	6.5	70	100

23.6 CORRELATIONS

Actinide cations interact with hard Lewis bases through strongly ionic bonds whose thermodynamic strength is dependent of the charges of the actinide cations and of the ligands and on any steric constraints imposed by the actinide ion or ligand (see Section 23.4). In the absence of steric effects, the predominance of ionic bonding in actinide complexes and the regular decrease in the size of actinide ions within an oxidation state as the atomic number increases are the basis for the systematics of actinide–ligand complexation, which can be exploited for important predictive capabilities. The stoichiometries, structures, and stability constants of actinide–ligand complexes in solution can often be predicted from the chemistry of related ligands or of other metal ions, including those in other oxidation states. Such empirical correlations can provide fairly accurate estimates of the properties of actinide–ligand complexes, although no correlation is universally applicable to all ligands, actinide ions, or actinide oxidation states because of electronic effects (e.g. covalency) or steric constraints. Given the large number of potential ligands, the ability to use such correlations to predict the strength of the interaction between a metal ion and a ligand accurately is very useful. The difficulties in working with radioactive materials further increase the value of these correlations.

The interactions of H^+ and An^{z+} with ligands are governed primarily by the same physical forces, electrostatics. Consequently, ligand basicity is often a good predictor of the relative thermodynamic strength of the interactions of ligands with actinide cations. In practice, ligand basicity may be expressed either in the Brønsted sense as the affinity of a ligand for protons or, more generally, as the affinity of a ligand for Lewis acids (i.e. other metal cations). Since both the pK_a and the logarithmic stability constant of a metal–ligand complex (M_nL_q), $\log \beta_{nq}$, are directly proportional to the Gibbs energy of reaction,

$$\Delta G_{\text{protonation}} = -2.303RT\,pK_a \tag{23.9}$$

$$\Delta G_{\text{complexation}} = -2.303RT \log \beta_{nq} \tag{23.10}$$

the correlation of stability constants with ligand basicity falls in the general category of linear Gibbs energy correlations.

The database of ligand pK_a values is the most extensive set of data available for correlating and interpreting actinide–ligand bonding. The logarithm of the stability constant for actinide–ligand complexation is expected to be directly proportional to the basicity of the ligand, expressed as the pK_a, within a series of ligands containing a single bonding functionality where variations in steric effects are negligible. Examples of this type of correlation for the formation of 1:1 UO_2^{2+}:monocarboxylate complexes and of both 1:1 and 1:2 NpO_2^+:β-diketonate complexes are shown in Fig. 23.16. The monocarboxylic acids could behave as monodentate or bidentate ligands (Howatson *et al.*, 1975; Denecke *et al.*, 1998; Rao *et al.*, 2002), while the β-diketonate ligands form bidentate six-membered chelate rings with the neptunyl(V) ion. The deviation of the $UO_2(O_2CCHCl_2)^+$ complex from the correlation likely arises from the formation of a mixture of inner and outer sphere dichloroacetate complexes (Section 23.5), while the other ligands form only inner sphere complexes with the uranyl(VI) cation.

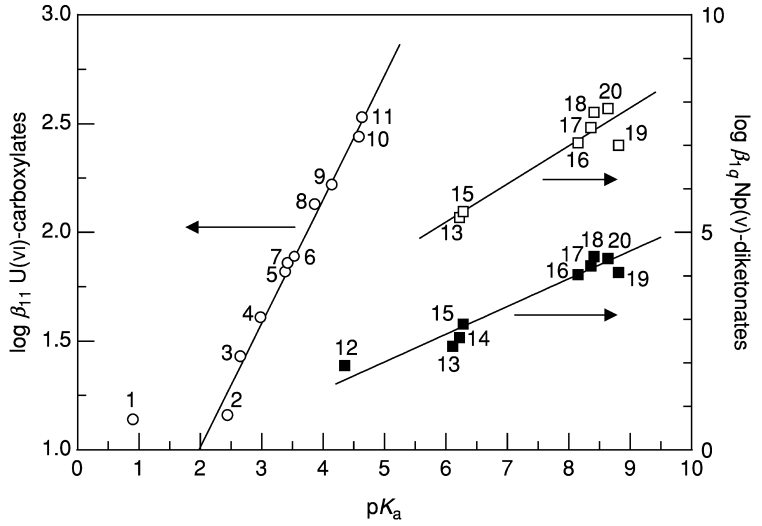

Fig. 23.16 *Linear Gibbs energy correlation of the stability constants of* 1:1 *uranyl(VI): monocarboxylate* (○), *and* 1:1 (■) *and* 1:2 (□) *neptunyl(V):β-diketonate complexes with the ligand basicity. Data from Martell* et al. (1998), *Gross and Keller* (1972), *and Sekine* et al. (1973). (1) *Dichloroacetate,* (2) *glycine,* (3) *chloroacetate,* (4) 2-*furoate,* (5) 2-*thenoate,* (6) *formate,* (7) *thioglycolate,* (8) 3,5-*dihydroxybenzenecarboxylate,* (9) *phenylacetate,* (10) *acetate,* (11) *propionate,* (12) *hexafluoroacetylacetone,* (13) 2-*furoyltrifluoroacetone,* (14) *trifluoroacetylacetone,* (15) 2-*thenoyltrifluoroacetone,* (16) *difuroylmethane,* (17) 2-*thenoylacetone,* (18) 2-*furoylacetone,* (19) *acetylacetone,* (20) *benzoylacetone.*

Using the pK_a to represent ligand basicity is straightforward for simple ligands, such as monocarboxylate and β-diketonate ligands (Fig. 23.16), where all of a ligand's donor atoms are available for coordination once the single ionizable proton is removed from the ligand. The correlation of actinide complexation constants to ligand basicity is more complicated when the ligand contains multiple basic sites or can form more than a single chelate ring. Summing the pK_a values for each of a ligand's donor groups yields a single parameter representing an effective, total basicity. These values, ΣpK_a, usually correlate fairly well with the stability constants, log β_{11}, of an actinide ion, as shown in Fig. 23.17. Such correlations between stability constants and ΣpK_a values is the strongest within groups of related ligands, as similarity of the structural features of the complex is more likely. In some cases, all of the

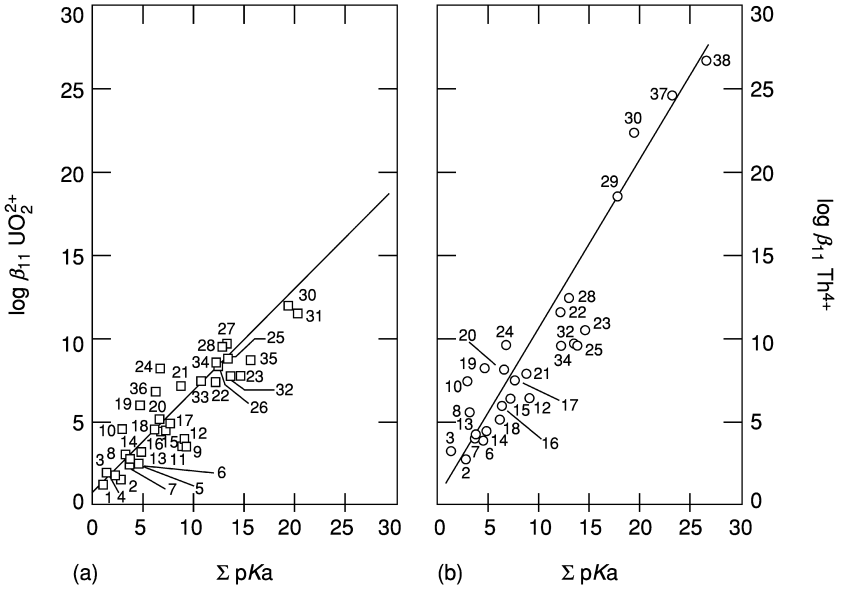

Fig. 23.17 *Linear Gibbs energy correlation between the stability constants and total ligand basicity for* (*a*) *uranyl*(*VI*) *and* (*b*) *thorium*(*IV*) *complexes.* (1) *Dichloroacetate,* (2) *chloroacetate,* (3) *sulfate,* (4) *nicotinate,* (5) *ascorbate,* (6) *acetate,* (7) *glycolate,* (8) *thiodiacetate,* (9) *adipate,* (10) *fluoride,* (11) *glutarate,* (12) *succinate,* (13) *lactate,* (14) α-*hydroxyisobutyrate,* (15) *maleate,* (16) *phthalate,* (17) *malonate,* (18) *picolinate,* (19) *oxalate,* (20) *oxydiacetate,* (21) *acetylacetonate,* (22) *citrate,* (23) *oxinate,* (24) *tropolonate,* (25) *iminodiacetate,* (26) *N*-(2-*hydroxyethyl*)*iminodiacetate,* (27) *N-methyliminodiacetate,* (28) *nitriliotriacetate,* (29) *N*-(2-*hydroxyethyl*)*ethylenediamine-N,N′,N′-triacetate–hedta*$^{3-}$, (30) *ethylenediaminetetraacetate–edta*$^{4-}$, (31) *ethylenediamine-N,N′-diacetate–edda*$^{2-}$, (32) *hydroxide,* (33) *monoprotonated ethylenediaminetetraacetate–H*(*edta*)$^{3-}$, (34) *sulfoxinate,* (35) *carbonate,* (36) *thenoyltrifluoroacetonate,* (37) *trans*-1,2-*diaminocyclohexane-N,N,N′,N′-tetraacetate–dcta*$^{4-}$, (38) *diethylenetriaminepentaacetate–dtpa*$^{5-}$, (39) *tetra*(2-*pyridylmethyl*)*ethylenediamine–tpen.*

potential donor atoms represented by the individual pK_a values do not bind the metal ion, either because of actinide- or ligand-based steric considerations, or because the donor atoms are not well matched to actinide chemistry (e.g. sulfur donors in aqueous solution). For such complexes, the actual An–L stability constant is smaller than predicted. In other cases, the assumption of An–L bonds being primarily ionic may be invalid, or the presence of a ligand containing donor atoms that are Lewis bases without appreciable Brønsted basicity (e.g. ether oxygens), would result in an An–L stability constant that is greater than that predicted by the ΣpK_a correlation.

Deviations from the expected correlation between a *measured* stability constant and ΣpK_a for a particular An–L pair can be a useful diagnostic for determining the denticity or coordination modes of ligands in actinide complexes (Jensen and Nash, 2001). The complexation of Np(v) by thiodiacetic acid (H_2tda) in 0.5 M $NaClO_4$ solution (Rizkalla *et al.*, 1990a) is a good example of this approach. Thiodiacetic acid (Fig. 23.18), is a potentially tridentate ligand, capable of forming two five-membered –S–C–C–O– chelate rings with metal ions of the proper size. However, the low affinity of actinide ions for ligands with sulfur donor atoms and the low effective charge of the neptunyl(v) cation, +2.2, combine to keep the ligand from forming such chelate rings. Based on the ΣpK_a (3.07 + 4.00 = 7.07), the correlation predicts a stability constant for $NpO_2(tda)^-$ of $\log\beta_{11} = 3.0$. A favorable Np–S interaction yielding a tridentate complex with two –S–C–C–O– chelate rings would make the stability constant still larger. However, the reported stability constant is much smaller ($\log\beta_{11} = 1.2$), indicating that the complex is not tridentate. The magnitude of the stability constant does match those of NpO_2^+ complexes with monofunctional carboxylic acid ligands ($\log\beta_{11} = 0.7$–1.3), and is only slightly larger than

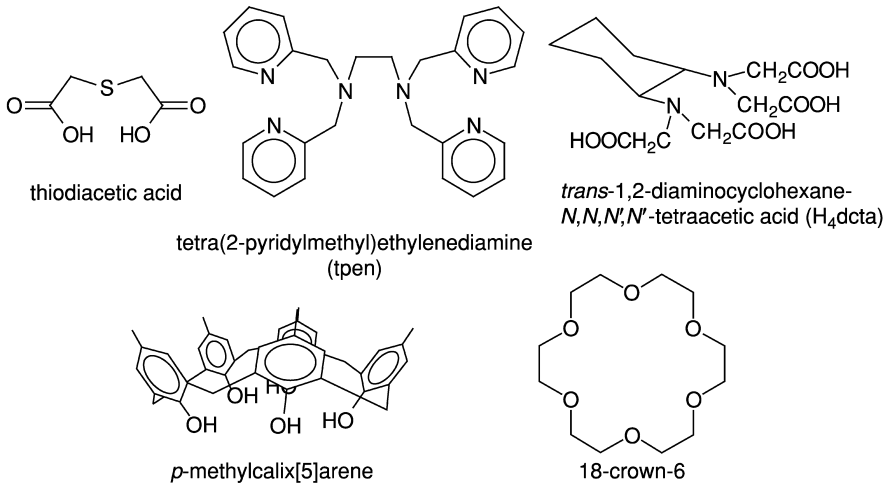

Fig. 23.18 *Ligand structures.*

the value predicted, $\log \beta_{11} = 0.8$, by considering NpO_2^+ complexation only at the most acidic site where $pK_a = 3.07$. The agreement of the experimental stability constant with that for a single ligand pK_a leads to the conclusion that there is no significant Np–S interaction and that tda^{2-} binds to NpO_2^+ only through a single carboxylate group. The lack of a Np–S bond also is consistent with the crystal structure of $NaNd(tda)_2$, in which only Nd–O bonds are observed (Kepert *et al.*, 1999).

The uncertainty in the nature of the interactions of certain actinide ions with particular ligands can make it difficult to understand or predict actinide complexation chemistry based solely on the basicity of a ligand, as the size and charge of the proton are very different from those of the actinide ions in solution. Using the Gibbs energies of complexation for other metal ions instead of pK_a values can overcome this limitation if the Lewis acids (metal ions) used for the correlations impose steric constraints, electrostatic fields, and degrees of covalency similar to those of the actinide ions under consideration. Since the lanthanide cations form metal–ligand bonds that are predominantly ionic and are of approximately the same size as actinide cations, they often are good models for actinide–ligand complexes. Hard transition metal cations, such as Fe^{3+} or Zn^{2+} (Hancock and Martell, 1989; Jarvis and Hancock, 1991), and alkaline earth cations, such as Ca^{2+} (Choppin *et al.*, 1992a), also can be used, with care, in some actinide–ligand bonding correlations. Figs. 23.18 and 23.19 compare the stability constants of actinide–ligand complexes of actinide cations in each of the common solution oxidation states (3+, 4+, 5+, and 6+) with the stability constants of the complexes formed by the same ligands with the trivalent lanthanide cations Nd^{3+} or Sm^{3+}. The correlations are considerably better than for the stability constants of the UO_2^{2+} –ligand or Th^{4+}–ligand complexes with the ΣpK_a values depicted in Fig. 23.17. However, as discussed in Section 23.4, the correlation fails when the assumption of similar steric constraints is incorrect for the complexes of actinyl ions with polydentate ligands containing more than three donor groups per ligand (Figs. 23.19a and 23.20a). In contrast, when the $Np(V)O_2^+$ complexes are compared to the complexes of $An(VI)O_2^{2+}$ cations, which are subject to similar steric constraints, the stability constants of polydentate ligands track the correlation well (Fig. 23.19b).

The stability constants of An(IV) cations, represented by Th^{4+}, and of An(III) cations, represented by Am^{3+}, track the Gibbs energies of trivalent lanthanide (Nd^{3+} or Sm^{3+}) complexation well (Fig. 23.20), indicating that any steric constraints imposed on the ligands by the trivalent and tetravalent actinide cations are similar to those of the lanthanide cations. However, one complex obviously deviates from the correlation. The stability constant of the $Am(tpen)^{3+}$ complex (Ligand #39, tetra(2-pyridylmethyl)ethylendiamine, Fig. 23.18) is two orders of magnitude larger than expected based on the stability constant of the $Sm(tpen)^{3+}$ complex, even though the larger radius of Am^{3+} suggests that the stability constant should be smaller for $Am(tpen)^{3+}$.

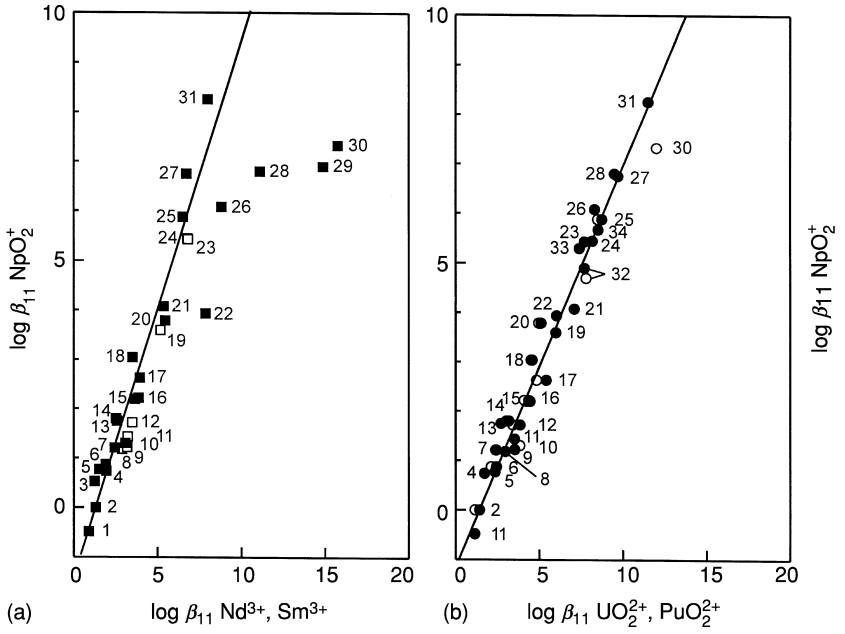

Fig. 23.19 *Correlation between the stability constants of neptunyl(v) complexes and the stability constants of the complexes of (a) the trivalent lanthanides* Nd^{3+} (■) *and* Sm^{3+} (□), *and (b) the hexavalent actinides* UO_2^{2+} (●) *and* PuO_2^{2+} (○). *See Fig.* 23.17 *for the ligands' numerical identities.*

(The crystal radius of Am^{3+} is 1.230 Å for coordination number 8, while for Sm^{3+} it is 1.219 Å under the same conditions [Shannon, 1976].) All six of the potential nitrogen donor atoms in the tpen ligand appear to be coordinated to both Ln^{3+} and An^{3+} cations, with some coordinated water molecules remaining in the inner coordination sphere of the metal ions in aqueous solution (Jensen *et al.*, 2000a). Based on the similar size and coordination environment of the two cations, steric constraints would be expected to play no role in this deviation of the Am^{3+}–Ln^{3+} correlation. The greater stability of the Am^{3+}–tpen complex most likely arises from an enhanced degree of covalence in the An–N bonds as compared to the Ln–N bonds (Choppin, 1983).

The size of the ligand chelate rings can also affect the stability of actinide–ligand complexes. Examining the Gibbs energy relationships for the complexes of two different ligands with numerous different metal ions can be instructive for understanding the interactions of actinide ions with ligands (Jensen and Nash, 2001). Five-membered chelate rings are the most stable ring size for complexes of actinide-sized cations (Hancock, 1992), and the strength of actinide–ligand interactions for chelating ligands usually decreases with ring size in the order $5 > 6 \gg 7 \sim 8$ for all actinide oxidation states (Stout *et al.*, 1989). If the

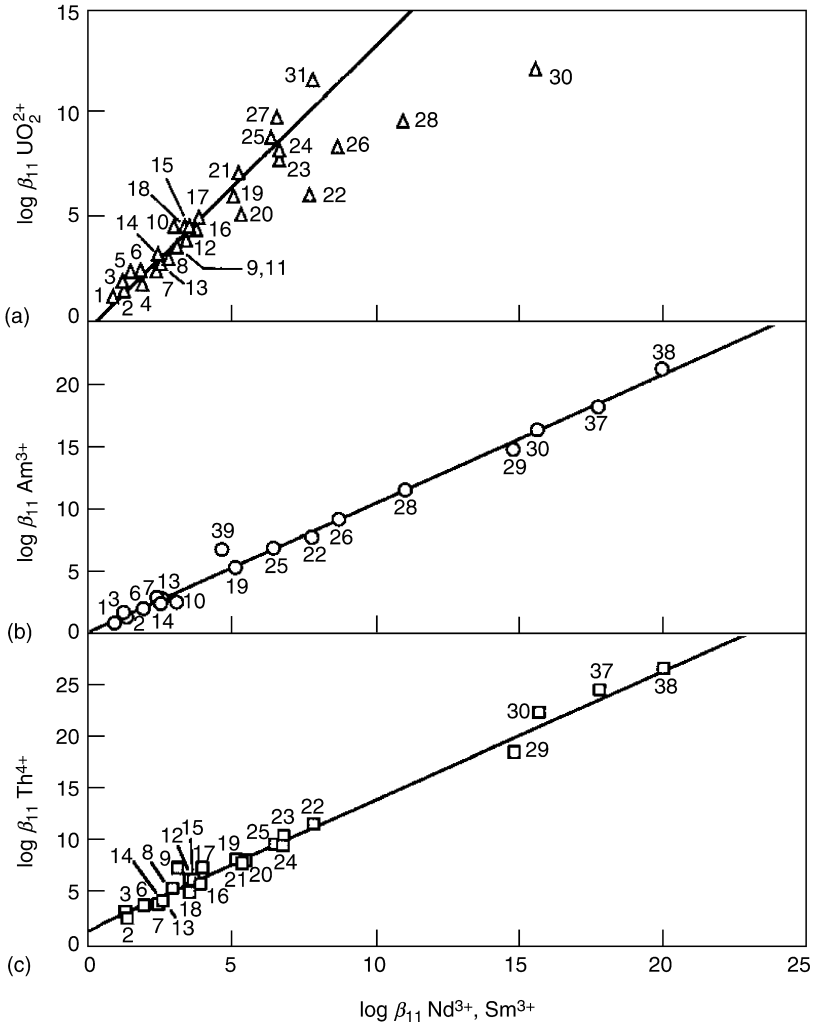

Fig. 23.20 *Correlation between the stability constants of trivalent lanthanide complexes and the stability constants of the complexes of* (*a*) *a hexavalent actinide,* (*b*) *a trivalent actinide, and* (*c*) *a tetravalent actinide. See Fig.* 23.17 *for the ligands' numerical identities.*

donor groups are strongly basic, ligands that form seven-membered rings can be quite stable. Presumably this is because the large size and non-directional electrostatic bonding of the actinide cations can accommodate the larger chelate ring (Rapko *et al.*, 1993). Complexes with eight-membered chelate rings formed by inter-ligand hydrogen bonding also are important species in non-aqueous

media, most notably for phosphoric acid based extractants such as bis(2-ethylhexyl)phosphoric acid (Ferraro and Peppard, 1963).

The basis for the empirical correlations between the stability constants of the actinide ion complexes with the acid constants of ligands or the stability constants of other metal ions is the strongly ionic character of the bonding in these systems. Born (1920) calculated the solvation energy of an ion in solution (M^{Z+}) from a model of a sphere of charge $+Z$ and radius R in a system with a dielectric constant, D, by the equation

$$\Delta G_{\text{solvation}}(M^{Z+}) \propto Z^2/DR \tag{23.11}$$

Modifications to the Born equation (Münze, 1972) have formed a useful basis for estimating and comparing actinide–ligand complexation constants (Choppin, 1983; Rizkalla *et al.*, 1990b), and may be useful for describing the entropies of complexation as well (Manning, 1996). For cations of the same charge (Z), the modified Born equation predicts a linear relationship between the logarithmic stability constant and $1/R_{\text{cation}}$, the reciprocal of the cation radii. This relationship holds over a range of cationic radii for numerous metal–ligand complexes, as shown for trivalent lanthanides and for trivalent and tetravalent actinides in Fig. 23.21. In systems where an approximately linear relationship does not hold for f-element complexes, such as citrate complexes (Fig. 23.21), significant steric effects or specific interactions (metal–solvent, ligand–solvent, complex–solvent, or ligand–ligand) are likely. However, it is not known if the order of magnitude deviation of the $Fm(dcta)^-$ and $Md(dcta)^-$ ($dcta^{4-}$ = *trans*-1,2-diaminocyclohexane-*N*,*N*,*N*′,N′-tetraacetate, Fig. 23.18) complexes from the correlation with $1/R_{\text{cation}}$ in Fig. 23.21 arises from such chemical factors or from the higher uncertainties associated with stability constant measurements of complexes involving high specific activity radionuclides.

The cationic charge used in the Born equation, Z, could be taken to be equal to the formal charge of An(III) and An(IV) cations, but it is less clear what the value of Z should be for AnO_2^+ and AnO_2^{2+} species since the oxo ligands appear to retain a partial negative charge. As discussed in Section 23.4, electrostatic correlations based on the Born equation for actinyl–fluoride complexes, suggest that the effective cationic charge experienced by a ligand bound to NpO_2^+ is $+2.2$, and for ligands bound to UO_2^{2+} is $+3.3$ (Choppin and Unrein, 1976; Choppin and Rao, 1984).

Defining the ligand charge in the cases of neutral ligands, polydentate ligands, or ligands containing both anionic functional groups (e.g., CO_2^- or PO_3^{2-}) and neutral donor sites (e.g. –N= or –O–) is also difficult. Effective anionic charges have been estimated for some organic ligands by assuming that the Born equation is valid for ligand protonation (Choppin, 1983), which results in a linear relationship between ΣpK_a and the effective anionic charge of a ligand,Z_{an},

$$Z_{an} = 0.208 \cdot \Sigma pK_a$$

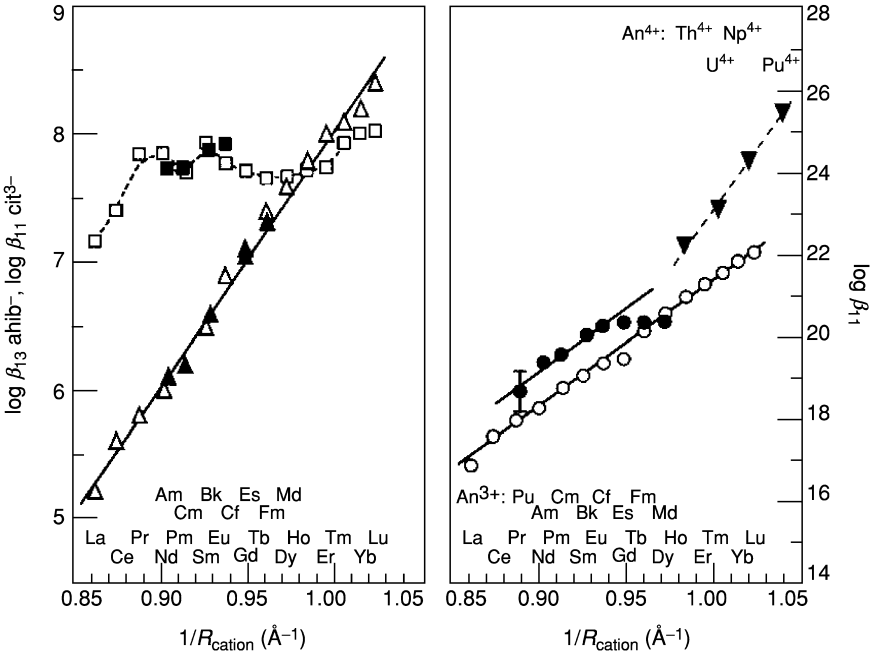

Fig. 23.21 *Dependence of the stability constants of actinide* (*solid symbols*) *and lanthanide* (*open symbols*) *complexes on cation size as dictated by a purely electrostatic bonding model:* (■, □) 1:1 *complexes of trivalent cations with citrate* (cit^{3-}), (▲, △) 1:3 *complexes of trivalent cations with* α*-hydroxyisobutyrate* ($ahib^{-}$), (●, ○) 1:1 *complexes of trivalent cations with trans*-1,2-*diaminocyclohexane-N,N,N′,N′-tetraacetate* ($dcta^{4-}$), (▼) 1:1 *complexes of tetravalent actinide cations with ethylenediaminetetraacetate* ($edta^{4-}$). *Stability constant data from* (▲) *Starý* (1966) *and Brüchle* et al. (1988) *at* $I = 0.5$ M; (△) *Martell* et al. (1998) *at* $I = 0.1$ M; (■, □) *Martell* et al. (1998) *at* $I = 0.1$ M (*ionic strength correction applied to* Pu^{3+}); (▼) *Martell* et al. (1998) *with Pu value average of Cauchetier and Guichard* (1973), *Krot* et al. (1962), *and Mikhailov* (1969) *at* $I = 0.5$ M (*ionic strength correction applied to* Np^{4+}, *and* Pu^{4+}). *Ionic radii from David* (1986) *for* $CN = 8$.

The Born approach has been useful in describing actinide–ligand complexation in solution, but there has been much discussion over the years about the proper form that an equation describing general electrostatic bonding interactions should take. This debate eventually waned due to the understanding that the general function, Z^n/r^m, is suitable (Huheey, 1976). The Brown–Sylva–Ellis equation, a semiempirical correlation using a complicated function of Z^2/r^2 coupled to a number of electronic corrections appears very successful for describing metal–ligand interactions for a wide range of metal ions, including the actinides (Brown *et al.*, 1985). Other electrostatic models that incorporate corrections for inter-ligand repulsion (Moriyama *et al.*, 1999, 2002; Neck and

Kim, 2000) into the general Born framework have been able to reproduce the stability complexes for higher mononuclear complexes of the actinides (i.e. β_{1q} with $q > 1$).

Inter-ligand interactions are not important for 1:1 An^{z+}:L^- complexes and the metal–ligand interactions can be represented by the simplest form of the coulombic attraction between a metal ion and a monovalent L^- ligand with $\log \beta_{11} \propto Z/d_{M-L}$ (d_{M-L} = the distance between the center of the metal ion and the ligand donor atom). Fig. 23.22 depicts this correlation for the 1:1 complexes of hydroxide and fluoride anions with neptunium in the trivalent, tetravalent, pentavalent, and hexavalent oxidation states, using estimates of the actinide–ligand bond distances derived from extended X-ray absorption fine structure measurements of aqueous actinide complexes (Allen *et al.*, 1997, 2000; Moll *et al.*, 1999; Vallet *et al.*, 2001) and effective charges of +2.2 and +3.2 for NpO_2^+ and NpO_2^{2+} cations, respectively. The correlation also holds for more complicated inorganic and organic ligands.

Correlations based on electrostatic considerations are important for understanding actinide–ligand bonding, but other correlations could also be used. Drago and Wayland (1965) used an empirical, four-parameter equation,

$$-\Delta H_{11} = E_A E_B + C_A C_B \tag{23.12}$$

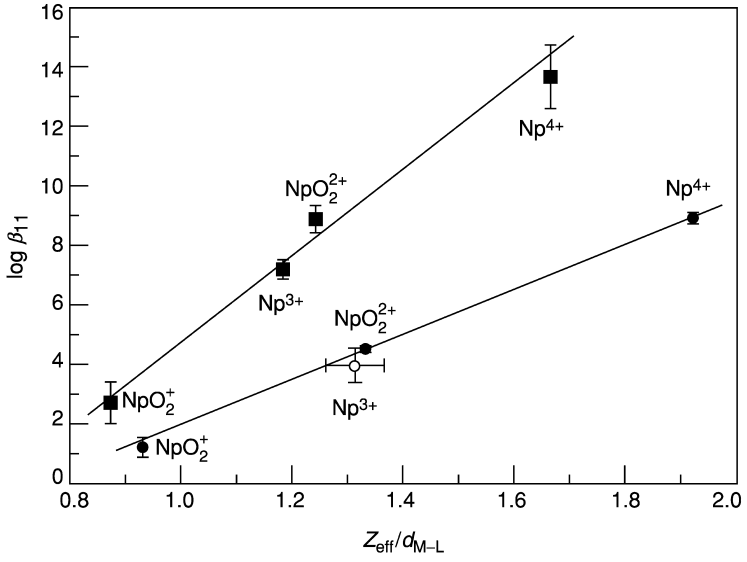

Fig. 23.22 *Dependence of the stability constants of neptunium fluoride* (●) *and neptunium hydroxide* (■) *on the effective ionic potential at* I = 0 M *and* 25°C. *Data from Lemire* et al. (2001) *with the value for* NpF^{2+} (○) *estimated from the* LnF^{2+} *stability constants of Martell* et al. (1998).

to describe the enthalpy of adduct formation between a Lewis acid (the E_A and C_A terms) and a Lewis base (the E_B and C_B terms). E_A and E_B are related to the tendency of an acid and base to form electrostatic bonds and C_A and C_B are related to their tendency to form covalent bonds. The equation was subsequently related to the molecular orbitals of the complexes formed (Marks and Drago, 1975). Hancock and Marsicano (1980) extended this approach to Gibbs energies of complexation using two additional parameters to include the steric constraints of the Lewis acid and base. Stability constants of aqueous Pu(IV) and U(VI) complexes with a number of ligands were estimated in this way (Hancock and Marsicano, 1980; Jarvis *et al.*, 1992; Jarvis and Hancock, 1994). This parameterization also has been used to understand bonding in lanthanide–ligand systems (Choppin and Yao, 1988; Carugo and Castellani, 1992). For a given lanthanide ion, the stability constants with oxygen donor ligands, which form strongly ionic bonds, were found to be well correlated to E_B, the ligand electrostatic parameter. In contrast, the stability constants of the complexes of the softer, nitrogen donor ligands were correlated with the ligand-based covalent parameter, C_B. Ionization potentials and electronegativities have also been used in correlations with the Gibbs energies of complexation of other families of metal ions (Hefter, 1974; Hancock and Martell, 1996).

The success of such correlations, whether based on linear Gibbs energy relationships of stability or protonation constants, on the Born solvation model, or on empirical parameterization is a reflection of the regularity of the solution chemistry of actinide cations and the strongly electrostatic nature of the bonding of their complexes.

23.7 ACTINIDE COMPLEXES

The complexes formed by actinide ions have been the focus of much research because of the importance of separating individual actinide elements from each other or from other elements in the nuclear fuel cycle, and of understanding the environmental chemistry of the actinide elements. A wide variety of experimental methods have been used to identify the stoichiometry or quantify the appropriate equilibrium constants of kinetically labile actinide complexes in solution. The accuracy of these studies depends strongly on the oxidation state purity of the actinide, which can be a problem for less stable oxidation states [e.g. U(III), U(V), Pu(V), Pu(VII), Am(IV), Am(V), or Am(VI)] and when multiple oxidation states can coexist in the same solution as is the case for neptunium and plutonium. The stoichiometry and strength of the actinide complexes with a given ligand are similar within a fairly narrow range for a particular oxidation state due to the predominantly ionic nature of the actinide–ligand bonds and the small differences in cationic radii. The consistent exception to this is Pa(V), which does not exist as an actinyl(V) cation.

23.7.1 Complexes with inorganic ligands

The reactions of actinide ions with halide and pseudohalide anions have been studied extensively. The complexes are, with the exception of the fluoro complexes, moderately weak in aqueous solution. As a consequence, measurements of the complexation constants often require high ligand concentrations (>1 M) and acidic media to allow sufficient amounts of the complexes to form and to avoid interference from hydrolysis reactions. This is most necessary for the tetravalent actinides which can undergo hydrolysis even when pH $\leq$ 1. Many of the halide complexes are sufficiently weak that outer sphere complexes are formed, particularly for the 1:1 (M:L) complexes.

Aqueous fluoro complexes of the actinide ions are known for the trivalent through the hexavalent oxidation states. The fluoride ligand has a much higher affinity for actinide cations than the heavier halides and all actinide fluoro complexes are inner sphere complexes. The neutral fluoro complexes of trivalent and tetravalent actinides, AnF_3 and AnF_4, are insoluble in aqueous solution ($pK_{sp} = 16.4$ for PuF_3 and 26.7 for PuF_4 at $I = 0$ M [Lemire *et al.*, 2001]). In contrast, all of the aqueous actinyl(V) and actinyl(VI) fluoro complexes are soluble. Separation of actinyl species from actinides in the lower oxidation states by fluoride precipitation is an effective method for determining the oxidation state speciation of trace actinides (Kobashi and Choppin, 1988). Cationic complexes formed in the equilibria

$$An^{z+} + qF^- \rightleftarrows AnF_q^{(z-q)+}$$

(An^{z+} = An(III), An(IV), An(V), and An(VI), and $q < z$) have been identified. Anionic complexes of AnO_2^+ and AnO_2^{2+} have also been studied (Ahrland and Kullberg, 1971b; Inoue and Tochiyama, 1985), and pentagonal bipyramidal $UO_2F_5^{3-}$ forms at high fluoride concentrations (Vallet *et al.*, 2002). Stability constants and thermodynamic parameters for the formation of the fluoro complexes of actinides in various oxidation states are summarized in Table 23.18. The stability constants of the 1:1 An:F complexes vary in the order $UO_2^{2+} > NpO_2^{2+} > PuO_2^{2+}$ for hexavalent actinides [see Section 23.4, and Choppin and Rao (1984)], $Th^{4+} < U^{4+} > Np^{4+} \geq Pu^{4+}$ for tetravalent actinides, and $Am^{3+} < Cm^{3+} < Bk^{3+} < Cf^{3+}$ for trivalent actinides (Chaudhuri *et al.*, 1999). Stability constants for the fluoro complexes of the pentavalent actinides have been reported only for protactinium (Guillaumont, 1966; Kolarich *et al.*, 1967) and neptunium (as assessed by Lemire *et al.*, 2001). The reversal in the sequence of the stability constants from the order expected based on the cationic radii of the tetravalent actinides is small, and the expected order is observed for AnF_2^{2+} and AnF_3^+. In each of these oxidation states, the stability of the actinide fluoro complexes is due to the highly favorable entropy contribution while the complexation enthalpies either oppose complex formation or are weakly favorable (Table 23.18). These ΔH and ΔS values reflect the importance of ion dehydration in the formation of inner sphere actinide complexes.

Table 23.18 *Stability constants, and Gibbs energies, enthalpies, and entropies of complexation for the reactions* $An^{z+} + qF^- \rightleftarrows AnF_q^{z-q}$ *and* $AnO_2^{z+} + qF^- \rightleftarrows AnO_2F_q^{z-q}$ *at* 25°C.

Number of F^-	*log* β_{1q}	ΔG ($kJ\,mol^{-1}$)	ΔH ($kJ\,mol^{-1}$)	ΔS ($JK^{-1}\,mol^{-1}$)	*References*
Am^{3+}, $I = 0.1$ M					
1[a]	2.49	−14.2	28	140	Choppin and Unrein (1976)
1	2.59	−14.8	23	126	Nash and Cleveland (1984a)
2	4.75	−27.1	24	170	Nash and Cleveland (1984a)
Th^{4+}, $I = 4$ M					
1	8.17	−46.6	−2.4	149	Ahrland *et al.* (1990)
2	14.57	−83.1	−3.3	120	Ahrland *et al.* (1990)
U^{4+}, $I = 4$ M					
1	9.02	−51.5	−5.6	154	Ahrland *et al.* (1990)
2	15.72	–89.7	−3.5	136	Ahrland *et al.* (1990)
3	21.18	−120.9	0.5	119	Ahrland *et al.* (1990)
Pu^{4+}, $I = 2$ M					
1	7.59	−43.3	5.6	164	Nash and Cleveland (1984b)
NpO_2^+, $I = 1$ M					
1	1.3	−7.4	–	–	Martell *et al.* (1998)
UO_2^{2+}, $I = 1$ M					
1	4.54	−25.9	1.7	92.5	Ahrland and Kullberg (1971c)
2	7.98	−45.5	2.1	160	Ahrland and Kullberg (1971c)
3	10.41	−59.5	2.4	207	Ahrland and Kullberg (1971c)
4	11.89	−67.9	0.3	229	Ahrland and Kullberg (1971c)
5	0.60[b]	–	–	–	Vallet *et al.* (2002)

[a] $I = 1.0$ M.
[b] K_5 for the reaction $UO_2F_4^{2-} + F^- \rightleftarrows UO_2F_5^{3-}$, $I = 1.0$ M, $T = -5$°C.

The actinide complexes of the heavier halides are much weaker than those of the fluoro complexes. They also are quite soluble. To the extent that equilibrium constants are available, the strength of the monohalogeno complexes decreases in the order $Cl^- > Br^- > I^-$ (Grenthe *et al.*, 1992) and they appear to be outer sphere under most circumstances (Section 23.2.6). Data on aqueous bromide complexation is scarce and the reducing power of iodide as well as the weakness of the complexes formed have limited studies of the iodide complexes to U(IV), Np(IV), and Pu(III) species (Vdovenko *et al.*, 1963; Khopkar and Mathur, 1974; Patil *et al.*, 1978). Stability constants for actinide complexation with chloride anions in aqueous solution are available for 1:1 and usually 1:2 species for trivalent (Ac, Pu–Es), tetravalent (Th–Pu), pentavalent (Np), and hexavalent

(U–Pu) actinides (Fuger *et al.*, 1992). For actinyl(VI) cations the complexation enthalpies for formation of the monochloro and dichloro complexes are endothermic in 2 M $HClO_4$ at 25°C ($\Delta H_{11} = +[9.2 \pm 0.5]$ and $\Delta H_{12} = +[18 \pm 1]$ kJ mol^{-1} for UO_2^{2+} and $\Delta H_{11} = +[14 \pm 2]$ kJmol^{-1} for PuO_2^{2+} (Rabideau and Masters, 1961; Awasthi and Sundaresan, 1981)). The values of the corresponding complexation entropies range from +26 to +50 $JK^{-1}mol^{-1}$.

Anionic chloro complexes are often used for separations purposes. Reliable stability constants are not known for these species, but anion exchanging resins or solvent extraction reagents promote the formation of these inner sphere complexes. The trivalent actinides form anionic $AnCl_4^-$ complexes in the resin or organic phase when the concentration of hydrochloric acid exceeds 8 M. Tetravalent uranium, neptunium, and plutonium form anionic chloro complexes with increasing ease, though anionic Th(IV) chloro complexes were reported as being only minor species in 12 M LiCl/0.1 M HCl (Kraus *et al.*, 1956). The actinyl(VI) cations also form anionic chloro complexes that absorb on anion exchange resins. Both the tetravalent and hexavalent actinides absorb as the doubly charged anionic complexes, $AnCl_6^{2-}$ and $AnO_2Cl_4^{2-}$, in 12 M HCl, while $AnCl_5^-$ and $AnO_2Cl_3^-$ are the likely species at lower chloride concentrations (Ryan, 1961; Allen *et al.*, 1997). Although anionic complexes form in the resin phase, in non-aqueous solvents (Marcus and Bomse, 1970) and in the solid state (Brown, 1972), anionic actinide chloro, bromo, and iodo complexes are not present in appreciable amounts in the aqueous phase, except at the highest halide concentrations (Marcus, 1966; Allen *et al.*, 2000). The stability constants for formation of the 1:1 complexes at $I = 1.0$ M are listed in Table 23.19.

The pseudohalides azide (N_3^-)and nitrogen-coordinated thiocyanate (NCS^-) form complexes with actinide cations that are moderately stronger than the equivalent chloro complexes (Table 23.19). The greater stability of the An(III) complexes with these softer ligands (i.e. Cl^-, N_3^-, and NCS^-) relative to that of the Ln(III) complexes has been the basis for group separations of the trivalent 5f elements from the 4f elements (Diamond *et al.*, 1954; Sekine, 1965; Starý, 1966; Musikas *et al.*, 1983; Borkowski *et al.*, 1994). Despite the greater strength of the pseudohalide complexes, spectroscopic measurements indicate that the 1:1 and, probably, the 1:2 An(III):SCN^- complexes are outer sphere complexes (Harmon *et al.*, 1972b). Strong evidence for the aqueous anionic complexes, $An(SCN)_4^-$, $AnO_2(SCN)_3^-$, and $AnO_2(N_3)_3^-$ and $AnO_2(N_3)_4^{2-}$ also have been reported (Ahrland, 1949; Sherif and Awad, 1961; Sekine, 1965; Kinard and Choppin, 1974; Chierice and Neves, 1983).

23.7.2 Complexes with inorganic oxo ligands

Actinides in the common oxidation states form complexes with inorganic oxo ligands. The complexes of the most common of these ligands, H_2O and OH^- are discussed in Sections 23.2 and 23.3, while the complexes of the halate ligands are considered in Section 23.5.

Table 23.19 *Stability of* 1:1 *actinide chloride, azide, and thiocyanate complexes at* I = 1 M *and* 25°C (*Martell* et al., 1998).

An^{z+}	$log\,\beta_{11}$ *chloride*	$log\,\beta_{11}$ *azide*	$log\,\beta_{11}$ *thiocyanate*
Ac^{3+}	−0.10	–	0.05
Pu^{3+}	−0.10	–	0.46
Am^{3+}	−0.1	0.67	0.43
Cm^{3+}	–	0.64	0.44
Bk^{3+}	−0.18[a]	–	0.49
Cf^{3+}	–	0.70	0.53
Es^{3+}	−0.18[a]	–	0.56
Th^{4+}	0.18	–	1.08
U^{4+}	0.40	–	1.49[c]
Pu^{4+}	0.14	–	–
NpO_2^+	−0.35[b]	–	0.32[b]
UO_2^{2+}	−0.10[c]	2.31[d]	0.74

[a] $I = 0.5$ M.
[b] $I = 2.0$ M.
[c] $T = 20$°C.
[d] $I = 0.1$ M.

The stabilities of the actinide complexes with inorganic oxo anions vary in the order $NO_3^- < SO_4^{2-} \ll CO_3^{2-} < PO_4^{3-}$, as expected from the increasing charge and basicity of the ligands. The actinide nitrato complexes are important in the processing of nuclear reactor fuel, especially in separations where the neutral actinide nitrates can be extracted into organic solvents and the anionic, hexanitrato actinide(IV) complexes are used in anion exchange separations. The reported stability constants of the 1:1 $An:NO_3^-$ complexes are slightly larger than those of the analogous chloro complexes, and the anionic nitrato species form more readily than the corresponding chloro complexes. For the actinides, nitrate ions usually act as bidentate chelating ligands with two oxygen atoms from each nitrate coordinated to an actinide.

Sulfate, carbonate, and phosphate complexes can be important in actinide processing, and, along with silicates, are important ligands in determining the environmental behavior of actinide cations. Normally, the stability constants of the complexes with these ligands increase in the usual sequence of $AnO_2^+ < An^{3+} < AnO_2^{2+} < An^{4+}$.

The trivalent actinides have been shown to form 1:1 and 1:2 $An:SO_4^{2-}$ complexes, while the trisulfato complexes also form for the tetravalent and hexavalent actinides. For the weakly complexing actinyl(V) cations, only $NpO_2SO_4^-$ has been reported (Halperin and Oliver, 1983). Stability constants for some actinide–sulfate complexes are summarized in Table 23.20. The thermodynamics of actinide–sulfate complexation are consistent with the formation of inner sphere

Table 23.20 *Stability constants of actinide sulfate complexes at* I = 2 M *and* 25°C (*De Carvalho and Choppin,* 1967*; Ahrland and Kullberg,* 1971*a; Halperin and Oliver,* 1983*; Nash and Cleveland,* 1983*; Martell* et al.*,* 1998) *and carbonate complexes at* I = 0 M *and* 25°C (*Grenthe* et al., 1992; *Silva* et al., 1995; *Lemire* et al., 2001).

	Sulfate (I = 2 M)		*Carbonate* (I = 0 M)		
An^{z+}	$log\,\beta_{11}$	$log\,\beta_{12}$	$log\,\beta_{11}$	$log\,\beta_{12}$	$log\,\beta_{13}$
Ac^{3+}	1.36[a]	2.68[a]			
Pu^{3+}	1.55	2.12			
Am^{3+}	1.43	1.85	7.8	12.3	15.2
Th^{4+}	3.25	5.53			
U^{4+}	3.48	5.82			
Np^{4+}	3.49	6.06			
Pu^{4+}	3.80	6.6			
UO_2^{+}					7.4
NpO_2^{+}	0.19		4.96	6.53	5.50
PuO_2^{+}					5.1
UO_2^{2+}	1.81[a]	2.76[a]	9.68	16.94	21.60
NpO_2^{2+}			9.3	16.5	19.37
PuO_2^{2+}			11.6	14.5	17.7

[a] $I = 1$ M.

Table 23.21 *Thermodynamic parameters for actinide sulfate complexation in* 2 M *perchlorate media at* 25°C (*Sullivan and Hindman*, 1954; *Zielen*, 1959; *Jones and Choppin*, 1969; *Ahrland and Kullberg*, 1971*a*; *Halperin and Oliver*, 1983).

Actinide ion	ΔG_{11} ($kJ\,mol^{-1}$)	ΔH_{11} ($kJ\,mol^{-1}$)	ΔS_{11} ($J\,K^{-1}\,mol^{-1}$)	ΔG_{12} ($kJ\,mol^{-1}$)	ΔH_{12} ($kJ\,mol^{-1}$)	ΔS_{12} ($J\,K^{-1}\,mol^{-1}$)
Am^{3+}	−8.4	18.4	90	–	–	–
Cm^{3+}	−7.5	17.2	83	–	–	–
Cf^{3+}	−7.9	18.8	90	–	–	–
Th^{4+}	−18.8	20.9	133	−32.6	40.4	245
Np^{4+}	−20.0	18.3	128	–	–	–
NpO_2^{+}	−1.1	19	66	–	–	–
UO_2^{2+}[a]	−10.3	18.2	96	−15.7	35.1	171

[a] $I = 1$ M $NaClO_4$.

complexes. The endothermic enthalpies of complexation vary little between actinides in different oxidation states and the strength of a particular actinide–sulfate complex relative to that of other actinide–sulfate species is determined mainly by the complexation entropies (Table 23.21). Sulfate complexes of uranyl(VI) can form polynuclear, ternary hydroxo-sulfato complexes in weakly acidic solutions (Grenthe and Lagerman, 1993; Moll *et al.*, 2000).

Carbonate complexes of the actinides have been investigated often, as reviewed by Newton and Sullivan (1985) and Clark *et al.* (1995). Although the solubility of neutral $AnO_2(CO_3)$ is low, the triscarbonato uranyl(VI) complex, $UO_2(CO_3)_3^{4-}$, is responsible for the relatively high concentration of uranium in seawater (Spence, 1968). The complexes $NpO_2(CO_3)_3^{4-}$ and $PuO_2(CO_3)_3^{4-}$ are less important in the environment because the stability constants of the actinyl (VI) triscarbonato complexes decrease by four orders of magnitude from UO_2^{2+} to PuO_2^{2+} as the effective charge on the actinide decreases (Table 23.20). Similar to nitrate, the carbonate ligands are bidentate, binding in the equatorial plane of the actinyl cations, forming triscarbonato actinyl complexes with hexagonal bipyramidal geometry. Carbonate complexes also are among the few soluble complexes of uranyl(V), plutonyl(V), and americyl(V) that have been quantitatively studied (Bennet *et al.*, 1992; Giffaut and Vitorge, 1993; Docrat *et al.*, 1999). The stabilities of the triscarbonato actinyl(V) complexes are roughly 13 orders of magnitude smaller than the corresponding actinyl(VI) complexes (Lemire *et al.*, 2001). Nevertheless, carbonate ligands stabilize actinyl(V) ions, especially in the solid state (Keenan and Kruse, 1964; Madic *et al.*, 1983a). Few measured stability constants for $An(IV)-CO_3^{2-}$ complexes have been reported, but those of the limiting solution species, $An(CO_3)_5^{6-}$ (Clark *et al.*, 1998), are large, exceeding 10^{35} M^{-5}. Well-characterized polynuclear complexes of the actinyl(VI) cations with bridging and terminal carbonate ligands have an $AnO_2^{2+}:CO_3^{2-}$ stoichiometry of 3:6 (Åberg *et al.*, 1983b; Allen *et al.*, 1995). Carbonate complexes of Np(VII) also have been proposed (Shilov *et al.*, 1976).

The actinide complexes of highly charged inorganic ligands, such as phosphates, arsenates, or silicates, can precipitate in a variety of different solid phases. Soluble, protonated complexes of these ligands, for example $AnO_2(HPO_4)_n^{2-2n}$, have lower stability constants than complexes of the fully deprotonated ligands because of the reduced charge of the protonated ligand. The actinyl(V) and actinyl(VI) cations form soluble 1:1 complexes with PO_4^{3-} that are strong enough to compete with carbonate complexation (Sandino and Bruno, 1992; Brendler *et al.*, 1996; Morgenstern and Kim, 1996).

Singly deprotonated orthosilicic acid, $H_3SiO_4^-$, forms complexes with trivalent and hexavalent actinides in solutions that are weakly acidic to neutral (Yusov and Fedoseev, 2003 and references therein), and the stability constants of the orthosilicate complexes are proportional to the hydrolysis constants of the metal cations (Jensen and Choppin, 1998).

Multicharged, complex inorganic oxides, such as polyphosphates, polymeric silicates, and polyoxometallates, with properties intermediate between those of simple ligands and of oxide or mineral surfaces also form complexes with actinide cations. Stability in acidic solution and the ability to create soluble, well-defined structures with extensive redox activity make the actinide polyoxometallates interesting complexes (Yusov and Shilov, 1999). The rich chemistry of polyoxometallates results in the complexation and stabilization of

transplutonium actinides in oxidation states usually not stable in aqueous solutions, for example Am(IV), Cm(IV), and Cf(IV) (Kosyakov *et al.*, 1977). Many common polyoxometallate anions, such as $SiW_{12}O_{40}^{4-}$, $P_2W_{18}O_{62}^{6-}$, $Nb_6O_{19}^{8-}$, and $NaP_5W_{30}O_{110}^{14-}$, form complexes with actinide cations, and both 1:1 and 1:2 complexes have been identified. The stability constants for the Th^{4+} complexes of $SiW_{12}O_{40}^{4-}$ are $\log \beta_{11} = 11.3$ and $\log \beta_{12} = 17.8$, and are characterized by large positive complexation entropies, $\Delta S_{11} = 232\ JK^{-1}mol^{-1}$ and $\Delta S_{12} = 356\ JK^{-1}mol^{-1}$ (Choppin and Wall, 2003). The binding sites on the surfaces of some polyoxometallate ligands can accommodate the steric requirements of the actinyl cations as well as the simple actinide cations (Gaunt *et al.*, 2002). Certain polyoxometallates, like the Preyssler anion $P_5W_{30}O_{110}^{15-}$, also can encapsulate actinide cations internally, forming inert, but soluble, compounds (Creaser *et al.*, 1993; Antonio *et al.*, 1998).

23.7.3 Complexes with organic ligands

The variety and strength of organic ligands that form complexes with actinide ions in aqueous solution are limited by the preference of the actinides for hard donor ligands and by the tendency of actinide cations toward hydrolysis. Consequently, ligands that bind actinide cations in aqueous solution usually contain some hard base, oxygen donor sites because the strength and basicity of organic ligands containing only softer donor groups, generally, are insufficient to suppress the precipitation of actinide hydroxides. In organic solvents, where actinide hydrolysis is not important, organic ligands with softer donors such as dithiophosphinic acids (Pinkerton *et al.*, 1984; Jensen and Bond, 2002), thiacrown ethers (Karmazin *et al.*, 2002), ethylenediamine (Cassol *et al.*, 1990), or tripyrazine (Drew *et al.*, 2000) form actinide complexes that are stable, although weaker than complexes of similar oxygen donor ligands.

The most commonly studied actinide–organic ligand complexes involve ligands bearing carboxylic acid groups. Actinide complexes with simple monocarboxylate ligands (i.e. those that contain no other actinide-binding groups) are not among the stronger actinide complexes (Table 23.22). Compared to common inorganic ligands, the actinide complexes of simple monocarboxylates are somewhat stronger than the equivalent SO_4^{2-} complexes, but weaker than the OH^- or CO_3^{2-} complexes. For acetic acid, the stability constants of the first and second acetate complexes, β_{11} and β_{12}, follow the expected order of effective cation charge and ionic radii for actinides in the different oxidation states. However, the 1:3 acetate complexes of the actinyl(VI) ions are stronger than expected from the stability constants of the An(III) and An(IV) complexes. The thermodynamics of actinide–monocarboxylate complexation are, like those of the simple inorganic ligands, entropy driven, with weakly positive or negative complexation enthalpies. Monocarboxylates with low pK_a values (e.g. dichloroacetate [$pK_a = 1.1$] and trichloroacetate [$pK_a = -0.5$]), form outer sphere complexes with the actinides (Section 23.5).

Table 23.22 *Stability constants of actinide carboxylate and phosphonate complexes in perchlorate media at* 25°C.

		I (M)	$log\,\beta_{11}$	$log\,\beta_{12}$	$log\,\beta_{13}$	$log\,\beta_{14}$	*References*
Acetate (ac^-) $CH_3CO_2^-$	Pu^{3+}	2[a]	2.02	3.34	–	–	Magon *et al.* (1968)
	Am^{3+}	0.5[a]	1.99	3.28	–	–	Grenthe (1962)
	Cm^{3+}	0.5[a]	2.06	3.09	–	–	Grenthe (1963)
	Th^{4+}	1	3.86	6.97	8.94	10.28[d]	Portanova *et al.* (1975)
	NpO_2^+	2	0.87	–	–	–	Rizkalla *et al.* (1990b)
	UO_2^{2+}	1	2.42	4.41	6.40	–	Ahrland and Kullberg (1971a)
	NpO_2^{2+}	1[a]	2.31	4.23	6.0	–	Portanova *et al.* (1970)
glycolate $HOCH_2CO_2^-$	Am^{3+}	0.5[a]	2.82	4.86	6.3	–	Grenthe (1962)
	Cm^{3+}	0.5[a]	2.85	4.75	–	–	Grenthe (1963)
	Bk^{3+}	2	2.65	4.69	–	–	Choppin and Degischer (1972)
	Th^{4+}	1	4.11	7.45	10.1	12.0[e]	Di Bernardo *et al.* (1978)
	NpO_2^+	2	1.43	1.90	–	–	Rizkalla *et al.* (1990b)
	UO_2^{2+}	1	2.35	3.97	5.17	–	Di Bernardo *et al.* (1976)
	NpO_2^{2+}	1[a]	2.37	3.95	5.00	–	Portanova *et al.* (1972)
	PuO_2^{2+}	0.1	2.43	3.79	–	–	Eberle and Schaefer (1968)
oxalate $(CO_2)_2^{2-}$	No^{2+}	0.5[b]	1.68		–	–	McDowell *et al.* (1976)
	Am^{3+}	1	4.63	8.35	11.15	–	Sekine (1964)
	Th^{4+}	1	8.23	16.77	22.77	–	Moskvin and Essen (1967)
	Np^{4+}	1	8.19	16.21	–	–	Bansal and Sharma (1964)
	NpO_2^+	1	3.71	6.12	–	–	Tochiyama *et al.* (1992)
	UO_2^{2+}	1[a]	5.99	10.64	11.0	–	Havel (1969)
malonate $CH_2(CO_2)_2^{2-}$	Th^{4+}	1	7.47	12.79	16.3	–	Di Bernardo *et al.* (1977)
	NpO_2^+	1	2.63	4.28	–	–	Jensen and Nash (2001)

Table 23.22 (*Contd.*)

		I (M)	$log\beta_{11}$	$log\beta_{12}$	$log\beta_{13}$	$log\beta_{14}$	*References*
	UO_2^{2+}	1	5.42	9.48	–	–	Di Bernardo *et al.* (1977)
succinate $(CH_2CO_2)_2^{2-}$	Th^{4+}	1	6.44	–	–	–	Di Bernardo *et al.* (1983)
	NpO_2^+	1[c]	1.51	2.14	–	–	Stout *et al.* (1989)
	UO_2^{2+}	1	3.85	–	–	–	Bismondo *et al.* (1981)
diglycolate $O(CH_2CO_2)_2^{2-}$	Th^{4+}	1	8.15	14.8	18.2	–	Di Bernardo *et al.* (1983)
	NpO_2^+	1	3.79	–	–	–	Jensen and Nash (2001)
	UO_2^{2+}	1	5.11	7.54	–	–	Di Bernardo *et al.* (1980)
	NpO_2^{2+}	1[a]	5.16	–	–	–	Cassol *et al.* (1973)
	PuO_2^{2+}	1[a]	4.97	–	–	–	Cassol *et al.* (1973)
phosphonoacetate $O_2CCH_2PO_3H^{2-}$	Th^{4+}	2	8.50	16.05			Nash (1991a)
	UO_2^{2+}	0.1	7.57	14.17			Nash (1993b)
methane-1,1-diphosphonate $CH_2(PO_3H)_2^{2-}$	Th^{4+}	2	8.34	15.44			Nash (1991a)
	UO_2^{2+}	0.1	7.82	13.82			Nash (1993b)
ethane-1,2-diphosphonate $(CH_2PO_3H)_2^{2-}$	UO_2^{2+}	0.1	5.34	8.31			Nash (1993b)

[a] 20°C.
[b] 0.5 M NH_4NO_3, no temperature given.
[c] 23°C.
[d] $\log \beta_{15} = 11.00$.
[e] $\log \beta_{15} = 13.4$.

Multifunctional ligands such as polycarboxylates, hydroxycarboxylates, and aminocarboxylates tend to form stronger actinide complexes than simple monocarboxylates due to the formation of chelate rings through coordination of multiple functional groups. This occurs because the affinity of carboxylate (or phosphonate) groups for actinide ions, and their very favorable complexation entropies, provide an anchor for the complexation of amines, ether oxygens, or other less effective donor atoms within the same ligand. For instance, simple

alcohols are not good ligands for actinides in aqueous solution. However, the stability constants of the 1:1 An:L complexes of α-hydroxycarboxylates like glycolate (Table 23.22) and α-hydroxyisobutyrate are stronger than that of acetate because of chelation via the α-hydroxy group (Ahrland, 1986; Stumpf *et al.*, 2002; Toraishi *et al.*, 2002), even though the pK_a values of the carboxylic group would indicate that they are less basic ligands.

Multifunctional ligands also form polynuclear complexes by bridging actinide ions, though this behavior is not unique to actinide cations. In some cases, for example $(UO_2)_2$(edta), $(UO)_2(\text{citrate})_2^{2-}$, or $Th_4(\text{glycolate})_n$ ($n = 8 \pm 1$) (Kozlov and Krot, 1960; Rajan and Martell, 1965; Fraústo da Silva and Simoes, 1968; Toraishi *et al.*, 2002), the polynuclear complexes are well defined and soluble, making measurement of the formation constants of the polynuclear species possible. The likelihood of polynuclear complex formation is usually favored by increasing metal concentrations and decreasing ligand:metal ratios. As the size of the polynuclear complexes increase, their precipitation becomes more likely.

Ethylenediaminetetraacetic acid (H_4edta) and the related multifunctional polyaminocarboxylate ligands are strong, but not very selective, complexants for An(III) and An(IV) cations. Steric constraints make them much poorer ligands for actinyl(V) and actinyl(VI) cations as discussed in Section 23.6. This has led to the use of polyaminocarboxylates as masking agents for interfering An(III) or An(IV) cations in the chemical analysis of actinyl ions. When fully coordinated, the most commonly used polyaminocarboxylate ligands, hexadentate edta^{4-} and dcta^{4-}, and octadentate dtpa^{5-} only partially envelope actinide cations, leaving one or more coordination sites for water molecules (Carey and Martell, 1968; Fried and Martell, 1971; Kimura and Choppin, 1994), or for other small ligands (Pachauri and Tandon, 1975). The strongest polyaminocarboxylate ligands complex An(III) and An(IV) cations over a wide range of acidities (Fig. 23.23). In moderately acidic media (pH 1–3), protonated actinide–polyaminocarboxylate complexes, for example An(Hedta), form. As the pH is increased, fully deprotonated complexes, such as An(edta)$^-$ form first, followed by the formation of ternary actinide–hydroxy-polyaminocarboxylate complexes, such as An(OH)(edta)$^{2-}$, in basic solutions. Increasing the hydroxide concentration further will eventually displace the organic ligand, but for strong polyaminocarboxylate ligands like edta^{4-} this occurs only in the most caustic solutions (>1 M NaOH) (Wang *et al.*, 2003).

Table 23.23 shows that the strength of actinide-polyaminocarboxylate complexes is principally due to large, positive complexation entropies, in common with other inner sphere actinide complexes. However, in contrast to the actinide complexes of inorganic or carboxylate ligands, most actinide–polyaminocarboxylate complexes are strengthened by substantially exothermic complexation enthalpies, which are commonly observed in metal–amine complexation.

Organophosphorus ligands with low water solubility are used widely in organic solvents for chemical separation or purification of the actinides by

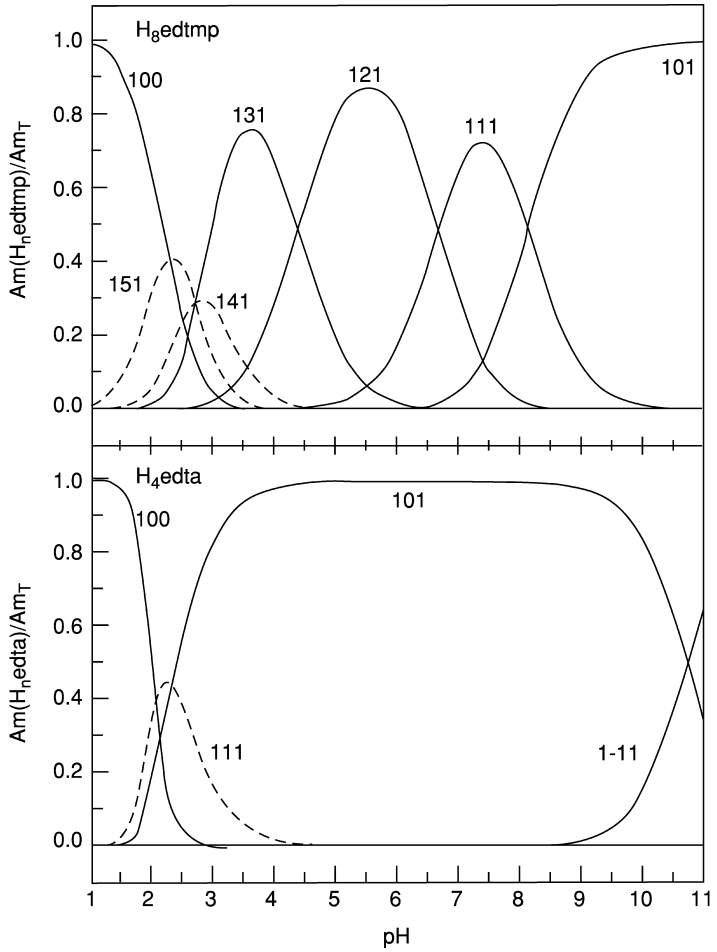

Fig. 23.23 *Speciation of Am(III) complexes of ethylenediaminetetraacetic acid (H_4edta) and ethylenediaminetetra(methylenephosphonic) acid (H_8edtmp) identified by the An:H:L stoichiometry as a function of pH for* 1×10^{-6} M *Am and* 1.2×10^{-4} M *ligand at* $I = 0.1$ M *and* 25°C. *Stability constants from Shalinets* (1972*a,b*).

solvent extraction. Water-soluble organophosphorus ligands based on phosphoric and phosphonic acids, $ROPO_3H_2$ and RPO_3H_2, are also important actinide complexants in nature (Panak *et al.*, 2002a,b) and in chemical separations (see Chapter 24). Compared to carboxylic acids, the phosphonic acids usually form f-element complexes with Gibbs energies of complexation that are larger than expected from the ligand basicity (Nash, 1993b), even when the ligands are partially protonated (e.g. RPO_3H^-) as illustrated in Table 23.22. The methane-1,1-diphosphonic acids, $RCH(PO_3H_2)_2$, analogs of malonic acid,

Table 23.23 *Thermodynamic parameters for actinide acetate and aminopolycarboxylate complexation at* 25°C.

		I (M)	ΔG_{11} (kJ mol^{-1})	ΔH_{11} (kJ mol^{-1})	ΔS_{11} (J K^{-1} mol^{-1})	*References*
ac^-	Am^{3+}	2	−11.2	6.8	60	Rizkalla *et al.* (1989)
	Cm^{3+}	2	−11.7	6.0	57	Choppin *et al.* (1985)
	Th^{4+}	1	−22.0	11.3	112	Portanova *et al.* (1975)
	UO_2^{2+}	1	−13.8	10.5	82	Ahrland and Kullberg (1971a)
ida^{2-}	Am^{3+}	0.5	−44.9	−4.6	136	Rizkalla *et al.* (1989)
	Th^{4+}	1	−55.3	6.5	207	Di Bernardo *et al.* (1983)
	NpO_2^+	0.5	−33.2	−16.4	56	Choppin *et al.* (1992a)
		1	−33.6	−16.0	59	Jensen and Nash (2001)
	UO_2^{2+}	1	−50.1	−2.2	161	Di Bernardo *et al.* (1980)
$edta^{4-}$	Pu^{3+}	0.1	−103.1	−17.7	287	Fuger and Cunningham (1965)
	Am^{3+}	0.1	−103.7	−19.5	282	Fuger and Cunningham (1965)
		0.5	−95.7	−23.9	241	Rizkalla *et al.* (1989)
	Cm^{3+}	0.5	−96.2	−29.3	225	Choppin *et al.* (1985)
	Th^{4+}	0.1	−132.5	−12.1	404	Kinard *et al.* (1989)
$dcta^{4-}$	Am^{3+}	0.5	−103.9	−10.8	312	Rizkalla *et al.* (1989)
	Cm^{3+}	0.5	−103.3	−9.7	314	Choppin *et al.* (1987)
$dtpa^{5-}$	Am^{3+}	0.5	−120.6	−39.5	272	Rizkalla *et al.* (1989)
	Th^{4+}	0.1	−163.8	−12	510	Kinard *et al.* (1989)

$CH_2(CO_2H)_2$, form quite strong complexes. Partially protonated complexes are believed to be a key factor in the strength of these diphosphonate complexes, stabilizing the 1:2 actinide:phosphonate complexes through inter-ligand, intra-complex hydrogen bonding (Nash *et al.*, 1995). The larger anionic charge of the fully deprotonated phosphonic acids, the presence of inter-ligand hydrogen bonding, and the enhanced dehydration of the metal cations on complexation (Jensen *et al.*, 2000b), contribute to the stability of actinide–diphosphonate complexes, as does the strength of the An–O=P bond. Complexation of An(IV) cations by neutral, fully protonated methanediphosphonic acid, $CH_2(PO_3H_2)_2$, persist in 2 M nitric acid at ligand concentrations as low as 0.05 M (Nash, 1991b).

Since monophosphonate and diphosphonate ligands form complexes with actinide ions more readily than the corresponding carboxylates, methylenephosphonic acid derivatives of H_4edta might be expected to be extremely powerful complexants. However, replacing the four acetic acid groups of H_4edta with

methylenephosphonic acid groups (H_8edtmp) yields slightly weaker An(III) complexes (Fig. 23.23), although the stability constants indicate that a range of $AnH_n edtmp^{n-5}$ complexes exist in 1 M NaOH for a concentration of 1×10^{-4} M edtmp (Shalinets, 1972b). Inter-ligand hydrogen bonding between the amines and the phosphonates (Jensen *et al.*, 2000b) and steric constraints (Shalinets, 1972c) apparently resist the formation of complexes in these aminomethylenephosphonates.

Anionic carboxylate and organophosphorus-based ligands are among the most studied organic actinide complexants in aqueous solution, but the actinide complexes of a variety of other organic ligands also have been studied. Stable actinide complexes form in weakly acidic aqueous solution (pH 3–6) with neutral ligands like tpen (Fig. 23.18), or polyamino(2-hydroxyalkyl) ligands (Jarvis *et al.*, 1992; Jarvis and Hancock, 1994; Jensen *et al.*, 2000a). The pK_a values of these neutral ligands are low enough that An(III), An(IV), or An(VI) cations can effectively compete with protons for the ligand binding sites in acidic solutions. However, the hydroxide concentration in nearly neutral solutions is sufficient to displace these neutral organic ligands and precipitate actinide hydroxides.

Competition of protons for the actinide binding sites is not a hindrance to the binding of crown ether ligands (e.g. 15-crown-5 or 18-crown-6, Fig. 23.18). Yet without chelating by other complexing groups such as carboxylic acids incorporated into the crown ether, these ligands are weak actinide complexants in aqueous solution (Brighli *et al.*, 1985), most likely forming outer sphere complexes (Guilbaud and Wipff, 1993b). In contrast, even the simplest phenol-based calix[5]- and calix[6]-arene macrocyclic ligands (Fig. 23.18) form strong actinyl(VI) complexes ($\log\beta_{11} = 19$ for UO_2^{2+} at 25°C, $I = 0.1$ M) with a selectivity ratio for UO_2^{2+} over divalent transition metal cations that exceeds 10^{10} (Shinkai *et al.*, 1987).

Naturally occurring ligands that efficiently bind metal cations are found throughout the biosphere. Hard transition metal cations are vital for many biological processes and there are many natural ligands that regulate their biochemistry. The actinides are also hard cations and the charge to radius ratio of the tetravalent actinides is similar to that of one of the most biologically important metal ions, Fe(III). Consequently, ligands that efficiently bind iron are expected to be efficient ligands for actinides. Desferrioxamine siderophores, a class of polyhydroxamic acid ligands used by microbes to scavenge and transport Fe(III), have proven to be equally efficient ligands for Pu(IV) (Jarvis and Hancock, 1991). X-ray crystallography of the Pu(IV) complex of desferrioxamine E shows that the Pu is nine-coordinated with three water molecules and six desferrioxamine oxygens in the inner coordination sphere (Neu *et al.*, 2000). Interestingly, the ligand is only slightly deformed when it complexes Pu(IV) rather than Fe(III), despite the 0.08 Å difference in ionic radii (CN = 6).

The complexing strength of naturally occurring hydroxamic and catechol (1,2-dihydroxybenzene) groups that siderophores use to sequester Fe(III) have

led to the design of catecholamide and hydroxypyridone ligands that strongly complex An(III) and An(IV) cations (Raymond, 1985). These ligands are highly selective for An(IV) over Fe(III) both *in vitro* (Romanovski *et al.*, 1999; Zhao *et al.*, 1999) and *in vivo* (Stradling *et al.*, 1992; Xu *et al.*, 1995), and are more efficient reagents for Pu decontamination than the polyaminocarboxylate, diethylenetriaminepentaacetate ($dtpa^{5-}$).

Humic and fulvic acids are naturally occurring polyelectrolytes resulting from the decay of natural matter. Their composition varies with the local geology, hydrology, and biology, resulting in fulvic acids with molecular weights as low as 300 and humic acids with molecular weights in excess of 100 000 (Choppin and Allard, 1985). These materials contain alcoholic, phenolic, and carboxylic acid groups, which result in an affinity for metal ion complexation. Actinide ions may interact with these ligands either through binding in specific sites (Marinsky, 1976) or through a generalized 'territorial' binding where the cation is attracted by multiple functional groups within one area of the ligand (Manning, 1979). Different modeling approaches have been proposed to calculate the stability constants for metal ions bound by these ligands (Choppin and Labonne-Wall, 1997). Stability constants of certain humic and fulvic acid complexes have been reported for the most common actinides (Choppin and Allard, 1985; Kim and Sekine, 1991; Moulin *et al.*, 1992; Kim *et al.*, 1993; Marquardt and Kim, 1998). In addition to complexation of actinide cations, humic and fulvic acids can also be redox active, reducing the hexavalent NpO_2^{2+} and PuO_2^{2+} (Dahlman *et al.*, 1976; Choppin, 1988; Jainxin *et al.*, 1993; Yaozhong *et al.*, 1993), and pentavalent PuO_2^{+} (André and Choppin, 2000) and NpO_2^{+} (Marquardt *et al.*, 1996). Both their redox and complexation properties can lead to significant effects on actinide behavior in environmental systems.

23.8 TERNARY COMPLEXES

In aqueous solution, most actinide–ligand complexes could be considered ternary complexes, as they have three components, an actinide ion (component 1), one or more ligands (component 2) and some number of inner sphere water molecules (component 3). It is common, however, to consider such metal cation + ligand anion + coordinated water complexes as a binary metal–ligand complexes. Therefore, our discussion of ternary (or mixed) complexes is limited to three-component complexes, such as AnX_qY_p or $AnO_2X_qY_p$, where X and Y are different ligands but not H_2O. Such ternary complexes may also have coordinated water molecules and varying degrees of protonation of the ligands. Bimetallic complexes, $An_nM_mX_q$ also are considered ternary complexes, but solution studies on such bimetallic complexes of actinide cations are rare (Stemmler *et al.*, 1996; Dodge and Francis, 1997). Despite the large literature on actinide–ligand complexation and the large number of possible complexes of

actinide ions in their various oxidation states, with two different ligands, the number of detailed experimental studies on ternary actinide complexation is limited.

The combination of the low polarity and hydrophobicity of organic solvents often results in the formation of ternary complexes in these solvents. As a consequence, the best documented and most extensively studied actinide ternary complexes are those present in the organic phases of liquid–liquid (solvent) extraction systems, which are described in detail in Chapter 24. In organic solvents, the ternary actinide complexes often form with neutral organophilic ligands, required to provide solubility, and anions, required to balance the positive charge of the actinide cations, in the inner coordination sphere. However, complexes containing different anions and no neutral ligands are also well known in such solvents (Ferraro and Peppard, 1963).

Ternary complexes of actinide salts have been important in actinide separations for more than a century, since the initial use of the extraction of $UO_2(NO_3)_2(Et_2O)_2$ into diethylether to purify uranium (Péligot, 1842). Industrial scale processing of the tetravalent and hexavalent actinides was built on this foundation, substituting methylisobutylketone, dibutylcarbitol (dibutoxydiethylene glycol), or tri(*n*-butyl)phosphate (and similar organophosphate-based ligands) for diethylether. The tri(*n*-butyl)phosphate (TBP) systems are particularly important since they have been adopted internationally for processing nuclear fuel in the PUREX process (Choppin *et al*., 2002). When actinides are extracted from nitric acid solutions into organic solutions containing TBP, the complexes $AnO_2(NO_3)_2(TBP)_2$ are formed in the organic phase for the hexavalent actinides, while the tetravalent actinides have the form $An(NO_3)_4(TBP)_p$ ($p = 2$ or 3). The nitrate groups are directly coordinated to the central actinide cation as bidentate ligands.

Given the propensity of the actinides to undergo hydrolysis reactions (Section 23.3), the single largest class of ternary complexes in aqueous solution are the mixed hydroxides, $An(OH)_qL_p$, which are readily encountered even in weakly acidic solutions for some species. This class of complexes was first reported almost 50 years ago (Hök-Bernström, 1956). The most extensively studied ternary actinide complexes remain the hydroxycarbonates, $An(OH)_q(CO_3)_p$ and $AnO_2(OH)_q(CO_3)_p$. The structural features and the formation constants of An^{3+}, An^{4+}, AnO_2^+, and AnO_2^{2+} hydroxycarbonates have been reported (Clark *et al*., 1995). The hydroxycarbonates of the pentavalent and hexavalent actinyl ions (Neck *et al*., 1997; Szabó *et al*., 2000) exhibit some solubility. In contrast, the neutral hydroxycarbonates, $An(OH)(CO_3)$, are the solubility-limiting species in near neutral aqueous solutions in equilibrium with atmospheric carbon dioxide when other ligands are absent (Bernkopf and Kim, 1984; Silva and Nitsche, 1984; Standifer and Nitsche, 1988; Felmy *et al*., 1990). Neutral 1:1:1 $An(OH)(CO_3)$ species do not exist in significant amounts in the solution phase (Felmy *et al*., 1990; Meinrath and Kim, 1991). Simple, mononuclear hydroxycarbonate complexes, as well as polynuclear species with average

stoichiometries of $Th_{16}(OH)_{20}(CO_3)_{16}^{12+}$ and $Th_8(OH)_{20}(CO_3)_2^{8+}$ have been reported at low metal concentrations (Grenthe and Lagerman, 1991).

Ternary U(VI)–fluoride–carboxylate ligand complexes have been used for systematic studies of the rates and mechanisms of intermolecular and intramolecular exchange reactions. Multinuclear NMR and potentiometric investigations of the complexes revealed a variety of stoichiometries and structures that depend on the nature of the carboxylic acid (Smith, 1959; Szabó *et al.*, 1997; Aas *et al.*, 1998; Szabó and Grenthe, 2000; Szabó, 2002). The presence of two types of ligands ($X = F^-$, $Y = RCOO^-$) and a variety of coordination geometries usually gave rise to a number of different ternary complexes that were simultaneously present in the solutions. In the presence of carbonate or glycolate ligands, the formation of dinuclear ternary complexes, $(UO_2)_2F_q(gly)_p^{4-q-p}$ and $(UO_2)_2F_q(CO_3)_p^{4-q-2p}$, was reported. Although a variety of species were present in the solutions studied, the rate constants and the activation parameters for fluoride exchange were not strongly dependent on the identity of the carboxylate ligand, even for chelating ligands containing other coordinating groups (e.g. picolinic acid, glycine, and *N*-(phosphonomethyl) glycine). Coordination of negatively charged carboxylate ligands (Y^{z-}) has little effect on the equilibrium constants for fluoride complexation by $UO_2Y_q^{2-qz}$ in contrast to fluoride complexation by $UO_2(H_2O)_q^{2+}$ (Aas *et al.*, 1998).

The small amount of quantitative information regarding ternary complexes in aqueous solution limits attempts to model the chemical speciation of actinides in chemical systems when many different ligands are present. Nevertheless, the regularity of electrostatic bonding in actinide complexes (Section 23.4) makes estimation of the formation constants possible, allowing evaluation of the possible importance of a hypothesized species to determine if additional experimental work would be justified. The thermodynamic parameters for the formation of simple 1:1:1 An(X)(Y) ternary complexes often can be estimated from the parameters of the binary AnX and AnY complexes (Grenthe and Puigdomenech, 1997); however, the uncertainty in an estimated formation constant for these complexes can approach an order of magnitude. The most accurate estimated equilibrium constants for the formation of ternary complexes should include corrections for the appropriate change in the effective charge of the actinide caused by the complexation of the first ligand and for the decrease in the number of available coordination sites, which is an entropic (statistical) factor.

23.9 CATION–CATION COMPLEXES

Most studies of actinide complexation have involved interaction of actinide cations with neutral or anionic ligands as nearly all of the known complexes are with such ligands. However, the cationic, *trans*-dioxoactinide(v) (i.e. actinyl(v)),

species form weak complexes with polyvalent metal cations in non-complexing, acidic solutions, as first observed for the complexes of NpO_2^+ with UO_2^{2+} (Sullivan *et al*., 1961). Cation–cation complexes of UO_2^+ (Newton and Baker, 1962), PuO_2^+ (Newton and Burkhart, 1971), and AmO_2^+ (Rykov and Frolov, 1975) with various cations have also been reported. Actinyl(v) cations are not the only dioxocation species that form cation–cation complexes. A complex of pentavalent *cis*-dioxovanadium(v), VO_2^+, with oxovanadium(IV), VO^{2+}, also has been reported (Madic *et al*., 1983b).The formation of cation–cation complexes is not an inherent property of all actinyl ions. The presence of a pentavalent actinyl(v) cation is required to form cation–cation complexes. The actinyl(VI) cations, which have the same structure as the actinyl(v) cations, form cation–cation complexes only with an actinyl(v) cation.

The nature of the species formed in cation–cation complexes has been a focus of investigation since their discovery. Three different models have been proposed. In one model, cation–cation complexes were treated as products of incomplete redox reactions accompanied by the formation of electron–hole pairs in the solvent (Rykov and Frolov, 1972a, 1974). However, this model postulated the formation of solvated electrons, which are not observed in the EPR spectrum of the Np(v)−U(VI) complex (Madic *et al*., 1979). Another model proposed that the cation–cation complexes are polynuclear, ligand-bridged complexes (Guillaume *et al*., 1982; Nagasaki *et al*., 1992) by analogy with oligomeric AnO_2^{2+} hydroxides such as $(UO_2)_2(OH)_2$. However, cation–cation complexes are stable in acidic solutions (2 M $HClO_4$), and it is not apparent why water molecules or perchlorate anions would be effective bridging ligands for polynuclear species requiring participation of AnO_2^+ cations, as these cations generally form comparatively weak complexes with normal ligands.

In the model most used, the cation–cation complexes are the result of bonding between AnO_2^+ cations either as inner sphere (Sullivan, 1962) or outer sphere complexes (Stout *et al*., 1993). Although the actinyl(v) cations possess a formal +1 charge, the effective charge of the actinide atom is approximately +2.2 (Choppin and Rao, 1984). This observation implies that each of the -yl oxygen atoms has a residual negative charge of ca. –0.6 that allows them to form moderately weak electrostatic bonds with other cations (Vodovatov *et al*., 1979). Relativistic spin–orbit configuration interaction calculations on NpO_2^+ resulted in a value for the residual negative charge of −0.48 on each of the neptunyl(v) oxygens while the calculated residual charge on the oxygen atoms of neptunyl(VI) was −0.17 (Matsika and Pitzer, 2000). If the residual negative charge on the oxygen atoms of actinyl(VI) cations is indeed so much smaller than it is for the actinyl(v) cations, the formation of cation–cation complexes by actinyl(v) ions but not by actinyl (VI) ions can be understood.

However, a different explanation for the lack of actinyl(VI) cation–cation complexes is required if the empirical effective positive charges on the actinyl (VI) (ca. +3.2) and actinyl(v) (ca. +2.2) cations are more accurate reflections of the electron distribution in the actinyl cations than are these theoretically

computed electron distributions. The effective positive charges measured for the pentavalent and hexavalent actinyl cations (Choppin and Rao, 1984) predict that the -yl oxygen atoms of actinyl cations carry approximately the same partial negative charge, –0.6, regardless of the oxidation state of the actinyl cation. Therefore, the attractive electrostatic force between the negatively charged -yl oxygen atoms and a given cation would be the same for both oxidation states. Under this model, the lack of actinyl(VI) cation–cation complexes must be attributed to the cancellation of the attractive electrostatic force between the cation and the -yl oxygen atoms by the larger repulsive force between the effective +3.2 charge of the central hexavalent actinide atom and the positive charge of the other cation.

Regardless of which mechanism is correct, the formally cationic actinyl(V) ions can assume the normal role of ligands, forming electrostatic bonds with other cations through the actinyl oxygen atoms, which carry a substantial, partial negative charge.

The actual structures of cation–cation complexes in solution can be surmised from the combination of several different lines of structural evidence. The magnetic splitting of the Np Mössbauer spectra of $NpO_2^+ - Cr^{3+}$ and $NpO_2^+ - Rh^{3+}$ adsorbed on cation exchange resin were interpreted as being consistent with axially symmetric NpO_2^+ (Karraker and Stone, 1977). Wide angle X-ray scattering measurements of solutions containing either $NpO_2^+ - NpO_2^+$ or $NpO_2^+ - UO_2^{2+}$ cation–cation complexes show a peak at 4.2 Å in the radial distribution function, which was assigned as the distance between nearest neighbor actinide atoms in the cation–cation complexes (Guillaume *et al.*, 1983). Also, inner sphere NpO_2^+–NpO_2^+ cation pairs have been observed in a number of crystalline neptunyl(V) complexes (Cousson *et al.*, 1984; Tomilin *et al.*, 1986; Grigor'ev *et al.*, 1993a–c, 1995). In the solid state, two structural motifs for $NpO_2^+ - NpO_2^+$ complexes, the staggered and the 'T-shaped' dimers (Fig. 23.24), with significantly different cation–cation distances, have been observed. The Np–Np distances of the T-shaped dimers, like those observed in $NpO_2ClO_4 \cdot 4H_2O$, 4.20 Å (Grigor'ev *et al.*, 1995), are excellent matches for the X-ray scattering results from aqueous solutions of $NpO_2^+ - NpO_2^+$ complexes (Guillaume *et al.*, 1983). Polymeric NpO_2^+ cation–cation structures have not been observed in solution. Taken together, these experiments confirm the T-shaped solution phase coordination geometry initially suggested by Sullivan (1962) and imply that these are inner sphere complexes.

The stability constants for the formation of cation–cation complexes are invariably small. Typical constants reported for the equilibrium

$$AnO_2^+ + M^{z+} \rightleftarrows AnO_2M^{(z+1)+}$$

range from 0.1 to 16 M^{-1} in aqueous solution, depending on the cations involved and the ionic strength. In organic media the equilibrium constants may be much larger (Rykov and Frolov, 1972b; Musikas, 1986). The enthalpies and entropies

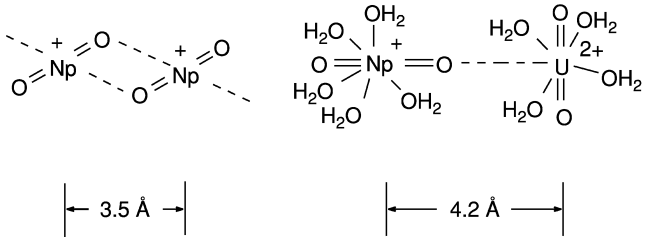

Fig. 23.24 *Inner sphere cation–cation interactions showing staggered* $NpO_2^+ - NpO_2^+$ *and T-shaped* $NpO_2^+ - UO_2^{2+}$ *complexes.*

Table 23.24 *Thermodynamic parameters of aqueous* NpO_2^+*–cation complexes at* 25°C. *Data taken from Sullivan* (1964), *Murmann and Sullivan* (1967), *Madic* et al. (1979), *and Stout* et al. (1993).

Cation	ΔG ($kJ\,mol^{-1}$)	ΔH ($kJ\,mol^{-1}$)	ΔS ($J\,K^{-1}\,mol^{-1}$)	*Ionic strength* (M)
Cr^{3+}	−2.96	−14	−38	8.0
Rh^{3+}	−2.37	−15	−42	8.0
NpO_2^{2+}	−2.01	0	+9	7
UO_2^{2+}	−2.72	−12	−34	6.0
NpO_2^+	−0.9	0	+3	6.0

of complexation in aqueous solutions also are relatively small (Table 23.24). Such small or negative ΔH and ΔS values often indicate outer sphere complexation (Choppin, 1997). However, the reported ΔH and ΔS values also would be in agreement with the accumulated structural data and the formulation of the complexes as inner sphere, $O{=}An{=}O^+{-}M^{z+}$, complexes if the hydration sphere about the resulting complex is more ordered than the hydration spheres of the individual cations are (Stout *et al.*, 1993).

The redox reaction rates of AnO_2^+ ions are often influenced by complex formation with other cations present in the solution. Despite the small stability constants of these complexes (<10), the oxidation of AnO_2^+ by several agents is slowed by the formation of cation–cation complexes. The stabilities of the complexes of AnO_2^+ with UO_2^{2+} decrease in the sequence $UO_2^+ > NpO_2^+ > AmO_2^+ > PuO_2^+$, with a stability constant of $\beta = 16$ for the most stable complex, $UO_2^+ - UO_2^{2+}$. The complexes $NpO_2^+ - UO_2^{2+}$ and $NpO_2^+ - NpO_2^{2+}$ have about the same stability (Madic *et al.*, 1979). Because the $UO_2^+ - UO_2^{2+}$ complex undergoes redox disproportionation at a much slower rate than the simple UO_2^+ aquo ion, solutions of the relatively unstable uranium(v) are significantly stabilized in the presence of UO_2^{2+}.

23.10 KINETICS OF REDOX REACTIONS

The redox reactions of the lighter actinides, which often have several oxidation states of almost equal reduction potentials (e.g. plutonium, Fig. 23.1) are particularly challenging systems. The An(IV)–An(III) and the An(VI)–An(V) couples involve simple electron loss or gain (Newton, 1975; Sullivan and Nash, 1986). The An(VI)–An(IV) and An(V)–An(IV) redox half-reactions include metal–oxygen bond formation or rupture, as well as electron gain or loss, because of the dioxo structure of the actinyl(V) and actinyl(VI) cations. The redox behavior of the actinides is complicated further by the possibility of disproportionation reactions at macro (but not at micro) concentrations.

23.10.1 Electron exchange reactions

Examples of reactions where the An–O bonds in the actinyl ions are not broken are processes such as

$$An(1)^{3+} + An(2)O_2^{2+} \rightleftarrows An(1)^{4+} + An(2)O_2^{+}$$

where An(1) and An(2) denote actinide ions that retain their structures (e.g. $An(1)^{z+}$ or $An(2)O_2^{z+}$). A number of such reactions, involving uranium, neptunium, and plutonium as reductants and oxidants, have been carefully studied (Table 23.25) (Fulton and Newton, 1970). Though these reactions are fast, the rates vary within wide limits; for example, the oxidation of U^{3+} by UO_2^{2+} or Np^{3+} by NpO_2^{2+}, respectively, are extremely fast while that of Np^{3+} by UO_2^{2+} or of Pu^{3+} by NpO_2^{2+} are much slower. The difference is not due to the fact that the latter reactions involve different actinides, since the oxidation of Pu^{3+} by $PuO_2{}^{2+}$ is even slower than the $Np^{3+} + UO_2^{2+}$ and the $Pu^{3+} + NpO_2^{2+}$ reaction rates.

The rates of reaction are closely connected with the Gibbs energies, enthalpies, and entropies of activation (ΔG^*, ΔH^*, and ΔS^*). These have been determined from the temperature dependence of the rate constants and are listed in Table 23.25 for the formation of the activated complex $[An(1)An(2)O_2^{5+}]^*$ along with the equilibrium thermodynamic reaction values ΔG°, ΔH°, and ΔS° for the redox reaction.

The equilibrium values of the entropy changes, ΔS°, are practically the same in all the reactions. This is because the hydration of the actinide ions in a particular oxidation state is fairly independent of the particular element involved. The values of ΔS° are very negative, implying that the formation of strongly hydrated M^{4+} ions brings about a considerable net increase of order in the solutions. However, the values of ΔH°, and, consequently, the values of ΔG°, differ considerably between the various systems in such a way that the fastest reactions are also the most exothermic. The reactions rate constants, k, do not decrease monotonically as the reactions become less exothermic.

The activation parameters provide insight into the source of the large differences in the reaction rates. The three reactions $U^{3+} + UO_2^{2+}$, $Np^{3+} + NpO_2^{2+}$, and $Pu^{3+} + PuO_2^{2+}$ are all first order in each of the reactants and independent of H^+ in the range of acidities measured (0.04–0.6 M, 0.01–0.1 M, and 0.1–1.0 M perchloric acid, respectively, at constant ionic strength) (Newton and Fulton, 1970). This implies that the reactions proceed via an activated complex $[An(1)An(2)O_2^{5+}]^*$. The reaction $Pu^{3+} + NpO_2^{2+}$, also progresses through formation of this activated complex. Since the rate depends upon the acidity, a parallel reaction path via a hydrolyzed complex $[Pu(OH)NpO_2^{4+}]^*$ was proposed (Fulton and Newton, 1970). In the case of $Np^{3+} + UO_2^{2+}$, the conditions are complicated by the presence of two parallel reactions following the initial reaction (Newton, 1970):

$$Np^{3+} + UO_2^+ + 4H^+ \rightarrow Np^{4+} + U^{4+} + 2H_2O$$

and

$$2UO_2^+ + 4H^+ \rightarrow UO_2^{2+} + U^{4+} + 2H_2O$$

At high acidities, these reactions are fast, despite the need to break the U–O -yl bonds in UO_2^+. As the reaction proceeds in 1.0 M acid, the concentration of uranyl(V) reaches a maximum, then decreases, while the concentration of uranium(IV) produced by the reaction of Np^{3+} with UO_2^+ steadily increases after a slow beginning. The activation parameters listed in Table 23.25 refer to the activated complexes $[An(1)An(2)O_2^{5+}]^*$.

The rates of the two fastest reactions are due to different causes. For $U^{3+} + UO_2^{2+}$, the rate is due to the less negative activation entropy while for $Np^{3+} + NpO_2^{2+}$, it is due to the less endothermic enthalpy. The values of ΔH^* are not very different for $U^{3+} + UO_2^{2+}$ and $Pu^{3+} + PuO_2^{2+}$, but the values of ΔS^* are quite different. The faster rates of the mixed systems $Np^{3+} + UO_2^{2+}$ and $Pu^{3+} + NpO_2^{2+}$ compared to $Pu^{3+} + PuO_2^{2+}$ are due primarily to the favorable values of ΔH^*.

23.10.2 Reactions of An–O bond breakage

Redox reactions in which An–O bonds are broken or formed are represented by

$$An(1)^{4+} + An(2)O_2^{2+} + 2H_2O \rightleftarrows An(1)O_2^+ + An(2)O_2^+ + 4H^+$$

in Table 23.26. Analogous to the oxidation of An^{3+} (Table 23.25), the rates have a first-order dependence on the concentrations of each of the actinide reactants. However, the rates of the An^{4+} oxidations also depend upon the H^+ concentrations with exponents that vary from –1 to –3. For some reactions, a non-integral exponent is found, indicating alternative paths with different orders of dependence on the acidity. The apparent second-order rate constants are generally much smaller than the rate constants of the An^{3+} oxidation reactions.

Table 23.25 *Rate constants* ($M^{-1}\ s^{-1}$), *activation parameters, and thermodynamic equilibrium parameters for the reaction* $An(1)^{3+} + An(2)O_2^{2+} \rightarrow An(1)^{4+} + An(2)O_2^{+}$ *in* 1.0 M $HClO_4$ *at* 25°C *from Fulton and Newton* (1970).

Reaction	k ($M^{-1}\ s^{-1}$)	ΔG^* ($kJ\,mol^{-1}$)	ΔH^* ($kJ\,mol^{-1}$)	ΔS^* ($J\,K^{-1}\,mol^{-1}$)	ΔG^o ($kJ\,mol^{-1}$)	ΔH^o ($kJ\,mol^{-1}$)	ΔS^o ($J\,K^{-1}\,mol^{-1}$)
$U^{3+} + UO_2^{2+}$	5.5×10^4	46.0	18.1	−93	−67	−112	−151
$Np^{3+} + NpO_2^{2+}$	1.05×10^5	44.4	4.2	−134	−95	−141	−159
$Pu^{3+} + PuO_2^{2+}$	2.7×10^0	70.5	20.2	−169	6.3	−40	−151
$Np^{3+} + UO_2^{2+}$	3.9×10^1	64.4	10.9	−178	8.6	−36	−151
$Pu^{3+} + NpO_2^{2+}$	3.55×10^1	64.2	14.6	−166	−15	−61	−153

Table 23.26 *Apparent second-order rate constants, activation parameters, and thermodynamic equilibrium parameters for the reaction* $An(1)^{4+} + An(2)O_2^{2+} + 2H_2O \rightarrow An(1)O_2^{+} + An(2)O_2^{+} + 4H^+$ *in perchlorate media with* 1.0 M H^+ *at* 25°C. *Data from Masters and Schwartz* (1961), *Newton and Baker* (1965), *Sullivan* et al. (1960), *Hindman* et al. (1954), *Newton and Montag* (1976), *and Rabideau* (1957).

Reaction	I (M)	n[a]	k ($M^{-1}\ s^{-1}$)	ΔG^* ($kJ\,mol^{-1}$)	ΔH^* ($kJ\,mol^{-1}$)	ΔS^* ($J\,K^{-1}\,mol^{-1}$)	ΔG^o ($kJ\,mol^{-1}$)	ΔH^o ($kJ^{-1}\,mol^{-1}$)	ΔS^o ($J\,K^{-1}\,mol^{-1}$)
$U^{4+} + UO_2^{2+}$	2	−3	4×10^{-7}	111	157	152	51.4	111	198
$U^{4+} + NpO_2^{2+}$	2	−1	22	66.9	76.1	31	−54.0	7.1	205
$U^{4+} + PuO_2^{2+}$	2	−1(−2)	3.1	69.5	73.6	14	−32.6	28.9	205
$Np^{4+} + NpO_2^{2+}$	2	−2(−1)	5×10^{-2}	80.8	102.9	74	−38.5	31.4	234
$Np^{4+} + PuO_2^{2+}$[b]	1	−2(−3)	7.5×10^{-4}	93	129	125	−17.2	–	–
$Pu^{4+} + PuO_2^{2+}$	1	−3	2×10^{-7}	111	158	159	24.3	79.5	184

[a] Order of the hydrogen ion dependence; if more than one reaction path was observed, the order of the less important path is given in parentheses.
[b] $T = 30$°C.

The strong tendency for hydrolysis of An^{4+} sets a lower limit on the acidity of the solutions which can be investigated, ca. 0.1 M.

Inverse acidity dependence is displayed by the reactions $U^{4+} + UO_2^{2+}$ and $Pu^{4+} + PuO_2^{2+}$, which have similar slow rates and almost equal activation parameters, indicating they proceed along analogous paths. By contrast, $U^{4+} + NpO_2^{2+}$ and $U^{4+} + PuO_2^{2+}$, which also display inverse linear acidity dependence, are the fastest of these reactions with similar values for the activation parameters. The large increase in the rate is due to the much more favorable values of ΔH^*. The values of ΔS^* are less favorable, reducing somewhat the influence of the more favorable values of ΔH^*.

Generally, the slow rates of An^{4+} oxidation are due to very positive values of ΔH^*. Positive values of ΔS^* favor the process but are insufficient to compensate for the influence of ΔH^*. Both the ΔH^* and ΔS^* values of An^{4+} oxidation differ significantly from those of An^{3+} oxidations (Table 23.25).

These trends are even more marked in the thermodynamic equilibrium parameters in Tables 23.25 and 23.26 for the two types of reactions. The values of ΔS^o are negative in An^{3+} oxidation reactions due to the formation of the strongly hydrated An^{4+} ions but they are positive for the oxidation reactions in the An^{4+} systems as this reaction is accompanied by release of water from the inner coordination sphere of the tetravalent cation. By contrast, the An^{3+} oxidations are exothermic, while the An^{4+} oxidations are endothermic. Thus, ΔH^o opposes ΔS° in both sets of reactions and the result is a mixture of values for the Gibbs energy changes of these oxidation reactions.

23.10.3 Redox disproportionation reactions

The disproportionation of actinyl(v) ions, AnO_2^+, is the reverse of the $An^{4+} + AnO_2^{2+}$ oxidation–reduction reactions. In Table 23.27, the rates and activation parameters of the disproportionation reactions of UO_2^+, NpO_2^+, and PuO_2^+ are listed. These rates vary from UO_2^+ reacting quite rapidly to NpO_2^+

Table 23.27 *Apparent second order rate constant and activation parameters for the disproportionation reaction* $2AnO_2^+ + 4H^+ \rightarrow An^{4+} + AnO_2^{2+} + 2H_2O$ *in perchlorate media,* $[H^+] = 1.0$ M *at* 25°C *from Ahrland* (1986).

	I (M)	n[a]	k ($M^{-1}\,s^{-1}$)	ΔG^* ($kJ\,mol^{-1}$)	ΔH^* ($kJ\,mol^{-1}$)	ΔS^* ($J\,K^{-1}\,mol^{-1}$)
UO_2^+	2	1	4×10^2	60	46	−46
NpO_2^+	2	2	9×10^{-9}	119	72	−159
PuO_2^+	1	1	3.6×10^{-3}	87	79	−24

[a] Acid dependence of the rate constant.

reacting extremely slowly. The fast reaction rate of UO_2^+ is due to a low value of ΔH^* while the slow rate of $NpO_2{}^+$ is due, to a large negative value of ΔS^*.

For both the redox and the disproportionation reactions, the lower the charge of the activated complex, the lower the ΔS^* value. For the formation of AnO_2^+ ions, the more negative the exponent of the hydrogen dependence, the more positive the ΔS^* value. For the disproportionation reactions, the more positive the exponent of the hydrogen dependence, the more negative the ΔS^* value. All of the AnO_2^+ ions listed disproportionate at a faster rate in D_2O (Rabideau, 1957; Hindman *et al.*, 1959). Also, the reaction rates of MO_2^+ ions are often influenced by complex formation with cations present in the reaction. These cation–cation complexes are discussed in Section 23.9. Their formation results in a slower rate of oxidation of the AnO_2^+ species by a number of oxidizing agents.

23.10.4 Effect of complexation

All reactions discussed so far take place between hydrated metal ions in non-complexing perchlorate media. In the presence of complex formation with anions, the reaction rates usually increase significantly. This was noticed initially for chloride and sulfate solutions. For example, plutonium(IV) disproportionates about five times faster in hydrochloric acid than in perchloric acid of the same concentration (Rabideau and Cowan, 1955). A study of sulfate media containing Np(IV), Np(V), and Np(VI) revealed that the rate of formation of neptunium(V) depends upon the concentration of the complexes $NpSO_4^{2+}$ and NpO_2SO_4, while disproportion depends upon the concentration of HSO_4^- (Sullivan *et al.*, 1957). For both reactions, the rate laws are not simple. With increasing sulfate concentration, the rate of formation initially increases, reaches a maximum, then decreases. The maximum coincides with the maximum concentration of $NpSO_4^{2+}$ as the higher sulfate complexes have no catalytic effect. The rate of disproportionation, by contrast, is a monotonically increasing function of the concentration of HSO_4^-. Table 23.28 lists the parameters for the reduction reactions of NpO_2^{2+} by complexing anions.

In the disproportionation of americium(V), analogous catalytic effects have been observed (Coleman *et al.*, 1963). In perchloric acid, the reaction

$$3AmO_2^+ + 4H^+ \rightleftarrows 2AmO_2^{2+} + Am^{3+} + 2H_2O$$

occurs, with a rate dependence on the hydrogen ion between 2 and 3. At 76°C, and an acidity of 2 M, the rates in nitric, hydrochloric, and sulfuric acids are 4, 4.6, and 24 times as great as that in perchloric acid. Similar effects have also been found for several other systems.

Comparison of the rate constants for the reaction of $[(NH_3)_6Co]^{3+}$ and $[(NH_3)_5CoX]^{2+}$ ($X = N_3^-, F^-, Cl^-, ac^-, Br^-, CN^-$, or NCS^-) with U^{3+} indicate that these reactions proceed by an inner sphere mechanism. The activation parameters for the analogous reaction of Np^{3+} with $(NH_3)_5RuX^{3+}$ ($X = H_2O$

Table 23.28 *Rate constant and activation parameters for the reduction of Np(VI). Data from Rao and Choppin* (1984), *Kim and Choppin* (1988), *and Choppin and Kim* (1989).

Reductant	*pH*	*T* (°C)	k_1 (s^{-1})	ΔH^* ($kJ\,mol^{-1}$)	ΔS^* ($J\,K^{-1}\,mol^{-1}$)
Dicarboxylic acids ($I = 0.10$ M NaCl)					
oxalic acid	1.1	33.7	1.30×10^{-3}	90 ± 7	-7 ± 21
malonic acid	2.2	34.2	2.70×10^{-3}	70 ± 10	-64 ± 25
methylmalonic acid	2.4	34.7	1.06×10^{-4}	88 ± 9	-16 ± 29
dimethylmalonic acid	3.0	35.2	3.10×10^{-5}	43 ± 13	-183 ± 33
succinic acid	3.0	34.0	1.50×10^{-4}	66 ± 9	-103 ± 42
maleic acid	3.0	35.9	1.00×10^{-4}	87 ± 12	-43 ± 42
phthalic acid	3.0	34.1	5.20×10^{-5}	38 ± 8	-209 ± 25
fumaric acid	3.0	23.1	1.80×10^{-5}	37 ± 23	-209 ± 84
Hydroxylic acids (I = 1.0 M NaCl)					
kojic acid	4.6	25.0	1.6	83 ± 3	34 ± 1
tropolone		25.0	70.8	67 ± 3	15 ± 12

and NH_3) (Espenson and Wang, 1970; Lavallee *et al.*, 1973) supported this proposal, indicating formation of a seven-coordinate Ru(III) intermediate. Other bridging ligands such as SO_4^{2-}, ClO_4^-, Cl^-, etc. have an accelerating effect on the reaction rate. This was attributed to a reduction in the cation–cation electrostatic repulsion through the formation of the intermediate $An^{3+}{-}X^{x-}{-}M^{z+}$.

23.11 KINETICS OF COMPLEXATION REACTIONS

The complexation and dissociation of actinide cations with anions of simple structure are more rapid than the analogous rates of reaction of the d-transition cations. These fast reaction rates are due to the strongly ionic nature of most actinide–ligand bonds, which results in a wide range of hydration and coordination numbers and symmetries. This structural versatility arises from the lack of strong crystal-field effects in 5f electronic configurations as well as from the relatively large ionic radii of these cations as the coordination numbers and symmetries are determined by steric and electrostatic factors (see Sections 23.4 and 23.6).

The complexation reactions usually proceed by the Eigen mechanism (Diebler and Eigen, 1959; Eigen and Tamm, 1962; Eigen, 1963). This mechanism involves two steps, the rapid formation of an outer sphere association complex (i.e. an ion pair) and the subsequent rate-determining step in which the ligand displaces one or more water molecules.

$$M(H_2O)_q^{m+} + L^{z-} \rightleftarrows M(H_2O)_q^{m+}{-}L^{z-} \rightleftarrows M(H_2O)_{q-1}L^{(m-z)} + H_2O$$

The actual ligand-interchange step may be dissociative or associative in character. For multidentate ligands, the associative steps with replacement of two-coordinated water can be represented as

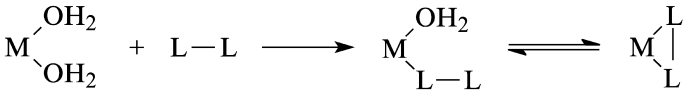

In the absence of any steric constraints, formation of the first M–L bond, generally, but not always, leads to rapid ring closure. As the chain distance separating the two donor atoms of the ligand increases, the rate (or probability) of ring closure decreases (Wilkins, 1974, Burgess, 1978). This is reflected in a decrease in $\log\beta_{11}$ and a deviation from linearity in plots of $\log\beta_{11}$ versus ΣpK_a (see Section 23.6). In some systems it is uncertain whether this increase in donor separation is accompanied by a change from chelation to monodentation. Microscopic reversibility requires that complex dissociation reactions follow the formation pathway in reverse. Complex dissociation is typically investigated by addition of a competing metal ion or of a chelating agent that binds more strongly to the cation. Complex dissociation reactions are often catalyzed by H^+ in acidic solution. A variety of experimental techniques have been used to study actinide complexation kinetics. These include stopped-flow spectrophotometry, pulse radiolysis, temperature-jump, NMR, solvent extraction separation methods, and conventional spectrophotometry.

According to the Eigen mechanism for complexation, the rate of solvent water exchange represents an upper limit to the rate of complex formation. Such rates are not available for the trivalent actinides but have been discussed for the chemically analogous lanthanides. Cossy *et al.* (1989) have reported that the second-order rate constants for water exchange are directly proportional to the cation radii of trivalent lanthanides. The water exchange rates for Am(III)–Cf(III) are estimated to range from 1×10^9 to 1×10^8 M^{-1} s^{-1} assuming a linear correlation with the lanthanides based on cation radius (Nash and Sullivan, 1998). Kiener *et al.* (1976) report that the water exchange rates for UO_2^{2+} are complex. Exchange rates for tetravalent and for pentavalent actinide cations have neither been reported, nor can they be estimated reliably. Bardin *et al.* (1998) have reported NMR data that give a first order rate constant for water exchange by UO_2^{2+} in d_6-acetone of 1×10^6 s^{-1} at 25°C.

The complexation kinetics of multidentate ligands are slower than for monodentate ligands due to the changes in ligand structural characteristics during the reactions. The aminopolycarboxylates have been used commonly in actinide separations, and, as a result, their kinetics of complexation with the An(III) cations have been studied in more depth than for any other An(III)–ligand system. Such studies usually involve metal exchange in which the An(III) cation displaces a trivalent lanthanide from complexation with an aminopolycarboxylate complex. For the reaction of An(III) with the Eu(III)–ethylenediaminetetraacetate complex (D'Olieslager *et al.*, 1970; Williams and Choppin, 1974), the rate was shown to be described by the equation:

$$\begin{aligned}\text{Rate} = {} & (k_a[\text{Eu(edta)}][\text{H}][\text{An}]/[\text{Eu}] + k_b[\text{Eu(edta)}][\text{An}]) \\ & - (k_c[\text{An(edta)}][\text{H}] + k_d[\text{An(edta)}][\text{Eu}])\end{aligned} \tag{23.14}$$

in which the ionic charges are omitted for simplicity. The specific rate constants k_a and k_c are associated with the hydrogen ion catalyzed forward and reverse terms, while k_b and k_d are specific rate constants for the respective acid-independent terms.

Below about pH 6 the hydrogen-catalyzed paths dominate the reaction. In these paths, the metal complex is protonated in a series of proton additions, leading ultimately to the decomposition of the complex and hence to metal exchange. The alternate acid-independent path in the exchange mechanism has been described by a metal ion-catalyzed decomposition of the complex in which the ligand serves as a bridge between the entering and exiting metal ions. The exchange reactions can be represented as follows ($Y = edta^{4-}$).

(A) *Acid-dependent mechanism*

$$\begin{array}{ccccccc} & & \overset{\text{Fast}}{} & & \overset{\text{Slow}}{} & & \overset{\text{Fast}}{} \\ \text{EuY} + \text{H} & \rightleftharpoons & \text{EuYH} & \rightarrow & [\text{EuYH}]^* & \rightleftharpoons & \text{Eu} + \text{H}_x\text{Y} + \text{An} \\ & & & & & & \downarrow\uparrow \text{ Fast} \\ & & \overset{\text{Fast}}{} & & & & \overset{\text{Slow}}{} \\ \text{AnY} + \text{H} & \rightleftharpoons & \text{AnYH} & & & \leftarrow & [\text{AnYH}]^* \end{array}$$

(B) *Acid-independent mechanism*

$$\begin{array}{ccccc} & & \overset{\text{Fast}}{} & & \overset{\text{Slow}}{} \\ \text{EuY} + \text{An} & \rightleftharpoons & \text{EuY–An} & \rightarrow & [\text{EuYAn}]^* \\ & & & & \downarrow \text{ Fast} \\ & & & \overset{\text{Fast}}{} & \\ & & \text{AnY} + \text{Eu} & \rightleftharpoons & \text{Eu-YAn} \end{array}$$

The formation and dissociation reactions of other aminopolycarboxylate complexes of Ln and An cations follow these general mechanisms. The rates of metal ion exchange for the trivalent actinides (Am, Cm, Bk, Cf) with $Eu(edta)^-$ indicate a similar dependence on acidity and, in cases where an acetate buffer was used, an additional dependence on free acetate concentration (Choppin and Williams, 1973; Williams and Choppin, 1974).

The rates of formation and dissociation of the Am(III) complex with $dcta^{4-}$ (*trans*-1,2-diaminocyclohexane-*N*,*N*,*N*′,*N*′-tetraacetate, Fig. 23.18) were determined using stopped-flow spectrophotometry to study the formation reaction and conventional spectrophotometry for the decomposition reaction (Sullivan *et al.*, 1978). The experimental results are consistent with the interpretation that a precursor between Am(III) and the ligand is formed. The rate-determining step in the reaction was postulated to be the formation of a bond between Am(III) and an imino nitrogen of $dcta^{4-}$.

The dissociation of the $Am(dcta)^-$ complex was studied by the metal ion exchange technique using Cu^{2+}, as was reported in an analogous study of the

$Ln(dcta)^-$ chelates (Nyssen and Margerum, 1970). No dependence on the copper concentration was observed, implying that any reaction rates measured were pertinent to either acid-induced or spontaneous dissociation of the complex. The results agree with studies on the rate of dissociation of trivalent actinides with a variety of aminopolycarboxylate complexants studied by solvent extraction or ion exchange separation techniques at radiotracer concentrations of the metal ion (D'Olieslager *et al.*, 1970; Choppin and Williams, 1973; El-Rawi, 1974; Williams and Choppin, 1974; Muscatello *et al.*, 1989). The rate-determining step for complex formation is an acid-dependent intramolecular process that appears to be limited by the rate of formation of An(III) bonding to the amine nitrogen. The activation parameters for the reaction were reported to be $E_a = +59.0\ kJ\,mol^{-1}$ and $\Delta S^* = -19\ JK^{-1}\,mol^{-1}$ (Sullivan *et al.*, 1978).

The rate of dissociation of trivalent actinide (Am, Cm, Bk, Cf) complexes with the aminopolycarboxylate ligands $hedta^{3-}$ (*N*-hydroxyethylethylenediaminetriacetate) and $tmdta^{4-}$ (trimethylenediaminetetraacetate) have been measured (El-Rawi, 1974; Muscatello *et al.*, 1989). As in the case for the edta complexes, the rate of the acid-catalyzed dissociation decreases with increasing cation atomic number (Fig. 23.25), which is consistent with a simple electrostatic model for the interactions of both lanthanides and actinides. The dissociation rate of $Am(dcta)^-$ was observed to be more similar to that of the isoelectronic $Eu(dcta)^-$ than to the dissociation rate of $Nd(dcta)^-$, whose cationic radius (and, hence, electrostatic attraction for the ligand) is closest to that of Am^{3+}.

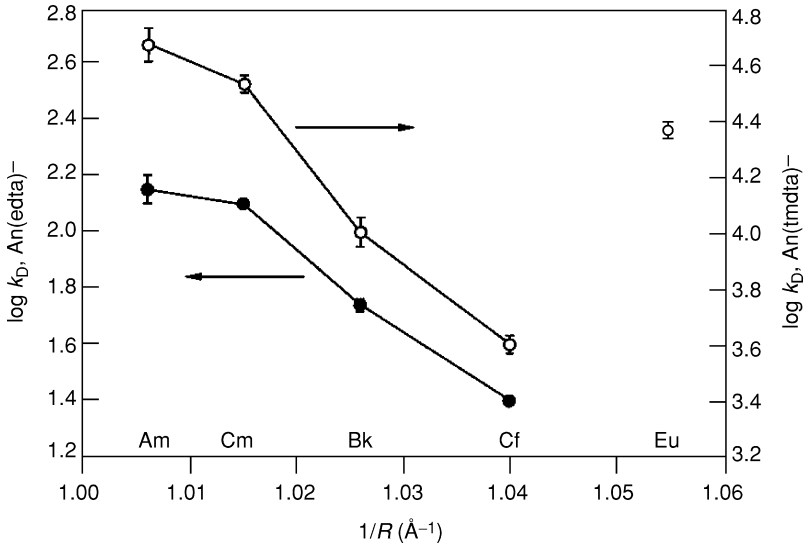

Fig. 23.25 *Correlation of the rate constant of the acid dependent dissociation pathway,* k_D, *of* MY^- ($Y = edta^{4-}$ *or* $tmdta^{4-}$) *and the reciprocal of the cation radius* ($CN = 6$).

Table 23.29 *Rate constants* (M^{-1} s^{-1}, 25°C) *for the reaction*

$$An^{3+} + HY^{3-} \underset{k_D}{\overset{k_F}{\rightleftharpoons}} AnY^{-} + H^{+}.$$

	tmdta^{4-}		*dcta*$^{4-}$		*edta*$^{4-}$	
Metal ion	$10^{-7}\,k_F$	$10^{-4}\,k_D$	$10^{-8}\,k_F$	k_D	$10^{-10}\,k_F$	$10^{-2}\,k_D$
Am	5.5 ± 0.9	4.78 ± 0.49	1.2	4.4	0.59	1.39
Cm	8.8 ± 1.2	3.52 ± 0.22	2.4	2.8	1.0	1.10
Bk	8.8 ± 1.6	0.95 ± 0.10	–	–	1.2	0.57
Cf	1.3 ± 1.0	0.39 ± 0.02	–	–	0.85	0.25
Eu	3.2 ± 0.4	2.29 ± 0.13	0.34	3.2	0.32	2.28

This result suggests a possible minor covalent contribution in the binding of Am(III) to the amine (Nash and Sullivan, 1998).

The dissociation rate constants for the trivalent actinide complexes with tmdta^{4-}, as seen in Fig. 23.25, are about two orders of magnitude larger than for the corresponding An(edta)$^{-}$ complexes. This is most probably due to the greater lability of the Am–N bonds in the six member N–Am–N ring of the tmdta complex when compared to the lability of the Am–N bonds in the five-membered N–Am–N ring of the edta chelate.

In contrast to the tmdta complex, the acid-dependent rate constant for the acid dissociation of the Am(dcta)$^{-}$ complex is $\log k_D = 0.64$, which is two orders of magnitude smaller than that for Am(edta)$^{-}$ (Sullivan *et al.*, 1978). This was attributed to the structural effect of the rigidity of the cyclohexyl ring. Table 23.29 lists the values for both the formation and dissociation rate constants for actinide(III) complexes of tmdta^{4-}, dcta^{4-}, and edta^{4-} from Muscatello *et al.* (1989).

23.12 SUMMARY

Although the aqueous complexes of the actinide elements has been a topic of continual interest for over half a century, puzzles remain to be solved and opportunities abound because such complexes are central to understanding the environmental, biological, and separations chemistry of the actinides. Historically, most of this work has involved studies of complexation strength, and to a lesser extent, studies of the kinetics of reactions. Many different techniques have been used. Unfortunately, the utility of such thermodynamic and kinetic measurements diminishes the farther system conditions deviate from those used in the laboratory measurements. The presence of new kinetic pathways, unforeseen equilibria, or solid phases that were not encountered in the laboratory studies can dominate the aqueous speciation when the concentrations of

the solution components or pH values are significantly different from the conditions that have been studied. For instance, the U–O bonds of the UO_2^{2+} cation are quite inert in acidic aqueous solutions with a half-life for oxygen exchange of 4×10^4 h in 1 M perchloric acid (Gordon and Taube, 1961), but in 3.5 M tetramethylammonium hydroxide, the exchange is complete in minutes (Clark *et al*., 1999). As a result, other techniques for studying actinide complexes, such as NMR, fluorescence spectroscopy, and EXAFS have become increasingly important sources of extra-thermodynamic information on dissolved actinide complexes in recent years.

While the information available on the solution complexation of the actinide elements covers a range of actinide ions, oxidation states, and ligands, it can usually be understood by several straightforward principles. The actinide cations are hard Lewis acids that interact preferentially with ligands that are hard Lewis base donors, in aqueous solution, forming strongly electrostatic bonds. Thus, the complexes generally become more stable as the effective charge of the actinide cation or ligand increases and as the size of the actinide cation decreases, if metal- or ligand-centered steric constraints are not important. This is best characterized for the An(III) and An(IV) oxidation states. However, the limited number of actinide cations that are stable in several of the oxidation states from 3+ to 6+, and the short half-lives of the *trans*-californium elements limit the number of actinide species that can be studied by many techniques for use in systematic, empirical comparisons of the metal ion properties. The electrostatic model of actinide–ligand bonding can be very useful despite its simplicity. However, accurate, quantitative, and non-empirical predictions of the strength and structure of actinide complexes are currently only possible for the simplest ligands because of ligand- and solvent-centered effects.

Many areas of actinide complexation chemistry remain relatively unexplored. Topics in actinide complexation which are only beginning to be defined include actinide complexation by neutral ligands in aqueous solutions, the formation of ternary complexes, and the behavior of actinide complexes in alkaline solutions. In addition, studies of ligands that are capable of stabilizing difficult to attain oxidation states; studies of ligands with well defined, pre-organized actinide binding sites; and studies of actinide–selective soft donor ligands have the potential to create new perspectives in actinide chemistry.

ACKNOWLEDGMENTS

This chapter incorporates portions of Chapter 21, Solution Chemistry and Kinetics of Ionic Reactions by Sten Ahrland from *The Chemistry of the Actinide Elements*, second edition. Preparation of this chapter was supported by the U.S. Department of Energy, Office of Basic Energy Sciences, Division of Chemical Sciences, Geosciences, and Biosciences at Argonne National Laboratory (Contract No. W-31-109-ENG-38) and at Florida State University.

REFERENCES

Aas, W., Moukhamet-Galeev, A., and Grenthe, I. (1998) *Radiochim. Acta*, **82**, 77–82.
Åberg, M. (1969) *Acta Chem. Scand.*, **23**, 791–810.
Åberg, M. (1970) *Acta Chem. Scand.*, **24**, 2901–15.
Åberg, M., Ferri, D., Glaser, J., and Grenthe, I. (1983a) *Inorg. Chem.*, **22**, 3986–9.
Åberg, M., Ferri, D., Glaser, J., and Grenthe, I. (1983b) *Inorg. Chem.*, **22**, 3981–5.
Ahrland, S. (1949) *Acta Chem. Scand.*, **3**, 1067–76.
Ahrland, S. and Kullberg, L. (1971a) *Acta Chem. Scand.*, **25**, 3677–91.
Ahrland, S. and Kullberg, L. (1971b) *Acta Chem. Scand.*, **25**, 3457–70.
Ahrland, S. and Kullberg, L. (1971c) *Acta Chem. Scand.*, **25**, 3471–83.
Ahrland, S. (1986) in *Chemistry of the Actinide Elements,* 2nd edn, vol. 2 (eds. J. J. Katz, G. T. Seaborg, and L. R. Morss), Chapman&Hall, New York, pp. 1480–546.
Ahrland, S., Hefter, G., and Norén, B. (1990) *Acta Chem. Scand.*, **44**, 1–7.
Alcock, N. W. and Esperås, S. (1977) *J. Chem. Soc., Dalton Trans.,* 893–6.
Allard, B., Kipatsi, H., and Liljenzin, J. (1980) *J. Inorg. Nucl. Chem.*, **42**, 1015–27.
Allard, B. and Rydberg, J. (1983) in *Plutonium Chemistry* (eds. W. T. Carnall and G. R. Choppin) (ACS Symp. Ser. 216), American Chemical Society, Washington, DC, pp. 275–95.
Allen, P. G., Bucher, J. J., Clark, D. L., Edelstein, N. M., Ekberg, S. A., Gohdes, J. W., Hudson, E. A., Kaltsoyannis, N., Lukens, W. W., Neu, M. P., Palmer, P. D., Reich, T., Shuh, D. K., Tait, C. D., and Zwick, B. D. (1995) *Inorg. Chem.*, **34**, 4797–807.
Allen, P. G., Bucher, J. J., Shuh, D. K., Edelstein, N. M., and Reich, T. (1997) *Inorg. Chem.*, **36**, 4676–83.
Allen, P. G., Bucher, J. J., Shuh, D. K., Edelstein, N. M., and Craig, I. (2000) *Inorg. Chem.*, **39**, 595–601.
André, C. and Choppin, G. R. (2000) *Radiochim. Acta*, **88**, 613–16.
Antonio, M. R., Williams, C. W., and Soderholm, L. (1998) *J. Alloys Compd.*, **271–273**, 846–9.
Antonio, M. R., Soderholm, L., Williams, C. W., Blaudeau, J.-P., and Bursten, B. E. (2001) *Radiochim. Acta*, **89**, 17–25.
Antonio, M. R., Williams, C. W., and Soderholm, L. (2002) *Radiochim. Acta*, **90**, 851–6.
Appelman, E. H., Kostka, A. G., and Sullivan, J. C. (1988) *Inorg. Chem.*, **27**, 2002–5.
Awasthi, S. P. and Sundaresan, M. (1981) *Indian J. Chem.*, **20A**, 378–81.
Baes, C. F. Jr, Norman, J., Meyer, N. J., and Roberts, C. E. (1965) *Inorg. Chem.*, **4**, 518–27.
Baes, C. F. Jr and Mesmer, R. E. (1976) *The Hydrolysis of Cations,* John Wiley, New York.
Bansal, B. M. L. and Sharma, H. D. (1964) *J. Inorg. Nucl. Chem.*, **26**, 799–805.
Bardin, N., Rubini, P., and Madic, C. (1998) *Radiochim. Acta*, **83**, 189–94.
Beck, M. T. (1968) *Coord. Chem. Rev.*, **3**, 91–113.
Beitz, J. V. and Hessler, J. P. (1980) *Nucl. Technol.*, **51**, 169–77.
Beitz, J. V., Bowers, D. L., Doxtader, M. M., Maroni, V. A., and Reed, D. T. (1988) *Radiochim. Acta*, **44/45**, 87–93.
Beitz, J. V. (1991) *Radiochim. Acta*, **52/53**, 35–9.
Beitz, J. V. (1994) *J. Alloys Compd.*, **207/208**, 41–50.

Bennet, D. A., Hoffman, D. C., Nitsche, H., Russo, R. E., Torres, R. A., Baisden, P. A., Andrews, J. E., Palmer, C. E. A., and Silva, R. J. (1992) *Radiochim. Acta*, **56**, 15–19.
Bernkopf, M. F. and Kim, J. I. (1984) *Hydrolyse-Reaktionen und Karbonat Komplexierung von Dreiwertigen Americium im NatÜrlichen Aquatischen System,* Institut fÜr Radiochemie, Technical University Munich Report RCM-02884.
Bismondo, A., Cassol, A., Di Bernardo, P., Magon, L., and Tomat, G. (1981) *Inorg. Nucl. Chem. Lett.*, **17**, 79–81.
Bjerrum, N. (1926) Kgl. Danske Vidensk. Selskab. Math.-fysike Medd, **7**(9), 1–48.
Bleaney, B., Llewellyn, P. M., and Jones, D. A. (1956) *Proc. Phys. Soc.*, **B69**, 858–60.
Bockris, J. O'M. and Reddy, A. K. D. (1970) *Modern Electrochemistry,* vol. I, Plenum Press, New York.
Bockris, J. O'M. and Saluja, P. P. S. (1972a) *J. Phys. Chem.*, **76**, 2140–51.
Bockris, J. O'M. and Saluja, P. P. S. (1972b) *J. Phys. Chem.* **76**, 2298–310.
Borkowski, M., Krejzler, J., and Siekierski, S. (1994) *Radiochim. Acta*, **65**, 99–103.
Born, M. (1920) *Z. Phys.*, **1**, 45–8.
Brand, J. R. and Cobble, J. W. (1970) *Inorg. Chem.*, **9**, 912–17.
Bratsch, S. G. (1983) *Chem. Phys. Lett.*, **98**, 113–17.
Bratsch, S. G. and Lagowski, J. J. (1985a) *J. Phys. Chem.*, **89**, 3310–16.
Bratsch, S. G. and Lagowski, J. J. (1985b) *J. Phys. Chem.*, **89**, 3317–19.
Bratsch, S. G. and Lagowski, J. J. (1986) *J. Phys. Chem.*, **90**, 307–12.
Brendler, V., Geipel, G., Bernhard, G., and Nitsche, H. (1996) *Radiochim. Acta*, **74**, 75–80.
Brennan, J. G., Stults, S. D., Andersen, R. A., and Zalkin, A. (1987) *Inorg. Chim. Acta*, **139**, 201–2.
Brennan, J. G., Green, J. C., and Redfern, C. M. (1989) *J. Am. Chem. Soc.*, **111**, 2373–7.
Brighli, M., Fux, P., Lagrange, J., and Lagrange, P. (1985) *Inorg. Chem.*, **24**, 80–4.
Brown, D. (1972) in *MTP International Review of Science, Lanthanides and Actinides*, Inorganic Chemistry, Ser. 1, vol. 7 (ed. K. W. Bagnall), University Park Press, Baltimore, MD, pp. 87–137.
Brown, P. L., Sylva, R. N., and Ellis, J. (1985) *J. Chem. Soc., Dalton Trans.*, 723–30.
Brüchle, W., Schädel, M., Scherer, U. W., Kratz, J. V., Gregorich, K. E., Lee, D., Nurmia, M., Chasteler, R. M., Hall, H. L., Henderson, R. A., and Hoffman, D. C. (1988) *Inorg. Chim. Acta*, **146**, 267–76.
Bünzli, J.-C. G., Metabanzoulou, J.-P., Froidevaux, P., and Jin, L. (1990) *Inorg. Chem.*, **29**, 3875–81.
Burgess, J. (1978) *Metal Ions in Solution,* John Wiley, New York.
Burns, J. H., Baldwin, W. H., and Stokely, J. R. (1973) *Inorg. Chem.*, **12**, 466–9.
Butler, R. N. and Symons, M. C. R. (1969) *Trans. Faraday Soc.*, **65**, 945–9.
Caceci, M. S. and Choppin, G. R. (1983a) *Radiochim. Acta*, **33**, 101–4.
Caceci, M. S. and Choppin, G. R. (1983b) *Radiochim. Acta*, **33**, 113–14.
Carey, G. H. and Martell, A. E. (1968) *J. Am. Chem. Soc.*, **90**, 32–8.
Carnall, W. T. (1989) *J. Less Common Metals*, **156**, 221–35.
Carugo, O. and Castellani, C. B. (1992) *Inorg. Chim. Acta*, **191**, 115–20.
Cassol, A., Magon, L., Tomat, G., and Portanova, R. (1972a) *Inorg. Chem.*, **11**, 515–19.
Cassol, A., Magon, L., Portanova, R., and Tondello, E. (1972b) *Radiochim. Acta*, **17**, 28–32.

Cassol, A., Di Bernardo, P., Portanova, R., and Magon, L. (1973) *Inorg. Chim. Acta*, **7**, 353–8.
Cassol, A., Di Bernardo, P., Portanova, R., Tolazzi, M., Tomat, G., and Zanonato, P. (1990) *Inorg. Chem.*, **29**, 1079–84.
Cauchetier, P. and Guichard, C. (1973) *Radiochim. Acta*, **19**, 137–46.
Chatterjee, A., Maslen, E. N., and Watson, K. J. (1988) *Acta Cryst. B*, **44**, 381–6.
Chaudhuri, N. K., Sawant, R. M., and Sood, D. D. (1999) *J. Radioanal. Nucl. Chem.*, **240**, 993–1011.
Chierice, G. O. and Neves, E. A. (1983) *Polyhedron*, **2**, 31–5.
Choppin, G. R. and Strazik, W. F. (1965) *Inorg. Chem.*, **4**, 1250–4.
Choppin, G. R. and Schneider, J. K. (1970) *J. Inorg. Nucl. Chem.*, **32**, 3283–8.
Choppin, G. R. (1971) *Pure Appl. Chem.*, **27**, 23–41.
Choppin, G. R. and Degischer, G. (1972) *J. Inorg. Nucl. Chem.*, **34**, 3473–7.
Choppin, G. R. and Williams, K. R. (1973) *J. Inorg. Nucl. Chem.*, **35**, 4255–69.
Choppin, G. R. and Unrein, P. J. (1976) in *Transplutonium Elements* (eds. W. Müller and R. Lindner), North-Holland, Amsterdam, pp. 97–107.
Choppin, G. R. and Ensor, D. D. (1977) *J. Inorg. Nucl. Chem.*, **39**, 1226–7.
Choppin, G. R. (1983) *Radiochim. Acta*, **32**, 43–53.
Choppin, G. R. and Rao, L. F. (1984) *Radiochim. Acta*, **37**, 143–6.
Choppin, G. R. and Allard, B. (1985) in *Handbook on the Physics and Chemistry of the Actinides,* vol. 3 (eds. A. J. Freeman and C. Keller), Elsevier, New York, pp. 407–29.
Choppin, G. R., Liu, Q., and Sullivan, J. C. (1985) *Inorg. Chem.*, **24**, 3968–9.
Choppin, G. R., Rizkalla, E. N., and Sullivan, J. C. (1987) *Inorg. Chem.*, **26**, 2318–20.
Choppin, G. R. and Yao, K. (1988) *Inorg. Chim. Acta*, **147**, 131–3.
Choppin, G. R. (1988) *Radiochim. Acta*, **44/45**, 23–8.
Choppin, G. R. and Kim, W. H. (1989) *Radiochim. Acta*, **48**, 153–7.
Choppin, G. R. (1991) *J. Radioanal. Nucl. Chem.*, **147**, 109–16.
Choppin, G. R., Rao, L. F., Rizkalla, E. N., and Sullivan, J. C. (1992a) *Radiochim. Acta*, **57**, 173–5.
Choppin, G. R., Khalili, F. I., and Rizkalla, E. N. (1992b) *J. Coord. Chem.*, **26**, 243–50.
Choppin, G. R. (1993) *Thermochim. Acta*, **227**, 1–7.
Choppin, G. R. and Rizkalla, E. N. (1994) in *Handbook on the Physics and Chemistry of Rare Earths,* vol. 18 (eds. K. A. Gschneidner Jr, L. Eyring, G. R. Choppin, and G. H. Lander), Elsevier, New York, pp. 559–90.
Choppin, G. R. (1997) *J. Alloys Compd.*, **249**, 9–13.
Choppin, G. R. and Labonne-Wall, N. (1997) *J. Radioanal. Nucl. Chem.*, **221**, 67–71.
Choppin, G. R., Liljenzin, J., and Rydberg, J.-O. (2002) *Radiochemistry and Nuclear Chemistry,* 3rd edn, Butterworth-Heinemann, Woburn, MA, p. 653.
Choppin, G. R. (2003) *Radiochim. Acta*, **91**, 645–9.
Choppin, G. R. and Wall, D. E. (2003) *J. Radioanal. Nucl. Chem.*, **255**, 47–52.
Clark, D. L., Hobart, D. E., and Neu, M. P. (1995) *Chem. Rev.*, **95**, 25–48.
Clark, D. L., Conradson, S. D., Keogh, D. W., Palmer, P. D., Scott, B. L., and Tait, C. D. (1998) *Inorg. Chem.*, **37**, 2893–9.
Clark, D. L., Conradson, S. D., Donohoe, R. J., Keogh, D. D., Morris, D. E., Palmer, P. D., Rogers, R. D., and Tait, C. D. (1999) *Inorg. Chem.*, **38**, 1456–66.
Coleman, J. S., Keenan, T. K., Jones, L. H., Carnall, W. T., and Penneman, R. A. (1963) *Inorg. Chem.*, **2**, 58–61.

Combes, J.-M., Chisholm-Brause, C. J., Brown, G. E. Jr, Parks, G. A., Conradson, S. D., Eller, P. G., Triay, I. R., Hobart, D. E., and Meijer, A. (1992) *Environ. Sci. Technol.*, **26**, 376–82.

Cossy, C., Barnes, A. C., Enderby, J. E., and Merbach, A. E. (1989) *J. Chem. Phys.*, **90**, 3254–60.

Coulter, L. V., Pitzer, K. S., and Latimer, W. M. (1940) *J. Am. Chem. Soc.*, **62**, 2845–51.

Cousson, A., Dabos, S., Abazli, H., Nectoux, F., Pagès, M., and Choppin, G. R. (1984) *J. Less Common Metals*, **99**, 233–40.

Cramer, R. E., Maynard, R. B., Paw, J. C., and Gilje, J. W. (1983) *Organometallics*, **2**, 1336–40.

Creaser, I., Heckel, M. C., Neitz, R. J., and Pope, M. T. (1993) *Inorg. Chem.*, **32**, 1573–8.

D'Olieslager, W., Choppin, G. R., and Williams, K. R. (1970) *J. Inorg. Nucl. Chem.*, **32**, 3605–10.

Dahlman, R. C., Bondietti, E. A., and Eyman, L. D. (1976) in *Actinides in the Environment* (ed. A. M. Friedman) (ACS Symp. Ser. 35), American Chemical Society, Washington, DC, pp. 47–81.

David, F., Fourest, B., and Duplessis, J. (1985) *J. Nucl. Mater.*, **130**, 273–9.

David, F. (1986) *J. Less Common Metals*, **121**, 27–42.

David, F. H. and Vokhmin, V. (2003) *New J. Chem.*, **27**, 1627–32.

Decambox, P., Mauchien, P., and Moulin, C. (1989) *Radiochim. Acta*, **48**, 23–8.

De Carvalho, R. G. and Choppin, G. R. (1967) *J. Inorg. Nucl. Chem.*, **29**, 725–35.

Dem'yanova, T. A., Stepanov, A. V., Babauer, A. S., and Aleksandruk, V. M. (1986) *Radiokhimiya*, **28**, 494–8.

Den Auwer, C., Charbonnel, M. C., Presson, M. T., Madic, C., and Guillaumont, R. (1997) *Polyhedron*, **16**, 2233–8.

Denecke, M. A., Reich, T., Bubner, M., Pompe, S., Heise, K. H., Nitsche, H., Allen, P. G., Bucher, J. J., Edelstein, N. M., and Shuh, D. K. (1998) *J. Alloys Compd.*, **271–273**, 123–7.

Denning, R. G., Green, J. C., Hutchings, T. E., Dallera, C., Tagliaferri, A., Giarda, K., Brookes, N. B., and Braicovich, L. (2002) *J. Chem. Phys.*, **117**, 8008–20.

Di Bernardo, P., Bismondo, A., Portanova, R., Traverso, O., and Magon, L. (1976) *Inorg. Chim. Acta*, **18**, 47–50.

Di Bernardo, P., Di Napoli, V., Cassol, A., and Magon, L. (1977) *J. Inorg. Nucl. Chem.*, **39**, 1659–63.

Di Bernardo, P., Roncari, E., Mazzi, U., Bettella, F., and Magon, L. (1978) *Thermochim. Acta*, **23**, 293–302.

Di Bernardo, P., Tomat, G., Bismondo, A., Traverso, O., and Magon, L. (1980) *J. Chem. Res. M*, 3144–71.

Di Bernardo, P., A., Cassol, G., Tomat, A., Bismondo, and L. Magon, (1983) *J. Chem. Soc., Dalton Trans.*, 733–5.

Diamond, R. M., Street, K., and Seaborg, G. T. (1954) *J. Am. Chem. Soc.*, **76**, 1461–9.

Diebler, H. and Eigen, M. (1959) *Z. Phys. Chem.* (Frankfurt), **20**, 299–309.

Docrat, T. I., Mosselmans, J. F. W., Charnock, J. M., Whiteley, M. W., Collison, D., Livens, F. R., Jones, C., and Edmiston, M. J. (1999) *Inorg. Chem.*, **38**, 1879–82.

Dodge, C. J. and Francis, A. J. (1997) *Environ. Sci. Technol.*, **31**, 3062–7.

Drago, R. S. and Wayland, B. B. (1965) *J. Am. Chem. Soc.*, **87**, 3571–7.

Drew, M. G. B., Iveson, P. B., Hudson, M. J., Liljenzin, J. O., Spjuth, L., Cordier, P.-Y., Enarsson, Å., Hill, C., and Madic, C. (2000) *J. Chem. Soc., Dalton Trans.*, 821–30.
Eberle, S. H. and Schaefer, J. B. (1968) *Inorg. Nucl. Chem. Lett.*, **4**, 283–7.
Eigen, M. and Tamm, K. (1962) *Z. Elektrochem.*, **66**, 93–107, 107–21.
Eigen, M. (1963) *Ber. Bunsenges Phys. Chem.*, **67**, 753–62.
Eigen, M. and Wilkins, R. G. (1965) *Adv. Chem. Ser.*, **49**, 55–67.
El-Rawi, H. (1974) *Complexing Kinetics of Transplutonium Elements*, Institut für Radiochemie, Kernforschungszentrum, Karlsruhe Report KFK-1927.
Ensor, D. D. and Choppin, G. R. (1980) *J. Inorg. Nucl. Chem.*, **42**, 1477–80.
Ernst, S. and Jezowska-Trzebiatowska, B. (1975a) *J. Phys. Chem.*, **79**, 2113–16.
Ernst, S. and Jezowska-Trzebiatowska, B. (1975b) *Z. Phys. Chem.* (Leipzig), **256**, 330–6.
Espenson, J. H. and Wang, R. T. (1970) *J. Chem. Soc., Chem. Commun.,* 207–8.
Fanghänel, T. and Kim, J. I. (1994) *Radiochim. Acta*, **66/67**, 81–7.
Felmy, A. R., Rai, D., and Fulton, R. W. (1990) *Radiochim. Acta*, **50**, 193–204.
Ferraro, J. R. and Peppard, D. F. (1963) *Nucl. Sci. Eng.*, **16**, 389–400.
Fourest, B., Duplessis, J., and David, F. (1984) *Radiochim. Acta*, **36**, 191–5.
Fratiello, A., Lee, R. E., and Schuster, R. E. (1970a) *Inorg. Chem.*, **9**, 391–2.
Fratiello, A., Kubo, V., Lee, R. E., and Schuster, R. E. (1970b) *J. Phys. Chem.*, **74**, 3726–30.
Fraústo da Silva, J. J. R. and Simoes, M. L. S. (1968) *Talanta*, **15**, 609–22.
Fried, A. R. and Martell, A. E. (1971) *J. Am. Chem. Soc.*, **93**, 4695–700.
Fuger, J. and Cunningham, B. B. (1965) *J. Inorg. Nucl. Chem.*, **27**, 1079–84.
Fuger, J. and Oetting, F. L. (1976) *The Chemical Thermodynamics of Actinide Elements and Compounds,* part 2, *The Actinide Aqueous Ions*, International Atomic Energy Agency, Vienna.
Fuger, J. (1982) in *Actinides in Perspective* (ed. N. M. Edelstein), Pergamon Press, New York, pp. 409–31.
Fuger, J., Khodakovsky, I. L., Sergeyava, E. I., Medvedev, V. A., and Navratil, J. D. (1992) *The Chemical Thermodynamics of Actinide Elements and Compounds,* part 12, *The Actinide Aqueous Inorganic Complexes*, International Atomic Energy Agency, Vienna.
Fulton, R. B. and Newton, T. W. (1970) *J. Phys. Chem.*, **74**, 1661–9.
Garnov, A. Y., Krot, N. N., Bessonov, A. A., and Perminov, V. P. (1996) *Radiochemistry*, **38**, 402–6.
Gaunt, A. J., May, I., Helliwell, M., and Richardson, S. (2002) *J. Am. Chem. Soc.*, **124**, 13350–1.
Giffaut, E. and Vitorge, P. (1993) in *Scientific Basis for Nuclear Waste Management XVI,* vol. 294 (eds. C. G. Interrante and R. T. Pabalan), Materials Research Society, Pittsburg, PA, pp. 747–51.
Gordon, G. and Taube, H. (1961) *J. Inorg. Nucl. Chem.*, **19**, 189–91.
Gordon, S., Mulac, W. A., Schmidt, K. N., and Sjoblom, R. K. (1978) *Inorg. Chem.*, **17**, 294–6.
Grenthe, I. (1962) *Acta Chem. Scand.*, **16**, 1695–712.
Grenthe, I. (1963) *Acta Chem. Scand.*, **17**, 1814–15.
Grenthe, I. (1964) *Acta Chem. Scand.*, **18**, 283–92.
Grenthe, I. and Lagerman, B. (1991) *Acta Chem. Scand.*, **45**, 231–8.

Grenthe, I., Fuger, J., Konings, R. J. M., Lemire, R. J., Muller, A. B., Nguyen-Trung, C., and Wanner, H. (1992) *Chemical Thermodynamics of Uranium,* North-Holland, Amsterdam.

Grenthe, I. and Lagerman, B. (1993) *Radiochim. Acta*, **61**, 169–76.

Grenthe, I. and Puigdomenech, I. (1997) *Modelling in Aquatic Chemistry,* Nuclear Energy Agency/Organisation for Economic Cooperation and Development, Paris.

Grigor'ev, M. S., Gulev, B. F., and Krot, N. N. (1986) *Radiokhimiya*, **28**, 690–4; *Sov. Radiochem.*, **28**, 630–3.

Grigor'ev, M. S., Baturin, N. A., Budantseva, N. A., and Fedoseev, A. M. (1993a) *Radiokhimiya*, **35**(2), 29–38; *Sov. Radiochem.*, **35**, 151–6.

Grigor'ev, M. S., Charushnikova, I. A., Krot, N. N., Yanovskii, A. I., and Struchkov, Y. T. (1993b) *Radiokhimiya*, **35**(4), 31–7; *Sov. Radiochem.*, **35**, 39–48.

Grigor'ev, M. S., Charushnikova, I. A., Krot, N. N., Yanovskii, A. I., and Struchkov, Y. T. (1993c) *Radiokhimiya*, **35**(4), 24–30; *Sov. Radiochem.*, **35**, 388–93.

Grigor'ev, M. S., Baturin, N. A., Bessonov, A. A., and Krot, N. N. (1995) *Radiochemistry*, **37**, 12–4.

Gritmon, T. F., Goedken, M. P., and Choppin, G. R. (1977) *J. Nucl. Inorg. Chem.*, **39**, 2021–3.

Gross, J. and Keller, C. (1972) *J. Inorg. Nucl. Chem.*, **34**, 725–38.

Guilbaud, P. and Wipff, G. (1993a) *J. Inclusion Phenom. Mol. Recognit. Chem.*, **16**, 169–88.

Guilbaud, P. and Wipff, G. (1993b) *J. Phys. Chem.*, **97**, 5685–92.

Guillaumont, R. (1966) *Rev. Chim. Minér.*, **3**, 339–73.

Guillaumont, R. (1968) *Bull. Soc. Chim. Fr.*, 168–70.

Guillaumont, R., Bouissières, G., and Muxart, R. (1968) *Actinides Rev.*, **1**, 135–63.

Guillaumont, R., Fanghänel, T., Fuger, J., Grenthe, I., Neck, V., Palmer, D., and Rand, M. H. (2003) *Update on the Chemical Thermodynamics of Uranium, Neptunium, Plutonium, Americium and Technetium,* Elsevier, Amsterdam.

Guillaume, B., Begun, G. M., and Hahn, R. L. (1982) *Inorg. Chem.*, **21**, 1159–66.

Guillaume, B., Hahn, R. L., and Narten, A. H. (1983) *Inorg. Chem.*, **22**, 109–11.

Gusev, N. I. (1971) *Russ. J. Phys. Chem.*, **45**, 1268–71, 1455–7, 1575–6.

Gusev, N. I. (1972) *Russ. J. Phys. Chem.*, **46**, 1034–7, 1657–9.

Gusev, N. I. (1973) *Russ. J. Phys. Chem.*, **47**, 52–5, 184–7, 687–90, 1309–12.

Habenschuss, A. and Spedding, F. H. (1979a) *J. Chem. Phys.*, **70**, 2797–806.

Habenschuss, A. and Spedding, F. H. (1979b) *J. Chem. Phys.*, **70**, 3758–64.

Habenschuss, A. and Spedding, F. H. (1980) *J. Chem. Phys.*, **73**, 442–50.

Halperin, J. and Oliver, J. H. (1983) *Radiochim. Acta*, **33**, 29–33.

Hancock, R. D. and Marsicano, F. (1980) *Inorg. Chem.*, **19**, 2709–14.

Hancock, R. D. and Martell, A. E. (1989) *Chem. Rev.*, **89**, 1875–914.

Hancock, R. D. (1992) in *Perspectives in Coordination Chemistry* (eds. A. F. Williams, C. Floriani, and A. E. Merbach), Springer-Verlag, New York, pp. 129–51.

Hancock, R. D. and Martell, A. E. (1996) *J. Chem. Educ.*, **73**, 654–63.

Harmon, H. D., Peterson, J. R., McDowell, W. J., and Coleman, C. F. (1972a) *J. Inorg. Nucl. Chem.*, **34**, 1381–97.

Harmon, H. D., Peterson, J. R., Bell, J. T., and McDowell, W. J. (1972b) *J. Inorg. Nucl. Chem.*, **34**, 1711–19.

Havel, J. (1969) *Collect. Czech. Chem. Commun.*, **34**, 3248–65.
Hay, P. J., Martin, R. L., and Schreckenbach, G. (2000) *J. Phys. Chem. A*, **104**, 6259–70.
Hefter, G. (1974) *Coord. Chem. Rev.*, **12**, 221–39.
Hietanen, S. (1954) *Acta Chem. Scand.*, **8**, 1626–42.
Hietanen, S. (1956) *Acta Chem. Scand.*, **10**, 1531–46.
Hietanen, S. and Sillen, L. G. (1968) *Acta Chem. Scand.*, **22**, 265–80.
Hinchey, R. J. and Cobble, J. W. (1970) *Inorg. Chem.*, **9**, 922–6.
Hindman, J. C., Sullivan, J. C., and Cohen, D. (1954) *J. Am. Chem. Soc.*, **76**, 3278–80.
Hindman, J. C., Sullivan, J. C., and Cohen, D. (1959) *J. Am. Chem. Soc.*, **81**, 2316–19.
Hinton, J. F. and Amis, E. S. (1971) *Chem. Rev.*, **71**, 627–74.
Hök-Bernström, B. (1956) *Acta Chem. Scand.*, **10**, 163–73.
Howatson, J., Grev, D. M., and Morosin, B. (1975) *J. Inorg. Nucl. Chem.*, **37**, 1933–5.
Huheey, J. E. (1976) *Inorganic Chemistry,* Harper and Row, New York.
Hulet, E. K., Lougheed, R. W., Baisden, P. A., Landrum, J. H., Wild, J. F., and Lundqvist, R. F. D. (1979) *J. Inorg. Nucl. Chem.*, **41**, 1743–7.
Inoue, Y. and Tochiyama, O. (1985) *Bull. Chem. Soc. Jpn.*, **58**, 2228–33.
Itagaki, H., Nakayama, S., Tanaka, S., and Yamawaki, M. (1992) *Radiochim. Acta*, **58/59**, 61–6.
Jainxin, T., Yaozhong, C., and Zhangji, L. (1993) *Radiochim. Acta*, **61**, 73–5.
Jarvis, N. V. and Hancock, R. D. (1991) *Inorg. Chim. Acta*, **182**, 229–32.
Jarvis, N. V., de Sousa, A. S., and Hancock, R. D. (1992) *Radiochim. Acta*, **57**, 33–9.
Jarvis, N. V. and Hancock, R. D. (1994) *Radiochim. Acta*, **64**, 15–22.
Jensen, M. P. and Choppin, G. R. (1998) *Radiochim. Acta*, **82**, 83–8.
Jensen, M. P., Morss, L. R., Beitz, J. V., and Ensor, D. D. (2000a) *J. Alloys Compd.*, **303/304**, 137–41.
Jensen, M. P., Beitz, J. V., Rogers, R. D., and Nash, K. L. (2000b) *J. Chem. Soc., Dalton Trans.*, 3058–64.
Jensen, M. P. and Nash, K. L. (2001) *Radiochim. Acta*, **89**, 557–64.
Jensen, M. P. and Bond, A. H. (2002) *J. Am. Chem. Soc.*, **124**, 9870–7.
Johansson, G. (1968) *Acta Chem. Scand.*, **22**, 399–409.
Johansson, L. (1971) *Acta Chem. Scand.*, **25**, 3569–76.
Johansson, G., Magini, M., and Ohtaki, H. (1991) *J. Solution Chem.*, **20**, 775–92.
Johnson, D. A. (1982) *Some Thermodynamic Aspects of Inorganic Chemistry,* 2nd edn, Cambridge University Press, Cambridge.
Jones, A. D. and Choppin, G. R. (1969) *Actinides Rev.*, **1**, 311–36.
Kaltsoyannis, N. (2000) *Inorg. Chem.*, **39**, 6009–17.
Karmazin, L., Mazzanti, M., and Pécaut, J. (2002) *Chem. Commun.*, 654–5.
Karraker, D. G. and Stone, J. A. (1977) *Inorg. Chem.*, **16**, 2979–80.
Keenan, T. K. and Kruse, F. H. (1964) *Inorg. Chem.*, **3**, 1231–2.
Kepert, C. J., Skelton, B. W., and White, A. H. (1999) *Aust. J. Chem.*, **52**, 617–20.
Khalili, F. I., Choppin, G. R., and Rizkalla, E. N. (1988) *Inorg. Chim. Acta*, **143**, 131–5.
Khopkar, P. K. and Mathur, J. N. (1974) *J. Inorg. Nucl. Chem.*, **36**, 3819–25.
Kiener, C., Folcher, G., Rigny, P., and Virlet, J. (1976) *Can. J. Chem.*, **54**, 303–12.
Kim, J. I. and Kanellakopulos, B. (1989) *Radiochim. Acta*, **48**, 145–50.
Kim, J. I. and Sekine, T. (1991) *Radiochim. Acta*, **55**, 187–92.
Kim, J. I., Wimmer, H., and Klenze, R. (1991) *Radiochim. Acta*, **54**, 35–41.

Kim, J. I., Rhee, D. S., Wimmer, H., Buckau, G., and Klenze, R. (1993) *Radiochim. Acta*, **62**, 35–43.
Kim, W. H. and Choppin, G. R. (1988) *Inorg. Chem.*, **27**, 2771–3.
Kimura, T. and Choppin, G. R. (1994) *J. Alloys Compd.*, **213–214**, 313–17.
Kimura, T., Choppin, G. R., Kato, Y., and Yoshida, Z. (1996) *Radiochim. Acta*, **72**, 61–4.
Kimura, T. and Kato, Y. (1998) *J. Alloys Compd.*, **271–273**, 867–71.
Kinard, W. F. and Choppin, G. R. (1974) *J. Inorg. Nucl. Chem.*, **36**, 1131–4.
Kinard, W. F., Grant, P. M., and Baisden, P. A. (1989) *Polyhedron*, **8**, 2385–8.
Kirby, H. W. (1959) *The Radiochemistry of Protactinium*, U.S. Atomic Energy Commission Report NAS-NS 3016. (*The Radiochemistry of. . .*" series can be found at http://lib-www.lanl.gov/radiochemistry/elements.htm).
Klenze, R., Kim, J. I., and Wimmer, H. (1991) *Radiochim. Acta*, **52/53**, 97–103.
Kobashi, A. and Choppin, G. R. (1988) *Radiochim. Acta*, **43**, 211–15.
Kolarich, R. T., Ryan, V. A., and Schuman, R. P. (1967) *J. Inorg. Nucl. Chem.*, **29**, 783–97.
Kolbe, W. and Edelstein, N. M. (1971) *Phys. Rev. B*, **4**, 2869–75.
Kosyakov, V. N., Timofeev, G. A., Erin, E. A., Andreev, V. I., Kopytov, V. V., and Simakin, G. A. (1977) *Sov. Radiochem.*, **19**, 418–23.
Kozlov, A. G. and Krot, N. N. (1960) *Russ. J. Inorg. Chem.*, **5**, 954–6.
Kraus, K. A. and Dam, J. R. (1949) in *The Transuranium Elements* (eds. G. T. Seaborg, J. J. Katz, and W. M. Manning), Natl. Nucl. En. Ser., Div. IV, 14B, part 1, McGraw-Hill, New York, pp. 528–49.
Kraus, K. A. and Holmberg, R. W. (1954) *J. Phys. Chem.*, **58**, 325–30.
Kraus, K. A., Moore, G. E., and Nelson, F. (1956) *J. Am. Chem. Soc.*, **78**, 2692–4.
Krot, N. N., Ermolaev, N. P., and Gel'man, A. D. (1962) *Russ. J. Inorg. Chem.*, **7**, 1062–6.
Krot, N. N., Shilov, V. P., Nikolaevskii, V. B., Pikaev, A. K., Gel'man, A. D., and Spitsyn, V. I. (1974) *Dokl. Acad. Sci. USSR*, **217**(3), 525–7.
Laidler, K. J. (1956) *Can. J. Chem.*, **34**, 1107–13.
Laubscher, A. E. and Fouché, K. F. (1971) *J. Inorg. Nucl. Chem.*, **33**, 3521–35.
Lavallee, D. K., Lavallee, C., Sullivan, J. C., and Deutsch, E. (1973) *Inorg. Chem.*, **12**, 570–4.
Lemire, R. J., Fuger, J., Nitsche, H., Rand, M. H., Potter, P., Rydberg, J., Spahiu, K., Sullivan, J. C., Ullman, W. J., Vitorge, P., and Wanner, H. (2001) *Chemical Thermodynamics of Neptunium and Plutonium,* Elsevier, New York.
Lundqvist, R. (1974) in *Proc. Int. Solvent Extr. Conf. 1974,* vol. 1 (ed. G. V. Jeffreys), Society of Chemical Industry, London, pp. 469–76.
Lundqvist, R., Hulet, E. K., and Baisden, P. A. (1981) *Acta Chem. Scand.*, **35A**, 653–61.
Madic, C., Guillaume, J. C., Morisseau, J. C., and Moulin, J. P. (1979) *J. Inorg. Nucl. Chem.*, **41**, 1027–31.
Madic, C., Hobart, D. E., and Begun, G. M. (1983a) *Inorg. Chem.*, **22**, 1494–503.
Madic, C., Begun, G. M., Hobart, D. E., and Hahn, R. L. (1983b) *Radiochim. Acta*, **34**, 195–202.
Magon, L., Cassol, A., and Portanova, R. (1968) *Inorg. Chim. Acta*, **2**, 285–8.
Makarova, T. P., Sinitsyna, G. S., Stepanov, A. V., Shestakova, I. A., and Shestakov, B. I. (1972) *Sov. Radiochem.*, **14**(4), 555–7.

Manning, G. S. (1979) *Acc. Chem. Res.*, **12**, 443–9.
Manning, T. J. (1996) *J. Chem. Educ.*, **73**, 661–3.
Marcus, Y. (1966) *J. Inorg. Nucl. Chem.*, **28**, 209–19.
Marcus, Y. and Bomse, M. (1970) *Israel. J. Chem.*, **8**, 901–11.
Marcus, Y. and Loewenschuss, A. (1986) *J. Chem. Soc., Faraday Trans.*, **82**, 2873–86.
Marinsky, J. A. (1976) *Coord. Chem. Rev.*, **19**, 125–71.
Marks, A. P. and Drago, R. S. (1975) *J. Am. Chem. Soc.*, **97**, 3324–9.
Marquardt, C., Herrmann, G., and Trautmann, N. (1996) *Radiochim. Acta*, **73**, 119–25.
Marquardt, C. and Kim, J. I. (1998) *Radiochim. Acta*, **81**, 143–8.
Martell, A. E., Smith, R. M., and Motekaitis, R. J. (1998) *Critically Selected Stability Constants of Metal Complexes Database Version 5.0,* NIST Standard Reference Data, Gaithersburg, MD.
Masci, B., Nierlich, M., and Thuéry, P. (2002) *New J. Chem.*, **26**, 120–8.
Masters, B. J. and Schwartz, L. L. (1961) *J. Am. Chem. Soc.*, **83**, 2620–4.
Matonic, J. H., Scott, B. L., and Neu, M. P. (2001) *Inorg. Chem.*, **40**, 2638–9.
Matsika, S. and Pitzer, R. M. (2000) *J. Phys. Chem. A*, **104**, 4064–8.
McDowell, W. J., Keller, Jr, O. J. Dittner, P. E., Tarrant, J. R., and Case, G. N. (1976) *J. Inorg. Nucl. Chem.*, **38**, 1207–10.
Meinrath, G. and Kim, J. I. (1991) *Radiochim. Acta*, **53**, 29–34.
Miguirditchian, M. (2003) PhD Dissertation, Paris XI University, Orsay.
Mikhailov, V. A. (1969) *Russ. J. Inorg. Chem.*, **14**, 1119–24.
Mikheev, N. B., Spitsyn, V. I., Kamenskaya, A. N., Konovalova, N. A., Rumer, I. A., Auerman, L. N., and Podorozhnyi, A. M. (1977) *Inorg. Nucl. Chem. Lett.*, **13**, 651–6.
Mikheev, N. B., Spitsyn, V. I., Kamenskaya, A. N., Mikulski, J., and Petryna, T. (1980) *Radiochem. Radioanal. Lett.*, **43**, 85–92.
Milic, N. B. (1981) *J. Chem. Soc.*, *Dalton Trans.*, 1445–9.
Milic, N. B. and Suranji, T. M. (1982) *Can. J. Chem.*, **60**, 1298–303.
Moll, H., Denecke, M. A., Jalilehvand, F., Sandström, M., and Grenthe, I. (1999) *Inorg. Chem.*, **38**, 1795–9.
Moll, H., Reich, T., Hennig, C., Rossberg, A., Szabó, Z., and Grenthe, I. (2000) *Radiochim. Acta*, **88**, 559–66.
Moon, H.-C. (1989) *Bull. Korean Chem. Soc.*, **10**, 270–2.
Morgenstern, A. and Kim, J. I. (1996) *Radiochim. Acta*, **72**, 73–7.
Moriyama, H., Kitamura, A., Fujiwara, K., and Yamana, H. (1999) *Radiochim. Acta*, **87**, 97–104.
Moriyama, H., Fujiwara, K., and Yamana, H. (2002) *J. Nucl. Sci. Technol.*, Suppl. **3**, 246–50.
Morse, J. W. and Choppin, G. R. (1991) *Rev. Aquat. Sci.*, **4**, 1–22.
Morss, L. R. (1976) *Chem. Rev.*, **76**, 827–41.
Morss, L. R. and McCue, M. C. (1976) *J. Chem. Eng. Data*, **21**, 337–41.
Morss, L. R. (1985) in *Standard Potentials in Aqueous Solutions* (eds. A. J. Bard, R. Parsons and J. Jordan), Marcel Dekker, New York, pp. 587–629.
Morss, L. R., Nash, K. L., and Ensor, D. D. (2000) *J. Chem. Soc.*, *Dalton Trans.*, 285–91.
Moskvin, A. I. and Essen, L. N. (1967) *Russ. J. Inorg. Chem.*, **12**, 359–62.
Moulin, V., Tits, J., and Ouzounian, G. (1992) *Radiochim. Acta*, **58–59**, 179–90.
Münze, R. (1972) *J. Inorg. Nucl. Chem.*, **34**, 661–8.
Murmann, R. K. and Sullivan, J. C. (1967) *Inorg. Chem.*, **6**, 892–900.

Muscatello, A. C., Choppin, G. R., and D'Olieslager, W. (1989) *Inorg. Chem.*, **28**, 993–7.
Musikas, C., Cuillerdier, C., Livet, J., Forchioni, A., and Chachaty, C. (1983) *Inorg. Chem.*, **22**, 2513–18.
Musikas, C. (1984) in *International Symposium on Actinide/Lanthanide Separations* (eds. G. R. Choppin, J. D. Navratil, and W. W. Schulz), World Scientific, Philadelphia, pp. 19–30.
Musikas, C. (1986) *J. Less Common Metals*, **122**, 107–23.
Nagasaki, S., Kinoshita, K., Enokida, Y., and Suzuki, A. (1992) *J. Nucl. Sci. Technol.*, **29**, 1100–7.
Nash, K. L. and Cleveland, J. M. (1983) in *Plutonium Chemistry* (eds. W. T. Carnall and G. R. Choppin) (ACS Symp. Ser. 216), American Chemical Society, Washington, DC, pp. 251–62.
Nash, K. L. and Cleveland, J. M. (1984a) *Radiochim. Acta*, **37**, 19–24.
Nash, K. L. and Cleveland, J. M. (1984b) *Radiochim. Acta*, **36**, 129–34.
Nash, K. L. (1991a) *Radiochim. Acta*, **54**, 171–9.
Nash, K. L. (1991b) *Eur. J. Solid State Inorg. Chem.*, **28**, 389–92.
Nash, K. L. (1993a) *Solvent Extr. Ion Exch.*, **11**, 729–68.
Nash, K. L. (1993b) *Radiochim. Acta*, **61**, 147–54.
Nash, K. L., Rao, L. F., and Choppin, G. R. (1995) *Inorg. Chem.*, **34**, 2753–8.
Nash, K. L. and Sullivan, J. C. (1998) *J. Alloys Compd.*, **271–273**, 712–18.
Neck, V., Kim, J. I., and Kanellakopulos, B. (1992) *Radiochim. Acta*, **56**, 25–30.
Neck, V., Fanghänel, T., and Kim, J. I. (1997) *Radiochim. Acta*, **77**, 167–75.
Neck, V. and Kim, J. I. (2000) *Radiochim. Acta*, **88**, 815–22.
Neck, V. and Kim, J. I. (2001) *Radiochim. Acta*, **89**, 1–16.
Nelson, D. M. and Lovett, M. B. (1978) *Nature*, **276**, 599–601.
Neu, M. P., Matonic, J. H., Ruggiero, C. E., and Scott, B. L. (2000) *Angew. Chem.*, **39**, 1442–4.
Newton, T. W. and Baker, F. B. (1962) *Inorg. Chem.*, **1**, 368–77.
Newton, T. W. and Baker, F. B. (1965) *Inorg. Chem.*, **4**, 1166–70.
Newton, T. W. (1970) *J. Phys. Chem.*, **74**, 1655–61.
Newton, T. W. and Fulton, R. B. (1970) *J. Phys. Chem.*, **74**, 2797–801.
Newton, T. W. and Burkhart, M. J. (1971) *Inorg. Chem.*, **10**, 2323–6.
Newton, T.W. (1975) *The Kinetics of the Oxidation–Reduction Reactions of Uranium, Neptunium, Plutonium, and Americium in Aqueous Solutions*, U.S. ERDA TID-26506.
Newton, T. W. and Montag, T. (1976) *Inorg. Chem.*, **15**, 2856–61.
Newton, T. W. and Sullivan, J. C. (1985) in *Handbook on the Physics and Chemistry of the Actinides,* vol. 3 (eds. A. J. Freeman and C. Keller), Elsevier, New York, pp. 387–406.
Nugent, L. J., Baybarz, R. D., Burnett, J. L., and Ryan, J. L. (1973a) *J. Phys. Chem.*, **77**, 1528–39.
Nugent, L. J., Burnett, J. L., and Morss, L. R. (1973b) *J. Chem. Thermodyn.*, **5**, 665–78.
Nyssen, G. A. and Margerum, D. W. (1970) *Inorg. Chem.*, **9**, 1814–20.
Pachauri, O. P. and Tandon, J. P. (1975) *J. Inorg. Nucl. Chem.*, **37**, 2321–3.
Palmer, D. A. and Nguyen-Trung, C. (1995) *J. Solution Chem.*, **24**, 1281–91.
Panak, P. J., Booth, C. H., Caulder, D. L., Bucher, J. J., Shuh, D. K., and Nitsche, H. (2002a) *Radiochim. Acta*, **90**, 315–21.
Panak, P. J., Knopp, R., Booth, C. H., and Nitsche, H. (2002b) *Radiochim. Acta*, **90**, 779–83.

Passynskii, A. (1938) *Acta Phys. Chim. USSR*, **8**, 385–418.
Patil, S. K., Ramakrishna, V. V., and Rananiah, M. V. (1978) *Coord. Chem. Rev.*, **25**, 133–71.
Péligot, E. (1842) *Ann. Chim. Phys. Ser. 3*, **5**, 1–6.
Pepper, M. and Bursten, B. E. (1991) *Chem. Rev.*, **91**, 719–41.
Peretrukhin, V. F., David, F., and Maslennikov, A. (1994) *Radiochim. Acta*, **65**, 161–6.
Perrin, A. (1976) *Acta Crystallogr. B*, **32**, 1658–61.
Pinkerton, A. A., Pisaniello, D. L., and Zonnevijlle, F. (1984) *Inorg. Chim. Acta*, **82**, 153–6.
Pocev, S. and Johansson, G. (1973) *Acta Chem. Scand.*, **27**, 2146–60.
Portanova, R., Tomat, G., Magon, L., and Cassol, A. (1970) *J. Inorg. Nucl. Chem.*, **32**, 2343–8.
Portanova, R., Tomat, G., Magon, L., and Cassol, A. (1972) *J. Inorg. Nucl. Chem.*, **34**, 1768–70.
Portanova, R., Di Bernardo, P., Traverso, O., Mazzocchin, G. A., and Magon, L. (1975) *J. Inorg. Nucl. Chem.*, **37**, 2177–9.
Rabideau, S. W. and Cowan, H. D. (1955) *J. Am. Chem. Soc.*, **77**, 6145–8.
Rabideau, S. W. (1957) *J. Am. Chem. Soc.*, **79**, 6350–3.
Rabideau, S. W. and Masters, B. J. (1961) *J. Phys. Chem.*, **65**, 1256–61.
Rai, D., Strickert, R. G., Moore, D. A., and Ryan, J. L. (1983) *Radiochim. Acta*, **33**, 201–6.
Rai, D., Felmy, A. R., Sterner, S. M., and Moore, D. A. (1997) *Radiochim. Acta*, **79**, 239–47.
Rajan, K. S. and Martell, A. E. (1965) *Inorg. Chem.*, **4**, 462–9.
Rao, L. F. and Choppin, G. R. (1984) *Inorg. Chem.*, **23**, 2351–4.
Rao, L., Jiang, J., Zanonato, P. L., Di Bernardo, P., Bismondo, A., and Garnov, A. Y. (2002) *Radiochim. Acta*, **90**, 581–8.
Rapko, B. M., Duesler, E. N., Smith, P. H., Paine, R. T., and Ryan, R. R. (1993) *Inorg. Chem.*, **32**, 2164–74.
Raymond, K. (1985) in *Environmental Inorganic Chemistry* (eds. K. J. Irgolic and A. E. Martell), VCH Publishers, Deerfield Beach, FL, pp. 331–47.
Reynolds, J. G., Zalkin, A., Templeton, D. H., and Edelstein, N. M. (1977) *Inorg. Chem.*, **16**, 1090–6.
Rinaldi, P. L., Khan, S. A., Choppin, G. R., and Levy, G. C. (1979) *J. Am. Chem. Soc.*, **101**, 1350–1.
Rizkalla, E. N., Sullivan, J. C., and Choppin, G. R. (1989) *Inorg. Chem.*, **28**, 909–11.
Rizkalla, E. N., Nectoux, F., Dabos-Seignon, S., and Pagès, M. (1990a) *Radiochim. Acta*, **51**, 151–5.
Rizkalla, E. N., Nectoux, F., Dabos-Seignon, S., and Pagès, M. (1990b) *Radiochim. Acta*, **51**, 113–17.
Rizkalla, E. N. and Choppin, G. R. (1994) in *Handbook on the Physics and Chemistry of Rare Earths,* vol. 18 (eds. K. A. Gschneidner Jr, L. Eyring, G. R. Choppin, and G. H. Lander), Elsevier, New York, pp. 529–58.
Romanovski, V. V., White, D. J., Xu, J. D., Hoffman, D. C., and Raymond, K. N. (1999) *Solvent Extr. Ion Exch.*, **17**, 55–71.
Ryan, J. L. (1960) *J. Phys. Chem.*, **64**, 1375–85.
Ryan, J. L. (1961) *J. Phys. Chem.*, **65**, 1856–9.

Rykov, A. G., Vasil'ev, V. Y., and Blokhin, N. B. (1971) *Russ. J. Inorg. Chem.*, **16**, 1539–40.
Rykov, A. G. and Frolov, A. A. (1972a) *Sov. Radiochem.*, **14**, 737–40.
Rykov, A. G. and Frolov, A. A. (1972b) *Sov. Radiochem.*, **14**, 729–36.
Rykov, A. G., Andreichuk, N. N., and Vasil'ev, V. Y. (1973) *Sov. Radiochem.*, **15**, 350–5.
Rykov, A. G. and Frolov, A. A. (1974) *Sov. Radiochem.*, **16**, 786–92.
Rykov, A. G. and Frolov, A. A. (1975) *Sov. Radiochem.*, **17**, 189–91.
Samhoun, K., David, F., Hahn, R. L., O'Kelley, G. D., and Tarrant, J. R. (1979) *J. Inorg. Nucl. Chem.*, **41**, 1749–54.
Sandino, A. and Bruno, J. (1992) *Geochim. Cosmochim. Acta*, **56**, 4135–45.
Ščavnicar, S. and Prodic, B. (1965) *Acta Crystallogr.*, **18**, 698–702.
Schedin, U. (1975) *Acta Chem. Scand.*, **29A**, 333–44.
Schmidt, K. H., Gordon, S., Thompson, R. C., and Sullivan, J. C. (1980) *J. Inorg. Nucl. Chem.*, **43**, 611–15.
Sekine, T. (1964) *J. Inorg. Nucl. Chem.*, **26**, 1463–5.
Sekine, T. (1965) *Bull. Chem. Soc. Jpn.*, **38**, 1972–8.
Sekine, T., Hasegawa, Y., and Ihara, N. (1973) *J. Inorg. Nucl. Chem.*, **35**, 3968–70.
Shalinets, A. B. (1972a) *Sov. Radiochem.*, **14**(2), 285–9.
Shalinets, A. B. (1972b) *Sov. Radiochem.*, **14**(2), 279–84.
Shalinets, A. B. (1972c) *Sov. Radiochem.*, **14**(1), 18–25.
Shalinets, A. B. and Stepanov, A. V. (1972) *Radiokhimiya*, **14**, 280–3; *Sov. Radiochem.*, **14**, 290–3.
Shannon, R. D. (1976) *Acta Crystallogr.*, **32A**, 751–67.
Shcherbakov, V. A., Jorga, E. V., and Mashirov, L. G. (1974) *Sov. Radiochem.*, **16**, 286–7.
Shcherbakov, V. A. and Shcherbakova, L. L. (1976) *Radiokhimiya*, **18**, 207–10; *Sov. Radiochem.*, **18**, 188–90.
Sherif, F. G. and Awad, A. M. (1961) *J. Inorg. Nucl. Chem.*, **19**, 94–100.
Shilov, V. P. (1976) *Sov. Radiochem.*, **18**, 567–8.
Shilov, V. P., Stepanova, E. S., and Krot, N. N. (1976) *Sov. Radiochem.*, **18**, 310–13.
Shinkai, S., Koreishi, H., Ueda, K., Arimura, T., and Manabe, O. (1987) *J. Am. Chem. Soc.*, **109**, 6371–6.
Siddall, T. H. and Stewart, W. E. (1967) *Inorg. Nucl. Chem. Lett.*, **3**, 279–84.
Silva, R. J. and Nitsche, H. (1984) in *NRC Nuclear Waste Geochemistry* (eds. D. H. Alexander and G. F. Birchard), NUREG/CR-0052, U.S. Nuclear Regulatory Commission, Washington, DC, pp. 70–93.
Silva, R. J., Bidoglio, G., Rand, M. H., Robouch, P. B., Wanner, H., and Puigdomenech, I. (1995) *Chemical Thermodynamics of Americium,* Elsevier, New York.
Smith, T. D. (1959) *J. Inorg. Nucl. Chem.*, **11**, 314–19.
Spence, R. (1968) *Talanta*, **15**, 1307–9.
Spencer, S., Gagliardi, L., Handy, N. C., Ioannou, A. G., Skylaris, C. K., Willetts, A., and Simper, A. M. (1999) *J. Phys. Chem. A*, **103**, 1831–7.
Spitsyn, V. I., Gelman, A. D., Krot, N. N., Mefodiyeva, M. P., Zacharova, F. A., Komkov, Y. A., Shilov, V. P., and Smirnova, V. I. (1968) *J. Inorg. Nucl. Chem.*, **31**, 2733–45.
Stadler, S. and Kim, J. I. (1988) *Radiochim. Acta*, **44–45**, 39–44.
Standifer, E. M. and Nitsche, H. (1988) *Lanthanide Actinide Res.*, **2**, 383–4.

Starý, J. (1966) *Talanta*, **13**, 421–37.
Stemmler, A. J., Kampf, J. W., and Pecoraro, V. L. (1996) *Angew. Chem. Int. Edn. Eng.*, **35**, 2841–3.
Stepanov, A. V. (1971) *Russ. J. Inorg. Chem.*, **16**, 1583–6.
Stout, B. E., Caceci, M. S., Nectoux, F., and Pagès, M. (1989) *Radiochim. Acta*, **46**, 181–4.
Stout, B. E., Choppin, G. R., Nectoux, F., and Pagès, M. (1993) *Radiochim. Acta*, **61**, 65–7.
Stradling, G. N., Gray, S. A., Ellender, M., Moody, J. C., Hodgson, A., Pearce, M., Wilson, I., Burgada, R., Bailly, T., Leroux, Y. G. P., Elmanouni, D., Raymond, K. N., and Durbin, P. W. (1992) *Int. J. Radiat. Biol.*, **62**, 487–97.
Stumpf, T., Fanghänel, T., and Grenthe, I. (2002) *J. Chem. Soc., Dalton Trans.*, 3799–804.
Sullivan, J. C. and Hindman, J. C. (1954) *J. Am. Chem. Soc.*, **76**, 5931–4.
Sullivan, J. C., Cohen, D., and Hindman, J. C. (1955) *J. Am. Chem. Soc.*, **77**, 6203–4.
Sullivan, J. C., Cohen, D., and Hindman, J. C. (1957) *J. Am. Chem. Soc.*, **79**, 4029–34.
Sullivan, J. C., Zielen, A. J., and Hindman, J. C. (1960) *J. Am. Chem. Soc.*, **82**, 5288–92.
Sullivan, J. C., Hindman, J. C., and Zielen, A. J. (1961) *J. Am. Chem. Soc.*, **83**, 3373–8.
Sullivan, J. C. (1962) *J. Am. Chem. Soc.*, **84**, 4256–9.
Sullivan, J. C. (1964) *Inorg. Chem.*, **3**, 315–19.
Sullivan, J. C. and Zielen, A. J. (1969) *Inorg. Nucl. Chem. Lett.*, **5**, 927–31.
Sullivan, J. C., Gordon, S., Cohen, D., Mulac, W. A., and Schmidt, K. H. (1976) *J. Phys. Chem.*, **80**, 1684–6.
Sullivan, J. C., Nash, K. L., and Choppin, G. R. (1978) *Inorg. Chem.*, **17**, 3374–7.
Sullivan, J. C. and Nash, K. L. (1986) in *Inorganic and Bioinorganic Reaction Mechanisms,* vol. 4 (ed. A. G. Sykes), Academic Press, London, pp. 185–213.
Sullivan, J. C., Choppin, G. R., and Rao, L. F. (1991) *Radiochim. Acta*, **54**, 17–20.
Sutton, J. (1952) *Nature*, **169**, 235–6.
Swift, T. J. and Sayre, W. G. (1966) *J. Chem. Phys.*, **44**, 3567–74.
Szabó, Z., Aas, W., and Grenthe, I. (1997) *Inorg. Chem.*, **36**, 5369–75.
Szabó, Z. and Grenthe, I. (2000) *Inorg. Chem.*, **39**, 5036–43.
Szabó, Z., Moll, H., and Grenthe, I. (2000) *J. Chem. Soc., Dalton Trans.*, 3158-61.
Szabó, Z. (2002) *J. Chem. Soc., Dalton Trans.*, 4242–7 .
Tochiyama, O., Inoue, Y., and Narita, S. (1992) *Radiochim. Acta*, **58/59**, 129–36.
Tochiyama, O., Siregar, C., and Inoue, Y. (1994) *Radiochim. Acta*, **66/67**, 103–8.
Tomilin, S. V., Volkov, Y. F., Kapshukov, I. I., and Rykov, A. G. (1981) *Sov. Radiochem.*, **23**, 570–4, 574–8, 695–9.
Tomilin, S. V., Volkov, Y. F., Melkaya, R. F., Spiryakov, V. O., and Kapshukov, I. I. (1986) *Sov. Radiochem.*, **28**(3), 272–8.
Toraishi, T., Farkas, I., Szabó, Z., and Grenthe, I. (2002) *J. Chem. Soc., Dalton Trans.,* 3805–12.
Tsushima, S. and Suzuki, A. (2000) *J. Mol. Struct.* (*THEOCHEM*), **529**, 21–5.
Vallet, V., Wahlgren, U., Schimmelpfennig, B., Moll, H., and Szabó, Z., Grenthe, I. (2001) *Inorg. Chem.*, **40**, 3516–25.
Vallet, V., Wahlgren, U., Szabó, Z., and Grenthe, I. (2002) *Inorg. Chem.*, **41**, 5626–33.
Vdovenko, V. M., Romanov, G. A., and Shcherbakov, V. A. (1963) *Sov. Radiochem.*, **5**, 624–7.

Vodovatov, V. A., Mashirov, L. G., and Suglobov, D. N. (1979) *Sov. Radiochem.*, **21**(6), 711–16.
Wahlgren, U., Moll, H., Grenthe, I., Schimmelpfennig, B., Maron, L., Vallet, V., and Gropen, O. (1999) *J. Phys. Chem. A*, **103**, 8257–64.
Walch, P. F. and Ellis, D. E. (1976) *J. Chem. Phys.*, **65**, 2387–92.
Wang, Z., Felmy, A. R., Xia, Y. X., and Mason, M. J. (2003) *Radiochim. Acta*, **91**, 329–37.
Werner, A. (1913) *Neu Anschauungen auf dem Gebiet der anorganischen Chemie,* 3rd edn, Vieweg Sohn, Braunschweig.
Wilkins, R. (1974) *The Study of Kinetics and Mechanisms of Reactions of Transition Metal Complexes,* Allyn and Bacon, Boston.
Williams, K. R. and Choppin, G. R. (1974) *J. Inorg. Nucl. Chem.*, **36**, 1849–53.
Williams, C. W., Blaudeau, J.-P., Sullivan, J. C., Antonio, M. R., Bursten, B. E., and Soderholm, L. (2001) *J. Am. Chem. Soc.*, **123**, 4346–7.
Wimmer, H., Kim, J. I., and Klenze, R. (1992) *Radiochim. Acta*, **58/59**, 165–71.
Xu, J., Kullgren, B., Durbin, P. W., and Raymond, K. N. (1995) *J. Med. Chem.*, **38**, 2606–14.
Yaozhong, C., Bingmei, T., and Zhangji, L. (1993) *Radiochim. Acta*, **62**, 199–201.
Yusov, A. B. and Shilov, V. P. (1999) *Radiochemistry*, **41**, 1–23.
Yusov, A. B. and Fedoseev, A. M. (2003) *Russ. J. Coord. Chem.*, **29**, 582–90.
Zhao, P. H., Romanovski, V. V., Whisenhunt, D. W., Hoffman, D. C., Mohs, T. R., Xu, J. D., and Raymond, K. N. (1999) *Solvent Extr. Ion Exch.*, **17**, 1327–53.
Zhu, Y., Chen, J., and Jiao, R. (1996) *Solvent Extr. Ion Exch.*, **14**, 61–8.
Zielen, A. J. (1959) *J. Am. Chem. Soc.*, **81**, 5022–8.
Zielen, A. J. and Cohen, D. (1970) *J. Phys. Chem.*, **74**, 394–405.

CHAPTER TWENTY FOUR

ACTINIDE SEPARATION SCIENCE AND TECHNOLOGY

Kenneth L. Nash, Charles Madic, Jagdish N. Mathur, and Jérôme Lacquement

24.1 INTRODUCTION

Both the science and technology of the actinides as we know them today owe much to separation science. Conversely, the field of metal ion separations, solvent extraction, and ion exchange in particular, would not be as important as it is today were it not for the discovery and exploitation of the actinides. Indeed, the synthesis of the actinides and the elucidation of their chemical and physical features required continuous development and improvement of chemical separation techniques. Furthermore, the diverse applications of solvent extraction and ion exchange for metal ion separations as we know them today received significant impetus from Cold War tensions (and the production of metric tons of plutonium) and the development of nuclear power for peaceful uses.

Solvent extraction, precipitation/coprecipitation, and ion exchange procedures have played a central role in the discovery and characterization of the 5f transition elements. Each of these separations techniques likewise has shaped progress in technological applications of actinides for electricity production and for nuclear weapons. Recent decades have seen the rise of pyroelectrometallurgical separations, wherein the long-term future of actinide separations may lie.

Efficient chemical separations are an essential feature of actinide science and technology because (1) aside from U and Th there are no primordial transuranic actinides and so no natural mineral deposits from which to isolate them and (2) the nuclear techniques employed to create actinides also induce fission in the heavy metal target atoms producing mixtures that can include up to one-third of the periodic table. Whether for scientific purposes or technological applications, high degrees of purification of actinides from diverse solid solutions containing small amounts of the desired material in a complex solid matrix are required. This chapter addresses the details of these chemical separation processes and describes what the exercise of these separation processes has taught us about the chemistry of the actinides.

Four specific separation tasks had to be accomplished to enable the discovery of the 5f elements and then to support creation of sufficient amounts of these elements to sustain their practical application: isolation of natural uranium from its mineral sources, isotope enrichment to increase the relative percentage of fissile ^{235}U above that of natural uranium, separation of actinides from a diverse mixture of fission products, and separation of individual members of the series. The accomplishment of these tasks required innovative solutions to demanding problems. Setting aside the technologically essential process of isotope enrichment (not discussed in this chapter), separations of actinides can be considered at two scales: analytical-scale separations conducted at low concentrations or with small amounts of the analyte, and large-scale separations conducted on kilogram quantities of materials in large shielded facilities. Each of these carries unique opportunities and challenges. Analytical separations are best served by reagents that are both highly specific and very efficient (i.e. capable of quantitatively separating the target species in a single (or small number of) contact(s)). Plant-scale separations also perform best with highly specific reagents, but extremely high phase-transfer efficiency typically is not preferred because materials must also be readily recovered from the separation matrix. Weak chemical separations processes can be overcome at plant scale by adding more repeat contacts (stages) of reagents.

In a once through nuclear fuel cycle, there are no large-scale separations subsequent to the preparation of the enriched uranium fuel. However, in the operation of a closed loop fuel cycle, it is necessary to separate the transuranium actinides individually or as a group from uranium and fission products. For the purpose of scientific discovery, it was (and is) necessary to isolate individual members of the series. The diverse redox chemistry of uranium, neptunium, and plutonium is the primary feature of processes for their isolation and purification. For the actinides beyond americium and in most applications for americium as well, the trivalent oxidation state predominates. The trivalent oxidation state is also prevalent in the lanthanides, which are produced in about one-third of thermal neutron-induced fission events in ^{235}U and ^{239}Pu. Most features of the chemistries of the trivalent transplutonium actinides and lanthanides are nearly identical.

Aside from the unique demands of trivalent actinide/lanthanide group separations, the discussions of separations systems below will consider features of lanthanide separations as representative of the behavior of trivalent actinides. The separation of individual trivalent actinides relies on the predominantly electrostatic bonding characteristics of the ions and on the steady reduction that is seen in the trivalent cation radii with increasing atomic number, a behavior paralleling that of the lanthanides. This small but (more-or-less) regular decrease in cationic radii provides an adequate driving force for ion exchange-based separations of the individual members of the series, as will be described below.

The actinides are as a group readily separated from most fission products, based on their unique chemistry as compared with the great diversity of species present. Typically, only Ru, Mo, Zr (under some circumstances), and the ubiquitous lanthanides represent a significant separations challenge. The isolation of individual trivalent transplutonium actinides from trivalent lanthanides can be readily achieved if the species to be separated are sufficiently differentiated based on cation radii. Specifically, the transplutonium elements can be readily separated from the light lanthanides, but with greater difficulty from those in the middle of the series. For an effective separation of the trivalent actinides from the lanthanides as a group or for ions having similar cation radii, it has proven essential to incorporate into the separation scheme donor atoms 'softer' than oxygen or fluoride. Poly-aza ligands of complex geometries, chloride ions, thiocyanate ions, or species containing sulfur donor atoms have proven the most viable candidates. These soft-donor reagents can appear in the separation schemes either as lipophilic extractant molecules or as water-soluble complexing agents.

Nearly 60 years of industrial scale implementation of aqueous processing schemes has produced both considerable insight into the ways and means of conducting these separations, and large waste disposal/environmental restoration challenges at the sites where such large-scale processing has been conducted. The legacy of the massive volume of waste generated during these many years of aqueous processing to recover actinides from spent fuel has spurred efforts to develop radically different approaches. In particular, separations developed conceptually in the 1960s based on molten salts, molten metal, including electrochemical processing in these media, have received considerable attention in recent years for their potential as alternative large-scale separations methods for spent fuel processing. Such methods tend to strongly favor reduced actinide species and radically different (though fundamentally simple) coordination chemistry for the actinide species in these media. Far less is known about the chemistry of actinides in supercritical fluids, room-temperature ionic liquids, or other non-conventional media, but any of these methods could play a central role in future nuclear fuel cycles. Processes based on volatility of certain actinide compounds have also received some attention and possess some interesting features. However, each of these concepts is far behind aqueous processing,

both because of the number of years of experience that have been accumulated for the aqueous option, and the unknowns always attendant to developing new science and technology.

24.1.1 Prior literature reviews/useful reference volumes

There are two categories of previous studies each serving a complementary role in describing actinide separation science: those providing 'recipes' for conducting separations of radioactive materials and those explaining the underlying principles. In the beginning, the chemical properties of the transuranium elements were a matter of informed speculation, so underlying principles were not known except by inference. Their discovery and the ultimate elucidation by Seaborg of the actinide hypothesis was a clear demonstration of the correctness (and utility) of Mendeleev's periodic table. The chemical separation procedures that enabled actinide science as we know it today were based on belief in chemical periodicity. One remarkable aspect of actinide separation science is the enduring quality of many of the separations developed during the days of actinide discovery. This is a tribute to the talents and abilities of those early practitioners of actinide separation science.

Perhaps the most useful (even today 40 or more years after their publication) detailed experimental separation procedures are those found in the National Academy of Science Series on radioanalytical chemistry. This series, published in the 1950s and 1960s, still constitutes a useful primary reference for formula separation schemes for the entire periodic table, including the actinides. Though individual bound volumes of these separation procedures are widely available, the series is long out of print. These volumes are however presently available online (http://lib-www.lanl.gov/radiochemistry/elements.htm).

Of course, the insights gained from these initial explorations have allowed the development of more general reference works and a better understanding of the chemical features of the processes. The classic reference book for aqueous separations chemistry (both ion exchange and solvent extraction) has long been *Ion Exchange and Solvent Extraction of Metal Complexes* by Marcus and Kertes (1969). In this book, the theory and practice of separation science is discussed in great detail. Solvent extraction chemistry has been reviewed by Sekine and Hasegawa (1977). In addition to concentrating on solvent extraction, this work differs from the Marcus and Kertes volume in that it has references to many more specific examples. Helfferich (1962) published a volume that is generally considered as the most authoritative discussion of the unique theoretical aspects of ion exchange-based separations. Two 'how-to' manuals have been published which describe in detail useful ion exchange separation procedures for the lanthanides and actinides (Korkisch, 1986a,b).

Updates on the state of the art of f-element separations have appeared in the literature at regular intervals. Jenkins (1979, 1984) reviewed ion exchange applications in the atomic energy industry. Symposium volumes entitled

Actinide Separations (Navratil and Schulz, 1980), *Lanthanide/Actinide Separations* (Choppin *et al.*, 1985) and *Separations of f Elements* (Nash and Choppin, 1995) are collections of papers from several authors covering various aspects of lanthanide and actinide separations. Additional specialized reviews of specific topics have also appeared frequently. Most of these are considered below.

The subject of lanthanide/trivalent actinide separations has been reviewed previously (Weaver, 1974; Nash, 1993a). Weaver's review is an excellent source for a comprehensive discussion of solvent extraction separations of the lanthanides and trivalent actinides. Weaver discusses many of the historical aspects of lanthanide/actinide separations, and considers both the successes and failures in the separation of trivalent lanthanides and actinides. Nash's review complements and updates the observations of Weaver, emphasizing the critical role played by soft-donor ligands in the development of efficient processes for the selective separations of the trivalent 4f and 5f elements.

Arguably, the most important reagent for actinide separations is tri(*n*-butyl) phosphate (TBP – structure a). This compound is the subject of a four-volume handbook entitled *The Science and Technology of Tributyl Phosphate* (Schulz *et al.*, 1990). Many chapters in this collection address important features of the application of TBP for nuclear fuel processing and actinide recovery. On the subject of large-scale separations of actinides, the current state of the art in hydrometallurgical processing of actinides from spent fuel or radioactive wastes has been reviewed recently (Horwitz and Schulz, 1999; Mathur *et al.*, 2001).

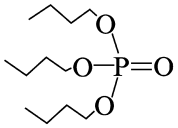

Structure a

These reports describe and critically evaluate water-based actinide partitioning research activities being conducted around the world. The diversity of activities being pursued worldwide is in some respects surprising. However, it does reflect the increasingly important nature of these separations. In truth, aqueous separations still dominate the actinide separations landscape. Contemporary research attempts to take a 21st century perspective on nuclear fuels processing, emphasizing the importance of closing the fuel cycle while minimizing the generation of wastes requiring geological disposal.

24.1.2 Scope of the chapter

The space available to this chapter simply does not allow for a comprehensive treatment of all aspects of the subject of actinide separations. Some selectivity will therefore be applied in the following discussion. All essential features of actinide separations will be discussed, but it will not be possible to include detailed step-by-step descriptions of all of the well-known separation systems.

The reader will find such information among the several reviews noted above. Greater emphasis will be placed on the details of newer science and technologies, those currently being considered for advanced applications, and on those most appropriate methods to preserve long-term options for nuclear fuels recycling in the 21st century.

Because chemical separations have played such an important role in the discovery of the actinides, the chapter begins with a discussion of the early history of actinide separations. This discussion will be followed by some consideration of the fundamental chemistry of separation systems and of actinide behavior in phase transfer systems. The fundamental chemistry of actinides in aqueous solutions has been described in the previous chapter. It will therefore not be necessary to address the details of actinide behavior in solution in detail here. However, some aspects of the aqueous chemistry of actinides (redox, solvation, complexation) do play an important role in actinide separations, and so will receive an appropriate emphasis wherever needed in this chapter. The general features of phase transfer reactions will be discussed briefly, focusing on the differences between the classic solvent extraction, ion exchange, and precipitation methods. Unconventional techniques, those still at the developmental/exploration stage, including those related to the use of supercritical fluids (mainly CO_2), molten metals/molten salts, and more exotic (and less extensively tested) techniques like those based on the use of room temperature ionic liquids (RTILs) or volatility will then be addressed. The issue of scale will be considered with coverage of analytical separations followed by a detailed description of the current state of the art in hydrometallurgical (industrial-scale) separations for actinide recovery, recycle, and transmutation. The chapter concludes with some consideration of future directions.

24.2 HISTORICAL DEVELOPMENT OF ACTINIDE SEPARATIONS

Actinide separations had its beginnings with the discovery of radioactivity. Crookes and Becquerel found that the addition of carbonate to a solution containing uranium caused the formation of a precipitate that contained the beta, gamma radioactivity while the uranium remained in the solution phase. Rutherford and Soddy made a similar observation for thorium. Marie and Pierre Curie began a program to separate the components of pitchblende. In 1898, they announced the discovery of the new element polonium, ''While carrying out these operations (separations by precipitation), more active products are obtained. Finally, we obtained a substance whose activity was 400 times larger than that of uranium. We therefore believe that the substance whose activity we have isolated from pitchblende is a hitherto unknown metal. If the existence of this metal can be affirmed, we suggest the name polonium'' (Choppin *et al.*, 2002). The separation method used by these pioneers was precipitation/coprecipitation, which remained the predominant

separation technique through the Manhattan Project of World War II. A historical perspective on the development of this science and technology through the end of World War II is available in *The Making of the Atomic Bomb* (Rhodes, 1986).

Between 1934 and 1939, about 50 research papers claimed the discovery and reported studies of transuranium elements with $Z = 93$, 94, 95, 96. In 1939, Hahn and Strassmann conducted very careful separations on neutron-irradiated uranium samples and proved that these 'transuranium elements' were, in fact, products of nuclear fission with atomic numbers below 60. This led to new experiments in 1940 in which neptunium ($Z = 93$) and plutonium ($Z = 94$) were synthesized and separated. These new elements were isolated using an oxidation–reduction cycle (with BrO_3^- as the oxidizing agent) followed by precipitation of the reduced metal ions with crystalline LaF_3, establishing a link with the 4f elements.

Within the context of world politics in the 1930s and 1940s (and as it turned out the following decades), it was perhaps inevitable that the discovery of fission would be first valued for its potential military applications. Two approaches to the assembly of a critical mass were immediately recognized: isotope enrichment to increase the atom percentage of the fissile uranium isotope ^{235}U and transmutation of ^{238}U by neutron capture and β^- decay to produce ^{239}Pu. The former option required a many theoretical plate isotope separation process wherein the stage-wise efficiency is limited by the small difference in mass of the two principal isotopes. Plutonium production instead relies on neutron capture in a reactor fueled by uranium (the ratio of ^{239}Pu production to fission of ^{238}U after capture of a thermalized neutron is about 14 to 1 (Choppin and Rydberg, 1980) and chemical separation of different elements. Differences in the redox chemistries of uranium and plutonium facilitate their mutual separation. Neither isotope enrichment nor plutonium production were considered to have an advantage in the race to produce a critical mass for the first nuclear weapon in time to affect the outcome of the war, so both methods were pursued with equal vigor in the Manhattan Project.

Two approaches to uranium isotope enrichment were proposed for full investigation and process development: electromagnetic isotope separation, proposed by E. O. Lawrence at Berkeley, and gaseous diffusion, championed by John Dunning at Columbia University (Rhodes, 1986). The latter was considered the more likely to succeed on an industrial scale because it was based on technology that was better established. It also offered the advantage of continuous operation, which was not deemed possible in the electromagnetic separation option. Electromagnetic isotope separation received equal consideration because of the greater per-stage separation potential of the technique. Each method relied on the low-temperature volatility of UF_6 (Cotton and Wilkinson, 1988).

As research continued on both approaches, groundbreaking occurred on the Clinch River in eastern Tennessee in 1942, leading to the establishment of the Clinton Engineering Works in Oak Ridge. The Gaseous Diffusion Plant (K-25)

required the co-siting of a dedicated coal-fired power plant and occupied about 0.2 sq. km under a four-stories-high roof. The electromagnetic isotope separations plant (Y-12) occupied half that space and required 13 tons of silver (borrowed from the U.S. Treasury) for the electromagnets. In the end, K-25 provided feedstock of up to 50% enriched ^{235}U to the Y-12 plant for completion of the high enrichment needed for weapons production. These two plants working in tandem produced the ^{235}U for the Hiroshima weapon (Rhodes, 1986).

Industrial scale plutonium production was first accomplished at the Hanford site on the Columbia River near Richland, Washington (Anonymous, 1996). It began with commissioning of B reactor in September 1944 and continued through the lifetimes of eight single-pass reactors, N reactor (the only dual-use Hanford reactor that produced both usable steam and Pu), and the fast flux test facility (FFTF) ending in the early 1980s. The isolation of plutonium from uranium and fission products was initially accomplished by precipitation with $BiPO_4$. The process, pioneered by S. G. Thompson (Thompson and Seaborg, 1956, 1957; Seaborg and Thompson, 1960), involves coprecipitation of Pu(IV) by $BiPO_4$ followed by oxidation to Pu(VI), which does not carry on $BiPO_4$. The process was repeated several times and followed by a LaF_3 precipitation to increase the purity of the product. This batch process is inherently inefficient and has the additional disadvantage of losing uranium to the waste stream. At the time, the loss of uranium to the waste stream was particularly damaging to process efficiency because of the limited amount of purified uranium that was available. However, precipitation/coprecipitation was the only viable technology that could be readily scaled up to production plant dimensions within the demanding time constraints of the Manhattan Project. In fact, the $BiPO_4$ coprecipitation process was first demonstrated using microgram quantities of plutonium, hence the scale-up was by a factor of 10^9. Because of the consistency and reproducibility of the chemistry involved, this scale-up occurred without significant complications. After the war, additional separations of $BiPO_4$ wastes were conducted to recover the rejected uranium for recycle to reactors.

$BiPO_4$ was eventually replaced at Hanford by solvent extraction processes based on the use of methyl(isobutyl)ketone (hexone, Structure b) for extraction of uranium and plutonium from slightly acidic $Al(NO_3)_3$ solutions (REDOX process) and later using TBP to selectively extract (and mutually separate) uranium and plutonium from nitric acid solutions (PUREX process). Great improvements in efficiency were achieved with each successive development, though the PUREX process produced a far smaller volume of secondary wastes than the REDOX process. Fifty years later, PUREX remains the principal method for processing of spent nuclear fuel.

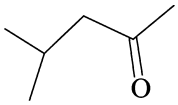

Structure b

In the spirit of scientific discovery and at several laboratories around the world, though primarily at Berkeley and under the supervision of Glenn Seaborg, research in the 1950s and 1960s continued to extend the actinide series from plutonium and americium towards the final element of the series ($Z = 103$). The identification of new elements demands satisfaction of "...The basic criterion for the discovery of a new element is the experimentally verified proof that the atomic number of the new element is different from the atomic numbers of all previous elements. Establishment of the atomic number can be by chemical means, by identification of the characteristic X-rays in the decay of the new species, or by establishment of genetic decay relationships through α-particle decay chains in which the new element is identified by the observation of previously known decay products" (Seaborg and Loveland, 1990). To respond to the demand for predictable chemistry, it was essential that the separations process behave in a systematic fashion.

As the postwar research on actinide syntheses progressed, it was quickly learned that the rich redox chemistry of the light actinides, which was central to most of the successful separations of the light members of the series, did not persist beyond americium. In aqueous solutions, the elements beyond americium behaved chemically more like the 4f analog lanthanides than the light members of the series, strongly preferring to remain in the trivalent oxidation state.

Because synthesis of successive members of the series (beyond Cm) required the isolation and irradiation of a previous member of the series, the task of identifying the later members of the series was hindered not only by the ability to analyze for new species produced, but also by the rate at which target elements could be produced (and how quickly they decayed). The difficulty is demonstrated in Table 24.1 in which the nuclear reaction, target element, and product are noted. The process was further complicated by the increasingly short half-lives of the elements produced, and the low efficiency of the reactions leading to their production. For the elements beyond einsteinium, only a few atoms at a time were created and detected. The procedures of one-atom-at-a-time chemistry have been described in some detail by Seaborg and Loveland (1990) and can be found in Chapters 13 and 14 of this work.

The particle capture reactions that yielded new elements were also always accompanied by some fission. Yields for lanthanides in heavy element fission are high thus the dissolution of irradiated targets led to the creation of solutions that contained not only small amounts of the target transamericium elements but also significant concentrations of lanthanides. This complication impacted both the identification of new elements and the creation of appropriate target materials.

Two challenging separation problems resulted from this circumstance: the need for mutual separation of the two groups (5f from 4f), and of adjacent metal ions (in the 5f series) of identical charge and similar cationic radii. Because

Table 24.1 *Summary of original actinide synthesis methods, means, and materials.*

Actinide	*Target*	*Half-life*[a] (*Target*)	*Half-life*[a] (*Product*)	*Projectile*	*Method*
^{239}Np	^{238}U	4.47×10^9 yr	2.35 d	n	cyclotron
^{238}Pu	^{238}U	4.47×10^9 yr	87.74 yr	^{2}H	cyclotron
^{241}Am	^{239}Pu	24 100 yr	432.7 yr	n	reactor
^{242}Cm	^{239}Pu	24 100 yr	162.7 d	^{4}He	cyclotron
^{243}Bk	^{241}Am	432.7 yr	4.5 h	^{4}He	cyclotron
^{245}Cf	^{242}Cm	162.9 d	43.6 min	^{4}He	cyclotron
^{253}Es	^{238}U	4.47×10^9 yr	20.47 d	n	fusion explosion
^{255}Fm	^{238}U	4.47×10^9 yr	20.47 h	n	fusion explosion
^{256}Md	^{253}Es	20.47 d	1.27 h	^{4}He	cyclotron
^{254}No	^{244}Cm	18.11 yr	55 s	^{12}C	HILAC[b]
^{258}Lr	$^{249–252}$Cf	351, 13.08	3.9 s	^{10,11}B	HILAC[b]
	–	898, 2.645 yr	–	–	–

[a] Appendix II.
[b] Heavy ion linear accelerator.

of the minute amounts of materials being used as targets and produced in irradiations, and the absence of multiple oxidation states, many standard separation procedures (e.g. precipitation/coprecipitation) were simply not useful. The emergence of polymeric ion exchange materials proved essential to accomplishing both of these separations.

Though cation exchange resins bearing readily deprotonated sulfonic acid groups adsorbed the trivalent f-elements strongly, even from moderately acidic solutions, these sorbents exhibited little inherent facility for accomplishing either separation, i.e. there was insufficient differentiation between cations of similar size. Lanthanides and trivalent actinides were absorbed by the resin under the same conditions and with most inorganic eluants exited the column together. The secret to attaining selectivity was proper choice of the eluting solution. Two distinctly different classes of eluting agents were applied to these separation problems, soft-donor ligands, and hydroxycarboxylate complexants. Their use enabled the positive identification of the remaining members of the series thus confirming the basic correctness of the actinide hypothesis. Each of these separations methods is discussed in greater detail in Section 24.3.3.

24.3 FUNDAMENTAL FEATURES OF ACTINIDE SEPARATION SYSTEMS

To isolate an actinide ion from a complex mixture, some procedure must be devised to transport the target metal ion from its starting condition into a separate phase and then recover the target metal ion from that separate phase. For analytical-scale separations, a highly efficient process that can be

accomplished in a single (or small number of) contact(s) between the phases is most desirable. For large-scale separations, complex series of processes are typically combined to accomplish the separation. As a result, less efficient single-stage chemical processes are acceptable (and in fact often preferred) for hydrometallurgical applications. Selectivity becomes a more important feature than extractant strength. The key features needed for large-scale separations of nuclear materials are: (1) reversibility of phase transfer (mass transport) reactions with a shift in extraction conditions, (2) sufficient reliability to be readily adaptable to remote (i.e. no human contact) operations, (3) rapid chemical reaction and phase-transfer kinetics, and (4) the ability to operate in a continuous rather than batch fashion. The first three features are absolutely essential; the fourth is highly desirable. Materials must also demonstrate physical and chemical stability in contact with strongly acidic aqueous solutions and in a high radiation environment. General features of selected separation techniques will be discussed in the following sections.

24.3.1 Volatility-based separations methods

Choppin (2002) has provided an overview of the subject of separation processes based on the volatility of actinides and selected fission products. He suggests possible approaches to selective removal of Zr, Tc, and Ru fission products (or cladding material) through their volatile oxides (Tc, Ru) or chlorides (Zr). There are also reports on the potential use of volatile β-diketone complexes of trivalent lanthanides for gas phase based separations. For example, tetra- and hexavalent actinide cations are known to form volatile compounds with FOD (6,6,7,7,8,8,8-heptafluoro-2,2-dimethyl-3,5-octanedione, Structure c), which could form the basis for a separation of uranium and plutonium from americium (Anonymous, 1995). This same reagent will appear again in the discussion of actinide separations methods based on supercritical CO_2 (Section 24.3.10). No separation system based on the volatility of either fission product oxides or β-diketonate complexes has received extensive development at the process scale.

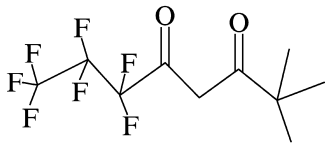

Structure c

The most extensively researched system for volatility separations is based on the same volatile fluorides that are the basis of isotope separations. A separation based on the volatility of uranium and plutonium fluorides was demonstrated by Hyman *et al.* (1956) and investigated in greater detail at Oak Ridge National Laboratory for reprocessing as a part of the molten salt reactor project (Rosenthal *et al.*, 1972). The overall effectiveness of the process is limited

principally by the simultaneous production of volatile fluorides of fission products Tc, Te, and I. The volatile fluorides can be separated by distillation, though the lower volatility of PuF_4 (arising from the decomposition of PuF_6) leads to Pu deposition problems. In principle, this approach should produce minimal volumes of wastes, though operations combining fluorine compounds and radioactive materials always present challenging materials handling and safety issues. The application of fluorinated compounds to volatility separations is mimicked in many separations that rely on supercritical CO_2, as will be discussed in Section 24.3.10.

24.3.2 Precipitation/coprecipitation methods

In the laboratory, precipitation and coprecipitation processes are a regular and accepted feature of radioanalytical chemistry. Several applications of precipitation and coprecipitation techniques for conducting investigations of the redox speciation of actinides at radiotracer concentrations are discussed in Section 24.4.1a. For the cleanup of aqueous media containing low concentrations of actinides, ultrafiltration has also been employed to collect ultrafine actinide-containing solids (Cecille *et al.*, 1987; Senentz and Liberge, 1998; Smith *et al.*, 1998, 1999; Bisset *et al.*, 2003). Though a number of precipitation processes have been advanced over the years to assist in selected actinide separation scenarios (Bertozzi *et al.*, 1976; Mousty *et al.*, 1977; Pietrelli *et al.*, 1987; Spurny and Heckmann, 1987; Grossi *et al.*, 1992a,b; Sinha *et al.*, 1992; Strnad and Heckmann, 1992; Felker *et al.*, 1995; Tomiyasu and Asano, 1995; Harada *et al.*, 2001), precipitation is no longer practiced as the primary means of separations for large-scale actinide production purposes.

Because the actinides are acidic cations, they readily undergo hydrolysis and precipitate as hydroxides. If complexing agents are kept from the solution, actinide hydroxides can be readily precipitated in the trivalent ($K_{sp} \approx 10^{-20}$), tetravalent ($K_{sp} \approx 10^{-54}$), pentavalent ($K_{sp} \approx 10^{-10}$), and hexavalent ($K_{sp} \approx 10^{-25}$) oxidation states (Martell and Smith, 1998). Hydroxides are generally avoided at the production scale and are unreliable for radioanalytical purposes, but often prove quite convenient avenues to the purification of actinide ions at the milligram to gram level for research purposes. Their most notable feature is the ready reversibility of the precipitation through the addition of mineral acid solutions, thus hydroxide precipitation can be used to readily convert from (for example) chloride to nitrate salts. The cautionary note here is to avoid the formation of tetravalent plutonium hydroxide, which has an extremely low K_{sp} and is redissolved only with difficulty, and often not cleanly, particularly if the precipitate is aged. The presence of carbonate or strong complexing agents (e.g. aminopolycarboxylates) can seriously interfere with hydroxide precipitation processes.

Other species that are readily precipitated are the phosphates of actinide ions in any oxidation state and under a wide range of conditions, and the fluorides

and the oxalates of trivalent and tetravalent actinide ions. The latter two reagents can be employed for oxidation state-based separations, as the pentavalent or hexavalent actinide cations do not form insoluble species under most conditions with these anions while both the trivalent and tetravalent ions precipitate readily from acidic solutions. In the remanufacture of plutonium from nuclear weapons pits (fission core of a thermonuclear device), the selective precipitation of tetravalent plutonium as the peroxide was an essential feature of operations at the Rocky Flats Plant (Cleveland, 1970).

The most technologically important coprecipitation process (no longer used in practice) is that based on bismuth phosphate, as noted above in Section 24.2 and again later in more detail in the discussion of process chemistry. For actinide oxidation state speciation in radioanalytical applications, the actinides themselves are present at concentrations too low to challenge solubility limits in a reliable fashion. The introduction of cations and anions that combine to form insoluble species that carry the actinides down are useful analytical or laboratory-scale purification procedures. This is the case of lanthanum fluoride (LaF_3) whose solubility product is reported as about $10^{-18.7}$ (Martell and Smith, 1998). This compound is readily precipitated from comparatively dilute acidic fluoride solutions. LaF_3 (actually, most any lanthanide will serve) quantitatively carries trivalent and tetravalent actinide ions. Care must be exercised for quantitative LaF_3 carrier precipitation to avoid excess HF, as the resultant formation of soluble metal fluoride complexes can interfere with the efficiency of precipitation. Partly as a result of the unique coordination geometry of the dioxo actinide (V) and (VI) cations, there are no reliable coprecipitation procedures for their analysis or macroscale separation, though there are a number of insoluble adsorbents that will remove these ions from solutions (though with limited selectivity). These adsorption reactions will be discussed in Section 24.4.1.

24.3.3 Ion exchange methods

The development of solid materials capable of capturing and reversibly releasing the metal ions back into the contacting solution, ion exchange materials, was a great step forward in separating elements with similar properties. The earliest non-crystallization separation processes for individual trivalent lanthanide ions based on inorganic ion exchangers demonstrated separation factors for adjacent ions of 1.01–1.05, barely acceptable for chromatographic separations using large columns. For the production of actinides in microscopic amounts, such separation factors are simply too low to be useful. The selectivity limitations of inorganic ion exchange materials were only slightly improved with the development of polymeric organic ion exchange materials, though the latter offered superior reproducibility and resistance to dissolution. Radiation stability is an issue for either class of sorbents, but more problematic for the polymeric

materials. Clearly, more efficient procedures were required to cope with submicroscopic amounts of the new transplutonium elements being produced.

The separation of trivalent actinides from lanthanides was first achieved by cation exchange from concentrated chloride media. Street and Seaborg (1950), Diamond *et al.* (1954), and later Choppin and Chetham-Strode (1960) demonstrated that the behavior of lanthanides and actinides on cation exchange columns was identical below 6 M HCl, but diverged between 6 and 12 M (as shown in Fig. 24.1). Separation factors of about 10 were achieved at 12 M HCl. Separation efficiency was increased when the separation was carried out from salt solutions (dilute acid) or from alcohol–water mixtures of HCl. Diamond and coworkers proposed that the separation of promethium and americium at high concentrations of HCl was a manifestation of f-orbital covalency to the bonding of Am^{3+} to Cl^{-} (which is not present in the Pm system). The origin of the effect is still a matter of discussion and debate, but it has become abundantly clear over the intervening decades that the most effective trivalent actinide and lanthanide separations are based on the contribution of ligand donor atoms softer (i.e. more polarizable) than oxygen.

Separation efficiency was slightly greater when anion exchange was employed. Thompson *et al.* (1954) found actinide/lanthanide separation factors above 10 for anion exchange separation from 10 M LiCl aqueous solutions.

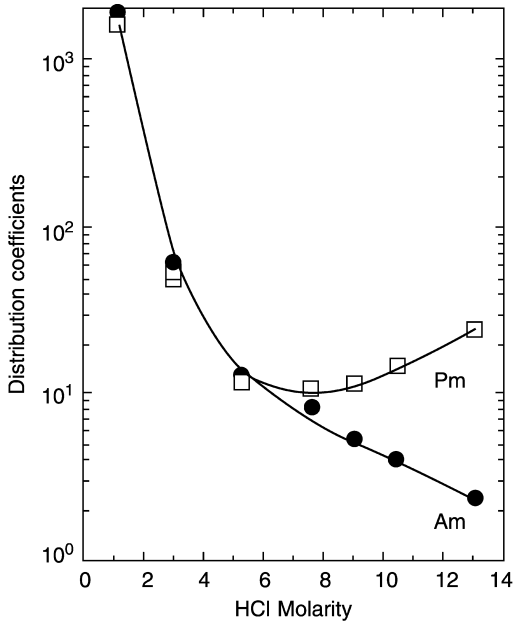

Fig. 24.1 *Distribution of Pm(III) and Am(III) onto Dowex* 50 *cation exchange resin as a function of hydrochloric acid concentration* (*Diamond* et al., 1954).

In this case, higher order (anionic) actinide chloride complexes are formed which preferentially associate with the resin. Introduction of 20% ethanol improved the separation factor, presumably through a modification of the hydration characteristics of the metal ions or their complexes. In this system, the actinides were eluted within a few column volumes while the lanthanides required much larger volumes. In another procedure using a Dowex 1 anion exchange resin column and eluting with 9.9 M LiCl (0.11 M HCl), Hulet *et al.* (1961) achieved an excellent separation of Ln–An. Surls and Choppin (1957) reported that similar results could be achieved in thiocyanate solution at significantly lower concentrations than is required for chloride (Fig. 24.2). This is a result of the increased interaction strength of the actinide with the 'less-soft' nitrogen donor atom of SCN^- relative to the very soft Cl^- anion. The LiCl anion exchange process is still used for actinide/lanthanide separation at Oak Ridge National Laboratory for actinide production (King *et al.*, 1981).

The results of Guseva and Tikhomirova (1972) indicate a significant improvement in the group separation from 4% cross-linked Dowex 50 using 10.5 M HCl

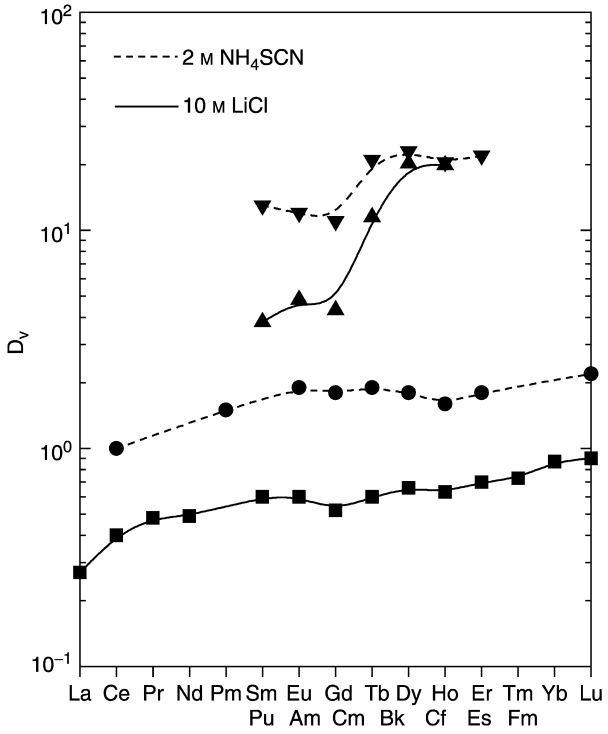

Fig. 24.2 *Partitioning of trivalent actinides and lanthanides onto Dowex* 1 *anion exchange resin from* 10 M *lithium chloride* (*Hulet* et al., 1961) *and* 2 M *ammonium thiocyanate* (*Surls and Choppin*, 1957) *solutions* (▼, ▲, *actinides*, ●, ■, *lanthanides*).

in 40% ethanol as the eluant as compared with 12.5 M HCl in water. Guseva *et al*. (1987a,b) subsequently demonstrated an efficient separation of trivalent actinides from all matrix elements (lanthanides and other fission products) with both cation and anion exchange from aqueous–ethanol solutions of sulfuric acid. Usuda and coworkers (Usuda, 1987, 1988; Usuda *et al*., 1987) have proposed a separation scheme for trivalent actinides using a three-step ion exchange partition from light actinides and fission products. Though little fundamental solution chemistry research has been done to probe the impact of alcohol–water mixtures on actinide separations, the effects cited above clearly indicate an important role for the interactions between solvent and solute molecules in these systems.

The separation of adjacent trivalent actinides represented an even more challenging task. The inherent selectivity of Dowex 50 cation exchange resin for adjacent lanthanide cations (in this case, behaving analogously with the trivalent actinides under all conditions) is demonstrated in Fig. 24.3. Separation factors for adjacent lanthanide cations average about 1.007. The coupling of water-soluble chelating agents (also demonstrated in Fig. 24.3) with the ion

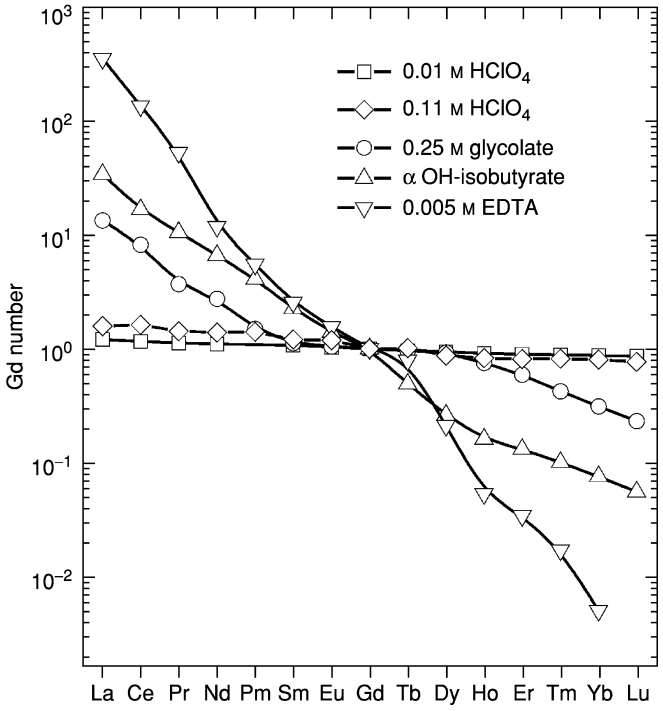

Fig. 24.3 *Partitioning of trivalent lanthanide ions onto Dowex* 50 *cation exchange resin from various aqueous acid solutions.* (*Gd number is the distribution ratio of the element normalized relative to* $D_{Gd} = 1.0$, *created from data in Marcus*, 1983.)

exchange systems by Thompson and coworkers (Thompson *et al.*, 1950, 1954; Choppin *et al.*, 1956) was the enabling science that made the identification of the new transplutonium elements possible.

The combination of a buffered solution of, in particular, a hydroxycarboxylic acid with a strong acid cation exchange resin like Dowex 50 made it possible to take advantage of the relative stability of the aqueous complexes of the actinide ions (which generally increase in proportion to those of the analogous lanthanide complexes across the series). This effect can be readily understood given a little consideration of the monophasic and biphasic equilibria involved in the process. Assuming that the water-soluble metal complexes present in the eluant are not sorbed by the resin, the distribution of the metal ion onto the acidic resin phase is governed by the following equilibrium (taking a trivalent cation as the example):

$$M^{3+} + 3H(\text{Resin}) \rightleftarrows M(\text{Resin}) + 3H^{+} \tag{24.1}$$

In the aqueous phase the metal complexation equilibria with a ligand HY can be written as:

$$M^{3+} + nHY \rightleftarrows MY_n^{(3-n)^+} + nH^{+} \tag{24.2}$$

The distribution ratio (D) for the metal ion is the ratio of the amount of metal species in the resin phase, $[M]_R$ to that in the aqueous phase $[M]_a$. Most commonly, these values are normalized to 1 ml of solution and 1 g of resin, respectively.

$$D = [M]_R/[M]_a = [M(\text{Resin})]/([M^{3+}] + \Sigma_1^n(MY_n^{(3-n)^+})) \tag{24.3}$$

The distribution ratio is directly proportional to the resin's affinity for the metal ion and inversely proportional to the degree of complex formation in the aqueous phase. In general, the separation factor (S), the ratio of distribution ratios, determines whether a separation of two species is successful or not. Written in terms of the respective one- and two-phase complexation equilibria, the separation factor is:

$$S_{M'}^{M} = \frac{D_M}{D_{M'}} = \frac{K_{ex}^{M}\ \cancel{[HR]^3}/\cancel{[H^+]^3}(1+\Sigma\ \beta_i^{M'}[Y]^i)}{K_{ex}^{M'}\ \cancel{[HR]^3}/\cancel{[H^+]^3}(1+\Sigma\ \beta_i^{M'}[Y]^i)} \tag{24.4}$$

wherein $K_{ex}^{M,M'}$ represents the equilibrium coefficient for the partitioning of the cation onto the resin phase, and $\beta_i^{M,M'}$ represents the complexation equilibrium constants for species present in the eluant solution. In fact, multiple complexants can be used in the aqueous phase to enhance separations, in which case additional complexation equilibria can be used to predict separation performance.

First attempts relied on citric acid (Structure d) as the eluant. As the synthesis of new actinides proceeded across the series, the product nuclides had progressively shorter half-lives, and in passing the middle of the series, the actinide equivalent of a gadolinium break (differentiation of the stability constants of

adjacent actinide complexes, predominant at the beginning and end of the lanthanide series, disappeared in the middle of the series) reduced the effectiveness of citrate as an eluant. These combined features resulted in smaller separation factors between the newest nuclides and in their early exit from the column, hampering analysis and detection. Substitution of lactic acid for citric acid improved performance. The comparative elution positions of Am, Cm, Bk, Cf, Es, and Fm from Dowex 50 cation exchange resin when the eluting solution was 0.25 M ammonium citrate or 0.4 M ammonium lactate are shown in Table 24.2.

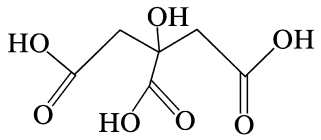

Structure d

Ultimately, the demands of the chemistry and the radiochemistry required a 'better' eluant (i.e. one yielding more consistent (i.e. linear) trends of elution with decreasing radii while retaining rapid kinetics). To satisfy this demand, Choppin and Silva (1956) introduced α-hydroxyisobutyric acid (Structure e), α-HIBA, which also came to be known colloquially as the 'BUTT' eluant. This complexant differs from lactate in the substitution of a second methyl group for H at the alpha position. The α-hydroxyisobutyric acid provides average separation factors for adjacent lanthanides or trivalent actinides of about 1.3–1.5 and very consistent elution positions even through the middle of the series where many reagents fail to give acceptable results. Parallel performance between trivalent lanthanides and actinides in cation exchange separations was a key factor in the identification of most of the transplutonium actinides. Fig. 24.4 shows the elution profile of trivalent actinides and lanthanides with ammonium α-hydroxyisobutyrate and shows the consistency in separation factors for adjacent cations across the series. It should be noted that if the data were plotted in terms of cationic radii rather than atomic number, the lanthanide and actinide results would overlap. Table 24.3 compares $S_M^{M'}$ of adjacent actinides with lactic acid, α-hydroxyisobutyrate, ethylenediamine-*N*,*N*,*N*′,*N*′-tetraacetic acid (EDTA) and further relates those data to the separation factors observed for

Table 24.2 *Elution of transplutonium elements from Dowex* 50 *cation exchange resin using ammonium carboxylate salts at* 87°C, pH 3.0–4.5, 2 min/drop, 2 mm *by* 10–20 mm *column* (*Thompson* et al., 1950, 1954).

			Retention time (*drop number*)			
Carboxylic acid	*Am*	*Cm*	*Bk*	*Cf*	*Es*	*Fm*
0.25 M ammonium citrate	94.0	80.8	56.0	38.3	32.5	26.7
0.4 M ammonium lactate	58.5	49.0	33.0	22.0	18.0	13.6

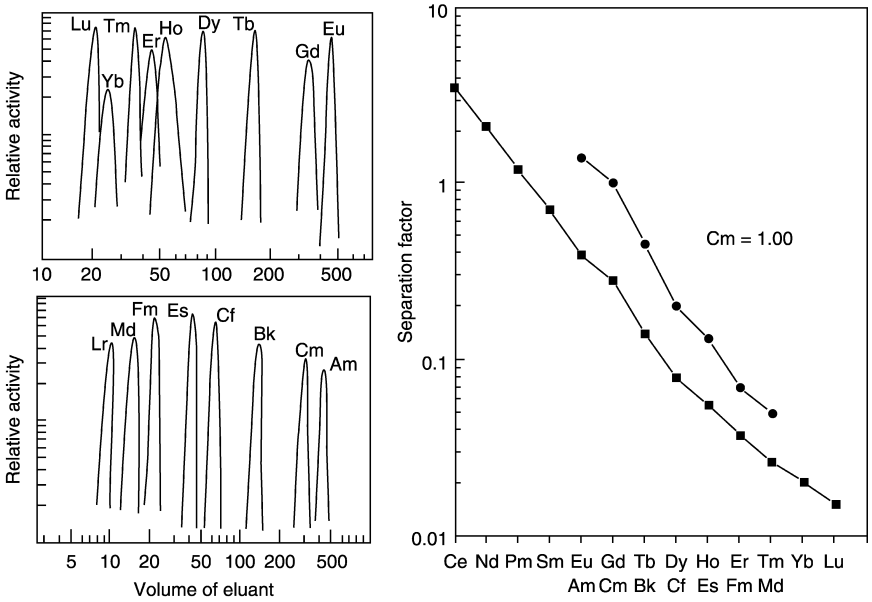

Fig. 24.4 *Elution profiles for trivalent lanthanide and actinide ions and separation factors (relative to Cm = 1.0) for α-hydroxyisobutyrate elution from Dowex 50 cation exchange resin* (*Choppin and Silva*, 1956).

solvent extraction separations using bis(2-ethylhexyl)phosphoric acid (HDEHP, Structure f), which will be considered further in Section 24.3.4a

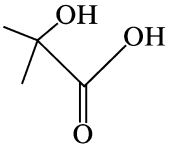

Structure e

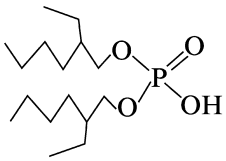

Structure f

Improvements in separations have been achieved with cation exchange systems of this type using very finely divided resin beds and high-pressure elutions (Campbell, 1970). Kilogram amounts of americium and gram amounts of curium have been purified from each other by using nitrilotriacetic acid (NTA) and diethylenetriamine-*N*,*N*,*N*′,*N*″,*N*″-pentaacetic acid (DTPA, Structure g) as

Table 24.3 *Separation factors for adjacent trivalent actinides with solvent extraction and cation exchange column using different reagents.*

	Reagents			
		Cation exchanger		
Element	*Solvent extration. HDEHP/HNO₃*	*EDTA*	*Lactic acid*	*α-HIBA*
Am/Cm	1.24	2.0	1.21	1.4
Am/Bk	8.3	3.1	1.54	1.7
Bk/Cf	2.7	2.0	1.55	2.2
Cf/Es	1.02	–	1.25	1.5
Es/Fm	2.2	–	1.45	1.7
Fm/Md	4.4	–	–	1.4

α-HIBA = α-hydroxyisobutyric acid.

the eluants (Baybarz, 1970). The kinetics of the metal complexation/ion exchange equilibration on the Dowex 50 column with α-hydroxyisobutyrate eluant was also found to be superior to that for the several other ligands that had been previously employed. For example, aminopolycarboxylic acid ligands like EDTA demonstrated comparable or even superior separation factors (to α-hydroxyisobutyrate; see Fig. 24.3), but slower equilibration rates, which required longer residence times for the solutions on the column. The need for longer equilibration times on the column was a definite handicap in the search for short-lived actinide species. Like TBP and PUREX, the BUTT column remains today one of the most effective ion exchange separation method for trivalent f-elements from a mixture of like elements (Nash and Jensen, 2000).

It should be noted that the intrinsic affinity of cation exchange resins increases for actinides in the order An(V) < An(III) < An(VI) < An(IV), in accord with the comparative electrostatic attraction of the cations for the anionic sulfonate functional groups of the resin. The differences are sufficiently large to allow the mutual separation of the ions in different oxidation states; however, all but the pentavalent oxidation state are bound too strongly for effective separation procedures to be routinely used. Where necessary and possible, sorption of strongly bound ions is generally reversed using oxidation state adjustment or chelating agents.

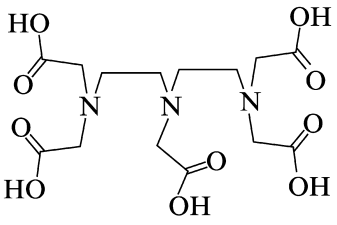

Structure g

To avoid the elution difficulties of the cation exchange resins, ion exchange separations for the purification of the tetravalent and hexavalent actinides more frequently rely on anion exchange techniques. A variety of separation methods based on the use of tetraalkylammonium or methyl pyridinium polymeric resins have been developed. Introduction of the Reillex resins, based on methylpyridinium functional groups, is among the more significant recent advances in anion exchange separations for actinides (Abney *et al.*, 1995). Perhaps the most important application of anion exchange resins is in the purification of plutonium. Pu(IV) is selectively sorbed onto Dowex 1 from 8 M HNO_3, allowing the passage of other contaminants through the resin. Pu(IV), which is retained on the resin as the hexanitrato complex ($Pu(NO_3)_6^{2-}$), is readily eluted using more dilute nitric acid. Anion exchange separations for An(IV) and An(VI) are facile because these cations readily form anionic complexes with simple inorganic anions like NO_3^- and Cl^-. However, higher order complexes are formed in the presence of the resin than are observed in the same solution in its absence. This is due to the superposition of the phase transfer equilibrium upon the typical aqueous phase complexation reactions, which tends to drive the process. In essence, anionic complexes are sorbed to the resin whether or not they are present in the aqueous solution phase contacting the resin.

A new chelating ion exchange resin (Diphonix) that exhibits high affinity for actinide cations in all oxidation states from strongly acidic solutions has been developed jointly at Argonne National Laboratory and the University of Tennessee as a spinoff of the development of the transuranium extraction (TRUEX) solvent extraction process (Alexandratos *et al.*, 1993; Chiarizia *et al.*, 1993, 1994, 1996, 1997; Horwitz *et al.*, 1993, 1994; Chiarizia and Horwitz, 1994, 2000; Trochimczuk *et al.*, 1994). Diphonix resin combines a methylenediphosphonic acid chelating group with carboxylic and benzene sulfonic acid groups in a styrene–divinylbenzene matrix. This combination results in a chelating resin that exhibits good metal ion uptake kinetics (Chiarizia *et al.*, 1994) and effectively sorbs actinide metal ions in all oxidation states from moderate to strong acid solutions and even in the presence of moderately strong complexants. The hexavalent and tetravalent species are so strongly retained by the resin even from 10 M HNO_3 that they can only be removed upon elution with a moderately concentrated solution of a structurally related diphosphonate chelating agent (1-hydroxyethane-1,1-diphosphonic acid, HEDPA; Structure h) or by applying a reducing agent. The distribution ratios for Am(III), U(VI), Pu(IV), Np(IV), and Th(IV) onto Diphonix as a function of [HNO_3] are shown in Fig. 24.5. The acid dependence for Am(III) uptake indicates normal cation exchange behavior while that for Th(IV) and U(VI) has been interpreted in terms of coordination of these cations by the phosphoryl oxygens of the fully protonated methylenediphosphonate groups. The principal feature of the Diphonix resin is the strength of cation uptake rather than selectivity, though the resin demonstrates significant selectivity for Pu(IV) and U(VI) over Am(III) from concentrated nitric acid media. The principal advantage of this resin may

be in the separation of actinides from less-strongly-bound fission product and cations present as a result of matrix dissolution.

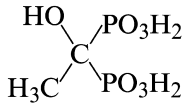

Structure h

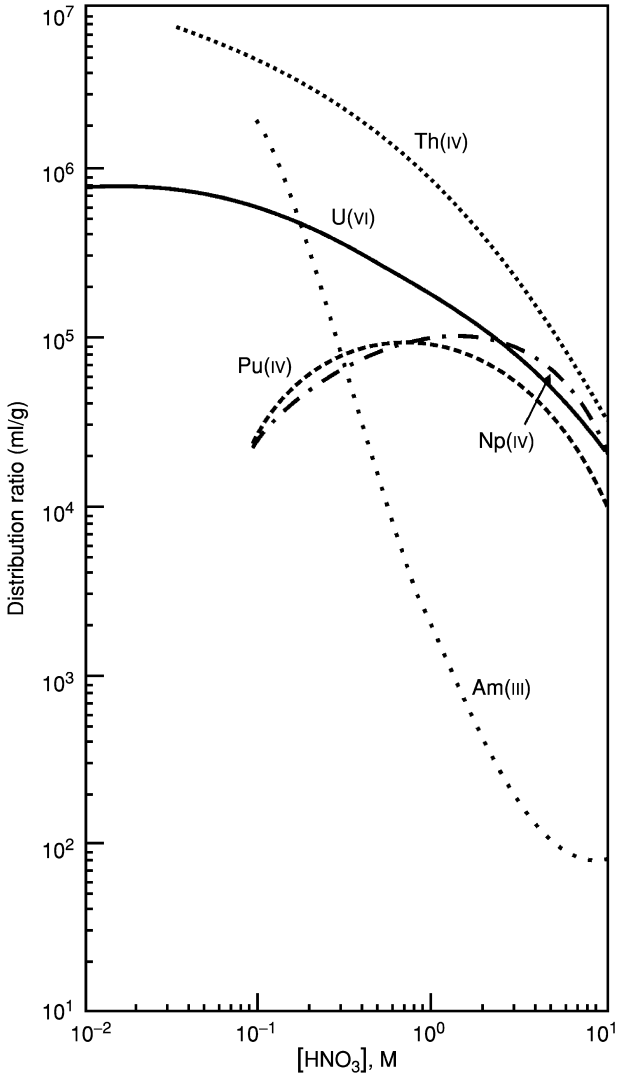

Fig. 24.5 *Distribution of selected actinide ions onto Diphonix resin from nitric acid solutions* (*Chiarizia* et al., 1997).

24.3.4 Solvent extraction methods

Successful solvent extraction processes depend on the *selective* transport of the target metal ion (or group of metal ions) from an aqueous solution containing contaminants into an immiscible organic solution. When the target metal ion is removed from that organic phase, it will have undergone some degree of purification, often characterized in terms of a 'decontamination factor' (D_f). Additional purification processes may subsequently be engaged, depending on the D_f required for the product. Strongly acidic, extensively hydrated metal ions like actinides and most of their complexes with typical mineral acid anions or other hydrophilic complexants have minimal intrinsic tendency to partition spontaneously from aqueous into non-polar organic solutions. The driving force for phase transfer is provided by the introduction of a lipophilic complexant (extractant) into the organic phase. Usually, new complexes possessing a hydrophobic external 'shell' are formed at the oil–water interface and transferred to the non-polar (or less polar) organic phase. Chemical reactions occurring in the aqueous phase, including oxidation–reduction, hydrolysis, and the formation of water-soluble complexes, all affect the phase transfer equilibrium position as well.

Of all separation techniques that have been applied for actinide separations, solvent extraction offers the greatest number of options and adjustable parameters to finetune performance. Further, it is perhaps the separations technique best adapted to the continuous operations, high throughput, and remote handling that are essential to the processing of nuclear fuels. Of course, this flexibility can also introduce complications, including rather long development time for the creation of a new solvent extraction-based process. Historically, industrial scale aqueous processes have also produced waste streams noteworthy for both their complexity and volume.

It is important at this stage to make the clear distinction between the chemistry of actinides in the organic media relevant to solvent extraction and the chemistry generally termed as organoactinide chemistry, which is covered in Chapters 25 and 26. In solvent extraction, metal ions in organic solutions *never* engage in bonding to *carbon* atoms, as they do in most true organometallic complexes. Direct bonding interactions between actinide ions and lipophilic complexants *do* play an important role in most solvent extraction systems, except for those based on molecules that organize in organic solutions to form reverse micelles. For the actinides in extraction processes, bonding is always to oxygen, nitrogen, or occasionally sulfur donor atoms in organic compounds or to chloride or thiocyanate anions, sometimes in combinations.

In solvent extraction, some dissolved water molecules are always present in the organic phase. For actinide separations, these solutions will often also bear mineral acid molecules that have been extracted by the same lipophilic reagents that remove the actinides from the aqueous phase. In some systems, a specific interaction can occur between the metal cation and solvent molecules, but only

with compounds like methyl(isobutyl)ketone (MIBK) or (neat) tri(*n*-butyl) phosphate (TBP) which are moderately strong Lewis bases and so capable of competing with adventitious water molecules in the organic phase of solvent extraction systems.

It would be impossible to catalog all of the various reagents whose actinide extraction properties have been investigated in the space allocated for this overview. In the following discussion, the general characteristics of the classes of selected extraction systems are considered. The objective here is to illustrate the general features of the techniques. There are at least five different classes of solvent extraction systems that have been employed for actinide separations. The classes and representative biphasic extraction equilibria are:

Liquid cation exchangers/chelating agents,

$$M^{3+}_{aq} + nHL_{org} \rightleftarrows ML_{n,org} + 3H^{+}_{aq} \tag{24.5}$$

Micellar extractants,

$$M^{3+}_{aq} + (HL)_{n,org} \rightleftarrows MH_{n-3}L_{n,org} + 3H^{+}_{aq} \tag{24.6}$$

Solvating extractants,

$$M^{3+}_{aq} + 3X^{-}_{aq} + nS_{org} \rightleftarrows MX_3S_{n,org} \tag{24.7}$$

Ion pair forming extractants (or liquid anion exchangers),

$$M^{3+}_{aq} + 3X^{-}_{aq} + A^{+}X^{-}_{org} \rightleftarrows MX_4A_{org} \tag{24.8}$$

Synergistic extractants,

$$M^{3+}_{aq} + 3HL_{org} + nS_{org} \rightleftarrows ML_3S_{n,org} + 3H^{+}_{aq} \tag{24.9}$$

Species present in the aqueous and organic solutions are designated by the subscripts aq and org, respectively. In solvent extraction systems, the metal ion distribution ratio is a dimensionless quantity defined as $D = [M]_{org}/[M]_{aq}$. D is not a species-specific term but rather defines the analytical concentrations of the metal ion in the aqueous and organic phases. The stoichiometric features of the equilibria outlined above are most relevant at low concentrations of the metal ions. Under conditions near the stoichiometric limits of concentrations, the phase transfer equilibria can be substantially more complex than these simple equilibria indicate.

Each class of extraction system accomplishes the phase transfer by a slightly different chemical process. However, these systems share the following general characteristic: while the high dielectric constant of water readily supports the presence of charged ionic species as discrete molecules, the low polarity of organic solutions demands close contact between cations and anions. Most solutes in most organic solvents are expected to be discrete electroneutral entities. The liquid cation exchangers, chelating agents, and micellar extractants each exchange a number of monovalent cations (usually H^{+}) equivalent to the

formal charge on the cation extracted to maintain electroneutrality in both phases. In these systems, transfer of the metal ion into the organic phase is favored by low acidity, implying that the metal ion can be stripped from the loaded organic solution into concentrated acid solutions (as H^+ competes with the metal ion for the extractant). Some acidic extractants have a tendency to self organize (aggregate), even in the absence of the extracted metal ion, to form dimers or higher order aggregates. Sulfonic acid extractants in particular behave in this manner, forming reverse micelles in the organic phase.

Solvating extractant systems are technologically the most important for actinide purification. They accomplish phase transfer by solvating electroneutral metal complexes with mineral acid anions, hence the net phase transfer reaction includes the necessity to dehydrate and resolvate in the organic phase both the metal ion and a sufficient number of conjugate base anions of mineral acids to neutralize the cation charge. In solvating extraction systems, the phase transfer reaction is favored by high concentrations of the counter-ion (preferably introduced as an acid solution to minimize the generation of secondary wastes) and stripped from the loaded organic solution by contact with dilute acid solutions, a change in oxidation state, or washing with a water-soluble complexant.

Primary among the solvating extractant systems that are technologically the most important actinide separations systems in operation today are those based on the solvating ability of TBP. More than 50 years of cumulative industrial scale experience exists on the PUREX process. This solvent extraction process accomplishes the selective removal of both plutonium [as Pu(IV)] and uranium [as U(VI)] from dissolved spent fuel solutions (3–6 M HNO_3) as their electroneutral nitrate salts with minimal complication (Fig. 24.6). Most fission products and the trivalent and pentavalent actinides [Am(III), Cm(III), Np(V)] are rejected by TBP.

Plutonium is selectively recovered from the extractant phase through its reduction to the trivalent oxidation state in which its extraction performance is comparable to that of Am(III). In PUREX processing, changes in neptunium oxidation state speciation causes partitioning of this element to undesirable locations within the process flow scheme. Until recent years, it has been most advantageous to try to maintain Np(V) in the aqueous phase so that it remains with the fission product raffinate. The emergence of full recycle fuel cycles for actinide transmutation in recent years has brought greater attention to the means of controlling Np speciation in PUREX-style separations. The details of neptunium's speciation complexity are discussed in Section 24.4.4f.

Synergistic systems generally combine acidic extractants, usually and most effectively multidentate chelating agents, with solvating extractants, hence they share some features of both liquid cation exchangers and solvating extractant molecules. Ion pair-forming extractants tend to be micellar in most organic solutions and to exchange simple anions for negatively charged metal coordination complexes. For actinide extraction by liquid anion exchangers, the

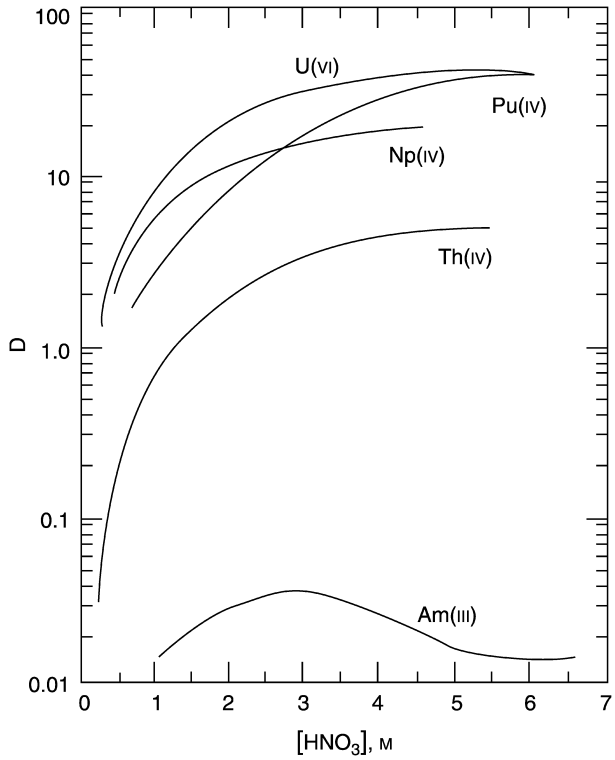

Fig. 24.6 *Extraction of actinides into tri*(n-*butyl*)*phosphate/dodecane as a function of nitric acid concentration*.

anionic complex (e.g. $AmCl_4^-$) exists only in the organic phase in the presence of the lipophilic counter-ion and is usually not an important species in the aqueous phase. These extractants are the soluble analogs of anion exchange resins and so exhibit relative actinide affinities in the order: An(IV) > An(VI) > An(III) > An(V).

As a general (though not universal) rule, the greatest selectivity for metal ions having similar properties (like adjacent trivalent lanthanides or actinides) is seen in acidic extractant systems, particularly those involving the formation of multidentate complexes. Solvating extractant systems tend to exhibit their greatest selectivity only for metal ions differing in charge (for interactinide separations, this implies the presence of the metal ions in different oxidation states), but extract chemically similar species without much selectivity. Such behavior is also generally seen for micellar reagents, i.e. minimal selectivity is demonstrated for series of closely related metal ions. Synergistic systems achieve increased extraction strength, usually at the price of decreased selectivity (though there are some exceptions).

Table 24.4 *Am and Eu extraction with* 20% *triisooctyl amine from* 11.9 M *LiCl*/0.1 M *HCl* (*Moore,* 1961).

Diluent	*Percent extracted*		*Separation factor* S_{Eu}^{Am}
	Am	*Eu*	
xylene	91.7	15.7	59
toluene	87.0	10.1	60
benzene	80.8	7.0	56
mesitylene	94.2	23.4	53
hexone	87.3	2.7	47
β,β′-dichloroethyl ether	97.1	63.1	20
o-Dichlorobenzene	80.6	7.5	51
nitrobenzene	87.2	11.8	51
n-Hexane	98.4	54.8	51
CH_2Cl_2	99.7	91.3	32
CCl_4	23.4	0.9	34
$CHCl_3$	0.6	<0.3	–
xylene-$CHCl_3$			
1:1	<1.0	<1.0	–
3:1	10.3	<0.5	–
20:1	71.2	4.3	55
50:1	83.4	8.7	53

$S_{Eu}^{Am} = D_{Am}/D_{Eu} =$ (% org Am/%AqAm)/(% org Eu/%AqEu)

The organic molecule almost always used to solubilize or dilute the extractant[1] is commonly considered to be 'inert', but, as the data in Table 24.4 indicates, this inertness is relative. Considering a single extractant system that transfers the metal ion in a straightforward equilibrium process, several orders of magnitude variation in extraction efficiency can be seen to result simply from a change in the diluent. For analytical separations, different classes of diluents can be employed, though many techniques favor volatile species like chloroform. For hydrometallurgical separations, issues of phase compatibility at high solute loading, low flammability, and low toxicity are primary considerations in the selection of a diluent.

Phase modifiers, secondary solute molecules that may or may not enter into specific interaction with the metal ion, the extracted complex, or the extractant itself are often employed simply to improve solubility characteristics. In hydrometallurgical separations of actinides, the phenomenon of third phase formation (also known as phase splitting), in which the biphasic system

[1] Typically this organic compound is referred to as the diluent for historic reasons – the solution containing the extractant molecule in a diluent is referred to as the "solvent" in solvent extraction.

becomes a ternary liquid system, complicates process operations under conditions of high solute loading of the organic phase. This phenomenon has been most extensively studied in the TBP–PUREX system from an operational perspective (Rao and Kolarik, 1996) and empirical correlations have been developed. More recent work by Chiarizia and coworkers (Borkowski *et al.*, 2002, 2003; Jensen *et al.*, 2002a; Chiarizia *et al.*, 2003a,b, 2004) and by Tondre and coworkers (Erlinger *et al.*, 1998; Lefrancois *et al.*, 2001a,b) has attempted to provide a more fundamental understanding of the physical chemistry of the phenomenon.

Subtle variations in the properties of the aqueous phase can alter both extraction efficiency and selectivity patterns, as illustrated by the work of Sekine on the TBP extraction of Am^{3+} and Eu^{3+} by tri(*n*-butyl)phosphate from thiocyanate and mixed thiocyanate/perchlorate solutions [Fig. 24.7 (Sekine, 1965)]. The salting out effect of added perchlorate reduces the degree of order in the aqueous solution, which leads to a more efficient phase transfer process. However, the penalty paid is a reduction in the selectivity of the thiocyanate extractant system for Am over Eu. This system is discussed in more detail in Section 24.3.9. Note that in this example, Am(III) and Eu(III) are extractable into TBP solution because the aqueous acid solution has been replaced by a salt solution of higher pH.

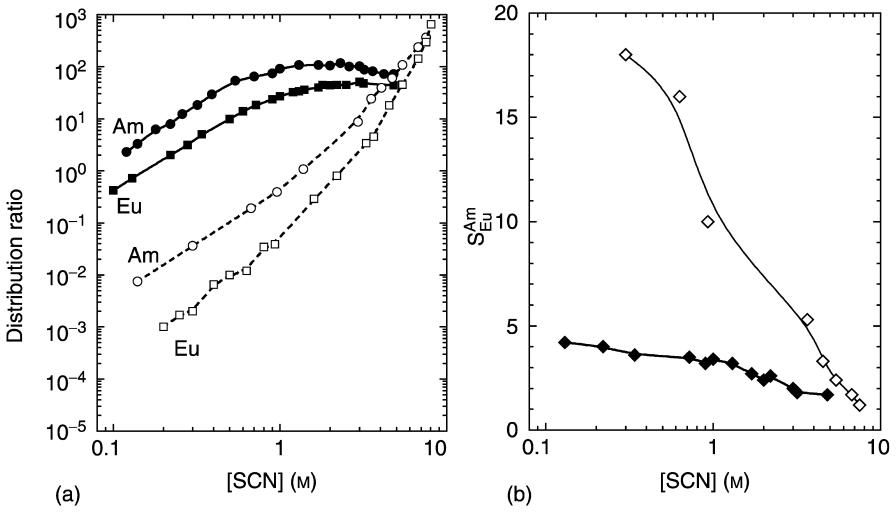

Fig. 24.7 (*a*) *Distribution of Am*(III) *and Eu*(III) *between sodium thiocyanate or sodium thiocyanate/perchlorate solutions and tri*(n-*butyl*)*phosphate/benzene solutions* (*open symbols thiocyanate only*, *closed symbols thiocyanate–perchlorate mixtures – from data in Sekine*, 1965); (*b*) *Am/Eu separation factors from thiocyanate alone* (◇) *and from thiocyanate/perchlorate mixtures* (◆).

(a) Acidic extractants

The extraction of actinides (and lanthanides) by thenoyltrifluoroacetone (TTA, Structure i) was one of the first solvent extraction methods for the isolation of individual An(III) ions (Stary, 1966). The separation factors for adjacent ions are slightly greater than in α-HIBA elution, but they are less constant throughout the series. TTA extraction from 1 M acid solutions is highly specific for tetravalent actinide ions, and is often employed in studies of oxidation state speciation of actinides in environmental samples (Choppin and Bond, 1996; Choppin and Wong, 1998; Nash *et al.*, 1988a; Rollin, 1999). Because of the photolytic instability of TTA and its appreciable solubility in aqueous solutions, it is employed almost exclusively in research rather than in hydrometallurgical separations. For analytical applications, this reagent should be prepared fresh frequently and always protected from ambient light and air. Structurally similar pyrazolone compounds extract actinide ions in patterns similar to those demonstrated by the β-diketones represented by TTA. They differ from β-diketones in that they are slightly more acidic, thus able to accomplish actinide phase transfer from more acidic solutions.

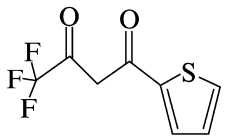

Structure i

Acidic organophosphorus extractant molecules have been used extensively in actinide separations. The first important acidic organophosphorus extractant was dibutylphosphoric acid (HDBP), which is produced spontaneously during the use of TBP (solvating-class extractant) for nuclear fuel processing. In TBP-based extraction systems, the presence of HDBP in the extractant phase caused considerable difficulty in the stripping of actinides from loaded and degraded TBP solutions into dilute acid solutions. From the above extraction equilibrium equations, it is clear that conditions needed for stripping of metal complexes from solvating extractants favor the phase transfer of the acidic analog, hence the simultaneous presence of both solvating and acidic extractants can have an important negative impact on the efficiency of solvent extraction separations. In the case of HDBP, the complications introduced by its presence were readily overcome by the development of careful procedures for removing HDBP from the TBP-extractant phase as its water-soluble sodium salt by scrubbing of recycled process solvent with sodium carbonate (Schulz *et al.*, 1990).

Realization of the special features of HDBP extraction touched off efforts to develop similar extractants less prone to degradation or able to function under different sets of conditions. One of the current principal methods for isolation of individual lanthanides commercially is solvent extraction with HDEHP mentioned above (Structure f), a reagent first reported by Peppard *et al.* (1957).

Adjacent lanthanide separation factors are up to twice as high for HDEHP separations as for α-hydroxyisobutyrate cation exchange. Trivalent actinides likewise are separated from one another by this reagent. A representative plot of actinide extraction in the most common oxidation states is shown in Fig. 24.8. This extractant is the phase transfer reagent for the TALSPEAK process for lanthanide/trivalent actinide separation (Weaver and Kappelmann, 1964, 1968).

Many long years of research were invested in systematic studies of monofunctional acidic organophosphorus extractants containing different alkyl groups designed to alter both the solubility of the reagent and the basicity of the functional group. Dialkylphosphoric acids like HDEHP [$(RO)_2P(O)(OH)$] are characterized by the presence of two alkyl ester bonds. The P–O–C linkage is far more susceptible to hydrolytic and radiolytic degradation than P–C bonds. To increase the long-term stability of the extractant (and its suitability for application to the separation of radioactive materials) while simultaneously modifying its basicity (and so the effective range of pH operation), phosphonic [$(RO)(R)P(O)(OH)$] and phosphinic [$(R)_2P(O)(OH)$] acids replace alkoxide groups with alkyl groups, resulting in reagents of steadily increasing hydrolytic stability and greater basicity of the functional groups. Higher basicity translates into stronger metal ion bonding but typically forces operation under less acidic conditions due to the increased affinity of the extractants for H^+.

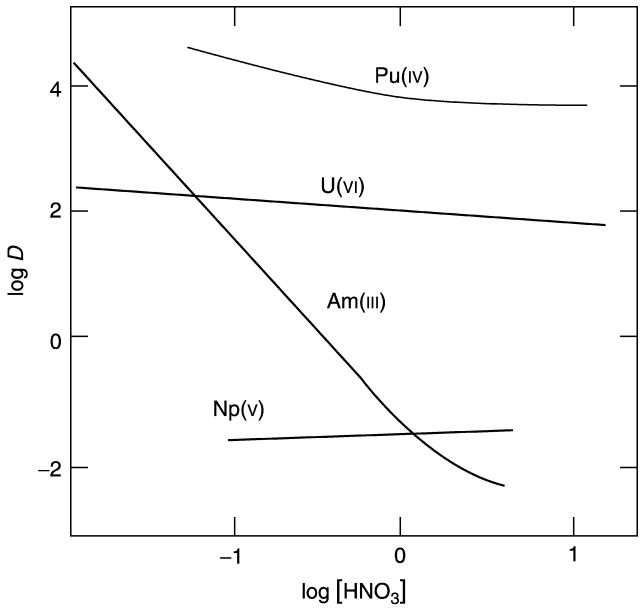

Fig. 24.8 *Dependence of extraction of Pu(IV), U(VI), Am(III), and Np(V) into* 0.5 M *HDEHP/iso-octane on nitric acid concentration* (*Myasoedov* et al., 1974).

Many variations on these general structures are commercially available. They have found application for actinide/lanthanide separation and for actinide partitioning, as will be described in Section 24.3.9.

If one acidic organophosphorus binding site is good, might not two be better? In the 1960s, work in the water-treatment/detergent industry led to the production of alkyldiphosphonic acid complexing agents as substitutes for pyrophosphates in detergent formulations (Irani and Moedritzer, 1962; Carroll and Irani, 1967, 1968; Elesin *et al.*, 1972; Wada and Fernando, 1972). These complexants followed the same operational philosophy as the extractant development activity discussed in the previous paragraph: replacement of P–O–C bonds with P–C bonds increases hydrolytic stability and thereby utility of this arrangement of ligand donor groups. During the development of CMPO (most typically referring to octyl(phenyl)-*N*,*N*-diisobutylcarbamoylmethylphosphine oxide, but the term CMPO is used to refer to carbamoylmethylphosphine oxide extractants generally; generic Structure j) and the TRUEX process, research at Argonne National Laboratory addressed the use of diphosphonate complexants as efficient actinide-stripping reagents (Nash and Horwitz, 1990; Nash, 1991, 1993b). An additional feature of these compounds is that selected representatives were devised to be readily decomposable to minimize waste volumes in process applications. The latter ligands were given the acronym TUCS, meaning thermally unstable complexants (Schulz and Kupfer, 1991; Horwitz *et al.*, 1992; Nash and Rickert, 1993).

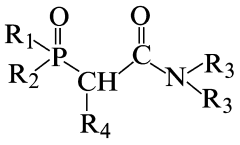

Structure j

Chiarizia and coworkers (Chiarizia *et al.*, 1998; McAlister *et al.*, 2002; Otu and Chiarizia, 2002; Otu *et al.*, 2002) have prepared and characterized a number of dialkyl diacidic actinide extractants based on diphosphonic acids, derived from symmetric partial esterification of water-soluble diphosphonates (Structure k). These extractants have proven uniquely capable actinide sequestrants, finding unique application in analytical separations. Neutron scattering and osmometric studies of these extractants reveal unexpected patterns of extractant aggregation and cation size selectivity as the length of the alkyl chain bridging the phosphonate monoester groups changes from 1 to 6.

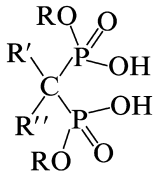

Structure k

(b) Solvating extraction systems

The ability of TBP to reject the so-called minor actinides (Np, Am, Cm) present in dissolved spent fuel was recognized as a desirable feature of this extractant system when maximizing production of plutonium and recovery of uranium were the primary motivations for processing spent nuclear fuels. However, for actinide separations in the 21st century, minimizing the toxicity of the wastes exiting a production facility must become an equally important factor in process operations. In most countries operating a closed loop nuclear fuel cycle today, recovery of the minor actinides for isolation or transmutation has become more desirable. To recover americium and curium from spent nuclear fuel using TBP would demand reduction of the acidity of the aqueous feed and the addition of salting out reagents like $NaNO_3$. Both of these actions will increase the volume of wastes and therefore are unacceptable. Neptunium can in principle be recovered as either Np(IV) or Np(VI), but neither oxidation state has adequate stability in nitric acid to prevent its dispersal to undesirable portions of the process under the ambient conditions prevailing in a process facility (i.e. moderate concentrations of nitric acid, radiolysis). Within the structure of a modern processing facility, what is needed is a reagent that will complement TBP (most probably a solvating extractant) by accomplishing the complete and selective recovery of the minor actinides from strongly acidic solutions. A significant fraction of research on actinide separations today seeks to develop such reagents and processes for their use.

In the early 1960s, a few bidentate carbamoyl phosphonate compounds (Structure l) were synthesized (Siddall, 1963a, 1964) and their utility for the extraction of trivalent americium, cerium, and promethium from moderately acidic solutions demonstrated. The bifunctional nature of the extractant reduces the impact of competition between HNO_3 and the target metal ion for the primary extractant binding site (P=O). Schulz and coworkers (Schulz and McIsaac, 1975; Schulz and Navratil, 1982) revived interest in synthesis of new compounds of this class and in their utilization for the extraction of actinides and lanthanides. Since that time, several groups in the United States (of greatest note, the Horwitz group at Argonne National Laboratory) and other parts of the world have synthesized numerous derivatives of CH_2-bridged (CMPs) and unbridged (CPs) extractants and studied the extraction behavior of hexavalent, tetravalent, and trivalent actinides and a few lanthanides using the extractant alone (Martella and Navratil, 1979; Navratil and Thompson, 1979; Petrzilova *et al.,* 1979; Horwitz *et al.*, 1981, 1982; Kalina *et al.*, 1981b; Hugen *et al.*, 1982; McIsaac, 1982; McIsaac and Baker, 1983; Kalina and Horwitz, 1985; Akatsu and Kimura, 1990; Rapko, 1995) or in combination with TBP in various diluents (Mathur *et al.*, 1991, 1992a).

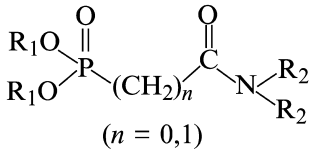

Structure 1

Slope analysis studies at radioanalytical concentrations established the stoichiometry of the extracted complexes of trivalent actinides and lanthanides from NO_3^- and SCN^- media, and those of U(VI) and Th(IV) from the NO_3^- medium by CMP from the equilibria:

$$M^{3+}_{aq} + 3NO^-_{3\,aq} + 3CMP_{org} \rightleftarrows M(NO_3)_3 \cdot 3CMP_{org} \tag{24.10}$$

$$M^{3+}_{aq} + 3SCN^-_{aq} + 4CMP_{org} \rightleftarrows M(SCN)_3 \cdot 4CMP_{org} \tag{24.11}$$

$$UO^{2+}_{2\,aq} + 2NO^-_{3\,aq} + 2CMP_{org} \rightleftarrows UO_2(NO_3)_2 \cdot 2CMP_{org} \tag{24.12}$$

$$Th^{4+}_{aq} + 4NO^-_{3\,aq} + 3CMP_{org} \rightleftarrows Th(NO_3)_4 \cdot 3CMP_{org} \tag{24.13}$$

where M^{3+} = trivalent actinides and lanthanides. In the case of the Am system, the slope of the straight line for log D vs log [CMP] plot was only 3.6 in the thiocyanate system implying the presence of both tri- and tetra-solvate complexes. However, while using the mixture of CMP and TBP, americium and promethium were extracted from a NO_3^- medium as $M(NO_3)_3 \cdot (2.6)$ CMP·0.4 TBP. Complete coordination of all possible ligand donor atoms (bidentate nitrate and CMP molecules) would require unusually large complex coordination numbers. It is believed in general that the denticity of the CMP ligands is less than two in most of these species with the P=O group preferentially coordinated.

Ultimately, the CMP and CP extractants proved inadequate for the task of trivalent actinide recovery from nitric acid solutions of moderate concentration as are encountered in the raffinate from the first stages of PUREX processing. Ligand development procedures conducted over an extended period led Horwitz and coworkers to conclude that the extractant CMPO represents the best combination of features around which to build an effective industrial-scale process for total actinide recycle, including their extraction in the trivalent oxidation state. The greater basicity of the phosphine oxide overcomes the principal weakness of the CP and CMP class of ligands.

The nature of U(VI) and Pu(IV) species extracted into the organic phase from NO_3^- medium with CMPO can be given by the following equilibria:

$$UO_{2\,aq}^{2+} + 2NO_{3\,aq}^{-} + 2CMPO_{org} \rightleftarrows UO_2(NO_3)_2 \cdot 2CMPO_{org} \quad (24.14)$$

$$Pu_{aq}^{4+} + 4NO_{3\,aq}^{-} + 2CMPO_{org} \rightleftarrows Pu(NO_3)_4 \cdot 2CMPO_{org} \quad (24.15)$$

There has been a lot of interest in the extraction of Am(III) and Eu(III) by CMPO from aqueous media containing NO_3^-, SCN^-, ClO_4^- or $NO_3^- + ClO_4^-$. The extraction equilibria can be given as:

$$M_{aq}^{3+} + 3NO_{3\,aq}^{-} + 3CMPO_{org} \rightleftarrows M(NO_3)_3 \cdot 3CMPO_{org} \quad (24.16)$$

$$M_{aq}^{3+} + 3SCN_{aq}^{-} + 3CMPO_{org} \rightleftarrows M(SCN)_3 \cdot 3CMPO_{org} \quad (24.17)$$

$$M_{aq}^{3+} + 3\,ClO_{4\,aq}^{-} + 3\,CMPO_{org} \rightleftarrows M(ClO_4)_3 \cdot 3CMPO_{org} \quad (24.18)$$

$$M_{aq}^{3+} + NO_{3\,aq}^{-} + 2ClO_{4\,aq}^{-} + 3CMPO_{org} \rightleftarrows M(NO_3)(ClO_4)_2 \cdot 3CMPO_{org} \quad (24.19)$$

The thermodynamic features of these reactions will be discussed in Section 24.3.5. The work of Dozol and coworkers (Delmau *et al*., 1998, 1999; Arduini *et al*., 2000; Dozol *et al*., 2000; Garcia-Carrera *et al*., 2001; Gruener *et al*., 2002; Teixidor *et al*., 2002; Arnaud-Neu *et al*., 2003; Schmidt *et al*., 2003) and of Scott (Peters *et al*., 2002) has sought to introduce an element of molecular recognition into CMPO–actinide coordination complexes with the creation of polydentate podand structures based on rigid alkyl backbones and calixarenes. These intriguing structures have yet to produce startling advances in actinide separations.

The process based on the use of CMPO is the TRUEX process (Vandegrift *et al*., 1984, 1993; Horwitz and Schulz, 1990; Horwitz and Chiarizia, 1996). The TRUEX process solvent consists of 0.2–0.25 M CMPO and 1.0–1.4 M TBP (depending on the nature of the diluent, with a normal paraffinic hydrocarbon preferred). Because this solvent can simultaneously extract the actinides in the oxidation states important in technological processes, it could have significant impact in the reduction of the volume of high-level waste requiring burial in a geological repository. There has been one report that proposes an oxidation state selective separation of actinides based on the use of TRUEX extraction and a diphosphonic acid complexant (Nash and Rickert, 1993).

The neutral bifunctional extractants (CMPs, CMPOs, and related compounds) have been applied to a few analytical-scale separations as well. Horwitz *et al*. (1981) studied the separation of the trivalent actinides from Am to Fm (Table 24.5) using dihexyl-*N*,*N*-diethylcarbamoylmethylphosphonate (DHDECMP) and aqueous nitrate solutions. Steadily decreasing distribution ratios are observed for the lanthanides, but a much smaller decrease is found for the trivalent actinides. These results suggest possible interlanthanide

Table 24.5 *Separation factors (relative to Am) for solvent extraction of trivalent lanthanides and actinides with* 0.817 M *DHDECMP/DIPB*/1.0 M HNO_3 *from* (*Horwitz* et al., 1981). *For separation factors of adjacent elements, M represents the higher, M′ the next lower value in the table.* (*i.e. next lower atomic number*).

Actinides	S_M^{Am}	$S_M^{M'}$	*Lanthanides*	S_M^{Am}	$S_M^{M'}$
Fm	0.575	–	Lu	0.048	–
	–	1.04		–	1.41
Es	0.595	–	Yb	0.067	–
	–	1.15		–	1.34
Cf	0.685	–	Tm	0.090	–
	–	1.05		–	1.15
Bk	0.719	–	Y	0.103	–
	–	0.90		–	1.29
Cm	0.649	–	Er	0.133	–
	–	1.54		–	1.40
Am	1.00	–	Ho	0.186	–
				–	1.43
			Dy	0.266	–
				–	1.32
			Tb	0.351	–
				–	1.15
			Gd	0.403	–
				–	1.49
			Eu	0.602	–
				–	1.22
			Sm	0.735	–
				–	1.16
			Pm	0.855	–
				–	1.12
			Nd	0.962	–
				–	1.26
			Pr	1.21	–
				–	1.12
			Ce	1.36	–
				–	1.04
			La	1.41	–

(but probably not interactinide) separations. The adaptation of CMPOs to extraction chromatography has led to the development of additional selective separations methods based on these reagents, to be discussed in Section 24.4.4b. Continued development of phosphine oxide ligand types and processes based on their use has produced a simplified version of the CMPO ligands (and an alternative TRUEX process, discussed in Sections 24.4.4b(i)–(iv)) and tridentate pyridine-*N*-oxide bisphosphine oxide reagents (Structure m) that exhibit useful actinide separations properties (Paine, 1995; Bond *et al.*, 1997, 1998; Nash *et al.*, 2002). Chmutova *et al.* (1975) have demonstrated that alkylene phosphine dioxides exhibit some ability to enhance the separation of californium from americium ($S_{Cf}^{Am} \approx 25$), and berkelium from curium ($S_{Bk}^{Cm} \approx 10$).

A considerable body of research has been developed by Karandashev and coworkers (Turanov *et al.*, 2000, 2002, 2004) on the subject of lanthanide extraction by bisphosphine oxide (and structurally similar) podands that should have strong analogies to actinide separations, though this latter opportunity has not been extensively investigated.

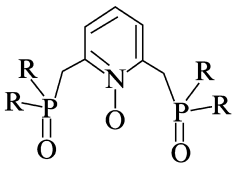

Structure m

A new class of solvating extractants has been introduced during the past decade as non-phosphorus-containing alternatives to CMPO for total actinide recycle. Amidation of the well-studied lanthanide/actinide complexant malonic acid yields lipophilic complexants that exhibit affinity for actinides in the trivalent, tetravalent, and hexavalent oxidation states. Malonamide extractants (Structure n) were proposed initially by Musikas and coworkers in the 1980s and have seen extensive investigation during the intervening years (Musikas, 1987; Cuillerdier *et al.*, 1991a; Nakamura *et al.*, 1995; Nigond *et al.*, 1995; Berthon *et al.*, 1996, 2001; Delavente *et al.*, 1998, 2001, 2003; Erlinger *et al.*, 1998, 1999; Mahajan *et al.*, 1998; Iveson *et al.*, 1999; Madic *et al.*, 2002). These extractants, functionalized at the α-carbon atom with either long chain alkyl groups or alkoxides to improve phase compatibility, compare favorably with CMPO in many respects. The process built around these extractants is referred to as the DIAMEX process.

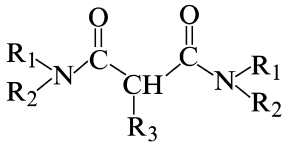

Structure n

The DIAMEX system has a steeper nitric acid dependence than is seen for CMPO, requiring that the aqueous feed be maintained above 3 M HNO_3 for adequate phase transfer. However, a steep acid dependence also implies more facile stripping of the actinides from the loaded organic phase. The primary advantage of this class of reagents, containing only carbon, hydrogen, oxygen, and nitrogen (CHON), is their ability to be completely incinerated leaving no ash behind when the end of their useful lifetime arrives. A further and in some respects equally important advantage of the malonamides is the innocuous character of the degradation products of diamides. Unlike the phosphinic acid, compounds that are produced as CMPO is degraded (to be discussed in Section 24.4.4b(iv)) or the dibutylphosphoric acid from TBP, the carboxylates

and amines resulting from the degradation of diamides do not appear to interfere appreciably with the ease of stripping of actinides from the loaded extractant phase. This positive feature is counterbalanced by a slightly faster rate of radiolytic degradation than is seen for CMPO or TBP. Phase compatibility issues in large-scale tests to date have indicated a moderate tendency toward (third-phase formation) and led to adjustments in both the extractant and diluent.

Extraction of Am(III), U(VI), Np(IV), Fe(III), Sr(II), and Cs(I) from solutions of different HNO_3 concentrations using 1 M dimethyldibutyltetradecylmalonamide (DMDBTDMA in *n*-dodecane and that of americium from a synthetic PHWR–HLW (pressurized heavy water reactor–high level waste) has been reported (Mahajan *et al.*, 1998). It is suggested that this amide is very promising for the extraction of americium and other actinides from 3–4 M HNO_3, particularly under high loading of Nd or a mixture of Nd and U. The extraction of trivalent, tetravalent, and hexavalent actinides from HNO_3 medium by DMDBTDMA/*n*-dodecane can be represented by the equilibria:

$$Am^{3+}_{aq} + 3NO^{-}_{3\,aq} + 2A_{org} \rightleftarrows Am(NO_3)_3 \cdot 2A_{org} \tag{24.20}$$

$$Pu^{4+}_{aq} + 4NO^{-}_{3\,aq} + 3A_{org} \rightleftarrows Pu(NO_3)_4 \cdot 3A_{org} \tag{24.21}$$

$$UO^{2+}_{2\,aq} + 2NO^{-}_{3\,aq} + 2A_{org} \rightleftarrows UO_2(NO_3)_2 \cdot 2A_{org} \tag{24.22}$$

These species have very similar stoichiometries to those observed for CMPO. The same diamide when adsorbed on an inert support is also efficient for the uptake of trace quantities of actinide ions from 3–5 M HNO_3. Batch studies show reasonable uptake of actinides from synthetic PHWR–HLW, only when it has been given two contacts with 20% TBP/*n*-dodecane (Mohapatra *et al.*, 2000).

Hydrolytic and radiolytic degradation of *n*-dodecane solutions of three malonamides, DMDBTDMA, *N*,*N*′-dimethyl-*N*,*N*′-dibutyldodecyloxyethyl malonamide (DMDBDDEMA), and *N*,*N*′-dimethyl-*N*,*N*′-dioctylhexyloxyethyl malonamide (DMDOHEMA), in the presence of HNO_3 have been conducted (Berthon *et al.*, 2001). The results of a similar investigation of *N*,*N*,*N*′,*N*′-tetraoctyl-3-oxapentane-1,5-diamide (TODGA) has also been reported (Sugo *et al.*, 2002). Degradation products were identified using gas chromatography coupled to Fourier transform infrared spectroscopy (FTIR) or mass spectrometry. The primary degradation products are a variety of amide–acid species and secondary amines R′–CH_3NH. The amide–acids are thermally unstable and decarboxylate to form monoamides. The other products such as amide–lactone, diamides, carboxylic acids, and alcohol are formed but their concentrations in the organic phase are much lower than the three mentioned above. It has been observed that D_{Am} and D_{Ln} values decrease with increasing irradiation doses. In a comparative study on the radiolysis of 1 M solution of

TBP, DMDBTDMA, and DMDOHEMA in TPH (hydrogenated tetrapropene or 4,4-dipropyl heptane) in contact with 4 M HNO_3 with an integrated dose of 0.7 M Gy, the concentrations found after radiolysis were respectively 0.95, 0.68, and 0.57 M. For these process representative conditions, the stability of malonamides is lower than that of TBP by a factor of 6–9.

DMDBTDMA/*n*-dodecane has been used as carrier in supported liquid membranes (SLM) studies for the facilitated transport of Am(III) using 1–5.5 M of HNO_3 as the feed solution and 0.01 M HNO_3 as the strip solution (Sriram *et al.*, 2000). It is interesting to note that under similar conditions, the permeability of Fe(III) was significantly lower than that of Am(III). In another study (Sriram and Manchanda, 2002), several other diluents apart from *n*-dodecane were used to prepare solutions of DMDBTDMA and the transport of U(VI), Pu(IV), Am(III), and Eu(III) from HNO_3 medium using a SLM technique was carried out. The stripping agent containing a mixture of 0.4 M formic acid, 0.4 M hydrazine hydrate, and 0.1 M DTPA was most promising.

Madic and coworkers (Spjuth *et al.*, 2000) have synthesized seven new compounds in the malonamide series by introducing an ether oxygen into the alkyl chain attached to the bridging methylene group or of phenyl substituents on the nitrogen. These modifications reduce the basicity of the new derivatives to less than that of DMDBTDMA. The extraction of Am from HNO_3 by different malonamides in *t*-butylbenzene diluent has shown that the D_{Am} is higher for the malonamides with low basicity than that for DMDBTDMA.

Taking the cue from the malonamide work, researchers at the Japan Atomic Energy Research Institute (JAERI) have synthesized six diglycolamides (Structure o) having the generic formula R,R–N–CO–CH_2–O–CH_2–CO–N–R,R where R is an alkyl group having carbon atoms ranging from 3 to 10 (Sasaki *et al.*, 2001). Of these, only two compounds, namely, *N*,*N*,*N*′,*N*′-tetra(octyl)-3-oxapentanediamide (TODGA) and *N*,*N*,*N*′,*N*′-tetradecyl-3-oxapentanediamide (TDDGA) showed adequate solubility in *n*-dodecane to be useful for process development. Using TODGA the *D* values of actinides increased with increasing HNO_3 concentrations and the number of diglycolamide molecules attached to the extracted actinide ions (derived from slope analysis at radioanalytical concentrations of the metal ions) were three for Th(IV), U(VI), and Pu(IV) and four for Am(III) and Cm(III). TODGA in *n*-dodecane has been shown to extract both actinides and lanthanides completely from HNO_3 solutions.

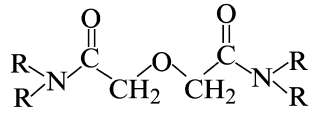

Structure o

Additional basic work continues on this class of reagents on many fronts in France, in Japan with the development of diglycolamide extractants (Sasaki *et al.*, 2001; Sasaki and Tachimori, 2002) and in the U.S., with the report of a

structurally–hindered diamide (Lumetta *et al.*, 2002, 2003) that exhibits greater affinity for trivalent actinides than the free rotation analogs (Structure p). Work also progresses on monoamides as possible replacements for TBP in a PUREX-like extraction system. The ultimate potential of this class of extractant molecules has perhaps not yet been reached.

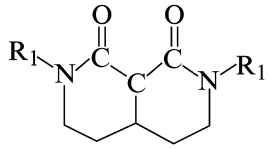

Structure p

(c) Ion pair formation systems

Two classes of alkyl amine extraction systems are known, tertiary and quaternary amines. Tertiary amines are electroneutral species that are readily protonated to form lipophilic salts ($R_3NH^+X^-$) while quaternary amines are tetraalkylammonium ions (R_4N^+) bearing a permanent positive charge and always associated with an anion in the organic phase. Both extractant classes have a tendency toward the formation of reverse micelles in organic solutions.

Tertiary amines require preequilibration with concentrated acid to create the ion pair. However, this protonation reaction introduces an additional means of adjusting the extraction chemistry of such systems. The efficiency of this class of extractants is impacted by both the salt concentration in the aqueous contacting solution and its acid concentration. Quaternary ammonium extractants are analogous to tetraalkylammonium based anion exchange resins and bear some kinship to the room temperature ionic liquids that will be discussed in Section 24.3.10.

Moore (1964) first applied quaternary amines to lanthanide/actinide group separations examining the system Aliquat 336[2]/xylene/H_2SO_4–NH_4SCN.

A principal advantage of this method is the relatively low concentration of salts required to attain a usable separation. Several other applications of the method have been summarized (Weaver, 1974). This class of extractants can be immobilized on an inert support to create extraction chromatographic materials that combine the best features of the extractants with the increased efficiency of extraction chromatography. Horwitz *et al.* (1995) have reported the application of the effect of thiocyanate for the selective separation of actinides from lanthanides using such resins (Fig. 24.9). When loaded from a solution 1.0 M NH_4SCN/0.1 M HCO_2H, trivalent actinides (represented by Am^{3+}) are quantitatively sorbed while lanthanides (from La to Eu) are rejected. Americium can be eluted from the column with 0.25 M HCl for a very selective actinide/lanthanide separation.

[2] Aliquat 336-nitrate is tri(C8-10 alkyl)methylammonium nitrate

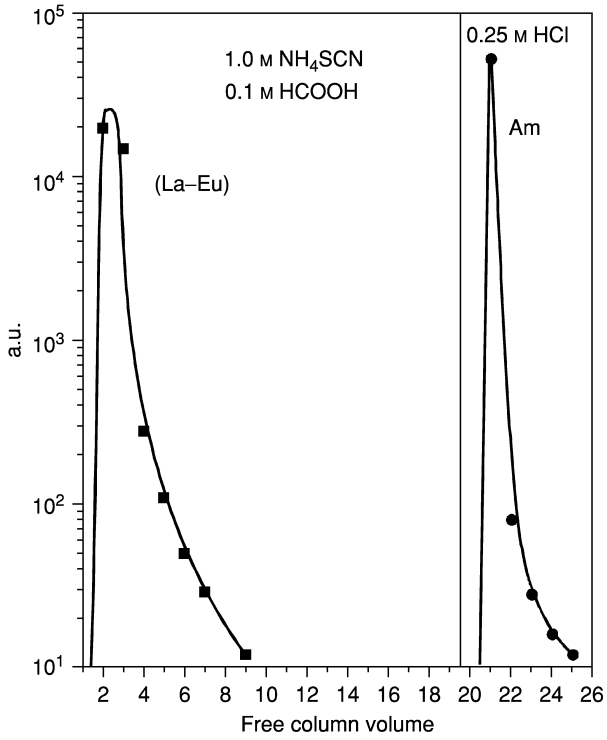

Fig. 24.9 *Partitioning of trivalent lanthanides and actinides on U-TEVA resin™* (*Horwitz* et al., 1995).

(d) Synergistic systems

The principal feature of synergistic extraction systems is increased extraction strength. Improved extraction efficiency often comes at the expense of selectivity. This is seen in the extraction of lanthanides from xylene solutions of TTA and TTA/TBP mixtures for which the separation factors (normalized to Lu^{3+}) are shown in Fig. 24.10. A linear correlation is observed between the separation factors and the position of the lanthanide ions through the series for the extraction of $Ln(TTA)_3$, whereas for extraction of $Ln(TTA)_3(TBP)_2$ separation of adjacent cations is observed for the light lanthanides only but not for the latter members of the series. The relevant literature on trivalent lanthanide/actinide separations by synergistic systems was reviewed by Mathur (1983).

Extensive investigations of 1-phenyl-3-methyl-4-benzoyl-5-pyrazolone (PMBP, Structure q) by Chmutova *et al.* (1973) indicate that the synergistic enhancement for TBP and TOPO adducts (in benzene) of the trivalent actinides (extracted from nitric acid) increase in the order Am < Cm < Bk < Cf. However, Khopkar and Mathur (1982) do not observe any particular order in

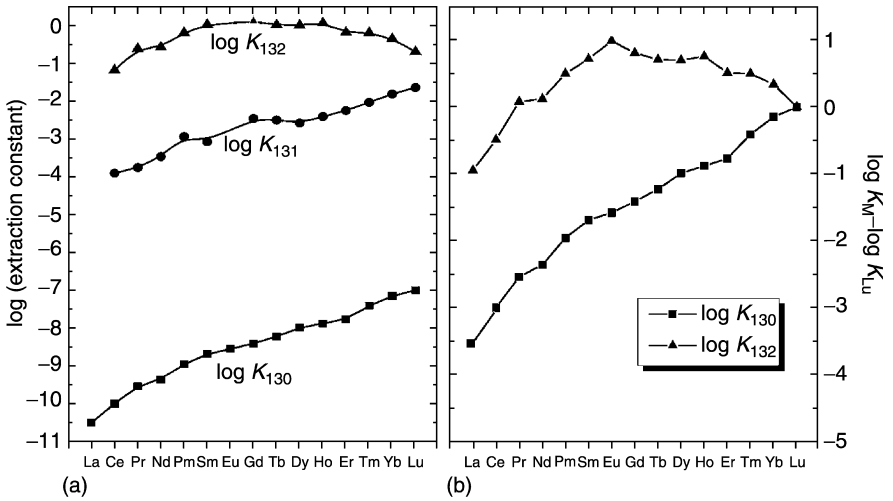

Fig. 24.10 *The effect of adding a synergist on extraction efficiency and comparative extraction of trivalent lanthanides in the TTA–TBP system*: (*a*) *extraction equilibrium constants for the reactions* $M^{3+} + 3\ HTTA \rightleftarrows M(TTA)_3 + 3\ H^+$ (K_{130}) (*Poskanzer and Foreman*, 1961), $M(TTA)_3 + TBP \rightleftarrows (M(TTA)_3TBP$ (K_{131}), *and* $M(TTA)_3 + 2\ TBP \rightleftarrows M(TTA)_3(TBP)_2$ (K_{132}) (*Farbu* et al., 1974). (*b*) *Comparative data normalized to log* $K_{Lu} = 0$.

the extraction of these metal ions from hydrochloric acid solutions into the same extractant mixtures with xylene as diluent.

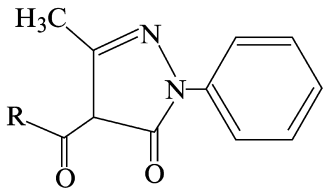

Structure q

While such reagents possess interesting cation coordination properties, ligands designed for size-selective metal ion coordination, the crown ethers (CE), calixarenes, and related species have been employed primarily as synergists for An(III) separations. As yet, no important separations of actinides have been developed based on the application of such species as a primary extractant. The use of benzo-15-crown-5 (Bz15-C-5), and dicyclohexano-18-crown-6 (DCH18-C-6) as synergists for lanthanide and actinide extraction with 1-phenyl-3-methyl-4-trifluoroacetyl-5-pyrazolone (PMPFT)/chloroform suggest some potential for such mixtures to accomplish certain specific group and inter-actinide separations (Mathur and Khopkar, 1988). Aly *et al.* (1985) studied synergistic extraction using TTA and 15-crown-5 synergist for lanthanide and trivalent actinide extraction. They found significant enhancement of the extraction, but

little separation of individual ions. The extracted complex is $M(TTA)_3(CE)_2$ for the 15-crown-5 synergist and $M(TTA)_3(CE)$ for the 18-crown-6.

There is also evidence that non-cyclic polyethers can function as synergists in lanthanide/actinide separations. Ensor and Shah (1983, 1984) report that 1,13-bis[8-quinolyl]-1,4,7,10,13-pentaoxatridecane (Kryptofix-5, or K-5) enhances the extraction of Ce(III), Eu(III), Tm(III), Am(III), Cm(III), and Bk(III) into chloroform solutions of TTA. The extracted complex has the stoichiometry $R(TTA)_3 \cdot K\text{-}5$, and the synergistic enhancement is comparable to that of TBP under the conditions studied. The separation factors reported for TTA alone are $S_{Am}^{Cm} = 1.1$, $S_{Am}^{Bk} = 5.25$, $S_{Am}^{Cf} = 11$, while for the mixture of TTA and K-5 the values are $S_{Am}^{Cm} = 0.87$, $S_{Am}^{Bk} = 3.4$, $S_{Am}^{Cf} = 2.5$, clearly indicating a decrease in separation efficiency.

24.3.5 Thermodynamic features of actinide solvent extraction reactions

The transfer of a metal ion from an aqueous medium to an organic extractant solution and back is governed by the relative positions of several competing reversible equilibria. In the aqueous phase, hydration and protonation equilibria of metal cations, chelating agents, and metal complexes, as well as the complexation equilibria of metal ions and ligands control the relative extractability of metal ions. In the organic phase, metal–ligand bonding, non-specific and specific solvation of complexes, and ligand–ligand interactions are the most important processes contributing to the net thermodynamics of phase transfer (Nash, 2001). Because solvent extraction reactions are fundamentally mass-transfer processes, they can be driven against an unfavorable Gibbs energy gradient by manipulation of phase transfer conditions, as will be demonstrated in the discussion of trivalent ion extraction by Cyanex 301 below.

Most investigations of the thermodynamics of f-element solvent extraction reactions have been performed relying on the change in the extraction equilibrium constant (K_{ex}) as a function of temperature with application of the Van't Hoff relationship $[\partial(\ln K_{ex})/\partial(1/T) = -\Delta H/R]$. Second order thermodynamic effects resulting from changes in ΔC_p generally do not complicate the application of this technique, as the temperature range is restricted by solubility and volatility considerations to the region of 0–60°C, often significantly less. There have been several reports of enthalpy changes measured calorimetrically in synergistic systems. In these experiments, measured enthalpies describe the addition of a co-extractant to the primary chelate complex of the extracted metal ion in a homogeneous organic phase. The experimental results described below are derived from a variety of literature reports. The reader is referred to the original references for details of the experimental procedures.

The most thoroughly investigated synergistic extraction systems involving f-elements are those in which TTA is the primary extractant. Neutral organophosphorus compounds, aliphatic amines, crown ethers, bipyridyl, phenanthroline, and aliphatic sulfoxide extractants have all been investigated

thermochemically as synergistic reagents for lanthanide and actinide extraction by TTA. Most of the thermodynamic data were determined using the temperature variation method, some were investigated by calorimetry, and a few systems have been studied using both techniques. Adduct formation reactions are generally exothermic (ΔH between –20 and –70 kJ mol^{-1}) while the entropies cover a wide range of both favorable and unfavorable contributions to the net equilibrium, dependent primarily on the nature of the synergist (Nash, 2001).

The tris-TTA complex of the lanthanides is a dihydrate or trihydrate in most organic diluents, thus the entropy change upon formation of the adduct partly reflects the ability of the synergist to displace this residual hydration. Using calorimetry, Choppin and coworkers (Caceci *et al.*, 1985) studied the addition of both TBP and trioctylphosphine oxide (TOPO, Structure r, where $R_1 = R_2 = R_3 =$ *n*-octyl) to the neutral TTA complexes of UO_2^{2+}, Nd^{3+}, and Th^{4+} in benzene. The enthalpies of adduct formation were 10–20 kJ mol^{-1} more exothermic in the dry solvent than the water-saturated equivalent. The corresponding variations in the entropy changes almost fully compensated the variations in enthalpy changes, resulting in a constant Gibbs energy of adduct formation. Crown ether adducts on the corresponding TTA complexes (Mathur and Choppin, 1993) were characterized by negligible entropy changes in the trivalent lanthanide adducts, but moderately unfavorable entropy changes for the UO_2^{2+} and Th^{4+} complexes.

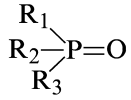

Structure r

Addition of pyridine-based donors like bipyridyl to lanthanide TTA complexes or dipivaloylmethane (also a β-diketone) is characterized by a strongly exothermic enthalpy (–40 to –70 kJ mol^{-1}) partially compensated by an unfavorable entropy change (Kassierer and Kertes, 1972; Kertes and Kassierer, 1972; Dakternieks, 1976). The synergistic extraction of lanthanides by mixtures of TTA and trialkyl amines exhibits no temperature dependence implying that the formation of the adduct from $Ln(TTA)_3$ is characterized by an enthalpy change of the same magnitude but opposite in sign to that of the extraction of the lanthanide by TTA alone. This curious observation has been made for the combination of tertiary amines and pyrazolone extractants as well.

The greater affinity of actinides for donor atoms softer than oxygen is at the heart of all successful separations of the trivalent ions of the transplutonium elements from the lanthanides (Nash, 1994). This difference in interaction strength has been attributed to a greater tendency for the actinides towards covalency in their bonding, which should, in principle, be manifested thermodynamically by exothermic complexation heats. Dithiophosphinic acid extractants [e.g. Cyanex 301, bis(2,4,4-trimethylpentyl)dithiophosphinic acid, Structure s] have been shown to exhibit separation factors of greater than 10^3 for

trivalent actinide ions over lanthanides of comparable size. Cyanex 301 when purified and used for the extraction of Am(III) and Eu(III) from nitrate medium gave an S_{Eu}^{Am} of 5.9×10^3 (Zhu *et al.*, 1996). The $S_M^{M'}$ for other lanthanides was found to be Am/La ~3500, Am/Ce ~1000, Am/Pr ~1000, Am/Nd ~1900, Am/Sm ~4500. The average Am/Ln $S_M^{M'}$ being greater than 2300.

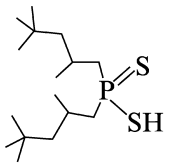

Structure s

The work of Tian *et al.* (2001) has demonstrated that Am/Eu separation factors above 10^3 can be seen even in partially degraded solvents when excess lanthanides are present in the aqueous phase. Excess non-radioactive lanthanides tend to mask the deleterious effect of degradation products of Cyanex 301 (oxygenated phosphinic acid extractant molecules in particular) on Am/Eu separation factors by competing more strongly than Am for the oxygenated species. Lanthanide saturation of the oxygenated degradation products allows the soft-donor interaction between Am and the thio phosphinates to be maintained.

These authors also have calculated thermodynamic parameters based on the measurement of distribution ratios as a function of temperature the enthalpy associated with extraction of Am^{3+} and Eu^{3+} from 1.0 M Na/HNO_3 by purified Cyanex 301. Tian *et al.* report $\Delta H_{Am} = +18.1$ kJ mol^{-1}, $\Delta H_{Eu} = +43.6$ kJ mol^{-1} with corresponding entropy changes of $\Delta S_{Am} = -87$ J K^{-1} mol^{-1}, $\Delta S_{Eu} = -66$ J K^{-1} mol^{-1}. Though both phase transfer reactions are characterized by unfavorable endothermic enthalpic effects and negative entropies, analysis of the data indicates that the enthalpy difference between the americium and the europium extraction is the principal source of the greater selectivity of Cyanex 301 for Am^{3+} [$(\Delta H_{Am} - \Delta H_{Eu}) = -25.5$ kJ mol^{-1}; $-T(\Delta S_{Am} - \Delta S_{Eu}) = +6.3$ kJ mol^{-1}]. Both the more exothermic heat and greater order implicit in the entropy contribution are consistent with increased strength of the Am–S bonding relative to that of Eu–S.

Jensen and Bond (2002a,b) have concluded based on a combination of EXAFS, osmometry, Karl Fisher titration, and UV–visible spectrophotometry that the complexes of lanthanide and trivalent actinide ions extracted into Cyanex 301 in xylene are octahedral containing no inner sphere water molecules. They interpret this result as indicating that the difference in thermodynamic parameters is most likely a result of increased Cm–S bonding strength relative to that of Sm. Tian *et al.* (2003) argue based on EXAFS, FTIR, and MS data for the presence of eight-coordination lanthanide and actinide complexes with Cyanex 301. The lanthanide complex contains an inner-sphere water molecule that is not present in the corresponding eight-coordinate Am complex.

The most common neutral extractants for f-elements are trialkyl-phosphates, -phosphonates, -phosphinates, and -phosphine oxides. As shown in equation (24.7) describing the extraction process for systems of this class, both an appropriate number of aqueous anions to neutralize the cation charge and a variable number of extractant molecules to make the complex lipophilic are needed. This assembly of a number of components to form a single product species suggests that the net extraction entropy for such reactions should be consistently negative. In fact, for extraction of trivalent lanthanides, actinides, Th^{4+}, and UO_2^{2+} by simple monodentate or complex bidentate organophosphorus extractants (which represent the bulk of such neutral extractant systems) the extraction entropies range between –40 and –150 J K^{-1} mol^{-1}independent of the nature of the counter ion X^-. Extraction enthalpies are exothermic and in the range of –30 to –90 kJ mol^{-1}, implying a net increase in bonding strength for the phase transfer reaction (though the origin of the increased bonding strength cannot be established from such investigations) (Nash, 2001).

The relative extraction of trivalent lanthanides and actinides in neutral systems has been examined by comparing Am^{3+} and Eu^{3+} extraction by CMPO (Mathur and Nash, 1998; Suresh *et al*., 2001) and DHDECMP (Horwitz *et al*., 1981; Muscatello *et al*., 1982). The stoichiometries of the extraction equilibria are as described above. The thermodynamic data (ΔG, ΔH, and ΔS) for the extraction of Am(III) and Eu(III) species from NO_3^- and SCN^- media with CMP and NO_3^-, SCN^-, ClO_4^-, and $ClO_4^- + NO_3^-$ media with CMPO are given in Table 24.6. The thiocyanate systems demonstrate a greater selectivity for americium corresponding to an increased Gibbs energy change of 4–5 kJ mol^{-1} (a separation factor of 5–7). Substantially more exothermic extraction enthalpies are observed in both the Eu^{3+} and Am^{3+} thiocyanate systems than is seen in the corresponding nitrate reactions. This difference has been attributed, based on data tabulated by Marcus (1997), to the greater exothermicity of the transfer three SCN^- ions from the aqueous to a normal alkane organic phase as compared with the transfer of three nitrate anions (Mathur and Nash, 1998). Differences in the enthalpy of extraction of americium relative to europium are not substantial or consistent enough to attribute the enhanced extraction of the actinide to a soft donor-effect.

24.3.6 Aqueous biphasic systems

Some research has been done on liquid–liquid extraction systems that seek to eliminate hydrophobic organic materials. For example, polyethylene glycols can produce two-phase systems (called aqueous biphases) when equilibrated with concentrated salt solutions of water-structuring anions (Rogers *et al*., 1993). The key characteristic of these systems is that the immiscible phases are both largely aqueous in nature. Myasoedov and Chmutova (1995) have reported conditions for the separation of transplutonium elements from uranium, thorium, and lanthanides. The aqueous biphase itself does not extract actinides

Table 24.6 *Thermodynamic parameters for Am(III) and Eu(III) extraction from nitrate, thiocyanate, perchlorate, and nitrate + perchlorate media using neutral donors CMPO and CMP at* 25°C.

System	ΔG (kJ mol^{-1})	ΔH (kJ mol^{-1})	ΔS (J mol^{-1} K^{-1})	*Reference*
$Am(NO_3)_3 \cdot 3$ CMPO	–24.3	–66.5	–142	Suresh *et al*. (2001)
$Eu(NO_3)_3 \cdot 3$ CMPO	–25.8	–65.3	–133	Suresh *et al*. (2001)
$Am(SCN)_3 \cdot 3$ CMPO	–42.3	–92.3	–168	Suresh *et al*. (2001)
$Eu(SCN)_3 \cdot 3$ CMPO	–37.8	–114.2	–256	Suresh *et al*. (2001)
$Am(ClO_4)_3 \cdot 3$ CMPO	–25.3	–39.1	–46	Suresh *et al*. (2001)
$Eu(ClO_4)_3 \cdot 3$ CMPO	–23.8	–67.4	–146	Suresh *et al*. (2001)
$Am(NO_3)(ClO_4)_2 \cdot 3$ CMPO	–32.3	–124.8	–310	Suresh *et al*. (2001)
$Eu(NO_3)(ClO_4)_2 \cdot 3$ CMPO	–30.6	–139.2	–365	Suresh *et al*. (2001)
$Am(NO_3)_3 \cdot 3$ CMPO	–32.2	–49.4	–58	Mathur and Nash (1998)
$Eu(NO_3)_3 \cdot 3$ CMPO	–32.8	–64.5	–106	Mathur and Nash (1998)
$Am(SCN)_3 \cdot 3$ CMPO	–57.4	–89.9	–109	Mathur and Nash (1998)
$Eu(SCN)_3 \cdot 3$ CMPO	–51.6	–83.8	–108	Mathur and Nash (1998)
$Am(NO_3)_3 \cdot 3$ CMP	–6.67	–42.3	–120	Horwitz *et al*. (1981)
$Eu(NO_3)_3 \cdot 3$ CMP	–6.68	–37.4	–103	Horwitz *et al*. (1981)
$Am(SCN)_3 \cdot 3.6$ CMP	–44.4	–87.4	–144	Muscatello *et al*. (1982)
$Eu(SCN)_3 \cdot 4$ CMP	–40.5	–94.1	–179	Muscatello *et al*. (1982)

strongly, but Arsenazo III (2,7-bis(2,2′-arsonophenylazo)-1,8-dihydroxy-naphthalene-3,6-disulfonic acid) is a highly effective carrier for these metal ions. A method for preparation of an isotope generator for ^{239}Np from ^{243}Am using an ammonium sulfate solution containing potassium phosphotungstate has also been reported (Molochnikova *et al*., 1995). Overall, while the aqueous biphasic extraction approach brings forward some interesting features, the high salt concentrations needed to generate the biphase work against its utility for large-scale separations. Polyethylene glycols remain useful compounds when employed as phase modifiers in conventional solvent extraction.

24.3.7 Actinide separations from Alkaline Solutions

Alkaline conditions tend, in general, to lead to the precipitation of actinide hydroxides. However, much of the actinide inventory within the waste system in the U.S. is found in (or in contact with) such solutions, and the tendency of actinides to precipitate from alkaline solutions can be overcome by

water-soluble chelating agents. There are a few examples of the separation of lanthanides and actinides from alkaline and carbonate solutions, as reviewed by Karalova *et al*. (1988). Both solvating and chelating extractants have been used in these studies. Ternary and quaternary amines, alkylpyrocatechols, β-diketones, pyrazolones, and *N*-alkyl derivatives of aminoalcohols are the extractants indicated as useful for alkaline extraction processes. A variety of diluents have been used, but their nature seems to have little effect on the extraction efficiency or separation factors.

The factors contributing to a successful separation procedure in alkaline media are not different from those relevant in acidic solutions, i.e. the efficiency is dependent on the nature of the extractant and the aqueous complexant, the pH of the aqueous solution, and the strength of aqueous complexes. Two advantages provided by this approach are the relative ease of back extraction (contact with neutral salt solutions is usually sufficient) and the potential for separations based on relative rates of phase transfer reactions. The disadvantage (from a practical standpoint) is the requirement of working with concentrated salt solutions, which creates waste disposal problems. However, the potential for reducing the transuranium element (TRU) content of alkaline wastes justifies a search for viable separation schemes based on alkaline solutions.

Extraction from alkaline and carbonate solutions is characterized by an unusual sequence of the distribution ratios favoring the trivalent oxidation state [in carbonate solutions the order of extraction is M(III) > M(IV) > M(V) > M(VI)]. A further benefit of operation in alkaline solutions is the greater tendency for air oxidation of some trivalent metal ions. Group separation factors for the trivalent actinides and lanthanides are about 2 for extraction by Aliquat 336-EDTA in contact with an alkaline EDTA aqueous solution (Bukina *et al*., 1983). Eu–Am separation factors of 70 have been reported for a non-equilibrium extraction in the system 4-(α,α-dioctylethyl)-pyrocatechol/NaOH/DTPA (or DTPMPA, diethylenetriamine-*N*,*N*,*N*′,*N*″,*N*″-pentamethylenephosphonic acid) (Karalova *et al*., 1982). In contrast with most acid-medium separation systems, the separation factors are based mainly on the difference in the *rates* of the metal–DTPA (or DTPMPA) complexation reactions for europium and americium rather than chemical equilibria. They are, therefore, highly dependent on the contact time. A principal limitation to the practical application of separation schemes based on alkaline solutions is the relatively long contact times (more than 10 min) required for extraction.

24.3.8 Separations of actinides involving natural agents

Several natural agents present in plants (Dushenkov *et al*., 1997; Huang *et al*., 1998; Thulasidas *et al*., 1999) or more generally biomass (Anonymous, 1951; Dhami *et al*., 1998a,b; Banaszak *et al*., 1999), jimson weeds (Anonymous, 1995), tannin biomolecules (Sakaguchi and Nakajima, 1987, Nakajima and Sakaguchi,

1990), siderophores (Whisenhunt *et al*., 1993), chitosan (a natural biopolymer derivative of chitin) (Anonymous, 1995; Park *et al*., 1999; Srinivasan *et al*., 2001) etc. have been considered for actinide separations from very dilute solutions. Our emphasis here will be on non-living microbial biomass, a common fungus *Rhizopus arrhizus* (*RA*), which has chitin chains inside its cell walls, and chitosan which is a natural biopolymer derivative of chitin extracted from crab shell.

A detailed study on the biosorption of uranium and thorium by *RA* has been carried out by Tsezos and coworkers (Tsezos and Volesky, 1981, 1982; Tsezos, 1983) where they have reported very high uptake of uranium from aqueous solutions to the extent of 180 mg U per gram of *RA*. The highest uptake of the metal ions was between pH 4 and 5. The presence of Cu^{2+}, Zn^{2+}, and Fe^{2+} ions interfered in the biosorption of uranium and thorium. The mechanism of uranium sequestering by *RA* has been studied by using techniques like electron microscopy, X-ray energy dispersion analysis, and IR spectroscopy. It has been proposed that the total sorption of uranium is the cumulative effect of three processes: formation of uranium coordination compounds with the amine nitrogen of the chitin chains, adsorption of uranium to the polyalcohol surface of the chitin matrix, and hydrolysis of the U–chitin complex formed, resulting in the precipitation of the hydrolysis product in the cell wall (Tsezos and Volesky, 1982). Sorption of radionuclides ^{233}U, ^{239}Pu, ^{241}Am, ^{144}Ce, ^{147}Pm, $^{152,154}Eu$, and ^{95}Zr from aqueous nitrate medium (pH 2–11) has been studied with *RA*: it was suggested that *RA* is an effective biomass for the removal of actinides and trivalent fission product lanthanides from low-level waste streams generated in PUREX process and also in the secondary wastes generated from the TRUEX process (Dhami *et al*., 1998a,b).

The adsorption of uranyl ion on powdered chitosan is characterized by a high affinity in neutral pH range; however the adsorption capacity of chitosan at relatively high pH decreases due to the presence of negatively charged uranyl species in the solution (Park *et al*., 1999). Chitosan has been found to be a good natural material for the sorption of ^{241}Am at a pH of 3 (Srinivasan *et al*., 2001).

24.3.9 Trivalent actinide/lanthanide separation systems

The classic historical methods of separating trivalent actinides from fission product lanthanides are based on ion exchange, as discussed in Section 24.2.4. However, as is seen in Section 24.3.4, solvent extraction techniques have a wider range of applications. One approach to accomplishing trivalent actinide/lanthanide separation by solvent extraction is to apply consecutively two unrelated separation processes in a complementary fashion. Sekine and Dyrssen (1964) reported Eu/Am separation factors for 12 acidic extractants covering the spectrum of available materials (Table 24.7 is adapted from their work). Based on their separation factors, one can envision a counter-current separation procedure involving first extraction by dibutylphosphoric acid (HDBP) to

Table 24.7 *Europium/americium separation factors for a series of acidic extractants* (*Sekine and Dyrssen,* 1964).

Extractant	*Diluent*	S_{Am}^{Eu}
dibutylphosphoric acid	$CHCl_3$	22.9
dioctylphosphoric acid	$CHCl_3$	14.1
1-phenyl-3-methyl-4-acetylpyrazolone-5	$CHCl_3$	3.47
thenoyltrifluoroacetone	$CHCl_3$	3.02
neocupferron	$CHCl_3$	1.74
N-benzoylphenylhydroxylamine	$CHCl_3$	1.66
N-2,4-dichlorobenzoylphenylhydroxylamine	$CHCl_3$	1.32
β-isopropyltropolone	$CHCl_3$	0.98
1-hydroxy-2-napthoic acid	hexone	1.07
2-hydroxy-1-napthoic acid	hexone	1.02
3-hydroxy-2-napthoic acid	hexone	0.95
5,7-dichloroxine	$CHCl_3$	0.10

preferentially remove americium, followed by contact of the aqueous phase with 5,7-dichloroxine to extract europium. Substituting bis(2-ethylhexyl)phosphoric acid (HDEHP) for HDBP, Kasting *et al*. (1979) suggest that such a separation procedure could give actinide/lanthanide separation factors of several thousand.

From a process-scale application perspective, combinations of extraction systems are generally considered undesirable because of the complexity they introduce into the separations process. The more widely accepted approach to the separation of trivalent actinides from lanthanides is to rely upon the slightly stronger interaction that the trivalent actinides exhibit with ligands containing soft-donor bases (S, Cl, or N), as reported by Diamond *et al*. (1954). The soft-donor atoms may be present as free ions (SCN^-, Cl^-) or in a complexant/extractant molecule either water-soluble or lipophilic. This condition was recognized early in the race to produce new actinides, and formed the basis of separations techniques developed between 1945 and 1960, several of which still constitute the 'state-of-the-art' in actinide separations. Both ion exchange and solvent extraction techniques figure prominently in these separations.

The efficiency of lanthanide/actinide separations through the agency of soft-donor complexants is highly dependent on the strength of the interaction between the hydrated metal cation and the bulk water structure in the aqueous phase as well. The results reported by Sekine (1965) illustrate this in showing the combined effect of soft-donor ligands (SCN^-) and of water-structure disrupting anions (both SCN^- and ClO_4^-) on Am/Eu separation using a solvating extractant (Fig. 24.7). Both the extraction and mutual separation of americium and europium with 5% TBP in hexane from 5.0 M $NaClO_4$/NaSCN, and from NaSCN solutions without supporting electrolyte (pH 4–5) exhibit strong dependence on the concentration of SCN^-. In each case, separations factors (S_{Eu}^{Am}) decline with increasing thiocyanate concentration, though they are

lower throughout the range of observation in the mixed salt system than in the thiocyanate-only system. However, in the thiocyanate-only system, distribution ratios overall are significantly lower for both metal ions, particularly at low total thiocyanate.

Distribution ratios are significantly higher in the mixed salt system due to the 'perchlorate effect' (Marcus and Kertes, 1969). The Gibbs energy for extraction of either Am or Eu in the presence of perchlorate (for example, at 1 M NaSCN) is 12–17 kJ mol^{-1} more favorable than when perchlorate is absent. At the highest SCN^- concentrations, separation factors are about unity because the disrupting effect of SCN^- and ClO_4^- on the water structure essentially diminishes the importance of the effect of the soft-donor interaction in actinide binding to the SCN^-. It appears that cation/complex solvation effects dominate the relative interactions under these conditions. Effectively, water activity is increased by the disruptive effect of the large anions and thus the soft-donor thiocyanate can no longer effectively distinguish between Am and Eu (as it clearly does at lower salt concentrations).

The bifunctional extractants (CMPs and CMPOs discussed in Section 24.3.4b) are designed for process applications to permit complete recovery of all actinides in oxidation states 3+, 4+, and 6+ from nitric acid solutions. Their extraction strength does not readily lend itself to selective separations. However, Muscatello *et al.* (1982) reported that substitution of dilute NH_4SCN for HNO_3, in the extraction of trivalent f-elements from 0.244 M DHDECMP (dihexyl)diethylcarbamoylmethylphosphonate) yielded americium/europium separation factors as high as 10.8. The thermodynamic features of these and related systems have been discussed in Section 24.3.5.

A more efficient, but considerably more complex, approach to actinide/lanthanide separation was developed by Weaver and Kappelmann (1964). If the normal mineral acid aqueous phase is replaced by a 1 M carboxylic acid (pH 1.8) solution, HDEHP extraction of Am is depressed relative to that for the lanthanides. At higher pH values (~3.0), the separation factors are increased, with the most consistent enhancement observed for lactic acid. Addition of only 0.05 M DTPA to the solutions of carboxylic acids at pH 3 resulted in dramatically improved separation factors. For extraction from 1 M lactic acid/0.05 M DTPA at pH 3 with 0.3 M HDEHP/diisopropylbenzene, the worst actinide/lanthanide separation factor is for $S_{Cf}^{Nd} \approx 10$. Separation factors for lanthanides over americium and curium were greater than 100. In this system, up to one lactic acid molecule appears in the extracted complex. The DTPA complexes remain in the aqueous phase.

This separation process has acquired the acronym TALSPEAK (Trivalent Actinide Lanthanide Separation by Phosphorus reagent Extraction from Aqueous Komplexes). The generic applicability of the concept is demonstrated by the work of Baybarz (1965), who finds only slightly reduced efficiency upon substitution of 2-ethylhexyl(phenyl)phosphonic acid/diethyl benzene (H(EH(Φ)P)/DEB) for HDEHP/DIPB. The impact of substitution of DTPA

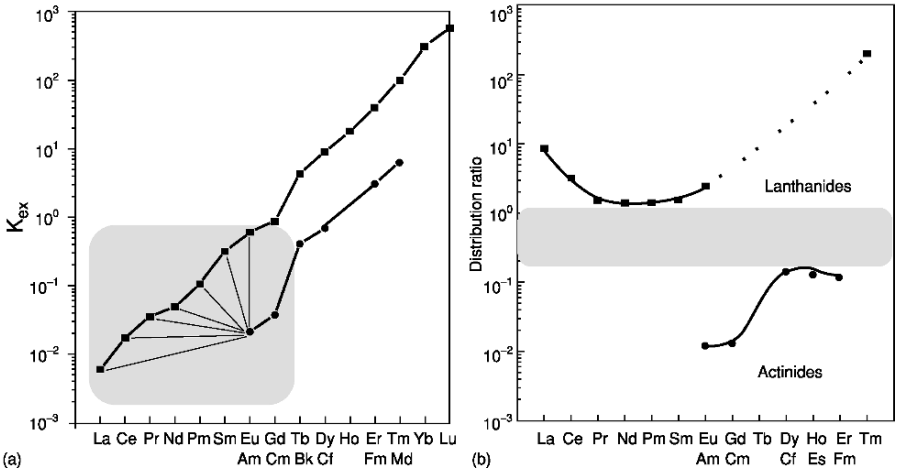

Fig. 24.11 *Distribution of lanthanide* (▪) *and trivalent actinide* (●) *cations between* (*a*) *nitric acid and* 0.5 M *HDEHP* (*Peppard* et al., 1957) *and* (*b*) 0.3 M *HDEHP/DIPB*, 1 M *lactic acid*, 0.05 M *DTPA at pH* 3 (*Weaver and Kappelmann*, 1964).

and lactate for nitric acid on group separations (as compared with HDEHP alone) is illustrated in Fig. 24.11. In a modification of the TALSPEAK process, known as the Reverse TALSPEAK process, trivalent actinides and lanthanides together are extracted by 1 M HDEHP from the 0.1 M HNO_3 feed solution. Americium and curium are then selectively stripped from the organic phase with a mixture of 0.05 M DTPA and 1.5 M lactic acid at a suitable pH adjusted with ammonia (Persson *et al*., 1984).

A number of other reports have discussed applications, process experience, and modifications of TALSPEAK. Kosyakov and Yerin (1980) report that for curium extraction with TALSPEAK-type aqueous solutions using HDEHP/decane solutions both extractant (HDEHP) and acid dependencies (i.e. the number of extractant molecule dimers in the complex and the number of H^+ ions released to the aqueous solution) decreased from 3 to 2. This reduction indicates the extraction of a 1:1 M–lactate complex for the aliphatic diluent. Similar extractant dependencies were reported for Bk, Eu, and Ce. Bourges *et al*. (1980) report a comparison of TALSPEAK with TBP-nitrate and trilauryl ammonium nitrate extraction for Am/Cm separations using DTPA as aqueous complexing agent (in extraction chromatographic mode). Though TALSPEAK gives higher lanthanide/actinide separation factors, these authors cite favorable chromatographic kinetics and improved Am/Cm separation as justification for the choice of TBP/DTPA over TALSPEAK. Ishimori finds higher distribution ratios in a TALSPEAK type system using di-isodecylphosphoric acid (DIDPA, Structure t) in place of HDEHP (Ishimori, 1980). Bond and Leuze (1980) describe a lanthanide/actinide removal and separation scheme using a 1 M lactic

acid–0.05 M DTPA stripping solution to separate trivalent actinides from the lanthanides.

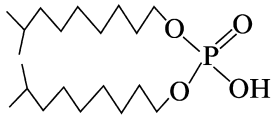

Structure t

The TALSPEAK process is adaptable to liquid membrane separations (Novikov and Myasoedov, 1987). These authors report the use of a 'supported liquid membrane' impregnated with HDEHP for the separation of Am/Cm, Eu/Tb, and Am/Eu using DTPA, citric acid, and the potassium salt of a heteropolyacid ($K_{10}P_2W_{17}O_{61}$) as aqueous complexants. The optimum separation factors reported are $S_{Cm}^{Am} = 5.0$, $S_{Tb}^{Eu} = 10.8$, and $S_{Am}^{Eu} > 10^2$. Elements of the TALSPEAK (or reverse) still get periodic consideration in process chemistry of actinide recycle, as will be discussed in Section 24.4.4 g.

French researchers have investigated the use of soft-donor extractants and complexants to enhance actinide/lanthanide group separations (Musikas *et al.*, 1980; Musikas, 1985; Vitorge, 1985). The relative stability constants for lanthanide and actinide azide complexes reported by Musikas *et al.* (1980) suggest that hydrazoic acid (HN_3) could function as a useful reagent for this separation. This is confirmed in a later report on Am/Eu separation (Musikas, 1985) in which americium extraction is suppressed by complex formation with azide. The separation factors are similar to those reported by Sekine (1965) using SCN^- as the complexant in TBP extraction. As to the thermodynamic factors describing this system, Choppin and Barber (1989) find that, while the trivalent actinide–azide stability constants are somewhat larger than those of the trivalent lanthanides, the complexation enthalpies (calculated from the temperature coefficient of the stability constants) do not support the existence of a covalent bonding contribution.

A soft-donor extractant system, mixtures of *o*-phenanthroline and nonanoic acid (Musikas, 1985), extracts americium in order of magnitude more strongly than europium from 0.1 M $NaNO_3$ solutions at pH 4.5–5.1 [$S_{Eu}^{Am} = (17.4 \pm 0.9)$]. To accomplish the separation at higher acidity, research has been conducted on the complexant/extractant 2,4,6-tris(2-pyridyl)-1,3,5-triazine (TPTZ, Structure u), used in conjunction with carboxylate and sulfonate co-extractants. The latter is necessary because of the hydrophilicity of the $Am(NO_3)_3TPTZ$ complex. Replacement of nitrate by α-bromocaprate (with decanol as diluent) gives group separation factors ≈ 10 with little apparent variation in the distribution ratios for the members of the groups (Am, Cm, or Eu, Nd, Tb, and Yb) (Table 24.8) in the pH range of 2–3. Substitution of dinonylnaphthalenesulfonic acid (HDNNS) for α-bromocapric acid gives similar performance at 0.1 M acid.

Table 24.8 *Extraction of selected trivalent actinides and lanthanides by* 2,4,6-*tris* (2-*pyridyl*)-1,3,5-*triazine* (*TPTZ*)/1 M α-*bromocapric acid* (*ABCA*)/*decanol*, *and TPTZ/HDNNS/t-butylbenzene*(*TBB*) *nitric acid* (*Musikas*, 1985).

Metal	*D*(*TPTZ/ABCA*) pH 2.2	*D*(*TPTZ*/(*TPTZ/HDNNS*) $[HNO_3] = 0.12$ M
Am	0.85	1.35
Cm	0.80	1.40
Ce	–	0.158
Nd	0.08	–
Eu	0.10	0.199
Gd	–	0.178
Tb	0.11	0.14
Yb	0.10	0.22

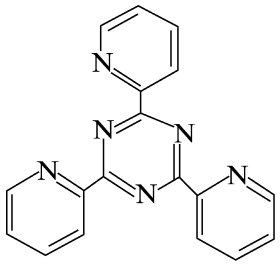

Structure u

Structurally, TPTZ is perhaps not ideally suited as an extractant for this separation. Though there are a number of nitrogen donor atoms present in TPTZ, the planar nature of the ligand demands that no more than three nitrogen atoms be coordinated to a metal ion, leaving three additional potential donor atoms available for interactions (quite probably non-productive interactions) with other solutes in the organic phase. Continued research on the design, synthesis, and characterization of polyaza extractants led ultimately to the development by Kolarik *et al*. (1999) of the bistriazinylpyridine (BTP) class of ligands (Structure v). Work continues on the adjustment of the structure and properties of these ligands (Hägstrom *et al*., 1999; Hudson *et al*., 2003; Drew *et al*., 2004a, b).

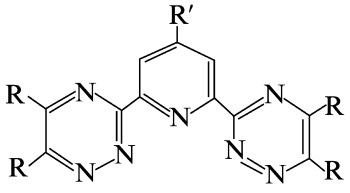

Structure v

In this ligand, pyridine rings have been substituted by triazines, in a geometry that favors at least tridentate coordination of the metal ion. Actinide/lanthanide

separation factors as high as 100 have been reported. This ligand is receiving considerable attention as a candidate for process-scale lanthanide/actinide reagent (Madic *et al.*, 2002). To date, 75 derivatives of this class of reagents have been prepared and have undergone some degree of characterization. Lipophilic co-extractants (carboxylic or organophosphoric acids) and/or long-chain alcohol diluents are often employed to minimize partitioning of the BTP extractant to the aqueous phase.

Another polyaza ligand that has received some attention for its potential to accomplish actinide/lanthanide separation is the EDTA structural analog *N*,*N*,*N*′,*N*′-tetra(methylpyridyl)ethylenediamine (TPEN, Structure w). Investigations of the structure of lanthanide complexes (Morss and Rogers, 1997) and the thermochemistry (Jensen *et al.*, 2000) of the corresponding aqueous species confirm the existence of a hexadentate coordination mode and an apparent 100-fold selectivity for actinides over lanthanides in aqueous solutions. Separation-specific studies have been conducted by Takeshita and coworkers (Watanabe *et al.*, 2002). These authors have reported separation factors greater than 70 in a synergistic extraction system analogous to that employed in the BTP system. As with all polyaza ligands, extractant partitioning to the aqueous phase is a complication in these systems.

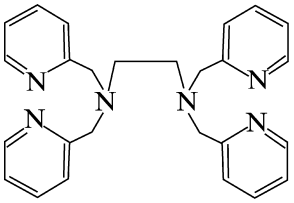

Structure w

In general, f-elements are poorly extracted by simple sulfur donor extractants. Furthermore, extractant molecules that incorporate sulfur as a donor atom are often plagued by poor stability when contacted with acidic (particularly nitrate) aqueous solutions. Certain types of extractants are more vulnerable to such attack, as results presented by Musikas (1985) indicate. His reports of good actinide/lanthanide separation factors for solvent extraction by thio derivatives of HDEHP were later dismissed (Freiser, 1988) as being the result of hydrolysis of the extractant to produce the oxygenated derivative. Because the oxygenated analogs of thiophosphorus ligands extract trivalent lanthanide/actinide cations very strongly, even very low concentrations of these degradation products profoundly compromise the ability of the soft-donor extractant to accomplish the separation.

Thiophosphinic acids like Cyanex 301 are slightly more resistant to hydrolytic degradation than the dialkyldithiophosphates though the oxygenated products of their hydrolysis are as damaging to a successful lanthanide/actinide separation as HDEHP is in the thiophosphate system. This extractant when employed for separations of d-transition metals (e.g. Cd^{2+}) is often used in a de-aerated

environment to reduce the impact of degradation of the extractant on separation efficiency. Unfortunately, for separations of radioactive materials, the effect of radiolysis (and the oxygenated by-products of water radiolysis) cannot be eliminated and degradation of the extractant will be problematic in process applications.

Other derivatives of dialkyl dithiophosphinic acids have also been prepared and evaluated as potential actinide/lanthanide separation reagents. Results from Jarvinen *et al.* (1995) indicate moderate separation factors for americium from europium using dithiophosphinic acid extractants (R_2PS_2H) Cyanex 301, dicyclohexyldithiophosphinic acid, and diphenyldithiophosphinic acids. Wang *et al.* (2001) have synthesized several dialkylthiophosphinic acids where 2,4,4-trimethylpentyl group present in Cyanex 301 was replaced with *n*-octyl, 1-methylheptyl, 2-ethylhexyl, heptyl, or hexyl groups. It has been observed that by using 0.5 M solution of the thiophosphinic acids, the pH for 50% extraction ($pH_{1/2}$) of americium and europium from 1 M sodium nitrate is 2.58, 2.63, 2.67, 3.19, and 3.94, 3.99, 4.06, 4.52, respectively, for R = *n*-octyl, 1-methylheptyl, 2-ethylhexyl, or 2,4,4-trimethylpentyl groups. The Am/Eu separation factors for the four extractants are $\sim 1 \times 10^4$. These authors suggest that di(2-ethylhexyl)dithiophosphinic acid is the most promising of these extractants because of its lower $pH_{1/2}$ and higher loading capacity of extraction of americium as compared to Cyanex 301 (Tian *et al.*, 2001). More data on extractions at macro concentrations of the lanthanides, S_{Eu}^{Am} mixer–settler or centrifugal contactor runs will be required to substantiate these studies.

In an attempt to lower the $pH_{1/2}$ of this class of extractants, Modolo and Odoj (1999) prepared bis(*p*-chlorophenyl)dithiophosphinic acid. This extractant in a process solvent that includes tri(*n*-butyl)phosphate or trioctylphosphine oxide as a co-extractant is able to selectively extract trivalent actinides from lanthanides with separation factors acceptable for process applications. This extractant is receiving attention for possible process application, as will be discussed in Section 24.4.5b.

The higher $S_M^{M'}$ between americium and europium has been suggested by Ionova *et al.* (2001) as being due to the strong coordination of M(III) to soft-donor sulfur atoms of Cyanex 301, covalent effect being significantly higher for Am–S as compared with Eu–S bonds. These authors have further shown that while using a mixture of Cyanex 301 and neutral O-bearing co-extractants, the extraction of M(III) and S_{Eu}^{Am} can be correlated with the effective charge on O atom of the neutral organophosphorus extractant molecule. The S_{Eu}^{Am} reported are 3200 for Cyanex 301 alone, 4700 for Cyanex 301 and TBP, 9100 for Cyanex 301 and tri-*tert*-butyl phosphate, 16 000 for Cyanex 301 and triphenyl phosphate, 0.45 for Cyanex 301 and TOPO/CMPO, 95 for Cyanex 301 and *N*, *N*′-dimethyl-*N*,*N*′-dibutyltetradecylmalonamide, and 17 000 for Cyanex 301 and *N*, *N*′-di (ethyl-2-hexyl)dimethyl-2,2-butanamide.

Other classes of sulfur donor extractants appear to be more resistant to hydrolysis, and have demonstrated some potentially useful selectivity for

Table 24.9 *Distribution ratios and separation factors for americium/europium extraction by 4-benzoyl-2,4-dihydro-5-methyl-2-phenyl-3H-pyrazol-3-thione/toluene* (0.0297 M)/0.1 M $NaClO_4$ *as a function of* 4,7-*diphenyl*-1,10-*phenanthroline* (*synergist*) *from* (*Ensor* et al., 1988).

[DPPHEN]	D_{Am}	S_{Eu}^{Am}
0.00269	25.3	183
0.00215	21.9	196
0.00144	14.8	192
0.00108	10.3	174
0.000718	6.1	156
0.000359	2.7	129

actinides over lanthanides. For example, the mixture of 0.3 M 4-benzoyl-2, 4-dihydro-5-methyl-2-phenyl-3H-pyrazol-3-thione (BMPPT)/0.01 M TOPO/benzene extracts (from 0.1 M $LiClO_4$, pH 3) americium preferentially over europium ($S_{Eu}^{Am} = 68$) (Smith *et al.*, 1987). The analogous system based on the oxygen-donor analog and TOPO (Chmutova and Kochetkova, 1970) gave stronger extraction but no significant separation of curium from europium. Further substitution of the soft-donor synergist 4,7-diphenyl-1,10-phenanthroline (DPPHEN, Structure x) for TOPO (Ensor *et al.*, 1988), results in even greater selectivity for americium ($S_{Eu}^{Am} = 190$, pH 3.7, 0.03 M HBMPPT/0.0027 M DPPHEN). The extracted species is $M(BMPPT)_3(DPPHEN)$ (Table 24.9). This is the only known example of a system that contains soft-donor atoms in both the primary extractant and in the synergist. Choppin *et al.* (1995) have reported on the separation of americium from europium using various combinations of thiothenoyltrifluoroacetone, tri(*n*-butyl)phosphate, tributylphosphine sulfide, and *N*,*N*-dimethyl-*N*,*N*′-dihexyl-3-oxapentanediamide as coextractant ligands in a synergistic extraction system. In this case, the soft-donor ligands show little enhancement of Am/Eu separation factors.

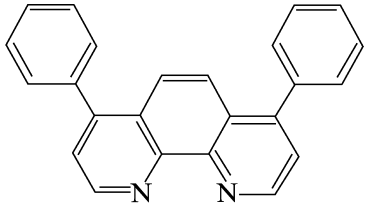

Structure x

24.3.10 Supercritical fluid extraction of actinides

The field of supercritical fluid extraction (SFE) of metal ions has been developed during the past decade. Among the first papers published, those by Wai and coworkers were the most important. In 1991, this group (Laintz *et al.*, 1991)

published a paper describing the solubility of fluorinated metal dithiocarbamates in supercritical carbon dioxide (sc-CO_2) wherein they demonstrated that the solubility of the fluorinated dithiocarbamates were two to three orders of magnitude higher than those of the corresponding non-fluorinated compounds. This technique was thus recognized as a promising new extraction method for metal ions from various sources. A year later, Wai and co-workers published a second paper (Laintz *et al.*, 1992) related to the SFE of metal ions from aqueous solutions and solid materials, and in 1993 they demonstrated the possibility of extracting lanthanide (Ln) and actinide (An) ions from solid materials with a fluorinated β-diketone (Lin *et al.*, 1993).

The rationale for the use of SFE of metal ions as an alternative to conventional liquid–liquid extraction (LLE) was mainly to minimize the generation of the secondary organic waste often encountered in LLE processes. Carbon dioxide was chosen as the most appropriate supercritical fluid because: (i) the values of the critical point (Darr and Poliakoff, 1999) were appropriate for a SFE application: $P_c = 72.9$ atm, $T = 304.2$ K, $\rho_c = 0.47$ g mL^{-1}; (ii) CO_2 can be considered as a green solvent for the environment; (iii) (aside from asphyxiation hazards) CO_2 is harmless to workers; (iv) CO_2 is almost inert with respect to radiolysis; (v) CO_2 is inexpensive. Moreover, the high diffusivity of sc-CO_2 means that rapid extraction of the metal ions from their sources can be expected. Since 1991, about 80 reports related to the SFE of metal ions have been published, most of them related to actinides. The most studied actinide ion is U(VI), with about 50 papers. This field was recently reviewed by Darr and Poliakoff (1999) and by Wai (2002). The sections to follow present the most important aspects of the SFE of actinide ions contained within various sources: (i) aqueous solutions, (ii) solid materials, (iii) pure actinide oxides. As most of the information available in the literature is related to U(VI), the examples discussed will predominantly concern this ion.

(a) Experimental setup and SFE procedures

Fig. 24.12 is a schematic of an experimental setup proposed by Tomioka *et al.* (2001a) for the SFE of metal ions from a metal oxide. A similar apparatus has been described by Wai and Laintz (1999). The carbon dioxide passes first through a vessel where it dissolves the contained ligand (solid or liquid). In the second vessel, the sc-CO_2 ligand solution then comes into contact with the actinide oxide to be extracted. Trofimov *et al.* (2001) recently showed that the use of ultrasound increases the solid dissolution rate. After extraction, the metal ion complex can be recovered by reducing both the pressure and temperature of the sc-CO_2 solution, leading to the precipitation of the metal ion complex and of the excess ligand. The CO_2 can subsequently be recycled. To perform this reduction of pressure and temperature, the loaded sc-CO_2 solution passes through a capillary restrictor made of silica or stainless steel. Wai *et al.* (1998) noted some drawbacks to using this technique, such as clogging of the capillary

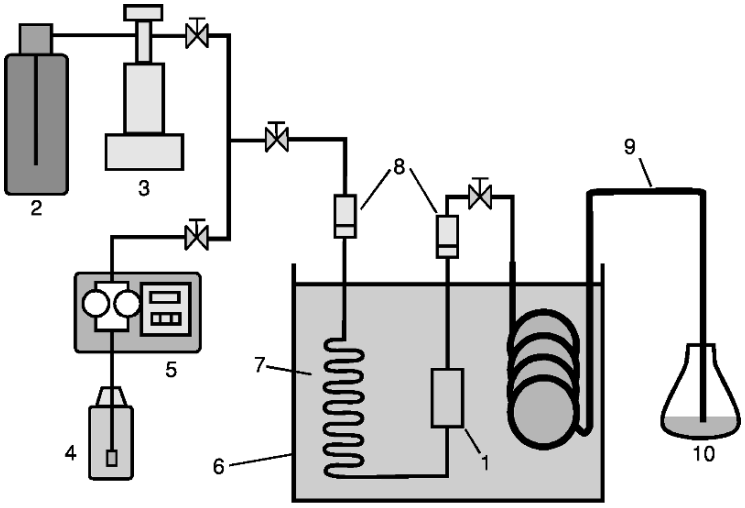

Fig. 24.12 *Apparatus for the dissolution of uranium oxide powder with supercritical CO_2 containing the HNO_3–TBP complex* (*adapted from Tomioka* et al., 2001*a*).

by the solutes, or breaking of the silica capillary in case of the use of sc-CO_2 modified with methanol. They therefore proposed an improved stripping method to eliminate these drawbacks by passing the loaded sc-CO_2 solution through an acidic aqueous solution while maintaining the pressure and temperature conditions of the SFE. Extraction of metal ions from aqueous solutions can be performed in such an apparatus with minor modifications.

Several systems have been developed to measure the concentration of the metal ion extracted into the sc-CO_2. The most popular uses a UV–visible spectrophotometric cell to measure colored metal ion complexes, as in the case of U(VI) (Furton *et al.*, 1995; Addleman *et al.*, 1998; Sasaki *et al.*, 1998). Recently, Wai and co-workers (Carrott and Wai, 1998; Hunt *et al.*, 1999) proposed sophisticated UV–visible measurement cells, with several light path lengths (38 μm, 733 μm, and 1 cm) coupled with optical fibers, the spectra being measured with a charge–coupled device array UV–visible spectrophotometer. In the case of SFE of U(VI), the same research group also proposed the use of a Raman measurement cell (Addleman *et al.*, 1998) or of a time-resolved laser-induced fluorescence spectrometry cell (TRLIFS) (Addleman *et al.*, 1998, 2000a,b; Addleman and Wai, 1999, 2000). The latter technique permits the measurement of U(VI) complexes under a wide range of concentrations.

The pressure and temperature conditions often chosen for SFE of metal ions are the following: pressure in the range 150–300 atm, temperature in the range 60–120°C. Frequently used conditions are 150 atm and 60°C. SFE of metal ions can be carried out in two modes:

(1) Static mode: The actinide containing sample and the sc-CO_2 fluid are placed in contact and stirred until the actinide distribution equilibrium is obtained. The actinide-loaded sc-CO_2 fluid is then removed from the extraction vessel.
(2) Dynamic mode: The sc-CO_2 fluid containing the extractant is continuously fed to the extraction vessel and the actinide-loaded sc-CO_2 fluid is then stripped online.

(b) SFE properties of actinide ions

(*i*) *Ligands*

Numerous ligands can be used for the SFE of actinide ions, most of which have also been used (or are structurally similar to reagents that have been used) in conventional solvent extraction. The most important ones are as follows.

β-Diketones

A ligand of this type, 2,2-dimethyl-6,6,7,7,8,8,8-heptafluoro-3,5-octanedione (FOD), was used by Wai and coworkers in the first article related to the SFE of actinide ions (Lin *et al.*, 1993). It was shown that about 99% of 10 μg of uranyl ion contained within uranyl acetate solutions at pH 1.0 or deposited on cellulose-based filter paper from a solution at pH 6.5, can be extracted under the following SFE conditions: 80 μg of FOD, sc-CO_2 containing 5% methanol, wet paper, 60°C; 150 atm. In another article, the same group (Lin *et al.*, 1994) studied the SFE efficiency of several β-diketones for Th(IV) and U(VI); the following ligands were studied: acetylacetone (AA), trifluoroacetylacetone (TAA), hexafluoroacetylacetone (HFA), thenoyltrifluoroacetone (TTA), and FOD. In the absence of methanol in the sc-CO_2 and all other SFE conditions being identical to those mentioned above, the extraction efficiency observed for U(VI) and Th(IV) were the following, respectively: 10 and 12% (AA), 15 and 22% (TAA), 40 and 69% (HFA), 51 and 80% (FOD), and 70 and 82% (TTA). The fluorinated β-diketones are the most effective ligands and among them TTA seems to be the best. Note that Th(IV) is slightly more strongly extracted than U(VI) under these conditions.

Neutral organophosphorous compounds

Organophosphates and phosphine oxides were the most studied neutral organophosphorous compounds for SFE of actinide ions. Work has principally focused on the use of TBP for the extraction of uranyl nitrate (Lin *et al.*, 1994, 1995; Iso *et al.*, 1995, 2000; Meguro *et al.*, 1996, 1997, 1998b, 2002;

Toews *et al*., 1996; Smart *et al*., 1997b; Carrott *et al*., 1998; Sasaki *et al*., 1998; Addleman *et al*., 2000a; Addleman and Wai, 2000, 2001; Enokida *et al*., 2000; Park *et al*., 2000; Tomioka *et al*., 2000, 2001a,b, 2002; Clifford *et al*., 2001; Shamsipur *et al*., 2001) This was certainly related to the observation of Toews *et al*. (1996) that of the three extractants TBP, tri-*n*-butylphosphine oxide (TBPO) and tri-*n*-octylphosphine oxide (TOPO), TBP was by far the most effective ligand for sc-CO_2 extraction and transport of uranyl nitrate. This is primarily a result of the greater solubility of TBP in sc-CO_2 relative to the phosphine oxides (Lin *et al*., 1995). Only a few reports concern the TBP-mediated SFE of other actinide ions: Th(IV) (Lin *et al*., 1995) and Pu(IV) (Iso *et al*., 2000). SFE of actinide ions (mostly U(VI) and Th(IV) by phosphine oxides has been the subject of a few reports (Lin *et al*., 1995; Toews *et al*., 1996; Wai *et al*., 1999; Addleman *et al*., 2000a; Shamsipur *et al*., 2001).

It should be noted that most of the research on the extraction of actinide ions by neutral organophosphorous ligands has been done by Wai (U.S.), Yoshida (Japan) and their coworkers. Some of the results related to the extraction of uranyl nitrate by TBP are presented here; other results related to this system will be presented later in this section. The extracted complex in sc-CO_2 has the same stoichiometry $[UO_2(NO_3)_2(TBP)_2]$ as is observed in conventional solvent extraction. The identity of the complex was established by Meguro *et al*. (1996) and confirmed by Wai *et al*. (1999) using the classical slope analysis method. This complex was characterized by UV–visible spectrophotometry (Addleman *et al*., 1998; Carrott *et al*., 1998; Sasaki *et al*., 1998), Raman spectrometry (Addleman *et al*., 1998), and TRLIFS (Addleman *et al*., 1998, 2000a,b; Addleman and Wai, 1999, 2000, 2001). TRLIFS was used in particular by Addleman and coworkers to determine the solubility of the U(VI) complex (Addleman *et al*., 2000a) and the $D_{U(VI)}$ values (Addleman and Wai, 2001), and for online measurement of the extracted U(VI) (Addleman *et al*., 2000b). The extraction kinetics of uranyl nitrate by TBP in sc-CO_2 are rapid (Wai *et al*., 1999) ($\sim$45 min) if the U(VI) source consists of aqueous solutions. With solid samples (tissue paper, soil, sand, etc.), the extraction of U(VI) requires more time. An efficient model for interpreting the kinetic aspects of the SFE extraction of uranyl nitrate by TBP in sc-CO_2 in dynamic mode was recently proposed by Clifford *et al*. (2001).

The value of $D_{U(VI)}$ is 2.0, for extraction by 0.3 mol L^{-1} TBP in sc-CO_2 at 60°C and 15 MPa from an aqueous solution of 3 mol L^{-1} HNO_3 (Iso *et al*., 2000). Under the same experimental conditions, the distribution ratio for Pu(IV) was found to be 3.1 (Iso *et al*., 2000). Other thermodynamic aspects of the extraction of uranyl nitrate by TBP are considered below in the discussion of the influence of pressure and temperature on the SFE of metal ions. Uranyl nitrate can be effectively extracted from various sources, such as aqueous solutions, whether acidic or neutral, and solid waste (cellulosic paper, contaminated soil or sand, metallic waste). The solubility of $UO_2(NO_3)_2(TBP)_2$ in sc-CO_2 was found to be the highest of all the metallic complexes studied so far (Meguro *et al*., 1996):

~0.43 mol L^{-1} at 40°C and 225 atm (Carrott *et al.*, 1998). This moderate solubility warrants consideration of process development for spent nuclear fuel reprocessing. Only a few reports have considered the use of bidentate neutral organophosphorous extractants. This is certainly due to the low solubility of these ligands in sc-CO_2, as shown by Meguro *et al.* (1998a) for dihexyl (*N,N,*-diethylcarbamoyl)methylphosphonate and for the octyl(phenyl)(*N,N*-diisobutyl)carbamoylmethylphosphine oxide (OΦCMPO).

Synergistic mixtures

In 1994, Lin *et al.* (1994) were the first to report the existence of synergistic phenomena for the SFE of U(VI) and Th(IV) ions. For example, with TTA and TBP extractants at 60°C and 150 atm, SFE was carried out in dynamic mode on samples consisting of sand (200 mg) contaminated with 10 μg of U and 10 μg of Th with the following results (U and Th extracted, respectively): TTA (80 μmol) = 72 and 74%; TBP (80 μmol) = 15 and 10%; TTA + TBP (40 μmol + 40 μmol) = 94 and 93%. A net synergistic effect was thus observed for the extraction of both actinide ions. Several papers related to SFE of actinide ions by diketones and neutral organophosphorous compound synergistic mixtures have been published since (Furton *et al.*, 1995; Lin *et al.*, 1998, 2001; Murzin *et al.*, 1998; Addleman *et al.*, 2000a, 2000b; Geertsen *et al.*, 2000).

(*ii*) *Modifiers*

The addition of a modifier can be an effective means of enhancing the extraction efficiency of sc-CO_2 extractant solutions. Methanol is the most widely used modifier. The use of methanol as an sc-CO_2 modifier was often reported when the ligands were β-diketones and their synergistic mixtures, but modifiers are not ordinarily used in the case of TBP alone. The following example illustrates the efficiency of methanol as an sc-CO_2 modifier. Lin *et al.* (1994) studied the SFE of U(VI) and Th(IV) with the β-diketones: AA, TAA, HFA, FOD, and TTA, with neat or 5% methanol-modified sc-CO_2. The following experimental conditions were chosen: 60°C, 150 atm, cellulose-based filter contaminated with 10 μg of U and 10 μg of Th, 80 μmol of ligand, dynamic extraction. The actinide ion extraction yields obtained for neat and 5% methanol-modified sc-CO_2, respectively, were as follows: AA (U = 10 and 45%; Th = 12 and 58%), TAA (U = 15 and 98%; Th = 22 and 95%), HFA (U = 40 and 95%; Th = 69 and 92%), FOD (U = 51 and 98%; Th = 80 and 97%), TTA (U = 70 and 96%; Th = 82 and 91%). The presence of methanol thus induces a net increase in uranium and thorium extraction efficiency, and this is certainly correlated to the increased polarity of the sc-fluid due to the presence of the modifier.

With SFE of solid samples, such as soil, sand or paper, it is also observed (Lin *et al.*, 1993) that a small amount of water must be added to obtain satisfactory metal ion extraction efficiency.

(c) Influence of pressure and temperature on SFE of actinide ions

The SFE efficiency of actinide ion complexes can be tuned by modifying the pressure and temperature conditions as well. To illustrate these properties, consider the TBP SFE of U(VI) and Pu(IV) nitrates from aqueous nitric acid solutions, as studied by Yoshida and coworkers (Iso *et al.*, 2000). At constant temperature and TBP concentration in sc-CO_2, an increase in pressure induces a decrease in $D_{U(VI)}$ and $D_{Pu(IV)}$ correlated with the higher density of the sc-fluid. A simple linear correlation between $D_{U(VI)}$ or $D_{Pu(IV)}$ and ρ is observed in log–log plots:

$$\log D = a \log \rho + b \qquad \text{(I)}$$

in which a is a proportionality constant related to the solvation characteristics of the metal complexes in sc-CO_2. The slopes a of the relationships were equal to $-(2.7 \pm 0.5)$ for U(VI) and $-(1.6 \pm 0.1)$ for Pu(IV). The differences in D as well as in the slope a between U(VI) and Pu(IV) make it possible to design a SFE scheme to separate uranium from plutonium. In the case of U(VI), for a temperature increase from 313 to 353 K and for a pressure of 40 MPa, $D_{U(VI)}$ decreases by a factor of about 2, as shown by Yoshida and coworkers (Meguro *et al.*, 1997; Iso *et al.*, 2000). Conversely, the same group (Iso *et al.*, 2000) has shown that $D_{Pu(IV)}$ increases with T, and the lower the pressure the greater the temperature effect.

The increase in the pressure of sc-CO_2 that induces an increase in the density of the sc-fluid has a large impact on the solubility of solutes. Chrastil (1982) demonstrated that the solubility S (g L^{-1}) of an organic solute in a sc-fluid is correlated with the density (g L^{-1}) of the sc-fluid by the following empirical relation

$$\ln S = \kappa \ln \rho + C \qquad \text{(II)}$$

where the value of k is related to the solute–solvent interactions and that of C to the volatility of the solute. Since then, equation (II) has also been found to represent variations of the solubility of metal ion complexes in sc-CO_2. A review of the solubility of chelating agents and their metal complexes has been published by Smart *et al.* (1997a). This equation was also shown to be usable to represent the solubility of actinide ion extractants and their complexes (Meguro *et al.*, 1998b). This is the case in particular for $UO_2(NO_3)_2(TBP)_2$ (Carrott *et al.*, 1998; Addleman *et al.*, 2000a) which, as noted above, is the metallic complex with the highest solubility in sc-CO_2.

(d) Sources of actinide ions for SFE

Several sources of actinide ions can be treated by SFE, including:

(1) Aqueous solutions: Acetate-buffered solution are often used when the extractants are β-diketones (Lin *et al.*, 1994), nitric acid, and nitric acid and alkali nitrate solutions (Lin *et al.*, 1995; Meguro *et al.*, 1996, 1997,

1998b; Smart *et al*., 1997b; Iso *et al*., 2000), uranium mine water (Lin *et al*., 1994).

(2) Solid matrices (surrogates or genuine wastes): Cellulosic filter paper (Lin *et al*., 1993, 1994; Brauer *et al*., 1994; Shamsipur *et al*., 2001; Kumar *et al*., 2002), sand (Tomioka *et al*., 2002), soil (Fox *et al*., 1999), kaolin (Furton *et al*., 1995), glass wool (Furton *et al*., 1995), metals (Murzin *et al*., 1998; Shadrin *et al*., 1998), asbestos (Murzin *et al*., 1998), rubber (Murzin *et al*., 1998), plastics (polyethylene, polyester) (Furton *et al*., 1995), contaminated with solid actinide compounds, such as nitrates or oxides,

(3) Actinide oxides: This case is particularly important in the light of the potential future applications, and is considered here in greater detail. Wai *et al*. (1997) filed a patent related to the SFE of metal ions directly from their oxides. They proposed as ligands numerous acidic compounds including β-diketones, phosphinic acids, and carboxylic acids. Better performance was seen for fluorinated derivatives. In 2000, Tomioka and coworkers (Enokida *et al*., 2000; Tomioka *et al*., 2000) described the dissolution of gadolinium and neodymium ions from their sesquioxides M_2O_3 (M=Gd and Nd) by the complex TBP–HNO_3 dissolved in sc-CO_2. Wai and Waller (2000) also demonstrated the efficiency of the SFE extraction of uranium from UO_3 by TTA or TTA + TBP synergistic mixtures. Several papers related to the dissolution of uranium oxides (UO_2, U_3O_8, and UO_3) by the TBP–HNO_3 complex have been published since then (Enokida *et al*., 2000; Samsonov *et al*., 2001; Tomioka *et al*., 2001a,b; Trofimov *et al*., 2001). The dissolution of UO_2 was less rapid than those of the two other oxides, but it is possible to increase the dissolution rates of oxides if the HNO_3/TBP molar ratio in sc-CO_2 is greater than 1. In a recent conference paper, Samsonov *et al*. (2002) reported the SFE of actinides from their oxides using TBP–HNO_3; the studied oxides were: ThO_2, UO_2, U_3O_8, and UO_3, NpO_2, and PuO_2. Under the experimental conditions [65°C, 250 atm, TBP–HNO_3 reagent in sc-CO_2, thrice-repeated alternation of static (10 min) and dynamic (15 min) extractions] it was shown that the extraction yields of U oxides were good (> 85% for the lowest value) while those of the oxides of Th, Np, and Pu were almost nil.

(e) Possible applications

(*i*) *Industrial processes*

(1) Spent nuclear fuel reprocessing: Smart and Clifford (2001) from BNFL (UK) filed an international patent in 2001 in which they claimed that the reprocessing of spent nuclear fuel will be possible using the SFE method. The several steps of the conceptual process flow sheet are the following: (i) oxidize decladding of spent fuel under oxygen at 600°C, (ii) SFE of uranium by treatment of the oxidized fuel with a sc-CO_2 solution containing

an acidic ligand like a β-diketone, (iii) separation of U from the other extracted ions in fractionation columns, and (iv) reduction of the volatile uranium complex by hydrogen to precipitate UO_2. Probably the most interesting reagent for such application is TBP–HNO_3 as noted by the teams of Wai and Yoshida.

(2) Actinide waste decontamination: As noted above, the efficiency of SFE extraction of actinides from miscellaneous solid wastes has been demonstrated. An interesting case was the demonstration by Shadrin *et al*. (1998) of the efficiency of SFE for decontamination (U, Np, Pu, and Am) of 'real-world' contaminated stainless steel. This could be a basis for further industrial developments.

(*ii*) *Analytical applications*

SF-chromatography has been used to develop analytical methods. Examples include the work of Martin-Daguet *et al*. (1997) and Geertsen *et al*. (2000) for the analysis of U(VI).

(f) Conclusions

SFE of actinide ions has been a very active research field since its inception a decade ago. Important nuclear applications may some day be developed, particularly in spent nuclear fuel reprocessing and nuclear waste decontamination. The observation by Wai *et al.* on dissolution of uranium oxides by sc-CO_2 solutions of HNO_3–TBP solutions is noteworthy. The Wipff group is examining the system using the techniques of computational chemistry (Baaden *et al*., 2002; Schurhammer and Wipff, 2003). However, fundamental understanding of the basic chemistry of actinide interactions in supercritical media lags far behind practical demonstrations. Considerable basic research and development studies are still required, but it is safe to say that the interest in this field is likely to increase in the future.

24.3.11 Actinides in room-temperature ionic liquids (RTILs)

Room temperature ionic liquids (RTILs) were discovered by Hurley and Wier (1951), who found that a mixture of $AlCl_3$ and ethylpyridinium bromide (EPB) in a 2:1 molar ratio melted at $-40°C$ and that this liquid is suitable for the electrodeposition of aluminum metal at room temperature. Research in this area has been pursued with two main objectives: the development of electrolytes for batteries, and the use of RTILs as 'green' liquids for the design of industrial processes for the synthesis of organic compounds. Though continuing research has established that this class of RTILs can indeed be quite toxic, these liquids are considered 'green' compared with traditional organic solvents used in the industry because they have no vapor pressure, hence no gaseous emissions, at

least from intact RTIL formulations. However, it should further be noted that many RTIL formulations are based on the use of hydrolytically unstable inorganic anions like PF_6^- (reacts with water to produce HF). For more information on the properties of these materials, see reviews by Hussey (1983) and Welton (1999). The interest in using RTILs to develop separation processes for metals, for example liquid–liquid extraction with hydrophobic RTILs, is quite recent, as noted in a review by Visser *et al.* (2002). This subject became a hot topic in the late 1990s.

The first paper dealing with an actinide in an RTIL, published in 1982 by De Waele *et al.* (1982), examined the electrochemical behavior of uranium(IV) in a Lewis acidic $AlCl_3$ + *N*(*n*-butyl)pyridinium chloride (BPC) RTIL. Since that time, about 20 papers including patents for separation applications related to the chemistry of actinides within RTILs have been published, most of them (16) being related to uranium. In this short review, after a brief presentation of RTILs, the main chemical properties of actinides in RTILs will be described and the possible uses of RTILs for actinide separation presented.

(a) A brief description of RTILs

RTILs (Carpio *et al.*, 1979; Hussey, 1983; Visser *et al.*, 2002) are salts made of organic cations, such as: (i) *N*-alkyl quaternary ammonium, R_4N^+, (ii) *N*-alkyl pyridinium, (iii) *N*-alkylisoquinolinium, (iv) 1-*N*-alkyl-3-methylimidazolium, (v) *N*-alkyl quaternary phosphonium, R_4P^+, associated with various anions, e.g. halides (Cl^-, Br^-), haloaluminates (chloro or bromo), chlorocuprate ($CuCl_2^-$), tetraalkylborides (R_4B^-), NO_3^-, $CF_3CO_2^-$, BF_4^-, PF_6^-, and $N(SO_2CF_3)_2^-$. With the anions BF_4^-, PF_6^-, $N(SO_2CF_3)_2^-$, the RTILs are most often hydrophobic and can be used, for example, for the development of liquid–liquid extraction separation processes (Visser *et al.*, 2002). Nevertheless, most of the work related to actinides concerns RTILs of $AlCl_3$ and *N*-alkylpyridinium or *N*-alkylmethylimidazolium chlorides (called APC and AMIC, respectively). Both classes are highly sensitive to moisture. Recent work concerning the use of RTILs for nuclear fuel reprocessing is based on an RTIL made of *N*-alkylmethylimidazolium nitrate (Thied *et al.*, 1999). RTILs with nitrate anions were mentioned for the first time by Lane (1953).

The physical properties, such as the density, viscosity, or electric conductivity of RTILs consisting of mixtures of $AlCl_3$ and APC or AMIC have been the subject of numerous measurements (Carpio *et al.*, 1979; Hussey, 1983; Fannin *et al.*, 1984). The density of these melts exceeds 1 kg dm^{-3}; although most of them are quite viscous, their conductivity is suitable for electrochemical applications. The chemistry of these melts is dominated by the Lewis chloro-acidity. Depending on the molar ratio (M_r) of $AlCl_3$ versus APC or AMIC, the chloro-acidity (which can be expressed as pCl^- with low and high pCl^- for basic and acidic melts, respectively) of the melts varies. For $M_r = 1, > 1$, and < 1, the melts are neutral, acidic, and basic, respectively. The main reactions between

aluminum chloride and the chloride ion occurring in these melts that control pCl^- are the following:

$$AlCl_3 + Cl^- \rightleftarrows AlCl_4^- \tag{24.23}$$

$$AlCl_4^- + AlCl_3 \rightleftarrows Al_2Cl_7^- \tag{24.24}$$

For these melts, pCl^- can vary between ~0 and 15 for highly basic and highly acidic melts, respectively, as shown by Schoebrechts and Gilbert (1985) for RTILs containing mixtures of $AlCl_3$ and *n*-butylpyridinium chloride. If oxygen-bearing compounds such as water are present in these melts, aluminum oxochloro complexes, e.g. $AlOCl_3^{2-}$, are formed that can influence the chemistry of the other metallic solutes. An ^{17}O NMR study of water in these melts was carried out by Zawodzinski and Osteryoung (1987a,b). One of the main advantages of these RTILs is the large electrochemical window available. For example, for melts made of mixtures of $AlCl_3$ and 1-ethyl-3-methylimidazolium chloride (EMIC), Gray *et al.* (1995) noted the following values for the electrochemical window (ΔV):

(i) neutral melt: $\Delta V = 4.7$ V, between the anodic $4\,AlCl_4^- \rightleftharpoons 2Al_2Cl_7^- + Cl_2 + 2\,e^-$ and cathodic $Na^+ + e^- \rightleftharpoons Na$ or ($EMI^+ + ne^- \rightarrow$ unknown coompound) reactions,

(ii) acidic melt: $\Delta V = 2.5$ V, between the anodic $4\,AlCl_4^- \rightleftharpoons 2Al_2Cl_7^- + Cl_2 + 2\,e^-$ and cathodic $4\,Al_2Cl_7^- + 3\,e^- \rightleftharpoons Al + 7AlCl_4^-$ reactions,

(iii) basic melt: $\Delta V = 3.3$ V, between the anodic $2\,Cl^- \rightleftharpoons Cl_2 + 2\,e^-$ and cathodic $Na^+ + e^- \rightleftharpoons Na$ (or $EMI^+ + ne^- \rightarrow$ unknown compound) reactions.

(b) Basic actinide properties in RTILs

Almost all studies of actinide chemistry in RTILs have been done in materials obtained by mixing $AlCl_3$ with APC or AMIC. The only exception is the work reported by Mohammed (1987) who also studied the properties of uranium within RTILs made of mixtures of $AlBr_3$ and EMI bromide. Most of the published work (16 papers) concerns uranium. Neptunium and plutonium were the subjects of only one and three papers, respectively. No work related to other actinides was found in the literature.

(c) Uranium chemistry in RTILs made of mixtures of $AlCl_3$ and APC or AMIC

The chemistry of uranium within these melts has been studied using electrochemical and spectrochemical methods. The most detailed spectrometric study by Costa and coworkers (Hopkins *et al.*, 2000, 2001) concerned the U(VI) chloro complex, $UO_2Cl_4^{2-}$, in basic ($AlCl_3$ + EMIC) RTIL, carried out by

UV–visible–NIR, Raman, and one-photon and two-photon excitation spectroscopy, and by luminescence lifetime measurements. As will appear from the references in the next sections, many research groups have been involved in the study of the properties of actinides in RTILs. A brief summary of the properties of U in basic or acidic ($AlCl_3$ + EMIC) RTILs, used as an example of this type of RTIL, is presented below.

(*i*) *Basic* (*$AlCl_3$ + EMIC*) *RTILs*

Uranium can exist in these basic ($AlCl_3$ + EMIC) RTILs as U(III), U(IV), and U(VI). U(V) was not stable in these basic melts as noted by Dai *et al.* (1997b). The chemical forms for the stable uranium solutes are the following: UCl_6^{3-} for U(III), UCl_6^{2-} for U(IV), and $UO_2Cl_4^{2-}$ for U(VI). These species have been characterized mainly by UV–visible–NIR spectroscopy. In the case of U(VI) species, Dai *et al.* (1997a) observed that it is certainly stabilized in the medium by establishing a hydrogen bond with the H born by the carbon in position 2 on the heterocycle ring of the EMI^+ cation.

The diffusion coefficients of U(III) and U(IV) chloro complexes have been determined electrochemically and both values were found to be similar (1.61 and 1.85×10^{-7} $cm^2\ s^{-1}$, respectively) and compatible with the 1:6 stoichiometry between U(III) or U(IV) ions and the Cl^- ligand within the complexes. The electrochemical reaction $UCl_6^{2-} + e^- \rightleftharpoons UCl_6^{3-}$ was found to be reversible. Conversely, no reduction of U(IV) to U(III) was observed in basic RTILs made of mixtures of $AlCl_3$ and BPC, as shown by Heerman *et al.* (1985). This difference is a result of the reduction potential of BP^+ being higher than that of EMI^+. Thus, BP^+ can oxidize U(III) to U(IV). The U(VI)/U(IV) electrochemical conversion in [$AlCl_3$ + EMIC] RTILs is irreversible. Moreover, no reduction of U(III) to U metal was observed.

(*ii*) *Acidic* (*$AlCl_3$ + EMIC*) *RTILs*

Owing to the large decrease of the concentration of Cl^- in the acidic ($AlCl_3$ + EMIC) RTILs compared with the basic melts, the chloro complexes of U(III), U(IV), U(VI) are destabilized. Note that U(VI) is not chemically stable in these media. It is converted to U(V) species, the ultimate complex being UCl_6^-, after reduction and loss of oxide ions (Anderson *et al.*, 1999). The UCl_6^- complex was also observed by Sinha (1986) in ($AlCl_3$ + BPC) RTIL. It should be noted that U(V) was found to be stable in these RTILs. Moreover, if oxide ions are present in these RTILs, mixed oxo-chloro complexes can be formed. The chemistry of these RTILs is thus more complex than for the basic melts. After extensive electrochemical and spectrochemical work, Costa *et al.* (2000) proposed a general scheme (Fig. 24.13) for the inter-conversion of U(VI), U(V), U(IV), and U(III) species by chemical and electrochemical equilibria in acidic ($AlCl_3$ + EMIC) RTILs.

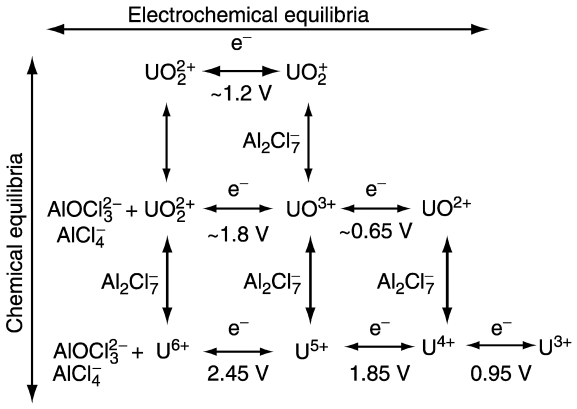

Fig. 24.13 *Mechanism for the inter-conversion of the different chemical forms of uranium within acidic RTILs* (*Costa* et al., 2000) (*note that the* Cl^- *ligands bound to the U ions are not shown for clarity*).

(d) Neptunium chemistry in basic and acidic ($AlCl_3$ + BPC) RTILs

Schoebrechts and Gilbert (1985) published the only paper on neptunium chemistry in ionic liquids. In acidic as well as in basic RTILs, the electrochemical reduction of Np(IV) to Np(III) is quasi-reversible on a glassy carbon electrode. UV–visible and Raman spectra indicated that Np(IV) and Np(III) both exist as hexachloro complexes in basic media. For acidic melts, these complexes are destabilized and Np(III) was found to lose more Cl^- ligands than Np(IV). These results are close to those observed for U in ($AlCl_3$ + EMIC) RTILs mentioned above.

(e) Plutonium chemistry in basic and acidic ($AlCl_3$ + EMIC) RTILs

Costa *et al*. (2000) published the only fundamental paper related to plutonium chemistry in basic and acidic ($AlCl_3$ + EMIC) RTILs. In basic RTIL, the reversible redox couple Pu(IV)/Pu(III) was observed at +0.37 V [the reference electrode being an aluminum metal wire in a 40/60 basic ($AlCl_3$ + EMIC) RTIL]. For acidic melts, the electrochemical behavior of plutonium resembles that described above for uranium, with the involvement of the plutonium oxidation states 6+, 5+, 5+, and 3+, and the existence of chloro and oxo-chloro complexes (Fig. 24.13). Further work is required for a more precise understanding of the chemistry of plutonium in these RTILs.

(f) Possible separation techniques for actinides using RTILs

The potential interest of using RTILs in the industrial processing of actinide nuclear materials is being tested by a team led by Costa at Los Alamos National Laboratory (USA) which studied plutonium processing (Costa *et al*., 2000;

Harmon *et al*., 2001). Another team in UK led by Seddon supported by British Nuclear Fuels Plc, proposes the use of RTILs for the reprocessing of commercial spent nuclear fuels and the treatment of nuclear wastes. In recent years, this team filed several patents in this area (Fields *et al*., 1998, 1999; Thied *et al*., 1999, 2001). Several techniques that could be used in processing nuclear materials within RTILs are briefly described in the following sections.

(*i*) *Dissolution*

Dissolution of solid actinide compounds in RTILs has been established. UO_3 readily dissolves in basic ($AlCl_3$ + BPC, Heerman *et al*., 1985; $AlCl_3$ + EMIC) RTILs (Anderson, 1990; Anderson *et al*., 1991). As shown by the patent of Fields *et al*. (1998), UO_2 dissolves in RTIL made of nitrates of BP^+ or EMI^+. This requires the presence of an oxidant to convert U(IV) (from UO_2) into soluble U(VI). Suitable oxidants include HNO_3, H_2SO_4, and $[NO][BF_4]$. These nitrate-based RTILs are the main new media proposed by BNFL for nuclear spent fuel reprocessing: in their patent, Thied *et al*. (2001) have shown that uranium and plutonium *metals* can be dissolved by anodic electrochemical oxidation in BMI nitrate (for U at room temperature) and EMIC (for Pu at 90°C).

(*ii*) *Precipitation*

U(VI) can be precipitated from an RTIL of BMI nitrate in the form of a crystalline compound (Bradley *et al*., 2002) with the formula $[\{(UO_2)(NO_3)_2\}_2(C_2O_4)][BMI]_2$. The source of the oxalate anion that induces the precipitation of U(VI) can be acetone, being oxidized to oxalate by the medium.

(*iii*) *Electrodeposition of metals*

Thied *et al*. (2001) claimed the feasibility of electrorefining uranium in molten hexylethylimidazolium (HEI) chloride at 70°C using a uranium metal rod anode and a copper cathode. During the experiment described, for a total of 236 Coulombs passed in the electrochemical cell, 193 mg of uranium metal was dissolved from the anode as U(III) species in the melt and 18.7 mg of uranium was deposited on the copper cathode. Solid material was found at the bottom of the cell, indicating that deposited uranium does not adhere well to copper. An identical experiment was performed for plutonium, but no plutonium deposit was observed on the cathode.

More work is necessary in the domain of electrodeposition of actinide metals from RTILs. The experience accumulated in the field of electrodeposition of metals could be used to select suitable systems. RTILs made of AMI^+ cations are preferable owing to the low potential required for the reduction of AMI^+. For example, in melts made of neutral ($AlCl_3$ + EMIC), the electrodeposition of

lithium and sodium metals can be performed if the solutes HCl (Gray *et al.*, 1995) or SO_2Cl_2 (Fuller *et al.*, 1995) are present in the melts. Tsuda *et al.* (2001, 2002) also studied the electrodeposition of lanthanum metal or Al–La alloy from ($AlCl_3$ + EMIC) RTIL.

(*iv*) *Liquid–liquid extraction*

Liquid–liquid extraction of metal ions is possible with hydrophobic RTILs based on the use of the anions: BF_4^-, PF_6^-, and $N(SO_2CF_3)_2^-$. The first work was published by Dai *et al.* (1999) who showed that Sr(II) can be very efficiently extracted from aqueous solutions by a crown ether dissolved in RTILs made of AMI^+ cations and the anions PF_6^- or $N(SO_2CF_3)_2^-$. Subsequent investigations (Jensen *et al.*, 2002b, 2003) have established that the elevated distribution ratios and resistance to back extraction exhibited by this system are at least in part a result of extraction occurring by a cation exchange mechanism in which the AMI^+ cation is transferred (irreversibly) to the aqueous phase. Since then, Rogers and his co-workers published several important papers in this field (Visser *et al.*, 2000a,b, 2001a,b) including a review paper (Visser *et al.*, 2002).

A few reports address features of the partitioning of actinides into RTILs (Davis, 2002; Visser and Rogers, 2002; Visser *et al.*, 2003). This system likewise is impacted by the problem of undesirable partitioning of the hydrophobic cation to the aqueous and irreversibility of the phase transfer reaction (Jensen *et al.*, 2003). Much additional work is required before this simple solvent-substitution approach to improving actinide separations with RTILs can be established.

(g) Conclusions

The chemistry of the actinides in RTILs is still in its infancy. Due to the recent impetus given by several research teams in the U.S. and UK, growing interest can be expected worldwide in this field owing, in particular, to the interesting practical applications that could be designed for the nuclear industry. Issues related to biphasic instability, generation of HF, the expense and toxicity of the RTILs may prove a significant obstacle to any efforts for an early implementation of these compounds in actinide process chemistry.

24.3.12 Pyrochemical processes

Pyrochemical processing involves the conduct of dry chemical reactions at high temperature in which the reactions occur in solid, liquid, and gas phases. Oxidation–reduction, volatilization (of halide or metal), slagging (melt refining, molten salt extraction, carbide slagging), liquid metal (melt refining, liquid metal extraction, liquation, precipitation), and electrolytic processes are the most common types.

Molten salts – or fused salts – lead to operating conditions that are constraining: high temperatures are required and corrosion effects are common, making identification of appropriate containers quite difficult. However, metallurgists use molten salts for electrolytic production of some metallic products, notably for refining very electropositive elements and strong reducing agent such as alkali metals. Potassium and sodium metals were first prepared in 1807 by using melt electrolysis of respectively potash and soda (Davy, 1808). Today melt electrolysis (alkali chloride) remains the only process for production of metallic sodium or lithium. Molten salt refining is also appropriate for aluminum, which is obtained by electrolytic decomposition of aluminum oxide in molten cryolite (Hall–Héroult process) (Grojtheim *et al.*, 1982).

Essential to the examples above, molten salts also have some properties which make them attractive for nuclear applications: (i) they are less subject to radiolytic degradation than aqueous media due to their ionic liquid structure; (ii) criticality concerns and problems are reduced due to the absence of neutron moderating elements and organic solvents. These properties in particular enable the processing of materials producing high radiation loadings, for example, high concentrations of fissile materials like spent nuclear fuels after a short cooling interval. In addition, it is possible to reduce the number of chemical conversion steps compared to those needed for aqueous processes. The first significant attempts at actinide metal production in molten salts started with the Manhattan Project in the 1940s (Rhodes, 1986). Significantly, Kolodney (1982) confirmed that uranium and plutonium could be electrodeposited from molten chlorides. The literature on U and Pu electrorefining in molten salts has been reviewed by Willit *et al.* (1992). Basic chemistry and technologies developed in Russia have been described by Bychkov and Skiba (1999).

Today, molten alkali and alkaline earth chlorides have been most extensively studied for plutonium conversion and separation. Three processes are in use throughout the world at significant scale-up (Moser and Navratil, 1983): (i) direct oxide reduction (DOR) process which consists of PuO_2 reduction by calcium in Ca-based chloride salt; (ii) molten salt extraction (MSE) process for ^{241}Am removal from weapon-grade plutonium by $MgCl_2$ in alkali chloride salt; (iii) electrorefining (ER) process for high plutonium purification using molten alkali and/or alkaline earth chloride electrolyte.

Pyroprocessing has also been proposed and developed for reducing the cost of fuel fabrication and fuel reprocessing (Motta, 1956). Between 1964 and 1969, a rudimentary process without molten salts – melt refining – was first demonstrated in Idaho Falls to recycle metallic fuel from the second experimental breeder reactor (EBR-II) (Trice and Chellew, 1961; Stevenson, 1987).

At the same time in the former USSR, emerged a concept of vibropacked fuel fabrication for fast reactors and pyroelectrochemical reprocessing based on electrolysis of oxide fuel in molten alkali chlorides. After being applied to UOX fuel, the Dimitrovgrad Dry Process (DDP) process has been adapted today for

MOX fuel reprocessing and weapon-grade plutonium conversion into plutonium oxide for civilian use in Russian fast reactors (Bychkov *et al.*, 1995; Skiba and Ivanov, 1995).

Due to the low burn-ups that have been achieved with EBR-II and for safety considerations, the interest in metal fuels declined in the U.S. for the next 15 years while ceramic fuel development, mainly oxides, increased (Burris, 1986). Consequently, molten salt process development slowed in the U.S. In the mid-1980s, interest of molten salts was renewed by the integral fast reactor concept proposed by Argonne National Laboratory (Till and Chang, 1988; Chang, 1989; Hannum, 1997). A combination of the electrometallurgical technology (EMT) and a set of molten salt/liquid alloy extractions was selected for overall actinide management purposes in the IFR fuel cycle (metallic alloy of U, Pu, and Zr) (Burris *et al.*, 1987). EMT consists of electrorefining the reactor fuel in LiCl–KCl melt at 500°C in an inert atmosphere: (i) the fuel in metallic form is dissolved at the anode, (ii) uranium, plutonium, and other transuranium elements are selectively deposited on solid or liquid cathode (e.g. cadmium), (iii) cladding material and fission products are left at the anode and/or in the electrolyte. In parallel, a pyrometallurgical process for the recovery of the transuranium elements from irradiated oxide fuels was initiated as a means of providing a source of plutonium for the start-up of additional IFRs (Pierce, 1991).

After the IFR program was stopped in 1994, EMT development was sufficiently advanced to be proposed for new applications: DOE spent nuclear fuel reconditioning (Laidler, 1994). A demonstration campaign (1996–1999) on spent EBR-II fuel in Idaho Falls used EMT for converting the fuel to a safe configuration by eliminating the sodium seal and recovering high enriched uranium for interim storage.

EMT is now being considered around the world for various fuel cycle concepts. Japan calls for the development of: (i) a global fuel cycle combining oxide fuel in pressurized water reactors (PWR) with transmutation of actinides as metal fuel in fast neutron reactors and (ii) a ^{15}N-enriched nitride fuel cycle involving molten salt reprocessing for ^{15}N management. For both projects, spent fuel reprocessing should take place in a LiCl–KCl melt using previous separation techniques: DOR process (lithium substituting calcium), ER process on solid or liquid cathode, and MSE process (Inoue *et al.*, 1991; Arai and Yamashita, 1997; Takano *et al.*, 1998).

Researchers in the U.S. recently have proposed a baseline process combining aqueous and pyrochemical processes in the framework of the preparation of a technology development roadmap for the accelerator transmutation of waste (ATW) Technology (ATW Separations, 1999). The process begins with an aqueous 'UREX' process that would produce from light water reactor (LWR) spent fuel a pure U stream for waste, technetium, and iodine streams for target fabrication and a transuranium elements–fission product oxide stream. Using pyroprocessing, this oxide stream would be treated for converting TRU elements to a metallic form suitable for fabrication of ATW fuel (based on Zr).

The pyroprocessing should involve two steps: (i) DOR process with Li in LiCl melt to reduce the actinide oxides to the metallic form and (ii) EMT in LiCl–KCl melt to separate transuranium elements from the remaining fission products. The baseline option for ATW irradiated fuel processing would rest on a chloride volatility process for zirconium separation coupled to an electrowinning process in LiCl–KCl for TRU and fission product separation.

Since the mid-1990s, countries of the European Community (Great Britain, France, Spain, Italy), the European Institute for Transuranium Elements (Karlsruhe, Germany), and the Czech Republic have launched research programs for the development of molten salt chemistry and technology for various applications (Partitioning & Transmutation, future fuel cycles). At present, these programs only involve work at the laboratory scale on fundamental aspects or small pilot projects.

Finally, a fused medium in which fuel and reprocessing are strongly connected concerns molten fluorides. In the past, molten fluorides have been developed as fuel and coolant in molten salt reactor systems. The development was largely carried out at Oak Ridge National Laboratory in the 1960s for the molten salt breeder reactor concept, using molten $LiF–BeF_2$ solutions. Today molten salt reactor development has been stopped, though some countries continue isolated investigations (e.g. Czech Republic or Russia).

(a) Chemistry of actinides in major salts – general considerations

As noted above, all the significant pyrochemical technology developments for plutonium conversion and for oxide, metal, or nitride fuel reprocessing call essentially for halide systems: molten chlorides of alkaline and alkaline earth metals, molten fluorides of different cation compositions. Other salt systems, based on oxy-anion salts, have been proposed as backup process or for exotic fuel processing. The most common salts of alkali metals are nitrates, sulfates, molybdates, and tungstates.

Both fundamental and technological progress was reported at the beginning of the 1990s. In this section, after a presentation of the main chemical properties of actinides in molten salts, the principles of separation techniques will be described and main ongoing work on pyroreprocessing in the nuclear industry will be presented. For more detailed information, the reader is referred to the literature cited herein. Molten salt chemistry of actinides has been reviewed previously by Martinot (1991).

(b) Molten chlorides

(*i*) *Thorium*

Anhydrous $ThCl_4$ is colorless and is prepared, among other techniques, by reacting a mixture of $CCl_4 + Cl_2$ gases on ThO_2 at 600°C (Cuthbert, 1958). Dissolved in a KCl melt, thorium exists in the tetravalent oxidation state.

The existence of Th(II) has been reported (Smirnov and Ivanovskii, 1957), but this conclusion also has been disputed (Martinot, 1991). Apparent standard potentials of Th(IV)/Th(0) (relative to the Cl_2/Cl^-, mole fraction couple) are –2.52, –2.50, and –2.47 V at 673, 723, and 773 K, respectively, in LiCl–KCl eutectic (Martinot *et al.*, 1977) and $-3.109 + 6.3810^{-4}T$ (923–973 K) (in volts) in NaCl–KCl eutectic (Srinivasan and Flengas, 1964). Activity coefficient at infinite dilution in LiCl–KCl and NaCl–KCl, solubility product of ThO_2 in LiCl–KCl and NaCl–KCl, potential–pO^{2-} diagram in LiCl–KCl with $[Th(IV)] = 10^{-2}$ M are given by Martinot (1986, 1991).

(*ii*) *Protactinium*

Anhydrous $PaCl_4$ is prepared from PaO_2 by reacting with CCl_4 at 300°C (Stein, 1964) while $PaCl_5$ is obtained from Pa_2O_5 reactions with $SOCl_2$ at 400°C (Brown and Jones, 1966; Hendricks *et al.*, 1971). Pa(V) is reduced in chloride melts to Pa(IV). Apparent standard potential of Pa(IV)/Pa(0) (referred to Cl_2/Cl^-, mole fraction) are –2.35, –2.32, and –2.29 V at 673, 723, and 773 K, respectively, in LiCl–KCl eutectic (Martinot *et al.*, 1980). Activity coefficient at infinite dilution, solubility product of PaO_2 and potential–pO^{2-} diagram in LiCl–KCl with $[Pa(IV)] = 10^{-2}$ M are given by Martinot and Fuger (1986, 1991).

(*iii*) *Uranium*

A great deal of work has been done in the past in binary melts (NaCl–KCl, LiCl–KCl, NaCl–CsCl), in NaCl–KCl–$BaCl_2$, NaCl–KCl–$MgCl_2$, LiCl–NaCl–$CaCl_2$–$BaCl_2$, and the results have been reviewed (Martinot, 1991; Willit *et al.*, 1992; Bychkov and Skiba, 1999). Some results in LiCl–KCl have been published as well (Roy *et al.*, 1996; Sakamura *et al.*, 1998; Shirai *et al.*, 1998). The reader is referred to these papers for more detailed information. Only values related to melts in use in the current EMT development are reported hereafter. It essentially concerns three alkali chloride eutectics: NaCl–KCl, NaCl–2CsCl, and 3LiCl–2KCl.

Uranium in NaCl–KCl

The first EMF measurements, referred to Ag/AgCl (5 mol%) or Cl_2/Cl^- electrodes, have been made from 700 to 850°C (Flengas, 1961; Smirnov and Skiba, 1963). These authors reported only the U(III)/U(0) and U(IV)/U(III) couples. Martinot and coworkers gave the temperature dependence of the several apparent standard potentials (referred to Cl_2/Cl^- electrode). At 700°C (Martinot and Ligot, 1989; Martinot, 1991), $E°[U(III)/U(0)] = -2.49$ V, $E°[U(IV)/U(III)] = -1.33$ V, and $E°[U(V)/UO_2] = -0.80$ V. A recent review (Bychkov and Skiba, 1999) reports 'formal electrode potential' at 727°C (referred to Cl_2/Cl^- electrode): $E°[U(III)/U(0)] = -2.19$ V, $E°[U(IV)/U(III)] = -1.39$ V, and $E°[U(VI)/UO_2] = -0.40$ V. Willit *et al.* (1992) report that the formal potential

incorporates both standard potential and ratio of activity coefficients of the oxidized and reduced species.

Activity coefficients for U(IV) and U(III) are available at various temperatures (Flengas, 1961; Martinot *et al.*, 1975; Martinot, 1991). Diffusion coefficients for U(IV) and U(III) at 700°C have been determined (Willit *et al.*, 1992). Martinot and Ligot (1989) and Martinot (1991) also report the temperature dependence of the solubility product of UO_2; a potential–pO^{2-} diagram has been calculated for [U(V)] = [U(IV)] = [U(III)] = 10^{-2} M. These authors claim that U(VI) does not exist at equilibrium and that the stability area of U(V) is very wide in comparison with the other chloride melts.

Uranium in NaCl–2CsCl

Investigations in the eutectic have been made in the framework of the DDP process development. Few data are available in the open literature. Formal electrode potentials (referred to Cl_2/Cl^- electrode) are given at 727°C: $E°$[U(III)/U(0)] = –2.39 V, $E°$[U(IV)/U(0)] = –1.45 V, and $E°$[U(VI)/UO_2] = –0.65 V (Bychkov and Skiba, 1999).

Uranium in 3LiCl–2KCl

U(III), U(IV), and U(VI) have been identified spectrophotometrically in LiCl–KCl melt (Gruen *et al.*, 1960). At present, the existence of U(V) is no longer considered in dispute (Martinot, 1991). As for the NaCl–KCl eutectic, historic background and basic data have been reported in previous reviews (Martinot, 1991; Willit *et al.,* 1992; Bychkov and Skiba, 1999). Several apparent standard potentials (referred to Cl_2/Cl^-, molar fraction) are available from Martinot (1991): at 450°C, $E°$[U(III)/U(0)] = –2.59 V, $E°$[U(IV)/U(III)] = –1.49 V, $E°$[U(VI)/U(V)] = –0.84 V, and $E°$[U(VI)/UO_2] = –0.81 V. Data from Russian studies are summarized at 500°C by Bychkov and Skiba (1999): $E°$[U(III)/U(0)] = –2.31 V, $E°$[U(IV)/U(III)] = –1.40 V, and $E°$[U(VI)/UO_2] = –0.50 V, all referred to Cl_2/Cl^-. Recent results on the U(III)/U(0) couple (Roy *et al.*, 1996; Sakamura *et al.*, 1998) give at 450°C $E°$ = –1.287 V vs Ag/AgCl (–2.498 V vs Cl_2/Cl^-), which is consistent with other reports.

Activity coefficients at infinite dilution for U(IV) and U(III) are given as a function of temperature (Martinot, 1975, 1991). New calculations have been made recently by Roy *et al.* (1996) and by Betchel and Storvick (1999). Roy and coworkers indicate non-ideal solution behavior for U(III) (activity coefficient is 3.1×10^{-3} at 450°C). Diffusion coefficients for U(IV), U(III) and U(VI) have been determined by Caligara *et al.* (1968) for the range of temperature 400–550°C; other studies of U(III) and U(IV) have been reviewed by Willit *et al.* (1992). $D_{U(III)}$ is typically between 4.1 and 10.3 $\times$ 10^{-3} cm^2s^{-1}. Using the values of UO_2 solubility product (Martinot and Fuger, 1986), Martinot (1991) has calculated potential–pO^{2-} diagram at 450°C (Fig. 24.14). The stability area of U(V) is rather narrow in comparison with NaCl–KCl eutectic.

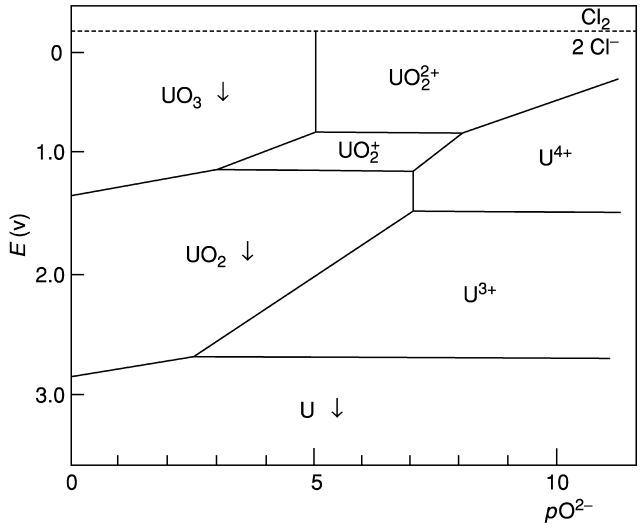

Fig. 24.14 *Potential–pO^{2-} diagram for* [*U*(*IV*)] = [*U*(*III*)] = [*U*(*IV*)] = [*U*(*V*)] = 10^{-2} M *in* 3*LiCl–2KCl at* 450°C (*Martinot*, 1991).

(*iv*) *Neptunium*

Neptunium has been the subject of fewer investigations than uranium. Its chemical behavior has been most extensively studied in alkali chloride melts. In the eutectic (3LiCl–2KCl), the 3+, 4+, and 5+ oxidation states have been identified spectrophotometrically (Gruen *et al.*, 1960). Np(IV), Np(III), and Np(V) are stable species while Np(VI) does not exist as a stable species. Np(VI) is reduced by chloride ions to Np(V) (Martinot, 1991). Standard potentials for Np(III)/Np(0), Np(IV)/Np(III), and Np(V)/NpO_2 have been measured (vs Cl_2/Cl^-, molar fraction) at various temperatures by Martinot and coworkers (Martinot *et al.*, 1967; Martinot and Duyckaerts, 1969a,b). At 450°C, the standard potentials are: E°[Np(III)/Np(0)] = –2.41 V, E°[Np(IV)/Np(III)] = –0.70 V, and E°[Np(V)/NpO_2] = –0.32 V (Martinot, 1991). Bychkov and Skiba (1999) report formal potentials (vs Cl_2/Cl^-, molar fraction) at 500°C: E°[Np(III)/Np(0)] = –2.315 V, E°[Np(IV)/Np(III)] = –1.51 V, and E°[Np(V)/NpO_2] = –0.32 V (450°C). The latest reports from Roy and coworkers (Roy *et al.*, 1996; Sakamura *et al.*, 1998) give for Np(III)/Np(0) E° = –1.487 V vs Ag/AgCl (i.e. –2.698V vs Cl_2/Cl^-). Discrepancies in the results could possibly be explained by the variety of experimental arrangements.

Activity coefficient of Np(III) and diffusion coefficients of Np(III), Np(IV), and Np(V) are available in the literature (Martinot, 1975, 1986, 1991). $D_{Np(III)}$ is equal to $(4.6 \pm 0.2) \times 10^{-6}$ cm^2 s^{-1} at 400°C. The solubility product of NpO_2 has also been measured as a function of temperature by Martinot and

Fuger (1986). Potential–pO^{2-} diagram has been calculated for [Np(V)] = [Np(IV)] = [Np(III)] = 10^{-2} M at 450°C (Martinot, 1986, 1991).

(*v*) *Plutonium*

The electrochemistry of plutonium in molten chlorides was studied early driven by the belief that electrorefining could be a method of purification of plutonium notably for military applications (Brodsky and Carleson, 1962; Mullins and Leary, 1965). Willit *et al*. (1992) have published a useful review on the technological aspects. The melts investigated include LiCl–KCl, NaCl–KCl, $BaCl_2$–KCl, $BaCl_2$–$CaCl_2$–LiCl—NaCl, and NaCl–$CaCl_2$. The most stable oxidation state of plutonium in alkali chloride melts is the trivalent state. Chronopotentiometric and potentiometric studies carried out in the 1960s and 1970s to understand the mechanism of Pu(III) reduction (Campbell and Leary, 1966; Nissen, 1966; Martinot, 1991; Bychkov and Skiba, 1999) have been recently repeated (Roy *et al*., 1996; Sakamura *et al*., 1998, 2001; Shirai *et al*., 1998, 2001). Campbell and Leary (1966) measured the standard potential of Pu(III)/Pu in 3LiCl–2KCl as a function of temperature using a Ag/AgCl reference electrode. Recent results with the same kind of reference electrode agree with the previous value within the uncertainties of the Ag/AgCl electrode potentials due certainly to the membrane potential: E°[Pu(III)/Pu(0)] = –2.204 + 0.000845T (vs Ag/AgCl, molar fraction, AgCl 1 wt%) (Sakamura *et al*., 2001). When adjusted to the Cl_2/Cl^- reference, the standard potential should be –2.775 V at 500°C (Roy *et al*., 1996). Bychkov and Skiba (1999) reports a similar result (–2.82 V) while Martinot (1991) gave a more positive potential.

The activity coefficient of Pu(III) in 3LiCl–2KCl is between 1.0×10^{-3} and 4.1×10^{-3} from 400 to 500°C (Roy *et al*., 1996). Diffusion coefficient $D_{Pu(III)}$ is equal to 12×10^{-6} cm^2 s^{-1} (Nissen, 1966; Willit *et al*., 1992). These data are similar to those of UCl_3. The Pu(IV)/Pu(III) couple has been investigated (Martinot and Duyckaerts, 1970, 1973; Landresse and Duyckaerts, 1974; Bychkov and Skiba, 1999). In common alkali chloride melts, the standard potential of the Pu(IV)/Pu(III) couple is very close to that of Cl_2/Cl^-. For example, in 3LiCl–KCl at 500°C, E°[Pu(IV)/Pu(III)] = +0.01 V, in NaCl–KCl at 727°C E°[Pu(IV)/Pu(III)] = +0.09 V, in NaCl–2CsCl at 600°C, E°[Pu(IV)/Pu(III)] = –0.05 V (Bychkov and Skiba, 1999).

In the presence of a chlorine–oxygen gas mixtures, oxygen-free trivalent and tetravalent forms of plutonium disappear while oxygenated ions of Pu(V) and Pu(VI) appear (Martinot, 1991; Bychkov and Skiba, 1999). The potential–pO^{2-} diagram in 3LiCl–2KCl at 450°C is available from Martinot and coworkers (Martinot and Duyckaerts, 1973; Martinot, 1991) but the authors indicate that it must be considered as a tentative diagram due to large uncertainties in solubility products of plutonium oxides. The NaCl–2CsCl eutectic has been well investigated and temperature dependencies of standard potentials of Pu(VI)/PuO_2 and Pu(V)/PuO_2 couples are known. A potential–pO^{2-}

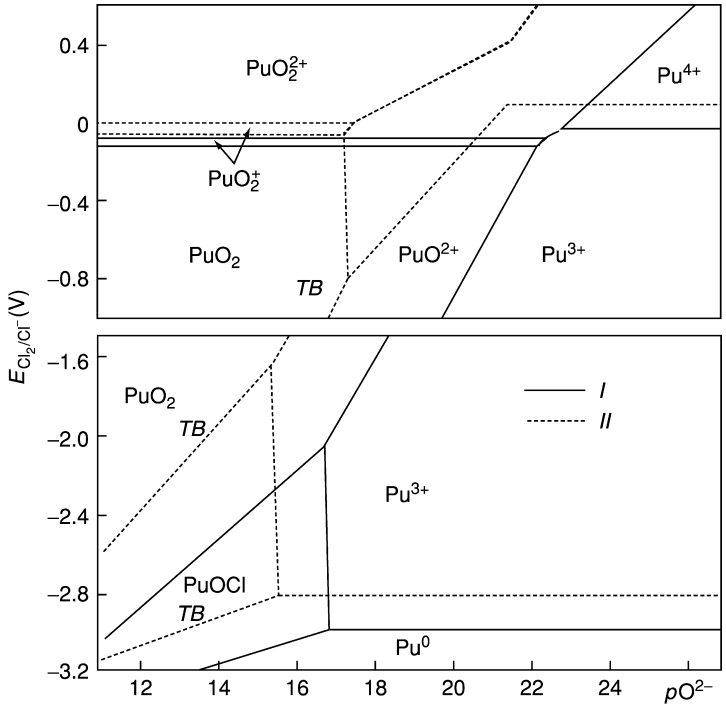

Fig. 24.15 *Potential–pO^{2-} diagram for* $[Pu(IV)] = [Pu(III)] = [PuO_2^+] = [PuO_2^{2+}] = [PuO^{2+}] = 10^{-3}$ M *in NaCl–2CsCl at* 600°C (*solid line*) *and* 800°C (*dashed line*). *Insoluble species are indicated with the TB notation.* (*Vavilov* et al., 1985).

diagram (Fig. 24.15) has been calculated for the medium NaCl–2CsCl (Vavilov *et al.*, 1985).

(*vi*) *Americium*

The existence of both trivalent and divalent americium in alkali chloride melts has been claimed. Initially, similarity in the spectrum of $AmCl_3$ dissolved in 3LiCl–KCl at 450°C obtained by Gruen *et al.* (1960) and the spectrum of Am(III) in concentrated HCl establish the existence of Am(III). Later, chronopotentiometric studies by Martinot *et al.* (1973) in the same eutectic confirmed the existence of the Am(III)/Am(0) couple. Leary and Mullins (1973) argued the existence of Am(II) in NaCl–KCl eutectic, while Kolesnikov *et al.* (1976), using measurements of polarization of various cathodes in $AmCl_3$–NaCl–KCl melts ($AmCl_3$ 1.1 wt%) at 700°C, just showed the wave of discharging of Am(III) to the metal. More recently, based on cyclic voltammetry at 450°C in 3LiCl–2KCl, Grimmett *et al.* (1994) proposed that deposition of Am proceeds in two steps: reduction of Am(III) to Am(II) and then Am(II) into Am metal. The two oxidation states have been confirmed by Lambertin *et al.* (2000).

Standard potentials vs Cl_2/Cl^- for Am(III)/Am(II) and Am(II)/Am(0) in 3LiCl–2KCl between 450 and 500°C reported by several authors (Bychkov and Skiba, 1999; Fusselman *et al.*, 1999; Lambertin *et al.*, 2001) are internally consistent. At 450°C, $E°$[Am(III)/Am(II)] = –2.83 V, $E°$[Am(II)/Am(0)] = –2.852 V (Fusselman *et al.*, 1999). The existence and solubility products of AmO^+, AmOCl, and Am_2O_3 in 3LiCl–2KCl have been determined by potentiometric titration and cyclic voltammetry; a potential–pO^{2-} diagram has been calculated at 470°C for [Am(III)] = [Am(II)] = 10^{-2} M (Lambertin *et al.*, 2000). Lambertin also reports disproportionation of divalent americium in 3LiCl–2KCl can be induced by addition of fluoride anion.

(*vii*) *Curium and transcurium elements*

There have been few studies on the chemistry of curium in chloride melts. Trivalent curium has been identified in 3LiCl–2KCl and NaCl–KCl (Martinot *et al.*, 1975; Kolesnikov *et al.*, 1976). In NaCl–KCl at 750°C, Kolesnikov and coworkers showed, as for americium, that the potential of discharging Cm(III) to Cm(0) is close to the potential of deposition of the alkali metal (difference 0.25–0.3 V) and claimed use of a liquid cathode for alloying americium or curium during recovery by electrolysis. Attempts have been carried out with a zinc cathode (Kolesnikov *et al.*, 1976). In their investigations on the lowest oxidation states of lanthanides and actinides, Kulyukhin *et al.* (1997) show that californium, einsteinium, and fermium in LiCl–$NdCl_2$–$NdCl_3$ melt can be reduced only to the 2+ oxidation state. This is also true for americium.

(c) Molten fluorides

The chemical development carried out in support of the molten salt breeder reactor (MSBR) at Oak Ridge National Laboratory (ORNL) has produced a quantitative description of the chemistry and thermodynamics of actinide and fission-product fluorides in molten LiF–BeF_2 solutions (Baes, 1966). The molten-salt technology was based on the concept of a high-temperature, thermal-neutron breeder reactor that operated on the ^{233}U–^{232}Th fuel cycle with ^{7}LiF–BeF_2–ThF_4–UF_4 (71.7–16–12–0.3 mol%) as reference fuel (Hightower, 1975). In that case, the nature of the fuel logically implies on-site reprocessing involving molten phases to minimize the number of conversion steps and to have low reprocessing costs. The processes that have been developed are described in numerous reports from ORNL. The chemistry of the actinides in molten fluorides has been reviewed (Martinot, 1991). We refer the reader to this comprehensive review as a source for quantitative data – in particular for solubility products, apparent standard potentials, and activity coefficients – of the actinides in molten fluorides. The basic chemical properties of actinides in MSBR melt and the principles of molten salt reactor processing are briefly described in the following sections.

(*i*) *Thorium and protactinium*

In $LiF–BeF_2$ (67–33 mol%), $LiF–BeF_2–ThF_4$ (72–16–12 mol%), and LiF–NaF–KF (46.5–11.5–42 mol%) melts, only the tetravalent oxidation state is observed for thorium. Coordination complexes are formed depending on the excess of free fluoride ions in the melt. The activity coefficient for ThF_4 has been measured as a function of the LiF mole fraction in various $LiF–BeF_2–ThF_4$ melts (Baes, 1974). In the MSBR fuel cycle, ^{233}Pa is formed as a result of neutron capture by ^{232}Th. In such a medium, tetravalent and pentavalent protactinium are potentially coexisting species. By controlling the pO^{2-} and the redox potential of the melt (i.e. U(IV)/U(III) ratio, if the MSBR operating conditions this ratio is ~100), it is possible to have protactinium only in the tetravalent oxidation state (Ross *et al.*, 1973; Tallent and Ferris, 1974).

(*ii*) *Uranium and plutonium*

Trivalent and tetravalent uranium are stable in MSBR melt. Apparent standard potentials have been experimentally measured in $LiF–BeF_2$ (67–33 mol%) as a function of temperature (Martinot, 1975). The chemistry of uranium has been largely investigated and equilibrium constants of interest have been determined in MSBR melt (Baes, 1969; Long and Blankenship, 1969; Toth and Gilpatrick, 1972) to control the redox potential of the fuel and undesirable reactions (e.g. corrosion). By fixing the ratio of U(IV)/U(III) to about 100, only the trivalent oxidation state is stable. Quantitative data (apparent standard potential of Pu(III)/Pu(0), solubility of PuF_3 and PuO_2) are available in $LiF–BeF_2$ (67–33 mol%) and $LiF–BeF_2–UF_4$ (70–10–20 mol%) (Baes, 1969; Toth and Gilpatrick, 1972).

(d) Processing requirements

If a thorium–uranium reactor is to operate as a breeder, ^{233}Pa must be isolated from the region of high neutron flux during its decay to ^{233}U. Also, the fission products must be removed in order to minimize neutron absorptions. The rare earths and zirconium are the principal fission products that must be removed. It also is necessary to remove the excess uranium that is produced to maintain the proper redox potential of the fuel salt and to maintain oxide and corrosion product concentrations at acceptable levels (Long and Blankenship, 1969).

(e) Molten-salt reactor processing

The reference flow sheet has been described (Bell and McNeese, 1971; Hightower, 1975) and was based upon a fluorination-reductive extraction and a metal-transfer process. The fuel salt containing 0.3 mol% of UF_4 and approximately 0.0035 mol% of PaF_4 is withdrawn from the reactor on a 10-day cycle. Uranium is first

removed as volatile UF_6 in a continuous fluorinator. The U-free salt is then fed to an extraction column where protactinium, zirconium, and the remaining uranium are extracted into a bismuth stream containing a reductant.

Subsequently, the bismuth stream is hydrofluorinated in the presence of a second salt stream, which results in transfer of the extracted materials to the salt. Reductant is added to recovered bismuth, and the resulting metal stream is recycled to the extraction column. The secondary salt stream is circulated through a hydrofluorinator, a fluorinator, and a protactinium decay tank. The fluorinator is used to maintain an acceptably low uranium concentration in the protactinium decay tank. The salt is withdrawn from the decay tank periodically to remove zirconium and other fission products that accumulate in the tank. The salt is held for a sufficient period before final discard to allow ^{233}Pa to decay to ^{233}U, which is recovered from the salt by batch fluorination.

Salt leaving the protactinium extraction column is essentially free of uranium and protactinium but contains the rare earths. It is fed to the metal transfer process (McNeese, 1971). This process for removal of rare earths and separating them from thorium is based upon the selective extraction of rare earths from bismuth into LiCl (Ferris *et al.*, 1970, 1972). Rare earths and thorium are extracted into bismuth containing elemental lithium reductant (0.2 at.%) and the rare earths are selectively removed from the bismuth by contact with LiCl. Divalent and trivalent rare earths are removed separately from the LiCl by extraction into Bi–Li streams containing 50 and 5 at.% Li, respectively. The bismuth stream used for the isolation of protactinium is actually fed to the recirculating bismuth stream in the rare earth removal system.

Uranium is returned to the fuel salt in a fuel reconstitution step before the salt is sent back to the reactor. The uranium addition is performed by absorbing the UF_6 stream coming from the fluorinators into a recycle salt stream containing dissolved UF_4. UF_6 reacts with UF_4 to give non-volatile UF_5, which is reduced by hydrogen gas into UF_4. At last a purification step is necessary to remove traces of bismuth before the salt is returned to the reactor.

(f) Molten oxy-anion salts

(*i*) *Molten molybdates*

Investigations of molten molybdates focus on recrystallization of uranium and plutonium oxides (Bychkov and Skiba, 1999). A MoO_3–Na_2MoO_4 melt could be a potential candidate. Ustinov (1995) studied various phase diagrams of binary and ternary systems: UO_2–MoO_3, PuO_2–MoO_3, UO_3–MoO_3, CeO_2–MoO_3, ZrO_2–MoO_3, BaO–MoO_3, RuO_2–MoO_3, UO_2–MoO_3–Na_2MoO_4, PuO_2–MoO_3–Na_2MoO_4 in the temperature range 1000–1200°C. Practically all the oxides are dissolved in molten MoO_3 except for RuO_2. The solubility of the oxides of fission products in MoO_3 is higher than those of oxides of uranium and plutonium. On the other hand, oxides of uranium and

plutonium have a low solubility in Na_2MoO_4. The solubility of molybdates of U and Pu increases with the temperature. From the experimental phase diagrams, various recrystallization methods are proposed for the production of: (i) UO_2, (ii) PuO_2, (iii) homogeneous solid solution of $(U–Pu)O_2$, and (iv) uranium molybdates.

(*ii*) *Molten tungstates*

Molten tungstates, M_2WO_4–$M_2W_2O_7$ where M = Li, Na, K, and Cs have some interesting physical properties: (i) high thermal stability, (ii) low volatility, (iii) relatively low melting points, and (iv) high values of decomposition voltage (Afonichkin and Komarov, 1995). Common working temperatures are in the range 700–900°C and an inert atmosphere is required (Afonichkin *et al*., 2001). Nevertheless, there have been few experiments on actinides. Afonichkin and coworkers investigated the electrodeposition of uranium oxide from Na_2WO_4–UO_2WO_4 and Na_2WO_4–$Na_2W_2O_7$–UO_2WO_4 melts. In the binary melt, an ionic model has been proposed to explain the dissolution of uranium oxide and the formation of UO_2, UO_{2+x}, U_4O_{9-y}, and U_3O_8 phases on the cathode (Afonichkin *et al*., 2001):

$$U_3O_8 + 2Na_2WO_4 + \frac{1}{2}O_2 \rightleftarrows Na_2[UO_2(WO_4)_2] + Na_2U_2O_7 \tag{24.25}$$

$$Na_2[UO_2(WO_4)_2] \rightleftarrows 2Na^+ + [UO_2(WO_4)_2]^{2-} \tag{24.26}$$

$$[UO_2(WO_4)_2]^{2-} \rightleftarrows UO_2^{2+} + 2WO_4^{2-} \tag{24.27}$$

$$2UO_2^{2+} + 2WO_4^{2-} \rightleftarrows U_2O_5^{2+} + W_2O_7^{2-} \tag{24.28}$$

and, in concentrated UO_2WO_4 solutions,

$$UO_2^{2+} + U_2O_5^{2+} + 2WO_4^{2-} \rightleftarrows U_3O_8^{2+} + W_2O_7^{2-} \tag{24.29}$$

Electrolysis:

$$UO_2^{2+} + 2e^- \rightleftarrows UO_2 \tag{24.30}$$

$$U_3O_8^{2+} + 2e^- \rightleftarrows U_3O_8 \tag{24.31}$$

$$(1-2x)UO_2^{2+} + xU_2O_5^{2+} + 2(1-x)e^- \rightleftarrows UO_{2+x} \tag{24.32}$$

$$2(1+y)UO_2^{2+} + (1-y)U_2O_5^{2+} + 2(3+y)e^- \rightleftarrows U_4O_{9-y} \tag{24.33}$$

If the ternary system allows a lower melting point, the resulting addition of $Na_2W_2O_7$ in the melt decreases the potential of the melt decomposition. However, it has been shown that the transition from the binary to the ternary melt

has minimal effect on the oxygen coefficient and on the main parameters of electrolysis. Current efficiency does not exceed 65% of theoretical value (Afonichkin and Komarov, 1995; Afonichkin *et al.*, 2001), indicating chemical interactions of the cathodic product with the electrolyte. With increasing temperature and $W_2O_7^{2-}$ concentration, the current efficiency decreases.

(*iii*) *Nitrates and sulfates*

Several authors (Morgan *et al.*, 1980; Martinot, 1991; Bychkov and Skiba, 1999) have prepared comprehensive reviews of pyroprocessing of actinides in nitrate and sulfate media. Such media create awkward operating conditions since nitrate melts are particularly hazardous and processes in molten sulfates involve corrosive gaseous phases. A distinctive feature of the molten alkali nitrate melts (300–450°C) is the ability to dissolve uranium oxide while PuO_2 remains insoluble. In molten sulfates (450–650°C), both uranium and plutonium oxides can be dissolved using gaseous sulfur oxides or vapor of sulfuric acid (Brambilla, 1984; Bychkov and Skiba, 1999). Uranium oxide could be recovered by electrolysis though PuO_2 is precipitated by decomposition of its sulfate at high temperature (Brambilla, 1984; Bychkov and Skiba, 1999).

(g) Separation techniques: principles, performances, and limitations

(*i*) *Oxide–oxide processes*

Since the 1960s, Research Institute of Atomic Reactors (RIAR, Dimitrovgrad), has been developing fabrication and reprocessing processes for oxide fast reactor fuel (Bychkov *et al.*, 1995; Skiba and Ivanov, 1995). It combines vibropacking fabrication of fuel rods and pyroelectrochemical technology of spent fuel in molten alkali chlorides. Original studies conducted at Hanford within the framework of the Salt Cycle Process development (for UO_2–PuO_2 fuel reprocessing) involved LiCl–KCl melts (Benedict *et al.*, 1963). Changing the melt composition and the electrolysis atmosphere allowed production of various oxides. For instance, highly enriched UO_2 was dissolved in equimolar LiCl–KCl with chlorine sparging and UO_2Cl_2 was then electroreduced at 550–800°C to UO_2 on the cathode, leaving plutonium and fission products in the melt. If one wanted a PuO_2–UO_2 solid solution, electrolysis was done in the same melt at 475–675°C under chlorine–oxygen gaseous mixture. If it was only necessary to recover plutonium, dissolution was performed in 2.5:1 LiCl–KCl melt and plutonium was precipitated as dioxide with chlorine–oxygen sparging. Since that time, RIAR has developed a similar process, named Dimitrovgrad dry process (DDP), at the semi-industrial scale, for spent UO_2 or MOX fuel reprocessing, in two other alkali melts: NaCl–2CsCl or NaCl–KCl–UO_2Cl_2 (Bychkov and Skiba, 1999).

(*ii*) *Basis of the DDP*

Dissolution

First, spent oxide fuel is dissolved in the melt by a strong oxidizing agent, chlorine gas at 650–700°C. Actinides are present either as chlorides or oxychlorides (see Section 24.3.12b). Uranium and plutonium behaviors can be explained by the following chemical reactions and equilibria:

$$UO_2 + Cl_2 \rightleftarrows UO_2Cl_{2\ melt} \tag{24.34}$$

$$PuO_2 + Cl_2 \rightleftarrows PuO_2Cl_{2\ melt} \tag{24.35}$$

$$PuO_2Cl_2 \rightleftarrows PuO_2Cl_{melt} + \frac{1}{2}Cl_2 \tag{24.36}$$

$$PuO_2Cl_2 + Cl_2 \rightleftarrows PuCl_{4\ melt} + O_2 \tag{24.37}$$

$$PuCl_4 \rightleftarrows PuCl_{3\ melt} + \frac{1}{2}Cl_2 \tag{24.38}$$

U(VI) present as uranyl species UO_2^{2+} is stable; treating the melt with chlorine–oxygen gaseous mixture will stabilize the highest oxidation states of plutonium, respectively PuO_2^+ and PuO_2^{2+}. The temperature dependence of equilibrium constants for plutonium species in NaCl–2CsCl is known for various partial pressures of chlorine gas (Vavilov *et al*., 1985).

Uranium and plutonium recovery

The recovery of uranium and plutonium as oxides at high temperature (> 400°C) works because UO_2 and PuO_2 conduct electricity and can be electrodeposited at a cathode like a metal. According to the formal potentials listed in Table 24.10, UO_2 and PuO_2 are reduced at more positive potentials than all the fission products, except for noble metals (Bychkov and Skiba, 1999; Bychkov *et al*., 2000). If plutonium recovery is not necessary, UO_2Cl_2 is electroreduced to UO_2 at the pyrolytic carbon cathode, leaving plutonium and the majority of fission products in the melt. Recovery efficiency is 99.0–99.5% (Bychkov and Skiba, 1999). At the anode, chloride ions are oxidized to chlorine gas.

Table 24.10 *Formal electrode potentials of actinides and fission products* (*vs* Cl_2/Cl^-, *molar fraction*) *in NaCl–2CsCl eutectic at* 600°C (*in* volts) (*Bychkov and Skiba*, 1999).

Sm(II)/Sm	–3.58	Pu(III)/Pu	–2.83	U(VI)/UO_2	–0.65
Eu(II)/Eu	–3.39	U(III)/U	–2.39	Pd(II)/Pd	–0.48
Ce(III)/Ce	–3.08	Zr(IV)/Zr	–2.17	Rh(III)/Rh	–0.44
		Fe(II)/Fe	–1.48	Ru(III)/Ru (510°C)	–0.413
		U(IV)/U(III)	–1.45	Np(V)/NpO_2	–
		Mo(III)/Mo	–0.97	Pu(IV)/Pu(III)	–0.05
		Ag(I)/Ag	–0.932	Pu(VI)/PuO_2	+0.12

If both uranium and plutonium recovery is desired, electrolysis must be carried out while sparging the melt with an oxygen–chlorine gaseous mixture (Bychkov and Skiba, 1999). The cathodic products are quasi-homogeneous (U, Pu)O_2 with two-phase composition: solid solution of PuO_2 in UO_2 crystals and solid solution of UO_2 in PuO_2 crystals. UO_2 deposition rate is pre-set by current density while PuO_2 deposition rate is limited by the diffusion of plutonyl ions to the cathode (Bychkov *et al.*, 2000). If it should be necessary to recover only PuO_2, dissolution is performed in NaCl–KCl and plutonium oxide is precipitated by oxygen gas (Bychkov and Skiba, 1999).

Behavior of minor actinides

(Np, Am, and Cm). After the dissolution step, neptunium is present in the melt as NpO_2^+. As a result, neptunium is electroreduced to NpO_2 and is co-deposited with uranium oxide (see Table 24.11). The behavior of americium and curium is not similar to that of neptunium; they remain as soluble species in the melt like other soluble fission products (alkaline elements, alkaline earth elements, and rare earth elements) (Kormilitzyn *et al.*, 1999).

Separation of americium and curium from the soluble fission products by carbonate precipitation has been proposed. Sodium carbonate is added to the spent melt (NaCl–2CsCl or NaCl–KCl) for fractional precipitation of americium and curium, probably as sesquioxides M_2O_3 (M = Am and Cm). Similar results were obtained for both media in terms of the possible separation of minor actinides and rare-earth elements (hereafter REE) (Kormilitzyn *et al.*, 1999, Fig. 24.16). Unfortunately, americium precipitates between lanthanide(III) and lanthanide(II), which makes it difficult to separate Am from REE. Even if a small part of the americium sesquioxide could be recovered by filtration at high temperature, the remaining americium precipitates as mixed oxide with REE. If the separation of americium from REE is not necessary, the melt can be purified by adding phosphate to precipitate americium (and curium) and fission products. Fission products in the trivalent oxidation state precipitate as insoluble double phosphates $Na_3M(PO_4)_2$, while many fission products in the divalent

Table 24.11 *Gibbs energies of formation of selected oxides at* 1700 K *compiled by Mullins* et al. (1960) *from* (*Glassner*, 1957) kJ (g atom O)$^{-1}$ (*Recalculated from values in* kcal (g atom O)$^{-1}$).

La_2O_3	–452	Pu_2O_3	–402	InO	–105
Ce_2O_3	–452	UO_2	–397	Sb_2O_3	–96
Nd_2O_3	–444	ZrO_2	–385	K_2O	–84
Y_2O_3	–439	MgO	–376	TcO_2	–67
SrO	–422	NbO	–268	Rh_2O	–8
		FeO	–151	Rb_2O	–8
		MoO_2	–134	RuO_2	0
				TeO_2	0

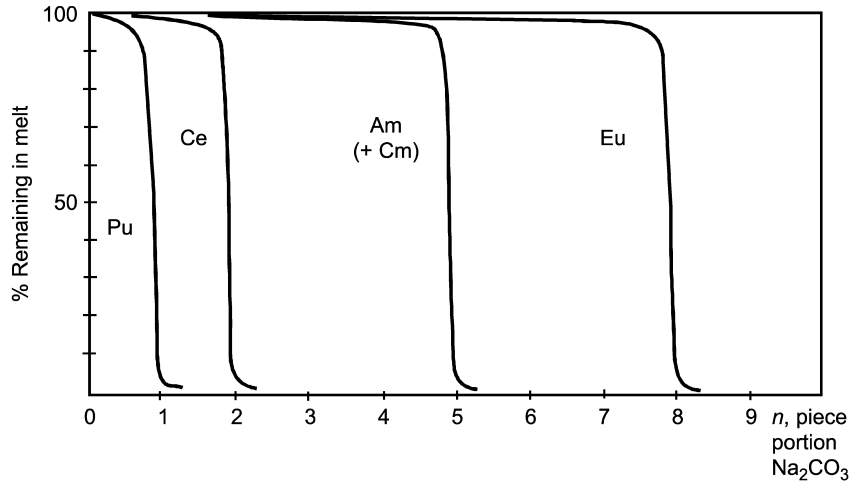

Fig. 24.16 *Relative contents for Pu, Am, Ce, Eu in NaCl–2CsCl melt during fractional carbonate precipitation coming just after electrolysis step* (*Kormilitzyn* et al., 1999).

oxidation state, including alkaline earth elements, also precipitate (Kormilitzyn *et al.*, 1999).

(h) Applications, separation efficiency in the DDP

A chlorinator–electrolyzer has been designed that will accommodate a volume of 40 L. It can reprocess a loading of about 30 kg of material. All the internal surfaces that come into contact with the salt and gaseous phases (anode-crucible, cathode, gas tube) are crafted of pyrolitic graphite. After pyroelectrochemical treatment, the cathodic deposits are crushed, purified from salts by distillation, dried, and classified for vibropac fabrication of fuel rods (Bychkov and Skiba, 1999). Since the 1970s about 3 metric tons of UO_2, 100 kg of PuO_2, and 1600 kg of $(U–Pu)O_2$ have been produced in molten alkali chlorides for BOR60, BN350, and BN600 reactors. From 1968 to 1973, 5.8 kg of spent UO_2 coming from VK-50 and BOR60 reactors were reprocessed while spent MOX fuel reprocessing began in the 1990s with 4.1 kg from BN350 (burn-up 4.7%) and 3.5 kg from BOR60 (burn-up 21–24%) (Bychkov and Skiba, 1999). For example, reprocessing of MOX fuel from BOR60 involved: (i) dissolution of the fuel in LiCl–4.53NaCl–4.88KCl–0.66CsCl; (ii) electrolysis to remove part of UO_2 free from Pu; (iii) PuO_2 precipitation; (iv) additional electrolysis for removing residual uranium as UO_2, and (v) melt purification by phosphates.

Mass balances give information on the behavior of actinides and fission products. It has been found that (Bychkov and Skiba, 1999; Bychkov *et al.*, 2000): (i) Zr, Nb, Ru, Rh, Pd, and Ag were located in the first UO_2 deposit; (ii) U/Pu separation factor in the first electrolysis is 120–140; (iii) most of the

Np is distributed between the two UO_2 deposits; (iv) Am is present in UO_2 deposits (~3.5 wt%), in PuO_2 precipitate (~18 wt%) and in phosphates (~73 wt%); (v) practically all the Cm is in phosphates though it has also been detected in the second UO_2 deposit; (vi) representatives of REE (Ce and Eu) are concentrated in phosphates, and (vii) Cs, Rb, and partially Sr remain in melt.

If a (U, Pu)O_2 deposit is desired, it will be necessary to perform a preliminary electrolysis for the removal of Ru, noble metals and Zr, before carrying out the main electrolysis under a chlorine–oxygen atmosphere. In tests on simulated materials in NaCl–2CsCl, the separation factors observed were: ~ 1000 for Cs, >100 for REE, ~1 for Ru and Zr without preliminary electrolysis, and ~10 with preliminary electrolysis (Kormilitzyn *et al.*, 1999).

DDP is currently used for oxide fuel reprocessing and for producing three oxides: UO_2, PuO_2, and (U–Pu)O_2. The latter one is mainly dedicated to MOX fuel fabrication for BOR-60 reactor. Research programs are now focused on conversion of weapon-grade plutonium into MOX fuel, development of a process for complete recycle of Pu, Np, Am and Cm (*D*ry reprocessing, *O*xide fuel, *V*ibro-compact, *I*ntegral, *T*ransmutation of *A*ctinides, DOVITA program) (Bychkov and Skiba, 1999).

(i) Metal–metal processes

(*i*) *Melt refining* (*or oxide slagging process*)

Early pyrometallurgical processes which have been developed for minimizing the cost of recycling were rudimentary. One example is the melt refining process, which was proposed to reprocess the metallic uranium fuel alloy used in the core of the second experimental breeder reactor (EBR-II) (Motta, 1956; Burris *et al.*, 1964). The fuel was an enriched uranium alloy (~52 wt% ^{235}U) containing 5 wt % *fissium* (mixture of molybdenum, ruthenium, rhodium, palladium, zirconium, and niobium) with sodium used as a thermal bond (Burris *et al.*, 1964; Steunenberg *et al.*, 1970). Melt refining is also named oxide slagging or oxide drossing. Fission products were removed by combining volatilization and selective oxidation.

After the mechanical removal of cladding and sodium bonds, the separation process consisted simply in melting the fuel at 1300–1400°C in a lime-stabilized zirconia crucible. Volatile fission products that are condensable, such as iodine and cesium, were trapped on alumina–silica fibers while gaseous fission products (krypton, xenon) were stored to allow decay of 5.3 day ^{133}Xe before being released into the atmosphere. Elements more electropositive than zirconium (see Table 24.11: alkali metals, alkaline earth, and rare earth elements) reacted with the zirconia to form an insoluble oxide slag. The other fission products (noble metals comprising the *fissium*) and the actinides remained with the uranium in the metallic form to be recycled. At this stage, the uranium recovery yield ranged from 90 to 95 wt% (Trice and Chellew, 1961; Burris *et al.*, 1964).

The melt refining process leaves a residue or skull (mixture of oxides and unpoured metal) at the bottom of the crucible, which represented about 5–10% of the loading. An auxiliary process had been proposed to recover uranium from the skull. After preliminary oxidation of the skull under oxygen–argon mixture at 700°C, the resulting oxides were dissolved into a chloride flux. Contact with liquid zinc between 700 and 800°C allowed the removal of noble metals (Ru, Mo, Rh, Pd) and Ag. Uranium was then extracted from the chloride flux by using Mg–Zn alloy (magnesium being the reducing agent and zinc the alloying agent). Combining this process with the melt refining increased the uranium recovery yield to about 99.5 wt%. The fission product removals that had been achieved (rare earths: 90%, Ru: 80%, Mo: 90%, Pd: >99%, Zr: 75%, Ba, and Sr: >99%) were sufficient to maintain the desired concentrations of the *fissium* alloying elements in the EBR-II fuel (Burris *et al*., 1964). The complementary process, named the skull reclamation process, has been studied only at the laboratory scale (Burris *et al*., 1964; Steunenberg *et al*., 1970).

Oxide slagging was also investigated for plutonium reactor fuels, for example with the proposed LAMPRE fuel (Los Alamos Molten Plutonium Reactor Experiment, 10 wt% Fe–Pu alloy) (Mullins *et al*., 1960). Tests on synthetic spent plutonium fuel have been performed in magnesia and zirconia crucibles. But this approach was rapidly abandoned because of numerous drawbacks: high temperature, slow reaction rates, and the creation of a plutonium-bearing residue.

(j) Melt refining under molten salts (or halide slagging processes)

In the halide slagging process, in particular chloride slagging, the active fission products were rapidly removed from the molten fuel as a result of chemical reactions occurring at the interface between two liquid phases. Moreover, the plutonium transfer was less than 1 wt%. The process consisted of contacting the molten fuel at 600–700°C with molten alkali chloride salts containing plutonium chloride or magnesium chloride as an oxidant. Used slags were $PuCl_3$–NaCl, $MgCl_2$–LiCl—KCl, or $MgCl_2$–NaCl–KCl (Leary *et al*., 1958; Mullins *et al*., 1960). Gibbs energies of formation of selected halides are shown in Table 24.12.

Results were in agreement with thermodynamic predictions: electropositive fission products (alkali and alkaline earth elements, rare earths) were oxidized and dissolved in the chloride slag. But, as in every melt refining process, the noble metal fission products were not removed from the spent fuel. Mullins *et al*. (1960) gave for $MgCl_2$–NaCl–KCl at 700°C the percentage transferred into the salt phase for the following elements: Pu 0.92, Fe 0.04, Zr < 0.04, Mo < 0.15, Ru < 0.20, Ce 98, La 100, Mg 26. In these experiments, the $MgCl_2$ exceeded by 10% the stoichiometric quantity needed to remove the rare earths. A similar process has been tested on (10–20 wt% plutonium)–uranium alloys with $BaCl_2$–$CaCl_2$ and $MgCl_2$ as oxidant (Glassner, 1957). The effect of the slag

Table 24.12 *Gibbs energies of formation*[a] *of selected chlorides at* 775 K. *Compiled by Ackerman* (1991) *from Pankratz* (1984) kJ (g atom Cl)$^{-1}$.

CsCl	–367.4	$CeCl_3$	–287.0	UCl_3	–231.0
KCl	–362.8	$NdCl_3$	–284.1	$ZrCl_4$	–195.0
$SrCl_2$	–354.4	YCl_3	–272.4	$CdCl_2$	–135.1
LiCl	–345.2	$AmCl_3$	–268[b]	$FeCl_2$	–122.3
NaCl	–339.3	$CmCl_3$	–268[b]	$MoCl_2$	–70.3
$LaCl_3$	–293.7	$PuCl_3$	–261.1[b]	$TcCl_3$	–46
$PrCl_3$	–288.7	$NpCl_3$	–242.7[b]		

[a] Recalculated from values in kcal (g atom Cl)$^{-1}$.
[b] Estimated values.

composition is minor. The criteria for slag selection must be melting point and high stability of halide components (alkali or alkaline earth elements).

(k) Molten metal-salt extraction processes

By combining liquid metal (or alloy) solvent with molten salts and using oxidation–reduction reactions, it is possible to accomplish separations that could not be achievable by melt refining. The elements are distributed in the two-phase solvent system and the distribution coefficients depend on the nature of the oxidizing and reducing agents and on the activities of the reacting species in solution. In general, chlorides are preferred because of their lower volatility, their compatibility with many containers, and favorable solubility relationships. Such separation techniques in various biphasic systems have been proposed in the past by several American laboratories: Brookhaven National Laboratory investigated Bi/$MgCl_2$–NaCl–KCl to reprocess bismuth–uranium fuel (Bennett *et al.*, 1964); the Hanford Works studied the actinide distribution in Al/$AlCl_3$–KCl (Dwyer, 1956); the Ames Laboratory examined the same in Zn/LiCl–KCl (Moore and Lyon, 1959); Los Alamos National Laboratory tested Hg/RbCl–LiCl–$FeCl_2$ for the reprocessing of LAMPRE fuel (Chiotti and Parry, 1962); Argonne National Laboratory proposed various applications in $MgCl_2$-based salt with Cu–Mg or Zn–Mg alloy. One of them is the Argonne salt transport process for the reprocessing of LMFBR fuels (Steunenberg *et al.*, 1970).

(*i*) *Argonne salt transport process*

The partitioning of element M between magnesium alloy and $MgCl_2$-based salt can be expressed by:

$$\mathrm{M(alloy)} + \tfrac{1}{2}n\mathrm{MgCl_2(salt)} \rightleftharpoons \mathrm{MCl}_n\mathrm{(salt)} + \tfrac{1}{2}n\mathrm{Mg\ (alloy)} \qquad (24.39)$$

If K_a is the equilibrium constant, a_i and γ_i respectively the activity and the activity coefficient of the reactants, the distribution ratio D_M for a metal M

(ratio of mole fraction of MCl_n in salt to atom fraction of M in alloy) will be expressed by:

$$\log D_M = (-\Delta G^\circ/2.3RT) + (-\tfrac{1}{2}n \log a_{Mg} + \log \gamma_M) - (-\tfrac{1}{2}n \log a_{MgCl_2} + \log \gamma_{MCl_n}) \quad (24.40)$$

where $\Delta G^\circ = -RT \ln K_a = \Delta G_f^\circ(MCl_n, T) - \frac{1}{2}n\Delta G_f^\circ(MgCl_2, T)$. The first term in brackets in equation (24.40) depends on temperature via the Gibbs energy of formation of MCl_n and $MgCl_2$. The second term depends on temperature and composition of the alloy while the third depends on temperature and composition of salt. Importance of these terms on D_M decreases from left to right when salt with $MgCl_2$ is used as the oxidizing agent (Bowersox and Leary, 1960).

The halides of the noble-metal fission products and the metals used for cladding (like Fe), have a less negative Gibbs energy of formation (see Table 24.12) the first term dominates the distribution ratio and they should be easily separated from actinides by remaining in the alloy. For actinides and rare earth elements, the two following terms cannot be ignored. Johnson (1974) has explained their effect on distribution coefficients.

Distribution ratios of actinides and rare earth elements between molten $MgCl_2$ and Mg-alloy (Mg–Zn, Mg–Cu) have been measured over a wide range of magnesium content (Knighton and Steunenberg, 1965; Knighton, 1969). They are at a minimum when a Zn–Mg alloy is used (Mg content is about 10 wt%). A similar effect is not observed when Cu–Mg alloy is used. These two alloys have been proposed by Argonne National Laboratory to separate uranium and plutonium from fission products. Salt transport separation is based on the selective transfer of uranium and plutonium from a donor alloy to an acceptor alloy via a saline phase (see Fig. 24.17):

$$Pu(\text{donor alloy}) + \tfrac{3}{2}MgCl_2(\text{salt}) \rightarrow PuCl_3(\text{salt}) + \tfrac{3}{2}Mg\ (\text{donor alloy}) \quad (24.41)$$

$$PuCl_3(\text{salt}) + \tfrac{3}{2}Mg(\text{acceptor alloy}) \rightarrow Pu(\text{acceptor alloy}) + \tfrac{3}{2}MgCl_2(\text{salt}) \quad (24.42)$$

When uranium and plutonium are salt-transported from the donor alloy to the acceptor alloy, noble fission product metals remain in the donor alloy and rare earth fission product are stabilized in the salt phase. Using 50 mol% $MgCl_2$–30 mol% NaCl–20 mol% KCl and Mg–44 at% Cu alloy at 650°C, the separation factor for Ce from Pu is about 1000.

Typical phase compositions for plutonium recovery and purification are: for the donor alloy, Cu–33wt% Mg; for the salt, 50 mol% $MgCl_2$–30 mol% NaCl–20 mol% KCl; for the acceptor alloy, Zn–5 wt% Mg. The solubility of the transported material in the donor alloy must be high enough to have a significant transfer rate. For example, the solubility of uranium at 600°C in Cu–33 wt% Mg alloy is very low (50 ppm) while it can reach 3.8 wt% in

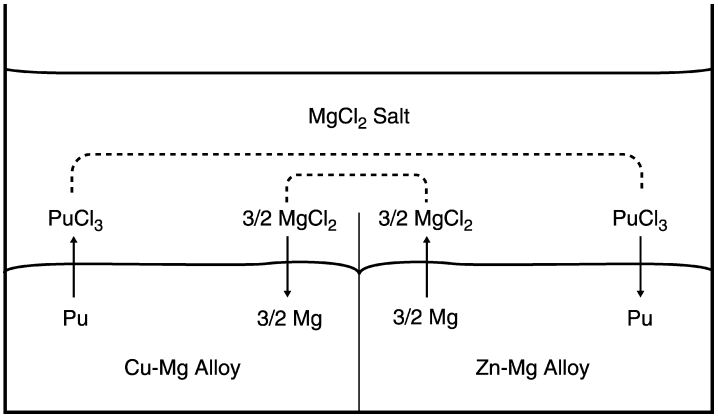

Fig. 24.17 *Scheme of salt transport process for plutonium* (*Steunenberg* et al., 1970).

Cu–6.5 wt% Mg alloy (Steunenberg *et al.*, 1970). Salt transport process has been developed at the laboratory scale, but no full scale application has yet been developed, though it was proposed in the mid-1990s in a conceptual flow sheet for recovering actinides from LWR fuels (Pierce *et al.*, 1993; Johnson *et al.*, 1994) (see Section 24.3.12n).

(*ii*) *Other applications of molten salt-metal extraction*

Development of this separation technique in molten fluorides has been carried out largely at Oak Ridge National Laboratory, in support of the molten salt breeder reactor (MSBR) concept for the reprocessing of fuel based on molten $LiF–BeF_2$ solutions (see Section 24.3.12**c**). In chlorides, molten salt-metal extraction has been proposed for enhanced recovery of actinides from spent salt generated during electrorefining of metallic fuel (see Section 24.3.12.l). It has also been developed as one process stage for actinide recovery from HLLW coming from PUREX (see Section 24.3.12m(i)).

(l) Electrorefining

Early work on electrorefining from molten salts was done to prepare either high-purity metallic uranium or plutonium separately. It began with investigations on uranium at small scale (Driggs and Lilliendahl, 1930; Marzano and Noland, 1953), at larger scale (Anonymous, 1951; Chauvin *et al.*, 1962, 1964), then with plutonium. A significant application is the recovery and purification of plutonium developed at Los Alamos National Laboratory (Mullins *et al.*, 1962) and used at Rocky Flats, Hanford and in various countries (Moser and Navratil, 1983). There has been little research and development related to the application of electrorefining techniques to the recovery and purification of spent fuels.

Investigations on irradiated uranium (Chauvin *et al*., 1964) and on Los Alamos Molten Plutonium Reactor Experiment (LAMPRE) fuel (Leary *et al*., 1958) have been carried out.

Interest in electrorefining was revived with the proposed advanced fast reactor concept called the integral fast reactor (IFR) (Burris, 1986; Till and Chang, 1988; Chang, 1989; Hannum, 1997) whose primary feature was an integral fuel cycle in which the core and blanket materials after discharging are to be processed and refabricated in an onsite facility. The fuel cycle was based on electrorefining with a molten salt electrolyte (LiCl–KCl–UCl_3/$PuCl_3$) at 500°C in an inert atmosphere. An abundant literature has appeared on the chemistry and technology of IFR (see in particular Burris *et al*., 1987; Willit *et al*., 1992; Hannum, 1997; Anonymous, 2000). In the discussion below, the following features of this system will be presented: (i) a brief description of the main steps of the pyro-process; (ii) the chemical basis for partitioning of actinides and fission products between metallic (solid or liquid) and salt phases; and (iii) the separation efficiencies obtained at laboratory scale and in the only engineering scale application (EBR-II spent fuel treatment demonstration) completed to date.

(*i*) *Reprocessing in the IFR fuel cycle*

After discharging the spent core fuel (alloy of U, Pu, and Zr) in its stainless cladding, the fuel is chopped and placed in an anode basket. The anode basket containing the chopped fuel is put into an electrorefiner containing molten LiCl–KCl electrolyte and a liquid cadmium pool under inert atmosphere. $CdCl_2$ is added in the electrolyte to oxidize electropositive fission-product metals (alkali, alkaline earths, and a large fraction of the rare earth metals) to their chlorides (see Table 24.12). The amount of oxidizing agent to be added is adjusted to maintain 2 mol% actinide chlorides in the salt phase. The basket is made anodic and the following sequence occurs: (i) nearly pure uranium is electro-transported to a solid mandrel cathode and (ii) transuranium elements and some uranium are transferred by electro-transport to a liquid cadmium cathode. Noble metal fission products remain in an unoxidized form and are removed from the basket with the cladding hulls, although some portion falls into the cadmium pool at the bottom of the electrolyzer. Electropositive fission products remain in the salt and build-up during the successive reprocessing batches and progressively modify the electrochemical and physical properties of the electrolyte. Periodic treatment is thus required to remove them and recycle the electrolyte.

The molten metal-salt extraction (using Li–Cd alloys) has been proposed for reduction and removal of transuranium elements (TRUs) from the electrolyte salt and for TRU reoxidation back into the salt to start the next electrorefining campaign. Moreover, the use of UCl_3 as oxidant makes it possible to avoid the introduction of cadmium in the electrorefiner and thus the lower cadmium pool can be eliminated. This approach avoids the deposition of cadmium and

makes easier the removal of solids that accumulate at the bottom of the electrolyzer.

Both types of cathode products are processed to distill off adhering salt and cadmium (in case a liquid cadmium cathode is used). Such a process produces three waste streams: fission product gases, metal waste stream that contains cladding hulls, and noble metal fission products, and salt waste stream (alkali, alkaline earth fission products). The treatment, the immobilization, and the disposal of these wastes are challenging, but their discussion is not within the scope of this chapter. These features have largely evolved during the laboratory-scale and engineering-scale developments depending on the applications. The lone large-scale feedback is the demonstration campaign on the treatment of spent metal fuel from the EBR-II fast reactor commenced in 1996 at the Argonne-West site in Idaho. Processes and results obtained are discussed in reference Anonymous (2000).

(*ii*) *Chemical basis of electro-transport in LiCl–KCl*

Johnson (1988) and Ackerman and coworkers (Ackerman, 1991, Tomczuk *et al*., 1992; Ackerman and Johnson, 1993) have described the chemistry that controls the electro-transport in LiCl–KCl electrolyte on solid or liquid cathode. The transfer of the element of interest (for example U or Pu) is done by electrolyzing (electrochemical oxidation) this element into the salt (electrolyte) at the anode and electrodepositing it as metal at the cathode. The element must be initially present in the electrolyte before starting electrolysis. Dissolution is facilitated by addition of a chemical oxidizing agent (i.e. a chemical agent whose the chloride is less stable than the chloride of the element one wishes to electro-transport). For uranium electro-transport, the oxidizing agent can be $CdCl_2$ (see Table 24.12).

In the electrorefiner, the salt is well stirred and is in contact with both metal (electrode) phases. When a predetermined number of moles of metal (of given composition) are removed from the anode to the cathode, the compositions of both electrodes and the salt change until the salt is in equilibrium. For both elements M and M′, the following equilibrium exists at each electrode:

$$n1(\mathrm{MCl}_{n2}) + n2(\mathrm{M}')_{\mathrm{alloy}} \rightleftarrows n1(\mathrm{M})_{\mathrm{alloy}} + n2(\mathrm{M}'\mathrm{Cl}_{n1})\mathrm{salt} \tag{24.43}$$

Equilibrium constant K_a can be expressed using mole fraction x_i and activity coefficient γ_i of M and M′ in metal phase(s) and salt by:

$$K_a(T) = [(\gamma\mathrm{M})^{n1}(\gamma\mathrm{M}'\mathrm{Cl}_{n1})^{n2}]/[(\gamma\mathrm{M}')^{n2}(\gamma\mathrm{MCl}_{n2})^{n1}] \cdot [(\mathrm{xM})^{n1}(\mathrm{xM}'\mathrm{Cl}_{n1})^{n2}]/[(\mathrm{xM}')^{n2}(\mathrm{xMCl}_{n2})^{n1}] \tag{24.44}$$

where $\Delta G^{\circ}(T) = -RT \ln K_a(T) = n_2 \Delta G_f^{\circ}(\mathrm{MCl}_{n1}, T) - n_1 \Delta G_f^{\circ}(\mathrm{M}'\mathrm{Cl}_{n2}, T)$. By writing donor alloy = anode and acceptor alloy = cathode (Johnson, 1988), the equations are similar to those written for salt transport description

(see Section 24.3.12.**k**). The metal (electrode) phases need not to be in equilibrium with each other in the classical sense which would mean that activity of each metal would be the same in all phases (Anonymous, 1951; Tomczuk *et al.*, 1992; Ackerman and Johnson, 1993).

Concentrations in the salt phase at equilibrium depend on activity coefficients in metal phases (solid or liquid) and salt. As the salt is diluted, the activity coefficients of MCl_{n2} and $M'Cl_{n1}$ are assumed to be constant. However, activity coefficients of M and M′ in metal phases can vary greatly when changing the metal phase and they can be greatly reduced by the formation of intermetallic compounds. For instance, the plutonium activity is reduced in cadmium by formation of $PuCd_6$ (Johnson *et al.*, 1965). A similar decrease for rare earth activity coefficients is observed with Cd (Johnson and Yonco, 1970). Uranium does not form intermetallic compounds with cadmium at the electrorefining temperature (500°C) (Martin *et al.*, 1961).

A reduction in the activity coefficient of an element (e.g. Pu) is equivalent to a reduction in the stability of the corresponding chloride. In presence of cadmium, plutonium behaves as its trichloride was about 3.3 kJ (equiv.)$^{-1}$ more stable than uranium trichloride whereas it is 30.1 kJ (equiv.)$^{-1}$more stable in absence of cadmium (Ackerman, 1991, see Table 24.12). This result also implies that the difference between the reduction potential of Pu(III)/Pu(0) and U(III)/U(0) is less negative at the liquid cadmium cathode than at the solid cathode. Sakamura *et al.* (1999) have summarized the reduction potential of actinide and rare earth elements in LiCl–KCl salt when the nature of the cathode change (see Fig. 24.18). These data are compiled from the literature (Martin *et al.*, 1961; Lebedev *et al.*, 1968, 1969; Krumpelt *et al.*, 1974; Ackerman and Johnson, 1993; Kurata *et al.*, 1996; Kinoshita *et al.*, 1999).

The removal of pure uranium on a solid mandrel electrode is possible because the reduction potential of U(III)/U(0) is far from those of the other actinides (see Fig. 24.18). The range of $PuCl_3/UCl_3$ ratios in the electrolyte within which pure uranium can be removed at a solid cathode has been determined by Tomczuk *et al.* (1992). At a liquid cadmium cathode, the reduction potentials of actinides are very similar and such a cathode should be suitable for recovery of all actinides together. However, the potentials are too close to those of rare earth elements to be suitable for an actinide/rare earth separation. The gap between actinides and rare earth elements is increased if bismuth is substituted for cadmium. This change could enable an actinide/RE separation (see Section 24.3.12 m(i)). The principal drawback of bismuth as an electrode material (compared to cadmium) is that it is not distillable and therefore difficult to purify.

(*iii*) *Separation efficiencies in EBR-II demonstration campaign* (2000)

From 1996 to 1999, a hot demonstration was conducted in the Fuel Conditioning Facility at Idaho Falls where 100 spent driver assemblies (410 kg of highly enriched uranium alloyed with ~10 wt% Zr, plus stainless steel cladding) and

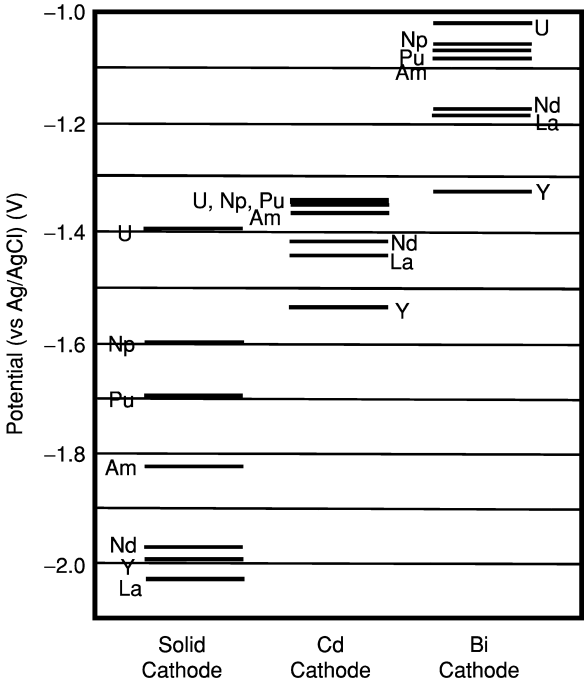

Fig. 24.18 *Reduction potential of actinide and rare earth elements at solid cathode, liquid cadmium cathode, and liquid bismuth cathode in LiCl–KCl eutectic salt at* 500°C, $x_{M\ in\ salt} = x_{M\ in\ Cd} = x_{M\ in\ Bi} = 0.001$. (*Figure created from information in Sakamura* et al., 1999.)

25 spent blanket assemblies (1200 kg of depleted-uranium with stainless steel cladding) from the Experimental Breeder Reactor-II have been treated by the electro metallurgical technology (EMT) developed by Argonne National Laboratory. The metallic fuel was separated into three components: metallic uranium, a metallic waste form from the anode, and a highly radioactive salt mixture. The global process involved the following steps: (i) chopping the fuel elements; (ii) electrorefining; (iii) removing entrained salt (about 20 wt%) from uranium deposits and consolidating dendritic deposits in a cathode processor; (iv) casting into ingots the uranium metal from the cathode; (v) casting into ingots the metal residue from the anode; and (vi) mixing, heating, and pressing the salt electrolyte with zeolite to form a ceramic waste.

The core of the process is the electrorefining step in LiCl–KCl melt at 500°C: the metallic fuel is selectively dissolved at the anode while nearly pure uranium metal is deposited at the cathode, leaving fission products, fuel cladding material, plutonium, and other transuranium elements partially at the anode and partially in the molten salt. In addition, the process neutralizes the reactive components (e.g. sodium-bonds) of the fuel. The distribution of actinides

(U, Np, and Pu) and some fission products in each flux has been calculated from material balance given by Mariani and coworkers (Anonymous, 2000; Mariani *et al.*, 2000) for spent driver fuel treatment (Table 24.13).

Two electrorefiners have been designed and developed. The first, Mark-IV, was used for driver elements and contained a cadmium pool. This pool was not used as cathode but acted as neutron absorber and corrosion-resistant barrier. $CdCl_2$ was added into the electrolyte to oxidize some of the U and other active metals before starting electrotransport. The anode assembly (four baskets) could hold about 8 kg of uranium. An overall anode batch size of 16 kg was achieved by using dual anode assemblies with a single cathode. Steel scrapers were placed near the cathode to control the growth of the uranium dendritic deposit and to allow the removal of the deposit through the cathode port. During the demonstration campaign, Mark-IV was used to treat 12 driver assemblies at an average rate of 24 kg of uranium per month over a 3-month period.

The second electrorefiner, Mark-V, cadmium free, was used for blanket elements (large quantities of depleted uranium). The throughput has been increased by using anode–cathode modules (ACMs) with a capacity of 37 kg per ACM. The overall anode batch size was about 150 kg when four ACMs are used. Each ACM would be able to produce about 87–100 kg of uranium per month. During the demonstration campaign, Mark-V was used to treat 4.3 blanket assemblies at an average rate of 206 kg of U per month over one month.

(m) Oxide–metal processes

A pyrometallurgical partitioning technology for the recovery of uranium and transuranium elements from high-level liquid waste (HLLW) has been developed by the Japanese Central Research Institute of Electric Power Industry (CRIEPI) (Inoue *et al.*, 1991), as described below.

(*i*) *Recovery of actinides from denitrated HLLW*

The process begins with a denitration step in which dehydration by heating converts all the elements in water to insoluble oxides (except for alkali metals which are removed by rinsing with water). The resulted oxides are chlorinated in molten LiCl–KCl eutectic melt. Kurata *et al.* (2000) argue that Cr, Fe, Zr, Mo, and Te are separated during the chlorination step. This is followed by a set of reductive extraction steps.

(*ii*) *Reductive extraction of noble metals*

The purpose of the first reductive extraction is to remove as much of the noble metals as possible while carrying less than 0.1% of each actinide into the reductive extraction product. Extraction step is performed by adding Cd–Li alloy. Laboratory-scale tests show that the amounts of neptunium, plutonium,

Table 24.13 *Actinide and fission product distribution (in %) in EBR-II spent driver fuel treatment.*

	U	*Pu*	*Np*	*Na*	*Ce*	*Cs*	*Ru*	*Sb*	*Tc*
cladding hulls[a]	2.4	11.6	8.5	8.1	10.5	7.8	100	100	99
uranium ingot for interim storage	91.9	0.3	2.1	<0.05	0	0	0	0	0.3
dross from cathode processor	1.3	0	0	0	0	0	0	0	0
remaining in electrorefiner salt[b]	3.6	87.8	88.0	88.4	89.5	91.5	0	0	0
remaining in electrorefiner hold-up, cadmium pool and plenum sections	0.8	0.3	1.4	3.5	0	0.7	0	0	0.7
total output	100	100	100	100	100	100	100	100	100

[a] To be converted to metal waste form.
[b] To be converted to ceramic waste form.

and americium extracted in cadmium alloy is less than 0.1% while a larger fraction of uranium is transferred to the alloy. The zirconium removal from the salt ranges from 50 to 95% (Fusselman *et al.*, 1997).

(*iii*) *Reductive extraction of actinides and rare earth elements*

The purpose of the second reductive extraction is to separate the actinides from alkaline earth elements with a recovery yield of each actinide higher than 99.9%. Uranium, transuranium elements are reduced by adding Cd–Li and transferred into Cd alloy, leaving alkaline earth elements in the salt phase. Laboratory-scale experiments indicate that the removal of U, Np, Pu, and Am from the melt is more than 99.9% but most of the rare earth elements are also reduced and so not separated from the actinides (Fusselman *et al.*, 1997).

(*iv*) *Separation of actinides from rare earth elements*

The cadmium phase coming from the second extraction step serves as an anode in an electrorefining step. The goal is to extract the actinides and rare earths from the cadmium alloy for recycling it and to deposit uranium onto the cathode as solid metal (Fusselman *et al.*, 1997, see also Section 24.3.12k). The salt coming from the electrorefining step is then introduced in a multistage extraction step for separating the transuranium elements (TRUs) from rare earths (REs). Distribution coefficients for actinides and rare earths in LiCl–KCl/Li–Cd system have been measured by numerous workers (Sakata *et al.*, 1991; Koyama *et al.*, 1992; Ackerman and Settle, 1993; Hijikata *et al.*, 1993; Sakamura *et al.*, 1994). The LiCl–KCl/Li–Bi system has been investigated by Kurata *et al.* (1995).

Liquid bismuth is used instead of cadmium because the LiCl–KCl/Li–Bi system provides better TRU/RE separation factors than the LiCl–KCl/Li–Cd system (see Table 24.14). Separation factors obtained in laboratory-scale tests performed as described in Fig. 24.19 at 500°C are constant at each extraction stage and are in good agreement with those given in the literature, except for uranium and zirconium whose separation factors vary and are higher than expected. This result could be explained by transfer of a part of uranium and zirconium to the salt phase as soluble oxygenated species due to traces of oxygen in the salt (Uozumi *et al.*, 2001).

(*v*) *Actinide electrorecovery*

Contrary to extraction in the LiCl–KCl/Cd system wherein the actinides can be recovered from the final metallic product (An–Cd alloy) by cadmium distillation, in the LiCl–KCl/Bi system bismuth is not easily distillable, as was noted above. It is therefore necessary to carry out a complementary oxidation–reduction step to separate actinides from bismuth and to recover them as metal.

Table 24.14 *Some separation factors of TRUs and trivalent REs relative to uranium* (*Kurata* et al., 1995).

Element	*LiCl–KCl/Bi at* 773 K, *Kurata* et al. (1995)	*LiCl–KCl/Cd at* 773 K, *Ackerman and Settle* (1993)	*LiCl–KCl/Cd at* 773 K, *Koyama* et al. (1992)	*LiCl–KCl/Cd at* 773 K, *Hijikata* et al. (1993)	*LiCl–KCl/Cd at* 723 K, *Sakamura* et al. (1994)
U	1	–	1	1	1
Np	1.1×10^1	–	2.2	2.1	2.9
Pu	1.3×10^1 [a]	1.9	1.9	–	3.6
Am	–	2.9	3.1	–	1.1[b]
Cm	–	–	3.5	–	–
Pr	9.22×10^2	4.3×10^1	–	–	–
Nd	9.33×10^2	4.4×10^1	3.9×10^1	4.9×10^1	6.4×10^1
Ce	8.34×10^2	4.9×10^1	–	5.2×10^1	–
La	2.53×10^3	1.3×10^2	–	1.26×10^2	–

[a] Estimated from γ_{Pu} in Bi.
[b] At $\log D_U = 0$.

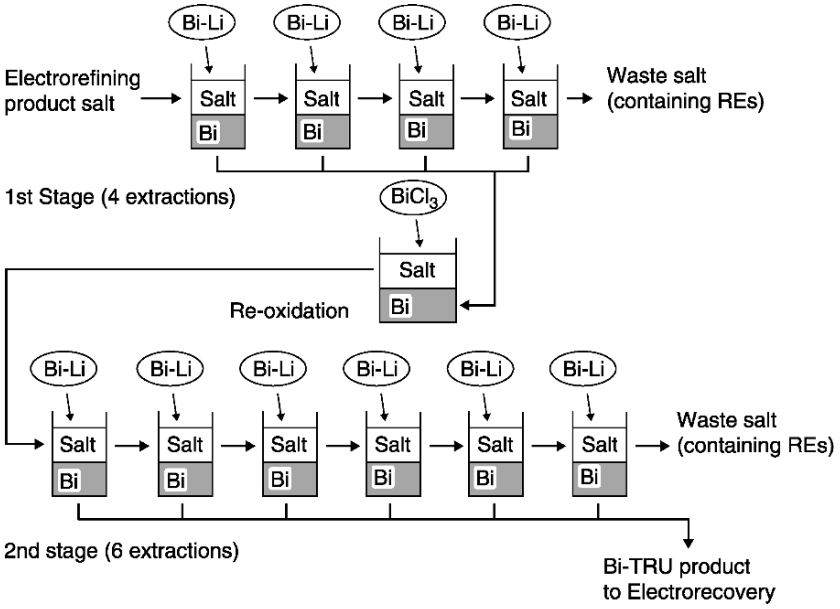

Fig. 24.19 *Schematic flow sheet tested for TRUs/REs separation.* (*Figure created from information in Uozumi* et al., 2001).

An electrolytic recovery in which actinides are stripped from bismuth used as anode and collected on a cathode has been proposed (Uozumi *et al.*, 2001). All the actinides are well stripped (97% for U and more than 99% for TRUs) from Bi. During the electrodeposition, 91–93% of each actinide – U, Np, and Pu – whose lowest stable oxidation state is 3+, are collected on a tantalum cathode. Americium exhibits a more complex behavior because of its two possible oxidation states (3+ and 2+). The recovery of americium is limited by the reproportionation reaction $2Am(III) + Am(0) \rightleftharpoons 3Am(II)$ (see Section 24.3.12b) and only 25% of the total is recovered. Reuse of the americium-bearing salt in the previous step has been proposed to avoid sending it to waste.

Laboratory-scale demonstration tests show that, by combining electrorefining and reductive extraction as described above, less than 0.1% of uranium and individual TRUs are transferred to waste salt. The weight ratio between TRUs and REs in the final product is 2.01 (larger than 1.0, the minimal value required ratio for transmutation strategies).

(n) Recovery of actinides from LWR fuels

Argonne National Laboratory has developed (and is still developing) oxide pyroprocessing compatible with the pyrochemical processes for metal fuels. One purpose is to recover actinides from spent light water reactor fuels to

introduce them into an integral fast reactor fuel cycle. Basically the process for oxide fuel involves the reduction of the oxides to metallic form, followed by either: (i) a combination of the salt transport and halide slagging for separation of fission products and the separation of the uranium from the transuranic elements (see Section 24.12k, (Pierce *et al.*, 1993; Johnson *et al.*, 1994) or (ii) the standard electrorefining process (see Section 24.3.12l) for the same purpose (Pierce, 1991; Laidler, 1994). Typically, the reducing agent is calcium or lithium.

(*i*) *Calcium reduction*

In the 1960s, the production of plutonium metal by direct calcium reduction of plutonium dioxide (direct oxide reduction or DOR process) was investigated. These efforts were reviewed by Moser and Navratil (1983). First attempts showed that molten salts were necessary for dissolving the CaO produced and for allowing plutonium metal consolidation. The first used salt was $CaCl_2$ at 800°C but the binary melt $CaCl_2$–CaF_2 with lower working temperature is efficient for minimizing corrosion and product contamination. Calcium reduction has been adapted for LWR fuel reduction when salt transport is used. The oxide fuel is reduced by a Ca–Mg–Cu alloy in contact with $CaCl_2$–CaF_2. Calcium plays the role of reducing agent while Mg–Cu alloy is the donor alloy for salt transport as described in Section 24.3.12k. Most of the reduced uranium and noble metals are insoluble in Mg–Cu alloy and thus precipitate while TRUs and trivalent REs are solubilized in the alloy. Alkali metals, alkaline earth elements, Sm, Eu, Se, Te, Br, and I remain in the salt phase (Pierce *et al.*, 1993; Johnson *et al.*, 1994).

Reduction experiments at laboratory scale have been carried out on high-fired UO_2, powders of PuO_2 and NpO_2, several representative fission product oxides, and simulated fuel pellets with non-radioactive fission products. Reduction yields obtained for the actinides are more than 99%. Neptunium coprecipitates with uranium (Pierce *et al.*, 1993; Johnson *et al.*, 1994). The salt is electrochemically treated for CaO decomposition and calcium regeneration. Oxygen is liberated at the carbon anode as CO and CO_2 and the calcium that is produced is dissolved in a liquid cathode of recycled Mg–Cu alloy. The feasibility of the electrochemical regeneration of the spent salt has been established at the laboratory scale. Current efficiency of 70% is reached when Mg–Cu alloy is used as cathode, but the current density of about 170 mA cm^{-2} is low for a full-scale process (Pierce *et al.*, 1993).

(*ii*) *Lithium reduction*

Reduction by lithium in chloride melts has been proposed when the objective of the process is electrorefining in LiCl–KCl melt (Johnson *et al.*, 1994; Laidler, 1994). In such reduction no metallic solvent is required and the temperature is

lower so that common construction materials can be used. The reduction produces lithium oxide in the salt. Lithium is a less effective reducing agent than calcium, thus the progress of the reduction depends greatly on the activity of Li_2O (i.e. its concentration in the salt) (Johnson *et al*., 1994). Moreover, it is necessary to maintain Li_2O dissolved in salt to avoid physical interactions between the reduced oxides and Li_2O. Reductions on UO_2 in various chloride melts between 500 and 750°C showed that reductions were complete, but Li_2O solubility was exceeded when low-temperature melts were used (Johnson *et al*., 1994). Pure LiCl, whose the melting point is 602°C, has been chosen as the medium for the reduction and Li_2O solubility has been measured in the range 600–750°C (Johnson *et al*., 1994; Usami *et al*., 2002). Johnson *et al*. (1994) gives 8.7 wt% at 650°C and 11.9 wt% at 750°C.

Experiments on mock fuel with TRU oxides in LiCl at 650, 700, and 750°C have shown poor reduction efficiencies for TRUs. The reduction efficiency decreases with increasing temperature. For instance, the amount of plutonium remaining in salt varies from 0.004 to 37.7% in the range 500–750°C while the americium remaining in the salt varies from 0.06 to 29.6%. To prevent this, LiCl–KCl (60–40 wt%) melt has been proposed as the medium for reduction at lower temperature (500°C) (Johnson *et al*., 1994). It has been claimed that PuO_2 is completely reduced by lithium at 650°C in LiCl with no intermediate product formation, even if Li_2O concentration is just below the solubility limit (Usami *et al*., 2002). In reduction tests performed at 500°C, alkaline earth elements and europium are in the salt presumably as chlorides while the other REs probably remain as precipitated sesquioxides in the salt phase (Pierce *et al.*, 1993). Laboratory-scale (50 to 100 g of simulated fuel) and engineering-scale (3.7 to 5.2 kg of simulated fuel) experiments are currently performed to determine and to master the parameters for process scale-up, taking into account the electrorefiners developed at Argonne National Laboratory (Karell *et al*., 2001). As was the case in calcium reduction, the spent reduction salt is decomposed electrochemically to recover the salt and the lithium metal. Laboratory-scale experiments showed that platinum is a suitable oxygen-evolving electrode that can be operated at high current densities (2 to 3 A cm^{-2}). Current efficiencies are reported at 50–80% (Karell *et al*., 2001).

(o) Nitride–nitride process

In the early 1990s, the Japan Atomic Energy Research Institute (JAERI) proposed a double strata fuel cycle concept for partitioning–transmutation strategies in which the minor actinides from the commercial fuel cycle go into a second-stratum transmutation ('actinide-burner') cycle. Dense fuel is preferable in the second-stratum and nitride fuel is regarded as the reference fuel (metallic fuel remaining an alternative) by JAERI (Mukaiyama *et al*., 1995; Ogawa *et al*., 1995). Having a high electrical conductivity, the molten salt

electrolytic process developed for metallic fuel (see Section 24.3.12l) can be applicable to mononitride fuel (Arai *et al.*, 1995).

(*i*) *Dissolution step*

The actinide nitrides are anodically dissolved in molten LiCl–KCl eutectic at 773 K as follows:

$$UN + 3Cl^- \rightleftarrows 3e^- + UCl_3 + \tfrac{1}{2}N_2 \qquad (24.45)$$

Actinides and most of fission products (except for zirconium) behave almost the same as in metallic fuel (Arai *et al.*, 1995; Kobayashi *et al.*, 1999). According to the above chemical reaction, nitrogen escapes from salt bath as N_2 gas so that such dissolution should facilitate the recycling of ^{15}N-enriched nitrogen, which would have to be used in nitride fuel to minimize the generation of ^{14}C (Ogawa *et al.*, 1995). The release of nitrogen has been studied during NdN dissolution by chemical oxidation (with $CdCl_2$). About 90% of the nitrogen is evolved as N_2 gas (Arai *et al.*, 1999; Kobayashi *et al.*, 1999).

The feasibility of the anodic dissolution has been demonstrated at the laboratory scale for UN (Kobayashi *et al.*, 1995), for NpN and PuN (Arai *et al.*, 1999; Shirai *et al.*, 2000). During the dissolution, a by-product (UNCl) can be formed at the anode. The stability diagram of the U–N–Cl system has been determined. This by-product can be decomposed by heating to high temperatures (Ogawa *et al.*, 1997). The chemistry of AnN in molten LiCl–KCl is still in its infancy and several unknowns remain: (i) the effect of partial pressure of released N_2 on the redox potential of AnN/An(III); (ii) the formation of AnNCl, and (iii) the behavior of transplutonium elements.

(*ii*) *Actinide nitride recovery*

Fission products and actinides are dissolved in the bath as chlorides. The actinides can be recovered as nitrides by either direct or indirect methods (Ogawa *et al.*, 1997):

(i) the actinide chlorides are directly converted to actinide nitrides in molten LiCl–KCl by using Li_3N (Lithium Nitride Extraction of actinides (LINEX process),
(ii) the actinide chlorides are first electro-reduced as actinide metals on a liquid cadmium cathode and then they are converted to nitrides in the liquid cadmium (with either N_2 gas or Li_3N).

The LINEX process is based on the comparable stability of mononitrides of actinides and lanthanides. As the Gibbs energies of formation of the lanthanide trichlorides are more negative than those of the actinide trichlorides

(see Table 24.12), the actinide nitrides should be preferentially formed and the following equilibrium should be displaced to the right:

$$AnCl_3 + Li_3N \rightleftarrows AnN + 3LiCl \tag{24.46}$$

In LiCl–KCl eutectic, the equilibrium constant must be expressed by taking into account the chemical activities of the various species. First attempts of nitridation by Li_3N have been performed on a $LiCl–UCl_3–NdCl_3$ mixture where preferential nitridation of UCl_3 has been observed (Ogawa *et al.*, 1997).

Nitridation in liquid cadmium has been tried on 2 wt%U–1 wt%Gd–1 wt% Ce–Cd mixtures with N_2 gas over the temperature range of 773–873 K (Akabori *et al.*, 1997). Uranium was preferentially nitrided to form U_2N_3, while almost all of Ce remained in the liquid Cd phase as $CeCd_{11}$. Gadolinium behavior is more complex and a small portion of Gd is precipitated (nitride or metallic forms). Nitridation in liquid cadmium appears efficient for light lanthanides (La–Nd).

24.4 APPLICATIONS OF SEPARATIONS IN ACTINIDE SCIENCE AND TECHNOLOGY

24.4.1 A question of scale and more – analytical separations and hydrometallurgical processing

Previous sections of this chapter have dealt with actinide separations emphasizing the basics of actinide solution chemistry in aqueous/organic media and molten salt/metallic phases, historical background, and emerging techniques that may figure prominently in future developments of actinide separations options. In this section, the focus will be on applications of the most extensively developed methods for analysis and industrial-scale processes.

(a) Separation techniques for actinide speciation in the environment

Development and validation of thermodynamic models for actinide behavior in nature require accurate information on oxidation state distribution of the actinides in natural samples. A major difficulty in the determination of (for example) plutonium oxidation states in groundwater samples is the relative ease of interconversion among the oxidation states. Because of the typically very low concentrations involved (generally below 10^{-8} M and often far less), conventional techniques (e.g. spectrophotometry) are not useful, except for the unique case of curium, which can be determined at extremely low concentrations through its fluorescence emissions (discussed in Chapter 9). For most laboratories, separation chemistry combined with radiometric or mass spectrometric analysis are the most appropriate techniques for such speciation at these

low concentrations. The key challenge is to determine the oxidation state using procedures that do not alter this oxidation state during the measurement. Time of analysis and efficient separation procedures are clearly the most important aspect of separation for this purpose. Several complementary separation methods can (and should) be applied to insure accuracy. Some examples of actinide oxidation state speciation methods based on sorption or solvent extraction are:

- LaF_3 coprecipitation in which a lanthanide fluoride carries An(III) and An(IV), leaving An(V) or An(VI) in the solution phase, a technique that traces its roots to the dawn of discovery of transuranium actinides. Care must be exercised during the application of this technique, as excess fluoride can promote reduction during the precipitation process (Choppin and Nash, 1996). Samples must be acidified as well, thus risking the chance of oxidation state change during analysis.
- Silica gel (SiO_2) selectively sorbs An(IV) and An(VI) from basic media leaving An(V) in solution (Inoue and Tochiyama, 1977).
- $CaCO_3$ selective sorbs An(V) and An(IV), leaving An(VI) in solution as the tris carbonato complex (Kobashi *et al.*, 1988).
- Thenoyltrifluoroacetone (TTA, 0.5 M in xylene) selectively extracts An(IV) from 0.25 to 1.0 M acid. The same extractant can then be used to extract An (VI) from acetate buffer at pH 4 (Bertrand and Choppin, 1982). Photolysis of this solution can be used to produce comparatively pure samples of Pu(V) in neutral solutions (Saito *et al.*, 1985).
- The β-diketone dibenzoylmethane (DBM, 0.2 M in xylene) selectively extracts An(IV) at pH<2.5, An(VI) at pH 5, An(III) at pH 7. An(V) is not extracted (Saito and Choppin, 1983).

Filtration of the sample should always be conducted prior to conducting the analysis to determine whether some portion of the material is being transported as colloidal material. Most of the analytical procedures require that the ambient conditions of the solution be altered. It has been suggested that acidification of the sample may be undesirable, as redox-active metals like Pu can undergo oxidation state change with a change in pH. However, there are situations under which acidification might be desirable, for example when appreciable concentration of organic complexing agents are present. In these cases, acidification can reduce the stability of the actinide complex, releasing the cation, and improving the accuracy of the analysis. The guiding principle in conducting such analyses is to never rely on a single observation by one technique to establish actinide oxidation state speciation in natural water samples. Multiple methods should be applied in tandem and some of the methods applied should include alteration of the solution conditions.

As discussed more extensively in Chapter 30, quantitative analysis of actinide concentrations in environmental or bioassay samples by standard methods requires extensive treatment to promote the release of the radionuclides from

the complex matrix. For such quantitative analysis, preserving the ambient condition of the sample is a less important consideration than assuring complete recovery of the sample and applying internal standards to trace yields of the separation processes. Analyses of such samples have required up to 24 h processing time. Standard ion exchange and solvent extraction have been used for these analyses. The recent development of more selective extraction chromatographic materials and the development of procedures for their use have greatly shortened the time required for these analyses (Horwitz *et al*., 1995). These extraction chromatographic materials are based on well-known solvent extraction methods, as follows:

- TRU® resin for selective sorption of An(III), An(IV), An(VI), Ln(III). The extractant is 0.75 M CMPO in TBP.
- TEVA® resin for sorption of An(IV). The extractant is $(C_{10}H_{21})_2(C_8H_{17})(CH_3)N^+$ (Aliquat 336, neat i.e. without diluent present).
- U/Teva® resin for sorption of U(VI), An(VI). The extractant is $(C_5H_{11}O)_2(C_5H_{11})P{=}O$ DP[PP], neat.

An example of an element-specific separation scheme of actinides using TRU® resin is as follows:

- load sample from 2 M HNO_3, rinse off non-TRUs with 1.0 M HNO_3 then 9 M HCl,
- elute Am^{3+} with 4 M HCl,
- elute Pu^{4+} with 4 M HCl/0.1 M hydroquinone,
- elute Th^{4+} with 2 M HCl,
- elute Np^{4+} with 1 M HCl/0.03 M oxalate,
- elute UO_2^{2+} with 0.1 M $NH_4HC_2O_4$,
- analyze fractions radiometrically.

Analytical methods of this sort are seeing increasing application for bioassay. In addition, instrumental analysis methods suitable for quantitation of lanthanides (Nash and Jensen, 2000) would be suitable for application to samples containing actinides at higher concentrations, but there are few examples of these techniques having been applied for actinide analysis.

24.4.2 Hydrometallurgy – industrial scale separations of actinides

The production of electricity by nuclear fission is, at present, nearly 366 gigawatts electric (GW_e), generated from 438 operating nuclear reactors. The spent fuel from power production reactors contains moderate amounts of transuranium (TRU) actinides and fission products in addition to the still slightly enriched uranium. As we noted previously, there are three choices for the management of the spent fuel: (a) recycle to recover valuable components; (b) direct geologic disposal as waste, or (c) long-term monitoring after stabilization for surface or near-surface storage. At present, both byproduct recycle and 'short-term'

monitoring are being practiced worldwide. After more than 30 years of continuous investigation, no repositories have been fully licensed to receive commercial reactor fuels. Yet safe disposal of either spent fuel or the high-level waste (HLW) generated during reprocessing of spent fuel is a matter of great environmental concern (Baetsle, 1992). The question of waste disposal has become the largest single issue standing in the way of further development of this otherwise environmentally friendly technology. Furthermore, a recent analysis projecting how fission-based nuclear power could favorably impact greenhouse gas emissions emphasizes the need for breeding additional fuel to satisfy a projected long-term shortage (Hoffert *et al.*, 2002). Satisfying this demand can only be accomplished by closing the loop of the fuel cycle by reprocessing spent fuel.

Though the pyrometallurgical processes described in Section 24.3.12 may ultimately prove the most efficient method for actinide recycle and transmutation, the nearly 60 years of industrial-scale experience that has been accumulated worldwide on aqueous-based processing of nuclear fuels clearly qualify these methods as the best approach to actinide recycle during at least the next 20 years. In this section, the ongoing research seeking new approaches to hydrometallurgical processing of nuclear fuels will be outlined.

(a) Statement of the problem

At present, half of the world's spent nuclear fuel is produced in a 'once-through cycle'. The other half is reprocessed to recycle uranium and plutonium. A deep geological repository is still considered the best option for the sequestration of either spent fuel or high-level waste by-products of reprocessing from the environment. Without actinide partitioning and transmutation, radioactivity levels in a repository will remain above natural backgrounds for several hundred thousand to several million years. How to accomplish long-term surveillance of a geologic repository to make reliable predictions on the projected lifetime of the engineered and natural barriers beyond a period of 10000 years (which time exceeds, that of all human history) and, above all, public acceptance of such repositories are key questions that impact the future of nuclear power.

The option of partitioning actinides from HLW represents an opportunity to reduce the uncertainties associated with geologic disposal. Partitioning followed by geologic disposal of the transplutonium actinides and long-lived fission products can reduce the volume of materials requiring this most expensive form of sequestration, allowing less expensive near-surface burial of shorter-lived fission products. Homogeneous feed streams for waste form production (for example, containing only actinides) would enable the use of waste forms specifically designed to accommodate the class of waste being sequestered (as opposed to demanding that one waste form be compatible with the largest part of the periodic table of species present in wastes). The long-term stability of such tailored waste forms would be easier to assure based on analogies with natural systems.

Table 24.15 *Long-lived actinides in HLW solution and their half-lives.*

Nuclide	^{237}Np	^{238}Pu	^{239}Pu	^{240}Pu	^{241}Am	^{243}Am	^{246}Cm
$t_{½}$ (yr)	2.144×10^6	87.74	24 411	8550	432.2	7370	4760

Exercise of the partitioning and transmutation (P&T) option seeks to convert all long-lived nuclides into short-lived radioactive (or stable) species. Successful application of this approach to radioactive waste management could substantially reduce the requirement for geologic repository capacity. The trade-offs are that a P&T approach to radioactive waste management could increase opportunities for Pu proliferation and will increase the *volumes* of some categories of high-level, intermediate-level, and low-level wastes. However, even if the cost of P&T exceeds the gain in energy from actinide incineration, the added safety margin for the repository could justify the expense. The important actinides from a waste management perspective are given in Table 24.15.

It should be noted that there are different degrees of difficulty associated with different processing options. Spent fuel freshly discharged from the reactor (or allowed only a short cool-down interval) is the most demanding because of the radiation, thermal heat, and diversity of materials to be separated. Long-term storage of these materials prior to reprocessing reduces these problems, as heat and the most intense radiation decline at a moderate rate. In plants designed to recycle purified materials that have not been irradiated (for example, decommissioned weapons), the radiation effects are significantly diminished and heat loads are minimal thus the processes are less damaging to materials and reagents. The aqueous processing of waste materials may approach either situation depending on the source. For tank wastes like those found in the DOE complex in the U.S., their long-term storage implies that most of the fission product radioactivity has decayed and heat loads are significantly reduced (though not eliminated). But for such materials, chemical diversity remains and challenging solid–liquid separations are needed prior to any processing.

24.4.3 Actinide production processes with considerable industrial experience

There are several coprecipitation and solvent extraction procedures that have been utilized to separate and recover actinides from different solutions including the dissolver solutions (resulting from dissolution of the spent fuel). Among the coprecipitation reagents, lanthanum fluoride and bismuth phosphate were widely used in the earlier times. As has been noted previously, bismuth phosphate has been used for plant-scale separation of Pu from dissolver solutions. Among the solvent extraction processes, REDOX, BUTEX, TLA, and PUREX processes have been demonstrated to the production scale, mainly for the separation of uranium and plutonium. A brief description of these processes,

and why they cannot be used for the recovery of minor actinides from high level waste or TRU waste solutions will be discussed below.

(a) Bismuth phosphate process

Bismuth phosphate is a highly specific carrier for Pu in the trivalent and tetravalent oxidation states. Pu(IV) is more efficiently carried on $BiPO_4$ than Pu(III). For separating Pu from dissolver solutions, free of UO_2^{2+} and with high D_f from the fission products, $BiPO_4$ precipitation from moderate HNO_3 solutions containing sulfuric acid can be used. Under such conditions, UO_2^{2+} is sufficiently complexed by sulfate ion to prevent precipitation of uranyl phosphate (Perlman, 1946; Lawroski, 1955; Thompson and Seaborg, 1956; Hill and Cooper, 1958; Stoller and Richards, 1961; Wick, 1967; Cleveland, 1970; Schulz and Benedict, 1972). Pu can be redissolved in ~10 M HNO_3. A few cycles of $BiPO_4$ precipitation and dissolution followed by a final LaF_3 precipitation considerably increases the concentration of Pu in the solution and final recovery can be accomplished by plutonium peroxide and then oxalate precipitations.

For large-scale isolation of plutonium at the Hanford site, the $BiPO_4$ process was employed by adding sodium nitrite in the dissolver solution to adjust the valency of plutonium to the 4+ state, while neptunium remains in the 5+ and uranium in the 6+ state. Plutonium is co-precipitated with $BiPO_4$, leaving behind all the actinides and fission products. $BiPO_4$ product precipitate is dissolved in ~10 M nitric acid and plutonium oxidized to 6+ state by strong oxidizing agents like $K_2Cr_2O_7$, $KMnO_4$, or sodium bismuthate. PuO_2^{2+} remains in the filtrate. It can then be reduced to Pu(IV) with Fe^{2+}. This cycle can be repeated several times. The flow sheet developed at Hanford gave an overall D_f of 10^7. This process was employed during the Manhattan Project because it was the only separation technology reliable enough to be scaled up quickly to meet wartime production demands. The inability to operate the process continuously (separations are made batch-wise) and its rejection of the still-useful enriched uranium caused the discontinuation of its application in favor of the solvent extraction processes, which overcame both of these limitations.

(b) REDOX process

This process, developed at the Argonne National Laboratory, utilizes methyl (isobutyl)ketone (hexone) as the extractant and dissolver solution as the aqueous phase. Plutonium is oxidized to the hexavalent state with $Na_2Cr_2O_7$. High nitrate salt concentrations are generated by addition of $Al(NO_3)_3$ under acid-deficient conditions. PuO_2^{2+} and UO_2^{2+} are extracted into the organic phase, leaving behind most of the fission products, corrosion products, and trivalent actinides in the raffinate (Anonymous, 1951; Merrill and Stevenson, 1955; Stoller and Richards, 1961). Uranium and plutonium are stripped from the hexone phase by water containing small amounts of $Na_2Cr_2O_7$ (to maintain

oxidizing conditions). This cycle is repeated two or three times to get a high D_f from the fission products. Finally, the feed solution containing uranium, plutonium, $Al(NO_3)_3$, acid, and $Na_2Cr_2O_7$ in the required quantity (for feed adjustment and keeping metal ions as PuO_2^{2+} and UO_2^{2+}) are contacted with the hexone solution. From the loaded organic phase, plutonium is stripped by an aqueous solution of $Al(NO_3)_3$ and ferrous sulfamate, which reduces Pu(VI) to Pu(III). Uranium is subsequently stripped with water. To obtain uranium and plutonium in high purity and with high D_f from the fission products, the entire cycle is repeated several times. The ability to run this process as a continuous operation and to recover uranium marked a major improvement for production efficiency over the $BiPO_4$ process. However, the process generated enormous volumes of moderately difficult wastes containing mixed fission products and minor actinides, and demanded procedures to accommodate the toxicity and flammability of the extractant. At Hanford, the process-generated aqueous wastes were made basic and stored in underground tanks. The Al_2O_3 that was generated as a by-product of this process complicates current efforts to remediate tank wastes.

(c) BUTEX process

This process, developed in the UK, utilizes the triether dibutylcarbitol, 'Butex' (C_4H_9O–$(C_2H_4O)_2$–C_4H_9; Structure y) as the main extracting agent. The primary advantage of this process as compared with REDOX is that it is possible to extract uranium and plutonium from HNO_3 solutions without the addition of a salting out agent (Howells *et al.*, 1958). The extraction order for actinides and a few fission products is $UO_2^{2+} > PuO_2^{2+} > Pu^{4+} > U^{4+} > Zr^{4+} > Ce^{4+} > Ru(NO)^{3+}$. Like the REDOX and $BiPO_4$ processes, BUTEX rejected neptunium and the transplutonium actinides to the waste stream. Because of several limitations including the high viscosity and density of the extractant, and the formation of crystalline uranyl nitrate–Butex compounds, this process was discontinued as more efficient processes emerged.

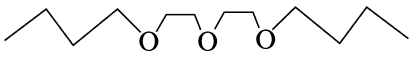

Structure y

(d) TLA process

Trilaurylamine (TLA, Structure z) is a highly specific extractant for Pu(IV) while the extration of U(VI) is very low. Thus the TLA process was suggested for a second-stage plutonium recovery process (Auchapt *et al.*, 1968). A solution of 7–20% TLA in diethylbenzene has been used to extract Pu from 1.25–3 M HNO_3. Plutonium was stripped with 3–4 M acetic acid (Coleman, 1964). From a solution formed as zircaloy-clad fuel element is dissolved in nitric acid, plutonium extraction has been shown to be highly effective by using 10% TLA in

t-butylbenzene (Haeffner *et al.*, 1965; Hultgren, 1967). With certain modifications, the TLA process has generated a $D_{f\,Pu}$ of 1.75×10^7 from uranium and of 8×10^7 from β and γ activities.

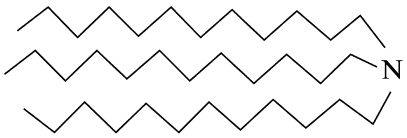

Structure z

(e) PUREX process

The PUREX (originally Plutonium Uranium Extraction but also found in the literature as Plutonium Uranium Recovery by Extraction or Plutonium Uranium Reduction Extraction) process used TBP dissolved in an inert aliphatic diluent as the extractant for uranium and plutonium from dissolver solution (Anonymous, 1951, 1955; McKay, 1956; Cooper and Walling, 1958; Mathieson and Nicholson, 1968; Koch *et al.*, 1977). Normally a solution of 20–30% TBP in *n*-dodecane, odorless kerosene, or another normal (or branched) paraffinic hydrocarbon (or mixture of hydrocarbons) is used as the diluent. This process was first developed at the Oak Ridge National Laboratory (Flanary, 1954). It has been employed at the industrial scale for nearly 50 years and remains the cornerstone of nuclear fuel reprocessing for both defense and power reactor fuels around the world. One of the major advantages of this process is that it selectively extracts $Pu(NO_3)_4$ and $UO_2(NO_3)_2$ from dissolved spent nuclear fuels from solutions of moderate nitric acid concentrations (2–3 M), requires no addition of any salts, and is plagued by few co-extracted impurities.

Both Pu(IV) and Pu(VI) are readily extracted into the organic phase, whereas Pu(III) extraction is comparable to that of americium (see Fig. 24.6). In the hexavalent state, the order of distribution ratio is U(VI) > Np(VI) > Pu(VI). Neptunium, normally maintained in the pentavalent oxidation state in PUREX processing, is extracted even less than the trivalent actinides. Neptunium redox chemistry in nitric acid solutions generally causes some more extractable neptunium species to be present, hence there is often 'leakage' of neptunium into undesirable process streams in a PUREX plant (Drake, 1990), as will be discussed further in Section 24.4.4f. As the detailed description of the PUREX flow sheet is given elsewhere, only the practical steps involved with this process are listed here:

(1) Feed preparation – fuel is decladded and dissolved, nitric acid concentration is adjusted to 2–3 M and plutonium valency is adjusted to 4+, most commonly with H_2O_2 or HNO_2.
(2) Co-decontamination cycle – U(VI) and Pu(IV) are co-extracted into the TBP phase leaving behind the fission products, trivalent actinides, and Np(V) in the aqueous raffinate.

(3) Partition cycle – Pu(IV) is reduced to Pu(III) using ferrous sulfamate, U(IV), or hydroxylamine, resulting in Pu(III) being stripped into the aqueous phase while uranium remains in the TBP phase; U(VI) is subsequently stripped with very dilute nitric acid solution; final cleanup of remaining traces of U(VI) occurs during extractant reconditioning with Na_2CO_3.
(4) A second uranium and plutonium extraction cycle follows step (3) for both the aqueous phases separately after feed adjustments to improve recovery.
(5) Final purification of plutonium is done in modern PUREX plants using additional TBP solvent extraction steps. Historically, pure plutonium has been prepared using anion exchange chromatography, as follows: the feed is adjusted to 7.1 M HNO_3 and the plutonium anionic species $Pu(NO_3)_6^{2-}$ is adsorbed strongly onto the column; remaining contaminants like U, Zr–Nb, Ru, and Fe are not adsorbed; after adequate washings, plutonium is eluted from the anion exchange resin with 0.5 M nitric acid.

The improved PUREX (IMPUREX) process operated at temperatures higher than 50°C suggests several advantages such as prevention of plutonium accumulation in the extractors, improvement in fission products and neptunium separations, etc. (Schmeider and Petrich, 1989) and is worth considering.

All of the processes mentioned above, particularly PUREX, have been operated on a production scale. However, none of these processes can be used to separate and recover trivalent actinides or Np(V) neither from HLW solutions nor from various TRU containing waste solutions, which are often moderately concentrated nitric acid solutions (2–4 M). TBP can be employed to extract trivalent actinides (as was indicated in the work of Sekine, 1965, discussed in Section 24.3.4), but only with the reduction of acidity of the aqueous stream and addition of salting out agents. Diluting the HLW solutions, decreasing the acidity by denitration, or partial neutralization to obtain dilute acid salt solutions will increase the volumes of by-product wastes and increase the difficulty of their disposal. If the so-called minor actinides are to be transmuted, there clearly is a need for developing full-fledged processes for recovery of these minor actinides from HLW and TRU wastes.

(f) THOREX process

In the 1960s and 1970s, great interest developed in the thorium fuel cycle as a supplement to limited uranium reserves. The slightly harder neutron spectrum of heavy water and gas-cooled/graphite-moderated reactors make such reactors reasonable centerpieces of a uranium–thorium breeder reactor cycle, though it has been shown that thorium can be used practically in any type of existing reactor. For example, Stewart *et al.* (1971) have described a thorium–uranium breeder fuel cycle designed around the now-decommissioned Fort St. Vrain gas-cooled reactor. Molten salt reactors have a similar favorable neutron spectrum

for this fuel cycle. These initiatives have been virtually brought to a halt for various reasons, except in India, where research has continued with its exploration of the thorium–uranium fuel cycle (Lung and Gremm, 1998).

The initial ^{233}U to operate this fuel cycle must be produced in a ^{235}U-fueled reactor, or with an initial ^{235}U or ^{239}Pu charge surrounded by a ^{232}Th breeding blanket. Two fundamental limitations of the U–Th fuel cycle are the creation of ^{228}Th ($t_{1/2} = 1.912$ years, 5.42 MeV α) and ^{232}U ($t_{1/2} = 68.9$ years, 5.32 MeV α) and their daughters as by-products, and the creation of ^{233}Pa ($t_{1/2} = 27$ days, 0.3 MeV γ, 0.6 MeV β^-) as parent of the desired ^{233}U product. The build-up of isotopic contaminants during successive irradiations of recycled ^{233}U–Th fuels can greatly affect the handling procedures used in fuel-element refabrication. Reactor-fuel elements containing ^{233}U may be fabricated semi-remotely provided that complete fabrication can be accomplished in 2 weeks or less. If ^{233}U contains more than 200 ppm ^{232}U, or if refabrication of fuel elements requires longer than 2 weeks, a shielded refabrication facility is necessary. Thorium fuels must be allowed to decay for 12 years if unshielded refabrication procedures are to be used (Arnold, 1962; Schlosser and Behrens, 1967). The fuel cycle has been advocated as non-proliferating on the basis of the presence of ^{232}U isotope and the energetic γ activity of its ^{208}Tl and ^{212}Bi daughters (Ragheb and Maynard, 1980). Another significant advantage of this fuel cycle is the reduced production of long-lived transuranium actinides.

Several approaches to fuel dissolution have been developed for this fuel cycle dependent in part on the reactor type used to breed ^{233}U. The oxide fuel and the breeding blanket used for gas-cooled reactor fuels are imbedded in a graphite matrix. In this cycle, the spent fuel is crushed and the carbon typically burned out prior to fuel reprocessing.

Stainless steel cladding from water-moderated reactors is easily dissolved with 4–6 M H_2SO_4 (Sulfex process) or 5 M HNO_3–2M HCl (Darex process) in low-carbon nickel alloy or titanium equipment, respectively. Uranium losses to the decladding solutions are readily recovered from the Darex decladding solutions in the acid THOREX extraction process. The ThO_2–UO_2 core can be dissolved in 13 M HNO_3–0.04 M NaF–0.1 M $Al(NO_3)_3$. Uranium and thorium can be recovered from graphite-based fuels by: (a) disintegration and leaching with 90% HNO_3; (b) grinding and leaching with 70% HNO_3; or (c) combustion followed by dissolution in fluoride-catalyzed HNO_3 (Blanco *et al.*, 1962). Irradiated Al-clad Th metal slugs are dissolved in HNO_3 containing Hg^{2+} and F^- as catalysts (Bruce, 1957).

The separation of thorium from uranium is most typically accomplished using the same basic chemistry that drives the PUREX process, i.e. extraction of Th(IV) and U(VI) from nitric acid solutions into TBP solutions with aliphatic hydrocarbon diluents. The use of an acid-deficient feed (0.15 M) induces high decontamination while injection of HNO_3 at the fourth extraction stage provides high salting strength and insures quantitative uranium and thorium extraction. Because thorium is extracted by TBP less effectively than Pu(IV) or

U(VI), the introduction of $Al(NO_3)_3$ (Oliver, 1958) or $Be(NO_3)_2$ (Farrell *et al.*, 1962) as salting out reagent has been demonstrated.

In the acid THOREX process, three solvent extraction cycles are used. In the first cycle, uranium and thorium are extracted away from most fission products by 30% TBP from 5 M HNO_3. Both are stripped into a dilute acid phase. In the second cycle, acid conditions are controlled for selective extraction of uranium while thorium remains in the aqueous raffinate. The extracted uranium is further purified by solvent extraction or ion exchange while the thorium is concentrated and stored for recycle.

The processing of short-cooled thorium metal results in the collection of a first cycle extraction column raffinate that contains 20–30% of the mass 233 as ^{233}Pa. Ultimate recovery of ^{233}U requires storage of the raffinate for decay of ^{233}Pa. During a THOREX pilot plant short-cooled scouting run, an estimated 27 g of ^{233}Pa was collected and stored as extraction column raffinate. A one-cycle solvent extraction flow sheet was used to separate ^{233}U from fission products and other contaminants contained in the raffinate. ^{233}U was extracted into 6% TBP in Amsco 125–82 and subsequently stripped into dilute HNO_3 (McDuffee and Yarbro, 1957, 1958).

Five thorium processing campaigns were conducted at the Savannah River Plant. Two different flow sheets were used and a total of about 240 metric tons of thorium and 580 kg of uranium was processed. In the first two campaigns on thorium oxide, uranium was recovered with a dilute 3.5% TBP flow sheet and the thorium was sent to waste. ^{232}U concentrations in these two campaigns were 40–50 ppm and 200 ppm. In the third campaign, thorium metal and thorium oxide were processed. ThO_2 was processed in the final two THOREX campaigns. The three THOREX campaigns used 30% TBP to recover both uranium and thorium. Irradiation conditions were set to produce a concentration of 4–7 ppm ^{232}U. Dissolving rates for thorium metal exceeded 4 metric tons per day and with thorium sent to waste, solvent extraction rates increased, and posed no limits. When Th oxide feed was used dissolving and THOREX solvent extraction rates were $\approx$1 metric ton per day. Satisfactory flow sheets were developed, losses were acceptable, and decontamination from fission products and Pa were adequate. Th–DBP precipitates did appear in the second Th cycle during the first THOREX campaign (Orth, 1978). Rainey and Moore (1962) demonstrated a laboratory-scale THOREX separation in which good decontamination factors were obtained, and U and Th losses were less than 0.01 and 0.3%. Watson and Rainey (1979a,b) have demonstrated a THOREX computer code.

When the fuel being irradiated contains appreciable amount of ^{238}U, the plutonium thus formed requires that a combination of the THOREX and PUREX processes must be applied. The THOREX process is technologically less advanced and principally hindered by the much lower distribution coefficient of Th nitrate relative to uranium and plutonium. To drive thorium into the

TBP phase, a strong salting agent is required. Aluminum nitrate is replaced by nitric acid to reduce the amount of radioactive waste. However, high acid concentrations are counter-effective in achieving high fission product decontamination. Therefore, several flow sheet variants with acid and acid-deficient feed solutions, respectively, have been investigated (Merz and Zimmer, 1984). To achieve high decontamination factors, a dual cycle THOREX process was developed. This process uses an acid feed solution in the first cycle and an acid-deficient feed in the second cycle. An immediate separation of thorium and uranium appears advisable in view of both fuel cycle strategy and process feasibility.

To test the separation of thorium, uranium, and plutonium from each other, Grant *et al.* (1980) developed a modified THOREX solvent extraction flow sheet using 30% TBP. Not surprisingly, the inclusion of plutonium in the fuel cycle increases complexity. The first and second stages are used as a decontamination cycle to remove most of the fission products from the actinides. After intermediate concentration and adjustment of plutonium valency [to Pu(III)], the next three stages comprise the primary separation system and are used to recover Pu(III), Th, and ^{233}U separately.

Finally, several alternative extractants and even extractant types have also been suggested as a means of separating ^{233}U from irradiated thorium. To overcome the comparatively weak extraction of Th by TBP, Siddall (1958, 1963b) suggests that diamyl(amyl)phosphonate (DAAP) should be considered as a replacement for TBP in Th processing. The separation factor between thorium and zirconium is at least ten times greater with DAAP than with TBP. A high degree of complexing of DAAP by thorium occurs even in dilute HNO_3. This extractant is also less prone to third phase formation.

The extraction behavior of 1 M solutions of tri-2-ethylhexyl phosphate (TEHP), di-2-ethylhexyl isobutyramide (D2EHIBA), and di-*n*-hexyl hexanamide (DHHA) in *n*-dodecane towards U(VI), Th(IV), and Pa(V) in the presence of 220 g L^{-1} of thorium from nitric acid medium also has been studied (Pathak *et al.*, 2000). Separation factors for U(VI) over Th(IV) consistently varied in the order: D2EHIBA > DHHA > TEHP > TBP under most conditions. The quantitative extraction of ^{233}U from a synthetic mixture containing $^{233}U(10^{-5}$ M), ^{233}Pa (10^{-11} M), and thorium (220 g L^{-1}) at 1 M HNO_3 using a 1 M solution of D2EHIBA in *n*-dodecane is achieved in three stages.

Detailed studies on the processing of irradiated thorium using an amine solvent at pilot plant scale have been reported (Awwal, 1971). In this process, the ^{233}U and thorium are coextracted with 0.1 M methyldidecylamine from a feed solution of 5.8 g Th L^{-1} having 2.5×10^{-3} M H_2SO_4. The extracted thorium is selectively stripped with 1M H_2SO_4 and ^{233}U is stripped with 0.5 M HNO_3. The final product is purified by anion exchange. The decontamination factor from fission products for ^{233}U and thorium are 3.2×10^4, 3.8×10^4, respectively, for the single cycle solvent extraction process. The separation factor of ^{233}U from thorium is 2×10^4.

24.4.4 Actinide production processes at the design and pilot stages

During the last two decades, concerted and mission-oriented research conducted around the world has identified a number of promising extractant systems for actinide separations using solvent extraction, extraction chromatography, supported liquid membrane, magnetically assisted chemical separations, or pyro-reprocessing. The pyrometallurgical options have been discussed in Section 24.3.12. Plant-scale demonstrations are yet to occur, partly because of materials/corrosion issues. Most aspects of separations in the IFR project have been demonstrated at the pilot scale. In the following discussion, the performance of the new extraction systems that have been developed for actinide partitioning will be compared. Many of the new extractant systems under development are based on bifunctional (or multifunctional) reagents, whose unique nature will become apparent in the discussion to follow. The chemical features of many of these systems have been considered above (see Section 24.3.4b). The emphasis in this section will be more on the status of process development. The reader is referred to the cited literature for detailed information on the chemistry of the extraction systems.

(a) Dihexyl-*N*,*N*-diethylcarbamoylmethylphosphonate (DHDECMP or CMP)

Navratil and coworkers (Martella and Navratil, 1979; Navratil and Thompson, 1979) conducted a preliminary feasibility study for separation of actinides from synthetic acidified waste solutions likely to be produced during nuclear fuel fabrication and reprocessing. The initial solution contained large quantities of Na_2CO_3, Na_3PO_4, NaCl, Na_2SO_4, and the actinides, plutonium, americium, and uranium. A first contact with 30% TBP/*n*-dodecane removed more than 99.99% of uranium and most of the plutonium. The aqueous raffinate was then contacted with 20–30% CMP/CCl_4 which removed more than 99.91% of americium and all the residual plutonium and other actinides.

Rapko and Lumetta (1994) have reported the extraction of U(VI), Pu(IV), Am (III), and important competing metal ions (e.g. Fe(III), Zr(IV), Bi(III)) from HNO_3 solutions using a mixture of CMP (0.75 M) and TBP (1.05 M) in an aliphatic diluent [normal paraffinic hydrocarbon (NPH) or isoparaffinic hydrocarbon (ISOPAR)]. Above 2M HNO_3, this organic phase splits into heavy and light fractions (third phase formation) even in the presence of $\sim$ 1 M TBP. Adjustment to about 2.0 M $NaNO_3$ is indicated as necessary to prevent third phase formation. At about 2 M (HNO_3, NO_3^-) in the absence of any aqueous complexing agent, a distribution ratio D_{Am} of about 5 is reasonably good. Though 0.1 M HF has no effect on D_{Am}, 0.05 M oxalic acid decreases D_{Am} to about 1. Salting out with $NaNO_3$ increased this value. D_{Pu} at radiotracer concentrations and D_U at 0.05 M ($\sim$12 g L^{-1} total uranium) have been reported. D_{Am} decreases in the presence of such moderate concentrations of uranium, presumably as a

result of the tying up of the free extractant by the macroscopic quantities of uranium present. Degradation products and acidic impurities in the CMP extractant can inhibit stripping of plutonium and uranium. The increased volume of wastes in all categories that would result from the introduction of a salting-out reagent required to maintain extraction efficiency and phase compatibility is a significant drawback to the application of this class of reagents.

(b) Octyl(phenyl)-*N*,*N*-di-isobutylcarbamoylmethylphosphine oxide (OϕDiBCMPO or CMPO)

To overcome the comparative weakness of the CMP-class extractants, structurally similar extractants containing the phosphine oxide functional group were prepared. Compounds with different substituents at the phosphoryl group and the amide nitrogen have been synthesized (Kalina *et al.*, 1981a; Chmutova *et al.*, 1983) and studied for extraction of transplutonium metal ions. Alterations have also been made at the bridge between the P=O and C=O groups (Rapko, 1995). Two detailed papers describe the synthesis and purification (Gatrone *et al.*, 1987) and the spectral properties of the carbamoylmethylphosphine oxides (Gatrone and Rickert, 1987). The extraction behavior of mainly trivalent actinides, lanthanides, and a few other metal ions has been studied with all the reagents synthesized in this class. Actinide extraction properties and phase compatibility varied significantly with the nature of the alkyl substituents on the carbamoylmethylphosphine oxide core. Of the compounds investigated, OΦCMPO was found to possess the best combination of properties for actinide extraction in a PUREX-compatible diluent system. The CMPO-type compounds have received the greatest attention of all potential actinide partitioning reagents developed over the past 20 years and as a result represent the best-understood hydrometallurgical reagents for total actinide partitioning from wastes.

Numerous investigations have attempted to demonstrate quantitative phase transfer of americium from HNO_3 or HCl solutions by CMPO into diluents like diethylbenzene, CCl_4, C_2Cl_4, and paraffinic hydrocarbons (Horwitz *et al.*, 1981, 1983, 1986; Kalina *et al.*, 1981a; Horwitz and Kalina, 1984). Extraction of Eu(III) from HNO_3 or HCl with CMPO alone or a mixture of CMPO and TBP in mesitylene or *n*-dodecane has been reported (Liansheng *et al.*, 1990) as has the extraction of neptunium and plutonium (Kolarik and Horwitz, 1988; Mincher, 1989; Nagasaki *et al.*, 1992) and Pm, U, Pu, Am, Zr, Ru, Fe, and Pd (Mathur *et al.*, 1992b) from HNO_3 into a mixture of CMPO and TBP in *n*-dodecane. Basic studies of CMPO have reported its activity coefficients (Diamond *et al.*, 1986), complexes formed with trivalent actinides and lanthanides (Mincher, 1992), electrochemistry of Ce(III) nitrate complex (Jiang *et al.*, 1994), and numerical modeling to predict operations in the TRUEX process (Regalbuto *et al.*, 1992; Vandegrift *et al.*, 1993; Vandegrift and Regalbuto, 1995) and for co-extraction of Tc(VII) with U(VI) (Takeuchi *et al.*, 1995).

The now well-known TRUEX process for the recovery of all the actinides from various types of highly acidic nuclear waste solutions is based on CMPO as the principal extractant. The TRUEX process solvent is 0.2–0.25 M CMPO + 1.0–1.4 M TBP in paraffinic hydrocarbon (linear or branched, though the process has been demonstrated in chlorinated diluents as well) (Vandegrift *et al.*, 1984; Horwitz *et al.*, 1985; Schulz and Horwitz, 1988; Horwitz and Schulz, 1990; Mathur and Nash, 1998; Suresh *et al.*, 2001). TBP hinders third-phase formation, contributes to better acid dependencies for D_{Am}, improves phase compatibility, and reduces hydrolytic and radiolytic degradation of CMPO. The basic actinide solvent extraction chemistry of TRUEX has been discussed in Sections 24.3.4b and 24.3.5. The ability to efficiently extract trivalent, tetravalent, and hexavalent actinides from solutions of moderate acid concentration and with good selectivity over *most* fission products (except lanthanides) is a key feature of this extractant. From an engineering perspective, the more-or-less constant D values of Pu(IV), U(VI), and Am(III) between about 1 and 6 M HNO_3 is important, as it allows efficient extraction of actinides from wastes or dissolved fuels with little or no need to adjust the acidity of the feed solution. This particular feature of TRUEX distinguishes this extraction system from other methods for TRU isolation. A sufficient volume of process-relevant thermodynamic data on CMPO extraction chemistry has been developed to support the existence of a computational model, the generic TRUEX model (GTM) that can be used to predict system performance over a wide range of conditions (Regalbuto *et al.*, 1992; Vandegrift *et al.*, 1993; Vandegrift and Regalbuto, 1995).

Russian chemists have independently developed a TRU extraction process based on a somewhat simpler (thus, less expensive) derivative of CMPO (diphenyl-*N*,*N*-di-*n*-butyl CMPO, DΦDBuCMPO) employing a fluoroether diluent (Fluoropol-732) (Myasoedov *et al.*, 1993). This process behaves similarly to the TRUEX process in terms of its efficiency for actinide extraction, shows little tendency toward third-phase formation, and avoids the interferences caused by degradation of TBP. It has been tested in centrifugal contactors and found to recover actinides with greater than 99.5% efficiency. The corrosive nature of aqueous effluents derived from degraded solvent (i.e. containing HF) is a potential drawback for this process.

Continuing exploration of this extractant has suggested a *un*iversal solvent *ex*traction (UNEX) process for the separation of cesium, strontium, and the actinides from nitric acid solutions and from actual acidic radioactive waste solutions (Law *et al.*, 2001, 2002; Romanovskiy *et al.*, 2001a,b, 2002; Herbst *et al.*, 2002, 2003; Romanovskiy, 2002a,b; Todd *et al.*, 2003). The composition of the UNEX solvent is 0.08 M chlorinated cobalt dicarbollide, 0.5 vol.% polyethylene glycol-400 (PEG-400) and 0.02 M DΦDBuCMPO in a phenyltrifluoromethyl sulfone (FS-13) diluent. Cobalt dicarbollide $[Co(B_9C_2H_8Cl_3)_2^-]$ is a lipophilic substitution-inert Co(III) complex that exhibits significant affinity for Cs^+. Using the Idaho National Engineering and Environmental Laboratory

(INEEL) tank waste, removal efficiencies of 99.4, 99.995, and 99.96% for ^{137}Cs, ^{90}Sr, and the actinides, respectively, have been demonstrated. Possible limitations of the process include corrosive products of diluent degradation (e.g. HF), difficult back extraction due to the requirement of very low acidity for low D_{Am}, and possibly complex solvent cleanup prior to recycle of the extractant (Horwitz and Schulz, 1999).

(*i*) *TRUEX demonstrations with HLW and simulants*

Decontamination of four types of actinide-bearing wastes (or waste simulants) from the Hanford site, plutonium finishing plant (PFP), complexant concentrate (CC), neutralized cladding removal waste (NCRW), and single-shell tank (SST) waste have been the subject of either bench-scale experiments or pilot-scale demonstrations using TRUEX with results as follows:

- The removal of americium and plutonium from the plutonium finishing plant (PFP) aqueous acidic waste [$HNO_3/Al(NO_3)_3$ at 3 M total nitrate with 0.09 M HF, 0–0.2 M U, 10^{-5} to 10^{-4} M Pu, 10^{-6} to 10^{-5} M Am, less than 6×10^{-4} M Be, Cr, Ni, Zn, Pb] was accomplished using the TRUEX solvent (0.25 M CMPO, 0.75 M TBP in C_2Cl_4). The first two highly successful counter-current runs with actual PFP waste employed a cross-flow microfilter unit to remove finely divided solids and 4 cm diameter centrifugal contactor equipment for the solvent extraction of TRU elements. Duplicate runs were completed with 10 L of the clarified waste in about 40 min. The α-activity of the aqueous raffinate was 1–2 $n\text{Ci} \cdot \text{g}^{-1}$ and a TRU D_f of 10^4 was obtained. A generic flow sheet of the TRUEX process for the removal of americium and plutonium from PFP waste is given in Fig. 24.20. A larger-scale demonstration using a 20-stage centrifugal contactor configuration achieved α-decontamination factors up to 6.5×10^4 (Chamberlain *et al.*, 1997).
- The CC waste is alkaline and contains high concentrations of Na^+, NO_3^-, NO_2^-, $Al(OH)_4^-$, CO_3^{2-}, organic complexants (EDTA, HEDTA, citric acid, and their radiolytic and hydrolytic degradation products), and moderate concentrations of Cs^+ and Sr^{2+}. After acidification, bench-scale batch extraction tests with synthetic and actual CC waste demonstrated that the $D_{f\ TRU}$ was on the order of 10^2 (Schulz and Horwitz, 1988). The TRU concentration in the effluent was 1 $n\text{Ci g}^{-1}$.
- NCRW consists of solids (principally $ZrO_2 \cdot xH_2O$) generated while treating Zircaloy-clad fuels. It contains moderate amounts of TRU elements. A preliminary test with actual NCRW dissolved in HNO_3 or HNO_3–HF solutions using the TRUEX solvent was reported to result in satisfactory uptake of the actinides (Schulz and Horwitz, 1988). At the Pacific Northwest National Laboratory (PNNL), highly encouraging results have been reported for actinide removal by TRUEX treatment of NCRW sludge and of PFP sludge (Swanson, 1991a–c; Lumetta and Swanson, 1993a–c).

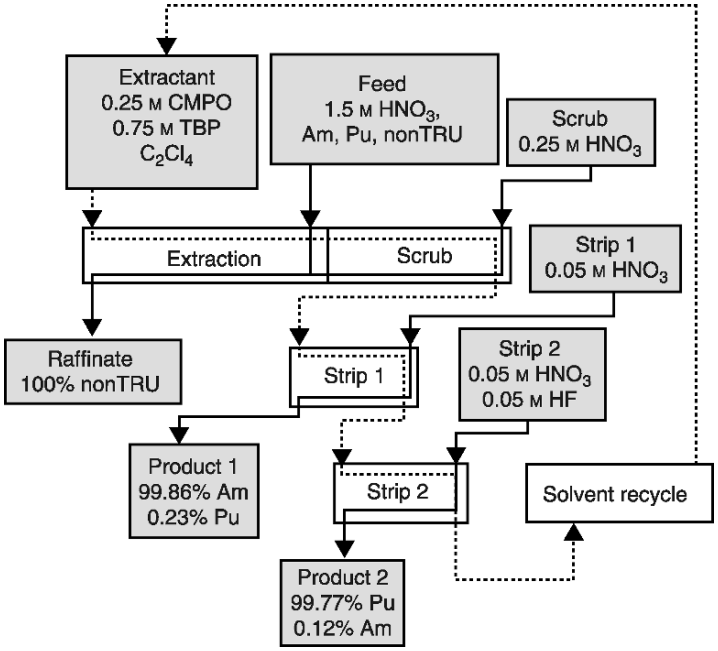

Fig. 24.20 *Generic flow sheet for TRUEX processing of plutonium finishing plant (PFP) wastes.*

- SST waste, a mixture of solid salt cake (e.g. water-soluble sodium salts), solid sludge [primarily hydrated Fe(III) oxide], and a small volume of interstitial liquid containing TRU elements, can also be treated and TRU removed from the acidic solutions, as has been demonstrated using TRUEX on simulated dissolved sludge waste (Schulz and Horwitz, 1988).

The most extensive pilot-scale testing of the TRUEX process has been done at the Idaho National Engineering and Environmental Laboratory under the auspices of the Lockheed Martin Idaho Technologies Co. Several TRUEX demonstration runs have been made on sodium-bearing wastes (Law *et al.*, 1998), a secondary acidic HLW. An optimized TRUEX flow sheet was tested in shielded hot cells at the Idaho Chemical Processing Plant (ICPP) Remote Analytical Laboratory using a 20-stage bank of 2 cm centrifugal contactors.

Stripping of actinides from the loaded process solvent was accomplished with 99.79% efficiency (99.84% for Am, 99.97% for Pu, 99.80% for U) using 1-hydroxyethane-1,1-diphosphonic acid (HEDPA) as the stripping agent. A second demonstration using a dissolved zirconium calcine feed recovered 99.2% of Am (Law *et al.*, 1998). In this case, the HEDPA stripping was less efficient due to problems created by precipitation of zirconium phosphate. The phosphate is believed to be present as an impurity in the HEDPA solution.

Literature reports indicate that such impurities are readily removed by recrystallization of HEDPA from glacial acetic acid (Nash and Horwitz, 1990). The radiolytic stability of this reagent has not been tested, but it is stable in acidic aqueous solutions.

At the Los Alamos National Laboratory (LANL) substantial amounts of waste chloride salts containing moderate concentrations of Pu and Am are generated. These salts, dissolved in HCl, can serve as feed for the separation of actinides using high concentration of CMPO (0.5 M) in C_2Cl_4. If the feed contains large amounts of metal ion impurities that are appreciably extracted by CMPO [e.g. U(VI)], a preceding solvent extraction process employing TBP, TOPO, quaternary ammonium compounds, or some other process must be applied. The D values of Th(IV), U(VI), Np(IV), Pu(IV), and Am(III) at varying HCl concentrations in contact with 0.5 M CMPO in tetrachloroethylene have been reported previously (Horwitz *et al.*, 1987). Initial counter-current studies using TRUEX solvent indicated the need for moderate chloride ion concentration in the feed solution for satisfactory extraction of plutonium and americium (Schulz and Horwitz, 1988). Flow sheet for the generic TRUEX process for the removal of actinides from aqueous chloride solutions is given in Fig. 24.21.

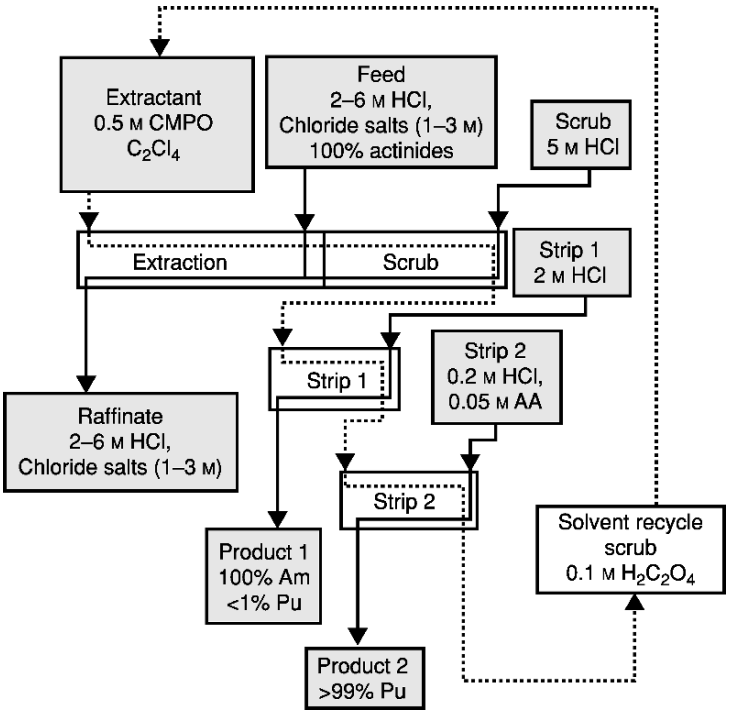

Fig. 24.21 *Generic flow sheet for TRUEX processing of chloride wastes.*

In the European Community R&D program on the management and disposal of radioactive wastes, the Fuel Cycle Dept. ENEA, Rome, Italy, reported that the mixture of TBP and CMPO in chlorinated or aliphatic hydrocarbons achieves a very high D_f for actinides. Batch and counter-current extraction experiments were performed with MOX fabrication liquid wastes. Only batch studies were conducted with simulated solutions of aluminum MTR CANDU high-level wastes of the EUREX reprocessing plant and with analytical wastes from control laboratories of a MOX fabrication plant. Very high D_f values for actinides were obtained without requiring any salting agents and in the presence of many potentially complexing anions (Casarci *et al.*, 1988, 1989).

At Japan's Power Reactor and Nuclear Fuel Development Corporation (PNC), batch and counter-current runs with real high-active raffinate from FBR spent fuel reprocessing have been carried out without adjusting acidity, using 0.2 M CMPO + 1.2 M TBP in *n*-dodecane. The mixer–settler employed in this study had 19 stages for extraction-scrubbing and 16 stages for stripping. The rare earths were extracted along with actinides and some fraction of ruthenium. The D_f for actinides was greater than 10^3. Oxalic acid was added in the feed and scrubbing solutions to improve ruthenium decontamination and effectively lower the D values of zirconium and molybdenum (Ozawa *et al.*, 1992). In another communication from the same laboratory, Ozawa *et al.* (1998) suggested improvements in the TRUEX process flow sheet, specifically, increasing the acidity of the feed to about 5 M to improve Ru decontamination in the actinide fraction, and using salt-free reagents like hydrazine oxalate, hydrazine carbonate, and tetramethylammonium hydroxide for stripping and cleanup steps to obtain a final raffinate that is α-inactive and salt-free. The improved TRUEX flow sheet utilized at PNC is given in Fig. 24.22.

A numerical simulation code for the TRUEX process has been developed to determine the optimum operational conditions for the separation and recovery of TRU elements (Takanashi *et al.*, 2000). With a view to minimize radioactive organic/inorganic waste released from TRUEX process, the electro-redox technique and mediatory electrochemical oxidation using Ag(II)/Ag(I) or Co(III)/Co(II) couples have shown great promise (Ozawa *et al.*, 2000).

At the Bhabha Atomic Research Centre in India, basic data were generated for the extraction of actinides and a few fission and corrosion products using TRUEX solvent (0.2 M CMPO + 1.2 M TBP in *n*-dodecane) (Mathur *et al.*, 1992b). Subsequent studies examined the extraction and separation of actinides from synthetic and actual high-level aqueous raffinate waste (HAW), sulfate-bearing high-level waste solutions (SBHLW) at low acidity of about 0.3 M, non-sulfate wastes originating from pressurized heavy water reactor (PHWR), and fast breeder reactor (FBR) both in about 3 M HNO_3, and actual HLW solutions generated from the reprocessing of research reactor fuels at this center. In each study, the compositions of the synthetic waste solutions were reported (Deshingkar *et al.*, 1993, 1994; Mathur *et al.*, 1993a, 1995, 1996a; Gopalakrishnan *et al.*, 1995). The results of batch studies on actual waste solutions are given below:

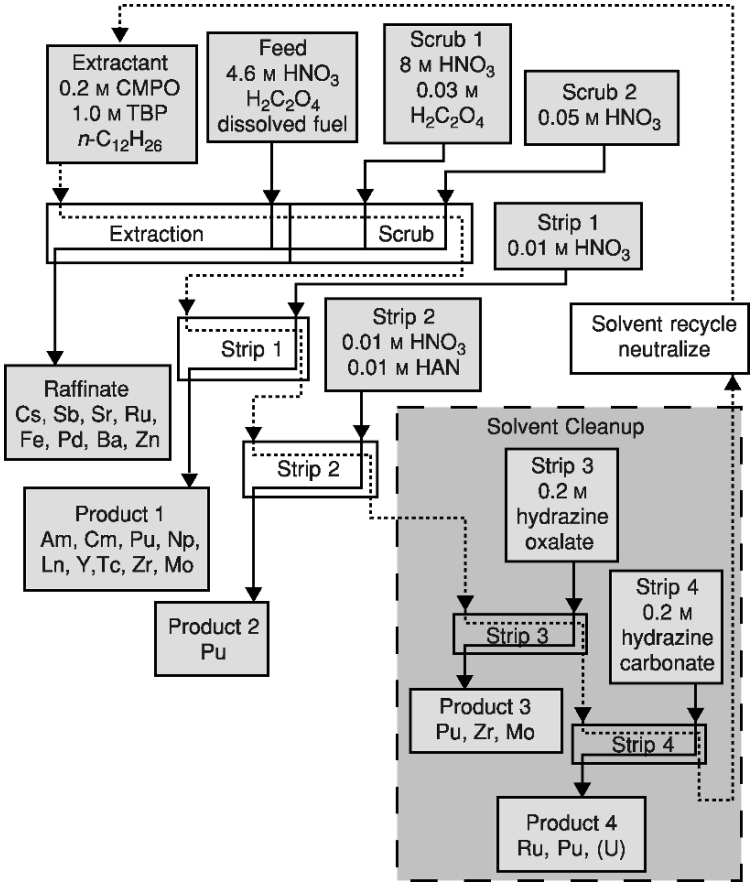

Fig. 24.22 *Generic TRUEX flow sheet for actinide partitioning at JNC.*

- Unmodified HAW was contacted twice with fresh lots of 0.2 M CMPO + 1.2 M TBP in *n*-dodecane in 1:1 ratio. After two contacts, 99.8% of the α-activity was found in the organic phase. The rare earths (Ce, Pm, Eu, etc.) followed americium, and ruthenium was partially extracted while cesium and strontium were not (Mathur *et al.*, 1993a).
- For extraction of HLW, the feed contains at least ten times higher concentration of uranium, fission and corrosion products than those in HAW. Therefore, one contact with 30% TBP/*n*-dodecane was made to deplete the uranium content. After this, four contacts were made with 0.2 M CMPO + 1.4 M TBP. The raffinate was found to contain $\sim$ 0.06% of the total α-activity (Mathur *et al.*, 1993a).

- With SBHLW, two contacts were made with 30% TBP followed by four contacts with 0.2 M CMPO + 1.2 M TBP in *n*-dodecane. Even at the low acidity of 0.3 M and ~ 0.16 M SO_4^{2-}, about 99.6% of the total α-activity was removed from the HLW solutions (Gopalakrishnan *et al*., 1995).

Mixer–settler experiments employing a six-stage unit with synthetic SB- and PHWR-HLW have been reported. After pretreatment with 30% TBP to reduce the concentrations of uranium, neptunium, and plutonium, the raffinate containing the remaining uranium, neptunium, and plutonium and the trivalent actinides and lanthanides (at total acidity of about 3 M) was the feed for a subsequent mixer–settler experiment using 0.2 M CMPO + 1.2 M TBP in *n*-dodecane. In all cases, the HLW raffinate leaving the extraction section showed α-activity near background level. Final analysis indicated that nearly 99.7% of the rare earths are extracted along with the actinides and with about 30% of the ruthenium (Deshingkar *et al*., 1993, 1994; Chitnis *et al*., 1998b). The combined flow sheet using 30% TBP and the TRUEX solvent (Fig. 24.23) has been tested with actual HAW solutions generated from the reprocessing of research reactor fuels.

In the first step, with 30% TBP U, Np, and Pu were recovered from HAW and then minor actinides left in the raffinate were extracted with the TRUEX solvent in the second step. Plutonium and neptunium extracted in TBP were stripped together using a mixture of H_2O_2 and ascorbic acid in 2 M HNO_3 and later uranium was stripped from the TBP phase with dilute HNO_3. Actinides extracted in TRUEX solvent were stripped together using a mixture of formic acid, hydrazine hydrate, and citric acid. The final raffinate analysis showed no alpha activity (Chitnis *et al*., 2000).

(*ii*) *Recovery of Pu from oxalate supernatant*

The solutions resulting from Pu oxalate precipitation (oxalate supernatants) are among the final liquid waste streams in conventional PUREX processing. This waste typically contains ~30 mg $L^{-1}$of plutonium in 3 M HNO_3 and about 0.1 M oxalic acid. TRUEX solvent has proven highly efficient for almost quantitative recovery of plutonium from such a solution in batch solvent extraction studies. Plutonium is stripped from the loaded CMPO phase by 0.5 M acetic acid or by a mixture of oxalic acid, calcium nitrate, and sodium nitrite (Mathur *et al*., 1994). Plutonium also could be recovered from such solutions utilizing the extraction chromatographic technique in which CMPO adsorbed on Chromosorb-102 (CAC) was used for batch and column studies (Mathur *et al*., 1993b). When the oxalate supernatant contained large amounts of uranium (10–12 g L^{-1}) along with plutonium, a TBP extraction step followed by TRUEX process solvent step has recovered uranium and plutonium almost quantitatively (Michael *et al*., 2000).

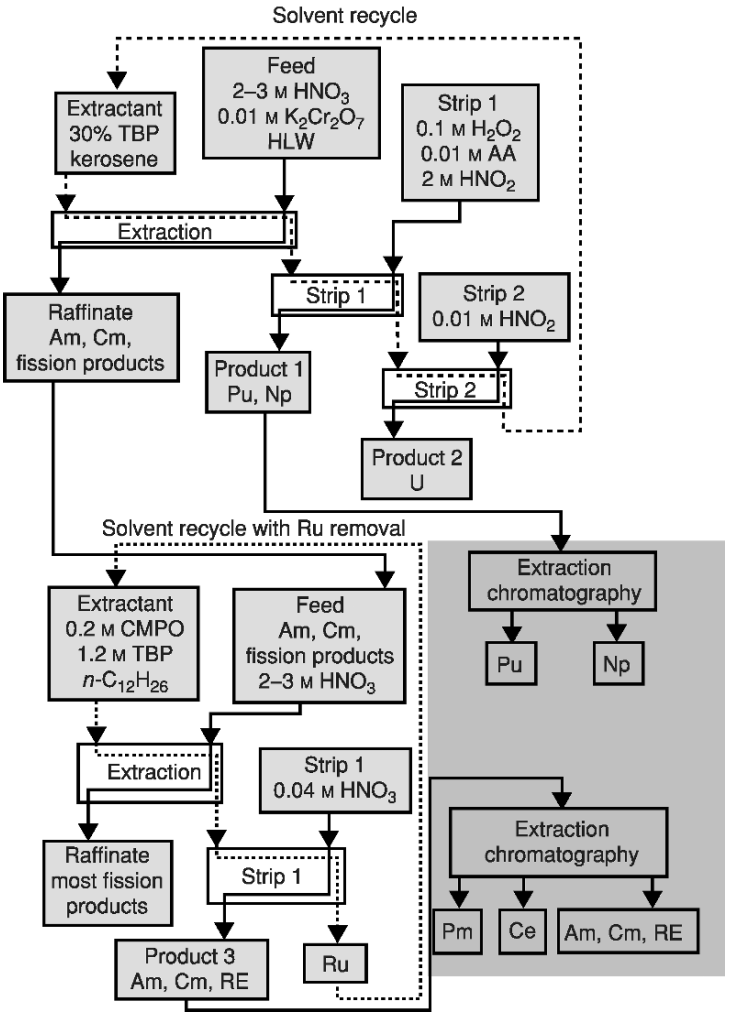

Fig. 24.23 *Generic TRUEX flow sheet for actinide partitioning at BARC.*

(*iii*) *Stripping of actinides from TRUEX solvent*

Oxidation state-specific stripping of actinides from loaded TRUEX solvent can be done in three steps: 0.04 M HNO_3 to remove trivalent actinides, dilute HNO_3–HF mixture (0.05M each), or dilute oxalic acid for selective stripping of tetravalent actinides, and 0.25 M Na_2CO_3 for uranium recovery (and simultaneous reconditioning of solvent for recycle). Horwitz and Schulz (1990)

recommend that a solution of either vinylidene-1,1-diphosphonic acid (VDPA) or HEDPA be used for stripping TRUs when they are directly to be vitrified. In similar fashion, coprecipitation of actinides, lanthanides, and a few other fission and corrosion products extracted into the TRUEX process solvent was achieved by using iron(III)ferricyanide as a carrier precipitant. The volume of the precipitate was very small and suitable for vitrification of TRUs (Rizvi and Mathur, 1997). In other reports (Chitnis *et al.*, 1999a,b), a mixture of formic acid, hydrazine hydrate, and citric acid have shown promise for efficient stripping of Am and Pu from TRUEX solvent loaded with simulated HLW in both batch and counter-current modes. Ozawa *et al.* (1998) report that hydrazine oxalate, hydrazine carbonate, and tetramethylammonium hydroxide for stripping of actinides from loaded TRUEX solvent and its cleanup will lead to a salt-free effluent.

(*iv*) *Degradation, cleanup, and reusability of TRUEX solvent*

The hydrolytic and radiolytic degradation of CMPO has been studied in CCl_4 and decahydronaphthalene (decalin) (Chiarizia and Horwitz, 1986), TCE, or a mixture of TBP and TCE (Nash *et al.*, 1988b). Hydrolytic and radiolytic degradation of TRUEX process solvent (0.2 M CMPO + 1.2 M TBP in *n*-dodecane) has been investigated in the presence of 5 M HNO_3 (Chiarizia and Horwitz, 1990) and under dynamic conditions in contact with 3 M HNO_3 or synthetic PHWR-HLW (Mathur *et al.*, 1988). The *G* values (molecules/100 eV deposited) for the disappearance of CMPO in CMPO–TBP mixture are (1.2 ± 0.3) in *n*-dodecane, (4.5 ± 0.3) in TCE, and (16.4 ± 1.7) in CCl_4 (Nash *et al.*, 1989; Chiarizia and Horwitz, 1990), indicating that more reactive conditions are created upon radiolysis of chlorinated diluents. Hydrolysis generates only acidic compounds while radiolysis produces both acidic and neutral compounds. The degradation products reported are methyl(octyl)phenylphosphine oxide, octyl(phenyl)-*N*-monoisobutylcarbamoylmethyl phosphine oxide, dibutylphosphoric acid, octyl(phenyl)phosphinic acid, octyl(phenyl)phosphinyl acetic acid (Chiarizia and Horwitz, 1990), methyl(phenyl)-*N*,*N*-diisobutylcarbamoylmethylphosphinic acid, and phenyl(diisobutyl) carbamoylnitromethylphosphine oxide (Mathur *et al.*, 1988).

The presence of the acidic extractants as degradation products increases D_{Am} under stripping conditions. Such impurities must be nearly completely removed from the used TRUEX solvent prior to recycle of the extractant. Table 24.16 gives the D_{Am} with an irradiated CMPO mixture under static conditions in contact with 5 M HNO_3 (Chiarizia and Horwitz, 1990) and under dynamic conditions in contact with 3 M HNO_3 (Mathur *et al.*, 1988). The *D* values at pH 2.0 are quite high and increase with absorbed dose. They also increase in the same fashion at 0.04 M HNO_3, but up to a dose of 200 kGy ($\sim$55 W h L^{-1} or 20 Mrad absorbed dose), *D* is less than 1, hence stripping with 0.04 M HNO_3 should still be possible. Up to an absorbed dose of about 200 kGy, primary cleanup

Table 24.16 *Partitioning of americium (D_{Am}) between* 0.2 M *CMPO* + 1.2 M *TBP in* n-*dodecane* and *HNO_3 as a function of absorbed gamma dose.*

	D_{Am}				
	Static condition 5.5 M *HNO_3 Chiarizia and Horwitz* (1990)			*Dynamic condition* 3 M *HNO_3 Mathur* et al. (1988)	
Dose (kGy)	pH 2.0	0.04 M	*Dose* (kGy)	pH 2.0	0.04 M
0	0.011	0.13	0	0.016	–
~70	0.87	0.72	~50	0.55	0.23
~130	0.91	0.61	~110	2.77	0.38
~200	1.33	0.59	~210	16.4	0.81
~280	1.42	0.58	~260	32.7	1.21

D_{Am} only after the wash with respective aqueous phase, no sodium carbonate or alumina treatment.

with 0.25 M Na_2CO_3 will remove most of the acidic impurities. Although the D_{Am} at pH = 2.0 may not match the reference condition, D_{Am} at 0.04 M HNO_3 suggests that continuous counter-current stripping of americium will be efficient. However, at high radiation doses, a secondary cleanup with macroporous anion exchange resin (Chiarizia and Horwitz, 1990) or with basic alumina (Mathur *et al.*, 1988) will restore TRUEX process solvent to near reference condition.

(*v*) *CMPO for extraction chromatography separation of actinides*

Extraction chromatography is fundamentally solvent extraction in which the extractant phase is 'immobilized' on a non-reactive solid support. The technique is generally considered to be most applicable for analytical purposes due to the tendency of the immobilized extractant to 'bleed' from the solid as the aqueous effuent transits the column. However, process-scale applications have been suggested.

The feasibility of using TRU-Resin™ (CMPO + TBP adsorbed on Amberchrom-CG-71 from Eichrom Industries Inc., Darien, Illinois, USA) for separating TRU elements from actual neutralized decladding waste solution (resulting from the removal of zirconium cladding from irradiated fuel) from the Hanford Waste tank has been demonstrated (Lumetta *et al.*, 1993). Actinides (U, Pu, Am) and lanthanides (Ce, Eu) were separated from nitric acid solutions using a column of 0.75 M CMPO in TBP adsorbed on XAD-7. They were subsequently eluted from the column with HCl, oxalic acid, and nitric acid solutions (Yamaura and Matsuda, 1999). Highly encouraging results have been reported for the separation of americium, plutonium, and uranium from acidic waste solutions using several types of extraction chromatographic supports

impregnated with CMPO (Barney and Covan, 1992; Schulte *et al.*, 1995a,b, 1996; Barr *et al.*, 2001).

Batch uptake studies have been carried out on the extraction chromatographic behavior of U(VI), Pu(IV), Am(III), and several fission and corrosion products from HNO_3 media using CMPO adsorbed on Chromosorb-102 (CAC) (Mathur *et al.*, 1995). Very high *D* values of actinides and lanthanides as compared to other fission products were obtained. For example, a small CAC column (containing 9.5 g of CAC) was prepared and about 0.5 L of the uranium depleted actual HAW at an acidity of ~1.7 M was passed through it. No α-activity was detected in the effluent. An americium and RE fraction, plutonium fraction, and uranium fraction were subsequently eluted with 0.04 M HNO_3, 0.01 M $H_2C_2O_4$, and 0.25 M Na_2CO_3, respectively. Comparable results were obtained while using a similar column and a synthetic SBHLW (Gopalakrishnan *et al.*, 1995).

A novel silica-based extraction chromatographic support has been prepared by immobilizing styrene–divinylbenzene copolymer in porous silica particles (SiO_2-P) (Wei *et al.*, 2000). Separation experiments using a CMPO/SiO_2–P resin packed column have given good separation of trivalent actinides and lanthanides from fission products like Cs, Sr, and Ru in simulated HLW solutions containing concentrated HNO_3. Also, it has been shown that, using a column packed with freshly purified Cyanex-301/SiO_2–P, americium was completely adsorbed by the resin and only about 1–2% of the Ln(III) were adsorbed from a 1 M $NaNO_3$ solution at pH 3.99 containing trace amounts of ^{241}Am, ^{153}Gd, ^{152}Eu (and 10^{-2} M Eu carrier), and ^{139}Ce. Americium was then eluted in a pure form with 0.1 M HNO_3.

(*vi*) *CMPO in supported liquid membrane separation of actinides*

Supported liquid membrane (SLM) is a technique wherein a microporous film (either as flat sheets or hollow tubes) is impregnated with an extractant and the transport of target metal ions is facilitated from the feed to the stripping solution. A simple schematic description of the SLM system is shown in Fig. 24.24. The salient features of the SLM processes are (1) extractant needed is in small quantities, (2) high feed/strip volume ratio, and (3) very simple

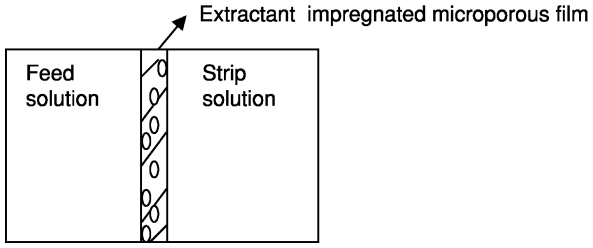

Fig. 24.24 *Schematic description of a supported liquid membrane (SLM) system.*

operation systems. Danesi *et al.* (1983) have used a solution of CMPO/DEB adsorbed onto a 48-μm thick microporous polypropylene film to facilitate the transport of Am(III) from aqueous nitrate solutions to the strip section containing formic acid solution. The transport mechanism suggested consists of a diffusion process in the feed compartment through an aqueous diffusion film followed by a fast interfacial chemical reaction and finally diffusion through the membrane itself to the stripping compartment. The membrane permeability coefficient has been correlated with the diffusional parameters and to the chemical composition of the system.

In another study from the same group (Danesi *et al.*, 1985), an SLM consisting of a mixture of 0.25 M CMPO and 0.75 M TBP in decalin adsorbed on thin microporous polypropylene supports in flat-sheet and hollow-fiber configurations was used for the selective separation and concentration of actinides (Am, Pu, U, and Np) and lanthanides from synthetic acidic nuclear wastes. It has been shown that actinides can be efficiently removed at a level sufficient to characterize the resulting solution as a non-TRU waste. An adjustment developed by Danesi *et al.* (1985) suggested an improvement in the efficiency of actinide removal from waste solutions. Incorporation of a double liquid membrane system, wherein a second SLM containing a primary amine that extracts only HNO_3 from the strip solution, allows near complete removal of actinide and lanthanide metal ions from the feed solution (Chiarizia and Danesi, 1987).

Ramanujam *et al.* (1999) have reported the transport of actinides from nitric acid and uranium-lean simulated samples as well as the actual HLW using CMPO/*n*-dodecane as a carrier and polytetrafluoroethylene as the support. The receiving phase was a mixture of citric acid, formic acid, and hydrazine hydrate. Very good transport of U(VI), Np(VI), Np(IV), Pu(IV), Am(III), and Ce (III) has been achieved. The TRUEX solvent (0.2 M CMPO + 1.2 M TBP/*n*-dodecane) has also been used as a carrier for the transport of Am(III) from nitrate–nitric acid solutions using track-etched polycarbonate plastic membranes (Pandey *et al.*, 2001). For Am(III) transport, these membranes performed at a level comparable to that obtained using commercial membranes.

(*vii*) *CMPO in magnetically assisted chemical separation of actinides*

Pioneering work on the separation and recovery of actinides from waste solutions using magnetically assisted chemical separation (MACS) was performed at the Argonne National Laboratory by Nunez *et al.* (1995a,b). This process gives a selective and efficient separation by chemical sorption followed by magnetic recovery. Magnetic particles (ferrite, magnetite, etc.) are coated with extractants and added to the treatment tank containing dilute TRU waste. The solution can be stirred mechanically or by any other method. Finally, the particles are magnetically separated by imposing a magnetic field around the tank, pumping the solution through a magnetic filter, or introducing a magnet into the tank. Actinide ions can be stripped from the loaded particles with small

volumes of suitable stripping agents. This process of recovery of actinides (or any other metal ions) from the waste streams seems to be very simple, compact and, in the proper application, is likely to be cost-effective. Like membrane-based separations, this approach does not involve large amounts of organic solvents and will not produce large volumes of secondary wastes. A conceptual diagram of the MACS process could be visualized as given in Fig. 24.25.

Nunez *et al.* (1995a,b) have used TRUEX solvent (CMPO in TBP) as the active coating on the magnetic particles. The extraction of americium and plutonium from HNO_3 solutions ranging in concentration from 2 to 8 M was found to decrease slowly with increasing acid concentration. The range of K_d values was between 400 and 3000 for americium and between 3900, and 46000 for plutonium. The uptake of the same nuclides was tested using synthetic dissolved sludge waste equivalent to the Hanford site waste. It was concluded that the MACS process could be applied to remediation problems at the Hanford site and other sites only if the waste streams contained low concentrations of TRU elements and lanthanides.

Kaminiski and Nunez (2000) have further studied the separation of U(VI) from HNO_3 and HCl solutions using extractants like CMPO, TBP, TOPO, and HDEHP employing the MACS technique. When magnetic particles were coated with TBP or a mixture of TOPO and HDEHP, partitioning of U(VI) was most efficient from dilute acid environments typical of contaminated ground water. From 2 to 8 M HNO_3, the 1.0 M CMPO in TBP-coated

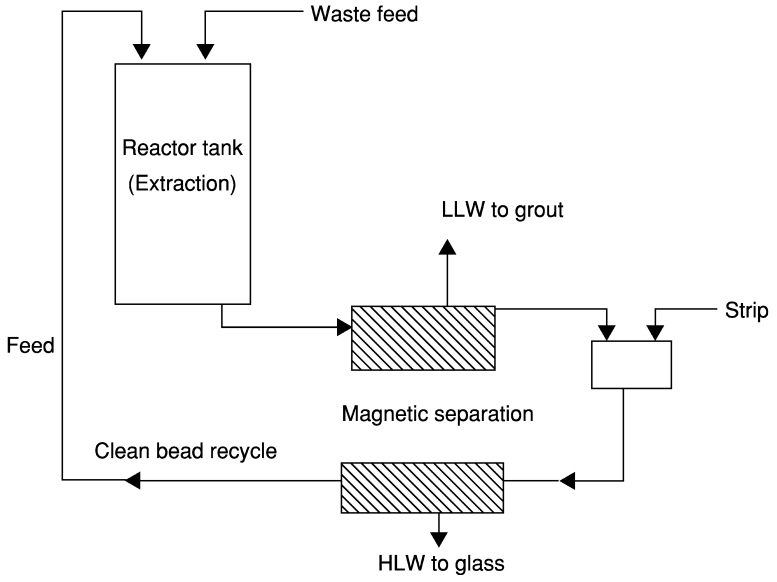

Fig. 24.25 *Schematic diagram of a magnetically assisted chemical separation system (MACS).*

particles gave the highest K_d values for U(VI). From these collected observations, it seems likely that MACS has potential for separating actinides from different actinide-bearing acidic waste solutions using various extractants coated on magnetic particles. Further studies are needed to demonstrate a full-scale operation. The same group has also shown a very high separation between Co and Ni while coating the magnetic particles with a mixture of 0.5 M Cyanex 272 and 0.5 M HDEHP (Kaminski and Nunez, 1999). The other uses of the MACS technique were in pre-analysis separation and concentration of actinides in groundwater (Navratil, 2001), capture of 0.2–0.8 μm PuO_2 particles from very dilute solutions (Worl *et al.*, 2001), and removal of Pu and Am from pH 12 waste waters using magnetic polyamine–epichlorohydrin (Ebner *et al.*, 1999).

(c) Trialkylphosphine oxide (TRPO)

Trialkylphosphine oxide, a mixture of seven alkyl phosphine oxides (Structure r), R being heptyl and octyl alone and a mixture of hexyl, heptyl, and octyl groups[3], has been tested initially in China at the Institute for Nuclear Energy and Technology (Tsinghua University) (Zhu *et al.*, 1983). Tests were continued in a collaborative effort with the European Institute for Transuranium Elements (Karsruhe, Germany) (Apostolidis *et al.*, 1991; Zhu and Song, 1992; Glatz *et al.*, 1993, 1995; Song *et al.*, 1994, 1996; Song and Zhu, 1994; Zhu and Jiao, 1994) for the extraction of actinides, lanthanides, and other fission products from HNO_3 and HLW solutions. The extraction equilibria for the actinide metal ions in their different valency states from nitrate solutions by TRPO can be represented as follows:

$$M^{3+}_{aq} + 3NO^{-}_{3\,aq} + 3TRPO_{org} \rightleftarrows M(NO_3)_3 \cdot 3TRPO_{org} \tag{24.47}$$

$$M^{4+}_{aq} + 4NO^{-}_{3\,aq} + 2TRPO_{org} \rightleftarrows M(NO_3)_4 \cdot 2TRPO_{org} \tag{24.48}$$

$$MO^{+}_{2\,aq} + NO^{-}_{3\,aq} + TRPO_{org} \rightleftarrows MO_2(NO_3) \cdot TRPO_{org} \tag{24.49}$$

$$MO^{2+}_{2\,aq} + 2NO^{-}_{3\,aq} + 2TRPO_{org} \rightleftarrows MO_2(NO_3)_2 \cdot 2TRPO_{org} \tag{24.50}$$

From studies in HNO_3 medium with 30% TRPO in *n*-dodecane as the extractant (Zhu and Song, 1992), it was observed that D_{Am} was less than 1 at 3 M and about 10 only at 1 M HNO_3. To achieve an acceptable D_f for Am, the acidity of HLW (typically 3–6 M) must be reduced to less than 1 M. Neptunium extraction is accomplished after electrolytic reduction to Np(IV) in HNO_3 and in simulated HAW solutions. During all of the experiments with concentrated wastes initially 3 M HNO_3, the waste was diluted ten times and the acidity

[3] Zhu and Song (1992) report approximate composition of 10% hexyl, 50% heptyl and 40% octyl.

then adjusted between 0.7 and 1.0 M. Under such conditions, the recovery of U, Np, Pu, Am, and Cm from HAW using a seven-stage mixer–settler was highly efficient (Zhu and Jiao, 1994). Centrifugal contactor runs (Glatz *et al.*, 1993, 1995; Song *et al.*, 1996) using a battery of 12 extractors with actual diluted HLW has given $D_{f\ \text{actinides}}$ between 10^3 and 10^5. The actinides have in all cases been stripped with 5 M HNO_3 (Am, Cm, rare earths), 0.5 M oxalic acid (Np, Pu), and 5% Na_2CO_3 (U).

Subsequent investigations applied the process to highly saline actual HLW from a Chinese reprocessing plant using 30% TRPO-kerosene. The feed was diluted 2.7 times and the HNO_3 concentration maintained at 1.08 M. This run using miniature centrifugal contactors gave a D_f for total α and ^{99}Tc activities of 588 and 125, respectively. It is claimed that after partitioning the HLW is a non-α waste (Jianchen and Chongli, 2001). The study of γ-irradiation of a 30% TRPO solution in kerosene has shown that above a dose of 2×10^6 Gy phosphonic and phosphinic acids are produced as the radiolytic degradation products along with the formation of polymeric products in the molecular weight range of 500–900 g mol^{-1}. The polymer forms strong complexes with plutonium from which the plutonium is not back-extracted even after five contacts with 0.6 M oxalic acid. This leads to the retention of plutonium in the organic phase (Morita and Kubota, 1987, 1988; Morita *et al.*, 1995; Zhang *et al.*, 2001).

Studies have been carried out with the commercially available TRPO (Cyanex-923, Cytec, Canada Inc., a mixture of four alkyl phosphine oxides R_3PO, R'_3PO, $R_2R'PO$ and RR'_2PO where R = hexyl and R′ = octyl group) to evaluate the effect of phase modifier, TBP, on the extraction of actinides from HNO_3 and synthetic PHWR-HLW solutions (Murali and Mathur, 2001). A series of experiments carried out under various conditions indicated that a mixture of 30% TRPO/20% TBP in *n*-dodecane, when contacted with PHWR-HLW containing ~18 g L^{-1} U at 1 M acidity and an organic to aqueous phase ratio of 5:1, gave highly encouraging results in batch studies. In these experiments, acidity was adjusted with ammonia (a 0.1 L solution of HLW required ~0.02 L of liquid ammonia).

The suitability of TRPO for the partitioning of actinides from HLW solutions has been summarized in Table 24.17. A generic flow sheet is shown in Fig. 24.26. A significant weakness of employing TRPO for actinide partitioning is its comparatively limited capacity and narrow range of nitric acid concentrations that will enable acceptable extraction of trivalent actinides. The dilution of HLW and adjustment of acidity increase waste volume that will create many problems when handling large volumes of HLW.

(d) Diisodecylphosphoric acid (DIDPA)

At the Japan Atomic Energy Research Institute, separation of metal ions from the HLW solutions has been classified into four groups: transuranium elements, Tc–platinum group metals, Sr–Cs, and other elements. For the separation of

Table 24.17 *Suitability of TRPO for the partitioning of actinides from HLW.*

HLW, condition	*Reagent composition*	*Inference*
In ~3.0 M acidity, as such	30% TRPO/*n*-dodecane	third phase formation, cannot be used
Zhu and Song (1992) 10 times diluted, $[H^+]$ adjusted, 0.7–1.0 M	30% TRPO/*n*-dodecane	extraction, reported satisfactory
Murali and Mathur (2001) $[H^+] = \sim 1.0$ M	30% TRPO + 20% TBP/*n*-dodecane, org:aq = 5:1	up to six successive contacts, no reflux, reasonably high *D*
Murali and Mathur (2001) $[H^+] = \sim 1.0$ M HLW, diluted in the ratio 1:2 with 1 M HNO_3	30% TRPO + 20% TBP/*n*-dodecane org:aq = 2:1	up to six successive contacts, no reflux, reasonably high *D*

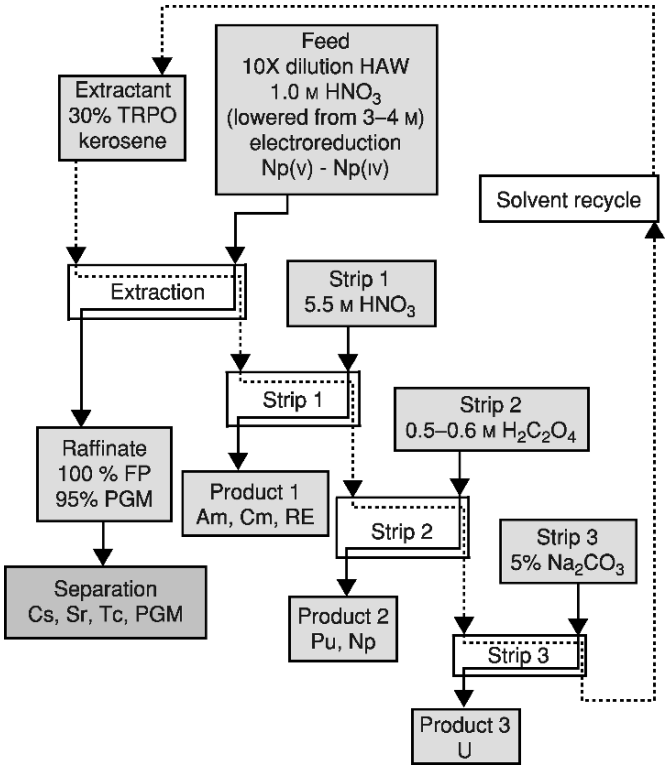

Fig. 24.26 *Generic flow sheet for actinide partitioning using TRPO.*

TRU elements, a mixture of 0.5 M DIDPA + 0.1 M TBP in *n*-dodecane has been proposed with the acidity of the HLW reduced to 0.5 M. Neptunium is reduced from Np(V) to Np(IV) using H_2O_2 and co-extracted with Pu(IV). DIDPA being in the dimeric form (H_2A_2) in *n*-dodecane, the species of the trivalent tetravalent, pentavalent and hexavalent actinides extracted in the organic phase are most likely the electroneutral complexes $M(HA_2)_3$, $M(HA_2)_4$, $MO_2(HA_2)$, and $MO_2(HA_2)_2$, respectively.

Batch as well as counter-current tests using a 16-stage miniature mixer–settler with conditioned synthetic HLW have given very high extraction of actinides including neptunium (flow sheet in Fig. 24.27). During stripping, batch studies with DTPA as a stripping agent gave an Am/rare earths separation factor of greater than 10. After selectively stripping trivalent actinides with DTPA, rare earths could be quantitatively removed with 4 M HNO_3. Neptunium and plutonium are stripped with 0.8 M oxalic acid (Morita and Kubota, 1987, 1988; Morita *et al.*, 1995). In this process, reduction of acidity to about 0.5 M

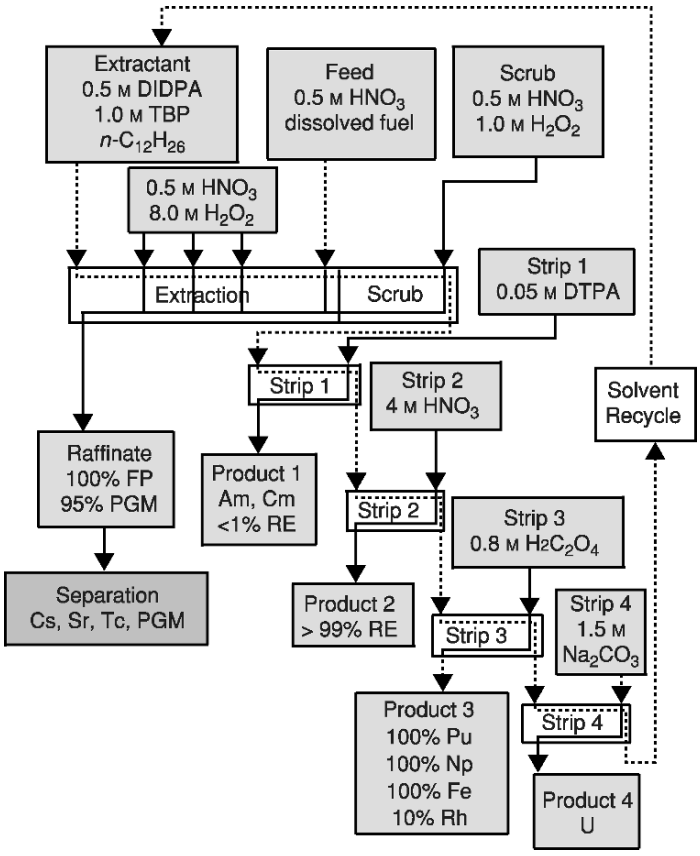

Fig. 24.27 *Generic flow sheet for actinide partitioning in the DIDPA process.*

is accomplished using formic acid. At such low acidity, molybdenum and zirconium precipitate out, carrying about 93% of the plutonium. Filtration units are needed to get a clean HLW solution.

(e) *N*,*N*′-Dimethyl-*N*,*N*′-dibutyltetradecylmalonamide (DMDBTDMA)

One drawback of using organophosphorus extractants is the solid residue that results upon their incineration at the end of their useful life. French researchers have championed the CHON (carbon, hydrogen, oxygen, nitrogen) principle of extractant design (avoiding the use of S or P containing reagents) to minimize the generation of wastes from extractant destruction. This approach to extractant design has generated a much interesting research on a diverse group of reagents.

Among the numerous diamides synthesized and employed for extraction of actinides from nitric acid solutions (Musikas and Hubert, 1983; Musikas, 1987, 1991, 1995; Cuillerdier *et al.*, 1991a,b, 1993; Nigond *et al.*, 1994a,b; Baudin *et al.*, 1995), *N*,*N*-dimethyl-*N*′,*N*′-dibutyl-2-tetradecylmalonamide (DMDBTDMA) has shown the greatest promise. This diamide dissolves in *n*-dodecane, does not give a third phase when in contact with 3–4 M HNO_3, and a 1 M solution gives a D_{Am} of about 10 at 3 M HNO_3. In France, this extractant has been strongly promoted for the partitioning of actinides from HLW solutions (the DIAMEX process).

Investigations of the extraction of uranium, plutonium, americium, and iron by DMDBTDMA at varying HNO_3 concentrations from medium activity liquid waste has given encouraging results. However, some problems have been reported while using this process on tests with high-activity liquid wastes (Baudin *et al.*, 1995). A counter-current centrifugal extractor experiment using a 16-stage battery has been carried out to investigate the hydraulic and extraction behavior of the DIAMEX process using a synthetic HLW solution (Courson *et al.*, 2000) and then finally used for the genuine HLW solution (Malmbeck *et al.*, 2000). With six extraction stages, decontamination factors between 100 and 230 were obtained for lanthanides and above 300 for minor actinides. For back-extraction, four stages were sufficient to recover more than 99.9% of both lanthanides and actinides. The kinetics of lanthanide/actinide extraction (Weigl *et al.*, 2001) and both transient and steady-state concentration profiles in DIAMEX counter-current processing (Facchini *et al.*, 2000) have also been studied. Detailed characterization of these materials and further development of the DIAMEX process continue under the auspices of the PARTNEW European Program (Madic *et al.*, 2002).

(f) Neptunium partitioning during processing

In PUREX processing, consistent control of the flow of neptunium through the system is much more difficult than that of uranium, plutonium, or the trivalent actinides. Dissolution of spent reactor fuel by nitric acid under reflux conditions yields a solution containing principally Np(V) and Np(VI). Flow of neptunium in

PUREX depends on what initial oxidation state adjustments are made to the feed and what steps are taken subsequently to partition plutonium and uranium. Drake (1990) has summarized both the chemistry and process aspects of neptunium control in PUREX. The distribution of neptunium remains a topic of interest in actinide partitioning.

At the Bhabha Atomic Research Centre, the recovery of neptunium from the HLW along with uranium was attempted using a 30% TBP extraction step. The sample was pretreated with 0.01 M $K_2Cr_2O_7$ to oxidize both neptunium and plutonium to the hexavalent state. Both are subsequently co-extracted with U (VI) into 30% TBP. The extraction behavior of neptunium was tested with three types of synthetic wastes and finally with an actual HLW solution. More than 90% of uranium, neptunium, and plutonium could be removed in a single contact. Stripping of neptunium was achieved using a mixture of 0.01 M ascorbic acid and 0.1 M H_2O_2 in 2 M HNO_3 (Mathur *et al.*, 1996b). The kinetics of Np(VI) extraction and stripping under the above conditions while taking synthetic PHWR-HLW as the feed using the AKUFVE technique (Andersson *et al.*, 1969; Johansson and Rydberg, 1969; Reinhardt and Rydberg, 1969; Rydberg, 1969) has demonstrated that the reaction kinetics are fast enough to avoid problems in mixer–settler contacts (Chitnis *et al.*, 1998a). A counter-current study using PHWR-HLW has confirmed the entire process of neptunium extraction and stripping (Chitnis *et al.*, 1998b).

Recent work at the British Nuclear Fuels Limited (BNFL) has focused on the development of an advanced PUREX process. Control of neptunium partitioning in such a system can be accomplished through its interactions with hydroxamic acids. Taylor *et al.* (1998, 2001a,b) report that both formo- and acetohydroxamic acids selectively complex tetravalent actinides and rapidly reduce Np(VI) to Np(V). These characteristics could be used to separate neptunium from plutonium or uranium depending on the approach taken for neptunium extraction. Selected alkyl hydroxylamine species have also been evaluated as reductants for Np(VI) and Pu(IV).

A similar approach to neptunium selectivity using reduction of Np(VI) by butyraldehydes has been suggested by Uchiyama *et al.* (1998). In the partitioning conundrum (PARC), process, the separation of neptunium from plutonium and uranium is proposed in steps prior to Pu/U partitioning in the first extraction cycle of PUREX. Np(VI) is rapidly reduced to Np(V) by *n*-butyraldehyde. This reagent has no effect on the oxidation state of either Pu(IV) or U(VI). Flow sheet development demonstrated partial success in neptunium, technetium, and uranium partitioning. Further work is required to optimize the process.

(g) Trivalent actinide/lanthanide group separation

As noted in Section 24.3.9, separation of trivalent actinides as a group from the lanthanides has been a topic of great interest since the time of discovery of the transplutonium elements. However, setting aside waste volume minimization

considerations, this separation is most important as a problem for hydrometallurgical separations only if the actinides are to be transmuted. Neutron economy in transmutation requires the substantial removal of neutron-absorbing lanthanides. In the PUREX process, as in most new processes being developed for actinide partitioning from HLW, the stripped fraction containing the trivalent actinides (Am and Cm) also contains the trivalent lanthanides. If all actinides are to be recycled as fuel (or targets for transmutation) in a current generation reactor, it is essential to separate americium and curium from trivalent lanthanides to avoid the strong absorption of thermalized neutrons by the lanthanides. Due to the similarities in chemical properties and behavior of Am(III) and Ln(III) reagents, extractants or complexing agents containing soft-donor atoms such as N, S, Cl, etc. are required for reliable group separations (Nash, 1994). A number of techniques and reagents have been developed to achieve separation of trivalent actinides and lanthanides. Among these, a few important existing methods and those being newly developed will be discussed.

(*i*) *TRAMEX process*

Solution of concentrated LiCl at an acidity of 0.02 M HCl in contact with a tertiary amine solution in kerosene or diethyl benzene is the basis of the TRAMEX process for plant-scale separation of trivalent actinides from fission-product lanthanides (Baybarz *et al*., 1963). In this process, the feed solution is 11 M LiCl (0.02 M HCl) containing trivalent actinides and the fission products; the organic phase employed is 0.6 M Alamine 336 (a mixture of tertiary C6–C8 alkyl amines) in diethyl benzene. The scrubbing solution is 11 M LiCl (0.02 M HCl). Trivalent actinides are extracted into the organic phase, while the trivalent lanthanide fission products remain in the raffinate. The actinides are subsequently stripped from the organic phase with 5 M HCl. The TRAMEX process flow sheet is shown in Fig. 24.28. In a single extraction contact, trivalent actinides (Am, Cm, Bk, Cf, Es, and Fm) as a group have a separation factor of about 100 from the trivalent lanthanides (Ce, Nd, Eu, Tb, Ho, and Tm). The order of extraction for the actinides is reported to be Cf > Fm > Es > Bk > Am > Cm.

Several tertiary amines also have been investigated for the extraction of americium and europium from 8 M LiCl/2 M $AlCl_3$/0.02 M HCl using 0.5 M amine in diethyl benzene. The separation factor between americium and europium followed the order: triisoheptyl- (151.7) > triisooctyl- (124.5) ~ trilauryl- (124.1) > Alamine 336 (108). The distribution ratios of americium and europium increased with a decrease in the carbon chain length of the amines. Although separation factor between americium and europium was lowest with Alamine 336, this extractant was preferred because of its easy availability and satisfactory extraction characteristics.

In another study, extraction of trivalent Pu, Am, Cm, Cf, Eu, and Tm from 11.9 M LiCl at pH 2.0 was done with quaternary amines (Aliquat-336 and

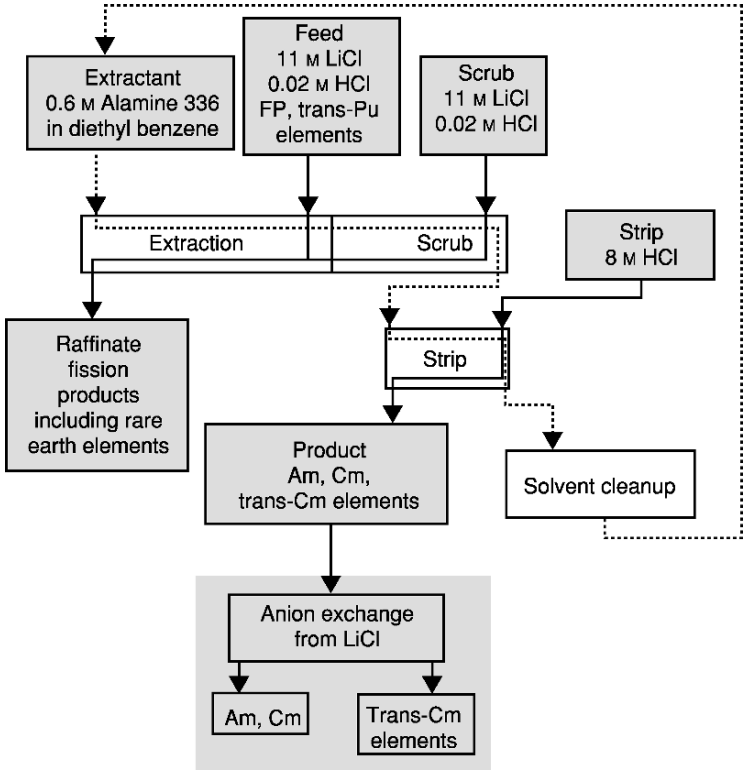

Fig. 24.28 *Generic flow sheet for the TRAMEX process* (*adapted from King* et al., 1981).

tetraheptyl ammonium chloride) and tertiary amines (triisooctyl amine, tri-*n*-octyl amine, Alamine-336 and trilauryl amine) in xylene (Khopkar and Mathur, 1981). The authors have obtained very low separation factors between trivalent actinides and lanthanides when quaternary amines were used whereas they are moderately high while using the tertiary amines. From the absorption spectra of americium and neodymium extracted by the above amines, it was established that the higher separation factors between actinides and lanthanides with tertiary amines are a result of the formation of octahedral hexachloro complexes as compared to the predominantly lower chloro-complexes extracted by the quaternary amines.

(*ii*) *Separation using LIX-63*

The extractant 5,8-diethyl-7-hydroxydodecane-6-one oxime (LIX 63, Structure aa) gave a separation factor (D_{Am}/D_{Eu}) of 2.9 in a batch extraction study (Hoshi *et al.*, 2001). Using this extractant, separation of americium from lighter

lanthanides has been achieved using high-speed counter-current chromatography with a small-coiled column. The coiled column was filled with polytetrafluoroethylene impregnated with a hexane solution of LIX 63. The mobile phase (0.1 M $NaNO_3$/0.01 M morpholinoethane sulfonic acid) contained neodymium and europium (each 10^{-5} M) and radiotracer ^{241}Am. The sample gave a very clear peak for lanthanides when the pH of the mobile phase was 5.60. ^{241}Am was eluted at a pH of 4.60.The authors claim that separation of micro amounts of americium from macro amounts of lanthanides (Hoshi *et al.*, 2001) is possible using this technique. Further work needs to be done to complete the evaluation of the method.

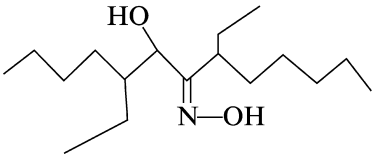

Structure aa

(*iii*) *TALSPEAK process*

The chemistry of the TALSPEAK process has been discussed in detail in Section 24.3.9. Though not deployed as such for accomplishing lanthanide–trivalent actinide separations at process scale, the critical reagent in TALSPEAK, aminopolycarboxylic acids, have repeatedly been employed in the conceptual development of actinide–lanthanide hydrometallurgical separation processes. In the DIDPA and SETFICS processes (described in the next section), the separation of 4f and 5f elements is accomplished in a reverse-TALSPEAK stripping with 0.05 M DTPA (see Fig. 24.11). In the context of modern process design, the aminopolycarboxylates are acceptable reagents, as they are composed of only C, H, O, and N, and hence are fully incinerable. It should be noted, however, that this class of compounds are known to cause difficulties in storage, as hydrogen generation in waste tanks at Hanford has taught (Babad *et al.*, 1991; Meisel *et al.*, 1991; Pederson *et al.*, 1992).

24.4.5 Methods under development

The considerable knowledge that has been developed during decades of fundamental studies of actinide separations supports a number of fresh approaches to important separations processes. It is expected that future efforts to minimize the volume of wastes derived from spent-fuel processing will benefit from this scientific legacy as well. An example of the use of well-understood science being applied in process development is the use of DTPA for La/An partitioning in the DIDPA extraction process for the TRU elements (Morita *et al.*, 1995, 2002). In this case, the stripping of trivalent actinides from the loaded 0.5 M

DIDPA + 0.1 M TBP solvent gave in a batch experiment (after adjustment to pH 3.6) a separation factor of americium from the lanthanides of 10.

A report from JNC has suggested the separation of trivalent actinides and lanthanides applying DTPA in a TRUEX-based process known as SETFICS (Solvent Extraction for Trivalent F-elements Intragroup Separation in CMPO-Complexant System) (Koma *et al*., 1998, 1999; Ozawa *et al*., 1998). Using this process, a counter-current experiment was done with an actual TRUEX product solution employing 0.05 M DTPA/4 M $NaNO_3$ (pH 2.0) as the strippant. Americium and curium were successfully recovered using SETFICS. $^{144}Ce/^{241}Am$ decontamination factor has been reported to be 72. Though 80% of the lanthanides were rejected from the Am–Cm fraction, samarium and europium were poorly separated from the actinide fraction (Koma *et al*., 1998).

(a) Employing soft-donor extractants

By comparison with oxygen donor extactants, soft-donor extractant molecules offer greater potential for more efficient trivalent actinide–lanthanide group separations. For example, Ensor *et al.* (1988) reported Am/Eu separation factors of greater than 100 using the synergistic combination of 4-benzoyl-2,4-dihydro-5-methyl-2-phenyl-3H-pyrazol-3-thione (BMPPT) and 4,7-diphenyl-1,10-phenanthroline (DPPHEN). Independently, neither extractant is particularly effective for the extraction of americium or europium. Musikas and Hubert (1983) reported a high $S_{Am}^{M'}$ between americium and rare earths for their extraction from dilute nitric acid into an extractant mixture of TPTZ and dinonylnaphthalenesulfonic acid (HDNNS) in CCl_4. It was further proposed that HDNNS could be replaced by α-bromocapric acid in an aliphatic diluent. Work on solvent extraction procedures using TPTZ (and related complexants) continues (Cordier *et al*., 1998; Drew *et al*., 1998, 2000).

To overcome the considerable aqueous solubility of TPTZ while conforming to the CHON principle, development of nitrogen-containing extractant molecules continues. In a multinational effort funded by the European Commission's research program on nuclear fuels reprocessing for the future (NEWPART), polyaza ligands, BTPs, have been characterized for selective extraction of trivalent actinides from 1.9 M HNO_3/NH_4NO_3 solutions (Kolarik *et al*., 1999). The extracted complexes have the stoichiometry $M(NO_3)_3 \cdot HNO_3 \cdot 3BTP$ and the Am/Eu separation factors average 100–120. The extraction and separation efficiency is strongly dependent on the diluent. The *n*-propyl derivative self-associates (forming dimers and trimers) in a solution of branched alkanes with 2-ethyl-1-hexanol present as a phase modifier. Counter-current testing of the SANEX-BTP process with real radioactive materials at the Atalante facility in France demonstrated that the *n*-propyl derivative was susceptible to air oxidation with HNO_2 catalysis. Branching in the hydrocarbon side chain improves stability.

(b) Employing Cyanex 301 and other dialkyldithiophosphinic acids

Though Musikas (1985) indicated potential for effective separation of trivalent actinides from lanthanides using thiophosphoric acid extractants, the instability of such extractants towards hydrolysis reduced their utility. However, dithiophosphinic acids, represented by the commercially available extractant Cyanex 301, are somewhat more stable (Sole *et al.*, 1993). Basic features of these systems have been discussed in Sections 24.3.5 and 24.3.9. In a counter-current fractional process having three extraction and two scrubbing stages, more than 99.99% of americium can be separated from a trace amount of europium with less than 0.1% extraction of the latter (Zhu, 1995; Zhu *et al.*, 1996; Chen *et al.*, 1997; Hill *et al.*, 1998).

In another study, a mixture of 0.5 M purified Cyanex 301 and 0.25 M TBP/kerosene has been used in a counter-current experiment to separate americium from lanthanides (Pr, Nd, and Eu) at concentrations of 0.1–0.6 M. A separation factor of around 200 between americium and the lanthanides has been obtained and the extraction can be performed at a pH of 2.7–2.8. This pH value is about 1 unit lower than that needed when Cyanex 301 is used alone. Americium was successfully (>99.998%) separated from macro amounts of lanthanides with only less than 0.04% lanthanides co-extracted (Wang *et al.*, 2001).

The alternative to the SANEX-BTP process that relies instead on dialkyldithiophosphinic acid extractants has been examined as the SANEX-DTP or ALINA process. Initial investigations with a solvent composed of Cyanex 301 in combination with TBP or TOPO as phase modifiers proved inadequate in testing due to the instability of Cyanex 301 under representative conditions. Aromatic derivatives were synthesized in an effort to enable the separation from more acidic media and improve radiation stability. The bis(*p*-chlorophenyl) dithiophosphinic acid (DClDPDTPA) synthesized by Modolo and Odoj (1999) accomplishes both of these objectives. The SANEX-IV process currently under development relies on DClDPDTPA in combination with TOPO as phase modifier. This solvent is reported to extract trivalent actinides from 0.5 to 1.5 M nitric acid.

Apart from the solvent extraction technique for the separation of trivalent actinides from the lanthanides employing Cyanex 301, other techniques like supported liquid membrane and column chromatography have also been utilized (Hoshi *et al.*, 2000; Mimura *et al.*, 2001). A selective and preferential transport of americium across a supported liquid membrane containing highly purified Cyanex 301 has been achieved in the product solution while most of europium remained in the feed solution (Hoshi *et al.*, 2000). Also, microcapsules enclosing Cyanex 301 were prepared by employing a biopolymer gel, alginic acid, as an immobilization matrix. The chromatographic separation of americium and europium was accomplished by gradient elution with 0.1 M (H, Na)NO_3 (pH 2.0) for europium and 0.1 M HNO_3 for americium while using the column packed with the above micro-capsule (Mimura *et al.*, 2001).

Although Cyanex 301 has not yet been used for the separation of americium and curium from the rare earths in the fraction stripped by 0.04 M HNO_3 in the TRUEX process, this process appears to have great potential, though radiation stability and the nature of degradation products represent a concern.

24.4.6 Comparison of extractants being proposed for actinide partitioning

A comparison of the different extractants, their concentration, diluent, phase modifier, best conditions for extraction and stripping of americium is given in Table 24.18. Each system has both positive and negative features. Based on cost of the extractant, the DIDPA and TRPO are clearly superior. However, processes based on the TRPO and DIDPA extractants require, respectively, a ten-fold dilution of the aqueous feed and/or denitration with formaldehyde impacting the volume of wastes generated. Only the DMDBTDMA extractant is completely incinerable. Furthermore, degradation products of DMDBTDMA do not interfere with stripping of americium, while those of CMP and CMPO can. However, the malonamide requires higher concentrations of HNO_3 for efficient extraction of americium, has a comparatively steep nitric acid dependence on the extraction side, and a lower radiolytic stability than that of TBP. Phase modifiers (TBP) are required for both CMP and CMPO extraction systems to prevent third-phase formation, but the TBP apparently increases the stability of the primary extractant. Extraction in the CMPO/TRUEX system is moderately independent of the concentration of HNO_3, simplifying feed preparation. As a complement to PUREX, TRUEX has an advantage, as no adjustment of the aqueous raffinate from PUREX would be required to

Table 24.18 *Comparative features of partitioning of actinides* (*with data for Am*(III)) *with various extractants.*

Extractant concentration (M)	*Diluent*	*HNO_3 conc., for extraction* (M)	*HNO_3 concentration for stripping* (M)
CMP, 0.75	aliphatic hydrocarbon + 0.5 M TBP	>2	<0.15
DIDPA, 0.5	*n*-dodecane + 0.1 M TBP	0.5, denitration or dilution of HLW	4
CMPO, 0.2	*n*-dodecane + 1.2 M TBP	2–3, any HLW as such	0.04
TRPO, 30% (V/V)	*n*-dodecane	0.7–1.0 M, HLW diluted 10 times	>4
TRPO, 30% (V/V)	*n*-dodecane + 20% TBP	~1.0 M, no major dilution	>4
DMDBTDMA, 1.0	*n*-dodecane	>2	<0.5

make successive TRUEX extraction stages compatible. Several new options for trivalent actinide/lanthanide separations by solvent extraction are also emerging. It is clear that, like the decision of whether to process irradiated fuels or not, countries having irradiated nuclear fuels clearly have numerous viable options for processing those fuels should the P&T option be pursued.

Actinide partitioning if and when incorporated at the back-end of the nuclear fuel cycle will considerably reduce the long-term radiological risks and therefore increase the safety of the disposal of nuclear wastes in a geologic repository. Whether actinides are recycled to a reactor (or accelerator) for transmutation or disposed of in a repository, a significant reduction in the hazard associated with the wastes (with transmutation) or the cost (without transmutation) can be achieved through the deployment of actinide partitioning technologies. Though there is no universal consensus on the desirability of actinide partitioning for radioactive waste disposal, continuing research around the world offers an ever-increasing number of potentially viable options for accomplishing partitioning based on solvent extraction, extraction chromatography, supported liquid membranes, or magnetically assisted chemical separations. The continued development of more options relying on the proven technology of solvent extraction may assist immeasurably in securing the public acceptability of nuclear power as the most viable strategy for combating global warming. More advanced options may emerge as work progresses on alternative media like supercritical fluids, room temperature ionic liquids, or the various pyrometallurgical processing options.

24.4.7 Actinide separations around the world – past, present, and future

In the last 20 years, significant emphasis has been put on partitioning and transmutation (P&T) of actinides present in TRU waste generated from various operations involving actinides and also from the HLW solution generated from the reprocessing of nuclear reactor fuels. The International Atomic Energy Agency (IAEA, Vienna) held several advisory group meetings and coordinated research programs on the P&T option. These meetings served as a forum for discussion among several participating countries regarding various extractants, processes developed earlier, or those being developed for partitioning of actinides from HLW solutions. Some of the extractants and developed processes have been discussed above. Here the work that has been carried out and brought to mixer–settler or centrifugal contactor stage of testing will be discussed emphasizing the status of activities in those countries involved in the process, noting that international collaboration is important in this field

(a) United States

In the U.S. after a large amount of work on the extraction of trivalent actinides and lanthanides with several carbamoylmethylphosphonate and phosphine oxides, OΦCMPO was adjudged as the best extractant for this purpose.

For process applications, a mixture of 0.2–0.25 M ОФCMPO and 1–1.4 M TBP in *n*-dodecane, called the TRUEX solvent has been judged as optimum. Although actual HLW generated from the fuel reprocessing plants have not been treated with TRUEX solvent on a large scale in the U.S., different TRU wastes generated have been treated. For example, large volumes of waste generated at the Argonne National Laboratory and the New Brunswick Laboratory have been treated. At Lockheed Martin Idaho Technologies Co., the TRUEX process has been evaluated for the separation of actinides from sodium-bearing waste and calcine waste. At the Oak Ridge National Laboratory, separation and recovery of macro quantities of americium and curium from highly irradiated (> 87% fission) ^{242}Pu targets has been achieved employing the TRUEX process. Other TRU wastes treated with TRUEX solvent at different laboratories in the U.S. are neutralized cladding removal waste (Pacific Northwest National Laboratory), plutonium finishing plant waste (Westinghouse Hanford Co.), and TRU wastes containing chloride salts (Los Alamos National Laboratory). Successful demonstration of a very high efficiency of recovery of TRU elements from the above-mentioned types of wastes is a unique feature for CMPO as an extractant.

Recently, new work has been initiated in the U.S. on the evaluation of possible future nuclear fuel cycles with the commencement of the Advanced Fuel Cycle Initiative. This program is progressing more-or-less in tandem with work on future reactor designs (Generation IV program). In addition, a considerable amount of work has been done in the U.S. investigating pyrometallurgical processing of spent nuclear fuels. Though much work remains to be done to fully enable pyroprocessing, there is no denying that this option has some attractive features and additional work to improve the process is justified.

(b) Japan

At the Japan Atomic Energy Research Institute, 0.5 M DIDPA + 0.1 M TBP in *n*-dodecane has been proposed for the separation of TRU elements from HLW solutions. To employ this acidic extractant for spent fuel reprocessing, the acidity must be reduced to 0.5 M to obtain an efficient recovery of actinides. Work has been done in batch and counter-current tests using synthetic HLW. At Power Reactor and Nuclear Fuel Development Corporation, the TRUEX solvent, i.e. 0.2 M CMPO + 1.2 M TBP in *n*-dodecane, has been utilized for actinide partitioning in batch and counter-current runs with a real high-active raffinate from FBR spent fuel reprocessing. Pyroprocessing and supercritical fluids extraction are also under active consideration in Japan, as are alternatives to the DIAMEX process.

(c) Russia

At the Khlopin Radium Institute, St. Petersburg, efforts have been directed towards using a modified PUREX process to recover actinides such as neptunium

and the other actinides, possibly including the trivalent ions by using a neutral organophosphorus extractant like isoamyldialkylphosphine oxide. Scientists in this laboratory have developed a Russian TRUEX process, based on diphenyl-*N*,*N*-dibutyl CMPO which is less expensive and gives higher D_{Am} values as compared to O(Φ)CMPO. It does not need TBP as the phase modifier but the diluent used is a fluoroether. Very high recoveries and separations of trivalent actinides have been achieved from waste solutions. A variation on this process has been incorporated by scientists in the U.S. at the Idaho National Engineering and Environmental Laboratory in the development of the UNEX process for radioactive waste processing.

(d) China

In China, the main emphasis has been on the extractant trialkylphosphine oxide (TRPO), which is easily synthesized and inexpensive. Actinide recovery and separation from HLW solutions carried out within international collaborations had to be done at acidity of $\leq$1 M and the HLW diluted considerably in this process. However, batch studies, mixer–settler, and centrifugal contactor runs have given highly encouraging results.

(e) France

French chemists have concentrated on the CHON (carbon, hydrogen, oxygen, and nitrogen) principle to design the new extractants of the class amides and diamides. After significant efforts in synthesizing various diamides with different combinations of substituents at R_1, R_2, and R_3 (Structure n), the compound DMDBTDMA was prepared, which is soluble in aliphatic diluent like *n*-dodecane and has respectable *D* values for trivalent actinides and lanthanides at 3–4 M HNO_3. More recently, the tetradecyl backbone substituent has been replaced (in the baseline process) by an ethoxy hexyl (ether) group to improve phase compatibility characteristics. Batch studies, mixer–settler, and centrifugal contactor runs with synthetic as well as actual high-active wastes have given satisfactory results for the recovery of actinides. A great deal of effort has been expended in France on new reagents and processes for minor actinide partitioning and lanthanide/actinide separations and on investigating phase compatibility issues in solvent extraction. Creativity and innovation highlight both the technology and R&D efforts in France on the closed-loop nuclear fuel cycle.

(f) India

Scientists at Bhabha Atomic Research Centre have tested the TRUEX solvent for batch and mixer–settler runs using synthetic high-active waste, stored sulfate bearing waste, and PHWR-HLW. A uranium depletion step with 30% TBP/*n*-dodecane followed by TRUEX process has been suggested for highly efficient

separation and recovery of all the actinides. Batch studies with actual HAW and HLW of research reactor fuels and mixer–settler runs with actual HAW of research reactor fuels have been performed. The raffinate from the mixer–settler runs with synthetic as well as actual wastes had α-activities at the background level. Also, work has been done with Cyanex 923 (a commercially available TRPO) and its mixture with TBP in *n*-dodecane. The batch studies suggest that even with the combination of Cyanex 923 and TBP, the acidity has to be brought down to about 1 M but it may not be necessary to dilute the HLW to a great extent for achieving high separation efficiencies of the actinides. Preliminary studies have been carried out on the extraction of Am(III), U(VI), and Pu(IV) with DMDBTDMA from nitric acid and PHWR-HLW solutions.

(g) Sweden

The research group at Chalmers University developed a three-stage process called CTH (Chalmers Tekniska Hogskola) for separation and recovery of all the actinides from HLW solutions (Svantesson *et al.*, 1979, 1980; Liljenzin *et al.*, 1980). In the first step, acidity of HLW is adjusted to 6 M and uranium, neptunium, and plutonium are extracted with 1 M HDEHP/kerosene. This step also extracts most of the Fe, Zr, Nb, and Mo. In the second step, the acidity of the raffinate is considerably reduced by contacting with 50% TBP/kerosene. Finally in the third step, americium, curium, and rare earths are extracted with 1 M HDEHP. From all the loaded organic phase, the actinides are stripped with suitable reagents. The entire process has been tried with synthetic waste using small-scale mixer–settlers. Because of the problems associated with significant acidity adjustment in the entire process, this may not be cost-effective on a plant scale.

(h) Other countries

In the UK, though British Nuclear Fuels Ltd. actively reprocesses commercial fuels to recover uranium and plutonium, little has been done in the field of actinide partitioning. It appears likely that if the United Kingdom ultimately decides to partition actinides, an appropriate process from the variety of options being developed elsewhere will most probably be adopted. Among the other countries, at the European Commission Joint Research Centre–Ispra Establishment, Italy, a process has been developed by first extracting uranium, neptunium, and plutonium with TBP or HDEHP, diluting the raffinate to a pH of 2 and extracting trivalent americium, curium, and rare earths with a mixture of 0.3 M HDEHP + 0.2 M TBP in *n*-dodecane (Cecille *et al.*, 1980). This process has the same limitations mentioned above for the CTH process. Within Europe, wide international collaboration on actinide partitioning is supported by the European Commission in the frame of its successive Research Framework Programs.

24.5 WHAT DOES THE FUTURE HOLD? FUTURE DIRECTIONS IN ACTINIDE SEPARATIONS

Actinide separations for plutonium processing (in connection with either weapons production or as a part of a plutonium recycle program) and uranium recovery involve primarily solvent extraction processes operating on acidic aqueous solutions. As a consequence of 50 years of both research and process experience, this technology must be considered mature, and has proven to be reliable, though its application has generated complex wastes. Partly as a result of this maturity, but also due to changes in world politics, acid processing to recover plutonium is no longer the principal driving force for development in actinide separations. The challenges attendant to the present status of actinide separations are determined by renewed interest in closing the fuel cycle and by the need for waste cleanup and environment restoration for legacy materials. Current issues in actinide separations are defined by the physical and chemical state of actinides as they occur and the motivation for carrying out the separation.

24.5.1 Alkaline wastes in underground storage tanks

One legacy of 50 years of plutonium production for defense purposes is a large volume of mixed wastes (containing TRUs, long-lived fission products, and non-radioactive but chemically hazardous materials) (Horwitz *et al.*, 1982). Their presence in underground waste tanks or storage bins represents a potential threat to the surrounding environment and so demands attention. These wastes take the form of sludges, solids, alkaline, or acidic solutions, and slurry phases in which actinides coexist with long-lived fission products and non-radioactive constituents. In the face of this complexity, how can the volume of waste going to a repository be minimized? Two potentially important areas for development are: improving sludge washing procedures that can selectively remove actinides from the solids or sludges (solid–liquid separation), and separation procedures suitable for plant-scale development which can operate in alkaline media.

24.5.2 Actinide burnup strategies

A 'permanent' remedy to the long-term hazard of actinides is to 'incinerate' them in advanced reactors or accelerators and thus transform them into short-lived fission products. An added advantage of this approach is the potential for recovery of the energy value of the actinides. Clearly, transmutation also eliminates weapons proliferation concerns as well. Because lanthanides have high cross sections for neutron capture and thus interfere with the neutron physics of actinide burnup, robust Ln/An separation methods are demanded, in particular, processes resistant to radiolysis effects. Two areas of actinide separations research relevant to this problem are the continued development

of fast reactor concept and pyrometallurgical separation process, and the development of new soft-donor extractants and aqueous complexants for actinide/lanthanide separations. Some of the less developed unconventional materials and techniques (RTILs and sc-CO_2, and volatility-based methods in particular) may ultimately have an important role to play in solving this challenging problem.

24.5.3 Actinides and the environment

Minor concentrations of actinides are present in the terrestrial environment as a result of atmospheric weapons testing, the Chernobyl accident, and actinide production activities (including both planned and accidental releases). Accurate speciation techniques, environment decontamination methods, and *in-situ* immobilization techniques are needed. Three generic areas for research, all of which involve some form of separation science, are pertinent to this subject: the development of reliable speciation techniques and thermodynamic models; solid-solution separation methods for removal of actinides from soils, contaminated process equipment, etc.; and solution–mineral conversion techniques to fix residual actinides *in-situ* and inhibit their entry into the hydrosphere/biosphere.

In the earliest days of actinides separations, discovery and plutonium production dominated the landscape. Sixty years later as we approach the end of the age of fossil fuels, actinide separation could play a central role in the preservation and restoration of the planetary environment. The major change in emphasis does not mean the end of the need for actinide separations, it indicates a shift toward new horizons. Many opportunities exist for improvements in existing procedures or the development of new methods for actinide isolation.

REFERENCES

Abney, K. D., Pinkerton, A. B., Staroski, R. C., Schroeder, N. C., Ashley, K. R., Adams, J. M., and Ball, J. R. (1995) in *Separations of f-Elements* (eds. K. L. Nash and G. R. Choppin), Plenum Press, New York, pp. 209–23.

Ackerman, J. P. (1991) *Ind. Eng. Chem. Res.*, **30**, 141–5.

Ackerman, J. P. and Johnson, T. R. (1993) Partition of Actinides and Fission Products Between Metal and Molten Salt Phases – Theory, Measurement and Application to IFR Pyroprocess Development, in *Int. Conf. Actinides 93,* Santa Fe, NM, Abstract 81.

Ackerman, J. P. and Settle, J. L. (1993) *J. Alloys Compd.*, **199**, 77–84.

Addleman, R. S., Hills, J. W., and Wai, C. M. (1998) *Rev. Sci. Instrum.*, **69**(9), 3127–31.

Addleman, R. S. and Wai, C. M. (1999) *Phys. Chem. Chem. Phys.*, **1**, 783–90.

Addleman, R. S., Carrott, M. J., and Wai, C. M. (2000a) *Anal. Chem.*, **72**, 4015–21.

Addleman, R. S., Carrott, M. J., Wai, C. M., Carleson, T. E., and Wenclawiak, B. W. (2000b) *Anal. Chem.*, **73**, 1112–19.

Addleman, R. S. and Wai, C. M. (2000). *Anal. Chem.* **72**, 2109–2116.
Addleman, R. S. and Wai, C. M. (2001) *Radiochim. Acta*, **89**, 27–33.
Afonichkin, V. K. and Komarov, V. E. (1995) Production of Granulated Uranium Oxides by Electrolysis of Molten Tungstate, Abstracts of the Molten Salt in Nuclear Technologies Seminar, Dimitrovgrad, Russia.
Afonichkin, V. K., Komarov, V. E., Khrustova, L. G., and Vakarin, S. V. (2001) *Radiochemistry*, **43**(3), 224–9.
Akabori, M., Itoh, A., and Ogawa, T. (1997) *J. Nucl. Mater.*, **248**, 338–42.
Akatsu, J. and Kimura, T. (1990) *J. Radioanal. Nucl. Chem.*, **140**, 195–203.
Alexandratos, S. D., Trochimczuk, A. Q., Crick, D. W., Horwitz, E. P., Gatrone, R. C., and Chiarizia, R. (1993) in *Emerging Separation Technology for Metallic Fuels, Proc. Symp.,* pp. 111–17.
Aly, H. F., Khalifa, S. M., Navratil, J. D., and Saba, M. T. (1985) *Solvent Extr. Ion Exch.*, **3**, 623–36.
Andersson, C., Andersson, S. O., Liljenzin, J. O., Reinhardt, H., and Rydberg, J. (1969) *Acta Chem. Scand., (1947–1973)*, **23**(8), 2781–96.
Anderson, C. J. (1990) PhD Dissertation, Chemistry Department, Florida State University.
Anderson, C. J., Deakin, M. R., Choppin, G. R., D'Olieslager, W., Heerman, L., and Pruett, D. J. (1991) *Inorg. Chem.*, **30**, 4013–16.
Anderson, C. J., Choppin, G. R., Pruett, D. J., Costa, D. A., and Smith, W. H. (1999) *Radiochim. Acta*, **84**, 31–6.
Anonymous (1951) *Hanford Redox Technical Manual*, Chemical Development Section, Separations Technology Division, Technical Divisions, Hanford Works, HW-18700 and declassified with deletions as HW-18700 DEL.
Anonymous (1955) *PUREX Technical Manual*, Chemical Development Subsection, Separations Technology Section, Engineering Department, Hanford Atomic Products Operation, declassified with deletion as HW-31000 DEL.
Anonymous (1995) *Nuclear Wastes*: *Technologies for Separation and Transmutation*, National Research Council, National Academy Press, Washington, DC.
Anonymous (1996) *Closing the Circle on the Splitting of the Atom: The Environmental Legacy of Nuclear Weapons Production in the United States and What the Department of Energy is Doing About It*, Report DOE/EM-0266, U.S. Department of Energy.
Anonymous (2000) *Committee on Electrometallurgical Techniques for DOE Spent Fuel Treatment Final Report*, National Academy Press, Washington, DC.
Apostolidis, C., De Meester, R., Koch, L., Molinet, R., Liang, J., and Zhu, Y. (1991) in *New Separation Chemistry Techniques for Radioactive Waste and Other Specific Applications* (eds. L. Cecille, M. Casarci, and L. Pietrelli), Elsevier Applied Science, London and New York, pp. 80–6.
Arai, Y., Suzuki, Y., and Handa, M. (1995) in *Proc. Inter. Conf. on Evaluation of Emerging Nuclear Fuel Cycle Systems* (*Global'95*), Versailles, France.
Arai, Y. and Yamashita, T. (1997) Overview of Activities on Plutonium and Minor Actinides Fuel Research in JAERI, 2nd Seminar on the New Fuel Cycle Technology Towards the 21st Century, Taejon, Korea.
Arai, Y., Iwai, T., Nakajima, K., Shirai, O., and Suzuki, Y. (1999) Experimental Research on Nitride Fuel Cycle in JAERI, in *Proc. Inter. Conf. on Future Nuclear Systems* (*Global'99*), Jackson Hole, Wyoming.

Arduini, A., Bohmer, V., Delmau, L., Desreux, J.-F., Dozol, J.-F., Carrera, M. A. G., Lambert, B., Musigmann, C., Pochini, A., Shivanyuk, A., and Ugozzoli, F. (2000) *Chem. Eur. J.*, **6** (12), 2135–44.

Arnaud-Neu, F., Barboso, S., Boehmer, V., Brisach, F., Delmau, L., Dozol, J.-F., Mogck, O., Paulus, E. F., Saadioui, M., and Shivanyuk, A. (2003) *Aust. J. Chem.*, **56**(11), 1113–19.

Arnold, E. D. (1962) *Radiation Hazards of Recycled ^{233}U-Th Fuels*, Report TID-7650 (Book 1), USAEC, Oak Ridge National Laboratory, pp. 253–84.

ATW Separations Technology and Waste Forms Technical Working Group (1999) *A Roadmap for Developing ATW Technology: Separations & Waste Forms Technology*, Report ANL-99-15, Argonne National Laboratory.

Auchapt, P., Giraud, J. P., Talmont, X., Bathellier, A., Grieneisen, A., and Plessy, L. (1968) *Energy Nucl.* (*Paris*), **10**(3), 181–91.

Awwal, M. A. (1971) *Aqueous Reprocessing of Thorium–Uranium-233 Fuel Cycle by Amine Solvent from Sulfate Media,* NTIS Report (A/CONF.49/P-650), Atomic Energy Center, Dacca, Pakistan.

Baaden, M., Schurhammer, R., and Wipff, G. (2002) *J. Phys. Chem. B*, **106**(2), 434–41.

Babad, H., Johnson, G. D., Lechelt, J. A., Reynolds, D. A., Pederson, L. R., Strachan, D. M., Meisel, D., Jonah, C., and Ashby, E. C. (1991) *Evaluation of the Generation and Release of Flammable Gases in Tank 241-SY-101,* Westinghouse Hanford, Richland, WA, WHC-EP-0517.

Baes, C. F. Jr (1966) *The Chemistry and Thermodynamics of Molten Salt Reactor Fluoride Solutions,* vol. 1, *Thermodynamics*, Vienna, IAEA.

Baes, C. F. Jr (1969) *Reprocessing of Nuclear Fuels*, Conf. 690-801, USAEC.

Baes, C. F. Jr (1974) *J. Nucl. Mater.*, **51**, 149–62.

Baetsle, L. H. (1992) International Atomic Energy Agency, Vienna, IAEA bull., **34**(3), pp. 32–4.

Banaszak, J. E., Rittmann, B. E., and Reed, D. T. (1999) *J. Radioanal. Nucl. Chem.*, **241**, 385–435.

Barney, G. S. and Covan, R. G. (1992) Separation of Actinide Ions from Radioactive Waste Solutions Using Extraction Chromatography, Presented at the American Chemical Society National Meeting, San Francisco, CA, April 5–10.

Barr, M. E., Schulte, L. D., Jarvinen, G. D., Espinoza, J., Ricketts, T. E., Valdez, Y., Abney, K. D., and Bartsch, R. A. (2001) *J. Radioanal. Nucl. Chem.*, **248**(2), 457–65.

Baudin, G., Lefevre, J., Prunier, C., and Salvatores, M. (eds.) (1995) in *Proc. Technical Committee on Safety and Environmental Aspects of Partitioning and Transmutation of Actinides and Fission Products*, 1993, IAEA, Vienna, p. 37.

Baybarz, R. D., Weaver, B. S., and Kuiser, H. B. (1963) *Nucl. Sci. Eng.*, **17**, 457–62.

Baybarz, R. D. (1965) *J. Inorg. Nucl. Chem.*, **27**, 1831–9.

Baybarz, R. D. (1970) *At. Energy Rev.*, **8**, 327–60.

Bell, J. R. and McNeese, L. E. (1971) Report ORNL-TM-3141, Oak Ridge National Laboratory.

Benedict, G. E., Harmon, K. M., Jansen, G. J., Mudge, L. K., and Scott, F. A. (eds.) (1963) in *New Nuclear Materials Including Non-Metallic Fuels*, vol 1, IAEA, Prague, pp. 21–37.

Bennett, G. A., Burris, L. J., and Vogel, R. C. (1964) *Halide Slagging for Uranium–Plutonium Alloys*, Report ANL-6895, USAEC, Argonne National Laboratory.

Berthon, C., Vaufrey, F., Livet, J., Madic, C., and Hudson, M. J. (1996) in *Proc. Inter. Solvent Extraction Conf. ISEC'96*, vol. 2 (eds. D. C. Shallcross, R. Paimin, and L. M. Prvcic), Melbourne, pp. 1349–54.

Berthon, L., Morel, J. M., Zorz, N., Nicol, C., Virelizier, H., and Madic, C. (2001) *Sep. Sci. Technol.*, **36** (5–6), 709–28.

Bertozzi, G., Girardi, F., and Mousty, F. (1976) *Transplutonium 1975*, in *Proc. 4th Int. Transplutonium Elem. Symp.*, pp. 449–57.

Bertrand, P. A. and Choppin, G. R. (1982) *Radiochim. Acta*, **31**, 135–7.

Betchel, T. B. and Storvick, T. S. (1999) *Ind. Eng. Chem. Res.*, **38**, 1723–8.

Bisset, W., Jacobs, H., Koshti, N., Stark, P., and Gopalan, A. (2003) *React. Funct. Polym.*, **55**(2), 109–19.

Blanco, R. E., Ferris, L. M., and Ferguson, D. E. (1962) *Aqueous Processing of Thorium Fuels*, Report ORNL-3219, USAEC, p. 35.

Bond, E. M., Engelhardt, U., Deere, T. P., Rapko, B. M., and Paine, R. T. (1997) *Solvent Extr. Ion Exch.*, **15**, 381–400.

Bond, E. M., Engelhardt, U., Deere, T. P., Rapko, B. M., and Paine, R. T. (1998) *Solvent Extr. Ion Exch.*, **16**, 967–83.

Bond, W. D. and Leuze R. E. (1980) in *Actinide Separations*, (eds. J. D. Navratil, and W. W. Schulz), (ACS Symposium Series 117) American Chemical Society, Washington, DC, pp. 441–54.

Borkowski, M., Ferraro, J. R., Chiarizia, R., and McAlister, D. R. (2002) *Solvent Extr. Ion Exch.*, **20**, 313–30.

Borkowski, M., Chiarizia, R., Jensen, M. P., Ferraro, J. R., Thiyagarajan, P., and Littrell, K. C. (2003) *Sep. Sci. Technol.*, **38**, 3333–51.

Bourges, J., Madic, C., and Koehly, G. (1980) in *Actinide Separations* (eds. J. D. Navratil and W. W. Schulz) (ACS Symp. Ser. 117), American Chemical society, Washington, DC, pp. 33–50.

Bowersox, D. F. and Leary, J. A. (1960) *Purification of Plutonium Fuels by Mercury Processing* (*Experimental Survey*), Report USAEC LAMS-2518, Los Alamos Scientific Laboratory.

Bradley, A. E., Hatter, J. E., Nieuwenhuyzen, M., Pitner, W. R., Seddon, K. R., and Thied, R. C. (2002) *Inorg. Chem.*, **41**, 1692–4.

Brambilla, G. (1984) *Radiochim. Acta*, **36**(1/2), 37–42.

Brauer, R. D., Carleson, T. E., Harrington, J. D., Jean, F. M., Jiang, H., Lin, Y., and Wai, C. M. (1994) EGG-WTD-10993, January 1994.

Brodsky, M. B. and Carleson, B. G. F. (1962) *J. Inorg. Nucl. Chem.*, **24**, 1675–81.

Brown, D. and Jones, P. J. (1966) *J. Chem. Soc.* (*A*), 874–8.

Bruce, F. R. (1957) *Ion-Exchange Isolation Processes*, Report TID-7534 (Book 1), USAEC, pp. 180–222.

Bukina, T. I., Karalova, Z. K., and Myasoedov, B. F. (1983) *Radiokhimiya*, **25**, 697–700.

Burris, L., Harmon, K. M., Brand, G. E., Murbach, E. W., and Steunenberg, R. K. (eds.) (1964) in *Proc. 3rd U.N. Int. Conf. on the Peaceful Uses of Atomic Energy*, vol. 10, United Nations, New York, pp. 501–7.

Burris, L. (1986) *Chem. Eng. Prog.*, **82**(2), 35–9.

Burris, L., Steunenberg, R., and Miller, W. E. (1987) *AIChE Symp. Ser.*, **83**(254), 135–42.

Bychkov, A. V., Vavilov, S. K., Porodnov, P. T., and Skiba, O. V. (1995) *Experience on Spent Oxide Fuel Reprocessing in Molten Chlorides,* Abstracts of the Molten Salt in Nuclear Technologies Seminar, Dimitrovgrad, Russia.

Bychkov, A. V. and Skiba, O. V. (1999) in *Chemical Separation Technologies and Related Methods of Nuclear Waste Management* (eds. G. R. Choppin and M. K. Khankhasayev), Kluwer Academic Publishers, Dordrecht, pp. 71–98.

Bychkov, A. V., Skiba, O. V., Vavilov, S. K., Kormilitzin, M. V., and Osipenko, A. G. (eds.) (2000) in *Proc. Workshop on Pyrochemical Separations*, OECD/NEA, Avignon, France, pp. 37–46.

Caceci, M., Choppin, G. R., and Liu, Q. (1985) *Solvent Extr. Ion Exch.*, **3**, 605–21.

Caligara, F., Martinot, L., and Duyckaerts, G. (1968) *J. Electroanal. Chem.*, **16**, 335–40.

Campbell, G. M. and Leary, J. A. (1966) *Thermodynamics Properties of Plutonium Compounds from EMF Measurements*, Report LA-3399, Los Alamos National Laboratory.

Campbell, D. O. (1970) *Ind. Eng. Chem., Process Des. Dev.*, **9**, 95–9.

Carpio, R. A., King, L. A., Lindstrom, R. E., Nardi, J. C., and Hussey, C. L. (1979) *J. Electrochem. Soc.*, **126**(10), 1644–50.

Carroll, R. L. and Irani, R. R. (1967) *Inorg. Chem.*, **6**, 1994–8.

Carroll, R. L. and Irani, R. R. (1968) *J. Inorg. Nucl. Chem.*, **30**, 2974–6.

Carrott, M. J. and Wai, C. M. (1998) *Anal. Chem.*, **70**, 2421–5.

Carrott, M. J., Waller, B. E., Smart, N. G., and Wai, C. M. (1998) *Chem. Commun.*, 373–4.

Casarci, M., Chiarizia, R., Gasparini, G. M., Puzzuoli, G., and Valeriani, G. (1988) *Separation and Recovery of Transuranium Elements from Liquid Wastes Produced by the Casaccia Plutonium Plant*, ISEC' 88, vol. IV, Moscow, p. 219.

Casarci, M., Gasparini, G. M., and Grossi, G. (1989) Actinide Recovery from Radioactive Liquid Wastes Produced by ENEA Experimental Fabrication and Reprocessing Plants by CMPO, Actinides-89, Tashkent, USSR.

Cecille, L., Dworschak, H., Girardi, F., Hunt, B. A., Mannove, F., and Mousty, F. (1980) in *Actinide Separations* (eds. J. D. Navratil and W. W. Schulz), American Chemical Society, Washington, DC, pp. 427–40.

Cecille, L., Gompper, K., Gutman, R., Halaszovich, S., Mousty, F., and Petteau, J. F. (1987) *Chemical Precipitation Processes for the Treatment of Low and Medium Level Liquid Waste,* CEC, Brussels, Belgium, Comm. Eur. Communities, [Rep.] EUR.

Chamberlain, D. B., Conner, C., Hutter, J. C., Leonard, R. A., Wygmans, D. G., and Vandegrift, G. F. (1997) *Sep. Sci. Technol.*, **32**, 303–26.

Chang, Y. (1989) *Nucl. Technol.*, **88**, 129–38.

Chauvin, G., Coriou, H., and Huré, J. (1962) *Métaux* (*Corrosion-Ind*), **37**, 112–26.

Chauvin, G., Coriou, H., Jabot, P., and Laroche, A. (1964) *J. Nucl. Mater.*, **11**, 183–92.

Chen, J., Jiao, R., and Zhu, Y. (1997) *Radiochim. Acta*, **76**, 129–30.

Chiarizia, R. and Horwitz, E. P. (1986) *Solvent Extr. Ion Exch.*, **4**, 677–723.

Chiarizia, R. and Danesi, P. R. (1987) *Sep. Sci. Technol.*, **22**, 641–59.

Chiarizia, R. and Horwitz, E. P. (1990) *Solvent Extr. Ion Exch.*, **8**, 907–41.

Chiarizia, R., Horwitz, E. P., Gatrone, R. C., Alexandratos, S. D., Trochimczuk, A. Q., and Crick, D. W. (1993) *Solvent Extr. Ion Exch.*, **11**(5), 967–85.

Chiarizia, R. and Horwitz, E. P. (1994) *Solvent Extr. Ion Exch.*, **12**(4), 847–71.

Chiarizia, R., Horwitz, E. P., and Alexandratos, S. D. (1994) *Solvent Extr. Ion Exch.*, **12**(1), 211–37.
Chiarizia, R., Horwitz, E. P., D'Arcy, K. A., Alexandratos, S. D., and Trochimczuk, A. W. (1996) *Solvent Extr. Ion Exch.*, **14**(6), 1077–100.
Chiarizia, R., Horwitz, E. P., Alexandratos, S. D., and Gula, M. J. (1997) *Sep. Sci. Technol.*, **32**(1–4), 1–35.
Chiarizia, R., Urban, V., Thiyagarajan, P., and Herlinger, A. W. (1998) *Solvent Extr. Ion Exch.*, **16**, 1257–78.
Chiarizia, R. and Horwitz, E. P. (2000) *Solvent Extr. Ion Exch.*, **18**(1), 109–32.
Chiarizia, R., Jensen, M. P., Borkowski, M., Ferraro, J. R., Thiyagarajan, P., and Littrell, K. C. (2003a) *Sep. Sci. Technol.*, **38**(12/13), 3313–32.
Chiarizia, R., Nash, K. L., Jensen, M. P., Thiyagarajan, P., and Littrell, K. C. (2003b) *Langmuir*, **19**(23), 9592–99.
Chiarizia, R., Jensen, M. P., Borkowski, M., Thiyagarajan, P., and Littrell, K. C. (2004) *Solvent Extr. Ion Exch.*, **22**(3), 325–51.
Chiotti, P. and Parry, S. F. S. (1962) *J. Less Common Metals*, **4**, 315–37.
Chitnis, R. R., Wattal, P. K., Murali, M. S., Nair, A. G. C., and Mathur, J. N. (1998a) *Solvent Extr. Ion Exch.*, **16**, 899–912.
Chitnis, R. R., Wattal, P. K., Ramanujam, A., Dhami, P. S., Gopalakrishnan, V., Mathur, J. N., and Murali, M. S. (1998b) *Sep. Sci. Technol.*, **33**, 1877–87.
Chitnis, R. R., Wattal, P. K., Ramanujam, A., Dhami, P. S., Gopalakrishnan, V., Bauri, A. K., and Banerji, A. (1999a) *J. Radioanal. Nucl. Chem.*, **240**, 727–30.
Chitnis, R. R., Wattal, P. K., Ramanujam, A., Dhami, P. S., Gopalakrishnan, V., Bauri, A. K., and Banerji, A. (1999b) *J. Radioanal. Nucl. Chem.*, **240**, 721–6.
Chitnis, R. R., Dhami, P. S., Gopalakrishnan, V., Wattal, P. K., Ramanujam, A., Murali, M. S., Mathur, J. N., Bauri, A. K., and Chattopadhyay, S. (2000) *Partitioning of Actinides from High Active Waste Solution of PUREX Origin: Counter Current Extraction Studies Using TBP and CMPO*, Report BARC/E – 031, Bhabha Atomic Research Centre.
Chmutova, M. K. and Kochetkova, N. E. (1970) *Zh. Anal. Khim.*, **25**, 710–14.
Chmutova, M. K., Pribylova, G. A., and Myasoedov, B. F. (1973) *Zh. Anal. Khim.*, **28**, 2340–3.
Chmutova, M. K., Nesterova, N. P., Koiro, O. E., and Myasoedov, B. F. (1975) *Zh. Anal. Khim.*, **30**, 1110–15.
Chmutova, M. K., Kochetkova, N. E., Koiro, O. E., Myasoedov, B. F., Medved, T. Y., Nesterova, N. P., and Kabachnik, M. I. (1983) *J. Radioanal. Nucl. Chem.*, **80**, 63–9.
Choppin, G. R., Harvey, B. G., and Thompson, S. G. (1956) *J. Inorg. Nucl. Chem.*, **2**, 66–8.
Choppin, G. R. and Silva, R. J. (1956). *J. Inorg. Nucl. Chem.* **3**, 153–154.
Choppin, G. R. and Chetham-Strode, A. (1960) *J. Inorg. Nucl. Chem.*, **15**, 377–83.
Choppin, G. R. and Rydberg, J. (1980) *Nuclear Chemistry, Theory and Applications,* Pergamon Press, Oxford.
Choppin, G. R., Navratil, J. D., and Schulz, W. W. (eds.) (1985) *Actinide/Lanthanide Separations,* World Scientific, Singapore.
Choppin, G. R. and Barber, D. W. (1989) *J. Less Common Metals*, **149**, 231–5.
Choppin, G. R., Yao, J., and Wharf, R. M. (1995) in *Separations of f-Elements* (eds. K. L. Nash and G. R. Choppin), Plenum Press, New York, pp. 31–42.

Choppin, G. R. and Bond, A. H. (1996) *J. Anal. Chem.* (Translation of Zhurnal Analiticheskoi Khimii), **51**(12), 1129–38.
Choppin, G. R. and Nash, K. L. (1996) *Radiochim. Acta*, **70/71**, 225–36.
Choppin, G. R. and Wong, P. J. (1998) *Aquat. Geochem.*, **4**(1), 77–101.
Choppin, G. R. (2002) in *Chemical Separations in Nuclear Waste Management* (eds. G. R. Choppin, M. K. Khankhasayev, and H. S. Plendl), Battelle Press, Columbus, OH, pp. 49–55.
Choppin, G. R. Liljenzin, J.-O., and Rydberg, J. (2002) *Radiochemistry and Nuclear Chemistry,* 3rd edn, Butterworth-Heinemann, Woburn, MA, p. 2.
Chrastil, J. (1982) *J. Phys. Chem.*, **86**, 3016–21.
Cleveland, J. M. (1970) *The Chemistry of Plutonium,* Gordon and Breach, New York.
Clifford, A. A., Zhu, S., Smart, N. G., Lin, Y., Wai, C. M., Yoshida, Z., Meguro, Y., and Iso, S. (2001) *J. Nucl. Sci. Technol.*, **38**(6), 433–8.
Coleman, C. F. (1964) *At. Energy Rev.*, **2**(2), 3–54.
Cooper, U. R. and Walling, M. T. Jr (1958) in *Proc. 2nd U.N. Int. Conf. on Peaceful Uses of Atomic Energy*, Geneva, 1958, vol. 17, pp. 291–373.
Cordier, P. Y., Hill, C., Baron, P., Madic, C., Hudson, M. J., and Liljenzin, J. O. (1998) *J. Alloys Compd.*, **271–273**, 738–41.
Costa, D. A., Smith, W. H., and Dewey, H. J. (2000) in *Molten Salts XII, Proc. Electrochem. Soc.*, pp. 80–99 and 99–41.
Cotton, F. A. and Wilkinson, G. (1988) in *Advanced Inorganic Chemistry,* 5th edn, John Wiley, New York, pp. 1004–5.
Courson, O., Lebrun, M., Malmbeck, R., Pagliosa, G., Romer, K., Satmark, B., and Glatz, J. P. (2000) *Radiochim. Acta*, **88**, 857–63.
Cuillerdier, C., Musikas, C., Hoel, P., Nigond, L., and Vitart, X. (1991a) *Sep. Sci. Technol.*, **26**, 1229–44.
Cuillerdier, C., Musikas, C., and Hoel, P. (1991b) in *New Separation Techniques for Radioactive Waste and Other Specific Applications* (eds. L. Cecille, M. Casarci, and L. Pietrelli) (*Proc. Tech. Semin.*), Elsevier Applied Science, New York and London, pp. 41–8.
Cuillerdier, C., Musikas, C., Hoel, P., and Nigond, L. (1993) *Sep. Sci. Technol.*, **28**, 155–75.
Cuthbert, F. L. (1958) *Thorium Production Technology,* Addison-Wesley, Reading, MA.
Dai, S., Shin, Y. S., Toth, L. M., and Barnes, C. E. (1997a) *Inorg. Chem.*, **36**, 4900–2.
Dai, S., Toth, L. M., Hayes, G. R., and Peterson, J. R. (1997b) *Inorg. Chim. Acta*, **256**, 143–5.
Dai, S., Ju, Y. H., and Barnes, C. E. (1999) *J. Chem. Soc., Dalton Trans.*, 1201–2.
Dakternieks, D. R. (1976) *J. Inorg. Nucl. Chem.*, **38**, 141–3.
Danesi, P. R., Horwitz, E. P., and Rickert, P. G. (1983) *J. Phys. Chem.*, **87**, 4708–15.
Danesi, P. R., Chiarizia, R., Rickert, P., and Horwitz, E. P. (1985) *Solvent Extr. Ion Exch.*, **3**, 111–47.
Darr, J. A. and Poliakoff, M. (1999) *Chem. Rev.*, **99**, 495–541.
Davis, J. H. Jr (2002) *ACS Symp. Ser.*, **818** (Ionic Liquids), 247–58.
Davy, H. (1808) *Philos. Trans. R. Soc. London,*
De Waele, R., Heerman, L., and D'Olieslager, W. (1982) *J. Electroanal. Chem.*, **142**, 137–46.

Delavente, F., Guillot, J. M., Thomas, O., Berthon, L., and Charbonnel, M. C. (1998) *Environ. Eng.* **3** (*Environ. Eng. Manage.*), 189–98.

Delavente, F., Guillot, J. M., Thomas, O., Berthon, L., and Nicol, C. (2001) *J. Anal. Appl. Pyrolysis*, **58–59**, 589–603.

Delavente, F., Guillot, J.-M., Thomas, O., Berthon, L., and Nicol, C. (2003) *J. Photochem. Photobiol. A*, **158**(1), 55–62.

Delmau, L. H., Simon, N., Dozol, J.-F., Eymard, S., Tournois, B., Schwing-Weill, M.-J., Arnaud-Neu, F., Bohmer, V., Gruttner, C., Musigmann, C., and Tunayar, A. (1998) *Chem. Commun.*, (16), 1627–8.

Delmau, L. H., Simon, N., Schwing-Weill, M.-J., Arnaud-Neu, F., Dozol, J.-F., Eymard, S., Tournois, B., Gruttner, C., Musigmann, C., Tunayar, A., and Bohmer, V. (1999) *Sep. Sci. Technol.*, **34**(6–7), 863–76.

Deshingkar, D. S., Chitnis, R. R., Theyyunni, T. K., Wattal, P. K., Ramanujam, A., Dhami, P. S., Gopalakrishnan, V., Rao, M. K., Mathur, J. N., Murali, M. S., Iyer, R. H., Badheka, L. P., and Bannerji, A. (1993) *Counter-Current Studies on Actinide Partitioning from Sulphate Bearing Simulated High-Level Wastes Using CMPO*, Report BARC/E-028, Bhabha Atomic Research Centre.

Deshingkar, D. S., Chitnis, R. R., Wattal, P. K., Theyyunni, T. K., Nair, M. K. T., Ramanujam, A., Dhami, P. S., Gopalakrishnan, V., Rao, M. K., Mathur, J. N., Murali, M. S., Iyer, R. H., Badheka, L. P., and Bannerji, A. (1994) *Partitioning of Actinides from Simulated High Level Wastes Arising from Reprocessing of PHWR Fuels: Counter-Current Extraction Studies Using CMPO*, Report BARC/E-014, Bhabha Atomic Research Centre.

Dhami, P. S., Gopalakrishnan, V., Kannan, R., Ramanujam, A., Salvi, N., and Udupa, S. R. (1998a) *Biotechnol. Lett.*, **20**, 225–8.

Dhami, P. S., Kannan, R., Gopalakrishnan, V., Ramanujam, A., Salvi, N., and Udupa, S. R. (1998b) *Biotechnol. Lett.*, **20**, 869–72.

Diamond, R. M., K., Street, J., and Seaborg, G. T. (1954) *J. Am. Chem. Soc.*, **76**, 1461–9.

Diamond, H., Horwitz, E. P., and Danesi, P. R. (1986) *Solvent Extr. Ion Exch.*, **4**, 1009–27.

Dozol, J. F., Carrera, A. G., and Rouquette, H. (2000) *AIP Conf. Proc.*, **532** (Plutonium Futures – The Science), 82–7.

Drake, V. A. (1990) in *Science and Technology of Tributyl Phosphate,* vol. III. (eds. W. W. Schulz, L. L. Burger, and J. D. Navratil), CRC Press, Boca Raton, FL, pp. 123–45.

Drew, M. G. B., Hudson, M. J., Iveson, P. B., Russell, M. L., Liljenzin, J. O., Skälberg, M., Spüth, L., and Madic, C. (1998) *J. Chem. Soc., Dalton Trans.*, 2973–80.

Drew, M. G. B., Iveson, P. B., Hudson, M. J., Liljenzin, J. O., Sputh, L., Cordier, P. Y., Enarsson, A., Hill, C., and Madic, C. (2000) *J. Chem. Soc., Dalton Trans.*, 821–30.

Drew, M.G. B., Hill, C., Hudson, M. J., Iveson, P. B., Madic, C., and Youngs, T. G. A. (2004a) *Dalton Trans.*, (2), 244–51.

Drew, M. G. B., Hill, C., Hudson, M. J., Iveson, P. B., Madic, C., Vaillant, L., and Youngs, T. G. A. (2004b) *New J. Chem.*, **28**(4), 462–70.

Driggs, F. D. and Lilliendahl, W. C. (1930) *Ind. Eng. Chem.*, **22**, 516–19.

Dushenkov, S., Vasudev, D., Kapulnik, Y., Gleba, D., Fleisher, D., Ting, K. C., and Ensley, B. D. (1997) *Environ. Sci. Technol.*, **31**, 3468–74.

Dwyer, O. E. (1956) *J. Am. Inst. Chem. Eng.*, **2**, 163–8.

Ebner, A. D., Ritter, J. A., Ploehn, H. J., Kochen, R. L., and Navratil, J. D. (1999) *Sep. Sci. Technol.*, **37**, 1277–300.

Elesin, A. A., Zaitsev, A. A., Kazakova, S. S., and Yakovlev, G. N. (1972) *Radiokhimiya*, **14**, 541–5.

Enokida, Y., Tomioka, O., Suzuki, M., and Yamamoto, I. (2000) in *Proc. 4th Japan-Korea Seminar on Advanced Reactors*, Bulletin of the Research Laboratory for Nuclear Reactors, Special Issue 3, pp. 145–52.

Ensor, D. D. and Shah, A. H. (1983) *Solvent Extr. Ion Exch.*, **1**, 241–50.

Ensor, D. D. and Shah, A. H. (1984) *Solvent Extr. Ion Exch.*, **2**, 591–605.

Ensor, D. D., Jarvinen, G. D., and Smith, B. F. (1988) *Solvent Extr. Ion Exch.*, **6**, 439–45.

Erlinger, C., Gazeau, D., Zemb, T., Madic, C., Lefrancois, L., Hebrant, M., and Tondre, C. (1998) *Solvent Extr. Ion Exch.*, **16**(3), 707–38.

Erlinger, C., Belloni, L., Zemb, T., and Madic, C. (1999) *Langmuir*, **15**(7), 2290–300.

Facchini, A., Amato, L., Modolo, G., Nannicini, R., Madic, C., and Baron, P. (2000) *Sep. Sci. Technol.*, **35**, 1055–68.

Fannin, A. A. J., Floreani, D. A., King, L. A., Landers, J. S., Piersma, B. J., Stech, D. J., Vaughn, R. L., Wilkes, J. S., and Williams, J. L. (1984) *J. Phys. Chem.*, **88**, 2614–21.

Farbu, L., Alstad, J., and Augustson, J. H. (1974) *J. Inorg. Nucl. Chem.*, **36**, 2091–5.

Farrell, M. S., Orrock, B. J., and Temple, R. B. (1962) *The Reprocessing of Beryllium-Based Reactor Fuels. A Chemical Feasibility Study of a Modified THOREX Process for the Recovery of the Uranium and Thorium*, Report AAEC/TM-146, USAEC, p. 12.

Felker, L. K., Benker, D. E., Chattin, F. R., and Stacy, R. G. (1995) *Sep. Sci. Technol.*, **30**(7–9), 1769–78.

Ferris, L. M., Mailen, J. C., Lawrence, J. J., Smith, F. J., and Nogueira, E. D. (1970) *J. Inorg. Nucl. Chem.*, **32**, 2019–35.

Ferris, L. M., Smith, F. J., Mailen, J. C., and Bell, M. J. (1972) *J. Inorg. Nucl. Chem.*, **34**, 313–20.

Fields, M., Hutson, G. V., Seddon, K. R., and Gordon, C. M. (1998) *Ionic Liquids as Solvents*, Patent WO98/06106.

Fields, M., Thied, R. C., Seddon, K. R., Pitner, W. R., and Rooney, D. W. (1999) *Treatment of Molten Salt Reprocessing Wastes*, Patent WO 99/14160.

Flanary, J. R. (1954) *Reactor Sci. Technol.*, **4**(1), 9–36.

Flengas, S. (1961) *Can. J. Chem.*, **39**, 773–83.

Fox, R. V., Mincher, B. J., and Holmes, R. G. G. (1999) Report INEEL/EXT-99-00870, Idaho National Engineering and Environmental Laboratory.

Freiser, H. (1988) *Solvent Extr. Ion Exch.*, **6**, 1093–108.

Fuller, J., Osteryoung, R. A., and Carlin, R. T. (1995) *J. Electrochem. Soc.*, **142**(11), 3632–6.

Furton, K. G., Chen, L., and Jaffé, R. (1995) *Anal. Chim. Acta*, **304**, 203–8.

Fusselman, S. P., Gay, R. L., Grimmett, D. L., Roy, J. J., Krueger, C. L., Nabelek, C. R., Storvick, T. S., Inoue, T., Kinoshita, K., and Takahashi, N. (1997) *Proc. Int. Conf. on Future Nuclear Systems* (*Global'97*), vol. 2, Yokohama, Japan.

Fusselman, S. P., Roy, J. J., Grimmett, D. L., Grantham, L. F., Krueger, C. L., Nabelek, C. R., Storvick, T. S., Inoue, T., Hijikita, T., Kinoshita, K., Sakamura, Y., Uozimi, K., Kawai, T., and Takahashi, N. (1999) *J. Electrochem. Soc.*, **146**, 2573–80.

Garcia-Carrera, A., Rouquette, H., Dozol, J. F., Bohmer, V., and Sastre, A. M. (2001) in *Solvent Extraction for the 21st Century, Proc. Int. Solvent Extraction Conf., ISEC'99* (eds. M. Cox, M. Hidalgo, and M. Valiente), Barcelona, Society of Chemical Industry, London, pp.1095–101.

Gatrone, R. C., Kaplan, L., and Horwitz, E. P. (1987) *Solvent Extr. Ion Exch.*, **5**, 1075–116.

Gatrone, R. C. and Rickert, P. G. (1987) *Solvent Extr. Ion Exch.*, **5**, 1117–139.

Geertsen, V., Chollet, H., Marty, P., and Moulin, C. (2000) *Ind. Eng. Chem. Res.*, **39**, 4877–81.

Glassner, A. (1957) *The Thermodynamics Properties of Oxides, Fluorides and Chlorides to 2500°K*, Report ANL-5750, Argonne National Laboratory.

Glatz, J. P., Song, C., He, X., Bokelund, H., and Koch, L. (1993) in *Partitioning of Actinides from HAW in a Continuous Process by Means of Centrifugal Extractors. Emerging Techniques in Hazardous Waste Management V,* American Chemical Society, Atlanta, GA, Sept. 27–29.

Glatz, J. P., Song, C., Koch, L., H., B., and He, X. M. (1995) Hot Tests of the TRPO Process for the Removal of TRU Elements from HLLW, in *Int. Conf. on Evaluation of Emerging Nuclear Fuel Cycle Systems* (*Global'95*),Versailles, France.

Gopalakrishnan, V., Dhami, P. S., Ramanujam, A., Balaramakrishna, M. V., Murali, M. S., Mathur, J. N., Iyer, R. H., Bauri, A. K., and Bannerji, A. (1995) *J. Radioanal. Nucl. Chem. Art.*, **191**, 279–89.

Grant, G. R., Morgan, W. W., Mehta, K. K., and Sargent, F. P. (1980) in *Actinide Separations* (eds. J. D. Navratil and W. W. Schulz) (ACS Symp. Ser. 117), American Chemical Society, Washington, DC, pp. 351–69.

Gray, G. E., Kohl, P. A., and Winninck, J. (1995) *J. Electrochem. Soc.*, **142**(11), 3636–42.

Grimmett, D. L., Roy, J. J., Grantham, L. F., Krueger, C. L., Storvick, T. S., Sharp, P. R., Sorrell, D. A., Cooper, J. W., Inoue, T., Sakamura, Y., and Takahashi, N. (1994) no 1396, Electrochemical Society Meetings Abstracts, Honolulu.

Grojtheim, K., Krohn, C., Malinovsky, M., Matiasovsky, K., and Thonstad, J. (1982) *Aluminium Electrolysis – Fundamentals of the Hall-Héroult Process,* 2nd edn, Aluminium-Verlag, Düsseldorf.

Grossi, G., Marrocchelli, A., Pietrelli, L., Calle, C., Gili, M., Luce, A., and Troiani, F. (1992a) *Selective Separation of Actinides and Long-Lived Fission Products from 1 AW MTR Liquid Waste: PilotPlant Tests. Part II*, Report EUR 13644/2, Nucl. Fuel Cycle Dep., ENEA, S. Maria di Galeria, Italy, Comm. Eur. Communities.

Grossi, G., Pietrelli, L., and Troiani, F. (1992b) *Selective Separation of Actinides and Long-Lived Fission Products from 1AW MTR Liquid Waste: Process Development. Part I*, Report EUR-13644/1, ENEA, Comm. Eur. Communities.

Gruen, D. M., McBeth, R. L., Kooi, J., and Carnall, W. T. (1960) *Ann. N. Y. Acad. Sci.*, **79**, 941–9.

Gruener, B., Plesek, J., Baca, J., Cisarova, I., Dozol, J. F., Rouquette, H., Vinas, C., Selucky, P., and Rais, J. (2002) *New J. Chem.*, **26**(10), 1519–27.

Guseva, L. I. and Tikhomirova, G. S. (1972) *Radiokhimiya*, **14**, 188–93.

Guseva, L. I., Tikhomirova, G. S., and Stepushkina, V. V. (1987a) *Radiokhimiya*, **29**, 211–16.

Guseva, L. I., Tikhomirova, G. S., and Stepushkina., V. V. (1987b) *Radiokhimiya*, **29**, 629–34.

Haeffner, E., Hultgren, A., and Larsen, A. (1965) in *Proc. 3rd Int. Conf. on Peaceful Uses of Atomic Energy*, Geneva, 1964, vol. 10, pp. 370–81.

Hägstrom, I., Spjuth, L., Enarsson, A., Liljenzin, J. O., Skälberg, M., Hudson, M. J., Iveson, P. B., Madic, C., Cordier, P. Y., Hill, C., and Francois, N. (1999) *Solvent Extr. Ion Exch.*, **17**(2), 221–42.

Hannum, W. H. (1997) The technology of the integral fast reactor and its associated fuel cycle, *Prog Nucl. Energy*, Special Issue, 31.

Harada, M., Varga, T., Tomiyasu, H., and Ikeda, Y. (2001) *Bull. Res. Lab. Nucl. Reactors* (*Tokyo Institute of Technology*), **25**, 76–8.

Harmon, C. D., Smith, W. H., and Costa, D. A. (2001) *Radiat. Phys. Chem.*, **60**, 157–9.

Heerman, L., De Waele, R., and D'Olieslager, W. (1985) *J. Electroanal. Chem.*, **193**, 289–94.

Helfferich, F. (1962) *Ion Exchange,* McGraw-Hill, New York.

Hendricks, M. E., Jones, E. R., Stone, J. A., and Karraker, D. G. (1971) *J. Chem. Phys.*, **55**, 2993–7.

Herbst, R. S., Law, J. D., Todd, T. A., Romanovskiy, V. N., Babain, V. A., Esimantovskiy, V. M., Smirnov, I. V., and Zaitsev, B. N. (2002) *Solvent Extr. Ion Exch.*, **20**(4–5), 429–45.

Herbst, R. S., Law, J. D., Todd, T. A., Romanovskiy, V. N., Smirnov, I. V., Babain, V. A., Esimantovskiy, V. N., and Zaitsev, B. N. (2003) *Sep. Sci. Technol.*, **38**(12–13), 2685–708.

Hightower, J. R. Jr (1975) Process Technology for The Molten Salt Reactor ^{233}U-Th Cycle Paper no 231, *Proc. ANS Winter Meeting*, San Francisco, CA.

Hijikata, T., Higashi, T., Kinoshita, K., and Miyasiro, H. (1993) in *Proc. Int. Conf. and Technology Exposition on Future Nuclear Systems: Emerging Fuel Cycles and Waste Disposal Options* (*Global '93*), vol. 2 (ed. J. A. Rawlins), Seattle, Washington, Sept. 12–17, 1993, American Nuclear Society, La Grange Park, IL.

Hill, O. F. and Cooper, V. R. (1958) *Ind. Eng. Chem.*, **50**, 599–602.

Hill, C., Madic, C., Baron, P., Ozawa, M., and Tanaka, X. (1998) *J. Alloys Compd.*, **271–273**, 159–62.

Hoffert, M. I., Caldeira, K., Benford, G., Criswell, D. R., Green, C., Herzog, H., Jain, A. K., Kheshgi, H. S., Lackner, K. S., Lewis, J. S., Lightfoot, H. D., Manheimer, W., Mankins, J. C., Mauel, M. E., Perkins, L. J., Schlesinger, M. E., Volk, T., and Wigley, T. M. L. (2002) *Science*, **298**, 981–7.

Hopkins, T. A., Berg, J. M., Costa, D. A., Smith, W. H., and Dewey, H. J. (2000) AIP Conference Proceedings 532, in *AIP Conf. Proc.*

Hopkins, T. A., Berg, J. M., Costa, D. A., Smith, W. H., and Dewey, H. J. (2001) *Inorg. Chem.*, **40**, 1820–5.

Horwitz, E. P., Muscatello, A. C., Kalina, D. G., and Kaplan, L. (1981) *Sep. Sci. Technol.*, **16**, 417–37.

Horwitz, E. P., Kalina, D. G., Kaplan, L., Mason, G. W., and Diamond, H. (1982) *Sep. Sci. Technol.*, **17**, 1261–79.

Horwitz, E. P., Diamond, H., and Kalina, D. G. (1983) in *Plutonium Chemistry* (eds. W. T. Carnall and G. R. Choppin) (ACS symp. Ser. no. 216), American Chemical Society, Washington, DC, pp. 433–50.

Horwitz, E. P. and Kalina, D. G. (1984) *Solvent Extr. Ion Exch.*, **2**, 179–200.
Horwitz, E. P., Kalina, D. G., Diamond, H., Vandegrift, G. F., and Schulz, W. W. (1985) *Solvent Extr. Ion Exch.*, **3**, 75–109.
Horwitz, E. P., Martin, K. A., Diamond, H., and Kaplan, L. (1986) *Solvent Extr. Ion Exch.*, **4**, 449–94.
Horwitz, E. P., Diamond, H., and Martin, K. A. (1987) *Solvent Extr. Ion Exch.*, **5**(3), 447–70.
Horwitz, E. P. and Schulz, W. W. (1990) The TRUEX Process: A Vital Tool for Disposal of U.S. Defense Nuclear Waste, New Separation Chemistry for Radioactive Waste and Other Specific Applications, Sponsored by the Commission of the European Communities and the Italian Commission for Nuclear and Alternative Energy sources, Rome, Italy, May 16–18.
Horwitz, E. P., Diamond, H., Gatrone, R. C., Nash, K. L., and Rickert, P. G. (1992) *Process Metall.*, **7A** (*Solvent Extr.*, 1990, Pt. A), 357–62.
Horwitz, E. P., Chiarizia, R., Diamond, H., Gatrone, R. C., Alexandratos, S. D., Trochimczuk, A. Q., and Crick, D. W. (1993) *Solvent Extr. Ion Exch.*, **11**(5), 943–66.
Horwitz, E. P., Chiarizia, R., and Alexandratos, S. D. (1994) *Solvent Extr. Ion Exch.*, **12**(4), 831–45.
Horwitz, E. P., Dietz, M. L., Chiarizia, R., Diamond, H., Maxwell, S. C. III, and Nelson, D. R. (1995) *Anal. Chim. Acta*, **310**, 63–78.
Horwitz, E. P. and Chiarizia, R. (1996) in *Separation Techniques in Nuclear Waste Management* (eds. T. E. Carlson, N. A. Chipman, and C. M. Wai), CRC Press, Boca Raton, FL, pp. 3–33.
Horwitz, E. P. and Schulz, W. W. (1999) in *Metal Ion Separation and Preconcentration: Progress and Opportunities* (eds. A. H. Bond, M. L. Dietz, and R. D. Rogers) (ACS Symp. Ser. 716), American Chemical Society, Washington, DC, pp. 20–50.
Hoshi, H., Tsuyoshi, A., and Akiba, K. (2000) *J. Radioanal. Nucl. Chem.*, **243**, 621–4.
Hoshi, H., Tsuyoshi, A., and Akiba, K. (2001) *J. Radioanal. Nucl. Chem.*, **249**, 547–50.
Howells, G. R., Hughes, T. G., and Saddington, K. (1958) in *Progress in Nuclear Energy,* Ser. III, *Process Chemistry*, vol. 2 (eds. F. R. Bruce, J. M. Fletcher, and H. H. Hyman), Pergamon Press, London, pp. 151–87.
Huang, J. W., Blaylock, M. J., Kapulnik, Y., and Ensley, B. D. (1998) *Environ. Sci. Technol.*, **32**, 2004–8.
Hudson, M. J., Foreman, M. R. St. J., Hill, C., Huet, N., and Madic, C. (2003) *Solvent Extr. Ion Exch.*, **21**(5), 637–52.
Hugen, Z., Yuxing, Y., and Xuexian, Y. (1982) in *Radioactive Waste Management* (eds. J. D. Navratil and W. W. Schulz), Academic Publishers, Harwood, pp. 227–44.
Hulet, E. K., Gutmacher, G. R., and Coops, M. S. (1961) *J. Inorg. Nucl. Chem.*, **17**, 350–60.
Hultgren, A. V. (1967) *Reprocessing of Fuel from Present and Future Power Reactors*, Norwegian Report, KR-126.
Hunt, F., Ohde, H., and Wai, C. M. (1999) *Rev. Sci. Instrum.*, **70**(12), 4661–7.
Hurley, F. H. and Wier, T. P. J. (1951) *J. Electrochem. Soc.*, **98**(5), 203–6.
Hussey, C. L. (1983) *Adv. Molten Salt Chem.*, **5**, 185–230.
Hyman, H. H., Vogel, R. C., and Katz, J. J. (1956) Fundamental chemistry of uranium hexafluoride distillation processes for the decontamination of irradiated reactor fuels, in *Progress in Nuclear Energy,* Ser. III, Process Chemistry, McGraw-Hill, New York.

Inoue, Y. and Tochiyama, O. (1977) *J. Inorg. Nucl. Chem.*, **39**, 1443–7.
Inoue, T., Sakata, M., Miyashiro, H. Matsumura, M. Sasashara, A., and Yoshiki, N. (1991) *Nucl. Technol.*, **69**, 206–21.
Ionova, G., Ionov, S., Rabbe, C., Hill, C., Madic, C., Guillaumont, R., and Krupa, J. C. (2001) *Solvent Extr. Ion Exch.*, **19**, 391–414.
Irani, R. R. and Moedritzer, K. (1962) *J. Phys. Chem.*, **66**, 1349–53.
Ishimori, T. (1980) in *Actinide Separations* (eds. J. D. Navratil and W. W. Schulz) (ACS Symp. Ser. vol. 117), American Chemical Society, Washington, DC, pp. 333–50.
Iso, S., Meguro, Y., and Yoshida, Z. (1995) *Chem. Lett.*, 365–6.
Iso, S., Uno, S., Meguro, Y., Sasaki, T., and Yoshida, Z. (2000) *Prog. Nucl. Energy*, **37**(1–4), 423–8.
Iveson, P. B., Drew, M. G. B., Hudson, M. J., and Madic, C. (1999) J. Chem. Soc., *Dalton Trans.*, (20), 3605–10.
Jarvinen, G. D., Barrans, R. E. Jr, Schroeder, N. C., Wade, K. L., Jones, M. M., Smith, B. F., Mills, J. L., Howard, G., Freiser, H., and Muralidharan, S. (1995) in *Separations of f-Elements* (eds. K. L. Nash and G. R. Choppin), Plenum Press, New York, pp. 43–62.
Jenkins, I. L. (1979) *Hydrometallurgy*., **5**, 1–13.
Jenkins, I. L. (1984) *Solvent Extr. Ion. Exch*., **2**, 1–27.
Jensen, M. P., Morss, L. R., Beitz, J. V., and Ensor, D. D. (2000) *J. Alloys Compd.*, **303–304**, 137–41.
Jensen, M. P. and Bond, A. H. (2002a) *J. Am. Chem. Soc.*, **124**(33), 9870–7.
Jensen, M. P. and Bond, A. H. (2002b) *Radiochim. Acta*, **90**(4), 205–9.
Jensen, M. P., Chiarizia, R., Ferraro, J. R., Borkowski, M., Nash, K. L., Thiyagarajan, P., and Littrell, K. C. (2002a) in *Proc. Int. Solvent Extraction Conf., ISEC 2002* (eds. K. C. Sole, P. M. Cole, J. S. Preston, and D. J. Robinson), Capetown, South Africa, Chris van Rensburg Publications, South African Institute of Mining and Metallurgy, Johannesburg, pp. 1137–42.
Jensen, M. P., Dzielawa, J. A., Rickert, P., and Dietz, M. L. (2002b) *J. Am. Chem. Soc.*, **124**(36), 10664–5.
Jensen, M. P., Neuefeind, J., Beitz, J. V., Skanthakumar, S., and Soderholm, L. (2003) *J. Am. Chem. Soc.*, **125**(50), 15466–73.
Jianchen, W. and Chongli, S. (2001) *Solvent Extr. Ion Exch.*, **19**, 231–42.
Jiang, P. I., Ikeda, Y., and Kumagai, M. (1994) *J. Nucl. Sci. Technol.*, **31**, 491–3.
Johansson, H. and Rydberg, J. (1969) *Acta Chem. Scand.* (*1947–1973*), **23**(8), 2797–807.
Johnson, I., Chasanov, M. G., and Yonco, R. M. (1965) *Trans. Metall. Soc. AIME*, **233** (July), 1408–14.
Johnson, I. and Yonco, R. M. (1970) *Metall. Trans.*, **1** (April), 905–10.
Johnson, I. (1974) *J. Nucl. Mater.*, **51**, 163–77.
Johnson, I. (1988) *J. Nucl. Mater.*, **154**, 169–80.
Johnson, G. K., Pierce, R. D., Poa, D. S., and McPheeters, C. C. (1994) *Pyrochemical Recovery of Actinide Elements from Spent Light Water Reactor Fuel, Proc. Int. Symp. on Actinide Process*, 123rd Annu. Meet. Miner., Met., Mat. Soc.
Kalina, D. G., Horwitz, E. P., Kaplan, L., and Muscatello, A. C. (1981a) *Sep. Sci. Technol.*, **16**, 1127–45.
Kalina, D. G., Mason, G. W., and Horwitz, E. P. (1981b) *J. Inorg. Nucl. Chem.*, **43**, 159–63.

Kalina, D. G. and Horwitz, E. P. (1985) *Solvent Extr. Ion Exch.*, **3**, 235–50.
Kaminski, M. D. and Nunez, L. (1999) *J. Magn. Magn. Mater.*, **194**, 31–6.
Kaminski, M. D. and Nunez, L. (2000) *Sep. Sci. Technol.*, **35**, 2003–18.
Karalova, Z. K., Rodionova, L. M., and Myasoedov, B. F. (1982) *Radiokhimiya*, **24**(2), 210–13.
Karalova, Z. K., Myasoedov, B. F., Bukhina, T. I., and Lavrinovich, E. A. (1988) *Solvent Extr. Ion Exch.*, **6**, 1109–35.
Karell, E. J., Gourishankar, K. V., Smith, J. L., Chow, L. S., and Redey, L. (2001) *Nucl. Technol.*, **136**, 342–53.
Kassierer, E. F. and Kertes, A. S. (1972) *J. Inorg. Nucl. Chem.*, **34**, 3221–31.
Kasting, G. B., Hulet, E. K., Heppert, J. A., and Wild, J. F. (1979) *Inorg. Nucl. Chem. Lett.*, **41**, 745–7.
Kertes, A. S. and Kassierer, E. F. (1972) *Inorg. Chem.*, **11**, 2108–11.
Khopkar, P. K. and Mathur, J. N. (1981) *J. Inorg. Nucl. Chem.*, **43**, 1035–41.
Khopkar, P. K. and Mathur, J. N. (1982) *Sep. Sci. Technol.*, **17**, 985–1002.
King, L. J., Bigelow, J. E., and Collins, E. D. (1981) in *Transplutonium Elements – Production and Recovery* (eds. J. D. Navratil and W. W. Schulz) (ACS Symp. Ser. vol. 161), American Chemical Society, Washington, DC, pp. 133–45.
Kinoshita, K., Inoue, T., Fusselman, S. P., Grimmett, D. L., Roy, J. J., Gay, R. L., Krueger, C. L., Nabelek, C. R., and Storvick, T. S. (1999) *J. Nucl. Sci. Technol.*, **36**(2), 189–97.
Knighton, J. B. and Steunenberg, R. K. (1965) *J. Inorg. Nucl. Chem.*, **27**, 1457–62.
Knighton, J. B. *et al.* (1969) *Nucl. Metall.*, **15**, 337.
Kobashi, A., Choppin, G. R., and Morse, J. W. (1988) *Radiochim. Acta*, **43**, 211–15.
Kobayashi, F., Ogawa, T., Akabori, M., and Kato, Y. (1995) *J. Am. Ceram. Soc.*, **78**(8), 2279–81.
Kobayashi, F., Ogawa, T., Takano, M., Akabori, M., Itoh, A., and Minato, K. (1999) Dissolution of Metal Nitrides in LiCl–KCl Eutectic Melt, in *Proc. Int. Conf. on Future Nuclear Systems* (*Global'99*), Jackson Hole, Wyoming.
Koch, G., Baumgartner, F., Goldacker, H., Ochsenfeld, W., and Schmieder, M. (1977) A Solvent Extraction Flowsheet for a Large-Scale LWR Fuel Reprocessing Plant, Report KFK-2557, Kernforschungszentrum Karlsruhe.
Kolarik, Z. J. and Horwitz, E. P. (1988) *Solvent Extr. Ion Exch.*, **6**, 247–63.
Kolarik, Z., Mullich, U., and Gassner, F. (1999) *Solvent Extr. Ion Exch.*, **17**, 1155–70.
Kolesnikov, V. P., Kazantsev, G. N., and Skiba, O. V. (1976) *Radiokhimiya*, **19**(4), 545–8.
Kolodney, M. (1982) *J. Electrochem. Soc.*, **129**(11), 2438–42.
Koma, Y., Watanabe, M., Nemoto, S., and Tanaka, Y. (1998) *Solvent Extr. Ion Exch.*, **16**, 1357–67.
Koma, Y., Koyama, T. M., Nemoto, S., and Tanaka, Y. (1999) *J. Nucl. Sci. Technol.*, **36**, 934–9.
Korkisch, J. (ed.) (1986a) in *Handbook of Ion Exchange Resins: Their Application to Inorganic Chemistry, Principles, Rare Earth Elements*, vol. 1, Chemical Rubber Company, Boca Raton, FL, pp. 115–271.
Korkisch, J. (ed.) (1986b) in *Handbook of Ion Exchange Resins: Their Application to Inorganic Chemistry, Actinides*, vol. 2, CRC, Boca Raton, FL, pp.

Kormilitzyn, M. V., Vavilov, S. K., Bychkov, A. V., Skiba, O. V., Chistyakov, V. M., and Tselichshev, I. V. (1999) personal communication.
Kosyakov, V. N. and Yerin, E. A. (1980) *J. Radioanal. Chem.*, **56**, 93–104.
Koyama, T., Johnson, T. R., and Fischer, D. F. (1992) *J. Alloys Compd.*, **189**, 37–44.
Krumpelt, M., Johnson, I., and Heiberger, J. J. (1974) *Metall. Trans.*, **5**, 65–70.
Kulyukhin, S. A., Mikheev, N. B., and Rumer, I. A. (1997) *Radiochemistry*, **39**(2), 134–6.
Kumar, R., Sivaraman, N., Srinivasan, T. G., and Vasudeva Rao, P. R. (2002) *Radiochim. Acta*, **90**, 141–5.
Kurata, M., Sakamura, Y., Hijikita, T., and Kinoshita, K. (1995) *J. Nucl. Mater.*, **227**, 110–21.
Kurata, M., Sakamura, Y., and Matsui, T. (1996) *J. Alloys Compd.*, **234**, 83–92.
Kurata, M., Kinoshita, K., Hijikata, T., and Inoue, T. (2000) *J. Nucl. Sci. Technol.*, **37**(8), 682–90.
Laidler, J. (1994) Pyrochemical Processing of DOE Spent Nuclear Fuel, Report ANL/CMT/CP-84355, Argonne National Laboratory.
Laintz, K. E., Wai, C. M., Yonker, C. R., and Smith, R. D. (1991) *J. Supercrit. Fluids*, **4**,194–8.
Laintz, K. E., Wai, C. M., Yonker, C. R., and Smith, R. D. (1992) *Anal. Chem.*, **64**, 2875–8.
Lambertin, D., Lacquement, J., Sanchez, S., and Picard, G. (2000) *Plasmas Ions*, **3**, 65–72.
Lambertin, D., Lacquement, J., Sanchez, S., and Picard, G. (2001) *Electrochem. Commun.*, **3**, 519–23.
Landresse, G. and Duyckaerts, G. (1974) *Anal. Chim. Acta*, **73**, 121–7.
Lane, E. S. (1953) *J. Chem. Soc.*, 1172–5.
Law, J. D., Brewer, K. N., Herbst, R. S., Todd, T. A., and Olsen, L.G. (1998) Demonstration of Optimized TRUEX Flowsheet for Partitioning of Actinides from Actual ICPP Sodium-Bearing Waste Using Centrifugal Contactors in a Shielded Cell Facility, Idaho National Engineering Laboratory, INEL/EXT-98-00004.
Law, J. D., Herbst, R. S., Todd, T. A., Romanovskiy, V. N., Babain, V. A., Esimantovskiy, V. M., Smirnov, I. V., and Zaitsev, B. N. (2001) *Solvent Extr. Ion Exch.*, **19**(1), 23–36.
Law, J. D., Herbst, R. S., Todd, T. A., Romanovskiy, V. N., Esimantovskiy, V. M., Smirnov, I. V., Babain, V. A., and Zaitsev, B. N. (2002) in *Proc. Int. Solvent Extraction Conf., ISEC 2002* (eds. K. C. Sole, P. M. Cole, J. S. Preston, and .D. J. Robinson), Capetown, South Africa, Chris van Rensburg Publications, South African Institute of Mining and Metallurgy, Johannesburg, pp. 1229–34.
Lawroski, S. (1955) in *Proc. First Int. Conf. on Peaceful Uses of Atomic Energy*, Geneva, vol. 9.
Leary, J. A., Benz, R., Bowersox, D. F., Bjorklund, C. W., Johnson, K. W. R., Maraman, W. J., Mullins, L. J., and Reavis, J. G. (1958) Pyrometallurgical Purification of Plutonium Reactor Fuels, in *Proc. 2nd U.N. Int. Conf. on the Peaceful Uses of Atomic Energy*, Geneva, vol. 17, pp. 376–82.
Leary, J. A. and Mullins, L. J. (1973) *J. Chem. Thermodyn.*, **6**, 103.
Lebedev, V. A., Nichkov, I. F., and Raspopin, S. P. (1968) *Russ. J. Phys. Chem.*, **42**, 363; *Zh. Fiz. Khim.*, 42 (3), 690–3.

Lebedev, V. A., Babikov, L. G., Vavilov, S. K., Nichkov, I., Raspopin, S. P., and Skiba, O. V. (1969) *Atomnaya Energiya*, **27**(1), 59–61.

Lefrancois, L., Belnet, F., Noel, D., and Tondre, C. (2001a) in *Solvent Extraction for the 21st Century, Proc. Int. Solvent Extraction Conf., ISEC'99* (eds. M. Cox, M. Hidalgo, and M. Valiente), Barcelona, Society of Chemical Industry, London, pp. 637–41.

Lefrancois, L., Delpuech, J.-J., Hebrant, M., Chrisment, J., and Tondre, C. (2001b) *J. Phys. Chem. B*, **105**(13), 2551–64.

Liansheng, W., Casarci, M., and Gasparini, G. M. (1990) *Solvent Extr. Ion Exch.*, **8**, 49–64.

Liljenzin, J. O., Rydberg, J., and Skarnemark, G. (1980) *Sep. Sci. Technol.*, **15**, 799–824.

Lin, Y., Brauer, R. D., Laintz, K. E., and Wai, C. M. (1993) *Anal. Chem.*, **65**, 2549–51.

Lin, Y., Wai, C. M., Jean, F. M., and Brauer, R. D. (1994) *Environ. Sci. Technol.*, **28**, 1190–3.

Lin, Y., Smart, N. G., and Wai, C. M. (1995) *Environ. Sci. Technol.*, **29**, 2706–8.

Lin, Y., Wu, H., Smart, N. G., and Wai, C. M. (1998) *J. Chromatogr. A*, **793**, 107–13.

Lin, Y., Wu, H., Smart, N. G., and Wai, C. M. (2001) *Sep. Sci. Technol.*, **36**(5–6), 1149–62.

Long, G. and Blankenship, F. (1969) Stability of Uranium Trifluoride. I. Stability in the Solid Phase, Report ORNL-TM-2065, Oak Ridge National Laboratory.

Lumetta, G. J. and Swanson, J. L. (1993a) *Sep. Sci. Technol.*, **28**, 43–58.

Lumetta, G. J. and Swanson, J. L. (1993b) Pretreatment of Neutralized Cladding Removal Waste (NCRW) Sludge – Results of FY 1991 Studies, Report PNL-8536, Pacific Northwest Laboratory.

Lumetta, G. J. and Swanson, J. L. (1993c) Pretreatment of Plutonium Finishing Plant (PFP) Sludge, Report for the period October 1990–March 1992, Report PNL-8601, Pacific Northwest Laboratory.

Lumetta, G. J., Wester, D. W., Morrey, J. R., and Wagner, M. J. (1993) *Solvent Extr. Ion Exch.*, **11**, 663–82.

Lumetta, G. J., Rapko, B. M., Garza, P. A., Hay, B. P., Gilbertson, R. D., Weakley, T. J. R., and Hutchison, J. E. (2002) *J. Am. Chem. Soc.*, **124**(20), 5644–5.

Lumetta, G. J., Rapko, B. M., Hay, B. P., Garza, P. A., Hutchison, J. E., and Gilbertson, R. D. (2003) *Solvent Extr. Ion Exch.*, **21**(1), 29–39.

Lung, M. and Gremm, O. (1998) *Nucl. Eng. Des.*, **180**(2), 133–46.

Madic, C., Hudson, M. J., Liljenzin, J.-O., Glatz, J.-P., Nannicini, R., Facchini, A., Kolarik, Z., and Odoj, R. (2002) *Prog. Nucl. Energy*, **40**(3–4), 523–6.

Mahajan, G. R., Prabhu, D. R., Manchanda, V. K., and Badheka, L. P. (1998) *Waste Manage. (Oxford)*, **18**(2), 125–33.

Malmbeck, R., Courson, O., Pagliosa, G., Romer, K., Sätmark, B., Glatz, J. P., and Baron, P. (2000) *Radiochim. Acta*, **88**, 865–71.

Marcus, Y. and Kertes, A. S. (1969) *Ion Exchange and Solvent Extraction of Metal Complexes,* Wiley-Interscience, London.

Marcus, Y. (1983) Sc, Y, La-Lu rare earth elements, part D6, ion exchange and solvent extraction reactions, organometallic compounds, in *Gmelin Handbook of Inorganic Chemistry,* 8th edn, Springer-Verlag, Berlin, pp. 1–136.

Marcus, Y. (1997) *Ion Properties,* Marcel Dekker, New York.

Mariani, R. D., Vaden, D., Westphal, B. R., Laug, D. V., Cunningham, S. S., Li, S. X., Johnson, T. A., Krsul, J. R., and Lambregts, M. J. (2000) *Process Description for Driver Fuel Treatment Operations,* ANL Technical Memorandum No 11, Argonne National Laboratory, Argonne, IL.

Martell, A. E. and Smith, R. M. (1998) *Critically Selected Stability Constants of Metal Complexes Database* Database 46, Gaithersburg, MD 20899, NIST.

Martella, L. L. and Navratil, J. D. (1979) *Waste Management Analysis for the Nuclear Fuel Cycle: I. Actinide Recovery from Aqueous Salt Wastes*, Report RFP-2812, Rocky Flats Plant.

Martin, A. E., Johnson, I., and Feder, H. M. (1961) *Trans. Metall. Soc. AIME*, **221** (August), 789–91.

Martin- Daguet, V., Gasnier, P., and Caude, M. (1997) *Anal. Chem.*, **69**, 536–41.

Martinot, L., Duyckaerts, G., and Caligara, F. (1967) *Bull. Soc. Chim. Belg.*, **76**, 211–20.

Martinot, L. and Duyckaerts, G. (1969a) *Inorg. Nucl. Chem. Lett.*, **5**, 909–19.

Martinot, L. and Duyckaerts, G. (1969b) *Bull. Soc. Chim. Belg.*, **78**, 495–502.

Martinot, L. and Duyckaerts, G. (1970) *Inorg. Nucl. Chem. Lett.*, **6**, 587–93.

Martinot, L. and Duyckaerts, G. (1973) *Anal. Chim. Acta*, **66**, 474–6.

Martinot, L., Spirlet, J. C., Duyckaerts, G., and Muller, W. (1973) *Anal. Lett.*, **6**(4), 321–6.

Martinot, L., Reul, J., and Duyckaerts, G. (1975) *Anal. Lett.*, **8**(4), 233–9.

Martinot, L. (1975) *J. Inorg. Nucl. Chem.*, **37**, 2525–8.

Martinot, L., Bohet, J., Duyckaerts, G., and Muller, W. (1977) *Inorg. Nucl. Chem. Lett.*, **13**, 315–19.

Martinot, L., Duyckaerts, G., Spirlet, J. C., and Muller, W. (1980) *Inorg. Nucl. Chem. Lett.*, **16**, 177–83.

Martinot, L. (1986) *J. Radioanal. Nucl. Chem. Lett.*, **106**(3), 135–44.

Martinot, L. and Fuger, J. (1986) *J. Less Common Metals*, **120**, 255–66.

Martinot, L. and Ligot, M. (1989) *J. Radioanal. Nucl. Chem. Lett.*, **136**(1), 53–60.

Martinot, L. (1991) in *Handbook on the Physics and Chemistry of Actinides* (eds. A. J. Freeman and C. Keller), Elsevier Science Publishers B.V., pp. 241–71.

Marzano, C. and Noland, R. A. (1953) The Electrolytic Refining of Uranium, Report ANL-5102, USAEC, Argonne National Laboratory.

Mathieson, W. A. and Nicholson, C. A. (1968) *PUREX* Chemical Flow Sheet-Processing of Aluminium Clad Uranium Fuels, Report ARH-214 DEL, Hanford Works.

Mathur, J. N. (1983) *Solvent Extr. Ion Exch.*, **1**, 349–412.

Mathur, J. N. and Khopkar, P. K. (1988) *Solvent Extr. Ion Exch.*, **6**(1), 111–24.

Mathur, J. N., Murali, M. S., Ruikar, P. B., Nagar, M. S., Sipahimalani, A. T., Bauri, A. K., and Banerji, A. (1988) *Sep. Sci. Technol.*, **33**, 2179–96.

Mathur, J. N., Murali, M. S., and Natarajan, P. R. (1991) *J. Radioanal. Nucl. Chem.*, **152**, 127–35.

Mathur, J. N., Murali, M. S., and Natarajan, P. R. (1992a) *J. Radioanal. Nucl. Chem.*, **155**, 195–200.

Mathur, J. N., Murali, M. S., Natarajan, P. R., Badheka, L. P., and Banerji, A. (1992b) *Talanta*, **39**, 493–6.

Mathur, J. N., Murali, M. S., Natarajan, P. R., Badheka, L. P., Banerji, A., Ramanujam, A., Dhami, P. S., Gopalakrishnan, V., Dhumwad, R. K., and Rao, M. K. (1993a) *Waste Manage.*, **13**, 317–25.

Mathur, J. N., Murali, M. S., Rizvi, G. H., Iyer, R. H., Michael, K. M., Kapoor, S. C., Ramanujam, A., Badheka, L. P., and Bannerji, A. (1993b) *J. Nucl. Sci. Technol.*, **30**, 1198–200.

Mathur, J. N. and Choppin, G. R. (1993) *Solvent Extr. Ion Exch.*, **11**, 1–18.

Mathur, J. N., Murali, M. S., Rizvi, G. H., Iyer, R. H., Michael, K. M., Kapoor, S. C., Dhumwad, R. K., Badheka, L. P., and Bannerji, A. (1994) *Solvent Extr. Ion Exch.*, **12**, 745–63.

Mathur, J. N., Murali, M. S., Iyer, R. H., Ramanujam, A., Dhami, P. S., Gopalakrishnan, V., Badheka, L. P., and Bannerji, A. (1995) *Nucl. Technol.*, **109**, 216–25.

Mathur, J. N., Murali, M. S., Balaramakrishna, M. V., Iyer, R. H., Chitnis, R. R., Wattal, P. K., Bauri, A. K., and Bannerji, A. (1996a) *J. Radioanal. Nucl. Chem. Lett.*, **213**, 419–29.

Mathur, J. N., Murali, M. S., Balaramakrishna, M. V., Iyer, R. H., Chitnis, R. R., Wattal, P. K., Theyyunni, T. K., Ramanujam, A., Dhami, P. S., Gopalakrishnan, V., Badheka, L. P., and Bannerji, A. (1996b) *Sep. Sci. Technol.*, **31**, 2045–63.

Mathur, J. N. and Nash, K. L. (1998) *Solvent Extr. Ion Exch.*, **16**, 1341–56.

Mathur, J. N., Murali, M. S., and Nash, K. L. (2001) *Solvent Extr. Ion Exch.*, **19**, 357–90.

McAlister, D. R., Dietz, M. L., Chiarizia, R., and Herlinger, A. W. (2002) in *Proc. Int. Solvent Extraction Conf., ISEC 2002* (eds. K. C. Sole, P. M. Cole, J. S. Preston, and D. J. Robinson), Capetown, South Africa, Chris van Rensburg Publications, South African Institute of Mining and Metallurgy, Johannesburg, pp. 390–5.

McDuffee, W. T. and Yarbro, O. O. (1957) Preparation of Thorium Oxide from ORNL THOREX Thorium Nitrate, Report CF-57-2-113, USAEC, Oak Ridge National Laboratory, p. 13.

McDuffee, W. T. and Yarbro, O. O. (1958) THOREX Pilot Plant Run AWD-1 Summary, Report CF-58-1-56, USAEC, Oak Ridge National Laboratory, p. 5.

McIsaac, L. D. (1982) *Sep. Sci. Technol.*, **17**, 387–405.

McIsaac, L. D. and Baker, J. D. (1983) *Solvent Extr. Ion Exch.*, **1**, 27–41.

McKay, H. A. C. (1956) in *Proc. Ist Int. Conf. on the Peaceful Uses of Atomic Energy*, Geneva, 1955, vol. 7, pp. 314–17.

McNeese, L. E. (1971) Report ORNL-TM-3140, Oak Ridge National Laboratory.

Meguro, Y., Iso, S., Takeishi, H., and Yoshida, Z. (1996) *Radiochim. Acta*, **75**, 185–91.

Meguro, Y., Sasaki, T., Iso, S., and Yoshida, Z. (eds.) (1997) in *The 4th Int. Symp. on Supercritical Fluids*, Sendaï, Japan, pp. 447–50.

Meguro, Y., Iso, S., Sasaki, T., and Yoshida, Z. (1998a) *Anal. Chem.*, **70**, 774–8.

Meguro, Y., Iso, S., and Yoshida, Z. (1998b) *Anal. Chem.*, **70**, 1262–7.

Meguro, Y., Iso, S., and Yoshida, Z. (2002) in *Proc. Int. Solvent Extraction Conf., ISEC 2002* (eds. K. C. Sole, P. M. Cole, J. S. Preston, and D. J. Robinson), Capetown, South Africa, Chris van Rensburg Publications, South African Institute of Mining and Metallurgy, Johannesburg, pp. 1131–6.

Meisel, D., Diamond, H., Horwitz, E. P., Jonah, C. D., Matheson, M. S., Sauer, M. C. Jr, and Sullivan, J. C. (1991) *Radiation Chemistry of Synthetic Waste,* Argonne National Laboratory, ANL-91/40.

Merrill, E. T. and Stevenson, R. L. (1955) *Redox Chemical Flow Sheet*, HW No. 5, HW-38684.

Merz, E. and Zimmer, E. (1984) *Aqueous Chemical Reprocessing of HTR Fuel*, Inst. Chem. Technol., Kernforsch. G.m.b.H., Juelich, Fed. Rep. Ger., Ber. Kernforschungsanlage Juelich.

Michael, K. M., Rizvi, G. H., Mathur, J. N., and Ramanujam, A. (2000) *J. Radioanal. Nucl. Chem.*, **246**, 355–9.

Mimura, H., Hoshi, H., Akiba, K., and Onodera, Y. (2001) *J. Radioanal. Nucl. Chem.*, **247**, 375–9.

Mincher, B. J. (1989) *Solvent Extr. Ion Exch.*, **7**, 645–54.

Mincher, B. J. (1992) *Solvent Extr. Ion Exch.*, **10**, 615–22.

Modolo, G. and Odoj, R. (1999) *Solvent Extr. Ion Exch.*, **17**(1), 33–53.

Mohammed, T. J. (1987) PhD Thesis, University of Sussex.

Mohapatra, P. K., Sriram, S., Manchanda, V. K., and Badheka, L. P. (2000) *Sep. Sci. Technol.*, **35**, 39–55.

Molochnikova, N. P., Shkinev, V. M., and Myasoedov, B. F. (1995) *Radiokhimiya*, **37**(6), 517–21.

Moore, R. H. and Lyon, W. L. (1959) Distribution of the Actinide Elements in the Molten System KCl-$AlCl_3$-Al, Report HW-59147, USAEC.

Moore, F. L. (1961) *Anal. Chem.*, **33**, 748–51.

Moore, F. L. (1964) *Anal. Chem.*, **36**, 2158–62.

Morgan, L. G., Burger, L. L., and Scheele, R. D. (1980) in *Actinide Separations* (eds. J. D. Navratil and W. W. Schulz) (ACS Symp. Ser. 117), American Chemical Society, Washington, DC, pp. 233–52.

Morita, Y. and Kubota, M. (1987) *J. Nucl. Sci. Technol.*, **24**, 227–32.

Morita, Y. and Kubota, M. (1988) *Solvent Extr. Ion Exch.*, **6**, 233–46.

Morita, Y., Yamaguchi, I., Kondo, Y., Shirahashi, K., Yamagishi, I., Fujiwara, T., and Kubota, M. (1995) Safety and Environmental Aspects of Partitioning and Transmutation of Actinides and Fission Products, IAEA, IAEA-TECDOC-783.

Morita, Y., Tachimori, S., Koma, Y., and Aoshima, A. (2002) *Studies on Actinide Separation Process from High-Level Liquid Waste*, JAERI-Research-2002-017, Tokai Research Establishment, Japan Atomic Energy Research Institute.

Morss, L. R. and Rogers, R. D. (1997) *Inorg. Chim. Acta*, **255**(1), 193–7.

Moser, W. S. and Navratil, J. D. (1983) Review of Major Plutonium Pyrochemical Technology, Report RFP-3686, Rocky Flats Plant.

Motta, E. E. (1956) High Temperature Fuel Processing Methods, in *Proc. Int. Conf. on the Peaceful Uses of Atomic Energy*, Geneva, Progress in Nuclear energy – Series 3: Process chemistry, pp. 309–15.

Mousty, F., Toussaint, J., and Godfrin, J. (1977) *Radiochem. Radioanal. Lett.*, **31**(1), 9–18.

Mukaiyama, T., Kubota, M., Takizuka, T., Ogawa, T., Mizumoto, M., and Yoshida, H. (1995) in *Proc. Int. Conf. on Evaluation of Emerging Nuclear Fuel Cycle Systems* (*Global'95*), vol 1, Versailles, France.

Mullins, L. J., Leary, J. A., and Maraman, W. J. (1960) *Ind. Eng. Chem.*, **52**(3), 227–30.

Mullins, L. J., Leary, J. A., Morgan, A. N., and Maraman, W. J. (1962) Plutonium Electrorefining, Report LA-2666, USAEC, Los Alamos National Laboratory.

Mullins, L. J. and Leary, J. A. (1965) *Ind. Eng. Chem.*, **4**, 394–400.

Murali, M. S. and Mathur, J. N. (2001) *Solvent Extr. Ion Exch.*, **19**, 61–77.

Murzin, A. A., Babain, V. A., Shadrin, A. Y., Smirnov, I. V., Romanovskii, V. N., and Muradymov, M. Z. (1998) *Radiochemistry*, **40**(1), 47–51.

Muscatello, A. C., Horwitz, E. P., Kalina, D. G., and Kaplan, L. (1982) *Sep. Sci. Technol.*, **17**, 859–75.

Musikas, C., Le Marois, G., Fitoussi, R., and Cuillerdier, C. (1980) in *Actinide Separations* (eds. J. D. Navratil and W. W. Schulz) (ACS Symp. Ser. vol. 117), American Chemical Society, Washington, DC, pp. 131–45.

Musikas, C. and Hubert, H. (1983) *Int. Solvent Extraction Conf., ISEC '83*, Denver, CO.

Musikas, C. (1985) in *Actinide/Lanthanide Separations, Proc. Int. Symp.* (eds. G. R. Choppin, J. D. Navratil, and W. W. Schulz), Honolulu, HI, World Scientific, Singapore, pp. 19–30.

Musikas, C. (1987) *Inorg. Chim. Acta*, **140**, 197–206.

Musikas, C. (1991) *Int. Symp. on Radiochemistry and Radiation Chemistry,* BARC, Mumbai, India.

Musikas, C. (1995) *Nuclear and Radiochemistry Symp.,* Indira Gandhi Centre for Atomic Research, Kalpakkam, India.

Myasoedov, B. F., Guseva, L. I., Lebedev, I. A., Milyukova, M. S., and Chmutova, M. K. (1974) *Analytical Chemistry of Transplutonium Elements,* John Wiley, New York.

Myasoedov, B. F., Chmutova, M. K., Smirnov, I. V., and Shadrin, A. U. (1993) in *Global '93. Future Nuclear Systems: Emerging Fuel Cycles and Waste Disposal Options,* American Nuclear Society, La Grange Park, IL, pp. 581–7.

Myasoedov, B. F. and Chmutova, M. K. (1995) in *Separations of f-Elements,* (eds. K. L. Nash and G. R. Choppin), Plenum Press, New York, pp. 11–29.

Nagasaki, S., Kurioshita, K., Wisnubroto, D. S., Enokida, Y., and Suzuki, A. (1992) *J. Nucl. Sci. Technol.*, **29**, 671–6.

Nakajima, A. and Sakaguchi, T. (1990) *J. Chem. Technol. Biotechnol.*, **47**, 31–8.

Nakamura, T., Matsuda, Y., and Miyake, C. (1995) *Mater. Res. Soc. Symp. Proc.*, **353** (Scientific Basis for Nuclear Waste Management XVIII, Pt. 2), 1293–300.

Nash, K. L., Cleveland, J. M., and Rees, T. F. (1988a) *J. Environ. Radioact.*, **7**(2), 131–57.

Nash, K. L., Gatrone, R. C., Clark, G. A., Rickert, P. G., and Horwitz, E. P. (1988b) *Sep. Sci. Technol.*, **23**, 1355–72.

Nash, K. L., Gatrone, R. C., Clark, G. A., Rickert, P. G., and Horwitz, E. P. (1989) *Solvent Extr. Ion Exch.*, **7**, 655–75.

Nash, K. L. and Horwitz, E. P. (1990) *Inorg. Chim. Acta*, **169**, 245–52.

Nash, K. L. (1991) *Radiochim. Acta*, **54**, 171–9.

Nash, K. L. (1993a) *Solvent Extr. Ion Exch.*, **11**, 729–68.

Nash, K. L. (1993b) *Radiochim. Acta*, **61**, 147–54.

Nash, K. L. and Rickert, P. G. (1993) *Sep. Sci. Technol.*, **28**, 25–41.

Nash, K. L. (1994) Separation chemistry for lanthanides and trivalent actinides, in *Handbook on the Physics and Chemistry of Rare Earths*, vol. 18 (eds. K. A. Gschneidner Jr, L. Eyring, G. R. Choppin, and G. H. Lander), pp. 197–235, ch. 121.

Nash, K. L. and Choppin, G. R. (eds.) (1995) in *Separations of f-Elements, Proc. Symp. at the 208th American Chemical Society Meeting*, San Diego, CA, March 1994, Plenum Press, New York.

Nash, K. L. and Jensen, M. P. (2000) in *Handbook on the Physics and Chemistry of Rare Earths,* vol. 28 (eds. K. A. Gschneidner and L. Eyring), North-Holland, Amsterdam, pp. 311–71.

Nash, K. L. (2001) in *Solvent Extraction for the 21st Century, Proc. Int. Solvent Extraction Conf., ISEC'99* (eds. M. Cox, M. Hidalgo and M. Valiente), Barcelona, Society of Chemical Industry, London, pp. 555–9.

Nash, K. L., Lavallette, C., Borkowski, M., Paine, R. T., and Gann, X. (2002) *Inorg. Chem.*, **41**, 5849–58.

Navratil, J. D. and Thompson, G. H. (1979) *Nucl. Technol.*, **43**, 136–45.

Navratil, J. D. and Schulz, W. W. (eds.) (1980) *Actinide Separations* (ACS Symp. Ser. 117), American Chemical Society, Washington, DC.

Navratil, J. D. (2001) *J. Radioanal. Nucl. Chem.*, **248**, 571–4.

Nigond, L., Musikas, C., and Cuillerdier, C. (1994a) *Solvent Extr. Ion Exch.*, **12**, 261–96.

Nigond, L., Musikas, C., and Cuillerdier, C. (1994b) *Solvent Extr. Ion Exch.*, **12**, 297–323.

Nigond, L., Condemns, N., Cordier, P. Y., Livet, J., Madic, C., Cuillerdier, C., Musikas, C., and Hudson, M. J. (1995) *Sep. Sci. Technol.*, **30**(7–9), 2075–99.

Nissen, D. A. (1966) *J. Inorg. Nucl. Chem.*, **28**, 1740–3.

Novikov, A. P. and Myasoedov, B. F. (1987) *Solvent Extr. Ion Exch.*, **5**, 111–27.

Nunez, L., Buchholz, B. A., and Vandegrift, G. F. (1995) *Sep. Sci. Technol.*, **30**, 1455–71.

Nunez, L. and Vandegrift, G. F. (1995) in *Separations of f-Elements* (eds. K. L. Nash and G. R. Choppin), Plenum Press, New York, pp. 241–56.

Ogawa, T., Yamagishi, S., Kobayashi, F., Itoh, A., Mukaiyama, T., Handa, M., and Haired, R. G. (1995) in *Proc. Int. Conf. on Evaluation of Emerging Nuclear Fuel Cycle Systems* (*Global'95*), vol. 1, Versailles, France.

Ogawa, T., Akabori, M., Suzuki, Y., and Kobayashi, F. (1997) in *Proc. Int. Conf. on Future Nuclear Systems* (*Global'97*), Yokohama, Japan.

Oliver, J. R. (1958) THOREX Process: Third Uranium Cycle Studies, Report ORNL-2473, USAEC, p. 15.

ORNL (1962) Annual Report for Period Ending June 30, 1962, ORNL-3314, Oak Ridge National Laboratory.

Orth, D. A. (1978) SRP (Savannah River Plant) thorium processing experience, Du Pont de Nemours (E.I.) and Co., Aiken, SC, Report DPSPU-78-30-3, CONF-780622-72, p. 16.

Otu, E. O. and Chiarizia, R. (2002) in *Proc. Int. Solvent Extraction Conf., ISEC 2002* (eds. K. C. Sole, P. M. Cole, J. S. Preston, and D. J. Robinson), Capetown, South Africa, Chris van Rensburg Publications, South African Institute of Mining and Metallurgy, Johannesburg, pp. 408–13.

Otu, E. O., Chiarizia, R., Rickert, P. G., and Nash, K. L. (2002) *Solvent Extr. Ion Exch.*, **20**, 607–32.

Ozawa, M., Nemoto, S., Togashi, A., Kawata, T., and Onishi, K. (1992) *Solvent Extr. Ion Exch.*, **10**, 829–46.

Ozawa, M., Koma, Y., Nomura, K., and Tanaka, Y. (1998) *J. Alloys Compd.*, **271–273**, 538–43.

Ozawa, M., Sano, Y., Ohara, C., and Kishi, T. (2000) *Nucl. Technol.*, **130**, 196–205.

Paine, R. T. (1995) in *Separations of f-Elements* (eds. K. L. Nash and G. R. Choppin), Plenum Press, New York, pp. 63–75.

Pandey, A. K., Gautam, M. M., Shukla, J. P., and Iyer, R. H. (2001) *J. Membr. Sci.*, **190**, 9–20.

Pankratz, L. B. (1984) *Thermodynamic Properties of Halides*, Bull. U.S. Bur Mines No 674.

Park, G. I., Park, H. S., and Woo, S. I. (1999) *Sep. Sci. Technol.*, **34**, 833–54.

Park, Y.-Y., Fazekas, Z., Yamamura, T., Harada, M., Ikeda, Y., and Tomiyasu, H. (2000) *Proc. 4th Japan-Korea Seminar on Advanced Reactors*, Bulletin of the Research Laboratory for Nuclear Reactors, Special Issue.

Pathak, P. N., Prabhu, D. R., and Manchanda, V. K. (2000) *Solvent Extr. Ion Exch.*, **18**(5), 821–40.

Pederson, L. R., Ashby, E. C., Jonah, C., Meisel, D., and Strachan, D. M. (1992) Gas Generation and Retention in Tank 101-SY: A Summary of Laboratory Studies, Tank Data, and Information Needs., Report PNL-8124, Pacific Northwest National Laboratory.

Peppard, D. F., Mason, G. W., Maier, J. L., and Driscoll, W. J. (1957) *J. Inorg. Nucl. Chem.*, **4**, 334–43.

Perlman, I. (1946) *Separations Process*, Report CN-3627.

Persson, G. E., Svantesson, S., Wingefors, S., and Liljenzin, J. O. (1984) *Solvent Extr. Ion Exch.*, **2**, 89–113.

Peters, M. W., Werner, E. J., and Scott, M. J. (2002) *Inorg. Chem.*, **41**(7), 1707–16.

Petrzilova, H., Binka, J., and Kuca, L. (1979) *J. Radioanal. Nucl. Chem.*, **51**, 107–17.

Pierce, R. D. e. a. (1991) Recycle of LWR actinides to an IFR, in *3rd Int. Conf. on Nuclear Fuel Reprocessing and Waste Management 1.*

Pierce, R. D., Johnson, T. R., McPheeters, C. C., and Laidler, J. J. (1993) *J. Metals*, **February**, 40–4.

Pietrelli, L., Grossi, G., Torri, G., and Donato, A. (1987) *Energia Nucleare* (*Rome*), **4**(3), 57–62.

Poskanzer, A. M. and Foreman, B. M. Jr (1961) *J. Inorg. Nucl. Chem.*, **16**, 323–36.

Ragheb, M. M. H. and Maynard, C. W. (1980) *Atomkernenergie/Kerntechnik*, **35**(2), 122–4.

Rainey, R. H. and Moore, J. G. (1962) Acid THOREX Process for Recovery of Consolidated Edison Th Reactor Fuel, Report ORNL-3155, USAEC, Oak Ridge National Laboratory, p. 29.

Ramanujam, A., Dhami, P. S., Gopalakrishnan, V., Dudwadkar, N. L., Chitnis, R. R., and Mathur, J. N. (1999) *Sep. Sci. Technol.*, **34**, 1717–28.

Rao, P. R. V. and Kolarik, Z. (1996) *Solvent Extr. Ion Exch.*, **14**(6), 955–93.

Rapko, B. M. and Lumetta, G. J. (1994) *Solvent Extr. Ion Exch.*, **12**, 967–86.

Rapko, B. M. (1995) in *Separations of f-Elements* (eds. K. L. Nash and G. R. Choppin), Plenum Press, New York, pp. 99–123.

Regalbuto, M. C., Misra, B., Chamberlain, D. B., Leonard, R. A., and Vandegrift, G. F. (1992) The Monitoring and Control of TRUEX Processes: Volume 1. The Use of Sensitivity Analysis to Determine Key Process Variables and Their Control Bounds, Report ANL-92/7, Argonne National Laboratory.

Reinhardt, H. and Rydberg, J. (1969) *Acta Chem. Scand. (1947–1973)*, **23**(8), 2773–80.

Rhodes, R. (1986) *The Making of the Atomic Bomb,* Simon & Schuster, New York.

Rizvi, G. H. and Mathur, J. N. (1997) Utilization of Ferrocyanide Ion for Stripping of Actinides and Lanthanides from CMPO Phase and Aqueous Complexing of these

Metal Ions with Ferrocyanide Ion, Report BARC/P/004/1997, Bhabha Atomic Research Centre.

Rogers, R. D., Bond, A. H., and Bauer, C. B. (1993) *Sep. Sci. Technol.*, **28**, 1091.

Rollin, S. (1999) On-Line Coupling of an Ion Chromatograph to the ICP-MS: Separations with a Cation Exchange Chromatography Column, SKB Technical Report Tr-99-35, Studsvik Nuclear AB, Sweden.

Romanovskiy, V. N., Smirnov, I. V., Babain, V. A., Todd, T. A., Herbst, R. S., Law, J. D., and Brewer, K. N. (2001a) *Solvent Extr. Ion Exch.*, **19**(1), 1–21.

Romanovskiy, V., Smirnov, I., Esimantovsky, V., Zaitsev, B., Babain, V., Dzekun, E., Todd, T., Herbst, S., Law, J., and Brewer, K. (2001b) *Proc. 9th Int. High-Level Radioactive Waste Management Conf.*, Las Vegas, NV, April 29-May 3, 2001, pp. 309–12.

Romanovskiy, V. N. (2002a) *J. Nucl. Sci. Technol.*, Suppl. 3, 8–13.

Romanovskiy, V. N. (2002b) Chemical Separations in Nuclear Waste Management: The State of the Art and a Look to the Future (International Workshop, Technologies for Nuclear Separations: A Look to the Future), Prague, Czech Republic, Sept. 11, 2000, pp. 57–66.

Romanovskiy, V. N., Babain, V. A., Esimantovskiy, V. M., Smirnov, I. V., Zaitsev, B. N., Herbst, R. S., Law, J. D., and Todd, T. A. (2002) in *JAERI-Conf*. 2002–2004 (*Proc. Int. Symp. NUCEF 2001*), pp. 247–53.

Rosenthal, M. W., Haubenreich, P. N., and Briggs, R. B. (1972) The Development Status of Molten Salt Breeder Reactors, Report ORNL-4812, Oak Ridge National Laboratory.

Ross, R., Bamberger, C., and Baes, C. F. Jr (1973) *J. Inorg. Nucl. Chem.*, **35**, 453.

Roy, J. J., Grantham, L. F., Grimmett, D. L., Fusselman, S. P., Krueger, C. L., Storvick, T. S., Inoue, T., Sakamura, Y., and Takahashi, N. (1996) *J. Electrochem. Soc.*, **143**(8), 2487–92.

Rydberg, J. (1969) *Acta Chem. Scand.* (*1947–1973*), **23**(2), 647–59.

Saito, A. and Choppin, G. R. (1983) *Anal. Chem.*, **55**, 2454–57.

Saito, A., Roberts, R. A., and Choppin, G. R. (1985) *Anal. Chem.*, **57**(1), 390–91.

Sakaguchi, T. and Nakajima, A. (1987) *Sep. Sci. Technol.*, **22**, 1609–23.

Sakamura, Y., Hijikita, T., Storvick, T. S., and Grantham, L. F. (eds.) (1994) in *Proc. 26th Symp. on Molten Salt Chemistry*, Sapporo, Japan, p. 101.

Sakamura, Y., Hijikata, T., Kinoshita, K., Inoue, T., Storvick, T. S., Krueger, C. L., Roy, J. J., Grimmett, D. L., Fusselman, S. P., and Gay, R. L. (1998) *J. Alloys Compd.*, **271–273**, 592–6.

Sakamura, Y., Inoue, T., Shirai, O., Iwai, T., Arai, Y., and Suzuki, Y. (eds.) (1999) in *Proc. Int. Conf. on Future Nuclear Systems* (*Global'99*), Jackson Hole, Wyoming, pp. 209–16.

Sakamura, Y., Shirai, O., Iwai, T., and Suzuki, Y. (2001) *J. Alloys Compd.*, **321**, 76–83.

Sakata, M., Hijikita, T., and Kurata, M. (1991) *J. Nucl. Mater.*, **185**, 56–65.

Samsonov, M. D., Wai, C. M., Lee, S.-C., Kulyako, Y., and Smart, N. G. (2001) *Chem. Commun.*, 1868–9.

Samsonov, M. D., Trofimov, T. I., Vinokurov, S. E., Lee, S. C., Myasoedov, B. F., and Wai, C. M. (2002) in *Proc. Int. Solvent Extraction Conf., ISEC 2002* (eds. K. C. Sole, P. M. Cole, J. S. Preston, and D. J. Robinson), Capetown, South Africa, Chris van

Rensburg Publications, South African Institute of Mining and Metallurgy, Johannesburg, pp. 1187–92.
Sasaki, T., Meguro, Y., and Yoshida, Z. (1998) *Talanta*, **46**, 689–95.
Sasaki, Y., Sugo, Y., Suzuki, S., and Tachimori, S. (2001) *Solvent Extr. Ion Exch.*, **19**, 91–103.
Sasaki, Y. and Tachimori, S. (2002) *Solvent Extr. Ion Exch.*, **20**(1), 21–34.
Schlosser, G. and Behrens, E. (1967) *Nukleonika*, **9**(1), 36–42.
Schmeider, H. and Petrich, G. (1989) *Radiochim. Acta*, **48**, 181–92.
Schmidt, C., Saadioui, M., Boehmer, V., Host, V., Spirlet, M.-R., Desreux, J. F., Brisach, F., Arnaud-Neu, F., and Dozol, J.-F. (2003) *Org. Biomol. Chem.*, **1**(22), 4089–96.
Schoebrechts, J. P. and Gilbert, B. (1985) *Inorg. Chem.*, **24**, 2105–10.
Schulte, L. D., Fitz Patrick, J. R., Salazar, R. R., Schake, B. S., and Martinez, B. T. (1995a) *Separations of f-Elements* (eds. K. L. Nash and G. R. Choppin), Plenum Press, New York, 199–208.
Schulte, L. D., FitzPatrick, J. R., Salazar, R. R., Schake, B. S., and Martinez, B. T. (1995b) *Sep. Sci. Technol.*, **30**(7–9), 1833–47.
Schulte, L. D., McKee, S. D., and Salazar, R. R. (1996) *Proc. Embedded Topical Meeting on DOE Spent Nuclear Fuel and Fissile Material Management*, Reno, Nev., June 16–20, 1996, pp. 418–27.
Schulz, W. W. and Benedict, G. E. (1972) *Neptunium-237 – Production and Recovery* (*AEC Critical Review Series*), Report TID-25955, 85 pp.
Schulz, W. W. and McIsaac, L. D. (1975) Removal of Actinides from Nuclear Fuel Reprocessing Waste Solutions with Bidentate Organophosphorus Extractants, Atlantic Richfield Hanford Co., Richland, Washington, ARH-SA-217.
Schulz, W. W. and Navratil, J. D. (1982) in *Recent Developments in Separation Science* (ed. N. N. Li), CRC Press, Boca Raton, FL, p. 31 and references therein.
Schulz, W. W. and Horwitz, E. P. (1988) *Sep. Sci. Technol.*, **23**, 1191–210.
Schulz, W. W., Burger, L. L., and Navratil, J. D. (eds.) (1990) *Science and Technology of Tributyl Phosphate,* CRC Press, Boca Raton, FL.
Schulz, W. W. and Kupfer, M. J. (1991) Candidate Reagents and Procedures for the Dissolution of Hanford Site Single-Shell Tank Sludges, Report WHC-EP-0451, Westinghouse Hanford Company.
Schurhammer, R. and Wipff, G. (2002) *New J. Chem.*, **26**, 229–33.
Schurhammer, R. and Wipff, G. (2003) in *ACS Symp. Ser.*, **860** (Supercritical Carbon Dioxide), pp. 223–44.
Seaborg, G. T. and Thompson, S. G. (1960) Concentration and Decontamination of Plutonium Solutions by Precipitation of the Bismuth Phosphate Carrier 2950168 Continuation-in-part of U.S. 2,785,951 (CA 51, 7898a).
Seaborg, G. T. and Loveland, W. D. (1990) *The Elements Beyond Uranium,* John Wiley, New York.
Sekine, T. and Dyrssen, D. (1964) *Talanta*, **11**, 867–73.
Sekine, T. (1965) *Bull. Chem. Soc. Jpn.*, **38**, 1972–8.
Sekine, T. and Hasegawa, Y. (1977) *Solvent Extraction Chemistry,* Marcel Dekker, New York.
Senentz, G. and Liberge, R. (1998) in *Proc. Waste Management Conf. WM'98*, Tucson, AZ, pp. 2126–32.

Shadrin, A., Babain, V., Starchenko, V., Murzin, A. A., Smirnov, I., and Smart, N. G. (1998) *Proc. Int. Conf. Decomm. Decontam. Nucl. Hazard Waste Manage.,* St. Petersburg, Russia, American Nuclear Society, La Grange Park, IL.

Shamsipur, M., Ghiasvand, A. R., and Yamini, Y. (2001) *J. Supercrit. Fluids*, **20**, 163–9.

Shirai, O., Iwai, T., Suzuki, Y., Sakamura, Y., and Tanaka, H. (1998) *J. Alloys Compd.*, **271–273**, 685–8.

Shirai, O., Iwai, T., Shiozawa, K., Suzuki, Y., Sakamura, Y., and Inoue, T. (2000) *J. Nucl. Mater.*, **277**, 226–30.

Shirai, O., Iizuka, M., Iwai, T., and Arai, Y. (2001) *Anal. Sci.*, **17**, 51–7.

Siddall, T. H. III (1958) *U. S. At. Energy Comm.* (BNL 483 (C-26)), 149–53.

Siddall, T. H. Jr (1963a) *J. Inorg. Nucl. Chem.*, **25**, 883–92.

Siddall, T. H. III (1963b) *Aqueous Reprocess. Chem. Irradiated Fuels, Symp.*: 57–79, discussion 79–81.

Siddall, T. H. Jr (1964) *J. Inorg. Nucl. Chem.*, **26**, 1991–2003.

Sinha, S. P. (1986) *Lanthanide Actinide Res.*, **1**(3), 195–6.

Sinha, P. K., Lal, K. B., Amalraj, R. V., and Krishnasamy, V. (1992) *Indian J. Chem., Sect A*, **31A**(10), 808–10.

Skiba, O. V. and Ivanov, V. B. (1995) *State and Prospects of the Fuel Cycle Development Using Pyroelectrochemical Processes in Molten Salts*, Abstracts of the Molten Salt in Nuclear Technologies Seminar, Dimitrovgrad, Russia.

Smart, N. G., Carleson, T. E., Kast, T., Clifford, A. A., Burford, M. D., and Wai, C. M. (1997a) *Talanta*, **44**, 137–50.

Smart, N. G., Yoshida, Z., Meguro, Y., Iso, S., Clifford, A. A., Lin, Y., Toews, K., and Wai, C. M. (1997b) in *Proc. Int. Conf. on Future Nuclear Systems* (*Global'97*), Yokohama, Japan.

Smart, N. G. and Clifford, A. A. (2001) *A Method of Separating Uranium*, WO 01/45115 A2.

Smirnov, M. V. and Ivanovskii, L. (1957) *Zh. Fiz. Khim.*, **31**, 801.

Smirnov, M. V. and Skiba, O. V. (1963) *Tr. Inst. Elektrokhim. (Sverdlovsk)*, **4**(3), 17–28.

Smith, B. F., Jarvinen, G. D., Miller, G. G., Ryan, R. R., and Peterson, E. J. (1987) *Solvent Extr. Ion Exch.*, **5**, 895–8.

Smith, B. F., Gibson, R. R., Jarvinen, G. D., Jones, M. M., Lu, M. T., Robison, T. W., Schroeder, N. C., and Stalnaker, N. (1998) *J. Radioanal. Nucl. Chem.*, **234**(1–2), 219–23.

Smith, B. F., Robison, T. W., and Jarvinen, G. D. (1999) in *Metal-Ion Separation and Preconcentration* (eds. A. H. Bond, M. L. Dietz, and R. D. Rogers) (ACS Symp. Ser. 716), pp. 294–330.

Sole, K. C., Hiskey, J. B., and Ferguson, T. L. (1993) *Solvent Extr. Ion Exch.*, **11**, 783–96.

Song, C., Glatz, J. P., He, X., Bokelund, H., and Koch, L. (1994) Actinide Partitioning by Means of the TRPO Process, in *The 4th Int. conf. on Nuclear Fuel Reprocessing and Waste Management*, RECORD' 94, London, April 24–28, 1994.

Song, C. and Zhu, Y. (1994) *J. Tsinghua Univ.*, **34**, 79–83.

Song, C., Glatz, J. P., Koch, L., Bokelund, H., and He, X. (1996) in *Proc. Int. Solvent Extraction Conf., ISEC'96*, vol. 2 (eds. D. C. Shallcross, R. Paimin, and L. M. Prvcic), Melbourne, pp. 1355–60.

Spjuth, L., Liljenzin, J. O., Hudson, M. J., Drew, M. G. B., Iveson, P. B., and Madic, C. (2000) *Solvent Extr. Ion Exch.*, **18**, 1–23.

Spurny, J. and Heckmann, K. (1987) *Chem-Ztg.*, **111**(10), 305–7.
Srinivasan, R. and Flengas, F. (1964) *Can. J. Chem.* **42**, 1315.
Srinivasan, P., Kunnaraguru, K., Pushparaja, and Mathur, J. N. (2001) Sorption Behaviour of Am (III) in Nitric Acid Medium Using Chitosan, in *Nuclear and Radiochemistry Symp. NUCAR-2001,* Pune University, Pune, India.
Sriram, S., Mohapatra, P. K., Pandey, A. K., Manchanda, V. K., and Badheka, L. P. (2000) *J. Membr. Sci.*, **177**, 163–75.
Sriram, S. and Manchanda, V. K. (2002) *Solvent Extr. Ion Exch.*, **20**(1), 97–114.
Stary, J. (1966) *Talanta*, **13**, 421–37.
Stein, L. (1964) *Inorg. Chem.*, **3**, 995–1001.
Steunenberg, R. K., Pierce, R. D., and Burris, L. (eds.) (1970) in *Progress in Nuclear Energy*, Ser. III, Pergamon Press, New York, pp. 461–504.
Stevenson, C. E. (ed.) (1987) *The EBR-II Fuel Cycle Story,* American Nuclear Society, LaGrange Park, IL.
Stewart, H. B., Dahlberg, R. C., Goeddel, W. V., Trauger, D. B., Kasten, P. R., and Lotts, A. L. (1971) *Utilization of the Thorium Cycle in the HTGR* (*High-Temperature Gas-Cooled Reactor*),USAEC, Gulf General Atomics, San Diego, CA.
Stoller, S. M. and Richards, R. B. (eds.) (1961) *Reactor Handbook,* 2nd edn, vol. II, Fuel Reprocessing, Interscience, New York.
Street, K. Jr and Seaborg, G. T. (1950) *J. Am. Chem. Soc.*, **72**, 2790–2.
Strnad, J. and Heckmann, K. (1992) *J. Radioanal. Nucl. Chem.*, **163**(1), 47–57.
Sugo, Y., Sasaki, Y., and Tachimori, S. (2002) *Radiochim. Acta*, **90**(3), 161–5.
Suresh, G., Murali, M. S., and Mathur, J. N. (2001) *Solvent Extr. Ion Exch.*, **19**, 947–64.
Surls, J. P. and Choppin, G. R. (1957) *J. Inorg. Nucl. Chem.*, **4**, 62–73.
Svantesson, I., Hagstrom, I., Persson, G., and Liljenzin, J. O. (1979) *Radiochem. Radioanal. Lett.*, **37**, 215–22.
Svantesson, I., Hagstrom, I., Persson, G., and Liljenzin, J. (1980) *J. Inorg. Nucl. Chem.*, **42**, 1037–43.
Swanson, J. L. (1991a) Initial Studies of Pretreatment Methods for Neutralized Cladding Removal Waste (NCRW) Sludge, Report PNL-7716, Pacific Northwest National Laboratory.
Swanson, J. L. (1991b) Use of TRUEX Process for the Pretreatment of Neutralized Cladding Removal Waste (NCRW) Sludge – Results of a Design Basis Experiment, Report PNL-7734, Pacific Northwest National Laboratory.
Swanson, J. L. (1991c) Use of the TRUEX Process for the Pretreatment of Neutralized Cladding Removal Waste (NCRW) Sludge – Results of FY 1990 Studies, Report PNL-7780, Pacific Northwest National Laboratory.
Takanashi, M., Koma, Y., Koyama, T., and Funasaka, H. (2000) *J. Nucl. Sci. Technol.*, **37**, 963–9.
Takano, H., Akie, H., Osugi, T., and Ogawa, T. (1998) *Prog. Nucl. Energy*, **32**(3/4), 373–80.
Takeuchi, M., Tanaka, S., Yamawaki, M., and Tachimori, S. (1995) *J. Nucl. Sci. Technol.*, **32**, 450–5.
Tallent, O. and Ferris, L. M. (1974) *J. Inorg. Nucl. Chem.*, **36**, 1277–83.
Taylor, R. J., May, I., Denniss, I. S., Wallwork, A. L., Hill, N. J., Galkin, B. Y., Zilberman, B. Y., and Fedorov, Y. S. (1998) *J. Alloys Compd.*, **271–273**, 534–7.

Taylor, R. J., May, I., and Hill, N. J. (2001a) in *Solvent Extraction for the 21st Century, Proc. Int. Solvent Extraction Conf., ISEC'99* (eds. M. Cox, M. Hidalgo, and M. Valiente), Barcelona, Society of Chemical Industry, London, pp. 1339–43.

Taylor, R. J., May, I., Denniss, I. S., Koltunov, V. S., Baranov, S. M., Marvhenko, V. I., Mezhov, E. A., Pastuschak, V. G., Zhuravleva, G. I., and Savilova, O. A. (2001b) in *Solvent Extraction for the 21st Century,* Proc. Int. Solvent Extraction Conf., ISEC'99 (eds. M. Cox, M. Hidalgo, and M. Valiente), Barcelona, Society of Chemical Industry, London, pp. 1381–5.

Teixidor, F., Casensky, B., Dozol, J. F., Gruener, B., Mongeot, H., and Selucky, P. (2002) Selective Separation of M(1+), M(2+) and M(3+) Radionuclides, Namely of Cs, Sr and Actinides, from Nuclear Waste by Means of Chelating Hydrophobic Cluster Anions, Report EUR 19956, Institut de Ciencia de Materials de Barcelona, European Commission.

Thied, R. C., Seddon, K. R., Pitner, W. R., and Rooney, D. W. (1999) Patent WO99/41752.

Thied, R. C., Hatter, J. E., Seddon, K. R., and Pitner, W. R. (2001) Patent WO01/13379 A1.

Thompson, S. G., Cunningham, B. B., and Seaborg, G. T. (1950) *J. Am. Chem. Soc.*, **72**, 2798–801.

Thompson, S. G., Harvey, B. G., Choppin, G. R., and Seaborg, G. T. (1954) *J. Am. Chem. Soc.*, **76**, 6229–36.

Thompson, S. G. and Seaborg, G. T. (1956) First use of bismuth phosphate for separating plutonium from uranium and fission products, in *Progress in Nuclear Energy – Series 3: Process Chemistry,* sect. 3, vol. I (eds. F. R. Bruce, J. M. Fletcher, H. H. Hyman, and J. J. Katz), McGraw-Hill, New York, pp. 163–71.

Thompson, S. G. and Seaborg, G. T. (1957) Bismuth phosphate process for the separation of plutonium from aqueous solutions, Patent 2785951.

Thulasidas, S. K., Kulkarni, M. J., Goyal, N., Murali, M. S., Mathur, J. N., Page, A. G., Chintalwar, G. J., and Banerji, A. (1999) Studies on the Uptake of U, Eu, Cs and Sr by Plant *Sesurium portulacastrum* for Bioremediation Using Analytical Spectroscopy, in *Nuclear and Radiochemistry Symp. NUCAR-99*, Bhabha Atomic Research Centre.

Tian, G., Zhu, Y., and Xu, J. (2001) *Solvent Extr. Ion Exch.*, **19**, 993–1015.

Tian, G., Zhu, Y., Xu, J., Zhang, P., Hu, T., Xie, Y., and Zhang, J. (2003) *Inorg. Chem.*, **42**(3), 735–41.

Till, C. and Chang, Y. (eds.) (1988) *The Integral Fast Reactor,* Advances in Nuclear Science and Technology, Plenum Publishing, New York.

Todd, T. A., Law, J. D., Herbst, R. S., and Peterman, D. R. (2003) in *American Institute of Chemical Engineers* (Spring National Meeting), New Orleans, LA, March 30–April 3, 2003, pp. 2349–55.

Toews, K. L., Smart, N. G., and Wai, C. M. (1996) *Radiochim. Acta*, **75**, 179–84.

Tomczuk, Z., Ackerman, J. P., Wolson, R. D., and Miller, W. E. (1992) *J. Electrochem. Soc.*, **139**(12), 3523–8.

Tomioka, O., Enokida, Y., and Yamamoto, I. (2000) *Prog. Nucl. Energy*, **37**(1–4), 417–22.

Tomioka, O., Meguro, Y., Enokida, Y., Yamamoto, I., and Yoshida, Z. (2001a) *J. Nucl. Sci. Technol.*, **38**(12), 1097–102.

Tomioka, O., Meguro, Y., Iso, S., Yoshida, Z., Enokida, Y., and Yamamoto, I. (2001b) *J. Nucl. Sci. Technol.*, **38**(6), 461–2.

Tomioka, O., Meguro, Y., Iso, S., Yoshida, Z., Enokida, Y., and Yamamoto, I. (2002) in *Proc. Int. Solvent Extraction Conf., ISEC 2002* (eds. K. C. Sole, P. M. Cole, J. S. Preston, and D. J. Robinson), Capetown, South Africa, Chris van Rensburg Publications, South African Institute of Mining and Metallurgy, Johannesburg, pp. 1143–7.

Tomiyasu, H. and Asano, Y. (1995) *Prog. Nucl. Energy*, **29** (Suppl.), 227–34.

Toth, L. and Gilpatrick, L. (1972) Report ORNL-TM-4056, Oak Ridge National Laboratory.

Trice, V. G. and Chellew, N. R. (1961) *Nucl. Sci. Eng.*, **9**, 55–8.

Trochimczuk, A. W., Horwitz, E. P., and Alexandratos, S. D. (1994) *Sep. Sci. Technol.*, **29**(4), 543–9.

Trofimov, T. I., Samsonov, M. D., Lee, S. C., Smart, N. G., and Wai, C. M. (2001) *J. Chem. Technol. Biotechnol.*, **76**, 1223–6.

Tsezos, M. and Volesky, B. (1981) *Biotechnol. Bioeng.*, **23**, 583–604.

Tsezos, M. and Volesky, B. (1982) *Biotechnol. Bioeng.*, **24**, 385–401.

Tsezos, M. (1983) *Biotechnol. Bioeng.*, **25**, 2025–40.

Tsuda, T., Nohira, T., and Ito, Y. (2001) *Electrochim. Acta*, **46**, 1891–7.

Tsuda, T., Nohira, T., and Ito, Y. (2002) *Electrochim. Acta*, **47**, 2817–22.

Turanov, A. N., Karandashev, V. K., Kharitonov, A. V., Yarkevich, A. N., and Safronova, Z. V. (2000) *Solvent Extr. Ion Exch.*, **18**(6), 1109–34.

Turanov, A. N., Karandashev, V. K., Kharitonov, A. V., Safronova, Z. V., and Yarkevich, A. N. (2002) *Radiochemistry* **44**(1), 18–25. (Moscow, Russian Federation) (Translation of *Radiokhimiya*).

Turanov, A. N., Karandashev, V. K., Yarkevich, A. N., and Safronova, Z. V. (2004) *Solvent Extr. Ion Exch.*, **22**(3), 391–413.

Uchiyama, G., Asakura, T., Hotoku, S., and Fujine, S. (1998) *Solvent Extr. Ion Exch.*, **16**, 1191–213.

Uozumi, K., Kinoshita, K., Inoue, T., Fusselman, S. P., Grimmett, D. L., Roy, J. J., Storvick, T. S., Krueger, C. L., and Nabelek, C. R. (2001) *J. Nucl. Sci. Technol.*, **38**(1), 36–44.

Usami, T., Kurata, M., Inoue, T., Sims, H. E., Beetham, S. A., and Jenkins, J. A. (2002) *J. Nucl. Mater.*, **300**, 15–26.

Ustinov, O. A. (1995) *Physical-Chemical Validation of Spent U-Pu Oxide Fuel Reprocessing by Recrystallization in Molten Molybdates*, Abstracts of the Molten Salt in Nuclear Technologies Seminar, Dimitrovgrad, Russia.

Usuda, S. (1987) *J. Radioanal. Nucl. Chem.*, **111**(2), 399–410.

Usuda, S., Shinohara, S. N., and Yosikama, H. (1987) *J. Radioanal. Nucl. Chem.*, **109**, 353–61.

Usuda, S. (1988) *J. Radioanal. Nucl. Chem.*, **123**, 619–31.

Vandegrift, G. F., Leonard, R. A., Steindler, M. A., Horwitz, E. P., Basile, L. J., Diamond, H., Kalina, D. G. and Kaplan, L. (1984) Transuranic Decontamination of Nitric Acid Solutions by the TRUEX Solvent Extraction Process – Preliminary Development Studies, Report ANL-84-85, Argonne National Laboratory, Argonne, IL.

Vandegrift, G. F., Chamberlain, D. B., Conner, C., Copple, J. M., Dow, J. A., Everson, L., Hutter, J. C., Leonard, R. A., Nunez, L., Regalbuto, M. C., Sedlet, J., Srinivasan, B., Weber, S. and Wygmans, D. G.. (1993) in *Proc. Symp. on Technology and Programs for Radioactive Waste Management and Environmental Restoration*, vol. 2, Tucson, AZ, pp. 1045–50.

Vandegrift, G. F. and Regalbuto, M. C. (1995) *Proc. 5th Int. Conf. on Radioactive Waste Management and Environmental Remediation*, vol. 1, Berlin, Sept. 3–7, 1995, pp. 457–62.

Vavilov, S. K., Porodnov, P. T., Savochkin, Y. P., Skiba, O. V., and Shishalov, O. V. (1985) *Radiokhimiya*, **27**(1), 116–21.

Visser, A. E., Swatloski, R. P., Reichert, W. M., Griffin, S. T., and Rogers, R. D. (2000a) *Ind. Eng. Chem. Res.*, **39**, 3596–604.

Visser, A. E., Swatloski, R. P., and Rogers, R. D. (2000b) *Green Chem.* **(February)**, 1–4.

Visser, A. E., Swatloski, R. P., Griffin, S. T., Hartman, D. H., and Rogers, R. D. (2001a) *Sep. Sci. Technol.*, **36**(5–6), 785–804.

Visser, A. E., Swatloski, R. P., Reichert, W. M., Mayton, R., Sheff, S., Wierzbicki, A., Davis, J. H. J., and Rogers, R. D. (2001b) *Chem. Commun.*, 135–6.

Visser, A. E., Holbrey, J. D., and Rogers, R. D. (2002) in *Proc. Int. Solvent Extraction Conf., ISEC 2002* (eds. K. C. Sole, P. M. Cole, J. S. Preston, and D. J. Robinson), Capetown, South Africa, Chris van Rensburg Publications, South African Institute of Mining and Metallurgy, Johannesburg, pp. 474–80.

Visser, A. E. and Rogers, R. D. (2002) *Proc. Electrochem. Soc.*, **2002–2019** (Molten Salts XIII), 516–29.

Visser, A. E., Jensen, M. P., Laszak, I., Nash, K. L., Choppin, G. R., and Rogers, R. D. (2003) *Inorg. Chem.*, **42**, 2197–99.

Vitorge, P. (1985) Report 1984, Commissariat a l'Energie Atomique (CEA), Report CEA-R-5270.

Wada, H. and Fernando, Q. (1972) *Anal. Chem.*, **44**, 1640–3.

Wai, C. M., Smart, N. G., and Phelps, C. (1997) Patent no. US005606724.

Wai, C. M., Smart, N. G., and Lin, Y. (1998) Patent no. WO 98/04754.

Wai, C. M. and Laintz, K. E. (1999) Patent no. US005965025.

Wai, C. M., Lin, Y., Ji, M., Toews, K. L., and Smart, N. G. (1999) in *Metal Ion Separations and Concentration* (eds. A. H. Bond, M. L. Dietz, and R. D. Rogers) (ACS Symp. Ser. 716), American Chemical Society, Washington, DC., pp. 390–40.

Wai, C. M. and Waller, B. E. (2000) *Ind. Eng. Chem. Res.*, **39**, 4837–41.

Wai, C. M. (2002) in *Supercritical Fluid Technology in Materials Science and Engineeering. Syntheses, Properties and Applications* (ed. V.-P. Sun), Marcel Dekker, New York; Basel, pp. 351–86.

Wang, X., Zhu, Y., and Jiao, R. (2001) *Solvent Extr Ion Exch.*, **19**, 1007–36.

Watanabe, M., Mirvaliev, R., Tachimori, S., Takeshita, K., Nakano, Y., Morikawa, K., and Mori, R. (2002) *Chem. Lett.*, **12**, 1230–1.

Watson, S. B. and Rainey, R. H. (1979a) Modeling the Effect of Temperature on Thorium and Nitric Acid Extraction and the Formation of Third Phase for Modification of the SEPHIS: THOREX Computer Program, Report ORNL/CSD/TM-69, Oak Ridge National Laboratory, 35 pp.

Watson, S. B. and Rainey, R. N. (1979b) User's Guide to the SEPHIS Computer Code for Calculating the THOREX Solvent Extraction System, Report ORNL/CSD/TM-70, Oak Ridge National Laboratory, 50 pp.

Weaver, B. and Kappelmann, F. A. (1964) A New Method of Separating Americium and Curium from Lanthanides by Extraction from an Aqueous Solution of Amino Polyacetic Acid Complex with a Monoacidic Phosphate, Report ORNL-3559, Oak Ridge National Laboratory.

Weaver, B. and Kappelmann, F. A. (1968) *J. Inorg. Nucl. Chem.*, **30**, 263–72.

Weaver, B. (1974) in *Ion Exchange and Solvent Extraction,* vol. 6 (eds. J. A. Marinsky and Y. Marcus), Marcel Dekker, New York, pp. 189–277.

Wei, Y., Kumagai, M., Takashima, Y., Modolo, G., and Odoj, R. (2000) *Nucl. Technol.*, **132**, 413–23.

Weigl, M., Geist, A., Gompper, K., and Kim, J. (2001) *Solvent Extr. Ion Exch.*, **19**, 215–29.

Welton, T. (1999) *Chem. Rev.*, **99**, 2071–83.

Whisenhunt, D. W. Jr, Neu, M. P., Xeu, J., Houk, Z., Hoffman, D. C., and Raymond, K. N. (1993) *Thermodynamic Formation Constants for Actinide(IV) Ions with Siderophores and Siderophore Analogs in Actinides 93, Int. Conf.*, Santa Fe, NM, Abstract P-127.

Wick, O. J. (ed.) (1967) *Plutonium Handbook, A Guide to the Technology,* American Nuclear Society, Reprint 1980, Gordon and Breach, New York.

Willit, J. L., Miller, W. E., and Battles, J. E. (1992) *J. Nucl. Mater.*, **195**, 229–49.

Worl, L. A., Devlin, D., Hill, D., Padilla, D., and Prenger, C. (2001) *Sep. Sci. Technol.*, **36**, 1335–49.

Yamaura, M. and Matsuda, H. T. (1999) *J. Radioanal. Nucl. Chem.*, **241**, 277–80.

Zawodzinski, T. A. J. and Osteryoung, R. A. (1987a) *Inorg. Chem.*, **26**, 2920–2.

Zawodzinski, T. A. J. and Osteryoung, R. A. (1987b) *Proc. Joint Int. Symp. on Molten Salts,* The Electrochemical Society, Pennington, NJ.

Zhang, P., Song, C. L., Liang, J. F., and Xin, R. X. (2001) *Solvent Extr. Ion Exch.*, **19**, 79–89.

Zhu, Y., Jiao, R., Wang, S., Fan, S., Liu, B., Zheng, H., S., Z., and Chen, S. (1983) An Extractant (TRPO) for the Removal and Recovery of Actinides from High Level Radioactive Liquid Waste, in *Proc. Int. Solvent Extraction Conf., ISEC'83*, Denver, CO.

Zhu, Y. and Song, C. (1992) Recovery of neptunium, plutonium and americium from high active waste, in *Transuranium Elements: A Half Century* (eds. Morss, R. Lester J. Fuger), American Chemical Society, Washington, DC, pp. 318–30.

Zhu, Y. and Jiao, R. (1994) *Nucl. Technol.*, **108**, 361–9.

Zhu, Y. (1995) *Radiochim. Acta*, **68**, 95–8.

Zhu, Y., Chen, J., and Jiao, R. (1996) *Solvent Extr. Ion Exch.*, **14**, 61–8.

SUBJECT INDEX

Vol. 1: 1–698, Vol. 2: 699–1395, Vol. 3: 1397–2111, Vol. 4: 2113–2798, Vol. 5: 2799–3440.

Page numbers suffixed by t and f refer to Tables and Figures respectively.

AUTHOR INDEX

Vol. 1: 1–698, Vol. 2: 699–1395, Vol. 3: 1397–2111, Vol. 4: 2113–2798, Vol. 5: 2799–3440.

Page numbers suffixed by t and f refer to Tables and Figures respectively.

CHAPTER TWENTY FIVE

ORGANOACTINIDE CHEMISTRY: SYNTHESIS AND CHARACTERIZATION

Carol J. Burns and Moris S. Eisen

25.1 INTRODUCTION

The advent of modern organometallic chemistry has often been cited as the report of the preparation of ferrocene, $(\eta^5\text{-}C_5H_5)_2Fe$, the first metallic complex containing a π-complexed ligand (Pauson, 1951). It was not long after the report of this compound that comparable analogs of the lanthanides and actinides were reported (Reynolds and Wilkinson, 1956). Since that time, the organometallic chemistry of the actinides has lagged in comparable developments to the chemistry of the transition metals. Recent years, however, have witnessed a resurgence of interest in the non-aqueous chemistry of the actinides, in part due to the availability of a much wider array of ancillary ligands capable of stabilizing new compounds and introducing new types of reactivity. Equally important in stimulating new interest has been the realization by numerous researchers that the organometallic chemistry of these elements provides types of chemical environments that effectively probe the metals' ability to employ valence 6d and 5f orbitals in chemical bonding. Modern organoactinide chemistry is now characterized by the existence not only of actinide analogs to many classes of d-transition metal complexes (particularly those of Groups 3 and 4), but increasingly common reports of compounds (and types of reactions) unique to the actinide series. Most developments in the non-aqueous chemistry of the

actinides have involved the use of thorium and uranium, both due to their lower specific activity, and to the apparent chemical similarity these elements bear to Group 4 metals in organometallic transformations. Uranium has further demonstrated the ability to access a wide range of oxidation states (3+ to 6+) in organic solvents, providing for greater flexibility in effecting chemical transformations.

The earliest technological interest in organometallic actinide chemistry focused on its potential for application in isotope separation processes (Gilman, 1968). More recent reports continue to discuss the volatility of organoactinide compounds as a possible benefit in separation processes (gas chromatography, fractional sublimation) or in chemical vapor deposition processes (Mishin *et al.*, 1986). At the same time, interest has emerged in the behavior of the actinide elements in stoichiometric and catalytic transformations, particularly in comparison to d-transition metal analogs. The relatively large size and abundance of valence orbitals associated with the actinide metals can facilitate transformations of substrates at the metal center, or enable new types of reactions. These reactions will be discussed further in Chapter 26.

This chapter will provide an overview of the preparation and properties of the major classes of actinide complexes; the material will be organized by major ancillary ligand type. Within a class of ligands, compounds will be discussed based upon assigned formal oxidation states. While earlier definitions of organometallic chemistry would restrict consideration to compounds exclusively containing metal–carbon σ- or π-bonds, for the purposes of this treatise we will briefly consider select classes of ancillary ligands based principally coordination of the metal center by elements of Group 15 or Group 16, particularly where these ligand sets serve to support novel molecular transformations at the metal center.

25.2 CARBON-BASED ANCILLARY LIGANDS

25.2.1 Cyclopentadienyl ligands

(a) Trivalent chemistry

The most common class of organoactinide complexes is that containing the cyclopentadienyl ligand ($C_5H_5^-$), or one of its substituted derivatives. The use of variants of the cyclopentadienyl ligand has dominated the field of organometallic chemistry over the past 50 years, given their ability to stabilize a wide variety of oxidation states and coordination environments (Cotton *et al.*, 1999). The cyclopentadienyl ligand itself dominated the early development of organoactinide chemistry. The coordination environment that likely has been reported for the largest number of the actinide elements is the homoleptic compound $(\eta^5\text{-}C_5H_5)_3An$ (An = actinide). This ligand set support most members of the actinide series from thorium to californium (Table 25.1).

A number of synthetic routes have been reported to generate these species and their tetrahydrofuran (THF) adducts, including direct metathesis with alkali

Table 25.1 *Tris(cyclopentadienyl)actinide complexes.*

Compound	*Color*	*Melting point* (°C)	*References*
$(\eta^5\text{-}C_5H_5)_3Th$[a]	Green	–	Kanellakopolous *et al.* (1974a)
$(\eta^5\text{-}C_5H_5)_3U$	Brown	>200	Kanellakopolus *et al.* (1970)
$(\eta^5\text{-}C_5H_5)_3Np$	Brown	–	Karraker and Stone (1972)
$(\eta^5\text{-}C_5H_5)_3Pu$	Green	180 (dec.)	Baumgärtner *et al.* (1965)
$(\eta^5\text{-}C_5H_5)_3Am$	Flesh	330 (dec.)	Baumgärtner *et al.* (1966)
$(\eta^5\text{-}C_5H_5)_3Cm$	Colorless	–	Laubereau and Burns (1970a)
$(\eta^5\text{-}C_5H_5)_3Bk$	Amber	–	Laubereau and Burns (1970b)
$(\eta^5\text{-}C_5H_5)_3Cf$	Red	–	Laubereau and Burns (1970b)

[a] Compound not fully characterized.

metal salts (Crisler and Eggerman, 1974; Kanellakopolus *et al.*, 1974a, 1980; Moody and Odom, 1979; Wasserman *et al.*, 1983), or transmetallation with Be $(\eta^5\text{-}C_5H_5)_2$ or $Mg(\eta^5\text{-}C_5H_5)_2$ (Fischer and Fischer, 1963; Baumgärtner *et al.*, 1965, 1966, 1967, 1970; Laubereau and Burns, 1970a,b). In addition, the trivalent compounds may be obtained from chemical (Crisler and Eggerman, 1974) or photochemical (Kalina *et al.*, 1977; Bruno *et al.*, 1982) reduction of suitable tetravalent actinide precursors (Karraker and Stone, 1972; Chang *et al.*, 1979; Zanella *et al.*, 1980). Examples of these preparations are given in equations (25.1)–(25.5).

$$UCl_3 \cdot n\text{THF} + 3Na(C_5H_5) \xrightarrow{\text{THF}} (\eta^5\text{-}C_5H_5)_3U(\text{THF}) + 3\text{NaCl} \quad (25.1)$$

$$2AnCl_3 + 3Be(C_5H_5)_2 \xrightarrow{70^\circ C} (\eta^5\text{-}C_5H_5)_3An + 3BeCl_2 \quad An = Pu,\ Am,\ Cm,\ Bk,\ Cf \quad (25.2)$$

$$2PuCl_3 + 3Mg(C_5H_5)_2 \xrightarrow{\text{THF}} (\eta^5\text{-}C_5H_5)_3Pu + 3MgCl_2 \quad (25.3)$$

$$(\eta^5\text{-}C_5H_5)_3U[(CH(CH_3)_2] \xrightarrow{h\nu, C_6H_6} (\eta^5\text{-}C_5H_5)_3U\text{-H} + CH_2{=}CHCH_3$$
$$(\eta^5\text{-}C_5H_5)_3U\text{-H} + (\eta^5\text{-}C_5H_5)_3U[CH(CH_3)_2] \longrightarrow (\eta^5\text{-}C_5H_5)_3U + CH_3CH_2CH_3 \quad (25.4)$$

$$Cs_2PuCl_6 + Mg(C_5H_5)_2 \xrightarrow{\text{THF}} (\eta^5\text{-}C_5H_5)_3Pu + \text{unknown} \quad (25.5)$$

More recently, a study was conducted on reduction products of $(\eta^5\text{-}C_5H_5)_3UCl$ with a variety of reducing agents (Le Marechal *et al.*, 1989). It was found that the composition of the product was a function of the reducing agent [equations (25.6)–(25.8)].

$$(\eta^5\text{-}C_5H_5)_3UCl + Na/Hg \xrightarrow{THF} (\eta^5\text{-}C_5H_5)_3U(THF) \quad (25.6)$$

$$(\eta^5\text{-}C_5H_5)_3UCl + Na/Hg + 18{-}crown{-}6 \xrightarrow{THF} [(18{-}crown{-}6)Na][(\eta^5\text{-}C_5H_5)_3UCl] \quad (25.7)$$

$$(\eta^5\text{-}C_5H_5)_3UCl + NaH \longrightarrow [Na(THF)_2]\{[(\eta^5\text{-}C_5H_5)_3U]_2(\mu\text{-}H)\} \quad (25.8)$$

Perhaps the most useful development in the synthetic chemistry of trivalent actinide complexes in recent years has been the development of the more soluble iodide starting materials (Karraker, 1987; Clark *et al.*, 1989) AnI_3L_4 (An = U, Np, Pu; L = THF, pyridine, DMSO). These species, generated from actinide metals and halide sources in coordinating solvents, are readily soluble in organic solvents, and serve as convenient precursors to a variety of trivalent actinide species [equations (25.9)–(25.10)] (Zwick *et al.*, 1992).

$$An + 3/2I_2 \xrightarrow[L = THF,\ pyridine,\ DMSO]{L} AnI_3L_4 \quad (25.9)$$

$$PuI_3(THF)_4 + Li(C_5H_5) \xrightarrow{THF} (\eta^5\text{-}C_5H_5)_3Pu(THF) + 3LiI \quad (25.10)$$

The solubility of the parent tris(cyclopentadienyl)actinide complexes is limited in non-polar media, presumably due to oligomerization through bridging cyclopentadienyl ligands. The molecular structures of these species have only been inferred by comparison of powder diffraction data with that obtained from known tris(cyclopentadienyl)lanthanide complexes. In response, a number of groups have explored the chemistry of substituted analogs of the cyclopentadienyl ligand for the light actinides (Th, U), including those with alkyl or silyl substituents, as well as the indenyl ligand. Tris(ligand) complexes have been reported and several examples have been structurally characterized. Tris(indenyl) complexes of thorium and uranium have been reported, and the complex $(\eta^5\text{-}C_9H_7)_3U$ was structurally characterized (Goffart, 1979; Meunier-Piret *et al.*, 1980). Several other trivalent substituted cyclopentadienyl complexes have been prepared by reduction of tetravalent precursors (Brennan *et al.*, 1986a; Zalkin *et al.*, 1988a; Stults *et al.*, 1990), as shown in equation (25.11).

$$(\eta^5\text{-}Me_3SiC_5H_4)_3UCl + {}^tBuLi \xrightarrow{Toluene} \quad (25.11)$$

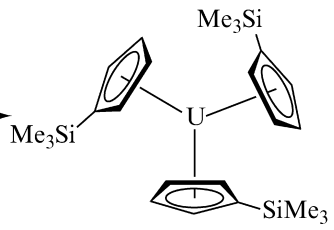

The complexes $[\eta^5\text{-}(Me_3Si)_2C_5H_3]_3U$ and $(\eta^5\text{-}C_5Me_4H)_3U$ have also been prepared by reduction of tetravalent precursors (del Mar Conejo *et al.*, 1999), although in the synthesis of $[\eta^5\text{-}(Me_3Si)_2C_5H_3]_3U$, ligand redistribution also takes place [equation (25.12)].

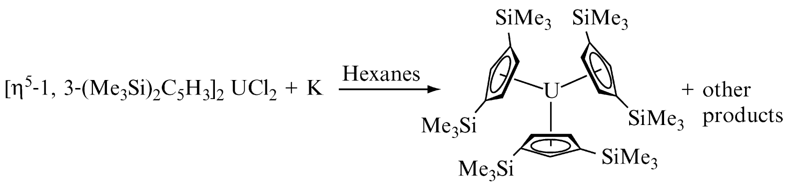

(25.12)

One of the more interesting members of the series of trivalent homoleptic cyclopentadienyl complexes is the well-characterized thorium example, $[\eta^5\text{-}(RMe_2Si)_2C_5H_3]_3Th$ (R = Me, ${}^tBu$) (Blake *et al.*, 1986a, 2001). This complex was prepared in a manner similar to that shown in equation (25.12), by reduction of the metallocene dichloride or the tris(cyclopentadienyl) chloride in toluene by Na–K alloy. The compound is isolated in good yield as a dark blue crystalline material, which has been structurally characterized (Fig. 25.1).

As for most base-free tris(cyclopentadienyl)actinide complexes, the compound crystallizes in a pseudo-trigonal planar structure, with averaged ligand centroid–thorium–centroid angles near 120°, and averaged $Th\text{–}C_{ring}$ distances of 2.80(2) Å. A particular element of interest for this complex has been its electronic structure. One of the most investigated aspects of actinide–cyclopentadienyl chemistry has been the nature of bonding between the metal and the ligand (Burns and Bursten, 1989). Most experimental studies of tris(cyclopentadienyl)actinide complexes, including ^{237}Np Mössbauer studies of $(\eta^5\text{-}C_5H_5)_3Np$ (Karraker and Stone, 1972) and infrared and absorption spectroscopic studies of plutonium, americium, and curium analogs (Baumgärtner *et al.*, 1965; Pappalardo *et al.*, 1969; Nugent *et al.*, 1971) suggest that while the bonding is somewhat more covalent than that in lanthanide analogs, the interaction between the metal and the cyclopentadienyl ring is still principally ionic. Theoretical treatments have suggested that the 6d orbitals are chiefly involved in interactions with ligand-based orbitals. While the 5f orbital energy drops across the series, creating an energy match with ligand-based orbitals, spatial overlap is poor, precluding strong metal–ligand bonding (Strittmatter and Bursten, 1991). Thorium lies early in the actinide series and the relatively high energy of the 5f orbitals (before the increasing effective nuclear charge across the series drops the energy of these orbitals) has lead to speculation that a Th(III) compound could in fact demonstrate a $6d^1$ ground state. In support of this, Kot *et al.* (1988) have reported the observation of an EPR spectrum with *g* values close to 2 at room temperature.

Despite the common use of the permethylated cyclopentadienyl ligand $(C_5Me_5^-)$ in actinide and lanthanide chemistry, it is only recently that a tris (cyclopentadienyl) actinide complex has been prepared with this ligand

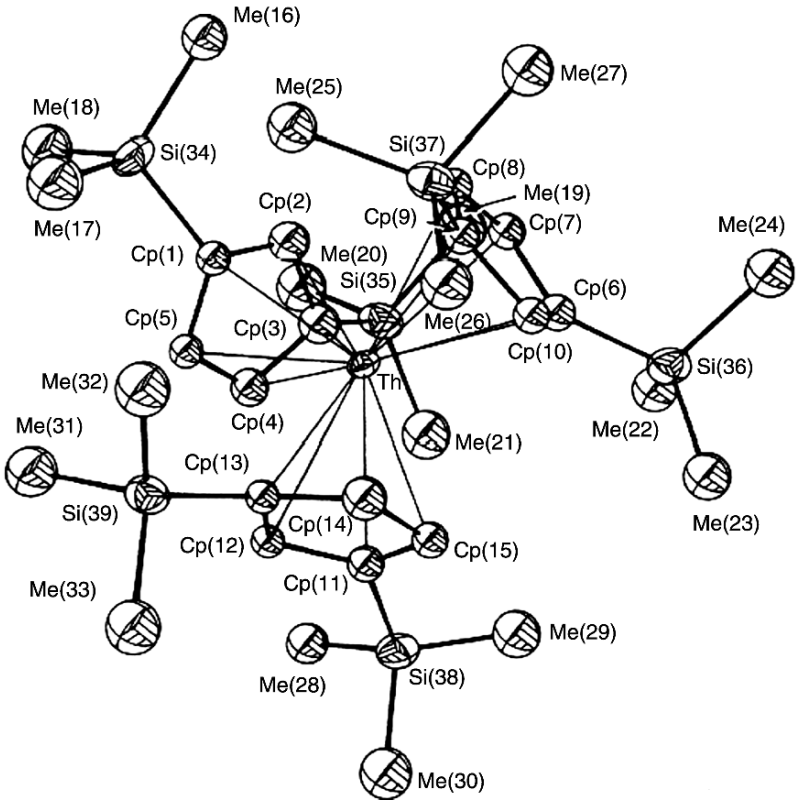

Fig. 25.1 *Crystal structure of* $[\eta^5\text{-}(Me_3Si)_2C_5H_3]_3Th$ (*Blake* et al., 1986a). (*Reproduced by permission of The Royal Society of Chemistry*.)

(Evans *et al.*, 1997). It was previously anticipated that the large steric bulk associated with this ligand would preclude incorporation of three pentamethylcyclopentadienyl groups in the coordination sphere of an actinide, and in fact direct metathesis routes had not proven successful. The complex $(\eta^5\text{-}C_5Me_5)_3U$ was instead initially prepared by reaction of a trivalent hydride complex with tetramethylfulvene [equation (25.13)].

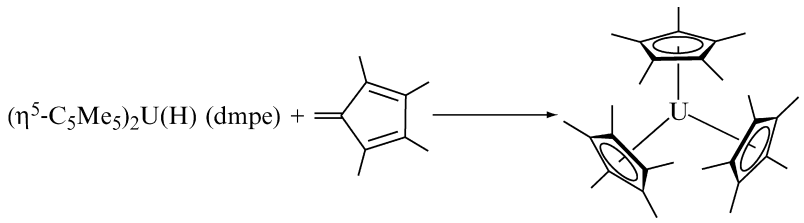

(25.13)

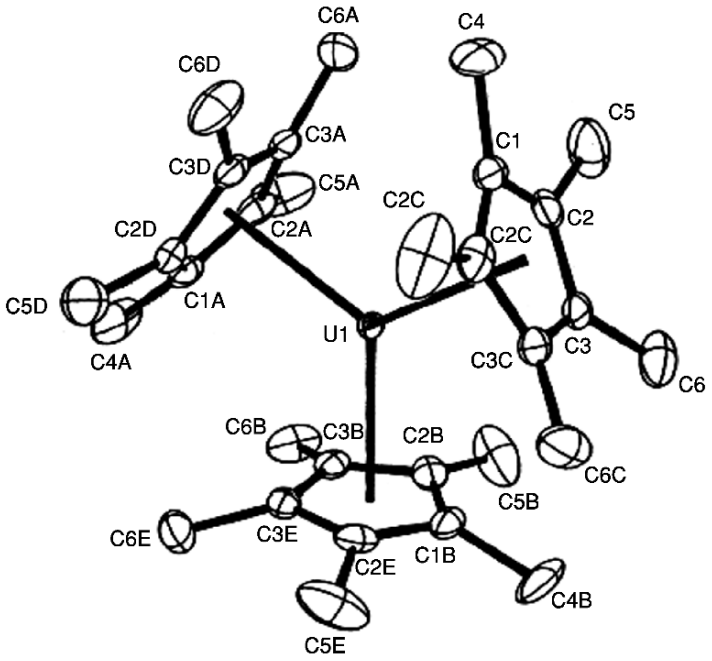

Fig. 25.2 *Crystal structure of* $(\eta^5\text{-}C_5Me_5)_3U$ (*Evans* et al., 1997). (*Reproduced with permission from John Wiley & Sons, Inc.*)

Since that time, however, several other routes have been reported to generate the compound (Evans *et al.*, 2002). The molecular structure is shown in Fig. 25.2.The average $U–C_{ring}$ bond distance in this compound [2.858(3) Å] is much larger than in other crystallographically characterized U(III) pentamethylcyclopentadienyl complexes (*ca.* 2.77 Å), suggesting a significant degree of steric crowding.

The tris(cyclopentadienyl)actinide complexes display a rich coordination chemistry, and one which sheds light on the nature of metal orbital participation in chemical bonding. Actinide metals generally are acidic and coordinate Lewis bases. As previously discussed, many of the tris(cyclopentadienyl)actinide complexes can be isolated as THF adducts directly from reactions carried out in that solvent. In addition, these complexes will coordinate other simple N-, O-, or P-donor bases. In most instances the complexes form simple 1:1 adducts [equation (25.14)] (Brennan and Zalkin, 1985; Brennan *et al.*, 1986b, 1988a; Zalkin and Brennan, 1987; Rosen and Zalkin, 1989; Adam *et al.*, 1993), while in select cases complexes have been isolated where two metal centers are bridged by a bidentate base [equation (25.15)] (Zalkin *et al.*, 1987b).

$$(\eta^5\text{–}MeC_5H_4)_3U + L \longrightarrow (\eta^5\text{–}MeC_5H_4)_3U\text{–}L \quad L=Ph_3P=O, \tag{25.14}$$

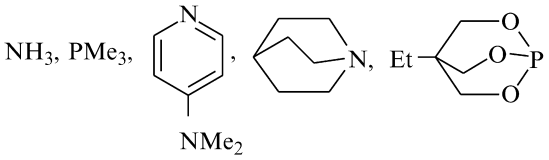

$$(\eta^5\text{-}C_5H_5)_3U(THF) + dmpe \xrightarrow{THF} Cp_3U\text{—}P \quad P\text{—}UCp_3 \tag{25.15}$$

Similarly, reaction of tris(cyclopentadienyl) complexes with anionic reagents has been shown to produce either anionic [equation (25.16)] or anion-bridged bimetallic complexes [equation (25.17)] (Stults *et al.*, 1989; Berthet *et al.*, 1991a, 1992a):

$$2(\eta^5\text{-}(SiMe_3)C_5H_4)_3U + NaN_3 + 18\text{-crown-6} \longrightarrow [Na(18\text{-crown-6})]\,[(\eta^5\text{-}(SiMe_3)C_5H_4)_3U\text{–}N{=}N{=}N\text{–}U(\eta^5\text{-}(SiMe_3)C_5H_4)_3U] \tag{25.16}$$

$$2(\eta^5\text{-}(SiMe_3)C_5H_4)_3U + NaH + 18\text{-crown-6} \longrightarrow [Na(18\text{-crown-6})]\,[(\eta^5\text{-}(SiMe_3)C_5H_4)_3U\text{–}H\text{–}U(\eta^5\text{-}(SiMe_3)C_5H_4)_3U] \tag{25.17}$$

Determination of the relative affinities of tris(cyclopentadienyl) complexes for various classes of ligands has been used to suggest the extent of metal-to-ligand π-back-donation. In order to compare the properties of actinides with lanthanides, ligand displacement series have been evaluated for the compounds $(RC_5H_4)_3M$ (M = U, Ce) (Brennan *et al.*, 1987). Both uranium and cerium complexes were found to have a preference for 'softer' phosphine donor ligands over 'harder' amine ligands, although in direct competition between the two metals, uranium always prefers the softer donors over cerium. Examination of the crystal structures of comparable uranium and cerium compounds reveals a slight shortening of the U–P bond (corrected for differences in metal radii); it has been suggested that this is a consequence of metal π-back-donation to phosphorus.

Another indication of the ability of low-valent early actinides to engage in π-back-donation may be found in the coordination of carbon monoxide to $(R_nC_5H_{5-n})_3U$ (Brennan *et al.*, 1986c; Parry *et al.*, 1995; del Mar Conejo *et al.*, 1999). Both structural and spectroscopic studies indicate that a strong degree of metal-to-ligand back donation occurs. The molecular structure of $(\eta^5\text{-}C_5Me_4H)_3U(CO)$ (Fig. 25.3) evidences a short $U\text{–}C_{CO}$ bond distance of 2.383(6) Å.

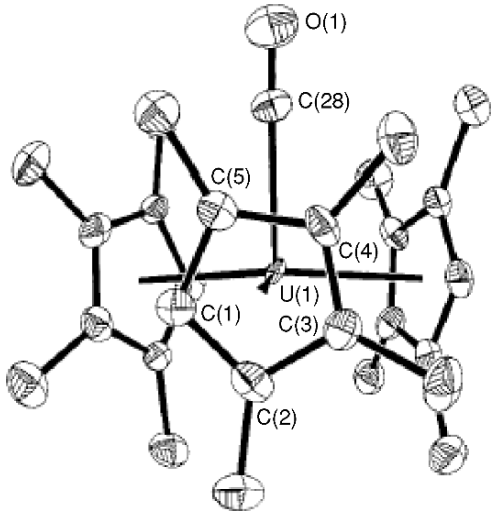

Fig. 25.3 *Crystal structure of* $[\eta^5\text{-}C_5Me_4H]_3U(CO)$ (*del Mar Conejo* et al., 1999). (*Reprinted with permission from John Wiley & Sons, Inc.*)

Table 25.2 *IR data of* $(\eta^5\text{-}R_nC_5H_{5-n})_3U(CO)$ *complexes.*

Compound	ν_{CO} (cm^{-1})
$(\eta^5\text{-}C_5Me_4H)_3U(CO)$	1880
$(\eta^5\text{-}Me_3CC_5H_4)_3U(CO)$	1960
$(\eta^5\text{-}Me_3SiC_5H_4)_3U(CO)$	1976
$[\eta^5\text{-}(Me_3Si)_2C_5H_3]_3U(CO)$	1988

Comparison of the ν_{CO} stretching frequencies for a series of compounds with varying ligand substituents (Table 25.2) demonstrates that electron-donating substituents on the ring contribute to increasing the electron density at the metal center, increasing metal-to-ligand back donation.

There is little comparable data for the heavier actinides, although the above bonding arguments would suggest that as the 6d orbital energy drops across the series, metal–ligand interactions would be weaker. Consistent with this picture, it has been reported that plutonium forms less robust adducts. While the complex $(\eta^5\text{-}C_5H_5)_3Pu(THF)$ can be isolated from solution, the THF is removed upon sublimation (Crisler and Eggerman, 1974); the analogous uranium compound remains intact upon sublimation (Wasserman *et al.*, 1983).

The early trivalent actinide cyclopentadienyl complexes are susceptible to one- and two-electron oxidation reactions. As an example, reaction of the tris (cyclopentadienyl) complexes have been reported to yield the corresponding U(IV) thiolate or selenolate complexes [equation (25.18)] (Leverd *et al.*, 1996).

$$\begin{aligned} &Cp_3U + R-E-E-R \longrightarrow Cp_3U-ER \\ &Cp = (\eta^5\text{-}C_5H_5),\ (\eta^5\text{-}C_5H_4Me),\ (\eta^5\text{-}C_5H_4SiMe_3); \\ &E = S,\ R = Me,\ Et,\ {}^{i}Pr,\ {}^{t}Bu,\ P;\ E = Se,\ R = Me \end{aligned} \tag{25.18}$$

Alkyl halides are similarly capable of oxidizing U(III) to generate equimolar mixtures of U(IV)–R and U(IV)–X as shown in equation (25.19) (Villiers and Ephritikhine, 1990).

$$2(\eta^5\text{-}C_5H_5)_3U(THF) + R-X \longrightarrow (\eta^5\text{-}C_5H_5)_3U-R + (\eta^5\text{-}C_5H_5)_3U-X \tag{25.19}$$

In the presence of sodium amalgam to reduce the uranium halide formed, the reaction can be made to be quantitative for formation of the alkyl species.

Reaction of $(\eta^5\text{-}C_5H_5)_3U(THF)$ with dioxygen produces the bridged bimetallic complex $[(\eta^5\text{-}C_5H_5)_3U]_2(\mu\text{-}O)$ (Spirlet *et al.*, 1996). The analogous μ-sulfido complex was produced by reaction of $(\eta^5\text{-}C_5H_5)_3UCl$ with freshly prepared K_2S. Chalcogen transfer reagents also oxidize tris(cyclopentadienyl) uranium complexes to yield bridged bimetallic species [equation (25.20)]; while most phosphine chalcogenides react readily, phosphine oxide does not oxidize U(III), but rather yields a base adduct (Brennan *et al.*, 1986b).

$$\begin{aligned} &(\eta^5\text{-}C_5H_4Me)_3U(THF) + E=PR_3 \longrightarrow \\ &(\eta^5\text{-}C_5H_4Me)_3U-E-U(\eta^5\text{-}C_5H_4Me)_3 \\ &\quad E = Se,\ Te,\ R = Bu;\ E = S,\ R = Ph \end{aligned} \tag{25.20}$$

An analogous bridging oxo complex has been generated by the reaction of $(\eta^5\text{-}C_5H_4SiMe_3)_3U$ with CO_2 or N_2O [equation (25.21)] (Berthet *et al.*, 1991b).

$$\begin{aligned} &(\eta^5\text{-}C_5H_4SiMe)_3U + CO_2 \text{ or } N_2O \longrightarrow \\ &(\eta^5\text{-}C_5H_4SiMe_3)_3U-O-U(\eta^5\text{-}C_5H_4SiMe_3)_3 \end{aligned} \tag{25.21}$$

This complex can also be prepared by the reaction of $(\eta^5\text{-}C_5H_4SiMe_3)_3U(OH)$ with $(\eta^5\text{-}C_5H_4SiMe_3)_3UH$ (Berthet *et al.*, 1993); pyrolysis of the hydroxide complex generates instead the trinuclear complex $[(\eta^5\text{-}C_5H_4SiMe_3)_2U(\mu\text{-}O)]_3$.

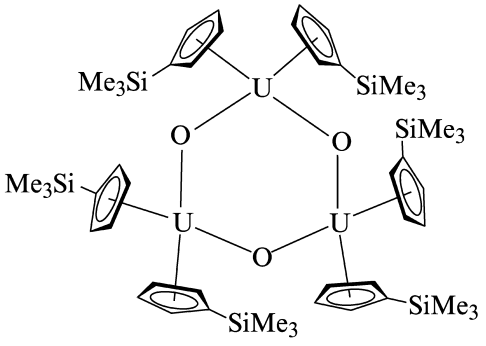

There are also a limited number of examples of two-electron oxidation reactions of tris(cyclopentadienyl)uranium compounds. Reaction of $(\eta^5\text{-}C_5H_4Me)_3U(THF)$ with organic azides (Brennan and Andersen, 1985) results in elimination of dinitrogen and formation of U(v) organoimido derivatives [equation (25.22)].

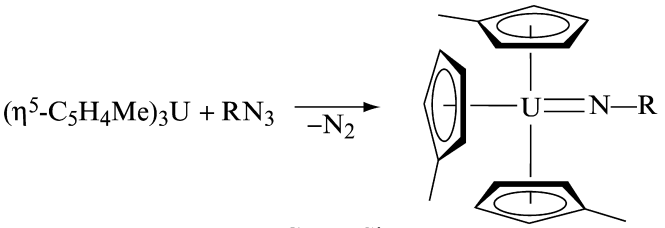

(25.22)

The related reaction with 1,3- or 1,4-diazidobenzene gives rise to bimetallic pentavalent products [equation (25.23)] (Rosen *et al.*, 1990).

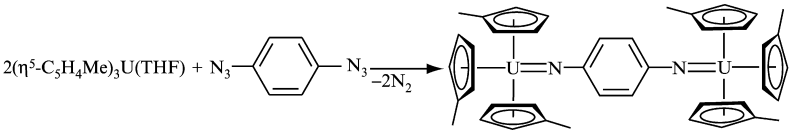

(25.23)

The product generated from 1,4-diazidobenzene supports electronic communication between the metal centers through an aromatic ligand conjugation-based superexchange pathway; antiferromagnetic coupling is observed between the unpaired spins on the two metal centers (Fig. 25.4). The compound derived from 1,3-diazidobenzene, however, cannot undergo similar conjugation, and the susceptibility data show no interaction between the metal centers.

There exist relatively fewer examples of trivalent actinide complexes with two cyclopentadienyl rings. Compounds of the parent cyclopentadienyl ion are somewhat rare. Examples include the reported compounds $(\eta^5\text{-}C_5H_5)_2ThCl$ (Kanellakopulos *et al.*, 1974a) and $(\eta^5\text{-}C_5H_5)_2BkCl$ (Laubereau, 1970), thought to exist as dimers. The compounds $(\eta^5\text{-}C_5H_4Me)_2NpI(THF)_3$ and $(\eta^5\text{-}C_5H_4Me)NpI_2(THF)_3$ were prepared by reactions of $NpI_3(THF)_4$ with $Tl(C_5H_4Me)$ in tetrahydrofuran (Karraker, 1987). Given the propensity of sterically smaller ligands to redistribute and generate multiple species in solution, most complexes have been generated with more highly substituted cyclopentadienyl ligands, particularly $(\eta^5\text{-}C_5Me_5)$, $[\eta^5\text{-}(Me_3Si)_2C_5H_3]$, and $[\eta^5\text{-}(Me_3C)_2C_5H_3]$. One of the most investigated of these complexes is the chloride-bridged trimeric complex $[(\eta^5\text{-}C_5Me_5)_2U(\mu\text{-}Cl)]_3$ (Manriquez *et al.*, 1979; Fagan *et al.*, 1982). The complex can be prepared by a number of routes as shown in equations (25.24)–(25.26).

$$(\eta^5\text{-}C_5Me_5)_2U(Cl)(R) + 3/2\ H_2 \longrightarrow 1/3[(\eta^5\text{-}C_5Me_5)_2U(\mu\text{-}Cl)]_3 + 3RH \quad (25.24)$$

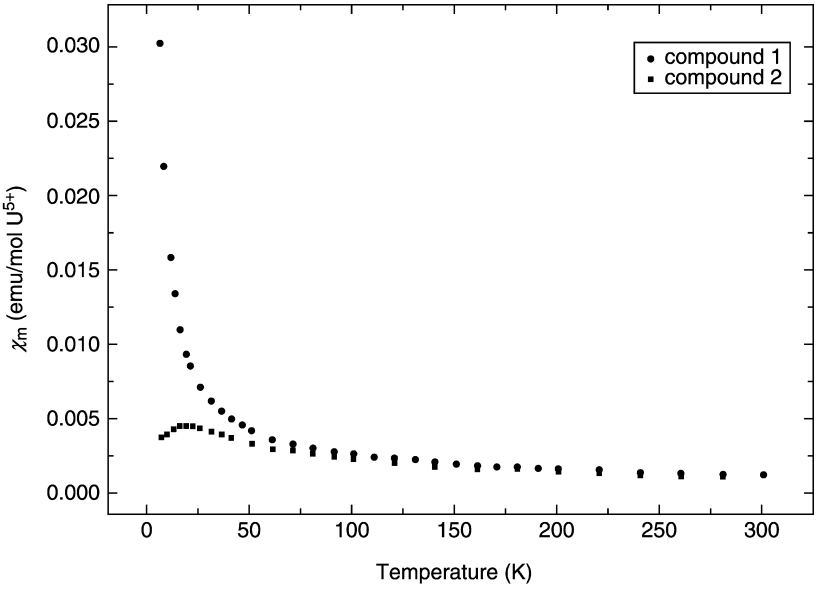

Fig. 25.4 *Magnetic susceptibility data for* 1,4-[(η^5-$C_5H_4Me)_3U$](=*N*-C_6H_4-*N*=)[*U*(η^5-$C_5H_4Me)_3$] (*compound* 1) *and* 1,3-[(η^5-$C_5H_4Me)_3U$](=*N*-C_6H_4-*N*=)[*U*(η^5-$C_5H_4Me)_3$] (*compound* 2). (*Reprinted with permission from Rosen* et al. (1990). *Copyright* 1990 *American Chemical Society.*)

$$(\eta^5\text{-}C_5Me_5)_2UCl_2 + {}^t\text{BuLi} \longrightarrow 1/3\ [(\eta^5\text{-}C_5Me_5)_2U(\mu\text{-}Cl)]_3 + \text{LiCl} + \text{organic products} \quad (25.25)$$

$$(\eta^5\text{-}C_5Me_5)_2UH_2 + (\eta^5\text{-}C_5Me_5)_2UCl_2 \longrightarrow 1/3[(\eta^5\text{-}C_5Me_5)_2U(\mu\text{-}Cl)]_3 \quad (25.26)$$

The reduction reaction shown in equation (25.24) has been extended to bis (alkyl) complexes to generate a stable mononuclear hydride complex stabilized by added ligand (Duttera *et al.*, 1982), as depicted in equation (25.27).

$$(\eta^5\text{-}C_5Me_5)_2UR_2 + 3/2\ H_2 + \text{dmpe} \longrightarrow (\eta^5\text{-}C_5Me_5)_2\ U(H)(P,P) + 2RH \quad (25.27)$$

The complex [(η^5-$C_5Me_5)_2U(\mu$-Cl)]$_3$ reacts with a variety of Lewis bases to generate monomeric adducts, and will undergo metathesis reactions (Fig. 25.5).

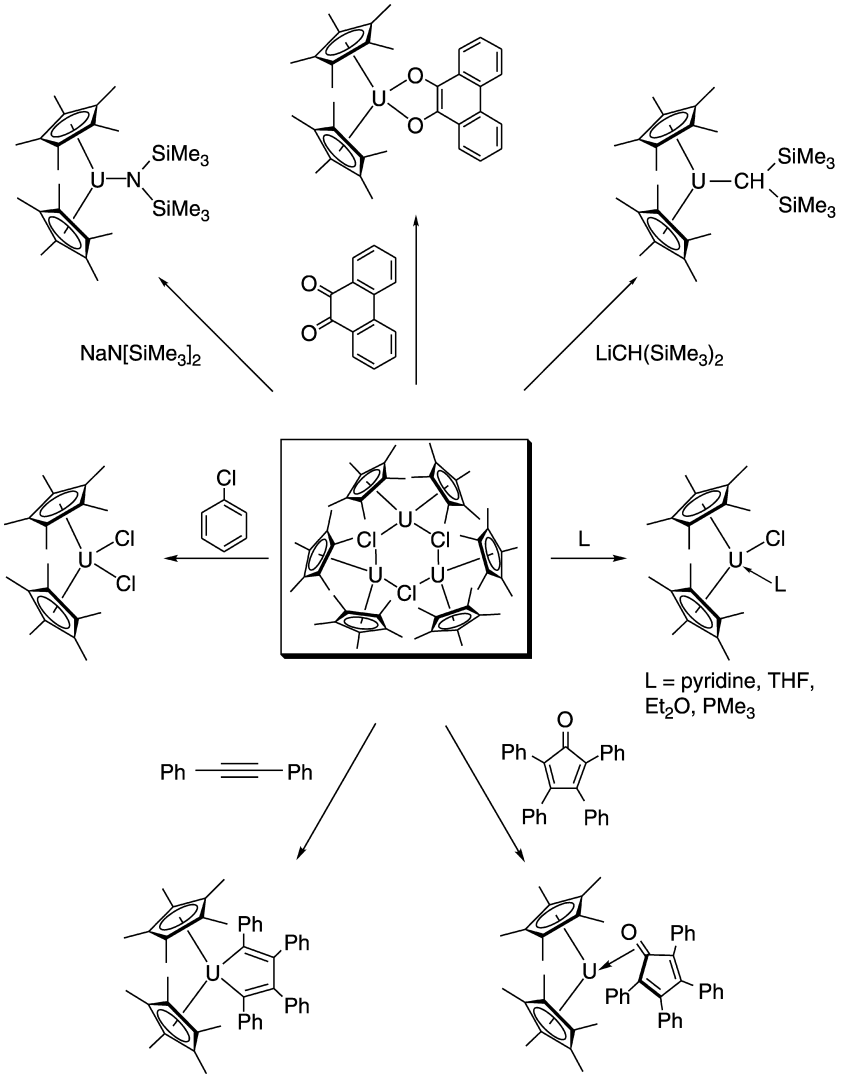

Fig. 25.5 *Reactions of* $[(\eta^5\text{-}C_5Me_5)_2U(\mu\text{-}Cl)]_3$ (*Fagan* et al., 1982).

Alkyl complexes have been prepared by reaction with alkyllithium reagents, but are unstable at room temperature, except for $R = CH(SiMe_3)_2$. One of the most interesting reactions is that of $[(\eta^5\text{-}C_5Me_5)_2U(\mu\text{-}Cl)]_3$ with unsaturated substrates such as diphenylacetylene. In an apparent disproportionation, the reaction products include the metallacycle complex resulting from coupling of two alkyne ligands, as well as an equivalent amount of $(\eta^5\text{-}C_5Me_5)_2UCl_2$. Finke *et al.* (1981a,b) have examined the oxidation of the base adduct

$(\eta^5\text{-}C_5Me_5)_2UCl(THF)$ with alkyl halides. Kinetic evidence supports an atom-abstraction oxidative addition mechanism to the coordinatively unsaturated $(\eta^5\text{-}C_5Me_5)_2UCl$. The rate of reaction is 10^4–10^7 faster than any known isolable transition metal system reacting by atom abstraction.

A cationic bis(pentamethylcyclopentadienyl)uranium(III) complex has been reported (Boisson *et al.*, 1997). The complex $[(\eta^5\text{-}C_5Me_5)_2U(THF)_2][BPh_4]$ is generated by protonation of the complex $(\eta^5\text{-}C_5Me_5)_2U[N(SiMe_3)_2]$ with $[NH_4][BPh_4]$.

A number of U(III) complexes containing the $[\eta^5\text{-}1,3\text{-}(Me_3Si)_2C_5H_3]$ ligand have been prepared (Blake *et al.*, 1986b, 1987) by reduction of U(IV) precursors with Na–Hg or *n*-BuLi in toluene or hexanes [equation (25.28)].

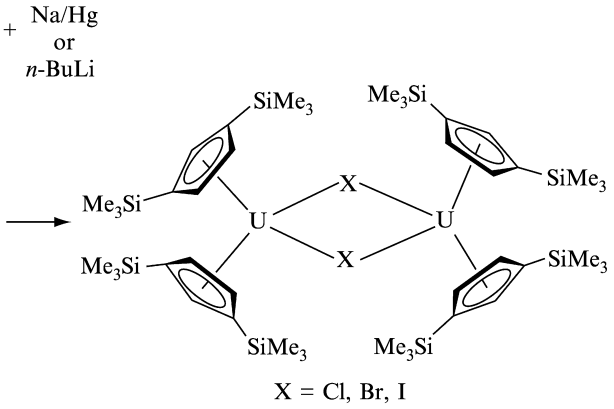

(25.28)

In the presence of a coordinating ligand (e.g. TMEDA), a uranate salt ($[\eta^5\text{-}(Me_3Si)_2C_5H_3](\mu\text{-}Cl)_2U(L)$) (L = ligand) is isolated (Blake *et al.*, 1988).

An expanded synthesis of these and related $[\eta^5\text{-}1,3\text{-}(Me_3C)_2C_5H_3]$ complexes has been reported involving reduction of tetravalent precursors by *t*-BuLi in hexanes (Lukens *et al.*, 1999b,c). A number of the dimeric complexes have been structurally characterized (Fig. 25.6) (Lukens *et al.*, 1999a). The solution behavior of a number of members of the class $[\{\eta^5\text{-}1,3\text{-}R_2C_5H_3\}_2U(\mu\text{-}X)]_2$ (R = Me_3Si or Me_3C) have been examined by variable temperature NMR (Lukens *et al.*, 1999b). The complexes exist as dimers in solution at all temperatures examined. The dimers react with Lewis bases to yield monomeric mono- or bis-ligand adducts (Blake *et al.*, 1987; Beshouri and Zalkin, 1989; Zalkin and Beshouri, 1989); these serve as reagents in subsequent metathesis reactions (Blake *et al.*, 1987).

The complexes $[\{\eta^5\text{-}1,3\text{-}R_2C_5H_3\}_2U(\mu\text{-}OH)]_2$ (R = Me_3Si or Me_3C) have been prepared by reaction of one equivalent of water with $[\eta^5\text{-}1,3\text{-}(Me_3Si)_2C_5H_3]_3U$ and $[\eta^5\text{-}1,3\text{-}(Me_3C)_2C_5H_3]_2UH$, respectively (Lukens *et al.*, 1996).

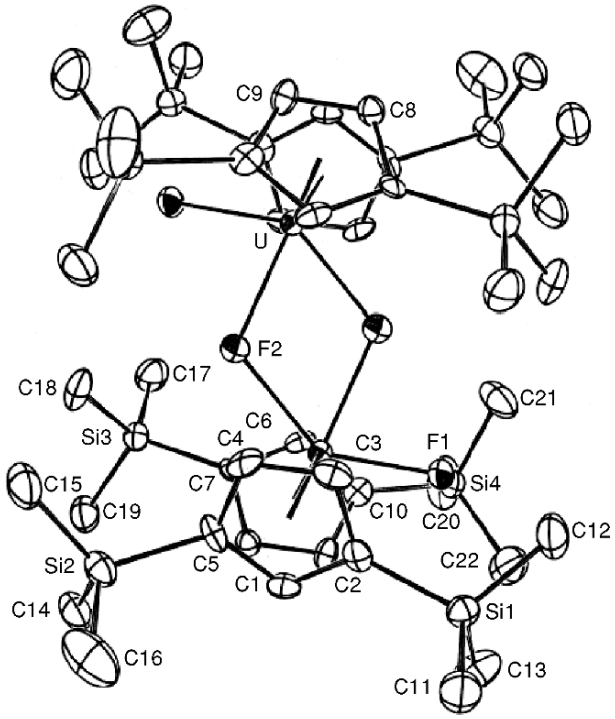

Fig. 25.6 *Crystal structure of* $[\{\eta^5\text{-}1,3\text{-}(Me_3Si)_2C_5H_3\}_2U(\mu\text{-}F)]_2$. (*Reprinted with permission from Lukens* et al. (1999a). *Copyright* 1999 *American Chemical Society*.)

Upon heating, these complexes have been observed to undergo an unusual 'oxidative elimination' to yield the corresponding μ-oxo complexes [equation (25.29)].

$$[\{\eta^5\text{-}1,3\text{-}R_2C_5H_3\}_2U(\mu\text{-}OH)]_2 \xrightarrow[-H_2]{100^\circ C} [\{\eta^5\text{-}1,3\text{-}R_2C_5H_3\}_2U\{\mu\text{-}O)]_2 \qquad (25.29)$$
$$R = Me_3Si \text{ or } Me_3C$$

The kinetics of this process have been examined, and the reaction is found to be intramolecular, probably involving a stepwise α-elimination process.

The reagent $UI_3(THF)_4$ has proven valuable in generating mono(cyclopentadienyl) uranium(III) complexes (Avens *et al.*, 2000). Reaction of one equivalent of $UI_3(THF)_4$ with $K(C_5Me_5)$ results in the formation of the complex $(\eta^5\text{-}C_5Me_5)UI_2(THF)_3$. In the solid state this complex exhibits a pseudo-octahedral *mer*, *trans* geometry, with the cyclopentadienyl group occupying the axial position.

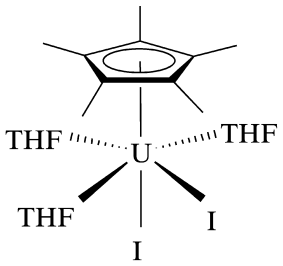

In the presence of excess pyridine, this complex can be converted to the analogous pyridine adduct, $(\eta^5\text{-}C_5Me_5)UI_2(py)_3$. $(\eta^5\text{-}C_5Me_5)UI_2(THF)_3$ will react further with $K(C_5Me_5)$ to generate the bis(ring) product, $(\eta^5\text{-}C_5Me_5)_2UI$ (THF), or will react with two equivalents of $K[N(SiMe_3)_2]$ to produce $(\eta^5\text{-}C_5Me_5)U[N(SiMe_3)_2]_2$. The solid state structure of the bis(trimethylsilyl)amide derivative reveals close contacts between the uranium center and two of the methyl carbons [2.80(2), 2.86(2) Å].

Oxidation of $(\eta^5\text{-}C_5Me_5)UI_2(THF)_3$ with CS_2 or ethylene sulfide produces a complex of the formula $[(\eta^5\text{-}C_5Me_5)UI_2(THF)_3]_2(S)$. This species undergoes slow decomposition in solution to yield a polynuclear complex (Clark *et al.*, 1995):

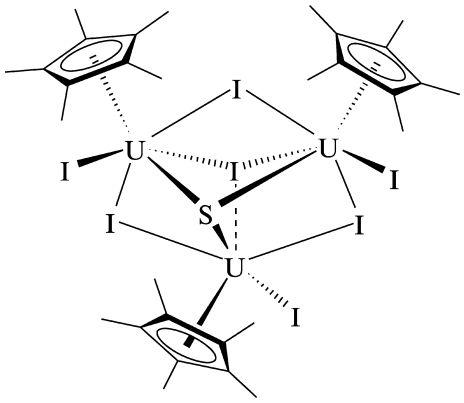

(b) Tetravalent chemistry

The tetravalent oxidation state dominates the cyclopentadienyl chemistry of the early actinide elements. Tetrakis(cyclopentadienyl) complexes were among the earliest actinide complexes prepared, and the complexes $(\eta^5\text{-}C_5H_5)_4An$ are known for Th (Fischer and Treiber, 1962), Pa (Baumgärtner *et al.*, 1969), U (Fischer and Hristidu, 1962), and Np (Baumgärtner *et al.*, 1968). Although only the uranium and thorium compounds have been structurally characterized (Burns, 1974; Maier *et al.*, 1993), IR spectral and X-ray powder data confirm

that all four complexes are isostructural. $(\eta^5\text{-}C_5H_5)_4U$ is found to be psuedo-tetrahedral, with a mean $U\text{–}C_{ring}$ bond distance of 2.81(2) Å. This is somewhat longer than average $U\text{–}C_{ring}$ distances for other U(IV) cyclopentadienyl complexes, reflecting the degree of steric crowding. The related tetrakis(indenyl) thorium compound has also been reported (Rebizant *et al.*, 1986). The thorium atom is bonded to the carbons of the five-membered ring portion of the indenyl ligand, although not in a η^5 fashion. The shortest Th–C bond distances [Th–C average = 2.83(3) Å vs 3.09(3) Å] are to the three non-bridging carbon atoms, leading to the overall designation of the rings as trihapto.

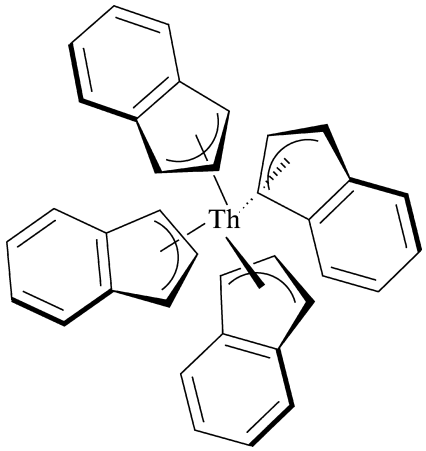

The first reported organoactinide complex was $(\eta^5\text{-}C_5H_5)_3UCl$ (Reynolds and Wilkinson, 1956), a member of the extensive class of complexes represented as Cp_3AnX. The complex was first prepared by the reaction of uranium tetrachloride with sodium cyclopentadienide in tetrahydrofuran. Comparable routes have been used to prepare $(\eta^5\text{-}C_5H_5)_3NpCl$ (Karraker and Stone, 1979), although this complex has also been prepared by reaction of $NpCl_4$ with $(C_5H_5)_2Be$ (Fischer *et al.*, 1966). Alternative routes have since been reported for the generation of $(\eta^5\text{-}C_5H_5)_3UCl$ (Marks *et al.*, 1976). Tris(indenyl)uranium and tris(indenyl)thorium complexes have been prepared by metathesis reactions with $K(C_9H_7)$ in THF (Burns and Laubereau, 1971; Laubereau *et al.*, 1971; Goffart *et al.*, 1975, 1981; Goffart and Duyckaerts, 1978).

Since the first report of cyclopentadienyl complexes, attempts have been made to assess the nature of the bonding in these complexes from their chemical reactivity. In contrast to complexes of lanthanides and Group 3 metals, $(\eta^5\text{-}C_5H_5)_3UCl$ does not react with $FeCl_2$ to produce ferrocene, and it decomposes relatively slowly in water. Although this is taken as some indication of increased covalency in chemical bonding, these complexes are still believed to be more ionic than the majority of d-transition metal cyclopentadienyl complexes (Burns and Bursten, 1989). The molecular structure of several Cp_3AnX complexes have

been determined, as well as several structures of closely related tris(indenyl) actinide halide complexes. Some comparative structural information is provided in Table 25.3, and a typical structure represented by $(\eta^5\text{-}C_5H_5)_3UBr$ is presented in Fig. 25.7.

Table 25.3 *Structural information for Cp_3AnX complexes.*

Compound	*M–C* (*average*) (Å)	*M–X* (Å)	*References*
$(\eta^5\text{-}C_5H_5)_3UCl$	2.74	2.559(16)	Wong *et al.* (1965)
$(\eta^5\text{-}C_5H_5)_3UBr$	2.72(1)	2.820(2)	Spirlet *et al.* (1989a)
$(\eta^5\text{-}C_5H_5)_3UI$	2.73(3)	3.059(2)	Rebizant *et al.* (1991)
$(\eta^5\text{-}C_5H_4CH_2Ph)_3UCl$	2.733(1)	2.627(2)	Leong *et al.* (1973)
$[\eta 5\text{-}(Me_3Si)_2C_5H_3]_3UCl$	2.77(1)	2.614(2)	Blake *et al.* (1998)
$(\eta^5\text{-}C_5Me_4H)_3UCl$	2.79(1)	2.637	Cloke *et al.* (1994)
$(\eta^5\text{-}C_5Me_5)_3UF$	2.829(6)	2.43(2)	Evans *et al.* (2000)
$(\eta^5\text{-}C_5Me_5)_3UCl$	2.833(9)	2.90(1)	Evans *et al.* (2000)
$[\eta^5\text{-}(Me_3Si)_2C_5H_3]_3ThCl$	2.84(1)	2.651(2)	Blake *et al.* (1998)
$[\eta^5\text{-}(Me_3Si)_2C_5H_3]_2(C_5Me_5)ThCl$	2.84(2)	2.657(5)	Blake *et al.* (1998)
$[\eta^5\text{-}(Me_2\text{-}^tBuSi)_2C_5H_3]_3ThCl$	2.85(1)	2.648(2)	Blake *et al.* (1998)
$\{\eta^5\text{-}[(Me_3Si)_2CH]C_5H_4\}_3ThCl$	2.83(1)	2.664(2)	Blake *et al.* (1998)
$(\eta^5\text{-}C_9H_7)_3UBr$	2.71(2), 2.85(2)	2.747(2)	Spirlet *et al.* (1987)
$(\eta^5\text{-}C_9H_7)_3UI$	2.68(2), 2.88(2)	3.041(1)	Rebizant *et al.* (1988)
$(\eta^5\text{-}C_9HMe_6)_3UCl$	–	2.621(1)	Spirlet *et al.* (1992a)
$(\eta^5\text{-}C_9H_6Et)_3ThCl$	2.78(1), 2.93(1)	2.673(3)	Spirlet *et al.* (1990)

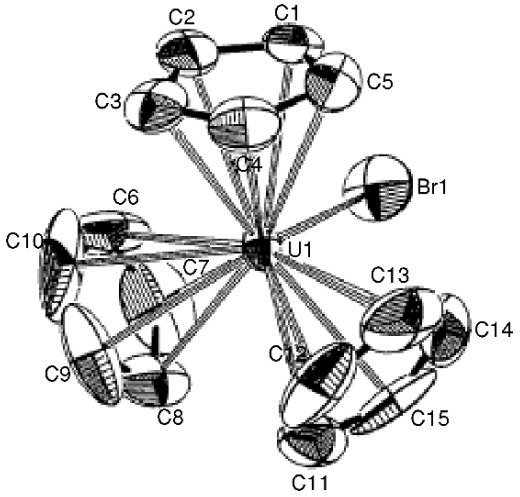

Fig. 25.7 *Crystal structure of $(\eta^5\text{-}C_5H_5)_3UBr$* (*Spirlet* et al., 1989a). (*Reprinted with permission of the International Union of Crystallography.*)

All complexes possess pseudo-tetrahedral geometry, with the halide ligand on an approximate three-fold axis of symmetry. The An–C and An–X bond lengths are consistent for most of the complexes; Th–C and Th–X values are slightly larger, as would be expected for the larger ionic radius. The average U–C_{ring} and U–X bond lengths are longer than would be expected in complexes $(\eta^5\text{-}C_5Me_5)_3UX$ (X = Cl, F); the U–Cl bond length in $(\eta^5\text{-}C_5Me_5)_3UCl$ is >0.15 Å longer than that for related complexes. The origin of this difference appears to be significant steric crowding in the molecule. Interligand repulsions between the bulky pentamethylcyclopentadienyl ligands results in the most signficant distortion from tetrahedral geometry; the cyclopentadienyl rings lie within a crystallographic plane of symmetry, requiring the angle X–U–$C_{centroid}$ to be rigorously 90°. This in turn results in repulsion between the rings and the halide, lengthening the bond.

As observed in the $An(indenyl)_4$ complexes, the tris(indenyl) complexes all evidence a 'slip' of the rings towards a trihapto bonding, resulting in two separate sets of U–C distances. The compound $(C_9HMe_6)_3UCl$ possesses a highly substituted hexamethylindenyl ligand (Spirlet *et al.*, 1992a). The steric encumbrance associated with this ligand induces a further slippage of the ring; the resulting complex has indenyl rings that are essentially monohapto towards the metal center, with mean U–C bonds of 2.622(6) Å (Fig. 25.8).

A number of approaches have been employed to generate derivatives of Cp_3AnX (von Ammon *et al.*, 1969; Kanellakopulos *et al.*, 1974b; Marks and Kolb, 1975; Fischer and Sienel, 1976, 1978; Bagnall *et al.*, 1982a,b; Spirlet *et al.*, 1996). Prototype reactions include protonation of $(\eta^5\text{-}C_5H_5)_4U$ [equation (25.30)] and metathesis [equation (25.31)].

$$(\eta^5\text{-}C_5H_5)_4U + HCN \longrightarrow (\eta^5\text{-}C_5H_5)_3U{-}CN + C_5H_6 \qquad (25.30)$$

$$(\eta^5\text{-}C_5H_5)_3An{-}Cl + KX \longrightarrow (\eta^5\text{-}C_5H_5)_3An{-}X + KCl \qquad (25.31)$$
$$An = U,\ Np,\ Pu;\ X = CN^-,\ CNBH_3^-,\ NCS^-$$

Reactions such as that between $(\eta^5\text{-}C_5H_5)_3UCl$ and KCN may be carried out in water (Bagnall *et al.*, 1982b), indicating the stability of the metal–ligand bonding in these complexes. In fact, it has been suggested that $(\eta^5\text{-}C_5H_5)_3UCl$ ionizes in water to yield the five-coordinate adduct $[(\eta^5\text{-}C_5H_5)_3U(H_2O)_2]^+$ (Fischer *et al.*, 1982). This spurred further interest in investigating other five coordinate species, e.g. $[(\eta^5\text{-}C_5H_5)_3UXY]^-$. The anionic complexes $[(\eta^5\text{-}C_5H_5)_3An(NCS)_2]^-$ (An = U, Np, Pu) can be isolated, provided that the cation is sufficently large (Bagnall *et al.*, 1982b). Spectrophotometric and other evidence indicates a trigonal–bipyramidal geometry for these species. The assignment of the geometry of these species is further supported by structural characterization of neutral base adducts $(\eta^5\text{-}C_5H_5)_3AnXL$, such as $(\eta^5\text{-}C_5H_5)_3U(NCS)(NCMe)$ (Fischer *et al.*, 1978; Aslan *et al.*, 1988) or $(\eta^5\text{-}C_5H_5)_3U(NCBH_3)(NCMe)$ (Adam *et al.*, 1990);

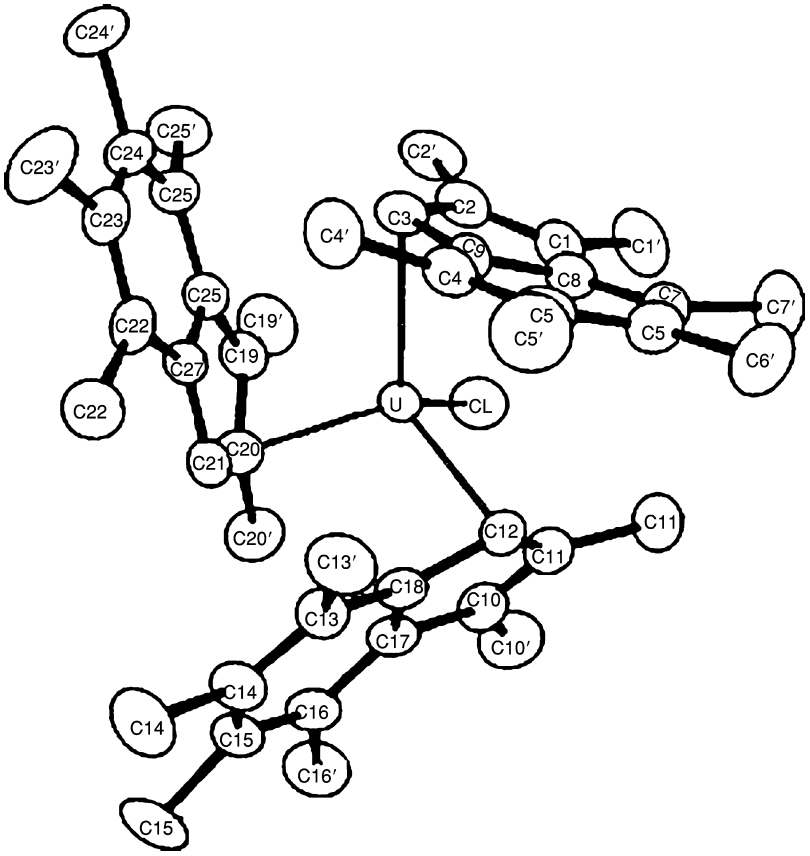

Fig. 25.8 *Crystal structure of* $(C_9HMe_6)_3UCl$ (*Spirlet* et al., 1992a). (*Reprinted with permission of the International Union of Crystallography*.)

these complexes exibit a trigonal-bipyramidal geometry, with the smaller ligands adopting the axial positions.

Cationic species can also be produced. The compound $[(\eta^5\text{-}C_5H_5)_3U(NCMe)_2]^+$ has been isolated as a $[BPh_4]^-$ salt by the reaction of $(\eta^5\text{-}C_5H_5)_3UCl$ and $NaBPh_4$ in water/acetonitrile mixtures (Aslan *et al.*, 1988). The cationic complex $[(\eta^5\text{-}C_5H_5)_3U(THF)]BPh_4$ was generated by protonation of the neutral amide precursor with $[NHEt_3]^+$ as illustrated in equation (25.32) (Berthet *et al.*, 1995).

$$(\eta^5\text{-}C_5H_5)_3U-NR_2 + [HNEt_3][BPh_4] \xrightarrow{THF} [(\eta^5\text{-}C_5H_5)_3U(THF)][BPh_4] + HNR_2 + NEt_3 \quad R = Me, Et \tag{25.32}$$

Similarly, treatment of precursor alkyl or amide complexes with pyridinium triflate gives rise to the triflate complex $(\eta^5\text{-}C_5H_5)_3U(O_3SCF_3)$ (Berthet *et al.*, 2002).

The crystal structure of the ^{t}BuCN adduct has also been determined (Berthet *et al.*, 1998).

Metathesis and protonation routes have been used to generate L_3An(IV) (L = cyclopentadienyl, indenyl) complexes containing alkoxide (OR), amide (NR_2), phosphide (PR_2), and thiolate (SR) ligands (Jamerson *et al.*, 1974; Goffart *et al.*, 1977; Karraker and Stone, 1979; Arduini *et al.*, 1981; Paolucci *et al.*, 1985; Leverd *et al.*, 1996; De Ridder *et al.*, 1996). Both magnetic susceptibility measurements and ^{237}Np Mössbauer spectroscopy have been employed to assess the qualitative order of ligand field strengths for a variety of ligands in the complexes $(\eta^5\text{-}C_5H_5)_3NpX$ (Karraker and Stone, 1979). The identified order of donor strength from this study is $X = Cl^- \sim BH_4^- > OR^- > R^- > C_5H_5^-$.

One of the best studied classes of $(\eta^5\text{-}C_5H_5)_3AnR$ (Th, U, Np) complexes is that containing alkyl or aryl ligands. The literature on alkyl complexes is extensive (e.g. Brandi *et al.*, 1973; Calderazzo, 1973; Gabala and Tsutsui, 1973; Marks *et al.*, 1973; Tsutsui *et al.*, 1975; Marks, 1979). The complexes are most often prepared by reaction of $(\eta^5\text{-}C_5H_5)_3AnX$ (X = halide) with Grignard [equation (25.33)] or alkyllithium [equation (25.34)] reagents.

$$(\eta^5\text{-}C_5H_5)_3An-X + RMgX' \longrightarrow (\eta^5\text{-}C_5H_5)_3An-R + MgXX' \quad (25.33)$$

$$(\eta^5\text{-}C_5H_5)_3An-X + LiR \longrightarrow (\eta^5\text{-}C_5H_5)_3An-R + LiX \quad (25.34)$$

Comparable indenylactinide derivatives have also been prepared (e.g. Goffart *et al.*, 1977). While there is a dearth of thermally stable U(IV) hydride complexes, the complexes $[\eta^5\text{-}(Me_3Si)C_5H_4]_3UH$ and $[\eta^5\text{-}(Me_3C)C_5H_4]_3UH$ can be obtained by reaction of the corresponding chlorides with $KBEt_3H$ (Berthet *et al.*, 1992b).

The molecular structures of several $(\eta^5\text{-}C_5H_5)_3AnR$ complexes have been determined; compounds display pseudo-tetrahedral geometries. Typical metal–carbon bond lengths for the alkyl ligand are 2.40 Å. All three cyclopentadienyl ligands are pentahapto, which nearly saturates the coordination environment of the metal center, as evidenced by the observation that allyl ligands can only be accomodated in a simple σ-bonded fashion (Halstead *et al.*, 1975) as shown in Fig. 25.9.

This monohapto geometry is also the low-temperature limiting structure for $(\eta^5\text{-}C_5H_5)_3U$(allyl) in solution (Marks *et al.*, 1973) although at room temperature the allyl ligand is fluxional, presumably interconverting sites by means of a π-bound intermediate. The relative coordinative saturation is reflected in the thermal stabilities of alkyl derivatives: primary > secondary > tertiary. Primary alkyl ligands are resistant to β-hydride elimination; thermal decomposition is presumed to take place through U–C bond homolysis and abstraction of a ring proton by the caged alkyl radical (although metal-containing products have not been definitively identified).

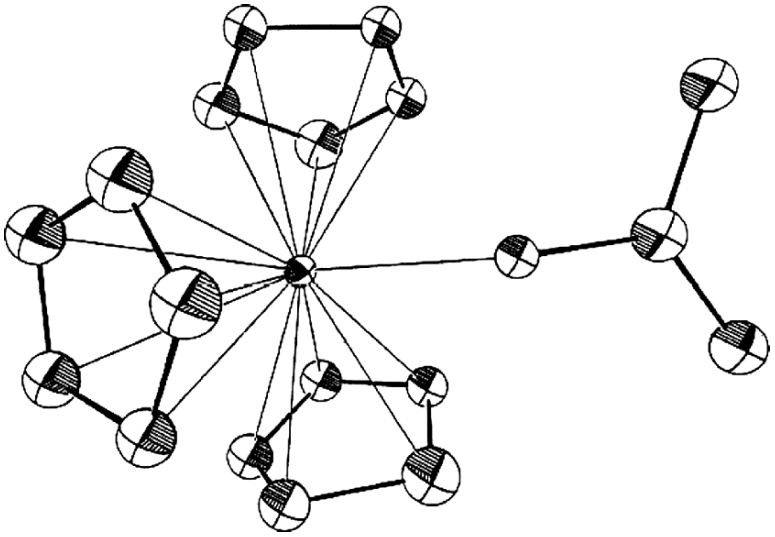

Fig. 25.9 *Crystal structure of* $(\eta^5\text{-}C_5H_5)_3U[CH_2C(CH_3)_2]$. (*Reprinted with permission from Halstead* et al. (1975). *Copyright* 1975 *American Chemical Society*.)

Further indication of the steric saturation of the complex may be found in the observation that reaction of $(\eta^5\text{-}C_5H_5)_3UR$ with excess alkyllithium does not result ultimately in the formation of anionic bis(alkyl) complexes. Rather, reaction products either result from alkyl exchange (Tsutsui *et al.*, 1975) or reduction of the metal center (Arnaudet *et al.*, 1983, 1986) as shown in equation (25.35).

$$(\eta^5\text{-}C_5H_5)_3U\text{–}R + LiR \longrightarrow Li[(\eta^5\text{-}C_5H_5)_3U\text{–}R] + \text{organic products} \tag{25.35}$$

It has been reported that the complex $[(\eta^5\text{-}C_5H_5)_3UMe_2]^-$ can be observed as an intermediate in solution by NMR spectroscopy (Villiers and Ephritikhine, 1991).

Other derivatives of the Group 14 elements have been prepared. Reaction of $(\eta^5\text{-}C_5H_5)_3UCl$ with $Li(EPh_3)$ affords the silyl- and germyluranium derivatives $(\eta^5\text{-}C_5H_5)_3U(EPh_3)$ [E = Si (Porchia *et al.*, 1986, 1989), E = Ge (Porchia *et al.*, 1987)], whereas the stannyl analog $(\eta^5\text{-}C_5H_5)_3U(SnPh_3)$ was best made from a the reaction of $(\eta^5\text{-}C_5H_5)_3U(NEt_2)$ with $HSnPh_3$. It can also be made from the transmetallation reaction of $HSnPh_3$ with $(\eta^5\text{-}C_5H_5)_3U(EPh_3)$ (E = Si, Ge) (Porchia *et al.*, 1989). The silyl compound is very reactive; under a number of conditions it can be transformed into $(\eta^5\text{-}C_5H_5)_3U(OSiPh_3)$. Insertion of xylylisocyanide into U–E bonds generates the corresponding η^2-iminoacyl complexes $[(\eta^5\text{-}C_5H_5)_3U\{C(EPh_3) = N(xylyl)\}]$ (E = Si, Ge).

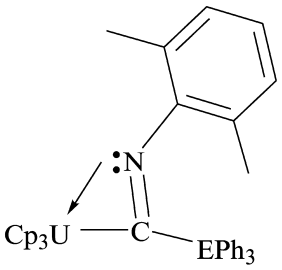

E = Si, Ge

Several groups have conducted investigations of the thermochemistry of organoactinide complexes in order to determine the enthalpies of metal–ligand bonds, and thereby shed light on the nature of bonding and the anticipated reaction patterns. An excellent overview of available data on organouranium complexes has appeared recently (Leal *et al.*, 2001). Data compiled for tris (cyclopentadienyl)uranium(IV) complexes are presented in Table 25.4. Values tabulated in Leal *et al.* (2001) are based upon several types of measurements: solution titration experiments involving reaction with iodine or alcohols, static bomb combustion calorimetry, or gas-phase or solution equilibrium experiments. A few general trends may be noted. The enthalpy values for all U–C (sp^3) bonds are relatively consistent; U–C(sp^2) and U–C(sp) bonds increase in strength, as might be expected for a bond involving a higher degree of s-orbital involvement. While the bonds involving all Group 14 element bonds are reasonably close in energy, uranium bonds to Group 16 or Group 17 elements are somewhat stronger. The reason for the disparity between D(U–S) for the EtS^- and $^tBuS^-$ may be due to the greater steric bulk associated with the latter.

Comparable experiments have been carried out for the complexes (η^5-$C_5H_5)_3$ThR (Sonnenberger *et al.*, 1985); results of these measurements are found in Table 25.5. The thorium–carbon bond strengths are found to be overall higher than for comparable uranium species. This has been rationalized in terms of the greater stability of the U(III) complexes, resulting from homolytic loss of an alkyl radical.

The reaction of carbon monoxide with (η^5-$C_5H_5)_3$AnR (An = Th, U; R = alkyl, hydride) yields an acyl complex as shown in equation (25.36).

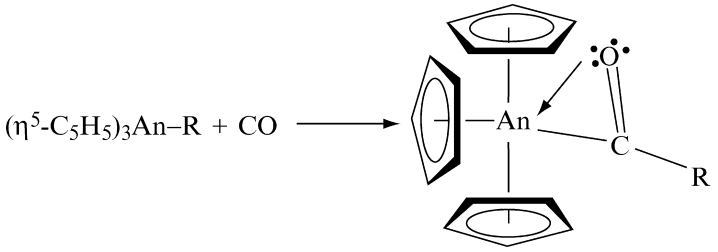

(25.36)

Table 25.4 *Bond dissociation enthalpies for Cp_3UX and $(indenyl)_3UX$ complexes.*[a]

Compound	*R*	*D*(*U–R*) (kJ mol^{-1})	*Reference*
$(\eta^5\text{-}C_5H_5)_3UR$	$SiPh_3$	156 ± 18	Nolan *et al.* (1991)
	$GePh_3$	163 ± 19	Nolan *et al.* (1991)
	$SnPh_3$	156 ± 17	Nolan *et al.* (1991)
	$Fe(CO)_2Cp$	129 ± 13	Nolan *et al.* (1991)
	$Ru(CO)_2Cp$	169 ± 17	Nolan *et al.* (1991)
	Cp	299 ± 10[b,c]	Telnoy *et al.* (1979)
	i-Bu	*D*[Cp_3U–Cp] – (70 ± 35)[c,d]	Telnoy *et al.* (1989)
	OBu	*D*[Cp_3U–Cp] + (247 ± 28)[c,d]	Telnoy *et al.* (1989)
	Cl	*D*[Cp_3U–Cp] + (73 ± 31)[c,d]	Telnoy *et al.* (1989)
$[\eta^5\text{-}(Me_3Si)C_5H_4]_3UR$	Me	185 ± 2	Schock *et al.* (1988)
	Bu	152 ± 8	Schock *et al.* (1988)
	CH_2SiMe_3	168 ± 8	Schock *et al.* (1988)
	CH_2Ph	149 ± 8	Schock *et al.* (1988)
	$CH{=}CH_2$	223 ± 10	Schock *et al.* (1988)
	CCPh	363	Schock *et al.* (1988)
	I	262 ± 1	Schock *et al.* (1988)
		265.6 ± 4.3	Jemine *et al.* (1992)
	SEt	266 ± 9	Jemine *et al.* (1994)
	S-*t*-Bu	158 ± 8	Jemine *et al.* (1994)
	H	253.7 ± 5.1	Jemine *et al.* (1992)
$[\eta^5\text{-}(Me_3C)C_5H_4]_3UR$	H	251.6 ± 5.7	Jemine *et al.* (1992)
	I	246.3 ± 5.3	Jemine *et al.* (1992)
	SEt	252 ± 8	Jemine *et al.* (1994)
$(\eta^5\text{-}C_9H_7)_3UR$	Me	195 ± 5	Bettonville *et al.* (1990)
	OCH_2CF_3	301 ± 9	Bettonville *et al.* (1989, 1990)
	I	267 ± 3	Bettonville *et al.* (1990)
$(\eta^5\text{-}C_9H_6Et)_3UR$	Me	187 ± 6	Bettonville *et al.* (1989, 1990)
$(\eta^5\text{-}C_9H_6SiMe_3)_3UR$	SEt	158 ± 8	Jemine *et al.* (1994)

[a] Determined using reaction–solution calorimetry unless otherwise indicated.
[b] Mean bond dissociation enthalpy.
[c] Static bomb combustion calorimetry.
[d] This notation means that the bond is the stated amount stronger or weaker than the first bond dissociation enthalpy in $U(\eta^5\text{-}C_5H_5)_4$.

These reactions have been studied mechanistically (Sonnenberger *et al.*, 1984) for a series of thorium deriatives (R = *i*-Pr, *s*-Bu, *neo*-C_5H_{11}, *n*-Bu, $CH_2Si(CH_3)_3$, Me, and $CH_2C_6H_5$). Under the conditions employed, insertion is first order in thorium complex and first order in CO. The relative rates of insertion for

Table 25.5 *Bond dissociation enthalpies for Cp_3ThR complexes.*

Compound	*R*	*D*(*Th–R*) (kJ mol^{-1})
$(\eta^5\text{-}C_5H_5)_3ThR$	CH_3	374.9 (4.6)
	$CH(CH_3)_2$	342.2 (10.9)
	$CH_2C(CH_3)_3$	333.0 (11.7)
	$CH_2Si(CH_3)_3$	367.8 (15.1)
	$CH_2C_6H_5$	315.1 (9.2)

the ligands was found to be *i*-Pr > *s*-Bu > *neo*-C_5H_{11} > *n*-Bu > $CH_2Si(CH_3)_3$ > Me > $CH_2C_6H_5$. The relative rates of insertion correlate reasonably well with the bond enthalpies reported in Table 25.5, and as expected, were accelerated by photolysis. Where R = *s*-Bu, *neo*-C_5H_{11}, *n*-Bu, Me, and $CH_2C_6H_5$, the chief isolated product was the insertion (η^2-acyl) product shown in equation (25.36). This complex has been discussed as having a 'carbene-like' resonance form:

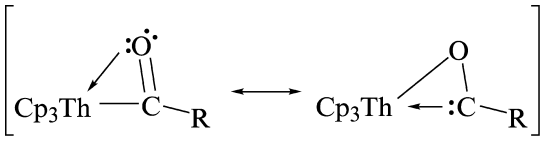

In the case of *i*-Pr and $CH_2Si(CH_3)_3$, however, the only products that could be isolated were those arising from 1,2-rearrangement [equations (25.37)–(25.38)].

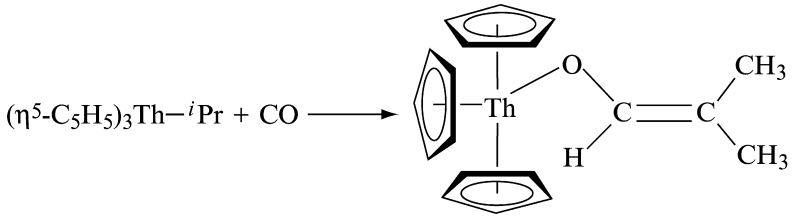

(25.37)

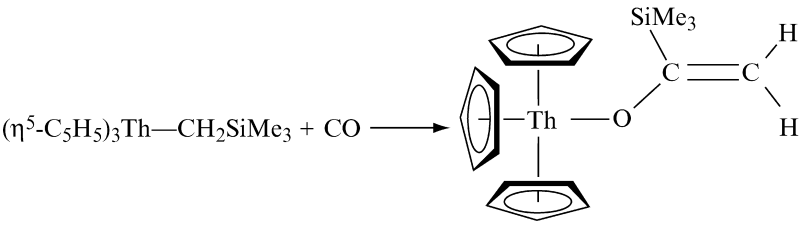

(25.38)

A comparative study of CO_2 insertion to generate carbonate complexes showed that carboxylation is significantly slower than carbonylation, and exhibits different trends in the dependence of rate on the alkyl ligand (Sonnenberger *et al.*, 1984).

Similar insertion reactions of carbon monoxide have been investigated for complexes of the type $(\eta^5\text{-}C_5H_4R)_3UR'$ (Paolucci *et al.*, 1984; Villiers and Ephritikhine, 1994). Villiers and Ephritikhine performed mechanistic studies, which showed that the insertion reaction appears first order under conditions of excess CO. The rate of insertion varies as a function of the cyclopentadienyl ring, with the rate decreasing in the order R = H > Me > ^{i}Pr > ^{t}Bu, as might be expected from steric considerations. The rate also depends on the identity of the alkyl ligand in the unusual order R′ = *n*-Bu > ^{t}Bu > Me > ^{i}Pr. The resulting η^2-acyl product was not stable and rearranged to yield alkylbenzenes C_6H_4RR', suggested to arise from ring enlargement of the cyclopentadienyl ligand by incorporation of the CR′ fragment. The reaction was observed to follow first-order kinetics, with the rate varying with the alkyl ligand in the order R′ = Me > *n*-Bu > ^{i}Pr > ^{t}Bu. In benzene solvent, the rates varied with R in the order ^{t}Bu > ^{i}Pr > Me > H, while the opposite order was observed in THF solvent. For a given solvent, the relative proportions of *meta*- and *para*-isomers were invariant with R and R′. The proposed mechanism involved a cyclopropyl intermediate, resulting from addition of the oxycarbene group to the cyclopentadienyl ligand.

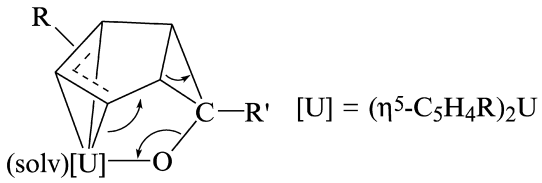

Carbon monoxide will also insert into the U–H bond of $(\eta^5\text{-}C_5H_4SiMe_3)_3UH$ (Berthet and Ephritikhine, 1992). As shown in equation (25.39), the initial product is believed to be a formate complex, which reacts further with the hydride to yield a dioxymethylene species.

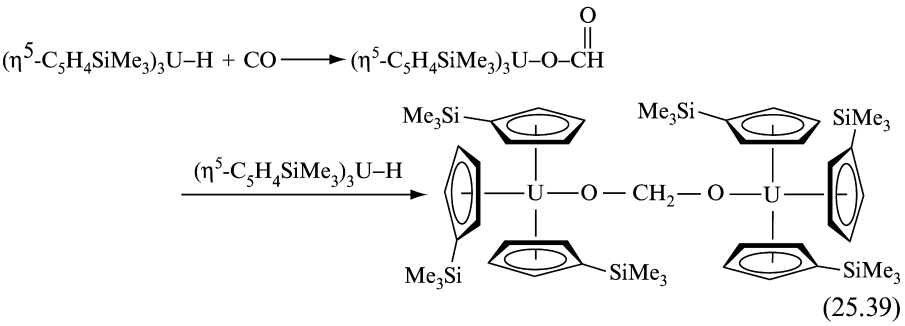

(25.39)

Isoelectronic isocyanide ligands will also undergo insertion into uranium–carbon or uranium–nitrogen bonds (Dormond *et al.*, 1984; Zanella *et al.*, 1987) to yield η^2-iminoalkyl and η^2-iminocarbamoyl adducts.

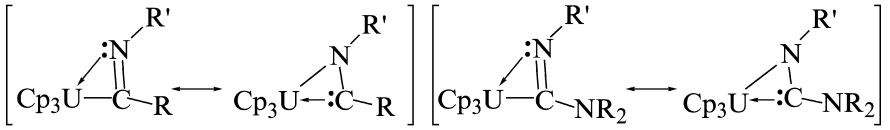

η^2-Iminoalkyl η^2-Iminocarbamoyl

A unique class of $(\eta^5\text{-}C_5H_5)_3AnR$ complexes has been generated by Cramer *et al.* (1981, 1983, 1988). Reaction of $(\eta^5\text{-}C_5H_5)_3AnCl$ with lithium ylide or phosphine imide salts yields the following species [equations (25.40) and (25.41)]:

$$(\eta^5\text{-}C_5H_5)_3U\text{–}Cl + Li[(CH_2)_2P(CH_3)(C_6H_5)] \longrightarrow (\eta^5\text{-}C_5H_5)_3U[(CH)P(CH_3)_2(C_6H_5)] \quad (25.40)$$

$$(\eta^5\text{-}C_5H_5)_3An\text{–}Cl + Li[NP(C_6H_5)_3] \longrightarrow (\eta^5\text{-}C_5H_5)_3An[NP(C_6H_5)_3] \quad (25.41)$$

An = Th, U

The molecular structure of the uranium phosphine imide complex is shown in Fig. 25.10.

While the overall geometry of these complexes is similar to most $(\eta^5\text{-}C_5H_5)_3AnX$ compounds, these species are characterized by unusually short U–C(N) bonds. The U–C(1) bond distance in the ylide complex is 2.29(3) Å [significantly shorter than the average uranium–alkyl bond in $(\eta^5\text{-}C_5H_5)_3UR$ complexes, *ca.* 2.43 Å], and the U–N bond distance in the phosphine imide complex is 2.07(2) Å. Two useful descriptions have been presented for the bonding in these complexes, consistent with the resonance forms depicted for the phosphoylide complex:

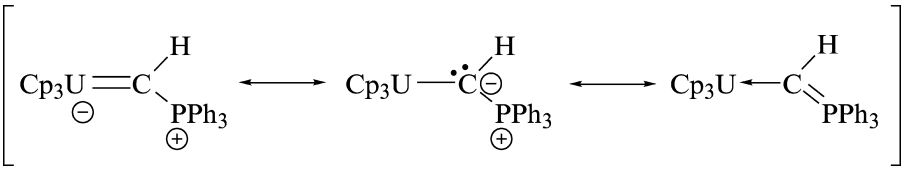

One model would suggest that a multiple bond is formed between the metal and the carbon. This is supported by theoretical calculations at the extended Hückel level (Tatsumi and Nakamura, 1984; Cramer *et al.*, 1988) that reveal an important overlap population in the U–C bond of the phosphoylide complex and U–N bond of the phosphine imine complex. A second description would

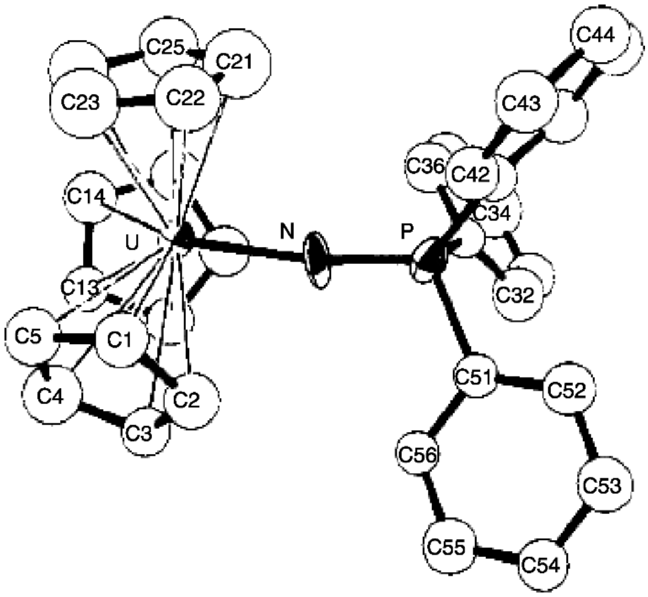

Fig. 25.10 *Crystal structure of* (η^5-C_5H_5)$_3$*U*[*NP*(C_6H_5)$_3$]. (*Reprinted with permission from Cramer* et al. (1988). *Copyright* 1988 *American Chemical Society.*)

suggest that the compounds are principally ionic, with the short U–C bond attributed to the Coulombic attraction between the electropositive metal and the residual charge on the ligand, as well as the smaller radial extent of the sp^2-hybridized ligand-based orbital. In reality, these models are probably merely extreme descriptions of the true bonding situation, and both are valid.

Unlike other complexes with metal–ligand multiple bonds (*vide infra*), the phosphoylide complex reacts as a U(IV) alkyl, however, undergoing a variety of insertion reactions (Cramer *et al.*, 1982, 1984a,b, 1986, 1987a,b) as shown in Fig. 25.11.

Complexes of the general formula (η^5-C_5H_5)$_2$AnX_2 have proven very difficult to synthesize, given the instability of the metallocene complex with respect to ligand redistribution to yield mono- and tris(ring) species (Kanellakopulos *et al.*, 1974c). Alternative approaches to generate complexes of this formula have generally involved introduction of the cyclopentadienyl ligands in the presence of other ligands that inhibit redistribution, as in equations (25.42)–(25.45) (Jamerson and Takats, 1974; Zanella *et al.*, 1977, 1987).

$U(NEt_2)_4$ + 2 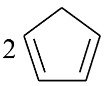 $\longrightarrow$ (η^5-C_5H_5)$_2$U(NEt_2)$_2$ + 2 $HNEt_2$ (25.42)

$$UCl_4 + NaBH_4 \longrightarrow (BH_4)_2UCl_2 + 2NaCl \qquad (25.43)$$

$$(BH_4)_2UCl_2 + 2Tl(C_5H_5) \longrightarrow (\eta^5\text{-}C_5H_5)_2U(BH_4)_2 + 2TlCl \qquad (25.44)$$

$$(dmpe)ThCl_4 + 2Na(C_5H_5) \longrightarrow (\eta^5\text{-}C_5H_5)_2Th(Cl)_2(dmpe) + 2NaCl \qquad (25.45)$$

The bis(indenyl) complex $(\eta^5\text{-}C_9H_7)_2U(BH_4)_2$ has been generated by the reaction of $Na(C_9H_7)$ with $U(BH_4)_2$, and the structure reported (Spirlet *et al.*, 1989b). Peralkylated indenyl ligands have also been used to produce metallocene derivatives. Reaction of $ThCl_4$ with $Li(C_9Me_7)$ yields the dichloride complex $(\eta^5\text{-}C_9Me_7)_2ThCl_2$ (Trnka *et al.*, 2001). This species serves as a reagent for the synthesis of a number of derivatives, including $(\eta^5\text{-}C_9Me_7)_2ThMe_2$, $(\eta^5\text{-}C_9Me_7)_2Th(NMe_2)_2$, $(\eta^5\text{-}C_9Me_7)_2Th(NC_4H_4)_2$, and $(\eta^5\text{-}C_9Me_7)_2Th(\eta^3\text{-}H_3BH)_2$. The permethylindenyl ligand in all of these derivatives binds with nearly an idealized η^5-coordination mode, with the Th–C bonds for the five-membered ring of the indenyl ligands varying by no more than 0.05 Å. The indenyl rings are not entirely planar, indicating that there are steric repulsions between the proximal methyl groups of the two $(\eta^5\text{-}C_9Me_7)$ ligands, although these distortions are smaller than in related zirconium compounds, consistent with the larger radius of the thorium ion.

The principal synthetic means employed to stabilize bis(cyclopentadienyl) actinide complexes against ligand redistribution has been to use substituted cyclopentadienyl ligands. The first reports of successfully stabilizing bis(cyclopentadienyl) complexes involved the use of peralkylated derivatives (C_5Me_5: Manriquez *et al.*, 1978; Fagan *et al.*, 1981a; C_5Me_4Et: Green and Watts, 1978). The pentamethylcyclopentadienyl ligand has come to be one of the most widely used ligands in organoactinide chemistry due to the thermal stability, solubility, and crystallinity of its compounds. Initial synthetic routes involved alkylation of the metal tetrahalides by Grignard [equation (25.46)] or tin [equation (25.47)] reagents:

$$AnCl_4 + 2(C_5Me_5)MgCl \cdot THF \longrightarrow (\eta^5\text{-}C_5Me_5)_2AnCl_2 + 2MgCl_2 \quad An = Th, U \qquad (25.46)$$

$$UCl_4 + 2(C_5Me_4Et)SnBu_3 \longrightarrow (\eta^5\text{-}C_5Me_4Et)_2UCl_2 + 2Bu_3SnCl \qquad (25.47)$$

The molecular structure of $(\eta^5\text{-}C_5Me_5)_2UCl_2$ has been determined (Spirlet *et al.*, 1992b; Fig. 25.12), as have those of $(\eta^5\text{-}C_5Me_5)_2ThX_2$ (X = Cl, Br, I) (Spirlet *et al.*, 1992b; Rabinovich *et al.*, 1997, 1998).

All exist as monomeric complexes with a pseudo-tetrahedral, 'bent metallocene' geometry. The complex $(\eta^5\text{-}C_5Me_5)_2NpCl_2$ was generated in a manner similar to that in equation (25.46) (Sonnenberger and Gaudiello, 1986); reaction of the tetrahalide with $Tl(C_5Me_5)$ had previously been reported to yield a THF

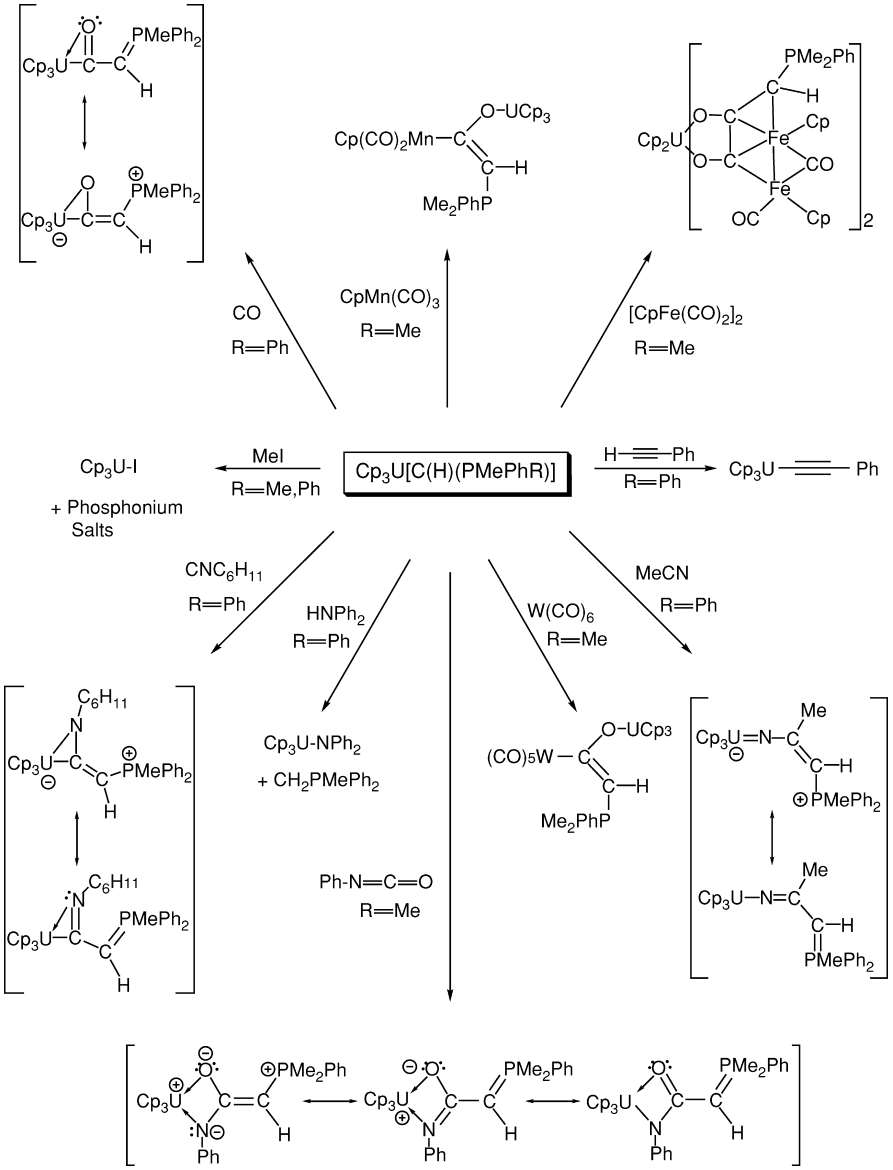

Fig. 25.11 *Reactions of* $(\eta^5\text{-}C_5H_5)_3U[(CH)P(CH_3)(C_6H_5)(R)]$, *where* $R = CH_3$, C_6H_5.

adduct (Karraker, 1983). The electrochemistry of $(\eta^5\text{-}C_5Me_5)_2NpCl_2$ reveals a reversible one-electron reduction wave at –0.68 V versus a ferrocene internal standard. A one-electron reversible reduction is also reported for $(\eta^5\text{-}C_5Me_5)_2UCl_2$ at –1.30 V (Finke *et al.*, 1982). Interestingly, the difference in

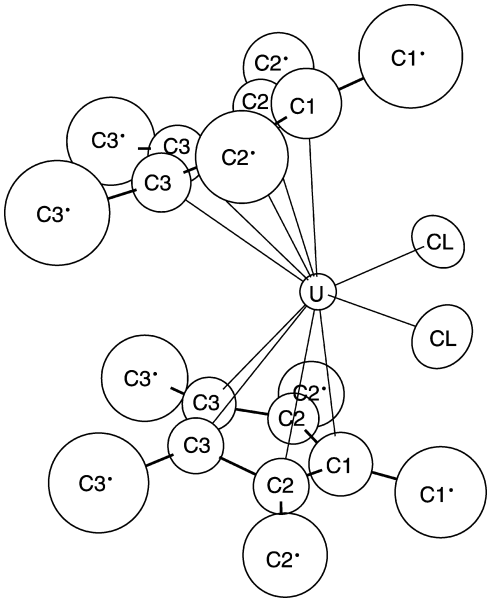

Fig. 25.12 *Crystal structure of* $(\eta^5\text{-}C_5Me_5)_2UCl_2$ (*Spirlet* et al., 1992b). (*Reprinted with permission of the International Union of Crystallography*.)

the U and Np non-aqueous reduction potentials is very close to the difference in their aqueous reduction potentials.

Other substituted cyclopentadienyl ligand sets have been generated and used to stabilize tetravalent metallocenes, particularly [1,3-$(Me_3Si)_2C_5H_3$] and [1,3-$(Me_3C)_2C_5H_3$]. The metal complexes have been prepared by reaction of the metal tetrahalides with either cyclopentadienyllithium reagents [equation (25.48)] (Blake *et al.*, 1995) or the substituted magnesocenes [equation (25.49)] (Lukens *et al.*, 1999a).

$$\mathrm{AnCl_4 + 2Li[1,3\text{-}(Me_3Si)_2C_5H_3] \longrightarrow [\eta^5\text{-}1,3\text{-}(Me_3Si)_2C_5H_3]_2AnCl_2 + 2LiCl} \quad \mathrm{An = Th,\ U} \tag{25.48}$$

$$\mathrm{UCl_4 + (1,3\text{-}R_2C_5H_3)_2Mg \longrightarrow (\eta^5\text{-}1,3\text{-}R_2C_5H_3)_2UCl_2 + MgCl_2} \quad \mathrm{R = SiMe_3,\ CMe_3} \tag{25.49}$$

In the latter case, all metatheses were performed with the chloride salt, and the chloride product was subsequently converted to other halides by reaction with $XSiMe_3$ (X = Br, I) or $BF_3 \cdot Et_2O$. The molecular structures of the complexes $[\eta^5\text{-}1,3\text{-}R_2C_5H_3]_2UX_2$ ($R = SiMe_3$, X = F, Cl, Br; R = ^{t}Bu, X = F, Cl) have

been reported, as has the structure of $[\eta^5\text{-}1,3\text{-}(Me_3Si)_2C_5H_3]_2ThCl_2$. All exist as monomers in the solid state, except for $[\{\eta^5\text{-}1,3\text{-}(Me_3Si)_2C_5H_3\}_2UF(\mu\text{-}F)]_2$, which is a dimer (see Fig. 25.6). A detailed study of the solution behavior of the complexes has been conducted (Lukens *et al.*, 1999a). Both fluoride complexes are found to display a monomer–dimer equilibrium in solution. The ^1H NMR chemical shifts and magnetic susceptibility data for the complexes further suggest that the ligands $[1,3\text{-}(Me_3Si)_2C_5H_3]$ and $[1,3\text{-}(Me_3C)_2C_5H_3]$ produce significantly different electronic environments at the metal center.

Despite the kinetic stability that the sterically larger cyclopentadienyl ligands provide, in a limited number of cases base adducts have been generated. The complex $(\eta^5\text{-}C_5Me_5)_2UCl_2(pz)$ (pz = pyrazole) has been reported (Eigenbrot and Raymond, 1982), as has the chelating phopshine adduct $[\eta^5\text{-}1,3\text{-}(Me_3Si)_2C_5H_3]_2ThCl_2(dmpe)$ (Edelman *et al.*, 1995). The complex $(\eta^5\text{-}C_5Me_5)_2U(OTf)_2(H_2O)$ (OTf = trifluoromethylsulfonate) was isolated in low yield from the reaction of $(\eta^5\text{-}C_5Me_5)_2UMe_2$ with triflic acid (Berthet *et al.*, 1998). In compounds of the formula $(\eta^5\text{-}C_5Me_5)_2UX_2(L)$ (L = neutral ligand), the coordinated base generally occupies the central position in the equatorial wedge.

A second strategy for kinetically stabilizing actinide metallocenes against redistribution reactions is to employ the chelate effect by linking the two cyclopentadienyl rings (*ansa* metallocenes). The most common of these ligands are the *ansa* ligand sets.

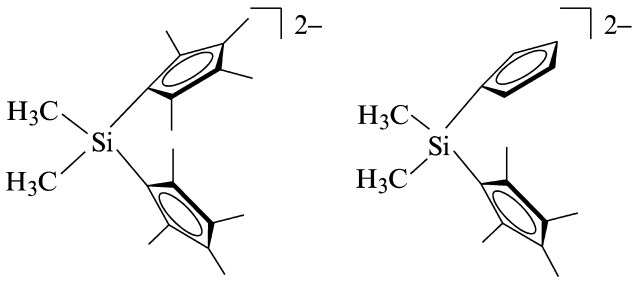

The molecular structure of $[(\eta^5\text{-}C_5Me_4)_2(\mu\text{-}SiMe_2)]U(\mu\text{-}Cl)_4[Li(TMEDA)]_2$ (TMEDA = *N*,*N*,*N*′,*N*′-tetramethylethylenediamine) is shown in Fig. 25.13.

As for most *ansa* metallocenes, the complex is characterized by a more acute centroid–metal–centroid angle (114.1°) than non-linked metallocenes (133–138°). This leaves more room in the equatorial wedge, accounting for the ability to accommodate four bridging chloride ligands. The more open coordination environment generated by 'tying' back the cyclopentadienyl ligands also enhances the reactivity of the resulting metal complex. The complex $[(\eta^5\text{-}C_5Me_4)_2(\mu\text{-}SiMe_2)]Th(n\text{-}Bu)_2$, generated by reaction of the structurally characterized precursor $[(\eta^5\text{-}C_5Me_4)_2(\mu\text{-}SiMe_2)]Th(\mu\text{-}Cl)_4[Li(DME)]_2$ with *n*-BuLi, was found to be a very active catalyst for the dimerization of terminal alkynes and the hydrosilylation of terminal alkynes or alkenes with $PhSiH_3$ (Dash *et al.*, 2001).

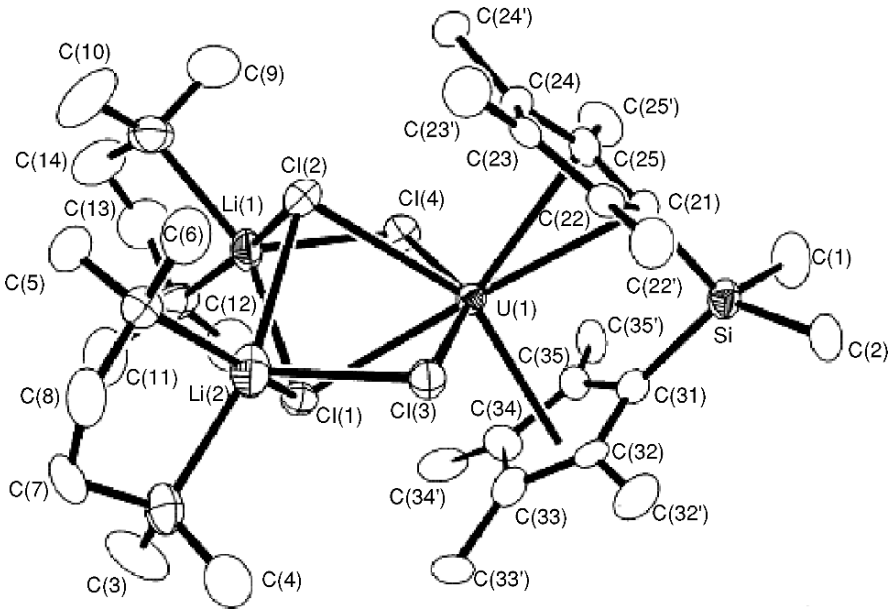

Fig. 25.13 *Crystal structure of* $[(\eta^5\text{-}C_5Me_4)_2(\mu\text{-}SiMe_2)]U(\mu\text{-}Cl)_4[Li(TMEDA)]_2$ (*Schnabel* et al., 1999). (*Reprinted with permission from Elsevier*.)

Other ligand sets have been explored that append Lewis base groups to the ring that will coordinate to the metal center to help prevent ring redistribution. A bis(cyclopentadienyl) substituted pyridine ligand has been used to generate the complex $[\eta^5\text{-}C_5H_4(CH_2)]_2(C_6H_5N)UCl_2$ (Paolucci *et al.*, 1991), and the pendant ether complex $[\eta^5\text{-}C_5H_4(CH_2CH_2OCH_3)]_2UCl_2$ has also been reported (Deng *et al.*, 1996):

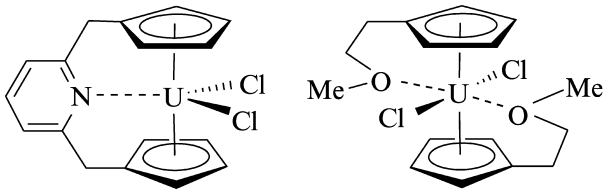

Metathesis and protonation reactions have been employed to produce a wide array of derivatives of the metallocene unit. A limited number of complexes exist with bonds to Group 14 elements other than carbon. Reaction of $(\eta^5\text{-}C_5Me_5)_2ThCl_2$ with the bulkyl silyl salt $(THF)_3Li[Si(SiMe_3)_3]$ yields an unstable complex $(\eta^5\text{-}C_5Me_5)_2Th(Cl)[Si(SiMe_3)_3]$ that could be trapped by reaction with two equivalents of carbon monoxide to produce a ketene complex $(\eta^5\text{-}C_5Me_5)_2Th(Cl)[O\text{–}C(=C=O)Si(SiMe_3)_3]$.

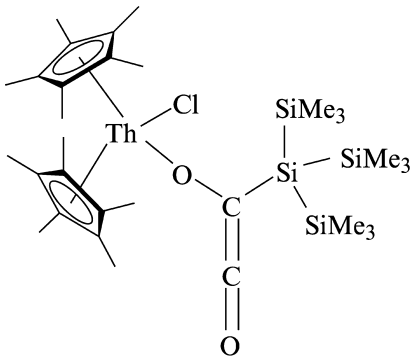

The analogous silyl compound $(\eta^5\text{-}C_5Me_5)_2ThCl(Si^tBuPh_2)$ could be isolated and its reaction with CO gave a similar silylthoroxyketene compound, and in this case the transient η^2-acyl complex $(\eta^5\text{-}C_5Me_5)_2ThCl[\eta^5\text{-}CO(Si^tBuPh_2)]$ could be detected (Radu *et al.*, 1995).

Metathesis [equations (25.50), (25.52), and (25.53)] and protonation [equations (25.42) and (25.51)] reactions are the most widely used routes to generate metallocene amide complexes (Fagan *et al.*, 1981a,b; Eigenbrot and Raymond; 1982).

$$(\eta^5\text{-}C_5Me_5)_2AnCl_2 + 2\,LiNMe_2 \xrightarrow[-2\ LiCl]{} (\eta^5\text{-}C_5Me_5)_2U(NMe_2)_2 \quad (25.50)$$
$$An = Th, U$$

$$(\eta^5\text{-}C_5Me_5)_2AnR_2 + 2\ HNEt_2 \xrightarrow[-2\ RH]{} (\eta^5\text{-}C_5Me_5)_2U(NEt_2)_2 \quad (25.51)$$
$$An = Th, U$$

$$(\eta^5\text{-}C_5Me_5)_2UCl_2 + Na(pz) \longrightarrow (\eta^5\text{-}C_5Me_5)_2U(Cl)(pz) + NaCl \quad (25.52)$$
$$pz = pyrazolate$$

$$(\eta^5\text{-}C_5Me_5)_2UCl_2 + 2\ Na(pz) \longrightarrow (\eta^5\text{-}C_5Me_5)_2U(pz)_2 + 2\ NaCl \quad (25.53)$$
$$pz = pyrazolate$$

Metallocene phosphide complexes have been generated by metathesis routes [equations (25.54) and (25.55)] (Wrobleski *et al.*, 1986a; Hall *et al.*, 1993).

$$(\eta^5\text{-}C_5Me_5)_2ThCl_2 + 2\ LiPR_2 \longrightarrow (\eta^5\text{-}C_5Me_5)_2Th(PR_2)_2 + 2\ LiCl \quad (25.54)$$
$$R = Ph, Cy, Et$$

$$(\eta^5\text{-}C_5Me_5)_2An(X)(Cl) + KP(SiMe_3)_2 \longrightarrow (\eta_5\text{-}C_5Me_5)_2An(X)[P(SiMe_3)_2] + KCl \quad (25.55)$$
$$An = Th, U;\ X = Cl, Me$$

For the bis(trimethylsilyl)phosphide substituent, a bis(phosphido) complex cannot be produced. Solution ^{1}H NMR spectra indicate that there is restricted rotation about the An–P bond at room temperature. The complexes $(\eta^5\text{-}C_5Me_5)_2AnMe[P(SiMe_3)_2]$ decompose thermally by elimination of methane to generate a metallacyclic complex:

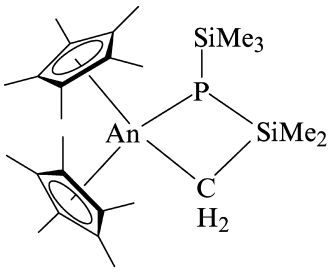

An = Th, U

The metallocene framework has also been integral to the isolation of organoimido and phosphinidene complexes. Comproportionation of U(III) and U(V) metallocenes results in the formation of uranium(IV) organoimido complexes [equation (25.56)] (Brennan *et al.*, 1988b).

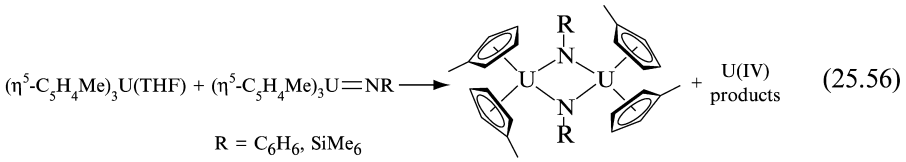

(25.56)

The molecular structure of $[(\eta^5\text{-}MeC_5H_4)_2U(\mu\text{-}NPh)]_2$ is shown in Fig. 25.14.

The complexes exist as centrosymmetric dimers with asymmetric bridging organoimido ligands; the degree of asymmetry in the U–N bonds depends on the identity of the imido substituent.

It is only recently that terminal organoimido complexes of U(IV) have been isolated (Arney and Burns, 1995). α-Elimination reactions have been employed to generate the monoimido complex $(\eta^5\text{-}C_5Me_5)_2U(=N\text{-}2,4,6\text{-}{}^tBu_3C_6H_2)$ [equation (25.57)].

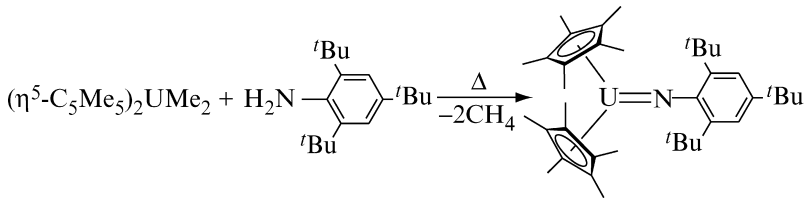

(25.57)

The complex is isolated even from ethereal solvents as a base-free species. The complex displays a very short U–N bond distance [1.95(1) Å], and a large

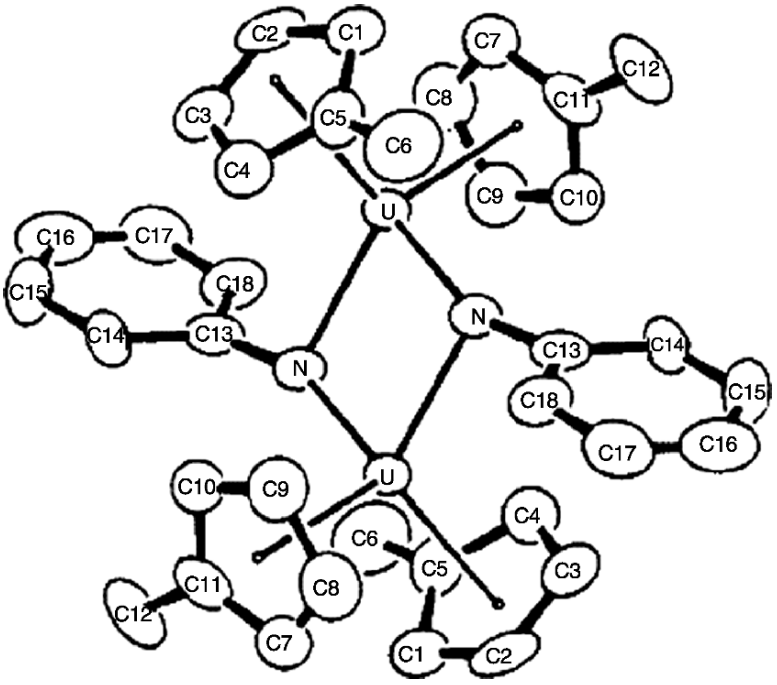

Fig. 25.14 *Crystal structure of* $[(\eta^5\text{-}MeC_5H_4)_2U(\mu\text{-}NPh)]_2$. (*Reprinted with permission from Brennan* et al. (1988b). *Copyright* 1988 *American Chemical Society.*)

U–N–C angle [162.3(10)°]. Unlike the phosphoylide and phosphine imide complexes described previously, the organoimido complex is relatively inert; it does not undergo insertion reactions, suggestive of a bond order greater than 1. The steric bulk of the aryl group is important in stabilizing a base-free organoimido complex; the smaller $(\eta^5\text{-}C_5Me_5)_2U(=N\text{-}2,6\text{-}{}^iPr_2C_6H_3)$ is best isolated as the THF adduct, and the parent phenylimido has only been isolated as a uranate salt, $[Li(TMEDA)][(\eta^5\text{-}C_5Me_5)_2U(=NC_6H_5)Cl]$. Organoimido complexes of U(IV) and Th(IV) have been implicated as intermediates in the catalytic intermolecular hydroamination of terminal alkynes (Straub *et al.*, 1996, 2001). It has been proposed that monoimido derivatives of the formula $(\eta^5\text{-}C_5Me_5)_2An(=NR')$ are formed in the reaction of $(\eta^5\text{-}C_5Me_5)_2AnMe_2$ with primary amines $R'NH_2$. These undergo metathesis reaction with alkynes to yield four-membered azametallacyclic intermediates, which can undergo subsequent amine protonation (with isomerization) to yield the product imines. The mechanism of this reaction is discussed further in Chapter 26. Although the organoimido intermediates involving aliphatic amines have not been isolated, analogs such as $(\eta^5\text{-}C_5Me_5)_2Th(=N\text{-}2,6\text{-}Me_2C_6H_3)(THF)$ have been structurally

characterized (Haskel *et al.*, 1996; Straub *et al.*, 2001). As in the case of the uranium organoimido complex, the thorium complex displays a short Th–N bond [2.045(8) Å] and a near-linear Th–N–C_{ipso} angle (171.5(7)°).

Similarly, bridging actinide phosphinidene complexes predated their terminal counterparts. The hydride complex $[(\eta^5\text{-}C_5Me_5)_2UH_2]_2$ reacts with $P(OMe)_3$ to generate a bridging phosphinide complex $[(\eta^5\text{-}C_5Me_5)_2U(OMe)]_2(\mu\text{-}PH)$ by P–O cleavage with sacrificial formation of $(\eta^5\text{-}C_5Me_5)_2U(OMe)_2$ [equation (25.58)] (Duttera *et al.*, 1984).

$$[(\eta^5\text{-}C_5Me_5)_2UH_2]_2 + P(OMe)_3 \longrightarrow (\eta^5\text{-}C_5Me_5)_2U(MeO)\text{–}P(H)\text{–}U(OMe)(\eta^5\text{-}C_5Me_5)_2 + (\eta^5\text{-}C_5Me_5)_2U(OMe)_2 \quad (25.58)$$

A terminal phosphinidene complex has also been reported (Arney *et al.*, 1996). Reaction of $(\eta^5\text{-}C_5Me_5)_2U(Me)Cl$ with $KPH(2,4,6\text{-}{}^tBu_3C_6H_2)$ in the presence of trimethylphosphine oxide yields the base adduct of the phosphinidene complex $(\eta^5\text{-}C_5Me_5)_2U(=P\text{-}2,4,6\text{-}{}^tBu_3C_6H_2)(OPMe_3)$ (Fig. 25.15).

The complex displays a short U–P distance [2.562(3) Å]. The U–P–C angle 143.7(3)°; the nonlinear angle is not unusual in comparison to d-transition metal terminal phosphinidene complexes. No product is isolated in the absence of coordinating base, except for when the ancillary ligand set is $[(\eta^5\text{-}C_5Me_4)_2(\mu\text{-}SiMe_2)]$. In the case of the less congested *ansa*-metallocene; a phosphinidene-bridged dimer $[\{(\eta^5\text{-}C_5Me_4)_2(\mu\text{-}SiMe_2)\}U(\mu\text{-}PR)]_2$ (R = 2,4,6-${}^tBu_3C_6H_2$) is generated.

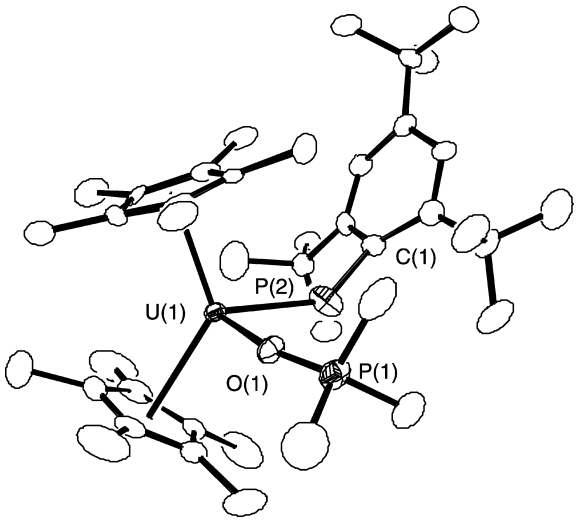

Fig. 25.15 *Crystal structure of* $(\eta^5\text{-}C_5Me_5)_2U(=P\text{-}2,4,6\text{-}t\text{-}Bu_3C_6H_2)(OPMe_3)$. (*Reprinted with permission from Arney* et al. (1996). *Copyright* 1996 *American Chemical Society*.)

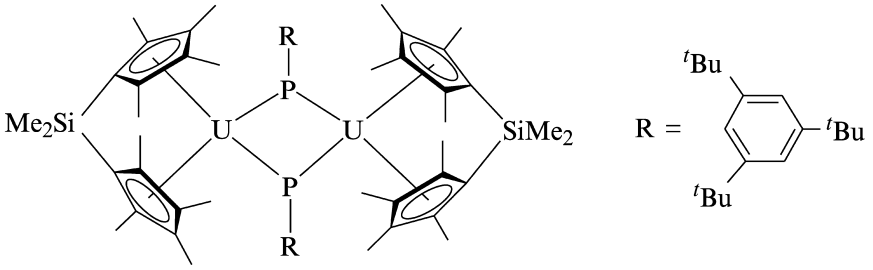

An interesting series of polypnictide complexes have been generated by the reaction of $(\eta^5\text{-}1,3\text{-}^t\text{Bu}_2\text{C}_5\text{H}_3)_2\text{Th}(\eta^4\text{-}\text{C}_4\text{H}_6)$ with P_4 or As_4. The main group elements react to generate a hexapnictide complex: $[(\eta^5\text{-}1,3\text{-}^t\text{Bu}_2\text{C}_5\text{H}_3)_2\text{Th}]_2(\mu,\eta^3,\eta^3\text{-}\text{E}_6)$ (E = P, As) (Scherer *et al.*, 1991, 1994).

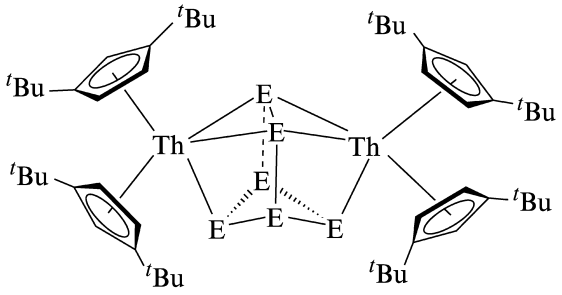

E = P, As

In the presence of magnesium chloride, however, only the complex: $[(\eta^5\text{-}1,3\text{-}^t\text{Bu}_2\text{C}_5\text{H}_3)_2\text{Th}](\mu,\eta^3\text{-}\text{P}_3)[\text{Th}(\text{Cl})(\eta^5\text{-}1,3\text{-}^t\text{Bu}_2\text{C}_5\text{H}_3)_2]$ is formed in the reaction with phosphorus.

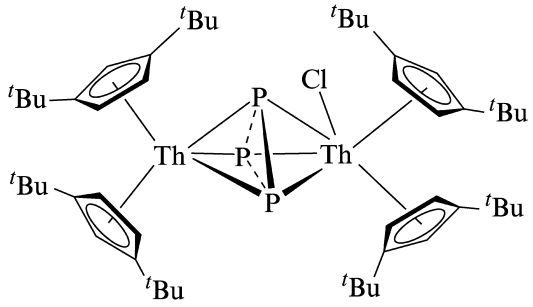

One of the earliest descriptions of metallocene thiolate complexes involved reactions of $(\eta^5\text{-}\text{C}_5\text{H}_5)_2\text{U}(\text{NEt}_2)_2$ with monothiols and dithiols (Jamerson and Takats, 1974). While compounds with the chelating thiols are stable (generally dimers), compounds of monodentate thiols $(\eta^5\text{-}\text{C}_5\text{H}_5)_2\text{U}(\text{SR})_2$ were reported to

be unstable and decomposed to form $(\eta^5\text{-}C_5H_5)_2U(SR)$. Two other reports of bis (pentamethylcyclopentadienyl) metallocene dithiolates have been appeared: $(\eta^5\text{-}C_5Me_5)_2Th(SPr)_2$ (Lin *et al.*, 1988) and $(\eta^5\text{-}C_5Me_5)_2U(SR)_2$ (R = Me, ^{i}Pr, ^{t}Bu, Ph) (Lescop *et al.*, 1999).

Two reports have appeared featuring cyclopentadienyl-supported actinide chalcogenide complexes. Reaction of $(\eta^5\text{-}C_5Me_5)_2ThCl_2$ with Li_2S_5 generates the compound $(\eta^5\text{-}C_5Me_5)_2Th(S_5)$ (Wrobleski *et al.*, 1986b); the molecular structure of this complex shows that the six-membered ring formed by the S_5 ligand and the Th has a twist-boat conformation. Bonding of the ligand was characterized as η^4 on the basis of close contacts between the β-sulfides and the metal center. Variable temperature NMR data show that the ligand is fluxional at room temperature.

The complex $(\eta^5\text{-}C_5Me_5)_2U(S^tBu)_2$ is reported to undergo reduction by Na–Hg with cleavage of a C–S bond (Ventelon *et al.*, 1999). The product was isolated with 18-crown-6 and proved to be a complex with a terminal sulfido ligand bound to the sodium counter-ion. The complex [Na(18-crown-6)][$(\eta^5\text{-}C_5Me_5)_2U(S^tBu)(S)$] possesses a short U–S bond distance [2.462(2) Å], which is significantly shorter than typical U–SR bond distances (*ca.* 2.64 Å).

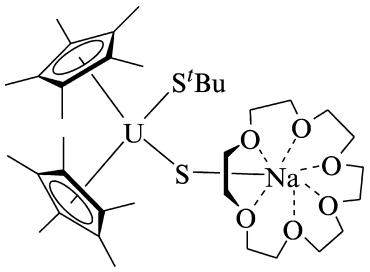

Given the relative importance of d-transition metal metallocene alkyl chemistry in Group 4 organometallic chemistry, it is to be expected that the alkyl chemistry of the actinide metallocene complexes would also be extensively studied. The majority of this chemistry has employed the more highly substituted ligand sets, although less sterically hindered metallocene frameworks can be alkylated in the presence of a stabilizing base as shown in equation (25.59) (Zalkin *et al.*, 1987a):

$$(\eta^5\text{-}C_5H_5)_2ThCl_2(dmpe) + 2LiR \longrightarrow (\eta^5\text{-}C_5H_5)_2ThR_2(dmpe) + 2LiCl \quad R = CH_3,\ CH_2Ph \tag{25.59}$$

Complexes employing the pentamethylcyclopentadienyl ligand can be prepared for a wide range of alkyl and aryl groups (Fagan *et al.*, 1981a; Erker *et al.*, 1986; Smith *et al.*, 1986), where the alkylating agents can be either alkyllithium, Grignard, or dialkylmagnesium reagents [equation (25.60)].

$$(\eta^5\text{-}C_5Me_5)_2AnCl_2 + 2R^- \longrightarrow (\eta^5\text{-}C_5Me_5)_2AnR_2 + 2Cl^-$$
$$An = Th,\ U;\ R = CH_3,\ CH_2SiMe_3,\ CH_2CMe_3,\ C_6H_5,\ CH_2C_6H_5 \qquad (25.60)$$

The corresponding mixed alkyl halide complexes can be prepared in most cases by reaction of $(\eta^5\text{-}C_5Me_5)_2AnCl_2$ with one equivalent of alkylating agent, although the methyl chloride complex is best prepared by redistribution from the dichloride and dimethyl complexes [equation (25.61)].

$$(\eta^5\text{-}C_5Me_5)_2AnCl_2 + (\eta^5\text{-}C_5Me_5)_2AnMe_2 \longrightarrow 2(\eta^5\text{-}C_5Me_5)_2An(Me)(Cl)$$
$$An = Th,\ U \qquad (25.61)$$

The complexes are generally thermally stable, although some undergo elimination reactions at elevated temperatures (*vide infra*). The dimethyl complexes react with acetone, alcohols, and iodine to produce the corresponding *t*-butoxide, alkoxides (with generation of methane), and iodides (with generation of methyl iodide) (Fagan *et al.*, 1981a). Competition experiments at –78°C indicate that the thorium complexes are more reactive than those of uranium, consistent with its larger ionic radius.

Two alternate descriptions have appeared for the complex $(\eta^5\text{-}C_5Me_5)_2Th(\eta^4\text{-}C_4H_6)$. The complex and its derivatives have been termed both butadiene and 2-buten-1,4-diyl complexes, although the latter description is generally favored. The molecular structure of $(\eta^5\text{-}C_5Me_5)_2Th(\eta^4\text{-}C_4H_6)$ is shown in Fig. 25.16.

The crystal structure supports the η^4-hapticity of the organic ligand, given that the average Th–C distance to the terminal carbon atoms of the ligand [2.57(3) Å] is only slightly smaller than that to the internal carbon atoms [2.74(2) Å], and are comparable to those found in other thorium alkyl complexes. The C(1)–C(2) and C(3)–C(4) average distances (average of four independent molecules in the unit cell) is 1.46(5) Å, and the average C(2)–C(3) distance is 1.44(3) Å. The complex displays fluxional behavior in solution, with equilibration of the cyclopentadienyl and α-methylene protons occurring via the intermediacy of a planar metallacyclopentene structure.

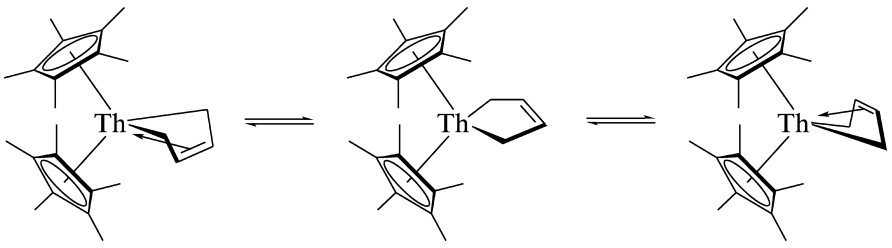

The actinide–carbon bonds in these complexes appear to be reasonably polar; they undergo hydrogenolysis under one atmosphere of dihydrogen to yield the dihydride complexes [equation (25.62)]:

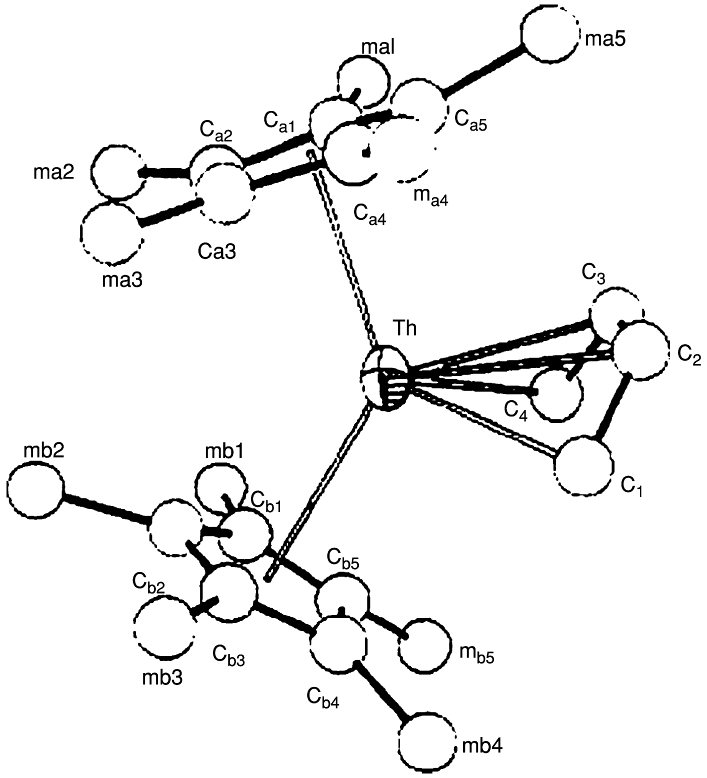

Fig. 25.16 *Crystal structure of* $(\eta^5\text{-}C_5Me_5)_2Th(\eta^4\text{-}C_4H_6)$. (*Reprinted with permission from Smith* et al. (1986). *Copyright* 1986 *American Chemical Society.*)

$$(\eta^5\text{-}C_5Me_5)_2AnR_2 + 2H_2 \longrightarrow \tfrac{1}{2}(\eta^5\text{-}C_5Me_5)_2An(H)(\mu\text{-}H)_2An(H)(\eta^5\text{-}C_5Me_5)_2 + 2RH \qquad (25.62)$$

An = Th, U

The dimeric formulation of the dihydride complexes is supported both by cryoscopic molecular weight determinations and a single-crystal neutron diffraction structure of the thorium compound (Broach *et al.*, 1979); ^{1}H NMR experiments indicate that the bridge and terminal hydrides exchange rapidly in solution to –85°C. Under an atmosphere of D_2, H/D exchange in the hydride positions is very rapid. In the case of uranium, the ring methyl protons appear to interchange rapidly with the hydrides, resulting in isotopic scrambling. The thorium complex is thermally stable; in contrast, the uranium complex loses dihydrogen at room temperature *in vacuo* over a period of 3 h to generate a U(III) hydride.

Dialkyl complexes of an *ansa*-metallocene [$(\eta^5\text{-}C_5Me_4)_2(\mu\text{-}SiMe_2)$]$ThR_2$ (R = CH_2SiMe_3, CH_2CMe_3, C_6H_5, *n*-C_4H_9, and $CH_2C_6H_5$) have also been reported (Fendrick *et al.*, 1988). The ring centroid-metal-centroid angle (118.4°) is again much reduced from that typically found in non-linked metallocene complexes (135–138°). The dialkyl complexes undergo rapid hydrogenolysis under H_2 to yield a light-sensitive dihydride complex [$\{(\eta^5\text{-}C_5Me_4)_2(\mu\text{-}SiMe_2)\}ThH_2]_2$. IR spectroscopy and structural data [a short Th···Th distance of 3.632(2) Å] are evidence cited in support of a formulation of the compound as one with four bridging hydride ligands.

Thermochemical investigations have tabulated the bond disruption enthalpies for a number of metallocene alkyl halide and dialkyl complexes; these values are given in Table 25.6 (Bruno *et al.*, 1983, 1986b). As noted previously, the Th–R bond enthalpies are uniformly larger than those for U–R. It has also been noted (Leal *et al.*, 2001) that there appears to be significantly different values for certain bond enthalpy values (e.g. U–Me in Tables 25.4 and 25.6). The authors note that these values are based upon different reactions (alcholysis vs reaction with iodine), and therefore are based upon different assumed enthalpy values for product species. A potential correction was proposed, leading to a more self-consistent description of uranium bond enthalpies.

A further observation from the thermochemistry of thorium complexes is that the bond dissociation enthalpy for Th–H in [$(\eta^5\text{-}C_5Me_5)_2Th(\mu\text{-}H)H]_2$ (407.9 ± 2.9 kJ/mol), while somewhat larger than typical Th–C values (300–380 kJ mol^{-1}), is not larger enough to produce as strong a driving force for the

Table 25.6 *Mean bond dissociation enthalpies for* $(\eta^5\text{-}C_5Me_5)_2AnR_2$ *and* $(\eta^5\text{-}C_5Me_5)_2AnRX$ *complexes* (*Bruno et al.,* 1983, 1986*b*).

Compound	*R*	*D*(*An–R*) (kJ mol^{-1})
$(\eta^5\text{-}C_5Me_5)_2UR_2$	Me	300 ± 11
	CH_2Ph	244 ± 8
	CH_2SiMe_3	307 ± 8
$(\eta^5\text{-}C_5Me_5)_2URCl$	Me	312 ± 8
	CH_2Ph	263 ± 12
	Ph	358 ± 11
$(\eta^5\text{-}C_5Me_5)_2ThR_2$	Me	345.2 ± 3.5
	Et	313.4 ± 6.7
	n-Bu	303.8 ± 9.2
	Ph	379.3 ± 10.3
	CH_2CMe_3	312.1 ± 15.7
	CH_2SiMe_3	339.3 ± 13.0
$(\eta^5\text{-}C_5Me_5)_2ThRCl$	Et	302.1 ± 7.5
	CH_2Ph	285.3 ± 5.9
	Ph	380.8 ± 16

formation of hydrides. Therefore, unlike mid- to late-transition metal compounds, reactions such as β-hydride elimination will not be strongly favored. This energetic situation, similar to that found for early transition metals, makes actinide metallocenes suitable species to effect C–C bond forming reactions, such as olefin polymerization (see Chapter 26).

One of the predominant reaction patterns of bis(cyclopentadienyl)actinide complexes is insertion chemistry. Insertion of unsaturated substrates such as CO, CNR, CO_2, and CS_2 into U–C, U–Si, U–N, and U–S bonds has been observed (Fagan *et al.*, 1981a,b; Erker *et al.*, 1986; Porchia *et al.*, 1989; Lescop *et al.*, 1999). The products of insertion generally display η^2-C(R) =E bonding. As an example, insertion of CO into An–R bonds yields η^2-acyl derivatives. Theoretical studies (Tatsumi *et al.*, 1985) have been conducted, both to explain the geometry of the η^2-complexes, as well as to understand the origin of the 'carbene-like' reactivity (Fig. 25.17).

A second common reaction pattern observed in metallocene complexes is thermally induced intramolecular elimination reactions. The dominant classes of elimination reactions are those involving formation of four-membered metallacyle complexes [equation (25.63)] (Bruno *et al.*, 1986a).

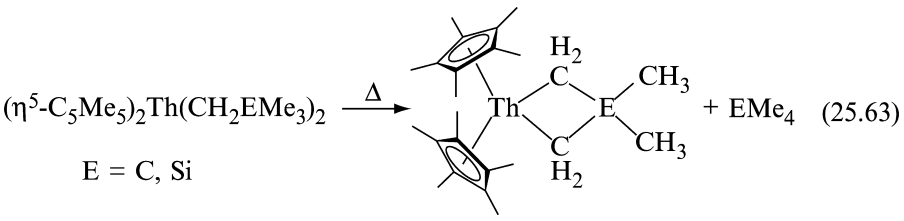

(25.63)

Kinetic and labeling studies in the cyclometallation reactions indicate that intramolecular γ-C–H activation is the rate-limiting step. It is believed that the reaction is chiefly entropically driven, with some driving force coming from relief of steric strain associated with the thorium dialkyl complex. The cyclometallated products have extensive reaction chemistry that is characterized by insertion of unsaturated substrates into Th–C bonds, as well as intermolecular activation of C–H bonds of other substrates, even saturated hydrocarbons such as methane [equation (25.64)] (Fendrick and Marks, 1986).

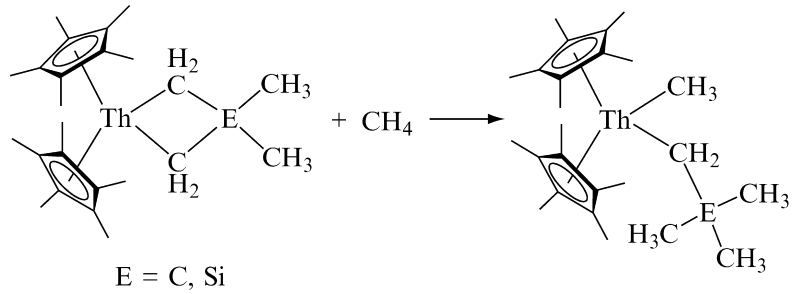

(25.64)

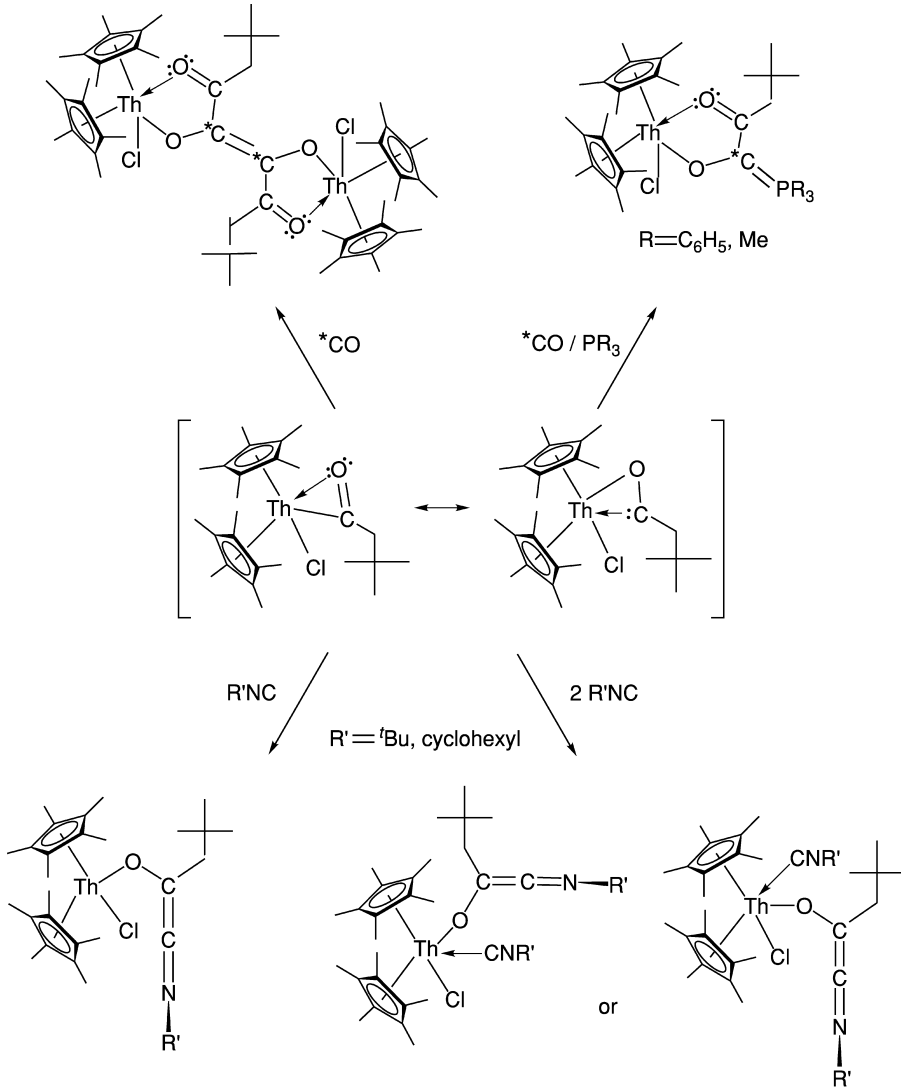

Fig. 25.17 *Reactivity of actinide η^2-Acyl complexes* (*Moloy* et al., 1983).

A second class of reactions is the elimination of benzene from diaryl complexes to form *o*-diphenylene, or benzyne-type complexes [equation (25.65)] (Fagan *et al.*, 1981a).

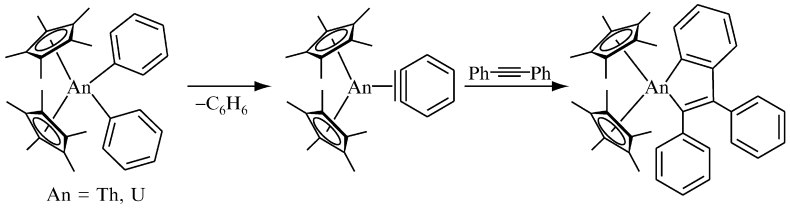

(25.65)

The uranium complexes undergo this *ortho*-activation process ($k_U \gg k_{Th}$); although the intermediate benzyne complex is not stable, it can be trapped with diphenylacetylene to yield a metallacyclopentadiene product.

Despite the early report of mono-ring complexes of the formula (η^5-C_5H_5)UCl_3(DME) (DME = 1,2-dimethoxyethane) (Doretti *et al.*, 1972), there are far fewer reports of compounds containing a single cyclopentadienyl ring. The complex was initially prepared by reaction of UCl_4 with $Tl(C_5H_5)$ in DME [equation (25.66)].

$$UCl_4 + Tl(C_5H_5) \xrightarrow{DME} (\eta^5\text{-}C_5H_5)UCl_3(DME) \qquad (25.66)$$

Since that time, a number of other base adducts of the uranium mono-ring compound have been prepared using both monodentate (Bagnall and Edwards, 1974; Bagnall *et al.*, 1978a; Bombieri *et al.*, 1978) and bidentate bases (Ernst *et al.*, 1979). The complex $U(BH_4)_4$ similarly reacts with $Tl(C_5H_5)$ to yield (η^5-C_5H_5)$U(BH_4)_3$ (Baudry and Ephritikhine, 1988), although base adducts of this compound are reported to redistribute to generate (η^5-C_5H_5)$_2U(BH_4)_2$ (Baudry *et al.*, 1988). The structure of the (η^5-C_5H_5)$U(BH_4)_3(THF)_2$ complex has been proposed to be *mer*-octahedral with *cis* THF ligands on the basis of solution NMR investigations with a pentahapto cyclopentadienyl ring; this structure was confirmed for the complex (η^5-MeC_5H_4)$UCl_3(THF)_2$.

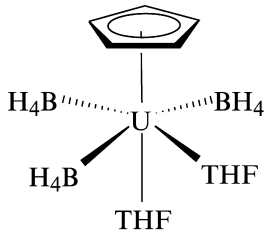

A later NMR study (Le Marechal *et al.*, 1986) reported an equilibrium between two isomers in solution for a variety of base adducts of (η^5-C_5H_5)UCl_3. Analogous compounds of the formula (η^5-C_5H_5)AnX_3L_2 (X = halide, NCS^-) have been produced for thorium (Bagnall and Edwards, 1974), neptunium (Karraker and Stone, 1972; Bagnall *et al.*, 1986), and plutonium (Bagnall *et al.*, 1985).

A variety of substituted cyclopentadienyl ligands have been introduced to generate cyclopentadienylthorium and cyclopentadienyluranium compounds by reaction with Grignard or alkali metal reagents. Indenyl complexes of the formula $(\eta^5\text{-}C_9H_7)AnX_3L$ (X = halide, L = base) can be prepared as shown in equations (25.67) and (25.68) (Goffart *et al.*, 1980; Meunier-Piret *et al.*, 1980).

$$AnX_4 + K(C_9H_7) \xrightarrow{THF} (\eta^5\text{-}C_9H_7)AnX_3(THF)_2 + KX \qquad (25.67)$$

An = Th, U, Np; X = Cl, Br

$$(\eta^5\text{-}C_9H_7)AnX_3(THF)_2 + Ph_3P{=}O \longrightarrow (\eta^5\text{-}C_9H_7)AnX_3(THF)(O{=}PPh_3) + THF \qquad (25.68)$$

An = Th, U, Np; X = Cl, Br

The use of alkali metal cyclopentadienyl reagents can lead to the formation of uranate-type complexes [equations (25.69) and (25.70)] (Edelman *et al.*, 1987, 1995):

$$UCl_4 + Li[1,2,4\text{-}(Me_3Si)_3C_5H_2] \xrightarrow{THF}$$

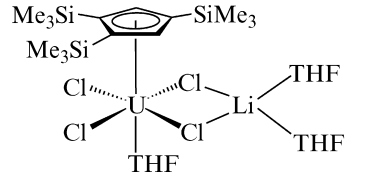

(25.69)

$$ThCl_4 + Na[1,2,4\text{-}(Me_3Si)_3C_5H_2] \xrightarrow{Et_2O}$$

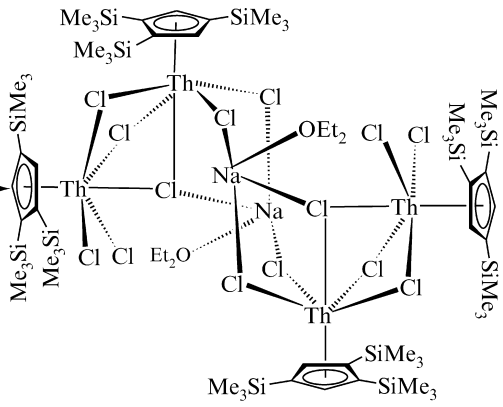

(25.70)

Mono-ring pentamethylcyclopentadienyl thorium and pentamethylcyclopentadienyl uranium complexes can also be synthesized from reaction of the tetrahalides with $(C_5Me_5)MgCl$ (Mintz *et al.*, 1982; Butcher *et al.*, 1996), and their base adducts prepared. Spectroscopic data would again indicate a meridional disposition of the chloride ligands in a pseudo-octahedral geometry. As described in equation (25.71), these complexes can be alkylated with either organolithium or Grignard reagents to yield a limited number of stable alkyl derivatives (Mintz *et al.*, 1982; Cymbaluk *et al.*, 1983a; Marks and Day, 1985; Marks, 1986).

$$(\eta^5\text{-}C_5Me_5)AnX_3(THF)_2 + RLi \text{ or } RMgX \longrightarrow (\eta^5\text{-}C_5Me_5)AnR_3$$

An = Th; R = allyl, $CH_2C_6H_5$, CH_2CMe_3, *o*-$C_6H_4NMe_2$ (25.71)

An = U; R = allyl, 2-methylallyl, $CH_2C_6H_5$

One study has been conducted of the metathesis chemistry of $(\eta^5\text{-}C_5Me_5)ThBr_3(THF)_3$ with aryloxide salts (Butcher *et al.*, 1996). Both the mono(aryloxide) and bis(aryloxide) complexes $(\eta^5\text{-}C_5Me_5)ThBr_2(OAr)(THF)$ and $(\eta^5\text{-}C_5Me_5)ThBr(OAr)_2$ (OAr = O-2,6-^{t}Bu$_2$C$_6$H$_3$) may be produced by reaction with one or two equivalents of KOAr. The dibromide complex may be further alkylated to generate $(\eta^5\text{-}C_5Me_5)Th(CH_2SiMe_3)_2(OAr)$. Thermolysis of this compound in the presence of triphenylphosphine oxide permits the isolation of a rare example of an f-element compound with a cyclometallated aryloxide ligand.

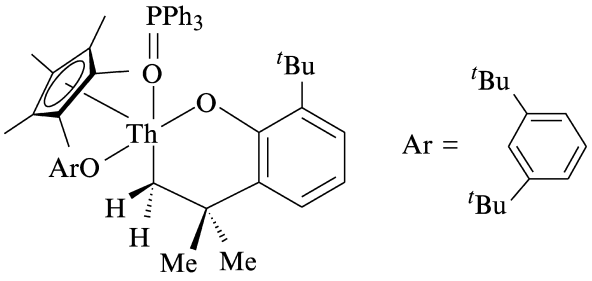

(c) Pentavalent chemistry

Pentavalent complexes of the actinides containing organic ligands are rare. They are anticipated to be limited to uranium, given the increasing stability of lower oxidation states for the later actinides. Most pentavalent organouranium complexes are supported by multiply bonded functional groups, such as those present in the complexes $(\eta^5\text{-}C_5H_4Me)_3U{=}NR$ previously described [see equation (25.22)]. The complex $[\eta^5\text{-}1,3\text{-}(Me_3Si)_2C_5H_3]_2UCl(THF)$ has been reported to react with Me_3SiN_3 to liberate N_2 and generate the U(v) organoimido complex $[\eta^5\text{-}1,3\text{-}(Me_3Si)_2C_5H_3]_2U(=NSiMe_3)(Cl)$ (Blake *et al.*, 1987). Oxo transfer has also been effected to a U(III) precursor; the complex $(\eta^5\text{-}C_5Me_5)U(OAr)(THF)$ (Ar = 2,6-^{i}Pr$_2$C$_6$H$_3$) reacts with pyridine *N*-oxide to yield the oxo derivative $(\eta\text{-}C_5Me_5)U(=O)(OAr)$ (Arney and Burns, 1993). The molecular structure of this complex has been determined. The complex exists as a typical pseudo-tetrahedral metallocene complex, with a U–O (oxo) bond length of 1.859(6) Å, slightly longer than that common for a mutliply-bonded oxo group in the uranyl ion (UO_2^{2+}).

Attempts to prepare U(VI) dioxo complexes supported by cyclopentadienyl groups has recently generated another rare example of a pentavalent oxo complex. Reaction of $(\eta^5\text{-}^t Bu_3C_5H_2)_2UCl_2$ with KC_8, followed by oxidation with pyridine N-oxide, results in the formation of the complex $(\eta^5\text{-}^t Bu_3C_5H_2)_4U_6O_{13}(bipy)_2$ (Duval *et al.*, 2001) (Fig. 25.18).

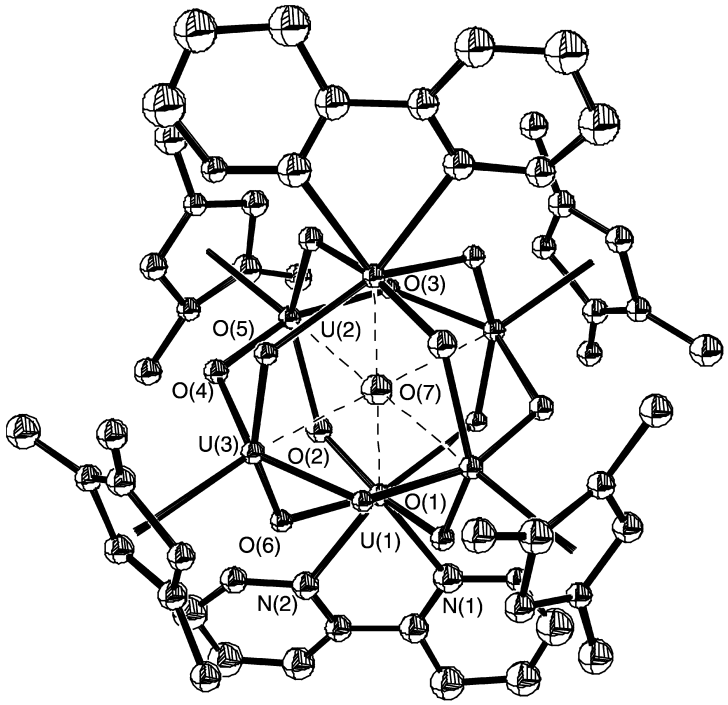

Fig. 25.18 *Crystal structure of* $(\eta^5\text{-}^t Bu_3C_5H_2)_4U_6O_{13}(bipy)_2$ (*methyl carbons of* tert-*butyl groups are omitted for clarity*) (*Duval* et al., 2001). (*Reprinted with permission from John Wiley & Sons, Inc.*)

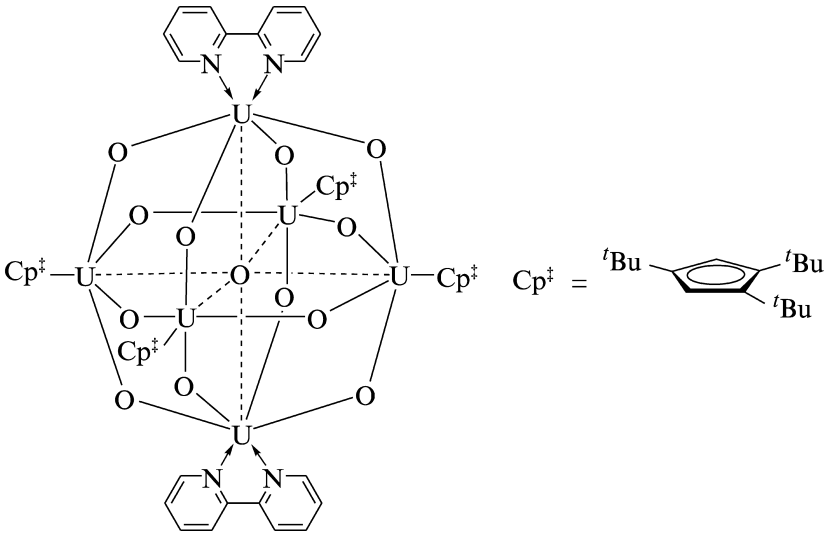

The core of the complex is a U_6O_{13} aggregate. Four uranium atoms in an equatorial plane are capped with a tri-*tert*-butylcyclopentadienyl ligand, while the two apical uranium atoms are ligated by 2,2′-bipyridine ligands, apparently derived from the by-product pyridine. The proposed mechanism for the formation of the aggregate is the generation and assembly of 'UO_2' and '$(\eta^5\text{-}^t Bu_3C_5H_2)_2UO_2$' fragments from homolytic ring loss. Although the central metal oxo unit is structurally similar to the Lindqvist class of polyoxometallate anions, there is no indication of electronic delocalization in the complex. Magnetic susceptibility measurements suggest that the uranium centers behave as independent U(v) f^1 paramagnets.

Another approach to U(v) organometallic complexes has recently been reported. Oxidation of neutral precursors $(\eta^5\text{-}C_5Me_5)U(NMe_2)_3(THF)$ and $(\eta^5\text{-}C_5Me_5)_2U(NEt_2)_2$ with $AgBPh_4$ gives rise to the corresponding cationic derivatives $[(\eta^5\text{-}C_5Me_5)U(NMe_2)_3(THF)][BPh_4]$ and $[(\eta^5\text{-}C_5Me_5)_2U(NEt_2)_2][BPh_4]$ (Boisson *et al.*, 1995). The electronic structure of these complexes was subsequently examined by EPR in frozen solution (Gourier *et al.*, 1997). It was shown that the interaction of the metal 5f orbitals with the cyclopentadienyl and amido ligands are sufficiently small and that the $J = 5/2$ ground state quantum number for U(v) remains a good quantum number for the complexes; the 5f orbitals are essentially nonbonding, and any covalent bonding interaction must therefore involve metal 6d orbitals.

(d) Hexavalent chemistry

Historically, there have been extremely few examples of non-aqueous compounds of hexavalent actinides, despite the prevalence of the actinyl ion (AnO_2^{2+}) for the elements U to Am. Attempts to prepare alkyl- or cyclopentadienyl compounds of the actinyl ions were met with reduction of the metal center (Seyam, 1982). In the last 10 years, a class of formally hexavalent cyclopentadienyluranium complexes has been prepared that is alternatively stabilized by the presence of organoimido substituents. The complex $(\eta^5\text{-}C_5Me_5)_2U(=NC_6H_5)_2$ was first prepared by the oxidation of $[Li(TMEDA)][(\eta^5\text{-}C_5Me_5)_2U(=NC_6H_5)Cl]$ with phenyl azide (Arney *et al.*, 1992; Arney and Burns, 1995), although other routes have since been devised (Fig. 25.19). The structure of the complex is shown in Fig. 25.20.

The complex has a pseudo-tetrahedral bent metallocene geometry, with a N–U–N angle of 98.7(4)°. This bent E=U=E moiety is quite different from the linear O=U=O angle found in the uranyl ion, and may be attributed to the strong donor character of the pentamethylcyclopentadienyl groups. The short uranium–nitrogen distances [1.952(7) Å], and the near-linear U–N–C bond angle [177.8(6)°] are consistent with the formulation of the ligands as organoimido groups. The organoimido ligands are remarkably unreactive in comparison with their Group 4 d-transition metal counterparts (Walsh *et al.*, 1988, 1992, 1993; Baranger *et al.*, 1993), showing no reaction with unsaturated

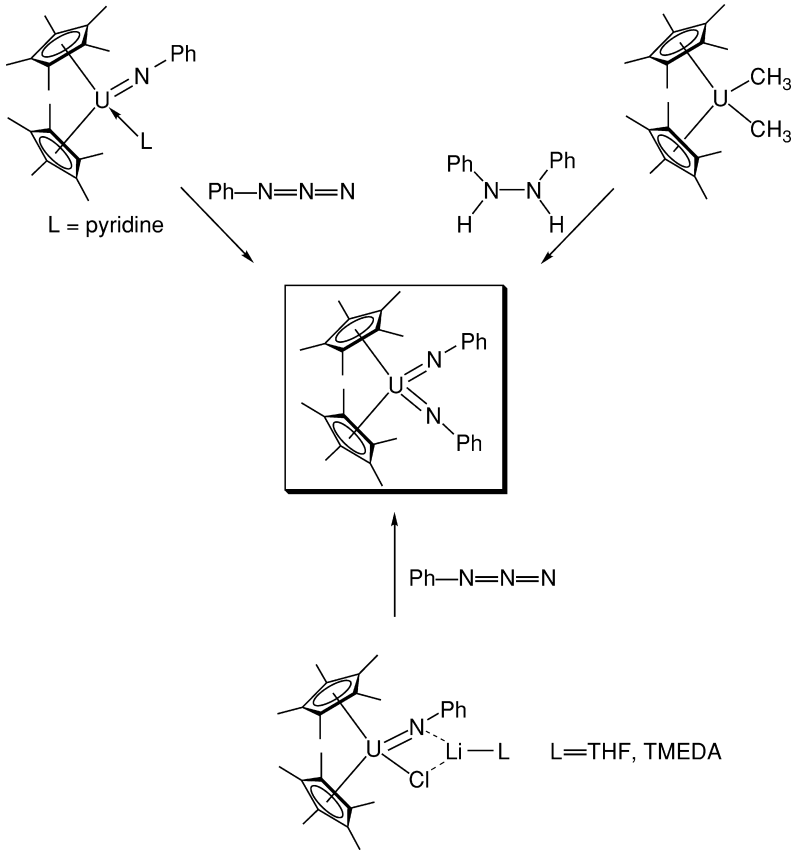

Fig. 25.19 *Synthetic pathways to* $(\eta^5\text{-}C_5Me_5)_2U(=NC_6H_5)_2$ (*Arney* et al., 1995).

substrates, MeI, or ammonia. This, coupled with the observation that the U–C_{ring} bond distances [2.72(1)–2.75(1) Å] are comparable with those found in typical U(IV) metallocenes, argues for some degree of covalency in the U–N bonding. In order to invoke a higher bond order, it is necessary to suggest the involvement of 5f orbitals in stabilizing the nitrogen 2p lone pair electrons, as there is no 6d orbital of the appropriate symmetry. The U(VI) character of the complex is demonstrated in the lack of observable metal-based electronic transitions (f–f, f–d) in the near-IR spectrum, as well as the observation in the ^{1}H NMR spectrum that the complex appears to act as a temperature-independent paramagnet (Arney *et al.*, 1992).

Since the initial report, other U(VI) bis(imido) compounds have been prepared with substituted arylimido and trimethylsilylimido ligands. In addition, U(VI) imido-oxo complexes $(\eta^5\text{-}C_5Me_5)_2U(=NAr)(=O)$ (Ar = 2,4,6-$Me_3C_6H_2$, 2,4,6-$^t Bu_3C_6H_2$, 2,6-$^i Pr_2C_6H_3$) have been synthesized (Arney and Burns, 1995). These complexes have similar geometries to the bis(imido)

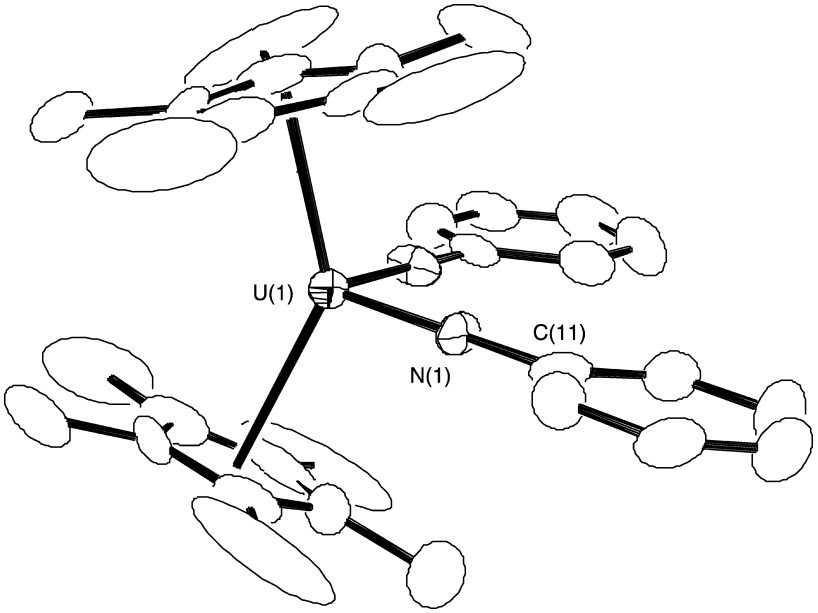

Fig. 25.20 *Crystal structure of* $(\eta^5\text{-}C_5Me_5)_2U(=NC_6H_5)_2$. (*Reprinted with permission from Arney* et al. (1992). *Copyright* 1992 *American Chemical Society*.)

derivatives, with a U–O bond length of 1.844(4) Å for the complex $(\eta^5\text{-}C_5Me_5)_2U(=N\text{-}2,6\text{-}{}^iPr_2C_6H_3)(=O)$. This bond length is significantly longer than that observed for uranyl ions, which may reflect a reduced bond order.

The ancillary ligand appears to make a difference in the accessibility of the U (VI) oxidation state. Complexes of uranium with the chelating ligand sets $[Me_2Si(\eta^5\text{-}C_5Me_4)_2]^{2-}$ and $[Me_2Si(\eta^5\text{-}C_5Me_4)(\eta^5\text{-}C_5H_4)]^{2-}$ have been prepared and employed in analogous reactions to prepare organoimido complexes (Schnabel *et al.*, 1999). While the bis(tetramethylcyclopentadienyl) *ansa*-metallocene successfully produces a bis(imido) compound, reaction of $[Me_2Si(\eta^5\text{-}C_5Me_4)(\eta^5\text{-}C_5H_4)]U(CH_2C_6H_5)_2$ with *N*,*N*′-diphenylhydrazine yields only the tetravalent bridging imido complex and $[\{Me_2Si(\eta^5\text{-}C_5Me_4)(\eta^5\text{-}C_5H_4)\}U(\mu\text{-}NPh)]_2$. Electrochemical investigations of the chloride compounds $[Me_2Si(\eta^5\text{-}C_5Me_4)_2]UCl_2 \cdot 2LiCl \cdot 4(Et_2O)$ and $[Me_2Si(\eta^5\text{-}C_5Me_4)(\eta^5\text{-}C_5H_4)]UCl_2 \cdot 2LiCl \cdot 4(THF)$ suggest that the ancillary ligands have the capacity to significantly alter the redox activity of the metal center; $[Me_2Si(\eta^5\text{-}C_5Me_4)(\eta^5\text{-}C_5H_4)]UCl_2 \cdot 2LiCl \cdot 4(THF)$ is more difficult to oxidize than $[Me_2Si(\eta^5\text{-}C_5Me_4)_2]UCl_2 \cdot 2LiCl \cdot 4(Et_2O)$ by ~ 0.24 V (vs $[Cp_2Fe]^{0/+}$). It has also been proposed that *ansa* bis(cyclopentadienyl) ligands sets generate more electrophilic metal centers (Lee *et al.*, 1998; Shin *et al.*, 1999).

As mentioned previously, the uranium imido complexes are generally unreactive, although a limited number of bond activation reactions have been

reported. The complex $(\eta^5\text{-}C_5Me_5)_2U(=NC_6H_5)_2$ will effect the homolytic cleavage of dihydrogen to yield a bis(amide) compound [equation (25.72)].

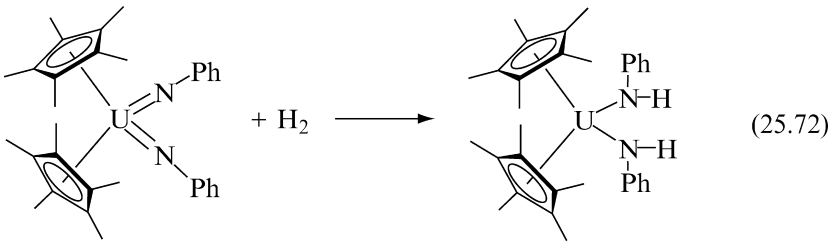

(25.72)

In an attempt to prepare more reactive organoimido functional groups, the more electron-rich adamantylimido complex $(\eta^5\text{-}C_5Me_5)_2U(=NAd)_2$ (Ad = Adamantyl) was prepared (Warner *et al.*, 1998). This complex undergoes decomposition under thermolysis to generate a complex derived from C–H activation of a pentamethylcyclopentadienyl methyl group (Peters *et al.*, 1999).

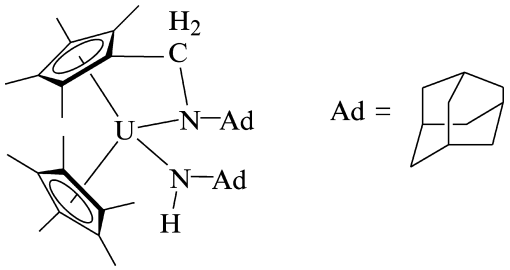

More reactive uranium–nitrogen multiple bonds may be generated by heteroatom substitution. The reaction of tetravalent $(\eta^5\text{-}C_5Me_5)_2U(=N\text{-}2,4,6\text{-}{}^tBu_3C_6H_2)$ with diphenyldiazomethane generates the mixed bis(imido) complex $(\eta^5\text{-}C_5Me_5)_2U(=N\text{-}2,4,6\text{-}{}^tBu_3C_6H_2)(=N\text{-}N{=}CPh_2)$, which undergoes a cyclometallation reaction upon mild thermolysis to generate a uranium(IV) bis(amide) complex that results from net addition of a C–H bond of an ortho *tert*-butyl group across the N=U=N core (Kiplinger *et al.*, 2002).

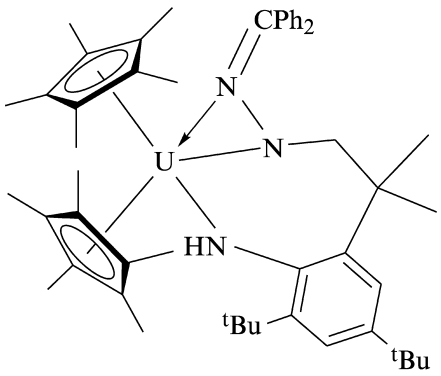

In select cases, U(VI) will catalyze chemical transformations; these will be discussed further in Chapter 26.

25.2.2 Cyclooctatetraenyl ligands

The chemistry of the cyclooctatetraenyl ligand and its substituted variants is significant in the development of actinide organometallic chemistry, and highlights differences between the f-elements and transition metals. The recognition that the lanthanides and actinides possess f-orbitals of the appropriate symmetry to interact with this carbocyclic ligand led to the theoretical prediction that a 'sandwich' compound could be prepared (Fischer, 1963). This prediction was subsequently validated by the preparation of $(\eta^8\text{-}C_8H_8)_2U$ (or 'uranocene') by the reaction of UCl_4 and the potassium salt of the dianion of cyclooctatetraene, $K_2(C_8H_8)$ [equation (25.73)] (Streitwieser and Müller-Westerhoff, 1968). Since that time, other synthetic routes to bis(cyclooctatetraenyl) complexes of the actinides have appeared [equations (25.74) and (25.75)] (Starks and Streitwieser, 1973; Starks *et al.*, 1974; Chang *et al.*, 1979; Rieke and Rhyne, 1979):

$$UCl_4 + 2K_2(C_8H_8) \xrightarrow{\text{THF}} (\eta^8\text{-}C_8H_8)_2U + 4KCl \qquad (25.73)$$

$$U\ (\text{powder}) + 2C_8H_{10} \xrightarrow{\text{Hg(cat.)}} (\eta^8\text{-}C_8H_8)_2U + 2H_2 \qquad (25.74)$$

$$UF_4 + 2Mg(C_8H_8) \longrightarrow (\eta^8\text{-}C_8H_8)_2U + 2MgF_2 \qquad (25.75)$$

Bis(cyclooctatetraenyl) complexes of a number of other actinide elements have also been prepared, including Th (Streitwieser and Yoshida, 1969; Goffart *et al.*, 1972; Starks and Streitwieser, 1973), Pa (Goffart *et al.*, 1974; Starks *et al.*, 1974), Np (Karraker *et al.*, 1970), and Pu (Karraker *et al.*, 1970). Most are prepared by the methods of equations (25.73) and (25.74), although the plutonium compound was prepared from Cs_2PuCl_6.

A large number of substituted (cyclooctatetraenyl) complexes have also been reported. The addition of substituents has been employed to improve solubility, alter electronic properties, or investigate the dynamics of ring rotation reactions. The largest class of these are the 1,1′-disubstituted derivatives (Harmon *et al.*, 1977; Spiegl, 1978; Miller and DeKock, 1979; Spiegl and Fischer, 1979) prepared by the method of equation (25.76):

$$UCl_4 + 2K_2(C_8H_7R) \longrightarrow (\eta^8\text{-}C_8H_7R)_2U + 4KCl \qquad (25.76)$$

R = Me, Et, *n*-Bu, cyclo-C_3H_5, $CH{=}CH_2$, C_6H_5, OMe, OEt, O^{t}Bu, CO_2Et, *p*-C_6H_4R, NR_2, *p*-$C_6H_4NMe_2$, PR_2, $SiMe_3$, $SnMe_3$

1,1′-Disubstituted derivatives (R = Et, *n*-Bu) of neptunium and plutonium have also been prepared (Karraker, 1973). A number of uranocene derivatives with higher degrees of substitution have been reported (Streitwieser *et al.*, 1971;

Streitwieser and Harmon 1973; Streitwieser and Walker, 1975; Solar *et al.*, 1980; LeVanda and Streitwieser, 1981; Miller *et al.*, 1981; Lyttle *et al.*, 1989), including several with exocyclic ligands (Luke *et al.*, 1981; Zalkin *et al.*, 1982; Streitwieser *et al.*, 1983). The silylated derivatives $[\eta^5\text{-}1,3,5\text{-}(SiMe_3)_3C_8H_5]_2An$ have been prepared for An = Th, U, and Np (Apostolidis *et al.*, 1999). There is also one example of a bridged, or linked uranocene, [η^8:η^8-1,2-bis(cyclooctatetraenyldimethylsilyl)ethane]uranium (Streitwieser *et al.*, 1993).

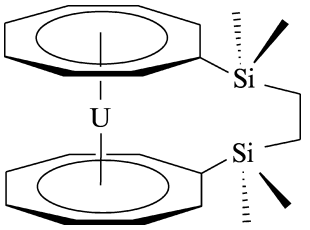

The molecular structure of many uranocene derivatives have been determined; the molecular structure of $(\eta^8\text{-}C_8H_8)_2U$ is shown in Fig. 25.21 (Zalkin and Raymond, 1969, Avdeef *et al.*, 1972).

The molecule possesses rigorous D_{8h} symmetry, with the eight-membered rings arranged in an eclipsed conformation. The averaged $U\text{–}C_{ring}$ bond distance is 2.647(4) Å; all atoms of the cyclooctatetraene ligand lie within the plane

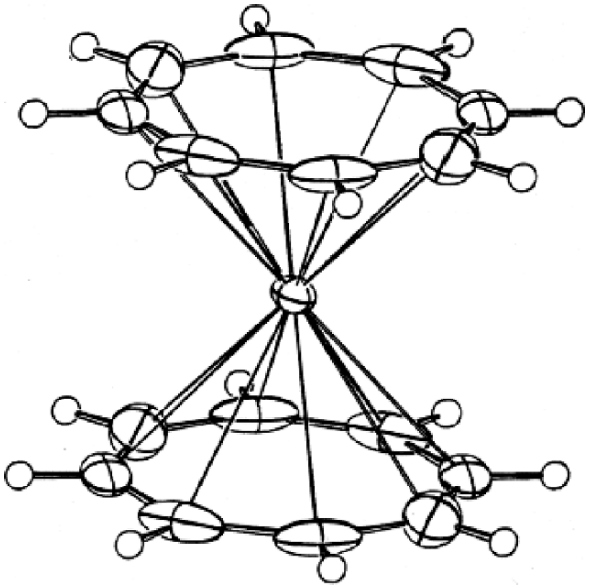

Fig. 25.21 *Crystal structure of* $(\eta^8\text{-}C_8H_8)_2U$. (*Reprinted with permission from Zalkin and Raymond* (1969). *Copyright* 1969 *American Chemical Society.*)

to 0.02 Å. A comparison of the average C–C bond lengths for alternate sets of four bonds within the rings [1.396(5) and 1.388(27) Å] confirms the aromatic nature of the ligand. Substituted uranocene derivatives can show staggered ring geometries in the solid state; the rings in the complex bis(η^8-1,3,5,7-tetraphenylcyclooctatetraene)uranium are eclipsed (Templeton *et al.*, 1976), while the structure of bis(η^8-1,3,5,7-tetramethylcycloctatetraene)uranium reveals two symmetry-independent molecules in the asymmetric unit: one with staggered rings and one in which the rings are nearly eclipsed (Hodgson and Raymond, 1973).

The bonding in these highly symmetric compounds has been studied extensively by theoretical and experimental methods. The first theoretical treatments assumed that the principal metal–ligand interactions occurred through 5f orbitals, and that 6d orbitals would be too high in energy to interact with ligand-based orbitals. Improvement in computation methods (such as the inclusion of spin–orbit coupling) and inclusion of relativistic corrections have amended this bonding description. An *ab initio* calculation on uranocene incorporating relativistic core potentials and spin–orbit CI calculations suggests a significant degree of covalency in metal–ligand bonding; the 6d orbitals play a primary role in these interactions, and the 5f orbital involvement is secondary (Chang and Pitzer, 1989). A qualitative molecular orbital diagram is shown in Fig. 25.22.

The principal bonding interaction involves the metal 6dδ and ligand $3e_{2g}$ orbitals, as well as the metal 5fδ and ligand $3e_{2u}$ combination. Minimal interaction also exists between the metal 5fϕ orbitals and the ligand-based e_{3u} orbitals. The dashed line in the figure shows the impact of including relativistic effects in the calculations, further stabilizing a d_{z^2} orbital, making it the lowest unoccupied molecular orbital, housing any unpaired metal electrons (the orbital is essentially metal–ligand nonbonding).

Experimental probes of bonding in actinocenes have included chemical reactivity, magnetism, NMR spectroscopy, optical spectroscopy, Np-237 Mössbauer spectroscopy, and photoelectron spectroscopy (PES) (Burns and Bursten, 1989, and references therein). The initial observation of the stability of (η^8-$C_8H_8)_2U$ to hydrolysis (relative to (η^8-$C_8H_8)_2Th$) suggested a higher degree of covalency in bonding in the uranium complex. Attempts have been made to derive the magnetic moment for bis(cyclooctatetraene) complexes of U, Np, and Pu. For example, (η^8-^{t}Bu$C_8H_7)_2Pu$ is reported to have a $J = 0$ ground state and exhibits temperature-independent paramagnetism (Karraker, 1973). The first predictions of the magnetism were based on the assumption of ionic bonding (weak crystal-field perturbations) and simple *L–S* coupling models (Karraker *et al.*, 1970). Deviations of the calculated moments from the observed were corrected by application of an empirical 'orbital reduction factor' described as a measure of covalency in bonding. Later non-relativistic calculations provided a better fit to experimentally observed magnetic moments between 10 and 80 K (Hayes and Edelstein, 1972). These calculations suggested a significant degree of covalency, but it was pointed out that the high value assumed for the

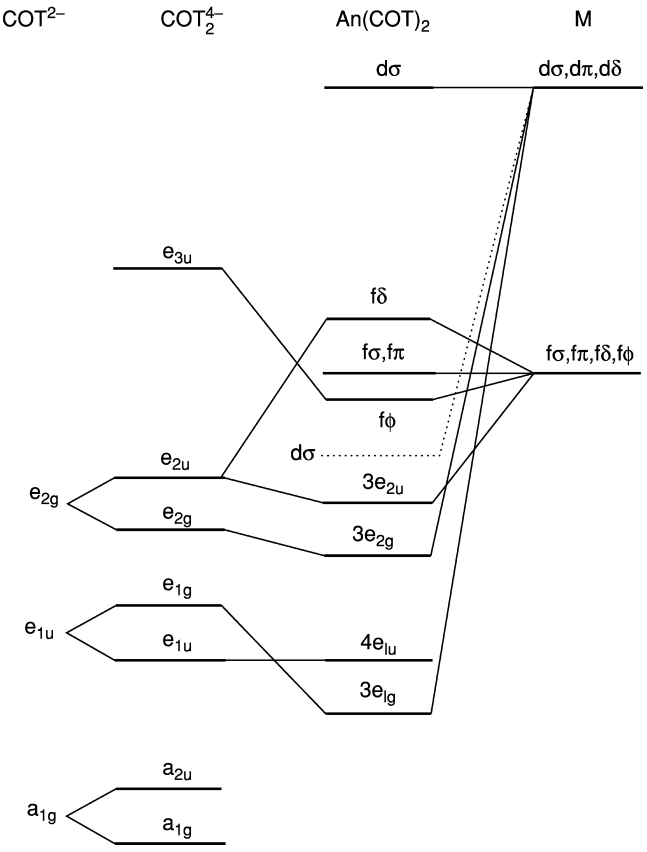

Fig. 25.22 *Molecular orbital diagram of* $(\eta^8\text{-}C_8H_8)_2U$. (*Reprinted with permission from Parry* et al. (1999). *Copyright* 1999 *American Chemical Society*.)

5f valence state ionization potential could cause an overestimation of the covalence in bonding.

Some of the most compelling evidence for the degree of covalency in uranocene (and particularly for a 5f orbital role) comes from variable energy photoelectron spectroscopy (Brennan *et al.*, 1989). In general, metal-based electrons are known to have an energy-dependent cross section. In $(\eta^8\text{-}C_8H_8)_2U$ (over the energy range 24–125 eV), the f-band shows cross-section features attributable to 5f resonant photoemission in the vicinity of the 5d–5f giant resonant absorption ($h\nu = 101$ and 110 eV). The e_{2g} and e_{2u} bands also show small cross-section maxima at these energies; that for the e_{2u} ionization being the more intense. The mapping of the intensity changes of the f-band by the e_{2u} band provides strong evidence for f-orbital contribution to valence orbitals in this molecule (Fig. 25.23).

Ring dynamics (rotation and exchange) have been studied by means of variable-temperature NMR spectroscopy for substituted derivatives. It is

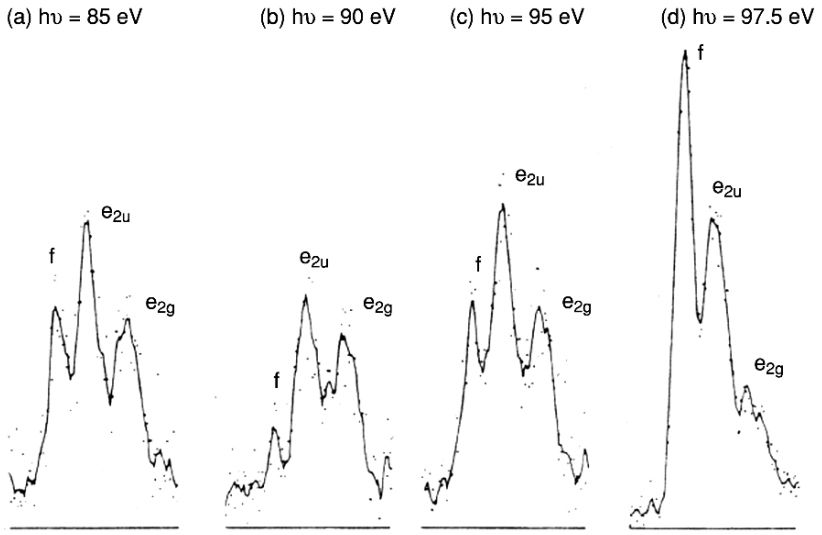

Fig. 25.23 *Variable energy photoelectron spectrum of* $(\eta^5\text{-}C_8H_8)_2U$. (*Reprinted with permission from Brennan* et al. (1989). *Copyright* 1989 *American Chemical Society*).

found that uranocenes undergo rapid ligand exchange with cyclooctatetraene dianions (LeVanda and Streitwieser, 1981). The barrier to ring rotation has been estimated at 8.3 kcal mol^{-1} for $(\eta^8\text{-}1,4\text{-}{}^t Bu_2C_8H_6)_2U$; this compares with a value of 13.1 kcal mol^{-1} for a d-transition metal metallocene analog $(\eta^5\text{-}1,3\text{-}{}^t Bu_2C_5H_3)_2Fe$ (Luke and Streitwieser, 1981).

In addition to the neutral tetravalent actinocenes, synthetic routes have been devised to anionic trivalent derivatives, $[(\eta^8\text{-}C_8H_8)_2An]^-$, either by treatment of trivalent precursors with $K_2(C_8H_8)$ [equation (25.77)], or by reduction of the actinocene [equation (25.78)] (Karraker and Stone, 1974; Billiau *et al.*, 1981; Eisenberg *et al.*, 1990).

$$\begin{aligned} &AnI_3 + 2K_2(C_8H_8) \xrightarrow{\text{THF}} K[(\eta^8\text{-}C_8H_8)_2An] \cdot 2THF \\ &An = Np, Pu \end{aligned} \tag{25.77}$$

$$\begin{aligned} &(\eta^8\text{-}C_8H_8)_2An + K/\text{Naphthalene} \longrightarrow K[(\eta^8\text{-}C_8H_8)_2An] \\ &An = U,\ Np,\ Pu \end{aligned} \tag{25.78}$$

The Mössbauer spectrum of the neptunium compound $[(\eta^8\text{-}C_8H_8)_2Np]^-$ confirms that the metal is in the trivalent oxidation state, and suggests a lower overall degree of covalency in metal–ligand bonding than in tetravalent derivatives. Most recently, the reduction route has been extended to generate trivalent actinocenes $K(DME)_2[\{\eta^8\text{-}1,4\text{-}({}^t BuMe_2Si)_2C_8H_6\}_2An]$ (An = Th, U), wherein the bulky silyl substituents are proposed to provide both kinetic and

thermodynamic stabilization of the Th(III) compound (Parry *et al.*, 1999). The complexes display asymmetric An–C_{ring} distances, owing to the 'capping' of one ring by close association with the potassium counter-ion. The observed magnetic moment for the thorium compound is $1.20\mu_B$ at 293 K, which is low when compared to the spin-only value for one unpaired electron ($1.73\mu_B$). It has been proposed that the low moment is due to mixing of the ground state magnetic component with low-lying excited states.

Intermolecular electron-transfer rates have been studied for uranocene and substituted derivatives of uranium, neptunium, and plutonium (Eisenberg *et al.*, 1990) by examining the variable-temperature NMR spectra of mixtures of $(\eta^8\text{-}C_8H_8)_2An$ and $[(\eta^8\text{-}C_8H_8)_2An]^-$. In all cases, electron transfer rates are rapid. Specific rates could not be derived for uranium and plutonium derivatives due to the small chemical shift differences between analogous An(IV) and An(III) compounds, but in the case of $(\eta^8\text{-}^tBuC_8H_7)_2Np$, the rate has been estimated to be of the same order of magnitude as comparable lanthanide cyclooctatetraene compounds ($\sim 10^7$ $M^{-1}s^{-1}$).

The chemistry of actinide complexes containing a single cyclooctatetraenyl ring began with a report of $(\eta^8\text{-}C_8H_8)NpI\cdot xTHF$, prepared by reaction of $NpI_3(THF)_4$ and $K_2(C_8H_8)$ in THF (Karraker and Stone, 1977). The first structurally characterized examples of this class of compounds included both derivatives of uranium [$(\eta^8\text{-}C_8H_8)UCl_2(pyridine)_2$ and $(\eta^8\text{-}C_8H_8)U(MeCOCHCOMe)_2$; Boussie *et al.*, 1990] and thorium [$(\eta^8\text{-}C_8H_8)ThCl_2(THF)_2$; Zalkin *et al.*, 1980]. Since these initial reports, other entries into mono-ring chemistry have been established, principally those involving redistribution [equations (25.79) and (25.80)] (LeVanda *et al.*, 1980; Gilbert *et al.*, 1988; Baudry *et al.*, 1990a), halogenation [equation (25.81)] (Berthet *et al.*, 1990), and metathesis [equations (25.82) and (25.83)] (Boisson *et al.*, 1996a).

$$\tfrac{1}{2}(\eta^8\text{-}C_8H_8)_2Th + ThCl_4 \longrightarrow (\eta^8\text{-}C_8H_8)ThCl_2 \qquad (25.79)$$

$$\tfrac{1}{2}(\eta^8\text{-}C_8H_8)_2U + \tfrac{1}{2}U(BH_4)_4 \longrightarrow (\eta^8\text{-}C_8H_8)U(BH_4)_2 \xrightarrow{L} (\eta^8\text{-}C_8H_8)U(BH_4)_2(L) \qquad L = THF,\ Ph_3P{=}O \qquad (25.80)$$

$$(\eta^8\text{-}C_8H_8)_2U + I_2 \xrightarrow{THF} (\eta^8\text{-}C_8H_8)UI_2(THF)_2 \qquad (25.81)$$

$$(NEt_2)_2UCl_2 + K_2(C_8H_8) \xrightarrow{THF} (\eta^8\text{-}C_8H_8)U(NEt_2)_2(THF) + 2KCl \qquad (25.82)$$

$$(\eta^8\text{-}C_8H_8)_2U + 3LiNEt_2 \longrightarrow Li[(\eta^8\text{-}C_8H_8)U(NEt_2)_3] \qquad (25.83)$$

Collectively, these complexes further serve as precursors to a variety of mono (cyclooctatetraenyl) derivatives, including alkyl (Berthet *et al.*, 1994), alkoxide (Arliguie *et al.*, 1992), amide (Gilbert *et al.*, 1988; Le Borgne *et al.*, 2000), and

thiolate (Leverd *et al.*, 1994; Arliguie *et al.*, 2000) complexes. Mixed-ring derivatives containing both cyclooctatetraenyl and cyclopentadienyl ligands have similarly been prepared by metathesis reactions (Gilbert *et al.*, 1989; Berthet *et al.*, 1994, Boisson *et al.*, 1996b). The complex $(\eta^8\text{-}C_8H_8)(\eta^5\text{-}C_5Me_5)Th[CH(SiMe_3)_2]$ undergoes hydrogenolysis to yield the hydride compound $(\eta^8\text{-}C_8H_8)(\eta^5\text{-}C_5Me_5)ThH$ (Gilbert *et al.*, 1989).

An interesting example of the introduction of a bridging cyclooctatetraenyl ligand is found in the reaction of $(\eta^5\text{-}C_5Me_5)_3U$ with cyclooctatetraene (Evans *et al.*, 2000). As previously discussed, the bulky tris(pentamethylcyclopentadienyl) complex can act as a multi-electron reductant. Reaction with C_8H_8 produces the complex $[(\eta^8\text{-}C_8H_8)(\eta^5\text{-}C_5Me_5)U]_2(\mu\text{-}C_8H_8)$, along with $(C_5Me_5)_2$. The complex consists of two mixed-ring U(IV) units coordinated to a bridging $C_8H_8^{2-}$ ligand (Fig. 25.24). The bridging ring is non-planar and appears bound to the two metal centers in an unusual $\eta^3{:}\eta^3$ manner, with one carbon in common.

Cationic derivatives of the formula $[(\eta^8\text{-}C_8H_8)U(NEt_2)(THF)_2][BPh_4]$ and $[(\eta^8\text{-}C_8H_8)U(BH_4)(THF)_2][BPh_4]$ may be produced by protonation of the respective tetravalent precursors $(\eta^8\text{-}C_8H_8)UX_2(THF)$ with $[NEt_3H][BPh_4]$ (Boisson *et al.*, 1996b; Cendrowski-Guillaume *et al.*, 2000). Reaction of the latter with additional ammonium salt in the presence of hexamethylphosphoramide (HMPA) yields the unique dicationic species $[(\eta^8\text{-}C_8H_8)U(HMPA)_3][BPh_4]_2$. The U–N bond in the complex $[(\eta^8\text{-}C_8H_8)U(NEt_2)(THF)_2][BPh_4]$ is susceptible to protonation by alcohols and thiols, and will insert CO_2, CS_2, or MeCN to generate the complexes $[(\eta^8\text{-}C_8H_8)U(E_2CNEt_2)(THF)_2][BPh_4]$ (E = O, S) and $[(\eta^8\text{-}C_8H_8)U(NC(Me)NEt_2)(THF)_2][BPh_4]$.

Few trivalent derivatives of mono(cyclooctatetraenyl)uranium have been isolated, likely due to the facile ligand redistribution and disproportionation

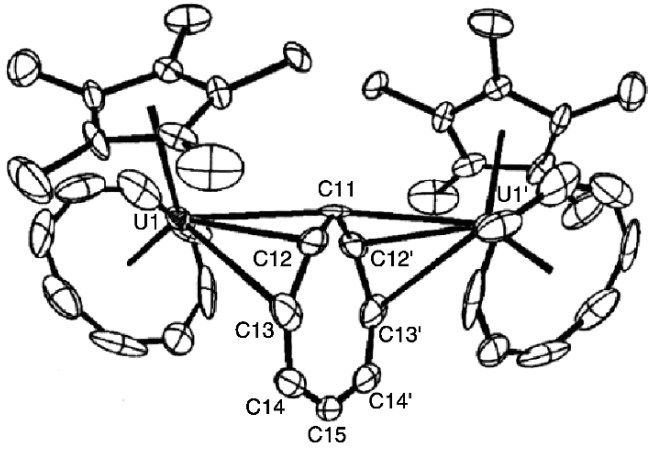

Fig. 25.24 *Crystal structure of* $[(\eta^8\text{-}C_8H_8)(\eta^5\text{-}C_5Me_5)U]_2(\mu\text{-}C_8H_8)$ (*Evans* et al., 2000). (*Reprinted with permission from John Wiley & Sons, Inc.*)

reactions that give rise to uranocene. The complex $(\eta^8\text{-}C_8H_8)(\eta^5\text{-}C_5Me_5)U(THF)$ is produced by reaction of $(\eta^5\text{-}C_5Me_5)UI_2(THF)$ with $K_2(C_8H_8)$ (Schake *et al.*, 1993); the 4,4′-dimethyl-2,2′-bipyridine adduct has been structurally characterized. The complex exists as a bent metallocene with a ring centroid–uranium–ring centroid angle of 138.2°. The average $M\text{–}C_{ring}$ distances are consistent with the larger ionic radius of U(III). The aforementioned dication $[(\eta^8\text{-}C_8H_8)U(HMPA)_3][BPh_4]_2$ can be reduced by sodium amalgam to generate a monocation $[(\eta^8\text{-}C_8H_8)U(HMPA)_3][BPh_4]$ (Cendrowski-Guillaume *et al.*, 2001).

An interesting new class of pentavalent complexes supported by the cyclooctatetraenyl ligand has recently been developed. Oxidation of anionic U(IV) mono-ring amide complexes with $TlBPh_4$ or $AgBPh_4$ generates the corresponding pentavalent amide complexes as shown in equations (25.84) and (25.85) (Berthet and Ephritikhine, 1993; Boisson *et al.*, 1995).

$$[(\eta^8\text{-}C_8H_8)U(NEt_2)_3]^- + TlBPh_4 \longrightarrow (\eta^8\text{-}C_8H_8)U(NEt_2)_3 \qquad (25.84)$$

$$(\eta^8\text{-}C_8H_8)U(NEt_2)_2(THF) + AgBPh_4 \longrightarrow [(\eta^8\text{-}C_8H_8)U(NEt_2)_2(THF)][BPh_4] \qquad (25.85)$$

The molecular structure of $[(\eta^8\text{-}C_8H_8)U(NEt_2)_2(THF)][BPh_4]$ has been determined (Boisson *et al.*, 1996a). The amide ligands are susceptible to protonation by alcohols to yield alkoxide complexes. Pentavalent cyclooctatetraenyluranium compounds have been studied by EPR (Gourier *et al.*, 1997) and X-ray absorption spectroscopy (Den Auwer *et al.*, 1997). Analysis of EPR spectra suggested that (as for cyclopentadienyl ligands) chemical bonding with the cyclooctatetraenyl ligand occurs principally with the uranium 6d orbitals, except in the case of the tris(*iso*-propoxide) complex $(\eta^8\text{-}C_8H_8)U(O^iPr)_3$. In this complex, it was proposed that the 5f–O interaction is strong, so that J is no longer a good quantum number, and the weak-field approximation can no longer be considered valid.

25.2.3 Other carbocyclic ligands

(a) Arene ligands

Although arene compounds of the d-transition metals were prepared early in the 20th century, their identity as η^6-ligands was not recognized until many years later. All previous carbocyclic ligands discussed in this article may be regarded to have a formal charge (e.g. $C_5H_5^-$, $C_8H_8^{2-}$), and so therefore may bind more strongly to actinide centers via Coulombic forces. In contrast, arenes are often regarded as neutral ligands, and so any interaction with a metal center might best be regarded as one involving significant electrostatic polarization of the ligand π-electrons, or alternatively, covalent bonding. Given the propensity of the later actinides to engage principally in ionic bonding, it is therefore not

surprising that arene complexes are restricted to the early actinides. Only uranium has been found to generate arene complexes. This suggests a greater propensity for uranium to engage in covalent bonding, consistent with the observation that U–C bonding in uranocene appears to be more covalent than in its thorium analog.

The initial method employed to prepare π-arene complexes of d-transition metals was the reducing Friedel–Crafts route developed by Fischer and Hafner (1955), involving reduction of a metal salt with aluminum powder, followed by reaction with an arene ligand. Extension of this method to reaction with UCl_4 produced the first π-arene complex, the trivalent species $(\eta^6\text{-}C_6H_6)U(AlCl_4)_3$ (Cesari *et al.*, 1971). The molecular structure of the complex consists of a pseudotetrahedral arrangement of the four ligands about uranium, with two bridging chlorides between each aluminum and uranium. The benzene ring was refined as an idealized model, with uranium–carbon distances of 2.91–2.92 Å. Toluene and hexamethylbenzene analogs have also been described (Cotton and Schwotzer, 1987; Garbar *et al.*, 1996). Subsequently, two polymetallic tetravalent complexes were prepared by a variant of this procedure as depicted in equation (25.86) (Cotton and Schwotzer, 1985; Campbell *et al.*, 1986):

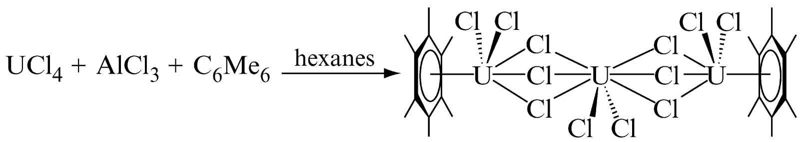

(25.86)

The complex $[(\eta^6\text{-}C_6Me_6)Cl_2U(\mu\text{-}Cl)_3UCl_2(\eta^6\text{-}C_6Me_6)][AlCl_4]$ was isolated by further reduction with zinc powder. Once isolated, the compounds are insoluble in non-coordinating solvents. The cation of the molecule $[(\eta^6\text{-}C_6Me_6)Cl_2U(\mu\text{-}Cl)_3UCl_2(\eta^6\text{-}C_6Me_6)][AlCl_4]$ is shown in Fig. 25.25.

The arene ligands in these complexes are all found to be weakly bound, and are readily displaced by other bases such as THF or acetonitrile. Detailed structural studies have been conducted on these arene complexes. In no case does the arene ring appear to significantly deviate from planarity. The $U\text{–}C_{arene}$ bond distances in these complexes are long for actinide–carbocyclic ligands; they fall in the range 2.89(2)–2.96(2) Å.

η^6-Arene complexes of trivalent uranium have also been isolated from the thermolysis of $U(BH_4)_4$ in aromatic solvents (Baudry *et al.*, 1989a). The mesitylene complex $(\eta^6\text{-mesitylene})U(BH_4)_3$ was initially isolated from that solvent. The weakly coordinated arene is readily displaced by other aromatic substrates, however, and the hexamethylbenzene complex is reported to be more stable to displacement in toluene solution.

More recently, reduction of tetravalent actinide amide complexes has been found to give rise to an interesting series of 'inverted sandwich', or bridging arene complexes (Diaconescu *et al.*, 2000; Diaconescu and Cummins, 2002). Reduction of $[N(^tBu)Ar]_3UI$ ($Ar = 3,5\text{-}Me_2C_6H_3$) by KC_8 in toluene generates the complex $[N(^tBu)Ar]_2U(\mu\text{-}\eta^6,\eta^6\text{-}C_7H_8)U[N(^tBu)Ar]_2$. The related compound

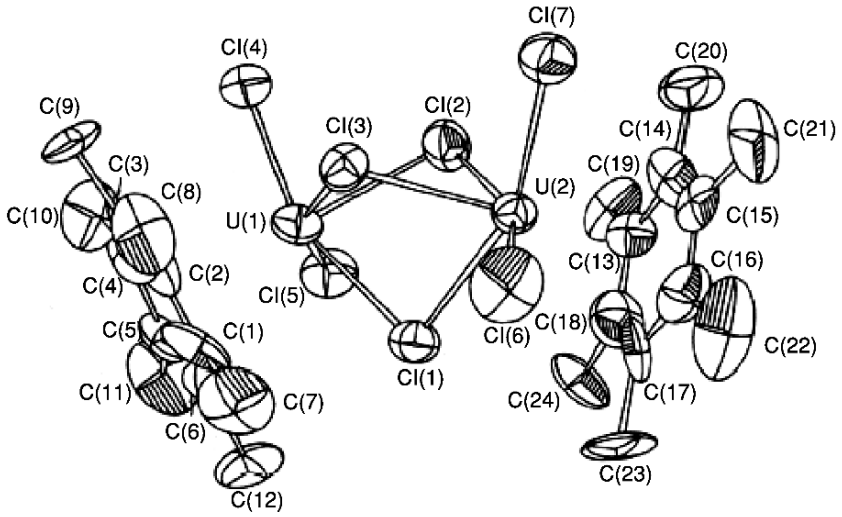

Fig. 25.25 *Molecular structure of* $[(\eta^6\text{-}C_6Me_6)Cl_2U(\mu\text{-}Cl)_3UCl_2(\eta^6\text{-}C_6Me_6)]^+$. (*Reprinted with permission from Campbell* et al. (1986). *Copyright* 1986 *American Chemical Society*.)

$[N(R)Ar]_2U(\mu\text{-}\eta^6,\eta^6\text{-}C_7H_8)U[N(R)Ar]_2$ (R = adamantyl; Ar = 3,5-$Me_2C_6H_3$), could also be generated in low yield by reaction of $UI_3(THF)_4$ with $(Et_2O)LiN(R)Ar$ in toluene. Structural characterization reveals that the complex contains a bridging toluene molecule bound symmetrically to the two metal centers (Fig. 25.26).

The U–C_{ring} distances are short relative to other η^6-arene complexes, ranging from 2.503(9) to 2.660(8) Å. In addition, there is a slight distortion in the bound toluene ligand; the average C–C distances increase by approximately 0.04 Å from that in free toluene. Density functional calculations carried out on the molecule suggest that four electrons are engaged in the formation of two δ-symmetry back-bonds involving U 6d and 5f orbitals and the LUMO of the bridging arene molecule. The complex acts as a 'uranium(II)' reagents in subsequent reactions, and can effect four-electron reduction of substrates.

(b) Other carbocyclic ligands (cycloheptatrienyl, pentalene, endohedral metallofullerenes)

Complexes of actinides with five-, six-, and eight-membered rings have already been described. It is only recently that this series has been completed with the preparation of complexes employing the cycloheptatrienyl ligand. Unlike the other members of this series, the first complex to be prepared was not the sandwich complex, but rather the 'inverse sandwich' compound $[X_3U(\mu\text{-}\eta^7,\eta^7\text{-}C_7H_7)UX_3]^-$ (X = NEt_2, BH_4), formed in the reaction of $U(NEt_2)_4$ or

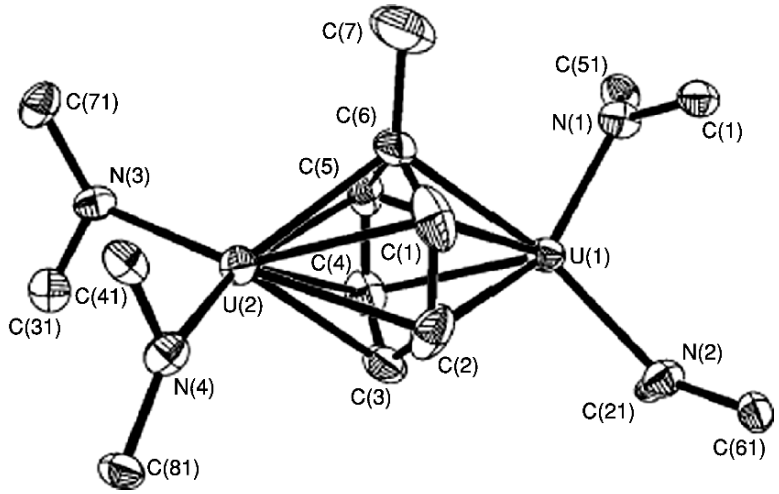

Fig. 25.26 *Molecular structure of* $[N(R)Ar]_2U(\mu\text{-}\eta^6,\eta^6\text{-}C_7H_8)U[N(R)Ar]_2$ (R = *adamantyl, Ar* = 3,5-$Me_2C_6H_3$). *Bulky peripheral substituents omitted for clarity*. (*Reprinted with permission from Diaconescu* et al. (2000). *Copyright* 2000 *American Chemical Society*.)

$U(BH_4)_4$ with $K(C_7H_9)$ (Arliguie *et al.*, 1994). The sandwich complex [K(18-crown-6)][$(\eta^7\text{-}C_7H_7)_2U$] has subsequently been prepared [equations (25.87) and (25.88)] (Arliguie *et al.*, 1995).

$$UCl_4 + K + \text{xs} \quad \xrightarrow[\text{18-crown-6}]{\text{THF}} \quad [K(18\text{-crown-6})][(\eta^7\text{-}C_7H_7)_7U] \tag{25.87}$$

$$UCl_4 + 4K(C_7H_7) \xrightarrow[18-\text{crown}-6]{\text{THF}} [K(18\text{-crown-6})][(\eta^7\text{-}C_7H_7)_2U] \tag{25.88}$$

The molecular structure of the anion $[(\eta^7\text{-}C_7H_7)_2U]^-$ is shown in Fig. 25.27.

The complex consists of a sandwich of crystallographic C_{2h} symmetry. The cycloheptatrienyl ligands are planar to within 0.02 Å, and display a regular heptagonal geometry. The two rings are staggered. The uranium–carbon bond distances average 2.53(2) Å, significantly shorter than those found for typical tetravalent uranium cyclopentadienyl and cyclooctatetraenyl complexes. Similar bond shortening has been observed in M–C bonds in early transition metal cycloheptatrienyl complexes, and has been explained as reflecting electron transfer from the metal to the ligand, with an increase in metal valency. Some attention has therefore been given to the assignment of oxidation state in this complex. A density functional study examined the question of bonding in the complexes $(\eta^7\text{-}C_7H_7)_2An$ (Li and Bursten, 1997). It was found that the 5f δ-symmetry orbitals not only participate in the bonding with e_2'' pπ orbitals of the C_7H_7 rings, but are as important as the

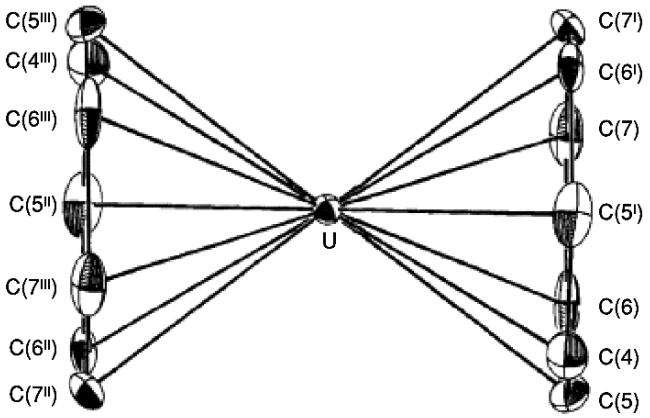

Fig. 25.27 *Molecular structure of* $[(\eta^7\text{-}C_7H_7)_2U]^-$ (*Arliguie* et al., 1995). (*Reproduced by permission of The Royal Society of Chemistry*.)

symmetry-appropriate 6d orbitals in stabilizing the ligand-based fragment orbitals. The 5f percentage in frontier e_2 molecular orbitals increases across the series, although not the energetic stabilization. The most important bonding interactions are shown in Fig. 25.28.

Although only one valence electron resides in a principally 5f localized orbital in the known uranium complex, a formal oxidation state of +3 ($5f^3$) was assigned to uranium, based on the fact that the $3e_2''$ molecular orbitals (occupied by four electrons) are nearly 50% 5f in character, and so two of these electrons were assigned to the metal. EPR and ENDOR studies of $[(\eta^7\text{-}C_7H_7)_2U]^-$ suggest that the complex could be treated as $5f^1$, with a ground state molecular orbital comprised of both $5f_\pi$ and $5f_\sigma$ orbitals (Gourier *et al*., 1998).

Although the cyclooctatetraenyl dianion has been extensively employed in actinide organometallic chemistry, another C8 ligand, the pentalene dianion ($C_8H_6^{2-}$) has been far less studied, due to the difficulty inherent in its preparation. The ligand may be considered to be derived from $C_8H_8^{2-}$ by removal of two hydrogen atoms with generation of a C–C bond to yield two fused five-membered rings.

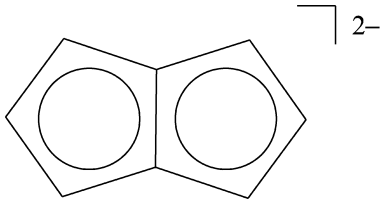

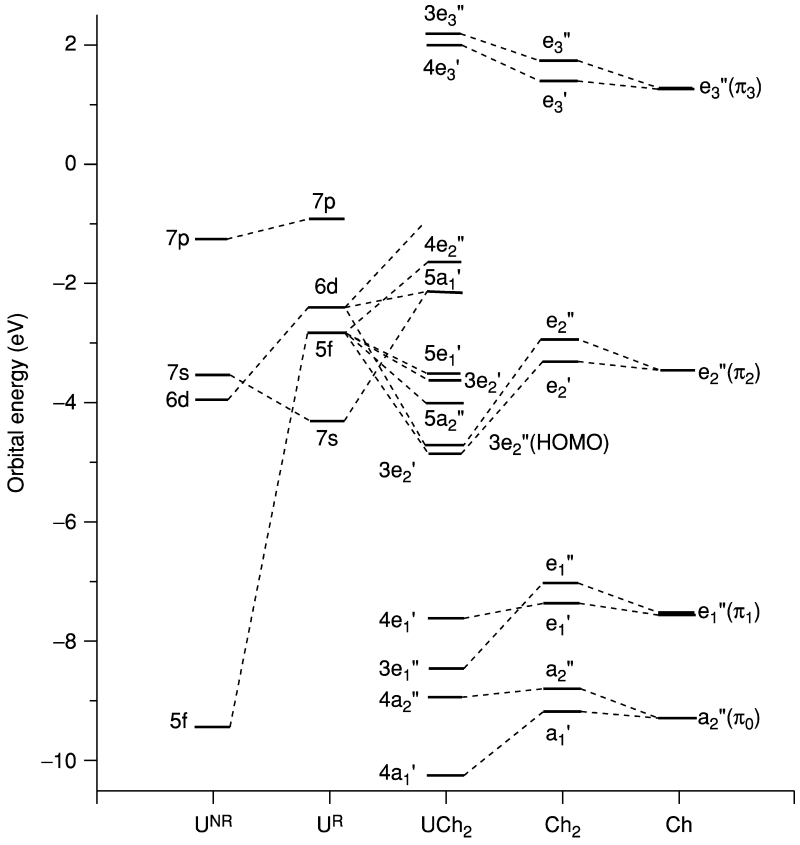

Fig. 25.28 *Bonding interactions in* $[(\eta^7\text{-}C_7H_7)_2U]^-$ *under* D_{7h} *symmetry.* U^{NR} *and* U^{R} *indicate atomic orbital energies at the nonrelativistic and relativistic levels, respectively.* $Ch = \eta^7\text{-}C_7H_7$. (*Reprinted with permission from Li and Bursten* (1997). *Copyright* 1997 *American Chemical Society.*)

A substituted derivative of the pentalene ligand, $[1,5\text{-}(Si^iPr_3)_2C_8H_4]^{2-}$, has been employed to generate the neutral bis(ligand) uranium and thorium compounds $[\eta^8\text{-}1,5\text{-}(Si^iPr_3)_2C_8H_4]_2Th$ and $[\eta^8\text{-}1,5\text{-}(Si^iPr_3)_2C_8H_4]_2U$, which are rare examples of η^8-coordinated pentalene ligands (Cloke and Hitchcock, 1997; Cloke *et al.*, 1999). The molecular structure of the thorium compound revealed it to be a near-equal mixture of staggered and eclipsed sandwich isomers in a disordered structure. The two isomers are generated by thorium binding to two different prochiral faces of the ligand; as such the isomers are not found in NMR studies to interconvert on any timescale in solution.

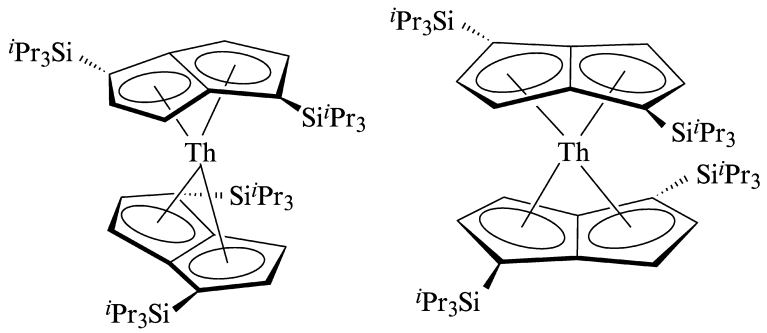

The larger actinide ion accommodates a smaller bending, or 'folding' angle about the bridgehead C–C bond (24°, compared to 33° in a related tantalum compound). The Th–C_{ring} bond lengths vary from 2.543(10) to 2.908(11) Å. Photoelectron spectroscopy studies and density functional calculations present a consistent picture of the bonding in these complexes. Metal–ligand bonding takes place chiefly through four molecular orbitals with both 6d and 5f orbital involvement (although 6d orbitals again make a larger contribution); the uranium compound further houses two unpaired electrons in 5f-based orbitals. Both the f-ionization and the highest lying ligand orbitals have lower ionization energies than uranocene or $(\eta^5\text{-}C_5H_5)_4U$, suggesting that the pentalene dianion is a stronger donor ligand than other carbocyclic groups.

Among the largest discrete organometallic ligands that could be identified would be fullerenes, and many metal-encapsulated derivatives, or endometallofullerene complexes have been identified. The first reports of possible uranium encapsulation (Haufler *et al.*, 1990; Guo *et al.*, 1992) suggested that the principal products from laser vaporization experiments with graphite and UO_2 in a supersonic cluster beam apparatus included $U@C_{60}$ and the product of the unusually small cage $U@C_{28}$. XPS studies of the bulk product suggested a uranium valence of 4+ in the complex. A subsequent report identified $U@C_{60}$ and $U@C_{82}$ in the sublimed soot (Diener *et al.*, 1997). Most recently, metallofullerenes of uranium, neptunium, and americium have been produced via arc-discharge using a carbon rod containing lanthanum as a carrier with ^{237}U, ^{239}Np, and ^{240}Am as radiotracers (Akiyama *et al.*, 2001). The metallofullerenes were purified by CS_2 extraction and toluene HPLC elution. The dominant products identified for neptunium and americium were $An@C_{82}$. Two uranium-containing metallofullerenes were identified, $U@C_{82}$ and $U_2@C_{80}$. Based upon comparison with the optical spectra of lanthanide analogs, it was suggested that the oxidation state in these complexes might best be regarded as +3.

Electronic structure calculations have been carried out on $U@C_{60}$, $U@C_{28}$, and $Pa@C_{28}$ (Chang *et al.*, 1994; Zhao and Pitzer, 1996). The ground state of $Pa@C_{28}$ was found to have one electron in a cage π^* orbital, suggested a higher overall oxidation state for the metal. Similarly, $U@C_{28}$ had a $(\pi^*)^1(5f)^1$

diamagnetic ground state. In all cases, the complexes show extensive mixing of π-orbitals with both 6d and 5f orbitals, suggesting strong bonding.

25.2.4 Allyl, pentadienyl and related π-ligands

Allyl complexes with associated cyclopentadienyl ligands have been discussed previously. There are, however, several classes of complexes reported for thorium and uranium that contain allyl or other 'open' π-system ligands. Tetrakis (allyl) and substituted allyl complexes of thorium and uranium can be prepared by the reaction of the tetrachloride complexes with the appropriate Grignard reagent (Wilke *et al.*, 1966; Lugli *et al.*, 1969; Brunelli *et al.*, 1973), although they are thermally unstable and decompose at temperatures greater than –20°C [equation (25.89)].

$$AnCl_4 + 4C_3H_5MgX \longrightarrow \text{An(allyl)}_4 + 4MgXCl \qquad (25.89)$$

An = Th, U

Mixed-ligand complexes are known to be somewhat more stable. As an example, the reaction of $(\eta^5\text{-}C_3H_5)_4U$ with aliphatic alcohols has been reported to generate the mixed-ligand complexes $[(\eta^5\text{-}C_3H_5)_2An(OR)_2]_2$ (Brunelli *et al.*, 1979); the structure of the isopropoxide derivative has been determined. The complex exists as a dimer in the solid state, with two bridging alkoxide ligands, although they are proposed to be monomeric in THF solution. The allyl ligands are bound trihapto, which is consistent with the proposed mode of coordination for allyl ligands in the homoleptic compounds, as determined by solution NMR studies. A further example is provided by the reaction of $(\eta^5\text{-}C_3H_5)_4U$ with 2,2′-bipyridine. The product generated is more thermally stable, likely due to the incorporation of three Lewis bases into the coordination sphere of the metal. It is proposed that this is made possible by the transfer of two of the allyl groups to one or more of the bipyridine ligands (Vanderhooft and Ernst, 1982).

A more stable 'open' π-system is provided by the pentadienyl ligand. Since pentadienyl complexes are generally considered to be more reactive than cyclopentadienyl ligands, it has often proven necessary to employ substituted derivatives. The 2,4-dimethylpentadienyl ligand was first used in the generation of a homoleptic compound of U(III) [equation (25.90)] (Cymbaluk *et al.*, 1983b).

$$UCl_3 \cdot n\text{THF} + 3K(2,4\text{-}Me_2C_5H_5) \longrightarrow \text{U(dienyl)}_3 + 3KCl \qquad (25.90)$$

The mixed-ligand complex [K(18-crown-6)][(η^5-2,4-$Me_2C_5H_5$)$_2$U(BH_4)$_2$] has been prepared either by reaction of (η^5-mesitylene)U(BH_4)$_3$ with K(2,4-$Me_2C_5H_5$), or by reaction of (η^5-2,4-$Me_2C_5H_5$)$_3$U with KBH_4 (Baudry *et al.*, 1989b). The reaction of (η^5-2,4-$Me_2C_5H_5$)$_3$U with [Et_3NH][BPh_4] has been reported to generate a cationic complex [(η^5-2,4-$Me_2C_5H_5$)$_2$U][BPh_4]. The tetravalent derivatives (η^5-2,4-$Me_2C_5H_5$)$_2$U(BH_4)$_2$ and (η^5-2,4-$Me_2C_5H_5$)U(BH_4)$_3$ have been generated by the reactions of (η^5-2,4-$Me_2C_5H_5$)$_3$U with $TlBH_4$ or U(BH_4)$_4$ with K(2,4-$Me_2C_5H_5$), respectively (Baudry *et al.*, 1989c).

Comparable reactions have also been carried out with the related 6,6-dimethylcyclohexadienyl ligand. Reaction of U(BH_4)$_4$ with K(6,6-$Me_2C_6H_5$) generates the bis(ligand) compound, (η^5-6,6-$Me_2C_6H_5$)$_2$U(BH_4)$_2$ as shown in equation (25.91) (Baudry *et al.*, 1990b).

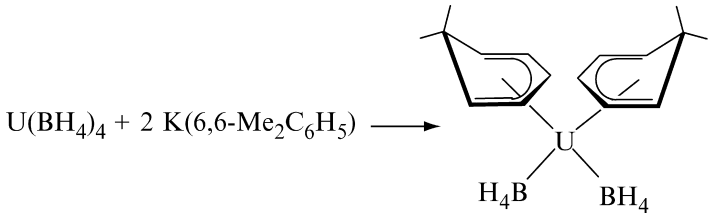

(25.91)

In order to generate the mono(ligand) compound, (η^5-6,6-$Me_2C_6H_5$)U(BH_4)$_3$, it is necessary to react U(BH_4)$_4$ with (η^5-6,6-$Me_2C_6H_5$)$_2$U(BH_4)$_2$ in a ligand redistribution reaction (Baudry *et al.*, 1990b). The anionic compounds [K(18-crown-6)][(η^5-6,6-$Me_2C_6H_5$)$_2$UX_2] (X = Cl, BH_4) were synthesized by treatment of UCl_4 or (η^6-mesitylene)U(BH_4)$_3$ with K(6,6-$Me_2C_6H_5$).

Although no alkyne coordination complex of an actinide has been isolated, alkyne complexes have been proposed as intermediates in the catalytic dimerization of terminal alkynes by cationic amide complexes, based upon spectroscopic evidence (Wang *et al.*, 1999; Dash *et al.*, 2000).

25.2.5 Alkyl ligands

Early attempts to prepare homoleptic alkyl complexes of the actinides resulted only in the formation of organic decomposition products and uranium metal, suggesting thermal instability (Gilman, 1968). Various methods of steric stabilization have been employed to enhance the stability of alkyl complexes, including reactions designed to generate uranate complexes, and the introduction of ancillary bases to block the elimination reactions believed to occur during decomposition.

The reactions of uranium and thorium tetrachlorides with excess alkyllithium reagents yield isolable products [equations (25.92) and (25.93)] (Andersen *et al.*, 1975; Sigurdson and Wilkinson, 1977; Lauke *et al.*, 1984).

$$\begin{aligned} &UCl_4 + XS\,RLi \xrightarrow{xs\,L} [Li(L)_n]_2[UR_6] \\ &R = CH_3,\ C_6H_5,\ CH_2(SiMe_3)_2 \\ &L = Et_2O,\ THF,\ n = 4;\ L = TMEDA,\ n = 3.5 \end{aligned} \tag{25.92}$$

$$ThCl_4 + xs\,CH_3Li + xs\,TMEDA \longrightarrow [Li(TMEDA)]_3[TH(CH_3)_7] \cdot TMEDA + 4LiCl \tag{25.93}$$

While the uranium compounds are reported to decompose above room temperature, the thorium compound is stable for hours at room temperature, and the crystal structure has been determined. The thorium is hepta-coordinate, with a monocapped trigonal prismatic geometry. Six of the methyl groups also bridge to the three lithium counter-ions [Th–C = 2.667(8)–2.765(9) Å], while the seventh methyl group is terminal [Th–C = 2.571(9) Å].

The other proven route to stabilization of alkyl complexes involves the use of coordinating phosphines to sterically saturate the coordination sphere. The bis (1,2-dimethylphosphino)ethane (dmpe) complexes of uranium and thorium tetrachloride have been prepared; metathesis reactions with these precursors yield thermally stable alkyl complexes [equations (25.94) and (25.95)] (Edwards *et al.*, 1981, 1984):

$$\begin{aligned} &(dmpe)_2AnCl_4 + 4RLi \longrightarrow (dmpe)_2AnR_4 \\ &An = Th,\ U \\ &R = CH_3,\ CH_2C_6H_5 \end{aligned} \tag{25.94}$$

$$(dmpe)_2AnCl_4 + 3Li(CH_2C_6H_5) + LiCH_3 \longrightarrow (dmpe)_2An(CH_3)(CH_2C_6H_5)_3 \quad An = Th,\ U \tag{25.95}$$

The only neutral homoleptic actinide complex characterized to date is $U[CH(SiMe_3)_2]_3$, produced by the reaction of $U(O\text{-}2,6\text{-}{}^tBu_2C_6H_3)_3$ with $Li[CH(SiMe_3)_2]$ in hexane (Van Der Sluys *et al.*, 1989). The molecular structure is shown in Fig. 25.29.

Unlike comparable first-row transition metal tris(alkyl) complexes, the compound has a pyramidal geometry, with a C–U–C angle of 107.7(4)°, and a U–C bond distance of 2.48(2) Å. The complex is thermally stable in the solid state at room temperature, but decomposes with loss of alkane at temperatures greater than 60°C. Reaction of $UCl_3(THF)_x$ with three equivalents of $Li[CH(SiMe_3)_2]$ does not generate the neutral complex, but rather an ionic complex formulated as $[Li(THF)_3][(Cl)U\{CH(SiMe_3)_2\}_3]$. The neptunium and plutonium analogs $An[CH(SiMe_3)_2]_3$ have been reported (Zwick *et al.*, 1992), although not fully characterized.

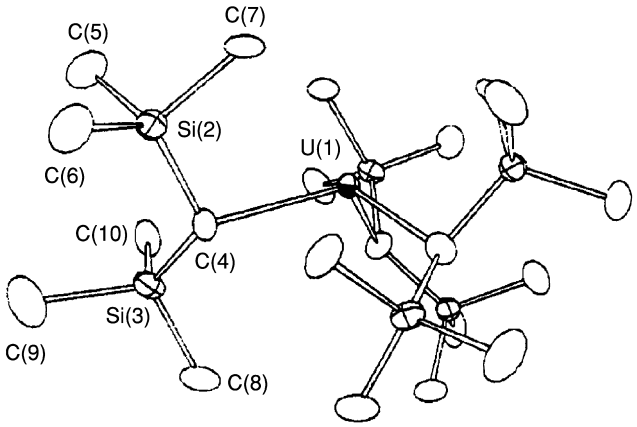

Fig. 25.29 *Molecular structure of* $[CH(SiMe_3)_2]_3U$. (*Reprinted with permission from Van Der Sluys* et al. (1989). *Copyright* 1989 *American Chemical Society*.)

25.3 HETEROATOM-CONTAINING π-ANCILLARY LIGANDS

25.3.1 Dicarbollide ligands

Although not strictly carbocyclic ligands, 1,2-dicarbollide groups ($C_2B_9H_{11}^{2-}$) have been employed as ancillary ligands in organoactinide chemistry, and deserve inclusion owing to their structural analogy to cyclopentadienyl groups. This ligand has been used in the synthesis of a number of mono- and bis-ligand analogs of cyclopentadienyl complexes. The first report of a dicarbollide complex was the generation of an anionic 'bent metallocene analog' [equation (25.96)] (Fronczek *et al.*, 1977).

$$UCl_4 + 2Li_2(C_2B_9H_{11}) \xrightarrow{\text{THF}} [Li(THF)_4]_2[(\eta^5\text{-}C_2B_9H_{11})_2UCl_2] + 2LiCl \tag{25.96}$$

The complex has a geometry analogous to a typical metallocene complex, with pentahapto dicarbollide ligands. The two carbons of the capping face could not be definitively distinguished, although a model was suggested that placed the carbon atoms closest to the coordinated chloride ligands. The U–B(C) bond distances range from 2.64(3) to 2.86(3) Å. The average value of 2.73(2) Å is similar to that found in typical U(IV) cyclopentadienyl complexes. A uranium(IV) dibromide analog has since been reported (Rabinovich *et al.*, 1996), as have thorium complexes $[Li(THF)_4]_2[(\eta^5\text{-}C_2B_9H_{11})_2ThX_2]$ (X = Cl, Br, I) (Rabinovich *et al.*, 1997). The uranium(IV) dibromide complex can be chemically reduced to generate a uranium(III) complex, $[Li(THF)_x]_2[(\eta^5\text{-}C_2B_9H_{11})_2UBr(THF)]$ (de Rege *et al.*, 1998). Trivalent mono-ligand complexes can also be generated by metathesis reactions with $UI_3(THF)_4$ [equation (25.97)]

(Rabinovich *et al.*, 1996):

$$UI_3(THF)_4 + 2Li_2(C_2B_9H_{11}) + TMEDA \xrightarrow{THF} [Li(TMEDA)][(\eta^5\text{-}C_2B_9H_{11})UI_2(THF)_2] + LiI \quad (25.97)$$

A single report has appeared on the complexation of uranium by another carborane anion [equation (25.98)] (Xie *et al.*, 1999).

$$UCl_3 + 12K + 4o\text{-}C_2B_{10}H_{12} \xrightarrow{THF} [\{K_2(THF)_5\}\{(\eta^7\text{-}C_2B_{10}H_{12})(\eta^6\text{-}C_2B_{10}H_{12})U\}]_2 + 8KCl \quad (25.98)$$

25.3.2 Phospholyl ligands

The closest π-ligand analogs to cyclopentadienyl groups in this class are phosphole compounds and their derivatives. Of these potential ligands, the tetramethylphospholyl group has been employed to generate actinide complexes. The initial report involved introduction of the phospholyl ligand to the metal center by metathesis [equations (25.99) and (25.100)] (Gradoz *et al.*, 1992a):

$$U(BH_4)_4 + 2K(Me_4C_4P) \longrightarrow (\eta^5\text{-}Me_4C_4P)_2U(BH_4)_2 \quad (25.99)$$

$$U(BH_4)_4 + K(Me_4C_4P) \longrightarrow (\eta^5\text{-}Me_4C_4P)U(BH_4)_3 \quad (25.100)$$

Reduction of these complexes in THF by sodium amalgam affords trivalent uranate anions. Reaction of trivalent uranium precursors with the phospholyl salt also yields the uranate species. The molecular structure of the U(IV) product $(\eta^5\text{-}Me_4C_4P)_2U(BH_4)_2$ has been described and is presented in Fig. 25.30 (Baudry *et al.*, 1990c).

The complex is structurally very similar to a bis(cyclopentadienyl) metallocene. The phospholyl ring remains planar upon coordination to the uranium center, and coordinates in a pentahapto manner. The average metal–carbon bond distance is 2.81(4) Å, comparable to that found in U(IV) metallocene complexes, and the U–P distance is 2.905(8) Å. The complex $(\eta^5\text{-}Me_4C_4P)_2UCl_2$ was subsequently generated from the reaction of UCl_4 with the potassium salt of the phospholyl (Gradoz *et al.*, 1994a).

The tris(phospholyl) complexes have been produced from uranium tetrachloride [equation (25.101)] (Gradoz *et al.*, 1992b):

$$UCl_4 + 3K(Me_4C_4P) \longrightarrow (\eta^5\text{-}Me_4C_4P)_3UCl + 3KCl \quad (25.101)$$

The chloride may be further substituted to generate alkyl, hydrido, and alkoxide species.

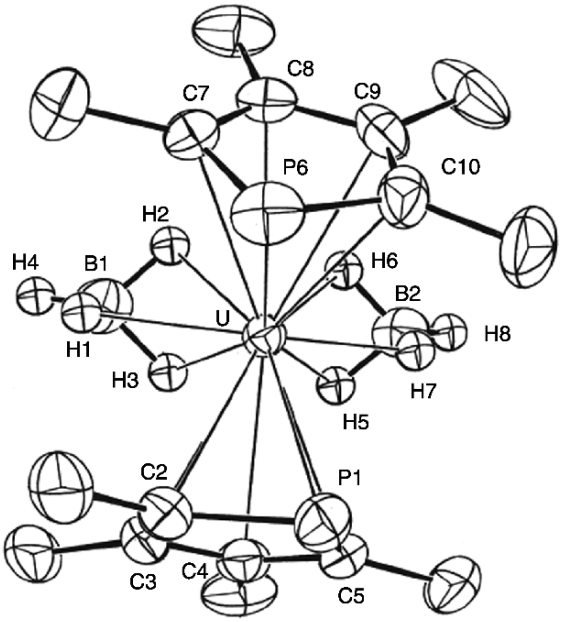

Fig. 25.30 *Molecular structure of* $(\eta^5\text{-}Me_4C_4P)_2U(BH_4)_2$ (*Baudry* et al., 1990*c*). (*Reprinted with permission from John Wiley & Sons, Inc.*)

Mono-ring complexes of the formula $(\eta^5\text{-}Me_4C_4P)UCl_3(DME)$ and $(\eta^5\text{-}Me_4C_4P)UCl_3(THF)_2$ are prepared by the reaction of UCl_4 and $K(Me_4C_4P)$ in the appropriate solvent (Gradoz *et al.*, 1994a). It is the borohydride derivative $(\eta^5\text{-}Me_4C_4P)U(BH_4)_3$ and its pentamethylcyclopentadienyl analog $(\eta^5\text{-}C_5Me_5)U(BH_4)_3$ that serve as reagents in most reported subsequent metathesis reactions as illustrated in equation (25.102) for the preparation of the mixed-ring complex $(\eta^5\text{-}C_5Me_5)(\eta^5\text{-}Me_4C_4P)U(BH_4)_2$:

$$(\eta^5\text{-}C_5Me_5)U(BH_5)_3 + K(Me_4C_4P) \longrightarrow \quad (25.102)$$

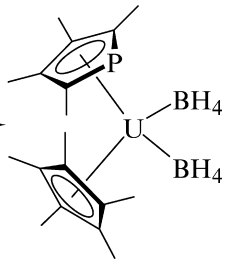

The complexes $(\eta^5\text{-}Me_4C_4P)_2U(BH_4)_2$, $(\eta^5\text{-}Me_4C_4P)U(BH_4)_3$, and $(\eta^5\text{-}C_5Me_5)(\eta^5\text{-}Me_4C_4P)U(BH_4)_2$ serve as precursors for a number of alkyl and alkoxide derivatives (R = Me, CH_2SiMe_3, OEt, O^{i}Pr, and O^{t}Bu).

The mixed-ring compounds $(\eta^8\text{-}C_8H_8)(\eta^5\text{-}Me_4C_4P)U(BH_4)(THF)$ and $K[(\eta^8\text{-}C_8H_8)(\eta\text{-}Me_4C_4P)_2U(BH_4)(THF)_x]$ can be generated by the reaction of

(η^8-C_8H_8)U(BH_4)$_2$(THF) or [(η^8-C_8H_8)U(BH_4)(THF)$_2$][BPh_4], respectively, with K(Me_4C_4P). The cationic complex [(η^8-C_8H_8)U(η^5-Me_4C_4P)(HMPA)$_2$][BPh_4] is isolated from the reaction of [(η^8-C_8H_8)U(HMPA)$_3$][BPh_4] with the potassium phospholyl salt (Cendrowski-Guillaume *et al.*, 2002).

The dimeric trivalent compound [(η^5-Me_4C_4P)(μ,η^5,η^1-Me_4C_4P)U(BH_4)]$_2$ constitutes a rare example of a dimeric phospholyl complex, in which each phospholyl ligand phosphorus atom serves as a donor to the other uranium atom (Gradoz *et al.*, 1994b). The molecular structure of the complex reveals pseudo-tetrahedral uranium coordination, with the borohydride ligands on the same side of the U_2P_2 plane (Fig. 25.31).

The metrical data indicate no apparent strain introduced by the dimer formation; U-ring atom bond distances and centroid-metal-centroid angles are not significantly distorted from the values found for (η^5-Me_4C_4P)$_2$U(BH_4)$_2$ [U–C_{ave} = 2.84(3) Å, U–P_{ave} = 2.970(3) Å] (Fig. 25.30). The bridging P→U distance is 2.996(3) Å. Although it has been suggested that the phosphorus lone pair of the phospholyl group should lie in the ring plane, the P→U-ring centroid angle in this complex is 159.0(3)°, suggesting that U_2P_2 'ring closure' imposes a steric requirement for bending about the donor phosphorus atom.

25.3.3 Pyrrole-based ligands

The nitrogen-based analog, the pyrrole ligand, has not been found by itself to support pentahapto coordination to actinide centers, presumably due to the relative 'hard' basic character of the nitrogen in the heterocycle. Examples of (η^5-C_4N) coordination may instead be found in the reaction products of uranium halides with the tetraanion of the macrocycle [{(–CH_2–)$_5$}$_4$-calix[4]tetrapyrrole] (Korobkov *et al.*, 2001a). As described in equation (25.103), the reaction of $UI_3(THF)_4$ with the potassium salt of the tetrapyrrolide in THF generates a dinuclear U(IV) complex, [{[{(–CH_2–)$_5$}$_4$-calix[4]tetrapyrrole]UK(THF)$_3$}$_2$(μ-O)]·2THF; the oxo group is proposed to come from deoxygenation of a THF molecule.

$UI_3(THF)_4$ + [$K(THF)_4$] [calix-[4]-tetrapyrrole] ⟶

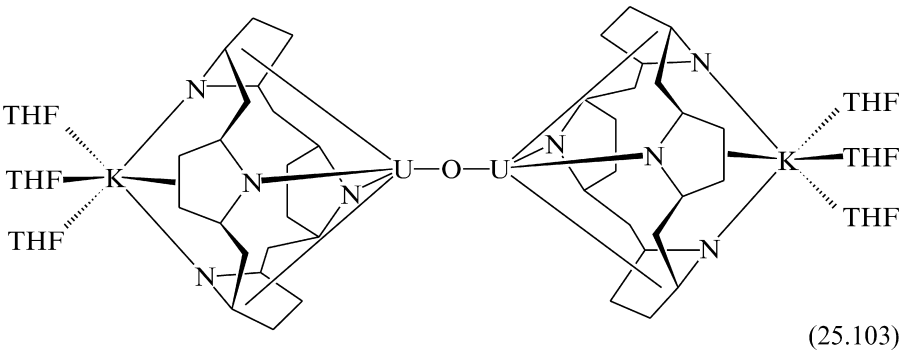

(25.103)

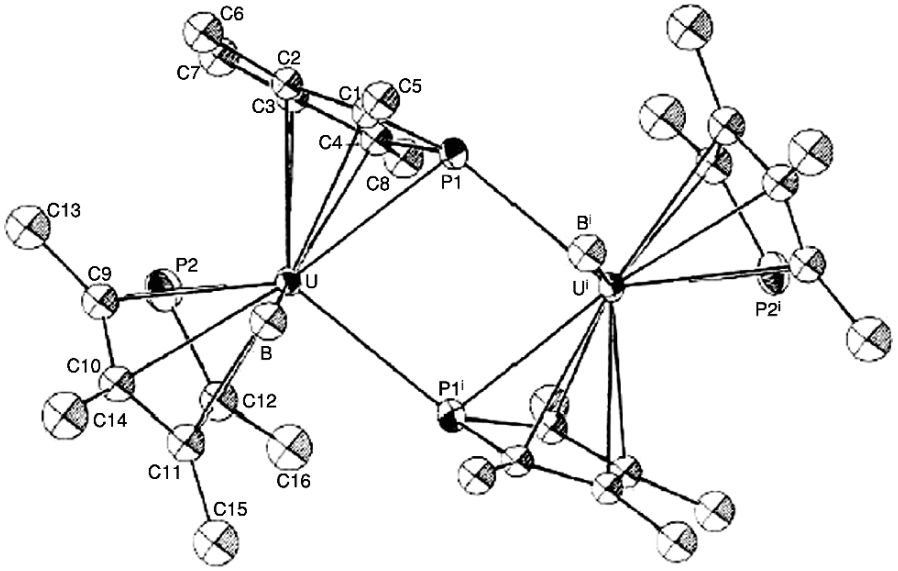

Fig. 25.31 *Molecular structure of* $[(\eta^5\text{-}Me_4C_4P)(\mu\eta^5\eta^1\text{-}Me_4C_4P)U(BH_4)]_2$. *The H atoms of the* BH_4 *ligand have been omitted for clarity* (*Gradoz* et al., 1994b). (*Reprinted with permission from Elsevier*.)

Reaction of $UI_3(THF)_4$ with the corresponding lithium tetrapyrrolide salt in a 1:2 ratio generates instead $[\{[(-CH_2-)_5]_4\text{-calix[4]tetrapyrrole}\}ULi(THF)_2]_2 \cdot$ hexane, in which the β-carbon of one of the pyrrole rings has undergone a metallation reaction (Fig. 25.32).

Reaction of the potassium salt with $UI_3(DME)_4$ avoids the complication of THF activation, and the simple trivalent uranate complex, $[\{[(-CH_2-)_5]_4\text{-calix[4]tetrapyrrole}\}U(DME)][K(DME)]$, is generated. The geometry about the metal center in these compounds is qualitatively similar to a metallocene complex. The ligand adopts a σ/π-bonding mode, in which two of the four pyrrole rings in the macrocycle are η^5-bonded to the uranium, and the other two rings are σ-coordinated only through the pyrrole nitrogen. The U–N (σ) bond lengths for the tetravalent derivatives range from 2.39 to 2.47 Å; these distances are slightly longer in the trivalent derivative (*ca*. 2.53 Å). The π-coordination of the pyrrole ring yields somewhat longer U–N bond distances (*ca*. 2.65 Å in tetravalent compounds, 2.74 Å in the trivalent compound), and $U-C_{pyrrole}$ bond distances that range from 2.68 to 2.88 Å.

Reaction of $UI_3(THF)_4$ with $[Li(THF)]_4\{[(-CH_2-)_5]_4\text{-calix[4]tetrapyrrole}\}$ in a substoichiometric (2:1) ratio generates the dinuclear complex $[Li(THF)_4]_2[U_2I_4\{[(-CH_2-)_5]_4\text{-calix[4]-tetrapyrrole}\}]$ (Fig. 25.33) in moderate yield (Korobkov *et al*., 2001b).

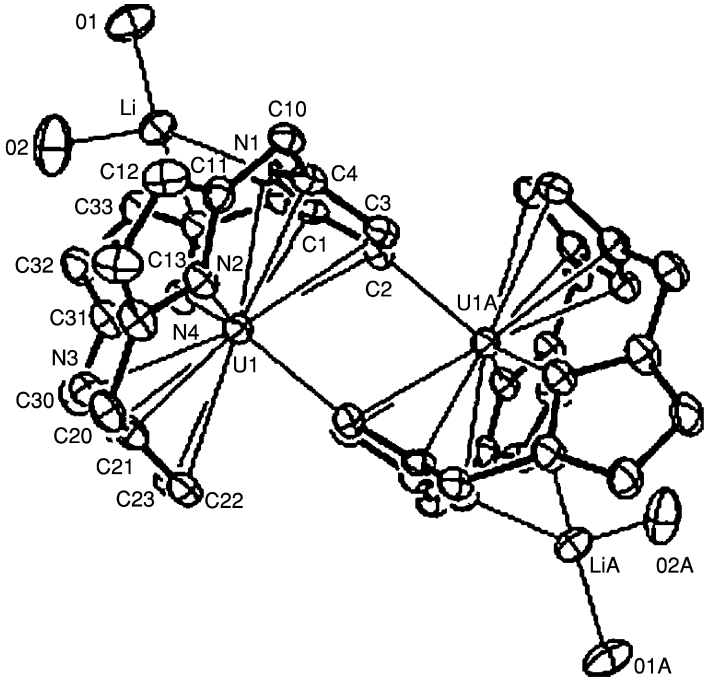

Fig. 25.32 *Molecular structure of* [{(–CH_2–)$_4$-*calix*[4]-*pyrrole*}*ULi*(*THF*)$_2$]$_2$. (*Reprinted with permission from Korobkov* et al. (2001*a*). *Copyright* 2001 *American Chemical Society*.)

Partial reduction of UCl_4, followed by reaction with one half of an equivalent of the lithium salt is reported to generate the mixed-valence compound [Li(THF)$_2$](μ-Cl)$_2${U$_2$[(–CH_2–)$_5$]$_4$-calix[4]tetrapyrrole}Cl$_2$·THF. Both of these complexes display alternate σ/η^5, π-coordination to opposite pairs of pyrrole ligands in a single tetrapyrrole group. The bridging nature of the macrocyclic ligand brings the uranium centers into relatively close proximity (3.4560(8) and 3.365(6) Å, respectively); magnetic susceptibility measurements on the U(III)/U(III) dimer suggests weak antiferromagnetic coupling occurs between metal centers.

25.3.4 Other nitrogen-containing π-ligands

Amidinate ligands have been employed as ancillary ligands in the generation of organometallic compounds of tetravalent uranium and thorium, as well as complexes with the uranyl ion. Reaction of Li[N(SiMe$_3$)$_2$] and Na[N(SiMe$_3$)$_2$] with *para*-substituted benzonitriles yields the benzamidinate ligands M[4-RC$_6$H$_4$C(NSiMe$_3$)$_2$] (M = Li, Na; R = H, Me, OMe, CF$_3$).

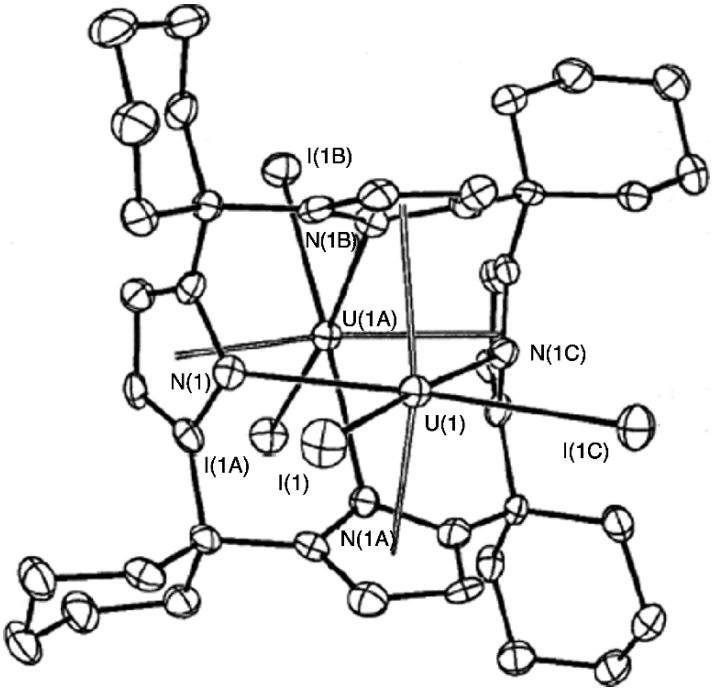

Fig. 25.33 *Molecular structure of* $[Li(THF)_4]_2[U_2I_4\{[(-CH_2-)_5]_4$-*calix*[4]-*tetrapyrrole*$\}]$. (*Reprinted with permission from Korobkov* et al. (2001b). *Copyright* 2001 *American Chemical Society*.)

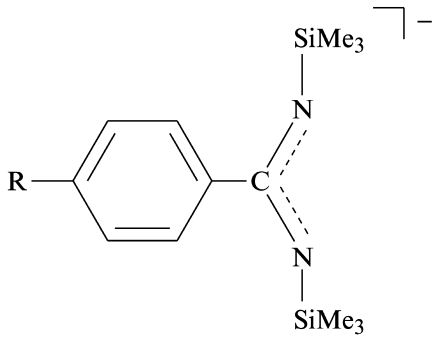

Alternatively, more substituted ligands $Li[2,4,6\text{-}R_3C_6H_2C(NSiMe_3)_2]$ (R = CF_3, Me) are generated by the addition of aryllithium reagents to $Me_3SiN{=}C{=}NSiMe_3$. The amidinate ligands (L) have been used to generate complexes of the formula L_2AnCl_2 (An = Th, U) and L_3AnCl (for less

sterically demanding substituents) by metathesis reactions (Wedler *et al.*, 1990). Substitution of the halide precursors has been reported to generate methyl and borohydride derivatives (Wedler *et al.*, 1992a). The molecular structure of the complex $[C_6H_5C(NSiMe_3)_2]_3UMe$ has been determined. The benzamidinate ligands coordinate to the metal center in a η^3-manner; the relatively long U–C σ bond of 2.498(5) Å is taken as an indication of steric crowding in the complex.

The benzamidinate ligands have been found to support a range of oxidation states in uranium chemistry. The uranyl complex $[C_6H_5C(NSiMe_3)_2]_2UO_2$ complex was prepared by a metathesis reaction with UO_2Cl_2 (Wedler *et al.*, 1988), and the interesting pentavalent derivative $[4\text{-}MeC_6H_4C(NSiMe_3)_2]_2UCl_3$ was produced by adventitious aerobic oxidation during reaction of UCl_4 with the corresponding silylated benzimidine [equation (25.104)] (Wedler *et al.*, 1992b).

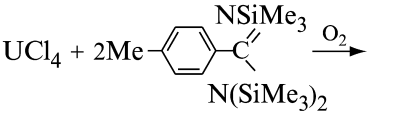

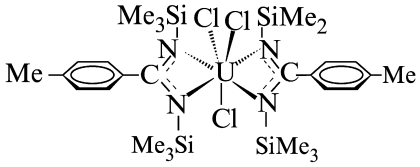

(25.104)

Related amidinate and 1-aza-allyl ligands also have been shown to generate bis(ligand)thorium dichloride complexes (Hitchcock *et al.*, 1997), as well as an interesting mixed-valence U(III)/U(VI) complex (Hitchcock *et al.*, 1995).

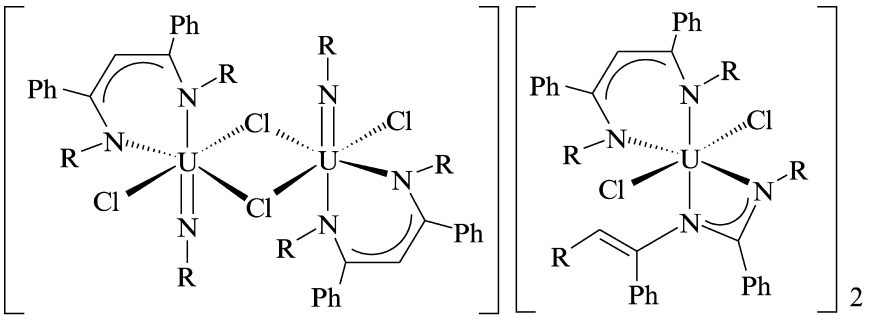

R = $SiMe_3$; Ph = C_6H_5

A rare example of a U–C interaction in hexavalent actinide chemistry is found in the isolation of a bis(iminophosphorano)methanide uranyl complex (Sarsfield *et al.*, 2002). Reaction of $[UO_2Cl_2(THF)_2]_2$ with $Na[CH(Ph_2P{=}NSiMe_3)_2]$ generates the dimer $[UO_2(\mu\text{-}Cl)\{CH(Ph_2P{=}NSiMe_3)_2\}]_2$.

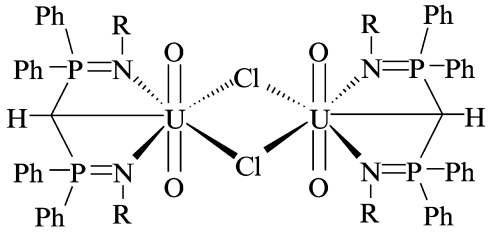

R = $SiMe_3$

The U–C distance is 2.691(8) Å; the length indicates a very weak interaction, although it falls within the sum of the van der Waals radii of the two atoms.

25.4 HETEROATOM-BASED ANCILLARY LIGANDS

Although complexes containing primarily heteroatom-donor ligands are less likely to be regarded as organometallic species, these ligands are playing an increasing important role in the development of non-aqueous f-element chemistry. The flexible steric and electronic characteristics of these ligands can stabilize unusual oxidation states and promote novel substrate activation reactions at actinide centers, making their study more attractive. Although not all 'inorganometallic' chemistry will be comprehensively reviewed here, discussion is warranted for certain classes of ligands that have played a significant role in the development of non-aqueous actinide chemistry.

25.4.1 Bis(trimethylsilyl)amide

As an ancilliary ligand, the bis(trimethylsilyl)amide ligand $[N(SiMe_3)_2]^-$ has been shown to support a wide array of oxidation states of uranium. It has further been used in tetravalent actinide chemistry (An = U, Th) to support metal centers that can effect a number of organic transformations.

Trivalent homoleptic complexes $[(SiMe_3)_2N]_3An$ have been prepared for uranium, neptunium, and plutonium (Andersen, 1979; Clark *et al.*, 1989; Zwick *et al.*, 1992) by metathesis reactions [equations (25.105) and (25.106)].

$$UCl_3 \cdot (THF)_x + 3Na[N(SiMe_3)_2] \xrightarrow{THF} [(SiMe_3)_2N]_3U \qquad (25.105)$$

$$AnI_3(THF)_4 + 3Na[N(SiMe_3)_2] \xrightarrow{THF} [(SiMe_3)_2N]_3An \qquad (25.106)$$
$$An = U, Np, Pu$$

The molecular structure of $[(SiMe_3)_2N]_3U$ has been determined (Stewart and Andersen, 1998). The geometry about the uranium center is trigonal pyramidal, with a U–N distance of 2.320(4) Å, and a N–U–N angle of 116.24(7)°. The

magnetic susceptibility shows that the complex has effective moments comparable to those determined for trivalent metallocenes and halides ($\mu_{eff} = 3.354(4)$, $\theta = -13$ K at 5 kG), consistent with a $5f^3$ electronic configuration. This is confirmed by the photoelectron spectroscopy, which demonstrates a low-energy 5f ionization band (Green *et al.*, 1982). The steric congestion about the metal center prohibits isolation of stable base coordination compounds.

Tetravalent complexes of the formula $[(SiMe_3)_2N]_3AnCl$ (An = Th, U) have been prepared (Turner *et al.*, 1979a) from the 3:1 reaction of $NaN(SiMe_3)_2$ with $AnCl_4$ [(equation (25.107)], and the complex $[(SiMe_3)_2N]_2UCl_2(DME)$ can be generated from a 2:1 reaction of ligand:halide salt (McCullough *et al.*, 1981).

$$AnCl_4 + 3Na[N(SiMe_3)_2] \xrightarrow{THF} [(SiMe_3)_2N]_3An-Cl \quad (25.107)$$
$$An = Th, U$$

Substituted complexes of the formula $[(SiMe_3)_2N]_3AnR$ (An = Th, U; R = Me, Et, ^{i}Pr, Bu, BH_4) are formed by the reaction of $[(SiMe_3)_2N]_3AnCl$ with the appropriate lithium or magnesium reagent (Turner *et al.*, 1979a; Dormond *et al.*, 1988). Unlike comparable cyclopentadienyl analogs, the methyl compound does not undergo ready insertion of CO, although a number of other insertion and protonation reactions have been reported, including insertion of ketones, aldehydes, isocyanides, and aliphatic nitriles (Dormond *et al.*, 1987b, 1988). The methyl ligand is further susceptible to removal by protic reagents such as secondary amines.

The hydride compounds $[(SiMe_3)_2N]_3AnH$ (An = Th, U) are the sole products of attempts to introduce an additional equivalent of the bis(trimethylsilyl) amide ligand to $[(SiMe_3)_2N]_3AnCl$ (Turner *et al.*, 1979b). Pyrolysis of the hydride results in the loss of dihydrogen and the formation of an unusual metallacycle (Simpson and Andersen, 1981a).

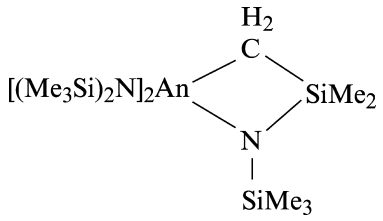

The metallacycles of uranium and thorium have been shown to undergo a large number of insertion and protonation reactions (Simpson and Andersen, 1981b; Dormond *et al.*, 1985, 1986a,b, 1987a,b, 1989a,b; Baudry *et al.*, 1995), as shown in Fig. 25.34.

In some cases these reactions (such as reduction of carbonyl-containing organic compounds) have been found to be stereoselective.

As in the case of substituted cyclopentadienyl complexes, the bis(trimethylsilyl)amide ligand is capable of supporting the formation of organoimido

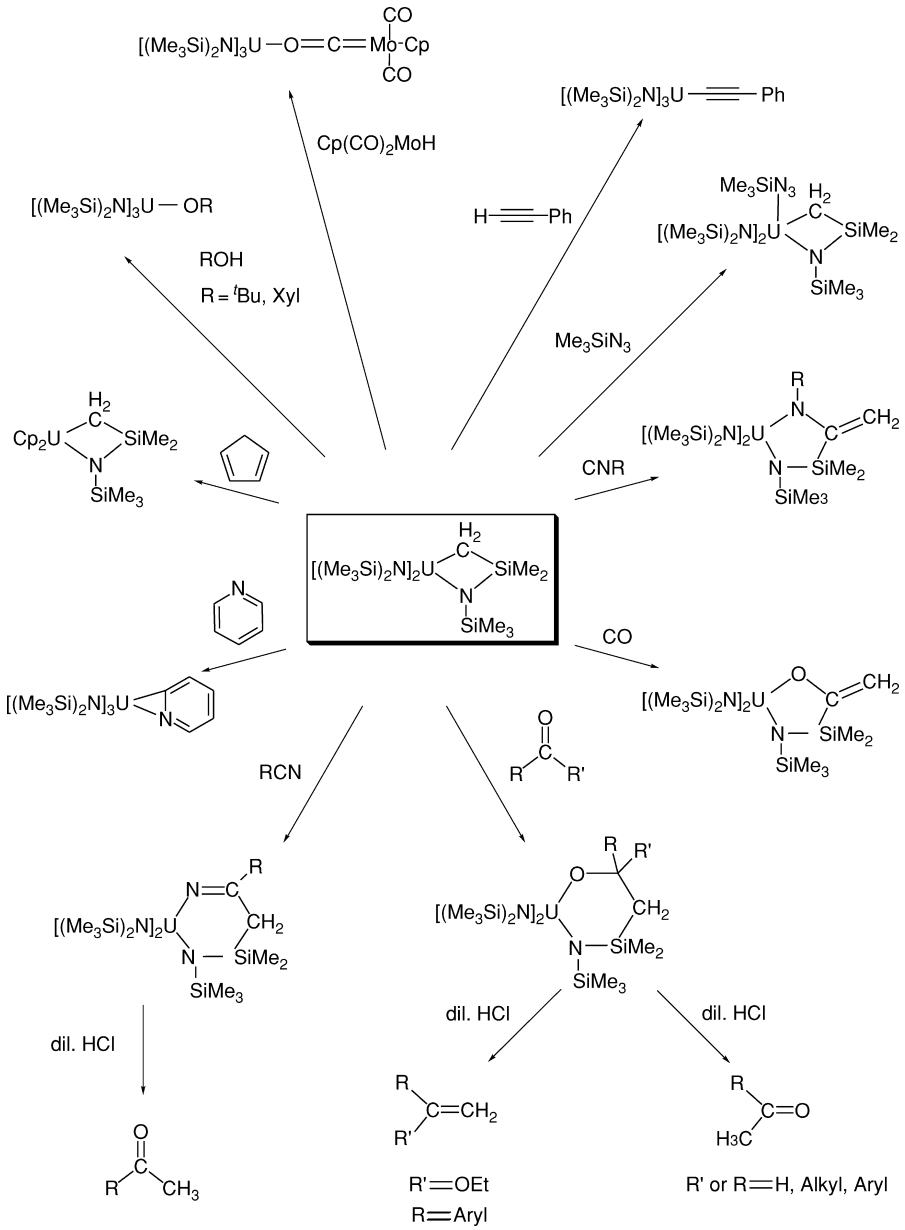

Fig. 25.34 *Reactions of uranium metallacycle.*

complexes. The tetravalent uranium dimer $[\{(SiMe_3)_2N\}_2U(\mu\text{-}N\text{-}p\text{-}C_6H_4Me)]_2$ was prepared by reaction of $[(SiMe_3)_2N]_3UCl$ with $Li[N(H)(p\text{-}C_6H_4Me)]$ [equation (25.108)] (Stewart and Andersen, 1995), presumably by α-elimination of $HN(SiMe_3)_2$ from an intermediate amide complex:

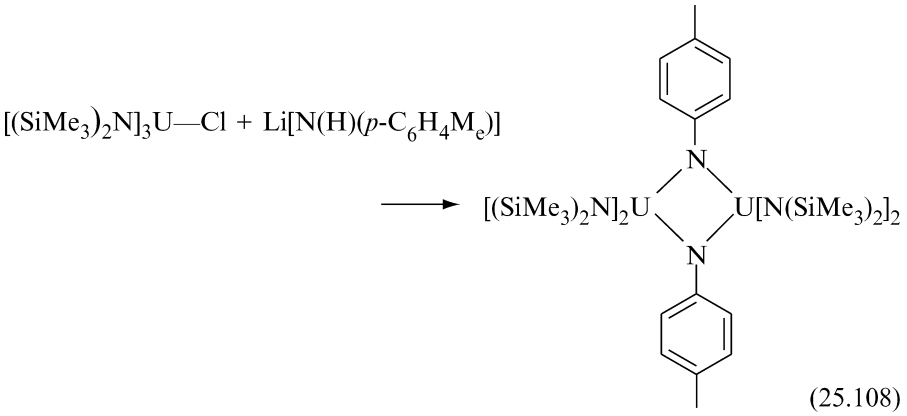

(25.108)

As in the case of the related cyclopentadienyl compound, the arylimido ligand bridges the two metal centers in an asymmetric fashion, with U–N bond distances of 2.378(3) and 2.172(2) Å.

Reaction of $[(SiMe_3)_2N]_3U$ with Me_3SiN_3 generates the uranium(V) organoimido complex $[(Me_3Si)_2N]_3U(=NSiMe_3)$ (Zalkin *et al.*, 1988b). Both this and the related phenylimido complex are oxidized by mild oxidants such as $AgPF_6$ or $[Cp_2Fe][PF_6]$ to generate the U(VI) imido fluoride complexes $[(Me_3Si)_2N]_3U(=NR)F$ (R = $SiMe_3$, Ph) as shown in equation (25.109) (Burns *et al.*, 1990).

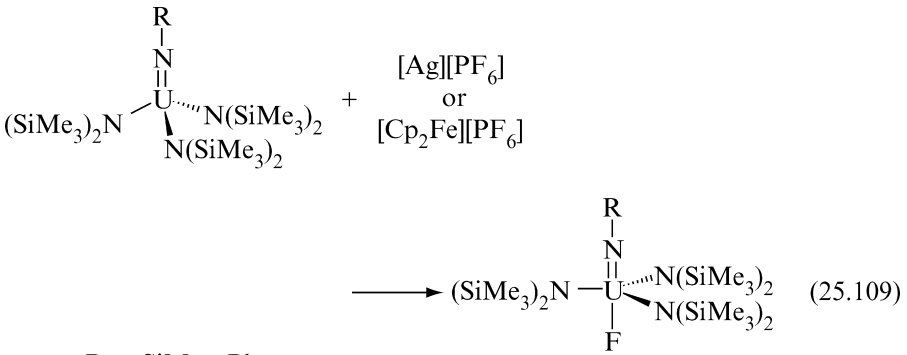

(25.109)

R = $SiMe_3$, Ph

Both U(VI) complexes are trigonal bipyramidal with the bis(trimethylsilyl) amido groups occupying the equatorial positions. The F–U–N_{imido} angles are near linear, as are the U–N–Si(C) angles. The U=N_{imido} bond lengths are 1.85 (2) and 1.979(8) Å, respectively, for the silylimido and phenylimido complexes.

25.4.2 Pyrazolylborate

Monoanionic poly(pyrazolyl)borate ligands ($B(pz)_4^-$, $HB(pz)_3^-$, $H_2B(pz)_2^-$, and substituted derivatives, pz = pyrazol-1-yl) have found broad application as ancillary ligands in d-transition metal chemistry as substitutes for cyclopentadienyl ligands (Trofimenko, 1993). Their σ-donor strength is comparable to that of a cyclopentadienyl ligand, although the precise ordering depends on the metal (Tellers *et al.*, 2000). These ligands most commonly bind to f-elements in either a trihapto or dihapto geometry through nitrogen atoms in the pyrazolyl substituents.

The first report of an actinide complex employing a poly(pyrazolyl)borate ligand was the preparation of complexes of the formula $[H_2B(pz)_2]_4U$, $[HB(pz)_3]_4U$, and $[HB(pz)_3]_2UCl_2$ by reaction of UCl_4 with the potassium salt of the appropriate ligand (Bagnall *et al.*, 1975). On the basis of ^{13}C NMR spectroscopy, the $HB(pz)_3$ ligands were assigned as bidentate in the complex $[HB(pz)_3]_2UCl_2$, while the complex $[HB(pz)_3]_4U$ was speculated to have two bidentate and two tridentate ligands (Bagnall *et al.*, 1976).

Since the initial identification of these compounds, the chemistry of poly(pyrazolyl)borate ligands has expanded to include representatives involving trivalent actinides, most encompassing the substituted ligand $HB(3,5\text{-}Me_2pz)_3$. The complex $[HB(3,5\text{-}Me_2pz)_3]UCl_2$ has been generated either by metathesis reaction of UCl_3 with $K[HB(3,5\text{-}Me_2pz)_3]$ (Santos *et al.*, 1985, 1986) or reduction of the U(IV) precursor $[HB(3,5\text{-}Me_2pz)_3]UCl_3$ with sodium naphthalenide (Santos *et al.*, 1987). The complex is somewhat unstable, and upon recrystallization can be oxidized to generate the tetravalent oxo complex $[\{HB(3,5\text{-}Me_2pz)_3\}UCl(\mu\text{-}O)]_4$ (Domingos *et al.*, 1992a).

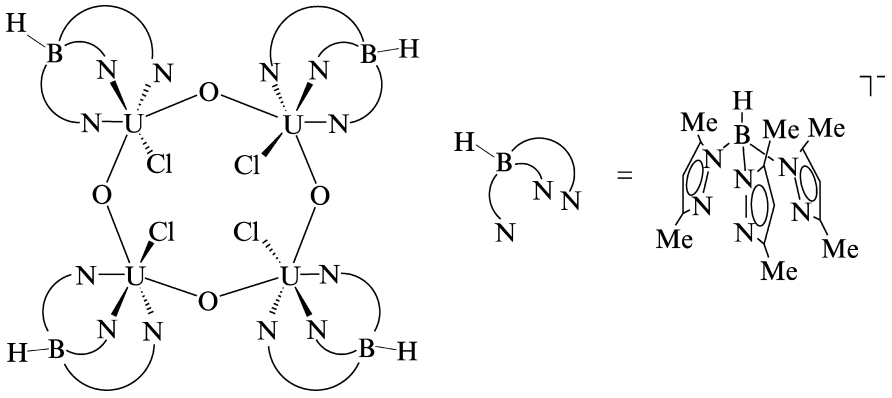

Recently, the use of uranium triiodide has become more common in the synthesis of trivalent complexes. Reaction of $UI_3(THF)_4$ with $M[HB(3,5\text{-}Me_2pz)_3]$ (M = Na, K) in a 1:1 or 1:2 ratio results in the formation of the compounds $[HB(3,5\text{-}Me_2pz)_3]UI_2(THF)_2$ and $[HB(3,5\text{-}Me_2pz)_3]_2UI$, respectively (McDonald *et al.*, 1994; Sun *et al.*, 1994). In the monoligand compound,

the pyrazolylborate ligand is tridentate, while the bis(ligand) compound demonstrates two different coordination modes for the two [$HB(3,5\text{-}Me_2pz)_3$] groups.

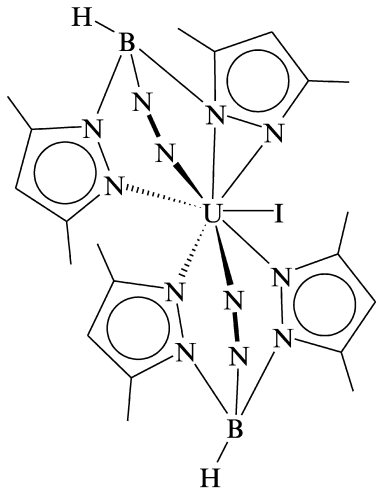

One of the ligands is η^3-coordinated to the metal center, while in the second ligand, one of the pyrazolyl rings appears to coordinate in a 'side-on' type of arrangement with the N–N bond of the ring within a bonding distance to the uranium atom. Upon abstraction of the iodide ligand with $TlBPh_4$, however, this ligand reverts to a conventional tridentate geometry; the uranium center is seven-coordinate in $[\{HB(3,5\text{-}Me_2pz)_3\}_2U(THF)]^+$, with the tetrahydrofuran ligand occupying the seventh site (McDonald *et al.*, 1994).

A limited number of U(III) complexes have been reported with other pyrazolylborate ligands. Uranium trichloride or triiodide reacts with the bis(pyrazolyl) borate ligands $H_2B(3,5\text{-}Me_2pz)_2$ and $H_2B(pz)_2$ to generate the species $[H(\mu\text{-}H)B(3,5\text{-}Me_2pz)_2]_3U$ and $[H(\mu\text{-}H)B(pz)_2]_3U(THF)$ (Carvalho *et al.*, 1992; Sun *et al.*, 1995). The coordinated tetrahydrofuran may be removed from the latter to yield the base-free complex $[H(\mu\text{-}H)B(pz)_2]_3U$. The solid state structure of $[H(\mu\text{-}H)B(3,5\text{-}Me_2pz)_2]_3U$ reveals that the metal lies in a trigonal prismatic arrangement of six pyrazole nitrogen atoms, with the three rectangular faces of the trigonal prism capped by three B–H bonds (Fig. 25.35).

When a related ligand devoid of B–H bonds is employed ($Ph_2B(pz)_2$), the resulting tris(ligand) complex $[Ph_2B(pz)_2]_3U$ contains a six-coordinate uranium center (Maria *et al.*, 1999). The lower coordination number is considered to be the origin of slightly shorter U–N bond distances (2.53(3) Å versus 2.59(3) or 2.58(3) Å in the ten- and nine-coordinate complexes, respectively). A mixed-alkyl substituted bis(pyrazolyl)borate complex has been produced by the reaction of $UI_3(THF)_4$ with $K[H_2B(3\text{-}^t\!Bu,5\text{-}Mepz)_2]$. The complex $[H_2B(3\text{-}^t\!Bu,5\text{-}Mepz)_2]UI_2(THF)_2$ reacts with $Ph_3P{=}O$ to yield the base adduct $[H_2B(3\text{-}^t\!Bu,5\text{-}Mepz)_2]UI_2(O{=}PPh_3)_2$ (Maria *et al.*, 1999).

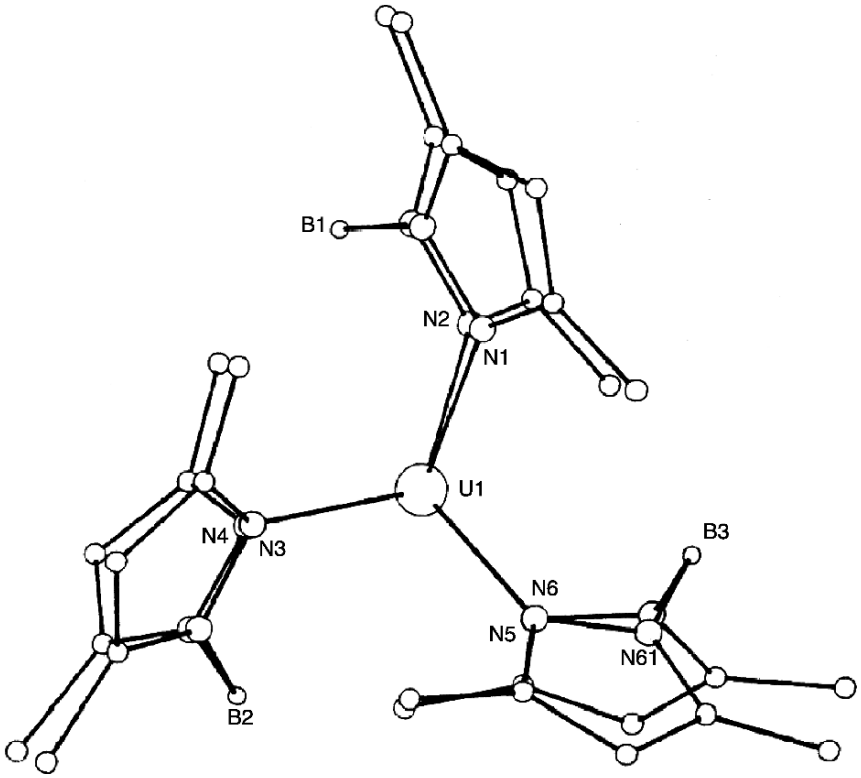

Fig. 25.35 *Molecular structure of* $[H(\mu\text{-}H)B(3,5\text{-}Me_2pz)_2]_3U$. *The PLUTO view is in the plane of one of the triangular faces of the trigonal prism* (*Carvalho* et al., 1992). (*Reprinted with permission from Elsevier.*)

Only one complex of a trivalent transuranic metal has been reported; reaction of $PuCl_3$ with $K[HB(3,5\text{-}Me_2pz)_3]$ in refluxing THF generates the dimeric complex $[PuCl(\mu\text{-}Cl)\{HB(3,5\text{-}Me_2pz)_3\}(3,5\text{-}Me_2pzH)]_2$ (Apostolidis *et al.*, 1991, 1998).

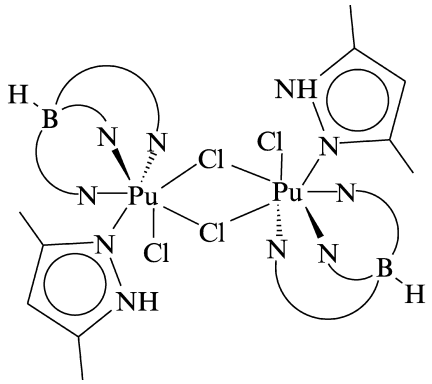

The chemistry of tetravalent actinides with poly(pyrazolyl)borates has been explored more extensively. The first report of metathesis reactions with thorium involved the preparation of the compounds $[HB(pz)_3]_{4-n}ThX_n$ ($n = 2$, X = Cl, Br; $n = 1$, X = Cl), $[HB(3,5\text{-}Me_2pz)_3]_2ThCl_2$, $[B(pz)_4]_2ThBr_2$, and base adducts of the complexes $[HB(pz)_3]ThCl_3$ and $[HB(pz)_3]_4Th$ (Bagnall *et al.*, 1978b), although subsequent reports have appeared describing other derivatives, including $[HB(3,5\text{-}Me_2pz)_3]ThCl_3$ (Ball *et al.*, 1987). The larger ionic radius of thorium enables higher coordination numbers; unlike the uranium complexes, the thorium derivatives $[HB(pz)_3]_2ThX_2$ (X = Cl, Br) were shown spectoscopically to possess tridentate pyrazolylborate ligands.

Several routes have been identified to produce $[HB(pz)_3]_2UI_2$, including reaction of UI_4 with two equivalents of $K[HB(pz)_3]$ in CH_2Cl_2 (Campello *et al.*, 1994), oxidation of $[HB(pz)_3]_2UI(THF)_2$ with iodine, and reaction of the tetravalent alkyl $[HB(pz)_3]_2U(CH_2SiMe_3)_2$ with iodine (Campello *et al.*, 1993). The reaction of UI_4 with two equivalents of $K[HB(pz)_3]$ in THF does not yield the same compound, however. Instead, the iodobutoxide complex $[HB(pz)_3]_2U(I)[O(CH_2)_4I]$ was isolated, presumably generated by ring-opening of solvent (Collin *et al.*, 1993; Campello *et al.*, 1994). The smaller size of the U(IV) ion, combined with the larger steric size of the $[HB(3,5\text{-}Me_2pz)_3]$ ligand, inhibits formation of bis(ligand) complexes of the substituted poly(pyrazolyl)borate; reaction of UCl_4 with two equivalents of $K[HB(3,5\text{-}Me_2pz)_3]$ leads to ligand degradation and the formation of $[HB(3,5\text{-}Me_2pz)_3]UCl_2(3,5\text{-}Me_2pz)$ [equation (25.110)] (Marques *et al.*, 1987a).

$$UCl_4 + 2K[HB(3,5\text{-}Me_2Pz)_3] \longrightarrow \quad (25.110)$$

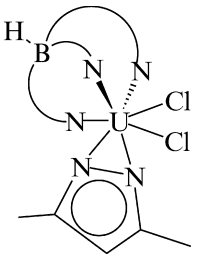

The complex $[HB(3,5\text{-}Me_2pz)_3]UCl_3(THF)$ contains a relatively weakly coordinated solvent molecule; the base-free complex can be isolated, and has been crystallographically characterized (Domingos *et al.*, 1990). The THF is also readily replaced by a number of other coordinating bases, permitting comparisons of relative ligand affinity. The relative affinities of a series of bases for $[HB(3,5\text{-}Me_2pz)_3]UCl_3$ was found to be

$$O{=}PPh_3 > C_6H_{11}NC > PhCN > MeCN > O{=}P(OEt)_3 > O{=}P(O{-}n\text{Bu})_3 > C_5H_5N > THF$$

Attempts to introduce a larger poly(pyrazolyl)borate ligand have established the steric limits of this system. Reaction of UCl_4 with one equivalent of the thallium salt of $[HB(3\text{-}Mspz)_3]^-$ (Ms = mesityl) generates only the product containing an isomerized ligand, $[HB(3\text{-}Mspz)_2(5\text{-}Mspz)]UCl_3$ (Silva *et al.*, 2000).

A variety of metathesis reactions have been carried out with the bis(ligand) actinide species $[HB(pz)_3]_2AnCl_2$ (An = Th, U) to generate complexes containing oxygen, nitrogen, or sulfur donors (Santos *et al.*, 1987; Domingos *et al.*, 1989a, 1992b,c), as depicted in Fig. 25.36.

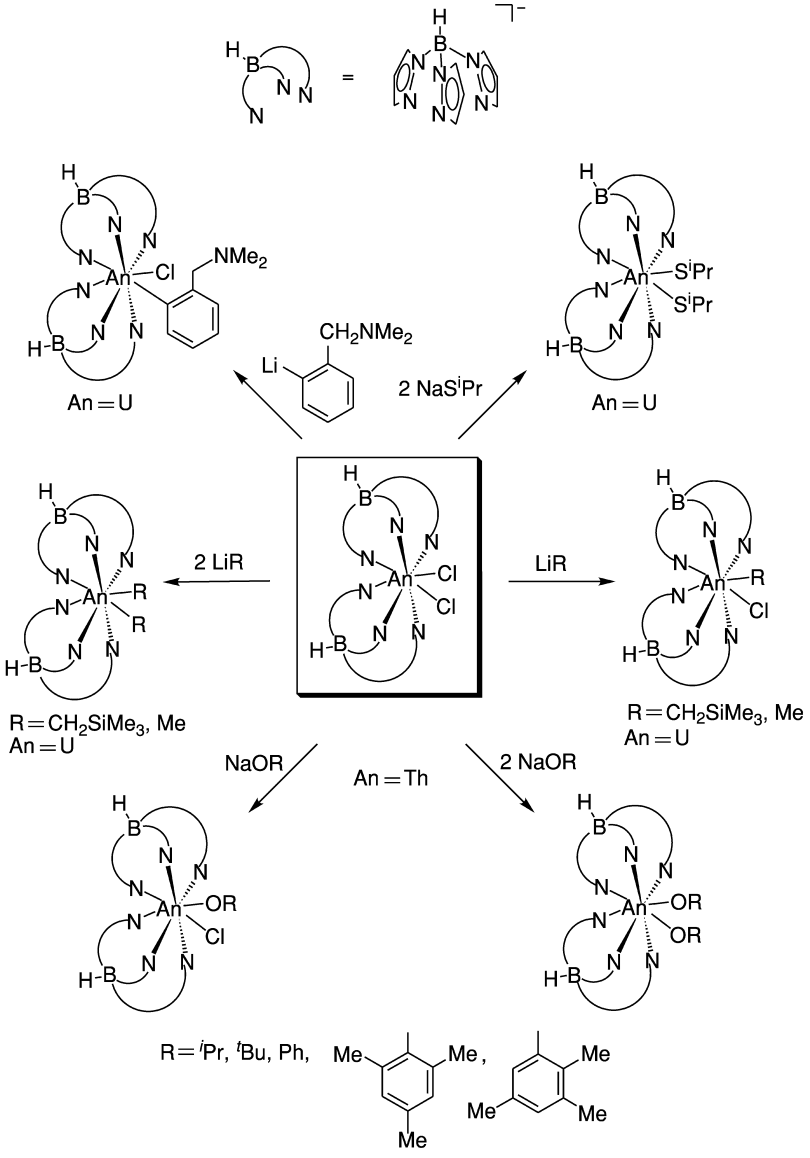

Fig. 25.36 *Chemical reactions of* $[HB(pz)_3]_2AnCl_2$ *(An = Th, U).*

Steric factors can be significant in these reactions. For example, reaction of bulky alkylamides with $[HB(pz)_3]_2UCl_2$ generates only the monoamide complexes $[HB(pz)_3]_2UCl(NR_2)$. These complexes display restricted rotation about the U–N bond at room temperature, indicating a significant degree of steric saturation. Relatively few complexes have been isolated containing alkyl ligands. Many reactions of U(IV) with alkyllithium reagents result in reduction of the metal center. The complexes $[HB(pz)_3]_2Th(CH_2SiMe_3)_2$, $[HB(pz)_3]_2U(R)Cl$ (R = Me, CH_2SiMe_3, *o*-$NMe_2CH_2C_6H_4$) and $[HB(pz)_3]_2UR_2$ (R = Me, CH_2SiMe_3) have been reported (Domingos *et al.*, 1992c; Campello *et al.*, 1997).

In an attempt to reduce the steric constraints of the ancillary ligand, derivatives of the mono(pyrazolylborate) complexes $[HB(3,5\text{-}Me_2pz)_3]AnCl_3(THF)$ (An = Th, U) have also been prepared (Marques *et al.*, 1987b; Domingos *et al.*, 1989b, 1992d; Leal *et al.*, 1992). As before, the degree of substitution is often dependent on the size of the ligand introduced; tris(amide) derivatives such as $[HB(3,5\text{-}Me_2pz)_3]An(NR_2)_3$ can be produced for R = Et, Ph, whereas for the larger ligand $[N(SiMe_3)_2]^-$, only a monoamide complex can be isolated. The monoalkoxide and monoaryloxide complexes of thorium have been reported to be unstable; uranium mono(phenoxide) and bis(phenoxide) complexes are only stable in the presence of a coordinating molecule of THF (Domingos *et al.*, 1989b). The complex $[HB(3,5\text{-}Me_2pz)_3]UCl_3(THF)$ is also susceptible to reduction by alkyllithium reagents; the full range of $[HB(3,5\text{-}Me_2pz)_3]U(Cl)_{3-x}(R)_x$ complexes have been prepared only for R = CH_2SiMe_3. Reaction of $[HB(3,5\text{-}Me_2pz)_3]UCl_3(THF)$ with phenyllithium results in the formation of U(III) species (Silva *et al.*, 1995), but the use of aryllithium reagents with bulky ortho-substituents permits isolation of mono(aryl) products, $[HB(3,5\text{-}Me_2pz)_3]UCl_2R$. The reactivity of $[HB(3,5\text{-}Me_2pz)_3]UCl_2(CH_2SiMe_3)$ and $[HB(3,5\text{-}Me_2pz)_3]UCl_2[CH(SiMe_3)_2]$ toward unsaturated substrates has been investigated (Domingos *et al.*, 1994); insertion similar to that reported in other alkyl complexes is observed. As an example, $[HB(3,5\text{-}Me_2pz)_3]UCl_2(CH_2SiMe_3)$ reacts with stoichiometric amounts of aldehydes, ketones, nitriles, and isonitriles to yield the corresponding secondary and tertiary alkoxide, azomethine, and iminoalkyl products.

The neptunium derivatives $[HB(pz)_3]_2NpCl_2$ and $[HB(3,5\text{-}Me_2pz)_3]NpCl_3(THF)$ have been produced from $NpCl_4$ (Apostolidis *et al.*, 1990).

The reaction of uranium tetrachloride with two equivalents of the bulky ligand $[B(pz)_4]^-$ as the potassium salt yields the complex $[B(pz)_4]_2UCl_2$ (Campello *et al.*, 1999). Although a limited number of derivatives of this compound could be produced, in general the ligand set provided less thermal stability than comparable complexes of the '$[HB(pz)_3]_2U$' fragment. The complex $[B(pz)_4]_2UCl_2$ displays eight-coordinate geometry in the solid state, in a distorted square antiprismatic arrangement of ligands (Fig. 25.37).

The complex is fluxional in solution; ^1H NMR spectra demonstrate that all coordinated pyrazolylborate rings are equivalent. For the derivatives $[B(pz)_4]_2UCl(O^tBu)$, $[B(pz)_4]_2UCl(O\text{-}2,4,6\text{-}Me_3C_6H_2)$, $[B(pz)_4]_2U(S^iPr)_2$, and

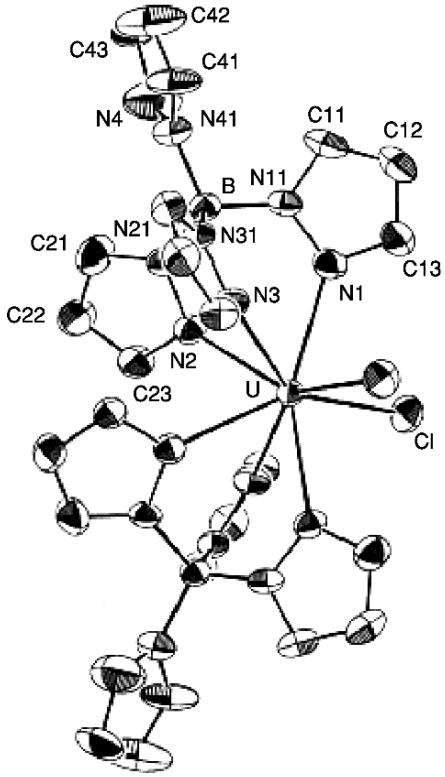

Fig. 25.37 *Molecular structure of* $[B(pz)_4]_2UCl_2$ (*Campello* et al., 1999). (*Reprinted with permission from Elsevier*.)

$[B(pz)_4]_2U(O^tBu)_2$, it is possible to slow down the interconversion of the typical eight-coordinate polyhedra (square antiprism ↔ dodecahedron ↔ bicapped trigonal prism). At higher temperatures, it was possible for some of these compounds to reach a regime where all pyrazolyl groups were equivalent on the NMR timescale, indicating dissociative exchange of free and coordinated rings.

25.4.3 Tris(amidoamine)

As in the case of early transition metals, the tris(amido)amine class of ligands, $[N(CH_2CH_2NR)_3]^{3-}$ (R = trialkylsilyl), has proven to be a versatile ligand set that supports unusual reactivity in the early actinides. Complexes of both thorium and uranium have been generated by metathesis reactions involving both the ligands $[N(CH_2CH_2NSiMe_3)_3]^{3-}$ and $[N(CH_2CH_2NSi^tBuMe_2)_3]^{3-}$. The complexes $[\{N(CH_2CH_2NSiMe_3)_3\}AnCl]_2$ (An = Th, U) were the first to be reported (Scott and Hitchcock, 1994); the molecular structure of the uranium complex demonstrated it was dimeric in the solid state. The chloride ligand may

be substituted, and derivatives incorporating cyclopentadienyl, borohydride, alkoxide, amide, and diazabutadiene derivatives have been characterized (Scott and Hitchcock, 1995a,b; Roussel *et al.*, 1997a, 1999). Attempts to alkylate the complex $[N(CH_2CH_2NSi^tBuMe_2)_3]UI$ with alkyllithium or alkylpotassium reagents resulted in the isolation of a metallacyclic product resulting from intramolecular activation of a methyl group, as shown in equation (25.111) (Boaretto *et al.*, 1999).

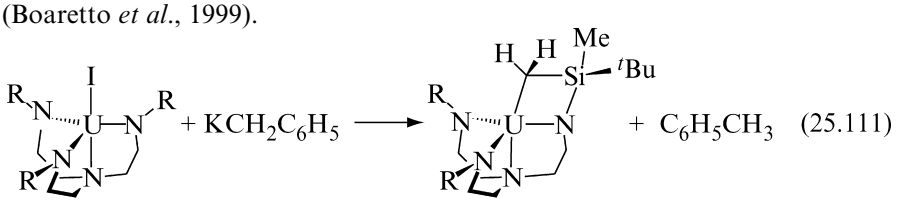

(25.111)

R = Si^tBuMe_2

The U–C bond length in the metallacyclic unit is unusually long [2.752(11) Å], and is susceptible to protonation by alcohols, amines, and terminal alkynes; reaction with pyridine leads to the generation of a η^2-pyridyl complex.

Initial attempts to reduce the complex $[N(CH_2CH_2NSi^tBuMe_2)_3]UCl$ resulted in the formation of a mixed-valence complex $[\{N(CH_2CH_2NSi^tBuMe_2)_3\}U]_2(\mu\text{-Cl})$ (Roussel *et al.*, 1996, 1997b). The complex is thought to possess electronically distinct U(III) and U(IV) centers. Fractional sublimation results in the isolation of a purple species, identified as the trivalent $[N(CH_2CH_2NSi^tBuMe_2)_3]U$ (Roussel *et al.*, 1997b). This complex can also be produced by reduction of $[N(CH_2CH_2NSi^tBuMe_2)_3]UI$ by potassium in pentane. A variety of base adducts of this complex have been reported (Roussel *et al.*, 2002). The U(III) complex can similarly be oxidized by trimethylamine *N*-oxide, trimethylsilyazide, and trimethylsilyldiazomethane to yield μ-oxo, imido, and hydrazido derivatives, respectively (Roussel *et al.*, 2002). One of the most unusual adducts isolated in this system is prepared by the reaction of the U(III) complex with dinitrogen [equation (25.112)].

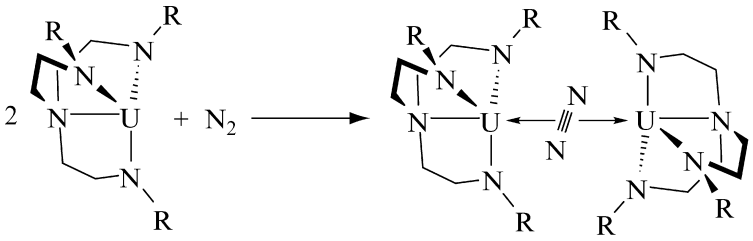

(25.112)

R = Si^tBuMe_2

The molecular structure of the complex has been reported (Roussel and Scott, 1998) (Fig. 25.38). The N–N distances in the dinitrogen unit are essentially unperturbed. Metrical data, along with magnetic data, suggest that the complex

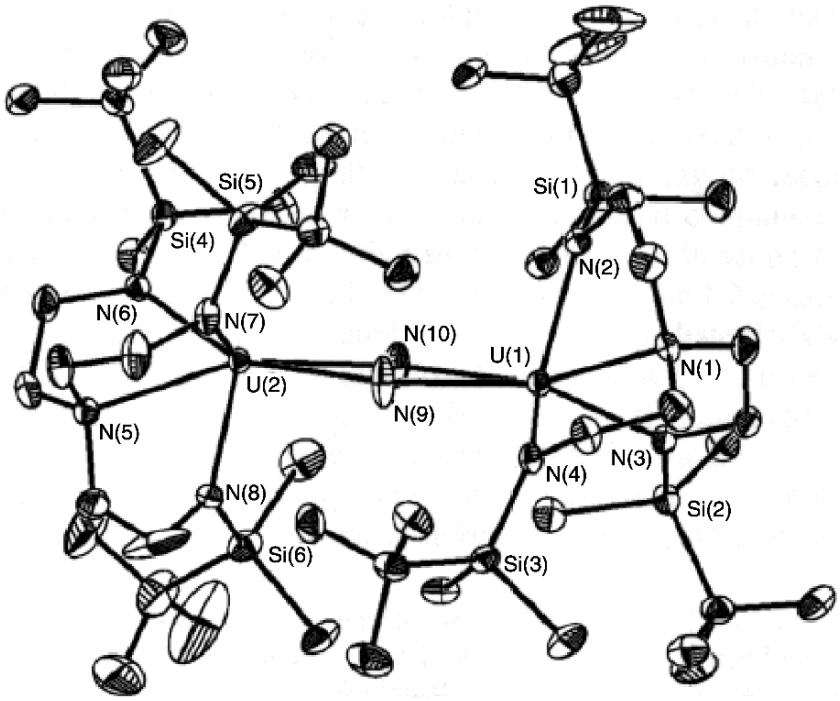

Fig. 25.38 *Molecular structure of* $[\{N(CH_2CH_2NSi^tBuMe_2)_3\}U](\mu^2\text{-}\eta^2\text{:}\eta^2\text{-}N_2)$. (*Reprinted with permission from Roussel and Scott* (1998). *Copyright* 1998 *American Chemical Society.*)

may be best formulated as a U(III) species. The electronic structure of this complex has been investigated; the only significant U–N_2–U interaction was found to consist of U→N_2 π-backbonding (Kaltsoyannis and Scott, 1998).

25.4.4 Other

Few other ligands have been developed with the steric bulk and solubility to stabilize mononuclear actinide complexes and support organometallic chemistry. A bulky amide ligand set has been developed for uranium that supports novel coordination complexes of lower valent uranium. Complexes of the formula $(NRAr)_3UI$ (R = ^{t}Bu, adamantyl; Ar = 3,5-$Me_2C_6H_3$) may be prepared by the reaction of $UI_3(THF)_4$ with Li[NRAr] (Odom *et al.*, 1998); oxidation of the uranium center is presumed to be accompanied by sacrificial generation of U(0). A limited number of tetravalent derivatives of this ligand set have been reported, including the silyl complex $(N^tBuAr)_3U[Si(SiMe_3)_3]$ (Diaconescu *et al.*, 2001) and the bridging cyanoimide complex $(N^tBuAr)_3U{=}N{=}C{=}N{=}U(N^tBuAr)_3$ (Ar = 3,5-$Me_2C_6H_3$) (Mindiola *et al.*, 2001).

Reduction of the uranium (IV) complex by sodium amalgam results in the isolation of $(N^tBuAr)_3U(THF)$ (Ar = 3,5-$Me_2C_6H_3$). Reaction of the trivalent complex with $Mo[N(Ph)(R')]_3$ (R′ = ^{t}Bu, adamantyl) under dinitrogen results in the formation of $[N^tBuAr]_3U(\mu\text{-}N_2)Mo[N(Ph)(R')]_3$, which contains a linear Mo–N–N–U unit. It is suggested that both metals are best regarded as tetravalent. As previously mentioned, reduction of $(N^tBuAr)_3UI$ also provides entry into an interesting class of μ-arene complexes (*vide supra*).

25.5 BIMETALLIC COMPLEXES

One of the least explored aspects of the non-aqueous chemistry of the actinides is that of complexes containing other metals. Bimetallic complexes have been studied with the intent of creating complexes with two centers of reactivity for effecting chemical transformations. In addition, interest has grown in creating true metal–metal bonds. These complexes are rare; metal–metal bonding is disfavored in the f-elements with respect to d-transition metals, perhaps due to the limited radial extent of valence d- and f-orbitals most likely to be employed in bonding between two metal centers.

Many of the early attempts to generate bimetallic complexes focused on metathesis reactions involving the introduction of anionic metal carbonylate ligands onto actinide cations (Bennett *et al.*, 1971; Dormond and Moise, 1985). These reactions invariably resulted in the isolation of isocarbonyl species in which the actinide was bound by the oxygen atom of one or more carbonyl ligands [equation (25.113)].

$$UCl_4 + 4Na[Mn(CO)_5] \xrightarrow{THF} U[Mn(CO)_5]_4 + 4NaCl \qquad (25.113)$$

More recently, synthetic efforts have been further expanded to include several classes of compounds in which bridging ligands hold two metal centers in close proximity, but no evidence exists for a metal–metal interaction. Bridging hydride complexes $(\eta^5\text{-}C_5H_5)_3UH_6ReL_2$ (L = PPh_3, P(*p*-F-C_6H_4)$_3$) have been prepared by the reaction of $(\eta^5\text{-}C_5H_5)_3UCl$ with $[K(THF)_2][L_2ReH_6]$ in THF (Baudry and Ephritikhine, 1986). The compounds are fluxional at room temperature in solution, judging from the equivalence of all hydride ligands in the ^{1}H NMR spectrum, but it has been hypothesized that the Re and U centers are bridged by multiple hydride ligands. Ring-substituted analogs $(\eta^5\text{-}C_5H_4R)_3UH_6Re(PPh_3)_2$ could not be prepared directly from $(\eta^5\text{-}C_5H_4R)_3UCl$; rather, the cationic reagent $[(\eta^5\text{-}C_5H_4R)_3U][BPh_4]$ was employed (Cendrowski-Guillaume and Ephritikhine, 1996). Reaction of $(\eta^5\text{-}C_5Me_5)_2UCl(THF)$ with $[K(THF)_2][(PPh_3)_2ReH_6]$ does not result in simple metathesis. Instead, an anionic product of the formula $[K(THF)_2][(\eta^5\text{-}C_5Me_5)_2U(Cl)H_6Re(PPh_3)_2]$ is obtained (Cendrowski-Guillaume *et al.*, 1994; Cendrowski-Guillaume and Ephritikhine, 1996). NMR data suggest that three hydride ligands bridge the two metal centers.

Other examples of bimetallic complexes are generated using ligands on the actinide center that have pendant phosphine groups capable of binding transition metal centers. The diphenylphosphidocyclopentadienyl ligand acts as an electron-poor carbocyclic ligand in the synthesis of bis- and tris-cyclopentadienyl uranium complexes $(\eta^5\text{-}C_5H_4PPh_2)_3UX$ and $(\eta^5\text{-}C_5H_4PPh_2)_2UX_2$ (X = Cl, OR, R, NEt_2, BH_4) (Dormond *et al.*, 1990; Baudry *et al.*, 1993). In reactions with suitable transition metal reagents, complexes can be prepared in which the diphenylphosphide group binds to a second metal center (Dormond *et al.*, 1990; Baudry *et al.*, 1993; Hafid *et al.*, 1994) (equation (25.114)).

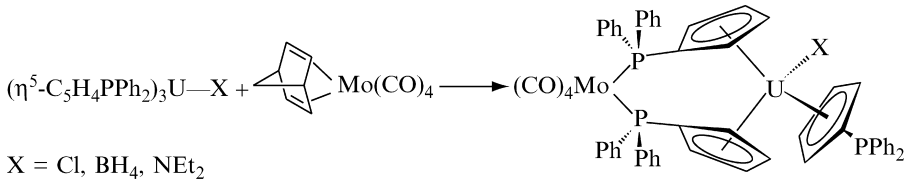

(25.114)

A second approach involves the use of cyclopentadienyl complexes in which the other substituents have pendant phosphine groups. A series of alkoxyphosphido complexes of uranium have been prepared for both bis- and tris-cyclopentadienyl frameworks: $(\eta^5\text{-}C_5Me_5)_2UCl[O(CH_2)_nPPh_2]$, $(\eta^5\text{-}C_5Me_5)_2U[O(CH_2)_nPPh_2]_2$, and $(\eta^5\text{-}C_5H_5)_3U[O(CH_2)_nPPh_2]$ (n = 0,1) (Dormond *et al.*, 1994). These species react with (norbornadiene)$M(CO)_4$ (M = Mo, W) to yield bimetallic compounds. The complexes $(\eta^5\text{-}C_5Me_5)_2U[O(CH_2)_nPPh_2]_2$ generate 1:1 (U:M) products in which both phosphorus atoms are bound to a single transition metal. As illustrated in equation (25.115), the complexes $(\eta^5\text{-}C_5Me_5)_2UCl[O(CH_2)_nPPh_2]$ and $(\eta^5\text{-}C_5H_5)_3U[O(CH_2)_nPPh_2]$ react to form 2:1 (U:M) adducts in which the metal carbonyl fragment is bound to one 'arm' of each of the uranium units:

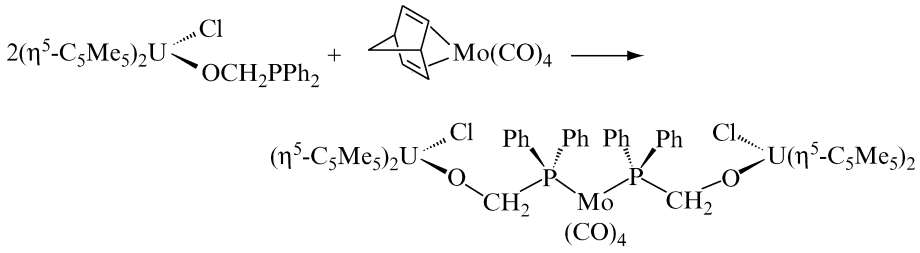

(25.115)

The compounds containing the sterically less hindered OCH_2PPh_2 ligand react more quickly in substitution reactions that their counterparts containing $OPPh_2$.

The phospholyl ligand has also demonstrated the ability to bridge two metal centers in a $\mu\text{-}\eta^5,\eta^1$ manner. Reduction of $NiCl_2$ in the presence of the previously mentioned uranium phospholyl compound $(\eta^5\text{-}C_5Me_4P)_2UCl_2$ yields the complex $Cl_2U(\mu\text{-}\eta^5,\eta^1\text{-}C_5Me_4P)_2Ni(\mu\text{-}\eta^5,\eta^1\text{-}C_5Me_4P)_2UCl_2$ in which the

central nickel atom is bound in a near-tetrahedral fashion by four phosphorus atoms from the four phospholyl ligands (Arliguie *et al.*, 1996).

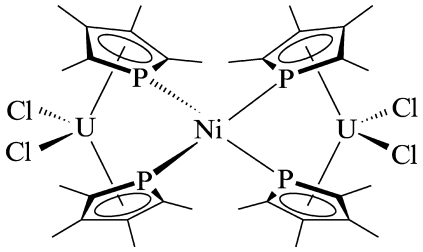

The dimeric nickel phospholyl complex $(\eta^5\text{-}C_5Me_4P)Ni(\mu\text{-}\eta^1\text{-}C_5Me_4P)_2Ni(\eta^5\text{-}C_5Me_4P)$ can also be prepared; reduction of this in the presence of two equivalents of $(\eta^5\text{-}C_5Me_4P)_2UCl_2$ yields a tetrametallic complex $[Cl_2U(\mu\text{-}\eta^5,\eta^1\text{-}C_5Me_4P)_2Ni(\mu\text{-}\eta^1\text{-}C_5Me_4P)_2Ni(\mu\text{-}\eta^5,\eta^1\text{-}C_5Me_4P)_2UCl_2]$ (Fig. 25.39). In these complexes, long U···Ni distances (>3.3 Å) preclude direct metal–metal interaction.

Select compounds have been prepared in which the bridging ligands appear to coexist with a direct metal–metal interaction. The phosphido-bridged complexes $(\eta^5\text{-}C_5Me_5)_2Th(\mu\text{-}PPh_2)_2ML_n$ [ML_n = $Ni(CO)_2$, $Pt(PMe_3)$] are prepared by the reaction of the thorium phosphide precursor, $(\eta^5\text{-}C_5Me_5)_2Th(PPh_2)_2$ with an olefin complex of the appropriate transition metal species in the presence of additional ligand [equations (25.116) and (25.117)] (Ritchey *et al.*, 1985; Hay *et al.*, 1986).

$$(\eta^5\text{-}C_5Me_5)_2\,Th(PPh_2)_2 + Ni(COD)_2 + 2CO \longrightarrow (\eta^5\text{-}C_5Me_5)_2Th\begin{array}{c}Ph_2\\P\\\diagup\quad\diagdown\\Ni(CO)_2\\\diagdown\quad\diagup\\P\\Ph_2\end{array} \qquad (25.116)$$

$$(\eta^5\text{-}C_5Me_5)_2Th(PPh_2)_2 + Pt(COD)_2 + PMe_3 \longrightarrow (\eta^5\text{-}C_5Me_5)_2Th\begin{array}{c}Ph_2\\P\\\diagup\quad\diagdown\\Pt\text{—}PMe_3\\\diagdown\quad\diagup\\P\\Ph_2\end{array} \qquad (25.117)$$

Calculations performed on both complexes suggest the presence of a direct M–Th interaction (Hay *et al.*, 1986; Ortiz, 1986). This contention appears to be supported both by ^{31}P NMR and structural evidence. The thorium–metal distance in each compound is shorter than that expected on the basis of metal radii derived from related structures without metal–metal nonbonded distances [Th–Ni = 3.206(2) Å, Th–Pt = 2.984(1) Å]. Furthermore, the Th–M–P_2 unit is 'folded' about the phosphide ligands in each case to bring the two metal atoms

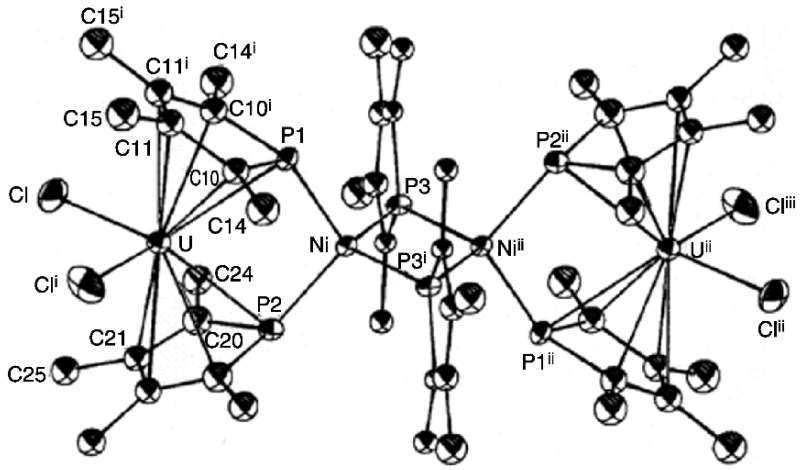

Fig. 25.39 *Molecular structure of* $[Cl_2U(\mu\text{-}\eta^5,\eta^1\text{-}C_5Me_4P)_2Ni(\mu\text{-}\eta^1\text{-}C_5Me_4P)_2Ni(\mu\text{-}\eta^5,\eta^1\text{-}C_5Me_4P)_2UCl_2]$ (*Arliguie* et al., 1996). (*Reprinted with permission from Elsevier.*)

in closer proximity. Theoretical examination of these compounds suggest that the interaction is essentially a M→Th (M = Ni, Pt) dative donor–acceptor bond, involving principally metal d-orbitals.

One class of compounds exist which possess an unsupported metal–metal interaction. Reaction of $(\eta^5\text{-}C_5Me_5)_2ThX_2$ (X = Cl, I) with $Na[(\eta^5\text{-}C_5H_5)Ru(CO)_2]$ produces the complexes $(\eta^5\text{-}C_5Me_5)_2Th(X)Ru(\eta^5\text{-}C_5H_5)(CO)_2$ [equation (25.118)] (Sternal *et al.*, 1985). This synthetic methodology has also been extended to include derivatives of the tris(cyclopentadienyl) framework [equation (25.119)] (Sternal and Marks, 1987).

$$(\eta^5\text{-}C_5Me_5)_2ThX_2 + Na[(\eta^5\text{-}C_5H_5)Ru(CO)_2] \longrightarrow (\eta^5\text{-}C_5Me_5)_2Th(X)Ru(CO)_2 + NaX \qquad X = Cl, I \qquad (25.118)$$

$$(\eta^5\text{-}C_5H_5)_3AnCl \; (An = Th, U) + Na[(\eta^5\text{-}C_5H_5)M(CO)_2] \; (M = Fe, Ru) \longrightarrow (\eta^5\text{-}C_5H_5)_3An\text{–}M(CO)_2 + NaX \qquad (25.119)$$

The molecular structure of $(\eta^5\text{-}C_5Me_5)_2Th(I)Ru(\eta^5\text{-}C_5H_5)(CO)_2$ has been determined (Fig. 25.40); it confirms the presence of a direct metal–metal interaction, with a Th–Ru bond length of 3.0277(6) Å.

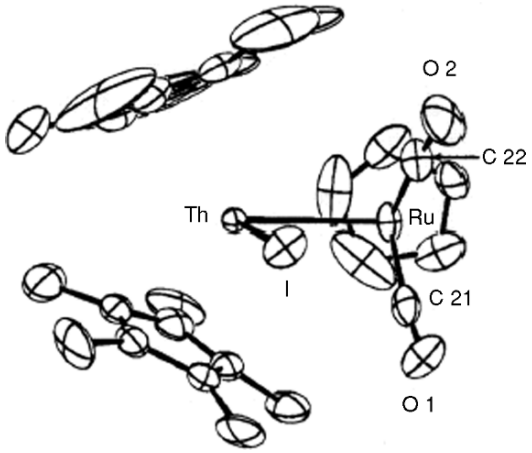

Fig. 25.40 *Molecular structure of* (η^5-C_5Me_5)$_2$*Th*(*I*)*Ru*(η^5-C_5H_5)(*CO*)$_2$. (*Reprinted with permission from Sternal* et al. (1985). *Copyright* 1985 *American Chemical Society*.)

The bond distance is sensitive to the identity of the metal; the Th–Fe distance in the complex (η^5-C_5H_5)$_3$ThFe(η^5-C_5H_5)(CO)$_2$ is 2.940(5) Å. Variable temperature NMR data for the complexes (η^5-C_5H_5)$_3$AnM(η^5-C_5H_5)(CO)$_2$ (M = Fe, Ru) suggest rotation about the metal–metal bond is hindered in solution at room temperature. Thermochemical measurements have determined U–M bond disruption enthalpies for the derivatives (η^5-C_5H_5)$_3$UM(η^5-C_5H_5)(CO)$_2$ [M = Fe, 30.9 (3.0) kcal/mol; M = Ru, 40.4 (4.0) kcal/mol], indicating relatively weak metal–metal interactions (Nolan *et al.*, 1991). Consistent with this observation, the An–M interactions are easily disrupted by protic reagents. In addition, reaction of (η^5-C_5Me_5)$_2$Th(Cl)Ru(η^5-C_5H_5)(CO)$_2$ with coordinating bases (such as ketones or acetonitrile) generates (η^5-C_5H_5)Ru(CO)$_2$H, along with thorium products arising from C–H activation of the Lewis base substrate, followed by insertion of a second (and third) equivalent of the Lewis base (Sternal *et al.*, 1987). Theoretical examination of the bonding (η^5-C_5Me_5)$_2$Th(I)Ru(η^5-C_5H_5)(CO)$_2$ (Bursten and Novo-Gradac, 1987) demonstrates that once again, the bonding is best described as a Ru→Th dative donor–acceptor bond, involving principally Th 6d and Ru 4d orbitals.

25.6 NEUTRAL CARBON-BASED DONOR LIGANDS

One of the most common ligands in d-transition metal organometallic chemistry, the carbonyl ligand, is virtually unknown in actinide chemistry. Aside from the carbon monoxide adducts of tris(cyclopentadienyl)uranium previously described (see Section 25.2.1.1), there are no actinide carbonyl complexes that are

isolable at room temperature and pressure. Uranium carbonyl complexes U $(CO)_n$ ($n = 1$–6) were first reported to form in matrix isolation experiments and were produced by the condensation of thermally generated uranium vapor with carbon monoxide in an argon matrix at 4 K (Slater *et al.*, 1971; Sheline and Slater, 1975). More recent studies indicate that thermal and pulsed-laser evaporated uranium atoms undergo reaction with CO in argon matrices to generate the linear triatomic species CUO (Tague *et al.*, 1993). Tague *et al.* (1993) indicate that higher uranium carbonyls ($n > 2$) are only produced upon subsequent annealing of the matrices to 15—30 K. Photolysis was reported to regenerate CUO from the carbonyls.

The most recent class of Group 14 donor ligands to be employed in actinide chemistry is that of *N*-heterocyclic carbenes. These ligands act as σ-donor bases toward a number of metals in coordination chemistry. Reaction of $[UO_2Cl_2(THF)_2]_2$ with 1,3-dimesitylimidazole-2-ylidene and its 4,5-dichloro-substituted derivative generate 1:2 (uranium:carbene) adducts $UO_2Cl_2(L)_2$ (Oldham *et al.*, 2001). Crystallographic characterization reveals an octahedral metal center with *trans* oxo, chloro, and carbene ligands. The uranium–carbon bond distances in these species are long at 2.626(7) and 2.609(4) Å, consistent with the formulation of the C–U bond as a dative interaction.

ACKNOWLEDGMENTS

C. J. Burns gratefully acknowledges support at LANL by the U.S. Department of Energy, Office of Science, Office of Basic Energy Sciences, Division of Chemical Sciences, Geosciences, and Biosciences. M. S. Eisen thanks the Fund for the Promotion of Research at The Technion. C. J. Burns thanks Dr. J. Kiplinger for intellectual input and technical assistance.

REFERENCES

Adam, M., Yunlu, K., and Fischer, R. D. (1990) *J. Organomet. Chem.*, **387**, C13–16.

Adam, R., Villiers, C., Ephritikhine, M., Lance, M., Nierlich, M., and Vigner, J. (1993) *J. Organomet. Chem.*, **445**, 99–106.

Andersen, R., Carmona-Guzman, E., Mertis, K., Sigurdson, E., and Wilkinson, G. (1975) *J. Organomet. Chem.*, **99**, C19–20.

Andersen, R. A. (1979) *Inorg. Chem.*, **18**, 1507–9.

Apostolidis, C., Kanellakopulos, B., Maier, R., Marques, N., Pires de Matos, A., and Santos, I. (1990) *20^e Journées des Actinides*, Prague.

Apostolidis, C., Kanellakopulos, B., Maier, R., Meyer, D., Marques, N., and Rebizant, J. (1991) *21^e Journées des Actinides*, Montechoro, Portugal.

Apostolidis, C., Carvalho, A., Domingos, A., Kanellakopulos, B., Maier, R., Marques, N., Pires de Matos, A., and Rebizant, J. (1998) *Polyhedron*, **18**, 263–72.
Apostolidis, C., Edelmann, F. T., Kanellakopulos, B., and Reissmann, U. (1999) *Z. Naturforsch., B: Chem. Sci.*, **54**, 960–2.
Arduini, A. L., Edelstein, N. M., Jamerson, J. D., Reynolds, J. G., Schmid, K., and Takats, J. (1981) *Inorg. Chem.*, **20**, 2470–4.
Arliguie, T., Baudry, D., Ephritikhine, M., Nierlich, M., Lance, M., and Vigner, J. (1992) *J. Chem. Soc.*, *Dalton Trans.*, 1019–24.
Arliguie, T., Lance, M., Nierlich, M., Vigner, J., and Ephritikhine, M. (1994) *J. Chem. Soc.*, *Chem. Commun.*, 847–8.
Arliguie, T., Lance, M., Nierlich, M., Vigner, J., and Ephritikhine, M. (1995) *J. Chem. Soc.*, *Chem. Commun.*, 183–4.
Arliguie, T., Ephritikhine, M., Lance, M., and Nierlich, M. (1996) *J. Organomet. Chem.*, **524**, 293–7.
Arliguie, T., Fourmigue, M., and Ephritikhine, M. (2000) *Organometallics*, **19**, 109–11.
Arnaudet, L., Charpin, P., Folcher, G., Lance, M., Nierlich, M., and Vigner, D. (1986) *Organometallics*, **5**, 270–4.
Arney, D. S. J., Burns, C. J., and Smith, D. C. (1992) *J. Am. Chem. Soc.*, **114**, 10068–9.
Arney, D. S. J. and Burns, C. J. (1993) *J. Am. Chem. Soc.*, **115**, 9840–1.
Arney, D. S. J. and Burns, C. J. (1995) *J. Am. Chem. Soc.*, **117**, 9448–60.
Arney, D. S. J., Schnabel, R. C., Scott, B. C., and Burns, C. J. (1996) *J. Am. Chem. Soc.*, **118**, 6780–1.
Aslan, H., Yunlu, K., Fischer, D., Bombieri, G., and Benetollo, F. (1988) *J. Organomet. Chem.*, **354**, 63–76.
Avdeef, A., Raymond. K. N., Hodgson, K. O., and Zalkin, A. (1972) *Inorg. Chem.*, **11**, 1083–8.
Avens, L. R., Burns, C. J., Butcher, R. J., Clark, D. L., Gordon, J. C., Schake, A. R., Scott, B. L., Watkin, J. G., and Zwick, B. D. (2000) *Organometallics*, **19**, 451–7.
Bagnall, K. W. and Edwards, J. (1974) *J. Organomet. Chem.*, **80**, C14–16.
Bagnall, K. W., Du Preez, J. G. H., and Warren, R. F. (1975) *J. Chem. Soc.*, *Dalton Trans.*, 140–3.
Bagnall, K. W., Edwards, J., and Heatley, F. (1976) *Transplutonium 1975*, *Proc. 4th Int. Transplutonium Elem. Symp.* (eds. W. Mueller and R. Lindner), North-Holland, Amsterdam, pp. 119–22.
Bagnall, K. W., Edwards, J., and Tempest, A. C. (1978a) *J. Chem. Soc.*, *Dalton Trans.*, 295–8.
Bagnall, K. W., Beheshti, A., and Heatley, F. (1978b) *J. Less Common Metals*, **61**, 171–6.
Bagnall, K. W., Plews, M. J., and Brown, D. (1982a) *J. Organomet. Chem.*, **224**, 263–6.
Bagnall, K. W., Plews, M. J., Brown, D., Fischer, R. D., Klahne, E., Landgraf, G. W., and Sienel, G. R. (1982b) *J. Chem. Soc.*, *Dalton Trans.*, 1999–2007.
Bagnall, K. W., Payne, G. F., and Brown, D. (1985) *J. Less Common Metals*, **113**, 325–9.
Bagnall, K. W., Payne, G. F., Alcock, N. W., Flanders, D. J., and Brown, D. (1986) *J. Chem. Soc.*, *Dalton Trans.*, 783–7.
Ball, R. G., Edelman, F., Matisons, J. G., Takats, J., Marques, N., Marçalo, J., Pires de Matos, A., and Bagnall, K. W. (1987) *Inorg. Chim. Acta*, **132**, 137–43.

Baranger, A. M., Walsh, P. J., and Bergman, R. G. (1993) *J. Am. Chem. Soc.*, **115**, 2753–63.
Baudry, D. and Ephritikhine, M. (1986) *J. Organomet. Chem.*, **311**, 189–92.
Baudry, D. and Ephritikhine, M. (1988) *J. Organomet. Chem.*, **349**, 123–30.
Baudry, D., Dorion, P., and Ephritikhine, M. (1988) *J. Organomet. Chem.*, **356**, 165–71.
Baudry, D., Bulot, E., Charpin, P., Ephritikhine, M., Lance, M., Nierlich, M., and Vigner, J. (1989a) *J. Organomet. Chem.*, **371**, 155–62.
Baudry, D., Bulot, E., and Ephritikhine, M. (1989b) *J. Chem. Soc.*, *Chem. Commun.*, 1316–17.
Baudry, D., Bulot, E., Charpin, P., Ephritikhine, M., Lance, M., Nierlich, M., and Vigner, J. (1989c) *J. Organomet. Chem.*, **371**, 163–74.
Baudry, D., Bulot, E., Ephritikhine, M., Nierlich, M., Lance, M., and Vigner, J. (1990a) *J. Organomet. Chem.*, **388**, 279–87.
Baudry, D., Bulot, E., and Ephritikhine, M. (1990b) *J. Organomet. Chem.*, **397**, 169–75.
Baudry, D., Ephritikhine, M., Nief, F., Ricard, L., and Mathey, F. (1990c) *Angew. Chem. Int. Edn Engl.*, **29**, 1485–6.
Baudry, D., Dormond, A., and Hafid, A. (1993) *New J. Chem.*, **17**, 465–70.
Baudry, D., Dormond, A., and Hafid, A. (1995) *J. Organomet. Chem.*, **494**, C22–23.
Baumgärtner, F., Fischer, E. O., Kanellakopulos, B., and Laubereau, P. (1965) *Angew. Chem. Inter. Edn*, **4**, 878.
Baumgärtner, F., Fischer, E. O., Kanellakopulos, B., and Laubereau, P. (1966) *Angew. Chem. Inter. Edn*, **5**, 134.
Baumgärtner, F., Fischer, E. O., and Laubereau, P. (1967) *Radiochim. Acta*, **7**, 188–97.
Baumgärtner, F., Fischer, E. O., Kanellakopulos, B., and Laubereau, P. (1968) *Angew. Chem. Inter. Edn*, **7**, 634.
Baumgärtner, F., Fischer, E. O., Kanellakopulos, B., and Laubereau, P. (1969) *Angew. Chem. Inter. Edn*, **8**, 202.
Baumgärtner, F., Fischer, E. O., Billich, H., Dornberger, E., Kanellakopulos, B., Roth, W., and Steiglitz, L. (1970) *J. Organomet. Chem.*, **22**, C17–19.
Bennett, R. L., Bruce, M. I., and Stone, F. G. A. (1971) *J. Organomet. Chem.*, **26**, 355–6.
Berthet, J. C., Le Marechal, J. F., and Ephritikhine, M. (1990) *J. Organomet. Chem.*, **393**, C47–8.
Berthet, J. C., Lance, M., Nierlich, M., Vigner, J., and Ephritikhine, M. (1991a) *J. Organomet. Chem.*, **420**, C9–11.
Berthet, J. C., Le Marechal, J.-F., Nierlich, M., Lance, M.., Vigner, J., and Ephritikhine, M. (1991b) *J. Organomet. Chem.*, **408**, 335–41.
Berthet, J. C. and Ephritikhine, M. (1992) *New J. Chem.*, **16**, 767–8.
Berthet, J. C., Villiers, C., Le Marechal, J.-F., Delavaux-Nicot, B., Lance, M., Nierlich, M., Vigner, J., and Ephritikhine, M. (1992a) *J. Organomet. Chem.*, **440**, 53–65.
Berthet, J. C., Le Marechal, J.-F., Lance, M., Nierlich, M., Vigner, J., and Ephritikhine, M. (1992b) *J. Chem. Soc.*, *Dalton Trans.*, 1573–7.
Berthet, J. C., Ephritikhine, M., Lance, M., Nierlich, M., and Vigner, J. (1993) *J. Organomet. Chem.*, **460**, 47–53.

Berthet, J. C. and Ephritikhine, M. (1993) *J. Chem. Soc*, *Chem. Commun.*, 1566–7.
Berthet, J. C., Le Marechal, J. F., and Ephritikhine, M. (1994) *J. Organomet. Chem.*, **480**, 155–61.
Berthet, J. C., Boisson, C., Lance, M., Vigner, J., Nierlich, M., and Ephritikhine, M. (1995) *J. Chem. Soc., Dalton Trans.*, **18**, 3027–33.
Berthet, J. C., Lance, M., Nierlich, M., and Ephritikhine, M. (1998) *Chem. Commun.*, 1373–4.
Berthet, J. C., Nierlich, M., and Ephritikhine, M. (2002) *Comptes Rendus Chimie*, **5**, 81–7.
Beshouri, S. M. and Zalkin, A. (1989) *Acta Crystallogr., Sect. C*, **45**, 1221–2.
Bettonville, S., Goffart, J., and Fuger, J. (1989) *J. Organomet. Chem.*, **377**, 59–67.
Bettonville, S., Goffart, J., and Fuger, J. (1990) *J. Organomet. Chem.*, **393**, 205–11.
Billiau, F., Folcher, G., Marquet-Ellis, H., Rigny, P., and Saito, E. (1981) *J. Am. Chem. Soc.*, **103**, 5603–4.
Blake, P. C., Lappert, M. F., Atwood, J. L., and Zhang, H. (1986a) *J. Chem. Soc.*, *Chem. Commun.*, 1148–9.
Blake, P. C., Lappert, M. F., Taylor, R. G., Atwood, J. L., Hunter, W. E., and Zhang, H. (1986b) *J. Chem. Soc.*, *Chem. Commun.*, 1394–5.
Blake, P. C., Lappert, M. F., Taylor, R. G., Atwood, J. L., and Zhang, H. (1987) *Inorg. Chim. Acta*, **139**, 13–20.
Blake, P. C., Lappert, M. F., Atwood, J. L., and Zhang, H. (1988) *J. Chem. Soc.*, *Chem. Commun.*, 1436–8.
Blake, P. C., Lappert, M. F., Taylor, R. G., Atwood, J. L., Hunter, W. E., and Zhang, H. (1995) *J. Chem. Soc.*, *Dalton Trans.*, 3335–41.
Blake, P. C., Edelman, M. A., Hitchcock, P. B., Hu, J., Lappert, M. F., Tian, S., Muller, G., Atwood, J. L., and Zhang, H. (1998) *J. Organomet. Chem.*, **551**, 261–70.
Blake, P. C., Edelstein, N. M., Hitchcock, P. B., Kot, W. K., Lappert, M. F., Shalimoff, G. V., and Tian, S. (2001) *J. Organomet. Chem.*, **636**, 124–9.
Boaretto, R., Roussel, P., Kingsley, A. J., Munslow, I. J., Sanders, C. J., Alcock, N. W., and Scott, P. (1999) *Chem. Commun*, 1701–2.
Boisson, C. J., Berthet, J. C., Lance, M., Nierlich, M., Vigner, J., and Ephritikhine, M. (1995) *J. Chem. Soc.*, *Chem. Commun.*, 543–4.
Boisson, C., Berthet, J. C., Lance, M., Vigner, J., Nierlich, M., and Ephritikhine, M. (1996a) *J. Chem. Soc.*, *Dalton Trans.*, 947–53.
Boisson, C., Berthet, J. C., Ephritikhine, M., Lance, M., and Nierlich, M. (1996b) *J. Organomet. Chem.*, **522**, 249–57.
Boisson, C., Berthet, J. C., Lance, M., Nierlich, M., and Ephritikhine, M. (1997) *Fr. Chem. Commun.*, 2129–30.
Bombieri, G., De Paoli, G., Del Pra, A., and Bagnall, K. W. (1978) *Inorg. Nucl. Chem. Lett.*, **14**, 359–61.
Boussie, T. R., Moore, R. M. Jr, Streitwieser, A., Zalkin, A., Brennan, J., and Smith, K. A. (1990) *Organometallics*, **9**, 2010–16.
Brandi, G., Brunelli, M., Lugli, G., and Mazzei, A. (1973) *Inorg. Chim. Acta*, **7**, 319–22.
Brennan, J. G. and Zalkin, A. (1985) *Acta Crystallogr., Sect. C*, **41**, 1038–40.
Brennan, J. G. and Andersen, R. A. (1985) *J. Am. Chem. Soc.*, **107**, 514–16.

Brennan, J. G., Andersen, R. A., and Zalkin, A. (1986a) *Inorg. Chem.*, **25**, 1756–60.
Brennan, J. G., Andersen, R. A., and Zalkin, A. (1986b) *Inorg. Chem.*, **25**, 1761–4.
Brennan, J. G., Andersen, R. A., and Robbins, J. L. (1986c) *J. Am. Chem. Soc.*, **108**, 335–6.
Brennan, J. G., Stults, S. D., Andersen, R. A. and Zalkin, A. (1987) *Inorg. Chim. Acta*, **139**, 201–2.
Brennan, J. G., Stults, S. D., Andersen, R. A., and Zalkin, A. (1988a) *Organometallics*, **7**, 1329–34.
Brennan, J. G., Andersen, R. A., and Zalkin, A. (1988b) *J. Am. Chem. Soc.*, **110**, 4554–8.
Brennan, J. G., Green, J. C., and Redfern, C. M. (1989) *J. Am. Chem. Soc.*, **111**, 2373–7.
Broach, R. W., Schultz, A. J., Williams, J. M., Brosn, G. M., Manriquez, J. M., Fagan, P. J., and Marks, T. J. (1979) *Science*, **203**, 172–4.
Brunelli, M., Lugli, G., and Giacometti, G. (1973) *J. Magn. Reson.*, **9**, 247–54.
Bruno, J. W., Kalina, D. G., Mintz, E. A. and Marks, T. J. (1982). *J. Am. Chem. Soc.*, **104**, 1860–9.
Bruno, J. W., Marks, T. J., and Morss, L. R. (1983) *J. Am. Chem. Soc.*, **105**, 6824–32.
Bruno, J. W., Smith, G. M., Marks, T. J., Fair, C. K., Schultz, A. J., and Williams, J. M. (1986a) *J. Am. Chem. Soc.*, **108**, 40–56.
Bruno, J. W., Stecher, H. A., Morss, L. R., Sonnenberger, D. C., and Marks, T. J. (1986b) *J. Am. Chem. Soc.*, **108**, 7275–80.
Burns, J. H. and Laubereau, P. G. (1971) *Inorg. Chem.*, **10**, 2789–92.
Burns, J. H. (1974) *J. Organomet. Chem.*, **69**, 235–43.
Burns, C. J. and Bursten, B. E. (1989) *Comments Inorg. Chem.*, **9**, 61–93.
Burns, C. J., Smith, W. H., Huffman, J. C., and Sattelberger, A. P. (1990) *J. Am. Chem. Soc.*, **112**, 3237–9.
Butcher, R. J., Clark, D. L., Grumbine, S. K., Scott, B. L., and Watkin, J. G. (1996) *Organometallics*, **15**, 1488–96.
Calderazzo, F. (1973) *Pure Appl. Chem.*, **33**, 453–74.
Campbell, G. C., Cotton, F. A., Haw, J. F., and Schwotzer, W. (1986) *Organometallics*, **5**, 274–9.
Campello, M. P. C., Domingos, A., and Santos, I. (1993) *X FECHEM Conf. on Organometallic Chemistry*, Crete.
Campello, M. P. C., Domingos, A., and Santos, I. (1994) *J. Organomet. Chem.*, **484**, 37–46.
Campello, M. P. C., Calhorda, M. J., Domingos, A., Galvao, A., Leal, J. P., Pires de Matos, A., and Santos, I. (1997) *J. Organomet. Chem.*, **538**, 223–40.
Campello, M. P., Domingos, A., Galvão, A., Pires de Matos, A., and Santos, I. (1999) *J. Organomet. Chem.*, **579**, 5–17.
Carvalho, A., Domingos, A., Gaspar, P., Marques, N., Pires de Matos, A., and Santos, I. (1992) *Polyhedron*, **11**, 1481–8.
Cendrowski-Guillaume, S. M., Lance, M., Nierlich, M., Vigner, J., and Ephritikhine, M. (1994) *J. Chem. Soc., Chem. Commun.*, 1655–7.
Cendrowski-Guillaume, S. M., and Ephritikhine, M. (1996) *J. Chem. Soc., Dalton Trans.*, 1487–91.
Cendrowski-Guillaume, S. M., Lance, M., Nierlich, M., and Ephritikhine, M. (2000) *Organometallics*, **19**, 3257–59.

Cendrowski-Guillaume, S. M., Lance, M., and Ephritikhine, M. (2001) *Eur. J. Inorg. Chem.*, 1495–8.
Cendrowski-Guillaume, S. M., Lance, M., and Ephritikhine, M. (2002) *J. Organomet. Chem.*, **643–644**, 209–13.
Cesari, M., Pedretti, U., Zazetta, A., Lugli, G., and Marconi, W. (1971) *Inorg. Chim. Acta.*, **5**, 439.
Chang, C. C., Sung- Yu, N. K., Hseu, C. S., and Chang, C. T. (1979) *Inorg. Chem.*, **18**, 885–6.
Chang, A. H. H. and Pitzer, R. M. (1989) *J. Am. Chem. Soc.*, **111**, 2500–7.
Chang, A. H. H., Zhao, K., Ermler, W. C., and Pitzer, R. M. (1994) *J. Alloys Compd.*, **213–214**, 191–5.
Clark, D. L., Sattelberger, A. P., Bott, S. G., and Vrtis, R. N. (1989) *Inorg. Chem.*, **28**, 1771–3.
Clark, D. L., Gordon, J. C., Huffman, J. C., Watkin, J. G., and Zwick, B. D. (1995) *New J. Chem.*, **19**, 495–502.
Cloke, F. G. N., Hawkes, S. A., Hitchcock, P. B., and Scott, P. (1994) *Organometallics*, **13**, 2895–7.
Cloke, F. G. N. and Hitchcock, P. B. (1997) *J. Am. Chem. Soc.*, **119**, 7899–900.
Cloke, F. G. N., Green, J. C., and Jardine, C. N. (1999) *Organometallics*, **18**, 1080–86.
Collin, J., Pires de Matos, A., and Santos, I. (1993) *J. Organomet. Chem.*, **463**, 103–7.
Cotton, F. A. and Schwotzer, W. (1985) *Organometallics*, **4**, 942–3.
Cotton, F. A. and Schwotzer, W. (1987) *Organometallics*, **6**, 1275–80.
Cotton, F. A., Wilkinson, G., and Murrillo, C. (1999) *Advanced Inorganic Chemistry,* John Wiley, New York.
Cramer, R. E., Maynard, R. B., Paw, J. C., and Gilje, J. W. (1981) *J. Am. Chem. Soc.*, **103**, 3589–90.
Cramer, R. E., Maynard, R. B., Paw, J. C., and Gilje, J. W. (1982) *Organometallics*, **1**, 869–71.
Cramer, R. E., Maynard, R. B., Paw, J. C., and Gilje, J. W. (1983) *Organometallics*, **2**, 1336–40.
Cramer, R. E., Panchanatheswaran, K., and Gilje, J. W. (1984a) *J. Am. Chem. Soc.*, **106**, 1853–54.
Cramer, R. E., Higa, K. T., and Gilje, J. W. (1984b) *J. Am. Chem. Soc.*, **106**, 7245–7.
Cramer, R. E., Jeong, J. H., and Gilje, J. W. (1986) *Organometallics*, **5**, 2555–7.
Cramer, R. E., Engelhardt, U., Higa, K. T., and Gilje, J. W. (1987a) *Organometallics*, **6**, 41–5.
Cramer, R. E., Jeong, J. H., and Gilje, J. W. (1987b) *Organometallics*, **6**, 2010–12.
Cramer, R. E., Edelmann, F., Mori, A. L., Roth, S., Gilje, J. W., Tatsumi, K., and Nakamura, A. (1988) *Organometalics*, **7**, 841–9.
Crisler, L. R. and Eggerman, W. G. (1974). *J. Inorg. Nucl. Chem.*, **36**, 1424–6.
Cymbaluk, T. H., Ernst, R. E., and Day, V. W. (1983a) *Organometallics*, **2**, 963–8.
Cymbaluk, T. H., Liu, J. Z., and Ernst, R. D. (1983b) *J. Organomet. Chem.*, **255**, 311–15.
Dash, A. K., Wang, J. X., Berthet, J. C., Ephritikhine, M., and Eisen, M. S. (2000) *J. Organomet. Chem.*, **604**, 83–98.
Dash, A. K., Gourevich, I., Wang, J. Q., Wang, J., Kapon, M., and Eisen, M. S. (2001) *Organometallics*, **20**, 5084–104.

del Mar Conejo, M., Parry, J. S., Carmona, E., Schultz, M., Brennan, J. G., Beshouri, S. M., Andersen, R. A., Rogers, R. D., Coles, S., and Hursthouse, M. (1999) *Chem. Eur. J.*, **5**, 3000–9.

Den Auwer, C., Madic, C., Berthet, J. C., Ephritikhine, M., Rehr, J. J., and Guillaumont, R. (1997) *Radiochim. Acta*, **76**, 211–18.

Deng, D. L., Zhang, X. F., Qian, C. T., Sun, J., and Zheng, P. J. (1996) *J. Chen, Chin. Chem. Lett.*, **7**, 1143–4.

De Rege, F. M., Smith, W. H., Scott, B. L., Nielsen, J. B., and Abney, K. D. (1998) *Inorg. Chem.*, **37**, 3664–6.

De Ridder, D. J. A., Apostolidis, C., Rebizant, J., Kanellakopulos, B., and Maier, R. (1996) *Acta Crystallogr., Sect. C*, **52**, 1436–8.

Diaconescu, P. L., Arnold, P. L., Baker, T. A., Mindiola, D. J., and Cummins, C. C. (2000) *J. Am. Chem. Soc.*, **122**, 6108–9.

Diaconescu, P. L., Odom, A. L., Agapie, T., and Cummins, C. C. (2001) *Organometallics*, **20**, 4993–5.

Diaconescu, P. L. and Cummins, C. C. (2002) *J. Am. Chem. Soc.*, **124**, 7660–1.

Diener, M. D., Smith, C. A., and Viers, D. K. (1997) *Chem. Mater.*, **9**, 1773–7.

Domingos, A., Pires de Matos, A., and Santos, I. (1989a) *J. Less Common Metals*, **149**, 279–85.

Domingos, A., Marçalo, J., Marques, N., Pires de Matos, A., Takats, J., and Bagnall, K. W. (1989b) *J. Less Common Metals*, **149**, 271–7.

Domingos, A., Marques, N., and Pires de Matos, A. (1990) *Polyhedron*, **9**, 69–74.

Domingos, A., Marques, N., Pires de Matos, A., Santos, I., and Silva, M. (1992a) *Polyhedron*, **11**, 2021–5.

Domingos, A., Pires de Matos, A., and Santos, I. (1992b) *Polyhedron*, **11**, 1601–6.

Domingos, A., Marçalo, J., and Pires de Matos, A. (1992c) *Polyhedron*, **11**, 909–15.

Domingos, A., Marçalo, J., Marques, N., and Pires de Matos, A. (1992d) *Polyhedron*, **11**, 501–6.

Domingos, A., Marques, N., Pires de Matos, A., Santos, I., and Silva, M. (1994) *Organometallics*, **13**, 654–62.

Dormond, A. and Moise, C. (1985) *Polyhedron*, **4**, 595–8.

Dormond, A., El Bouadili, A. A., and Moise, C. (1984) *J. Chem. Soc., Chem. Commun.*, 749–51.

Dormond, A., El Bouadili, A. A., and Moise, C. (1985) *J. Chem. Soc., Chem. Commun.*, 914–16.

Dormond, A., Aaliti, A., and Moise, C. (1986a) *Tetrahedron Lett.*, **27**, 1497–8.

Dormond, A., El Bouadili, A. A., and Moise, C. (1986b) *J. Less Common Metals*, **122**, 159–66.

Dormond, A., El Bouadili, A. A., and Moise, C. (1987a) *J. Org. Chem.*, **52**, 688–9.

Dormond, A., Aaliti, A., Elbouadili, A., and Moise, C. (1987b) *J. Organomet. Chem.*, **329**, 187–99.

Dormond, A., Aaliti, A., and Moise, C. (1988) *J. Org. Chem.*, **53**, 1034–7.

Dormond, A., El Bouadili, A. A., and Moise, C. (1989a) *J. Org. Chem.*, **54**, 3747–8.

Dormond, A., El Bouadili, A. A., and Moise, C. (1989b) *J. Organomet. Chem.*, **369**, 171–85.

Dormond, A., Hepiegne, P., Hafid, A., and Moise, C. (1990) *J. Organomet. Chem.*, **398**, C1–3.
Dormond, A., Baudry, D., Vissequx, M., and Hepiegne, P. (1994) *J. Alloys Compd.*, **213/214**, 1–7.
Doretti, L., Zanella, P., Faraglia, G., and Faleschini, S. (1972) *J. Organomet. Chem.*, **43**, 339–41.
Duttera, M. R., Fagan, P. J., Marks, T. J., and Day, V. W. (1982) *J. Am. Chem. Soc.*, **104**, 865–7.
Duttera, M. R., Day, V. W., and Marks, T. J. (1984) *J. Am. Chem. Soc.*, **106**, 2907–12.
Duval, P. B., Burns, C. J., Clark, D. L., Morris, D. E., Scott, B. L., Werkema, E. L., Jia, L., and Andersen, R. A. (2001) *Angew. Chem. Int. Edn*, **40**, 3358–61.
Edelman, M. A., Lappert, M. F., Atwood, J. L., and Zhang, H. (1987) *Inorg. Chim. Acta*, **139**, 185–6.
Edelman, M. A., Hitchcock, P. B., Hu, J., and Lappert, M. F. (1995) *New J. Chem.*, **19**, 481–9.
Edwards, P. G., Andersen, R. A., and Zalkin, A. (1981) *J. Am. Chem. Soc.*, **103**, 7792–4.
Edwards, P. G., Andersen, R. A., and Zalkin, A. (1984) *Organometallics*, **3**, 293–8.
Eigenbrot, C. W. Jr, and Raymond, K. N. (1982) *Inorg. Chem.*, **21**, 2653–60.
Eisenberg, D. C., Streitwieser, A., and Kot, W. K. (1990) *Inorg. Chem.*, **29**, 10–14.
Erker, G., Mühlenbernd, T., Benn, R., and Rufinska, A. (1986) *Organometallics*, **5**, 402–4.
Ernst, R. D., Kennelly, W. J., Day, C. S., Day, V. W., and Marks, T. J. (1979) *J. Am. Chem. Soc.*, **101**, 2656–64.
Evans, W. J., Forrestal, K. J., and Ziller, J. W. (1997) *Angew. Chem. Int. Edn. Engl.*, **36**, 774–6.
Evans, W. J., Nyce, G. W., and Ziller, J. W. (2000) *Angew. Chem. Int. Edn. Engl.*, **39**, 240–2.
Evans, W. J., Nyce, G. W., Forrestal, K. J., and Ziller, J. W. (2002) *Organometallics*, **21**, 1050–5.
Fagan, P. J., Manriquez, J. M., Maata, E. A., Seyam, A. M., and Marks, T. J. (1981a) *J. Am. Chem. Soc.*, **103**, 6650–67.
Fagan, P. J., Manriquez, J. M., Vollmer, S. H., Day, C. S., Day, V. W., and Marks, T. J. (1981b) *J. Am. Chem. Soc.*, **103**, 2206–20.
Fagan, P. J., Manriquez, J. M., Marks, T. J., Day, C. S., Vollmer, S. H., and Day, V. W. (1982) *Organometallics*, **1**, 170–80.
Fendrick, C. M. and Marks, T. J. (1986) *J. Am. Chem. Soc.*, **108**, 425–37.
Fendrick, C. M., Schertz, L. D., Day, V. W., and Marks, T. J. (1988) *Organometallics*, **7**, 1828–38.
Finke, R. G., Schiraldi, D. A., and Hirose, Y. (1981a) *J. Am. Chem. Soc.*, **103**, 1875–6.
Finke, R. G., Hirose, Y., and Gaughan, G. (1981b) *J. Chem. Soc*, *Chem. Commun.*, 232–4.
Finke, R. G., Gaughan, G., and Voegli, R. (1982) *J. Organomet. Chem.*, **229**, 179–84.
Fischer, E. O. and Hafner, W. (1955) *Z. Naturforsch.*, **10b**, 665.
Fischer, E. O. and Hristidu, Y. (1962) *Z. Naturforsch.*, **17b**, 275–6.
Fischer, E. O. and Treiber, A. (1962) *Z. Naturforsch.*, **17b**, 276.

Fischer, E. O. and Fischer, H. (1963) *J. Organomet. Chem.*, **6**, 141–50.
Fischer, E. O., Laubereau, P., Baumgärtner, F., and Kanellakopulos, B. (1966) *J. Organomet. Chem.*, **5**, 583–4.
Fischer, R. D. (1963) *Theor. Chim. Acta*, **1**, 418.
Fischer, R. D. and Sienel, G. R. (1976) *Z. Anorg. Allg. Chem.*, **419**, 126–38.
Fischer, R. D. and Sienel, G. R. (1978) *J. Organomet. Chem.*, **156**, 383–8.
Fischer, R. D., Klähne, E., and Köpf, J. (1978) *Z. Naturf.*, **33b**, 1393–7.
Fischer, R. D., Klähne, E., and Köpf, J. (1982) *J. Organomet. Chem.*, **238**, 99–111.
Fronczek, F. R., Halstead, G. W., and Raymond, K. N. (1977) *J. Am. Chem. Soc.*, **99**, 1769–75.
Gabala, A. E. and Tsutsui, M. (1973) *J. Am. Chem. Soc.*, **95**, 91.
Garbar, A. V., Leonov, M. R., Zakharov, L. N., and Struchkov, Y. T. (1996) *Russ. Chem. Bull.*, **45**, 451–4.
Gilbert, T. M., Ryan, R. R., and Sattelberger, A. P. (1988) *Organometallics*, **7**, 2514–18.
Gilman, H. (1968) *Adv. Organomet. Chem.*, **7**, 33.
Goffart, J., Fuger, J., Gilbert, B., Kanellakopulos, B., and Duyckaerts, G. (1972) *Inorg. Nucl. Chem. Lett.*, **8**, 403–12.
Goffart, J., Fuger, J., Brown, D., and Duyckaerts, G. (1974) *Inorg. Nucl. Chem. Lett.*, **10**, 413–19.
Goffart, J., Fuger, J., Gilbert, B., Hocks, L., and Duyckaerts, G. (1975) *Inorg. Nucl. Chem. Lett.*, **11**, 569–83.
Goffart, J., Gilbert, B., and Duyckaerts, G. (1977) *Inorg. Nucl. Chem. Lett.*, **13**, 186–96.
Goffart, J. and Duyckaerts, G. (1978) *Inorg. Nucl. Chem. Lett.*, **14**, 15–20.
Goffart, J. (1979) in *Organometallics of the f-Elements* (eds. T. J. Marks and R. D. Fischer), Reidel, Dordrecht.
Goffart, J., Meunier-Piret, J., and Duyckaerts, G. (1980) *Inorg. Nucl.Chem. Lett.*, **16**, 233–44.
Goffart, J., Desreux, J. F., Gilbert, B. P., Delsa, J. L., Renkin, J. M., and Duyckaerts, G. (1981) *J. Organomet. Chem.*, **209**, 281–96.
Gourier, D., Caurant, D., Berthet, J. C., Boisson, C., and Ephritikhine, M. (1997) *Inorg. Chem.*, **36**, 5931–6.
Gourier, D., Caurant, D., Arliguie, T., and Ephritikhine, M. (1998) *J. Am. Chem. Soc.*, **120**, 6084–92.
Gradoz, P., Baudry, D., Ephritikhine, M., Nief, F., and Mathey, F. (1992a) *J. Chem. Soc., Dalton Trans.*, 3047–51.
Gradoz, P., Boisson, C., Baudry, D., Lance, M., Nierlich, M., Vigner, J., and Ephritikhine, M. (1992b) *J. Chem. Soc., Chem. Commun.*, 1720–1.
Gradoz, P., Baudry, D., Ephritikhine, M., Lance, M., Nierlich, M., and Vigner, J. (1994a) *J. Organomet. Chem.*, **466**, 107–18.
Gradoz, P., Ephritikhine, M., Lance, M., Vigner, J., and Nierlich, M. (1994b) *J. Organomet. Chem.*, **481**, 69–73.
Green, J. C. and Watts, O. (1978) *J. Organomet. Chem.*, **153**, C40.
Green, J. C., Payne, M., Seddon, E. A., and Andersen, R. A. (1982) *J. Chem. Soc., Dalton Trans.*, 887–92.
Guo, T., Diener, M. D., Chai, Y., Alford, M. J., Haufler, R. E., McClure, S. M., Ohno, T., Weaver, J. H., Scuseria, G. E., and Smalley, R. E. (1992) *Science*, **257**, 1661–4.

Hafid, A., Dormond, A., and Baudry, D. (1994) *New J. Chem.*, **18**, 557–9.
Hall, S. W., Huffman, J. C., Miller, M. M., Avens, L. R., Burns, C. J., Arney, D. S. J., England, A. F., and Sattelberger, A. P. (1993) *Organometallics*, **12**, 752–8.
Halstead, G. W., Baker, E. C., and Raymond, K. N. (1975) *J. Am. Chem. Soc.*, **97**, 3049–52.
Harmon, C. A., Bauer, D. P., Berryhill, S. R., Hagiwara, K., and Streitwieser, A. J. (1977) *Inorg. Chem.*, **16**, 2143–7.
Haskel, A., Straub, T., and Eisen, M. S. (1996) *Organometallics*, **15**, 3773–6.
Haufler, R. E., Conceicao, J., Chibante, L. P. F., Chai, Y., Byrne, N. E., Flanagan, S., Haley, M. M., O'Brien, S. C., Pan, C., Xiao, Z., Billups, W. E., Cuifolini, M. A., Hauge, R. H., Margraves, J. L., Wilson, L. J., Curl, R. F., and Smalley, R. E. (1990) *J. Phys. Chem.*, **94**, 8634–6.
Hay, P. J., Ryan, R. R., Salazar, K. V., Wrobleski, D. A., and Sattelberger, A. P. (1986) *J. Am. Chem. Soc.*, **108**, 313–15.
Hayes, R. G. and Edelstein, N. (1972) *J. Am. Chem. Soc.*, **94**, 8688.
Hitchcock, P. B., Lappert, M. F., and Liu, D.-S. (1995) *J. Organomet. Chem.*, **488**, 241–8.
Hitchcock, P. B., Hu, J., Lappert, M. F., and Tian, S. (1997) *J. Organomet. Chem.*, **536/537**, 473–80.
Hodgson, K. O. and Raymond, K. N. (1973) *Inorg. Chem.*, **12**, 458–66.
Jamerson, J. D., Masino, A. P., and Takats, J. (1974) *J. Organomet. Chem.*, **65**, C33–6.
Jamerson, J. D. and Takats, J. (1974) *J. Organomet. Chem.*, **78**, C23–5.
Jemine, X., Goffart, J., Berthet, J. C., and Ephritikhine, M. (1992) *J. Chem. Soc., Dalton Trans.*, 2439–40.
Jemine, X., Goffart, J., Leverd, P. C., and Ephritikhine, M. (1994) *J. Organomet. Chem.*, **469**, 55–7.
Kalina, D. G., Marks, T. J., and Wachter, W. A. (1977) *J. Am. Chem. Soc.*, **99**, 3877–9.
Kaltsoyannis, N. and Scott, P. (1998) *Chem. Commun.*, 1665–6.
Kanellakopulos, B., Dornberger, E., and Baumgärtner, F. (1974a) *Inorg. Nucl. Chem. Lett.*, **10**, 155–60.
Kanellakopulos, B., Dornberger, E., and Billich, H. (1974b) *J. Organomet. Chem.*, **76**, C42–4.
Kanellakopulos, B., Aderhold, C., and Dornberger, E. (1974c) *J. Organomet. Chem.*, **66**, 447–51.
Kanellakopulos, B., Fischer, E. O., Dornberger, E., and Baumgärtner, F. (1980). *J. Organomet. Chem.*, **24**, 507–14.
Karraker, D. G., Stone, J. A., Jones, E. R. Jr, and Edelstein, N. (1970) *J. Am. Chem. Soc.*, **92**, 4841–5.
Karraker, D. G. and Stone, J. A. (1972) *Inorg. Chem.*, **11**, 1742–6.
Karraker, D. G. (1973) *Inorg. Chem.*, **12**, 1105–8.
Karraker, D. G. and Stone, J. A. (1974) *J. Am. Chem. Soc.*, **96**, 6885–8.
Karraker, D. G. and Stone, J. A. (1977) *J. Inorg. Nucl. Chem.*, **39**, 2215–17.
Karraker, D. G. and Stone, J. A. (1979) *Inorg. Chem.*, **18**, 2205–7.
Karraker, D. G. (1983) *Inorg. Chem.*, **22**, 503–6.
Karraker, D. G. (1987) *Inorg. Chim. Acta*, **139**, 189–91.
Kiplinger, J. K., Morris, D. E., Scott, B. L., and Burns, C. J. (2002) *Chem. Commun*, 30–2.

Korobkov, I., Gambarotta, S., and Yap, G. P. A. (2001a) *Organometallics*, **20**, 2552–9.
Korobkov, I., Gambarotta, S., Yap, G. P. A., Thompson, L., and Hay, P. J. (2001b) *Organometallics*, **20**, 5440–5.
Kot, W. K., Shalimoff, G. V., Edelstein, N. M., Edelman, M. A., and Lappert, M. F. (1988) *J. Am. Chem. Soc.*, **110**, 986–7.
Laubereau, P. (1970) *Inorg. Nucl. Chem. Lett.*, **6**, 611.
Laubereau, P. and Burns, J. (1970a) *Inorg. Nucl. Chem. Lett.*, **6**, 59–63.
Laubereau, P. and Burns, J. (1970b) *Inorg. Chem.*, **9**, 1091–5.
Laubereau, P. G., Ganguly, L., Burns, J. H., Benjamin, B. M., Atwood, J. L., and Selbin, J. (1971) *Inorg. Chem.*, **10**, 2274–80.
Lauke, H., Swepston, P. N., and Marks, T. J. (1984) *J. Am. Chem. Soc.*, **106**, 6841–3.
Le Borgne, T., Lance, M., Nierlich, M., and Ephritikhine, M. (2000) *J. Organomet. Chem.*, **598**, 313–17.
Le Marechal, J.-F., Ephritikhine, M., and Folcher, G. (1986) *J. Organomet. Chem.*, **299**, 89–95.
Le Marechal, J.-F., Villiers, C., Charpin, P., Lance, M., Nierlich, M., Vigner, J., and Ephritikhine, M. (1989) *J. Chem. Soc., Chem. Commun.*, 308–10.
Leal, J. P., Marques, N., Pires de Matos, A., Calhorda, M. J., Galvao, A. M., and Simoes, J. A. M. (1992) *Organometallics*, **11**, 1632–7.
Leal, J. P., Marques, N., and Takats, J. (2001) *J. Organomet. Chem.*, **632**, 209–14.
Lee, H., Desrosiers, P. J., Guzei, I., Rheingold, A. L., and Parkin, G. (1998) *J. Am. Chem. Soc.*, **120**, 3255–6.
Leong, J., Hodgson, K. O., and Raymond, K. N. (1973) *Inorg. Chem.*, **12**, 1329–35.
Lescop, C., Arliguie, T., Lance, M., Nierlich, M., and Ephritikhine, M. (1999) *J. Organomet. Chem.*, **580**, 137–44.
Le Vanda, C., Solar, J. P., and Streitwieser, A. (1980) *J. Am. Chem. Soc.*, **102**, 2128–9.
Le Vanda, C. and Streitwieser, A. J. (1981) *Inorg. Chem.*, **20**, 656–9.
Leverd, P. C., Arliguie, T., Lance, M., Nierlich, M., Vigner, J., and Ephritikhine, M. (1994) *J. Chem. Soc., Dalton Trans.*, 501–4.
Leverd, P. C., Ephritikhine, M., Lance, M., Vigner, J., and Nierlich, M. (1996) *J. Organomet. Chem.,* **507**, 229–37.
Li, J. and Bursten, B. E. (1997) *J. Am. Chem. Soc.*, **119**, 9021–32.
Lin, Z. R., Brock, C. P., and Marks, T. J. (1988) *Inorg. Chim. Acta*, **141**, 145–9.
Lugli, G., Marconi, W., Mazzei, A., Palladino, N., and Pedretti, U. (1969) *Inorg. Chim. Acta*, **3**, 253–4.
Luke, W. D. and Streitwieser, A. J. (1981) *J. Am. Chem. Soc.*, **103**, 3241–3.
Luke, W. D., Berryhill, S. R., and Streitwieser, A. Jr (1981) *Inorg. Chem.*, **20**, 3086–9.
Lukens, W. W. Jr, Beshouri, S. M., Blosch, L. L., and Andersen, R. A. (1996) *J. Am. Chem. Soc.*, **118**, 901–2.
Lukens, W. W. Jr, Beshouri, S. M., Blosch, L. L., Stuart, A. L., and Andersen, R. A. (1999a) *Organometallics*, **18**, 1235–46.
Lukens, W. W. Jr, Beshouri, S. M., Stuart, A. L., and Andersen, R. A. (1999b) *Organometallics*, **18**, 1247–52.
Lukens, W. W. Jr, Allen, P. G., Bucher, J. J., Edelstein, N. M., Hudson, E. A., Shuh, D. K., Reich, T., and Andersen, R. A. (1999c) *Organometallics*, **18**, 1253–9.
Lyttle, M. H., Streitwieser, A. Jr, and Miller, M. J (1989) *J. Org. Chem.*, **54**, 2331–5.

Maier, R., Kanellakopulos, B., Apostolidis, C., Meyer, D., and Rebizant, J. (1993) *J. Alloys Compd.*, **190**, 269–71.
Manriquez, J. M., Fagan, P. J., and Marks, T. J. (1978) *J. Am. Chem. Soc.*, **100**, 3939–41.
Manriquez, J. M., Fagan, P. J., Marks, T. J., Vollmer, S. H., Day, C. S., and Day, V. W. (1979) *J. Am. Chem. Soc.*, **101**, 5075–8.
Maria, L., Campello, M. P., Domingos, A., Santos, I., and Andersen, R. (1999) *J. Chem. Soc.*, *Dalton Trans.*, 2015–20.
Marks, T. J., Seyam, A. M., and Kolb, J. R. (1973) *J. Am. Chem. Soc.*, **95**, 5529.
Marks, T. J. and Kolb, R. J. (1975) *J. Am. Chem. Soc.*, **97**, 27–33.
Marks, T. J., Seyam, A. M., and Wachter, W. A. (1976) *Inorg. Synth.*, **XVI**, 147–51.
Marks, T. J. (1979) *Prog. Inorg. Chem.*, **25**, 224–333.
Marks, T. J. and Day, V. W. (1985) in *Fundamental and Technological Aspects of Organo-f-Element Chemistry* (eds. T. J. Marks and I. Fragalà), Reidel, Dordrecht, ch. 4.
Marks, T. J. (1986) in *The Chemistry of the Actinide Elements,* 2nd edn (eds. J. J. Katz, G. T. Seaborg, and L. R. Morss), Chapman&Hall, London, ch 23.
Marques, N., Marçalo, J., Pires de Matos, A., Bagnall, K. W., and Takats, J. (1987a) *Inorg. Chim. Acta*, **139**, 79–81.
Marques, N., Marçalo, J., Pires de Matos, A., Santos, I., and Bagnall, K. W. (1987b) *Inorg. Chim. Acta*, **139**, 309–14.
McCullough, L. G., Turner, H. W., Andersen, R. A., Zalkin, A., and Templeton, D. H. (1981) *Inorg. Chem.*, **20**, 2869–71.
McDonald, R., Sun, Y., Takats, J., Day, V. W., and Ebersprachер, T. A. (1994) *J. Alloys Compd.*, **213/214**, 8–10.
Meunier-Piret, J., Declercq, J. P., German, G., and van Meersche, M. (1980) *Bull. Soc. Chim. Belg.*, **89**, 121–4.
Miller, J. T. and De Kock, C. W. (1979) *Inorg. Chem.*, **18**, 1305–6.
Miller, M. J., Lyttle, M. H., and Streitwieser, A. Jr (1981) *J. Org. Chem.*, **46**, 1977–84.
Mindiola, D. J., Tsai, Y.-C., Hara, R., Chen, Q., Meyer, K., and Cummins, C. C. (2001) *Chem. Commun*, 125–6.
Mintz, E. A., Moloy, K. G., Marks, T. J., and Day, V. W. (1982) *J. Am. Chem. Soc.*, **104**, 4692–5.
Mishin, V. Ya., Sidorenko, G. V., and Suglobov, D. N. (1986) *Radiokhimiya*, **28**, 293–300.
Moloy, K. G., Marks, T. J., and Day, V. W. (1983) *J. Am. Chem. Soc.*, **105**, 5696–8.
Moody, D. C. and Odom, J. D. (1979) *J. Inorg. Nucl. Chem.*, **41**, 533–5.
Nolan, S. P., Porchia, M., and Marks, T. J. (1991) *Organometallics*, **10**, 1450–7.
Odom, A. L., Arnold, P. L., and Cummins, C. C. (1998) *J. Am. Chem. Soc.*, **120**, 5836–7.
Parry, J., Carmona, E., Coles, S., and Hursthouse, M. (1995) *J. Am. Chem. Soc.*, **117**, 2649–50.
Paolucci, G., Rossetto, R., Zanella, R., Yünlü, K., and Fischer, R. D. (1984) *J. Organomet. Chem.*, **272**, 363–83.
Paolucci, G., Rossetto, R., Zanella, R., and Fischer, R. D. (1985) *J. Organomet. Chem.*, **284**, 213–28.
Paolucci, G., Fischer, R. D., Benetollo, F., Seraglia, R., and Bombieri, G. (1991) *J. Organomet. Chem.*, **412**, 327–42.

Parry, J. S., Cloke, F. G. N., Coles, S. J., and Hursthouse, M. B. (1999) *J. Am. Chem. Soc.*, **121**, 6867–71.
Pauson, P. (1951) *Nature*, **168**, 1039.
Peters, R. G., Warner, B. P., Scott, B. L., and Burns, C. J. (1999) *Organometallics*, **18**, 2587.
Porchia, M., Casellato, U., Ossola, F., Rossetto, G., Zanella, P., and Graziani, R. (1986) *J. Chem. Soc., Chem. Commun.*, 1034–5.
Porchia, M., Ossola, F., Rossetto, G., Zanella, P., and Brianese, N. (1987) *J. Chem. Soc., Chem. Commun.*, 550–1.
Porchia, M., Brianese, N., Casellato, U., Ossola, F., Rossetto, G., Zanella, P., and Graziani, R. (1989) *J. Chem. Soc., Dalton Trans.*, 677–81.
Rabinovich, D., Haswell, C. M., Scott, B. L., Miller, R. L., Nielsen, J. B., and Abney, K. D. (1996) *Inorg. Chem.*, **35**, 1425–6.
Rabinovich, D., Chamberlin, R. M., Scott, B. L., Nielsen, J. B., and Abney, K. D. (1997) *Inorg. Chem.*, **36**, 4216–17.
Rabinovich, D., Schimek, G. L., Pennington, W. T., Nielsen, J. B., and Abney, K. D. (1997) *Acta Crystallogr., Sect. C*, **53**, 1794–7.
Rabinovich, D., Bott, S. G., Nielsen, J. B., and Abney, K. D. (1998) *Inorg. Chim. Acta*, **274**, 232–5.
Radu, N., Engeler, M. P., Gerlach, C. P., and Tilley, T. D. (1995) *J. Am. Chem. Soc.*, **117**, 3621–2.
Rebizant, J., Spirlet, M.-R., Kanellakopulos, B., and Dornberger, E. (1986) *J. Less Common Metals*, **122**, 211–14.
Rebizant, J., Spirlet, M.-R., Van den Bossche, G., and Goffart, J. (1988) *Acta Crystallogr., Sect. C*, **44**, 1710–12.
Rebizant, J., Spirlet, M.-R., Apostolidis, C., and Kanellakopulos, B. (1991) *Acta Crystallogr., Sect. C*, **47**, 854–6.
Reynolds, L. T. and Wilkinson, G. (1956) *J. Inorg. Nucl. Chem.*, **2**, 246.
Rieke, R. D. and Rhyne, L. D. (1979) *J. Org. Chem.*, **44**, 3445–6.
Ritchey, J. M., Zozulin, A. J., Wrobleski, D. A., Ryan, R. R., Wasserman, H. J., Moody, D. C., and Paine, R. T. (1985) *J. Am. Chem. Soc.*, **107**, 501–3.
Rosen, R. K. and Zalkin, A. (1989) *Acta Crystallogr., Sect. C*, **45**, 1139–41.
Rosen, R. K., Andersen, R. A., and Edelstein, N. M. (1990) *J. Am. Chem. Soc.*, **112**, 4588–90.
Roussel, P., Hitchcock, P. B., Tinker, N. D., and Scott, P. (1996) *Chem. Commun.*, 2053–4.
Roussel, P., Hitchcock, P. B., Tinker, N. D., and Scott, P. (1997a) *Inorg. Chem.*, **36**, 5716–21.
Roussel, P., Hitchcock, P. B., Tinker, N. D., and Scott, P. (1997b) *J. Am. Chem. Soc.*, **36**, 5716–21.
Roussel, P. and Scott, P. (1998) *J. Am. Chem. Soc.*, **120**, 1070–1.
Roussel, P., Alcock, N. W., Boaretto, R., Kingsley, A. J., Munslow, I. J., Sanders, C. J., and Scott, P. (1999) *Inorg. Chem.*, **38**, 3651–6.
Rousssel, P., Boaretto, R., Kingsley, A. J., Alcock, N. W., and Scott, P. (2002) *J. Chem. Soc., Dalton Trans.*, 1423–8.
Santos, I., Marques, N., and Pires de Matos, A. (1985) *Inorg. Chim. Acta*, **110**, 149–51.

Santos, I., Marques, N., and Pires de Matos, A. (1986) *J. Less Common Meals*, **122**, 215–18.
Santos, I., Marques, N., and Pires de Matos, A. (1987) *Inorg. Chim. Acta*, **139**, 87–8.
Schake, A. R., Avens, L. R., Burns, C. J., Clark, D. L., Sattelberger, A. P., and Smith, W. H. (1993) *Organometallics*, **12**, 1497–8.
Scherer, O. J., Werner, B., Heckmann, G., and Wolmershäuser, G. (1991) *Angew. Chem. Int. Edn Engl.*, **30**, 553–5.
Scherer, O. J., Schultze, J., and Wolmershäuser, G. (1994) *J. Organomet. Chem.*, **484**, C5–7.
Schnabel, R. C., Scott, G. L., Smith, W. H., and Burns, C. J. (1999) *J. Organomet. Chem.*, **591**, 14–23.
Scott, P. and Hitchcock, P. B. (1994) *Polyhedron*, **13**, 1651–3.
Scott, P. and Hitchcock, P. B. (1995a) *J. Chem. Soc., Dalton Trans.*, 603–9.
Scott, P. and Hitchcock, P. B. (1995b) *J. Chem. Soc., Chem. Commun.*, 579–80.
Seyam, A. M. (1982) *Inorg. Chim. Acta*, **58**, 71–4.
Sheline, R. K. and Slater, J. L. (1975) *Angew. Chem. Int. Edn Engl.*, **14**, 209–13.
Shin, J. H., Hascall, T., and Parkin, G. (1999) *Organometallics*, **18**, 6–9.
Sigurdson, E. R. and Wilkinson, G. (1977) *J. Chem. Soc., Dalton Trans.*, 812–18.
Silva, M., Marques, N., and Pires de Matos, A. (1995) *J. Organomet. Chem.*, **493**, 129–32.
Silva, M., Domingos, A., Pires de Matos, A., Marques, N., and Trofimenko, S. (2000) *J. Chem. Soc., Dalton Trans.*, 4628–34.
Simpson, S. and Andersen, R. A. (1981a) *Inorg. Chem.*, **20**, 2991–5.
Slater, J. L., Sheline, R. K., Lin, K. C., and Weltner, W. J. (1971) *J. Chem. Phys.*, **55**, 5129.
Simpson, S. and Andersen, R. A. (1981b) *J. Am. Chem. Soc.*, **103**, 4063–6.
Smith, G. M., Suzuki, H., Sonnenberger, D. C., Day, V. W., and Marks, T. J. (1986) *Organometallics*, **5**, 549–61.
Solar, J. P., Burghard, H. P. G., Banks, R. H., Streitwieser, A. Jr, and Brown, D. (1980) *Inorg. Chem.*, **19**, 2186–8.
Sonnenberger, D. C., Mintz, E. A., and Marks, T. J. (1984) *J. Am. Chem. Soc.*, **106**, 3484–91.
Sonnenberger, D. C., Morss, L. R., and Marks, T. J. (1985) *Organometallics*, **4**, 352–5.
Sonnenberger, D. C. and Gaudiello, J. (1986) *J. Less Common Metals*, **126**, 411–14.
Spiegl, A. (1978) Ph.D. dissertation, University of Erlangen-Nürnberg Erlangen 1978.
Spiegl, A. and Fischer, R. D. (1979) *Chem. Ber.*, **112**, 116.
Spirlet, M.-R., Rebizant, J., Apostolidis, C., Andreetii, G. D., and Kanellakopulos, B. (1989a) *Acta Crystallogr., Sect. C*, **45**, 739–41.
Spirlet, M.-R., Bettonville, S., and Goffart, J. (1989b) *Acta Crystallogr., Sect. C*, **45**, 1509–11.
Spirlet, M.-R., Rebizant, J., Bettonville, S., and Goffart, J. (1992a) *Acta Crystallogr., Sect. C*, **48**, 1221–3.
Spirlet, M.-R., Rebizant, J., Apostolidis, C., and Kanellakopulos, B. (1992b) *Acta Crystallogr., Sect. C*, **48**, 2135–7.
Spirlet, M.-R., Rebizant, J., Apostolidis, C., Dornberger, E., Kanellakopulos, B., and Powietzka, B. (1996) *Polyhedron*, **15**, 1503–8.

Starks, D. F. and Streitwieser, A. Jr (1973) *J. Am. Chem. Soc.*, **95**, 3423–4.
Starks, D. F., Parson, T. C., Streitwieser, A. Jr, and Edelstein, N. (1974) *Inorg. Chem.*, **13**, 1307–8.
Sternal, R. S., Brock, C. P., and Marks, T. J. (1985) *J. Am. Chem. Soc.*, **107**, 8270–2.
Sternal, R. S. and Marks, T. J. (1987) *Organometllics*, **6**, 2621–3.
Sternal, R. S., Sabat, M., and Marks, T. J. (1987) *J. Am. Chem. Soc.*, **109**, 7920–1.
Stewart, J. L. and Andersen, R. A. (1995) *New J. Chem.*, **19**, 587–95.
Stewart, J. L. and Andersen, R. A. (1998) *Polyhedron*, **17**, 953–8.
Straub, T., Frank, W., Reiss, G. J., and Eisen, M. S. (1996) *J. Chem. Soc.*, *Dalton Trans.*, 2541–6.
Straub, T., Haskel, A., Neyroud, T. G., Kapon, M., Botoshansky, M., and Eisen, M. S. (2001) *Organometallics*, **20**, 5017–35.
Streitwieser, A. Jr and Müller-Westerhoff, U. (1968) *J. Am. Chem. Soc.*, **90**, 7364.
Streitwieser, A. Jr and Yoshida, N. (1969) *J. Am. Chem. Soc.*, **91**, 7528.
Streitwieser, A. Jr, Dempf, D., La Mar, G. N., Karraker, D. G., and Edelstein, N. M. (1971) *J. Am. Chem. Soc.*, **93**, 7343–4.
Streitwieser, A. Jr and Harmon, C. A. (1973) *Inorg. Chem.*, **12**, 1102–4.
Streitwieser, A. Jr and Walker, R. (1975) *J. Organomet. Chem.*, **97**, C41–2.
Streitwieser, A. Jr, Kluttz, R. Z., Smith, K. A., and Luke, W. D. (1983) *Organometallics*, **2**, 1873–7.
Streitwieser, A. Jr, Barros, M. T., Wang, H. K., Boussie, T. R. (1993) *Organometallics*, **12**, 5023–4.
Strittmatter, R. J and Bursten, B. E. (1991) *J. Am. Chem. Soc.*, **113**, 552–9.
Stults, S. D., Andersen, R. A., and Zalkin, A. (1989) *J. Am. Chem. Soc.*, **111**, 4507–8.
Stults, S. D., Andersen, R. A., and Zalkin, A. (1990) *Organometallics*, **9**, 1623–9.
Sun, Y., McDonald, R., Takats, J., Day, V. W., and Eberspracher, T. A. (1994) *Inorg. Chem.*, **33**, 4433–4.
Sun, Y., Takats, J., Eberspracher, T., and Day, V. (1995) *Inorg. Chim. Acta*, **229**, 315–22.
Tague, T. J. Jr, Andrews, L., and Hunt, R. D. (1993) *J. Phys. Chem.*, **97**, 10920–4.
Tatsumi, K. and Nakamura, A. (1984) *J. Organomet. Chem.*, **272**, 141–54.
Tatsumi, K., Nakamura, A., Hofmann, P., Stauffert, P., and Hoffmann, R. (1985) *J. Am. Chem. Soc.*, **107**, 4440–51.
Tellers, D. M., Skoog, S. J., Bergman, R. G., Gunnoe, T. B., and Harman, W. D. (2000) *Organometallics*, **19**, 2428–32.
Telnoy, V. I., Rabinovich, I. B., Leonov, M. R., Solov'yova, G. V., and Gramoteeva, N. I. (1979) *Dokl. Akad. Nauk. SSSR*, **245**, 1430–2.
Telnoy, V. I., Rabinovich, I. B., Larina, V. N., Leonov, M. R., and Solov'yova, G. V. (1989) *Sov. Radiochem.*, **31**, 654–6.
Templeton, L. K., Templeton, D. H., and Walker, R. (1976) *Inorg. Chem.*, **15**, 3000–3.
Trnka, T. M., Bonanno, J. B., Bridgewater, B. M., and Parkin, G. (2001) *Organometallics*, **20**, 3255–64.
Trofimenko, S. (1993) *Chem. Rev.*, **93**, 943–80.
Tsutsui, M., Ely, N., and Gebala, A. (1975) *Inorg. Chem.*, **14**, 78–81.
Turner, H. W., Andersen, R. A., Zalkin, A., and Templeton, D. H. (1979a) *Inorg. Chem.*, **18**, 1221–4.
Turner, H. W., Simpson, S. J., and Andersen, R. A. (1979b) *J. Am. Chem. Soc.*, **101**, 2782.

Van Der Sluys, W. G., Burns, C. J., Huffman, J. C., and Sattelberger, A. P. (1989) *Organometallics*, **8**, 855–7.
Vanderhooft, J. C. and Ernst, R. D. (1982) *J. Organomet. Chem.*, **233**, 313–19.
Ventelon, L., Lescop, C., Arliguie, T., Ephritikhine, M., Leverd, P. C., Lance, M., and Nierlich, M. (1999) *Chem. Commun.*, 656–60.
Villiers, C. and Ephritikhine, M. (1990) *J. Organomet. Chem.*, **393**, 339–42.
Villiers, C. and Ephritikhine, M. (1991) *New J. Chem.*, **15**, 559–63.
Villiers, C. and Ephritikhine, M. (1994) *J. Chem. Soc., Dalton Trans.*, 3397–403.
von Ammon, R., Kanellakopulos, B., and Fischer, R. D. (1969) *Inorg. Nucl. Chem. Lett.*, **5**, 219–24.
Walsh, P. J., Hollander, F. J., and Bergman, R. G. (1988) *J. Am. Chem. Soc.*, **110**, 8729–31.
Walsh, P. J., Baranger, A. M., and Bergman, R. G. (1992) *J. Am. Chem. Soc.*, **114**, 1708–19.
Walsh, P. J., Hollander, F. J., and Bergman, R. G. (1993) *Organometallics*, **12**, 3705–23.
Wang, J. Q., Dash, A. K., Berthet, J. C., Ephritikhine, M., and Eisen, M. S. (1999) *Organometallics*, **18**, 2407–9.
Warner, B. P., Scott, B. L., and Burns, C. J. (1998) *Angew. Chem. Int. Edn Engl.*, **37**, 959–60.
Wasserman, H. J., Zozulin, A. J., Moody, D. C., Ryan, R. R., and Salazar, K. V. (1983) *J. Organomet. Chem.*, **254**, 305–11.
Wedler, M., Roesky, H. W., and Edelmann, F. (1988) *J. Organomet. Chem.*, **345**, C1–3.
Wedler, M., Knoesel, F., Noltemeyer, M., Edelmann, F. T., and Behrens, U. (1990) *J. Organomet. Chem.*, **388**, 21–45.
Wedler, M., Knoesel, F., Edelmann, F. T., and Behrens, U. (1992a) *Chem. Ber.*, **125**, 1313–18.
Wedler, M., Noltemeyer, M., and Edelmann, F. T. (1992b) *Angew. Chem. Int. Edn Engl.*, **31**, 72–3.
Wilke, G., Bogdanovic, B., Hardt, P., Heimbach, P., Keim, W., Kroner, M., Oberkirch, W., Tanaka, K., Steinrücke, E., Walter, D., and Zimmermann, H. (1966) *Angew. Chem. Int. Edn Engl.*, **5**, 151–64.
Wong, C. H., Yesn, T. M., and Lee, T. Y. (1965) *Acta Crystallogr.*, **18**, 340–5.
Wrobleski, D. A., Ryan, R. R., Wasserman, H. J., Salazar, K. V., Paine, R. T., and Moody, D. C. (1986a) *Organometallics*, **5**, 90–4.
Wrobleski, D. A., Cromer, D. T., Ortiz, J. V., Rauchfuss, T. B., Ryan, R. R., and Sattelberger, A. P. (1986b) *J. Am. Chem. Soc.*, **108**, 174–5.
Xie, Z., Yan, C., Yang, Q., and Mak, T. C. W. (1999) *Angew. Chem. Int. Edn Engl.*, **38**, 1761–3.
Zalkin, A. and Raymond, K. N. (1969) *J. Am. Chem. Soc.*, **91**, 5667–8.
Zalkin, A., Templeton, D. H., Le Vanda, C., and Streitwieser, A. (1980) *Inorg. Chem.*, **19**, 2560–3.
Zalkin, A., Templeton, D. H., Luke, W. D., and Streitwieser, A. Jr (1982) *Organometallics*, **1**, 618–22.
Zalkin, A. and Brennan, J. G. (1987) *Acta Crystallogr., Sect. C*, **43**, 1919–22.
Zalkin, A., Brennan, J. G., and Andersen, R. A. (1987a) *Acta Crystallogr., Sect. C*, **43**, 418–20.

Zalkin, A., Brennan, J. G., and Andersen, R. A. (1987b) *Acta Crystallogr., Sect. C*, **43**, 1706–7.

Zalkin, A., Brennan, J. G., and Andersen, R. A. (1988a) *Acta Crystallogr., Sect. C*, **44**, 2104–5.

Zalkin, A., Brennan, J. G., and Andersen, R. A. (1988b) *Acta Crystallogr., Sect. C*, **44**, 1553–4.

Zalkin, A. and Beshouri, S. M. (1989) *Acta Crystallogr., Sect. C*, **45**, 1219–20.

Zanella, P., De Paoli, G., DelPra, A., and Bagnall, K. W. (1977) *J. Organomet. Chem.*, **142**, C21–4.

Zanella, P., Rossetto, G., DePaoli, G., and Traverso, O. (1980) *Inorg. Chim. Acta*, **44**, L155–6.

Zanella, P., Brianese, N., Casellato, U., Ossola, F., Porchia, M., Rossetto, G., and Graziani, R. (1987) *J. Chem. Soc., Dalton Trans.*, 2039–43.

Zhao, K. and Pitzer, R. M. (1996) *J. Phys. Chem.*, **12**, 4798–802.

Zwick, B. D., Sattelberger, A. P., and Avens, L. R. (1992) in *Transuranium Elements: A Half Century* (eds. L. R. Morss and J. Fuger), American Chemical Society, Washington, DC, p. 239, ch. 25.

CHAPTER TWENTY SIX

HOMOGENEOUS AND HETEROGENEOUS CATALYTIC PROCESSES PROMOTED BY ORGANOACTINIDES

Carol J. Burns and Moris S. Eisen

26.1 INTRODUCTION

During the last two decades, the chemistry of organoactinides has flourished, reaching a high level of sophistication. The use of organoactinide complexes as stoichiometric or catalytic compounds to promote synthetically important organic transformations has matured due to their rich, complex, and

uniquely informative organometallic chemistry. Compared to early or late transition metal complexes, the actinides sometimes exhibit parallel and sometimes totally different reactivities for similar processes. In many instances the regiospecific and chemical selectivities displayed by organoactinide complexes are complementary to that observed for other transition metal complexes. Several recent review articles (Edelman *et al.*, 1995; Edelmann and Gun'ko, 1997; Ephritikhine, 1997; Hitchcock *et al.*, 1997; Berthet and Ephritikhine, 1998; Blake *et al.*, 1998; Edelmann and Lorenz, 2000), dealing mostly with the synthesis of new actinide complexes, confirm the broad and rapidly expanding scope of this field.

The aim of this chapter is to survey briefly and in a selective manner the catalytic chemistry of organoactinide complexes in homogeneous and heterogeneous catalytic reactions. A comprehensive review of the reactivities of actinide compounds has been published covering the literature until 1992 (Edelmann, 1995). This chapter reviews the new literature for the last decade. The treatment of this chapter is necessarily concise. We encourage the reader to seek the recent review articles and additional references given as an integral part of the subchapters for additional details and background material.

26.2 REACTIVITY OF ORGANOACTINIDE COMPLEXES

26.2.1 Modes of activation

Interest in the reactivity of organoactinide complexes is based on their ability to effect bond-breaking and bond-forming of distinctive moieties. The factors influencing these processes are both steric and electronic. A number of articles have been devoted to the steric control in organo-5f-complexes. Xing-Fu *et al.* (1986a) have proposed a model for steric saturation, suggesting that the stability of a complex is governed by the sum of the ligand cone angles (Xing-Fu *et al.*, 1986a,b; Xing-Fu and Ao-Ling, 1987). In this model, highly coordinated 'oversaturated' complexes will display low stability. An additional model concerning steric environments has been proposed by Pires de Matos (Marçalo and Pires de Matos, 1989). This model assumes pure ionic bonding, and is based on cone angles defining the 'steric coordination number'. A more important and unique approach to the reactivity of organo-5f-complexes regards the utilization of thermochemical studies. The knowledge of the metal–ligand bond enthalpies is of fundamental importance to allow the estimation of new reaction pathways (Marks *et al.*, 1989; Jemine *et al.*, 1992, 1993; King *et al.*, 1992; Leal *et al.*, 1992; Leal and Martinho Simões, 1994; King and Marks, 1995; Leal *et al.*, 2001). In addition, neutral organoactinides have been shown to follow a four-center transition state in insertion reactions [equation (26.1)], suggesting that prediction of new actinide patterns of reactivity is possible taking into account the negatives entropies of activation (Marks and Day, 1985).

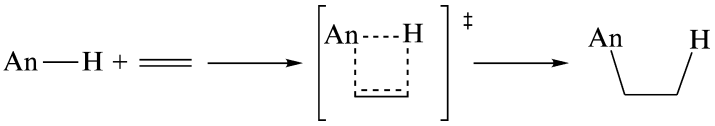

(26.1)

This chapter deals with the reactions of organoactinide complexes that comprise intermediate and key steps in catalytic processes, whereas the preceding chapter focuses in a more detailed and comprehensive fashion on the synthesis and characterization of similar complexes.

26.2.2 Stoichiometric reactions of organoactinide complexes of the type $(C_5Me_5)_2AnMe_2$

The different catalytic reactivity found for similar organoactinides, previously unprecedented in the chemistry of organoactinides, was the driving force for Haskel *et al.* (1999) to study the stoichiometric reactivity of organoactinide complexes of the type $(C_5Me_5)_2AnMe_2$ (An = Th, U). These complexes have been widely used for the hydrogenation of olefins under homogeneous conditions (Fagan *et al.*, 1981a; Fendrick *et al.*, 1988; Lin and Marks, 1990). The reactivity of the actinide complexes towards alkynes and/or amines is outlined in Schemes 26.1 and 26.2 for Th and U, respectively.

$(C_5Me_5)_2ThMe_2$ (**1**) was found to react with terminal alkynes producing the bisacetylide complexes $(C_5Me_5)_2Th(C{\equiv}CR)_2$ (**2**) (R = ^{t}Bu, TMS). The reaction of these bisacetylide complexes **2** with equimolar amounts of amine yielded half of an equivalent of the corresponding bisamido complexes $(C_5Me_5)_2Th(NHR)_2$ (**5**) and half of an equivalent of the starting bisacetylide complex, indicating that the second amine insertion into the thorium monoamido monoacetylide complex **4** was faster than the first insertion. The reaction of $(C_5Me_5)_2Th(CH_3)_2$ (**1**) with an equimolar amount of amine resulted in the formation of the monoamido thorium methyl complex **3**, which upon subsequent reaction with another equivalent of amine produced the bisamido complex **5**. Heating complex **5**, in THF, allowed the elimination of an amine molecule producing the formation of the thorium–imido complex **7**. This complex also was formed by eliminating methane by heating complex **3** (Haskel *et al.*, 1996). In the presence of an excess of amine, the bisamido complex **5**, was found to be in rapid equilibrium with the bisamido–amine complex **6** (Straub *et al.*, 1996), resembling lanthanide complexes (Gagné *et al.*, 1992a,b; Giardello *et al.*, 1994) though the equilibrium was investigated and found to lie towards the bisamido complex.

Similar reactivity has been found for the corresponding uranium complex, **8** (Scheme 26.2). The reaction with alkynes produced the bisacetylide complexes $(C_5Me_5)_2U(C{\equiv}CR)_2$ (**9**) (R = Ph, TMS) but in contrast to the thorium species, these bisacetylide complexes are extremely stable and the bisamido complex **12** can be formed only by adding large excess of the amine, indicating that the

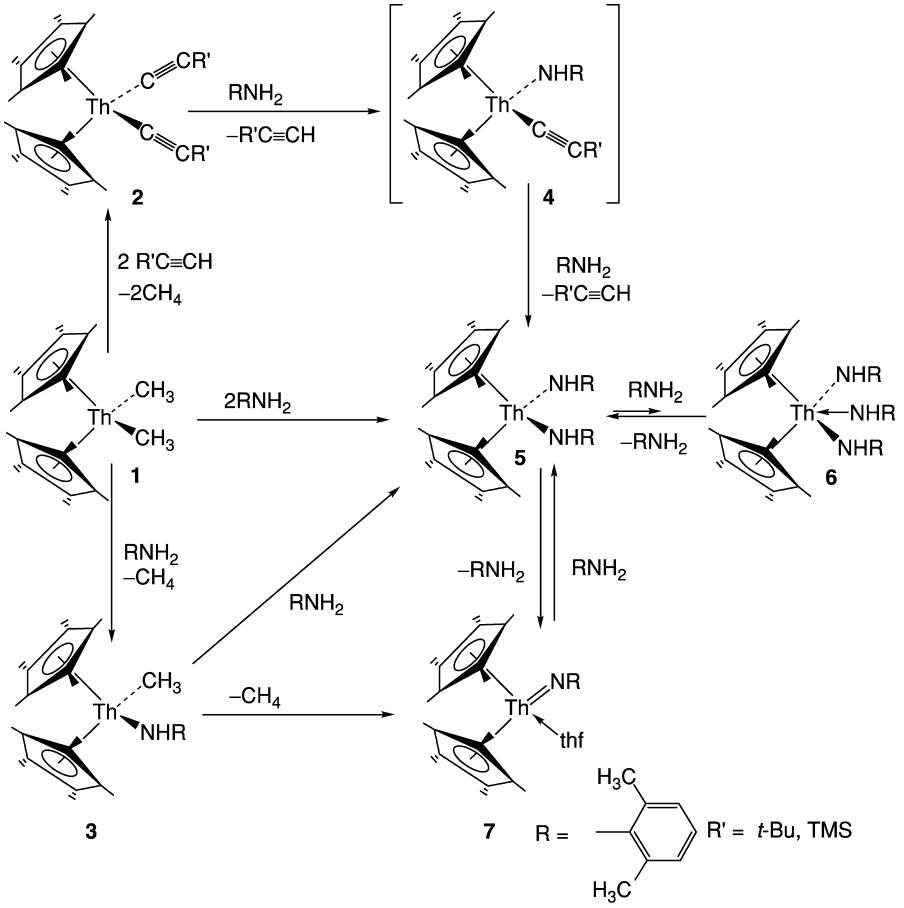

Scheme 26.1 *Stoichiometric reactions of the complex* $(C_5Me_5)_2ThMe_2$ *with amines and terminal alkynes.*

equilibrium between complexes **9** and **12** lies preferentially towards the bisacetylide complexes, instead of either the monoamido monoacetylide **11** or the bisamido complexes **12**. Attempts to isolate the monomethyl–amido complex **10**, by reacting one equivalent of amine with complex **8**, yielded only half of an equivalent of the bisamido complex **12**. Similar to the reactivity of the thorium complex, in the presence of an excess of amine, complex **12** was found to be in fast equilibrium with complex **13**, with the equilibrium favoring the bisamido complex. By heating the bisamido complex **12** in THF, elimination of an amine molecule was observed allowing the formation of the corresponding uranium–imido complex **14** (Eisen *et al.*, 1998). The U(IV) arene–imido complexes have also been prepared following a parallel pathway through a potassium salt [equation (26.2)] (Arney and Burns, 1995).

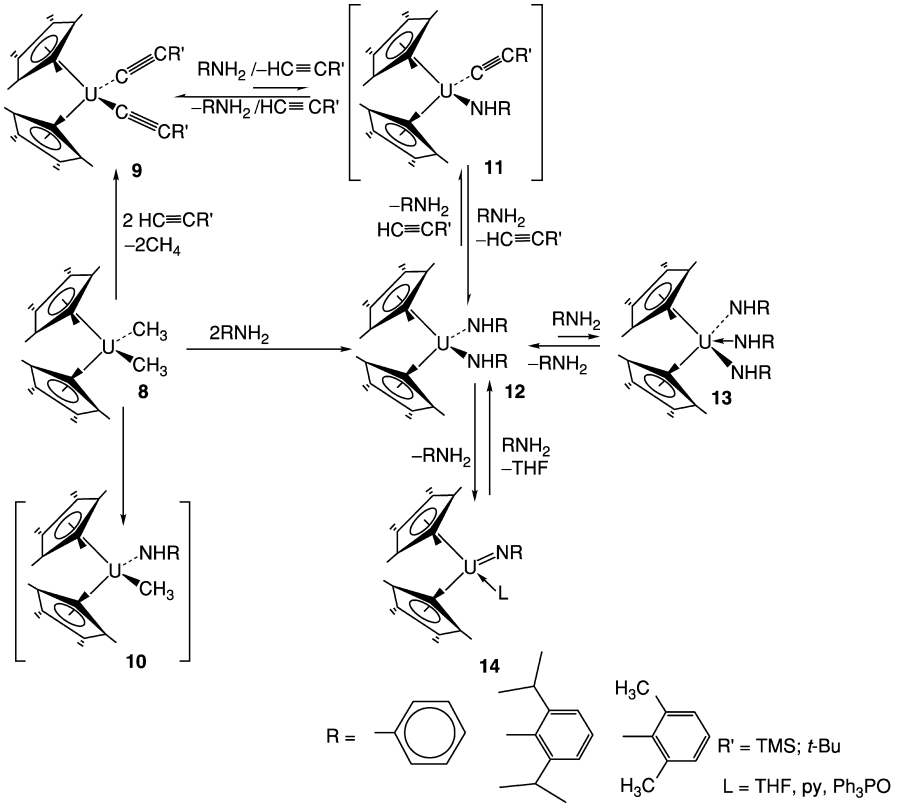

Scheme 26.2 *Stoichiometric reactions of the complex* $(C_5Me_5)_2UMe_2$ *with amines and terminal alkynes.*

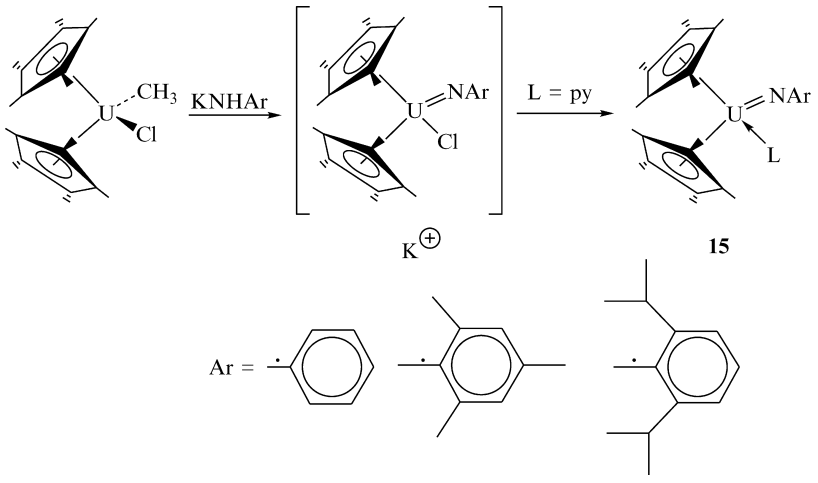

(26.2)

The only base-free monomeric organo-imido complex of U(IV) has been obtained for the bulky tris-*tert*-butyl phenyl amine derivative [equation (26.3)] [32].

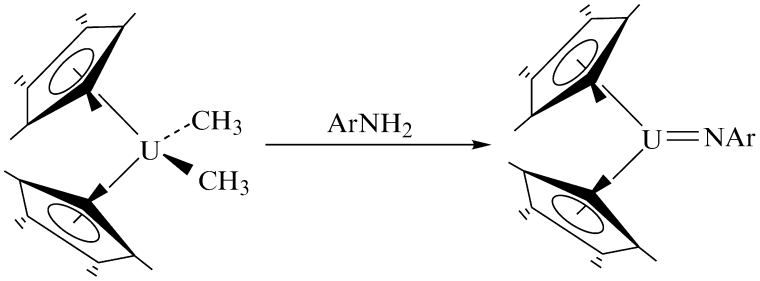

(26.3)

Ar = 2,4,6-^{t}Bu$_3$C$_6$H$_2$

16

The crystal structure of this coordinatively unsaturated organoimido uranium (IV) complex (**16**) exhibits almost a linear U–N-*ipso*-C linkage with and almost C_2 symmetry along the U–N bond. The U–N-*ipso*-C angle is 162.30(10), with the aryl substituent canted towards the uranium through the methyl group in the *ortho*- position of the aromatic ring. Interestingly, besides this close disposition, no chemical evidence was found regarding any agostic interactions. The remarkable feature in this complex was found to be the extremely short U–N bond length of 1.952(12) Å resembling the distance of aryl–imido complexes of U(V) and U(VI) (Brennan and Andersen, 1985; Burns *et al.*, 1990; Arney and Burns, 1993) when the differences in ionic radii due to the variation in the U oxidation states were taken into account (Shannon, 1976). Thus, it was suggested that in this aryl–imido uranium (IV) complex **16**, there is a high formal bond order presumably formed by donation of a lone pair of electrons from the nitrogen to the uranium center.

26.2.3 Stoichiometric reactions between $(C_5Me_5)_2AnMe_2$ (An = Th, U), alkynes and silanes

In order to detect the key organometallic intermediates in the hydrosilylation process (*vide infra*), a consecutive series of stoichiometric reactions were investigated, using the organoactinide precursor $(C_5Me_5)_2AnMe_2$ (An = Th, U), reacting with ^{t}PrC≡CH and $PhSiH_3$. The stoichiometric reaction of $PhSiH_3$ with $(C_5Me_5)_2UMe_2$ induced the dehydrogenative coupling of the silane ($PhSiH_3$) to give oligomers, but the reaction $PhSiH_3$ with $(C_5Me_5)_2ThMe_2$ produced only the dimer and the corresponding $[(C_5Me_5)_2ThH(\mu\text{-}H)]_2$, as described in the literature (Fagan *et al.*, 1981b; Aitken *et al.*, 1989). The reaction of the organoactinide complexes $(C_5Me_5)_2AnMe_2$ (An = Th, U) with alkynes in stoichiometric amounts allowed the preparation and characterization of monoacetylide and bisacetylide complexes of organoactinides as described in Scheme 26.3.

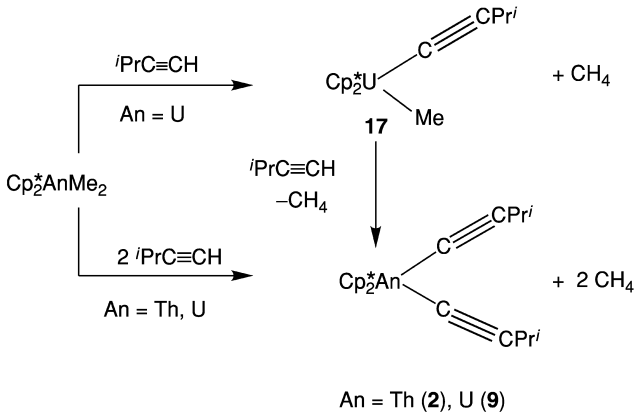

Scheme 26.3 *Stoichiometric reactivity of the organoactinide complexes* $(C_5Me_5)_2AnMe_2$ *(An = Th, U) with terminal alkynes.*

In stoichiometric reactions of ^{i}PrC≡CH with $(C_5Me_5)_2UMe_2$, methane gas was evolved leading to the formation of the orange (mono)acetylide methyl complex, $(C_5Me_5)_2U(C{\equiv}CPr^i)(Me)$ (**17**). This transient species was found to be very reactive, and the addition of a second equivalent of ^{i}PrC≡CH converted complex **17** rapidly into the deep red brown bisacetylide complex $(C_5Me_5)_2U(C{\equiv}CPr^i)_2$ (**9**). Addition of one equivalent of $PhSiH_3$ at room temperature to a benzene solution of any of the bisacetylide organoactinide complexes resulted in the quantitative formation of the silylalkenyl acetylide actinide complexes $(C_5Me_5)_2An(PhSiH_2C{=}CH^iPr)(C{\equiv}C^iPr)$ (An = Th (**18**), U (**19**)), which were found to be intermediates in the catalytic cycle for the hydrosilylation reactions [equation (26.4)].

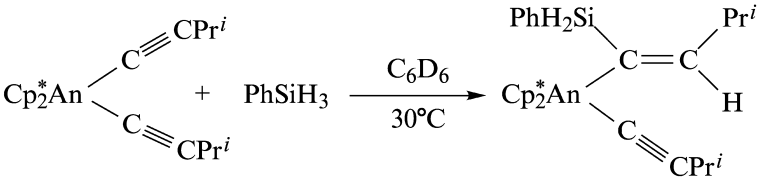

(26.4)

An = Th (**2**), U (**9**) An = Th (**18**), U (**19**)

Formation of the intermediate was indicated by the change in color of the reaction from pale yellow to dark red for **18**, and orange to dark orange brown for complex **19**. The structure of **18** and **19** were unambiguously confirmed by ^{1}H-, ^{13}C-, ^{29}Si-NMR spectroscopy as well as by nuclear overhauser effect (NOE) experiments. The silyl group was found to be in the *cis*-configuration with respect to the *iso*-propyl group in the organometallic

complex. Corroboration of this stereochemistry of the organometallic intermediate **18** was found by the quenching of **18** with H_2O producing the corresponding *cis*-vinylsilane product **20** [equation (26.5)].

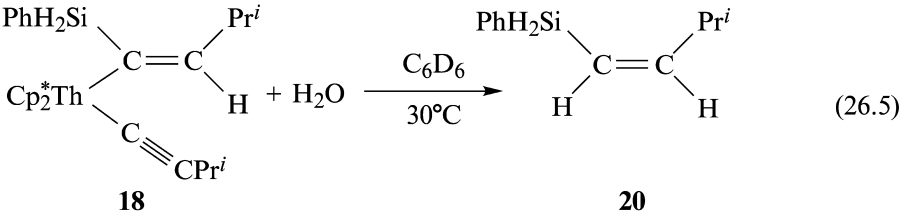

18 **20** (26.5)

Intriguingly, no further reaction was observed with an excess of $PhSiH_3$ with complexes **18** or **19**, strongly suggesting that at room temperature, neither the silane nor the alkyne is able to induce the σ-bond metathesis or the protonolysis of the hydrosilylated alkene or the alkyne. The addition of an excess of alkyne at room temperature to complex **18** in the presence of $PhSiH_3$ yielded the unexpected *trans*-hydrosilylated alkyne, in addition to the corresponding alkene, silylalkyne, and the bis(acetylide) complex.

26.2.4 Synthesis of *ansa*-organoactinide complexes of the type $Me_2Si(C_5Me_4)_2AnR_2$

Stoichiometric and catalytic properties of organo-f-element complexes are profoundly influenced by the nature of the π ancillary ligands (Bursten and Strittmatter, 1991; Edelmann, 1995a,b; Anwander, 1996; Anwander and Herrmann, 1996; Edelmann, 1996; Molander, 1998). It has proven possible to generate a more open coordination sphere at the metal center by introducing a bridge metallocene ligation set as in the complex *ansa*-$Me_2SiCp''_2MR_2$ ($Cp'' = C_5Me_4$) (Fendrick *et al.*, 1984; Jeske *et al.*, 1985a,b; Fendrick *et al.*, 1988). The effect of opening the coordination sphere of organolanthanides in some catalytic processes resulted in an increase (10-fold to 100-fold) in rates for the olefin insertion into the M–R bond (Jeske *et al.*, 1985a,b; Gagné and Marks, 1989; Giardello *et al.*, 1994). In organoactinides, this modification was shown to cause an increase (10^3-fold) in their catalytic activity for the hydrogenation of 1-hexene (Fendrick *et al.*, 1984). The syntheses of the complexes $Me_2Si(C_5Me_4)_2ThCl_2$ (**21**) and $Me_2Si(C_5Me_4)_2Th^nBu$ (**22**) have been reported as presented in equation (26.6) (Gagné and Marks, 1989; Dash *et al.*, 2001). The complex $Me_2Si(C_5Me_4)_2ThCl_2$ was isolated in 82% yield as a lithium chloride adduct. The single-crystal X-ray diffraction revealed a typical bent metallocene complex. The ring–centroid–Th–centroid angle (113.3°) is smaller than that observed in unbridged bis(pentamethylcyclopentadienyl) thorium complexes (130–138°) (Bruno *et al.*, 1986), and slightly smaller than the angle determined for the bridged thorium dialkyl complex $Me_2Si(C_5Me_4)_2Th$

$(CH_2Si(CH_3)_3)_2$ (118.4°) (Fendrick *et al.*, 1984). The thorium–carbon (carbon = cyclopentadienyl ring carbons) bond lengths are not equidistant; the complex displays a shorter distance between the metal and the first carbon adjacent to the silicon bridge because of the strain generated by the Me_2Si-bridge, similar to that reported for other *ansa* types of complexes (Bajgur *et al.*, 1985).

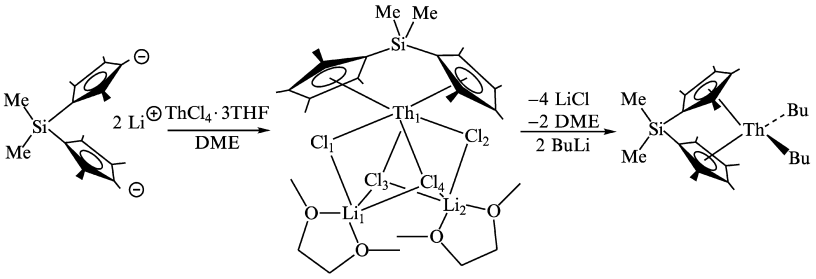

(26.6)

21 **22**

The X-ray analysis of complex **21** showed that two of the thorium–chloride bonds are shorter than the other two Th(1) – Cl(1) = 2.770(2)Å, Th(1) – Cl(2) = 2.661(2)Å, Th(1) – Cl(3) = 2.950(2)Å, and Th(1) – Cl(4) = 2.918(2)Å. The longer Th–Cl distances are those corresponding to the chlorine atoms disposed in the three-fold bridging positions and coordinated to both lithium atoms. Each of the other two chlorine atoms is coordinated only to one lithium atom. All the Th–Cl distances are longer than those observed for terminal Th–Cl distances (Th–Cl = 2.601Å for $Cp^*_2ThCl_2$ or 2.65Å for $Cp^*_2Th(Cl)Me$). *ansa*-Chelating bis(cyclopentadienyl) complexes of uranium have been prepared as presented in Scheme 26.4. Schnabel *et al.* (1999) have described an effective high yield procedure for these desired U(IV) complexes (Schnabel *et al.*, 1999).

The uranium complexes (**23–25**) were obtained as dark-red air- and moisture-sensitive materials. The complexes are soluble in aromatic solvents but insoluble in hexane. In solution, these complexes have shown no dynamic behavior. The molecular structure of complex **23** reveals a normal bent metallocene with an angle of 114.1° for the ring centroid–metal–ring centroid. This angle is smaller as compared to the non-bridged uranium complexes (133–138°) (Fagan *et al.*, 1981b; Eigenbrot and Raymond, 1982; Duttera *et al.*, 1984; Cramer *et al.*, 1989a,b). The uranium atom is bound to four bridging chloride ligands; two bonds are much longer than the others U–(Cl(1)) = 2.885(3), U–(Cl(2)) = 2.853(3), U–(Cl(3)) = 2.760(3), U–(Cl(4)) = 2.746(3)Å, the longer U–Cl bonds are those associated with chlorides that bridge to one lithium atom. For the preparation of the dialkyl complexes, the corresponding chloride–TMEDA complex **24** was used as a precursor. The alkylation of the halide precursors with Grignard reagents produced the corresponding alkyl complexes using a large excess of dioxane as the precipitating solvent for the magnesium salts.

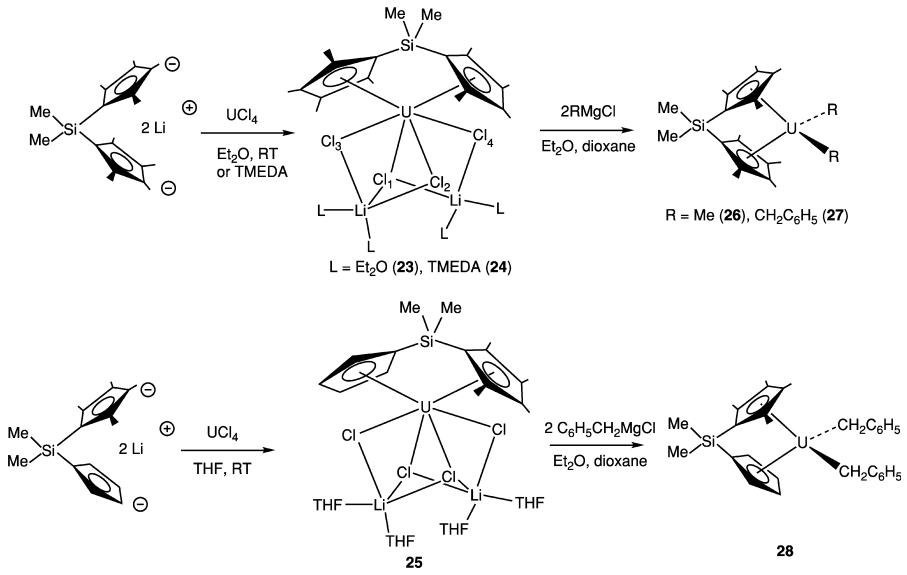

Scheme 26.4 *Synthetic pathway for the preparation of* ansa*-organouranium complexes.*

Interestingly, complex **28** is very stable in comparison to the corresponding dimethyl thorium complex (Fendrick *et al.*, 1984). The dimethyl complex of the mixed cyclopentadienyl precursor **25** could not be isolated. Instead, the precipitation of insoluble material and the evolution of gas were observed. In contrast, the dibenzyl complexes **27** and **28** were obtained in high yields. The mixed benzyl–chloride complex was obtained by protonation of the dibenzyl complex **27** with $[HNMe_3]Cl$ as described in equation (26.7).

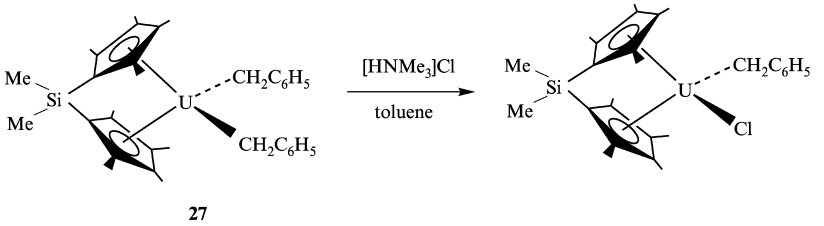

(26.7)

26.2.5 Synthesis of high-valent organouranium complexes

The reactivity of organoactinide (IV) alkyl, amido, or imido complexes towards unsaturated organic substrates such as olefin, alkynes, and nitriles follows a four-center transition state as described in equation (26.1). These complexes

display this type of reactivity due to the high-energy orbital impediment to oxidative addition and reductive elemination. Consequently, the synthesis, characterization, and reactivity studies of high-valent organouranium complexes are of primary importance. The ability to transform U(IV) to U(VI) and vice versa can create complementary modes of activation inducing unique and novel reactivities.

The first high-valent organouranium(VI) bis(imido) complex **29** was prepared by Arney *et al.* (1992) by the oxidation of a lithium salt of an organoimido uranium chloride complex with phenylazide [equation (26.8)] (Arney *et al.*, 1992).

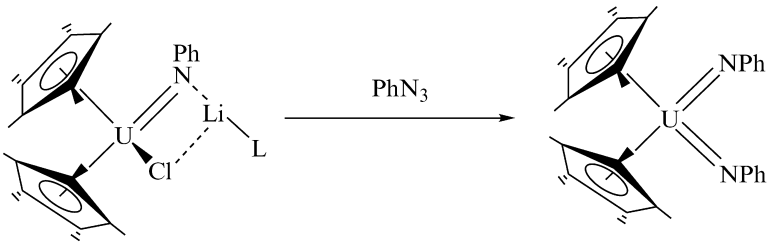

(26.8)

29

Other bis(imido) organouranium (VI) complexes have been prepared as described in Scheme 26.5. The reactions involve the oxidation of uranium (IV)

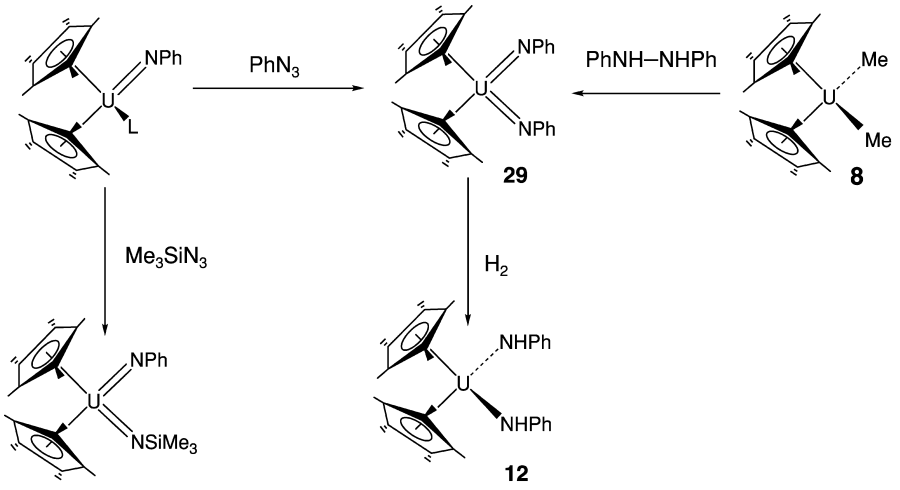

Scheme 26.5 *Alternative synthetic pathways for the preparation of high-valent organouranium–imido complexes and their reactivity with dihydrogen.*

bis(alkyl) or uranium (IV) imido complexes with the two-electron atom transfer reagents in high yield (Brennan and Andersen, 1985).

A very elegant and simple procedure for the generation of high-valent bis (imido) organouranium (VI) complexes has been described starting from an organometallic uranium (III) species. The reaction involves the direct reduction of diazenes or azides [equation (26.9)] (Warner *et al.*, 1998). Complex **30** was found to react at elevated temperature activating one methyl of the cyclopentadienyl ring (Peters *et al.*, 1999a) [equation (26.10)].

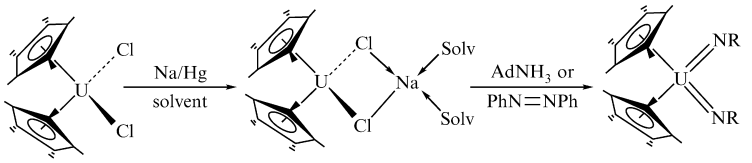

(26.9)

31 R = Ph (**29**), Ad (**30**)

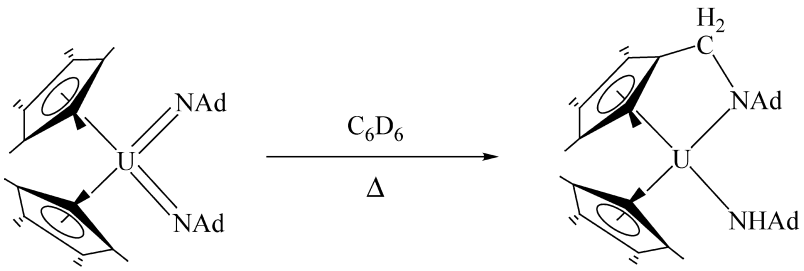

(26.10)

30 **32**

26.2.6 Reactivity of the cationic complex $[(Et_2N)_3U][BPh_4]$ with primary amines

As will be presented in the course of this chapter, a large amount of work has been dedicated towards catalytic reactions using the cationic complex $[(Et_2N)_3U][BPh_4]$ (Berthet *et al.*, 1995). In order to tailor the possibilities of such cationic complexes, stoichiometric reactions with amines have been studied. Under mild conditions (room temperature in benzene), the amido ligands of $[(Et_2N)_3U][BPh_4]$ were straightforwardly activated. The reaction of $[(Et_2N)_3U][BPh_4]$ with *n*-propylamine yielded an organoactinide intermediate that upon consecutive quenching reaction with water, after all volatiles were removed, yielded *n*-propylamine with no traces of Et_2NH. This result indicated that all three amido groups were easily transaminated [equation (26.11)] (Wang *et al.*, 2000). NMR spectroscopy has indicated that complexes

of the type $[(R_2N)_3U][BPh_4]$ normally adopts a zwitterionic structure in non-coordinating solvents, with two phenyl groups of BPh_4 coordinated to the metal center (Wang *et al.*, 2002a).

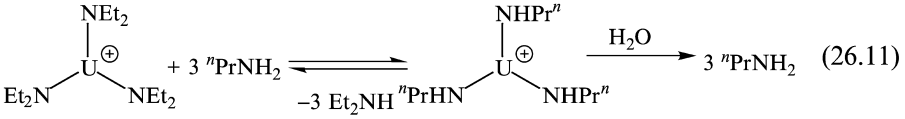

(26.11)

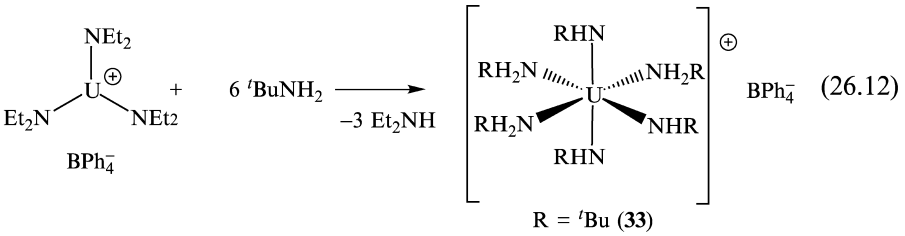

(26.12)

Similarly reaction of $[(Et_2N)_3U][BPh_4]$ with ^{t}butylamine allowed the formation of the complex $[(t\text{BuNH}_2)_3(t\text{BuNH})_3U][BPh_4]$ (**33**) [equation (26.12)]. The X-ray diffraction analysis of **33** revealed a uranium atom in a slightly distorted octahedral environment, with the three amido and three amine ligands arranged in a *mer* geometry. The U–N(amido) bond lengths average 2.20(2)Å and were similar to those determined in the distorted facial octahedral cation $[(Et_2N)_3(THF)_3U]^+$ (mean value of 2.18(1)Å) (Wang *et al.*, 2002a). The complex $[(t\text{BuNH}_2)_3(t\text{BuNH})_3U][BPh_4]$ is a unique uranium(IV) complex with primary amine ligands that have been crystallographically characterized (Wang *et al.*, 2002a). The mean U–N(amino) bond distance of 2.67(3)Å can be compared with the average U–N bond length of 2.79(2)Å in $[UCl_4(Me_2NCH_2CH_2NMe_2)_2$ (Zalkin *et al.*, 1986). The shorter U–N(amido) bond length (U–N = 2.185(7) Å) and the longer U–N(amine) bond length (U–N = 2.705(8) Å) were found to be those which are in *trans* positions. The small octahedral distortion was manifested in the different angles between the amine–amido, amine—amine, and amido–amido groups.

26.3 OLIGOMERIZATION OF ALKYNES

The last decade has witnessed an intense investigation of the chemistry of electrophilic d^0/f lanthanide and actinide metallocenes (Edelmann, 1995a,b). A substantial impact was encountered in diverse catalytic areas, where the key step is an insertion of an olefinic (alkene or alkyne) functionality into a metal–alkyl, metal—hydride, or metal–heteroatom moiety [equation 26.13; $Cp^* = \eta^5$-C_5Me_5; X = alkyl, H, NR_2).

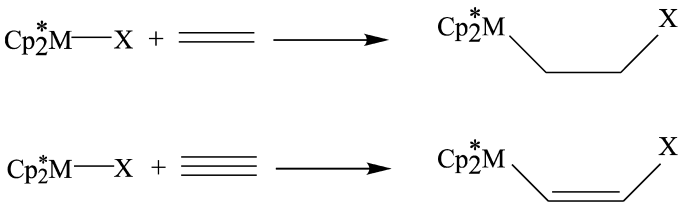

(26.13)

For organolanthanides, such processes include hydrogenation (Molander and Hoberg, 1992; Giardello *et al.*, 1994; Haar *et al.*, 1996; Molander and Winterfeld, 1996; Roesky *et al.*, 1997a,b), dimerization (Heeres *et al.*, 1990), oligomerization/polymerization (Jeske *et al.*, 1985c; Watson and Parshall, 1985; Heeres and Teuben, 1991; Schaverien, 1994; Fu and Marks, 1995; Ihara *et al.*, 1996; Mitchell *et al.*, 1996), and other related reactions that will be discussed later in this chapter, whereas for organoactinides, until 1991 C–H activation (Smith *et al.*, 1986a; Fendrick *et al.*, 1988) and hydrogenation (Fagan *et al.*, 1981a,b; Fendrick *et al.*, 1988; Lin and Marks, 1990) comprised all such processes. Mechanistically, these insertion reactions are not in general well understood and are certainly more efficient in very different metal–ligand environments than the more extensive studied analogs of the middle- and late-transition metals (Collman *et al.*, 1987; Elschenbroich and Salzer, 1989; Hegedus, 1995). Hence, the d^0/f metal ions are likely to be in a high formal oxidation state, and in neutral complexes are expected to be electronically unsuitable for π-back-donation. In addition, these types of complexes are unlikely to form stable olefin/alkyne complexes, due to the relatively polar metal–ligand bonding with strong affinity for 'hard' ligands, and to feature startling M–C/M–H bond disruption enthalpy patterns as compared with those of the late transition elements (Marthino Simões and Beauchamp, 1990; Nolan *et al.*, 1990; King and Marks, 1995).

26.3.1 Bisacetylide organoactinide complexes

Organometallic complexes containing an acetylide moiety have played an important role in the development of organolanthanide chemistry (Evans *et al.*, 1983, 1989; Den Haan *et al.*, 1987; Shen *et al.*, 1990). A number of synthetic routes applicable to the preparation of this class of compounds have been developed, examples of which include the salt metatheses between lanthanide halides with main group acetylides, and the σ-bond metatheses between lanthanide alkyl or hydrides and terminal alkynes.

Bisacetylide organoactinide complexes can be synthesized at room temperature by the reaction of $(C_5Me_5)_2AnMe_2$ (An = Th, U) with either stoichiometric or excess amounts of the corresponding terminal alkynes (Schemes 26.1 and 26.2). The reaction is faster for the organoactinide uranium complex than for the corresponding thorium complex. In all cases, the bisacteylide complexes

were obtained instead of the uranium methyl acetylide complex (**34**) [equation (26.14)], indicating that the metathesis substitution of the second methyl ligand by the terminal alkyne is normally much faster than the first σ-bond metathesis.

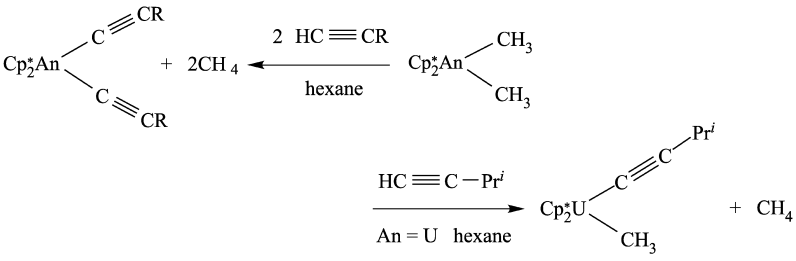

(26.14)

An = Th (**2**), U (**9**)

34

$An = Th, R = TMS, {}^{i}Pr; An = U, R = Ph, {}^{t}Bu, {}^{i}Pr$

Due to the paramagnetism of the $5f^2$ uranium (IV) center and its rapid electron spin–lattice relaxation times, the chemical shifts of the magnetically non-equivalent ligand protons were found to be generally sharp, well-separated, and readily resolved in the ^{1}H-NMR spectra.

26.3.2 Oligomerization of terminal alkynes catalyzed by neutral organoactinide complexes of the type $(C_5Me_5)_2AnMe_2$

The reaction of $(C_5Me_5)_2AnMe_2$ (An = Th, U) with an excess of *tert*-butylacetylene yielded the regioselective catalytic formation of the head-to-tail dimer, 2,4-di-*tert*-butyl-1-butene-3-yne (Th = 99%; U = 95%), whereas with trimethylsilylacetylene the head-to-tail geminal dimer, 2,4-bis(trimethylsilyl)-1-butene-3-yne (Th = 10%; U = 5%), and the head-to-tail-to-head trimer, (*E,E*)-1,4,6-tris(trimethylsilyl)-1-3-hexadiene-5-yne (Th = 90%; U = 95%), were the exclusive products [equation (26.15)] (Straub *et al.*, 1995):

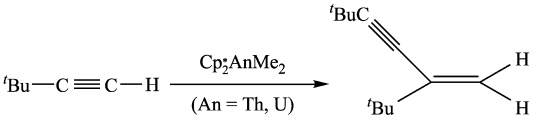

(26.15)

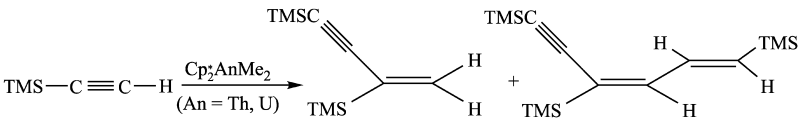

head-to-tail dimers and the formation of higher oligomers with no specific regio-selectivity and chemo-selectivity. For the bulky 4-Me-PhC≡CH, a different reactivity was found for the different organoactinide complexes. Whereas $(C_5Me_5)_2ThMe_2$ generated a mixture of dimers and trimers, the corresponding $(C_5Me_5)_2UMe_2$ afforded *only* the head-to-head *trans*-dimer. In contrast to the reactivity of lanthanide complexes, the organoactinides did not induce the formation of allenic compounds. Although the turnover frequencies for both of the organoactinide complexes were in the range of the 1–10 h^{-1}, the turnover numbers were found to be higher, in the range of 200–400.

26.3.3 Key intermediate complex in the oligomerization of terminal alkynes promoted by neutral $(C_5Me_5)_2AnMe_2$ organoactinides

When the reaction of TMSC≡CH with $(C_5Me_5)_2ThMe_2$ was followed spectroscopically, two different compounds were observed. The first compound observed at room temperature was the bisacetylide complex. The oligomerization reaction started only upon heating the reaction mixture to 70°C, whereupon the bisacetylide complex disappeared and the new complex **35** (Fig. 26.1) was spectroscopically characterized, indicating that both acetylide positions at the metal center were active sites.

26.3.4 Kinetic, thermodynamic, and thermochemical data in the oligomerization of terminal alkynes promoted by neutral $(C_5Me_5)_2AnMe_2$ organoactinides

A kinetic study of the trimerization of TMSC≡CH with $Cp^*_2UMe_2$ was monitored *in situ* by ^{1}H-NMR spectroscopy. From the kinetic data, the empirical rate law for the organoactinide-catalyzed oligomerization of TMSC≡CH is given by equation (26.16). The derived rate constant at 70°C for the production

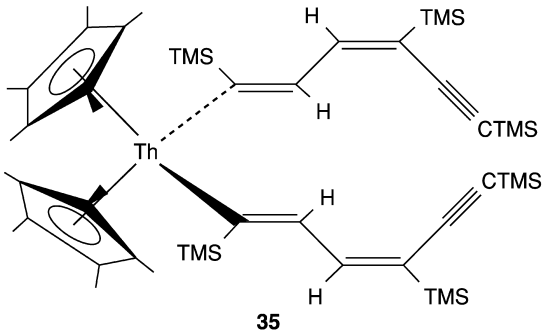

35

Fig. 26.1 *Bis*(*dienyne*) *organoactinide complex* **35** *found in the linear oligomerization of terminal alkynes.*

of the corresponding trimer was found to be $k = 7.6 \times 10^{-4}$ (6) s^{-1}.

$$v = k[\text{alkyne}]^1[\text{U}]^1 \tag{26.16}$$

A similar kinetic dependence on alkyne and catalyst concentration was observed over a range of temperatures permitting the derivation of the activation parameters from the corresponding Eyring analysis. The values measured were $E_a = 11.8(3)$ kcal mol^{-1}, $\Delta H^{\ddagger} = 11.1(3)$ kcal mol^{-1}, and $\Delta S^{\ddagger} = -45.2(6)$ eu, respectively (Straub *et al.*, 1999).

Thermodynamically, higher oligomers and even polymers were expected (Ohff *et al.*, 1996; Wang and Eisen, 2003). The reaction of either the Th or U organoactinide complex with acetylene (HC≡CH) resulted in the precipitation of black *cis*-polyacetylene. The *cis*-polyacetylene was thermally converted to the corresponding *trans*-polyacetylenes at 80°C. The enthalpies of reaction may be calculated for the addition of triple bonds in a conjugated manner (Scheme 26.6), The ΔH_{calc} for the dimer formation is exothermic by 27 kcal mol^{-1}, whereas additional insertions are calculated to be exothermic by an additional 20 kcal mol^{-1}. Thus, ΔH_{calc} for the trimer formation is exothermic by 47 kcal mol^{-1}, supporting the results in which non-bulky terminal alkynes were oligomerized with no chemoselectivity.

A plausible pathway was proposed for the organoactinide-oligomerization of terminal alkynes, presented in Scheme 26.7. The mechanism is a sequence of well-established reactions such as insertion of an alkyne into a M–C σ-bond and

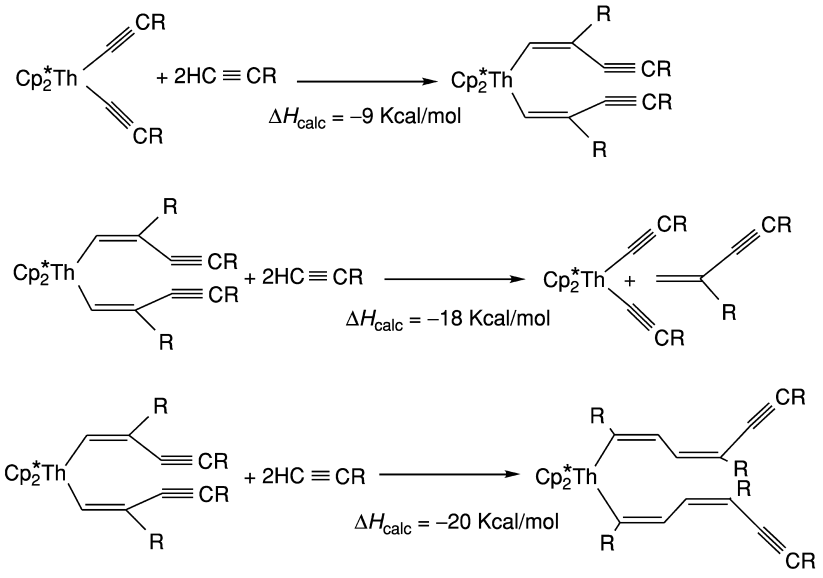

Scheme 26.6 *Calculated enthalpies of reaction for the oligomerization of terminal alkynes.*

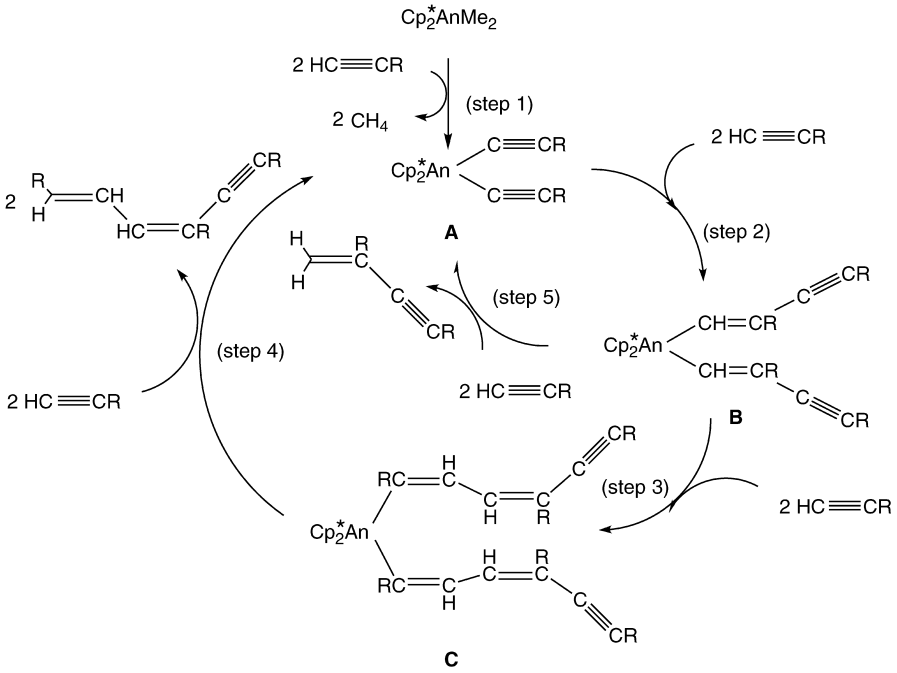

Scheme 26.7 *Proposed mechanism for the linear oligomerization of terminal alkynes catalyzed by organoactinide bisacetylide complexes.*

σ-bond metathesis. The first step in the catalytic cycle involves the protonation of the alkyl groups in the organoactinide precatalyst at room temperature, yielding the bisacetylide complexes $(C_5Me_5)_2An(C{\equiv}CR)_2$ (**A**), with the concomitant elimination of methane (step 1). In general, this is a very rapid reaction extremely exothermic as calculated for the reaction of the organoactinides with PHC≡CH [equation (26.17)]

The 1,2-head-to-tail-insertion of the alkyne into the actinide–carbon σ-bond was proposed to yield the plausible bisalkenyl actinide complex **B** (step 2). Complex **B** may undergo either a σ-bond metathesis with the C–H bond of another alkyne producing the corresponding geminal dimer and **A** (step 5), or an additional 2,1-tail-to-head-insertion of an alkyne, with the expected regioselectivity (for TMSC≡CH), into the organoactinide alkenyl complex **B**, yielding the bis(dienyl)organoactinide complex **C** (step 3). The reaction of complex **C** with an incoming alkyne was proposed to yield the corresponding trimer and regenerating the active actinide bisacetylide complex **A** (step 4). The turnover-limiting step for the catalytic trimerization was identified to be the elimination of the organic trimer from the organometallic complex **C**. This result indicated that the rate for σ-bond metathesis between the actinide–carbyl and the alkyne and the rate of insertion of the alkyne into the metal–acetylide (steps 1 and 2)

were much faster than the rate for σ-bond metathesis of the alkyne with the metal–dialkenyl bond in the catalytic cycle (step 4).

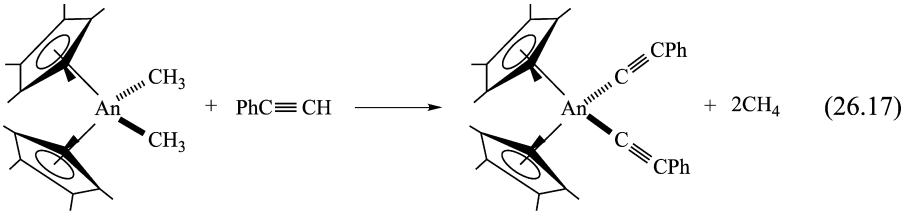

$\Delta H_{\text{Th (calc)}} = -18$ kcal mol^{-1}
$\Delta H_{\text{U (calc)}} = -48$ kcal mol^{-1}

26.3.5 Cross oligomerization of ^{t}BuC≡CH and TMSC≡CH promoted by $(C_5Me_5)_2UMe_2$

In the oligomerization of ^{t}BuC≡CH with $(C_5Me_5)_2UMe_2$, the geminal dimer was found to be the major product, indicating that the addition of the alkyne to the metal acetylide was regioselective with the bulky group pointing away from the cyclopentadienyl groups (Fig. 26.2).

The reaction of equimolar amounts of ^{t}BuC≡CH and TMSC≡CH with $(C_5Me_5)_2UMe_2$ produced two dimers (14%) and three specific trimers (86%). The dimers generated in the reaction were characterized to be the geminal dimer **36** (10%) and the cross geminal dimer **37** (4%), resulting from the insertion of a ^{t}BuC≡CH with the same regioselectivity as observed in Fig. 26.2 into the uranium bis(trimethylsilylacetylide) complex. The trimers obtained were the head-to-tail-to-head trimer, (*E,E*)-1,4,6-tris(trimethylsilyl)-1-3-hexadiene-5-yne (**38**), as the major product (43%), the trimer **39** (15%), resulting from the insertions of two TMSC≡CH into the *tert*-butylacetylide complex, and the unexpected trimer **40** (27%) [equation (26.18)]. Trimer **40** was

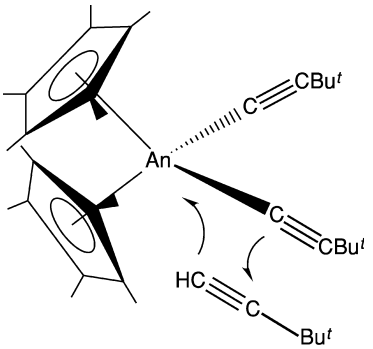

Fig. 26.2 *Regioselectivity of the insertion of* ^{t}*BuC≡CH into an organoactinide acetylide bond.*

formed by the consecutive insertion of ^{t}BuC≡CH after the TMSC≡CH insertion. These results indicated that in the formation of trimers, the last insertion rate must be fast and competitive for both alkynes, and that the metathesis of the free alkyne is the rate-determining step.

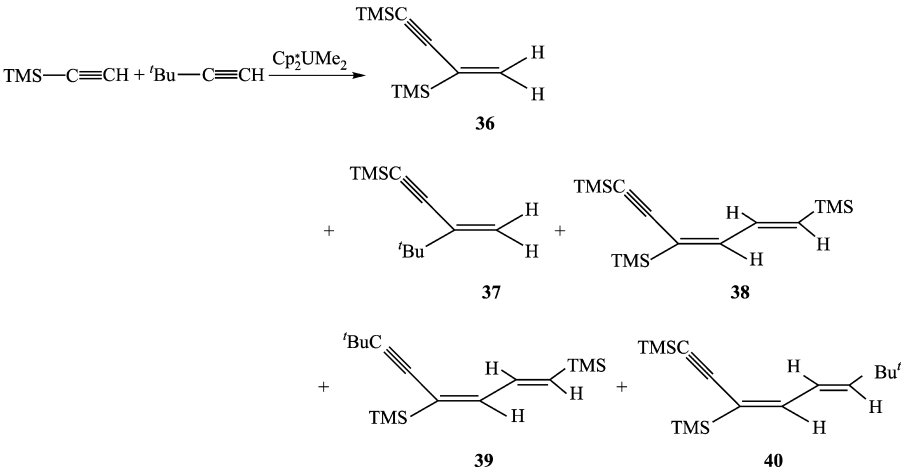

(26.18)

26.4 DIMERIZATION OF TERMINAL ALKYNES

Due to the different reactivities displayed in the selective dimerization of terminal alkynes by different neutral and cationic organo-5f-complexes, this topic will be divided based on the nature of the catalytic species.

26.4.1 Dimerization of terminal alkynes promoted by neutral $(C_5Me_5)_2AnMe_2$ complexes in the presence of amines

An interesting rationale has been presented in connection with the proposed mechanism, suggesting the means to permit the formation of a specific dimer while limiting the formation of higher oligomers. This would, in effect block steps 3 and 4 in Scheme 26.7 and restrict the reaction to follow steps 2 and 5. Haskel *et al.* (1999) have reported a principle for the selective control over the extent of the oligomerization of terminal alkynes by using an acidic chain-transfer agent. The basic approach employs a chain transfer reagent not ending up in the product and not involving subsequent elimination from the product to release the unsaturated oligomer (in contrast to e.g. ethene oligomerization by metallocene catalysts or magnesium reagents) (Samsel, 1993; Pelletier *et al.*, 1996). The dimerization was performed in the presence of an amine (primary or

secondary); this resulted in minimal alteration of the turnover frequencies compared with the non-controlled process. The selectivity control (i.e. the amount of the different oligomers obtained by the different complexes (Th, U)) of the new catalytic cycle is explained by considering the difference in the calculated bond-disruption energies between an actinide–alkenyl- and an actinide–amido-bond, and combining non-selective catalytic pathways with individual stoichiometric reactions.

Organoactinide complexes of the type $(C_5Me_5)_2AnMe_2$ (An = Th, U) reacted with terminal alkynes in the presence of primary amines yielding preferentially alkyne dimers [equation (26.19)] and for certain alkynes small amounts of regioselective trimers [equation (26.20)]. This selectivity was opposite to that found in the oligomerization of alkynes under the same conditions in the absence of amines. In general, the initial reaction of $(C_5Me_5)_2AnMe_2$ (An = Th, U) with an alkyne yielded the bisacetylide complex, though in the presence of amines, for the thorium complex, the corresponding $(C_5Me_5)_2Th(NHR)_2$ (**5**) was formed. For the uranium complex, no bisamido complex is observed unless large excess of the amine was used.

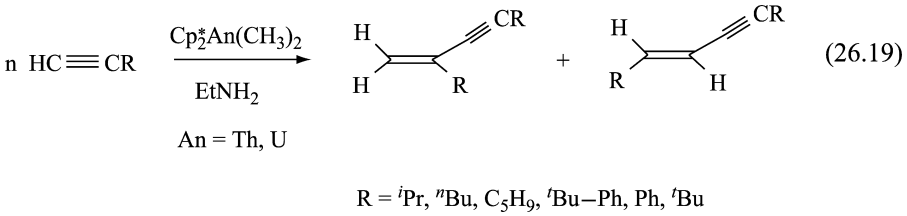

(26.19)

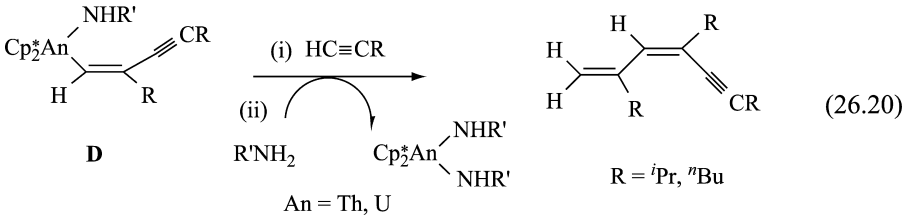

(26.20)

When comparing the oligomerization of terminal alkynes promoted by the thorium complex in the presence of amines as to the results obtained without amines, a dramatic reduction in the extent of oligomerization was observed. When $EtNH_2$ or other primary amines were used with aliphatic alkynes, mixtures of the corresponding *geminal* and *trans* dimer were produced, while for aromatic alkynes, just the *trans* dimer was formed. Increasing the bulkiness of the primary amine for aliphatic alkynes allowed only the formation of the *geminal* dimer, and the specific trimer as represented in equation (26.20). These results indicated that the insertion of the second alkyne into the metalla–eneyne **D** complex and the trimer elimination [equation (26.20)] are faster than either the insertion of an alkyne into the intermediate complex **E**,

and/or the protonolysis of **E** by either the alkyne or the amine, eliminating the corresponding isomeric trimer and/or dimer, respectively [equation (26.21)]. Reactions of the thorium precursor with secondary amines allowed the formation of higher oligomers (up to pentamers), however in lower yields, as compared with the results obtained in the reactions in the absence of amines. It was proposed that for secondary amines, the protonolysis of the growing oligomer from the metal was much slower as compared to the insertion of the alkynes and cutting the oligomer chain by the alkyne itself.

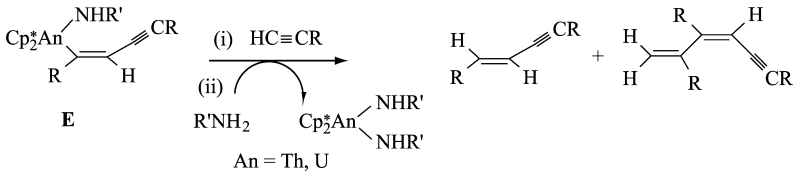

(26.21)

For uranium, the oligomerization of non-bulky alkynes with secondary amines showed no control whereas for primary amines ($R'NH_2$), the intermolecular hydroamination product obtained was exclusively ($RCH_2CHN{=}R'$) (Haskel *et al.*, 1996). While the dimerization of ^{t}BuC≡CH produced the *geminal* dimer, in the presence of ^{t}BuNH$_2$, a mixture of both dimers were obtained, which suggested the attachment of the amine to the metal center at the time of the alkyne insertion allowing different regioselectivities. Previously, for the non-controlled oligomerization reactions, the actinide–bisacetylide complex was proposed as the active species in the catalytic cycle. In the controlled oligomerization reaction, the formation of the organoactinide bisamido complex, which was the predominant species, provided strong evidence that the amine was the major protonolytic agent. A novel strategy was implemented in support of the protonolytic theory to increase the selectivity towards the trimeric isomer. Enhanced selectivity was attained by providing a kinetic delay for the fast protonolysis using deuterated amine. The kinetic effect allowed more trimer formation, in a reaction producing both dimer and trimer [equation (26.22)]. The strategy biased the chemoselectivity of the oligomerization increasing the trimer:dimer ratio.

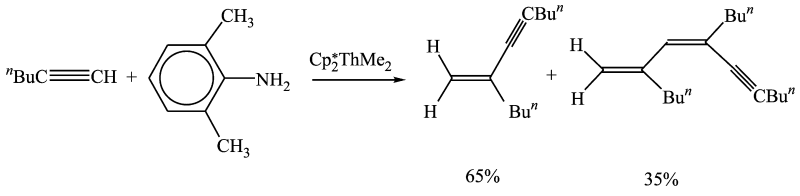

(26.22)

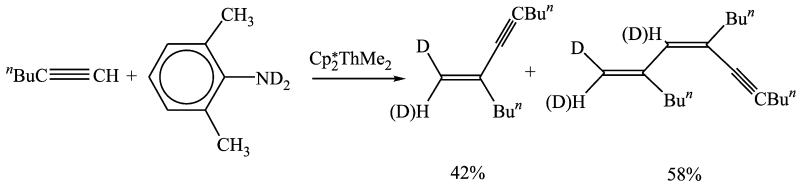

When the product formation was followed as a function of time, the first deuterium was observed at the geminal position, but at higher conversions, more olefinic positions were deuterated, suggesting that the alkyne and the deuterated amine were in equilibrium through a metal complex only exchanging hydrogen/deuterium atoms.

(a) Kinetic, thermodynamic, and mechanistic studies of the controlled oligomerization of terminal alkynes

Kinetic measurements of the controlled oligomerization reaction of ^{n}BuC≡CH with ^{i}BuNH$_2$ promoted by $(C_5Me_5)_2ThMe_2$ revealed a first-order dependence of the catalytic rate on substrate concentration, an inverse first-order in amine and first-order dependence in precatalyst. Thus, the rate law for the controlled oligomerization of terminal alkynes promoted by organoactinides can be written as presented in equation (26.23).

$$v = k\,[\mathrm{Th}]^1\ [\mathrm{alkyne}]^1\ [\mathrm{amine}]^{-1} \tag{26.23}$$

The derived $\Delta H^{\dagger}$ and $\Delta S^{\dagger}$ values from an Eyring analysis were measured to be 15.1(3) kcal mol^{-1} and –41.2(6) eu, respectively.

An inverse proportionality in catalytic systems is consistent with a rapid equilibrium before the rate-limiting step. For this reaction, it was consistent with the equilibrium between the bisamido complex and a bisamido–amine complex, as found in the hydroamination of terminal alkynes promoted by early transition complexes (Walsh *et al.*, 1992; Baranger *et al.*, 1993) and in the hydroamination of olefins promoted by organolanthanide complexes (Gagné *et al.*, 1992a,b; Molander and Hoberg, 1992).

A reasonable mechanism for the controlled oligomerization of terminal alkynes is described in Scheme 26.8.

The mechanism presented in Scheme 26.8 consists of a sequence of simple reactions, such as insertion of acetylene into an M–C σ-bond, and σ-bond metathesis. The starting complex $(C_5Me_5)_2ThMe_2$ reacts fast with amines to the bisamido complex **G** and the bisamido–amine complex **F**. These complexes were found to be in rapid equilibrium and responsible for the inverse proportionality in the kinetic dependence of the amine (Straub *et al.*, 1996). Complex **G**, which was found to be the resting state for the catalytic species, reacted with one equivalent of alkyne in the rate-limiting step, producing complex **H** (step 1). Comparison of the results obtained for the oligomerization of phenylacetylene in the absence of amines (with amines only a dimer was obtained), in which both dimers and higher oligomers were obtained, indicated that an amido acetylide and not the bisacetylide complex was responsible for the regio-differentiation. Complex **H** reacts with an alkyne, yielding the actinide–alkenyl amido complex **I** (step 2), which may undergo either a σ-bond protonolysis with the amine to yield the corresponding dimer and the bisamido complex **G** (step 3), or another

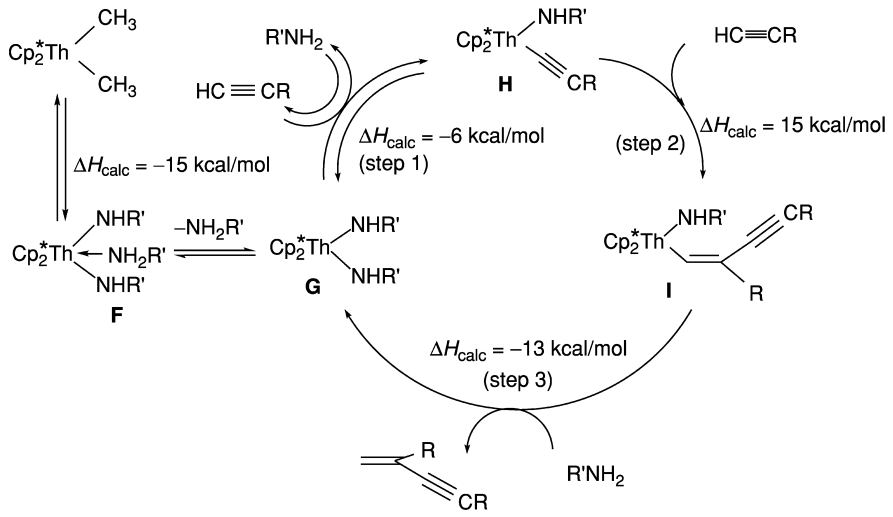

Scheme 26.8 *Plausible mechanism for the oligomerization of terminal alkynes, in the presence of amines, promoted by organothorium complexes.*

insertion of an alkyne and concomitant σ-bond protonolysis by the amine, yielding the oligomeric trimer and the bisamido complex **G**. Thus the reaction rate law presented in equation (26.23) was compatible with rapid, irreversible alkyne insertion (step 2), rapid σ-bond protonolysis of the oligomer by the amine (step 3), a slow pre-equilibration involving the bis-amido **G** and the mono amido-acetylide complex (**H**) (step 1), and a rapid equilibrium between the bisamido complex **G** and the bisamido–amine complex **F**.

Control over the oligomerization was accomplished by a kinetic competition between the insertion reaction of a new alkyne molecule into the metal–alkenyl bond [equation (26.24)] and the protonolysis by the amine [equation (26.25)]. The insertion reaction produces a larger metalla–oligomer complex, whereas the competing protonolysis produces the organic product and the bisamido organometallic complex. The difference in selectivity found for the thorium and uranium complexes was corroborated using bond disruption energy data (Bruno *et al.*, 1983; Smith *et al.*, 1986b; Marthino Simões and Beauchamp, 1990; Giardello *et al.*, 1992). For thorium, both reactions [equations (26.24) and (26.25)] were calculated to be exothermic by almost equal amounts generating control over the extent of oligomerization. For the corresponding uranium complex, where no control over chain length was observed, the formation of the bisamido complex was calculated to be endothermic, limiting the control over the degree of oligomerization.

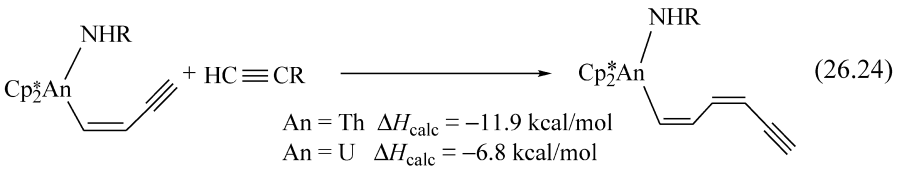

(26.24)

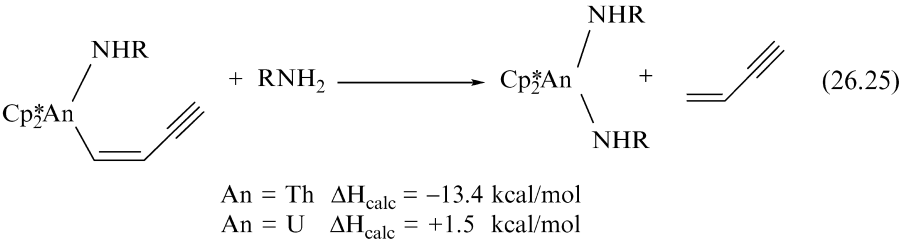

(26.25)

26.4.2 Dimerization of terminal alkynes promoted by the *ansa*-organothorium complex $Me_2Si(C_5Me_4)_2ThBu_2$

The *ansa*-bridged organoactinide complex $Me_2Si(C_5Me_4)_2Th^nBu_2$ was found to be an excellent precatalyst for the chemo- and regio-selective dimerization of terminal alkynes. At room temperature, head-to-tail geminal dimers were obtained, whereas at higher temperature (78°C), the geminal dimer and some minor amounts of the specific head-to-tail-to-tail trimer (up to 5%) were also observed particularly for the specific alkynes ^{i}PrC≡CH and ^{n}BuC≡CH [equation (26.26)] (Dash *et al.*, 2001). Although no large difference was observed among similar alkyne substituents, the dimerization reaction of either ^{i}PrC≡CH or ^{n}BuC≡CH with $Me_2Si(C_5Me_4)_2Th^nBu_2$ was much faster and more selective than the dimerization with $Cp^*_2ThMe_2$. The most striking result regarding the dimerization/oligomerization of terminal alkynes was found for TMSC≡CH (TMS = Me_3Si). No catalytic reaction was observed by using the *ansa*-bridged complex (butane was evolved), in contrast to the results obtained in the reaction of TMSC≡CH with $Cp^*_2ThMe_2$, in which the geminal dimer (10%) and the head-to-tail-to-head trimer (90%) were obtained with high regioselectivity (Straub *et al.*, 1995).

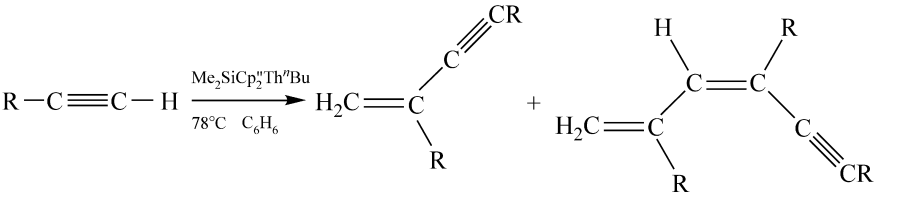

R = ^{t}Bu, ^{i}Pr, H_2C=C(Me), ^{n}Bu, Me R = ^{i}Pr, ^{n}Bu

(26.26)

A domino reaction was observed in the dimerization of the alkene-functionalized alkyne producing dimer **41**, which undergoes a quantitative intermolecular Diels–Alder cyclization to produce compound **42** [equation (26.27)].

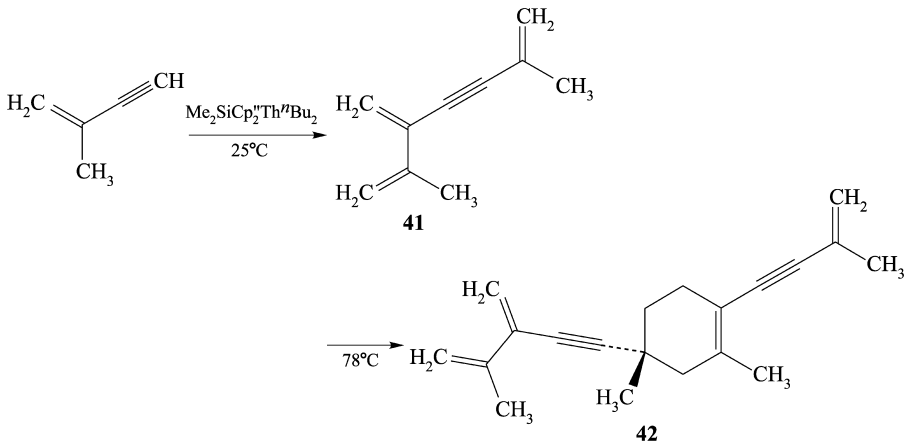

(26.27)

(a) Kinetic studies of the dimerization of terminal alkynes promoted by $Me_2Si(C_5Me_4)_2Th''Bu_2$

The kinetics for the dimerization of $^{i}PrC{\equiv}CH$ promoted by $Me_2Si(C_5Me_4)_2Th''Bu_2$ were studied. The reaction displayed a first-order dependence in precatalyst, and two different kinetic domains were observed, with differing alkyne dependence (Fig. 26.3). At low concentrations of alkyne, an inverse proportionality was observed indicating that the reaction is in an inverse first-order, but at higher concentrations, the reaction exhibited a zero order in alkyne (Eisen *et al.*, 1998). The change from an inverse rate to a zero rate was rationalized by invoking two equilibrium processes. In one of these equilibrium processes, the complex was removed from the catalytic cycle (inverse order), whereas the second equilibrium was found to be the rate-determining step in the dimer formation. The latter was measured only at high alkyne concentrations. The derived activation parameters E_a, $\Delta H^{\ddagger}$, and $\Delta S^{\ddagger}$ from an Eyring analysis were 11.7(3) kcal mol^{-1}, 11.0(3) kcal mol^{-1}, and 22.6(5) eu, respectively.

Given that the stereochemical approach of the alkyne to the organometallic moiety is likely side-on, the highly regioselective production of the geminal dimers was rationalized by suggesting that the insertion of the alkyne occurs with the substituent away from the metal center. The methyl groups of the cyclopentadienyl spectator ligand also disfavor the disposition of the alkyne substituent facing the metal center.

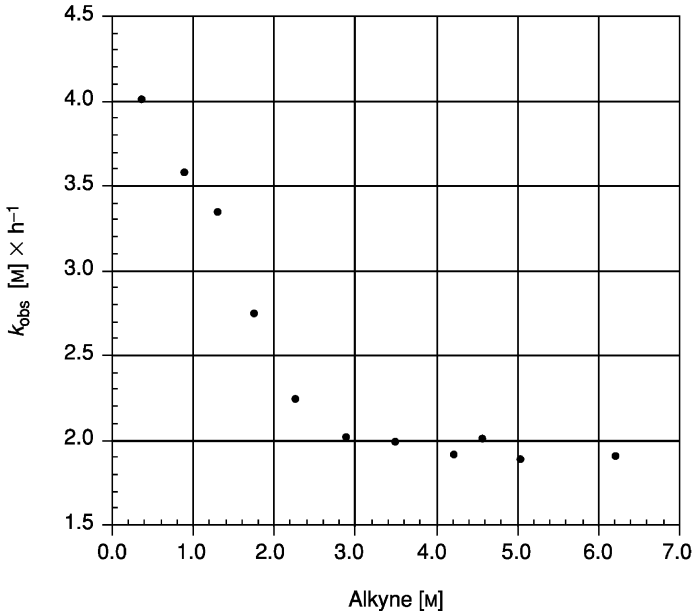

Fig. 26.3 *Alkyne dependence in the dimerization of* $^{i}PrC{\equiv}CH$ *promoted by* $Me_2Si(C_5Me_4)_2Th^{n}Bu_2$.

A plausible mechanism for the selective dimerization of $^{i}PrC{\equiv}CH$ promoted by $Me_2Si(C_5Me_4)_2Th^{n}Bu_2$ is presented in Scheme 26.9. The initial step in the catalytic cycle is the alkyne C–H activation by the complex $Me_2Si(C_5Me_4)_2Th^{n}Bu_2$ and the formation of the bisacetylide complex **J** together with butane (step 1). Complex **J** is proposed to be in equilibrium with an alkyne, forming the proposed π-alkyne acetylide complex **K**, which removes the active species from the catalytic cycle (inverse rate dependence). Alternatively, **J** undergoes a head-to-tail insertion with another alkyne into the thorium–carbon σ-bond, producing the substituted alkenyl complex **L** (step 2). Complex **L** goes through a σ-bond protonolysis with an additional alkyne (step 3), yielding the corresponding dimer and regenerating the active acetylide complex **J.** In contrast to the general expectations for organoactinides, complex **K** was the first π-olefin intermediate complex (*vide infra*) exhibiting new rich and versatile reactivity for actinide complexes.

The turnover-limiting step for the catalytic dimerization was measured to be the insertion of the alkyne into the thorium–acetylide complex **J** (step 2). Thus, the derived rate law based on the mechanism proposed in Scheme 26.9 for the oligomerization of terminal alkynes promoted by the complex $Me_2SiCp''_2Th^{n}Bu_2$ is given by equation (26.28), fitting the kinetic performances of the alkyne and catalysts.

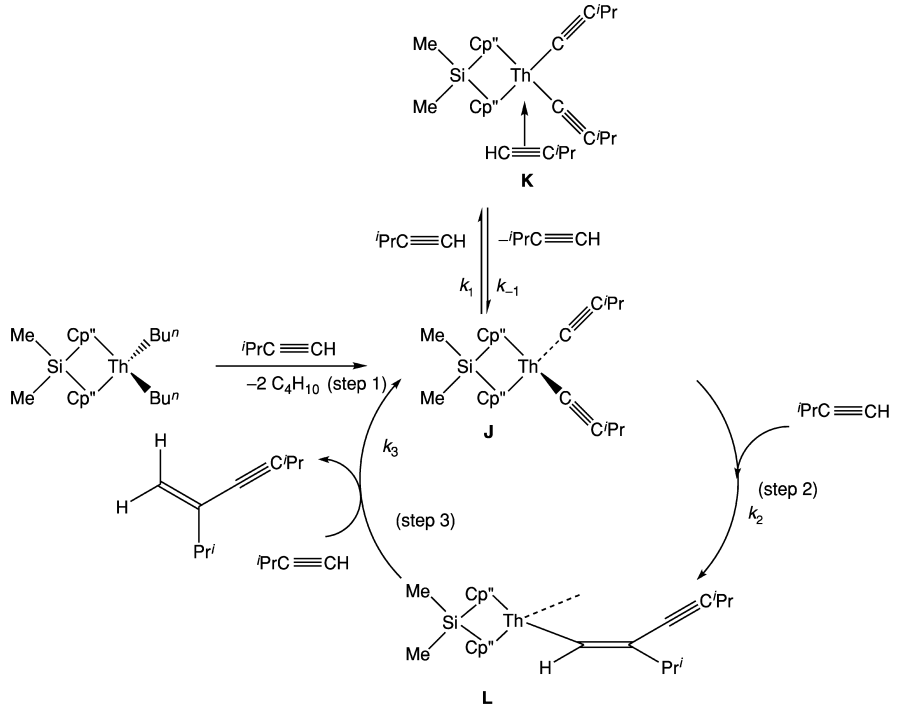

Scheme 26.9 *Proposed mechanism for the dimerization of terminal alkynes promoted by* $Me_2SiCp''_2Th^nBu_2$.

$$v = \frac{k_{-1}k_2[\text{Cat}]}{k_1 + k_2 - \frac{k_2k_{-2}}{k_3[\text{alkyne}]}} \tag{26.28}$$

26.4.3 Catalytic dimerization of terminal alkynes promoted by the cationic actinide complex $[(Et_2N)_3U][BPh_4]$. First f-element alkyne π-complex $[(Et_2N)_2U(C{\equiv}C^tBu)(\eta^2\text{-}HC{\equiv}C^tBu)][BPh_4]$

Unlike neutral organoactinide complexes, homogeneous cationic d^0/f^n actinide complexes have been used as catalysts for the polymerization of α-olefins (Jia *et al.*, 1997; Chen *et al.*, 1998), as have their isolobal group 4 complexes. The alkyne oligomerization reaction has been mentioned as a useful probe for the insertion and σ-bond metathesis reactivity of organoactinide complexes. For the corresponding cationic actinide complexes, little was known regarding their reactivity with terminal alkynes (Wang *et al.*, 1999). Reaction of the cationic complex $[(Et_2N)_3U][BPh_4]$ (Berthet *et al.*, 1995) with the terminal alkynes RC≡CH, (R = Me, ^{n}Bu, ^{i}Pr) resulted in the chemo- and regio-selective catalytic formation of the head-to-tail *gem*-dimers without the formation of the *trans* dimer or any other major oligomers [equation (26.29)]. For PhC≡CH, the

reaction was less chemoselective, allowing the formation of some trimers (dimer:trimer ratio = 32:58). For TMSC≡CH, besides the formation of the geminal head-to-tail dimer, the *trans*-head-to-head dimer, and the regioselective head-to-tail-to-head-trimer (*E,E*)-1,4,6-tris(trimethylsilyl)1-3-hexadien-5-yne, the unexpected head-to-head *cis* dimer was also formed [equation (26.30)]. For ^{t}BuC≡CH, besides the geminal dimer also the unexpected *cis*-dimer was formed [equation (26.31)].

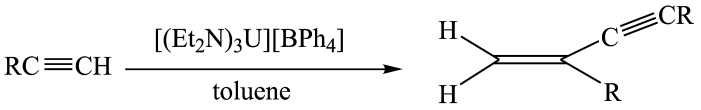

(26.29)

R = Me, ^{n}Bu, ^{i}Pr

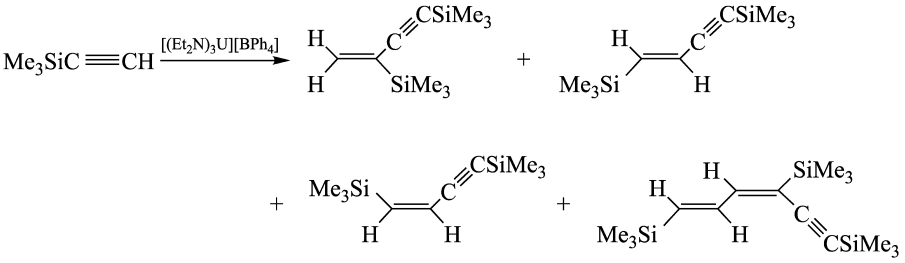

(26.30)

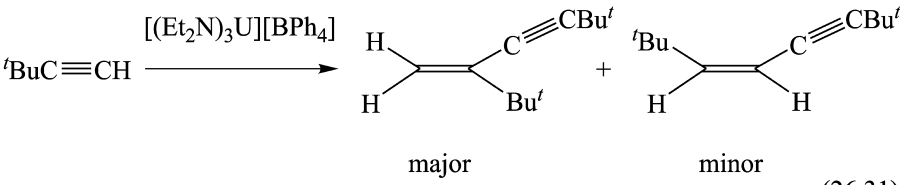

(26.31)

As already mentioned, mechanistically, the relatively polar metal–ligand bonds, the absence of energetically accessible metal oxidation states for oxidative addition/reductive elimination processes and the presence of relatively low-lying empty σ-bonding orbitals, implicate a 'four-center' heterolytic transition state in the metal–carbon bond cleavage (Marks and Day, 1985; Marks, 1986a,b). The reaction of the metal acetylide with a terminal alkyne occurs in a *syn* mode and the σ-bond protonolysis of the resulting alkenyl complex will be expected to maintain the *cis*-stereochemistry at the product (Fig. 26.4).

Hence, the formation of the *trans* dimers [equations (26.30) and (26.31)] argued for an isomerization pathway before the products were released from the metal center. For comparison, in the oligomerization of terminal alkynes promoted by the cationic complexes $[Cp^*_2AnMe][B(C_6F_5)_4]$ (An = Th, U), the

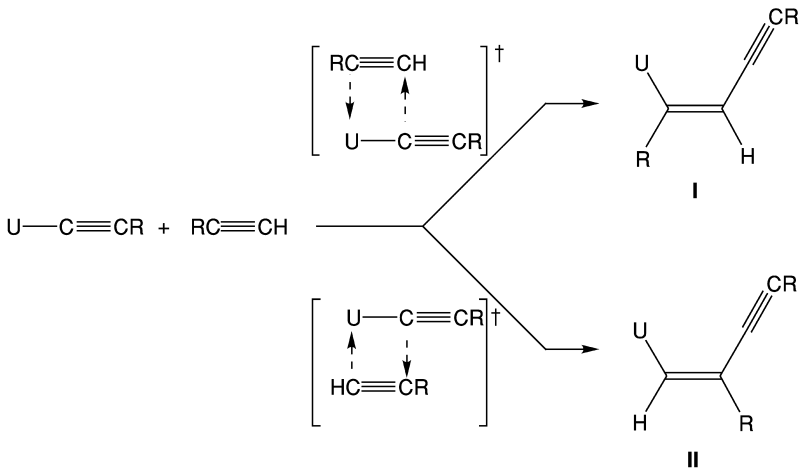

Fig. 26.4 *Modes of activation of an actinide–acetylide complex with an alkyne through a* syn *four-centered transition state pathway towards the formation of the intermediates* I *or/and* II.

geminal dimer was chemoselectively formed with no trace formation of either *cis* or *trans* dimers (Haskel *et al*., 1999).

Mechanistically, in the reaction of $[(Et_2N)_3U][BPh_4]$ with terminal alkynes, one equivalent of the Et_2NH amine was released in solution, forming the bisamido acetylide cationic complex $[(Et_2N)_2U–C{\equiv}CR][BPh_4]$. This reaction was shown to be a slow equilibrium, and the addition of different equimolar amounts of external Et_2NH to the reaction mixture led to a linear lowering of the reaction rate (Fig. 26.5).

Considering that in the reactions with alkynes, the amount of the released free amine was stoichiometric, it was deduced that the free terminal alkyne was also the major protonolytic agent. The confirmation of this protonolytic hypothesis was obtained by generating a kinetic delay for the presumed fast protonolysis by the alkyne to allow trimer formation, through replacement of the terminal hydrogen with deuterium [equation (26.32)]. By using that strategy, the chemoselectivity of the oligomerization was altered allowing formation of the deuterated geminal dimer, and some trimer (Dash *et al*., 2000).

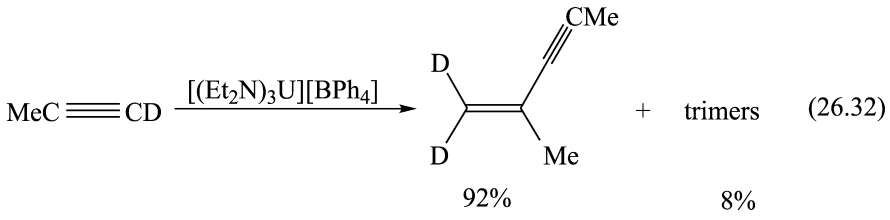

The kinetics of the dimerization reaction of $^{n}BuC{\equiv}CH$ was studied, indicating that the reaction behaved with a first-order dependence in precatalyst, and as

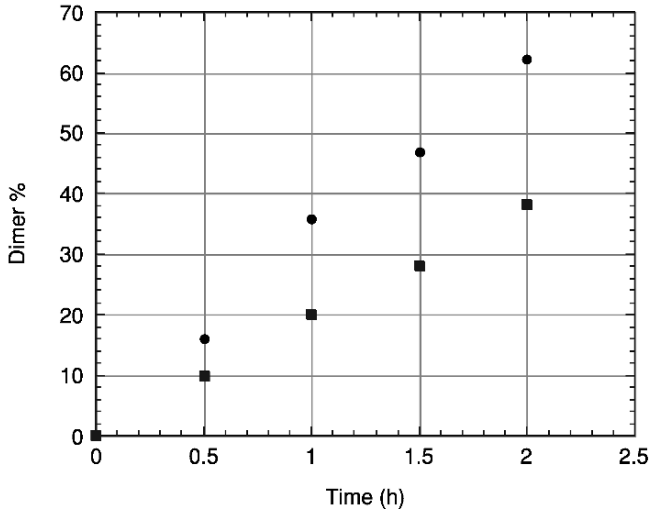

Fig. 26.5 *Following the dimer formation as a function of time in the reaction of* $^{i}PrC{\equiv}CH$ *catalyzed by* $[(Et_2N)_2U{-}C{\equiv}CR][BPh_4]$. *Absence of external amine* (●), *presence of one equivalent of external* Et_2NH (▪).

a function of alkyne, the kinetic plots showed two domains (Fig. 26.6). At low alkyne concentrations, an inverse proportionality was observed, indicating that the reaction was inverse first-order, and at higher concentrations, the reaction exhibits a zero-order in alkyne, similar to the behavior displayed in Fig. 26.3.

The activation parameters derived for the dimerization of ^{n}BuC≡CH were characterized by a small enthalpy of activation ($\Delta H^{\dagger} = 15.6(3)$ kcal mol^{-1}) and a negative entropy of activation ($\Delta S^{\dagger} = -11.4(6)$ eu). The proposed mechanism for the dimerization of ^{n}BuC≡CH is presented in Scheme 26.10. The initial step in the catalytic cycle is the alkyne C–H activation by the cationic uranium amide complex and the formation of the bisamido carbyl complex $[(Et_2N)_2U\text{-}C{\equiv}C^{n}Bu][BPh_4]$ (**M**) together with Et_2NH. Complex **M** can be in equilibrium with an alkyne forming the π-alkyne acetylide uranium complex **N**, which drives the active species out of the catalytic cycle (inverse rate dependence), or undergoes with an alkyne a head-to-tail insertion into the uranium–carbon σ-bond, yielding the substituted uranium alkenyl complex **O**. Complex **O** may undergo a σ-bond metathesis with an additional alkyne, leading to the corresponding dimer and regenerating the active carbyl complex **M**.

Complex **N** (for R = ^{t}Bu) was trapped and its structure spectroscopically determined. The ^{1}H- and ^{13}C-NMR spectra of complex **N** showed sharp lines as found for other actinide-IV type of complexes. The ^{1}H-NMR spectrum exhibited the acetylide signal (≡C–H) at $\delta = -2.14$ which correlated in the distortionless enhancement by polarization transfer (DEPT) and in the 2D C–H correlation NMR experiments to the carbon having the signal at $\delta = -19.85$

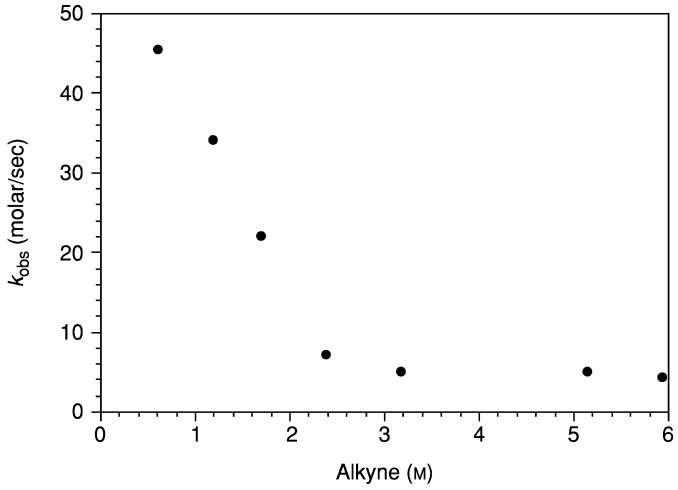

Fig. 26.6 *Alkyne dependence in the dimerization of* $^{n}BuC{\equiv}CH$ *promoted by* $[(Et_2N)_3U][BPh_4]$.

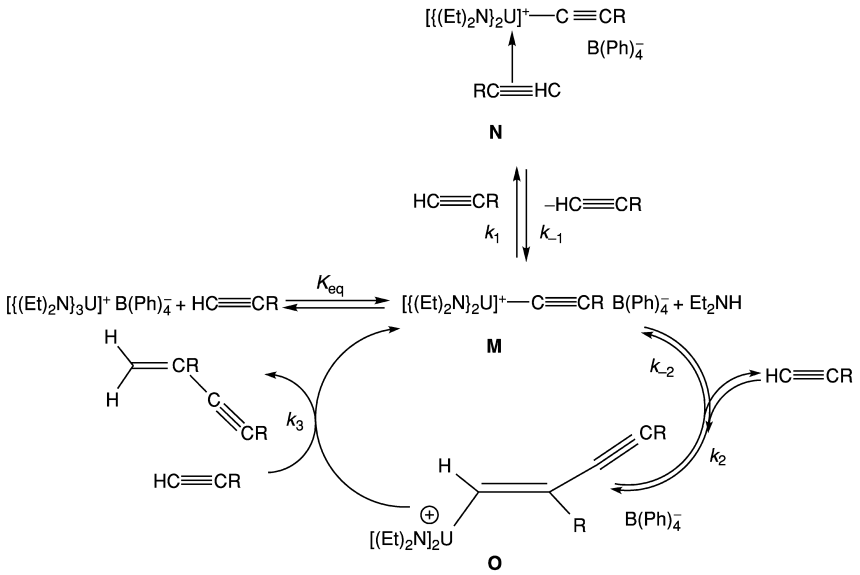

Scheme 26.10 *Proposed mechanism for the dimerization of terminal alkynes promoted by* $[(Et_2N)_3U][BPh_4]$.

ppm, with a coupling constant of $^{1}J = 250$ Hz. A confirmation of the formation of an alkyne η^2-complex, as compared to an acetylide complex or to a free alkyne was also obtained by FT-IR spectroscopy. The C≡C stretching of the free alkyne (2108 cm^{-1}) disappeared, giving rise to two signals at lower

frequencies, as expected for η^2-transition metal complexes, one at 2032 cm^{-1} similar to acetylide lanthanides, and the second one at 2059 cm^{-1}. The turnover-limiting step for the catalytic dimerization was found to be the insertion of the alkyne into the uranium–carbyl complex **M**. The proposed mechanism also agreed with the formation of trimer oligomers, which are only expected if a kinetic delay in the protonolysis was operative [equation (26.32)].

For sterically demanding alkyne substituents (TMS, ^{t}Bu), it was proposed that the rate of the protonolysis step is lower than that of the isomerization of the metalla–alkenyl complex **43**, producing the unexpected *cis*-dimer **45**, probably through the metalla–cyclopropyl cation (**44**), via the 'envelope isomerization' [equation (26.33)] (Faller and Rosan, 1977). The preference for the *cis*-isomer was suggested to arise from an agostic β-hydrogen interaction to the metal center (Wang *et al.*, 1999; Dash *et al.*, 2000).

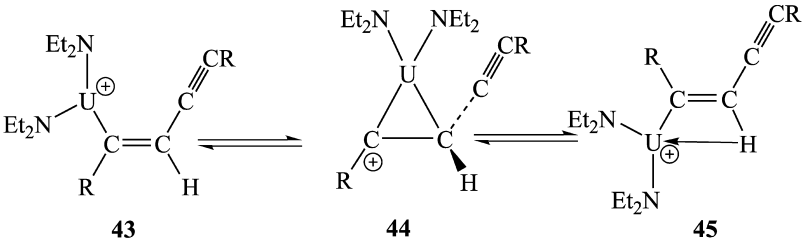

(26.33)

(a) Effect of external amines in the dimerization of alkynes promoted by the cationic complex $[(Et_2N)_3U][BPh_4]$

Since the formation of the cationic complex **M** is an equilibrium reaction (Scheme 26.10), it was possible to tailor the regiochemistry of the dimerization by using external amines. The expectation was that the amine would be bonded to the cationic metal center, causing a kinetic delay, but also allowing unique regiochemistry. As presented above in the reaction of 1-hexyne with a catalytic amount of the cationic complex $[(Et_2N)_3U][BPh_4]$ [equation (26.29)] the geminal dimer was chemoselectively obtained. However, when the reaction was carried out in a polar solvent like THF, the reaction was much slower, yielding besides the dimer a mixture of trimers [equation (26.34)]. The result was rationalized by the lower reactivity of the THF adduct $[(Et_2N)_3(THF)_3U]^+$ resulting in slower protonolysis of the corresponding alkenyl intermediate $[(Et_2N)_2(THF)_3U(C{=}C(H)C{\equiv}CR)]^+$ (R = ^{n}Bu), and allowing further alkyne insertion with the formation of trimers, but with a total lack of regioselectivity.

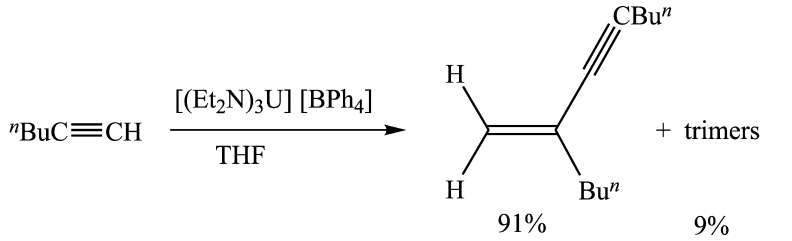

(26.34)

For 1-hexyne, the addition of equimolar amounts of the external amine $EtNH_2$ (alkyne:amine = 1:1) to the reaction mixture impeded the occurrence of the dimerization process. The same behavior was found for propyne [equation (26.35)]. This lack of reactivity for these alkynes was proposed to be a consequence of either their inability to engage in the equilibrium reaction (Scheme 26.10), resulting in the formation of the acetylide complex **M** in the presence of external $EtNH_2$, or the formation of an inactive π-alkyne complex, similar to **N** in Scheme 26.10. When 1-hexyne was reacted in the presence of an equimolar amount of the bulkier amine $^{t}BuNH_2$, the *gem* dimer and the unexpected *cis* dimer were obtained [equation (26.36)], indicating that the bulky amine probably allowed the formation of the acetylide intermediate $[(^{t}BuNH_2)_x(^{t}BuNH)_2U(C{\equiv}C^{n}Bu)]^{+}$ by the reaction of $^{n}BuC{\equiv}CH$ with the trisamido cation $[(^{t}BuNH_2)_3(^{t}BuNH)_3U]^{+}$. This acetylide would then undergo insertion of an alkyne molecule to give the corresponding alkenyl species and dimerization products.

$$RC{\equiv}CH + EtNH_2 \xrightarrow[\text{benzene}]{[(Et_2N)_3U]\,[BPh_4]} \text{no reaction} \qquad (26.35)$$

$R = CH_3,\ ^{n}Bu$

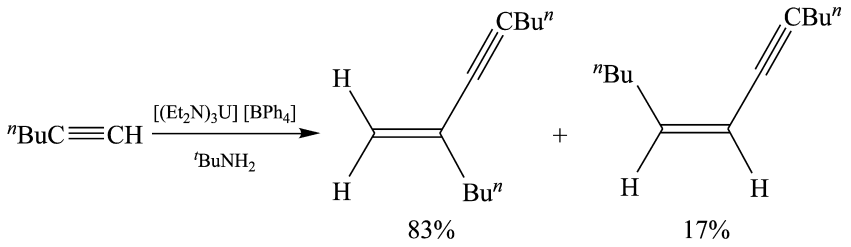

(26.36)

(b) Dimerization and hydroamination of $^{i}PrC{\equiv}CH$ and $^{t}BuC{\equiv}CH$ catalyzed by $[(Et_2N)_3U][BPh_4]$ in the presence of amines

Unpredictably, the reactions of $^{i}PrC{\equiv}CH$ and $^{t}BuC{\equiv}CH$ followed a quite distinct course. These alkynes were found to be more reactive than 1-hexyne or propyne in the presence of different amines. The nature of the diverse products were found to be strongly dependent on the size or steric encumbrance of the amine. The reaction of $^{i}PrC{\equiv}CH$ with $[(Et_2N)_3U][BPh_4]$ in the presence of $EtNH_2$ or $^{i}PrNH_2$ afforded the *cis* dimer, trace amounts of the *gem* dimer, and depending on the amine, one or both of the two corresponding hydroamination products were generated. By using the bulkier amine $^{t}BuNH_2$ both dimers and only one hydroamination product were observed [equation (26.37)] (Wang *et al.*, 2002a).

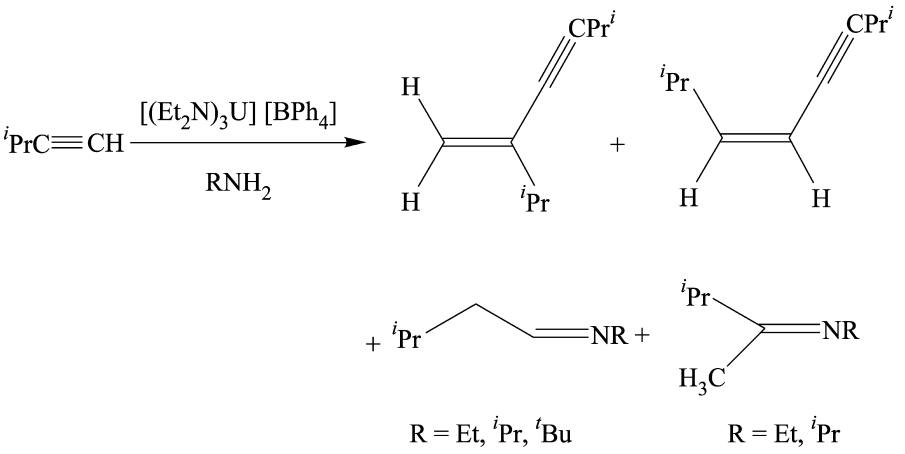

(26.37)

The rather large effect of alkyne concentration on the distribution of the products was revealed by the relative proportions of the dimers (*gem* to *cis*), which vary from 40:24 in the reaction of ^{t}BuND$_2$ with two equivalents of ^{i}PrC≡CH to 70:8 in the reaction of ^{t}BuNH$_2$ with one equivalent of ^{i}PrC≡CH. The results agreed with a dimerization mechanism such as that in Scheme 26.11. The mechanism consists of the formation of complex **Q** by the reaction of the cationic complex **P** with the alkyne (step 1). The acetylide complex reacts with an additional alkyne, producing the mixture of alkenyl compounds **R** and **S** (step 2). Isomerization of complex **R** through an envelope mechanism [equation (26.33)] allowed the formation of complex **T** (step 3) that by protonolysis yielded the unexpected *cis*-dimer (step 4). The addition of a large amount of alkyne in combination with a source of deuterium (as ^{t}BuND$_2$) removed complex **S** from the catalytic cycle as the *geminal* product (step 5). This latter species was found partially deuterated since the alkyne served also as a protonolytic reagent. The rate-determining step in the reaction was proposed to be the isomerization reaction (step 3).

(c) Regioselective oligomerization of ^{t}BuC≡CH promoted by [(Et$_2$N)$_3$U][BPh$_4$] in the presence of amines

Reaction of the bulkier alkyne ^{t}BuC≡CH with the cationic uranium complex [(Et$_2$N)$_3$U][BPh$_4$] in the presence of ethylamine gave mainly the *cis* dimer and small amounts of the *gem* isomer (up to 2%), showing the remarkable influence of the nature of the amine on the dimerization reaction, by transposing the regioselectivity [see equation (26.31)]. With other primary or secondary amines, the *cis* dimer was the major product although the concomitant formation of one regiospecific trimer and one regiospecific tetramer were also observed.

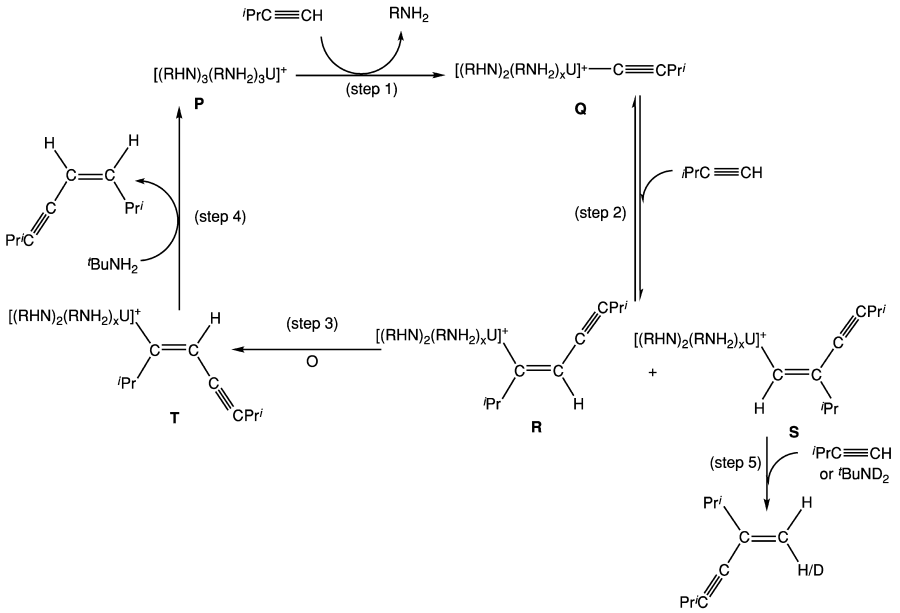

Scheme 26.11 *Proposed mechanisms for the formation of the* gem- *and* cis-*dimers, promoted by the cationic complex* $[(Et_2N)_3U][BPh_4]$ *in the reaction of* $^{i}PrC{\equiv}CH$ *with primary amines.*

The most remarkable result, aside from the formation of only one trimer and one tetramer, was the fact that the regiochemistry of these oligomers was unpredictable, regardless of amine [equation (26.38)]. The trimer and the tetramer corresponded to the consecutive insertions of an alkyne molecule into the vinylic CH bond *trans* to the bulky *tert*-butyl group.

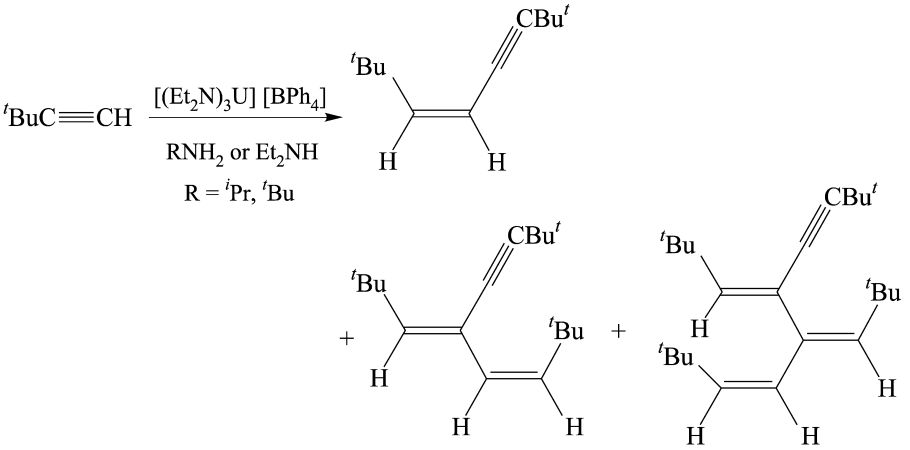

(26.38)

To reveal the role of the amine, and to examine the possibility that the initially *cis* isomer was reactivated to yield the regioselective trimer and tetramer, the reactions with deuterated amine ^{t}BuND$_2$ and deuterated alkyne ^{t}BuC≡CD were performed (Scheme 26.12). The reaction of ^{t}BuC≡CD with ^{t}BuNH$_2$ gave the products with *no* deuterium, indicating that ^{t}BuC≡CD was transformed into ^{t}BuC≡CH. The reaction for the H/D exchange between ^{t}BuC≡CH and ^{t}BuND$_2$ was found to be active in the presence of the catalyst, to give ^{t}BuC≡CD and ^{t}BuNHD. These compounds were also observed at early stages of the catalytic oligomerization of ^{t}BuC≡CH in the presence of ^{t}BuND$_2$, which afforded the *cis* dimer as a mixture of mono- and non-deuterated compounds. The amount of the non-deuterated dimer was always larger than that of the mono-deuterated dimer. The deuterium atom in the dimer was found only in the *trans* position relative to the ^{t}Bu group. Mixtures of non- and mono-deuterated compounds were also obtained for the trimer and tetramer having the deuterium atom always in the internal position, *trans* to the ^{t}Bu group. The presence of only one deuterium atom in the oligomers, in unique positions, strongly suggested that this D atom was introduced during the protonolysis steps of the catalytic cycle. In agreement with this hypothesis was the increasing proportion of the trimer and dimer, which likely results from the slower cleavage of the alkenyl intermediate by the deuterated amine or alkyne, permitting further insertion of an alkyne molecule into the U–C bond.

The proposed mechanism for the regiospecific formation of the trimer and tetramer is described in Scheme 26.13. The same intermediate **44**, which was proposed to explain the *trans–cis* isomerization of the alkenyl intermediate by the envelope mechanism [equation (26.33)] was proposed to explain conceptually the regiospecific formation of one trimer and one tetramer. The mechanism is based on the 1,2-hydride shift isomerization of the metal–alkenyl complex **44**, leading to the isomeric compound **U** (step 1). Deuterolysis at this stage liberates the deuterated dimer regioselectively (step 2). Insertion of an alkyne molecule into the U–C bond of **U** leads to the formation of complex **V**. The regioselectivity of this insertion (step 3) results from the steric hindrance between the alkyne substituent at the α-position of the metal–alkenyl chain and the incoming alkyne. The same isomerization process as before converts complex **V** into the *syn* complex **W** (step 4). Protonolysis of **W** regenerates the catalyst and produces the specific trimer (step 5), whereas the additional insertion of the alkyne, envelope isomerization, and protonolysis yielded the specific tetramer.

26.5 CROSS DIMERIZATION OF TERMINAL ALKYNES CATALYZED BY $[(Et_2N)_3U][BPh_4]$

Based on the different regioselectivities observed for the cationic complex $[(Et_2N)_3U][BPh_4]$, it was proposed that selective cross dimerization of alkynes could be induced. In the reaction of an equimolar mixture of ^{t}BuC≡CH

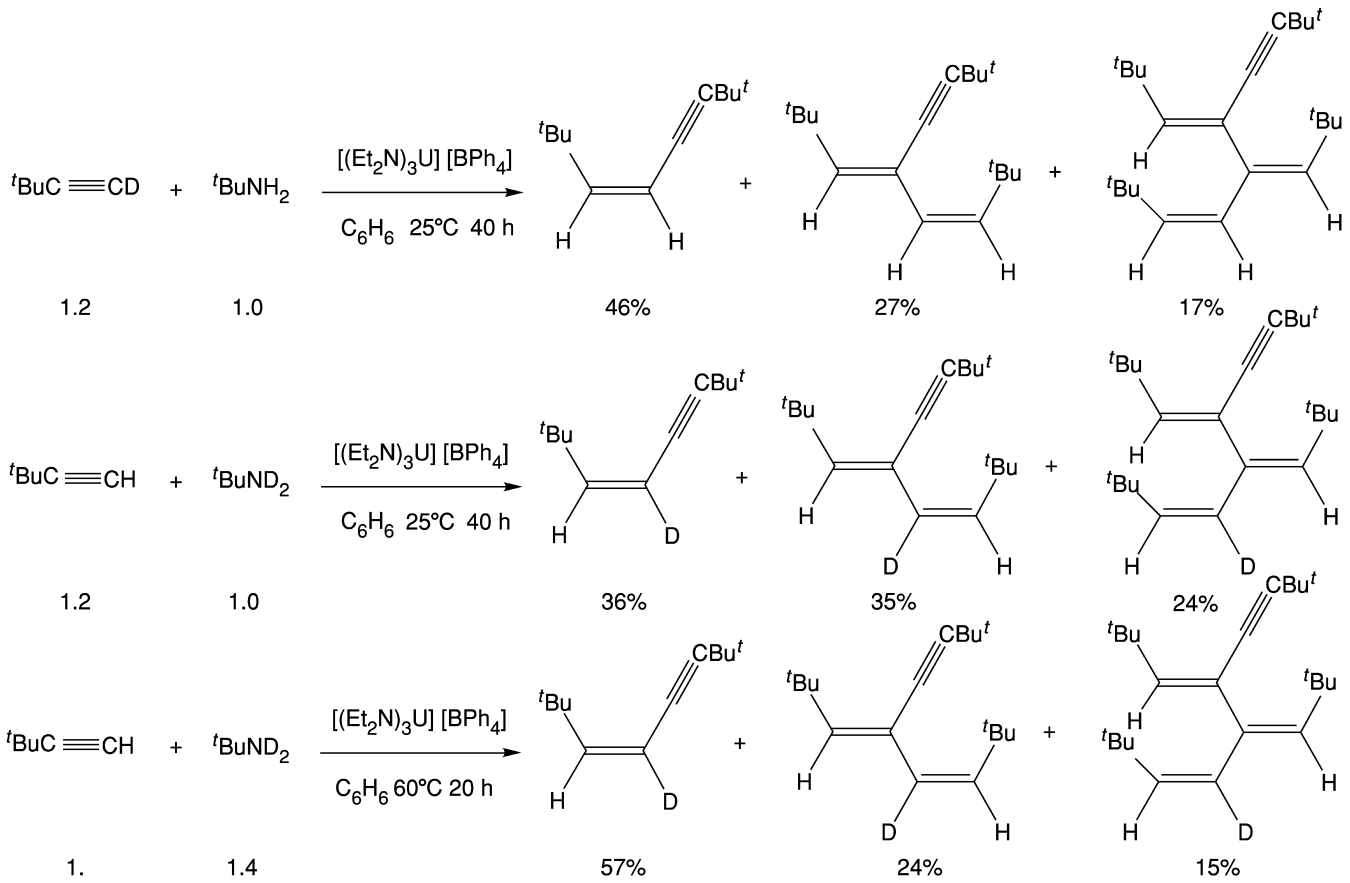

Scheme 26.12 *Deuterium labeling experiments in the oligomerization of* $^{t}BuC{\equiv}CH$ *with* $^{t}BuND_2$ *and* $^{t}BuC{\equiv}CD$ *with* $^{t}BuNH_2$ *promoted by* $[(Et_2N)_3U][BPh_4]$.

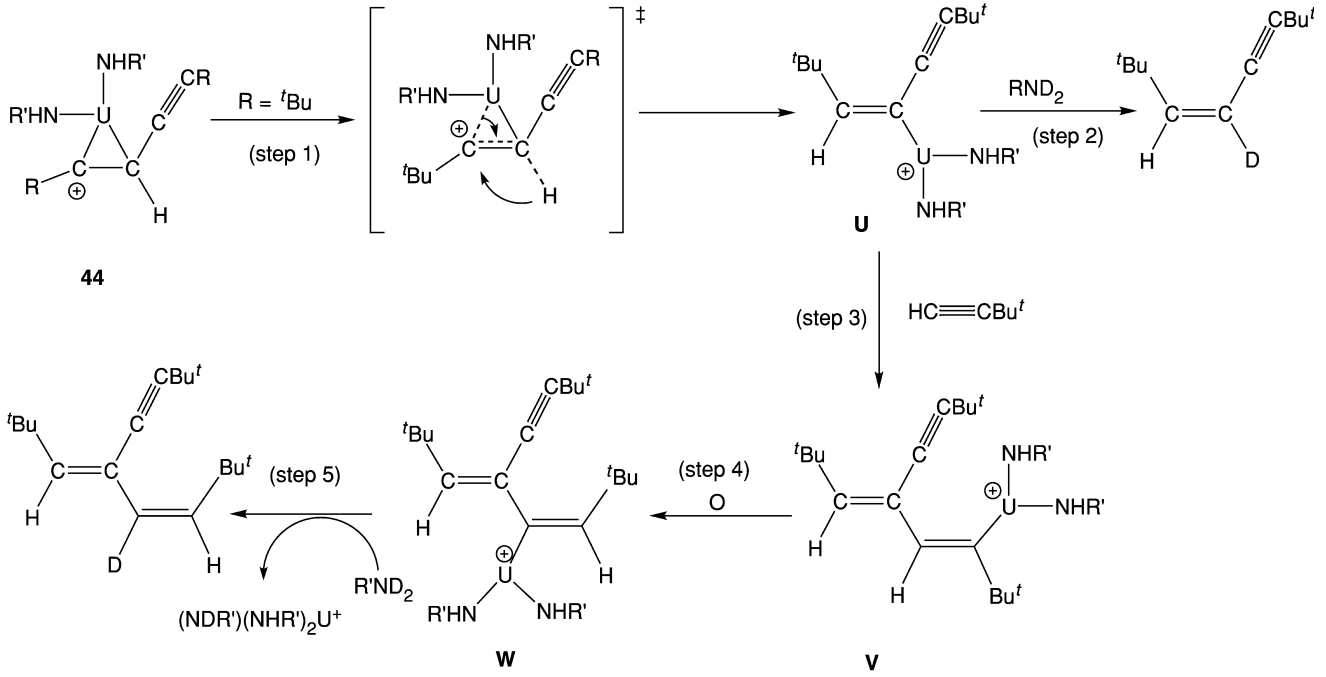

Scheme 26.13 *Proposed mechanism for the regioselective dimerization and trimerization of* $^{t}BuC{\equiv}CH$ *promoted by* $[(Et_2N)_3U][BPh_4]$ *in the presence of* $^{t}BuNH_2$.

and ^{i}PrC≡CH with [$(Et_2N)_3U$][BPh_4], the *gem*-dimer of ^{i}PrC≡CH and the *gem*-codimer were obtained [equation (26.39)] (Wang *et al.*, 2002b).

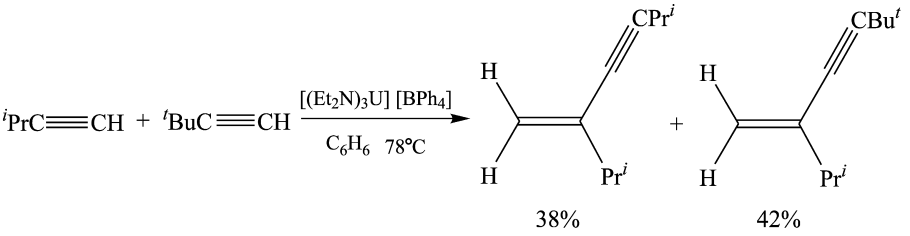

(26.39)

This result was extremely important, since it pointed out that the formation of both metal–acetylide complexes, M–C≡CR (R = ^{i}Pr, ^{t}Bu), was rapid and of comparable rates, although the insertion of ^{i}PrC≡CH into both M–C≡CR (R = ^{i}Pr, ^{t}Bu) moieties was much faster than that of ^{t}BuC≡CH. The lack of any trimer formation implied that the protonolysis of the metal–alkenyl fragments by either one of the terminal alkynes was faster than any additional alkyne insertion.

When a mixture of ^{i}PrC≡CH and PhC≡CH was reacted at room temperature (to avoid trimers), the *gem*-codimer was obtained. This codimer was the result of the protonolysis of the metal–alkenyl fragment produced from the insertion of ^{i}PrC≡CH into the M–C≡CPh moiety. Along with the codimer, a small amount of the *gem*-dimer of PhC≡CH was also produced by the insertion of PhC≡CH into the M–C≡CPh moiety before the protonolysis [equation (26.40)]. This result showed that PhC≡CH preferentially reacted with the precatalyst [$(Et_2N)_3U$][BPh_4] forming the acetylide complex U–C≡CPh into which ^{i}PrC≡CH inserted faster as compared with the aromatic alkyne. To shed light on which of the alkynes is the major protonolytic reagent the reaction of a mixture of ^{i}PrC≡CD and PhC≡CH was performed [equation (26.41)].

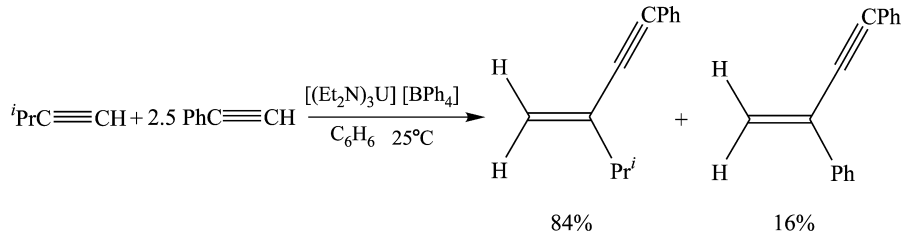

(26.40)

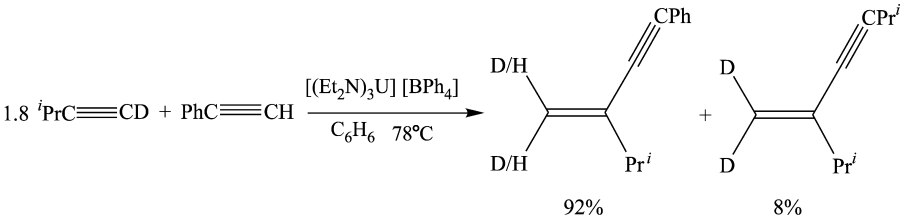

(26.41)

The favored formation of the codimer was substantiated with the following observations: (i) the aromatic metal–acetylide moiety was initially formed; (ii) ^{i}PrC≡CD inserted faster than the corresponding aromatic alkyne; (iii) the protonolysis by PhC≡CH was faster than that of the aliphatic alkyne; (iv) the formation of the deuterated *gem*-dimer was obtained due to some excess of the aliphatic alkyne that was present in the reaction. The scrambling of the deuterium atom at the geminal position (only one deuterium at each dimer) was the result of the exchange of acidic H/D atoms between the two aliphatic and aromatic alkynes through the metal center. With an excess of the aliphatic alkyne, the deuterolysis of the most stable U–C≡CPh by ^{i}PrC≡CD produced PhC≡CD and U–C≡CPr^{i} that reacted again with the aromatic alkyne yielding back U–C≡CPh and ^{i}PrC≡CH. The intermediate U–C≡CPr^{i} was the fragment responsible for the formation of the *gem* unlabelled dimer when the aliphatic alkyne was present in excess. The absence of trimers was an indication that the protonolysis by the PhC≡CH/D was much faster than any alkyne insertion, aromatic or aliphatic, into the metal–alkenyl complex.

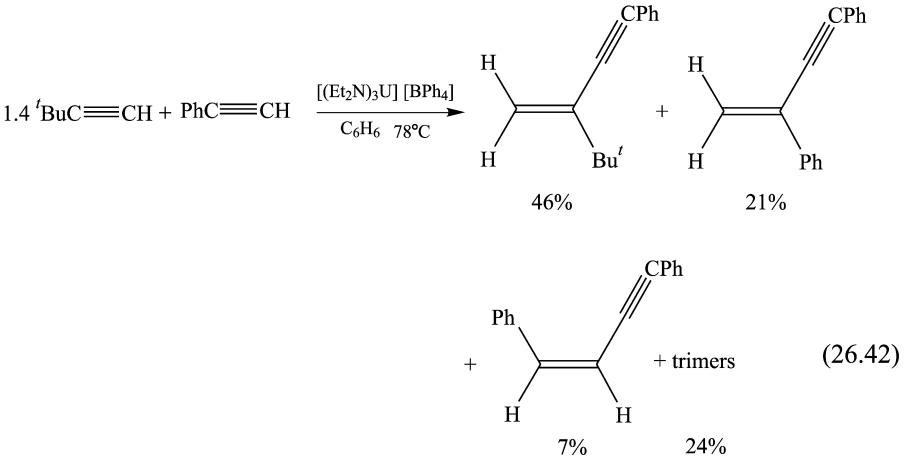

(26.42)

As mentioned above, when the bulkier alkyne ^{t}Bu≡CH was dimerized, the *cis* product was formed in addition to the *geminal* dimer [equation (26.31)]. Thus, in the codimerization of ^{t}Bu≡CH with PhC≡CH [equation (26.42)], the

gem-codimer and the two dimers (*gem* and *cis*) of the aromatic alkyne were characterized as products. This result argued once more for the preferred formation of the aromatic metal–acetylide U–C≡CPh into which both ^{t}BuC≡CH or PhC≡CH are able to insert. PhC≡CH inserted in this codimerization with low regioselectivity and the protonolysis was found to be not as fast as the insertion, since mixtures of trimers of PhC≡CH were also found in trace quantities.

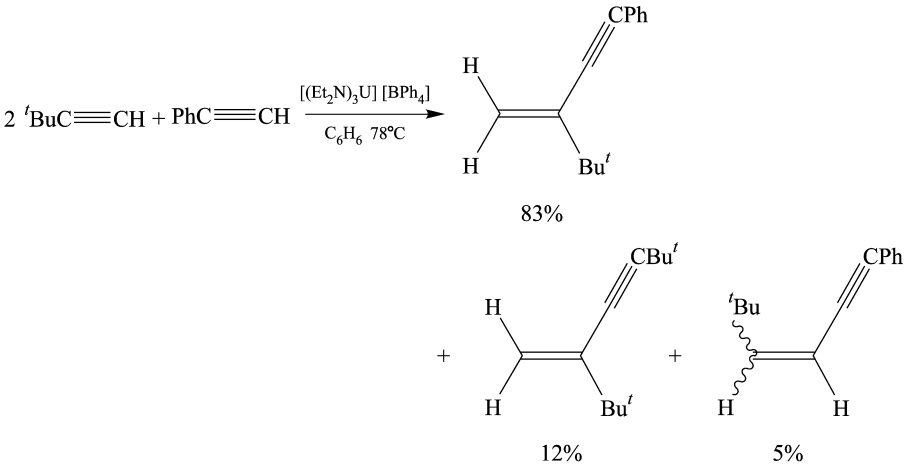

(26.43)

To avoid the trimers and to allow a better regioselectivity a larger excess (two equivalent) of ^{t}BuC≡CH and one equivalent of PhC≡CH were used in the cross dimerization [equation (26.43)] producing the *gem*-codimer as the major isomer (83%), the *gem*-dimer of the aliphatic alkyne (12%), and small amounts of the codimer (5%). This result indicated again that the U–C≡CPh moiety was the first intermediate formed. To this acetylide intermediate, ^{t}BuC≡CH inserts preferentially in the head-to-tail manner to obtain the precursor of the codimer.

The effect of external amines in the cross dimerization of terminal alkynes with the cationic complex $[(Et_2N)_3U][BPh_4]$ was investigated by the reaction of an excess of PhC≡CH with ^{i}PrC≡CH in the presence of $EtNH_2$. The reaction generated low yields of the codimer $CH_2{=}C(^{i}Pr)C{\equiv}CPh$ (17%), as compared with the reaction without external amine, and remarkably the *cis* aromatic dimer, was the major product [equation (26.44)].

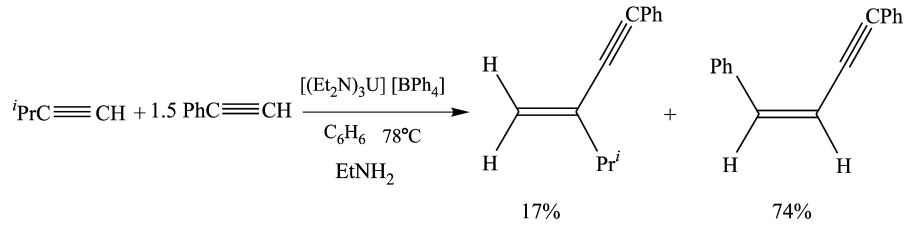

(26.44)

26.6 CATALYTIC HYDROSILYLATION OF OLEFINS

26.6.1 Catalytic hydrosilylation of terminal alkynes promoted by neutral organoactinides

The metal-catalyzed hydrosilylation reaction, which is the addition of a Si–H bond across a carbon–carbon multiple bond, is one of the most important reactions in organosilicon chemistry and has been studied extensively for half a century. The hydrosilylation reaction is used in the industrial production of organosilicon compounds (adhesives, binders, and coupling agents), and in research laboratories, as an efficient route for the syntheses of a variety of organosilicon compounds, silicon-based polymers, and new type of dendrimeric materials. The versatile and rich chemistry of vinylsilanes has attracted considerable attention in recent years as they are considered important building blocks in organic synthesis (Chan, 1977; Colvin, 1988; Fleming *et al.*, 1989).

The syntheses of vinylsilanes have been extensively studied and one of the most convenient and straightforward methods is the hydrosilylation of alkynes (Esteruelas *et al.*, 1993; Takeuchi and Tanouchi, 1994; Asao *et al.*, 1996). In general, hydrosilylation of terminal alkynes produces the three different isomers, *cis*, *trans*, and *geminal*, as a result of both 1,2 (*syn* and *anti*) and 2,1 additions, respectively, as shown in equation (26.45). The distribution of the products is found to vary considerably with the nature of the catalyst, substrates, and the specific reaction conditions.

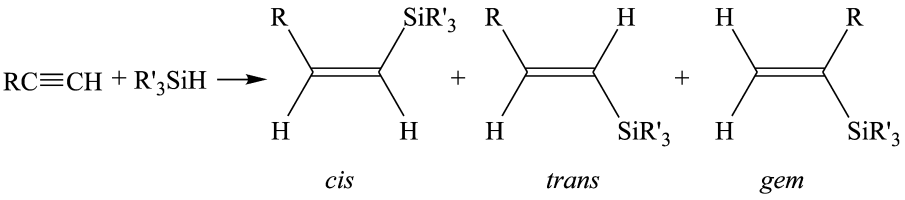

(26.45)

(a) Hydrosilylation of terminal alkynes: scope at room temperature by $(C_5Me_5)_2AnMe_2$ complexes

The room temperature reaction of $(C_5Me_5)_2AnMe_2$ (An = Th, U) with an excess of terminal alkynes RC≡CH (R = ^{t}Bu, ^{i}Pr, ^{n}Bu) and $PhSiH_3$ resulted in the catalytic formation of the corresponding *trans*-vinylsilanes RCH = $CHSiH_2Ph$, the dehydrogenative silylalkyne RC≡$CSiH_2Ph$ and alkenes RCH=CH_2 (R = ^{t}Bu, ^{i}Pr, ^{n}Bu) [equation (26.46)] (Dash *et al.*, 1999).

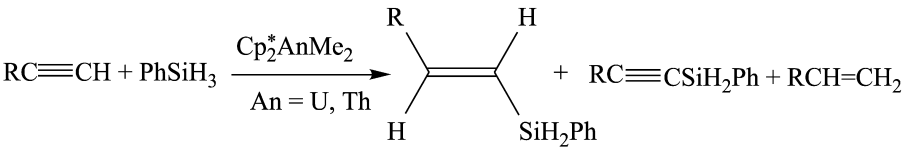

$R = {}^{t}Bu, {}^{i}Pr, {}^{n}Bu$ (26.46)

Irrespective of the alkyl substituents and the metal center, the major product in the hydrosilylation reaction was the regio- and stereoselective *trans*-vinylsilane without any trace formation of the other two hydrosilylation isomers (*geminal* or *cis*). For bulky alkynes (^{t}BuC≡CH), the product distribution was nearly the same for both catalytic systems, whereas for other terminal alkynes, it varies from one catalytic system to another. In the hydrosilylation reaction of the alkynes with $(C_5Me_5)_2ThMe_2$ and $PhSiH_3$, similar amounts of the alkene and the silylalkyne were obtained. This result suggested a mechanistic pathway involving two organometallic complexes formed possibly in a consecutive manner, each species being responsible for each one of the products.

The reaction of $(C_5Me_5)_2UMe_2$ with TMSC≡CH (TMS = Me_3Si) and $PhSiH_3$ was slow producing the *trans*-TMSCH = $CHSiH_2Ph$ and the silylalkyne $TMSC{\equiv}CSiH_2Ph$ respectively, whereas for the analogous $(C_5Me_5)_2ThMe_2$, no hydrosilylation or dehydrogenative coupling products were observed [equation (26.47)].

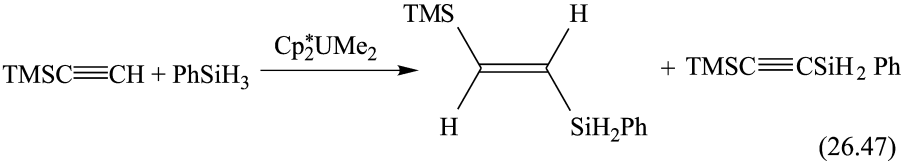

(26.47)

(b) Hydrosilylation of terminal alkynes: scope of catalysis at high temperature by $(C_5Me_5)_2AnMe_2$ complexes

The chemoselectivity and the regioselectivity of the vinylsilanes formed in the organoactinide-catalyzed hydrosilylation of terminal alkynes with $PhSiH_3$ at high temperature (65–78°C) were found to be diverse, as compared to the hydrosilylation results obtained at room temperature. The hydrosilylation of RC≡CH (R = ^{t}Bu, ^{i}Pr, ^{n}Bu) with $PhSiH_3$ catalyzed by $(C_5Me_5)_2UMe_2$, produced in addition to the hydrosilylation products at room temperature [equation (26.46)] the corresponding *cis*-hydrosilylated compounds, *cis*-$RCH{=}CHSiH_2Ph$, and small to moderate yields of the *unexpected* double hydrosilylation products $RCH{=}C(SiH_2Ph)_2$ (R = ^{t}Bu, ^{i}Pr, ^{n}Bu), in which the

two silyl moieties are attached to the same carbon atom [equation (26.48)] (Dash *et al.*, 1999).

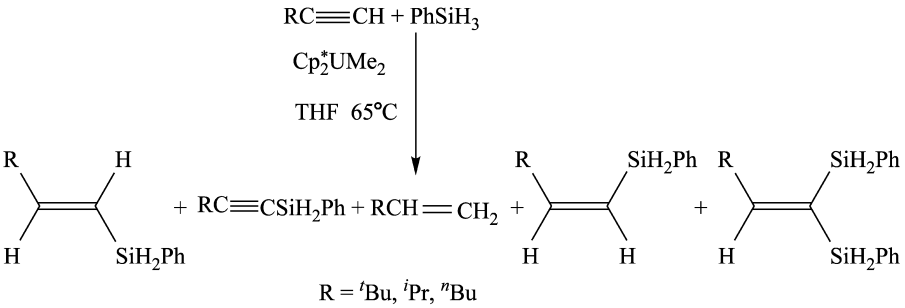

(26.48)

Whereas $(C_5Me_5)_2UMe_2$ catalyzed the hydrosilylation yielding a mixture of both *cis*- and *trans*-vinylsilane, remarkably, $(C_5Me_5)_2ThMe_2$ afforded only the *trans*-vinylsilane.

In the hydrosilylation reaction of TMSC≡CH with $PhSiH_3$ catalyzed by $(C_5Me_5)_2UMe_2$, besides the *trans*-vinylsilane and the silylalkyne products, which were also obtained at room temperature [equation (26.47)], the *cis*-vinylsilane and the olefin $TMSCH{=}CH_2$ were also observed [equation (26.49)]. For $(C_5Me_5)_2ThMe_2$, the same products as in the hydrosilylation reaction promoted by $(C_5Me_5)_2UMe_2$ were formed except for the *cis*-vinylsilane, in contrast to the room temperature reaction, in which no products were found.

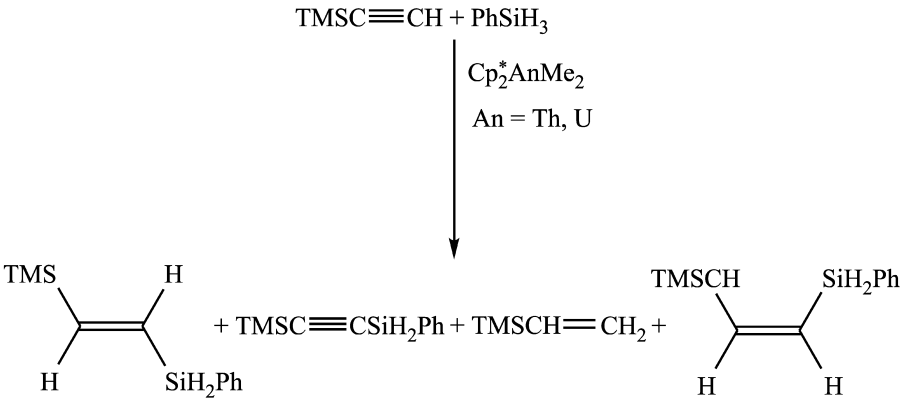

(26.49)

(c) Effect of the Ratio Alkyne:Silane and the Silane Substituent in the Hydrosilylation Reaction

The effect of $PhSiH_3$ on the formation of the different products was studied by performing comparative experiments. Large chemoselectivity and regioselectivity dependence of the products on the silane concentrations was observed [equation (26.50)].

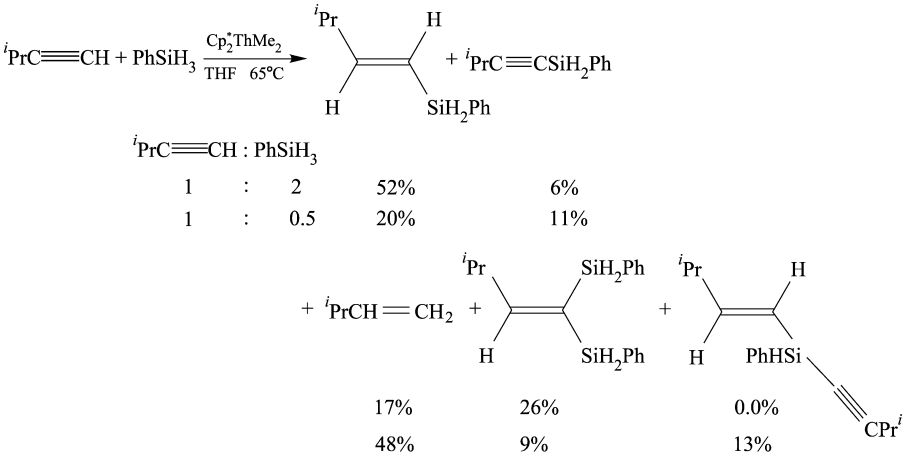

(26.50)

When the hydrosilylation reaction was carried out using a 1:2 ratio of $^{i}PrC{\equiv}CH$:$PhSiH_3$ with $(C_5Me_5)_2ThMe_2$, the *trans*-vinylsilane was found to be the major product. When the reaction was conducted with the opposite ratio between the substrates ($^{i}PrC{\equiv}CH$:$PhSiH_3 = 0.5$), the olefin $^{i}PrCH{=}CH_2$ was found to be the major product, in addition to the other products (*trans*-$^{i}PrCH{=}CHSiH_2Ph$, $^{i}PrC{\equiv}CSiH_2Ph$, the double hydrosilylated olefin, and the tertiary silane *trans*-$^{i}PrCH{=}CHSiH(Ph)(C{\equiv}C^{i}Pr)$). The tertiary silane was obtained by the dehydrocoupling metathesis between the *trans*-alkenylsilane and the metal acetylide complex.

The replacement of a hydrogen atom on $PhSiH_3$ by either an alkyl or a phenyl group generated a reduction in the hydrosilylation reaction rate when compared to the rate obtained utilizing phenylsilane. The selectivities of the products were appreciably different when compared to those obtained using $PhSiH_3$ as the hydrosilylating agent [equation (26.51)].

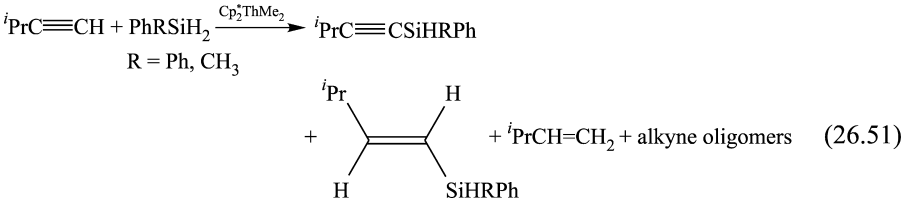

(26.51)

(d) Kinetic studies on the hydrosilylation of ^{i}PrC≡CH with $PhSiH_3$ catalyzed by $(C_5Me_5)_2ThMe_2$

The kinetic study of the hydrosilylation of ^{i}PrC≡CH with $PhSiH_3$ catalyzed by $(C_5Me_5)_2ThMe_2$ shows a first-order dependence in alkyne, silane, and catalyst. The empirical rate law expression for the $(C_5Me_5)_2ThMe_2$ catalyzed hydrosilylation of ^{i}PrC≡CH with $PhSiH_3$ is given by equation 26.52.

$$v = k[^{i}\mathrm{PrC}{\equiv}\mathrm{CH}][\mathrm{PhSiH_3}][(\mathrm{C_5Me_5})_2\mathrm{ThMe_2}] \qquad (26.52)$$

From the Eyring analysis, the derived activation parameters, E_a, $\Delta H^{\dagger}$, and $\Delta S^{\dagger}$ values are 6.9 (3) kcal mol^{-1}, 6.3(3) kcal mol^{-1}, and 51.1(5) eu, respectively.

(e) Formation of active species, mechanism, and thermodynamics in the hydrosilylation of alkynes

We have already seen that in the reaction of either bisacetylide organoactinide complex with $PhSiH_3$ the quantitative isolation of complexes **18** and **19**, for thorium and uranium, respectively, was observed [equation (26.4)]. These complexes were formed by the σ-bond metathesis with the silane forming the corresponding actinide hydrides and the silylalkyne, which rapidly reinsert producing **18** or **19 [**equation (26.53)].

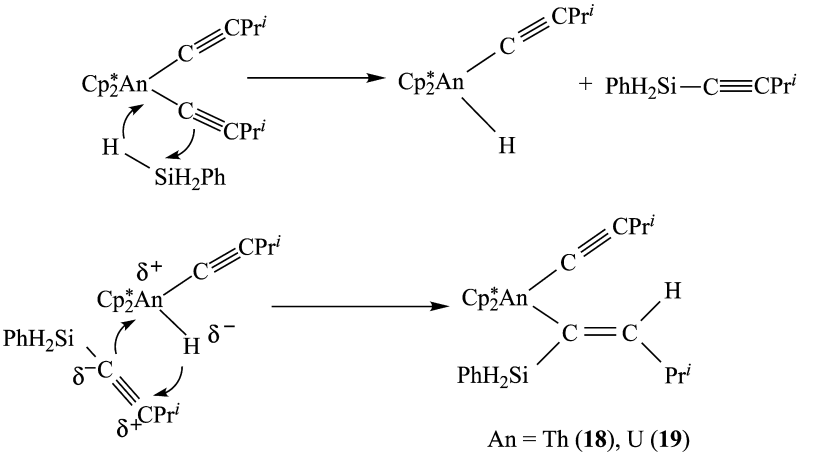

(26.53)

The regioselectivity of the insertion of $PhSiH_2C{\equiv}CPr^i$ into the actinide hydride bond is electronically favored, driven by the polarity of the organoactinides and the π* orbital of the alkyne (Apeloig, 1989). In addition, since the insertion occurs through a four-center transition state mechanism, the *cis*-stereochemistry is expected, as corroborated by the H_2O poisoning experiment and the high-temperature reactions with alkyne or silane [equation (26.5)]. The same regioselective insertion of TMSC≡CH into an organothorium

alkenyl complex Th–C bond was observed in the organoactinide-catalyzed oligomerization of alkynes (Straub *et al.*, 1995, 1999).

The formation of an organoactinide–silane intermediate **46** as described in Scheme 26.14 was shown to be not operative by the following experiments: (1) quenching experiments with water gave exclusively the *cis* vinylsilane; (2) under stoichiometric conditions, the addition of silane did not induce the protonolysis of the acetylide–alkenylsilane complex (**18** or **19**), to yield complex **46**; (3) no geminal hydrosilylated products were obtained (as would be expected were complex **48** an intermediate); (4) no *cis* hydrosilylated products can be obtained from complex **46**, and (5) no *cis* double hydrosilylated product was observed (if σ-bond metathesis occurred from complex **47** or **48**) (Dash *et al.*, 1999).

The reactions of complexes **18** or **19** yielding the double hydrosilylated product [equation (26.54)] were proposed to be stereoselectively favored, due to the assumed polarization of the $PhSiH_3$ towards the metal center, as well as the preferred thermodynamics, as compared to the protonolysis by the silane producing complex **46** and the *cis* hydrosilylated product ($\Delta H_{(Th)} = +15$ (4) kcal mol^{-1}; $\Delta H_{(U)} = -3$ (2) kcal mol^{-1}).

The most remarkable observation concerned the reaction products of complexes **18** or **19** with alkyne at either low or high temperatures. At elevated temperatures, the expected *cis*-hydrosilylated product was obtained, but at low temperatures, the unexpected *trans* isomer was achieved. These results have been explained through a competitive mechanism in which an equilibrium gives the different hydrosilylation products at different temperatures.

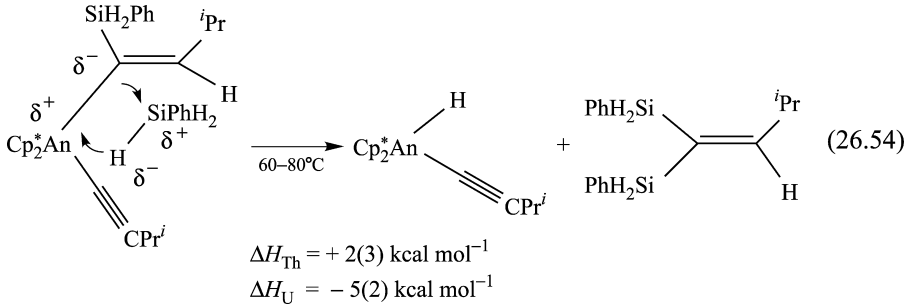

(26.54)

Different alkynes displayed different reactivities. TMSC≡CH exhibited a total lack of reactivity with $PhSiH_3$ in the presence of $(C_5Me_5)_2ThMe_2$ at room temperature. However, at high temperature, the *trans* vinylsilane, the silylalkyne, and the alkene were obtained. This type of reactivity was explained, in general, as the result of a kinetic effect suggesting also an equilibrium between the organometallic complexes **50** and **51** (Scheme 26.15). Complex **51** was obtained by the insertion of the silylalkyne into a hydride complex. Complex **51** is able to react with another alkyne, yielding the alkene and the bis(acetylide) complex (protonolysis route) or react with a silane producing the organometallic hydride and the *trans*-product (σ-bond metathesis route). The low activity

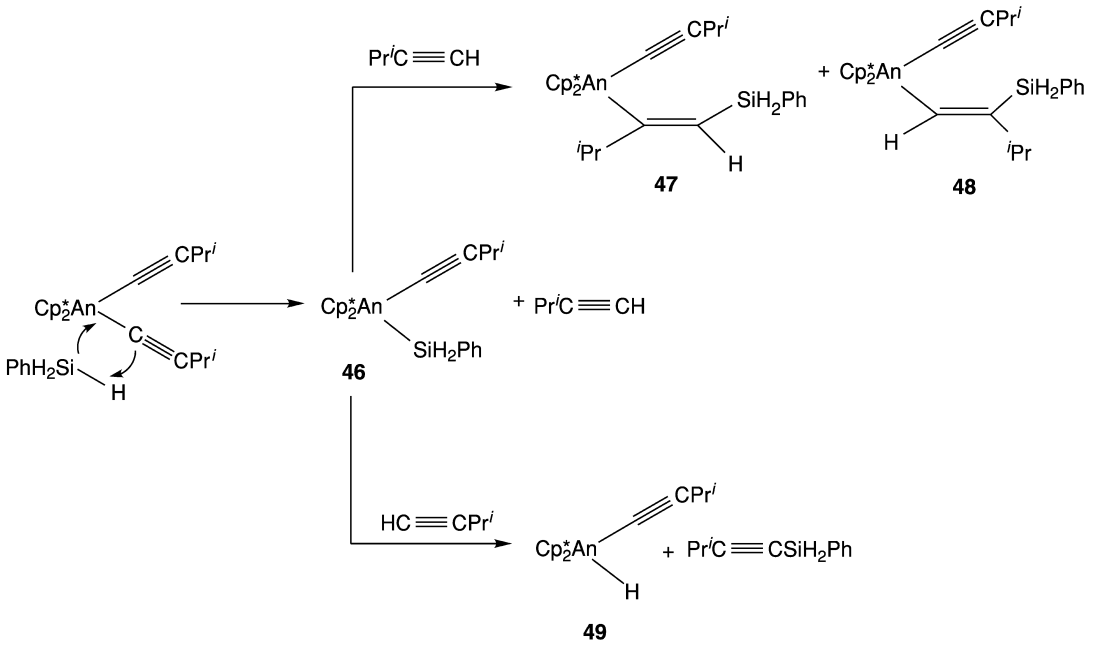

Scheme 26.14 *Expected organoactinide intermediates in the stoichiometric hydrosilylation of terminal alkynes through a transient organoactinide–silicon bond.*

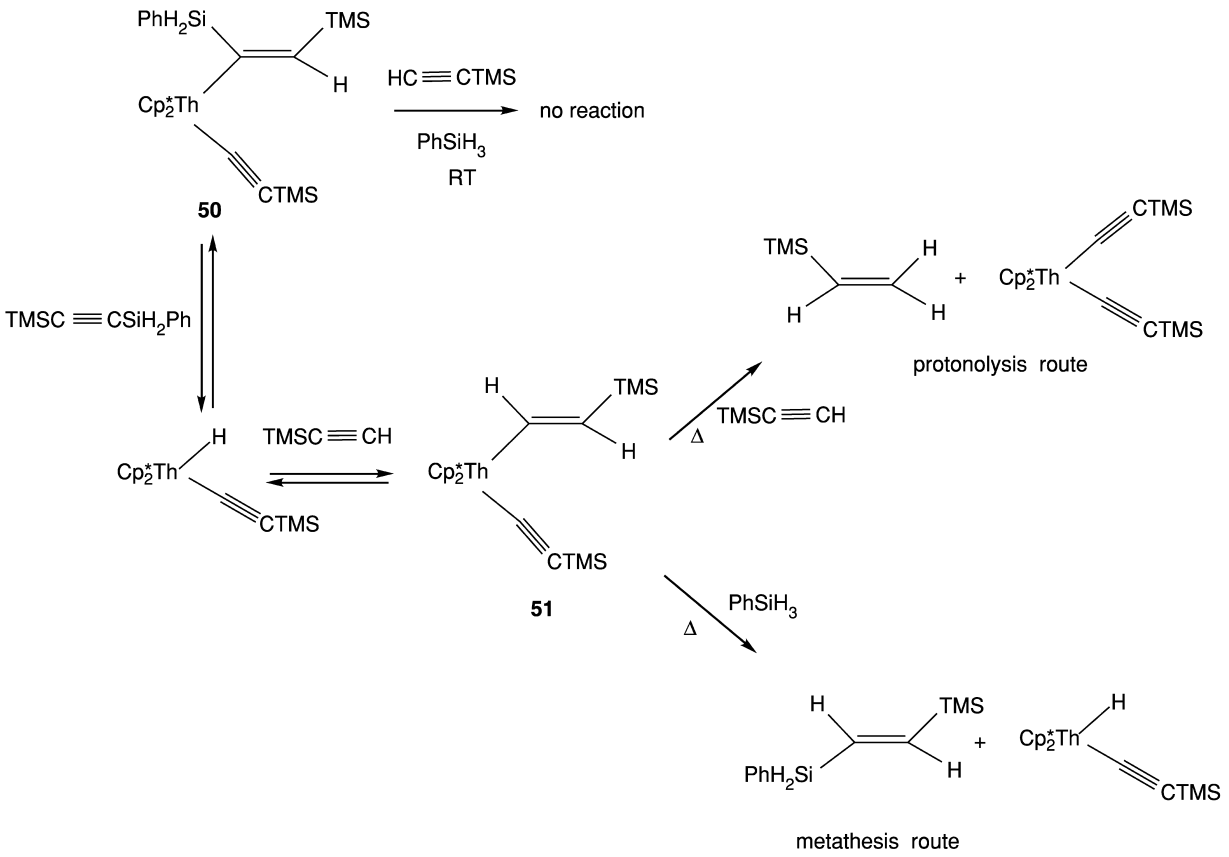

Scheme 26.15 *Protonolysis and σ-bond metathesis routes for the high-temperature hydrosilylation of TMSC≡CH with $PhSiH_3$ catalyzed by $(C_5Me_5)_2ThMe_2$.*

obtained for TMSC≡CH was explained by an elevated activation energy to perform both the metathesis or protonolysis of complex **51**, as compared with other alkynes (Dash *et al.*, 1999).

The ratio between the silane and the alkyne were found to govern the kinetics leading to the different products. Thus, when the $PhSiH_3$:$^{i}PrC{\equiv}CH$ ratio was two, the *trans*- and the double-hydrosilylation products were the major products (metathesis route). Increasing the alkyne concentration routed the reaction towards the alkene and the bis(acetylide) complex (protonolysis route).

A likely mechanism for the hydrosilylation of terminal alkynes catalyzed by $Cp^{*}_{2}ThMe_2$ was proposed and described in Scheme 26.16.

The mechanism presented in Scheme 26.16 consists of insertion of acetylene into a metal–hydride σ-bond, σ-bond metathesis by a silane, and protonolysis by an acidic alkyne hydrogen. The precatalyst $(C_5Me_5)_2ThMe_2$ in the presence of alkyne was converted to the bis(acetylide) complex **Z**. Complex **Z** reacts with $PhSiH_3$ towards the silylalkyne and the organoactinide hydride **X** (step 1), which was found to be in equilibrium with the intermediate **AA** after reinsertion of the silylalkyne with the preferential stereochemistry (step 2). Complex **AA** was found to be the principal complex under silane and alkyne starvation. Complex **X** will react with an alkyne producing the alkenyl acetylide organothorium complex **Y** (step 3), which is presumably in equilibrium with complex **X** (first-order in alkyne). Complex **Y** was proposed to react with $PhSiH_3$, as the rate-determining step, regenerating the hydride complex **X** and the *trans*-hydrosilylated product (step 4). Under the catalytic conditions, complex **Y** may also react with a second alkyne producing the alkene and the bis (acetylide) complex **Z** (step 5). A similar insertion of the alkene into complex **X** with the concomitant reaction with an additional alkyne produced the double hydrogenated product, as found for isopropylacetylene. At high temperature, complex **AA** may react with a silane (step 6), yielding complex **X** and the double hydrosilylation product or with an alkyne (step 7), yielding complex **Z** and the *cis*-isomer. Thus, the reaction rate law [equation (26.52)] was rationalized with rapid irreversible phenylsilane metathesis with complex **Z**, rapid pre-equilibrium involving the hydride, and alkenyl complexes **X** and **Y**, and a slow metathesis by the $PhSiH_3$. For the thorium complex, step 6 was found to be much faster than step 7 since the amounts of the *cis*-product were obtained in trace amounts.

The mechanistic pathway as proposed, takes into the account comparable yields for the alkene and silylalkyne even when the alkyne concentration was in excess (the sum of the silylated products must equal the amount of the alkene). For the thorium or uranium complexes, the amount of the hydrosilylated product was always similar to or larger than that of the alkene, indicating that a competing equilibrium should be operative, responsible for the transformation of the hydride complex back to the bisacetylide complex, allowing the production of the silylalkyne without producing the alkene [equation (26.55)].

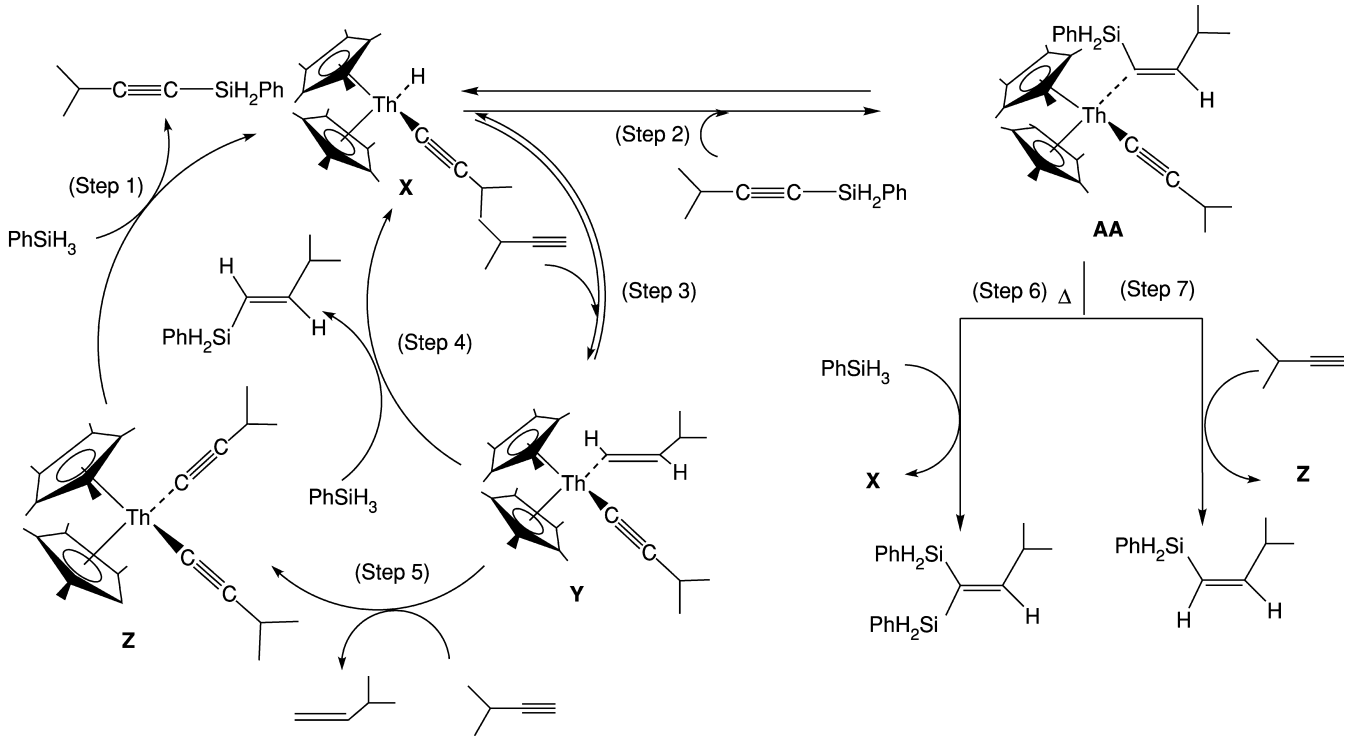

Scheme 26.16 *Proposed mechanism for the room- and high-temperature hydrosilylation of isopropylacetylene with* $PhSiH_3$ *promoted by* $(C_5Me_5)_2ThMe_2$.

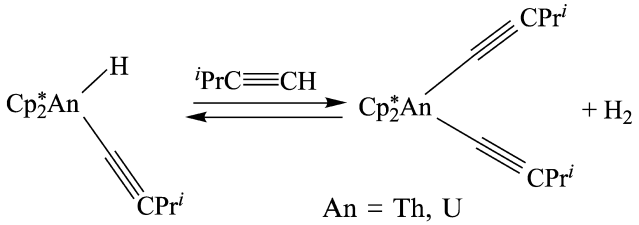

(26.55)

Thermodynamically, it is very interesting to compare the possible mechanistic silane and hydride intermediates towards the possible hydrosilylation *trans*-product as presented in equations (26.56) and (26.57), respectively.

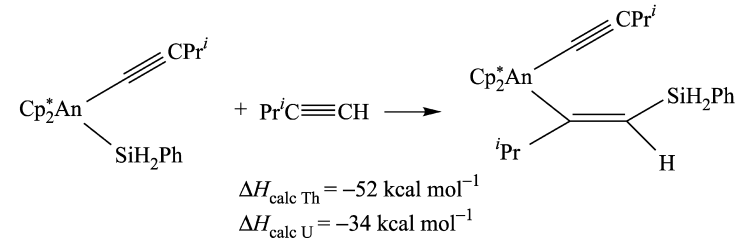

$\Delta H_{\text{calc Th}} = -52$ kcal mol^{-1}

$\Delta H_{\text{calc U}} = -34$ kcal mol^{-1}

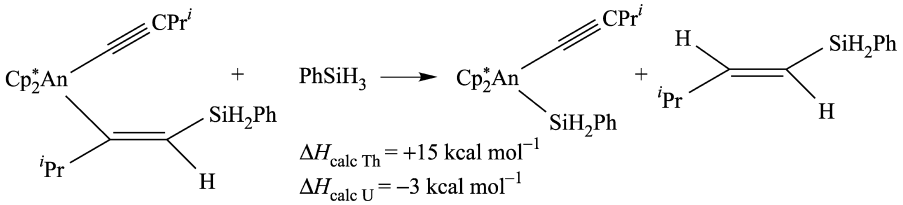

$\Delta H_{\text{calc Th}} = +15$ kcal mol^{-1}

$\Delta H_{\text{calc U}} = -3$ kcal mol^{-1}

(26.56)

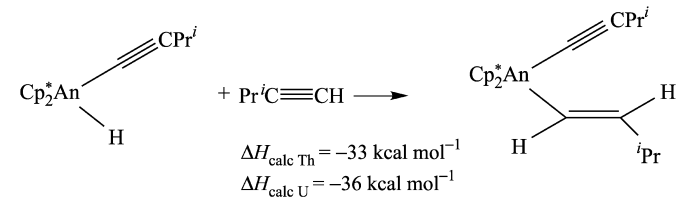

$\Delta H_{\text{calc Th}} = -33$ kcal mol^{-1}

$\Delta H_{\text{calc U}} = -36$ kcal mol^{-1}

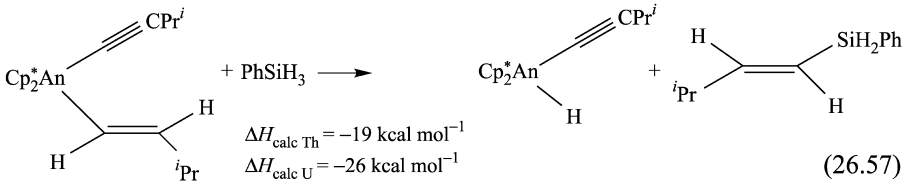

$\Delta H_{\text{calc Th}} = -19$ kcal mol^{-1}

$\Delta H_{\text{calc U}} = -26$ kcal mol^{-1}

(26.57)

The calculated enthalpy of reaction for the insertion of an alkyne into an actinide–silane bond [equation (26.56)] ($\Delta H_{Th} = -52$ kcal mol^{-1}, $\Delta H_U = -34$ kcal mol^{-1}) or into an actinide hydride bond [equation (26.57)] ($\Delta H_{Th} = -33$ kcal mol^{-1}, $\Delta H_U = -36$ kcal mol^{-1}) was expected to be exothermic. However, the protonolysis by the silane yielding the An-Si bond and the *trans*-product [equation (26. 56)] was for thorium an endothermic process ($\Delta H_{Th} = +15$ kcal mol^{-1}), as compared to the exothermicity of the σ-bond metathesis [equation (26.57) of the thorium alkenyl complex with the silane ($\Delta H_{Th} = -19$ kcal mol^{-1}), yielding the corresponding Th–H bond and the *trans*-product. For the corresponding uranium complexes, the latter processes were calculated to be exothermic although the σ-bond metathesis route [equation (26.57)] was more exothermic ($\Delta H_U = -26$ kcal mol^{-1}) than the protonolysis route [equation (26.56)] ($\Delta H_U = -3$ kcal mol^{-1}).

26.6.2 Catalytic hydrosilylation of terminal alkynes promoted by the bridged complex $Me_2SiCp''_2Th^nBu_2$

The hydrosilylation reaction of terminal alkynes and $PhSiH_3$ catalyzed by $Me_2SiCp''_2Th^nBu_2$ resulted in the speedy and regioselective formation of the hydrosilylated *trans*-vinylsilane as the unique product regardless of the alkyne substituent [equation (26.58)].

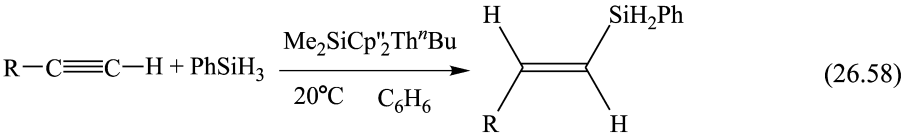

(26.58)

R = ^{t}Bu, ^{i}Pr, ^{n}Bu, Ph, 4-^{t}Bu-Ph

When an olefin-functionalized alkyne was used for the reaction with $PhSiH_3$, the alkyne moiety was regioselectively hydrosilylated to yield the corresponding *trans*-diene [equation (26.59)]. Addition of an excess of $PhSiH_3$ did not induce any subsequent hydrosilylation.

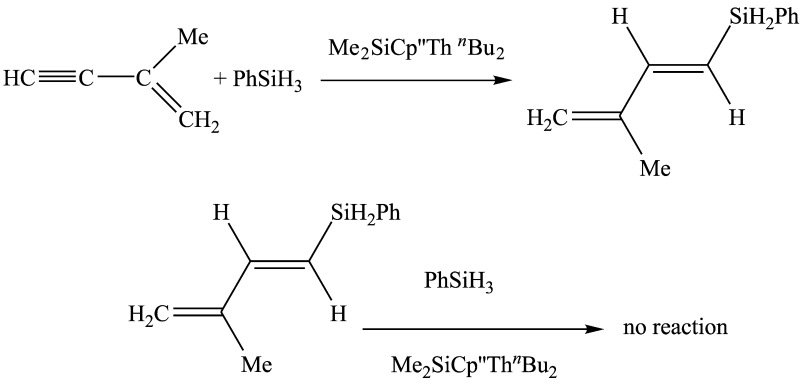

(26.59)

The addition of an excess of $PhSiH_3$ to any of the vinylsilane products did not induce further hydrosilylation. However, addition of a second equivalent of an alkyne to a hydrosilylation product allowed the formation of the corresponding alkene and the dehydrogenative coupling of the alkyne with the *trans*-vinylsilane [equation (26.60)] (Forsyth *et al.*, 1991; Harrod, 1991; Corey *et al.*, 1993; Tilley, 1993).

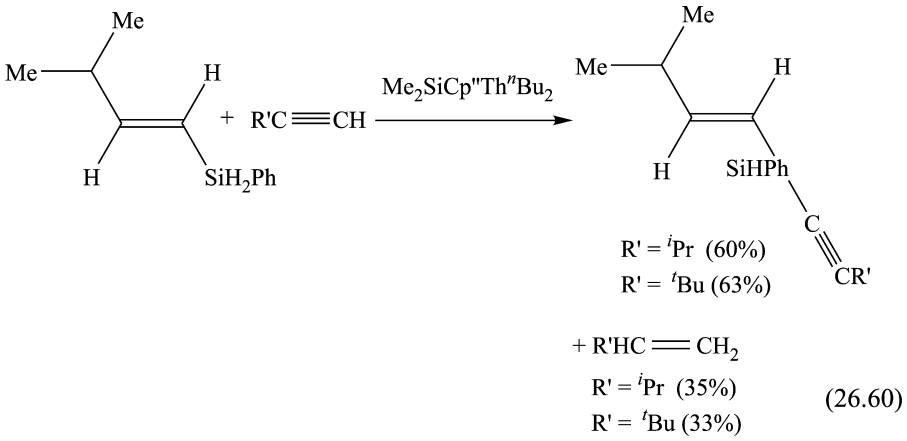

(26.60)

(a) Kinetic and thermodynamic studies for the hydrosilylation of terminal alkynes with primary silanes promoted by the bridged complex $Me_2Si(C_5Me_4)_2Th^nBu_2$

Kinetic measurements on the hydrosilylation ^{i}PrC≡CH with $PhSiH_3$ catalyzed by $Me_2Si(C_5Me_4)_2Th^nBu_2$ indicated that the reaction behaved with a first-order dependence in precatalyst and silane, and exhibited an inverse proportionality (inverse first-order) in alkyne [equation (26.61)]. The inverse proportionality was consistent with a rapid equilibrium before the turnover limiting-step, removing one of the key organoactinide intermediates from the catalytic cycle.

$$v = k[Me_2Si(C_5Me_4)_2Th^nBu_2][\text{silane}]^1[\text{alkyne}]^{-1} \qquad (26.61)$$

The derived $\Delta H^{\ddagger}$ and $\Delta S^{\ddagger}$ parameter values from a thermal Eyring analysis were measured to be 10.07(5) kcal mol^{-1} and –22.06(5) eu, respectively (Dash *et al.*, 2001).

It is important to note the difference between the kinetic behavior of the alkyne in the hydrosilylation reaction and that in the dimerization process (*vide supra*). In the latter process, the alkyne was involved in two parallel routes, both sensitive to the alkyne concentration. In one route, the alkyne exhibited an inverse kinetic order (removing one of the active compounds from catalytic cycle), whereas in the second pathway the alkyne was involved in the rate-determining step. Thus, at high alkyne concentrations the overall dependence

on alkyne is cancelled out. In the hydrosilylation process, the alkyne was proposed to be only involved in routing an active compound out of the catalytic cycle, with the silane presumably reacting in the rate-limiting step. Thus, modification of the alkyne order was observed.

In the hydrosilylation reactions of organo-f-element complexes, two Chalk–Harrod mechanisms have been proposed as plausible routes, differing in the inclusion of a σ-bond metathesis instead of the classical oxidative addition–reductive elimination processes. The two mechanisms differ in the reactive intermediates; the hydride (M–H) route and the silane ($M–SiR_3$) route (Chalk and Harrod, 1965; Harrod and Chalk, 1965; Ruiz *et al.*, 1987; Seitz and Wrighton, 1988; Tanke and Crabtree, 1991; Duckett and Perutz, 1992; Marciniec *et al.*, 1992; Takeuchi and Yasue, 1996; Bode *et al.*, 1998; Ojima *et al.*, 1998; Reichl and Berry, 1998; Sakaki *et al.*, 1998). The use of terminal alkynes with bridged organoactinides was an excellent probe to investigate which of the two routes was the major pathway followed. Thus, taking into account that the alkyne was expected to insert with the substituent group pointing away from the metal center (as observed in the dimerization) the following mechanistic insights were obtained. If the hydrosilylation reaction goes through a $M–SiR_3$ intermediate, the *gem*-hydrosilylated vinyl isomer will be formed, whereas only the *trans*-isomer will be obtained via the M–H route (if the insertion stereochemistry is not maintained, the *cis* product will be observed). The exclusive selectivity obtained for $Me_2Si(C_5Me_4)_2Th^nBu_2$ towards the *trans* hydrosilylated isomer argued that the hydride route was acting as the major mechanistic pathway.

(b) Hydrosilylation of terminal alkynes with primary silanes promoted by the bridged complex $Me_2Si(C_5Me_4)_2Th^nBu_2$: scope and mechanism

The hydrosilylation of terminal alkynes with $PhSiH_3$ promoted by the bridged complex $Me_2Si(C_5Me_4)_2Th^nBu_2$ produced regioselectively and chemoselectively the *trans*-hydrosilylated vinylsilane without any other by-products. The lack of silylalkynes, the dehydrogenative silane coupling products, or any other geometrical isomer of the vinylsilane strongly indicated that the Th–H pathway was the major operative route in the hydrosilylation reaction. A plausible mechanism for the hydrosilylation of terminal alkynes towards *trans*-vinylsilanes was proposed and is presented in Scheme 26.17.

The precatalyst $Me_2Si(C_5Me_4)_2Th^nBu_2$ in the presence of silane and alkyne was converted into the hydride complex **BB** (step 1), as observed by the stoichiometric formation of n-$BuSiH_2Ph$. Rapid insertion of an alkyne into complex **BB** allows the formation of the vinylic complex **CC** (step 2). Complex **CC** was found to be in rapid equilibrium with the proposed π-complex **DD** (step 3), responsible for the inverse order in alkyne, and undergoes a σ-bond metathesis with $PhSiH_3$, as the rate-determining step (step 4), producing selectively the *trans*-hydrosilylated vinyl product and regenerating complex **BB**. Since no

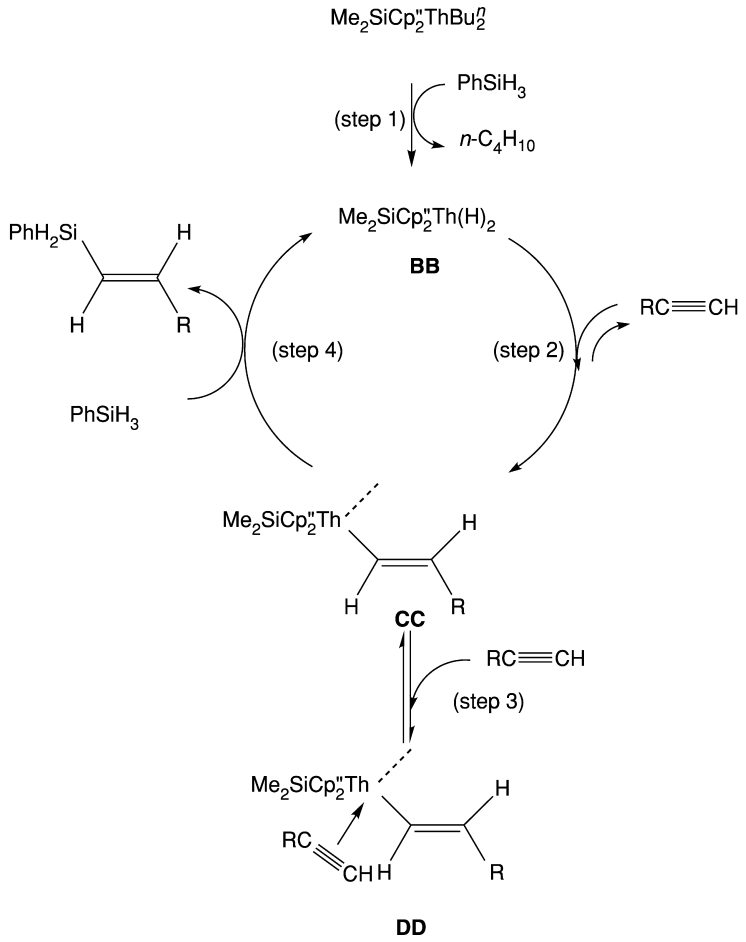

Scheme 26.17 *Proposed mechanism for the hydrosilylation of terminal alkynes with* $PhSiH_3$ *promoted by the bridged complex* $Me_2Si(C_5Me_4)_2Th^nBu_2$.

geometrical isomers or different products were observed by adding an excess of $PhSiH_3$ to any of the vinylsilanes, neither the hydride complex **BB** nor the alkenyl complex **CC** were found to be the resting catalytic state, indicating complex **DD** is the resting state. However, the subsequent addition of a second equivalent of an alkyne to the reaction mixture formed the corresponding alkene and the silylalkyne. The formation of these two compounds was proposed to follow the mechanistic pathway as shown in Scheme 26.18. Complex **CC** reacts, in the absence of a primary silane, with another alkyne (step 5) producing the corresponding alkene and the acetylide complex **EE.** A σ-bond metathesis with the Si–H bond of the vinylsilane (step 6) formed the

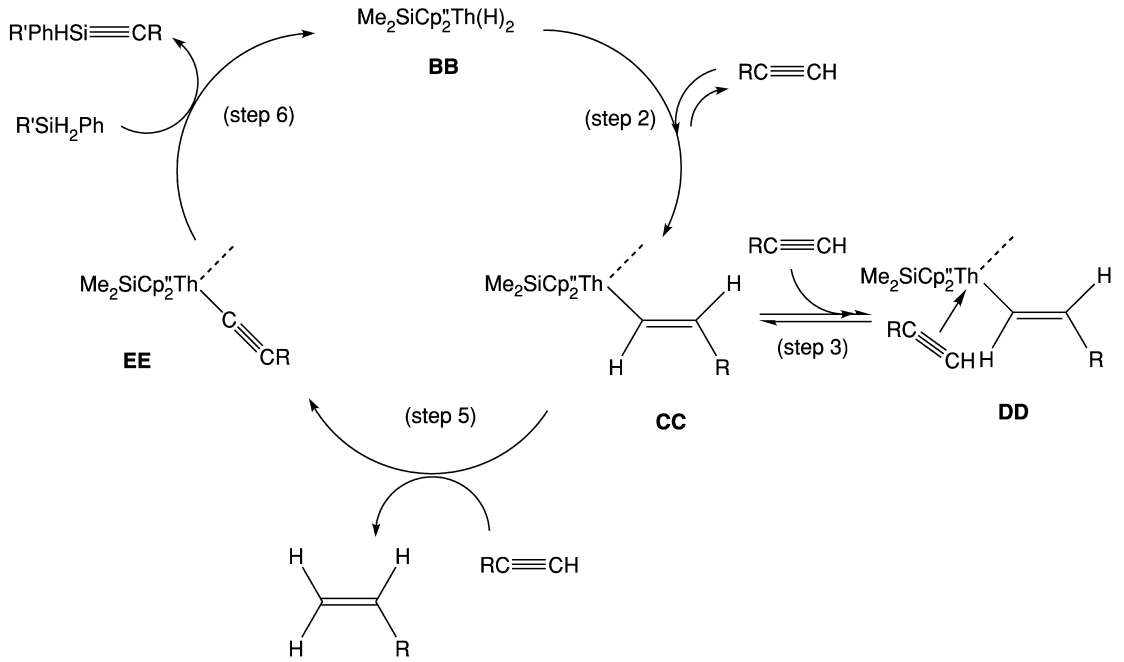

Scheme 26.18 *Proposed mechanism for the formation of alkene and silylalkyne in the presence of vinylsilanes and terminal alkynes promoted by* $Me_2Si(C_5Me_4)_2Th^nBu_2$. *Only one of the equatorial ligations at the metal center is shown for clarity.*

dehydrogenative coupling product and regenerated the hydride complex **BB** (Dash *et al*., 2001).

The yield of the alkene was found to be lower than that of the silylalkyne product. Therefore, an additional equilibrium reaction was proposed to exist, responsible for the transformation of complex **BB** into the acetylide complex **EE**, allowing the formation of the silylalkyne without forming the alkene. This pathway was also observed for non-bridged organoactinides [equation (26.55)] (Dash *et al*., 1999, 2001). Examination of the measured rates of the hydrosilylation process catalyzed by the bridged complex revealed larger turnover frequencies as compared to $(C_5Me_5)_2YCH_3 \cdot THF$ or other lanthanide complexes (Schumann *et al*., 1999). The yttrium complex was found to induce the hydrosilylation reaction of internal alkynes preferentially towards the *E*-isomer, although in some case the *Z*-isomer was found in comparable amounts. Mechanistically, the active species for the yttrium hydrosilylation of internal alkynes was proposed to be the corresponding hydride (Molander and Knight, 1998). It is well known that the hydrosilylation of alkynes is induced either by radical initiators (Selin and West, 1962) or by transition metal catalysts (Weber, 1983; Hiyama and Kusumoto, 1991; Sudo *et al*., 1999). The radical procedure often provides a mixture of *trans*- and *cis*-hydrosilylation products. In contrast, the transition metal catalyzed reaction proceeds with high stereoselectivity via a *cis*-hydrosilylation pathway usually producing a mixture of two regio-isomers (terminal and internal adducts). Thus, the organoactinide process seems to contain a unique chemical environment allowing the production of the *trans*-vinylsilane, complementing the chemistry of other transition metal complexes.

26.6.3 Catalytic hydrosilylation of alkenes promoted organoactinide complexes

The organoactinide complexes $(C_5Me_5)_2ThMe_2$ and $Me_2Si(C_5Me_4)_2Th^nBu_2$ were also found to be good precatalysts for the highly regio-selective hydrosilylation of alkenes. The chemoselectivity of the reactions was moderate since the hydrogenated alkane was always encountered as a concomitant product. The reactions of $(C_5Me_5)_2ThMe_2$ and $Me_2Si(C_5Me_4)_2Th^nBu_2$ with an excess of an alkene and $PhSiH_3$ resulted in the formation of the regioselective 1,2-addition hydrosilylated alkene and the alkane with no major differences between the two organoactinides [equation (26.62)] and Table 26.1 (Dash *et al*., 2001).

$$RHC{=}CH_2 + PhSiH_3 \xrightarrow{Cat.} RH_2C{-}\underset{\displaystyle SiH_2Ph}{CH_2} + RH_2C{-}CH_3 \qquad (26.62)$$

$$R = {}^n\!Bu,\ {}^n\!C_6H_{13},\ PhCH_2$$

Table 26.1 *Activity data for the hydrosilylation of alkenes promoted by* $(C_5Me_5)_2ThMe_2$ *and* $Me_2Si(C_5Me_4)_2Th^nBu_2$.[a]

Entry	*Cat.*[b]	*R in RHC=CH*	*Temperature* (°C)	*Time* (*h*)	*Yield of* 1-*silylalkane* (%)	*Yield of alkane* (%)	Nt[c] (h^{-1})
1	NB	^{n}Bu	20	12	54	44	1.5
2	B	^{n}Bu	20	12	63	35	5.5
3	NB	^{n}Bu	78	6	57	41	3.2
4	B	^{n}Bu	78	1	62	36	64.5
5	NB	$^nC_6H_{13}$	20	12	68	30	1.9
6	B	$^nC_6H_{13}$	20	12	65	33	4.6
7	NB	$PhCH_2$	78	6	61	38	4.8
8	B	$PhCH_2$	78	1	71	29	83.1
9	NB	Ph	78	36	65(6)[d]	28	0.9
10	B	Ph	78	36	31(30)[d]	37	1.9

[a] Solvent = benzene.
[b] B = $Me_2Si(C_5Me_4)_2Th^nBu_2$, NB = $(C_5Me_5)_2ThMe_2$.
[c] Turnover frequency for the hydrosilylation process.
[d] The number in parentheses corresponds to the 2,1-addition hydrosilylation product, 2-(phenylsilyl)ethylbenzene.

Since for the substrate allyl benzene only one hydrosilylated product was formed, a comparison of the effect of distance between the aromatic ring and the metal center was performed. In the hydrosilylation of styrene with each of the organoactinides [equation (26.63)], both 1,2- and 2,1-hydrosilylation products were obtained, in addition to ethylbenzene. For $(C_5Me_5)_2ThMe_2$, a small amount of the branched silane was obtained whereas for the coordinatively unsaturated complex $Me_2Si(C_5Me_4)_2Th^nBu_2$ equal amounts of both (linear and branched) isomers were found (entries 9,10 in Table 26.1).

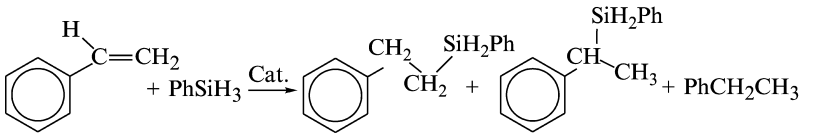

(26.63)

The presence of the two major products (hydrosilylation and hydrogenation) indicated the existence of two parallel catalytic pathways. The formation of the hydrogenation products required considering the possibility that intermediates with Th–Si/Th–H bonds were formed [equation (26.64)]. Thus, the production of alkanes might be considered, to some extent, as indirect evidence of the existence of complexes containing an actinide–Si bond. Protonolysis of a Th–alkyl by the silane will yield the Th–Si bond and the hydrogenation product, whereas metathesis of the Th–alkyl by the silane will produce the hydrosilylated compound regenerating the hydride complex.

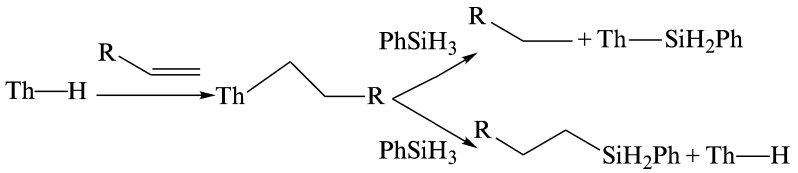

(26.64)

Another pathway to obtain a hydrogenation product from a Th–alkyl complex may be proposed, consisting of cutting the alkyl chain with an additional alkene, forming a transient vinyl complex. Therefore, the reaction between $(C_5Me_5)_2ThMe_2$ and an excess of 1-octene was studied. Although no hydrogenation product was observed, ruling out the protonolysis by an alkene, a stoichiometric reaction, resulting in the production of 2-methyl-1-octene, 2-nonene, and 3-nonene in almost equal amounts, and the additional slow catalytic isomerization of the starting 1-octene to *E*-4-octene (3.8%), *E*-3-octene (39.4%), *E*-2-octene (13.0%), and *Z*-2-octene (41.8%), was observed [equation (26.65)] (Dash *et al.*, 2001).

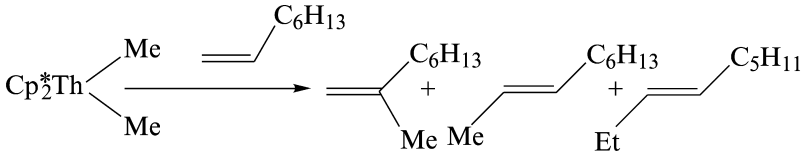

(26.65)

This result indicated that the Th–Me bond underwent insertion by the alkene moiety, forming a Th–alkyl complex, followed by a β-hydrogen elimination to the corresponding metal–hydride (Th–H) and equimolar amounts of all three isomeric nonenes. The hydride was proposed to be the active species in the isomerization of 1-octene. The same reaction with 2-octene showed a slower reaction and different product ratios (*E*-3-octene (11.2%), *E*-2-octene (82.2%), and *Z*-2-octene (6.6%)), indicating a non-equilibrium process between 1-octene and 2-octene. In order to study the resting state of the organoactinide catalyst given that only two complexes with either a thorium hydride (Th–H) or a thorium–alkyl (Th–R) were expected, the isomerization reaction was followed until full conversion of 1-octene (>98%) was obtained. All the volatiles were removed under vacuum and new solvent was reintroduced. The ratio between the products that remained in the reaction mixture was measured by gas chromatography, demonstrating the disappearance of 1-octene. Quenching of the reaction mixture with a slight excess of D_2O at low temperatures, and analysis of the solution showed the presence of a mono-deuterated 1-*d*-octane, indicating that the Th–alkyl moiety was the resting organoactinide. The most astounding result was the presence of equimolar amounts of 1-octene, based on the metal complex. This result indicated that a *π-alkene thorium–alkyl* complex (**HH** in Scheme 26.19) was the resting catalytic state of the organoactinide complex; addition of D_2O liberated the alkene and the alkane from the metal.

(a) Kinetic studies of the hydrosilylation of alkenes with $PhSiH_3$

Kinetic measurements of the hydrosilylation of allylbenzene with $PhSiH_3$ catalyzed by $(C_5Me_5)_2ThMe_2$ were performed. The reaction was found to follow a first-order dependence in precatalyst and silane, and exhibits an inverse first-order dependence in alkene. The inverse proportionality as described for alkynes is consistent with a rapid equilibrium before the rate-determining step, steering an intermediate out of the catalytic cycle. Thus, the rate law for the hydrosilylation of alkenes with $PhSiH_3$ promoted by $(C_5Me_5)_2ThMe_2$ can be expressed as presented in the following equation:

$$v = k[(C_5Me_5)_2ThMe_2][\text{silane}]^1[\text{alkene}]^{-1} \tag{26.66}$$

The derived E_a, $\Delta H^{\ddagger}$, and $\Delta S^{\ddagger}$ parameter values from an Arrhenius and a thermal Eyring analysis were measured to be 11.0(4) kcal mol^{-1}, 10.3(4) kcal mol^{-1}, and –45 eu, respectively.

A comparison of the product distribution for both bridged and non-bridged organoactinides revealed that no special effects were introduced by increasing the coordinative unsaturation of the organothorium complex. The presence of double hydrosilylation products suggested the presence of two parallel interconnecting competing pathways. The formation of the alkane required the presence of the intermediate Th–H/Th–Si moieties (Eisen, 1997, 1998). The only evidence available so far for the formation of a Th–Si bond was obtained

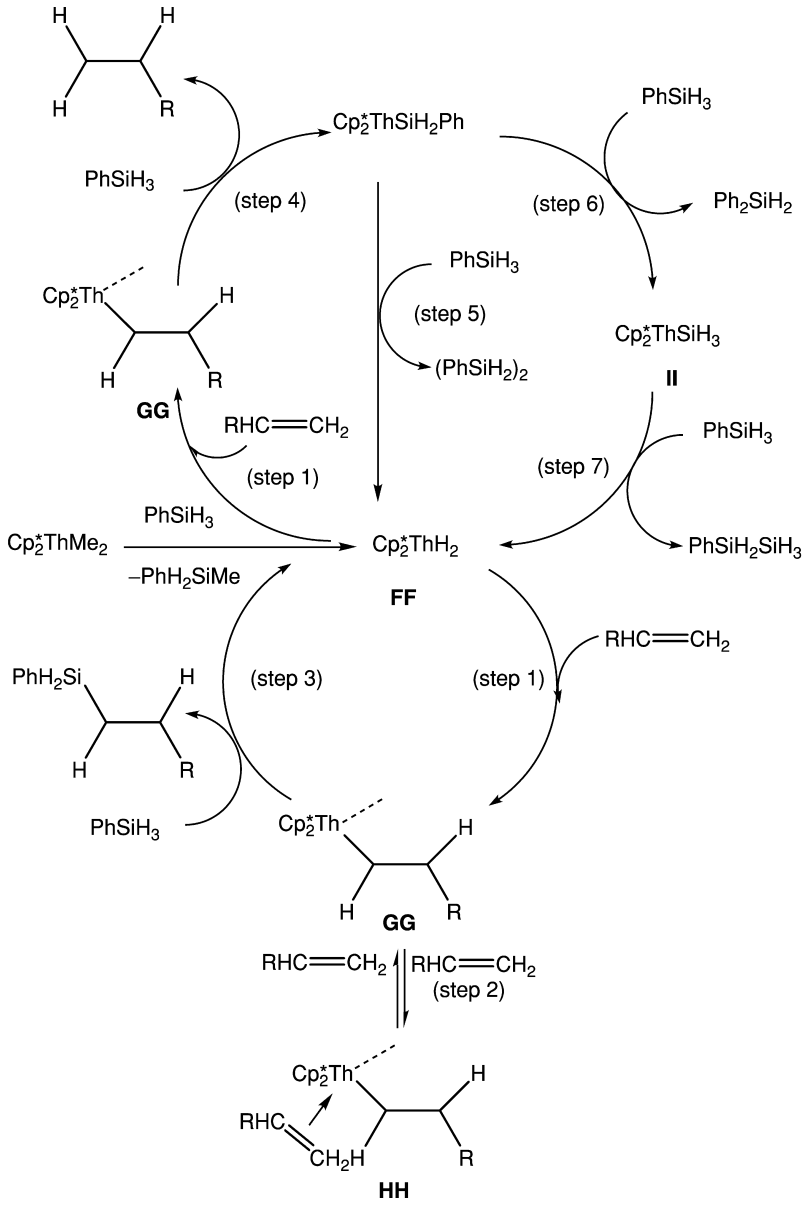

Scheme 26.19 *Proposed mechanism for the hydrosilylation of alkenes with $PhSiH_3$ promoted by $(C_5Me_5)_2ThMe_2$ or $Me_2Si(C_5Me_4)_2Th^nBu_2$. The scheme depicts the mechanism for the unbridged metallocene. Only one of the equatorial ligations at the metal center is shown for clarity.*

from the formation of a metalloxy ketene via the double insertion of carbon monoxide into a Th–Si bond (Radu *et al.*, 1995). The proposed mechanism for the hydrosilylation of alkenes promoted by organoactinides is described in Scheme 26.19.

The first step in the proposed mechanism is the reaction of the precatalyst $(C_5Me_5)_2ThMe_2$ with $PhSiH_3$, yielding the hydride complex **FF** and $PhSiH_2Me$. Complex **FF** may react with an alkene producing the alkyl complex **GG** (step 1), which can undergo three parallel pathways. The first route is a reaction with an alkene, to produce a π-alkene complex **HH**, removing the complex **GG** from the catalytic cycle (step 2), and giving rise to the inverse order in alkene. The second and third paths are metathesis and protonolysis reactions between the Th–alkyl fragment and the Si-H moiety, yielding in the former case the substituted silane and regenerating complex **FF** (step 3), and yielding in the latter process the Th–SiH_2Ph complex and the alkane (step 4). The proposed scheme also takes into account the formation of materials in trace amounts.

For styrene, the formation of both hydrosilylation products in similar amounts indicates comparable activation energy for both processes, differing only in the disposition of the silane with respect to the thorium alkyl complex. The Th–SiH_2Ph bond can be activated by two different paths. The metathesis reaction with the Si–H bond in $PhSiH_3$ produces the dehydrogenative dimer and the hydride **FF** (step 5), whereas in the reaction with a Si–Ph bond, Ph_2SiH_2, and a complex containing the Th–SiH_3 (**II**) moiety will be obtained (step 6), which will then rapidly react with an additional silane yielding the oligomeric dehydrogenative coupling of silanes (step 7). In the hydrosilylation of styrene, the formation of the branched isomer was rationalized by the stereochemistry of the insertion reaction of the styrene with the metal hydride complex (Scheme 26.20); the alkyl formed is presumably stabilized by the π-arene interaction (**JJ′**).

For alkenes, the hydrosilylation reaction promoted by organolanthanides of the type $(C_5Me_5)_2LnR$ (Ln = Sm, La, Lu) or $Me_2Si(C_5Me_4)_2SmR$ are much faster (by one order of magnitude) than those obtained with organoactinides. The major difference is found for linear α-alkenes, which lanthanides will hydrosilylate forming both isomers, whereas actinides will exclusively yield the 1,2-adduct product (Harrod, 1991; Ojima *et al.*, 1998; Schumann *et al.*, 1999). Mechanistically, the lanthanide hydrides have been proposed as the primary pathway towards the hydrosilylated products. Thus, organoactinides represent again complementary catalysts to organolanthanides and other transition metal complexes for the regioselective hydrosilylation of α-olefins.

26.6.4 Catalytic hydrosilylation of alkynes promoted by the cationic complex $[(Et_2N)_3U][BPh_4]$

The hydrosilylation reactions of terminal alkynes promoted by neutral organoactinides has motivated similar studies whose goal is the formation of a cationic hydride complex as an intermediate in the catalytic hydrosilylation of

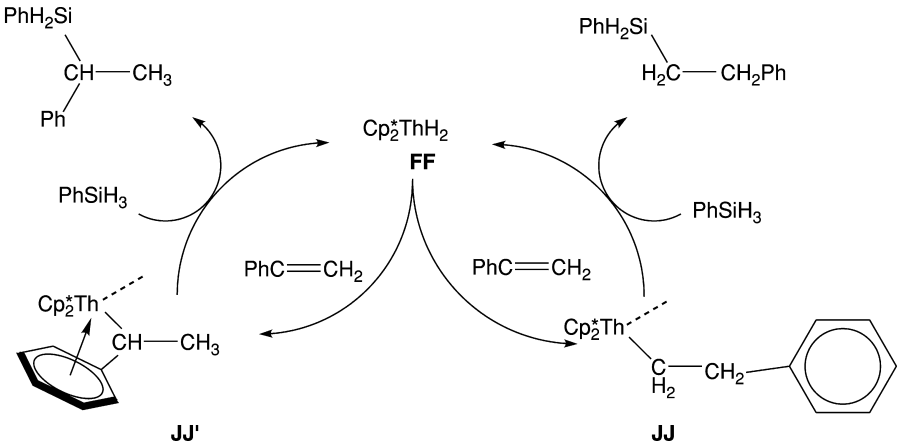

Scheme 26.20 *Proposed mechanism for the hydrosilylation of styrene and $PhSiH_3$ promoted by $(C_5Me_5)_2ThMe_2$ or $Me_2Si(C_5Me_4)_2Th^nBu_2$.*

terminal alkynes. Reactions promoted by the cationic complex $[(Et_2N)_3U][BPh_4]$ were studied (Dash *et al.*, 2000). The reaction of $[(Et_2N)_3U][BPh_4]$ with terminal alkynes RC≡CH (R = ^{i}Pr, ^{t}Bu) and $PhSiH_3$ resulted in the catalytic formation of a myriad of products. The observed products *cis*- and *trans*-vinylsilane ($RCH{=}CHSiH_2Ph$), the dehydrogenative silylalkyne ($RC{\equiv}CSiH_2Ph$), alkenes ($RCH{=}CH_2$) (R = ^{i}Pr, ^{t}Bu), and the aminosilane Et_2NSiH_2Ph were found to account for 100% conversion with respect to the alkyne. For the bulky ^{t}BuC≡CH, the tertiary silanes *trans*-^{t}BuCH=CHSi(HPh)(C≡C^{t}Bu), and ^{t}BuCH=C(SiH_2Ph)Si(HPh)(C≡C^{t}Bu) were also observed [equation (26.67)]. Formation of the tertiary silanes can be accounted for by metathesis reactions of the *trans*-alkenylsilane and the double hydrosilylated compound with the metal acetylide complex **52**, respectively, as shown in equations (26.68) and (26.69).

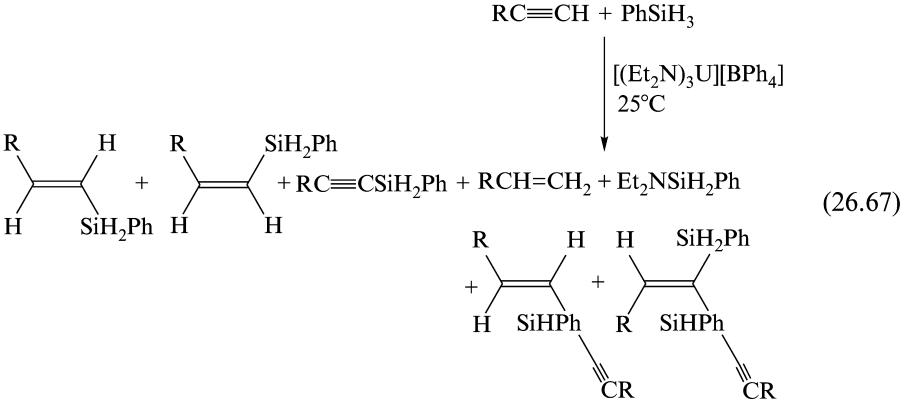

(26.67)

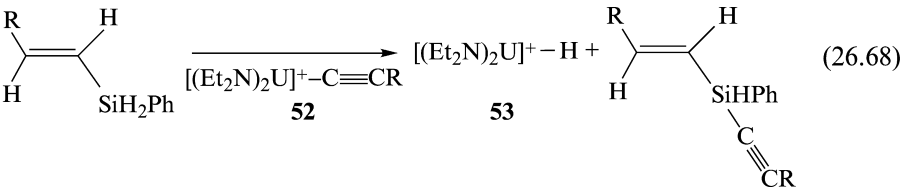

(26.68)

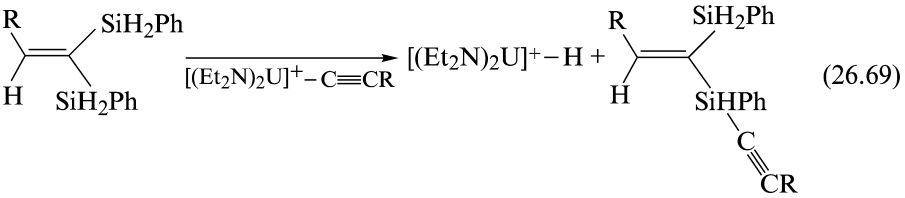

(26.69)

At high temperatures (65–78°C), the chemoselectivity and regioselectivity of the products formed in the cationic organouranium-catalyzed hydrosilylation of terminal alkynes with $PhSiH_3$ were found to be different in comparison to those obtained at room temperature. The hydrosilylation of RC≡CH (R = ^{n}Bu, ^{i}Pr, ^{t}Bu) with $PhSiH_3$ catalyzed by $[(Et_2N)_3U][BPh_4]$ produced, in addition to the hydrosilylation products at room temperature [equation (26.67)], the corresponding double hydrosilylated compounds: $RCH{=}C(SiH_2Ph)_2$ (R = ^{n}Bu, ^{i}Pr, ^{t}Bu), and small amounts of the corresponding geminal dimers and trimers. A similar type of mechanism as observed for the neutral organoactinides was proposed, based on kinetic data and product distributions.

The formation of an active uranium hydride complex **53** was proposed to occur either by the reaction of the cationic complex with a silane molecule, giving the corresponding aminosilane, and/or by the reaction of the acetylide complex **52** with a silane, producing the corresponding silylalkyne [equations (26.70) and (26.71), respectively).

$$[(Et_2N)_3U]^+ \xrightarrow{PhSiH_3} [(Et_2N)_2U]^+{-}H + PhSiH_2NEt_2 \qquad (26.70)$$

$$\underset{\mathbf{52}}{[(Et_2N)_2U]^+{-}{\equiv}CR} \xrightarrow{PhSiH_3} \underset{\mathbf{53}}{[(Et_2N)_2U]^+{-}H} + RC{\equiv}CSiH_2Ph \qquad (26.71)$$

The proposed mechanism, which takes into account the formation of all products, is described in Scheme 26.21 (Dash *et al.*, 2000).

The precatalyst $[(Et_2N)_3U][BPh_4]$ in the presence of alkyne was converted to the acetylide complex **52** by removal of one of the amido ligands. Complex **52** was proposed to react with $PhSiH_3$ to give the silylalkyne and the actinide hydride **53** (step 1). The hydride **53** may reinsert the silylalkyne forming complex **55** (step 2) or react with the alkyne to produce the alkenyl uranium complex **54** (step 3). Complex **54** is then proposed to react with $PhSiH_3$, regenerating the organouranium hydride complex **53** and the *trans*-hydrosilylated product

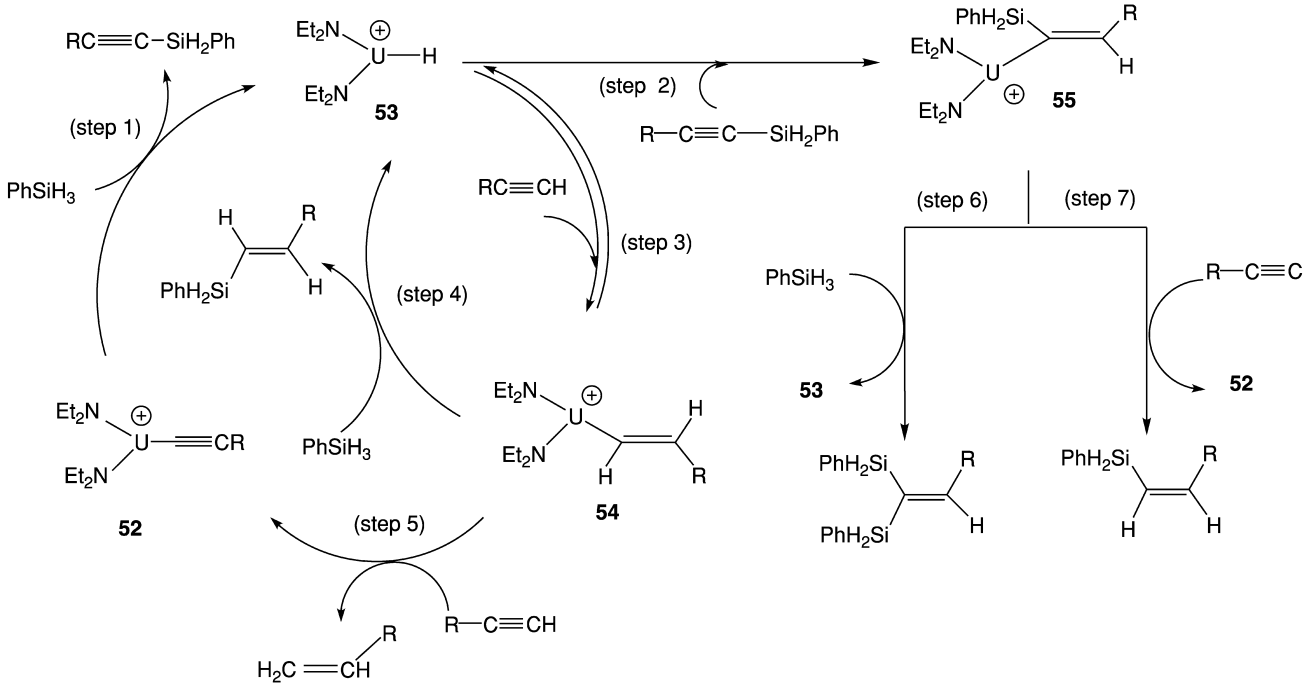

Scheme 26.21 *Proposed mechanism for the room- and high-temperature hydrosilylation of terminal alkynes promoted by* $[(Et_2N)_3U][BPh_4]$. *The transformation of the starting complex into the acetylide complex* $[(Et_2N)_2U{-}C{\equiv}CR][BPh_4]$ (**52**) *was described in Scheme* 26.10, *and is omitted here for clarity.*

(step 4). Under catalytic conditions, complex **54** may also react with a second alkyne giving the alkene and the acetylide complex **52** (step 5). Complex **55** may react with a silane (step 6) yielding complex **53** and the double hydrosilylation product, or with an alkyne (step 7) yielding complex **52** and the *cis*-isomer.

This mechanistic scenario took into account the higher yields observed for the alkene compound as compared with those obtained for the silylalkyne. For TMSC≡CH and ^{i}PrC≡CH at high temperature, the amount of the hydrosilylated products is larger than that of the alkenes, indicating that a competing equilibrium route was present. This would again involve the transformation of the hydride **53** back into the acetylide complex **52** by reaction with the alkyne [equation (26.72)], allowing the production of more silylalkyne without producing the alkene. The hydride **53** could alternatively react with $PhSiH_3$ to give the organometallic silyl compound $[(Et_2N)_2USiH_2Ph][BPh_4]$ [equation (26.73)], which would further react with $PhSiH_3$ or RC≡CH to regenerate the hydride **53** and $PhH_2Si\text{-}SiH_2Ph$ or $PhH_2SiC{\equiv}CR$, respectively.

$$\underset{\mathbf{53}}{(Et_2N)_2U^{\oplus}\text{—}H} \underset{}{\overset{HC{\equiv}CTMS}{\rightleftharpoons}} \underset{\mathbf{52}}{(Et_2N)_2U^{\oplus}\text{—}C{\equiv}CTMS} + H_2 \qquad (26.72)$$

$$(Et_2N)_2U^{\oplus}\text{—}H \xrightarrow{PhSiH_3} (Et_2N)_2U^{\oplus}\text{—}SiH_2Ph + H_2$$

$$\xrightarrow{PhSiH_3} PhH_2Si\text{—}SiH_2Ph + (Et_2N)_2U^{\oplus}\text{—}H$$

$$\xrightarrow{HC{\equiv}CTMS} (Et_2N)_2U^{\oplus}\text{—}H + PhH_2SiC{\equiv}CTMS \qquad (26.73)$$

In the hydrosilylation reaction of ^{t}BuC≡CH at high temperature, a small amount of the dehydrogenative coupling of phenylsilane was observed. This product argued for the formation of a compound with an uranium–silicon bond, although not as a major intermediate. The compound $[(Et_2N)_2USiH_2Ph][BPh_4]$ can be theoretically postulated instead of the hydride complex **53** either from steps 1, 4, or 6 in the catalytic cycle (Scheme 26.21). In these steps, the silane would act as the protonolytic source.

26.7 DEHYDROCOUPLING REACTIONS OF AMINES WITH SILANES CATALYZED BY $[(Et_2N)_3U][BPh_4]$

The catalytic processes involving the cationic uranium amide complex, $[(Et_2N)_3U][BPh_4]$, have been found to be particularly efficient in the controlled dimerization of terminal alkynes and in the hydrosilylation reactions of terminal alkynes and alkenes with $PhSiH_3$. These processes have been characterized

through the activation of the corresponding amido uranium–acetylide or the amido uranium–hydride species that were the active intermediates, respectively. A conceptual question that arose from those studies concerned the possibility of activating the amido ancillary ligands in $[(Et_2N)_3U][BPh_4]$ with a silane molecule producing the corresponding aminosilane and an organometallic hydride complex. The ability to transform the hydride into the starting amido complex using another amine with the attendant elimination of dihydrogen would give a way to perform the catalytic dehydrogenative coupling of amines and silanes. Thermodynamic calculations have predicted this process as plausible (King and Marks, 1995). The dehydrogenative coupling of amines and silanes has been performed by either late transition metal catalysts (Blum and Laine, 1986; Biran *et al*., 1988; Wang and Eisenberg, 1991) or early transition metal complexes (Liu and Harrod, 1992; He *et al*., 1994; Lunzer *et al*., 1998). These reactions are an alternate route to silazanes, which are precursors for the synthesis of silicon nitride materials. The reaction of $^{n}PrNH_2$ and $PhSiH_3$ promoted by the cationic complex $[(Et_2N)_3U][BPh_4]$ produced dihydrogen and the aminosilanes $PhSiH(NHPr^{n})_2$ and $PhSi(NHPr^{n})_3$ [equation (26.74)]. The use of a large excess of amine allowed for full conversion of the silane into the di- and tri-aminosilanes. The monoaminosilane, $PhSiH_2(NHPr^{n})$, was not detected, indicating that in this compound the Si–H hydride bonds were more reactive than those in the starting $PhSiH_3$ (Wang *et al*., 2000).

The reaction of $^{i}PrNH_2$ and $PhSiH_3$ gave dihydrogen together with $PhSiH_2NHPr^{i}$ (33%) and $PhSiH(NHPr^{i})_2$ (56%) with a total conversion of 89% for $PhSiH_3$. The use of large amine excess promoted the reaction towards the bisaminosilane $PhSiH(NHPr^{i})_2$. The bulky $^{t}BuNH_2$ reacted with $PhSiH_3$ producing $PhSiH_2NHBu^{t}$ quantitatively. This monoaminosilane reacted further with an excess of amine to produce an additional equivalent of dihydrogen and exclusively the bisaminosilane $PhSiH(NHBu^{t})_2$. This latter compound was transformed back slowly into the mono aminosilane, $PhSiH_2NHBu^{t}$, after the addition of one equivalent of $PhSiH_3$ [equation (26.75)], which indicated that the production of aminosilanes promoted by the cationic complex $[(Et_2N)_3U][BPh_4]$ was in equilibrium.

$$RNH_2 + PhSiH_3 \xrightarrow[-H_2]{[(Et_2N)_3U][BPh_4]} PhSiH_2NHR$$

$$R = {}^{n}Pr;\ {}^{i}Pr;\ {}^{t}Bu$$

$$PhSiH_2NHR \xrightarrow[-H_2]{[Cat]\ RNH_2} PhSiH(NHR)_2 \xrightarrow[-H_2]{[Cat]\ RNH_2} PhSi(NHR)_3 \qquad (26.74)$$

$$PhSiH_2(NHBu^{t}) \underset{[(Et_2N)_3U][BPh_4]\ PhSiH_3}{\overset{[(Et_2N)_3U][BPh_4]\ {}^{t}BuNH_2}{\rightleftharpoons}} PhSiH(NHBu^{t})_2 \qquad (26.75)$$

Ethylenediamine $H_2NCH_2CH_2NH_2$ reacted with $PhSiH_3$ in the presence of the catalyst, yielding dihydrogen and the spiro chelated complex $PhSi(\eta^2\text{-}NHCH_2CH_2NH)(\eta^2\text{-}NHCH_2CH_2NH_2)$ quantitatively. When the spiro product was heated at 25°C under vacuum, ethylenediamine was removed and $PhSi(\eta^2\text{-}NHCH_2CH_2NH)(\eta^2\text{-}NHCH_2CH_2NH_2)$ was transformed into a mixture of oligomers [equation (26.76)].

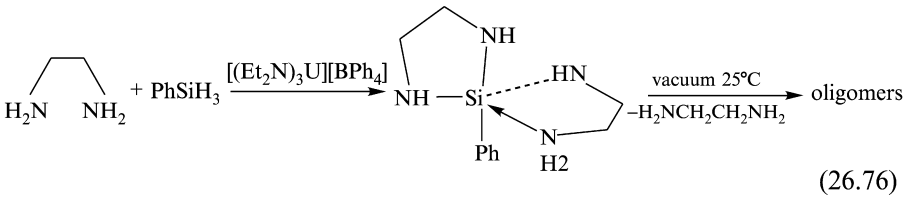

(26.76)

From these results it was concluded that the reactivity of primary amines RNH_2 in the formation of aminosilanes with $PhSiH_3$ catalyzed by the cationic uranium complex $[(Et_2N)_3U][BPh_4]$ follows the order primary > secondary > tertiary.

Secondary amines and secondary silanes were found to be less reactive than the corresponding primary amine and silanes. The reaction of Et_2NH with $PhSiH_3$ produced H_2 and a mixture of $PhSiH(NEt_2)_2$ and $PhSiH_2NEt_2$. No reaction was observed between $(^{i}Pr)_2NH$ and $PhSiH_3$, presumably because of the steric hindrance of the amine. The bulk of the silane was also found to have an effect. $^{n}PrNH_2$ reacted with the secondary silane $PhSiMeH_2$, generating H_2, $PhSiHMe(NHPr^{n})$ and $PhSiMe(NHPr^{n})_2$.

$[(Et_2N)_3U][BPh_4]$ reacted directly with stoichiometric or excess amounts of $PhSiH_3$, creating in both cases one equivalent of the corresponding aminosilane $PhSiH_2NEt_2$ and $[(Et_2N)UH][BPh_4]$; when an excess of silane was used, trace formation of the homodehydrogenative coupling product of the silane was observed. These results identified the monohydride complex as the active intermediate, since no other amido moieties were found to react with the phenylsilane. Therefore, the synthesis of a uranium hydride was accomplished by treatment of the corresponding amide with a silane, as has been reported in zirconium chemistry. Similar exchange reactions with boranes, alanes, and stannanes have been observed (Lappert *et al.*, 1980; Hays and Fu, 1997; Liu *et al.*, 1999).

A plausible mechanism for the dehydrocoupling of amines with silanes promoted by the cationic complex $[(Et_2N)_3U][BPh_4]$ is described in Scheme 26.22. The first step of the mechanism was proposed to be the transamination reaction of $[(Et_2N)_3U][BPh_4]$ with RNH_2 giving $[(NHR)_3U][BPh_4]$ (**KK**) (step 1). Complex **KK** may react with $PhSiH_3$ to afford the monoaminosilane $PhSiH_2NHR$ and the corresponding hydride $[(NHR)_2UH][BPh_4]$ (**LL**) (step 2). The last step of the catalytic cycle (step 3) is the reaction of **LL** and the amine, regenerating **KK** with the concomitant elimination of dihydrogen.

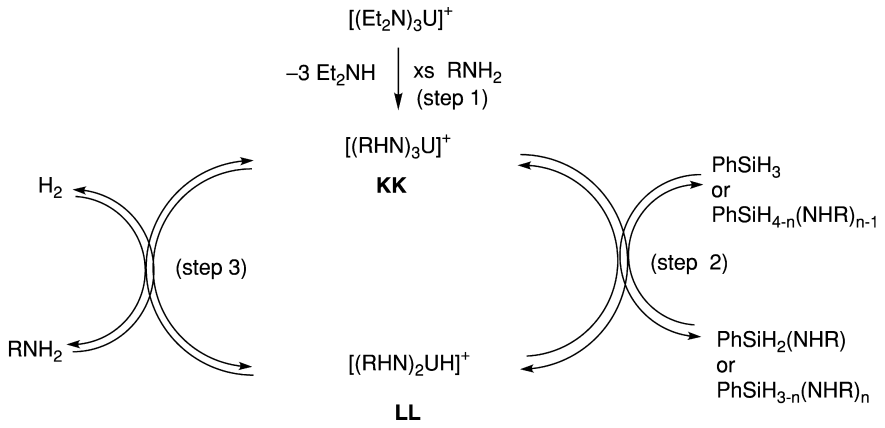

Scheme 26.22 *Proposed mechanism for the coupling of amine with silanes promoted by* $[(Et_2N)_3U][BPh_4]$.

The different polyaminosilanes $PhSiH_{3-n}(NHR)_n$ are obtained by replacing $PhSiH_3$ with $PhSiH_{4-n}(NHR)_{n-1}$ ($n \geq 1$) in step 2.

Since in the presence of an excess of amine the reactive hydrogen atoms were found to be those of the silane, a study of the reactivity of the aminosilane products towards a silane was conducted. The reaction of $PhSi(NHPr^n)_3$ with an excess of $PhSiH_3$ in the absence of amine was considered in order to determine a possible equilibrium and/or a tailoring approach to specific products by activation of the amine hydrogen atoms of the aminosilane. $PhSi(NHPr^n)_3$ reacted with an excess of $PhSiH_3$ in the presence of $[(Et_2N)_3U][BPh_4]$ to give a mixture of four compounds (**MM, NN, OO, PP)** (Scheme 26.23).

The explanation of how only four compounds were obtained may be found by consideration of the formation of all possible compounds as outlined in Scheme 26.24.

These results show how a cationic organoactinide complex offered an alternative route for the dehydrogenative coupling of amines with silanes by a mechanism consisting of activation of an amido ligand by a silane, producing the aminosilane and an organometallic hydride, which was recycled by addition of amine.

26.8 INTERMOLECULAR HYDROAMINATION OF TERMINAL ALKYNES

26.8.1 Intermolecular hydroamination of terminal alkynes catalyzed by neutral organoactinide complexes: scope and mechanistic studies

Catalytic C–N bond formation is a process of cardinal importance in organic chemistry, and the hydroamination of unsaturated substrates by the catalytic addition of a N–H moiety epitomizes a desirable atom-economic transformation

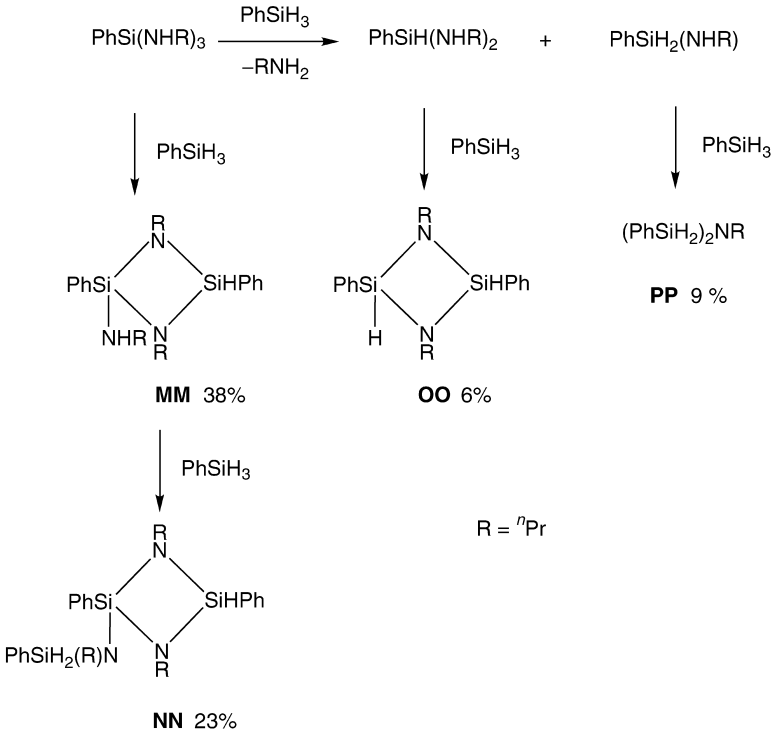

Scheme 26.23 *Reactivity of PhSi(NHPr^n)$_3$ with an excess of PhSiH$_3$ in the presence of* [$(Et_2N)_3U$][BPh_4].

with no by-products. This reaction remains a challenge [equation (26.77)] and current catalytic research activities in this area is widespread and spans to the entire periodic table (Nobis and Driessen-Hölscher, 2001; Molander and Romero, 2002; Pohlki and Doye, 2003; Seayad *et al.*, 2003; Trost and Tang, 2003; Utsunoyima *et al.*, 2003). The intermolecular functionalization of olefins and alkynes with amines has been mentioned as one of the ten most important challenges in catalysis (Haggin, 1993).

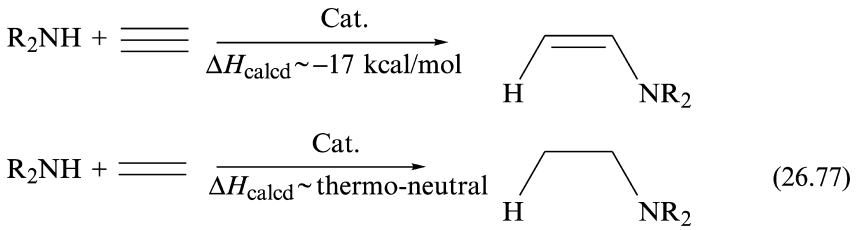

(26.77)

Thermodynamically, the addition process of amines to alkenes is close to thermoneutral whereas the addition to alkynes is more enthalpically favored.

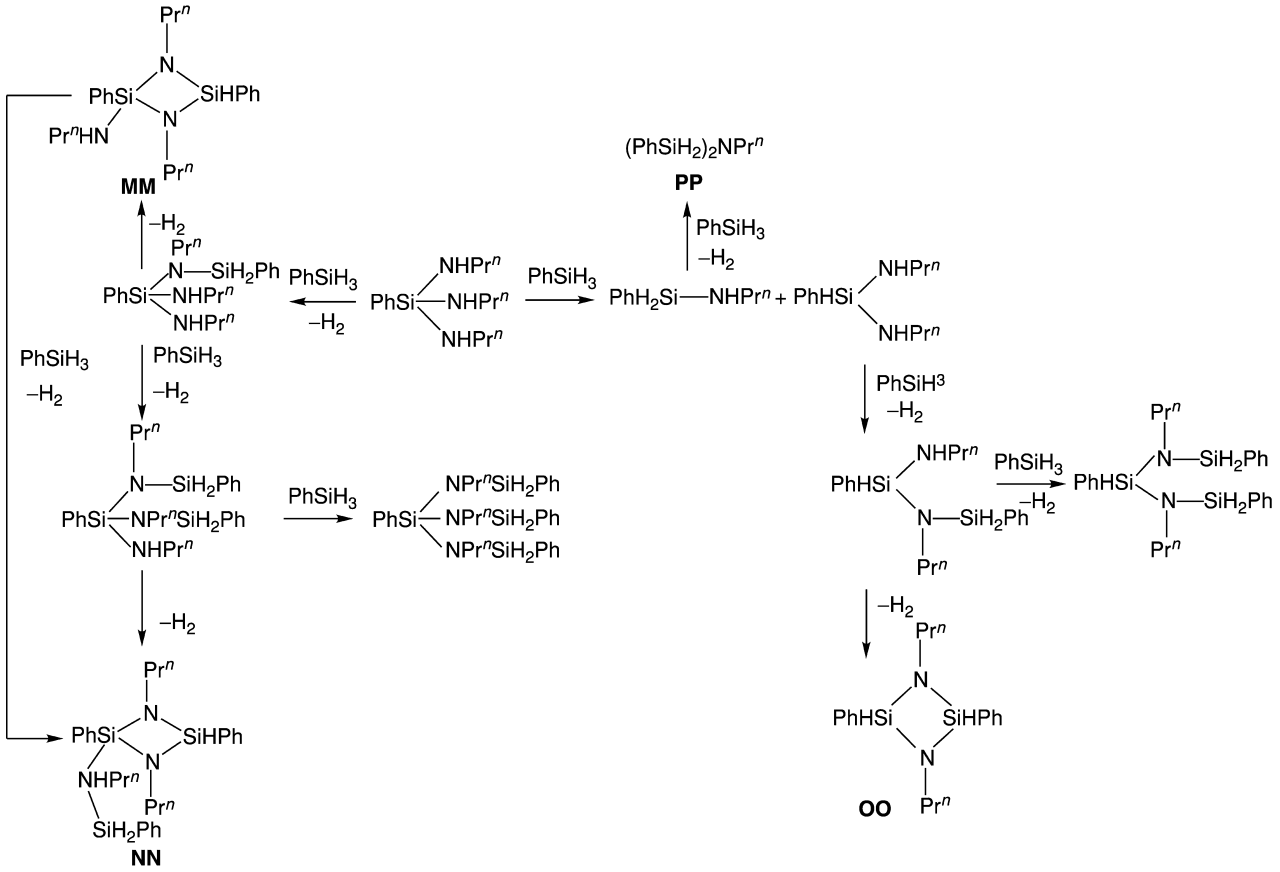

Scheme 26.24 *Formation of compounds **MM, NN, OO**, and **PP** in the coupling of amine and silanes catalyzed by* $[(Et_2N)_3U][BPh_4]$.

Because of the mode of activation of these organoactinides, the negative entropy of the reaction thwarts the use of high temperatures. Organolanthanide complexes have been found to be extremely good catalysts for the intramolecular hydroamination/cyclization of aminoalkenes, aminoalkynes, and aminoallenes (Gagné *et al.*, 1992a,b; Li and Marks, 1996; Roesky *et al.*, 1997b; Buergstein *et al.*, 1998; Li and Marks, 1998; Arredondo *et al.*, 1999a,b; Molander and Dowdy, 1999; Tian *et al.*, 1999; Ryu *et al.*, 2001; Douglass *et al.*, 2002; Hong and Marks, 2002; O'Shaughnessy *et al.*, 2003), and enantioselective intramolecular amination reactions have been performed using chiral organolanthanide precatalysts (Gagné *et al.*, 1992a).

The organoactinide complexes $(C_5Me_5)_2AnR_2$ (An = Th, U, R = Me, NHR′ R′ = alkyl) were found to be excellent precatalysts for the intermolecular hydroamination of terminal aliphatic and aromatic alkynes in the presence of primary aliphatic amines yielding the corresponding imido compounds (Haskel *et al.*, 1996; Straub *et al.*, 2001). The reactivity exhibited for the uranium complexes was different, depending on the alkynes, when compared to organothorium complexes [equations (26.78) and (26.79)].

The intermolecular process [equations (26.78) and (26.79)] showed two hydroamination regioselectivities depending on the precatalyst. The intermolecular hydroamination catalyzed by the uranium compound exhibited large regioselectivity and chemoselectivity with the *E*-isomer of the imine usually formed. For the thorium catalyst, the methyl alkyl-substituted imines were obtained. In the latter case, the imines were produced in moderate yields with the concomitant formation of the alkyne *gem* dimer.

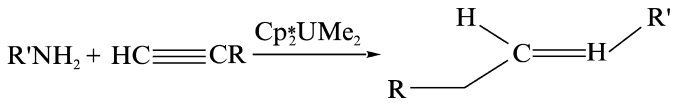

R = TMS, ^{t}Bu; R' = Me, Et, ^{n}Pr, ^{i}Pr, ^{n}Bu, ^{i}Bu
R = ^{n}Bu; R' = Me, Et, ^{n}Pr, ^{i}Pr, ^{i}Bu
R = Ph; R' = Me, Et
R = ^{i}Bu; R' = Et
R = C_5H_{11}; R' = Et

(26.78)

For R = TMS the imines are obtained as mixtures of E and Z isomers.

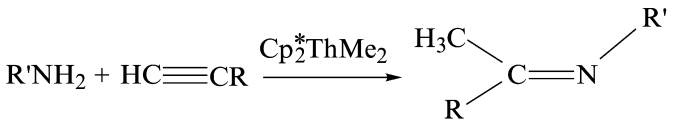

R = H; R' = Et
R = ^{n}Bu; R' = Me, Et
R = Ph; R' = Et
R = ^{i}Pr; R' = Ph

(26.79)

When the alkyne reactions catalyzed by the uranium complexes were performed using the bulky $^{t}BuNH_2$ as the primary amine, no hydroamination products were obtained. The products observed were only the selective *gem* dimers corresponding to the starting alkyne. This result has indicated that with $^{t}BuNH_2$, the proposed active species responsible for the intermolecular hydroamination was not generated. Using this bulky amine, the observed organouranium complexes in solution were the corresponding uranium bis(acetylide) (**9**) and the uranium bis(amido) (**12**) complexes. These two compounds were found to be in rapid equilibrium with the monoamido acetylide complex (**56**), responsible for the oligomerization of alkynes in the presence of amines [equation (26.80)].

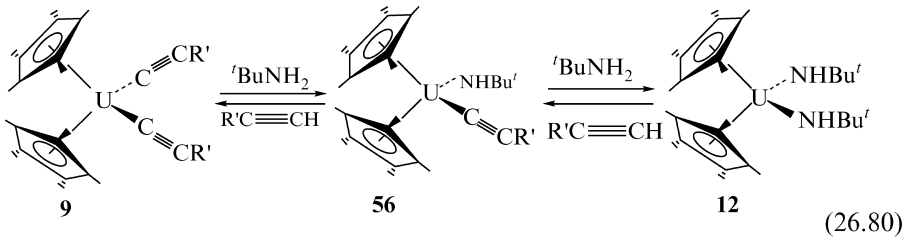

9 **56** **12** (26.80)

When comparing the hydroamination rates for a specific alkyne utilizing the various amines, the bulkier the amines, the lower the turnover frequency, and when comparing the hydroamination rates for a particular amine ($MeNH_2$) using various alkynes, similar turnover frequencies were observed. The lack of effect on the turnover frequency suggested no steric effect of the alkynes on the hydroamination process.

The intermolecular hydroamination catalyzed by the analogous organothorium complex $(C_5Me_5)_2ThMe_2$ exhibited similar reactivities with TMSC≡CH and $MeNH_2$ or $EtNH_2$ [equation (26.78)]. However, in the intermolecular hydroamination with ^{n}BuC≡CH or PhC≡CH and $MeNH_2$ or $EtNH_2$ a dramatic change in the regioselectivity was obtained, generating the unexpected imines [equation (26.79)]. For all the organoactinides, no hydroamination products were formed by using either secondary amines or internal alkynes. With secondary amines, the chemoselective alkyne dimers and in some cases trimers were obtained.

The catalytic hydroamination of ^{n}BuC≡CH or TMSC≡CH with $EtNH_2$ with either the organothorium complexes **1** or **5** gave identical results (rate, yields, stereochemistry of the products, and kinetic curves) indicating that both reactions occurred through a common active species, in a similar manner to that observed for the uranium complexes. It is interesting to point out that when the mixture of imines **57** and **58** were obtained, **57** was found to undergo a noncatalyzed Brook silyl rearrangement to form the corresponding enamine **59** [equation (26.81)] (Brook and Bassindale, 1980). The rearrangement followed

first-order kinetics with direct conversion of **57** to **59**, leaving the concentration of **58** unaffected:

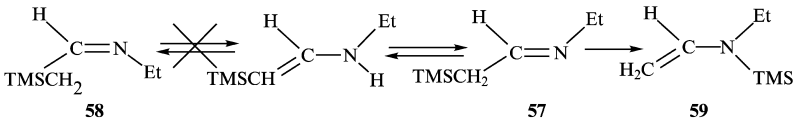

(26.81)

The formation of the corresponding oligomers in the hydroamination reactions catalyzed by the thorium complexes indicated that two different complexes were active in solution, possibly interconverting, resulting in two parallel processes. It was possible to discriminate between the two most probable mechanistic pathways to find the key organometallic intermediate responsible for the hydroamination process (Scheme 26.25). The first route proposed involved the insertion of an alkyne into a metal–amido bond, as found in lanthanide chemistry (Gagné *et al.*, 1992a,b; Roesky *et al.*, 1997a,b; Tian *et al.*, 1999). The second route consisted of insertion of an alkyne into a metal–imido (M=N) bond, as observed for early transition metal complexes (Walsh *et al.*, 1992, 1993).

26.8.2 Kinetic studies of the hydroamination terminal alkynes with primary amines

Kinetic measurements of the hydroamination of TMSC≡CH with $EtNH_2$ revealed that the reaction has a inverse first-order dependence in amine, first-order dependence in precatalyst, and zero-order dependence in alkyne

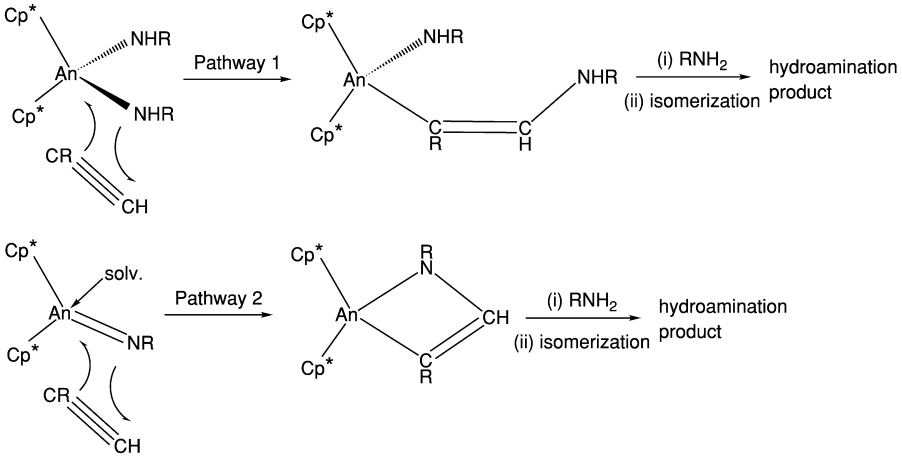

An = U;
For An = Th, the stereochemistry approach for some alkynes was inverted before insertion

Scheme 26.25 *Expected pathways for the organoactinide-catalyzed intermolecular hydroamination of primary amines with terminal alkynes.*

concentration. Thus, the rate law for the hydroamination of terminal alkynes promoted by organoactinides can be formulated as presented in equation (26.82). The derived $\Delta H^{\ddagger}$ and $\Delta S^{\ddagger}$ parameter values (in the range 60–120°C) (error values are in parenthesis) from a thermal Eyring analysis were 11.7(3) kcal mol^{-1} and –44.5(8) eu, respectively.

$$v = k[\mathrm{An}][\mathrm{amine}]^{-1}[\mathrm{alkyne}]^{0} \tag{26.82}$$

Since the approach of either alkyne or an amine to the organometallic catalyst is expected to occur in a side-on manner in the metallocene, the lack of alkyne concentration dependence in the kinetic hydroamination rate suggested that the proposed pathway 1 (Scheme 26.25) was not a major operative route. The zero kinetic order on alkyne suggests pathway 2 (Scheme 26.25) is consistent with the high coordinative unsaturation of the imido complexes that allows a fast insertion of the different alkynes with indistinguishable rates. When bulky amines were utilized, the formation of the corresponding imido complexes was hindered due to the encumbered transition state [equation (26.83)], reaching the highest steric hindrance with $^{t}BuNH_2$

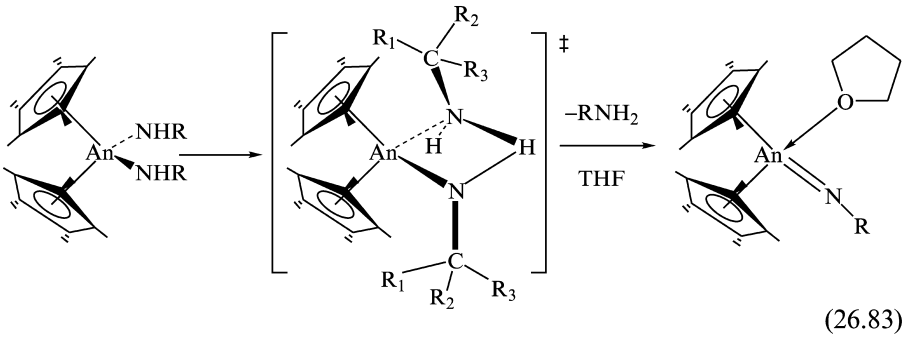

(26.83)

The different activation mode for the two organoactinides is very unusual. For both organoactinide–imido complexes, a selective metathesis with the π-bond of the alkyne was found to exist (demonstrated by the production of hydroamination products), whereas for the thorium complex a protonolysis reaction was observed as a competing reaction. The competing reaction was found to be responsible for the selective dimerization of the terminal alkynes (Scheme 26.26).

A likely scenario for the intermolecular hydroamination of terminal alkynes promoted by the organothorium complex is shown in Scheme 26.27. The first step in the catalytic cycle involved the N–H σ-bond activation of the primary amine by the starting organoactinide, yielding methane and the bisamido–amine complex $(C_5Me_5)_2Ac(NHR')_2 \cdot H_2NR'$ **6** (step 1), which was found to be in rapid equilibrium with the corresponding bis(amido) complex **5** (step 2) (Straub *et al.*, 1996; Eisen *et al.*, 1998) An additional starting point

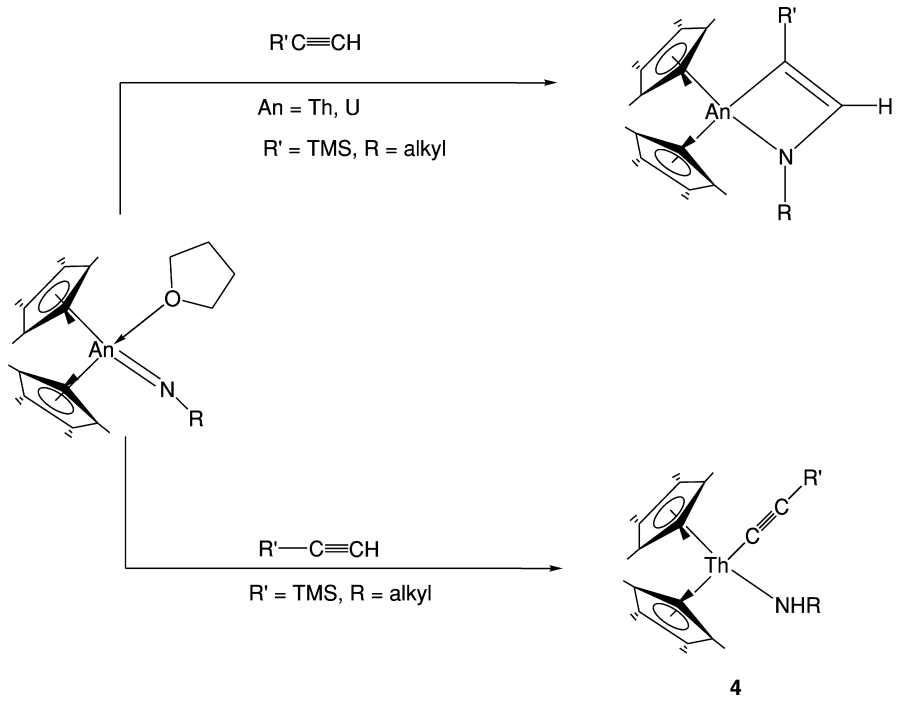

4

Scheme 26.26 *Distinctive modes of activation for organoactinide–imido complexes in the presence of terminal alkynes.*

involved a similar C–H activation of an alkyne with the organoactinide yielding methane and the bis(acetylide) complex **2** (step 3). This complex may react rapidly in the presence of amines either in equivalent amounts (step 4) or with an excess (step 5) yielding complexes **4** or **6**, respectively. Complex **5** followed two competitive equilibrium pathways. The σ-bond metathesis with a terminal alkyne yielded complex **4** (step 6), which induced the production of selective dimers (step 13). The second pathway (step 7), as the rate-limiting step, involves elimination of an amine molecule producing the corresponding imido complex **7**. The imido complex participated in a rapid π-bond metathesis with an incoming alkyne, yielding the metallacycle **60** (step 8). Rapid protonolytic ring opening of complex **60** by an amine yielded the actinide–enamine amido complex **61** (step 9). Complex **61** rapidly isomerized to the actinide–alkyl(imine) amido, **62**, by an intramolecular 1,3 sigmatropic hydrogen shift (step 10), which upon a subsequent protonolysis by an additional amine (step 11) produced the imine and regenerates the bis(amido) complex **5**.

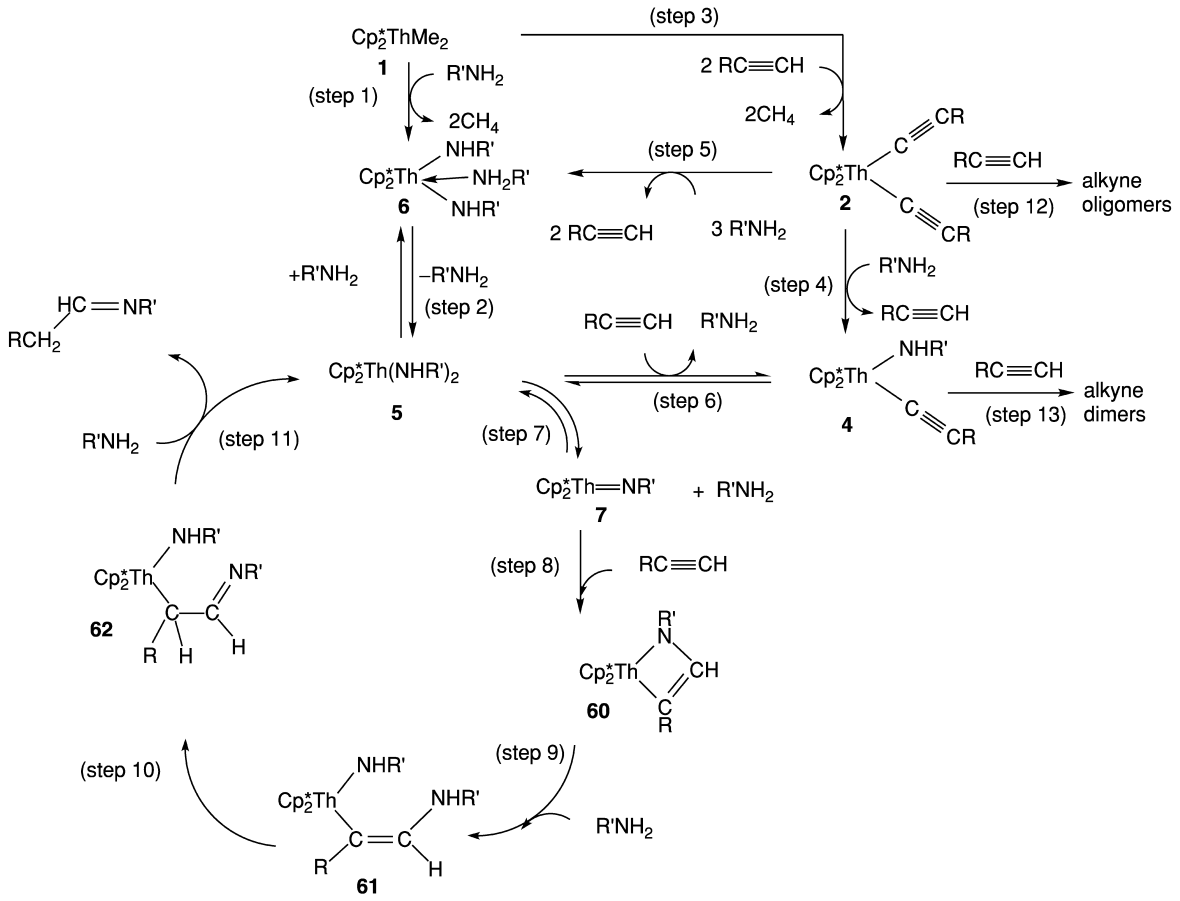

Scheme 26.27 *Proposed mechanism for the intermolecular hydroamination of terminal alkynes and primary amines promoted by neutral organoactinide complexes.*

The preferential formation of the *E* imine isomer as compared to that of the *Z* isomer may be explained by the steric hindrance of the amine substituents in the isomerization pathway as described in Scheme 26.28.

The distinct products formed by the two organoactinide catalysts in the hydroamination reaction are a result of a stereochemical difference in the approach of the alkyne to the imido complex (Scheme 26.29). It has been proposed that the regiochemistry of the intermolecular hydroamination between U and Th is driven by the differences in their electronic configurations, rather than the difference in their thermochemistry (potentially the f^2 electronic configuration of the uranium complex).

26.9 INTRAMOLECULAR HYDROAMINATION BY CONSTRAINED-GEOMETRY ORGANOACTINIDE COMPLEXES

Recently novel types of constrained-geometry actinide complexes were synthesized by the amine elimination syntheses using a protic ligation and the corresponding homoleptic amido-actinide precursor (Scheme 26.30) (Stubbert *et al.*, 2003). The equilibrium position of the elimination reaction was controlled by the dialkylamine concentration, whereas the removal of this by-product was the key step to obtain good yields for both actinide metals (Th, U). A slight excess of the ancillary ligand was used to obtain the complexes under mild conditions in up to 77% yield.

All three uranium complexes were crystallized as well as the $(CGC)Th(NMe_2)_2$ ($CGC{=}Me_2Si(\eta^5\text{-}Me_4C_5)\text{-}(^t BuN)$). The observed trends for the Cp(centroid)–metal–nitrogen angles for the actinide complexes and their respective comparison to lanthanides are Th > U > Sm > Yb, indicating a more open coordination for the 5f elements (Tian *et al.*, 1999; Stubbert, *et al.*, 2003). The *tert*-butylamido-metal bond length in all the complexes was found to be larger than the corresponding metal–NR_2 bond. The longer bonds are plausibly due to the lower basicity of the (Me_2Si *tert*-ButylN) as compared to that of the NR_2 moieties. Table 26.2 shows the turnover frequency for the hydroamination/cyclyzation of aminoalkenes and aminoalkynes. In addition, a nice comparison for the different abilities of the constrained geometry complexes with organoactinide metallocenes $Cp^*_2AnMe_2(An = Th, U)$ in the hydroamination is illustrated.

Kinetic studies on the hydroamination/cyclization reaction shows similar behavior as found for lanthanides. The kinetic rate law exhibits a first-order dependence on the precatalyst and zero order on the substrate i.e. rate α $[precatalyst]^1[substrate]^0$. This result argues that the protonolysis of the precatalyst amido moieties by the substrate is rapid, and that the rate determining step of the reaction is the olefin (alkene or alkyne) insertion into the An–NHR bond. For aminoalkenes, faster reactions are observed for the organoactinide

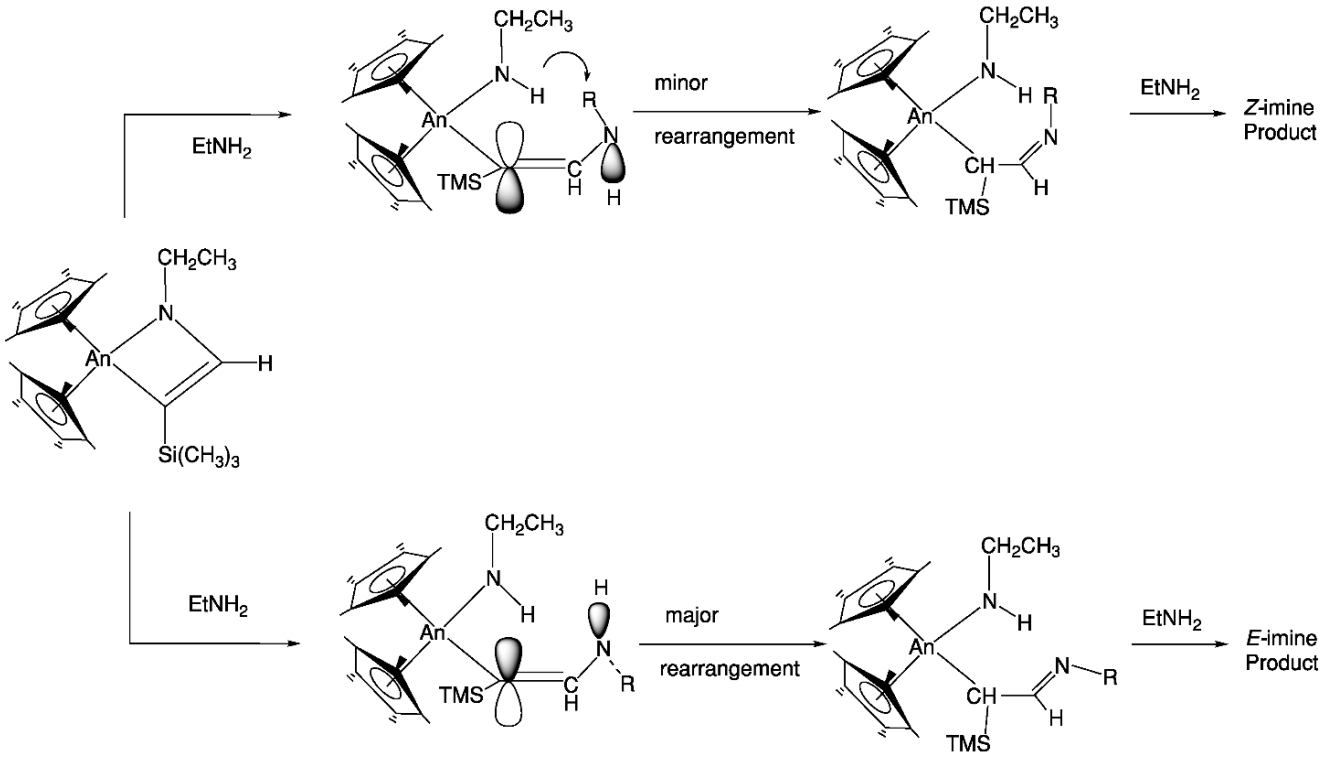

Scheme 26.28 *Formation of imines* E *and* Z *by a* 1,3*-sigmatropic hydrogen shift from the two possible organoactinide complexes. The curved arrow shows the steric interaction between the amine substituents present in the top route as compared to the bottom route.*

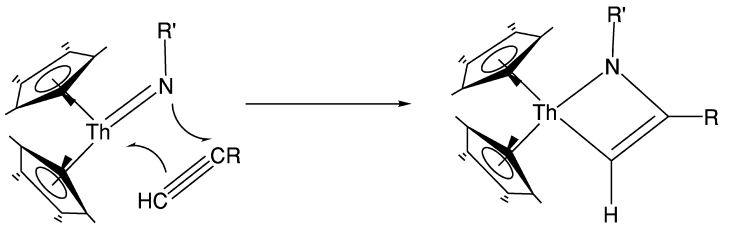

7

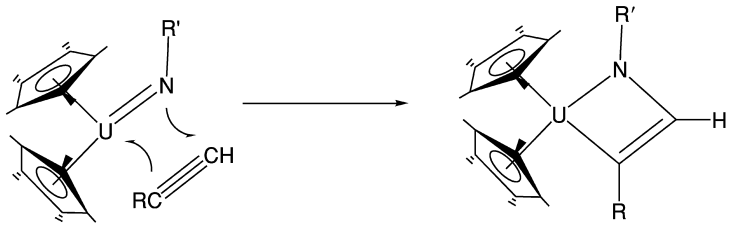

14

Scheme 26.29 *Opposite reactivity exhibited in the reaction of organoactinide–imido complexes with terminal alkynes.*

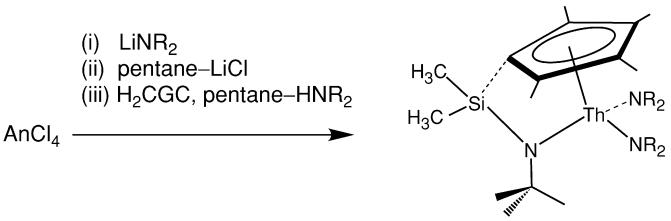

(An = Th; $NR_2 = NMe_2$ = 33.1%; NEtMe = 20.7%; NEt_2 = 22.1%
(An = U; $NR_2 = NMe_2$ = 57.9%; NEtMe = 77.1%; NEt_2 = 26.0%)

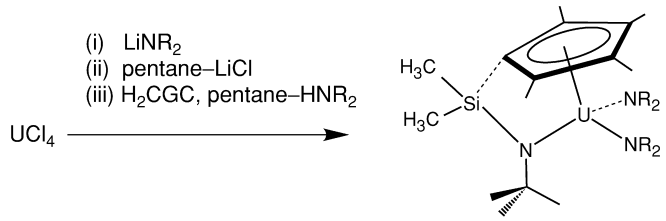

($NR_2 = NMe_2$ = 33%; NEtMe = 20.7%; NEt_2 = 22.1%)

Scheme 26.30 *Synthetic route towards constrained geometry organoactinides.*

Table 26.2 *Catalytic hydroamination/cyclization by various organoactinide complexes.*

Entry	*Precatalyst*	*Substrate*	*Product*	N_t (h^{-1})
1	(CGC)Th(NR_2)$_2$	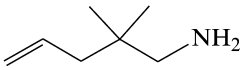	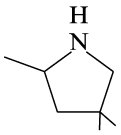	15
2	(CGC)U(NR_2)$_2$			2.5
3	$Cp^*_2ThMe_2$			0.4
4	(CGC)Th(NR_2)$_2$	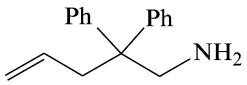	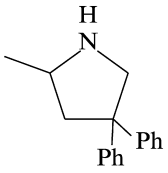	1460
5	(CGC)U(NR_2)$_2$			430
6	(CGC)Th(NR_2)$_2$	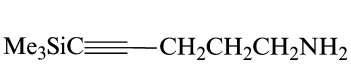	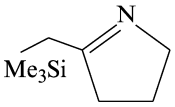	82
7	(CGC)U(NR_2)$_2$			>1600
8	(CGC)Th(NR_2)$_2$	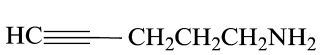	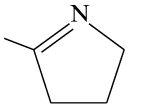	7.8
9	(CGC)Th(NR_2)$_2$			1210
10	$Cp^*_2UMe_2$			26
11	(CGC)Th(NR_2)$_2$		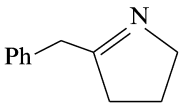	4.3
12	(CGC)Th(NR_2)$_2$			51
13	$Cp^*_2ThMe_2$			0.8

with a larger ionic radius, while for aminoalkynes, the faster reactions are observed for the organoactinide with the smaller ionic radius. A plausible mechanism for the hydroamination/cyclization is presented in Scheme 26.31.

It can be seen that the more sterically open environment of the constrained geometry complexes induces to a greater turnover frequencies for the aminoalkene substrates by allowing a greater access to the metal center without interfering with the kinetics and the stability of the complexes. For both aminoalkene and aminoalkynes, the constrained geometry complexes react much faster than the corresponding organoactinide metallocenes.

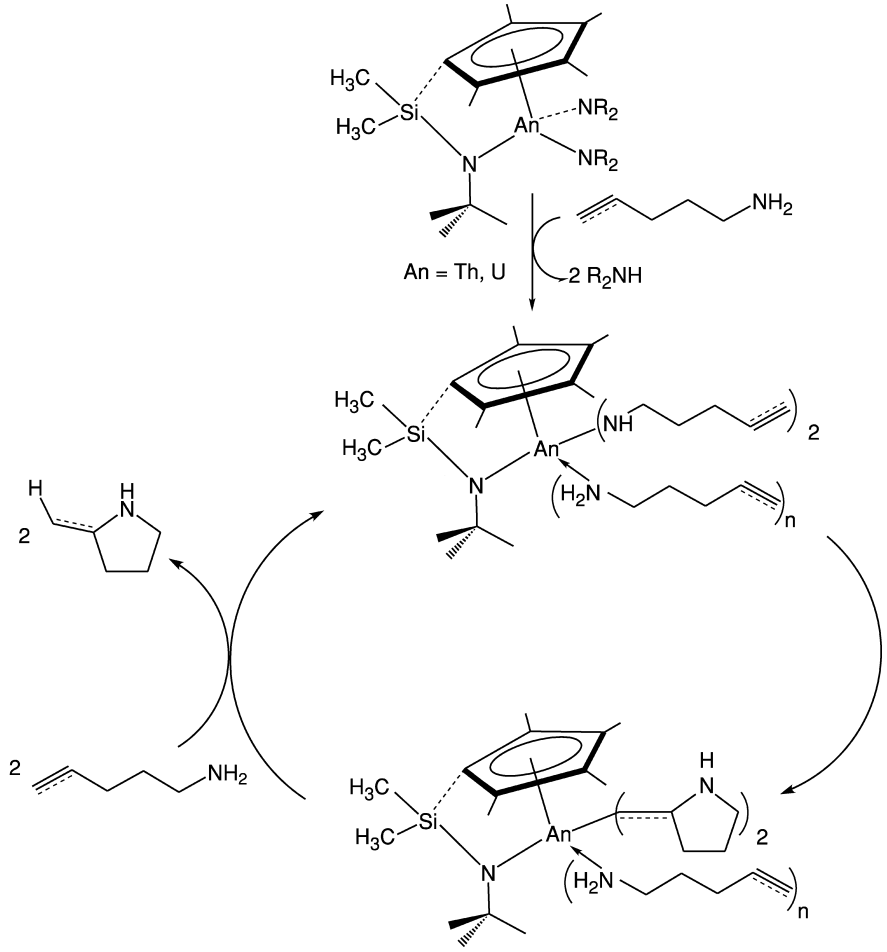

Scheme 26.31 *Plausible mechanism for the intramolecular hydroamination/cyclization of aminoolefins promoted by constrained geometry organoactinide complexes.*

26.10 THE CATALYTIC REDUCTION OF AZIDES AND HYDRAZINES BY HIGH-VALENT ORGANOURANIUM COMPLEXES

U(IV) metallocene compounds frequently show reactivities comparable to lanthanide and group IV transition metal metallocenes. Common types of processes among these metals (as demonstrated above) include olefin insertion, σ-bond metathesis, and protonolysis. In contrast to the lanthanides and group IV metals, however, uranium can also access the 6+ oxidation state, giving rise to the possibility of two-electron (4+/6+) redox processes. When the complexes $(C_5Me_5)_2U(=NR)_2$ (R = Ph, **29**; R = Ad = 1-adamantyl), **30**; are exposed to an

atmosphere of hydrogen, they are reduced to the corresponding bis(amide) complexes $(C_5Me_5)_2U(NHR)_2$ (**12**) (R = Ph, Ad,) [equation (26.84)]. The rate of hydrogenation of complex **30** was found to be much faster than that of complex **29**. When AdN_3 was added to a solution of the bis(amide) **12**, the bis (imido) **30** and $AdNH_2$ were formed [equation (26.85)]. Therefore, when complex **12** (R = Ad) was reacted with AdN_3 under an atmosphere of dihydrogen, catalytic hydrogenation of AdN_3 to $AdNH_2$ was observed (Scheme 26.32) (Peters *et al.*, 1999b).

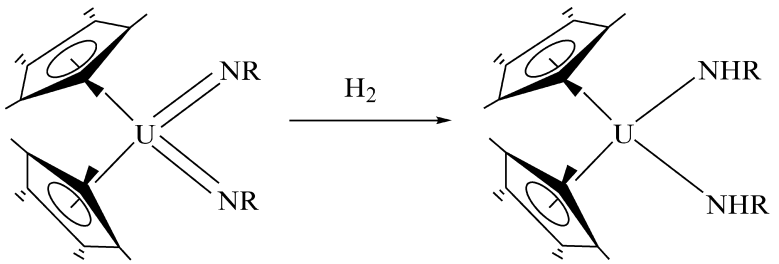

(26.84)

R = Ph, Ad

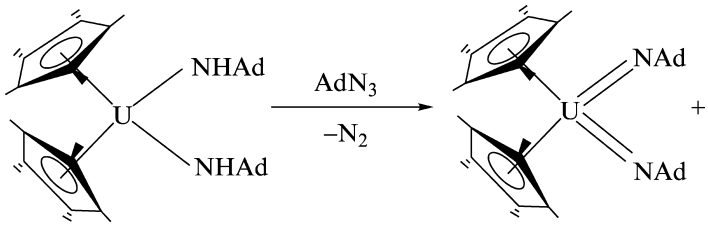

+ $AdNH_2$ (26.85)

30

N,*N*′-diphenylhydrazine was also used as the oxidant converting $(C_5Me_5)_2UMe_2$ (**8**) to **29**. This reaction was shown to occur by the protonation of the methyl groups, liberating methane. When $(C_5Me_5)_2U(=NPh)_2$ was treated with an excess of *N*,*N*′diphenylhydrazine in the absence of hydrogen, the substrate was entirely consumed, and aniline and azobenzene were observed to form in a 2:1 ratio [equation (26.86)]. This disproportionation indicated that the *N*,*N*′-diphenylhydrazine functioned as both oxidant and reductant. The formation of aniline during this reaction suggested that the U(IV) bis(amide) **12** is formed and serves to reduce the hydrazine, although the only observed uranium species in solution throughout the reaction was $(C_5Me_5)_2U(=NPh)_2$, indicating that the oxidation from U(IV) to U(VI) is faster than the subsequent reduction (Peters *et al.*, 1999b).

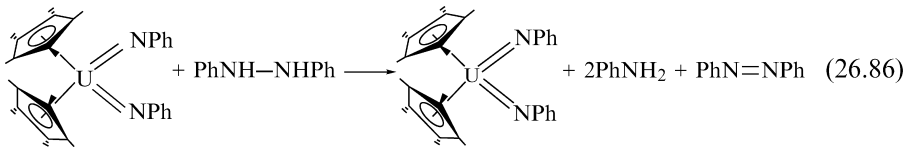

(26.86)

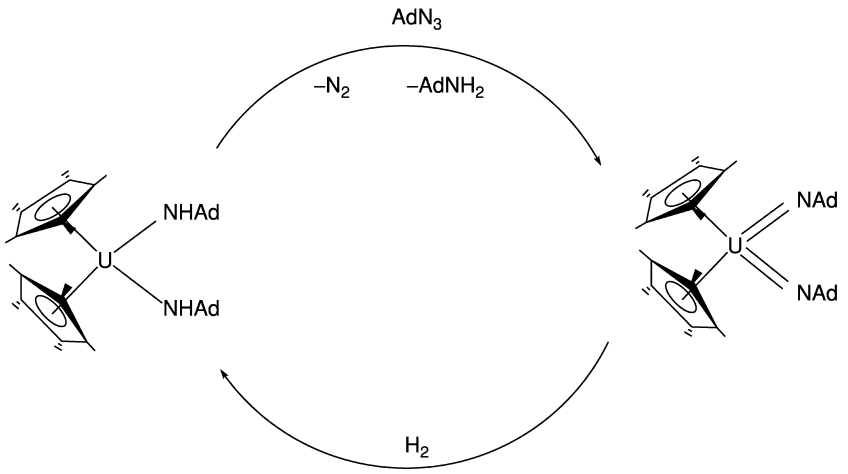

Scheme 26.32 *Catalytic reduction of azides by organouranium complexes.*

This reaction is favored both enthalpically and entropically. The calculated ΔH_f for converting two molecules of *N*,*N*'-diphenylhydrazine to two molecules of aniline and one molecule of azobenzene is –14.6 kcal/mol. Entropy considerations also qualitatively favor product formation; two molecules of starting material are converted to three molecules of product.

The catalytic activity of $(C_5Me_5)_2U(=NAd)_2$ (**30**) was also examined. The expectation was that if the mechanism of catalysis proceeds by protonation of the U(IV) bis(amide) by *N*,*N*′-diphenylhydrazine, similar to the reaction of *N*,*N*′-diphenylhydrazine with $(C_5Me_5)_2UMe_2$, initial product formation would include adamantylamine and azobenzene, with the concomitant formation of $(C_5Me_5)_2U(=NPh)_2$. However upon performing that reaction, $(C_5Me_5)_2U(=NAd)_2$, aniline and azobenzene were the only products observed, indicating that the imido ligands plausibly operated as sites for mediating H-atom transfer. No reaction was observed in the stoichiometric reaction of **29** with 1-adamantanamine ruling out the possibility of U–N bond rupture in which compound **29** is formed and undergoes subsequent rapid reaction with 1-adamantanamine regenerating **30** (Peters *et al.*, 1999a,b).

The catalytic transformations of substrates by two-electron processes are a novel type of reactivity for f-element complexes. The involvement of U(VI) species strongly argued for the requirement of f-orbital participation.

26.11 HYDROGENATION OF OLEFINS PROMOTED BY ORGANOACTINIDE COMPLEXES

The insertion of olefinic functionalities into metal–hydride bonds is an important step in various stoichiometric and homogeneous catalytic processes. A rich and versatile chemistry of organoactinide hydride complexes has been observed

for the complexes $(C_5Me_5)_2AnR_2$ (An = Th, U; R = alkyl). The formation of the hydride complexes has been obtained by hydrogenolysis of the corresponding organoactinide hydrocarbyl bonds [equations (26.87) and (26.88)] (Fagan *et al.*, 1981a,b; Marks, 1982, 1986a,b).

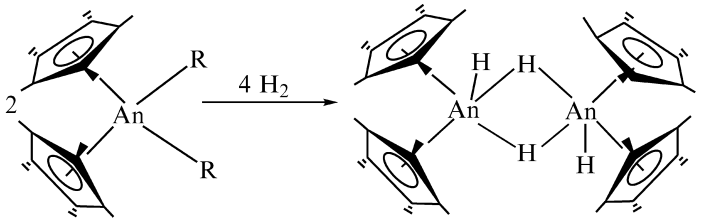

(26.87)

An = Th, U; R = alkyl

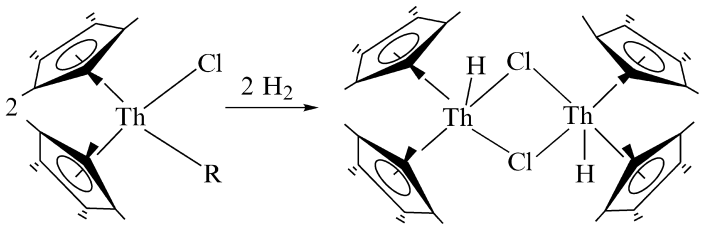

(26.88)

R = alkyl

These reactions have been studied thoroughly, mechanistically following a four-center transition state. Kinetic studies show that the reaction displays a first-order dependence in both actinide complex and in dihydrogen (Lin and Marks, 1987, 1990).

The organoactinide hydrides of the type $[(C_5Me_5)_2AnH_2]_2$ react rapidly and quantitatively with olefins yielding the corresponding 1,2-addition product. For example, the hydride complex $[(C_5Me_5)_2UH_2]_2$ catalyzes the hydrogenation of 1-hexene at 25°C and 1 atm of H_2 in toluene with a turnover frequency of 63000 h^{-1}. Scheme 26.33 shows the proposed hydrogenation mechanism of alkenes. The mechanism was derived from kinetic investigations similar to the hydrogenations promoted by the organolanthanide hydride $[(C_5Me_5)_2Lu(\mu\text{-}H)]_2$.

26.12 POLYMERIZATION OF α-OLEFINS BY CATIONIC ORGANOACTINIDE COMPLEXES

The synthesis of the cationic actinide complexes $[(C_5Me_5)_2ThMe][BPh_4]$ and $[(C_5Me_5)_2ThMe][B(C_6F_5)_4]$ has led to their study for the polymerization of ethylene and 1-hexene (Yang *et al.*, 1991). Mechanistically, the complexes $(C_5Me_5)_2AnMe_2$ (An = Th, U) react with a strong Lewis acid, like methylalumoxane (MAO), resulting in the formation of a cationic complex of the type $[(C_5Me_5)_2AnMe]^+[MAO\text{–}Me]^-$. These cationic complexes insert α-olefins many

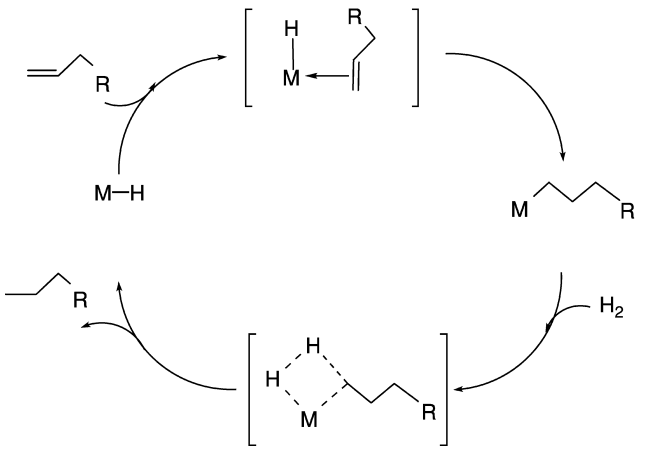

Scheme 26.33 *Proposed mechanism for the catalytic hydrogenation of alkenes promoted by* $[(C_5Me_5)_2UH_2]_2$.

times before a β-hydrogen elimination or a β-methyl elimination occurs, producing polymers. For ethylene, high-density polyethylene has been obtained whereas for propylene, atactic polypropylene was the product. The search for different cocatalysts (instead of MAO) has brought the development of new and versatile perfluoroaromatic boron compounds. These highly coordinative unsaturated cationic organothorium complexes have been recently prepared and found active for the polymerization of olefins [equation (26.89)] (Jia *et al.*, 1994, 1997).

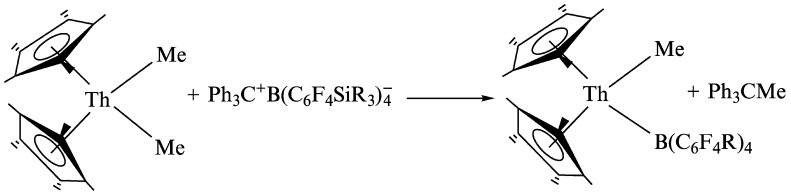

(26.89)

R = F, TBS, TIPS

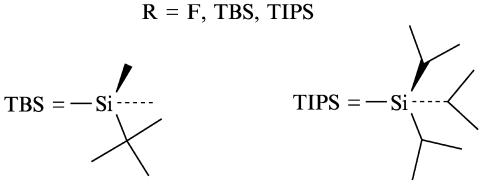

The reactivity of the organothorium complexes for the polymerization of ethylene follows the order: $[(C_5Me_5)_2ThMe][B(C_6F_5)_4] > [(C_5Me_5)_2ThMe]$

$[B(C_6F_4TIPS)_4] > [(C_5Me_5)_2ThMe][B(C_6F_4TBS)_4]$; however, their activity is an order of magnitude lower that observed for the corresponding zirconium complexes.

26.13 HETEROGENEOUS SUPPORTED ORGANOACTINIDE COMPLEXES

26.13.1 Hydrogenation of arenes by supported organoactinide complexes, kinetic, and mechanistic studies

Supporting homogeneous complexes on metal oxides creates a substantial alteration in their activity as compared to that observed in solutions (Iwasawa and Gates, 1989). For early transition metals (Yermakov *et al.*, 1981) and actinide alkyl complexes (Burwell and Marks, 1985; Finch *et al.*, 1990; Gillespie *et al.*, 1990; Marks, 1992) adsorbed upon metal oxide (e.g. alumina), large enhancements in the activities for catalytic hydrogenation were observed. The increase in coordinative unsaturation in metallocene organometallic-f-complexes generates a remarkable increase in the reactivity of these adsorbed complexes towards polymerization and hydrogenation of simple olefins, rivaling the activity of supported rhodium (He *et al.*, 1985; Marks, 1992), although these complexes are inefficient for the hydrogenation of arenes. Chemisorption of organoactinides involves the transfer of an alkyl group to the Al^{3+} (coordinatively unsaturated surfaces) sites and the formation of a 'cation–like' organothorium center as shown schematically in equation (26.90) (Jia *et al.*, 1997).

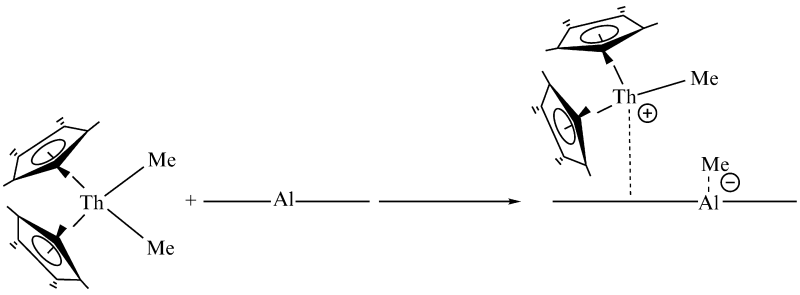

(26.90)

To address the question of how coordinatively unsaturated an organometallic-f-element complex was needed for the efficient reduction of arenes, a series of complexes of the type $R^1R^2_3Th(R^1 = \eta^5 - (CH_3)_5C_5; R^2 = CH_2C_6H_5; R^1 = R^2 = 1,3,5 - (CH_3)_3C_6H_2, R^1 = R^2 = \eta^3 - C_3H_5)$chemisorbed on highly dehydroxilated γ-alumina (DA) were prepared (Eisen and Marks, 1992a). Presumably, the adsorption of these organometallic-f-complexes is similar as displayed in equation (26.90), transferring an allyl group from the

thorium coordination to the strong Lewis acid site at the surface [equation (26.91)].

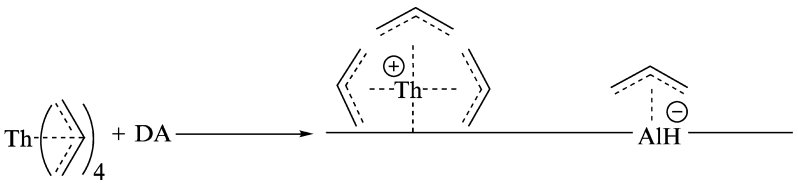

(26.91)

The hydrogenation reactivity of the latter complexes towards the hydrogenation of arenes (Table 26.3) shows that faster rates of hydrogenation are observed for less sterically hindered substrates.

26.13.2 Assessment of the percentage of $Th(\eta^3\text{-}C_3H_5)_4$/DA active sites

The percentage of supported organoactinide sites active in the olefin hydrogenation was estimated by dosing the catalyst with measured quantities of CO in a H_2 stream, measuring the amount of CO adsorbed by the catalyst, and determining the effect on subsequent catalytic activity. Similar results were found for H_2O/D_2O, and CH_3Cl poisoning experiments. The CO poisoning chemistry presumably involved migratory insertion equation (26.92) to produce surface η^2-formyl, which may then undergo various possible subsequent reactions.

Table 26.3 *Product and kinetic data for the $Th(\eta^3\text{-}C_3H_5)_4$/DA catalyzed hydrogenation of various arenes*[a]

Substrate	*Product*	*Turnover frequency* (s^{-1})
C_6H_6	C_6H_{12}	6.80
C_6D_6	$C_6H_6D_6$	6.78
$CH_3C_6H_5$	$CH_3C_6H_{11}$	4.05[b]
$CD_3C_6D_5$	$CD_{3-x}H_xC_6H_6D_5$	3.98[b]
1,4-$(CH_3)_2C_6H_4$	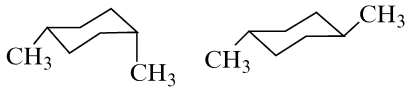 3 : 1	0.65[b]
Naphthalene	 5 : 1	8.3×10^{-3}

[a] pH_2 = 190 psi; [arene] = 10 mmol. Temp = 90°C.
[b] = values at 100% yield.

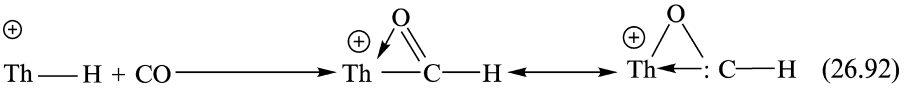

(26.92)

Additional confirmation of the estimated number of active sites was provided by measurement of the metal–hydride content by adding aliquots of D_2O, and studying the catalytic activity after each addition. This stepwise titration of active sites indicated that $8 \pm 1\%$ of the total $Th(\eta^3\text{-}C_3H_5)_4/DA$ sites present on the support were responsible for the majority of the catalysis [equation (26.93)].

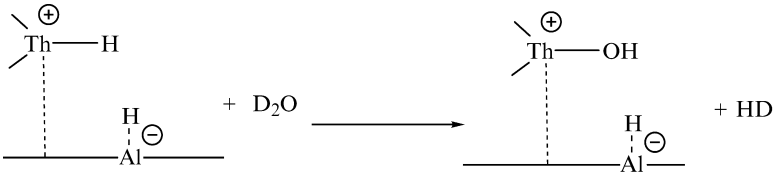

(26.93)

Another additional complementary experiment for measuring the number of hydrides was undertaken by reacting the adsorbed $Th(\eta^3\text{-}C_3H_5)_4/DA$ with hydrogen and measuring the amount of organic gas recovery from the reaction. The amount of propane per thorium was found to be only 10% of the total amount expected [equation (26.94)]. No propylene was released from the reaction, indicating that the hydrogenation of propylene was extremely fast, and indeed, the turnover frequency for the hydrogenation of propylene was measured separately to be ($N_t(25^\circ C) = 25\ s^{-1}$).

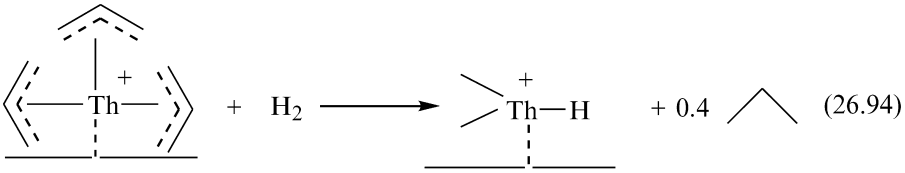

(26.94)

The number of thorium hydride sites formed was confirmed to be the same by reaction with methyl chloride and measurement of the amount of methane per Th that was evolved from the reaction [equation (26.95)].

(26.95)

The importance of these poisoning experiments is that they indicate that only a very small fraction of the organothorium adsorbate sites on dehydroxylated alumina were responsible for the bulk of the catalytic reactivity. It is likely that one or more different structures of the suggested 'cation-like' organothorium moieties constitute the catalytic sites on alumina, but the exact structural characteristics defining these structures remain to be elucidated.

For arene hydrogenation, the kinetic data can be accommodated by three repetitions of a two-step sequence: (i) arene insertion (olefin insertion for the subsequent step) into a Th–H bond; (ii) hydrogenolysis of the resulting Th–alkyl bond. The kinetic data measured for benzene conforms to the rate law $N_t = k$ [benzene]^0[pH_2]^1[Th]^1 (Th = tetraallyl complex). The kinetic isotope measurements for the hydrogenation of benzene indicated $N_t(H_2)/N_t(D_2) = 3.5 \pm 0.3$ at 90°C and 180 psi of H_2. In the hydrogenation reaction of benzene with D_2, the product $C_6H_6D_6$ was obtained as a mixture of two geometric isomers as refers to the disposition of the deuterium atoms: *all cis* and *cis*, *cis*, *trans*, *cis*, *trans* in a ratio of 1:3 respectively. The Arrhenius activation energies for the catalytic hydrogenation of benzene was measured to be 16.7 ± 0.3 kcal mol^{-1} and the corresponding thermodynamic activation parameters were $\Delta H^{\ddagger} = 16.0 \pm 0.3$ kcal/mol and $\Delta S^{\ddagger} = 32.3 \pm 0.6$ eu (Eisen and Marks, 1992).

The mechanism proposed for the hydrogenation of arenes is described in Scheme 26.34. The process takes into account the lack of facial selectivity by which the ratio 1:3 among the geometrical isomers were formed. As a function of substrate, the relative rates of Th(η^3-C_3H_5)$_4$/DA-catalyzed hydrogenation of arenes was found to be in the order benzene > toluene > *p*-xylene > naphthalene.

In the hydrogenation of benzene no H/D scrambling is observed during the process but H/D scrambling is observed after complete hydrogenation of the starting material. In the reaction between toluene-d_8 and H_2 or toluene and D_2 significant C–H/C–D exchange at the benzylic positions was observed during the hydrogenation. Significant incorporation of deuterium atoms into the starting toluene and subsequently into the cyclohexane product was observed at partial conversions. The C–H/C–D exchange was suggested to occur through a benzylic activation as shown in equation (26.96).

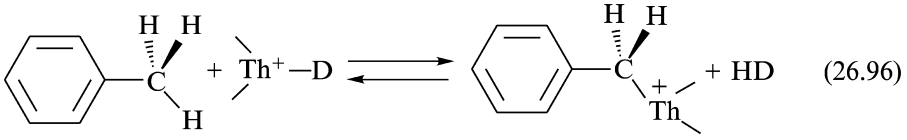

(26.96)

Competition experiments confirmed the large kinetic discrimination for the different arenes. The hydrogenation reaction of equimolar quantities of *p*-xylene and benzene yielded cyclohexane with almost complete selectivity (97%) and a mixture of 3:1 *cis*:*trans* 1,4-dimethylcyclohexane (3%).

26.13.3 Facile and selective alkane activation by supported tetraallylthorium

C–H activation processes involving alkanes are considered high-energy demanding transformations. Although significant advances have been made in the functionalization of C–H bonds by f- and early transition complexes (Shilov, 1984; Gillespie *et al.*, 1990; Ryabov, 1990; Watson, 1990; Basset *et al.*, 1998;

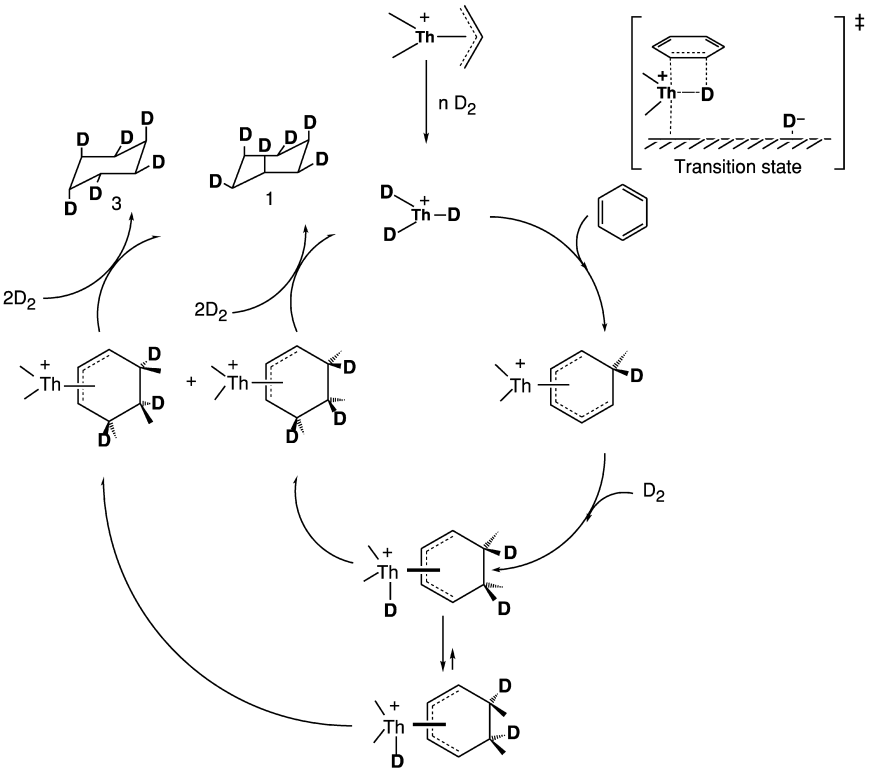

Scheme 26.34 *Proposed mechanism for the hydrogenation of arenes by cationic supported organoactinide complexes.*

Schneider *et al.*, 2001), the catalytic intermolecular activation of inert alkane molecules with favorable rates and selectivities is still a major challenge. As noted above, studies on benzene reduction with D_2 revealed C–H/C–D exchange in the cyclohexane product only after benzene conversion was complete. This observation prompted detailed studies of the activation of hydrocarbons. The results from slurry reaction studies of C–H/C–D exchange for a variety of alkanes catalyzed by thorium tetraallyl complex/DA under a D_2 atmosphere are summarized in Table 26.4 (Eisen and Marks, 1992b).

Rapid C–H/C–D exchange was promoted by the tetraallyl complex/DA, with turnover frequencies comparable to or exceeding those of conventional group 9 heterogeneous alkane activation catalysts (Butt and Burwell, 1992). C–H functionalization occurred with substantial selectivity and in an order which does not parallel the C–H bond dissociation energies: primary > secondary > tertiary,

Table 26.4 *Kinetic and product structure/deuterium distribution data for Th(η^3-C_3H_5)$_4$/DA catalyzed C–H/C–D fuctionalization.*

Substrate	*Deuterium distribution in product* (%)	*Turnover frequency* (h^{-1})
$CH_3CH_2CH_2CH_2CH_3$	$CH_2DCHDCHDCHDCH_2D$	778
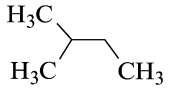	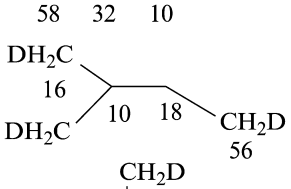	879
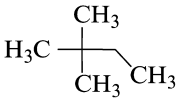	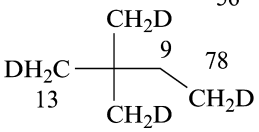	825
C_6H_{12}	$C_6H_{12-x}D_x$	1285
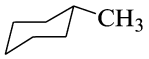	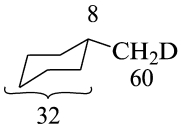	1113
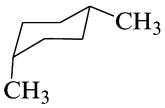	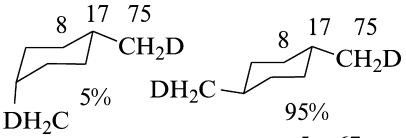	884
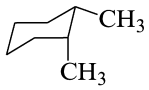	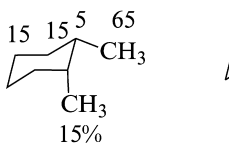 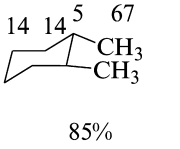	834

and sterically less hindered > sterically more hindered. NMR and GC-MS measurements as a function of conversion indicated single C-H exchanges, with no evidence for multiple exchange processes (e.g. non-statistical amounts of RD_2 species). Unexpectedly, the CH/CD exchange reaction of *cis*-dimethylcyclohexanes produced isomerization towards a *cis–trans* mixture. Based on the same two reasonable assumptions as for the arene hydrogenation, a plausible mechanistic scenario for the activation and isomerization of alkanes was proposed and summarized in Scheme 26.35. The mechanistic sequence invokes presumably endothermic Th–C bond formation and HD elimination via a 'four- center', heterolytic 'σ-bond metathesis' (step 1), followed by deuterolysis

(step 2). Cycloalkane skeletal isomerization would then occur via a β-H elimination (step 3) and re-addition of the Th^{+}–H to the opposite face of the double bond (step 4). This process would involve the rapid dissociation and re-addition of the alkene, although other mechanisms have been proposed as conceivable. Insertion (step 5) and deuterolysis (step 6) produced the isomerized cycloalkane. The isotopic labeling experiments revealed little D incorporation at the dimethylcyclohexane tertiary carbon centers and negligible differences in the D label distribution of the isomerized and un-isomerized hydrocarbons. These results indicated that the ancillary ligands L and L′ in Scheme 26.35 are either non-D in identity (e.g. η^3-allyl or oxide), or that such Th–D functionalities were chemically and stereochemically inequivalent to that formed in a β-H abstraction, since they do not compete for olefin addition.

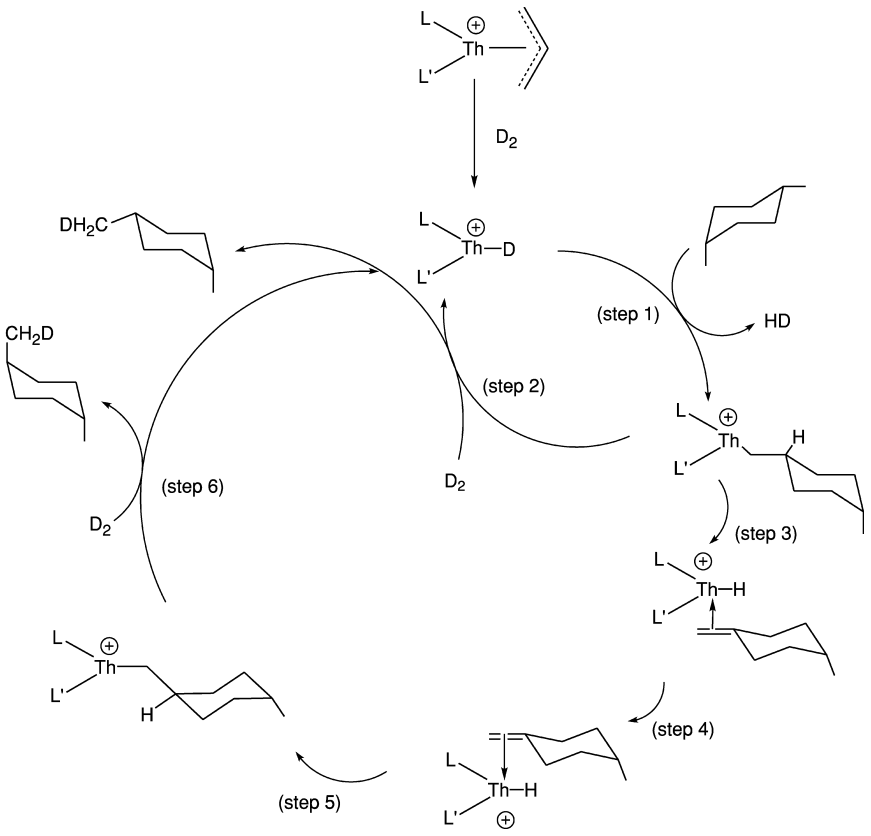

Scheme 26.35 *Proposed scenario for the Th(η^3-allyl)$_4$/DA-catalyzed C–H activation and isomerization of alkanes.*

In summary, these results demonstrate that supported organo-f-complexes are extremely active catalysts for a number of high-energy organic chemistry transformations.

ACKNOWLEDGMENTS

C. J. B. gratefully acknowledges support at LANL by the U.S. Department of Energy, Office of Science, Office of Basic Energy Sciences, Division of Chemical Sciences, Geosciences, and Biosciences. M. S. E. thanks the Fund for the Promotion of Research at The Technion.

REFERENCES

Aitken, C., Barry, J. P., Gauvin, F. G., Harrod, J. F., Malek, A., and Rousseau, D. (1989) *Organometallics*, **8**, 1732–6.

Anwander, R. (1996) in *Applied Homogeneous Catalysis with Organometallic Compounds,* vol. 2 (eds. B. Cornils and W. A. Herrmann) VCH Publishers, New York.

Anwander, R. and Herrman, W. A. (1996) *Top. Curr. Chem.*, **179**, 1–32.

Apeloig, Y. (1989) in *The Chemistry of Organic Silicon Compounds* (eds. S. Patai and Z. Rappoport), Wiley-Interscience, New York, pp. 57—225.

Arney, D. S. J., Burns, C. J., and Smith, D. C. (1992) *J. Am. Chem. Soc.*, **114**, 10068–9.

Arney, D. S. J. and Burns, C. J. (1993) *J. Am. Chem. Soc.*, **115**, 9840–1.

Arney, D. S. J. and Burns, C. J. (1995) *J. Am. Chem. Soc.*, **117**, 9448–60.

Arredondo, V. M., Tian, S., McDonald, F. E., and Marks, T. J. (1999a) *J. Am. Chem. Soc.*, **121**, 3633–9.

Arredondo, V. M., McDonald, F. E., and Marks, T. J. (1999b) *Organometallics*, **18**, 1949–60.

Asao, N., Sudo, T., and Yamamoto, Y. (1996) *J. Org. Chem.*, **61**, 7654–5.

Bajgur, C. S., Tikkanen, W. R., and Petersen, J. L. (1985) *Inorg. Chem.*, **24**, 2539–46.

Baranger, A. M., Walsh, P. J., and Bergman, R. G. (1993) *J. Am. Chem. Soc.*, **115**, 2753–63.

Basset, J. M., Lefebvre, F., and Santini, C. (1998) *Coord. Chem. Rev.*, **178–180**, 1703–23.

Berthet, J. C., Boisson, C., Lance, M., Vigner, J., Nierlich, M., and Ephritikhine, M. (1995) *J. Chem. Soc., Dalton Trans.*, 3019–25.

Berthet, J. C. and Ephritikhine, M. (1998) *Coord. Chem. Rev.*, **178–180**, 83–116.

Biran, C., Blum, Y. D., Glaser, R., Tse, D. S., Youngdahl, K. A., and Laine, R. M. (1988) *J. Mol. Catal.*, **48**, 183–97.

Blake, P. C., Edelman, M. A., Hitchcock, P. B., Hu, J., Lappert, M. F., Tian, S., Müller, G., Atwood, J. L., and Zhang, H. (1998) *J. Organomet. Chem.*, **551**, 261–70.

Blum, Y. and Laine, R. M. (1986) *Organometallics*, **5**, 2081–6.

Bode, B. M., Day, P. N., and Gordon, M. S. (1998) *J. Am. Chem. Soc.*, **120**, 1552–5.

Brennan, J. G. and Andersen, R. A. (1985) *J. Am. Chem. Soc.*, **107**, 514–16.

Brook, A. G. and Bassindale, A. R. (1980) in Rearrangements in Ground and Excited States, vol. 2, Academic Press, New York.

Bruno, J. W., Marks, T. J., and Morss, L. R. (1983) *J. Am. Chem. Soc.*, **105**, 6824–32.
Bruno, J. W., Smith, G. M., and Marks, T. J. (1986) *J. Am. Chem. Soc.*, **108**, 40–56.
Buergstein, M. R., Berberich, H., and Roesky, P. W. (1998) *Organometallics*, **17**, 1452–4.
Burns, C. J., Smith, W., Huffman, J. C., and Sattelberger, A. P. (1990) *J. Am. Chem. Soc.*, **112**, 3237–9.
Bursten, B. E. and Strittmatter, R. J. (1991) *Angew. Chem. Int. Edn. Engl.*, **30**, 1069–85.
Burwell, R. L. Jr and Marks, T. J. (1985) in *Catalysis of Organic Reactions* (ed. R. L. Augustine), Marcel Dekker, New York, pp. 207—24.
Butt, J. B. and Burwell, R. L. Jr (1992) *Catal. Today*, **12,**177—88.
Chalk, A. J. and Harrod, J. F. (1965) *J. Am. Chem. Soc.*, **87**, 16–21.
Chan, T. H. (1977) *Acc. Chem. Res.*, **10**, 442–8.
Chen, Y.-X., Metz, M. V., Li, L., Stern, C. L., and Marks, T. J. (1998) *J. Am. Chem. Soc.*, **120**, 6287–305.
Collman, J. P., Hegedus, L. S., Norton, J. R., and Finke, R. G. (1987) *Principles and Applications of Organotransition Metal Chemistry,* University Science, Mill Valley, CA, chs 6, 10, and 13.
Colvin, E. W. (1988) *Silicon Reagents in Organic Synthesis,* Academic Press, London.
Corey, J. Y., Huhmann, J. L., and Zhu, X.-H. (1993) *Organometallics*, **12**, 1121–30.
Cramer, R. E., Roth, S., and Gilje, J. W. (1989a) *Organometallics*, **8**, 2327–30.
Cramer, R. E., Roth, S., Edelmann, F., Bruck, M. A., Cohn, K. C., and Gilje, J. W. (1989b) *Organometallics*, **8**, 1192–9.
Dash, A. K., Wang, J. Q., and Eisen, M. S. (1999) *Organometallics*, **18**, 4724–41.
Dash, A. K., Wang, J. X., Berthet, J. C., Ephritikhine, M. and Eisen, M. S. (2000) *J. Organomet. Chem.*, **604**, 83–98.
Dash, A. K., Gourevich, I, Wang, J. Q., Wang, J., Kapon, M., and Eisen, M. S. (2001) *J. Am. Chem. Soc.*, **20**, 5084–104.
Den Haan, K. H., Wielstra, Y., and Teuben, J. H. (1987) *Organometallics*, **6**, 2053–60.
Douglass, M. R., Ogasawara, M., Hong, S., Metz, M. V., and Marks, T. J. (2002) *Organometallics*, **21**, 283–92.
Duckett, S. B. and Perutz, R. N. (1992) *Organometallics*, **11**, 90–98.
Duttera, M. R., Day, V. W., and Marks, T. J. (1984) *J. Am. Chem. Soc.*, **106**, 2907–12.
Edelman, M. A., Hitchcock, P. B., Hu, J., and Lappert, M. F. (1995) *New. J. Chem.*, **19**, 481–9.
Edelmann, F. T. (1995b) in *Comprehensive Organometallic Chemistry II* (eds. E. W. Abel, F. G. A. Stone, and G. Wilkinson), Pergamon Press, Oxford, ch. 4.
Edelmann, F. T. (1996) *Top. Curr. Chem.*, **179**, 247–76.
Edelmann, F. T. and Gun'ko, Y. (1997) *Coord. Chem. Rev.*, **165**, 163–237.
Edelmann, F. T. and Lorenz, V. (2000) *Coord. Chem. Rev.*, **209**, 99–160.
Eigenbrot, C. W. and Raymond, K. N. (1982) *Inorg. Chem.*, **21**, 2653–60.
Eisen, M. S. and Marks, T. J. (1992a) *J. Am. Chem. Soc.*, **114**, 10358–68.
Eisen, M. S. and Marks, T. J. (1992b) *Organometallics*, **11**, 3939–41.
Eisen, M. S. (1997) *Rev. Inorg. Chem.*, **17**, 25–52.
Eisen, M. S. (1998) in *The Chemistry of Organosilicon Compounds,* vol. 2 (eds. Y. Apeloig, and Z. Rappoport), John Wiley, Chichester, pp. 2038–122, part 3, ch. 35.
Eisen, M. S., Straub, T., and Haskel, A. (1998) *J. Alloys Compd.*, **271–273**, 116–22.
Elschenbroich, Ch. and Salzer, A. (1989) *Organometallics,* VCH, Weinheim, Germany, ch. 17.

Ephritikhine, M. (1997) *Chem. Rev.*, **97**, 2193–242.
Esteruelas, M. A., Nurnberg, O., Olivian. M., Oro, L. A. and Werner, H. (1993) *Organometallics*, **12**, 3264–72.
Evans, W. J., Bloom, I., Hunter, W. E., and Atwood, J. L. (1983) *Organometallics*, **2**, 709–14.
Evans, W. J., Drummond, D. K., Hanusa, T. P., and Olofson, J. M. (1989) *J. Organomet. Chem.*, **376**, 311–20.
Fagan, P. J., Manriquez, J. M., Maata, E. A., Seyam, A. M., and Marks, T. J. (1981a) *J. Am. Chem. Soc.*, **103**, 6650–67.
Fagan, P. J., Manriquez, J. H., Vollmer, S. H., Day, C. S., Day, V. W., and Marks, T. J. (1981b) *J. Am. Chem. Soc.*, **103**, 2206–20.
Faller, J. W. and Rosan, A. M. (1977) *J. Am. Chem. Soc.*, **99**, 4858–9.
Fendrick, C. M., Mintz, E. A., Schertz, L. D., Marks, T. J., and Day, V. W. (1984) *Organometallics*, **3**, 819–21.
Fendrick, C. A., Schertz, L. D., Day, V. W., and Marks, T. J. (1988) *Organometallics*, **7**, 1828–38.
Finch, W. C., Gillespie, R. D., Hedden, D., and Marks, T. J. (1990) *J. Am. Chem. Soc.*, **112**, 6221–32.
Fleming, I., Dunogues, J., and Smithers, R. H. (1989) *Org. React.*, **37**, 57–575.
Forsyth, C. M., Nolan, S. P., and Marks, T. J. (1991) *Organometallics*, **10**, 2543–5.
Fu, P.-F. and Marks, T. J. (1995) *J. Am. Chem. Soc.*, **117**, 10747–8.
Gagné, M. R. and Marks, T. J. (1989) *J. Am. Chem. Soc.*, **111**, 4108–9.
Gagné, M. R., Stern, C. L., and Marks, T. J. (1992a) *J. Am. Chem. Soc.*, **114**, 275–94.
Gagné, M. R., Brard, L., Conticello, V. P., Giardello, M. A., Stern, C. L., and Marks, T. J. (1992b) *Organometallics*, **11**, 2003–5.
Giardello, M. A., King, W. A., Nolan, S. P., Porchia, M., Sishta, C., and Marks, T. J. (1992) in *Energetics of Organometallic Species* (ed. J. A. Martinho Simões), Kluwer Academic Press, Dodrecht, The Netherlands, pp. 35—51.
Giardello, M. A., Conticello, V. P., Brard, L., Gagné, M. R., and Marks, T. J. (1994) *J. Am. Chem. Soc.*, **116**, 10241–54.
Gillespie, R. D., Burwell, R. L. Jr, and Marks, T. J. (1990) *Langmuir*, **6**, 1465–77.
Haar, C. M., Stern, C. L., and Marks, T. J. (1996) *Organometallics*, **15**, 1765–84.
Haggin, J. (1993) *Chem. Eng. News*, **17(22)**, 23.
Harrod, J. F. and Chalk, A. J. (1965) *J. Am. Chem. Soc.*, **87**, 1133–5.
Harrod, J. F. (1991) in *Inorganic and Organometallic Polymers with Special Properties* (ed. R. M. Lain), Kluwer Academic Publishers, Amsterdam, ch. 14.
Haskel, A., Straub, T., and Eisen, M. S. (1996) *Organometallics*, **15**, 3773–6.
Haskel, A., Wang, J. Q., Straub, T., Gueta-Neyroud, T., and Eisen, M. S. (1999) *J. Am. Chem. Soc.*, **121**, 3025–34.
Hays, D. S. and Fu, G. C. (1997) *J. Org. Chem.*, **62**, 7070–1.
He, M.-Y., Xiong, G., Toscano, P. J., Burwell, R. L. Jr, and Marks, T. J. (1985) *J. Am. Chem. Soc.*, **107**, 641–52.
He, J., Liu, H. Q., Harrod, J. F., and Hynes, R. (1994) *Organometallics*, **13**, 336–43.
Heeres, H. J., Heeres, A., and Teuben, J. H. (1990) *Organometallics*, **9**, 1508–10.
Heeres, H. J. and Teuben, J. H. (1991) *Organometallics*, **10**, 1980–6.
Hegedus, L. S. (1995) in *Comprehensive Organometallic Chemistry II,* vol. 12 (eds. E. W. Abel, F. G. A. Stone, and G. Wilkinson), Pergamon Press, Oxford.

Hitchcock, P. B., Hu, J., Lappert, M. F., and Tian, S. (1997) *J. Organomet. Chem.*, **536–537**, 473–80.
Hiyama, T. and Kusumoto, T. (1991) in *Comprehensive Organic Synthesis,* vol 8 (eds. B. M. Trost and I. Fleming), Pergamon Press, Oxford.
Hong, S. and Marks, T. J. (2002) *J. Am. Chem. Soc.*, **124**, 7886–7.
Ihara, E., Nodono, M., Yasuda, H., Kanehisa, N., and Kai, Y. (1996) *Macromol. Chem. Phys.*, **197**, 1909–17.
Iwasawa, Y. and Gates, B. C. (1989) *CHEMTEC*, **3**, 173–81.
Jemine, X., Goffart, J., Berthet, J.-C., and Ephritikhine, M., Fuger, J. (1992) *J. Chem. Soc.*, *Dalton Trans.*, 2439–44.
Jemine, X., Goffart, J., Ephritikhine, M., and Fuger, J. (1993) *J. Organomet. Chem.*, **448**, 95–8.
Jeske, C., Lauke, H., Mauermann, H., Schumann, H., and Marks, T. J. (1985a) *J. Am. Chem. Soc.*, **107**, 8111–18.
Jeske, C., Schock, L. E., Mauermann, H., Swepston, P. N., Schumann, H., and Marks, T. J. (1985b) *J. Am. Chem. Soc.*, **107**, 8103–10.
Jeske, G., Schock, L. E., Swepson, P. N., Schumann, H., and Marks, T. J. (1985c) *J. Am. Chem. Soc.*, **107**, 8091–103.
Jia, J., Yang, X., Stern, C. L., and Marks, T. J. (1994) *Organometallics*, **13**, 3755–7.
Jia, J., Yang, X., Stern, C. L., and Marks, T. J. (1997) *Organometallics*, **16**, 842–57.
King, W. A., Marks, T. J., Anderson, D. M., Duncalf, D. J., and Cloke, F. G. N. (1992) *J. Am. Chem. Soc.*, **114**, 9221–3.
King, W. and Marks, T. J. (1995) *Inorg. Chim. Acta.*, **229**, 343–54.
Lappert, M. F., Power, P. P., Sanger, A. R., and Srivastava, R. C. (1980) in *Metal and Metalloid Amides: Synthesis*, *Structures*, *and Physical and Chemical Properties*, Ellis Horwood-Wiley, Chichester, New York, chs 12 and 13.
Leal, J. P., Marquez, N., Pires de Matos, A., Caldhorda, M. J., Galvão, J. A., and Martinho Simões, J. A. (1992) *Organometallics*, **11**, 1632–7.
Leal, J. P. and Martinho Simões, J. A. (1994) *J. Chem. Soc.*, *Dalton Trans.*, 2687–91.
Leal, J. P., Marquez, N., and Takats, J. (2001) *J. Organomet. Chem.*, **632**, 209–14.
Li, Y. and Marks, T. J. (1996) *Organometallics*, **15**, 3770–3.
Li, Y. and Marks, T. J. (1998) *J. Am. Chem. Soc.*, **120**, 1757–71.
Lin, Z. and Marks, T. J. (1987) *J. Am. Chem. Soc.*, **109**, 7979–85.
Lin, Z. and Marks, T. J. (1990) *J. Am. Chem. Soc.*, **112**, 5515–25.
Liu, H. Q. and Harrod, J. F. (1992) *Organometallics*, **11**, 822–7.
Liu, X., Wu, Z., Peng, Z., Wu, Y-D., and Xue, Z. (1999) *J. Am. Chem. Soc.*, **121**, 5350–1.
Lunzer, F., Marschner, C., and Landgraf, S. (1998) *J. Organomet. Chem.*, **568**, 253–5.
Marçalo, J. and Pires de Matos, A. (1989) *Polyhedron*, **8**, 2431–7.
Marciniec, B., Gulinsky, J., Urbaniak, W., and Kornetka, Z. W. (1992) *Comprehensive Handbook on Hydrosilylation* (ed. B. Marciniec), Pergamon, Oxford.
Marks, T. J. (1982) *Science*, **217**, 989–97.
Marks, T. J. and Day, V. W. (1985) in *Fundamental and Technological Aspects of Organo-f-Element Chemistry* (eds. T. J. Marks and I. L. Fragalà), Reidel, Dodrecht, ch 4.
Marks, T. J. (1986a) in *The Chemistry of the Actinide Elements,* vol. 2 (eds. J. J. Katz, J. T. Seaborg, and L. R. Morss), Chapman & Hall, London; New York, ch. 22.

Marks, T. J. (1986b) in *The Chemistry of the Actinide Elements,* vol. 2 (eds. J. J. Katz, J. T. Seaborg, and L. R. Morss), Chapman & Hall, London; New York, ch. 23.
Marks, T. J., Gagné, M. R., Nolan, S. P., Schock, L. E., Seyam, A. M., and Stern, D. (1989) *Pure Appl. Chem.*, **61**, 1665–72.
Marks, T. J. (1992) *Acc. Chem. Res.*, **25**, 57–65.
Marthino Simões, J. A. and Beauchamp, J. L. (1990) *Chem. Rev.*, **90**, 629–88.
Mitchell, J. P., Hajela, S., Brookhart, S. K., Hardcastle, K. I., Henling, L. M., and Bercaw, J. E. (1996) *J. Am. Chem. Soc.*, **118**, 1045–53.
Molander, G. A. and Hoberg, J. O. (1992) *J. Am. Chem Soc.*, **114**, 3123–5.
Molander, G. A. and Winterfeld, J. (1996) *J. Organomet. Chem.*, **524**, 275–9.
Molander, G. A. and Knight, E. E. (1998) *J. Org. Chem.*, **63**, 7009–12.
Molander, G. A. (1998) *Chemtracs: Org. Chem.*, **11**, 237–63.
Molander, G. A. and Dowdy, E. D. (1999) *J. Org. Chem.*, **64**, 6515–17.
Molander, G. A. and Romero, J. A. C. (2002) *Chem. Rev*., **102**, 2161–86.
Nobis, M. and Driessen-Hölscher, B. (2001) *Angew. Chem., Int. Edn.*, **40**, 3983–5.
Nolan, S. P., Stern, D., Hedden, D., and Marks, T. J. (1990) *ACS Symp. Ser.*, **428**, 159–74.
Ohff, A., Burlakov, V. V., and Rosethal, U. (1996) *J. Mol. Catal.*, **108**, 119–23.
Ojima, I., Li, Z., and Zhu, J. (1998) in *The Chemistry of Organic Silicon Compounds* (eds. Z. Rappoport and Y. Apeloig), John Wiley, New York, ch. 29, and references therein.
O'Shaughnessy, P. N., Knight, P. D., Morton, C., Gillespie, K. M., and Scott, P. (2003) *Chem. Commun.*, **14**, 1770–1.
Pelletier, J.-F., Mortreux, A., Olonde, X., and Bujadoux, K. (1996) *Angew. Chem. Int. Edn. Engl.*, **35**, 1854–6.
Peters, R. G., Warner, B. P., Scott, B. L., and Burns, C. J. (1999a) *Organometallics*, **18**, 2587–9.
Peters, R. G., Warner, B. P., and Burns, C. J. (1999b) *J. Am. Chem. Soc.*, **121**, 5585–6.
Pohlki, F. and Doye, S. (2003) *Chem. Soc. Rev.*, **32**, 104–14.
Radu, N. S., Engeler, M. P., Gerlach, C. P., Tilley, T. D., and Rheingold, A. L. (1995) *J. Am. Chem. Soc.*, **117**, 3621–2.
Reichl, J. and Berry, D. H. (1998) *Adv. Organomet. Chem.*, **43**, 197–265.
Roesky, P. W., Denninger, U., Stern, C. L., and Marks, T. J. (1997a) *Organometallics*, **16**, 4486–92.
Roesky, P. W., Stern, C. L., and Marks, T. J. (1997b) *Organometallics*, **16**, 4705–11.
Ruiz, J., Bentz, P. O., Mann, B. E., Spencer, C. M., and Taylor, B. F., Maitlis, P. M. (1987) *J. Chem. Soc., Dalton Trans.*, 2709–13.
Ryabov, A. D. (1990) *Chem. Rev.*, **90**, 403–24.
Ryu, J. S., Marks, T. J., and McDonald, F. E. (2001) *Org. Lett.*, **3**, 3091–4.
Sakaki, S., Mizoe, N., and Sugimoto, M. (1998) *Organometallics*, **17**, 2510–23.
Samsel, E. G. (1993) Patent Application EP 574854.
Schaverien, C. J. (1994) *Organometallics*, **13**, 69–82.
Schnabel, R. C., Scott, B. L., Smith, W. H., and Burns, C. J. (1999) *J. Organomet. Chem.*, **591**, 14–23.
Schneider, H., Puchta, G. T., Kaul, F. A. R., Raudaschl- Sieber, G., Lefebvre, F., Saggio, G., Mihalios, D., Hermann, W. A., and Basset, J. M. (2001) *J. Mol. Catal. A*: *Chem.*, **170**, 127–41.

Schumann, H., Keitsch, M. R., Demtschuk, J., and Molander, G. A. (1999) *J. Organomet. Chem.*, **582**, 70–82.
Seayad, A. M., Selvakumar, K., Ahmed, M., and Beller, M. (2003) *Tetrahedron Lett.*, **44**, 1679–83.
Seitz, F. and Wrighton, M. S. (1988) *Angew. Chem., Int. Edn. Engl.*, **27**, 289–91.
Selin, T. J. and West, R. (1962) *J. Am. Chem. Soc.*, **84**, 1860–3.
Shannon, R. D. (1976) *Acta Crystallogr.*, **A32**, 751–67.
Shen, Q., Zheng, D., Lin, L., and Lin, Y. (1990) *J. Organomet. Chem.*, **391**, 307–12.
Shilov, A. E. (1984) *Activation of Saturated Hydrocarbons by Transition Metal Complexes,* Reidel, Hingham, MA.
Smith, G. M., Carpenter, J. D., and Marks, T. J. (1986a) *J. Am. Chem. Soc.*, **108**, 6805–7.
Smith, G. M., Susuki, H., Sonnenberg, D. C., Day, V. W., and Marks, T. J. (1986b) *Organometallics*, **5**, 549–61.
Straub, T., Haskel, A., and Eisen, M. S. (1995) *J. Am. Chem. Soc.*, **117**, 6364–5.
Straub, T. R. G., Frank, W., and Eisen, M. S. (1996) *J. Chem. Soc., Dalton Trans.*, 2541–6.
Straub, T., Haskel, A., Dash, A. K., and Eisen, M. S. (1999) *J. Am. Chem. Soc.*, **121**, 3014–24.
Straub, T., Haskel, A., Neyroud, T. G., Kapon, M., Botoshansky, M., and Eisen, M. S. (2001) *Organometallics*, **20**, 5017–35.
Stubbert, B. D., and Stern, C. L., Marks, T. J. (2003) *Organometallics*, **22**, 4836–8.
Sudo, T., Asao, N., Gevorgyan, V., and Yamamoto, Y. (1999) *J. Org. Chem.*, **64**, 2494–9.
Takeuchi, R. and Tanouchi, N. (1994) *J. Chem. Soc., Perkin Trans. 1*, 2909–13.
Takeuchi, R. and Yasue, H. (1996) *Organometallics*, **15**, 2098–102.
Tanke, R. S. and Crabtree, R. H. (1991) *Organometallics*, **10**, 415–18.
Tian, S., Arredondo, V. M., Stern, C. L., and Marks, T. J. (1999) *Organometallics*, **18**, 2568–70.
Tilley, T. D. (1993) *Acc. Chem. Res.*, **26**, 22–9.
Trost, B. M. and Tang, W. J. (2003) *J. Am. Chem. Soc.*, **125**, 8744–5.
Utsonomiya, M., Kuwano, R., Kawatsura, M., and Hartwig, J. F. (2003) *J. Am. Chem. Soc.*, **125**, 5608–9.
Walsh, P. J., Baranger, A. M., and Bergman, R. G. (1992) *J. Am. Chem. Soc.*, **114**, 1708–19.
Walsh, P. J., Hollander, F. J., and Bergman, R. G. (1993) *Organometallics*, **12**, 3705–23.
Wang, W. D. and Eisenberg, R. (1991) *Organometallics*, **10**, 2222–7.
Wang, J. Q., Dash, A. K., Berthet, J. C., Ephritikhine, M., and Eisen, M. S. (1999) *Organometallics*, **18**, 2407–9.
Wang, J. X., Dash, A. K., Berthet, J. C., Ephritikhine, M., and Eisen, M. S. (2000) *J. Organomet. Chem.*, **610**, 49–57.
Wang, J., Dash, A. K., Kapon, M., Berthet, J. C., Ephritikhine, M., and Eisen, M. S. (2002a) *Chem. Eur. J.*, **8**, 5384–96.
Wang, J., Kapon, M., Berthet, J. C., Ephritikhine, M., and Eisen, M. S. (2002b) *Inorg. Chim. Acta*, **344**, 183–92.
Wang, J. Q. and Eisen, M. S. (2003) unpublished results.
Warner, B. P., Scott, B. L., and Burns, C. J. (1998) *Angew. Chem., Int. Edn. Engl.*, **37**, 959–60.

Watson, P. L. and Parshall, G. W. (1985) *Acc. Chem. Res.*, **18**, 51–6.
Watson, P. L. (1990) in *Selective Hydrocarbon Activation* (eds. J. A. Davies, P. L. Watson, J. F. Liebman, and A. Greenberg), VCH, New York, ch. 4.
Weber, W. P. (1983) *Silicon Reagents for Organic Synthesis,* Springer-Verlag, Berlin.
Xing-Fu, L., Xi-Zhang, F., Ying-Ting, X., Hai-Tung, W., Jie, S., Li, L., and Peng-Nian, S. (1986a) *Inorg. Chim. Acta*, **116**, 85–93.
Xing-Fu, L., Ying-Ting, X., Xi-Zhang, F., and Peng-Nian, S. (1986b) *Inorg. Chim. Acta*, **116**, 75–83.
Xing-Fu, L. and Ao-Ling, G. (1987) *Inorg. Chim. Acta*, **134**, 143–53.
Yang, X., Stern, C. L., and Marks, T. J. (1991) *Organometallics*, **10**, 840–2.
Yermakov, Y. I., Kuznetsov, B. N., and Zakharov, V. A. (1981) *Catalysis by Supported Complexes,* Elsevier, Amsterdam.
Zalkin, A., Edwards, P. G., Zhang, D., and Andersen, R. A. (1986) *Acta Crystallogr.*, **C42**, 1480–2.

CHAPTER TWENTY SEVEN

IDENTIFICATION AND SPECIATION OF ACTINIDES IN THE ENVIRONMENT

Claude Degueldre

27.1 BACKGROUND

All actinide isotopes are radioactive. Since the middle of the last century, new actinide and transactinide isotopes have been artificially produced and the use of several of the naturally occurring actinide isotopes has increased. This production is due to the nuclear power industry and the military fabrication and use of nuclear weapons. These activities have created anxiety about the introduction of actinide elements into the environment. Consequently, environmental systems that contain or are exploited for natural actinides, or, are potentially contaminated by anthropogenic actinides, must be investigated. The analytical techniques introduced in this chapter are used, after sampling when required, to identify and quantify the actinide isotopes and to determine the species in which they are present.

The amounts or concentrations of actinide elements or isotopes in the environmental samples need to be identified and quantified. Moreover, since transport properties and bioavailability are closely linked to species and atomic environment of the actinide elements, both radiotoxicity and speciation of actinides in the studied phases must be determined to understand the behavior of these elements in the environment (Livens, 2001). In this chapter, analysis of a broad range of environmental systems are considered such as fluid phases from air or waters from surface to subsurface, samples from terrestrial

to oceanic, and samples from rocks to organic or bio-related phases. These samples range from depleted to rich in actinides and from inorganic to organic or bioorganic. The actinides are either dissolved in solid or liquid solutions, or associated with particles dispersed in the sample phase: in air or water, or in heterogeneous solids. Actinide species may also be located at phase boundaries such as rock–water or dispersed *in vivo*, associated with biofunctional environments. The phases of interest range from the nanometer to the kilometer in size, in surface or in volume.

In all cases, accurate or quantifiable sampling is required, together with identification, quantification, and determination of the redox states or of the complexes in the phases or at the interfaces, as well as characterization of the molecular environment, or emphasis on the crystalline or the amorphous phases that contain actinide isotopes, elements, or species. This information is required to understand how actinide species will behave in the environment and the way in which actinides can migrate or be retained. However, contamination may concentrate via bioaccumulation mechanisms (Holm and Fukai, 1986; Skwarzec *et al.*, 2001) or a geochemical process specific to a local hydrogeochemical environment (Bundt *et al.*, 2000). Spatial information is needed, ranging from the subnanometer to the micrometer size to understand migration behavior from the microscopic to the geographic scale, and temporal information is needed, ranging from second fractions to millions of years.

Figure 27.1 schematizes the source, location, or occurrence of natural actinides and of present or potential contamination including man-made actinide elements in the environment. The actinide elements and isotopes considered are the natural ones, with Th and U (primordial nuclides formed in the buildup of the terrestrial matter and still present today) being the major elements at the 10^{13} ton level in the Earth's crust (Wasserburg *et al.*, 1964) and with Ac and Pa being the trace elements formed by decay of the major natural actinide isotopes. Naturally occurring Np and Pu are present at the ultratrace level generated by nuclear reactions in the environment, and are also residual traces of primordial actinides, or produced man-made, as discussed below.

Natural actinide isotopes are present in rocks or minerals, e.g. phosphates containing uranium or thorium (^{232}Th and ^{235}U, ^{238}U) (Heier and Rogers, 1963; Khater *et al.*, 2001). The minor components (^{227}Ac, ^{228}Ac, ^{227}Th, ^{228}Th, ^{230}Th, ^{231}Th, ^{234}Th, ^{231}Pa, ^{234m}Pa, ^{234}U) are produced by decay of the major actinide isotopes (e.g. Murray *et al.*, 1987; Arslanov *et al.*, 1989). Natural ^{236}U has been detected at an atomic ratio, ^{236}U/^{238}U, of 6×10^{-10} in uranium deposits such as at the Cigar Lake, Saskatchewan, Canada (Zhao *et al.*, 1994). It may be generated by neutron capture on ^{235}U. Similarly, a long-lived actinide such as ^{237}Np was found in ultratrace levels (^{237}Np/^{238}U: 2×10^{-12}) in uranium ores from Katanga (Myers and Lindner, 1971). Ultratrace components such as ^{239}Np or ^{239}Pu are also generated by neutron capture (Curtis *et al.*, 1987; Barth *et al.*, 1994), with typical concentrations in the order of 10^{-12} g Pu per gram sample

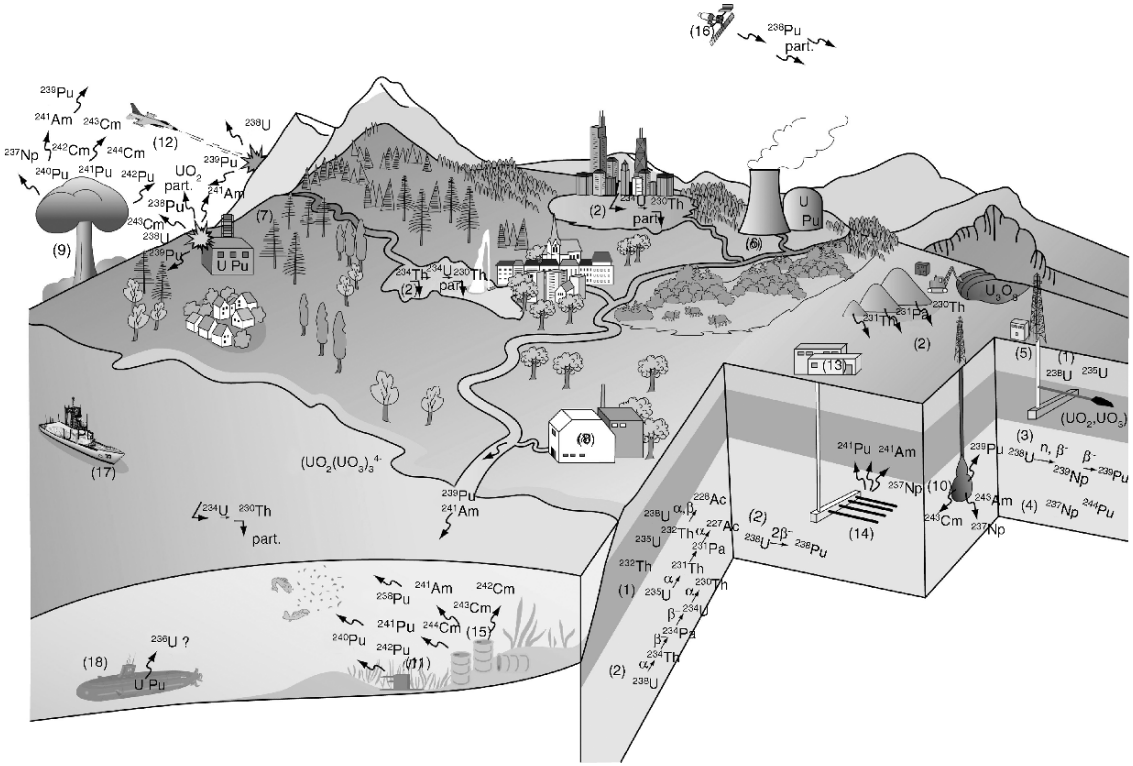

Fig. 27.1 *Natural and anthropogenic actinide species in the environment.* (1) *Natural major actinides,* (2) *minor actinides,* (3) *actinides at the ultratrace level generated from the majors by neutron capture in environment,* (4) *actinides of primordial origin,* (5) *natural actinide contamination around uranium mining and milling plants. Anthropogenic actinides:* (6) *released intentionally below legal norms from nuclear power plants,* (7) *by accident, or* (8) *reprocessing facilities. Actinides released from military activities, e.g. weapons production:* (9) *atmospheric tests,* (10) *underground detonations, or* (11) *objects from nuclear naval vessels, or* (12) *depleted uranium warheads. Waste management activities:* (13) *intermediate or* (14) *geologic and* (15) *oceanic disposal. Unexpected events from nuclear power sources, e.g.* (16) *satellite reentry in atmosphere,* (17) *nuclear icebreaker, or* (18) *nuclear submarine sinking; 'part' stands for colloidal particles.*

in pitchblende, 10^{-14} g Pu per gram U ore, and maximum concentrations in the order of 5×10^{-15} g Pu per gram lava (Hawaiian), 10^{-15} to $3 \times 10^{—17}$ g Pu per gram granite (Kontinentales Tiefbohrprogramm). ^{244}Pu, which was found in a rare earth mineral to the extent of 1 part per 10^{18}, is likely to have been produced during Earth formation (Hoffman *et al.*, 1971). As identification techniques become increasingly sensitive, it may be possible that specific isotopes such as heavy curium isotopes may be found at the ultratrace level as natural components as it was targeted in a study about supernova producing long-living radionuclides in terrestrial archives (Wallner *et al.*, 2000).

The specific case of the natural fossil reactors in the Oklo region (e.g. Oklo, Oklobonde, Bagombe), which underwent spontaneous chain neutronic reaction some 2×10^9 years ago, was studied extensively and revealed the buildup of large quantities of transuranium elements during chain reactions. However, most of them have now decayed. Natural plutonium has been produced and has remained in the environment even before it was produced artificially. It remains the heaviest natural element found in the environment at the level of milligrams per 100 tons of uranium ore residues (Peppard *et al.*, 1951).

Artificial or anthropogenic actinides are those generated by civilian and military activities. Actinide isotopes that have been artificially produced in significant amounts are ^{233}Pa, ^{233}U, ^{236}U, ^{237}Np, ^{238}Pu, ^{239}Pu, ^{240}Pu, ^{241}Pu, ^{242}Pu, ^{241}Am, ^{243}Am, ^{242}Cm, ^{243}Cm, and ^{244}Cm (Mitchell *et al.*, 1995b; Lujaniene *et al.*, 1999), with about 2000 tons Pu produced until now, which some groups would like to reuse in a very pragmatic way (Degueldre and Paratte, 1999). The amount of artificially produced actinides is larger than that occurring naturally. Actinide isotopes such as ^{239}Np and ^{239}Pu belong to both classes and are qualified as natural or anthropogenic according to their origin. Recently, attention has also been drawn to depleted uranium and its use in projectiles. Its dispersal in the environment has been the subject of investigations with regard to its toxic potential.

Natural processes typically disperse, transport, and dilute contaminants. Some local geophysical, hydrochemical, or bioorganic processes can concentrate them. Usually, however, atmospheric flow transports particulate contaminants through the atmosphere or the stratosphere. Water flows allow contaminants to migrate to the geosphere or at its surface. In these systems, naturally occurring actinides may be used as tracers to estimate element residence time in particulate form in air or in water systems. For example, ^{234}Th is used as a natural marker to study particles in Lake Michigan (Nelson and Metta, 1983) or Lake Geneva (Dominik *et al.*, 1989). Similarly, Th isotopes may be used to investigate their scavenging by colloidal mechanisms in seawater (Baskaran *et al.*, 1992). Similar studies may be applied to study actinides in particulate phases, or aerosols, in the atmosphere (Salbu, 2001). The naturally occurring actinides U and Th, as well as Ra, may be utilized in studies of paleoclimate, dating old groundwaters, rock–water interaction processes (Ivanovich, 1994), and geochronology systems (Balescu *et al.*, 1997), using

$^{234}U/^{238}U$ or $^{230}Th/^{234}U$ ratios. Anthropogenic actinides may also be used as markers; for example, the use of $^{239+240}Pu$ to replace ^{137}Cs as an erosion tracer in agricultural landscapes contaminated with the Chernobyl fallout (Schimmack *et al.*, 2001) was recently suggested.

Actinides from human activities have also been occasionally released into the environment. The potential of contamination begins at the uranium mine with tailings and the problems associated with, for example, the release of U and Th, and their daughter products (e.g. Winkelmann *et al.*, 2001); hazards continue all along the nuclear fuel cycle with research, commercial, or military activities and the potential for real spread and contaminations of the environment, as for example, the Irish Sea, Semipalatinsk, and Maralinga (Kim *et al.*, 1992; Cooper *et al.*, 1994; Kazachevskiy *et al.*, 1998), due to commercial or military activities or accidental events. Actinides may be dispersed, at restricted levels and below legal limits, from electric power utilities during operations (Mátel *et al.*, 1993), or may be instantaneously dispersed in large doses, for example, as a consequence of an accident involving a reactor (Holm *et al.*, 1992), an aircraft carrying nuclear weapons (Mitchell *et al.*, 1995a; Rubio Montero and Martin Sánchez, 2001a,b), or during nuclear bomb testing (Wolf *et al.*, 1997; Kudo, 1998). These actinide releases contaminate the environment, such as desert (Church *et al.*, 2000) or forest soil, but contaminate flora specimens such as mushrooms insignificantly (Mietelski *et al.*, 1993). However, diluted in water, actinides undergo bioaccumulation, e.g. in a marine environment (Baxter *et al.*, 1995), within phytoplankton and macro algae (Holm and Fukai, 1986), crustacean (Swift and Nicholson, 2001a,b), and fish (Skwarzec *et al.*, 2001). The reentry of a satellite equipped with a ^{238}Pu power source in the atmosphere and its disintegration through the stratosphere has been a source of contamination. In the ocean the leakage of objects from naval reactor pressure vessels in submarines (Mount *et al.*, 1995) or waste dumping on the seabed (Rastogi and Sjoeblom, 1999) are also potential sources of actinide contamination. In the geosphere, contaminants may affect the saturated or the unsaturated zones (Penrose *et al.*, 1990). All these cases schematized in Fig. 27.1 depict situations for which actinides are present as a main or a diluted phase. They also may be in a 'dissolved' state or present as colloidal particles in the liquid or gas environment. Consequently, the analytical techniques used range from major component quantitative analysis to detection at the ultratrace level. The analytical methods used to identify and characterize, i.e. provide speciation information for the actinides, must be efficient, accurate, very sensitive, and able to provide information on the chemical characterization of the environment of the actinide. This allows the reconstruction of the history of the actinide-loaded phases and consequently the prediction of actinide behavior in the environment to be made. For example, an oxide phase produced at low temperature will dissolve faster in water than a high-temperature oxide phase. Size distribution of these particles is a relevant parameter to estimate dissolution or transport behavior.

Before analysis, sampling and/or sample treatment, with separation if needed, must be utilized when the analytical technique is not applied *in situ*.The investigated analytical techniques are classified according to the interaction (if any) between irradiation particles or reagent and the analyzed sample, and for the signal detected or recorded (see Table 27.1). For passive techniques, excitations are absent. For interactive techniques, irradiations or reagent additions are made with phonons, photons, electrons, neutrons, or ions with a known energy, flux, chemical affinity, or mass. The irradiation or injection is done locally while the reception may be carried out in a given space at a given angle from the stimuli direction or the incident beam, instantaneously or after a certain time after irradiation. The detection tools are spectroscopy (S), microscopy (M), or radiography (RAD) instruments. The reaction takes place within or without a specific field such as electrical and magnetic flow or mechanical acceleration. The detected signal may be the same in nature as the incident one, with the same energy, or a signal with lower energy, with particles being phonons, photons, electrons, neutrons, or ions. In addition to these analytical tools or techniques, neutral species such as atoms or molecules may also be used to interrogate the material. They are treated in this chapter as ions (from a mass point of view). The techniques are classified according to increasing energy of reagents or incident particles. The combination of all excitation or reagent addition and reception or product detections makes the analytic potential very rich for identification of elements or isotopes, quantitative determination, and spatial speciation in a broad way.

The sensitivity κ (units of $M \cdot au^{-1}$, with M: $mol \cdot L^{-1}$, and au: arbitrary unit), and detection limit DL of the concentration C(M) of isotope, element, or species, or their amount N(mol) must be discussed at both theoretical and experimental levels. From the experimental side these concentration and amount limits are given by:

$$C_{DL} = 3\sigma\kappa \tag{27.1}$$

$$N_{DL} = V_{min} C_{DL} \tag{27.2}$$

where σ(au) is the standard deviation of the limiting noise and V_{min}(L) is the minimum volume that can be analyzed (e.g. 1 mL). From the theoretical side, a detection limit may be evaluated from the physical–chemical process and from the performance of the analytical unit, while it remains usually an experimental limit.

For all analyses, sample volume, mass, or amount, the flux of the reagent, the size of the analyzed part of the sample, and the acquisition time or time of analysis are key parameters linked to the detection limit. The nature and origin of the environmental sample dictate the size of the sample. However, the size of the sample is also coupled with the analytical technique for which time and detection limits (DLs) are key parameters for its application. DL is a function of the number

Table 27.1 *Analytical techniques including excitation (if any) and detection for isotope, element, or species characterization (see list of abbreviations in the glossary). Note: excitation or detection is performed with phonons, photons, electrons, neutrons, ions (or atoms or molecules) considering the particles (plain, solvated, or cluster) or their associated waves.*

Detection / *Excitation*	*Phonon*	*Photon*	*Electron*	*Neutron*	*Ion*
–	–	XS, γS, MBES	EHE, RAD, LSC, βS	NS	GRAV, ISE RAD, LSC, αS
Phonon	SR, aAFM	–	–	–	–
Photon	LIPAS, (LIPDS), LIBD	IRFT, DRS, AAS NIR-VIS-UVS, COL, RAMS TRLITS, PHOS, PCS, XAS, XRF, TOM, PHOTA	UPS, XPS, SEXAS	NPHOT	TIMS, RIMS, LAMMA, LAICPMS
Electron	SEAM	EDS, EMPA	eAFM, SEM, TEM, AES, EELS	–	DPP, DPV, COUL, ESMS, SSMS
Neutron	–	NAA	NAA	DNAA	NAA, RAD
Ion	–	ICPOES, PIXE, PIGE	–	NRA	VOL, AFM ICPMS, SIMS, AMS, RBS, ERDA, NRA

of actinide atoms, the volume of the sample, the subsample excitation conditions (see Section 27.2), and the acquisition quality of the detector, and interferences such as quenching or peak overlapping. It may, however, be desirable to split the speciation range according to 'macro concentration' $> 10^{-6}$ M $>$ 'trace concentration'. Analysis may be performed in-line, on-line, on a flow bypass with direct detection of activity, for example, or at-line with intermediate samples, or off-line with the transfer of the sample in the laboratory. The analysis may be carried out *in situ*, for example using an atmospheric balloon, or in an underground rock laboratory in the considered phase, or *ex situ* with transfer of the sample and separation. To complete the picture it must be mentioned that separation techniques such as filtration, centrifugation, diffusion, electrodiffusion, electroplating, partitioning (liquid–liquid or solid–liquid) may also be applied, making the analysis more specific or efficient.

Information required such as activity (chemical, radioisotopic), amount (mass), concentration (fraction), and structures of the actinides in the studied phases have to be determined at the nuclear (pm), atomic, molecular (nm), microscopic (μm), macroscopic structural (mm), bulk scale (cm), at the component or system scale (m), or at environmental or geographic scale (km) according to the requirements of the study. Identification concerns the actinide elements and isotopes, but speciation may be understood not only at the molecular scale but also in a broader sense such as at the environmental scale. Understanding in the macroscopic scale by plain washing, leaching, or extraction tests would be a step for remediation investigations. In many types of soil the mitigation approach could be some type of soil washing to remove selectively the contaminating species (Burnett *et al.*, 1995). The selective extraction tests are also discussed in this chapter; the phases are, however, analyzed using the techniques discussed below.

Passive and active analytical methods will be reviewed (Table 27.1) through Sections 27.2 and 27.3, with examples of their utilization in transmission, injection diffusion, or reflective modes. The sampling area, beam size, and reagent quantities are macroscopic, microscopic, or nanoscopic in nature, while spatial–temporal conditions make excitation vs detection direction through solid angle, with synchronous detection or with temporal delay, possible. In Section 27.4, combinations of techniques are discussed. For example, seismic reflection (SR), which cannot be used by itself for identifying thorium or uranium, can be used in combination with other techniques as a prospecting tool. Atomic force microscopy (AFM) morphological studies also provide useful information; however, they must be complemented with other technique results to provide the required identification result (e.g. Walther, 2003). Similarly, *Eh* electrode (EHE) measurements may contribute to the speciation of redox-sensitive actinides such as U, Np, or Pu in waters. They are, however, generally completed by spectroscopic investigations. Chromatography, which is basically a separation technique, must be combined with detectors and is also studied in this chapter.

Separation of elements of interest, which are later analyzed by different analytical techniques, is an important prerequisite of any analytical method, as discussed in Section 27.2. The analytical procedure typically includes sampling or sample preparation (e.g. decomposition), separation, and/or enrichment before analysis in either a passive or an interactive way.

27.2 SAMPLING, HANDLING, TREATMENT, AND SEPARATION

In environmental systems, actinides may sometimes be analyzed on site. This requires a probe or detector installation *in situ* and direct detection or measurement of actinide concentration, activity, or amount. This is an ideal case. Because of interferences, low levels of concentrations, or difficulties in transporting the analytical unit, sampling is generally the best solution, with transfer of samples or subsamples to the laboratory for further analysis. The sampling and sample handling are performed taking into account (Salbu, 2000):

- representative samples and fractionation of samples,
- treatment *in situ*, at-site, or shortly after sampling, and
- dilution or pre-concentration, and chemical yield (efficiency of handling).

Sampling, pretreatment, shipment to laboratory, and analysis are areas where contaminations, losses, or speciation changes can occur (Harvey *et al.*, 1987). Corrections for these artifacts must be applied by using isotopic tracers or specific handling conditions.

27.2.1 Sample and data collection of compounds

The two main strategies are either to make measurements on site without sampling and adapting the probe *in situ* or to collect samples and then perform the analysis *ex situ*, as discussed below.

Sample amounts and collection techniques are dependent on the nature of the sample and on its actinide content. Samples with high actinide contents do not generally need enrichment phases, while very dilute actinide samples may require treatment, enrichment, and other time-consuming protocols. The strategy may be very different for fluids (such as air or water) than for solids (such as rock or biospecimen).

In air samples, actinides are usually present as liquid aerosols or particles since their partial pressure as gaseous species is insignificant. A particulate phase must be characterized in terms of size distribution and nature, because its behavior in the environment may be function of production mode and history, which have a direct impact on composition, nature, specific size distribution, and actinide-release properties.

In water samples, the actinides may be present as truly dissolved species, as separate particulate, and/or as colloidal phases. Here again the particle structure and size distribution must be determined to understand the actinide migration potential.

In solid samples, actinides are either present as constituents of solid solutions or as phases that are heterogeneously dispersed within the matrix phases. This is also valid for biospecimens. The sample in all cases must be preserved from degradation, contamination, or other physicochemical changes. Specific protocols such as collection under a controlled atmosphere, a preservative reagent, and storage in the dark and at a reduced temperature may be required. The larger the sample volume and the corresponding contact area of the vessel, the smaller will be the loss by sorption on the vessel wall and the shorter the storage time, and the less will be degradation of the sample by contamination or particle aggregation.

As an example, typical air sample volumes range over several hundred meters (Iwatschenko-Borho *et al.*, 1992). Rainwaters, for example, require collectors of $\sim$1 m^2 active surface, and water samples of the order of 100 L (Rubio Montero and Martin Sánchez, 2001b). Analysis of river water may also require some 100 L (Garcia *et al.*, 1996) for Pu and Am determination. Seawater sampling also requires very large volumes, processed up to 6000 L (Livingston and Cochran, 1987; Robertson, 1985), in order to achieve concentration measurements of trace level of Th, Pu, and Am isotopes. Rock samples may be as large as the 100 kg amount that was required for the detection of ^{244}Pu (Hoffmann *et al.*, 1971) in nature.

27.2.2 Sample treatment and separation

Sample preparation and separation of ions or other species of interest, which are later analyzed by different analytical techniques, are usually important prerequisite steps of any analytical method. Radiotracer techniques may be applied for each step of the separation: sample decomposition, trace–matrix separation (precipitation, ion exchanger, solvent extraction), volatilization, and other treatment without any restriction on the chemical and physical forms of sample. All these techniques may be quantitatively applied using isotope dilution, e.g. with ^{235}Np, ^{236}Pu (Bellido *et al.*, 1994), or ^{244}Pu spikes according to the specific requirements.

Air samples are generally treated in a way such that their particulate content may be collected on filters or impactors (Iwatschenko-Borho *et al.*, 1992). Aerosol analysis generally requires treatment of a very large volume of air.

Aqueous solutions are generally filtered, typically through a 0.45 μm pore membrane, followed by a series of ultrafiltration (Orlandi *et al.*, 1990; Francis *et al.*, 1998) or centrifugation (Kim *et al.*, 1997; Dominik *et al.*, 1989; Itagaki *et al.*, 1991) steps. Centrifugation requires larger instrumentation compared to filtration. This limits the use of centrifugation on site and

furthermore *in situ*. The two new samples produced are: (1) single particle or colloid cake on the collector surface, or colloid concentrate; and (2) the filtered liquid phase with its soluble content. Treatments of restricted volumes of water are required, depending on the level of contamination of the water. For example, observation of chemical speciation of plutonium was carried out after filtration of Irish Sea and western Mediterranean Sea waters (Mitchell *et al.*, 1995). The redox state distribution of ^{239,240}Pu and ^{238}Pu in these waters shows little variation with 87% as Pu(V). Pu(IV) is mostly associated with particles.

In situ dialysis has also been applied to concentrate the colloid phase associated with actinides. Extraction of an actinide from the particulate phase or from a rock sample may be carried out by applying a successive leaching technique (e.g. Szabó *et al.*, 1997; Nagao *et al.*, 1999), with reagents successively more and more aggressive such as, for example, the following:

1. water at 25°C to desorb exchangeable actinides;
2. sodium acetate at pH 5 and 25°C to dissolve carbonate phases;
3. ammonium oxalate at pH 3 and 25°C to separate reducible phases, i.e. (Fe, Mn);
4. sodium hydroxide 0.3 M at 60°C to leach actinide associated with organics;
5. hydrogen peroxide at pH 1 and 60°C to dissolve sulfide phases;
6. nitric acid 8 M at 80°C to leach mineralized phases including actinide oxides.

Each step must be characterized by a reagent, a pH value, a temperature, a sample/reagent volume or mass ratio, and a given time. Each extraction step may be repeated several times before the next extraction step in order to follow the reversibility of the desorption or leaching process (Salbu, 2000). Sequential leaching has been applied to perform speciation of uranium associated with particulates in seawater (Hirose, 1994). The major species consists of an insoluble complex that dissolves by leach test at pH 1.

Co-precipitation is usually applied as an enrichment technique of an actinide from an aqueous solution with $Fe(OH)_3$ (Morello *et al.*, 1986), LaF_3 (Nelson and Lovett, 1978), or $Ba(SO_4)$ for Ac assay on Ra (Niese, 1994), as a carrier phase, followed by dissolution and separation.

Electroplated sources are very useful for alpha spectroscopy (αS). Electroplating is the preparation of very thin and uniform actinide films obtained by electrodeposition onto stainless steel disks. The literature on electrodeposition describes the procedure (see Chapter 30), which remains empirical, perhaps because electrodeposition is a multiparametric process that includes the electrolyte solution (concentration, pH), the hydrodynamic profile in the cell, the nature and geometry of the electrodes, the deposition current and potential, and the electrodeposition time. The electrodeposition of americium was reviewed with emphasis on the physicochemical behavior of the solution (Becerril-Vilchis *et al.*, 1994). The use of a tracer may be required to evaluate losses by adsorption of the studied actinides, or a quantitative method is

followed such as the use of a hydrogen sulfate–sodium sulfate buffer (Bajo and Eikenberg, 1999). The effect of a counter-ion was also studied in detail (Zarki *et al.*, 2001). Recently, however, specific microprecipitation followed by ultrafiltration has been used as an alternative for source preparation.

The separation and/or concentration of elements or species as soluble entities may be performed by applying partitioning between two phases such as:

- liquid–liquid, with specific complexes soluble in an organic phase: e.g. 2,4-pentanedione (Haa) in toluene (Engkvist and Albinsson, 1992), thenoyltrifluoroacetone (TTA) in xylene for Np extraction (Dupleissis *et al.*, 1974), tri-*n*-octylphosphine oxide (TOPO) in toluene for Pu, Am, and Cm extraction (Kosyakov *et al.*, 1994), and solvent liquid extraction can be used for the analytical determination of actinides in urine (Harduin *et al.*, 1993);
- liquid–solid, with specific polymers: anionic or cationic, organic (Qu *et al.*, 1998) or inorganic (Kobashi *et al.*, 1988). For example, actinides from contaminated soil samples can be separated by use of anion-exchanger columns for Am, Cm, and Pu spectroscopy (Michel *et al.*, 1999), and uranium from waters may be pre-concentrated using an ion exchanger and filtered off before desorption in small aliquot acidic solution and analyzed using inductively coupled plasma optical emission spectroscopy (ICPOES) (Van Britsom *et al.*, 1995).

Chromatography is discussed in combination with detections in Section 27.4.

The separation of colloidal species may be performed by applying specific techniques such as:

- field-free techniques: ultrafiltration, gel permeation, or size exclusion chromatography (Taylor and Farrow, 1987; Hafez and Hafez, 1992), or
- within a controlled field: flow-field fractionation (Bouby *et al.*, 2002), density gradient fractionation (Mohan *et al.*, 1991), or capillary or gel electrophoresis.

The latter technique has been performed for actinide separation by applying an electrical field during liquid–solid distribution. Speciation and solubility of neptunium has been studied in an underground environment by paper electrophoresis, ion exchange, and ultrafiltration (Nagasaki *et al.*, 1988). Gradient gel electrophoresis was used to characterize 13 kDa polysaccharide ligands complexing ^{234}Th from marine organic matter (Quigley *et al.*, 2002). Capillary electrophoresis is growing in importance as a versatile assay for speciation; however, there are still major challenges that limit the practical acceptance of the technique. The potential problems are inadequate attention to sample preparation (species stability, matrix effect), ignoring possible change in speciation during electrophoresis, inappropriate treatment on method validation and system suitability, and no sample enrichment methodology. Recommendations have recently been suggested (Timerbaev, 2001).

27.3 IDENTIFICATION AND SPECIATION

27.3.1 Passive techniques

Radiometric techniques dominate the analyses of short- and medium-lived actinide nuclides. The passive techniques currently used for actinide detection are summarized in Table 27.2. They include spectroscopy (S) or RAD of X-rays or gamma photons, along with Mössbauer emission spectroscopy (MBES), conversion electrons or β^-, neutrons, and ions such as alpha or spontaneous fission products that are emitted during decay of actinide nuclides. The investigated systems range from geographic to microscopic in size and the detection tool may also be adapted to these scales. The actinide isotopes considered in the environmental studies are not β^+ emitters; they may be neutron emitters that can consequently be detected by neutron spectroscopy (NS). Nothing is reported so far for the detection of the phonons generated by the actinide decays. Ion-selective electrodes (ISEs) may be used to detect actinide elements in a passive way, while gravimetry (GRAV) may be applied for concentrated phases.

The passive techniques and more especially the radiometric techniques remain widely used for the analysis of actinides because they utilize low-cost instrumentation, are simple to operate, achieve low-cost of analysis per sample, and have the possibility to perform non-destructive sample analysis.

In X-ray spectroscopy (XS) and γ-ray spectroscopy (γS), the most important developments include the production of high-efficiency coaxial and well-type detectors operating with anti-cosmic ray or anti-Compton shielding. Detection is currently carried out using a semiconductor crystal or by scintillation. Typical analytes include natural actinides such as ^{234}Th or anthropogenic actinides with detection limits of the order of 1 mBq. Based on this activity limit, the detection limits for actinide isotope amounts are calculated for relevant isotopes in Table 27.2. Sample preparation may require classical specific treatments before radioanalysis, such as separation or enrichment, as treated in Section 27.2.

Measurements of transuranics, in particular several isotopes of plutonium, are especially difficult to carry out due to the low-penetrating nature of their radiations (α- and X-rays). Direct alpha detection is difficult; therefore thin scintillators that rely on the detection of L-shell X-rays (13–21 keV) are used for survey work (Miller, 1994). These instruments may be used for environmental detection and for X-ray astronomical measurements in space. Theoretical detection limits for thin-layer samples are given in Table 27.2. Determination of actinides in solution may also be carried out by using a high-purity germanium crystal detector, allowing for plutonium a detection limit near 10^{-10} mol (Gatti *et al.*, 1994).

Classically, ^{227}Ac may be determined in environmental samples from the beta or gamma activity of its daughter products (Khokhrin and Denisov, 1995). Gamma-ray spectroscopy was used *in situ* and in the laboratory to determine

Table 27.2 *Passive analytical techniques used for actinide isotope, element, or species identification. Detection limit (DL) in mol recalculated from DL in Bq.*

Detection	*Goal*	*Sample*	*$^{A}An(Y)$*	*Detection limit*	*Remarks*
Photon					
XS, γS, MBES, RAD	determination of isotope activity and identification of isotope	solid or liquid bulk or film	^{227}Ac	2×10^{-14}	γS, *DL*: 1 mBq
			^{230}Th, ^{232}Th	1×10^{-11}, 5×10^{-7}	
			^{231}Pa	2×10^{-14}	
			^{234} U, ^{238}U	2×10^{-11}, 2×10^{-8}	
			^{237}Np	2×10^{-12}	
			^{239} Pu, ^{240}Pu	7×10^{-12}, 1×10^{-12}	(Bojanoswki, 1987)
			^{241}Am	1×10^{-16}	(Guillot, 2001)
			^{242}Cm, ^{244}Cm	5×10^{-15}, 1×10^{-16}	
Electron					
βS, LSC, RAD	concentration or activity determination	solid film electroplated or liquid bulk scintillation	^{228}Ac	5×10^{-22}	β LSC, *DL*: 10 mBq, in 1 mL
			^{234}Th	5×10^{-20}	
			^{233}Pa	5×10^{-20}	
			U	–	
			Np	–	
			^{241}Pu	1×10^{-17}	(Yu-fu, 1990)
			Am	–	
			Cm	–	
Ion					
GRAV, ISE, αS, LSC, RAD	determination of mass or of isotope activity and identification of isotope	solid film electroplated or liquid bulk scintillation	^{227}Ac	4×10^{-18}	αS, *DL*: 10 μBq
			^{228}Th, ^{230}Th, ^{232}Th	1×10^{-21}, 6×10^{-17}, 1×10^{-11}.	
			^{231}Pa	2×10^{-17}	
			^{234}U, ^{235}U, ^{238}U	2×10^{-21}, 4×10^{-17}, 3×10^{-11}	
			^{237}Np	2×10^{-15}	(Bojanoswki, 1987)
			^{238}Pu, ^{239}Pu, ^{240}Pu	7×10^{-20}, 2×10^{-17}, 5×10^{-18}	(Yu-fu, 1990)
			^{241}Am	3×10^{-19}	(Degueldre, 1994)
			^{242}Cm, ^{248}Cm	3×10^{-22}, 10^{-20}	

^{228}Ac activities in eight sites around the proposed Yucca Mountain repository in Nevada (Benke and Kearfott, 1997). The *in situ* determined specific activities were consistently within the ±15% of the laboratory soil sample results. Despite the good correlation between field and laboratory results, *in situ* counting with calibrated detector was recommended.

Gamma-ray spectroscopy has been systematically used to detect ^{232}Th or ^{238}U from environmental samples. The detection of these isotopes may be done using gamma photons from daughter nuclides. *In situ* determination of uranium in surface soil was performed by gamma spectroscopy measuring ^{234}Th and ^{234m}Pa using a high-resolution γ-ray spectrometer and assuming secular equilibrium (Miller *et al*., 1994). On the other hand, uranium and thorium were also detected in soil samples by measuring ^{208}Tl and ^{214}Bi (LaBreque, 1994), respectively, which were as well assumed to be in secular equilibrium with their respective parents. The determination of the specific activity of these major natural actinides may be carried out by airborne gamma spectroscopy using the above key nuclides, or other nuclides, e.g. U by Ra (Kerbelov and Rangelov, 1997). This method enables analysis during fixed-wing aircraft or helicopter flight (Guillot, 2001). The sensitivity of the spectral analysis of windows at 2615 and 1764 keV for ^{232}Th (by ^{208}Tl) and ^{238}U (by ^{214}Bi), respectively, was optimized by subtraction of the Compton continuum in the detection window. The detection of ^{232}Th and ^{238}U is possible in their natural background of 33 Bq kg^{-1} in a large-volume NaI detector (16 L) and a short sampling time (1–5 s) at 40 m ground clearance. The calculation of the concentrations is then simple and reliable. A quantitative estimate of radioactive anomalies can also be obtained easily. The spectral profile analysis is of great interest and has been applied within the framework of environmental monitoring studies. Fig. 27.2(a) shows a map obtained for ^{232}Th during a mapping exercise. Similarly, aerial measurements above uranium mining and milling area have also been reported (Winkelmann *et al.*, 2001).

A gamma-logging (γS) probe has been used to monitor thorium and uranium as a function of depth in a borehole (Nagra, 1991; Mwenifumbo and Kjarsgaard, 1999), as presented in Fig. 27.2(b). The technique is used for uranium exploration; it discriminates between valuable uranium ore and other radioactive material of little value. Here again, lateral resolution is linked to detector geometry and improvements, e.g. coaxial logging cables are suggested (Conaway *et al.*, 1980). Gamma logging has been used recently in a well contaminated with plutonium (Hartman and Dresel, 1998). In addition, the use of gamma spectroscopy for identifying and measuring plutonium isotopes in contaminated soil samples has been reported (Kadyrzhonov *et al.*, 2000).

The application of marine γ-ray measurements follows similar principles. The difference from the aerial technique is that water absorbs γ-rays rather strongly and that the detector must move at the surface of the seabed while being towed. The emitters are detectable if they are present in sufficient quantities and have energies above 100 keV. Consequently, if ^{238}U and ^{232}Th are

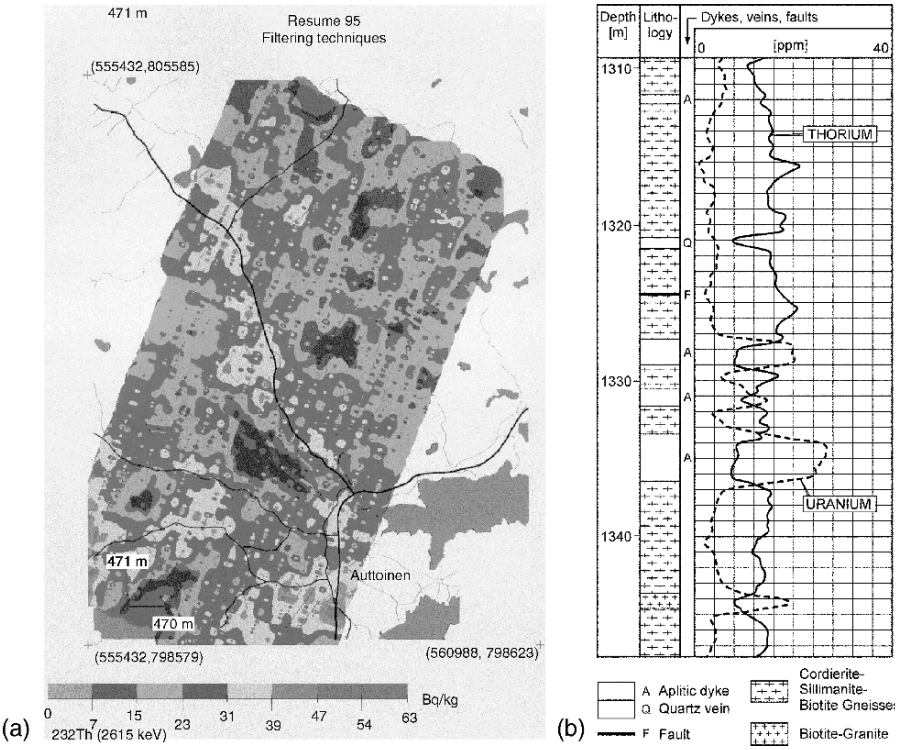

Fig. 27.2 (*a*) ^{232}*Th maps* (*from exercise in Finland, Area* 2) *processed by the filtering and window methods* (*Guillot,* 2001). (*b*) *Th and U profiles from gamma spectroscopic* (γS) *instrumental analysis in Leuggern borehole* (*north Switzerland*). *Note the uranium* (*opposite scale*) *depletion through defined faults in formation* (*Nagra,* 1991).

detectable with daughter isotopes, low-energy γ emitters such as ^{241}Am and the plutonium isotopes are very difficult to measure by applying this *in situ* technique (Jones, 2001).

The radiometric technique alone is not effective for speciation. Only MBES, a resonant emission of gamma photons, can provide information. Among the actinide isotopes, ^{231}Pa, ^{232}Th, ^{238}U, ^{237}Np, and ^{243}Am are active as the Mössbauer nucleus. While ^{237}Np is an excellent Mössbauer nuclide, little speciation has been done for environmental samples, perhaps because Mössbauer spectroscopy requires macroconcentrations.

In the field of beta spectroscopy (βS), introduction of a very low background liquid scintillation counting (LSC) spectrometer enables the analysis of soft β emitters such as ^{241}Pu with detection limits of the order of 10 mBq (Yu-fu *et al.*, 1990). This makes it possible to estimate the detection limit for beta

spectroscopy in Table 27.2. However, since the beta spectrum is continuous, application of beta spectroscopy cannot be directly used for the identification of actinides in environmental samples without the use of specific separation techniques. The counting yield of beta scintillation counting is always smaller than 100%.

NS can be applied in a plain counting mode to detect spontaneously fissile actinides in the environment and in the framework of trafficking. Plutonium-239 is hard to detect by means of its α-, x-, or γ-rays, but neutrons are more penetrating and can be specifically detected. Recently, sensitive neutron detectors including ^{3}He proportional counter tubes moderator and integrated electronic have been developed to detect ^{239}Pu down to the gram (5×10^{-3} mol) level at 20 cm in 5 s (Klett, 1999).

GRAV belongs to the last class of passive techniques. Actinide GRAV, e.g. from ore samples, may be carried out after dissolution and separation with, for example, oxalate or oxinates at pH 5–9. Uranium in neutral conditions gives a red precipitate with oxine, $UO_2(C_9H_6NO)_2 \cdot (C_9H_7NO)$ (Hecht and Reich-Rohrwig, 1929), which should be washed with oxine solution (Claassen and Vissen, 1946). However, this technique suffers from a lack of specificity.

ISEs belong to the class of electron detection passive tools for species analysis, and while the hydrated electrons themselves are not detected, the electronic exchange remains the driving force. Poly(vinyl chloride) matrix membrane uranyl ion-sensitive electrodes based on organophosphorous sensors were successfully tested (Moody *et al.*, 1988). Recently, multi-sensors were developed for the determination of Fe(II), Fe(III), U(VI), and U(IV) in complex solutions (Legin *et al.*, 1999). Twenty-nine different sensors (selective electrodes) with various solid-state crystalline and vitreous materials with enhanced electronic conductivity and redox and ionic cross-sensitivity have been incorporated into the sensor array. The system was tested for Fe(II) and Fe(III) concentrations in the range 10^{-7} to 10^{-4} M, as well as for U(VI) and U(IV), the latter being determined with a precision of 10–40%, depending on the concentration. The developed multi-sensor system could be applied in the future for the analysis of mining and borehole waters, and other contaminated natural media; it can include on-site measurements.

For alpha spectroscopy, the high-resolution silicon detectors have proved to be sensitive down to 10 μBq levels for analysis of both natural Th and U isotopes and daughter nuclides, as well as for the anthropogenic actinides. The isotope ^{227}Ac was quantitatively determined in environmental samples after sample treatment and electrodeposition: a first alpha count at 4.85–4.95 MeV for the 1.38% alpha decay of ^{227}Ac and a second at 5.5–6.1 MeV after ^{227}Th buildup to equilibrium (Bojanowski *et al.*, 1987) were obtained. After sample treatment ^{232}Th and ^{238}U from environmental samples are better characterized by alpha spectroscopy than by gamma spectroscopy as, for example, in urine analysis (Eikenberg *et al.*, 1999) (Fig. 27.3(a)). Natural (U, Th) and anthropogenic (Pu, Am) actinides were, for example, determined and their

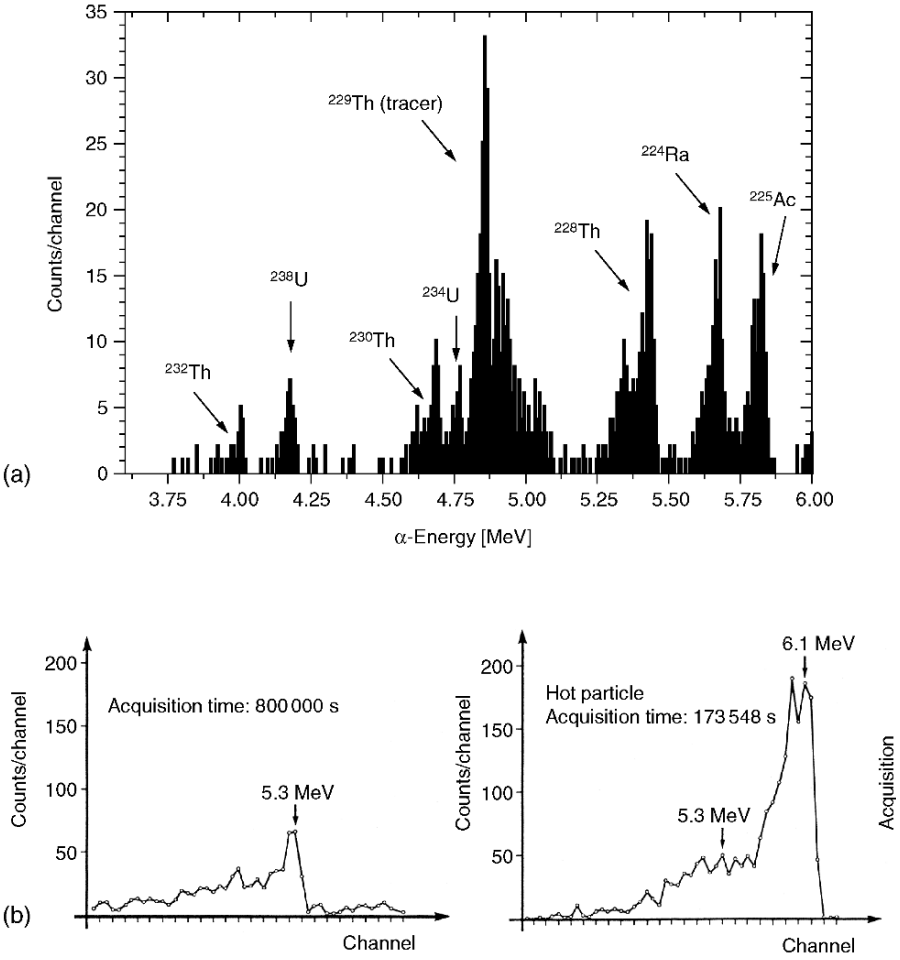

Fig. 27.3 (*a*) *An alpha spectrum of naturally occurring nuclides in urine with an added* ^{229}*Th spike for determination of the chemical recovery of Th. At high energy, the peaks of* ^{224}*Ra and* ^{225}*Ac are daughter products of* ^{228}*Th and* ^{229}*Th, respectively. Isotopes of U are also present because the fast procedure for actinide extraction does not separate between Th and U* (*Eikenberg* et al., 1999). (*b*) *Alpha spectrum obtained for an air filter;* ^{242}*Cm is identified at* 6.1 MeV*; the sampling was* 960 m^3 *air through a* 154 cm^2 *filter, without hot spot and with a hot spot* (0.03 Bq α, ~10^{-21} mol ^{242}*Cm*), *note the* 5.3 MeV *peak is due to natural* ^{210}*Po* (*Gäggeler* et al.,1986).

speciation determined in Venice canal sediment samples (Testa *et al.*, 1999). Here sequential extraction was applied before extraction chromatography, followed by electroplating and alpha spectroscopy. Pu and Am were found at the 1.0 and 0.3 Bq kg^{-1} level, respectively, with a ^{241}Am/$^{239+240}$Pu ratio of 0.3,

while Th and U were at the 20 and 30 Bq kg^{-1} levels. These isotopic analyses show that the sediments were not affected by the Chernobyl fallout but have been contaminated by nuclear weapon test fallout.

An activity may be measured after separation of the sample on a membrane after filtration or ultrafiltration. This may be applied for electrolytic fluids, solutions, or gas. Activity measurements on size-fractionated aerosols indicate different transport mechanisms for I and Ru, Cs (gaseous), or actinides (particulate) released during the Chernobyl accident. A hot particle found by autoradiography on an air filter sample was measured with a surface barrier detector (Gäggeler *et al.*, 1986). Its alpha activity was identified to be mainly due to ^{242}Cm (Fig. 27.3(b)).

Alpha LSC is attractive because it offers a nearly 4π geometry and because the counting yield for an actinide α emitter is about 100%, but with a lower energy resolution than for alpha spectroscopy. Improvements for alpha energy resolution and background reduction are key needs. An improvement of alpha energy resolution for determining low-level plutonium has been achieved using combined solvent extraction low-level liquid scintillation counter (Yu-fu *et al.*, 1990) and can also be applied for $^{239+40}$Pu and ^{241}Pu activity measurements in seawater (Irish Sea and North Sea) and soils (Cumbria and Belorussia) (Yu-fu *et al.*, 1990). Resolution of the order of 275 keV for liquid scintillation spectra can be achieved, which allows low-level determination of plutonium (see Fig. 27.4(a)).

Autoradiography (RAD) consists of using a photographic film or an organic-sensitive polymer to record tracks induced by the decay products from hot spots or contaminated phases in seawater, sediments, or marine organisms (Wong, 1971; Baxter *et al.*, 1995) (e.g. Fig. 27.4(b)) or, for example, natural rock samples sorbed with uranium and americium (Smyth *et al.*, 1980). After development, quantification of the tracks can be performed by counting the tracks or using a densitometer. Extensive work has also been performed with rock samples contacted with actinide solutions or simply contaminated (e.g. Fig. 27.4(c)). ^{241}Am and ^{233}U sorbed onto the rock cause tracks in the autoradiographic emulsions, which may be revealed and observed with an optical microscope. Direct detection with a grid detector and an image reconstruction of the source can also be carried out (Ward *et al.*, 1998).

In all passive techniques, geometrical parameters such as size of the system analyzed, size of the detector, and object–detector distance are key parameters, which, together with acquisition time, rule the detection limit for actinide identification.

Radon and helium contents in groundwater, rock, or soil may be analyzed as actinide by-products to identify uranium- or thorium-rich phase locations. Radon and uranium contents may be correlated (Virk, 1997). However, radon data need to be correlated with helium to yield more accurate results (Virk *et al.*, 1998). It must be noted that radon emanations and helium data are controlled not only by the uranium content of the rock and soil but also by structural zones (thrust, fault, etc.) that help in the easy migration of helium and radon from

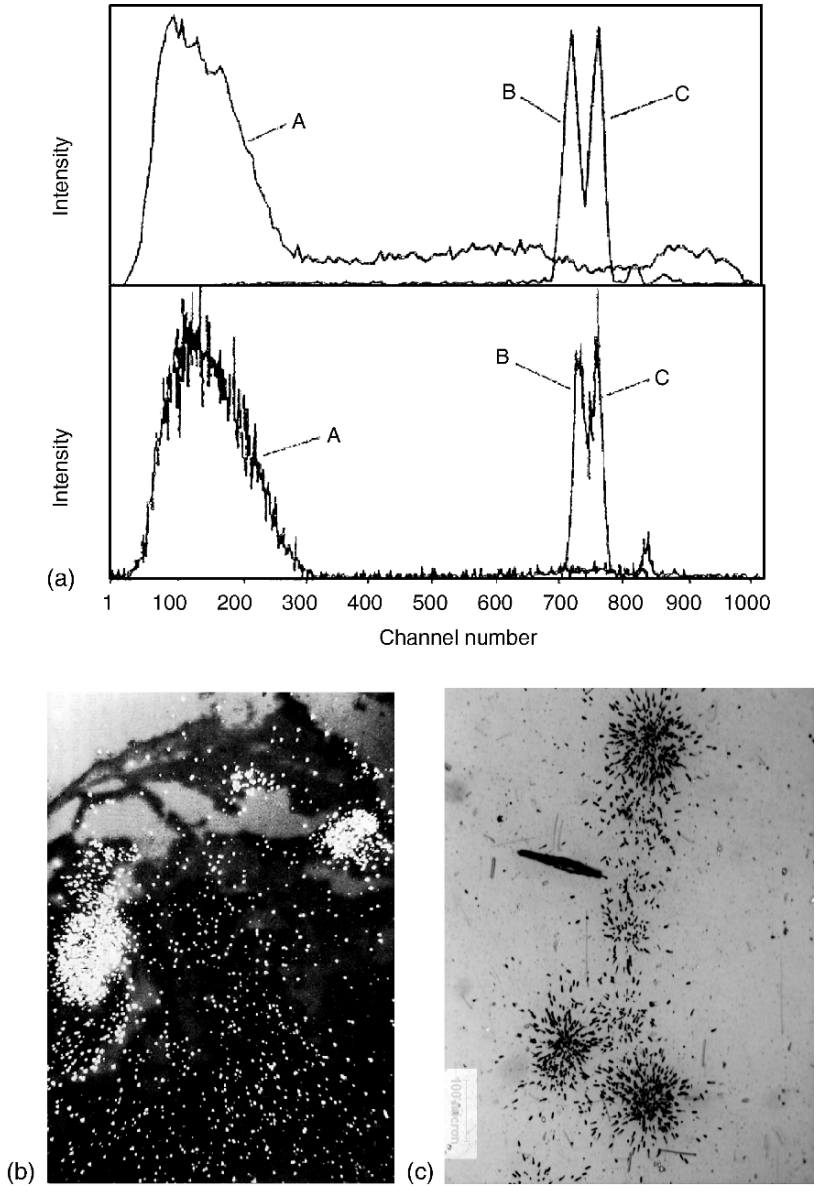

Fig. 27.4 (*a*) *Liquid scintillation counting spectrum from a soil layer, showing* (*A*) ^{241}Pu (β) *and alpha activities including both* $^{239}Pu + {}^{240}Pu$ (*B*) *and the* ^{236}Pu *tracer* (*C*) (*Yu-fu* et al., 1990). *Note that compared to alpha spectrometry, LSC resolution is lower.* (*b*) *Heterogeneous alpha-track distribution in the digestive gland of the winkle following* 13 day *uptake of* ^{239}Pu *from labeled food. A 19* day *exposure* (3 cm = 500 μm) (*Baxter* et al., 1995). (*c*) *Alpha tracks of a hot spot from the analysis of the humus layer, exposure time* 46 days*, total number of alpha tracks about* 600*, corresponding to an activity of* ~0.5 mBq (*Carbol* et al., 2003).

deeper parts of the Earth's crust. Consequently, for uranium prospection, the use of helium and radon data must be verified by combining other techniques, as discussed in Section 27.4.

27.3.2 Interactive photon–photon techniques

The techniques derived from the interaction of photons with a sample and subsequent detection and spectral analysis of photons are numerous, taking advantage of the potential of the large energy spectrum available. They are listed by increasing energy of the incident photon beam as follows: nuclear magnetic resonance (NMR), electron paramagnetic resonance (EPR), infrared Fourier transform spectroscopy (IRFT), diffuse reflection spectroscopy (DRS), near-infrared and visible spectroscopy (NIR-VIS), or spectrophotometry, or colorimetry (COL), Raman spectroscopy (RAMS), atomic absorption spectroscopy (AAS), laser ablation inductively coupled plasma optical emission spectroscopy (LAICPOES), time-resolved laser-induced fluorescence spectroscopy (TRLIFS), phosphometry (PHOS), ultraviolet spectroscopy (UVS), X-ray absorption spectroscopy (XAS), X-ray fluorescence spectroscopy (XRF), X-ray tomography (TOM), Mössbauer absorption spectroscopy (MBAS), and photoactivation (PHOTA). Table 27.3 depicts the way in which these techniques may be used in spatial (transmission, reflection) and temporal (with or without delay) modes when applied to actinide identification or speciation.

In transmission mode, single- or double-beam techniques are applied, the second technique subtracting automatically the blank. In reflection or scattering mode the axis along the detection probe forms an angle with the incident beam. In the delayed mode, detection is carried out at a specific time after excitation of the sample.

NMR is a radiofrequency spectroscopy method that utilizes the interaction of a nuclear magnetic dipole or an electric quadrupole moment with an external or internal magnetic field. Information collected from these investigations characterizes chemical atomic environments. Actinide isotopic species such as ^{229}Th(IV), ^{233}U(VI), and ^{235}U(VI) are active in NMR (Fisher, 1973) at concentration above 10^{-2} M, and for ^{231}Pa(V) and ^{237}Np(VII) above 10^{-4} M. However, very little NMR is done in actinide environmental science except using the NMR signals of actinide neighbor nuclides (^{1}H, ^{17}O,...). EPR is a spectroscopy involving the interaction of electrons in magnetic field, allowing magnetic characterization and indirectly speciation. This technique has been mostly used to study the effect of actinide decay on the magnetic properties dictated by the paramagnetic center concentration of the sample, e.g. soil matrix (Rink and Odom, 1991; Li and Li, 1997; Kadyrzhanov *et al.*, 2000).

Infrared spectroscopy (IRS) has occasionally been used for the study of actinides under environmental conditions. It has been used in the transmission mode as well as in the diffuse reflectance mode, both with and without the

Table 27.3 *Interactive analytical techniques including photon–photon for actinide isotope, element, or species characterization.*

Detection	*Goal*	*Sample*	*^{A}An (Y)*	*Detection limit*	*Remarks*
Transmitted photon					
IRS, IRFT, NIR-VIS, PCS, COL, AAS, UVS, XAS, TOM, MBAS	identification and determination of species	solid or liquid bulk, or interphases	Ac(III)	–	VIS or COL
			Th(IV)	3×10^{-8} M COL	
			Pa(V)	–	
			U(VI)	4×10^{-8} M COL	(Keil, 1981)
			Np(V)	1×10^{-7} M VIS	(Keil, 1979)
			Pu(IV–VI)	–	(Gauthier *et al.*, 1983)
			Am(III–VI)	–	
			Cm(III)	–	
Reflected scattered photon					
NMR, EPR, DRS, RAMS, PHOS, UVF, XRF	determination of species	solid bulk or liquid bulk	Ac(III)	–	XRF
			Th(IV)	–	
			Pa(IV,V)	–	
			U(IV–VI)	6×10^{-10} mol	
			Np(IV–VI)	2×10^{-9} mol	(Civici, 1997)
			Pu(IV–VI)	1×10^{-9} mol	(Akopov *et al.*, 1988)
			Am(III–V)	1×10^{-9} mol	
			Cm(III)	–	
Delayed photon					
LAICPOES, TRLIFS, PHOTA	determination of elements species or isotopes	liquid bulk or solid bulk	Ac(III)	–	TRLIFS
			$^{227–232}$Th(IV)	–	
			$^{2331–234}$Pa(V)	–	
			$^{234–238}$U(VI)	1×10^{-12} M	(Moulin *et al.*, 1991)
			^{237,239}Np(IV–VI)	1×10^{-9} M	(Stepanov, 1990)
			$^{238–244}$Pu(IV–VI)	4×10^{-8} M	(Moulin, 1995)
			^{241,243}Am(III)	4×10^{-9} M	(Beitz, 1980, 1988)
			$^{242–250}$Cm(III)	4×10^{-11} M	

application of the Fourier transform. IRS may provide useful information on the speciation of an actinide when present in relatively large concentrations. For example the complexation and reduction of uranium by lignite was determined with site-specific material (Nakashima, 1992). An alternative way to determine actinide speciation may be obtained applying RAMS. The vibrational frequencies concerned are assigned to AnO_2^{i+}, which yields a peak near 870 nm for U(VI) to 860 nm for Np(VI), 767 nm for Np(V), and 835 for Pu(VI) and for actinide concentrations above 10^{-3} M (Basile *et al.*, 1978; Maya and Begun, 1981). The speciation of uranyl in water and sorbed on a smectite (see Fig. 27.5 (a) and (b)) was investigated by Raman vibrational spectroscopy (Morris *et al.*, 1994). The uranium loading was from 0.1 to about 50% of the cation-exchange capacity. The spectral peaks varied in shape and morphology, suggesting speciation changes during the loading. RAMS may be applied at the macroscale (cubic millimeter) as well as at the microscale (cubic micrometer).

NIR-VIS of the 5f elements is a powerful technique for the characterization of oxidation state (e.g. Gauthier *et al.*, 1983) for Np and complexes (e.g. Runde *et al.*, 1997) of actinides. Molar absorptivities (ε) of actinide ions are however smaller than 500 M^{-1} cm^{-1}, limiting the detection limit of the actinide solutions to ~10^{-5} M. Consequently, for actinide ion speciation in natural waters ((An) $<10^{-6}$ M), classical NIR-VIS is not sufficiently sensitive. Addition of a specific complexing dye is required, as described in the next paragraph.

COL, which is a specific application of absorption spectroscopy, has been applied to analyze actinide ions. This technique remains a powerful one despite the emergence of new techniques. This method requires in principle addition of an absorbent specific complex before spectrochemical analysis in the domain 300–1000 nm. Arsenazo-III has been used in the past for the determination of Th and U after extraction (Keil, 1979, 1981) with DL = 7 ng·mL^{-1} (3×10^{-11} mol·mL^{-1}) and 10 ng·mL^{-1} (4×10^{-11} mol·mL^{-1}), respectively. Pyrocatechol violet (3,3′,4′-trihydroxyfuchson–2″-sulfonic acid) has been used recently in a competitive complexation to derive speciation data of uranyl with respect to orthosilicic acid (Jensen and Choppin, 1998). Silicate complexes of uranyl are derived from these tests, allowing estimate of uranyl in silica-rich groundwaters such as those found in the tuff formations in Nevada. (Hydroxy-2-disulfo-3-6-naphtylazo-1)-2 benzene arsonic acid (Thoron) was used at 540 nm for Th quantification in various waters and rocks, e.g. sand (Bhilare and Shinde, 1994). Recently, the use of coumarine azo dyes was suggested for the determination of thorium by spectrophotometry (El-Ansary *et al.*, 1998). DRS has been used to detect uranium down to 35 ng (1.5×10^{-11} mol) on gel by specific complex with 2-(5-bromo-2-pyridylazo)-5-(diethylamino)phenol (5Br-PADAP) in a 10 mL volume of solution (Ivanov *et al.*, 1995).

Actinide colloids may be characterized by photon correlation spectroscopy (PCS). This technique makes use of the light scattered from a laser beam in a colloidal suspension and of dynamic analysis of the scattered light by

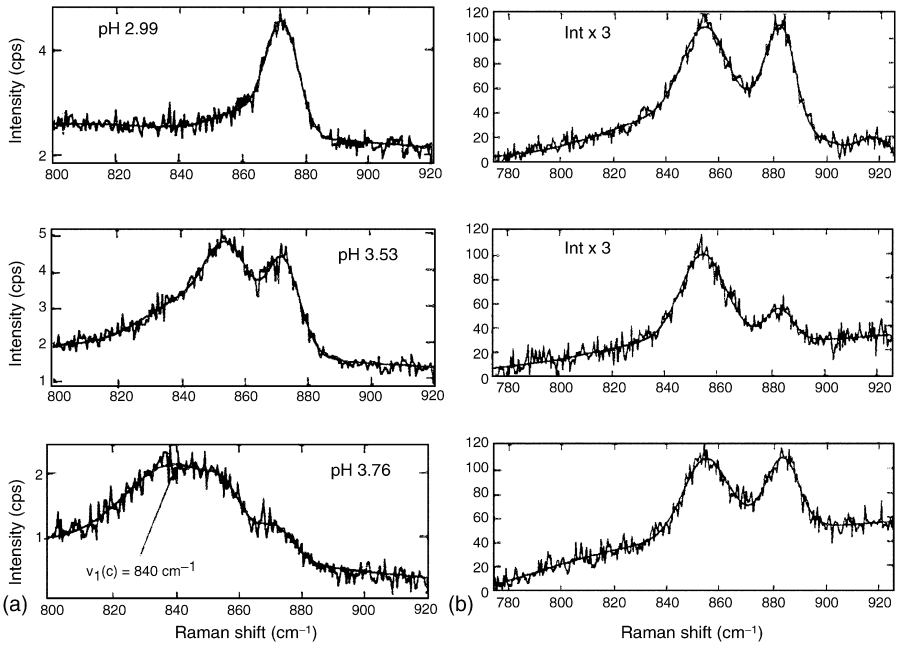

Fig. 27.5 (*a*) *Raman spectrum of U(VI) in water as function of pH, and* (*b*) *spectra of air-dried smectite samples loaded with U(VI) form uranyl solutions from alpha. Conditions: intensities are in arbitrary units, fits were obtained from combinations of Gaussian and linear terms, and spectra were generated with* 363.8 nm *Ar laser excitation* (*Morris* et al., 1994).

deconvolution. Little has been done with actinide colloids apart from analysis of their size as reported for thorium colloids (Walther, 2003) or for plutonium colloids (Triay *et al.*, 1991).

AAS is based on the metal-ion absorption of light in a flame or furnace atmosphere. AAS has occasionally been applied for uranium analysis but the detection limit is relatively high, e.g. 7 ppm in flame or 31 ppb in furnace (Goltz *et al.*, 1995).

LAICPOES applies the combination of sample vaporization by a laser ablation process followed by ICPOES (see Section 27.3.5). LAICPOES has been applied in the field in a mobile laboratory for the *in situ* determination of uranium in soil from sites suspected to contain uranium (Zamzow *et al.*, 1994). The optical emission spectroscopy (OES) detection uses the U line at 409.014 nm, with a detection limit for uranium around 5 ppm. Concentration of uranium determined for 15 sites ranged from <20 to 285 ppm. For these concentrations, uncertainty is very large (2σ: 85 ppm). It is, however, reduced

when performing the analysis in the laboratory (2σ: 10 ppm). For 10 ppm C (DL) and a 10 μm^3 crater the N(DL) is around 10^{-18} mol.

UVS may occasionally be used for actinide analysis, but has poor detection limits. It has however been used for speciation studies with Np(V) in carbonate solutions (Neck *et al.*, 1994) and with Am(III) in the micrometer range (Kim *et al.*, 1993).

Detection in a fluorescence mode improves the speciation method and allows trace analysis in liquid or solid samples. Classically, the excitation is carried out in the UV domain, around 340 nm, e.g. with a mercury lamp or with a laser, and the detection performed in the visible region, e.g. from 490 to 570 nm for U(VI), and near 600 nm for Cm(III). Although this technique may be applied to aqueous solutions, it was developed for pellet samples of fluorite salt solid solutions. Salt mixtures, e.g. NaF–LiF, as fluxes with the sample (an aliquot containing U) are melted, e.g. at 1000°C, and examined with a fluorimeter (fluorometer) after cooling at room temperature (Price *et al.*, 1953; Veselsky and Ratsimandresy, 1979). This technique, which is not limited by the interference effect of organics, is however limited by the quenching effect due to the presence of absorbing elements (e.g. Veselsky and Ratsimandresy, 1979; Veselsky and Degueldre, 1986). Structural characterization of Cm(III) on phosphate mineral surfaces was carried out using laser spectrofluorimetry (Cavellec *et al.*, 1998). This technique also allows characterizing the surface complexes of Cm on the mineral surface. Future improvements may include the use of microchip lasers and *in situ* measurements.

TRLIFS, like kinetic PHOS, applies detection temporal windows during fluorescence decay after decrease of organic impurities fluorescence. Pioneering studies demonstrated the powerfulness of this technique for actinide analysis in aqueous solutions (Beitz and Hessler, 1980; Beitz *et al.*, 1988). It is a very versatile tool to achieve speciation of actinides such as uranium and curium (see Fig. 27.6). It has been used successfully to characterize U(IV) hydroxide complexes in environmental conditions (Moulin *et al.*, 1995), occasionally doped with phosphates (Eliet *et al.*, 1995), and for uranium speciation in waters from different mining areas (Bernard *et al.*, 1998). Direct speciation of Cm(III) in natural aquatic system shows that the method is applicable at concentrations down to 7×10^{-9} M (Wimmer *et al.*, 1992) (see Fig. 27.6). The technique can also be applied to gain surface speciation information.

XAS today takes advantage of third-generation high-brilliance synchrotron radiation sources fitted with insertion devices such as wigglers and undulators. This technique has revived interest in the field of hard X-rays in macro- and microprobes. Recent developments are based on the use of Fresnel zone plates and containment techniques such as taped glass capillaries and plastic films, which allow microanalysis to be performed. Typical performance of synchrotron microprobes corresponds to a photon flux of 10^{10} $s^{-1} \cdot \mu m^{-2}$, with minimum

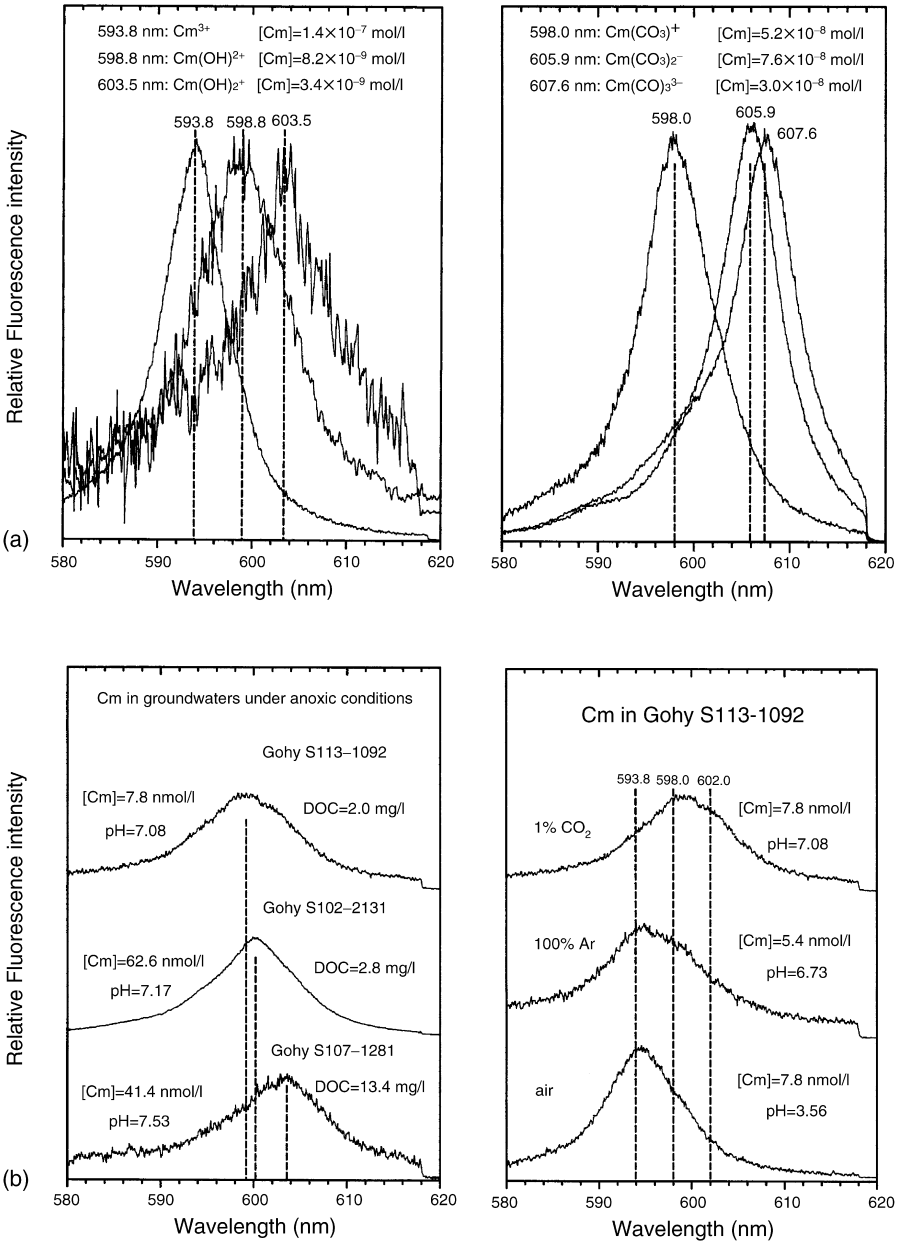

Fig. 27.6 *Time-resolved fluorescence spectrum of Cm(III) in water samples.* (*a*) *Cm in solution to identify the hydroxo and carbonato species and* (*b*) *Cm in groundwater with various dissolved organic carbon DOC concentration and pH. Conditions: the intensities are scaled to be the same height* (*Wimmer* et al., 1992).

detection limits ~10^{-15} g (~4×10^{-18} mol). Analyses are performed by X-ray absorption near-edge spectroscopy (XANES) methods to map elemental distribution and to determine the oxidation states, and extended X-ray absorption fine structure spectroscopy (EXAFS) method to determine the coordination environment of the atoms in question.

Several authors (Nitsche, 1995; Hess *et al.*, 1997; Antonio *et al.*, 2001) suggested recently the use of X-rays provided by synchrotron beams in absorption spectroscopy (XAS) as a new tool for actinide speciation in solids (soils) and liquid (waters) as well as at their interface. This technique is quasi non-destructive, element-specific (L edges for actinides), and very attractive for actinide speciation and for the definition of their atomic environment (Conradson, 1998; Degueldre *et al.*, 2004) and redox state (see Fig. 27.7). It makes use of monoenergetic beams in the range up to (100 keV, focusing a very intense beam over a small area. The micro X-ray absorption beam may be used to focus on local details, for example to better understand the sorption of uranium in soil sediments (Bertsch *et al.*, 1994). In addition, comparison of fine structure for various valence state of uranium (IV) and (VI) was for example recently reported (Hunter and Bertsch, 1998).

XRF is based on the measurement of the fluorescent characteristic radiation emitted by an element when its inner shell electrons are excited. Technically the method is applied in two different spectroscopy modes called wavelength-dispersive spectrometry (WDS) and energy-dispersive X-ray spectroscopy (EDS) modes. The energy-dispersive system is a multielemental technique that can determine the elements in a wide range of concentration from 10^{-6} to 1 $g \cdot g^{-1}$ (ppm). It is non-destructive, with minimum spectral interference. The analysis is very fast and in many cases the sample preparation requires only grinding and pelletizing. The recent use of detectors with better energy resolution down to 10 eV (superconducting tunnel junction) makes this technique even more promising. XRF is also a technique that can be applied in the field with portable units. It may be applied for mineral exploration, mining, monitoring of polluted areas, and other environmental studies.

Aerosol deposits on a filter create homogeneous and thin layers, which result in negligible matrix effects during XRF analysis. The most recent advances are the application of synchrotron-induced XRF. In water, suspended matter can be separated on a filter and analyzed by XRF. Actinides in samples like soils, sediments, rocks, minerals, fly ash, and solid waste are often detected at the 10^{-6} $g \cdot g^{-1}$ level when applying an XRF method. This technique has been applied for analysis of particles from waters, sediments, and waste phases. (see Fig. 27.8) and may also be applied for determination in biological tissues, analysis of airborne particles, and foodstuffs (Akopov *et al.*, 1988; Misaelides *et al.*, 1995; Hunter and Bertsch, 1998). Uranium can be determined in water by precipitation with a non-specific chelating reagent and collection on a filter, which is analyzed by XRF (Civici, 1997). The detection limit is 0.15 μg U (6×10^{-10} mol) or 10^{-9} mol for a 500 mL sample. It can be improved with a microbeam.

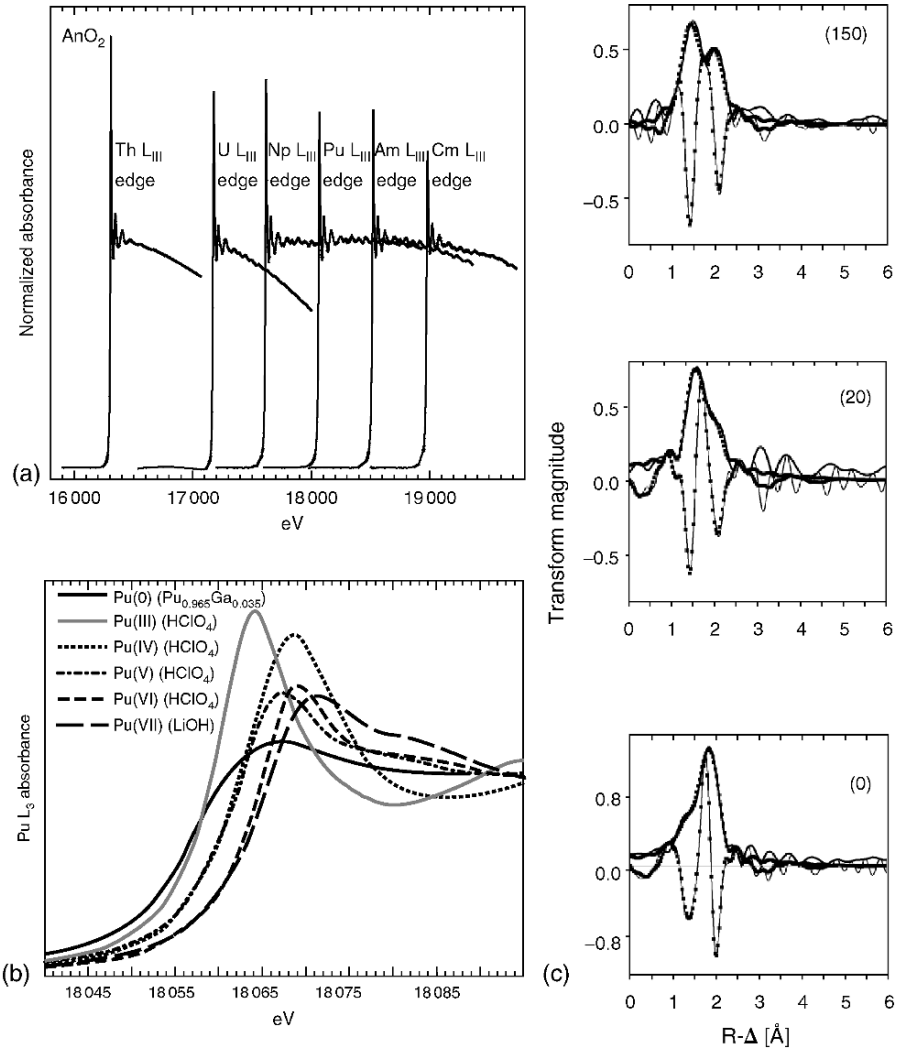

Fig. 27.7 (*a*) *Normalized L3 edge XAS spectrum of Th, U, Np, Pu, Am, and Cm from their dioxides,* (*b*) *XANES of Pu*(0), *Pu*(III), *Pu*(IV), *Pu*(V), *Pu*(VI), *and Pu*(VII) (*derived from* (*Conradson,* 1998)) *showing the shift induced by the oxidation, and* (*c*) *Np L3EXAFS magnitudes and imaginary part of the Fourier transform recorded for a Np*(IV) *acidic solution during* in situ *photooxidation of Np*(IV), *initial result compared after* 20 *and* 150 min, *note the presence of Np*(V) *formation* (*Denecke* et al., 2004).

X-ray TOM investigations have been carried out to identify and locate the spatial extension of phases. When used with dichromatic or dual-energy mode for the element discrimination, the irradiation is first performed below the element edge and then above the edge. This mode of TOM allows analyzing a specific

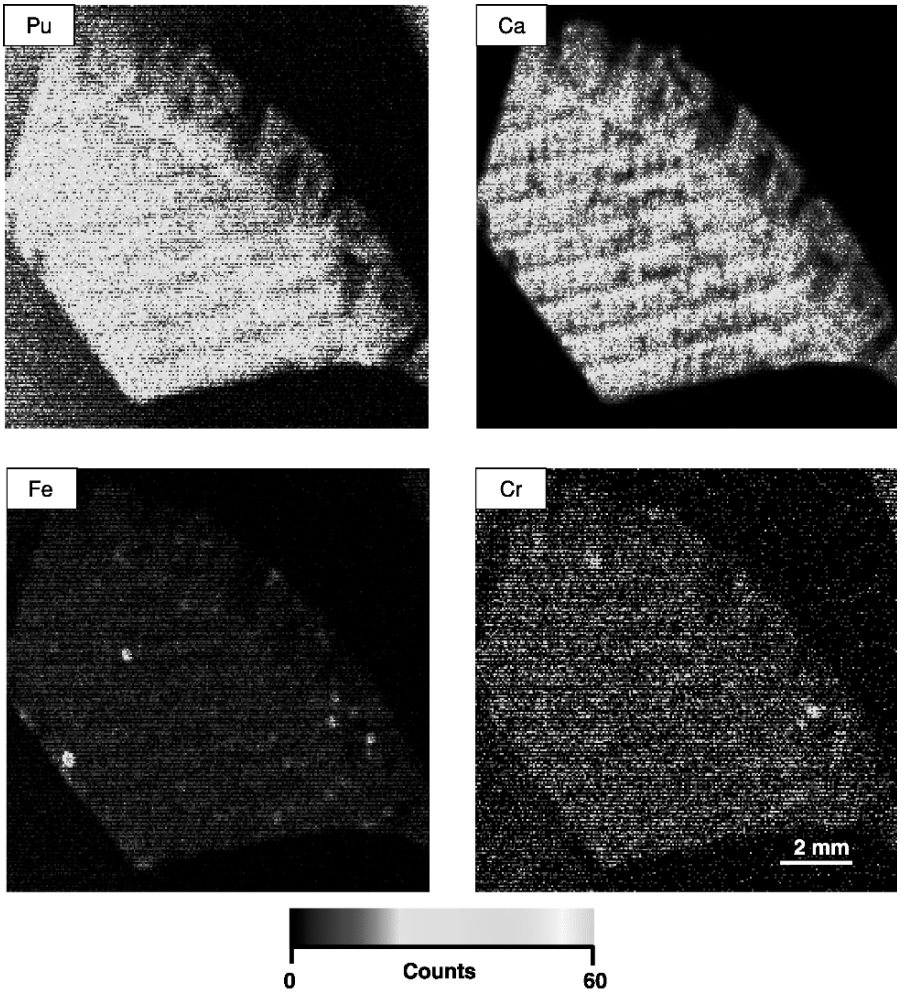

Fig. 27.8 *Micro X-ray fluorescence maps for a precipitate sample filtered from a test container showing Pu- and Sr-enriched phases. Conditions: the thermal scale represents higher concentration of the particular elements; a* 100 μm *aperture that restricts the output beam is used* (*Schoonover and Havrilla,* 1999).

element by comparing the intensity of X-ray absorption below and above the edge. Since the actinide atomic number is high, the energy of the X-ray absorption K edge is rather high too. The sample is placed on a rotation table; the beam is several millimeters in size, with photon intensity of the order of 10^8 mm^{-2} s^{-1}. The detector is a charge-coupled device (ccd) camera that records the image obtained on an X-ray converter screen. Images collected are translated into a 3D tomogram of the element considered, visualizing the element densities. Fig. 27.9 presents

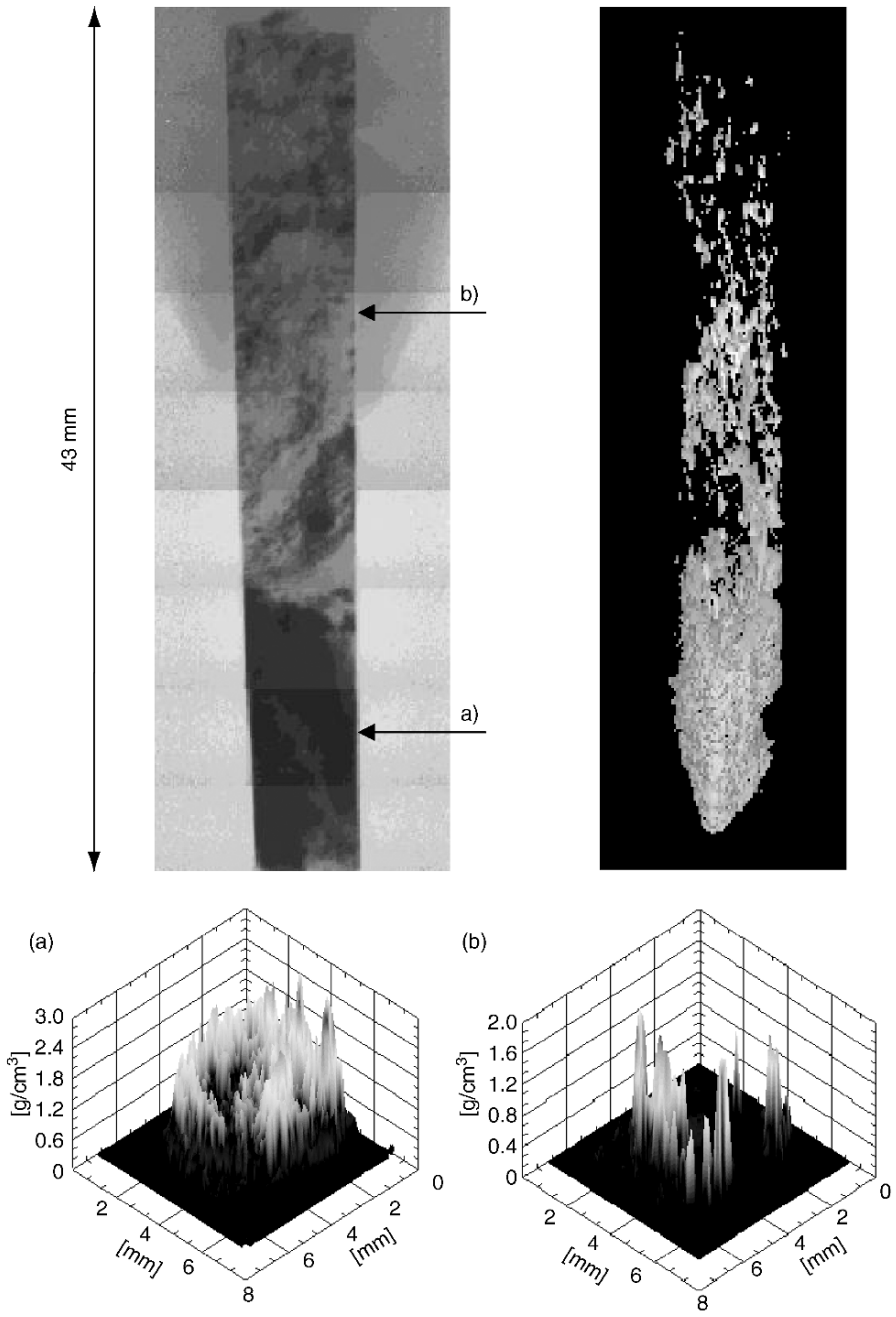

Fig. 27.9 *Single radiograph of Okelobondo* (*top left*) *sample with synchrotron radiation at* 87 keV *and iso-density surfaces* (*top right*) *showing the uranium distribution in the sample; tomograms* (*a*) *and* (*b*) *of the U phase recorded with two light energies* 114.6 *and* 116.6 keV (*Baechler* et al., 2001).

typical radiograms and tomograms obtained for a sample from Okelobondo, Oklo, Gabon (Baechler *et al.*, 2001).

MBAS is a resonant absorption of gamma photons that may be applied to provide information on several actinide isotopes: ^{231}Pa, ^{232}Th, ^{238}U, ^{237}Np, and ^{243}Am. Recently, preparation details of source and sealed absorption holders for ^{237}Np and ^{238}U Mössbauer measurements were reported (Nakada *et al.*, 1998). However, little has been done for actinide speciation of environmental samples, perhaps because this technique requires macro quantities. However, the study of the interaction of Pu(IV) and Np(IV,V,VI) with iron hydroxides has been performed by Fe Mössbauer spectroscopy in order to predict the behavior of actinides in environmental media (Grigoriev *et al.*, 2001).

PHOTA, which involves γ-ray absorption by nuclides, has not yet been used for actinide characterization so far.

27.3.3 Interactive photon–phonon, –electron, –neutron, –ion techniques

Interactive techniques implying photon irradiation and detection of other signals such as phonons, electrons, neutrons, and ions are also used to identify or analyze the actinides. The techniques described below are laser-induced photoacoustic spectroscopy (LIPAS), laser-induced thermal lensing, laser-induced photothermal displacement spectroscopy (LIPDS), laser-induced breakdown detection (LIBD), ultraviolet photoelectron spectroscopy (UPS), X-ray photoelectron spectroscopy (XPS), secondary electron X-ray absorption spectroscopy (SEXAS), laser ablation micro mass analysis (LAMMA), laser ablation inductively coupled plasma mass spectroscopy (LAICPMS), resonance-induced mass spectroscopy (RIMS), and neutron photoactivation (NPHOT), the latter being only occasionally used. They are listed in Table 27.4 on the basis of the particle detected.

Photoacoustic spectroscopy (PAS) is based on the detection of the acoustic signal during photon absorption in the system. PAS has been applied for speciation studies of uranium and transuranium species in aqueous solution as well as in precipitates. LIPAS has been adapted for the UV–VIS and NIR photon energy, as well as for the infrared, domain. The technique applies the absorption of light that creates locally a thermal shock wave, which is detected through a piezoelectric crystal using a dual-beam system (Pollard *et al.*, 1988; Klenze *et al.*, 1991). LIPAS permits identification of U, and its speciation may be performed down to 10^{-6} M. It may be used to achieve speciation of uranium ions in mill tailing water (Geispel *et al.*, 1998). This technique may be used for the speciation of uranium in solution or in precipitates (Kimura *et al.*, 1992). LIPAS has also been used to characterize plutonium species as Pu(VI) in slightly acidic solutions (Okajima *et al.*, 1991) and in neutral solutions (Neu *et al.*, 1994), as well as to generate americium colloids (Buckau *et al.*, 1986). This was carried out for various actinide speciation tests in solution that simulate environmental conditions (see Fig. 27.10). Using an optical heterodyne interferometer, the

Table 27.4 *Interactive analytical techniques including photon–phonon, –electron, or –ion for actinide isotope element or species characterization.*

Detection	*Goal*	*Sample*	*$^{A}An(Y)$*	*Detection limit*	*Remarks*
Phonon					
LIPAS, LIPDS, LIBD	speciation complexes or redox and determination	liquid bulk	Ac(III)	–	LIPAS
			Th(IV)	–	
			Pa(V)	–	(Geipel *et al.*, 1998)
			U(VI)	5×10^{-6} M	(Pollard, 1988)
			Np(V)	1×10^{-7} M	(Okajima, 1991)
			Pu(VI)	2×10^{-5} M	(Klenze and Kim, 1988)
			Am(III)	1×10^{-8} M	
			Cm(III)	–	
Electron					
UPS, XPS, SEXAS	speciation at interfaces	solid surface film	Ac(III)	–	estimated for XPS
			Th(IV)	4×10^{-11} mol	with 10 nm × 1 cm × 1 cm
			Pa(IV,V)	–	sample of density 1 g cm^{-3}
			U(IV–VI)	4×10^{-11} mol	and 1% An weight fraction
			Np(IV–VI)	–	
			Pu(IV–VI)	–	
			Am(III–V)		
			Cm(III)		
Ion					
TIMS, RIMS, LAICPMS, LAMMA	analysis of isotopes elements, chemical species	solid film or bulk nano-micro	Ac	–	RIMS, DL
			$^{227–232}$Th(IV)	3×10^{-18} mol	
			$^{2331–234}$Pa(IV,V)	–	
			$^{234–238}$U(IV–VI)	3×10^{-18} mol	
			^{237,239}Np(IV–VI)	3×10^{-18} mol	(Trautmann, 1992)
			$^{238–244}$Pu(IV–VI)	3×10^{-18} mol	(Trautmann *et al.*, 1986)
			^{241,243}Am(III–V)	3×10^{-18} mol	
			$^{242–250}$Cm(I–II)	3×10^{-18} mol	

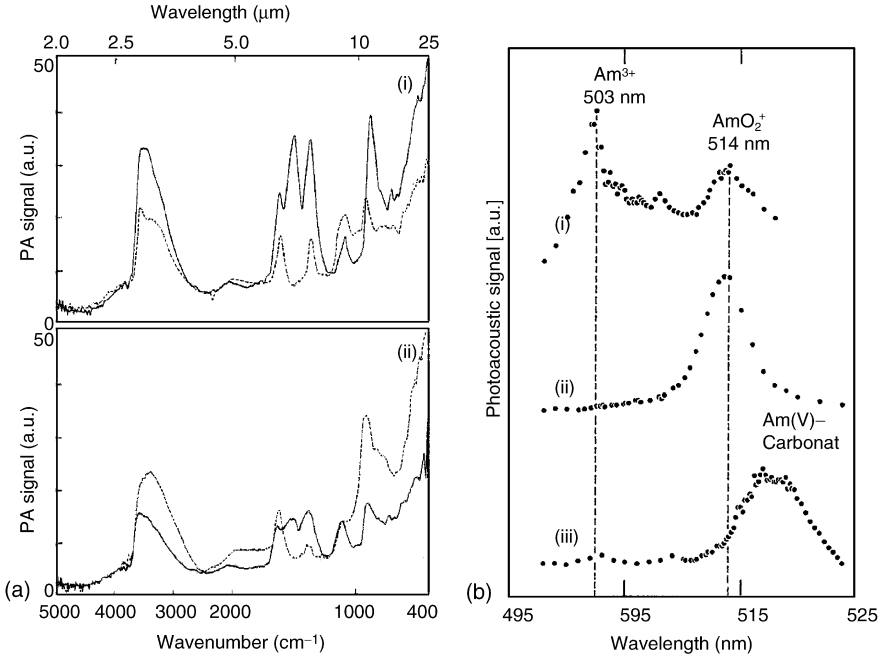

Fig. 27.10 (*a*) *IR-LIPAS spectrum of uranium precipitate* (*i*) *in* 1 M $NaHCO_3$ (*bold line*) *and* 1 M $NaClO_4$ (*broken line*) *solutions, and* (*ii*) *in* 0.05 M (*bold line*) *and* 0.02 M (*broken line*) $NaHCO_3/NaClO_4$ *solutions from* (*Kimura* et al., 1992). *Note solutions simulating groundwaters; absorption bands: OH:* 3521 *and* 1632 cm^{-1}, CO_3: 1098, 1383, *and* 1524 cm^{-1}, *OUO:* 907 cm^{-1}. (*b*) *Speciation of autoradiolytic oxidation process of Am*(III) *during the dissolution of* $Am(OH)_3(s)$ *in* 5 M *NaCl, spectrum after* (*i*) 3.6×10^{-6} M *after* 1 day *dissolution at* $pH = 8.3$, (*ii*) 10^{-4} M *after* 7 days *at* $pH = 8.3$ (*iii*) 10^{-5} M *after* 7 days *at* $pH = 10.7$ *from* (*Klenze and Kim,* 1988). *Note solutions simulating salt dome brine.*

LIPAS unit can be modified in a photothermal displacement instrument (LIPDS), which can be used for the speciation of lanthanides and actinides (Kimura *et al.*, 1998).

When the laser intensity is increased, phase breakdown occurs. Instead of a simple thermal shock, the material is atomized (breaks down). Laser-induced breakdown spectroscopy (LIBS) is used to detect colloidal particles (Gutmacher *et al.*, 1987) and allows the detection of actinide colloids or actinide-associated particles. LIBS was applied to determine the solubility product of Th(IV) colloids (Bundschuh *et al.*, 2000; Bitea *et al.*, 2003).

UPS and XPS applies to spectroscopy of electrons excited by UV or X-ray photons from samples under vacuum. UPS was not applied to environmental samples but to thin-layer actinide research only (Gouder, 1998).

XPS techniques have occasionally been used to characterize actinides associated with environmental samples. They help to understand how uranium is sorbed onto phosphate (Drot *et al.*, 1998) or calcite (Geipel *et al.*, 1997) surfaces, as well as how actinides behave in contaminated soil (Dodge *et al.*, 1995) in the presence of microbes (Francis *et al.*, 1994). In all cases XPS allows redox and spatial speciation of the actinides by the use of energy shifts. For XPS, the detection limit may be estimated as 4×10^{-11} mol for a sample of 1 cm^2 with a 10 nm thickness and a density of 1 g cm^{-3} and 1% actinide mass. This detection limit can be upgraded for microbeam units.

SEXAS could be used to study particles on filters, but nothing has been reported on actinide investigations with this technique. In this case a layer of the order of 100 nm is analyzed and the DL for a 1 to a 10 μm size XAS would be 10^{-11} to 10^{-19} mol, respectively.

Other photon–particle interactive techniques include production of neutrons or ions. Photoneutron logging (PHOTN) was discussed for uranium detection in boreholes in the frame of rock and ore analysis in their occurrence site (Burmistenko, 1986).

Thermal ionization mass spectroscopy (TIMS) applies thermal ionization by evaporating a sample from a heated metal surface and simultaneous measurement of all isotopes of an actinide, using up to nine Faraday detectors. These conditions lead to high precision of isotope ratio measurements ($\leq$0.01%). Due to isobaric interferences, a chemical separation of the interfering elements must be performed before analysis. Therefore, isotopic dilution analysis mass spectroscopy coupled with TIMS represents one of the most accurate methods for the determination of the content of actinides and their isotopic composition. TIMS is currently applied to analyze actinide isotopic composition. The analysis of ^{230}Th distribution in the waters of a North Atlantic site (Vogler *et al.*, 1998), as well as the study of the origin of initial Th from Lake Lahontan, Nevada (Lin *et al.*, 1996), was performed by TIMS. The isotopic measurements of rock samples from the Oklo uranium ore deposit (Ohnuki *et al.*, 1996), as well as a wide variety of environmental samples (Buesseler, 1989), were analyzed by TIMS. Isotope dilution can provide for concentration determination down to the 10^{-15} to 10^{-18} g (4×10^{-18} to 4×10^{-21} mol) range.

LAMMA could be used to study particles on filters or directly on solid samples, but very little has been reported on actinide investigations with this technique. As an example, LAMMA has been applied to fingerprinting coal constituents in bituminous coal. Uranium phases were detected (Lyons *et al.*, 1987). Laser desorption ionization mode of matrix-assisted laser desorption ionization (MALDI) time-of-flight mass spectrometry (TFMS) analysis of U(VI) leads to the formation of uranium oxide clusters (Soto-Guerrero *et al.*, 2001). The formation of clusters can be eliminated using selected matrices, and a more sensitive uranium determination with a detection limit down to 10^{-12} M is possible.

LAICPMS has been used for determination of elemental concentration (in ppm range) and their isotopic composition in solid samples (conducting or not

conducting). It can be done without time-consuming sample preparations. The beam diameter can vary from ~10 to 300 μm. The method allows a depth profile analysis in the range from about 10 μm to several millimeters. The inductively coupled plasma mass spectroscopy (ICPMS) technique is described and illustrated in Section 27.3.5. LAICPMS has been applied for the *in situ* determination of thorium and uranium in silicate rocks and soils (Perkins *et al.*, 1993). Powdered geological materials have been prepared both as pressed powder disks and as fused glasses. Detection limits are better than routine XRF, but comparable with instrumental neutron activation analysis (NAA). For a 10 μm^3 crater and a 1 ppm C(DL) the N(DL) would be 10^{-19} mol. Uranium was analyzed successfully by LAICPMS in various geological samples such as in Neo-Proterozoic or older zircons or baddeleyite with U contents $\geq$65–270 ppm (Horn *et al.*, 2000), in a coral colony (*Porites lobata*) (Fallon *et al.*, 1999) and in the chalcopyrite wall of a black smoker chimney (Butler and Nesbitt, 1999). Dating of the normal faulting along the Indus Suture in the Pakistan Himalayas has also been performed by analyzing ^{231}Pa–^{235}U disequilibrium by LAICPMS (Anczkiewicz *et al.*, 2001).

In resonance ionization spectroscopy (RIS), atoms or molecules are excited stepwise from a defined state, normally the ground state, to highly excited states by resonant absorption of photons followed by an ionization process. An additional mass separation step completes the method of resonance ionization mass spectroscopy (RIMS). Spectroscopic study of thorium using continuous-wave RIMS with ultraviolet ionization provided sufficient signal for isotopic analysis of volcanic-like samples containing as little as 1–5 ng of thorium. The ability to determine accurately and precisely the ^{230}Th/^{232}Th isotopic ratios for 1 ng samples represented an improvement over TIMS (Johnson and Feary, 1993). Detection and speciation of trace amounts of neptunium and plutonium is possible by RIMS, with a three-step photoionization in combination with TFMS (Trautmann, 1992). The detection efficiency allows analysis of 10^7 atoms (2×10^{-17} mol) of an actinide, allowing identification at very low concentrations (see Fig. 27.11). RIMS has been applied to plutonium and transplutonium elements and should allow detection down to 10^6 atoms (3×10^{-18} mol) (Trautmann *et al.*, 1986; Erdmann *et al.*, 1998).

27.3.4 Interactive electron–photon, –electron, –ion techniques

Several techniques using electrons as incident beam or reagent are also applied to identify or characterize actinides. They are summarized in Table 27.5: electron–photon, such as EDS or wavelength-dispersed spectroscopy (electron microprobe analysis, EMPA); electron–electron, such as scanning electron microscopy (SEM) or transmission electron microscopy (TEM), Auger electron spectroscopy (AES), and electron energy loss spectroscopy (EELS); electron–ion, such as electrospray ionization mass spectroscopy (ESMS), and spark

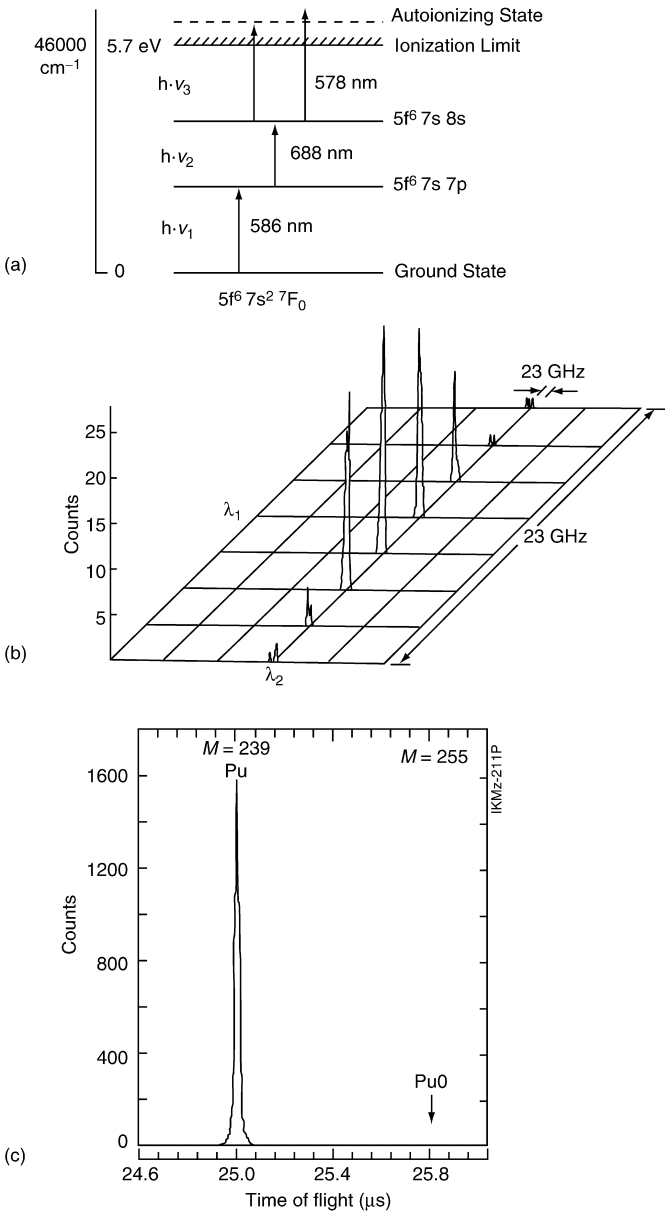

Fig. 27.11 *RIMS of plutonium.* (*a*) *Excitation scheme used for resonance ionization of plutonium.* (*b*) *Plutonium resonance measured by scanning the dye lasers for the first two steps with* λ_3 *fixed.* (*c*) *Time-of-flight mass spectrum of* ^{239}*Pu with two wavelengths in resonance, from* (*Trautmann* et al., 1986).

Table 27.5 *Interactive analytical techniques including electron–photon, –electron, or –ion for actinide isotope element or species characterization.*

Detection	*Goal*	*Sample*	*$^{A}An(Y)$*	*Detection limit*	*Remarks*
Photon					
EDS, EMPA	identification and composition of microphases determination	solid bulk subsurface	Ac(III)	5×10^{-16} mol	estimated for EDS and EMPA with $1 \times 1 \times 1$ μm sample of density 3 g cm^{-3} and 5% An weight fraction
			Th(IV)	5×10^{-16} mol	
			Pa(IV,V)	5×10^{-16} mol	
			U(IV–VI)	5×10^{-16} mol	
			Np(IV–VI)	5×10^{-16} mol	
			Pu(IV–VI)	5×10^{-16} mol	
			Am(III–V)	5×10^{-16} mol	
			Cm(III)	5×10^{-16} mol	
Electron					
SEM, TEM, AES, EELS	morphologic investigations and nanophase speciation	solid, film, or bulk subsurface	Ac(III)	1×10^{-22} mol	estimated for EELS with $2 \times 2 \times 50$ nm sample of density 3 g cm^{-3} and 10% An weight fraction
			Th(IV)	1×10^{-22} mol	
			Pa(IV,V)	1×10^{-22} mol	
			U(IV–VI)	1×10^{-22} mol	
			Np(IV–VI)	1×10^{-22} mol	
			Pu(IV–VI)	1×10^{-22} mol	
			Am(III–V)	1×10^{-22} mol	
			Cm(III)	1×10^{-22} mol	
Ion					
ESMS, SSMS DPV, DPP, COUL	molecular speciation element-isotope speciation and quantitative analysis	solid and solutions solutions	Ac(III)	–	DPV, DPP in solution
			Th(IV)	–	
			Pa(IV,V)	–	
			U(IV–VI)	4×10^{-9} M	(Keil, 1978)
			Np(IV–VI)	2×10^{-8} M	(Kuperman *et al.*, 1989)
			Pu(IV–VI)	2×10^{-8} M	
			Am(III)	–	
			Cm(III)	–	

source mass spectroscopy (SSMS). Electron–phonon methods such as scanning electron acoustic microscopy (SEAM) have not been reported for the identification of actinides. Electroanalytical techniques such as differential pulse voltammetry (DPV) or differential pulse polarography (DPP) may also be applied to characterize the actinides and are treated below.

In the field of structural analysis, microscopic techniques such as TEM, SEM, and high-resolution electron microscopy (HREM) are powerful imaging techniques with nano-scale resolution as well as microprobe capabilities using electron excitation and XS, electron loss spectroscopy, or time-of-flight atom probing. With EDS, high-resolution semiconductor detectors capable of spectral resolution of X-ray lines of neighboring elements made possible the construction of energy-disperse systems. SEAM studies of actinide-doped samples are not reported so far in the literature.

EMPA applies a WDS of the X-rays produced by interaction in the sample. Radiation from the sample is resolved by crystal diffraction, and the monochromatic photons are measured at different angles, assuming a very good resolution of the lines. EMPA is well established and used mainly for elemental analysis in industrial and environmental fields. This technique is used for actinide characterization in environmental samples with a lateral resolution better than 1 μm (Berry *et al.*, 1989, 1994).

Inhalation of respirable particles of uranium is a radiological concern. An investigation of some exposures to low enriched uranium indicated that intakes occurred from the inhalation of surface oxide (UO_x) particles, for example, above low enriched uranium metal plates. Measurements of the size distributions of these particles were made by SEM image analysis (Linauskas *et al.*, 1996). The size distribution analysis from 0.05 to 50 μm allowed a better understanding of the inhalation properties of these uranium oxide particles. As is known, inhaled particles with size <1 μm may be retained in the lungs. SEM allows excellent morphological analysis, which can be completed by backscattered electron analysis to complement the phase study, such as the actinide-doped phase (uranpyrochlore) vs the actinide-depleted phase (baddeleyite), as presented in Fig. 27.12.

X-ray analyses by EDS associated with SEM or TEM enable the investigation at the subcellular level. Since actinides have been introduced in marine environments, their bioavailability to marine organisms is of economic and ecological interest. Cellular and subcellular distributions of ^{238}U, ^{239}Pu, and ^{241}Am have been examined by means of microanalytical techniques, i.e. EDS in organisms: oysters, mussels, shrimps, crabs, and sea spiders (Chassard-Bouchaud and Galle, 1988). Actinide bioaccumulation was detected in target organs, cells, and organelles for every species. The process of the physiological strategies involved in the uptake, storage, and elimination of these actinides was elucidated. The concentration factors range from 10 to 2×10^3. If detection is performed in a cubic micrometer phase with 2% actinide doping, the detection limit DL calculated is reported in Table 27.5. This detection limit is reduced by

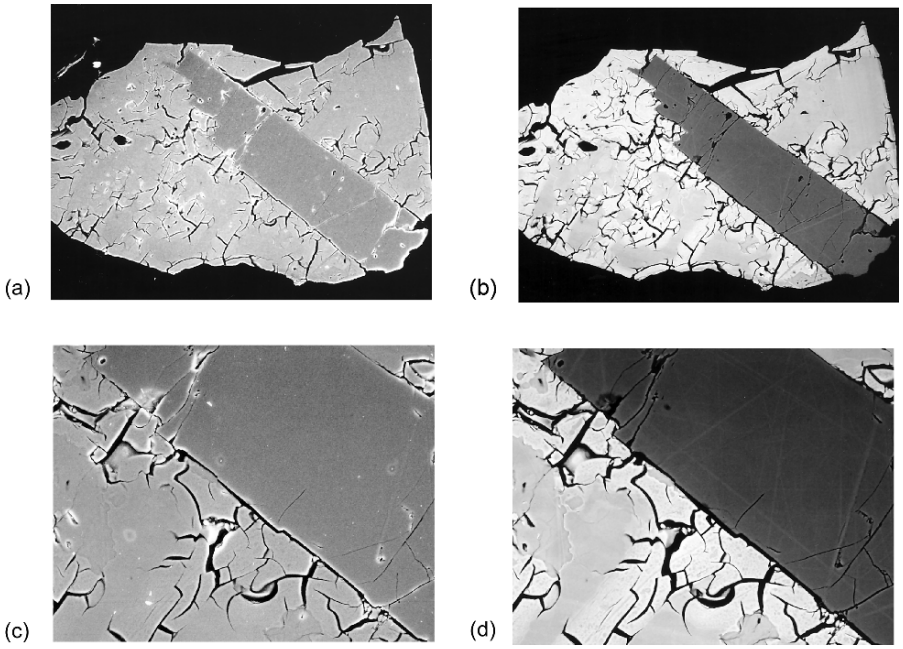

Fig. 27.12 *SEM comparison of secondary* (*a,c*) *and backscattered* (*b,d*) *electron images* (*Lumpkin,* 1999). *Conditions: pairs of intergrowth between uranpyrochlore and baddeleyite from Jacupiranga carbonatite complex, Brazil. Micrograph widths* (*a*) & (*b*) 500 μm; (*c*) & (*d*) 200 μm. *Images taken at low magnification* (*a,b*) *show the general features, including microfracturing and alteration in the uranpyrochlore* (*lighter gray,* $(U,Ca,Ce)_2(Nb,Ta)_2O_6(OH,F)$) *and the platy habit of the baddeleyite* (*darker gray,* ZrO_2).

a factor of 10^3 in a 10^6–10^7 nm^3 phase for an EDS adapted to a TEM unit. However, overlapping of peaks from L and K edges of elements may reduce the accuracy of the analysis.

AES is a technique yielding results similar to XPS. However, AES makes use of the electron as an excitation tool. AES has not been utilized for characterizing actinides in environmental samples. The only AES studies in this field concern the oxygen states in the oxides of uranium and their Auger spectra (Teterin *et al.*, 1997; Gouder, 1998).

EELS may be coupled to TEM or to scanning transmission electron microscopy (STEM) analysis. It is based on spectroscopy of the electron energy after passing through the microscopic specimen. EELS allows study of the oxidation state and the chemical coordination of lanthanides and actinides to be performed in host materials. The speciation may be derived from the M4/M5 edges position and structure. Low levels of transuranics may be characterized with a lateral resolution of the order of 1 nm and concentrations of <200 ppm (Buck and Fortner, 1997). This was applied to redox studies in glasses for plutonium

immobilization (Fortner *et al.*, 1997), in uranium pyrochlore and uraninite as natural analogs of Pu- and U-bearing waste forms (Xu and Wang, 1999), as well as to test the role of alveolar macrophages in the dissolution of different industrial uranium oxide phases (Henge Napoli *et al.*, 1996). The characterization of zirconia–thoria–urania ceramics by X-ray and electron interaction has recently been performed, bridging for actinides EELS and X-ray absorption fine structure spectroscopy (XAFS) potential (Curran *et al.*, 2003). The comparison of EELS spectra collected for these ceramics with spectra recorded for UO_2 and U_3O_8 reference materials also allows assessing U oxidation state at the nanometer-size level in these samples.

Because of its excellent lateral resolution ($2 \times 2 \times 10$ nm) and high sensitivity (1–0.1%), EELS has a demonstrated superior detection limit vs EDS for elements with absorption edges <1000 eV (see Table 27.5).

DPV and DPP are based on electron exchanges between polarizable electrodes and a solution containing redox-sensitive actinides such as U, Np, and Pu (Fig. 27.13). Uranium can be analyzed in U–Fe mixtures by DPV routinely at the 20 μg mL^{-1} (10^{-4} M) level in phosphate solution (Sreenivasan and Srinivasan, 1995) and down to 0.3 μg mL^{-1} (10^{-6} M) level without a preconcentration step in the processing and waste streams of a uranium plant (Sawant *et al.*, 1996). Submicrogram quantities of neptunium and plutonium may be determined by potentiometric voltammetry down to 2×10^{-8} M (Kuperman *et al.*, 1989). Investigations of the redox behavior and the speciation of plutonium in concentrated NaCl solutions with respect to an intermediate-level waste repository were carried out with a rotating disk electrode (Marx *et al.*, 1992). Concentrations of Pu(IV) may be determined quantitatively from the peak height while the shifts in potential are due to speciation changes (complexation) within the solution. In addition, simultaneous determination of U(VI), Pu(VI), and Pu(V) in 0.5–4.0 M NaOH was reported by DPV (Abuzwida *et al.*, 1991). U(VI) is detected at the dropping mercury electrode in the range 10^{-7} to 3×10^{-3} M. Pu(VI) and Pu(V) at the platinum electrode were analyzed at concentrations from 4×10^{-6} to 10^{-3} M even in the presence of various potential interfering ions such as Mo(VI), W(VI), V(V), and Cu(II) in salts such as $NaNO_3$, $NaNO_2$, and NaI.

On non-polarizable electrodes, quantitative electroanalytical methods can also be applied, taking advantage of the rich redox chemistry of the actinide elements. Numerous controlled potential coulometry (COUL) studies have been reported in the literature. For example, neptunium determination is possible at as low as the 2 mg level with a precision of 0.2% (Kasar *et al.*, 1991), even in the presence of interfering elements such as Pu, U, Ce, Cr, Fe, or Mn (1000-fold) (Karelin *et al.*, 1991).

ESMS is a recently developed analytical technique that seems promising for speciation studies. This technique applies a spray of electrons on a material surface followed by mass spectrometry of the cluster ions formed in 'soft conditions'. First developed for biological samples, it is now used for direct

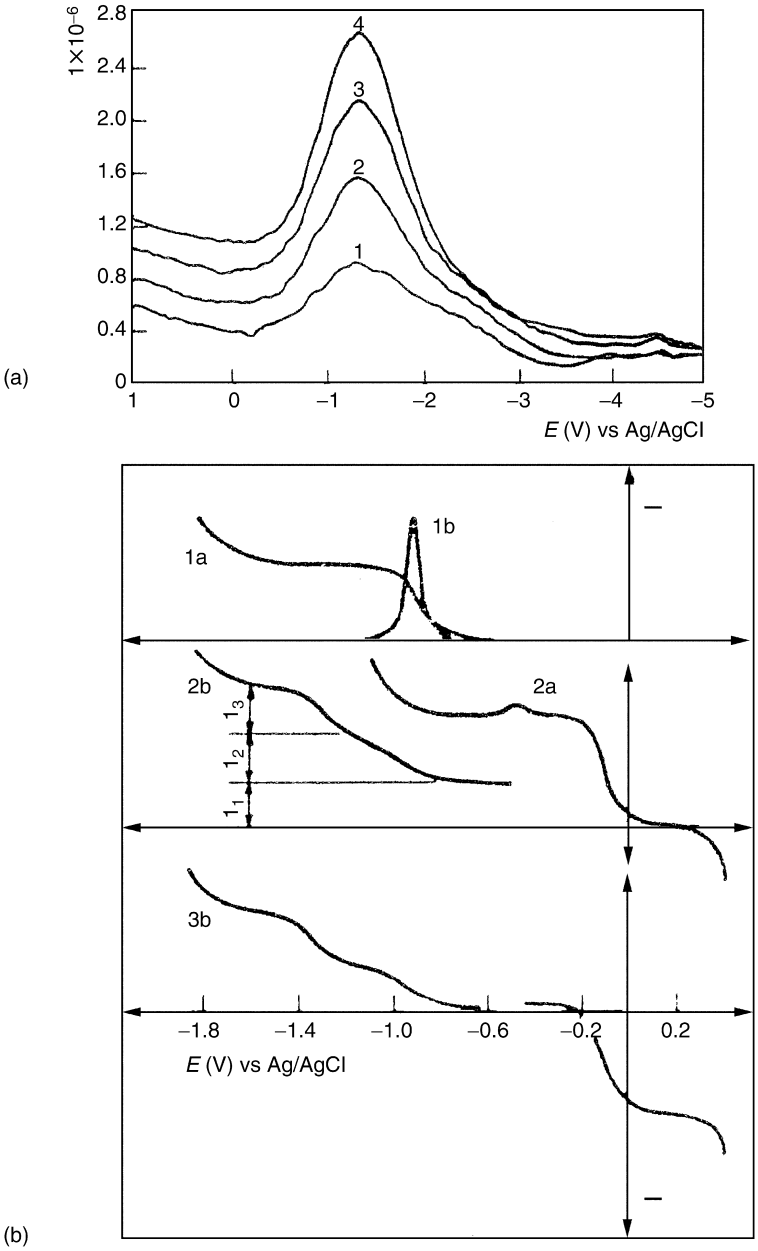

Fig. 27.13 (*a*) *Differential pulse polarogram* (*DPP*) *of U* 1.5 *to* 6×10^{-5} M *at dropping mercury electrode* (*Sawant* et al., 1996)*, possible down to* 10^{-6} M *level without a pre-concentration step in the processing and waste streams of a uranium plant, and* (*b*) *DPV of U and Pu* 10^{-4} M *on Pt electrode* (*Abuzwida* et al., 1991) *in* 1 M *NaOH.*

speciation studies in solution. It is now possible to directly couple a liquid at atmospheric pressure to mass detection at reduced pressure, even if the mechanisms taking place are rather complex. ESMS investigations were adapted for the speciation of Th(IV) hydrolysis species (Moulin *et al.*, 2001) and U(VI) in neutral solutions (Moulin *et al.*, 2000). Fig. 27.14 shows a typical spectrum obtained

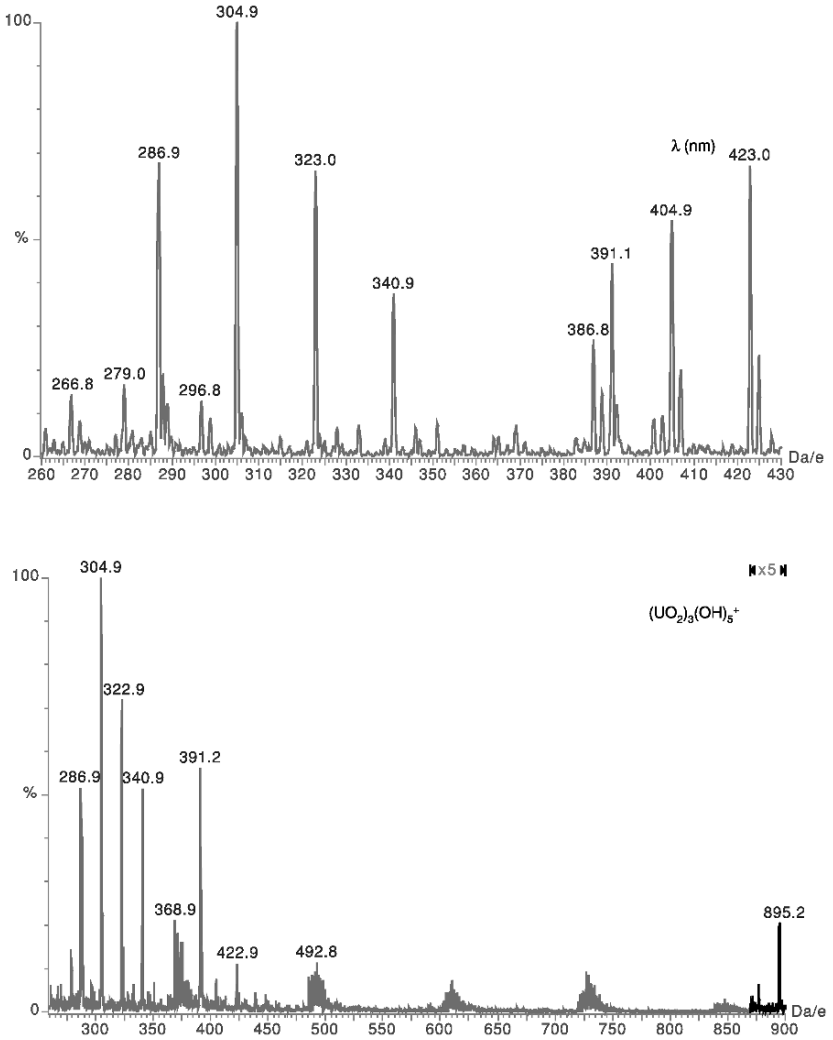

Fig. 27.14 *Electrospray mass spectrum of uranium at* 10 mg L^{-1} *at pH* 3.5 *and at pH* 6.5 (*Moulin* et al., 2000). *Note the presence of species such as* (*a*) $(UO_2OH(H_2O)_n)^+$ *with masses* 286.9 + n·18 *at pH* 3.5 *and* (*b*) *at pH* 6.5, *where* $((UO_2)_3(OH)_5)^+$ *with mass* 895.2 *is also observed.*

for a uranyl solution at pH 3.5. Peaks can be interpreted for the species $((UO_2)_i(OH)_j\,(H_2O)_n)^{(2i-j)+}$.

Increasing the energy of the electronic stimuli permits the technique to be extended from molecular to atomic analysis. SSMS is similar to the former technique but the source of electrons is driven at higher potential. This allows direct quantitative analysis of elements and isotopes of the material. SSMS was used to determine trace elements in the U_3O_8 standard (Li *et al.*, 1991) as well as in other actinide oxides. In a complementary way SSMS may be used to analyze uranium from environmental samples.

27.3.5 Interactive neutron–photon, –electron, –neutron, –ion techniques

Neutron-interactive techniques make use of neutron scattering or absorption in the studied environmental samples. Absorption may be specific to actinide isotopes. The nuclide generated by neutron capture may be detected for its emission of gamma photon, neutron, or ion (fission products or alpha). Its detection is performed as described in Section 27.3 using spectrometric (S) or radiographic (RAD) techniques such as fission track (FT) techniques. Analytical data are given in Table 27.6.

Neutrons are ideal probes for the study of condensed matter, having important advantages over other radiation types. The outstanding feature of neutrons as probes is their high penetration (~10 cm) in materials, while the non-systematic variation of scattering length and absorption cross section from element to element makes its use versatile for actinide analysis. However, neutron RAD has not found applications for actinide speciation in environmental samples but may be used to characterize nuclear fuel pellets in segments of rods (e.g. Groeschel *et al.*, 2003).

NAA, being essentially an isotopic and not an elemental method of analysis, is capable of determining a number of actinide nuclides of radioecological interest by transformation of a nuclide into a radionuclide more quantifiable. The nuclear characteristics that favor this technique may be summarized in an advantage factor relative to radiometric analysis of the original radioanalyte. NAA can be performed by means of several kinds of sources such as nuclear reactors for cold, thermal, epithermal, and fast neutrons, portable isotopic sources such as Am–Be neutron sources, actinide (^{252}Cf) sources, and accelerator/generator or spallation sources with which originally fast neutrons can be thermalized. After activation, the nuclides that are produced are detected by gamma, beta, or alpha spectrometry. Its advantage is that NAA is a multielement, very highly sensitive, not handling intensive, efficient, instrumental, quasi non-destructive, and isotopic technique. On the other hand, it suffers from high costs, nuclear interferences, and residual radioactive wastes. NAA is a sensitive and accurate method for bulk analysis. NAA has been widely used for actinide analysis, in particular in the field of uranium prospecting. Nowadays it

Table 27.6 *Interactive analytical techniques including neutron–photon, –electron, or –ion for actinide isotope element or species characterization.*

Detection	*Goal*	*Sample*	*$^{A}An(Y)$*	*Detection limit*	*Remarks*
Photon					
NAA	isotopic analysis	liquid bulk	^{232}Th	2×10^{-15} mol	NAA *DL* for 1 h
			^{231}Pa	2×10^{-15} mol	irradiation at 4×10^{12} cm^{-2}s^{-1}
			^{238}U	2×10^{-15} mol	(May, 1987)
			^{237}Np	2×10^{-15} mol	(Byrne, 1999)
			Pu	–	
			Am	–	
			Cm	–	
Neutron					
DNAA	isotopic analysis	solid subsurface film bulk depth profiling	^{232}Th	–	
			^{231}Pa	–	DNAA
			^{235}U	–	(Jaiswal *et al.*, 1987)
			^{237}Np	–	(Alfassi, 1990)
			^{239}Pu	–	
			^{241}Am	–	
			^{244}Cm	–	
Ion					
NAA, FTRAD	elemental or isotopic analysis	solid film or bulk nano microdepth profiling	^{232}Th	–	Fission Track *DL* for 7 h
			^{231}Pa	–	irradiation in neutron
			^{235}U	4×10^{-18} mol	flux of 4×10^{12} cm^{-2}s^{-1}
			^{237}Np	2×10^{-16} mol	(Hursthouse *et al.*, 1992)
			^{239}Pu	2×10^{-18} mol	(Johanson, 1996)
			^{241}Am	–	
			^{244}Cm	–	

is applied to determine concentrations in environmental, geological, and biological samples. NAA has also the advantage of being well suited for routine analysis.

Since neutrons activate almost all elements present in the sample, it is necessary to resolve the activity generated by actinides from activities of other elements. Separations are achieved through instrumentation or chemical methods.

The application of NAA to determine ^{230}Th, ^{232}Th, ^{235}U, ^{238}U, and ^{237}Np quantitatively provides an independent quantification that complements the conventional radiometric techniques (Byrne, 1993). NAA was used to determine, in the presence of other elements, Th distribution in geological material (Castillo *et al.*, 1996), ^{231}Pa in environmental and biological samples (Byrne and Benedik, 1999), ^{235}U and ^{238}U in geological samples (Sheng *et al.*, 1985), and ^{237}Np in sediments (Byrne, 1986) (Fig. 27.15) and in biological samples (May *et al.*, 1987), the latter with detection limits down to 5×10^{-13} g Np (2×10^{-15} mol) corresponding to 2.5×10^{-9} mg kg^{-1} for a 200 mL seawater sample.

NAA is currently used for solid samples. However, it has also been successfully applied to the analysis of waters. For example, the effect of humic material on the dissolution of natural trace elements, especially of actinide homologs, and on the sorption behavior of Np, Pu, Am, and Cm has been determined (Probst *et al.*, 1995). The groundwater constituents have been analyzed by applying NAA as well as other analytical techniques. Fractions of fluid samples were obtained by ultrafiltration and by ultracentrifugation. The study showed that trace actinides were associated with the colloidal phase (Kim *et al.*, 1987).

Delayed neutron activation analysis (DNAA) applies delayed neutron detection (see Section 27.3.1) after nuclide activation by neutrons. This technique is very sensitive to the detection of fissile isotopes. It has been compared to other techniques for ^{232}Th, ^{238}U, ^{239}Pu, and ^{240}Pu analysis (Alfassi, 1990; Jaiswal *et al.*, 1994). DNAA was performed for isotopic analysis of uranium in safeguard studies (Papadopulos and Tsagas, 1994), and was applied to uranium analysis in sediments (Noller andHart, 1993), in vegetal specimens (Apps *et al.*, 1988), and in human tissues (Gonzales *et al.*, 1988).

Track-etching is a form of RAD that may also be applied for localizing phases rich in fissile actinides (Fernandez-Valverde *et al.*, 1988). This technique has been applied for ^{235}U and ^{238}U quantification. Different kinds of polycarbonates were used as fission fragment detectors. Sample solutions, with U at the ppm level, dried on the detector are neutron irradiated for a given fluence and fission fragment tracks are microscopically counted (Berry *et al.*, 1989). FT detection is appropriate for the detection of ^{239}Pu in, for example, biological and environmental samples (Johansson and Holm, 1996). The lower detection limit is a few microbecquerel ($2\ \mu$Bq $= 4 \times 10^{-18}$ mol), which is comparable to the detection limit of mass spectroscopy and more sensitive than the alpha spectroscopic method. It must, however, include a removal of uranium from the sample.

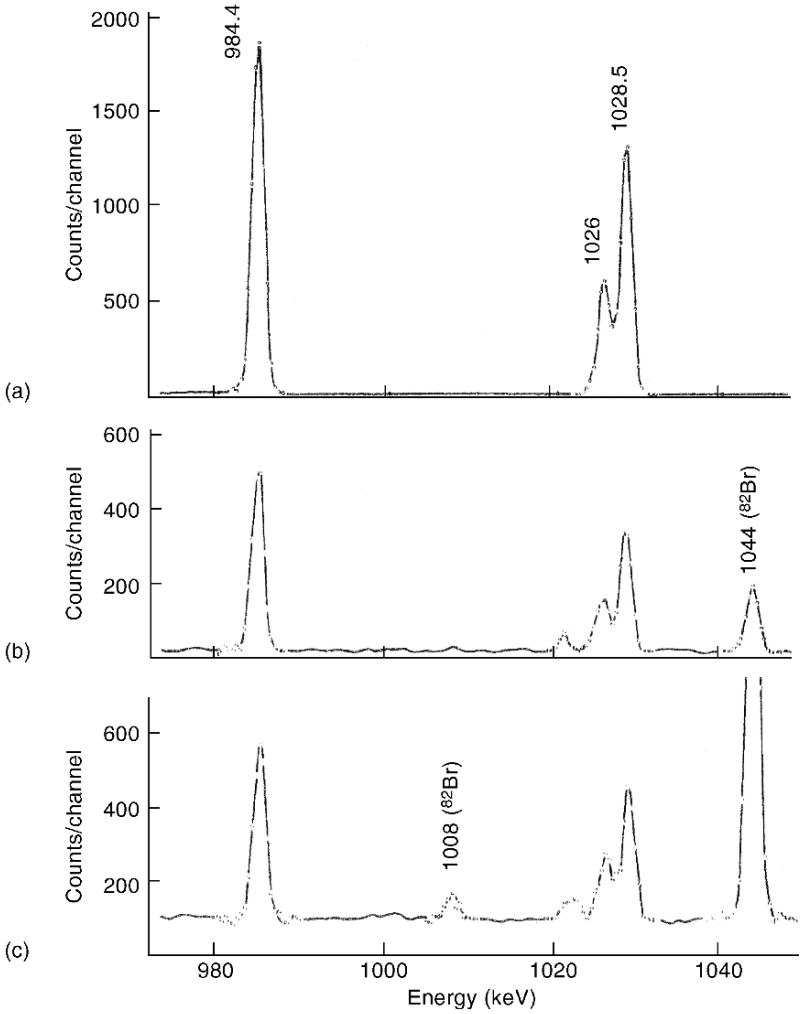

Fig. 27.15 *NAA: partial gamma spectra of* ^{238}*Np from standard and Cumbrian sediments* (*Byrne,* 1986): (*a*) 26.8 ng ^{237}*Np standard, counted* 600 s*; and* (*b*) *Ravenglass sediment* 2 g, 0.2 ng *Np* g^{-1} *counted* 10 000 s*: and* (*c*) *Grange-over-Sands sediment,* 5 g, 20 pg *Np* g^{-1} *counted* 50 000 s. *Conditions: sediment irradiation in Triga Mark II reactor at a neutron flux of* 2×10^{12} cm^{-2} s^{-1} *for about* 20 h *with Np standards.*

27.3.6 Interactive ion–photon, –electron, –neutron, –ion techniques

The techniques derived from the ion reaction/interaction with sample particle detection make use of the large potential of the spectrum of particles produced or reemitted. They are listed as follows: ion–photon, ion–phonon, ion—electron, and ion–ion (Table 27.7). The ion–photon techniques are LAICPOES,

Table 27.7 *Interactive ion–photon, –electron or –ion techniques for actinide isotope element or species characterization.*

Detection	*Goal*	*Sample*	*$^{A}An(Y)$*	*Detection limit*	*Remarks*
Photon					
ICPOES	concentration determination	liquid	^{227}Ac	–	ICPOES
			^{232}Th	4×10^{-9} M	*DL*
			$^{231–234}$Pa	–	(Miekeley *et al.*, 1987)
			^{238}U	8×10^{-9} M	
			^{237}Np	2×10^{-7} M	(Van Britsom *et al.*, 1995)
PIXE, PIGE	identification depth profile	solid subsurface	^{239}Pu	1×10^{-7} M	
			^{241}Am	8×10^{-9} M	(Huff and Bowers, 1990)
			^{248}Cm	1×10^{-8} M	
Neutron					
NRA	elemental and isotopes analysis		^{227}Ac		NRA not recommended for actinide analysis, see text
			$^{231–234}$Th	–	
			$^{231–234}$Pa	–	
			$^{234–238}$U	–	
			^{237,239}Np	–	
			$^{238–244}$Pu	–	
			^{241,243}Am	–	
			$^{242–244}$Cm		
Ion					
VOL, ICPMS	concentration determination	solid surface or bulk nano microdepth profiling	^{227}Ac(III)	4×10^{-14} M[a]	ICPMS
			$^{227–232}$Th(IV)	4×10^{-14} M[a]	*DL* estimated
SIMS, AMS, RBS, ERDA, NRA	elemental or isotopic analysis, also depth profiling		$^{2331–234}$Pa(IV,V)	4×10^{-14} M[a]	
			$^{234–238}$U(IV–VI)	4×10^{-14} M[a]	
			^{237}Np(IV–VI)		(Kim, 1989)
			$^{238–244}$Pu(IV–VI)	4×10^{-14} M[a]	(Hursthouse *et al.*, 1992)
			^{241,243}Am(III–V)		
			$^{242–250}$Cm(III)		(Agaranda, 2001)

[a]Occasionally down to 4×10^{-16} M.

proton (particle)-induced X-ray emission spectroscopy (PIXE), and particle (proton)-induced gamma radiation emission (PIGE). Both ion–phonon and ion–electron techniques have not been applied so far. However, the ion–ion analytical mode is adapted by several powerful techniques such as ICPMS, secondary ion mass spectroscopy (SIMS), accelerator mass spectroscopy (AMS), Rutherford backscattering (RBS), elastic recoil detection analysis (ERDA), and nuclear reaction analysis (NRA). Finally, volumetry (VOL) is added as representative for the ion reaction with ions in solution.

The methods that utilize low-energy ions are dominated by inductively coupled plasma (ICP) techniques. In ICP an inductively coupled argon plasma is used to ionize an aerosol from the finely dispersed matrix and an optical emission spectrometer (ICPOES) detects the emitted light intensities. ICPOES allows, in principle, analysis of actinides at ~2 to 20 ppb levels (~10^{-8} to 10^{-7} M) (Van Britsom *et al.*, 1995; Huff and Bowers, (1990)). It has been used to analyze uranium (at 385.96 nm) at low levels (<100 ppm) in raw phosphoric acid from leachate of phosphate rocks (Waqar *et al.*, 1995). High-resolution (HR) ICPOES has also been used in the nuclear field to analyze fuel burn-up and to analyze samples for major uranium isotopes. The determination of the $^{235}U/^{238}U$ isotopic ratio demonstrates the versatility of the HR-ICPOES technique (Johnson *et al.*, 1998).

Other methods that employ high-energy ions use accelerator-based techniques to generate these ions. The ion accelerators provide a variety of ion beams with energies from a few keV to a few hundred MeV, and beam size ranges from the nanometer to the millimeter scale. Ion beams are applied to trace element determination using X-rays produced in the ionization process or nuclear reactions, including elastic or inelastic scattering or Coulomb excitation to measure actinides or isotopes in the sample. Detection limits are typically of the order of 10^{-6} g g^{-1} mass ratio (~4×10^{-9} mol g^{-1}), or much lower when detection is performed by mass spectroscopy. Ion microbeam analysis uses an ion beam focused to micrometer dimensions for elemental imaging at sample surfaces. This can be performed by measuring secondary radiation induced by the primary ion beam, such as X-rays and nuclear reaction products, or by measuring the energy loss of transmitted primary ions. This technique is very powerful in combination with electron microscopy for investigations of dust and soil particles, particularly those loaded with actinides.

PIXE is typically based on the use of MeV protons and allows the quantification of trace elements ranging from Na to actinides with sensitivities in the range from 10^{-6} – to 10^{-3} $g \cdot g^{-1}$, depending on element and matrices. The μPIXE detection limit is about 5×10^{-16} mol for a $5 \times 5 \times 5$ μm phase depending on the actinide detected. PIXE was, for example, used to determine qualitatively and quantitatively the distribution of uranium and plutonium sorbed onto a variety of rocks and their constituent minerals (Berry *et al.*, 1994). Both surface and subsurface concentrations of actinides were measurable. This identified which minerals are important for the sorption of uranium and plutonium for a given

rock. U and Pu were detected by PIXE in particle grains from contaminated soils (Kadyrzhanov *et al.*, 2000).

PIGE is normally used to detect light elements but cannot be applied to detect actinides.

NRA may be applied with neutron detection, e.g. (d,n). This method is used for elements for which PIXE analysis is unfavorable (e.g. $Z < 20$) but is not applicable to actinides, perhaps because of their larger Coulomb barrier.

VOL analyses such as complexometry and redox titration are two methods in which actinide ions react with other ions in solution to determine the actinide element concentration. For example, Th(IV) can be titrated by ethylenediaminetetracetic acid (EDTA) for the estimation of thorium concentration in low-grade ores (Strelow, 1961), or thorium-rich minerals. This complexation titration is carried out at pH 9–9.5, using Eriochrome Black T as an indicator (Negi and Malhotra, 1980). EDTA complexometry for Np(IV) was reported at pH from 1.3 to 2.0 with xylenol orange as indicator (Rykov *et al.*, 1975). Plutonium and uranium may also be titrated by the same complexation reagent.

Redox titrations are only possible for U, Np, and Pu. Volumetric determination of uranium is classically carried out by reduction using titanous sulfate as reducing reagent before oxidimetric titration (Wahlberg *et al.*, 1957). Ce(IV) (Moss, 1960) or AgO (Godbole and Patil, 1979) may be used to oxidize Np(V) to Np(VI), and Fe(II) to titrate Np(VI) to Np(V). Assay of uranium and plutonium in the same aliquot is possible by potentiometric titration (Nair and Kumar, 1986). The Macdonald method, rescaled down to milligrams of plutonium, was applied using an electrochemical process for each step; the end point of the final titration was determined potentiometrically (Kuvik *et al.*, 1992). Here again, as for GRAV, chemical separation may be required in order to avoid specific complexometric or redox interferences.

In ICPMS the analysis of assayed ions generated in an argon-ion plasma torch is carried out in a quadrupole or a magnetic mass spectrometer. The low detection limits for a large number of elements and the possibility to measure isotopic ratios have established ICPMS as a powerful analytical tool. The advantages are clearly a large dynamic range, 10^{-6} to 10^{-12} g·g^{-1} (4×10^{-14} M: see Table 27.7), occasionally down to 10^{-14} g·g^{-1} (4×10^{-16} M), and the use of various sample introduction techniques with the possibility to measure liquid or solid samples. Nevertheless, the numerous molecular and isobaric overlaps restrict the direct analysis of some elements. The latter problem may be overcome by using a higher-resolution unit (sector spectrometer) or separation (see Section 27.4). Precise and accurate analysis and isotope ratio measurement of long-lived actinides at trace and ultratrace concentration levels in environmental samples can be carried out by ICPMS. This technique allows the analysis of isotopic ratio variation in environmental materials and can provide evidence of contamination from radioactive wastes. The technique is widely used today and is routinely applied for age dating, as well as characterization of samples from the environment and from nuclear reactor materials. The determination of

precise isotopic ratio of uranium, thorium, and plutonium samples with relative standard deviation of the order of 0.05% can be achieved by utilizing a quadrupole mass spectrometer, a direct-injection high-efficiency nebulizer (Becker and Dietze, 1999a), and optimal isotope analysis (Becker and Dietze, 1999b). For actinides, ICPMS has been used to analyze Th and U in soil and plants (e.g. Yukawa *et al.*, 1999), neptunium (Kim *et al.*, 1989) in contaminated soil (Igarashi *et al.*, 1990), and transuranium elements (Agarande *et al.*, 2001) up to Cm (Barrero Moreno *et al.*, 1996). In addition to the large variety of injector, nebulizer, and torch design, electrothermal vaporization (ETV) allows direct introduction of solid samples (such as in a fine suspension) in the plasma. The advantage of the ETV is that there is no need for dilution. ETV–ICPMS was used to determine $^{240}Pu/^{239}Pu$ atomic ratios and ^{237}Np concentrations in marine sediments (Sampson *et al.*, 1991). Determination of a small volume of Am solution, e.g. 20 μl, can be performed using a micronebulizer and a minicyclonic spray chamber (Becker and Dietze, 1999a). Recently ICPMS has been used to analyze colloids in a single-particle mode. This method was applied for the analysis of thorium colloids (Degueldre and Favarger, 2004) and uranium colloids (Degueldre *et al.*, 2005).

SIMS is used for isotopic analysis with high sensitivity and micron-size space resolution. It makes use of a sputter-ion source and a mass spectrometer for analysis and detection of keV secondary particles (positive, negative, or neutral) produced. SIMS may be used in a static way for ion imaging of a surface or in a dynamic way by sputtering for depth profiling. The use in a SIMS system of an accelerator mass spectrometer improves the detection limit for many elements by several orders of magnitude. This technique is sometimes referred to as super-SIMS. Super-SIMS systems that allow bulk sensitivities of 10^{13} atoms per cm^3 (2×10^{-11} mol per cm^3) have been developed, which may be used for both bulk and depth profile measurements.

Micro-SIMS was used to characterize and map actinides ingested in marine organisms, allowing isotopic measurement and cellular images (Chassard-Bouchaud and Galle, 1988) (see Fig. 27.16). Concentrations of uranium and plutonium sorbed onto minerals can be routinely determined with sensitivities down to 1 ng cm^{-2}. Data obtained have been used to identify the minerals in a rock that are relevant to actinide sorption. The age determination of Pu particles was demonstrated by SIMS images (Wallenius *et al.*, 2001). This age is highly important in view of the pending cut-off treaty for nuclear weapon materials. By collecting particles from the vicinity of or inside the nuclear facilities and determining their ages, it is possible to monitor the observance of the agreement. SIMS was also used to measure qualitatively the distribution of sorbing actinides and their penetration rates into minerals after sorption tests (Berry *et al.*, 1993). SIMS has excellent spatial resolution (less than micrometer scale) and achieves some depth profiling to a few micrometers beneath a surface.

AMS incorporates an ion accelerator and its beam transport system as elements of an ultrasensitive mass and charge spectrometer. Isotopic ratios of

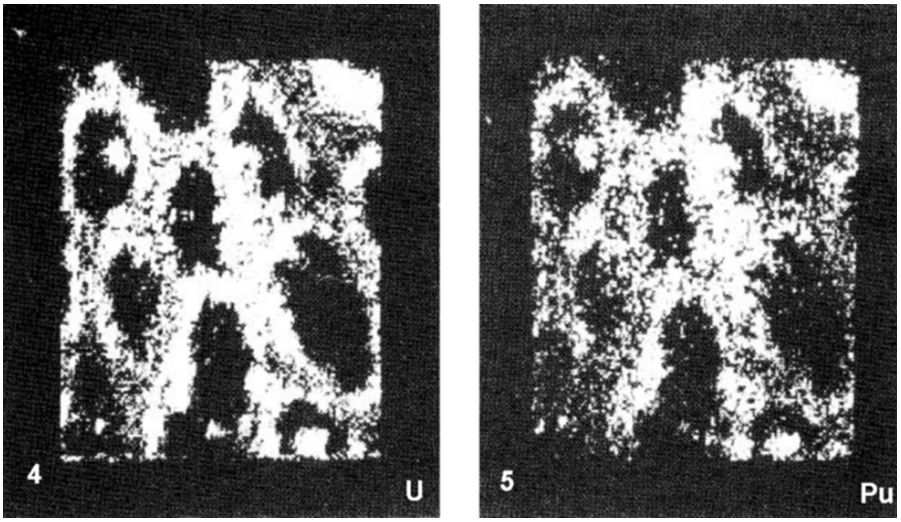

Fig. 27.16 *SIMS pictures of U and Pu from subcellular features of a mussel* Mytilus edulis *digestive gland* (*Chassard-Bouchaud and Galle,* 1988) (200 mm *full horizontal scale*).

less than 1 part in 10^{15} can be measured for some actinide isotopes. This is four or five orders of magnitude smaller than possible with conventional mass spectroscopy. Negative ions produced by a sputter-ion source (e.g. Cs or Ga) can be detected using an AMS system. AMS assay of ^{229}Th, ^{230}Th, ^{233}U, ^{236}U, ^{237}Np, ^{239}Pu, and ^{244}Pu are reported (Zhao *et al.*, 1994a,b; Purser *et al.*, 1996; Zhao *et al.*, 1997). The theoretical detection limit is determined by the overall efficiency of the system: the product of the AnO^- negative ion formation, which ranges from 0.15 for ThO^- to 1.0% for PuO^- (Fifield *et al.*, 1997), multiplied by the transmission efficiency through the accelerator to the detector. The overall efficiency is 1×10^{-6}, so that the sensitivity is 1 count for 1.7×10^4 atoms or 2.8×10^{-20} mol with an extremely small background (virtually zero). Among the lowest-level samples analyzed recently were the river waters downstream from the Mayak plant (Oughton *et al.*, 2000). A sample containing 6×10^7 atoms of ^{239}Pu yielded 63 counts in 15 min in a sample of 3 mg Fe_2O_3. The extreme case was described recently (Wallner *et al.*, 2000) for the detection of supernova-produced long-lived actinide nuclei.

RBS measures the composition profile of a material near the surface. Conventional RBS is performed using helium ions, while heavy-ion RBS has the advantage of a better mass resolution for heavy elements, being able to separate isotopes in some cases. Sensitivity increases for higher masses. Depth resolutions down to 1 nm can be obtained with Si surface barrier detectors in optimized setups, leading to quantitative studies of surface interface mixing and interdiffusion (see Fig. 27.17). The scavenging properties of inorganic particles towards heavy elements such as actinides may be studied by RBS

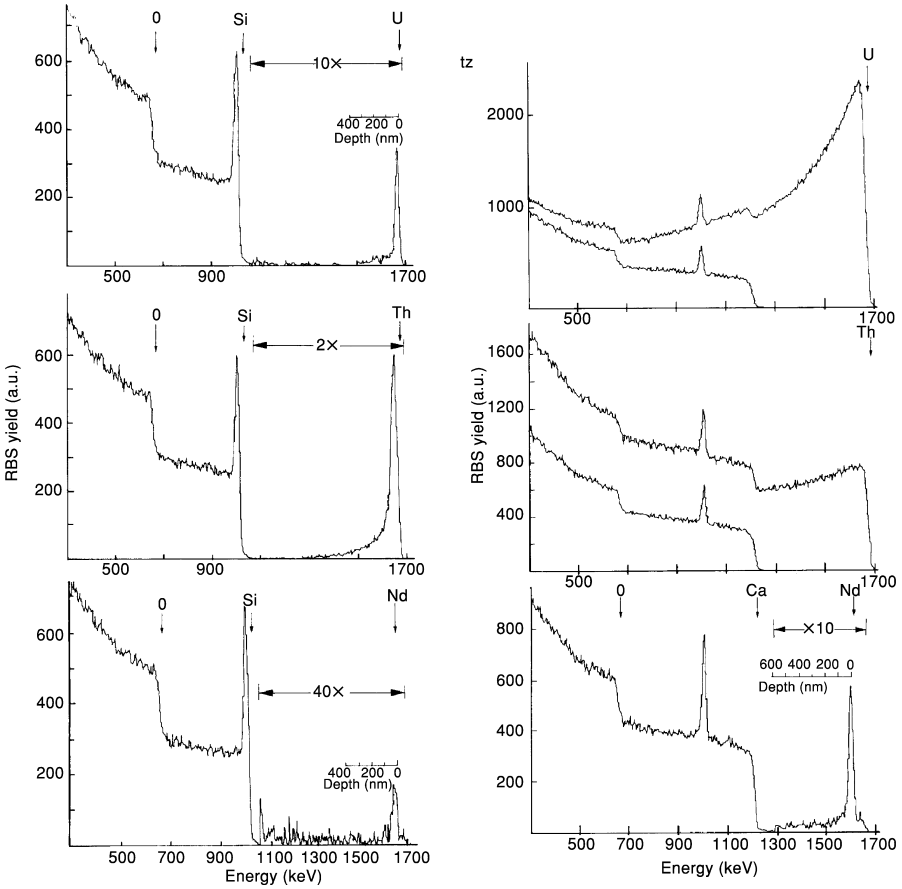

Fig. 27.17 *RBS spectra of U and Th sorbed* (*a*) *on quartz on the surface at* 100°C *and* (*b*) *on calcite at* 50°C *with diffusion in the bulk* (*below the spectra of calcite leached with DI-water*). *Conditions:* 2.2 MeV $^4He^{2+}$. *Note the thin actinide layer on quartz and the diffuse profile in calcite* (*Dran* et al., 1988).

(Della Mea *et al.*, 1992). The interactions of U(VI) and Th(IV) at the calcite–solution interface have been investigated by RBS; it was observed that uranium forms a solid solution while Th yields precipitates (Carroll *et al.*, 1992). Sorption of these actinides was also studied on silica and granite by this technique (Dran *et al.*, 1988). Further sorption work was carried out with uranium and plutonium on minerals with loadings of the order of 1 ng cm^{-2} (Berry *et al.*, 1993). This technique remains a very powerful tool for the identification of the actinides on light-element matrices (soil, bioorganic material).

ERDA makes use of glancing angle heavy-ion irradiation to extract light-element ions from a matrix. This technique is not used to identify actinides but to contribute to light element speciation studies in actinide compounds. ERDA was used to quantitatively measure hydration and hydrogen profiles in the near surface of UO_2 for spent nuclear fuel direct storage, and for a tailor-made titanium-based ceramic that was developed to incorporate radioactive waste for safe and long-term underground storage (Matzke *et al.*, 1990; Matzke and Turos, 1991). In these specimens, no hydrogen uptake was observed at temperatures below 100°C, but for higher leaching temperatures up to 200°C and for longer times, hydrogen profiles could be measured for both materials.

With NRA, specific (d,p), (d,α), (p,α), and other nuclear reactions are used to make sensitive determination of many specific isotopes. In general this method is used for elements for which PIXE analysis is unfavorable (e.g. $Z < 20$) but is not applied for actinides, perhaps because of their larger Coulomb barrier.

27.4 COMBINING AND COMPARING ANALYTICAL TECHNIQUES

The sequential and comparative use of analytical techniques is an important way to improve the quality of any analytical investigations. This has been widely applied to actinide characterization. Combination of techniques is a useful strategy to optimize and confirm information on species. Physical or chemical separation followed by applying one or several identification or speciation techniques is a key route for performing specific and accurate analysis.

SR has become a valuable tool for uranium ore body prospecting. SR is applied in a high-resolution mode, by the action of vibroseis (acoustic source emitters) at a low frequency (10–80 Hz) that are separated by, for example, 10 m, and an array of receivers (geophones) (Phelps and Davis, 1981). Seismic waves can respond specifically to uranium-bearing ore deposits (Liu *et al.*, 1985). SR data incorporate the mapping of geophysical features with radon/helium detection, transient electromagnetic (EM) sounding (Rozenberg and Hoektra, 1982), gravity anomalies, airborne gamma spectroscopy, and gamma logging, to identify high-grade uranium deposits (Dong, 1990; Poty and Roux, 1998). Often the confidential aspect of seismic studies does not allow their use to be made public. Uranium deposit exploration requires, consequently, extensive studies of empirical regional parameters including relationship to geophysical and geochemical records. X-ray diffraction (XRD) and IRS in a reflective mode provide useful lithogeochemical data. These need also to be combined with an EM survey that can be obtained by airborne scanning. Conductive zones that could be key indicators and uranium-rich features may be detected in these bodies. Radiometric survey, gravity mapping, and resistivity measurements complete the later studies. Geochemical and geophysical signatures are correlated in a semiempirical way to guide exploration before uranium ore body identification (Matthews *et al.*, 1997).

AFM has been used to characterize thorium oxyhydroxide colloids (Walther, 2003). This technique, being non-specific for an element, must be combined with others such as SEM/EDS and TEM/EDS to identify the actinide colloidal species. However, AFM is very powerful for determining the morphology and the size of these actinide colloids. The derived techniques such as acoustic AFM (aAFM) and electrochemical AFM (eAFM) allow characterization of specific properties. The latter was recently applied for nanoscopic observation of U(IV) oxide surface dissolution and remineralization (Römer *et al.*, 2003).

EHE may be used for speciation of redox-sensitive actinides such as U, Np, or Pu in waters. Groundwater redox conditions and oxidation state of dissolved uranium were studied in natural water samples from the Palmottu uranium deposit, Finland (Ahonen *et al.*, 1994). Good correlations were observed between the dissolved U(IV)/U(VI) ratio and the measured redox value. The latter, however, requires careful measurements, as recently reported (Degueldre *et al.*, 1999).

The technique of alpha and beta counting by a phoswich detector for simultaneous counting of α- and β-ray (including γ-ray) and determination of actinides is feasible by multi-interface (ZnS(Ag)/NE102A) detectors. Such systems have been developed for complementary actinide α- and β-emitter analysis (Usuda *et al.*, 1997, 1998) and are applicable for actinide identification under high background conditions.

The combination of chemical separation and radioanalysis is classical. Sequential separation combined with photon electron rejecting alpha liquid scintillation (PERALS™) is currently applied for measuring ^{228}Th, ^{230}Th, ^{232}Th, ^{234}U, and ^{238}U in soil samples without tracers (Füeg *et al.*, 1997) (see Fig. 27.18). The minimal detectable concentration ranges between 0.2 and 0.8 Bq kg^{-1} for a 1 g aliquot and 80 000 s counting time. Determination of ^{239}Pu + ^{240}Pu, and ^{241}Pu in environmental samples has been achieved (Yu-fu *et al.*, 1990). After pretreatment of the sample, the plutonium nuclides are co-precipitated with iron(III) hydroxide and calcium oxalate and isolated further from impurities by means of anion-exchange chromatography. Plutonium isotopes are extracted before spectrometric measurement with an ultra low-level liquid scintillation spectrometer. Counting efficiency of plutonium for 100 L of seawater or 40 g of soil sample was about 50%. The detection limit was 0.2 mBq (4×10^{-16} mol) for ^{239,240}Pu.

Extraction may also be used as a separation and a pre-concentration step before polarographic investigations of uranium. This protocol was applied for the determination of U(VI) (Degueldre and Taibi, 1996): the actinide was quantitatively extracted in a hydrocarbon–diethyl-2-hexyl phosphoric acid–TOPO or in hydrocarbon –tri-*n*-octylamine, the organic phase was diluted into the same volume of alcohol and spiked with H_2SO_4 (0.1 M) before electroanalytical investigation by direct current polarography and by DPP. The pulse polarographic peak allowed determination of U(VI) down to 10^{-6} M in the organic phase, which would be impossible without pre-concentration by

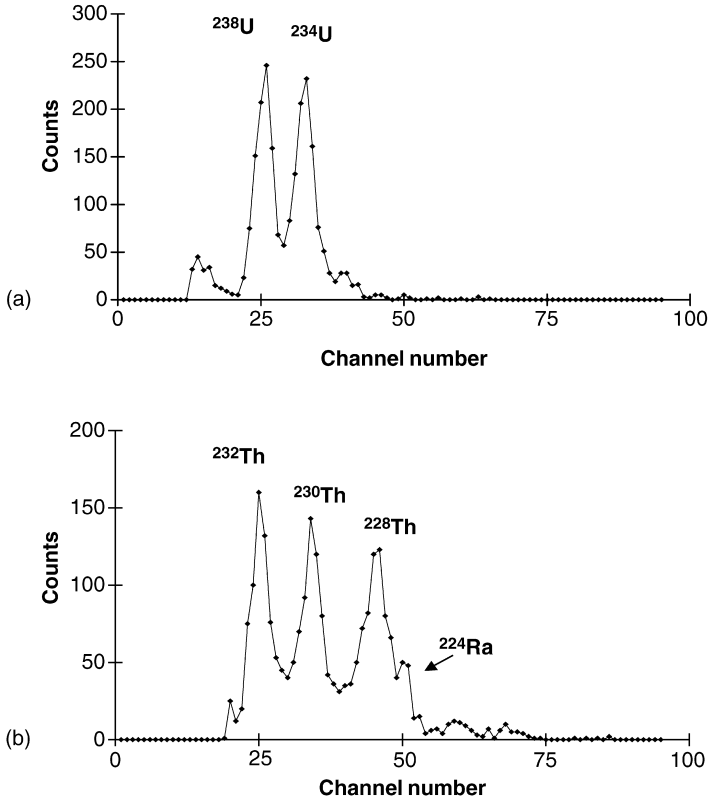

Fig. 27.18 *Typical PERALS™ spectra for the determination of uranium and thorium by extraction and counting.* (*a*) *U in reference soil IAEA*-375, (*b*) *Th in reference soil IAEA*-375*; data from* (*Füeg* et al., 1997).

extraction. This protocol of extraction and analysis is currently applied, for example, with ICPOES for the determination of uranium and thorium in apatite minerals after solvent extraction into diisobutyl ketone using 1-phenyl-3-methyl-4-trifluoroacetyl-5-pyrazolone (Fujino *et al.*, 2000).

Chromatography is basically a separation technique that needs to be completed by applying analytical sensors after the separation step. Chromatography may be performed with an ion-exchange column or by extraction with partitioning onto a liquid phase; spectroscopy and conductivity sensors are generally used for detection. Extraction chromatography was applied for the determination of plutonium and americium in soil samples from Semipalatinsk (Kazachevskij *et al.*, 1999). Ion chromatography was used to perform speciation of plutonium in natural groundwater using anion-exchange resin (Cooper *et al.*, 1995). In most cases actinides are detected using alpha spectroscopy (e.g. Morello *et al.*, 1986). Occasionally, UVS–VIS has been applied to identify actinides eluted.

The determination of actinides (U, Np, Pu, Am, and Cm) is very sensitive and accurate by combining high-performance ion chromatography and ICP quadrupole mass spectrometric detection (Garcia Alonso *et al.*, 1995; Röllin *et al.*, 1996) (see Fig. 27.19). This separation technique followed by mass spectroscopic detection allows the elimination of isobaric interferences such as from one

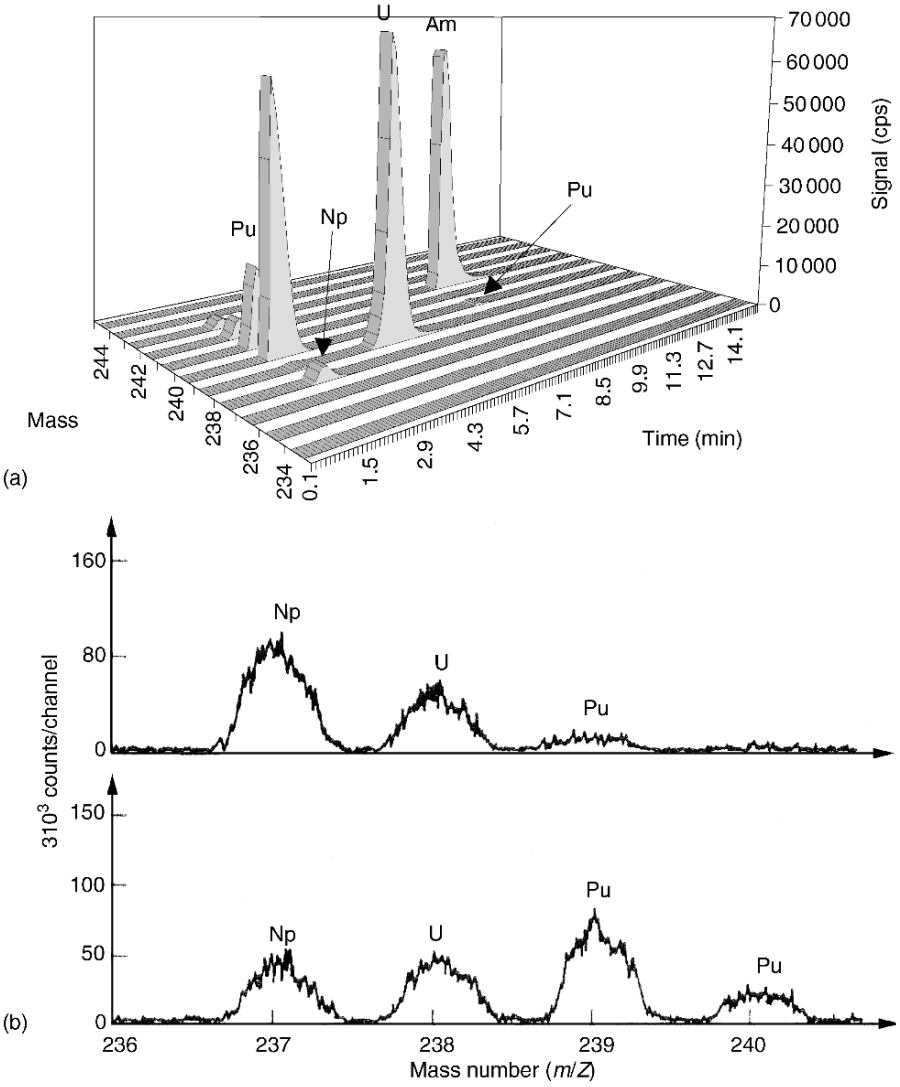

Fig. 27.19 (*a*) *Separation of U, Np, Pu, and Am in* 200 µl *of* 1% HNO_3 *solution containing* 100 ng mL^{-1} *U, Pu, and Am by HPLC-ICPMS* (*Röllin* et al., 1996). (*b*) *Result of actinide analysis by ETV-ICPMS scan of* 1 g *marine sediment collected near a nuclear discharge and subsequently chemically extracted in the laboratory* (*Kim* et al., 1989).

actinide element, e.g. ^{243}Am and ^{243}Cm, or from cluster ions, e.g. $^{155}Gd^{40}Ar_2^+$ or $^{207}Pb^{16}O^{12}C^+$ for $^{235}U^+$, $^{238}U^1H^+$ for $^{239}Pu^+$ (Moreland *et al.*, 1970), $^{232}Th^{12}C^+$ for $^{244}Cm^+$ (e.g. from ETV), or $^{232}Th^{16}O^+$ for $^{248}Cm^+$ (Becker *et al.*, 1999c).

Physical separation techniques such as filtration or ultracentrifugation may be used to enhance actinide speciation. Ultrafiltration or dialysis may be used with alpha spectroscopy for actinides associated with particles or colloids (Degueldre *et al.*, 1994). Combination of ultrafiltration and ICPMS offers also a very sensitive means for colloid analysis, as was the case for groundwater sampling around the fossil reactor of Bagombé (Pedersen, 1996).

Recently, capillary electrophoresis was coupled to ICPMS in order to combine the good performance of this separation technique with the high sensitivity of the ICPMS for the analysis of plutonium and neptunium states (Kuczewski *et al.*, 2003). It was possible to separate a model element mixture containing NpO_2^+, UO_2^{2+}, La^{3+}, and Th^{4+} in 1 M acetic acid. All separations were obtained in less than 15 min and a detection limit of 2×10^{-7} M was achieved. To verify the good speciation performances for plutonium and neptunium during the separation, capillary electrophoresis ICPMS was compared with the result of UV-VIS.

Combining XRF with micro-Raman and IR spectroscopies is a powerful experimental approach in providing information on components present in highly heterogeneous materials, which contain or have been in contact with actinides (Schoonover and Havrilla, 1999). XRF mapping allows identification of plutonium-contaminated regions, while vibrational microspectroscopy provides information on molecular species present and their spatial distribution. This approach provides insight into very complex samples and provides a technique capable of exploring the interaction of molecular components with actinides in complex environmental media. For example, XANES and XPS are combined to confirm uranium reduction from VI to IV by *Clostridium* sp. (Francis *et al.*, 1994). Speciation of uranium complexes in solutions at low ionic strength containing phosphate such as those of seepage waters from old uranium mill tailings was performed by combining data provided by potentiometric and spectroscopic investigations (Brendler *et al.*, 1996).

The feasibility of using the combination of PIXE and RBS to measure uranium and thorium in environmental and biological samples has been demonstrated for environmental studies (Paschoa *et al.*, 1987). The microdistribution of uranium-bearing particles in biological tissues was performed in order to evaluate local irradiation doses in the lungs of former and present uranium miners and millers. These particles have been localized in lungs using neutron-induced uranium FTs registered in solid-state nuclear track detectors in association with a microPIXE and RBS combination. Similarly, RBS and microPIXE have been recently used combined for the study of uranium diffusion in granitic rock matrices analyzing the effect of the presence of bentonite clay (Alonso *et al.*, 2003).

The analysis of the structure of layers on UO_2 leached in H_2O was performed by combining nuclear techniques including RBS-channeling, resonance

scattering, and ERDA using energetic He ions (Matzke, 1996). They were used for the analysis of a UO_2 single crystal leached in demineralized water with different pH values at temperatures up to 200°C. For growth of a U_3O_7 layer, the rate law for layer growth followed a $t^{1/2}$ trend for temperatures between 150 and 200°C and pH in the range 6–10.

Experiments investigating the migration behavior of Th, U, Np, Pu, and Am and the influence of smectite colloids by *in situ* tracer experiment in fractured rock have been performed in dipole mode (Möri *et al.,* 2003). The colloid determination was carried out by LIBD, PCS, and single-particle counting (SPC), while the actinides were determined by the radiochemical techniques after physical separation. Colloid recovery was comparable for these detection techniques.

A comparison of techniques for the analysis of uranium from uraniferrous coal-bearing clays has been reported (Ochsenkuehn Petropulu and Parissakis, 1993). It was carried out using separation techniques, including leaching in carbonate solution, enrichment through an ion exchanger, and elution of Mo and V with EDTA. Uranium is quantitatively eluted by HNO_3 and precipitated by NH_4OH. DPP, atomic absorption analysis (AAS), XRF, instrumental NAA, and ICPMS have been used to determine the uranium content in the raw materials and to investigate the various steps of the process.

Comparison of sensitive techniques such as ICPMS and radiometric alpha and beta spectroscopy has been systematically explored by authors (e.g. Solatie *et al.*, 2000). ICPMS remains very sensitive for the long-lived actinides while radiometric techniques are more suited for short-lived actinides. The half-lives of actinides that are appropriate for analysis by ICPMS may be estimated from Table 27.2 (DL = 10 μBq) and Table 27.7. The detection limits for ICPMS range from 4×10^{-17} to 4×10^{-19} mol in 1 mL depending on the methodology, which correspond to half-lives of 10^4 to 10^2, respectively.

Table 27.8 presents a summary of detection limits estimated for a large number of the sensitive techniques discussed in this chapter. The passive radioanalytical techniques are very sensitive to short-lived nuclides. Alpha spectroscopy has better performance than gamma spectroscopy because of the more efficient detection yield and better background conditions. NAA may improve the sensitivity but its use becomes increasingly limited. Visible spectrophotometry (VIS) is less sensitive than COL but fluorescence (TRLIFS) techniques, allowing speciation, are much more powerful. DPP and XAS provide data for actinide speciation in solution, the latter method in the solid phase also at the 10^{-9} mol level (upgraded to ~4×10^{-18} mol for microXAS, see Section 27.3.2). ICPMS, SIMS, RIMS, and AMS are all very sensitive. The latter reaches DLs better than 10^{-20} mol. Finally, EELS associated with STEM is the most sensitive identification and speciation technique. The detection limit is estimated to be of the order of 10^{-22} mol but it applies to specific small specimens in vacuum, which require extensive preparation and time-consuming analysis and interpretation. EELS has however proved its superior detection.

Table 27.8 *Comparison of detection limits for actinide isotope element or species, all data given in* mol, *normalized to* 1 mL *fluid analysis for VIS/COL, TRLIFS, DPP, and ICPMS. Note:* **bold** *figures for experimental data, and regular figures for theoretical or estimated data,* γS *from slim-layer source and from Table* 27.2, αS *from electroplated sources and from Table* 27.2*; VIS/COL: for* 1 mL *sample and from Table* 27.3*; TRLIFS: for* 1 mL *and from Table* 27.3*; DPP for* 1 mL *and from Table* 27.5*; EELS from Table* 27.5*; NAA from Table* 27.6*; AMS from Section* 27.3.6*; ICPMS for* 1 mL *and from Table* 27.7.

$^{A}An(Y)$	γS	αS	*VIS/COL*	*TRLIFS*	*DPP*	*EELS*	*NAA*	*AMS*	*ICPMS*
^{227}Ac(III)	4×10^{-14}	4×10^{-18}	–	–	–	1×10^{-22}	–	–	4×10^{-17}
^{230}Th(IV)	1×10^{-11}	6×10^{-17}	$\mathbf{3 \times 10^{-11}}$	$\mathbf{1 \times 10^{-17}}$	–	1×10^{-22}	–	$\sim 3 \times 10^{-20}$	$\mathbf{4 \times 10^{-17}}$
^{232}Th(IV)	5×10^{-7}	1×10^{-11}			–		$\mathbf{\sim 2 \times 10^{-15}}$		
^{231}Pa(V)	2×10^{-14}	2×10^{-17}	–	–	–	1×10^{-22}	$\mathbf{\sim 2 \times 10^{-15}}$	–	4×10^{-17}
^{234}U(VI)	2×10^{-11}	2×10^{-21}					–		
^{235}U(VI)	–	5×10^{-13}	$\mathbf{2 \times 10^{-11}}$	$\mathbf{1 \times 10^{-15}}$	$\mathbf{4 \times 10^{-12}}$	1×10^{-22}	–	$\sim 3 \times 10^{-20}$	$\mathbf{4 \times 10^{-17}}$
^{238}U(VI)	2×10^{-8}	3×10^{-11}					$\mathbf{\sim 2 \times 10^{-15}}$		
^{237}Np(V)	2×10^{-12}	2×10^{-15}	$\mathbf{1 \times 10^{-10}}$	$\mathbf{1 \times 10^{-12}}$	$\mathbf{2 \times 10^{-11}}$	1×10^{-22}	$\mathbf{\sim 2 \times 10^{-15}}$		$\mathbf{4 \times 10^{-17}}$
^{238}Pu(IV)	–	7×10^{-22}					–		
^{239}Pu(IV)	7×10^{-12}	2×10^{-17}		$\mathbf{4 \times 10^{-11}}$	$\mathbf{2 \times 10^{-11}}$	1×10^{-22}	–	$\sim 3 \times 10^{-20}$	4×10^{-17}
^{240}Pu(IV)	1×10^{-12}						–		
^{241}Am(III)	1×10^{-16}	3×10^{-19}		$\mathbf{4 \times 10^{-12}}$	–	1×10^{-22}	–	–	4×10^{-17}
^{242}Cm(III)	5×10^{-15}	3×10^{-22}	–	$\mathbf{4 \times 10^{-14}}$	–	1×10^{-22}	–	–	4×10^{-17}
^{244}Cm(III)	1×10^{-16}	1×10^{-20}			–		–	–	

27.5 CONCLUDING REMARKS

For the past 50 years, actinide identification and speciation in environmental samples has been a topic of growing interest. Techniques required to perform the characterization of actinides that will have better performance in terms of capacity, realization, precision, and detection limit are needed. This will remain a challenge for this century. Detection limits are compared in Tables 27.2–27.7 and summarized in Table 27.8.

Since most of the actinides are α emitters, development of separation techniques coupled with highly sensitive alpha spectroscopy or LSC allows their detection below the 10 mBq level. LSC allows a fast analysis while alpha spectroscopy requires more experimental efforts but permits higher resolution and more sensitive analysis (10 μBq). An alternative to conventional alpha spectrometry may be NAA for which limitations of low counting rates on the non-activated actinide-bearing samples should be improved by their activation; the background is, however, also enhanced. NAA has been found to be particularly prone to interference especially from uranium nuclides.

The trend today is to use advanced ICPMS techniques instead of separation, electroplating, and alpha spectroscopy because ICPMS uses less material and is a less time-consuming technique. ICPMS may, however, require the use of a separation technique, as discussed in Section 27.4, which may advantageously be performed on-line because ICPMS is fast enough, compared to NAA or alpha spectroscopy, to analyze the eluant on-line. Evaluation of NAA and ICPMS methods for the assay of neptunium and other long-lived actinides in environmental matrices has been discussed (Hursthouse *et al.*, 1992). ICPMS offers suitable sensitivity, precision, and accuracy compared to other techniques, with considerably faster sample throughput relative to radiometric and activation approaches. Added advantages of ICPMS include the abilities to determine concentrations of several long-lived actinides simultaneously and to quantify $^{239}Pu/^{240}Pu$ ratios.

ICPMS, NAA, and alpha spectrometry were compared (Kim *et al.*, 1989) for the determination of ^{237}Np in environmental samples. The accuracy and precision of ICPMS was assessed by comparison with that obtained by NAA and alpha spectrometry. Results are in good agreement at a relative deviation of 2–9%. The routine analysis detection limit is 0.02 mBq mL^{-1} or 4×10^{-15} mol (comparable with the estimated data in Table 27.8) calculated with the specific activity of 26 Bq per ng of ^{237}Np.

Plutonium is somewhat difficult to analyze quantitatively by γ-ray spectroscopy because all the commonly encountered isotopes ^{236}Pu, ^{238}Pu, ^{239}Pu, ^{240}Pu, ^{242}Pu, and ^{244}Pu have very low γ-ray abundance emissions, making conventional 4π α-γ coincidence counting techniques impractical. ^{241}Pu is a low-energy β emitter with low (20 keV) end point energy and no associated γ-ray. ^{241}Pu is best analyzed using LSC by calibration with ^{3}H with some corrections for differing end-point energies and beta spectrum shapes.

Several of the advanced analytical techniques described in this chapter are very powerful methods for the determination and characterization of actinides in environmental systems. Better standards and reference materials, as well as intercomparison exercises, are required. For some techniques, standards are occasionally unavailable, for example for SIMS, EMPA, LAICPMS, XRF, and some surface analyses. Other techniques such as RBS, AMS, and EELS under vacuum and XAS in solution require internal calibrations; the sensitivity of the latter is expected to improve in the future. However, the techniques presented are often complementary; in many cases they provide unique information that cannot be obtained with alternative methods. Consequently, their continued and expanded utilization is required for actinide identification and speciation in the environment. Development of analytical techniques such as MBE/AS or EPR, which is more sensitive than NMR for actinide identification and speciation, may be suggested in future research programs.

As far as the environment is concerned, one has to think the way the analyst and the environmental scientist would collaborate together to produce data that can be used by modelers or authorities. The challenge is however to understand the behavior of actinide elements in the environment. Biogeochemical pathways have to be described, quantified, and understood. The contaminated systems interact with the local environment that may modify actinide speciation by physical–chemical processes, which need to be studied. Simple processes such as actinide association with biofilm, bioaccumulation, specific co-precipitation, or sorption onto soil or rock require detailed and full quantification and speciation for the understanding of process mechanism. Transport of actinides in fluids such as air or water includes particulate or colloidal phases. These analyses must be integrated in the analytical strategy as specific species for modeling their biogeochemical affinity.

The challenge will be to find and develop direct analytical probes for actinide speciation at very low concentration to provide data that will better characterize the actinide species to predict their behavior in heterogeneous and complex natural systems.

GLOSSARY

aAFM	Acoustic AFM
AAS	Atomic absorption spectroscopy
AES	Auger electron spectroscopy
AFM	Atomic force microscope
AMS	Accelerator mass spectroscopy
COL	Colorimetry
COUL	Coulometry
DNAA	Delay neutron activation analysis
DPP	Differential pulse polarography

DPV	Differential pulse voltammetry
DRS	Diffuse reflection spectroscopy
eAFM	Electrochemical AFM
EDS	Energy-dispersive X-ray spectroscopy
EELS	Electron energy loss spectroscopy
EMPA	Electron microprobe analysis
EPR	Electron paramagnetic resonance
ERDA	Elastic recoil detection analysis
ESMS	Electrospray ionization mass spectroscopy
ETV	Electrothermal vaporization
EXAFS	Extended X-ray absorption fine structure spectroscopy
FTRAD	Fission track radiography
GRAV	Gravimetry
HPLC	High-pressure liquid chromatography
ICPOES	Inductively coupled plasma optical emission spectroscopy
ICPMS	Inductively coupled plasma mass spectroscopy
IRFT	Infrared Fourier transform spectroscopy
IRS	Infrared spectroscopy
ISE	Ion-selective electrode
LAICPMS	Laser ablation inductively coupled plasma mass spectrometry
LAICPOES	Laser ablation inductively coupled plasma optical emission spectrometry
LAMMA	Laser ablation micro mass analysis
LSC	Liquid scintillation counting
LIBD	Laser-induced breakdown detection
LIPAS	Laser-induced photoacoustic spectroscopy
LIPDS	Laser-induced photothermal displacement spectroscopy
MALDI	Matrix-assisted laser desorption ionization
MBAS	Mössbauer absorption spectroscopy
MBES	Mössbauer emission spectroscopy
MS	Mass spectroscopy
NAA	Neutron activation analysis
NIRS	Near-infrared spectroscopy
NMR	Nuclear magnetic resonance
NPHOT	Neutron photolysis
NRA	Nuclear reaction analysis
NS	Neutron spectroscopy
PAS	Photoacoustic spectroscopy
PCS	Photon correlation spectroscopy
PERALS	Photon electron-rejecting alpha liquid scintillation
PHOS	Phosphometry
PHOTA	Photoactivation
NPHOT	Neutron photoactivation
PIGE	Particle (proton)-induced gamma emission

PIXE	Proton (particle)-induced X-ray emission
RAD	Radiography, autoradiography
RAMS	Raman spectroscopy
RBS	Rutherford backscattering
RIS	Resonance ionization spectroscopy
RIMS	Resonance ionization mass spectroscopy
RMA	Raman microprobe analysis
SEAM	Scanning electron acoustic microscopy
SEM	Scanning electron microscopy
SEXAS	Secondary electron X-ray absorption spectroscopy
SIMS	Secondary ion mass spectroscopy
SNMS	Sputtered neutral mass spectroscopy
SPC	Single-particle counting
SR	Seismic reflection
SSMS	Spark source mass spectroscopy
STEM	Scanning transmission electron microscopy
TEM	Transmission electron microscopy
TFMS	Time-of-flight mass spectroscopy
TIMS	Thermal ionization mass spectroscopy
TOM	Tomography
TRLIFS	Time-resolved laser-induced fluorescence spectroscopy
VIS	Visible spectroscopy
UPS	Ultraviolet photoelectron spectroscopy
UVS	Ultraviolet spectroscopy
VOL	Volumetry
WDS	Wavelength-dispersive spectrometry
XANES	X-ray absorption near-edge spectroscopy
XAS	X-ray absorption spectroscopy
XPS	X-ray photo-electron spectroscopy
XRF	X-ray fluorescence spectroscopy
XS	X-ray conversion spectroscopy
αS	Alpha spectroscopy
βS	Beta spectroscopy
γS	Gamma spectroscopy

REFERENCES

Abuzwida, M. A., Maslennikov, A. G., and Peretrokhin, V. F. (1991) *J. Radioanal. Nucl. Chem.,* **147**, 41–50.

Agarande, M., Benzoubir, S., Bouisset, P., and Calmet, D. (2001) *Appl. Radiat. Isot.,* **55**, 161–5.

Ahonen, L., Ervanne, H., Jaakkola, T., and Blomqvist, R. (1994) *Radiochim. Acta,* **66/7**, 115–21.

Akopov, G. A., Krinitsyn, A. P., and Tikhonova, A. E. (1988) *Radiokhimiya,* **30**, 578–83.

Alfassi, Z. B. (1990) *Activation Analysis* (vol. 1), CRC Press, Boca Raton, FL, pp. 97–109.

Alonso, U., Missana, T., Patelli, A., Ravagnan, J., and Rigato, V. (2003) *Nucl. Instrum. Met. B,* **207**, 195–204.

Anczkiewicz, R., Oberli, F., Burg, J. P., Villa, I. M., Guenther, D., and Meier, M. (2001) *Earth Planet. Sci. Lett.,* **191**, 101–14.

Antonio, M. R., Soderholm, L., Williams, C. W., Blaudeau, J.-Ph., and Bursten, B. E. (2001) *Radiochim. Acta,* **89**, 17–25.

Apps, M. J., Duke, M. J. M., and Stephens-Newsham, L. G. (1988) *J. Radioanal. Nucl. Chem.,* **123**, 133–47.

Arslanov, K. A., Kuznetsov, V., Yu., Lokshin, N. V., and Pospelov, Yu. N. (1989) *Sov. Radiochem.,* **30**, 378–82.

Baechler, S., Materna, Th., Jolie, J., Cauwels, P., Crittin, M., Honkimaki, V., Johner, H. U., Masschaele, B., Mondelaers, W., Kern, J., and Piboule, M. (2001) *J. Radiochem. Nucl. Chem.,* **250**, 39–45.

Bajo, S. and Eikenberg, J. (1999) *J. Radioanal. Nucl.Chem.,* **242**, 745–51.

Balescu, S., Dumas, B., Gueremy, P., Lamothe, M., Lhenaff, R., and Raffy, J. (1997) *Paleogeogr. Paleoclimat. Paleoecol.,* **130**, 25–41.

Barrero Moreno, J., Garcia Alonso, J. I., Arbore, Ph., Nicolaou, G., and Koch, L. (1996) *J. Anal. At. Spectrom.,* **11**, 929–35.

Barth, H., Ganz, M., and Brandt, R. (1994) *Geochim. Cosmochim. Acta,* **58**, 4759–65.

Basile, L. J., Ferraro, J. R., Mitchell, M. L., and Sullivan, J. C. (1978) *Appl. Spectrosc.,* **32**, 535–7.

Baskaran, M., Santschi, P. H., Benoit, G., and Honeyman, B. D. (1992) *Geochim. Cosmochim. Acta,* **56**, 3375–88.

Baxter, M. S., Fowler, S. W., and Povinec, P. P. (1995) *Appl. Radiat. Isot.,* **46**, 1213–23.

Becerril- Vilchis, A., Meas, Y., and Rojas-Hernández, A. (1994) *Radiochim. Acta,* **64**, 99–105.

Becker, S. and Dietze, H.-J. (1999a) *Fresenius J. Anal. Chem.,* **364**, 482–8.

Becker, S. and Dietze, H.-J. (1999b) *J. Anal. At. Spectrom.,* **14**, 1493–500.

Becker, J. S., Dietze, H.-J., McLean, J. A., and Montaser, A. (1999c) *Anal. Chem.,* **71**, 3077–84.

Beitz, J. V. and Hessler, J. P. (1980) *Nucl. Technol.,* **51**, 169–77.

Beitz, J. V., Bowers, D. L., Doxater, M. M., Maroni, V. A., and Reed, D. T. (1988) *Radiochim. Acta,* **44/5**, 87–93.

Bellido, L. F., Robinson, V. J., and Sims, H. E. (1994) *Radiochim. Acta,* **64**, 11–4.

Benke, R. R. and Kearfott, K. J. (1997) *Health Phys.,* **73**, 350–61.

Bernard, G., Geipel, G., Brendler, V., and Nitsche, H. (1998) *J. Alloys Compds,* **271/3**, 201–5.

Berry, J. A., Jefferies, N. L., and Littleby, A. K. (1989) *Proc. Water – Rock Interact.*, Balkema, Rotterdam, 75–8.

Berry, J. A., Bishop, H. E., Cowper, M. M., Fozard, P. R., McMillan, J. W., and Mountfort, S. A. (1993) *Analyst,* **118**, 1241–6.

Berry, J. A., Bishop, H. E., Cowper, M. M., Fozard, P. R., McMillan, J. W., and Mountfort, S. A. (1994) *Radiochim. Acta,* **66/7**, 243–50.

Bertsch, P. M., Hunter, D. B., Sutton, S. R., Bajt, S., and Rivers, M. L. (1994) *Environ. Sci. Technol.,* **28**, 980–4.
Bhilare, N. G. and Shinde, V. M. (1994) *J. Radioanal. Nucl. Chem.,* **185**, 243–50.
Bitea, C., Müller, R., Neck, V., Walther, C., and Kim, J. I. (2003) *Coll. Surf. A,* **217**, 63–70.
Bojanowski, R., Holm, E., and Whitehead, N. E. (1987) *J. Radioanal. Nucl. Chem.,* **115**, 23–37.
Bouby, M., Ngo-Munh, Th., Geckeis, H., Scheibaum, F. J., and Kim, J. I. (2002) *Radiochim. Acta,* **90**, 727–32.
Brendler, V., Geipel, G., Bernhard, G., and Nitsche, H. (1996) *Radiochim. Acta,* **74**, 75–80.
Buck, E. C., and Fortner, J. A. (1997) *Ultramicroscopy,* **67**, 69–75.
Buckau, G., Stumpe, R., and Kim, J. I. (1986) *J. Less Common Metals,* **122**, 555–62.
Buesseler, K. O. (1989) *Development and Evaluation of Alternative Radioanalytical Methods, Including Mass Spectrocopy for Marine Material. Proc. Adv. Group Meet.,* Monaco, June 6–9 1989, TECDOC-683, IAEA, pp. 45–51.
Bundschuh, T., Knopp, R., Müller, R., Kim, J. I., Neck, V., and Fanghänel, Th. (2000) *Radiochim. Acta,* **88**, 625–9.
Bundt, M., Albrecht, A., Froidevaux, P., Blaser, P., and Flühler, H. (2000) *Environ. Sci. Technol.,* **34**, 3895–9.
Burmistenko, Yu. N. (1986) *Photonuclear analysis of substance composition*, Ehnergoatomizdat, pp. 153–7.
Burnett, W. C., Schultz, M., Inn, K. G. W., and Thomas, W. (1995) *Radioact. Radiochem.,* **6**, 46.
Butler, I. B. and Nesbitt, R. W. (1999) *Earth Planet. Sci. Lett.,* **167**, 335–45.
Byrne, A. R. (1986) *J. Environ. Radioact.,* **4**, 133–44.
Byrne, A. R. (1993) *Fresenius J. Anal. Chem.,* **345**, 144–51.
Byrne, A. R. and Benedik, L. (1999) *Czech. J. Phys.,* **49**, 263–70.
Carbol, P., Solatie, D., Erdmann, N., Betty, M., and Nylén, T. (2003) *J. Environ. Radioact.,* **68**, 27–46.
Carroll, S. A., Bruno, J., and Petit, J. C. (1992) *Radiochim. Acta,* **58/9**, 245–52.
Castillo, M. K., Santos, G. P., Ramos, A. F., and Teherani, D. K. (1996) *Nucleus,* **32**, 17–23.
Cavellec, R., Lucas, C., Simoni, E., Hubert, S., and Edelstein, N. (1998) *Radiochim. Acta,* **82**, 221–5.
Chassard-Bouchaud, C., and Galle, P. (1988) *Radiation Protection Practice,* Pergamon Press, Sydney, pp. 656–9.
Church, B. W., Shinn, J. H., Williams, G. A., Martin, L. J., O'Brien, R. S., and Adams, S. R. (2000) *Nuclear Physical Methods in Radioecological Investigations of Nuclear Test Sites.* (eds. S. S. Hecker, C. F. V. Mason, K. K. Kadyrzhanov and S. B. Kislitsin), Kluwer Academic Publishers, Dordrecht, pp. 203–19.
Civici, N. (1997) *J. Nat. Tech. Sci.,* **3**, 43–8.
Claassen, A., and Vissen, J. (1946) *Rec. Trav. Chim.,* **65**, 211–5.
Conaway, J. G., Bristow, Q., and Killeen, P. G. (1980) *Geophysics,* **45**, 292–311.
Conradson, S. (1998) *Appl. Spectrosc.,* **52**, 252A–79A.
Cooper, M. B., Burns, P. A., Tracy, B. L., Wilks, M. J., and Williams, G. A. (1994) *J. Radioanal. Nucl. Chem.,* **177**, 161–84.
Cooper, E. L., Haas, M. K., and Mattie, J. F. (1995) *Appl. Radiat. Isot.,* **46**, 1159–73.

Curran, G., Sevestre, Y., Rattray, W., Allen, P., and Czerwinski, K. R. (2003) *J. Nucl. Mater.,* **323**, 41–48.

Curtis, D. B., Cappis, J. H., Perrin, R. E., and Rokop, D. J. (1987) *Appl. Geochem.,* **2**,133.

Degueldre, C., Ulrich, H. J., and Silbi, H. (1994) *Radiochim. Acta,* **65**, 173–9.

Degueldre, C. and Taibi, K. (1996) *Anal. Chim. Acta,* **321**, 201–7.

Degueldre, C. and Paratte, J. M. (1999) *J. Nucl. Mater.,* **273**, 1–6.

Degueldre, C., Rochicoli, F., and Laube, A. (1999) *Anal. Chim. Acta,* **834**, 23–31.

Degueldre, C. and Favarger, P. Y. (2004) *Talanta,* **62**, 1051–54.

Degueldre, C., Reed, D., Kroft, A. J., and Mertz, C. (2004) *J. Synchrotron. Rad.,* **11**, 198–203.

Degueldre, C., Favarger, P.-Y., Rosser, R., and Wold, S. (2005) *Talenta*.

Della Mea, G., Dran, J.-C., Moulin, V., Petit, J.-C., Theyssier, M., and Ramsay, J. D. F. (1992) *Radiochim. Acta,* **58/9**, 219–23.

Denecke M., Dardenne, K., and Maquart, Ch. (2004) *Talanta*.

Dodge C. J., Francis, A. J., and Clayton, C. R. (1995) in *Emerging Technologies in Hazardous Waste Management*, ACS, CONF 9509139, 1352–77.

Dominik, J., Schuler, Ch., and Santschi, P. H. (1989) *Earth Planet. Sci. Lett.,* **93**, 345–57.

Dong, Z. (1990) *Uranium Geology Youkuang Dizhi China,* **6**, 291–6.

Dran, J. C., Della Mea, G., Paccagnella, A., Petit, J. C., and Menager, M.-Th. (1988) *Radiochim. Acta,* **44/5**, 299–304.

Drot, R., Simoni, E., Alnot, M., and Ehrhart, J. J. (1998) *J. Colloid Interface Sci.,* **205**, 410–6.

Dupleissis, J., Genet, M., and Guillaumont, R. (1974) *Radiochim. Acta,* **21**, 21–8.

Eikenberg, J., Zumsteg, I., Bajo, S., Vezzu, G., and Fern, M. (1999) *Radioact. Radiochem.,* **10**, 31–40.

El- Ansary, A. L., Issa, Y. M., Kandil, A. T., and Soliman, M. H. (1998) *Asian J. Chem.,* **10**, 86–98.

Eliet, V., Bidoglio, G., Omenetto, N., Parma, L., and Grenthe, I. (1995) *J. Chem. Soc. Faraday Trans.,* **91**, 2275–85.

Engkvist, I. and Albinsson, Y. (1992) *Radiochim. Acta,* **58/9**, 109–12.

Erdmann, N., Nunnemann, M., Eberhardt, K., Herrmann, G., Huber, G., Köhler, S., Kratz, J. V., Passler, G., Peterson, J. R., Trautmann, N., and Waldek, A. (1998) *J. Alloys Compds,* **271/3**, 837–40.

Fallon, S. J., McCulloch, M. T., van Woesik, R., and Sinclair, D. J. (1999) *Earth Planet. Sci. Let.,* **172**, 221–38.

Fernandez-Valverde, S., Bulbulian, S., and Segovia, N. (1988) *Nucl. Chem. Technol.,* **30**, 1–45.

Fifield, L. K., Clacher, A. P., Morris, K., King, S. J., Cresswell, R. G., Day, J. P., and Livens, F. R. (1997) *Nucl. Instrum. Methods B,* **123**, 400–4.

Fisher, R. D. (1973), in *NMR of Paramagnetic Molecules, Principes and Applications* (eds. G. D. La Mar, W. D. Horrocks, and R. H. Holm), Academics, New York, pp. 521–53.

Fortner, J. A., Buck, E. C., Ellison, A. J. G., and Bates, J. K. (1997) *Ultramicroscopy,* **67**, 77–81.

Francis, A. J., Dodge, C. J., Lu, F., Halada, G. P., and Clayton, C. R. (1994) *Environ. Sci. Technol.,* **28**, 636–9.

Francis, A. J., Gillow, J. B., Dodge, C. J., Dunn, M., Mantione, K., Strietelmeier, B. A., Pansoy-Hjelvic, M. E., and Papenguth, H. W. (1998) *Radiochim. Acta,* **82**, 347–54.
Füeg, B., Tschachtli, T., and Krähenbühl, U. (1997) *Radiochim. Acta,* **78**, 47–51.
Fujino, O., Umetani, S., Ueno, E., Shigeta, K., and Matsuda, T. (2000) *Anal. Chim. Acta,* **420**, 65–71.
Gäggeler, H., Baltensperger U., Haller P., Jost D., and Zinder, B. (1986) *Tagungsberichte Radioaktivitaetsmessungen in der Schweiz nach Tschernobyl und Ihre Wissenschafliche Interpretation*, BGW, Bern 20–22 Oct. 1986.
Garcia Alonso, J., Sena, F., Arbode, Ph., Betti, M., and Koch, L. (1995) *J. Anal. At. Spectrom.,* **10**, 381–93.
Garcia, K., Boust, D., Moulin, V., Douville, E., Fourest, B., and Guillaumont, R. (1996) *Radiochim. Acta,* **74**, 165–70.
Gatti, R. C., Carpenter, S. A., Roberts, K. E., Bescraft, K. A., Prussin, T. G., and Nitsche, H. (1994) *Proc. Fifth Conf. High Level Radioact. Waste Manage.*, 2719–29.
Gauthier, R., Ilmstädter.V., and Lieser, K. H. (1983) *Radiochim. Acta,* **33**, 35–39.
Geipel, G., Reich, T., Brendler, V., Bernard, G., and Nitsche, H. (1997) *J. Nucl. Mater.,* **248**, 408–11.
Geipel, G., Bernhard, G., Brendler, V., and Nitsche, H. (1998) *Radiochim. Acta,* **82**, 59–62.
Godbole, A. G. and Patil, S. K. (1979) *Talanta,* **26**, 330–2.
Goltz, D. M., Grégoire, D. C., Byrne, J. P., and Chakrabarti, C. L. (1995) *Spectrochim. Acta,* **50B**, 803–14.
Gonzales, E. R., Gladney, E. S., Boyd, H. A., McInroy, J. F., Muller, M., and Palmer, P. D. (1988) *Health Phys.,* **55**, 927–32.
Gouder, T. (1998) *J. Alloys Compds,* **271/3**, 841–45.
Grigoriev, M. S., Fedoseev, M., Gelis, A. V., Budantseva, N. A., Shilov, V. P., Perminov, V. P., Nikonov, M. V., and Krot, N. N. (2001) *Radiochim. Acta,* **89**, 95–100.
Groeschel, F., Bart, G., Montgomery, R., and Yagnik, S. K. (2003) *IAEA TECDOC* **1345**, 188–202.
Guillot, L. (2001) *J. Environ. Radioact.,* **53**, 381–98.
Gutmacher, R. G., Cremers, D. A., and Wachter, Z. (1987) *Trans. Am. Nucl. Soc.,* **55**, 19–20.
Hafez, M. B. and Hafez, N. (1992) *J. Radioanal. Nucl. Chem. Lett.,* **166**, 203–10.
Harduin, J. C., Peleau, B., and Piechowski, J. (1993) *Radioprot. Bull. Soc. Radioprot. Fr.,* **28**, 291–301.
Hartman, M. J. and Dresel, P. E. (1998) Report PNNL-11793.
Harvey, B. R., Lovett, M. B., and Boggis, S. J. (1987) *J. Radioanal. Nucl. Chem.,* **115**, 357–68.
Hecht, F. and Reich-Rohrwig, W. (1929) *Monatsh. Chem.,* **53/4**, 596.
Heier, K. S., and Rogers, J. J. W. (1963) *Geochim. Cosmochim. Acta,* **27**, 137–54.
Henge Napoli, M. H., Ansoborlo, E., Claraz, M., Berry, J. P., and Cheynet, M. C. (1996) *Cell. Mol. Biol.,* **42**, 413–20.
Hess, N. J., Felmy, A. R., Rai, D., and Conradson, S. D. (1997) *Mat. Res. Soc. Symp. Proc.,* **465**, 729–34.
Hirose, K. (1994) *J. Radioanal. Nucl. Chem.,* **181**, 11–24.
Hoffman, D. C., Lawrence, F. O., Merwerter, J. L., and Rourke, F. M. (1971) *Nature,* **234**, 132–34.

Holm, E. and Fukai, R. (1986) *J. Less Common Metals,* **122**, 487–97.
Holm, E., Rioseco, J., and Pettersson, H. (1992) *J. Radioanal. Nucl. Chem.,* **156**, 183–200.
Horn, I., Rudnick, R. L., and McDonough, W. F. (2000) *Chem. Geol.,* **164**, 281–301.
Huff, E. A. and Bowers, D. L. (1990) *Appl. Spectrosc.,* **44**, 728–29.
Hunter, D. B. and Bertsch, P. M. (1998) *J. Radioanal. Nucl. Chem.,* **234**, 237–42.
Hursthouse, A. S., Baxter, M. S., McKay, K., and Livens, F. R. (1992) *J. Radiochem. Nucl. Chem.,* **157**, 281–94.
Igarashi, Y., Shiraishi, K., Kim, Ch. K., Takaku, Y., Yamamoto, M., and Ikeda, N. (1990) *Anal. Sci.,* **6**, 157–64.
Itagaki, H., Tanaka, S., and Yamawaki, M. (1991) *Radiochim. Acta,* **52/3**, 91–4.
Ivanov, V. M., Morozko, S. A., and Massud, S. (1995) *J. Anal. Chem.,* **50**, 1171–8.
Ivanovich, M. (1994) *Radiochim. Acta,* **64**, 81–94.
Iwatschenko-Borho, M., Frenzel, E., and Kreiner, H. J. (1992) *Am. Chem. Soc.,* **49**, 507–14.
Jaiswal, D. D., Dang, H. S., Pullat, V. R., and Sharma, R. C. (1994) *Bull. Radiat. Prot.,* **17**, 44–7.
Jensen, M. P. and Choppin, G. R. (1998) *Radiochim. Acta,* **82**, 83–8.
Johansson, L. and Holm, E. (1996) *Nucl. Instrum. Methods A,* **376**, 242–7.
Johnson, S. G. and Feary, B. L. (1993) *Spectrochim. Acta,* **48B**, 1065–77.
Johnson S. G., Giglio J. J., Goodall P. S., and Cummings D. G. (1998) ANL report 95703, 11 p.
Jones, D. G. (2001) *J. Environ. Radioact.,* **53**, 313–33.
Kadyrzhanov, K. K. *et al*., (2000) in *Nuclear Physical Methods in Radioecological Investigations of Nuclear Test Sites* (eds. S. S. Hecker, C. F. V. Mason, K. K. Kadyrzhanov and S. B. Kislitsin), Kluwer Academics Publishers, Dordrecht, 17–42.
Karelin, A. I., Semenov, E. N., and Mikhailova, N. A. (1991) *J. Radioanal. Nucl. Chem.,* **147**, 33–40.
Kasar, U. M., Joshi, A. R., and Patil, S. K. (1991) *J. Radioanal. Nucl. Chem.,* **150**, 369–76.
Kazachevskiy, I. V., Solodukhin, V. P., Khajekber, S., Smirin, L. N., Chumikov, G. N., and Lukashenko, S. N. (1998) *J. Radioanal. Nucl. Chem.,* **235**, 145–9.
Kazachevskij, I. V., Lukashenko, S. N., Chumikov, G. N., Chakroya, E. T., Smirin, L. N., Solodukhin, V. P., Khaekber, S., Berdinova, N. M., Ryazanova, L. A. Bannyh, V. I., and Muratova, V. M. (1999) *Czech. J. Phys.,* **49**, 445–60.
Keil, R. (1978) *Fresenius Z. Anal. Chem.,* **292**, 13–9.
Keil, R. (1979) *Fresenius Z. Anal. Chem.,* **297**, 384–7.
Keil, R. (1981) *Fresenius Z. Anal. Chem.,* **305**, 374–8.
Kerbelov, L. M., and Rangelov, R. (1997) *Uranium Exploration Data and Techniques Applied to the Preparation of Radioelement Maps, IAEA TECDOC* **980**, 299–304.
Khater, A. E., Higgy, R. H., and Pimpl, M. (2001) *J. Environ. Radioact.,* **55**, 255–67.
Khokhrin, V. M. and Denisov, A. F. (1995) *Zadodskaya Laboratoriya,* **61**, 15–7.
Kim, Ch. K., Takaku, A., Yamamoto, M., Kawamura, H., Shiraishi, K., Igarashi, Y., Igarashi, S., Takayama, H., and Ikeda, N. (1989) *J. Radioanal. Nucl. Chem.,* **132**, 131–7.
Kim, Ch. K., Morita, S., Seki, R., Takaku, Y., Ikeda, N., and Assinder, D. J. (1992) *J. Radioanal. Nucl. Chem.,* **156**, 201–3.

Kim, J. I., Buckau, G., and Klenze, R. (1987) Natural Colloids and Generation of Actinide Pseudocolloids in Groundwater, in *Natural Analogues in Radioactive Waste Disposal* (eds. B. Come and N. Chapman), Graham and Trottman, London.
Kim, J. I., Rhee, D. S., Buckau, G., and Morgenstern, A. (1997) *Radiochim. Acta,* **79**, 173–81.
Kimura, T., Serrano, J., Nakayama, S., Takahashi, K., and Takeishi, H. (1992) *Radiochim. Acta,* **58/9**, 173–8.
Kimura, T., Kato, Y., and Yoshida, Z. (1998) *Radiochim. Acta,* **82**, 141–5.
Klenze, R. and Kim, J. I. (1988) *Radiochim. Acta,* **44/5**, 77–85.
Klenze, R., Kim, J. L., and Wimmer, H. (1991) *Radiochim. Acta,* **52/3**, 97–103.
Klett, A. (1999) *IEEE Trans. Nucl. Sci.,* **46**, 877–9.
Kobashi, A., Choppin, G. R., and Morse, J. W. (1988) *Radiochim. Acta* **43**, 211–5.
Kosyakov, V. N., Yakovlev, N. G., Vlasov, M. M., and Piskarev, P. E. (1994) *Radiokhimiya,* **36**, 175–8.
Kuczewski, B., Marquardt, Ch., Seibert, A., Geckeis, H., Kratz, J. V., and Trautmann, N. (2003) *Anal. Chem.,* **75**, 6769–6774.
Kudo, A. (1998) *Radiochim. Acta,* **82**, 159–66.
Kuperman, A., Ya., Smirnov, Yu. A., Fedotov, S. N., Nikol'skaya, T. L., and Efimova, N. S. (1989) *Sov. Radiochem.,* **30**, 750–5.
Kuvik, V., Lecouteux, N., Doubek, N., Ronesch, K., Jammet, G., Bagliano, G., and Deron, S. (1992) *Anal. Chim. Acta,* **256**, 163–76.
La Breque, J. J. (1994) *J. Radioanal. Nucl. Chem.,* **178**, 327–36.
Legin, A. V., Seleznev, B. L., Rudnitskaya, A. M., Vlasov, Yu. G., Tverdokhlebov, S. V., Mack, B., Abraham, A., Arnold, T., Baraniak, L., and Nitsche, H. (1999) *Czech. J. Phys.,* **49**, 679–85.
Lierse, G., Pomar, C., and Rugel, G. (2000) *Nucl. Instrum. Methods B* **172**, 333–37.
Li, B., Wang, M., Lu, B., and Wu, J. (1991) *At. Energy. Sci. Technol.,* **25**, 66–70.
Li, R. and Li, Yu. (1997) *Uranium Geology Youkuang Dizhi,* **13**, 359–63.
Liu, Ch. Yu., Ngian, F. H. M., Kuo, Sh. Y., Northrup, D. R., and Huffman, A. C. (1985) *Soc. Exploration Geophys.,* **1**, 163–5.
Lin, J. C., Broecker, W. S., Anderson, R. F., Hemming, S., Rubenstone, J. L., and Bonani, G. (1996) *Geochim. Cosmochim. Acta,* **60**, 2817–32.
Linauskas, S. H., Szostak, F., and Trivedi, A. (1996) *Health Phys.,* **70**, 85–6.
Livens, F. (2001) *J. Environ. Radioact.,* **55**, 1–3.
Livingston, H. D. and Cochran, J. K. (1987) *J. Radioanal. Nucl. Chem.,* **115**, 299–308.
Lujaniene, G., Lujanas, V., Jankunaite, D., Ogorodnikov, B., Mastauskas, A., and Ladygiene, R. (1999) *Czech. J. Phys.,* **49**, 107–14.
Lumpkin, G. R. (1999) *J. Nucl. Mater.* **274**, 206–17.
Lyons, P. C., Hercules, D. M., Morelli, J. J., Sellers, G. A., Mattern, D., Thomson Rizer, C. L., Brown, F. W., and Millay, M. A. (1987) *Intern. J. Coal Geol.* **7**, 185–94.
Marx, G., Esser, V., Bischoff, H., and Xi, R. H. (1992) *Radiochim. Acta,* **58–9**, 199–204.
Mátel, L., Mikulaj, V., and Rajec, P. (1993) *J. Radioanal. Nucl. Chem.,* **175**, 41–6.
Matthews, R., Koch, R., and Leppin, M. (1997) in *Proc. Exploration* 97 (ed. A. Gubins), pp. 993–1024.
Matzke, H. and Turos, A. (1991) *Solid State Ionics,* **49**, 189–94.
Matzke, H., Della-Mea, G., Freire, F. L., Jr., and Rigato, V. (1990) *Nucl. Instrum. Method B,* **45**, 194–8.

Matzke, H. (1996) *J. Nucl. Mater.,* **238**, 58–63.
May, S., Engelmann, Ch., and Pinte, G. (1987) *J. Radioanal. Nucl. Chem.,* **113**, 343–50.
Maya, L. and Begun, G. M. (1981) *J. Inorg. Nucl. Chem.,* **43**, 2827–32.
Michel, H., Gasparro, J., Barci-Funel, G., Dalmasso, J., Ardisson, G., and Sharovarov, G. (1999) *Talanta,* **48**, 821–5.
Mietelski, J. W., LaRosa, J., and Ghods, A. (1993) *J. Radioanal. Nucl. Chem.,* **170**, 243–58.
Miller, K. M. (1994) *Trans. Am. Nucl. Soc.,* **70**, 47–8.
Miller, K. M., Shebell, P., and Klemic, G. A. (1994) *Health. Phys.,* **67**, 140–50.
Misaelides, P., Godelitsas, A., Charistos, D., Filippidis, A., and Anousis, I. (1995) *Sci. Total Environ.,* **173**, 237–46.
Mitchell, P. I., Vinto, L. L., Dahlgaard, H., Gasco, C., and Sanchez Cabeza, J. A. (1995a) *Environmental Radioactivity in the Artic* (eds. P. Strand and A. Cooke), pp. 339–45.
Mitchell, P. I., Batlle, J. V., Downes, A. B., Condren, O. M., León Vintró, L. L., and Sánchez Cabeza, J. A. (1995b) *Appl. Radiat. Isot.,* **46**, 1175–90.
Mohan, M. S., Ilger, J. D., and Zingaro, R. A. (1991) *Energy and fuels U.S.,* **5**, 568–573.
Moody, G. J., Slater, J. M., and Thomas, J. D. R. (1988) *Analyst,* **113**, 699–703.
Moreland, P. E., Rokop, D. J., and Stevens, C. M. (1970) *Int. J. Mass Spectrom. Ion Phys.,* **5**, 127–36.
Morello, M., Colle, C., and Bernard, J. (1986) *J. Less Common Metals,* **122**, 569–76.
Möri, A., Alexander, W. R., Geckeis, H., Hauser, W., Schäfer, T., Eikenberger, J., Fierz, Th., Degueldre, C., and Missana, T. (2003) *Coll. Surf. A,* **217**, 33–47.
Morris, D. E., Chilsholm-Brause, C. J., Barr, M. E., Conradson, S. G., and Eller, P. G. (1994) *Geochim. Cosmochim. Acta,* **58**, 3613–23.
Moss, J. H. (1960) AERE report 3214.
Moulin, C., Decambox, P., Mauchien, P., Moulin, V., and Theyssier, M. (1991) *Radiochim. Acta,* **52/3**, 119–25.
Moulin, C., Decambox, P., Moulin, V., and Decaillon, J. G. (1995) *Anal. Chem.,* **67**, 348–53.
Moulin, C., Charron, N., Plancque, G., and Virelizier, H. (2000) *Appl. Spectrosc.,* **54**, 843–8.
Moulin, C., Amekraz, B., Hubert, S., and Moulin, V. (2001) *Anal. Chim. Acta,* **21**, 1–11.
Mount, M. E., Sheaffer, M. K., and Abbott, D. T. (1995) *J. Environ. Radioact.,* **25**, 11–9.
Murray, A. S., Marten, R., Johnston, A., and Martin, P. (1987) *J. Radioanal. Nucl. Chem.,* **115**, 263–88.
Mwenifumbo, C. J. and Kjarsgaard, B. A. (1999) *Exploration Mining Geol.,* **8**, 137–147.
Myers, W. A., and Lindner, M. (1971) *J. Inorg. Nucl. Chem.,* **33**, 3233–8.
Nagao, S., Matsunaga, T., and Muraoka, S. (1999) *J. Radioanal. Nucl. Chem.,* **239**, 555–59.
Nagasaki, S., Tanaka, S., and Takahashi, Y. (1988) *J. Radioanal. Nucl. Chem.,* **124**, 383–95.
NAGRA (1991) *Sondierbohrung Leuggern*, Technischer Bericht 88–10, Beilage Band 5.16, Wettingen, Switzerland.
Nair, G. M. and Kumar, P. C. (1986) *J. Radioanal. Nucl. Chem.,* **107**, 297–22.
Nakada, M., Saeki, M., Masaki, N. M., and Tsutsui, S. (1998) *J. Radioanal. Nucl. Chem.,* **232**, 201–7.

Nakashima, S. (1992) *Sci. Total Environ.,* **117/8**, 425–37.
Neck, V., Runde, W., Kim, J. I., and Kanellakopulos, B., (1994) *Radiochim. Acta,* **65**, 29–37.
Negi, R. S. and Malhotra, R. K. (1980) *Proc. Symp. Chem. Anal. Geol. Mater.*, **1**, 33–5.
Nelson, D. M. and Metta, D. N. (1983) *Radiol. Environ. Res. Div. Ann. Rep.* 42–7.
Nelson, D. M. and Lovett, M. B. (1978) *Nature,* **276**, 599–601.
Neu, M., Hoffman, D., Roberts, K. E., Nitsche, H., and Silva, R. J. (1994) *Radiochim. Acta,* **66/7**, 251–8.
Niese, S. (1994) *Zhurn. Analit. Khim.,* **49**, 132–4.
Nitsche, H. (1995) *J. Alloys Compds,* **223**, 274–9.
Noller, B. N. and Hart, B. T. (1993) *Environm. Technol.,* **14**, 649–56.
Ochsenkuehn Petropulu, M. and Parissakis, G. (1993) *J. Anal. Chem.,* **345**, 43–7.
Ohnuki, T., Isobe, H., and Hidaka, H. (1996) *Hoshasei Haikibutsu Kenkyu,* **2**, 145–51.
Okajima, S., Reed, D. T., Beitz, J. V., Sabau, C. A., and Bowers, D. L. (1991) *Radiochim. Acta,* **52/3**, 111–7.
Orlandi, K. A., Penrose, W. R., Harvey, B. R., Lovett, M. B., and Findlay, M. W. (1990) *Environ. Sci. Technol.,* **24**, 706–12.
Oughton, D. H., Fifield, L. K., Day, J. P., Cresswell, R. G., Skipperud, L., Di Tada, M. L., Salbu, B., Strand, P., Drozcho, E., and Morrov, Y. (2000) *Environ. Sci. Technol.,* **34**, 1938–45.
Papadopulos, N. N. and Tsagas, N. F. (1994) *J. Radioanal. Nucl. Chem.,* **179**, 35–43.
Paschoa, A. S., Cholewa, M., Jones, K. W., Singh, N. P., and Wrenn, M. E. (1987) *J. Radioanal. Nucl. Chem.,* **115**, 231–40.
Pedersen, K. (ed.) (1996) *Bacteria, Colloids and Organic Carbon in Groundwater at the Bagombé Site in the Oklo Area*. SKB Technical report 96–01, Stockholm, Sweden.
Penrose, W., Polzer, W., Essington, E., Nelson, D., and Orlandi, K. (1990) *Environ. Sci. Technol.,* **24**, 228–34.
Peppard, D. F., Studier, M. H., Gergel, M. V., Mason, G. W., Sullivan, J. C., and Mech, J. F. (1951) *J. Am. Chem. Soc.,* **73**, 2529–31.
Perkins, W. T., Pearce, N. J. G., and Jefferies, T. E. (1993) *Geochim.Cosmochim. Acta,* **57**, 475–82.
Phelps, W. T., Jr. and Davis, T. L. (1981) *Soc. Exploration Geophys.,* **1**, 89.
Pollard, P. M., Liezers, M., McMillan, J. W., Phillips, G., Thomason, H. P., and Ewart, F. T. (1988) *Radiochim. Acta,* **44/5**, 95–101.
Poty, B. and Roux, J. (1998) *Uranium Ores*, EDF Publisher, Paris, p. 610.
Price, G. R., Ferretti, R. J., and Schwartz, S. (1953) *Anal. Chem.* **25**, 322–31.
Probst, T., Zeh, P., and Kim, J. I. (1995) *Fresenius. J. Anal. Chem.,* **351**, 745–51.
Purser, K. H., Litherland, A. E., and Zhao, X. (1996) *Nucl. Instrum. Methods B,* **113**, 445–52.
Qu, H., Stuit, D., Glover, S. E., Love, S. F., and Filby, R. H. (1998) *J. Radioanal. Nucl. Chem.,* **234**, 175–81.
Quigley, M. S., Santschi, P. H., and Hung, C. C. (2002) *Limnol. Oceanogr.,* **47**, 367–77.
Rastogi, R. C. and Sjoeblom, K. L. (1999) *Inventory of Radioactive Waste Disposal at SeaI,* IAEA-TECDOC–1105.
Rink, W. J., and Odom, A. L. (1991) *Nucl. Track Rad. Meas. Inter., J. Rad. Appl. Inst.,* **18**, 163–73.

Robertson, D. E. (1985) *Speciation of Fission and Activation Products in the Environment*, Elsevier Science, New York, pp. 47–57.
Röllin, S., Kopajtic, Z., Wernli, B., and Magyar, B. (1996) *J. Chromatogr. A,* **739**, 139–49.
Römer, J., Plaschke, M., Beuchle, G., and Kim, J. I. (2003) *J. Nucl. Mater.,* **322**, 80–6.
Rozenberg, G. and Hoektra, P. (1982) *Soc. Exploration Geophys.,* **1**, 376–8.
Rubio Montero, M. P. and Martin Sánchez, A. (2001a) *J. Environ. Radioact.,* **55**, 157–65.
Rubio Montero, M. P. and Martin Sánchez, A. (2001b) *Appl. Radiat. Isot.,* **55**, 99–102.
Runde, W., Neu, M. P., Conradson, S. D., Clark, D. L., Palmer, P. D., Reilly, S. D., Scott, B. L., and Tait, C. D. (1997) *Mat. Res. Soc. Symp. Proc.,* **465**, 693–703.
Rykov, A. G., Piskunov, E. M., and Timofeev, G. A. (1975) *J. Anal. Chem. USSR,* **30**, 598–601
Salbu, B. (2000) in *Speciation of radionuclides in the environment. Encyclopedia of analytical chemistry,* (ed. R. A. Meyers, John Wiley, Chichester, pp. 12993–3016.
Salbu, B. (2001) *J. Environ. Radioact.,* **53**, 267–8.
Sampson, K. E., Scott, R. D., Baxter, M. S., and Hutton, R. C. (1991) in *Proc. Radionuclide in the Study of Marine process*, Elsevier, London, pp. 177–86.
Sawant, L. R., Kalsi, P. K., Kulkarni, A. V., and Vaidyanathan, S. (1996) *J. Radioanal. Nucl. Chem.,* **207**, 39–43.
Schimmack, W., Auerswald, K., and Bunzl, K. (2001) *J. Environ. Radioact.,* **53**, 41–57.
Schoonover, J. R. and Havrilla, G. L. (1999) *Appl. Spectrosc.,* **53**, 257–65.
Sheng, Z., Zhao, Y., and Gu, D. (1985) *Ti Ch'iu Hua Hsueh,* **2**, 188–95.
Skwarzec, B., Struminska, D., and Borylo, A. (2001) *J. Environ. Radioact.,* **55**, 167–78.
Smyth, J. R., Thomson, J., and Wolfberg, K. (1980) *Radioact. Waste Manage.,* **1**, 13–24.
Solatie, D., Carbol, P., Betti, M., Bocci, F., Hiernaut, T., Rondinella, V., and Cobos, J. (2000) *Fresenius J. Anal. Chem.,* **368**, 88–94.
Soto-Guerrero, J., Gajdosova, D., and Havel, J. (2001) *J. Radioanal. Nucl. Chem.,* **249**, 139–43.
Sreenivasan, N. L. and Srinivasan, T. G. (1995) *J. Radioanal. Nucl. Chem.,* **201**, 391–9.
Stepanov, A. V., Aleksandruk, V. M., Babaev, A. S., Demyanova, T. A., Nikitina, S.-A., and Preobrazhenskaya, E. B. (1990) *Radioisot. Czech.,* **31**, 267.
Strelow, F. W. (1961) *Anal. Chem.,* **33**, 1648–50.
Swift, D. J. and Nicholson, M. D. (2001) *J. Environ. Radioact.,* **54**, 311–26.
Szabó, G., Guczi, J., and Nisbet, A. (1997) *J. Radioanal. Nucl. Chem.,* **226**, 255–9.
Taylor, D. M. and Farrow, L. C. (1987) *Nucl. Med. Biol. Inter. J. Rad. Appl. Instrum.,* **14**, 27–31.
Testa, C., Desideri, D., Guerra, F., Meli, M. A., Roselli, C., and Degetto, S. (1999) *Czech. J. Phys.,* **49**, 649–56.
Teterin, Yu. A., Ivanov, K. E., Teterin, A. Yu., Lebedev, A. M., and Vukcevic, L. (1997) *Yugoslav Nucl. Soc.*, CONF 961055, pp. 449–52.
Timerbaev, A. (2001) *Anal. Chim. Acta,* **433**, 165–80.
Trautmann, N., Peuser, P., Rimke, H., Sattelberger, P., Herrmann, G., Ames, F., Krönert, U., Ruster, W., Bonn, J., Kluge, H.-J., and Otten, E.-W. (1986) *J. Less-Common Metals,* **122**, 533–8.
Trautmann, N. (1992) in *Proc. of Transuranium Elements. A Half Century*, Washington, DC, pp. 159–67.

Triay, I. R., Hobart, D. E., Mitchell, A. J., Newton, T. W., Ott, M. A., Palmer, P. D., Rundberg, R. S., and Thompson, J. L. (1991) *Radiochim. Acta,* **52/3**, 127–31.
Usuda, S., Sakurai, S., and Yasuda, K. (1997) *Nucl. Instrum. Methods A,* **388**, 193–8.
Usuda, S., Yasuda, K., and Sakurai, S. (1998) *Appl. Radiat. Isot.,* **49**, 1131–7.
Van Britsom, G., Slowikowski, B., and Bickel, M. (1995) *Sci. Total Environ.,* **173**, 83–9.
Veselsky, J. C. and Ratsimandresy, Y. (1979) *Anal. Chim. Acta,* **104**, 345.
Veselsky, J. C. and Degueldre, C. (1986) *Analyst,* **111**, 535–8.
Virk, H. S. (1997) *Bull. Radiat. Prot.,* **20**, 139–42.
Virk, H. S., Sharma, A. K., and Naresh, K. (1998) *J. Geol. Soc. India,* **52**, 523–8.
Vogler, S., Scholten, J., Rutger, van-der-Loeff, M., and Mangini, A. (1998) *Earth Planet. Sci. Lett.,* **156**, 61–74.
Wahlberg, J., Skinner, D. L., and Rader, L. F., Jr. (1957) *Anal. Chem.,* **29**, 954–7.
Wallenius, M., Tamborini, G., and Koch, L. (2001) *Radiochim. Acta,* **89**, 55–8.
Wallner, C., Faestermann, T., Gerstmann, U., Hillebrandt, W., Knie, K., Korshinek, G., Lierse, C., Pomar, C., and Rugel, G. (2000) *Nucl. Instrum. Methods B,* **172**, 333–37.
Walther, C. (2003) *Coll. Surf. A,* **217**, 81–92.
Waqar, F., Jan, S., Mohammad, B., and Ahmed, M. (1995) in *Spectroscopy for Material Analysis*, PINSTECH, Islamabad, pp. 189–93.
Ward, W. C., Martinez, H. E., Abeyta, C. L., Morgan, A. N., and Nelson, T. O. (1998) *J. Radioanal. Nucl. Chem.,* **235**, 5–10.
Wasserburg, G. T., McDonald, G. J. F., Hoyle, F., and Fowler, W. A. (1964) *Science,* **143**, 465–7.
Wimmer, H., Kim, J. I., and Klenze, R. (1992) *Radiochim. Acta,* **58–9**, 165–71.
Winkelmann, I., Thomas, M., and Vogl, K. (2001) *J. Environ. Radioact.,* **53**, 301–11.
Wolf, S. F., Bates, J. K., Buck, E. C., Dietz, N. L., Fortner, J. A., and Brown, N. R. (1997) *Environ. Sci. Technol.,* **31**, 467–71.
Wong, K. (1971) *Anal. Chim. Acta,* **56**, 355
Xu, H. and Wang, Y. (1999) *J. Nucl. Mater.,* **265**, 117–123.
Yu-fu, Y., Salbu, B.Bjørnstad, H. E., and Lien, H. (1990) *J. Radioanal. Nucl. Chem.,* **145**, 345–53.
Yu-fu, Y., Bjørnstad, H. E., and Salbu, B. (1992) *Analyst,* **117**, 439–42.
Yukawa, M., Watanabe, Y., Nishimura, Y., Guo, L., Yongru, Z., Lu, H., Zhang, W., Wei, L., and Tao, Z. (1999) *Fresenius J. Anal. Chem.,* **363**, 760–6.
Zamzow, D., Baldwin, D., Weeks, S., Bajic, S., and D'Silva, A. (1994) *Environ. Sci. Technol.,* **28**, 352–8.
Zarki, R., Elyahyaoui, A., and Chiadli, A. (2001) *Appl. Radiat. Isot.,* **55**, 164–74.
Zhao, X., Nadeau, M. J., Garwan, M. A., Kilius, L. R., and Litherland, A. E. (1994) *Nucl. Instrum. Methods B,* **92**, 258–64.
Zhao, X. L., Nadeau, M. J., Kilius, L. R., and Litherland, A. E. (1994) *Earth Planet. Sci. Lett.,* **124**, 241–4.
Zhao, X., Kilius, L. R., Litherland, A. E., and Beasley, T. (1997) *Nucl. Instrum. Methods B,* **126**, 297–300.

CHAPTER TWENTY EIGHT

X-RAY ABSORPTION SPECTROSCOPY OF THE ACTINIDES

Mark R. Antonio and Lynda Soderholm

28.1 INTRODUCTION

The recent availability of synchrotron radiation has revolutionized actinide chemistry. This is particularly true in environmental studies, where heterogeneous samples add to the already multifaceted chemistry exhibited by these ions. Environmental samples are often inhomogeneous, chemically diverse, and amorphous or poorly crystalline. Even surrogates prepared in the laboratory to simplify the natural complexity are plagued by multiple oxidation state and varied coordination polyhedra that are a reflection of inherent 5f chemistry. For example, plutonium can be found as Pu^{3+}, Pu^{4+}, $Pu(V)O_2^+$, and $Pu(VI)O_2^{2+}$ within naturally occurring pH–Eh conditions, consequently complex equilibria are found between these oxidation states in one solution. In addition, dissolved actinides have significant affinities for various mineral surfaces, to which they can adsorb with or without concomitant reduction–oxidation (redox) activity, depending on details of the solution and surface conditions.

A molecular level understanding of this diverse chemistry is necessary if predictive modeling of the fate and transport of these biohazardous ions is to be attained. Synchrotron studies are rapidly becoming a workhorse in the effort to chemically characterize 5f, actinide pollutants, their speciation, and their complexation at a molecular level. Synchrotrons are proving ideal for the task for several reasons: (1) they provide a high flux of tunable, high-energy

radiation; (2) highly focused beams allow for small (<1 mg) sample sizes; (3) the energy range permits excitation of the M- and L-adsorption edges of the actinides; (4) the penetrating nature of X-rays allows sample encapsulation and containment; and (5) a wide variety of spectroscopy, scattering, and imaging experiments are available.

Most of the synchrotron studies published to date have focused on X-ray absorption spectroscopy (XAS). This technique has found widespread use as a speciation probe for several reasons: (1) it is a single-ion probe that can be used to study one element from a complex mixture; (2) it is sensitive to both the oxidation state and to the coordination environment of the ion, and (3) it can be used for solution, surface, or solid samples. As a result, XAS has been able to answer a variety of important fundamental chemistry questions about actinide-ion speciation in solution and in the solid-state that have direct relevance to environmentally germane problems. Very recent trends indicate that these studies will expand to include other X-ray techniques and that more studies will focus on transuranics as the scientific community becomes more aware of the vast potential of synchrotron radiation as a molecular-level probe.

XAS itself is often artificially divided into two experiments, X-ray absorption near-edge structure (XANES), and extended X-ray absorption fine structure spectroscopy (EXAFS) because of the two different modes employed for analyses (Koningsberger and Prins, 1988; Bertagnolli and Ertel, 1994; Zubavichus and Slovokhotov, 2001). From a practical perspective they both arise from the same response about an absorption edge as a function of energy, as shown in Fig. 28.1. The absorption about the edge, or XANES data, provides information about the valence of the central ion by comparison to standards of known oxidation states. Often there is a shift of the absorption edge to higher energy that can be correlated to an increase in valence. This shift can be quite pronounced, as seen for example in Fig. 28.2a for Eu, which shows a 8 eV difference in absorption energy between Eu^{2+} and Eu^{3+} (Antonio *et al.*, 1997; Rakovan *et al.*, 2001). Shifts with oxidation state are often less definitive for the actinides and are complicated by the significant change in coordination environment that occurs in the 4+/5+ couple with the formation of the actinyl ion for U–Am (Ankudinov *et al.*, 1998; Conradson *et al.*, 1998; Antonio *et al.*, 2001) as shown in Fig. 28.2b. The dioxo coordination manifests itself as a predominant shoulder on the high-energy side of the absorption edge (Hudson *et al.*, 1995a) and a shift to somewhat lower energy (Soderholm *et al.*, 1999). This feature is even more enhanced for tetraoxo coordination, as seen in $[Np(VII)O_4]^-$ (Williams *et al.*, 2001) and demonstrated in Fig. 28.2c. Therefore, although XANES is primarily used for determining oxidation states, in specific situations it can be used to infer something about the absorbing ion's coordination environment.

Detailed coordination information is determined by fitting the EXAFS oscillations above the absorption edge (Lee *et al.*, 1981; Teo, 1986; Filipponi, 2001). The discovery of EXAFS was made in the 1920s (Lytle, 1999); however, it was

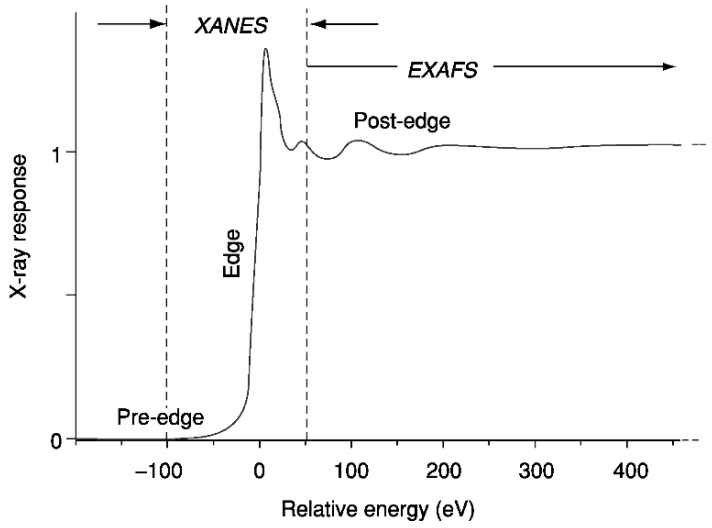

Fig. 28.1 *A* X*-ray absorption spectrum after background subtraction and normalization. The XANES region is usually considered to be the data from about* 100 eV *below the absorption edge to about* 50 eV *above the edge. The higher-energy data are considered to be the EXAFS spectrum. This distinction is somewhat arbitrary and reflects the different methods used to analyze the data. The XANES are considered to be electronic in origin and are often plotted as their derivative in order to clearly define the absorption edge for use in oxidation state assignment. The EXAFS data are re-configured into momentum space* ($Å^{-1}$) (*Teo,* 1986) *and then may be Fourier transformed to obtain a real-space* (Å) *spectrum. Data are fit for distances from the central absorbing ion and number of coordinating ligands using either* k*-space or FT data, as shown in Fig.* 28.3.

not until the 1970s that three pivotal developments set the foundation for the practice and acquisition of EXAFS. The first was the direct application of Fourier transform (FT) analysis to invert experimental data to obtain structural information about the near-neighbor coordination environment of a selected absorbing element in amorphous and crystalline materials alike (Sayers *et al.*, 1971). The second was the advent of intense synchrotron radiation of X-ray wavelengths that immensely facilitated the collection of data. Throughout the past three decades, the unique properties of synchrotron radiation available at some 30 operational facilities (as of 2003) throughout the world (Winick and Nuhn, 2003) has been exploited for EXAFS experiments that would be impossible to perform with conventional sources of x-radiation.

One important property – polarization – of the synchrotron radiation, was exploited for what was the first publication (Templeton and Templeton, 1982) about X-ray experiments with an actinide-bearing material, rubidium uranyl nitrate, $RbUO_2(NO_3)_3$, at a synchrotron facility. U L_3- and L_1-edge XANES

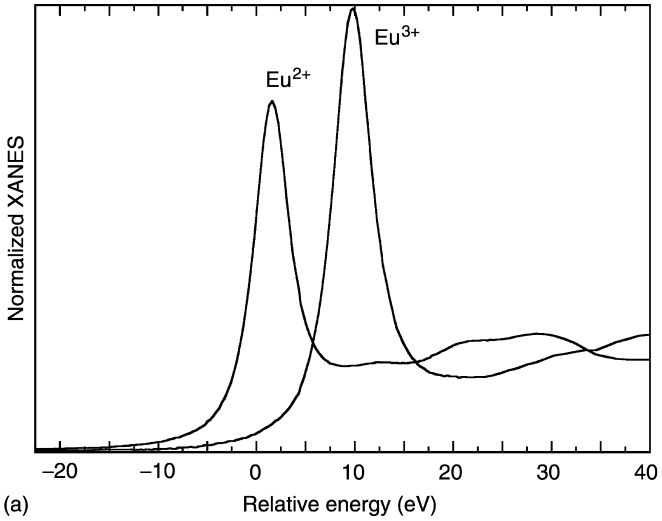

Fig. 28.2 (a) *Eu L_3-edge XANES demonstrating the* 8 eV *difference between the divalent and trivalent absorption maximum. Less obvious from the spectra is the slightly different FWHMs and integrated intensities of the two spectra, which is important to take into account when determining relative oxidation states from XANES* (*Antonio* et al., 1997; *Newville* et al., 1999).

data were acquired for a single-crystal with the electric vector of the linearly polarized synchrotron radiation both parallel and perpendicular to the linear, *trans*-dioxo uranyl {O–U–O} axis. At the time, the interpretation of the 'substantial dichroism' effects posed "...a challenge which we hope will stimulate further theoretical work" (Templeton and Templeton, 1982). This theoretical challenge, and the third pivotal development of EXAFS, was largely met in the 1990s with the release of the general-purpose XAS *ab initio* code known as FEFF (de Leon *et al*., 1991; Rehr *et al*., 1991, 1992; Zabinsky *et al*., 1995). The theoretical algorithms available with FEFF6 were first brought to bear upon spectroscopic features in U L_3-edge XANES of oxides and intermetallics (Hudson *et al*., 1995a). Together with other results, this benchmark study established the origin – a localized multiple-scattering resonance attributable to the linear $[O{=}U{=}O]^{2+}$ group – of the absorption resonance observed some 15 eV above the U edge peak in uranyl fluoride, UO_2F_2, in particular, and for uranyl compounds, in general. The calculations provided the initial successful interpretation of the substantial linear X-ray dichroism effects observed some 13 years earlier in the original U L_1- and L_3-eges XANES (Templeton and Templeton, 1982) and the subsequent U L_3-edge XANES and EXAFS of uranyl acetate dihydrate, $[UO_2(OOCCH_3)_2]\cdot 2H_2O$ (Hudson *et al*., 1996).

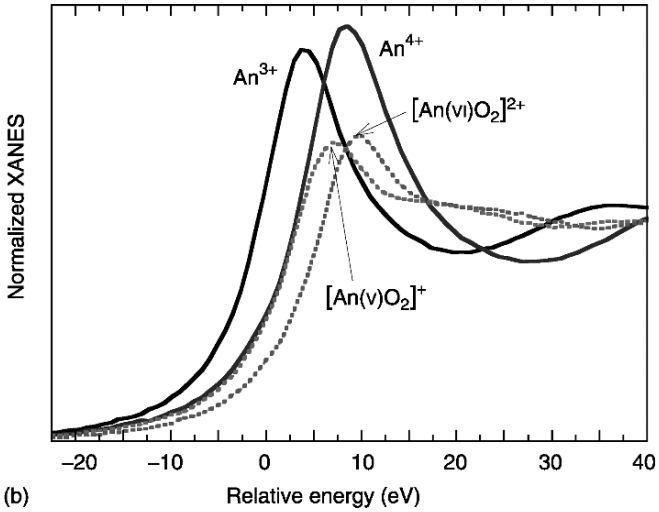

Fig. 28.2 (b) *Representative XANES data as a function of oxidation state and coordination environment. The trivalent and tetravalent spectra show about a* 4 eV *difference in the edge energy, as do the pentavalent and hexavalent dioxo moieties. However, a comparison of tetravalent with pentavalent dioxo spectra show very small, sometimes negative shifts in the edge energies, as shown. In addition, the shapes of the spectra are different. The trivalent and tetravalent species tend to have a larger white-line feature whereas the dioxo coordination of the higher oxidation states produces multiple-scattering that results in the shoulder to higher energy of the edge peak itself* (*Hudson* et al., 1995a).

Today EXAFS is widely used to determine the coordination environment of an actinide in a non-crystalline sample. All measurements of the EXAFS response, including the use of both primary (e.g. transmission, fluorescence, electron-yield) and secondary (e.g. optical luminescence, ion-yield, photoconductivity, photoacoustic) detection schemes, are made as a function of incident X-ray energy, E, in electron volts. Following a number of data reduction treatments, the EXAFS signal, χ, is plotted as a function of the photoelectron wave vector k (Å^{-1}), which is obtained according to:

$$k = \frac{2\pi}{\lambda_e} = \sqrt{\frac{2m}{\hbar^2}(E - E_0)} = \sqrt{0.263(E - E_0)} \tag{28.1}$$

Here, E_0 is the experimental energy threshold chosen to define the energy origin of the EXAFS spectrum in k-space. That is, $k = 0$ Å^{-1} when the X-ray energy E equals E_0, and the photoelectron of wavelength λ_e has no kinetic energy. Examples of representative data, $\chi(k)$ vs k, and their corresponding FTs are shown in Fig. 28.3. Under favorable conditions, the number, distance, and identity of the coordinating ion can be determined and, together with XANES

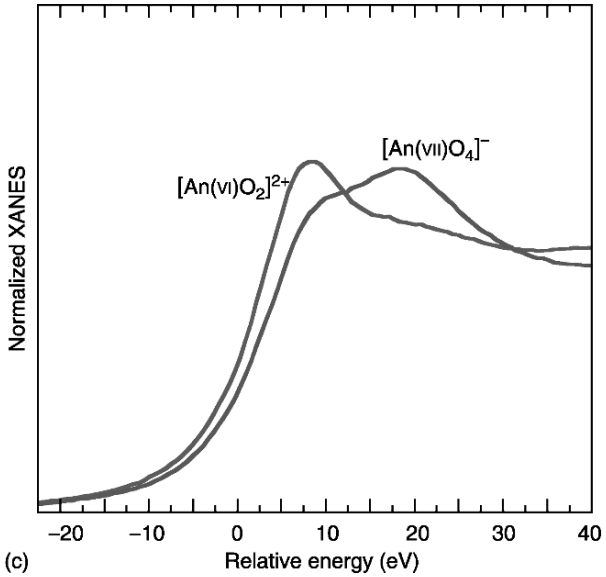

Fig. 28.2 (c) *A comparison of XANES spectra from an An(VI) dioxo-coordinated ion with that of a tetraoxo An(VII)-coordinated ion. The increased shoulder intensity for the latter coordination is presumed to arise from an increased number of multiple-scattering pathways.*

data, provide metrics on actinide-ion speciation. FEFF plays a very important role by providing element-specific phase and amplitude functions, thereby eliminating the need for obtaining these quantities from standard compounds. Until FEFF was in common use, the need for standard compounds to study actinides was a significant problem because of the very limited number of transuranic compounds with well-known structures and because of the radically different coordination environments, including dioxo coordination, which was difficult to resolve well enough experimentally to obtain adequate independent phase and amplitude functions.

In most cases, non-linear least squares minimization techniques are applied to fit the EXAFS or FT data with a semiempirical, phenomenological model of short-range, single-scattering according to (Teo, 1986):

$$\chi(k) = S_0^2 \sum_{i=1}^{n} \frac{N_i F_i(k, r_i)}{k r_i^2} \exp\left(-2k^2\sigma_i^2\right) \exp\left(\frac{-2r_i}{\lambda_e(k)}\right) \sin\left(2kr_i + \varphi_i(k, r_i) + \varphi_c(k)\right) \tag{28.2}$$

The backscattering amplitude, $F_i(k, r_i)$, and phase, $\varphi_i(k, r_i)$, as well as the central atom phase, $\varphi_c(k)$, are typically obtained from the FEFF and used as input for the iterative refinement procedures. An overall amplitude reduction

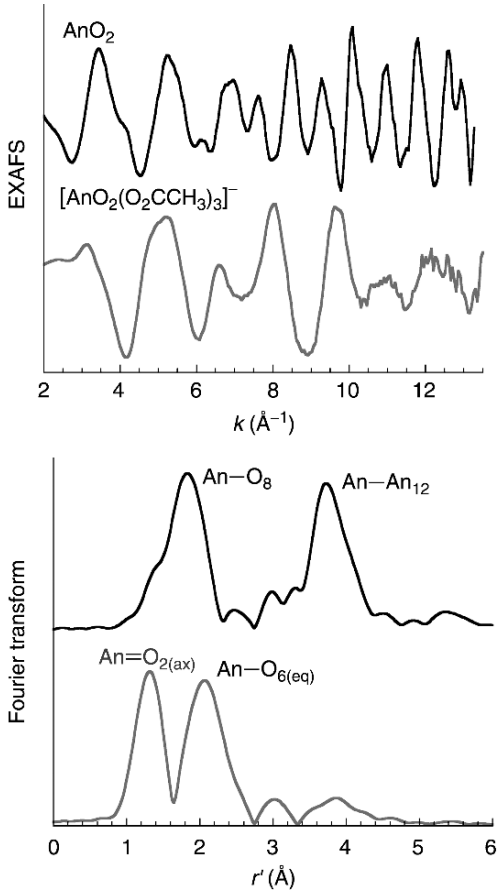

Fig. 28.3 *Representative L_3 EXAFS data comparing tetravalent and dioxo-hexavalent absorbers. Data are plotted as $k^3\chi(k)$, and their corresponding Fourier transforms (FTs) for a tetravalent oxide, AnO_2, and a hexavalent actinyl absorber with acetate ligation, $[AnO_2(O_2CCH_3)_3]^-$. The FT data for the dioxide shows a singe peak at* 1.83 Å (*before phase shift correction*) *due to O backscattering, whereas the dioxo complex anion shows two strong peaks due to O at* 1.32 *and* 2.07 Å (*before phase shift correction*) *that are diagnostic of the axial* (*ax*) *and equatorial* (*eq*) *backscattering, beyond which there is little response. In contrast, the strong, distant peak at* 3.73 Å (*before phase shift correction*) *observed in the FT data for the dioxide is diagnostic of An–An backscattering.*

factor, S_0^2, is normally a fixed input parameter too. The exponential term that includes the photoelectron mean free path, $\lambda_e(k)$, is not explicitly used for a standard analysis. The three principal structure parameters obtained from the fitting include the coordination number, N_i, interatomic distance, r_i, and the Debye–Waller factor, σ_i, for each of the i-th scattering shells about the central absorbing ion out to about 4 Å. An energy scale (ΔE_0) parameter is also fitted to

account for differences between the experimental and theoretical values of E_0. The distances and energy scale both depend on the period of EXAFS oscillations and are therefore correlated, as are the coordination number and Debye–Waller factor, which both depend on the amplitude of the oscillations. The number of parameters that can be determined from a data set, N_p depend on the k- and r-ranges over which the data are fit, and can be calculated according to: $N_p = 2\Delta k \Delta r/\pi$ (Teo, 1986). A rule-of-thumb error estimate is that the fitted distances are precise to about $\pm 1\%$ whereas the coordination numbers can be quoted to ± 1.

It has been understood for some time that correlations exist between the bond distance, coordination number, and oxidation state for a metal species, M^{n+}. A quantitative, electrostatic model for coordination environments in complex ionic solids was proposed in 1929 (Pauling, 1929). Improvements in X-ray diffraction techniques have allowed significant refinement of this original model, and the development of an empirical correlation between valence and the length of a bond (Brown, 1981, 1987, 2002). This correlation, built up by examining the published X-ray structures now available, has been approximated by a simple, two-parameter expression for the experimental bond-valence, S_{ij} :

$$S_{ij} = \exp\left(\frac{R_0 - R_{ij}}{B}\right)$$

where R_{ij} is the distance between atoms i and j. R_0 is an empirically derived parameter, determined such that it represents the length of the bond of unit valence. Its value is dependent on the two ions involved in the bond, and has been tabulated for a variety of bond pairs (Brown, 1996, 2002). Unless otherwise noted, B is generally assumed to be very close to 37 pm. The valence sum rule:

$$V_i = \sum S_{ij}$$

states that the sum of the experimental bond-valences around ith atom is equal to the atomic valence (Brown, 2002). In this way, the bond distance, coordination number, and metal-ion valence can all be correlated.

This concept has been nicely realized for the hexavalent uranyl ion (Burns *et al.*, 1997), for which Brown's R_0 and B parameters have been established from a wide range of X-ray single-crystal structural refinements. A representative plot of bond-valence sum (BVS) versus bond distance is shown in Fig. 28.4, for which the BVS for hexavalent U has been optimized to six. These results can be used in several ways, including confirmation of a coordination number from EXAFS data when a bond distance has been determined. This concept is a useful added tool because the coordination numbers are often not adequately determined from EXAFS alone to answer a question in hand. Likewise, confirmation of oxidation state can come from correlations between bond distances

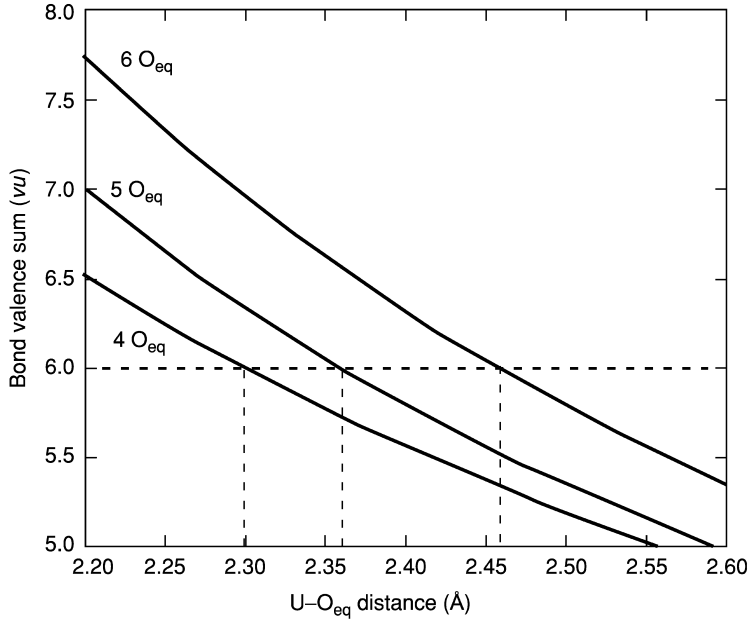

Fig. 28.4 *Bond-valence sums* (*Brown,* 2002) *calculated for the uranyl*(*VI*) *ion with ligating oxygen ions. Parameters used in the calculation* (*Burns* et al*.,* 1997) *were derived from an extensive analysis of available single-crystal structures. Whereas O=U=O bonds are seen to be invariant to changes in coordination environment, the distances to the* O_{eq} *are seen to be dependent on the number of coordinating ions in the equatorial plane. For* $U(VI)O_2^{2+}$ *the average bond distances are* 2.29(5), 2.37(9), *and* 2.47(12) Å *for* 4, 5, *and* 6 *equatorial ligation. These distances can be compared with those obtained from fitting EXAFS data to support a determination of the equatorial coordination environment. Unfortunately, the good quality, single-crystal X-ray structural data necessary to determine a similar plot for transuranic ions is not currently available.*

and XANES data. Interpretation of the XAS data can be further checked by comparison with a variety of published data on similar systems. Published compendia of XAS spectra and analyses for a variety of Th- and U-containing mineral and related phases facilitate these comparisons (Farges, 1991; Thompson *et al*., 1997; Hanchar, 1999). Unfortunately, the use of well-established trends in bond distances and oxidation states or coordination numbers for transuranic studies is limited by the paucity of well-determined single-crystal structures for these ions.

XAS is a single-ion probe that can be tuned to an energy that selects the absorption edge of an ion of interest, an essential attribute when studying an ion's speciation in chemically complex samples. Unfortunately, the spectrum that is obtained is the sum of all the oxidation states and coordination

environments that occur in the sample. This can be particularly problematic for actinide-containing samples in which multiple redox states and coordination environments often occur within one sample. Although difficult to ascertain from simple data analysis, there are two recent developments that are proving to be powerful tools to assess and overcome this problem. The increased brightness afforded by the newer generation synchrotrons has made microsynchrotron-X-ray fluorescence (μ-SXRF) particularly valuable for examining inhomogeneous natural samples. The utility of this technique was clearly demonstrated in seminal experiments examining Pu speciation when adsorbed onto natural tuff samples (Duff *et al.*, 1999a). The results of the experiments demonstrated that Pu was preferentially associated with Mn phases, as opposed to Fe-bearing phases as had been hypothesized, and that some of the Pu had been oxidized. The observation of Pu in multiple oxidation states, and its association with Mn phases were made possible by the use of a very small, focused beam. The second development is the application of principal component analysis (PCA) to XAS data (Wasserman, 1997; Wasserman *et al.*, 1999). PCA can be used on a series of data to determine how many different independent species are required to account for all of the spectra. This mathematical approach provides an estimate of the number of species present in the samples, information that is not otherwise available. Together with model compound spectra, PCA can suggest which of a variety of chemically possible species are present in different samples.

This chapter presents an overview of synchrotron studies on actinide species in environmentally relevant samples. The discussion is organized into solution studies in aqueous acid and base media, sorption studies onto mineral, natural soil, and bacterial surfaces. With the exception of selected experiments on μ-SXRF, almost all of the work has involved XAS studies.

28.2 THE TERRESTRIAL AQUATIC ENVIRONMENT

Since the discovery of the anthropogenic transuranium elements in the 1940s to 1950s, massive efforts have been directed at preventing the despoliation of the environment, particularly the ground- and surface-water supplies, fresh and saline alike, with radionuclide ions. Because of the legacy of the Cold War, the fate and migration of actinide (An) ions presently in the geosphere is a subject of intense interest (Lieser, 1995; Silva and Nitsche, 1995; Nitsche, 1997; Sterne *et al.*, 1998). In terms of its sheer abundance and essentially isotropic distribution on Earth, water is viewed as the principal dispersant of radionuclide pollution. Moreover, because potable water is vital to humanity and all its activities, especially agriculture and aquaculture, fundamental research about An speciation in aqueous media is of historical and contemporary significance.

From a science perspective too, water is the single-most important system with dual benchmark properties of solvent and coordinating ligand. Insofar as both hydration and coordination influence reactivity as well as spectro- and electrochemical responses of 5f-ions in aquatic environments, information about An aquo ions is pivotal to a thorough and predictive understanding of basic chemical phenomena involving migration, absorption, solvation, complexation, exchange, electron transfer, and hydrolysis behaviors, just to name a few, pertinent to hydrologic and geochemical processes. By comparison with the extent of knowledge about An oxidation states and their well-known redox activity (Morss, 1994), metrical details about the coordination of water with the trans-uranium elements are generally sparse. Despite the availability of potential–pH (Pourbaix) equilibrium diagrams for Th, U, Np, Pu, and Am in aqueous solutions at 25°C (Pourbaix, 1974), these do not provide quantitative information about bond lengths and coordination numbers as a function of oxidation state, the so-called An redox speciation. Nor do these diagrams apply to ligands other than H_3O^+, H_2O, and OH^-, and no diagrams are available to describe the redox equilibrium behavior of Ac, Pa, and the trans-Am elements in aqueous solution.

To build a foundation for a thorough understanding of An redox speciation in aqueous media containing environmentally relevant ligands that are known An complexants, e.g. HCO_3^-, CO_3^{2-}, Cl^-, NO_3^-, and SO_4^{2-}, it is first important to understand the structure of the pure molecular An aquo ions and the nature of the An–OH_2 interactions in each of their accessible oxidation states without other interference. In order to suppress and eliminate possible complicating effects of hydrolysis, disproportionation, oligomerization, precipitation, etc., experiments have been routinely performed at low pH in aqueous non-complexing mineral acids. Perchloric acid is the system of choice because the ClO_4^- anion does not participate in direct, inner-sphere interactions with An ions, thereby providing immediate access to the hydrated An species in the absence of competitive binding effects.

Within the domain of the thermodynamic stability of water, which consists of a small (1.229 V) polarization window (Bratsch, 1989), all An electrochemical equilibria are limited by the pH-dependent reduction and oxidation of water itself. Under standard conditions at 25°C that include no complexing ions and 1 atm partial pressures of H_2 and O_2, the potential limits of water with respect to the standard hydrogen electrode (SHE) are imposed by the following reactions:

$$\text{Reduction of } H^+(\text{and } H_2O) \text{ to } H_2 - E^\circ(\text{V}) = 0.000 - 0.0591 \times \text{pH}$$
$$H^+ + e^- \rightarrow {}^1\!/_2H_2 \uparrow \quad \text{and} \quad H_2O + e^- \rightarrow {}^1\!/_2H_2 \uparrow + OH^- \tag{28.3}$$

$$\text{Oxidation of } H_2O \text{ (and } OH^-) \text{ to } O_2 - E^\circ(\text{V}) = +1.229 - 0.0591 \times \text{pH}$$
$${}^1\!/_2H_2O \rightarrow {}^1\!/_4O_2 \uparrow + H^+ + e^- \quad \text{and} \quad OH^- \rightarrow {}^1\!/_4O_2 \uparrow + {}^1\!/_2H_2O + e^- \tag{28.4}$$

The linear and parallel potential, E° (V), dependencies for the reactions (28.3) and (28.4) as a function of pH are conveniently visualized in the Pourbaix diagrams for all elements from $Z=1$ to 95 (Am) such as is illustrated in Fig. 28.5 for Fe. As can be seen from Table 28.1, there are a number of solution-stable An species under both acid and alkaline conditions that exhibit redox activity within the electrochemical window afforded by water. In fact, some transuranium ions, notably Np and Pu, are known to have a remarkable variety of solution species as well as intricacies and ambiguities of valence with five accessible oxidation states – III, IV, V, VI, and VII. In this regard, electrochemical research has played a central role in the advancement of actinide science. And, in the field of equilibrium electrochemistry, the cornerstone of all practical, thermodynamic applications of electroanalytical techniques, e.g. potentiometry and polarography, is the Nernst equation (28.5). (Archer, 1989):

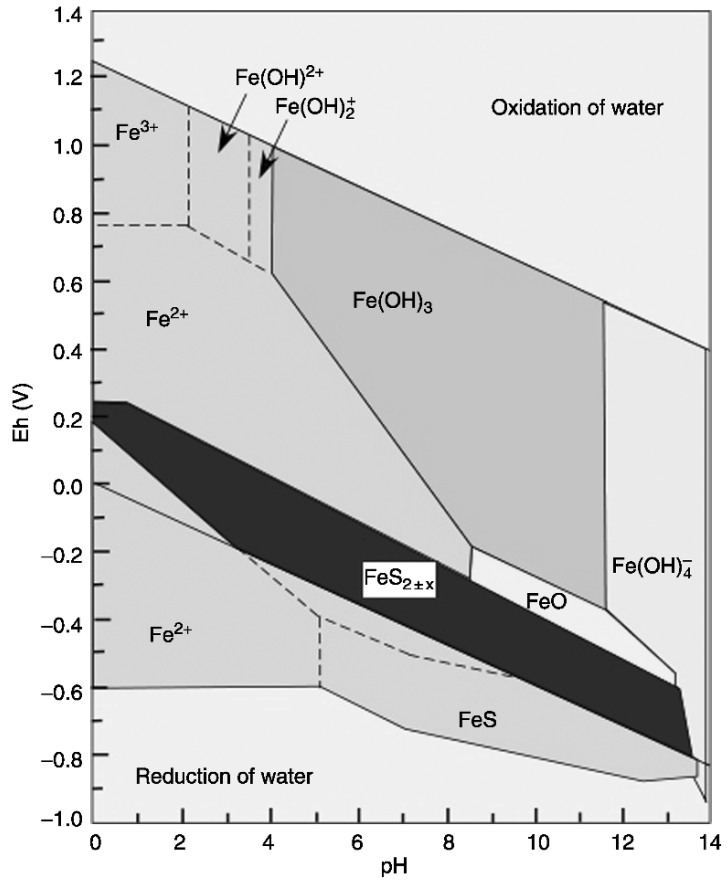

Fig. 28.5 *The complex behavior of iron in an aqueous environment, showing both changes in oxidation state and ligation as a function of solution Eh and pH* (*Hem*, 1985).

Table 28.1 *The standard reduction potentials (E°, V vs SHE) for some one- and two-electron half-reactions of selected ions. The more positive the potential, the more favored the reaction as written. Except where noted, all values are from Bratsch* (1989).

Reduction half-reaction couples	E°
acid solutions	
$U^{4+} + e^- \rightarrow U^{3+}$	–0.577
$Eu^{3+} + e^- \rightarrow Eu^{2+}$	–0.35
$H^+ + e^- \rightarrow \frac{1}{2}H_2\uparrow$	0.0000
$Np^{4+} + e^- \rightarrow Np^{3+}$	+0.157
$CO_2\uparrow + 8H^+ + 8e^- \rightarrow CH_4\uparrow + 2H_2O$	+0.1694
$[UO_2]^{2+} + 4H^+ + 2e^- \rightarrow U^{4+} + 2H_2O$	+0.273
$[NpO_2]^+ + 4H^+ + e^- \rightarrow Np^{4+} + 2H_2O$	+0.567
$Fe^{3+} + e^- \rightarrow Fe^{2+}$	+0.771
$Hg^{2+} + 2e^- \rightarrow Hg\downarrow$	+0.852
$[PuO_2]^{2+} + e^- \rightarrow [PuO_2]^+$	+0.966
$[PuO_2]^{2+} + 4H^+ + 2e^- \rightarrow Pu^{4+} + 2H_2O$	+1.000
$[PuO_2]^+ + 4H^+ + e^- \rightarrow Pu^{4+} + 2H_2O$	+1.035
$\frac{1}{4}O_2\uparrow + H^+ + e^- \rightarrow \frac{1}{2}H_2O$	+1.2291
$[NpO_2]^{2+} + e^- \rightarrow [NpO_2]^+$	+1.236
$Bk^{4+} + e^- \rightarrow Bk^{3+}$	+1.67
$Ce^{4+} + e^- \rightarrow Ce^{3+}$	+1.72
alkaline solutions	
$H_2O + e^- \rightarrow \frac{1}{2}H_2\uparrow + OH^-$	–0.8280
$[SO_4]^{2-} + 8e^- + 5H_2O \rightarrow SH^- + 9OH^-$	–0.683
$[Fe(OH)_4]^- + e^- \rightarrow [Fe(OH)_4]^{2-}$	–0.68
$[NpO_2(OH)_4]^{2-} + e^- \rightarrow [NpO_2(OH)_4]^{3-}$	+0.17[a]
$[PuO_2(OH)_4]^{2-} + e^- \rightarrow [PuO_2(OH)_4]^{3-}$	+0.27[a]
$\frac{1}{4}O_2\uparrow + \frac{1}{2}H_2O + e^- \rightarrow OH^-$	+0.4011
$[NpO_4(OH)_2]^{3-} + 2H_2O + e^- \rightarrow [NpO_2(OH)_4]^{2-} + 2OH^-$	+0.58
$[PuO_4(OH)_2]^{3-} + 2H_2O + e^- \rightarrow [PuO_2(OH)_4]^{2-} + 2OH^-$	+0.95

[a] From (Shilov, 1998).

$$E_p = E^{\circ\prime} + \frac{RT}{nF}\ln\frac{[\Re_{ox}]}{[\Re_{rd}]} \tag{28.5}$$

Derived in 1888 by W. H. Nernst (1864–1941), his eponymous equation establishes the equality between an electrode potential, E_p, and the formal electrode potential, $E^{\circ\prime}$, which is a thermodynamic value, for a redox reaction, such as shown in Table 28.1, under any conditions of pH, electrolyte, ionic strength, etc. In general, for a reversible electrode couple involving n electrons, as illustrated by equation (28.6), the extent of the forward and reverse redox reactions can be manipulated by the application of an applied potential in the vicinity, typically ± 0.20 V, of $E^{\circ\prime}$:

$$\Re_{ox} + ne^- \leftrightarrows \Re_{rd} \tag{28.6}$$

Through measurement of the solution concentrations of both the oxidized and reduced ions, $[\Re_{ox}]$ and $[\Re_{rd}]$, respectively, at a series of selected potentials, a so-called Nernst plot can be prepared in the form of E_p vs $\ln([\Re_{ox}]/[\Re_{rd}])$. An example of a Nernst plot for the one-electron reaction of equation (28.7) for the neptunium redox couple is shown in Fig. 28.6:

$$Np^{4+} + e^- \leftrightarrows Np^{3+} \tag{28.7}$$

For this so-called Nernstian process, meaning that the reaction (28.7) is thermodynamically reversible, wherein the reactant, Np^{4+}, and electrogenerated product, Np^{3+}, maintain equilibrium concentrations at the electrode surface with variation of E_p, a linear plot results. The x-axis intercept is obtained when $[\Re_{ox}]=[\Re_{rd}]$ and provides the formal potential, $E^{\circ\prime}$. The slope, RT/nF, of the plot provides the number of electrons, n, transferred in the redox reaction. For measurements at room temperature, $T=298.15$ K, it is a matter of convenience to simplify equation (28.5) with numerical substitutions for the constants, where R is the universal gas constant, 8.314570 J K^{-1} mol^{-1}, and F is the Faraday constant, 96485 C mol^{-1}, and by conversion from the natural logarithm, ln, to the common logarithm, log, as shown in the following equation:

$$E_p = E^{\circ\prime} + \frac{0.05915}{n} \log \frac{[\Re_{ox}]}{[\Re_{rd}]} \tag{28.8}$$

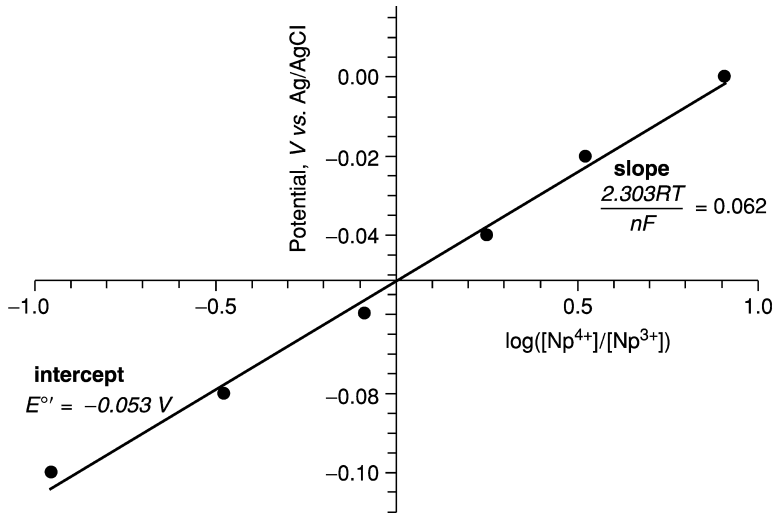

Fig. 28.6 *Nernst plot for the* Np^{4+}/Np^{3+} *redox reaction* (28.7). *The experimental data* (*circles*) *were obtained through use of XANES spectroelectrochemistry*. (*Soderholm* et al., 1999) *The linear least-squares fit shown as a line* ($R^2 = 0.994$) *provides a slope that corresponds to a* 1 e^- *couple, and an intercept of* –0.053 V, *which compares favorably with published values* (*Cohen and Hindman*, 1952*; Riglet* et al., 1989*; Li* et al., 1993).

In the plot of Fig. 28.6, the relative concentrations of the oxidized and reduced Np species were determined by use of XANES spectroscopy (Soderholm *et al.*, 1999). Optical, vibrational, and nuclear magnetic resonance (NMR) probes of concentration are more typically employed in experimental combinations of spectroscopy and electrochemistry, shortened to spectroelectrochemistry in common usage, than are X-ray techniques (Gale, 1988). Regardless of the method, a range of controlled electrochemical potentials must be selected at which the forward and reverse reactions provide sufficient concentration variations of admixtures of $\Re_{ox}$ and $\Re_{rd}$ to perform a Nernst analysis. A typical abscissa range extends between log values of –1 and +1, corresponding to concentration ratios, $[\Re_{ox}]/[\Re_{rd}]$, of 1/10 and 10/1, respectively.

In 1980, XAS, consisting of the methods of XANES and EXAFS, was first brought to bear upon the issue of An speciation in aqueous solutions. This section contains a review of the results published since then for the An aquo species of Th and U–Cf, inclusive (there are no published reports for Ac, Pa, Es, and beyond) with particular emphasis on hydration numbers and inner-sphere An–O interatomic distances with the neutral water molecule. The results are discussed in Section 28.2.2. The interactions of An ions in solution and as solid-state complexes with anionic ligands of mono- and multidentate organic anions are treated separately in Section 28.3.4.

28.2.2 Acid redox speciation

Because of their high charge, small size, and oxophilicity, the 5f-elements are especially prone to hydrolysis reactions and precipitation in neutral and alkaline media. Their solubility and stability in aqueous acid media of $pH \leq 2$ facilitates spectroscopic research, especially the EXAFS work reviewed here whose origins can be attributed to the study of what is now considered to be a concentrated (0.2 M) hexavalent U sample dissolved in 0.2 M HNO_3 (Karim *et al.*, 1980). The L_3-edge EXAFS was acquired with a rotating anode X-ray source and, despite the low signal-to-noise (S/N) quality, provided 'striking' information about the uranyl moiety, $[UO_2]^{2+}$, in solution. The two resolved peaks of the FT data, which are immediately recognized in modern EXAFS research, were attributed to a combination of backscattering from the O nearest atoms of the linear *trans*-dioxo cation, $[O{=}U^{6+}{=}O]^{2+}$, and the next-nearest O atoms of an equatorial arrangement of ligands typical of a hydrolysis complex or, alternatively, the H_2O molecules of a hydration shell. The comparison of the solution FT with that for crystalline UO_2F_2 (a known structure) confirmed the existence of the 'ubiquitous' uranyl group upon dissolution of the solid. At the time in 1980, the theoretical central atom phase function for U was not available. As a result, the functions of Teo and Lee (1979) were extrapolated to simulate the U L_3 $k\chi(k)$ EXAFS with two O atoms at 1.77 Å and five O atoms at 2.38 Å. As shown in Table 28.2, these distances, especially that for the close O atoms of the

Table 28.2 *Uranium redox speciation for U(III), U(IV), U(V), and U(VI). For the spherical ions, the hydration numbers* (n, n′, *coordinated* H_2O) *and U–*OH_2 *interatomic distances are listed. For the uranyl ions, the axial* (*ax.*) *oxygen coordination numbers and U=O distances precede the equatorial* (*eq.*) *hydration numbers* (n″, n‴) *and the U–*OH_2 *bond lengths. Estimated standard deviations, where available, are obtained from the primary sources and are given after the ± sign or within parentheses.*

Aquo ion	*CN, O/*H_2O	*Distance*(*s*)	*Technique/Conditions*	*References*
U(III)·$n$$H_2O$	8.7(9)	2.56(1)	EXAFS/1 M HCl	David *et al.* (1998)
U(IV)·$n'$$H_2O$	8	nd[a]	Optical/≤ 6 M HNO_3; organic-1 M HNO_3(aq.) mixtures	Rykov *et al.* (1973); Vasil'ev *et al.* (1974)
	5.9 – 10.1	2.419–2.519	X-ray scattering/1 M $HClO_4$	Pocev and Johansson (1973)
	9.4 ± 1.1	2.42	EXAFS/pH = 2	Charpin *et al.* (1985)
	11.0 ± 0.8	2.39	EXAFS/1.5 M $HClO_4$	Moll *et al.* (1998)
	10 ± 1	2.42(1)	EXAFS/1.5 M $HClO_4$	Moll *et al.* (1999)
$[U(V)O_2]^{+}\cdot n''H_2O$	2 ax. O + 4.5 eq. H_2O	nd	geometric modeling	Mauerhofer *et al.* (2004)
$[U(VI)O_2]^{2+}\cdot n'''H_2O$[b]	2 ax. O + 5 eq. H_2O	1.77, 2.38	EXAFS/0.2 M HNO_3[c]	Karim *et al.* (1980)
	2 ax. O + 5 eq. H_2O	nd	Optical MCD[d]/H_2O	Görller-Walrand and Colen (1982)
	2 ax. O + 5 eq. H_2O	1.702(5), 2.421(5)	X-ray scattering, ^{1}H NMR/0.09 M $HClO_4$	Aberg *et al.* (1983)
	2 ax. O + 5 eq. H_2O	1.75–1.77, 2.42–2.48	EXAFS/pH = 2	Charpin *et al.* (1985)
	2 ax. O + 5–6 eq. H_2O	1.77(1), 2.40(2)	EXAFS/HNO_3, pH = 1.8	Dent *et al.* (1992)
	2 ax. O + 5 eq. H_2O	nd	molecular dynamics	Guilbaud and Wipff (1993)
	2 ax. O + 5 eq. H_2O	1.78(2), 2.46(2)	EXAFS/HNO_3, pH = 2	Chisholm-Brause *et al.* (1994)
	2 ax. O + 5 eq. H_2O	1.78, 2.41	EXAFS/0.5 M HCl	Hudson *et al.* (1995b)

Table 28.2 (*Contd.*)

Aquo ion	*CN, O/H_2O*	*Distance(s)*	*Technique/Conditions*	*References*
	2 ax. O + 4.8(3) eq. H_2O	1.77, 2.42	EXAFS/H_3CCO_2H, pH = 0.5	Reich *et al.* (1996a)
	2 ax. O + 5 eq. H_2O	1.77, 2.42	EXAFS/HNO_3 pH < 1	Thompson *et al.* (1997)
	2 ax. O + 5 eq. H_2O	1.76(1), 2.41(1)	EXAFS/0 M HCl	Allen *et al.* (1997)
	2 ax. O + 4.5(4) eq. H_2O	1.78, 2.41	EXAFS/0.1 M $HClO_4$	Moll *et al.* (1998)
	2 ax. O + 5 eq. H_2O	nd	^{1}H NMR/$HClO_4$	Bardin *et al.* (1998)
	2 ax. O + 5 eq. H_2O	1.77, 2.42	EXAFS/0.2, 1.0 M $[NO_3]^-$, 25–250°C	Schofield *et al.* (1999)
	2 ax. O + 5 eq. H_2O	1.7477, 2.502	density functional theory	Spencer *et al.* (1999)
	2 ax. O + 4.5(4) eq. H_2O	1.78, 2.41	EXAFS/0.1 M $HClO_4$	Wahlgren *et al.* (1999)
	2 ax. O + 5 eq. H_2O	1.756, 2.516	density functional theory	Hay *et al.* (2000)
	2 ax. O + 5 eq. H_2O	1.76, 2.42	Hartree–Fock/MP2, B3LYP	Tsushima and Suzuki (2000); Tsushima *et al.* (2002)
	2 ax. O + 4.2–4.9 eq. H_2O	1.75–1.76, 2.40–2.43	EXAFS/0.1–11.5 M $HClO_4$	Sémon *et al.* (2001)
	2 ax. O + 4.5–4.8 eq. H_2O	1.75–1.76, 2.41–2.42	EXAFS/5–10 M CF_3SO_3H	Sémon *et al.* (2001)
	2 ax. O + 5.2(4) eq. H_2O	1.77, 2.41	EXAFS/0.1 M $HClO_4$	Vallet *et al.* (2001)
	1.8 ax. O + 5.5 eq. H_2O	1.77(1), 2.41(2)	EXAFS/0.1 M $HClO_4$	Rao *et al.* (2002)
	2 ax. O + 5.0 eq. H_2O	1.76, 2.40(1)	EXAFS/1 M $HClO_4$	Moll *et al.* (2003)
	2 ax. O + 5 eq. H_2O	1.76, 2.43	density functional theory	Bridgeman and Cavigliasso (2003)
	2 ax. O + 5.2 eq. H_2O	nd	geometric modeling	Mauerhofer *et al.* (2004)

[a] Not determined.
[b] Citations to literature published from 1980 only.
[c] Rotating anode X-ray tube source.
[d] Magnetic circular dichromism.

uranyl group, are precisely comparable with numerous subsequent synchrotron radiation measurements.

In the historic work of Karim *et al.* (1980), the exact extent of equatorial O coordination could not be determined because of S/N complications and the imprecise knowledge of Debye–Waller factors and electron mean-free-path terms. Now, decades later, and despite remarkable advances in the theory of EXAFS (Rehr and Albers, 2000), similar problems with scattering losses, amplitude reduction effects, etc. continue to plague aspects of the precision and accuracy of coordination numbers extracted from EXAFS data by curve-fitting methods (Allen *et al.*, 2000). This is especially true for distant, next-nearest neighbors in multi-shell systems wherein spectral congestion and phase cancellation effects can make analyses difficult. Uncertainties can also arise in the determination of the coordination numbers for the simple trivalent and tetravalent hydrated cations, $An^{3+}\cdot nH_2O$ and $An^{4+}\cdot n'H_2O$, where n and n' are the numbers of water molecules directly bound to the An ions in the immediate hydration sphere. The case in point is illustrated by the results of Table 28.3 for the Th^{4+} aquo ion in 1–1.5 M $HClO_4$.

(a) The monatomic spherical An(III) and An(IV) ions

Under conditions that pertain to most ecological habitats, the low-valent 3+ oxidation states of the 5f-elements would not be stable until Am ($Z=95$) and beyond. This is one of the obvious contrasts with lanthanide coordination chemistry wherein stability is dominated by the spherical, monatomic, tripositive ions. Actinide coordination chemistry in natural systems may, however, be influenced by the 4+ oxidation states that are stabilized in anoxic, subsurface aquifers and lacustrine and marine basins wherein redox processes are mediated by species other than O_2, such as S-bearing entities. Under such reducing conditions, An(IV) interactions with H_2O are largely driven by classical, electrostatic forces. This facilitates various approaches in the modeling of thermodynamic properties for the aquo species of the two spherical, monatomic

Table 28.3 *Thorium speciation with hydration numbers (n, coordinated H_2O) and Th–OH_2 interatomic distances obtained from literature sources. Estimated standard deviations, where available, are given after the ± sign or within parentheses.*

Aquo ion	*CN, H_2O*	*Distance(s)*	*Technique/ Conditions*	*References*
Th(IV)$\cdot n H_2O$	8.0±0.5	2.485±0.010	X-ray scattering/1 M $HClO_4$	Johansson *et al.* (1991)
	11.0±0.7	2.43	EXAFS/1 M $HClO_4$	Moll *et al.* (1998)
	10±1	2.45(1)	EXAFS/1.5 M $HClO_4$	Moll *et al.* (1999)
	12.7	2.45	EXAFS/1.5 M $HClO_4$	Rothe *et al.* (2002)
	12.7	2.45	EXAFS/1.5 M $HClO_4$	Neck *et al.* (2002)

An(III) and An(IV) cations (David and Vokhmin, 2003). These efforts incorporate or rely upon the significant body of metrical information obtained from the An EXAFS reviewed below.

(*i*) *Thorium*(*IV*)

The initial analysis of Th L_3 EXAFS for a 0.055 M solution of Th^{4+} in 1 M $HClO_4$ provided an O coordination number of 11.0 ± 0.7, which at the 95% confidence level means that hydration numbers of 10, 11, and 12 are statistically equivalent (Moll *et al*., 1998). In a more rigorous follow-up study with two solutions – 0.03 and 0.05 M – of Th^{4+} in 1.5 M $HClO_4$, hydration numbers of 11.0 ± 0.9 and 11.2 ± 0.9 and corresponding distances of 2.43 and 2.45 Å, respectively, were obtained from curve-fitting analyses of the L_3-edge EXAFS with and without the use of cumulant methods, which account for an asymmetrical distribution of distances about Th^{4+} (Moll *et al*., 1999). Despite the evidence for an asymmetric distribution of H_2O about Th^{4+}, the effects of pair asymmetry on the Th–OH_2 interatomic distance were small, 0.01–0.02 Å, and of approximately the same magnitude as the experimental error itself.

Based upon a combination of results from the primary (Th EXAFS) data and a variety of other metrical comparisons, Moll *et al*. (1999) concluded that the EXAFS results were compatible with hydration numbers of 9–11, and they ultimately "...selected 10 ± 1 as the most likely coordination number" for the Th^{4+} (and U^{4+}) aquo ion in perchloric acid. The addition of fluoride ion in the form of NaF at the same concentration (0.05 M) as that for Th^{4+} in the acid solution was shown to have a significant effect on the coordination environment, but not on the total coordination number. The EXAFS data were analyzed to reveal a pair distribution (Th–F and Th–O) asymmetry with 1 F^- at 2.14 Å and 10 H_2O at 2.48 Å. The subsequent Th L_3-edge results (Neck *et al*., 2002; Rothe *et al*., 2002) for a 0.055 M Th^{4+} solution in 1.5 M $HClO_4$ indicate that the aqueous speciation consists of 12.7 O atoms at an average distance of 2.45 Å about Th^{4+}. Although the interstudy agreement of Th–O distances is better than 1%, there is an approximately 25% study-to-study variation of coordination number. Because of the experimental conditions employed and the interatomic distances obtained, the results of the four studies (Moll *et al*., 1998, 1999; Neck *et al*., 2002; Rothe *et al*., 2002) are essentially the same. Thus the coordination number discrepancy may not arise from genuine variations of sample condition. Rather, it appears to stem from different approaches to the curve-fitting analyses including, in addition to a host of other factors, the choice of amplitude reduction factor, S_0^2, which has direct impact on the absolute accuracy of EXAFS determinations of coordination numbers (Allen *et al*., 2000).

A final comment about the nature of the Th^{4+} aquo ion in these different experiments is necessary. The EXAFS results in each of the three aforementioned studies (Moll *et al*., 1999; Neck *et al*., 2002; Rothe *et al*., 2002) on the

dilute and similar Th^{4+} solutions as summarized in Table 28.3 are contrasted with those from large-angle X-ray scattering studies (Johansson *et al.*, 1991) that reveal a less populated hydration sphere of 8.5 ± 0.5 water molecules at an average distance of 2.485 ± 0.010 Å. In the extremely concentrated solutions, ≈ 1 M Th^{4+}, required for the scattering measurements, it is reasonable to expect that inter-ion aggregation phenomena can lead to a different form of the aquo ion from the significantly less concentrated (18–33 times less) solutions of the EXAFS studies (Moll *et al.*, 1999). At high concentration, the Th^{4+} cations may be partially dehydrated because of an insufficient number of H_2O molecules to satisfy their own solvation requirements as well as those for the (5 M) $[ClO_4]^-$ anions. There is also the possibility for some degree of nucleation and contact through cation–anion and cation–cation interactions. Until one (or both) of the experiments can be repeated under identical conditions, comparisons are not reliable, and it certainly is not obvious that either one (or more) of the studies is in error. In the interim, results from DFT calculations indicate that the first hydration shell about Th^{4+} contains 9 H_2O molecules with Th–O bond lengths of 2.54–2.55 Å (Yang *et al.*, 2001).

(*ii*) *Uranium*(*IV*)

The first U L_3-edge EXAFS results for a dilute, acidic (pH = 2) solution of the U^{4+} aquo ion revealed a hydration number of nine with an average U–O interatomic distance of 2.42 Å (Charpin *et al.*, 1985). The earliest structure report using X-ray scattering was ultimately interpreted to show that the coordination number of U^{4+} in $HClO_4$ was "not significantly different from eight" (Pocev and Johansson, 1973). The indefinite nature of this phrase may reflect the variations in coordination number (between six and ten) obtained with different analysis procedures, especially data set length, and numerical modeling treatments of the data for the acid solution of concentrated (2.044 M) U^{4+} in which about 2% (0.035 M) was present as uranyl(VI). The low-limit value of the reported range of U–O distances, 2.42–2.52 Å (Pocev and Johansson, 1973) is the same as the EXAFS-determined distance (Charpin *et al.*, 1985). The initial work on a dilute (0.05 M) solution of U^{4+} in 1.5 M $HClO_4$ revealed an O coordination number of 11 ± 1 and, moreover, that the hydration numbers of U^{4+} and Th^{4+} are the same (Moll *et al.*, 1998). In a subsequent and more extensive paper on the subject of the tetravalent aquo ion, including the effects of fluoride ion, an EXAFS-determined value of 10.8 ± 0.5 water molecules about U^{4+} at an average distance of 2.41–2.42 Å was reported (Moll *et al.*, 1999). The presence of F^- at concentrations equal to (0.055 M) and greater than that for $[U^{4+}]$ (0.09 M) was shown to affect the speciation, wherein the immediate coordination environment was shown to consist of ca. one F^- at 2.10 Å and 8.2–8.7 H_2O at 2.45–2.46 Å.

Additional insights about the magnitude of the 10.8 ± 0.5 hydration number for the pure aquo ion were provided by comparison of the U–O interatomic

distance with the previously reported Er–O distance (2.36 Å) (Johansson and Wakita, 1985) for the Er^{3+} aquo ion, which has an exact hydration number of eight. The comparison is appropriate because the ionic radii of U^{4+} and Er^{3+} (1.00 and 1.004 Å, respectively, for CN 8) (Shannon, 1976) are essentially identical. Because An–OH_2 bond lengths are mainly influenced by electrostatic effects, the extent of such interatomic interactions is known to increase with increasing coordination number. It is argued that the 0.06 Å longer distance for the U^{4+} aquo species "...can only be explained by a coordination number larger than eight" (Moll *et al.*, 1999). Based upon this and other comparisons with available U–O distances in solid-state crystal structures, they suggested that coordination numbers of either nine or ten are possible and ultimately selected ten as the most likely one. The fact that the larger value (≈ 11) obtained from the actual analyses of the data can be so readily disregarded with sound arguments based upon EXAFS-determined distances further underscores the generally recognized problems with the accuracy of EXAFS coordination number determinations mentioned above. Similar selections of coordination numbers other than those obtained from analysis of the primary data are scattered throughout the literature reviewed here for aqueous An species.

(*iii*) *Neptunium*(*IV*)

Neptunium is considered to be the most problematic of the transuranium elements for waste storage because of its high solubility in groundwater (Viswanathan *et al.*, 1998; Kaszuba and Runde, 1999) and the projected dose commitments to the public that would arise from its breach of long-term containment (Hursthouse *et al.*, 1991). The aquo ion of tetravalent ^{237}Np has been the subject of three independent EXAFS investigations (Allen *et al.*, 1997; Reich *et al.*, 2000; Antonio *et al.*, 2001). Well before these, optical data were interpreted to reveal a hydration number of eight (Rykov *et al.*, 1973). Neptunium L_3-edge measurements of dilute (0.005 M) Np^{4+} were originally obtained in various concentrations of HCl from 1–10 M (Allen *et al.*, 1997). No inner-sphere Cl^- complexation was noted for the solution of Np^{4+} in 1 M HCl, and the EXAFS data for the aquo ion were analyzed to reveal 11.2 O neighbors at an average distance of 2.40 Å. Comparisons of this interatomic distance with a selection of related Np^{4+} and Pu^{4+} species suggested "...that the number of waters around the Np^{4+} ion lies in the range of 9–11." On increasing HCl concentrations from 5 to 10 M, the data analysis revealed a systematic replacement of inner-sphere H_2O molecules by inner-sphere Cl^- ions (reaching values of 7.7 and 2.0, respectively) that was accompanied by a 0.04 Å elongation of the Np–O bond length. The trends were interpreted to indicate the formation of a mixture of multi-aquo-chloro complexes of the general form $[Np(OH_2)_xCl_y]^{4-y}$, for $y \geq 2$.

In the second study (Reich *et al.*, 2000), a dilute (0.05 M) solution of Np^{4+} in 0.1 M HNO_3 was stabilized by the addition of 2 M H_2SO_4 to suppress the

spontaneous oxidation reaction,

$$Np^{4+} + 2H_2O \rightarrow [Np^{5+}O_2]^+ + e^- + 4H^+. \quad (28.9)$$

Analysis of the L_3-edge EXAFS revealed an O coordination number of 11 with an average Np–O distance of 2.39(1) Å, both of which bear close resemblance to the initial results (Allen *et al.*, 1997). Upon further analysis of distant features in the FT data, evidence was found for the inner-sphere coordination that contains two $[SO_4]^{2-}$ groups bound to Np^{4+} in a bidentate fashion (Reich *et al.*, 2000). So, the total O coordination number of 11 is the sum of four O from two sulfate groups and seven from H_2O molecules and, despite the agreement with the earlier work (Allen *et al.*, 1997), the mixed sulfate–hydrate of Np^{4+} species is not a pure aquo ion.

In order to avoid such troublesome effects of complexation as well as those from oxidation, hydrolysis, disproportionation, and precipitation reactions, a dilute (0.0047 M) solution of Np in the non-complexing, supporting electrolyte of perchloric acid (1 M) was used for *in situ* L_2-edge EXAFS spectroelectrochemical measurements of all four – III, IV, V, and VI–aquo ion species (Antonio *et al.*, 2001). The *in situ* technique eliminates interferences from chemical reductants/oxidants that may be required to produce and maintain a specific Np oxidation state during the time required to perform a conventional *ex situ* experiment. Moreover, the use of the non-complexing, supporting electrolyte of perchloric acid further assures that all inner-sphere Np–O bonding is free of interferences from Np–$[ClO_4]^-$, Np–$[SO_4]^{2-}$, Np–$[Cl]^-$, etc., interactions. The EXAFS analyses of the data for the Np^{4+} aquo ion revealed a coordination number of 9(1) O atoms at an average distance of 2.37(2) Å. Comparison of this solution Np^{4+}–O distance with the corresponding distance for crystalline NpO_2, containing eight-coordinate Np^{4+}, reveals that the average distance for the aquo ion is 0.02 Å longer. Insofar as interatomic distances can be used to estimate coordination numbers, it was concluded that "...hydration numbers of either 8 or 9 are more realistic than hydration numbers of either 10 or 11" for the Np^{4+} aquo ion (Antonio *et al.*, 2001). In support of this conclusion, a simple numerical model, based upon an adaptation of the original method of Egami and Aur (1987) used previously with success for metal-ions in glass matrices, was introduced for estimating An ion coordination numbers. The number calculated for Np^{4+} was eight.

The *in situ* X-ray absorption technique was further developed as a means to determine the formal electrode potential ($E^{\circ\prime}$) of Np redox reactions (Soderholm *et al.*, 1999), including the Np^{4+}/Np^{3+} couple of equation (28.7). As discussed previously, for reversible reduction–oxidation reactions of An ions in general, the measurement of thermodynamic formal potentials is important from fundamental and practical perspectives concerning An mobility and reactivity in the geosphere. Whereas the equipment and methods of X-ray absorption spectroelectrochemistry have evolved since the first description of its use (Smith *et al.*, 1984), none of the myriad of multipurpose cell designs (Sharpe *et al.*, 1990;

Igo *et al.*, 1991; Farley *et al.*, 1999) were directly suitable to achieve the application-specific containment and safety standards necessary for *in situ* experiments with radionuclides. This led to the design of a purpose-built system (Antonio *et al.*, 1997), which by facilitating the simultaneous combination of electrochemistry and XANES, provides direct access to the formal electrode potentials of redox reactions of An ions. For example, by use of a series of controlled electrochemical potentials (E_p) at which the forward and reverse reactions of equation (28.7) provide concentration variations of Np^{4+} and Np^{3+}, sufficient XANES data were acquired (Soderholm *et al.*, 1999) to perform a Nernst analysis according to equation (28.8). The spectra for the admixtures of the two solution species were analyzed using standard linear regression analysis as well as PCA with the valence-pure Np^{4+} and Np^{3+} spectra to provide the relative partial concentrations used for the Nernst plot of potential, E_p, vs $\log[Np^{4+}]/[Np^{3+}]$ shown in Fig. 28.6. In this analysis, the slope (0.062 V) corresponds to $n = 1$ e^-. The x-axis intercept provides the formal potential, $E^{\circ\prime} = -0.053$ V. Besides the Np^{4+}/Np^{3+} reaction of equation (28.7), the method was successfully applied to the Bk^{4+}/Bk^{3+} (Antonio *et al.*, 2002) and Np^{6+}/Np^{5+} (Soderholm *et al.*, 1999) aquo ion redox reactions as well as with the IV/III couples of Np and Pu in complexes with the electroactive, Wells–Dawson heteropolyoxoanion ligand, $[P_2W_{17}O_{61}]^{10-}$, which obscures the optical and electrochemical response of the An-ion itself (Chiang *et al.*, 2003). In this situation, the *in situ* XANES approach provides information about formal electrode potentials that is not obtainable from conventional spectrophotometric measurements, cyclic voltammetry, or potentiometric titrations alone.

(*iv*) *Plutonium*(IV)

Metrical aspects of the speciation of the $^{242}Pu^{4+}$ aquo ion came to light in three papers (Ankudinov *et al.*, 1998; Conradson, 1998; Conradson *et al.*, 1998). The experimental Pu XANES at the L_1 (Ankudinov *et al.*, 1998) and L_3 (Conradson *et al.*, 1998) edges for a 0.10 M Pu^{4+} solution in 1 M $HClO_4$ were compared with theoretical spectra obtained from multiple-scattering XANES calculations using the *ab initio* code known as FEFF (Rehr and Albers, 2000). Although these efforts provided no quantitative information about the Pu^{4+} coordination environment in terms of bond distances and hydration numbers, structural parameters for Pu^{4+} as well as for the three other Pu aquo ions were provided in an appendix (Ankudinov *et al.*, 1998). The primary source of the supplementary results was attributed to, at that time, an unpublished study. These structure details appear to be the same as those subsequently published in the review article (Conradson, 1998), which shows the FT data and the results from the curve-fitting analysis of the L_3 EXAFS. The Pu^{4+} aquo ion in 1 M $HClO_4$ was shown to consist of eight or nine water molecules at an average distance of 2.39 Å. A similar hydration structure was found for the Np^{4+} aquo ion species that was also studied in 1 M $HClO_4$ (Antonio *et al.*, 2001).

Independent EXAFS measurements of aqueous solutions of 0.05 M $^{239}Pu^{4+}$ in 3 and 8 M HNO_3 revealed an O coordination number of 11 with best fit Pu–O distances of 2.41 and 2.45 Å, respectively (Allen *et al*., 1996b). Analysis of the distant peaks in the FT data revealed N backscattering that increased with the HNO_3 concentration. The N coordination numbers and Pu–N interatomic distances, in combination with results from ^{15}N NMR and optical spectroscopies (Veirs *et al*., 1994), revealed the formation of di- and tetra-nitrato complexes with decreasing water content, $[Pu(NO_3)_2(H_2O)_7]^{2+}$ and $[Pu(NO_3)_4(H_2O)_3]$, respectively, wherein each $[NO_3]^-$ acts as a bidentate ligand. At 13 M HNO_3, the Pu coordination sphere was fully dehydrated, consisting of a 12 O coordinate hexanitratro complex, $[Pu(NO_3)_6]^{2-}$, with an average Pu–O distance of 2.49 Å for the bidentate $[NO_3]^-$ bonds (Veirs *et al*., 1994; Allen *et al*., 1996b).

The discovery of significant oxygen hyperstoichiometry in the binary Pu^{4+}–O system, e.g., PuO_{2+x} for $0.0 \leq x \leq 0.27$ (Haschke *et al*., 2000), has sparked something of a revolution in the oxide chemistry of plutonium. Even though similar hyperstoichiometry is well-known and of considerable practical importance in the binary fluorite-type oxygen-excess uranium oxides, a similar situation was not recognized with plutonium oxides. It is only now clear that the fluorite lattice of PuO_2 ($Fm3m$) can accommodate excess O as well (Haschke *et al*., 2001; Haschke and Allen, 2002; Haschke and Oversby, 2002). Considerable international interest in the PuO_{2+x} system has arisen vis-à-vis actinide environmental science because of the possibility that the oxidized Pu ions, either Pu^{5+} and/or Pu^{6+} required for charge compensation, might be easily leached out of the otherwise water-insoluble PuO_2. Although the precise location of the excess O^{2-} in these materials is still open to question, the Pu L_3-edge X-ray absorption work (Conradson *et al*., 2003, 2004) provides valuable insights about the Pu valence and speciation. Most important, and contrary to initial suggestions (Haschke *et al*., 2000), the XANES and EXAFS "...results indicate that the excess O in PuO_2 occurs as localized Pu^{5+}–oxo moieties" with distances of 1.83–1.91 Å, and not as localized Pu^{6+} sites (Conradson *et al*., 2003). Also contrary to initial concern, the unusual stability of the PuO_{2+x} system suggests that the Pu^{5+} ions in the bulk solid of PuO_{2+x} may not have any higher solubility than the Pu^{4+} ions (Conradson *et al*., 2003). Still, many pieces of this new puzzle in plutonium chemistry remain, and until the time that additional definitive and conclusive evidence is reported, many of the issues opened up in the landmark publication (Haschke *et al*., 2000) will continue to fuel contemporary research interests.

(*v*) *Berkelium*(*IV/III*)

Of the trans-plutonium elements, only Bk has a comparatively stable, tetravalent aquo ion. Because of their spontaneous reactivity with water ($E^\circ > +2.6$ V), (Bratsch, 1989) the tetravalent aquo ions of Am, Cm, and Cf have, as yet, to be

stabilized for detailed physical, spectroscopic, and structure characterization. In comparison to the extensive volume of results for the aquo ions of Th, U, Np, and Pu (see Tables 28.2–28.5), there are significantly fewer metrical details about the coordination of water with the trans-plutonium elements (cf. Tables 28.2 to 28.6). For example, despite significant research in the years since the discovery of Bk in 1949, no direct structural information about the aquo ion of Bk^{4+} as well as that of Bk^{3+} was available until 2002. At that time, the simultaneous combination of XAS and electrochemical methods was used to probe the redox speciation of ^{249}Bk (Antonio *et al.*, 2002). Through use of *in situ* L_3-edge measurements of a dilute (0.47 mM) Bk solution in a non-complexing aqueous mineral acid electrolyte (1 M $HClO_4$) the inner-sphere hydration environments were found to undergo reorganization, with regard to the average Bk–OH_2 interatomic distances and the number of coordinated H_2O molecules, corresponding to controlled variation of redox state. Bk^{4+} was found to be eight-coordinate with an average Bk–O distance of 2.32(1) Å, whereas Bk^{3+} was found to be nine-coordinate with an average Bk–O distance of 2.43(2) Å. The change in hydration was shown to have a number of parallels with the well-recognized change between the aquo ions of the large, light trivalent lanthanide ions, e.g. La–Pm, and the small heavy ones, e.g. Tb–Lu (Habenschuss and Spedding, 1980; Cossy *et al.*, 1995).

(*vi*) *Curium*(III)

The trivalent aquo ions of ^{248}Cm and ^{249}Cf, the elements adjacent to Bk, have been independently investigated in HCl media through use of L_3-edge EXAFS. The spectrum for a 0.01 M solution of Cm^{3+} in 0.25 M HCl was fit to reveal 10.2 O at an average distance of 2.45 Å (Allen *et al.*, 2000). The single sinusoidal-like variation of the EXAFS data was interpreted to indicate an inner-sphere coordination of water molecules without interference from Cl^- complexation. No compelling evidence for inner-sphere Cm–$[Cl]^-$ interactions was obvious from the FT data and the curve-fitting results until surprisingly high LiCl concentrations, $\geq$ 8.7 M. Although the EXAFS data suggest that little chloride complexation occurs at low $[Cl^-]$ ($\sim$5 M or less), this absence of evidence may reflect, in part, general problems with the method itself concerning resolution and detection limitations of Cl backscattering in a dilute admixture of one (or more) chloro complex(es) in an aquo ion system.

(*vii*) *Californium*(III)

In the highest Z (98) EXAFS yet reported, a multinational effort on a dilute (0.007 M) solution of $^{249}Cf^{3+}$ in 1 M HCl led to the publication of two reports (David *et al.*, 1998; Revel *et al.*, 1999). The initial one (David *et al.*, 1998) contained metrical results from EXAFS analyses that revealed 9.5(9) O around

Table 28.4 *Neptunium redox speciation for Np(III), Np(IV), Np(V), Np(VI), and Np(VII). For the spherical ions, the hydration numbers* (n, n′, *coordinated* H_2O) *and Np–*OH_2 *interatomic distances are listed. For the neptunyl ions, the axial* (*ax.*) *oxygen coordination numbers and Np=O distances precede the equatorial* (*eq.*) *hydration numbers* (n″, n‴) *and the Np–*OH_2 *bond lengths. Estimated standard deviations, where available, are obtained from the primary sources and are given after the ± sign or within parentheses.*

Aquo ion	*CN, O/*H_2O	*Distance*(*s*)	*Technique/Conditions*	*References*
$Np(III)\cdot nH_2O$	9.8(9)	2.52(1)	EXAFS/1 M HCl	David *et al.* (1998)
	8–9	2.48(2)–2.51	EXAFS/1 M $HClO_4$, DFT	Antonio *et al.* (2001)
$Np(IV)\cdot n'H_2O$	8	nd[a]	Optical/$\leq$ 6 M HNO_3	Rykov *et al.* (1973)
	11	2.40(1)	EXAFS/1 M HCl	Allen *et al.* (1997)
	11±1	2.39(1)	EXAFS/0.1 M HNO_3 + 2 M H_2SO_4	Reich *et al.* (2000)
	8–9	2.37(2)	EXAFS/1 M $HClO_4$, DFT	Antonio *et al.* (2001)
$[Np(V)O_2]^{+}\cdot n''H_2O$	2 ax. O + 6 eq. H_2O	nd	NMR/0–8 M LiCl, NH_4NO_3	Glebov *et al.* (1977)
	1.6 ax. O + 5.2 eq. H_2O	1.83(2), 2.52(2)	EXAFS/$HClO_4$, pH = 2	Combes *et al.* (1992)
	2 ax. O + 5 eq. H_2O	nd	optical/H_2O–organic mixtures	Garnov *et al.* (1996)
	2 ax. O + 5 eq. H_2O	1.85(1), 2.50(2)	EXAFS/3 M LiCl	Allen *et al.* (1997)
	1.9(2) ax. O + 3.6(6) eq. H_2O	1.822(3), 2.488(9)	EXAFS/0.1 M HNO_3	Reich *et al.* (2000)
	2 ax. O + 5 eq. H_2O	1.81, 2.61	density functional theory	Hay *et al.* (2000)
	2 ax. O + 5 eq. H_2O	1.81, 2.52	Hartree-Fock/MP2	Tsushima and Suzuki (2000)
	2 ax. O +5 eq. H_2O	1.80(2), 2.44(3)	EXAFS/1 M $HClO_4$	Antonio *et al.* (2001)
	2 ax. O + 4.8(10) eq. H_2O	1.82(2), 2.51(2)	EXAFS/$HClO_4$, pH = 1	Den Auwer *et al.* (2003a)
	2 ax. O + 3.9 eq. H_2O	nd	geometric modeling	Mauerhofer *et al.* (2004)
$[Np(VI)O_2]^{2+}\cdot n'''H_2O$	2 ax. O + 6 eq. H_2O	nd	^{1}H, ^{17}O NMR/H_2O-organic mixtures	Shcherbakov *et al.* (1974); Mashirov *et al.* (1975); Shcherbakov and Iorga (1975)

Table 28.4 (*Contd.*)

Aquo ion	*CN, O/H_2O*	*Distance(s)*	*Technique/Conditions*	*References*
	2 ax. O + 5 eq. H_2O	nd	optical/H_2O–organic mixtures	Garnov *et al.* (1996)
	2 ax. O + 5 eq. H_2O	nd	^1H NMR/$HClO_4$	Bardin *et al.* (1998)
	2.0(1) ax. O + 4.6(6) eq. H_2O	1.754(3), 2.414(6)	EXAFS/0.1 M HNO_3	Reich *et al.* (2000)
	2 ax. O + 5 eq. H_2O	1.752, 2.50	density functional theory	Hay *et al.* (2000)
	2 ax. O + 5 eq. H_2O	1.67, 2.50	Hartree–Fock	Tsushima and Suzuki (2000)
	2 ax. O + 5 eq. H_2O	1.73(2), 2.36(3)	EXAFS/1 M $HClO_4$	Antonio *et al.* (2001)
	2 ax. O + 5.3 eq. H_2O	nd	geometric modeling	Mauerhofer *et al.* (2004)
Np(VII)	2 ax. O + 4 eq. OH^-	1.85(2), 2.18(3)	EXAFS/2.5 M NaOH	Clark *et al.* (1997)
	4 eq. O + 2 ax. OH^-	1.86–1.87(1), 2.24(4)	EXAFS/1 M NaOH, DFT	Williams *et al.* (2001)
	4 eq. O + 2 ax. OH^-	1.89–1.90, 2.32–2.33	EXAFS/2.5 M NaOH, DFT	Bolvin *et al.* (2001)

[a] Not determined.

Table 28.5 *Plutonium redox speciation for Pu(III), Pu(IV), Pu(V), and Pu(VI). For the spherical ions, the hydration numbers* (n, n′, *coordinated* H_2O) *and Pu–*OH_2 *interatomic distances are listed. For the plutonyl ions, the axial* (*ax.*) *oxygen coordination numbers and Pu=O distances precede the equatorial* (*eq.*) *hydration numbers* (n″, n‴) *and the Pu–*OH_2 *bond lengths. Estimated standard deviations, where available, are obtained from the primary sources and are given after the* ± *sign or within parentheses.*

Aquo ion	*CN, O/*H_2O	*Distance*(s)	*Technique/Conditions*	*References*
$Pu(III)\cdot nH_2O$	10.2[a]	2.51(1)	EXAFS/0.01 M LiCl	Allen *et al.* (1997)
	9.9(9)	2.51(1)	EXAFS/1 M HCl	David *et al.* (1998)
	9	2.48	EXAFS/ns[b]	Ankudinov *et al.* (1998)
	8–9	2.49	EXAFS/ns[b]	Conradson (1998)
	8–9	2.51–2.55	density functional theory	Blaudeau *et al.* (1999)
$Pu(IV)\cdot n'H_2O$	8	nd[c]	Optical/$\leq$ 6 M HNO_3	Rykov *et al.* (1973)
	8	2.39	EXAFS/ns[b]	Ankudinov *et al.* (1998)
	8–9	2.39	EXAFS/ns[b]	Conradson (1998)
	nd	2.41	hydration free energy	Babu and Lim (1999)
$[Pu(V)O_2]^{+}\cdot n''H_2O$	2 ax. O + 5 eq. H_2O	nd	Optical/H_2O–organic mixtures	Garnov *et al.* (1996)
	2 ax. O + 4 eq. H_2O	1.84, 2.45	EXAFS/ns[b]	Ankudinov *et al.* (1998)
	2 ax. O + 4 eq. H_2O	1.81, 2.47	EXAFS/ns[b]	Conradson (1998)
	2 ax. O + 5 eq. H_2O	1.808, 2.61	density functional theory	Hay *et al.* (2000)
	2 ax. O + 5 eq. H_2O	1.65, 2.36	Hartree–Fock	Tsushima and Suzuki (2000)
	2 ax. O + 3.6 eq. H_2O	nd	geometric modeling	Mauerhofer *et al.* (2004)
$[Pu(VI)O_2]^{2+}\cdot n'''H_2O$	2 ax. O + 5 eq. H_2O	nd	optical/H_2O–organic solutions	Garnov *et al.* (1996)
	2 ax. O + 5 eq. H_2O	1.75, 2.45	EXAFS/1 M $HClO_4$	Runde *et al.* (1997)
	2 ax. O + 6 eq. H_2O	1.74, 2.45	EXAFS/ns[b]	Ankudinov *et al.* (1998)
	2 ax. O + 6 eq. H_2O	1.74, 2.40	EXAFS/ns[b]	Conradson (1998)
	2 ax. O + 5 eq. H_2O	1.7568, 2.523	density functional theory	Spencer *et al.* (1999)
	2 ax. O + 5 eq. H_2O	1.742, 2.485	density functional theory	Hay *et al.* (2000)
	2 ax. O + 5 eq. H_2O	1.59, 2.29	Hartree–Fock	Tsushima and Suzuki (2000)
	2 ax. O + 5.5 eq. H_2O	nd	geometric modeling	Mauerhofer *et al.* (2004)

[a] Subsequently adjusted to 9.2 (Allen *et al.*, 2000).
[b] Although the conditions were not specified in the primary sources cited here, it is likely that the conditions were the same as those of the XANES study of the Pu aquo ions in 1 M $HClO_4$ (Conradson *et al.*, 1998).
[c] Not determined.

Table 28.6 *Americium, curium, berkelium, and californium redox speciation with hydration numbers* (n, n′, *coordinated* H_2O) *and An-*OH_2 *interatomic distances obtained from literature sources. For the two americyl ion entries, the axial* (*ax.*) *oxygen coordination numbers precede the equatorial* (*eq.*) *hydration numbers* (n″, n‴). *Estimated standard deviations, where available, are given after the* ± *sign or within parentheses.*

Aquo ion	*CN, O/*H_2O	*Distance*(*s*)	*Technique/Conditions*	*References*
$Am(III)\cdot nH_2O$	9.5(9)	2.51(1)	EXAFS/1 M HCl	David *et al.* (1998)
	10.3	2.48	EXAFS/0.25 M HCl	Allen *et al.* (2000)
	8–9	2.47–2.49	EXAFS/$HClO_4$ pH ≈ 0.5	Stumpf *et al.* (2004)
$[Am(V)O_2]^{+}\cdot n''H_2O$	2 ax. O + 3.8 eq. H_2O	nd[a]	Geometric Modeling	Mauerhofer *et al.* (2004)
$[Am(VI)O_2]^{2+}\cdot n'''H_2O$	2 ax. O + 5.9 eq. H_2O	nd	Geometric Modeling	Mauerhofer *et al.* (2004)
$Cm(III)\cdot nH_2O$	10.2	2.45	EXAFS/0.25 M HCl	Allen *et al.* (2000)
$Bk(III)\cdot nH_2O$	9	nd	Diffusion/$HClO_4$ pH = 2.5	Latrous and Oliver (1999)
	9.0(6)	2.43(2)	EXAFS/1 M $HClO_4$	Antonio *et al.* (2002)
$Bk(IV)\cdot n'H_2O$	7.9(5)	2.32(1)	EXAFS/1 M $HClO_4$	Antonio *et al.* (2002)
$Cf(III)\cdot nH_2O$	9.5(9)	2.44(1)	EXAFS/1 M HCl	David *et al.* (1998)
	8.5 ± 1.5	2.42(2)	EXAFS/1 M HCl	Revel *et al.* (1999)

[a] Not determined.

Cf^{3+} at an average distance of 2.44(1) Å. For ensuing calculations of the molecular radius of H_2O and comparison with that obtained from an ionic model, the authors selected 8.5 as the O coordination number, which is the value inferred from previous conductivity measurements (Fourest *et al.*, 1995) because the EXAFS-determined coordination number was "measured with insufficient accuracy." The second note (Revel *et al.*, 1999) contains, in addition to the $L_{1,2,3}$-edge Cf XANES data, the $k^3\chi(k)$ EXAFS curve-fitting results for a single shell of 8.5 ± 1.5 O atoms at 2.42(2) Å. It is not clear if the coordination number, which is described as an indicative value, was refined in the fitting procedure. Despite the concentration (1 M) of the HCl solution, there was no evidence for the formation of an inner-sphere chloro complex of Cf^{3+}. This result is consistent with the aforementioned EXAFS conclusions (Allen *et al.*, 2000) for Cm^{3+} in chloride media of < 5 M.

(*viii*) *Americium*(*III*)

The aquo ions of the trivalent actinides have been of particular interest for comparison with those of the trivalent lanthanides in order to address fundamental issues about the nature of An–O bonding, i.e. the comparative extent of 5f versus 4f orbital overlap with O orbitals. Because the ionic radius (IR) of Am^{3+} (1.09 Å for CN = 8) (Shannon, 1976) is intermediate of those for Nd^{3+} (1.109 Å) and Sm^{3+} (1.079 Å), this similarity facilitates direct comparisons of the coordination environments of the Am^{3+} aquo ion and the nine-coordinate Nd^{3+} and Sm^{3+} aquo ions. Although no metrical details were reported, the FT data obtained from the EXAFS for an Am^{3+} solution of unspecified concentration in 1 M $HClO_4$ indicate that the Am^{3+}–OH_2 bond distance for the pure aquo ion decreases slightly with the addition of Cl^-, suggesting a subtle reorganization of either of its inner- and/or outer-hydration sphere (Runde *et al.*, 1997). The results of the analysis of the EXAFS data for an Am^{3+} solution (also of unspecified concentration) in 1 M HCl were reported to reveal 9.5(9) O atoms at 2.51(1) Å (David *et al.*, 1998). For subsequent modeling and calculations of the molecular radius of H_2O, the coordination number of nine was selected largely on the basis of other indirect measurements (Fourest *et al.*, 1995). The L_3-edge EXAFS data of a 0.01 M solution of ^{243}Am in 0.25 M HCl were fit to show that the aquo ion has 10.2 O at 2.45 Å (Allen *et al.*, 2000). The O coordination number decreases to 8.9 and 6.4 at Cl^- concentrations of 8 and 12.5 M, respectively, as the number of Am–Cl interactions simultaneously grow in, reaching a maximum of ca. 2. Remarkably, there is essentially no effect on the Am–O interatomic distances, which range from 2.48–2.51 Å in no particular order with $[Cl^-]$, which is qualitatively different from the preliminary observations of Am^{3+} (Runde *et al.*, 1997).

(*ix*) *Uranium*(*III*)

The significant amount of work on the tripositive aquo ions of Np and Pu (Tables 28.4 and 28.5) stands in obvious contrast with the sole study of the U^{3+} aquo ion in 1 M HCl (David *et al.*, 1998; see Table 28.2). Although the concentration is not specified and despite the notorious instability of U^{3+} to oxidation upon contact with air, EXAFS data were acquired and analyzed to provide a coordination number of 8.7(9) and an average U–O distance of 2.56(1) Å, which sets the benchmark as the longest one of the entire An^{3+} series for which data are available. This result is consistent with the effects of the contraction of 5f-element IR with increasing Z, where near the beginning of the series, i.e. U^{3+}, the interatomic distances are longer than for those ions near the end of the series, for example Cf^{3+} mentioned above, which has a distance of 2.42–2.44 Å (David *et al.*, 1998; Revel *et al.*, 1999) for its aquo ion. Curiously, the experimental An^{3+}–O bond length variation between U ($Z=91$) and Cf ($Z=98$) of 0.12–0.14 Å is nearly twice (1.6 to 1.9 times) the difference between their ionic radii, 0.075 Å, for CN = 6.

Concurrent with the measurements of the U^{3+} aquo ion and in the same manner, EXAFS data were collected and analyzed for the aquo ions of Np^{3+} and Pu^{3+}, which were also of unspecified concentration in 1 M HCl and of considerable reactivity with respect to oxidation (David *et al.*, 1998). The metrical details were reported as, in order of Np^{3+} and Pu^{3+}, 9.8(9) O at 2.52 (1) Å and 9.9(9) O at 2.51(1) Å. As expected, both interatomic distances are within the aforementioned scale and, moreover, are near to that for U^{3+}–O. The collective results of David *et al.* (1998) indicate that the trivalent aquo ions of U, Np, Pu, Am, and Cf are either nine or ten-coordinate with O atoms of water molecules. For the most part, the results of the comparable studies of Tables 28.2 and 28.4–28.6 as discussed separately in sections above and below bear this out.

(*x*) *Neptunium*(*III*)

The *in situ* L_3 EXAFS data for the aquo ion of Np^{3+} (0.0047 M in 1 M $HClO_4$), in which the oxidation state was precisely maintained by electrochemical methods, were best fit with 9(1) O atoms at 2.48(2) Å (Antonio *et al.*, 2001). The corresponding results from density functional theory (DFT) methods, including relativistic effects, indicate that coordination numbers of either eight or nine lead to the most stable conformations. In addition, the coordination number calculated from a simple geometric model was eight. The combination of the EXAFS, DFT, and modeling results led to the conclusion that Np^{3+} has a coordination number of eight or nine in aqueous perchloric acid. The same conclusion was obtained for Np^{4+}. The 0.04 Å difference in the experimental, average Np^{3+}–O distances of 2.48(2) Å (Antonio *et al.*, 2001) and 2.52 Å (David *et al.*, 1998) may reflect the influence of the (1 M) chloride ion on the hydration sphere in the solution of the latter experiment. The perchlorate anion is known

to be significantly less interacting, essentially non-complexing, with cations than is Cl^- and, moreover, $[ClO_4]^-$–H_2O interactions are less well-defined than those for $[Cl]^-$–H_2O (Neilson *et al.*, 1985).

(*xi*) *Plutonium*(*III*)

The speciation of the Pu^{3+} aquo ion and the surprising results about the effects of Cl^- on the Pu hydration sphere were addressed in two provocative reports (Allen *et al.*, 1997, 2000). In the first, for a solution of 0.02 M $^{242}Pu^{3+}$ in dilute (0.01 M) LiCl at pH = 3, the L_2-edge EXAFS was best fit to show an environment that consisted of 10.2 ± 1 O at 2.51 Å. In the subsequent work, the value of the O coordination number was refined to 9.2 by use of a larger amplitude reduction factor than fixed previously. The independent investigation (David *et al.*, 1998) for an aqueous Pu^{3+} solution of unspecified concentration in 1 M HCl confirmed the original Pu–O distance exactly and, within the error of the measurement, the O coordination numbers too (see Table 28.5). A remarkable aspect of the results is that the Pu EXAFS "...showed no evidence for the formation of inner-sphere chloro complexes up to a Cl^- concentration of 12.3 M" (Allen *et al.*, 1997). Although the O coordination number was shown to decrease from 9.2 to 5.2 with increasing $[Cl^-]$, there was no systematic change in the Pu–O distance, which held constant at 2.50–2.51 Å. The apparent dehydration of the Pu^{3+} aquo ion was not simultaneously compensated by the addition of Cl^-, thereby leading to the formation of some type of coordinately unsaturated Pu^{3+} aquo ion in the 12.3 M $[Cl^-]$ medium. What seems odd about this behavior is the insensitivity of the Pu–O bond length to the significant change in O coordination number. The combination of this observation with the contradictory behavior noted for the effects of Cl^- on the aquo ions of Am^{3+} and Cm^{3+} presents something of a quandary. There is the possibility that the EXAFS method itself may be the source of inherently misleading information for this Pu^{3+} system, wherein, for example, the apparent absence of Pu–Cl backscattering and the reduction of the Pu–O backscattering arise from cancellation effects. The confluence of coincidental phase and amplitude differences relating to the O and Cl interatomic distances, their Debye–Waller factors, and their coordination numbers, may lead to a significant degree of destructive interference and, ultimately signal cancellation. Such problems with EXAFS have been noted beforehand with multi-shell systems (Antonio *et al.*, 1983; Goulon *et al.*, 1983; Martens *et al.*, 1985; Roehler, 1992; Zhang *et al.*, 1998). Whether it applies to the Pu^{3+} system described here is, of course, unknown and requires independent confirmation of the experimental results.

Two other associated EXAFS studies of the Pu^{3+} aquo ion provide experimental results, i.e. eight to nine O at 2.48–2.49 Å (Ankudinov *et al.*, 1998; Conradson, 1998) that are in reasonable accord with the aforementioned ones (see Table 28.5) obtained in chloride media. Although details about the composition of the Pu^{3+} specimen were not included in either report, the EXAFS data

are likely to have been collected on the very same sample, 0.10 M Pu^{3+} in the non-complexing aqueous mineral acid solution of 1 M $HClO_4$, from which the XANES was acquired (Conradson *et al.*, 1998). If true, the shorter bond lengths (2.48–2.49 Å) for the Pu^{3+} aquo ion in the perchlorate solution compared with that (2.51 Å) for the chloride-containing solutions are consistent with subtle differences in the hydration of Pu^{3+}. Additional studies would be beneficial in this regard. Nevertheless, all of the EXAFS metrical information (Allen *et al.*, 1997; Ankudinov *et al.*, 1998; Conradson, 1998; David *et al.*, 1998; Allen *et al.*, 2000) are in reasonable accord with the relativistic DFT investigation (Blaudeau *et al.*, 1999) showing that the first solvation shell of Pu^{3+} contains eight or possibly nine H_2O molecules with Pu–O bond lengths of 2.51–2.55 Å.

(b) The triatomic An(V) and An(VI) ions

Up to this point, the discussions have focused on the spherical, monatomic trivalent and tetravalent An ions involving only An–OH_2 bonding. We now turn attention to the penta- and hexavalent An ions, which in acidic aqueous solution invariably take the form of the linear, triatomic *trans*-dioxocations, $[O{=}An^{5+}{=}O]^{+}$ and $[O{=}An^{6+}{=}O]^{2+}$. In these so-called actinyl cations, the terminal O interactions with the An ions have double bond character as indicated and, moreover, the An ions are coordinately unsaturated. Their coordination spheres are completed by the complexation of H_2O molecules that encircle the An ions in an equatorial plane perpendicular to the axial O=An=O moiety. The exact degree of hydration of the actinyl cations $[AnO_2]^{+}$ and $[AnO_2]^{2+}$ has been the subject of decades-long study and debate. The extent that the results from An EXAFS experiments have provided insights into the structure of these hydrated ions is summarized below. Additional aspects of actinyl electronic properties and coordination in molecular complexes as probed by XAS have been reviewed elsewhere (Den Auwer *et al.*, 2003b).

(*i*) *Uranyl*(VI)

The aqueous uranyl ion, $[UO_2]^{2+}$, with formally hexavalent U is the most studied system, whereas its pentavalent homolog, $[UO_2]^{+}$ is the least studied because of its limited stability and susceptibility to disproportionation. Even before the first U EXAFS measurements were recorded with a laboratory spectrometer (Karim *et al.*, 1980), the consensus from a number of structural experiments was that, in the solid-state, the $[UO_2]^{2+}$ ion exhibits a preference for five equatorial ligands thereby forming a pentagonal bipyramid (Evans, 1963). More contemporary compilations of structural data bear this out (Burns *et al.*, 1997). In the solid-state, the pentagonal bipyramidal polyhedron of $[UO_2]^{2+}$ is more common than either of the square or hexagonal bipyramidal coordination polyhedra. From the survey of solution EXAFS results presented in Table 28.2, the consensus is clear. The *trans*-dioxo $[UO_2]^{2+}$ cation exists in acidic aqueous

solution just as it does in the solid-state and that it has a hydration number of five. It is generally assumed that the U coordination geometry in dilute (<0.25 M) solutions is the same as that in the solid-state with an equatorial arrangement of five H_2O molecules between the two axial O atoms, wherein U^{6+} is seven-coordinate in the form of a pentagonal bipyramid, which is illustrated below. The selection of results shown in Table 28.2 from a number of theoretical calculations and other spectroscopic measurements are in agreement about the structure of the $[UO_2]^{2+} \cdot 5H_2O$ aquo ion.

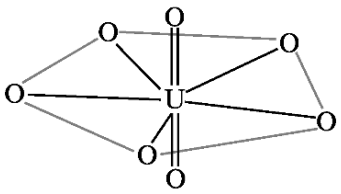

For the uranyl cation, the EXAFS-determined axial U=O distances of Table 28.2, 1.75–1.78 Å, have a small (0.03 Å) dispersion, and are essentially independent of differences in experimental conditions. By comparison, the 1.702(5) Å U=O bond length obtained for a concentrated (1 M) $[UO_2]^{2+}$ solution through use of X-ray scattering is anomalously short (Aberg *et al.*, 1983). The bond length dispersion is more than twice as large (0.08 Å) for the EXAFS-determined U–OH_2 distances, which for the synchrotron radiation studies exhibit a range of 2.40–2.48 Å. This suggests that the equatorial hydration of $[UO_2]^{2+}$ is sensitive to experimental variations, such as pH as well as the nature and concentration of the anion in the inorganic and organic acids.

To address aspects of these issues, an exhaustive series of U L_3-edge EXAFS measurements have demonstrated that the perchlorate anion does not coordinate directly to the $[UO_2]^{2+} \cdot 5H_2O$ aquo cation even in 11.5 M $HClO_4$ (Sémon *et al.*, 2001). The average, equatorial U–OH_2 distances (2.40–2.43 Å) for the $[UO_2]^{2+}$ aquo ions in perchloric acid are independent of concentration, and are at the short end of the range of distances for the mineral acid aquo ion systems of Table 28.2. In contrast, the systematic U L_3 EXAFS studies of the $[UO_2]^{2+}$ ion in 0–10 M solution concentrations of HCl reveal inner-sphere Cl^- complexation at and above 4 M, which is accompanied by expansion of the U–OH_2 bond lengths (Allen *et al.*, 1997). The total equatorial coordination number remained constant at five, suggesting a simple replacement of H_2O with Cl^- as the concentration of HCl increased. Subsequent treatments of the ten EXAFS spectra in the $[Cl^-]$ series through principal component (factor) analysis revealed the presence of three distinct species (Wasserman *et al.*, 1999). Two of these reflect the inner-sphere replacement of H_2O by Cl^- at the equatorial position in the 1–10 M HCl solutions. The third species, significant only for the $[UO_2]^{2+}$ ion in 12 and 14 M solutions of LiCl, was attributed to a product resulting from the use of the Dowex anion-exchange resin for the preparative chemistry.

In acidic solutions (pH ≈ 5) of 0.052 M $[UO_2]^{2+}$ with excess fluoride ion (0.21 and 0.45 M), the equatorial coordination number was also found to be five, consisting of a combination of U–F and U–OH_2 interactions that were not resolved in the FT data (Vallet *et al.*, 2001). The F^- and H_2O coordination numbers were determined from the combined results of equilibrium measurements and the U L_3-edge EXAFS analysis to reveal tri- and tetrafluoride complexation, $[UO_2F_3(H_2O)_2]^-$ and $[UO_2F_4(H_2O)]^{2-}$, with average U–F and U–OH_2 distances of 2.25–2.26 and 2.47–2.48 Å, respectively. At 3 M [F^-], water does not participate in the equatorial coordination, which was shown to consist of five F^- anions at 2.26 Å, of the uranyl(VI) pentafluoride complex, $[UO_2F_5]^{3-}$ (Vallet *et al.*, 2001). Solution EXAFS and quantum chemical methods have been brought to bear upon the nature of aqueous uranyl(VI) complexes with fluoride and oxalate, $[C_2O_4]^{2-}$, ligands (Vallet *et al.*, 2003). At pH = 4.2 in the absence of F^-, the equatorial bonding in the $[UO_2(O_2C_2O_2)_2H_2O]^{2-}$ complex was determined to consist of five O atoms of which four are attributable to the two symmetric oxalate ligands, wherein each carboxylate group chelates to U in a monodentate fashion with one O, and the fifth is from H_2O. In this molecular complex, whose structure is illustrated below (left), the average equatorial U–O distance is 2.38 Å. Upon the addition of F^- at a concentration slightly in excess of that (0.06 M) for $[UO_2]^{2+}$, the fluoride ion displaces the water molecule without any effect on the nature of the oxalate chelation, thereby maintaining the five-coordinate equatorial ligation, $[UO_2(O_2C_2O_2)_2F]^{3-}$. With excess (1.68 M) oxalate at pH = 6.5, a five-coordinate complex with three oxalate ligands, $[UO_2(O_2C_2O_2)_3]^{4-}$, is formed. In this structure (illustrated below, right) two of the oxalates are chelate-bonded exactly as in the aquo and fluoride complexes and the third is bound to U through a single carboxylate O.

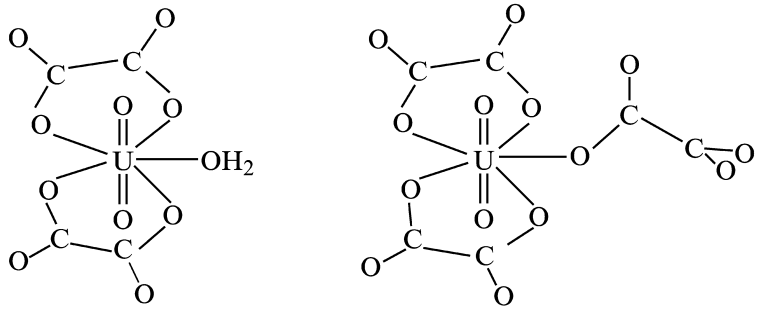

The early EXAFS experiments indicated that the dissolution of solid uranyl nitrate, $UO_2(NO_3)_2 \cdot 6H_2O$, and sodium uranyl acetate, $NaUO_2(CH_3CO_2)_3$, at concentrations of 0.25 M and less in acidic media leads to their complete dissociation and formation of the pentahydrate aquo ion, $[UO_2]^{2+} \cdot 5H_2O$ (Charpin *et al.*, 1985). In subsequent concentration- and temperature-dependent U L_3-edge EXAFS measurements (Schofield *et al.*, 1999), no evidence was found for equatorial ligand replacement of H_2O with $[NO_3]^-$ in acidic solutions of 1 M nitrate and less at 150°C and below. In related *in situ*,

temperature-dependent U L_3-edge EXAFS studies of the uranyl ion speciation in acidic acetate solutions with different concentration ratios, $[CH_3CO_2^-]$: $[UO_2^{2-}]$, (Mosselmans *et al.*, 2001), little direct evidence was apparent in the FT data for $[CH_3CO_2]^-$ coordination to the pentahydrate $[UO_2]^{2+}$ cation at low ratios. Whereas the equatorial coordination number was also found to be five at high ratios, the evidence for distant U–C backscattering suggests the coordination of at least two bidentate acetate ligands even at temperatures as high as 250°C. The presence of one H_2O molecule is presumed to complete the equatorial O coordination in a neutral aquo species, $[UO_2(CH_3CO_2)_2H_2O]$.

For the binary, aqueous $[UO_2]^{2+}$–$[SO_4]^{2-}$ system in acidic solution pH$\leq$2, bidentate O coordination of the sulfate ligand to $[UO_2]^{2+}$ was evident through observation of distant S backscattering in the U L_3-edge EXAFS data for each of two solution species identified as UO_2SO_4(aq) and $[UO_2(SO_4)_2]^{2-}$ in the equilibrium distribution diagram (Moll *et al.*, 2000a). Both were shown to have an equatorial O coordination number of five, meaning that in addition to the two O atoms from the bidentate $[SO_4]^{2-}$ groups, the former has three H_2O molecules, i.e. $[UO_2SO_4(H_2O)_3]$, and the latter has one H_2O molecule, i.e. $[UO_2(SO_4)_2H_2O]^{2-}$, in the inner-sphere equatorial coordination environment of $[UO_2]^{2+}$. At the higher pH of 5.25, obtained by adjustment with NaOH, the EXAFS metrical results showing bidentate sulfate chelation in the $[UO_2]^{2+}$–$[SO_4]^{2-}$–$[OH]^-$ system were used to verify the previously proposed structure models for the tri- and pentanuclear complex anions, $[(UO_2)_3O(OH)_2(SO_4)_3(H_2O)_2]^{4-}$ and $[(UO_2)_5O_3(OH)_2(SO_4)_4(H_2O)_2]^{6-}$, respectively. For a related sulfur-bearing oxoanion in acidic aqueous solutions, the triflate anion, $[CF_3SO_3]^-$, was found to act as a monodentate ligand by inner-sphere coordination to U through one O atom at high (>8 M) concentrations of the anion (Sémon *et al.*, 2001). The total equatorial O coordination number is approximately five, suggesting the displacement of one H_2O molecule from the pentahydrate aquo species and the formation of $[UO_2(CF_3SO_3)_1(H_2O)_4]^+$.

(*ii*) *Neptunyl*(*v*)

Although there are, as yet, no experimental structural details for the aqueous uranyl ion of U^{5+}, $[UO_2]^+$, the calculated structure (Hay *et al.*, 2000) using DFT methods is, not surprisingly, a pentagonal bipyramid with U=O and U–OH_2 bond lengths of 1.810 and 2.616 Å, respectively. Unlike U, the most stable form of Np in acidic aqueous solution is the pentavalent neptunyl ion, $[NpO_2]^+ \cdot n''H_2O$. It can be conveniently and reversibly interconverted to the hexavalent form, $[NpO_2]^{2+} \cdot n'''H_2O$, by electrochemical means, suggesting that the one-electron redox reaction is either independent of possible differences in the hydration of Np or, alternatively, that the hydration numbers n'' and n''' for $[Np^{5+}O_2]^+$ and $[Np^{6+}O_2]^{2+}$, respectively, are equivalent. This has been an issue of some controversy since the 1970s, when original work involving NMR

studies of perchlorate salt solutions of $[NpO_2]^{2+}$ was interpreted to provide a mean number of six-coordinated water molecules (Shcherbakov *et al.*, 1974; Mashirov *et al.*, 1975; Shcherbakov and Iorga, 1975). Similarly, based upon ^1H NMR experiments, a hydration number of six was proposed for $[NpO_2]^+$ (Glebov *et al.*, 1977). Recent interpretations of electronic absorption spectra suggest that the hydration number for both neptunyl species, $[NpO_2]^+$ and $[NpO_2]^{2+}$, is five and, furthermore, that their coordination polyhedra are pentagonal bipyramids (Garnov *et al.*, 1996). This interpretation is consistent with the accepted coordination of the pentahydrate, hexavalent uranyl ion, $[UO_2]^{2+} \cdot 5H_2O$.

As shown in Table 28.4, the first Np L_3-edge EXAFS brought to bear upon the $[NpO_2]^+ \cdot n''H_2O$ ion indicated that $^{237}Np^{5+}$ has an equatorial coordination of five H_2O molecules at 2.52(2) Å (Combes *et al.*, 1992). Two subsequent, independent EXAFS investigations (Allen *et al.*, 1997; Antonio *et al.*, 2001) as well as the results from two theoretical calculations (Hay *et al.*, 2000; Tsushima and Suzuki, 2000) confirmed the hydration number of five. A lower value of four H_2O molecules was extracted from the analysis of the EXAFS data for an aqueous solution of 0.05 M $[NpO_2]^+$ in 0.1 M HNO_3, the sole exception (Reich *et al.*, 2000). Although the exact reasons for the variance are not known, the complex hydrolytic behavior of Np^{5+}, particularly at pH $\approx$ 1, might have some bearing upon this as well as the unusually large (0.08 Å) range of average interatomic distances, 2.44–2.52 Å, involving the equatorial coordination of water molecules. Alternatively, it may suggest that the hydration sphere of $[NpO_2]^+$ has substantial sensitivity to experimental conditions, such as pH, counter-anion, ionic strength, etc., whereas the axial Np=O interactions (1.80–1.85 Å) are less sensitive. In either case, complicating chemical behaviors, e.g. hydrolysis, disproportionation, complexation, oligomerization, precipitation, etc., are generally suppressed in a highly acidic (pH $\approx$ 0) non-complexing perchloric acid medium. The EXAFS experimental conditions cover a range of pH values starting from effectively 0 in 1 M $HClO_4$ (Antonio *et al.*, 2001) to pH $\approx$ 1 in 0.1 M HNO_3 (Reich *et al.*, 2000), to pH $\approx$ 2 in perchloric acid (Combes *et al.*, 1992) and, finally, to pH $\approx$ 3 in hydrochloric acid with excess (3 M) chloride as LiCl (Allen *et al.*, 1997). At Cl^- concentrations of ca. 6 M and above, the equatorial coordination number remains constant at five, but whereas one (or more) Cl^- ions displace and replace an equal number of H_2O molecules about $[NpO_2]^+$ (Allen *et al.*, 1997). This is accompanied by an elongation of the Np–OH_2 bond lengths.

(*iii*) *Neptunyl*(*VI*)

The two independent Np L_3-edge EXAFS studies (Reich *et al.*, 2000; Antonio *et al.*, 2001) and the two independent theoretical studies (Hay *et al.*, 2000; Tsushima and Suzuki, 2000) of the hexavalent neptunyl ion are in consensus

about the hydration number (five). The EXAFS results reveal axial Np=O bond lengths (1.73–1.75 Å) and equatorial Np–OH_2 bond lengths (2.36–2.41 Å) that are consistently shorter (ca. 0.03–0.16 Å) than the corresponding interactions for the pentavalent neptunyl aquo ion $[NpO_2]^+ \cdot 5H_2O$. The shorter bond distances for the hexavalent species $[NpO_2]^{2+} \cdot 5H_2O$ are consistent with the expected decrease in the Np IR with increasing oxidation state. The well-known ionic radii (IR) tabulations of Shannon (1976) are limited to the comparison between Np^{5+} (0.75 Å) and Np^{6+} (0.72 Å) for CN = 6. The 0.03 Å difference is considerably smaller than the corresponding IR contraction of 0.14 Å between Np^{3+} (1.01 Å) and Np^{4+} (0.87 Å), which is clearly borne out in the Np–OH_2 distances of Table 28.4 for the $Np^{3+} \cdot nH_2O$ and $Np^{4+} \cdot n'H_2O$ systems. The absence of experimental detail for the pentavalent uranyl aquo ion prevents the analogous metrical comparisons between it and the hexavalent uranyl aquo ion. Because the Pu aquo system has stable pentavalent and hexavalent plutonyl ions, additional comparisons, both absolute and relative, can be drawn with regard to the data of Table 28.5.

(*iv*) *Plutonyl*(*VI/V*)

Two reports of Pu L_3-edge EXAFS measurements (Ankudinov *et al.*, 1998; Conradson, 1998) constitute the full extent of experimental investigation of the $[Pu^{5+}O_2]^+ \cdot n''H_2O$ system and the majority of that for $[Pu^{6+}O_2]^{2+} \cdot n'''H_2O$. For plutonyl(V), the curve-fitting analysis furnished axial Pu=O bond lengths of 1.81–1.84 Å and an equatorial coordination number of four with Pu–OH_2 bond lengths of 2.45–2.47 Å. This hydration number (four) stands in contrast to that (five) obtained from the results of two different levels of calculation with DFT (Hay *et al.*, 2000) and Hartree–Fock (Tsushima and Suzuki, 2000) methods. The theoretical investigations of the hexavalent plutonyl aquo ion reach the same conclusion, namely that $[PuO_2]^{2+}$ forms the most stable and strongly bound complexes with five H_2O molecules in the equatorial coordination (Spencer *et al.*, 1999; Hay *et al.*, 2000; Tsushima and Suzuki, 2000). Whereas the optical spectroscopy (Garnov *et al.*, 1996) and the early EXAFS experiments (Runde *et al.*, 1997) are in agreement, showing an O coordination number of five, the later EXAFS work (Ankudinov *et al.*, 1998; Conradson, 1998) provides an O coordination number of six. The fact that the average Pu–OH_2 distances of 2.45 Å (Runde *et al.*, 1997) for the pentahydrate plutonyl(VI) and 2.40–2.45 Å (Ankudinov *et al.*, 1998; Conradson, 1998) for the hexahydrate plutonyl(VI) species are overlapping despite the unit difference in hydration number remains something of a quandary. In strongly acidic (1 M $HClO_4$ and 1 M HCl) $[PuO_2]^{2+}$ solutions with aqueous chloride concentrations of 5 M and above, Pu EXAFS data reveal the formation of plutonyl(VI) chloro complexes, wherein some number of inner-sphere H_2O are replaced by Cl^- ions (Runde *et al.*, 1997). Although the exact extent of the

Cl^- substitution was not determined, the effects include a weakening and elongation (0.01 to 0.06 Å) of the remaining equatorial Pu–OH_2 interactions as well as the axial Pu=O bonds.

According to the data of Table 28.5, the axial Pu–O interatomic distance contraction between the plutonyl(v) and (vi) aquo ions amounts to 0.06–0.10 Å. This is more than twice that expected based upon the difference in the Pu^{5+} (0.74 Å) and Pu^{6+} (0.71 Å) IR for CN=6 (Shannon, 1976). As mentioned previously, the same phenomenon was observed for the neptunyl(v) and (vi) aquo ions. This behavior is to be contrasted with that between the aquo ions of Pu^{3+} and Pu^{4+}, which exhibit a 0.09–0.12 Å Pu–OH_2 interatomic distance contraction that is consistent in magnitude with the 0.14 Å difference of IR for CN = 6. In view of the apparent difference in the equatorial coordination number between $[PuO_2]^+$ and $[PuO_2]^{2+}$, it is difficult to ascribe any significance to the 0.0–0.07 Å difference between the Pu–OH_2 distances of Table 28.5. Comparisons with corresponding Am species, $[AmO_2]^+$ and $[AmO_2]^{2+}$, would be informative but are not possible because of the present lack of metrical information for these two aquo ions.

28.2.3 Base redox speciation

The aqueous actinide chemistry of the four oxidation states – iii, iv, v, and vi – described above for acidic solutions have been complemented by studies, albeit far fewer in number, of the same four states plus the heptavalent (vii) one in alkaline and carbonate solutions (Shilov and Yusov, 2002). In particular, the An^{7+} ions of Np, Pu, and Am are extremely unstable species under all but the most alkaline of conditions. Concentrated carbonate solutions too have been shown to facilitate studies of the otherwise unstable Am^{4+}, Cf^{5+}, and Cm^{6+} ions. Aspects of An redox speciation in hydroxide and carbonate media as obtained by use of EXAFS spectroscopy are surveyed in this section.

(a) Hydroxide solution systems

(*i*) *Neptunium*(*vii/vi*)

A longstanding problem in actinide science about the nature of the Np^{7+} species in aqueous, basic solutions was resolved through use of EXAFS and quantum chemistry. Since the first report of its preparation (Krot and Gelman, 1967), the coordination environment of Np^{7+} has remained controversial, in part because of the technical difficulties associated with the stabilization of the high-valent ion. The existence of an anionic species of Np^{7+} in alkaline solution was proposed early on (Spitsyn *et al.*, 1969), "...and its formula is believed by most researchers to be NpO_5^{3-}" (Fahey, 1986). Still, equally probable trianionic

forms include $[NpO_4(OH)_2]^{3-}$ (Burns *et al.*, 1973) and $[NpO_2(OH)_6]^{3-}$, among others. In order to address this speciation issue, Np L_3-edge EXAFS was brought to bear upon a 0.03 M solution of Np^{7+} in 2.5 M NaOH prepared by ozonation of the neptunyl(VI) hydroxide, $NpO_2(OH)_2$ (Clark *et al.*, 1997). The analysis provided evidence for a linear, *trans*-dioxo species of Np^{7+}, which has an overall pentagonal bipyramidal coordination consisting of the two axial O atoms at 1.85(2) Å and five equatorial O atoms attributed to four OH^- at 2.18(3) Å and one H_2O at 2.43(3) Å. This environment is consistent with the formation of a monoanionic neptunyl(VII) species, $[NpO_2(OH)_4(H_2O)]^-$, whose coordination polyhedron is similar, albeit with different Np–O distances, to those for the *bona fide* dioxo species of $[Np^{5+}O_2]^+$ and $[Np^{6+}O_2]^{2+}$ that are ubiquitous in acid solution.

In contrast, two subsequent Np EXAFS and DFT studies (Bolvin *et al.*, 2001; Williams *et al.*, 2001) of the coordination geometry of Np^{7+} in alkaline solution came to the conclusion that Np^{7+} has a tetraoxo square planar coordination environment. The presence of two distant, axial O atoms, presumably hydroxide ligands, completes the coordination sphere, which has a square bipyramid structure. In one study (Williams *et al.*, 2001), bulk electrolysis techniques in simultaneous combination with ozonation were utilized to control the Np valence in a freshly prepared suspension of Np^{5+} (0.0065 M) in 1 M NaOH for *in situ* Np L_3-edge EXAFS of the Np^{7+} and Np^{6+} ions, whose electrochemical interconversion is facile (Zielen and Cohen, 1970). The Np^{6+} EXAFS was fit to reveal a typical *trans*-dioxo species with two close, axial O atoms at 1.82(2) Å and an equatorial coordination of four distant O atoms at 2.21(3) Å, in what would likely be a square bipyramidal polyhedron, $[NpO_2(OH)_4]^{2-}$. Geometry optimizations at the B3LYP level using a CPCM solvent model confirm this neptunyl(VI) structure and stoichiometry (Bolvin *et al.*, 2001). In contrast, the Np^{7+} EXAFS was fit to reveal four close O atoms at 1.87(1) Å and two distant ones at 2.24(4) Å, consistent with a polyhedron that could also be a square bipyramid. The accompanying DFT calculations predicted a slightly distorted square-planar geometry for the tetraoxo, $[NpO_4]^-$, anion (Williams *et al.*, 2001). The geometry was further elucidated at the DFT level using the hybrid functional B3LYP and a CPCM solvent model to reveal a six-coordinate Np^{7+} in the square bipyramid polyhedron, $[NpO_4(OH)_2]^{3-}$ (Bolvin *et al.*, 2001). The associated Np L_3-edge EXAFS acquisition and analysis for a solution of Np^{7+} (0.015 M) in 2.5 M NaOH revealed a coordination of 3.6 ± 0.3 O atoms at 1.89 Å and 3.3 ± 1.3 O atoms at 2.33 Å. The large error on the distant O coordination number was attributed to the low backscattering amplitude and the interference from the four close O atoms. From the combination of theoretical results and experimental data (including solid-state structural and solution electrochemical information) (Shilov, 1998), it was concluded "...that the predominant Np(VII) complex found in solutions with high concentration of OH^- is indeed $NpO_4(OH)_2^{3-}$" (Bolvin *et al.*, 2001).

(*ii*) *Plutonium*(*VII/VI*)

Although no EXAFS results have been published about the corresponding Pu^{7+}/Pu^{6+} and Am^{7+}/Am^{6+} redox speciation in alkaline solutions, the plutonium electrochemical behavior as a function of hydroxide ion activity is very much like that for neptunium, except for the more positive electrode potentials for Pu (Shilov, 1998). This suggests that the six O, tetragonal bipyramidal coordination environments for both Np^{7+} and Np^{6+} are likely to be obtained for the corresponding Pu species. In these, the absence of a substantial structural rearrangement between the hexa- and heptavalent species would explain the reversible and generally facile redox reaction:

$$[An^{7+}O_4(OH)_2]^{3-} + 2H_2O + e^- \leftrightarrow [An^{6+}O_2(OH)_4]^{2-} + 2OH^- \qquad (28.10)$$

The formulas shown in this equation are presently accepted by actinide electroanalytical chemists in general (for An ≡ Np, Pu, and Am) and this An^{7+}/An^{6+} redox speciation appears, exactly as written, in contemporary compilations of standard electrode potentials (Bratsch, 1989). The estimated potential for the Pu^{8+}/Pu^{7+} couple (>3V) (Shilov and Yusov, 2002) is well beyond the polarization window of aqueous solutions. The existence of Pu^{8+} will have to be confirmed in other solvents, such as newly designed ionic liquids with immense (ca. 5V) polarization windows (Quinn *et al.*, 2002), or in the solid-state.

(*iii*) *Uranyl*(*VI*)

Because of practical and technological issues in nuclear waste storage and processing, the speciation and structure of U^{6+} complexes in strongly alkaline solutions has been investigated with U L_3-edge EXAFS, quantum chemical calculations, and other spectroscopic and physical methods (Moll *et al.*, 1998; Schreckenbach *et al.*, 1998; Clark *et al.*, 1999; Wahlgren *et al.*, 1999; Moll *et al.*, 2000b; Vallet *et al.*, 2001). Driven by implications of serious environmental concern, i.e. aging tanks of alkaline high-level waste, the original work (Clark *et al.*, 1999) on $[UO_2]^{2+}$ (≈0.10 M) in a 3.5 M tetramethylammonium hydroxide, $[(CH_3)_4N]OH$, solution sparked interest of theoretical, applied, and fundamental importance. The FT data revealed a single asymmetric peak, which was shown to include backscattering contributions from axial and equatorial O coordination. The $k^3\chi(k)$ EXAFS was fit to expose two nearest O atoms at 1.79(1) Å, attributed to axial U=O bonding, and 5.2(5) O atoms at 2.22(1) Å, attributed to equatorial U–OH bonding. This seven O pentagonal bipyramidal coordination of U^{6+} is not unusual on its own and, except for the relatively long and short axial and equatorial bonds, respectively, it is the prevalent structure in acid solution. Yet, comparison of the solution environment with that for the solid uranyl(VI) salt, $[Co(NH_3)_6]_2[UO_2(OH)_4]_3 \cdot H_2O$, crystallized from 3.5 M $[(CH_3)_4N]OH$ revealed unexpected detail that has been the source of multinational debate. The single-crystal structure shows a six O pseudo-octahedral

coordination of U^{6+} with two *trans*-oxo atoms at 1.82(1) Å and four OH^- ligands at 2.26(2) Å. The corresponding EXAFS data for the crystalline compound, collected and analyzed in the same manner as for the solution sample, are in agreement with the X-ray diffraction data. The $k^3\chi(k)$ EXAFS were best fit with two O atoms with an average U=O distance of 1.81(1) Å and 3.9(5) O atoms with an average U–O distance of 2.21(1) Å (Clark *et al.*, 1999). The pivotal difference between the solid and solution structures is the OH^- coordination number, which is four in the solid and five in solution.

Although such differences in coordination upon dissolution of a solid are not extraordinary, the remarkable aspect here is the observation of essentially identical, within experimental error, average U=O and U–OH distances despite the coordination number difference in the solution (7) and solid (6) uranyl hydroxide complexes. Based upon a comparison of the U^{6+} IR for CN=6 and 7 (0.73 and 0.81 Å, respectively) (Shannon, 1976), the U–O distances for the seven-coordinate solution sample are anticipated to be 0.08 Å longer than those for the corresponding six-coordinate solid sample. An expansion of this magnitude is not evident, suggesting that a simple ionic, electrostatic model of the U=O and U–OH interactions is inappropriate for these systems. Alternatively, it may be an indication of some degree of covalency and the participation of f-electrons in the U–O bonding, or that the solution coordination number is in error because of, for example, the effects of an equilibrium distribution of two monomeric uranyl(VI) species, a pentahydroxide, $[UO_2(OH)_5]^{3-}$, and a tetrahydroxide, $[UO_2(OH)_4]^{2-}$ (Clark *et al.*, 1999). These intriguing results, in particular, the equatorial coordination number (5) in highly alkaline solution conditions, have been experimentally confirmed through EXAFS (Moll *et al.*, 1998; Wahlgren *et al.*, 1999). Yet, remarkably, and as developed below, the EXAFS-determined value was set aside in favor of that (4) from bond length comparisons and theoretical and geometrical optimizations.

Uranium L_3-edge EXAFS was used to elucidate the coordination of $[UO_2]^{2+}$ (0.055 M) in solutions of $[(CH_3)_4N]OH$. The results obtained from the curve-fitting analyses are indistinguishable and reveal two axial O atoms at 1.82 Å as well as 5.0 ± 0.5 and 5.2 ± 0.5 equatorial O atoms at 2.24 Å in 1 and 3 M $[(CH_3)_4N]OH$, respectively (Moll *et al.*, 1998; Wahlgren *et al.*, 1999). This latter coordination number was subsequently reevaluated to be 4.6 ± 0.6 (Moll *et al.*, 2000b). A number of factors combine to cast doubt on the EXAFS result for the equatorial coordination number, including the general difficulty and large uncertainty associated with such determinations for uranyl complexes at ambient temperature. (Thompson *et al.*, 1995, 1997; Barnes *et al.*, 2000) Insofar as bond lengths generally increase with coordination number (Shannon, 1976), it is also peculiar that the average U–OH distance (2.24 Å) for a purportedly five-coordinate hydroxo anion of $[UO_2]^{2+}$ in solution is the same as that (2.26(2) Å) for the four OH^--coordinated $[UO_2]^{2+}$ complex anion, $[UO_2(OH)_4]^{2-}$, in a crystallographically characterized solid (Clark *et al.*, 1999). Despite the higher coordination number indicated by the EXAFS data, it was concluded "...that

the coordination number of uranyl(VI) ion in strongly alkaline solution is four, not five. . .'' and that the mononuclear, tetrahydroxide species, $[UO_2(OH)_4]^{2-}$, is the dominant complex in strongly alkaline solutions (Wahlgren *et al.*, 1999). This suggestion was corroborated by the results of geometry optimizations obtained through a number of *ab initio* quantum chemical calculations (Moll *et al.*, 1998; Schreckenbach *et al.*, 1998; Wahlgren *et al.*, 1999; Vallet *et al.*, 2001).

At the time of this publication, issues about the form of $[UO_2]^{2+}$ in alkaline solution were most recently revisited with regard, again, to its speciation in 0.5 and 3 M $[(CH_3)_4N]OH$ by use of U L_3-edge EXAFS and ^{17}O NMR (Moll *et al.*, 2000b). The results serve to resolve, in part, the controversy generated by the watershed report (Clark *et al.*, 1999), whose experimental evidence indicated the formation of a pentahydroxide species, and the approximately coincident work (Wahlgren *et al.*, 1999), whose evidence was interpreted in favor of a tetrahydroxide species. The latest research has found evidence for the latter, $[UO_2(OH)_4]^{2-}$, species from the primary EXAFS analysis of data obtained in a dilute (0.05 M) solution of $[UO_2]^{2+}$ in 0.5 M $[(CH_3)_4N]OH$ at pH = 13.7 (Moll *et al.*, 2000b). The pseudo-octahedral environment of U^{6+} was shown to consist of 1.8 ± 0.3 O atoms at 1.83 Å and 4.2 ± 0.6 O atoms at 2.26 Å. In the concentrated, 3 M solution of $[(CH_3)_4N]OH$ of the original studies (Clark *et al.*, 1999), the presence of a fifth OH^- ligand in association with $[UO_2(OH)_4]^{2-}$ was unambiguously established by use of ^{17}O NMR (Wahlgren *et al.*, 1999). A $[UO_2(OH)_5]^{3-}/[UO_2(OH)_4]^{2-}$ ratio of ≈ 0.3 in a 3 M solution of $[(CH_3)_4N]OH$ was calculated based upon an estimation of the equilibrium constant for the aqueous reaction,

$$[UO_2(OH)_4]^{2-} + OH^- \leftrightarrow [UO_2(OH)_5]^{3-} \qquad (28.11)$$

The EXAFS results for this mixture of solution species provide a site-averaged coordination environment of 1.8 ± 0.3 O at 1.83 Å and 4.6 ± 0.6 O at 2.25 Å (Wahlgren *et al.*, 1999).

Since the publication of the results from the pioneering X-ray scattering experimentation (Aberg, 1970; Musikas and Narten, 1978), metrical details about the solution structures of polynuclear hydrolysis products of uranyl(VI) have been few and far between. At least, there is a dearth of EXAFS research, other than the investigation of an acidic solution (pH = 4.1) of dilute (0.05 M) $[UO_2]^{2+}$ in 0.05 M $[(CH_3)_4N]OH$ (Moll *et al.*, 2000b). In these conditions, the formation of the triangular, trinuclear complex, $[(UO_2)_3(OH)_5]^+$, was confirmed on the basis of the 3.80 Å U–U interatomic distance. The U coordination number for a pure specimen of this trinuclear hydrolysis complex is two. The lower, EXAFS-determined values of $1.3–1.4\pm0.4$ are consistent with an admixture of the trinuclear complex and the binuclear one, $[(UO_2)_2(OH)_2]^{2+}$, whose structure has been optimized at several levels of theory (Tsushima and Reich, 2001) and which is presumed to have the core structure of the solid-state hydroxo compound $[(UO_2)_2(OH)_2Cl_2(H_2O)_4]$, with a U coordination number of one and a U–U interatomic distance of 3.94 Å (Aberg, 1970).

The EXAFS-measured distribution of equatorial U–O interactions, which involve a combination of bridging as well as terminal oxo and hydroxide ligation and bond lengths, are also consistent with a mixed speciation of polynuclear complexes. The site- and species-averaged, axial U=O bond length of the uranyl ion was 1.79 Å (Moll *et al.*, 2000b).

(*iv*) *Thorium*(IV)

The hydrolysis of the tetravalent actinides leads to a complicated distribution of species with different degrees of aggregation, the exact extent of which hinges upon the solution conditions (Neck and Kim, 2001). For example, even below the onset of oligomerization, in the narrow (2 unit) pH range of 3–5, the calculated Th^{4+} speciation already indicates appreciable amounts of bi- and tetranuclear species, such as $[Th_2(OH)_2]^{6+}$ and $[Th_4(OH)_8]^{8+}$, in addition to the mononuclear ones, e.g. $[Th(OH)]^{3+}$, $[Th(OH)_2]^{2+}$, $[Th(OH)_3]^{+}$ (Neck *et al.*, 2002). In view of the complexity for such an assortment of multi-site, polynuclear complexation, the use of EXAFS for studies of the aqueous speciation of suspended colloids above the onset of hydrolysis has been limited. The available studies concern the use of Th L_3-edge EXAFS for coulometrically titrated solutions (pH = 1.38–3.67) of 0.0043–0.028 M Th^{4+} in 0.5 M NaCl (Neck *et al.*, 2002; Rothe *et al.*, 2002). The FT data for the aqueous solutions of pH $\leq$ 3 (below the onset of colloid formation) exhibit a strong, nearly symmetric peak due to O backscattering, fit as 11.6–12.7 O at 2.45–2.46 Å, that is typical of the Th^{4+} aquo ion. In contrast, the FT data for the aqueous suspension of colloidal species at pH = 3.50 and 3.62 exhibit a weak, highly asymmetric peak due to O backscattering, fit as 10.5–10.6 O at 2.51 Å, that is expected for a broad distribution of Th–O interactions arising from the presence of a mixture of ultrafine (i.e. nanosize), polynuclear species and amorphous Th^{4+} colloids. The EXAFS data for the aqueous suspension at pH = 3.67 also reveals a weak, distant peak attributed to Th–Th interactions. The structural parameters and Th^{4+} coordination environment for this specimen are similar to those for the carefully prepared amorphous hydrated oxyhydroxide solid, $ThO_n(OH)_{4-2n} \cdot xH_2O$ (Neck *et al.*, 2002; Rothe *et al.*, 2002).

(b) Carbonate solution systems

A large part of the interest and activity in environmental and molecular sciences of the actinide elements concerns their interactions with carbonate, $[CO_3]^{2-}$, and bicarbonate, $[HCO_3]^{-}$, anions in hydrologic and geochemical processes. Besides H_2O (including hydroxide) itself, these are the predominant ligands for An-ion complexation found in fresh and saline waters alike. Of the Earth's estimated total water volume, approximately 97% or 317×10^6 mi^3 is attributed to seawater alone (Nace, 1967), which is known to contain an essentially uniform, worldwide distribution of uranium at $3.35 \pm 0.2 \times 10^{-9}$ g/cm^3 (Ku *et al.*, 1977).

An estimate of the total amount of dissolved U in the oceans (4.43×10^{12} kg) provides a glimpse of the enormity of scale and the correspondingly keen interest in its aqueous speciation. From decades of experimental study, it is generally accepted that U takes the form of the mononuclear anionic, uranyl(VI) tris(carbonato) complex, $[UO_2(CO_3)_3]^{4-}$, in the slightly alkaline (pH$\approx$8) ocean waters (Djogic and Branica, 1991). Despite comprehensive studies of actinide carbonate chemistry, which are very well reviewed elsewhere (Clark *et al.*, 1995), the field of synchrotron radiation research of An carbonate complexes was late to break open with the report on uranyl carbonate complexes in near-neutral aqueous solution (Allen *et al.*, 1995). In this section, we describe the results obtained from EXAFS studies of the carbonate solution chemistry of the trivalent and tetravalent An ions as well as for the actinyl, $[AnO_2]^{n+}$, carbonates of the pentavalent ($n=1$) and hexavalent ($n=2$) An ions.

(*i*) *Uranyl*(VI)

The apparent simplicity of the $[CO_3]^{2-}$ anion belies its flexibility in the formation of coordination compounds with $[UO_2]^{2+}$ in various degrees of polynuclear association. In addition to serving conventional mono- and symmetrical bidentate structural roles, it may serve to bridge and link metal-ions. Although some 14 modes of carbonate ligation with two, three, four, and six metal-ions are known (Cotton *et al.*, 1999), its service as a molecular bridge between uranyl cations is relatively rare (Allen *et al.*, 1995; Clark *et al.*, 1995). To elucidate aspects of such aggregation behavior, a multipronged approach was taken to unravel the solution species distribution of the monomeric tris(carbonato) complex, $[UO_2(CO_3)_3]^{4-}$, and the trimeric complex, $[(UO_2)_3(CO_3)_6]^{6-}$. The unusual structure of the trimer, schematically illustrated below without the axial O atoms, is built up of three bis(carbonato) monomers of empirical formula

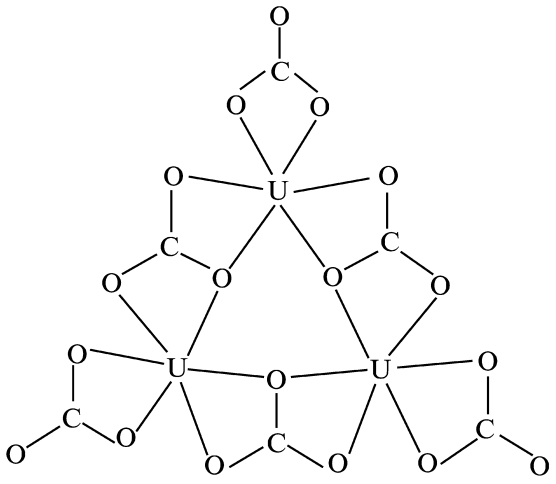

$[UO_2(CO_3)_2]^{2-}$ with three bridging carbonate ligands linking three U^{6+} ions in a fashion (i.e. six-bond $-(U-O)_3-$ ring) not depicted in Cotton *et al.* (1999).

A 0.2 M aqueous solution (pH = 5.7) of this crystallographically characterized triangular, trinuclear uranyl(VI) carbonate, $[(UO_2)_3(CO_3)_6]^{6-}$ as the guanidinium salt $[C(NH_2)_3]^+$, was studied by U L_3-edge EXAFS (Allen *et al.*, 1995). The data analysis provided O, C, and U coordination numbers and interatomic distances consistent with the trimeric structure of the solid salt, $[C(NH_2)_3]_6[(UO_2)_3(CO_3)_6]\cdot 6.5H_2O$, suggesting that the oligomeric anionic unit is maintained upon dissolution of the solid under the selected conditions. The analysis was confirmed by the presence of a distant, 4.92 Å U–U interaction that was not evident in the EXAFS data for the corresponding monomeric species, $[UO_2(CO_3)_3]^{4-}$, which has an otherwise identical, eight O coordination of U^{6+} in a hexagonal bipyramid polygon (Reeder *et al.*, 2000). The two closest, axial O atoms are bonded at 1.79 Å in both the monomeric and trimeric anions. The six equatorial O atoms arise from the symmetrical bidentate coordination of three carbonate groups, with an average U–O distance of 2.42 Å for the monomer and 2.45–2.46 Å for the trimer. The EXAFS data for the trimer and the monomer alike provide evidence for distant backscattering that was fit to reveal three C at 2.89–2.90 Å as well as three O at 4.12 Å (monomer) and at 4.16–4.17 Å (trimer), which are attributed to the terminal O atoms of the three carbonate ligands.

The recent discovery and characterization of the aqueous, neutral dicalcium uranyl(VI) tris(carbonato) complex, $[Ca_2UO_2(CO_3)_3]$, in natural, mining-related waters (Bernhard *et al.*, 1996) reinvigorates interest with the ages-old anionic species, $[UO_2(CO_3)_3]^{4-}$, particularly with regard to issues of ion-pairing. The combination of experimental (Bernhard *et al.*, 2001) and theoretical (Tsushima *et al.*, 2002) results reveal that counter-cations can play a significant role in the aqueous speciation and structure of the otherwise ordinary $[UO_2(CO_3)_3]^{4-}$ complex anion. The solution (pH = 8) U L_2- and L_3-edge EXAFS for $[Ca_2UO_2(CO_3)_3]$ (0.0005 M) and $[UO_2(CO_3)_3]^{4-}$ (0.001 M) do not differ significantly and, moreover, the carbonate coordination of uranyl(VI) in both is the same as that for the natural mineral liebigite, $Ca_2UO_2(CO_3)_3\cdot 10H_2O$, which has two axial O at 1.78 Å, six equatorial O at 2.43 Å, three C at 2.86, and three O at 4.12 Å. In addition, the crystallographic structure of liebigite reveals a 4.07 Å U–Ca interaction arising from two Ca–O polyhedra in the equatorial plane. These distant Ca interactions are difficult to identify in the U EXAFS data of the $[Ca_2UO_2(CO_3)_3]$ aqueous species and solid mineral specimens at ambient temperature because of spectral congestion and overlap with the nearly equidistant interactions of the terminal O atoms (3) of the symmetrical, bidentate carbonate ligands. Nevertheless, based upon a rigorous analysis of the available EXAFS and in combination with other physical and spectroscopic evidence, Bernhard *et al.* (2001) concluded "...that the calcium atoms are likely to be in the same positions both in the solution complex and in the solid." Structure optimizations of the neutral $[Ca_2UO_2(CO_3)_3]$ aquo species were subsequently

calculated at different levels (HF, MP2, and B3LYP) of theory with and without Ca^{2+}, i.e., $[UO_2(CO_3)_3]^{4-}$, and with and without hydration (Tsushima *et al.*, 2002). The calculated structure that included two Ca^{2+} and ten H_2O molecules is in good agreement with that deduced by EXAFS measurement and, thereby, demonstrates the need to explicitly incorporate counter-cations and water molecules to obtain accurate geometrical structures from theory.

Uranium L_3-edge EXAFS was used to probe the coordination environment of the uranyl(VI) tris(carbonato) complex, $[UO_2(CO_3)_3]^{4-}$, before and after a stoichiometric, one-electron electrochemical reduction (Docrat *et al.*, 1999). In aqueous electrolytes of 1 M Na_2CO_3 at pH = 11.95 (Docrat *et al.*, 1999) and 0.1 M Na_2CO_3/0.1 M $NaNO_3$ at pH = 11.3 (Morris, 2002), the cyclic voltammetry data for $[UO_2(CO_3)_3]^{4-}$ (0.0022–0.010 M) show one electrochemically irreversible couple attributed to U^{6+}/U^{5+} redox activity. The metastable reduced species formed by controlled potential coulometry was ascribed to the uranyl(V) tris (carbonato) complex, $[UO_2(CO_3)_3]^{5-}$. The U L_3-edge position for the reduced species was 2.4 eV lower than that for the oxidized form, consistent with the reduction of $[U^{6+}O_2]^{2+}$ to $[U^{5+}O_2]^{+}$. The EXAFS analysis revealed that the basic geometry of the U coordination environment is essentially the same for both solution complexes, except for the expected variation of interatomic distances with change of U oxidation state. The average axial dioxo distance increases by 0.10 Å from 1.80(2) to 1.90(2) Å upon reduction. Elongations of similar magnitude (0.05–0.10 Å) are found for the six equatorial O bonds, the three C, and the three terminal O interactions with the carbonate ligands. These three distances increase, in order, from 2.43(2), 2.89(4), and 4.13(4) Å in the oxidized form to 2.50(2), 2.94(4), and 4.23(4) Å, respectively, in the reduced form. The absence of significant conformational variation between $[UO_2(CO_3)_3]^{4-}$ and $[UO_2(CO_3)_3]^{5-}$ makes it difficult to rationalize the less than ideal electrochemical response and the relative instability of the reduced species (Docrat *et al.*, 1999).

Four different isomers have been proposed for the binuclear complex anion, $[(UO_2)_2(CO_3)(OH)_3(H_2O)_n]^-$, in solution (Szabo *et al.*, 2000). This variety of bridge isomers is largely attributable to the assortment of different carbonate bonding modes (Cotton *et al.*, 1999) that can be envisioned to link the two $[UO_2]^{2+}$ groups in this ternary species. Although the use of U EXAFS alone is not sufficient to provide an unambiguous identification of the predominant isomer, the EXAFS results in combination with multinuclear (^{13}C and ^{17}O) NMR measurements have provided conclusive insight about the speciation. The U L_3-edge EXAFS of a 0.05 M solution of $[(UO_2)_2(CO_3)(OH)_3(H_2O)_n]^-$ (pH $\approx$ 7–8) was analyzed with multi-shell models of axial and equatorial O, U–C, and U–U interactions (Szabo *et al.*, 2000). The pivotal aspect of the analyses was the identification of terminal, equatorial OH^- bonding (1.3 ± 0.3 at 2.26 Å) and distant U interactions (0.5 ± 0.1 at 3.90 Å). The equatorial coordination sphere is completed by 3.9 ± 0.6 O atoms at 2.47 Å. This is consistent with a pentagonal bipyramidal uranyl(VI) environment, wherein the two axial O atoms are bonded

at 1.81 Å. The isomer structure consistent with the combined EXAFS and NMR data is suggested to consist of two $[UO_2]^{2+}$ groups that are bridged by two O atoms, one from hydroxide and one from the lone carbonate ligand that is in bidentate coordination with one uranyl unit. The terminal equatorial coordination is completed by a combination of the two remaining hydroxide ligands and three water molecules, $[(H_2O)(OH)_2UO_2(OH)(CO_3)UO_2(H_2O)_2]^-$, as illustrated below.

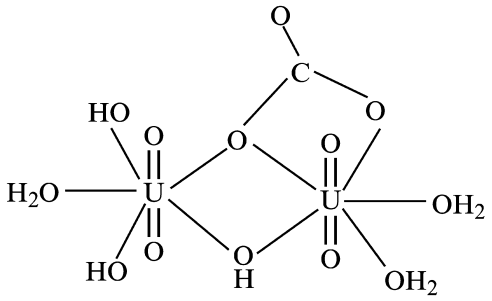

(*ii*) *Neptunyl*(V)

The study of neptunium in aqueous carbonate solutions provides fundamental information that can be applied to intricate environmental problems and to solving difficult issues with regard to the treatment of alkaline, high-level tank waste. Concerns about pentavalent neptunyl carbonate complexation, particularly the aqueous speciation, solubility, redox, and sorption behaviors, also relate to its fate and transport in subsurface geologic repositories (Efurd *et al.*, 1998; Kaszuba and Runde, 1999).

Three environmentally relevant neptunyl(V) carbonato complexes of general composition $[NpO_2(CO_3)_n]^{(2n-1)-}$ for $n=1$ $[NpO_2(CO_3)]^-$, $n=2$ $[NpO_2(CO_3)_2]^{3-}$, and $n=3$ $[NpO_2(CO_3)_3]^{5-}$, have long been of interest. Information about their molecular structures and the extent of hydration became available through Np L_3-edge EXAFS and complementary spectroscopic work on single-component solutions of the anions with unprecedented solubilities (0.001 M) achieved by use of the large, bulky tetra-*n*-butylammonium, $[(n\text{-}Bu)_4N]^+$, counter-cations in place of alkali-metal cations (Clark *et al.*, 1996a,b). For the tris(carbonato) complex ($n=3$) in a Na_2CO_3 solution (of unspecified concentration), the EXAFS spectra show "...unequivocally that the carbonate ligands must be coordinated in a bidentate fashion due to the combination of six Np–O and three Np–C distances of 2.52 and 2.98 Å", (Clark *et al.*, 1996a) respectively. The overall eight-coordinate geometry of Np^{5+} is hexagonal bipyramidal, in which the two *trans*-neptunyl O atoms at 1.86(2) Å occupy the usual axial positions with respect to the six equatorial O atoms. Much less definitive information about the equatorial coordination was provided for the mono- and bis

(carbonato) species, $n=1$, and 2, respectively, in $[(n\text{-Bu})_4N]_2CO_3$ solutions (unspecified concentrations) because of curve-fitting difficulties and metrical uncertainties. What seems clear "... is a distinct change in coordination geometry about the neptunyl ion, from six O atoms in the tris- and bis-carbonato complexes, to five O atoms in the mono(carbonato) complex" (Clark *et al.*, 1996b). The five O atoms of the equatorial ligation for the mono(carbonato) complex are attributed to the coordination of three H_2O molecules and two O atoms from the $[CO_3]^{2-}$ anion in a symmetrical bidentate mode. The overall stereochemistry of Np^{5+} is expected to be a pentagonal bipyramid that has an average Np–O equatorial distance of 2.49(3) Å. This bond length is shorter than that (2.53(3) Å) for the 6-O equatorial coordination of the tris(carbonato) species, a detail that is consistent with the 5-O equatorial coordination of $[NpO_2]^+$ in $[NpO_2(CO_3)(H_2O)_3]^-$. Similarly, the six O atoms of the equatorial ligation for the bis(carbonato) complex are attributed to the coordination of two H_2O molecules and four O atoms from the two bidentate $[CO_3]^{2-}$ anions, as $[NpO_2(CO_3)_2(H_2O)_2]^{3-}$, with an average distance of 2.48(3) Å. It seems counter-intuitive that the higher coordination number for the bis(carbonato) complex does not correlate with a larger average equatorial Np–O distance, e.g. like that for the unequivocally characterized tris(carbonato) neptunyl(v) complex with six O atoms in the equatorial plane.

(*iii*) *Plutonyl*(*VI*)

The aqueous speciation of the plutonyl and americyl cations, $[AnO_2]^{n+}$ for $n=1$ and 2, in carbonate media has not been examined through XAS. Solid-state EXAFS studies of actinyl carbonates are similarly absent, except for the sole work in which $^{239}Pu^{6+}$ was precipitated from an acid solution of pH=4 with CO_2 over the course of 3–5 days (Runde *et al.*, 1999). The washed solids, identified as PuO_2CO_3 from powder X-ray diffraction measurements, were examined by Pu EXAFS to reveal the typical FT data with contributions from axial (1.74 Å) and equatorial O atoms (2.45 Å) as well as a distant, 4.2 Å Pu–Pu interaction. No coordination numbers were reported for this monocarbonate phase.

(*iv*) *Tetravalent An*

The tetravalent An carbonate series, $[An(CO_3)_n]^{4-2n}$ for An ≡ Th, U, Np, and Pu, has been the subject of systematic and comprehensive EXAFS investigations. In this collection of results, the predominant aqueous species is, by far, the pentacarbonato ($n=5$) complex, $[An(CO_3)_5]^{6-}$. For example, the extensive L_3-edge EXAFS measurements of U^{4+}, Np^{4+}, and Pu^{4+} in the aqueous $K^+ - HCO_3^- - CO_3^{2-} - OH^- - H_2O$ system (Rai *et al.*, 1998, 1999a,b) can be succinctly summarized as follows: The aqueous An^{4+} complexes in carbonate (5.4–6.0 M K_2CO_3) and bicarbonate (0.9–1.0 M) solutions were found to be

$[An(CO_3)_5]^{6-}$. Despite the excess concentrations of $[HCO_3]^-$, with respect to $[An^{4+}]$, no evidence was ever found for its complexation. This may reflect an inherent limitation of the technique, wherein the effects of protonation on the average An–O and An–C distances would be insignificant in comparison with the measurement error, and therefore extremely difficult to determine. In this regard, the detection of appreciably more coarse and substantial structural variations, especially the equatorial O coordination number, can be problematic and fraught with uncertainty. This, in turn, can make it difficult to determine the exact number of bicarbonate and carbonate groups, as well as their identity, involved in the complexation of tetravalent An ions.

(*v*) *Neptunium*(*IV*)

A case that illustrates this complicated issue as regards An^{4+} EXAFS in general concerns the investigation of the pure Np^{4+} ion (of unspecified milli-molar concentration) in 0.93 M $KHCO_3$ (Rai *et al.*, 1999a). In the FT data, the Np–O and Np–C interactions are not resolved, and correlation effects in the curve-fitting leads to metrical parameters that are not diagnostic of a unique structure. For example, from the nearest O and C coordination numbers, 11.0 ± 2.8 and 5.8 ± 1.8, respectively, alone, it is difficult to establish the presence of tetra-, penta-, hexa-, or heptacarbonato complexation. In this situation, fortunately, the magnitude of the average Np–O and Np–C interatomic distances, 2.43(2) and 2.84(2) Å, respectively, is known to be diagnostic of bidentate carbonate coordination (Denecke *et al.*, 1997b). To provide added quantitative insights about the Np carbonate species, a distant and well-resolved peak in the FT data attributed to the distal O atoms of the bidentate $[CO_3]^{2-}$ groups was subjected to analysis. The coordination number obtained, 5.4 ± 1.6 O atoms, is a conclusive indicator "...that five carbonate groups were involved, and the complexed Np^{4+} species therefore is $Np(CO_3)_5^{6-}$" in 0.93 M $KHCO_3$ (Rai *et al.*, 1999a).

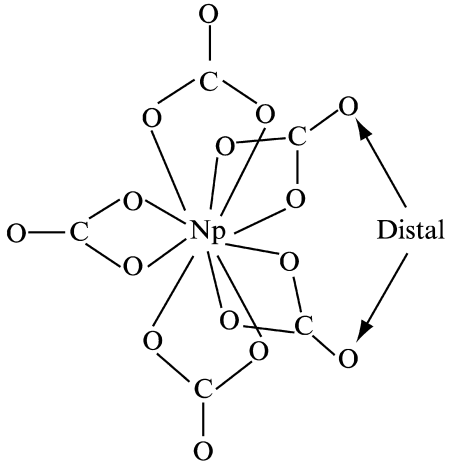

The structure is illustrated above in which two of the five distal O atoms at 4.16 (2) Å are identified. For the corresponding 5.4 M K_2CO_3 solution, the unintended, partial oxidation of Np^{4+} leads to neptunyl(V) contamination and additional uncertainties with the EXAFS analyses. Nevertheless, the data are consistent with the suggestion that $[Np(CO_3)_5]^{6-}$ is the dominant species in carbonate solution.

(*vi*) *Uranium*(*IV*) *and plutonium*(*IV*)

From EXAFS acquisition and analyses (Rai *et al.*, 1998, 1999b), the speciation of U^{4+} and Pu^{4+} (of unspecified milli-molar concentrations) in 0.9 and 1.0 M $KHCO_3$ solutions, respectively, was shown to be like that for Np^{4+}. Namely, the three An^{4+} solution species are the anionic (6–) penta(carbonato) complexes, wherein the five carbonate groups are in bidentate coordination consisting of 9.5 O at 2.46 Å and 5.2 C at 2.90 Å for U (Rai *et al.*, 1998) and 9.8 ± 2.5 O at 2.41(2) Å and 5.5 ± 1.7 C at 2.88 Å for Pu (Rai *et al.*, 1999b). The corresponding distal O interactions consist of 4.1 O at 4.18 Å for U and 5.0 ± 1.5 O at 4.14(2) Å for Pu. Because of the presence of oxidation state impurities, e.g. uranyl(VI) and plutonyl(V), and the low S/N ratio of the primary data due to minuscule solubility, the EXAFS spectra for the U^{4+} and Pu^{4+} carbonate species in 5.4–6.0 M solutions of K_2CO_3 were not adequate for detailed analysis. Despite the uncertainties with the available EXAFS, it was concluded largely based upon other comparisons that $[An(CO_3)_5]^{6-}$ is the dominant An^{4+} species in concentrated carbonate solutions. Other complementary research (Clark *et al.*, 1998) provides thorough and convincing evidence in this regard. The Pu L_3-edge EXAFS of the limiting $^{242}Pu^{4+}$ (ca. 0.1 M) ion in an aqueous solution of 2.5 M Na_2CO_3 was fit to reveal 10.0 ± 1.2 O atoms at 2.42(1) Å; 5.0 ± 0.6 C atoms at 2.88(2) Å; 5.0 ± 0.6 O atoms at 4.16(2) Å. These values are consistent with the formation of a monomeric penta(carbonato) anion, $[Pu(CO_3)_5]^{6-}$, that is essentially identical to the one found in the solid-state, single-crystal X-ray structure of $[Na_6Pu(CO_3)_5]_2 \cdot Na_2CO_3 \cdot 33H_2O$ (Clark *et al.*, 1998). In this anion, each of the five $[CO_3]^{2-}$ groups has bidentate coordination in a pseudo-hexagonal bipyramid polygon about Pu^{4+} with three in equatorial positions and two in axial ones. This definitive structure sets to rest a decade-long debate about the molecular structure of the limiting complex in the Pu^{4+} carbonate system under high $[CO_3^{2-}]$ in both solution- and solid-states.

(*vii*) *Thorium*(*IV*)

EXAFS investigations of the Th^{4+} carbonate system show that a penta(carbonato) $[Th(CO_3)_5]^{6-}$ solution species is obtained at high concentrations of carbonate (1–2 M Na_2CO_3 with 0.1–1.0 M NaOH) and bicarbonate (0.17–1.0 M $NaHCO_3$) (Felmy *et al.*, 1997; Hess *et al.*, 1997). Curve-fitting analysis of Th

L_3-edge EXAFS data for solutions of 0.001–0.009 M Th^{4+} reveals ten O atoms at 2.49–2.50 Å, a distance that is consistent with bidentate coordination of $[CO_3]^{2-}$. Because the C backscattering is weaker than that for the nearer O and because the Th–C peak cannot be resolved from the Th–O peak in the FT data, the Th–C metrical parameters are subject to large uncertainties. For example, coordination numbers of 3.1–5.2 and distances of 2.97–3.01 Å make it difficult to be specific about the character of the carbonate complexation. The number of coordinated carbonate groups was determined through the analysis of the signal for the well-resolved distal O peak in the FT data to reveal 5 ± 1 O atoms at 4.21–4.26 Å, as expected for the $[Th(CO_3)_5]^{6-}$ anion. In contrast, for solutions with a bicarbonate concentration of 0.1 M and less, "...the thorium speciation changes dramatically" (Felmy *et al.*, 1997; Hess *et al.*, 1997). The specific and exact nature of this change was not conclusively established from the EXAFS analysis because of data quality limitations, i.e. low S/N ratio, of the primary spectra for the dilute (≤ 0.0001 M) Th^{4+} solutions at pH = 9.39–9.43. Although the issue is open to question, the initial EXAFS results suggest a contraction of the Th–O bond length (from ca. 2.50 Å for $[Th(CO_3)_5]^{6-}$ to 2.46 Å) accompanied by a decrease in the number of nearest O atoms (from 10 for $[Th(CO_3)_5]^{6-}$ to 8). Based upon this information, a mixed carbonate hydroxide species was proposed (Felmy *et al.*, 1997), wherein three $[CO_3]^{2-}$ groups are in bidentate coordination around Th^{4+} along with two OH^- groups (Hess *et al.*, 1997).

28.2.4 Organic acids

EXAFS analyses provide an average structure of all the element-selected An ions in solution, regardless of their state of speciation – monomer, dimer, trimer, ..., polymer – and their possible combined and simultaneous presence as hydrolysis products, intermediates, non-complexed aquo ions, etc. As such, the short-range metrical results for An materials containing an assortment of bonding sites and mixtures of phases are difficult to use for definitive comparisons with individual structures proposed in speciation diagrams. In these cases, additional spectroscopic information, such as from, for example, NMR, optical, vibrational, fluorescence, etc., experiments is necessary to confirm the available EXAFS results. For example, the use of EXAFS alone to study the coordination and binding stoichiometry of An ions in natural materials like organic macromolecules known as humic substances, which contain multiple coordination sites, different functional groups (i.e. carboxyl, carbonyl, hydroxyl, thiol, amido, etc.), and bonding modes, can be a difficult and intricately complicated problem. Fortunately, the carboxylate anions, $-COO^-$, of organic acids are the most important and widespread functional group for An complexation in the surface-waters and in the subsurface geologic fluids of the terrestrial aquatic environment (Pittman and Lewan, 1994). Moreover, the use of EXAFS has been developed for such challenging environmental research thorough analysis and understanding of the spectra for smaller, molecularly characterized

An carboxylate complexes of common organic, carboxylic acids both aliphatic (R-COOH) and aromatic (Ar-COOH), including the di- and tricarboxylic acids.

Tables 28.7 and 28.8 contain the structures of the mono-, di-, and tricarboxylate ligands as well as several phenolate ligands that are relevant with regard to their presence in natural waters and materials. Except for two publications, one about Th^{4+} (Denecke *et al*., 1999) and the other on Np^{4+} (Denecke *et al*., 2002), the EXAFS research available in time for this publication is exclusively focused on the uranyl(VI) ion, $[UO_2]^{2+}$, complexes of these organic anions. Though large, the extent of the EXAFS structure investigations is dwarfed by the number of crystal and molecular structures studies that have been completely reviewed and discussed in the light of the complexation of radionuclides with humic substances, particularly the humic and fulvic acids, elsewhere (Leciejewicz *et al*., 1995; Denecke *et al*., 1997a).

(a) Model systems

Despite early success at probing the bonding of $[UO_2]^{2+}$ with the aliphatic, monobasic acetate ligand through use of U L_3-edge EXAFS (Charpin *et al*., 1985), research on An complexes of organic acids was not immediately impacted by the method. More than a decade later, three EXAFS studies were reported (Allen *et al*., 1996a; Pompe *et al*., 1996; Reich *et al*., 1996a) with results for uranyl(VI) solutions and solids containing organic carboxylate ligands that set the groundwork for EXAFS measurements that continue today. A pivotal development was realized when the results from EXAFS were demonstrated to be diagnostic of carboxylate coordination (Denecke *et al*., 1997a,b, 1998a,b). In particular, the distinction between mono- and bidentate O coordination is plainly reflected in the U–O interatomic distance, wherein long U–O distances of ca. 2.5 Å are indicative of bidentate coordination and shorter ones of ca. 2.3 Å suggest monodentate coordination. Oftentimes, the bidentate mode of coordination is corroborated by the appearance of either one or two U–C interactions. The first one with a U–C interaction of ca. 2.85 Å arises from the nearest C atom that is bonded to the two O atoms and the second oftentimes weak one at ca. 4.4 Å arises from the next nearest, the so-called distal C atom that is collinear with the nearest C and absorbing An atoms. Because these two U–C interactions occur at significantly longer distances for the monodentate-bonding mode, e.g. the first and closest U–C distance is ca. 3.5 Å, they are rarely observed in the FT data of An EXAFS. A schematic representation of these two binding forms is shown below. Similar schemes and interatomic distances apply for the bidentate and monodentate coordination of the carbonate ligand discussed above.

Despite the extensive research with the model ligands (L) of Tables 28.7 and 28.8, the results from EXAFS are not sufficient on their own to provide conclusive speciation information about the equatorial coordination of $[UO_2]^{2+}$ and other An moieties. The An:L complexation ratio, e.g. 1:1, 1:2,

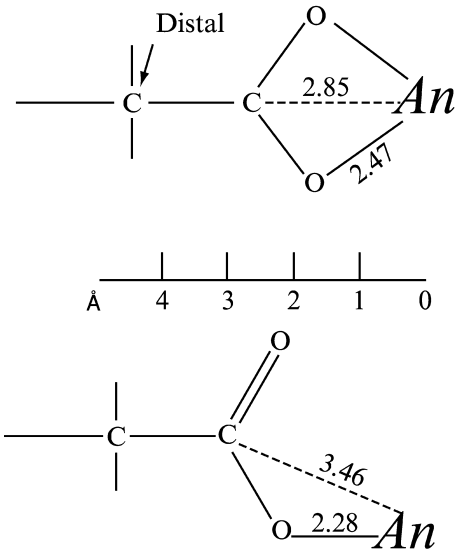

1:3, and 2:2, 2:3, etc., is especially difficult to determine from one-dimensional metrical information largely because of spectral congestion. For example, the identification of typically weak and distant U–U interactions that are expected for the 2:2 complexes is oftentimes complicated. Peaks that are purported to arise from U–U interactions can be essentially identical to the O–O peak (i.e. the U–O–U–O–U backscattering pathway) that arises from multiple-scattering within a single uranyl group, which is a common structural feature of the monomeric (1:1, 1:2, ...) and dimeric (2:2, 2:3, ...) complexes. Fortunately, in this regard, the U–U assignment can be convincingly made by use of low-temperature EXAFS (Thompson *et al.*, 1995, 1997; Barnes *et al.*, 2000; Hennig *et al.*, 2001b). Another difficulty arises in the identification of all of the equatorial O ligands in the molecular complexes of $[UO_2]^{2+}$ that contribute to the total coordination number of which five is the most common one of all the entries of Tables 28.7 and 28.8. For example, the O equatorial responses from carboxylate, phenolate, water, and hydroxide are difficult, oftentimes impossible, to distinguish from EXAFS alone. The use of vibrational spectroscopies, particularly FT-infrared, is especially useful with regard to information about the coordination of $R–COO^-$ and $Ar–COO^-$ moieties.

(b) Natural systems

Both humic and fulvic acids play key roles that are not very well understood in the biological and environmental sciences. Humic acid is, in large part, responsible for the immobilization of An ions and heavy metals in soils. The complexation of metals with reactive functional groups is an important regulatory

process of the solubility and fate of soil contaminants. As such, the identity of potential binding sites of 'hard' and 'soft' functional groups, including ligands of N (e.g. amino), O (e.g. hydroxyl, carboxyl, carbonyl), and S (e.g. thiol, sulfide, thiol-ether, sulfonyl) on the outer and inner surfaces of humic acid that would accommodate An ions with different charge/IR ratios has been a subject of practical concern. The difficulties in this area of research stem from uncertainties about the nature of humic acid itself. The diversity of the chemical building blocks that combine in their assembly to form humic acid is well-known and remains a matter of significant interest (Giordano, 1994; Silva and Nitsche, 1995; Nitsche, 1997; Paciolla *et al.*, 1999). In particular, the primary and secondary molecular and crystal structures of humic acid and its conformers, which are believed to vary with ancestry, are not known. Yet, despite the existing gap in knowledge about the specific formula and stereochemistry of humic acid, in general, and about the metal-binding sites of humic acid, in particular, the obvious strength of the EXAFS work is that it provides direct insight about the An coordination. The results of exhaustive U L_3-edge EXAFS data acquisition and analysis of humic and fulvic acids of both natural and synthetic origin, and under the neutral to slightly acidic conditions of pH and Eh that are of environmental relevance, are in consensus (Denecke *et al.*, 1997a, 1998a,b; Reich *et al.*, 1998a; Nitsche *et al.*, 1999; Schmeide *et al.*, 2003). The bonding of the uranyl ion is predominantly associated with carboxylate functional groups. Moreover, the U–O interatomic distances are consistent with the monodentate coordination structure shown above. Under alkaline conditions, the bonding appears to involve some degree of interaction with phenolic –OH groups (Reich *et al.*, 1996a), which are deprotonated at $8 \leq \text{pH} \leq 10$. The pH-dependent bonding of $[UO_2]^{2+}$ to carboxylate and phenolate functionalities has been demonstrated in several model systems (Rossberg *et al.*, 2000, 2003; Moll *et al.*, 2003). Additional work has been proposed to clarify this possibility with natural humic acids (Reich *et al.*, 1996a; Schmeide *et al.*, 2003).

28.3 SORPTION STUDIES

Chemical reactions that take place at the particle–water interface play a large role in controlling environmental speciation, bioavailability, and transport of ions. For example, adsorption/desorption equilibria and redox reactions can be significantly influenced by the nature of the surfaces seen by the solution. Simple solution solubilities may be altered in the presence of a mineral surface that can preferentially adsorb, and thereby concentrate and precipitate metal-ions at solution concentrations well below their solubility limits. In addition, surface redox reactions can also reduce metal solubility and result in mineral incorporation or crystallization reactions that would not occur in the absence of the active surface (Breit, 1995). In this manner, the mobility of radionuclides through the environment is strongly influenced by their interactions at water–mineral

Table 28.7 *Uranyl(VI) complexes of low-molecular weight aliphatic carboxylate ligands (L) with axial (ax.) oxygen coordination numbers and U=O distances as well as equatorial (eq.) coordination numbers and U–O bond lengths. The L stick structures do not represent the true stereochemistry. Estimated standard deviations, where available, are obtained from the primary sources and are given after the ± sign or within parentheses.*

Ligand (L) structure	*Name/Formula*	*An*	*Coordination*	*Phase An:L speciation*	*References*
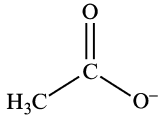	acetate CH_3COO^-	U^{6+}	2 ax. O^{2-}, 1.75–1.76 Å 6 eq. O, 2.46–2.48 Å	solids and solutions $Na[UO_2(L)_3]$ and $[P(C_6H_5)_4]UO_2(L)_3$	Charpin *et al.* (1985)
		U^{6+}	2 ax. O^{2-}, 1.77 Å 4.8(4) eq. O, 2.41 Å	solid $UO_2(L)_2 \cdot 2H_2O$	Reich *et al.* (1996a)
			2 ax. O^{2-}, 1.78 Å 4.7(5) eq. O, 2.46 Å	aqueous solution pH = 3.7, $[UO_2(L)_3]^-$	
		U^{6+}	∥ 4 ax. O^{2-}, 1.787(1) Å 2.5 eq. O, 2.331(5) Å ⊥ 1 ax. O^{2-}, 1.717(4) Å 6 eq. O, 2.378(3) Å 2 ax. O^{2-}, 1.768(1) Å 5 eq. O, 2.384(2) Å	oriented single-crystal $UO_2(L)_2 \cdot 2H_2O$ parallel (∥) and perpendicular (⊥) to $[O=U=O]^{2+}$. polycrystalline solid	Hudson *et al.* (1996); Reich *et al.* (1998a)

Table 28.7 (*Contd.*)

Ligand (L) structure	*Name/Formula*	*An*	*Coordination*	*Phase An:L speciation*	*References*
		U^{6+}	2 ax. O^{2-}, 1.78 Å 4.3(6) eq. O, 2.49 Å	solid $Na[UO_2(L)_3]$	Denecke *et al.* (1997b)
		U^{6+}	2 ax. O^{2-}, 1.78 Å 5.2 eq. O, 2.48 Å	solid $Na[UO_2(L)_3]$	Denecke *et al.* (1998a,b)
		U^{6+}	2 ax. O^{2-}, 1.78 ± 0.02 Å 6 eq. O, 2.44 ± 0.02 Å	aqueous solution pH = 3.7, $[UO_2(L)_3]^-$	Reich *et al.* (1998a); Nitsche *et al.* (1999)
		U^{6+}	2 ax. O^{2-}, 1.76–1.79 Å 3.9–5.2 eq. O, 2.36–2.44 Å	aqueous solutions pH = 1.8–2.6 T = 25–250°C $[UO_2]^{2+}$:L = 0.01–2.0	Mosselmans *et al.* (2001)
		U^{6+}	2 ax. O^{2-}, 1.78(1) Å 2.8 eq. O, 2.36(2) Å 1.8 eq. O, 2.49(2) Å 1.7 ax. O^{2-}, 1.78(1) Å 6.4 eq. O, 2.48(2) Å	solids $UO_2(L)_2 \cdot 2H_2O$ $Na[UO_2(L)_3]$	Jiang *et al.* (2002)

		U^{6+}	2 ax. O^{2-}, 1.78(1) Å 4 eq. O, 2.38(2) Å 2 eq. O, 2.50(2) Å	aqueous solutions $[UO_2(L)_1]^+$, pH = 2.84	Jiang *et al.* (2002); Rao *et al.* (2002)
			2 ax. O^{2-}, 1.78(1) Å 5.9 eq. O, 2.42(2) Å	$UO_2(L)_2$, pH = 3.46	
			2 ax. O^{2-}, 1.78(1) Å 1.9 eq. O, 2.34(2) Å 4.1 eq. O, 2.48(2) Å	$[UO_2(L)_3]^-$, pH = 3.85, 4.5	
		U^{6+}	2 ax. O^{2-}, 1.81 Å 6 eq. O, 2.50 Å	DFT, COSMO solvation model	Vazquez *et al.* (2003)
		U^{6+}	2 ax. O^{2-}, 1.77–1.80 Å 3.3–5.4 eq. O, 2.39–2.46 Å	aqueous solutions pH = 1.8–3.8 T = 25–250°C $[UO_2]^{2+}$: L = 0.01–2.0	Bailey *et al.* (2004)
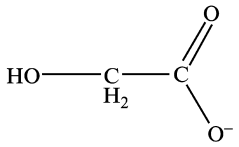	glycolate $HOCH_2COO^-$	U^{6+}	2 ax. O^{2-}, 1.77–1.80 Å 4.8–5.5 eq. O, 2.37–2.40 Å	aqueous solutions pH = 2–8	Moll *et al.* (2003)
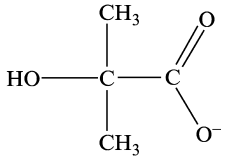	α-hydroxyisobutyrate $HOC(CH_3)_2COO^-$	U^{6+}	2 ax. O^{2-}, 1.77–1.80 Å 4.4–5.4 eq. O, 2.36–2.43 Å	aqueous solution, pH = 2–8	Moll *et al.* (2003)

Table 28.7 (*Contd.*)

Ligand (L) structure	*Name/Formula*	*An*	*Coordination*	*Phase An:L speciation*	*References*
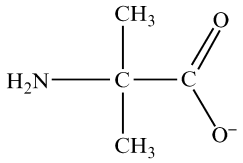	α-aminoisobutyrate $H_2NC(CH_3)_2COO^-$	U^{6+}	2 ax. O^{2-}, 1.77 Å 5.1–5.6 eq. O, 2.39–2.40 Å	aqueous solutions pH = 3, 4	Moll *et al.* (2003)
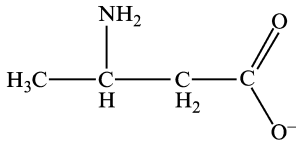	β-aminobutyrate $H_3CCHNH_2CH_2COO^-$	U^{6+}	2 ax. O^{2-}, 1.77 Å 5.5 eq. O, 2.43 Å	aqueous solution pH = 4	Moll *et al.* (2003)
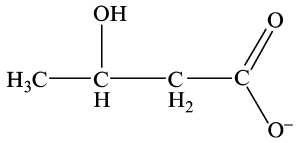	β-hydroxybutyrate $H_3CCHOHCH_2COO^-$	U^{6+}	2 ax. O^{2-}, 1.78 Å 5.4–5.5 eq. O, 2.41–2.453 Å	aqueous solutions pH = 2.5, 6	Moll *et al.* (2003)
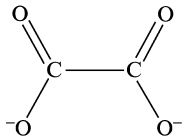	oxalate $^-OOCCOO^-$	U^{6+}	2 ax. O^{2-}, 1.78–1.79 Å 5.1 ± 0.7 eq. O, 2.37–2.38 Å	aqueous solutions pH = 4.4, 6.5 $[UO_2(L)_2]^{2-}$, $[UO_2(L)_3]^{4-}$	Vallet *et al.* (2003)

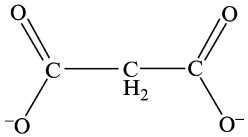	malonate $^{-}OOCCH_2COO^{-}$	U^{6+}	2 ax. O^{2-}, 1.79 Å 4.6(3) eq. O, 2.37 Å	aqueous solution pH = 4.0, $[UO_2(L)_2]^{2-}$	Reich *et al.* (1996a)
		U^{6+}	2 ax. O^{2-}, 1.78 ± 0.02 Å 5 eq. O, 2.36 ± 0.02 Å	aqueous solution pH = 3.9, $[UO_2(L)_2]^{2-}$	Reich *et al.* (1998a); Nitsche *et al.* (1999)
		U^{6+}	2 ax. O^{2-}, 1.78(1) Å 3.9 eq. O, 2.34(2) Å 1.9 eq. O, 2.40(2) Å 2.3 ax. O^{2-}, 1.79(1) Å 5.2 eq. O, 2.39(2) Å	aqueous solutions $[UO_2(L)_2]^{2-}$, pH = 3.5 $[UO_2(L)_1]$, pH = 5.2	Rao *et al.* (2002)
		U^{6+}	2 ax. O^{2-}, 1.79–1.82 Å 5–6 eq. O, 2.41–2.52 Å	DFT, COSMO solvation model 8 optimized structures	Vazquez *et al.* (2003)
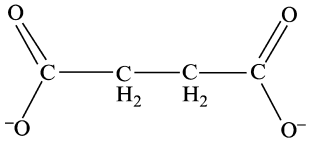	succinate $^{-}OOC(CH_2)_2COO^{-}$	U^{6+}	2 ax. O^{2-}, 1.78 ± 0.02 Å 5 eq. O, 2.48 ± 0.02 Å	aqueous solution pH = 4.0, $UO_2(L)$	Reich *et al.* (1998a)
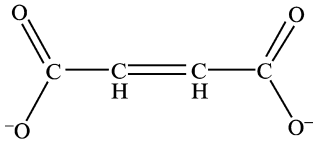	maleate $^{-}OOC(CH)_2COO^{-}$	U^{6+}	2 ax. O^{2-}, 1.78 ± 0.02 Å 6 eq. O, 2.37 ± 0.02 Å	aqueous solution pH = 4.2, $UO_2(L)$	Reich *et al.* (1998a); Nitsche *et al.* (1999)

Table 28.7 (*Contd.*)

Ligand (L) structure	*Name/Formula*	*An*	*Coordination*	*Phase An:L speciation*	*References*
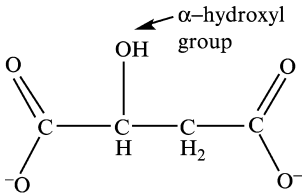	malate $^{-}OOCCH_2CHOHCOO^{-}$	U^{6+}	2 ax. O^{2-}, 1.78 ± 0.02 Å 2.7 eq. O, 2.33 ± 0.02 Å 2.7 eq. O, 2.45 ± 0.02 Å	aqueous solution pH = 2.0, $(UO_2)_2(L)_2$	Allen *et al.* (1996a)
		U^{6+}	2 ax. O^{2-}, 1.78 ± 0.02 Å 5 eq. O, 2.37 ± 0.02 Å	aqueous solution pH = 3.2, $(UO_2)_2(L)_2$	Reich *et al.* (1998a)
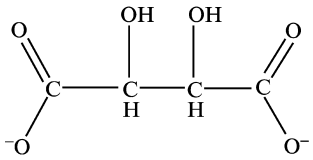	tartrate $^{-}OOCCHOHCHOHCOO^{-}$	U^{6+}	2 ax. O^{2-}, 1.78 ± 0.02 Å 3.1 eq. O, 2.35 ± 0.02 Å 2.3 eq. O, 2.47 ± 0.02 Å	aqueous solution pH = 2.2, $(UO_2)_2(L)_2$	Allen *et al.* (1996a)
		U^{6+}	2 ax. O^{2-}, 1.78 ± 0.02 Å 4 eq. O, 2.36 ± 0.02 Å	aqueous solution pH = 3.2, $(UO_2)_2(L)_2$	Reich *et al.* (1998a)
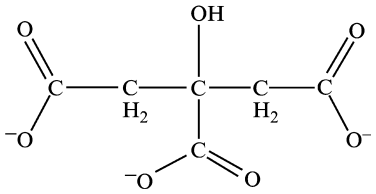	citrate $^{-}OOCCH_2COHCO_2^{-}$ CH_2COO^{-}	U^{6+}	2 ax. O^{2-}, 1.78 ± 0.02 Å 5 eq. O, 2.38 ± 0.02 Å	aqueous solution pH = 3.8–3.9, $[(UO_2)_2(L)_2]^{2-}$	Allen *et al.* (1996a); Reich *et al.* (1998a)
		U^{6+}	2 ax. O^{2-}, 1.77 Å 5.0–5.3 eq. O, 2.36–2.37 Å	solid and aqueous solution, pH = 6 $2[UO_2]^{2+}$:$2Fe^{3+}$:4*L* $[Na(UO_2)_2$ $Fe_2(L)_4$ $O(OH)_2$ $(OH_2)]^{5-}$	Dodge and Francis (1997, 2003)

Table 28.8 *Uranyl(VI), thorium(IV), and neptunium(IV) complexes of low-molecular weight, aromatic carboxylate ligands (L) and high-molecular weight fulvates and humates of both natural and synthetic origin, including axial (ax.) oxygen coordination numbers and U=O distances as well as equatorial (eq.) coordination numbers and U–O bond lengths. The L stick structures do not represent the true stereochemistry. Estimated standard deviations, where available, are obtained from the primary sources and are given after the ± sign or within parentheses.*

Ligand (L)				*Phase An:L*	
Structure	*Name*	*An*	*Coordination*	*Speciation*	*References*
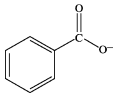	benzoate $C_6H_5COO^-$	U^{6+}	2 ax. O^{2-}, 1.76 Å 4.1–4.5 eq. O, 2.29 Å	solid $UO_2(L)_2$	Denecke *et al.*, 1997b, 1998a,b)
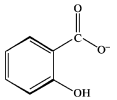	salicylate *o*-$HOC_6H_4COO^-$	U^{6+}	2 ax. O^{2-}, 1.78 Å 3.6(2) eq. O, 2.32 Å	solid $UO_2(L)_2$	Reich *et al.* (1996a)
		U^{6+}	2 ax. O^{2-}, 1.77 Å 5.6(6) eq. O, 2.42 Å	solid $UO_2(L)_2$	Denecke *et al.* (1998a)
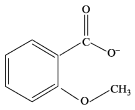	*o*-methoxybenzoate o-$CH_3OC_6H_4COO^-$	U^{6+}	2 ax. O^{2-}, 1.78 Å 4.3(5) eq. O, 2.44 Å	solid $UO_2(L)_2$	Reich *et al.* (1996a)
		U^{6+}	2 ax. O^{2-}, 1.77 Å 4.4(2) eq. O, 2.29 Å	solid $UO_2(L)_2$	Denecke *et al.* (1998a)
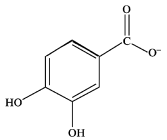	protocatechuate 3,4-dihydroxybenzoate	U^{6+}	2 ax. O^{2-}, 1.79–1.81 Å 4.6–6.3 eq. O, 2.366–2.460 Å	aqueous solutions pH = 4.3, 5.5, 10.0	Rossberg *et al.* (2000)

Table 28.8 (*Contd.*)

Ligand (*L*) *Structure*	*Name*	*An*	*Coordination*	*Phase An:L Speciation*	*References*
				see original article for $[UO_2]^{2+}$ speciation	
		U^{6+}	2 ax. O^{2-}, 1.784–1.805 Å 5.0–6.7 eq. O, 2.357–2.457 Å	aqueous solutions pH = 4.0–6.8.	Rossberg *et al.* (2003)
				see original article for $[UO_2]^{2+}$ speciation	
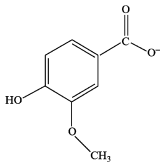	vanillate 3-methoxy,4-hydroxybenzoate	U^{6+}	2 ax. O^{2-}, 1.78 ± 0.02 Å 4.7(8) eq. O, 2.437(8) Å	aqueous solution, pH = 4.1.	Rossberg *et al.* (2000)
				see original article for $[UO_2]^{2+}$ speciation	
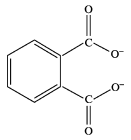	phthalate *o*-carboxybenzoate	U^{6+}	2 ax. O^{2-}, 1.78 ± 0.02 Å 6 eq. O, 2.37 ± 0.02 Å	aqueous solution, pH = 4.6. $UO_2(L)_1$	Reich *et al.* (1998a)

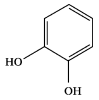	catechol *o*-hydroxyphenol	U^{6+}	2 ax. O^{2-}, 1.78–1.82 Å 5.9–6.1 eq. O, 2.374–2.391 Å	aqueous solutions pH = 5.0, 10.0. see original article for $[UO_2]^{2+}$ speciation.	Rossberg *et al.* (2000)
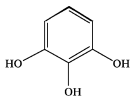	pyrogallol *o,m*-dihydroxyphenol	U^{6+}	2 ax. O^{2-}, 1.80–1.81 Å 4.8–5.1 eq. O, 2.383–2.396 Å	aqueous solutions pH = 4.8, 8.0 see original article for $[UO_2]^{2+}$ speciation.	Rossberg *et al.* (2000)
	fulvate	Np^{4+}	2–4 OH^-, 2.24–2.27 Å 5–7 O, 2.41–2.44 Å	wet pastes, Gorleben, boom clay	Denecke *et al.* (2002)
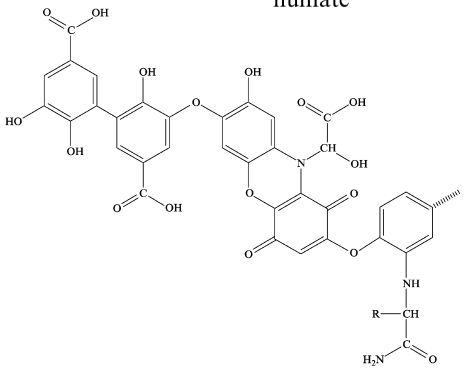	humate[a,b]	Th^{4+}	9–10 O, 2.44 ± 0.01 Å	dry solid and wet paste	Denecke *et al.* (1999)
		U^{6+}	2 ax. O^{2-}, 1.78 ± 0.02 Å 5 eq. O, 2.38 ± 0.02 Å	dry solids and wet pastes. $[UO_2]^{2+}$ sorbed on solid HA and precipitated out of HA solution at pH ≤ 5.4.	Reich *et al.* (1996a)
			2 ax. O^{2-}, 1.83 ± 0.02 Å 5 eq. O, 2.30 ± 0.02 Å	$[UO_2]^{2+}$ precipitated out of HA solution at pH = 8–10.	

Table 28.8 (*Contd.*)

Ligand (*L*) *Structure*	*Name*	*An*	*Coordination*	*Phase An:L Speciation*	*References*
		U^{6+}	2 ax. O^{2-}, 1.78 ± 0.02 Å 4–5 eq. O, 2.38 ± 0.02 Å	wet pastes, $[UO_2]^{2+}$ on natural and synthetic humics	Pompe *et al.* (1996)
		U^{6+}	2 ax. O^{2-}, 1.77–1.78 Å 5 eq. O, 2.37–2.39 Å	dry solids and wet pastes with $[UO_2]^{2+}$, see original article.	Denecke *et al.* (1997a)
		U^{6+}	2 ax. O^{2-}, 1.78 ± 0.02 Å 4–5 eq. O, 2.38 ± 0.02 Å	solution $[UO_2]^{2+}$ HA	Reich *et al.* (1998a); Nitsche *et al.* (1999)
		U^{6+}	2 ax. O^{2-}, 1.78 Å 5.3(5) eq. O, 2.39 Å	dry solid $[UO_2]^{2+}$ HA	Denecke *et al.* (1998a)
		U^{6+}	2 ax. O^{2-}, 1.77–1.78 Å 5 ± 0.7 eq. O, 2.37–2.39 Å	solutions and aqueous solid suspensions with $[UO_2]^{2+}$. see original article.	Denecke *et al.* (1998b)
		U^{6+}	2 ax. O^{2-}, 1.78 ± 0.02 Å 5 eq. O, 2.39 ± 0.02 Å	dry solids $[UO_2]^{2+}$ HA	Schmeide *et al.* (2003)

[a] HA = humic acid.
[b] Partial building block structure of humic acid adapted from (Sonnenberg *et al.*, 1989; Giordano, 1994; Stevenson, 1994; Paciolla *et al.*, 1999).

interfaces. For example, uranium mobility in oxic groundwater is dominated by adsorption of U(VI) onto mineral surfaces. The sorption of uranyl on to organic and inorganic surfaces plays a major role in preconcentrating low-temperature sedimentary uranium and the formation of uranium-bearing minerals, such as uraninite, through reduction following adsorption from groundwater. To predict mobility, it is necessary to have a fundamental understanding of interaction processes including surface complexation and precipitation as well as radionuclide incorporation into mineral phases. Among physical factors that influence partitioning between solution and metal surface are the specific actinide involved, its concentration, coordinating ligands such as dissolved carbonate, phosphate, and other complexing ions, solution pH, and mineral surface contamination.

Published synchrotron studies examining actinide interactions on mineral surfaces focus on valence and structural details of binding. Questions to be answered have centered on the valence state of the actinide and its coordination environment, including the presence of mineral-phase atoms visible in the coordination sphere that may help to distinguish inner- from outer-sphere interactions. The presence of actinide–actinide interactions may indicate clustering or the formation of oligomers on the mineral surface. Such oligomers may represent precursors to mineral-phase formation.

Synchrotron work to date has focused on XAS and microprobe studies of U, Np, or Pu adsorption onto silicate, phosphate or iron-based mineral phases and onto more complex soil samples. Work has also been published that looks at sorption onto bacterial surfaces as well as incorporation into mineral phases. These topics will be reviewed in the following subsections.

28.3.1 Silicates

Silicates are the largest and most complicated class of minerals, with estimates that as much as 90% of the Earth's crust is composed of silicates. These complicated structures can form as single units, double units, chains, sheets, rings, and frameworks. Phyllosilicates are a silicate subclass in which rings of tetrahedra are linked by shared oxygens to other rings in a two-dimensional plane that produces a sheet-like structure. The silicon to oxygen ratio is generally 2:5, with the sheets typically connected to each other by cation layers. The cation layers are weakly bound and often have water and other moieties trapped between the sheets. Clays are a group of phyllosilicates that contain large percentages of water trapped between the silicate sheets. Most clays are chemically and structurally analogous to other phyllosilicates but contain varying amounts of water and allow facile ion-exchange of interlayer ions. It is the physical characteristics of clays, more so than their chemical and structural characteristics, which defines this group.

Clay minerals are further divided into four groups, one of which is the montmorillonite/smectite group. Montmorillonites differ mostly in chemical

content. The general formula is $(Ca,Na,H)(Al,Mg,Fe,Zn)_2(Si,Al)_4O_{10}(OH)_2 \cdot nH_2O$. The water content is variable, and in fact when water is absorbed, the crystals tend to swell to several times their original volume. The effect of montmorillonite is to slow the progress of water through soil or rocks.

There have been several studies of the adsorption of actinide ions onto silicate surfaces, as summarized in Table 28.9. These studies are driven by the realization that the surfaces of these mineral phases have a discernable influence on the migration of ions in natural environments. Silicates have been proposed to have two surface sites onto which an adsorbed ion can bind. Numerous experiments explore specific models which address these two broad classes of binding sites: external amphoteric 'edge' sites whose properties are pH-dependent, and fixed-charge, basal-plane 'exchange' sites whose reactivity is independent of pH (Sposito, 1984, 1990; Weiland *et al.*, 1994). Unlike many transition-metal mineral phases, the silicate surface itself shows no redox chemistry. This simplifies the types of interactions that can be expected on the surface to complexation,

Table 28.9 *Published studies of thorium and uranium surface sorption onto silicate phases.*

Common name	*Formula*	*Sorbed ion*	*References*
silica gels	$SiO_2 \cdot nH_2O$ amorphous	Th(IV)	Oesthols *et al.* (1997)
		U(VI)	Dent *et al.* (1992); Michard *et al.* (1996); Reich *et al.* (1996b, 1998b); Allard *et al.* (1999); Sylwester *et al.* (2000)
montmorillonite	$(Ca,Na,H)(Al,Mg,Fe,Zn)_2(Si,Al)_4O_{10}(OH)_{2-x}H_2O$	Th(IV)	Giaquinta *et al.* (1997a); Daehn *et al.* (2002)
		U(VI)	Dent *et al.* (1992); Chisholm-Brause *et al.* (1992); Chisholm-Brause *et al.* (1994); Thompson *et al.* (1997); Sylwester *et al.* (2000); Hennig *et al.* (2002)
	bentonite	U(VI), U(IV)	Giaquinta *et al.* (1997a,b)
	vermiculite: $Mg_{0.7}(Mg,Fe,Al)_6(Si,Al)_8O_{22}(OH)_2 \cdot 8H_2O$	U(VI)	Hudson *et al.* (1999)
mica	hydrobiotite: $K(Mg,Fe)_6(Si,Al)_8O_{20}(OH)_4 \cdot xH_2O$	U(VI)	Hudson *et al.* (1999)
kaolinite	$Al_2Si_2O_5(OH)_4$	U(VI)	Thompson *et al.* (1998)

precipitation, and incorporation, and thereby providing simple model for study. The main question that has been addressed to date is the mechanism by which the ion binds to a silicate surface. As demonstrated in Fig. 28.7 for an actinyl ion, surface binding can include mononuclear or polynuclear inner- or outer-sphere complexation. Inner-sphere complexes can bind with either monodentate or bidentate ligation with surface sites.

The simplest of the silica phases to be studied are silica gels, amorphous $SiO_2 \cdot nH_2O$. Non-porous pyrogenic silica samples, consisting of spherical particles amorphous by X-ray diffraction, were used in a study of Th adsorption in order to determine the molecular details of the adsorption (Oesthols *et al.*, 1997). Wet samples of Th sorbed onto amorphous silica were studied using Th L_3-edge EXAFS. Solution pH values in the study were in the range of 2.8–4.0, which corresponded to the adsorption edge in the pH region of 2–3 that had previously been determined potentiometrically (Oesthols, 1995). Th surface coverages were

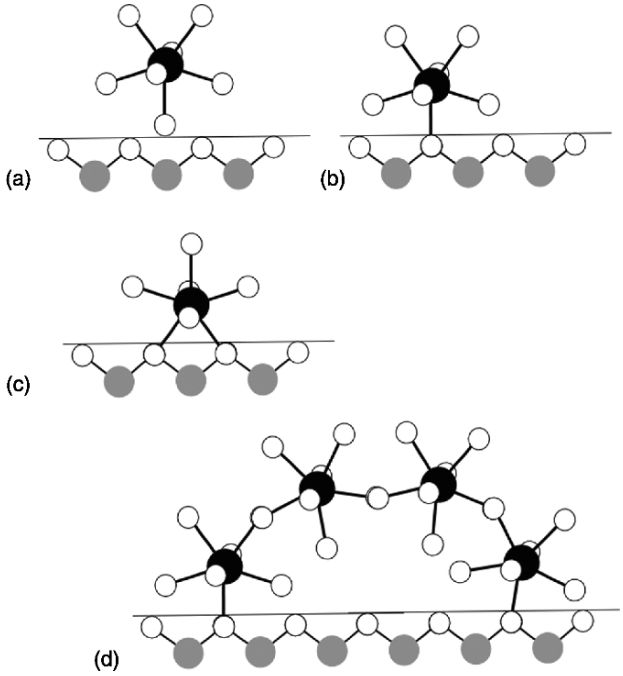

Fig. 28.7 *Binding modes for a metal-ion to a mineral surface. The binding can be* (*a*) *outer sphere, in which the metal ion's first coordination sphere is not a bulk-surface ion;* (*b*) *a mononuclear, monodentate, inner-sphere complex, in which the metal-ion's first coordination sphere includes an ion from the bulk-surface;* (*c*) *mononuclear, bidentate coordination, in which the complexing metal-ion shares two ligands with the surface; and* (*d*) *polynuclear, bidentate coordination, in which the metal-ion has coordination to other metal-ions as well as the surface.*

determined to be 3.8–230%. The spectra showed a decrease in structural order with increasing surface coverage. For lower surface coverage, 3.8–75.5%, two oxygen coordination shells were seen at approximately 2.28 and 2.54 Å with coordination numbers of about 2–2.7 and 5, respectively. These samples also showed about 2(1) Th–Si interactions at 3.85 Å. Samples with higher Th surface coverage, that is 92.7 and 230%, also showed two oxygen shells, with about two O at 2.33 Å and 4.5 O at 2.54 Å and 2.3 and 1.3 Th–Si interactions at 3.84 and 3.79 Å, respectively. None of the samples showed evidence of any Th–Th interactions, even the sample reported to have 230% surface coverage, suggesting that the surface layer resembles amorphous thorium hydroxide, which also shows no significant Th–Th correlations. The absence of Th–Th correlations, even in amorphous $Th(OH)_4$ was attributed to a high degree of disorder (Oesthols *et al.*, 1997). The EXAFS data were consistent with Th adsorption onto the amorphous silica surface via bidentate inner-sphere complexation, in which Th has a double corner-sharing bond with two different SiO_4 surface tetrahedra. Four to eight oxygen atoms are shared with coordinated solution–water molecules, which account for the longer Th–O correlations at 2.55 Å.

Uranium sorption by silica gels has also been shown to be pH sensitive (Michard *et al.*, 1996), increasing with increasing pH over the range of about 3–5. This pH interval corresponds approximately to that over which there are hydrolyzed uranyl species present in solution. A two-phase process has been proposed that involves an external mass transfer and an intra-particle mass transfer, of which only the former is strongly pH-dependent. Earlier, Raman studies had suggested that uranyl sorbs as an inner-sphere surface complex (Maya, 1982). This suggestion has been confirmed by EXAFS studies of UO_2^{2+} sorption products for samples prepared at pH 3 and 5 (Dent *et al.*, 1992), which were noted to be indistinguishable, but no detailed analysis was provided. Coordination information of uranyl sorbed to silicic acid and silica gel samples prepared at pH 4 was determined by EXAFS (Reich *et al.*, 1996b). The two materials are distinguished by different surface areas, 80 vs 470 mg/g for silicic acid and silica gel respectively, as determined by BET measurements. An analysis of EXAFS data showed the expected dioxo coordination with a $U–O_{ax}$ distance of 1.78 Å for both samples. Two silicic acid samples, prepared with different solution uranyl concentrations, were examined. The sample, obtained from a 0.01 M UO_2^{2+} solution, has two resolvable O coordination shells in the equatorial plane with 2.6(4) O at a distance of 2.27 Å and 1.8 O at a distance of 2.50 Å. The sample obtained from a more concentrated uranyl solution, 0.05 M, has 2.1(4) equatorial O at a distance of 2.27 Å and 2.25 O at a distance of 2.48 Å. Both samples show a total equatorial O coordination of slightly less than 5. These results compare to those determined for silica gel samples obtained from a 0.05 M uranyl solution, which also have two equatorial O shells, one with 4(1) O at 2.29 Å and the other with 1.6(7) O at a distance of 2.50 Å, for a total O coordination greater than five. Similar results were determined for a sample prepared at pH 3.4 (Sylwester *et al.*, 2000).

The observation of two O coordination shells separated by about 0.2 Å, coupled by the absence of an EXAFS feature attributable to U–U interactions, is strong evidence that, at pH values 3.4 and 4, uranyl undergoes inner-sphere, mononuclear, bidentate surface complexation (Reich *et al*., 1996b; Sylwester *et al*., 2000). In contrast, samples prepared at higher pH values show additional U–Si and U–U coordination shells (Allard *et al*., 1999; Sylwester *et al*., 2000). For example, at pH 6.24 additional coordination shells are observable in the data, with one Si at 3.1 Å and about two U at 4 Å (Sylwester *et al*., 2000). This result indicates some form of oligomeric uranyl phase, either a surface complex or a precipitate. The U–Si atomic distance and coordination number would imply a surface adsorption via bidentate complexation to two surface O associated with the same Si. Monodentate complexation with surface O would be expected to result in a longer U–Si distance of about 3.8 Å (Burns *et al*., 1997).

EXAFS spectra of uranyl-loaded montmorillonite, which contains aluminol as well as silanol sites, are clearly different from that of the metal adsorbed onto silica (Chisholm-Brause *et al*., 1992, 1994; Thompson *et al*., 1997; Sylwester *et al*., 2000; Hennig *et al*., 2002). The degree of complexation at the edge aluminol or silanol sites should rise with increasing pH because these sites become increasingly deprotonated and therefore available for cation complexation. In studies with pH values in the range of about 3 (Chisholm-Brause *et al*., 1994) to 5 (Dent *et al*., 1992; Sylwester *et al*., 2000), the data contain an unresolvable single-shell structure similar to those seen in aqueous solution and consistent with outer-sphere coordination. The observed $U–O_{eq}$ bond distances of 2.41–2.43 Å support this finding. In contrast, studies at higher pH (5–7) indicate that an inner-sphere complexation process dominates the sorption. Although the short data range (3.1–11.4 $Å^{-1}$) prohibited the observation of a splitting in the shell attributed to equatorial ligation, large Debye–Waller factors (0.013–0.017 $Å^2$) together with much shorter bond distances observed at higher pH, 2.34–2.38 Å, were used to support models for binding to amphoteric surface hydroxyl sites (Hennig *et al*., 2002).

Another interesting study was published concerning the role of montmorillonite surface coverage on the local structure about the uranyl (Chisholm-Brause *et al*., 1994). There were three samples studied whose final pH values decreased with increasing surface coverage, from 5.6 to 4.4 and finally to 3.4. At low surface coverage, 0.0103 mmol/g, the ratio of the integrated EXAFS amplitude from the equatorially bound O to that found in solution is only 0.58. The bond distance is also short at 2.391 Å. As the solution concentration was increased, the surface coverage also increased from 0.044 to 0.208 mmol/g, there was a higher ratio of uranyl ligation in the equatorial plane (0.65 and 0.77) and these O occurred at longer distances, specifically 2.414 and 2.444 Å, respectively. This same observation has been previously quantified in terms of significant differences in equatorial O coordination as a function of solution U concentration (Chisholm-Brause *et al*., 1992; Dent *et al*., 1992). The authors argue that these data suggest that uranyl forms at least three distinct sorption

complexes on montmorillonite, a result that is consistent with previously published modeling (Zachara and McKinley, 1993). Using simple bond-length to coordination-number correlations, it was also argued that the observed increase in amplitude of the EXAFS spectra with increasing surface coverage must be due, at least in part, to decreasing disorder, and not just an increase in the number of coordinating ligands (Chisholm-Brause *et al*., 1994). An independent study (Hennig *et al*., 2002) on samples with uranium loading of 1751–2473 ppm did not support this finding. These EXAFS data show no evidence of U–U interactions, even at pH values >5.4, where thermodynamic modeling predicts the formation of solid-hydrated uranyl oxides, indicating that surface complexation may be kinetically favored relative to precipitation under the conditions employed. It should be noted that molecular dynamics simulations of uranyl sorption onto a quartz surface find that water oxygen atoms and surface oxygen atoms are equidistant to the metal-ion. Equatorial splitting of the bond distances is caused not by inner-sphere coordination, but instead by the presence of other ligands in the first coordination sphere of the UO_2^{2+}, such as the carbonate anion (Greathouse *et al*., 2002).

Uranyl sorption complexes on two related phyllosilicates, vermiculite, which is a montmorillonite, and hydrobiotite, which is a mica, were studied to gain further information on binding to different surface sites (Hudson *et al*., 1999). Samples were prepared that favored fixed-charge, ion-exchange sites, or amphoteric surface hydroxyl sites. Samples made under conditions that significantly favored the ion-exchange sites had EXAFS spectra with one resolvable equatorial O distance, consistent with outer-sphere uranyl complexation. Upon dehydration, the EXAFS data are consistent with inner-sphere uranyl coordination. In addition to the standard EXAFS experiments, the local structure about the uranyl ion in the hydrated sample was also studied using polarized L_1- and L_3-edge XANES. Polarized X-ray absorption data have been demonstrated to yield information about the spatial orientation of the linear dioxo group (Hudson *et al*., 1996). Polarization data were used to probe the orientation of the linear dioxo-groups with respect to the silicate surface in the vermiculite sample (Hudson *et al*., 1999). The ion-exchanged sites, with outer-sphere coordination, showed a preferred orientation of the dioxo moiety parallel to the silicate layers. Samples that significantly favored the hydroxy sites have EXAFS spectra that show the uranyl ion in a highly distorted equatorial shell with the detection of a U–U interaction, which suggests the formation of surface precipitates and/or oligomeric complexes.

The reports on sorption onto montmorillonite have been extended by experiments on uptake at initial Th concentrations representing undersaturation (pH 2 and 3) and oversaturation (pH 5) with respect to amorphous ThO_2 (Daehn *et al*., 2002). The sorption experiments were conducted with Th concentrations in the range of 2.7×10^{-6} to 4×10^{-4} M and under an N_2 atmosphere. At low and intermediate surface coverage, 1–34 and 157 μmol/g, two coordinating oxygen shells were observed, with about three O at 2.24 Å, six to

eight O at 2.45–2.48 Å, and one Si shell at 3.81–3.88 Å. Any attempt to include Th–Th interactions into the fit failed. The same coordination environment was observed for both pH values. The pH = 5 samples had Th–O coordination similar to those observed at the lower pH. For the samples with lower Th loading (14 and 40 μmol/g), data analyses suggested a reduced number of Th–Si pairs, 1.4–1.7 at a distance of 3.87 Å, compared to the sorption samples prepared at pH = 3, which had 2.5–2.9 Si at 3.83 Å. The reduced Th–Si coordination number at the higher pH could be explained by assuming that a fraction of Th is no longer directly bonded to the montmorillonite surface, but instead forms an outer-sphere complex. It could also indicate destructive interference with the EXAFS generated by the Th–Si pairs at 3.9 Å (Daehn *et al.*, 2002). This latter hypothesis is supported by the data from the pH = 5 sample with the highest Th loading (166 μmol/g), which was satisfactorily fit with neither a Th–Si nor a Th–Th interaction. However, the similarity of EXAFS data from this sample with those obtained from a Th amorphous precipitate suggests the surface formation of similar precipitates at high Th concentrations and high pH.

Polarized EXAFS measurements were also obtained from Th-treated oriented films, prepared at pH values of 2 and 3, to investigate whether the sorbed Th was oriented with respect to the octahedral sheets of the clay (Daehn *et al.*, 2002). The spectra were recorded with an electric field vector at 10°, 35°, 55°, and 80° with respect to the clay-film plane. No significant polarization effects were observed in the spectra obtained from the pH = 2 or 3 samples. It was postulated that Th adsorbs to the montmorillonite at its edge sites, by sharing double corners with Si tetrahedra, and that these sites are saturated when the concentration of Th is greater than 32 μmol/g. This hypothesis is supported by the observed difference in EXAFS spectra of the lower concentration samples compared with the higher surface-coverage samples, which look more similar to solution Th spectra. This result may indicate that Th is sorbed as an outer-sphere complex after the clay edge sites are saturated.

Studies on Th- (Giaquinta *et al.*, 1997a) and uranyl-exchanged bentonite (Giaquinta *et al.*, 1997a,b), a smectite clay, and zeolite (Wasserman *et al.*, 2000) samples extended previous work on two aspects: (1) the exchanged clays were coated with hydrophobic silanes in order to inhibit interlayer-water exchange and (2) uranyl-exchanged samples were subjected to hydrothermal conditions. The uranyl-ion-exchanged samples were thoroughly washed in an effort to produce samples with single-interlayer binding sites. The EXAFS from the simple, untreated samples were analyzed, assuming only one site. The results from Th L_3-edge EXAFS (Giaquinta *et al.*, 1997a) showed that Th had a single hydration sphere with approximately 11 O at a distance of 2.49 Å and 2.7(6) O at 3.66 Å. In contrast, EXAFS spectra from the hydrothermally treated samples were similar to that obtained from ThO_2. The first O shell shifted to a slightly shorter distance, 2.39 Å and there were two additional peaks present. The peak at 3.93 Å, present only in the treated sample, was attributed to a Th–Th

interaction and consistent with the formation of a thoria-like hydrous polymer (Baes and Mesmer, 1976). The EXAFS from the UO_2^{2+} exchanged sample, before treatment, was analyzed with 2.2 O at 1.77 Å, 5 O at 2.43 Å, and 2.6 O at 3.45 Å (Giaquinta *et al*., 1997b). This result is consistent with outer-sphere uranyl complexation as seen for other montmorillonite samples.

In contrast to the Th samples, the uranyl-loaded clays from hydrothermally treated samples produced EXAFS spectra that were different from those obtained before treatment. The silane-treated uranyl samples also showed no change to the uranyl environment compared to those obtained before hydrothermal treatment, except that the spectra showed that the coordination shells were at longer distances. The methoxysilane data revealed dramatic changes in the uranium environment. The dioxo coordination environment disappeared and was replaced by a single oxygen shell at 2.33 Å. There was also an additional peak observed at 3.36 Å and another at 3.92 Å, determined to be a U–U interaction. This coordination is suggestive of small particle uraninite formation, which implies the reduction of U(VI) to tetravalent U. This suggestion was confirmed by U L_3 XANES experiments. The observation of uranyl reduction in the presence of an organic and under elevated temperature and pressure is important in terms of uranium migration under geological conditions.

Dissolved CO_2 is also believed to significantly influence uranium adsorption on mineral surfaces with a maximum at near-neutral pH, and decreasing sharply toward more acidic (pH $<$ 6) and more alkaline (pH $>$ 7) conditions. The mechanism behind this influence was studied using EXAFS to probe uranyl sorption onto the clay-mineral kaolinite (Thompson *et al*., 1998). The combination of uranium concentrations and pH values used in these experiments were such that complex uranyl oxyhydroxides would be expected. Indeed U–U interactions were observed.

In addition to the work on the aluminosilicate clays, there have been limited EXAFS studies of actinide sorption onto aluminates, specifically uranyl onto γ-Al_2O_3 and α-Al_2O_3. The former study was done on two samples with contact solution pH values of 3.48 and 6.50 (Sylwester *et al*., 2000). EXAFS data from both samples demonstrated the standard dioxo uranium(VI) coordination at 1.78 Å. There were also two equatorial shells, the first with about 2.8 O at 2.37 Å and about 2.0 O at 2.53 Å, whereas the second had about 2.6 O at 2.34 Å and 3.1 O at 2.50 Å. The splitting of the equatorial coordination shell is again used as evidence for inner-sphere coordination to the alumina surface. The sample at near-neutral pH also showed a U–U interaction at 4.10 Å corresponding to about 0.5 U near-neighbors, which indicated the coordination of a mixture of mononuclear and polynuclear surface complexes. The study of uranyl sorption on α-Al_2O_3 (Denecke *et al*., 2003) examined the polarization dependence of uranyl ions sorbed onto a single-crystal (110) surface under different loading conditions. Although the authors indicate the potential of polarization experiments, no definitive information about uranyl coordination to the α-Al_2O_3 surface was provided.

28.3.2 Carbonate incorporation

Carbonate minerals are among the most common secondary phases that form in near-surface environments. There are three main sedimentary carbonate minerals: calcite, aragonite, and dolomite, as listed in Table 28.10. Of these mineral phases, calcite is one of the most abundant of the non-silicate minerals, comprising about 4% by weight of the Earth's crust. Aragonite is a less common polymorph of calcite and is a major constituent of invertebrate skeletons that, in most environments, eventually converts to calcite. Carbonate minerals are known to incorporate trace amounts of uranium, an attribute that has been utilized for the U-series age determinations of ancient calcites and as marine paleoenvironmental (Brannon *et al.*, 1996) and diagenetic indicators (Russell *et al.*, 1994). In addition, the carbonate mineral class itself includes a variety of stable uranyl carbonates (Reeder, 1983). The studies of actinide interactions with carbonate phases have focused on incorporation studies.

It is important to develop a molecular level understanding of the speciation of actinides sequestered in carbonate phases in order to assist in the assessment of these ubiquitous minerals in actinide mobility and sequestration. The mechanism(s) of actinide incorporation into carbonates, particularly calcium carbonates, for which the actinide can substitute for Ca^{2+}, has been the source of significant recent study when the substituting ion is uranium (Shen and Dunbar, 1995). The structural work published to date has focused on uranium substitution and has not directly addressed the issue of transuranic substitution into a calcium carbonate lattice. U^{4+} is approximately the right size to substitute for Ca^{2+} in the calcite lattice, but there are two problems to this simple ion replacement. First, the substitution of a tetravalent ion for a divalent one requires some stable charge-balance mechanism available in the lattice. Second, U^{4+} has a low groundwater solubility because of the precipitation of insoluble uranous phases and as a result U is present in most natural waters as the dioxo uranium(VI) ion. Although $U(VI)O_2^{2+}$ is divalent, its configuration and size would be expected to cause significant local structural disruption if it were to substitute directly for Ca^{2+} (Langmuir, 1978; Reeder, 1983).

Table 28.10 *Carbonate mineralogy. The common carbonate mineral phases studied for actinide incorporation using synchrotron radiation.*

Mineral	*Formula*	*Crystallographic group*	*References*
calcite	$CaCO_3$	trigonal ($R\bar{3}c$)	Effenberger *et al.* (1981)
aragonite	$CaCO_3$	orthorhombic (Pmcn)	Dal Negro and Ungaretti (1971); de Villiers (1971)
dolomite	$CaMg(CO_3)_2$	trigonal ($R\bar{3}$)	Effenberger *et al.* (1981)
strontianite	$SrCO_3$	orthorhombic (Pmcn)	de Villiers (1971)
siderite	$FeCO_3$	trigonal ($R\bar{3}c$)	Effenberger *et al.* (1981)

The structural details of uranium incorporation into calcite and dolomite were first probed by performing EXAFS experiments on powdered samples exposed to a uranyl perchlorate solution (Geipel *et al.*, 1997). The adsorption experiments were done with no external pH control and under atmospheric conditions, that is, without excluding CO_2. The final solution pH values, after equilibration, were measured to be between 8 and 9 and the final samples had loadings of about 12.8 to 66.3 mg U/g. XPS studies on the samples indicated that the uranyl ions displace Ca at the mineral surface. There was no chlorine-containing surface species detected, indicating that the perchlorate anion did not participate in the surface reaction. The U EXAFS of all the samples studied were indistinguishable and consistent with uranyl coordination. The uranyl equatorial shell was characterized by a broad distribution of U–O distances, with an average of 2.34(2) Å. These results support conclusions of earlier studies that uranyl carbonates and hydroxides form at the grain surfaces of calcite (Carroll and Bruno, 1991; Carroll *et al.*, 1992).

More recent studies have focused on the incorporation of uranyl into synthetic aragonite (Reeder *et al.*, 2000) and calcite (Reeder *et al.*, 2000, 2001). Several previous studies have shown uranyl to be preferentially taken up by aragonite relative to calcite (Kitano and Oomori, 1971; Meece and Benninger, 1993), which points to underlying important mechanistic or structural differences for its incorporation into these two polymorphs. This issue was directly examined by comparing synthetic samples of the two phases (Reeder *et al.*, 2000) that were formed under similar conditions, that is U concentrations were held in the range 10–82 mM, the pH values were maintained at about 8.2–8.3, and air was bubbled through the solutions. Because of the deleterious effects of Sr incorporation on XAS data collection, efforts were made to ensure its exclusion during sample preparation. The final aragonite samples had 985 and 10810 ppm U whereas the calcite samples had 700 and 1890 ppm U in agreement with previous findings that uranyl is preferentially taken up by the orthorhombic phase. U L_3 XANES data indicate the presence of uranyl(VI) in the samples. Fits to the EXAFS data for all uranyl-containing aragonite and calcite samples showed the typical dioxo-coordination environment.

The results of a detailed analysis of the EXAFS data are given in Table 28.11. The most significant differences between U in the two mineral phases were evident in the first equatorial shell. For the aragonite sample, a fit to the data determined that the uranyl ion in aragonite has the same coordination environment as the uranyl triscarbonato solution complex, which was also measured during the same experiment (Reeder *et al.*, 2000, 2001). The O_{eq} distances from aragonite compare to the U–O average distance of 2.47 Å determined for the uranyl coordination by six equatorial oxygens (Burns *et al.*, 1997). In addition to oxygen scattering, a correlation attributed to U–C_3, from carbonate at 2.89 Å is in the range characteristic of bidentate coordination by three carbonate groups (Allen *et al.*, 1995). A further correlation attributed to distal oxygens of carbonate groups at 4.1 Å was also observed, as was a linear

Table 28.11 *Comparisons of coordination numbers (CN), distance from uranium (R), and Debye-Waller factor (σ^2) determined for the best fits of U L_3 EXAFS data from synthetic aragonite and calcite that were precipitated from solutions containing the uranyl ion (Reeder* et al.*, 2000). Multiple values for one parameter indicate fits from different samples. Underlined values indicate that the parameter was fixed during fitting.*

	Aragonite			*Calcite*		
Shell	**CN**	**R (Å)**	**σ^2 (Å^2)**	**CN**	**R (Å)**	**σ^2 (Å^2)**
O_{ax}	2	1.80, 1.81	.003, .002	2	1.80	.002, .003
O_{eq}	5.9, 6.0	2.44, 2.42	.004, .005	5.2, 5.3	2.33	.009, .010
C	3.2	2.90, 2.89	.002, .003	2.1, 1.9	2.91, 2.81	.003, .005
C				1.6, 1.3	3.22	.005
Ca	2.8, 1.7	3.82, 3.78	.004			
Ca	2.9, 3.2	4.03, 3.96	.007, .006			
Ca	0.9, 1.0	4.75	.003, .004			
O_{dist}	3.9, 5.3	4.22, 4.10	.004			

Estimated errors are CN (±20%), R (±0.01 Å, first 2 shells; ±0.02–0.03 Å).

three-legged multiple-scattering path (O_{dist}–C–U) at essentially the same distance. The observation of bidentate coordination of U by three carbonate ions was supported by Raman and luminescence spectroscopies. There was no unambiguous evidence of any U–U interactions that would indicate clustering or co-precipitation of a uranyl mineral phase. In addition, evidence of U–Ca correlation was observed that was dependent on U concentration.

The same basic structural unit was determined for the uranyl incorporation into aragonite as was observed in the growth solution, which was also measured and analyzed (Reeder *et al.*, 2000). The EXAFS results, supported by Raman data, were used to postulate an incorporation mechanism for uranyl into aragonite. EXAFS show that the predominant aqueous uranyl species is $UO_2(CO_3)_3^{4-}$ and that this configuration is preserved in aragonite. The authors suggest that the entire solution species is incorporated into the mineral phase essentially intact (Reeder *et al.*, 2000).

In contrast to the well-defined coordination environment observed for uranyl in aragonite, the coordination environment of uranyl in calcite appears significantly more disordered (Reeder *et al.*, 2000, 2001). The second FT peak from the U EXAFS data, attributable to U–O_{eq}, is significantly less intense and at a smaller U–O distance, relative to the dioxo peak, in the calcite sample. This observation is manifested in the fit, which has fewer, about five, equatorial O with significantly larger Debye–Waller factors (0.009–0.010 Å^2). Weak peaks in the FT suggest that there are carbon atoms coordinated at 2.9 and 3.2 Å with more than one type of U coordination by carbonate, indicating both mono and bidentate interactions. The luminescence data are also different for calcite, indicating the possibility of uranyl hydroxide formation on mineral surfaces, a postulate previously made from an independent study (Geipel *et al.*, 1997).

The work on powder-samples of calcite has been augmented by further work, on single-crystals, designed to address the issue of whether incorporation occurs at structurally distinct surface sites (Reeder *et al.*, 2001). The single crystals were grown at slightly lower pH values (7.5–7.6) than were the powder samples. Luminescence lifetime measurements indicated that more than one solution species was present in the growth solution. The average U concentrations in the crystals were rather low, about 15 and 225 ppm. Micro synchrotron X-ray fluorescence (μ-SXRF) and micro X-ray absorption near-edge structure (μ-XANES) data were obtained from the single-crystals using a monochromatic beam with spot size 15×15 μm^2 or 5×6 μm^2. The as-grown $(10\overline{1}4)$ face was examined, and had a single, polygonized growth hillock composed of four uniform vicinal faces that differed by the orientation of their growth steps and the direction of their advancement during growth. The presence of this hillock is significant because uranyl species can become incorporated into structurally distinct steps of the non-equivalent vicinal faces during crystal growth processes. The μ-SXRF data reveal a striking difference in the distribution of uranium corresponding precisely to the non-equivalent vicinal faces. The $[4\overline{4}1]_+$ and $[4\overline{4}1]_-$ surfaces were highly enriched in uranium relative to the $[48\overline{1}]_+$ and $[48\overline{1}]_-$ surfaces. The magnitude of differential uptake was approximately a factor of 6 to 10. The implications of these findings are that surface controls are significant and therefore that the relative proportions of crystal surface morphologies can strongly influence uranyl incorporation. Polarized μ-XANES revealed neither a discernible difference between the spectra obtained from the non-equivalent vicinals nor any orientational dependence. Fits to the EXAFS data were similar to those from the powder samples, listed in Table 28.11, with two axial O at 1.80 Å, 5.7 O at 2.36 Å, and 3.2 C at 2.92 Å. Weak features observed at higher *r* could be fit with minor contributions from a distal oxygen and a multiple-scattering path at 4.15 and 4.18 Å, respectively. The results indicate that there is no preferred orientation of the uranyl moiety within the single-crystal, and would be consistent with multiple uranium species, as suggested by luminescence and supported by the apparent disorder seen by EXAFS beyond the first coordination shell.

The uranyl concentrations in the synthetic calcite and aragonite samples far exceed that normally found in natural samples, raising the possibility that the obtained coordination environments do not reflect the environments seen in natural samples, which equilibrate over long time frames, and may undergo repeated dissolution/precipitation or structural transformations. Unfortunately, the low concentrations of U typically found in natural calcium carbonate mineral samples, combined with the presence of large amounts of Sr^{2+}, either substituting directly for Ca^{2+} ion in the lattice or as partially segregated into stronitianite (Greegor *et al.*, 1997) complicate the acquisition of EXAFS data with adequate statistics for useful analyses. One study looked at U incorporation into natural coral skeletal aragonite (Pingitore *et al.*, 2002). Two live coral samples, collected from the Galapagos Islands, and one dead sample,

obtained from an exposed reef terrace on Guadeloupe were used in the study. Radiocarbon dating from nearby reefs yielded the age of the Guadeloupe sample as about 25000–30000 years old. The U content, determined from inductively coupled plasma-mass spectrometry (ICP-MS) was low, approximately 3 ppm. In contrast, the Sr concentrations were approximately 7000 ppm in all three samples, requiring XAS data acquisition at the U L_2-edge. XANES edge energies and shapes were used to infer that the U in the two live samples was present as uranyl(VI) whereas that in the dead sample from the exposed reef on Guadeloupe was predominately U^{4+}. Unfortunately, the EXAFS data were not of sufficient quality to confirm this observation and furthermore it should be noted that XANES data can sometimes be misleading when distinguishing between tetra- and hexavalent U (Eller *et al.*, 1985; Calas *et al.*, 1987; Greaves *et al.*, 1989; Biwer *et al.*, 1997; Hess *et al.*, 1998; Sturchio *et al.*, 1998).

There have been two reports published on natural calcite samples that contain uranium. The first looked at a natural sample of spar calcite from a Mississippi Valley-type zinc ore deposit (Sturchio *et al.*, 1998). This sample has a relatively high U concentration (5–35 ppm). The sample also included a high concentration of Sr, necessitating data collection at the U L_2-edge. The XANES data are inconclusive with respect to the U oxidation state. In contrast, the EXAFS data fit well with a single coordination environment. The missing peak at 1.8 Å in the FT confirms the absence of a uranyl ion and the overall coordination environment confirms the incorporation of tetravalent U into the calcite lattice. Although the EXAFS results show an important difference for the U coordination over that of Ca^{2+}, it is clear that the U does directly substitute for Ca^{2+} in the lattice. In calcite, the Ca^{2+} has a first coordination shell of octahedral O about Ca^{2+} at a distance of 2.36 Å (Effenberger *et al.*, 1981). In contrast the incorporated U is best fit with two shells: one at 2.21 and one at 2.78 Å. More distant shells were also observed, including six C at 3.26 Å, six Ca^{2+} at 4.02 Å, and six Ca^{2+} at 4.98 Å. These distances are indistinguishable from those observed in calcite itself. An X-ray synchrotron microprobe analysis of the same sample confirms the substitution of U into the calcite structure and is inconsistent with inclusions of distinct U-rich phases. The simultaneous presence of sulfide minerals and hydrocarbon inclusions indicates that this calcite sample was formed in a reducing environment. This may explain the high concentration of U in this sample, and indicates that U^{4+} is preferentially incorporated into calcite in such environments. In contrast, U^{6+} is generally excluded from calcite. These results provide insight into the geochemical cycle of U in deep groundwater aquifers and anoxic lacustrine and marine basins. The incorporation of U into calcite gives a potentially stable host for dispersed U^{4+} over geological time scales.

The second report of an XAS study of uranium in natural calcite (Kelly *et al.*, 2003) involved the use of XAS and X-ray microprobe to look at a sample relatively rich in U (about 360 μg/g) from a 13700-year-old speleothem deposit

in northern Italy (Spoetl *et al.*, 2002). X-ray fluorescence (XRF) mapping was done with a monochromatic beam (17.3 keV) focused to 5×5 μm^2. Fluorescence emission from U, Sr, and Ca were monitored. XRF mapping indicated that uranium concentrations vary between 80 and 500 ppm that were homogeneous on the 100-μm scale. The data were considered consistent with a dilute solid solution. It is interesting to note that there is petrographic evidence that this natural sample of calcite formed by recrystallization of a U-rich aragonite sample, which may explain the high uranium substitution. In contrast to the previous data on the natural calcite sample from the Mississippi valley, the XANES data from the northern Italy calcite sample indicated uranium is predominately hexavalent. The EXAFS data confirmed a hexavalent, dioxouranyl coordination that is monodentate to four carboxylates with U–O distances from the EXAFS fit of 2.41 Å. These results are similar, although more detailed, than those previously reported for synthetic calcite samples (Reeder *et al.*, 2000, 2001) but the interpretation is different. The authors of the paper, reporting uranyl incorporation into natural calcite (Kelly *et al.*, 2003), propose a direct substitution into the calcite lattice that involves the replacement by UO_2^{2+} of one Ca and two carbonate anions. Charge balance then requires the non-local substitution of excess Na^+, which is observed in the chemical analysis. Overall, the reported EXAFS analyses are not inconsistent with their proposed model, although the complexity of the uranyl site requires eight scattering contributions with 19 variable parameters to adequately fit the data. Considering the reported *k*-range, only 15 parameters should have been used in the fit (Teo, 1986). Thus, although the proposed model for uranyl substitution into calcite is interesting, further experimental work is required for its confirmation.

The overall conclusion that the uranyl ion is more effectively incorporated into the aragonite than the calcite structure raises an environmental issue (Reeder *et al.*, 2000). Prevalent geological conditions at or near the Earth's surface favor the transformation of aragonite, which is metastable, into calcite. However, the uranyl ion does not fit into the calcite lattice as well as it does into the aragonite lattice. The UO_2^{2+} coordination environment is more clearly defined in the latter material, which is known to incorporate a significantly higher concentration of uranyl. Therefore the transformation of aragonite into calcite destabilizes the uranyl incorporated into the phase. As a result, $CaCO_3$ may not be an effective sequestering agent for U(VI) under geologic conditions and over long timescales.

28.3.3 Fe-bearing mineral phases

Iron and its compounds play an important environmental role in both biotic and abiotic processes. Its complex redox and solubility behavior is a function of solution Eh and pH, as sketched in Fig. 28.5 (Hem, 1985). Fe^{2+} is generally soluble in groundwater systems whereas most iron minerals and insoluble complexes contain Fe^{3+}. Iron oxides in particular are ubiquitous in soils and

sediments where they play an important, although not well understood, role in regulating metal-ion distribution through chemical, adsorption, and redox mechanisms. Iron sulfides also play a role in more anoxic environments. Oxidation state properties of Fe can play an important role in actinide speciation and transport, especially in reducing environments. Simple solution redox reactions may be directly affected by the presence of a redox-active surface, or they may be altered in the presence of a mineral surface that can preferentially adsorb, and thereby concentrate metal-ions at solution concentrations that are well below their solubility limits.

In order to understand the results of experiments designed to study actinide speciation on Fe surfaces, which are conducted at a macroscopic level, it is necessary to elucidate a molecular level model for the solid/surface reactivity. Several studies, using EXAFS spectroscopy, have been undertaken to probe actinide speciation on carefully prepared Fe samples, as listed in Table 28.12. Most, although not all of these experiments have focused on uranyl adsorption onto mineral phases, although the occlusion of U by Fe-oxide mineral coatings has also been reported (Jenne, 1977). In the absence of high solution concentrations of complexing ligands, U has been shown to complex to Fe minerals such

Table 28.12 *Published studies of uranium and neptunium binding to Fe mineral surfaces. These studies focus on inner- versus outer-sphere coordination of actinide with mineral surface as well as any evidence of redox chemistry.*

Actinide	*Mineral name*	*Chemical formula*	*References*
uranium (VI)	hydrous Fe oxide, ferrihydrate	microcrytalline hydrous $Fe_2O_3 \cdot nH_2O$	Manceau *et al*. (1992)
			Waite *et al*. (1994); Reich *et al*. (1998b)
	goethite	α-FeOOH	Moyes *et al*. (2000); Reddon *et al*. (2001); Walter *et al*. (2003)
	hematite	α-Fe_2O_3	Reich *et al*. (1998b); Bargar *et al*. (1999a, 2000)
	lepidocrocite	γ-FeOOH	Moyes *et al*. (2000)
	mackinawite	FeS_{1-x}	Moyes *et al*. (2000)
	schwertmannite	$Fe_{16}O_{16}(OH)_{12-9}(SO_4)_{2-3.5} \cdot 10H_2O$	Walter *et al*. (2003)
	green rust	mixed Fe(II)/Fe(III) hydroxides	O'Loughlin *et al*. (2003)
		U-Fe oxide co-precipitates	Duff *et al*. (2002)
neptunium (V)	goethite	α-FeOOH	Combes *et al*. (1992)
	mackinawite	FeS_{1-x}	Moyes *et al*. (2002)

as hematite and goethite over a wide range of solution pH conditions (Hsi and Langmuir, 1985; Waite *et al.*, 1994; Duff and Amrhein, 1996), making these reactions of significant importance to its environmental behavior. For the most part, these studies involve Fe(III) phases and are therefore unlikely to involve redox activity because the studies have utilized the fully oxidized UO_2^{2+} ion in solution.

Among the relevant experiments are those that probe the interaction of uranyl with hydrous ferric oxide (HFO) because the enrichment factor for uranyl on the HFO surface is about 500 times greater than on well-crystallized goethite, and about 10^5 times greater than on clay surfaces (Szalay, 1991). EXAFS data, obtained from samples prepared at pH 5 with an 8.2% surface coverage (Manceau *et al.*, 1992), show uranyl coordination with about five equatorial oxygens at 2.2–2.4 Å and an additional broad peak corresponding to one Fe at about 3.4 Å and another 0.5 Fe at about 3.3 Å. These distances are consistent with uranyl bonding as a mononuclear bidentate inner-sphere complex, sharing edges with the Fe–O, OH surface octahedra. The authors note the excellent match between the unshared edges of the Fe–O octahedra and of the O–O distance of the equatorial uranyl ligands. They use this match to explain the unusually high affinity of uranyl for HFO as compared to crystalline phases such as goethite. The structural relationship between the sorbent and the sorbate is used to explain, at a molecular level, why uranyl complexes inhibit the HFO to crystalline oxide transformation (Manceau *et al.*, 1992).

A related study involved U L_3-XAFS studies of U(VI) adsorption onto ferrihydrate over a wide range of solution and adsorption conditions (Waite *et al.*, 1994). Ferrihydrate is an amorphous or poorly crystalline hydrous Fe(III) oxide that exhibits a stoichiometry near $Fe_2O_3 \cdot H_2O$. EXAFS experiments were performed on ferrihydrite samples that had been aged for 65 h at 25°C and pH 6, after which the pH was adjusted to 5 or 5.5 and held for a further 24 h before adding U(VI). There were two samples made with U/Fe molar ratios of 0.044 and 0.077. Data, collected over a k-range of 3–16 $Å^{-1}$, required three U–O and one U–Fe shells to obtain the best fit. The results, using integral coordination numbers for the U–O fits, were two axial O at 1.80 Å, three equatorial O at 2.34 Å, two O at 2.52 Å, and about 0.5–1 Fe at a distance of approximately 3.4 Å. The authors conclude from their fits that the O at 2.52 Å is an inner-sphere O sorbed to the ferrihydrate surface. The Fe is coordinated in a bidentate fashion with the U, and, within a 10% error margin, there are no sorbed multinuclear uranyl complexes. These results are very similar to those reported in the previous study (Manceau *et al.*, 1992), although the latter study shows a split equatorial oxygen shell. The EXAFS results, supported by model simulations, suggest that the major U(VI) species at the ferrihydrite surface in the acidic pH range is an inner-sphere, bidentate complex that involves two surface hydroxyls of an Fe octahedral edge and the uranyl cation. Later work on very similar samples (Reich *et al.*, 1998b) failed to confirm the split oxygen shells at 2.34 and 2.52 Å, but instead found a single shell with five O coordinating at 2.36–2.39 Å

with a large Debye–Waller factor, consistent with the earlier work (Manceau *et al.*, 1992). Despite the absence of evidence for a split equatorial oxygen shell, inner-sphere complexation was proposed (Reich *et al.*, 1998b), and the authors noted that the difference in the equatorial oxygen coordination cannot be explained by the shorter *k*-range of their data.

Uranium uptake was studied from solutions at various pH values in the presence of the iron-bearing mineral phases goethite, lepidocrocite, and mackinawite (Moyes *et al.*, 2000). Refinements of EXAFS data show the U coordination at the surface to be very similar to those reported previously for U bound to other Fe–O and Fe–S mineral surfaces (Waite *et al.*, 1994; Reich *et al.*, 1998b). Binuclear, bidentate surface complexes are present together with monodentate, mononuclear coordination to the structural sulfate for the $FeSO_4$ oxide, schwertmannite (Walter *et al.*, 2003).

The EXAFS results from uranyl adsorbed on HFO and other mineral samples, together with modeling, show that the adsorbed complex is a unique product of the coordination environment at the surface, and appears independent of the predominant U(VI) speciation in solution, as was previously suggested (Waite *et al.*, 1994). A diffuse double-layer, two-site model with two proposed surface species provided excellent agreement with all data over a range of pH, U(VI) concentration, and two dissolved CO_2 concentrations. This conclusion contradicts several previously published modeling approaches to uranyl surface speciation (Hsi and Langmuir, 1985).

It has been previously reported that dissolved carbonate, ubiquitous in groundwater, plays a crucial role in the distribution of U(VI) between solution and Fe oxide surfaces (Ho and Doern, 1985; Hsi and Langmuir, 1985). EXAFS studies have focused on the molecular influence of carbonato complexation on U sorption onto Fe oxide surfaces. U complexed to ferrihydrite shows a U–C distance of 2.93(2) Å (Reich *et al.*, 1998b), which matches the U–C distance previously reported for a bidentate coordination of the CO_3^{2-} group to uranyl (Coda *et al.*, 1981; Allen *et al.*, 1995), and is consistent with the proposed formation of $(\equiv FeO_2)UO_2CO_3^{2-}$ (Waite *et al.*, 1994), an inner-sphere structure. U coordinated to hematite shows a similar behavior (Bargar *et al.*, 1999a,b). EXAFS fits indicate that U(VI) has five to six equatorial oxygens. Since two of these should be hematite-surface oxygens, it is argued that there are at most two carbonate ligands and the complex should have a composition similar to $FeO_2UO_2(CO_3)_x$, where $x \leq 2$. The absolute coordination numbers for carbonate in all samples imply that $\geq$ 50% of adsorbed U was complexed, even at pH 4.75. This finding contradicts predictions that U(VI)–carbonato ternary complexes should predominate only above pH 6 (Waite *et al.*, 1994). In addition, at pH values $\leq$ 6.5, there was no evidence from the EXAFS data for second-neighbor U(VI), indicating that the adsorbates were monomeric (Bargar *et al.*, 2000).

Also ubiquitous in the environment is the citrate anion. EXAFS was used to characterize the coordination environment of uranyl adsorbed onto goethite in

the presence of citrate under aqueous conditions where uranyl is strongly sorbed (Reddon *et al.*, 2001). A PCA showed that two major constituents should account for all the data. Unlike other Fe-mineral adsorption studies, there was no evidence of a Fe-neighbor in the U EXAFS. The authors concluded that the adsorption of uranyl does not follow a simple, stoichiometric relationship between the total U and citrate in the sample, and that under the conditions employed the adsorption of citrate on goethite appears to be favored over the formation of a uranyl–citrate–goethite complex.

In addition to the adsorption of uranyl onto mineral phases, EXAFS structural data were reported for U trapped in Fe-rich gels that are formed during the oxidative weathering of a granitic U deposit in the context of acid-mine drainage (Allard *et al.*, 1999). These natural samples, from the Massif Central in France, were in water that was close to saturation with respect to amorphous silica and crystalline-hydrated U-hydroxides and silicates. This effort addressed the elementary processes implied in U sorption and the trapping mechanism of U by natural short-range ordered phases. They investigated samples obtained at the fissure outlets on the walls of the galleries. These include hydrated amorphous products that are referred to as gels. XANES data confirm that the U was found to be present as hexavalent uranyl. The EXAFS on the Fe-rich gels found that uranyl is mainly present either as an outer-sphere complex or as an inner-sphere complex unresolved by EXAFS. No U–Fe, U–Si/Al, or U–U interactions were evident from the gel samples. The absence of U–Fe contributions to the data, despite the high affinity of uranyl for hydrous Fe oxides, suggests that U may be trapped in a two-step process involving the early complexation of U and Si/Al followed by the transport of Fe as ferrous in fissure water, with the ultimate precipitation of Fe in Si/Al-containing solutions at a redox front.

Green rusts, which are mixed Fe(II)/Fe(III) hydroxides, are formed by a number of abiotic and biotic processes under circumneutral to alkaline conditions in suboxic environments. The interaction of hydroxysulfate green rust, in which SO_4^{2-} is an interlayer anion was studied to examine its influence on the redox behavior of U(VI) (O'Loughlin *et al.*, 2003). L_3-edge XANES spectra show that U(VI) was readily reduced to U(IV) at a pH of 7.3 in the presence of green rust. EXAFS data indicate an average U local environment similar to that in UO_2. The decreased FT amplitude in the green rust sample compared to a UO_2 standard probably indicates small particle size and/or increased disorder.

The co-precipitation of uranium with iron-oxide minerals was studied with a series of co-precipitates with mole fractions of U in the range of 0.35–5.4% (Duff *et al.*, 2002). Although the XANES spectra are consistent with U(VI), EXAFS results show U to be in a highly distorted environment, in agreement with XRD, FT-infrared, XANES, and luminescence studies. Fits to the data for samples with <1 mol% U indicate no axial O, instead there are about four O at 2.21–2.36 Å. The model fits also indicate that at least one Fe atom exists in the uranium second-coordination shell at 3.19 Å. However, details of the fit suggest that there are multiple shell environments. Overall, the results are interpreted as

consistent with the incorporation of U(VI), minus the dioxo coordination, into the Fe oxides. This situation does not apply for co-precipitated samples with > 1 mol% U, which exhibit uranyl coordination and evidence of a second shell U backscatterer. These data are consistent with XRD, FT-infrared and luminescence data, which taken together show evidence of a U(VI) oxide hydrated phase such as schoepite, $UO_2(OH)_2 \cdot 2H_2O$.

There have been few reports of synchrotron studies centered on the sorption of transuranics onto Fe-bearing mineral phases. Despite its low affinity for complexation, Np(V) has been reported to sorb onto mineral surfaces with the decreasing affinity: calcite > goethite >> $MnO_2 \approx$ clays. The sorption of Np(V) onto these phases may involve its reduction to yield the much less soluble Np^{4+}, which has much high binding affinities and generally lower solubility. An early study of Np(V) on an iron-bearing mineral involved goethite, which has fully oxidized Fe (Combes *et al.*, 1992). XANES spectra confirm the presence of neptunyl groups. Fitting the EXAFS data results in 2.2 O at 1.85 Å and 5.5 O at 2.51 Å for Np adsorbed onto goethite, compared with the fit obtained from Np (V) in solution of 1.6 O at 1.83 Å and 5.2 O at 2.52 Å. This coordination environment for solution Np(V) compares with more recent comparative studies of Np coordination in solution, which are listed in Table 28.4. The only observed difference between the spectra obtained directly from solution and the goethite-sorbed spectrum is the presence of high-amplitude structure between 2.5 and 4 Å in the FT of the latter. Although these data may indicate Np–Fe interactions, the short *k*-range prohibits a full analysis. The authors claim that their data rule out diffusion into the solid and precipitation or coprecipitation of ordered solids onto the goethite surface. A more recent study (Moyes *et al.*, 2002) looked at solution Np(V) sorption onto microcrystalline mackinawite (FeS) at pH values in the range 7–8 and 3, and Np solution concentrations of 0.27, 0.68, and 2.74 mM. XANES spectra indicate limited sorption coupled with a reduction to Np(IV) that is confirmed by EXAFS. The coordination environment of Np in all samples is indistinguishable, with four O at 2.25 Å, three S at 2.63 Å, two Fe at 3.92 Å, and six Fe at 4.15 Å. The absence of two axial O atoms at about 1.85 Å supports the XANES finding for the reduction of Np(V). The short Np–S distances suggest a direct coordination with mineral surface S.

28.3.4 Phosphates

The phosphate class of minerals are made up of $(MO_4)^{3-}$ units in which M^{5+} can be P, As, Sb, or V (Deer *et al.*, 1992). Although apatites are the most common subclass of the phosphates, monazites are important here because of the insolubility of rare-earth and actinide phases. Thorium and uranium are common impurity phases in monazite.

Uranium sorption on the surface of hydroxyapatite, $Ca_5(PO_4)_3OH$, was studied as a removal mechanism for heavy metals from groundwater, either

by precipitating as a phosphate or by ion-exchange for Ca^{2+} (Fuller *et al*., 2002). Samples with less than 4700 ppm surface-sorbed uranium(VI) were studied by EXAFS and found to have the standard axial dioxo coordination. In addition, a broad equatorial shell was observed that, for two of the three samples studied could not be resolved by the fit. The single, unresolved shell was fit to a distance of about 2.313 Å by employing large Debye–Waller factors and fixing the coordination number to six. The most concentrated sample (4700 ppm) showed a resolvable two-shell equatorial coordination with 3.6(6) O at 2.338(8) Å and 2.1(2) O at 2.51 Å. Two of the three samples also had U–Ca interactions that fit to about one Ca at 3.8 Å, a distance consistent with bidentate edge sharing and/or monodentate corner-sharing coordination between the equatorial oxygens of the uranyl ion and the Ca–O polyhedra on the hydroxyapatite surface. In contrast, the U(VI) coordination environment is inconsistent with its incorporation into the mineral phase. One of the samples, exposed to dissolved carbonate, showed a U–C interaction implying U–carbonate ternary complexes. There were also indications of a more distant coordination shell that was fit as either a Ca atom at 4.55 Å or a U atom at 4.09 Å, with no independent evidence presented that could distinguish between the two fits. As the uranyl coverage on the hydroxyapatite surface increased above 4700 ppm, the EXAFS spectra began to resemble that of a U(VI) phosphate, notably chernikovite, $(H_3O)_2(UO_2)_2(PO_4)_2 \cdot 6H_2O$. The uranyl uptake at the onset of chernikovite precipitation corresponds to a surface coverage of about 6% of a monolayer.

An independent study was also conducted on the incorporation of U(VI) into synthetic fluorapatite (Rakovan *et al*., 2002). XAS together with luminescence and diffuse reflectance were used to determine the local structure of U(VI) in a powder sample. The sample had a concentration of 2.3 wt% U. Optical luminescence data, including lifetime measurements, combined with diffuse reflectance data indicate that although the U appears hexavalent in the fluorapatite sample, it does not have the standard dioxo coordination environment. This finding is supported by U L_3-edge XANES spectra, which confirms that uranium is hexavalent. However, the XANES data do not show the small shoulder feature indicative of dioxo coordination about uranium (Hudson *et al*., 1995a), but instead are similar to the spectra observed for U(VI) in Li_4UO_5 (Locock and Burns, unpublished) and Np(VII) in solution (Williams *et al*., 2001). Both of these ions exhibit an unusual tetraoxo coordination environment of four short and two longer oxygen distances. This coordination environment is confirmed by a simple inspection of the U EXAFS data, which are also inconsistent with a dioxo coordination environment. An analysis revealed that U is coordinated to six equidistant oxygens at 2.06 Å. With respect to the host fluorapatite sample, the U EXAFS fit shows a similarity to the coordination environment of the Ca1 site (space group $P6_3/m$, No 176; Wyckoff position 4*f*; 3 symmetry) (Comodi *et al*., 2001). Attempts to fit the data assuming Ca2 substitution (Wyckoff position 6*h*, *m* symmetry) were unsuccessful. The finding of 6 oxygen at 2.06 Å is in agreement with the average U–O distances for

six-coordinate, tetraoxo- (Hoekstra and Siegel, 1964) or near-cubic (Bawson *et al*., 1956) coordination. This work clearly demonstrates that fluorapatite can accommodate large concentrations of U(VI) into the lattice, with a coordination environment that is very similar to that found in perovskites, another common mineral class. Therefore, the determination of significant uranium incorporation into fluorapatite may point to an important sequestration mechanism for high-valent actinides in the environment.

Uranyl sorption onto the lanthanide phosphates $LaPO_4$ and $La(PO_3)_3$ has also been studied as a function of pH (Ordonez-Regil *et al*., 2002). The study included pH values of 1, 2, and 3, which compare to the isoelectric point of about 4 for $LaPO_4$ and 3 for $La(PO_3)_3$. The fitted parameters for the EXAFS spectra from the two samples were statistically indistinguishable. In addition to the dioxo-shell, there were two equatorial O shells, with 2.4 O at 2.31 Å, and 1.8 O at 2.47 Å, distances consistent with bidentate, inner-sphere coordination. The observation of a U–P interaction at 2.74 Å is used to argue that the uranyl is complexed to a single surface phosphate group.

28.3.5 Natural soil samples

The understanding and prediction of actinide speciation in natural soil samples comes from a synthesis of the published studies of actinide speciation and coordination under laboratory conditions. The challenge encountered when characterizing naturally occurring samples is the length scale of potential inhomogeneities. Depending on their origins, soil samples can have fine grain sediments that present chemical inhomogeneities on the micron or smaller length scale. Micro techniques that have been used to study such samples, including scanning tunneling microscopy (STM) (Yanase *et al*., 2002) uranyl fluorescence (Joergensen, 1977) and micro-Raman (Allen *et al*., 1987; Biwer *et al*., 1990; Palacios and Taylor, 2000) that produce important, but limited, information about uranium speciation.

Until the development of specialized μ-XAS and μ-SXRF capabilities, synchrotron-based spectroscopic studies were limited by beam sizes on the order of mm^2 or larger. Various micro-focusing techniques have reduced the beam size to about 50×50 μm^2 or larger, depending on energy ranges and flux requirements. Unfortunately, the focusing optics work over limited energy ranges, so that for work on the actinide L_3-edges, XAS energy scans are limited to 200–300 eV, sufficient only for XANES spectroscopy. Nevertheless, information has been obtained by these μ-XAS techniques that have significantly broadened the knowledge of actinide speciation in these complex samples.

A conventional XAS study on uranium-contaminated soil samples showed the potential for XAS to contribute information necessary to the development of a rational remediation scheme (Morris *et al*., 1996). This study examined samples from the Fernald Environmental Restoration Management Company, a U.S. DOE facility that once served as one of the principal processing centers

for uranium. The soil matrix consists primarily of quartz, calcite, dolomite, and the clay minerals illite and chlorite, with the pH of the topsoils in the range of about 5.4–6.3 (Elless and Lee, 1994). Background levels of U in uncontaminated reference topsoils near the production facility are typically about 3–5 ppm. There were many different source terms for the contaminants including both aqueous waste and airborne particulate. U concentrations from production range from about 10 to 8000 ppm at pH values of 7–8.5. Only about the top 0.25–0.3 m were contaminated.

XANES studies of both bulk and size-selected samples showed that most of the U exists in the hexavalent oxidation state, a finding that was confirmed by EXAFS. EXAFS data showed that the equatorial uranyl coordination varied significantly between samples and indicated variation in speciation. Independent optical, microscopy, and diffraction (Elless and Lee, 1994) data indicated the presence of autunite-like, $Ca(UO_2)_2(PO_4)_2 \cdot 2–6H_2O$, and schoepite-like, $UO_3 \cdot 2H_2O$, phases in the samples, consistent with the variation in EXAFS coordination. The goethite (FeOOH) that is naturally present in the soil should require U(VI) if equilibrium is reached because the Fe(III)/Fe(II) reduction potential is considerably lower than the corresponding U(VI)/U(IV) potential. The XAS used in this study, together with other spectroscopies, confirmed that 75–95% U was hexavalent. Based on this speciation, the authors were able to make specific recommendations about site remediation, including the need for near-term action based on the solubility and mobility of U(VI). A later study, in which U was added to natural subsurface soil samples from Hanford, SRS, and Oak Ridge produced similar results (Bostick and Fendorf, 2002).

Micro-XAS and synchrotron X-ray fluorescence (SXRF) studies on soil and sediment samples from Fernald and the Savannah River Site (SRS) offer a different perspective (Bertsch *et al.*, 1994; Hunter and Bertsch, 1998). The samples from the SRS differ from those of Fernald in that the U contamination was discharged as aqueous waste. This study used a micro-focused synchrotron beam with spot sizes that varied from 50×50 to 300×300 μm^2. The focusing optics utilized limit the energy range over which data was collected to approximately 200–300 eV, which restricted spectra to the XANES region only. Under the experimental configuration employed, it was possible to simultaneously collect a full SXRF spectrum to provide specific information on associated elemental distributions that is coupled to speciation data from XAS. The objective of the study was to determine U speciation in localized regions within inhomogeneous samples. XANES of clay fractions from both sites indicated $> 90\%$ hexavalent U, with no evidence of spatial variability of the U speciation within the clay fraction. This result was expected because the beam size was much bigger than individual clay particles and was consistent with the large number of size-fractionated sediment samples from SRS even though some of these latter samples were collected in seasonally reduced environments from wetland areas. No observation of significant biotic or abiotic U reduction was observed, as had been previously suggested (Lovley *et al.*, 1991; Nagy *et al.*, 1991), from samples

with high organic content that were in reducing environments. In contrast, sand and sediment fractions showed significant spatial variation using a 50 μm beam. The XRF signal was monitored, looking for areas concentrated in U, and then XANES spectra collected. Two types of populations were discernable: (1) those highly enriched in U and depleted in other elements such as Fe and Mn. For Fernald soil samples, U-rich regions were often relatively enriched in Ca, Cu, and Zn, whereas for SRS sediment these regions were highly enriched in Ni, and (2) U was concentrated and co-associated with regions relatively enriched in Fe and Mn. The U-rich region represented about 25% of the observations and may represent discrete U-containing phases either originally deposited as a component of the source term, or subsequently precipitated as a secondary phase. The zones of lower U concentration may represent either U co-precipitated with or sorbed to the Fe, Al, and Mn oxyhydroxides indigenous to the samples. XANES data, obtained using a 50 μm beam, from various regions within the sand fraction of Fernald soils provided evidence of varying oxidation states. Two of the 22 regions sampled showed predominantly U(IV) whereas other regions showed U(VI). There appeared to be discrete regions of U(IV) surrounded by a larger number of U (VI)-containing particles or surface-associated U(VI) phases. In contrast, when operating with a beam size of 300 μm, there was no evidence of pure or predominantly U(VI) speciation because of spatial averaging, pointing out the clear advantage of microprobe studies of natural, spatially inhomogeneous samples. The sand fractions from SRS did not display spectral differences indicative of varying oxidation states and were consistent with U(VI). However, post edge features indicated significant differences in the coordination environments within various regions of the sample.

During the 1999 global conflicts in the Balkan states, ammunitions were expended containing large amounts of depleted uranium (DU) that remains as an environmental pollutant with unknown health risks (Fetter and von Hippel, 1999; Priest, 2001; Bleise *et al.*, 2003). A series of studies was devised to investigate the oxidation state of particles dispersed into the geosphere in order to assess the fate and transport of this introduced pollutant (Shaughnessy *et al.*, 2003). The samples used in the analyses were collected at Ceja Mountain, Kosovo. Analytical results revealed U in soils with concentrations exceeding 2–3 ppm. Scanning electron microscopy (SEM) showed that most of the particles were present in the respiratory fraction, that is less than 5 μm (Danesi *et al.*, 2003). Micro-XANES data from the samples, obtained over an energy range of 300 eV using an X-ray beam spot size of 20×20 μm^2, were compared with U standards. SXRF data indicated the simultaneous presence of U and Ti, in accord with other analytical techniques and the known sample histories. The U L_3-edge data from the samples indicated that the U was oxidized, i.e. that there was no metal present. Depending on sample details, the U was consistent with either tetravalent U, as UO_2, or U_3O_8, or mixed samples. Hexavalent U was not observed. This finding is interpreted as DU particles with tetravalent

cores and oxidized surfaces, indicating weathering. This study revealed important factors for further assessing the environmental and health impacts of munitions-generated depleted U.

Elevated levels of U occur in natural soils and evaporation ponds that are associated with agricultural irrigation activities in the southwestern U.S. Evaporation ponds are periodically filled and evaporated to dryness, a process that can significantly influence redox processes. Most soils in the area are derived from marine Cretaceous shale that is known to contain high levels of U, with total concentrations as high as 280 ppm. A synchrotron-based study has been published that focuses on natural uranium speciation in evaporation ponds located in the San Joaquin Valley (SJV), CA (Duff *et al.*, 1997). Sediment samples, obtained from depths of 0–5 cm, were collected on two different occasions, one when the pond was nearly dry and the other when it was partially filled with drainage water. Suspension pH and Eh measurements were obtained at the time of sampling. There were no observable trends in U concentration with depth of sample, however the aqueous concentrations of U(IV) decreased with increasing Eh whereas dissolved U(VI) concentrations increased greatly with increasing Eh.

Micro-XANES data were obtained over a 130 eV range with a $200 \times 200\ \mu m^2$ beam size and SXRF data were collected at the U L_3-edge energy. XANES spectra were fitted using those obtained from standard spectra to assess relative ratios of reduced to oxidized U. These data showed that the amount of reduced U relative to oxidized U increases with increasing sample depth. The deepest samples (about 5 cm) showed that about 25% of the U in the measured samples was tetravalent. No changes were observed in the U concentration as the beam was scanned across the sample. Whereas the samples did not appear to contain any U hotspots, it should be noted that the particle sizes less than 2 μm were considerably smaller than the beam size, which was about 200 μm. A scenario for the fate of U in the SJV evaporation pond was proposed based on XANES and SXRF data that were complemented by other analytical techniques. It was proposed that U enters the pond in the drainage water, probably as a carbonate anionic species. Some of the U is accumulated by algae that creates a biomass with reducing conditions in which U(VI) reduction takes place. The precipitation of mixed U(VI)/U(IV) in organic matter then brings the U into the sediment. Over time, with increasing burial, the increasingly anoxic environment further reduces the U(VI). As the ponds drain, the soil aerates and the reduced U is reoxidized, resolublized, and thus remobilized. A follow-up study was published that addressed samples obtained over a wider depth range, 0–40 cm (Duff *et al.*, 2000). Microprobe (300 μm^2 spot size) XANES measurements, over a 140 eV range, were used to infer the relative amount of U(VI) by comparing edge position with known standards. This study found that the relative percentage of U(VI) appeared to decrease with increasing sampling depth and correlated with a decreasing total organic content.

The power of synchrotron-based microprobe spectroscopies to provide unique speciation information was clearly demonstrated in a series of experiments designed to probe plutonium adsorbed to natural tuff samples from the Yucca Mountain site (Duff *et al.*, 1999a,b, 2001). Tuff is rock composed of compacted volcanic ash that varies in size from fine particulate to gravel. These studies were performed to assist in the modeling of Pu speciation and groundwater transport in the event of a release of stored radioactive waste into the environment. The solubility of Pu in groundwater varies greatly, with 3+ and 4+ states being significantly more sorptive and less soluble than their higher valent counterparts. This discrepancy occurs because the higher valent ions form dioxo moieties, which have lower overall ionic charges. Under acidic conditions, Pu(v) undergoes disproportionation, to form Pu(iv) and Pu(vi), whereas in neutral to basic oxic solutions $Pu(v)O_2^+$ dominates speciation. The synchrotron microprobe studies were designed to determine what Pu species are adsorbed to natural tuff samples using spatially resolved μ-SXRF to determine Pu distribution and μ-XANES to determine oxidation states. All oxidation states of Pu have been reported to sorb to smectites and iron- and manganese-bearing oxyhydroxides (Keeney-Kennicutt and Morse, 1985; Sanchez *et al.*, 1985). A question addressed by these studies is whether minerals, particularly those with redox-active surfaces, can influence the redox chemistry of Pu in solution. The tuff samples, analyzed by X-ray diffraction, were predominantly zeolitic phases, specifically clinoptilolite 80 wt%, smectite 2%, opal 8%, feldspar 7%, and quartz 3%. Further work on the smectite isolates showed them to contain rancieite, a mineral with mixed manganese content, (Ca, Mn^{2+}) $Mn_4^{4+}O_9 \cdot 3H_2O$.

Information on the average oxidation state of sorbed Pu on tuff was obtained on the spatial scale of about 140 μm^2. The Pu-sorbed samples were prepared using 10^{-4} M, $^{239}Pu(v)$ spiked, synthetic groundwater meant to mimic deep tuffaceous aquifers such as those found below Yucca Mountain. About 92–98% of the initial Pu(v) in solution was sorbed to the samples. SXRF was done for elements with absorption energies below 18.5 keV. The problem in resolving the Pu and Sr signals was circumvented by obtaining one elemental map just below the Pu L_3-edge and another just above the edge. The Pu elemental map was then obtained by subtracting the images. Contrary to expectations based on previous work (Triay *et al.*, 1997), the mapping showed that Pu is predominately associated with manganese oxides, specifically rancieite, and smectites but not with iron oxides. Fractures and pore spaces from Yucca Mountain tuff samples contain highly reactive surfaces that can sorb a variety of differently charged and sized ions from fracture- and pore-space fluids. Rancieite comprises less than a percent of the mineral distribution in the tuff, but its presence at primary flow paths makes it highly accessible to dissolved species in the groundwater (Duff *et al.*, 2001). Several other elements in addition to Pu were co-associated with the manganese oxide and not with hematite. It is postulated that the iron mineral surfaces appear to be passivated and thus inaccessible to sorption.

Why the iron oxide, and not the manganese oxide, surfaces were passivated is not understood. Modeling and surface calculations based on experimentally determined concentrations suggest that multiple binding sites are present on the Mn–O/smectite phase.

μ-XANES was obtained from the same samples at two different 10×15 μm^2 spots that appeared to contain the highest level of Pu as determined by the SXRF mapping. Unfortunately, XANES was not definitive in determining the oxidation state. Although the Pu L_3-edge position indicates the presence of primarily Pu(VI), the post edge feature associated with multiple-scattering from the plutonyl was not observed. The FT of a short EXAFS spectrum ($k_{max} = 8$ Å^{-1}) did not show evidence of the two-shell first coordination sphere that is expected for plutonyl coordination (Duff *et al*., 1999b). A single peak at 1.65 Å (uncorrected for phase shift) was observed but not fit. In addition, there was no evidence of a Pu–Pu interaction, which would have signaled Pu precipitation on the tuff surface. The authors conclude only that there may have been some oxidation of their Pu upon sorption to the Mn^{4+}-rich phase. It should be noted that tuff samples have been shown to oxidize Ce(III) to Ce(IV) (Vaniman *et al*., 2002), an oxidation that was attributed to its association with rancieite, which contains an oxidized fraction of Mn.

These seminal papers clearly demonstrate the importance of a molecular level understanding of sorption on natural samples. That Pu should sorb preferentially to a Mn-oxide phase was not expected. Such information is very important in modeling actinide migration through the geosphere. In addition, it supports previous findings that actinide sorption is governed by the solid–water interface rather than solution speciation (Waite *et al*., 1994). The results show that predictive remediation requires a more comprehensive understanding of Mn–Pu interactions.

Toward this end, a study was undertaken (Shaughnessy *et al*., 2003) of interfacial reactions between aqueous Pu(VI) species and Mn oxyhydroxide mineral surfaces, notably manganite (MnOOH) and hausmannite (Mn_3O_4), which serve as representative examples of Mn phases typically found in the vadose zone. Note that manganite has a rutile-related structure, with trivalent Mn whereas hausmannite is a spinel-related structure with mixed di- and trivalent Mn. These two phases were from commercial stock and size selected for particles in the range of 63–212 μm. The pH of the point of zero surface charge (pH_{pzc}) was determined to be 7.4(3) for manganite and greater than 10 for hausmannite. Sorption studies were done as a function of pH over the range 3–10, a function of Pu concentration, and as a function of solution exposure time at a fixed pH. Pu solution concentrations ranged from 1×10^{-7} to 1×10^{-4} M. There was an initial rapid sorption step that occurred within the first 24 h of contact, followed by a much slower sorption process. This two-step process for actinide adsorption onto mineral phases has been previously reported (Keeney-Kennicutt and Morse, 1985; Waite *et al*., 1994). All XAS data reported in the Mn work were limited to samples that had a 24 h contact time with the soak-Pu

solutions. The sorbed Pu oxidation states were determined by a combination of optical absorption methods and XAS. A comparison of the Pu L_3-edge XANES data from the mineral-adsorbed phase with those from oxidation-state specific solution phases showed that the Pu sorbed to the Mn phases had been reduced from Pu(VI) in the initial solutions to Pu(IV) on the sorbed surface. Optical spectra on the remaining solutions determined the presence of Pu(V). In other words, all of the initial solution phase Pu(VI) had been reduced to either Pu(V), which remained in solution, or Pu(IV), which remained sorbed on manganite or hausmannite. There was no reduction observed for a blank Pu(VI) solution over the same time frame. The reductant in this redox reaction was not clearly evident from the experiment, but the authors conjecture that there may have been dissolved Mn(II) in solution. It should be noted that the reduction of Pu(VI) observed in this study is in contrast to the work on natural tuff, in which Pu (V) was seen to oxidize (Duff *et al*., 1999a,b, 2001). The similarity in redox couples for Pu(IV), Pu(V), and Pu(VI) clearly complicates the chemistry in these redox-active mineral systems. EXAFS data from the same Mn samples (Shaughnessy *et al*., 2003) were analyzed to determine the Pu coordination onto the mineral surfaces. The data were analyzed over a short *k*-range (2.5–10 $Å^{-1}$), significantly limiting the allowable number of variable parameters in the fitting. The data do not indicate dioxo coordination of the Pu, supporting the XANES interpretation of Pu reduction to tetravalent. The best fit was consistent with a single O shell at distances of 2.28–2.36 Å and with coordination numbers in the range of 7–9. The values may vary with the pH of the soak solution used for the sorption experiments. The fitted distances compare well with those expected for Pu(IV)–O interactions, as exemplified by the 2.337 Å one found in PuO_2 (Haschke *et al*., 2000). In addition, Pu–Mn interactions were observed at about 3.37 Å for all samples, indicating that, like other adsorbed actinides, the sorbed Pu has an inner-sphere coordination with the mineral surface. These results support the finding that Mn-based mineral phases may serve to sequester Pu under natural groundwater conditions.

28.3.6 Bacterial interactions

It has been recently realized that microbes can actively influence actinide chemistry in the environment. Although much less studied than processes involving inorganic constituents, biotic interactions can have a marked influence on actinide speciation. Microbes are ubiquitous in the environment and therefore their influence must be included when developing predictive modeling for actinide fate and transport. Microbial processes can cause either mobilization or immobilization of radionucludes, that is actinides may be stabilized in solution or precipitated by direct processes, such as respiration, or indirect processes, such as the biotic modification of solution constituents.

XAS is developing into a cornerstone technique for discerning the influence of bacteria on actinide speciation, as indicated by the published work referenced in

Table 28.13. XAS is often used together with other physical techniques, such as optical and/or infrared spectroscopies, X-ray diffraction, microscopy (TEM, SEM), EDS (energy dispersive X-ray spectroscopy). These results augment the standard chemical analyses, such as titrations and solvent extraction. The advantage afforded by XAS is that it can probe metal-ion speciation *in situ*, that is in the presence of bacterial cells, cell growth media, and other metal-ions, with no necessity for chemical pretreatment. Its sensitivity to oxidation state is particularly important for probing redox effects of microbial interactions. Among its most significant disadvantages are its sensitivity, often requiring ppm or higher concentrations for meaningful data acquisition, and the propensity for beam-induced redox chemistry (Skanthakumar *et al.*, 2004) that can vitiate speciation, especially at low metal concentrations.

There are several questions that arise concerning microbial influence on actinide speciation. These all center on solubility and transport issues, and include precipitation, adsorption to the bacterial surface, incorporation into the cell, and solubilization of mineral phases. Precipitation can occur either through a change in redox state or through chelation. Generally, the higher oxidation states, including U(VI), Np(V), and Pu(V), (VI) are soluble in acidic and near-neutral pH, whereas their tetravalent analogs are relatively insoluble. Therefore, processes that control oxidation state are particularly important to quantify. Compounds or ions in solution may be used as electron acceptors in energy metabolism, a process referred to as dissimilative metabolism. The reduced species is excreted in the environment. Microbes are known to involve metal-ions, such as Fe(III) or Mn(III,IV), directly in their respiratory processes as electron acceptors. Aerobic respiration involves O_2 as the electron acceptor. Some microbes are capable of anaerobic respiration, in which they use nitrate, sulfate, carbonate, ferric iron or even certain organic compounds as the electron acceptor. Because these ions have lower reduction potentials than O_2, less energy is released. However, the use of alternate electron acceptors in their respiratory process allows microorganisms to live in environments that contain too little oxygen to support life.

Dissimilatory metal-reducing bacteria (DMRB) are able to couple the oxidation of organic matter to the reduction of Fe(III) or Mn(III/IV). Under anoxic conditions, DMRB have been shown to readily reduce U(VI) to precipitate UO_2 solid (Lovley *et al.*, 1991; Gorby and Lovley, 1992). XANES spectroscopy was used to probe U(VI) reduction, either as an aqueous species $[UO_2(CO_3)^{4-}_{3(aq)}]$ or as metaschoepite $[UO_3 \cdot 2H_2O_{(s)}]$ (Fredrickson *et al.*, 2000). The results showed that the DMRB bacterium *Shewanella putrefaciens* reduced UO_2^{2+} in complex mineral suspensions via a combination of direct enzymatic or indirect mechanisms to insoluble U(IV) species. U reduction occurred whether the U(VI) was in solution or associated with a solid phase. The studies further showed that *S. putrefaciens* could reduce U(VI) in complex suspensions that included Fe(III) as an alternative electron acceptor, despite the lower standard potential of the U (VI) couple, as shown in Table 28.1. Further experiments, involving Mn K-edge

Table 28.13 *Published studies of actinide-ion sorption onto bacterial surfaces. These studies involve actinide redox speciation studies and efforts to define active binding sites on bacterial surfaces.*

	Strain	*Gram*	*Growth conditions*	*pH*	*Comment*	*Metal*	*References*
Clostridium sp.	ATCC 53464		anaerobe	6.8		U(VI)	Francis *et al*. (1994) Francis *et al*. (2002) Francis (2002)
Clostridium sp.			anaerobe		inactive uranium mine	U(VI)	Suzuki *et al*. (2003)
Pseudomonas fluorescens	ATCC 55241		aerobe	6.1	citrate, Fe(III) complexes	U(VI)	Dodge and Francis (1997)
Halomonas sp.	WIPP1A	+	(an)aerobe	about 9.1		U(VI)	Gillow *et al*. (1999) Francis *et al*. (2000)
Desulfovibrio desulfuricans	ATCC 29577		anaerobe	6.1		Np(V)	Soderholm *et al*. (2000)
Shewanella putrefaciens	CN32		aerobe	about 7		U(VI)	Fredrickson *et al*. (2000)
Bacillus cereus	JG-A30 4415	+	aerobe		vegetative cells, spores	U(VI)	Hennig *et al*. (2001a)
Bacillus sphaericus	JG-A12 9602	+	aerobe			U(VI)	Hennig *et al*. (2001a)
Acidithiobacillus ferrooxidans				2		U(VI)	Merroun *et al*. (2002a)
Shewanella putrefaciens	CN32		anaerobe		Mn(III,IV)	U(VI)	Fredrickson *et al*. (2002)
Pseudomonas fluorescens	ATCC 55241	–		variable		Np(V)	Songkasiri *et al*. (2002)
Bacillus sphaericus	ATCC 14577	+	aerobe		vegetative, heat killed cells, spores	U(VI)	Panak *et al*. (2002b)
Bacillus sphaericus	ATCC 14577	+	aerobe	4.4		Pu(VI)	Panak *et al*. (2002a)
Acidithiobacillus ferrooxidans	D2				recovered from U mining waste	U(VI)	Merroun *et al*. (2002a)
Pseudomonas stutzeri	DSMZ 7136 DSMZ 5190					U(VI)	Merroun *et al*. (2002a)

Table 28.13 (*Contd.*)

	Strain	*Gram*	*Growth conditions*	*pH*	*Comment*	*Metal*	*References*
Pseudomonas migulae	CIP 105470					U(VI)	Merroun *et al*. (2002a)
Desulfosporosinus ssp.		+	anaerobe		inactive uranium mine	U(VI)	Suzuki *et al*. (2002, 2003)
Bacillus subtilis				variable		U(VI)	Kelly *et al*. (2002)
Shewanella putrefaciens	CN32		aerobe anaerobe			U(VI)	Brooks *et al*. (2003)
Desulfovibrio desulfuricans			anaerobe			U(VI)	Brooks *et al*. (2003)
Geobacter sulfurreducens			aerobe			U(VI)	Brooks *et al*. (2003)

XANES, showed that the presence of Mn(III/IV) oxides may impede the reduction of U(VI), by *S. putrefaciens* (Fredrickson *et al*., 2002), in soils. Independent studies use U L_3 XANES to determine that *Desulfosporosinus* ssp, a Gram positive sulfate reducer, is able to reduce U(VI) to U(IV) (Suzuki *et al*., 2002, 2003). These studies used organic substrates to create anaerobic conditions to stimulate growth of *Desulfosporosinus* ssp in natural U-contaminated sediments from the Midnite Mine, WA, USA. After 1 month, the U concentrations were reduced from 20 to 0.3 ppm. EXAFS-determined coordination numbers were used to infer an average particle size of about 1.5 nm. XAS, together with TEM data show the particles to be uraninite. The authors conclude that the small particle size of biogentic UO_2 may not significantly limit its mobility. This has important implications for the use of bacteria in environmental remediation.

A review of the standard reduction potentials listed in Table 28.1 shows that both Np(V) and Pu(VI), (V) are more easily reduced than is U(VI), suggesting that microbial reduction may play an important role in the aquatic environmental chemistry of dissolved or sorbed actinide ions. In addition, bacteria can be viewed as generating a biopotential through their surfaces and through enzymes, such as siderophores, that they excrete into their environment. In this way, bacteria compete with dissolved ions to influence the solution's effective reduction potential, or Eh. There are very few studies focused on their microbial reduction, even though Pu(VI) and (V) are both more easily reduced than Fe(III). Published work investigating Np(V) reduction by *Desulfovibrio desulfuricans* (Soderholm *et al*., 2000) and by an anaerobic methanogenic microcosm (Banaszak *et al*., 1999) indicate that Np(V) is reduced abiotically in the growth medium necessary to sustain the organism.

The solubility and mobility of actinide ions can also be significantly influenced by biosorption. In addition to living cells and spores, dead and decomposed cells are present in natural systems, and can play a role in complexation. Actinides can be complexed with the amino, carboxylate, hydroxyl, and phosphate functional groups that are present on the cell surface. These negatively charged groups are capable of complexation with actinide cations to form biocolloids that have their own chemistry and transport properties. EXAFS spectroscopy has been used to develop an understanding of the functional groups responsible for complexation. XAS studies of actinide biocolloid formation are largely limited to L_3-edge U data. EXAFS of biocolloids formed in brine by halophilic bacteria (WIPP 1A) indicate that bulk samples contain more than one U-containing phase (Francis *et al*., 1998). TEM and EDS analyses supported this result, showing that U was accumulated intracellularly in addition to being bound to the cell surface. In another study (Hennig *et al*., 2001a), Gram-positive strains of *Bacillus cereus* and *Bacillus sphaericus* were recovered from a U waste pile, the 'Haberlandhalde' in Germany. The vegetative cells and spores of these isolates were compared with cells and spores of two reference strains, *B. cereus* 4415 and *B. sphaericus* 9602. The structure of the spore coat is completely different from that of the cell wall. The studies showed that the

bacteria selectively accumulate a large variety of heavy metals, specifically these strains accumulate large amount of U. L_3- and L_2-edge XANES spectra obtained from all the bacilli samples were consistent with U(VI). The EXAFS parameters from all the samples, including both vegetative cells and spores, were very similar, indicating that a structurally similar U complex is formed in all cases. The structural parameters exclude the presence of hydrolysis species but coordination numbers and bond lengths compare well with inorganic 1:1 uranyl phosphate phases. U–P interactions at 3.61–3.63 Å in all samples, which are typical distances for monodentate-bound phosphate phases. After 8 weeks, vegetative cells of *B. sphaericus*, lysing cells, and the activity of enzymes lead to the release of $H_2PO_4^-$ that caused quantitative precipitation of bacterial U(VI) as $UO_2(H_2PO_4)_2$ (Panak *et al.*, 2002b). This complex differs significantly from those of the bacterial surface complexes. The results confirm that surface complexes are formed without metabolic activity.

Similar results were obtained from studies of U complexes formed by *Acidithiobacillus ferrooxidans* (Merroun *et al.*, 2002a), which accumulate U as phosphate compounds. EXAFS data, supported by EDX and infrared spectroscopy (Merroun *et al.*, 2002b) were used to suggest that U accumulates within extracellular polysaccharides and as dense granules in the cell cytoplasm. On the basis of these results it was suggested that these bacteria use polyphosphates to detoxify and remove U when it enters the cells and is present at toxic levels.

In order to quantitatively assess the effects of changing chemical conditions on actinide adsorption/desorption on bacterial surfaces, a surface complexation model for U complexation for Gram-positive cells has been developed (Fein *et al.*, 1997). This model treats surface complexation as a series of thermodynamic equilibria that are dependent on binding geometry and may be pH-dependent. XAS spectroscopy has been used to test this uranyl–bacterial surface speciation model (Kelly *et al.*, 2002). In general, the data are consistent with the model, although a large number of parameters were used to treat the EXAFS data.

Np(V) was determined to adsorb on the facultative, gram negative soil bacterium *Pseudomonas fluorescens* without significant reduction (Songkasiri *et al.*, 2002). The adsorption of 15–20% of the available NpO_2^+ onto the bacterial surface at pH 7 is contrary to expectations based on solution Np(V) chemistry. The situation is more complex for Pu. Sorption studies with Pu(VI) on aerobic soil bacteria showed the reduction of Pu upon complexation, as determined by optical absorption spectroscopy and solvent extraction techniques (Panak and Nitsche, 2001). Follow-up studies, employing XANES spectroscopy in conjunction with solvent extraction, showed that after 9 days of contact with *B. sphaericus*, 32(10)% of the Pu(VI) remained, whereas 28(12)% and 40(6)% were reduced to Pu(V) and Pu(IV), respectively (Panak *et al.*, 2002a). EXAFS data were used to show that Pu(VI) forms strong surface complexes with *B. sphaericus*. These complexes mainly involve phosphate groups, similar to earlier U work (Panak *et al.*, 2000). These results are consistent with a model of

the different interaction processes of Pu(VI) with aerobic soil bacteria (Panak and Nitsche, 2001). This process involves (i) the complexation of Pu(VI) with phosphate groups on the cell wall, (ii) reduction of Pu(VI) followed by the dissolution of Pu(V), and (iii) disproportionation of Pu(V) to tetravalent and hexavalent Pu, followed by the complexation of Pu(IV) with the biomass. These interactions may have important implications for the migration behavior of Pu in natural systems.

Overall, the role of bacteria on the chemistry of actinides and their impact on speciation and transport remains unclear. There is certainly evidence of actinide reduction and precipitation; it remains unclear if these small particles remain mobile through some biocolloid transportation mechanisms. In addition, the particles are so small that re-dissolution reactions may be important. The development of predictive models for the mechanisms of actinide complexation with bacterial surfaces (Fein *et al.*, 1997) and actinide redox reactions (Panak and Nitsche, 2001) are important steps toward a predictive understanding of bacterial influences on actinide mobility. XAS is playing a crucial role in the development and testing of these models.

28.4 FUTURE DIRECTION

XAS and μ-SXRF capabilities have proven to be important synchrotron tools applied to the study of actinide chemistry. The information obtained has significantly improved, and is still improving, our understanding of environmental actinide chemistry. The direction of future actinide studies is closely tied with the operation of existing synchrotrons and with the development of the so-called fourth generation facilities. The availability of new beamlines will open scientific vistas heretofore unavailable with regard to time, energy, and spatial resolution, including the study of dynamic processes and reactions with unprecedented temporal sensitivity; high-energy resolution measurements throughout the electromagnetic spectrum from the infrared through the visible, vacuum ultraviolet, and deep into the X-ray region; and microanalysis of materials on the nanometer length scale.

There are a variety of other synchrotron techniques that are currently under development and are beginning to find use for answering outstanding issues in environmental science (Fenter *et al.*, 2002). Although XAS and microprobe experiments are expected to continue playing a central role in discerning actinide speciation, several relatively new synchrotron techniques, including small-angle X-ray scattering (SAXS), high-energy X-ray scattering (HES), standing wave, and reflectivity measurements are expected to play a growing role in unraveling ever more complex problems posed by actinides in the environment.

Although it is always more convenient to conduct experiments in one's own laboratory than at a synchrotron radiation facility, conventional tube-sources

of X-rays do not provide properties, such as polarization and pulsed-time structure to name just two, that arise naturally from the continuum radiation produced at bending magnets and from the tuned radiation produced from insertion devices. Without exception, synchrotron light is a probe with which actinide science will advance in ways that would be impossible otherwise.

ACRONYMS, ABBREVIATIONS, AND SYMBOLS

An	actinide
Ar	aromatic/aryl functional group
ATCC	American-Type Culture Collection
B	empirical constant, 0.37, in Brown's BVS equation
B3LYP	hybrid Hamiltonian of Becke's 3 parameter exchange functional and correlation functional of Lee-Yang-Parr
BET	Brunauer-Emmett-Teller, adsorption method for surface area measurement
BVS	bond-valence sum
COSMO	conductor-like screening model
CPCM	conductive polarizable continuum model
CN	coordination number
DFT	density functional theory
DMRB	dissimilatory metal-reducing bacteria
DU	depleted uranium
e^-	electron
E	X-ray energy, eV
E_p	applied/controlled electrode potential, V
E°	standard electrode potential, V
E°'	formal electrode potential, V
E_0	energy threshold for k-space conversion, eV
ΔE_0	energy scale parameter
Eh	redox potential
EDS	energy dispersive X-ray spectroscopy
EDX	energy dispersive X-ray analysis
EXAFS	extended X-ray absorption fine structure
F	Faraday's constant
$F(k, r)$	back-scattering amplitude function
FEFF	effective curved-wave scattering amplitude, $F_{\text{eff}}(k, r)$, computer code
FT	Fourier transform
$\hbar$	Planck's constant
HES	high-energy X-ray scattering
HFO	hydrous ferric oxide

ICP-MS	inductively coupled plasma-mass spectrometry
IR	ionic radius/radii
k	photoelectron wave vector, $Å^{-1}$
λ_e	photoelectron wavelength
m	electron mass
MCD	magnetic circular dichroism
MP2	2^{nd} order Moller Plesset perturbation theory
n	number of electrons
N	coordination number
N_p	number of independent parameters
μ-SXRF	micro synchrotron-X-ray fluorescence
μ-XANES	micro X-ray absorption near-edge structure
$\varphi(k, r)$	backscattering atom phase function
$\varphi_c(k)$	central atom phase function
pH	negative log of the hydrogen ion concentration
PCA	principal component analysis
R	aliphatic/alkyl functional group
r	interatomic distance
R	gas constant
R_0	empirical radius parameter in Brown's BVS equation
$\Re_{ox}$	oxidized form of reagent
$\Re_d$	reduced form of reagent
σ	Debye–Waller factor
S_0^2	amplitude reduction factor
SJV	San Joaquin Valley
SRS	Savannah River Site
SEM	scanning electron microscopy
S/N	signal to noise
SAXS	small-angle X-ray scattering
SHE	standard hydrogen electrode
SXRF	synchrotron X-ray fluorescence
T	temperature
TEM	transmission electron microscopy
WIPP	waste isolation pilot plant
XANES	X-ray absorption near-edge structure
XAS	X-ray absorption spectroscopy
$\chi(k)$	EXAFS signal

ACKNOWLDEGMENTS

This work is supported by the U.S. DOE, OBES – Chemical Sciences, under Contract W-31-109-ENG-38.

REFERENCES

Aberg, M. (1970) *Acta Chem. Scand.,* **24**, 2901–15.

Aberg, M., Ferri, D., Glaser, J., and Grenthe, I. (1983) *Inorg. Chem.,* **22**, 3986–9.

Allard, T., Ildefonse, P., Beaucaire, C., and Calas, G. (1999) *Chem. Geol.,* **158**, 81–103.

Allen, G. C., Butler, I. S., and Tuan, N. A. (1987) *J. Nucl. Mater.,* **144**, 17–19.

Allen, P. G., Bucher, J. J., Clark, D. L., Edelstein, N. M., Ekberg, S. A., Gohdes, J. W., Hudson, E. A., Kaltsoyannis, N., Lukens, W. W., Neu, M. P., Palmer, P. D., Reich, T., Shuh, D. K., Tait, C. D., and Zwick, B. D. (1995) *Inorg. Chem.,* **34**, 4797–807.

Allen, P. G., Shuh, D. K., Bucher, J. J., Edelstein, N. M., Reich, T., Denecke, M. A., and Nitsche, H. (1996a) *Inorg. Chem.,* **35**, 784–7.

Allen, P. G., Veirs, D. K., Conradson, S. D., Smith, C. A., and Marsh, S. F. (1996b) *Inorg. Chem.,* **35**, 2841–5.

Allen, P. G., Bucher, J. J., Shuh, D. K., Edelstein, N. M., and Reich, T. (1997) *Inorg. Chem.,* **36**, 4676–83.

Allen, P. G., Bucher, J. J., Shuh, D. K., Edelstein, N. M., and Craig, I. (2000) *Inorg. Chem.,* **39**, 595–601.

Ankudinov, A. L., Conradson, S. D., de Leon, J. M., and Rehr, J. J. (1998) *Phys. Rev. B,* **57**, 7518–25.

Antonio, M. R., Teo, B. -K.,Cleland, W. E., and Averill, B. A. (1983) *J. Am. Chem. Soc.,* **105**, 3477–84.

Antonio, M. R., Soderholm, L., and Song, I. (1997) *J. Appl. Electrochem.,* **27**, 784–92.

Antonio, M. R., Soderholm, L., Williams, C. W., Blaudeau, J. P., and Bursten, B. E. (2001) *Radiochim. Acta,* **89**, 17–25.

Antonio, M. R., Williams, C. W., and Soderholm, L. (2002) *Radiochim. Acta,* **90**, 851–6.

Archer, M. D. (1989) *ACS Symp. Ser.,* **390**, 115–26.

Babu, C. S. Lim, C. and (1999) *J. Phys. Chem. B,* **103**, 7958–68.

Baes, C. E. and Mesmer, R. F. (1976) *The Hydrolysis of Cations,* John Wiley, New York.

Bailey, E. H., Mosselmans, J. F. W., and Schofield, P. F. (2004) *Geochim. Cosmochim. Acta,* **68**, 1711–22.

Banaszak, J. E., Webb, S. M., Rittmann, B. E., Gaillard, J. F., and Reed, D. T. (1999) *Mater. Res. Soc. Symp. Proc.,* **556**, 1141–9.

Bardin, N., Rubini, P., and Madic, C. (1998) *Radiochim. Acta,* **83**, 189–94.

Bargar, J. R., Reitmeyer, R., and Davis, J. A. (1999a) *Environ. Sci. Technol.,* **33**, 2481–4.

Bargar, J. R., Reitmeyer, R. L., and Davis, J. A. (1999b) *Abstr. Pap. Am. Chem. Soc.,* **217**, 143-NUCL

Bargar, J. R., Reitmeyer, R., Lenhart, J. J., and Davis, J. A. (2000) *Geochim. Cosmochim. Acta,* **64**, 2737–49.

Barnes, C. E., Shin, Y., Saengkerdsub, S., and Dai, S. (2000) *Inorg. Chem.,* **39**, 862–4.

Bawson, J. K., Wait, Z., Alcock, K., and Chilton, D. R. (1956) *J. Chem. Soc.,* **1956**, 3531–40.

Bernhard, G., Geipel, G., Brendler, V., and Nitsche, H. (1996) *Radiochim. Acta,* **74**, 87–91.

Bernhard, G., Geipel, G., Reich, T., Brendler, V., Amayri, S., and Nitsche, H. (2001) *Radiochim. Acta,* **89**, 511–18.

Bertagnolli, H. and Ertel, T. S. (1994) *Angew. Chem. Int. Edn. Engl.,* **33**, 45–66.

Bertsch, P. M., Hunter, D. B., Sutton, S. R., Bajt, S., and Rivers, M. L. (1994) *Environ. Sci. Technol.,* **28**, 980–4.
Biwer, B. M., Ebert, W. L., and Bates, J. K. (1990) *J. Nucl. Mater.,* **175**, 188–93.
Biwer, B. M., Soderholm, L., Greegor, R. B., and Lytles, F. W. (1997) *Mater. Res. Soc. Symp. Proc.,* **465**, 229–36.
Blaudeau, J. P., Zygmunt, S. A., Curtiss, L. A., Reed, D. T., and Bursten, B. E. (1999) *Chem. Phys. Lett.,* **310**, 347–54.
Bleise, A., Danesi, P. R., and Burkart, W. (2003) *J. Environ. Radioact.,* **64**, 93–112.
Bolvin, H., Wahlgren, U., Moll, H., Reich, T., Geipel, G., Fanghaenel, T., and Grenthe, I. (2001) *J. Phys. Chem. A,* **105**, 11441–5.
Bostick, B. C. and Fendorf, S. (2002) *Soil Sci. Soc. Am. J.,* **66**, 99–108.
Brannon, J. C., Cole, S. C., Podosek, F. A., Ragan, V. M., Coveney, R. M. J., Wallace, M. W., and Bradley, A. J. (1996) *Science,* **271**, 491–3.
Bratsch, S. G. (1989) *J. Phys. Chem. Ref. Data,* **18**, 1–21.
Breit, G. N. (1995) *Econ. Geol.,* **90**, 407–17.
Bridgeman, A. J. and Cavigliasso, G. (2003) *Faraday Discuss.,* **124**, 239–58.
Brooks, S. C., Fredrickson, J. K., Carroll, S. L., Kennedy, D. W., Zachara, J. M., Plymale, A. E., Kelly, S. D., Kemner, K. M., and Fendorf, S. (2003) *Environ. Sci. Technol.,* **37**, 1850–8.
Brown, I. D. (1981) in *Structure and Bonding in Crystals,* vol. 2 (eds. M. O'Keeffe and A. Navrotsky), Academic Press, New York, pp. 1—52.
Brown, I. D. (1987) *Phys. Chem. Miner.,* **15**, 30–4.
Brown, I. D. (1996) *J. Appl. Crystallogr.,* **29**, 479–80.
Brown, I. D. (2002) *The Chemical Bond in Inorganic Chemistry: The Bond Valence Model,* Oxford University Press, Oxford.
Burns, J. H., Baldwin, W. H., and Stokely, J. R. (1973) *Inorg. Chem.,* **12**, 466–9.
Burns, P. C., Ewing, R. C., and Hawthorne, F. C. (1997) *Can. Mineral.,* **35**, 1551–70.
Calas, G., Brown, G. E. Jr, Waychunas, G. A., and Petiau, J. (1987) *Phys. Chem. Miner.,* **15**, 19–29.
Carroll, S. A. and Bruno, J. (1991) *Radiochim. Acta,* **52–53**, 187–93.
Carroll, S. A., Bruno, J., Petit, J. C., and Dran, J. C. (1992) *Radiochim. Acta,* **58–59**, 245–52.
Charpin, P., Dejean, A., Folcher, G., Rigny, P., and Navaza, P. (1985) *J. Chim. Phys. Phys.-Chim. Biol.,* **82**, 925–32.
Chiang, M.-H., Soderholm, L., and Antonio, M. R. (2003) *Eur. J. Inorg. Chem.*, 2929–36.
Chisholm-Brause, C., Conradson, S., Eller, P. G., and Morris, D. E. (1992) *Mater. Res. Soc. Symp. Proc.,* **257**, 315–22.
Chisholm-Brause, C., Conradson, S. D., Buscher, C. T., Eller, P. G., and Morris, D. E. (1994) *Geochim. Cosmochim. Acta,* **58**, 3625–31.
Clark, D. L., Hobart, D. E., and Neu, M. P. (1995) *Chem. Rev.,* **95**, 25–48.
Clark, D. L., Conradson, S. D., Ekberg, S. A., Hess, N. J., Janecky, D. R., Neu, M. P., Palmer, P. D., and Tait, C. D. (1996a) *New J. Chem.,* **20**, 211–20.
Clark, D. L., Conradson, S. D., Ekberg, S. A., Hess, N. J., Neu, M. P., Palmer, P. D., Runde, W., and Tait, C. D. (1996b) *J. Am. Chem. Soc.,* **118**, 2089–90.
Clark, D. L., Conradson, S. D., Neu, M. P., Palmer, P. D., Runde, W., and Tait, C. D. (1997) *J. Am. Chem. Soc.,* **119**, 5259–60.

Clark, D. L., Conradson, S. D., Keogh, D. W., Palmer, P. D., Scott, B. L., and Tait, C. D. (1998) *Inorg. Chem.,* **37**, 2893–9.

Clark, D. L., Conradson, S. D., Donohoe, R. J., Keogh, D. W., Morris, D. E., Palmer, P. D., Rogers, R. D., and Tait, C. D. (1999) *Inorg. Chem.,* **38**, 1456–66.

Coda, A., Giusta, A. D., and Tazzoli, V. (1981) *Acta Crystallogr. B,* **37**, 1496–500.

Cohen, D. and Hindman, J. C. (1952) *J. Am. Chem. Soc.,* **74**, 4679–82.

Combes, J. M., Chisholm-Brause, C. J., Brown, G. E. Jr, Parks, G. A., Conradson, S. D., Eller, P. G., Triay, I. R., Hobart, D. E., and Miejer, A. (1992) *Environ. Sci. Technol.,* **26**, 376–82.

Comodi, P., Liu, Y., Zanazzi, P. F., and Montagnoli, M. (2001) *Phys. Chem. Miner.,* **28**, 219–24.

Conradson, S. D. (1998) *Appl. Spectrosc.,* **52**, 252A–79A.

Conradson, S. D., Al Mahamid, I., Clark, D. L., Hess, N. J., Hudson, E. A., Neu, M. P., Palmer, P. D., Runde, W. H., and Tait, C. D. (1998) *Polyhedron,* **17**, 599–602.

Conradson, S. D., Begg, B. D., Clark, D. L., Den Auwer, C., Espinosa-Faller, F. J., Gordon, P. L., Hess, N. J., Hess, R., Keogh, D. W., Morales, L. A., Neu, M. P., Runde, W., Tait, C. D., Veirs, D. K., and Villella, P. M. (2003) *Inorg. Chem.,* **42**, 3715–17.

Conradson, S. D., Abney, K. D., Begg, B. D., Brady, E. D., Clark, D. L., Den Auwer, C., Ding, M., Dorhout, P. K., Espinosa-Faller, F. J., Gordon, P. L., Haire, R. G., Hess, N. J., Hess, R. F., Keogh, D. W., Lander, G. H., Lupinetti, A. J., Morales, L. A., Neu, M. P., Palmer, P. D., Paviet-Hartmann, P., Reilly, S. D., Runde, W. H., Tait, C. D., Veirs, D. K., and Wastin, F. (2004) *Inorg. Chem.,* **43**, 116–31.

Cossy, C., Helm, L., Powell, D. H., and Merbach, A. E. (1995) *New J. Chem.,* **19**, 27–35.

Cotton, F. A., Wilkinson, G., Murillo, C., and Bochmann, M. (1999) *Advanced Inorganic Chemistry,* John Wiley, New York.

Daehn, R., Scheidegger, A. M., Manceau, A., Curti, E., Baeyens, B., Bradbury, M. H., and Chateigner, D. (2002) *J. Colloid Interface Sci.,* **249**, 8–21.

Dal Negro, A. and Ungaretti, L. (1971) *Am. Mineral.,* **56**, 768–72.

Danesi, P. R., Markowicz, A., Chinea-Cano, E., Burkart, W., Salbu, B., Donohue, D., Ruedenauer, F., Hedberg, M., Vogt, S., Zahradnik, P., and Ciurapinski, A. (2003) *J. Environ. Radioact.,* **64**, 143–54.

David, F., Revel, R., Fourest, B., Hubert, S., Le Du, J. F., Den Auwer, C., Madic, C., Morss, L. R., Ionova, G., Mikhalko, V., Vokhmin, V., Nikonov, M., Berthet, J. C., and Ephritikhine, M. (1998) in *Speciation, Techniques and Facilities for Radioactive Materials at Synchrotron Light Sources,* Nuclear Energy Agency: Organisation for Economic Co–Operation and Development, Grenoble, France, pp. 95–100.

David, F. H. and Vokhmin, V. (2003) *New J. Chem.,* **27**, 1627–32.

de Leon, J. M., Rehr, J. J., Zabinsky, S. I., and Albers, R. C. (1991) *Phys. Rev.,* **B44**, 4146–56.

de Villiers, J. P. R. (1971) *Am. Mineral.,* **56**, 758–66.

Deer, W. A., Howie, R. A., and Zussman, J. (1992) *The Rock Forming Minerals,* Longman Scientific and Technical, Hong Kong.

Den Auwer, C., Grégoire-Kappenstein, A. C., and Moisy, P. (2003a) *Radiochim. Acta,* **91**, 773–6.

Den Auwer, C., Simoni, E., Conradson, S., and Madic, C. (2003b) *Eur. J. Inorg. Chem.*, 3843–59.

Denecke, M. A., Pompe, S., Reich, T., Moll, H., Bubner, M., Heise, K. H., Nicolai, R., and Nitsche, H. (1997a) *Radiochim. Acta,* **79**, 151–9.

Denecke, M. A., Reich, T., Pompe, S., Bubner, M., Heise, K. H., Nitsche, H., Allen, P. G., Bucher, J. J., Edelstein, N. M., and Shuh, D. K. (1997b) *J. Phys. IV,* **7**, 637–8.

Denecke, M. A., Reich, T., Bubner, M., Pompe, S., Heise, K. H., Nitsche, H., Allen, P. G., Bucher, J. J., Edelstein, N. M., and Shuh, D. K. (1998a) *J. Alloy. Compd.,* **271**, 123–7.

Denecke, M. A., Reich, T., Pompe, S., Bubner, M., Heise, K. H., Nitsche, H., Allen, P. G., Bucher, J. J., Edelstein, N. M., Shuh, D. K., and Czerwinski, K. R. (1998b) *Radiochim. Acta,* **82**, 103–8.

Denecke, M. A., Bublitz, D., Kim, J. I., Moll, H., and Farkes, I. (1999) *J. Synchrotron. Radiat.,* **6**, 394–6.

Denecke, M. A., Marquardt, C. M., Rothe, J., Dardenne, K., and Jensen, M. P. (2002) *J. Nucl. Sci. Technol.,* **Suppl. 3**, 410–13.

Denecke, M. A., Rothe, J., Dardenne, K., and Lindqvist-Reis, P. (2003) *Phys. Chem. Chem. Phys.,* **5**, 939–46.

Dent, A. J., Ramsay, J. D. F., and Swanton, S. W. (1992) *J. Colloid Interface Sci.,* **150**, 45–60.

Djogic, R. and Branica, M. (1991) *Mar. Chem.,* **36**, 121–35.

Docrat, T. I., Mosselmans, J. F. W., Charnock, J. M., Whiteley, M. W., Collison, D., Livens, F. R., Jones, C., and Edmiston, M. J. (1999) *Inorg. Chem.,* **38**, 1879–82.

Dodge, C. J. and Francis, A. J. (1997) *Environ. Sci. Technol.,* **31**, 3062–7.

Dodge, C. J. and Francis, A. J. (2003) *Radiochim. Acta,* **91**, 525–32.

Duff, M. C. and Amrhein, C. (1996) *Soil Sci. Soc. Am. J.,* **60**, 1393–400.

Duff, M. C., Amrhein, C., Bertsch, P. M., and Hunter, D. B. (1997) *Geochim. Cosmochim. Acta,* **61**, 73–81.

Duff, M. C., Hunter, D. B., Triay, I. R., Bertsch, P. M., Reed, D. T., Sutton, S. R., Shea-Mccarthy, G., Kitten, J., Eng, P., Chipera, S. J., and Vaniman, D. T. (1999a) *Environ. Sci. Technol.,* **33**, 2163–9.

Duff, M. C., Newville, M., Hunter, D. B., Bertsch, P. M., Sutton, S. R., Triay, I. R., Vaniman, D. T., Eng, P., and Rivers, M. L. (1999b) *J. Synchrotron. Radiat.,* **6**, 350–2.

Duff, M. C., Morris, D. E., Hunter, D. B., and Bertsch, P. M. (2000) *Geochim. Cosmochim. Acta,* **64**, 1535–50.

Duff, M. C., Hunter, D. B., Triay, I. R., Bertsch, P. M., Kitten, J., and Vaniman, D. T. (2001) *J. Contam. Hydrol.,* **47**, 211–18.

Duff, M. C., Coughlin, J. U., and Hunter, D. B. (2002) *Geochim. Cosmochim. Acta,* **66**, 3533–47.

Effenberger, H., Mereiter, K., and Zemann, H. (1981) *Z. Kristallogr.,* **156**, 233–43.

Efurd, D. W., Runde, W., Banar, J. C., Janecky, D. R., Kaszuba, J. P., Palmer, P. D., Roensch, F. R., and Tait, C. D. (1998) *Environ. Sci. Technol.,* **32**, 3893–900.

Egami, T. and Aur, S. (1987) *J. Non-Cryst. Solids*, **89**, 60–74.

Eller, P. G., Jarvinen, G. D., Purson, J. D., Penneman, R. A., Ryan, R. R., Lytle, F. W., and Greegor, R. B. (1985) *Radiochim. Acta,* **39**, 17–22.

Elless, M. P. and Lee, S.-Y. (1994) *Physicochemical and Mineralogical Characterization of Transuranic Contaminated Soils for Uranium Soil Integrated Demonstration,* ORNL/TM-12848, Oak Ridge National Laboratory, Oak Ridge, TN.

Evans, H. T. Jr (1963) *Science,* **141**, 154–8.

Fahey, J. A. (1986) in *The Chemistry of the Actinide Elements,* vol. 1 (eds. J. J. Katz, G. T. Seaborg, and L. R. Morss), Chapman & Hall, London, pp. 443–98.
Farges, F. (1991) *Geochim. Cosmochim. Acta,* **55**, 3303–19.
Farley, N. R. S., Gurman, S. J., and Hillman, A. R. (1999) *Electrochem. Commun.*, **1**, 449–52.
Fein, J. B., Daughney, C. J., Yee, N., and Davis, T. A. (1997) *Geochim. Cosmochim. Acta,* **61**, 3319–28.
Felmy, A. R., Rai, D., Sterner, S. M., Mason, N. J., Hess, N. J., and Conradson, S. D. (1997) *J. Solution Chem.,* **26**, 233–48.
Fenter, P. A., Rivers, M. L., Sturchio, N. C., and Sutton, S. R. (eds.) (2002) *Applications of Synchrotron Radiation in Low-Temperature Geochemistry and Environmental Science,* Reviews in Mineralogy and Geochemistry, Mineralogical Society of America, Washington DC.
Fetter, S. and von Hippel, F. N. (1999) *Sci. Globe Security,* **8**, 125–61.
Filipponi, A. (2001) *J. Phys.: Condens. Matter,* **13**, R23–R60.
Fourest, B., Morss, L. R., Blain, G., David, F., and M'Halla, J. (1995) *Radiochim. Acta,* **69**, 215–19.
Francis, A. J., Dodge, C. J., Lu, F. L., Halada, G. P., and Clayton, C. R. (1994) *Environ. Sci. Technol.,* **28**, 636–9.
Francis, A. J., Gillow, J. B., Dodge, C. J., Dunn, M., Mantione, K., Strietelmeier, B. A., Pansoy-Hjelvik, M. E., and Papenguth, H. W. (1998) *Radiochim. Acta,* **82**, 347–54.
Francis, A. J., Dodge, C. J., Gillow, J. B., and Papenguth, H. W. (2000) *Environ. Sci. Technol.,* **34**, 2311–17.
Francis, A. J. (2002) in *Uranium in the Aquatic Environment* (eds. B. J. Merkel, B., Planer-Friedrich, and C. Wolkersdorfer), Springer-Verlag, Berlin, pp. 451–8.
Francis, A. J., Joshi-Tope, G. A., and Dodge, C. J., Gillow, J. B. (2002) *J. Nucl. Sci. Technol.*, **Suppl. 3**, 935–8.
Fredrickson, J. K., Zachara, J. M., Kennedy, D. W., Duff, M. C., Gorby, Y. A., Li, S.-M. W., and Krupka, K. M. (2000) *Geochim. Cosmochim. Acta,* **64**, 3085–98.
Fredrickson, J. K., Zachara, J. M., Kennedy, D. W., Liu, C., Duff, M. C., Hunter, D. B., and Dohnalkova, A. (2002) *Geochim. Cosmochim. Acta,* **66**, 3247–62.
Fuller, C. C., Bargar, J. R., Davis, J. A., and Piana, M. J. (2002) *Environ. Sci. Technol.,* **36**, 158–65.
Gale, R. J. (ed.) (1988) *Spectroelectrochemistry: Theory and Practice,* Plenum Press, New York.
Garnov, A. Y., Krot, N. N., Bessonov, A. A., and Perminov, V. P. (1996) *Radiochem., Engl. Transl.,* **38**, 402–6.
Geipel, G., Reich, T., Brendler, V., Bernhard, G., and Nitsche, H. (1997) *J. Nucl. Mater.,* **248**, 408–11.
Giaquinta, D. M., Soderholm, L., Yuchs, S. E., and Wasserman, S. R. (1997a) *J. Alloys. Compd.,* **249**, 142–5.
Giaquinta, D. M., Soderholm, L., Yuchs, S. E., and Wasserman, S. R. (1997b) *Radiochim. Acta,* **76**, 113–21.
Gillow, J. B., Francis, A. J., Dodge, C. J., Harris, R., Beveridge, T. J., Brady, P. V., and Papenguth, H. W. (1999) *Mater. Res. Soc. Symp. Proc.,* **556**, 1133–40.
Giordano, T. H. (1994) in *Organic Acids in Geological Processes* (eds. E. D. Pittman and M. D. Lewan), Springer-Verlag, Berlin, pp. 319–54.

Glebov, V. A., Nikitina, T. M., and Tikhonov, M. R. (1977) *Sov. Radiochem., Engl. Transl.* **19**, 231–2.
Gorby, Y. A. and Lovley, D. R. (1992) *Environ. Sci. Technol.,* **26**, 205–7.
Görller-Walrand, C. and Colen, W. (1982) *Chem. Phys. Lett.,* **93**, 82–5.
Goulon, J., Goulon-Ginet, C., Friant, P., Poncet, J. L., Guilard, R., and Battioni, J. P., Mansuy, D. (1983) *Proc. 4th Int. Conf. on Organic Chemistry of Selenium and Tellurium*, Birmingham, England, 1983: pp. 379–90.
Greathouse, J. A., O'Brian, R. J., Bemis, G., and Pabalan, R. T. (2002) *J. Phys. Chem. B,* **106**, 1546–655.
Greaves, G. N., Barrett, N. T., Antonini, G. M., Thronley, F. R., Willis, B. T. M., and Steel, A. (1989) *J. Amer. Chem. Soc.,* **111**, 4313–20.
Greegor, R. B., Pingitore, N. E. Jr., and Lytle, F. W. (1997) *Science,* **275**, 1452–5.
Guilbaud, P. and Wipff, G. (1993) *J. Phys. Chem.,* **97**, 5685–92.
Habenschuss, A. and Spedding, F. H. (1980) *J. Chem. Phys.,* **73**, 442–50.
Hanchar, J. M. (1999) in *Uranium: Mineralogy, Geochemistry and the Environment,* vol. 38 (eds. P. C. Burns and R. Finch), Mineralogical Society of America, Washington DC, pp. 500–19.
Haschke, J. M., Allen, T. H., and Morales, L. A. (2000) *Science* **287**, 285–7.
Haschke, J. M., Allen, T. H., and Morales, L. A. (2001) *J. Alloys Compd.,* **314**, 78–91.
Haschke, J. M. and Allen, T. H. (2002) *J. Alloys Compd.,* **336**, 124–31.
Haschke, J. M. and Oversby, V. M. (2002) *J. Nucl. Mater.,* **305**, 187–201.
Hay, P. J., Martin, R. L., and Schreckenbach, G. (2000) *J. Phys. Chem. A,* **104**, 6259–70.
Hem, J. D. (1985) Study and Interpretation of the Chemical Characteristics of Natural Water, U.S. Geological Survey Water Supply Paper 2254, U.S. Geological Survey.
Hennig, C., Panak, P. J., Reich, T., Rossberg, A., Raff, J., Selenska-Pobell, S., Matz, W., Bucher, J. J., Bernhard, G., and Nitsche, H. (2001a) *Radiochim. Acta,* **89**, 625–31.
Hennig, C., Reich, T., Funke, H., Rossberg, A., Rutsch, M., and Bernhard, G. (2001b) *J. Synchrotron. Radiat.,* **8**, 695–7.
Hennig, C., Reich, T., Daehn, R., and Scheidegger, A. M. (2002) *Radiochim. Acta,* **90**, 653–7.
Hess, N. J., Felmy, A. R., Rai, D., and Conradson, S. D. (1997) *Mater. Res. Soc. Symp. Proc.,* **465**, 729–34.
Hess, N. J., Weber, W. J., and Conradson, S. (1998) *J. Alloys Compd.,* **271–273**, 240–3.
Ho, C. H. and Doern, D. C. (1985) *Can. J. Chem.,* **63**, 1100–4.
Hoekstra, H. and Siegel, S. (1964) *J. Inorg. Nucl. Chem.,* **26**, 693–700.
Hsi, C. K. D. and Langmuir, D. (1985) *Geochim. Cosmochim. Acta,* **49**, 1931–41.
Hudson, E. A., Rehr, J. J., and Bucher, J. J. (1995a) *Phys. Rev. B,* **52**, 13815–26.
Hudson, E. A., Terminello, L. J., Viani, B. E., Reich, T., Bucher, J. J., Shuh, D. K., and Edelstein, N. M. (1995b) *Mater. Res. Soc. Symp. Proc.,* **375**, 235–40.
Hudson, E. A., Allen, P. G., Terminello, L. J., Denecke, M. A., and Reich, T. (1996) *Phys. Rev. B,* **54**, 156–65.
Hudson, E. A., Terminello, L. J., Viani, B. E., Denecke, M., Reich, T., Allen, P. G., Bucher, J. J., Shuh, D. K., and Edelstein, N. M. (1999) *Clays Clay Miner.,* **47**, 439–57.
Hunter, D. B. and Bertsch, P. M. (1998) *J. Radioanal. Nucl. Chem.,* **234**, 237–42.

Hursthouse, A. S., Baxter, M. S., Livens, F. R., and Duncan, H. J. (1991) *J. Environ. Radioact.,* **14**, 147–74.
Igo, D. H., Elder, R. C., Heineman, W. R., and Dewald, H. D. (1991) *Anal. Chem.,* **63**, 2535–9.
Jenne, E. A. (1977) in *Molybdenum in the Environment* (eds.. W. Chappel and K. Peterson), Marcel Dekker, New York, pp. 425–553.
Jiang, J., Rao, L., Bernardo, P. D., Zanonato, P., and Bismondo, A. (2002) *J. Chem. Soc., Dalton Trans.*, 1832-8.
Joergensen, C. K. (1977) *Rev. Chim. Miner.,* **14**, 127–38.
Johansson, G. and Wakita, H. (1985) *Inorg. Chem.,* **24**, 3047–52.
Johansson, G., Magini, M., and Ohtaki, H. (1991) *J. Solution Chem.,* **20**, 775–92.
Karim, D. P., Georgopoulos, P., and Knapp, G. S. (1980) *Nucl. Technol.,* **51**, 162–8.
Kaszuba, J. P. and Runde, W. H. (1999) *Environ. Sci. Technol.,* **33**, 4427–33.
Keeney-Kennicutt, W. L. and Morse, J. W. (1985) *Geochim. Cosmochim. Acta,* **49**, 2577–88.
Kelly, S. D., Kemner, K. M., Fein, J. B., Fowle, D. A., Boyanov, M. I., Bunker, B. A., and Yee, N. (2002) *Geochim. Cosmochim. Acta,* **66**, 3855–71.
Kelly, S. D., Newville, M. G., Cheng, L., Kemner, K. M., Sutton, S. R., Fenter, P., Sturchio, N. C., and Spoetl, C. (2003) *Environ. Sci. Technol.,* **37**, 1284–7.
Kitano, Y. and Oomori, T. J. (1971) *J. Oceanogr. Soc. Jpn.,* **27**, 34–42.
Koningsberger, D. C. and Prins, R. (1988) *X-Ray Absorption: Principles, Applications, Techniques of EXAFS, SEXAFS, and XANES,* John Wiley, New York.
Krot, N. N. and Gelman, A. D. (1967) *Dokl. Akad. Nauk. SSSR, Engl. Transl.,* **177**, 124–6.
Ku, T.-L., Knauss, K. G., and Mathieu, G. G. (1977) *Deep-Sea Res.,* **24**, 1005–17.
Langmuir, D. (1978) *Geochim. Cosmochim. Acta,* **42**, 547–69.
Latrous, H. and Oliver, J. (1999) *J. Mol. Liq.,* **81**, 115–21.
Leciejewicz, J., Alcock, N. W., and Kemp, T. J. (1995) *Struct. Bond.,* **82**, 43–84.
Lee, P. A., Citrin, P. H., Eisenberger, P., and Kincaid, B. M. (1981) *Rev. Mod. Phys.,* **53**, 769–806.
Li, Y., Kato, Y., and Yoshida, Z. (1993) *Radiochim. Acta,* **60**, 115–19.
Lieser, K. H. (1995) *Radiochim. Acta,* **70–71**, 355–75.
Locock, A. J. and Burns, P. C. unpublished data.
Lovley, D. R., Phillips, E. J. P., Gorby, Y. A., and Landa, E. R. (1991) *Nature,* **350**, 413–16.
Lytle, F. W. (1999) *J. Synchrotron. Radiat.,* **6**, 123–34.
Manceau, A., Charlet, L., Boisset, M. C., Didier, B., and Spadini, L. (1992) *Appl. Clay Sci.,* **7**, 201–23.
Martens, G., Rabe, P., and Wenck, P. (1985) *Phys. Status Solidi A: Appl. Res.,* **88**, 103–11.
Mashirov, L. G., Suglobov, D. N., and Shcherbakov, V. A. (1975) *Sov. Radiochem., Engl. Transl.,* **17**, 768–70.
Mauerhofer, E., Zhernosekov, K., and Rösch, F. (2004) *Radiochim. Acta,* **92**, 5–10.
Maya, L. (1982) *Radiochim. Acta,* **31**, 147–51.
Meece, D. E. and Benninger, l. K. (1993) *Geochim. Cosmochim. Acta,* **57**, 1447–58.
Merroun, M., Hennig, C., Rossberg, A., Geipel, G., Reich, T., and Selenska- Pobell, S. (2002a) *Biochem. Soc. Trans.,* **30**, 669–72.

Merroun, M., Hennig, C., Rossberg, A., Reich, T., Nicolai, R., Heise, K. H., and Selenska-Pobell, S. (2002b) in *Uranium in the Aquatic Environment* (eds. B. J. Merkel, B. Planer-Friedrich, and C. Wolkersdorfer), Springer-Verlag, Berlin, pp. 509–15.

Michard, P., Guibal, E., Vincent, T., and Le Cloirec, P. (1996) *Microporous Mater.,* **5**, 309–24.

Moll, H., Farkas, I., Jalilehvand, F., Sandström, M., Szabó, Z., Grenthe, I., Denecke, M. A., and Wahlgren, U. (1998) in *Speciation, Techniques and Facilities for Radioactive Materials at Synchrotron Light Sources,* Organisation for Economic Co–Operation and Development, Nuclear Energy Agency, Grenoble, France: pp. 261–8.

Moll, H., Denecke, M. A., Jalilehvand, F., Sandstrom, M., and Grenthe, I. (1999) *Inorg. Chem.,* **38**, 1795–9.

Moll, H., Reich, T., Hennig, C., Rossberg, A., Szabo, Z., and Grenthe, I. (2000a) *Radiochim. Acta,* **88**, 559–66.

Moll, H., Reich, T., and Szabo, Z. (2000b) *Radiochim. Acta,* **88**, 411–15.

Moll, H., Geipel, G., Reich, T., Bernhard, G., Fanghänel, T., and Grenthe, I. (2003) *Radiochim. Acta,* **91**, 11–20.

Morris, D. E., Allen, P. G., Berg, J. M., Chisholm-Brause, C., Conradson, S., Donohoe, R. J., Hess, N. J., Musgrave, J. A., and Tait, C. D. (1996) *Environ. Sci. Technol.,* **30**, 2322–31.

Morris, D. E. (2002) *Inorg. Chem.,* **41**, 3542–7.

Morss, L. R. (1994) in *Handbook on the Physics and Chemistry of Rare Earths,* vol. 18 (eds. K. A. Gschneidner Jr, L. Eyring, G. R. Choppin, and G. H. Lander), Elsevier Science, Amsterdam, pp. 239–91.

Mosselmans, J. F., Bailey, E., and Schofield, P. (2001) *J. Synchrotron Radiat.,* **8**, 660–2.

Moyes, L. N., Parkman, R. H., Charnock, J. M., Vaughan, D. J., Livens, F. R., Hughes, C. R., and Braithwaite, A. (2000) *Environ. Sci. Technol.,* **34**, 1062–8.

Moyes, L. N., Jones, M. J., Reed, W. A., Livens, F. R., Charnock, J. M., Mosselmans, J. F. W., Hennig, C., Vaughan, D. J., and Pattrick, R. A. D. (2002) *Environ. Sci. Technol.,* **36**, 179–83.

Musikas, C. and Narten, A. H. (1978) *Inorg. Nucl. Chem. Lett.,* **14**, 283–5.

Nace, R. L. (1967) *Are We Running Out of Water?*, U.S. Geological Survey Circular 536.

Nagy, B., Gauthier-Lafaye, F., Holliger, P., Davis, D. W., Mossman, D. J., Leventhal, J. S., Rigali, M. J. and Parnell, J. (1991) *Nature,* **354**, 472–4.

Neck, V. and Kim, J. I. (2001) *Radiochim. Acta,* **89**, 1–16.

Neck, V., Müller, R., Bouby, M., Altmaier, M., Rothe, J., Denecke, M. A., and Kim, J. I. (2002) *Radiochim. Acta,* **90**, 485–94.

Neilson, G. W., Schioeberg, D., and Luck, W. A. P. (1985) *Chem. Phys. Lett.,* **122**, 475–9.

Newville, M., Sutton, S., Rivers, M., and Eng, P. (1999) *J. Synchrotron. Radiat.,* **6**, 353–5.

Nitsche, H. (1997) in *The Robert A. Welch Foundation,* Proc. 41st Conf. on Chemical Research. The Transactinide Elements, Robert A. Welch Foundation, Houston, TX, ch. 5.

Nitsche, H., Silva, R. J., Brendler, V., Geipel, G., Reich, T., Teterin, Y. A., Thieme, M., Baraniak, L., and Bernhard, G. (1999) in *Actinide Speciation in High Ionic Strength Media* (eds. D. T. Reed, S. B. Clark, and L. Rao), Kluwer Academic Publishers, New York, pp. 11–38.

Oesthols, E. (1995) *Geochim. Cosmochim. Acta,* **59**, 1235–49.
Oesthols, E., Manceau, A., Farges, F., and Charlett, L. (1997) *J. Colloid Interface Sci.,* **194**, 12–21.
O'Loughlin, E. J., Kelly, S. D., Cook, R. E., Csencsits, R., and Kemner, K. M. (2003) *Environ. Sci. Technol.,* **37**, 721–7.
Ordonez-Regil, E., Drot, R., Simoni, E., and Ehrhardt, J. J. (2002) *Langmuir,* **18**, 7977–84.
Paciolla, M. D., Davies, G., and Jansen, S. A. (1999) *Environ. Sci. Technol.,* **33**, 1814–18.
Palacios, M. L. and Taylor, S. H. (2000) *Appl. Spectrosc.,* **54**, 1372–8.
Panak, P. J., Raff, J., Selenska-Pobell, S., Geipel, G., Bernhard, G., and Nitsche, H. (2000) *Radiochim. Acta,* **88**, 71–6.
Panak, P. J. and Nitsche, H. (2001) *Radiochim. Acta,* **89**, 499–504.
Panak, P. J., Booth, C. H., Caulder, D. L., Bucher, J. J., Shuh, D. K., and Nitsche, H. (2002a) *Radiochim. Acta,* **90**, 315–21.
Panak, P. J., Knopp, R., Booth, C. H., and Nitsche, H. (2002b) *Radiochim. Acta,* **90**, 779–83.
Pauling, L. (1929) *J. Am. Chem. Soc.,* **51**, 1010–26.
Pingitore, N. E. Jr., Iglesias, A., Lytle, F., and Wellington, G. M. (2002) *Microchem. J.,* **71**, 261–6.
Pittman, E. D. and Lewan, M. D. (eds) (1994) *Organic Acids in Geological Processes,* Springer-Verlag, Berlin.
Pocev, S. and Johansson, G. (1973) *Acta Chem. Scand.,* **27**, 2146–60.
Pompe, S., Bubner, M., Denecke, M. A., Reich, T., Brachmann, A., Geipel, G., Nicolai, R., Heise, K. H., and Nitsche, H. (1996) *Radiochim. Acta,* **74**, 135–40.
Pourbaix, M. (1974) *Atlas of Electrochemical Equilibria in Aqueous Solutions,* Cebelcor, Brussels.
Priest, N. D. (2001) *Lancet,* **357**, 244–6.
Quinn, B. M., Ding, Z., Moulton, R., and Bard, A. J. (2002) *Langmuir,* **18**, 1734–42.
Rai, D., Felmy, A. R., Hess, N. J., Moore, D. A., and Yui, M. (1998) *Radiochim. Acta,* **82**, 17–25.
Rai, D., Hess, N. J., Felmy, A. R., Moore, D. A., and Yui, M. (1999a) *Radiochim. Acta,* **84**, 159–69.
Rai, D., Hess, N. J., Felmy, A. R., Moore, D. A., Yui, M., and Vitorge, P. (1999b) *Radiochim. Acta,* **86**, 89–99.
Rakovan, J., Newville, M., and Sutton, S. (2001) *Am. Mineral.,* **86**, 697–700.
Rakovan, J., Reeder, R. J., Elzinga, E. J., Cherniak, D. J., Tait, C. D., and Morris, D. E. (2002) *Environ. Sci. Technol.,* **36**, 3114–17.
Rao, L., Jiang, D. L., Zanonato, P., Di Bernardo, P., Bismondo, A., and Garnov, A. Y. (2002) *Radiochim. Acta,* **90**, 581–8.
Reddon, G., Bargar, J. R., and Bencheikh-Latmani, R. (2001) *J. Colloid. Interface Sci.,* **244**, 211–19.
Reeder, R. J. (1983) in *Reviews of Mineralogy,* vol. 23 (ed. R. J. Reeder), Mineralogical Society of America, Washington DC, pp. 1–47.
Reeder, R. J., Nugent, M., Lamble, G. M., Tait, C. D., and Morris, D. E. (2000) *Environ. Sci. Technol.,* **34**, 638–44.

Reeder, R. J., Nugent, M., Tait, C. D., Morris, D. E., Heald, S. M., Beck, K. M., and Hess, W. P. (2001) *Geochim. Cosmochim. Acta,* **65**, 3491–503.

Rehr, J. J., de Leon, J. M., Zabinsky, S. I., and Albers, R. C. (1991) *J. Am. Chem. Soc.,* **113**, 5135–40.

Rehr, J. J., Albers, R. C., and Zabinsky, S. I. (1992) *Phys. Rev. Lett.,* **69**, 3397–400.

Rehr, J. J. and Albers, R. C. (2000) *Rev. Mod. Phys.,* **72**, 621–54.

Reich, T., Denecke, M. A., Pompe, S., Bubner, M., Heise, K.-H., Schmidt, M., Brendler, V., Baraniak, L., Nitsche, H., Allen, P. G., Bucher, J. J., Edelstein, N. M., and Shuh, D. K. (1996a) in *Synchrotron Radiation Techniques in Industrial, Chemical, and Materials Science* (eds. K. L. D'Amico, L. J. Terminello, and D. K. Shuh), Plenum Press, New York, pp. 215–28.

Reich, T., Moll, H., Denecke, M. A., Geipel, G., Bernhard, G., Nitsche, H., Allen, P. G., Bucher, J. J., Kaltsoyannis, N., Edelstein, N. M., and Shuh, D. K. (1996b) *Radiochim. Acta,* **74**, 219–23.

Reich, T., Hudson, E. A., Denecke, M. A., Allen, P. G., and Nitsche, H. (1998a) *Poverkhnost* (*4–5*), *1997, pp 149–57* **13**, 557–68.

Reich, T., Moll, H., Arnold, T., Denecke, M. A., Hennig, C., Geipel, G., Bernhard, G., Nitsche, H., Allen, P. G., Bucher, J. J., Edelstein, N. M., and Shuh, D. K. (1998b) *J. Electron Spectrosc. Relat. Phenom.,* **96**, 237–43.

Reich, T., Bernhard, G., Geipel, G., Funke, H., Hennig, C., Rossberg, A., Matz, W., Schell, N., and Nitsche, H. (2000) *Radiochim. Acta,* **88**, 633–7.

Revel, R., Den Auwer, C., Madic, C., David, F., Fourest, B., Hubert, S., Le Du, J. F., and Morss, L. R. (1999) *Inorg. Chem.,* **38**, 4139–41.

Riglet, C., Robouch, P., and Vitorge, P. (1989) *Radiochim. Acta,* **46**, 85–94.

Roehler, J. (1992) in *Lattice Effects in High-Tc Superconductors: Proceedings of the Conference: Santa Fe, New Mexico, January 13–15, 1992* (eds. Y. Bar-Yam, T. Egami, J. Mustre-de Leon, and A. R. Bishop) World Scientific, Singapore, pp. 77-83.

Rossberg, A., Baraniak, L., Reich, T., Hennig, C., Bernhard, G., and Nitsche, H. (2000) *Radiochim. Acta,* **88**, 593–7.

Rossberg, A., Reich, T., and Bernhard, G. (2003) *Anal. Bioanal. Chem.,* **376**, 631–8.

Rothe, J., Denecke, M. A., Neck, V., Mueller, R., and Kim, J. I. (2002) *Inorg. Chem.,* **41**, 249–58.

Runde, W., Neu, M. P., Conradson, S. D., Clark, D. L., Palmer, P. D., Reilly, S. D., Scott, B. L., and Tait, C. D. (1997) *Mater. Res. Soc. Symp. Proc.,* **465**, 693–703.

Runde, W., Neu, M. P., and Reilly, S. D. (1999) in *Actinide Speciation in High Ionic Strength Media* (eds. D.T. Reed, S. B. Clark, and L. Rao), Kluwer Academic Publishers, New York, pp. 141–51.

Russell, A. D., Emerson, S., Nelson, B. K., Erez, J., and Lea, D. W. (1994) *Geochim. Cosmochim. Acta,* **58**, 671–81.

Rykov, A. G., Andreichuk, N. N., and Vasil'ev, V. Y. (1973) *Sov. Radiochem., Engl. Transl.,* **15**, 350–5.

Sanchez, A. L., Murray, J. W., and Silbley, T. H. (1985) *Geochim. Cosmochim. Acta,* **49**, 2297–307.

Sayers, D. E., Stern, E. A., and Lytle, F. W. (1971) *Phys. Rev. Lett.,* **27**, 1204–7.

Schmeide, K., Sachs, S., Bubner, M., Reich, T., Heise, K. H., and Bernhard, G. (2003) *Inorg. Chim. Acta,* **351**, 133–40.

Schofield, P. F., Bailey, E. H., and Mosselmans, J. F. W. (1999) in *Geochemistry of the Earth's Surface* (ed. H. Armannsson), Proc. 5th Int. Symp. on Geochemistry of the Earth's Surface Balkema, Rotterdam, pp. 465–8.

Schreckenbach, G., Hay, P. J., and Martin, R. L. (1998) *Inorg. Chem.,* **37**, 4442–51.

Sémon, L., Boehme, C., Billard, I., Hennig, C., Lutzenkirchen, K., Reich, T., Rossberg, A., Rossini, I., and Wipff, G. (2001) *Chem. Phys. Chem.,* **2**, 591–8.

Shannon, R. D. (1976) *Acta Crystallogr.,* **A32**, 751–67.

Sharpe, L. R., Heineman, W. R., and Elder, R. C. (1990) *Chem. Rev.,* **90**, 705–22.

Shaughnessy, D. A., Nitsche, H., Booth, C. H., Shuh, D. K., Waychunas, G. A., Wilson, R. E., Gill, H., Cantrell, K. J., and Serne, R. J. (2003) *Environ. Sci. Technol.*, **37**.

Shcherbakov, V. A., Iorga, E. V., and Mashirov, L. G. (1974) *Sov. Radiochem., Engl. Transl.,* **16**, 286–7.

Shcherbakov, V. A. and Iorga, E. V. (1975) *Sov. Radiochem., Engl. Transl.,* **17**, 763–7.

Shen, G. T. and Dunbar, R. B. (1995) *Geochim. Cosmochim. Acta,* **59**, 2009–24.

Shilov, V. P. (1998) *Radiochem., Engl. Transl.,* **40**, 11–16.

Shilov, V. P. and Yusov, A. B. (2002) *Russ. Chem. Rev., Engl. Transl.,* **71**, 465–88.

Silva, R. J. and Nitsche, H. (1995) *Radiochim. Acta,* **70–71**, 377–96.

Skanthakumar, S., Gorman-Lewis, D., Locock, A., Chiang, M.-H., Jensen, M. P., Burns, P. C., Fein, J. B., Jonah, C. D., Attenkofer, K., and Soderholm, L. (2004) *Mater. Res. Soc. Symp. Proc.,* **802**, 151–6.

Smith, D. A., Heeg, M. J., Heineman, W. R., and Elder, R. C. (1984) *J. Am. Chem. Soc.,* **106**, 3053–4.

Soderholm, L., Antonio, M. R., Williams, C., and Wasserman, S. R. (1999) *Anal. Chem.,* **71**, 4622–8.

Soderholm, L., Williams, C. W., Antonio, M. R., Tischler, M. L., and Markos, M. (2000) *Mater. Res. Soc. Symp. Proc.,* **590**, 27–32.

Songkasiri, W., Reed, D. T., and Rittmann, B. E. (2002) *Radiochim. Acta,* **90**, 785–9.

Sonnenberg, L. B., Johnson, J. D., and Christman, R. F. (1989) in *Aquatic Humic Substances. Influence on Fate and Treatment of Pollutants* (eds. I. H. Suffet and P. MacCarthy) (ACS Symp. Ser. 219), American Chemical Society, Washington, DC, pp. 3–23.

Spencer, S., Gagliardi, L., Handy, N. C., Ioannou, A. G., Skylaris, C.-K., Willetts, A., and Simper, A. M. (1999) *J. Phys. Chem. A,* **103**, 1831–7.

Spitsyn, V. I., Gelman, A. D., Krot, N. N., Mefodiyeva, M. P., Zakharova, F. A., Komkov, Y. A., Shilov, V. P., and Smirnova, I. V. (1969) *J. Inorg. Nucl. Chem.,* **31**, 2733–45.

Spoetl, C., Unterwurzacher, M., Mangini, A., and Longstaffe, F. J. (2002) *J. Sediment. Res.,* **72**, 793–808.

Sposito, G. (1984) *The Surface Chemistry of Soils,* Oxford University Press, Oxford.

Sposito, G. (1990) in *Reviews in Mineralogy,* vol. 23 (eds. M. F. Hochellaand A. F. White), Mineralogical Society of America, Washington DC, pp. 259–79.

Sterne, P. A., Gonis, A., and Borovoi, A. A. (eds.) (1998) *Actinides and the Environment,* Kluwer Academic Publishers, Dordrecht.

Stevenson, F. J. (1994) *Humus Chemistry: Genesis, Composition, Reactions,* John Wiley, New York.

Stumpf, T., Hennig, C., Bauer, A., Denecke, M. A., and Fanghaenel, T. (2004) *Radiochim. Acta,* **92**, 133–8.

Sturchio, N. C., Antonio, M. R., Soderholm, L., Sutton, S. R., and Brannon, J. C. (1998) *Science,* **281**, 971–3.

Suzuki, Y., Kelly, S. D., Kemner, K. M., and Banfield, J. F. (2002) *Nature (London),* **419**, 134.

Suzuki, Y., Kelly, S. D., Kemner, K. M., and Banfield, J. F. (2003) *Appl. Environ. Microbiol.,* **69**, 1337–46.

Sylwester, E. R., Hudson, E. A., and Allen, P. G. (2000) *Geochim. Cosmochim. Acta,* **64**, 2431–8.

Szabo, Z., Moll, H., and Grenthe, I. (2000) *J. Chem. Soc.*, *Dalton Trans.*, 3158-61.

Szalay, A. (1991) *Geochim. Int.,* **6**, 1605–14.

Templeton, D. H. and Templeton, L. K. (1982) *Acta Crystallogr.,* **A38**, 62–7.

Teo, B. K. (1986) *EXAFS: Basic Principles and Data Analysis,* Springer-Verlag, Berlin.

Teo, B. K. and Lee, P. A. (1979) *J. Am. Chem. Soc*., **101**, 2815–32.

Thompson, H. A., Brown, G. E., and Parks, G. A. (1995) *Physica B,* **209**, 167–8.

Thompson, H. A., Brown, G. E., and Parks, G. A. (1997) *Am. Mineral.,* **82**, 483–96.

Thompson, H. A., Parks, G. A., and Brown, G. E. (1998) in *Adsorption of Metals by Geomedia* (ed. E. A. Jenne), Academic Press, San Diego, pp. 349–70.

Triay, I. R., Meijer, A., Conca, J. L., Kung, K. S., Rundberg, R. S., Strietelmeier, B. A., and Tait, C. D.(1997) *Summary and Synthesis Report on Radionuclide Retardation for the Yucca Mountain Site Characterization Project*, LA-13262, Los Alamos National Laboratory.

Tsushima, S. and Suzuki, A. (2000) *J. Mol. Struct. (Theochem),* **529**, 21–5.

Tsushima, S. and Reich, T. (2001) *Chem. Phys. Lett.,* **347**, 127–32.

Tsushima, S., Uchida, Y., and Reich, T. (2002) *Chem. Phys. Lett.,* **357**, 73–7.

Vallet, V., Wahlgren, U., Schimmelpfennig, B., Moll, H., Szabo, Z., and Grenthe, I. (2001) *Inorg. Chem.,* **40**, 3516–25.

Vallet, V., Moll, H., Wahlgren, U., Szabo, Z., and Grenthe, I. (2003) *Inorg. Chem.,* **42**, 1982–93.

Vaniman, D. T., Chipera, S. J., Bish, D. L., Duff, M. C., and Hunter, D. B. (2002) *Geochim. Cosmochim. Acta,* **66**, 1349–74.

Vasil'ev, V. Y., Andreichuk, N. N., and Rykov, A. G. (1974) *Sov. Radiochem., Engl. Transl.,* **16**, 583–6.

Vazquez, J., Bo, C., Poblet, J. M., de Pablo, J., and Bruno, J. (2003) *Inorg. Chem.,* **42**, 6136–41.

Veirs, D. K., Smith, C. A., Berg, J. M., Zwick, B. D., Marsh, S. F., Allen, P., and Conradson, S. D. (1994) *J. Alloys Compd.,* **213**, 328–32.

Viswanathan, H. S., Robinson, B. A., Valocchi, A. J., and Triay, I. R. (1998) *J. Hydrol.,* **209**, 251–80.

Wahlgren, U., Moll, H., Grenthe, I., Schimmelpfennig, B., Maron, L., Vallet, V., and Gropen, O. (1999) *J. Phys. Chem. A,* **103**, 8257–64.

Waite, T. D., Davis, J. A., Payne, T. E., Waychunas, G. A., and Xu, N. (1994) *Geochim. Cosmochim. Acta,* **58**, 5465–78.

Walter, M., Arnold, T., Reich, T., and Bernhard, G. (2003) *Environ. Sci. Technol.,* **37**, 2898–904.

Wasserman, S. R. (1997) *J. Phys. IV,* **7**, 203–5.

Wasserman, S. R., Allen, P. G., Shuh, D. K., Bucher, J. J., and Edelstein, N. M. (1999) *J. Synchrotron Radiat.,* **6**, 284–6.

Wasserman, S. R., Soderholm, L., and Giaquinta, D. M. (2000) *Mater. Res. Soc. Symp. Proc.,* **590**, 39–44.

Weiland, E., Wanner, H., Albinsson, Y., Wersin, P., and Karnland, O. (1994) SKB Technical Report 94-26, 64 pp.

Williams, C. W., Blaudeau, J.-P., Sullivan, J. C., Antonio, M. R., Bursten, B. E., and Soderholm, L. (2001) *J. Am. Chem. Soc.,* **123**, 4346–7.

Winick, H. and Nuhn, H.-D. (2003) http://www.lightsources.org

Yanase, N., Isobe, H., Sato, T., Sanada, Y., Matsunaga, T., and Amano, H. (2002) *J. Radioanal. Nucl. Chem.,* **252**, 233–9.

Yang, T., Tsushima, S., and Suzuki, A. (2001) *J. Phys. Chem. A*, **105**, 10439–45.

Zabinsky, S. I., Rehr, J. J., Ankudinov, A., Albers, R. C., and Eller, M. J. (1995) *Phys. Rev.,* **B52**, 2995–3009.

Zachara, J. M. and McKinley, J. P. (1993) *Aquat. Sci.,* **55**, 250–61.

Zhang, L., Crossley, M. J., Dixon, N. E., Ellis, P. J., Fisher, M. L., King, G. F., Lilley, P. E., Mac Lachlan, D., Pace, R. J., and Freeman, H. C. (1998) *J. Biol. Inorg. Chem.,* **3**, 470–83.

Zielen, A. J. and Cohen, D. (1970) *J. Phys. Chem.,* **74**, 394–405.

Zubavichus, Y. V. and Slovokhotov, Y. L. (2001) *Russ. Chem. Rev., Engl. Transl.,* **70**, 373–403.

CHAPTER TWENTY NINE

HANDLING, STORAGE, AND DISPOSITION OF PLUTONIUM AND URANIUM

John M. Haschke and Jerry L. Stakebake

29.1 INTRODUCTION

The need to address topics of handling, storage, and disposal of plutonium and uranium is driven by concern about hazards posed by the element and by the worldwide quantity of civilian and military materials. The projected inventory of separated civilian plutonium for use in fabricating mixed-oxide (MOX) reactor fuel during initial decades of this century is constant at about 120 metric tons and a comparable amount of excess military plutonium is anticipated from reductions in nuclear weapon stockpiles (IAEA Report, 1998). Although inventories of civilian material are in oxide form, Pu from weapons programs exists primarily as metal. Plutonium is a radiological toxin (Voelz, 2000); its management in a safe and secure manner is essential for protecting workers, the public, and the environment.

The focus of this chapter is on plutonium handling and storage, which are operations required for both civilian and weapons materials. Plutonium dioxide for MOX fabrication is processed and stored on an interim basis. The spent fuel formed during power generation is considered suitable for disposal. Excess Pu from military sources must be extracted, prepared, and stored until disposal options are investigated and evaluated. Storage periods of several decades may

be required until disposal methods are selected and implemented. This chapter centers on handling and storage of plutonium metal and oxide, and where information is available, on handling and storage of uranium metal and oxide.

Hazards associated with Pu and U strongly depend on the material form and are substantially altered by chemical reaction. Atmospheric dispersal of particles is the primary mechanism for large-scale environmental distribution of actinide-containing materials such as oxide (Mishima and Pinkston, 1994). Entrainment and dispersal of oxide particles with geometric dimensions less than 10 μm is anticipated under normal aerodynamic conditions. The source term for environmental release is determined by the mass fraction of particles within the aerosolizable size range. Oxide particles in the respirable fraction have geometric dimensions less than 3 μm and are retained in a human respiratory system if inhaled. Metal is not highly dispersible, but its release is facilitated by corrosion reactions that transform metal into powdered forms and contribute to loss of containment by generating heat and pressure. Therefore, corrosion reactions of Pu and U are important considerations, especially in light of pyrophoric tendencies exhibited by metal fines and corrosion products such as the hydrides.

In addition to an inherent source term for dispersal, oxides of Pu and U chemically interact with environmental gases during handling and storage in ways that significantly alter the potential hazard. This statement conflicts with the widely held view that PuO_2 is stable and unreactive. Because oxides and other compounds exist as adherent layers on the surfaces of Pu and U, a thorough understanding of the chemistry is necessary to determine their properties and influence on behavior of the metals. Some product layers are protective and slow the corrosion of the metal, but others catalyze rapid reaction. Such a 'runaway' reaction occurred during a seemingly routine operation in which a failed storage vessel containing a Pu casting was examined in a gloved box filled with a nitrogen-rich atmosphere normally used for handling metal (Haschke and Martz, 2000). After the partially disassembled package had been exposed to that atmosphere for 3 h, workers discovered that the vessel was hot and that its diameter had increased by 50% in the region around the metal. Subsequent investigation showed that a spontaneous reaction had advanced into the metal at more than 1 cm h^{-1}, a rate that is 10^{10} faster than normal corrosion of Pu in dry air at room temperature.

Unanticipated behavior is a consistent feature of plutonium chemistry. As described in a review by Waber (1980) early experience with handling and storage of plutonium and uranium revealed perplexing and unexplained observations. Reports suggest that corrosion rates of metal are markedly enhanced by moisture, by storage in Ar, or other inert gases with low oxygen content, and by confinement in a sealed vessel, but are slow in open air or a large amount of oxygen. Pyrophoric products are often present on Pu after extended storage in a closed container. Metal pyrophoricity and ignition behavior are unpredictable.

In a later review (Stakebake, 1971), proposed corrosion mechanisms and possible involvement of hydrogen are described, as well as instances of container pressurization that correlate with adsorption of atmospheric gases such as H_2O and CO_2 and with their subsequent radiolysis or thermal desorption. Other reviews describe kinetics (Colmenares, 1975) and mechanisms (Colmenares, 1984) of U and Pu oxidation, as well as physicochemical properties of the oxides. Material properties and kinetics, as well as conditions for safe handling and storage of plutonium metal and oxide, are discussed in more recent reviews (Haschke and Martz, 1998a; IAEA Report, 1998).

In this chapter, we describe relevant chemistry of plutonium metal, oxide, hydride, and other compounds and apply observations in interpreting the complex behavior of Pu and PuO_2 during handling and storage. Recent identification of key gas–solid and solid-state reactions that were not recognized in early studies show the importance of both rapid and slow reactions. Processes occurring over periods of years form highly catalytic surfaces that promote metal corrosion. The importance of minor chemical constituents such as water, of catalytic cycles, and of synergistic reactions is recognized. We describe and evaluate incidents involving containment failure and release of nuclear material with the objective of identifying conditions that alter chemical reactivity and the potential hazard. Existence of multiple hazards and multiple paths to the same potentially hazardous state suggests that unrecognized pathways probably exist and that knowledge is incomplete. Although current understanding of behavior is adequate for recommending procedures that significantly increase safety during handling and extended storage of metals and oxides, definition of general comprehensive requirements is precluded by substantial uncertainty about behavior of Pu-containing residues.

29.2 KINETIC CONSIDERATIONS

29.2.1 Scope of concerns

Chemical reactions that create hazards during handling differ in one important way from those encountered during storage. Reactions during handling are typically of concern only if they are rapid enough to create a direct hazard, such as pyrophoric ignition, during that operation. In contrast, reactions of concern during extended storage may occur slowly with cumulative effects resulting in a hazard such as progressive pressurization and containment failure over time. Gas–solid and liquid–solid reactions are of primary concern because rates of solid–solid reactions are typically insignificant, but exceptions to this general rule cannot be excluded.

The scope of the review is confined to hazards associated with separated plutonium and uranium, not those posed by spent fuel. Three material

categories are identified and addressed: metals, oxides, and residues. Metallic forms are typically from weapons sources. They generally include unalloyed and Ga-containing alloys of typical weapons-grade Pu (initially 0.04% ^{238}Pu, 93.3% ^{239}Pu, 6.0% ^{240}Pu, 0.6% ^{241}Pu, 0.04% ^{242}Pu) (IAEA Report, 1998), as well as highly enriched (>90% ^{235}U) and depleted (<0.72% ^{235}U) U. Oxides are derived from both weapons and civilian sources. The isotopic distribution of Pu depends on the level of fuel burnup and is typically about 1% ^{238}Pu, 60–70% ^{239}Pu, 20–25% ^{240}Pu, 5–10% ^{241}Pu, and 1–5% ^{242}Pu for civilian sources (IAEA Report, 1998). Unirradiated MOX fuel for light-water reactors typically contains 5–7% Pu. Residues are poorly defined and include a broad spectrum of wastes produced by processing activities.

29.2.2 Rate-controlling factors and mechanisms

A negative Gibbs energy change is necessary for any reaction, either rapid or slow. The potential hazard existing during handling depends on both the rate and the enthalpy of reaction. Factors that determine the reaction rates of liquids and gases with metals or ionic compounds are suggested by consideration of likely mechanistic steps. Reacting molecules must (1) reach the solid interface, (2) adsorb on that surface, and (3) dissociate to form a monatomic anion by interaction with electrons from the solid. Resulting anions must (4) enter the solid lattice, (5) be transported through the layer of product solid while electrons move toward the surface, and (6) ultimately react at the product–reactant interface. The rate of reaction is determined by the slowest step or the combined effect of steps.

A general expression for the rate, R, of a gas–solid reaction includes dependencies on temperature and on partial pressures $P_1, P_2, P_3, \ldots$ of gaseous reactants $1, 2, 3, \ldots$.

$$R = k \exp(-E_a/R^*T)(P_1)^{n_1}(P_2)^{n_2}(P_3)^{n_3} \ldots .$$

This equation includes the proportionality constant (k) and an Arrhenius term defined by the activation energy (E_a), the gas constant (R^*), and temperature. The rate is normalized for surface area of the reacting solid using geometric areas of massive solids or molecular-scale (BET) areas of powders. Dependencies of R on gas concentrations are described by the pressure exponents $n_1, n_2, n_3, \ldots$. Experimental valuation of k, E_a, and n are important in identification of rate-determining steps.

Different rate-controlling steps are encountered during corrosion of solids at different conditions (Haschke *et al.*, 2000a). During reaction of a mixture of reactive and inert gases, the rate may be controlled by transport of reactive gas through a layer of unreactive gas that accumulates at the gas–solid interface. In some cases, the rate is determined by the concentration of reactant molecules adsorbed on the surface. In other cases, R is determined by diffusion of the reacting anion through an adherent product layer on the reacting solid, as

indicated by a parabolic time dependence of the extent of reaction. Parabolic dependence is observed only as long as the product adheres and the thickness of the diffusion barrier increases. If spallation of product particles begins, the layer is thin in some locations and the rate increases at those sites. Although rates vary across the surface, continuing reaction and spallation maintain a constant average thickness and results in a linear dependence of extent on time. The combined process of parabolic and linear steps is described as 'paralinear' behavior. In the linear step, the diffusion-controlled rate is constant at fixed temperature and reactant pressure. The diffusion rate is usually increased by increasing temperature or by increasing pressure until the surface becomes saturated with reactant molecules. The reaction rate is dramatically increased and becomes temperature independent if the surface layer catalytically dissociates and transports reactant to the product–reactant interface. In that case, the rate is determined solely by the concentration of adsorbed reactant and depends only on gas pressure.

The preceding discussion of rate-controlling processes implies that the product layer on the surface of a reacting solid may be protective or catalytic depending on its ability to form and transport the diffusing species. The structure of the product formed on the reacting solid (metal or compound) is important in determining its nature. A surprising feature of plutonium compounds formed by atmospheric constituents is the pervasive presence of plutonium in cubic ($Fm3m$ symmetry) structures in which Pu occupies face-centered cubic (fcc) positions (Haschke *et al.*, 2000a). The fcc cation lattice has two tetrahedral interstitial sites per cation and one interstitial octahedral site per cation, features that allow for a variety of compositions and accommodation of up to three anions per Pu. Maintenance of charge balance in the lattice is enhanced by the ability to include anions with different charges and Pu cations in different oxidation states in solids.

This structural flexibility facilitates formation of various products at low temperature by decreasing or increasing the anion/cation ratio or by replacing existing anions. Such reactions of solid phases usually occur at elevated temperatures because of the high activation energies associated with rearrangement of the cationic lattice. The NaCl-type structure is formed by anion occupation of octahedral sites in the fcc lattice, the CaF_2-type structure is formed by occupation of the tetrahedral sites, and the anti-Fe_3Al structure is formed by occupation of both sites. Extended solid solutions form as the anion/cation ratio and the average oxidation state of Pu progressively change.

Transport rates of reactant ions in the product layer appear strongly dependent on deviations from ideal stoichiometry (Haschke *et al.*, 2000a). At low temperatures, transport of ions through a rigid CaF_2-type lattice like PuO_2 or UO_2 occurs by hopping of reactant ions between octahedral sites. Vacant tetrahedral sites formed in substoichiometric compounds share faces with normally vacant octahedral sites and create channels that facilitate anion movement. In a similar way, occupation of octahedral sites in compositions with

anion:cation ratios greater than 2 tends to hinder anion movement because diffusion channels are occupied. However, markedly different behavior is encountered with superionic conductors in which the cation lattice is rigid and the anions (e.g. O^{2-}, F^-, Cl^-, I^-) are highly mobile (Boyce and Huberman, 1979). These solids frequently have NaCl-type, CaF_2-type, or related structures; their ionic conductivities are comparable to those of molten salts and typically exceed those of ordinary ionic solids by more than 10^8.

In large measure, plutonium reactivity and its perplexing behavior are determined by fundamental properties of the product compound(s) existing on the metal surface, not by the properties of Pu. The only important property of plutonium is its chemical potential that drives reaction. Interpretation of Pu corrosion hinges on understanding the behavior of hydride, oxide, and other surface compounds. Therefore, relevant fundamental properties of these materials are reviewed as a basis for describing reactivities of metals and compounds.

29.3 FORMATION AND PROPERTIES OF COMPOUNDS

29.3.1 Plutonium hydrides

As shown by the phase diagram in Fig. 29.1, the complex plutonium–hydrogen system is dominated by the existence of a fcc PuH_x solid solution that is stable from $PuH_{1.95}$ to $PuH_{2.7}$ at room temperature and extends to PuH_3 above 300°C. This simplified diagram does not indicate regions of apparent structural ordering outlined in comprehensive reviews of hydride properties (Flotow *et al.*, 1984; Haschke *et al.*, 1987; Ward and Haschke, 1994). At high compositions, the fcc CaF_2-related hydride coexists with the PuH_y ($2.8<y<3.0$ at 25°C) solid solution, a substoichiometric phase derived from the hexagonal LaF_3-related PuH_3 phase by formation of anion vacancies. Hydrides are obtained by reaction of metal with H_2 or with elemental hydrogen derived from other sources. Hexagonal hydride is formed by reaction of Pu with H_2 at several bar pressure and temperatures above 400°C (Haschke *et al.*, 1987) and its appearance is unlikely unless these conditions exist. Transformation of the Pu cations from the fcc arrangement of PuH_x to the hcp arrangement of PuH_y at low temperatures is apparently precluded by a high activation energy. Therefore, metastable PuH_x forms beyond the $PuH_{2.7}$ composition as hydrogen occupies vacant octahedral sites in the cubic structure. The value of x exceeds 2.9 as the H_2 pressure is increased to 1 bar (Haschke *et al.*, 1980). The cubic PuH_x powder formed by slow reaction at low temperatures is pyrophoric in air at room temperature, but the hexagonal PuH_y only ignites in air when heated above 270°C (Haschke *et al.*, 1987).

Stoichiometric PuH_2 is frequently formulated as a distinct binary phase, but reference to Fig. 29.1 shows that the dihydride exists only as a composition within the PuH_x continuum. The hydride at the lower phase boundary has a

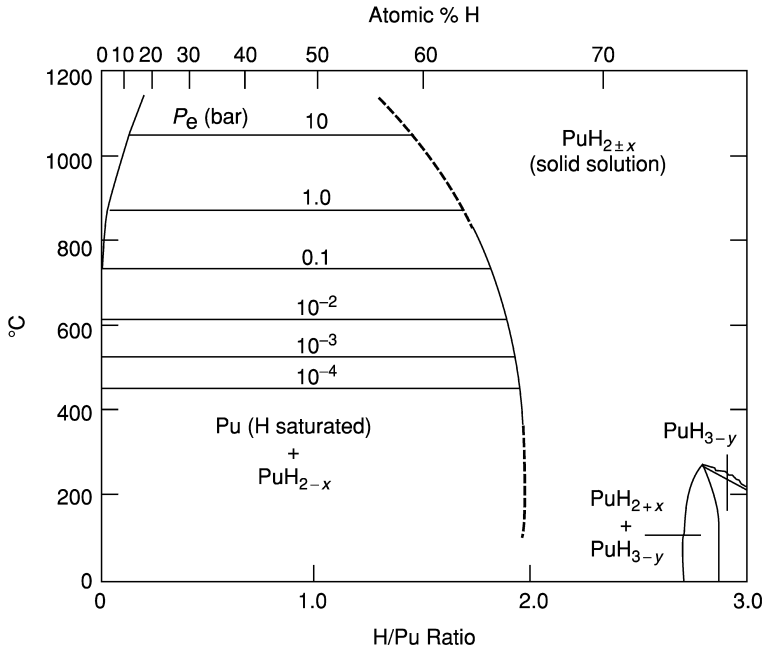

Fig. 29.1 *Proposed phase diagram of the Pu–H system. Data are from Flotow* et al. (1984).

progressively decreasing x with increasing temperature and coexists with hydrogen-saturated metal (Allen, 1991). Temperatures and corresponding equilibrium H_2 pressures within the two-phase region (Fig. 29.1) show that the hydride decomposes to metal upon heating in vacuum. The extrapolated equilibrium hydrogen pressure at room temperature is 10^{-21} bar (Flotow *et al.*, 1984) and the estimated H/Pu ratio in the metal is 10^{-9} (Allen, 1991). ΔH_f° (298 K) and ΔG_f° (298 K) for cubic PuH_x vary regularly with x between values for terminal compositions in Table 29.1 (Flotow *et al.*, 1984).

Electrical properties of PuH_x are inconsistent with those of ionic insulators having CaF_2-type structures (Haschke *et al.*, 1987; Ward and Haschke, 1994). Whereas compositions less than PuH_2 are consistent with forming vacancies on anion sites, x values in the 2–3 range are apparently attained by progressive occupation of additional anion sites by H^-. The PuH_2 formula implies that plutonium is present as the divalent cation, an unknown oxidation state of Pu in solids. The color of PuH_x changes from silver at $x = 2$ to black at high x; hydride conductivity is comparable to that of α-phase Pu at x near 2 and decreases to the semiconductor range at high x. Magnetic data show that Pu in PuH_x is present in the trivalent state. PuH_2 is most easily viewed as a Pu(III) lattice in which anion sites are occupied by H^- in a 2:1 H/Pu ratio and a

Table 29.1 *Thermodynamic data for selected plutonium compounds.*[a]

Compound	ΔH_f°(298 K) (kJ mol^{-1})	ΔG_f°(298 K) (kJ mol^{-1})	*References* [b]
fcc PuH_2	–164	–135	A
fcc PuH_3	–211	–156	A
α-$PuO_{1.5}$[c]	(–828)	(–787)	B
PuO_2	–1056	–998	C
$PuO_{2.1}$	(–1088)	(–1032)	D
$PuO_{2.5}$	(–1209)	(–1146)	D
PuN	–299	–274	C

[a] Estimated values are in parenthesis.
[b] References: A, Flotow *et al*. (1984); B, Morss (1986); C, Lemire *et al*. (2001); D, Haschke and Allen (2002).
[c] Values are normalized to $PuO_{1.500}$ using data for $PuO_{1.515}$ (Morss, 1986).

conduction band is occupied by one electron per Pu (Haschke *et al*., 1987). The hydride color changes from silver to black with increasing PuH_x composition as conduction electrons are progressively bound as H^- on anion sites.

High mobility of hydrogen in PuH_x is indicated by proton nuclear magnetic resonance (NMR) data showing that resonance lines are motionally narrowed and the diffusion of hydrogen is 'too fast' for measurements at room temperature (Cinader *et al*., 1976). At and below 190 K (–83°C), line shapes of PuH_x correspond to a rigid lattice with hydrogen occupying all tetrahedral sites and the appropriate fraction of octahedral sites required by x. A previously unexplained broad peak in the C_p curve for hydride (Flotow *et al*., 1984) at 200–270 K coincides with freezing-in of H^- on lattice sites. This peak is identified as the transition from ionic to superionic conduction above 0°C (Haschke and Allen, 2001) and implies that hydrogen transport in PuH_x is extremely rapid at 25°C and higher temperatures.

29.3.2 Plutonium oxides

The partial plutonium–oxygen phase diagram in Fig. 29.2 is based on phase relationships presented in prior reviews of oxide chemistry (Colmenares, 1975; Weigel *et al*., 1986) and in a more recent assessment of high-temperature data (Wriedt, 1990). Three oxides are stable at room temperature: hexagonal La_2O_3-type sesquioxide (identified as β-Pu_2O_3), bcc Mn_2O_3-related $PuO_{1.515}$ (identified as α-Pu_2O_3), and PuO_2. According to the diagram, β-Pu_2O_3 coexists with oxygen-saturated Pu and α-Pu_2O_3 coexists with PuO_2 below 335°C with a narrow two-phase region separating the $PuO_{1.50}$ and $PuO_{1.515}$ compositions at low temperatures. Assignment of this unusual relationship is based on coexistence of the two phases, failure to observe the hexagonal to cubic transition, and a reported lack of overlap in their compositions (Wriedt, 1990). This basis seems tenuous because dimorphic relationships of hexagonal and cubic oxides exist for

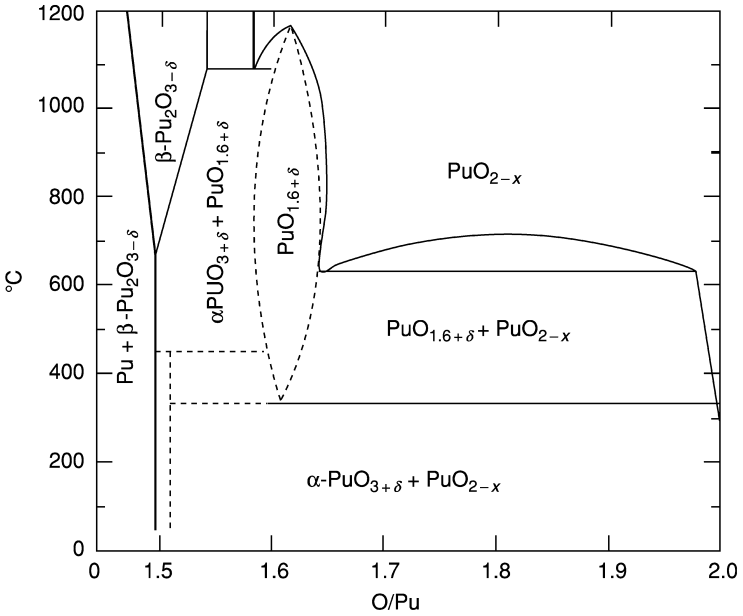

Fig. 29.2 *Partial Pu–O phase diagram based on high-temperature studies with O_2.*

lanthanide analogs (Eyring, 1979) and transformation is likely to be slow at low temperatures. The composition of the cubic oxide ($PuO_{1.46 \pm 0.04}$) formed during slow oxidation of Pu by water at room temperature (Haschke *et al.*, 1983) suggests that composition ranges of the two oxides are not significantly different. A reason to expect enhanced stability for a stoichiometric Mn_2O_3-related phase at the Pu_2O_3 composition with 3% occupancy of the cation sites by Pu(IV) is not apparent. In addition, both α- and β-forms of the sesquioxide are reportedly prepared by carbon reduction of PuO_2 at 1500–2000°C (Haire and Haschke, 2001), a temperature range in which α-Pu_2O_3 is unstable (Fig. 29.2) (Weigel *et al.*, 1986; Wriedt, 1990).

Concern about the precise phase relationships of sesquioxide may seem unmerited, but the nature of the oxide layer on Pu is apparently a key factor in determining metal reactivity. Data in Fig. 29.2 imply that β-Pu_2O_3 should exist on the metal surface, but analysis of Pu surfaces shows that only PuO_2 is detectable after exposure to air at room temperature (Terada *et al.*, 1969; Stakebake, 1971; Colmenares, 1984). Kinetic control of oxidation is implied (Haschke, 1992a) and supported by X-ray diffraction (XRD) measurements showing that heating of dioxide-coated Pu in vacuum results in reduction of the PuO_2 surface layer to α-Pu_2O_3 by the underlying metal (Terada *et al.*, 1969). The α-Pu_2O_3 readily appears at 150°C, is completely formed within minutes at 200°C, and persists when heated at 420°C. Appearance of a NaCl-type phase

at higher temperatures is attributed to formation of PuO (Cleveland, 1979). Subsequent X-ray photoelectron spectroscopy and atomic emission spectroscopy (XPS/AES) investigation confirms the facile reduction of PuO_2 to Pu_2O_3 at 200°C, but shows that the product observed at high temperatures is an oxide carbide (nominally $Pu(III)O_{0.5 \pm 0.1}C_{0.5 \pm 0.1}$) formed by reaction of free carbon with oxide and metal (Larson and Haschke, 1981). The spectroscopic data also show that plutonium oxide is extensively contaminated with unbound C after exposure to air or CO_2 and that the C(1s) peak shifts to a lower binding energy characteristic of carbide (C^{4-}) at temperatures in the range reported for PuO formation. Although plutonium monoxide is frequently reported in the literature, those products are most likely ternary compounds stabilized by carbon or nitrogen (Larson and Haschke, 1981; Weigel *et al.*, 1986).

Formation of an α-Pu_2O_3 layer on Pu at 200°C does not agree with phase relationships in Fig. 29.2, but is consistent with facile movement of oxide ions in fcc Pu cations lattice. The bcc Mn_2O_3-type structure (Wells, 1975) is derived by ordered removal of O^{2-} from one-fourth of the tetrahedral sites of CaF_2-type PuO_2 and occupation of all cation sites by Pu(III). The superstructure of anion vacancies results in a doubled cubic cell (a_0 bcc $= 2\ a_0$ fcc). Electrons move into the PuO_2 layer and reduce Pu(IV) to Pu(III) as O^{2-} ions move from the oxide layer to the oxide–metal interface and form additional α-Pu_2O_3.

In air or O_2, the steady-state chemical composition of the oxide layer on the Pu surface is determined by the relative rates of competing reactions (Haschke and Allen, 2001). Formation of α-Pu_2O_3 at the oxide–metal interface is countered by its oxidation to PuO_2 by oxygen. The relatively rapid rate of PuO_2 formation at 25°C yields a layer that is primarily dioxide, even though a thin sesquioxide layer must exist at the oxide–metal interface. These reactions have different activation energies and the rate of reduction increases more rapidly with increasing temperature than the rate of oxidation, as demonstrated by XRD and XPS analysis of the product layer formed in water vapor at 250°C (Stakebake *et al.*, 1993). The α-Pu_2O_3 layer is detectable beneath a relatively thin double layer composed of an inner PuO_2 layer and an outer layer of a previously unidentified higher oxide with a CaF_2-related structure. The dominant oxide layer on Pu surface in air progressively changes from PuO_2 at 25°C to α-Pu_2O_3 with increasing temperature (Haschke and Allen, 2001). The rate reduction becomes increasingly rapid with increasing temperature and formation of sesquioxide is kinetically favored above 500°C.

Additional complexity of the Pu–O phase diagram is suggested by results of water titration measurements in which Pu was submerged in salt solution at room temperature (Haschke *et al.*, 1983; Haschke, 1992a). Ionic radii of Pu(III) and Pu(IV) and relative free energies of Pu_2O_3 and PuO_2 correspond closely with those of Pr, suggesting that stable mixed-valence intermediate oxides like the CaF_2-related phases in the Pr–O system (Eyring, 1979) are to be expected for Pu. The titration (Haschke *et al.*, 1983), which is monitored by measuring hydrogen production, shows that the H_2 generation rate progressively decreases

Table 29.2 *Sequence of reactions derived from cumulative H_2/Pu ratios at intersection points of linear segments during reaction of Pu with water at* 23°C (*Haschke*, 1992*a*).

Reaction	*Cumulative H_2/Pu ratio*[a]	
	Theoretical	*Experimental*
$Pu + H_2O \rightarrow PuOH + 1/2H_2$	0.500	0.507(6)
$PuOH + 2/7H_2O \rightarrow 1/7Pu_7O_9H_3 + 4/7H_2$	1.071	1.078(23)
$1/7Pu_7O_9H_3 + 3/14H_2O \rightarrow 1/2Pu_2O_3 + 3/7H_2$	1.500	1.455(38)
$1/2Pu_2O_3 + 3/14H_2O \rightarrow 1/7Pu_7O_{12} + 3/14H_2$	1.714	1.716(170)
$1/7Pu_7O_{12} + 4/63H_2O \rightarrow 1/9Pu_9O_{16} + 4/63H_2$	1.778	1.763(118)
$1/9Pu_9O_{16} + 1/45H_2O \rightarrow 1/10Pu_{10}O_{18} + 1/45H_2$	1.800	1.803(2)
$1/10Pu_{10}O_{18} + 1/30H_2O \rightarrow 1/12Pu_{12}O_{22} + 1/30H_2$	1.833	1.831(181)
$1/12Pu_{12}O_{22} + 1/6H_2O \rightarrow PuO_2 + 1/6H_2$	2.000	1.993(16)

[a] Uncertainties in measured values are given in parenthesis.

over a year-long period in a sequence of constant-rate steps with intersection points at well-defined molar ratios of H_2:Pu associated with completion points of successive reactions. Intersection points corresponding to changes in rate (Table 29.2) are assigned to formation of oxide hydrides (PuOH and $Pu_7O_9H_3$), Pu_2O_3, members of the Pu_nO_{2n-2} homologous series with $n = 7$, 9, 10, and 12, and PuO_2. Continued generation of pure H_2 beyond the dioxide composition could not be explained. XRD data for initial and terminal products show CaF_2-related structures and imply that all intermediate products have fcc Pu lattices that do not transform at 25°C. Members of the homologous series presumably have CaF_2-related structures like those of intermediate praseodymium oxides (Eyring, 1979).

Formation of a high-composition plutonium oxide, PuO_{2+x}, by reaction of PuO_2 with H_2O or with O_2 in the presence of water is indicated by microbalance and pressure–volume–temperature measurements at 25–250°C (Haschke *et al.*, 2000b). The oxide–water reaction proceeds with H_2 formation and a mass increase corresponding to stoichiometric incorporation of oxygen in the solid:

$$PuO_2(s) + xH_2O(l, g) \rightarrow PuO_{2+x}(s) + xH_2(g).$$

Dry O_2 (air) does not react with PuO_2 at a detectable rate, but is preferentially consumed in forming PuO_{2+x} via a water-catalyzed cycle if water is present. Catalyzed reaction of O_2 forms PuO_{2+x} at the same rate as the oxide–water reaction, but H_2 is not formed. The catalytic cycle is established as water reacts with the oxide at its characteristically more rapid rate and atomic H formed on the surface combines with dissociatively adsorbed oxygen to re-form water. In the absence of O_2, high-purity (>99.99%) H_2 is produced according to the above reaction as H atoms associate and desorb.

XRD data for solid products of the oxide–water reaction show a single CaF_2-related phase with a lattice parameter that increases by 0.4 pm as reaction

initiates and thereafter has a linear dependence on composition, a_0 (nm) = 0.53643 + 0.001764(2+x), consistent with the formation of an extended solid solution. Results account for earlier observations of H_2 generation beyond the PuO_2 composition in liquid water (Haschke *et al.*, 1983; Haschke, 1992a) and show that oxide stoichoimetries approach $PuO_{2.3}$ (Haschke *et al.*, 2000b), but do not define the upper phase boundary of PuO_{2+x}. The area-normalized rate of H_2 formation by the PuO_2–water reaction is temperature-dependent (E_a = 39.3 kJ mol^{-1}), implying that the reaction is chemical, not radiolytic. Self-induced radiation damage does not account for the expansion of a_0 (Haschke and Allen, 2002) and radiolysis of H_2O fails to account for either the observed H_2 formation rate or for absence of O_2 as a gaseous product (Haschke *et al.*, 2001a).

As implied by extended X-ray absorption fine structure (EXAFS) and X-ray absorption near edge structure (XANES) results showing Pu(V) in PuO_{2+x} (Conradson *et al.*, 2003, 2004; Paffett *et al.*, 2003a), formation of this UO_{2+x} analog occurs by substitution of Pu(V) for Pu(IV) on cation lattice sites and accommodation of additional O^{2-} on octahedral interstices of the lattice (Haschke *et al.*, 2000b). EXAFS results show nearest-neighbor Pu–O distances of 0.183–0.193 nm for a range of PuO_{2+x} compositions (Conradson *et al.*, 2003, 2004). This value is significantly shorter than the characteristic Pu–O distance of 0.233 nm for O in tetrahedral sites of PuO_2. Evaluation of parameters affecting XANES edge energies indicates that observations are most consistent with the presence of Pu(V) in PuO_{2+x}.

The highest PuO_{2+x} possible composition is identified as $PuO_{2.5}$, the maximum attainable stoichiometry of the $Pu(IV)_{1-2x}Pu(V)_{2x}O_{2+x}$ solid solution (Haschke and Allen, 2002). Lattice parameters of steady-state solids formed after placing Pu(IV) hydrous oxide in aqueous solution are consistent with formation of cubic PuO_{2+x} with x-values that vary from 0 near pH 10 to 0.5 near pH 3 (Haschke and Oversby, 2002). Stability of PuO_{2+x} is demonstrated by extraction of oxygen from water during formation and is supported by thermodynamic assessment (Haschke and Allen, 2002). Results indicating that the phase is stable to $x = 0.5$ in air at temperatures of 350–400°C and that x approaches zero at 600°C are not confirmed by experiment. ΔH_f°(298 K) and ΔG_f°(298 K) for α-Pu_2O_3, PuO_2, and selected PuO_{2+x} compositions are given in Table 29.1.

Further EXAFS investigation of hydrothermal products and other compounds formed by aging precipitates from neutral Pu(IV) and Pu(VI) solutions shows the 0.183–0.193 nm Pu–O distances characteristic of PuO_{2+x} (Conradson *et al.*, 2004). These compounds, as well as those formed by reaction of PuO_2 with water vapor, have slightly increased fcc lattice parameters relative to PuO_2 and are identified as $PuO_{2+x-y}(OH)_{2y}$. Interpretation of EXAFS and XANES results leads to a structure described as a conglomeration of oligomerized Pu(IV) and PuO_2^+ oxo-hydroxide-aquo moieties with the same average Pu sublattice locations as in PuO_2. Other workers suggest that additional oxygen is

accommodated in the lattice predominately as hydroxyls, not as oxide and describe the phase as $PuO_{2+x} \cdot H_2O$ (Paffett *et al.*, 2003a).

Results of thermal decomposition and chemical analyses (Haschke, 1992a) of the product subsequently identified as $PuO_{2.27}$ on the basis of H_2 generation (Haschke *et al.*, 2000b) are most consistent with an anhydrous product, but stabilization of the higher oxide by hydroxide cannot be excluded. A first-principles quantum mechanical calculation of the PuO_{2+x} electronic structure (Petit *et al.*, 2003) indicates that a delicate energy balance does not favor PuO_{2+x} formation, but might be altered if interstitial species other than O^{2-} are present. The predicted composition dependence of the cubic PuO_{2+x} lattice parameter is consistent with the observed insensitivity of a_0 to x. Incorporation of hydroxyl in the lattice during exposure of oxide to moisture may account for the mass loss observed above 700°C during calcination (Stakebake, 1973).

Although behavior of plutonium oxides is generally consistent with a recently proposed Pu–O phase diagram (Haire and Haschke, 2001), the alternative diagram in Fig. 29.3 shows overlapping compositions for α-Pu_2O_3 and β-Pu_2O_3. Transformation of α into β near 450°C (Wriedt, 1990) is consistent with behavior of lanthanide oxides (Eyring, 1979). Thermodynamic data do not resolve the issue because the difference in free energies of formation of the two oxides is small. The $\Delta G_f^\circ(298\ K)$ of –1580 kJ mol^{-1} recommended for β-Pu_2O_3

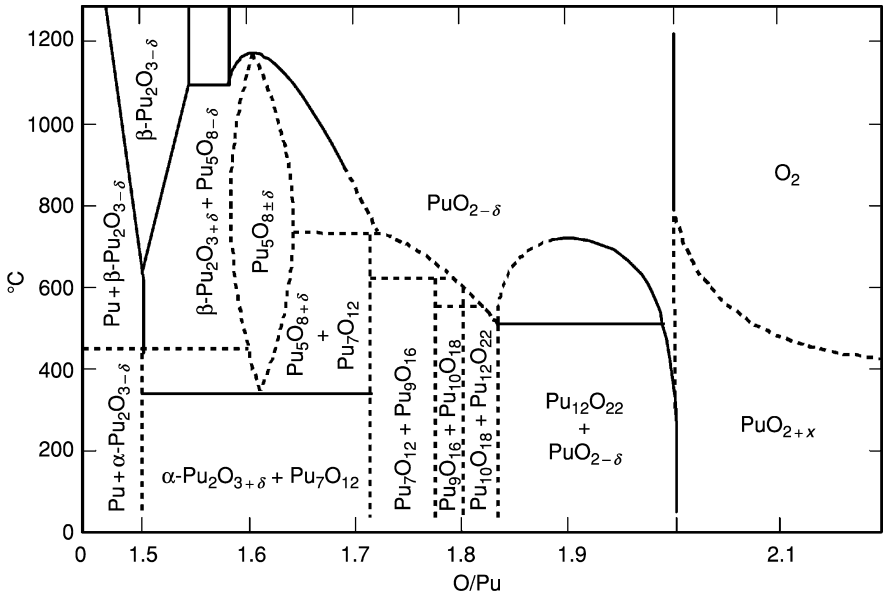

Fig. 29.3 *Partial PuO–phase diagram based on studies with O_2 at high temperatures and on studies with H_2O at low temperatures.*

(Morss, 1986) overlaps with the composition-adjusted value (–(1574 ± 11) kJ mol^{-1}) for stoichiometric α-Pu_2O_3. Formation of α-Pu_2O_3 in water at low temperatures may result from favorable kinetics of a preexisting fcc Pu lattice, but the reported preparation of bcc $PuO_{1.515}$ by reduction of PuO_2 above 1600°C (Weigel *et al.*, 1986) cannot be explained because that composition is within the phase field of β-Pu_2O_3 (Figs. 29.2 and 29.3), a solid that apparently does not transform into α-Pu_2O_3 on cooling (Wriedt, 1990).

A major difference between Figs. 29.2 and 29.3 is the existence of homologous series oxides containing fixed ratios of Pu(III) and Pu(IV) (Haschke, 1992a). Observed compositions correspond to those of Pr–O (Eyring, 1979) plus an additional member at $n = 5$ ($PuO_{1.6}$). Intermediate oxides apparently form during reaction of α-Pu_2O_3 with water at room temperature because rates of the oxide–water reactions are sufficiently slow that conditions are isothermal and differences in rates of successive reactions are resolved (Haschke *et al.*, 1983; Haschke, 1992a). Failure to observe intermediate oxides in studies with O_2 is attributed to the catalytic nature of α-Pu_2O_3 and rapid exothermic reaction of the bcc oxide with oxygen (Haschke and Allen, 2001). Rapid reaction heats the oxide beyond the stability ranges of the Pu_nO_{2n-2} phases and terminates at PuO_2. Unlike the dioxides of Ce, Pr, and Tb (Eyring, 1979), PuO_2 does not desorb oxygen and equilibrate with $Pu_{12}O_{22}$ when heated to 500°C, but vaporized incongruently at 1500–2000°C with the formation of PuO_2 (g), PuO (g), O (g), and O_2 (g) (Cleveland, 1979; Weigel *et al.*, 1986).

As defined by estimated equilibrium oxygen pressures (Haschke and Allen, 2001), the phase boundary of the PuO_{2+x} solid solution is indicated in Fig. 29.3. Data suggest that the stable solution extends to $PuO_{2.5}$ at temperatures up to 400°C and imply that a very narrow two-phase region exists between PuO_2 and PuO_{2+x}. Behavior is uncertain and additional work is needed to resolve the controversy over existence of PuO_{2+x} (Ronchi *et al.*, 2000) and define equilibria in the Pu–O and Pu–O–H systems.

29.3.3 Other plutonium compounds

As the major constituent of air, nitrogen is an important potential reactant in corrosion. The only binary compound of plutonium is the mononitride, PuN, which has a variable composition ($PuN_{1-\delta}$) attributed to formation of anion vacancies in the fcc NaCl-type structure (Cleveland, 1979; Weigel *et al.*, 1986). Reaction of N_2 with Pu initiates at about 300°C, but is slow and only 80% complete after 17 h at 1000°C (Brown *et al.*, 1955). The nitriding rate is markedly increased by reacting N_2 with PuH_x in a process that initiates at temperatures as low as 230°C. A rapid initial reaction is about 60% complete and followed by a slower second step that results in 97% of theoretical PuN formation after several hours. Nitriding of Pu is promoted if the metal is coated with hydride and then exposed to N_2 at 250°C (Cleveland, 1979). The reaction apparently proceeds as nitrogen displaces hydrogen in the fcc Pu lattice of PuH_x

and as product H atoms advance into the metal to re-form hydride (Haschke and Allen, 2001). Values of $\Delta H_f^\circ(298\ K)$ and $\Delta G_f^\circ(298\ K)$ for PuN are given in Table 29.1 (Lemire *et al.*, 2001).

Reaction of plutonium metal with water in near-neutral solutions at room temperature proceeds by a stoichiometric reaction that forms 0.5 mol H_2 per mol of Pu and a hydridic black solid identified as plutonium monoxide monohydride, PuOH (Haschke *et al.*, 1983; Haschke, 1992a). Formation of this compositional analog of PuOCl is suppressed at high pH (Haschke, 1995) and catalyzed by chloride and other salts in solution, but those anions are not incorporated in the solid (Haschke, 1992a). The product forms an adherent layer on the metal and spalls as particles with average dimensions of about 7 nm (Haschke *et al.*, 1983). PuOH crystallizes in a CaF_2-related structure and XPS data indicates that plutonium is trivalent, implying that cation sites are occupied by Pu(III) and anion sites are occupied by O^{2-} and H^-. Thermal decomposition of PuOH at 105–195°C in vacuum results in stoichiometric loss of hydrogen and formation of a violently reactive solid at the PuO composition. The oxide hydride is insoluble in dilute HCl and continued exposure to liquid water produces additional H_2 and a sequence of solid products identified in Section 29.3.2.

29.3.4 Plutonium alloys

As shown by phase diagrams for binary and higher systems of plutonium (Ellinger *et al.*, 1968), formation of intermetallic compounds is an extensive and important aspect of Pu chemistry. Alloying of Pu with 3–9 at% (1–3 wt%) Ga expands the thermal stability range of the fcc δ-phase from the 310–452°C span of pure metal to a range extending from about 100 to 600°C (Hecker, 2001) and substantially reduces the corrosion rate in air (Waber, 1980). Although the Ga alloy is apparently unstable at room temperature, the rate of transformation is extremely slow. Addition of Al has comparable effects on δ-phase stability and corrosion, and forms a $PuAl_2$ intermetallic compound that melts congruently at 1540°C (Ellinger *et al.*, 1968). Alloying with Fe forms a eutectic composition (10 at% Fe) that melts at 410°C and Pu_6Fe, an intermetallic phase that melts at 428°C (Ellinger *et al.*, 1968). Other metals, such as Nb and V, do not form compounds with Pu and are relatively insoluble in molten Pu (Ellinger *et al.*, 1968). At 1200–1300°C, the saturated Pu-rich liquid contains about 10 at% of these metals.

29.3.5 Uranium compounds

Like plutonium, uranium forms compounds with constituents of the atmosphere and of environments for handling and storage. A single stoichiometric hydride, UH_3, formed by reaction of the elements exists in two cubic modifications (Ward, 1985). The low-temperature α-UH_3 is difficult to prepare and is not expected to form during routine operations. The β-UH_3 phase crystallizes in a

structure identified as β-tungsten-type, but the correct structure is apparently anti-type W_3O (Wells, 1975). All H-atoms occupy distorted tetrahedral sites that are formed by four U-atoms and share a face with another occupied tetrahedron and edges with three occupied tetrahedra. Edge-shared octahedral vacancies formed by six edge-shared tetrahedra provide the most likely pathway for H-transport. The measured activation energy for hydrogen self-diffusion in β-UH_3 is (30 ± 5) kJ mol^{-1} (Ward and Haschke, 1994). The electrical conductivity at 25°C (1×10^{-3} ohm^{-1} cm^{-1}) indicates metallic behavior. The hydride is highly reactive and ignites spontaneously when exposed to air. Thermodynamic properties of the hydride are reviewed (Flotow *et al.*, 1984; Grenthe *et al.*, 1992): $\Delta H_f^\circ(298\ K)$ and $\Delta G_f^\circ(298\ K)$ for β-UH_3 are –127 and –73 kJ mol^{-1}, respectively.

The U–O_2 system is also complex (Keller, 1973; Colmenares, 1975). Studies cited in these reviews indicate that reaction of U with O_2 successively forms UO_2, UO_{2+x} ($x < 0.2$), U_4O_9, U_3O_7, U_2O_5, and U_3O_8, the stable oxide in air with U in U(IV) and U(VI) oxidation states. UO_2 is prepared by reducing higher oxides with H_2 (Anderson *et al.*, 1955). The highest oxide, UO_3, is obtained in five crystallographic forms by heating U_3O_8 in 40 bar O_2 at 500°C or in NO_2 at (115 ± 60)°C and by ignition of oxygen-rich precipitates such as the hydrated nitrate ($UO_2(NO_3)_2 \cdot 6H_2O$) at 400–600°C (Hoekstra *et al.*, 1961). UO_{2+x} forms by accommodating oxygen on octahedral sites of CaF_2-type UO_2. UO_{2+x} is stable only at temperatures above 300°C, but may form as a metastable phase at lower temperatures. The CaF_2-related structure of U_4O_9 results from long-range ordering of oxygen on octahedral sites. The structure of low-temperature orthorhombic α-U_3O_8 (Wells, 1975) contains chains of vertex-shared pentagonal–bipyramidal (UO_7) coordination polyhedra. The structure, which is formed by sharing edges of polyhedral chains, has narrow channels that may restrict oxygen transport (Haschke *et al.*, 2001b). $\Delta H_f^\circ(298\ K)$ and $\Delta G_f^\circ(298\ K)$ for UO_2, U_4O_9, and U_3O_8 are –1085 and –1032 kJ mol^{-1}, –4511, and –4276 kJ mol^{-1}, and –3575 and –3369 kJ mol^{-1}, respectively (Grenthe *et al.*, 1992).

Hydrothermal studies indicate that U_3O_7, U_2O_5, and $UO_3 \cdot nH_2O$ form by spontaneous reaction of UO_2 with water at 130–200°C (Matzke and Turos, 1991). Rutherford backscattering (RBS) and elastic recoil detection analysis (ERDA) show that a layer of hydrogen-free higher oxide forms on the dioxide surface and imply that H_2 is produced.

$$3UO_2(s) + H_2O(l) \rightarrow U_3O_7(s) + H_2(g).$$

Experimental conditions preclude the presence of significant amounts of O_2. Hydrated UO_3 ($UO_3 \cdot nH_2O$) apparently forms at 200°C via a complex process involving oxidation of UO_2, leaching of U(VI) from the higher oxide product, and precipitation of hydrated UO_3. However, thermodynamic data for uranium oxides (Grenthe *et al.*, 1992) indicate that oxidation of UO_2 by H_2O is unfavorable at standard conditions. Because changes in heat capacities are small over a limited temperature range, ΔG° for the reaction at 130°C is approximately equal

to that for 25°C (+92 kJ mol^{-1}) and ΔG at 2.7 bar H_2O pressure remains positive unless the H_2 pressure is less than 10^{-12} bar, a condition that is difficult to maintain in an autoclave system as H_2 is apparently produced. Behavior parallels that for PuO_2–H_2O (see Section 29.3.2) and additional work is needed.

Uranium reacts with N_2 or NH_3 to form sesquinitride, U_2N_3, at temperatures above 400°C (Dell, 1973). The phase is non-stoichiometric with compositions typically ranging from $UN_{1.6}$ to $UN_{1.7}$. Below 1100°C, the α-U_2N_3 product has the bcc Mn_2O_3-related structure like that of α-Pu_2O_3 (Wells, 1975). The NaCl-type mononitride, UN, obtained by decomposing the sesquinitride in vacuum above 1100°C has a room-temperature conductivity (6.7×1^{-3} ohm^{-1} cm^{-1}) similar to that of Bi and Pb (Keller, 1973). The tendency to form sesquinitride during reaction of the elements is consistent with autocatalysis of nitriding by UN. Behavior appears similar to autocatalysis of hydriding by PuH_x and to the catalyzed oxidation of α-Pu_2O_3 by O_2. Values of $\Delta H_f^\circ(298\ K)$ and $\Delta G_f^\circ(298\ K)$ for UN and α-$U_2N_{3.18}$ are –290 and –265 kJ mol^{-1} and –758 and –676 kJ mol^{-1}, respectively (Grenthe *et al.*, 1992).

29.4 REACTION KINETICS OF PLUTONIUM COMPOUNDS

29.4.1 Hydride reactions

(a) Relevant hydride properties

Reaction rates of PuH_x ($1.95<x<3$) with gases and liquids depend on the size distribution of hydride particles and are proportional to surface area (Haschke, 1991). Size distributions of PuH_x vary with preparative conditions; fine powders are formed during slow reaction at low temperatures (Stakebake, 1981a,b) and coarse particles with dimensions up to 1 cm are produced during rapid reaction at temperatures above 400°C (Haschke *et al.*, 1980). Specific surface areas of the low-temperature hydride are in the 0.15–0.25 m^2 g^{-1} range and equal those (0.1–0.2 m^2 g^{-1}) of Pu powders prepared by thermal dehydriding of the powder (Stakebake, 1981c). Therefore, the size distribution of metal particles prepared by a hydride–dehydride process is adopted for low-temperature PuH_x (Haschke, 1992b). Geometric areas of a few cm^2 per gram for hydride prepared at high temperatures are comparable to those of massive Pu.

(b) Reaction of PuH_x with hydrogen

The reaction of PuH_x with H_2 is an important process in ignition and corrosion of Pu metal, but has not been extensively studied. Compositions measured by microbalance methods at constant pressures in the 1–400 mbar range as PuH_x was heated at 2°C min^{-1} in the 25–500°C range agree with isothermal x-values at equilibrium (Haschke, 1981). In addition to indicating that the rates of

hydrogen absorption and desorption by cubic PuH_x are rapid, these results imply that formation of atomic H at the gas–solid interface and transport of hydrogen in the hydride are facile, even at room temperature. The rate of hydrogen absorption by PuH_x is comparable to the rate of the Pu–H_2 reaction and is essentially constant for compositions in the $PuH_{1.9}$–$PuH_{2.7}$ range (Haschke *et al.*, 1980). After adjustment of the surface area to account for a two- to three-fold increase during hydriding, the area-normalized rate at 1 bar H_2 pressure is 1–3 mmol H_2 cm^{-2} min^{-1} (geometric area).

Accommodation of additional hydrogen in the hydride structure is facile and has important kinetic consequences (Haschke and Allen, 2001). Product hydrogen accumulates in the solid and is released as H_2 after x of the PuH_x cores inside reacting hydride particles approach 3. Therefore, reactions of PuH_x with liquids and gases initiate without counter-current flow of hydrogen out of the solid or formation of H_2 at the gas–solid interface.

(c) Reaction of PuH_x with oxygen

Because exposure of hydride to oxygen is expected to result in pyrophoric reaction, observations made during microbalance studies in which PuH_x ($2.0<x<2.7$) at 50–360°C was exposed to O_2 at 13.3 mbar are perplexing (Stakebake, 1981a,b). Reaction initiated immediately at 50°C, essentially ceased after 2 min (20% completion), and completely transformed the hydride to PuO_2 only after the temperature was increased to 315°C in several steps. After each step, the microbalance system was evacuated and the sample temperature was increased before O_2 was reintroduced. During the initial stage of each step, the oxidation rate of oxide-coated hydride was similar to that observed during initial exposure of PuH_x to O_2. Within each step, the rate progressively decreased during an intermediate stage and continued at a slow temperature-dependent rate after entry into a final stage. Results show that reaction at 360°C proceeds via these stages with 95% transformation to PuO_2 after 90 min. XRD data verify that PuO_2 is the product layer on the hydride during the final stage. Kinetic analysis shows that E_a for the initial spontaneous PuH_x–O_2 reaction is negative (–9 kJ mol^{-1}), a result that is inconsistent with the expectation of high activation energies for autothermic processes. Evaluation of linear rates R, in mg O_2 (mg PuH_x)$^{-1}$ min^{-1}, for the final stage shows an Arrhenius dependence ($\ln R = 8.75 - 5050/T$) and an E_a (42 kJ mol^{-1}) consistent with diffusion control of oxygen through a protective PuO_2 film.

In a more recent study of hydride pyrophoricity and catalysis (Haschke and Allen, 2001), the stages of PuH_x oxidation observed in earlier work (Stakebake, 1981a,b) are correlated with chemistry of the oxide layer on the hydride. During heating in vacuum, PuH_x spontaneously reduces the PuO_2 layer to α-Pu_2O_3, a product that rapidly dissociates O_2, and transports oxygen to the oxide–hydride interface. The initial linear oxidation rates of PuH_x and α-Pu_2O_3-coated PuH_x form a single data set with values (88 μg Pu cm^{-2} min^{-1} at 50°C to

21 μg Pu cm^{-2} min^{-1} at 360°C, BET area) and yield an E_a of –8 kJ mol^{-1}. Results imply that α-Pu_2O_3 and PuH_x are equally reactive toward O_2. A negative E_a is consistent with a decrease in concentration of adsorbed reactant on a catalytic ($E_a = 0$) solid as temperature increases at constant pressure. Oxidation of the Pu_2O_3 surface to PuO_2 competes with reduction of PuO_2 by hydride during the intermediate stage, a process apparently triggered as x in PuH_x approaches 3 and product hydrogen flows out of the solid. The diffusion-controlled final stage is entered as the surface is covered by protective PuO_2.

The PuH_x–O_2 reaction is not autothermic, but is controlled by the oxygen pressure, P_{O_2} (Haschke and Allen, 2001). The rate equation is based on data for a range of temperatures because E_a is essentially zero:

$$R \text{ (in g Pu cm}^{-1}\text{min}^{-1}) = 0.37(P_{O_2})^2 \text{ (BET area, } P \text{ in bar)}.$$

The reason for a squared pressure dependence is unknown. The equation accurately predicts temperature-independent rates and is applied in interpreting hydride pyrophoricity and its dependence on temperature. Oxidation is rapid when the hydride is covered by α-Pu_2O_3 and is markedly slowed by a layer of PuO_2. Contrary to expectation, increasing the O_2 pressure does not favor formation of PuO_2. As with the oxide layer on Pu, high temperatures result in reduction of PuO_2 to α-Pu_2O_3 on PuH_x instead of PuO_2 formation (see Section 29.3.2). The large increase in the rates of oxidation and heat generation induced by a small increase in P_{O_2} drives up the temperature, promotes transformation of the oxide surface into catalytic α-Pu_2O_3, and results in continued oxidation at a rate equal to that of freshly prepared PuH_x. E_a for the PuH_x–O_2 reaction is zero, but pyrophoric oxidation of hydride depends indirectly on temperature as the pressure-dependent reaction heats the solid and maintains the catalytic surface.

Consistent failure of PuH_x to oxidize completely upon exposure to 13 mbar O_2 (Stakebake, 1981b) suggests that this P_{O_2} is below a threshold ignition pressure required for generating heat at a rate sufficient to form Pu_2O_3 and sustain rapid oxidation (Haschke and Allen, 2001). Complete oxidation of hydride within minutes at 0.13 bar O_2 (Stakebake, 1981a) implies that the threshold ignition pressure is 13–130 mbar, a range consistent with spontaneous ignition in air (0.21 bar O_2). The estimated threshold O_2 pressure for ignition of PuH_x is 40 mbar.

(d) Reaction of PuH_x with N_2

A facile PuH_x–N_2 reaction is implied by the use of hydride as an intermediate in preparing PuN (see Section 29.3.3), but kinetic data are limited. In an early study, nitriding initiated abruptly at 230°C during heating at 2.7°C min^{-1} in 1 bar N_2, transformed 60% of the PuH_x to PuN within minutes, and continued in a slow stage that approached completion (97%) after several hours (Brown *et al.*, 1955). XRD analysis of PuN products showed the presence of PuO_2 that

may have formed on the PuH_x before nitriding or on the nitride during handling. Effects of surface oxide in preventing reaction at temperatures below 230°C are uncertain.

A microbalance investigation of the PuH_x–N_2 reaction (Muromura and Ouchi, 1974) shows that rapid initial reactions of PuH_2 and PuH_3 at 282°C and 1 bar N_2 pressure are followed by progressively slower reactions that are about 60% complete after 2 h. Data for the initial stage at 225–268°C and 10^{-3}–1 bar N_2 are evaluated using a model based on rate control by chemisorption of nitrogen or hydrogen. Results indicate that the initial rate is controlled by slow association of product H-atoms at the gas–solid interface, a conclusion that seems inconsistent with measured E_a values of 150–297 kJ mol^{-1} for the initial stage of reaction.

Subsequent microbalance results for PuH_x–N_2 at 67 mbar (Stakebake, 1988) are consistent with early observations (Brown *et al.*, 1955). Mass–time data for reaction at 275°C show an initial linear rate (0.2 mg Pu cm^{-2} min^{-1}, BET area) stage resulting in 30% reaction, an intermediate stage in which the rate became progressively slower over time, and a slow constant-rate final stage entered after 85% reaction. Linear rates for the slow stage at 270–445°C (0.14–0.37 μg Pu cm^{-2} min^{-1}, BET area) yield an activation energy of 18 kJ mol^{-1}. Each temperature increase was followed by a brief, but rapid initial reaction. The initial rate at 275°C (1.6 mg Pu cm^{-2} min^{-1}) is comparable to that for the α-Pu_2O_3-catalyzed PuH_x–O_2 reaction at 67 mbar.

(e) Reaction of PuH_x with air

Exposure of PuH_x to air at 25°C results in spontaneous reaction of O_2 and N_2 and a thermal spike (Haschke *et al.*, 1998a). PuH_x was exposed to air supplied from a reservoir connected to a reactor. After reaction ceased, the residual gas was 50–75% H_2 plus 25–50% N_2. Product mole fractions in the solid were 0.80–0.95 PuH_x, 0.03–0.15 PuN, and 0.20–0.5 Pu_2O_3. N_2 and O_2 were consumed in a (1.6 ± 0.5) ratio (3.71 N_2/O_2 ratio in air) during reaction, showing that temperatures generated by hydride oxidation were sufficient to initiate the PuH_x–N_2 reaction. Product hydrogen accumulated in the hydride cores of reacting particles until x approached 3 and was thereafter released as H_2, a product that pressurized the reactor and subsequently prevented access of additional O_2.

The preceding results show that pyrophoric PuH_x–air reaction involves both O_2 and N_2, but are skewed by an experimental configuration in which accumulation of H_2 prevents continuing access of air (O_2) to the sample. Experience shows that unconfined reaction of hydride in air typically continues to completion and is accompanied by burning of H_2 as a pale flame above the solid. Water may have existed as a transient species in the closed system, but is probably formed in open systems. Unlimited access to air may also result in a secondary reaction in which the Pu_2O_3 and PuN products are oxidized to PuO_2.

(f) Reaction of PuH_x with H_2O

Reaction of PuH_x with liquid water at 25°C proceeds at a surprisingly slow rate (Haschke, 1995). The proposed reaction is based on simultaneous generation of H_2 and increase in composition of hydride cores of reacting particles until $x+\delta$ approaches 3:

$$PuH_x(s) + y\ H_2O(l) \rightarrow y\ PuOH(s) + (1-y)\ PuH_{x+\delta}(s) + (y(1+x+\delta)-\delta)/2\ H_2(g).$$

Production of H_2 is observed and XRD data for the product show an increase in hydride composition, but the oxidation product is not identified. Formation of PuOH is assumed by analogy to the reaction of liquid water with Pu metal.

Measurements of the H_2 formation rate show that a moderately rapid reaction occurs during the 0.5 h period after immersion of PuH_2 in 1 M $CaCl_2$ solution (Haschke, 1995). This initial stage is followed by one in which the rate has a parabolic time dependence, characteristic of a diffusion-controlled reaction. Based on H_2 generation and the above equation, the derived linear rate for the initial stage (0.3 μg Pu cm^{-2} min^{-1}, BET area) is 100-fold less than that for corrosion of Pu in 1 M $CaCl_2$ (Haschke, 1992a).

29.4.2 Oxide reactions

(a) Reactions of α-Pu_2O_3

Contrary to early reports that describe the bcc sesquioxide as protective and the source of parabolic oxidation kinetics during metal corrosion (Schnizlein and Fischer, 1967; Lindsay *et al.*, 1972), recent studies suggest that α-Pu_2O_3 is highly reactive and catalyzes reactions of Pu with H_2, O_2, and N_2 (Haschke and Allen, 2001). Kinetic data are available for the reaction of sesquioxide with liquid water (Haschke *et al.*, 1983; Haschke, 1992a). During formation of Pu_7O_{12} at 25°C, α-Pu_2O_3 reacts with H_2O at a slow constant rate of 10 nmol H_2 per g Pu_2O_3 per min or about 2 pg Pu_2O_3 cm^{-2} min^{-1} (BET area) according to the reaction shown in Table 29.2.

(b) Reactions of PuO_2

Reactions of PuO_2 with liquids and gases also depend on surface area, a property that varies substantially depending on the oxide source and preparative conditions (Haschke and Ricketts, 1995). Specific areas of oxides obtained by firing oxygenated precipitates at 400–500°C vary from 10 m^2 g^{-1} for nitrate to as much as 60 m^2 g^{-1} for oxalate and those from oxidation of Pu are 5–15 m^2 g^{-1}. Specific areas decrease upon firing above 600°C and consistently fall to 1–5 m^2 g^{-1} during calcining at 950°C.

Chemical behavior of plutonium dioxide is altered over broad ranges of temperature and humidity by chemisorption and physisorption of water

(Stakebake and Steward, 1973; Benhamou and Beraud, 1980, Haschke and Ricketts, 1997). Dissociative chemisorption occurs at low humidity by reaction of H_2O with O^{2-} ions to form two OH^- ions that bind strongly to the surface (Haschke and Ricketts, 1997). This reaction occurs at low H_2O concentrations (<300 ppm or <0.3 mbar H_2O) via two first-order steps that each adds one monolayer of hydroxide corresponding to a mass gain of 0.11 mg H_2O m^{-2} of oxide surface (3 μmol H_2O m^{-2}) and transforms the surface stoichiometry to $PuO(OH)_2$. Measurements with $U_{0.75}PuO_{0.25}O_{2-x}$ ($0.02<x<0.05$) suggest that the oxide surface is saturated by chemisorbed water at a gas-phase concentration of 10–20 ppm H_2O (Woodley and Gibby, 1973). Adsorbate-free (calcined) oxide tenaciously getters water and maintains a low H_2O pressure at 25°C and 10–15% coverage by the initial hydroxide layer (Haschke *et al*., 2001b). The chemisorption rate in air at 25°C and 0.3 mbar H_2O (1% relative humidity at 25°C) is approximately 10 μmol H_2O m^{-2} h^{-1} (Haschke *et al*., 2001a).

Additional water physisorbs on the $PuO(OH)_2$ surface of the oxide at progressively slower rates in discrete first-order steps corresponding to layers of molecular H_2O (0.22 mg H_2O m^{-2} per layer) as water pressure increases (Haschke and Ricketts, 1997). At 25°C and relative humidities in the 10–60% range, the equilibrium water concentration, $[H_2O]$, is (0.4 ± 0.1) mg H_2O m^{-2}, corresponding to two OH^- layers plus approximately one H_2O layer. The $[H_2O]$ increases sharply above 70% relative humidity and approaches a total of ten layers at saturation. The water content of oxide equilibrated with moist air at a given temperature and relative humidity is readily estimated if the specific surface area of the oxide is known. Although the distribution of water between adsorbed and gaseous states in a closed container depends on specific conditions, more than 99% of available H_2O resides on the oxide surface in a typical storage configuration at 25–75°C (Haschke *et al*., 2001a).

Thermal studies show that water desorbs from PuO_2 in two temperature ranges (Stakebake, 1973). Desorption enthalpies derived from kinetic data for removal of water in the 100–150 and 300–350°C ranges are 84 and 285 kJ mol^{-1}, respectively, if reversible adsorption is assumed to be a nonactivated process. Gravimetric data show a third mass loss above 700°C, but that process is not characterized. Adsorption–desorption measurements in a closed system at 25–260°C indicate that desorption is complete within that temperature range (Paffett *et al*., 2003b). Desorption enthalpies derived from non-isothermal adsorption data vary from 51 to 44 kJ mol^{-1} depending on adsorbate coverage and are consistent with values for UO_2 and other metal oxides. Further work is needed to resolve the differences between results of these studies and to account for a significant mass loss at 700–1000°C (Stakebake, 1973).

Slow reaction of PuO_2 with liquid or gaseous water forms PuO_{2+x} and H_2 via a temperature-dependent process (see Section 29.3.2). The rate of H_2 formation (or oxygen accommodation in the dioxide structure) is described by an Arrhenius equation derived from data for gaseous and liquid water at 25–350°C (Haschke *et al*., 2000b):

$$\ln R \text{ (mol } H_2 \text{ m}^{-2} \text{ h}^{-1}) = -6.441 - (4706/T) \text{ (BET area)}.$$

This reaction also defines R (in mol O m^{-2} h^{-1}) for PuO_{2+x} formation by water-catalyzed reaction of O_2. The rate is independent of water concentration at room temperature (Haschke *et al.*, 2001b), but behavior at high temperatures is unknown.

Radiolytic decomposition of adsorbed water by alpha particles from decay of Pu isotopes occurs simultaneously with the formation of PuO_{2+x} and H_2. As with gamma radiolysis of liquid water (Draganić and Draganić, 1971), alpha radiolysis (Christensen, 1998) proceeds with formation of free radicals such as hydroxyl (OH) and atomic hydrogen (H). Association of radicals leads to formation of H_2 and H_2O_2, a product that accumulates in solution and decomposes with the formation of O_2. The radiochemical yield (G_{H_2}) for hydrogen production is 0.45 H_2 per 100 eV of energy absorbed by water for gamma radiation and approximately 1.3 H_2 per 100 eV of energy absorbed by water for alpha particles. If water is irradiated in a closed system, a steady-state pressure of 1–2 atm is established as rates of radiolysis and re-formation of water become equal (Allen *et al.*, 1952). Similar dissociation reactions occur during radiolysis of adsorbed water, but differences are expected because absence of a liquid phase prevents formation and accumulation of products in solution. A review of observations during gamma irradiation of water adsorbed on non-radioactive oxides (Haschke *et al.*, 2001a) shows variable behavior and imbalance in the hydrogen–oxygen inventory, a condition attributed to reaction of gaseous product (usually loss of oxygen) with substrate solids. Radiochemical yields of adsorbed H_2O are reduced by factors of 10^3 in some cases and increased by up to 10^2 in others. Difficulties in balancing the radiolytic inventory and determining the radiolysis rate for H_2O on PuO_2 are likely because radiolytic oxygen is scavenged by PuO_{2+x} formation and because H_2 is independently produced by the oxide–water reaction (Haschke *et al.*, 2001a).

Studies of alpha-particle radiolysis of water by ^{244}Cm in solution show a H_2/O_2 ratio of 1.86 in the product gas (Kalinichenko *et al.*, 1987). Results of companion studies with $^{238}PuO_2$ immersed in water or exposed to steam at 60–140°C (0.2–3.6 bar H_2O pressure) imply that H_2 is the only gaseous product because G_{H_2} values for alpha radiolysis of water (1.05 and 5.8 H_2/100 eV absorbed by liquid and vapor, respectively) are based on measured (total) rates of gas evolution. The chemical fate of oxygen is not addressed. H_2 generation rates measured during exposure of mixed residues containing PuO_2 and MgO, $Ca(OH)_2$, or CaF_2 to moist air in closed containers at ambient temperature and 90°C are compared with predictions based on the rate of energy release by alpha decay, G_{H_2}, and composition-weighted stopping powers of water in the mixture (Livingston, 1999). On average, observed rates exceed predictions by a factor of 10. Evaluation (Haschke *et al.*, 2001a) of data from tests with only PuO_2 (Livingston, 1999) shows consumption of O_2, formation of N_2, and a temperature-dependent process that is inconsistent with radiolysis.

An estimate of the radiolysis rate ((9 ± 4) pmol H_2 m^{-2} h^{-1}) for oxide exposed to 50% humid air at 25°C (Haschke *et al.*, 2001a) indicates that radiolysis neither accounts for observed H_2 generation rates during exposure of PuO_2 to H_2O nor for a temperature dependence of the rate (Haschke *et al.*, 2000b). Particle-size distribution and self-absorption of alpha energy by the oxide, specific area of the oxide, thickness and alpha particle range of the absorbed water layer, and G_{H_2} for liquid H_2O are included in the derivation. Observed rates exceed estimated values by factors of 10 at 25°C and 10^5 at 350°C. A rate equation is derived assuming a linear dependence on water concentration and a zero rate in the absence of water:

$$R\ (\text{pmol H}_2\ \text{m}^{-2}\ \text{h}^{-1}) = 0.37\ (\text{mol H}_2\ (\text{mol H}_2\text{O})^{-1}\ \text{h}^{-1})[\text{H}_2\text{O}](\mu\text{mol H}_2\text{O}\ \text{m}^{-2}).$$

Observations with CeO_2–H_2O show that G_{H_2} is strongly dependent on $[H_2O]$ if less than—two to three water layers are adsorbed and remains essentially constant if more than three layers are adsorbed (LaVerne and Tandon, 2002). Therefore, proportionality of R and $[H_2O]$ may be limited to water concentrations less than 15 μmol H_2O m^{-2}.

Exposure of H_2–O_2 mixtures to calcined (water-free) PuO_2 at 25–300°C results in surface-catalyzed combination as H_2O (Haschke *et al.*, 1996, 2001b; Morales, 1998). The spontaneous reaction apparently proceeds by dissociative adsorption of H_2 and O_2 and combination of the atomic species. Behavior at 25°C is consistent with first-order kinetics controlled by the concentration of active sites on the oxide surface and progressive blockage of those sites by chemisorption of product water as OH^- (Haschke *et al.*, 2001b), but R is less sensitive to $[H_2O]$ at 100–300°C (Morales, 1998). Combination rates on water-free PuO_2 at 25 and 100–300°C are 30 nmol H_2O m^{-2} h^{-1} and 50 μmol m^{-2} h^{-1} (BET areas), respectively (Haschke *et al.*, 2001a). Adsorption of product H_2O sharply reduces the rate at 25°C, but only causes a 50-fold reduction above 100°C. The combination rate on stainless steel at 25°C (100 nmol H_2O m^{-2} h^{-1}, geometric area) is comparable to that for PuO_2 (Haschke *et al.*, 2001a). The combination reactions on both solids compete with radiolytic decomposition of water, but the extent of reaction on the relatively small area of steel in a typical storage configuration is negligible compared to that on calcined oxide ((3 ± 2) m^2 g^{-1}).

29.4.3 Nitride reactions

Plutonium nitride is readily oxidized to hydrous oxide ($PuO_2 \cdot xH_2O$) by water and reacts more slowly with oxygen to form dioxide (Brown *et al.*, 1955). The oxidation rate in O_2 is increased by moisture (Cleveland, 1979). Reaction with O_2 in air initiates below 100°C and rapidly goes to completion by 150°C with apparent formation of a hydrous intermediate that decomposes on heating above 800°C (Brown *et al.*, 1955). An effect of residual hydrogen on the reactivity of PuN formed via hydride is suggested by absence of pyrophoric

behavior after the product was heated in vacuum and N_2 at 700°C (Leary *et al.*, 1967). This result is confirmed by a study in which nitride from a PuH_x–N_2 reaction was heated at 700°C in N_2 atmospheres that were repeatedly replaced until H_2 could not be detected (<0.01%) in the static gas (Allen, 2001). The product was unreactive in 1 bar O_2 at temperatures up to 700°C, suggesting that residual hydrogen or moisture formed by hydrogen is involved in promoting oxidation of PuN.

29.5 CORROSION KINETICS OF PLUTONIUM METAL

29.5.1 Reaction of Pu with hydrogen

As with the U–H_2 reaction (Haschke, 1991), hydriding of PuO_2-coated Pu proceeds through several stages that culminate in rapid corrosion of the metal (Haschke *et al.*, 2000a). Pu is inherently coated with oxide unless the surface is prepared in ultra-high vacuum by abrasion/scraping or sputter etching. At room temperature, a variable induction period, during which reaction is not detected, is followed by nucleation and growth of reactive hydride sites that ultimately cover the metal surface and induce the maximum hydriding rate. Kinetic studies are facilitated using Pu samples that are covered by PuH_x before testing (Ogden *et al.*, 1980; Haschke and Allen, 2001). Uncertainty is inherent in rate measurements because variation in x of the PuH_x product alters the amount of Pu consumed by a given quantity of H_2. Although PuH_2 is not a distinct phase, use of that hydride composition facilitates evaluation.

Data from pressure–volume–temperature (PVT) in Fig. 29.4 show the dependence of the Pu hydriding rate, R, on H_2 pressure between –18 and 300°C (Haschke and Allen, 2001). The $\ln R - \ln P_{H_2}$ slopes define the pressure exponents, n, of H_2 (see Section 29.2.2). The dependence of R on temperature and P_{H_2} are described by a general rate equation:

$$R\,(\text{g Pu cm}^{-2}\ \text{min}^{-1}) = 0.0567\exp(805/T)(3.75P_{H_2})^n\ (\text{geometric area},\ P \text{ in bar}).$$

The pressure exponent is 1 for P_{H_2} less than 0.27 bar and 0.5 for higher pressures. These pressure exponents are consistent with the Langmuir model and control of the rate by the concentration of adsorbed hydrogen at the gas–hydride interface. The progressive decrease in the rate with increasing temperature in Fig. 29.4 gives an E_a of –7 kJ mol^{-1}, a result attributed to a decrease in the concentration of adsorbed hydrogen with increasing temperature at constant P_{H_2}. The hydriding rate is 1–2 g Pu cm^{-2} min^{-1} or 4–8 mmol H_2 cm^{-2} min^{-1}at 1 bar H_2 (geometric area), a value that is close to the rate (1–3 mmol H_2 cm^{-2} min^{-1}) of the PuH_x–H_2 reaction.

Results for reaction of H_2 with metal powder (0.1–0.3 m^{-2} g^{-1}) from unalloyed Pu (Stakebake, 1992a) and the δ-phase Ga alloy (Stakebake, 1981c) are consistent with findings for massive metal. The pressure exponent is 1 at low

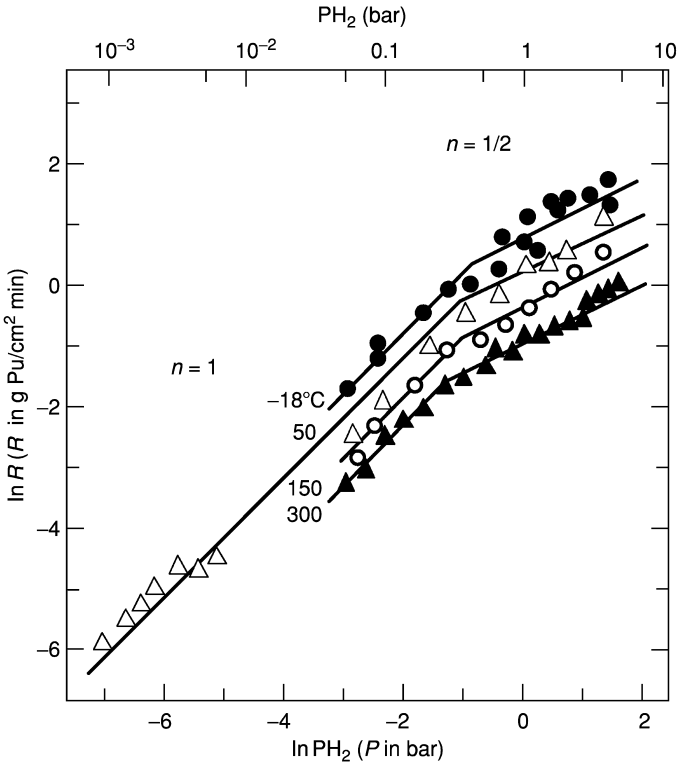

Fig. 29.4 *Dependence of* ln R *on* ln P_{H_2} *for the Pu–H_2 reaction at selected temperatures between* –18 *and* 300°C.

P_{H_2}, but the transition to $n = 1/2$ occurs near 5 mbar H_2. Activation energies are negative (–0.2 to –0.6 kJ mol^{-1}). The initial linear hydriding rate at 30°C and 10.6 mbar H_2 (1.7 mg Pu cm^{-2} min^{-1}, BET area) is less than calculated for massive Pu (32 mg cm^{-2} min^{-1}, geometric area) by the above equation. The ratio of the rates implies that the true (BET) area of hydride surface on massive metal is 20 times greater than the geometric area (Haschke and Allen, 2001).

In early hydriding rate measurements, massive metal was attached to heat sinks and the extent of reaction was controlled in an effort to limit thermal excursion and minimize error in the E_a determination. Pressure exponents of 0.6 (Bowersox, 1977) and 0.7 (Ogden *et al.*, 1980) are determined for experimental P_{H_2} ranges spanning the transition pressure from $n = 1$ to 0.5 in Fig. 29.4, but Arrhenius evaluations give positive E_a values of 8 kJ mol^{-1} (Ogden *et al.*, 1980) and 25 kJ mol^{-1} (Bowersox, 1977) inconsistent with negative values obtained without thermal control. A negative activation energy cannot result from autothermic effects. Self-heating always drives E_a to more positive values regardless

of its sign and cannot cause E_a to be negative, only less negative. Mass–time data for an extended test at 40°C and 9.0 bar H_2 (Ogden *et al.*, 1980) are inconsistent with a positive E_a. The temperature of the sample and sink rose by about 100°C during the measurement. Although a two-fold rate increase is anticipated if E_a is 8 kJ mol^{-1} as a result of the temperature increase, microbalance data show a two-fold rate decrease consistent with –8 kJ mol^{-1}.

Kinetics of the Pu–H_2 reaction are altered by the type of oxide on the metal surface (Haschke and Allen, 2001). Induction periods are absent and maximum hydriding rates are observed immediately upon exposure of the metal to H_2 at all temperatures if the PuO_2 layer is reduced to α-Pu_2O_3 by heating to 200°C in vacuum before reaction. Catalytic properties of PuH_x and α-Pu_2O_3 are implied by the rates at which those materials dissociate and transport hydrogen. At room temperature and 1 bar H_2, the corrosion rates of unalloyed and alloyed Pu are about 1.7 g Pu cm^{-2} min^{-1} and correspond to advancement of the reaction front into the metal at about 6 cm h^{-1}, a rate that is unusually rapid for a gas–solid reaction. The rate is essentially independent of temperature, but goes to zero if equilibrium conditions in the Pu–PuH_x two-phase region (Fig. 29.1) are satisfied. As indicated by curve 11 in Fig. 29.5, corrosion of Pu by H_2 at 1 bar ceases at the 850°C equilibrium point (Flotow *et al.*, 1984).

29.5.2 Reaction of Pu with oxygen, water, and air

(a) Overview of kinetic behavior

Plutonium ignites in air and oxidizes via a self-sustaining reaction if the temperature exceeds 500°C or the corrosion rate exceeds 0.07 g Pu cm^{-2} min^{-1}, the approximate R required for self-heating of Pu to that autothermic temperature (Haschke and Allen, 2001). The Arrhenius evaluation of Pu corrosion reactions in Fig. 29.5 shows three sets of rate curves. Curves 1–7 show strong temperature dependence characteristic of rate control by diffusion of reactant through a protective PuO_2 layer. Curves 8 and 9 are consistent with onset of self-sustaining oxidation at high temperatures. Reaction becomes self-sustaining when the metal is heated above the ignition temperature, T_i, by an external or internal heat source. The set formed by curves 10–12 are independent of temperature and rates of these catalyzed reactions inherently exceed that required for ignition, regardless of initial temperature. Equations (Haschke *et al.*, 1998a; Haschke and Allen, 2001) for the curves in Fig. 29.5 are given in Table 29.3.

A variety of parameters participate in controlling the corrosion rate of thermally driven processes described by curves 1–6 in Fig. 29.5 (Haschke *et al.*, 1996, 1998a). Reactions in this set are temperature-dependent and exhibit paralinear behavior, implying that rates are controlled by diffusion of reactant through the product layer on the metal (Haschke *et al.*, 2001b). Parabolic kinetics are observed only during the formation of the initial oxide layer at temperatures below 400°C and are typically not encountered during routine

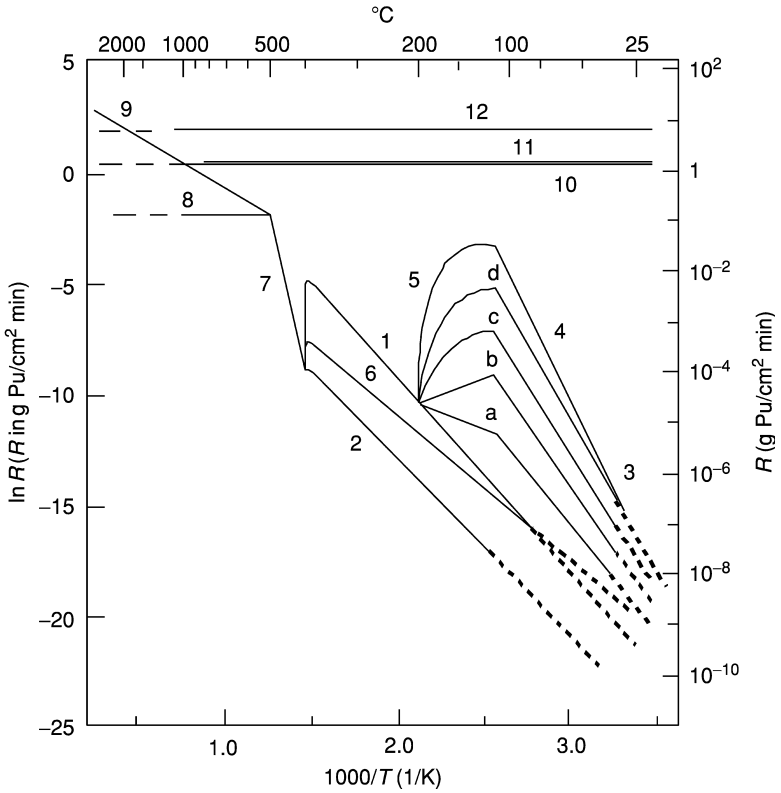

Fig. 29.5 *Arrhenius curves for corrosion of unalloyed Pu and δ-phase Ga alloy. Curves* 1 *and* 2 *describe the oxidation rates of unalloyed metal and alloy in dry air, respectively. Curves* 3–5, *and a–d describe oxidation of unalloyed Pu in moist air or water vapor. Curves a, b, c, and d are for* 10, 10^2, 10^3, *and* 10^4 ppm H_2O, *respectively. Curve* 6 *describes the oxidation of alloy by water vapor. Curve* 7 *defines behavior in a region where effects of alloying and water are absent. Curves* 8 *and* 9 *describe behavior of static metal in air and of ignited Pu droplets during free fall in air, respectively. Curves* 10, 11, *and* 12 *describe catalyzed corrosion of hydride-coated Pu by air,* H_2, *and* O_2, *respectively. Detailed descriptions of the curves are given in the text and in Tables* 29.3 *and* 29.4.

handling and storage. Rates indicated by curves 1–6 in Fig. 29.5 are for the linear (constant-rate) stage of corrosion maintained by continuous spallation of product and diffusion of reactant through a product layer of constant average thickness. Assessment of behavior in air is facilitated by normalization of data to 0.21 bar oxidant (O_2 or H_2O) pressure.

Influence of parameters other than temperature is shown by effects of moisture and alloying on corrosion rates described by curves 1–6. Therefore, corrosion kinetics of unalloyed and alloyed Pu in dry air, water vapor, and moist air are discussed separately. Attainment of moisture levels at which the corrosion

Table 29.3 *Arrhenius equations*[a] *for corrosion of Pu in H_2, O_2, air, or H_2O vapor.*[b]

Curve	*Reaction*	*T range* (K)	*A*	*B*	*References*[c]
1	Unalloyed Pu + dry[d] air	<673	8.78	9010	A
2	Alloyed Pu + dry[d] air	<673	6.40	9560	A,B
3	Unalloyed Pu + H_2O at P_e[e]	248–334	41.47	17120	A
4	Unalloyed Pu + H_2O at 0.21 bar	334–383	40.74	16880	A
6	Alloyed Pu + H_2O at 0.21 bar	334–673	4.29[f]	7850	A,C
7	Pu + air or H_2O at 0.21 bar	673–773	44.51	35940	A
8	Static Pu + air	>773	–1.97	0	A,D
9	Dynamic Pu + air	773–3773	4.21	4830	A,E
10	Coated[g] Pu + H_2 at 1 bar	289–890	0.53	0	F
11	Coated[g] Pu + air at 1 bar	>298	0.53	0	F
12	Coated[g] Pu + O_2 at 1 bar	>298	2.00	0	A,F

[a] Equations are for the linear stage of corrosion and have the form $\ln R$ (g Pu cm^{-2} min^{-1}) $= A - B/T$ (geometric area of Pu).
[b] The oxidant pressure is 0.21 bar O_2 or H_2O, unless otherwise specified.
[c] References: A, Haschke *et al.* (1998a); B, Stakebake and Saba (1990); C, Stakebake and Lewis (1988); D, Haschke and Martz (1998b); E, Martz and Haschke (1998); F, Haschke and Allen (2001).
[d] Dry conditions are less than 0.5 ppm H_2O at 1 bar pressure.
[e] P_e is the equilibrium pressure of H_2O at T.
[f] The value of A has been changed to correct an error (Haschke *et al.*, 1996).
[g] The Pu surface is coated with PuH_x or a double layer of α-Pu_2O_3 and PuH_x.

rate of unalloyed Pu in air or oxygen is insensitive to water concentration at low temperatures is difficult. Results of many studies with 'dry' gases appear inaccurate because residual H_2O concentrations exceeded the 0.5 ppm level required to avoid moisture enhancement of corrosion (Haschke *et al.*, 1996).

(b) Dry oxidation of unalloyed and alloyed Pu

Linear oxidation of unalloyed Pu in dry (<0.5 ppm H_2O) air or 0.21 bar O_2 proceeds as described by curve 1 in Fig. 29.5 and Table 29.3 (Haschke *et al.*, 1996, 1998a). Behavior is defined by a single Arrhenius curve for temperatures up to 400°C, implying that the same reaction occurs over that range (Haschke *et al.*, 2001b). Oxidation of Pu in dry air forms PuO_2 (Colmenares, 1984), a product that persists at the gas–solid interface even though the thickness of the α-Pu_2O_3 layer at the product–metal interface increases with increasing temperature. The E_a for oxidation is 75 kJ mol^{-1} (Haschke *et al.*, 1996), but the temperature dependence for autoreduction at the interface is unknown. The penetration rate by oxidation in dry air at 25°C is about 20 pm h^{-1}.

Control of oxidation by the rate of O^{2-}-ion diffusion through the dioxide layer is supported by paralinear kinetics and agreement of E_a values for oxidation and oxygen self-diffusion in nonstoichiometric dioxide (Haschke *et al.*, 1996, 2001b). Dependence of electrical conductivity on P_{O_2}, positron annihilation data for UO_2 (Colmenares, 1984), and close correspondence of the Pu and

U systems suggest that the oxidation is a concerted process in which electrons move toward the gas–solid interface as Pu(v) ions simultaneously migrate toward the product–metal interface. Data suggest that O^{2-} ions form clusters by associating with Pu(v) and move by hopping between octahedral sites in the fluorite structure. Migration of O^{2-} through the oxide layer is driven by the gradient in oxygen concentration between the gas–oxide and oxide–metal interfaces.

Arrhenius results for oxidation of δ-phase Ga alloy in dry air or O_2 are shown by curve 2 in Fig. 29.5 and Table 29.3 (Stakebake and Saba, 1990; Haschke *et al.*, 1998a). The pressure exponent of O_2 varies from near zero to 0.5 (Stakebake and Lewis, 1988). The activation energy (79 kJ mol^{-1}) agrees with that (75 kJ mol^{-1}) for unalloyed Pu, suggesting that the oxidation mechanism is essentially identical for the two metals. The only obvious difference is that oxidation of the alloy is a factor of 70 slower than that of unalloyed Pu. Because the rate is apparently controlled by diffusion of oxygen through the oxide layer in both cases, the slower oxidation rate of the alloy apparently results from a reduced rate of oxygen transport through PuO_2 formed by that metal. The chemical fate of gallium during oxidation of the alloy is uncertain. Ga may occupy octahedral anion sites in the PuO_2 structure and slow diffusion of oxygen or reside on cation sites and restrict the flow of electrons to the surface.

In addition to the parabolic and linear stages of reaction, a second linear stage appears after 1–2 days during oxidation of alloyed Pu at 275–300°C (Stakebake, 1986; Stakebake and Lewis, 1988). A similar rapid third stage is observed for unalloyed Pu (Stakebake, 1992b). This more rapid corrosion results in 1.5- to three-fold rate increases and is attributed to the formation of cracks in the adherent surface layer of oxide.

(c) Oxidation of unalloyed and alloyed Pu by water vapor

As shown by curves 3–5 in Fig. 29.5, the corrosion rate of unalloyed Pu in water vapor at temperatures below 200°C is more rapid than that in dry air (Haschke *et al.*, 1996, 1998a; Haschke and Allen, 2001). Curves 3 and 4 differ slightly because P_{H_2O} is fixed at 0.21 bar above 61°C and equals the value for liquid–gas equilibrium at lower temperatures. As shown by curve 5, the progressive decrease in R between 110 and 200°C is consistent with a mechanism change in which effects of moisture enhancement are lost (Haschke and Allen, 2001). At temperatures above 200°C, the corrosion rate in water at 0.21 bar is indistinguishable from that in dry air. Moisture enhancement of the Pu corrosion rate is confined to the envelope bounded by curves 1, 3, and 5. Relative to dry oxidation, R is increased by 10^2 at room temperature and by 10^4 at 100°C.

Kinetic data show that the corrosion rate of unalloyed Pu by water depends on temperature and is proportional to $(P_{H_2O})^{1/2}$ (Haschke *et al.*, 1996). As shown by data in Table 29.4, experimental E_a values are a linear function of $\ln P_{H_2O}$. The systematic set of Arrhenius equations derived from these data

Table 29.4 *Arrhenius equations*[a] *for reaction of unalloyed Pu with water vapor at selected pressures or with air at* 1 bar *pressure and the corresponding partial pressures of water* (*Haschke* et al., 1996).[b]

P_{H_2O} (bar)	*H_2O concentration* (ppm)	E_a (kJ mol^{-1})	*A*	*B*
4.7×10^{-7}	0.46	75	8.90	9050
1×10^{-6}	1	79	10.72	9480
1×10^{-5}	10	89	16.16	10760
1×10^{-4}	10^2	100	21.58	12030
1×10^{-3}	10^3	111	27.29	13310
1×10^{-2}	10^4	121	32.43	14580
0.1	10^5	132	37.89	15850
1	10^6, $(P_{H_2O})_e$[c]	142	42.76	17130

[a] The form of the Arrhenius equations is $\ln R$ (g Pu cm^{-2} min^{-1}) $= A - B/T$ (T in K, geometric area of Pu). Note that rate units are mg O cm^{-2} min^{-1} in the original report, but are reported here as g Pu cm^{-2} min^{-1} to facilitate comparison with data in Table 29.3.
[b] Each equation is valid for T between 383 K and the point at which P_{H_2O} equals the equilibrium pressure $(P_{H_2O})_e$.
[c] The maximum P_{H_2O} at each T is $(P_{H_2O})_e$ below 373 K and equals 1 bar at higher temperatures.

describes the dependence of R on T within the envelope. Curves a, b, c, and d in Fig. 29.5 indicate behavior at 0.01, 0.1, 1, and 10 mbar H_2O, respectively. Rate equations for any water concentration within the envelope are readily derived by interpolation of equations in Table 29.4. Values in the region of decreasing rates between 110 and 200°C may be estimated using curves in the figure.

Although formation of PuO_2 and PuH_2 is reported in early studies of the Pu–H_2O reaction, PuO_2 and H_2 are the only detectable products below 100°C (Stakebake, 1971; Colmenares, 1984). Because production of hydride is thermodynamically favorable in the presence of metal, formation of H_2 implies that hydrogen is not readily transported through the oxide product layer at low temperatures (Haschke *et al.*, 2001b). Increasingly larger amounts of hydrogen are apparently transported with increasing temperature, but the observed product fraction of about 0.15 PuH_x after extended reaction of H_2O at 250°C (Stakebake *et al.*, 1993) is substantially less than the 0.67 fraction expected for complete reaction of hydrogen. As described in Section 29.5.2(d), stoichiometric amounts of PuH_x form at all temperatures via a secondary reaction if excess metal and H_2O are confined in a closed system for an extended period.

The oxide product of the Pu–H_2O reaction is chemically identical to that formed by dry O_2 and kinetics are paralinear, implying diffusion control of O^{2-} transport through an oxide layer (Haschke *et al.*, 2001b). The rapid oxidation rate (curve 3) relative to that by dry air/O_2 (curve 1) is attributed to the combined effect of a high concentration of chemisorbed OH^- at the gas–solid

interface, to facile formation of O^{2-} by interaction of OH^- ions with electrons, and the resulting increase in oxide concentration that produced PuO_{2+x} at the surface (Stakebake *et al.*, 1993). The oxidation rate is enhanced by H_2O because the steady-state oxygen gradient across the constant thickness oxide layer is larger than with dry oxygen. Whereas O^{2-} is formed by transferring one electron to OH^-, the probability of transferring two electrons to dissociatively adsorbed O atoms is low and results in slow oxidation. Enhancement of the Pu oxidation rate by H_2O is attributed to the relatively rapid rates of forming oxide ions from hydroxide ions at the gas–oxide interface. Closure of the rate–temperature envelope (curve 5) is consistent with progressive desorption of water at 110–200°C.

Comparison of curves 6 and 2 in Fig. 29.5 shows the oxidation rate of δ-phase Ga alloy in 0.21 bar water vapor is about a factor of 10 faster than in dry air (Stakebake and Saba, 1990; Haschke *et al.*, 1996). Kinetics of the alloy–water reaction are paralinear and the linear stage is followed by a third stage. At 305°C, the third-stage rate progressively increases by 100 fold and results in complete reaction of 1-mm-thick unalloyed Pu over a 10 h period (Stakebake, 1992b). At that temperature and 20 mbar H_2O, the maximum rate is about 0.01 g Pu cm^{-2} min^{-1} (geometric area). The activation energy (65 kJ mol^{-1}) and the pressure exponent ($n = 0.15$–0.23) of the linear stage are similar to those for oxidation in dry conditions, but E_a is low (11 kJ mol^{-1}) and $n = 1$ for the third stage. Behavior parallels that encountered with hydride-catalyzed oxidation of metal by air (see Section 29.4.1b), suggesting that more rapid diffusion of hydrogen through the oxide layer at elevated temperatures results in the accumulation of hydride at the product–metal interface and catalytic enhancement of reaction by α-Pu_2O_3 and PuH_x layers (Haschke and Allen, 2001). Formation of cracks in the oxide product should enhance this process.

Mixtures of oxide and hydride are formed during reaction of Pu skulls and turnings with flowing mixtures of 25% steam and 75% Ar at 400–800°C (Smith, 1960). After initiation by external heating, reaction becomes self-sustaining and is controlled by adjusting the steam–argon ratio at 1 bar total pressure. The reported corrosion rate of 250 g Pu h^{-1} and the approximate specific area (10 cm^2 g^{-1}) of turnings (Martz *et al.*, 1994) yield an area-normalized value of 0.4 g Pu cm^{-2} min^{-1} (geometric area). Prediction of the third-stage rate at 0.25 bar H_2O pressure using the rate based on data for at 305°C (Stakebake, 1992b) and first-order dependence on P_{H_2O} (Stakebake and Saba, 1990) yields 0.1 g Pu cm^{-2} min^{-1}. Similarity of the rates suggests that the self-sustaining process corresponds to the third stage of the Pu–H_2O reaction, that E_a is zero, and that rate is controlled by P_{H_2O} after a hydride layer is formed at the product–metal interface. As observed during oxidation of PuH_x, a protective PuO_2 layer apparently forms unless the water pressure, heat-generation rate, and resulting temperature are adequate to maintain an α-Pu_2O_3 surface that catalyzes the reactions of H_2 and O_2.

(d) Oxidation of unalloyed Pu by moist air

At a given water pressure and temperatures less than 110°C, the corrosion rate of unalloyed Pu in moist air is more rapid than in dry air and indistinguishable from that observed during oxidation in water vapor at corresponding conditions (Haschke *et al.*, 1996). The pressure exponent for H_2O is 0.5; activation energies and Arrhenius equations vary with humidity as defined by data for water vapor in Table 29.4. Curves a, b, c, and d in Fig. 29.5 indicate corrosion behavior in 1 bar air at 10, 100, 10^3, and 10^4 ppm H_2O. The effect of 1 ppm water is clearly evident and reliability of many kinetic studies at 'dry' conditions appears doubtful.

Although corrosion kinetics in moist air and water vapor are indistinguishable, the chemistry of moisture-enhanced oxidation in moist air below 110°C is different from that for water vapor because O_2 is consumed and H_2 is not produced. Failure to observe H_2 has apparently resulted in proposal of various mechanisms to account for moisture enhancement of corrosion in air. As discussed in a review of proposed mechanisms (Haschke *et al.*, 2001b), two primary explanations are suggested: (1) disruption of the protective oxide layer by formation of hydride or hydrogen at the product–metal interface and (2) rapid transport of oxygen through the oxide as OH^- or H_2O. The validity of such mechanisms is questioned because formation of PuO_2 as the only product at low temperatures requires that product H either form PuH_x or return to the gas–solid interface and re-form H_2O. Because hydride is not observed and decomposition back to metal and hydrogen is prevented by thermodynamic stability of PuH_x, mechanisms involving migration of hydrogen or hydrogen-containing species through the oxide layer appear unlikely.

Modification of the mechanisms for oxidation in dry air and water vapor (see Sections 29.5.2(b) and 29.5.2(c)) accounts for all observations with moist air, including appearance of linear kinetics and absence of physical disruption of the oxide layer (Haschke *et al.*, 2001b). As shown by the following sequence of reactions, chemical behavior is described by a water-catalyzed cycle like that for formation of PuO_{2+x} in air (Haschke *et al.*, 2000b):

$$\begin{aligned}
&Pu(s) + 2H_2O(ads) \rightarrow PuO_2(s) + 4H(ads)\\
&O_2(g) \leftrightarrow 2O(ads)\\
&\underline{4H(ads) + 2O(ads) \rightarrow 2H_2O(ads)}\\
&Pu(s) + O_2(g) \rightarrow PuO_2(s)
\end{aligned}$$

Adsorbed water reacts at the relatively rapid rate of Pu–H_2O reaction. In the presence of O_2, product H-atoms combine with dissociative adsorbed oxygen to re-form H_2O instead of associating as H_2. The net reaction accounts for the disappearance of O_2, formation of PuO_2, and absence of PuH_x or H_2 products. As with reaction of Pu with water vapor, adsorption of H_2O and formation of PuO_{2+x} at the gas–solid interface apparently create an oxygen gradient that

enhances corrosion by driving more rapid transport of oxide ions through the PuO_2 layer.

Mixtures of oxide and hydride are formed by reaction of Pu (and U) with water vapor or moist air at low temperatures if three conditions are satisfied: the system is closed, the time period is sufficiently long, and excess metal is present. In moist air, O_2 is first consumed by the above cycle and H_2O then reacts via the second step to form additional oxide and H_2 (Haschke *et al.*, 2001b). Oxide is formed at equal rates during those reactions. If the system remains closed, H_2 produced by the second step reacts with available Pu (U) to form hydride after H_2O is depleted. Hydriding of Pu is facile if the oxide surface on the metal is transformed to α-Pu_2O_3 by autoreduction.

(e) Thermal ignition and self-sustained oxidation of Pu

As shown by curves 1, 2, and 6 in Fig. 29.5, all effects of water vapor and alloying cease abruptly near 400°C (Haschke *et al.*, 1996; Haschke and Allen, 2001). The origin of the rate decrease for unalloyed Pu and of the convergence of Arrhenius curves for all metal forms is uncertain. A reasonable suggestion consistent with the sharpness of the step is the stoichiometry-dependent transition of $PuO_{2-\delta}$ from n-type to p-type semiconduction (Stakebake and Lewis, 1988). The ensuing rate increase indicated by curve 7 leads to self-sustained oxidation reactions defined by curves 8 and 9.

A sharp increase in corrosion rate at 400–500°C is shown by measurements with the Ga alloy in 0.67 bar air (Stakebake and Lewis, 1988). High E_a values (205–226 kJ mol^{-1}) are observed during both the second and third stages of reaction. As indicated by the average oxide thickness at which kinetic behavior deviates from parabolic behavior, the PuO_2 diffusion barrier progressively decreases in thickness over the 400–450°C range and is not discernable at higher temperatures. Behavior implies that the rate of sesquioxide formation by the Pu–PuO_2 reaction at the product–metal interface approaches and exceeds that for dioxide formation at the gas–solid interface as temperature increases (Haschke and Allen, 2001). The proposed transformation of surface oxide to α-Pu_2O_3 near 500°C is consistent with the onset of self-sustained corrosion in air at (500 ± 25)°C (Martz *et al.*, 1994). The high E_a (298 kJ mol^{-1}) for curve 7 (Fig. 29.5 and Table 29.3), which is based on well-defined rates at 400 and 500°C (Haschke *et al.*, 1998a), agrees with measured results and reflects the change from a protective to a catalytic surface.

Ignition and onset of self-sustained oxidation of unalloyed and alloyed Pu at 500°C are shown by results of several studies cited in a review of plutonium pyrophoricity (Martz *et al.*, 1994). If determined under conditions of dynamic heating, the ignition temperature, T_i, is correlated with geometric specific area, S, of the metal as shown in Fig. 29.6. Whereas Pu powder, chips, turnings ignite at (150 ± 50)°C, foil and bulk metal with thicknesses greater than 0.2 mm ignite at (500 ± 25)°C. As outlined in the preceding paragraph, T_i apparently corresponds

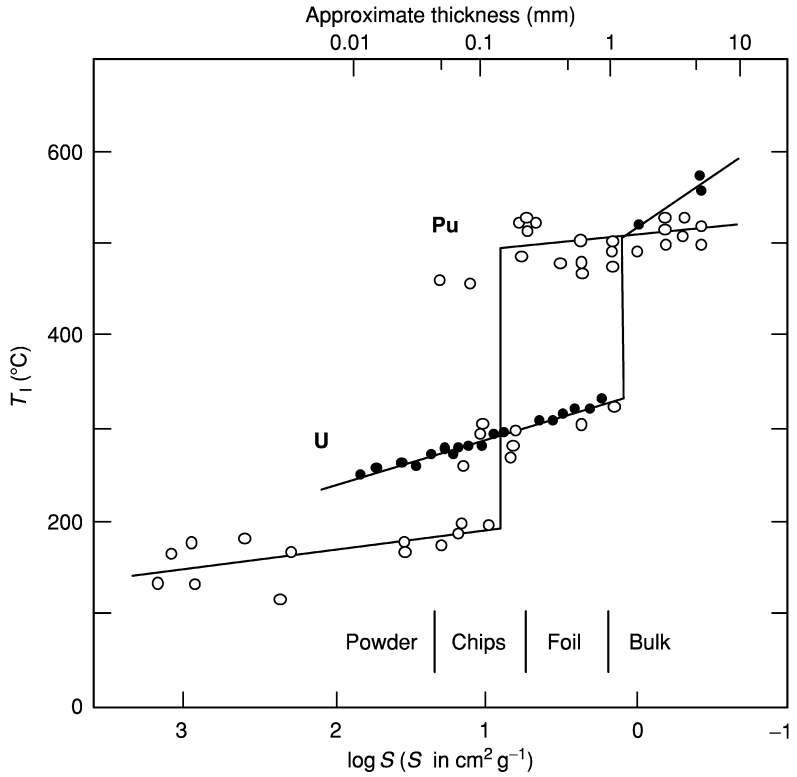

Fig. 29.6 *Correlation of reported ignition temperatures, T_i, for Pu and U with specific surface area, S, of the metal.*

to the temperature at which autoreduction transforms the oxide layer to α-Pu_2O_3, but low-temperature ignition of powder and turnings seems inconsistent with that interpretation. Appearance of large pre-ignition exotherms at 200–300°C during studies with bulk metal samples (Pitts, 1968; Schnizlein and Fischer, 1968) suggests that substantial amounts of heat are generated by a rapid chemical reaction at the Pu surface. If a fixed amount of heat is produced per unit area of metal, the self-heating effect is much larger for powders and turnings with high specific area than for massive pieces of Pu. A likely exothermic source is rapid re-oxidation of the Pu_2O_3 layer at the oxide–metal interface. A thermal model based on this concept and retention of all heat by the metal and reaction products predicts ΔT for rapid reoxidation of the Pu_2O_3 layer (5 μm thick) formed in the oxide–metal interface at 150°C (Martz *et al.*, 1994). ΔT values equaling or exceeding the 350° increment required to reach 500°C are predicted for spherical Pu particles with diameters less than 0.25 mm and foils

with thicknesses less than 0.088 mm, agreeing with the observed specific area for transition from $T_i = 150°C$ to $T_i = 500°C$ in Fig. 29.6.

The thermal model for low-temperature ignition (Martz *et al.*, 1994) accounts for unanticipated observation of lower T_i values in air than in 1 bar O_2 (Schnizlein and Fischer, 1968). Although conventional logic suggests that foils and powders should oxidize more readily in oxygen than in air, an increase in P_{O_2} favors formation of protective PuO_2 while suppressing Pu_2O_3 formation and onset of ignition. This explanation seems to contradict the conclusion that increasing P_{O_2} promotes Pu_2O_3 formation during oxidation of PuH_x (see Section 29.4.1(b)) and PuH_x-coated Pu (see Section 29.5.2(f)), but differences in the dependence of rate on P_{O_2} must be considered. Rates of reaction and heat production are proportional to $(P_{O_2})^n$ with $n = 2$ for the PuH_x–O_2 reaction and with $0<n<0.5$ for the Pu–O_2 reaction (see Section 29.5.2(b)). If PuH_x is present, increasing P_{O_2} from 0.2 to 1 bar increases the rate of heat production by a factor of 25. In the absence of PuH_x, the resulting rate change is less than two-fold.

Effects of other counter-intuitive observations (Pitts, 1968) are also consistent with Pu_2O_3 formation at the ignition point. T_i values for Pu powder (100–250 μm diameter) are 392, 189, and 152°C for 0.03, 0.12, and 0.60 g specimens, respectively. The steady-state O_2 concentration within the porosity of a powder bed decreases with increasing sample size because the area of reactive surface is larger and oxygen diffusion into the powder is increasingly restricted. Low P_{O_2} in the bed promotes formation of catalytic α-Pu_2O_3 and reduces T_i. Similar decreases in T_i of foil (0.06 mm thick) after folding and compressing are probably not due to stress in the metal, but to fracture of the PuO_2 layer during deformation and to reduction of the O_2 concentration within folds of the sample. A decrease in T_i with increasing extent of surface oxidation before testing is consistent with formation of a thicker Pu_2O_3 layer and a larger ΔT during reoxidation (Martz *et al.*, 1994).

The 500°C ignition point of Pu is observed under dynamic conditions in which heat is supplied at a rate that causes a temperature increase in excess of 10°C min^{-1} (Pitts, 1968; Schnizlein and Fischer, 1968; Musgrave, 1971). Studies show that T_i of massive Pu is progressively decreased by reducing the heating rate and reaches 355°C at about 0.1°C min^{-1} (Pitts, 1968). During constant-temperature experiments, samples ignited after 0.5 h at 400°C and after 3 h at 375°C, but oxidized completely without igniting at 350°C. Results are consistent with thermal calculations indicating that the static ignition point of massive Pu is near 300°C, the temperature at which the rates of heat generation by the Pu oxidation in air and heat loss from the metal surface are equal (Haschke *et al.*, 2000c). Autothermic behavior is possible above 300°C, but experiments suggest that static ignition is likely to occur only at above 350°C.

As indicated by curve 8 in Fig. 29.5, self-sustained oxidation of Pu in static air is independent of temperatures above 500°C (Haschke and Martz, 1998b). The average rate at 500–1000°C is (0.14 ± 0.07) g Pu cm^{-2} min^{-1}, corresponding to a

linear corrosion rate of about 5 mm Pu per hour. E_a for the process ((9.6 ± 6.3) kJ mol^{-1}) is effectively zero, but the dependence on P_{O_2} is unknown. The zero E_a is attributed to the formation of an O_2-depleted boundary layer of unreactive N_2 that controls the oxidation rate by limiting the O_2 flux to the metal surface, causing the burning metal to glow with a steady charcoal-like orange color during reaction (Haschke *et al.*, 2000a). However, analogy to results for other reactions involving catalytic α-Pu_2O_3 (Haschke and Allen, 2001) suggests that the rate might be invariant because E_a is zero and P_{O_2} of air is constant.

Curve 9 in Fig. 29.5 shows the Arrhenius relationship derived for dynamic Pu in air after ignition (Martz and Haschke, 1998). The kinetic assessment is based on studies in which laser-ignited metal particles (0.07–0.6 mg) incandesced with increasing brightness and ultimately 'exploded' during free fall in air (Nelson, 1980). The time in free fall before explosion increased with increasing particle mass. Vaporization and oxidation of residual Pu during the nonviolent explosions produced hollow oxide spherules with one or more vent holes plus an aerosol that accounted for up to 77% of the Pu. Conceptually, oxide-coated metal spheres form upon melting of the Pu at 640°C and react at an increasing rate during free fall because an O_2-depleted layer cannot form (Martz and Haschke, 1998). Progressive heating increases the particle temperature, melts the oxide coat at 2300–2400°C, and results in venting of residual metal as vapor above the 3230°C boiling point of Pu. The 'explosion' results from rapid oxidation of vented Pu vapor in air.

A quantitative thermal model based on the above concept includes correction for thermal losses by the falling particle and fitting of the activation energy (Martz and Haschke, 1998). The model accurately predicts time intervals to explosion and fractions of aerosolized Pu as a function of Pu particle size. The effective E_a (40 kJ mol^{-1}) for reaction of ignited Pu in free fall suggests a temperature-dependent process that is evident for dynamic conditions in which the N_2 boundary layer is swept away. However, self-sustained oxidation of α-Pu_2O_3-coated PuH_x by O_2 (see Section 29.4.1(b)) and of Pu by H_2O (see Section 29.5.2(c)) has zero activation energy. Because α-Pu_2O_3-coated Pu may behave in a similar way, the apparent E_a might be a consequence of P_{O_2} dependence and the increasing O_2 impingement rate as the particle accelerates during free fall.

Ignition studies with samples of Pu powder are relevant to anecdotal reports that kilogram-sized pieces (Martz *et al.*, 1994), as well as chips and turnings (Stakebake, 1992c), spontaneously ignite in air at room temperature. Specimens of Pu powder (50–100 μm size) used in ignition studies were prepared by filing metal and sieving the fines in dried (200–700 ppm H_2O) air (Musgrave, 1971). If fine Pu particles were pyrophoric, they would ignite during this preparation. The filings apparently oxidized slowly in air at room temperature and ignited only upon heating to 175–200°C, suggesting that other reactive materials such as α-Pu_2O_3 and PuH_x participate in initiation of self-sustained reactions of both finely divided and massive metal at room temperature (see Section 29.8.4b).

(f) Catalyzed ignition and self-sustained reaction of Pu

Involvement of reactive materials in initiating self-sustained oxidation of Pu is supported by results of kinetic studies with Ga alloy coated with PuH_x or a double layer of α-Pu_2O_3 and PuH_x (Haschke *et al.*, 1998a; Haschke and Allen, 2001). Oxidation of a 1.5 mm thick Pu sample coated with the double layer was complete in less than 1 s and produced gas-phase temperatures in excess of 1000°C after exposure to O_2 at a median pressure of 3.2 bar (Haschke *et al.*, 2000a). The solid product expanded in the shape of the Pu sample during reaction and consisted of a PuH_x core surrounded by a thick Pu_2O_3 layer. Product hydrogen was accommodated as PuH_x during advancement of oxidation into the metal and was not detectable in the gas phase after reaction. As with the PuH_x–O_2 reaction, oxidation of hydride-coated metal has zero activation energy, a property that allows the dependence of rate on P_{O_2} to be evaluated without regard for the temperature.

Rate data for oxidation of Pu coated with the α-Pu_2O_3–PuH_x double layer are consistent with those for reaction of O_2 with PuH_x and α-Pu_2O_3-coated PuH_x (Haschke and Allen, 2001). If the factor of 20 between geometric and BET areas of the metal is included, evaluation shows that the oxidation rate of hydride-coated Pu with O_2 is proportional to P_{O_2} squared as indicated by the following equation.

$$R \text{ (in g Pu cm}^{-2} \text{ min}^{-1}) = 7.4(P_{O_2})^2 \text{ (geometric area, } P \text{ in bar).}$$

The rate in 1 bar O_2 is indicated by curve 12 in Fig. 29.5. Hydride-catalyzed oxidation is apparently independent of alloying and penetrates the metal at more than 25 cm h^{-1} at 1 bar O_2 and by almost 3 m h^{-1} at 3 bar O_2, a value corresponding to the interfacial hydriding rate expected for the metal–hydrogen reaction at 1 kbar H_2. Rapid oxidation of Pu is attributed to a two-part catalytic process in which α-Pu_2O_3 dissociatively adsorbs and transports oxygen to the oxide–hydride interface and PuH_x transports product hydrogen to the hydride–metal interface. Transport of anions in the fixed fcc Pu lattice of product compounds and formation of PuH_x at the product–metal interface are extremely rapid. Zero activation energy and the dependence of R on P_{O_2} imply that the corrosion rate is controlled by dissociative adsorption of O_2.

Exposure of PuH_x-coated Pu or PuOH-coated Pu to air at room temperature results in rapid corrosion that parallels behavior of the PuH_x–air reaction (see Section 29.4.1c) and indiscriminately consumes N_2 and O_2 at the 3.7:1 ratio of air (Haschke *et al.*, 1998a; Haschke and Allen, 2001). Stoichiometry data show that reaction is described by formation of PuN:Pu_2O_3 in a 5.57:1 ratio plus PuH_x with x near 3 and consumes 1.86 moles of Pu per mol of air. The solid product may be a mixture of nitride and sesquioxide or contain a NaCl-related oxide nitride, $PuN_{1-v}O_v$, having a maximum v of 0.13 (Jain and

Ganguly, 1993). Reaction continues until all Pu is consumed and forms solids with PuH_x cores similar to those observed during reaction of O_2. H_2 is produced if spalled hydride powder is present (Haschke *et al.*, 1998a). Reaction of PuOH-coated metal apparently proceeds through an initial stage in which the surface layer reacts with metal to form α-Pu_2O_3 and PuH_x (Haschke and Allen, 2001).

Kinetic data for substantial ranges of air pressure, P_a, and temperature show that the corrosion rate of Pu coated by the α-Pu_2O_3–PuH_x double layer is independent of temperature and proportional to P_a squared (Haschke and Allen, 2001).

$$R \text{ (in g Pu cm}^{-2} \text{ min}^{-1}) = 1.72(P_a)^2 \text{ (geometric area, } P_a \text{ in bar)}.$$

Behavior is indicated by curve 11 in Fig. 29.5. Fortuitously, the corrosion rate in 1 bar air is coincident with that for the Pu–H_2 reaction at 1 bar pressure (see Section 29.5.1) and advances into the metal at about 6 cm h^{-1}. Dissociation and transport of nitrogen and oxygen are catalyzed by the PuN–α-Pu_2O_3 corrosion product covering the PuH_x layer. Involvement of PuH_x in catalyzing the Pu–N_2 reaction is evident because N_2 does not react with Pu_2O_3-coated Pu following thermal ignition (see Section 29.5.2(e)). Reactions of PuH_x-coated Pu and PuH_x in air are similar and suggest that involvement of N_2 is contingent on generation of sufficient heat by the initial PuH_x–O_2 reaction to form Pu_2O_3 and to initiate the PuH_x–N_2 reaction. Both the amount and partial pressure of O_2 are important factors in hydride-catalyzed ignition of self-sustained corrosion in air.

The importance of O_2 in initiating and sustaining catalyzed corrosion of Pu in air is shown by derivation of the rate equation for reaction in air from that for oxidation of PuH_x in O_2 (Haschke and Allen, 2001). That relationship is obtained by assuming that the oxidation kinetics of hydride (see Section 29.4.1(c)) and hydride-coated plutonium by O_2 are identical. If reaction of N_2 is driven by the thermal effect of O_2 reaction, the squared dependence of R on P_a arises only from the partial pressure of O_2, while the pressure exponent for N_2 is zero. The rate equation for air is derived from that for oxidation in O_2 by including the metal consumption ratio (5.57:1) for indiscriminate reaction of air and by substituting $0.21P_a$ for P_{O_2}.

$$R \text{ (in g Pu cm}^{-2}\text{min}^{-1}) = 1.8(P_a)^2 \text{ (geometric area, } P_a \text{ in bar)}.$$

Agreement of this derived equation with the experiment result presented above supports the conclusion that the kinetics the PuH_x–air and hydride-catalyzed Pu–air reactions are controlled by the O_2 partial pressure. As with the PuH_x–O_2 reaction, oxygen pressures below a threshold value have an insufficient heat generation rate for maintaining a catalytic α-Pu_2O_3 surface and result in the formation of a protective PuO_2 layer.

(g) Salt-catalyzed corrosion of Pu in liquid water

Formation of PuOH by reaction of Pu with water is strongly dependent on the anion concentration, [X], in solution (Haschke, 1992a). Data for [X] in the 10^{-7} ($[OH^-]$ in distilled H_2O) to 2 M ($[Cl^-]$ in $CaCl_2$ solution) at 25°C (Haschke, 1995) show that $\ln R$ is a linear function of ln[X] as described by the dependence of corrosion rate, R, on salt concentration in moles per liter.

$$R \text{ (in g Pu cm}^{-2}\text{ h}^{-1}) = 0.0073[\text{X}]^{0.43} \text{ (geometric area)}.$$

Measured corrosion rates in distilled water, typical tap water, and synthetic seawater are 7×10^{-3}, 0.52, and 6.3 mg Pu cm^{-2} h^{-1}, respectively. If a 1 mm thick piece of Pu is submerged in seawater at room temperature, corrosion on both surfaces results in transformation to PuOH powder within 5–6 days. The dependence of R on salt concentration suggests that anions catalyze the reaction by facilitating electron transfer at the surface.

Data indicate that the corrosion rate in water is sensitive to pH and temperature (Haschke, 1995). The corrosion rate at pH 10 is 10^4 slower than at pH 7 and freshly burnished metal is untarnished after 3 weeks in solution at pH 13.7. Relative to the corrosion rate in 1 M $CaCl_2$ solution, the 50-fold more rapid rates in 1 M $FeCl_3$ and $NiCl_2$ solutions are attributed to H^+ formation by cation hydrolysis. Evaluation of limited data gives an E_a of 25 kJ mol^{-1} for corrosion in near-neutral solutions.

29.5.3 Reaction of Pu with steel

Molten plutonium aggressively dissolves all types of iron and steel (Haschke and Martz, 1998a). If excess Pu is present, corrosion penetrates a 1.5 mm thick stainless steel barrier within a few minutes at 700–900°C. Although a eutectic near the Pu_6Fe composition melts at 410°C, the Pu–Fe reaction is slow below the 640°C melting point of Pu because reaction proceeds by inter-diffusion of the solid metals. The intimate contact required for that process is further hindered by the presence of oxide layers on the metals.

The extent of corrosion at temperatures below the 1230°C melting point of $PuFe_2$ is limited by the equilibrium composition of the Pu-rich liquid coexisting with that intermetallic compound (Ellinger *et al.*, 1968). At 1000°C, the iron-saturated solution contains 33 at% Fe, the composition formed by reaction of 6.8 g Pu with a 1 cm^2 area of 1 mm thick steel. Complete dissolution of Fe is expected at 1000°C if the thickness-normalized ratio of g Pu per cm^2 of steel surface approaches or exceeds 6.8 at any point of contact. The corrosion rate decreases as the molar ratio of Fe:Pu exceeds 1:2 (33 at% Fe) and reaction of residual Fe is slowed by formation of a protective $PuFe_2$ layer. The likelihood of penetration is low if the Fe:Pu ratio exceeds 2:1, but failure of a steel container is possible at high Fe:Pu ratios if corrosion of the steel is localized. In typical storage configurations, the Fe:Pu ratio is low and rapid loss of containment is likely if the temperature exceeds 700°C.

29.6 CORROSION KINETICS OF URANIUM COMPOUNDS AND URANIUM METAL

29.6.1 Reaction of UO_2 with water

Formation of higher-oxide layers on the surface of UO_2 during exposure to water and aqueous solutions in the absence of O_2 at 130–200°C (Matzke and Turos, 1991) implies that H_2 is produced by chemical reaction. The kinetics in pH 10 solution are parabolic over the 170–200°C range as indicated by proportionality of the product layer thickness (τ in nm) to the square root of reaction time (t in hours) at constant temperature: $\tau = kt^{1/2}$. Arrhenius evaluation of published data shows that $2\ln k$ (nm $h^{-0.5}$) = 31.75 –(10100/T) and that E_a (84 kJ mol^{-1}) is consistent with self-diffusion of oxygen in the oxide. If the product layer is U_3O_7, each nm of oxide thickness formed by reaction of H_2O corresponds to generation of 1.4 nmol H_2 per cm^2 of oxide (BET area).

The corrosion rate and the mechanism of the UO_2–H_2O reaction are sensitive to solution pH and temperature (Matzke and Turos, 1991). The rate is apparently not controlled by diffusion below 170°C or in neutral solutions because the layer growth is linear with time at those conditions. Although kinetic data are not reported for the linear regime, reaction apparently proceeded with formation of higher oxide and H_2 over a broad parametric range. Consequences of the UO_2–H_2O reaction during storage of uranium oxide merit consideration and further evaluation even though thermodynamic data indicate that the process is not favorable.

29.6.2 Reaction of U with hydrogen

Kinetics of the U–H_2 reaction are outlined in earlier reviews describing quantitative rate data and models for hydriding are proposed (Haschke, 1991; Ward and Haschke, 1994). Hydriding of oxide-coated U proceeds sequentially through induction, nucleation, and acceleration stages as localized hydride sites initiate and grow. Under certain conditions, a parabolic stage appears in the window bounded by complete surface coverage by UH_3 and onset of the final linear (constant-rate) stage. As with Pu, nucleation of hydride sites on U is slowed by oxide on the metal surface and preferential site growth implies that hydriding is promoted by UH_3. Appearance of a parabolic stage indicates the rate is controlled by diffusion of hydrogen through a UH_3 layer and that the hydriding mechanisms of U and Pu differ.

Adequate kinetic data are available only for the terminal constant-rate stage of hydriding with a fully active surface covered by UH_3. The $\ln R$–$\ln P_{H_2}$ isotherms in Fig. 29.7 derived (Ward and Haschke, 1994) from measurements at low (10^{-7}–0.1 bar) (Powell *et al.*, 1991) and high (0.01–50 bar) (Block and Mintz, 1981) H_2 pressures show that the area-normalized rate during the linear stage of the U–H_2 reaction depends on both T and P_{H_2} as described by $R = k\exp(-E_a/R^*T)(P_{H_2})^n$. Three regions with distinctly different pressure

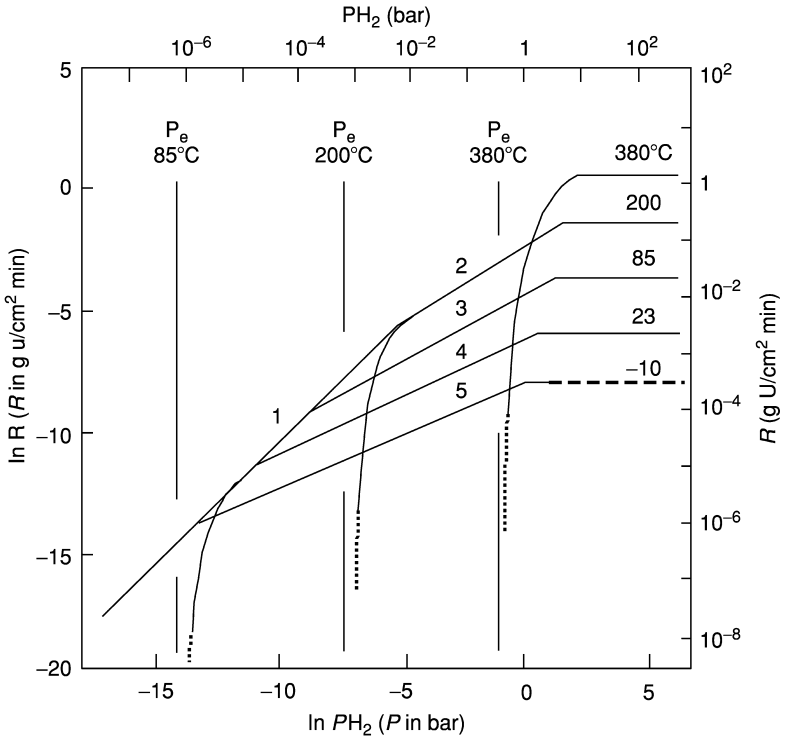

Fig. 29.7 *Dependence of* ln R *on* ln P_{H_2} *for the U–H_2 reaction at selected temperatures between* –10 *and* 380°C.

exponents consistent with Langmuir adsorption theory are identified: a low-pressure region in which the surface concentration of adsorbed hydrogen, θ, is negligible and proportional to P_{H_2} ($n = 1$); an intermediate-pressure region in which θ is proportional to $(P_{H_2})^n (n = 0.5 \pm 0.1)$, and a high-pressure region in which θ is 1 and independent of $P_{H_2} (n = 0)$. At low P_{H_2} and temperatures below 200°C, rates for all temperatures converge to a single line with a slope of 1 (curve 1 in Fig. 29.7) consistent with rate control by impingement of H_2 on the surface. In the absence of a dependence on T, $E_a = 0$ and $R = kP_{H_2}$. As shown by data in Table 29.5, the general equation also applies to curves 2–5 with n values near 0.5, implying that R depends on the concentration of adsorbed H_2 and that reaction involves dissociation into atomic H. Pressure independence at high P_{H_2} is attributed to hydrogen saturation of the surface.

Arrhenius results in Table 29.6 show that the hydriding rate is dependent on temperature at intermediate and high P_{H_2} (Ward and Haschke, 1994). In the pressure-independent ($n = 0$) region, R depends only on temperature. As shown by E_a values in Table 29.6, activation energies coincide with the

Table 29.5 *Rate equations describing the dependence of the U hydriding rate on H_2 pressure for curves in Fig.* 29.7.[a]

Curve	T (°C)	*Applicable* P_{H_2} *range* (bar)	k	n
1	<200	–[b]	0.75	1.0
2	200	5×10^{-3}–5	0.067	0.61
3	85	2×10^{-4}–3	0.012	0.53
4	23	2×10^{-5}–1	1.7×10^{-3}	0.46
5	–10	2×10^{-6}–0.7	3.2×10^{-4}	0.40

[a] Rate equations have the form R(in g U cm^{-2} min^{-1}) $= k(P_{H_2})^n$ (P_{H_2} in bar, geometric area of U). Reference to Fig. 29.7 may be necessary to verify validity of the equation.
[b] The applicable P_{H_2} range of curve 1 depends on temperature and expands to higher pressures with increasing temperature. Curve 1 is not applicable above 200°C because the required P_{H_2} approaches P_e for UH_3 formation. Reference to a detailed analysis of applicable kinetic regimes (Ward and Haschke, 1994) may be necessary.

Table 29.6 *Arrhenius equations*[a] *for hydriding of U along selected H_2 isobars in Fig.* 29.7 (*Haschke*, 1998).

P_{H_2} (bar)	*Applicable* T *range*[b] (°C)	E_a (kJ mol^{-1})	A	B
10	<425	32	6.40	3815
1	0–325	27	4.32	3270
0.1	–50 to 250	25	2.36	2995
10^{-2}	<200	24	0.82	2865
10^{-3}	<70	23	–0.49	2730

[a] Rate equations have the form $\ln R$ (R in g U cm^{-2} min^{-1}) $= A-(B/T)$ (T in K, geometric area of U).
[b] Temperature limits are based on kinetic regimes defined in a $P_{H_2} - T$ diagram (Ward and Haschke, 1994).

(30 ± 5) kJ mol^{-1} E_a for hydrogen self-diffusion in UH_3 (see Section 29.3.4), implying that R is controlled by diffusion of hydrogen through the adherent hydride layer at high P_{H_2} and is determined by the combined effects of the adsorbed H_2 concentration and diffusion at intermediate pressures. Rates in the intermediate-pressure ($n \sim 0.5$) region vary with T, as well as with P_{H_2}, showing that R depends on both parameters. Systematic variations of n with T (Table 29.5) and E_a with P_{H_2} (Table 29.6) suggest that parameters are not independent. In part, the dependence of E_a on P_{H_2} accounts for the large range of activation energies (8–33 kJ mol^{-1}) cited in early studies (Haschke, 1991); the observed value depends on the isobaric H_2 pressure present during measurement.

Involvement of thermodynamic rate control is shown in Fig. 29.7 by abrupt decreases in rate as P_{H_2} approaches the equilibrium pressure, P_e, for UH_3 formation at 85, 200, and 380°C. Values of R consistently deviate from control by other parameters for $P_{H_2} < 10P_e$. Values of P_e are defined by $\ln P_e$ (in bar) $= 14.54-(10233/T)$ (Flotow *et al.*, 1984). A diagram identifying the

$P_{H_2} - T$ regimes in which different parameters determine the rate of U–H_2 reaction (Ward and Haschke, 1994) shows that impingement control is not possible above 200°C because the P_{H_2} required to drive that process is greater than P_e. In a similar way, existence of the regime involving combined effects of P_{H_2} and T is precluded by thermodynamic control above 400°C. The 85°C isotherm in Fig. 29.7 exhibits all four types of control. Although several models have been proposed to describe and predict the hydriding kinetics of U (Haschke, 1991), results suggest that accounting for behavior over the full parametric range with a single model is unlikely unless all control mechanisms and their relationships are included.

Kinetic studies with high surface area (0.5–3 $m^2\ g^{-1}$) U prepared by hydriding and dehydriding cycles (Condon and Larson, 1973; Stakebake, 1979) suggest that reaction of H_2 with powdered metal differs from that of massive uranium. Studies with U-powder at 75–200°C and 5×10^{-4}–0.13 bar H_2 show that $n = 0.5$ (Condon and Larson, 1973), that E_a is –7 kJ mol^{-1} (Condon and Larson, 1973; Stakebake, 1979), and that R depends on the amount of unreacted metal, not on the surface area. Proposed models in both studies are based on rapid diffusion of hydrogen and formation of hydride within the U-particles. Mass–time data for reaction of U-powder (0.6 $m^2\ g^{-1}$) with H_2 at 0.13 bar and 100°C (Stakebake, 1979) yield a linear rate of 2×10^{-4} g U $cm^{-2}\ min^{-1}$ (BET area). The value of R calculated for massive U at 100°C using the equation for 0.1 bar in Table 29.6 and a specific area that is 10–20 times the geometric value yields a rate of $(2 \pm 1) \times 10^{-4}$ g U $cm^{-2}\ min^{-1}$ (BET area), suggesting that hydriding kinetics of powdered and massive U are similar.

Compared to the penetration rate of Pu by H_2 at 1 bar and 25°C (6 cm h^{-1}), corrosion of massive U by H_2 at those conditions is relatively slow (40 μm h^{-1}) and is consistent with differences in hydrogen-transport properties of the hydrides. Although the corrosion rate of finely divided uranium appears to be indistinguishable from that of massive metal, the rate of heat generation is enhanced because of the larger surface area. The UH_3 product has a specific area of about 1 $m^2\ g^{-1}$ (Condon and Larson, 1973) and is pyrophoric in air. Studies of the reaction between UH_3 and saturated H_2O vapor at 100°C show that UO_2 and H_2 form at a constant rate until the process is approximately 65% complete after 20 h (Baker *et al.*, 1966). Subsequent reaction continues at a progressive slower rate and becomes immeasurably slow at about 80% completion after 50–60 h.

29.6.3 Reaction of U with oxygen, water, and air

As shown in a recent review (Haschke, 1998), oxidation kinetics of U in dry air and water vapor closely parallel those of Pu, but diverge in moist air below the ignition point and in static air at temperatures above the ignition point. The kinetic behavior of U (Fig. 29.8) is similar to that of unalloyed Pu in Fig. 29.5. Arrhenius curves for U form an envelope bounded by slow rates in dry air and

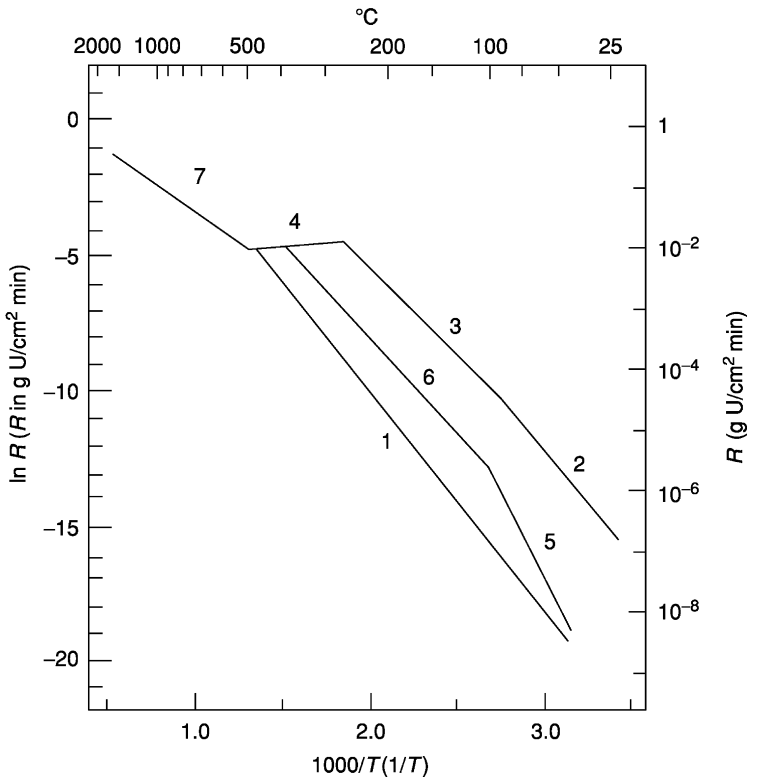

Fig. 29.8 *Arrhenius curves for corrosion of U in air and water vapor. Curve* 1 *describes behavior in dry air. Curves* 2, 3, *and* 4 *are for corrosion in water vapor at the equilibrium pressure below* 100°C *and in* 1 bar *steam at higher temperatures. Curve* 5 *shows behavior in air at all humidity levels and curve* 6 *describes the behavior at* 0.053 bar *water pressure. Curve* 7 *describes the corrosion in air above* 500°C. *Detailed descriptions of the curves are given in the text and in Table* 29.7.

rapid rates in water vapor at low temperatures and closed by convergence of rates at high temperatures. Respective rates for U and Pu in dry air at 25°C are 8 and 5 ng metal cm^{-2} min^{-1}. The oxidation rates of both metals in saturated water vapor are approximately 250 times faster than in dry air at room temperature.

Oxidation of uranium in dry air proceeds with formation of an adherent product layer on the metal surface and with paralinear kinetics (Haschke *et al.*, 2001b). The chemical composition of the layer during the linear stage was identified as UO_2 below 275°C and an outer layer of U_3O_8 was observed in air at higher temperatures (Colmenares, 1975). Spalled oxide continues to react and form U_3O_8 in air. Curve 1 in Fig. 29.8 for the constant-rate stage of oxidation (Haschke, 1998) is based on measurements in dry air at 40–350°C (McGillivray

Table 29.7 *Arrhenius equations*[a] *for corrosion of U in air and H_2O vapor.*

		Applicable range				
Curve	*Reaction*	*T* (K)	P_{H_2O} (bar)	*A*	*B*	*References*[b]
1	U + dry air	<773	0	6.19	8 077	A,B
2	U + H_2O vapor	<373	P_e[c]	10.64	7 725	A,C
3	U + H_2O vapor	373–623	1.01	8.33	6 860	A,D
4	U + H_2O vapor	623–773	1.01	–4.92	0	A,D
5	U + humid air	<373	0.003–0.5	22.96	13 285	A,C,E
6	U + humid air	372–673	0.053[d]	5.09	6 765	A,B,C
7	U + dry/humid air	>773	1.01	1.21	4 655	A,F

[a] Arrhenius equations have the form R (in g U cm^{-2} min^{-1}) = $A - B/T$ (T in K, geometric area).
[b] References: A, Haschke (1998); B, McGillivray *et al.* (1994); C, Colmenares (1984); D, Huddle (1953); E, Ritchie *et al.* (1986); F, Hilliard (1958).
[c] P_e is the H_2O pressure in equilibrium with water at T.
[d] The 0.053 bar H_2O pressure corresponds to a median value of the measurements. Rates at other conditions are derived using the temperature-dependent exponent of P_{H_2O}, n, which varies from 0 at 100°C to a maximum of 1 at 250°C and decreases to 0.6 at 350°C (Haschke, 1998).

et al., 1994). The Arrhenius equation describing curve 1 appears in Table 29.7. E_a (67 kJ mol^{-1}) is consistent with rate control by diffusion of oxygen through the adherent oxide layer. As shown by curves 2 and 3 in Fig. 29.8, corrosion of uranium in water vapor is more rapid than in dry air (curve 1). Contrary to reports that UH_3 is formed by the U–H_2O reaction, products are identified as H_2 and UO_{2+x} with values of x varying from 0 to 0.2 (Haschke *et al.*, 2001b). Curve 2 (Table 29.7) describes the reaction rate for equilibrium vapor pressures, P_e, of water at temperatures up to 100°C (Haschke, 1998). The pressure exponent is 0.5 and E_a is 64 kJ mol^{-1}, implying that the rate is controlled by diffusion of oxygen through the product layer of constant average thickness (Haschke *et al.*, 2001b). The derived rate equation for 100–250°C given by curve 3 in Fig. 29.8 and Table 29.7 is derived using R at 100°C and 1.01 bar H_2O and on experimental data (curve 4) for the uranium-steam reaction at 200–500°C (Huddle, 1953). Those data describe a temperature-independent process that results in closure of the rate envelope near 500°C and absence of moisture-enhanced corrosion above that point.

Curves 5 and 6 in Fig. 29.8 and Table 29.7 describe the corrosion of uranium in moist air (Ritchie *et al.*, 1986; McGillivray *et al.*, 1994; Haschke, 1998). At 100°C, R for U at O_2 concentrations less than 20 ppm is proportional to $(P_{H_2O})^{0.5}$(Colmenares, 1984). This behavior is like that observed for Pu at all O_2 pressures (see Section 29.5.2(c)). If P_{O_2} exceeds 0.15 mbar (150 ppm), R exceeds the rate in dry air, but remains fixed as P_{H_2O} is varied from 3 to 130 mbar. Curve 5 describes the humidity-independent corrosion rate (E_a = 110 kJ mol^{-1}) in air at 40–100°C. At 100–400°C, the corrosion rate is dependent on H_2O pressure with values of n increasing linearly from 0 at 100°C to a maximum

of 1 at 250°C and decreasing linearly to 0.6 at 350°C (Haschke, 1998). Curve 6 defines R for a median H_2O pressure of 0.053 bar and an E_a equal to 56 kJ mol^{-1}. Rates, $R(P_{H_2O})_T$, at other values of T and P_{H_2O} are derived using $R(0.053)_T$ from curve 6 and the equation: $R(P_{H_2O})_T = R(0.053)_T((P_{H_2O})^n/0.053^n)$. Enhancement of the rate in moist air is attributed to the same water-catalyzed cycle as proposed for plutonium (see Section 29.5.2d) (Haschke *et al.*, 2001b). Attenuation of enhancement by O_2 suggests that the oxide surface is chemically altered by the formation of a higher oxide or other change that reduces the rate of O^{2-} formation or transport. Convergence of curves 5 and 1 at 35–40°C indicates that corrosion of U in air is insensitive to humidity at room temperature or that curve 1 describes the corrosion rate in air with significant residual moisture.

At temperatures above 500°C, the corrosion rate of U is humidity-independent and described by curve 7 (Hilliard, 1958; Haschke, 1998). The convergence of curves 1, 4, and 7 in Fig. 29.8 at this temperature suggests that measurements are consistent and implies a significant change in chemical behavior. Corrosion rates exceed that required to form a N_2-rich boundary layer with Pu (curve 8, Fig. 29.5) (Haschke and Martz, 1998b), are insensitive to an increase of 10^4 in the flow rate of air during reaction, and show that reaction slows slightly after O_2 is depleted from static air at 805°C (Hilliard, 1958). Unlike Pu, corrosion of U at high temperatures apparently proceeds with facile reaction of both O_2 and N_2. E_a (39 kJ mol^{-1}) is comparable to that (40 kJ mol^{-1}) observed for ignited Pu during free fall in air.

29.6.4 Thermal ignition and self-sustained oxidation of U

The ignition behavior of U is uncertain because of conflicting observations. Reported ignition temperatures of U in air (Fig. 29.6) indicate that the ignition behavior is similar to that of Pu. Ignition temperatures, T_i, extracted from an early review (Wilkinson, 1962) show that powder, chips, and foils with dimensions less than 1 mm ignite at 250–325°C and that pieces with larger dimensions ignite at 500–600°C. Behavior suggests that rapid reoxidation of a UO_2 layer at the oxide–metal interface to U_3O_8 might provide sufficient heat to raise the temperatures of powder and chips to the ignition point in a process similar to that described for Pu (see Section 29.5.2(e)).

Questions about the T_i data in Fig. 29.6 are raised by results of other studies (Hilliard, 1958). Exposure of burnished and preheated U samples to flowing air resulted in three types of behavior depending on initial temperature. At temperatures below 400°C, attainment of a stable temperature after 1–2 h is followed by a continuing reaction at a constant rate. At temperatures of 400–650°C, an initial thermal spike is followed by a period in which the sample temperature remained near the furnace temperature. Successive periods (0.3–0.5 h) of such slow reaction were followed by a thermal spike that exceeded 1000°C in some cases. This cyclic process continued until the metal was consumed.

At initial temperatures above 650°C, a sharp initial thermal spike was followed by a period (0.5–1 h) in which the sample temperature remained relatively constant at a value above the furnace temperature.

Thermal excursions attributed to ignition may correspond to spikes induced by periodic spallation of a thick oxide layer (Hilliard, 1958), not with onset of autothermic reaction. That possibility is supported by failure of samples at 1250°C to continue reacting in air after removal from the furnace (Hilliard, 1958). Corrosion rates derived for isothermal reactions during extended (>1 h) tests at 440 (365°C furnace) and 810°C (710°C furnace) are 0.006 and 0.05 g U cm^{-2} min^{-1}, respectively. The corresponding rates calculated for curves 1 and 7 (Table 29.7) are 0.0059 and 0.045 g U cm^{-2} min^{-1}. Observation of a stable rate over a long time period at 810°C is inconsistent with onset of autothermic behavior at 500–600°C. The autothermic behavior of U remains uncertain.

29.6.5 Reactions of U and UH_3 with water

A review and assessment of chemistry and reaction kinetics for reactions of U and UH_3 with water (Haschke, 1995) suggest that the solid products may be oxide hydrides ($UO_{1.5 \pm 0.3}H_{0.5 \pm 0.2}$), not mixtures of UO_2 and UH_3. The corrosion rate of U in distilled water at 25°C (0.5 μg U cm^{-2} min^{-1}, geometric area) is similar to that for Pu, but the U–H_2O rate in synthetic seawater is a factor of 20 slower than in distilled water. The reaction rate of UH_3 (2 μg U cm^{-2} min^{-1}, BET area) is modest for small samples, but violent exothermic reaction is reported for samples greater than 25 g (Newton *et al.*, 1949).

29.7 RADIOLYTIC REACTIONS

Radiolysis of organic and molecular compounds in close proximity to radioactive materials provides an important source of chemical reactants capable of altering properties and behavior of materials, especially during periods of extended storage. The extent of radiolysis is a function of specific alpha activity, which is negligible for ^{238}U and varies significantly for the common Pu isotopes (IAEA Report, 1998). Respective values for ^{238}Pu, ^{239}Pu, ^{240}Pu, ^{241}Pu, and ^{242}Pu are 600, 2, 8, 3700 (beta decay), and 0.1 GBq g^{-1}. The alpha activity of ^{241}Am formed by beta decay of ^{241}Pu is 120 GBq g^{-1}. The isotopic distribution of Pu varies markedly with the level of fuel burnup. An activity of 8×10^{-5} GBq g^{-1} for ^{235}U indicates that radiolytic processes are relatively insignificant for highly enriched uranium.

Formation of H_2, CH_4, and other gaseous products by alpha-induced radiolytic decomposition of hydrocarbons (–CH_2–) and other organic materials is especially important:

$$-CH_2- \ (s, l, g) + \alpha\text{-particle energy} \rightarrow C(s) + H_2(g).$$

Hydrocarbon oils polymerize and polyethylene plastics are embrittled by this reaction. Alpha radiolysis of oxygenated organic compounds also generates CO and CO_2 (Kazanjian, 1976). Radiolysis of polyvinyl chloride (PVC) and chlorinated solvents produces HCl. Rates progressively decrease over time from 'burnout' as a layer of carbon-rich residue forms adjacent to the Pu-containing source. Studies in which liquid and solid organic materials (oil, ethylene glycol, silicone rubber) were placed in contact with oxide-coated Pu show that H_2 is the primary (>99%) gaseous product and that gas generation rates are surprisingly similar for all organic materials in the tests (Haschke *et al*., 2001c). Respective rates after 0.01, 0.5, and 2.5 years are 4, 0.07, and 0.04 nmol H_2 cm^{-2} min^{-1} (geometric Pu area). Corresponding H_2-generation rates for plutonium oxide powders in contact with organic materials are expected to vary from 0.2 to 0.002 nmol H_2 cm^{-2} min^{-1} (BET area).

Formation of gaseous products is reported for tests in which cellulose, plastics, hydrocarbon oils, latex rubber, and chlorocarbon solvents were exposed to $^{238}PuO_2$ or $^{239}PuO_2$ in closed containers with air atmospheres (Kazanjian, 1976). Derived *G*-values for total gas generation vary from 0.4 to 3 molecules per 100 eV of absorbed energy. As shown by a linear time dependence of moles H_2 produced, rates of hydrogen production were essentially constant over 1-year test periods and show no evidence for decreases associated with burnout. O_2 was consumed at a constant rate over a period of 20–60 days, suggesting that observed rates of H_2 production during the initial period were reduced by formation of H_2O. These results and consistent evidence for water in gas analyses indicate that H_2 does not accumulate as predicted by *G*-values if O_2 is present, but that water is formed by surface-catalyzed combination of the elements. Continuing formation of CO_2 after depletion of O_2 suggests a radiolytic or catalytic reaction of H_2O with C-rich residues.

Radiolytic reactions of Pu also form highly reactive and corrosive products in other systems. In the absence of organic compounds, radiolysis of air in a confined volume produces mixtures containing up to 10% N_2O and NO_2 within 2–3 years (Haschke and Martz, 1998a). NO_2 is corrosive to steel at moisture levels above 3% relative humidity. Radiolysis of air-exposed aqueous solutions produces HNO_3 (Rai *et al*., 1980; Rai and Ryan, 1982). The pH of a solution containing about 1 mg $^{238}PuO_2$ per ml decreased from neutral to 1.5 within a 3.5-year period. N_2 atmospheres are not inert if aqueous solutions are present because HNO_3 is formed from oxygen produced by radiolysis of water. Radiation-promoted nitration of organic materials such as ion-exchange resins in nitric acid solution forms solids that may react violently when dry (Cleveland, 1979).

Mention of an important nonradiolytic process related to alpha decay of Pu isotopes is merited because of its apparent involvement in movement of submicrogram-size oxide particles. Observation indicates that spreading of radioactive contamination occurs spontaneously during operations with oxide. Movement of $^{238}PuO_2$ is noticeably more rapid than in similar operations with $^{239}PuO_2$. The unquantified process, which is attributed to air entrainment

of small particles by recoil energy from alpha decay, is apparently an important factor in transport of finely divided powders and spread of contamination over time.

29.8 HAZARD ASSESSMENT

29.8.1 Synergistic reactions

The chemistry of Pu metal and oxide, and to a lesser extent that of U, is unusually complex and reactivities of systems containing those materials may be dramatically altered by changes in surface chemistry. Slow processes that normally do not merit consideration may become important during an extended storage period. Trace amounts of hydrogen, water, and other gases are important constituents because of their chemical properties. For example, H_2 reacts with O_2 to form water and with Pu to form hydride. Both products catalyze specific reactions. In some cases, transport of oxide particles is a key step in radiolytic formation of H_2. Entrainment of submicrogram-size particles is promoted by alpha recoil. Synergistic convergence of several processes like these may produce unanticipated behavior.

Synergistic interaction is demonstrated by considering a hypothetical storage configuration in which oxide-coated Pu metal and a high-purity Ar atmosphere are sealed for an extended period in a steel container with an elastomeric *o*-ring closure. A potentially hazardous situation is created by occurrence of parallel and sequential reactions. In the absence of oxygen, the oxide layer is reduced to α-Pu_2O_3 over time. Small oxide particles entrained by alpha recoil are simultaneously dispersed throughout the container via thermal currents created by heat from radioactive decay. Hydrogen formed by radiolytic decomposition of elastomer by alpha particles from oxide particles deposited on the *o*-ring reacts with the sesquioxide-coated Pu to form a Pu_2O_3–PuH_x double layer. Catalytic initiation of self-sustained oxidation and nitriding (see Section 29.5.2(f)) is possible and likely upon exposure of the metal to air.

A significant constraint on assessment of hazards for Pu exists because all pathways that lead to potentially hazardous situations are not defined. In light of limited understanding of synergistic interactions, subsequent discussions of hazards cannot be considered exhaustive.

29.8.2 Potential hazards

(a) Formation of gases

Concern focuses on the formation of potentially explosive gases and generation of static pressures that might result in loss of containment and dispersal of Pu-containing particles. H_2 produced by chemical or radiolytic processes is

highly reactive and forms explosive mixtures with O_2. Gas pressures generated by chemical reaction, radiolysis, or thermal decomposition may rupture a container.

Contrary to widely held views that PuO_2 is inert and the ideal storage form for plutonium, observations (see Sections 29.3.2 and 29.4.2) show that dioxide tenaciously adsorbs water and reacts with H_2O to form PuO_{2+x} and H_2. If air or O_2 is sealed in the storage container with moisture-equilibrated oxide, the water-catalyzed PuO_2–O_2 reaction (Haschke *et al.*, 2000b) proceeds via a mechanism like that for water-catalyzed oxidation of Pu by O_2 (see Section 29.5.2d).

$$\begin{aligned}
&PuO_2(s) + x\ H_2O(ads) \rightarrow PuO_{2+x}(s) + 2x\ H(ads)\\
&x/2\ O_2\ (g) \leftrightarrow x\ O(ads)\\
&\underline{2x\ H(ads) + x\ O(ads) \rightarrow x\ H_2O(ads)}\\
&PuO_2(s) + x/2\ O_2(g) \rightarrow PuO_{2+x}(s)
\end{aligned}$$

Occurrence of this process in storage is shown by initial disappearance of O_2 from air-filled storage containers at the rate predicted for kinetic control by the first step of this cycle (Haschke *et al.*, 2001a). Calculations indicate that O_2 in a typical air-filled container is consumed after about 1.5 years. After O_2 is depleted, H_2O reacts via the initial step with association of H atoms as H_2.

The maximum H_2 pressure from chemical reaction of water in a closed, air-filled system is determined by several factors: amount of oxide, specific area of the oxide, initial concentration of adsorbed water, oxide mass, free volume of the container, and rate of the oxide–water reaction. These factors are included in a quantitative model for calculating the time dependence of pressure in a sealed oxide container (Haschke *et al.*, 2001a). Thermodynamic assessment indicates that reaction of water is not limited by attainment of the equilibrium H_2 pressure and that the oxide–water reaction proceeds to completion (Haschke and Allen, 2002).

An important consequence of the water-catalyzed cycle is the sequential nature of the catalytic cycle. Depletion of O_2 before onset of H_2 formation is observed for water-enhanced oxidation of Pu and U, implying that corrosion is controlled by the oxide surface. Therefore, formation of H_2–O_2 mixtures by chemical reaction is apparently precluded. That assessment is tempered by the requirement that formation of H_2 by radiolysis of H_2O or some other process is slow relative to the rate of O_2 consumption (Haschke *et al.*, 2001a). Although formation of H_2 by weapons-grade plutonium oxide appears sufficiently slow, the radiolysis rate must be considered in each case because rapid formation of H_2 may result in the formation of a transient explosive mixture.

As implied by preceding discussion, H_2 is produced by radiolysis of organic materials in close proximity to oxide or metal. The process is under kinetic control and is capable of generating high pressures. Formation of H_2 is limited only by the amount of organic material available, but its rate of formation is slowed by kinetic factors such as 'burnout' around the radiation source

(see Section 29.7) and by formation of H_2O in the presence of O_2. The rates at which H_2 and O_2 dissociatively adsorb and form H_2O on various surfaces are unknown, but may be important in determining the H_2 inventory and pressure.

H_2 is also generated by reaction of H_2O with metallic Pu and U. Measurements with Pu in moist air show that the pressure in a sealed container decreases as O_2 is consumed and then increases at essentially the same rate as H_2 is formed (Haschke *et al.*, 2001b). However, as discussed in Section 29.5.2d, hydrogen is a transient species in the presence of Pu and is expected to ultimately react with available metal to form PuH_x. Measurements show that the reaction proceeds as expected if H_2O is the only source of H_2 or if solid organic materials are radiolyzed. Hydride formation does not initiate immediately and the H_2 pressure may continue to increase over time if volatile organic liquids are present.

The course of the Pu–H_2O reaction in low-O_2 atmospheres is altered and the rate of H_2 generation is increased if small amounts of gaseous HCl are present (Haschke *et al.*, 1998b). $PuCl_3$ formed by rapid Pu–HCl reaction is deliquescent, forms a concentrated chloride solution on the metal surface, and apparently catalyzes the formation of PuOH plus H_2, as observed in aqueous chloride solution (see Section 29.5.2(g)). Chloride catalysis increases the H_2 formation rate of alloyed Pu by approximately 10^3 at room temperature.

Thermodynamic data derived for PuO_{2+x} suggest that the higher oxide is a thermally activated source of high-O_2 pressure (Haschke and Allen, 2002). Results indicate that $PuO_{2.2}$ is the equilibrium composition formed by calcination of oxalate, peroxide, nitrate, or other oxygenated solids at 400–450°C in air and that PuO_2 is stable above 650°C. Predictions are consistent with formation of $PuO_{2.3}$ during heating of $PuO_3 \cdot 0.7H_2O$ in vacuum at 200–250°C. Pressurization of storage containers may result from decomposition of PuO_{2+x} upon heating to 450–500°C (Bagnall and Laidler, 1964), as well as from generation of gases by pyrolysis of anion residues in low-fired solids (see Section 29.8.3(b)). Generation of O_2 pressures approaching 50 bar is possible if a typical sealed storage vessel containing low-fired (400–450°C) $PuO_{2.2}$ is heated above 650°C. Formation of O_2–H_2 mixtures is possible during heating if higher oxide was formed *in situ* by reaction of adsorbed H_2O.

Other possible methods of generating O_2 and other noncondensable gases exist if the storage container for low-fired oxide is involved in a fire. Pressurization may occur as gases are formed by thermal decomposition of residual oxygen-containing anions or anion fragments remaining in the oxide.

A minor contribution to the pressure is made by accumulation of helium produced by alpha decay in oxide. For short time periods (several hundred years) compared to the half-life of ^{239}Pu, the He production rate is approximately constant at 0.10 mmol He per kg $^{239}PuO_2$ per year. Although a comparable rate of 0.11 mmol He per kg ^{239}Pu per year exists for Pu, He is retained in the metal (Hecker and Martz, 2000) and is released only upon heating. Results

indicate that, except for a near surface layer from which alpha particles escaped, all He produced in bulk ^{239}Pu over a 40 year period remains in the metal.

Although generation of gas pressures during storage of UO_2 has not been of concern, questions are raised by the reported reaction of UO_2 with liquid water and solutions (Matzke and Turos, 1991). Additional investigation is needed to determine if uranium dioxide reacts with water vapor and adsorbed water, to define kinetic behavior over a broad range of conditions, and to assess potential consequences for handling and storage.

(b) Thermal hazards

In addition to the thermal hazard posed by reaction of hydrogen from radiolytic and chemical interactions, large amounts of heat are produced over short time periods by rapid, self-sustained corrosion of Pu metal. As described in Sections 29.5.2e and 29.5.2f, autothermic reactions are initiated in two ways: thermally and catalytically. Thermal sources may be external or exist within the chemical system. As discussed in Section 29.5.2e, Pu powder does not spontaneously ignite in air at room temperature, implying that spontaneous ignition of the metal at 25°C is driven by reaction of coexisting pyrophoric or catalytic materials. Formation of catalytic surface layers on Pu may result in spontaneous ignition upon exposure to air at room temperature. Self-sustained reaction during both thermal and catalytic processes is apparently contingent on attainment of a temperature required to maintain an α-Pu_2O_3 surface, but PuH_x is also necessary for catalyzed reaction and results in simultaneous reaction of both O_2 and N_2.

Highly reactive and pyrophoric compounds of plutonium are potential thermal sources for heating Pu above the 500°C ignition point. The α-Pu_2O_3 layer formed on Pu by autoreduction of the oxide surface is identified as the ignition source for Pu chips and fines (Martz *et al.*, 1994). PuH_x is considered pyrophoric because of its unique ability to accommodate product H_2 and consume N_2 (Haschke and Allen, 2001). In concert, these processes promote pyrophoric reaction by facilitating transport of O_2 to the hydride surface and preventing formation of a N_2/H_2 boundary layer at the hydride surface. The heat-generation rate of 10–15 kJ g^{-1} PuH_x per min for the hydride–air reaction is substantially larger than the 0.1–0.5 kJ g^{-1} Pu per min rate required for self-sustained reaction of massive metal in air because the hydride surface area is relatively high. Thermal calculations show that more than 30 mass% of a hypothetical mixture containing substoichiometric dioxide ($PuO_{1.98}$), 5% hydride, and 0.5% Pu powder must be present and react to adiabatically heat the co-existing metal (70 mass%) to 500°C (Haschke and Allen, 2001).

Catalyzed corrosion of Pu by H_2 is initiated by an α-Pu_2O_3 surface layer, as well as by a layer of PuH_x. As discussed in Section 29.5.2f, Pu coated with an α-Pu_2O_3–PuH_x double layer spontaneously reacts with O_2 and N_2 upon exposure

to air at room temperature. The catalytic double layer forms on the Pu surface via several pathways, including exposure of PuH_x-coated metal to air or O_2. Other known routes to the catalytically active surface include exposure of α-Pu_2O_3-coated Pu to a small amount of H_2 and formation of a PuOH precursor by immersion of the metal in water (Haschke and Allen, 2001). When altered by traces of gaseous HCl, the water vapor–metal reaction also produces a reactive PuOH surface (see Section 29.8.2a). Existence of additional routes to the catalytically active surface is likely. On the basis of rate equations and enthalpy data, rates of heat generation by self-sustained oxidation of static Pu in air, by the autocatalytic Pu–H_2 (1 bar H_2) reaction, and by the catalyzed Pu–air reaction are 0.5, 1.1, and 2.7 kJ cm^{-2} min^{-1}, respectively. If the surface of a 2 kg Pu casting (5 cm diameter, 1.3 cm high) is fully active and all heat is retained in the metal, a 1.0 kJ cm^{-2} min^{-1} generation rate produces a temperature increase of 490° per min.

Secondary consequences of thermal excursions of internal or external origin are also of concern because temperatures frequently exceed the 640°C melting point of Pu. If the metal is in a steel container, rapid corrosion of the vessel by molten Pu (see Section 29.5.3) may result in catastrophic release to the environment (Haschke and Martz, 1998a). A substantial increase in the surface area of the metal is possible upon release and may cause a noticeable increase in the corrosion rate.

As discussed in Section 29.6.2, the ignition characteristics of U are uncertain. Behavior seems most consistent with rate control by a protective UO_2 product layer that is not capable of forming a catalytic oxide like α-Pu_2O_3. If sharp thermal spikes are caused by periodic spallation of the uranium oxide, onset of self-sustained reaction of massive metal is unlikely. However, exposure of UH_3 powder to air is likely to result in pyrophoric ignition and a large thermal excursion.

(c) Release and dispersal of nuclear material

For humans, the primary health hazard of plutonium is radiation exposure from small Pu-containing particles retained in the respiratory system (Voelz, 2000). Airborne particles with aerodynamic diameters, D_A, less than 10 μm are deposited in significant quantities in the lungs (Luna *et al.*, 1971). D_A is the diameter of a unit-density (1 g cm^{-3}) sphere with the same terminal velocity in air as a particle of arbitrary size, shape, and density. Because effects of shape and air resistance are small, $D_A \sim (\rho_p)^{0.5} D_G$, where D_G is the geometric diameter of a particle with density ρ_p (Mishima and Pinkston, 1994). The density of PuO_2 is 11.46 g cm^{-3} and the combined mass of oxide particles with geometric diameters less than 3 μm constitutes the respirable release fraction (RRF) of an oxide powder. The aerosol release fraction (ARF) is the mass fraction of powder comprised of particles that are likely to become airborne. Because aerodynamic diameters of particles in ARF are less than 30 μm, PuO_2 particles

in this mass fraction typically have geometric diameters less than 10 μm, but entrainment studies during metal oxidation suggest that D_G may extend to 20 μm (Stewart, 1963).

The source term (ST) for the airborne release of respirable particles is usually defined by the source strength of aerosolizable particles in units of grams (Luna *et al.*, 1971). ST is a function of the quantity, Q, of material at risk, ARF, and RF, the respirable fraction of ARF:

$$\mathrm{ST} = Q \times \mathrm{ARF} \times \mathrm{RF} = Q \times \mathrm{RRF}.$$

Note that RF is a fraction of ARF and that RRF is a fraction of Q because these quantities are easily confused.

The risk of releasing and dispersing respirable particles is significantly enhanced by corrosion reactions that simultaneously transform metal into powder and promote loss of containment (Haschke *et al.*, 1998a). Reactions of oxide do not detectably alter the source term, but generate gases that pressurize the container. Consequences of solid expansion during metal corrosion are surprising because solid products do not move to occupy free volume within the container. After the solid product expands to the container wall, further reaction compresses the product, prevents movement that would relieve radial pressure, and leads to rupture of the container (Haschke and Martz, 1998a).

Assessment of the dispersal hazard is contingent on availability of source-term data, and in some cases, on the corrosion rate, R, of metal at conditions of interest (Haschke and Martz, 1998b). If corrosion continues during the dispersal incident, the material at risk increases as metal is progressively transformed into product. The dependence of ST on R, surface area of metal involved, and time period of the incident are incorporated into the above source-term equation by replacing Q with the product of R, surface area, and time. Values of R are defined for Pu and U in Sections 29.5 and 29.6. Alternatively, the measured airborne release rate, which inherently equals $R \times$ ARF, may be included along with SA and time to define the source term for a dynamic event.

Cumulative mass fractions of particles with geometric sizes less than 3, 10, and 30 μm for oxides from corrosion of Pu and calcination of precipitates are listed in Table 29.8 (Pritchard *et al.*, 1963; Stewart, 1963; Stakebake and Robinson, 1977; Giacomini, 1985; Ricketts, 1995; Machuron-Mandard and Madic, 1996; Haschke *et al.*, 1998a; Martz and Haschke, 1998c; Szempruch, 2001). Respirable release fractions are indicated by cumulative fractions for 3 μm size particles. Because RRF varies by as much as 10^5 depending on preparative method, reliable assessment of the dispersal hazard is unlikely unless the oxide source is considered. RRF for oxide from corrosion of metal is decreased by increasing temperature and humidity or by the presence of hydride catalyst, but is increased by alloying (Stewart, 1963; Haschke *et al.*, 1998a). These correlations suggest that the size distribution of a spalled corrosion product is determined by the relative rates of corrosion and crack formation in the density-stressed product layer on the metal surface (Haschke *et al.*, 1998a). Nucleation

Table 29.8 *Size distribution data for plutonium oxide prepared at different conditions.*[a,b]

Preparative history of PuO_2	*Cumulative mass fraction at specified size* (μm)			*References*[c]
	3	10	30	
unalloyed Pu, air, room temperature	0.03	0.05	>0.95	A
Pu, air, 100–400°C	0.02	0.07	0.2	B
Pu, air, >500°C	6×10^{-6}	5×10^{-4}	0.01	A
Pu, air, >500°C	1×10^{-3}	5×10^{-3}	–	B
Pu + PuH_x, air, low temperature	6×10^{-3}	0.2	0.8	A
Pu + PuH_x, air, >500°C	5×10^{-5}	2×10^{-4}	2×10^{-3}	A
Pu droplets, air, >3300°C	0.7	0.8	0.8	A,C
PuH_x + air, <800°C	0.02	0.25	0.8	D,E
Pu(III)oxalate, 950°C calcination	1×10^{-4}	8×10^{-3}	0.2	F
Hanford production oxide	<0.01	0.25	>0.95	G
peroxide, 950°C calcination	0.05	0.2	–	H
Pu(III)oxalate, 950°C calcination	0.05	0.4	–	H
Pu(IV)oxalate, 950°C calcination	0.30	0.95	1.0	I
PuO_2 in Rocky Flats process residue	3×10^{-3}	0.03	0.2	J

[a] Particle sizes are geometric.
[b] In several cases, values were extracted from graphical data. In some instances, values are estimated upper limits determined by precision of the data.
[c] References: A, Haschke *et al.* (1998a); B, Stewart (1963); C, Martz and Haschke (1998); D, Haschke (1992b); E, Stakebake and Robinson (1977); F, Ricketts (1995); G, Szempruch (2001); H, Pritchard *et al.* (1963); I, Machuron-Mandard and Madic (1996); J, Giacomini (1985).

and propagation of cracks appear rather insensitive to parameters that increase the corrosion rate; slow reaction at room temperature promotes formation of small particles by allowing time for extensive crack formation and spallation before a thick product layer is formed. Size distributions of products formed at temperatures above the 500°C ignition point of Pu and by rapid catalyzed reactions are bimodal, suggesting that particles form by two processes (Haschke, 1992b). A second distribution of small fragments is apparently produced during spallation of large particles. A bimodal distribution also results from formation of small oxide particles during oxidation of PuH_x.

The RRF for ignited Pu droplets (Table 29.8) is approximately 0.7 for all droplets with diameters greater than 100 μm if the free-fall period is sufficient for the temperature to exceed the boiling point of Pu (Martz and Haschke, 1998). Electron micrographs of oxide formed by oxidation of the vapor show a fume aerosol containing web-like chains of particles with diameters of 5–100 nm (Raabe *et al.*, 1978). *In vitro* dissolution rates of the fume aerosol are higher than normally observed for PuO_2. Data from tests to simulate dispersal of Pu by accidental detonation of high explosive show that particles collected in downwind air samplers were primarily spheres or spheroids with average densities of ~2.8–4.9 g cm^{-3} (Friend and Thomas, 1965), suggesting that metal particles

were heated above the melting point during detonation and that hollow oxide spherules were formed by venting of metal vapor (see Section 29.5.2(e)). Size distribution data for collected particles show that RRF is approximately 0.2 and that the mass fraction of particles with aerodynamic diameters below 0.1 μm (geometric diameter <0.03 μm) is less than 0.005 (Friend and Thomas, 1965; Luna *et al*., 1971; Stephens, 1995). Trimodal distributions correlate with three size-determining processes: fragmentation of metal, surface oxidation of fragments, and oxidation of Pu vapor. Average spherule densities of 3–5 g cm^{-3} correspond to release of 55–75% of the mass as fume aerosol and suggest that the aerosol release fraction may far exceed the 0.5% value derived from collection data.

RRF values for PuO_2 prepared by calcination of precipitates such as oxalate and peroxide in Table 29.8 vary by a factor of 10^2, even for the same chemical process. Although differences are inherently introduced by different methods of size measurement, that possibility is unlikely to account for these observations and suggests that specific preparative procedures are important in determining the source term of the oxide product. Adoption of a single conservative value of RRF for all situations seems inappropriate. Characterization of the specific material at risk appears necessary for a meaningful assessment of the dispersal hazard.

Uranium oxide particles produced by oxidation of U in a fuel fire are significantly larger than those from oxidation of Pu under similar conditions (Stewart, 1961; Haschke, 1998). Size data are described by a bimodal distribution and estimated cumulative mass fractions with dimensions less than 3, 10, and 30 μm are 1×10^{-4}, 5×10^{-4}, and 5×10^{-3}, respectively.

(d) Uncertainty of chemical properties

A serious hazard associated with the variety of Pu-containing materials is uncertainty about chemical composition and reactivity. Certain process residues such as chloride-rich pyrochemical salts have been characterized (Haschke and Phillips, 2000) and their chemical reactivity has been evaluated (Haschke *et al*., 2000c). However, numerous potential vulnerabilities cited in an assessment of weapons-related facilities (DOE Report, 1994) derive from lack of knowledge about properties of residues containing several metric tons of Pu. Vulnerabilities are likely to exist worldwide for residues from both military and civilian operations.

(e) Nuclear criticality

Radiation levels produced by fission of ^{239}Pu or ^{235}U in a nuclear chain reaction present a severe potential hazard during operations involving these isotopes. Criticality is controlled by complex relationships that depend on the amount, density, and geometry of fissionable isotopes, as well as on moderation and

reflection of neutrons and interactions with other neutron sources. Criticality assessment is beyond the scope of this review and must be made by expert evaluation for each specific handling or storage configuration.

29.8.3 Case studies

(a) Incidents with metal

Several incidents involving spontaneous ignition and reaction of kilogram-size Pu metal castings have resulted in contamination of workers and facilities by nuclear materials (Haschke and Martz, 1998a, 2000). In at least two cases, storage of metal in unsealed storage containers and sealed plastic contamination barriers resulted in rupture of the container by expansion of the solid and release of material to the environment. Assessment of the previously mentioned incident (see Section 29.1) (Haschke *et al*., 2000a) is especially useful because the package involved in the incident appeared stable over an 11-year storage period. The package consisted of an inner cylindrical steel container with 2.5 kg of rod-shaped Pu castings and welded closures at both ends, two sealed plastic contamination barriers, and an outer steel can with a slip-lid closure covered by plastic tape. A worker became highly contaminated with Pu-containing particles during routine handling of the package.

Inspection of the package in a nitrogen-rich gloved box atmosphere routinely used for handling Pu metal showed that the outer can contained a fine oxide-like powder, that the plastic barriers had embrittled and failed surrounding the lower weld, and that the end of the inner can had been torn open by formation and expansion of a solid reaction product around the Pu castings. Product particles had apparently been released as air was expelled by flexing and volume change as the can was handled. During a 3 h period after exposure of the inner container to the gloved box atmosphere, a rapid reaction caused significant bulging and heating of the inner container. Reaction ceased after the container was transferred to an argon-filled gloved box.

Assessment suggests the occurrence of two important processes: (1) autoreduction of oxide on the metal surface to α-Pu_2O_3 over a period of years and (2) simultaneous transport and deposition of oxide particles on the plastic bagging, resulting in radiolytic production of H_2 and embrittlement of the plastic. Movement of oxide from the inner container, through the constriction of a faulty weld, and onto the plastic barrier is attributed to recoil entrainment of small particles and pumping of gas by action of atmospheric pressure changes on the plastic bagging. Reaction of hydrogen with the activated metal surface produced a Pu_2O_3–PuH_x double layer and resulted in catalyzed reaction of O_2 and N_2 after the plastic failed and air entered the package. This reaction led to failure of an inner metal container. The rate of rapid corrosion observed after the inner container was placed in a reduced-oxygen gloved box corresponds to that for indiscriminate reaction of Pu with air (Haschke *et al*., 1998a).

Formation of the catalytic double layer by different pathways is suggested by observations with other massive samples (Martz *et al.*, 1994). Spontaneous ignition of a massive Pu casting in air after exposure to hydrocarbon oil in a closed container is consistent with reaction of radiolytic H_2 to form a PuH_x surface layer followed by catalyzed reaction upon exposure to air. Similar reaction of Pu after opening of a container that had been immersed in water during criticality measurements is consistent with formation of PuOH on the metal surface and ignition in air (see Section 29.5.2(f)). Water apparently entered the steel container through a faulty seal.

Involvement of catalytic surfaces is also suggested by exothermic reaction of a Ga alloy casting during annealing in a N_2 atmosphere at temperatures in the δ-phase stability range (Haschke, 1986). As the alloy was heated during the initial processing operation in a newly constructed annealing furnace, the temperature greatly exceeded the programmed value and continued to rise after the furnace had been shut down. Exothermic reaction ceased after the casting was consumed, but resumed when the furnace was opened to air. The initial exothermic reaction is attributed to PuH_x-catalyzed nitriding. Surface hydride was apparently formed by high-temperature reaction of water driven from a furnace hearth plate of asbestos fiberboard containing hydrated aluminosilicates. The second exotherm resulted from oxidation of the nitride. In addition to showing that hydrogen originates from unexpected sources, these observations demonstrated that N_2 is not an inert gas for operations with Pu metal at elevated temperatures. Inertness is unlikely even at room temperature where nitriding of PuH_x-coated metal is documented (Haschke *et al.*, 2001c).

(b) Incidents with oxide

The hazard associated with organic material in contact with oxide is shown by violent rupture of a sealed container with only 225 g of PuO_2 after less than 2 years in storage (Haschke and Martz, 1998a). The oxide compact was contaminated with a die lubricant containing aluminum stearate and dodecane. When the package failed, it was propelled out of a criticality well and onto the floor of the storage vault, resulting in extensive contamination of the facility. Examination of a companion container showed that high H_2 pressures were generated by radiolysis of the organic material.

In another incident (Haschke and Martz, 1998a), a storage container of oxide with a relatively high ^{238}Pu content ruptured during transport in an insulated shipping container certified for the existing heat load. The multi-kilogram charge had been prepared by calcination of plutonium nitrate. Alpha contamination was discovered in the shipping container during unpacking. Inspection showed that an inner slip-lid container, a sealed plastic contamination barrier, and an outer rim-seal can had all failed due to internal pressure. Pressurization was attributed to thermal desorption of water and other gases from the oxide, but a high adsorbate concentration would have been necessary. As outlined in

Section 29.8.2a, formation of O_2 by thermal decomposition of PuO_{2+x} and of anion residues may also have contributed to pressurization.

The possibility for PuO_{2+x} involvement in pressurization is supported by analytical data for the Pu and O content of oxides prepared by calcination of oxalate, peroxide, and nitrate precipitates using production procedures (Moseley and Wing, 1965). Materials were heated to the indicated temperatures, but heating periods are not specified. Results (Table 29.9) derived from reported analytical data show that O/Pu ratios in the products generally decrease with increasing temperature and that mass fractions of Pu plus O approach 1.00, suggesting that other constituents remain after calcination at low temperatures. Oxide compositions in excess of the PuO_2 are consistently indicated and are likely to be present unless oxides are thoroughly calcined at high temperature.

(c) Incidents with residues

Although photographs of numerous corroded and failed containers of Pu metals and compounds are presented in a U.S. DOE vulnerability study (DOE Report, 1994), information and documentation of the failures are unavailable. The difficulty associated with residues is demonstrated by severe bulging of rim-seal cans containing reacted ash, a residue produced by firing hydroxide precipitates of Pu and other metals with filter paper and other organic materials at 400–450°C (Van Konynenburg *et al.*, 1996). Residues prepared over a period of 20 years before repackaging were removed from storage in unsealed containers with plastic contamination barriers, homogenized by blending in air, and sealed in food-pack cans. Bulging of cans was observed after 13 months and subsequent analysis of several containers showed that pressure increases up to 5 bar resulted from two distinctly different processes (Haschke and Martz,

Table 29.9 *Analytical data for oxides prepared by calcination of plutonium-containing precipitates* (*Moseley and Wing*, 1965).[a,b]

Initial precipitate	*Calcination temperature* (°C)	(g *Pu* + g *O*)/g	*O/Pu ratio*
Pu(III) oxalate	400	0.893	3.21
	600	0.983	2.48
	800	0.991	2.06
	1000	1.000	2.09
Pu peroxide	400	0.961	2.33
	600	0.983	2.17
	1000	1.000	2.04
Pu nitrate	600	0.997	2.06
	800	0.974	2.18
	1000	0.999	2.14

[a] Calcination times are not specified and may vary.
[b] Pu contents were determined by Ce titration and emission spectrography; O contents were determined by vacuum fusion with carbon.

1998a). For cases in which large amounts of free C was apparently present, N_2 appeared stable, O_2 was depleted, H_2 and CO_2 were formed, and a pH of 4 was measured after the solid residue was placed in water. In other cases, N_2 plus O_2 were formed and the observed pH was 10. A qualitative explanation for some observations is proposed (Van Konynenburg *et al.*, 1996), but proposed processes do not account for production of N_2 and O_2. Formation of N_2 parallels that observed with air-exposed oxide in radiolysis studies (Livingston, 1999) and suggests involvement of radiolytic nitrogen oxides that form on the oxide surface during exposure to air (Stakebake *et al.*, 1970).

Large variations in the chemistry of a relatively well-characterized residue such as reacted ash are surprising. Confidence in estimation of the potential hazard must be tempered by recognition of uncertainty and lack of knowledge. Assessment of hazards for poorly characterized plutonium-bearing residues is especially difficult.

29.9 MITIGATION OF HAZARDS

29.9.1 Atmospheres for safe handling of plutonium

Control of oxygen and moisture levels in the gloved box atmosphere is essential for preventing excessive corrosion of Pu metal and adsorption of water on the oxide. As shown by retention of H_2O formed by combination of H_2 and O_2 on PuO_2 (Haschke *et al.*, 2001b), water tenaciously adsorbs on oxide and oxide-coated metal. Use of an argon atmosphere is desirable because radiolytic formation of nitrogen oxides and nitrates is curtailed, but maintenance of low ($<$10 ppm) O_2, H_2O, and N_2 concentrations is challenging. Use of nitrogen atmospheres is less desirable because N_2 is not radiolytically (see Section 29.7) or chemically (see Sections 29.4.1(e) and 29.8.3(a)) inert at room temperature.

A perplexing observation reported by early workers is that corrosion of Pu by moisture is as much as 60 times more rapid in argon or helium than in air at the same humidity level (Waber, 1980). Suggestions that this behavior parallels that of U and that H_2O corrosion is suppressed by O_2 are not supported by results for the Pu–H_2O reaction (Haschke *et al.*, 1996). Another possibility is suggested by enhancement of Pu corrosion by traces of HCl in an Ar atmosphere (Haschke *et al.*, 1998b). At 25°C, the estimated corrosion rate of alloyed Pu in saturated H_2O is 0.2 ng Pu cm^{-2} min^{-1}; the derived rate with ppm levels of HCl and P_{H_2O} less than 0.1 mbar is 0.5 μg Pu cm^{-2} min^{-1} (Haschke *et al.*, 2001c). The likely source of HCl is radiolysis of polymerized residues formed during prolonged use of chlorinated organic solvents in the gloved box. Enhanced corrosion in He or Ar atmospheres during early studies may have resulted from a similar synergistic interaction.

Dry air is suitable for handling plutonium metal and oxide if adequate controls are exercised. Metal powder and chips do not spontaneously ignite in

air at room temperature (see Section 29.5.2e) and corrosion of Pu is suppressed by formation of a protective PuO_2 layer, but ignition is likely if reactive and catalytic compounds such as PuH_x and Pu_2O_3 are present. Effects of water concentration on the corrosion rate of unalloyed Pu are evident at 1 ppm H_2O and maintenance of 0.5 ppm is apparently necessary to prevent moisture enhancement (Haschke *et al.*, 1996). The water-catalyzed cycle for the Pu–O_2 reaction (see Section 29.5.2d) is almost insidious. H_2O is not consumed during corrosion as long as O_2 is present, but remains tenaciously adsorbed and accumulates on the oxide surface over time at low equilibrium pressure. The surface of freshly calcined PuO_2 has a stronger affinity for water than many commonly used desiccants (molecular sieves, $CaSO_4$, and $CaCl_2$) and will extract water from them.

Use of dry N_2-enriched atmospheres containing less than 3–5% O_2 is advantageous because pyrophoric materials such as PuH_x do not spontaneously ignite at this condition (Haschke and Allen, 2001). Experiments show that preheated (>500°C) Pu specimens rapidly cool instead of oxidizing when exposed to N_2–O_2 mixtures with 7–9% O_2, but burn in a self-sustaining reaction when exposed to mixtures containing 10% or more O_2 (Musgrave, 1971). Predictions based on corrosion rates show that thermal ignition of Pu is prevented by maintaining the O_2 percentage below 9.6% and that pyrophoric reactions of PuH_x and PuH_x-coated Pu are prevented by maintaining the O_2 percentage below 4.2% (Haschke and Allen, 2001). Results are consistent with observations indicating that the threshold O_2 pressures for self-sustained reactions of Pu and PuH_x are 90 and 40 mbar, respectively.

29.9.2 Conditions for safe storage of metals and oxides

(a) Packaging and storage of plutonium

General requirements for storage of plutonium metals and oxides are outlined in safety guidelines (IAEA Report, 1998) and in a recent review (Haschke and Martz, 1998a). Specific recommendations for storage periods up to 50 years are presented in a U.S. DOE standard (DOE Standard, 2000a). In addition to outlining criteria for design, construction, and testing of storage containers, the DOE publication includes recommendations for material stabilization, packaging, quality assurance, documentation, and surveillance. The standard applies to Pu-containing metals and oxides containing at least 30 mass% Pu plus U and unirradiated MOX fuel, but not to residues, wastes, spent nuclear fuels, radiation sources, or solutions.

Packaging recommendations in the DOE standard include double confinement of materials in nested cylindrical containers constructed of a durable, corrosion-resistant metal such as 300 series stainless steel (Fig. 29.9) and sealed by welding (DOE Standard, 2000a). An unsealed convenience can be used to facilitate loading without contamination of the inner container or the weld

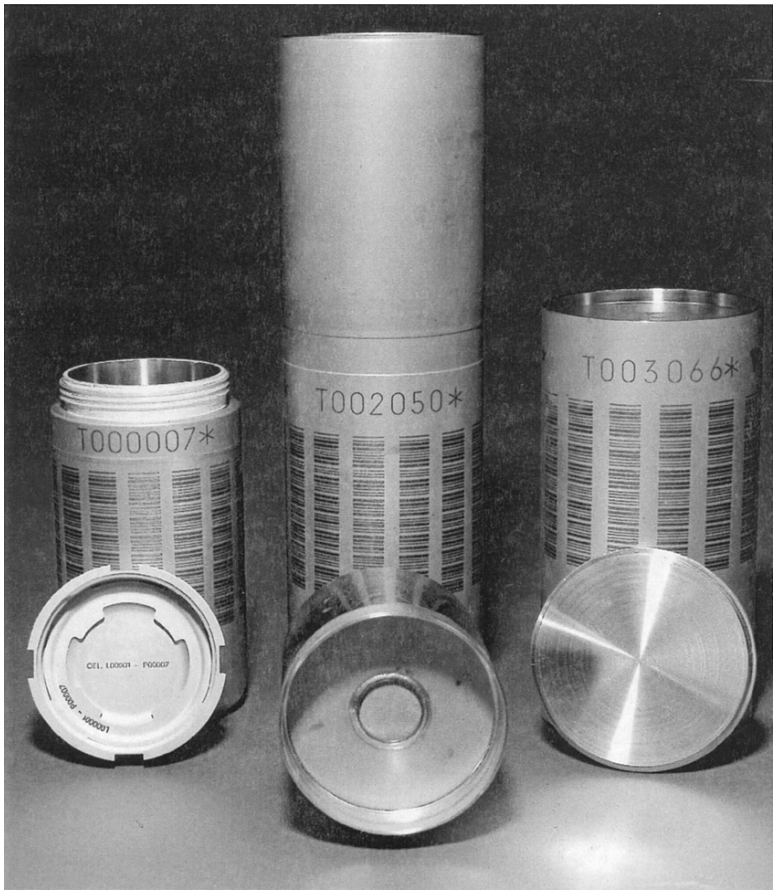

Fig. 29.9 *Plutonium storage containers fabricated in accordance with DOE Standard* 3013. *Convenience can* (*left*), *inner welded can* (*center*), *and outer welded can* (*right*) *are shown.*

zone. The inner container is designed to deform if the internal pressure reaches 8 bar; the minimum design pressure of the outer container is 50 bar. Welds are certified to have leak rates less than 10^{-7} std cm^3 s^{-1} using standard leak-test procedures. Rigorous exclusion of organic materials such as elastomeric gaskets, organic coatings, and plastic contamination barriers from the storage package is essential to prevent formation of radiolytic gases during storage.

Recommendations for stabilization of metals are simple compared to those for oxides (DOE Standard, 2000a). Metal pieces weighing more than 50 g are considered suitable for storage because ignition at 150–200°C is unlikely (see Section 29.5.2(e)). Metal surfaces should be visibly free of non-adhering corrosion products (including oxide) and organic materials. Stabilization of oxides is

accomplished by calcination at 950°C in an oxidizing atmosphere such as air for a minimum of 2 h or until the loss-on-ignition (LOI) criterion or other suitable method indicates that residual moisture level is sufficiently low. LOI is a gravimetric analysis that measures the loss of volatile species from a calcined oxide sample during heating at 1000°C for 1 h. The acceptance criterion for oxide at the time of packaging is a maximum LOI of 0.5 mass%, a level that limits the H_2 pressure from the oxide–water reaction (see Sections 29.3.2 and 29.4.2b) to a value below the design pressure of the package. In addition to removing moisture, calcination at 950°C consistently reduces the specific area of PuO_2 to below 5 $m^2\ g^{-1}$ (Haschke and Ricketts, 1995; Machuron-Mandard and Madic 1996), an area that prevents re-adsorption of H_2O in excess of the 0.5 mass% criterion during exposure to air (Haschke and Ricketts, 1997).

The combined mass of Pu and other fissile materials such as ^{235}U stored as metal or oxide in each package is limited to 4.40 kg (DOE Standard, 2000a). The container may be filled with any gas (air, argon, or a He-rich mixture for leak testing) that does not react adversely with the container or contained materials. Surveillance is based on initial and periodic measurements of package properties. Onset of pressurization may be detected by radiographic indication of a deformed inner container. Recommended non-destructive surveillance activities also include periodic verification of package mass and leak rate.

(b) Packaging and storage of uranium

The standard for storage of ^{233}U (DOE Standard, 2000b) is similar to that for plutonium, but is much less restrictive.

29.10 DISPOSITION OPTIONS

29.10.1 Issues

Reduction in nuclear arsenals and dismantlement of nuclear weapons creates the problem of what to do with excess plutonium and enriched uranium. In addition to issues of environmental aspects, safety, and health, the proliferation risk posed by surplus nuclear material is of concern. An ideal disposition method would eliminate the possibility of reusing such materials in weapons applications. Because total elimination is unrealistic, the U.S. National Academy of Sciences has proposed the 'spent-fuel standard' as a concept for minimizing accessibility to plutonium and uranium (National Academy of Sciences Report, 1994). The concept, which has been accepted by the U.S., Russia, and seven other stakeholder nations, defines 'minimized accessibility' as equivalent to that of Pu in spent reactor fuel. In cooperative agreements endorsed by other countries, the U.S. and Russia will investigate and demonstrate disposition technologies for use in subsequent disposal of 68 metric tons of weapons-grade Pu.

Studies to define the best disposal options for excess fissile materials are concentrated in three main areas:

- immobilization with high-level waste (HLW) (treating plutonium as waste);
- conversion to a mixed oxide (MOX) for burning in existing reactors;
- use in fueling fast-neutron reactors.

Russia, for example, is focusing on disposal of surplus Pu by burning MOX fuel in reactors. The hybrid United States strategy attempts to insure against possible difficulties by including both irradiation of MOX and immobilization (DOE, 1996, 1997a,b). The approach allows for immobilization of some relatively impure Pu in glass or ceramic material and disposal in a geologic repository, as well as for burning MOX in existing commercial reactors with subsequent geologic disposal as spent fuel. Low-grade Pu-containing materials may be disposed of as nuclear waste. As implied in following sections, implementation of disposal options will require extensive processing capability to separate and prepare materials for disposal. Construction of dedicated facilities to accomplish these tasks will probably be necessary.

29.10.2 Disposition of metals and oxides

(a) Disposition of plutonium metal

Implementation of disposal options requires that Pu metal be converted to oxide. Consideration has been given to pyrochemical processes in which preparation of plutonium hydride is followed by direct conversion to the oxide or by a two-step method involving formation of nitride and subsequent oxidation to PuO_2. In an alternative method, oxide can be produced directly by somewhat slower oxidation of metal, but hazards associated with handling hydrogen and plutonium hydride are avoided. An intriguing one-step process for separation and oxidation employs formation of the α-Pu_2O_3–PuH_x double layer on the metal and controlled oxidation with O_2 (see Section 29.5.2f). An advanced recovery and integrated extraction system (ARIES) is being developed to demonstrate requisite process technologies (Rofer *et al.*, 2000).

(b) Disposition as plutonium as MOX fuel

One disposal pathway for plutonium is irradiation of MOX fuel ($\sim$5% PuO_2) in commercial light-water reactors. The fissile content is similar to that of enriched uranium fuels in which the Pu content reaches about 1% during normal operation. Civilian plutonium is currently being recycled in European light-water reactors in this way, and MOX usage is expected to expand to Japan and other countries. Burning military plutonium as MOX fuel minimizes accessibility in two important ways: (1) formation of the Pu-containing matrix of highly

radioactive fission products and (2) alteration of the isotopic distribution from weapons-grade to reactor-grade plutonium.

Opponents of using military Pu in MOX fuels contend that substantial proliferation risk exists because the plutonium is considered 'weapons-usable' after irradiation. As noted in Section 29.2.1, weapons-grade plutonium typically contains 93–94% of the fissile ^{239}Pu isotope, whereas reactor-grade plutonium usually contains less than 70% ^{239}Pu. Irradiation of 'weapons-grade' plutonium as MOX fuel increases the difficulty of using high-burnup material in weapons applications by increasing the fraction of non-fissile Pu isotopes. Burning weapons Pu as MOX has limited effect on the proliferation risk because extensive spent-fuel sources of Pu exist worldwide.

(c) Plutonium immobilization

Immobilization of plutonium oxide in a suitable glass or ceramic material and placement in a geological repository achieves the spent-fuel standard by encapsulating plutonium in a waste form with a radiological barrier to reduce accessibility. The radiological barrier can be either internal or external to the plutonium packages. 'Homogeneous' and 'can-in-can' (CIC) are two types of immobilization packaging concepts that have been evaluated (Gray and Gould, 1997). In both concepts the fission products in the canister generate a radiation barrier of at least 100*R* per hour at a distance of 1 m from the package over 30 years and would mimic the characteristics of spent fuel.

The homogeneous package is formed by incorporating HLW or ^{137}Cs as an internal radiation barrier along with Pu in a glass or ceramic. In a batch process, plutonium oxide is melted directly with fission products such as ^{137}Cs or HLW to form a single highly radioactive glass product that is placed in a large stainless steel canister. This type of package may also be prepared in a two-stage process that first forms a Pu-containing glass. In the second step, glass and fission products are heated and the molten mixture is poured into the storage canister.

The CIC package has a radiation barrier that is external to the plutonium-bearing material (Gray and Gould, 1997). Small cans of Pu-containing glass or ceramic matrix are placed in a rack within a large (0.6 m in diameter, 3 m high) stainless steel canister that is then filled with HLW glass as an external radiation barrier. Although the homogeneous concept has a slight advantage from a non-proliferation standpoint because of the intimate mixing of the plutonium with fission products, the CIC option is preferred over the homogeneous designs from an operational perspective because of higher technical viability and ease of implementation. Both concepts meet the 'spent fuel' criterion, but extensive fabrication facilities and potentially hazardous process operations are required to produce a form that is inherently obtained by burning MOX fuel.

(d) Immobilization of plutonium by vitrification

Vitrification of HLW and placement in a packaging configuration is a disposal option that has been extensively studied and evaluated for 30 years (McKibbon and Wicks, 1995). Early studies show that plutonium can be safely incorporated into a high-level plutonium borosilicate glass at concentrations up to at least 4–5 wt% (Matzke and van Geel, 1995). Another candidate matrix is an alkali–tin–silicate (ATS) glass for incorporating ^{137}Cs as an internal radiation barrier. However, work on this glass has essentially stopped because of interest in the CIC option.

The glass proposed for the CIC option is similar to commercial Löffler optical glasses that contain up to 55 wt% rare-earth oxide. This glass is a single-phase lanthanide borosilicate (LaBS) formulated to accommodate up to 16 wt% actinide (Gould *et al.*, 1988). Highly volatile cesium cannot be incorporated as an internal radiation barrier because of the high melting temperature (1500°C) of these glasses (Science and Technology Review, 1997). Leaching tests show that LaBS is more durable than typical borosilicate glass and has outstanding chemical resistance. Excellent performance of glass systems and general improvement with time were observed in laboratory tests and actual field experiments in Sweden, Belgium, England, and the U.S. (Wicks, 1999).

(e) Immobilization of plutonium by ceramification

Ceramic waste forms have been considered for use in immobilizing HLW since the late 1970s. The most advanced ceramic formulation to date is a synthetic rock (Synroc) developed by the Australian Nuclear Science and Technology Organization (ANSTO) in 1978 (Jostons, 1994). A demonstration plant completed in 1987 operated at a commercial scale of approximately 10 kg of Synroc per hour. The proposed plutonium immobilization ceramic form is Synroc-F, a pyrochlore-rich ceramic that also contains zirconolite, brannerite, and rutile as secondary and tertiary phases (Gould *et al.*, 1988). This titanate ceramic was chosen for Pu immobilization to accommodate high loadings of plutonium and uranium, as well as the neutron absorbers gadolinium and hafnium that are added to ensure criticality control in the repository. Plutonium and uranium are interchangeable in pyrochlore with nominal actinide loadings of 10 wt% Pu and 20 wt% U. The preferred titanate-based ceramic can be formulated as $ABTi_2O_7$ where Ca and half of the Gd are in the A-position, and Pu, U, Hf, and the remainder of the Gd occupies the B-position. Calcium and titanium oxide are the mineral formers. Natural pyrochlore is calcium zirconate titanate ($CaZrTi_2O_7$), but the pyrochlore selected for immobilizing Pu has the chemical formula: $(Ca_{0.89}Gd_{0.11})(Hf_{0.23}U_{0.44}Pu_{0.22}Gd_{0.11})Ti_2O_7$. The molar ratio of neutron poison to Pu is 1:1; the molar ratio of U to Pu is 2:1 (Rankin and Gould, 1999).

Assessment of current information indicates that both ceramic and glass are acceptable forms for Pu immobilization. Ceramic technology is recommended for the CIC packaging option because of superior proliferation resistance, repository performance and acceptability, potential worker dose, and cost effectiveness (Cohran *et al.*, 1997; Macfarlane, 1998).

29.10.3 Interim storage

At the present time, the path forward for disposition of weapons plutonium is uncertain. In some cases, the method of disposition has not been conclusively determined and/or requisite processing facilities do not exist. Placing these materials in a final disposition condition (either by immobilization or burning as MOX fuel) will most likely take longer than weapons dismantlement. Therefore, safe interim storage of excess plutonium must be considered for both short and extended periods.

Likewise, interim storage of highly enriched uranium and separated reactor-grade plutonium oxide for use in MOX fuel fabrication will be necessary. It is hoped that use of the fundamental and applied information presented in this chapter will facilitate safe handling, storage, and disposition of these nuclear materials.

REFERENCES

Allen, A. O., Hochanadel, C. J., Ghormley, J. A., and Davis, T. W. (1952) *J. Phys. Chem.*, **56**, 575–81.

Allen, T. H. (1991) *The Solubility of Hydrogen in Plutonium in the Temperature Range 475 to 826 Degrees Centigrade*, Thesis, University of Colorado at Denver, Denver, CO.

Allen, T. H. (2001) personal communication unpublished data, Los Alamos National Laboratory.

Anderson, J. S., Roberts, L. E. J., and Harper, E. A. (1955) *J. Chem. Soc.*, **1955**, 3946–59.

Bagnall, K. W. and Laidler, J. B. (1964) *J. Chem. Soc.*, **1964**, 2693–6.

Baker, M. McD., Less, N. L., and Orman, S. (1966) *Trans. Faraday Soc.*, **62**, 2513–24.

Benhamou, A. and Beraud, J. P. (1980) *Analysis*, **A8**, 376–80.

Block, J. and Mintz, M. H. (1981) *J. Less Common Metals*, **81**, 301–20.

Bowersox, D. F. (1977) *The Reaction Between Plutonium and Deuterium Part II. Rate Measurements by Weight Changes*, Los Alamos Scientific Laboratory Report LA-6681-MS.

Boyce, J. B. and Huberman, B. A. (1979) *Phys. Rep., Phys Lett.*, **51**, 189–265.

Brown, F., Ockenden, H. M., and Welch, G. A. (1955) *J. Chem. Soc.*, **1955**, 4196–201.

Christensen, H. (1998) *Nucl. Technol.*, **124**, 165–74.

Cinader, G., Zamir, D., and Hadari, Z. (1976) *Phys. Rev. B.*, **14**, 912–20.

Cleveland, J. M. (1979) *The Chemistry of Plutonium*, American Nuclear Society, La Grange Park, IL, pp. 291–322.

Cohran, S. G., Dunlop, W. H., Edmunds, T. A., Mac Lean, L. M., and Gould, T. H. (1997) *Final Immobilization Form Assessment and Recommendation*, Lawrence Livermore National Laboratory Report UCRL-ID-128705.

Colmenares, C. A. (1975) *Prog. Solid State Chem.*, **9**, 139–239.

Colmenares, C. A. (1984) *Prog. Solid State Chem.*, **15**, 257–364.

Condon, J. B. and Larson, E. A. (1973) *J. Phys. Chem.*, **59**, 855–65.

Conradson, S. D., Begg, B. D., Clark, D. L., den Auwer, C., Espinosa-Faller, F. J., Gordon, P. L., Hess, N. J., Hess, R., Keogh, D. W., Morales, L. A., Neu, M. P., Runde, W., Tait, C. D., Veirs, D. K., and Villella, P. M. (2003) *Inorg. Chem.*, **42**, 3715–17.

Conradson, S. D., Abney, K. D. Begg, B. D., Brady, E. D., Clark, D. L., den Auwer, C., Ding. M., Dorhaut, P. K., Espinosa-Faller, F. J., Gordon, P. L., Haire, R. G., Hess, N. J., Hess, R., Keogh, D. W., Lander, G. H., Lupinetti, A. J., Morales, L. A., Neu, M. P., Palmer, P. D., Paviet-Hartmann, P., Reilly, S. D., Runde, W., Tait, C. D., Veirs, D. K., and Wastin, F. (2004) *Inorg. Chem.*, **43**, 116–31.

Dell, R. M. (1973) in *Comprehensive Inorganic Chemistry*, vol. 5 (eds. J. C. Bailar, H. J. Emeléus, Sir R. Nyholm, and A. F. Trotman-Dickenson), Pergamon, Oxford, pp. 319–55.

DOE Report (1994) *Plutonium Working Group Report on Environmental, Safety and Health Vulnerabilities Associated with the Department's Plutonium Storage*, U.S. Department of Energy, Report DOE/EH-0145.

DOE Report (1996) *Storage and Disposition of Weapons – Usable Fissile Materials Final Programmatic Environmental Impact Statement*, U.S. Department of Energy, Report DOE/EIS-0299.

DOE Report (1997a) *DOE Announces Decision on the Storage and Disposition of Surplus Nuclear Weapons Materials*, U.S. Department of Energy, Press Release R-97-001.

DOE Report (1997b) *Record of Decision for the Storage and Disposition of Weapons-Usable Fissile Materials Final Programmatic Environmental Impact Statement*, U.S. Department of Energy.

DOE Standard (2000a) *Stabilization, Packaging and Storage of Plutonium-Bearing Materials*, U.S. Department of Energy Standard DOE-STD-3013-2000.

DOE Standard (2000b) *Criteria for Packaging and Storing* ^{233}U *– Bearing Materials*, U.S. Department of Energy Standard DOE-STD-3028-2000.

Draganić, I. G. and Draganić, Z. D. (1971) *The Radiation Chemistry of Water*, Academic Press, New York, pp. 23–197.

Ellinger, F. H., Miner, W. N., O'Boyle, D. R., and Schoenfeld, F. W. (1968) *Constitution of Plutonium Alloys*, Los Alamos Scientific Laboratory, Report LA-3870.

Eyring, L. (1979) in *Handbook on the Physics and Chemistry of Rare Earths*, vol. 3, *The Binary Rare Earth Oxides*, ch. 27 (eds. K. A. Gschneidner Jr and L. Eyring), North-Holland, Amsterdam, pp. 337–99.

Flotow, H. E., Haschke, J. M., and Yamauchi, S. (1984) *The Chemical Thermodynamics of Actinide Elements and Compounds*, part 9, The Actinide Hydrides, International Atomic Energy Agency, Vienna.

Friend, J. P. and Thomas, D. M. C. (1965) *The Determination of the Particle Size Distribution of the Particulate Material Collected During the Double Tracks and Clean Slate 1 Events of Operation Roller Coaster*, United Kingdom Atomic Weapons Research Establishment Report AWRE O-20/65.

Giacomini, J. J. (1985) *Particle Size Determinations of MMEC Oxide*, Rocky Flats Report SA/85-026.

Gould, T., Meyers, B., Gray, L., and Edmunds, T. (1988) *Evaluation of Candidate Glass and Ceramic Forms for Immobilization of Surplus Plutonium*, Lawrence Livermore National Laboratory, Report UCRL-JC-130952, pp. 366–73.

Gray, L. and Gould, T. (1997) *Immobilization Technology Down-Selection Radiation Barrier Approach,* Lawrence Livermore National Laboratory Report UCRL-ID-127320.

Grenthe, I., Fuger, J., Konings, R. J. M., Lemire, R. J., Muller, A. B., Nguyen-Trung, C., and Wanner, H., (1992) *Chemical Thermodynamics of Uranium*, North-Holland, Amsterdam, pp. 30–60.

Haire, R. G. and Haschke, J. M. (2001) *MRS Bull.*, **26**, 689–96.

Haschke, J. M., Hodges, A. E. III, Smith, C. M., and Oetting, F. L. (1980) *J. Less Common Metals*, **73**, 41–8.

Haschke, J. M. (1981) *Thermodynamic Properties of the Cubic Plutonium Hydride Solid Solution*, Rocky Flats Report RFP-3099.

Haschke, J. M., Hodges, A. E. III, Bixby, G. E., and Lucas, R. L. (1983) *The Reaction of Plutonium with Water: Kinetic and Equilibrium Behavior of Binary and Ternary Phases in the Pu-O-H System*, Rocky Flats Plant Report RFP-3416.

Haschke, J. M. (1986) unpublished results, Rocky Flats Plant.

Haschke, J. M., Hodges, A. E. III, and Lucas, R. L. (1987) *J. Less Common Metals*, **133**, 155–66.

Haschke, J. M. (1991) in *Synthesis of Lanthanide and Actinide Compounds* (eds. G. Meyer and L. R. Morss), Kluwer Academic Publishers, Dordrecht, pp. 1–53.

Haschke, J. M. (1992a) in *Transuranium Elements A Half Century*, ch. 40 (eds. L. R. Morss and J. Fuger), American Chemical Society, Washington DC, pp. 416–25.

Haschke, J. M. (1992b) *Evaluation of Source-Term Data for Plutonium Aerosolization*, Los Alamos National Laboratory Report LA-12315-MS.

Haschke, J. M. (1995) *Reactions of Plutonium and Uranium with Water: Kinetics and Potential Hazards*, Los Alamos National Laboratory Report LA-13069-MS.

Haschke, J. M. and Ricketts, T. E. (1995) *Plutonium Dioxide Storage: Conditions for Preparation and Handling*, Los Alamos National Laboratory Report LA-12999-MS.

Haschke, J. M., Allen, T. H., and Stakebake, J. L. (1996) *J. Alloys Compds*, **243**, 23–35.

Haschke, J. M. and Ricketts, T. E. (1997) *J. Alloys Compds*, **252**, 148–56.

Haschke, J. M. (1998) *J. Alloys Compds*, **278**, 149–60.

Haschke, J. M. and Martz, J. C. (1998a) in *Environmental Analysis and Remediation* (ed. R. A. Meyer), John Wiley, New York, pp. 3740–55.

Haschke, J. M. and Martz, J. C. (1998b) *J. Alloys Compds*, **266**, 81–9.

Haschke, J. M., Allen, T. H., and Martz, J. C. (1998a) *J. Alloys Compds*, **271–273**, 211–15.

Haschke, J. M., Allen, T. H., Morales, L. A., Jarboe, D. M., and Puglisi, C. V. (1998b) *Chloride-Catalyzed Corrosion of Plutonium in Glovebox Atmospheres*, Los Alamos National Laboratory Report LA-13428-MS.

Haschke, J. M. and Phillips, A. G. (2000) *J. Nucl. Mater.*, **277**, 175–83.

Haschke, J. M. and Martz, J. C. (2000) in *Los Alamos Science*, no. 26 (ed. N. G. Cooper), Los Alamos National Laboratory, Los Alamos, pp. 266–7.

Haschke, J. M., Allen, T. H., and Morales, L. A. (2000a) in *Los Alamos Science*, no. 26 (ed. N. G. Cooper), Los Alamos National Laboratory, Los Alamos, pp. 252–73.
Haschke, J. M., Allen, T. H., and Morales, L. A. (2000b) *Science*, **287**, 285–7.
Haschke, J. M., Fauske, H. K., and Phillips, A. G. (2000c) *J. Nucl. Mater.*, **279**, 127–38.
Haschke, J. M. and Allen, T. H. (2001) *J. Alloys Compds*, **320**, 58–71.
Haschke, J. M., Sherman, M. P., and Stakebake, J. L. (2001a) *Conceptual and Quantitative Models for Gas Generation During Transport and Storage of Plutonium Dioxide*, Rocky Flats Plant Report RFP-5390.
Haschke, J. M., Allen, T. H., and Morales, L. A. (2001b) *J. Alloys Compds*, **314**, 78–91.
Haschke, J. M., Martinez, R. J., Pruner, R. E., Martinez, B., and Allen, T. H. (2001c) *Interactions of Plutonium with Diverse Materials in Moist Air and Nitrogen–Argon, Mixtures at Room Temperature*, Los Alamos National Laboratory Report LA-12739-MS.
Haschke, J. M. and Allen, T. H. (2002) *J. Alloys Compds*, **336**, 124–31.
Haschke, J. M. and Oversby, V. M. (2002) *J. Nucl. Mater.*, **305**, 187–201.
Hecker, S. S. and Martz, J. C. (2000) in *Los Alamos Science*, no. 26 (ed. N. G. Cooper), Los Alamos National Laboratory, Los Alamos, pp. 238–43.
Hecker, S. S. (2001) *MRS Bull.*, **26**, 672–8.
Hilliard, R. J. (1958) *Oxidation of Uranium in Air at High Temperatures*, Hanford Atomic Products Operation Report HW-58022.
Hoekstra, H. R., Santoro, A., and Siegel, S. (1961) *J. Inorg. Nucl. Chem.*, **18**, 166–78.
Huddle, R. A. U. (1953) *The Uranium Steam Reaction*, Atomic Energy Research Establishment Report AERE-M/R-1281.
IAEA Report (1998) *Safety Reports Series No. 9, Safe Handling and Storage of Plutonium*, International Atomic Energy Agency, Vienna.
Jain, G. C. and Ganguly, C. (1993) *J. Nucl. Mater.*, **202**, 245–51.
Jostons, A. (1994) *Status of Synroc Development, Proc. 9th Pacific Basin Nucl. Conf.*, Sydney, Australia.
Kalinichenko, B. S., Kulazhko, V. G., Kalashnikov, N. A., Shvetsov, I. K., and Sersbryakov, V. N. (1987) *Radiokhimiya*, **29**, 675–81; English translation, Plenum, 1988, pp. 647–52.
Kazanjian, A. R. (1976) *Radiolytic Gas Generation in Plutonium Contaminated Waste Materials*, Rocky Flats Plant Report RFP-2469.
Keller, C. (1973) in *Comprehensive Inorganic Chemistry*, vol. 5 (eds. J. C. Bailar, H. J. Emeléus, Sir R. Nyholm, and A. F. Trotman-Dickenson), Pergamon, Oxford, pp. 219–76.
Larson, D. T. and Haschke, J. M. (1981) *Inorg. Chem.*, **20**, 1945–50.
La Verne, J. A. and Tandon, L. (2002) *J. Chem. Phys. B*, **106**, 380–6.
Leary, J. A., Prichard, W. C., Nance, R. L., and Shupe, W. M. (1967) in *Plutonium 1965* (eds. A. E. Kay and M. B. Waldron), Barnes and Nobel, New York, pp. 639–53.
Lemire, R., Fuger, J., Nitsche, H., Rand, M., Potter, P., Rydberg, J., Spahiu, K., Sullivan, J., Ullman, W., Vitorge, P., and Wanner, H., (2001) *Chemical Thermodynamics of Neptunium and Plutonium*, Elsevier, Amsterdam, pp. 55–64.
Lindsay, J. W., Terada, K., and Thompson, M. A. (1972) *J. Electrochem. Soc.*, **119**, 726–9.
Livingston, R. R. (1999) *Gas Generation Test Support for Transportation and Storage of Plutonium Residue Materials*, Savannah River Site Report WSRS-TR-99-00223.

Luna, R. E., Church, H. W., and Shreve, J. D. (1971) *Atmospheric Environ.*, **5**, 579–97.
Macfarlane, A. (1998) *Sci. Global Security*, **7**, 271–309.
Machuron-Mandard, X. and Madic, C. (1996) *J. Alloys Compds*, **235**, 216–14.
Martz, J. C., Haschke, J. M., and Stakebake, J. L. (1994) *J. Nucl. Mater.*, **210**, 130–42.
Martz, J. C. and Haschke, J. M. (1998) *J. Alloys Compds*, **266**, 90–103.
Matzke, Hj. and Turos, A. (1991) *Solid State Ionics*, **49**, 189–94.
Matzke, Hj. and van Geel, J. (1995) *Incorporation of Plutonium and Other Actinides in Borosilicate Glass and in Waste Ceramics*, NATO Advanced Workshop on Disposition of Weapons Plutonium – Approaches and Prospects, St. Petersburg, Russia.
McGillivray, G. W., Geeson, D. A., and Greenwood, R. C. (1994) *J. Nucl. Mater.*, **208**, 81–97.
McKibbon, J. M. and Wicks, G. W. (1995) *Technical Aspects of the Plutonium Vitrification Option*, Westinghouse Savannah River Company Report WSRC-MS-95-0200.
Mishima, J. and Pinkston, D. (1994) *Airborne Release Fractions/Rates and Respirable Fractions for Nonreactor Nuclear Facilities*, DOE-HDBK-3010-94.
Morales, L. (1998) *Preliminary Report on the Recombination Rates of Hydrogen and Oxygen over Pure and Impure Plutonium Oxides*, Los Alamos National Laboratory Report LA-UR-98-5200.
Morss. L. R. (1986) in *Chemistry of the Actinide Elements*, vol. 2, ch. 17 (eds. J. J. Katz, G. T. Seaborg, and L. R. Morss), Chapman and Hall, London, pp. 1278–360.
Moseley, J. D. and Wing, R. O. (1965) *Properties of Plutonium Dioxide*, Rocky Flats Report RFP-503.
Muromura, T. and Ouchi, K. (1974) *J. Inorg. Nucl. Chem.*, **36**, 2525–30.
Musgrave, L. E. (1971) *Effect of Water Vapor, Reduced Oxygen Concentrations, and Solvent Vapors on Plutonium Ignition*, Rocky Flats Plant Report RFP-1566.
National, Academy of Sciences, Report (1994) *Management and Disposition of Excess Weapons Plutonium*, National Academy of Sciences Committee on International Security and Arms Control, National Academy Press, Washington DC.
Nelson, L. S. (1980) *High Temp. Sci.*, **12**, 297–303.
Newton, A. S., Warf, J. C., Spedding, F. H., Johnson, O., Johns, I. B., Nottorf, R. W., Ayres, J. A., Fisher, R. W., and Kant, A. (1949) *Nucleonics*, 17–24.
Ogden, J., Alexander, C., and Colmenares, C. A. (1980) *Isothermal and Isobaric Studies of the Pu–H_2 Reaction*, Lawrence Livermore Laboratory Report UCRL-84307.
Paffett, M. T., Farr, D., and Kelly, D. (2003a) *Am. Inst. Phys. Proc.*, **673**, 193–5.
Paffett, M. T., Kelly, D., Joyce, S. A., Morris, J., and Veirs, K. (2003b) *J. Nucl. Mater.*, **322**, 45–56.
Petit, L., Svane, A., Szotek, Z., and Temmerman, W. M. (2003) *Science*, **301**, 498–501.
Pitts, S. H. Jr (1968) *Nucl. Safety*, **9**, 112–19.
Powell, G. L., Harper, L. W., and Kirkpatrick, J. R. (1991) *J. Less Common Metals*, **172–174**, 116–23.
Pritchard, W. C., Johnson, K. A., and J. A. Leary (1963) *Compaction and Sintering of PuO_2-Type 302B Stainless Steel Powder Mixtures*, Los Alamos National Laboratory Report LAMS-2898.
Raabe, O. G., Teague, S. V., Richardson, N. L., and Nelson, L. S. (1978) *Health Phys.*, **35**, 663–74.
Rai, D., Strickert, R. G., and Ryan, J. L. (1980) *Inorg. Chem. Nucl. Lett.*, **16**, 551–5.
Rai, D. and Ryan, J. L. (1982) *Radiochim. Acta.*, **30**, 213–16.

Rankin, D. T. and Gould, T. H. Jr (1999) *Plutonium Immobilization Program: Can-In-Canister*, Westinghouse Savannah River Technology Center Report WSRC-MS-99-00349.

Ricketts, T. E. (1995) Personal communication of unpublished data, Los Alamos National Laboratory.

Ritchie, A. G., Greenwood, R. C., Randles, S. R., Netherton, D. R., and Whitehorn, J. P. (1986) *J. Nucl. Mater.*, **140**, 197–201.

Rofer, C. K., Martinez, D. A., and Trujillo, V. L. (2000) *NATO Sci. Ser.*, **29**, 131–6.

Ronchi, C., Capone, F., Colle, J. Y., and Hiernaut, J. P. (2000) *J. Nucl. Mater.*, **280**, 111–15.

Schnizlein, J. G. and Fischer, D. F. (1967) *J. Electrochem. Soc.*, **114**, 23–9.

Schnizlein, J. G. and Fischer, D. F. (1968) *J. Electrochem. Soc.*, **115**, 462–6.

Science and Technology Review (1997) *Dealing with a Dangerous Surplus from the Cold War* (1997), April.

Smith, R. C. (1960) *Plutonium: Steam Oxidation and Oxide Dissolution*, Hanford Report HW-66431.

Stakebake, J. L., Loser, R. W., and Chamber, C. A. (1970) *Appl. Spectrosc.*, **25**, 70–6.

Stakebake, J. L. (1971) *J. Nucl. Mater.*, **38**, 241–59.

Stakebake, J. L. (1973) *J. Phys Chem.*, **77**, 581–6.

Stakebake, J. L. and Steward, L. M. (1973) *J. Colloid Interface Sci.*, **42**, 328–33.

Stakebake, J. L. and Robinson, H. R. (1977) *Nucl. Technol.*, **33**, 30–9.

Stakebake, J. L. (1979) *J. Electrochem. Soc.*, **126**, 1596–601.

Stakebake, J. L. (1981a) *Reaction of Oxygen with Plutonium Hydride*, Rocky Flats Report RFP-3096.

Stakebake, J. L. (1981b) *Nucl. Sci. Eng.*, **78**, 386–92.

Stakebake, J. L. (1981c) *J. Electrochem Soc.*, **128**, 2383–8.

Stakebake, J. L. (1986) *J. Less Common Metals*, **123**, 185–97.

Stakebake, J. L. (1988) *Semi-Annual Report; July–December 1978*, Rocky Flats Plant Report RFP-2883.

Stakebake, J. L. and Lewis, L. A. (1988) *J. Less Common Metals*, **136**, 349–66.

Stakebake, J. L. and Saba, M. A. (1990) *J. Less Common Metals*, **158**, 221–37.

Stakebake, J. L. (1992a) *J. Alloys Compds*, **187**, pp. 271–83.

Stakebake, J. L. (1992b) in *Transuranium Elements A Half Century*, ch. 27 (eds. L. R. Morss and J. Fuger), American Chemical Society, Washington DC, pp. 251–9.

Stakebake, J. L. (1992c) *Plutonium Pyrophoricity*, Rocky Flats Report RFP-4517.

Stakebake, J. L., Larson, D. T., and Haschke, J. M. (1993) *J. Alloys Compds*, **202**, 251–63.

Stephens, D. R. (1995) *Source Terms for Aerosolization from Nuclear Weapon Accidents*, Lawrence Livermore National Laboratory Report UCRL-ID-119303.

Stewart, K, (1961) *Vixen A Trials: Experiments to Study the Release of Particulate Material During the Combustion of Plutonium, Uranium and Beryllium in a Petrol Fire*, United Kingdom Atomic Weapons Research Establishment Report AWRE T15/60.

Stewart, K. (1963) *Prog. Nucl. Energy, Ser. IV*, **5**, 535–79.

Szempruch, R. (2001) *Particle Sizes and Respirable Fractions from MIS Samples*, MIS Meeting, Los Alamos National Laboratory, Los Alamos, NM, October 23–5.

Terada, K., Meisel, R. L., and Dringman, M. R. (1969) *J. Nucl. Mater.*, **30**, 340–2.

Van Konynenburg, R. A., Wood, D. H., Condit, R. H., and Shikany, S. D. (1996) *Bulging of Cans Containing Plutonium Residues – Summary Report*, Lawrence Livermore National Laboratory Report UCRL-ID-125115.

Voelz, G. L. (2000) in *Los Alamos Science*, no. 26 (ed. N. G. Cooper), Los Alamos National Laboratory, Los Alamos, pp. 74–89.

Waber, J. T. (1980) in *Plutonium Handbook* (ed. O. J. Wick), American Nuclear Society, La Grange Park, IL, pp.145–89.

Ward, J. W. (1985) in *Handbook on the Physics and Chemistry of Actinides*, ch. 1 (eds. A. J. Freeman and C. Keller), Elsevier Science, Amsterdam, pp. 1–74.

Ward, J. W. and Haschke, J. M. (1994) in *Handbook on the Physics and Chemistry of Rare Earths*, vol. 18, *Lanthanides/Actinides: Chemistry*, ch. 123 (eds. K. A. Gschneidner Jr, L. Eyring, G. R. Choppin, and G. H. Lander), Elsevier Science, Amsterdam, pp. 194–363.

Weigel, F., Katz, J. J., and Seaborg, G. T. (1986) in *Chemistry of the Actinide Elements*, vol. 1, ch. 7 (eds. J. J. Katz, G. T. Seaborg, and L. R. Morss), Chapman and Hall, London, pp. 499–869.

Wells, A. F. (1975) *Structural Inorganic Chemistry*, Clarendon Press, Oxford, pp. 450–8.

Wicks, G. W. (1999) *Nuclear Waste Glasses – Suitability, Surface Studies, and Stability*, Westinghouse Savannah River Technology Center Report WSRC-MS-99,000082.

Wilkinson, W. D. (1962) *Uranium Metallurgy*, vol. II, ch. 7, Interscience Publishers, New York, pp. 757–853.

Woodley, R. E. and Gibby, H. (1973) *Room-Temperature Oxidation of* $(U,Pu)O_{2-x}$, Westinghouse Hanford Company Report HEDL-SA-592.

Wriedt, H. A. (1990) *Bull. Alloy Phase Diagr.*, **11**, 184–202.

CHAPTER THIRTY

TRACE ANALYSIS OF ACTINIDES IN GEOLOGICAL, ENVIRONMENTAL, AND BIOLOGICAL MATRICES

Stephen F. Wolf

30.1 INTRODUCTION

Actinide elements are ubiquitous in nature. Uranium and thorium are present in the Earth's crust with average concentrations of 1–10 μg g^{-1}, making them more abundant than Ag, Sb, Cd, or Hg. While U and Th can even be found as major or minor mineral constituents in a variety of geochemical environments, typically they are highly dispersed and present only at trace or ultra-trace concentrations in most natural materials. Because ^{238}U, ^{235}U, and ^{232}Th are the parents of the three naturally occurring non-extinct radioactive decay chains, they are always accompanied by lower concentrations of their radioactive progeny, many of which are also actinides (Table 30.1). The chemical behavior of ^{238}U, ^{235}U, ^{232}Th, and their progeny have been studied for years because accurate determination of their relative abundances can provide geochronological information on a variety of geological/environmental processes. Careful analyses have revealed that trace amounts of the transuranic actinides ^{237}Np and ^{239}Pu occur naturally and are present in U ores with mass ratios of

Table 30.1 *Nuclear data for naturally occurring actinides, their decay products, as well as nuclides used as analytical isotopic tracers. The abundances, half-life* ($t_{1/2}$)*, and primary decay mode data are taken from Firestone and Shirley* (1996)*. The thermal-neutron cross section* (σ_n) *data are taken from Erdtmann* (1976).

Nuclide	*Abundance*	$t_{1/2}$	*Specific activity* (Ci g^{-1})	*Decay modes*	σ_n (b)	*Comments*
^{227}Ac		21.773 y	72.328	β^- (98.620%) α (1.380%)	(n,γ) 762 ± 29 (n,f) <0.002	b
^{228}Ac		6.15 h	2.23×10^6	β^- (100%)	–	c
^{227}Th		18.72 d	2.391×10^4	α (100%)	(n,f) 200 ± 20	b
^{228}Th		1.9116 y	820.20	α (100%)	(n,γ) 123 ± 15 (n,f) <0.3	c
^{229}Th		7340 y	0.205	α (100%)	(n,γ) 54 ± 6 (n,f) 30.5 ± 3.0	d
^{230}Th		7.538×10^4 y	0.02062	α (100%)	(n,γ) 23.2 ± 0.6 (n,f) <0.0012	a
^{232}Th	100%	1.405×10^{10} y	1.097×10^{-7}	α (100%)	(n,γ) 7.40 ± 0.08	c
^{233}Th		22.3 m	3.54×10^7	β^- (100%)	(n,γ) 1500 ± 100 (n,f) 15 ± 2	e
^{234}Th		24.10 d	2.276×10^4	β^- (100%)	(n,γ) 1.8 ± 0.5 (n,f) <0.01	a

^{231}Pa		3.276×10^4 y	0.04585	α (100%)	(n,γ) 210 ± 20 (n,f) 0.010 ± 0.005	b
^{233}Pa		26.967 d	2.0343×10^4	β^- (100%)	(n,γ) 21 ± 3 (n,f) <0.1	d
^{234m}Pa		1.17 m	6.75×10^8	β^- (99.84%) IT (0.16%)	–	a
^{232}U		68.9 y	21.8	α (100%)	(n,γ) 73.1 ± 1.5 (n,f) 75.2 ± 4.7	d
^{233}U		1.592×10^5 y	9.435×10^{-3}	α (100%)	(n,γ) 47.7 ± 2.0 (n,f) 531.1 ± 1.3	d,f
^{234}U	0.0055%	2.455×10^5 y	6.118×10^{-3}	α (100%)	(n,γ) 100.2 ± 1.5 (n,f) <0.65	a
^{235}U	0.7200%	7.038×10^8 y	2.134×10^{-6}	α (100%)	(n,γ) 98.6 ± 1.5 (n,f) 582.2 ± 1.3	b
^{236}U		2.342×10^7 y	6.413×10^{-5}	α (100%)	(n,γ) 5.2 ± 0.3	e
^{238}U	99.2745%	4.468×10^9 y	3.361×10^{-7}	α (100%) SF (0.0000545%)	(n,γ) 2.70 ± 0.02	a
^{239}U		23.45 m	3.369×10^7	β^- (100%)	(n,γ) 22 ± 5 (n,f) 14 ± 3	e

Comments: a, ^{238}U series; b, ^{235}U series; c, ^{232}Th series; d, isotopic tracer; e, NAA product; f, anthropogenic.

$<2 \times 10^{-12}$ and $<1 \times 10^{-11}$ for ^{237}Np/U and ^{239}Pu/U, respectively (Levine and Seaborg, 1951; Peppard *et al.*, 1952). Once considered extinct, the long-lived plutonium isotope ^{244}Pu was first proposed to have existed in the early solar system by Kuroda (1960). The presence of this nuclide in the early solar system was first confirmed via its signature of fissiogenic Xe isotopes (Rowe and Kuroda, 1965). The nuclide was eventually found to be non-extinct by direct detection in Precambrian bastnasite (Hoffman *et al.*, 1971).

Although the existence of some of the naturally occurring actinides has been known for more than two centuries, the use of actinides reached a new era with the discovery of nuclear fission in 1938. The development of nuclear fission as an energy source and weapon have led to the production and subsequent global spread of both natural and artificial actinide elements in the environment at ultra-trace levels. Fallout from nuclear weapon testing represents the highest contributor to the global spread of transuranic actinides with cumulative levels of the most abundant transuranic actinide Pu averaging approximately 1 mCi km^{-2} (Kim, 1986, and references therein). For the transuranic actinides, of particular concern are the nuclides that will linger in the environment due to long half-lives (Table 30.2). The more than 50 years of nuclear weapons production, testing, and energy generation has left a worldwide legacy of environmental contamination. As strategies for environmental remediation and disposal of actinide-contaminated materials are developed and implemented, the ability to perform accurate and precise determinations of trace level actinides in a variety of natural matrices has become increasingly important.

Accurate determination of trace actinides in geological, environmental, and biological materials represents a significant challenge due to their extremely low concentrations and the diverse matrix chemistry of these samples. Concentrations of the environmental transuranic actinides are frequently <1 fg g^{-1} sample and require accurate determination of less than 10^6 atoms of actinide. To perform these types of measurements, the modern analytical chemist can select from a variety of procedures and techniques encompassing sample decomposition, chemical separation, as well as analytical instruments, and calibration methods for the determination of concentration. The specific approach selected is dependent on several factors: sample matrix, sample size, analyte concentration, the need to determine multiple analytes, cost of analysis, time of analysis, equipment available, and the skill and training of the analyst. Any of these factors can influence the selection of an analytical method. The purpose of this chapter is to review and assess those procedures and techniques that are currently the state-of-the-art for trace actinide determination in geological, environmental, and biological matrices. This chapter emphasizes the procedures and techniques that are used specifically for the determination of the naturally occurring actinides and the long-lived environmental transuranic actinides at concentrations <1 μg g^{-1}.

Table 30.2 *Nuclear data for the environmental transuranic nuclides as well as nuclides used as analytical isotopic tracers. The half-life* ($t_{1/2}$) *and primary decay mode data are taken from Firestone and Shirley* (1996). *The thermal-neutron cross section* (σ_n) *data are taken from Erdtmann* (1976).

Nuclide	$t_{1/2}$	*Specific activity* (Ci g^{-1})	*Decay modes*	σ_n (b)	*Comments*
^{237}Np	2.144×10^6 y	7.006×10^{-4}	α (100%)	(n,γ) 169 ± 3 (n,f) 0.019 ± 0.003	
^{238}Np	2.117 d	2.592×10^5	β^- (100%)	(n,f) 2070 ±30	a
^{239}Np	2.3565 d	2.3280×10^5	β^- (100%)	(n,γ) 31 ± 6 (n,f) 14 ± 14	a
^{236}Pu	2.858 y	525.5	α (100%)	(n,f) 165 ± 20	a
^{238}Pu	87.7 y	17.1	α (100%)	(n,γ) 574 ± 20 (n,f) 16.5 ± 0.5	
^{239}Pu	2.411×10^4 y	0.06230	α (100%)	(n,γ) 268.8 ± 3.0 (n,f) 742.5 ± 3.0	
^{240}Pu	6563 y	0.2288	α (100%)	(n,γ) 289.5 ± 1.4 (n,f) 0.030 ± 0.045	
^{241}Pu	14.35 y	104.7	β^- (99.998%) IT (0.00245%)	(n,γ) 368 ± 10 (n,f) 1009 ± 8	
^{242}Pu	3.733×10^5 y	0.004024	α (100%) SF (0.000554%)	(n,γ) 18.5 ± 0.4 (n,f) <0.2	a
^{244}Pu	8.08×10^7 y	1.86×10^{-5}	α (99.879%) SF (0.121%)	(n,γ) 1.7 ± 0.1	a
^{241}Am	432.2 y	3.475	α (100%)	(n,γ) 832 ± 20 (n,f) 3.15 ± 0.10	b
^{242m}Am	141 y	10.65	IT (99.541%) α (0.459%)	(n,γ) 1400 ± 860 (n,f) 6600 ± 300	
^{243}Am	7370 y	0.2038	α (100%)	(n,γ) 79.3 ± 2.0 (n,f) <0.07	a
^{242}Cm	162.8 d	3370	α (100%)	(n,γ) 16 ± 5 (n,f) <5	c
^{243}Cm	29.1 y	51.6	α (99.71%) EC (0.2%)	(n,γ) 225 ± 100 (n,f) 600 ± 50	
^{244}Cm	18.10 y	80.90	α (100%) SF (0.0001371%)	(n,γ) 13.9 ± 1.0 (n,f) 1.2 ± 0.1	

Comments: a, isotopic tracer; b, ^{241}Pu daughter; c, ^{242m}Am daughter.

30.2 CHEMICAL PROCEDURES

30.2.1 Sample decomposition

Most modern instrumental analytical techniques first require the preparation of a homogeneous, stable, aqueous solution that possesses a known matrix. For aqueous samples, the actinides may be present as dissolved species or adsorbed on the surfaces of suspended solid materials. In many cases these actinides can be solubilized and stabilized via acidification. Environmental aqueous samples such as natural waters are simply acidified with HNO_3 or HCl soon after collection to eliminate and/or prevent the formation of Fe or Al hydroxides (Lally, 1992). Simple acidification, however, may not decompose all suspended solid materials. Urine samples are acidified and decomposed with heat after addition of an inactive carrier and isotopic spikes (Wyse *et al*., 1998). For solid samples, complete decomposition of the sample matrix is typically performed; this requires more aggressive chemical treatment. Samples possessing organic matrices are typically dried thermally and ashed as a first step. Complete dissolution of actinides in solid samples may be complicated due to the presence of refractory oxide actinide phases. Selection of the appropriate sample decomposition method is an important factor in performing an accurate determination of actinide concentration. Selection of a sample decomposition method is dependent on the sample matrix, the chemical state of the actinide, and the chosen method of actinide determination. The decomposition step may be followed by separation, purification, and conversion of the actinide to a chemical form that is appropriate with the requirements of the method of determination. Decomposition of solid materials can be accomplished by either fusion or acid decomposition.

(a) Fusion decomposition

Fusion decomposition is extremely aggressive and is used primarily for decomposition of geological and solid environmental materials. Fusions are performed by heating a mixture of the sample with a flux reagent at atmospheric pressure in a graphite, zirconium, or platinum crucible. The method is well suited for large samples (several grams). The wide variety of sample matrices in each case requires a careful selection of the flux reagent. Selection of the appropriate flux material can result in both acid–base and oxidation–reduction-based decompositions (Dolezal *et al*., 1968). Common fluxes are hydroxides, peroxides, carbonates, bisulfates, hydrosulfates, pyrosulfates, tetraborates, and metaborates (Dean, 1995). For fusion decompositions, 0.1–10 g of a dried, homogenized, and powdered solid sample is mixed with flux at a sample to flux ratio ranging from 1:2 to 1:20. Isotopic spikes and elemental carriers, if required, are added at this stage. The mixture is heated to a temperature above the melting point of the flux over a Meker burner or in a muffle furnace until the

mixture forms a well-mixed molten mass. After cooling, the resulting fusion bead is dissolved with a dilute acid such as HNO_3 or HCl.

Fusion with $NaOH–Na_2O_2$ is a standard geochemical procedure that is extremely effective in decomposing silica-containing matrices. The effectiveness of the method is due to the high temperatures and oxidizing conditions that can be achieved. This method was used to decompose gram quantities of U-ore materials for determination of naturally produced Pu and Tc (Dixon *et al.*, 1997). The oxidizing conditions of the fusion mixture ensured reproducible decomposition and equilibration of a ^{242}Pu isotopic spike. The method yielded a precision of 1.6% and a blank of (0.17 ± 0 .15) pg for ^{239}Pu in Canadian Reference Material BL-5. Comparison of ^{239}Pu results with results from acid-decomposed samples (Attrep *et al.*, 1992) indicates that the fusion method may be more effective in totally dissolving trace Pu in U ore samples than acid decomposition. Croudace *et al.* (1998) used a metaborate–tetraborate flux for fusion of soil and sediments contaminated with weapons Pu and U. The American Society for Testing and Materials (ASTM) has published a standard procedure for fusion decomposition of solid materials (ASTM C1342-96, 1996b).

The major disadvantage to fusion decomposition is that the large mass of flux material yields a solution with high total dissolved solids (TDS). Chemical separation of the analyte from the dissolved flux material is typically required. Additionally, trace analysis of naturally occurring actinides may be complicated due to trace impurities in the flux. The aggressiveness of the reaction can also result in the attack of the mass of the crucible, leading to contamination of the sample. Despite these disadvantages, fusion decomposition is one of the most effective methods of decomposing refractory mineral phases in geological and environmental samples.

(b) Acid decomposition

Acid decompositions have been adapted for virtually all sample matrices. Acid decompositions yield solutions with low TDS that can be used for direct determination of many elements, including actinides, without subsequent chemical treatment. The availability of ultrahigh purity acids makes acid decomposition ideal for determination of trace U and Th. Acid decompositions are performed in a chemically resistant beaker on a hotplate at atmospheric pressure or in a closed digestion bomb at elevated pressures and temperatures in a convection or microwave oven.

For open-vessel acid decompositions a dried, homogenized, and powdered solid sample is mixed with several milliliters of one or more concentrated acids in a glass, polytetrafluoroethylene (PTFE), or perfluoroalkoxy (PFA) beaker and heated in a fume hood on a hotplate at atmospheric pressure. Several grams of material can be decomposed in an open vessel. For closed-vessel acid decompositions, the sample and acids are mixed in a PTFE-lined pressure vessel.

Water can be added to increase the solubility and prevent temperature spikes due to exothermic reactions. The vessel is sealed tightly and heated in a convection oven. The effectiveness of closed-vessel system results from the higher pressures and temperatures under which the decomposition takes place. Closed-vessel decompositions are typically restricted to <1 g of inorganic material or <0.1 g of organic material for a 23 mL closed vessel (Dean, 1995).

The types of acids selected depend on the chemical properties of the sample matrix as well as the elements to be determined. Actinides are soluble in HNO_3 and HCl so most procedures for the decomposition of actinide-containing samples utilize these acids. The ASTM has published a set of standard procedures for hotplate and convection-oven digestion of water and solid samples with HNO_3 and HCl (ASTM D1971-95, 1995a). These procedures are applicable to wastewaters, sludges, river and lake waters, and plant and animal tissues.

A HF–HNO_3 mixture is required for acid decomposition of silicates. After decomposition, HF must be removed so that insoluble actinide fluorides are converted to a soluble form either by fuming with $HClO_4$ or H_2SO_4 or by complexation with H_3BO_3. Beasley *et al.* (1998) used open vessels for the decomposition of soil samples for U, Np, and Pu determinations. Samples weighing 1–3 g were ash dried at 600°C to remove organic matter and were dissolved in a mixture of HF–HCl. The residue was fumed to dryness in an open vessel three times to remove residual HF and then dissolved in 6 M HCl–H_3BO_3 mixture to solubilize actinide fluorides.

The addition of H_2O_2 in small or catalytic quantities aids in oxidizing organic matter. A HNO_3–H_2O_2 mixture has been used for decomposition of plant material (Testa *et al.*, 1998) as well as animal and human whole organs and bones (USTUR 100, 1995; Glover *et al.*, 1998b).

Recently, specially designed microwave sample decomposition systems have become a routine analytical tool for decomposition of geological, environmental, and biological samples (Lamble and Hill, 1998). Microwave systems provide high-heating efficiency and programmability for unattended operation. The resulting decomposition procedures are reproducible and rapid. Specially designed closed PTFE or PFA vessels minimize sample contamination. Standard procedures for microwave-heated, closed-vessel decomposition with HCl and HNO_3 for the determinations of metals in groundwater have been published (ASTM D4309-91, 1991a). These procedures are applicable for digestion of suspended solids in water and leaching elements from most solid materials but would not yield total dissolution of silica-containing materials. The United States Environmental Protection Agency (U.S. EPA) has developed Method 3052 (U.S. EPA, 1996) for total microwave-heated, closed-vessel decomposition of ashes, biological tissues, oils, oil-contaminated soils, sediments, sludges, and soils. This method has been validated for U determinations on the Standard Reference Material (SRM) 2704 Buffalo River Sediment. Attrep *et al.* (1992) used a microwave system for the decomposition of U-ore materials for the determination of naturally produced Pu and Tc. Alvarado *et al.* (1996) have

developed a microwave procedure for the rapid decomposition of plant tissue for the purpose of actinide analysis using a $HNO_3-H_2O_2$ mixture. An overview of microwave digestion techniques can be found in Kingston and Haswell (1997).

30.2.2 Chemical separation

The accuracy and precision of most methods of actinide determination are influenced both by nonspecific interferences from more abundant sample matrix species and by specific spectroscopic or isobaric interferences from other actinides. These interferences often necessitate chemical separation of the actinide from the interfering species before determination. Additionally, chemical separations preconcentrate the analyte. Preconcentration is especially useful for actinides because of their ultralow concentrations in the environment. Chemical separations can enhance the sensitivity, accuracy, and precision of the overall analytical method.

Actinides are amenable to a variety of chemical separation methods including: coprecipitation, adsorption, chelation, liquid–liquid extraction, column ion-exchange chromatography, column extraction chromatography, or a combination of two or more of these methods. Procedures for the separation and purification of environmentally important actinides have been compiled (Kirby, 1959; Hyde, 1960; Penneman and Keenan, 1960; Stevenson and Nervik, 1961; Gindler, 1962; Coleman, 1965; Burney and Harbour, 1974). Many of these methods are applicable here. Recently, flow injection (FI) analysis and high-performance liquid chromatography (HPLC) have been utilized for online actinide separation with radiometric or mass spectrometric detection. In this section, we review the methods that have been used specifically for analytical-scale separations of trace actinides for the purpose of concentration determination. Because of the common desired goal, i.e. separation of the actinide from more abundant matrix elements and/or other actinides, most of the procedures below can be adapted to geological, environmental, and biological samples.

(a) Coprecipitation

Actinides can be preconcentrated from a large solution volume by coprecipitation. The most frequently used anions for actinide coprecipitation are fluorides, hydroxides, and phosphates. Actinides in the trivalent and tetravalent states are efficiently scavenged from solution by addition of a rare-earth element carrier with precipitation as a fluoride (Magnusson and LaChapelle, 1948). Actinides can also be coprecipitated as a group with $Fe(OH)_3$ (Lally, 1992) from a carbonate-free solution. Carbonate must be removed by boiling under acidic conditions due to its ability to complex with actinides and prevent quantitative precipitation. Coprecipitation is performed by adding a macroscopic amount of $FeCl_3$ to an acidified sample digest solution and adjusting the solution pH to basic by the addition of NH_4OH. The precipitate can then be filtered, washed,

and dissolved with HCl or HNO_3 before further separation and purification of the actinides. Coprecipitation of actinides can also be performed with Ca(II) as $Ca_3(PO_4)_2$ from an acidic digest solution with the addition of NH_4OH to a pH 8–9. This procedure is used for group actinide precipitation from digested soils (Kim *et al.*, 2000) and from urine for bioassay (Maxwell and Fauth, 2000). Direct coprecipitation with MnO_2(s) and adsorption onto MnO_2(s) have been extensively used for preconcentration of actinides from large-volume freshwater and seawater samples (Wong *et al.*, 1978; Bowen *et al.*, 1980). Sidhu and Hoff (1999) describe a procedure in which Pu was preconcentrated *in situ* from 2001 samples of fresh- and seawater. In this method, $KMnO_4$ solution was added to an acidified water sample and MnO_2(s) was precipitated with the addition of $NaHSO_3$. The resulting solid was filtered and the Pu was further purified before determination.

(b) Liquid–liquid extraction

Liquid–liquid extraction of actinides can be accomplished with a wide range of organic acids, ketones, ethers, esters, alcohols, and phosphoric acid derivatives (Lally, 1992). Methyl isobutyl ketone has been used to extract U(VI) from aqueous solutions. U(IV) can be extracted with ethyl acetate after treatment of an acidified solution with $Al(NO_3)_3 \cdot 9H_2O$ (Guest and Zimmerman, 1955). U(VI) can be extracted with 25% tributylphosphate (TBP) in toluene (Mair and Savage, 1986). A standard test method for the determination of U in water by high-resolution α-liquid-scintillation spectrometry utilizes a selective extractive scintillator solution containing dialkylphosphoric acid (ASTM D6239-98, 1998). Interfering radionuclides (Am, Pu, Po, Ra, Rn, and Th) are masked from extraction by diethylenetriaminepentaacetic acid (DTPA). Attrep *et al.* (1992) described a method for the determination of ultralow levels of natural ^{239}Pu in U ores in which Pu was extracted with 0.5 M thenoyltrifluoroacetone (TTA) in *o*-xylene and back-extracted into 8 M HNO_3. Bis(2-ethylhexyl)phosphoric acid (HDEHP) in toluene and dibutyl-*N*,*N*-diethylcarbamylphosphonate (DDCP) have both been used to separate Am from Pu for bioassay measurements (Filipy *et al.*, 1998). Triisooctylamine (TIOA) in xylene has been used to selectively extract Np from U and Pu (Novikov *et al.*, 1972). Whereas liquid–liquid extraction methods are very effective, in general they are being replaced due to the volume and classification of waste products that are produced by their use.

(c) Ion exchange

Ion-exchange resins are typically high-molecular-weight organic polymers containing a large number of functional groups that provide the basis for the separation of the analyte from undesired species. Cation exchange can be performed on resins possessing functional groups such as the strongly acidic

sulfonate group $-SO_3^-$. A cation-exchange resin composed of spherical polystyrene–divinylbenzene polymer substrate containing geminally substituted diphosphonic and sulfonic groups capable of selectively binding actinides and lanthanides from common matrix elements has been developed. This resin, Diphonix, allows preconcentration of actinides from large samples (Horwitz *et al.*, 1993a). Actinides can be recovered from Diphonix resin by elution with 1-hydroxyethylidenediphosphonic acid (HEDPA) or by complete decomposition of the resin (Chiarizia *et al.*, 1997). This method has been applied to separations of transuranic radionuclides in urine (Eikenberg *et al.*, 1999a) and for separation of Th from dietary samples, urine, and feces (Eikenberg *et al.*, 1999b).

Most ion-exchange methods for the separations of actinides utilize anion exchange. Anion exchange is performed on resins possessing functional groups such as the strongly basic quaternary ammonium salt $-NR_3^+$. Uranium can be separated from a variety of ions by the use of basic anion-exchange resins such as Bio-Rad AG1X8. Uranyl ions form strong anionic sulfate and chloride complexes that can be the basis for U separations. A standard test method for the determination of U in water uses coprecipitation of U spiked with ^{232}U-tracer with $Fe(OH)_3$ (ASTM D3972-90, 1990). After dissolution of the precipitate, U is separated from Th, Po, Pu, and Am by adsorption from a HCl solution onto an anion-exchange resin. Separation of ^{231}Pa is not achieved by this method and this nuclide could potentially cause spectroscopic interference with ^{234}U when alpha spectrometry is employed for U determination.

Anion exchange is also used for the separation of Pu from solution. Determination of Pu in water can be performed by coprecipitation of Pu and ^{242}Pu-tracer with Fe(III) as $Fe(OH)_3$ (ASTM D3865-97, 1997a). After dissolution of the precipitate, Pu is separated from Th and Am by anion exchange. Separation of ^{238}Pu from ^{228}Th and ^{241}Am is necessary due to α-spectroscopic interference.

A specialized anion-exchange resin called TEVA·Resin (EIChroM Industries Inc., Darien, IL, USA) is capable of separating actinides in different oxidation states from common matrix elements. The resin is composed of a liquid aliphatic quaternary amine incorporated onto an inert polymeric substrate, Amberchrom CG-71ms. Specifically, this resin allows the separation of the tetravalent actinides Pu(IV), Np(IV), and Th(IV) from hexavalent U(VI) and trivalent Am(III) in HNO_3 solutions (Horwitz *et al.*, 1995). Th(IV) that has sorbed onto TEVA·Resin can be preferentially eluted with 3 M HCl. Separation of Pu from Np is also feasible with this material. Addition of hydroquinone reduces Pu(IV) to Pu(III), allowing Pu elution with 9 M HCl whereas Np is retained. Np can then be eluted with 0.5 M HCl or 0.02 M HNO_3–0.02 M HF. Lanthanide elements are difficult to separate from Am(III) and may interfere with preparation of a sample for α-spectrometric analysis. Am can be separated from lanthanide elements on TEVA·Resin by complexation with thiocyanate.

(d) Extraction chromatography

Several extraction chromatographic resins have been developed specifically for the separation and preconcentration of actinides from acidic matrices such as acid-stabilized groundwaters and dissolved environmental and geological solids. These resins are composed of an inert support material that has been impregnated with an actinide-selective organic extractant. Whereas these resins function by passing actinide-containing solutions down to an exchange column containing the material, the separation is based on liquid–liquid extraction. These commercially available extraction resins named Actinide-CU, UTEVA·Spec, and TRU·Spec (EIChroM Industries Inc.) provide an extremely valuable tool for the preconcentration and separation of actinide elements from elements common to natural matrices and for separation of individual actinide elements from each other.

Preconcentration of Am and Pu from human tissue samples has been performed using Actinide-CU resin (Qu *et al.*, 1998). This resin is composed of bis(2-ethylhexyl)methanediphosphonic acid (H_2DEH[DMP] or DIPEX) supported by an inert polymeric substrate, Amberlite XAD-7. This resin has a strong affinity for actinides in strongly acid solutions and, thus, stripping of the actinide–organophosphonate complex with isopropanol is required to recover the actinides. This resin is appropriate only for preconcentration of actinides and not separation of individual elements.

The resin U/TEVA·Spec demonstrates specificity for U and tetravalent actinides. It is composed of diamylamylphosphonate (DAAP) sorbed on Amberlite XAD-7 (Horwitz *et al.*, 1992). Preconcentration and separation of U from common geological and environmental matrix elements such as Fe, Ca, Al, Na, and K and other actinides can be achieved from HNO_3 solutions. Separation of U from Th can be accomplished with a 2 M HNO_3 whereas separation of U from Np or Pu can be accomplished with a HNO_3–oxalic acid mixture.

TRU·Spec resin demonstrates high retention of tri-, tetra-, and hexavalent actinides. It is composed of octyl(phenyl)-*N*,*N*-diisobutylcarbamoylmethylphosphine oxide (CMPO) in TBP supported by Amberlite XAD-7 (Horwitz *et al.*, 1993b). In HNO_3 solutions, preconcentration and separation of all actinides from matrix elements common to geological and environmental samples can be achieved with TRU·Spec. Additionally, TRU·Spec allows for sequential elution of Am, Pu, Th, Np, and U using a scheme that incorporates HNO_3 and HCl rinse steps in combination with complexation and oxidation-state adjustments. Common matrix elements can be eluted before the actinides, providing for separation of these matrix elements. A method for preconcentration and separation of actinides from urine by this method was first described by Horwitz *et al.* (1990). Separations with applications to geochemistry have also been developed. TRU·Spec resin has been used for the separation of Th and U from geological samples (Pin and Zalduegui, 1997) and for the separation of

U and Th, from Pa in shells and minerals for geochronological measurements (Burnett and Yeh, 1995).

Many highly effective, flexible, and efficient methods for the separation of actinides from their sample matrix, as well as from each other, have been devised by combining anion exchange with one or more extraction chromatography steps. Croudace *et al.* (1998) described a procedure for the determination of Pu and U in soils and sediments that utilizes a combination of anion exchange and extraction chromatography (U/TEVA·Spec) to isolate Pu and Th from U and purify the U fraction. Maxwell (1997) devised a rapid-actinide separation method for environmental samples that utilizes anion exchange with TEVA·Spec resin and extraction chromatography with U/TEVA·Spec resin for the separation of U, Np, Pu, Am, and Cm.

Yokoyama *et al.* (1999) used extraction chromatography with U/TEVA·Spec resin and anion exchange with TEVA·Spec resin to separate Th and U before mass spectrometric determination of Th/U isotopic content of silicate rock samples. The recovery yields for Th and U were >90% and the total blanks were <19 pg for Th and <10 pg for U. Dual sequential columns and vacuum extraction were used to increase sample throughput. Separations by anion exchange with TEVA·Spec resin and extraction chromatography with TRU·Spec have been applied to separation of actinides from urine (Maxwell and Fauth, 2000), soil (Smith *et al.*, 1995), and soft human tissue (Moody *et al.*, 1998). A general radiochemical method that utilizes anion exchange and extraction chromatography for separating Th, U, Np, Pu, and Am from each other and matrix elements is shown in Fig. 30.1.

The use of extraction chromatographic resins configured as a continuous low-pressure FI or HPLC system, in series with the appropriate detector, can potentially enhance the selectivity, sensitivity, and speed of the detection method. Egorov *et al.* (1998) have developed a multieluant FI scheme utilizing TRU·Spec resin and off-line radiometric counting for quantitation. This system is capable of performing automated separations of Am from Pu including on-column Pu oxidation and reduction. FI has also been used with mass spectrometric detection of actinides (ASTM C1310-95, 1995c).

(e) Speciation separations

The most commonly used method for the determination of concentrations of actinides with oxidation-state specificity is direct spectrometric analysis in the visible and near IR spectral regions (see Chapter 27, section 27.3.2, of this book). Spectroscopic methods, however, typically require actinide concentrations that are higher than those found in most environmental and biological samples. To solve the problem of low concentration, indirect methods have been developed. These indirect methods use oxidation-state selective chemical separation of actinide species followed by radiometric or mass spectrometric

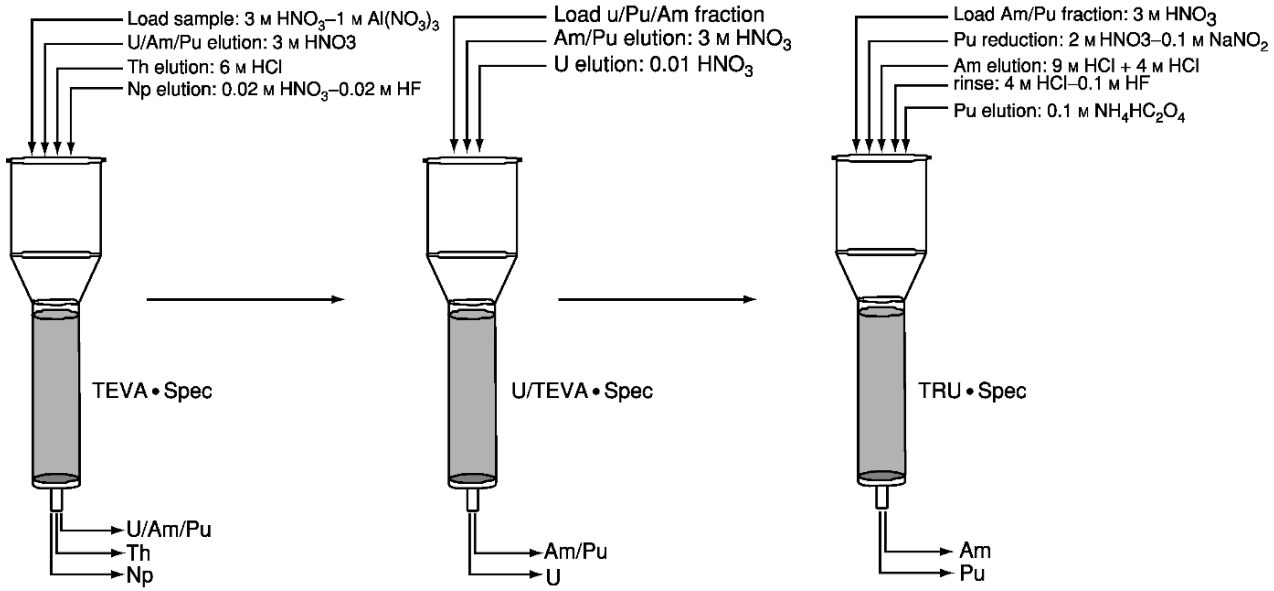

Fig. 30.1 *Schematic representation of a method for sequential separation of Th, Np, U, Am, and Pu using sequential anion exchange and extraction chromatography (after Horwitz* et al.*, 1995). In this procedure analyte and yield tracers are initially co-precipitated as a group from a dissolved or digested sample using one of the common carriers such as Ca(II). The precipitate is separated, washed, and dissolved with* 3 M HNO_3–1.0 M $Al(NO_3)_3$ *and loaded on the first column. The method is applicable to geological, environmental, and biological materials.*

determination. These chemical separation methods are based on the same fundamental principles of actinide separation used for interference removal.

Solvent extraction has been used for separating trace actinides possessing different oxidation states (Foti and Freiling, 1964). Saito and Choppin (1983) developed a solvent extraction-based methodology for the separation of trace level actinide elements in the III, IV, V, and VI oxidation states in solutions possessing pH 6–8. Dibenzoylmethane (DBM) in benzene was used as an extractant for actinides in 0.7 M NaCl aqueous solutions. The pH dependence of the extraction was determined for Am(III), Th(IV), Np(V), U(VI), and the method was demonstrated on systems containing mixtures of Pu(IV) and Pu (VI). The solvent extraction method can be applied to solutions possessing pH < 4 by using thenoyltrifluoroacetone (TTA) as the extractant (Bertrand and Choppin, 1982). Actinides in the V oxidation state were extracted from 0.1 M acetate buffer whereas actinides in the VI state were extracted from 0.6 M perchloric acid.

Oxidation state-specific adsorption has been used for separating trace actinide species. Inoue and Tochiyama (1977) used adsorption on silica gel to distinguish between Np(V) and Np(VI). Bondietti and Trabalka (1980) used differential adsorption to TiO_2 as a method to determine Pu(V) in natural waters with pH 9–11. Orlandini *et al*. (1986) used selective adsorption of Pu(VI) on silica gel and adsorption of Pu(V) on $CaCO_3$ for the determination of Pu oxidation state in Lake Michigan Water.

Coprecipitation has also been used to separate actinides possessing different oxidation states. The most widely used adsorption and coprecipitation method is the rare-earth fluoride technique that was adapted from the classical separation of reduced Pu(III + IV) from oxidized Pu(VI) by the coprecipitation of the former on a rare-earth fluoride (Magnusson and LaChapelle, 1948). This method was used for the determination of the oxidation state of Pu in filtered and unfiltered seawater samples from the Irish Sea (Nelson and Lovett, 1978a; Nelson *et al*., 1984) and the Pacific Ocean (Nelson and Lovett, 1978b). Samples were made 0.8 M in HNO_3, 0.25 M in H_2SO_4, 0.5 mM in $K_2Cr_2O_7$, and 0.7 mM in $Nd(NO_3)_3$. Sufficient HF was added to raise the total fluoride concentration to 0.25 M and the precipitated NdF_3, along with the coprecipitated Pu(III + IV), was filtered. The unprecipitated Pu(V) and Pu(VI) was treated with $(NH_4)_2SO_4 \cdot FeSO_4 \cdot 6H_2O$ to reduce the remaining Pu and a second NdF_3 step was performed. The Pu in each fraction was purified by anion exchange and Pu isotopes were quantified by alpha spectrometry.

The association of actinides with organic and inorganic aqueous colloidal materials is an important factor that controls the mobility of the actinide in the environment. The determination of the concentrations of actinides associated with aqueous colloids is typically performed by physically separating aqueous colloids by ultrafiltration with subsequent analysis of the filtrate. Ultrafiltration separation of actinide-associated colloidal materials in natural waters has been performed by passing solutions through flat membrane filters possessing specific nominal pore sizes (Nelson and Lovett, 1978a; Nelson *et al*., 1984), by

tangential-filtration with hollow-fiber cartridge filters (Marley *et al.*, 1991; Kaplan, *et al.*, 1994), and by size-exclusion chromatography (SEC) (Cooper *et al.*, 1995). Porcelli *et al.* (1997) used the tangential-flow hollow-fiber technique to separate U and other elements associated with colloids >10 kDa and >3 kDa in a study of the transport of U isotopes through the Kalix River watershed and Baltic Sea. Kersting *et al.* (1999) characterized Pu-associated colloidal material in groundwater from the Nevada Test Site by sequentially filtering aqueous samples with 1000, 50, and approximately 7 nm pore size filters. Tangential filtration was employed for the 7 nm size filtration. The $^{240}Pu/^{239}Pu$ ratio of the collected particulate material (>1000 nm), two colloidal fractions (1000–50 nm and 50–7 nm), and the ultrafiltrate (<7 nm) was determined by mass spectrometry. The measurements had a reported precision of ±1.5% and a procedural blank of <2 pg Pu. The Pu isotopic signature allowed the identification of the source of the Pu as a specific nuclear event. The authors noted, however, that the high pumping rates employed could potentially generate higher colloidal concentrations due to shear stress. The chemical form of the colloid could not be identified by this method.

30.3 NUCLEAR TECHNIQUES

The radioactive properties intrinsic to all actinides allow their direct detection by using radiometric techniques. In principle, the α-particles, β-particles, and γ-rays emitted by any radionuclide can be used for quantitative analysis (see Chapter 27, section 27.3.1, of this book). An examination of the radioanalytical literature reveals that a variety of mathematical criteria have been used to establish levels at which a radionuclide can be considered to be qualitatively detected or quantitatively determined with a given relative standard deviation (RSD). The minimum concentration level that leads to detection is generally defined as the minimum detection limit (MDL). The minimum concentration level that leads to quantitative determination with satisfactory precision is generally defined as the limit of quantitation (LOQ). Currie (1968) developed working expressions for the MDL as 3.29σ and the LOQ as 10σ where σ is the statistically defined standard deviation for the well-determined blank of the method. The confidence limits are assumed to be 95% for these values. These expressions have been widely adopted by the analytical community.

The natural abundances, half-lives ($t_{1/2}$), specific activities, modes of decay, and thermal-neutron capture cross sections (σ_n) for the naturally occurring actinides, their decay products, and several isotopic tracer nuclides are given in Table 30.1. The half-lives, specific activities, modes of decay, and thermal-neutron capture cross sections, for the environmental transuranic actinides and several of their tracers are given in Table 30.2.

Neutron activation analysis (NAA) techniques are based on the transmutation of nuclei to radionuclei or excited nuclear states by capture of neutrons.

Qualitative and quantitative analysis can be performed by detecting the α-particles, β-particles, γ-rays, delayed neutrons, or fission products that are produced as the excited nuclei relax. The emitted radiation or particles can be measured during irradiation or after a delay. Because all actinides are already radioactive the objective of NAA is to produce radionuclides with higher activities thus, improving the measurement sensitivity relative to alpha, beta, or gamma spectrometry of the unirradiated actinide.

Because quantitative analysis using radiometric and NAA techniques are based on the measurement of disintegration rates of radionuclides, the MDL is related to the specific activity of the determined radionuclide, the number of atoms of the radionuclide, counting time, and detection efficiency. The long half-lives and, therefore, low specific activities of the parents of the three non-extinct natural decay chains as well as several of the environmental transuranic nuclides complicates determination using radiometric techniques. Samples containing low concentrations of an actinide need to be counted for relatively long times on extremely stable spectrometers possessing low backgrounds to obtain precision adequate for detection and accurate determination. Whereas there are many radiometric procedures that are amenable to the determination of actinides at trace concentrations, the procedures that are the most generally applicable and commonly used are high-resolution alpha and gamma spectrometries.

30.3.1 Alpha spectrometry

Alpha spectrometry allows the analyst to identify and quantify individual α-emitting radionuclides based on the detection of emitted α-particles and determination of α-particle energies specific to the radionuclide of interest. Detection of α-particles with specific energies allows isotopic discrimination for most actinides. Nuclear data for naturally occurring actinides, environmental transuranic actinides, as well as nuclides utilized as isotopic tracers in α-spectrometric determinations are given in Table 30.3.

Despite the short range of α-particles through matter, analyses based their detection possess advantages as compared to the detection of β-particles and γ-rays due to the extremely low backgrounds that are achievable. However, accurate and precise α-spectrometric analysis typically requires chemical separation of actinide to eliminate sources of α-particles with energies similar to the analyte, correction for the recovery of the chemically separated actinide with an isotopic spike, and preparation of a thin source. Despite the necessity of these chemical procedures, alpha spectrometry is one of the most frequently utilized techniques for the routine determination of actinides in geological, environmental, and biological samples. The requirement of chemical separations can be used to the analyst's advantage by performing preconcentration from large samples. The instrumentation used in high-resolution alpha spectrometry is not extremely complex or expensive and

Table 30.3 *Nuclear data for naturally occurring actinides, environmental transuranic actinides, as well as nuclides utilized as isotopic tracers in alpha-spectrometric determinations. The principal α-particle energies (E_α) and yields (I_α) are taken from Firestone and Shirley* (1996).

Nuclide	$t_{1/2}$	E_α (keV)	I_α (%)	*Nuclide*	$t_{1/2}$	E_α(keV)	I_α (%)
^{228}Th	18.72 d	5340.31	28.2	^{237}Np	2.144×10^6 y	4771.0	25
		5423.20	71.1			4788.0	47
^{229}Th	1.9116 y	4814.6	9.30	^{236}Pu	2.858 y	5721.00	30.56
		4845.3	56.2			5767.66	69.26
		4901.0	10.20				
^{230}Th	7340 y	4621.2	23.4	^{238}Pu	87.7 y	5456.3	28.98
		4687.7	76.3			5499.03	70.91
^{232}Th	7.538×10^4 y	3954	21.1	^{239}Pu	2.411×10^4 y	5105.5	11.5
		4013	77.9			5144.3	15.1
						5156.59	73.3
^{231}Pa	3.276×10^4 y	4951.3	22.8	^{240}Pu	6563 y	5123.68	27.1
		5013.8	25.4			5168.17	72.8
		5028.4	20.0				
		5058.6	11.0				
^{232}U	68.9 y	5263.41	31.7	^{242}Pu	3.733×10^5 y	4856.2	22.4
		5320.17	68.0			4900.5	77.5
^{233}U	1.592×10^5 y	4783.5	13.2	^{244}Pu	8.08×10^7 y	4546	19.4
		4824.2	84.4			4589	80.6
^{234}U	2.455×10^5 y	4722.4	28.42	^{241}Am	432.2 y	5442.90	12.8
		4774.6	71.38			5485.60	85.2
^{235}U	7.038×10^8 y	4366.1	17	^{242}Cm	162.8 d	6069.42	25.0
		4397.8	55			6112.72	74.0
^{236}U	2.342×10^7 y	4445	25.9	^{243}Cm	29.1 y	5742.1	11.5
		4494	73.8			5785.2	72.9
^{238}U	4.468×10^9 y	4151	20.9	^{244}Cm	18.10 y	5762.70	23.6
		4198	79.0			5804.82	76.4

can be used on a routine basis. Alpha spectra are reasonably simple and allow straightforward quantitative analysis.

(a) Alpha-spectrometry fundamentals

Alpha spectrometry can be performed using ionization chambers, magnetic spectrometers, scintillation detectors, and semiconductor detectors. Because of the combination of high resolution, sensitivity, compactness, and relative ease of use, alpha spectrometry is most frequently performed utilizing spectrometers that incorporate ion-implanted Si semiconductor detectors.

A typical alpha spectrometer with a 450 mm^2 ion-implanted Si detector has an energy resolution $<$20 keV, an efficiency $>$25% for source-to-detector spacing $>$1 cm, an energy range from 3 to 8 MeV, and a background $<1 \times 10^{-4}$ Bq. The detector is part of an integrated spectrometer that includes a vacuum chamber, bias supply for the detector, complete amplification system (preamplifier and amplifier), and calibration pulser. Data acquisition is controlled by a personal computer equipped with a multichannel analyzer for pulse height analysis along with data acquisition and processing software. A schematic diagram of a typical alpha-spectrometry system is illustrated in Fig. 30.2. A more detailed discussion of the theory and operation of alpha spectrometers can be found in Ehman and Vance (1991) and in Ivanovich and Murray (1992).

For accurate determination by high-resolution alpha spectrometry the α-emitting radionuclide must be prepared as a thin, flat, uniform source. To minimize the inelastic scattering of α-particles that degrade peak resolution the ideal source consists of a monolayer of the actinide. Three methods have generally been used for source preparation: evaporation, microprecipitation with a rare-earth fluoride, and electrodeposition (ASTM D3084-95, 1995b). The method most often employed is electrodeposition. In this method actinides are electrochemically deposited quantitatively from an electrolyte solution onto a polished stainless steel or platinum cathode planchet. The deposition is non-selective. Prior chemical separation of the actinides from matrix elements may be required so that the total mass of electrodeposited material is $<$10 $\mu g\ cm^{-2}$. Additionally, chemical separation of the analyte from other

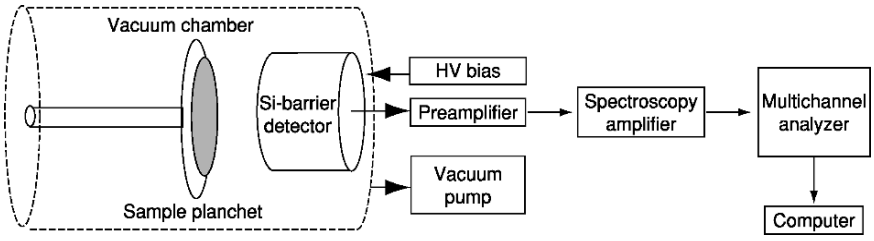

Fig. 30.2 *Schematic diagram of a alpha-spectrometry system.*

actinides that decay with similar α-particle energies is required to minimize spectroscopic interferences. A variety of electrolytes have been used in the preparation of electrodeposited actinide sources: $NaHSO_4$–Na_2SO_4, KOH–KCO_3, NH_4HCOO_2, NH_4Cl–HCl, NH_4Cl–NH_4I, NH_4Cl–$H_2C_2O_4$, $(NH_4)_2SO_4$, $(NH_4)_2SO_4$–H_2SO_4–NH_4OH, isopropanol, and dimethyl sulfoxide (DMSO) (Kressin, 1977 and references therein). The anode is typically Pt wire or gauze. Rotating the anode provides stirring for a more uniform deposit. Electrodeposition is performed at a constant current density (0.5 A cm^{-2}) and low voltage for approximately 2 h. Recent work on optimizing the $(NH_4)_2SO_4$–H_2SO_4–NH_4OH buffer system by Glover *et al.* (1998c) has demonstrated nearly 100% recoveries of Th, U, Pu, and Am in only 1 h. A standard procedure for electrodeposition of actinides from a solution of $(NH_4)_2SO_4$ has been published (ASTM D1284-00, 2000b).

Alpha-spectrometric measurement is performed by placing the actinide-containing planchet in a vacuum chamber at a fixed distance from a detector with a known background and efficiency. The air in the chamber is evacuated and the sample is counted for a time sufficient to attain desired statistical uncertainty. A total of 10000 counts would be required for 1% uncertainty (1σ) due to counting statistics alone (Friedlander *et al.*, 1981). The background is determined by separately counting a chemically prepared experimental blank. The efficiency of the detector for a given geometry is determined by counting a calibrated source at the same geometry that samples are counted. After counting the sample, the alpha spectrum is corrected for background and detector efficiency. Correction for losses incurred during radiochemical procedures are made based on the recovery of the isotopic spike. Spike recovery can be determined as determined from the alpha spectrum or by separate alpha-spectrometric analysis. The number of counts per second (cps) of each nuclide can then be related to the activity of the sample according to the following equation:

$$a = \frac{N}{\varepsilon_d r t_s d_s} \tag{30.1}$$

where a is the activity of the nuclide of interest (Bq), N is the total number of counts in the energy region of interest, ε_d is the detector efficiency, r is the fraction of isotopic tracer recovered, t_s is the analysis live-time (s), and d_s is the sample decay fraction from the time of sample collection to the midpoint of the counting period.

(b) Alpha-spectrometry applications

Because the analyte elements have typically been chemically separated (see Section 30.2.2) and prepared as a thin-layer source on a planchet before alpha-spectrometric analysis, the details of the actual analysis by alpha-spectrometric measurement are essentially independent of the initial source

matrix material. The nature of the source of the actinides (natural and/or anthropogenic) will dictate what spectral interferences may be present in the sample. There are numerous examples in the literature of applications of alpha spectrometry for the determination of trace actinide content in a variety of matrices. The following examples describe some specific details of these applications and give an overview of the breadth of applications.

Alpha spectrometry has historically been one of the most frequently utilized techniques for uranium-series disequilibria measurements particularly for ^{234}U and ^{238}U (Ivanovich and Murray, 1992). Complete isotopic analysis of the naturally occurring isotopes ^{238}U, ^{235}U, and ^{234}U can be performed with ion-implanted Si detectors because of complete resolution of their peaks. Uranium-232, a commonly used recovery spike, can also be completely resolved. ^{236}U has also been used as a recovery spike. However, tailing from the higher energy ^{236}U α-particles can potentially overlap with those of ^{235}U and a correction for this contribution may need to be performed. Samples must be counted soon after chemical separation due to the ingrowth of short-lived daughters whose α-particle energies overlap with U isotopes. To achieve a 1% counting uncertainty U isotope determination using a 7 day count and a 25% efficiency detector would require a sample containing 5.3 μg, 830 ng, and 290 pg of ^{238}U, ^{235}U, and ^{234}U, respectively. Alpha-spectrometric determination of U in geological and environmental samples require, therefore, long counting times and/or preconcentration from large samples to obtain sufficient amounts of U (see Section 30.2.2). For these reasons there has been great impetus for development of mass spectrometric methods for U isotopic analysis.

Maxwell and Fauth (2000) have recently demonstrated that alpha spectrometry possesses the sensitivity and low background sufficient for U isotope bioassay. By utilizing appropriate chemical procedures and a ^{232}U spike, they demonstrated analytical biases of +7.8% and +1.5% for ^{234}U and ^{238}U, respectively. Typical U levels in urine were found to be 0.003–0.03 Bq L^{-1} and 0.002–0.05 Bq L^{-1} for ^{234}U and ^{238}U, respectively. The method demonstrated blanks of 0.1 mBq L^{-1} for ^{234}U and 0.4 mBq L^{-1} for ^{238}U, sufficiently low for routine assay.

The determination of Th isotopes, specifically ^{230}Th and ^{232}Th, is an important component of uranium-series disequilibria measurements (Ivanovich and Murray, 1992). For the determination of ^{230}Th and ^{232}Th, chemical separation of Th from U is required due to the spectral interference between ^{230}Th and ^{234}U (Table 30.3). As with U, complete isotopic analysis of the naturally occurring Th isotopes ^{232}Th, ^{230}Th, and ^{228}Th can be performed because their peaks can be completely resolved using an ion-implanted Si detector. ^{229}Th, a commonly used recovery spike, can also be completely resolved. Alpha-spectrometric determination of Th isotopes can be complicated due to the ingrowth of ^{224}Ra interfering with ^{228}Th determination (Ivanovich and Murray, 1992). This parent–daughter relationship can be exploited for the determination of ^{224}Ra via alpha-spectrometric determination of ^{228}Th (Noyce, 1981). Eikenberg *et al.* (1999b) have recently utilized alpha spectrometry for the determination of Th

isotopic ratios in human diet as well as urine and feces achieving MDLs as low as 0.04 mBq L^{-1} for ^{232}Th, ^{230}Th, and ^{228}Th.

Protactinium-231 is a daughter product of ^{235}U that is used in soil and sediment dating (Ivanovich *et al.*, 1992). ^{231}Pa is typically determined via isotope dilution with ^{233}Pa followed by chemical separation and alpha-spectrometric determination. Chemical recovery is determined via by gamma-spectrometric determination of ^{233}Pa (Lally, 1992). High radiochemical purity is required to minimize spectral interferences from the typically more abundant ^{230}Th and ^{234}U (Table 30.3).

High-resolution alpha spectrometry is one of the most common methods for the determination of the environmental transuranic actinides in environmental and biological samples. When chemically separated as a group, the transuranic actinides can be determined with only a few spectral interferences, most notably: ^{240}Pu–^{239}Pu, ^{238}Pu–^{241}Am, and ^{243}Cm–^{244}Cm. Fig. 30.3 shows an alpha spectrum from a sample containing long-lived actinide and transuranic nuclides produced by the irradiation of UO_2 nuclear fuel.

Neptunium-237 is essentially free of spectral interferences from other transuranic actinides although separation from U and Th isotopes is required due to potential spectral interferences (Table 30.3). Neptunium-237 determination is complicated because it possesses a long half-life and is typically at much lower concentrations in nuclear fuel cycle source materials (Wolf, 1998). The general

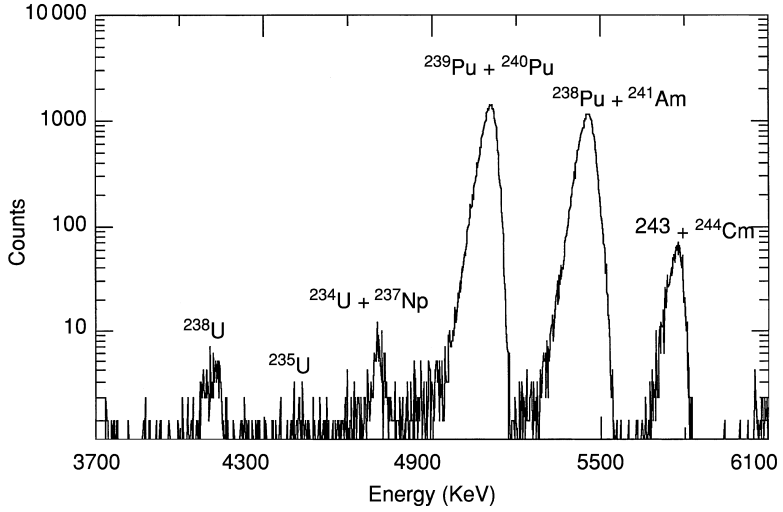

Fig. 30.3 *An alpha spectrum from the author's laboratory of an electrodeposited source containing actinides with E_α between* 3700 and 6100 keV *that are present in irradiated UO_2 nuclear fuel after a cooling period of* 20 years. *The spectrum contains prominent peaks from $^{243}Cm+^{244}Cm$, $^{238}Pu+^{241}Am$, and $^{240}Pu+^{239}Pu$ (listed from high to low energy). Also detectable at lower energies are minor contributions from long-lived nuclide $^{234}U+^{237}Np$, ^{235}U, and ^{238}U.*

reverse relationship between radionuclide half-life and α-particle energy (the Geiger–Nuttall relationship) complicates ^{237}Np determination when higher activities of high-energy α-emitters are present. High-accuracy alpha-spectrometric determination of ^{237}Np can be achieved via isotope dilution with ^{239}Np followed by chemical separation (Horwitz *et al.*, 1995). Chemical recovery is determined via by gamma-spectrometric determination of ^{239}Np. Examples of the routine application of alpha spectrometry to the determination of ^{237}Np in environmental and biological samples are given by Maxwell (1997) and Maxwell and Fauth (2000). Levels as low as 0.017 mBq of ^{237}Np were measured in Irish Sea sediment (Yamamoto *et al.*, 1998). Analogous to natural U and Th isotopes, the low specific activity of ^{237}Np complicates determination via alpha spectrometry and this has led to an effort to develop mass spectrometric methods of determination.

Alpha spectrometry is routinely used for the determination of Pu isotopes in environmental and biological samples. Plutonium-238 is particularly amenable to alpha-spectrometric determination because of its relatively high specific activity (for example, Cooper *et al.*, 2000). Chemical separation of Pu from Am must be performed due to spectral interferences between ^{238}Pu and ^{241}Am (Table 30.3). Thorium-228 will also interfere if present at sufficient concentrations. Unambiguous determination of both ^{240}Pu and ^{239}Pu cannot be performed due to near identical α-particle energies. For this reason it is common to report the combined $^{240+239}$Pu activity. Determination of individual ^{239}Pu and ^{240}Pu activities from an alpha-spectrometric measurement requires an independent mass spectrometric analysis determination of the ^{240}Pu/^{239}Pu atom ratio. Complete resolution of the ^{236}Pu, ^{238}Pu, $^{240+239}$Pu, and ^{242}Pu can be achieved with ion-implanted Si detectors. Plutonium-241 is not determined via alpha spectrometry because it does not decay by α-emission (Table 30.2). Standard methods for the determination of Pu in water (ASTM D3865-97, 1997a) and soil (ASTM C1001-00, 2000a) by alpha spectrometry have been published. These methods utilize either ^{236}Pu or ^{242}Pu as isotopic spikes. The procedure for determination of Pu in water demonstrates biases of less than ±10% whereas the procedure for determination of Pu in soil demonstrates biases of less than ±26% for soil samples containing 0.00188–0.150 Bq Pu g^{-1}.

Americium-241 is similar to ^{238}Pu in that it also possesses a relatively high specific activity compared to many of the environmental transuranic actinides. Frequently, Americium-241 is determined concurrently in a chemically separated aliquot of a sample. Americium-241 must be separated chemically from ^{238}Pu and ^{228}Th to remove spectral interferences. Accurate and precise determination of ^{241}Am via alpha spectrometry is performed using ^{243}Am as an isotopic spike. A routine procedure for ^{241}Am determinations in soil has been published (ASTM C1205-97, 1997b). Alpha spectrometry has been used extensively for the determination of anthropogenic Pu and Am isotopes in the environment including seawater (see for example, Nelson and Lovett, 1978a,1978b; Bowen *et al.*, 1980; Nelson *et al.*, 1984; Plutonium in the Environment, 1995), Antarctic

snow (Holm and Persson, 1978), and plant samples grown in a contaminated lake bed (Whicker *et al.*, 1999). Alpha spectrometry has been used for the determination of Pu and Am isotopes in biological samples such as human tissue (Moody *et al.*, 1998; Qu *et al.*, 1998), and urine (Maxwell and Fauth, 2000). It has also been used to determine concentrations of natural ^{239}Pu in geological samples (Ganz *et al.*, 1991).

The short half-lives of ^{243}Cm and ^{244}Cm essentially preclude their determination by any method other than alpha spectrometry at environmental levels. Spectral deconvolution is required to separate the ^{243}Cm and ^{244}Cm α-peaks due to low concentrations and similar energies (Mitchell *et al.*, 1998). Studies have utilized alpha spectrometry to search for ^{242m}Am via detection of daughter ^{242}Cm as well as ^{243}Cm and ^{244}Cm in lichen samples (Murray *et al.*, 1979).

A recent study of the application of alpha spectrometry to the transuranic actinides by Wolf (1998) achieved 10σ LOQ for ^{237}Np, ^{239}Pu, ^{241}Am, and ^{244}Cm of 40, 0.4, 0.008, and 0.0003 pg, respectively (1 mBq). These analyses were performed using relatively short counting periods (<48 h) under routine conditions with 450 mm^2 ion-implanted Si detectors possessing 25% relative efficiency and backgrounds (1×10^{-4} Bq). Activities over an order of magnitude have been quantified with dedicated low-level detectors and extremely long (>30 days) counting periods (Yamamoto *et al.*, 1998; Eikenberg *et al.*, 1999b; Cooper *et al.*, 2000; Maxwell and Fauth, 2000). The U.S. EPA and ASTM have published standard methods for the determination of actinides in water (U.S. EPA, 1979; ASTM D3084-95, 1995b).

30.3.2 Gamma spectrometry

Gamma spectrometry allows the analyst to identify and quantify individual actinide nuclides based on the detection of emitted γ-rays possessing energies that are specific to nuclear transitions in the actinide of interest. γ-Rays are highly penetrating and their measurement is relatively straightforward because essentially all γ-ray peaks can be individually resolved by high-resolution detectors. X-ray spectrometry is a related technique in which X-rays produced by a daughter atom after decay is detected. These X-rays are element-specific. Lower photon energies, sample self-shielding, lack of isotope specificity, and difficulty in calibrating efficiency curves at low energies complicate X-ray spectrometric determination. For these reasons, gamma spectrometry is a more commonly used than X-ray spectrometry for quantitation of specific actinide nuclides.

Gamma spectrometry requires minimal sample preparation, particularly when compared to the chemical procedures required for the preparation of a source for alpha spectrometric analysis. Gamma spectrometry is non-destructive and multiple radionuclides can be measured simultaneously. In some cases quantitation of actinides by gamma spectrometry can be performed based on the activity of one or more daughter products of the parent actinide. Quantitation based on daughter product activity requires an assumption of

radioactive equilibrium in the sample. However, daughter product analysis is the only route for determining ^{238}U and ^{232}Th by gamma spectrometry at their naturally occurring concentrations. Gamma spectrometry is frequently employed to measure recovery of long-lived actinides by way of spiking with a short-lived, γ-ray-emitting isotope. The sensitivity of the technique is dependent primarily on the half-life of the radionuclide and the percent γ-ray intensity (I_γ). Nuclear data for naturally occurring actinides, environmental transuranic actinides, as well as nuclides utilized as isotopic tracers in gamma-spectrometric determinations are given in Table 30.4.

(a) Gamma-spectrometry fundamentals

Several types of detectors can be used for gamma spectrometry. They can be classified as gas-filled, scintillation, and semiconductor. Gas-filled detectors are essentially a chamber filled with a gas mixture, such as 90% Ar–10% CH_4, that contains a positively biased anode. Depending on the bias voltage of the anode, gas-filled detectors can function as ionization chambers, proportional counters, or Geiger–Müller counters. Ionization chambers are used for high-radiation fluxes and are typically not suitable for trace analysis. Proportional counters are used for X-ray measurements where only moderate resolution is required (>1 keV at 5.9 keV). Geiger–Müller counters do not allow the energy of the γ-ray to be determined. Scintillation detectors function because γ-rays interacting with a scintillator produce a pulse of light that can be detected by a photomultiplier tube. A variety of plastics as well as Tl-activated NaI and CsI crystals are capable of detecting γ-rays with energies >1000 keV and have found applications as γ-ray detectors. The 7.6 × 7.6 cm NaI(T1) detector is the benchmark standard for the calculation of efficiency of γ-ray detectors. These detectors possess absolute efficiencies between 20 and 40% for the energies typical for most actinide γ-rays. Most analytically important actinide γ-rays and X-rays are in the 3–300 keV region. The low cost-to-size ratio of NaI and its ability to be configured into extremely large detector systems has enabled its use as anti-coincidence shields. One such environmental radionuclide detector system is described by Wogman (1970). However, the energy resolution of scintillator detectors (>10 keV at 100 keV) is typically insufficient to allow deconvolution of complex actinide γ-ray spectra.

Because of their superior resolution, most gamma-spectrometry systems currently utilize a high-purity germanium (HPGe) detector biased with a power supply, a preamplifier, spectroscopy amplifier, and pulse height analyzer. Most HPGe detectors are configured as a junction between n- and p-type semiconductor materials and come in a variety of geometries, sizes, and shapes. The selection of a specific detector depends on the types of samples measured. The most common geometry is a coaxial HPGe detector. Typical HPGe detectors used in geochemical and environmental analysis have volumes 100–200 cm^3, possess efficiencies of approximately 30–40% relative to a 7.6 × 7.6 cm NaI

Table 30.4 *Nuclear data for naturally occurring actinides, environmental transuranic actinides, as well as daughter nuclides and isotopic tracers utilized as in γ-spectrometric determinations. The principal γ-ray energies (E_γ) and yields (I_γ) are taken from Firestone and Shirley (1996).*

Nuclide	$t_{1/2}$	E_γ (keV)	I_γ (%)	*Nuclide*	$t_{1/2}$	E_γ (keV)	I_γ (%)
^{212}Pb	10.64 h	238.632	43.3	^{232}Th	1.405×10^{10} y	63.81	0.267
		300.087	3.28			140.88	0.018
^{214}Pb	26.8 m	351.921	35.8	^{234}Th	24.10 d	62.86	0.021
		295.213	18.5			63.29	4.8
		241.981	7.50			92.38	2.81
		53.226	1.11			92.80	2.77
^{214}Bi	19.9 m	609.312	44.8	^{234}U	2.455×10^5 y	53.20	0.123
		1120.287	14.8			120.90	0.0342
		1764.494	15.36				
^{226}Ra	1600 y	186.10	3.50	^{235}U	7.038×10^8 y	143.76	10.96
		262.27	0.0049			185.715	57.2
^{227}Ac	21.773 y	69.21	0.0071	^{238}U	4.468×10^9 y	49.55	0.064
		160.26	0.0063			113.5	0.0102
^{228}Ac	6.15 h	338.322	11.3	^{239}U	23.45 m	74.664	48.1
^{231}Pa	3.276×10^4 y	283.69	1.70	^{237}Np	2.144×10^6 y	29.374	15.0
		300.07	2.46			86.477	12.4
^{233}Pa	26.967 d	312.17	38.6	^{238}Np	2.117 d	984.45	27.8
						1028.54	20.3
^{234m}Pa	1.17 m	1001.03	1.34	^{239}Np	2.3565 d	106.123	27.2
						228.183	10.76
						277.599	14.38
^{227}Th	18.72 d	50.13	8.0	^{239}Pu	2.411×10^4 y	129.296	0.00631
		235.971	12.3			144.201	0.000283
^{228}Th	1.9116 y	84.373	1.266	^{240}Pu	6563 y	104.234	0.00708
						160.308	0.000402
^{230}Th	7.538×10^4 y	67.672	0.377	^{241}Am	432.2 y	59.537	35.9

(Tl) detector, and have resolutions <1 keV at 122 keV. These systems are useful for a wide spectrum of applications and are normally calibrated in the range from approximately 50 to 2000 keV. Larger detectors with relative efficiencies >150% are available but at the expense of slightly lower relative resolutions (<2 keV at 122 keV). These high-efficiency detectors are useful for counting larger-volume, low-activity environmental samples. Another approach to high-efficiency gamma spectrometry is to use a well-type HPGe. Well-type detectors offer the ultimate absolute counting efficiency for small samples. The name 'well type' is given because this type of detector possesses a cavity that can surround a small sample. A typical well only has an available volume of <10 cm^3, which precludes the analysis of very large-volume samples. Finally, thin planar HPGe detectors equipped with a beryllium window offer high resolutions for the measurement of γ-rays and X-rays with energies between 3 and 300 keV. The thin beryllium window minimizes attenuation of these low-energy photons. These thin detectors have the additional benefit of being transparent to higher energy γ-rays and thus possess lower background from Compton scattering of high-energy γ-rays.

HPGe detectors are required to be at liquid-nitrogen temperature when they are under high-voltage bias and are connected to a liquid N_2-containing Dewar via a cryostat. The detector and sample are normally shielded with alternating layers of lead, copper, and a low-Z material such as plastic. This graded shielding system minimizes the X-rays scattered from the lead shielding and shields the detector from external sources. Data acquisition and spectral analysis can be controlled by a personal computer equipped with data acquisition and processing software for quantitative analysis. A schematic diagram of a typical gamma-spectrometry system is illustrated in Fig. 30.4. A more detailed discussion of gamma-spectrometry systems can be found in Friedlander *et al.* (1981) and Ehman and Vance (1991).

Typically, all that is required is that the sample be placed in front of the detector of a calibrated gamma-spectrometry system. The detector needs to be

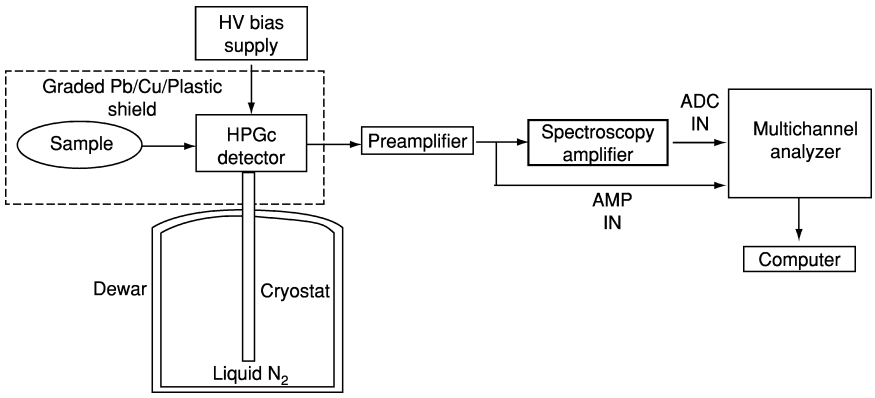

Fig. 30.4 *Schematic diagram of a gamma-spectrometry system* (*after Wolf,* 1999).

calibrated for energy and efficiency at the geometry at which the sample is counted. Additionally, the sample size and matrix of the sample need to be similar to that of the standardization source. This is typically achieved by preparing a mock-up sample that has been spiked with known amounts of radionuclides that emit γ-rays with energies comparable to those of interest.

(b) Gamma-spectrometry applications

Extensive work has been performed to develop gamma-spectrometric analysis methods for the determination of the naturally occurring long-lived actinides ^{238}U, ^{235}U, ^{232}Th, and their progeny for both environmental and geochemical studies. A review of this application of gamma spectrometry to U-series disequilibria has been published (Ivanovich and Murray, 1992).

In the ^{238}U-series nuclides, determination of ^{238}U is usually based on the measurement of short-lived daughter ^{234}Th due to the lack of an intense γ-ray for ^{238}U (Harbottle and Evans, 1997). ^{234}Th is essentially always in equilibrium with ^{238}U in geological and environmental samples such as minerals and soils unless the material has been recently chemically treated or the U has been recently deposited. Determination is typically based on the measurement of the 92.6 or the 63.3 keV γ-ray doublets. Measurement of the 63.3 keV γ-ray generally can be improved by using a planar HPGe with a thin Be window. A gamma spectrum of a UO_2 sample collected on a high-resolution planar HPGe detector is given in Fig. 30.5. Determination of ^{238}U can also be performed by measurement of the 1001 keV γ-ray from the decay of ^{234m}Pa. The low I_γ for this γ-ray precludes its use for samples with U concentrations $<10\ \mu g\ g^{-1}$. A recently published example of the application of gamma spectrometry for the determination of actinides is that of Gu *et al*. (1997). In a study of the deposition of dust in the Chinese loess plateau, activities of ^{238}U, as well as ^{232}Th and several of their daughter products were determined non-destructively using a low background well-type HPGe detector. Uranium-234 can potentially be determined by measuring its 53.23 keV γ-ray; however, this line is weak and spectral interference from ^{214}Pb at 53.2 keV essentially precludes direct determination of ^{234}U via gamma spectrometry. Determination of the ^{238}U daughter ^{230}Th can be accomplished by measuring its 67.8 keV emission. The low I_γ of this transition precludes its measurement in samples with only trace ^{238}U content. Harbottle and Cumming (1994) report a MDL of 4.4 μg for ^{238}U in 3 g environmental samples using a Compton suppression well counter.

In the ^{235}U-series, identification and quantitation can be performed directly on the parent nuclide via measurement of its strong 185.7 keV γ-ray. A correction for interference from the ^{238}U daughter ^{226}Ra is required for samples in secular equilibrium. However, this interference can be corrected by indirectly determining the contribution of ^{226}Ra based on measurement of γ-rays from ^{214}Pb and ^{214}Bi. The α-decay of ^{226}Ra produces ^{222}Rn ($t_{1/2}$ = 3.8235 days), which rapidly establishes equilibrium with both ^{214}Pb and ^{214}Bi. The short

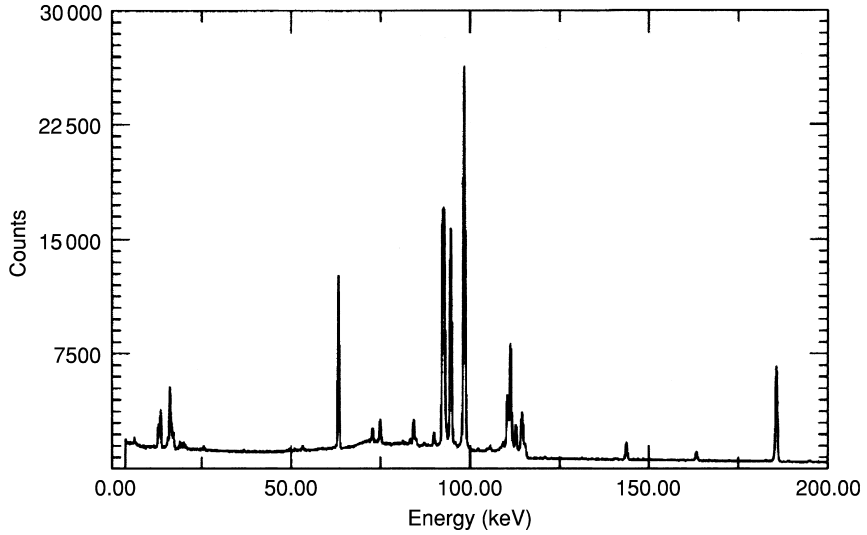

Fig. 30.5 *Gamma spectrum of an isotopically enriched U sample counted for 1 day. The spectrum was collected on a high-resolution planar HPGe detector possessing a thin Be window. The spectrum illustrates prominent peaks from* ^{234}*Th and* ^{235}*U* (*after Wolf,* 1999).

half-lives and abundance of γ-rays emitted by these two progeny make it possible to correct for ^{226}Ra in samples containing total U at concentrations <1 μg g^{-1} when secular equilibrium can be assumed (Harbottle and Evans, 1997). The total mass of U in the sample can be calculated from the determination of ^{235}U if a natural or other known isotopic distribution is assumed. Harbottle and Cumming (1994) report a MDL of 50 ng for ^{235}U in 3 g environmental samples using a Compton suppression well counter.

Direct determination of ^{231}Pa is difficult due to its complex γ-ray spectrum at relevant higher energies (280–300 keV). Indirect determination via the 50.14 keV γ-ray of short-lived daughter ^{227}Th is complicated due to sample shielding at lower energies. The availability of commercially available gamma-spectrometry software to enable the deconvolution of the 235.97 keV ^{227}Th peak from a quartet of peaks due to the presence of ^{212}Pb, ^{224}Ra, and ^{214}Pb (Harbottle and Evans, 1997). ^{233}Pa, an isotopic tracer for ^{231}Pa determinations, can be quantified directly by gamma spectrometry.

In the ^{232}Th-series, ^{232}Th cannot be determined directly via gamma spectrometry due to its long half-life and lack of an intense γ-ray. ^{232}Th can be determined indirectly by measuring one of several γ-rays emitted by short-lived daughters ^{228}Th, ^{228}Ac, or ^{212}Pb provided that equilibrium can be assumed.

In the transuranic actinides ^{237}Np, ^{239}Pu, ^{240}Pu, and ^{241}Am, typically only ^{241}Am is determined via gamma spectrometry. Americium-241 is a daughter of

^{241}Pu, a minor isotope of weapons-grade Pu, and has been used as a convenient qualitative signature for the presence of Pu (Burns *et al.*, 1995; Jerome *et al.*, 1995; Wolf *et al.*, 1997). Americium-241 can be readily be determined directly through measurement of its 59.54 keV γ-ray. Use of ^{241}Am as a signature for Pu, however, requires subsequent laboratory determination of Pu by other techniques to ensure that chemical fractionation of Am and Pu has not occurred in the environment.

Neptunium-237 can be determined directly via measurement of a pair of low-energy γ-rays at 29.4 and 86.5 keV or indirectly via daughter product ^{233}Pa after secular equilibrium has been achieved. The low specific activity of ^{237}Np essentially precludes its determination in environmental samples by gamma spectrometry. Chemical recovery of ^{237}Np can be monitored with the isotope spike ^{239}Np. Neptunium-239 can be determined directly by gamma spectrometry via any of its relatively intense γ-rays.

Plutonium isotopes ^{239}Pu and ^{240}Pu have numerous γ-rays that potentially allow their determination by gamma spectrometry (Gunnick, 1991). Most of these γ-rays have $I_\gamma < 1 \times 10^{-3}$, making their direct determination in environmental samples impossible. Alternatively, Pu can be determined by measuring U L-shell X-ray emissions associated with its decay. This method has been applied to chemically pure Pu standards achieving MDLs of 20 pg (Nitsche *et al.*, 1992). A recent study of the application of gamma spectrometry to the transuranic actinides by Wolf (1998) achieved LOQs for ^{237}Np, ^{239}Pu, and ^{241}Am of 100 ng, 1500 ng, and 5 pg, respectively. These analyses were performed under routine conditions using a 104% relative efficiency HPGe detector. These results correspond to LOQs of 1.0, 3500, and 0.5 Bq and MDLs of 0.3, 1100, and 0.2 Bq for ^{237}Np, ^{239}Pu, and ^{241}Am, respectively.

A standard method for the determination of γ-ray emitters in water has been published (ASTM D3649-91, 1991c). This method reports that with typical gamma spectrometers activities of approximately 40 Bq can be measured under routine conditions and activities of 0.4 Bq can be determined for many nuclides. Application of gamma spectrometry to most naturally occurring actinides and the environmentally important transuranic actinides, however, are limited by typical long half-lives and/or low intensities for emitted γ-rays. The limitations of radiometric determination via gamma spectrometry are particularly apparent when sensitivity is considered on a mass basis.

30.3.3 Neutron activation analysis

(a) NAA fundamentals

Analysis of trace actinide content by NAA has been performed on the naturally occurring actinides as well as on transuranic actinides (see Chapter 27, section 27.3.5, of this book). The most frequently used method of NAA is activation with thermal neutrons. Typically, NAA is performed using neutrons produced in a nuclear reactor or by an isotopic source such as ^{252}Cf and subsequently

thermalized (most probable energy of 0.025 eV). Samples and flux monitor standards are typically irradiated simultaneously and analyzed for high-precision quantitative analysis. After the irradiation, measurement of the α-particles, β-particles, γ-rays, delayed neutrons, or fission products are performed using an appropriate spectrometer. If no chemical treatment is performed after irradiation, the technique is called instrumental neutron activation analysis (INAA). If chemical separations are performed after irradiation, the technique is called radiochemical neutron activation analysis (RNAA). If chemical methods are used to preconcentrate the element of interest before activation the technique is called preconcentration neutron activation analysis (PCNAA). NAA employing epithermal neutrons, i.e. neutrons with energies of 0.1–1 eV, is called epithermal neutron activation analysis (ENAA). Finally, if the concentration of the nuclide is determined by using an isolated solid detector to quantify the number of tracks produced by neutron-induced fission, the method is known as fission track analysis (FTA).

The basic equation that governs all NAA methods is:

$$R = \frac{m}{M} N\phi\, \sigma_n \varepsilon (1 - \mathrm{e}^{-\lambda t}) \tag{30.2}$$

where R (Bq) is the count rate of a sample containing a mass m (g) of a given nuclide with molecular weight M (g mol^{-1}) at the end of irradiation, and N is Avogadro's constant. The thermal-neutron flux density (ϕ) is the number of thermal neutrons incident on a unit area of sample per unit time (n cm^{-2} s^{-1}). The thermal-neutron capture cross section (σ_n) is a measure of the probability that the nuclide of interest will capture a neutron and be activated and has unit surface area (cm^2). The term ε is the efficiency of the detector measuring the count rate (absolute number of decays per number of decays counted) for the decaying radionuclide. The final set of terms in parentheses corrects the activity for the duration of irradiation t (s) and the decay constant λ (s^{-1}) of the specific nuclide. This equation is valid for samples thin enough that attenuation of the neutron flux can be ignored. Examination of equation (30.2) shows that the absolute sensitivity of NAA is dependent on the flux ϕ, the cross section σ_n for the nuclear reaction, the decay constant λ of the nuclide of interest, and the irradiation duration t. An overview of the fundamentals of NAA can be found in texts such as Friedlander *et al.* (1981) and Ehman and Vance (1991).

(b) INAA applications

Non-destructive INAA determination of U in geological and environmental materials can be performed in several ways (Parry, 1991). One approach is NAA with subsequent detection of delayed neutrons. This method possesses a high specificity for U and has been used for many years in the exploration of U ores. The method is based on the measurement of delayed neutrons following a short irradiation with thermal neutrons. Uranium-235 undergoes thermal-neutron-induced fission. The resulting neutron-rich fission products undergo β^- decay.

While most of the fissiogenic daughter nuclei are in excited states and relax via γ-ray emission, some daughter nuclei possess sufficient energy for relaxation to occur via delayed-neutron emission. The delayed neutrons are emitted instantaneously after β^--decay with the half-life of the β^--decaying parent. The neutrons are detected with polyethylene-moderated BF_3 proportional counter systems. The BF_3 detector is extremely sensitive to neutrons and insensitive to the γ-rays and β^--particles emitted by other activated elements in the sample. The technique, therefore, is highly selective with respect to ^{235}U. If the sample is irradiated with a neutron flux possessing an appreciable fast-neutron component, there will be a contribution from fast-neutron fissions of ^{238}U. This condition is not problematic because this nuclide is still U. If the sample contains significant amount of ^{232}Th, a correction for fast-neutron fissions is required for accurate U determination. The dominant ^{235}U fission products that decay via delayed-neutron emission are ^{89}Br ($t_{1/2} = 4.4$ s), ^{87}Br ($t_{1/2} = 55.6$ s), ^{94}Rb ($t_{1/2} = 2.8$ s), ^{137}I ($t_{1/2} = 24.5$ s), and ^{135}Sb ($t_{1/2} = 1.7$ s). For example, the decay scheme for ^{87}Br is

$$^{87}_{35}\mathrm{Br} \xrightarrow{55.60\ \mathrm{s}} {}^{87}_{36}\mathrm{Kr} + {}^{0}_{-1}\beta^- + \bar{\nu} \xrightarrow{76.3\ \mathrm{min}} {}^{86}_{36}\mathrm{Kr} + {}^{1}_{0}n + {}^{0}_{-1}\beta^- + \bar{\nu}$$

NAA with delayed-neutron detection can be automated for online and unattended determination of U content in solid and liquid samples. A system described by Rosenberg *et al.* (1977) determines the U content in 10 g samples that have been packed in polyethylene containers and irradiated for 60 s in a flux of 10^{16} *n* cm^{-2} s^{-1}. Samples are counted for 60 s after a 20 s decay. Even though natural U is only 0.720% ^{235}U, and less than 1% of the neutrons released in the fission are from delayed-neutron emitters, the thermal cross section of ^{235}U is so large that the technique possesses sufficient sensitivity for routine analysis of U-containing materials with a reported MDL of 0.6 μg g^{-1}. This method can also be coupled with gamma spectrometry for the determination of additional elements in the sample.

A second and more common pathway for INAA of U is use of the (n,γ) reaction. For ^{238}U this method consists of determining the intensity of the 105 keV γ-ray from the decay of ^{239}Np. ^{239}Np is produced from the decay of ^{239}U that results from thermal-neutron capture by ^{238}U according to the following reaction:

$$^{238}_{92}\mathrm{U} + {}^{1}_{0}\mathrm{n} \longrightarrow {}^{239}_{92}\mathrm{U} \xrightarrow{23.5\mathrm{min}} {}^{239}_{93}\mathrm{Np} + {}^{0}_{-1}\beta^- + \bar{\nu} \xrightarrow{2.33\ \mathrm{days}} {}^{239}_{93}\mathrm{Pu} + {}^{0}_{-1}\beta^- + \bar{\nu}$$

The amount of ^{239}U and ^{239}Np produced is directly related to, and therefore a measure of, the amount of ^{235}U present in the original sample. At high concentrations U can be determined by measurement of the 74 keV γ-ray from the decay of ^{239}U immediately after sample irradiation. MDLs are enhanced with the use of a detector sensitive to low-energy photons such as a planar HPGe with a thin Be window. Both of these methodologies are enhanced with a higher ratio of epithermal neutrons. INAA of ^{232}Th is based on gamma-spectrometric

determination of ^{233}Pa produced by the following reaction:

$$^{232}_{90}\mathrm{Th} + ^{1}_{0}\mathrm{n} \longrightarrow ^{233}_{90}\mathrm{Th} \xrightarrow{22.3\mathrm{min}} ^{233}_{91}\mathrm{Pa} + ^{0}_{-1}\beta^{-} + \bar{\nu} \xrightarrow{27.0\ \mathrm{days}} ^{233}_{92}\mathrm{U} + ^{0}_{-1}\beta^{-} + \bar{\nu}$$

INAA determination of trace U and Th is that the analysis can be performed simultaneously with a suite of other elements. Routine applications of INAA for the determination of trace elements including U and Th in the recent literature include the analysis of oceanic basalts (Joron *et al*., 1997) and precious and common opals (McOrist and Smallwood, 1997). Joron *et al*. (1997) reported detection limits of 6.9 and 1.7 ng g^{-1} for U and Th, respectively. Samples weighing 150 mg were irradiated for 8–15 h at a flux of 1.1×10^{13} *n* cm^{-2} s^{-1} followed by a 1-week sample cooling and 3000 s count time for U determination. Samples were counted second time for 40000 s after a 30-day cooling period for the Th determination.

The high sensitivity of INAA makes this technique ideal for the analysis of minute amounts of material such as individual phases, minerals, and crystals separated from bulk material. Schrauder *et al*. (1966) used INAA to determine U and Th along with a suite of trace elements in 13 micro-inclusion-bearing fibrous diamonds from Botswana to constrain the composition of fluids in the mantle (Schrauder *et al*., 1996). Raimbault *et al*. (1997) developed a technique to extract single crystals and perform multielemental analysis, including U and Th, with INAA. The INAA technique required only a few micrograms of mineral and facilitated the measurement of more than 30 elements in multiple samples from the Oklo U deposit in Gabon. This work utilized the presence of epithermal neutrons in the reactor flux producing (n,p) reaction products, extending the number of elements determined. This methodology was able to detect low μg g^{-1} concentrations of U and Th in single-crystal samples in a variety of minerals.

A non-destructive method for the determination of ^{239}Pu by INAA in contaminated soils has been developed by Fuller *et al*. (1965). This method utilized the fission product ^{140}La to quantify ^{239}Pu. Because ^{140}La is produced by the fission of both ^{239}Pu and ^{235}U, the ^{235}U contribution needs to be subtracted from the total activity. This was accomplished by first directly determining the ^{235}U content of the unirradiated soil via gamma spectrometry. Soil samples were irradiated with thermal neutrons for 60 s and counted twice after decay periods of 3–4 and 10–14 days. The ^{238}U content was determined after the first cooling period via the ^{239}Np 74 keV γ-ray. Lanthanum-140 was determined after the second cooling period by measuring its 1.6 MeV γ-ray. The MDL for ^{239}Pu in soil sample was reported to be 5 ng.

(c) RNAA applications

With respect to NAA techniques, RNAA offers lower MDLs for actinides than INAA due to virtual elimination of activated matrix elements. RNAA has traditionally been used for trace U and Th determinations in a variety of

matrices (Parry, 1991) from the first lunar samples (Wänke *et al.*, 1970) to biological materials (Picer and Strohal, 1968). Typically, the irradiated sample is decomposed and equilibrated with a milligram amount of the element of interest known as the carrier. The carrier element, along with the radionuclide produced during sample irradiation, is then chemically separated and purified. The amount of radionuclide recovered from the chemical separation is determined gravimetrically from the amount of carrier element recovered. For RNAA determination of U, the quantitation is based on the radiochemical analysis of one or more fission products arising from the thermal-neutron-induced fission of ^{235}U. RNAA determination of ^{232}Th is complicated due to lack of a stable isotopic carrier for the determination of the recovery yield. In this case, ^{231}Pa can be used as a recovery tracer for the activation product ^{233}Pa (Glover *et al.*, 1998a and references therein). The purified elemental sample can then be radiometrically assayed by gamma spectrometry. RNAA is a destructive technique that is more time-consuming and requires greater analytical and chemical laboratory skills than does INAA. The chemical separation of the element of interest, however, results in a sample possessing a gamma spectrum with virtually no background from other γ-ray-emitting species. Procedures for the determination of trace U in geological materials via the ^{235}U(n,f)^{132}Te reaction are given in Anders *et al.* (1988). Using a thermal-neutron flux of 1×10^{14} *n* cm^{-2} s^{-1}, this methodology can achieve MDLs as low as 10 pg g^{-1} for U. Filby (1975) used the ^{235}U(n,f)^{135}I reaction to determine U in human lung samples, coal dust, coal filters, rat lung tissue, animal diets, and minerals. The reported MDLs for U in these matrices were as low as 5 ng g^{-1} depending on the sample matrix and final radiochemical purity.

A comparison of INAA and RNAA analyses for ^{232}Th show that up to two orders of magnitude improvement in MDLs can be achieved when RNAA is employed. RNAA has been used for the analysis of ^{232}Th in human tissue samples with a MDL of 10 pg (Picer and Strohal, 1968).

Recently, a procedure for PCNAA of ^{232}Th in human tissues has been developed (Glover *et al.*, 1998a). The method used ^{227}Th to determine the yield of the preconcentration process. Removal of the matrix elements before irradiation greatly lowers the dose to the radiochemist processing the sample. This method resulted in a MDL of 10^{-4} Bq per sample ($\sim$20 ng ^{232}Th), an order of magnitude lower than the MDL for direct alpha-spectrometric determination. PCNAA has the advantage in that very large samples can be processed. Th isotopic composition (^{228}Th, ^{230}Th, and ^{232}Th) can be determined when this PCNAA procedure is combined with alpha spectrometry (Glover *et al.*, 1998b). Thorium isotopes ^{228}Th and ^{230}Th can be determined before irradiation by electroplating the separated Th onto a V planchet and counting it on a alpha spectrometer. The electroplated sample can then be irradiated for ^{232}Th determination. This method has been used to measure the Th isotopic composition of human tissues with MDLs of 1×10^{-8}, 4×10^{-4}, and 1 ng for ^{228}Th, ^{230}Th, and

^{232}Th, respectively. A PCNAA method has been adapted for the determination of ^{237}Np via the ^{237}Np(n,γ) ^{238}Np reaction (Byrne, 1986). This method was used to determine ^{237}Np in contaminated sediments from the Esk estuary and the foreshore at Grange-over-Sands, Cumbria. The sediment samples were ashed and the Np separated by ketone extraction. Recovery of the ^{237}Np was monitored with a ^{239}Np isotopic spike. The reported MDL for ^{237}Np was 4 pg g^{-1} for a 5 g sample. This MDL could be improved to $<$0.4 pg g^{-1} if higher neutron fluences were used.

(d) FTA applications

If a sample is irradiated in close proximity to a glassy or plastic material, the heavy nuclides generated from thermal-neutron-induced fission will produce submicroscopic tracks in the material. The measurement of these tracks after etching is the basis for FTA and was first reported in 1958 by Young (1958). Moorthy *et al*. (1988) describe the application of FTA to the analysis of ^{239}Pu in urine. Because ^{235}U will also undergo thermal-neutron-induced fission the Pu is first isolated by anion-exchange chromatography. An aliquot of the separated sample was transferred to a fused silica slide. Samples and standards were irradiated for 10 min for a neutron fluence of 10^{17} *n* cm^{-2}. After cooling for 2 days the slide is washed and etched with HF. Fission track density is determined under a bright-field microscope. The reported LOQ was 5 fg ^{239}Pu per sample. Recently FTA has been used for the measurement of U in pore water (Barnes and Cochran, 1990). The FTA method can be performed with small samples but generally only gives precisions of 6–15%. Love *et al*. (1998) recently have described a novel approach to determine ^{240}Pu/^{239}Pu ratios in human tissue samples by combining alpha spectrometry and FTA.

30.4 ATOMIC SPECTROMETRIC TECHNIQUES

Atomic spectrometric techniques are based on the absorption and emission of electromagnetic radiation from atoms or ions. Information specific to the electronic structure of individual elements is manifested in the ultraviolet and X-ray regions (see Chapter 27, section 27.3.2, of this book) of the electromagnetic spectrum. Each element possesses a unique electronic structure and, therefore, unique atomic spectra. The absorption and emission of electromagnetic radiation of a wavelength specific to an electronic transition of a particular element can serve as the basis for analysis and determination of that element. The actinides are amenable to analysis and determination via several atomic absorption/emission-based techniques including atomic absorption spectrometry (AAS), atomic emission spectrometry (AES), flame emission spectrometry (FES), and inductively coupled plasma atomic emission spectrometry (ICPAES). The

application of these techniques for U determination has recently been reviewed (Wolf, 1999). The application of these techniques to trace analysis of actinides has been limited due to the complexity of actinide ultraviolet absorption/emission spectra, lack of sensitivity, and lack of isotopic specificity. Atomic spectrometric methods based on fluorescence or phosphorescence generally possess lower MDLs. The actinides U, Am, and Cm are relatively unique among most elements in that they can be determined directly via fluorometry without the addition of a fluorescent chelating agent. Even lower MDLs can be achieved by utilizing the ability of uranyl ions to phosphoresce when excited to a triplet state. Because of this, the techniques of fluorometry, and phosphorimetry, have been employed for trace U determination.

30.4.1 Fluorometry

(a) Fluorometry fundamentals

In the fluorometric determination of U, an aliquot of a decomposed solid sample or digested aqueous liquid sample is pipetted onto a Pt disk containing a NaF–LiF flux and is evaporated and fused in a furnace. The fused disk is then exposed to an ultraviolet source such as a mercury-arc lamp in combination with a filter or monochromator at 365 nm. Laser excitation with time-resolved detection can increase the sensitivity of the technique by two orders of magnitude. The intensity of the fluorescence is measured at 560 nm. The presence of ionic species of Cd, Cl, Cr, Co, Cu, Fe, Mg, Mn, Ni, Pb, Pt, Si, Th, and Zn quench U fluorescence and lower the sensitivity of the technique. Nb and Ta are reported to enhance U fluorescence. In samples containing significant quantities of these elements, analyses can be performed after chemical separation of the U or dilution of the sample if sufficient concentrations of U are present. The fluorometric method is a single-element method dedicated to the determination of U.

(b) Fluorometry applications

Fluorometry has also been applied to the determination of U in geological, environmental, and biological materials. The ASTM has published a standard test method for determining traces of U in water by fluorometry (ASTM D2907-91, 1991b). This method can determine U concentrations as low as 5 ng mL^{-1}. A procedure has recently been developed for the determination of trace U rocks, minerals, and soils by laser fluorometry after low-temperature dissolution with a HF–HNO_3 mixture for economical high-throughput analyses (Ramdoss *et al.*, 1997). Time-resolved laser fluorometry can attain MLDs as low as 50 pg mL^{-1} (Ghods-Esphahani *et al.*, 1990 and references therein).

30.4.2 Phosphorimetry

(a) Phosphorimetry fundamentals

The uranyl ion can be directly determined phosphorimetrically in a H_3PO_4 or H_2SO_4 solution. The acid is added to protect the uranyl ion from various intermolecular mechanisms that quench luminescence. The sample is excited at 254 nm, and the intensity of the yellow-green emission can be measured in a fluorimeter and related to concentration. Use of a pulse-laser excitation source can increase the sensitivity of this method greatly. In the pulsed-laser phosphorimetric method, an aliquot of sample is pipetted into a glass vial, mixed with HNO_3 and H_2O_2, and taken to dryness. The residue is dissolved in HNO_3 and a complexant such as H_3PO_4. The phosphorimetric method is a single-element method dedicated to the determination of U. The technique determines total U concentration independent of the specific isotopic composition of U.

(b) Phosphorimetry applications

The ASTM has published a standard test method for determining trace U in water by pulsed-laser phosphorimetry (ASTM D5174-91, 1991d). This technique can be used to determine U concentrations as low as 50 pg mL^{-1}.

30.5 MASS SPECTROMETRIC TECHNIQUES

In contrast to radiometric techniques, quantitative analysis by mass spectrometry is based only on counting the number of atoms of the nuclide of interest as opposed to counting randomly occurring radioactive decay events (see Chapter 27, section 27.3.3, of this book). The precision of the measurement is, therefore, independent of the specific activity of the radionuclide. The long half-lives and low specific activities of the parents of the three non-extinct natural decay chains and several of the environmental transuranic nuclides (^{231}Pa, ^{237}Np, ^{239}Pu, ^{240}Pu) make them ideal candidates for determination by mass spectrometry. Mass spectrometric techniques are based on the separation of gas-phase analyte ions (either molecular or atomic) on the basis of their mass-to-charge ratio (m/z) so that they can be separately detected. The technique can, therefore, provide isotopic information of the element of interest. The first mass spectroscopic measurement of a U compound was demonstrated by F. W. Aston in 1931 (Aston, 1931). The first accurate mass spectrometric measurement of the isotopic composition of U was performed by A. O. Nier in 1939 (Nier, 1939). Technological advancements have since resulted in highly automated, commercially available inorganic mass spectrometers that, in many laboratories, have

replaced radiometric and other nuclear-based techniques for the trace analysis of actinides.

Mass spectrometric measurements require the atomization and ionization of the analyte from a solid sample or solution in the ion source. Ions are electrostatically extracted from the source and focused with a system of electrostatic ion lenses into the mass analyzer. The mass analyzer disperses the ions in space or time based on m/z. Several types of mass analyzers have been utilized for inorganic mass spectrometry including single focusing static magnetic sectors, double focusing tandem magnetic/electrostatic sectors, dynamic time-of-flight (TOF) mass analyzers, and quadrupole mass analyzers (Becker and Dietze, 1998). A limitation to the magnetic-sector mass analyzer is that it does not focus on the basis of velocity for an ion with a given mass. Velocity focusing can be achieved with the addition of an electrostatic sector to form a double focusing tandem magnetic/electrostatic sector mass analyzer. The dynamic TOF mass analyzer functions by accelerating all ions to the same kinetic energy and allowing ions with different masses to disperse along a flight tube. Quadrupole mass analyzers function as a high-pass, low-pass mass filter. This is achieved by placing a direct current (dc) voltage and a radiofrequency (rf) voltage on two pairs of parallel rods. For a given set of dc and rf voltages, only ions with a specific m/z possess a stable path through the filter. A m/z scan can be performed by varying the dc and rf voltages. After dispersion by the mass analyzer ions are detected. High precision can be achieved on systems that disperse the ions in space by configuring multiple detectors to simultaneously detect ions with different m/z (multicollector systems). The detector and mass analyzer are both pumped to a very low pressure so that collisions with gas molecules are minimized. More details of the various configurations of sources, mass analyzers, and detectors can be found in Platzner *et al*. (1997).

Mass spectrometric techniques are defined primarily by the ion source. Mass spectrometers utilized for inorganic trace analysis include the spark source mass spectrometer (SSMS), the glow discharge mass spectrometer (GDMS), the laser ablation mass spectrometer (LAMS), the resonance ionization mass spectrometer (RIMS), the accelerator mass spectrometer (AMS), the secondary ion mass spectrometer (SIMS), the thermal ionization mass spectrometer (TIMS), and the inductively coupled plasma mass spectrometer (ICPMS). Mass spectrometric determination of trace actinides requires the spectrometer to produce actinide ions with high efficiency, and the capability of selectively separating the nuclide of interest from interfering isobars, molecules, and backgrounds caused by higher abundance isotopes. The most commonly used mass spectrometric techniques for trace actinide analysis are TIMS and ICPMS. AMS, and RIMS, although less routine than TIMS and ICPMS, have the potential for ultrahigh-sensitivity determination of actinides. Fundamentals and application of TIMS, AMS, RIMS, and ICPMS for trace actinide determinations are discussed below.

30.5.1 Thermal ionization mass spectrometry

Thermal ionization sources produce an extremely stable, relatively intense supply of ions with a minimal energy spread, and minimal molecular and atomic interferences. When coupled with an appropriate mass analyzer and multicollector detector system, the resulting TIMS instrument is capable of measuring elemental isotopic ratios with precisions $<0.01\%$ while requiring only nanograms of material (Becker and Dietze, 1998). However, the high first ionization potential for the actinides complicates their determination by TIMS due to the lower efficiency of the thermal ionization process. Despite this, methods have been developed so that as little as 40 fg of an actinide can be determined (Chen and Wasserburg, 1981). The main disadvantage of TIMS is that extensive sample preparation is required. Whereas the thermal ionization source is moderately selective with respect to some interfering atomic and organic molecular species, chemical procedures are required to separate individual actinides to minimize the presence of interfering isobars. Additionally, TIMS is typically used to determine only one element per prepared sample. Despite these disadvantages, TIMS has been used nearly exclusively in geochronological studies where high-precision isotope ratio determinations are required (Chen *et al.*, 1992). In some cases TIMS has been replacing alpha spectrometry in environmental studies where extremely low concentrations of long-lived transuranic actinides are being determined (Cooper *et al.*, 2000). TIMS analysis of actinides is also applicable for the purpose of bioassay (Maxwell, 1997).

(a) TIMS fundamentals

TIMS instruments that are used for actinide analysis consist of the following principal components: a thermal ionization source that produces positively charged actinide ions; ion extraction and focusing optics and source slit; mass analyzer; collector slit and detection system (Platzner *et al.*, 1997). These components and their arrangement are illustrated in Fig. 30.6.

Trace analysis of an element by TIMS first requires sample dissolution and chemical separation of the analyte element from sample matrix components as well as potentially interfering isobars (see Section 30.2.2). A small aliquot of solution containing the chemically separated actinide (typically <1 μg of actinide) is deposited onto a filament composed of a clean, degassed refractory metal such as Re or W that possesses a high-electron work function. The most frequently used method utilizes two filaments arranged opposite to each other. Single, double, and triple filament designs have been utilized. In a double filament configuration, one filament is used for evaporative heating of the atoms and the second for ionization. Arden and Gale (1974) and Chen and Wasserburg (1981) have developed a method using graphite to enhance U^+ emission by loading an aqueous colloidal suspension of graphite onto a Re filament. The solution is evaporated, producing a thin graphite film. The

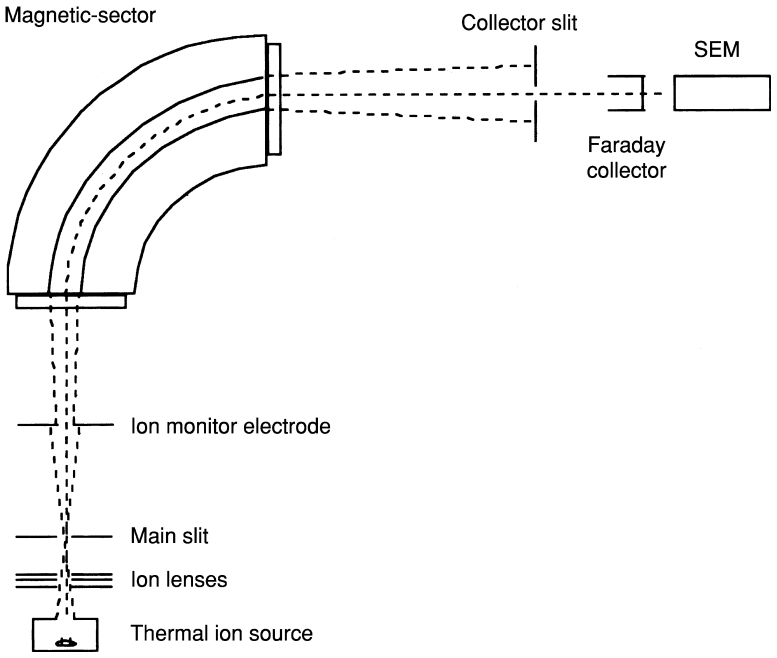

Fig. 30.6 *Schematic representation of a* 90° *single-collector TIMS* (*after Platzner* et al., 1997).

separated U sample is loaded onto the filament, evaporated, and a second graphite film is applied. The geometry of the filament was either V-shaped or dimpled. The ionization efficiencies with this method were determined to be 0.6–1.2% for standards and the source produced very stable ion beams. This method has also been utilized for the preparation of a ^{231}Pa source yielding efficiencies of 0.7% (Pickett *et al.*, 1994). A second method of source preparation directly uses an anion-exchange resin bead onto which U, Th, or Pu has been adsorbed (Walker *et al.*, 1974). This resin bead source has also been used for the determination of Am and Cm by TIMS (Poupard and Jouniaux, 1990). Perrin *et al.* (1985) developed a surface ionization-diffusion-type ionization (SID) source for the analysis of Pu, which uses a Re filament onto which Pu has been electroplated followed by an overplating with Pt.

Ions produced in the source are accelerated to approximately 10 kV, focused with a series of ion lenses, and pass through a source slit to enter the mass analyzer. The most common method of mass analysis for TIMS measurements of actinides is the single-focusing static magnetic sector (Chen *et al.*, 1992). The magnetic-sector mass analyzer disperses ions by m/z according to the following equation:

$$\frac{m}{z} = \frac{H^2 r^2}{2V} \tag{30.3}$$

where m is the ion mass, z is the ion charge, V is the potential to which the ion has been accelerated, H is the strength of the magnetic field, and r is the radius of the circular path followed by the ion. A magnet with a radius of 30 cm requires a field strength of 0.7 T to achieve beam separation of 0.255 cm for m/z 236 and 235 (Platzner *et al*., 1997). Double focusing tandem magnetic/electrostatic sector instruments (Palacz *et al*., 1992) as well as three-stage instruments (Lagergren and Stoffels, 1970) have also been utilized for actinide determination. In a single detector system, after dispersion by the magnetic sector, the ion beam is scanned across the collector slit so that only one isotope reaches the detector at any one time. Because of the low ion currents generated during trace analysis a detector that enhances the signal at each m/z such as a secondary electron multiplier (SEM) or Daly detector is used. Larger currents from major isotopes are measured with Faraday ion collectors. On a typical modern system, instrument control, data acquisition and analysis are computer-controlled.

Quantitative trace analysis by TIMS is typically performed via isotope dilution (ID). Accurate results require corrections for time-dependent and time-independent biases in the ion source, mass analyzer, and detector system. The rate of evaporation of isotopes of an element from any thermal ionization source is mass dependent so bias corrections are required. These mass fractionation discrimination effects limit the accuracy of determination. Correction for biases can be made in part by the use of internal isotopic standards and performing analysis of well-determined standards.

(b) TIMS applications

The analysis of trace concentrations of actinides by TIMS has been demonstrated for essentially all of the long-lived actinides including ^{234}U, ^{235}U, ^{238}U, ^{230}Th, ^{232}Th, ^{231}Pa, ^{237}Np, ^{239}Pu, ^{239}Pu, ^{240}Pu, ^{241}Pu, and ^{241}Am and has been utilized for measurements of geological, environmental, and biological samples. TIMS is currently one of the most frequently utilized techniques for U-series disequilibria measurements. Procedures and applications of TIMS to U measurements are summarized in Chen *et al*. (1992) and references therein. Chen and Wasserburg (1981) utilized their graphite-coated filament in a methodology for the determination of ^{238}U abundances, ^{238}U/^{235}U ratios, and ^{234}U/^{238}U ratios in small cosmochemical samples. The method utilized a ^{233}U–^{236}U double spike to correct for instrumental fractionation, high-yield, low-background chemical separation procedures, and filament-loading techniques. This methodology could determine ^{234}U/^{238}U ratios with a precision of 0.5% (2σ) for a sample size of 5×10^9 ^{234}U atoms and accurate U concentration measurements could be made with as little as 20 fg of U. This method has also been adapted for the determination of Th isotopes (Cheng *et al*., 2000). The high-precision and

sensitivity of TIMS has been used to redetermine the half-lives of ^{234}U and ^{230}Th by precisely determining $^{234}U/^{238}U$ and $^{230}Th/^{238}U$ ratios in many geological materials that have behaved as closed systems $>10^6$ years (Bourdon *et al*., 1999).

Naturally occurring ^{231}Pa, a nuclide that has traditionally been determined radiometrically, has recently been determined in geological and seawater samples by TIMS. Pickett *et al*. (1994) determined ^{231}Pa in geological samples by ID–TIMS. ^{233}Pa was separated from a ^{237}Np source and was utilized as the isotopic spike. The authors estimated that as little as 30 fg of ^{231}Pa under routine analysis conditions and achieved an external reproducibility better than $\pm 1\%$. The preferred sample size was stated to be >100 fg ^{231}Pa. A similar method has been developed by Bourdon *et al*. (1999) that utilizes a ^{233}Pa spike produced *in situ* from neutron activation of ^{232}Th. The application of TIMS to ^{231}Pa, ^{230}Th, and ^{232}Th determination in seawater yielded decreased sample size (100–1000-fold), increased precision (5–10% vs. 20–40%), and decreased measurement time (hours vs. weeks) when compared to traditional alpha-spectrometric determination (Edmonds *et al*., 1998).

A typical TIMS system and method used for the determination of transuranic actinides has been described by Perrin *et al*. (1985). The method utilized a modified instrument developed at the National Bureau of Standards (NBS, currently National Institute of Standards and Technology, NIST). This spectrometer is a 30.5 cm radius 90° deflection magnetic-sector mass analyzer equipped with a 17-stage electron multiplier. The dark current of the detector system is 0.05 cps. Application to Pu isotopic determination demonstrated the capability of measuring the $^{240}Pu/^{239}Pu$ atom ratio in samples of 0.5–2 ng with 0.07% precision and accuracy at the 95% confidence level. Chemical separation of Pu from U and Am is required to minimize isobaric interferences from ^{238}U and ^{241}Am on ^{238}Pu and ^{241}Pu, respectively. Plutonium-242 (Cooper *et al*., 2000) is typically used as an isotope spike in the ID–TIMS determination of Pu. Plutonium-244 has also been used as an isotope spike in an investigation of sources of transuranic elements in artic marine sediments where ^{242}Pu was one of the target analytes (Curtis *et al*., 1999). When combined with the appropriate analytical separations and clean room techniques the TIMS methodology has a ^{239}Pu blank of (17 ± 0.15) pg and MDL of 440 fg (Cooper *et al*., 2000). This method has been used to determine concentrations of naturally occurring ^{239}Pu in U ores (Attrep *et al*., 1992; Dixon *et al*., 1997) as well as measure colloidal transport of Pu in groundwater that originated from the testing of nuclear weapons at the Nevada Test Site (Kersting *et al*., 1999). The groundwater measurements had a reported precision of $\pm 1.5\%$ and a procedural blank of <2 pg Pu. These figures of merit allowed the identification of the source of the Pu as a specific nuclear event. A related ID–TIMS procedure for ^{237}Np in soil and in human tissue samples has been developed (Efurd *et al*., 1986). This ID–TIMS method used ^{236}Np was used as an isotope spike and is optimized for samples containing 100 pg ^{237}Np. Although ^{237}Np does not possess any isobaric interferences, chemical separation must be performed to

minimize the amount of ^{238}U in the sample due to the tail of the ^{238}U peak adding counts at $m/z = 237$. This type of interference results from limitations in a performance characteristic called abundance sensitivity. Abundance sensitivity is defined as the ratio of the signal at the mass of interest resulting from the presence of a major abundance peak to the signal of the major peak. This characteristic is inherent to each individual mass spectrometer. Interference is caused when ions possessing a higher m/z inelastically scatter with components of the spectrometers or residual gas in the spectrometer. This scattering causes ions to have decreased kinetic energies and produces a signal in the low m/z region of tail of the higher-mass isotope peak. The contribution of this signal becomes increasingly significant as the ratio of the minor to the major isotope decreases. Lagergren and Stoffels (1970) describe a three-stage TIMS that has been used for the low-level determination of actinides. This instrument is equipped with a sliding-shaft vacuum lock for precise positioning of the ion source, two magnetic sectors followed by an electrostatic sector, and a pulse-counting ion detection system. The instrument has good sensitivity for minor isotope determination and is capable of determining even the minor Pu isotopes ^{241}Pu and ^{242}Pu in environmental samples. This TIMS instrument has been used to assess the production of ^{237}Np from above-ground nuclear testing by determining $^{237}Np/^{239}Pu$ ratios in northern hemisphere soil samples. An essential component to this work is that it was performed in a dedicated low-level laboratory. Laboratory blank levels did not exceed approximately 10^4 atoms. Highly reproducible and accurate results were achieved at $<10^6$ atoms of transuranic actinide (^{237}Np, ^{239}Pu, ^{240}Pu, ^{241}Pu, ^{242}Pu).

Extremely high sensitivity and the capability of providing isotopic information makes TIMS an extremely effective tool for trace actinide determination. In general TIMS can be applied to actinide determination in geological, environmental, and biological samples. The technique can also be applied to routine actinide bioassay determination (Maxwell, 1997) although alpha spectrometry and ICPMS are typically used due to their greater cost effectiveness. The technique is highly selective due primarily to chemical procedures performed before analysis. The technique is applicable to isotopes of all the naturally occurring actinides and environmental transuranic actinides. Calculations based solely on counting statistics indicate that under routine conditions radionuclides with half-lives $\sim$70 years and greater can be determined more precisely by TIMS (Chen *et al.*, 1992). These calculations indicate that ^{238}Pu is the actinide with the half-life that is the lower limit for which TIMS is more precise than alpha spectrometry.

30.5.2 Accelerator mass spectrometry

Accurate determination of trace concentrations of any nuclide by mass spectrometric techniques requires the ability to discriminate between the analyte signal and the signal from interfering species possessing near-identical m/z ratios.

These interfering species may either be molecules, isobars, or species resulting from inelastic scattering of ions possessing higher m/z ratios. Theoretically, discrimination of molecules and isobars possessing near-identical m/z ratios may be achieved by increasing the resolution of the spectrometer to a level sufficient for discrimination on the basis of m/z. This approach, however, decreases ion transmission efficiency and thus, instrumental sensitivity. The determination of a minor isotope can be complicated if it possesses a lower mass than the most abundant isotope due to limitations in abundance sensitivity. All of these interferences result in limiting the ability of a mass spectrometer to precisely and accurately determine concentrations of trace elements and trace isotopes of elements. Acceleration of analyte ions to potentials >1 MV offers several unique mechanisms that together allow for the elimination of both of these types of interfering species. The utilization of high-energy accelerators for ultrahigh-sensitivity mass spectrometric analysis is called AMS.

(a) AMS fundamentals

The high sensitivity and specificity of AMS is achieved with control and manipulation of a combination of experimental parameters depending on mass (m), charge (z), and energy (E) of the analyte ion combined with unique advantages that high-energy acceleration introduces. The first significant experiment using AMS was reported by Alvarez and Cornog (1939) who used a cyclotron to assist in the discovery of ^{3}He in He. The AMS technique was reintroduced in the 1970s and developed for the measurement of long-lived ($t_{1/2}$ = 2.73 y – 16 My) cosmogenically produced radionuclides such as ^{3}H, ^{10}Be, ^{14}C, ^{26}Al, ^{32}Si, ^{36}Cl, ^{41}Ca, ^{53}Mn, ^{55,60}Fe, ^{59,63}Ni, ^{81,85}Kr, and ^{129}I (Vogel *et al.*, 1995). The primary strength of the AMS technique is the ability to measure the abundance of minor isotopes in the presence of major isotopes in the range 10^{-12} to 10^{-15}. Modern AMS instruments that have used for actinide analysis typically consist of the following components: a pre-accelerator system consisting of a negative ion source, pre-accelerator, and a mass analyzer; a tandem-based accelerator with a gas-based or foil-based electron stripper; and a post-accelerator analysis and detection system (Litherland, 1987). These components and their arrangement are illustrated in Fig. 30.7. Negative ions, either atomic or molecular, are extracted from the ion source at a potential of several kV. This potential allows the initial energy distribution of the ions extracted from the source to be sufficiently overwhelmed so that unit mass resolution analysis of the ions may be achieved before introduction into the accelerator. The ions accelerate toward the terminal of the accelerator that is at a high-positive electrostatic potential of several MV. At the terminal the ions pass through either a low-pressure gas or thin foil that strips one or more electrons from the ions. Typically beam conditions are optimized so that two or more electrons are stripped from the analyte ions. Multiply charged molecular ions fragment due to coulombic repulsion. Thus, essentially all molecules can be destroyed. These positively charged ions now

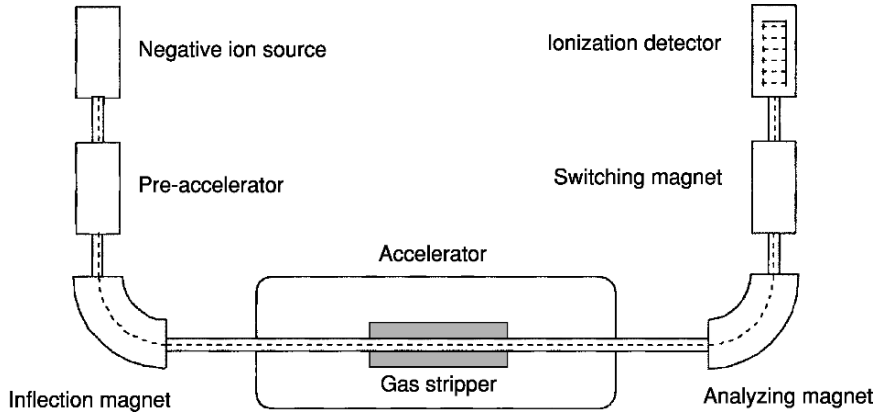

Fig. 30.7 *Schematic representation of the AMS based on the* 14UD *Pelletron accelerator at the Australian National University* (*after Fifield* et al., 1996).

accelerate away from the terminal with an increased energy. These ions, which can possess energies as high as several GeV, are subjected to further mass analysis and detection. The high energies that can be achieved in such a system allows utilization of rate of energy loss-range detection, a detection system that allows separation of isobars due to differing average nuclear charge as ions pass through a gas.

An important requirement for an AMS ion source is the ability to produce an intense beam of negative ions (>1 μA) with low memory effect. The most common ion source utilized for AMS is a Cs sputter ion source. Zhao *et al.* (1994a) studied the production of negative atomic and molecular ions from a Cs sputter ion source for introduction of ions into the accelerator for subsequent analysis and detection of the isotopes of interest. Samples were prepared as compressed as either mixtures of original sample material (Th metal or U ore); mixtures of actinide, C, and Al; or a mixture of actinide oxide and Nb. The authors concluded that a dicarbide was an effective molecule for the analysis of Th and Pa whereas a monoxide was superior for U and Pu.

Many of the facilities that developed AMS for the determination of these radionuclides utilized tandem-based accelerators originally constructed for nuclear physics experiments. However, the analysis of actinides by AMS was initially restricted due to limitations in the maximum achievable terminal potential of most tandem-based accelerators. Lower terminal potentials result in substantially higher backgrounds due to the higher cross sections of both elastic scattering and charge-changing collisions at these energies. Background can be particularly problematic for actinide analysis due to the large number of mass combinations of lighter atoms at heavier masses. Lower terminal potentials also result in decreased transmission efficiencies due to the lower yield of higher

charge states of heavier ions during charge-changing collisions. However, several instrumental advances resulting in improved background control now allow the analysis of actinides with tandem-based accelerators at moderate (1–3 MeV) energies (Kilius *et al*., 1990).

(b) AMS applications

AMS has been demonstrated for several actinide elements, in particular Th, Pa, U, and Pu. The first detection of the naturally occurring U isotope ^{236}U by AMS was achieved by Zhao *et al*. (1994b) at the IsoTrace Laboratory in Ontario, Canada. This nuclide is produced by the (n,γ) reaction on ^{235}U in U ore deposits. The production of ^{236}U can be significantly increased in U ore deposits saturated with water due to the production and subsequent thermalization of MeV neutrons from the fission of ^{238}U. Analysis of ^{236}U by conventional low-energy mass spectrometric methods is problematic due to the background resulting from elastic scattering of the intense ^{238}U signal and the molecular species ^{235}UH. The AMS instrument used in this work was composed of a Cs sputter source; an injection system consisting of a 45° electrostatic analyzer ($E/\Delta E \sim 400$) and a 90° magnet ($m/\Delta m \leq 400$); a tandem accelerator operating at a potential of $\leq$2MV; a post-accelerator system consisting of a 15° electrostatic analyzer ($E/\Delta E \sim 300$), a 90° magnet ($m/\Delta m \leq 2600$), a 45° electrostatic analyzer ($E/\Delta E \leq 900$); and an ionization chamber detection system. Molecular interferences were minimized by selecting an ion charge state of +5. This system determined a ^{236}U/^{234}U ratio of $(1.0 \pm 0\ .27) \times 10^{-5}$ in a sample of U ore from Cigar Lake, Saskatchewan, Canada. This ratio corresponds to a ^{236}U/^{238}U ratio of $(5.6 \pm 0\ .15) \times 10^{-10}$ under the assumption of secular equilibrium. This measurement demonstrated the capability of small tandem-based AMS systems for analyzing actinides.

Purser *et al*. (1996) proposed the configuration of a broad-range precision AMS system for the measurement of ^{229}Th, ^{230}Th ^{233}U, and ^{236}U. The authors proposed using ^{236}U as a thermal-neutron monitor with an integration period >100 My. The AMS instrument proposed by the authors consists of a Cs sputter source; an injection system consisting of a 90° magnet ($m/\Delta m \sim 800$) and a 90° electrostatic analyzer ($E/\Delta E \sim 120$); a tandem accelerator with a terminal stripping tube operating at a potential of 3 MV; a post-accelerator system consisting of two electrostatic analyzers, a second stripper to remove E/z ambiguities, a 90° magnet ($m/\Delta m > 1000$) equipped so that the energy of the ions can be bounced at the source to select individual masses, and a focal-plane detection system.

The measurement of Pu isotopes by AMS has been demonstrated by Fifield *et al*. (1996). A simplified schematic representation of the AMS system is shown in Fig. 30.7. The instrument consisted of a high-intensity negative ion source that produced PuO^-; an injection system consisting of a 125 kV preaccelerator and a 90° magnet; a 14 UD Pelletron accelerator operating with a terminal

voltage of 3.5 MV with a gas stripper; a post-accelerator system consisting of a 90° magnet and a switching magnet; and a longitudinal-field ionization heavy-ion detector. This instrument had a limit of detection of approximately 10^6 atoms of Pu and was capable of determining $^{240}Pu/^{239}Pu$ ratios.

The ability to measure isotopic ratios in the range 10^{-12} to 10^{-15} potentially makes AMS an extremely powerful technique, particularly for the determination of naturally occurring minor actinide isotopes such as ^{230}Th in the presence of ^{232}Th and ^{236}U as well as in the presence of the more abundant isotope ^{238}U. Despite the demonstrated high sensitivity of AMS it has not become a widely used method for the determination of trace levels of actinide elements. AMS requires dedicated accelerator facilities and personnel. Whereas several AMS user facilities exist, none of these facilities perform trace actinide analyses routinely.

30.5.3 Resonant ionization mass spectrometry

High ionization efficiency and extremely low interferences from isobars and molecular ions are important factors for the measurement of low concentrations of actinides by mass spectrometric techniques. The availability of high-intensity narrow-bandwidth tunable lasers has enabled the application of laser spectroscopic techniques for highly efficient and selective ionization of specific elements. RIMS is the name given for the technique in which photons from laser light sources are used to selectively excite and ionize atoms before mass spectrometric analysis. The resonant ionization process is theoretically achievable for every actinide element (Hurst, 1987).

(a) RIMS fundamentals

Ambartzumian and Letokhov (1972) were the first to describe the process by which neutral atoms are selectively excited and ionized via a two-step photon absorption process. The primary strength of this technique as a source of ions for mass spectrometric analysis is the high selectivity in which atoms of a selected element are ionized. A laser is tuned to a wavelength that will promote a valence electron in a Z-selected atom from its ground state to an excited state. Additional resonance or non-resonance steps are then used to achieve nearly 100% ionization efficiency. Hence, by selecting a laser or lasers with energies matching specific bound electronic transitions of the atoms of interest, saturated resonant excitation and ionization can be achieved provided that the sum of the energies of the photons exceed the ionization potential of the element. Two simplified resonance ionization schemes that have been used for RIMS analysis of actinides are illustrated in Fig. 30.8. These discrete resonant transitions are critical for the RIMS technique because they are highly specific and extremely efficient processes, as high as 10^9 times as that for non-resonant background

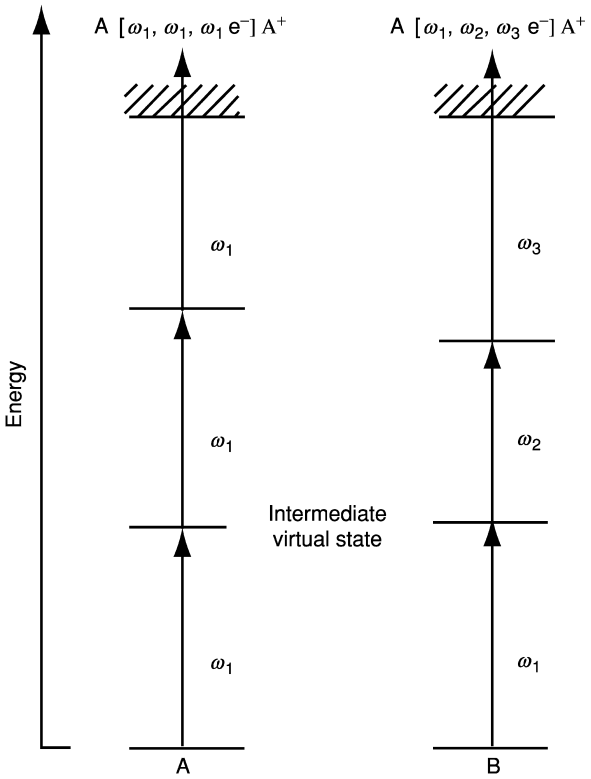

Fig. 30.8 *Simplified energy diagrams for two pathways that have used for RIMS analysis of actinide elements* (*after Krönert* et al., 1985*; Peuser* et al., 1985*; Trautmann,* 1992). *Pathway A is a two-photon transition followed by photoionization by a photon of the same energy. This resonance ionization pathway has been demonstrated for U* (*Krönert* et al., 1985). *Pathway B shows a three-step excitation and photoionization process using three photons possessing different energies. Pathway B has been demonstrated for Pu* (*Peuser* et al., 1985) *and Np* (*Trautmann,* 1992).

nuclides (Fassett *et al.*, 1983). In a typical two-photon process, an atom is first resonantly excited from the ground state to an excited electronic state and then subsequently ionized by absorbing a second photon. Some elements require a three-photon process: two photons for excitation to consecutive excited electronic states followed by a third photon for ionization. Multiple isotopes of a given element may be excited and ionized simultaneously, but not equally, by selecting broad bandwidth lasers. In RIMS, ionization is followed by mass spectrometric analysis for unambiguous identification on the basis of m/z. Mass analysis is typically performed using either magnetic sector or TOF mass spectrometers. Detection of ions is typically performed by a secondary electron multiplier or channel plate detectors.

(b) RIMS applications

Analysis by RIMS has been demonstrated for several actinides including Th, U, Np, and Pu. Detection of Pu isotopes by RIMS was first demonstrated by Donohue and Young (1983). A sample consisting of a mixture of NBS SRM 947e (^{238}Pu, ^{239}Pu, ^{240}Pu, and ^{241}Pu) and a ^{242}Pu standard was loaded onto a single Re thermal ionization source filament, atomized, and then excited and ionized with a nitrogen pumped dye-laser system. Several potential two-photon RIMS-active wavelengths in the excitation range of 431–451 nm were identified. After ionization, Pu ions were analyzed with a single-stage magnetic sector mass spectrometer that was scanned across the 238–250 amu mass range. The mass spectrum of this sample appeared with approximately the same abundances as it did when ionized by thermal ionization demonstrating that resonance ionization of Pu. This initial work with Pu did not, however, have sufficient sensitivity to achieve precision sufficient for analysis within a reasonable time. Further development of this method resulted in a methodology that, in addition to virtually eliminating isobaric interferences, demonstrated the potential of being at least as precise as TIMS (Donohue *et al.*, 1984). Improvements included the use of a single-wavelength RIMS process that used low-energy photons in the 590 nm region for resonant ionization of both U and Pu. A pulsed-heated filament synchronized with a 30 Hz pulsed-laser system resulted in a ten-fold improvement in sensitivity. Analysis was performed with a high-sensitivity tandem magnetic sector mass spectrometer.

Continued development and improvements in pulsed-laser systems have resulted in the ability to detect trace amounts of Pu by RIMS (Krönert *et al.*, 1985; Peuser *et al.*, 1985). Sensitivity was improved by applying a high-repetition pulsed-laser three-photon excitation and ionization scheme. A laser system was developed that consisted of a 6.5 kHz 30 ns pulse width Cu vapor laser for simultaneously pumping of three dye lasers. The dye lasers were scanned for the first two steps $\lambda_1 = 586.5$ nm and $\lambda_2 = 688.2$ nm using wavelength intervals of 0.05 nm whereas the third was made with part of the laser pump beam at $\lambda_3 = 578.2$ nm. TOF mass spectrometry was used for mass analysis and to minimize the background from non-resonantly produced ions. These improvements resulted in the ability to detect as few as 10^8 Pu atoms by RIMS and also demonstrated the capability to detect ^{237}Np (Trautmann, 1992). More recently RIMS has been applied to Pu and transplutonium elements with the potential of detecting 10^6 atoms in environmental samples (Erdmann *et al.*, 1998).

The RIMS method has been used for the measurement of U isotope ratios in several NBS standards. The ^{234}U/^{235}U ratio of NBS U930 and ^{235}U/^{238}U ratios of natural U, NBS U930, NBS U500, and NBS U750 were measured via resonant ionization followed by TOF mass spectrometry with a gated pulse counter designed specifically for the processing transient signals generated by the pulsed multiphoton ionization process. Replicate measurements of ^{235}U/^{238}U ratios in NBS U500 demonstrated accuracy and precision of 0.4%

(Green and Sopchyshyn, 1989). This work, however, was performed on relatively high concentrations of pure U samples.

Fearey *et al*. (1992) have developed a RIMS method for the determination of $^{230}Th/^{232}Th$ ratios for application in U-disequilibrium dating of geological samples. The use of both a broadband standing wave dye laser to excite both isotopes simultaneously and a scanned narrowband Ti:sapphire laser for excitation of each individual isotope was investigated. Mass spectrometry was performed with a single magnetic sector mass analyzer. Results indicated that the superior frequency stability of the narrowband Ti:sapphire laser compared to the broadband dye laser resulted in both higher accuracy and precision of the $^{230}Th/^{232}Th$ ratio determination. The method demonstrated a higher ionization efficiency than thermal ionization.

The extremely high efficiency and specificity of the resonant ionization process possesses enormous potential for high-sensitivity analysis of actinide elements. Single atom counting would be possible providing that suitably sensitive detection technologies could be developed and applied. The primary drawback of the technique is that ion signals generated by pulsed multiphoton ionization processes are inherently difficult to quantify with high precision. Despite its potential for high sensitivity RIMS has not become a widely used method for the determination of trace levels of actinide elements. The instrumentation for RIMS analysis is complex and is not well suited for routine analysis of geological, environmental, and biological samples. Further development of laser technologies may provide for less complex and less expensive RIMS instruments for routine analysis in the future. Application to complex geological, environmental, and biological samples will require utilization of chemical sample preparation procedures.

30.5.4 Inductively coupled plasma mass spectrometry

The ICP source is an effective and efficient atomization and ionization source that allows convenient introduction of aqueous samples. The high temperature of the ICP source efficiently ionizes actinide elements. When coupled with a quadrupole mass analyzer, the large dynamic range, nominal resolution, high-sample throughput and relatively simple spectra make ICPMS an extremely useful analytical tool for performing rapid trace analysis with <1 pg of an actinide. ICPMS instruments equipped with quadrupole mass analyzers became commercially available in the early 1980s and have since gained wide acceptance as a sensitive and accurate method for geoanalytical and environmental chemists. Actinides can be determined along with a suite of other trace elements simultaneously. Most aqueous samples can be analyzed with minimal pretreatment. ICPMS has rapidly emerged as one of the most versatile analytical techniques for trace actinide analysis.

(a) ICPMS fundamentals

Analysis by ICPMS typically requires a liquid sample. Bulk elemental analysis of solid materials by ICPMS requires the dissolution of the material followed by direct analysis. Acid dissolutions are usually performed so that the TDS values do not exceed 0.2%. In many cases ICPMS analysis can be performed directly on aqueous samples such as water and urine. Chemical preconcentration and separation of the actinides of interest from matrix elements can also be performed before analysis. Laser ablation (LA) has been used for direct sampling of solid materials. The analytical capabilities of LA–ICPMS have been described in Longerich *et al.* (1996). The focus of this section is aqueous sample ICPMS.

In ICPMS, a solution of the sample is introduced as an aerosol into the ICP source by a nebulizer in combination with spray chamber. Nebulization converts the liquid sample to an aerosol with a stable and reproducible size distribution. Because instrumental sensitivity and background values in ICPMS are dependent on the method of sample introduction, a variety of approaches have been designed to increase efficiency, reduce sample volume requirements, and reduce the effect of solvent loading on the plasma (Montaser *et al.*, 1998). Several types of nebulizers have been utilized with ICPMS including pneumatic, ultrasonic (USN), and electrothermal vaporization (ETV). Matrix reduction methods include FI as well as desolvation. The most common sample introduction method is pneumatic nebulization. Crain and Mikesell (1992) demonstrated that the higher efficiency of the USN system yielded improved sensitivity of ICPMS for the determination of U in industrial wastewater by an order of magnitude. FI preconcentrates analyte elements and reduces matrix effects. FI–ICPMS has been demonstrated for U analysis in environmental samples (Aldstadt *et al.*, 1996).

The aerosolized sample is swept into the ICP with a stream of Ar called the sample carrier gas. A typical ICP source contains a torch that is configured as three concentric quartz tubes through which Ar is flowing. The diameter of the largest tube is approximately 2 cm, and the Ar that flows through it at a rate of approximately 14 L min^{-1} is called the cooling gas. The middle tube contains Ar flowing at a rate of 0–1 L min^{-1}. This auxiliary flow can be used to affect the shape of the plasma and extend the torch life. The aerosol sample and carrier gas is introduced into the center tube with a flow of approximately 1 L min^{-1}. The torch is surrounded by a water-cooled induction coil that is powered by a radio frequency generator that creates the plasma. Typical frequencies are 27.5 and 40 MHz with a power of 1.3 kW. An impedance matching circuit is used to maintain a stable plasma. The source is called an inductively coupled plasma because the coil acts as an inductor. The ICP atomizes molecular species and ionizes the atoms.

The most critical component of an ICPMS is the interface that samples these ions and allows their transfer to a lower pressure region without significant bias.

Sampling is achieved by a sampling cone with an orifice approximately 1 mm in diameter. Ions flow through this orifice into an expansion chamber that is mechanically pumped to lower the pressure. The sampled material forms a supersonic jet. The jet flows through a skimmer cone also with an approximately 1 mm diameter orifice. Ions are extracted and focused toward the mass analyzer with a series of electrostatic ion lenses. Most commercial ICPMS instruments use a fast-scanning quadrupole mass analyzer operated at nominal mass resolution. Typical multielemental survey scan rates are 100 ms for a continuous scan from ^{6}Li to ^{238}U. Dedicated trace actinide analysis use programmed peak jumping with longer dwell times. Ions transmitted through the mass analyzer are typically detected with a channel electron multiplier. A schematic diagram of typical ICPMS instrumentation is given in Fig. 30.9. A thorough description of the principles of ICPMS operation and instrumentation can be found in Jarvis *et al.* (1991). Instrument control and data acquisition is controlled with a personal computer equipped with a software interface. For transuranic actinide analysis, the ion source or the entire instrument may be contained in a fume hood or gloved box.

Spectra generated by ICPMS are relatively simple, primarily singly charged ions with some additional doubly charged ions, oxides, and hydrides. The doubly charged ions, hydrides, and oxides can be minimized to approximately $<1\%$ of the parent ion. Actinide determination is straightforward due to the virtual absence of isobaric or molecular interferences in typical environmental and geological samples. Modern state-of-the-art ICPMS instruments possess 100 MHz μg^{-1} mL^{-1} sensitivity with backgrounds <0.5 cps. These figures correspond to a MDL <100 fg mL^{-1} for an actinide in solution, approximately 2.5×10^{8} atoms in a 1 mL sample, or 50 pg g^{-1} in solid samples assuming a typical 0.2% TDS sample dissolution. Equivalent MDLs are readily achievable for all other actinides.

Perhaps the technique that shows the most promise for improvements in routine actinide analysis is high resolution (HR)-ICPMS. This technique

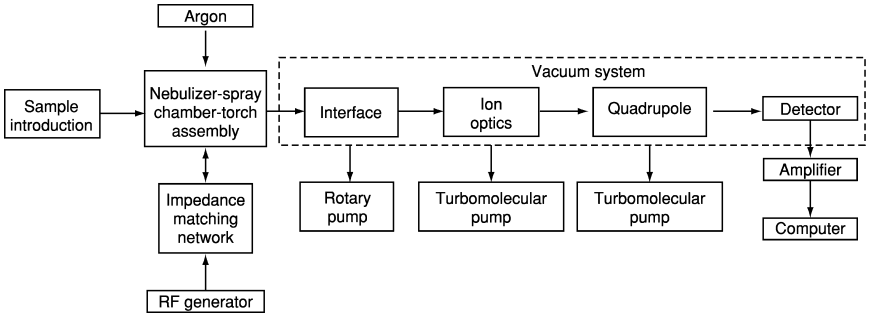

Fig. 30.9 *Schematic diagram of an ICPMS* (*after Wolf,* 1999).

combines an ICP source with a high-precision, double-focusing, mass analyzer. A review of HR-ICPMS instrumentation and applications has been published by Moens and Jakubowski (1998). The technique was first introduced in 1988 and the availability of commercial second- and third-generation HR-ICPMS instruments has made a significant impact on planetary, earth, and environmental chemistry. Commercial HR-ICPMS instruments, when operated at resolutions >2000, are capable of separating many interfering polyatomic ions from isotopes of interest. However, when operated at lower resolutions, a HR-ICPMS equipped with a single detector is capable of measurement with higher sensitivities, lower backgrounds, and higher precisions than typical quadrupole-based ICPMS instruments. A mass spectrum of a 1 ng mL^{-1} U- and Th-containing solution measured on a VG Elemental Axiom HR-ICPMS is given in Fig. 30.10. The spectrum was collected by the author using instrumental resolution setting of 460. Essentially all of the U and Th isotopes are isobar-free; however, ^{232}ThH and ^{238}UH can potentially bias ^{233}U and ^{239}Pu determinations if high ^{232}Th and ^{238}U concentrations are present. This instrument possesses a 2 GHz μg^{-1} mL^{-1} sensitivity and a <0.1 cps background corresponding to a MDL of <1 fg mL^{-1} for U in solution, approximately 2.5×10^{6} atoms of

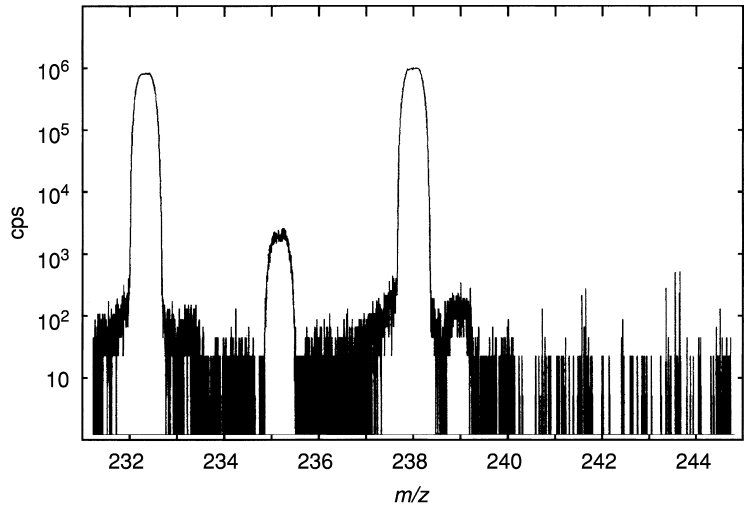

Fig. 30.10 *Spectrum of a* 1 ng mL^{-1} *U- and Th-containing sample. The spectrum was analyzed using conventional liquid sample introduction, pneumatic nebulization and a HR-ICPMS in the author's laboratory. The sample was prepared from NIST SRM* 3164 *and NIST SRM* 3159. *Note that even at these low concentrations, peaks from naturally occurring minor U isotopes* ^{234}U *and* ^{236}U *are evident. Also apparent is the contribution from the major* ^{238}U *peak to m/z* = 237 *and the contribution of* ^{238}UH *to m/z* = 239.

U in a 1 mL sample, or 1 pg g^{-1} in solid samples with assuming a typical 0.2% TDS sample dissolution. Equivalent MDLs are readily achievable for all other actinides. In addition to higher sensitivities, superior precisions can be achieved on HR-ICPMS instrumentation designed in a multicollector (MC) configuration. In this configuration, the precision of MC-ICPMS is comparable to TIMS.

(b) ICPMS applications

ICPMS can be used to determine total actinide element concentration, concentration of individual nuclides, and isotope ratios. The technique has been applied to the analysis of all of the long-lived naturally occurring actinides and environmental transuranic actinides. Elemental analysis of U and Th in geological samples with ICPMS requires the determination of the concentration of at least one isobar-free isotope and known isotopic distribution for the element. This is accomplished by direct determination of $m/z = 232$ for Th and $m/z = 238$ for U. Total U is calculated using the natural isotopic composition of U. Quantitative trace analysis of U and Th can be performed using internal standardization, external calibration, or isotope dilution. The most common approach to calibration is external calibration followed by linear regression. Internal standards such as ^{209}Bi (for ^{235}U, ^{238}U) (Wolf, 1998), another actinide (i.e. ^{232}Th for U analysis) (Crain and Mikesell, 1992), or an isotopic spike (i.e. ^{233}U, ^{235}U, or ^{236}U for U analysis) (Eggins *et al*., 1997) have been used to compensate for variations in instrumental response. These calibration methods typically yield uncertainties less than $\pm 10\%$ for a wide variety of matrices even at ultra-trace concentrations.

Isotope dilution (ID) is commonly employed to improve the accuracy of elemental ICPMS determinations. The suitability of ID-ICPMS analysis was evaluated for U determinations (Joannon *et al*., 1997). Uranium concentrations were measured in two separate solutions of six international rock reference materials, and the results differed by 1–3% for concentrations in the range of 10–400 ng g^{-1}. Isotope dilution ICPMS analysis can yield uncertainties less than $\pm 1\%$ in a wide variety of matrices.

Uranium and thorium isotope ratio measurements for U-disequilibrium studies using ICPMS and HR-ICPMS are straightforward because of the availability of the isobar-free nuclides ^{230}Th, ^{232}Th, ^{234}U, ^{235}U, and ^{238}U. Typical precisions for quadrupole-based ICPMS instruments range from 0.1 to 1.0%. These precisions limit its usefulness for measurement of many of the geologically important isotopic systems. Despite these limitations, the ease at which ICPMS is able to measure isotope ratios makes it useful for a few selected isotopic systems that do not require precisions better than approximately 0.1%. Superior precision can be achieved on HR-ICPMS instrumentation designed in a multicollector (MC) configuration. When used in the MC configuration, the precision of ICPMS is comparable to that of TIMS. A review of MC-ICPMS

instrumentation and applications including U and Th isotopic analysis has been reported (Halliday *et al*., 1998). This paper reviews results of replicate analysis of NIST SRM-906 measured by TIMS and MC-ICPMS. Precisions of approximately 1δ unit (2σ), comparable to the best achievable TIMS precision, were achieved. The external reproducibility of MC-ICPMS was superior to TIMS. Multicollector ICPMS will undoubtedly be established as the preferred method for U and Th isotopic determinations due to its high precision, ease of sample introduction, high sample throughout, and user-friendly interface.

ICPMS has been used to determine concentrations of U and Th in geological, environmental, and biological materials. A review of applications of ICPMS to geological materials has been published (Lipschutz *et al*., 2001). Environmental matrices such as wastewaters (Crain and Mikesell, 1992) and soils (Crain *et al*., 1995) have been analyzed by ICPMS. Biological materials studied include plant tissues (Alvarado *et al*., 1996), urine and lung fluid (Wyse *et al*., 1998), and fecal material (Twiss *et al*., 1994). Standard methods for the determination of ^{238}U and ^{232}Th in water (ASTM D5673-96, 1996a) and in soils (ASTM C1345-96, 1996c) have been published. The estimated MDLs for ^{238}U and ^{232}Th in water by ICPMS are 20 and 30 pg mL^{-1}, respectively. The ICPMS MDL for ^{238}U and ^{232}Th in soil are both 500 ng g^{-1}. These MDLs take into consideration a dilution factor of 200 from the soil dissolution procedures. A standard method for the determination of ^{234}U and ^{230}Th in soil by FI-ICPMS has also been published (ASTM C1310-95, 1995c). The estimated FI-ICPMS MDL for ^{234}U and ^{230}Th in soil are 2 and 5 pg g^{-1}, respectively.

The capabilities of both ICPMS and HR-ICPMS can easily be expanded to the determination of the transuranic actinides. In contrast to TIMS, direct analysis of actinides can be performed without any chemical separations. This approach can be complicated due to backgrounds caused by limitations in the mass analyzer, molecular interferences, and isobars. Chemical separation of U must be performed to minimize the contribution of ^{238}U to $m/z = 237$ during ^{237}Np determinations. ^{238}UH can interfere with trace determinations of ^{239}Pu particularly when the U/Pu ratio is $>10^6$. Chemical separation of U from Pu minimizes this effect. Isobaric interferences complicate total Pu isotopic analysis: ^{238}U interferes with ^{238}Pu, and ^{241}Am interferes with ^{241}Pu. Essentially all of these interferences can be minimized by utilizing one of the chemical separation procedures outlined in Section 30.2.2.

Vance *et al*. (1998) have recently assessed and reviewed the application of ICPMS for the routine determination of ^{237}Np in a variety of matrices and found that ICPMS achieves MDLs 1–2 orders of magnitude lower than alpha spectrometry. Yamamoto *et al*. (1994) used HR-ICPMS to measure fallout ^{237}Np in soil samples with concentrations as low as 15 fg g^{-1} of soil. Chemical separations were used to preconcentrate ^{237}Np from 10–40 g samples and ^{239}Np was used as a recovery spike. Crain *et al*. (1995) used ICPMS to determine concentrations of several long-lived actinides including ^{237}Np and ^{239}Pu in soil leachates with MDLs of 20 fg mL^{-1} of solution sample. These MDLs were

achieved using an USN and peak jumping for maximum sensitivity. ICPMS has also been used for the determination of ^{239}Pu in urine for bioassay (Wyse *et al.*, 1998). A recent study of the application of IDMS to the transuranic actinides achieved LOQs for ^{237}Np, ^{239}Pu, ^{239}Pu, ^{241}Am, and ^{244}Cm of 20 pg for each nuclide (Wolf, 1998). These analyses were performed using pneumatic nebulization on a quadrupole-based ICPMS designed in a containment hood. Considering the sensitivities of modern state-of-the-art instruments, MDLs of $<$100 fg in a 1 mL sample are readily attained for isobar-free actinides by ICPMS (Brenner *et al.*, 1998). If 1 mBq is assumed to be the MDL for routine alpha-spectrometric actinide determination, then ICPMS should possess higher sensitivities than alpha spectrometry for actinides with $t_{1/2} > 1400$ years.

HR-ICPMS and MC-ICPMS are capable of even greater sensitivities and precisions for trace transuranic actinide determination. HR-ICPMS has been used for the determination of ^{239}Pu, ^{240}Pu, and ^{242}Pu isotope ratios in soils from the former Semipaltinsk nuclear test site in the former USSR (Yamamoto *et al.*, 1996). Ratio measurements with precision of 5% could be achieved with as little as 100 fg mL^{-1} of solution. However, to discriminate between different source materials on the basis of Pu isotopic ratios requires precisions $<$1% at ultra-trace concentrations. Taylor *et al.* (2001) have determined Pu isotope ratios in solutions containing $<$100 fg mL^{-1} with precisions of 1.4% (2σ). These high precisions were achieved utilizing a MC-ICPMS along with a ^{236}U/^{233}U double spike to correct for instrument drift. High sensitivity of MC-ICPMS allowed the determination of ^{242}Pu/^{239}Pu ratios. MDLs $<$1 fg mL^{-1} that can be attained for isobar-free actinides by HR-ICPMS and MC-ICPMS. The addition of USN or other low-flow nebulizers to such systems could lower these MDLs by an order of magnitude. Again, if 1 mBq is assumed to be the MDL for routine alpha-spectrometric actinide determination, then HR-ICPMS should possess higher sensitivities than alpha spectrometry for actinides with $t_{1/2} > 14$ years.

30.6 SUMMARY

The development of standard methods, improvements in chemical procedures, and technological advances in instrumentation have significantly enhanced capabilities in trace actinide determination. There are many methods available for the determination of trace concentrations of actinides in geological, environmental, and biological materials. A substantial database of standard analytical methods for actinide determinations has been compiled and is maintained by the ASTM. In the area of chemical procedures, the development of actinide-specific anion and extraction chromatographic resins has greatly simplified actinide chemical separations. These procedures are used in most laboratories that specialize in the determination of actinides in geological,

environmental, and biological samples. The impact that improved chemical procedures have on the sensitivity, precision, and accuracy of analytical methods cannot be underestimated.

Because of the numerous and complex factors involved in the overall quality of an analytical approach, direct comparison of the different techniques is difficult. A few general observations can be made. The actinides are the only family of elements whose concentrations can be determined entirely by direct radiometric counting techniques. Gamma spectrometry has the advantage of being the only non-destructive radiometric technique but it is limited in general applicability to all the actinides due to the absence of intense γ-rays. Essentially all but a few of the naturally occurring actinides and environmental transuranic actinides can be determined by gamma spectrometry. Alpha spectrometry can provide complete isotopic information for U and Th. However, alpha spectrometry, like all radiometric techniques, is fundamentally limited by the low specific activity of most of the naturally occurring actinides and environmental transuranic. Despite this limitation, alpha spectrometry has been one of the most frequently utilized techniques for the routine determination of actinides in geological, environmental, and biological samples. The principal reasons for this are experimentally adequate sensitivity and selectivity as well as instrumentation well adapted to high-throughput routine analyses. In cases where higher sensitivity and higher precision are required, TIMS has typically been employed. The primary drawback to routine utilization of TIMS is that the instrumentation is more complex than in alpha spectrometry and is less suited to routine high-throughput analysis. In theory, both AMS and RIMS have the potential for improved sensitivity and selectivity over TIMS. In practice, however, the complexity of the instrumentation required for actinide determination by AMS and RIMS have so far prevented their adaptation as routine methods.

Perhaps the most significant technological advancement in the area of trace element analysis has been the continuing development of ICPMS and its application to actinide determinations. The strength of ICPMS resides in its high sensitivity, multielement capability, and high-sample throughput. ICPMS has replaced INAA as the standard method for trace element analysis of geological materials. Commercially available quadrupole-based ICPMS instruments are well suited for routine determination of actinides in a variety of sample matrices. The sensitivity and precision of ICPMS is comparable to that of alpha spectrometry for all but the shortest-lived actinides. When configured as a multicollector instrument the sensitivity and precision of MC-ICPMS is comparable to TIMS. The sensitivity of MC-ICPMS is comparable to, or superior to that of RNAA, for the determination of ultra-trace elements. Both ICPMS and MC-ICPMS are supplanting other methods in laboratories that need to determine trace actinide concentrations with isotopic specificity. Further development of applications of the more recently available HR-ICPMS and

MC-ICPMS instruments for ultra-trace actinide determinations will certainly improve our understanding of the chemistry of the actinide and transuranic actinide elements in the environment.

LIST OF ABBREVIATIONS

AAS	atomic absorption spectrometry
AES	atomic emission spectrometry
AMS	accelerator mass spectrometry
ASTM	American Society for Testing and Materials
Bq	Becquerel
CMPO	octyl(phenyl)-*N*,*N*-diisobutylcarbamoylmethylphosphine oxide
cps	counts per second
Da	Dalton, unified atomic mass unit
DAAP	diamylamylphosphonate
DBM	dibenzoylmethane
dc	direct current
DDCP	dibutyl-*N*,*N*-diethylcarbamylphosphonate
DTPA	diethylenetriaminepentaacetic acid
ENAA	epithermal neutron activation analysis
EPA	Environmental Protection Agency
ETV	electrothermal vaporization
FES	flame emission spectrometry
FI	flow injection
FTA	fission track analysis
GDMS	glow discharge mass spectrometry
HDEHP	bis(2-ethylhexyl)phosphoric acid
H_2DEH[DMP]	bis(2-ethylhexyl)methanediphosphonic acid
HEDPA	1-hydroxyethylidenediphosphonic acid
HPGe	high-purity germanium
HPLC	high-performance liquid chromatography
HR-ICPMS	high resolution-inductively coupled plasma mass spectrometry
ICPAES	inductively coupled plasma atomic emission spectrometry
ICPMS	inductively coupled plasma mass spectrometry
ID	isotope dilution
ID-ICPMS	isotope dilution-inductively coupled plasma mass spectrometry
ID-TIMS	isotope dilution-thermal ionization mass spectrometry
INAA	instrumental neutron activation analysis

LA	laser ablation
LA-ICPMS	laser ablation-inductively coupled plasma mass spectrometry
LAMS	laser ablation mass spectrometry
LOQ	limit of quantitation
MC-ICPMS	multicollector-inductively coupled plasma mass spectrometry
MDL	minimum detection limit
NAA	neutron activation analysis
NBS	National Bureau of Standards
NIST	National Institute of Standards and Technology
PCNAA	preconcentration neutron activation analysis
PFA	perfluoroalkoxy
PTFE	polytetrafluoroethylene
rf	radio frequency
RIMS	resonance ionization mass spectrometry
RNAA	radiochemical neutron activation analysis
RSD	relative standard deviation
SEC	size exclusion chromatography
SEM	secondary electron multiplier
SID	surface ionization diffusion
SIMS	secondary ion mass spectrometry
SRM	standard reference material
SSMS	spark source mass spectrometry
TBP	tributyl phosphate
TDS	total dissolved solids
TIMS	thermal ionization mass spectrometry
TIOA	triisooctylamine
TOF	time-of-flight
TTA	thenoyltrifluoracetone
USN	ultrasonic nebulization
USTUR	United States Transuranium and Uranium Registries

ACKNOWLEDGMENTS

The author would like to thank his colleagues at Argonne National Laboratory for many informative discussions on the chemistry of actinide elements and his colleagues at Indiana State University for encouragement and support during the writing of this work. The author is especially grateful to his wife Heather for her assistance and support through the many evenings and weekends that were used to produce this work.

REFERENCES

Aldstadt, J. H., Kuo, J. M., Smith, L. L., and Erickson, M. D. (1996) *Anal. Chim. Acta*, **319**, 135–43.

Alvarado, J. S., Neal, T. J., Smith, L. L., and Erickson, M. D. (1996) *Anal. Chim. Acta*, **322**, 11–20.

Alvarez, L. W. and Cornog, R. (1939) *Phys. Rev.*, **56**, 379.

Ambartzumian, R. V. and Letokhov, V. S. (1972) *Appl. Optics*, **11**, 354–8.

American Society for Testing and Materials (1990) ASTM D3972-90, *Annual Book of ASTM Standards*, vol 11.02.

American Society for Testing and Materials (1991a) ASTM D4309-91, *Annual Book of ASTM Standards*, vol 11.01.

American Society for Testing and Materials (1991b) ASTM D2907-91, *Annual Book of ASTM Standards*, vol 11.02.

American Society for Testing and Materials (1991c) ASTM D3649-91, *Annual Book of ASTM Standards*, vol 11.02.

American Society for Testing and Materials (1991d) ASTM D5174-91, *Annual Book of ASTM Standards*, vol 11.02

American Society for Testing and Materials (1995a) ASTM D1971-95, *Annual Book of ASTM Standards*, vol 11.01.

American Society for Testing and Materials (1995b) ASTM D3084-95, *Annual Book of ASTM Standards*, vol 11.02.

American Society for Testing and Materials (1995c) ASTM C1310-95, *Annual Book of ASTM Standards*, vol 12.01.

American Society for Testing and Materials (1996a) ASTM D5673-96, *Annual Book of ASTM Standards*, vol 11.02.

American Society for Testing and Materials (1996b) ASTM C1342-96, *Annual Book of ASTM Standards*, vol. 12.01.

American Society for Testing and Materials (1996c) ASTM C1345-96, *Annual Book of ASTM Standards*, vol 12.01.

American Society for Testing and Materials (1997a) ASTM D3865-97, *Annual Book of ASTM Standards*, vol 11.02.

American Society for Testing and Materials (1997b) ASTM C1205-97, *Annual Book of ASTM Standards*, vol 12.01.

American Society for Testing and Materials (1998) ASTM D6239-98, *Annual Book of ASTM Standards*, vol 11.02.

American Society for Testing and Materials (2000a) ASTM C1001-00, *Annual Book of ASTM Standards*, vol 12.01.

American Society for Testing and Materials (2000b) ASTM D1284-00, *Annual Book of ASTM Standards*, vol 12.01.

Anders, E., Wolf, R., Morgan, J. Ebihara, W., M., Woodrow, A. B., Janssens, M.-J., and Hertogen, J. (1988) NAS-NS-3117, Office of Scientific and Technical Information, USDOE.

Arden, J. W. and Gale, N. H. (1974) *Anal. Chem.*, **46**, 687–91.

Aston, F. W. (1931) *Nature*, **128**, 725.

Attrep, M. Jr, Roensch, F. R., Aguilar, R., and Fabryka-Martin, J. (1992) *Radiochim. Acta*, **57**, 15–20.
Barnes, C. E. and Cochran, J. K. (1990) *Earth Planet. Sci. Lett.*, **97**, 94–101.
Beasley, T. M., Kelley, J. M., Orlandini, K. A., Bond, L. A., Aarkrog, A., Trapeznikov, A. P., and Pozolotina, V. N. (1998) *J. Environ. Radioact.*, **2**, 215–30.
Becker, J. S. and Dietze, H.-J. (1998) *Spectrochim. Acta*, **52B**, 177–87.
Bertrand, P. A. and Choppin, G. R. (1982) *Radiochim. Acta*, **31**, 135–7.
Bondietti, E. A. and Trabalka, J. R. (1980) *Radiochem. Radioanal. Lett.*, **42**, 169–76.
Bourdon, B., Joron, J.-L., and Allegre, C. J. (1999) *Chem. Geol.*, **157**, 147–51.
Bowen, V. T., Noskin, V. E., Livingston, H. D., and Volchok, H. L. (1980) *Earth Planet Sci. Lett.*, **49**, 411–34.
Brenner, I. B., Liezers, M., Godfrey, J., Nelms, S., and Cantle, J. (1998) *Spectrochim. Acta*, **53**, 1087–107.
Burnett, W. C. and Yeh, C.-C. (1995) *Radioact. Radiochem.*, **6**, 22–6.
Burney, G. A. and Harbour R. M. (1974) *Radiochemistry of Neptunium*, NAS-NS-3060, Technical Information Center, USAEC.
Burns, P. A., Cooper, M. B., Lokan, K. H., Wilks, M. J., and Williams, G. A. (1995) *Appl. Radiat. Isot.*, **46**, 1099–107.
Byrne, A. R. (1986) *J. Environ. Radioact.*, **4**, 133–44.
Chen, J. H. and Wasserburg, G. J. (1981) *Anal. Chem.*, **53**, 2060–7.
Chen, J. H., Edwards, R. L., and Wasserburg, G. J. (1992) in *Uranium Series Disequilibrium Applications to Earth, Marine, and Environmental Sciences* (eds. M. Ivanovich and R. S. Harmon), Clarendon Press, Oxford, pp. 174–206.
Cheng, H., Edwards, R. L., Hoff, J., Gallup, C. D., Richards, D. A., and Asmerom, Y. (2000) *Chem. Geol.*, **169**, 17–33.
Chiarizia, R., Horwitz, E. P., Alexandratos, S. D., and Gula, M. J. (1997) *Sep. Sci. Technol.*, **32**, 1–35.
Coleman, G. H. (1965) *The Radiochemistry of Plutonium*, NAS-NS-3058, Technical Information Center, USAEC.
Cooper, E. L., Haas, M. K., and Mattie, J. F. (1995) *Appl. Radiat. Isot.*, **46**, 1159–90.
Cooper, L. W., Kelly, J. M., Bond, L. A., Orlandini, K. A., and Grebmeier, J. M. (2000) *Mar. Chem.*, **69**, 253–76.
Crain, J. S. and Mikesell, B. I. (1992) *Appl. Spectrosc.*, **46**, 1498–502.
Crain, J. S., Smith, L. L., Yaeger, J. S., and Alvarado, J. A. (1995) *J. Radioanal. Nucl. Chem.*, **194**, 133–9.
Croudace, I., Warwick, P., Taylor, R., and Dee, S. (1998) *Anal. Chim. Acta*, **371**, 217–25.
Currie, L. A. (1968) *Anal. Chem.*, **40**, 586–93.
Curtis, D. B., Fabbryka-Martin, J., Dixon, P., and Cramer, J. (1999) *Geochim. Cosmochim. Acta*, **63**, 275–85.
Dean, J. A. (1995) *Analytical Chemistry Handbook,* McGraw-Hill, New York.
Dixon, P., Curtis, D. B., Musgrave, J., Roensch, F., Roach, J., and Rokop, D. (1997) *Anal. Chem.*, **69**, 1692–9.
Dolezal, J., Povondra, P., and Sulcek, Z. (1968) *Decomposition Techniques in Inorganic Analysis,* London Iliffe Books, London.
Donohue, D. L. and Young, J. P. (1983) *Anal. Chem.*, **55**, 378–9.

Donohue, D. L., Smith, D. H., Young, J. P., McKown, H. S., and Pritchard, C. A. (1984) *Anal. Chem.*, **56**, 379–81.

Edmonds, H. N., Moran, S. M., Hoff, J. A., Smith, J. N., and Edwards, R. L. (1998) *Science*, **280**, 405–7.

Efurd, D. W., Drake, J., Roensch, F. R., Cappis, J. H., and Perrin, R. E. (1986) *Int. J. Mass Spectrom. Ion Phys.*, **74**, 309–15.

Egorov, O., Grate, J. W., and Ruzicka, J. (1998) *J. Radioanal. Nucl. Chem.*, **234**, 231–5.

Eggins, S. M., Woodhead, J. D., Kinsley, L. P. J., Mortimer, G. E., Sylvester, P., McCulloch, M. T., Hergt, J. M., and Handler, M. R. (1997) *Chem. Geol.*, **134**, 311–26.

Ehman, W. D. and Vance, D. E. (1991) *Radiochemistry and Nuclear Methods of Analysis,* Wiley Interscience, New York.

Eikenberg, J., Zumsteg, I., Rüthi, M., Bajo, S., Fern, M. J., and Passo, C. J. (1999a) *Radioact. Radiochem.*, **10**, 19–30.

Eikenberg, J., Zumsteg, M., Bajo, S., Vezzu, G., and Fern, M. J. (1999b) *Radioact. Radiochem.*, **10**, 31–40.

Erdmann, N., Nunnemann, M., Eberhardt, K., Herrmann, G., Huber, G., Köhler, S., Kratz, J. V., Passler, G., Peterson, J. R., Trautman, N., and Waldek, A. (1998) *J. Alloys Compds*, **271/3**, 837–40.

Erdtmann, G. (1976) *Neutron Activation Tables,* vol. 6, Verlag Chemie, Weinheim.

Fassett, J. D., Moore, L. J., Travis, J. C., and Lytle, F. E. (1983) *Anal. Chem.*, **55**, 765–70.

Fearey, B. L., Tissue, B. M., Olivares, J. A., Loge, G. W., Murrell, M. T., and Miller, C. M. (1992) LA-UR-92-1841.

Fifield, L. K., di Cresswell, R. G., Tada, M. L., Ophel, T. R., Day, J. P., Clacher, A. P., King, S. J., and Priest, N. D. (1996) *Nucl. Instrum. Methods*, **B 117**, 295–303.

Filby, R. H. (1975) NIOSH Technical Information, U.S. Department of Health, Education, and Welfare, U.S. Government Printing Office, Washington DC.

Filipy, R. E., Khokhryakov, V. F., Suslova, K. G., Romanov, S. A., Stuit, D. B., Aladova, E. E., and Kathren, R. L. (1998) *J. Radioanal. Nucl. Chem.*, **234**, 171–4.

Firestone, R. B. and Shirley, V. A. (1996) *Table of Isotopes,* 8th edn, John Wiley, New York.

Foti, S. C. and Freiling, E. C. (1964) *Talanta*, **11**, 385–92.

Friedlander, G., Kennedy, J. W., Macias, E. S., and Miller, J. M. (1981) *Nuclear Chemistry,* 3rd edn, Wiley Interscience, New York.

Fuller, R. K., O'Conner, J. D., Lukens, H. R., and Fleishman, D. (1965) in *Modern Trends in Activation Analysis*, National Bureau of Standards Special Publication 312.

Ganz, M., Barth, H., Fuest, M., Molzahn, D., and Brandt, R. (1991) *Radiochim. Acta*, **52/53**, 403–4.

Ghods-Esphahani, A., Veselsky, J. C., Zeoeda, E., and Peiris, M. A. R. K. (1990) *Radiochim. Acta*, **50**, 155–8.

Gindler, G. E. (1962) *Radiochemistry of Uranium,* NAS-NS-3050, Technical Information Center, USAEC.

Glover, S. E., Filby, R. H., and Clark, S. B. (1998a) *Radioanal. Nucl. Chem.*, **234**, 65–70.

Glover, S. E., Filby, R. H., and Clark, S. B. (1998b) *J. Radioanal. Nucl. Chem.*, **234**, 201–8.

Glover, S. E., Filby, R. H., Clark, S. B., and Grytdal, S. P. (1998c) *J. Radioanal. Nucl. Chem.*, **234**, 213–18.

Green, L. W. and Sopchyshyn, F. C. (1989) *Int. J. Mass Spectrom. Ion Processes*, **89**, 81–95.

Gu, Z. Y., Lal, D., Liu, T. S., Guo, Z. T., Southon, J., and Caffee, M. W. (1997) *Geochim. Cosmochim. Acta*, **61**, 5221–31.

Guest, R. J. and Zimmerman, J. B. (1955) *Anal. Chem.*, **27**, 931–6.

Gunnick, R. (1991) *MGA: A Gamma-ray Spectrum Analysis Code for Determining Plutonium Isotopic Abundances*, vol. 1, Report UCRL-LR-103220.

Halliday, A. N., Lee, D.-C., Christensen, J. N., Rehkämper, M., Yi, W., Luo, X., Hall, C. M., Ballentine, C. J., Pettke, T., and Stirling, C. (1998) *Geochim. Cosmochim. Acta*, **62**, 919–40.

Harbottle, G. and Cumming, J. B. (1994) *Nucl. Instrum. Methods*, **A353**, 503–7.

Harbottle, G. and Evans, C. V. (1997) *Radioact. Radiochem.*, **8**, 38–46.

Hoffman, D. C., Lawrence, F. O., Mewherter, J. L., and Rourke, F. M. (1971) *Nature*, **234**, 132–4.

Holm, E. and Persson, B. R. R. (1978) *Nature*, **273**, 289–90.

Horwitz, E. P., Dietz, M. L., Nelson, D. M., La Rosa, J. J., and Fairman, W. D. (1990) *Anal. Chim. Acta*, **238**, 263–71.

Horwitz, E. P., Chiarizia, R., Dietz, M. L., Diamond, H., Essling, A. M., and Graczyk, D. (1992) *Anal. Chim. Acta*, **266**, 25–37.

Horwitz, E. P., Chiarizia, R., Diamond, H., Gatrone, R. C., Alexandratos, S. D., Trochimczuk, A. Q., and Crick, E. W. (1993a) *Solvent Extr. Ion Exch.*, **11**, 943–66.

Horwitz, E. P., Dietz, M. L., Chiarizia, R., Diamond, H., and Nelson, D. M. (1993b) *Anal. Chim. Acta*, **281**, 361–72.

Horwitz, E. P., Dietz, M. L., Chiarizia, R., Diamond, H., Maxwell, S. L., and Nelson, M. R. (1995) *Anal. Chim. Acta*, **310**, 63–8.

Hurst, G. S. (1987) *Phil. Trans. R. Soc. Lond.*, **A323**, 155–70.

Hyde, E. K. (1960) *The Radiochemistry of Thorium,* NAS-NS-3004, Technical Information Center, USAEC.

Inoue, Y. and Tochiyama, O. J. (1977) *Inorg. Nucl. Chem.*, **39**, 1443–7.

Ivanovich, M. and Murray A. (1992) in *Uranium Series Disequilibrium Applications to Earth, Marine, and Environmental Sciences* (eds. M. Ivanovich and R. S. Harmon), Clarendon Press, Oxford, pp. 127–73.

Ivanovich, M., Latham, A. G., and Ku, T.-L. (1992) in *Uranium Series Disequilibrium Applications to Earth, Marine, and Environmental Sciences* (eds. M. Ivanovich and R. S. Harmon), Clarendon Press, Oxford, pp. 62–94.

Jarvis, K. E., Gray, A. L., and Houk, R. S. (1991) *Handbook of Inductively Coupled Plasma Mass Spectrometry,* Chapman and Hall, New York.

Jerome, S. M., Smith, D., Woods, M. J., and Woods, S. A. (1995) *Appl. Radiat. Isot.*, **46**, 1145–50.

Joannon, S., Telouk, P., and Pin, C. (1997) *Spectrochim. Acta*, **52**, 1783–9.

Joron, J. L., Treuil, M., and Raimbault, L. (1997) *Radioanal. Nucl. Chem.*, **216**, 229–35.

Kaplan, D. I., Bertsch, P. M., Adriano, D. C., and Orlandini, K. A. (1994) *Radiochim. Acta*, **66/67**, 181–7.

Kersting, A. B., Efurd, D. W., Finnigan, D. L., Rokop, D. J., Smith, D. K., and Thompson, J. L. (1999) *Nature*, **397**, 56–9.

Kilius, L. R., Baba, N., Garwan, M. A., Litherland, A. E., Nadeau, M.-J., Rucklidge, J. C., Wilson, G. C., and Zhao, X.-L. (1990) *Nucl. Instrum. Methods*, **B52**, 337–65.
Kim, G., Burnett, W. C., and Horwitz, E. P. (2000) *Anal. Chem.*, **72**, 4882–7.
Kim, J. I. (1986) in *Handbook on the Physics and Chemistry of the Actinides* (eds. A. J. Freeman and C. Keller), Elsevier Science, Amsterdam, pp. 413–55.
Kingston, H. M. and Haswell S. J. (eds.) (1997) *Microwave-Enhanced Chemistry Fundamentals, Sample Preparation, and Applications,* American Chemical Society, Washington DC.
Kirby, H. W. (1959) *The Radiochemistry of Protactinium,* NAS-NS-3016, Technical Information Center, USAEC.
Kressin, I. K. (1977) *Anal. Chem.*, **49**, 842–5.
Krönert, U., Bonn, J., Kluge, H.-J., Ruster, W., Wallmeroth, K., Peuser, P., and Trautmann, N. (1985) *Appl. Phys.*, **38B**, 65–70.
Kuroda, P. K. (1960) *Nature*, **187**, 36–8.
Lagergren, C. R. and Stoffels, J. J. (1970) *Int. J. Mass Spectrom. Ion Phys.*, **3**, 429–38.
Lally, A. E. (1992) in *Uranium Series Disequilibrium Applications to Earth, Marine, and Environmental Sciences* (eds. M. Ivanovich and R. S. Harmon), Clarendon Press, Oxford, pp. 94–126.
Lamble, K. J. and Hill, S. J. (1998) *Analyst*, **123**, 103R–33R
Levine, C. A. and Seaborg, G. T. (1951) *J. Am. Chem. Soc.*, **73**, 3278–83.
Lipschutz, M. E., Wolf, S. F., Hanchar, J. M., and Culp, F. B. (2001) *Anal. Chem.*, **73**, 2687–700.
Litherland, A. E. (1987) *Phil. Trans. R. Soc. Lond.*, **A323**, 5–21.
Longerich, H. P., Jackson, S. E., and Günther, D. (1996) *J. Anal. At. Spectrom.*, **11**, 899–904.
Love, S. F., Filby, R. H., Glover, S. E., Kathren, R. L., and Stuit, D. B. (1998) *Radioanal. Nucl. Chem.*, **234**, 189–93.
Magnusson, L. B. and La Chapelle, T. J. (1948) *J. Am. Chem. Soc.*, **70**, 3534–8.
Mair, M. A. and Savage, D. J. (1986) UK Atomic Energy Agency Report ND-R-134.
Marley, N. A., Gaffney, J. S., Orlandini, K. A., and Dugue, C. P. (1991) *Hydrol. Process.*, **5**, 291–5.
Maxwell, S. L. (1997) *Radioact. Radiochem.*, **8**, 36–44.
Maxwell, S. L. and Fauth, D. J. (2000) *Radioact. Radiochem.*, **11**, 28–34.
McOrist, G. D. and Smallwood, A. (1997) *Radioanal. Nucl. Chem.*, **223**, 9–15.
Mitchell, P. I., Holm, E., Leon Vintro, L., and Condren, O. M. (1998) *Appl. Radiat. Isot.*, **49**, 1283–8.
Moens, L. and Jakubowski, N. (1998) *Anal. Chem.*, **70**, 251A–6A
Montaser, A., Minnich, M. G., McLean, J. A., Liu, H., Caruso, J., McLeod, C. W. (1998) in *Inductively Coupled Plasma Mass Spectrometry* 2nd edn (ed. A. Montaser), VCH Publishers, New York.
Moody, C. A., Glover, S. E., Stuit, D. B., and Filby, R. H. (1998) *J. Radioanal. Nucl. Chem.*, **234**, 183–7.
Moorthy, A. R., Schopfer, C. J., and Benerjee, S. (1988) *Anal. Chem.*, **60**, 857A–60A
Murray, C. N., Kautsky, H., and Eicke, H. F. (1979) *Nature*, **279**, 628–9.
Nelson, D. M. and Lovett, M. B. (1978a) *Nature*, **276**, 599–601.
Nelson, D. M. and Lovett, M. B. (1978b) in *Impacts of Radionuclide Release into the Marine Environment,* IAEA-SM-248/145, Vienna, Austria, pp. 105–18.

Nelson, D. M., Carey, A. E., and Bowen, V. T. (1984) *Earth Planet Sci. Lett.*, **68**, 422–30.
Nier, A. O. (1939) *Phys. Rev.*, **55**, 150–3.
Nitsche, H., Gatti, R. C., and Lee, Sh. C. (1992) *J. Radioanal. Nucl. Chem.*, **161**, 401–11.
Novikov, Y. P., Myasoedov, B. V., and Margorian, M. N. (1972) *Radiochem. Radioanal. Lett.*, **10**, 11–17.
Noyce, J. R. (1981) National Bureau of Standards Report TN 1137.
Orlandini, K. A., Penrose, W. R., and Nelson, D. M. (1986) *Mar. Chem.*, **18**, 49–57.
Palacz, Z. A., Freedman, P. A., and Walder, A. J. (1992) *Chem. Geol.*, **101**, 157–65.
Parry, S. J. (1991) in *Activation Spectrometry in Chemical Analysis* (eds. J. D. Winefordner and I. M. Kolthoff), John Wiley, New York, pp. 206–7.
Penneman, R. A. and Keenan T. K. (1960) *The Radiochemistry of Americium and Curium,* NAS-NS-3006, Technical Information Center, USAEC.
Peppard, D. F., Mason, G. W., Gray, P. R., and Mech, J. F. (1952) *J. Am. Chem. Soc.*, **70**, 6081–7.
Perrin, R. E., Knobeloch, G. W., Armijo, V. M., and Efurd, D. W. (1985) *Int. J. Mass Spectrom. Ion Phys.*, **64**, 17–24.
Peuser, P., Herrmann, G., Rimke, H., Sattelberger, P., Trautmann, N., Ruster, W., Ames, F., Kluge, H.-J. Kroenert, U., and Otten, E.-W. (1985) *Appl. Phys.*, **38B**, 249–53.
Picer, M. and Strohal, P. (1968) *Anal. Chim. Acta*, **40**, 131–6.
Pickett, D. A., Murrell, M. T., and Williams, R. W. (1994) *Anal. Chem.*, **66**, 1044–9.
Pin, C. and Zalduegui, J. F. S. (1997) *Anal. Chim. Acta*, **339**, 79–89.
Platzner, I. T., Habfast, K., Walder, A. J., and Goetz, A. (1997) *Modern Isotope Ratio Mass Spectrometry* (ed. J. D. Weinfordner), John Wiley, New York.
Plutonium in the Environment (1995) *Proc. Symp.*, 6–8 July 1994, Ottawa, Canada; *Appl. Radiat. Isot.,* 46, 1089–293.
Porcelli, D., Andersson, P. S., Wasserburg, G. J., Ingri, J., and Baskaran, M. (1997) *Geochim Cosmochim. Acta*, **61**, 4095–113.
Poupard, D. and Jouniaux, B. (1990) *Radiochim. Acta*, **49**, 25–8.
Purser, K. H., Kilius, L. R., Litherland, A. E., and Zhao, X.-L. (1996) *Nucl. Instrum. Methods*, **B113**, 445–52.
Qu, H., Stuit, D., Glover, S. E., Love, S. F., and Filby, R. H. (1998) *J. Radioanal. Nucl. Chem.*, **234**, 175–81.
Raimbault, L., Peycelon, H., and Joron, J. L. (1997) *Radioanal. Nucl. Chem.*, **216**, 221–8.
Ramdoss, K., Gomathy Amma, B., Umashankar, V., and Rangaswamy, R. (1997) *Talanta*, **44**, 1095–8.
Rosenberg, R. J., Pitkanen, V., and Sorsa, A. (1977) *J. Radioanal. Chem.*, **37**, 169–79.
Rowe, M. W. and Kuroda, P. K. (1965) *J. Geophys. Res.*, **70**, 709–14.
Saito, A. and Choppin, G. R. (1983) *Anal. Chem.*, **55**, 2454–7.
Schrauder, M., Koeberl, C., and Navon, O. (1996) *Geochim. Cosmochim Acta*, **60**, 4711–24.
Sidhu, R. S. and Hoff, P. (1999) *Radiochim. Acta*, **84**, 89–93.
Smith, L. L., Crain, J. S., Yaeger, J. S., Horwitz, E. P., Diamond, H., and Chiarizia, R. (1995) *J. Radioanal. Nucl. Chem.*, **194**, 151–6.
Stevenson, P. C. and Nervik, W. E. (1961) *The Radiochemistry of the Rare Earths: Scandium, Yttrium, and Actinium,* NAS-NS-3020, Technical Information Center, USAEC.

Taylor, R. N., Warneke, T., Milton, J. A., Croudace, I. W., Warwick, P. E., and Nesbitt, R. W. (2001) *J. Anal. At. Spectrom.*, **16**, 279–84.
Testa, C., Degetto, S., Jia, G., Gerdol, R., Desideri, D., Meli, M. A., and Guerra, F. (1998) *J. Radioanal. Nucl. Chem.*, **234**, 273–6.
Trautmann, N. (1992) in *Transuranium Elements, A Half Century* (eds. L. R. Morss and J. Fuger), American Chemical Society, Washington DC, pp. 159–67.
Twiss, P., Watling, R. J., and Delev, D. (1994) *At. Spectrosc.*, **15**, 36–9.
United States Environmental Protection Agency (1979) EPA-600/7-79-093.
United States Environmental Protection Agency (1996) EPA Method 3052.
United States, Transuranium and Uranium Registries, Radiochemical Analytical Procedure, Manual (1995) USTUR 100, Washington State University, Pullman, WA.
Vance, D. E., Belt, V. F., Oatts, T. J., and Mann, D. K. (1998) *J. Radioanal. Nucl. Chem.*, **234**, 143–6.
Vogel, J. S., Turteltaub, K. W., and Nelson, D. E. (1995) *Anal. Chem.*, **67**, 353A–9A
Walker, R. L., Eby, R. E., Pritchard, C. A., and Carter, J. A. (1974) *Anal. Lett.*, **7**, 563–74.
Wänke, H., Begemann, F., Vilcsek, E., Rieder, R., Teschke, F., Born, W., Quijano- Rico, M., Voshage, H., and Wlotzka, F. (1970) Science, 167, 523–5.
Whicker, F. W., Hinton, T. G., Orlandini, K. A., and Clark, S. B. (1999) *J. Environ. Radioact.*, **45**, 1–12.
Wogman, N. A. (1970) *Nucl. Instrum. Methods*, **83**, 277–82.
Wolf, S. F., Bates, J. K., Buck, E. C., Dietz, N. L., Fortner, J. A., and Brown, N. R. (1997) *Environ. Sci. Technol.*, **31**, 467–71.
Wolf, S. F. (1998) *J. Radioanal. Nucl. Chem.*, **234**, 207–12.
Wolf, S. F. (1999) in *Reviews in Mineralogy,* vol. 38 (eds. P. C. Burns and R. Finch), Mineralogical Society of America, Washington DC, pp. 623–53.
Wong, K. M., Brown, G. S., and Noshkin, V. E. (1978) *J. Radioanal. Chem.*, **42**, 7–15.
Wyse, E. J., Mac Lellen, J. A., Lindenmeier, C. W., Bramson, J. P., and Koppenaal, D. W. (1998) *J. Radioanal. Nucl. Chem.*, **234**, 165–70.
Yamamoto, M., Kofuji, H., Tsumura, A., Yamasaki, S., Yuita, K., Komamura, M., and Komura, K. (1994) *Radiochim. Acta*, **64**, 217–24.
Yamamoto, M., Tsumura, A., Katayama, Y., and Tsukatani, T. (1996) *Radiochim. Acta*, **72**, 209–15.
Yamamoto, M., Kuwabara, J., and Assinder, D. J. (1998) *Radiochim. Acta*, **83**, 121–6.
Yokoyama, T., Makishima, A., and Nakamura, E. (1999) *Anal. Chem.*, **71**, 135–41.
Young, D. A. (1958) *Nature*, **182**, 315–17.
Zhao, X.-L., Nadeau, M.-J., Garwan, M. A., Kilius, L. R., and Litherland, A. E. (1994a) *Nucl. Instrum. Methods*, **B92**, 258–64.
Zhao, X.-L., Nadeau, Kilius, L. R., and Litherland, A. E. (1994b) *Nucl. Instrum. Methods*, **B92**, 249–53.

CHAPTER THIRTY ONE

ACTINIDES IN ANIMALS AND MAN

Patricia W. Durbin

31.1 INTRODUCTION

Protection of workers and the public has been the main objective of actinide biology research since its beginning in early 1942. It was recognized even before the fission chain reaction was demonstrated that nearly all of the isotopes of the newly created elements heavier than radium would be radioactive and emit alpha particles, and that, if taken into the body, they would be as damaging in the tissues as radium (Stone, 1951). Biological research with the actinides concentrated on quantifying their uptake and retention in tissues after introduction into the body by ingestion, inhalation, or injection (biokinetics, metabolism); identifying the nature of the radiation and/or chemical damage in the tissues with the greatest initial uptake, concentration, and longest retention; defining the radiation dose-dependent relationships between toxicity and actinide intake to blood.

Actinide biokinetics studies now include many species and the actinide sequence from $^{227}Ac^{3+}$ to $^{253}Es^{3+}$. Whole-body retention of several actinides has been measured in long-lived animals, in some cases for life span. Microscopic localization of actinides in the tissues has been investigated autoradiographically. Significant advances in the methods of aerosol preparation and inhalation exposure allowed quantification of deposition and retention of inhaled actinide particles in the lungs. Most of the biological investigations of internally

deposited actinides were undertaken to define their dose-dependent chronic radiotoxicity, which is manifested mainly as functional impairment and/or cancer induction in bone, liver, kidneys, and lung (when actinide aerosols are inhaled). Many of the actinide biology studies have been summarized (Zirkle, 1947; Voegtlin and Hodge, 1949, 1953; Thompson, 1962, 1989; Stover and Jee, 1972; Thompson and Bair, 1972; Hodge *et al.*, 1973; Nenot and Stather, 1979; Stannard, 1988; Lloyd *et al.*, 1993, 1994). As they became available, the data generated by those investigations were used to set and refine protection limits for actinide intakes into the body, both for workers and the public (Chalk River, 1949; NBS, 1953; ICRP, 1959, 1979, 1980, 1986, 1993, 1995). An introduction to the actinide biology literature is provided as an Appendix.

The biokinetic and toxicological data have generally been considered sufficient for radiation protection purposes, and with the exception of uranyl ion, less attention was given to understanding the chemical reactions of the actinides in the special chemical environments of the blood, tissue fluid, and tissues of the mammalian body.

Some of the aspects of actinide chemistry relevant to their uptake, distribution, and retention in the tissues of mammals have been reviewed (Durbin, 1962, 1975; Gindler, 1973; Taylor, 1973a,b; Bulman, 1978, 1980; Raymond and Smith, 1981; Duffield and Taylor, 1986; Katz *et al.*, 1986).

The chemical reactions of actinide ions in warm (37°C), nearly neutral (pH 7.4), dilute saline fluids of the mammalian body are dominated by hydrolysis and complexation (ICRP, 1972, 1986; Durbin, 1975; Duffield and Taylor, 1986; Taylor, 1998). After intake of an actinide in solution into the blood, ligand competition and exchange, in some cases facilitated by changes in local pH, determine its distribution among the tissues, presumably favoring those tissues or structural elements that contain or display the most stably binding bioligands on their surfaces.

31.2 INITIAL DISTRIBUTION OF ACTINIDES IN MAMMALIAN TISSUES

Access of foreign metal ions, in this case actinides, is most likely to occur by absorption from inhaled particles deposited in the lungs and from ingested food and water. Less likely modes of intake are through a contaminated wound or the broken skin. Once solubilized and transported into the blood, deposition in tissues and excretion of the absorbed actinides are essentially independent of the route of entry, for example, tissue deposition is equivalent for injected, inhaled, or ingested $^{239}Pu^{4+}$ citrate (Ballou *et al.*, 1972) and for a wide variety of uranium compounds (Voegtlin and Hodge, 1949, 1953; Tannenbaum, 1951b; Durbin and Wrenn, 1975). Parenteral injection (intravenous, iv; intraperitoneal, ip; intramuscular, im; subcutaneous, sc) has been a useful tool for investigating the chemically related factors that determine the disposition of actinides in the animal body. By placing solutions of actinide salts or complexes directly into the

blood or tissue fluid the experimental variables introduced by the efficient lung and gastrointestinal (GI) tract barriers are avoided. Comparable studies of the same actinide in several animal species help to differentiate between the chemical factors that are common across species and the biological factors that are species- or age-specific.

The initial distribution and excretion of soluble forms of the first ten actinides (Th through Es) plus Ac have been defined, in some cases in several animal species. Those basic biological data are collected in Tables 31.1–31.6; seven trivalent actinides including Pu^{3+} (rats, Table 31.1); five actinides injected in oxidation states greater than trivalent (rats, Table 31.2); actinide ions representing the four major oxidation states (mature female mice, Table 31.3); seven actinides considered to be long-term health hazards or with special radiological characteristics (young adult beagle dogs, Table 31.4); actinides in four major

Table 31.1 *Initial distribution of injected trivalent actinides in rats.*[a]

			Fractions of absorbed actinide (%)[b]				
			Tissues			*Excreta*	
Nuclide	*Mass injected* ($\mu g\ kg^{-1}$)	*Time* (days)	*Skeleton*	*Liver*	*Other tissues*[c]	*Urine*	*Feces and GI tract*
$^{227}Ac^{3+}$[d]	0.019	4	27	56	4	5	8
$^{239}Pu^{3+}$[e]	67	4	51	23	9	1	17
$^{241}Am^{3+}$[f]	0.12	4	35	42	3	10	10
$^{242}Cm^{3+}$[g]	1.6×10^{-3}	4	31	36	8	1	24
$^{249}Bk^{3+}$[h]	4×10^{-3}	5	54	16	9	15	6
$^{249,252}Cf^{3+}$[i]	0.02	4	64	14	4	7	11
$^{253}Es^{3+}$[j]	2.2×10^{-3}	7	69	7	2	11	11

[a] Investigators in the different laboratories used several strains of Wistar-derived albino rats. Ages at the time of injection were rarely stated; however, the reported body weights indicate a range of age from 60 to 150 days. For some incompletely reported studies, sex and body weight and/or age were obtained from archived data. Rats of both sexes are sexually mature at about 60 days, but this species does not achieve skeletal maturity. Because active growth centers remain at the ends of some long bones and vertebrae after 150 days of age, the skeletons of the rats used in these studies must be considered to be still growing (Simpson *et al.*, 1950).

[b] Data are normalized to 100% absorption and 100% material recovery; discrepancies are due to rounding.

[c] Includes kidneys, range 0.6 to 2.2%; ^{249}Bk and ^{253}Es studies also include full GI tract.

[d] Hamilton (1956); 180 g females; im injection of $^{227}Ac^{3+}$ in 0.1 M Na citrate (73% absorbed).

[e] Carritt *et al.* (1947); 225 g young males; iv injection of $^{239}Pu^{3+}$ in 0.14 M NaCl.

[f] Durbin *et al.* (1969); Durbin (1973); 240 g, 110-day-old females; im injection of $^{241}Am^{3+}$ in 0.1 M Na citrate (99% absorbed).

[g] Scott *et al.* (1949b); 190 g females; im injection of $^{242}Cm^{3+}$ in 0.14 M NaCl, pH 5 (92% absorbed).

[h] Hungate and Baxter (1972); 400 g males; iv injection of $^{249}Bk^{3+}$ in 0.01 M HCl.

[i] Durbin (1973); 250 g, 130-day-old females; im injection of $^{249,252}Cf^{3+}$ in 0.1 M Na citrate (98% absorbed).

[j] Smith (1972); 300 g females; iv injection of $^{253}Es^{3+}$ in HNO_3, pH 2.

Table 31.2 *Initial distribution of injected tetravalent, pentavalent, and hexavalent actinides in rats.*[a]

			Fraction of absorbed actinide (%)[b]					
			Tissues				*Excreta*	
Nuclide	*Mass injected* ($\mu g\ kg^{-1}$)	*Time* (days)	*Skeleton*	*Liver*	*Kidneys*	*Other tissues*	*Urine*	*Feces and GI tract*
$^{227}Th^{4+}$[c]	2×10^{-4}	8	66	4	3	10	9	7
$^{233}Pa^{5+}$[d]	5×10^{-3}	4	46	8	4	18	9	16
$^{239}Np^{4+}$[e]	3×10^{-6}	4	56	4	1	1	24	14
$^{237,238}Pu^{4+}$[f]	0.04	3	64	17	1	8	3	7
$^{239}Pu^{4+}$[g]	0.14	6	69	8	1	10	2	9
$^{239}Pu^{4+}$[g]	67	4	67	10	2	8	1	11
$^{237}NpO_2^{+}$[h]	360	3	45	5	3	6	36	5
$^{230}UO_2^{2+}$[i]	3×10^{-5}	4	11	0.2	12	0.9	76	–
$^{233}UO_2^{2+}$[j]	200	4	21	0.2	20	2	56	–
$^{238}PuO_2^{2+}$[k]	0.04	15	64	7	1	4	5	19
$^{239}PuO_2^{2+}$[l]	67	4	66	10	2	8	8	6

[a] Investigators in the different laboratories used several strains of Wistar-derived albino rats. Ages at the time of injection were rarely stated; however, the reported body weights indicate a range of age from 60 to 150 days. For some incompletely reported studies, sex and body weight and/or age were obtained from archived data. Rats of both sexes are sexually mature at about 60 days, but this species does not achieve skeletal maturity. Because active growth centers remain at the ends of some long bones and vertebrae after 150 days of age, the skeletons of the rats used in these studies must be considered to be still growing (Simpson *et al.*, 1950).

[b] Data are normalized to 100% absorption and 100% material recovery; discrepancies are due to rounding.

[c] Hamilton (1953); 215 g females; im injection of $^{227}Th^{4+}$ in 0.05 M Na citrate (94% absorbed).

[d] Hamilton (1948a); 190 g females; im injection of $^{233}Pa^{5+}$ in 0.14 M NaCl, pH 1.9 (42% absorbed).

[e] Lanz *et al.* (1946); 270 g males; im injection of $^{239}Np^{4+}$ in 0.14 M NaCl, pH 2.6 (64% absorbed).

[f] Talbot *et al.* (1990); 300 g, 140-day-old males; iv injection of $^{237}Pu^{4+}$ plus 30 Bq of other alpha-emitting Pu isotopes, 'impure ^{237}Pu', in citrate buffer.

[g] Carritt *et al.* (1947); 225 g, young males; iv injection of $^{239}Pu^{4+}$ in citrate buffer.

[h] Morin *et al.* (1973); 275 g, sex not specified; im injection of $^{237}NpO_2^{+}$ in HNO_3, pH 1.5 (43% absorbed).

[i] Hamilton (1948b); 190 g females; im injection of $^{230}UO_2^{2+}$ in 0.14 M NaCl (94% absorbed).

[j] Hamilton (1947a); 180 g males; im injection of $^{233}UO_2^{2+}$ in 0.14 M NaCl (97% absorbed).

[k] J. G. Hamilton (unpublished data); 200 g females; im injection of $^{238}PuO_2^{2+}$ in 0.1 M Na citrate and 0.01 M Na bromate (71% absorbed).

[l] Carritt *et al.* (1947); 225 g, young males; iv injection of $^{239}PuO_2^{2+}$ in dilute HNO_3.

oxidation states (mature Macaque monkeys, Table 31.5; mature Kenya baboons, Table 31.6); isotopes of industrially important Pu^{4+} and UO_2^{2+} and results from a $^{241}Am^{3+}$ accident case (adult human males, Table 31.7).

The data sets selected for inclusion in Tables 31.1–31.7 met the following criteria: The actinide studied was injected as an ultrafilterable citrate complex or a chloride or nitrate solution sufficiently acidic to avoid hydrolysis and colloid

Table 31.3 *Initial distribution of intravenously injected actinides in mice.*[a]

		Fraction of injected actinide at 1 day (%)[b]					
		Tissues				*Excreta*	
Nuclide	*Mass injected* ($\mu g\ kg^{-1}$)	*Skeleton*	*Liver*	*Kidneys*	*Other tissues*	*Urine*	*Feces and GI tract*
$^{241}Am^{3+}$[c]	0.23	27	50	1	6	14	3
$^{238}Pu^{4+}$[c]	0.09	31	50	2	8	4	5
$^{237}NpO_2^+$[d]	200	37	14	2	6	39	2
$^{232,234,235}UO_2^{2+}$[e]	100	17	1	19	3	58	2

[a] Sexually and skeletally mature female Swiss-Webster mice 90 to 160 days old (35 g body weight) (Durbin *et al.*, 1992).
[b] Data are normalized to 100% material recovery; discrepancies are due to rounding.
[c] Durbin *et al.* (1994); $^{241}Am^{3+}$ or $^{238}Pu^{4+}$ in 0.008 M Na citrate and 0.14 M NaCl, pH 3.5.
[d] Durbin *et al.* (1994); $^{237}NpO_2^+$ in 0.14 M NaCl, pH 3.5.
[e] Durbin *et al.* (1994); $^{232}UO_2^{2+}$ plus $^{234,235}UO_2^{2+}$ in 0.14 M NaCl, pH 3.5.

Table 31.4 *Initial distribution of intravenously injected actinides in beagle dogs.*[a]

			Fraction of injected actinide (%)[b]					
			Tissues				*Excreta*	
Nuclide	*Mass injected* ($\mu g\ kg^{-1}$)	*Time* (days)	*Skeleton*	*Liver*	*Kidneys*	*Other tissues*	*Urine*	*Feces*
$^{241}Am^{3+}$[c]	0.54	1–21	31	52	0.7	5	10	1
$^{243,244}Cm^{3+}$[d]	0.042	6–20	44	38	0.7	6	8	4
$^{249}Cf^{3+}$, $^{252}Cf^{3+}$[e]	0.0005–0.7	1–21	49	18	1	10	16	7
$^{253}Es^{3+}$[f]	10^{-4}	21	54	12	0.6	7	19	7
$^{228}Th^{4+}$[g]	3×10^{-3}	1–23	66	4	3	15	10	2
$^{239}Pu^{4+}$[h]	2.2	1–22	51	34	0.5	2	5	8
$^{233}UO_2^{2+}$[i]	300	7	8	1	7	2	83	~0

[a] Beagle dogs were bred and raised in the University of Utah colony (Rehfield *et al.*, 1972; Stover and Stover, 1972). Both sexes, 15 to 18 months old (mean body weight 10 kg), were sexually mature at the time of injection. Skeletal growth centers were united except in the ribs, but bone remodeling was still active in the spongy (trabecular) bone sites at the ends of some long bones and in the ribs and vertebrae (Dougherty, 1962).
[b] All actinides were injected iv in 0.08 M Na citrate buffer, pH 3.5; data are normalized to 100% material recovery.
[c] Lloyd *et al.* (1970); average dosage shown for dogs given 0.26 to 0.81 $\mu g\ kg^{-1}$.
[d] Lloyd *et al.* (1974).
[e] Lloyd *et al.* (1972a, 1976); Atherton *et al.* (1972); injected either $^{249}Cf^{3+}$ or $^{252}Cf^{3+}$.
[f] Lloyd *et al.* (1975).
[g] Stover *et al.* (1960), Lloyd *et al.* (1984a).
[h] Stover *et al.* (1959, 1972); average dosage shown for dogs given 0.25 to 4.85 $\mu g\ kg^{-1}$.
[i] Stevens *et al.* (1980).

Table 31.5 *Initial distribution of injected actinides in Macaque monkeys.*[a]

			Fractions of absorbed actinide (%)[b]					
			Tissues				*Excreta*	
Nuclide	*Mass injected* ($\mu g\ kg^{-1}$)	*Time* (days)	*Skeleton*	*Liver*	*Kidneys*	*Other tissues*	*Urine*	*Feces and GI tract*
$^{241}Am^{3+}$[c]	0.12	8	25	56	0.6	7	9	2
$^{238}Pu^{4+}$[d]	0.04	8	28	61	0.6	5	3	2
$^{237}NpO_2^+$[e]	42	4	42	10	1	3	43	0.5
$^{233}UO_2^{2+}$[f]	18	3	3	0.5	9	2	84	1

[a] Macaque monkeys (*Macaca mulatta*, *Macaca fasicularis*) were caught in the wild. Both sexes were used (about 80% were females), and injected at 5 to 15 years of age (2.5–11 kg body weight). They were sexually and skeletally mature; skeletal maturity was verified roentgenographically (Van Wagenen and Asling, 1958).
[b] Data are normalized to 100% absorption and 100% material recovery; discrepancies are due to rounding.
[c] Durbin (1973); im injection of $^{241}Am^{3+}$ in 0.08 M Na citrate buffer, pH 3.5 (98% absorbed); average dosage shown for monkeys given 0.03 to 0.17 $\mu g\ kg^{-1}$.
[d] Durbin *et al.* (1985); iv or im injection of $^{238}Pu^{4+}$ in 0.08 M Na citrate buffer, pH 3.5 (91% absorbed); average dosage shown for monkeys given 0.017 to 0.112 $\mu g\ kg^{-1}$.
[e] Durbin *et al.* (1987); im injection of ^{237}Np in 0.08 M Na citrate buffer, pH 3.5, probably a mixture of NpO_2^+ and Np^{4+} (99% absorbed).
[f] P. W. Durbin and N. Jeung unpublished data; im injection of $^{233}UO_2^{2+}$ in 0.14 M NaCl (100% absorbed).

formation in the medium; values were reported for the actinide content of all soft tissues, the whole skeleton, and the separated urine and feces; the fraction retained at the wound site was reported for im injection studies.

The skeleton is a major deposition site for the actinides in all of the oxidation states that have been administered to animals. Liver is the most important soft tissue deposition site for all of the actinides except UO_2^{2+}. Shortly after intake to blood, the skeleton and liver (skeleton and kidneys in the case of UO_2^{2+}) account for about 90% of the actinide in the body (Tables 31.1–31.6; ICRP, 1972). It is clear that both bone and liver possess appropriate binding sites and ligands with high affinities for actinide ions, but the partitioning of the individual actinides between deposition in bone and liver varies with their chemical properties, most importantly electronic charge and ionic radius.

The initial partitioning of an actinide between deposition in bone and liver is likely to depend primarily on the relative affinities of the ligands on the anatomical surfaces of bone and on liver cell membranes for binding that actinide in competition with the ligands that transport it in the blood. The outcome of those competitions will be modulated by the relative abundances of ligands (binding sites) on the bone surfaces and hepatic cell membranes that are exposed

Table 31.6 *Initial distribution of injected actinides in Kenya baboons.*[a]

			Fraction of injected actinide (%)[b]					
			Tissues				*Excreta*	
Nuclide	*Mass injected* ($\mu g\ kg^{-1}$)	*Time* (days)	*Skeleton*	*Liver*	*Kidneys*	*Other tissues*	*Urine*	*Feces and GI tract*
$^{241}Am^{3+}$[c]	0.06	1	35	31	0.7	22	10	1
$^{243,244}Cm^{3+}$[d]	3×10^{-3}	16	43	26	–	12[e]	17	3
$^{239}NpO_2^{2+}$[f]	4×10^{-4}	1	54	3	0.5	2	40	~0
$^{237}UO_2^{2+}$[g]	2×10^{-6}	4	~6	0.5	5	1	87	0.1

[a] Female Kenya baboons (*Papio anubis*, *Papio cynocephalus*) were caught in the wild. They were injected when 7 to 16 years old (12–15 kg body weight) and were sexually and skeletally mature. Skeletal maturity and ages were estimated from data on molar tooth eruption and wear, estrus cycles, and body weight (Guilmette *et al.*, 1980).
[b] Data are normalized to 100% absorption and 100% material recovery; discrepancies are due to rounding.
[c] Guilmette *et al.* (1980); iv injection of $^{241}Am^{3+}$ in 0.08 M Na citrate, pH 3.5.
[d] Lo Sasso *et al.* (1981); iv injection of $^{243,244}Cm^{3+}$ in 0.08 M Na citrate buffer, pH 3.5.
[e] Includes kidneys.
[f] Ralston *et al.* (1986); iv injection of $^{239}NpO_2^{2+}$ in 0.01 M $NaHCO_3$.
[g] Lipsztein (1981); iv injection of $^{237}UO_2^{2+}$ in HNO_3, pH 1.6.

to the circulating fluids, the relative rates of blood flow through those tissues, and the concentrations of the transport ligands.

31.2.1 Trivalent actinides

The initial distributions of Am^{3+} in the tissues of the six mammals (Tables 31.1–31.7) agree well with one another, as do the overall distributions of Cm^{3+} in the rats, dogs, and baboons (Tables 31.1, 31.4, and 31.6), and those of Cf^{3+} and Es^{3+} in the rats and dogs (Tables 31.1 and 31.4). Bone and liver are the major initial deposition sites. The larger animals (dog, baboon) retained more Am^{3+}, Cm^{3+}, Cf^{3+}, and Es^{3+} in the bulk soft tissues, mainly muscle and pelt, than did the rats and mice. Renal excretion of the trivalent actinides is limited. It tended to be somewhat greater for the heavier than for the lighter members of the series, and to be greater for the dogs, who were given iv injections of actinide solutions containing large excesses of citrate buffer. Impeded filtration through the kidneys into urine indicates that uptake of the trivalent actinides in the target tissues is rapid and/or that the major fraction of circulating actinide is bound to nonfilterable protein.

In both the rats (Table 31.1) and the dogs (Table 31.4), and similarly to the behavior of the lanthanides, the initial skeletal deposition of the trivalent actinides increases and the partitioning between deposition in bone and liver

Table 31.7 *Initial distribution of absorbed actinides in adult men.*

			Fraction of absorbed actinide (%)					
			Tissues				*Excreta*	
Nuclide	*Mass* ($\mu g\ kg^{-1}$)	*Time* (days)	*Skeleton*	*Liver*	*Kidneys*	*Other tissues*	*Urine*	*Feces*
$^{241}Am^{3+a}$	~0.04	4	~31	~69	–	–	–	–
$^{237}Pu^{4+b}$	4×10^{-8}	~20	~32	~59	–	~6[c]	2	2
$^{234,235,238}U^{4+d}$	700	21	12	11	1	8	68	–
$^{234,235,238}UO_2^{2+d}$	105	18	14	1	7	6	72	–

[a] Robinson *et al.* (1983); 64-year-old man; accidental high-level skin burns and abrasions contaminated with ~3 mCi of ^{241}Am in hot 7 M HNO_3; 10 μCi absorbed and retained as estimated from external photon measurements.
[b] Talbot *et al.* (1993); two male volunteers, average age 66 years, average body weight 73 kg; iv injection of $^{237}Pu^{4+}$ in 0.03 M Na citrate; tissue distribution estimated from collected excreta and external photon measurements.
[c] Includes kidneys.
[d] Original data of Bernard and Struxness (1957) normalized to 100% material recovery; bedridden terminally ill adult males with inoperable brain tumors; tissue distributions estimated from autopsy specimens. Case 6, iv injection of $UO_2(NO_3)_2$ enriched with $^{234,235}UO_2^{2+}$, age 60 years, body weight 57 kg. Case 8, iv injection of UCl_4 enriched with $^{234,235}U^{4+}$in in 0.2 M acetate buffer, pH 4.7, age 56 years, body weight 63 kg; most of the U detected in 'other tissues' was in the spleen (6.7%).

shifts from favoring liver to favoring bone with the decrease in ionic radius (r) that accompanies the addition of f-shell electrons (Durbin, 1962, 1973). Within each series, that is also the trend of increasing stability of complexes.

Within the lanthanide and actinide series, the stabilities of complexes with the same ligand increase with decreasing ionic radius (Cotton and Wilkinson, 1980), as illustrated for the actinide oxalate and citrate complexes in Table 31.8. It is reasonable to expect that the stabilities of their complexes with other biologically important ligands such as phosphate, for which stability constants are unavailable, will exhibit a similar trend. For the same ligand, complexes of the trivalent actinides tend to be more stable than those of their lanthanide analogs with the same ionic radii. For example, the EDTA complexes of the trivalent actinides are, on average, one to two orders of magnitude greater than those of the EDTA complexes with lanthanides of the same ionic radii (Sillen and Martell, 1964; Ahrland, 1986; Hulet, 1986).

For the purposes of this discussion, initial skeletal deposition is expressed as the skeletal fraction of the initial body burden ($BB_{0,\%}$ of injected amount), where BB_0=skeleton + soft tissue + $liver_{max}$=100% – Σ (urine). Skeleton, soft tissue, and urine are the measured amounts of actinide in those specimens (Table 31.1), and $liver_{max}$ is the sum of the measured amounts of actinide in the liver, GI tract plus contents, and passed feces. Biliary excretion of liver actinide into the GI tract and feces will be discussed in the context of actinides in

Table 31.8 *Ionic radii and stabilities of complexes of some actinides with the low molecular weight ligands in mammalian plasma and tissues.*

		Stability constant ($\log \beta_1$)[a]					
	Ion radius (nm)[b]	OH^-	CO_3^{2-}	HPO_4^{2-}	*Acetate*[c]	*Oxalate*	*Citrate*
Trivalent actinides (CN6)							
Ac^{3+}[d]	0.112	(4.7)	(5.6)		–	(4.7)	(7.6)
Pu^{3+}	0.100	6.7[e]	–		2.0[f]	7.3[g]	8.7[g]
Am^{3+}	0.098	7.9[e]	5.8[e]		2.0[f]	4.8[f]	7.1[g]
Cm^{3+}	0.097	7.9[e]	–		2.1[f]	4.8[f]	7.7[h]
Bk^{3+}	0.096	8.2[e]	–		2.1[f]	5.4[h]	7.9[h]
Cf^{3+}	0.095	8.2[e]	–		2.1[f]	5.5[h]	7.9[h]
Es^{3+}	0.094	8.9[j]	–		–	–	11[i]
Tetravalent actinides (CN8)							
Th^{4+}	0.105	9.6[e]	–	11[g]	3.9[f]	11[g]	13[g]
U^{4+}	0.100	12[e]		12[g]		12[g]	
Np^{4+}	0.098	12[e]	–	12[j]	–	11[g]	15[g]
Pu^{4+}	0.096	12[e]	–	13[g]	4.9[g]	11[g]	15[g]
Pentavalent actinides (CN8)							
Pa^{5+}	0.091	15					
Actinide dioxo cations (CN6)							
NpO_2^+	0.075	4.2[k]	4.5[l]	3.0[l]	1.9[g]	3.7[f]	3.7[g]
UO_2^{2+}	0.073	8.0[e]	9.3[m]	7.2[m]	2.4[f]	6.4[h]	7.4[h]
NpO_2^{2+}	0.072	8.6[e]			2.3[h]	7.2[h]	
PuO_2^{2-}	0.071	7.8[e]	–	8.2[g]	2.3[f]	9.4[h]	–

[a] Where available, values used were determined at or corrected to 25°C, ionic strength 0.1 to match 0.14 M NaCl in mammalian body fluids; reported values rounded to two significant figures.
[b] Shannon (1976); Katz *et al* (1986).
[c] Acetate is included as a representative monocarboxylic acid.
[d] Stability constants of La^{3+} complexes shown in parentheses are from Smith and Martell (1976, 1989) and Martell and Smith (1977). Ac^{3+} complexes are expected to be somewhat less stable. Log β, for HPO_4^{2-} complex from Kirby (1986a).
[e] Smith and Martell (1976).
[f] Ahrland (1986).
[g] Moskvin (1971).
[h] Martell and Smith (1977).
[i] Hulet (1986).
[j] Sillen and Martell (1971).
[k] Smith and Martell (1989).
[l] Lemire *et al.* (2001).
[m] Grenthe *et al.* (1992).

the liver. The initial skeletal fraction, skeleton/BB_0, normalizes the data by accounting for the somewhat variable early urinary excretion. Initial skeletal fractions of the trivalent lanthanides and actinides in rats are plotted vs ionic radius in Fig. 31.1. The straight-line segments were fitted by linear regression analysis to serve as eye guides. The initial skeletal fraction of Pu^{3+} lies so far

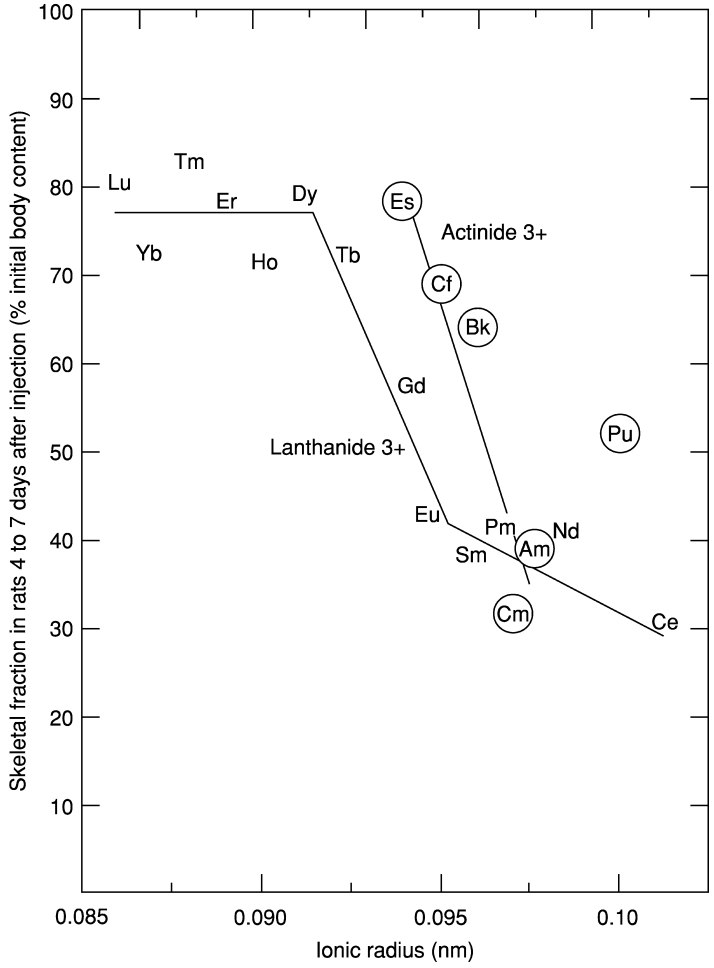

Fig. 31.1 *Deposition of trivalent actinides and lanthanides in the skeleton of rats at* 4 *to* 7 *days after injection, expressed as percent of initial body content* (%BB_0), *and shown as functions of their six-coordinate ionic radii. Lanthanide data from Durbin* (1973); *actinide data from Table* 31.1; *ionic radii from Shannon* (1976) *and Katz* et al. (1986).

from the trend line for the other trivalent actinides that it was not included in determining the regression line for the trivalent actinides. The aberrant behavior of Pu^{3+} supports the view that Pu^{3+} will be oxidized to Pu^{4+} *in vivo* (Carritt *et al.*, 1947; Scott *et al.*, 1948b).

The plot of initial skeletal fraction vs ionic radius for the trivalent actinides and lanthanides in rats (Fig. 31.1) is discontinuous. Six-coordinate ionic radii are those reported by Shannon (1976). Fig. 31.1 exhibits three distinct regions,

as follows: For the lanthanides, there is a plateau from Lu^{3+} to Tb^{3+} ($r < 0.0925$ nm), followed by a steeply declining region from Tb^{3+} to Eu^{3+} ($r = 0.0925$–0.095 nm), and a less steeply declining segment from Eu^{3+} to Ce^{3+} ($r \geq 0.095$ nm). For the trivalent actinides, Es^{3+} to Am^{3+} ($r = 0.094$–0.0975 nm), only the steeply declining central region was observed.

The initial skeletal fractions of Am^{3+} and Cm^{3+} in rats lie in the region defined by the larger lighter lanthanides; they resemble Pm^{3+}, which has about the same ionic radius, but two less f-shell electrons. The initial skeletal fraction of Es^{3+} lies within the region defined by the smaller heavier lanthanides; the initial skeletal fractions of Bk^{3+}, Cf^{3+}, and Es^{3+} most closely resemble the lanthanides, Gd^{3+}, Tb^{3+}, and Dy^{3+}, respectively, which have ionic radii 0.0025 nm smaller, on average, and one less f-shell electron.

If the increase in initial skeletal fraction with decreasing ionic radius found for the lanthanides and trivalent actinides depended only on their affinities for bone surface ligands (bone mineral and/or protein), a more gradual trend would be expected. The discontinuous pattern observed resembles the relationship between the size of a multivalent cation and its ability to occupy both of the similar but unequal metal-binding sites of transferrin (Tf), the iron-transport protein of mammalian blood plasma (Pecoraro *et al.*, 1981). The combined data for the skeletal deposition of the trivalent actinides and lanthanides in rats and metal binding to Tf suggest that the stabilities of their Tf complexes strongly influence the skeletal deposition of these trivalent metal ions.

Studies in several animal species show that a number of soft tissues other than liver accumulate radiologically significant concentrations of trivalent actinides (Lloyd *et al.*, 1970, 1974, 1975, 1976; Atherton and Lloyd, 1972; Durbin, 1973; Guilmette *et al.*, 1980). Autoradiographs of soft tissues of rats, dogs, monkeys, and baboons show that the initial actinide deposits are located extracellularly in the connective tissue components (Taylor *et al.*, 1969a,b, 1972a; Lloyd *et al.*, 1970; Durbin, 1973; Guilmette *et al.*, 1980). The connective tissue at most, but not all, of the sites of actinide deposition was shown histochemically to contain substances that react positively to the periodic-acid Schiff (PAS) stain for mucins, glycogen, and glycoproteins (Pearse, 1961; Taylor *et al.*, 1972a). The trivalent actinides were found deposited in the intertubular connective tissue of the kidneys of all of the species, and in the dogs, also in the capillary tufts and in or on the basement membrane of the glomerular capsule.

The most widely distributed deposition site identified in all of the tissues examined from all of the animals studied is the medial layer of the small arterioles, where the nuclides appeared to be localized in the connective tissue and not the smooth muscle layers. There was also some selective localization in specialized connective tissue components of the aorta, coronary arteries, and heart valves. Skeletal muscle and pelt contribute 43 and 14%, respectively, of the body weight of the study animals (Tables 31.1–31.6). Although the concentrations of the trivalent actinides in those tissues are low (0.5–2.5% per kg), most of the actinide in the body, apart from liver and skeleton, is associated with those

large tissue masses. Actinides in the walls of their abundant blood vessels can account for much of the early actinide content of these tissue masses.

All of the investigated trivalent actinides concentrated in the interfollicular connective tissue of the thyroid glands of the dogs, but not the primates. The stability of that binding was demonstrated by prolonged retention of $^{241}Am^{3+}$ (Lloyd *et al.*, 1970) and $^{249}Cf^{3+}$–$^{249}Bk^{3+}$ (Taylor *et al.*, 1972a) and by the recovery with the insoluble connective tissue fraction of 95% of ^{241}Am in a homogenate of the thyroid of a $^{241}Am^{3+}$ injected dog (Stevens *et al.*, 1969). Combined, all of these observations suggest that the trivalent actinides bind to glycoprotein in the connective tissue ground substance, a hypothesis supported by the affinity of purified bone glycoprotein for $^{241}Am^{3+}$ *in vitro* (Chipperfield and Taylor, 1968, 1972).

31.2.2 Tetravalent and pentavalent actinides

Thorium, protactinium, and plutonium were injected in animals as Th^{4+}, Pa^{5+}, and Pu^{4+}, respectively, their most stable states in biological systems (dilute saline solution, mild redox conditions, nearly neutral pH). The biological data indicate that Np^{4+} and U^{4+} tend to be unstable *in vivo* (Tables 31.2 and 31.7).

(a) Th^{4+}

Tracers of citrate complexes of two shorter-lived Th isotopes were injected im in rats ($^{227}Th^{4+}$, Table 31.2) and iv in dogs ($^{228}Th^{4+}$, Table 31.4). Absorption of Th^{4+} from the im injection site in the rats was nearly complete in 8 days. There was no evidence of intravascular colloid formation in the iv-injected dogs. The initial distributions of Th^{4+} in the rats and dogs agreed well. Bone is the predominant deposition site of Th^{4+}. Liver deposition is low, but soon after injection, kidneys and other soft tissues account for a substantial fraction of the body content (13 to 18% at 1 to 23 days). About 10% of the injected Th^{4+} is excreted in the urine, mainly in the first 24 h. Fecal excretion is low for the rats and negligible for the dogs.

Autoradiographs were prepared from the soft tissues of a dog that died 10 days after sc injection of a lethal dose of $^{228}Th^{4+}$ (10 μCi kg^{-1} of $^{228}ThCl_4$, pH 4–5) (Erleksova, 1960). The published autoradiographs are overexposed, and the distribution of the $^{228}Th^{4+}$ is obscured by tracks from the ingrown $^{224}Ra^{2+}$ and ^{220}Rn daughters. There is phagocytized radiation-damaged cell debris in many of the tissues. However, the general pattern of Th^{4+} distribution in the soft tissues can be discerned, and it is nearly the same as that described above for Am^{3+} and Cf^{3+} in dogs (Taylor *et al.*, 1969b, 1972a; Lloyd *et al.*, 1970). Some Th^{4+} in the liver was contained within hepatic cells. In the kidneys, Th^{4+} was associated with the tubular epithelium and with cell debris in collecting tubules. Combined, these observations were taken as evidence for the intratubular dissociation of an ultrafilterable low molecular weight Th^{4+} complex present

in the plasma. The $^{228}Th^{4+}$ alpha tracks appeared mainly, if not entirely, to be located in the connective tissue components of the organs examined, including thyroid, testis, and adrenal glands, and in the medial layers of arterioles. In the lungs, the Th^{4+} was accumulated in the bronchiolar cartilages. Slow release of $^{228}Th^{4+}$ from the soft tissues of the dogs (Stover *et al.*, 1960) and the great affinity of bone glycoproteins for Th^{4+} *in vitro* (Chipperfield and Taylor, 1972) suggest that Th^{4+} can bind stably to PAS-positive proteins in connective tissue.

(b) U^{4+}

The initial distribution of U after iv injection of U^{4+} has been reported for rats (Neuman, 1949) and an adult man (Bernard and Struxness, 1957). The details of the human study are given in Table 31.7. The rats (63 days old males and 112 days old females, 200 g body weight) were injected iv with natural UCl_4 in 0.2 M acetate buffer, pH 4.6, at doses ranging from 1.5 to 3 mg U per kg. Excreta and all tissues were analyzed for U by a fluorometric method (Flagg, 1949). In the female rats killed at 5 days, the injected U was distributed as follows [original data of Neuman (1949) normalized to 100% material recovery]: liver and spleen 59%, kidneys 4%, skeleton 7%, urine 21%, feces 6%.

The initial distributions of U injected iv as U^{4+} in the rats and the man can be compared with those of soluble Pu^{4+} and UO_2^{2+} (Tables 31.2 and 31.7). The initial urinary excretion of the U was much greater than for Pu^{4+}, but much less than for UO_2^{2+}. Deposition of the U in bone was much less than for Pu^{4+} and about the same as for UO_2^{2+}. Deposition of the U in the kidneys was much less than would be expected for UO_2^{2+}. The U retained in the liver and spleen of the man was less than for Pu^{4+}, but much greater than for UO_2^{2+}; in the rats, retention of the U in liver and spleen was much greater than would be expected for either soluble Pu^{4+} or UO_2^{2+}.

Several U compounds, including UCl_4, are unstable *in vivo*, and are slowly oxidized to UO_2^{2+} in 0.025 M HCO_3^- pH 7.4 (Dounce, 1949). If, similarly to Th^{4+} and Pu^{4+}, U^{4+} circulated as a nonfilterable plasma protein complex that was cleared slowly from the plasma, only a small amount would be excreted by the kidneys. However, an important fraction of the U injected as U^{4+} was excreted in the urine during the first day (14 and 24% by the rats and the man, respectively). The presence of filterable U in the circulation is evidence that some of the U^{4+} was oxidized to UO_2^{2+} within minutes after the injection. The rats excreted an additional 7% of the U in the urine in days 2 to 5 (Neuman, 1949), and the man excreted an additional 44% in the interval 2 to 21 days, (Table 31.7), providing evidence of slow continuous oxidation to UO_2^{2+} of U^{4+} initially sequestered in the tissues. Parenterally injected UCl_4 is only about one-tenth as toxic to the kidneys of rats as $UO_2(NO_3)_2$; the LD_{50s} at 14 to 21 days are 25 and 2.5 mg U per kg body weight, respectively (Yuile, 1973). *In vivo* oxidation of U^{4+} and release of UO_2^{2+} into the circulation apparently proceed sufficiently slowly that the kidneys are not exposed to a toxic level of UO_2^{2+}.

(c) Np^{4+}

Tetravalent $^{239}Np^{4+}$ and $^{237}Np^{4+}$ have been studied in rats (Table 31.2; Moskalev *et al.*, 1979; Paquet *et al.*, 1996; Ramounet *et al.*, 1998). The biological behavior of Np^{4+} would be expected to resemble Pu^{4+}, based on similar chemical properties. Deposition of Np^{4+} in the skeleton is about the same as that of Pu^{4+} and within the range of values reported for initial skeletal Pu^{4+} content of rats (ICRP, 1972). However, the Np^{4+} content of the liver was well below that expected based on similarity to Pu^{4+}. Urinary excretion of Np^{4+} was 24% in 4 days, more than 10 times that found for Pu^{4+}, but less than the early urinary excretion of NpO_2^+ (36% in 3 days, Table 31.2). Uptake of iv-injected $^{237}Np^{4+}$ citrate in the skeleton was significantly faster than for $^{238}Pu^{4+}$, but significantly slower than for $^{237}NpO_2^+$ (Ramounet *et al.*, 1998).

(d) Pu^{4+}

Most of the biological studies of Pu have been performed with $^{239}Pu^{4+}$, however, other Pu isotopes have been used to take advantage of their special physical properties – the photon emissions of $^{237}Pu^{4+}$, the greater specific radioactivity of $^{238}Pu^{4+}$, and the beta particle emissions of ^{241}Pu. In addition to the numerous studies of injected Pu^{4+}, various chemical forms of Pu^{4+} have been administered to animals by inhalation to measure absorption into the body and assess the local radiotoxicity of the Pu alpha particles in the tissues of the respiratory tract, and by mouth to measure absorption from the GI tract. Chemical forms of Pu that have been investigated in those studies range from soluble complexes to insoluble PuO_2 particles. In addition to the animal species represented in Tables 31.1–31.7, distribution, retention, and toxicity of injected Pu^{4+} have also been studied in rabbits, chinchillas, swine, and sheep (Buldakov *et al.*, 1969; Taylor, 1969; ICRP, 1972, 1986; Bair *et al.*, 1973; Vaughan *et al.*, 1973).

Overall, the initial distributions of injected Pu^{4+} in rats, mice, dogs, monkeys, and human adults are similar (Tables 31.1–31.5 and 31.7). On average, skeleton plus liver accounts for 85% of the injected Pu^{4+}, and soft tissues other than liver and early urinary and fecal excretion, for 7, 4, and 5%, respectively. The initial Pu^{4+} distributions in the rats and dogs are nearly the same as those of the heavier trivalent actinides, Bk^{3+}, Cf^{3+}, and Es^{3+}, whereas the Pu^{4+} distributions in the mice, monkeys, and human adults closely resemble Am^{3+}. The combined data for the initial Pu^{4+} distributions in the five species may be compared to those for the trivalent actinide(s) they resemble most closely. The Pu^{4+} contents of the soft tissues other than liver, as well as the early fecal Pu^{4+} excretion are nearly the same as the best matched trivalent actinide(s). About 10% more of the injected Pu^{4+} is deposited in the skeleton plus liver (85%) than is found for the matched trivalent actinide(s) (75%), and that difference is accounted for by the smaller amount of early Pu^{4+} excretion in urine (4%, on average) compared with an average early excretion of 15% for the matched trivalent actinides.

Although the initial Pu^{4+} content of skeleton plus liver is nearly the same for all five species, the partitioning of the Pu^{4+} between those two tissues favors skeletal deposition in the rats and dogs, and liver in the mice, monkeys, and human adults. That species difference may be attributed in part to the less mature and/or more reactive skeletons of the rats and dogs at the time of Pu^{4+} injection (Durbin, 1975). The male rat skeleton grows slowly until late in life (Simpson *et al.*, 1950). In dogs, the degree of skeletal maturity (age at the time of Pu^{4+} injection) alters the proportions of Pu in the skeleton and liver in a reciprocal manner, favoring deposition in bone of juvenile dogs (3 months old) and young adult dogs (18 months old) and in the liver in older dogs (5 years old) (Bruenger *et al.*, 1983).

Autoradiographs of soft tissues of several species show that initially, soluble Pu^{4+} is prominently deposited in hepatic cells and to a lesser degree in the renal papillae, on nonskeletal mineralized structures both physiological (calcifying tracheal cartilages) and ectopic (calcified renal stones and scar tissue), and occasionally in involuting ovarian follicles and corpora lutea. Low concentrations are seen in the medial layer of arteries and arterioles and in the connective tissue of all tissues and organs examined, including bronchiolar cartilages, heart, testis, and thyroid gland (Painter *et al.*, 1946; Bloom, 1948; Erleksova, 1960; Cochran *et al.*, 1962; Jee and Arnold, 1962; Durbin, 1975; Green *et al.*, 1977; Miller *et al.*, 1980; Durbin *et al.*, 1985). Concentrations of Pu^{4+} in connective tissue are much less than those found for the heavier trivalent actinides. Those observations suggest that Pu^{4+} complexes with connective tissue glycoproteins are not as stable as the circulating Pu^{4+} complexes with plasma proteins, particularly Tf, or the complexes that Pu^{4+} forms at binding sites on the surfaces of hepatic cells and bone.

Carritt *et al.* (1947) studied groups of rats injected iv with $^{239}Pu^{4+}$ citrate at doses ranging from 0.14 to 231 μg kg^{-1} (data for the 0.14 and 67 μg kg^{-1} groups are included in Table 31.2), and Talbot *et al.* (1990) injected rats iv with 0.04 μg kg^{-1} of $^{237,238}Pu^{4+}$ citrate. The results are essentially the same over the entire range of iv-injected Pu^{4+} doses indicating that, although limited in quantity, a sufficient number of Tf-binding sites were available to accommodate the largest amount of $^{239}Pu^{4+}$ (0.97 μmo1 kg^{-1}) injected.

(e) Pa^{5+}

The stable state of this poorly studied actinide appears to be Pa^{5+} *in vivo*. The eight-coordinate ionic radius of Pa^{5+}, 0.091 nm (Shannon, 1976), is smaller and the charge/radius ratio is larger than those of its quadrivalent neighbors, and it is more acidic and hydrolyzes at a lower pH (Smith and Martell, 1976; Katz *et al.*, 1986). Stability constants are not available for Pa^{5+} complexes with the low molecular weight ligands shown in Table 31.8, but complexes with those ligands and with Tf and tissue and bone glycoproteins should be as stable, if not more stable, than those formed by Pu^{4+}. Complete distribution and excretion

studies of Pa^{5+} have been conducted only in rats (Table 31.2). Distribution of the absorbed fraction of im-injected $^{233}Pa^{5+}$ in the tissue of rats – predominant deposition in the skeleton and low uptake in liver – closely resembles that of Th^{4+}. These results in rats are similar to those reported by others for im-injected $^{233}PaCl_5$ (Lanz *et al.*, 1946) or iv-injected, ultra filtered $^{233}Pa^{5+}$ citrate (Schuppler *et al.*, 1988).

There are incomplete data for the tissue distribution in baboons of iv-injected $^{233}Pa^{5+}$ (10^{-6}μg kg^{-1}) in 0.08 M citrate buffer, pH 3.2 (Ralston *et al.*, 1986). Initial excretion in urine was low (6% in 24 h). At 24 h, the Pa^{5+} content of the skeleton is estimated to be about 50% of the amount injected. Because plasma clearance of the Pa^{5+} is slow (Cohen and Ralston, 1983), much of the Pa^{5+} associated with soft tissue at early times can be accounted for by contained blood. By 21 days, when the plasma Pa^{5+} has been reduced to about 2% of the amount injected, measurements of excreta and *in vivo* γ-ray counting of the whole body indicate the following distribution of Pa^{5+} in this large animal: cumulative urine and feces 15 and 3%, respectively, skeleton 65%, all soft tissue 13%.

Ralston *et al.* (1986) reported that they also prepared an injection solution similar to the $^{233}Pa^{5+}$ described above, in which Pa was in the 6+ oxidation state. There is no evidence for the existence of a stable state of Pa higher than Pa^{5+} (Kirby, 1986b; Katz *et al.*, 1986), so it is reasonable to conclude that the procedures used to prepare the second solution made no change, and the oxidation state was Pa^{5+} in both injection media. Furthermore, the plasma clearances and whole-body retentions of the two preparations were identical, indicating that the oxidation state was the same, Pa^{5+}, in both cases.

31.2.3 The dioxo ions

(a) UO_2^{2+}

Hexavalent uranium, UO_2^{2+}, is the most stable state of U in the animal body. Many U compounds with broad ranges of composition and solubility have been fed to or inhaled by animals, and U metal fragments have been implanted in wounds. The fractions of the U that dissolve and are absorbed to blood are distributed in the tissues (skeleton and kidneys) and excreted in the urine similarly to injected $UO_2(NO_3)_2$ (Hodge, 1949; Maynard and Hodge, 1949; Stokinger *et al.*, 1949; Stradling *et al.*, 1985a,b, 1987, 1988; Hahn *et al.*, 2002).

Kidney is the only organ in which histopathological changes are seen consistently in U-poisoned animals. The nature and location of the renal injury (predominantly in the last third of the proximal tubules) are diagnostic of intake of UO_2^{2+} to blood (Voegtlin and Hodge, 1949, 1953; Hodge, 1949; Yuile, 1973). All of the U compounds studied that have any degree of dose-dependent toxicity exhibit the renal injury typical of UO_2^{2+}. The similarities to UO_2^{2+} (tissue distribution, urinary excretion, and kind and site of renal pathology) led to

the conclusion that the absorbed fractions of U compounds are converted to UO_2^{2+} under physiological conditions (Hodge, 1949; Dounce and Flagg, 1949).

The initial tissue distributions of U injected as UO_2^{2+} in the six mammalian species shown in Tables 31.2–31.7 agree well with one another, even though the sampling (postinjection) time ranged from 1 to 7 days and the UO_2^{2+} dose ranged from 2×10^{-6} μg kg^{-1} of $^{237}UO_2^{2+}$ (baboon) to 300 μg kg^{-1} of $^{233}UO_2^{2+}$ (dog). Skeleton and kidneys are the main sites of UO_2^{2+} deposition. They each contain about 12% at 4 days, on average, 3.5% is present in all other soft tissues; about 73% has been excreted, almost entirely in the urine. Linear regression analysis indicates weak correlations of tissue deposition and urinary excretion with UO_2^{2+} dosage; weakly positive for U deposition in skeleton and kidneys and weakly negative for urinary excretion. Linear regression analysis of tissue deposition and urinary excretion with time after injection predicts that at 24 h after a UO_2^{2+} injection, the U will be distributed, as follows: skeleton 15%, kidneys 18%, other tissues 5%, and urine 63%. That predicted distribution is in essential agreement with the parameters of the biokinetic model for U most recently adopted by the ICRP (1995).

The U initially deposited in the kidneys passes into the urine with a half-time of about 7 days (ICRP, 1995), until nearly all of the original U deposit has been eliminated. Nearly all of the long-retained U in the body is in the skeleton (Neuman, 1949; Yuile, 1973; Stevens *et al.*, 1980; Wrenn *et al.*, 1985).

In young rapidly growing rats, UO_2^{2+} is less toxic to the kidneys than in adults, and it is less toxic in adult male rats than in females of the same age (Haven and Hodge, 1949). Neuman (1949) observed that growing rats stored more U administered as UO_2^{2+} in their skeletons than adults and that the incomplete skeletons of adult male rats took up more U than adult females. The relative proportion of the U dose deposited in the kidneys varied inversely with U storage in bone; the kidneys of the growing rats and adult male rats were spared by diversion of larger fractions of the injected U to the skeleton.

(b) NpO_2^+, NpO_2^{2+}

The initial distributions in the tissues of im- or iv-injected $^{237}NpO_2^+$ in rats, mice, and monkeys agree well with one another (Tables 31.2, 31.3, and 31.5). Skeleton is the main site of Np deposition. Filtration into urine is the main excretory pathway, but little Np is deposited in the kidneys. At 1 to 4 days after injection, on average, 41% of the Np is in the skeleton, and the remainder is distributed as follows: liver 10%, kidneys 2%, other soft tissues 5%, urine 39%, and feces 2%. The initial distribution of circulating NpO_2^+ in the animals appears to be the result of competition between skeletal uptake and urinary excretion.

The initial distribution of Np in the tissues of a baboon-injected iv with $^{239}NpO_2^{2+}$ in 0.01 M $NaHCO_3$ was reported by Ralston *et al.* (1986), and those data are included in Table 31.6. The initial distributions of tracer quantities of $^{239}NpO_2^{2+}$ and $^{237}UO_2^{2+}$ in the baboon can be compared directly; the early

urinary excretion of the Np is much less, the skeletal deposition of Np is much greater, and Np deposition in the kidneys is much less than UO_2^{2+}. Distributions in the tissues and early urinary excretion of the dioxo Np ions are nearly the same regardless of the animal (rat, mouse, monkey, baboon), the reported valence state of the Np (NpO_2^+, NpO_2^{2+}), the injected dose of Np (range, 4×10^{-7} μg kg^{-1} of $^{239}NpO_2^{2+}$ or $^{239}NpO_2^+$ in baboons to 360 μg kg^{-1} of $^{237}NpO_2^+$ in rats), or the chemical composition of the injection medium (dilute nitric acid, isotonic saline, or citrate or bicarbonate buffer). Combined, these observations indicate that NpO_2^{2+} is unstable *in vivo* with respect to reduction to NpO_2^+.

Under the conditions of poorly oxygenated, slowly flowing tissue fluid at an im wound site in rats, 200 μg kg^{-1} of $^{233}UO_2^{2+}$ was rapidly and quantitatively absorbed (Table 31.2). In contrast, absorption of 360 μg kg^{-1} of $^{237}NpO_2^+$ injected im was slow (22% at 1 day and 62% at 30 days, Morin *et al.*, 1973). Those results suggest some reduction to Np^{4+} at the wound site.

(c) PuO_2^{2+}

In several early studies of Pu distribution in animal tissues, mice, rats, rabbits, and dogs were injected iv or im with $^{239}PuO_2^{2+}$ (Finkle *et al.*, 1946; Painter *et al.*, 1946; Van Middlesworth, 1947; Carritt *et al.*, 1947; Kisieleski and Woodruff, 1948, Scott *et al.*, 1948b). Complete data sets are available only for rats, and those shown in Table 31.2 are representative for rats injected im with $^{238}PuO_2^{2+}$ citrate or iv with $^{239}PuO_2(NO_3)_2$. The deposition pattern of PuO_2^{2+} in rats (Table 31.2) can be compared with data for both Pu^{4+} and UO_2^{2+} in several animal species (Tables 31.2–31.7). The initial tissue distribution of Pu given as PuO_2^{2+} does not resemble that of its analog UO_2^{2+}, but is nearly the same as that of Pu^{4+}.

The early association of about 5% of iv-injected PuO_2^{2+} with red blood cells (Painter *et al.*, 1946) resembles UO_2^{2+} (Lipsztein, 1981), but not Pu^{4+} (Stover *et al.*, 1959). Urinary excretion of PuO_2^{2+} in the first 24 h was much less than for PuO_2^{2+} and only somewhat greater than for Pu^{4+}. Retention of Pu in the kidneys after injection of PuO_2^{2+} was much less than for UO_2^{2+} and about the same as that of Pu^{4+}. Absorption of Pu after im injection of $^{239}PuO_2Cl_2$ was slower and much less efficient than for UO_2^{2+}, but faster than for the same mass of im-injected $^{239}PuCl_4$ (Scott *et al.*, 1948b). Combined, these results indicate that PuO_2^{2+} is unstable *in vivo* with respect to reduction to Pu^{4+}.

31.3 ACTINIDE TRANSPORT IN BODY FLUIDS

31.3.1 Composition of mammalian plasma and tissue fluid

The concentrations of the major electrolytes in normal human blood plasma listed in Table 31.9 include cations that compete with actinide ions for circulating bioligands and low molecular weight anions with the potential for actinide

Table 31.9 *Concentrations of low molecular weight electrolytes in human plasma and urine, and estimated concentrations in fluid entering last third of proximal ural tubules.*

	Concentration (mM)		
Electrolyte	*Plasma and tissue fluid*	*Late proximal tubule fluid*[a]	*Bladder urine*[b]
Na^+	140[b]	140	130
K^+	5[b]	5	44
Ca^{2+}	1.5[c]	2	4
Cl^-	110[b]	110	140
HCO_3^-	25[b]	8.8	1.6
HPO_4^{2-}[d]	1[d]	0.5	20
Citrate	0.1[d]	0.1[e]	4
pH	7.4	6.5[e]	6.0

[a] Calculated from human plasma concentrations and data of Wong *et al.* (1986) for electrolyte concentrations at last accessible micropuncture site in proximal tubules of *Cercopithicus aethiops* monkey kidneys.
[b] Altman and Dittmer (1971); Gamble (1954).
[c] Ultrafilterable fraction of plasma Ca^{2+} (Neuman and Neuman, 1958; Bronner, 1964).
[d] Total phosphate; distribution in plasma is 81% HPO_4^{2-} and 19% HPO_4^- (Neuman and Neuman, 1958; Youmans and Siebens, 1973).
[e] Estimated.

complexation. The concentrations of the major electrolytes in the plasma of the laboratory animals used in the studies of tissue distribution (Tables 31.1–31.7) differ little from each other or from those in human plasma (Altman and Dittmer, 1971; Loeb and Quimby, 1999).

Table 31.10 lists the fluid volumes (plasma, interstitial fluid) and the concentrations of proteins and iron in the plasma of the laboratory animals and human adults. Even though there is a 2000-fold range of body weight from mouse to man, their fractional plasma and tissue fluid volumes are similar. The mean fractional plasma and tissue fluid volumes of the animals are 43 ± 8 and 210 ± 39 mL kg^{-1} body weight, respectively, similar to those of human adults. The concentrations of albumin, globulins, and Tf, the iron-transport protein of mammalian plasma, do not vary greatly among the animals and man. However, the concentration of plasma iron and the numbers of Tf-binding sites normally occupied by iron (saturation) differ among the species. Tf Fe-saturation, which ranges from 33 to 44% for the larger animals (beagle, nonhuman primates, man) and from 59 to 74% for the small rodents, is inversely correlated with body weight (Table 31.10) and directly correlated with metabolic rate (Brody, 1945).

31.3.2 Circulation of extracellular fluid

Foreign ions taken into the mammalian body are transported in the circulating extracellular fluid (ECF), which is actually two communicating compartments. The plasma is the fluid phase of the blood, and it is confined within the blood

Table 31.10 *Fluid volumes and protein and iron concentrations in plasma of mature laboratory animals and human adults.*

	Mouse	*Rat*	*Beagle dog*	*Macaque monkey*	*Human adult*
Body weight (kg)[a]	0.035[b]	0.25	10	6.2	70[c]
Plasma (mL kg^{-1})	50[b]	36[d]	49[e]	36[f]	43[c]
Interstitial water (mL kg^{-1})	180[b]	250[g]	230[g]	170[g]	200[c]
Serum albumen (mM L^{-1})[a]	0.56	0.60	0.52	0.64	0.65[g]
Serum globulins (mM L^{-1})[a]	0.14	0.22	0.19	0.25	0.21[g]
Transferrin (mM L^{-1})[h]	0.036	0.033	0.032	0.040	0.027
Serum iron (mM L^{-1})[a]	0.053[i]	0.039	0.025	0.032	0.018[j]
Transferrin saturation (%)[k]	74	59	39	40	33[i]

[a] Loeb and Quimby (1999). Body weights and serum protein and iron concentrations for all animals unless otherwise noted.
[b] Durbin *et al.* (1992).
[c] ICRP (1974). Reference man.
[d] Everett *et al.* (1956).
[e] Stover *et al.* (1959).
[f] Gregerson *et al.* (1959).
[g] Altman and Dittmer (1971).
[h] LeBoeuf *et al.* (1995).
[i] Fairbanks and Beutler (1995).
[j] Transferrin concentration calculated from total iron binding capacities of mouse (Durbin *et al.*, 1992); human adult (Fairbanks and Beutler, 1995); other animals (Loeb and Quimby, 1999).
[k] Calculated from serum iron and transferrin concentrations, assuming 2 moles iron bound by 1 mole transferrin.

vessels. The interstitial (tissue) fluid is outside the vascular system, and it bathes the body cells and their supporting connective tissue.

Mammalian plasma is a steadily flowing, well-mixed, nearly neutral (pH 7.4), dilute saline solution containing numerous solutes (electrolytes and proteins) at closely regulated concentrations. The plasma water and filterable (low molecular weight, nonprotein constituents) are in steady-state exchange with the tissue fluid by outward diffusion though the arterial ends of the capillaries and inward diffusion at the venous ends, at a rate in human adults of about one plasma volume per min. The capillary walls are not completely impermeable, and between 50 and 100% of plasma proteins escape through the capillaries and reenter the blood via the lymphatic circulation daily (Cronkite, 1973). The composition of the tissue fluid approximates an ultrafiltrate of the plasma. It contains small molecules and electrolytes at about the same concentrations as the plasma, but the protein concentration is less than 20% of that in the plasma. The tissue fluid is the medium that transports the filterable dissolved solutes of the plasma to the body cells, and it transports cell products and wastes back into the plasma.

More tissue fluid is produced at the arterial ends of the capillaries than is withdrawn by diffusion back into the venous capillaries. That excess fluid and

the escaped protein are drained away and returned to the plasma by colocated lymph capillaries. The concentration of protein in lymph is somewhat greater than that in the tissue fluid.

31.3.3 Loose connective tissue

Tissue fluid does not flow freely; it penetrates and is confined within the loose connective tissue that fills the spaces between the capillaries and the cells of most tissues and organs. Loose connective tissue is composed of fine collagen and elastin fibers embedded in a colloidal gel hydrated by the tissue fluid. The solids of the gel are hydrated high molecular weight mucopolysaccharides (hyaluronic and chondroitin sulfuric acids) and glycoprotein. Both the structural proteins and the components of the connective tissue gel contain potential metal-binding sites – the carboxyl groups of the mucopolysaccharides, the carboxyl (aspartic and glutamic acid) and hydroxyl (tyrosine) side chains of the proteins, and the sialic acid side chains of the glycoproteins (Dounce and Lan, 1949; Passow *et al.*, 1961; Rothstein, 1961; Taylor, 1973a,b; Ham, 1974; Luckey and Venugopal, 1977; Pecoraro *et al.*, 1981).

31.3.4 Distribution of actinides in plasma

Trace quantities of multivalent cations circulate in the body fluids as complexes (Taylor, 1972, 1998; Luckey and Venugopal, 1977). Any complexing species such as citrate ion injected with a foreign cation is rapidly diluted and removed from the circulation, and the cation must form new complexes with the filterable low molecular weight plasma constituents (Table 31.9) or with nonfilterable plasma proteins (Table 31.10) or both.

Distribution of actinide ions among the constituents of mammalian blood plasma has been studied in plasma and serum (plasma minus fibrinogen and clotting factors) of rats and dogs injected iv with soluble actinides (*in vivo*) and in whole blood, plasma or serum of rats, dogs, and human adults and purified plasma constituents incubated with actinide solutions (*in vitro*).

The analytical techniques have included: ultrafiltration, electrophoresis, electrodialysis, size exclusion and ion-exchange chromatography, immunochromatography, immunoprecipitation, protein precipitation, and spectroscopy. The information provided by those studies is mainly semiquantitative, because each procedure tends to disturb the natural speciation of the system (reviewed by Taylor, 1998). Furthermore, in the living animal competition for injected actinide ions among the plasma constituents and between the plasma constituents and the tissue ligands continually shifts the chemical speciation in the plasma compartment in favor of the most stable complex(es) (Dounce, 1949; Stevens *et al.*, 1968; Turner and Taylor, 1968a,b; Durbin *et al.*, 1972; Durbin, 1973; Ramounet *et al.*, 1998).

(a) Filterable low molecular weight ligands

The stabilities of actinide complexes with a given ligand, including the OH of water, increase in the order: $MO_2^+ < MO_2^{2+} \sim M^{3+} < M^{4+}$. For actinides of the same electric charge, e^-, the stabilities of complexes with the same ligand generally increase with decreasing ionic radius, r. The net effect is increased stabilities of complexes with the increasing ratio of electric charge to ionic radius, e/r. The most stable complexes formed by the 'hard' actinide ions are those with ligands that contain oxygen as the electron donor group. In general, the stabilities of the actinide complexes with such groups are in the order: $SO_4^{2-} < CO_2^- < CO_3^{2-} \sim PO_4^{3-}$ (Ahrland, 1986).

Most of the actinide ions introduced into mammalian plasma *in vivo* or *in vitro* tend to associate predominantly with plasma proteins, but in all cases an ultrafilterable low molecular weight fraction has been identified, ranging from small (<10%) for the trivalent, tetravalent, and pentavalent actinides (Stevens *et al.*, 1968; Popplewell and Boocock, 1968; Turner and Taylor, 1968a,b; Bruenger *et al.*, 1971a) to large (≥50%) for UO_2^{2+} and NpO_2^+ (Dounce, 1949; Bruenger *et al.*, 1971b; Stevens *et al.*, 1980; Guilmette *et al.*, 1982).

Stability constants (log K_1) of one-to-one complexes with several of the low molecular weight ligands present in mammalian plasma are shown in Table 31.8 for the actinides that have been studied in animals and humans (Tables 31.1–31.7). Table 31.8 also includes the ionic radii of those actinide species (Shannon, 1976), assigning coordination number 6 (CN 6) for the trivalent actinides and the dioxo actinide cations, MO_2^+ and MO_2^{2+}, and CN 8 for the tetravalent and pentavalent actinides. The ionic radii are included to emphasize the relationships among ionic charge and ionic radius (charge–radius ratio, e/r) and the tendencies of the metal ions to hydrolyze and form stable complexes. The first hydrolysis constants for the actinides are shown for comparison with the other ligands, because at the nearly neutral pH of mammalian plasma, in the absence of stable complexing ligands, all of the actinides that have been administered to animals, with the possible exception of NpO_2^+, would be expected to hydrolyze and form colloidal hydroxides intravascularly.

(*i*) *Citric and other alpha-hydroxy dicarboxylic acids*

Citrate ion is the only low molecular weight ligand in mammalian plasma that is competitive with OH^- for all of the actinides studied (Table 31.9), and it is the only competitive ligand for the trivalent actinides. Dicarboxylic acids and phosphate may also compete with OH^- for the tetravalent actinides, and carbonate is competitive for the MO_2^{2+} dioxo actinide ions.

In addition to citrate, other alpha-hydroxy 3- and 4-carbon dicarboxylic acids (malic, oxaloacetic, tartaric) stably bind UO_2^+. These tridentate ligands bind

metal ions through the alpha OH group as well as the two carboxylate groups, forming stable five- and six-membered chelate rings. Those ligands form UO_2^{2+} complexes that are stable enough to prevent and to reverse the inhibitory binding of UO_2^{2+} to protein enzymes (Singer *et al.*, 1951). Low concentrations of three alpha-hydroxy dicarboxylic acids (malic, oxaloacetic, isocitric) are present in human plasma (Table 31.9), and their combined concentration is about the same as that of citrate ion. Those organic acids may also participate in actinide complexation in the plasma.

A small fraction of the filterable plasma Ca^{2+} circulates as a citrate complex (concentration about 7×10^{-5} M, Neuman and Neuman, 1958). The concentration of plasma citrate is about 10^{-4} M (Table 31.9), so nearly 70% of the circulating citrate ion is bound to Ca^{2+}. The stabilities of the citrate complexes with trivalent and tetravalent actinides (Table 31.8) are several orders of magnitude greater than that of Ca-citrate (log K_f=3.2, Martell and Smith, 1977), and they can be expected to compete with Ca^{2+} for citrate *in vivo*.

When citrate complexes of the tri- and tetravalent actinides are injected iv, the subsequent behavior of the metal ion demonstrates that the injected complexes are transient and less stable than the complexes that the metal ions can form with plasma protein(s) and tissue ligands. In rats and dogs within 2 h after iv injection of the Pu–citrate complex, 90% of the Pu^{4+} in the plasma was found by gel chromatography to be bound to nonfilterable protein(s); by 24 h after the injection less than 5% of the circulating Pu^{4+} was associated with filterable low molecular weight species. Concurrently, excretion of Pu^{4+} in the urine, which is a modified, concentrated ultrafiltrate of plasma, declined rapidly demonstrating the disappearance of the originally ultrafilterable citrate complex from the plasma (Stevens *et al.*, 1968; Turner and Taylor, 1968a; Durbin *et al.*, 1972).

The presence of low concentrations of ultrafilterable citrate complexes of Pu^{4+}, Am^{3+}, and Cm^{3+} in plasma was shown indirectly through identification of their citrate complexes as the major, if not the only, species of those actinides in urine (Popplewell *et al.*, 1975; Stradling *et al.*, 1976). It is reasonable to assume that small amounts of other actinides and foreign metal ions circulate as citrate complexes that can be ultrafiltered by the kidneys and excreted in the urine.

Citrate ion, injected locally soon after Pu^{4+} is deposited in an im wound, is capable of complexing and hastening Pu^{4+} absorption (Volf, 1975).

(*ii*) *Carbonate and bicarbonate*

Most carbonates are sparingly soluble, but the actinide dioxo ions form stable carbonate complexes at physiological pH (Smith and Martell, 1976; Ahrland, 1986). The special cases of *in vivo* transport of UO_2^{2+} and NpO_2^{+} as carbonate complexes are discussed below.

3.4.2 Nonfilterable plasma proteins

(a) Albumin and the globulins

Serum albumin and globulin are globular proteins that are soluble in dilute saline. In normal human plasma, albumin transports about 26% of Ca^{2+} and globulins transport about 7%. Ca^{2+} has low affinity for amino groups and monocarboxylic acids like acetate, but it is strongly chelated by polycarboxylic and hydroxycarboxylic acids like citrate (Neuman and Neuman, 1958). The serum proteins contain abundant amino acids with –COOH side chains (aspartic acid, glutamic acid, cystine), –OH side chains (serine, threonine, hydroxyproline), and phenolic side chains (tyrosine) (Hawk *et al.*, 1947). However, only carboxylate or hydroxyl side chains of the amino acids in close proximity to one another in the protein structure are able to bind Ca^{2+} and other multivalent cations.

The affinities of the serum proteins for cations depend on both their amino acid composition and the spatial arrangement of those amino acids and the binding units of their residues. The globular structures of the serum proteins are determined and maintained by the continuous coiling, bending, and folding of the polypeptide chains, which provide close approach of amino acid side chains that are widely separated in the primary (elongated) structure. That folded lattice-like three-dimensional structure provides numerous carboxyl and hydroxyl groups positioned suitably for metal binding (Schwartz and Fien, 1973). Nonspecific binding to serum proteins has been described for UO_2^{2+}, the trivalent lanthanides, and other multivalent metal ions (Painter *et al.*, 1946; Dounce and Lan, 1949; Gurd and Wilcox, 1956; Clarkson, 1961; Passow *et al.*, 1961; Rothstein, 1961; Kyker, 1962; Stevens *et al.*, 1965, 1968; Popplewell and Boocock, 1968; Stover *et al.*, 1968a; Bruenger *et al.*, 1969b, 1971b; Taylor, 1973a,b; Ham, 1974; Luckey and Venugopal, 1977).

The total concentrations of Ca^{2+} and Mg^{2+} in normal human plasma are about 2.5 and 1.0 mM, respectively. Assuming that Ca^{2+} and Mg^{2+} are distributed similarly among the constituents of plasma and that the strengths of their binding to the plasma proteins are similar, the fractions of the metal-binding sites of the plasma proteins normally occupied by the alkaline earth elements can be estimated. In human plasma, about 0.65 mM of Ca^{2+} is bound to albumin and about 0.17 mM is bound to the globulins; 0.26 and 0.07 mM of plasma Mg^{2+} are assumed to be associated with albumin and the globulins, respectively. The maximum Ca^{2+} and Mg^{2+} binding capacities of the plasma albumin and globulins are, on average, 11 and 6 moles of metal per 10^5 g of protein, respectively (Neuman and Neuman, 1958). The concentrations of albumin and the globulins in plasma are 6.5×10^{-4} and 21.0×10^{-4} M, respectively (Table 31.8). The mean molecular weights of serum albumin and the globulins are about 67 000 and 160 000, respectively (Hawk *et al.*, 1947). Calculations suggest that about 22% of the potential metal-binding sites of the plasma

proteins are normally occupied. Thus, binding sites are available for occupancy by foreign cations without need to displace their normal loads of Ca^{2+} and Mg^{2+}.

Nonspecific binding of the actinides by the plasma proteins is likely to be stronger than that of the alkaline earths, but weaker than specific binding to Tf (see below). The abundances of the plasma proteins and their potential binding sites may favor nonspecific actinide binding strong enough to withstand renal filtration, but too weak to compete with the ligands in liver, bone, and connective tissue.

(b) Transferrin

(*i*) *Structure*

Iron is transported in the plasma of mammals as Fe^{3+} bound to Tf, a specialized glycoprotein of molecular weight 79.6 kDa that migrates electrophoretically with the β-globulins. The amino acid sequence of transferrin has been defined. Each end of the Tf molecule has a globular sialoprotein moiety at which one Fe^{3+} atom may be bound in association with one bicarbonate molecule. The two iron-binding sites of Tf differ slightly. The C-terminal site is larger and binds Fe^{3+} more tightly than the smaller N-terminal site. At pH 7.4, the C-terminal site has an affinity for Fe^{3+} about five times greater than that of the N-terminal site. However, the weaker N-terminal site is preferentially occupied by Fe^{3+}, so kinetic and/or access factors may be more important than thermodynamic effects. Iron binding by Tf is pH-dependent, and Fe^{3+} is released at pH < 7.4.

(*ii*) *Function*

Tf is a true carrier molecule in that it is conserved for many cycles of Fe^{3+} delivery to the erythroblasts and reticulocytes (early and late stages of developing red cells) in the red bone marrow. Iron-bearing Tf, preferentially diferric Tf, binds to cell surface Tf receptors, forming clusters in surface pits, and these are internalized by endocytosis. Inside the developing red cells, the Fe–Tf receptor complex is contained in coated vesicles, which fuse with endosomes. Within the endosomes, the low pH ($\sim$5) releases one Fe^{3+} presumably from the N-terminal site. Release of a second Fe^{3+} may be mediated by other molecules and may involve reduction of Fe^{3+} to Fe^{2+}. Neither the Tf nor the Tf-receptor is degraded in the process. The Tf–Tf-receptor complex minus one or two Fe^{3+} atoms is returned to the cell membrane where, at pH 7.4, apotransferrin (iron-free Tf, apoTf) and/or monoferric Tf are released to the interstitial fluid and ultimately reenter the plasma to take up more Fe^{3+}. In addition to the developing red blood cells, hepatic cells and to a lesser degree most other cells possess surface Tf receptors and are able to endocytose Tf. When Tf is fully saturated with iron,

the iron absorbed from the GI tract is deposited in the liver (Katz, 1970; Aisen and Listowsky, 1980; Fairbanks and Beutler, 1995).

Tf is synthesized mainly in the parenchymal cells of the liver. At any time about 50% of the exchangeable Tf is located extravascularly in interstitial fluid, and it is returned to the plasma compartment with a half-time of about 17 h. As is the case with the other serum proteins, Tf is destroyed at a first-order rate. Its survival half-time of about 9 days is significantly shorter than that of serum albumin. The sites of Tf destruction are believed to be liver and kidneys (Katz, 1970).

(*iii*) *Binding of foreign metal ions*

Tf binds Fe^{3+} ($r = 0.0645$ nm, $e/r = 46.5$ e nm^{-1}) in preference to other biologically essential metal ions. Iron binding at both sites involves deprotonation of two tyrosine moieties and the association of one bicarbonate molecule. If a foreign multivalent cation is to occupy either binding site, it must be small enough to fit into the Fe-binding cavity, and have sufficient charge density (e/r) to deprotonate both of the two tyrosine phenols required for stable binding (Luk, 1971; Harris *et al.*, 1981).

Metal coordination with apoTf was investigated by spectrophotometric titration of the Tf complexes of metal ions with a broad range of electric charge and ionic radius. Two tyrosines were coordinated at both binding sites by the small transition metal ions and the smaller lanthanides; each Tf molecule bound two metal ions and released four tyrosine protons (Fig. 31.2, Pecoraro *et al.*, 1981). The larger lanthanide ions were able to fit only into one Fe-binding site, presumably the larger C-terminal site, and the number of coordinated tyrosines per Tf molecule decreased from four to two. Because of the size difference in the two sites, the larger Th^{4+} ion is bound stably at one site and weakly at the other, whereas the smaller Zr^{4+} and Pu^{4+} ions are expected to be bound stably at both sites. Europium appears to be an indicator of the maximum size (0.095 nm) of a multivalent cation that can fit into and bind stably at both Tf-binding sites, whereas the larger La^{3+}, Am^{3+}, and Cm^{3+} ions are expected to bind only at the larger C-terminal site.

(c) Actinide binding by transferrin

Under appropriate experimental conditions all of the actinides investigated, except NpO_2^+ form variably stable complexes with plasma Tf (Popplewell and Boocock, 1968; Stevens *et al.*, 1968; Stover *et al.*, 1968a; Turner and Taylor, 1968a,b; Bruenger *et al.*, 1969b, 1971b; Taylor, 1970, 1998; Stevens and Bruenger, 1972; Durbin *et al.*, 1976; Cooper and Gowing, 1981; Peter and Lehmann, 1981; Guilmette *et al.*, 1982; Wirth *et al.*, 1985; Taylor and Farrow, 1987; Paquet *et al.*, 1996). The apparent stabilities of those actinide Tf

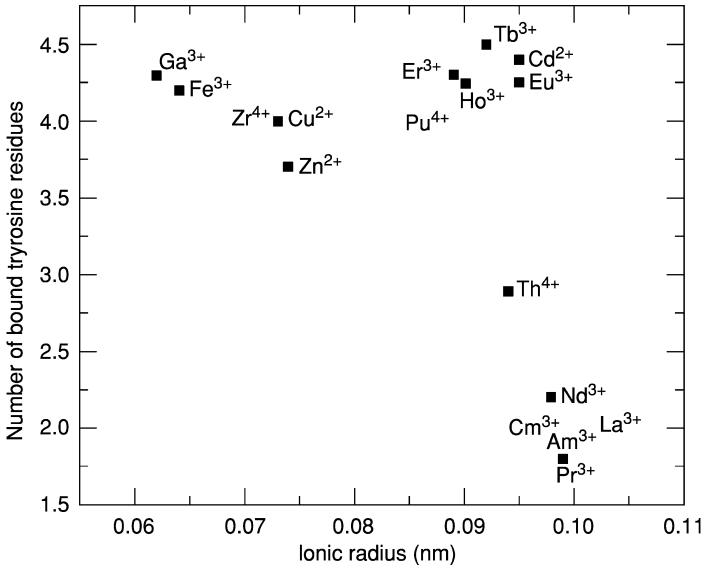

Fig. 31.2 *Number of tyrosine moieties engaged in binding metal ions as related to their six-coordinate radii* (*Shannon*, 1976). *Data of Harris* et al. (1981) *and Pecoraro* et al. (1981). *Not measured but noted by their elemental abbreviations are* Zr^{4+} *and* Pu^{4+}, *which are small enough to fit into both Fe-binding sites and displace four tyrosine protons, and* La^{3+}, Am^{3+}, *and* Cm^{3+}, *which are too large to occupy the smaller N-terminal site and would be expected to displace only two tyrosine protons per transferrin molecule.*

complexes is in the order expected based on their tendencies to form stable complexes:

$$Pa^{5+} > Pu^{4+} > Th^{4+} > Np^{4+} \gg UO_2^{2+} > Cf^{3+} > Am^{3+} > Cm^{3+}$$

Each Tf molecule possesses only two Fe-binding sites, and the concentrations of Tf in mammalian plasma are low (Table 31.10). Thus, the capacity of circulating Tf for transporting actinide ions is limited by both the total number of binding sites and the number of sites not already occupied by Fe^{3+}, that is, the degree of Fe saturation of the Tf. Stover *et al.* (1968a,b) showed that Tf binding of Pu^{4+} in plasma varied inversely with Fe–Tf saturation, and that relationship has also been demonstrated for Th^{4+} and Np^{4+} (Peter and Lehmann, 1981; Wirth *et al.*, 1985).

The actinide Tf complexes, with the possible exception of Pa^{5+}–Tf, are less stable than Fe–Tf, and the actinides are readily displaced from Tf by adding Fe^{3+} to the reaction medium (Popplewell and Boocock, 1968; Stover *et al.*, 1968a; Peter and Lehmann, 1981; Wirth *et al.*, 1985). Similarly to Fe–Tf, the Pu^{4+}, Th^{4+}, and UO_2^{2+} Tf complexes are pH-dependent and they begin to dissociate at pH < 7 (Bruenger *et al.*, 1971b). Presumably, the stabilities of the

Tf complexes with the other actinides are similarly pH-dependent (Popplewell and Boocock, 1968; Bruenger *et al.*, 1971b; Stevens *et al.*, 1980).

(d) Association of actinides with erythrocytes

The trivalent and tetravalent actinides form variably stable complexes with the Fe-transport protein, Tf, and the iron storage protein, ferritin, but they are not incorporated into hemoglobin or associated with the stroma of erythrocytes (red blood cells).

The primary function of Tf is delivery of iron to the developing erythroblasts in the red bone marrow for synthesis of hemoglobin. Iron-bearing Tf binds to specific Tf-receptors on the erythroblast surfaces, and the complete complex, Fe–Tf–Tf-receptor, is internalized by endocytosis. Within the erythroblasts, the complex is taken up by lysosomes, where the reduced pH (5 to 5.5) causes dissociation of the complex and release of Fe^{3+}. The released Tf is extruded from the cells for reuse (Aisen and Listowsky, 1980).

The simplest explanation for the absence from the interior of the erythroblasts of actinides and other multivalent cations that bind to Tf is that the foreign metal ions bound to Tf induce a conformational change in the protein structure that is not recognized by the erythroblast Tf-receptor. It is possible, but less likely, that foreign metal ions like Pu^{4+}, freed from their pH-dependent Tf complexes at the low lysosomal pH, are rapidly shuttled out of the erythroblasts, bound to new Tf molecules, extruded at the cell surface, and recirculated. However, because the latter mechanism probably would be imperfect, small amounts of residual foreign metal ions could be left in the red cells, perhaps bound to the stroma, and that is not observed.

There is evidence that some actinides can bind transiently to the red cell membrane. Actinides in the 3+, 4+, 5+, MO_2^+, and MO_2^{2+} oxidation states were equilibrated with aliquots of whole blood *in vitro*. Except for $^{239}Pu^{3+}$ and UO_2^{2+}, the actinide concentrations in the washed red cells were $\leq$10% of those in the plasma (Chevari and Likhner, 1968; Bruenger *et al.*, 1971b; Stevens *et al.*, 1980).

Small fractions ($\leq$4%) of iv-injected UO_2^{2+} and PuO_2^{2+} are transiently associated with the red cell membrane (Painter *et al.*, 1946; Lipsztein, 1981; Durbin *et al.*, 1997a). Clearance of UO_2^{2+} from the plasma volume is much faster than the rate of release of UO_2^{2+} from the red cell membrane. Consequently, most of the U in samples of whole human blood from individuals in equilibrium with their normal daily intakes of U in drinking water and foods is associated with the red cells (Hursh and Spoor, 1973; Wrenn *et al.*, 1985).

Evaluation of the clearance of iv-injected $^{228}Th^{4+}$ citrate from the blood of beagles included measurements of the Th^{4+} bound to centrifugally separated red cells (Lloyd *et al.*, 1984a). The association of the Th^{4+} with red cells is

greater and somewhat more persistent than, but otherwise similar to, that of UO_2^{2+}. The red cell associated Th^{4+} rose rapidly from zero at the time of the injection to about 8% at 1 min and 30% at 6 h; at that time the blood Th^{4+} was about equally divided between plasma and cells. From 6 to 48 h, red cells accounted for as much as two-thirds of the Th^{4+} in whole blood, and the red cell fraction was being cleared with a half-time of about 14 h, one-half of the plasma clearance rate. By 30 days, the Th^{4+} associated with red cells was nearly 100 times that of the plasma. Between 2 and 30 days, a small fraction of the Th^{4+} was released from the red cells (3.5%) with a half-time of about 15 days. In the special case of Th^{4+}, binding to the red cell membrane is competitive with complexation by plasma Tf. Binding to the membrane is the most likely mechanism for the association of actinides with red cells. If, for example, Th^{4+} had entered the red cell interior, a much larger fraction of the 6 h maximum amount of the Th^{4+} associated with red cells would be expected to remain with the circulating red cells for a longer time (the life span of mammalian red cells is about 90 days (Cronkite, 1973)).

31.4 CLEARANCE OF ACTINIDES FROM THE CIRCULATION

Data for plasma clearances and early urinary excretion of the actinides in laboratory animals and man can be combined with the information developed for their reactions with the plasma constituents to assess their status in the circulation.

Plasma clearances of nine actinides injected iv in soluble form have been investigated in at least one mammalian species (data are not available for Ac^{3+} or Bk^{3+}). Industrially important UO_2^{2+}, Pu^{4+}, and Am^{3+} have been studied in several species. Plasma clearance data are available for two valence states of U (U^{4+}, UO_2^{2+}), two of Pu (Pu^{4+}, PuO_2^{2+}), and three of Np (Np^{4+}, NpO_2^{+}, NpO_2^{2+}). Plasma clearance curves of the actinides are shown in Figs. 31.3–31.7, in rats, mice, beagles, nonhuman primates, and human adults, respectively. The plasma clearances of iv-injected Pu^{4+}, Am^{3+}, and UO_2^{2+} in the laboratory animals and human adults are compared in Figs. 31.8, 31.9, and 31.10, respectively.

The rates of clearance of the several actinides from mammalian plasma are determined largely by their chemical properties, in particular by their tendencies to form stable complex(es) with plasma Tf. The actinides that form the most stable Tf complexes are cleared slowly, whereas those that form only weak Tf complexes are cleared at much faster rates. The order of disappearance of the actinides introduced into mammalian plasma is independent of the animal used for study (Figs. 31.3–31.7). Combining the data for all of the animals, and based

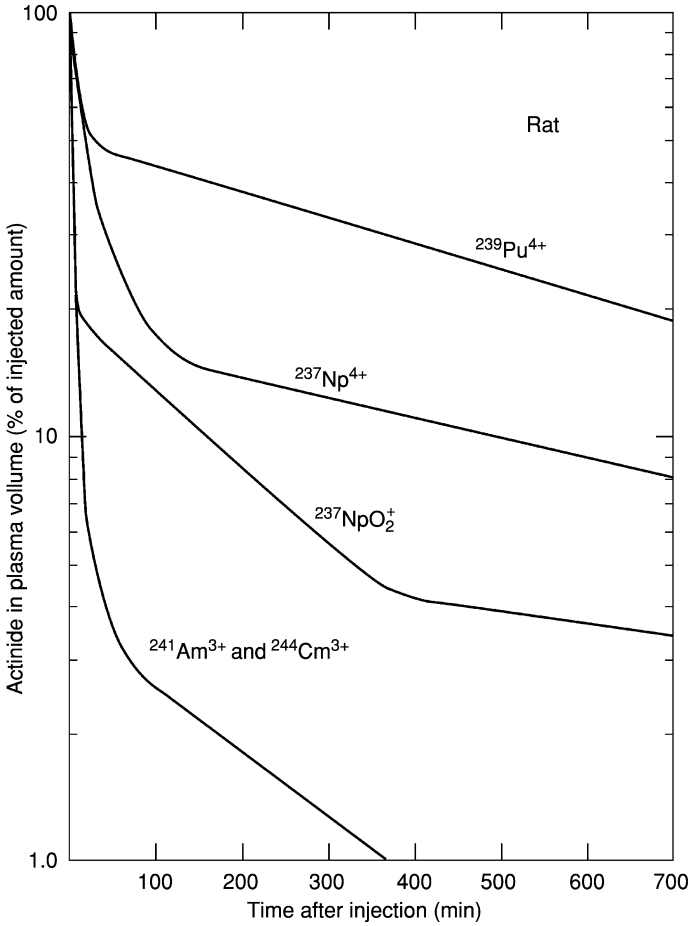

Fig. 31.3 *Clearance of iv-injected actinides from plasma volume of rats:* $^{239}Pu^{4+}$ (*Durbin* et al., 1972); $^{241}Am^{3+}$ *and* $^{244}Cm^{3+}$ (*Turner and Taylor*, 1968a); $^{237}Np^{4+}$ *and* $^{237}NpO_2^+$ (*Ramounet* et al., 1998).

on the time (min) required to clear 90% of the iv-injected actinide from the plasma volume, plasma clearance rates are in the order:

$$[UO_2^{2+}, Am^{3+}, Cm^{3+}, NpO_2^+] > [Cf^{3+}, Es^{3+}] \gg [Th^{4+}, Np^{4+}, Pa^{5+}, Pu^{4+}].$$

Note that the 90% plasma clearance measure does not differentiate among the rapidly clearing lighter trivalent actinides and the actinide dioxo ions, which are all cleared at about the same rate, but by different mechanisms.

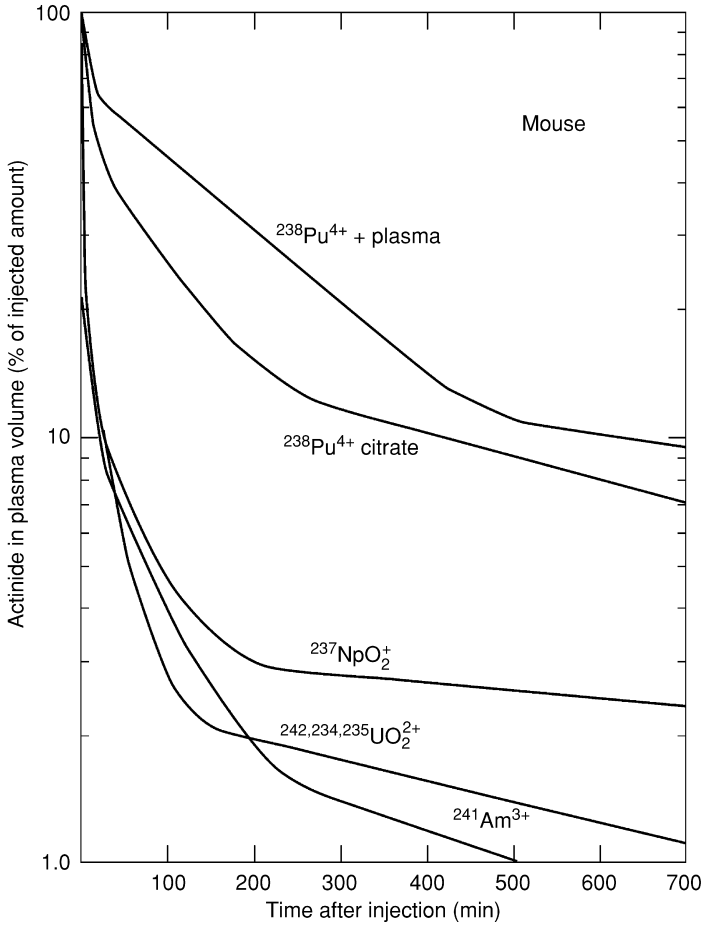

Fig. 31.4 *Clearance of iv-injected actinides from plasma volume of mice*: $^{238}Pu^{4+}$ *citrate* (*Durbin* et al., 1997b); $^{237}NpO_2^+$ (*Durbin* et al., 1998b); $^{232,234,235}UO_2^{2+}$ (*Durbin* et al., 1997a); $^{241}Am^{3+}$ and $^{238}Pu^{4+}$ + *plasma* (*P. W. Durbin and B. Kullgren, unpublished data*).

Plasma clearance of the actinides is modulated by the physiology of the animals used for study. Plasma retention of Pu^{4+}, Am^{3+}, and UO_2^{2+} in the different animals, as illustrated in Figs. 31.8–31.10, is in the order:

$$\text{adult man} > \text{dog} > \text{baboon} \geq \text{monkey} > \text{rat} > \text{mouse}.$$

Plasma actinide retention among the different animals is directly related to body size and inversely related to metabolic rate, renal filtration rate, and the degree of Fe saturation of the plasma Tf (Brody, 1945; Durbin *et al.*, 1997b; Table 31.10).

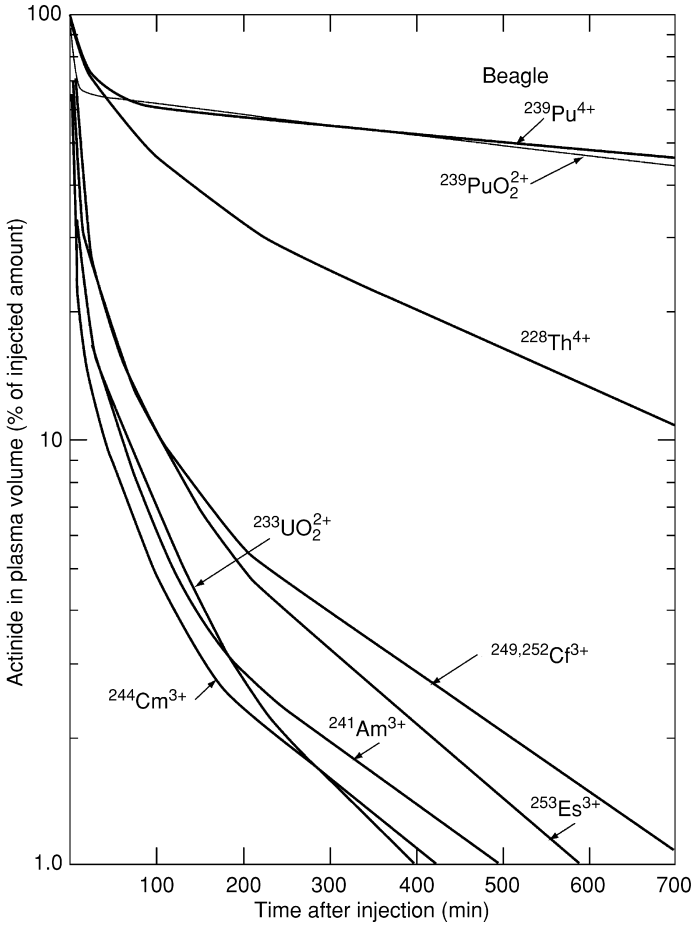

Fig. 31.5 *Clearance of iv-injected actinides from plasma volume of beagles:* $^{239}Pu^{4+}$, $^{228}Th^{4+}$, $^{241}Am^{3+}$, $^{249}Cf^{3+}$, and $^{252}Cf^{3+}$ (*Stevens and Bruenger,* 1972); $^{244}Cm^{3+}$ (*Atherton* et al., 1973); $^{253}Es^{3+}$ (*Atherton* et al., 1974); $^{233}UO_2^{2+}$ (*Stevens* et al., 1980); $^{239}PuO_2^{2+}$ (*Painter* et al., 1946).

31.4.1 Trivalent actinides

(a) Ac^{3+}

Timed plasma data for Ac^{3+} injected iv in rats are insufficient to define a clearance curve, however, the pattern of disappearance of $^{227}Ac^{3+}$ from the plasma is similar to Am^{3+} and Cm^{3+} in the same animals (Fig. 31.3). Clearance was 90% complete in about 50 min and 99% complete in about 400 min. Also

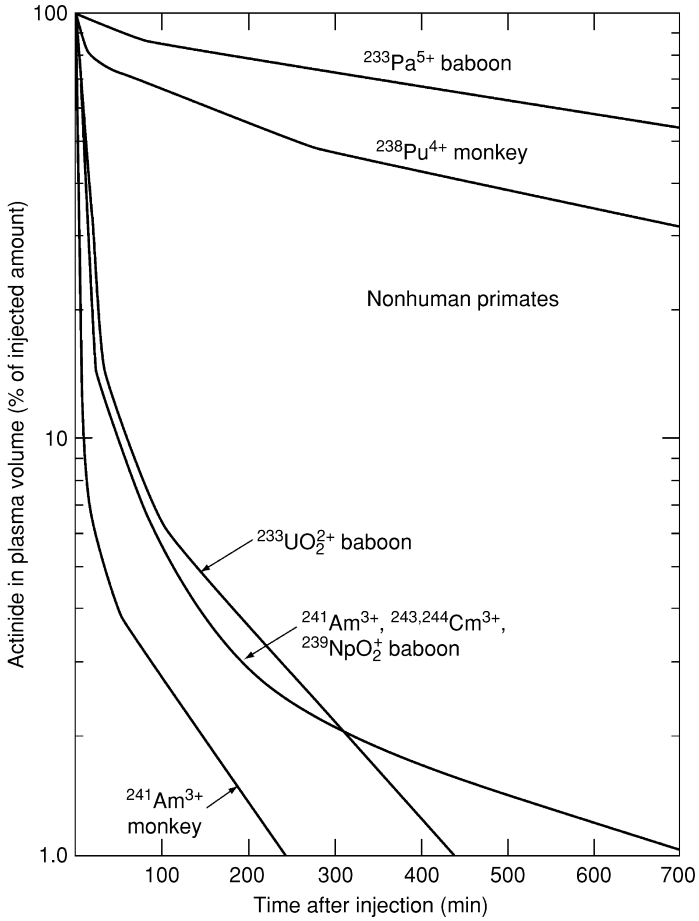

Fig. 31.6 *Clearance of iv-injected actinides from plasma volume of nonhuman primates: monkey* – $^{238}Pu^{4+}$ (*Durbin* et al., 1985), $^{241}Am^{3+}$ (*Durbin,* 1973); *baboon* – $^{241}Am^{3+}$ (*Guilmette* et al., 1980), $^{243,244}Cm^{3+}$ (*Lo Sasso* et al., 1981), $^{233}UO_2^{2+}$ (*Lipsztein,* 1981), $^{239}NpO_2^{+}$ and $^{233}Pa^{5+}$ (*Ralston* et al., 1986). (*Note: The curves for* $^{241}Am^{3+}$, $^{243,244}Cm^{3+}$, and $^{239}NpO_2^{+}$ *in the baboons coincide, and a single curve is shown for all three nuclides.*)

similarly to Am^{3+} and Cm^{3+}, tissue uptake was fast, and early urinary excretion was negligible (Taylor, 1970).

(b) Am^{3+}, Cm^{3+}, Cf^{3+}, Es^{3+}

Plasma clearances of iv-injected $^{241}Am^{3+}$ citrate or nitrate have been studied in five laboratory animals (Figs. 31.3–31.6, 31.9), and $^{243}Cm^{3+}$ or $^{244}Cm^{3+}$ citrate have been studied in three (Figs. 31.3, 31.5, and 31.6). Separate plasma curves

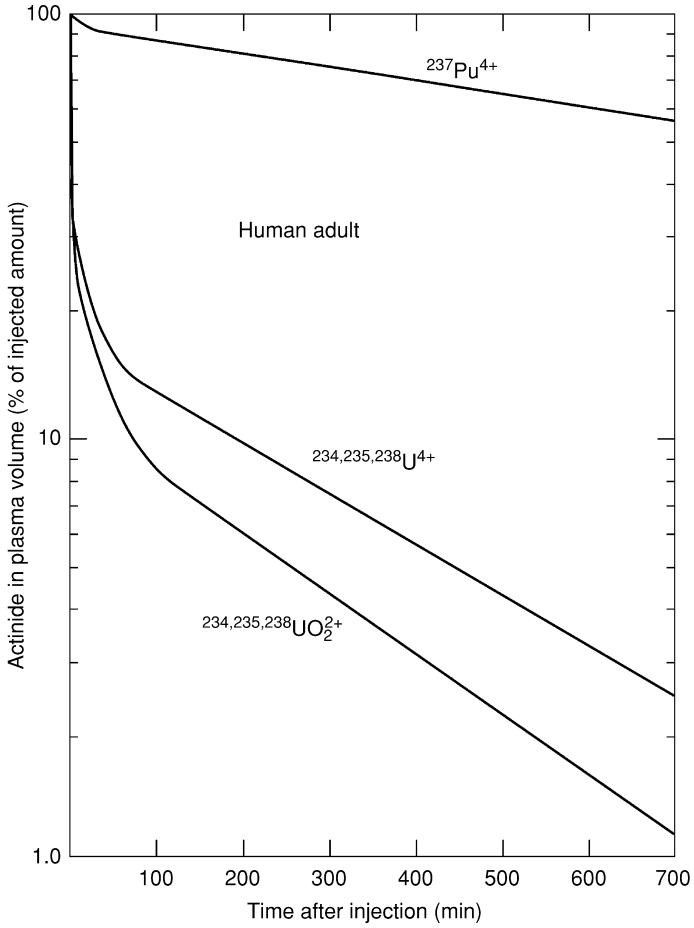

Fig. 31.7 *Clearance of iv-injected actinides from blood volume of adult human males:* $^{237}Pu^{4+}$ (*Talbot* et al., 1993); $^{234,235,238}U^{4+}$ *and* $^{234,235,238}UO_2^{2+}$ (*Bernard and Struxness*, 1957).

are not shown for Cm^{3+} in the rats (Fig. 31.3) or the baboons (Fig. 31.6), because they are indistinguishable from those for Am^{3+} in those animals. Clearances of Am^{3+} and Cm^{3+} from the plasma are fast: in all of the animals studied, they were 90% complete in 60 min and 99% complete in $\leq$600 min. Tissue uptake of both trivalent actinides is fast, and only small amounts are excreted in urine in the first 24 h (Taylor, 1962; Turner and Taylor, 1968a; Belyayev, 1969; Durbin, 1973).

Clearances of $^{249,252}Cf^{3+}$ and $^{253}Es^{3+}$ from the plasma of beagles was 90% complete in about 100 min, compared with 60 min for the two lighter larger

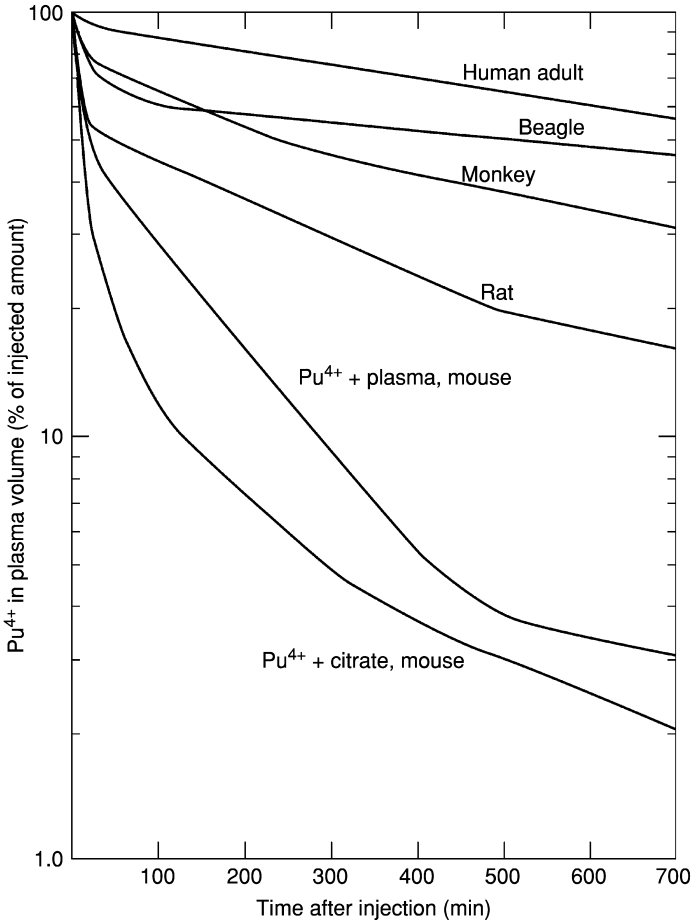

Fig. 31.8 *Clearance of iv-injected* Pu^{4+} *from plasma volume of animals and man:* $^{239}Pu^{4+}$, *rat* (*Durbin* et al., 1972); $^{238}Pu^{4+}$, *mouse* (*Durbin* et al., 1997b); $^{239}Pu^{4+}$, *beagle* (*Stevens and Bruenger,* 1972); $^{238}Pu^{4+}$, *monkey* (*Durbin* et al., 1985); $^{237}Pu^{4+}$, *adult human male* (*Talbot* et al., 1993); $^{238}Pu^{4+}$ + *plasma, mouse* (*P. W. Durbin and B. Kullgren, unpublished data*).

trivalent actinides, and the time required for 99% clearance of Cf^{3+} and Es^{3+} was about 200 min longer (Fig. 31.5). The slower plasma clearances of Cf^{3+} and Es^{3+}, compared with Am^{3+} and Cm^{3+}, confirmed the expectation that the two heavier smaller trivalent actinides would form more stable plasma protein complexes (Stevens and Bruenger, 1972; Atherton *et al.*, 1974).

Immediately after iv injection, the plasma contains rapidly declining fractions of the trivalent actinides in the form of the filterable low molecular weight complex injected (Turner and Taylor, 1968a). The major fraction apparently

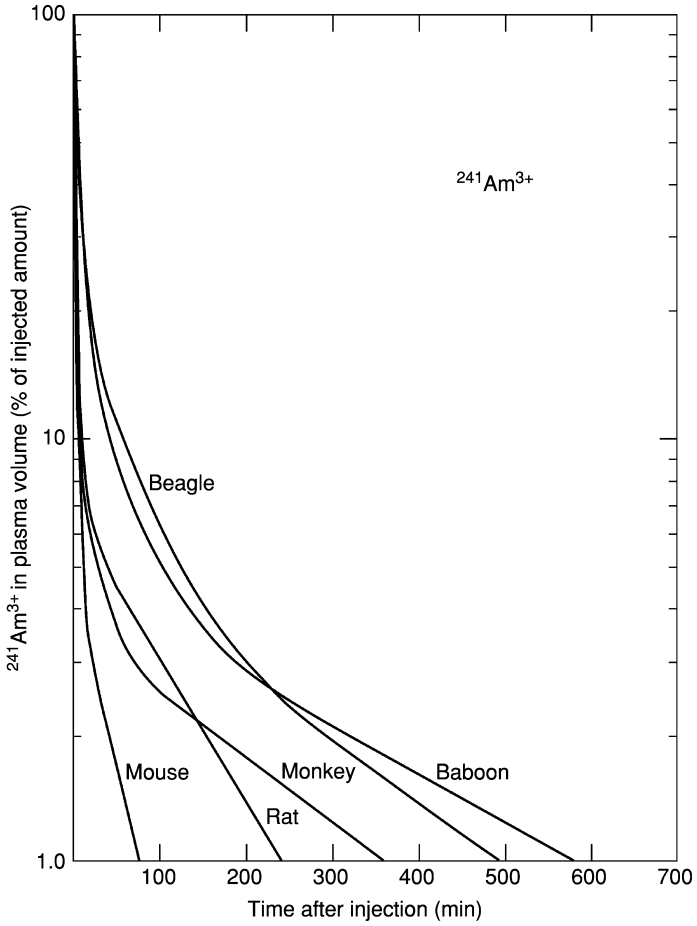

Fig. 31.9 *Clearance of iv-injected* $^{241}Am^{3+}$ *from the plasma volume of animals: rat* (*Turner and Taylor,* 1968a); *mouse* (*P. W. Durbin and B. Kullgren, unpublished data*); *beagle* (*Stevens and Bruenger,* 1972); *monkey* (*Durbin,* 1973); *baboon* (*Guilmette* et al., 1980).

forms weak nonfilterable complex(es) with Tf and other plasma proteins, which prevent renal filtration into urine, but are much less stable than the complexes that the trivalent actinides can form with ligands on hepatic cell and bone surfaces and in connective tissue.

In rats injected iv with Am^{3+} or Cm^{3+} citrate, about 50% was protein bound at 1 min and 95% was bound at 60 min (Turner and Taylor, 1968a). *In vivo* and *in vitro* studies of the associations of Ac^{3+}, Am^{3+}, Cm^{3+}, and Cf^{3+} with plasma proteins show that Tf is a major carrier of the trivalent actinides in mammalian plasma, however, those complexes are weak, and they do not survive the more

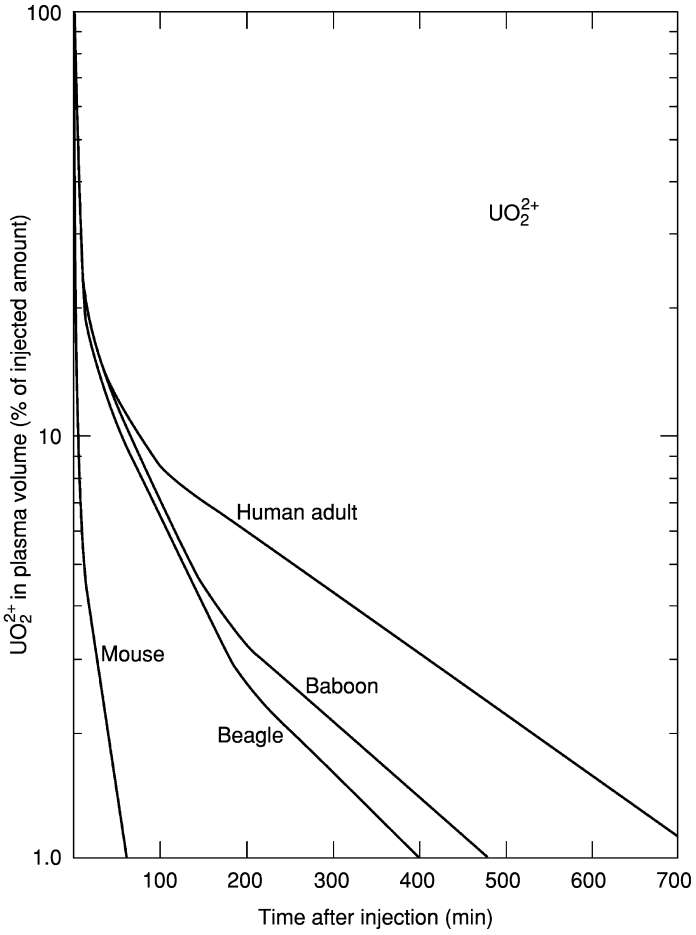

Fig. 31.10 *Clearance of iv-injected* UO_2^{2+} *from the plasma volume of animals and man:* $^{232}UO_2^{2+}$ *mouse* (*Durbin* et al., 1997a); $^{233}UO_2^{2+}$ *beagle* (*Stevens* et al., 1980); $^{233}UO_2^{2+}$ *baboon* (*Lipsztein,* 1981); $^{234,235,238}UO_2^{2+}$ *adult human male* (*Bernard and Struxness,* 1957).

rigorous analytical procedures (Popplewell and Boocock, 1968; Turner and Taylor, 1968a; Bruenger *et al.*, 1969b, 1971b; Taylor, 1970; Stevens and Bruenger, 1972; Cooper and Gowing, 1981). Provisional formation constants (log K_1) have been calculated, 5.3 and 6.5 for Am^{3+} and Cm^{3+}, respectively (Taylor, 1998), and these are similar to the value of the apparent stability constant for binding of Gd^{3+} to the C-terminal site of human Tf (Zak and Aisen, 1988).

Binding of Am^{3+} by Tf is reduced when Fe^{3+} saturation of Tf is high and eliminated altogether by addition of Fe^{3+} in excess of the Tf iron-binding

capacity (Popplewell and Boocock, 1968; Bruenger *et al.*, 1969b). The trivalent actinides also bind to plasma proteins other than Tf. Depending on the experimental conditions and the analytical methods, variable fractions of the trivalent actinides in plasma associate with the heaviest proteins and with albumin (Turner and Taylor, 1968a; Bruenger *et al.*, 1969b, 1971b; Stevens and Bruenger, 1972).

31.4.2 Tetravalent and pentavalent actinides

(a) Th^{4+}

Clearance of iv-injected $^{228}Th^{4+}$, studied only in beagles, is somewhat faster than, but comparable to that of $^{239}Pu^{4+}$ in the same animal (Fig. 31.5). Reduction to 10% occurred in 0.5 day, and 99% of the injected Th^{4+} had disappeared from the plasma in 1.5 days. A larger fraction of the Th^{4+} was excreted in 21 days than was found for Pu^{4+} (Table 31.4).

Transferrin is the main protein carrier of Th^{4+} in the plasma. The larger Th^{+} ion forms a Tf complex that appears to be less stable than the Pu^{4+}–Tf complex. Similarly to Pu^{4+}, the Th^{4+}–Tf complex is destabilized by excess Fe^{3+}. Binding of Th^{4+} to Tf is suppressed in Fe^{3+}-saturated plasma, permitting formation of less stable complexes with the heavier plasma proteins and small filterable ligands (Bruenger *et al.*, 1971a; Peter and Lehmann, 1981; Pecoraro *et al.*, 1981).

(b) U^{4+}

Clearance from the blood of iv-injected $^{234,235,238}U^{4+}$ was studied in rats (data not shown, Neuman, 1949) and an adult man (Table 31.7, Fig. 31.7; Bernard and Struxness, 1957). Based on their similar properties, the disposition of U^{4+} *in vivo* would be expected to resemble Th^{4+} and Pu^{4+}, with stable binding to plasma protein and delayed blood clearance (Tables 31.4, 31.7; Figs. 31.5, 31.7). However, disappearance from the blood of both the rats and man of U injected iv as U^{4+} was fast. In humans, it was 90% complete in 200 min and 99% complete in 24 h. During the first hour after injection, clearance from the blood of U injected as U^{4+} was nearly the same as that of UO_2^{2+} (Fig. 31.7). Thereafter, U in the blood declined at nearly the same rate as UO_2^{2+}, but the U concentration in the blood was about 1.7 times greater that of UO_2^{2+}. Overall, the clearance of U^{4+} from human blood closely resembled that of UO_2^{2+} and differed markedly from the plasma clearances of Th^{4+} and Pu^{4+} in the dogs and Pu^{4+} in adult men.

By analogy to Th^{4+} and Pu^{4+}, binding of U^{4+} by circulating Tf would be expected, but there is little evidence for such stable binding *in vivo*. The absence from the U^{4+} blood curve of a major rapidly forming and slowly clearing component argues against formation of a stable U^{4+}–Tf complex *in vivo*.

When $^{233}U^{4+}$ citrate was added to plasma *in vitro* and chromatographed on G-25 Sephadex, <10% of the U eluted with the plasma proteins (Bruenger *et al.*, 1971b).

(c) Np^{4+}

Plasma clearance of Np^{4+} was studied in rats injected iv with about 310 μg kg^{-1} (0.4 μmol per rat) of $^{237}Np^{4+}$ citrate, and plasma was sampled at 1, 2, 6, and 24 h (Fig. 31.3, Ramounet *et al.*, 1998). Paquet *et al.* (1996) injected rats iv with a tracer of $^{239}Np^{4+}$ citrate (17 pg kg^{-1}) or 1.2 mg kg^{-1} (1.1 μmol per rat) of $^{237}Np^{4+}$ citrate. Blood was sampled only at 24 h, at which time the plasma volumes of both groups contained 4 to 5% of the injected Np, in good agreement with the data of Fig. 31.3. Because no blood samples were taken sooner than 60 min after injection, the earliest phases of the plasma clearance curve for Np^{4+} are poorly defined. Renal excretion of Np at 24 h was about 20% of the amount injected regardless of the mass of Np^{4+} injected.

Based on their similar chemical properties, plasma clearances of Np^{4+} and Pu^{4+} would be expected to be similar, that is, slow clearance accompanied by slow tissue uptake and little early urinary excretion (Table 31.2). In the rats, plasma clearances of Np^{4+} and Pu^{4+} were 90% complete in 500 and 1150 min, respectively. After 2 h, their clearance rates were similar, and 99% of both actinides disappeared from the blood in 2 days. Extrapolation of the terminal slope of the Np^{4+} plasma curve (Fig. 31.3) to $t = 0$ suggests that about 16% of the injected Np^{4+} circulated bound to nonfilterable protein, compared with stable protein binding of ≥50% of the Pu^{4+}.

Sephacryl S-300 and DEAE-cellulose chromatography were used to investigate protein binding of Np in the plasma taken from rats 30 min after iv injection of 10 μCi of $^{239}NpO_2^+$ nitrate. At 30 min after injection, based on the plasma clearances of NpO_2^+ in other animals (Figs. 31.3, 31.4, and 31.6), it may be estimated that about 5% of the injected Np would still be in the plasma, most likely bound to protein. Both chromatographic techniques showed that ≥95% of the Np applied to the columns colocated with the Fe–Tf peak. Results were essentially the same when $^{239}NpO_2^+$ was incubated with rat serum *in vitro*, except that the fraction of Np applied to the columns eluting with the Tf peak was reduced to about 70%. Specific Np binding to Tf was confirmed by manipulation of the Fe saturation of the Tf; the association of the Np with the Tf peak decreased as the iron saturation of the Tf was increased. In highly Fe^{3+}-saturated preparations, larger fractions of the Np tended to be associated with both the heavier plasma proteins and with the low molecular weight solutes (Wirth *et al.*, 1985). These studies demonstrated binding of Np to Tf, but as Wirth *et al.* (1985) and Taylor (1998) suggest, it is likely to be complexation of Np^{4+} rather than of the weakly complexing NpO_2^+. These results also imply that some of the $^{239}NpO_2^+$ injected in the rats or added to rat serum *in vitro* was reduced to Np^{4+}.

(d) Pu^{4+}

Plasma clearances of iv-injected Pu^{4+} citrate are shown in Figs. 31.3–31.7 for rats, mice, beagles, monkeys, and human adults, respectively, and Fig. 31.8 compares the clearances of Pu^{4+} in all of these animals. Clearance of Pu^{4+} from the plasma is slow in all of the mammals studied. It was 90% complete in 0.2 to 0.75 day in mice and rats and 1.5 to 5 days in monkeys, beagles, and human adults. Reduction of plasma Pu^{4+} to 1% of its initial value required from 0.7 to 1 day in the rodents and 2.5 to 21 days in the larger animals and man.

Delayed clearance from the plasma of rats and dogs of iv-injected $^{239}Pu^{4+}$ or $^{239}PuO_2^{2+}$ and minimal amounts of urinary Pu excretion in the first 24 h were indications that Pu introduced into mammalian plasma was rapidly and almost quantitatively bound to nonfilterable plasma protein (Finkle *et al.*, 1946; Painter *et al.*, 1946; Muntz and Guzman-Barron, 1947; Stevens *et al.*, 1968). Slow plasma clearance of Pu^{4+} along with minimal renal excretion is evidence for rapid formation of a stable Pu^{4+} complex with plasma protein and for the slow kinetics of the exchanges of Pu^{4+} between Tf and the tissue ligands.

Transferrin is the main, if not the only, protein carrier of Pu^{4+} in normal mammalian plasma (Popplewell and Boocock, 1968; Stevens *et al.*, 1968, 1975; Stover *et al.*, 1968a; Turner and Taylor, 1968a,b; Bruenger *et al.*, 1971a; Durbin *et al.*, 1976; Lehmann *et al.*, 1983; Taylor, 1998). A provisional stability constant derived for Pu^{4+}–Tf (log K_1=21.8, Taylor, 1998) is close to but less than that derived for Fe^{3+}–Tf (log K_1=24; Raymond *et al.*, 1980). Pu–Tf is destabilized by reduction of the pH, by addition of excess Fe^{3+}, and by increasing the concentration of citrate ion to ten times that of normal plasma. The latter two reactions may contribute to the release of Pu^{4+} from Tf to competing tissue ligands.

A small fraction ($\leq$5%) of circulating Pu^{4+} is associated with low molecular weight plasma ligands, suggesting that an equilibrium exists between those ligands and the Tf-bound fraction of circulating Pu^{4+}. In highly Fe^{3+}-saturated plasma, Pu^{4+} can bind to the heavier proteins, and a larger than usual fraction associates with the low molecular weight ligands (Popplewell and Boocock, 1968; Stover *et al.*, 1968a).

(e) Pa^{5+}

Baboons were injected iv with 10^{-6} μg kg^{-1} of $^{233}Pa^{5+}$ in 0.08 M Na citrate pH 3.2, and blood was sampled frequently for 21 days (Fig. 31.5, Cohen and Ralston, 1983; Ralston *et al.*, 1986). Clearance of the Pa^{5+} from the plasma was slower than that of $^{239}Pu^{4+}$ citrate in beagles (Figs. 31.5 and 31.8), and comparable to that of $^{237}Pu^{4+}$ in adult men (Figs. 31.7 and 31.8). Plasma clearance was 90% complete in 6 days and 99% complete in 21 days. It was as slow as the plasma clearances of Pu^{4+} and Th^{4+} in the beagles, and along with low early urinary excretion, a good indication of the formation of a stable Pa^{5+} plasma protein complex.

Pa^{5+}, incubated with normal human plasma *in vitro*, was associated with the Tf peak, indicating that the stable complex was Pa^{5+}–Tf (Bruenger *et al.*, 1971b). Taylor and Farrow (1987) prepared a solution for animal injection by diluting a stock solution of $^{233}Pa^{5+}$ in 8 M HCl with normal saline and adjusting to pH 7 with $NaHCO_3$. The distribution of the Pa^{5+} in the serum from rats killed and bled at 5 and 50 min after injection was investigated by gel and ion-exchange chromatography and electrophoresis. In all procedures, the $^{233}Pa^{5+}$ was associated only with the Tf fraction of the serum proteins.

In normal mammalian plasma, Tf binds Th^{4+}, Np^{4+}, and Pu^{4+} (Peter and Lehmann, 1981; Lehmann *et al.*, 1983; Wirth *et al.*, 1985). Binding of those tetravalent actinides by Tf is reduced in Fe-saturated serum, and they are all released from their Tf complexes by treatment with excess Fe^{3+}. These findings are regarded as evidence that Fe^{3+}–Tf is more stable than the actinide^{4+}–Tf complexes. In contrast, Tf binding of Pa^{5+} was not prevented by presaturation of Tf with Fe^{3+}, nor was it reversed by addition *in vitro* of excess iron to rat serum containing Pa^{5+} (Taylor and Farrow, 1987). Those findings suggest that the Pa^{5+}–Tf complex is more stable than the Tf complexes of the tetravalent actinides and also more stable than Fe^{3+}–Tf.

(f) Summary

The charge/radius ratios of ferric iron and the tetra- and pentavalent actinides are, in units of e nm^{-1}, as follows: Pa^{5+}, 54.9; Fe^{3+}, 46.2; Pu^{4+}, 41.7; Np^{4+}, 40.8; Th^{4+}, 38.1 (eight-coordination is assumed for the actinides, six-coordination is assumed for Fe^{3+}, Table 31.8) (Shannon, 1976). Based on the positive correlation of the stabilities of actinide complexes and their charge/radius ratios, the stabilities of their Tf complexes would be predicted to be in the above order. The apparent stabilities of their Tf complexes in normal mammalian plasma relative to one another and to Fe^{3+} are in that expected order.

31.4.3 The dioxo ions

(a) UO_2^{2+}

Plasma clearance of iv-injected UO_2^{2+} has been studied in mice, beagles, baboons, and human adults (Figs. 31.4–31.7, 31.10). It was fast in all of the species studied; clearance was 90% complete in 10 to 80 min, and 99% was cleared in 60 to 700 min. Urinary excretion and uptake of UO_2^{2+} in the tissues are fast, as illustrated by measurements in mice (Durbin *et al.*, 1997a). Both processes begin immediately after the UO_2^{2+} is introduced into the blood and continue until the plasma is cleared (about 100 min). Diffusion of filterable low molecular weight complexes between the plasma and tissue fluid and weak binding to plasma protein briefly delay, but do not otherwise interfere with renal filtration of UO_2^{2+} or its deposition in the skeleton.

During the first few days after intake to blood about 85% of absorbed UO_2^{2+} is filtered through the kidneys, about 85% of the filtered fraction is eliminated in passed urine, but about 12% of the injected UO_2^{2+} is deposited in the kidneys (Tables 31.2–31.7). The UO_2^{2+} retained in the kidneys is bound mainly to the brush border of the luminal surfaces of the cells that line the proximal tubules, the site of the renal injury (Tannenbaum, 1951a,b). Binding of UO_2^{2+} to cell membranes is the presumed cause of the cell damage, but the mechanism – conformational changes, blockage of ion channels that interfere with the cell's absorptive functions, and/or inhibition of membrane enzymes required for cell respiration – is not certain (Dounce, 1949; Kirschbaum and Oken, 1979; Kirschbaum 1982; Leggett, 1989).

The large fraction of circulating UO_2^{2+} that is rapidly excreted in urine is indicative of formation of ultrafilterable UO_2^{2+} complexes with low molecular weight ligands in the plasma. Uranyl ion is rapidly and quantitatively absorbed from an im or sc injection site (Tables 31.2 and 31.5), even though formation of *in situ* poorly transportable hydrolysis products is expected at physiological pH, indicating that sufficient concentrations of ligands for UO_2^{2+} are also present in tissue fluid. Bicarbonate was presumed to be the dominant ligand for UO_2^{2+} in the body fluids; UO_2^{2+} complexes with phosphate and organic acids were considered to be of lesser importance (Dounce and Flagg, 1949; Muntz and Guzman-Barron, 1951).

The evidence for bicarbonate as the principal low molecular weight ligand for UO_2^{2+} in body fluids was indirect. Addition of HCO_3^- greatly increased the ultrafilterability of UO_2^{2+} added to blood serum. Protein precipitated with UO_2^{2+} redissolved, and enzymes inhibited with UO_2^{2+} were reactivated by addition of HCO_3^-. The urinary pH of cats and rabbits was lowered or raised by manipulation of their diets: acidification of the urine reduced UO_2^{2+} excretion and increased UO_2^{2+} deposition in the kidneys. Conversely, alkalinization increased urinary UO_2^{2+} excretion and reduced UO_2^{2+} deposition in the kidneys. Infusion of excess HCO_3^- in rabbits injected iv with UO_2^{2+} resulted in more and more rapid urinary UO_2^{2+} excretion and even less UO_2^{2+} retention in the kidneys than increasing urinary pH alone. The stability of the filtered UO_2^{2+} complex was more dependent on the concentration of HCO_3^- in the filtrate than on the pH (Dounce, 1949; Dounce and Flagg, 1949; Wills, 1949; Muntz and Guzman-Barron, 1951).

The abundance of HCO_3^- in both plasma and tissue fluid greatly exceeds those of the other low molecular weight ligands (phosphate, organic acids, Table 31.9). Uranyl carbonate complexes are more stable than those with phosphate and citric acid (Table 31.8; Grenthe *et al.*, 1992). The circulating filterable UO_2^{2+} complex is pH-dependent, whereas UO_2 citrate is stable over the physiological pH range (Dounce and Flagg, 1949).

About 40% of circulating UO_2^{2+} is bound to nonfilterable plasma protein. Based on estimated molecular weight and electrophoretic properties, the protein that bound UO_2^{2+} was originally thought to be serum albumin (Dounce, 1949;

Dounce and Flagg, 1949; Muntz and Gurman-Barron, 1951). Stevens *et al.* (1980) demonstrated that the protein that binds UO_2^{2+} in plasma is Tf. The UO_2^{2+}–Tf complex is demonstrably weaker than the complexes that UO_2^{2+} forms with carbonate. As the plasma UO_2^{2+} is depleted by glomerular filtration of the low molecular weight complexes, the equilibrium between the filterable and nonfilterable complexes is continuously reestablished by dissociation of the nonfilterable protein complex and shift to the filterable complex until UO_2^{2+} has been cleared from the plasma by renal filtration and binding to bone.

As the plasma ultrafiltrate formed by the renal glomeruli is converted to bladder urine >99% of the water and electrolytes are reabsorbed, mainly in the proximal tubules, and the pH is reduced. Bicarbonate and phosphate are preferentially reabsorbed as the fluid passes through the proximal tubule, and by the time the tubular fluid enters the last third of the proximal tubule (the site of UO_2^{2+} deposition and renal injury), their concentrations are 0.35 and 0.50, respectively, of those in the plasma (Wong *et al.*, 1986). Under these conditions UO_2^{2+} carbonate complexes formed in the plasma will become less stable.

The concentration of HCO_3^- in bladder urine is usually <1% of that in plasma, and the pH is about 6, whereas the concentrations of phosphate and citrate are slightly greater than in the plasma (Table 31.9). The UO_2^{2+} carbonate complexes formed in the plasma cannot survive the transit through the entire renal tubule system to the bladder, and the chemical form of UO_2^{2+} in urine is not likely to be the same as in the circulating fluids.

Speciation calculations can be used to identify and provide estimates of the relative concentrations of the UO_2^{2+} complexes that are likely to form in biological fluids. Concentrations of the important constituents of human plasma and bladder urine are shown in Table 31.9. The concentrations of these constituents in the fluid entering the last third of the proximal renal tubules (site of UO_2^{2+} deposition and renal injury) were estimated from the renal micropuncture data of Wong *et al.* (1986) (Table 31.9). Concensus values are available for the formation constants of the UO_2^{2+} complexes with the ligands in biological fluids at $T = 25°C$ and ionic strength $I = 0.1$ M, the closest match to the conditions in biological fluids. A very stable soluble neutral dicalcium uranyl triscarbonate complex, $Ca_2UO_2(CO_3)_3(aq)$, was shown to influence the speciation of UO_2^{2+} in the region pH 6 to 10 of calcite-rich U mining waters (Bernhard *et al.*, 2001). That complex was included in the present calculations, because the chemical conditions in the mine waters resemble those in blood plasma and renal tubular fluid, both of which are nearly neutral and contain significant concentrations of Ca^{2+} and HCO_3^-.

(*i*) *Complexes in plasma*

The conditions for the plasma calculations were, as follows: Data for the human UO_2^{2+} injection case (Table 31.7) were combined with human data for fluid volumes and Tf concentrations (Table 31.10) to calculate an initial UO_2^{2+}

concentration in plasma of 10^{-5} M and a concentration of available Tf-binding sites of 3.6×10^{-5} M. The partitioning of UO_2^{2+} in the plasma was set at 60% associated with ultrafilterable ligands and 40% bound to nonfilterable Tf (Stevens *et al.*, 1980). No correction was made for the small fraction of newly injected UO_2^{2+} ($\leq$4%) that is transiently associated with red blood cells (Dounce, 1949; Stevens *et al.*, 1980; Lipsztein, 1981; Durbin *et al.*, 1997a).

The set of equations for the competing reactions was solved simultaneously. The predominant filterable UO_2^{2+} complex in the plasma, identified as $Ca_2UO_2(CO_3)_3(aq)$, can account for 86% of the filterable UO_2^{2+}, with 13% in the form of the triscarbonate complex, and about 1% as the biscarbonate (Table 31.11). The selected concentration of Tf-binding sites and fraction of UO_2^{2+} bound to Tf yielded a value for the formation constant of UO_2^{2+}–Tf, $\log K_f = 14.5$, which agrees reasonably well with a reported value of $\log K_f = 16$ determined in a solution much more dilute than 0.1 M NaCl (Ansoborlo *et al.*, 2003).

(*ii*) *Complexes in proximal renal tubular fluid*

Only a crude estimate can be made of the speciation of the UO_2^{2+} complexes that exist in the chemical milieu of the fluid flowing through the late proximal renal tubules, because the fluid in the last third of the proximal tubules is not accessible to micropuncture sampling. The composition of the tubular fluid shown in

Table 31.11 UO_2^{2+} *complexes with the low molecular weight ligands of biological fluids as identified by speciation calculations.*[a,b]

	Distribution of UO_2^{2+} *complex species* (% *of total*)			
UO_2^{2+} *complex*	$\log K_f$	*Plasma ultrafiltrate*	*Late proximal tubule fluid*[c]	*Bladder urine*
$UO_2(CO_3)_2^{2-}$	16.2[c]	0.6	7.0	0.2
$UO_2(CO_3)_3^{4-}$	21.6[c]	13	6.3	<0.1
$Ca_2UO_2(CO_3)_3(Aq)$	28.1[d]	86	73	0.4
UO_2HPO_4	7.2[c]	<0.1	0.3	77
UO_2 citrate	7.4[e]	<0.1	0.5	22
'Tubule protein'[f]	–	–	13	–

[a] Values for formation constants at T=25°C and ionic strength I=0.1 used as best match to 0.14 M NaCl in biological fluids.
[b] The ionization constant for HCO_3^- given in Grenthe *et al.* (1992) was recalculated to $\log K_{i=}$–9.9 at ionic strength I=0.1 M.
[c] NEA (1992). Calculated from composition of fluid entering last third of proximal tubules.
[d] Bernhard *et al.* (2001).
[e] Martell and Smith (1977).
[f] Membrane of proximal tubule microvilli.

Table 31.9 is the set of measurements made closest to the beginning of the last third of the proximal tubules (Wong *et al.*, 1986). The concentration of HCO_3^- and the tubular fluid pH continue to be reduced during the traverse of the last portion of the proximal tubule, but by how much before the fluid enters the more distal nephron cannot be estimated, because Wong *et al.* (1986) did not report measurements of the concentration of HCO_3^- in the distal tubules.

Specification of chemical conditions for the tubular fluid calculations introduces additional uncertainty. During its transit through the last third of the proximal tubules, about 13% of the injected UO_2^{2+} is lost from the fluid phase and is deposited on the membrane of the brush border microvilli. To take account of that loss to protein binding, it was assumed that the contact between the tubular fluid and the membrane of the microvilli was so intimate that the membrane protein could be considered to be 'virtually' in solution. The concentration of membrane protein-binding sites was set at 10^{-4} M, assuming that the binding sites for UO_2^{2+} were three times more abundant than those of Tf. The concentrations of the UO_2^{2+} complexes calculated for the plasma ultrafiltrate were used as starting conditions for the UO_2^{2+} content of the tubular fluid.

The dominant complex is still $Ca_2UO_2(CO_3)_3(aq)$ (Table 31.11), which can account for 73% of the UO_2^{2+} entering the system, 13% is bound to kidney protein (fixed by starting conditions), the biscarbonate (7%) is more important than in the plasma, whereas the triscarbonate (6.3%) is less important than in plasma. In addition, about 1% of the UO_2^{2+} in this system is predicted to be associated with phosphate and citrate. The selected concentration and fractional binding of UO_2^{2+} to tubule membrane protein yielded a value for a 'formation constant' of UO_2^{2+}-membrane protein, $\log K_f = 9.6$. The fixed protein 'concentration' and $\log K_f$ are coupled, and both are uncertain.

(*iii*) *Complexes in bladder urine*

The conditions for the urine calculations were as follows: The human UO_2^{2+} injection case (Table 31.7) excreted 59% of the injected UO_2^{2+} (14 μmol) in 1.4 L of urine in the first 24 h (Hursh and Spoor, 1973), and the concentration of UO_2^{2+} in urine was 10^{-5} M. The concentrations of the constituents of urine of humans consuming an ordinary diet are those given in Table 31.9. The speciation calculations indicate that only 1% of the excreted UO_2^{2+} would still be a carbonate complex, and 99% would be present as phosphate and citrate complexes (Table 31.11). Diets that raise the pH and/or increase HCO_3^- in urine and HCO_3^- infusion, which increases both the HCO_3^- concentration and the pH of the urine, would allow survival of greater fractions of the carbonate complexes filtered from plasma and their excretion in the urine.

Two questions that have received little attention are the near absence at low UO_2^{2+} intakes to blood of significant UO_2^{2+} deposition in portions of the renal tubular system distal to the proximal tubules and the spreading out of the renal injury at toxic UO_2^{2+} doses. The degree and extent of renal injury

caused by UO_2^{2+} are dose-dependent. At low to moderately toxic intakes to blood, cell damage is limited to the later portion of the proximal tubules, seen in microscopic sections as occupying the region near the cortico-medullary junction. With increasing doses of UO_2^{2+}, the cellular injury becomes progressively more widespread, extending proximally to the earlier portions of the proximal tubules and the distal tubules in the cortical region and distally to the loops of Henle in the medulla (Barnett and Metcalf, 1949). Autoradiographs of the kidneys of rodents given low doses of $^{232}UO_2^{2+}$ or $^{233}UO_2^{2+}$ verified that deposition of the UO_2^{2+} coincided with the zone of low-dose cellular injury. When the shorter-lived U isotopes were given augmented with toxic amounts of $^{238}UO_2^{2+}$, autoradiographs showed more U deeper in the cortex (earlier portions of the proximal tubules and distal tubules) and deeper into the medulla (loops of Henle) than were seen with the lower doses of UO_2^{2+}.

In chemical terms, when high concentrations of UO_2^{2+} (10^{-3} M) were circulating, the carbonate complexes filtered from the plasma apparently begin to destabilize at the conditions of the earlier portions of the proximal tubules (Table 31.9), and the concentrations of phosphate and citrate are insufficient to prevent UO_2^{2+} binding to the presumably lower affinity proteins of the membrane of the later segments of the renal tubule system.

The microvilli of the proximal tubule brush border are specialized for absorption, and the brush border presents a surface area many orders of magnitude greater than the luminal surface of the more distal portions of the renal tubule system (Berliner, 1973). Combined, the lower concentrations of potential UO_2^{2+} binding sites and lower affinities for UO_2^{2+} of these sites (less than those of phosphate and citrate) could account for the apparent lack of binding of low doses of UO_2^{2+} in the more distal tubule segments.

(b) NpO_2^+

Plasma clearance of iv-injected $^{237}NpO_2^+$ was studied in rats and mice (Figs. 31.3 and 31.4). Clearance of NpO_2^+ from mouse plasma was fast, with 90% clearance in 10 min and 99% clearance in 60 min. At 100 min, skeletal uptake and urinary excretion accounted for 80% of the injected Np (Table 31.3). Plasma clearance of Np was also investigated in baboons injected iv with 1 ng kg^{-1} of ^{239}Np or 100 μg kg^{-1} of ^{237}Np reported as NpO_2^+ or NpO_2^{2+} in solutions of Na citrate, $NaHCO_3$, or $NaNO_3$ (Ralston *et al.*, 1986). No differences were found in the plasma clearances, urinary excretion rates, or whole-body retentions of the differing masses of Np or Np oxidation states or chemical compositions of the injection media. Those findings indicate that either NpO_2^{2+} had not been formed or that it was promptly reduced to NpO_2^+ *in vivo*. Plasma clearance of NpO_2^+ was fast in the baboons; it was 90% complete in about 45 min and 99% complete in about 300 min (Fig. 31.6).

The plasma clearance of iv-injected $^{237}NpO_2^+$ nitrate in the rats differs somewhat from those of the other animals (Figs. 31.3, 31.4, and 31.6). About 80% of

the injected Np was cleared from the plasma as rapidly as in the mice and baboons (in about 20 min, Figs. 31.4 and 31.6), but clearance of the remaining 20% was slow and resembled that of Np^{4+} in the same animal models. Overall clearance was slow; it was 90% complete in 160 min and 99% complete only after 1.7 days. In the three animals, a small fraction of the iv-injected NpO_2^+ was cleared from the plasma as slowly as Pu^{4+} (0.5% in the mice, 2% in the baboons, and 5.5% in the rats). The complexes of NpO_2^+ are weak (Table 31.8), and it is reasonable to consider that these small slowly clearing fractions of the injected Np had been reduced to Np^{4+} *in vivo* and were circulating complexed with serum proteins.

Human plasma was incubated with ^{237}Np as Np^{4+}, NpO_2^+, or NpO_2^{2+} in 0.08 M Na citrate buffer pH 3.2. Chromatography on G-25 Sephadex indicated that about 20% of the Np in all these preparations was associated with serum proteins. Chromatography on G-100–200 Sephadex indicated that the ^{237}Np, applied as NpO_2^+, was distributed among the heavy proteins (22%), the albumin-Tf peak (33%), and low molecular weight species (44%). Re-chromatography of the albumin-Tf peak on DEAE-Sephadex showed only a moderate tendency of the Np to be associated with the Tf peak (Bruenger *et al.*, 1971b).

Protein precipitation, dialysis, ultrafiltration, and gel chromatography (150-Sephadex) were used to study protein binding of $^{239}NpO_2^+$ incubated with dog serum. All of those procedures indicated that about 50% of the Np was associated with protein, but no specific protein(s) could be identified. Protein binding was weak, and gel chromatography showed that about 20% of the applied Np was associated with the heaviest proteins and 80% eluted with the low molecular weight species in the same fraction as NpO_2NO_3 (Guilmette *et al.*, 1982).

Intravenously injected NpO_2^+ is rapidly cleared from the plasma of mice, rats, and baboons, mainly to urinary excretion and uptake in bone (Tables 31.2, 31.3, 31.5, and 31.6; Figs. 31.3, 31.4, and 31.6). There is little evidence for protein binding of NpO_2^+ in the plasma. Combined, these observations are good indicators that, in accord with its tendency to form only weak complexes, NpO_2^+ does not form stable complexes with plasma protein (Bruenger *et al.*, 1971b; Guilmette *et al.*, 1982). Stable binding of Np to Tf apparently requires that the injected NpO_2^+ be reduced *in vivo* to Np^{4+}, which forms complexes as stable as those of Pu^{4+}. *In vivo* reduction of NpO_2^+ to Np^{4+} is likely to be slow, because it involves the breaking of M–O bonds, but as Durbin *et al.* (1998b) and Taylor (1998) point out, at pH 7.4 in the presence of ligands with great affinity for Pu^{4+} and Np^{4+} but little affinity for NpO_2^+ and an average eH in mammalian plasma of about 270 mV (Van Rossum and Schamhart, 1991), such reduction is theoretically possible.

The low molecular weight NpO_2^+ species transported in the plasma, filtered by the kidneys into the urine, and rapidly deposited in bone (Tables 31.2, 31.3, and 31.5) have not been identified. Hydrolysis of NpO_2^+ is not expected at physiological pH. Some of the NpO_2^+, which behaves like a large monovalent

cation, may exist as a hydrated ion, and carbonate is known to stabilize NpO_2^+ (Ahrland, 1986). Both an aqueous ion and a NpO_2^+ carbonate complex should be ultrafilterable and excreted by the kidneys into the urine.

The identities of the NpO_2^+ species that may be expected in mammalian plasma can be calculated for the specific set of conditions in the plasma volume of a 6.2 kg monkey immediately after iv injection of 42 μg kg^{-1} of $^{237}NpO_2^+$ (Table 31.5); the concentration of the NpO_2^+ would be 4.5×10^{-6} M in 0.025 M HCO_3^- at pH 7.4 (Tables 31.8 and 31.9). The stability constants of the NpO_2^+ carbonate, phosphate, and citrate complexes are as shown in Table 31.8.

The speciation calculations predict that in mammalian plasma hydrolysis of NpO_2^+ is negligible, and about 20% of the injected NpO_2^+ circulates as a hydrated ion, $NpO_2^+(aq)$, 50% as $NpO_2CO_3^-$, 20% as $NpO_2HPO_4^-$, and 10% as a NpO_2^+ citrate complex. The concentration of HCO_3^- and the pH are too low to allow formation of a biscarbonate.

The $NpO_2CO_3^-$ complex is unstable at the reduced HCO_3^- and pH in the renal tubules (Table 31.9). In the urine, NpO_2^+ is likely to be about equally divided between its HPO_4^{2-} and citrate complexes.

The fraction of iv-injected NpO_2^+ that deposits in the kidneys is $\leq$3% (Tables 31.2, 31.3, and 31.6), the tendency of NpO_2^+ to bind to kidney tissue protein is apparently much less than that of UO_2^{2+}. However, if the amount of Np injected (oxidation state not certain) is in the toxic range ($\geq$6 mg kg^{-1}), even that small fractional kidney deposit will result in renal tubular injury of the same nature at the same anatomical location that is typically seen with much smaller doses of UO_2^{2+} (Maynard and Hodge, 1949; Ballou *et al.*, 1962; Mahlum and Clarke, 1966).

(c) PuO_2^{2+}

A dog was injected iv with 0.84 μg Pu per kg of $^{239}PuO_2^{2+}$ in a solution containing 0.01 M Na citrate and 0.14 M NaCl, pH 7 (Painter *et al.*, 1946). About 35% of the injected Pu was cleared from the plasma in the first 20 min, but in contrast to its analog, UO_2^{2+}, clearance of about 65% of the injected PuO_2^{2+} from the plasma was as slow as that of Pu^{4+} in beagles (Fig. 31.5). Comparisons of the plasma clearance pattern and early urinary excretion in the dog and the tissue distributions in rats of Pu injected as PuO_2^{2+} with those of Pu^{4+} and UO_2^{2+} in the same animals (Tables 31.2 and 31.4) show that the disposition of PuO_2^{2+} does not resemble that of UO_2^{2+}, but is similar to that of Pu^{4+}. Combined, these observations indicate reduction of PuO_2^{2+} to Pu^{4+} *in vivo*. Where in the body that reduction occurs is not known, but because it is rapid, it is likely to take place in the circulating fluids.

The stabilities of the biscarbonate complexes of UO_2^{2+} and PuO_2^{2+} are similar (Table 31.8). However, after iv injection of $^{239}PuO_2^{2+}$ in rats little Pu was excreted in the urine, and the distribution of the Pu was nearly the same as that of iv-injected $^{239}Pu^{4+}$ citrate (Table 31.2; Carritt *et al.*, 1947). These results

also suggest that PuO_2^{2+} is rapidly reduced to Pu^{4+} in the circulation (Table 31.2). However, when $^{239}PuO_2Cl_2$ was injected im in rats, Pu absorption was greater and faster than when the same mass of Pu was injected im as $^{239}PuCl_4$ or $^{239}PuCl_3$, suggesting that some PuO_2^{2+} was mobilized from the wound site in a transportable form before it could be reduced to Pu^{4+} and hydrolyzed *in situ* (Scott *et al.*, 1948b).

31.5 TISSUE DEPOSITION KINETICS

The kinetics of the tissue uptake of some actinides and lanthanides have been studied to relate differences in their biological behavior to their chemical properties, to aid in developing procedures for the therapeutic removal of actinides from the body, to identify the biological processes underlying the several components of the plasma clearance curves, and to determine whether the target tissues take up actinide bound to plasma protein or complexed by low molecular weight plasma ligands or both. The experimental design of the kinetic studies, which as a practical matter have been conducted only in rats and mice, involves killing groups of animals at intervals from 1 min to 24 h after iv injection of an actinide and measuring the nuclide content of the blood, and/or plasma, tissues, and excreta.

31.5.1 Tissue deposition kinetics in rats

Tissue uptake data have been reported for iv-injected $^{241}Am^{3+}$ by Belyayev (1969), for $^{239}Pu^{4+}$ by Schubert *et al.* (1950) and Rosenthal and Schubert (1957), and for four representative lanthanides (Durbin *et al.*, 1955). Taylor (1962) reported that the pattern of uptake of iv-injected $^{241}Am(NO_3)_3$ or $^{241}Am^{3+}$ citrate in the bones of growing rats more closely resembled that of Ca^{2+} than Pu^{4+}. The data from those studies were recalculated to account for nuclide in the contained plasma of the tissues (Durbin *et al.*, 1972; Durbin, 1973). Within the first 5 min after iv injection of Ca^{2+}, Ce^{3+}, Eu^{3+}, Am^{3+}, or Pu^{4+} in rats, as much as 50% of the injected nuclide disappeared from the plasma, but could not be accounted for by excretion or uptake in bones and liver. Material balance studies with Ca^{2+} and four lanthanides demonstrated that at that time 75 to 90% of the missing nuclide was present transiently in the bulk soft tissue, indicating association with interstitial water (ISW) rather than with cellular components. The light lanthanides, Ce^{3+} and Eu^{3+}, Ca^{2+}, and Am^{3+} bind weakly to plasma proteins, and 50 to 60% of the injected amounts of those nuclides had diffused into ISW (Durbin, 1973). Plasma Tf binds stably to Pu^{4+}, and only 20 to 40% of iv-injected Pu^{4+} diffused into ISW, depending on whether the Pu^{4+} was administered as the nitrate or complexed with citrate (Durbin *et al.*, 1972).

The fraction of iv-injected nuclide diffusing into ISW depends on the stability of its protein complex(es). The less stable the protein binding, the more slowly the complex forms, and the larger is the fraction that promptly leaves the plasma by diffusion into ISW or immediate uptake by bone and/or liver or urinary excretion.

These kinetic studies of Am^{3+} and lanthanides demonstrated that the initial fast decline in the plasma clearance curves (first exponential component) was the combined result of rapid early deposition in the target tissues and urinary excretion and diffusion of filterable nuclide from the plasma to ISW, most of which is associated with the bulk soft tissues. Delayed return to the plasma compartment from ISW contributes to the second and third components of the plasma clearance curves and supports continued, but slower, uptake in the tissues. The multiexponential equations that describe the uptake of Am^{3+} in the bone and liver of rats have rate terms in common with each other and with the equations of clearance from the plasma and the soft tissues (ISW). Common terms in the transport equations are expected for two communicating fluid compartments (Durbin *et al.*, 1997b). The common rate terms in the liver and skeleton uptake equations indicated that Am^{3+} was being accumulated in both tissues from common pools – initially, from complexes with low molecular weight plasma ligands, and later from the weak plasma protein complexes (Durbin, 1973).

The recalculated data for Pu^{4+} clearance from the plasma and the uptake kinetics of Pu^{4+} in rat skeleton and liver (Schubert *et al.*, 1950; Rosenthal and Schubert, 1957) were combined with data for protein binding of Pu^{4+} in rat and dog plasma measured at times from a few minutes to 24 h after injection of Pu^{4+} citrate (Stevens *et al.*, 1968; Turner and Taylor, 1968a). These data were used to solve a biokinetic compartment model of circulatory transport and tissue uptake (Durbin *et al.*, 1972). The Pu^{4+} complexed with Tf and the Pu^{4+} complexed with filterable low molecular weight plasma ligands were designated as bound or free, respectively. The model structure consisted of four interconnecting transport compartments – plasma-bound, plasma-free, ISW-bound, and ISW-free. The plasma-bound and plasma-free compartments communicated with four effectively nonreturning sinks – liver, skeleton, soft tissue, and excreta. The numerical solutions of the model implied the following: Pu^{4+}-free binds to protein, mainly to Tf, in the ISW as well as in the plasma; little, if any Pu^{4+}-bound is excreted or deposited in the liver; which suggests that Tf binding is not a necessary precondition for liver uptake of Pu^{4+}; both Pu^{4+}-bound and Pu^{4+}-free are taken up by bone.

31.5.2 Tissue deposition kinetics in mice

Detailed studies of tissue uptake kinetics were conducted in mice injected iv with $^{232,235}UO_2Cl_2$ (Fig. 31.11, Durbin *et al.*, 1997a) , $^{237}NpO_2Cl$ (Fig. 31.12, Durbin *et al.*, 1998b) , $^{241}Am^{3+}$ citrate (Fig. 31.13, P. W. Durbin and B. Kullgren,

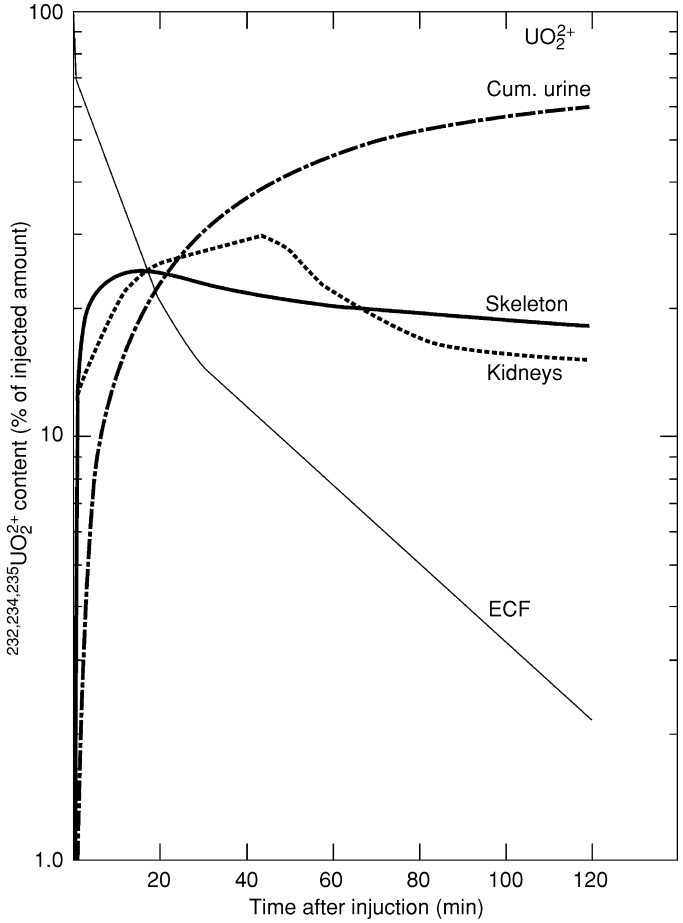

Fig. 31.11 *Clearance from extracellular fluid* (*ECF*) of mice, uptake in EFC-free skeleton and ECF-free kidneys, and cumulated urinary excretion of iv-injected $^{232,234,235}UO_2Cl_2$ (100 μg kg^{-1} *of U*). *Data of Durbin* et al. (1997a).

unpublished data) , or $^{238}Pu^{4+}$ citrate (Fig. 31.14, Durbin *et al.*, 1997b, P. W. Durbin and B. Kullgren unpublished data) . These studies provide useful comparisons of the deposition kinetics of actinides in their four biologically important oxidation states that form complexes with plasma constituents ranging in stability from very weak to strong. In all of these studies, female mice of the same strain and age were used. Nuclides were injected iv, and data were taken from groups of five mice killed at 16 timed intervals from 1 min to 24 h. Actinide content of plasma and all tissues of each mouse (including its entire skeleton) and pooled excreta of each five-mouse group were determined by

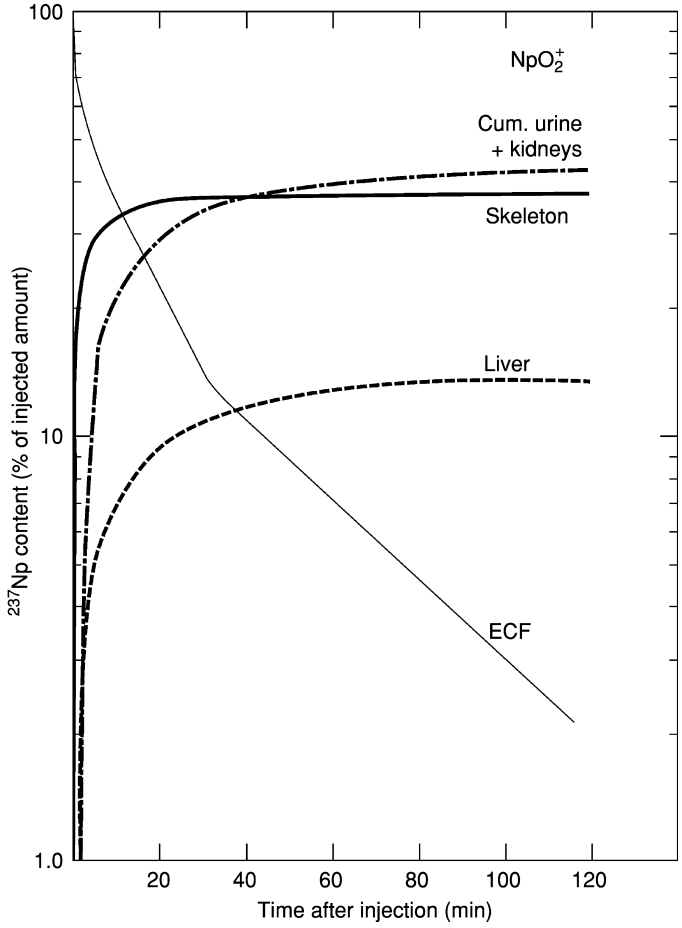

Fig. 31.12 *Clearance from extracellular fluid (ECF) of mice, uptake in ECF-free skeleton and ECF-free liver, and cumulated urinary excretion plus ECF-free kidneys of iv-injected* $^{237}NpO_2Cl$ (200 μg kg^{-1} *of Np*). *Data of Durbin* et al. (1998b).

scintillation counting. On average, 95% of the injected actinide was recovered in these material balance studies.

The fractional volumes of plasma and ECF in the tissues and whole body had been measured in similar mice (Durbin *et al.*, 1992). Those fluid distributions were used to calculate and apportion among its tissues the actinide removed in the plasma sample of each mouse, approximately recreating the total in-life actinide content of each tissue. The amounts of actinide deposited in the target tissues at each time (t), ECF-free tissue (t), was estimated by subtracting the amount of actinide calculated to be in their contained plasma [P(t)] and

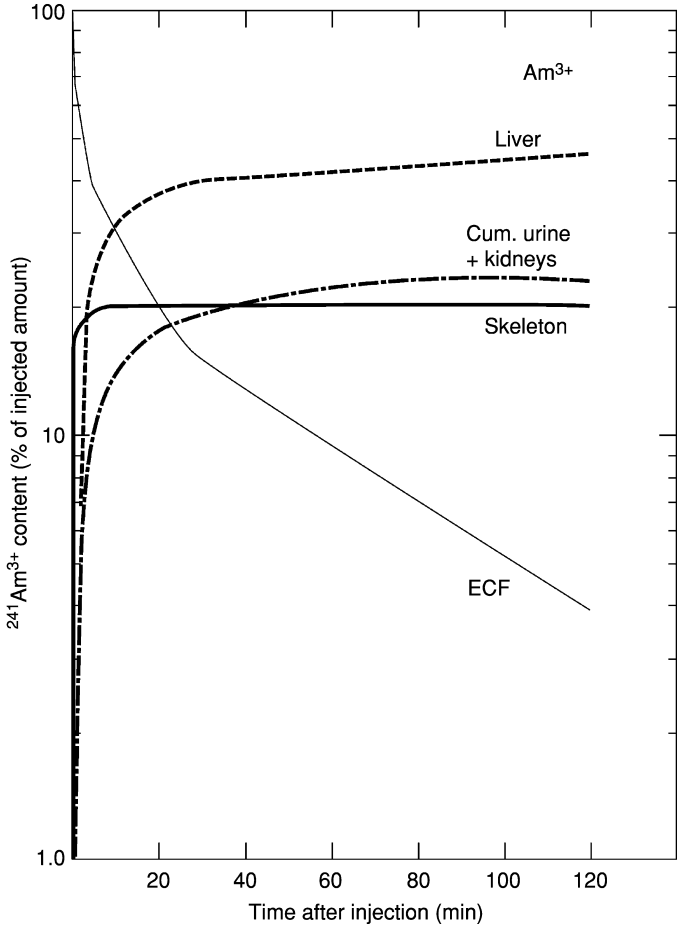

Fig. 31.13 *Clearance from extracellular fluid (ECF) of mice, uptake in ECF-free skeleton and ECF-free liver, and cumulated urinary excretion plus ECF-free kidneys of iv-injected* $^{241}Am^{3+}$ *citrate* (0.23 μg kg^{-1} *Am*). *Unpublished data of P. W. Durbin and B. Kullgren.*

ISW [I(t)] from their measured values that had been corrected for blood loss; skeleton [Sk(t)], liver [L(t)], and kidneys [K(t)] (Durbin *et al.*, 1992, 1997a,b, 1998b),

$$\text{ECF-free skeleton} = [\text{Sk}(t) - \text{P}_{\text{Sk}}(t) - \text{I}_{\text{Sk}}(t)]$$
$$\text{ECF-free liver} = [\text{L}(t) - \text{P}_{\text{L}}(t) - \text{I}_{\text{L}}(t)]$$
$$\text{ECF-free kidneys} = [\text{K}(t) - \text{P}_{\text{K}}(t) - \text{I}_{\text{K}}(t)].$$

The tissue uptake data (deposited fractions), expressed as percent of injected actinide in ECF-free tissues, are plotted vs time to 120 min after injection in Figs. 31.11–31.14. Those curves and the parameters of their multiexponential

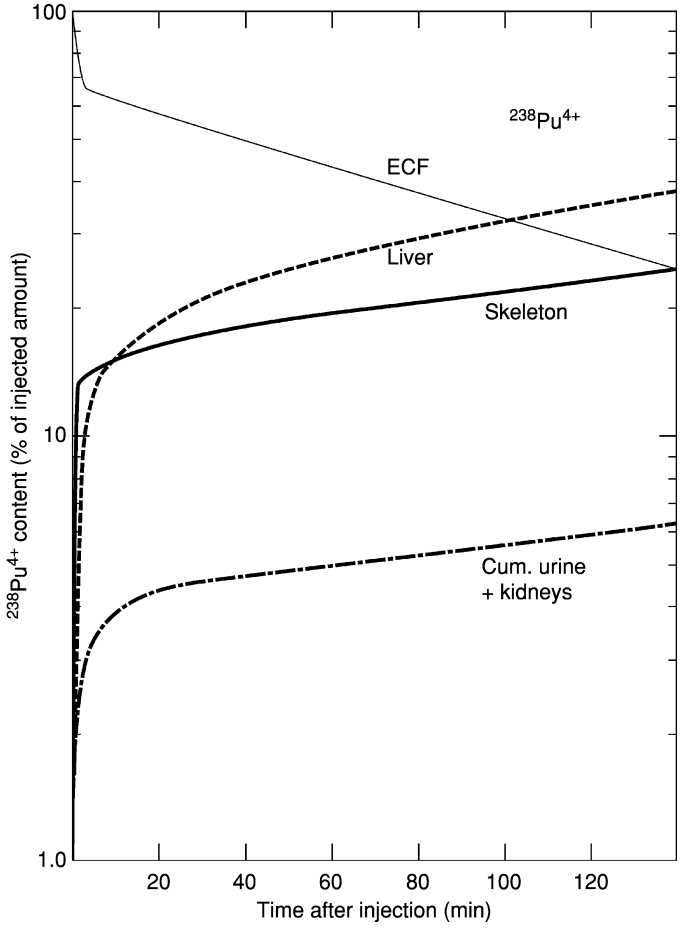

Fig. 31.14 *Clearance from extracellular fluid (ECF) of mice, uptake in ECF-free skeleton and ECF-free liver, and cumulated urinary excretion plus ECF-free kidneys of iv-injected* $^{238}Pu^{4+}$ *citrate* (0.09 μg kg^{-1} *Pu*). *Data of Durbin* et al. (1997b) *and unpublished data of P. W. Durbin and B. Kullgren.*

equations were obtained by log-linear regression analysis. The curves were plotted for clearance of actinides from the plasma (Fig. 31.4) and ECF (Figs. 31.11–31.14) of mice, and their equations were calculated to 120 min after injection for UO_2^{2+}, NpO_2^{+}, and Am^{3+} and to 480 min for Pu^{4+}. Each has three exponential components,

Plasma (t) or ECF(t) = $\sum A_i e^{-\lambda_i t}$(% of amount injected), t is min after injection.

Maximum actinide accumulations in the ECF-free tissues and urinary excretion were estimated from the tabular data. Equations were derived to describe

the actinide uptake in the target tissues and cumulated urinary excretion using published methods (Comar, 1955; Durbin, 1973). The exponential tissue uptake equations were calculated to 120 min for UO_2^{2+}, NpO_2^{+}, and Am^{3+} and to 480 min for Pu^{4+}. Nearly all of the tissue uptake equations also have three negative exponential terms,

Tissue(t) or cum. urine(t) $= \sum A_i(1 - e^{-\lambda_i t})$ (% of injected amount), t is min after injection.

The parameters, coefficients (A_i,%), and rate constants (λ_i, min^{-1}) of the plasma and ISW clearance equations and the equations describing actinide uptake in the ECF-free tissues and cumulated urinary excretion are collected in Table 31.12. Table 31.12 also includes the maximum values of the ECF-free tissue deposits and total urinary excretion and the approximate postinjection times of maximum accumulation. This table also includes, for comparison, the parameters of the two-component plasma clearance curves determined in similar mice for the organic tracers, $CaNa_3$–^{14}C–DTPA and ^{3}H-inulin, which are freely diffusible, do not accumulate in any tissue, and are quantitatively filtered into the urine (Durbin *et al.*, 1997b). The deposition kinetics studies of Am^{3+} and Pu^{4+} in the mouse confirmed the findings for those actinides in rats, and deposition kinetic studies were extended to include UO_2^{2+} and NpO_2^{+}.

In the mice, the first two exponential terms of the plasma clearance equations of Am^{3+}, UO_2^{2+}, and NpO_2^{+} are similar to those of the diffusible tracers, $CaNa_3$–^{14}C–DTPA and ^{3}H-inulin (Table 31.12). Within 5 min, about 85% of those injected actinides and the organic molecules have diffused into ISW, been filtered by the kidneys, and, for the actinides, been taken up by the skeleton and liver.

Immediate diffusion of large fractions of these three injected actinides into ISW and some early urinary excretion show that upon introduction into the plasma they exist mainly as 'free' filterable complexes with small ligands (either plasma constituents or, in the case of Am^{3+} with the injected excess citrate). Initially, large fractions of these actinides are taken up in the liver or kidneys and skeleton at very fast rates. The coefficients of the first components of their uptake equations (A_1) account for accumulation of 40–80% of the maximum deposits in the skeleton and about 30% of the maximum liver deposits. The rate constants (λ_1) imply uptake half-times of 0.3 to 0.8 min in bone and 1 to 1.4 min in liver (Table 31.12). Tissue uptake and urinary excretion persist, but more slowly at times longer than 5 min postinjection as is shown by the rate constants of the second and third components of their uptake equations (λ_2 and λ_3).

The deposition kinetics of Pu^{4+} differ quantitatively from those of the other three actinides of differing oxidation state, mainly because Pu^{4+} forms a stable complex with plasma Tf, while the complexes that NpO_2^{+}, UO_2^{2+}, and Am^{3+} form with Tf and other plasma proteins are very weak. In the mice, about 75% of Fe-binding sites of plasma Tf are occupied by Fe^{3+} (Table 31.10). During the first few minutes after iv injection of Pu^{4+} citrate, about one-half of the Pu^{4+} appeared to be 'free' and circulating as a filterable low molecular weight species.

Table 31.12 *Exponential equations describing clearance from plasma and ISW, accumulation in ECF-free tissues, and urinary excretion of iv-injected actinides in mice.*[a,b]

	Compartment maximum		*Parameters of clearance and accumulation equations*[c]					
Compartment	(%)*	min	A_1 (%)	λ_1 (min^{-1})	A_2 (%)	λ_2 (min^{-1})	A_3 (%)	λ_3 (min^{-1})
$^{232,234,235}UO_2Cl_2$								
Plasma			82	1.6	14	0.1	3.6	0.02
ISW[d]			–	–	25	0.1	25	0.02
Skeleton	25	20	10	2.1	15	0.3	–	–
Cum. urine + kidneys[e]	76	120	12	0.5	41	0.06	23	0.02
$^{237}NpO_2Cl$								
Plasma			84	1.5	13	0.08	3.0	0.01
ISW[d]			–	–	16	0.06	25	0.03
Skeleton	36	60	24	0.9	10	0.1	2.3	0.02
Liver	14	60	4.0	0.7	–	–	10	0.04
Cum. urine + kidneys[e]	42	90	3.0	1.2	26	0.07	14	0.02
$^{241}Am^{3+}$ citrate								
Plasma			86	0.8	10	0.08	4	0.02
ISW[d]			–	–	12	0.07	19	0.02
Skeleton	20	10	17	2.3	3.2	0.4	–	–
Liver	47	150	19	0.5	0.13	0.2	15	0.02
Cum. urine + kidneys[e]	22	60	9.5	0.6	12	0.05	–	–
$^{238}Pu^{4+}$citrate								
Plasma			43	1.2	27	0.04	30	0.006
ISW[d]			–	–	–	–	24	0.004
Skeleton	40	720	13	1.6	7.4	0.02	20	0.002
Liver	42	240	12	0.4	31	0.01	–	–
Cum. urine + kidneys[e]	8.8	480	2.0	1.8	2.5	0.1	4.3	0.002
^{14}C-DTPA								
Plasma[f]	–	–	86	1.3	14	0.08	–	–
^{3}H-inulin								
Plasma[f]	–	–	82	1.0	18	0.08	–	–

* % of injected nuclide and minutes (min) is time after injection.

[a] Data sources are as follows: $^{232,234,235}UO_2Cl_2$, Durbin *et al.* (1997a); $^{237}NpO_2Cl$, Durbin *et al.* (1998b); $^{241}Am^{3+}$ citrate, P. W. Durbin and B. Kullgren (unpublished data); $^{238}Pu^{4+}$ citrate, Durbin *et al.* (1997b) and P. W. Durbin and B. Kullgren (unpublished data).

[b] Equations for plasma and ISW clearance were fitted from $t(0)$ to $t(120$ min), and those for tissue accumulation and urinary excretion were fitted from $t(0)$ to t(maximum). Maximum tissue accumulation and cumulated urinary excretion values and the postinjection times at which those maxima were attained were estimated from Figs. 31.11–31.14.

[c] Clearance equations are of the form, plasma(t) or ISW(t)$=\sum A_i e^{-\lambda_i t}$, and those for accumulation in the tissues and cumulated urinary excretion are of the form, tissue(t) or cum. urine(t)$=\sum A_i(1-e^{-\lambda_i t})$, where plasma ($t$), ISW ($t$), tissue($t$), and cum. urine($t$) are expressed as % of injected actinide and t is min. after injection.

[d] Actinide calculated to have diffused into interstitial water (ISW).

[e] ECF-free kidneys (t) are combined with cum. urine (t) to account for all actinide filtered by the kidneys.

[f] Durbin *et al.* (1997b).

Only about 25% of the injected Pu^{4+} diffused into ISW, and skeleton and liver uptakes were about 30% of their maximum accumulated amounts (Table 31.12). The initial rates of Pu^{4+} deposition in liver and skeleton were about the same as those for the other study actinides (half-times 0.4 and 1.7 min, respectively, for skeleton and liver).

Subsequently, return of Pu^{4+} from ISW was slower than for the other actinides. Plasma Pu^{4+} retention was prolonged, renal excretion was negligible, and uptake in the target tissues proceeded at rates 1/3 to 1/10 as fast as those observed for the other actinides. Skeletal uptake persisted for about 24 h or until nearly all of the Pu^{4+} had been cleared from the plasma, during which time nearly all of the Pu^{4+} in the plasma was likely to be bound to Tf (components 2 and 3). Renal filtration, although small, also persists, indicating the continuous presence of a small fraction of 'free' Pu^{4+}. Net uptake in liver essentially stops when the 'free' Pu^{4+} has been reduced to a low level.

31.5.3 Summary

Bone and liver cell surfaces have great affinities for actinides (except that liver does not accumulate UO_2^{2+}), and those tissues take up (bind) actinides rapidly during the first few minutes after iv injection, when substantial fractions of the actinides are likely to be circulating as weak complexes with small filterable ligands. The reduced rates of tissue uptake and renal filtration that emerged in the mice at postinjection times longer than 5 min were not likely to be caused by sudden changes in the tissue affinities for actinides or the saturation of metal-binding sites. Alteration of the renal filtration rate is scarcely possible, because that rate is a species-specific constant (Smith, 1951; Durbin and Schmidt, 1989; Durbin *et al.*, 1997b). The reductions in tissue uptake and renal excretion rates and their related plasma clearance rates appear to be due to changes taking place in the transport system. Rapid diffusion of actinides from plasma to ISW and slow return reduce the rate at which the actinides are presented to the tissues. Protein binding, most importantly for Pu^{4+}, decreases the differences between the stabilities of the actinide complexes with the tissue ligands and those with the plasma ligands, effectively reducing the competitiveness of the tissue ligands and delaying or preventing the transfer of actinide from plasma ligands to tissue ligands.

31.6 ACTINIDES IN THE LIVER

Large fractions of injected soluble trivalent and tetravalent actinides are taken up by the liver, and their retention in liver has been studied because of its importance for tumor induction and radiation dosimetry (Tables 31.1–31.7; Finkle *et al.*, 1946; Painter *et al.*, 1946; Hamilton, 1947b, 1948c; ICRP, 1959,

1972, 1986; Durbin 1960, 1962, 1973; Cochran *et al.*, 1962; Stover *et al.*, 1968b, 1971; Taylor and Bensted, 1969; Mewhinney *et al.*, 1972; McKay *et al.*, 1972; Lloyd *et al.*, 1972b, 1984b; Taylor *et al.*, 1972b; Guilmette *et al.*, 1980; Lo Sasso *et al.*, 1981; Durbin *et al.*, 1985; NCRP, 2001).

Autoradiographic studies show that the actinides initially are distributed nearly uniformly in liver cells. With the passage of time after injection, actinide retained in the liver of rats, dogs, and monkeys tends to be located mainly in the Kupffer cells as aggregates associated with hemosiderin (Cochran *et al.*, 1962; Durbin, 1973, 1975; Durbin *et al.*, 1985).

31.6.1 Liver microanatomy

The initial binding sites in the liver for soluble blood-borne metal ions including the tri- and tetravalent actinides are the two sinusoidal membrane surfaces of the one-cell thick sheets of hepatocytes. The membranes facing the sinusoidal blood spaces possess numerous microvilli that project into the fluid-filled space. The microvilli are rich in receptors, enzymes, and transport proteins, and they provide an enormous surface area for absorption of blood-borne substances. Bile is secreted at the canalicular hepatic surfaces between the cells into minute ducts that ultimately coalesce and empty into the common bile duct (Ham, 1974; Ballatori, 1991).

31.6.2 Liver blood supply

The liver has an abundant blood supply; it receives about 20% of the cardiac output (Detweiler, 1973). Two-thirds of liver blood is delivered by the portal vein, which transports blood from the GI tract. The hepatic artery supplies the remainder. The two sets of blood vessels branch into capillaries that end in blood-filled spaces (sinusoids), where the venous and arterial blood mix. The thin flat lining cells that separate the sinusoidal hepatic cell surfaces from the sinusoidal blood are porous (pore size about 0.1 μm in diameter), thereby excluding red blood cells and larger particles while allowing access of the whole plasma to the hepatocyte microvilli. The sinusoidal lining contains fixed phagocytes (Kupffer cells) that recognize and ingest colloidal particles (Ham, 1974; Ballatori, 1991).

31.6.3 Transport of metals into liver cells

Entry of metal ions into hepatic cells may be via facilitated diffusion and/or by liquid phase, adsorptive, and receptor-mediated endocytosis, followed by temporary residence in the cytosol as complexes formed with binding proteins or in the lysosomes. In endocytosis, a vesicle of membrane envaginates into a sac, which sinks into the cytoplasm matrix. These vesicles fuse with each other or with other vesicles or with lysosomes. It has recently been shown that the liver

cell internalizes more than 20% of its volume and between 5 and 50% of its surface area each hour by a process termed membrane recycling. Rapid membrane recycling is likely to be a major contributor to the hepatic intake of metals that have high affinities for membrane-binding sites (Ballatori, 1991).

Iron is transported into hepatocytes by at least two independent pathways. The dominant mechanism is receptor-mediated endocytosis in which Fe–Tf binds to specialized Tf-receptors on the hepatocyte surface. Membrane binding is followed similarly to the delivery of Fe–Tf to developing erythrocytes, by endocytosis, and internalization of the Fe–Tf–Tf-receptor complex, fusion of the endocytotic vesicle with other vesicles, release of the Fe within the acidic vesicles, and extrusion of the iron-depleted Tf (Ballatori, 1991). Hepatic uptake of the normally very small fraction of Fe^{3+} circulating as a low molecular weight complex has been shown to occur by direct binding to integral membrane protein. Membrane binding is probably followed by internalization in the energy-dependent membrane recycling process (Planas-Bohne *et al.*, 1985, 1989; Planas-Bohne and Duffield, 1988; Planas-Bohne and Rau, 1990).

31.6.4 Iron storage

(a) Ferritin

Ferritin serves as a source of stored iron that can be mobilized for red cell production. It is a large water-soluble complex of protein (apoferritin, molecular weight about 450 kDa) and ferric oxyhydroxide. At the usual level of iron saturation (18%), the weight of the complex is about 620 kDa. The protein forms a shell within which crystals of iron hydroxide and phosphate are dispersed in a lattice-like relationship. Apoferritin is synthesized in response to intracellular iron by the ribosomes of nearly all mammalian cells, but liver, spleen, and bone marrow are especially rich in stored ferritin. At low iron levels, new iron is incorporated into existing apoferritin molecules, particularly those with a partially iron-filled core. Elevated iron stimulates production of apoferritin, which rapidly takes up excess iron. The residence time of ferritin in the cell cytosol is brief, and it tends to accumulate within lysosomes.

Iron is incorporated into and stored in ferritin as Fe^{3+}, but to break the coordination bonds and be released from the ferritin complex, the iron must be reduced to Fe^{2+}. It is then reoxidized in the cytosol and bound by intracellular Tf (Aisen and Listowsky, 1980; Fairbanks and Beutler, 1995).

(b) Hemosiderin

The other iron storage compound, hemosiderin, is found mainly in the macrophages of the bone marrow, the Kupffer cells of the liver, and phagocytic cells in the spleen. It is not water-soluble. It is composed of ferritin partially stripped of the protein component and contains 25 to 35% iron by weight. Much

hemosiderin appears to consist of ferric hydroxide core crystals (Fairbanks and Beutler, 1995).

31.6.5 Actinide association with stored iron

Investigations of actinide retention in the whole liver were extended to include identification of the constituents of hepatic cells that bind and store them (Taylor, 1972; Duffield and Taylor, 1986). Preliminary analysis of clear, particle-free homogenates of the livers of dogs injected iv with $^{239}Pu^{4+}$ citrate indicated that the Pu^{4+} was associated with ferritin (Bruenger *et al.*, 1969a). Competitive binding studies showed that the ferritin complexes of Pu^{4+} and Am^{3+} are more stable than their Tf complexes (Bruenger *et al.*, 1969a; Stover *et al.*, 1970).

The subcellular distributions of soluble iv-injected actinides in the livers of several animal species have been investigated using a variety of techniques. The actinides ($^{227}Ac^{3+}$,$^{233}Pa^{5+}$,$^{238}Pu^{4+}$,$^{239}Pu^{4+}$,$^{241}Am^{3+}$,$^{244}Cm^{3+}$,$^{249}Cf^{3+}$, $^{237}NpO_2^+$, and $^{239}NpO_2^+$) were studied in rats, mice, dogs, rabbits, baboons, and/or hamsters. Homogenates were prepared from the livers, and the subcellular organelles were separated from each other and from the filterable cytosol by means of differential centrifugation and centrifugation through sucrose or salt density gradients into nuclei plus cell debris, mitochondria, lysosomes, microsomes, and cytosol. Marker enzymes were used to identify mitochondria and lysosomes, and ^{59}Fe was used to identify ferritin. The nature of the actinide-binding protein(s) in the cytosol was investigated using gel chromatography and electrophoresis (Taylor, 1969, 1970, 1972; Taylor *et al.*, 1969a,b; Boocock *et al.*, 1970; Stover *et al.*, 1970; Bruenger *et al.*, 1971a, 1972, 1976; Grube *et al.*, 1978; Schuppler *et al.*, 1988; Paquet *et al.*, 1995, 1996, 1998). These methods did not provide clear separation of 'iron-rich' heavy lysosomes from the mitochondria.

In more recent studies, actinide-injected animals were pretreated with Triton WR 1339, which causes liver lysosomes to imbibe water and swell, thus reducing their density enough to allow clean separation from the mitochondria (Gruner *et al.*, 1981; Winter and Seidel, 1982; Sutterlin *et al.*, 1984). Carrier-free electrophoresis has also been used to obtain a clear separation of lysosomes from all other organelles (Seidel *et al.*, 1986). Most of those studies were conducted using liver material from rats injected with ultrafilterable $^{239}Pu^{4+}$ citrate, and the results agree with supporting studies of liver material from rats and other animals injected iv or im with other soluble actinides and $^{141}Ce^{3+}$.

Combined, all of the studies of subcellular distribution of actinides in the liver show that ferritin is the predominant actinide-binding protein within the hepatocytes, and the lysosomes are the main subcellular storage organelles. Actinides that have entered the hepatocytes are initially mainly associated with the soluble lighter 'apoferritin-rich' ferritin in the cytosol, and to a lesser degree, they are sequestered in lysosomes. With time, the actinide associated with the soluble ferritin in the cytosol declines and the lysosomal actinide fraction, which includes the heavier 'iron-rich' ferritin, increases (Boocock *et al.*, 1970; Bruenger

et al., 1971a; Grube *et al.*, 1978; Seidel *et al.*, 1986). That is the same time-dependent pattern followed by newly acquired hepatic iron – initial incorporation into freshly synthesized apoferritin in the cytosol followed by gradual accumulation in lysosomes of ferritin that has acquired more iron (Aisen and Listowsky, 1980; Fairbanks and Beutler, 1995). At times longer than 70 days in dogs injected iv with $^{239}Pu^{4+}$ citrate, the concentration of the Pu^{4+} in the nuclei-cell debris fraction increased, and it was shown autoradiographically that the Pu^{4+} was contained in the Kupffer cells in association with hemosiderin (Cochran *et al.*, 1962; Taylor *et al.*, 1969a,b; Bruenger *et al.*, 1971a).

In addition to their presence in the cytosol and lysosomes in association with ferritin, and depending on the mass injected or used to incubate cultured hepatocytes, lower specific activity $^{237}NpO_2^+$, and $^{239}Pu^{4+}$ localized in the hepatic cell nuclei in association with an as yet unidentified nuclear matrix protein (Schuler and Taylor, 1987; Paquet *et al.*, 1995, 1996).

31.6.6 Actinide uptake by liver cells

The multivalent lanthanides and actinides, particularly Pu^{4+}, share some metabolic properties of iron. They form variably stable complexes with Tf in the plasma and are stored in the liver associated with ferritin. It was reasonable to postulate that, like iron, these metals would be bound to and be taken into hepatic cells by a Tf-mediated receptor mechanism. However, in a series of elegant experiments using cultured liver cells (primary rat hepatocytes and human hepatoma Hep-G2 cells) and isolated rat hepatocyte membrane, Planas-Bohne and coworkers demonstrated that the mechanism by which Pu^{4+} (and presumably other trivalent and tetravalent metals) are bound to and taken into liver cells is not only independent of, but is actually hampered by, Tf binding (Planas-Bohne *et al.*, 1985, 1989; Schuler and Taylor, 1987; Schuler *et al.*, 1987; Planas-Bohne and Duffield, 1988; Planas-Bohne and Rau, 1990).

Uptake of Pu^{4+} from a medium containing Pu^{4+} citrate into liver cells was not influenced substantially by the Pu^{4+} concentration or the molar ratio, citrate: Pu^{4+}, suggesting a nonspecific nonsaturatable mechanism. Cell uptake of Pu^{4+} was much reduced at 4°C, compared with 37°C, suggesting that transport into the cells was energy dependent. Cells incubated with $^{239}Pu^{4+}$–^{14}C-citrate did not bind or take in the ^{14}C-citrate suggesting ligand exchange between the Pu^{4+} citrate and the Pu^{4+} receptor complex(es). If the Pu^{4+} was prebound to Tf, uptake of Pu^{4+} into the cells and by isolated perfused rat liver was very low, only about 10% of the uptakes from Pu^{4+} citrate.

Liver cell intake of Pu^{4+} from its citrate complex requires a high activation energy and can be prevented by inhibition of oxidative phosphorylation; other processes seem not to be important. Uptake of Pu^{4+} by liver cells from the Pu^{4+} citrate complex can be prevented by chelators (EDTA, DFO) and by unsaturated Tf suggesting that the Pu^{4+} reacts directly with constituents of the liver cell

membrane. The stabilities of the Pu^{4+} receptor complex(es) appear to be greater than that of Pu^{4+} citrate but less than that of Pu^{4+}–Tf or Pu^{4+}–EDTA.

Fragments of purified rat hepatocyte membrane were incubated with Pu^{4+} citrate. Binding of Pu^{4+} to the membrane was pH-dependent (optimal at pH 7.4), saturatable, and independent of temperature, suggesting direct binding of Pu^{4+} at a limited number of sites. Binding of Pu^{4+} was prevented by the presence of unsaturated Tf, EDTA, or DFO, indicating that membrane binding of Pu^{4+} involved Pu^{4+} complexation with a spatially suitable arrangement of amino acid residues at the binding sites. The two kinds of binding sites found for Pu^{4+} were shown not to be phospholipids or glycoproteins, but large integral membrane proteins (molecular weight between 150 and 400 kDa), and they are different from the two kinds of binding sites identified with direct uptake of iron. When membrane was incubated with Pu^{4+}–^{125}I–Tf and then solubilized and subjected to gel filtration, the Pu^{4+} eluted in fractions different from those containing ^{125}I–Tf bound to membrane protein receptors or unbound ^{125}I–Tf, indicating dissociation of the Pu^{4+}–Tf complex.

31.6.7 Summary

From the standpoint of actinide biology, the most important results are that Pu^{4+} can bind directly to a limited number of sites on the hepatic cell membrane and be internalized, that transport of the Pu^{4+} into hepatic cells is not mediated by Tf, and that complexation of Pu^{4+} by Tf suppresses Pu^{4+} binding to hepatic cell membrane. It is reasonable to assume that the elements of group III and subgroup IV and the lanthanides and other actinides can also bind directly, possibly at the same or similar hepatocyte-binding sites as Pu^{4+}. Direct metal binding in the liver and its suppression by competition with Tf suggest an explanation for the observed direct correlation between the fractional deposition of the lanthanides and actinides in the liver and the instabilities of their Tf complexes (for which increasing ionic radius and plasma clearance rates are crude proxies) (Tables 31.1–31.7; Figs. 31.3–31.7; Durbin, 1962, 1973). The hepatic cell metal-binding sites compete successfully with bone surfaces for multivalent cations like Ce^{3+} and Am^{3+} that circulate complexed with small plasma ligands like citrate or as weak complexes with Tf or other plasma proteins. However, competition for metals that form more stable Tf complexes, like Th^{4+} and Pu^{4+}, favors bone, and the source of the uptake in liver may be mainly the small fraction that circulates as low molecular weight complexes (Durbin *et al.*, 1972; Planas-Bohne *et al.*, 1989).

31.7 ACTINIDES IN BONE

The defining characteristic of the biological behavior of the actinides in mammals, and the chemically similar elements of group III, subgroup IV, and the lanthanides, is their intraskeletal distribution. As soon as suitable radioisotopes

became available, autoradiographs were prepared from undecalcified sections of the femora of rats injected with fission products ($^{91}Y^{3+}$, $^{95}Nb^{3+}$, $^{95}Zr^{4+}$, $^{144}Ce^{3+}$, $^{147}Pm^{3+}$, $^{152,154}Eu^{3+}$) and five actinides ($^{227}Ac^{3+}$, $^{234}Th^{4+}$, $^{239}Pu^{4+}$, $^{241}Am^{3+}$, $^{242}Cm^{3+}$) (Axelrod, 1947; Hamilton, 1947b). Autoradiographs of five representative radioelements were included in the original reports; the remainder was published later as a complete set (Durbin, 1962).

The deposition patterns of $^{45}Ca^{2+}$ and $^{89}Sr^{2+}$ in rat bones had already been studied autoradiographically, and it was shown that the alkaline earth elements penetrated into and were nearly uniformly distributed throughout the bone mineral volume (Hamilton, 1941; Pecher, 1942). The internal distribution of the multivalent cations was markedly different. None was initially incorporated into the bone volume. The tetravalent elements (Zr^{4+}, Th^{4+}, and Pu^{4+}) were deposited at endosteal surfaces, particularly on the trabeculae of the spongy bone and beneath the periosteum. The distribution patterns of the trivalent cations generally resembled the tetravalent elements, but there was also substantial spotty deposition in the compact bone, which was later shown to be on the mineralized walls of vascular channels.

The radioisotopes of all of the trivalent and tetravalent elements have been classified for the purposes of radiation dosimetry as 'bone surface seekers'. The methods used for calculating radiation doses to the bone cells and marrow surrounding the deposits of these nuclides in the skeleton have taken into account their nonuniform intraskeletal distribution (ICRP, 1959, 1967, 1979).

Actinide binding to the calcified bone surfaces is the net result of several biological and chemical processes: the nature of the bone mineral crystals and the organic bone matrix, the relative affinities of the individual actinides for the mineralized surface and the plasma ligands, the ability of the circulating actinide complexes to pass through or between the cells on resting surfaces and penetrate the osteoid and active osteoblasts on growing surfaces, and the richness of the blood supply and its proximity to the bone surfaces.

31.7.1 Bone surfaces

Detailed descriptions of the microanatomy of the skeleton and of bone growth and maintenance remodeling are available in specialized works (Bourne, 1956; Frost, 1963; Ham, 1974). The periosteal surface is beneath the outer tissue layer that envelops the whole bones. The endosteal surface is the inner aspect of whole bones plus the much larger surface of the three-dimensional interconnected network of the fine bony bars, rods, and plates of the spongy (trabecular) bone. The vascular (Haversian) surface is the cylindrical lining of the numerous vascular channels that penetrate and nourish the compact (cortical) bone. The large anatomical surface of the mammalian skeleton – about 12 m^2 in an adult human male – is about equally divided between the endosteal and Haversian surfaces (Spiers, 1968; Lloyd and Marshall, 1972; ICRP, 1979).

Three general bone surface types are recognizable histologically: actively growing, resting, and resorbing. Depending on age and stage of skeletal maturity, the abundances of the three surface types vary in individual bones and in the whole skeleton. New bone is laid down at the active surfaces, which are recognized by the presence of regular rows of tall columnar cells (active osteoblasts) located just above a variably thick layer of uncalcified or poorly calcified bone matrix (osteoid). A thin strongly PAS-positive margin marks the line of calcification. The cell and osteoid layers covering sites of active bone formation make these sites the least accessible to circulating metal ions. Resting surfaces are covered with a layer of thin flattened cells, which line the adjacent calcified surface. The bone beneath the resting cells is usually more calcified than that beneath the cells on the growing surfaces. The mineral–organic interface stains PAS-positive. Resting bone surface sites, which are predominant in human adults, are well mineralized, but their accessibility is somewhat hindered by the overlying cell layer. Resorbing surfaces are recognized by their irregular outline, their high degree of mineralization, the intense PAS-positive stain at the calcified margin, the absence of covering cells, and the presence of the large multinuclear osteoclasts that dissolve and digest bone. The resorbing sites are exposed directly to the circulating blood and/or tissue fluid, making them the most accessible.

The vascular channels of cortical bone (horizontal Volkmann's canals and longitudinal Haversian systems) are short cylindrical tunnels in the well-mineralized compact bone. They are lined with a layer of flattened endosteal cells, so their inner aspect resembles resting bone surface. The central space is filled with loose connective tissue and one large capillary or two small arterial and venous capillaries.

31.7.2 Bone blood supply

The blood supplies to the periosteum, the internal skeletal sites containing fatty marrow, and the vascular channels of cortical bone are closed capillary beds that effectively retain the red cells and nearly all of the plasma protein and allow only filterable low molecular weight plasma constituents and filterable metal complexes access to the bone surfaces. Erythropoietic marrow contains large vascular sinusoids with a discontinuous lining that permits whole plasma to pass into the extravascular space. The bony trabeculae embedded in the red marrow are exposed not only to metal ions complexed with the low molecular weight constituents of tissue fluid but also their nonfilterable complexes with plasma proteins (Ham, 1974; Wronski *et al.*, 1980; Miller *et al.*, 1982).

31.7.3 Intraskeletal distribution of actinides

More refined and definitive autoradiographic techniques confirmed the early observations of the surface-limited deposition of actinides in bone. Sectioning and autoradiography of undecalcified bone are difficult, and later studies

focused on $^{233}UO_2^{2+}$,$^{239}Pu^{4+}$,$^{241}Am^{3+}$, and most recently ^{237}Np. In addition to revealing important details of the initial distribution of these actinides in bone, they have helped to define the mechanisms of release of actinides bound to bone and the kinds and extent of local radiation damage.

(a) $^{241}Am^{3+}$

The initial intraskeletal distribution of $^{241}Am^{3+}$ was investigated autoradiographically in rats (Taylor *et al.*, 1961; Durbin *et al.*, 1969; Durbin, 1973; Priest *et al.*, 1983), dogs (Herring *et al.*, 1962; Lloyd *et al.*, 1972b; Polig *et al.*, 1984), and monkeys (Durbin, 1973, 1975). $^{241}Am^{3+}$ is initially deposited nearly uniformly on all types of bone surfaces – endosteal, periosteal, and Haversian canals. Deposition is somewhat more intense on resorbing and resting surfaces than on actively growing surfaces. No $^{241}Am^{3+}$ was found initially as a diffuse distribution in the bone volume (Herring *et al.*, 1962; Priest *et al.*, 1983). Results for $^{249,252}Cf^{3+}$ in rats were essentially the same as for $^{241}Am^{3+}$ (Durbin, 1973).

(b) Pu^{4+}

Initial intraskeletal distribution of Pu^{4+} ($^{238}Pu^{4+}$ or $^{239}Pu^{4+}$) was studied autoradiographically in rats (Arnold and Jee, 1957; Taylor *et al.*, 1961; Priest and Giannola, 1980), dogs (Arnold and Jee, 1959, 1962; Herring *et al.*, 1962; Wronski *et al.*, 1980), and monkeys (Durbin, 1975). Soluble Pu^{4+} is initially deposited almost entirely on endosteal surfaces, in particular, the surfaces of the trabeculae of spongy bone closest to the sinusoidal circulation of the erythropoietic marrow that surrounds them. In the beagles, the initial surface concentrations of $^{239}Pu^{4+}$ on the fine trabeculae in vertebral bodies, pelvis, and proximal humerus (sites in spongy bone containing red marrow) were four to eight times greater than on the coarser trabeculae in the proximal ulna and distal humerus (sites containing fatty marrow) (Wronski *et al.*, 1980). Endosteal deposition is not uniform, and Pu^{4+} concentrations on endosteal surfaces decrease generally in the order: resorbing > resting > actively growing. Deposits of Pu^{4+} on periosteal surfaces are less intense, and those on Haversian canal surfaces are very low. There is no initial diffuse distribution of Pu^{4+} in the bone volume.

(c) UO_2^{2+}

The initial intraskeletal distribution of UO_2^{2+} ($^{232}UO_2^{2+}$ or $^{233}UO_2^{2+}$) was studied autoradiographically in rats (Priest *et al.*, 1982) and dogs (Rowland and Farnham, 1969; Stevens *et al.*, 1980). Uranyl ion is initially deposited on all bone surface types, but it is found preferentially on actively growing surfaces that are laying down new bone. Similarly to Ra^{2+}, UO_2^{2+} is deposited in the calcifying zones of skeletal cartilage. In the dogs, a detectable fraction diffused into the bone volume.

(d) $^{237}NpO_2^+$

The intraskeletal distribution of ^{237}Np, injected iv as $^{237}NpO_2NO_3$, was investigated autoradiographically in rats (Wirth and Volf, 1984; Sontag, 1993). The initial distribution appears to be nearly uniform on all endosteal and periosteal surfaces and the vascular canal surfaces of compact bone. There is no evidence for early diffusion of Np into the bone volume.

(e) $^{91}Y^{3+}$, $^{144}Ce^{3+}$, $^{170}Tm^{3+}$

The initial intraskeletal distribution of these three trivalent metal ions was studied autoradiographically in growing dogs (Jowsey *et al.*, 1958), and $^{91}Y^{3+}$ was also investigated in rachitic young dogs and weanling rabbits (Herring *et al.*, 1962). The distributions of these trivalent elements in bone were similar to $^{241}Am^{3+}$. They were located on all bone surfaces, with the greatest concentrations associated with highly mineralized surfaces of resorbing or resting bone. There was little or no deposition in areas of active bone formation, and no deposition in osteoid tissue. All three radioisotopes were deposited on the mineralized surfaces of the resting and resorbing Haversian systems in cortical bone, but at intensities less than on the endosteal surfaces.

(f) Summary

Within the skeleton, deposition of multivalent cations is initially limited to the anatomical surfaces in the order: endosteal > periosteal >cortical vascular channels, and among the bone surfaces in the order: resorbing >resting > actively growing.

The intensities of the local surface deposits are positively correlated with accessibility to the blood supply, the nature of the local blood supply, the degree of mineralization of the surface, and the instability of the complexes formed with Tf and other plasma proteins.

31.7.4 Retention – remodeling and redistribution

Prolonged skeletal retention is a distinguishing feature of the actinides (ICRP, 1959, 1972, 1979, 1993, 1995; Leggett, 1985, 1989, 1992a,b). The actinides (except UO_2^{2+}), once deposited on bone surfaces, appear to be released only when the bone containing them is physically destroyed (Arnold and Jee, 1957, 1959). There are long-term skeletal retention data for several actinides in beagles. The terminal slope of the skeletal retention function for UO_2^{2+} in the beagles has a half-time of about 3 years: UO_2^{2+} is lost from bone by chemical processes as well as by structural remodeling, and because it is efficiently excreted in the urine, little is redeposited in bone (Rowland and Farnham, 1969; Stevens *et al.*, 1980; Leggett, 1989). Retention of the trivalent and tetravalent actinides in the

beagle skeleton is much more prolonged. The half-times of the terminal slopes of the skeletal retention equations for $^{241}Am^{3+}$, $^{249}Cf^{3+}$, and $^{228}Th^{4+}$ are 15 to 18 years (Stover *et al.*, 1960; Lloyd *et al.*, 1972b, 1976, 1984a,b). About 56% of the initial skeletal deposit of $^{239}Pu^{4+}$ is cleared with a half-time of about 1.6 years; later measurements of $^{239}Pu^{4+}$ in the skeletons of individual dogs at postinjection times as long as 4400 days yielded a curve with a slope that could not be distinguished from zero (Stover *et al.*, 1962, 1972; Stover and Atherton, 1974).

The mature mammalian skeleton is not static, and it undergoes much internal structural change throughout the life span. During growth, structural remodeling (both resorption and accretion) is vigorous and extensive, and there is a net increase in bone mass. After skeletal growth is complete, remodeling and bone turnover involve only small fractions of the skeleton at any time, and there is little change in skeletal mass. During the last years of life of some mammals, resorption exceeds replacement leading to a slow decrease in skeletal mass (Bourne, 1956; Frost, 1963).

Bone resorption and accretion are surface-limited processes (Bourne, 1956; Ham, 1974). In the mature skeleton, turnover of bone (resorption and accretion) at the surfaces of the fine trabeculae of spongy bone is faster than at the surfaces of the larger trabeculae in the flat and membranous bones and in the distal ends of the long bones and the surfaces of the cortical bone vascular channels (about eight times faster in young adult beagles and four times faster in human adults) (Arnold and Jee, 1962; Arnold and Wei, 1972; ICRP, 1973; Wronski *et al.*, 1980).

Actinide-labeled bone surfaces may be resorbed by osteoclasts or be buried beneath new bone in the course of structural remodeling, or they may remain unaltered (Copp *et al.*, 1946; Arnold and Jee, 1962; Durbin *et al.*, 1969; Durbin, 1973; Wronski *et al.*, 1980; Sontag, 1993). The actinide content of the resorbed bone is eventually dissolved by the osteoclasts and/or marrow macrophages, released into the circulation, and redistributed among the target tissues (Arnold and Jee, 1962; Priest and Giannola, 1980; Priest *et al.*, 1983; Durbin and Schmidt, 1985; Durbin *et al.*, 1985). There is evidence indicating that solubilized actinide released from bone (or any other body site) is complexed and transported by the same plasma ligands (mainly Tf) and distributed among the same target tissues in the same proportions as the soluble form originally injected (Arnold and Jee, 1962; Durbin *et al.*, 1969; Jee, 1972a,b; Durbin, 1973; Priest and Giannola, 1980; Leggett, 1985, 1989, 1992a,b).

Redeposition in the skeleton can occur on both old (preinjection) surfaces augmenting their existing actinide concentrations and on new (postinjection) surfaces, which will acquire a lighter more diffuse label than those labeled immediately after the injection. With the passage of time, resorption of actinide-labeled bone surfaces (mainly trabeculae at red marrow sites) and redeposition of substantial fractions of the released and solubilized actinide will reduce the concentrations at the bone surfaces and increase the concentration in the

bone volume, tending to equalize the concentration in bones containing red marrow sites (vertebral bodies, ribs, sternum, pelvis, proximal ends of humerus and femur) and those that are mainly cortical bone (Durbin, 1973; Durbin *et al.*, 1985; Durbin and Schmidt, 1985; Sontag, 1993).

31.7.5 Summary

Prolonged retention of actinides deposited in the skeleton is the combined result of redeposition in bone of actinide released from soft tissues, removal from bone only by the relatively slow process of bone resorption, recirculation after release bound mainly to plasma proteins (which severely impedes excretion), and redeposition at new bone sites of large fractions of the actinide released from initially labeled bone sites.

31.8 ACTINIDE BINDING IN BONE

The specific nature of the initial chemical reactions underlying the fixation of actinides in living bone is incompletely understood.

31.8.1 Composition of bone

The compositions of mature mammalian cortical and trabecular bone are, on average, about 61, 26, and 13% by weight and 40, 35, and 27% by volume, mineral, organic matrix, and water, respectively (Gong *et al.*, 1964). The mineral phase [hydroxyapatite, $Ca_{10}(PO_4)_6(OH)_2$] exists as minute tablet-shaped crystals 2 to 2.5 μm wide, 3.5 μm long, and 0.25 to 0.5 μm thick, and these are aligned parallel to the longitudinal direction of the collagen fibers of the matrix (Neuman and Neuman, 1958). At the microscopic level, bone is not homogeneous, but it is reasonable to assume that the proportions of mineral and matrix on fully mineralized bone surfaces are about the same as the bulk volume composition, that is, that the exposed surface area is about equally divided between mineral crystals and organic matrix along with some bound water. By the same reasoning, bone that is not fully developed would be expected to have a smaller proportion of mineral exposed on the surface.

31.8.2 Actinide binding to bone *in vivo*

There is good, if inferential, evidence for *in vivo* actinide binding to bone mineral. In living mammals, the initial skeletal binding site of the actinides and their trivalent and tetravalent chemical analogs is at the mineral–organic interface. Actinide deposition is greatest on bare, fully mineralized resorbing surfaces and least on growing surfaces covered by a layer of bone matrix

(osteoid) (Jowsey *et al.*, 1958; Herring *et al.*, 1962). In rachitic animals, bone continues to grow but is very poorly mineralized: In such animals, Pu^{4+} passed through the nonmineralized osteoid and deposited on the first available mineralized structures (Jee and Arnold, 1962). Actinides also accumulate on calcified nonskeletal structures such as renal calculi, calcified scar tissue, and calcified tracheal and bronchial cartilage (Painter *et al.*, 1946; Jee and Arnold, 1962; Durbin, 1973; Durbin *et al.*, 1985).

31.8.3 Actinide binding to bone mineral *in vitro*

Neuman (1953) demonstrated that binding of UO_2^{2+} by bone mineral *in vitro* was a reversible ion-exchange process: One UO_2^{2+} displaced two Ca^{2+} ions and immobilized two PO_4^{3-} moieties. *In vivo*, UO_2^{2+} deposits at growth sites in the skeleton, and it accompanies hydroxyapatite crystal growth *in vitro*. However, the evidence indicates that UO_2^{2+} is limited to the crystal surfaces, presumably because it is too large and too polar to 'fit' into the crystal lattice (Neuman and Neuman, 1958).

Jowsey *et al.* (1958) prepared solutions of $^{91}Y^{3+}$, $^{144}Ce^{3+}$, and $^{170}Tm^{3+}$ in human plasma reconstituted with water or with 0.0034 M sodium citrate. Bovine cortical bone was used to prepare the following dry powders (particle size not specified): fat-free whole bone, ED-bone (bone powder heated in ethylenediamine to digest the organic matrix); bone ash (heated at 600°C to destroy the organic matrix); EDTA-bone (bone powder treated with EDTA to remove the mineral fraction). Calcium phosphate [$Ca_3(PO_4)_2$] was included as a bone mineral surrogate, and charcoal and glass wool were included as nonspecific particulate controls. The dry powders (250 mg each) were placed in small paper thimbles, a solution of lanthanide in plasma or in citrated plasma was percolated through the solids, and two rinses of isotope-free media were applied. On average, uptake of the lanthanides by ED-bone, whole bone, $Ca_3(PO_4)_2$, and bone ash was 42, 40, 33, and 19% respectively, of the amounts present in the plasma media. Uptakes were about 30% greater from citrated plasma. The powdered organic matrix, charcoal, and glass wool did not take up the lanthanides from plasma, with or without added citrate. Thin sections of bone embedded in methylmethacrylate were incubated in a solution containing $^{91}Y^{3+}$, and autoradiographs showed that all of the calcified surfaces took up the lanthanide.

Foreman (1962) prepared a solution of $^{239}Pu^{4+}$ in 0.05 M lactate buffer pH 7. Bovine cortical bone was used to prepare the following dry powders (particle size not specified in most cases): fat-free whole bone, bone ash (700°C, 100–200 mesh), coarse bone ash (>100 mesh); KOH-bone (bone powder heated in KOH and ethylene glycol to digest the organic matrix); EDTA-bone (decalcified organic matrix). Carborundum, alundum, and pumice were included as particulate controls. Samples of each powder were shaken for 24 h with 100 to 200 mL of the Pu^{4+}-lactate buffer solution, and the clear supernatant was sampled periodically after allowing the solids to settle. After 24 h, the four particulates

containing bone mineral had taken up $\geq$95% of the Pu^{4+} in the medium. The initial uptake rates of the bone mineral samples were in the order: bone ash (fine) > bone ash (coarse) $\gg$ KOH-bone $\gg$ whole bone. At equilibrium, the EDTA-decalcified organic fraction took up $\leq$10% of the available Pu^{4+}. The Pu^{4+} did not adhere to the three inert mineral powders. Addition of 0.2 M Ca^{2+} or 0.2 M Na^{+} to the buffer medium did not change either the rates or 24 h uptakes of Pu^{4+} by the whole bone or bone ash powders.

Foreman (1962) also prepared whole rat femora, as follows: fresh bone cleaned of adhering soft tissue; bone ash (700°C furnace); KOH-bone; and EDTA-bone. Four replications of each femur preparation were sealed in cellophane bags and surgically implanted in the peritoneal cavities of 'host' rats. The 'host' rats were injected iv with $^{239}Pu^{4+}$ citrate 24 h later and killed 48 h after the Pu^{4+} injection. Uptake of the Pu^{4+} in the living femora of the 'host' rats was reproducible, on average, 164 400 $\pm$ 66 000 cpm per whole bone. Uptakes of Pu^{4+} in the implanted femora that had been heat or chemically ashed were nearly the same, about 40% of that in the living bone of their 'hosts', while Pu^{4+} uptakes in the implanted fresh bone and EDTA-decalcified bone were 15 and 6%, respectively. The chemically or heat ashed bone preparations that were essentially free of organic tissue barriers had the greatest affinities for the Pu^{4+}, while the affinity of the decalcified bone matrix was the least. An important outcome of this experiment was the demonstration of the passage of Pu^{4+} through the semipermeable cellophane membrane, implying the presence of a filterable Pu^{4+} complex in the interstitial fluid of the peritoneal cavity.

Chipperfield and Taylor (1972) prepared dilute solutions of $^{239}Pu^{4+}$, $^{241}Am^{3+}$, and $^{244}Cm^{3+}$ nitrates, each of these was mixed with 3 mL of solutions of tris buffer pH 7.2 containing chelators, including: 3.4×10^{-4} M sodium citrate, 3.2×10^{-4} M EDTA, 2.4×10^{-4} M DTPA, 3.4×10^{-6} M Tf, or 4×10^{-6} M bone sialoprotein or bone chondroitin sulfate–protein complex. Fine cortical bone ash powder (200–300 mesh) was added (10 mg) to each actinide-chelator solution and stirred vigorously for 1 h. Supernatant containing unbound actinide and solids containing bound actinide were separated by centrifugation. In the absence of a chelator, all three actinides were quantitatively associated with the bone mineral fraction. The fractions bound to the bone mineral (100% – reported solution content) for Pu^{4+}, Am^{3+}, and Cm^{3+}, respectively, were as follows: Tf (98, 99, 84); citrate (73, 100, 100); bone glycoproteins, on average (79, 92, 92); EDTA (91, 70, 61); DTPA (14, 0, 0). Effectiveness for preventing actinide binding to bone mineral, which can be viewed as the stabilities of their complexes with the chelators relative to those formed with the bone ash is in the order: Tf $\leq$ citrate < bone glycoproteins < EDTA < DTPA. Binding of Am^{3+} and Cm^{3+} to bone mineral was the same in this test system and nearly quantitative in the presence of Tf, citrate, or the bone glycoproteins; it was partially prevented by EDTA and completely prevented

by DTPA. Binding of Pu^{4+} to bone mineral was nearly quantitative in the presence of Tf, partially prevented by EDTA, the bone glycoproteins, or citrate, and incompletely prevented by DTPA.

Guilmette *et al.* (1998, 2003) prepared solutions of $^{238}Pu^{4+}$, $^{239}Pu^{4+}$, and $^{241}Am^{3+}$ in 0.0034 to 0.005 M sodium citrate. Finely ground bovine bone ash and synthetic bone mineral (hydroxyapatite, HAP) were characterized by X-ray diffraction, and their measured specific surface areas were 10.7 and 65 $m^2\ g^{-1}$, respectively. Each actinide was stirred for 24 h with 10 mg of a mineral powder in 0.1 M HEPES buffer pH 7.2. The solid and supernatant were separated by ultrafiltration. Under these conditions $\geq$99% of the actinide was bound to the minerals. Varying masses of $^{238}Pu^{4+}$ and $^{239}Pu^{4+}$ (0.001–100 μg) and $^{241}Am^{3+}$ (0.001–1.0 μg) were added to 10 mg of bone ash or HAP to characterize the relationships between actinide binding and mineral surface area, that is, the binding capacity. For Pu^{4+}, masses $\leq$10 μg, and for all $^{241}Am^{3+}$ masses studied, binding to both minerals was $\geq$99% in 24 h. However, when the mass of $^{239}Pu^{4+}$ was 100 μg, more than 50% incubated with bone ash and 20% incubated with HAP remained unbound at 24 h. The data are consistent with the larger specific surface area of HAP presenting more binding sites, and they may also be interpreted as signifying that the mineral surfaces contain a saturatable number of potential metal-binding sites per unit area. The DTPA chelates of $^{238}Pu^{4+}$ and $^{241}Am^{3+}$ were incubated with 10 mg of HAP. There was no indication that the $^{241}Am^{3+}$–DTPA complex dissociated in favor of mineral binding. In contrast, 50% of the $^{238}Pu^{4+}$–DTPA complex dissociated in 24 h in favor of binding to the bone mineral. The stability of $^{241}Am^{3+}$–DTPA is evidently greater, while that of $^{238}Pu^{4+}$–DTPA is somewhat less, than the stabilities of their respective bone mineral complexes.

Guilmette *et al.* (2003) investigated removal of $^{238}Pu^{4+}$ and $^{241}Am^{3+}$ from bone mineral by 24 h incubation of those actinides prebound to HAP by chelators in solutions of 0.1 M HEPES buffer pH 7.2. Binding of $^{238}Pu^{4+}$ and $^{241}Am^{3+}$ by HAP is sufficiently stable that $ZnNa_3$–DTPA removed only 1.4% of the Am^{3+} and $\leq$0.1% of the Pu^{4+} sorbed to the mineral. Actinide removal from HAP was tested with a set of tetra-, hexa-, and octadentate ligands with linear or branched backbones containing bidentate catecholate (CAM) or hydroxypyridinonate (HOPO) metal-binding groups. Removal of Pu^{4+} (4–54%) was achieved only by the linear octadentate CAM and HOPO ligands. Removal of Am^{3+} (5–21%) was achieved with several linear or branched tetra-, hexa-, or octadentate ligands.

Bostick *et al.* (2000), Moore *et al.* (2003), and Thomson *et al.* (2003) conducted investigations in support of the management and remediation of actinide-contaminated groundwaters, sediments, and wastewaters. Batch sorption and column tests demonstrated the great affinities of UO_2^{2+}, NpO_2^{+}, Pu^{4+}, Am^{3+}, and stable Ce^{3+} for natural and synthetic apatites, including hydroxyapatite, $Ca_3(PO_4)_2$, and bone ash.

31.8.4 Actinide binding by bone glycoproteins

A case can be made for the participation of some low abundance organic matrix constituents in the binding of actinides in living bone (reviewed by Duffield and Taylor, 1986). *In vitro* complexation of Th^{4+} and Pu^{4+}, and to a lesser degree, Am^{3+} and Cm^{3+} by isolated mucoprotein substituents of bone matrix has been demonstrated.

All of the multivalent lanthanides and actinides studied autoradiographically deposit most intensely on fully mineralized bone surfaces, anatomical sites that also stain positively with PAS for the presence of mucosubstances (Jowsey, 1956; Herring *et al.*, 1962; Williamson and Vaughan, 1964; Vaughan *et al.*, 1973). Paraphrasing Jowsey (1956) in response to a conference participant's question: In areas of bone resorption, the PAS staining is the result of the depolymerized state of the mucopolysaccharides in the ground substance (matrix). In such state there are presumably free side chains of the mucopolysaccharide molecules (containing potentially chelating 1,2-hydroxy groups), which are oxidized by the periodic acid to aldehydes and take up the Schiff stain.

Nearly 90% of the organic bone matrix is collagen, which contributes about 20% of the weight of native bone. Five distinct glycoprotein fractions were extracted from bovine cortical bone. Their designations and weight fractions of native bone (% by weight) are, as follows: bone sialoprotein, 0.25%; bone chondroitin sulfate–protein complex, 0.18%; three less well-characterized glycoprotein fractions – glycoprotein I and II, 1.57% combined; cetylpyridonium chloride (cpc) soluble glycoprotein, 0.1%. While not regarded as conclusive, supporting experiments indicate that the sialoprotein content (and perhaps also the other mucosubstances) of bone are formed and laid down in the matrix during bone formation. The functions of the mucosubstances of mature bone are not known (Herring, 1964). Bone sialoprotein contains large proportions of sialic, glutamic, and aspartic acids; 15, 20, and 15 moles of acids per mole of protein, respectively.

Chipperfield and Taylor (1968, 1970, 1972) used gel filtration (Sephadex G-25 and G-50) to investigate the bonding of ultrafiltered dilute solutions of $^{228}Th^{4+}$, $^{239}Pu^{4+}$, $^{241}Am^{3+}$, and $^{244}Cm^{3+}$ nitrates incubated with the isolated bone glycoproteins noted above. The proteins were dissolved in tris buffer pH 7.2, and the protein:metal molar ratios were 1:1 for Pu^{4+} and 10:1 for the higher specific activity radionuclides. The results of those studies are collected in Table 31.13. Those results, although variable and regarded by the authors as semiquantitative, indicate that at physiological pH the isolated glycoprotein fractions of bone matrix can form complexes with Th^{4+} and Pu^{4+}, and to a lesser degree, with Am^{3+} and Cm^{3+}. Under these experimental conditions, the affinities of the bone glycoprotein fractions for Th^{4+} and Pu^{4+} apparently exceed the affinities for these actinides of reconstituted human Tf or apo-Tf. Two of the bone glycoproteins, bone sialoprotein and bone chondroitin sulfate–protein

Table 31.13 *Collected data for association of selected actinides with isolated bone glycoproteins, human transferrin, and poly-L-glutamic acid.*[a]

Protein	*Percent of applied actinide eluted with protein*			
	$^{228}Th^{4+}$	$^{239}Pu^{4+}$	$^{241}Am^{3+}$	$^{244}Cm^{3+}$
Bone sialoprotein	96[d]	71[b], 52[c], 55[d]	30[b], 10[d]	12[d]
Bone chondroitin sulfate–protein complex	78[d], 22[e]	72[b], 49[d], 13[e]	5.0[b], 15[d], 0.3[e]	10[d], 0.3[e]
Glycoprotein I	13[d]	30[d]	2.8[d]	38[d]
Glycoprotein II	72[d]	50[d]	5.1[d]	8.2[d]
Cpc-soluble glycoprotein	83[d]	37[d]	4.6[d]	8.7[d]
Human transferrin	61[c,e]	24[b,c], 19[e]	0.17[b], 0.2[e]	0[e]
Apotransferrin	30[c]	43[c]	–	–
Soluble collagen	–	2.8[b], 23[d]	0.6[d], 0[e]	0.9[d]
Poly-L-glutamic acid	80[e]	69[e]	8.0[e]	27[e]

[a] Reported values of protein binding rounded to two significant figures. Ultrafiltered actinide nitrates incubated with proteins dissolved in tris buffer at pH 7.2. Mixtures eluted with buffer from G-25 or G-50 Sephadex gel columns to determine amount bound to protein.
[b] Chipperfield and Taylor (1968).
[c] Chipperfield and Taylor (1970).
[d] Table I of Chipperfield and Taylor (1972).
[e] Table II of Chipperfield and Taylor (1972).

complex, were about as effective as EDTA in competing with bone ash for Pu^{4+}, Am^{3+}, and Cm^{3+}.

Supporting studies demonstrated that actinide binding by the bone glycoproteins was pH dependent; maximum binding of Pu^{4+} by bone sialoprotein is at pH 6, and of Am^{3+} and Cm^{3+} at pH 8. These results were interpreted by the authors to mean that Pu^{4+} was bound by the abundant carboxyl groups of the protein's amino acid side chains, but that those carboxyl groups were less important for binding the trivalent actinides. Binding of Pu^{4+} by bone sialoprotein was reduced, but not abolished, by mild acid hydrolysis (removal) of the terminal sialic acid moieties, which suggests that the sialic acid groups may also participate in metal binding.

31.8.5 Summary

Actinide binding in bone is a surface phenomenon. However, except for UO_2^{2+}, binding of the trivalent and tetravalent actinides and NpO_2^+ to bone surfaces is so stable that those metals neither migrate into the bone volume via the canaliculi nor are released back into the circulation by ion exchange or complexation with the ligands of the constantly flowing plasma and tissue fluid.

At physiological pH, trivalent and tetravalent lanthanides and actinides, UO_2^{2+} and NpO_2^+, bind stably to native and synthetic bone mineral *in vitro*. Actinide uptake by various bone mineral preparations was nearly quantitative

from buffered solutions (lactate, tris, HEPES, pH 7–7.4) even from those solutions that also contained 0.3 to 0.5 mM citrate, whole plasma, or human Tf. In general, actinide uptake by the crystalline bone mineral preparations (synthetic HAP, chemically ashed KOH-glycol bone, or ED-bone) was faster than for bone ash, $Ca_3(PO_4)_2$, or powdered defatted whole bone, in which about one-half of the exposed particle surface is organic matrix. Actinide uptake by bone mineral is positively correlated with the surface area of the particles and appears to be saturable, indicating a fixed number of binding sites per unit surface area.

Hydroxyapatite [$Ca_{10}(PO_4)_6(OH)_2$] presents an organized Ca^{2+}-poor negatively charged surface with unsatisfied negative charges on adjacent phosphates. If Ca^{2+} is replaced, as is the case for UO_2^{2+}, there is access to the oxygens of two and perhaps three phosphates. The complexes of Th^{4+} and Pu^{4+} with bone mineral are more stable than the complexes that these metal ions form with $ZnNa_3$-DTPA, indicating that the crystals themselves provide spatially suitable multidentate binding sites.

The PAS-positive staining at the organic–mineral interface of bone surfaces, which are the actinide deposition sites in the skeleton, suggested that bone glycoproteins may participate in actinide binding, even though powdered decalcified bone matrix does not bind actinides. Five isolated low abundance bone glycoproteins form variably stable actinide complexes. The binding units of these proteins are considered to be mainly free sialic acid, the monodentate carboxyl groups of glutamic acid, and the bidentate alpha-hydroxy-carboxyl groups of aspartic acid.

The mineral crystals of native bone are sandwiched between layers of matrix collagen fibers, and the exposed bone surfaces do not present as many metal-binding sites as isolated bone mineral crystals. The most stable complexes of the trivalent lanthanides and actinides are six-coordinate (six M–O bonds), and those of the tetravalent actinides are eight-coordinate (eight M–O bonds). It would seem that *in situ* the number and configuration of the exposed potential binding groups of the glycoproteins alone would be insufficient to provide enough suitably arranged binding groups for stable actinide complexation. However, in living bone, both the mineral crystals and the neighboring matrix constituents (glycoproteins) combined may furnish sufficient numbers of binding groups suitably arranged in three-dimensional space for rapid stable actinide complexation *in situ*.

31.9 *IN VIVO* CHELATION OF THE ACTINIDES

The potential hazards to human health of the radioactive fission products and new heavy elements created by nuclear fission were recognized early, stimulating the search for effective ways to remove internally deposited radioelements

from the body (Schubert, 1955; Voegtlin and Hodge, 1949, 1953; Stone, 1951). Chemical agents that form stable excretable actinide complexes were soon recognized as the only practical therapy for internal contamination (decorporation) (Voegtlin and Hodge, 1949, 1953; Schubert, 1955; Rosenthal, 1956; Catsch, 1964). Such agents should have greater affinity for actinides at physiological pH than the biological ligands, low affinities for essential divalent metals, and low toxicity at effective dose. Reviews and proceedings of conferences on the development of chelators suitable for removal of internally deposited actinides have dealt with the chemistry of metal chelates, animal studies to determine ligand effectiveness for reducing actinide burdens in the tissues and amelioration of actinide-induced chemical and radiation damage, ligand toxicity, and clinical applications (Rosenthal, 1956; Seven and Johnson, 1960; Kornberg and Norwood, 1968; Volf, 1978; NCRP, 1980; Raymond and Smith, 1981; Taylor, 1991; Bhattacharyya *et al.*, 1992; Durbin *et al.*, 1997a, 1998a,b; Stradling *et al.*, 2000a,b; Wood *et al.*, 2000; Gorden *et al.*, 2003).

31.9.1 Polyaminopolycarboxylic acids

The first chelating agent investigated was ethylenediaminetetraacetic acid (H_4-EDTA). Its Ca^{2+} salt, $CaNa_2$–EDTA, was introduced to avoid toxic depletion of serum Ca^{2+}. It enhanced excretion of $^{91}Y^{3+}$, $^{144}Ce^{3+}$, and $^{239}Pu^{4+}$ in rats (Foreman and Hamilton, 1951; Hamilton and Scott, 1953). But $CaNa_2$–EDTA is a poor actinide decorporation agent: it is renally toxic at effective dose; it depletes essential Zn^{2+} and other divalent metals; its efficacy cannot be improved except by increasing the administered dose.

Pentacarboxyl diethylenetriaminepentaacetic acid (H_5-DTPA) and its Ca^{2+} and Zn^{2+} salts ($CaNa_3$–DTPA introduced in 1957 and $ZnNa_3$–DTPA introduced in 1965) improved lanthanide and actinide decorporation compared with $CaNa_2$–EDTA (Catsch and Lê, 1957; Kroll *et al.*, 1957; Smith, 1958; Catsch and von Wedelstaedt, 1965). Those clinically approved DTPA salts are effective decorporation agents for the trivalent lanthanides and actinides, less effective for Pu^{4+} and Th^{4+}, and nearly ineffective for reducing the body content of UO_2^{2+} or NpO_2^+. [See references cited in Volf, 1978; Durbin *et al.*, 1997a, 1998a,b; Gorden *et al.*, 2003]. Although nominally octadentate, $CaNa_3$–DTPA appears not to coordinate fully with Pu^{4+}, and it does not remove Pu^{4+} bound to bone mineral *in vitro* (Raymond and Smith, 1981; Guilmette *et al.*, 2003).

Several variants and derivatives of DTPA have been prepared and tested in animals, including polyaminopolycarboxylic acids with longer central bridges or additional carboxyl groups (Catsch, 1964); a dihydroxamic acid derivative, ZnNa–DTPA–DX (Durbin *et al.*, 1989b; Stradling *et al.*, 1991; Volf *et al.*, 1993); lipophilic derivatives containing long alkane side chains (Volf, 1978; Raymond and Smith, 1981; Miller *et al.*, 1993). None of those DTPA-based

ligands was substantially more effective for *in vivo* chelation of lanthanides or Pu^{4+} or less toxic than native $CaNa_3$–DTPA, and most have been abandoned.

31.9.2 Desferrioxamine

Desferrioxamine (DFO), a linear tris-hydroxamate ligand, is a member of a class of compounds (siderophores) elaborated by microorganisms to obtain iron from the environment (Raymond and Smith, 1981). *In vivo* Pu^{4+} chelation is hampered by the weak acidity of the hydroxamic groups, which are not ionized at pH < 8; they are deprotonated only slowly at pH 7.4 by Fe^{3+} and Pu^{4+} but not by trivalent actinides (Taylor, 1967; Durbin *et al.*, 1980, 1989b; Rodgers and Raymond, 1983).

31.9.3 Siderophores as model chelators

Investigations of the siderophores and their structures and coordination chemistry identified the powerful hexadentate iron-sequestering agent, enterobactin (EB). EB is produced by enteric bacteria (*E. coli*) to obtain Fe^{3+} from the nearly neutral contents of the mammalian intestine (see references in Raymond and Smith, 1981 and Gorden *et al.*, 2003). It contains three bidentate catecholate binding groups attached through amide linkages to a cyclic 1-serine backbone and is preorganized for binding. The properties and structure of EB and similarities in the coordination properties of Pu^{4+} and Fe^{3+} provided the basis for rational design of highly selective multidentate actinide chelators that would be effective at physiological pH.

(a) Catecholate ligands

Multidentate catecholate ligands based on the EB model (denticity 4–8) were prepared containing catechol (CAM), sulfocatechol [CAM(S)], carboxycatechol [CAM(C)], or catecholamide (TAM) metal-binding groups (Fig. 31.15) attached through amide linkage to linear (LI-), cyclic (CY-), aromatic (ME-), or branched (TREN-, H(2,2)-) backbones. Syntheses and structures of the CAM ligands are collected in Gorden *et al.* (2003). All of those ligands were evaluated for promotion of excretion of $^{238}Pu^{4+}$ from mice (30 μmol kg^{-1} ligand ip 1 h after iv injection of $^{238}Pu^{4+}$ citrate, kill at 24 h). Catecholate ligands of denticity <8 and those containing only CAM groups were marginally effective for *in vivo* Pu^{4+} chelation. The water-soluble octadentate ligands with flexible linear backbones based on spermine were more effective than octadentate ligands with attached lipophilic side chains or those with cyclic backbones. Reduction of skeleton Pu^{4+} by 3,4,3-LICAM(S) and of liver Pu^{4+} by 3,4,3-LICAM(C) were greater than obtained with an equimolar amount of $CaNa_3$–DTPA (Durbin *et al.*, 1980, 1984, 1989a,b, 1996; Lloyd *et al.*, 1984c). Those

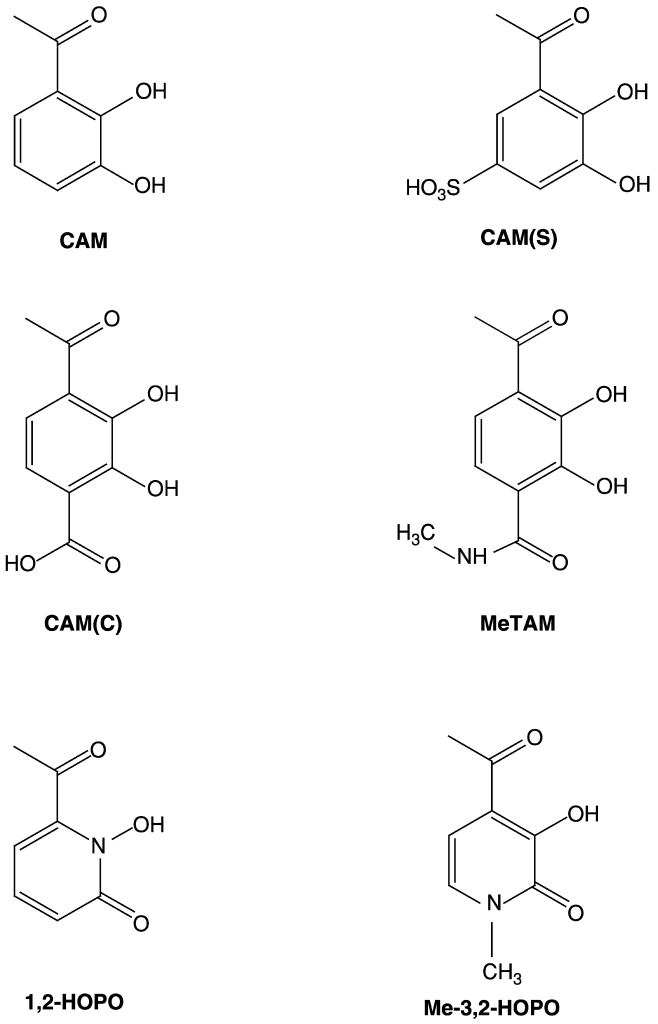

Fig. 31.15 *Catecholate and hydroxypyridonate metal-binding units incorporated into multidentate ligands for* in vivo *chelation of actinides. Catechol* (*CAM*), 5-*sulfocatechol* (*CAM*(*S*)), 4-*carboxycatechol* (*CAM*(*C*)), *methylterephthalamide* (*METAM*), 1,2 *hydroxypyridinone* (1,2-*HOPO*), *Me*-3,2-*hydroxypyridinone* (*Me*-3,2-*HOPO*).

ligands were much more effective than $CaNa_3$–DTPA at doses $\leq$30 μmol kg^{-1}, and they were orally active.

Although some of the *in vivo* properties of the two octadentate catecholate ligands are favorable, both are defective. *In vivo* chelation of Am^{3+} (and presumably other trivalent actinides and lanthanides) was significantly less than with $CaNa_3$–DTPA (Lloyd *et al.*, 1984c; Stradling *et al.*, 1986, 1989;

Volf, 1986; Volf *et al.*, 1986). The specific electric charge (e/r) of Am^{3+} is not great enough to deprotonate more than three of the eight OH groups of the tetracatecholate ligands at pH 7.4 (Kappel *et al.*, 1985). Furthermore, both of these nominally octadentate ligands are only functionally hexadentate at pH < 12. As the pH is reduced below 7.4, binding of Pu^{4+} by the more lipophilic 3,4,3-LICAM(C) becomes progressively less stable, and at pH 6 to 6.5 (the ambient pH of the lungs and renal tubules), the tetradentate species of the Pu^{4+}–3,4,3-LICAM(C) complex dominates (Kappel *et al.*, 1985; Durbin *et al.*, 1989a). Chelation of inhaled Pu^{4+} deposited in the lungs is weak and less effective than with $CaNa_3$–DTPA. The Pu^{4+} complex with 3,4,3-LICAM(C) that formed in the blood at pH 7.4 partially dissociates at the reduced pH of the kidneys depositing Pu^{4+} residues (Stradling *et al.*, 1986, 1989; Volf, 1986; Volf *et al.*, 1986; Durbin *et al.*, 1989a). 3,4,3-LICAM(S) was found to be renally toxic in dogs at the effective dose (Lloyd *et al.*, 1984c).

At pH 7.4, methylterephthalamide (MeTAM) forms a more stable ferric complex than any other catecholate-binding group (Durbin *et al.*, 1996). MeTAM was introduced into three octadentate ligands with differing backbones; the MeTAM group was attached to the N-terminal of DFO, and four MeTAM groups were incorporated into linear spermine (3,4,3-LIMeTAM) and branched PENTEN [H(2,2)-MeTAM]. Reductions of body Pu^{4+} by these octadentate ligands were similar to each other, somewhat greater than for 3,4,3-LICAM(C), and significantly greater than for $CaNa_3$–DTPA. Their Pu^{4+} complexes are stable over the physiological pH range, and no Pu^{4+} residues were left in the kidneys. These lipophilic ligands are sparingly soluble at pH < 8, their solutions are rapidly air oxidized, and their reductions of body Pu^{4+} in mice, similar to that obtained with 3,4,3-LICAM(C), suggested that they were also functionally hexadentate at pH 7.4.

(b) Hydroxypyridinonate ligands

Bidentate metal-binding groups more acidic than derivatized catechol and were required to achieve full eight-coordination with Pu^{4+} and to stably bind trivalent actinides in dilute aqueous solution at physiological pH. Highly selective HOPO metal-binding units occur in a few siderophores. The 1,2-HOPO and Me–3,2-HOPO isomers (Fig. 31.15) are structural and electronic analogs of hydroxamic acid and catechol, respectively. Their Fe^{3+} complexes are exceptionally stable, and both isomers are deprotonated and ready for metal binding at physiological pH (Scarrow *et al.*, 1985).

The 1,2-HOPO and Me–3,2-HOPO binding units were derivatized by attaching a carboxyl group adjacent to the OH group on the pyridinone ring; the COOH group can then be attached to amines on the selected molecular backbones through amide linkages. An important feature of the 1,2-HOPO and Me–3,2-HOPO complexes is that, as is observed in the catecholamide complexes, strong hydrogen bonds between the amide proton and the adjacent oxygen

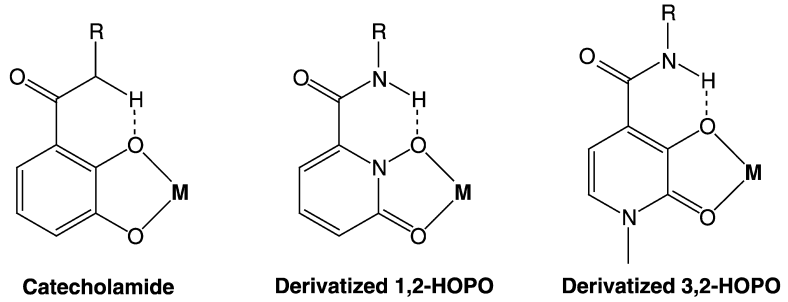

Fig. 31.16 *Strong hydrogen bonds between the amide proton and the adjacent oxygen donor enhance the stabilities of the metal complexes of the catecholate and hydroxypyridinonate ligands* (*Xu* et al., 2001).

donor increase the stabilities of their metal complexes (Fig. 31.16) (Xu *et al.*, 1995, 2001). Sets of multidentate 1,2-HOPO and Me–3,2-HOPO ligands were prepared, as follows: tetradentate with linear backbones (α-ω-alkanediamines – 3-LI-, 4-LI-, 5-LI- 6-LI- and 2-aminoethylether, 5-LIO-); hexadentate with a linear spermidine backbone (3,4-LI-) or with a tripodal branched backbone triethyleneamine (TREN-); octadentate with a linear spermine backbone (3,4,3-LI-), or through attachment of one HOPO group to the N-terminal of DFO (DFO-), (Fig. 31.17) (White *et al.*, 1988; Xu *et al.*, 1995; Xu and Raymond, 1999; Durbin *et al.*, 2000b).

Ligand efficacies were assessed for *in vivo* Pu^{4+} chelation by administering them to mice that had been injected iv with $^{238}Pu^{4+}$ citrate, as follows: ligand injected ip (30 μmol kg^{-1}) at 1 h (prompt injection), variable ligand dose at 1 h (dose effectiveness), ligand ip at 24 h (delayed effectiveness), ligand given orally at 5 min (oral activity). The ferric complexes of some ligands were administered promptly by ip injection or orally to assess competition between the ferric and Pu^{4+} complexes. Mice were killed 24 h after the ligand administration, and all tissues and excreta were radioanalyzed for Pu^{4+} (White *et al.*, 1988; Xu *et al.*, 1995; Durbin *et al.*, 2000b; Gorden *et al.*, 2003). Selected ligands were also assessed for *in vivo* chelation of $^{241}Am^{3+}$,$^{232}UO_2^{2+}$ or $^{233}UO_2^{2+}$, and $^{237}NpO_2^{+}$ (Durbin *et al.*, 1994, 1997a, 1998b, 2000a).

(c) Ligands for Pu^{4+}

1,2-HOPO and Me–3,2-HOPO ligands (tetradentate with 4-LI-, 5-LI-, 5-LIO-backbones, hexadentate with a TREN- backbone, and octadentate with a 3,4,3-LI- or H(2,2)- backbone) given ip or orally after the Pu^{4+} iv injection at doses ranging from 0.1 to 100 μmol kg^{-1} were significantly and markedly superior to equimolar amounts of $CaNa_3$–DTPA for promoting Pu^{4+} excretion. Promotion of Pu^{4+} excretion by ip injection of 30 μmol kg^{-1} of the linear 1,2-HOPO ligands (injected ip 1 h after the Pu^{4+} injection) was positively correlated with

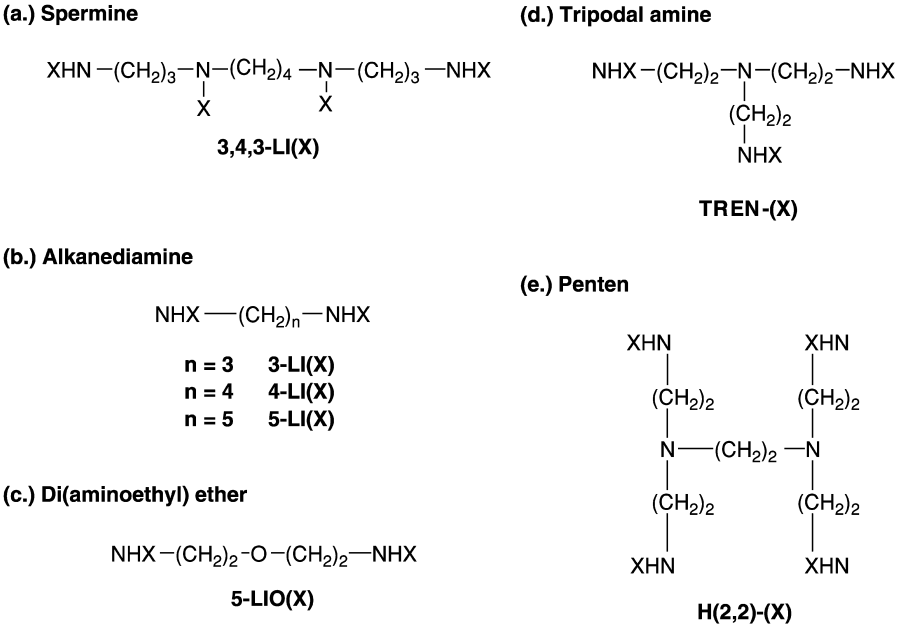

Fig. 31.17 *Linear and branched molecular backbones used for multidentate actinide chelating agents: tetradentate* (*b, alkanediamines; c, di*(*aminoethyl*)*ether*); *hexadentate* (*d, tripodal amine*); *octadentate* (*a, spermine; e, penten*).

ligand denticity, indicating formation of a complete eight-coordinate complex with octadentate 3,4,3-LI(1,2-HOPO) (White *et al.*, 1988; Gorden *et al.*, 2003).

At the standard 30 μmol kg^{-1} dose given to mice ip at 1 h after the Pu^{4+} injection, the tetra-, hexa-, and octadentate Me–3,2-HOPO ligands all promoted nearly the same amount of Pu^{4+} excretion. Apparently, the stabilities of the Pu^{4+} complexes with the tetradentate and hexadentate Me–3,2-HOPO ligands and the ligand concentrations established in the blood at this dose level are large enough to allow those ligands to compete for Pu^{4+} with the bioligands. However, when the Me–3,2-HOPO ligands were given orally, at lower doses, or as ferric complexes, the octadentate ligands, which have 1:1 stoichiometry for binding Pu^{4+}, were clearly more effective for *in vivo* Pu^{4+} chelation than the ligands of lesser denticity (Durbin *et al.*, 1989b, 2000b; Xu *et al.*, 1995; Gorden *et al.*, 2003).

The efficacies of the structurally analogous pairs of 1,2-HOPO and Me–3,2-HOPO ligands were compared in several Pu^{4+} removal protocols in mice. Overall, the Me–3,2-HOPO ligands were more effective for *in vivo* Pu^{4+} chelation than their structural 1,2-HOPO analogs (Durbin *et al.*, 2000b). The greater affinity of Me–3,2-HOPO for Pu^{4+} *in vivo* agrees with the greater stabilities of

the Me–3,2-HOPO complexes with other 'hard' metal ions like Fe^{3+} and Th^{4+} (Scarrow *et al.*, 1985; Veeck *et al.*, 2004).

Both octadentate HOPO ligands with the branched H(2,2)-backbone were highly effective for *in vivo* Pu^{4+} chelation, but they were considered to be too toxic to warrant further investigation (Durbin *et al.*, 1997a, 2000b). Low-toxicity DFO-(1,2-HOPO) given by ip injection is about as effective as 3,4,3-LI(1,2,-HOPO) for *in vivo* Pu^{4+} chelation, and it is moderately effective when given orally or at low dose (White *et al.*, 1988; Durbin *et al.*, 1989b). However, the weak acidity of the three hydroxamate groups prevents that ligand from competing effectively for inhaled Pu^{4+} deposited in the lungs and from stably binding Am^{3+} (Stradling *et al.*, 1991; Volf *et al.*, 1993, 1996a). *In vivo* Pu^{4+} chelation by DFO-(Me-3,2-HOPO) was significantly poorer than was obtained with its analog, DFO-(1,2-HOPO), but better than with native DFO. The lower than expected efficacy of DFO-(Me-3,2-HOPO) may be attributed to its lower aqueous solubility and the instability of its Pu^{4+} complex at the lower end of the physiological pH range (Xu *et al.*, 1995).

Among the ligand sets, the most effective for *in vivo* Pu^{4+} chelation is linear octadentate 3,4,3-LI(1,2-HOPO). Although it contains the less stably binding 1,2-HOPO unit, it has good aqueous solubility, and the flexible linear spermine backbone apparently confers advantages for Pu^{4+} binding by allowing a more favorable spatial arrangement of the four binding groups around the Pu^{4+} center. The 3,4,3-LI(1,2-HOPO) ligand is markedly superior to $CaNa_3$–DTPA for reducing Pu^{4+} in all tissues when given by injection, oral administration, or subcutaneous infusion after an iv or im injection or inhalation of Pu^{4+} nitrate or citrate in rats and mice (White *et al.*, 1988; Durbin *et al.*, 1989b, 2000b; Stradling *et al.*, 1992, 1993; Volf *et al.*, 1993, 1996a,b; Gray *et al.*, 1994). It is effective at doses as low as 0.03 μmol kg^{-1} in mice. When injected or infiltrated into an im wound site, it is more effective than $CaNa_3$–DTPA for reducing the body and wound site content of Th^{4+} (Stradling *et al.*, 1995a).

It was considered that the effectiveness of the octadentate 3,4,3-LI(1,2-HOPO) ligand might be improved, if the thermodynamically more potent Me-3,2-HOPO were introduced. Concerns about toxicity, lipophilicity, and aqueous solubility of a tetra-Me-3,2-HOPO ligand led to the synthesis of the mixed ligand, 3,4,3-LI(1,2-Me-3,2-HOPO). Two 1,2-HOPO units occupy the central secondary amines and two Me-3,2-HOPO units are attached to the terminal primary amines of spermine. Substitution of the two Me-3,2-HOPO groups for 1,2-HOPO slightly increased the stability of the Pu^{4+} complex at pH 7.4 and the lipophilicity and oral activity of the ligand, while somewhat reducing acute toxicity at high dose (Xu *et al.*, 2002). However, the modest thermodynamic gain was offset by the reduction in hydrophilicity, which appears to be an important property of 3,4,3-LI(1,2-HOPO), most likely facilitating its access to Pu^{4+} in the skeleton (Durbin *et al.*, 2000b, 2003).

Crystals have been prepared from water of structurally analogous Ce^{4+}[5-LI-(Me–3,2-HOPO)$_2$] and Pu^{4+}[5-LIO-(Me–3,2-HOPO)$_2$] complexes (Fig. 31.18).

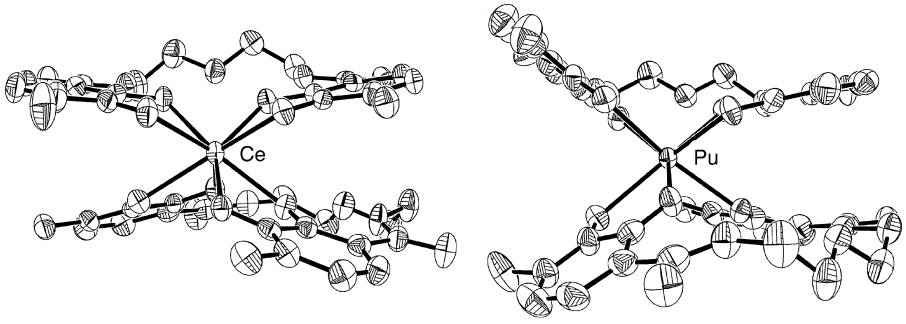

Fig. 31.18 *Molecular structures* (*viewed from the side*) *of Ce*(IV)[5-*LIO*(*Me*-3,2-*HOPO*)]$_2$ (*left side, Xu* et al., 2000) *and Pu*(IV)[5-*LIO*(*Me*-3,2-*HOPO*)]$_2$ (*right side, Gorden* et al., 2005).

In both cases the 2:1 structure is demonstrated. The overall ligand geometries resemble sandwich structures that are defined by the oxygen atoms coordinating to the Ce^{4+} and Pu^{4+} centers (Xu *et al.*, 2000; Gorden *et al.*, 2005). Solution thermodynamic studies of the Ce^{4+} complex system gave an overall formation constant of the complex (log β_2) of 41.6, and the formation constant of the analogous Pu^{4+} complex is expected to be essentially the same.

(d) Ligands for Am^{3+}

The efficacies of ligands containing HOPO groups for *in vivo* chelation of Am^{3+} and for removing Am^{3+} from bone mineral are generally in the order: octadentate > hexadentate > tetradentate (Guilmette *et al.*, 2003). The octadentate ligands more than satisfy the requirement for six-coordination preferred by Am^{3+}, and if three of their bidentate metal-binding units can bind to Am^{3+} without steric hindrance, the extra binding group appears to enhance the stabilities of their Am^{3+} complexes. As noted above, *in vivo* chelation of Am^{3+} by the octadentate ligands containing carboxy- or sulfocatechol [CAM (C), CAM(S)] or by hydroxamate (as in the octadentate ligands with the DFO-backbone) is weak because too few of the hydroxyl groups of those ligands can be deprotonated by Am^{3+} (and presumably other trivalent actinides) to form stable complexes at physiological pH (Lloyd *et al.*, 1984c; Kappel *et al.*, 1985; Stradling *et al.*, 1986, 1989; Volf, 1986; Volf *et al.*, 1986; Zhu *et al.*, 1988).

Four HOPO ligands have been investigated in rats and mice for *in vivo* chelation of Am^{3+}: octadentate 3,4,3-LI(1,2-HOPO), hexadentate TREN-(Me–3,2-HOPO), tetradentate 5-LI(Me–3,2-HOPO), and 5-LIO(Me–3,2-HOPO). When given by injection or orally (30 μmol kg^{-1}) to rats or mice contaminated with $^{241}Am^{3+}$ by injection or infiltration into a wound, all four of those ligands were more effective than an equimolar amount of

$CaNa_3$–DTPA. Octadentate 3,4,3-LI(1,2-HOPO) was about as effective as $CaNa_3$–DTPA, while the other HOPO ligands of lesser denticity were less effective than $CaNa_3$–DTPA for reducing body and lung Am^{3+} when the Am^{3+} had been inhaled (Stradling *et al.*, 1992; 1993, 1995b; Volf *et al.*, 1993, 1996; Durbin *et al.*, 1994; Gray *et al.*, 1994; Volf, 1996; Gorden *et al.*, 2003).

(e) Ligands for UO_2^{2+}

Soluble uranyl ion, UO_2^{2+}, is nephrotoxic, and because bone is the major storage organ for UO_2^{2+}, the high specific activity uranium isotopes also induce bone cancer (Voegtlin and Hodge, 1949, 1953; Finkel and Biskis, 1968; Hodge, 1973). Although sought since the 1940s, no multidentate ligand was identified that would efficiently bind UO_2^{2+} *in vivo*, promote its excretion, and reduce deposits in kidneys and bone (reviewed by Durbin *et al.*, 1997a). The modest reductions of acute UO_2^{2+} poisoning obtained with tiron, a bidentate sulfocatecholate, suggested that multidentate ligands containing similar binding groups would be effective *in vivo* UO_2^{2+} chelators.

Representative tetra-, hexa-, and octadentate ligands with linear or branched backbones containing CAM(S), CAM(C), MeTAM, 1,2-HOPO, or Me-3,2-HOPO groups (20 in all) were evaluated in mice for *in vivo* chelation of UO_2^{2+}. Experimental conditions were: $^{232\,+\,235}UO_2Cl_2$ or $^{233}UO_2Cl_2$ pH 4 injected iv, 30 μmol kg^{-1} of ligand injected ip at 5 min (see Fig. 31.11), ligand: U molar ratio 75 to 91, kill at 24 h. All of the test chelators were screened for acute toxicity. Except for the two tetradentate 1,2-HOPO ligands and $CaNa_3$–DTPA, all of the injected test chelators significantly reduced UO_2^{2+} in the kidneys compared with controls, and ligands containing CAM(S), CAM(C), or MeTAM groups also significantly reduced UO_2^{2+} in the skeleton. Administered orally at molar ratios from 90 to 300, the linear tetradentate ligands containing Me-3,2-HOPO, CAM (S), or CAM(C) and 3,4,3-LI(1,2-HOPO) significantly reduced UO_2^{2+} binding in the kidneys, but not in the skeleton. The combined assessments of ligand efficacy and acute toxicity identified tetradentate 5-LIO(Me-3,2-HOPO) and 5-LICAM(S) as the most effective low toxicity agents for UO_2^{2+}. They efficiently removed circulating UO_2^{2+} at molar ratios as low as 20, removed useful amounts of newly deposited UO_2^{2+} from kidneys and/or bone at molar ratios $\geq$100, and reduced kidney UO_2^{2+} significantly when given orally at molar ratios $\geq$100. 5-LIO(Me-3,2-HOPO) has greater affinity for UO_2^{2+} in the kidneys, 5-LICAM(S) has greater affinity for UO_2^{2+} in bone, and a 1:1 mixture of the two ligands (total ligand: U molar ratio 91) reduced kidney and bone UO_2^{2+} to 15 and 58% of control, respectively – more than an equimolar amounts of either ligand alone (Durbin *et al.*, 1989b; 1997a, 2000a; Gorden *et al.*, 2003).

Crystals of uranyl chelates with the set of linear tetradentate Me–3,2-HOPO ligands demonstrate a 1:1 structure and show that those ligands bind in a nearly planar ring perpendicular to the plane of the dioxo oxygens (Fig. 31.19) (Xu and Raymond, 1999).

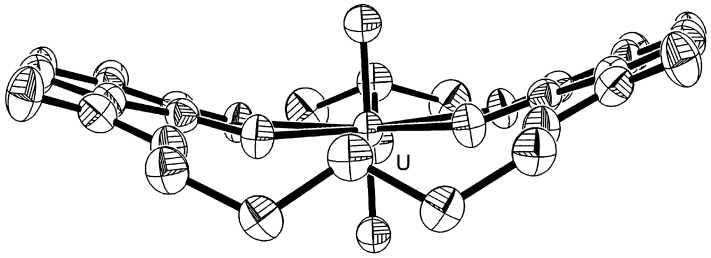

Fig. 31.19 *Molecular structure of* UO_2[5-*LI*(*Me*-3,2,-*HOPO*)] (*Xu and Raymond*, 1999).

(f) Ligands for NpO_2^+

As noted above in the sections dealing with tissue distribution, circulatory transport, and tissue uptake kinetics, the oxidation state of Np *in vivo* is uncertain and probably variable. Rapid plasma clearance and substantial urinary excretion of NpO_2^+ resemble the behavior of UO_2^{2+}, while the deposition in the skeleton of nearly one-half of Np taken into blood and its prolonged retention resemble Pu^{4+}. Redox conditions *in vivo* range from an oxidizing environment in the lungs to more reducing environments in the tissues. Depending on the oxidation state of the Np introduced into the blood (Np^{4+}, NpO_2^+, NpO_2^{2+}), the local conditions in the blood and tissues, and the availability of stabilizing bioligands, both reduction of NpO_2^+ and oxidation of Np^{4+} may be expected (Duffield and Taylor, 1986; NCRP, 1988; Taylor, 1998). The complexes formed by NpO_2^+ are weak, while those of Np^{4+} are about as stable as those of Pu^{4+} with the same ligands (Table 31.8).

$CaNa_3$–DTPA was injected ip at ligand:Np molar ratios $\geq$50 in rats that had been injected iv with ^{237}Np or ^{239}Np citrate solutions (oxidation states uncertain). Excretion of both Np isotopes was increased, the Np content of liver and kidneys was reduced, but there was little reduction in skeleton Np (Smith, 1972b). Effective reduction of ^{239}Np in the body of rats was achieved by ip injection of octadentate 3,4,3-LICAM(C), given at very large ligand:Np molar ratios 1 h after iv injection of $^{239}NpO_2NO_3$. But similarly to the experience with *in vivo* chelation of Pu^{4+} by that ligand, the Np complex formed in the blood partially dissociated leaving a residue of Np in the kidneys (Volf and Wirth, 1986). These observations were taken as an indication of the presence *in vivo* of chelatable Np^{4+}.

Based on that encouraging result, a systematic investigation was undertaken of the *in vivo* chelation of Np by a set of representative multidentate ligands. The ligands assessed for Np chelation were tetra-, hexa-, and octadentate with linear or branched backbones containing CAM(C), CAM(S), 1,2-HOPO, or Me-3,2-HOPO binding groups. Mice were injected ip with a ligand (30 μmol kg^{-1},

ligand:Np molar ratio 22) 5 min after the iv injection of $^{237}NpO_2Cl$ (see Fig. 31.12) and killed at 24 h. All 10 test ligands, but not $CaNa_3$–DTPA, significantly reduced body Np, regardless of denticity or the identity of the binding group. Most ligands significantly reduced Np in the liver, and except for 3,4,3-LICAM (C), also in the kidneys. Significant reduction of Np in the skeleton was also achieved with tetradentate 5-LIO(Me-3,2-HOPO) and 5-LI(Me-3,2-HOPO), and octadentate H(2,2)-(1,2-HOPO), H(2,2)-(Me-3,2-HOPO), and 3,4,3-LICAM(C). Except for tetradentate 5-LI(Me-3,2-HOPO), which was orally active at lower dose, ligand:Np molar ratios $\geq$22 were required to obtain significant reductions in body Np, when the test ligands were given orally at 5 min (Durbin *et al.*, 1994, 1998a,b).

Experiments were undertaken to examine the efficacy of 3,4,3-LI(1,2-HOPO) for *in vivo* chelation of ^{237}Np in contaminated wounds in rats. Ligand:Np molar ratios ranged from 4.3 to 285. Early infiltration of the wound site with the ligand was effective, but delayed treatments were progressively less effective. 3,4,3-LI (1,2-HOPO) was able to complex the Np at the wound site before it was translocated to blood, but Np deposited in the tissues became progressively less accessible to the ligand (Paquet *et al.*, 1997, 2000).

Based on the combined considerations of ligand efficacy and acute ligand toxicity, the most promising ligands for *in vivo* chelation of Np are in order: tetradentate 5-LIO(Me-3,2-HOPO) and 5-LI(Me-3,2-HOPO), octadentate 3,4,3-LI(1,2-HOPO), and hexadentate TREN-(Me-3,2-HOPO).

ACKNOWLEDGMENTS

The author wishes to thank the following members of the Lawrence Berkeley National Laboratory, Chemical Sciences Division, for their essential contributions to the preparation of this manuscript: Dr. Wayne W. Lukens, Jr. for the speciation calculations for UO_2^{2+} and NpO_2^+ in blood plasma; Lindarae M. Aubert and Lynne A. Dory for manuscript preparation; and Dr. Norman M. Edelstein for his patience and assistance. Flavio Robles of the Creative Services Group and Dr. Jide Xu of the U. C. Department of Chemistry provided the illustrations.

APPENDIX: SOURCES OF MATERIALS ON ACTINIDE BIOLOGY

The pioneering biological studies with actinides conducted during World War II (1942–1946) encompassed the following: pharmacology and toxicology of injected, ingested, and inhaled uranium compounds (Tannenbaum, 1951a,b; Voegtlin and Hodge, 1949, 1953); biokinetics of injected and ingested fission products, plutonium, and actinide fission by-products (Lanz *et al.*, 1946; 1947a,b, 1948a,b, 1949b; Carritt *et al.*, 1947; Finkle *et al.*, 1946; Hamilton,

1947b, 1948c); acute toxicity of injected fission products and plutonium (Painter *et al.*, 1946; Bloom, 1948; Fink, 1950); biokinetics and acute toxicity of inhaled or intratracheally intubated fission products and plutonium (Abrams *et al.*, 1946a,b, 1947; Scott *et al.*, 1947b, 1949a). Stannard (1988) summarized the designs and major findings of those studies and provided the tables of contents for the otherwise unpublished Plutonium Project documents and reports.

Actinide biology summaries and reviews include: General reviews – (Durbin, 1960, 1962), Finkel and Biskis (1968), Stover and Jee (1972), Nenot and Stather (1979), ICRP (1972, 1986), Duffield and Taylor (1986), Stannard (1988), Thompson (1989); Element-specific reviews, uranium – Hursh and Spoor (1973), Yuile (1973), Durbin and Wrenn (1975); neptunium – Thompson (1982), NCRP (1988); plutonium – Bair *et al.* (1973), Vaughan *et al.* (1973), Bair (1974), Durbin (1975); transplutonium elements – Durbin (1973); conference proceedings – Rosenthal (1956), Dougherty *et al.*, 1962), Thompson (1962), Mays *et al.* (1969), Thompson and Bair (1972), Healy (1975), Wrenn (1975), Jee (1976), Wrenn (1981), Gerber *et al.* (1989), Stather and Karaoglou (1994), Métivier *et al.* (1998), Stather *et al.* (2003); databases compiled for radiation protection guidance – ICRP (1959, 1972, 1979, 1980, 1986).

The bibliographies of three reports dealing with the deposition and biological effects of plutonium and other selected radionuclides provide an introduction to the large research program on internally deposited radionuclides undertaken in the USSR (Buldakov *et al.*, 1969; Moskalev *et al.*, 1969; Moskalev, 1972).

LIST OF ABBREVIATIONS

CN	coordination number
d	days
DFO	desferrioxamine
DTPA	diethylenetriaminepentaacetic acid
EB	enterobactin
ECF	extracellular fluid
EDTA	ethylenediaminetetraacetic acid
GI	gastrointestinal
h	hours
HAP	synthetic hydroxyapatite
HEPES	4-(2-hydroxyethyl)1-piperazine ethanesulfonic acid
ICRP	International Commission on Radiological Protection
im	intramuscular
ip	intraperitoneal
ISW	interstitial water
iv	intravenous
min	minutes
NCRP	National Council on Radiation Protection

PAS	periodic-acid Schiff
r	ionic radius
s	seconds
sc	subcutaneous
Tf	transferrin
tris	tris-(hydroxy methyl) aminomethane hydrochloride
y	years

REFERENCES

Abrams, R., Seibert, H. C., Forker, L., Greenberg, D., Lisco, H., Jacobson, L. O., and Simmons, E. L. (1946a) *Acute Toxicity of Intubated Plutonium*, USAEC, CH-3875.

Abrams, R., Seibert, H. C., Potts, A. M., Lohr, W., and Postel, S. (1946b) *Metabolism of Inhaled Fission Products*, CH-3485 MDDC-248.

Abrams, R., Seibert, H. C., Potts, A. M., Forker, L. L., Greenberg, D., Postel, S., and Lohr, W. (1947) *Metabolism and Distribution of Inhaled Plutonium in Rats CH-3655 MDDC-677*.

Ahrland, S. (1986) Solution chemistry and kinetics of ionic reactions, in *The Chemistry of the Actinide Elements* (eds. J. J. Katz, G. T. Seaborg, and L. R. Morss), Chapman and Hall, London, pp. 1480–546.

Aisen, P. and Listowsky, I. (1980) *Ann. Rev. Biochem.*, **49**, 357–93.

Altman, P. L. and Dittmer, D. S. (1971) *Blood and Other Body Fluids*, Federation of American Societies for Experimental Biology, Bethesda, MD.

Ansoborlo, E., Chiappini, R., and Moulin, V. (2003) *Clefs CEA*, **48**, 14–18.

Arnold, J. S. and Jee, W. S. S. (1957) *Am. J. Anat.*, **101**, 367–418.

Arnold, J. S. and Jee, W. S. S. (1959) *Lab. Invest.* **8**, 194–204.

Arnold, J. S. and Jee, W. S. S. (1962) *Health Phys.*, **8**, 705–8.

Arnold, J. S. and Wei, C.-T. (1972) Quantitative morphology of vertebral trabecular bone, in *Radiobiology of Plutonium* (eds. B. J. Stover and W. S. S. Jee), The J. W. Press, University of Utah, pp. 333–54.

Atherton, D. R. and LLoyd, R. D. (1972) *Health Phys.*, **22**, 675–8.

Atherton, D. A., Bruenger, F. W., and Stevens, W. (1974) On the early retention and distribution of 253Es by the beagle, in *Research in Radiobiology*, University of Utah School of Medicine Annual Report COO-119-249, pp. 247–54.

Atherton, D. A., Stevens, W., and Bruenger, F. W. (1973) Early retention and distribution of curium in soft tissues and blood of the beagle, in *Research in Radiobiology*, University of Utah School of Medicine Annual Report COO-119-248, pp. 178–85.

Axelrod, D. (1947) *Anat. Rec.*, **98**, 19–24.

Bair, W. J. (1974) Toxicology of plutonium, in *Advances in Radiation Biology*, vol. 4, Academic press, New York, pp. 255–315.

Bair, W. J., Ballou, J. E., Park, J. F., and Sanders, C. L. (1973) Plutonium in soft tissue with emphasis on the respiratory tract, in *Uranium, Plutonium, Transplutonic Elements* (eds. H. C. Hodge, J. N. Stannard, and J. B. Hursh), Springer-Verlag, New York, pp. 503–68.

Ballatori, N. (1991) *Drug Metabol. Rev.*, **23**, 83–132.

Ballou, J. E., Bair, W. J., Case, A. C., and Thompson, R. C. (1962) *Health Phys.*, **8**, 685–8.

Ballou, J. E., Park, J. F., and Morrow, W. G. (1972) *Health Phys.*, **22**, 857–62.

Barnett, T. B. and Metcalf, R. G. (1949) Pathological anatomy following uranium poisoning, in *Pharmacology and Toxicology of Uranium Compounds*, vol. 1 (eds. C. Voegtlin and H. C. Hodge), McGraw-Hill, New York, pp. 207–36.

Belyayev, Y. A. (1969) *Americium-241 Distribution in Rats and the Effect of Complexing Substances on Its Elimination*, AEC-tr-7195, pp. 168-74.

Berliner, R. W. (1973) The excretion of urine, in *Best and Taylor's Physiological Basis of Medical Practice* (ed. J. R. Brobeck), Williams and Williams, Baltimore, 5-1–5-37.

Bernard, S. R. and Struxness, E. G. (1957) *A Study of the Distribution and Excretion of Uranium in Man*, ORNL-2304.

Bernhard, G., Geipel, G., Reich, T., Brendler, V., Amayri, S., and Nitsche, H. (2001) *Radiochim. Acta*, **89**, 511–18.

Bhattacharyya, M. H., Breitenstein, B. D., Metivier, H., Muggenburg, B. A., Stradling, G. N., and Volf, V. (1992) *Radiat. Protect. Dosim.*, **41**, 1–49.

Bloom, W. (ed.) (1948) *Histopathology of Irradiation from External and Internal Sources*, McGraw-Hill, New York.

Boocock, G., Danpure, C. J., Popplewell, D. S., and Taylor, D. M. (1970) *Radiat. Res.*, **42**, 381–96.

Bostick, W. D., Stevenson, R. J., Jarabek, R. J., and Conca, J. L. (2000) *Adv. Environ. Res.*, **3**, 488–98.

Bourne, G. H. (ed.) (1956) *The Biochemistry and Physiology of Bone*, Academic Press, New York.

Brody, S. (1945) *Bioenergetics and Growth*. Reinhard Publications, New York.

Bronner, F. (1964) Dynamics and function of calcium, in *Mineral Metabolism*, vol. II, Part A (eds. C. L. Comar and F. Bronner), Academic Press, New York, pp. 342–5.

Bruenger, F. W., Stover, B. J., Stevens, W., and Atherton, D. R. (1969a) *Health Phys.*, **16**, 339–40.

Bruenger, F. W., Stevens, W., and Stover, B. J. (1969b) *Radiat. Res.*, **37**, 349–60.

Bruenger, F. W., Stover, B. J., and Stevens, W. (1971a) *Health Phys.*, **21**, 679–87.

Bruenger, F. W., Atherton, D. R., Stevens, W., and Stover, B. J. (1971b) Interaction between blood constituents and some actinides, in *Research in Radiobiology, Annual Report*, COO-119-244, University of Utah College of Medicine, pp. 212–27.

Bruenger, F. W., Atherton, D. R., and Stevens, W. (1972) *Health Phys.*, **22**, 685–9.

Bruenger, F. W., Grube, B. J., Atherton, D. R., Taylor, G. N., and Stevens, W. (1976) *Radiat Res.*, **66**, 443–52.

Bruenger, F. W., Smith, J. M., Atherton, D. R., Jee, W. S. S., Lloyd, R. D., and Stevens, W. (1983) *Health Phys.*, **44**(Suppl. 1), 513–27.

Buldakov, L. A., Lyubchanskii, Moskalev, Y. I., and Nifatov, A. P. (1969) *Problems of Plutonium Toxicology*. Atom Publications, Moscow (English translation).

Bulman, R. A. (1978) *Struct. Bonding*, **34**, 39–77.

Bulman, R. A. (1980) *Coord. Chem. Rev.*, **31**, 221–50.

Carritt, J., Fryxell, R., Kleinschmidt, J., Kleinschmidt, R., Langham, W., San Pietro, A., Schaffer, R., and Schnap, B. (1947) *J. Biol. Chem.*, **171**, 273–83.

Catsch, A. (1964) *Radioactive Metal Mobilization in Medicine*, Charles C. Thomas, Springfield, IL.

Catsch, A. and Lê, D. K. (1957) *Strahlentherapie*, **104**, 494–506.
Catsch, A. and von Wedelstaedt, E. (1965) *Experientia*, **21**, 210.
Chalk River (1949) *Permissible Doses Conference*, September 29–30, 1949, pp. 17.1–17.38.
Chevari, S. and Likhner, D. (1968) *Med. Radiol. ANL-trans-898*, **13**, 53–7.
Chipperfield, A. R. and Taylor, D. M. (1968) *Nature*, **219**, 609–10.
Chipperfield, A. R. and Taylor, D. M. (1970) *Radiat. Res.*, **43**, 393–402.
Chipperfield, A. R. and Taylor, D. M. (1972) *Radiat. Res.*, **51**, 15–30.
Clarkson, T. W. (1961) Discussion: the interaction of metals with epithelia, in *University of Rochester*, *Atomic Energy Project*, *UR-549*, pp. 37–47.
Cochran, T. H., Jee, W. S. S., Stover, B. J., and Taylor, G. N. (1962) *Health Phys.*, **8**, 699–704.
Cohen, N. and Ralston, L. (1983) Actinide biokinetics in man and the baboon: a comparison, in *Proceedings of the Seventh International Congress of Radiation Research*, Amsterdam, E5-02.
Comar, C. L. (1955) *Radioisotopes in Biology and Agriculture*, McGraw-Hill, New York.
Cooper, J. R. and Gowing, H. S. (1981) *Int. J. Radiat. Biol. Relat. Study Phys. Chem. Med.*, **40**, 569–72.
Copp, D. H., Greenberg, D. M., Hamilton, J. G., Chace, M. J., Middlesworth, L. V., Cuthbertson, E. M., and Axelrod, D. J. (1946) *The Deposition of Plutonium and Certain Fission Products in Bone as a Decontamination Problem*, *CH-3591*, AECD-2483.
Cotton, F. A. and Wilkinson, G. (1980) The actinide elements, chap. 24, in *Advanced Inorganic Chemistry*, Wiley, New York, pp. 1005–84.
Cronkite, E. P. (1973) Blood and lymph, in *Best and Taylor's Physiological Basis of Medical Practice*, 9th edn (ed. J. R. Brobeck), Williams and Wilkins, Baltimore, pp. 4-1–4-113.
Detweiler, D. K. (1973) Circulation, in *Best and Taylor's Physiological Basis of Medical Practice*, 9th edn (ed. J. R. Brobeck), Williams and Wilkins, Baltimore, pp. 3-1–3-24.
Dougherty, T. F., Jee, W. S. S., Mays, C. W., and Stover, B. J. (eds.) (1962) *Some Aspects of Internal Irradiation*, Pergamon Press, Oxford.
Dounce, A. L. (1949) The mechanism of action of uranium compounds in the animal body, in *Pharmacology and Toxicology of Uranium Compounds*, vol. 2 (eds. C. Voegtlin and H. C. Hodge), McGraw-Hill, New York, pp. 951–92.
Dounce, A. L. and Flagg, J. F. (1949) The chemistry of uranium compounds, in *Pharmacology and Toxicology of Uranium Compounds*, vol. 1 (eds. C. Voegtlin and H. C. Hodge), McGraw-Hill, New York, pp. 55–146.
Dounce, A. L. and Lan, T. H. (1949) The action of uranium on enzymes and proteins, in *Pharmacology and Toxicology of Uranium Compounds*, vol. 2 (eds. C. Voegtlin and H. C. Hodge), McGraw-Hill, New York, pp. 759–888.
Duffield, J. R. and Taylor, D. M. (1986) The biochemistry of the actinides, in *Handbook on the Physics and Chemistry of the Actinides*, (eds. A. J. Freeman and C. Keller), vol. 4 North-Holland, Amsterdam, pp. 129–57.
Durbin, P. W. (1960) *Health Phys.*, **2**, 225–38.
Durbin, P. W. (1962) *Health Phys.*, **8**, 665–71.
Durbin, P. W. (1973) Metabolism and biological effects of the transplutonium elements, in *Uranium, Plutonium, Transplutonic Elements* (eds. H. C. Hodge, J. N. Stannard, and J. B. Hursh), Springer-Verlag. Berlin, pp. 739–896.
Durbin, P. W. (1975) *Health Phys.*, **29**, 495–510.

Durbin, P. W. and Schmidt, C. T. (1985) *Health Phys.*, **49**, 623–61.
Durbin, P. W. and Schmidt, C. T. (1989) *Health Phys.*, **57**(Suppl. 1), 165–74.
Durbin, P. W. and Wrenn, M. E. (1975) Metabolism and effects of uranium in animals, in *Conference on Occupational Health Experience with Uranium* (ed. M. E. Wrenn), ERDA Report 93, pp. 67–129.
Durbin, P. W., Asling, G. W., Johnston, M. E., Hamilton, J. G., and Williams, M. H. (1955) The metabolism of the lanthanons in the rat, in *Rare Earths in Biochemical and Biomedical Research*, October 1955, Oak Ridge, TN, ORINS-12, pp. 171–92.
Durbin, P. W., Jeung, N., and Williams, M. H. (1969) Dynamics of ^{241}Am in the skeleton of the rat, in *Delayed Effects of Bone-seeking Radionuclides* (ed. C. W. Mays), University of Utah Press, Salt Lake City, pp. 137–56.
Durbin, P. W., Horovitz, M. W., and Close, E. R. (1972) *Health Phys.*, **22**, 731–41.
Durbin, P. W., Heavy, L. R., and Garcia, J. F. (1976) *Radiat. Res.*, **67**, 578[Abstract].
Durbin, P. W., Jones, E. S., Raymond, K. N., and Weitl, F. L. (1980) *Radiat. Res.*, **81**, 170–87.
Durbin, P. W., Jeung, N., Jones, E. S., Weitl, F. L., and Raymond, K. N. (1984) *Radiat. Res.*, **99**, 85–105.
Durbin, P. W., Jeung, N., and Schmidt, C. T. (1985) ^{238}*Pu(IV) in Monkeys; Overview of Metabolism*, U.S. Nuclear Regulatory Commission Report NUREG/CR-4355.
Durbin, P. W., Jeung, N., and Bucher, J. J. (1987) Initial distribution of neptunium-237 in a monkey, in *Division of Biology and Medicine Annual Report*, Lawrence Berkeley Laboratory, LBL-22300, pp. 78–86.
Durbin, P. W., White, D. L., Jeung, N. L., Weitl, F. L., Uhlir, L. C., Jones, E. S., Bruenger, F. W., and Raymond, K. N. (1989a) *Health Phys.*, **56**, 839–55.
Durbin, P. W., Jeung, N., Rodgers, S. J., Turowski, P. N., Weitl, F. L., White, D. L., and Raymond, K. N. (1989b) *Radiat. Protect. Dosim.*, **26**, 351–8.
Durbin, P. W., Jeung, N., Kullgren, B., and Clemons, G. K. (1992) *Health Phys.*, **63**, 427–41.
Durbin, P. W., Kullgren, B., Xu, J., and Raymond, K. N. (1994) *Radiat. Protect. Dosim.*, **53**, 305–9.
Durbin, P. W., Kullgren, B., Jeung, N., Xu, J., Rodgers, S. J., and Raymond, K. N. (1996) *Human Experiment. Toxicol.*, **15**, 352–60.
Durbin, P. W., Kullgren, B., Xu, J., and Raymond, K. N. (1997a) *Health Phys.*, **72**, 865–79.
Durbin, P. W., Kullgren, B., and Schmidt, C. T. (1997b) *Health Phys.*, **72**, 222–35.
Durbin, P. W., Kullgren, B., Xu, J., and Raymond, K. N. (1998a) *Radiat. Protect. Dosim.*, **79**, 433–43.
Durbin, P. W., Kullgren, B., Xu, J., Raymond, K. N., Allen, P. G., Bucher, J. J., Edelstein, N. M., and Shuh, D. K. (1998b) *Health Phys.*, **75**, 34–50.
Durbin, P. W., Kullgren, B., Ebbe, S. N., Xu, J., and Raymond, K. N. (2000a) *Health Phys.*, **78**, 511–21.
Durbin, P. W., Kullgren, B., Xu, J., and Raymond, K. N. (2000b) *Int. J. Radiat. Biol.*, **76**, 199–214.
Durbin, P. W., Kullgren, B., Xu, J., Raymond, K. N., Henge- Napoli, M. H., Bailly, T., and Burgada, R. (2003) *Radiat. Protect. Dosim.*, **105**, 503–8.
Erleksova, E. V. (1960) *Distribution of Radioactive Elements in the Animal Organism*, Megziz English Translation, AEC-tr-6982 (1969), Moscow.

Everett, N. B., Simmons, B., and Lasher, E. P. (1956) *Circ. Res.*, **4**, 419–24.
Fairbanks, V. F. and Beutler, E. (1995) Iron metabolism, in *Williams Hematology*, 5th edn (eds. E. Beutler, M. A. Lichtman, B. S. Coller, and T. J. Kipps), McGraw-Hill, New York pp. 369–80.
Fink, R. M. (ed.) (1950) *Biological Studies with Polonium, Radium, and Plutonium*, McGraw-Hill, New York.
Finkel, M. P. and Biskis, B. O. (1968) *Prog. Exp. Tumor Res.*, **10**, 72–111.
Finkle, R. D., Snyder, R. H., Jacobson, L. O., Kisieleski, W., Lawrence, B., and Simmons, E. L. (1946) *The Toxicity and Metabolism of Plutonium in Laboratory Animals*, CH-3783 MDDC-1140.
Flagg, J. F. (1949) Analytical methods for determining uranium and fluorine, in *Pharmacology and Toxicology of Uranium Compounds*, vol. 1 (eds. C. Voegtlin and H. C. Hodge), McGraw-Hill, New York, pp. 147–94.
Foreman, H. (1962) *Health Phys.*, **8**, 713–16.
Foreman, H. and Hamilton, J. G. (1951) *The Use of Chelating Agents for Accelerating Excretion of Radionuclides*, UCRL–1351. University of California Radiation Laboratory, Berkeley, CA.
Frost, H. M. (ed.) (1963) *Bone Biodynamics*, Little, Brown, Boston, MA.
Gamble, J. L. (1954) *Chemical Anatomy, Physiology, and Pathology of Extracellular Fluid*, Harvard University Press, Cambridge, MA.
Gerber, G. B., Metivier, H., and Stather, J. W. (eds.) (1989) Biological assessment of occupational exposure to actinides, *Radiat. Protect. Dosim.*, **26**, 1–4.
Gindler, J. E. (1973) Physical and chemical properties of uranium. in *Uranium, Plutonium, Transplutonic Elements* (eds. H. C. Hodge, J. N. Stannard, and J. B. Hursh), Springer-Verlag, New York, pp. 69–164.
Gong, J. K., Arnold, J. S., and Cohn, S. H. (1964) *Anat. Rec.*, **149**, 325–31.
Gorden, A. E. V., Xu, J. D., Raymond, K. N., and Durbin, P. (2003) *Chem. Rev.*, **103**, 4207–82.
Gorden, A. E. V., Shuh, D. K., Tiedemann, B. E. F., Wilson, R. E., Xu, J. D., and Raymond, K. N. (2005) *Chem. Eur. J.*, **11**, 2842–8.
Gray, S. A., Stradling, G. N., Pearce, M. J., Wilson, I., Moody, J. C., Burgada, R., Durbin, P. W., and Raymond, K. N. (1994) *Radiat. Protect. Dosim.*, **53**, 319–22.
Green, D., Howells, G., Vennart, J., and Watts, R. (1977) *Int. J. Appl. Radiat. Isot.*, **28**, 497–501.
Gregersen, M. I., Sear, H., Rawson, R. A., Chien, S., and Saiger, G. L. (1959) *Am. J. Physiol.*, **196**, 184–7.
Grenthe, I., Fuger, J., Konings, R. J. M., Lemire, R. J., Muller, A. B., Nguyen- Trung, C., and Wanner, H. (1992) *Chemical Thermodynamics of Uranium*, North-Holland, Amsterdam.
Grube, B. J., Stevens, W., and Atherton, D. R. (1978) *Radiat. Res.*, **73**, 168–79.
Gruner, R., Seidel, A., and Winter, R. (1981) *Radiat. Res.*, **85**, 367–79.
Guilmette, R. A., Cohen, N., and Wrenn, M. E. (1980) *Radiat. Res.*, **81**, 100–19.
Guilmette, R. A., Medinsky, M. A., and Petersen, D. A. (1982) *Binding of Neptunium to Serum Proteins* In vitro, Annual Report of the Inhalation Toxicology Research Institute, Lovelace Biomedical and Environmental Research Institute, LMF-102, pp. 209–11.
Guilmette, R. A., Lindhorst, P. S., and Hanlon, L. L. (1998) *Radiat. Protect. Dosim.*, **79**, 453–8.

Guilmette, R. A., Hakimi, R., Durbin, P. W., Xu, J., and Raymond, K. N. (2003) *Radiat. Protect. Dosim.*, **105**, 527–34.
Gurd, F. R. N. and Wilcox, P. E. (1956) *Adv. Protein Chem.*, **11**, 311–427.
Hahn, F. F., Guilmette, R. A., and Hoover, M. D. (2002) *Environ. Health Perspect.*, **110**, 51–9.
Ham, A. W. (1974) *Histology*, 7th edn. J. B. Lippincott, Philadelphia.
Hamilton, J. G. (1941) *J. Appl. Phys.*, **12**, 440–60.
Hamilton, J. G. (1947a) Medical and Health Physics Quarterly Report UCRL-41, University of California Radiation Laboratory, p. 15.
Hamilton, J. G. (1947b) *Radiology*, **49**, 325–43.
Hamilton, J. G. (1948a) Medical and Health Physics Quarterly Report UCRL-157, University of California Radiation Laboratory, pp. 6–11.
Hamilton, J. G. (1948b) Medical and Health Physics Quarterly Report UCRL-193, University of California Radiation Laboratory, p. 13.
Hamilton, J. G. (1948c) *Rev. Mod. Phys.*, **20**, 718–28.
Hamilton, J. G. (1953) Medical and Health Physics Quarterly Report UCRL-2553, University of California Radiation Laboratory, pp. 28–30.
Hamilton, J. G. (1956) Medical and Health Physics Quarterly Report UCRL-3268, University of California Radiation Laboratory, pp. 5–10.
Hamilton, J. G. and Scott, K. G. (1953) *Proc. Soc. Exp. Biol. (N.Y.)* **83**, 301–5.
Harris, W. R., Carrano, C. J., Pecoraro, V. L., and Raymond, K. N. (1981) *J. Am. Chem. Soc.* **103**, 2231–7.
Haven, F. and Hodge, H. C. (1949) Toxicity following parenteral administration of certain soluble uranium salts, in *Pharmacology and Toxicology of Uranium Compounds*, (eds. C. Voegtlin and H. C. Hodge), vol. 1 , McGraw-Hill, New York, pp. 281–308.
Hawk, P. B., Oser, B. L., and Summerson, W. H. (1947) *Practical Physiological Chemistry*, 12th edn, The Blakiston Co., Philadelphia.
Healy, J. W. (ed.) (1975) Plutonium — health implications for man. *Health Phys.*, **29**, 441–632.
Herring, G. M. (1964) Mucosubstances of cortical bone, in *Bone and Tooth* (ed. H. J. J. Blackwood), Pergamon, London, pp. 263–8.
Herring, G. M., Vaughan, J., and Williamson, M. (1962) *Health Phys.*, **8**, 717–24.
Hodge, H. C. (1949) Introduction to part I. The pharmacology and toxicology of uranium compounds, in *Pharmacology and Toxicology of Uranium Compounds*, (eds. C. Voegtlin and H. C. Hodge), vol. 1 , McGraw-Hill, New York, pp. 15–54.
Hodge, H. C. (1973) A history of uranium poisoning (1824–1942), in *Uranium, Plutonium, Transplutonic Elements* (eds. H. C. Hodge, J. N. Stannard, and J. B. Hursh), Springer-Verlag, New York, pp. 5–68.
Hodge, H. C., Stannard, J. N., and Hursh, J. B. (eds.) (1973) *Uranium, Plutonium, Transplutonic Elements*, Springer-Verlag, New York.
Hulet, E. K. (1986) Einsteinium, in *The Chemistry of the Actinide Elements* (eds. J. J. Katz, G. T. Seaborg, and L. R. Morss), Chapman and Hall, London, pp. 1071–84.
Hungate, F. P. and Baxter, D. W. (1972) 253-Es and 249-Bk Distribution in rat tissues following intragastric and intravenous administration, in *Pacific Northwest Laboratory Annual Report for 1971*, BNWL-1650 PT1, pp. 88–92.

Hursh, J. B. and Spoor, N. L. (1973) Data on man, in *Uranium, Plutonium, Transplutonic Elements* (eds. H. C. Hodge, J. N. Stannard, and J. B. Hursh), Springer-Verlag. New York, pp. 197–240.

ICRP. (1959) *Health Phys.*, **3**, 1–380.

ICRP. (1967) *A Review of the Radiosensitivity of Tissues in Bone, ICRP Pub. 11*, International Commission on Radiological Protection.

ICRP. (1972) *The Metabolism of Compounds of Plutonium and Other Actinides, ICRP Pub. 19*, Pergamon Press, Oxford.

ICRP. (1973) *Alkaline Earth Metabolism in Adult Man. ICRP Pub. 20*, *Health Phys.*, **24**, 125–221.

ICRP (1974) *Report of the Task Group on Reference Man*, ICRP Pub. 23, Pergamon Press, Oxford.

ICRP. (1979) *Limits for intakes of radionuclides by workers*, ICRP Pub. 30, Part 1. Ann. ICRP 2: (3–4).

ICRP. (1980) *Limits for intakes of radionuclides by workers*, ICRP Pub. 30, Part 2. Ann. ICRP 4: (3–4).

ICRP. (1986) *The metabolism of plutonium and related elements*. ICRP Pub. 48. Ann. ICRP 16: (2–3).

ICRP. (1993) Age-dependent doses to members of the public from intake of radionuclides: part 2 ingestion dose coefficients. ICRP Pub. 67, part 2. Ann. ICRP 23: (3–4).

ICRP. (1995) Age-dependent doses to members of the public from intake of radionuclides: Part 3. Ingestion dose coefficients. Ann. ICRP 25. (1).

Jee, W. S. S. (1972a) *Health Phys.*, **22**, 583–96.

Jee, W. S. S. (1972b) ^{239}Pu in bones as visualized by photographic and neutron-induced autoradiography, in *Radiobiology of Plutonium* (eds. B. J. Stover and W. S. S. Jee), The J. W. Press, University of Utah, Salt Lake City, pp. 171–94.

Jee, W. S. S. (ed.) (1976) *The Health Effects of Plutonium and Radium*, The J. W. Press, University of Utah Press, Salt Lake City.

Jee, W. S. S. and Arnold, J. S. (1962) *Health Phys.*, **8**, 709–12.

Jowsey, J. (1956) The localization of yttrium in bone, in *Rare Earths in Biochemical and Medical Research: A Conference ORINS-12* (eds. G. C. Kyker and E. B. Anderson), Oak Ridge Institute of Nuclear Studies, Oak Ridge, TN, pp. 311–22.

Jowsey, J., Rowland, R. E., and Marshall, J. H. (1958) *Radiat. Res.*, **8**, 490–501.

Kappel, M. J., Nitsche, H., and Raymond, K. N. (1985) *Inorg. Chem.*, **24**, 605–11.

Katz, J. H. (1970) Transferrin and its functions in the regulation of iron metabolism, in *Regulation of Hematopoiesis*, vol. I (ed. A. S. Gordon), Appleton-Century-Crofts, New York, pp. 539–77.

Katz, J. J., Seaborg, G. T., and Morss, L. R. (1986) Summary and comparative aspects of actinide elements, in *The Chemistry of Actinide Elements* (eds. J. J. Katz, G. T. Seaborg, and L. R. Morss), Chapman and Hall, London, pp. 1121–95.

Kirby, H. W. (1986a) Actinium, in *The Chemistry of the Actinide Elements* (eds. J. J. Katz, G. T. Seaborg,, and L. R. Morss), Chapman and Hall, London, pp. 14–40.

Kirby, H. W. (1986b) Protactinium, in *The Chemistry of the Actinide Elements* (eds. J. J. Katz, G. T. Seaborg, and L. R. Morss), Chapman and Hall, London, pp. 102–68.

Kirschbaum, B. B. (1982) *Toxicol. Appl. Pharmacol.*, **64**, 10–19.

Kirschbaum, B. B. and Oken, D. E. (1979) *Exp. Mol. Pathol.*, **31**, 101–12.

Kisieleski, W. E. and Woodruff, L. (1948) Studies on the distribution of plutonium in the rat, in *Quarterly Report, Biology Division, August 1947 to November 1947*, Argonne National Laboratory, ANL-4108, pp. 86–103.

Kornberg, and H. A. Norwood, W. D. (eds.) (1968) *Diagnosis and Treatment of Deposited Radionuclides*, Excerpta Medica Foundation, Amsterdam.

Kroll, H., Korman, S., Siegel, E., Hart, H. E., Rosoff, B., Spencer, H., and Laszlo, D. (1957) *Nature (Lond.)* **180**, 919–20.

Kyker, G. R. (1962) Rare earths, in *Mineral Metabolism*, vol. 2, Part B (eds. C. L. Comar and F. Bronner), Academic Press. New York, pp. 499–541.

Lanz, H., Scott, K. G., Crowley, J., and Hamilton, J. G. (1946) *The Metabolism of Thorium, Protactinium, and Neptunium in the Rat*, USAEC MDDC-648 (CH-3606).

Leboeuf, R. C., Tolson, D., and Heinecke, J. W. (1995) *J. Lab. Clin. Med.*, **126**, 128–36.

Leggett, R. W. (1985) *Health Phys.*, **49**, 1115–37.

Leggett, R. W. (1989) *Health Phys.*, **57**, 365–83.

Leggett, R. W. (1992a) *Health Phys.*, **62**, 288–310.

Leggett, R. W. (1992b) *Radiat. Protect. Dosim.*, **41**, 183–98.

Lehmann, M., Culig, H., and Taylor, D. M. (1983) *Int. J. Radiat. Biol.*, **44**, 65–74.

Lemire, R. J., Fuger, J., Nitsche, H., Potter, P., Rand, M. H., Rydberg, J., Spahiu, K., Sullivan, J. C., Ullman, W. J., Vitorge, P., and Wanner, H. (2001) *Chemical Thermodynamics of Neptunium and Plutonium*, Elsevier, Amsterdam.

Lipsztein, J. L. (1981) *An Improved Model for Uranium Metabolism in the Primate*, New York University.

Lloyd, E. and Marshall, J. H. (1972) Toxicity of ^{239}Pu relative to ^{226}Ra in man and dog, in *Radiobiology of Plutonium* (eds. B. J. Stover and W. S. S. Jee), The J. W. Press, University of Utah, pp. 377–84.

Lloyd, R. D., Mays, C. W., Taylor, G. N., and Atherton, D. R. (1970) *Health Phys.*, **18**, 149–56.

Lloyd, R. D., Mays, C. W., Taylor, G. N., and Williams, J. L. (1972a) *Health Phys.*, **22**, 667–73.

Lloyd, R. D., Jee, W. S. S., Ratherton, D., Taylor, G. N., and Mays, C. W. (1972b) Americium–241 in beagles: biological effects and skeletal distribution, in *Radiobiology of Plutonium* (eds. B. J. Stover and W. S. S. Jee), The J. W. Press, University of Utah, pp. 141–8.

Lloyd, R. D., Atherton, D. R., Mays, C. W., McFarland, S. S., and Williams, J. L. (1974) *Health Phys.*, **27**, 61–7.

Lloyd, R. D., Dockum, J. G., Atherton, D. R., Mays, C. W., and Williams, J. L. (1975) *Health Phys.*, **28**, 585–9.

Lloyd, R. D., Mays, C. W., McFarland, S. S., Atherton, D. R., and Williams, J. L. (1976) *Radiat Res.*, **65**, 462–73.

Lloyd, R. D., Jones, C. W., Mays, C. W., Atherton, D. R., Bruenger, F. W., and Taylor, G. N. (1984a) *Radiat. Res.*, **98**, 614–28.

Lloyd, R. D., Mays, C. W., Jones, C. W., Atherton, D. R., Bruenger, F. W., Shabestari, L. R., and Wrenn, M. E. (1984b) *Radiat. Res.*, **100**, 564–75.

Lloyd, R. D., Bruenger, F. W., Mays, C. W., Atherton, D. R., Jones, C. W., Taylor, G. N., Stevens, W., Durbin, P. W., Jeung, N., Jones, E. S., Kappel, M. S., Raymond, K. N., and Weitl F. L. (1984c) *Radiat. Res.*, **99**, 106–28.

Lloyd, R. D., Taylor, G. N., Angus, W., Bruenger, F. W., and Miller, S. C. (1993) *Health Phys.*, **64**, 45–51.

Lloyd, R. D., Miller, S. C., Taylor, G. N., Bruenger, F. W., Jee, W. S. S., and Angus, W. (1994) *Health Phys.*, **67**, 346–53.

Lo Sasso, T., Cohen, N., and Wrenn, M. E. (1981) *Radiat. Res.*, **85**, 173–83.

Loeb, W. F. and Quimby, F. W. (1999) *The Clinical Chemistry of Laboratory Animals*, Taylor and Francis, Philadelphia, PA.

Luckey, T. D. and Venugopal, B. (1977) *Metal Toxicity in Mammals*, vol. 1. *Physiologic and Chemical Basis for Metal Toxicity*, Plenum Press, New York.

Luk, C. K. (1971) *Biochemistry*, **10**, 2838–43.

Mahlum, D. D. and Clarke, W. J. (1966) *Health Phys.*, **12**, 7–13.

Martell, A. E. and Smith, R. M. (1977) *Critical Stability Constants*, vol. 3. *The Organic Ligands*, Plenum Press, New York.

Maynard, E. A. and Hodge, H. C. (1949) Studies of toxicity of various uranium compounds when fed to experimental animals, in *Pharmacology and Toxicology of Uranium Compounds*, vol. 1 (eds. C. Voegtlin and H. C. Hodge), McGraw-Hill, New York, pp. 309–76.

Mays, C. W., Jee, W. S. S., Lloyd, R. D., Stover, B. J., Dougherty, J. H., and Taylor, G. N. (eds.) (1969) *Delayed Effects of Bone-seeking Radionuclides*, The University of Utah Press, Salt Lake City.

McKay, L. R. (1972) *Health Phys.*, **22**, 633–40.

Métivier, H., Kaul, A., Menzel, H.-G., and Stather, J. W. (eds.) (1998) *Radiat. Protect. Dosim.*, **79**, 1–4.

Mewhinney, J. A., Brooks, A. L., and McClellan, R. O. (1972) *Health Phys.*, **22**, 695–700.

Miller, S. C., Bowman, B. M., and Rowland, H. G. (1980) Comparison of the autoradiographic localization of plutonium in the testes of rats and dogs, in *Research in Radiobiology*, University of Utah School of Medicine Report COO-119-264, pp. 91–101.

Miller, S. C., Smith, J. M., Rowland, H. G., Bowman, B. M., and Jee, W. S. S. (1982) The relationship of bone marrow microvasculature with plutonium incorporation into bone, in *Research in Radiobiology*, University of Utah School of Medicine Report COO-119-257, pp. 63–71.

Miller, S. C., Bruenger, F. W., Kuswik- Rabiega, G., Liu, G., and Lloyd, R. D. (1993) *J. Pharmacol. Exp. Ther.*, **267**, 548–54.

Moore, R. C., Holt, K., Zhao, H. T., Hasan, A., Awwad, N., Gasser, M., and Sanchez, C. (2003) *Radiochim. Acta*, **91**, 721–7.

Morin, M., Nenot, J. C., and Lafuma, J. (1973) *Health Phys.*, **24**, 311–15.

Moskalev, Y. I. (1972) *Health Phys.*, **22**, 723–9.

Moskalev, Y. I., Buldakov, L. A., Zhuravelova, A. K., Zalikin, G. A., Karpova, V. M., Kreslov, V. V., Levdik, T. I., Lemberg, V. K., Lyubchanskiy, E. R., Miushkacheva, G. S., Sevast'yanova, Yl. P., and Khalturin, G. V. (1979) *Toxicology and Radiobiology of Neptunium–237*, Atomizdat Publishers, Moscow (Eng. trans. ORNL-tr–4936).

Moskvin, A. I. (1971) *Radiokhimiya*, **13**, 230–8 (Engl. trans.).

Muntz, J. A. and Guzman-Barron, E. S. (1947) *Combination of Plutonium with Plasma Proteins*, USAEC MDDC-1268, pp. 1–23.

Muntz, J. A. and Guzman- Barron, E. S. (1951) The transport of uranium in the tissues, in *Toxicology of Uranium* (ed. A. Tannenbaum), McGraw-Hill, New York, pp. 182–98.

NBS Handbook 52. (1953) *Maximum Permissible Amounts of Radioisotopes in the Human Body and Maximum Permissible Concentrations in Air and Water*. U.S. Government Printing Office.

NCRP. (1980) *Management of Persons Accidentally Contaminated with Radionuclides*, NCRP Report No. 65. National Council on Radiation Protection and Measurements, Bethesda, MD.

NCRP. (1988) *Neptunium: Radiation Protection Guidelines*, NCRP Pub. 90. National Council on Radiation Protection, Bethesda, MD.

NCRP. (2001) *Liver Cancer Risk from Internally-deposited Radionuclides*, NCRP Report No. 135. National Council on Radiation Protection and Measurements, Bethesda, MD.

Nenot, J. C. and Stather, J. W. (1979) *The Toxicity of Plutonium, Americium, and Curium*, Pergamon Press, New York.

Neuman, W. F. (1949) The distribution and excretion of uranium, in *Pharmacology and Toxicology of Uranium Compounds*, vol. 2 (eds. C. Voegtlin and H. C. Hodge), McGraw-Hill, New York, pp. 701–28.

Neuman, W. F. (1953) Deposition of uranium in bone, in *Pharmacology and Toxicology of Uranium Compounds*, vol. 4 (eds. C. Voegtlin and H. C. Hodge), McGraw-Hill, New York, pp. 1911–91.

Neuman, W. F. and Neuman, M. W. (1958) *The Chemical Dynamics of Bone Mineral*, University of Chicago Press, Chicago.

Painter, E., Russell, E., Prosser, C. L., Swift, M. N., Kisieleski, W., and Sacher, G. (1946) *Clinical Physiology of Dogs Injected with Plutonium*, AECD-2042.

Paquet, F., Verry, M., Grillon, G., Landesman, C., Masse, R., and Taylor, D. M. (1995) *Radiat Res.*, **143**, 214–18.

Paquet, F., Ramounet, B., Metivier, H., and Taylor, D. M. (1996) *Radiat. Res.*, **146**, 306–12.

Paquet, F., Metivier, H., Poncy, J. L., Burgada, R., and Bailly, T. (1997) *Int. J. Radiat. Biol.*, **71**, 613–21.

Paquet, F., Ramounet, B., Metivier, H., and Taylor, D. M. (1998) *J. Alloys Compds.*, **271–273**, 85–8.

Paquet, F., Montegue, B., Ansoborlo, E., Henge- Napoli, M. H., Houpert, P., Durbin, P. W., and Raymond, K. N. (2000) *Int. J. Radiat. Biol.* **76**, 113–17.

Passow, H., Rothstein, A., and Clarkson, T. W. (1961) *Pharmacol. Rev.*, **13**, 185–224.

Pearse, A. G. E. (1961) *Histochemistry, Theoretical and Applied.* Little, Brown, Boston, MA.

Pecher, C. (1942) *Univ. Calif. Pub. Pharmacol.*, **2**, 117–39.

Pecoraro, V. L., Harris, W. R., Carrano, C. J., and Raymond, K. N. (1981) *Biochemistry*, **20**, 7033–9.

Peter, E. and Lehmann, M. (1981) *Int. J. Radiat. Biol.*, **40**, 445–50.

Planas-Bohne, F. and Duffield, J. (1988) *Int. J. Radiat. Biol.*, **53**, 489–500.

Planas-Bohne, F. and Rau, W. (1990) *Hum. Exp. Toxicol.*, **9**, 17–24.

Planas-Bohne, F., Jung, W., and Neu-Muller, M. (1985) *Int. J. Radiat. Biol.*, **48**, 797–805.

Planas-Bohne, F., Kampmann, G., and Olinger, H. (1989) *Sci. Total Environ.*, **83**, 263–71.

Polig, E., Smith, J. M., and Jee, W. S. (1984) *Int. J. Radiat. Biol.*, **46**, 143–60.

Popplewell, D. S. and Boocock, G. (1968) Distribution of some actinides in blood serum proteins, in *Diagnosis and Treatment of Deposited Radionuclides* (eds. H. A. Kornberg and W. D. Norwood), Excerpta Medica Foundation. Richland, WA, pp. 45–55.

Popplewell, D. S., Stradling, G. N., and Ham, G. J. (1975) *Radiat. Res.*, **62**, 513–19.

Priest, N. D. and Giannola, S. J. (1980) *Int. J. Radiat. Biol.*, **37**, 281–98.

Priest, N. D., Howells, G. R., Green, D., and Haines, J. W. (1982) *Hum. Toxicol.*, **1**, 97–114.

Priest, N. D., Howells, G., Green, D., and Haines, J. W. (1983) *Hum. Toxicol.*, **2**, 101–20.

Ralston, L. G., Cohen, N., Bhattacharyya, M. H., Larsen, R. P., Ayres, L., Oldham, R. D., and Moretti, E. S. (1986) The metabolism and gastrointestinal absorption of neptunium and protactinium *n* adult baboons, in *Speciation of Fission and Activation Products in the Environment* (eds. R. A. Bulman and J. R. Cooper), Elsevier Applied Science, Oxford, p. 191.

Ramounet, B., Matton, S., Grillon, G., and Fritsch, P. (1998) *J. Alloys Compds.*, **271–273**, 103–5.

Raymond, K. N. and Smith, W. L. (1981) *Struct. Bond.*, **43**, 159–86.

Raymond, K. N., Harris, W. R., Carrano, C. J., and Weitl, F. L. (1980) The synthesis, thermodynamic behavior, and biological properties of metal-ion-specific sequestering agents for man and the actinides, in *Inorganic Chemistry in Biology*, (ed. A. E. Martell), ACS Symposium Series No. 140, pp. 313–32.

Rehfield, C. E., Blomquist, J. A., and Taylor, G. N. (1972) The beagles, in *Radiobiology of Plutonium* (eds. B. J. Stover and W. S. S. Jee), The J. W. Press, The University of Utah, pp. 47–58.

Robinson, B., Heid, K. R., Aldridge, T. L., and Glenn, R. D. (1983) *Health Phys.*, **45**, 911–22.

Rodgers, S. J. and Raymond, K. N. (1983) *J. Med. Chem.*, **26**, 439–42.

Rosenthal, M. W. (ed.) (1956) Therapy of radioelement poisoning, ANL-5584, Argonne National Laboratory.

Rosenthal, M. W. and Schubert, J. (1957) *Radiat. Res.*, **6**, 349–54.

Rothstein, A. (1961) *The Cell Membrane as the Site of Action of Heavy Metals*, University of Rochester, Atomic Energy Project, UR-549, pp. 2–36.

Rowland, R. E. and Farnham, J. E. (1969) *Health Phys.*, **17**, 139–44.

Scarrow, R. C., Riley, P. E., Abu–Dari, K., White, D., and Raymond, K. N. (1985) *Inorg. Chem.*, **24**, 954–67.

Schubert, J. (1955) *Ann. Rev. Nucl. Sci.*, **5**, 369–412.

Schubert, J., Finkel, M. P., White, M. R., and Hirsch, G. M. (1950) *J. Biol. Chem.*, **182**, 635–42.

Schuler, F. and Taylor, D. M. (1987) *Radiat. Res.*, **110**, 362–71.

Schuler, F., Csovcsics, C., and Taylor, D. M. (1987) *Int. J. Radiat. Biol*., **52**, 883–92.

Schuppler, U., Planas-Bohne, F., and Taylor, D. M. (1988) *Int. J. Radiat. Biol*. **53**, 457–66.

Schwartz, J. L. and Fien, M. (1973) Amino acids and proteins. The molecular framework and machinery of living systems, in *Best and Taylor's Physiologic Basis of Medical Practice*, 9th edn (ed. J. R. Brobeck), pp. 1-114–1-141.

Scott, K. G., Overstreet, R., Jacobson, L., Hamilton, J. G., Fisher, H., Crowley, J., Chaikoff, I. L., Entenman, C., Fishler, M., Barber, A. J., and Loomis, F. (1947a) *The Metabolism of Carrier-Free Fission Products in the Rat*, USAEC MDDC-1275.

Scott, K. G., Axelrod, D., Crowley, J., Lenz, H. C., Jr. and Hamilton, J. G. (1947b) *Studies on the Inhalation of Fissionable Materials and Fission Products and Their Subsequent Fate in Rats and Man*, USAEC MDDC-1276.

Scott, K. G., Copp, D. H., Axelrod, D. J., and Hamilton, J. G. (1948a) *J. Biol. Chem.*, **175**, 691–703.

Scott, K. G., Axelrod, D. J., Fisher, H., Crowley, J. F., and Hamilton, J. G. (1948b) *J. Biol. Chem.*, **176**, 283–93.

Scott, K. G., Axelrod, D., Crowley, J., and Hamilton, J. G. (1949a) *Arch. Pathol.*, **48**, 31–54.

Scott, K. G., Axelrod, D. J., and Hamilton, J. G. (1949b) *J. Biol. Chem.*, **177**, 325–35.

Seidel, A., Wiener, M., Kruger, E., Wirth, R., and Haffner, H. (1986) *Int. J. Rad. Appl. Instrum. B*, **13**, 515–18.

Seven, M. J. and Johnson, L. A. (eds.) (1959) *Metal Binding in Medicine*, J. B. Lippincott, Philadelphia, PA.

Shannon, R. D. (1976) *Acta Crystallog.*, **A32**, 751–67.

Sillen, L. G. and Martell, A. E. (1964) *Stability Constants of Metal-ion Complexes*, The Chemical Society, London, Special Publ. 17.

Sillen, L. G. and Martell, A. E. (1971) *Stability Constants of Metal-ion Complexes*, The Chemical Society, London, Suppl. 1. Special Publ. 25.

Simpson, M. E., Asling, C. W., and Evans, H. M. (1950) *Yale J. Biol. Med.*, **23**, 1–27.

Singer, T. P., Muntz, J. A., Meyer, J., Gasvoda, B., and Guzman-Barron, E. S. (1951) The reversible inhibition of enzymes by uranium, in *Toxicology of Uranium* (ed. A. Tannenbaum), McGraw-Hill, New York, pp. 208–45.

Smith, H. W. (1951) *The Kidney: Structure and Function in Health and Disease*, Oxford University Press, New York.

Smith, V. H. (1958) *Nature*, 1792–3.

Smith, V. H. (1972a) The biological disposition of $Es(NO_3)_3$ in rats after intravenous, intramuscular, subcutaneous, and transcutaneous administration, in *Pacific Northwest Laboratory Annual Report for 1971*, BNWL-1650 PT1, pp. 279–83.

Smith, V. H. (1972b) *Health Phys.*, **22**, 765–78.

Smith, R. M. and Martell, A. E. (1976) *Critical Stability Constants*, vol. 4. Inorganic Complexes, Plenum Press, New York.

Smith, R. M. and Martell, A. E. (1989) *Critical Stability Constants*, vol. 6. Second Supplement, Plenum Press, New York.

Sontag, W. (1993) *Int. J. Radiat. Biol.*, **63**, 383–93.

Spiers, F. W. (1968) *Radioisotopes in the Human Body: Physical and Biological Aspects.* Academic Press, New York.

Stannard, J. N. (1988) *Radioactivity and Health. A History*, Pacific Northwest Laboratory, Batelle Memorial Institute, Richland, WA.

Stather, J. W. and Karaoglou, A. (eds.) (1994). *Radiat. Protect. Dosim.*, **53**, 1–4.

Stather, J. W., Bailey, M. R., Harrison, J. D., Menze, H.-G., and Métivier, H., eds. (2003) Internal Dosimetry of Radionuclides: Occupational, Public and Medical Exposure. Radiat. Prot. Dosim. 105, Nos. 1–4, 1–662.

Stevens, W. and Bruenger, F. W. (1972) *Health Phys.*, **22**, 679–83.
Stevens, W., Bruenger, F. W., and Stover, B. J. (1965) *Radiat. Res.*, **26**, 114–23.
Stevens, W., Bruenger, F. W., and Stover, B. J. (1968) *Radiat. Res.*, **33**, 490–500.
Stevens, W., Stover, B. J., Bruenger, F. W., and Taylor, G. N. (1969) *Radiat. Res.*, **39**, 201–6.
Stevens, W., Stover, B. J., Atherton, D. R., and Bruenger, F. W. (1975) *Health Phys.*, **28**, 387–94.
Stevens, W., Bruenger, F. W., Atherton, D. R., Smith, J. M., and Taylor, G. N. (1980) *Radiat. Res.*, **83**, 109–26.
Stokinger, H. E., Rothstein, A., Roberts, E., Spiegl, C. J., Dygert, H. P., La Bille, C. W., and Sprague, J., G. F. (1949) Toxicity following inhalation, in *Pharmacology and Toxicology of Uranium Compounds*, vols 1 & 2 (eds. C. Voegtlin and H. C. Hodge), McGraw-Hill, New York, pp. 423–700.
Stone, R. S. (1951) *Industrial Medicine on the Plutonium Project*, McGraw-Hill, New York.
Stover, B. J. and Atherton, D. R. (1974) *Radiat. Res.*, **60**, 525–35.
Stover, B. J. and Jee, W. S. S. (eds.) (1972) *Radiobiology of Plutonium*, The J. W. Press, University of Utah.
Stover, B. J. and Stover, J. C. N. (1972) The laboratory for radiobiology at the University of Utah, in *Radiobiology of Plutonium* (eds. B. J. Stover and W. S. S. Jee), The J. W. Press, University of Utah, pp. 29–46.
Stover, B. J., Atherton, D. R., and Keller, N. (1959) *Radiat. Res.*, **10**, 130–47.
Stover, B. J., Atherton, D. R., Keller, N., and Buster, D. S. (1960) *Radiat. Res.*, **12**, 657–71.
Stover, B. J., Atherton, D. R., Bruenger, F. W., and Buster, D. S. (1962) *Health Phys.*, **8**, 589–97.
Stover, B. J., Bruenger, F. W., and Stevens, W. (1968a) *Radiat. Res.*, **33**, 381–94.
Stover, B. J., Atherton, D. R., Bruenger, F. W., and Buster, D. S. (1968b) *Health Phys.*, **14**, 193–7.
Stover, B. J., Bruenger, F. W., and Stevens, W. (1970) *Radiat. Res.*, **43**, 173–86.
Stover, B. J., Atherton, D. R., and Buster, D. S. (1971) *Health Phys.*, **20**, 369–74.
Stover, B. J., Atherton, D. R., and Buster, D. S. (1972) Retention of ^{239}Pu(IV) in the beagle, in *Radiobiology of Plutonium* (eds. B. J. Stover and W. S. S. Jee), The J. W. Press, University of Utah, Salt Lake City, p. 149.
Stradling, G. N., Popplewell, D. S., and Ham, G. J. (1976) *Health Phys.*, **31**, 517–19.
Stradling, G. N., Stather, J. W., Ellender, M., Sumner, S. A., Moody, J. C., Towndrow, C. G., Hodgson, A., Sedgwick, D., and Cooke, N. (1985a) *Hum. Toxicol.*, **4**, 563–72.
Stradling, G. N., Stather, J. W., Strong, J. C., Sumner, S. A., Towndrow, C. G., Moody, J. C., Lennox, A., Sedgwick, D., and Cooke, N. (1985b) *Hum. Toxicol.*, **4**, 159–68.
Stradling, G. N., Stather, J. W., Gray, S. A., Moody, J. C., Ellender, M., and Hodgson, A. (1986) *Hum. Toxicol.*, **5**, 77–84.
Stradling, G. N., Stather, J. W., Gray, S. A., Moody, J. C., Ellender, M., Hodgson, A., Sedgwick, D., and Cooke, N. (1987) *Hum. Toxicol.*, **6**, 385–93.
Stradling, G. N., Stather, J. W., Gray, S. A., Moody, J. C., Hodgson, A., Sedgwick, D., and Cooke, N. (1988) *Hum. Toxicol.*, **7**, 133–9.
Stradling, G. N., Stather, J. W., Gray, S. A., Moody, J. C., Ellender, M., Hodgson, A., Volf, V., Taylor, D. M., Wirth, P., and Gaskin, P. W. (1989) *Int. J. Radiat. Biol.*, **56**, 503–14.

Stradling, G. N., Gray, S. A., Moody, J. C., Hodgson, A., Raymond, K. N., Durbin, P. W., Rodgers, S. J., White, D. L., and Turowski, P. N. (1991) *Int. J. Radiat. Biol.*, **59**, 1269–77.

Stradling, G. N., Gray, S. A., Ellender, M., Moody, J. C., Hodgson, A., Pearce, M., Wilson, I., Burgada, R., Bailly, T., Leroux, Y. G., El Manouni, Raymond, K. N., and Durbin, P. N. (1992) *Int. J. Radiat. Biol.*, **62**, 487–97.

Stradling, G. N., Gray, S. A., Moody, J. C., Pearce, M. J., Wilson, I., Burgada, R., Bailly, T., Leroux, Y., Raymond, K. N., and Durbin, P. W. (1993) *Int. J. Radiat. Biol.*, **64**, 133–40.

Stradling, G. N., Gray, S. A., Pearce, M. J., Wilson, I., Moody, J. C., Burgada, R., Durbin, P. W., and Raymond, K. N. (1995a) *Hum. Exper. Toxicol.*, **14**, 165–9.

Stradling, G. N., Gray, S. A., Pearce, M. J., Wilson, I., Moody, J. C., Hodgson, A., and Raymond, K. N. (1995b) *Efficacy of TREN-(Me-3,2-HOPO), 5-LI-(Me-3,2-HOPO) and DTPA for Removing Plutonium and Americium from the Rat after Inhalation and Wound Contamination as Nitrates: Comparison with 3,4,3-LI(1,2-HOPO) NRPB-M534.* National Radiological Protection Board, Chilton, Didcot.

Stradling, G. N., Henge-Napoli, M. H., Paquet, F., Poncy, J. L., Fritsch, P., and Taylor, D. M. (2000a) *Radiat. Protect. Dosim.*, **87**, 19–27.

Stradling, G. N., Henge-Napoli, M. H., Paquet, F., Poncy, J. L., Fritsch, P., and Taylor, D. M. (2000b) *Radiat. Protect. Dosim.*, **87**, 29–40.

Sutterlin, U., Thies, W. G., Haffner, H., and Seidel, A. (1984) *Radiat. Res.*, **98**, 293–306.

Talbot, R. J., Knight, D. A., and Morgan, A. (1990) *Health Phys.*, **59**, 183–7.

Talbot, R. J., Newton, D., and Warner, A. J. (1993) *Health Phys.*, **65**, 41–6.

Tannenbaum, A. (1951a) Reversible inhibition of enzymes by uranium, in *Toxicology of Uranium* (ed. A. Tannenbaum), McGraw-Hill, New York, pp. 236–44.

Tannenbaum, A. (ed.) (1951b) *Toxicology of Uranium*, McGraw-Hill, New York.

Taylor, D. M. (1962) *Health Phys.*, **8**, 673–7.

Taylor, D. M. (1967) *Health Phys.*, **13**, 135–40.

Taylor, D. M. (1969) *Br. J. Radiol.*, **42**, 44–50.

Taylor, D. M. (1970) *Health Phys.*, **19**, 411–18.

Taylor, D. M. (1972) *Health Phys.*, **22**, 575–81.

Taylor, D. M. (1973a) Chemical and physical properties of plutonium, in *Uranium, Plutonium, Transplutonic Elements* (eds. H. C. Hodge, J. N. Stannard, and J. B. Hursh), Springer-Verlag, New York, pp. 323–48.

Taylor, D. M. (1973b) Chemical and physical properties of the transplutonium elements, in *Uranium, Plutonium, Transplutonic Elements* (eds. H. C. Hodge, J. N. Stannard, and J. B. Hursh), Springer-Verlag, New York, pp. 717–38.

Taylor, D. M. (1991) Acceleration of the natural rate of elimination of transuranium elements from the mammalian body, in *Handbook on the Physics and Chemistry of the Actinides*, (eds. A. J. Freeman and C. Keller), vol. 6 , North-Holland, Amsterdam, pp. 533–49.

Taylor, D. M. (1998) *J. Alloys Compds.*, **271–273**, 6–10.

Taylor, D. M. and Bensted, J. P. M. (1969) Long-term biological damage from plutonium-239 and americium-241 in rats, in *Delayed Effects of Bone-seeking Radionuclides* (ed. C. W. Mays), The University of Utah Press, Salt Lake City, pp. 357–70.

Taylor, D. M. and Farrow, L. C. (1987) *Int. J. Rad. Appl. Instrum. B*, **14**, 27–31.

Taylor, D. M., Sowby, F. D., and Kember, N. F. (1961) *Phys. Med. Biol.*, **6**, 73–86.

Taylor, G. N., Jee, W. S., Dockum, N., and Hromyk, E. (1969a) *Health Phys.*, **17**, 723–5.

Taylor, G. N., Jee, W. S. S., Williams, J. L., Burggraft, B., and Angus, W. (1969b) Microscopic distribution of ^{241}Am in the beagle, in *Research in Radiobiology. University of Utah School of Medicine Annual Report COO-119-240*, pp. 97–118.

Taylor, G. N., Jee, W. S., Mays, C. W., Dell, R. B., Williams, J. L., and Shabestari, L. (1972a) *Health Phys.*, **22**, 691–3.

Taylor, G. N., Jee, W. S. S., Williams, J. L., and Shabestari, L. (1972b) Hepatic changes induced by ^{239}Pu, in *Radiobiology of Plutonium* (eds. B. J. Stover and W. S. S. Jee), The J. W. Press, University of Utah. Salt Lake City, p. 105.

Thompson, R. C. (ed.) (1962) *Proceedings of the Hanford Symposium on the Biology of the Transuranic Elements, Health Phys.*, 8, 561–780.

Thompson, R. C. (1982) *Radiat. Res.*, **90**, 1–32.

Thompson, R. C. (1989) *Life Span Effects of Ionizing Radiation in the Beagle Dog.* USDOE, Pacific Northwest Laboratory, Richland, WA.

Thompson, R. C., Bair, W. J. (eds.) (1972) *Proceedings of the Hanford Symposium on the Biological Implications of the Transuranium Elements, Health Phys.*, 22, 6.

Thomson, B. M., Smith, C. L., Busch, R. D., Siegel, M. D., and Baldwin, C. (2003) *J. Environ. Eng.-ASCE*, **129**, 492–9.

Turner, G. A. and Taylor, D. M. (1968a) *Phys. Med. Biol.*, **13**, 535–46.

Turner, G. A. and Taylor, D. M. (1968b) *Radiat. Res.*, **36**, 22–30.

Van Middlesworth, L. (1947) *Study of Plutonium Metabolism in Bone MDDC-1022*. USAEC Oak Ridge, TN.

Van Rossum, J. P. and Schamhart, D. H. (1991) *Exp. Gerontol.*, **26**, 37–43.

Van Wagenen, G. and Asling, C. W. (1958) *Am. J. Anat.*, **103**, 163–186.

Vaughan, J., Bleaney, B., and Taylor, D. M. (1973) Distribution, excretion and effects of plutonium as bone-seekers, in *Uranium, Plutonium, Transplutonic Elements* (eds. H. C. Hodge, J. N. Stannard, and J. B. Hursh), Springer-Verlag, New York, pp. 349–502.

Veeck, A. C., White, D. J., Whisenhunt, D. W., Xu, J. D., Gorden, A. E. V., Romanovski, V., Hoffman, D. C., and Raymond, K. N. (2004) *Solv. Extract. Ion Exchange*, **22**, 1037–68.

Voegtlin, C. and Hodge, H. C. (eds.) (1949) *Pharmacology and Toxicology of Uranium Compounds*, vols 1 and 2, , McGraw-Hill, New York.

Voegtlin, C. and Hodge, H. C. (eds.) (1953) *Pharmacology and Toxicology of Uranium Compounds*, vols 3 and 4, , McGraw-Hill, New York.

Volf, V. (1975) *Health Phys.*, **29**, 61–8.

Volf, V. (1978) Treatment of incorporated transuranium elements, *IAEA Technical Report 184*.

Volf, V. (1986) *Int. J. Radiat. Biol.*, **49**, 449–62.

Volf, V. and Wirth, R. (1986) *Int. J. Radiat. Biol.*, **50**, 955–9.

Volf, V., Taylor, D. M., Brandau, W., and Schlenker, P. (1986) *Int. J. Radiat. Biol.*, **50**, 205–11.

Volf, V., Burgada, R., Raymond, K. N., and Durbin, P. W. (1993) *Int. J. Radiat. Biol.*, **63**, 785–93.

Volf, V., Burgada, R., Raymond, K. N., and Durbin, P. W. (1996a) *Int. J. Radiat. Biol.*, **70**, 765–72.

Volf, V., Burgada, R., Raymond, K. N., and Durbin, P. W. (1996b) *Int. J. Radiat. Biol.*, **70**, 109–14.
White, D. L., Durbin, P. W., Jeung, N., and Raymond, K. N. (1988) *J. Med. Chem.*, **31**, 11–18.
Williamson, M. and Vaughan, J. (1964) A preliminary report on the sites of deposition of Y, Am, and Pu in cortical bone and in the region of the epiphyeal cartiledge plate, in *Bone and Tooth* (ed. H. J. J. Blackwood), Pergamon Press, London.
Wills, J. H. (1949) Characteristics of uranium poisoning, in *Pharmacology and Toxicology of Uranium Compounds*, vol. 1 (eds. C. Voegtlin and H. C. Hodge), McGraw-Hill, New York, pp. 237–280.
Winter, R. and Seidel, A. (1982) *Radiat. Res.*, **89**, 113–23.
Wirth, R. and Volf, V. (1984) *Int. J. Radiat. Biol.*, **46**, 787–92.
Wirth, R., Taylor, D. M., and Duffield, J. (1985) *Int. J. Nucl. Med. Biol.*, **12**, 327–30.
Wong, N. L., Reitzik, M., and Quamme, G. A. (1986) *Renal Physiol.*, **9**, 29–37.
Wood, R., Sharp, C., Gourmelon, P., Le Guen, B., Stradling, G. N., Taylor, D. M., and Hengé-Napoli, M.-H. (2000) *Radiat. Protect. Dosim.*, **87**, 51–6.
Wrenn, M. E. (ed.) (1975) *Conference on Occupational Health Experience with Uranium*, ERDA Report 93.
Wrenn, M. E. (ed.) (1981) *Actinides in Man and Animals*, RD Press, University of Utah, Salt Lake City.
Wrenn, M. E., Durbin, P. W., Howard, B., Lipsztein, J., Rundo, J., Still, E. T., and Willis, D. L. (1985) *Health Phys.*, **48**, 601–33.
Wronski, T. J., Smith, J. M., and Jee, W. S. (1980) *Radiat. Res.*, **83**, 74–89.
Xu, J. D. and Raymond, K. N. (1999) *Inorg. Chem.*, **38**, 308–15.
Xu, J., Kullgren, B., Durbin, P. W., and Raymond, K. N. (1995) *J. Med. Chem.*, **38**, 2606–14.
Xu, J., Radkov, E., Ziegler, M., and Raymond, K. N. (2000) *Inorg. Chem.*, **39**, 4156–64.
Xu, J., Durbin, P. W., and Raymond, K. N. (2001) Actinide sequestering agents: design, structural, and biological evaluations, in *Nuclear Science – Evaluation of Speciation Technology – Workshop Proceedings Tokai-mura*, Ibaraki, Japan, 26-28 October 1999, OECD, pp. 247–54.
Xu, J., Durbin, P. W., Kullgren, B., Ebbe, S. N., Uhlir, L. C., and Raymond, K. N. (2002) *J. Med. Chem.*, **45**, 3963–71.
Xu, J. D., Whisenhunt, D. W., Veeck, A. C., Uhlir, L. C., and Raymond, K. N. (2003) *Inorg. Chem.*, **42**, 2665–74.
Youmans, W. B. and Siebens, A. A. (1973) 'Respiration' in Best and Taylor's Physiological Basis of Medical Practice, 9th edition, (Brobeck, J. R., ed.), pp. 6–1 to 6–90, The Williams and Wilkins Co., Baltimore.
Yuile, C. L. (1973) Animal experiments, in *Uranium, Plutonium, Transplutonic Elements* (eds. H. C. Hodge, J. N. Stannard, and J. B. Hursh), Springer-Verlag, New York, pp. 165–96.
Zak, O. and Aisen, P. (1988) *Biochemistry*, **27**, 1075–80.
Zhu, D.-H., Kappel, M. J., and Raymond, K. N. (1988) *Inorg. Chim. Acta*, **147**, 115–21.
Zirkle, R. E. (1947) *Radiology*, **49**, pp. 269–365.

APPENDIX I

NUCLEAR SPINS AND MOMENTS OF THE ACTINIDES

Nuclear spins and nuclear moments are used to test the single-particle models and nuclear quadrupole moments provide the deformation of the nucleus. In the following table, we present measured values of ground state spin in units of $\hbar$, magnetic dipole moment (μ) in units of nuclear magneton, and spectroscopic quadrupole moment (Q) in units of barns. The data have been taken from Raghavan (1989) and Firestone and Shirley (1996).

Nuclide	*Nuclear spin* ($\hbar$)	*Nuclear magnetic moment* (nuclear magneton)	*Electric quadrupole moment* (barns)
^{217}Ac	9/2	+3.825(45)	
^{227}Ac	3/2	+1.1(1)	+1.7(2)
^{229}Th	5/2	+0.46(4)	+4.3(9)
^{228}Pa	3	+3.48(33)	
^{230}Pa	2	+2.00(29)	
^{231}Pa	3/2	+2.01(2)	–1.72(5)
^{233}Pa	3/2	+3.39(70)	−3.0
^{233}U	5/2	0.59(5)	3.663(8)
^{235}U	7/2	−0.38(3)	4.936(6)
^{237}Np	5/2	+3.14(4)	+3.886(6)
^{238}Np	2		
^{239}Np	5/2		
^{239}Pu	1/2	+0.203(4)	
^{241}Pu	5/2	−0.683(15)	+5.6(20)
^{241}Am	5/2	+1.61(3)	+4.2(13)
^{242}Am	1	+0.3879(15)	−2.4(7)
^{242m}Am	5	+1.00(5)	+6.5(20)
^{243}Am	5/2	+1.61(4)	+4.30(3)
^{243}Cm	5/2	0.41	
^{245}Cm	7/2	0.5 (1)	
^{247}Cm	9/2	0.37	
^{249}Bk	7/2	2.0(4)	+5.79
^{249}Cf	9/2	−0.28	
^{253}Es	7/2	+4.10(7)	6.7(8)
^{254m}Es	2	2.90(7)	3.7(5)

Firestone, R.B. and Shirley, V.S. (eds.) (1996). *Table of Isotopes,* 8th edn. John Wiley, New York.
Raghavan, P. (1989) *At. Nucl. Data Tables*, **42**, 189–291.

APPENDIX II

NUCLEAR PROPERTIES OF ACTINIDE AND TRANSACTINIDE NUCLIDES

Irshad Ahmad

DISCUSSION

In this appendix, an elementary discussion of the nuclear properties of heavy elements is presented. For a better understanding of the subject, the reader should refer to nuclear chemistry textbooks (Krane, 1988; Choppin *et al*., 2002) and for the information on decay data, the *Table of Isotopes* (Firestone and Shirley, 1996) or the *Table of Radioactive Isotopes* (Browne and Firestone, 1986) or *Nuclear Data Sheets* (Tuli, 2004) should be consulted.

Isotopes of all elements with $Z \geq 89$ are radioactive. The most common mode of decay for these nuclei is by the emission of alpha particles (^{4}He ions). Alpha decay energies have been experimentally measured (Browne and Firestone, 1986; Firestone and Shirley, 1996) for most nuclides and these can also be calculated from atomic masses (Wapstra *et al*., 2003). The α decay of a nucleus with atomic number Z and atomic mass A produces a daughter nucleus with atomic number Z–2 and atomic mass A–4. During the α decay, about 2% of the available decay energy is imparted to the recoiling daughter nucleus and the remaining energy is carried off by the fast moving α-particle. Several groups of α-particles are emitted by a sample of a nuclide, each with a definite energy. For the actinide nuclides, α-particle energies range from about 4 to 11 MeV. As a rule, α-particle energy increases with increasing Z, and for a given element, it decreases with increasing mass number.

The α-decay half-life decreases exponentially with increasing energy. As a guide, every 50 keV increase in the decay energy reduces the half-life by a factor of ~2. The dependence of the α-decay half-life on the decay energy is given by the well-known Geiger–Nuttall law and more recently by Viola–Seaborg formula. A very useful quantity that facilitates the understanding of the mechanism of α-decay is the concept of hindrance factor. It is defined as the ratio of the experimental partial α-decay half-life to the theoretical half-life calculated on the assumption that the α-particle pre-exists in the nucleus and during its emission, it carries no angular momentum. An alpha transition in which the

ground state configuration of the parent nucleus remains unchanged is called 'favored transition'. All alpha transitions between the ground states of even–even nuclei are favored transitions and are assigned a hindrance factor of one.

Like elements of lower Z, each actinide element has one or more β-stable isotopes. Isotopes heavier than the β-stable isotope decay by the emission of β^- particles (electrons) and isotopes lighter than the β-stable isotopes decay by electron capture (EC). Electron capture decay is usually accompanied by the emission of K x-rays of the daughter nuclide. These x-rays provide a signature of the decaying nuclide. In heavy nuclei, β^+/EC ratio is very small and, as a consequence, positron (β^+) emission has been observed only in a few nuclei. The β-decay energy increases as the mass of the isotope gets further away from the line of β-stability. A quantity denoted by log ft is very useful in classifying the β transitions and estimating the β-decay half-lives of unknown nuclei. The ft value, also called the reduced β transition probability, is the energy-independent transition rate.

Spontaneous fission is a decay process in which a nucleus breaks up into two almost equal fragments. Each fission event is accompanied by the release of about 200 MeV energy and the emission of two to four neutrons. More than hundred nuclides are produced in fission of a nuclide sample and the mass yields and charge distributions have been measured for many fissioning systems (Wahl, 1989; Ahmad and Phillips, 1995). The fission half-life depends on the fissility parameter Z^2/A and is the major decay mode for many isotopes of element 100 and beyond. Nuclides with reasonable fission branch and available for experiments and industrial use are ^{248}Cm ($t_{1/2} = 3.40 \times 10^5$ years) and ^{252}Cf ($t_{1/2} = 2.64$ years). The isotope ^{252}Cf is widely used as a neutron source in industry and research.

Another rare mode of decay for heavy elements is the decay by the emission of intermediate mass fragments. These fragments are heavier than α particles but smaller than fission fragments. The branching ratio for this kind of radioactivity is extremely small ($\sim 10^{-10}$). Examples of such radioactivity are the ^{24}Ne emission by ^{231}Pa and ^{232}U (Price, 1989).

Alpha and β transitions usually populate excited states in addition to the ground states of the daughter nuclei. The excited states then decay to the ground state by emission of γ rays and conversion electrons. Typical half-lives of the excited states range from 10^{-9} to 10^{-14} s. However, in some cases, the decay of an excited state is forbidden for fast magnetic dipole ($M1$), electric dipole ($E1$), or electric quadrupole ($E2$) transitions because of the angular momentum selection rule. Such states have half-lives between nanoseconds and years. An excited state that has a half-life value greater than a nanosecond is called a 'metastable' state or 'isomer'. The isomeric state either de-excites to the ground state of the same nucleus by an internal transition (IT) or it decays by the usual mode of disintegration.

Most isomers occur because of the large difference between the spins of the excited state and the ground state. However, there are isomers which result not

by the difference in the spins of the states but by the difference in the shapes. These isomers decay by fission and are called 'fission isomers' or 'shape isomers' and have half-lives between 10^{-9} and 10^{-3} s. These isomers have deformations that are twice as large as the deformations of the ground states. More than 50 fission isomers have been discovered (Vandenbosch, 1977).

Very neutron-deficient nuclides decay predominantly by electron capture (EC). In some of these nuclei, the EC decay energy is quite large (> 4 MeV) and hence states at high excitation energy are populated in the daughter nucleus and a small fraction of these excited states decay by fission. Delayed fission of many nuclei has been observed (Hall and Hoffman, 1992).

Nuclear structure studies of actinide nuclides have been performed using a variety of techniques. These include high-resolution alpha, electron and gamma-ray spectroscopy, charged-particle transfer reaction spectroscopy, and Coulomb excitation studies. These investigations have provided significant information on the shape, size, and single-particle potential of actinide nuclei. The available data establish a spheroidal shape for nuclei with $A \geq 225$, with major to minor axes ratio of $\sim$1.25. The intrinsic quadrupole moments of actinide nuclei have been measured to be about 10^{-23} e cm^2 and the nuclear radii are about 10^{-12} cm.

Although most actinide nuclei have spheroidal shapes, there are indications that some neutron-deficient Ac and Pa nuclei have small octupole deformation in their ground states. These nuclei are pear-shaped and are axially symmetric but they are reflection asymmetric. Examples of such nuclei are ^{229}Pa and ^{225}Ac (Ahmad and Butler, 1993).

In nuclei, nucleons (neutrons and protons) move in orbits under the influence of the central nuclear potential. Nilsson (1955) and others (Chasman *et al.*, 1977) have calculated the eigenvalues and eigenfunctions of nucleons in a deformed potential as a function of the deformation β. Plots of the eigenvalues versus the deformation, commonly known as Nilsson diagrams, are extremely useful in understanding the single-particle properties of actinide nuclei. Each Nilsson state is characterized by a set of quantum numbers Ω π, N, N_z, and Λ. The quantum number Ω is the projection of the single-particle angular momentum on the nuclear symmetry axis and π is the parity of the wavefunction. The asymptotic quantum numbers N, N_z and Λ denote the oscillator shell number, the number of the oscillator quanta along the symmetry axis, and the projection of the orbital angular momentum on the symmetry axis, respectively. In heavy nuclei, neutrons (protons) fill each orbital above the closed shell of 126 (82) pairwise and thus the ground state of an odd-mass nucleus is simply the orbital occupied by the last unpaired nucleon. All even–even nuclei have ground state spin-parity of 0^+.

A spheroidal nucleus rotates about an axis perpendicular to the nuclear symmetry axis. The projection, K, of the total angular momentum, I, on the symmetry axis is the same as Ω. The rotation of a spheroidal nucleus generates a rotational band with spin sequence K, $K+1$, $K+2, \ldots$. The

rotational energy E_I of a level with spin I is given by the expression

$$E_I = \frac{\hbar^2}{2\Im} I(I+1),$$

where $\hbar$ is Planck's constant and $\Im$ is the nuclear moment of inertia. Typical values of $\hbar^2/2\Im$ are 7.0 keV for even–even actinide nuclei and 6.0 keV for odd-mass nuclei. The ground state band of an even–even nucleus has spin-parity sequence 0^+, 2^+, 4^+ . . .; odd spin values are not allowed.

Qualitative and quantitative analysis of actinide samples can be performed by using a variety of techniques (Knoll, 2000). Gross counting with a 2π (50%) geometry gas proportional counter can be used to determine the α or β^- count rate in a sample. These counters have very low background for α particles but somewhat higher background for electrons. Background of $\sim$0.1 α count per minute can be easily achieved for these counters.

Alpha pulse height analysis can be used to identify nuclides in a sample. Alpha spectra are measured either by Au–Si surface barrier detectors or passivated implanted planar silicon (PIPS) detectors. For best resolution (full width at half maximum), which can be as low as 9.0 keV, extremely thin sources are required. Precise energies and intensities of alpha groups have been tabulated by Ritz (1991).

Gamma-ray spectroscopy with high-resolution germanium spectrometers provides a powerful technique for qualitative and quantitative analysis of actinide samples. For high-energy γ rays in the range of 200 keV to 1.5 MeV, large volume Ge detectors provide the best sensitivity. Resolutions (FWHM) of less than 2.0 keV at the ^{60}Co 1332.5 keV line are easily achieved. In actinide nuclei, K x-ray energies lie in the 80–160 keV range and can be measured with high-resolution low-energy planar spectrometers (LEPS). K x-rays are produced when a vacancy in the K shell of an atom, created by electron capture or internal conversion, is filled by an electron from a higher shell. These K x-rays energies depend on the atomic number and there is sufficient separation between the energies of adjacent elements for them to be clearly identified. The Cm K x-ray spectrum produced in the alpha decay of ^{251}Cf and measured with a high-resolution LEPS is displayed in Fig. A.2.1. The resolution (FWHM) of the spectrometer is about 500 eV. Measurements of gamma ray spectrum and K x-ray spectrum are very useful in identifying and quantifying odd-mass nuclei.

L x-rays of actinide nuclei, which are produced when a vacancy in the L subshell of an atom is filled by an electron from a higher shell, have energies in the 10–30 keV range. Spectra of L x-rays can be measured with lithium-drifted silicon, Si(Li), detectors with resolutions (FWHM) of $\sim$300 eV. A Np L x-ray spectrum from ^{241}Am alpha decay, measured with a Si(Li) spectrometer, is shown in Fig. A.2.2. These spectra are also characteristic of the element but are more complex. The definition of x-ray components is given in (Firestone and Shirley, 1996). Even–even nuclei decay to excited levels of daughter nuclei which de-excite by highly L converted transitions generating L x-rays. Thus even–even

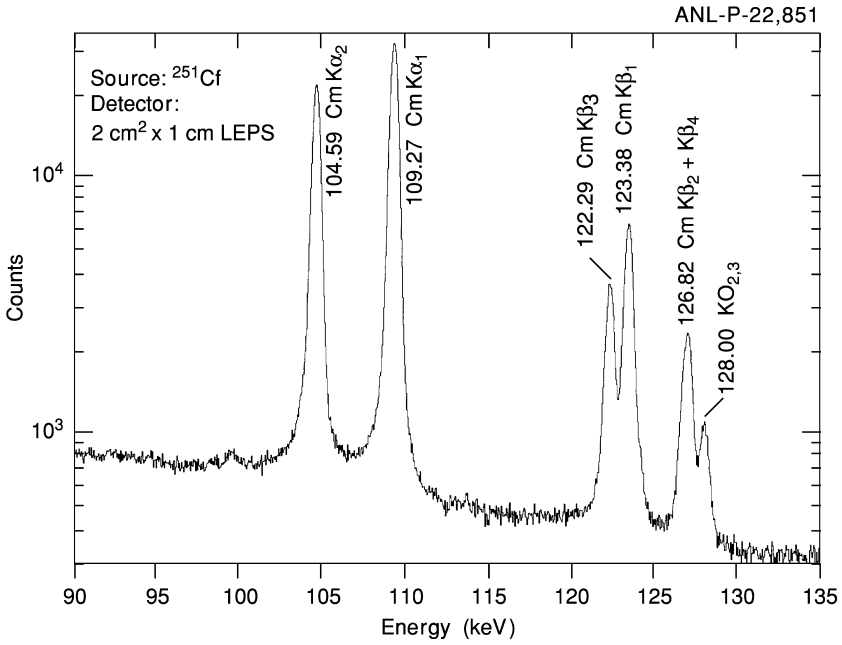

Fig. A.2.1 *K X-ray spectrum of Cm, produced in the alpha decay of* ^{251}*Cf, measured with a* 2 cm^2 × 1 cm *LEPS spectrometer.*

nuclei, which do not have any intense γ rays, can be analyzed by L X-ray spectroscopy.

Fissioning nuclides like ^{252}Cf can be assayed by measuring the gamma-ray spectrum with large-volume Ge detectors and using the intensities of gamma rays emitted in the decay of the abundant fission fragments (Ahmad *et al.*, 2003).

Some actinide nuclides have very long half-lives and hence they occur in nature. These include ^{232}Th, ^{235}U and ^{238}U which decay through a series of isotopes terminating at stable Pb isotopes. Isotopes of Ac, Th, and Pa are usually separated from the parent nuclides and used in the chemical and nuclear studies of these elements.

Transuranium isotopes are produced by long irradiations in nuclear reactors. In the US, there is a national program for the production and isolation of transuranium isotopes utilizing the High Flux Isotope Reactor (HFIR) at the Oak Ridge National Laboratory. The heaviest nuclide produced in this program is the 100 day ^{257}Fm. Neutron-deficient actinide isotopes are usually produced by nuclear reactions in charged particle accelerators.

All data in the tables of nuclear properties given in the preceding chapters and in this appendix have been taken from Browne and Firestone (1986), Firestone and Shirley (1996), Nuclear Data Sheets (Tuli, 2004) and from the

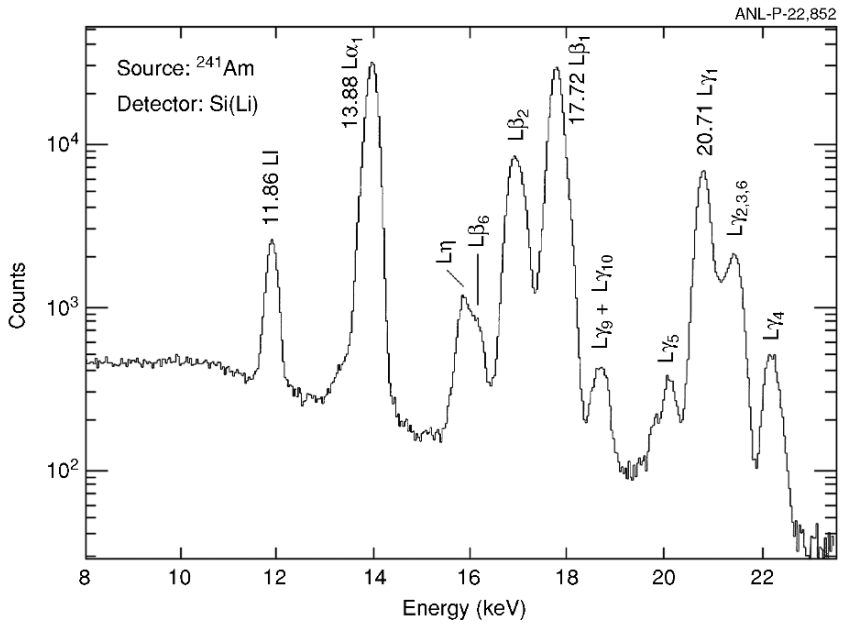

Fig. A.2.2 *L X-ray spectrum of Np, produced in the alpha decay of* ^{241}*Am, measured with a* 1 cm *diameter and* 5 mm *thick Si*(*Li*) *detector*.

web sites at the Isotope Project, Lawrence National Berkeley Laboratory (http://www.lbl.gov) and at the Nuclear Data Center, Brookhaven National Laboratory (http://www.nndc.bnl.gov). For the heaviest elements, data were taken from Armbruster (2000) and Hofmann and Münzenberg (2000). The cut-off date for literature survey was June 2004.

The notations for decay modes in the tables are: α for alpha decay, β^- for β^- decay, β^+ for positron decay, EC for electron capture decay, IT for isomeric transition, and SF for spontaneous fission. The letter m after a mass number represents an isomer. Isomers with half-lives of less than 1 s (except for the heaviest elements) and fission isomers are omitted from the tables. Energies and intensities are given for the most abundant α groups and most intense γ rays; for β^- particles, the maximum energy β_{max} is given. In the last column of Table A2.1, only the convenient methods of production are given; 'nature' denotes that the nuclide occurs in nature and 'multiple neutron capture' means that the nucleus is produced by multiple neutron capture in a high-flux reactor such as HFIR.

The specific activity S in disintegrations per minute per microgram was calculated using the expression

$$S = \frac{4.17449 \times 10^{17}}{t_{1/2}A},$$

where $t_{1/2}$ is half-life of the nuclide in minutes and A is the atomic mass in atomic mass units. The half-lives and atomic masses were taken from the references mentioned earlier in this text.

REFERENCES

Ahmad, I. and Butler, P. A. (1993) *Annu. Rev. Nucl. Part. Sci.,* **43**, 71–117.

Ahmad, I. and Phillips, W. R. (1995) *Rep. Prog. Phys.,* **58**, 1415–63.

Ahmad, I., Moore, E. F., Greene, J. P., Porter, C. E., and Felker, L. K. (2003) *Nucl. Instrum. Methods,* **A505**, 389–92.

Armbruster, P. (2000) *Annu. Rev. Nucl. Part. Sci.,* **50**, 411–79.

Browne, E. and Firestone, R. B. (1986) *Table of Radioactive Isotopes* (ed. V. S. Shirley), John Wiley, New York.

Chasman, R. R., Ahmad, I., Friedman, A. M., and Erskine, J. R. (1977) *Rev. Mod. Phys.,* **49**, 833–91.

Choppin, G. R., Liljenzin, J.-O., and Rydberg, J. (2002) *Radiochemistry and Nuclear Chemistry,* 3rd edn., Butterworth-Heinemann, Woburn.

Firestone, R. B. and Shirley, V. S. (eds.) (1996) *Table of Isotopes,* 8th edn., John Wiley, New York.

Hall, H. L. and Hoffman, D. C. (1992) *Annu. Rev. Nucl. Part. Sci.,* **42**, 147–75.

Hofmann, S. and Münzenburg, G. (2000) *Rev. Mod. Phys.,* **72**, 733–67.

Knoll, G. F. (2000) *Radiation Detection and Measurement,* John Wiley, New York.

Krane, K. S. (1988) *Introductory Nuclear Physics,* John Wiley, New York.

Nilsson, S. G. (1955) *Kgl. Dansk Videnskab. Selskab. Matt.-Fys. Medd.,* **29**, 16.

Price, P. B. (1989) *Annu. Rev. Nucl. Part. Sci.,* **39**, 19–42.

Ritz, A. (1991). *At. Data Nucl. Data Tables,* **47**, 205–39.

Tuli, (ed.) J. K. (2004) *Nuclear Data Sheets,* Academic Press, San Diego, CA.

Vandenbosch, R. (1977) *Annu. Rev. Nucl. Sci.,* **27**, 1–35.

Wahl, A. C. (1989) *At. Nucl. Data Tables,* **39**, 1–156.

Wapstra, A. H., Audi, G., and Thibault, C. (2003) *Nucl. Phys.,* **A729**, 129–336.

TABLES

In the following tables we reproduce the tables in each of the chapters 2 through 14 that contain the nuclear properties of the actinide and transactinide isotopes. We then give a table of specific activities of these isotopes.

Nuclear properties of actinium isotopes.

Mass number	*Half-life*	*Mode of decay*	*Main radiations* (MeV)	*Method of production*
206	33 ms	α	α 7.750	^{175}Lu(^{40}Ar,9n)
	22 ms	α	α 7.790	
207	22 ms	α	α 7.712	^{175}Lu(^{40}Ar,8n)
208	95 ms	α	α 7.572	^{175}Lu(^{40}Ar,7n)
	25 ms	α	α 7.758	
209	0.10 s	α	α 7.59	^{197}Au(^{20}Ne,8n)
210	0.35 s	α	α 7.46	^{197}Au(^{20}Ne,7n)
				^{203}Tl(^{16}O,9n)
211	0.25 s	α	α 7.48	^{197}Au(^{20}Ne,6n)
				^{203}Tl(^{16}O,8n)
212	0.93 s	α	α 7.38	^{203}Tl(^{16}O,7n)
				^{197}Au(^{20}Ne,5n)
213	0.80 s	α	α 7.36	^{197}Au(^{20}Ne,4n)
				^{203}Tl(^{16}O,6n)
214	8.2 s	α ≥ 86%	α 7.214 (52%)	^{203}Tl(^{16}O,5n)
		EC ≤ 14%	7.082 (44%)	^{197}Au(^{20}Ne,3n)
215	0.17 s	α 99.91%	α 7.604	^{203}Tl(^{16}O,4n)
		EC 0.09%		^{209}Bi(^{12}C,6n)
216	∼0.33 ms	α	α 9.072	^{209}Bi(^{12}C,5n)
216 m	0.33 ms	α	α 9.108 (46%)	
			9.030 (50%)	
217	69 ns	α	α 9.650	^{208}Pb(^{14}N,5n)
218	1.08 μs	α	α 9.20	^{222}Pa daughter
219	11.8 μs	α	α 8.66	^{223}Pa daughter
220	26.4 ms	α	α 7.85 (24%)	^{208}Pb(^{15}N,3n)
			7.68 (21%)	^{224}Pa daughter
			7.61 (23%)	
221	52 ms	α	α 7.65 (70%)	^{205}Tl(^{22}Ne,α2n)
			7.44 (20%)	^{208}Pb(^{18}O,p4n)
222	5.0 s	α	α 7.00	^{226}Ra(p,5n)
				^{208}Pb(^{18}O,p3n)
222 m	63 s	α > 90%	α 7.00 (15%)	^{208}Pb(^{18}O,p3n)
		EC ∼ 1%	6.81 (27%)	^{209}Bi(^{18}O,αn)
		IT < 10%		
223	2.10 min	α 99%	α 6.662 (32%)	^{227}Pa daughter
		EC 1%	6.647 (45%)	
224	2.78 h	EC ∼ 90%	α 6.211 (20%)	^{228}Pa daughter
		α ∼ 10%	6.139 (26%)	

Nuclear properties of actinium isotopes. (*Contd.*)

Mass number	*Half-life*	*Mode of decay*	*Main radiations* (MeV)	*Method of production*
225	10.0 d	α	α 5.830 (51%) 5.794 (24%) γ 0.100 (1.7%)	^{225}Ra daughter
226	29.37 h	β^- 83% EC 17% α 6×10^{-3}%	α 5.399 β^- 1.10 γ 0.230 (27%)	^{226}Ra(d,2n)
227	21.772 yr	β^- 98.62% α 1.38%	α 4.950 (47%) 4.938 (40%) β^- 0.045 γ 0.086	nature
228	6.15 h	β^-	β^- 2.18 γ 0.991	nature
229	62.7 min	β^-	β^- 1.09 γ 0.165	^{229}Ra daughter ^{232}Th(γ,p2n)
230	122 s	β^-	β^- 1.4 γ 0.455	^{232}Th(γ,pn)
231	7.5 min	β^-	β^- 2.1 γ 0.282	^{232}Th(γ,p) ^{232}Th(n,pn)
232	119 s	β^-		^{238}U + Ta
233	145 s	β^-		^{238}U + Ta
234	44 s	β^-		^{238}U + Ta

Nuclear properties of thorium isotopes.

Mass number	*Half-life*	*Mode of decay*	*Main radiations* (MeV)	*Method of production*
209	3.8 ms	α	α 8.080	^{32}S + ^{182}W
210	9 ms	α	α 7.899	^{35}Cl + ^{181}Ta
211	37 ms	α	α 7.792	^{35}Cl + ^{181}Ta
212	30 ms	α	α 7.82	^{176}Hf(^{40}Ar,4n)
213	140 ms	α	α 7.691	^{206}Pb(^{16}O,9n)
214	100 ms	α	α 7.686	^{206}Pb(^{16}O,8n)
215	1.2 s	α	α 7.52 (40%) 7.39 (52%)	^{206}Pb(^{16}O,7n)
216	28 ms	α	α 7.92	^{206}Pb(^{16}O,6n)
217	0.237 ms	α	α 9.261	^{206}Pb(^{16}O,5n)
218	0.109 μs	α	α 9.665	^{206}Pb(^{16}O,4n) ^{209}Bi(^{14}N,5n)
219	1.05 μs	α	α 9.34	^{206}Pb(^{16}O,3n)
220	9.7 μs	α	α 8.79	^{208}Pb(^{16}O,4n)
221	1.68 ms	α	α 8.472 (32%) 8.146 (62%)	^{208}Pb(^{16}O,3n)
222	2.8 ms	α	α 7.98	^{208}Pb(^{16}O,2n)

Nuclear properties of thorium isotopes. (Contd.)

Mass number	*Half-life*	*Mode of decay*	*Main radiations* (MeV)	*Method of production*
223	0.60 s	α	α 7.32 (40%) 7.29 (60%)	^{208}Pb(^{18}O,3n)
224	1.05 s	α	α 7.17 (81%) 7.00 (19%) γ 0.177	^{228}U daughter ^{208}Pb(^{22}Ne,α2n)
225	8.0 min	α ≈ 90% EC ≈ 10%	α 6.478 (43%) 6.441 (15%) γ 0.321	^{229}U daughter ^{231}Pa(p,α3n)
226	30.57 min	α	α 6.335 (79%) 6.225 (19%) γ 0.1113	^{230}U daughter
227	18.68 d	α	α 6.038 (25%) 5.978 (23%) γ 0.236	nature
228	1.9116 yr	α	α 5.423 (72.7%) 5.341 (26.7%) γ 0.084	nature
229	7.340×10^3 yr	α	α 4.901 (11%) 4.845 (56%) γ 0.194	^{233}U daughter
230	7.538×10^4 yr	α	α 4.687 (76.3%) 4.621 (23.4%) γ 0.068	nature
231	25.52 h	β^-	β^-0.302 γ 0.084	nature ^{230}Th(n,γ)
232	1.405×10^{10} yr $> 1 \times 10^{21}$ yr	α SF	α 4.016 (77%) 3.957 (23%)	nature
233	22.3 min	β^-	β^-1.23 γ 0.086	^{232}Th(n,γ)
234	24.10 d	β^-	β^- 0.198 γ 0.093	nature
235	7.1 min	β^-		^{238}U(n,α)
236	37.5 min	β^-	γ 0.111	^{238}U(γ,2p) ^{238}U(p,3p)
237	5.0 min	β^-		^{18}O + ^{238}U
238	9.4 min	β^-		^{18}O + ^{238}U

Nuclear properties of protactinium isotopes.

Mass number	*Half-life*	*Mode of decay*	*Main radiations* (MeV)	*Method of production*
212	5.1 ms	α	α 8.270	^{182}W(^{35}Cl,5n)
213	5.3 ms	α	α 8.236	^{170}Er(^{51}V,8n)
214	17 ms	α	α 8.116	^{170}Er(^{51}V,7n)

Nuclear properties of protactinium isotopes. (*Contd.*)

Mass number	*Half-life*	*Mode of decay*	*Main radiations* (MeV)	*Method of production*
215	14 ms	α	α 8.170	^{181}Ta(^{40}Ar,6n)
216	0.2 s	α	α 7.865	^{197}Au(^{24}Mg,5n)
217	4.9 ms	α	α 8.340	^{181}Ta(^{40}Ar,4n)
	1.6 ms	α	α 10.160	
218	0.12 ms	α	α 9.614 (65%)	^{206}Pb(^{16}O,4n)
219	53 ns	α	α 9.900	^{204}Pb(^{19}F,4n)
220	0.78 μs	α	α 9.15	^{204}Pb(^{19}F,3n)
221	5.9 μs	α	α 9.080	^{209}Bi(^{16}O,4n)
222	5.7 ms	α	α 8.54 (∼30%)	^{209}Bi(^{16}O,3n)
			∼8.18 (50%)	^{206}Pb(^{19}F,3n)
223	6 ms	α	α 8.20 (45%)	^{208}Pb(^{19}F,4n)
			8.01 (55%)	^{205}Tl(^{22}Ne,4n)
224	0.9 s	α	α 7.49	^{208}Pb(^{19}F,3n)
225	1.8 s	α	α 7.25 (70%)	^{232}Th(p,8n)
			7.20 (30%)	^{209}Bi(^{22}Ne,α2n)
226	1.8 min	α 74%	α 6.86 (52%)	^{232}Th(p,7n)
		EC 26%	6.82 (46%)	
227	38.3 min	α ∼85%	α 6.466 (51%)	^{232}Th(p,6n)
		EC ∼15%	6.416 (15%)	
			γ 0.065	
228	22 h	EC ∼98%	α 6.105 (12%)	^{232}Th(p,5n)
		α ∼2%	6.078 (21%)	^{230}Th(p,3n)
			γ 0.410	
229	1.5 d	EC 99.5%	α 5.669 (19%)	^{230}Th(d,3n)
		α 0.48%	5.579 (37%)	^{229}Th(d,2n)
230	17.7 d	EC 90%	α 5.345	^{230}Th(d,2n)
		β^- 10%	β^- 0.51	^{232}Th(p,3n)
		α 3.2×10^{-3}%	γ 0.952	
231	3.28×10^4 yr	α	α 5.012 (25%)	nature
			4.951 (23%)	
			γ 0.300	
232	1.31 d	β^-	β^- 1.29	^{231}Pa(n,γ)
			γ 0.969	^{232}Th(d,2n)
233	27.0 d	β^-	β^- 0.568	^{233}Th daughter
			γ 0.312	^{237}Np daughter
234	6.75 h	β^-	β^- 1.2	nature
			γ 0.570	
234 m	1.175 min	β^- 99.87%	β^- 2.29	nature
		IT 0.13%	γ 1.001	
235	24.2 min	β^-	β^- 1.41	^{235}Th daughter
				^{235}U(n,p)
236	9.1 min	β^-	β^- 3.1	^{236}U(n,p)
			γ 0.642	^{238}U(d,α)
237	8.7 min	β^-	β^- 2.3	^{238}U(γ,p)
			γ 0.854	^{238}U(n,pn)
238	2.3 min	β^-	β^- 2.9	^{238}U(n,p)
			γ 1.014	
239	106 min	β^-		^{18}O + ^{238}U

Nuclear properties of uranium isotopes.

Mass number	*Half-life*	*Mode of decay*	*Main radiations* (MeV)	*Method of production*
217	16 ms	α	α 8.005	^{182}W(^{40}Ar,5n)
218	1.5 ms	α	α 8.625	^{197}Au(^{27}Al,6n)
219	42 μs	α	α 8.680	^{197}Au(^{27}Al,5n)
222	1.0 μs	α	α 9.500	W(^{40}Ar,xn)
223	18 μs	α	α 8.780	^{208}Pb(^{20}Ne,5n)
224	0.9 ms	α	α 8.470	^{208}Pb(^{20}Ne,4n)
225	59 ms	α	α 7.879	^{208}Pb(^{22}Ne,5n)
226	0.35 s	α	α 7.430	^{232}Th(α,10n)
227	1.1 min	α	α 6.87	^{232}Th(α,9n) ^{208}Pb(^{22}Ne,3n)
228	9.1 min	α ≥ 95% EC ≤ 5%	α 6.68 (70%) 6.60 (29%) γ 0.152	^{232}Th(α,8n)
229	58 min	EC ∼ 80% α ∼ 20%	α 6.360 (64%) 6.332 (20%) γ 0.123	^{230}Th(^{3}He,4n) ^{232}Th(α,7n)
230	20.8 d	α	α 5.888 (67.5%) 5.818 (31.9%) γ 0.072	^{230}Pa daughter ^{231}Pa(d,3n)
231	4.2 d	EC > 99% α 5.5×10^{-3}%	α 5.46 γ 0.084	^{230}Th(α,3n) ^{231}Pa(d,2n)
232	68.9 yr $\sim 8 \times 10^{13}$ yr	α SF	α 5.320 (68.6%) 5.264 (31.2%) γ 0.058	^{232}Th(α,4n)
233	1.592×10^{5} yr 1.2×10^{17} yr	α SF	α 4.824 (82.7%) 4.783 (14.9%) γ 0.097	^{233}Pa daughter
234	2.455×10^{5} yr 2×10^{16} yr	α SF	α 4.777 (72%) 4.723 (28%)	nature
235	7.038×10^{8} yr 3.5×10^{17} yr	α SF	α 4.397 (57%) 4.367 (18%) γ 0.186	nature
235 m	25 min	IT		^{239}Pu daughter
236	2.3415×10^{7} yr 2.43×10^{16} yr	α SF	α 4.494 (74%) 4.445 (26%)	^{235}U(n,γ)
237	6.75 d	β$^-$	β$^-$ 0.519 γ 0.060	^{236}U(n,γ) ^{241}Pu daughter
238	4.468×10^{9} yr 8.30×10^{15} yr	α SF	α 4.196 (77%) 4.149 (23%)	nature
239	23.45 min	β$^-$	β$^-$ 1.29 γ 0.075	^{238}U(n,γ)
240	14.1 h	β$^-$	β$^-$ 0.36 γ 0.044	^{244}Pu daughter
242	16.8 min	β$^-$	β$^-$ 1.2 γ 0.068	^{244}Pu(n,2pn)

Nuclear properties of neptunium isotopes.

Mass number	*Half-life*	*Mode of decay*	*Main radiations* (MeV)	*Method of production*
226	31 ms	EC, α	α 8.044	^{209}Bi(^{22}Ne,5n)
227	0.51 s	EC, α	α 7.677	^{209}Bi(^{22}Ne,4n)
228	61.4 s	EC, α		^{209}Bi(^{22}Ne,3n)
229	4.0 min	α ≥ 50% EC ≤ 50%	α 6.890	^{233}U(p,5n)
230	4.6 min	α > 99% EC ≤ 0.97%	α 6.66	^{233}U(p,4n)
231	48.8 min	EC < 99% α > 1%	α 6.28 γ 0.371	^{233}U(d,4n) ^{235}U(d,6n)
232	14.7 min	EC	γ 0.327	^{233}U(d,3n)
233	36.2 min	EC < 99% α∼10^{-3}%	α 5.54 γ 0.312	^{233}U(d,2n) ^{235}U(d,4n)
234	4.4 d	EC 99.95% β^+ 0.05%	γ 1.559	^{235}U(d,3n)
235	396.1 d	EC > 99% α 1.6×10^{-3}%	α 5.022 (53%) 5.004 (24%)	^{235}U(d,2n)
236[a]	22.5 h	β^- 50% EC 50%	β^- 0.54 γ 0.642	^{235}U(d,n)
236[a]	1.54×10^5 yr	EC 87% β^-13%	γ 0.163	^{235}U(d,n)
237	2.144×10^6 yr $>1 \times 10^{18}$ yr	α SF	α 4.788 (51%) 4.770 (19%) γ 0.086	^{237}U daughter ^{241}Am daughter
238	2.117 d	β^-	β^- 1.29 γ 0.984	^{237}Np(n,γ)
239	2.3565 d	β^-	β^- 0.72 γ 0.106	^{243}Am daughter ^{239}U daughter
240	1.032 h	β^-	β^- 2.09 γ 0.566	^{238}U(α,pn)
240 m	7.22 min	β^-	β^- 2.05 γ 0.555	^{240}U daughter ^{238}U(α, pn)
241	13.9 min	β^-	β^- 1.31 γ 0.175	^{238}U(α,p) ^{244}Pu(n,p3n)
242 g or m	5.5 min	β^-	β^- 2.7 γ 0.786	^{244}Pu(n,p2n) ^{242}Pu(n,p)
242 g or m	2.2 min	β^-	β^- 2.7 γ 0.736	^{242}U daughter
243	1.85 min	β^-	γ 0.288	^{136}Xe + ^{238}U
244	2.29 min	β^-	γ 0.681	^{136}Xe + ^{238}U

[a] Not known whether ground-state nuclide or isomer.

Nuclear properties of plutonium isotopes.

Mass number	*Half-life*	*Mode of decay*	*Main radiations* (MeV)	*Method of production*
228	1.1 s	α	α 7.772	^{198}Pt(^{34}S,4n)
229	–	α	α 7.460	^{207}Pb(^{26}Mg,4n)
230	2.6 min	EC, α	α 7.055	^{208}Pb(^{26}Mg,4n)
231	8.6 min	EC 90% α 10%	α 6.72	^{233}U(^{3}He,5n)
232	33.1 min	EC ≥80% α ≤20%	α 6.600 (62%) 6.542 (38%)	^{233}U(α,5n)
233	20.9 min	EC 99.88% α 0.12%	α 6.30 γ 0.235	^{233}U(α,4n)
234	8.8 h	EC 94% α 6%	α 6.202 (68%) 6.151 (32%)	^{233}U(α,3n)
235	25.3 min	EC > 99.99% α 3×10^{-3}%	α 5.85 γ 0.049	^{235}U(α,4n) ^{233}U(α,2n)
236	2.858 yr 1.5×10^{9} yr	α SF	α 5.768 (69%) 5.721 (31%)	^{235}U(α,3n) ^{236}Np daughter
237	45.2 d	EC > 99.99% α 4.2×10^{-3}%	5.356 (∼17.2%) 5.334 (∼43.5%) γ 0.059	^{235}U(α,2n) ^{237}Np(d,2n)
238	87.7 yr 4.77×10^{10} yr	α SF	α 5.499 (70.9%) 5.457 (29.0%)	^{242}Cm daughter ^{238}Np daughter
239	2.411×10^{4} yr 8×10^{15} yr	α SF	α 5.157 (70.77%) 5.144 (17.11%) 5.106 (11.94%) γ 0.129	^{239}Np daughter
240	6.561×10^{3} yr 1.15×10^{11} yr	α SF	α 5.168 (72.8%) 5.123 (27.1%)	multiple n capture
241	14.35 yr	β^- > 99.99% α 2.4×10^{-3}%	α 4.896 (83.2%) 4.853 (21.1%) β^- 0.021 γ 0.149	multiple n capture
242	3.75×10^{5} yr 6.77×10^{10} yr	α SF	α 4.902 (76.49%) 4.856 (23.48%)	multiple n capture
243	4.956 h	β^-	β^- 0.58 γ 0.084	multiple n capture
244	8.08×10^{7} yr 6.6×10^{10} yr	α 99.88% SF	α 4.589 (81%) 4.546 (19%)	multiple n capture
245	10.5 h	β^-	β^- 0.878 (51%) γ 0.327 (25.4%)	^{244}Pu(n,γ)
246	10.84 d	β^-	β^- 0.15 (91%) γ 0.224 (25%)	multiple n capture
247	2.27 d	β^-		multiple n capture

Nuclear properties of americium isotopes.

Mass number	*Half-life*	*Mode of decay*	*Main radiations* (MeV)	*Method of production*
232	1.4 min	SF isomer		^{230}Th(^{10}B, 8n)
233	3.2 min	α	α 6.780	^{238}U(^{6}Li, 6n)
234	2.6 min	EC		^{230}Th(^{10}B, 6n)
235	15 min	EC		^{238}Pu(^{1}H, 4n)
236	4.4 min	EC		^{235}U(^{6}Li, 5n)
	3.7 min	EC		^{237}Np(^{6}He, 4n)
237	1.22 h	EC > 99%	α 6.042	^{237}Np(α, 4n)
		α 0.025%	γ 0.280 (47%)	^{237}Np(^{3}He, 3n)
238	1.63 h	EC > 99%	α 5.94	^{237}Np(α, 3n)
		α 1.0×10^{-4}%	γ 0.963 (29%)	
239	11.9 h	EC > 99%	α 5.776 (84%)	^{237}Np(α, 2n)
		α 0.010%	5.734 (13.8%)	^{239}Pu(d, 2n)
			γ 0.278 (15%)	
240	50.8 h	EC > 99%	α 5.378 (87%)	^{237}Np(α, n)
		α 1.9×10^{-4}%	5.337 (12%)	^{239}Pu(d, n)
			γ 0.988 (73%)	
241	432.7 yr	α	α 5.486 (84%)	^{241}Pu daughter
	1.15×10^{14} yr	SF	5.443 (13.1%)	multiple n capture
			γ 0.059 (35.7%)	
242	16.01 h	β$^-$ 82.7%	β$^-$ 0.667	^{241}Am(n, γ)
		EC 17.3%	γ 0.042 weak	
242 m	141 yr	IT 99.5%	α 5.207 (89%)	^{241}Am(n, γ)
	9.5×10^{11} yr	SF α (0.45%)	5.141 (6.0%)	^{241}Am(n, γ)
			γ 0.0493 (41%)	
243	7.38×10^{3} yr	α	α 5.277 (88%)	multiple
	2.0×10^{14} yr	SF	5.234 (10.6%)	n capture
			γ 0.075 (68%)	
244	10.1 h	β$^-$	β$^-$ 0.387	^{243}Am(n, γ)
			γ 0.746 (67%)	
244 m	26 min	β$^-$ > 99%	β$^-$ 1.50	^{243}Am(n, γ)
		EC 0.041%		
245	2.05 h	β$^-$	β$^-$ 0.895	^{245}Pu daughter
			γ 0.253 (6.1%)	
246[a]	25.0 min	β$^-$	β$^-$ 2.38	^{246}Pu daughter
			γ 0.799 (25%)	
246[a]	39 min	β$^-$	γ 0.679 (52%)	^{244}Pu(α, d)
				^{244}Pu(^{3}He, p)
247	24 min	β$^-$	γ 0.285 (23%)	^{244}Pu(α, p)

[a] Not known whether ground-state nuclide or isomer.

Nuclear properties of curium isotopes.

Mass number	*Half-life*	*Mode of decay*	*Main radiations* (MeV)	*Method of production*
237	–	EC, α	α 6.660	^{237}Np (^{6}Li,6n)
238	2.3 h	EC < 90% α > 10%	α 6.52	^{239}Pu(α,5n)
239	2.9 h	EC	γ 0.188	^{239}Pu(α,4n)
240	27 d	α	α 6.291 (71%)	^{239}Pu(α,3n)
	1.9×10^6 yr	SF	6.248 (29%)	
241	32.8 d	EC 99.0% α 1.0%	α 5.939 (69%) 5.929 (18%) γ 0.472 (71%)	^{239}Pu(α,2n)
242	162.8 d	α	α 6.113 (74.0%)	^{239}Pu(α,n)
	7.0×10^6 yr	SF	6.070 (26.0%)	^{242}Am daughter
243	29.1 yr	α 99.76% EC 0.24%	α 5.785 (73.5%) 5.741 (10.6%) γ 0.278 (14.0%)	^{242}Cm(n,γ)
244	18.10 yr	α	α 5.805 (76.7%)	multiple n capture
	1.35×10^7 yr	SF	5.764 (23.3%)	^{244}Am daughter
245	8.5×10^3 yr	α	α 5.362 (93.2%) 5.304 (5.0%) γ 0.175	multiple n capture
246	4.76×10^3 yr	α	α 5.386 (79%)	multiple n capture
	1.80×10^7 yr	SF β stable	5.343 (21%)	
247	1.56×10^7 yr	α	α 5.266 (14%) 4.869 (71%) γ 0.402 (72%)	multiple n capture
248	3.48×10^5 yr	α 91.61% SF 8.39%	α 5.078 (82%) 5.034 (18%)	multiple n capture
249	64.15 min	β^-	β^- 0.9 γ 0.634 (1.5%)	^{248}Cm(n,γ)
250	$\sim 8.3 \times 10^3$ yr	SF		multiple n capture
251	16.8 min	β^-	β^- 1.42 γ 0.543 (12%)	^{250}Cm(n,γ)

Nuclear properties of berkelium isotopes.

Mass number	*Half-life*	*Mode of decay*	*Main radiations* (MeV)	*Method of production*
238	2.4 min	EC		^{241}Am(α,7n)
240	4.8 min	EC		^{232}Th(^{14}Ne,6n)
241	4.6 min	EC	γ 0.2623	^{239}Pu(^{6}Li,4n)
242	7.0 min	EC		^{232}Th(^{14}N,4n) ^{232}Th(^{15}N,5n)
243	4.5 h	EC 99.85% α 0.15%	α 6.758 (15%) 6.574 (26%)	^{243}Am(α,4n)

Nuclear properties of berkelium isotopes. (*Contd.*)

Mass number	*Half-life*	*Mode of decay*	*Main radiations* (MeV)	*Method of production*
			γ 0.755	
244	4.35 h	EC > 99% α 6×10^{-3}%	α 6.667 (~50%) 6.625 (~50%) γ 0.218	^{243}Am(α,3n)
245	4.94 d	EC 99.88% α 0.12%	α 6.349 (15.5%) 6.145 (18.3%) γ 0.253 (31%)	^{243}Am(α,2n)
246	1.80 d	EC	γ 0.799 (61%)	^{243}Am(α,n)
247	1.38×10^3 yr	α	α 5.712 (17%) 5.532 (45%) γ 0.084 (40%)	^{247}Cf daughter ^{244}Cm(α,p)
248[a]	23.7 h	β⁻ 70% EC 30%	β⁻ 0.86 γ 0.551	^{248}Cm(d,2n)
248[a]	> 9 yr	decay not observed		^{246}Cm(α,pn)
249	330 d	β⁻ > 99% α 1.45×10^{-3}%	α 5.417 (74.8%) 5.390 (16%) β⁻ 0.125 γ 0.327 weak	multiple n capture
250	3.217 h	β⁻	β⁻ 1.781 γ 0.989 (45%)	^{254}Es daughter ^{249}Bk(n,γ)
251	55.6 min	β⁻	β⁻ ~1.1 γ 0.178	^{255}Es daughter

[a] Not known whether ground-state nuclide or isomer.

Nuclear properties of californium isotopes.

Mass number	*Half-life*	*Mode of decay*	*Main radiations* (MeV)	*Method of production*
239	39 s	α	α 7.63	^{243}Fm daughter
240	1.1 min	α	α 7.59	^{233}U(^{12}C,5n)
241	3.8 min	α	α 7.335	^{233}U(^{12}C,4n)
242	3.5 min	α	α 7.385 (~80%) 7.351 (~20%)	^{233}U(^{12}C,3n) ^{235}U(^{12}C,5n)
243	10.7 min	EC ~86% α ~14%	α 7.06	^{235}U(^{12}C,4n)
244	19.4 min	α	α 7.210 (75%) 7.168 (25%)	^{244}Cm(α,4n) ^{236}U(^{12}C,4n)
245	43.6 min	EC ~70% α ~30%	α 7.137	^{244}Cm(α,3n) ^{238}U(^{12}C,5n)
246	35.7 h 2.0×10^3 yr	α SF β stable	α 6.758 (78%) 6.719 (22%)	^{244}Cm(α,2n) ^{246}Cm(α,4n)
247	3.11 h	EC 99.96% α 0.035%	α 6.296 (95%) γ 0.294 (1.0%)	^{246}Cm(α,3n) ^{244}Cm(α,n)

Nuclear properties of californium isotopes. (*Contd.*)

Mass number	*Half-life*	*Mode of decay*	*Main radiations* (MeV)	*Method of production*
248	334 d	α	α 6.258 (80.0%)	^{246}Cm(α,2n)
	3.2×10^4 yr	SF	6.217 (19.6%)	
		β stable		
249	351 yr	α	α 6.194 (2.2%)	^{249}Bk daughter
	6.9×10^{10} yr	SF	5.812 (84.4%)	
			γ 0.388 (66%)	
250	13.08 yr	α	α 6.031 (83%)	multiple n capture
	1.7×10^4 yr	SF	5.989 (17%)	
251	898 yr	α	α 5.851 (27%)	multiple n capture
			5.677 (35%)	
252	2.645 yr	α 96.91%	α 6.118 (84%)	multiple n capture
		SF 3.09%	6.076 (15.8%)	
253	17.81 d	β 99.69%	α 5.979 (95%)	multiple n capture
		α 0.31%	5.921 (5%)	
254	60.5 d	SF 99.69%	α 5.834 (83%)	multiple n capture
		α 0.31%	5.792 (17%)	
255	1.4 h	β^-		^{254}Cf(n,γ)
256	12.3 min	SF		^{254}Cf(t,p)

Nuclear properties of einsteinium isotopes.

Mass number	*Half-life*	*Mode of decay*	*Main radiations* (MeV)	*Method of production*
241	8 s	α	α 8.11	^{245}Md daughter
242	13.5 s	α	α 7.92	^{233}U(^{14}N,5n)
243	21 s	α	α 7.89	^{233}U(^{15}N,5n)
244	37 s	EC 96%	α 7.57	^{233}U(^{15}N,4n)
		α ∼ 4%		^{237}Np(^{12}C,5n)
245	1.1 min	EC 60%	α 7.73	^{237}Np(^{12}C,4n)
		α 40%		
246	7.7 min	EC 90%	α 7.35	^{241}Am(^{12}C,α3n)
		α 10%		
247	4.55 min	EC ∼ 93%	α 7.32	^{241}Am(^{12}C,α2n)
		α ∼ 7%		^{238}U(^{14}N,5n)
248	27 min	EC 99.7%	α 6.87	^{249}Cf(d,3n)
		α ∼ 0.3%	γ 0.551	
249	1.70 h	EC 99.4%	α 6.770	^{249}Cf(d,2n)
		α 0.57%	γ 0.380	
250[a]	8.6 h	EC	γ 0.829	^{249}Cf(d,n)
250[a]	2.22 h	EC	γ 0.989	^{249}Cf(d,n)

Nuclear properties of einsteinium isotopes. (Contd.)

Mass number	*Half-life*	*Mode of decay*	*Main radiations* (MeV)	*Method of production*
251	33 h	EC 99.5% α 0.49%	α 6.492 (81%) 6.463 (9%) γ 0.177	^{249}Bk(α,2n)
252	471.7 d	α 78% EC 22%	α 6.632 (80%) 6.562 (13.6%) γ 0.785	^{249}Bk(α,n)
253	20.47 d 6.3×10^5 yr	α SF β stable	α 6.633 (89.8%) 6.592 (7.3%) γ 0.389	multiple n capture
254 g	275.7 d $> 2.5 \times 10^7$ yr	α SF	α 6.429 (93.2%) 6.359 (2.4%) γ 0.062	multiple n capture
254 m	39.3 h $> 1 \times 10^5$ yr	β^- 99.6% SF α 0.33% EC 0.08%	α 6.382 (75%) 6.357 (8%)	^{253}Es (n,γ)
255	39.8 d	β^- 92.0% α 8.0% SF 4×10^{-3}%	α 6.300 (88%) 6.260 (10%)	multiple n capture
256[a]	25.4 min	β^-		^{255}Es(n,γ)
256[a]	~7.6 h	β^-		^{254}Es(t,p)

[a] Not known whether ground-state nuclide or isomer.

Nuclear properties of fermium isotopes.

Mass number	*Half-life*	*Mode of decay*	*Main radiations* (MeV)	*Method of production*
242	0.8 ms	SF		^{204}Pb(^{40}Ar,2n)
243	0.18 s	α	α 8.546	^{206}Pb(^{40}Ar,3n)
244	3.3 ms	SF		^{206}Pb(^{40}Ar,2n) ^{233}U(^{16}O,5n)
245	4.2 s	α	α 8.15	^{233}U(^{16}O,4n)
246	1.1 s	α 92% SF 8%	α 8.24	^{235}U(^{16}O,5n) ^{239}Pu(^{12}C,5n)
247[a]	35 s	α ≥ 50% EC ≤ 50%	α 7.93 (~ 30%) 7.87 (~70%)	^{239}Pu(^{12}C,4n)
247[a]	9.2 s	α	α 8.18	^{239}Pu(^{12}C,4n)
248	36 s	α 99.9% SF 0.1%	α 7.87 (80%) 7.83 (20%)	^{240}Pu(^{12}C,4n)
249	2.6 min	α	α 7.53	^{238}U(^{16}O,5n) ^{249}Cf(α,4n)
250	30 min	α SF 5.7×10^{-4}%	α 7.43	^{249}Cf(α,3n) ^{238}U(^{16}O,4n)
250 m	1.8 s	IT		^{249}Cf(α,3n)

Nuclear properties of fermium isotopes. (*Contd.*)

Mass number	*Half-life*	*Mode of decay*	*Main radiations* (MeV)	*Method of production*
251	5.30 h	EC 98.2% α 1.8%	α 6.834 (87%) 6.783 (4.8%)	^{249}Cf(α,2n)
252	25.39 h	α SF 2.3×10^{-3}%	α 7.039 (84.0%) 6.998 (15.0%)	^{249}Cf(α,n)
253	3.0 d	EC 88% α 12%	α 6.943 (43%) 6.674 (23%) γ 0.272	^{252}Cf(α,3n)
254	3.240 h	α > 99% SF 0.0592%	α 7.192 (85.0) 7.150 (14.2%)	^{254m}Es daughter
255	20.07 h	α SF 2.4×10^{-5}%	α 7.022 (93.4%) 6.963 (5.0%)	^{255}Es daughter
256	2.63 h	SF 91.9% α 8.1%	α 6.915	^{256}Md daughter ^{256}Es daughter
257	100.5 d	α 99.79% SF 0.21%	α 6.695 (3.5%) 6.520 (93.6%) γ 0.241	multiple n capture
258	0.37 ms	SF		^{257}Fm(d,p)
259	1.5 s	SF		^{257}Fm(t,p)
260	4 ms	SF		^{260}Md decay product

[a] Not known whether ground-state nuclide or isomer.

Nuclear properties of mendelevium isotopes.

Mass number	*Half-life*	*Mode of decay*	*Main radiations* (MeV)	*Method of production*
245	0.4 s 0.9 ms	α SF	α 8.680	^{209}Bi(^{40}Ar,4n)
246	1.0 s	α	α 8.740	^{209}Bi(^{40}Ar,3n)
247	1.12 s 0.27 s	α 80% SF	α 8.424	^{209}Bi(^{40}Ar,2n)
248	7 s	EC ~ 80% α ~ 20%	α 8.36 (~25%) 8.32 (~75%)	^{241}Am(^{12}C,5n) ^{239}Pu(^{14}N,5n)
249	24 s	EC ≤ 80% α ≥ 20%	α 8.03	^{241}Am(^{12}C,4n)
250	52 s	EC 94% α 6%	α 7.830 (~25%) 7.750 (~75%)	^{243}Am(^{12}C,5n) ^{240}Pu(^{15}N,5n)
251	4.0 min	EC ≥ 94% α ≤ 6%	α 7.55	^{243}Am(^{12}C,4n) ^{240}Pu(^{15}N,4n)
252	2.3 min	EC > 50% α < 50%	α 7.73	^{243}Am(^{13}C,4n)
253	6 min	EC		^{238}U(^{19}F,4n)
254[a]	10 min	EC		^{253}Es(α,3n)
254[a]	28 min	EC		^{253}Es(α,3n)
255	27 min	EC 92%	α 7.333	^{253}Es(α,2n)

Nuclear properties of mendelevium isotopes. (*Contd.*)

Mass number	*Half-life*	*Mode of decay*	*Main radiations* (MeV)	*Method of production*
		α 8%	γ 0.453	^{254}Es(α,3n)
256	1.27 h	EC 90.7% α 9.9%	α 7.205 (63%) 7.139 (16%)	^{253}Es(α,n)
257	5.52 h	EC 90% α 10%	α 7.069	^{254}Es(α,n)
258[a]	51.5 d	α	α 6.790 (28%) 6.716 (72%)	^{255}Es(α,n)
258[a]	57.0 min	EC ?		^{255}Es(α,n)
259	1.60 h	SF		^{259}No daughter
260	31.8 d	SF > 73% EC < 15%		^{254}Es(^{18}O,^{12}C)

[a] Not know whether ground state nuclide or isomer.

Nuclear properties of nobelium isotopes.

Mass number	*Half-life*	*Mode of decay*	*Main radiations* (MeV)	*Method of production*
250	0.25 ms 39.2 ms	SF SF		^{233}U(^{22}Ne,5n)
251	0.76 s	α	α 8.68 (20%) 8.60 (80%)	^{244}Cm(^{12}C,5n)
252	2.27 s	α 73% SF 27%	α 8.415 (∼ 75%) 8.372 (∼ 25%)	^{244}Cm(^{12}C,4n) ^{239}Pu(^{18}O,5n)
253	1.62 min	α	α 8.01	^{246}Cm(^{12}C,5n) ^{242}Pu(^{16}O,5n)
254	51 s	α	α 8.086	^{246}Cm(^{12}C,4n) ^{242}Pu(^{16}O,4n)
254 m	0.28 s	IT		^{246}Cm(^{12}C,4n) ^{249}Cf(^{12}C,α3n)
255	3.1 min	α 61.4% EC 38.6%	α 8.121 (46%) 8.077 (12%)	^{248}Cm(^{12}C,5n) ^{249}Cf(^{12}C,α2n)
256	2.91 s	α ∼ 99.7% SF ∼ 0.3%	α 8.43	^{248}Cm(^{12}C,4n)
257	25 s	α	α 8.27 (26%) 8.22 (55%)	^{248}Cm(^{12}C,3n)
258	1.2 ms	SF		^{248}Cm(^{13}C,3n)
259	58 min	α ∼ 75% EC ∼ 25%	α 7.551 (22%) 7.520 (25%)	^{248}Cm(^{18}O,α3n)
260	106 ms	SF, α		^{254}Es(^{18}O,x)
262	5 ms	SF		^{262}Lr daughter

Nuclear properties of lawrencium isotopes.

Mass number	*Half-life*	*Mode of decay*	*Main radiations* (MeV)	*Method of production*
252	0.36 s	α	α 9.018 (75%)	^{256}Db daughter
253 m	1.5 s	α	α 8.722	^{257}Db daughter
253	0.57 s	α	α 8.794	^{257}Db daughter
254	13 s	α	α 8.460 (64%)	^{258}Db daughter
255	21.5 s	α, EC	α 8.43 (40%)	^{243}Am(^{16}O,4n)
			8.37 (60%)	^{249}Cf(^{11}B,5n)
256	25.9 s	α, EC	α 8.52 (19%)	^{243}Am(^{18}O,5n)
			8.43 (37%)	^{249}Cf(^{11}B,4n)
257	0.65 s	α, EC	α 8.86 (85%)	^{249}Cf(^{11}B,3n)
			8.80 (15%)	^{249}Cf(^{14}N,α2n)
258	3.9 s	α	α 8.621 (25%)	^{248}Cm(^{15}N,5n)
			8.595 (46%)	^{249}Cf(^{15}N,α2n)
259	6.2 s	α, SF	α 8.45	^{248}Cm(^{15}N,4n)
260	3.0 min	α, EC	α 8.03	^{248}Cm(^{15}N,3n)
261	39 min	SF		^{254}Es(^{22}Ne,x)
262	3.6 h	SF, EC		^{254}Es(^{22}Ne,x)

Nuclear properties of transactinide elements.

Mass number	*Half-life*	*Mode of decay*	*Main radiations* (MeV)	*Method of production*
rutherfordium (Rf)				
253	~ 48 μs	SF		^{206}Pb(^{50}Ti,3n)
254	22.3 μs	SF		^{206}Pb(^{50}Ti,2n)
255	1.64 s	α 48%	α 8.722 (94%)	^{207}Pb(^{50}Ti,2n)
		SF 52%		
256	6 ms	SF, α	α 8.79	^{208}Pb(^{50}Ti,2n)
257	4.7 s	α ~80%	α 9.012 (18%)	^{208}Pb(^{50}Ti,n)
		SF ~2%	8.977 (29%)	^{249}Cf(^{12}C,4n)
		EC ~18%		
258	12 ms	SF		^{246}Cm(^{16}O,4n)
259	3.1 s	α 93%	α 8.87 (~40%)	^{249}Cf(^{13}C,3n)
		SF 7%	8.77 (~60%)	^{248}Cm(^{16}O,5n)
260	20 ms	SF		^{248}Cm(^{16}O,4n)
261	75.5 s	α	α 8.28	^{248}Cm(^{18}O,5n)
	4.2 s	α, SF	8.52	
262	2.1 s	SF		^{248}Cm(^{18}O,4n)
	47 ms	SF		

Nuclear properties of transactinide elements. (*Contd.*)

Mass number	*Half-life*	*Mode of decay*	*Main radiations* (MeV)	*Method of production*
dubnium (Db)				
256	1.6 s	EC, α	α 9.014 (∼67%)	^{209}Bi(^{50}Ti,3n)
257	1.5 s	α, SF	α 8.967, 9.074	^{209}Bi(^{50}Ti,2n)
257 m	0.76 s	α, SF	9.163	^{209}Bi(^{50}Ti,2n)
258	4.4 s	α	α 9.19 9.07	^{262}Bh daughter
259	0.51 s	α	α 9.7	^{241}Am(^{22}Ne,4n)
260	1.5 s	α ≥ 90% SF ≤ 9.6% EC ≤ 2.5%	α 9.082 (25%) 9.047 (48%)	^{249}Cf(^{15}N,4n) ^{243}Am(^{22}Ne,5n)
261	1.8 s	α ∼ 75% SF ∼ 25%	α 8.93	^{243}Am(^{22}Ne,4n) ^{249}Bk(^{16}O,4n)
262	34 s	α > 67% SF + EC < 33%	α 8.66 (∼20%) 8.45 (∼80%)	^{249}Bk(^{18}O,5n)
263	27 s	α, SF	α 8.36	^{249}Bk(^{18}O,4n)
268	16 h	SF		115 decay product
seaborgium (Sg)				
258	2.9 ms	SF		^{209}Bi(^{51}V,2n)
259	0.48 s	α	α 9.62 (78%)	^{208}Pb(^{54}Cr,3n)
260	3.6 ms	α, SF	α 9.77 (83%)	^{208}Pb(^{54}Cr,2n)
261	0.23 s	α, SF	α 9.56 (60%)	^{208}Pb(^{54}Cr,n)
262	6.9 ms	α ≤ 22% SF > 78%		^{270}110 decay product
263	0.9 s	α	α 9.06 (90%)	^{249}Cf(^{18}O,4n)
	0.3 s	α	α 9.25	
265	7.4 s	α	α 8.84 (46%)	^{248}Cm(^{22}Ne,5n)
266	21 s	α	α 8.77, 8.52	^{248}Cm(^{22}Ne,4n)
bohrium (Bh)				
261	12 ms	α	α 10.10 (40%)	^{209}Bi(^{54}Cr,2n)
262	0.1 s	α	α 10.06, 9.91, 9.74	^{209}Bi(^{54}Cr,n)
	8.0 ms	α	α 10.37, 10.24	^{209}Bi(^{54}Cr,n)
264	1.0 s	α	α 9.48, 9.62	111 decay product
266	∼1 s	α	α 9.3	^{249}Bk(^{22}Ne,5n)
267	17 s	α	α 8.85	^{249}Bk(^{22}Ne,4n)
272	9.8 s	α	α 9.02	115 decay product
hassium (Hs)				
264	0.26 ms	α, SF	α 10.43	^{207}Pb(^{58}Fe,n)
265	1.7 ms	α	α 10.30 (90%)	^{208}Pb(^{58}Fe,n)
	0.8 ms	α	α 10.57 (63%)	^{208}Pb(^{58}Fe,n)

Nuclear properties of transactinide elements. (*Contd.*)

Mass number	*Half-life*	*Mode of decay*	*Main radiations* (MeV)	*Method of production*
266	2.3 ms	α	α 10.18	^{270}110 daughter
267	59 ms	α	α 9.88, 9.83, 9.75	^{271}110 daughter
269	14 s	α	α 9.23, 9.17	112 decay product
270	~4 s	α		^{248}Cm(^{26}Mg,4n)
meitnerium (Mt)				
266	1.7 ms	α	α 10.46, 11.74	^{209}Bi(^{58}Fe,n)
268	42 ms	α	α 10.10, 10.24	111 daughter
276	0.72 s	α	α 9.71	115 decay product
darmstadtium (Ds)				
267	3.1 μs	α	α 11.6	^{209}Bi(^{59}Co,n)
269	0.17 ms	α	α 11.11	^{208}Pb(^{62}Ni,n)
270	0.10 ms	α	α 11.03	^{207}Pb(^{64}Ni,n)
	6.0 ms	α	α 12.15	^{207}Pb(^{64}Ni,n)
271	56 ms	α	α 10.71	^{208}Pb(^{64}Ni,n)
	1.1 ms	α	α 10.74, 10.68	
273	0.15 ms	α	α 11.08	112 daughter
280	7.6 s	SF		114 decay product
roentgenium (Rg)				
272	1.6 ms	α	α 11.0	^{209}Bi(^{64}Ni,n)
280	3.6 s	α	α 9.75	115 decay product
element 112				
277	0.6 ms	α	α 11.65, 11.45	^{208}Pb(^{70}Zn,n)
283	3 min	α, SF		^{238}U(^{48}Ca,3n); 114 daughter
284	0.75 min	α	α 9.15	114 daughter
element 113				
284	0.48 s	α	α 10.00	115 daughter
element 114				
287	5 s	α	α 10.29	^{242}Pu(^{48}Ca,3n)
288	2.6 s	α	α 9.82	^{244}Pu(^{48}Ca,4n)
element 115				
288	87 ms	α	α 10.46	^{243}Am(^{48}Ca,3n)
element 116				
292	53 ms	α	α 10.53	^{248}Cm(^{48}Ca,4n)

Specific activities of actinide and transactinide nuclides.

Nuclide		*Major decay mode*[a]	*Half-life*[b]	S[c] (dis min^{-1} μg^{-1})	S[d] (Ci g^{-1})
Ac	206	α	33 ms	3.68×10^{18}	
		α	22 ms	5.50×10^{18}	
	207	α	22 ms	5.50×10^{18}	
	208	α	95 ms	1.27×10^{18}	
		α	25 ms	4.82×10^{18}	
	209	α	0.10 s	1.20×10^{18}	
	210	α	0.35 s	3.41×10^{17}	
	211	α	0.25 s	4.75×10^{17}	
	212	α	0.93 s	1.27×10^{17}	
	213	α	0.80 s	1.47×10^{17}	
	214	α	8.2 s	1.43×10^{16}	
	215	α	0.17 s	6.85×10^{17}	
	216	α	$\sim$ 0.33 ms	3.51×10^{20}	
	216 m	α	0.33 ms	3.51×10^{20}	
	217	α	69 ns	1.67×10^{24}	
	218	α	1.08 μs	1.06×10^{23}	
	219	α	11.8 μs	9.69×10^{21}	
	220	α	26.4 ms	4.31×10^{18}	
	221	α	52 ms	2.18×10^{18}	
	222	α	5.0 s	2.26×10^{16}	
	222 m	α	63 s	1.79×10^{15}	
	223	α	2.10 min	8.91×10^{14}	
	224	EC	2.78 h	1.12×10^{13}	
	225	α	10.0 d	1.29×10^{11}	5.80×10^{4}
	226	β^-	29.37 h	1.048×10^{12}	
	227	β^-	21.772 yr	1.6058×10^{8}	72.332
	228	β^-	6.15 h	4.96×10^{12}	
	229	β^-	62.7 min	2.91×10^{13}	
	230	β^-	122 s	8.92×10^{14}	
	231	β^-	7.5 min	2.41×10^{14}	
	232	β^-	119 s	9.67×10^{14}	
	233	β^-	145 s	7.41×10^{14}	
	234	β^-	44 s	2.43×10^{15}	
Th	209	α	3.8 ms	3.15×10^{19}	
	210	α	9 ms	1.3×10^{19}	
	211	α	37 ms	3.21×10^{18}	
	212	α	30 ms	3.94×10^{18}	
	213	α	140 ms	8.40×10^{17}	
	214	α	100 ms	1.17×10^{18}	
	215	α	1.2 s	9.71×10^{16}	
	216	α	28 ms	4.14×10^{18}	
	217	α	0.237 ms	4.87×10^{20}	
	218	α	0.109 μs	1.05×10^{24}	
	219	α	1.05 μs	1.09×10^{23}	
	220	α	9.7 μs	1.17×10^{22}	
	221	α	1.68 ms	6.75×10^{19}	

Specific activities of actinide and transactinide nuclides. (*Contd.*)

Nuclide		*Major decay mode*[a]	*Half-life*[b]	S^c (dis min^{-1} μg^{-1})	S^d (Ci g^{-1})
	222	α	2.8 ms	4.03×10^{19}	
	223	α	0.60 s	1.87×10^{17}	
	224	α	1.05 s	1.06×10^{17}	
	225	α	8.0 min	2.32×10^{14}	
	226	α	30.57 min	6.042×10^{13}	
	227	α	18.68 d	6.836×10^{10}	
	228	α	1.9116 yr	1.8208×10^{9}	820.20
	229	α	7.340×10^{3} yr	4.721×10^{5}	0.2127
	230	α	7.538×10^{4} yr	4.577×10^{4}	0.02062
	231	β^-	25.52 h	1.180×10^{12}	
	232	α	1.405×10^{10} yr	0.2435	1.097×10^{-7}
	233	β^-	22.3 min	8.03×10^{13}	
	234	β^-	24.10 d	5.140×10^{10}	
	235	β^-	7.1 min	2.50×10^{14}	
	236	β^-	37.5 min	4.72×10^{13}	
	237	β^-	5.0 min	3.52×10^{14}	
	238	β^-	9.4 min	1.87×10^{14}	
Pa	212	α	5.1 ms	2.32×10^{19}	
	213	α	5.3 ms	2.22×10^{19}	
	214	α	17 ms	6.88×10^{18}	
	215	α	14 ms	8.32×10^{18}	
	216	α	0.2 s	5.8×10^{17}	
	217 g	α	3.8 ms	3.04×10^{19}	
	217 m	α	1.08 ms	1.07×10^{20}	
	218	α	0.12 ms	9.57×10^{20}	
	219	α	53 ns	2.16×10^{24}	
	220	α	0.78 μs	1.46×10^{23}	
	221	α	5.9 μs	1.92×10^{22}	
	222	α	2.9 ms	3.89×10^{19}	
	223	α	5.1 ms	2.20×10^{19}	
	224	α	0.79 s	1.42×10^{17}	
	225	α	1.7 s	6.55×10^{16}	
	226	α	1.8 min	1.03×10^{15}	
	227	α	38.3 min	4.80×10^{13}	
	228	EC	22 h	1.39×10^{12}	
	229	EC	1.50 d	8.44×10^{11}	
	230	EC	17.4 d	7.24×10^{10}	
	231	α	3.276×10^{4} yr	1.049×10^{5}	0.04724
	232	β^-	1.31 d	9.54×10^{11}	
	233	β^-	26.967 d	4.6129×10^{10}	2.0779×10^{4}
	234	β^-	6.70 h	4.44×10^{12}	
	234m	β^-	1.17 min	1.52×10^{15}	
	235	β^-	24.5 min	7.25×10^{13}	
	236	β^-	9.1 min	1.94×10^{14}	
	237	β^-	8.7 min	2.02×10^{14}	

Specific activities of actinide and transactinide nuclides. (*Contd.*)

Nuclide		*Major decay mode*[a]	*Half-life*[b]	S[c] (dis min^{-1} μg^{-1})	S[d] (Ci g^{-1})
	238	β^-	2.3 min	7.62×10^{14}	
	239	β^-	106 min	1.64×10^{13}	
U	217	α	16 ms	7.21×10^{18}	
	218	α	1.5 ms	7.66×10^{19}	
	219	α	42 μs	2.72×10^{21}	
	222	α	1.0 μs	1.13×10^{23}	
	223	α	18 μs	6.24×10^{21}	
	224	α	0.9 ms	1.2×10^{20}	
	225	α	59 ms	1.89×10^{18}	
	226	α	0.35 s	3.17×10^{17}	
	227	α	1.1 min	1.67×10^{15}	
	228	α	9.1 min	2.01×10^{14}	
	229	EC	58 min	3.14×10^{13}	
	230	α	20.8 d	6.06×10^{10}	
	231	EC	4.2 d	2.99×10^{11}	
	232	α	68.9 yr	4.96×10^{7}	22.4
	233	α	1.592×10^{5} yr	2.139×10^{4}	9.724×10^{-3}
	234	α	2.455×10^{5} yr	1.381×10^{4}	6.223×10^{-3}
	235	α	7.038×10^{8} yr	4.798	2.161×10^{-6}
	235 m	IT	25 min	7.10×10^{13}	3.20×10^{7}
	236	α	2.3415×10^{7} yr	1.4361×10^{2}	6.4687×10^{-5}
	237	β^-	6.75 d	1.81×10^{11}	
	238	α	4.468×10^{9} yr	0.7462	3.361×10^{-7}
	239	β^-	23.45 min	7.447×10^{13}	
	240	β^-	14.1 h	2.06×10^{12}	
	242	β^-	16.8 min	1.03×10^{14}	
Np	226	EC, α	31 ms	3.57×10^{18}	
	227	EC, α	0.51 s	2.16×10^{17}	
	228	EC, α	61.4 s	1.79×10^{15}	
	229	α	4.0 min	4.56×10^{14}	
	230	α	4.6 min	3.94×10^{14}	
	231	EC	48.8 min	3.70×10^{13}	
	232	EC	14.7 min	1.22×10^{14}	
	233	EC	36.2 min	4.95×10^{13}	
	234	EC	4.4 d	2.82×10^{11}	
	235	EC	396.1 d	3.114×10^{9}	
	236	EC, β^-	22.5 h	1.31×10^{12}	
	236	EC	1.54×10^{5} yr	2.18×10^{4}	
	237	α	2.144×10^{6} yr	1.562×10^{3}	7.035×10^{-4}
	238	β^-	2.117 d	5.752×10^{11}	
	239	β^-	2.3565 d	5.1461×10^{11}	
	240	β^-	1.032 h	2.808×10^{13}	
	240 m	β^-	7.22 min	2.41×10^{14}	
	241	β^-	13.9 min	1.25×10^{14}	
	242	β^-	5.5 min	3.14×10^{14}	

Specific activities of actinide and transactinide nuclides. (*Contd.*)

Nuclide		*Major decay mode*[a]	*Half-life*[b]	S^c (dis min^{-1} μg^{-1})	S^d (Ci g^{-1})
	242	β^-	2.2 min	7.83×10^{14}	
	243	β^-	1.85 min	9.28×10^{14}	
	244	β^-	2.29 min	7.47×10^{14}	
Pu	228	α	1.1 s	1.0×10^{17}	
	230	EC, α	2.6 min	6.98×10^{14}	
	231	EC, α	8.6 min	2.10×10^{14}	
	232	EC	33.1 min	5.44×10^{13}	
	233	EC	20.9 min	8.57×10^{13}	
	234	EC	8.8 h	3.38×10^{12}	
	235	EC	25.3 min	7.02×10^{13}	
	236	α	2.858 yr	1.177×10^{9}	
	237	EC	45.2 d	2.71×10^{10}	
	238	α	87.7 yr	3.80×10^{7}	17.1
	239	α	2.411×10^4 yr	1.377×10^{5}	0.06203
	240	α	6.564×10^3 yr	5.037×10^{5}	0.2269
	241	β^-	14.35 yr	2.295×10^{8}	103.4
	242	α	3.733×10^5 yr	8.784×10^{3}	3.957×10^{-3}
	243	β^-	4.956 h	5.776×10^{12}	
	244	α	8.08×10^7 yr	4.02×10^{1}	1.81×10^{-5}
	245	β^-	10.5 h	2.70×10^{12}	
	246	β^-	10.84 d	1.087×10^{11}	
	247	β^-	2.27 d	5.17×10^{11}	
Am	232	EC	1.32 min	1.36×10^{15}	
	233	EC, α	3.2 min	5.60×10^{14}	
	234	EC, α	2.32 min	7.69×10^{14}	
	235	EC, α	10.3 min	1.72×10^{14}	
	236	EC, α	3.6 min	4.91×10^{14}	
	236	EC	2.9 min	6.10×10^{14}	
	237	EC	1.22 h	2.41×10^{13}	
	238	EC	1.63 h	1.79×10^{13}	
	239	EC	11.9 h	2.45×10^{12}	
	240	EC	50.8 h	5.71×10^{11}	
	241	α	432.2 yr	7.618×10^{6}	3.432
	242	β^-	16.02 h	1.794×10^{12}	
	242 m	IT	141 yr	2.33×10^{7}	
	243	α	7.37×10^3 yr	4.43×10^{5}	0.1996
	244	β^-	10.1 h	2.82×10^{12}	
	244 m	β^-	26 min	6.58×10^{13}	
	245	β^-	2.05 h	1.38×10^{13}	
	246	β^-	25.0 min	6.79×10^{13}	
	246	β^-	39 min	4.35×10^{13}	
	247	β^-	23.0 min	7.35×10^{13}	
Cm	238	EC	2.3 h	1.27×10^{13}	
	239	EC	2.9 h	1.00×10^{13}	

Specific activities of actinide and transactinide nuclides. (*Contd.*)

Nuclide		*Major decay mode*[a]	*Half-life*[b]	S^c (dis min^{-1} μg^{-1})	S^d (Ci g^{-1})
	240	α	27 d	4.47×10^{10}	
	241	EC	32.8 d	3.67×10^{10}	
	242	α	162.8 d	7.356×10^{9}	3.314×10^{3}
	243	α	29.1 yr	1.12×10^{8}	50.5
	244	α	18.10 yr	1.797×10^{8}	80.93
	245	α	8.5×10^{3} yr	3.81×10^{5}	0.172
	246	α	4.76×10^{3} yr	6.78×10^{5}	0.305
	247	α	1.56×10^{7} yr	2.06×10^{2}	9.28×10^{-5}
	248	α	3.48×10^{5} yr	9.19×10^{3}	4.14×10^{-3}
	249	β^-	64.15 min	2.613×10^{13}	
	250	SF	$\sim 8.3 \times 10^{3}$ yr	$\sim 3.82 \times 10^{5}$	
	251	β^-	16.8 min	9.10×10^{13}	
Bk	238	EC	2.4 min	7.31×10^{14}	
	240	EC	4.8 min	3.62×10^{14}	
	241	EC	4.6 min	3.8×10^{14}	
	242	EC	7.0 min	2.46×10^{14}	
	243	EC	4.5 h	6.36×10^{12}	
	244	EC	4.35 h	6.55×10^{12}	
	245	EC	4.94 d	2.39×10^{11}	
	246	EC	1.80 d	6.55×10^{11}	
	247	α	1.38×10^{3} yr	2.33×10^{6}	1.05
	248	β^-	23.7 h	1.18×10^{12}	
	248	decay not observed	>9 yr	$< 3.6 \times 10^{8}$	
	249	β^-	330 d	3.53×10^{9}	1.59×10^{3}
	250	β^-	3.217 h	8.648×10^{12}	
	251	β^-	55.6 min	2.99×10^{13}	
Cf	237	EC, SF	2.1 s	5.03×10^{16}	
	238	EC, SF	21 ms	5.01×10^{18}	
	239	α	39 s	2.69×10^{15}	
	240	α	1.06 min	1.64×10^{15}	
	241	α	3.8 min	4.56×10^{14}	
	242	α	3.7 min	4.66×10^{14}	
	243	EC	10.7 min	1.61×10^{14}	
	244	α	19.4 min	8.82×10^{13}	
	245	EC	45.0 min	3.79×10^{13}	
	246	α	35.7 h	7.92×10^{11}	
	247	EC	3.11 h	9.05×10^{12}	
	248	α	333.5 d	3.504×10^{9}	
	249	α	351 yr	9.08×10^{6}	4.09
	250	α	13.08 yr	2.426×10^{8}	109.3
	251	α	898 yr	3.52×10^{6}	1.59
	252	α	2.645 yr	1.190×10^{9}	536.2
	253	β^-	17.81 d	6.431×10^{10}	
	254	SF	60.5 d	1.89×10^{10}	

Specific activities of actinide and transactinide nuclides. (*Contd.*)

Nuclide		*Major decay mode*[a]	*Half-life*[b]	S^c (dis min^{-1} μg^{-1})	S^d (Ci g^{-1})
	255	β^-	1.4 h	1.95×10^{13}	
	256	SF	12.3 min	1.33×10^{14}	
Es	241	α	8 s	1.3×10^{16}	
	242	α	13.5 s	7.66×10^{15}	
	243	α	21 s	4.91×10^{15}	
	244	EC	37 s	2.77×10^{15}	
	245	EC	1.1 min	1.55×10^{15}	
	246	EC	7.7 min	2.20×10^{14}	
	247	EC	4.55 min	3.71×10^{14}	
	248	EC	27 min	6.23×10^{13}	
	249	EC	1.70 h	1.64×10^{13}	
	250[a]	EC	8.6 h	3.24×10^{12}	
	250[a]	EC	2.22 h	1.25×10^{13}	
	251	EC	33 h	8.40×10^{11}	
	252	α	471.7 d	2.438×10^{9}	1.098×10^{3}
	253	α	20.47 d	5.596×10^{10}	2.521×10^{4}
	254 g	α	275.7 d	4.138×10^{9}	1.864×10^{3}
	254 m	β^-	39.3 h	6.97×10^{11}	
	255	β^-	39.8 d	2.86×10^{10}	1.286×10^{4}
	256	β^-	25.4 min	6.42×10^{13}	
	256	β^-	7.6 h	3.57×10^{12}	
Fm	242	SF	0.8 ms	1.3×10^{20}	
	243	α	0.18 s	5.72×10^{17}	
	244	SF	3.3 ms	3.11×10^{19}	
	245	α	4.2 s	2.43×10^{16}	
	246	α	1.1 s	9.25×10^{16}	
	247	α	35 s	2.90×10^{15}	
	247	α	9.2 s	1.10×10^{16}	
	248	α	36 s	2.80×10^{15}	
	249	α	2.6 min	6.45×10^{14}	
	250	α	30 min	5.56×10^{13}	
	250 m	IT	1.8 s	5.56×10^{16}	
	251	EC	5.30 h	5.23×10^{12}	
	252	α	25.39 h	1.087×10^{12}	
	253	EC	3.0 d	3.82×10^{11}	
	254	α	3.240 h	8.451×10^{12}	
	255	α	20.07 h	1.359×10^{12}	6.122×10^{5}
	256	SF	2.63 h	1.03×10^{13}	
	257	α	100.5 d	1.122×10^{10}	5.054×10^{3}
	258	SF	0.37 ms	2.62×10^{20}	
	259	SF	1.5 s	6.44×10^{16}	
	260	SF	4 ms	2.4×10^{19}	
Md	245	α	0.4 s	2.6×10^{17}	
		SF	0.9 ms	1.14×10^{20}	

Specific activities of actinide and transactinide nuclides. (*Contd.*)

Nuclide		*Major decay mode*[a]	*Half-life*[b]	S^c (dis min^{-1} μg^{-1})	S^d (Ci g^{-1})
	246	α	1.0 s	1.02×10^{17}	
	247	α	1.12 s	9.05×10^{16}	
	248	EC	7 s	1.4×10^{16}	
	249	EC	24 s	4.19×10^{15}	
	250	EC	52 s	1.93×10^{15}	
	251	EC	4.0 min	4.16×10^{14}	
	252	EC	2.3 min	7.20×10^{14}	
	253	EC	6 min	2.8×10^{14}	
	254	EC	10 min	1.64×10^{14}	
	254	EC	28 min	5.87×10^{13}	
	255	EC	27 min	6.06×10^{13}	
	256	EC	1.27 h	2.14×10^{13}	
	257	EC	5.52 h	4.90×10^{12}	
	258	α	51.5 d	2.18×10^{10}	
	258	EC	57.0 min	2.84×10^{13}	
	259	SF	1.60 h	1.68×10^{13}	
	260	SF	31.8 d	3.50×10^{10}	
No	250	SF	0.25 ms	4.01×10^{20}	
		SF	39.2 ms	2.55×10^{18}	
	251	α	0.76 s	1.25×10^{17}	
	252	α	2.27 s	4.38×10^{16}	
	253	α	1.62 min	1.02×10^{15}	
	254	α	51 s	1.93×10^{15}	
	254 m	IT	0.28 s	3.52×10^{17}	
	255	α	3.1 min	5.28×10^{14}	
	256	α	2.91 s	3.36×10^{16}	
	257	α	25 s	3.90×10^{15}	
	258	SF	1.2 ms	8.09×10^{19}	
	259	α	58 min	2.78×10^{13}	
	260	SF, α	106 ms	9.08×10^{17}	
	262	SF	5 ms	1.9×10^{19}	
Lr	252	α	0.36 s	2.76×10^{17}	
	253 m	α	1.5 s	6.60×10^{16}	
	253	α	0.57 s	1.74×10^{17}	
	254	α	13 s	7.58×10^{15}	
	255	α, EC	21.5 s	4.57×10^{15}	
	256	α, EC	25.9 s	3.78×10^{15}	
	257	α, EC	0.65 s	1.50×10^{17}	
	258	α	3.9 s	2.49×10^{16}	
	259	α, SF	6.2 s	1.56×10^{16}	
	260	α, EC	3.0 min	5.35×10^{14}	
	261	SF	39 min	4.10×10^{13}	
	262	SF, EC	3.6 h	7.37×10^{12}	
Rf	253	SF	$\sim$ 48 μs	$\sim 2.1 \times 10^{21}$	
	254	SF	22.3 μs	4.42×10^{21}	

Specific activities of actinide and transactinide nuclides. (*Contd.*)

Nuclide		*Major decay mode*[a]	*Half-life*[b]	S^c (dis min^{-1} μg^{-1})	S^d (Ci g^{-1})
	255	α	1.64 s	5.99×10^{16}	
	256	SF, α	6 ms	1.63×10^{19}	
	257	α	4.7 s	2.07×10^{16}	
	258	SF	12 ms	8.08×10^{18}	
	259	α	3.1 s	3.12×10^{16}	
	260	SF	20 ms	4.82×10^{18}	
	261	α	75.5 s	1.271×10^{15}	
		α, SF	4.2 s	2.28×10^{16}	
	262	SF	2.1 s	4.55×10^{16}	
		SF	47 ms	2.03×10^{18}	
Db	256	EC, α	1.6 s	6.11×10^{16}	
	257	α, SF	1.5 s	6.50×10^{16}	
	257 m	α, SF	0.76 s	1.28×10^{17}	
	258	α	4.4 s	2.21×10^{16}	
	259	α	0.51 s	1.90×10^{17}	
	260	α	1.5 s	6.42×10^{16}	
	261	α	1.8 s	5.33×10^{16}	
	262	SF	34 s	2.81×10^{15}	
	263	α, SF	27 s	3.53×10^{15}	
	268	SF	16 h	1.62×10^{12}	
Sg	258	SF	2.9 ms	3.35×10^{19}	
	259	α	0.48 s	2.01×10^{17}	
	260	α	3.6 ms	2.67×10^{19}	
	261	α, SF	0.23 s	4.17×10^{17}	
	262	SF	6.9 ms	1.38×10^{19}	
	263	α	0.9 s	1.06×10^{17}	
		α	0.3 s	3.2×10^{17}	
	265	α	7.4 s	1.28×10^{16}	
	266	α	21 s	4.48×10^{15}	
Bh	261	α	12 ms	8.0×10^{18}	
	262	α	0.1 s	9.6×10^{17}	
		α	8.0 ms	1.19×10^{19}	
	264	α	1.0 s	9.5×10^{16}	
	266	α	~1 s	9.4×10^{16}	
	267	α	17 s	5.52×10^{15}	
	272	α	9.8 s	9.40×10^{15}	
Hs	264	α	0.26 ms	3.65×10^{20}	
	265	α	1.7 ms	5.56×10^{19}	
		α	0.8 ms	1.18×10^{20}	
	266	α	2.3 ms	4.09×10^{19}	
	267	α	59 ms	1.59×10^{18}	
	269	α	14 s	6.65×10^{15}	
	270	α	~4 s	$\sim 2.3 \times 10^{16}$	

Specific activities of actinide and transactinide nuclides. (*Contd.*)

Nuclide		*Major decay mode*[a]	*Half-life*[b]	S^c (dis min^{-1} μg^{-1})	S^d (Ci g^{-1})
Mt	266	α	1.7 ms	5.54×10^{19}	
	268	α	42 ms	2.22×10^{18}	
	276	α	0.72 s	1.26×10^{17}	
Ds	267	α	3.1 μs	3.02×10^{22}	
	269	α	0.17 ms	5.47×10^{20}	
	270	α	0.10 ms	9.27×10^{20}	
		α	6.0 ms	1.54×10^{19}	
	271	α	56 ms	1.65×10^{18}	
		α	1.1 ms	8.40×10^{19}	
	273	α	0.15 ms	6.11×10^{20}	
	280	SF	7.6 s	1.18×10^{16}	
Rg	272	α	1.6 ms	5.75×10^{19}	
	280	α	3.6 s	2.48×10^{16}	
112	277	α	0.6 ms	1.51×10^{20}	
	283	SF	3 min	4.9×10^{14}	
	284	α	0.75 min	1.96×10^{15}	
113	284	α	0.48 s	1.84×10^{17}	
114	287	α	5 s	1.7×10^{16}	
	288	α	2.6 s	3.34×10^{16}	
115	288	α	87 ms	1.00×10^{18}	
116	292	α	53 ms	1.62×10^{18}	

[a] Decay modes are denoted by: α for alpha decay, β^- for beta decay, EC for electron capture, IT for isomeric transition, and SF for spontaneous fission. The decay mode given in this column represents either the major decay mode or the only observed decay mode.
[b] 1 year = 365.243 days.
[c] Specific activity is given in units of disintegrations per minute per microgram and contains one more significant figure than the half-life in order to avoid rounding-off errors.
[d] For commonly used isotopes, specific activities are also given in units of Curies per gram. 1 Ci = 2.22×10^{12} disintegrations per minute = 3.7×10^{10} Bq.

SUBJECT INDEX

Vol. 1: 1–698, Vol. 2: 699–1395, Vol. 3: 1397–2111, Vol. 4: 2113–2798, Vol. 5: 2799–3440.

Page numbers suffixed by t and f refer to Tables and Figures respectively.

Vol. 1: 1–698, Vol. 2: 699–1395, Vol. 3: 1397–2111, Vol. 4: 2113–2798, Vol. 5: 2799–3440

Vol. 1: 1–698, Vol. 2: 699–1395, Vol. 3: 1397–2111, Vol. 4: 2113–2798, Vol. 5: 2799–3440

AUTHOR INDEX

Vol. 1: 1–698, Vol. 2: 699–1395, Vol. 3: 1397–2111, Vol. 4: 2113–2798, Vol. 5: 2799–3440.

Page numbers suffixed by t and f refer to Tables and Figures respectively.